Polyhedron Vol. 7, No. 1, pp. 1–4, 1988
Printed in Great Britain

0277–5387/88 $3.00+.00
© 1988 Pergamon Journals Ltd

ALKALI METAL COMPLEXES: MIXED LIGAND COMPLEXES OF ALKALI METAL SALTS OF SOME ORGANIC ACIDS WITH PICOLINIC ACID N-OXIDE AND QUINALDINIC ACID N-OXIDE

DHARM PRAKASH* and SHANKAR PRASAD SINGH

Department of Chemistry, Patna University, Patna-5, India

(*Received* 5 *February* 1987; *accepted after revision* 10 *June* 1987)

Abstract—A number of mixed ligand complexes of alkali metal salts of *o*-nitrophenol, 1-nitroso-2-naphthol and 8-hydroxyquinoline has been synthesized and characterized. IR studies indicate the presence of hydrogen bonding. Ease of complexation as well as the yield has been found to increase with the increase in radius of alkali metal cations. Low values of their molar conductivities suggest that they are non-electrolytes.

In an attempt to explore the mechanism of selective absorption of alkali metal ions by plants, with the assumption that a knowledge of coordination chemistry of the alkali metals would facilitate fuller understanding of the mechanism, our attention has been drawn to the ligands, picolinic acid N-oxide and quinaldinic acid N-oxide. Previous authors have reported the behaviour of picolinic acid N-oxide[1–5] (henceforth designated as HPicO) with various transition and non-transition metals; but no alkali metal complex with this ligand has been reported as yet. A literature survey also reveals that the ligand quinaldinic acid N-oxide (hereafter abbreviated as HQuinO), which has two possible coordination sites, has remained neglected and no attempt has yet been made to examine its chelating ability. The present investigation has been undertaken to examine the behaviour of these N-oxides towards alkali metal salts and also to study whether they are more selective in comparison to the parent acids.

We have obtained a number of mixed ligand complexes with these ligands having the general formula $ML \cdot nHL'$ where M = Li, Na or K; L = deprotonated *o*-nitrophenol, 1-nitroso-2-naphthol or 8-hydroxyquinoline; HL′ = HPicO or HQuinO behave as bidentate ligands.

* Author to whom correspondence should be addressed.

EXPERIMENTAL

Preparation of HPicO

The ligand picolinic acid N-oxide was prepared by the method as described in the literature.[6]

Preparation of HQuinO

5 g of quinaldinic acid was dissolved in 20 cm^3 glacial acetic acid and 40 cm^3 hydrogen peroxide (30%) was added to it. The contents were refluxed on a water bath for about 2 h. On cooling, a voluminous light yellow precipitate was obtained. The contents were evaporated to dryness and the residue was recrystallized from methanol, when shining light yellow needles of quinaldinic acid N-oxide were obtained. These were filtered, washed with the solvent and dried in an electric oven at about 80°C.

Authenticity of the product so obtained was established by its m.p. determination, analytical data and IR spectrum. The decomposition temperature of the sample comes out to be 168–170° dec. which is in consonance with the reported value.[6–8] A very high yield (*ca.* 96%) was obtained and it took only 2 h to complete the reaction.

Preparation of the complexes

The complexes were synthesized by taking equimolar proportions of the alkali metal salt (ML) and

the ligand (HL′) in absolute ethanol with the ligand in slight excess. On refluxing with continuous stirring, a clear solution was obtained. On cooling it, the adduct separated and was filtered, washed with absolute ethanol and then dried in an electric oven at 80°C.

No adduct separated in the case of lithium salts of *o*-nitrophenol and 1-nitroso-2-naphthol. Our attempts to synthesize adducts of the title ligands with the corresponding alkali metal salts did not succeed, although such adducts have been obtained from picolinic acid[9] and quinaldinic acid.[10]

RESULTS AND DISCUSSION

The complexes of these ligands with alkali metal salts are characteristically coloured. Ease of their complexation with these salts was found to increase with the increase in radius of the alkali metal ions. Yield too showed similar trends. The colours, the decomposition/transition temperatures, conductivity values as well as the analytical data of these complexes are listed in Table 1.

These complexes are soluble in most polar solvents such as methanol, but are insoluble in non-polar solvents such as benzene, toluene and diethylether. They are stable when kept *in vacuo* or in a desiccator over anhydrous $CaCl_2$. On exposure to moisture, they appear to decompose rapidly to give the free ligand and the alkali metal salt.

They either decompose or undergo a transformation at temperatures which are considerably higher than the melting point of the corresponding ligand, indicating thereby their greater thermal stability.

Infrared spectra

Infrared measurements for the title ligands and their hitherto unknown mixed ligand complexes with alkali metals were made between 4000–650 cm^{-1} in Nujol mulls. Pertinent IR data for these compounds are recorded in Table 2.

The multiple bands that occur in the spectrum of the ligands HPicO and HQuinO indicate that in the solid state, they contain strong hydrogen bonds, possibly of the symmetrical type resulting in the dimer.[11] In the spectra of the complexes, these multiple bands have disappeared.

The spectra of all the complexes of HPicO contain a broad band in the region 2420–2320 cm^{-1}, while those of HQuinO exhibit the broad band in the region 2340–1850 cm^{-1}. The complex KONP·HPicO exhibits a broad band at 2700 cm^{-1} also. Likewise the IR spectrum of the complex Na1N2N·HQuinO exhibits two broad bands at

Table 1

Compound	Colour	M.p./decomp./ transition temp. (°C)	Conductivity (Ohm^{-1} cm^2 mol^{-1})	(%) Found				(%) Calculated			
				C	H	N	M	C	H	N	M
HPicO	Pale yellow	161 m	—	51.7	3.7	10.5	—	51.8	3.6	10.1	—
NaONP·HPicO	Yellow	202 t	3.0	48.4	3.5	9.3	7.6	48.0	3.0	9.3	7.7
KONP·HPicO	Orange	275 d	5.0	45.6	2.8	8.8	12.2	45.5	2.8	8.9	12.3
KONP·2HPicO	Yellow	185 t	7.0	48.0	3.5	9.2	8.8	47.4	3.1	9.2	8.5
Na1N2N·HPicO	Brown	200 t	4.0	57.6	3.5	8.3	7.0	57.4	3.3	8.3	6.9
K1N2N·HPicO	Brown	135 d	4.5	55.3	3.3	8.0	11.2	54.9	3.1	8.0	11.1
Li8HQ·HPicO	Cream coloured	172 t	3.5	62.0	3.8	9.8	—	62.0	3.8	9.6	—
Na8HQ·HPicO	Cream coloured	168 t	4.0	58.9	4.0	9.7	7.5	58.8	3.6	9.1	7.5
K8HQ·HPicO	Cream coloured	165 t	4.5	56.1	3.4	8.8	12.0	56.0	3.4	8.7	12.1
HQuinO	Light yellow	168–170 d	—	63.7	3.8	7.4	—	63.5	3.7	7.4	—
NaONP·HQuinO	Yellow	205 d	2.0	54.9	3.8	8.0	6.5	54.8	3.1	8.0	6.6
KONP·HQuinO	Deep yellow	215 t	2.5	52.0	3.5	7.6	10.5	52.4	3.0	7.6	10.6
KONP·2HQuinO	Yellow	202 d	3.5	56.9	3.6	7.5	7.0	56.2	3.2	7.5	7.0
Na1N2N·HQuinO	Brown	185 d	3.5	63.0	3.9	7.2	6.2	62.5	3.3	7.3	6.0
K1N2N·HQuinO	Brown	178 d	1.0	59.9	3.8	7.0	9.8	60.0	3.2	7.0	9.7
Li8HQ·HQuinO	Cream coloured	190 t	1.0	66.6	4.5	8.2	—	67.0	3.8	8.2	—
Na8HQ·HQuinO	Pale yellow	185 d	3.0	63.7	4.2	7.8	6.4	64.0	3.6	7.8	6.4
K8HQ·HQuinO	Pale yellow	180 d	3.5	61.2	4.0	7.5	10.5	61.2	3.5	7.5	10.4

HPicO = picolinic acid N-oxide; HQuinO = quinaldinic acid N-oxide; ONP = *o*-nitrophenol; 1N2N = 1-nitroso-2-naphthol, and 8HQ = 8-hydroxyquinoline.

Table 2

Compound	Selected IR absorption bands (cm^{-1})					
HPicO	2800–1850 w	1720 s	1680 s	1620 s	1295 s	1267 s
NaONP·HPicO	2300 br	1710 m	1670 m	1615 m	1290 s	1255 s
KONP·HPicO	2350 br	1710 m		1620 s	1280 m	1250 m
KONP·2HOicO	2320 br	1685 sh	1680 m	1620 s	1285 m	1240 m
Na1N2N·HPicO	2320 br	1690 s	1640 s	1602 s	1285 sh	1242 m
K1N2N·HPicO	2340 br	1700 s	1660 s	1605 s	1290 s	1250 s
Li8HQ·HPicO	2340 br	1715 m	1680 m	1620 m	1295 s	1260 s
Na8HQ·HPicO	2340 br	1715 m	1660 m	1615 m	1295 s	1265 m
K8HQ·HPicO	2400 br	1720 m	1660 m	1615 m	1290 s	1275 m
HQuinO	2800–1900 br		1680 br	1610 m	1300 m	1280 m
NaONP·HQuinO	2340 br	1	1660 sh	1620 m	1295 w	1280 m
KONP·HQuinO	1850 br		1650 sh	1615 m	1295 sh	1280 m
Na1N2N·HQuinO	2320 br		1640 s	1598 sh	1290 m	1270 s
K1N2N·HQuinO	2320 br		1625 s	1598 sh	1285 m	1268 s
Li8HQ·HQuinO	2340 br		1660 s	1615 m	1290 sh	1275 m
Na8HQ·HQuinO	1950 br		1660 sh	1610 br	1290 w	1275 m
K8HQ·HQuinO	—		1630 s	1610 sh	1290 sh	1275 s

2350 and 1950 cm^{-1}. Such a band is completely absent in the spectrum of the complex K8HQ·HQuinO. These bands could be assigned to O···H—O/N···H—O absorptions and suggest hydrogen bonding to be an essential feature of these complexes, which is in conformity with the observation of Nyholm *et al.*[12]

The bands at 1720 cm^{-1} and 1680 cm^{-1} that occur in the ligand HPicO have been assigned to asymmetric —COOH absorptions;[5] while the band at 1295 cm^{-1} is, in all probability, due to symmetrical stretching —COOH vibrations. The shifting of all these bands to lower frequencies by 5–30, 10–40 and 5 cm^{-1} respectively in almost all the complexes is indicative of the coordination through the oxygen atom of the —COOH group of the ligand. The 1680 cm^{-1} band, that occurs in the spectrum of the ligand HQuinO, may, in analogy with the assignments in the case of picolinic acid N-oxide,[5] be attributed to asymmetric CO_2 vibrations of the —COOH group. On complexation, this band shows a negative shift of 20–50 cm^{-1}. The 1280 cm^{-1} band of the spectrum of HQuinO, due to symmetrical stretching —COOH vibrations, has either remained unaffected or has shifted to lower frequencies by 5 cm^{-1}.

In the spectra of the HPicO complexes, the 1620 cm^{-1} band of the ligand, assigned to $\nu CC + \nu CN$ absorption,[5] has shifted to lower frequencies by 5–18 cm^{-1}; while in those of HQuinO complexes, the 1610 cm^{-1} band of the ligand has either remained unaffected or shifted to higher frequency by 5–10 cm^{-1}.

The 1267 cm^{-1} band of the ligand HPicO, which is attributed to the stretching N–oxide vibrations, has shifted to lower frequencies in the complexes by 7–17 cm^{-1}. Likewise, the 1300 cm^{-1} band of medium intensity in the HQuinO spectrum ascribed to the stretching N—O vibrations has shifted to lower frequencies by 5-10 cm^{-1}. These features suggest the coordination of these ligands with the alkali metals.

The 1267 cm^{-1} band of the ligand HPicO, which is attributed to the stretching N-oxide vibrations, has shifted to lower frequencies in the complexes by 7–17 cm^{-1}. Likewise, the 1300 cm^{-1} band of medium intensity in the HQuinO spectrum ascribed to the stretching N—O vibrations has shifted to lower frequencies by 5–10 cm^{-1}. These features suggest the coordination of these ligands with the alkali metals through the oxygen atom of the N-oxide moiety. Similar shifts have also been observed in the case of complexes of the ligand picolinic acid N-oxide with transition metal cations.[3–5]

The band at 847 cm^{-1}, that occurs in the spectrum of HPicO, has been assigned to the bending N—O vibrations,[5] but no appreciable change in the position of this band appears to take place on complexation.

Conductivities

Molar conductivities of all the complexes were measured in methanol at 25°C at a concentration of 10^{-3} M.

A value of *ca.* 35–40 Ohm^{-1} cm^2 mol^{-1} cor-

responds to a 1 : 1 electrolyte.[13] From the results (Table 1), it is evident that the molar conductivity values of none of the complexes approach either ideal or 1 : 1 electrolytes. However, fairly low values of molar conductivities of these complexes suggests that they are non-electrolytes.

REFERENCES

1. B. Chatterjee, *J. Ind. Chem. Soc.* 1976, **53**, 1212.
2. Heller, *Bull. Res. Coun. Israel* 1960, **9A**, 245; 1961, **10A**, 7.
3. A. B. P. Lever, J. Lewis and R. S. Nyholm, *Proc. 7ICCC*, Stockholm and Uppsala, Sweden, 1962, 49.
4. A. B. P. Lever, J. Lewis and R. S. Nyholm, *J. Chem. Soc.* 1962, 5262.
5. T. J. Delia, M. A. Little and D. X. West, *J. Inorg. Nucl. Chem.* 1973, **35**, 1400.
6. Otto Diels, Kurt Adler, W. Friedrichsen, Petersen, Brodersen and Kech, *Ann.* 1934, **510**, 87.
7. Yoshiki Hamada, *Yakugaku Zasshi* 1959, **79**, 908.
8. M. Hamana and M. Yamazaki, *Chem. Pharm. Bull. (Tokyo)* 1962, **10**, 51; *Chem. Abstr.* 1963, **58**, 504d.
9. A. K. Banerjee, D. Prakash and S. K. Roy, *J. Ind. Chem. Soc.* 1976, **53**, 773.
10. D. Prakash and S. P. Singh, *Polyhedron* 1984, **3**, 243.
11. M. Szafran, *Bull. Acad. Polon Sci. Ser. Sci. Chim.* 1965, **13**, 245.
12. A. K. Banerjee, A. J. Layton, R. S. Nyholm and M. R. Truter, *J. Chem. Soc. (A)* 1970, 292.
13. A. K. Banerjee, A. J. Layton, R. S. Nyholm and M. R. Truter, *J. Chem. Soc. (A)* 1969, 2536.

Polyhedron Vol. 7, No. 1, pp. 5–9, 1988
Printed in Great Britain

0277–5387/88 $3.00+.00
© 1988 Pergamon Journals Ltd

COMPLEX FORMATION BETWEEN In(III) AND 2-MERCAPTOPROPANOIC ACID IN 3.0 M $NaClO_4$ AT 25°C

M. AGUILAR and A. FLORIDO*

Departament de Química, Escola Tècnica Superior d'Enginyers Industrials, Universitat Politècnica de Catalunga, E-08028 Barcelona, Spain

and

S. ALEGRET and M. VALIENTE*

Departament de Química, Facultat de Ciències, Universitat Autònoma de Barcelona, E-08193 Bellaterra, Spain

(*Received* 28 *May* 1987; *accepted* 10 *June* 1987)

Abstract—Complex formation reactions between In(III) and 2-mercaptopropanoic acid (H_2A) have been studied in 3.0 M $NaClO_4$ at 25°C, by measuring the EMF of the glass and In(Hg) electrodes as a function of the acidity of the solution. At $-\log|H^+| > 5.5$ the formation of a precipitate is observed. The EMF data obtained in the range $1 < -\log|H^+| < 5.5$, treated by the general minimizing program LETAGROP, can be explained by assuming the formation of the species InA^+, $InA(OH)$ and $InA(OH)_2^-$. A reaction equation is proposed and the formation constants for these species are given.

Simple aliphatic mercaptoacids have been studied as possible masking agents in analytical processes, sometimes as substitutive of potassium cyanide,[1–6] as well as simple coordination models which are present in some complex molecules of biological interest.[7]

The analytical work so far published deals mainly with qualitative aspects of many reactions with metals which are very interesting from the analytical point of view.

The information on the stoichiometry and equilibrium constants of these reactions is scanty. Studies of complex formation with divalent ions, which favour the formation of mononuclear species, show a high stability of the reaction products.[8,9] In other cases,[10,11] a precipitate appears which can be redissolved via polynuclear complex formation.

The existence of different reaction products introduces some difficulties in the analytical applications of this type of reaction. However, a detailed study of the system will elucidate the conditions where the analytical applications are successful.

In this context, a detailed study on the complexation of these acids with mono or trivalent cations has been undertaken in our laboratory.[12] The results on In(III)-2-mercaptopropanoic acid are reported here. Mono and trivalents cations have been chosen because of the lack of information in these systems which are of great analytical interest.

EXPERIMENTAL

Reagents, solutions and electrodes

2-Mercaptopropanoic acid, $CH_3CH(SH)COOH$, Fluka, p.a., was purified and determined as reported before.[10] A $In(ClO_4)_3$ stock solution was prepared as described elsewhere.[13] This solution was analysed by electrodeposition of metallic In on a Pt net coated with Cu[14] in a buffered oxalic acid/oxalate medium. The H^+ content of the $In(ClO_4)_3$ solution was determined potentiometrically. $NaClO_4$, $HClO_4$ and NaOH solutions were prepared and analysed according to recommended methods.[15]

Ag(s)/AgCl(s) reference electrode was prepared according to Brown.[16] The In(Hg) electrode was

* Authors to whom correspondence should be addressed.

prepared *in situ* for each titration by electrolytic reduction of In^{3+} in a mercury cathode,[17] until the indium concentration in the amalgam attained 0.02% (w/w). A glass electrode Radiometer G202C was used.

Apparatus

The EMF measurements were carried out with a Radiometer PHM 64 potentiometer with an accuracy of ± 0.1 mV. These measurements were monitored by means of an automatic system controlled by a microprocessor made in our laboratory. The equilibrium was considered when two consecutive EMF readings within 10 min did not differ by more than ± 0.2 mV. A Metrohm Herisau E211A coulometer was used for the "E_{oA} titration". All measurements were carried out in a thermostated bath at 25 ± 0.1°C.

EMF measurements

The complex formation equilibria were studied from EMF measurements using potentiometric titration techniques. The composition of the test solutions can be represented as:

$$TS = \mathbf{B}\,\text{mM In(III)}, \mathbf{A}\,\text{mM } H_2A, \mathbf{H}\,\text{mM } H^+, 3.0\,\text{M } ClO_4^-.$$

In each experiment the total concentration of In(III) and 2-mercaptopropanoic acid were kept constant while the H^+ concentration varied stepwise from $10^{-5.5}$ to 10^{-1} M. To vary $[H^+]$, equal volumes of the following solutions were added:

$$T_1 = 2\mathbf{B}\,\text{mM In(III)}, \mathbf{H}_1\,\text{mM } H^+, 3.0\,\text{M } ClO_4^-$$

$$T_2 = 2\mathbf{A}\,\text{mM } H_2A, \mathbf{H}_2\,\text{mM } H^+, 3.0\,\text{M } ClO_4^-.$$

The free concentrations of In^{3+} and H^+ of the test solution *TS* were determined by measuring the EMF of the cells:

$$\text{R.E./3.0 M } NaClO_4\,//\,\text{TS/G.E.} \quad \text{(I)}$$

$$\text{In(Hg)/TS}\,//\,\text{3.0 M } NaClO_4\text{/R.E.} \quad \text{(II)}$$

where R.E. is the reference electrode:

Ag(s), AgCl(s)/2999 mM $NaClO_4$, 1 mM $AgClO_4$,

G.E. is the glass electrode and In(Hg) the In(s) amalgam electrode. The sign // denotes the presence of a salt bridge of the Wilhelm type.[18]

The EMF of the cells I and II in mV at 25°C can be written as:

$$E_A = E_{oA} + 59.16 \log [H^+] + E_{jA} = E_{oA} + 59.16 \log \mathbf{h} + E_{jA} \quad (1)$$

$$E_B = E_{oB} + 19.72 \log [In^{3+}] + E_{jB} = E_{oB} + 19.72 \log \mathbf{b} + E_{jB}. \quad (2)$$

E_{oA} and E_{oB} were determined coulometrically and volumetrically, respectively, at the beginning of each experiment using the Gran functions.[19] E_{jB} and E_{jA} were determined in free ligand test solutions. E_{jB} was negligible in our experimental conditions while E_{jA} had only a significant value when $-\log \mathbf{h} < 2$.

Dissociation equilibrium of 2-mercaptopropanoic acid

The study of the dissociation equilibria of 2-mercaptopropanoic acid in 3.0 M $NaClO_4$ at 25°C was carried out previously to study complex formation.

This study was done following an experimental technique similar to the formerly explained. In this case measurements were done in absence of metal.

The data collected in the form (V_{T1}, V_{T2}, E_A) were treated by means of LETAGROP program[20] and could be explained by the following reactions:

$$H^+ + A^{2-} \rightleftharpoons HA^- \quad \log \beta_{101} = 10.12 \pm 0.02$$

$$2H^+ + A^{2-} \rightleftharpoons H_2A \quad \log \beta_{201} = 14.06 \pm 0.02.$$

These values agree with those obtained by us under another condition.[21]

RESULTS AND CALCULATIONS

Complex formation equilibria

Different titrations were carried out in which the analytical concentration of In(III) and 2-mercaptopropanoic acid were varied (2, 5 and 10 mM, and 15, 25 and 40 mM, respectively). The experimental data were taken in the form of (V_{T1}, V_{T2}, E_A, $E_B)_{B,A}$. The reversibility of the chemical equilibria was tested by titrating the test solution *TS* in two ways, i.e. first with an acid and then with an alkali, until a white precipitate was observed. The potential values agreed for each $-\log [H^+]$.

The complex formation equilibria between In(III) and 2-mercaptopropanoic acid can be written as follows:

$$pH^+ + qIn^{3+} + rA^{2-} \rightleftharpoons H_pIn_qA_r. \quad (3)$$

The formation constants for the different species can be defined as:

$$\beta_{pqr} = [H_pIn_qA_r]\mathbf{h}^{-p}\mathbf{b}^{-q}\mathbf{a}^{-r} \quad (4)$$

where **b**, **a** and **h** represent the free concentrations of In^{3+}, A^{2-} and H^+, respectively.

The experimental data were converted into

$(\eta, -\log \mathbf{h})_A$ pairs, being:

$$\eta = \log(\mathbf{B}/\mathbf{b}) \quad (5)$$

where **b** was calculated from eq. 2.

Mass equilibrium equations give the following general equation:

$$\eta = \log(1 + \Sigma q\beta_{pqr}\mathbf{b}^{q-1}\mathbf{a}'\mathbf{h}^p). \quad (6)$$

If η is plotted vs $-\log \mathbf{h}$ when the total concentration of the ligand is constant, the curves superimpose practically for low metal concentrations. It infers that η is independent of **b**, and this happens when $q = 1$ (mononuclear species) (cf. eq. 6). When the total concentration of the metal is increased, at $-\log h > 3$ the curves present a small deviation. This indicates that from this value the formation of polynuclear complexes is probable.

Numerical analysis of the data

In order to ascertain the composition of the different complexes, i.e. the different (p, q, r) values, as well as the best values for the formation constants, numerical calculations were performed using the NYTIT version[22] of the general minimizing program LETAGROP.[20] Taking sets of data $(V_{T1}, V_{T2}, E_A, E_B)_{B,A}$ and the composition of the T_i solutions of the different burets as input data, the program considered that the best set of equilibrium constants is that which minimizes the error square sum U:

$$U = \Sigma_{Np} w(E_{B,calc} - E_{B,exp})^2. \quad (7)$$

In this equation Np represents the number of experimental points, w is the statistical weight ($w = 1$, in our case), $E_{B,calc}$ is the corresponding quantity calculated by the computer by assuming a set of chemical species and equilibrium constants, and $E_{B,exp}$ is the experimental EMF value.

Taking into account the preliminary results obtained from graphical treatment of the data, different sets of complexes were chosen in order to fit the experimental data. In this way, the value of U at the minimum and the mean standard deviation in E_B, $\sigma(E_B)$, were calculated for each set. The best models were chosen as those which gave the lowest values for U and $\sigma(E_B)$. The results of these calculations are given in Table 1. It can be seen that the combination of complexes (0, 1, 1), (−1, 1, 1) and (−2, 1, 1) gave the best values for U and $\sigma(E_B)$. It can also be seen that inclusions of protonated or polynuclear species in the calculation implied that they were rejected by the computer or that they led to a considerable increase in the U and $\sigma(E_B)$ values.

Table 1. U and $\sigma(E_B)$ values for the different (p, q, r) models tried by the program LETAGROP-NYTIT

Model	Complexes (p, q, r)	U	$\sigma(E_B)$ (mV)	Rejected species
1	(0, 1, 1)	0.431E+5	8.26	
2[a]	(0, 1, 1) (−1, 1, 1) (−2, 1, 1)	0.676E+2	1.59	
3	(0, 1, 1) (−1, 1, 1) (−2, 1, 1) (−1, 2, 1) (−4, 3, 1)	0.130E+4	4.60	(−1, 2, 1)
4	(1, 1, 2) (0, 1, 1) (−1, 1, 1) (−2, 1, 1)	0.672E+2	1.59	(1, 1, 2)

[a] This model represents the best fit of the experimental data.

The value of $\sigma(E_B) = 1.59$ mV indicates that the model represented by the equations:

$$In^{3+} + A^{2-} \rightleftharpoons InA^+$$

$$\log \beta_{011} = 13.12 \pm 0.09 \quad (8)$$

$$H_2O + In^{3+} + A^{2-} \rightleftharpoons InA(OH) + H^+$$

$$\log \beta_{-111} = 10.69 \pm 0.16 \quad (9)$$

$$2H_2O + In^{3+} + A^{2-} \rightleftharpoons InA(OH)_2^- + 2H^+$$

$$\log \beta_{-211} = 8.21 \pm 0.06 \quad (10)$$

refers to a 99.9% confidence level.

The fit to experimental data is illustrated graphically in Fig. 1, where the value $(E_{B,calc} - E_{B,exp})$ is plotted as a function of the $-\log \mathbf{h}$ for different

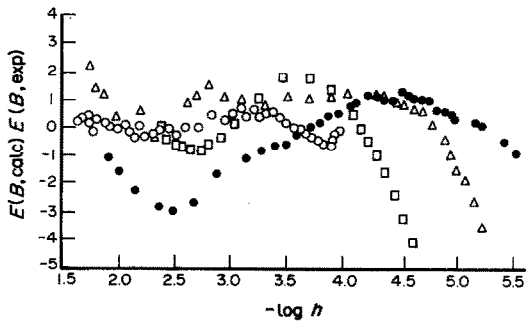

Fig. 1. $(E_{B,calc} - E_{B,exp})$ plotted as a function of $-\log \mathbf{h}$ at different metal to ligand ratios (○: **B** = 2 mM, **A** = 25 mM; ●: **B** = 2 mM, **A** = 40 mM; △: **B** = 5 mM, **A** = 40 mM; □: **B** = 10 mM, **A** = 41 mM).

concentrations of In(III). The EMF values represented in this figure seems to indicate the absence of any systematic deviation. It can be seen, however, that when the In(III) concentration exceeds the value of 5 mM, the deviations observed are higher than the mean values and this ratifies the fact, that for higher concentrations levels, the existence of polynuclear species is possible.

DISCUSSION

From the values of equilibrium constants reported in eqs (8–10), α_{pqr} was computed. The calculations performed with the program HALTAFALL,[23] are illustrated graphically in Fig. 2. This figure shows that the hydrolysis reactions of In(III) in the presence of 2-mercaptopropanoic acid in the range $1 < -\log \mathbf{h} < 5$ leads to soluble mixed hydrolytical species formally derived from the InA^+ complex, with the following general formula $InA(OH)_n^{1-n}$, with $n = 1$ or 2 in the present experimental conditions. These results follow the pattern postulated by Biedermann for the hydrolysis of In(III).[13] This author found the existence of mononuclear ions of the type $In(OH)_n^{3-n}$ ($n = 1$ or 2) which are formally similar to those found in present work.

The results of the present work can be easily expressed in terms of hydrolysis instead of formation constants. That is to say:

$$InA^+ + H_2O = InA(OH) + H^+ \qquad \log K_{-111} = -2.43$$

$$InA^+ + 2H_2O = InA(OH)_2^- + 2H^+ \qquad \log K_{-211} = -4.91$$

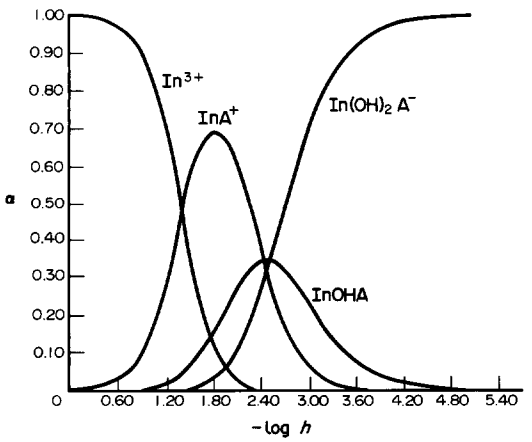

Fig. 2. Distribution of the species of the system In(III)-2-mercaptopropanoic acid in the form α_{pqr} vs $-\log \mathbf{h}$ when $\mathbf{B} = 2$ mM and $\mathbf{A} = 15$ mM.

because $\log K_{-n11} = \log \beta_{-n11} - \log \beta_{011}$ ($n = 1$ or 2). If we compare these values with the corresponding constants of hydrolysis of In(III) reported by Biederman:

$$In^{3+} + H_2O = In(OH)^{2+} + H^+ \quad \log K_{-110} = -4.25$$

$$In^{3+} + 2H_2O = In(OH)_2^+ + 2H^+ \quad \log K_{-210} = -8.53$$

we can conclude that the acidic properties of In^{3+} are enlarged when 2-mercaptotropanoic acid takes part in the coordination sphere of this ion. This fact has been observed in other systems.[24]

These results differ from those of Sarin and Munshi.[25] They claimed the formation of a series of complexes of general composition InA_n; n being 1, 2, 3. Although the formation constant for the first complex is of the same order of magnitude as that determined in this work [*vide* eq. (8)], the different experimental approach may explain the discrepancies. While, these authors titrated the metal solution up to pH = 10, we found around pH = 6 the formation of a white precipitate makes the EMF measurements extremely difficult. As the solid formation proceeds slowly it may be probable that under too fast titration procedures this reaction was not observed. This could indicate that Sarin and Munshi's data were collected before equilibrium was attained and consequently their results must be viewed with caution.

REFERENCES

1. E. Casassas and F. Buscarons, *Chim. Anal.* 1962, **44**, 20.
2. F. Buscarons and E. Casassas, *An. Quím.* 1959, **55B**, 655.
3. F. Buscarons and E. Casassas, *An. Quím.* 1959, **55B**, 663.
4. E. Casassas and J. Alsina, *An. Quím.* 1963, **59B**, 59.
5. A. M. Cabrera and T. S. West, *Talanta* 1962, **9**, 730.
6. R. Pribil and V. Vesely, *Talanta* 1961, **8**, 880.
7. M. Lamache-Duhameaux, *J. Inorg. Nucl. Chem.* 1976, **38**, 1979.
8. E. Casassas, *Arxius de la Secció de Ciències*, I.E.C. (1971).
9. W. Stricks, I. M. Kolthoff and A. Heyndrickx, *J. Am. Chem. Soc.* 1954, **76**, 1515.
10. M. Aguilar, S. Alegret and E. Casassas, *J. Inorg. Nucl. Chem.* 1977, **39**, 733.
11. M. Aguilar, S. Alegret and E. Casassas, *J. Inorg. Nucl. Chem.* 1978, **40**, 1903.
12. M. Valiente, M. Aguilar and E. Casassas, *Quím. Anal.* 1984, **3**, 71.
13. G. Biedermann, *Arkiv Kemi* 1956, **9**, 277.
14. H. Terrey and J. Thabit, *J. Chem. Soc.* 1958, 1303.
15. *Some Laboratory Methods*, Mimeograph, Department Inorg. Chem., Royal Inst. Technology, Stockholm (1959).
16. A. S. Brown, *J. Am. Chem. Soc.* 1934, **56**, 646.

17. D. Ferri, *Acta Chem. Scand.* 1972, **26**, 733.
18. W. Forsling, S. Heitanen and L. G. Sillén, *Acta Chem. Scand.* 1952, **6**, 901.
19. G. Gran, *Analyst* 1952, **77**, 661.
20. N. Ingri and L. G. Sillén, *Arkiv Kemi* 1965, **97**, 23.
21. M. Aguilar, M. Valiente and E. Casassas, *An. Quím.* 1978, **74**, 253.
22. B. Warnqvist, personal communication, 1974.
23. N. Ingri, W. Kakolowicz, L. G. Sillén and B. Warnqvist, *Talanta* 1967, **14**, 1261.
24. G. R. Lenz and A. E. Martell, *Inorg. Chem.* 1965, **4**, 378.
25. R. Sarin and K. N. Munshi, *J. Inorg. Nucl. Chem.* 1973, **35**, 201.

Polyhedron Vol. 7, No. 1, pp. 11–15, 1988
Printed in Great Britain

0277–5387/88 $3.00+.00
© 1988 Pergamon Journals Ltd

KINETICS AND MECHANISM OF THE OXIDATION OF L-METHIONINE BY AQUEOUS SOLUTION OF CHROMIUM(VI)

M. ADEGBOYEGA OLATUNJI* and G. ADEFIKAYO AYOKO

Department of Chemistry, Ahmadu Bello University, Zaria, Nigeria

(*Received* 7 *January* 1987; *accepted after revision* 19 *June* 1987)

Abstract—The kinetics of the reduction of Cr(VI) by L-methionine (represented by $RSCH_3$) have been studied in aqueous perchloric acid. The data are consistent with the rate law:

$$\frac{-d[Cr(VI)]}{dt} = (k_1 + k_2[H^+]^2[RSCH_3])[Cr(VI)]$$

with $k_1 = (3.1 \pm 0.5) \times 10^{-4}$ s^{-1}; $k_2 = 12.3 \pm 1.1$ mol^{-3} dm^9 s^{-1} at I = 1.0 mol dm^{-3} ($NaClO_4$), $[H^+] = 0.04$–0.10 mol dm^{-3} and T = 25.1°C. The corresponding activation parameters are $\Delta H_1^{\ddagger} = 26.2 \pm 0.4$ kJ mol^{-1}; $\Delta S_1^{\ddagger} = -224 \pm 1$ JK^{-1} mol^{-1}; $\Delta H_2^{\ddagger} = 33.9 \pm 0.01$ KJ mol^{-1}; $\Delta S_2^{\ddagger} = -111 \pm 1$ JK^{-1} mol^{-1}. The above rate is very much slower than those of other related reactions. This is interpreted in terms of a rate-determining Cr—S bonded intermediate which undergoes hydrolysis after electron transfer to yield Cr(III) and methionine sulphoxide. The significance of pathways involving second-order substrate dependence is also discussed.

Chromate ester formation is a common feature of chromium(VI) reduction by electron pair donors.[1–7] Presumably because of their medical significance,[8] more attention has been given to sulphur-bonded esters which are characterized by their formation constants and electronic spectra.[6,9] These intermediates are thought to provide low energy pathways for subsequent electron-transfer. Thus any factor that inhibits their formation is known to affect the reduction markedly.[10,11]

The reaction of Cr(VI) with L-methionine was investigated for several reasons. Firstly, L-methionine like L-cysteine[4] and other related thiols[1,2] has three coordinating centres *viz*: O, N and S. Of these, sulphur has been established as the most susceptible to attack by Cr(VI). However, this site is partially blocked by a methyl group within the substrate and it is therefore of interest to study the effect of this on the reactivity of the substrate. Secondly, although the reaction had been investigated by different workers[12,13] in the past, conflicting views had been expressed as to the nature of one of the final products. While one group[12] postulated a disulphide as one of the products of the reaction, the other group[13] was able to establish a sulphoxide as the corresponding final product. It is thought that the present investigation would be able to resolve the conflict and throw more light on the mechanism of the reaction.

EXPERIMENTAL

L-methionine (Koch-Light, Pure) was used without further purification. Potassium dichromate (Analar grade) was used for the kinetic runs while the sodium salt (B.D.H. Reagent) was used for the product analysis where concentrations were such as to cause precipitation of potassium perchlorate had the potassium salt been used. Mixtures of sodium perchlorate (Fluka, puriss) and perchloric acid (Analar Reagent) were used to maintain a constant ionic strength of 1.0 mol dm^{-3} at varying hydrogen ion concentrations $[H^+]$. Stock solutions of perchloric acid were analysed by titration against weighed quantities of sodium tetraborate.

* Author to whom correspondence should be addressed. Present address: Department of Chemistry, School of Science and Science Education, Federal University of Technology, Minna, Nigeria.

Kinetics

Under the conditions used for the kinetics $HCrO_4^-$ has been established[4] as the reacting species of the oxidant. Kinetic measurements were therefore made at 350 and 420 nm by monitoring the absorbance changes due to it on a Pye Unicam SP 8000 spectrophotometer with fully thermostated cell compartments. The concentration of the oxidant was kept constant at 4.0×10^{-4} mol dm^{-3} while L-methionine concentrations were varied between $(5.0–25.0) \times 10^{-3}$ mol dm^{-3} and the ionic strength of the medium was kept constant at 1.0 mol dm^{-3} using sodium perchlorate. Pseudo first-order plots were linear to more than three half lives and duplicate measurements agreed to $\pm 2\%$.

Products

The main product methionine sulphoxide was characterized as follows:

A reaction mixture containing 2.0×10^{-3} mol sodium dichromate, 2.5×10^{-2} mol methionine and 5.0×10^{-3} mol perchloric acid in a 50 cm^3 solution was allowed to stand for about 2 h. Thereafter 10 cm^3 of 0.4 mol dm^3 sodium bicarbonate was added and stirred vigorously followed by dropwise addition of benzoyl chloride solution until precipitation was completed. The precipitate obtained *N*-benzoyl methionine sulphoxide which is a derivative of methionine sulphoxide was confirmed by its melting point 183°C.[13] The yield obtained was about 70%.

A second method[14] for the characterization of the product was employed by adding an acetone–ethanol mixture (1 : 1 vol. ratio) to a similar reaction mixture as above which had previously been brought to pH 4. The precipitate of methionine sulphoxide was identified by its melting point which was found to be 238°C.[14] The yield obtained was about 86%.

RESULTS AND DISCUSSION

The linearity of the pseudo first-order plots implies that the reaction is first-order in Cr(VI). Representative values of the pseudo first-order constant, k_{obs} obtained at different methionine concentrations, hydrogen ion concentrations $[H^+]$, wavelength and ambient temperatures are shown in Table 1.

Plots of k_{obs} as a function of methionine concentration for different $[H^+]$ at constant temperature were linear with a common positive intercept (Fig. 1). The slopes of these lines vary linearly with the square of the hydrogen ion concentration $[H^+]^2$ (Fig. 2).

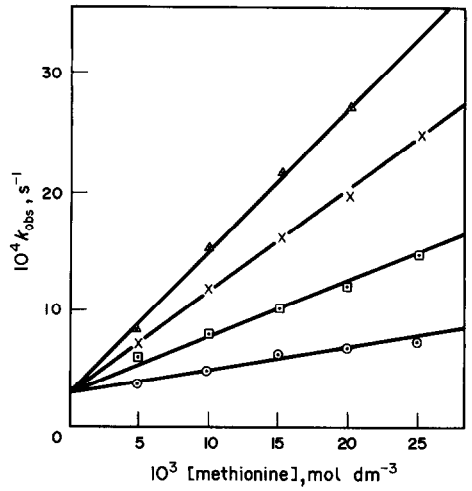

Fig. 1. The dependence of observed rate constant (k_{obs}) on the concentration of methionine at 25.1°C. $[Cr(VI)] = 4.0 \times 10^{-4}$ mol dm^{-3}; $I = 1.0$ mol dm^{-3} ($NaClO_4$); $[H^+] = 0.04$ mol dm^{-3} (⊙); $[H^+] = 0.06$ mol dm^{-3} (⊡); $[H^+] = 0.08$ mol dm^{-3} (×); $[H^+] = 0.10$ mol dm^{-3} (△).

From these results, the reaction is considered to proceed via two parallel pathways and the overall mechanism for the reaction can be represented by eqs (1)–(5). Under the conditions of the experiment, protonated methionine $CH_3SCH_2CH_2CH(\overset{+}{N}H_3)CO_2H$ represented as $RSCH_3$ is the predominant species in line with the argument presented elsewhere.[1,2,4,12] The mechanism is therefore given as:

$$HCrO_4^- + RSCH_3 \underset{}{\overset{K}{\rightleftharpoons}} R^1(CH_3)SCRo_3^- + H_2O \quad (1)$$

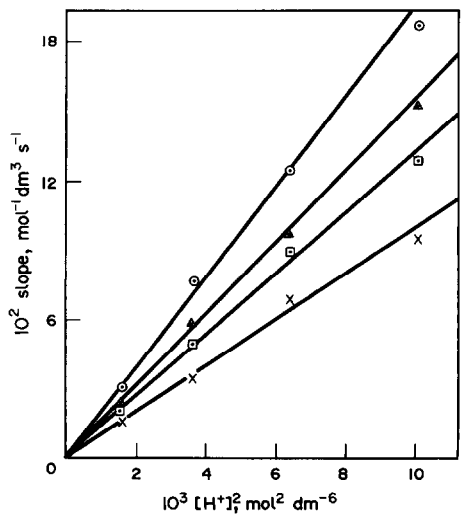

Fig. 2. Plots of slope [eq. (9)] as a function of $[H^+]^2$. = 20.1°C (⊙); 25.1°C (⊡); 30.1°C (△); 35.0°C (×).

Table 1. Observed rate constant (k_{obs}) for the reaction of Cr(VI) and L-methionine [$RSCH_3$] at different hydrogen ion concentrations [H^+] and temperatures. [Cr(VI)] = 4×10^{-4} mol dm^{-3}, I = 1.0 mol dm^{-3} ($NaClO_4$) and λ = 420 nm

10^3 [$RSCH_3$] (mol dm^{-3})	[H^+] (mol dm^{-3})	$10^4 k_{obs}$, s^{-1} 0.04	0.06	0.08	0.10
T = 20.1°C					
5.0		2.5	3.6	5.6	6.6
10.0		3.9	5.8	9.6	11.8
15.0		4.8	7.8	12.3	17.0
20.0		5.4	8.5	16.0	18.8
25.0		5.8	10.6	18.8	25.1
T = 25.1°C					
5.0		3.0 (3.0)	4.7	6.7	8.4 (8.4)
10.0		4.8 (4.9)	8.0	12.0 (12.0)	15.6
15.0		6.4 (6.2)	10.3 (10.0)	16.5 (16.2)	22.2
20.0		6.9	11.8 (11.6)	19.9 (19.2)	27.5 (27.4)
25.0		7.2	14.8 (14.7)	25.1	30.4
T = 30.1°C					
5.0		3.9	5.8	8.3	11.0
10.0		5.6	10.0	14.0	18.9
15.0		7.2	12.2	18.9	25.7
20.0		7.7	15.4	21.5	31.9
25.0		8.1	17.6	25.7	35.5
T = 35.1°C					
5.0		4.8	7.8	9.8	13.1
10.0		7.6	11.1	16.7	21.4
15.0		8.3	16.0	26.9	32.1
20.0		10.5	20.6	29.6	39.2
25.0		11.3	21.8	34.0	49.1

( ) Values at λ = 350 nm.

$$R^1(CH_3)SCrO_3^- \xrightarrow[H_2O]{k_1} Cr(IV) + R^1(CH_3)S{=}O \quad (2)$$

$$R^1(CH_3)SCrO_3^- + RSCH_3 \xrightarrow[2H_3O^+]{k_2} Cr(IV) + R^1(CH_3)S{=}O + RSCH_3 + 2H^+ \quad (3)$$

where $R^1(CH_3)SCrO_3^-$ is

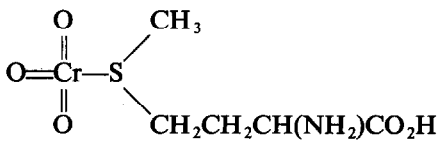

other contributing steps are as in (4)–(5).

$$2Cr(IV) \xrightarrow{fast} Cr(III) + Cr(V) \quad (4)$$

$$Cr(V) + RSCH_3 \xrightarrow[H_2O]{fast} Cr(III) + R^1(CH_3)S{=}O. \quad (5)$$

On the basis of this scheme the rate of loss of [$HCrO_4^-$] can be readily derived [eq. (6)]

$$\frac{-d[HCrO_4^-]_T}{dt} = \frac{K[RSCH_3](k_1 + k_2[RSCH_3][H^+]^2)[HCrO_4]_T}{1 + K[RSCH_3]}. \quad (6)$$

But

$$\frac{-d[HCrO_4^-]_T}{dt} = k_{obs}[HCrO_4^-]_T \quad (7)$$

therefore

$$k_{obs} = \frac{K[RSCH_3](k_1 + k_2[RSCH_3][H^+]^2)}{1 + K[RSCH_3]}. \quad (8)$$

If $K[RSCH_3] \gg 1$, eq. (8) becomes

$$k_{obs} = k_1 + k_2[H^+]^2[RSCH_3]. \quad (9)$$

Table 2. Rate constants k_1 and k_2 for the reaction of Cr(VI) with L-methionine at different temperatures

T/°C	[a]k_1/s^{-1}	[a]k_2/Mol^{-3} dm^9 s^{-1}
20.1	2.5±0.3	9.4±0.8
25.1	3.1±0.5	12.3±1.1
30.1	3.8±0.5	15.3±1.2
35.0	4.5±0.5	19.3±1.4

$\Delta H_1^{\ddagger} = 26.2 \pm 0.4$ kJ mol^{-1};

$\Delta S_1^{\ddagger} = -224 \pm 1$ JK^{-1} mol^{-1}

$\Delta H_2^{\ddagger} = 33.9 \pm 0.01$ kJ mol^{-1};

$\Delta S_2^{\ddagger} = -111 \pm 1$ JK^{-1} mol^{-1}

[a] Error expressed as standard deviation.

The observation that plots of k_{obs} vs [$RSCH_3$] gave good straight lines at constant [H^+] and temperature is consistent with the above mechanism. The various rate constants k_1, derived from the intercepts of such plots and k_2, obtained from the graph of slope vs [H^+] at different temperatures are shown in Table 2 together with their corresponding activation parameters.

Our observed rate law eq. (6) differs only slightly from those derived for other related reactions[1-4] with the predominant path involving two substrate molecules. A comparison of the activation parameters for the predominant path in this and similar Cr(VI) reductions[1,2,4] reveals that such routes involve essentially similar processes. There is a change in coordination number from four in Cr(VI) to six in the kinetically stable Cr(III) products. Therefore, an expansion of coordination shell has to occur somewhere between the two states. It is thought that the coordination of a second substrate facilitates the expansion of Cr(VI) which occurs in reactions (3) where there is a two electron reduction from Cr(VI) to Cr(IV). This requirement for reorganization may account for the slowness and rate-determining character of the step. Another argument that could be advanced in favour of the second substrate is that the substrate being positively charged under the experimental conditions used, would make the central chromium ion more positive and thereby increase the tendency of the metal to oxidize the coordinated substrate. This is very similar to the observation made in the reaction of the same reductant with the $[AuCl_4]^-$ anion.[14]

Interestingly, the reduction of Cr(VI) by methionine is much slower than the corresponding reductions of the same oxidant by penicillamine[1,2] glutathione[1,2] and cysteine[4] under the same experimental conditions. This is consistent with the postulate[5] that the formation of an intermediate complex is a prerequisite for these redox processes. It also supports reports by McAuley and his coworkers[1,2,4] that the site most susceptible to attack by Cr(VI) in these substrates is sulphur. The presence of an alkyl group at the site appears to inhibit but not totally prevent the coordination of sulphur to the chromium centre. Although the formation of an intermediate complex could not be established from repeated scanning of reaction mixtures, this does not invalidate the postulate that some form of complex formation is involved before electron-transfer.

Comparison of the rate constants k_1 and k_2 in this reaction with those of similar reactions involving the oxidant with penicillamine[2] and cysteine,[4] show that the former rate constants are two orders of magnitude greater than those of cysteine[4] and comparable with those of penicillamine.[2] This is not very surprising judging from the fact that the presence of the methyl group in methionine (which is retained after the electron-transfer process) and two methyl groups attached to the adjacent carbon atom in the case of penicillamine would aid the rapid release of the electrons from sulphur to the oxidant much more than in the case of cysteine[4] (inductive effect). However, in spite of this, the overall rate of oxidation of methionine is slower than those of the latter under the same experimental conditions. This would tend to suggest that substitution into the inner coordination sphere of chromium(VI) is likely to be the rate-determining step in these reactions.

The fate of the intermediate Cr(IV) produced in reactions (2–4) has generated a lot of debate in the past. Westheimer and Watanabe[10,15] considered several possible paths involving the subsequent reactions of Cr(IV), citing experimental evidence that in dilute $HClO_4$ one subsequent step must involve Cr(VI). However, addition of 0.04 mol dm^{-3} of Mn(II) had no effect on the rate of the reaction. This would suggest that the oxidant in this investigation is not involved after the rate-determining steps. Rather, a disproportionation of Cr(IV) is assumed to take place followed by a two electron reduction of the Cr(V) produced to give the final products Cr(III) and methionine sulphoxide. A similar observation was made by Haight and his coworkers[16] in the oxidation of hydrazine by Cr(VI).

Srivastava and coworkers[13] in their own investigation of the title reaction have proposed a direct linkage between the sulphur atom in methionine and one of the oxygen atoms in $HCrO_4^-$ rather than the metal centre in an attempt to rationalize the formation of a sulphoxide as one of the final products. It is difficult to see how this could possibly

be the case given the fact that both sulphur and oxygen are highly electronegative elements. On the other hand, Petri and Baldea[12] in their own studies, postulated that the title reaction proceeded via the hydrolysis of H_3C—S group in methionine leading to the formation of the sulphur-bonded $HO_2CCH(NH_2)CH_2CH_2SCrO_3^-$ intermediate before electron transfer. No alcohol was obtained as a product in our own investigation to make us reach such a conclusion. Moreover, the hydrolysis of the H_3C—S group leading to the fission of the C—S bond is highly unlikely in the acid medium used.

In conclusion, the oxidation of methionine is assumed to take place through the formation of a sulphur-bonded intermediate complex which undergoes hydrolysis after the electron transfer to give Cr(III), methionine sulphoxide and possibly substituted $[Cr^{III}(RSCH_3)]$ as the products in line with the suggestion elsewhere.[17,18] The formation of the sulphur-bonded intermediate complex is assumed to be the rate determining step in these reactions.

Acknowledgements—We thank Ahmadu Bello University, Zaria for providing the necessary facilities for the work and Dr J. O. Amupitan for useful discussions.

REFERENCES

1. M. A. Olatunji and A. McAuley, *Can. J. Chem.* 1977, **55**, 3335.
2. M. A. Olatunji and A. McAuley, *Can. J. Chem.* 1977, **55**, 3328.
3. M. A. Olatunji and A. McAuley, *J. Chem. Soc., Dalton Trans* 1975, 682.
4. A. McAuley and J. P. McCann, *J. Chem. Soc., Dalton Trans.* 1975, 783.
5. J. K. Beattie and G. P. Haight, *Prog. Inorg. Chem.* 1972, **17**, 93.
6. K. A. Muirhead, G. P. Haight and J. K. Beattie, *J. Am. Chem. Soc.* 1972, **94**, 3006.
7. (a) G. P. Haight, D. C. Richardson and N. H. Colburn, *Inorg. Chem.* 1964, **3**, 1777; (b) G. P. Haight, E. Perchonock, Emmenegger and G. Gordon, *J. Am. Chem. Soc.* 1965, **87**, 3835.
8. (a) Y. Sugiura, Y. Hojo and H. Tanaka, *Chem. Pharm. Bull.* 1972, **20**, 1362; (b) J. M. Walshe, *Chim. Sci.* 1964, **20**, 401.
9. I. Baldea and G. Niac, *Inorg. Chem.* 1968, **7**, 1232.
10. F. H. Westheimer, *Chem. Rev.* 1964, **45**, 419.
11. G. P. Haight, F. Smentowski, M. Rose and C. Heller, *J. Am. Chem. Soc.* 1968, **90**, 6325.
12. A. Petri and I. Baldea, *Stud. Univ. Babes-Bolyai, Ser. Chem.* 1975, **20**, 67.
13. K. B. Goswami, G. Chandra and S. N. Srivastava, *J. Ind. Chem. Soc.* 1981, **LVIII**, 252.
14. G. Natile, E. Bordigum and L. Cattalin, *Inorg. Chem.* 1976, **15**, 246.
15. W. Watanabe and F. H. Westheimer, *J. Chem. Phys.* 1949, **17**, 61.
16. G. P. Haight, T. J. Huang and B. Z. Shakhashiri, *J. Inorg. Nucl. Chem.* 1971, **33**, 2169.
17. J. N. Cooper, G. E. Staudt, M. L. Smalser, L. M. Settzo and G. P. Haight, *Inorg. Chem.* 1973, **12**, 2075.
18. D. W. J. Kwong and D. E. Pennington, *Inorg. Chem.* 1984, **23**, 2528.

Polyhedron Vol. 7, No. 1, pp. 17–23, 1988
Printed in Great Britain

0277–5387/88 $3.00+.00
© 1988 Pergamon Journals Ltd

THE FORMATION OF THE $[7\text{-}SeB_{10}H_{11}]^-$ ANION FROM 1-$SeB_{11}H_{11}$ AND THE STRUCTURE OF THE ANION STUDIED BY BORON-11 COSY NMR AND X-RAY CRYSTALLOGRAPHY

DAVID REED

Department of Chemistry, University of Edinburgh, Edinburgh EH9 3JJ, U.K.

GEORGE FERGUSON* and BARBARA L. RUHL

Department of Chemistry, University of Guelph, Guelph N1G 2W1, Canada

and

ORLA NI DHUBHGHAILL and TREVOR R. SPALDING*

Chemistry Department, University College, Cork, Ireland

(*Received* 5 *January* 1987; *accepted* 19 *June* 1987)

Abstract—The $[7\text{-}SeB_{10}H_{11}]^-$ anion has been prepared by the degradation of 1-$SeB_{11}H_{11}$ with NaOEt in ethanol. Data from ^1H, ^{11}B and ^{11}B–^{11}B COSY NMR spectra have enabled the structure of the anion in solution to be assigned. An X-ray diffraction study of $[Et_4N][7\text{-}SeB_{10}H_{11}]$ showed the crystals to be monoclinic, space group $P2_1/c$ with two formula units in each unit cell of dimensions $a = 8.485(2)$, $b = 10{,}654(2)$, $c = 10.078(2)$ Å, $\beta = 91.10(2)°$. 1985 unique reflections were measured, but only the 547 with $I > 3\sigma(I)$ were labelled "observed" and used in the structure solution and refinement. Both cation and anion lie on independent inversion centres and are disordered. In the anion, the Se atom was scrambled unequally over 12 sites. The final R value is 0.12. An analysis of the MNDO calculated composition of the five lowest energy unoccupied m.o's. of the sulphur analogue of $SeB_{11}H_{11}$ was carried out. The results suggest that the B-atom lost in the nucleophilic degradation reaction will be from a position adjacent to S(Se). This is supported by experimental data.

Most of the reported work on heteroboranes has concerned carbaboranes.[1] Cage substituted heteroboranes which contain Main Group elements other than C have received less attention although research groups in the U.S.A.[1,2] and Czechoslovakia[3] have made many notable contributions in this field. The relative lack of interest in heteroboranes is surprising since, where comparisons are available, there are clear differences in the reactions of isostructural and isoelectronic boranes, carbaboranes and heteroboranes. For example whilst $[B_{12}H_{12}]^{2-}$ and 1,2-$C_2B_{10}H_{12}$ failed to react with Pt(0) complexes of the type $[Pt(PR_3)_4]$,[4,5] both 1-$SB_{11}H_{11}$[6] and 1-$SeB_{11}H_{11}$[7] reacted with $[Pt(PPh_3)_4]$ in refluxing EtOH but gave different products namely *nido* $[9,9\text{-}(PPh_3)_2\text{-}6,9\text{-}SPtB_8H_{10}]$ and *closo* $[2,2\text{-}(PPh_3)_2\text{-}1,2\text{-}SePtB_{10}H_{10}]$. In our work we have decided to focus attention on heteroboranes containing S, Se or Te. In this paper we discuss the formation of the $[7\text{-}SeB_{10}H_{11}]^-$ anion from 1-$SeB_{11}H_{11}$ and the elucidation of its structure in solution by ^{11}B COSY NMR spectroscopy and in the solid state by X-ray crystallography.

Boron-11 COSY NMR spectroscopy has recently been shown to be an important new method of analysis of boron cluster systems in solution and is particularly useful when combined with other techniques such as $^1H\{^{11}B\}$ NMR.[8] These tech-

* Authors to whom correspondence should be addressed.

niques have been used in the present work to fully assign the ^{11}B and ^{1}H NMR spectra of $[SeB_{10}H_{11}]^-$.

Three solid state structures of selenium containing heteroborane cages are in the literature. Of these, the structure of 1-$SeB_{11}H_{11}$ showed crystallographic disorder[7] but *nido*-[7-(η^5-C_5H_5)-7,8,12-$CoSeB_9H_9$][9] and *closo*-[2,2-$(PPh_3)_2$-1,2-$SePtB_{10}H_{10}$][7] were not disordered. It was hoped that a crystal structure analysis of $[Et_4N][SeB_{10}H_{11}]$ would provide the first example of a non-disordered cage containing only Se and B.

RESULTS AND DISCUSSION

The $[SeB_{10}H_{11}]^-$ anion was first prepared by Todd *et al.*[10] by the reaction of a freshly prepared aqueous ammonia solution of Na_2Se_4 with decaborane. The alternative preparation presented here is the nucleophilic degradation of 1-$SeB_{11}H_{11}$ by NaOEt in refluxing ethanolic solution followed by precipitation of the anion with aqueous $[Et_4N]I$ solution, Fig. 1. By this method $[Et_4N][SeB_{10}H_{11}]$ was obtained in 55% yield. The reaction is comparable to the reported degradation of $SB_{11}H_{10}(Ph)$ by methanolic sodium hydroxide to give $[Me_4N][SB_{10}H_{10}(Ph)]$ (38% yield),[11] or the degradation by ethanolic potassium hydroxide of 1,2- or 1,7-$C_2B_{10}H_{12}$ to give the corresponding (3)-1,2- and (3)-1,7-$[C_2B_9H_{11}]^-$ anions.[12]

The anions $[B_{11}H_{13}]^{2-}$,[11] $[C_2B_9H_{12}]^-$,[12] and $[SeB_{10}H_{11}]^-$ are isoelectronic and by Wade's rules would be expected to be isostructural, that is based on an icosahedron with one apex missing, Fig. 1. In common with most other known heteroboranes containing main group atoms the heteroatom would be expected to occupy a position where it will have the minimum number of B atoms as neighbours, i.e. in the open face of a SeB_4 ring. The solution structure of $[SeB_{10}H_{11}]^-$ can be interpreted on this basis.

The $^{11}B\{^1H\}$ spectrum of $[SeB_{10}H_{11}]^-$ has been described before[10] and comprises six singlet signals; δ (ppm) -5.6(2B), -9.2(2B), -14.6(1B), -16.3(2B), -17.6(2B) and -35.6(1B). The assignment of these signals was carried out using $^1H\{^{11}B\}$ NMR results in conjunction with ^{11}B–^{11}B COSY data, Fig. 2. The $^1H\{^{11}B\}$ spectrum, with single frequency decoupling at $\delta(^{11}B) = -17.6$ showed sharpening of the B—H—B signal. Hence, the signal at δ -17.6 ppm in the ^{11}B spectrum arises from B(9,10). The ^{11}B–^{11}B COSY spectrum shows the signal at δ -17.6 couples to that at δ -14.6. This then must be due to B(5). Thus, the signal at δ -35.6 must be due to B(1). The COSY spectrum shows the signal at δ -5.6 displays coupling to every other signal. This could only be explained if this signal arose from B(4,6). In addition, the signal due to B(9,10) shows coupling to that at δ -9.2. Of the two remaining possibilities, only B(8,11) are adjacent to B(9,10), and so we assign the signal at δ -9.2 to B(8,11). Thus, the signal at δ -16.3 must be due to B(2,3). This signal shows two of the three interactions expected, i.e. to B(4,6) and B(1) though not to B(8,11). The boron NMR assignments are quoted in Table 1, together with proton NMR assignments as elicited from selective $^1H\{^{11}B\}$ experiments.

Table 1. NMR chemical shifts for $[SeB_{10}H_{11}]^-$ [a]

B—H site	δ ^{11}B[b]	δ ^1H[c]
8,11	−9.2	2.05
2,3	−16.3	1.67
9,10	−17.6	1.26 (also μ-H, −4.11)
4,6	−5.6	2.37
1	−35.6	1.05
5	−14.6	1.83

[a] Numbering of sites as in Fig. 1.
[b] Determined by ^{11}B–^{11}B COSY.
[c] Determined by ^1H–$\{^{11}B$ selective$\}$.

In order to establish the solid state structure of $[SeB_{10}H_{11}]^-$, a X-ray crystallographic study of the $[Et_4N]^+$ salt was undertaken. With $Z = 2$ in space group $P2_1/c$, both cation and anion must lie about

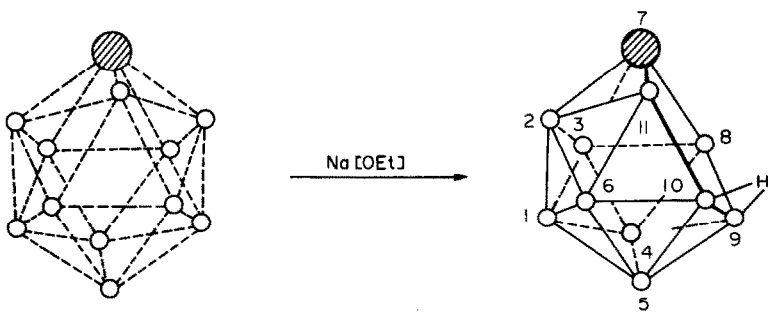

Fig. 1. Degradation of 1-$SeB_{11}H_{11}$ to $[7\text{-}SeB_{10}H_{11}]^-$.

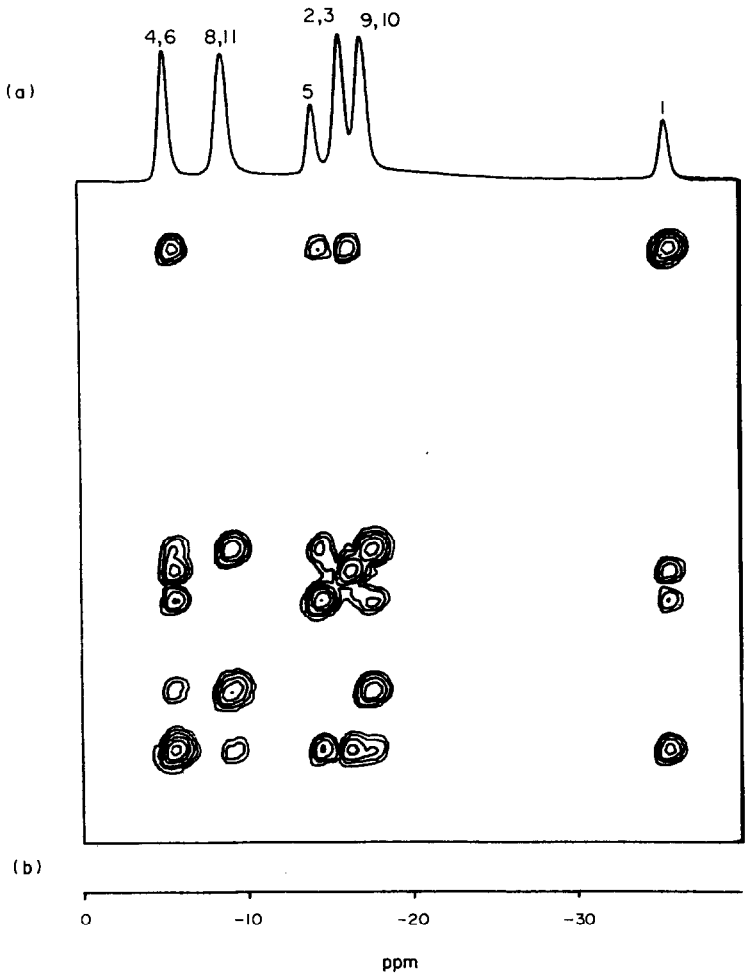

Fig. 2. (a) $^{11}B\{^1H\}$ and (b) ^{11}B–^{11}B COSY NMR of $[7\text{-}SeB_{10}H_{11}]^-$.

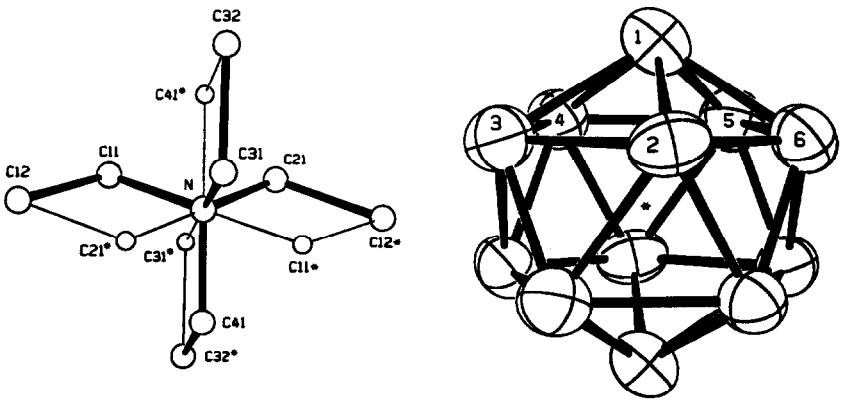

Fig. 3. A view of the $[Et_4N]^+$ and $[SeB_{10}H_{11}]^-$ ions. The anion lies on a crystallographic inversion centre denoted *; the Se and B atoms are mutually scrambled over the 12 sites. For clarity atoms in the disordered cation are shown as spheres of arbitrary radius. The bonds in one of the two $[NEt_4]^+$ moieties are shown as thick black lines.

Table 2. Bond distances in $[Et_4N][SeB_{10}H_{11}]$ (A) with estimated standard deviations in parentheses[a]

Atom 1	Atom 2	Distance	Atom 1	Atom 2	Distance
SE/B-1	SE/B-2	1.853(6)	N	C11	1.539(10)
SE/B-1	SE/B-3	2.003(6)	N	C21	1.500(10)
SE/B-1	SE/B-4	1.978(7)	N	C31	1.502(10)
SE/B-1	SE/B-5	1.965(6)	N	C41	1.589(11)
SE/B-1	SE/B-6	1.942(9)	C11	C12	1.619(11)
SE/B-2	SE/B-3	1.980(6)	$C12^{I}$	C21	1.675(14)
SE/B-2	$SE/B-4^{I}$	1.893(7)	C31	C32	1.708(13)
SE/B-2	$SE/B-5^{I}$	2.012(7)	$C32^{II}$	C41	1.551(15)
SE/B-2	SE/B-6	1.717(9)			
SE/B-3	SE/B-4	2.053(7)			
SE/B-3	$SE/B-5^{I}$	1.823(7)			
SE/B-3	$SE/B-6^{I}$	2.103(8)			
SE/B-4	SE/B-5	2.012(7)			
SE/B-4	$SE/B-6^{I}$	1.796(9)			
SE/B-5	SE/B-6	2.156(8)			

[a] The superscripts refer to the following equivalent positions: $^{I}-x, -y, -z$; $^{II}1-x, 1-y, -z$.

inversion centres and be disordered (Fig. 3). The non-hydrogen atoms of the $[SeB_{10}H_{11}]^-$ cage are scrambled over twelve sites with the Se scrambled unequally. Bond distances are given in Table 2. Previous values for Se—B bonds were in the ranges 2.098(9)–2.210(9) Å in *closo*-[2,2-$(PPh_3)_2$-1,2-$SePtB_{10}H_{10}$][7] and 2.004(5)–2.160(5) Å in *nido*-[7-(η^5-C_5H_5)-7,8,12-$CoSe_2B_9H_9$].[9]

To establish which boron site in 1-$SeB_{11}H_{11}$ had been removed in the degradation reaction, a partially deuterated derivative of 1-$SeB_{11}H_{11}$ was prepared with deuteration (74% by IR) in the six sites B(7)–B(12) only. The stereospecificity of the deuteration was established by comparison of ^{11}B and ^{1}H spectra of the undeuterated and deuterated samples of 1-$SeB_{11}H_{11}$. Degradation of the partially deuterated sample by ethanolic NaOEt as described above yielded partially deuterated (77% by IR) $[SeB_{10}H_{11}]^-$. Hence the degradation was stereospecific and involved the removal of a boron atom which was attached to Se i.e. one of B(2)–B(6). The bridged B(7)–B(8) bond had 100% B—H—B composition.

To gain some insight into the degradation reaction we have attempted to correlate the experimental observations with the MNDO m.o. model of the closely related compound 1-$SB_{11}H_{11}$. A recent analysis of the electrophilic substitution of 1-SB_9H_9 in terms of the atomic charges and composition of the five highest lying filled m.o.s. has produced a rationalization of the observed substitution patterns.[13] The icosahedral cage compound 1-$SB_{11}H_{11}$ could be analysed similarly. Unfortunately the MNDO calculations used in the above analysis do not as yet incorporate data for selenium but the previous results for the S-containing clusters are entirely consistent with electrophilic substitution of 1-$SeB_{11}H_{11}$. Hence they may be used to interpret some aspects of the present reaction of nucleophilic degradation of 1-$SeB_{11}H_{11}$ to $[SeB_{10}H_{11}]^-$. This reaction cannot be analysed in as much detail as the electrophilic substitutions mainly because the addition of electrons would cause a substantial change in structure (*closo*-$XB_{11}H_{11}$ to *nido*-$[XB_{11}H_{11}]^{2-}$ or to *arachno*-$[XB_{11}H_{11}]^{4-}$). However a few comments relating to the MNDO calculated 1-$SB_{11}H_{11}$ model would be appropriate here. First, the atomic charges are calculated to be 0.27 for S, −0.12 for each B atom in the B_5-ring adjacent to S and 0.07 for each H atom attached, −0.09 for each B atom in the lower B_5-ring and 0.08 for each H atom attached, −0.07 for the B atom opposite S and 0.06 for the H atom attached. Hence the sulphur atom is clearly positively charged and the BH units have slight negative charge but are very similar. On this basis nucleophilic attack may be expected to occur initially at S. The composition of the five lowest lying unoccupied m.o.s would suggest that the strongest interaction between 1-$SB_{11}H_{11}$ and an incoming nucleophile would occur in the region around the S and the B_5H_5-ring adjacent to S. The orbitals are

Table 3. Contributions of cluster units to the five l.u.m.o.s in $1\text{-}SB_{11}H_{11}$

Position	Unit	Molecular orbitals a_1	e_2		e_1	
1-S	S	0.39	—	—	0.29	0.29
B(2)–B(6)	B	0.39	0.59	0.59	0.40	0.40
	H	0.07	0.15	0.15	0.03	0.03
B(7)–B(11)	B	0.09	0.19	0.19	0.19	0.19
	H	0.04	0.07	0.07	0.03	0.03
B(12)	B	0.01	—	—	0.06	0.06
	H	0.01	—	—	—	—
		a_1	e_2		e_1	
Energy gap (eV)			0.94		0.08	

grouped as one of symmetry a_1 and two pairs (e_2, e_1) respectively, Table 3. The energy separations are a_1 to e_2 0.94 and e_2 to e_1 0.08 eV respectively with these five m.o.s. 1.4 eV lower in energy than the next unoccupied orbital. Contributions to the composition of the a_1 l.u.m.o. are 39% from S and 46% from the B_5H_5-ring attached to sulphur, ie. 85% on SB_5H_5. The nature of the orbital is essentially antibonding between S and the B_5H_5 ring but contains weakly bonding interactions between the B atoms. Addition of two electrons from a nucleophile would be expected therefore to weaken the S to B_5 bonding but slightly enhance B to B bonding. The e_2 pair of orbitals have no S component but have a large (74% each) contribution from the B_5H_5 ring adjacent to S. They are essentially antibonding between the B atoms of this ring and the lower one and hence addition of electrons would weaken the B to B bonding in this region. The e_1 pair of orbitals are constructured with 29% from S and 43% from B_5H_5 adjacent to S and are antibonding between the S and B_5H_5 units. It is clear from these comments that the addition of up to four electrons to $1\text{-}SB_{11}H_{11}$ would weaken the B—S and B—B bonds in the B_5 ring adjacent to S making these atoms more susceptible to further nucleophilic attack. If the structure was not constrained to remain icosahedral, then it would distort to a more open structure in which the B atoms adjacent to S would experience weakened cage bonding possibly leading to their excision. These conclusions are in general agreement with the experimental findings for the nucleophilic degradation of $1\text{-}SeB_{11}H_{11}$, Fig. 1. However both the structure of the intermediates and the mechanism of the reaction remain open to question. It is noteworthy that from the study of the degradation of $1,2\text{-}C_2B_{10}H_{12}$ it would appear that two nucleophiles per carbaborane are involved in a complex series of steps. Such complex interactions would be difficult to model by MNDO calculations.

EXPERIMENTAL

Infrared spectra were recorded as KBr discs on Perkin–Elmer 257 and 1310 spectrometers. Mass spectra were recorded on an AEI-Kratos MS 3074 double beam spectrometer. NMR spectra were recorded at 360 MHz (^{11}B) on a Bruker WH360 Spectrometer fitted with an Aspects 3000 computer at the University of Edinburgh, Scotland. A frequency lock was achieved on the deuterium resonance of the deuterated solvent. $^1H\{^{11}B$, broad band$\}$ and $^1H\{^{11}B$, selective$\}$ spectra were recorded and the proton shift data abstracted by difference from off resonance decoupled spectra. Chemical shifts δ are reported relative to $SiMe_4$ (^1H), and BF_3OEt_2 (external) (^{11}B); positive values represent shifts to high frequency ("low field") of the standards. Two dimensional ^{11}B–^{11}B (COSY) spectra were recorded using the Jeneer pulse sequence, Relaxation Delay-90°-t_1-90°-acquire, with a sequence repetition rate 0.14 s. The data gave a 256×256 matrix which was symmetrized prior to plotting.

Reactions were carried out under dry oxygen-free nitrogen, although manipulations and separation procedures were carried out in air. Solvents were dried and distilled under nitrogen before use. The compound *closo*-$1\text{-}SeB_{11}H_{11}$ was prepared by a literature method[7] and characterized spectroscopically; IR ν_{max} at 2585 s (BH), 2567 s (BH), 2530 s (BH), 2512 s (BH), 1014 s, 910 s, 853 m, 770 m, 722 s cm^{-1}. Mass spectrum cut-off at m/z 214 (P^+) calc. ($^{82}Se^{11}B_{11}{}^1H_{11}$) 214.

Reaction of closo-1-$SeB_{11}H_{11}$ *with* NaOEt *in* EtOH

1-$SeB_{11}H_{11}$ (0.1 g, 0.48 mmol) was added to a solution of NaOEt in EtOH which had been freshly prepared from sodium (0.012 g, 0.522 g atom) in EtOH (12 cm^3). The reaction was stirred at room temperature for 23 h and refluxed for 1 h. On cooling, excess aqueous $[Et_4N]I$ was added and the resultant white precipitate (0.087 g, 55.3%) was characterized spectroscopically as $[Et_4N][SeB_{10}H_{11}]$; IR ν_{max} at 2970 w (CH), 2920 w (CH), 2510 s (BH), 1475 s, 1450 s, 1438 s, 1415 s, 1395 m, 1360 m, 1175 s, 1115 w, 1055 m, 1015 w, 100 s, 930 vw, 910 m, 880 w, 790 s, 740 vw, 695 w cm^{-1}. $^{11}B\{^1H\}$ NMR (CD_2Cl_2, 115.5 MHz, 25°C) δ −5.6 (s, 2B), −9.2 (s, 2B), −14.6 (s, 1B), −16.3 (s, 2B), −17.6 (s, 2B), −35.6 (s, 1B).

Reaction of closo-1-$SeB_{11}H_{11}$ *with* DCl

DCl was generated from benzoyl chloride and D_2O. A 3 l three-necked flask was filled with DCl to 1 atm. To this was added 1-$SeB_{11}H_{11}$ (0.25 g, 1.19 mmol), freshly sublimed $AlCl_3$ and CS_2 (200 cm^3). The sealed reaction was stirred for 10 days at room temperature. The solution was evaporated giving a beige solid which was sublimed at 90°C *in vacuo* yielding a white solid (0.11 g, 43%). This was identified spectroscopically as partially deuterated 7,8,9,10,11,12-D_6-1-Se-$B_{11}H_5$; IR ν_{max} at 2590 s (BH), 2550 s (BH), 1915 s (BD), 1290 w, 1220 vw, 1165 w, 1100 m, 1055 vw, 990 w, 960 s, 910 m, 868 s, 830 m cm^{-1}. $^{11}B\{^1H\}$ NMR (CD_2Cl_2, 115.5 MHz, 25°C) 23.4* (s, 1B), −2.6 (s, 5B), −3.8* (s, 5B).

The reaction of partially deuterated $SeB_{11}H_{11}$ with NaOEt in EtOH was carried out as described above. The product was identified spectroscopically as partially deuterated (77%) $[Et_4N][1\text{-}SeB_{10}(H/D)_{11}]$; IR ν_{max} at 2970 m (CH), 2920 w (CH), 2850 vw (CH), 2510 (BH), 1885 (BD), 1475 s, 1455 s, 1438 s, 1410 m, 1392 w, 1360 w, 1314 w, 1260 m, 1180 s, 1170 s, 1100 m, 1059 vw, 1025 w, 1000 m, 950 w, 865 w, 795 s cm^{-1}.

X-ray analysis of $[Et_4N][SeB_{10}H_{11}]$—*crystal data*

$C_8H_{31}SeB_{10}N$, FW = 328.41, monoclinic, $a = 8.485(2)$, $b = 10.654(2)$, $c = 10.078(2)$ Å, $\beta = 91.10(2)°$, $U = 910.8$ Å^3, $Z = 2$, $D_c = 1.20$ g cm^{-3}, $F(000) = 340$, $\lambda(Mo\text{-}K_\alpha) = 0.71073$ Å, $\mu(Mo\text{-}K_\alpha) = 20.2$ cm^{-1}. Space group $P2_1/c$ (No. 14). A crystal measuring approximately $0.35 \times 0.40 \times 0.10$ mm was grown which was suitable for X-ray data collection with an Enraf-Nonius CAD 4 diffractometer. Following machine location and centring of 25 reflections with θ in the range $10 < \theta < 14$, cell constants and an orientation matrix were determined by least squares refinement. A total of 2279 reflections were collected with $2 < \theta < 27°$ of which 1985 were unique. Lorentz, polarization and absorption corrections were applied to the data. Maximum and minimum values of transmission coefficients were 0.718 and 0.675 respectively. The crystal diffracted so poorly that only 547 of these data could be labelled "observed" and used in structure solution and refinement.

In space group $P2_1/c$ with $Z = 2$, both cation and anion must lie on independent inversion centres (and be disordered). The structure was solved with the aid of Multan 82[14] which revealed positions for the non-hydrogen atoms of the scrambled $[SeB_{10}H_{11}]^-$ cage. Subsequent structure-factor and electron-density calculations[15] allowed us to deduce coordinates for the disordered $[Et_4N]^+$ group and also showed that the Se atom in the $[SeB_{10}H_{11}]^-$ cage was scrambled unequally over 12 sites. The initial refinement was by full-matrix least-squares calculation with isotropic thermal parameters; the atoms of the $[SeB_{10}H_{11}]^-$ cage were assigned as Se atoms with appropriate occupancy factors which were then refined. In the final rounds of calculations the atoms were allowed anisotropic vibrations. At convergence R was 0.121 and wR 0.153. The high R factors are undoubtedly caused by the partial scrambling of the BH and Se sites. Final difference maps had maxima of 0.33 e Å^{-3} around the disordered methyl groups of the cation but no features of chemical significance. In the refinement cycles, scattering factor data were taken from International Tables[16] and weights were derived from the counting statistics.

Table 2 lists bond distances and Fig. 3 shows views[17] of the cation and anion. A complete list of dimensions, structure factors, atomic positional and thermal parameters has been deposited as supplementary material with the Editor, from whom copies are available on request. Atomic coordinates have also been deposited with the Cambridge Crystallographic Data Centre.

If the observed "halving" of the $0k0$ reflections was "accidental" not "systematic", then the space group would become Pc with no crystallographically imposed disorder. Structure solution and refinement in this system still led to a disordered model not significantly different from that

* From a comparison of the ^{11}B and $^{11}B\{^1H\}$ spectra, these sites only are found to be partially deuterated (74%).

obtained in $P2_1/c$, as anticipated,[18] and was abandoned. The final R factors are higher than normal undoubtedly because the poor packing of the almost spherical ions, leading to the observed disorder, and the paucity of observable data.

REFERENCES

1. E. L. Meutterties (ed.), *Boron Hydride Chemistry*. Academic Press, New York (1975); G. Wilkinson (ed.), *Comprehensive Organometallic Chemistry*, Vol. 1. Pergamon Press, Oxford (1982).
2. L. J. Todd in *Metal Interactions with Boron Clusters* (Edited by R. N. Grimes). Plenum, New York (1982); W. R. Pretzer, T. K. Hilty and R. W. Rudolph, *Inorg. Chem.* 1975, **14**, 2459.
3. J. Plesek and S. Hermanek, *J. Chem. Soc., Chem. Commun.* 1975, 127; K. Base and B. Stibr, *Chem. Ind.* 1977, 919; K. Base, *Coll. Czech. Chem. Commun.* 1983, **48**, 2593.
4. N. N. Greenwood, personal communication, 1984.
5. J. L. Spencer, M. Green and F. G. A. Stone, *J. Chem. Soc., Chem. Commun.* 1972, 1178.
6. T. K. Hilty, D. A. Thompson, W. M. Butler and R. W. Rudolph, *Inorg. Chem.* 1979, **18**, 2642.
7. G. Ferguson, M. Parvez, J. MacCurtain, O. Ni Dhubhghaill, T. R. Spalding and D. Reed, *J. Chem. Soc., Dalton Trans.* 1987, 699.
8. W. C. Hutton, R. N. Grimes and T. L. Venable, *J. Am. Chem. Soc.* 1982, **104**, 4716; *ibid.* 1984, **106**, 29; D. Reed, *J. Chem. Res.* 1984, **(S)**, 198; G. B. Jacobsen, D. G. Meina, J. H. Morris, C. Thompson, S. J. Andrews, D. Reed, A. J. Welch and D. F. Gaines, *J. Chem. Soc., Dalton Trans.* 1986, 1645.
9. G. D. Friesen, A. Barriola, P. Daluga, P. Ragatz, J. C. Huffman and L. J. Todd, *Inorg. Chem.* 1980, **19**, 458.
10. J. L. Little, G. D. Friesen and L. J. Todd, *Inorg. Chem.* 1977, **16**, 869.
11. W. R. Hertler, F. Klanberg and E. L. Meutterties, *Inorg. Chem.* 1967, **6**, 1696.
12. M. F. Hawthorne, D. C. Young, P. M. Garrett, D. A. Owen, S. G. Schwerin, F. N. Tebbe and P. A. Wegner, *J. Am. Chem. Soc.* 1968, **90**, 862.
13. J. MacCurtain, P. Brint and T. R. Spalding, *J. Chem. Soc., Dalton Trans.* 1985, 2591.
14. P. Main, S. J. Fiske, S. E. Hull, L. Lessinger, G. Germain, J.-P. Declercq and M. M. Woofson, Multa-82. Universities of York, England and Louvain, Belgium (1982).
15. B. Frenz and Associates Inc., SDP-Plus. College Station, Texas 77840 and Entraf-Nonius, Delft, Holland (1983).
16. *International Table for X-ray Crystallography*, Vol. IV. Kynoch Press, Birmingham. (Present distributor D. Reidel, Dordrecht) (1974).
17. C. K. Johnson, Ortep II Report ORNL-514-38. Oak Ridge National Laboratory, Tennessee (1976).
18. R. E. Marsh, *Acta Cryst.* 1986, **B42**, 193.

Polyhedron Vol. 7, No. 1, pp. 25–28, 1988
Printed in Great Britain

0277–5387/88 $3.00+.00
© 1988 Pergamon Journals Ltd

ESR STUDY ON SILVER(II) DITHIOCARBAMATE COMPLEXES IN NEMATIC LIQUID CRYSTAL

PIOTR CHMIELEWSKI* and ADAM JEZIERSKI

Institute of Chemistry, University of Wrocław, 14 Joliot-Curie Street, Wrocław, Poland

(*Received* 22 *January* 1987; *accepted* 24 *June* 1987)

Abstract—$Ag(dtc)_2$ and $[Ag(dtc)_2py]$ complexes, (where dtc = dithiocarbamate ligand, py = pyridine) were investigated by ESR in MBBA oriented nematic glasses and organic solvents (MBBA = *N*-(4-methoxybenzylidene)-4′-butylaniline). On the basis of experimental ESR parameters and simulation procedure the stoichiometry of the complex $[Ag(dtc)_2py]$ was found. The dependences of the spin Hamiltonian parameters on the organic substituents in the dtc ligands and solvents were established and discussed.

In 1959 Vänngård and Åkerström reported the reaction of silver(I)–dtc complexes with thiuram disulphide yielding Ag(II)–dtc complexes.[1] Zhukov *et al.*[2] observed adduct formation for $Ag(dtc)_2$ with nitrogen bases and Ag(II) complexes have been applied in chemical analysis[3] and oxidation reactions.[4] Recently the Ag(II) complexes were widely revived, but no new results concerned Ag(II)–dtc complexes appeared.[5]

Here we report the results of an ESR investigation on the $Ag(dtc)_2$ complexes in oriented nematic glasses and organic solvents. We also present here our studies on equilibrium in the system $Ag(dtc)_2$ + py and the adduct $[Ag(dtc)_2py]$.

EXPERIMENTAL

The complexes $Ag(dtc)_2$ with dtc =

(1) di-*n*-propyl-dithiocarbamate (*n*-Pr_2dtc),
(2) di-*i*-propyl-dithiocarbamate (*i*-Pr_2dtc),
(3) di-cyclohexyl-dithiocarbamate (chx_2dtc)

were obtained by reaction of the Ag(I)–dtc complex with an appropriate thiuram disulphide as white powders by the method described in Ref. 1. Analytical data confirmed the formula $Ag(dtc)_2$. In the case of the pyrrolidine–carbodithioate ligand and mono-alkyl dithiocarbamates the synthesis method[1] was unsuccessful; the piperidine–carbodithioate–Ag(II) complex $[Ag(pipdtc)_2]$ was obtained, but partially decomposed.

ESR spectra were recorded on a JES-ME X-band spectrometer with proton magnetometer and ESR standards. The spectra were simulated using a computer program written by us in Pascal language taking the natural abundance of $^{107,109}Ag$ isotopes into account. The orthorhombic symmetry of the magnetic centre and coaxiality of the Zeeman and hyperfine tensors were assumed. The program summed spectra due to all possible orientations of the molecules weighted by the solid angle element $-1/2\Delta\cos\Theta\Delta\varphi$ and the orientation-dependent transition probability was calculated according to Aasa and Vänngård[6] for each particular transition. The best fit was obtained with Gaussian lineshape.

The MBBA liquid crystal (MBBA = *N*-(4-methoxybenzylidene)-4′-butylaniline) was used as a solvent for the Ag(II)–dithiocarbamate complexes. The oriented nematic glasses were obtained according to the method described by Fackler *et al.*[7] Samples were heated to obtain isotropic phase and oriented by applying a magnetic field of 8000 G while cooling to the nematic temperature range. The temperature was then lowered quickly to 130 K to produce a glass. Samples were rotated around the axis perpendicular to the magnetic field direction to obtain the angular dependence of line intensities.

RESULTS AND DISCUSSION

No ESR spectra for solid complexes were obtained; it is probably due to the polymeric structure of such complexes. These white substances dissolved in organic solvents gave blue-coloured solutions. Intense ESR signals were obtained at room

* Author to whom correspondence should be addressed.

Table 1. ESR parameters for $Ag(dtc)_2$ complexes in various solvents, $T = 295$ K; A in 10^{-4} cm^{-1} units. Maximal experimental error in $g \pm 0.001$, in $A \pm 0.1$

dtc = solvent[a]	pipdtc		n-Pr_2dtc		i-Pr_2dtc		chx_2dtc	
	g_{iso}	A_{iso}	g_{iso}	A_{iso}	g_{iso}	A_{iso}	g_{iso}	A_{iso}
n-heptane	2.020	28.2	2.020	28.2	2.020	28.0	2.020	28.0
toluene	2.020	28.2	2.020	28.2	2.020	28.0	2.020	27.9
nitrobenzene	2.019	28.2	2.020	28.2	2.019	28.1	2.019	27.9
acetone	2.019	28.2	2.020	28.1	2.020	28.1	2.019	28.0
THF	2.020	28.1	2.020	28.1	2.020	28.0	2.020	27.9
acetylacetone	2.019	28.2	2.019	28.1	2.019	28.1	2.019	28.1
DMF	2.020	28.2	2.020	28.2	2.020	28.2	2.019	28.0
DEF	2.020	28.2	2.020	28.2	2.020	28.1	2.019	28.0
DMSO	2.020	28.3	2.020	28.2	2.019	28.0	2.019	28.0
acetonitryl	2.019	28.2	2.020	28.2	2.019	28.2	2.019	28.1
MBBA[b]	—	—	2.020	28.1	2.020	27.9	2.019	27.9
quinoline	2.020	28.0	2.020	28.0	2.020	27.7	2.020	27.6
N-MeIm	2.020	28.0	2.020	28.0	2.020	27.8	2.019	27.7
pyridine	2.020	27.8	2.020	27.8	2.019	27.5	2.019	27.5

[a] THF = tetrahydrofuran, DMF = dimethylformamide, DEF = diethylformamide, DMSO = dimethylsulphoxide, N-MeIm = N-methylimidazole.

[b] Isotropic phase, $T = 320$ K.

temperatures for the solutions (see Table 1). The g_{iso} parameters lie between 2.019–2.020 and do not depend on the kind of dtc ligand or solvent. The A_{iso} parameters are generally smaller for N-coordinating solvents in comparison with non-coordinating or potentially O-coordinating solvents; a tendency of A_{iso} to diminish was observed in the order: pipdtc ~ n-Pr_2dtc > i-Pr_2dtc > chx_2dtc. The changes in A_{iso} are close to the error limit, but these are reproducible and are observed in all solvents. The tendency may be connected with the variation of ligand field strength in this row; it has been observed for magnetic moments of iron(III)–dtc complexes[8] and ESR hyperfine constants for iron and manganese dtc complexes.[9,10] Our results obtained for the Ag(II)–dtc complexes in oriented nematic glasses confirmed the effect of the substituents (see Table 2). Anisotropic data for the dtc complexes are presented in Tables 2–4.

The ESR spectra were obtained both for oriented frozen nematic MBBA glass (Fig. 1) and non-oriented MBBA glass (Fig. 2). ESR parameters calculated from the oriented nematic glass spectra and obtained from the randomly oriented samples (checked by simulation procedure) were the same (Table 2).

Experiments with oriented samples allow us to establish the in-plane and out-of-plane components of **g** and **A** tensors. At 0° orientation (no rotation) the out-of-plane component (z) intensity is a minimum, while the intensity of one of the in-plane components at the intermediate g value (labelled by x; in our coordinate scheme the x axis bisects the S–C–S angle in the complex plane) is a maximum. The reversed relation of intensities is observed after 90° rotation. The "y" component intensity (at the smallest g value) changes only slightly during rotation having its maximum at 0°. The similar

Table 2. ESR parameters for $Ag(dtc)_2$ complexes in MBBA [data obtained both from oriented nematic glass and non-oriented glass (simulated)], $T = 77$ K; A in 10^{-4} cm^{-1} units. Maximal experimental error in $g \pm 0.001$, in $A_z \pm 0.1$, in $A_{x,y} \pm 0.2$

dtc	g_x	g_y	g_z	A_x	A_y	A_z	g_{av}	A_{av}
n-Pr_2dtc	2.014	2.007	2.039	26.6	25.4	38.3	2.020	30.1
i-Pr_2dtc	2.013	2.006	2.039	26.4	25.2	38.2	2.019	29.9
chx_2dtc	2.013	2.006	2.038	26.3	25.1	37.7	2.019	29.7

Table 3. ESR parameters for $Ag(i\text{-}Pr_2dtc)_2$ in dimethylformamide (DMF) and tetrahydrofuran (THF), $T = 77$ K; A in 10^{-4} cm^{-1} units. Maximal experimental error in $g \pm 0.001$, in $A_z \pm 0.1$, in $A_{x,y} \pm 0.2$

	g_x	g_y	g_z	A_x	A_y	A_z	g_{av}	A_{av}
DMF	2.013	2.007	2.037	26.0	25.3	39.0	2.019	30.1
THF	2.013	2.006	2.038	26.8	25.3	38.8	2.019	30.3

Table 4. ESR parameters for $Ag(i\text{-}Pr_2dtc)_2py$ adduct in non-oriented glasses, $T = 77$ K; A in 10^{-4} cm^{-1} units. Maximal experimental error in $g \pm 0.001$, in $A_z \pm 0.1$ in $A_{x,y} \pm 0.2$, unless otherwise stated

Solvent	g_x	g_y	g_z	A_x	A_y	A_z	g_{av}	A_{av}
DMF	2.016	2.008	2.050	23.4	22.0	34.6	2.025	26.7
MBBA	2.015	2.008	2.049	21.5[a]	21.5[a]	34.6	2.024	25.9
pyridine	2.015	2.008	2.049	23.8[b]	22.0[b]	34.6[b]	2.024	26.8

[a] Error ± 0.5, parameters obtained from a mixture of $Ag(dtc)_2$ and $Ag(dtc)_2Py$.
[b] Error ± 0.3.

angular variations of the x and y components intensities were observed for the rhombic cobalt(II) complexes in liquid crystals.[11]

Analysis of the ESR parameters for dtc-complexes in MBBA and organic solvents (Tables 2 and 3) shows that the MBBA-potentially N-coordinating solvent does not coordinate to $Ag(dtc)_2$. This conclusion is supported by comparison of the parameters for $Ag(dtc)_2$ in MBBA with the data obtained for adducts with nitrogen-coordinating bases (see Table 4). ESR spectrum for the adducts is given in Fig. 3.

Stoichiometry of these adducts was established using the ESR technique. To the liquid solution of $Ag(dtc)_2$ in DMF (concentration about 0.001 M) the pyridine was added gradually and frozen solution spectra were recorded. The intensity ratio (I_n/I_4) of the lines from "z" orientation was calculated and its logarithm was plotted against $\log C(\text{py})$ [I_n—the intensity for adduct, I_4—for $Ag(dtc)_2$] (Fig. 4). The slope of the $\log(I_n/I_4)$ vs $\log C(\text{py})$ line is close to 1 as it was stated on the basis of three independent experiments. It shows 1 : 1 $Ag(dtc)_2$: py stoichiometry.

ESR spectra of the pure $[Ag(dtc)_2py]$ complex were obtained in DMF and pyridine solution, while in MBBA only a mixture with the parent complex exists even at high pyridine concentration. The

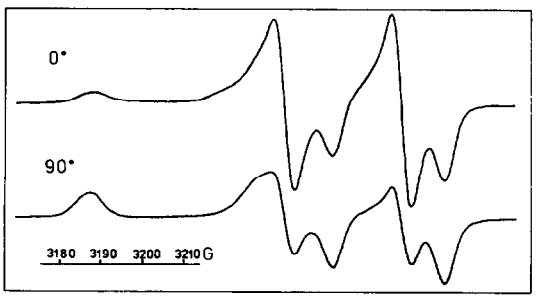

Fig. 1. ESR spectra of $Ag(i\text{-}Pr_2dtc)_2$ in oriented MBBA; upper trace—no rotation, lower trace—90° rotation. Microwave frequency $\nu = 9.155$ GHz, $T = 77$ K.

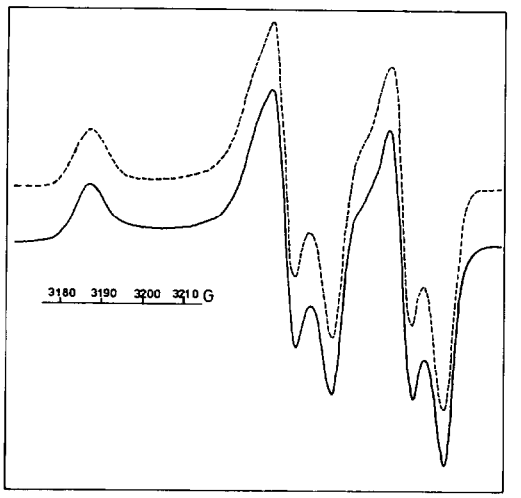

Fig. 2. ESR spectrum of $Ag(i\text{-}Pr_2dtc)_2$ in non-oriented MBBA; experimental—solid line, simulated—dashed line. Microwave frequency $\nu = 9.155$ GHz, $T = 77$ K.

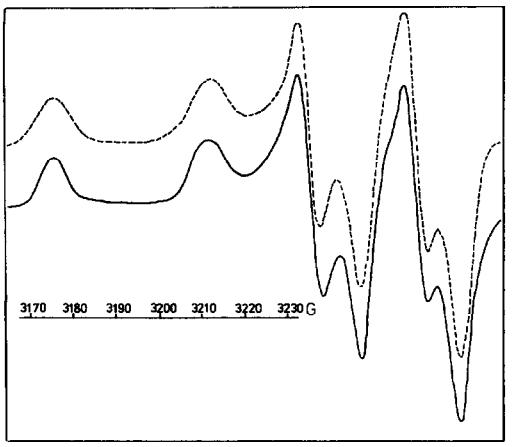

Fig. 3. ESR spectrum of Ag(*i*-Pr_2dtc)$_2$py in DMF; experimental—solid line, simulated—dashed line. Microwave frequency $\nu = 9.159$ GHz, $T = 77$ K.

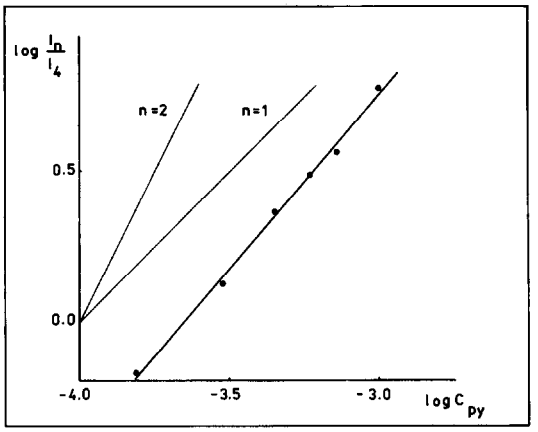

Fig. 4. Dependence of $\log(I_n/I_4)$ vs $\log C$(py) for Ag(*i*-Pr_2dtc)$_2$–py–DMF system.

ESR parameters, however, for the adduct in the latter solvent, were obtained by a simulation procedure made for the mixture (Table 4).

It is noteworthy that g_{iso} and g_{av} parameters for Ag(dtc)$_2$ are the same within experimental error; A_{iso} and A_{av} parameters differ for the Ag(dtc)$_2$ ($A_{av} > A_{iso}$). For the adducts Ag(dtc)$_2$py there are significant differences between g_{iso} and g_{av} ($g_{av} > g_{iso}$) and A_{iso} and A_{av} ($A_{iso} > A_{av}$). These effects are connected probably with different structures of the complexes in the liquid and frozen solutions. Distinct differences between Ag(dtc)$_2$ and [Ag(dtc)$_2$py] in frozen solutions and similarity between these complexes in liquids are particularly worth emphasizing.

REFERENCES

1. T. Vänngård and S. Åkerström, *Nature* 1959, **184**, 183.
2. V. V. Zhukov, I. N. Marov, O. M. Petrukhin and A. N. Ermakov, *Zh. Neorg. Khim.* 1973, **18**, 2863.
3. V. M. Byr'ko, *Ditiokarbamaty*. Nauka, Moskva (1984) and references therein.
4. E. Mentasti, C. Baiocchi and J. S. Coe, *Coord. Chem. Rev.* 1984, **54**, 131.
5. W. Levason and M. D. Spicer, *Coord. Chem. Rev.* 1987, **76**, 45.
6. R. Aasa and T. Vänngård, *J. Mag. Res.* 1975, **19**, 308.
7. J. P. Fackler, Jr., J. D. Levy and J. A. Smith, *J. Am. Chem. Soc.* 1972, **94**, 2436.
8. R. R. Eley, R. R. Myers and N. V. Duffy, *Inorg. Chem.* 1972, **11**, 1128.
9. A. Jezierski and B. Jezowska-Trzebiatowska, *Polyhedron* 1984, **3**, 1065.
10. A. Jezierski, *J. Mol. Struc.* 1984, **115**, 11.
11. (a) F. L. Urbach, R. D. Bereman, J. A. Topich, M. Hariharan and B. J. Kalbacher, *J. Am. Chem. Soc.* 1974, **96**, 5063; (b) B. M. Hoffman, F. Basolo and D. L. Diemente, *ibid*, 1973, **95**, 6497.

Polyhedron Vol. 7, No. 1, pp. 29–36, 1988
Printed in Great Britain

0277–5387/88 $3.00+.00
© 1988 Pergamon Journals Ltd

PLATINUM GROUP METAL COMPLEXES OF TRIS(2-(DIPHENYLPHOSPHINO)ETHYL)AMINE

M. M. TAQUI KHAN* and E. RAMA RAO

Discipline of Coordination Chemistry and Homogeneous Catalysis,
Central Salt and Marine Chemicals Research Institute, Bhavnagar 364 002, India

(*Received* 2 *June* 1987; *accepted* 1 *July* 1987)

Abstract—A mixed donor potential tetradentate ligand tris(2-(diphenylphosphino) ethyl)amine (TPEA) was synthesised by a modified procedure and characterized by ^{1}H, ^{13}C and ^{31}P NMR spectral data. Ru(II) complexes of TPEA were prepared by its interaction with $RuCl_2(PPh_3)_3$ and $RuCl_2(DMSO)_4$ to give $[RuCl_2(TPEA)]$ and $RuCl_2$ (DMSO)(TPEA) respectively. Ru(III) complexes of the composition $RuX_3(TPEA)$ or $[RuX_2(AsPh_3)(TPEA)]X$ were obtained by the reaction of TPEA with $RuX_3(AsPh_3)_2 \cdot$ MeOH ($X = Cl^-$, Br^-). A neutral Rh(I) complex of the composition RhCl(TPEA) was obtained by the reaction of $[RhCl(COD)]_2$ with TPEA. Cationic metal carbonyl complexes of the type [M(CO)(TPEA)]Cl (M = Rh, Ir) were obtained by the interaction of $[M(CO)Cl(PPh_3)_2]$ with TPEA. The reaction of hydrated $RhCl_3$ with TPEA gave $[RhCl_2(TPEA)]Cl$ in methanol. A five coordinated cationic complex [PdCl(TPEA)]Cl was obtained by the reaction of $PdCl_4^{2-}$ with TPEA. Interaction of $PtCl_2(COD)$ with TPEA however gave the square planar complex [PtCl(TPEA)]Cl. All the complexes were characterized by physico-chemical and spectroscopic methods.

In recent years there has been much emphasis on the synthesis of complexes with chelating ligands possessing mixed donor functionality due to their importance in structural chemistry as well as catalytic activity.[1–3] The chemistry of the metal complexes is governed[4–9] by the electronic and steric properties of the ligands and the oxidation state and coordination number of the complexes metal ion.

In our earlier communication,[3] we have reported the mononuclear and polynuclear platinum group metal complexes of bis(2-(diphenylphosphino) ethyl)amine. In the present communication we report some novel complexes of Ru(II), Ru(III), Rh(I), Rh(III), Ir(I), Ir(III), Pd(II) and Pt(II) with the tripod tetradentate mixed donor ligand tris(2-(diphenylphosphino)ethyl)amine (TPEA). In these complexes TPEA acts both as a tetradentate ligand with the coordination of N and three phosphorous atoms to a metal ion or terdentate with the coordination of only the phosphorous atoms. The complexes have been characterized on the basis of elemental analysis, conductivity, IR, NMR and EPR spectral data.

EXPERIMENTAL

The hydrated metal chlorides $RuCl_3 \cdot 3H_2O$, $RhCl_3 \cdot 3H_2O$, $IrCl_3 \cdot 3H_2O$, $PdCl_2$ and K_2PtCl_4 were obtained from Johnson Matthey (England), complexes $RuCl_2(PPh_3)_3$,[10] $RuCl_2(DMSO)_4$,[11] $RuX_3(AsPh_3)_2 \cdot MeOH$ (X = Cl, Br),[10] $MCl(CO)(PPh_3)_2$ (M = Rh, Ir),[12] $[RhCl(COD)]_2$[13] and $PtCl_2(COD)$[14] were prepared by published procedures. Triethanolamine and thionylchloride were of Analar grade and used without further purification. All metal complexes were prepared in a dry nitrogen atmosphere. Microanalysis, melting point, infrared spectra and conductivity measurement were done as reported earlier.[3,15] The ^{1}H NMR spectra were recorded on a Jeol FX100 spectrometer using TMS as an internal standard. The $^{13}C\{^{1}H\}$ spectrum of the ligand was taken at 24.99 MHz with TMS as internal standard. The proton noise-decoupled ^{31}P NMR spectra of the complexes were taken at 40.3 MHz in the FT mode using a deuterium lock. 85% H_3PO_4 was used as an exter-

* Author to whom correspondence should be addressed.

nal reference. The EPR spectra of Ru(III) complexes were recorded on a Bruker ESP-300 spectrometer in the solid state. The magnetic field calibration was checked with TCNE with a g value of 2.0028.

Synthesis of the ligand tris(2-(diphenylphosphino) ethyl)amine (TPEA)

The ligand TPEA was prepared by the reaction of tris(2-chloroethyl)amine with $KPPh_2$ (Scheme 1).

$$N(CH_2CH_2OH)_3 + 3SOCl_2 \xrightarrow{CHCl_3} Cl^-\overset{+}{H}N(CH_2CH_2Cl)_3 + 3SO_2 + HCl$$

$$Cl^-HN^+(CH_2CH_2Cl)_3 \xrightarrow{10\%\ NaOH} N(CH_2CH_2Cl)_3 + 3NaCl + 3H_2O$$

$$N(CH_2CH_2Cl)_3 + 3KPPh_2 \xrightarrow{1,4\text{-dioxane-THF}} N(CH_2CH_2PPh_2)_3 + 3KCl \quad (1)$$

TPEA

Tris(2-chloroethyl)amine hydrochloride was prepared by the published procedure.[16] The free amine tris(2-chloroethyl)amine was liberated by the action of 10% NaOH from its hydrochloride solution as an insoluble oil. The oil was extracted with diethylether and dried over anhydrous Na_2SO_4. A THF solution of the above oil was added dropwise with stirring to an orange–red suspension of $KPPh_2$[17] in dioxane in a stoichiometric amount under ice-cold conditions. The reaction mixture was then allowed to warm for 30 min under stirring and refluxed for about an hour. The reaction contents were poured into an ice-cold water–methanol mixture to get a dense oil, which solidified when kept in a freezer for 24 h. The filtered ligand was then washed with water, ethanol, petroleum ether, dried and purified by recrystallization from hot ethanol. Yield 22 g (70%).

Preparation of metal complexes

Dichlorotris (2 - (*diphenylphosphino*) *ethyl*) *amine*) *ruthenium* (II) $RuCl_2$ (TPEA) **1**. $RuCl_2(PPh_3)_3$ (0.29 g, 0.31 mmol) in benzene was refluxed with the ligand TPEA (0.20 g, 0.31 mmol) for 6 h. After the addition of the ligand the colour of the solution changed from brown to brownish-yellow and finally to yellow. The resulting yellow solution was cooled, filtered and concentrated to a small volume on a rotavapor. On the addition of ether a crystalline compound separated which was filtered and washed with ether. Yield 0.18 g (50%).

Dichlorodimethylsulphoxidetris (2 - (*diphenylphosphino*)*ethyl*)*aminеruthenium*(II) $RuCl_2$(DMSO) (TPEA) **2**. The complex $RuCl_2(DMSO)_4$ (0.15 g, 0.31 mmol) was dissolved in hot acetone. An acetone solution of TPEA (0.2 g, 0.31 mmol) was added to this solution and the solution refluxed for about 6 h. The resulting yellow solution was evaporated to half of its volume. Compound **2** separated on the addition of n-hexane. The compound was washed with n-hexane and recrystallized from dichloromethane-n-hexane mixture. Yield 0.19 g (66%).

Trichlorotris(2-(*diphenylphosphino*)*ethyl*)*amineruthenium*(III) $RuCl_3$(TPEA) **3** *and dichlorotriphenylarsinetris*(2 - (*diphenylphosphino*)*ethyl*)*amineruthenium*(III) *chloride* $[RuCl_2(AsPh_3)(TPEA)]Cl$ **4**. To the refluxing benzene solution of the complex $RuCl_3(AsPh_3)_2 \cdot MeOH$ (0.26 g, 0.31 mmol) was added a solution of the ligand TPEA (0.20 g, 0.31 mmol) in benzene. The solution was refluxed for 7 h. On cooling the solution a yellow crystalline complex separated which was filtered. This complex analysed as $[RuCl_3(TPEA)]$ **3** (Yield 0.18 g 40%). The filtrate was concentrated to a small volume and a yellow complex was isolated by the addition of pet. ether. The yellow complex analysed as $[RuCl_2(AsPh_3)(TPEA)]Cl$. Yield 0.14 g 40%.

Tribromotris (2 - (*diphenylphosphino*) *ethyl*) *amineruthenium* (III) $RuBr_3$(TPEA) **5** *and dibromotriphenylarsinetris*(2 - (*diphenylphosphino*)*ethyl*)*amineruthenium*(III) *bromide* $RuBr_2(AsPh_3)(TPEA)Br$ **6**. The complex $RuBr_3$(TPEA) **5** was obtained by a method similar to that used for the preparation of complexes **3** and **4** but with $RuBr_3(AsPh_3)_2 \cdot MeOH$ instead of $RuCl_3(AsPh_3)_2 \cdot MeOH$ as a starting material. Complex **5** was obtained as a brownish-violet solid with the composition $RuBr_3$(TPEA). Yield 0.12 g (40%). From the filtrate of complex **5**, a green crystalline solid was obtained with the composition $[RuBr_2(AsPh_3)$ (TPEA)]Br. Yield 0.15 g (39%).

Chlorotris(2-(*diphenylphosphino*)*ethyl*)*aminerhodium*(I) RhCl(TPEA) **7**. The complex $[RhCl(COD)]_2$ (0.07 g, 0.15 mmol) was suspended in ethanol and a hot ethanolic solution of the ligand TPEA (0.2 g, 0.31 mmol) was added to this suspension. The resulting reaction mixture was refluxed for 7 h and the mother liquor evaporated to about half of its original volume. The addition of diethylether to this solution gave a yellow precipitate which was filtered and washed repeatedly with diethylether. The complex was recrystallized from ethanol–petroleum ether mixture. Yield 0.13 g (53%).

Carbonyltris(2-(*diphenylphosphino*)*ethyl*)*amine-*

rhodium (I) *chloride* [Rh(CO)(TPEA)]Cl **8**. To a refluxing benzene solution of $RhCl(CO)(PPh_3)_2$ (0.16 g, 0.23 mmol) was added the ligand TPEA in equimolar quantities (0.15 g, 0.23 mmol) and further refluxed for 6–7 h. The solution was then concentrated to a small volume by a vacuum rotary evaporator and when petroleum ether was added a yellow precipitate was obtained. The complex was filtered, washed with petroleum ether and recrystallized from ethanol–petroleum ether mixture. Yield 0.12 g (66%).

Dichlorotris(2-(diphenylphosphino)ethyl)amine-rhodium (III) *chloride* $[RhCl_2(TPEA)]Cl$ **9**. $RhCl_3xH_2O$ (0.08 g, 0.31 mmol) was dissolved in methanol and the ligand TPEA (0.2 g, 0.31 mmol) was added in powder form. The resulting solution was refluxed for 4–5 h and was concentrated to a small volume by a vacuum evaporator. The compound was precipitated by the addition of diethyl ether. The resulting yellow complex was filtered, washed with diethyl ether and recrystallized from CH_2Cl_2-*n*-hexane mixture. Yield 0.23 g (87%).

Carbonyltris(2-(diphenylphosphino)ethyl)amine-iridium (I) *chloride* [Ir(CO)(TPEA)]Cl **10**. $IrCl(CO)(PPh_3)_2$ (0.18 g, 0.23 mmol) was added to a benzene solution of TPEA (0.15 g, 0.23 mmol) and the resulting solution refluxed for 5–6 h. The solution was then concentrated and when petroleum ether (60–80°) was added a lemon–yellow precipitate was obtained. The complex was filtered and washed with petroleum–ether. Yield 0.18 g (80%).

Chlorotris (2 - (*diphenylphosphino*) *ethyl*) *amine-palladium* (II) *chloride* [PdCl(TPEA)]Cl **11**. To a methanolic solution (15 cm^3) of Na_2PdCl_4 (0.11 g, 0.38 mmol) the ligand TPEA was added (0.25 g, 0.38 mmol) dissolved in 15 cm^3 dichloromethane. The resulting reaction mixture was stirred for 5 h and a yellow precipitate was obtained on the slow addition of diethylether. The compound was filtered, washed with water, benzene and finally with petroleum ether. Yield 0.24 g (75%).

Chlorotris (2 - (*diphenylphosphino*) *ethyl*) *amine-platinum* (II) *chloride* [PtCl(TPEA)]Cl **12**. To the refluxing acetone solution of $PtCl_2(COD)$ (0.11 g, 0.3 mmol) was added the ligand TPEA (0.2 g, 0.31 mmol) and the solution refluxed for 4–5 h. On cooling a crystalline white compound **12** was obtained. The compound was filtered, washed several times with acetone and recrystallized from methanol–diethylether mixture. Yield 0.28 g (98%).

RESULTS AND DISCUSSION

The PMR spectrum of TPEA exhibits resonance from the phenyl protons around 7.3 ppm as an intense broad peak. The methylene protons give complex multiplets centred at 1.97 ppm and 2.53 ppm assigned to $N—CH_2$ and $—CH_2P$ protons respectively. The obseved multiplet nature is due to the interaction of neighbouring protons followed by spin interaction with ^{31}P ($I = \frac{1}{2}$). The $^{13}C\{^1H\}$ spectrum gave two doublets centred at 49.14 ppm and 25.15 ppm with J(C—P) coupling constant value equal to 23.45 and 11.72 Hz. The doublet centred at 49.14 ppm is assigned to a methylene carbon attached to phosphorus and another doublet at 25.15 ppm to a methylene carbon attached to the nitrogen atoms. The aromatic carbons C-2, C-6 gave a doublet at 138.21 ppm with J(C—P) = 13.9 Hz. The C-1 (attached to phosphorus) gave another doublet at 132.54 ppm with J(C—P) = 19.05 Hz and carbon atoms C-3(5) and C-4 gave singlets at 128.43 ppm and 128.12 ppm respectively. The $^{31}P\{^1H\}$ spectrum gave an intense singlet at −19.07 ppm due to equivalence of three phosphorus atoms.

Metal complexes of TPEA

Ru(III) complexes of TPEA were prepared by the interaction of $RuCl_2(PPh_3)_3$ and $RuCl_2(DMSO)_4$ with TPEA. The interaction of TPEA with $RuX_3(AsPh_3)_2 \cdot MeOH$ (X = Cl, Br) gave Ru(III) complexes. Complexes **1** and **2** are found to be non-electrolytes thereby supporting their formulation as $RuCl_2(TPEA)$ and $RuCl_2(DMSO)(TPEA)$, respectively. Complexes **3** and **5** have the composition $RuX_3(TPEA)$ (X = Cl, Br) and are non-electrolytes. Complexes **4** and **6** are 1 : 1 electrolytes suggesting their formulation as $[RuX_2(AsPh_3)(TPEA)]X$ (X = Cl, Br) respectively[18] (Table 1).

The IR spectra of complexes **1** and **2** exhibit bands at 350, 327 cm^{-1} due to ν(Ru—Cl) thereby indicating a *cis* disposition of chlorides. In the octahedral complexes **3** and **5** of the composition $RuX_3(TPEA)$, the disposition of the halo group is *fac* since these complexes gave two bands in the far-infrared spectrum due to ν(Ru—X) (X = Cl, Br) (Table 2). Complexes **4** and **6** of the composition $RuX_2(TPEA)(AsPh_3)]X$ also gave two bands for ν(Ru—X) in the far IR spectral region thereby indicating a *cis*-disposition of the halide ions (Table 2) in the complexes.

The $^{31}P\{^1H\}$ NMR spectra of complexes **1**, **4** and **6** are comparable to each other as these complexes have two types of phosphorus atoms, which give rise to a doublet and triplet with $J_{P_a-P_b} = 29 \pm 0.5$ Hz. The phosphorus atom *trans* to chloride experiences a more down-field shift than the other phosphorus atoms (Table 3). The $J_{P_a-P_b}$ observed are in agreement with the *cis*-disposition of phosphorus atoms.[19] The $^{31}P\{^1H\}$ signals of

Table 1. Analytical and other data of metal complexes

	Complex[a]	Colour	M.p.[b]	Elemental analysis[c] C	H	N	Cl	Conductivity[d] $Ohm^{-1}\,cm^2mol^{-1}$
1	$Ru(L)Cl_2$	Yellow	250[b]	61.1 (61.0)	4.9 (4.8)	1.6 (1.6)	—	03[e]
2	$Ru(L)(DMSO)Cl_2$	Yellow	202	61.8 (61.5)	5.6 (5.5)	1.6 (1.6)	—	02[e]
3	$Ru(L)Cl_3$	Yellow	228[b]	58.5 (58.5)	4.9 (4.8)	1.6 (1.6)	—	—
4	$[Ru(L)(AsPh_3)Cl_2]Cl$	Yellow	232	61.7 (61.6)	4.9 (4.9)	1.2 (1.2)	—	61[f]
5	$Ru(L)Br_3$	Violet	226[b]	50.6 (50.3)	4.2 (4.2)	1.4 (1.3)	—	42[f]
6	$[Ru(L)(AsPh_3)Br_2]Br$	Green	250	55.3 (55.1)	5.3 (5.2)	1.1 (1.0)	—	77[f]
7	Rh(L)Cl	Yellow	172[b]	63.6 (63.6)	5.3 (5.3)	1.8 (1.7)	—	27
8	[Rh(L)(CO)]Cl	Yellow	176[b]	63.2 (62.9)	5.2 (5.1)	1.7 (1.7)	—	78
9	$[Rh(L)Cl_2]Cl$	Yellow	234	58.4 (58.3)	4.9 (4.9)	1.6 (1.6)	—	75
10	[Ir(L)(CO)]Cl	Lemon Yellow	250[b]	56.8 (56.5)	4.6 (4.6)	1.5 (1.4)	—	76
11	[Pd(L)Cl]Cl	Yellow	203	60.4 (60.0)	5.0 (5.0)	1.7 (1.7)	8.5 (8.5)	75
12	[Pt(L)Cl]Cl	White	244	54.8 (54.1)	4.5 (4.3)	1.5 (1.5)	7.7 (7.6)	71

[a] L = tris(2-(diphenylphosphino)ethyl)amine. [b] Decomposition temperature. [c] Found values are in parentheses. [d] Conductivity measurements were performed in methanol at room temperature except where mentioned. [e] Dichloromethane. [f] Dimethylformamide.

complexes **4** and **6** are broader than those of complex **1** because of the presence of the paramagnetic Ru(III) centre.

The $^{31}P\{^1H\}$ spectrum of **2** is of complicated nature and suggests the formation of two isomers since in the complex the ligand TPEA is coordinating in its tridentatemonoligate fashion by utilizing three phosphorus or two phosphorus and nitrogen for coordination. The isomer which coordinates with two P and N of TPEA gave two doub-

Table 2. IR and far-IR data of metal complexes

	Complex	(M—C═O, S═O) cm^{-1}	(M—X) cm^{-1} (X = Cl or Br)		(M—P) cm^{-1}
1	$Ru(L)Cl_2$	—	350(w),	327(w)	542(s)
2	$RuCl_2(DMSO)(L)$	1080	350(w),	327(w)	540(s)
3	$Ru(L)Cl_3$	—	325(b),	302(w)	535(s)
4	$[Ru(L)(AsPh_3)Cl_2]Cl$	—	325(s),	300(s)	540(s)
5	$Ru(L)Br_3$	—	302(m),	277(m)	539(s)
6	$[Ru(L)(AsPh_3)Br_2]Br$	—	299(m),	279(m)	540(s)
7	Rh(L)Cl	—	350(m)	—	540(s)
8	[Rh(L)(CO)]Cl	1970(s)	—	—	539(s), 562(s)
9	$[Rh(L)Cl_2]Cl$	—	325(m),	305(m)	539(s)
10	[Ir(L)(CO)]Cl	1945(s)	—	—	539(b)
11	[Pd(L)Cl]Cl	—	350(m)	—	525(s)
12	[Pt(L)Cl]Cl	—	350(m)	—	527(s)

L = tris(2-(diphenylphosphino)ethyl)amine. s = strong; b = broad; m = medium; w = weak.

Table 3. $^{31}P\{^1H\}$ spectral data of TPEA and its metal complexes

	Complex	Solvent	Chemical shift[a] (ppm) P_a	P_b	Coupling constants (Hz) $J_{(M-P_a)}$	$J_{(M-P_b)}$	$J_{(P_a-P_b)}$
	L	$CHCl_3$	−19.07(s)	—	—	—	—
1	$Ru(L)Cl_2$	$CHCl_3$	47.82(t)	27.18(d)	—	—	28.62
2	$Ru(L)(DMSO)Cl_2$	$CHCl_3$					
	(A)		33.87(d)	27.64(d)	—	—	29.6
	(B)		47.41(t)	30.09(d)	—	—	29.3
4	$[Ru(L)(AsPh_3)Cl_2]Cl$	$CHCl_3$	47.83(t)	27.18(d)	—	—	29.0
6	$[Ru(L)(AsPh_3)Br_2]Br$	$CHCl_3$	47.17(t)	22.61(d)	—	—	29.42
7	Rh(L)Cl	CH_2Cl_2	42.93(t)	30.77(d)	105	43	20.15
			40.33(t)	30.33(d)			
8	[Rh(L)(CO)]Cl	$CHCl_3$	44.20(t)	43.29(d)	134.28	134.28	19.54
			40.87(t)	39.96(d)			
9	$[Rh(L)Cl_2]Cl$	$CHCl_3$	32.57(t)	24.06(d)	117.19	91.55	21.97
			29.67(t)	21.80(d)			
10	[Ir(L)(CO)]Cl	$CHCl_3$	31.06(t)	30.28(d)	—	—	19.53
11	[Pd(L)Cl]Cl	MeOH	32.3(t)	29.76(d)	—	—	20.13
			19.19(t)				
12	[Pt(L)Cl]Cl	MeOH	−4.54(t)	+31.97(d)	3305.61	2729.48	20.76

[a] Positive chemical shifts down field flow from 85% H_3PO_4.
L = TPEA. s = singlet; d = doublet; t = triplet.

lets in 1 : 1 ratio, centred at 27.64 ppm and 33.87 ppm. The doublet centred at 27.64 ppm is assigned to P_a *trans* to DMSO and the other doublet centred at 33.87 ppm is assigned to P_b *trans* to chloride (Structure 1). The uncoordinated phosphorus atoms in this isomer displays a singlet at −19.3 ppm. The second isomer which is coordinated through all the phosphorus atoms gave a triplet and doublet (Table 3), since it contains two different P atoms in a 1 : 2 ratio. The ligand TPEA is coordinated in a *fac* manner in the first isomer and in a *mer* manner in the second (Structure 1). Due to low solubility and broadening of the ^{31}P peaks, the $^{31}P\{^1H\}$ data for complexes **3** and **5** could not be taken.

The PMR spectrum of complex **2** exhibits a singlet at 2.84 ppm due to the methyl proton of DMSO. The infrared spectrum of **2** gives a sharp band at 1080 cm^{-1} assigned to $\nu(S{=}O)$. The structure of complex **2** is shown in Structure 1.

The structure of complexes **3** and **5** are shown in Structure 2 and complexes **4** and **6** in Structure 3.

The EPR spectra of the Ru(III) complexes **3**, **4**, **5** and **6** with a $(t_2g)^5$ electronic configuration recorded in the solid phase gave three values of g tensor 2.45, 2.3 and 1.78 for complex **3**, and 2.45, 2.31 and 1.77 for complex **4** corresponding to g_1, g_2 and g_3 indicating a rhombic distorted configuration.[20,21] g tensors for complex **5** are

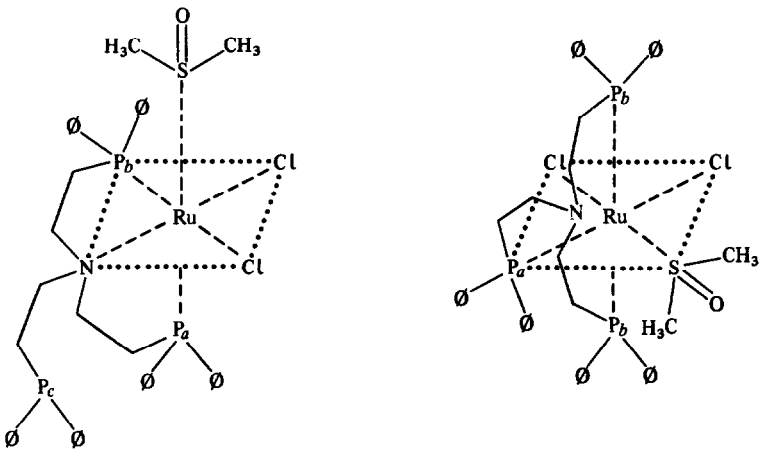

Structure 1. $RuCl_2(DMSO)(TPEA)$.

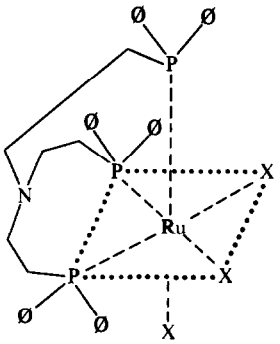

Structure 2. $RuX_3(TPEA)$, X = Cl, Br.

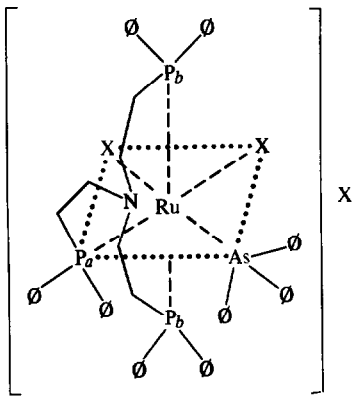

Structure 3. $[RuX_2(AsPh_3)(TPEA)]X$, X = Cl, Br.

$g_1 = 3.19, g_2 = 2.37$ and $g_3 = 1.96$ and for complex **6** are $g_1 = 1.74$, $g_2 = 2.31$ and $g_3 = 2.62$. These complexes gave large differences in their g_{11} value indicating different kinds of distortions in their geometry. The g value of complex **5** indicates an axial distortion in its octahedral geometry,[21] whereas complexes **3**, **4** and **6** gave equatorial distortion corresponding to a compressed octahedron.[20] The difference in the distortion pattern of complexes **3** and **5** arise due to a difference in the size of the meridionally coordinated halo group in these complexes.

The Rh(I) complexes of TPEA are prepared by the interaction of $[RuCl(COD)]_2$ and $[RhCl(CO)(PPh_3)_2]$ with TPEA. Complex **7** of the composition RhCl(TPEA) is a non-electrolyte and gives ν(Rh—Cl) at 350 cm^{-1}. Complex **8** is a 1 : 1 electrolyte with the formulation [Rh(CO)TPBA]Cl and gives an intense band at 1970 cm^{-1} due to ν(Rh—CO) (Table 1).

In both complexes **7** and **8** the ligand TPEA coordinates as a tridentate ligand with three phosphorus atoms coordinated in the metal ion in a triligated monometallic manner and the nitrogen atoms remain uncoordinated. These complexes appear to

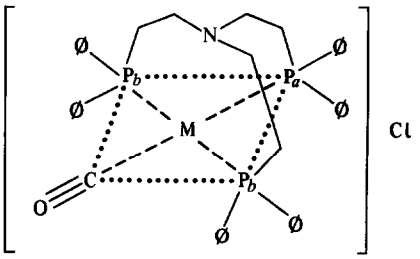

Structure 4. [M(CO)(TPEA)]Cl, M = Rh, Ir.

be pseudo square pyramid in structure (Structure 4).

The $^{31}P\{^1H\}$ spectra of complexes **7** and **8** exhibit a A_2MX pattern. Both the complexes contain two types of phosphorus atom P_a and P_b in a 1 : 2 ratio. The P_a atom is *trans* to chloride in **7** and carbonyl in **8**. The phosphorus atoms P_b are *trans* to each other. The phosphorus atom P_a gave two triplets at the downfield side in complex **7** since it is *trans* to chloride. There is a very little difference in the chemical shift values of P_a and P_b in complex **8** with a merging of the two peaks (Fig. 1). The interesting feature of ^{31}P NMR spectral data of **7** is the $J_{(Rh—P_b)}$ coupling constant which is very low about 43 Hz. However the $J_{(Rh—P_b)}$ value is found to be 134 Hz (Table 3). In complex **8** the metal phosphorus coupling constants $J_{(Rh—P_a)}$ and $J_{(Rh—P_b)}$ are found to be equal to 134.28 Hz. The $J_{(P_a—P_b)}$ values of 20 Hz found in **7** and **8** are characteristic of *cis*-disposition of different phosphorus atoms.[22]

Complex **9** of the composition $RhCl_3(TPEA)$ was obtained by the reaction of $RhCl_3xH_2O$ with TPEA in methanol. The far-infrared spectrum of the complex gave two bands at 325 and 305 m^{-1} corresponding to ν(Rh—Cl), and conductivity data is consistent with a 1 : 1 electrolyte, therefore the complex is formulated as $[RhCl_2(TPEA)]Cl$ with *cis*-disposition of two chlorides.

The $^{31}P\{^1H\}$ spectrum of complex **9** is also of A_2MX pattern and contains two different phosphorus atoms in 1 : 2 ratio. Since it is a Rh(III) complex, it gives lower $J_{(M—P)}$ values (Table 3). In this complex the ligand TPEA coordinates in a tetradentate monoligated fashion.[22]

The Ir(I) complex **10** was obtained by the interaction of $IrCl(CO)(PPh_3)_2$ and TPEA. The complex is a 1 : 1 electrolyte and gives a carbonyl stretching frequency at 1940 cm^{-1}. The $^{31}P\{^1H\}$ spectrum of **10** gave a triplet at 31.06 ppm due to the phosphorus atom *trans* to CO_2 and a doublet at 30.28 ppm due to mutually *trans* phosphorus atoms (P_b). The value $J_{(P_a—P_b)}$ is found to be 19.53 Hz. The complex is depicted in Structure 4.

A palladium(II) complex **11** of the composition $PdCl_2(TPEA)$ (Table 1) is prepared by the reaction

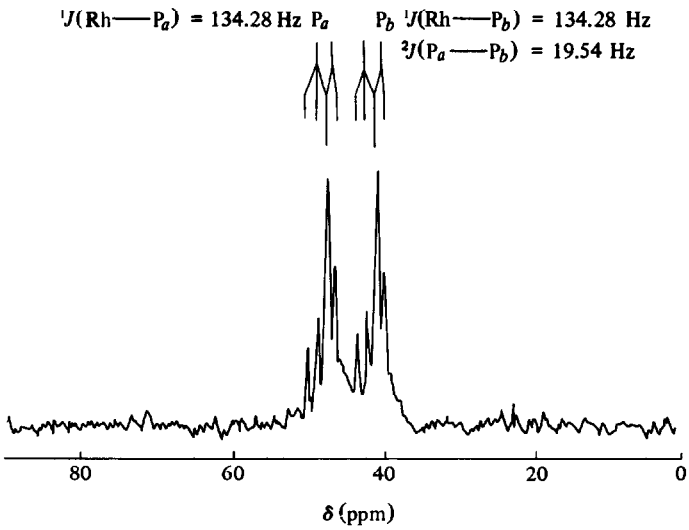

Fig. 1. ^{31}P $\{^1H\}$ NMR spectrum of [Rh(CO)(TPEA)]Cl **8**.

of Na_2PdCl_4 with the ligand TPEA in methanol–dichloromethane mixture. The complex is a 1 : 1 electrolyte. The far-infrared spectrum of **11** gave a band at 350 cm^{-1} due to ν(Pd—Cl). The ^{31}P $\{^1H\}$ spectrum of **11** shows a dynamic nature of the complex.[23] At room temperature it gives a broad peak centred at 34.09 ppm, doublet at 32.61 ppm and a triplet centred at 21.74 ppm. The spectrum recorded at −50°C gives a triplet at 32.3 ppm, a doublet at 29.76 ppm and a triplet at 19.19 ppm. The observation of two triplets is due to the dynamic nature of the complex between two possible structures with different modes of ligation of TPEA (Structure 5). Structure 5a, where phosphorus P_a is *trans* to the chloride and the two phosphorus P_b are *trans* to each other, exhibits a triplet centred at 32.3 ppm due to P_a and doublet at 29.70 ppm due to P_b with $J_{(P—P)} = 20.13$ Hz. In the second structure 5b, phosphorus P_a is at the axial position of the square pyramid and exhibits a triplet at 19.19 ppm, whereas the two phosphorus P_b, again *trans* to each other, gave a doublet, which overlaps with the doublet at the P_b of Structure 5a (Table 3).

Reaction of $PtCl_2$(COD) with the ligand TPEA gave a complex of the composition $PtCl_2$(TPEA) **12**. The conductivity data in methanol corresponds to a 1 : 1 electrolyte. The far IR spectra gave a band around 352 cm^{-1} assigned to ν(Pt—Cl). The ^{31}P $\{^1H\}$ spectrum of **12** gives a well defined triplet centred at −4.54 ppm and a doublet centred at 31.97 ppm with ^{195}Pt satellites indicating the presence of two types of phosphorus atoms in a 1 : 2 ratio. The metal–phosphorus coupling constant values observed are in agreement with the nature of the groups *trans* to phosphorus, the value $J_{(Pt—P_a)}$ (= 3305.6 Hz) is more since the P_a atom is *trans* to chloride and $J_{(Pt—P_b)}$ (= 2729.48 Hz) is less since two P_b atoms are *trans* to each other[24] (Table 3). $J_{(P_a—P_b)}$ is equal to 20.76 Hz characteristic of the *cis*-disposition of phosphorus atoms.

The electronic spectral data of the complexes **1**–**12** is given in Table 4, with molar extinction values. The bands with lower molar extinction values are assigned to a *d–d* transition and those with higher molar extinction values are assigned to LMCT transitions.

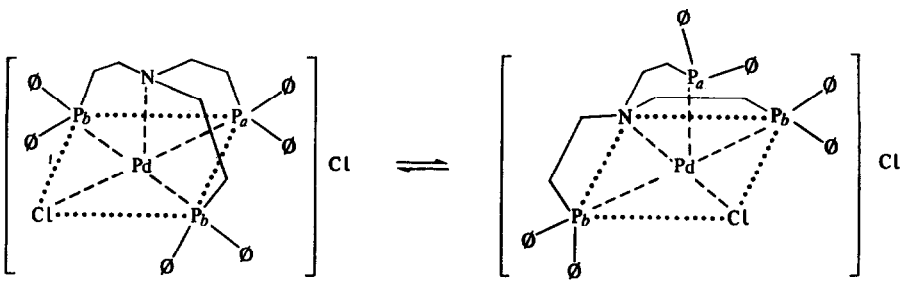

Structure 5. [Pd(TPEA)Cl]Cl.

Table 4. Electronic spectral data of metal complexes[a]

	Complex	$\lambda_{max, nm}$
1	$Ru(L)Cl_2$	410(406), 325(875), 240(7812)
2	$Ru(L)(DMSO)Cl_2$	400(786), 354(Sh)(900), 310(2400), 267(26,100)
4	$[Ru(L)(AsPh_3)Cl_2]Cl$	475(372), 402(1760), 330(3200), 265(27,200)
5	$Ru(L)Br_3$	530(1173), 455(1893), 300(25,200), 266(51,600)
6	$[Ru(L)(AsPh_3)Br_2]Br$	520(220), 450(960), 415(2240), 355(2640), 330(3360), 267(29,000)
7	Rh(L)Cl	357(1489), 310(3418), 264(9615), 220(41,660), 209(44,300)
8	[Rh(L)(CO)]Cl	375(5700), 285(17,384), 223(Sh)(40,460), 210(53,500)
9	$[Rh(L)Cl_2]Cl$	420(1470), 390(Sh)(2460), 298(22,160), 222(Sh)(46,700), 211(55,900)
10	[Ir(L)(CO)]Cl	355(4780), 315(Sh)(13,500), 285(14,800), 222(Sh)(41,600), 210(51,200)
11	[Pd(L)Cl]Cl	419(832), 355(9360), 295(10,600), 222(S)(41,600), 210(51,000)
12	[Pt(L)Cl]Cl	355(520), 265(19,500), 255(21,000), 210(49,400)

[a] Molar extinction values (m^{-1} cm^{-1}) are given in parentheses. Sh = Shoulder.

REFERENCES

1. M. M. Taqui Khan and B. Swamy, *Inorg. Chem.* 1987, **26**, 178.
2. M. M. Taqui Khan, B. T. Khan, Safia Begum and S. M. Ali, *J. Mol. Cat.* 1986, **34**, 283 and references therein.
3. M. M. Taqui Khan and E. Rama Rao, *Polyhedron* 1987, **6**, 1727.
4. G. Booth, *Advances in Inorganic Chemistry and Radio Chemistry*, Vol. 6. Academic Press, New York (1964).
5. L. M. Venanzi, *Angew. Chem. Int. Edn (Engl.)* 1964, **3**, 453.
6. R. B. King, *Acc. Chem. Res.* 1972, **5**, 177 and references therein.
7. M. M. Taqui Khan and A. E. Martell, *Inorg. Chem.* 1975, **14**, 676.
8. L. Sacconi and R. Morassi, *J. Chem. Soc. A* 1968, 2997.
9. L. Sacconi, *J. Chem. Soc. A*. 1970, 248.
10. T. A. Stephenson and G. Wilkinson, *J. Inorg. Nucl. Chem.* 1966, **28**, 945.
11. I. P. Evans, A. Spencer and G. Wilkinson, *J. Chem. Soc., Dalton Trans.* 1973, 204.
12. W. L. Jolly, Ed., *Inorganic Synthesis*, Vol. XI. McGraw Hill, New York.
13. J. Herde, J. Lambert and C. V. Senott, *Inorg. Synth.* 1974, **15**, 18.
14. J. Chatt, L. M. Vallarino and L. M. Venanzi, *J. Chem. Soc.* 1957, 3413.
15. M. M. Taqui Khan and K. Veera Reddy, *J. Coord. Chem.* 1982, **12**, 71.
16. E. Kimaru, Stefan Young and J. P. Collman, *Inorg. Chem.* 1970, **9**, 1183.
17. K. Isslieb and A. Tzschach, *Chem. Ber.* 1979, **92**, 1118.
18. M. M. Taqui Khan and V. Vijay Sen Reddy, *Inorg. Chem.* 1986, **25**, 208.
19. J. C. Briggs, C. A. McAuliffe and D. Dyer, *J. Chem. Soc., Dalton Trans.* 1984, 423.
20. Y. Arun Kumar, Ph.D. Thesis, Osmania University, Hyderabad (1984).
21. V. Vijay Sen Reddy, Ph.D. Thesis. Bhavnagar University (1985).
22. A. R. Sanger, *J. Chem. Soc., Dalton Trans.* 1977, 120.
23. M. Habid, H. Trujillo, C. A. Alexander and B. M. Storhoff, *Inorg. Chem.* 1985, **29**, 2344.
24. C. E. Johnson and R. Eisenberg, *J. Am. Chem. Soc.* 1985, **107**, 3148.
25. M. M. Taqui Khan, V. Vijay Sen Reddy and H. C. Bajaj, *Polyhedron* 1987, **6**, 921.

Polyhedron Vol. 7, No. 1, pp. 37–42, 1988
Printed in Great Britain

0277–5387/88 $3.00+.00
© 1988 Pergamon Journals Ltd

PREPARATION OF NEW MONO AND POLYNUCLEAR BIS(TRIPHENYLPHOSPHINE) COPPER(I) DERIVATIVES CONTAINING MONO AND BIDENTATE N-HETEROCYCLES, 8-HYDROXYQUINOLINE AND OXALATE LIGANDS

JOSEFINA DÍEZ, SANTIAGO FALAGÁN, PILAR GAMASA and JOSÉ GIMENO*

Departamento de Química Organometálica, Universidad de Oviedo, 33071 Oviedo, Spain

(*Received* 5 *January* 1987; *accepted* 10 *July* 1987)

Abstract—Novel mono and binuclear complexes of the type $Cu\{H(N—N)_2\}(PPh_3)_2$ [$H(N—N)_2^-$ = Hbibzim$^-$ (bibenzimidazolate), Htmbiim$^-$(tetramethylbiimidazolate)], $Cu(oxine)(PPh_3)_2$ and $Cu_2(\mu\text{-}C_2O_4)(PPh_3)_4$ [oxine = $C_9NH_6O^-$, $C_2O_4^{2-}$ = oxalate] have been obtained by reaction of $Cu(acac)(PPh_3)_2$ with the corresponding ligands. The reaction of $[Cu(CH_3CN)_2(PPh_3)_2]BF_4$ with imidazole or pyrazole derivatives renders tetrahedral mononuclear cationic complexes $[Cu(N—N)_x(PPh_3)_2]BF_4$ [$x = 1$, (N—N) = 2,2′-biimidazol (H_2biim), (H_2bibzim), (H_2tmbiim); $x = 2$, (N—N) = imidazole (Him), pyrazole (Hpz)]; the neutral tetranuclear complexes $[Cu_2\{\mu\text{-}(N—N)_2\}(PPh_3)_2]_2$ are formed when the corresponding bibenzimidazolate or tetramethylbiimidazolate are used as ligands. The structures of the resulting complexes have been elucidated by IR spectroscopy, ^1H, $^{31}P\{^1H\}$ NMR, molecular weight and conductance studies.

Copper(I) coordination chemistry is currently receiving much attention due mainly to the role of the metal in biological systems.[1] Copper(I) complexes, relevant to the understanding of copper-containing enzymes, are potentially air-sensitive, labile in solution and in some instances disproportionate to copper(0) and copper(II), but a large number of them have been described recently.[2] Recent structural studies in mononuclear Cu(I) complexes, namely $[CuL_n]^+$ (n = 2, 3, 4) or $CuXL_n$ (X = chloride, bromide, iodide) show their ability to adopt a range of different geometries. Thus, copper(I) complexes are known exhibiting di,[2] tri,[3] tetra[4] and penta[5] coordination which basically depends upon the bulk as well as the electronic properties of the N and/or P ligands.

Following our interest on coordination properties of N-donor heterocycles of the type of 2,2′-biimidazole and its derivatives[6] we describe in this paper the synthesis and characterization of novel copper(I) complexes containing Cu—N and/or Cu—O bonds, which are obtained by reactions of the type:

$$Cu(acac)(PPh_3)_2 + Y—H \rightarrow CuY(PPh_3)_2 + Hacac$$

[acac = acetylacetonate, Y—H = acidic N—H and O—H bidentate chelating ligands].

A method widely used by us, previously, for other M(acac) derivatives M = Rh,[7] Pd,[8] Au.[9] Thus, by reactions in appropriate conditions of $Cu(acac)(PPh_3)_2$ (**B**) with $H_2(N—N)_2$ (bibenzimidazole = H_2bibzim; 2,2′,4,4′-tetramethylbiimidazole = H_2tmbiim), mononuclear $Cu\{H(N—N)_2\}(PPh_3)_2$ and tetranuclear $[Cu_2\{\mu\text{-}(N—N)_2\}(PPh_3)_2]_2$ complexes are prepared. Similarly, $Cu(C_9NH_6O)(PPh_3)_2$ and $Cu_2(\mu\text{-}C_2O_4)(PPh_3)_4$ are obtained by reactions of (**B**) with 8-hydroxyquinoline and oxalic acid, respectively. This method of synthesis has only revealed to be of general utility with mild acidic ligands.

New tetrahedral mononuclear cationic copper(I) complexes of general formula $[Cu\{(N—N)_x\}(PPh_3)_2]BF_4$, $x = 1$, (N—N) = 2,2′-biimidazole (H_2biim), H_2bibzim, H_2tmbiim; $x = 2$, (N—N) = imidazole(Him), pyrazole (Hpz) are also described. These complexes can be of potential interest since photocatalytic reduction of dicationic methylviologen by similar copper(I) derivatives, namely $[Cu(N—N)(PPh_3)_2]^+$ (N—N = 1,10-phenanthroline, 2,2′-bipyridine and their derivatives) has been recently reported.[10] Table 1 lists the copper(I)

* Author to whom correspondence should be addressed.

complexes synthesized along with analytical, conductance and molecular weight data.

RESULTS AND DISCUSSION

(a) *Neutral complexes* (I–VI)

Reaction between dichloromethane solutions of $Cu(acac)(PPh_3)_2$ (acac = acetylacetonate) and $H_2(N—N)_2$, in 1/1 molar ratio leads according to eq. 1

$$Cu(acac)(PPh_3)_2 + H_2(N—N)_2 \xrightarrow{H_2CCl_2} Cu\{H(N—N)_2\}(PPh_3)_2 + Hacac \quad (1)$$

$[H(N—N)_2 = Hbibzim^-$ **(I)**, $Htmbiim^-$ **(II)**$]$

to a colourless solution from which complexes **(I)** and **(II)** can be obtained.

However, the reaction with H_2biim (2,2′-biimidazole) leads to a solid characterized as a mixture of the corresponding mononuclear and tetranuclear $[Cu_2(\mu\text{-biim})(PPh_3)_2]_2$ complexes, in a similar way as is described below (eq. 2). IR spectra of **(I)** and **(II)** (KBr mulls) show a ν(N—H) broad absorption band at *ca* 3000 cm^{-1} suggesting[8a] some intermolecular association via hydrogen protons of the ligands. (Fig. 1.)

^1H NMR spectra in $CDCl_3$ show resonances which are characteristic for aromatic protons along with two single peaks, in the case of the complex **(II)**, at δ 1.6 and 2.1 ppm assigned to the two chemically non-equivalent *exo* and *endo* methyl groups of the imidazole rings. The spectrum of **(II)** also shows a resonance at δ 5.2 ppm due to the presence of dichloromethane of crystallization.

Attempts to obtain binuclear derivatives of the type "$Cu[\mu\text{-}(N—N)_2]Cu$" by using the appropriate stoichiometric amounts (1/0.5) were unsuccessful, the reaction leading instead to a complex mixture. Thus, when $H_2tmbiim$ is used, a white solid is isolated which is characterized by ^1H NMR ($CDCl_3$ solution) as a mixture of $Cu(Htmbiim)(PPh_3)_2$ **(II)** and $[Cu_2(\mu\text{-tmbiim})(PPh_3)_2]_2$ **(VI)**. The spectrum

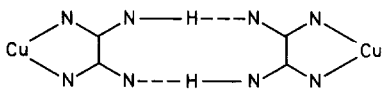

Fig. 1.

Table 1. Analytical data, colours, conductivity and molecular weight measurements of the novel complexes

	Compound	Found (Calc.) C	N	H	Colour	Λ_M or M.W[a]
(I)	$[Cu(Hbibzim)(PPh_3)_2]$	72.5 (73.2)	6.3 (6.8)	4.9 (4.7)	yellow	890 (821)[a]
(II)	$[Cu(Htmbiim)(PPh_3)_2]$	67.8 (67.7)[b]	6.9 (6.9)[b]	5.5 (5.5)[b]	white	890 (776)[a]
(III)	$[Cu(oxine)(PPh_3)_2]$	72.9 (73.8)	2.3 (1.9)	5.1 (4.9)	yellow	710 (732.2)[a]
(IV)	$[Cu_2(\mu\text{-}C_2O_4)(PPh_3)_4]$	69.7 (69.2)		5.2 (4.7)	white	1056 (1264)[a]
(V)	$[Cu_2(\mu\text{-bibzim})(PPh_3)_2]_2$	66.8 (64.4)	6.3 (6.3)	4.5 (4.3)	cream	1941 (1766)[a]
(VI)	$[Cu_2(\mu\text{-tmbiim})(PPh_3)_2]_2$	65.6 (65.8)	6.5 (6.7)	5.6 (5.0)	green	1570 (1678)[a]
(VII)	$[Cu(H_2biim)(PPh_3)_2]BF_4$	62.6 (62.4)	7.1 (6.9)	4.4 (4.5)	white	121[c]
(VIII)	$[Cu(H_2bibzim)(PPh_3)_2]BF_4$	65.0 (66.1)	5.9 (6.8)	4.8 (4.4)	yellow	111[c]
(IX)	$[Cu(H_2tmbiim)(PPh_3)_2]BF_4$	63.6 (63.9)	6.8 (6.5)	5.1 (5.1)	white	113[c]
(X)	$[Cu(Him)_2(PPh_3)_2]BF_4$	61.1 (62.3)	6.6 (6.9)	4.8 (4.7)	white	113.5[c]
(XI)	$[Cu(Hpz)_2(PPh_3)_2]BF_4$	60.9 (62.2)	6.9 (6.9)	4.6 (4.7)	white	126[c]
(XII)	$[Cu(3,5\text{-}Me_2Hpz)(CH_3CN)(PPh_3)_2]BF_4$	63.9 (63.7)	4.9 (5.2)	5.0 (5.0)	white	132.7[c]

[a] Molecular weight, ($CHCl_3$): Found (Calc.). [b] Calculated with $\frac{1}{2}H_2CCl_2$ of crystallization. [c] Acetone solutions ($\Omega^{-1}\,cm^2\,mol^{-1}$).

shows in the methyl protons range, four single peaks located at identical frequencies to those exhibited by pure samples of complexes (**II**) and (**VI**) (see below). No differences have been observed by increasing the time of reaction (30 min, 3 h), thus pointing to a process such as:

$$4Cu(acac)(PPh_3)_2 + 3H_2(N{-}N)_2 \xrightarrow{H_2CCl_2} 2Cu[H(N{-}N)_2](PPh_3)_2 + \tfrac{1}{2}[Cu_2\{\mu\text{-}(N{-}N)_2\}(PPh_3)_2]_2 + 2PPh_3 + 4Hacac \quad (2)$$

$[(N{-}N)_2^{2-}$ = biim^{2-}, tmbiim^{2-}].

A variety of other acid ligands Y—H react similarly through elimination of acetylacetone and lead to the formation of copper(I) complexes. Thus, previously known trigonal complexes, Cu(imide)$(PPh_3)_2$[11] [imide = $C_2H_4(CO)_2N^-$, $(C_6H_4)(CO)_2N^-$] and the tetrahedral $Cu(O_2CH)(PPh_3)_2$[12] (HCO_2^- = formiate) or novel ones, Cu(oxine)$(PPh_3)_2$ (**III**) (oxine = $C_9NH_6O^-$) and $Cu_2(\mu\text{-}C_2O_4)(PPh_3)_4$ (**IV**) ($C_2O_4^{2-}$ = oxalate) can be prepared in high yields by reaction with succinimide, phtalimide, formic acid, 8-hydroxiquinoline and oxalic acid, respectively.

IR spectra of (**III**) and (**IV**) show absorptions due to the presence of the ligands:[13] (**III**), 1560 (m), 1490 (w), 1455 (s) and 1110 cm^{-1}; (**IV**), 1600 (s) $\nu(CO_2)$ asym., 1300 (m) $\nu(CO_2)$ sym. cm^{-1}. Molecular weight determinations (see Table 1) reveals the chelate character of both anions and so forming, respectively, mono and binuclear derivatives. In contrast, the reaction with weaker acidic ligands such as pyrazole, imidazole and *o*-aminophenol do not take place, recovering the starting copper–acac complex unchanged. The chelate effect, which is supposedly acting in the reactions with H_2biim and their derivatives (eq. 1, see also below), can explain the reactivity of these very weak acid ligands.

Solutions of $[Cu(CH_3CN)_2(PPh_3)_2]BF_4$ in THF or CH_2Cl_2 react in 1/0.5 mol ratio with K_2bibzim and K_2tmbiim[$K_2(N{-}N)_2$] (prepared from $H_2(N{-}N)_2$ and an excess of potassium hydroxide in *ca* 3 : 1 THF/MeOH or CH_2Cl_2/MeOH) to give, respectively, cream and light green complexes (**V–VI**). The absence of ν(N—H) absorptions in the IR spectra and the values of molecular weights (determined osmometrically in chloroform, see Table 1) indicate a tetranuclear molecular structure of the type shown in Fig. 2.

The ^{1}H NMR ($CDCl_3$) spectrum of (**VI**) confirms the proposed structure, since it shows two single resonances at δ 2.3 and 1.7 ppm as expected for the two chemically non-equivalent methyl protons.

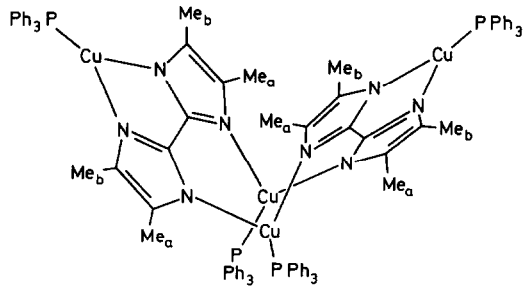

(*VI*)

Fig. 2.

Similar tetranuclear structures have been found in related Pd(II),[8a] Rh(I),[14] and Ir(I)[14] complexes. $^{31}P\{^1H\}$ NMR spectrum of (**VI**) shows one broad singlet at δ −4.28 ppm indicating possibly a fast intramolecular exchange process of phosphines (on the NMR time scale) which makes them chemically equivalent. These structures are further examples of the ability of copper(I) to adopt trigonal geometries in the presence of either a bulky S-donor[15a] or N-donor, with mild bulky substituents[15b] ligands.

Cationic complexes. (**VII–XII**)

Addition of stoichiometric amounts of the N-donor ligands $H_2(N{-}N)_2$ (H_2biim, H_2bibzim, H_2tmbiim) or H(N—N) (Hpz, Him) to dichloromethane solutions of $[Cu(CH_3CN)_2(PPh_3)_2]BF_4$ leads to the displacement of acetonitrile ligands to give tetrahedral cationic complexes (**VII–XII**), which can be precipitated as white or light yellow (**VIII**) solids by addition of diethyl ether to the partially evaporated solutions. (Fig. 3.)

Conductance data of all the complexes (Table 1) are typical of uni–univalent electrolytes and IR spectra (KBr pellets) show a broad ν(N—H) absorption band at *ca* 3360 cm^{-1} and strong broad absorption at 1150 cm^{-1} assigned to ν(B—F) vibrations. ^{1}H NMR spectra reveal resonaces of aromatic protons along with those expected for the corresponding in heterocyclic rings (see experimental).

Unexpectedly, the reaction with an excess of 3,5-dimethylpyrazole proceeds in a different way, to give a white solid formulated as $[Cu(3,5\text{-}Me_2Hpz)(CH_3CN)(PPh_3)_2]BF_4$ (**XII**), in which only one of the two originally coordinated acetonitrile ligands, has been substituted. The IR spectrum shows typical absorptions of the dimethyl pyrazol ligand (see experimental) and a weak $\nu(C{\equiv}N)$ band at 2260 cm^{-1} due to the still coordinated acetonitrile ligand, which is confirmed by the presence of a methyl single resonance at δ 1.95 ppm in the ^{1}H NMR spectrum ($CDCl_3$). In

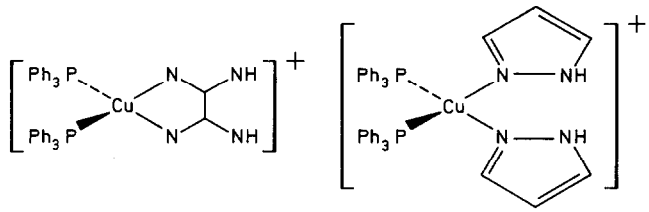

(VII - VIII - IX) *(X)*

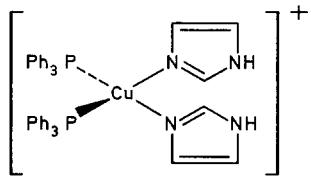

(XI)

Fig. 3.

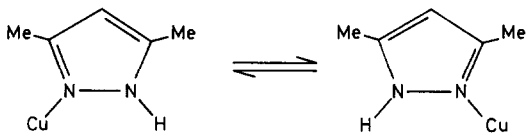

Fig. 4.

addition, instead of the two expected signals for the two methyl pyrazole groups only one slightly broad signal at δ 2.05 ppm is observed. This behaviour may be due to a rapid interexchange of pyrazole, in a dissociative process or "shuttling" of the H and the metal atom between the pair of N atoms.[16] (Fig. 4).

All the complexes described herein are air-stable in the solid state but their solutions are rapidly oxidized in air and decompose before melting. Table 1 lists their analytical data, molecular weights of the neutral complexes along with the conductivity data of the cationic complexes. Other relevant information on IR and ^1H or $^{31}P\{^1H\}$ NMR ($CDCl_3$) spectra are given in the experimental section.

EXPERIMENTAL

Measurements

C, H, N analyses were carried out with a Perkin–Elmer 240 microanalyzer. The IR spectra were recorded over the 4000–200 cm^{-1} range on a Perkin–Elmer 577 spectrophotometer using KBr discs or Nujol mulls between NaCl plates. Conductivities were measured at room temperature, in *ca* 10^{-3} mol dm^3 acetone solutions, with a Jenway PCM3 conductimeter. NMR spectra were recorded on a Varian FT-80A spectrometer at 79.54 MHz (^1H) or 32.20 MHz (^{31}P) using $SiMe_4$ and 85% H_3PO_4 respectively, as internal or external standard references. The molecular weights were determined in chloroform solutions with a Knauer vapour pressure osmometer (2×10^{-3} M solutions).

Synthesis

All reactions were performed under argon and the solvents were dried and deoxygenated before use. The ligands were used as purchased, except H_2biim, H_2bibzim and H_2tmbiim which are prepared as described elsewhere.[17,18] The reactions were carried out using 1 mmol of $Cu(acac)(PPh_3)_2$[19] or $[Cu(CH_3CN)_2(PPh_3)_2]BF_4$ as starting materials. The preparation of the acetonitrile complex is described below, since as far as we know it has not been isolated previously.

Neutral complexes

$Cu\{H(N—N)_2\}(PPh_3)_2$; $H(N—N)_2^-$ = Hbibzim$^-$ (**I**), Htmbiim$^-$ (**II**). A mixture of $Cu(acac)(PPh_3)_2$ and $H_2(N—N)_2$ (1 : 1 mol ratio) was stirred in dichloromethane at room temperature for 12 h. After filtration the resulting solution was concentrated and hexane was added yielding by precipitation a yellow (**I**) or white (**II**) solid. (**I**) yield: 60%. M.W.($CHCl_3$) Found(Calc.): 890(821). ^1H NMR ($CDCl_3$): δ 7.3 (m, 38H, Ph) ppm. $^{31}P\{^1H\}$ NMR ($CDCl_3$): δ −1.3(s) ppm. (**II**) yield: 65%. M.W.($CHCl_3$) Found(Calc.): 890(776). ^1H NMR ($CDCl_3$): δ 7.2 (s, 30H, C_6H_5), 5.2 (s, 1H, $\frac{1}{2}CH_2Cl_2$

crystallization), 2.1 (s, 6H, *exo* CH_3), 1.6 (s, 6H, *endo* CH_3) ppm. $^{31}P\{^1H\}$ NMR ($CDCl_3$): δ −1.5 (s) ppm. IR ν(N—H) (KBr) (**I**, **II**): 3000–2800 cm^{-1}.

Cu(oxine)$(PPh_3)_2$ (**III**) *and* $Cu_2(\mu\text{-}C_2O_4)(PPh_3)_4$ (**IV**). A mixture of Cu(acac)$(PPh_3)_2$ and 8-hydroxyquinoline (1:1 mol ratio) or $H_2C_2O_4 \cdot 2H_2O$ (1:0.5 mol ratio) were respectively stirred in dichloromethane or H_2CCl_2/MeOH (10:1) at room temperature for 24 h. The corresponding complexes were obtained from the filtered solutions as follows: (**III**) by precipitation after partial evaporation and addition of hexane. Yield: 90% M.W. ($CHCl_3$) Found (Calc.): 710(732.2). $^{31}P\{^1H\}$ NMR ($CDCl_3$): δ −2.5(s) ppm. (**IV**) dryness evaporation, extraction of solid residue with dichloromethane and addition of diethylether to the partially evaporated resulting solution. Yield: 90% M.W.($CHCl_3$) Found (Calc.): 1056 (1264). $^{31}P\{^1H\}$ NMR ($CDCl_3$): δ −3.9(s) ppm.

$[Cu_2\{\mu\text{-}(N—N)_2\}(PPh_3)_2]_2$; $(N—N)_2$ = bibzim^{2-}(**V**), tmbiim^{2-}(**VI**). A mixture of $H_2(N—N)$ (0.5 mmol) and KOH (2 mmol) in 30 ml of THF/MeOH (*ca* 3:1) was stirred for 0.5 h at room temperature and then $[Cu(CH_3CN)_2(PPh_3)_2]BF_4$ (1 mmol) was added. After stirring for 24 h the suspension was dryness evaporated and the solid residue extracted with 2×20 ml of H_2CCl_2. Partial evaporation under reduced pressure and addition of hexane led to the precipitation of cream (**V**) and light green (**VI**) microcrystalline solids. (**V**) Yield: 60%. M.W. ($CHCl_3$) Found (Calc.): 1941 (1766). ^1H NMR ($CDCl_3$) δ 7.1 (m, Ph) ppm. (**VI**) Yield: 75%. M.W. ($CHCl_3$) Found (Calc.): 1570 (1678). ^1H NMR ($CDCl_3$): δ 7.1 (m, 30H, Ph) δ 2.3 (s, 6H, CH_3), δ 1.7 (s, 6H, CH_3) ppm. $^{31}P\{^1H\}$ NMR ($CDCl_3$): δ −4.3 (s) ppm.

Reactions of $[Cu(CH_3CN)_2(PPh_3)_2]BF_4$ *with* H_2biim/KOH *and of* Cu(acac)$(PPh_3)_2$ *with* H_2biim (1:1 *mol ratio*). Reactions were carried out as described above for the preparation of (**I**) and (**II**) or (**V**) and (**VI**). Working up analogously, a white solid was obtained for both reactions. Both solids show identical IR (KBr pellet) spectra (ν(N—H) = 3000–2800 (m,br) cm^{-1}, biim, ring st, 1400(s), 1130(s) cm^{-1}) and elemental C, H, N analyses identified them as a mixture of Cu(Hbiim)$(PPh_3)_2$ and $[Cu_2(\mu\text{-biim})(PPh_3)_2]_2$.

Reaction of Cu(acac)$(PPh_3)_2$ *with* H_2tmbiim (1:0.5 *mol ratio*). A mixture of Cu(acac)$(PPh_3)_2$ and H_2tmbiim (1:0.5 mol ratio) was stirred in dichloromethane at room temperature for 24 h. Working up as described above for (**I**) and (**II**), a white microcrystalline solid was obtained. This was characterized as a mixture of (**II**) and (**VI**) by comparison of the ^1H NMR spectrum with those of the original samples.

Cationic complexes

$[Cu(CH_3CN)_2(PPh_3)_2]BF_4$. A mixture of $[Cu(CH_3CN)_4]BF_4$[20] and PPh_3 in dichloromethane (1:2 molar ratio) was stirred at room temperature for 6 h. After filtration a white microscrystalline solid is obtained by addition of hexane to the partially evaporated solution. Yield: 90%. C, N, H, Analyses: Found (Calc.): C 64.0 (63.5); N 3.8 (3.7); H 4.9 (4.8). Conductivity $\Lambda_M(\Omega^{-1}\,cm^2\,mol^{-1})$ (acetone): 132. ^1H NMR ($CDCl_3$): δ 7.18 (m, 30H, Ph), δ 2.07 (s, 6H, Me) ppm. IR (Nujol) μ(C≡N): 2285(vw), 2250(w) cm^{-1}.

$[Cu\{H_2(N—N)_2\}(PPh_3)_2]BF_4$; $H_2(N—N)_2$ = H_2biim (**VII**), H_2bibzim (**VIII**), H_2tmbiim (**IX**). To a dichloromethane solution of $[Cu(CH_3CN)_2(PPh_3)_2]BF_4$ (1 mmol), $H_2(N—N)_2$ (1 mmol) was added and then stirred at room temperature for 24 h. Complexes (**VII–IX**) were obtained from the filtered solutions after partial evaporation of the solvent and addition of diethylether. (**VII**) Yield: 75%. ^1H NMR ($CDCl_3$): δ 6.5–7.5 (m, Ph) ppm. $^{31}P\{^1H\}$ NMR ($CDCl_3$): δ 1.05(s) ppm. (**VIII**) Yield: 60%. ^1H NMR ($CDCl_3$): δ 7.2 (m, Ph) ppm. $^{31}P\{^1H\}$ NMR ($CDCl_3$): δ 0.0 (s) ppm. (**IX**) Yield: 90%. ^1H NMR ($CDCl_3$): δ 7.1 (m, Ph), δ 2.2 (s, 6H, *exo* CH_3), δ 1.75 (s, 6H, *endo* CH_3) ppm. $^{31}P\{^1H\}$ NMR ($CDCl_3$): δ −1.5 (s) ppm.

$[Cu\{H(N—N)\}_2(PPh_3)_2]BF_4$; H(N—N) = Him (**X**), Hpz (**XI**) *and* $[Cu(3,5\text{-}Me_2Hpz)(CH_3CN)(PPh_3)_2]BF_4$ (**XII**). To a dichloromethane solution of $[Cu(CH_3CN)_2(PPh_3)_2]BF_4$ (1 mmol), H(N—N) (2 mmol) was added and then stirred at room temperature for 24 h. Working up as above, complexes (**X**) and (**XI**) were obtained as white microcrystalline solids. (**X**) Yield: 80%. ^1H NMR ($CDCl_3$): δ 7.2, 7.1 (m, Ph) ppm. $^{31}P\{^1H\}$ NMR ($CDCl_3$): δ −2.5 (s) ppm. (**XI**) Yield: 70%. ^1H NMR ($CDCl_3$): δ 7.1 (m, Ph) ppm. $^{31}P\{^1H\}$ NMR ($CDCl_3$): δ −0.65 (s) ppm. (**XII**) Yield: 75%. IR (Nujol mull): ν(N—H) 3360 (m, br) cm^{-1}, ν(C≡N) 2260 (w) cm^{-1}, ν(C—N) ring 1580 (s) cm^{-1}. ^1H NMR ($CDCl_3$): δ 7.30, 7.15 (m, 30H, Ph), δ 2.05 (s, 6H, Me_2-pz), δ 1.95 (s, 3H, MeCN) ppm. $^{31}P\{^1H\}$ NMR ($CDCl_3$): δ −0.65 (s) ppm.

Acknowledgement—We thank the Comision Asesora de Investigación Científica y Técnica (CAICYT) for financial support.

REFERENCES

1. (a) *Metal Ions in Biological Systems*, Vol. 13, Copper Proteins (Edited by H. Siegel). Marcel Dekker, New

York (1981); (b) *Copper Coordination Chemistry: Biochemical Inorganic Perspectives* (Edited by K. D. Karlin and J. Zubieta). Academic Press, Guilderland, New York (1983); (c) *Biological and Inorganic Copper Chemistry* (Edited by K. D. Karlin and J. Zubieta). Adenine Press, Guiderland, New York (1986).
2. (a) T. N. Sorrell and D. L. Jameson, *J. Am. Chem. Soc.* 1983, **105**, 6013; (b) L. M. Engelhardt, C. Pakawatchai, A. H. White and P. C. Healy, *J. Chem. Soc., Dalton Trans.* 1985, 117 and refs therein.
3. J. C. Dyason, P. C. Healy, C. Pakawatchai, V. A. Patrick and A. L. White, *Inorg. Chem.* 1985, **24**, 1957 and refs therein.
4. L. M. Engelhardt, C. Pakawatchai, A. L. White and P. C. Healy, *J. Chem. Soc., Dalton Trans.* 1985, 125 and refs therein.
5. B. C. Green, C. H. L. Kennard, G. Smith, M. M. Elcombe, F. H. Moore, B. D. James and A. H. White, *Inorg. Chim. Acta.* 1984, **83**, 177; R. R. Gagné, J. C. Allison and G. L. Lisenski, *Inorg. Chem.* 1978, **17**, 3563.
6. M. P. Gamasa, E. García, J. Gimeno and C. Ballesteros, *J. Organomet. Chem.* 1986, **307**, 39 and refs therein.
7. R. Usón, L. A. Oro, J. Gimeno, M. A. Ciriano, J. Cabeza, A. Tiripicchio Camellini and M. Tiripicchio Camellini, *J. Chem. Soc., Dalton Trans.* 1983, 323.
8. (a) R. Usón, J. Gimeno, L. A. Oro, J. M. Martinez de Ilarduya, J. Cabeza, A. Tiripicchio and M. Tiripicchio Camellini, *J. Chem. Soc., Dalton Trans.* 1983, 1729; (b) R. Usón, J. Gimeno, J. Fornies and F. Martinez, *Inorg. Chim. Acta* 1981, **50**, 173.
9. R. Usón, J. Vicente and M. T. Chicote, *J. Organomet. Chem.* 1981, **209**, 271.
10. S. Sakaki, G. Koga and K. Ohkuto, *Inorg. Chem.* 1986, **25**, 2330.
11. T. Yamamoto, Y. Ehara, M. Kubota and A. Yamamoto, *Bull. Chem. Soc. Jpn.* 1980, **53**, 1299.
12. B. Hammond, F. J. Jardine and A. G. Vohra, *J. Inorg. Nucl. Chem.* 1971, **33**, 1017; C. Bianchini, C. Ghilardi, A. Meli, S. Midollini and A. Orlandini, *Inorg. Chem.* 1985, **24**, 924.
13. K. Nakamoto, *Infrared Spectra of Inorganic and Coordination Compounds*, pp. 210, 226. John Wiley, New York (1963).
14. S. W. Kaiser, R. B. Saillant, W. M. Butler and P. G. Rasmussen, *Inorg. Chem.* 1976, **15**, 2688.
15. (a) J. A. Tiethof, A. T. Hetey and D. W. Meek, *Inorg. Chem.* 1974, **13**, 2505; (b) P. C. Healey, C. Pakawatchai and A. L. White, *J. Chem. Soc., Dalton Trans.* 1985, 2531.
16. N. F. Borkett and M. J. Bruce, *J. Organomet. Chem.* 1974, **65**, C51.
17. B. F. Fieselmann, D. N. Hendrickson and G. B. Stucky, *Inorg. Chem.* 1978, **17**, 2078.
18. R. Kuhn and W. Blann, *Liebigs Ann. Chem.* 1975, **605**, 32.
19. D. Gibson, B. F. G. Johnson and J. Lewis, *J. Chem. Soc. A* 1970, 367.
20. G. J. Kubas, B. Monzyk and A. L. Crumbliss, *Inorg. Synth.* 1979, **19**, 90.

Polyhedron Vol. 7, No. 1, pp. 43–47, 1988
Printed in Great Britain

0277–5387/88 $3.00+.00
© 1988 Pergamon Journals Ltd

METAL DERIVATIVES OF 1,3-BIS(2-PYRIDYL)-1,3-PROPANEDIONE AND *N,N'*-DIMETHYL-1,3-BIS(2-PYRIDYL)-1,3-PROPANEDIONE

FRANCESC TEIXIDOR,* RAFAEL GARCIA, JOSEFINA PONS and JAUME CASABÓ

Institut de Ciència dels Materials, (C.S.I.C) i Departament de Química, Universitat Autònoma de Barcelona, Bellaterra 08193, Barcelona, Spain

(*Received* 24 *March* 1987; *accepted* 10 *July* 1987)

Abstract—Complexes of transition metal ions with the oxygen–nitrogen containing ligand 1,3-bis(2-pyridyl)-1,3-propanedione (bpypH) have been synthesized. These present stoichiometries which do not conform with the usual tendency manifested by β-diketones, since molecular formulas with the composition M(bpyp)X are found. A nitrogen methylated ligand *N,N'*-dimethyl-1,3-bis(2-pyridyl)-1,3-propanedione methyl sulphate [dimebpypH] $(MeSO_4)_2$ has also been synthesized and its complexes with transition metal ions studied. The stoichiometries now, resemble those of typical β-diketones, namely $[dimepyp]_2MX_4$ with four anions because of the dicationic nature of the original ligand. This, together with IR evidence suggests a dual type of coordination by bpip via the β-diketone and the pyridyl moieties.

Trinuclear metal complexes have been known for a long time, but most of them are the fortunate result of an unexpected synthesis such as $Ni_3(acac)_6$ or the complexation of a metal by two metal complexes acting as ligands such as $[Ni(MEA)_2]$ to give $[M(Ni(MEA)_2)]X_2$[1] or in few cases the complexation of two metal ions by one metal complex acting as a ligand.[2] These last two cases permit, *a priori*, the synthesis of heterotrinuclear complexes such as MM'M or M'MM'. We have chosen this last type of approach to the heterotrinuclear complexes by using a polynucleating β-diketone (1,3-bis-2-hydroxyphenyl)-1,3-propanedione ($bhppH_3$).[3] With it we envisaged the possibility of getting trinuclear complexes with a metal distribution that could be arranged as MM'M or M'MM', depending on the metal which had been inserted first. The different reactivity of the β-diketone vs the ketophenol group permitted the synthesis of isomerically pure mononuclear complexes,[4] which upon the addition of a different metal salt and an appropriate base would yield the heterotrinuclear complex. One of the major problems other research groups have encountered consisted of the synthesis of isomerically pure mononuclear complexes. Fortunately, this has not been our case. Due to the greater reactivity of the β-diketone vs the ketophenol moiety, pure mononuclear complexes have in all cases been found. However, upon the addition of the second two metals, a metal redistribution has been observed in the synthesis of $(UO_2)Co(UO_2)$ complexes, where CoCoCo and $(UO_2)Co(UO_2)$ complexes have been found.[5] This is due to the fact that the reacting conditions have to be forced to overcome the low reactivity of the ketophenol moiety.

With the aim of getting new polynucleating ligands which would enhance the reactivity of the outer reacting sites with respect to those in $bhppH_3$, we have synthesized the ligand bpypH 1,3-bis-(2-pyridyl)-1,3-propanedione. This ligand would not permit a metal linearity such as is presented by the other ligand $bhppH_3$, described in Fig. 1, but it was interesting to know its possibilities, especially the competition between both types of reacting sites.

The present paper concentrates on the synthesis of 1,3-bis-(2-pyridyl)-1,3-propanedione (bpypH), *N,N'*-dimethyl-1,3-bis-(2-pyridyl)-1,3-propanedione methyl sulphate $(dimebpypH)(MeSO_4)_2$ and their metal complexes. The complexes present different stoichiometries depending upon whether

* Author to whom correspondence should be addressed.

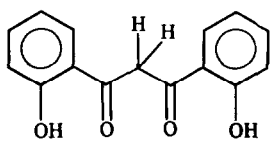

Fig. 1. The ligand $bhppH_3$ 1,3-bis-(2-hydroxyphenyl)-1,3-propanedione.

bpypH or dimepypH has been used as a ligand. We conclude that in the first case the ligand has coordinated to the metal via the pyridine nitrogen and the β-diketone units, while in the second case it only coordinates through the β-diketone unit.

EXPERIMENTAL

Starting materials

All reagents and solvents were commercial grade materials and were used after drying them with Na/benzophenone (toluene); Mg (ethanol) or without further purification. Methyl picolinate was synthesized from picolinic acid (FLUKA) following Sneed's procedure.[6] It was extremely important to have this compound very dry, otherwise the reaction did not occur.

Synthesis of 1,3-*bis*-(2-*pyridyl*)-1,3-*propanedione* (bpypH)

Sodium (0.67 g, 29.1 mmol) was placed in a round bottom flask, equipped with a magnetic stirrer and blanketed with dinitrogen, containing dry and degassed ethanol (20 cm^3). Once the sodium had been consumed the ethanol was evaporated off at the vacuum line. A white solid corresponding to sodium ethoxide was obtained.

Dry toluene (25–30 cm^3) and methyl picolinate (4 g, 29.1 mmol) were added to the flask, and very slowly, α-Pyridyl methyl ketone (4.95 g, 40.9 mmol) was added. During the addition care was taken to ensure that the temperature would be kept between 45–60°C. In this period the mixture changed from yellow to dark red. Without heating, the semi-solid mass was stirred for 30 min, until an off-white solid appeared. It was again gently warmed for 15 min, cooled at room temperature, filtered and dried.

The solid was slowly poured with constant and vigorous stirring into a mixture containing 30 cm^3 of acetic acid, 30 cm^3 of water and 100 g of ice, yielding a white solid, which was filtered and recrystallized in ethanol (yield 5.3 g, 80%) (m/e 226 corresponding to M). IR ν(C=O) 1600 cm^{-1}, ν(py) = 1580–1530 cm^{-1}.

Found: C, 68.9; H, 4.5; N, 12.4. Calc. for $C_{13}H_{10}N_2O_2$: C, 69.0; H, 4.5; N, 12.4%.

Synthesis of complexes with the general formula (bpyp)M(AcO)·xH_2O

To a three-necked flask equipped with a reflux condenser and two additional funnels containing, in the first 1,3-bis-(2-pyridyl)-1,3-propanedione (bpyp) (0.4 g, 1.77 mmol) in isopropanol (20 cm^3), and in the second the appropriate metal acetate (1.77 mmol) in methanol (20 cm^3), was added isopropanol (80 cm^3). The isopropanol was refluxed and the contents of the two additional funnels were added drop by drop at the same speed. The reaction proceeded differently as a function of the metal M, yielding solids (M = Cu, Zn) or solutions (M = Co, Ni).

When solids were obtained these were filtered and washed with isopropanol. In the other cases solids were obtained upon the addition of acetone, which were filtered and washed with isopropanol/acetone. Finally, all were dried *in vacuo*.

Analysis: For M = Zn; Found: C, 49.3; H, 3.6; N, 7.6; Zn, 17.8. Calc. for $C_{15}H_{12}N_2O_4Zn$: C, 49.0; H, 3.8; N, 7.6; Zn, 17.8%. For M = Cu; Found: C, 48.9; H, 3.6; N, 7.6; Cu, 17.0. Calc. for $C_{15}H_{12}N_2O_4Cu$: C, 49.2; H, 3.9; N, 7.7; Cu, 17.4%. For M = Co; Found: C, 45.6; H, 4.4; N, 6.8; Co, 14.9. Calc. for $C_{15}H_{12}N_2O_4Co$: C, 45.4; H, 4.7; N, 7.1; Co, 14.8%. For M = Ni; Found: C, 45.3; H, 4.3; N, 6.9; Ni, 15.1. Calc. for $C_{15}H_{12}N_2O_4Ni$: C, 45.4; H, 4.6; N, 7.1; Ni, 14.8%.

Synthesis of complexes with general formula (bpyp)MX·xH_2O (X = Cl, Br, SCN)

To a three-necked flask equipped with a reflux condenser and two additional funnels containing, in the first 1,3-bis-(2-pyridyl)-1,3-propanedione (bpyp) (0.4 g, 1.77 mmol) in isopropanol (20 cm^3), and in the second the appropriate metal salt (1.77 mmol) in methanol (20 cm^3), was added isopropanol (80 cm^3). The isopropanol in the flask was refluxed and the contents of the two additional funnels were added drop by drop at the same speed. A solid appeared in all cases, which was filtered, washed with isopropanol and dried *in vacuo*.

Analysis: For M = Cu; Found: C, 46.9; H, 3.0; N, 8.2; Cu, 18.8. Calc. for $C_{13}H_9N_2O_2$·$CuCl·0.5H_2O$: C, 46.9; H, 3.0; N, 8.4; Cu, 19.1%. For M = Co; Found: C, 41.8; H, 3.7; N, 7.5; Co, 15.5. Calc. for $C_{13}H_9N_2O_2CoCl·3H_2O$: C, 41.7; H, 4.0; N, 7.5; Co, 15.8%. For M = Ni; Found: C, 41.5; H, 3.7; N, 7.3; Ni, 15.4. Calc. for $C_{13}H_9N_2O_2NiCl·3H_2O$: C, 41.8; H, 4.0; N, 7.5; Ni, 15.7%. For M = Zn; Found: C, 42.0; H, 2.5; N, 7.8; Zn, 17.6. Calc. for $C_{13}H_9N_2O_2ZnBr$: C, 42.1; H, 2.4; N, 7.6; Zn, 17.6%. For M = Cu;

Found: C, 40.1; H, 2.5; N, 7.3; Cu, 16.3. Calc. for $C_{13}H_9N_2O_2CuBr \cdot H_2O$: C, 40.4; H, 2.9; N, 7.2; Cu, 16.4%. For M = Ni; Found: C, 46.5; H, 3.0; N, 11.9; Ni, 16.2. Calc. for $C_{14}H_9N_3O_2SNi \cdot H_2O$: C, 46.7; H, 3.1; N, 11.7; Ni, 16.3%. For M = Co; Found: C, 46.4; H, 3.0; N, 11.8; Co, 16.4. Calc. for $C_{14}H_9N_3O_2SCo \cdot H_2O$: C, 46.7; H, 3.1; N, 11.7; Co, 16.4%.

Synthesis of N,N'-dimethyl-1,3-bis-(2-pyridyl)-1,3-propanedione (dimebpypH) *methyl sulphate*

To a warm solution of 1,3-bis-(2-pyridyl)-1,3-propanedione (0.5 g, 2.2 mmol) in acetonitrile (10 cm^3) was added dimethyl sulphate (0.781 g, 6.2 mmol). After refluxing the resulting solution for 1 h, a yellow solid precipitated. The heating was continued for an additional 0.5 h and after cooling to room temperature the solid was filtered, washed with isopropanol/ether and dried *in vacuo*.

Analysis: Found: C, 37.4; H, 4.5; N, 5.9. Calc. for $C_{17}H_{22}N_2S_2O_{10}$: C, 37.7; H, 4.6; N, 5.9%.

Synthesis of complexes with general formula (dimebpyp)MX_4 (M = Zn, Cd, Cu, Mn, Ni, Co; X = $MeSO_4$, MeCOO).

A warm solution of the appropriate metal acetate (a 20% in excess of the stoichiometric amount) in methanol (5 cm^3), was added to a flask containing dimebpyp (0.2 g, 0.42 mmol) in warm methanol (10 cm^3) (isopropanol when M = Cd). The solution was refluxed yielding a solid in each case. The mixture was kept at 60°C for one day and was filtered, washed with isopropanol and dried *in vacuo*.

Analysis: For M = Zn, X = CH_3SO_4; Found: C, 39.9; H, 4.3; N, 5.2. Calc. for $C_{34}H_{42}N_4S_4O_{20}Zn$: C, 40.0; H, 4.1; N, 5.5%. For M = Cd, X = CH_3SO_4; Found: C, 37.9; H, 3.9; N, 5.0. Calc. for $C_{34}H_{42}N_4S_4O_{20}Cd$: C, 38.3; H, 3.9; N, 5.3%. For M = Cu, X = CH_3SO_4; Found: C, 39.5; H, 4.0; N, 6.4. Calc. for $C_{34}H_{42}N_4S_4O_{20}Cu$: C, 40.0; H, 4.1; N, 6.3%. For M = Mn, X = CH_3SO_4; Found: C, 39.8; H, 4.1; N, 5.2. Calc. for $C_{34}H_{42}N_4S_4O_{20}Mn$: C, 40.4; H, 4.2; N, 5.5%. For M = Ni, X = CH_3COO; Found: C, 56.4; H, 5.1; N, 6.8. Calc. for $C_{38}H_{42}N_4O_{12}Ni$: C, 56.6; H, 5.2; N, 7.0%. For M = Co, X = CH_3COO; Found: C, 56.3; H, 5.1; N, 6.7. Calc. for $C_{38}H_{42}N_4O_{12}Co$: C, 56.6; H, 5.2; N, 7.0%.

RESULTS

The reaction of methyl picolinate with α-pyridyl methyl ketone in the presence of sodium ethanolate gives the sodium salt of 1,3-bis-(2-pyridyl)-1,3-propanedione (bpypH). Further treatment of this with acetic acid yields the corresponding β-diketone with a good overall yield (eq. 1).

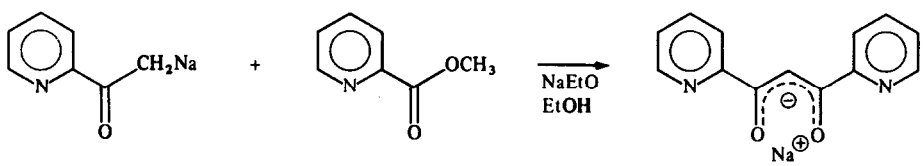

(1)

Further reaction of bpypH with dimethyl sulphate in acetonitrile afforded *N,N'*-dimethyl-1,3-(2-pyridyl)-1,3-propanedione (dimebpypH) methyl sulphate (eq. 2).

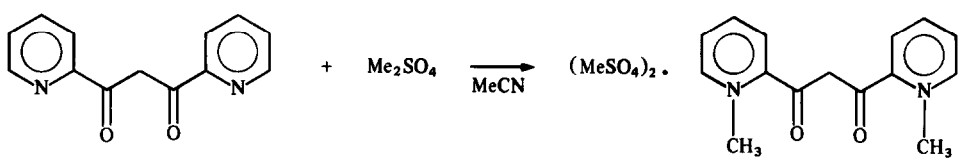

(2)

Reaction of bpypH with metal acetates, chlorides, bromides or thiocyanates in alcohols afforded compounds with general formula (bpyp)$MX \cdot xH_2O$ where M = Cu, Co, Ni, Zn, X = $MeCO_2$, Cl, Br, SCN.

$$\text{bpypH} + MX_2 \xrightarrow[\text{alcohol}]{} (\text{bpyp})MX + HX. \quad (3)$$

Reaction of [dimebpypH]X_2 with metal acetates yielded compounds with general formula (dimebpyp)$_2MX_4 \cdot xH_2O$, X being acetate or $MeSO_4^-$.

$$2[\text{dimebpypH}]X_2 + MX_2 \xrightarrow[\text{alcohol}]{} (\text{dimebpyp})_2MX_4 + 2HX. \quad (4)$$

The ^{1}H-NMR spectrum of bpypH clearly evidences the coexistence in chloroformic solution of the

β-diketone and the enolic forms in approximately 74 to 26 molar ratio.

DISCUSSION

The general tendency exhibited by β-diketones when they are complexed with metals, is to present stoichiometries with as many β-diketone ligands as the value of the metal charge. Surprisingly, this was not found in any of the bpyp complexes we synthesized, where stoichiometries (bpyp)MX have been found.[7] This tendency can be attributed to the greater reactivity of the pyridyl group as compared to the phenol group which was a part of the ligand $bhppH_3$ and to the comparable reactivity of the pyridyl and β-diketone groups towards first series transition metal ions.

It is clear the β-diketone coordinates to the metal, as indicated by the IR-spectrum (ν(C=O) in complexes 70 cm^{-1} lower than in the free ligand), but it is more difficult to prove the pyridyl linkage to the metal. We have observed in other pyridine compounds a larger splitting of the two pyridine bands near 1600 cm^{-1}, when this is metal coordinated than when the pyridine is free. In this case, even though there are other bands in the free ligand (C=O, pyridine) that appear at the same IR position, we observe a well resolved fine structure at 1600 cm^{-1} that is not observed in the free ligand, which suggests pyridine coordination to the metal.

Another support of the pyridine coordination is given by the visible spectrum of the copper complexes in pyridine solution, which are the same colour as the solid. A band at 730 nm is observed which can be attributed to a copper in a square pyramidal environment with oxygen and nitrogen.[8] Attempting to get more information than this may be risky because of the interaction of the solid with the coordinating solvents, which clearly can modify the stereochemistry and the environment of the metal.

Unfortunately, all attempts to get crystals suitable for an X-ray diffraction analysis failed, so in order to get more evidence on the nitrogen coordination to the metal, the nitrogen methylated derivative was synthesized. This would prevent nitrogen coordination and a new type of stoichiometry was expected. This indeed happened and stoichiometries $M(dimebpyp)_2X_4$ were found. Even though we do not have any crystal structures of these compounds (cobalt crystals were obtained but they broke down immediately they were taken out of the mother liquor) their structure is presumed to be similar to that found in $M(bhppH_2)_2$ compounds[3,4] namely to say, octahedral for Zn, Ni, Co and square planar for Cu^{2+}, with both β-diketone

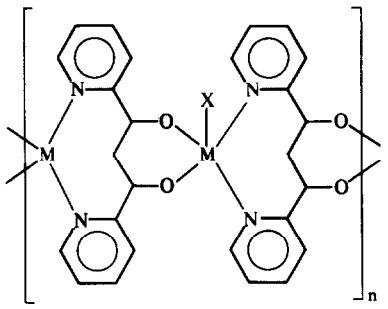

Fig. 2. A polymer like structure for M(bpyp)X not acceptable because of the long M—N distance.

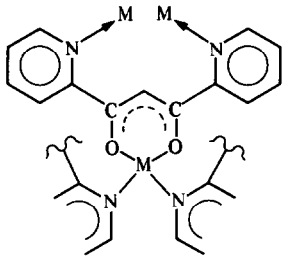

Fig. 3. Polymer structure proposed for M(bpyp)X.

ligands placed in the same plane.[9] We assume these structures on the basis of their IR, colour (Co, Mn = Orange; Zn, Cd = Yellow; Ni, Cu = Green) and UV-visible that correspond very well with those found in the aforementioned $M(bhppH_2)_2$ compounds.[3,4] Indirectly, the stoichiometries obtained with dimebpyp, prove the nitrogen coordination to the metal in bpyp, but do not give any more information on how this coordination takes place.

A polymer like structure such as that depicted in Fig. 2 is not acceptable because of the long M—N distance, so we propose a type of coordination where the ligand acts as chelating via the β-diketone but as monodentate via every pyridine nitrogen (Fig. 3).

Acknowledgement—We thank the C.A.I.C.Y.T. (Ministerio de Educación y Ciencia) for support of this research (grant 409/84).

REFERENCES

1. (a) D. C. Jicha and D. H. Busch, *Inorg. Chem.* 1968, **1**, 872, 878; (b) D. H. Busch, D. C. Jicha, M. C. Thompson, J. W. Wrathall and E. Blinn, *J. Am. Chem. Soc.* 1964, **86**, 3642.
2. (a) R. L. Lindvedt, B. A. Schoenfelner, C. Cercarelli and M. D. Glick, *Inorg. Chem.* 1984, **23**, 2867; (b) J. Colomer, J. Casabó, F. Teixidor, C. Miravitlles, E. Molins and J. Rius, submitted for publication.
3. F. Teixidor, A. Llobet, L. Escriche and J. Casabó, *Polyhedron* 1984, **3**, 1017.

4. F. Teixidor, A. Llobet, L. Escriche and J. Casabó, *Polyhedron* 1985, **4**, 215.
5. J. Colomer, J. Casabó and F. Teixidor, submitted for publication.
6. R. Levine and J. K. Sneed, *J. Am. Chem. Soc.* 1951, **73**, 5614.
7. R. C. Mehrota, R. Bohra and D. P. Gaur, *Metal β-diketone and allied derivatives*. Academic Press, New York (1978).
8. B. J. Hathaway and A. A. G. Tomlinson, *Coord. Chem. Rev.* 1970, **5**, 1.
9. X. Solans, M. Font-Altaba, J. L. Briansó, A. Llobet, F. Teixidor and J. Casabó, *Acta Cryst.*, 1983, **C39**, 1512.

Polyhedron Vol. 7, No. 1, pp. 49–55, 1988
Printed in Great Britain

0277–5387/88 $3.00+.00
© 1988 Pergamon Journals Ltd

THE DIRECT ELECTROCHEMICAL SYNTHESIS OF ADDUCTS OF BIS(DIPHENYLPHOSPHINO)METHANE (dppm) WITH COPPER(I) THIOLATES AND THE X-RAY CRYSTAL STRUCTURE OF $Cu_4(\mu\text{-}SC_5H_{11})_4(dppm)_2$

MASOOD A. KHAN, RAJESH KUMAR and DENNIS G. TUCK*

Department of Chemistry and Biochemistry, University of Windsor, Windsor, Ontario, Canada N9B 3P4

(*Received* 14 *May* 1987; *accepted* 10 *July* 1987)

Abstract—Adducts of bis(diphenylphosphino)methane (dppm) with copper(I) thiolates can be prepared by oxidizing anodic copper into an acetonitrile solution of dppm and RSH (R = *n*-C_4H_9, C_5H_{11}, C_6H_5, *o,m,p*-$CH_3C_6H_4$, 2-naphthyl). The products are $(CuSR)_2 \cdot$ dppm for R = *n*-C_4H_9, C_5H_{11} or C_6H_5, and $CuSR \cdot 1.5$dppm for R = *o*-$CH_3C_6H_4$ or 2-naphthyl. No adducts were obtained for R = *m*- or *p*-$CH_3C_6H_4$. Reaction between $(CuSC_5H_{11})_2 \cdot$dppm ($C_5H_{11} = C_2H_5C(CH_3)_2$-) and CS_2 gives the insertion product $CuS_2CSC_5H_{11} \cdot$dppm. An X-ray crystallographic study of $(CuSC_5H_{11})_2 \cdot$dppm reveals the presence of a novel Cu_4S_4 ring, in which sulphur atoms are below a Cu_4 plane; this Cu_4S_4 ring is capped by two six-membered Cu_2SCP_2 rings in the boat form.

The direct electrochemical synthesis of thiolato complexes of zinc,[1,2] cadmium,[1,2] mercury,[1] tin,[3] lead[3] and indium[4] has been the subject of recent papers from this laboratory. As in the other applications of this technique, which involves the anodic oxidation of a metal in a non-aqueous solution of the ligand precursor, the most important advantages are the simplicity of the technique and the high product yield. In the case of copper or silver, solutions of either alkyl or aryl thiols give rise to the MSR compounds in a one-step synthesis and adducts of CuSR with donors such as 1,10-phenanthroline are also accessible by the electrochemical route.[5,6] The reaction of $CuSC_5H_{11}$ with carbon disulphide gave the unusual copper(I)–thiolato–thioxanthato cage complex $Cu_8(SC_5H_{11})_4(S_2CSC_5H_{11})_4$.[5]

We now report an extension of this work to the preparation of adducts of various copper(I) thiolates with the bidentate phosphorus donor bis(diphenylphosphino)methane(dppm). The crystal structure of the adduct formed with $CuSC_5H_{11}$ reveals the presence of a central Cu_4S_4 ring, capped by Cu_2SCP_2 boat-form rings. The reaction between this compound and carbon disulphide results in the insertion of CS_2 into the Cu—S bond.

EXPERIMENTAL

General

Solvents were distilled from calcium hydride and stored over molecular sieves. Copper was used as foils, 0.25 mm thick, which were washed successively with conc. nitric acid and distilled water then dried before use. Thiols and dppm (Aldrich) were used as supplied.

Copper analysis was by atomic absorption spectrophotometry then microanalyses were carried out by Guelph Chemical Laboratories Ltd. Infrared spectra were recorded on a Nicolet 5DX instrument. Proton NMR spectra were obtained with a Bruker WP-80, and ^{31}P spectra with a Bruker 90 spectrometer. Mass spectra were recorded on a Varian MAT CH-5 spectrometer operating in the E.I. mode.

Electrochemical procedures

The general method was that described in previous papers,[1–3,6,7] using a cell of the form:

$$Pt_{(-)}/CH_3CN + RSH + dppm/Cu_{(+)}.$$

* Author to whom correspondence should be addressed.

Table 1. Experimental conditions for the electrochemical synthesis of dppm (= L) adducts of copper(I) thiolates

Thiol	Quantity[a] (cm^3)	dppm[a] (g)	Initial[b] voltage (v)	Time of electrolysis (h)	Metal dissolved (g)	Product
n-C_4H_9SH	1.5	0.9	25	4.3	0.32	$(CuSR)_2 \cdot L$
$C_5H_{11}SH$[c]	1	0.8	5	2.5	0.18	$(CuSR)_2 \cdot L$
C_6H_5SH	1	1.0	10	3	0.22	$(CuSR)_2 \cdot L$
o-$CH_3C_6H_4SH$	1	1.0	10	4	0.29	$CuSR \cdot 1.5L$
m-$CH_3C_6H_4SH$	1.5	0.8	20	3.3	0.26	CuSR
p-$CH_3C_6H_4SH$	0.5	0.9	5	5	0.36	See text
2-$C_{10}H_7SH$	0.5(g)	0.7	10	2.5	0.19	$CuSR \cdot 1.5L$

[a] In 50 cm^3 acetonitrile, plus *ca* 25 mg Et_4NClO_4.
[b] Voltage required to produce an initial current of 30 mA.
[c] $C_5H_{11}SH$ = 2-methyl-2-butanethiol.

Details of solution composition, etc. are given in Table 1. All operations were carried out under a flow of dry nitrogen, which bubbled through the solution thereby mixing the contents of the cell. As the experiment proceeded, hydrogen was evolved at the cathode and the solution became yellow as soluble products formed. Yellow solids eventually precipitated as the nitrogen flow continued and were collected, washed with *n*-pentane and dried *in vacuo*. In the case of $(CuSR)_2 \cdot$dppm, with R = *n*-C_4H_9, C_5H_{11} (= $C_2H_5C(CH_3)_2$-) and 2-$C_{10}H_7$, precipitation continued over a period of 12 h after the end of electrolysis, whereas for $(CuSC_6H_4CH_3$-*o*$) \cdot 1.5$ dppm and $(CuSC_6H_5)_2 \cdot$dppm, precipitation was essentially complete at the end of the electrolysis. No adducts were obtained with R = *m*- or *p*-$CH_3C_6H_4$. In the former case, the product was CuSR (Found: Cu, 33.8%, Calc. for $CuSC_6H_4CH_3$: Cu, 34.0%); with the *para* compound, the infrared spectrum showed the presence of dppm in the product, but copper analysis (Found: Cu, 28.5%) suggested that the product was a mixture of CuSR and a dppm adduct. These systems were not investigated further. Yields were generally better than 90%, based on the quantity of metal dissolved from the anode.

These dppm addition compounds are soluble in benzene and chlorinated hydrocarbons, and in some cases react with carbon disulphide (see below). The products were characterized by elemental analysis (Table 2), and by infrared and ^1H NMR spectroscopy (Table 3) which established the presence of the RS^- and dppm ligands. The spectra reported in Table 3 refer to freshly prepared solutions; in the case of the arylthiolato derivatives slow decomposition occurred, as evidenced by the appearance of the blue–green colour of copper(II) in the solution.

Reaction with carbon disulphide

$(CuSC_5H_{11})_2 \cdot$dppm (0.5 g, 0.70 mmol) was dissolved in CS_2 (40 cm^3), giving a red–brown solution which was stirred for 2 h, during which time an orange solid began to precipitate. The mixture was stirred for 3 days at ambient temperature, after which the solid was collected, washed with CS_2 and then *n*-pentane, and dried *in vacuo*. Found: Cu, 9.5. Calc. for $CuS_2CSC_5H_{11} \cdot$dppm, $C_{31}H_{33}CuP_2S_3$, Cu, 10.1%. The mass spectrum showed prominent peaks at m/e = 666 $(CuSC_5H_{11})_4^+$: 595 $Cu_4(SC_5H_{11})_3S^+$: 524 $(CuSC_5H_{11} \cdot CuS)_2^+$: 453

Table 2. Analytical results for dppm adducts of copper(I) thiolates

Compound	Found (%) Cu	C	H	N	Calc. (%) Cu	C	H	N
$(CuSC_4H_9$-*n*$)_2 \cdot$dppm	18.8				18.4			
$(CuSC_5H_{11})_2 \cdot$dppm	18.1	58.8	6.47		17.7	58.6	6.14	
$(CuSC_6H_5)_2 \cdot$dppm	17.2	61.5	4.88		17.4	60.9	4.39	
$(CuSC_6H_4CH_3$-*o*$) \cdot$1.5dppm	8.2	70.2	5.70		8.4	70.0	5.24	
$CuSC_{10}H_7 \cdot$1.5dppm	7.4	71.4	5.10		8.0	71.1	5.41	

Table 3. ^1H and ^{31}P NMR spectra of dppm adducts of copper(I) thiolates[a]

Compound	^1H Aromatic[b]	^1H CH_2(dppm)	^1H Alkyl Thiolate[c]	^{31}P
dppm	7.25 m(10)	2.76 t(1)	—	−22.93[d]
$(CuSC_4H_9\text{-}n)_2 \cdot$ dppm	7.15 m(10)	3.25 t(1)	2.42 t, 1.16m, 0.65 t(10)	−14.73
$(CuSC_5H_{11})_2 \cdot$ dppm	7.22 m(10)	2.95 t(1)	1.49 q, 1.30 s, 0.88 t(11)	−17.23
$(CuSC_6H_5)_2 \cdot$ dppm	6.98 m,br	2.73 s,br[e]	—	−14.17
$(CuSC_6H_4CH_3\text{-}o) \cdot$ 1.5dppm	7.01 m,br(11.5)	2.66 s,br(1)	2.38 s(1)(o-CH_3)	−18.93
$CuSC_{10}H_7 \cdot$ 1.5dppm	7.38 m,br	2.48 s,br[e]	—	−18.76
$CuS_2CSC_5H_{11} \cdot$ dppm	—	—	—	−36.86

[a] In CD_2Cl_2 solution. Frequencies for ^1H, ppm from Me_4Si and for ^{31}P, ppm for 85% H_3PO_4. Integrated relative intensities in parentheses. m = multiple, q = quartet, t = triplet, s = singlet, br = broad.

[b] Frequency at most intense peak.

[c] Total relative intensity of alkyl hydrogens.

[d] Lit. value −23.00 ppm (T. G. Appleton, M. A. Bannett and I. B. Tomkins, *J. Chem. Soc., Dalton Trans.* 1976, 439).

[e] Poor integration: see text.

$CuSC_5H_{11}$ $(CuS)_3$: 421 $Cu_4SC_5H_{11}S_2^+$: 382 $(C_6H_5)_4P_2CH_2^+$: 262 Ph_3P^+: 199 $(C_6H_5)_2PCH_2^+$. When these experiments were repeated with $(CuSC_6H_4CH_3\text{-}o) \cdot$ 1.5dppm (0.24 g, 0.31 mmol) and excess CS_2 using similar procedures, identical colour changes were observed and a precipitate was obtained. This was dissolved in benzene (10 cm^3), ethanol (30 cm^3) added to this solution and the mixture left overnight. The yellow solid which then appeared was shown to be the starting material (Found: Cu, 8.1. Calc. Cu, 8.3%) recovered in 70% yield.

Decomposition of $CuS_2CSC_5H_{11} \cdot$ dppm

(i) $CuS_2CSC_5H_{11} \cdot$ dppm (0.25 g, 0.40 mmol) was added to benzene (20 cm^3) and the solvent brought to reflux, to give a dark red–brown solution. After about 15 min, the colour changed to pale yellow. After a further 2 h reflux, the solution was taken to dryness, yielding a yellow gummy solid; addition of n-pentane (15 cm^3) caused this material to decompose, with traces of a green solid being formed. We were unable to characterize the yellow solid obtained.

(ii) A similar treatment of a suspension of $CuS_2CSC_5H_{11} \cdot$ dppm (0.29 g) in refluxing n-hexane (30 cm^3) underwent a colour change within the first hour to give a deep red–brown mixture. On further refluxing, much of the red suspended solid dissolved. After 18 h, the mixture was filtered and the filtrate taken to dryness *in vacuo*; the resultant red–brown residue was dissolved in acetonitrile (3 cm^3) and reprecipitated by the addition of methanol (20 cm^3) followed by slow evaporation. The final solid consisted of a mixture of colourless and red crystals. The former melted at 118–122°C (c.f. dppm, M.p. 121°C), and the latter at 135–142°C (c.f. $CuS_2CSC_5H_{11} \cdot$ dppm, m.p. 140°C). The ^1H NMR spectrum of the red crystals confirmed the presence of dppm.

Crystallography

A pale yellow crystal of $(CuSC_5H_{11})_2 \cdot$ dppm (**1**), dimensions 0.15 × 0.15 × 0.20 mm, was mounted in a Syntex $P2_1$ diffractometer, and data collected by the methods normally used in this laboratory.[8] The results were corrected for Lorentz and polarization effects; absorption was judged to be negligible, and no such corrections were made. Table 4 gives the appropriate experimental details.

The intensity statistics suggested a centric space group and the space group $P\bar{1}$ was assumed and subsequently confirmed by the successful refinement. The structure was solved by direct methods (SHELX-76)[9] and refined by a least-squares method, minimizing the function $\Sigma w(|F_o|-|F_c|)^2$, where $w = [\sigma^2(F_o)+0.0001F_o^2]^{-1}$. When the positional and anisotropic parameters of the non-hydrogen atoms were refined in two blocks, the carbon atoms of the thiolato ligands, and especially C(9) and C(10), showed large thermal parameters, suggesting a significant disorder for these atoms. In the final cycles of refinement, hydrogen atoms were only included on the phenyl and C(01) methylene carbon atoms; an idealized geometry, with r(C—H) = 0.95 Å, was assumed and individual iso-

Table 4. Summary of crystal data, intensity collection and structural refinement for **1**

Formula, *fw*	$C_{70}H_{88}Cu_4P_4S_4$, 1435.81
Cell constants[a] at 22°C	*a*, 12.350(2) Å; α, 63.97(1)°
	b, 14.143(3) Å; β, 102.71(2)°
	c, 12.430(3) Å; γ, 113.21(1)°
Cell volume (Å^3)	1790 (1)
Space group	$P\bar{1}$
Z	1
d (calc.), (exp.) (g cm^{-3})	1.332, 1.35[b]
Absorption coefficient (cm^{-1})	13.5
Radiation	MoK_α (λ = 0.71069 Å)
2θ (max) for data collection	45°
Scan width	Kα_1 − 0.8° to Kα_2 + 0.8°
Total reflections measured	
$(-h, \pm k, \pm l)$	4764
Unique "observed" reflections	
$(I \geqslant 2\Sigma(I))$	3108
$R = (\Sigma \|\|F_o\| - \|F_c\|\|)/\Sigma\|F_o\|)$	0.056
$R_w = (\Sigma w(\|F_o\| - \|F_c\|)^2/\Sigma w\|F_o\|^2)^{1/2}$	0.058
$S = [\Sigma(w(\|F_o\| - \|F_c\|)^2/(m-n)]^{1/2}$	1.6
Shift/e.s.d. (max) in the final cycle	0.4
Max (e Å^{-3}) in the final dimap	0.7

[a] Cell constants were derived by least-squares analysis of the diffractometer angular setting of 28 well-centred reflections (2θ range = 20–26°).

[b] Measured in a mixture of cyclohexane and CCl_4.

tropic temperature factors were refined for each of these hydrogen atoms. The final *R* value was 0.056, with $R_w = 0.058$.

The source of atomic scattering factors and the computer programmes used in the calculations, were those used previously.[10] Selected bond distances and angles are given in Table 5, and Fig. 1 shows the molecular structure with the atomic numbering scheme. Tables of atom coordinates, anisotropic thermal parameters, bond lengths and angles in the phenyl and thiolato groups, and observed and calculated structure factors, are available as supplementary material from the Editor.

RESULTS AND DISCUSSION

Preparative and spectroscopic

The results show that the preparation of dppm adducts of various copper(I) thiolates is readily achieved by the one-step high yield syntheses described. The stoichiometry clearly depends on the nature of the organic group attached to the thiolato sulphur atom, since both 1 : 1 and 1 : 1.5 adducts

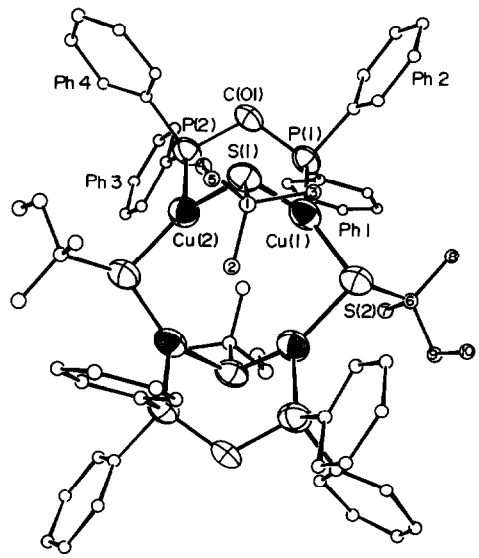

Fig. 1. Structure of the centrosymmetric molecule of **1**. For clarity, hydrogen atoms are omitted and the carbon atoms of the phenyl and thiol groups are plotted as spheres of arbitrary size. All the other atoms are plotted as 50% probability thermal ellipsoids. The numbering scheme for the phenyl carbon atoms follows that for the corresponding rings (C11, C12, . . . etc.).

Table 5. Selected bond lengths (Å) and angles (°) for **1**

(a) Bond lengths			
Cu(1)—S(1)	2.268(2)	S(2)—C(6)	1.884(10)
Cu(1)—S(2)	2.221(2)	P(1)—C(01)	1.861(7)
Cu(1)—P(1)	2.246(1)	P(1)—C(11)	1.825(9)
Cu(2)—S(1)	2.241(3)	P(1)—C(21)	1.834(10)
Cu(2)—S(2)[a]	2.253(3)	P(2)—C(01)	1.862(8)
Cu(2)—P(2)	2.301(2)	P(2)—C(31)	1.821(10)
S(1)—C(1)	1.876(8)	P(2)—C(41)	1.844(10)
(b) Angles			
S(1)—Cu(1)—S(2)	119.5(1)	Cu(1)—P(1)—C(11)	123.2(3)
S(1)—Cu(1)—P(1)	103.3(1)	Cu(1)—P(1)—C(21)	110.5(2)
S(2)—Cu(1)—P(1)	135.8(1)	C(01)—P(1)—C(11)	105.9(4)
S(2)[a]—Cu(2)—S(1)	141.8(1)	C(01)—P(1)—C(21)	97.8(4)
S(1)—Cu(2)—P(2)	100.5(1)	C(11)—P(1)—C(21)	102.3(4)
S(2)[a]—Cu(2)—P(2)	117.2(1)	Cu(2)—P(2)—C(01)	113.5(2)
Cu(1)—S(1)—Cu(2)	85.9(1)	Cu(2)—P(2)—C(31)	124.7(3)
Cu(1)—S(1)—C(1)	113.3(3)	Cu(2)—P(2)—P(41)	106.2(2)
Cu(2)—S(1)—C(1)	119.0(4)	C(01)—P(2)—C(31)	105.3(4)
Cu(2)[a]—S(2)—Cu(1)	98.5(1)	C(01)—P(2)—C(41)	100.9(4)
Cu(1)—S(2)—C(6)	118.0(3)	C(31)—P(2)—C(41)	103.1(4)
Cu(2)[a]—S(2)—C(6)	106.8(4)	P(1)—C(01)—P(2)	116.7(4)
Cu(1)—P(1)—C(01)	113.7(2)		

[a] Symmetry equivalent position is $2-x$, $1-y$, $-z$.

were obtained (see Table 2), but these differences are not the result of any electrochemical effect, since in each of the preparations reported in Table 1, the electrochemical efficiency, defined as moles metal dissolved per Faraday of charge, is 1.04 ± 0.03 mol F^{-1}. As in similar studies of the synthesis of metal thiolates,[1-6] the mechanism can be written as

$$\text{cathode:} \quad RSH + e \rightarrow RS^- + 1/2H_2(g)$$

$$\text{anode:} \quad RS^- + Cu \rightarrow CuSR + e$$

and this clearly is also valid for R = *m*-$CH_3C_6H_4$, where only CuSR was recovered, and R = *p*-$CH_3C_6H_4$ where the product was apparently a mixture of CuSR and CuSR · *x*dppm. The relative stability of crystalline CuSR · *x*dppm complexes ($x = 0$, 0.5, 1.5) must therefore be a function of the properties of R and not of the method of preparation. Given the variety of structures found for adducts and anionic complexes of the copper(I) thiolates, it would be premature to attempt any discussion of the nature of the relationship between R and the stoichiometry of the adducts.

While the infrared and ^{1}H NMR results confirm the presence of both R and dppm in the products, the most useful structural information is found in the ^{31}P NMR spectra (Table 3). Each of the adducts shows a ^{31}P resonance in the region +4 to +7 ppm from that in dppm itself. A number of previous studies[11-13] have established that the ^{31}P resonance frequency can be used diagnostically to distinguish bridging dppm from the chelated ligand, with the former all showing shifts to more positive frequencies compared to the free ligand. By this criterion, we conclude that all the CuSR adducts prepared involve bridging dppm and this has been formed by X-ray crystallography in the case of $(CuSC_5H_{11})_2 \cdot$dppm.

The amylthiolate complex undergoes an easy insertion reaction with carbon disulphide to give the corresponding thioxanthate complex. Similar *in situ* formation of the $RSCS_2^-$ derivative has been found in the case of $CuSC_5H_{11}$ itself[5] and with $Cd(SR)_2$ (R = *n*-C_4H_9, C_6H_5).[14] The obvious contrast between $CuSC_5H_{11}$ and its dppm adduct lies in the formation of $Cu_8(SR)_4(S_2CSR)_4$ in the first case as against $CuS_2CSR \cdot$dppm in the second, again implying different structures. With the 1 : 1.5 adduct of $CuSC_6H_4CH_3$-*o*, no insertion product was obtained on working up the CS_2 reaction mixture and to this extent the behaviour of CuSR species appears to parallel that of $Cd(SR)_2$ (R = *n*-C_4H_9, C_6H_5). The colour changes observed with $CuSC_6H_4CH_3$-*o* suggest that an unstable intermediate is formed when this molecule is in contact with CS_2. With the thioxanthato derivatives then, as with the dppm adducts of CuSR, changes in the properties of the R group produce significant

changes in the stability and structure of the molecules concerned.

We have not been able to elucidate the structure of $CuS_2CSC_5H_{11}$·dppm, but the ^{31}P NMR spectrum (CH_2Cl_2) shows a broad singlet at −36.86 ppm from 85% H_3PO_4, which establishes that in this compound dppm is acting as a chelating ligand;[11–13] further work on this structure is planned. The mass spectra of this compound and of $CuSC_5H_{11}$, are essentially identical, as is the spectrum of $Cu_8(SC_5H_{11})_4(S_2CSC_5H_{11})_4$, indicating that the processes in the ion source involve loss of CS_2 and dppm, leaving CuSR which then gives rise to a series of low intensity ions.

The structure of $(CuSC_5H_{11})_2$·dppm, $Cu_4(\mu\text{-}SC_5H_{11})_4(dppm)_2$ (**1**)

The structures of copper(I) thiolate derivatives provide one of the most intriguing problems of stereochemistry amongst the derivatives of the d^{10} metal ions. The present results identify a novel arrangement involving a Cu_4S_4 ring capped with two six-membered Cu_2SCP_2 rings. The four copper atoms of the central Cu_4S_4 ring are in a crystallographically imposed plane and sufficiently far apart as to exclude Cu—Cu bonding Cu(1)···Cu(2) = 3.071(1) Å, Cu(1)···Cu(2)* = 3.389(1) Å (c.f. ref. 6). The sulphur atoms S(1) and S(1)* are −1.52 Å from this Cu_4 plane, and S(2) and S(2)* −0.42 Å from it. Each copper atom has a CuS_2P coordination kernel and is almost trigonally planar, with a deviation of 0.11 Å for Cu(1) from the Cu(1), P(1), S(1), S(2) plane, and 0.07 Å from Cu(2), P(2), S(1), S(2)* in the case of Cu(2). The sum of the bond angles at copper is 358.6° [Cu(1)] and 359.5° [Cu(2)] respectively. The Cu—S bond distances of 2.268(2) and 2.221(2) Å at Cu(1), and 2.253(3) and 2.241(3) Å at Cu(2), are in the range reported for the $Cu(SPh)_3^-$ anion, which has Cu—S bond lengths of 2.274(4)–2.335(4) Å in the PPh_4^+ salt[15] and 2.239(2)–2.258(2) Å with the Et_4N^+ cation.[16] In the octacopper cage structure[5] $Cu_8(SC_5H_{11})_4(S_2CSC_5H_{11})_4$, there is a wide variety of Cu—S interactions, with mono-, bi- and tridentate sulphur ligands and as a result a direct comparison with the present values is difficult, especially since the thiolato sulphur atoms in that compound are all triply bridging. Nevertheless, the range of Cu—S(thiolate) distances in this cage is 2.237(5)–2.301(5) Å, in good agreement with the values reported above. There seems to be no benefit at this point in further comparisons with the Cu—S distances in other cage structures of different stereochemistry.

Copper–phosphorus bond lengths have been reported for a number of compounds. With triphenylphosphine acting as a terminal ligand to the (Cu—μ-SPh)$_2$ ring, the Cu—P distances are 2.308(2) and 2.304(2) Å,[17] while in $(\mu_2\text{-}SPh)_2(\mu\text{-}SPh)_2(CuPPh_3)_4$·toluene, the corresponding values are 2.238(2) and 2.217(2) Å.[18] The Cu—P distances in **1** are 2.301(2) and 2.246(2) Å, in reasonable agreement with the results quoted. The only example of a dppm complex is the cage structure $Cu_4(dppm)(CS_3)_2$,[19] where the Cu—P bond lengths are 2.272(7), 2.277(8), 2.286(7) and 2.347(8) Å, again in agreement with the bond distances in **1**. As with the Cu—S bonds, it is not helpful to attempt any detailed analysis in view of the different structural types involved.

The unique feature of the molecule is the eight-membered ring, for which there is apparently no analogue in other copper(I)–thiolate complexes. Cubanoid copper(I) structures are known, as is the step or chair version of the cube (c.f. ref. 18). The molecule $(\mu\text{-}SBu^t)_4Cu_4(PPh_3)_2$ is quoted as an example of the open eight-membered ring,[18] but no details are yet available. Several examples of six-membered Cu_2SCP_2 rings in the boat form are to be found among copper(I) thiolate cage structures and especially in $Cu_4(dppm)_2(CS_3)_2$, where the identical sub-unit occurs, albeit with small differences in the bond distances and angles.[19] Finally we note that there is only one tetrameric molecule per unit cell, with Van der Waals interactions between units.

Acknowledgement—This work was supported in part by Operating Grants (to DGT) from the Natural Sciences and Engineering Research Council of Canada.

REFERENCES

1. F. F. Said and D. G. Tuck, *Inorg. Chim. Acta* 1982, **59**, 1.
2. J. L. Hencher, M. A. Khan, F. F. Said and D. G. Tuck, *Polyhedron* 1985, **4**, 1263.
3. J. L. Hencher, M. A. Khan, F. F. Said, R. Sieler and D. G. Tuck, *Inorg. Chem.* 1982, **21**, 2787.
4. J. H. Green, R. Kumar and D. G. Tuck, unpublished results.
5. R. K. Chadha, R. Kumar and D. G. Tuck, *J. Chem. Soc., Chem. Commun.* 1986, 188.
6. R. K. Chadha, R. Kumar and D. G. Tuck, *Can. J. Chem.* 1987, **65**, 1336.
7. C. Oldham and D. G. Tuck, *J. Chem. Ed.* 1982, **59**, 420.
8. M. A. Khan, R. S. Steevensz, D. G. Tuck, J. G. Noltes and P. W. R. Corfield, *Inorg. Chem.* 1980, **19**, 3407.
9. G. M. Sheldrick, *Computing in Crystallography*

(Edited by G. Schlenk), pp. 34–42. Delft University Press (1978).
10. M. A. Khan, C. Peppe and D. G. Tuck, *Acta Cryst.* 1983, **C39**, 1339.
11. G. K. Anderson, H. C. Clark and J. A. Davies, *J. Organomet. Chem.* 1981, **210**, 135.
12. S. J. Cooper, M. P. Brown and R. J. Puddephatt, *Inorg. Chem.* 1981, **20**, 1374.
13. A. R. Sanger, *J. Chem. Soc., Dalton Trans.* 1981, 228.
14. S. J. Black, F. W. B. Einstein, P. C. Hayes, R. Kumar and D. G. Tuck, *Inorg. Chem.* 1986, **25**, 4181.
15. D. Coucouvanis, C. N. Murphy and S. K. Karodia, *Inorg. Chem.* 1980, **19**, 2993.
16. C. D. Garner, J. R. Nicholson and W. Clegg, *Inorg. Chem.* 1984, **23**, 2148.
17. I. G. Dance, P. J. Guerney, A. D. Rae and M. L. Scudder, *Inorg. Chem.* 1983, **22**, 2883.
18. I. G. Dance, M. L. Scudder and L. J. Fitzpatrick, *Inorg. Chem.* 1985, **24**, 2547.
19. A. M. M. Lanfredi, A. Tiripicchio, A. Camus and N. Marsich, *J. Chem. Soc., Chem. Comm.* 1983, 1126.

Polyhedron Vol. 7, No. 1, pp. 57–61, 1988
Printed in Great Britain

0277–5387/88 $3.00+.00
© 1988 Pergamon Journals Ltd

X-RAY CRYSTAL STRUCTURE OF 2,3,7,8,12,13,17,18-OCTAETHYLPORPHYRINATOPLATINUM(II) (PtOEP): POTENTIAL FOR CORRELATION OF MESO-CARBON BOND-ANGLE ($\hat{C}_m$) WITH ONE-BOND $^{13}C_{MESO}$—$^{1}H_{METHINE}$ COUPLING CONSTANT IN SOME DIAMAGNETIC METAL COMPLEXES OF OEP

LIONEL R. MILGROM*
School of Inorganic and Physical Chemistry, Kingston Polytechnic, Penrhyn Road, Kingston-upon-Thames KT1 2EE, U.K.

and

RICHARD N. SHEPPARD, ALEXANDRA M. Z. SLAWIN and DAVID J. WILLIAMS

Department of Chemistry, Imperial College of Science and Technology, Exhibition Road, London SW7 2AZ, U.K.

(*Received* 7 *April* 1987; *accepted* 24 *July* 1987)

Abstract—The X-ray crystal structure of the title compound is reported. Crystals of PtOEP are triclinic, $a = 8.165(1)$, $b = 10.042(2)$, $c = 10.069(2)$ Å, $\alpha = 84.42(2)$, $\beta = 81.02(1)$, $\gamma = 67.05(1)°$, space group $P\bar{1}$, $Z = 1$. The structure was refined on 2009 independent reflections to $R = 0.018$. Comparisons of crystallographically-determined C_a—C_{meso}—C_a bond angle ($\hat{C}_m$) of PtOEP and other diamagnetic metalloporphyrins, with the one-bond $^{13}C_{meso}$—$^{1}H_{methine}$ coupling constant (^{1}J) indicate a possible inverse relationship provided the macrocycle remains planar. For Ag(III)OEP^{+}CLO$_4^{-}$ and H_4OEP^{2+}, an increase in ^{1}J, by about 10 Hz, is attributed to delocalization of central positive charge onto the porphyrin meso-carbons, via the porphyrin π-system. The consequences this may have for the biological functioning of haemoproteins are discussed.

NMR spectroscopy has proved invaluable in the study of porphyrins and metalloporphyrins.[1] Recently, we described the use of proton-coupled ^{13}C-NMR in elucidating "through-space" intramolecular interactions in dihydroxo-5,10,15,20-tetraphenylporphyrinatotin(IV).[2] Also, measurement of the $^{13}C_{meso}$—$^{1}H_{methine}$ one-bond coupling constant (^{1}J) in 2,3,7,8,17,18-octaethylporphyrinatoplatinum(II) (PtOEP)[3] raised the question whether ^{1}J might correlate with the C_a—C_{meso}—$C_a(\hat{C}_m)$ bond angle in this and other metalloOEPs. In order to investigate this, we have determined the X-ray crystal structure of PtOEP and ^{1}J coupling constants for other diamagnetic metalloOEPs. We report this data here.

*Author to whom correspondence should be addressed.

EXPERIMENTAL

X-ray studies

PtOEP was prepared and purified by literature methods.[3,4] Bright orange–red crystals, suitable for X-ray crystallography, were grown by slow evaporation of a dilute ethanol solution of PtOEP.

Crystal data. $C_{36}H_{44}N_4Pt$, triclinic, $a = 8.165(1)$, $b = 10.042(2)$, $c = 10.069(2)$ Å, $\alpha = 84.42(2)$, $\beta = 81.02(1)$, $\gamma = 67.05(1)°$, $U = 750$ Å^3, space group $P\bar{1}$, $Z = 1$, $M = 727.8$, $D_c = 1.62$ g cm^{-3}, μ(Cu-K$_\alpha$) = 90 cm^{-1}, $F(000) = 366$.

Measurements. Refined unit cell parameters were obtained by centring 20 reflections on a Nicolet R3m diffractometer. Using the ω-scan measuring routine, 2009 independent reflections ($\delta \leqslant 58°$) were measured with Cu-K$_\alpha$ radiation (graphite monochromator), all of which had $|F_0| > \sigma(|F_0|)$ and were

considered to be observed. The data were corrected for Lorentz and polarization factors, and a numerical absorption correction (face-indexed crystal) was applied.

Structure analysis. The structure was resolved by the heavy atom method, with inspection of the vector map giving the positions of all the non-hydrogen atoms. These were refined anisotropically. The positions of the hydrogen atoms were idealized, C—H = 0.96 Å, assigned isotropic thermal parameters, $U(H) = 1.2U_{eq}(C)$, and allowed to ride on their parent carbon atoms. The methyl groups were refined as rigid bodies. Refinement was by block-cascade full-matrix least-squares and converged to give $R = 0.018$, $R_w = 0.018$ ($w^{-1} = \sigma^2(F) + 0.00007F^2$). Computations were carried out on an Eclipse S140 computer using the SHELXTL program system.[5] Scattering factors were taken from the *International Tables for X-Ray Crystallography*.[6]

Final atomic coordinates, thermal parameters and structure factors have been deposited with the Editor as supplementary data. Atomic coordinates have also been deposited with the Cambridge Crystallographic Data Centre

NMR studies

All ^{1}H- and ^{13}C-NMR spectra were obtained in the FT mode, using a Bruker WM 250 NMR spectrometer at 250 and 62.9 MHz, respectively. All spectra were recorded at ambient temperatures.

Ag(III)OEP$^+$ClO$_4^-$ was prepared via a literature method[7] and gave one base-line spot on tlc (alumina, eluting with chloroform) ie, there is no paramagnetic Ag(II)OEP present. The previous report of the preparation of this compound[7] did not cite its NMR spectra, so we report it here.

^{1}H-*NMR.* ($CDCl_3$, TMS internal reference), $-CH_2-CH_3$, 1.71 ppm (24H, triplet); $-CH_2-CH_3$, 4.17 ppm (16H, broad); methine-*H*, 9.95 ppm (4H, broad), TMS peak is sharp.

^{13}C-*NMR.* (Proton-decoupled, $CDCl_3$, TMS internal reference), $-CH_2-CH_3$, 18.14 ppm; $-CH_2-CH_3$, 19.32 ppm (broad); meso-C, 99.43 ppm (broad); C_a and C_b carbon resonances appear as very weak, broad lines about 140 ppm.

RESULTS AND DISCUSSION

There is a crystallographic centre of symmetry, coincident with the Pt atom, at the centre of the porphyrin ring (Fig. 1). The porphyrin ring is essentially planar, with the greatest deviations from the least squares plane of all the non-hydrogen atoms being 0.017 and 0.016 Å for C_m1 and C_b4, respectively; all the remaining atoms are within 0.009 Å of this plane.

The Pt—N bond lengths are equal [2.012(3) Å] and less than that typically found in Pt—N complexes (e.g. 2.1–2.14 Å[8]). The Pt(II) cation is thus "squeezed" within the central porphyrin hole, by the four macrocyclic nitrogens. This compression is effectively reduced by d–π^* backbonding into available porphyrin π^* orbitals, as observed by the shift

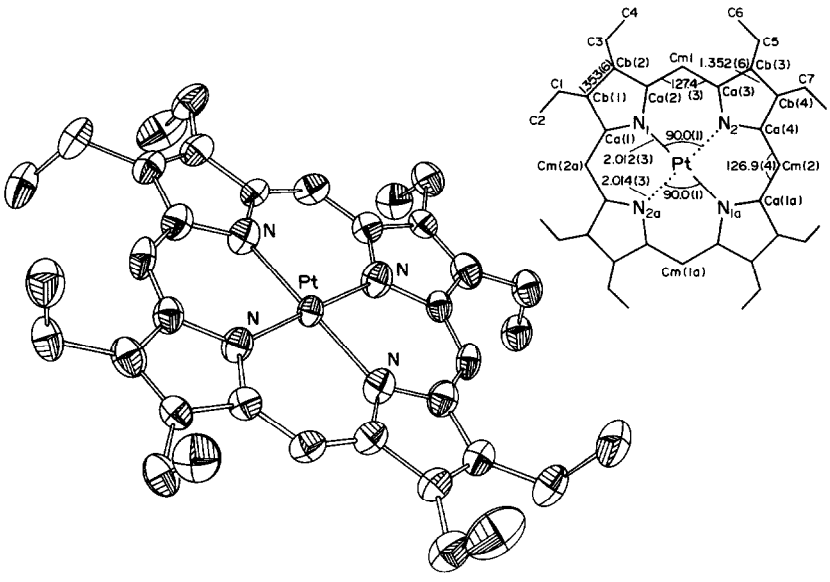

Fig. 1. Perspective drawing of PtOEP with 50% probability ellipsoids: inset, atomic nomenclature referred to in Table 1 with bond lengths and bond angles referred to in text.

Table 1. Bond lengths (Å) and bond angles (°) for PtOEP

Pt—N(1)	2.012(3)	Pt—N(2)	2.013(2)
Pt—N(1a)	2.012(3)	Pt—N(2a)	2.014(3)
N(1)—C_a(1)	1.377(5)	N(1)—C_a(2)	1.381(5)
C_a(1)—C_b(1)	1.452(5)	C_a(1)—C_m(2a)	1.376(6)
C_b(1)—C_b(2)	1.353(6)	C_b(1)—C(1)	1.504(6)
C_b(2)—C_a(2)	1.440(5)	C_b(2)—C(3)	1.508(5)
C_a(2)—C_m(1)	1.380(6)	C_m(1)—C_a(3)	1.364(5)
N(2)—C_a(3)	1.380(4)	N(2)—C_a(4)	1.382(5)
C_a(3)—C_b(3)	1.448(6)	C_b(3)—C_b(4)	1.352(5)
C_b(3)—C(5)	1.511(6)	C_b(4)—C_a(4)	1.446(6)
C_b(4)—C(7)	1.506(6)	C_a(4)—C_m(2)	1.369(5)
C_m(2)—C_a(1a)	1.376(6)	C(1)—C(2)	1.514(6)
C(3)—C(4)	1.511(6)	C(5)—C(6)	1.516(5)
C(7)—C(8)	1.520(6)		
N(1)—Pt—N(2)	90.0(1)	N(1)—Pt—N(1a)	180.0
N(2)—Pt—N(1a)	90.0(1)	N(1)—Pt—N(2a)	90.0(1)
N(2)—Pt—N(2a)	180.0	N(1a)—Pt—N(2a)	90.0(1)
Pt—N(1)—C_a(1)	126.9(2)	Pt—N(1)—C_a(2)	127.0(3)
C_a(1)—N(1)—C_a(2)	106.1(3)	N(1)—C_a(1)—C_b(1)	109.6(3)
N(1)—C_a(1)—C_m(2a)	124.7(3)	C_b(1)—C_a(1)—C_m(2a)	125.6(4)
$C_{a(1)}$—C_b(1)—C_b(2)	107.1(4)	C_a(1)—C_b(1)—C(1)	125.6(4)
C_b(2)—C_b(1)—C(1)	127.3(3)	C_b(1)—C_b(2)—C_a(2)	107.2(3)
C_b(1)—C_b(2)—C(3)	128.0(4)	C_a(2)—C_b(2)—C(3)	124.8(4)
N(1)—C_a(2)—C_b(2)	110.0(4)	N(1)—C_a(2)—C_m(1)	124.1(3)
C_b(2)—C_a(2)—C_m(1)	125.9(3)	C_a(2)—C_m(1)—C_a(3)	127.4(3)
Pt—N(2)—C_a(3)	127.0(3)	Pt—N(2)—C_a(4)	126.8(2)
C_a(3)—N(2)—C_a(4)	106.2(3)	C_m(1)—C_a(3)—N(2)	124.5(4)
C_m(1)—C_a(3)—C_b(3)	125.9(3)	N(2)—C_a(3)—C_b(3)	109.7(3)
C_a(3)—C_b(3)—C_b(4)	107.3(3)	C_a(3)—C_b(3)—C(5)	124.8(3)
C_b(4)—C_b(3)—C(5)	127.9(4)	C_b(3)—C_b(4)—C_a(4)	107.1(4)
C_b(3)—C_b(4)—C(7)	128.0(4)	C_a(4)—C_b(4)—C(7)	124.8(3)
N(2)—C_a(4)—C_b(4)	109.8(3)	N(2)—C_a(4)—C_m(2)	124.6(4)
C_b(4)—C_a(4)—C_m(2)	125.6(4)	C_a(4)—C_m(2)—C_a(1a)	126.9(4)
C_b(1)—C(1)—C(2)	112.9(4)	C_b(2)—C(3)—C(4)	113.2(3)
C_b(3)—C(5)—C(6)	112.7(3)	C_b(4)—C(7)—C(8)	113.4(3)

to shorter wavelengths of Pt porphyrin B bands in their UV/visible spectra,[9] and in upfield shifts of ^{1}H- and ^{13}C-resonances in their NMR spectra.[10]

PtOEP is isostructural with NiOEP[11] but differs significantly from PdTPP.[12] Thus, although, the Pd—N bond length (2.009(9) Å) in PdTPP is within statistical significance, identical to the Pt—N bond length in PtOEP, there is an appreciable puckering of the porphyrinato core in PdTPP, with the meso-carbons displaced by ± 0.38 Å from the mean plane of the ring. The principal macrocyclic bond lengths and bond angles are shown in Fig. 1 and Table 1.†

The mean C_b—C_b bond length is 1.353(8) Å. Previous work on the NMR of platinum deuteroporphyrin IX dimethyl ester[13] indicated a significantly diminished bond order for the C_b—C_b pyrrolic linkage. This implicates the periphery of the molecule in the delocalization pathway. The usual representation of the metalloporphyrin macrocyclic π-system as an 18π dianion delocalized over 16 atoms excludes the C_b—C_b double bonds from the delocalization path.[14] This situation is confirmed by an observed[14] C_b—C_b bond length of 1.34 Å, close to the carbon–carbon bond distance in ethylene. On the other hand, inclusion of the peripheral C_b—C_b bonds in the delocalization path increases the predicted C_b—C_b distance to 1.37 Å.[15] Our observed C_b—C_b bond length of 1.353(8) Å in PtOEP, therefore, reinforces the notion of some inclusion of the peripheral C_b—C_b bonds in the delocalization pathway.

The proton-coupled ^{13}C-NMR spectra of some diamagnetic metalloporphyrins in the main, only

† A librational analysis indicated that corrections to bond lengths due to thermal motion are less than 1 esd.

recorded the meso-carbon doublet[3] between 90–110 ppm. The ^1J coupling constants were measured from the spectrum. However, in two cases the whole of the spectrum was recorded and the results given. In NiOEP, for example, the proton-coupled ^{13}C-NMR spectrum of the β-ethyl groups was observed as a quartet of triplets (–CH_2–CH_3, centred on 18.7 ppm; $^1J_{^{13}C-^1H} = 126$ Hz, $^2J_{^{13}C-^1H} = 5$ Hz) overlapping a triplet of quartets (–CH_2–CH_3, centred on 20.0 ppm; $^1J_{^{13}C-^1H} = 126$ Hz, $^2J_{^{13}C-^1H} = 5$ Hz). In $MgOEP(Py)_2$, the proton-decoupled ^{13}C-NMR resonances of the pyridine axial ligands are shifted upfield compared to free pyridine, presumably due to coordination to the central magnesium atom, e.g. *C*-2, 146.5 ppm; *C*-3, 122.5 ppm; and *C*-4, 135.4 ppm (*cf.* 150.6, 124.5, and 136.4 ppm in free pyridine). In the proton-*coupled* ^{13}C-NMR spectrum of this metalloporphyrin, the pyridine carbon resonances are split into doublets of triplets for the C-3 ($^1J_{^{13}C-^1H} = 163$ Hz; $^2J_{^{13}C-^1H} = 7$ Hz) and the C-4 carbons ($^1J_{^{13}C-^1H} = 162$ Hz; $^2J_{^{13}C-^1H} = 6$ Hz), while the C-2 carbon resonances are split into a doublet of multiplets ($^1J_{^{13}C-^1H} = 180$ Hz). The more complicated secondary splitting is due to overlapping ^2J and ^3J couplings from neighbouring H atoms, and the proximity of the ^{14}N atom with its broadening nuclear quadrapole.

The ^1J coupling constant for PtOEP (155.6 ± 0.3Hz)[3] is close to that found for benzene (157.65 Hz[16]). The latter has an internal bond angle of 120°. The mean bond angle about the meso-carbons ($\hat{C}_m$) in PtOEP is 127.2 Å. Table 2 gives ^1J values measured for a series of diamagnetic metalloporphyrins, compared with the crystallographic values of $\hat{C}_m$. In Fig. 1, we investigate the possible correlations of ^1J with $\hat{C}_m$.

When the macrocycle is planar (e.g. in the Ni, Pt and Sn complexes) then an apparent inverse relationship exists between ^1J and $\hat{C}_m$ (see dotted line). Points off this line may be interpreted as due to:

(a) puckering of the macrocycle (e.g. in $MgOEP(Py)_2$[17] and to some extent, H_2OEP[18]): this appears to shift points to the left of the line,

(b) delocalization of central positive charge onto the meso-carbons, via the porphyrin π-system (H_4OEP^{2+})[19] which shifts the points to the right of the line.

A precedent for (b) exists with the tropylium cation,[16] where an increase in $^1J_{^{13}C-^1H}$, in going from cycloheptane to tropylium (156 to 166.8 Hz) is associated with the presence of delocalized positive charge.

A similar argument could also explain the unusually high ^1J value for Ag(III)OEP^+ClO_4 (161.7 ± 2 Hz). Here, the Ag(III) cation has a d^8 electronic configuration and spectroscopically[7] closely resembles Pd and PtOEP. The Ag(III) cation is of similar size to Pd(II) and Pt(II) cations (0.81 Å compared to 0.78 and 0.74 Å, respectively[20]) so that $\hat{C}_m$ should not differ significantly from that in PtOEP (backbonding from Ag(III) metal *d* orbitals into porphyrin π^* orbitals should adequately take care of this cation's slightly greater size).† The Ag(III)

Table 2. Comparison of meso-carbon bond angles with one-bond $^{13}C_{meso}$—$^1H_{methine}$ coupling constants in some diamagnetic metalloporphyrins

Porphyrin	Mean $\hat{C}_m$ (degrees)	^1J(Hz)
PtOEP	127.4(3)	155.6 ± 0.3
PdOEP	—	155.4 ± 1.2
NiOEP	125.1(1), 124.1(1)[a]	157.9 ± 0.6
$SnOEPCl_2$	129.5(4)[b]	153.5 ± 0.3
H_2OEP	127.6(3)[c]	153.7 ± 1.0
H_4OEP^{2+}	127.5(9)[d]	161.2 ± 0.4
$MgOEP(Py)_2$	129.3(2)[e]	150.3 ± 0.4
$AgOEPClO_4$	—	161.7 ± 1.8

[a] These bond angles are for the triclinic and tetragonal forms of NiOEP, respectively, see ref. 11.

[b] See D. L. Cullen and E. F. Meyer, Jr., *Acta Cryst. Sect. B* 1973, **29**, 2507.

[c] See ref. 18.

[d] See ref. 19.

[e] See ref. 17.

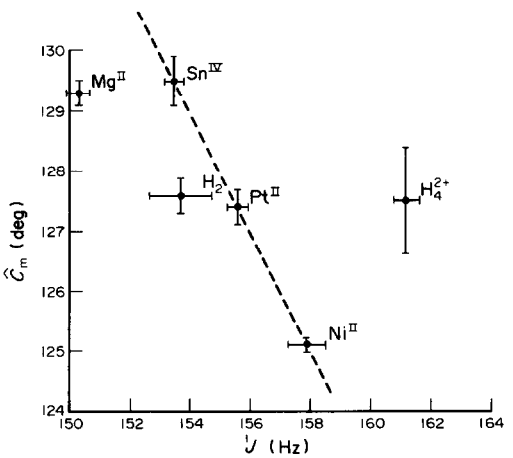

Fig. 2. Correlation of meso-carbon bond-angle ($\hat{C}_m$) with one-bond $^{13}C_{meso}$—$^1H_{methine}$ coupling constants (^1J) in some diamagnetic metalloporphyrins.

† We have not yet succeeded in acquiring crystals of $Ag(III)OEP^+$ suitable for X-ray crystallographic analysis.

cation, however, carries an additional positive charge that is not balanced by the (formal) porphyrin dianion. Also, because of the strong d-π^* back-bonding that exists in d^8 metalloporphyrins, this extra positive charge should be delocalized onto the macrocyclic meso-carbons. This could lead to solution dimerization (*cf.* $MgOEP^+$, radical cation[21]) which could induce some low-level paramagnetism or lead to slower molecular motion in solution. In either case, this would be expressed as broadening of NMR resonances. In fact, in the ^1H- and ^{13}C-NMR spectra of $Ag(III)OEP^+ClO_3^-$, peaks assigned to $-CH_2-$, methine-*H*, $-CH_2-$, meso-carbons and C_a and C_b carbons, are all broadened. We take this as evidence for Ag(III) metal charge delocalization onto the porphyrin macrocycle.

Such metal charge delocalization may be occurring in other biologically important metalloporphyrins, where the metal *d* orbitals are known to be strongly coupled to the porphyrin system, e.g. Fe(III) porphyrins.[22] Where a porphyrin bound iron atom is alternating between Fe(II)/Fe(III) oxidation states, e.g. in cytochrome c, changes in central metal positive charge could be mediated and transmitted, via the porphyrin π-system, to the close-packed amino-acid side-chains of the protein's haem pocket.[23] Similarly, in haemoglobin, the formation of a putative Fe(III)—O_2^- adduct (one interpretation of the haem—O_2 interaction[24]) would also lead to changes in positive charge on the porphyrin macrocycles that could affect surrounding amino-acids. In both cases, this mechanism could be one of the contributing factors leading to changes in protein conformation.

In conclusion, the results of this study, though not giving definitive evidence for a general correlation between $\hat{C}_m$ and $^1J_{^{13}C-^1H}$ in metalloporphyrins, under certain circumstances (e.g. when the metallomacrocycle is planar) a linear inverse relationship does appear to exist. Clearly, more data is required, though this has to date been restricted by the difficulties in obtaining metalloporphyrin complexes suitable for X-ray crystallographic analysis. Nevertheless, this type of correlation could be a potentially very powerful diagnostic tool in structural studies of these and related compounds.

Acknowledgement—We thank the SERC for support.

REFERENCES

1. (a) H. Scheer and J. J. Katz in *Porphyrins and Metalloporphyrins* (Edited by K. M. Smith) p 399. Elsevier, Amsterdam (1975); (b) T. R. Janson and J. J. Katz in *The Porphyrins* (Edited by D. Dolphin) Vol. IV, p. 1. Academic Press (1978).
2. L. R. Milgrom and R. M. Sheppard, *J. Chem. Soc., Chem. Commun.* 1985, 350.
3. L. R. Milgrom, *Polyhedron*, 1985, **4**, 1279.
4. J. W. Büchler and L. Puppe, *Ann. Chem.* 1974, 1046.
5. G. M. Sheldrick, *SHELXTL, An Integrated System for Resolving, Refining and Displaying Crystal Structures from Diffraction Data*, Revision 4.1.
6. *International Tables for X-Ray Crystallography*, Vol. IV, p. 99–149. Kynoch Press, Birmingham, U.K.
7. J.-H. Fühlrop, K. Kadish and D. G. Davies, *J. Am. Chem. Soc.* 1973, **95**, 5140.
8. For example see, G. B. Young, V. Sutcliffe and A. Skapski, *J. Chem. Soc., Chem. Commun.* 1986, 609.
9. J. W. Büchler in *The Porphyrins* (Edited by D. Dolphin) Vol. I, p. 472. Academic Press, New York (1978).
10. L. R. Milgrom, *Polyhedron* 1984, **3**, 879.
11. D. L. Cullen and E. F. Meyer Jr., *J. Am. Chem. Soc.* 1974, **96**, 2095.
12. E. B. Fleischer, C. K. Miller and L. E. Webb, *J. Am. Chem. Soc.* 1964, **86**, 2342.
13. L. R. Milgrom, *Polyhedron* 1985, **4**, 1661.
14. E. B. Fleischer, *Acc. Chem. Res.* 1970, 105.
15. M. J. S. Dewar and H. N. Schmeising, *Tetrahedron* 1959, **5**, 166.
16. H. Günther, H. Seel and M.-E. Günther, *Org. Mag. Res.* 1978, **11**, 97.
17. R. Bonnett, M. B. Hursthouse, K. M. Abdul Malik and B. Mateen, *J. Chem. Soc., Perkin Trans. II.* 1977, 2072.
18. J. W. Lauker and J. A. Ibers, *J. Am. Chem. Soc.* 1973, **95**, 5148.
19. E. Cetinkaya, A. W. Johnson, M. F. Lappert, G. M. McLaughlin and K. Muir, *J. Chem. Soc., Dalton Trans.* 1974, 1236.
20. J. E. Huheey, *Inorganic Chemistry* pp. 73–76. Harper International, London (1983).
21. J. K. M. Sanders and I. Baxter, *Tetrahedron Lett.* 1974, 4543.
22. M. Gouterman in *The Porphyrins* (Edited by D. Dolphin) Vol. III, p. 62. Academic Press, New York (1978).
23. R. Timkovich in *The Porphyrins* (Edited by D. Dolphin) Vol. VII, p. 271. Academic Press, New York (1978).
24. D. W. Smith and R. J. P. Williams, *Struc. Bonding* 1970, **7**, 1.

Polyhedron Vol. 7, No. 1, pp. 63–66, 1988
Printed in Great Britain

0277–5387/88 $3.00+.00
Pergamon Journals Ltd

REACTIONS OF $[WI_2(CO)(NCMe)(\eta^2\text{-}RC_2R)_2]$ (R = Me or Ph) WITH 1,4-DIAZA-1,3-BUTADIENES

PAUL K. BAKER* and ELAINE M. ARMSTRONG

Department of Chemistry, University College of North Wales, Bangor, Gwynedd LL57 2UW, U.K.

(*Received* 9 *July* 1987; *accepted* 24 *August* 1987)

Abstract—Reaction of $[WI_2(CO)(NCMe)(\eta^2\text{-}RC_2R)_2]$ (R = Me or Ph) in CH_2Cl_2 at room temperature with an equimolar quantity of R′N : CHCH : NR′ (R′ = Cy, ^{i}Pr, Ph, *p*-MePh or *p*-MeOPh) gave high yields of the new cationic bisalkyne complexes [WI(CO)(R′N : CHCH : NR′)$(\eta^2\text{-}RC_2R)_2$]I via successive displacement of acetonitrile and an iodide ligand. The cationic compounds [WI(CO)(CyN : CHCH : NCy)$(\eta^2\text{-}RC_2R)_2$][BPh_4] were also prepared by reaction of $[WI_2(CO)(NCMe)(\eta^2\text{-}RC_2R)_2]$ with CyN : CHCH : NCy in the presence of Na[BPh_4] in order to confirm the ionic nature of these complexes. ^{13}C NMR spectroscopy indicated that the two alkyne ligands are donating a total of six electrons to the metal in these complexes.

Cationic alkyne complexes of molybdenum(II) and tungsten(II) have proved to be important in recent years mainly due to the susceptibility of the coordinated alkyne ligand to nucleophilic attack.[1] Some examples of cationic alkyne complexes of molybdenum(II) and tungsten(II) are: $[Mo(CO)(\eta^2\text{-}RC_2R')_2(\eta^5\text{-}C_5H_5)][BF_4]$ (R = R′ = Me or Ph, R = H, R′ = Me; R = H, R′ = Bu^t);[2] $[M(CO)(\eta^2\text{-}MeC_2Me)_2(\eta^5\text{-}C_5H_5)][PF_6]$ (M = Mo or W);[3] $[Mo(CO)L(\eta^2\text{-}RC_2R')(\eta^5\text{-}C_5H_5)][BF_4]$ (L = CO, $P(OPh)_3$, PEt_3 or PPh_3; R = R′ = H, Me or Ph; R = H; R′ = Ph);[4] $[MoLL'(\eta^2\text{-}RC_2R')(\eta^5\text{-}C_5H_5$ or $\eta^5\text{-}C_9H_7)][BF_4]$ (L,L′ = CO and PR_3; L = L′ = $P(OMe)_3$; R,R′ = Me, Ph etc.);[5] $[MoI(CNR)_4(\eta^2\text{-}Bu^tNHC_2NHBu^t)]I$ (R = Me or Bu^t).[6] Hitherto, there have been no examples of cationic alkyne complexes of molybdenum(II) or tungsten(II) containing 1,4-diaza-1,3-butadienes as attached ligands. Hence in this paper we wish to report the synthesis and spectral properties of some new cationic bisalkyne complexes [WI(CO)(R′N : CHCH : NR′)$(\eta^2\text{-}RC_2R)_2$]I (R = Me or Ph; R′ = Cy, ^{i}Pr, Ph, *p*-MePh or *p*-MeOPh) and [WI(CO)(CyN : CHCH : NCy)$(\eta^2\text{-}RC_2R)_2$][BPh_4].

*Author to whom correspondence should be addressed.

EXPERIMENTAL

All preparations were carried out under an atmosphere of dry nitrogen using standard Schlenk line techniques. CH_2Cl_2 was dried over P_4O_{10} and distilled before use.

The complexes $[WI_2(CO)(NCMe)(\eta^2\text{-}RC_2R)_2]$ (R = Me or Ph) were prepared by literature methods[7] and the ligands R′N : CHCH : NR′ (R′ = Cy, ^{i}Pr, Ph, *p*-MePh or *p*-MeOPh) were also prepared by standard literature methods.[8–12] $[W(CO)_6]$, RC_2R etc were all purchased from commercial sources.

^{1}H and ^{13}C NMR spectra were recorded on either a Jeol FX 60 MHz spectrometer or a Bruker WH-400 MHz spectrometer (all spectra were calibrated against tetramethylsilane). IR spectra were recorded on a Perkin–Elmer 197 IR spectrophotometer. Elemental analyses for carbon, hydrogen and nitrogen were recorded on a Carlo Erba Elemental Analyser MOD 1106 (using helium as a carrier gas).

[WI(CO)(CyN : CHCH : NCy)$(\eta^2\text{-}MeC_2Me)_2$]I (1)

To $[WI_2(CO)(NCMe)(\eta^2\text{-}MeC_2Me)_2]$ (0.500 g, 0.813 mmol) dissolved in CH_2Cl_2 (15 cm^3) with continuous stirring under a stream of dry nitrogen was

added CyN : CHCH : NCy (0.179 g, 0.813 mmol). After stirring for 17 h, filtration, removal of the solvent *in vacuo* gave dark red crystals of [WI(CO)(CyN : CHCH : NCy)(η^2-MeC_2Me)$_2$]I (yield = 0.57 g, 88%), which were recrystallized from CH_2Cl_2/Et_2O.

Similar reactions of [WI_2(CO)(NCMe)(η^2-RC_2R)$_2$] (R = Me or Ph) with R'N : CHCH : NR' (R' = Cy, ^{i}Pr, Ph, *p*-MePh or *p*-MeOPh) afford the new complexes [WI(CO)(R'N : CHCH : NR')(η^2-RC_2R)$_2$]I (**2–10**). (See Table 1 for colours and yields.)

[WI(CO)(CyN : CHCH : NCy)(η^2-MeC_2Me)$_2$][BPh_4] · $\frac{1}{2}CH_2Cl_2$ (**11**)

To [WI_2(CO)(NCMe)(η^2-MeC_2Me)$_2$] (0.500 g, 0.813 mmol), dissolved in CH_2Cl_2 (15 cm^3) with continuous stirring under a stream of dry nitrogen was added CyN : CHCH : NCy (0.179 g, 0.813 mmol) followed by Na[BPh_4] (0.278 g, 0.813 mmol) and the mixture was stirred for 17 h. Filtration, to remove NaI and removal of the solvent *in vacuo* gave brown crystals of [WI(CO)(CyN : CHCH : NCy)(η^2-MeC_2Me)$_2$][BPh_4] · $\frac{1}{2}CH_2Cl_2$ (yield = 0.64 g, 76%), which were recrystallized from CH_2Cl_2/Et_2O.

In a similar reaction of [WI_2(CO)(NCMe)(η^2-PhC_2Ph)$_2$] with CyN : CHCH : NCy followed by Na[BPh_4] gave the new compound [WI(CO)(CyN : CHCH : NCy)(η^2-PhC_2Ph)$_2$][BPh_4] (**12**). (See Table 1 for colour and yield.)

RESULTS AND DISCUSSION

Equimolar quantities of [WI_2(CO)(NCMe)(η^2-RC_2R)$_2$] (R = Me or Ph) and R'N : CHCH : NR' react in CH_2Cl_2 at room temperature to give high yields of the new cationic bisalkyne complexes [WI(CO)(R'N : CHCH : NR')(η^2-RC_2R)$_2$]I. Reaction of [WI_2(CO)(NCMe)(η^2-RC_2R)$_2$] with CyN : CHCH : NCy in CH_2Cl_2 followed by Na[BPh_4] in a 1 : 1 : 1 molar ratio gave after filtration good yields of [WI(CO)(CyN : CHCH : NCy)(η^2-RC_2R)$_2$][BPh_4]. All the new complexes (**1–12**) described in this paper have been fully characterized by elemental analysis (C, H and N) (Table 1), IR (Table 2), and ^{1}H and ^{13}C NMR spectroscopy (Tables 3 and 4). Complexes (**3, 8** and **11**) are either CH_2Cl_2 or $\frac{1}{2}CH_2Cl_2$ solvates which were confirmed by repeated elemental analyses and ^{1}H NMR spectroscopy. The complexes are soluble in polar solvents such as CH_2Cl_2 and $CHCl_3$, and as expected, since the complexes are cationic they are insoluble in diethylether and hydrocarbon solvents. The complexes are all moderately stable in the solid state

Table 1. Physical and analytical[a] data for the complexes [WI(CO)(Rdab)(η^2-RC_2R)$_2$][X]

	Complex	Colour	Yield %	C	H	N
(**1**)	[WI(CO)(Cydab)(η^2-MeC_2Me)$_2$]I	dark red	88	35.2 (34.8)	4.7 (4.6)	3.4 (3.5)
(**2**)	[WI(CO)(Cydab)(η^2-PhC_2Ph)$_2$]I	dark green	80	49.7 (49.5)	4.5 (4.3)	2.3 (2.7)
(**3**)	[WI(CO)(^{i}Prdab)(η^2-MeC_2Me)$_2$]I · CH_2Cl_2	dark red	64	26.8 (27.1)	3.7 (3.8)	3.3 (3.5)
(**4**)	[WI(CO)(^{i}Prdab)(η^2-PhC_2Ph)$_2$]I	dark green	69	45.8 (46.2)	4.0 (3.8)	2.7 (2.9)
(**5**)	[WI(CO)(MePhdab)(η^2-MeC_2Me)$_2$]I	dark red	80	37.6 (37.1)	3.7 (3.5)	3.1 (3.5)
(**6**)	[WI(CO)(MePhdab)(η^2-PhC_2Ph)$_2$]I	dark green	70	51.5 (51.1)	3.8 (3.4)	2.6 (2.7)
(**7**)	[WI(CO)(Phdab)(η^2-MeC_2Me)$_2$]I	brown	75	35.3 (35.3)	3.0 (3.1)	3.4 (3.6)
(**8**)	[WI(CO)(Phdab)(η^2-PhC_2Ph)$_2$]I · $\frac{1}{2}CH_2Cl_2$	brown	71	48.7 (48.7)	3.3 (3.1)	2.4 (2.6)
(**9**)	[WI(CO)(MeOPhdab)(η^2-MeC_2Me)$_2$]I	red–brown	72	35.4 (35.7)	3.6 (3.4)	2.9 (3.3)
(**10**)	[WI(CO)(MeOPhdab)(η^2-PhC_2Ph)$_2$]I	brown	84	49.8 (49.6)	3.7 (3.3)	2.3 (2.6)
(**11**)	[WI(CO)(Cydab)(η^2-MeC_2Me)$_2$][BPh_4] · $\frac{1}{2}CH_2Cl_2$	brown	76	54.9 (55.4)	5.9 (5.6)	2.9 (2.7)
(**12**)	[WI(CO)(Cydab)(η^2-PhC_2Ph)$_2$][BPh_4]	dark green	78	64.9 (65.2)	5.3 (5.2)	2.3 (2.3)

[a] Calculated values in parentheses.

Table 2. IR data[a] for the complexes $[WI(CO)(Rdab)(\eta^2\text{-}RC_2R)_2][X]$

Complex	νCO (cm^{-1})	νC≡C (cm^{-1})
(1)	2052(s)	1648(vw)
(2)	2090(s)	1660(vw)
(3)	2060(s)	1640(vw)
(4)	2095(s)	1640(vw)
(5)	2050(s)	1690(w)
(6)	2090(s)	1695(w)
(7)	2047(s)	1692(vw)
(8)	2085(s)	1660(vw)
(9)	2050(s)	1652(vw)
(10)	2095(s)	1650(vw)
(11)	2052(s)	1638(vw)
(12)	2087(s)	1650(vw)

[a] Spectra recorded as $CHCl_3$ films between NaCl plates.

and can be stored under nitrogen for several weeks in the dark.

The reaction of the complexes $[WI_2(CO)(NCMe)(\eta^2\text{-}RC_2R)_2]$ with an equimolar amount of R′N:CHCH:NR′ probably proceeds via an initial displacement of an acetonitrile ligand since the reactions of $[WI_2(CO)(NCMe)(\eta^2\text{-}RC_2R)_2]$ (R = Me or Ph) with one equivalent of pyridine (L) give $[WI_2(CO)L(\eta^2\text{-}RC_2R)_2]$.[13] This is followed by displacement of iodide by the other nitrogen atom to give the observed products. It is interesting to note that the reaction of $[WI_2(CO)(NCMe)(\eta^2\text{-}RC_2R)_2]$ with bidentate phosphine ligands (LL) gives the neutral mono-alkyne complexes $[WI_2(CO)(LL)(\eta^2\text{-}RC_2R)]$[14] with no evidence for the formation of any cationic intermediates. DAB's (1,4-diaza-1,3-butadienes) are poorer π-acceptor and better σ-donor ligands than phosphines and hence these more electron-rich ligands can stabilize the formation of the cationic bisalkyne complexes.

Since the X-ray crystal structure of the closely related 2,2′-bipyridyl(bipy) complex $[WI(CO)(bipy)(\eta^2\text{-}MeC_2Me)_2][BPh_4]$ has been determined[13] and has very similar spectroscopic properties to the DAB complexes **(1)**–**(12)**, the structures of the bisalkyne complexes **(1)**–**(12)** are likely to be very similar (Fig. 1).

The IR spectra of the complexes **(1)**–**(12)** all show a single carbonyl band in the IR spectrum well above 2000 cm^{-1}. Since the tungsten(II) complexes are cationic and have two alkyne ligands which are competing for electron density to back-bond into their π*-orbitals there is little electron density available on the metal for back donation to the π*-

Table 3. ^1H NMR spectra[a] for the complexes $[WI(CO)(Rdab)(\eta^2\text{-}RC_2R)_2][X]$

Complex	^1H (δ) ppm
(1)[b]	8.74 (s, 2H, C*H*); 3.32 (d, 6H, *Me*C_2); 2.98 (d, 6H, *Me*C_2); 1.78, 1.71, 1.69, 1.57, 1.21, 1.12, 1.09 (brm, 22H, *Cy*).
(2)[b]	8.3 (s, 2H, CH); 7.54, 7.52, 7.36, 7.35, 7.33, 7.30 (brm, 20H, *Ph*); 2.0, 1.78, 1.2 (brm, 22H, *Cy*).
(3)	8.85 (s, 2H, C*H*); 7.78, 7.51 (d, 2H, C*H*$(Me)_2$), 5.3 (s, 2H, CH_2Cl_2); 3.37 (s, 6H, *Me*C_2); 3.06 (s, 6H, *Me*C_2); 1.42, 1.37, 1.21 (t, 12H,. *Me*).
(4)[b]	8.36 (s, 6H, C*H*); 7.57 (s, 2H, C*H*,$(Me)_2$); 7.54, 7.52, 7.36, 7.33 (brm, 20H, *Ph*C_2); 1.65, 1.63 (d, 6H, *Me*); 1.54, 1.52 (d, 6H, *Me*).
(5)[b]	7.64 (s, 2H, C*H*); 7.35, 7.25 (brm, 8H, *Ph*); 2.98 (s, 12H, *Me*C_2); 2.35, 2.16 (d, 6H, *Me*Ph).
(6)[b]	7.84, 7.82 (d, 2H, C*H*); 7.55, 7.53, 7.47, 7.41, 7.38 (brm, 20H, *Ph*C_2 and 8H, *Ph*); 2.30, 1.99 (d, 6H, *Me*Ph).
(7)[b]	7.49 (s, 2H, C*H*); 7.25 (brm, 10H, *Ph*); 3.22, 2.98 (d, 12H, *Me*C_2).
(8)	7.81 (s, 2H, C*H*); 7.4, 7.22 (brm, 20H, *Ph*C_2 and 10H, *Ph*); 5.26 (s, 1H, CH_2Cl_2).
(9)[b]	8.23 (s, 2H, C*H*); 7.76, 7.74, 7.69, 7.53 (brm, 8H, *Ph*); 3.83, 3.79 (d, *Me*O); 2.98 (s, 12H, *Me*C_2).
(10)[b]	8.31 (s, 2H, C*H*); 7.54, 7.52, 7.42, 7.35, 7.33 (brm, 20H, *Ph*C_2 and 8H, *Ph*); 3.87, 3.8 (m, 6H, *Me*O).
(11)	7.78 (s, 2H, C*H*); 7.49, 7.01, 6.9 (brm, 20H, *Ph*), 5.17 (s, 1H, CH_2Cl_2); 3.24 (s, 6H, *Me*C_2); 2.8 (s, 6H, *Me*C_2); 1.74, 1.20 (brm, 22H, *Cy*).
(12)	8.32 (bs, 2H, C*H*); 7.54, 7.01 (brm, 40H, *Ph*C_2 and *Ph*); 1.93, 1.43 (brm, 22H, *Cy*).

[a] Spectra run in $CDCl_3$ (+25°C) referenced to Me_4Si.
[b] Spectra run on a Bruker WH 400.

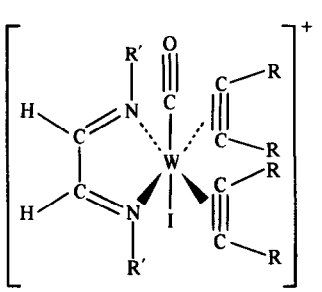

Fig. 1. Proposed structure of $[WI(CO)(R'N:CHCH:NR')(\eta^2\text{-}RC_2R)_2]^+$

Table 4. Selected ^{13}C NMR spectra[a] for the complexes $[WI(CO)(Rdab)(\eta^2\text{-}RC_2R)_2][X]$

Complex	^{13}C (δ) ppm
(1)[b]	203.18 (s, *C*O); 172.06, 161.91 (s, *C*≡*C*); 161.8, 120.0 (s, C*H*); 34.05, 30.61, 25.42, 25.06, 24.57, 24.23, 23.43 (brm, CH_2); 16.99 (s, *Me*C_2).
(2)[b]	188.61, 162.27 (s, *C*≡*C*); 143.6, 142.0 (s, C*H*); 136.98, 136.47, 131.34, 128.88, 128.08, 127.99, 127.85, 127.11 (brm, *Ph*); 35.61, 33.64, 33.51, 30.77, 25.77, 25.1, 24.56 (brm, CH_2).
(3)	203.76 (s, *C*O); 172.18, 162.05 (s, *C*≡*C*); 143.2, 120.2 (s, C*H*); 61.99 (s, C*H*$(Me)_2$); 52.11 (s, CH_2Cl_2); 23.78 (s, *Me*); 19.88, 17.57 (s, *Me*C_2).
(4)[b]	188.70, 141.81 (s, *C*≡*C*); 139.88 (s, C*H*); 131.27, 128.90, 128.02, 127.93, 127.07 (m, *Ph*); 89.01 (s, C*H*$(Me)_2$); 23.02, 20.97 (s, *Me*).
(6)[b]	208.00 (s, *C*O); 188.60, 156.40 (s, *C*≡*C*); 144.80, 139.90 (s, C*H*); 136.85, 131.25, 129.88, 129.52, 128.49, 128.0, 127.91 (brm, *Ph*), 20.89 (s, *Me*).
(7)[b]	208.15 (s, *C*O); 198.15, 158.8 (s, *C*≡*C*); 151.64 (s, C*H*); 134.0, 130.9, 129.37 (brm, *Ph*); 29.5, 18.9 (s, *Me*C_2).
(8)[b]	222.6 (s, *C*O), 174.78, 163.86 (s, *C*≡*C*); 137.23, 135.4 (s, C*H*); 131.51, 129.82, 128.78, 128.52, 128.0, 127.73 (brm, *Ph*); 52.1 (s, CH_2Cl_2).
(9)[b]	192.6, 161.01 (s, *C*≡*C*); 151.6, 140.51 (s, C*H*); 136.93, 127.86, 126.91, 125.45, 123.71 (brm, *Ph*); 29.39 (s, *Me*); 18.85 (s, *Me*C_2).
(10)[b]	208.03 (s, *C*O); 161.16 (s, *C*≡*C*); 136.9 (s, C*H*); 131.32, 128.53, 128.07, 127.98 (brm, *P*H); 29.40 (s, *Me*).

[a] Spectra run in $CDCl_3$ (+25°C) referenced to Me_4Si.
[b] Spectra run on a Bruker WH 400.
Carbonyl carbon is not seen in some of spectra as no relaxing agent $Cr(acac)_3$ was added to the solutions.

orbitals of the carbon monoxide ligand. The ^1H NMR spectra all show resonances expected for the static structures shown in Fig. 1. The ^{13}C NMR spectra of **(1)**–**(12)** all show resonances in the range 198.15–141.81 ppm for the alkyne contact carbon atoms. Templeton and Ward[15] have shown how ^{13}C NMR chemical shifts of coordinated alkynes can be related to the number of electrons donated to the metal centre. The range of values from 198.15 to 141.81 ppm in these complexes indicate that the alkyne ligands are donating an average of "three electrons" each to the tungsten atom. However it is highly likely that one alkyne ligand is donating four electrons and the other two electrons with rapid equilibration of these hybrids occurring (faster than the NMR time scale).

The complexes $[WI(CO)(CyN:CHCH:NCy)(\eta^2\text{-}RC_2R)_2]I$ were refluxed in $CHCl_3$ for 8 h in an attempt to afford the neutral "four electron" alkyne complexes $[WI_2(CO)(CyN:CHCH:NCy)(\eta^2\text{-}RC_2R)]$ analogous to the bidentate phosphine compounds $[WI_2(CO)(LL)(\eta^2\text{-}RC_2R)]$[14] without success. Also the complex $[WI(CO)(CyN:CHCH:NCy)(\eta^2\text{-}MeC_2Me)_2]I$ does not appear to react with $P(OMe)_3$ even after refluxing in $CHCl_3$ for 24 h.

Acknowledgements—We wish to thank Dr O. W. Howarth for running several ^1H and ^{13}C NMR spectra of samples at the University of Warwick and we thank the SERC for support. We also thank Miss Jane E. Barfield for preparing the R'N:CHCH:NR' ligands.

REFERENCES

1. M. Green, *J. Organomet. Chem.* 1986, **300**, 93 and refs cited therein.
2. M. Bottrill and M. Green, *J. Chem. Soc., Dalton Trans.* 1977, 2365.
3. P. L. Watson and R. G. Bergman, *J. Am. Chem. Soc.* 1980, **102**, 2698.
4. K. Sünkel, U. Nagel and W. Beck, *J. Organomet. Chem.* 1981, **222**, 251.
5. S. R. Allen, P. K. Baker, S. G. Barnes, M. Green, L. Trollope, L. M. Muir and K. W. Muir, *J. Chem. Soc., Dalton Trans.* 1981, 873.
6. S. Warner and S. J. Lippard, *Organometallics* 1986, **5**, 1716.
7. E. M. Armstrong, P. K. Baker and M. G. B. Drew, *Organometallics* (in press), 1988.
8. J. M. Kliegman and R. K. Barnes, *Tetrahedron Lett.* 1969, **24**, 1953.
9. V. C. Barry and P. W. D. Mitchell, *J. Chem. Soc.* 1953, 3610.
10. L. A. Cort and N. R. Francis, *J. Chem. Soc.* 1964, 2799.
11. J. M. Kliegman and R. K. Barnes, *Tetrahedron Lett.* 1970, **22**, 1859.
12. A. T. T. Hsieh and B. O. West, *J. Organomet. Chem.* 1976, **112**, 285.
13. E. M. Armstrong, P. K. Baker, M. B. Hursthouse and M. Harman, submitted to *J. Chem. Soc., Dalton Trans.*
14. E. M. Armstrong, P. K. Baker and M. G. B. Drew, submitted to *Inorg. Chem.*
15. J. L. Templeton and B. C. Ward, *J. Am. Chem. Soc.* 1980, **102**, 3288.

Polyhedron Vol. 7, No. 1, pp. 67–75, 1988
Printed in Great Britain

0277–5387/88 $3.00+.00
© 1988 Pergamon Journals Ltd

2,2′-BIPYRIDYL AND N,N,N′,N′-TETRAMETHYLETHYLENEDIAMINE DERIVATIVES OF MOLYBDENUM(V), NIOBIUM(V) AND TANTALUM(V) *t*-BUTYLIMIDO COMPLEXES

ALASTAIR J. NIELSON

Department of Chemistry, University of Auckland, Private Bag, Auckland, New Zealand

(*Received* 3 *June* 1987; *accepted* 24 *August* 1987)

Abstract—$MoCl_5$ reacts with two equivalents of $Me_3SiNHCMe_3$ in benzene to give $[Mo(NCMe_3)Cl_3(NH_2CMe_3)]_2 \cdot \frac{1}{6}C_6H_6$ (**1**) and with six equivalents of *t*-butylamine to give $[Mo(NCMe_3)(NHCMe_3)Cl_2(NH_2CMe_3)]_2 \cdot \frac{1}{6}C_6H_6$ (**2**). Complex (**1**) reacts with PMe_3 to give $[Mo(NCMe_3)Cl_3(PMe_3)_2]$ (**3**), with 2,2′-bipyridyl (bipy) to give $[Mo(NCMe_3)Cl_3(bipy)]$ (**4**) and with N,N,N′,N′-tetramethylethylenediamine (tmed) to give $[Mo(NCMe_3)Cl_3(tmed)] \cdot \frac{1}{3}C_6H_6$ (**5**). The IR spectra suggest *mer*-trichloro ligands. Complex (**2**) reacts with bipy in benzene to give $[Mo(NCMe_3)(NHCMe_3)Cl_2(bipy)]$ (**6**) for which the IR spectrum suggests *trans*-chloro ligands. In benzene, $[Nb(NCMe_3)Cl_3(NH_2CMe_3)]_2$ reacts with 4-picoline (pic) to give $[Nb(NCMe_3)Cl_3(pic)_2]$ (**7**), with bipy to give $[Nb(NCMe_3)Cl_3(bipy)] \cdot \frac{1}{12}C_6H_6$ (**8**) and with tmed to give $[Nb(NCMe_3)Cl_3(tmed)]$ (**9**). The tantalum complexes $[Ta(NCMe_3)Cl_3(bipy)] \cdot \frac{1}{3}C_6H_6$ (**10**), $[Ta(NCMe_3)Cl_3(tmed)] \cdot \frac{1}{6}C_6H_6$ (**11**), $[Ta(NCMe_3)(NHCMe_3)Cl_2(bipy)] \cdot \frac{1}{2}C_6H_6$ (**12**) were also prepared. $[Ta(NEt)Cl_3(NH_2Et)]_2$ (**13**) and $[Ta(NCHMe_2)(NHCHMe_2)Cl_2(bipy)]$ (**15**) were characterized by NMR spectroscopy. The NMR spectra of complexes (**7**), (**9**), (**11**) (**12**) and (**15**) show different coordination environments for the two nitrogen donor atoms of the bipy or tmed ligands.

In the early studies of reactions between primary amines and the high valent transition metal halides of groups V and VI, the products obtained have been formulated as amido complexes, $M(NHR)_x$.[1–3] We have recently shown however that when two such amido groups are present, intramolecular proton transfer occurs to give imido (M≡NR) and amine (M—NH_2R) groups. For example WCl_6 reacts with *t*-butylamine or N(trimethylsilyl)*t*-butylamine to give bis-organoimido complexes (eqs 1 and 2).[4]

$$WCl_6 + 7Me_3CNH_2 \rightarrow [W(NCMe_3)_2Cl_2(NH_2CMe_3)] + 4Me_3CNH_3Cl \quad (1)$$

$$WCl_6 + 4Me_3SiNHCMe_3 \rightarrow [W(NCMe_3)_2Cl_2(NH_2CMe_3)] + 4Me_3SiCl. \quad (2)$$

The pentachlorides of niobium and tantalum react with N(trimethylsilyl)*t*-butylamine to give the mono-organoimido complexes $[M(NCMe_3)Cl_3(NH_2CMe_3)]$ (eq. 3) and with a range of primary amines to form the complexes $[M(NR)(NHR)Cl_2(NH_2R)]$ (eq. 4) which contain imido, amido and amine ligands coordinated around the same metal centre.[5,6]

$$MCl_5 + 2Me_3SiNHCMe_3 \rightarrow [M(NCMe_3)Cl_3(NH_2CMe_3)] + 2Me_3SiCl \quad (3)$$

$$MCl_5 + 6RNH_2 \rightarrow [M(NR)(NHR)Cl_2(NH_2R)] + 3RNH_3Cl \quad (4)$$

(M = Nb, Ta).

Our attempts to use the niobium and tantalum complexes for the preparation of the phosphine derivatives $[M(NCMe_3)Cl_3P_2]$ and $[M(NR)(NHR)Cl_2P_2]$, invariably led to non-crystalline materials which could not be adequately characterized.[6] As part of a continuing interest in organoimido complexes, we wished to establish if

other metal pentachlorides would react similarly and whether nitrogen donors could be used successfully to prepare derivatives. Molybdenum complexes were the initial aim of these studies as preparative routes to mono-organoimido complexes of this metal[7,8] are less well developed than those of tungsten.[9,10] The present work details the preparation and characterization of Mo(V), Nb(V) and Ta(V) *t*-butylimido complexes containing the bidentate donor ligands 2,2′-bipyridyl and N,N,N′,N′-tetramethylethylenediamine.

RESULTS AND DISCUSSION

Reaction of $MoCl_5$ with two or more equivalents of $Me_3SiNHCMe_3$ in benzene led to dissolution of the molybdenum halide and after 18 h a purple–grey precipitate had formed. The solid analysed as the amido complex $[Mo(NHCMe_3)_2Cl_3]\cdot\frac{1}{12}C_6H_6$ but formulation as the imido complex $[Mo(NCMe_3)Cl_3(NH_2CMe_3)]_2\cdot\frac{1}{6}C_6H_6$ (**1**) is preferred. The complex is paramagnetic (d^1 system) so that ^{13}C NMR spectral data could not be used to establish the presence of the *t*-butylimido and amine ligands. However the IR spectrum is similar to the complexes $[M(NCMe_3)Cl_3(NH_2CMe_3)]_2$ (M = Nb, Ta), showing NH absorptions (3240, 3160 and 3090 cm^{-1}), bands characteristic of an imido function (ν_s\{Mo—N—C\} 1365, ν_{as}\{Mo—N—C\} 970 and δ\{Mo—N—C\} 680 cm^{-1}),[11] and several Mo—Cl vibrations in the far IR (350–285 cm^{-1}). The complexity of the metal–halogen stretches suggested the presence of more than one species and these are proposed as the chloro-bridged complexes (**a**) and (**b**).

When $MoCl_5$ was reacted with excess *t*-butylamine or complex (**1**) reacted with two equivalents of Me_3CNH_2 a brown solution formed and Me_3CNH_3Cl was precipitated. The complex obtained from the former reaction analysed as $[Mo(NHCMe_3)_3Cl_3]\cdot\frac{1}{12}C_6H_6$ but the alternative formulation $[Mo(NCMe_3)(NHCMe_3)Cl_2(NH_2CMe_3)]_2\cdot\frac{1}{6}C_6H_6$ (**2**) is preferred, again on the basis of IR spectral comparison with $[Ta(NCMe_3)(NHCMe_3)Cl_2(NH_2CMe_3)]_2$ for which an X-ray structure has been determined.[5] The chloro-bridge structure (**c**) is thus proposed for (**2**).

Complex (**1**) reacted with PMe_3 to give a non-crystalline solid which analysed closely as the bis phosphine complex $[Mo(NCMe_3)Cl_3(PMe_3)_2]$ (**3**) but further characterization was precluded by failure to obtain a suitable IR spectrum. Similarly when (**1**) was reacted with diphenylphosphinoethane (dppe) a non-crystalline complex was obtained which has not yet given a sufficiently pure product. The failure of these reactions to give clean products thus parallels the niobium and tantalum chemistry.[6]

Reaction of complex (**1**) with 2,2′-bipyridyl (bipy), however, produced dark green microcrystals of $[Mo(NCMe_3)Cl_3(bipy)]$ (**4**). The complex is insoluble in organic solvents and has an IR spectrum consistent with the formulation as a *t*-butylimido complex. The NH bands characteristic of the amine ligand of the parent complex were absent and there were absorptions consistent with the presence of an imido function. In the far IR three Mo—Cl stretches were present (335, 320 and 308 cm^{-1}) which suggest a *mer* configuration of the three chloro ligands.[12] Thus a *mer* configuration of chloro ligands (structure **d**) which could arise directly from both (**a**) and (**b**), is preferred to the *fac* structure (**e**).

To overcome solubility problems associated with the bipy complex, N,N,N′,N′-tetramethylethylene diamine (tmed) was added to complex (**1**) which led to the more soluble species $[Mo(NCMe_3)Cl_3(tmed)]\cdot\frac{1}{3}C_6H_6$ (**5**). In the IR spectrum NH bands were again absent, there were absorptions characteristic of the imido function and three Mo—Cl stretches were present in the vicinity of 300 cm^{-1} indicative of a *mer*-trichloro structure.

A reaction between $[Mo(NCMe_3)(NHCMe_3)Cl_2(NH_2CMe_3)]_2\cdot\frac{1}{6}C_6H_6$ (**2**) and bipy in benzene solution resulted in precipitation of the orange microcrystalline complex $[Mo(NCMe_3)(NHCMe_3)Cl_2(bipy)]$ (**6**). In the IR spectrum the amido NH absorption occurred at 3100 cm^{-1}, bands characteristic of the imido function were present, and in the far IR there was a single strong Mo—Cl stretch (325 cm^{-1}) consistent with *trans*-orientated dichloro ligands.[12] The *trans*-chloro structure (**f**) is thus preferred for this complex.

The molybdenum complexes are all paramagnetic and give rise to very broad NMR resonances where solubility is not a problem. Suitable NMR spectra are however obtainable for the d^0 complexes $[M(NCMe_3)Cl_3(NH_2CMe_3)]_2$ and $[M(NCMe_3)(NHCMe_3)Cl_2(NH_2CMe_3)]_2$ (M = Nb, Ta)[6] so derivatives were prepared which could be studied by NMR spectroscopy.

$[Nb(NCMe_3)Cl_3(NH_2CMe_3)]_2$ reacts with four equivalents of 4-picoline (pic) to give the non-crystalline *t*-butylimido complex $[Nb(NCMe_3)Cl_3(pic)_2]$ (**7**) for which a *mer*-trichloro structure (**g**) is proposed, again on the basis of three Nb—Cl stretches in the IR spectrum. Further evidence comes from the NMR spectra (Table 2) in which the *t*-butylimido ligand methyl protons appear in the ^1H NMR spectrum as a singlet while there are two singlets for the methyl groups of the 4-picoline ligands. While the β-protons of these ligands appear

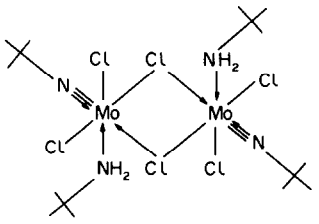

(a)

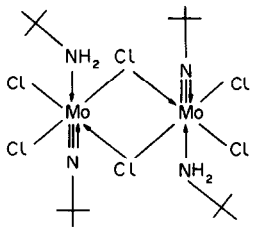

(b)

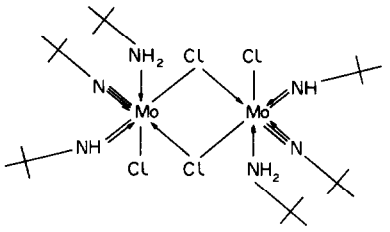

(c)

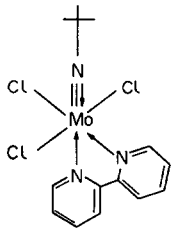

(d)

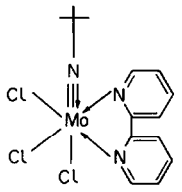

(e)

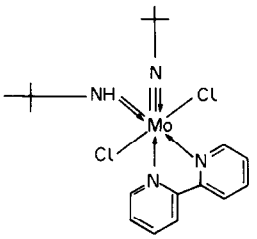

(f)

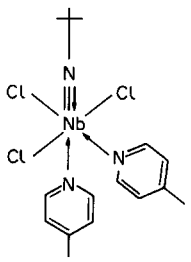

(g)

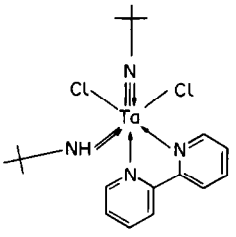

(h)

as a doublet, the α-protons appear as two superimposed doublets. In the ^{13}C NMR spectrum the *t*-butyl group methyl and quaternary carbons appear as single resonances characteristic of a *t*-butylimido group (*ca.* 30.0 and 70.0 ppm, respectively) while for the 4-picoline ligands the α- and β-carbons each appear as two resonances and the γ-carbon as a single resonance. The NMR spectral features thus indicate that the 4-picoline ligands are inequivalent which is consistent with the *cis*-configuration of pic ligands of structure (**g**).

Addition of bipy to a benzene solution of $[Nb(NCMe_3)Cl_3(NH_2CMe_3)]_2$ caused the microcrystalline complex $[Nb(NCMe_3)Cl_3(bipy)]\cdot\frac{1}{12}C_6H_6$ (**8**) to precipitate out. The complex is insoluble in a range of organic solvents so that NMR data could not be obtained, but a structure similar to that of the molybdenum complex (**4**) [structure (**d**)] is proposed on the basis of similarities in the IR spectra of the two complexes. In particular absorptions at 345, 340 and 320 cm^{-1} are consistent with a *mer*-trichloro structure.

When $[Nb(NCMe_3)Cl_3(NH_2CMe_3)]_2$ was reacted with tmed a more soluble derivative $[Nb(NCMe_3)$

Cl_3(tmed)] (**9**) was obtained. The IR spectrum is similar to the molybdenum analogue (**5**), containing absorptions characteristic of the imido function and Nb—Cl stretches indicating a *mer*-trichloro structure. In the ^1H NMR spectrum the *t*-butyl group methyl protons appeared as a singlet and there were two sets of resonances for the methyl and methylene protons of the tmed ligand. The ^{13}C NMR spectrum contained one resonance each for the *t*-butylimido group methyl and quaternary carbons while there were two sets of methyl and methylene carbon resonances for the tmed ligand. The spectra thus suggest that the tmed ligand nitrogens coordinate in a similar manner to the pic ligands in complex (**7**) (structure **g**).

Analogues similar to the niobium complexes can also be prepared for tantalum. $[Ta(NCMe_3)Cl_3(NH_2CMe_3)]_2$ reacts with bipy to produce the insoluble complex $[Ta(NCMe_3)Cl_3(bipy)]\cdot\frac{1}{3}C_6H_6$ (**10**) and with tmed to form $[Ta(NCMe_3)Cl_3(tmed)]\cdot\frac{1}{6}C_6H_6$ (**11**) which is soluble in a range of solvents. Both complexes have similar IR spectra to the respective niobium analogues and the NMR characteristics of the tmed complexes are the same apart from the position of the *t*-butyl group quaternary carbon resonance which lies slightly to higher field in the niobium complex (70.7 ppm compared with 65.8 ppm for the Ta complex). This change corresponds to a small decrease in the charge at the nitrogen atom on going from tantalum to niobium.[13]

When $[Ta(NCMe_3)(NHCMe_3)Cl_2(NH_2CMe_3)]_2$ was reacted with bipy in benzene, $[Ta(NCMe_3)(NHCMe_3)Cl_2(bipy)]\cdot\frac{1}{2}C_6H_6$ (**12**) precipitated from the reaction solution. The complex had an identical IR spectrum to the molybdenum analogue (**6**) and was sufficiently soluble for NMR spectra to be run. The ^1H NMR spectrum showed separate singlets for the *t*-butylimido and amido group methyl protons while there were two doublets for the α-protons of the bipy ligand. A *trans*-chloro structure similar to that proposed for the molybdenum analogue [structure (**f**)] is preferred for this complex on the basis of the single strong Ta—Cl stretch at 314 cm^{-1}. For this structure the two α-protons of the bipy ligands would be influenced by different molecular environments leading to different chemical shifts. It is noted however that the X-ray crystal structure of the parent complex $[Ta(NCMe_3)(NHCMe_3)Cl_2(NH_2CMe_3)]_2$ shows *cis*-chloro ligands.[5] In the absence of isomerization, reaction with bipy would be expected to give rise to a *cis* chloro complex, structure (**h**), but in this case the bipy α-protons would still experience different chemical shifts.

The ^{13}C NMR spectrum of (**12**) also shows the effect of the molecular environment. There is a single resonance for both the *t*-butylimido and amido methyl and quaternary carbon resonances, the characteristic quaternaries[6] occurring at 63.9 and 56.3 ppm, respectively, and there was a set of resonances for each ring of the bipyridyl ring. In other work we have shown that two sets of bipy resonances are present in the ^{13}C NMR spectrum of $[W(NCMe_3)(NPh)Cl_2(bipy)]$ when one $M—N_{bipy}$ bond is lengthened as a result of steric interaction between *t*-butylimido methyl groups and the bipy α-proton.[14] However, it is not clear in the present case whether the *t*-butylimido or amido methyl groups are involved.

A preliminary study was also made of several tantalum complexes containing smaller alkylimido ligands. $TaCl_5$ reacts with two equivalents of $Me_3SiNHEt$ to give a complex characterized by NMR spectroscopy as $[Ta(NEt)Cl_3(NH_2Et)]_2$ (**13**). On reaction with bipy the insoluble complex $[Ta(NEt)Cl_3(bipy)]$ (**14**) was formed. $[Ta(NCHMe_2)(NHCHMe_2)Cl_2(NH_2CHMe_2)]_2$,[6] reacts with bipy to give $[Ta(NCHMe_2)(NHCHMe_2)Cl_2(bipy)]$ (**15**) for which characterization was also made by NMR spectroscopy. In the ^1H NMR spectrum the α-protons of the bipy ligand appeared as two doublets, the isopropyl methine protons as two septets and there were two sets of doublets for the methyl groups of the isopropylimido and amido ligands. The ^{13}C NMR spectrum showed a separate set of resonances for each ring of the bipy ligand, two isopropyl methine carbon resonances and two resonances of equal intensity for the isopropylimido and amido methyl carbons. Asymmetry in the molecule is thus reflected by the non-equivalence of the isopropyl methyl groups.[15] The far IR, however, does not clearly show the expected *cis*-chloro groups, there being a very broad absorption between 320 and 280 cm^{-1}. This contrasts with the *t*-butyl analogues where a single sharp absorption suggests *trans*-chloro groups.

EXPERIMENTAL

t-Butylamine, 4-picoline and N,N,N′,N′-tetramethylethylenediamine were dried over and distilled from calcium hydride. N(trimethylsilyl)*t*-butylamine and N(trimethylsilyl)ethylamine were prepared by treating trimethylsilyl chloride with two equivalents of the appropriate amine and distilling the product.[16] Trimethylphosphine was prepared by a literature method.[17] $NbCl_5$ and $TaCl_5$ were sublimed prior to use and $MoCl_5$ was used as supplied. $[Nb(NCMe_3)Cl_3(NH_2CMe_3)]_2$, $[Ta(NCMe_3)Cl_3(NH_2CMe_3)]_2$, $[Ta(NCMe_3)(NHCMe_3)$

$Cl_2(NH_2CMe_3)]_2$ and $[Ta(NCHMe_2)(NHCHMe_2)Cl_2(NH_2CHMe_2)]_2$ were prepared as previously reported.[6] Petroleum ether (b.p. 40–60°C), benzene and toluene were distilled over sodium wire and dichloromethane over calcium hydride. All distillations and bench-top manipulations were carried out under N_2 treated to remove oxygen and water.[18] IR spectra were recorded on a Perkin–Elmer 597 spectrometer, ^1H NMR spectra on a Varian T60 Model spectrometer and ^{13}C NMR spectra on a JEOL FX60 spectrometer. Analytical data were obtained by Prof. A. D. Campbell and his associates, University of Otago, New Zealand. Melting points were determined in sealed tubes under N_2 on an electrothermal melting point apparatus and are uncorrected.

bis - t - Butylaminebis - t - butylimidohexachlorodimolybdenum(V) (**1**)

A solution of N(trimethylsilyl)*t*-butylamine (2 cm^3, 10.35 mmol) in benzene (30 cm^3) was slowly added to a suspension of molybdenum pentachloride (1.4 g, 5.1 mmol) in benzene (50 cm^3) cooled to ice-water temperature. The mixture was stirred for 18 h and the solution filtered, leaving the complex as a purple–grey microcrystalline solid which was washed twice with benzene (30 cm^3) and dried *in vacuo* (1.6 g, 88%).

IR (Nujol) bands at 3240w, 3160m, 3090m, 1590w, 1560m, 1400m, 1365s, 1340w, 1288s, 1220s, 1205s, 1178s, 1145m, 1030w, 970w, 928w, 890m, 845w, 800w, 745m, 720w, 680s, 590w, 550m, 530w, 445w, 422m, 370m, 350s, 340s, 320s, 305s and 285s cm^{-1}.

bis-t-Butylamidobis-t-butylaminebis-t-butylimidohexachlorodimolybdenum(V) (**2**)

A solution of *t*-butylamine (4.6 cm^3, 43.9 mmol) in benzene (30 cm^3) was added to a suspension of molybdenum pentachloride (2.0 g, 7.3 mmol) in benzene (80 cm^3) and the mixture was stirred for 3 h. The solution was filtered and the residue washed with benzene (5 cm^3). The filtrates were combined and the solvent removed to give the complex as a yellow–brown crystalline solid, which was washed with petroleum ether (60 cm^3) and dried *in vacuo* (2.5 g, 88%).

IR (Nujol) bands at 3300w, 3170m, 3100w, 2700w, 2600w, 2500w, 1605w, 1565m, 1402m, 1355s, 1300w, 1278m, 1240s, 1210s, 1165s, 1135m, 1100m, 1025m, 930w, 895m, 800m, 750w, 725w, 680w, 610m, 588m, 565w, 470w, 450w, 422w, 380w, 350w, 320s and 305s cm^{-1}.

t-Butylimidotrichlorobis(trimethylphosphine)molybdenum(V) (**3**)

A solution of trimethylphosphine (0.25 cm^3, 2.3 mmol) in dichloromethane (30 cm^3) was added to a suspension of bis-*t*-butylaminebis-*t*-butylimidohexachlorodimolybdenum (V) (0.4 g, 0.6 mmol) in dichloromethane (25 cm^3) and the mixture was stirred for 3 h. The solution was filtered and the solvent rermoved to give a flaky yellow solid which was washed with petroleum ether (60 cm^3) and dried *in vacuo*. The complex did not mull in Nujol or KEL-F.

(2,2′ - *Bipyridyl*)*t* - *butylimidotrichloromolybdenum*(V) (**4**)

A solution of 2,2′-bipyridyl (0.25 g, 1.6 mmol) in benzene (30 cm^3) was added to bis-*t*-butylaminebis-*t*-butylimidohexachlorodimolybdenum(V) (**1**) (0.5 g, 1.5 mmol) suspended in benzene and the mixture was stirred for 18 h. The solution was filtered and the solid washed with benzene (2 × 30 cm^3) and dried *in vacuo*. Yield 0.46 g (74%).

IR (Nujol) bands at 1595s, 1568w, 1490m, 1400w, 1360s, 1308m, 1240m, 1222s, 1178w, 1160w, 1105w, 1060w, 1042w, 1022m, 1010m, 970w, 890w, 878w, 800w, 758s, 725s, 680w, 655m, 650w, 635m, 570m, 565m, 445w, 415w, 370w, 335s, 320s and 308s cm^{-1}.

t - Butylimidotrichloro(N,N,N′,N′ - tetramethylethylenediamine)molybdenum(V) (**5**)

A solution of N,N,N′,N′-tetramethylethylenediamine (0.5 cm^3, 3.4 mmol) in benzene (30 cm^3) was added to bis-*t*-butylaminebis-*t*-butylimidohexachlorodimolybdenum(V) (**1**) (1.0g, 2.9 mmol) suspended in benzene (60 cm^3) and the mixture was stirred for 10 min. The solution was warmed to *ca.* 50°C, the volume reduced by 10 cm^3 to remove liberated *t*-butylamine, and the stirring continued for a further 2 h. The green solution was filtered, the solvent removed and the green complex washed with toluene (20 cm^3) followed by petroleum ether (30 cm^3) and dried *in vacuo* (0.85 g, 71%).

IR (Nujol) bands at 2720m, 2605m, 2505w, 2095m, 1618w, 1575w, 1514m, 1405m, 1310m, 1290w, 1235s, 1225s, 1180w, 962w, 940w, 895w, 860w, 835w, 809m, 730w, 605w, 535w, 464m, 430w, 355m, 340m, 305m and 290 m cm^{-1}.

(2,2′-Bipyridyl)t-butylamido-t-butylimidodichloromolybdenum(V) (**6**)

A solution of 2,2′-bipyridyl (0.8 g, 5.1 mmol) in benzene (40 cm^3) was added to a solution of

bis-*t*-butylamidobis-*t*-butylaminebis-*t*-butylimidohexachlorodimolybdenum(V) (1.9 g, 2.5 mmol) in benzene (60 cm^3) and the mixture was stirred for 2 h. The solution was filtered and the complex washed several times with benzene (20 cm^3) giving the complex as an orange–yellow microcrystalline solid (1.6 g, 70%).

IR (Nujol) 3100w, 1602s, 1580w, 1570w, 1495w, 1465s, 1460s, 1362s, 1316m, 1250s, 1210s, 1180m, 1160m, 1112s, 1080w, 1065w, 1050w, 1025s, 1020s, 975w, 910w, 900w, 805m, 773s, 750w, 740s, 655m, 633w, 609m, 580m, 473m, 425w, 385w, 362w and 325s cm^{-1}.

t-Butylimidotrichlorobis(4-picoline)niobium(V) (**7**)

t-Butylamine-*t*-butylimidotrichloroniobium(V) dimer (0.75 g, 1.1 mmol) was dissolved in benzene (80 cm^3) and the solution filtered. 4-Picoline (0.45 g, 4.8 mmol) in benzene (30 cm^3) was added and the mixture was refluxed for 2 h. The solution was filtered, the solvent removed and the residue washed with petroleum ether (50 cm^3). The complex was ground to a fine powder, washed with further petroleum ether (100 cm^3) and dried *in vacuo*.

IR (Nujol) bands at 2700w, 2600w, 2510w, 2075w, 1622s, 1508m, 1465s, 1405w, 1370s, 1305w, 1255s, 1238s, 1218s, 1072m, 1032m, 1020m, 935m, 880m, 850m, 820s, 758s, 730s, 690m, 570m, 555m, 542m, 530w, 500s, 460w, 378w, 330s, 315s and 294m cm^{-1}.

(2,2′-*Bipyridyl*)*t-butylimidotrichloroniobium*(V) (**8**)

N(trimethylsilyl)*t*-butylamine (2.6 cm^3, 13.5 mmol) in benzene (30 cm^3) was added slowly to a suspension of niobium pentachloride (1.8 g, 6.7 mmol) in benzene (70 cm^3) and the mixture was stirred for 17 h. The solution was filtered from the yellow precipitate which was washed with benzene (5 cm^3) and dried *in vacuo*. The complex (1 g, 1.5 mmol) was dissolved in benzene (60 cm^3) and the solution filtered several times until a clear light yellow solution was obtained. 2,2′-Bipyridyl (0.5 g, 3.2 mmol) in benzene (30 cm^3) was added and the mixture was stirred for 2 h during which time the complex precipitated out. The solution was filtered and the yellow solid washed with benzene (5 cm^3) followed by petroleum ether (30 cm^3) and dried *in vacuo*. Yield 1.1 g, 79%.

IR (Nujol) bands at 1603s, 1575w, 1517w, 1500m, 1409m, 1370m, 1318m, 1245s, 1222m, 1185w, 1168w, 1115w, 1070w, 1052w, 1030m, 1020m, 978w, 900w, 890w, 850w, 810w, 770s, 740s, 730w, 684w, 662m, 642m, 570m, 458m, 422w, 382m, 370w, 345s, 340s and 320s cm^{-1}.

t - Butylimidotrichloro(N,N,N′,N′ - tetramethylethylenediamine)niobium(V) (**9**)

N,N,N′,N′-tetramethylenediamine (0.2 g, 1.7 mmol) in benzene (30 cm^3) was added to bis-*t*-butylaminebis - *t* - butylimidohexachlorodiniobium(V), (0.5 g, 0.7 mmol) in benzene (60 cm^3) and the mixture was refluxed for 1 h. The solution was filtered and the solvent removed to give an oil which was allowed to stand under petroleum ether (50 cm^3) for 24 h. The solid was filtered, crushed to a powder and washed with further portions of petroleum ether (2×30 cm^3) and dried *in vacuo*. Yield 0.5 g, 89%.

IR (Nujol) bands at 1475s, 1404w, 1360s, 1290w, 1245s, 1222s, 1200w, 1160w, 1145w, 1120w, 1105w, 1068w, 1045w, 1010s, 985w, 955s, 920m, 845w, 804s, 772m, 730m, 595w, 565w, 550w, 525w, 490w, 460w, 390w, 338s, 315s and 290 m cm^{-1}.

(2,2′ - *Bipyridyl*)*t - butylimidotrichlorotantalum*(V) (**10**)

N(trimethylsilyl)*t*-butylamine (1.9 cm^3, 9.8 mmol) in benzene (50 cm^3) was added slowly to a suspension of tantalum pentachloride (1.7 g, 4.8 mmol) in benzene (50 cm^3) and the mixture was stirred for 16 h. The solution was filtered from a small amount of colourless solid and 2,2′-bipyridyl (0.8 g, 5.1 mmol) in benzene (30 cm^3) added. The mixture was stirred rapidly whereupon a light yellow solid was precipitated. After stirring for 2 h the solution was filtered and the solid washed with benzene (2×20 cm^3) and dried *in vacuo*. Yield 2.0 g, 82%.

IR (Nujol) bands at 1605s, 1575w, 1515w, 1500m, 1409m, 1375s, 1348m, 1280s, 1248w, 1222m, 1188w, 1170w, 1118w, 1081w, 1072w, 1055w, 1037m, 1025m, 982w, 900w, 894w, 850w, 812w, 770s, 742m, 687w, 666w, 645w, 570m, 462m, 428w, 358w, 330s and 308s cm^{-1}.

t - Butylimidotrichloro(N,N,N′,N′ - tetramethylethylenediamine)tantalum(V) (**11**)

N,N,N′,N′-tetramethylethylenediamine (0.3 g, 2.6 mmol) in benzene (30 cm^3) was added to *bis-t* - butylaminebis - *t* - butylimidohexachloroditantalum(V) (1.0 g, 1.2 mmol) in benzene (50 cm^3) and the mixture was refluxed for 2 h. The solution was filtered and the solvent removed to give an oil which solidified on standing under petroleum ether (50 cm^3) for 24 h. The complex was crushed to a powder, washed with petroleum ether (2×30 cm^3) and dried *in vacuo*. Yield 0.9 g, 80%.

IR (Nujol) bands at 1470s, 1405w, 1358s, 1285s, 1252m, 1222m, 1200w, 1175w, 1155w, 1120m,

Table 1. Physical data

Complex	Colour	m.p. (°)[a]	Analytical data[b] C	H	N	Infrared data (cm^{-1}) ν_s(M—N—C)	ν(M—Cl)
$[Mo(NCMe_3)Cl_3(NH_2CMe_3)]_2 \cdot \frac{1}{6}C_6H_6$ (**1**)	grey–purple	[c]	29.0	5.6	8.0	1365	350,340,320
			(28.9)	(5.9)	(7.9)		305,285
$[Mo(NCMe_3)(NHCMe_3)Cl_2(NH_2CMe_3)]_2 \cdot \frac{1}{6}C_6H_6$ (**2**)	yellow	—	38.7	7.8	10.8	1355	320,305
			(38.5)	(7.9)	(10.8)		
$[Mo(NCMe_3)Cl_3(PMe_3)_2]$ (**3**)	light yellow	—	31.4	7.3	3.7	[d]	[d]
			(28.2)	(6.4)	(3.3)		
$[Mo(NCMe_3)Cl_3(bipy)]$ (**4**)	dark green	> 185d	37.5	4.5	9.0	1360	335,320,308 (*mer*)
			(39.1)	(4.0)	(9.8)		
$[Mo(NCMe_3)Cl_3(tmed)] \cdot \frac{1}{3}C_6H_6$ (**5**)	green	> 120d	34.9	6.8	10.3	[e]	340,305,290 (*mer*)
			(34.7)	(6.3)	(10.1)		
$[Mo(NCMe_3)(NHCMe_3)Cl_2(bipy)]$ (**6**)	orange	252	45.8	5.9	12.1	1362	325 (*trans*)
			(46.3)	(5.8)	(12.0)		
$[Nb(NCMe_3)Cl_3(pic)_2]$ (**7**)	light yellow	148–150	42.0	5.8	8.7	1370	330,315,294 (*mer*)
			(42.1)	(5.1)	(9.2)		
$[Nb(NCMe_3)Cl_3(bipy)] \cdot \frac{1}{12}C_6H_6$ (**8**)	yellow	> 230d	40.4	4.4	9.3	1370	345,340,320 (*mer*)
			(40.2)	(4.1)	(9.7)		
$[Nb(NCMe_3)Cl_3(tmed)]$ (**9**)	light yellow	130	31.1	6.8	10.6	1360	338,315,290 (*mer*)
			(31.1)	(6.5)	(10.9)		
$[Ta(NCMe_3)Cl_3(bipy)] \cdot \frac{1}{3}C_6H_6$ (**10**)	light yellow	274–276	35.4	3.9	7.6	1370	340,330,310 (*mer*)
			(35.5)	(3.5)	(7.8)		
$[Ta(NCMe_3)Cl_3(tmed)] \cdot \frac{1}{6}C_6H_6$ (**11**)[f]	colourless	131–133	27.3	5.6	8.5	1358	338,310,290 (*mer*)
			(27.1)	(5.4)	(8.6)		
$[Ta(NCMe_3)(NHCMe_3)Cl_2(bipy)] \cdot \frac{1}{2}C_6H_6$ (**12**)[f]	colourless	115–118	42.1	5.3	9.1	1370	314 (*trans*)
			(42.7)	(5.1)	(9.5)		

[a] d = decomposition.
[b] Calculated figures in parentheses.
[c] Colour of complex prevents accurate determination of decomposition point.
[d] Suitable IR spectrum not obtained.
[e] Band obscured by Nujol.
[f] Benzene verified by NMR spectra.

Table 2. NMR spectra

Complex	^{13}C NMR[a,b] α-carbon	β-carbon	Others	^{1}H NMR[a,b,c]
$[Nb(NCMe_3)Cl_3(pic)_2]$ (7)	70.6	29.3 (Me_3)	21.1 and 21.4 (γ-CH_3, pic), 124.8 and 125.1 (β-CH, pic); 150.4 and 151.9 (α–CH, pic); 152.4 (γ-C, pic).	1.44 (s, 9H, CMe_3); 2.35 and 2.40 (2s, 6H, 2Me); 7.00–7.32 (d, 4H, β-Hs, pic); 8.50–8.95 (m, 4H, α-Hs, pic).
$[Nb(NCMe_3)Cl_3(tmed)]$ (9)	70.7	29.5 (Me_3)	49.3 and 55.4 (NMe, tmed); 56.9 and 59.7 (NCH_2, tmed).	1.45 (s, 9H, CMe_3); 2.88 and 3.10 (2s, 12H, 4Me); 2.94 and 3.00 (2s, obscured, 4H, $2CH_2$).
$[Ta(NCMe_3)Cl_3(tmed)] \cdot \frac{1}{6}C_6H_6$ (11)[d]	65.8	31.8 (Me_3)	49.6 and 55.6 (NMe, tmed); 57.1 and 59.7 (NCH_2, tmed).	1.42 (s, 9H, CMe_3); 2.90 and 3.15 (2s, 12H, 4Me); 2.92 and 3.04 (2s, obscured, 4H, $2CH_2$).
$[Ta(NCMe_3)(NHCMe_3)Cl_2(bipy)] \cdot \frac{1}{2}C_6H_6$ (12)[d]	56.3 (NHC) 63.9 (NC)	32.0 (Me_3) 34.5 (Me_3)	122.8 and 123.2, 126.0 and 126.4 (β-CHs, bipy); 128.2 (benzene); 140.2 and 140.7 (γ-CH, bipy); 151.3 and 152.8 (α-CHs, bipy); 151.8 and 152.4 (α-Cs, bipy).	0.85 (s, 9H, $NHCMe_3$); 1.59 (s, 9H, $NCMe_3$); 7.35 (benzene); 7.50–7.75 (m, 2H, γ-Hs, bipy); 7.90–8.64 (m, 4H, β-Hs, bipy); 9.35 and 9.80 (2d, 2H, α-CHs, bipy).
$[Ta(NEt)Cl_3(NH_2Et)]$ (13)	43.5 (NH_2C) 57.2 (NC)	17.7 (Me)	—	0.95–1.51 (m, 6H, 2Me); 2.75-3.81 and 4.53–5.11 (several m, 6H, $2CH_2$ and NH_2).
$[Ta(NCHMe_2)(NHCHMe_2)Cl_2(bipy)]$ (15)	59.0 (NCH) 59.2 (NHCH)	25.6 and 25.8 27.4 and 28.3	122.8 and 123.2, 126.2 and 126.3 (β-CHs, bipy); 140.3 and 140.7 (γ-CHs, bipy); 152.0 and 152.3 (α-Cs, bipy).	0.50–0.85 (2d, J = 6Hz, 6H, Me_2); 1.10–1.58 (2d, J = 6Hz, 6H, Me_2); 4.25 (sept, 1H, CH); 4.50–5.15 (b. sept, 1H, CH); 7.52–7.80 (m, 2H, γ-Hs, bipy); 8.05–8.65 (m, 4H, β-Hs, bipy); 9.10 and 9.50 (2d, J = 6Hz, 2H, α-CHs, bipy).

[a] Spectra obtained in $CDCl_3$.
[b] Assignments for pic, bipy and tmed made by comparison with the free ligand.
[c] b = broad, d = doublet, m = multiplet, s = singlet.
[d] Spectra show benzene consistent with formulation.

1105w, 1068m, 1048m, 1015s, 982m, 955s, 922m, 845m, 804s, 775m, 735m, 700w, 595w, 564w, 548w, 525w, 490w, 470w, 455w, 390w, 338s, 310s and 290m cm^{-1}.

(2,2′ - Bipyridyl)t - butylamido - t - butylimidodichlorotantalum(V) **(12)**

2,2′-Bipyridyl (0.8g, 5.1 mmol) in benzene (30 cm^3) was added to bis-*t*-butylamidobis-*t*-butylaminebis - *t* - butylimidotetrachloroditantalum(V), (2.0 g, 2.1 mmol) in benzene (60 cm^3) and the mixture was stirred for 4 h. The solution was filtered and the residue washed several times with benzene (20 cm^3) giving the complex as a colourless solid. Yield 2.3 g (92%).

IR (Nujol) bands at 1608m, 1575w, 1565w, 1370s, 1360s, 1318w, 1289m, 1274s, 1224m, 1183w, 1162w, 1118w, 1082w, 1068w, 1052w, 1036m, 985w, 811w, 798w, 785s, 755w, 742m, 730w, 690s, 660w, 568m, 425w and 314s cm^{-1}.

(2,2′ - Bipyridyl)dichloroethylimidotantalum(V) **(14)**

N(trimethylsilyl)ethylamine (1.34 cm^3, 9.5 mmol) in benzene (30 cm^3) was added to tantalum pentachloride (1.7 g, 4.8 mmol) suspended in benzene (60 cm^3) and the mixture was stirred for 16 h. The solution was filtered and the solvent removed to give a flaky solid which was washed with petroleum ether (50 cm^3) and dried *in vacuo*. ^1H and ^{13}C NMR spectra (Table 1) showed the material to be $[Ta(NEt)\ Cl_3(NH_2Et)]_2$ **(13)**. The complex (1.6 g, 2.1 mmol) was dissolved in benzene (50 cm^3) and the solution filtered. 2,2′-Bipyridyl (0.7 g, 4.5 mmol) in benzene (30 cm^3) was added and the mixture was stirred for 3 h. The solution was filtered and the complex washed with benzene (2×30 cm^3) followed by petroleum ether (30 cm^3) and dried *in vacuo*.

IR (Nujol) bands at 1602s, 1570w, 1365s, 1328w, 1317m, 1280s, 1242w, 1222w, 1195w, 1178w, 1158w, 1118w, 1105w, 1070w, 1050w, 1032w, 1020w, 900w, 854w, 800w, 772s, 738s, 690w, 665m, 642m, 500w, 425m, 390m, 330s, 318s and 295m cm^{-1}.

(2,2′ - Bipyridyl)dichloroisopropylamidoisopropylimidotantalum(V) **(15)**

2,2′-Bipyridyl (0.6 g, 3.8 mmol) in benzene (40 cm^3) was added slowly to a solution of bis(isopropylamido) bis (isopropylamine) bis (isopropylimido)tetrachloroditantalum(V), (1.6 g, 1.9 mmol) in benzene (60 cm^3) and the mixture was stirred for 5 h. The solution was filtered and the solvent removed to give a flaky solid which was washed with warm petroleum ether (50 cm^3). The complex was crushed to a powder, washed with petroleum ether (2×30 cm^3) and dried *in vacuo*.

IR (Nujol) bands at 1600m, 1560m, 1460s, 1350s, 1308s, 1270s, 1230m, 1160s, 1110s, 1068w, 1050w, 1030m, 1022m, 990w, 890w, 848w, 770s, 738s, 650m, 638m, 550w, 480w, 425w, 365w and 312vb cm^{-1}.

REFERENCES

1. G. W. A. Fowles and C. M. Pleass, *J. Chem. Soc.* 1957, 2078.
2. P. J. H. Cornell and G. W. A. Fowles, *J. Chem. Soc.* 1959, 4113.
3. D. A. Edwards and G. W. A. Fowles, *J. Chem. Soc.* 1961, 24.
4. B. R. Ashcroft, D. C. Bradley, G. R. Clark, R. J. Errington, A. J. Nielson and C. E. F. Rickard, *J. Chem. Soc., Chem. Commun.* 1987, 170.
5. T. C. Jones, A. J. Nielson and C. E. F. Rickard, *J. Chem. Soc., Chem. Commun.* 1984, 205.
6. P. A. Bates, A. J. Nielson and J. M. Waters, *Polyhedron* 1985, **4**, 1391.
7. W. A. Nugent and B. L. Haymore, *Coord. Chem. Rev.* 1980, **31**, 123.
8. C. Y. Chou, J. C. Huffman and E. A. Maatta, *J. Chem. Soc., Chem. Commun.* 1984, 1184.
9. D. C. Bradley, M. B. Hursthouse, K. M. A. Malik, A. J. Nielson and R. L. Short, *J. Chem. Soc., Dalton Trans.* 1983, 2651.
10. B. R. Ashcroft, G. R. Clark, A. J. Nielson and C. E. F. Rickard, *Polyhedron* 1986, **5**, 2081.
11. J. H. Osborne and W. C. Trogler, *Inorg. Chem.* 1985, **24**, 3098; W. P. Griffith, A. J. Nielson and M. J. Taylor, *J. Chem. Soc., Dalton Trans.* (in press).
12. K. Nakamoto, *Infrared and Raman Spectra of Inorganic and Coordination Compounds*, 3rd Edn, p 317. John Wiley, New York (1978).
13. W. A. Nugent, R. J. McKinney, R. V. Kasowski and F. A. Van-Catledge, *Inorg. Chim, Acta* 1982, **65**, L91.
14. G. R. Clark, A. J. Nielson and C. E. F. Rickard (unpublished results).
15. D. C. Bradley, R. C. Mehrotra and D. P. Gaur, *Metal Alkoxides*, p.125. Academic Press, London (1978).
16. R. M. Pike, *J. Org. Chem.* 1961, **26**, 232.
17. W. Wolfsberger and H. Schmidbaur, *Synth. React. Inorg. Metal-Org. Chem.* 1974, **4**, 149.
18. A. J. Nielson, *Chem. N.Z.* 1985, **49**, 11.

Polyhedron Vol. 7, No. 1, pp. 77–78, 1988
Printed in Great Britain

0277–5387/88 $3.00+.00
© 1988 Pergamon Journals Ltd

COMMUNICATION

PREPARATION AND STRUCTURAL CHARACTERIZATION OF A STIBIDO–INDIUM DIMER

ANDREW R. BARRON, ALAN H. COWLEY,* RICHARD A. JONES,* CHRISTINE M. NUNN and DONALD L. WESTMORELAND

Department of Chemistry, The University of Texas at Austin, Austin, TX 78712, U.S.A.

(*Received* 15 *June* 1987; *accepted* 24 *August* 1987)

Abstract—The interaction of $InCl_3$ with $tBu_2SbSiMe_3$ affords the partially substituted compound, $[(tBu_2Sb)(Cl)In(\mu\text{-}Sbt Bu_2)]_2$ (**1**). The dimeric nature of **1** was established by X-ray crystallography.

There has been a recent rekindling of interest in phosphido and arsenido complexes of the heavier group 13 elements.[1] Much of this effort has been prompted by the search for new precursors to semiconducting materials such as gallium arsenide and indium phosphide. Interestingly, however, the corresponding stibido (R_2Sb) complexes do not appear to have been prepared. We report the synthesis and characterization of the first stibido derivative of In(III).

EXPERIMENTAL

A suspension of $InCl_3$ (0.784 g, 3.54 mmol) in 100 cm^3 of toluene was cooled to −78°C and treated with a solution of $tBu_2SbSiMe_3$[2] (3.3 g, 11.0 mmol) in 6 cm^3 of hexane. The stirred reaction mixture was allowed to warm slowly to room temperature. The resulting red–brown solution was filtered through celite and stored at −20°C to promote the crystallization of **1**.

NMR (C_6D_6, 25°C): ^1H (300 MHz) 1.31 ppm (s, *t*-Bu); $^{13}C\{^1H\}$ (75.4 MHz) 35.2 ppm (s, CMe_3), 3.19 ppm (s, CCH_3).

The structure of **1** was determined by X-ray crystallography: $C_{16}H_{36}ClInSb$, $M_r = 622.24$, monoclinic, $P2_1/n$, $a = 11.854(6)$, $b = 12.767(4)$, $c = 16.505(4)$ Å, $\beta = 106.75(2)°$, $V = 2392.0$ Å^3, $Z = 4$, $D_c = 1.728$ g cm^{-3}, $\mu = 33.1$ cm^{-1} for Mo-K_α radiation ($\lambda = 0.71073$ Å). Intensity data: Enraf–Nonius diffractometer, $\theta/2\theta$ scan mode, 4207 reflections in the range $3.0 \leqslant 2\theta \leqslant 50.0°$. The structure of **1** was solved by direct methods and refined (full matrix, least squares) by using 2965 reflections with $I > 3\sigma(I)$. The final residuals were $R = 0.050$ and $R_w = 0.057$.† Disorder was observed in the positions of the In, Cl and Sb(2) atoms.

RESULTS AND DISCUSSION

Even though a 3:1 mole ratio of $tBu_2SbSiMe_3$ to $InCl_3$ was employed, only disubstitution occurred, the overall reaction being

$$4tBu_2SbSiMe_3 + 2InCl_3 \rightarrow [(tBu_2Sb)_2InCl]_2 + 4Me_3SiCl.$$

It is possible that this reaction proceeds via formation of donor-acceptor complexes, $(tBu)_2(Me_3Si)Sb \rightarrow In(Sbt Bu_2)_nCl_{3-n}$, $n = 0$, 1, 2, followed by the 1, 2 elimination of Me_3SiCl. When $n = 2$ dimerization occurs in preference to further coordination of $tBu_2SbSiMe_3$.

Unfortunately, it was not possible to characterize the product by EI-MS (70 eV) because of thermal decomposition to tBu_4Sb_2 in the inlet system. X-ray analysis revealed that the solid state comprises centrosymmetric bis(stibido)-bridged dimers,

* Authors to whom correspondence should be addressed.

† Supplementary material available: Atomic coordinates have been deposited with the Director, Cambridge Crystallographic Centre.

$[(t\mathrm{Bu}_2\mathrm{Sb})(\mathrm{Cl})\mathrm{In}(\mu\text{-}\mathrm{Sb}t\mathrm{Bu}_2)]_2$ (**1**), with an overall diborane-like skeleton. The terminal $t\mathrm{Bu}_2\mathrm{Sb}$ groups adopt a mutually *trans* arrangement. As noted in the Experimental section, the position of the In, Cl and Sb(2) atoms are disordered. The more abundant (80%) structure is shown in Fig. 1. The metric parameters for both structures are similar.

At first sight it seems surprising that stibido rather than chloride ligands should occupy bridging positions. However, the use of models reveals that placement of the bulky $t\mathrm{Bu}_2\mathrm{Sb}$ moieties in equatorial and terminal positions minimizes steric repulsions. We are not aware of any previous report on an In(III)—Sb bond length. However, the average bond length of 2.844(1) Å for **1** compares well with the value of 2.84 Å for the sum of covalent radii.

The dimeric nature of **1** in solution was confirmed by molecular weight measurement. However, at ambient temperature only one type of tBu resonance is apparent in both the ^{1}H and ^{13}C{^{1}H} NMR spectra. The implied rapid interchange of bridging the terminal groups is a common facet of group 13 dimers.[3]

Finally, we note that a somewhat similar compound, $\{[(\mathrm{Me}_3\mathrm{SiCH}_2)_2\mathrm{As}]_2\mathrm{GaCl}\}_2$ has been prepared.[1c] However, no crystal structure was reported.

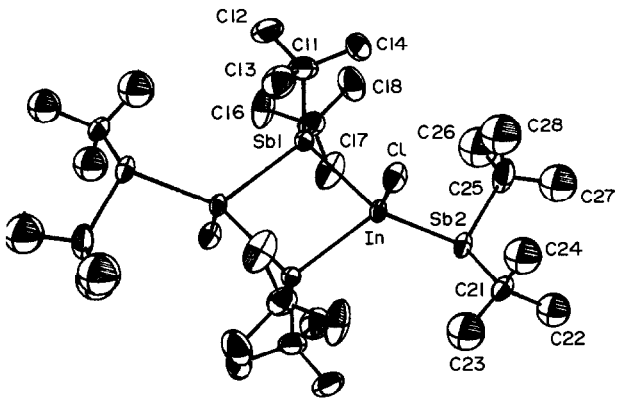

Fig. 1. Structure of $[(t\mathrm{Bu}_2\mathrm{Sb})(\mathrm{Cl})\mathrm{In}(\mu\text{-}\mathrm{Sb}t\mathrm{Bu}_2)]_2$ (**1**). Important parameters: Sb(1)—In 2.865(1), Sb(2)—In 2.797(1), In—Cl 2.407(2) Å, In—Sb(1)—In′ 94.93(2)°, Sb(1)—In—Sb(1)′ 85.07(2)°.

Acknowledgements—We are grateful to the National Science Foundation, the Robert A. Welch Foundation and the Texas Advanced Technology Research Program for financial support. R.A.J. thanks the Alfred P. Sloan Foundation for a fellowship (1985–1987).

REFERENCES

1. (a) R. L. Wells, A. P. Purdy, A. T. McPhail and C. G. Pitt, *J. Chem. Soc., Chem. Commun.* 1986, 487; (b) A. M. Arif, B. L. Benac, A. H. Cowley, R. Geerts, R. A. Jones, K. B. Kidd, J. M. Power and S. T. Schwab, *J. Chem. Soc., Chem. Commun.* 1986, 1543; (c) C. G. Pitt, A. P. Purdy, K. T. Higa and R. L. Wells, *Organometallics* 1986, **5**, 1266; (d) C. G. Pitt, K. T. Higa, A. T. McPhail and R. L. Wells, *Inorg. Chem.* 1986, **25**, 2483; (e) R. L. Wells, A. P. Purdy, A. T. McPhail and C. G. Pitt, *J. Organomet. Chem.* 1986, **308**, 281; (f) O. T. Beachley, J. P. Kopasz, H. Zhang, W. E. Hunter and J. L. Atwood, *J. Organomet. Chem.* 1987, **325**, 69; (g) R. L. Wells, A. P. Purdy, K. T. Kiga, A. T. McPhail and C. G. Pitt, *J. Organomet. Chem.* 1987, **325**, C7.
2. H. J. Breuning and T. Sevenergiz, *Z. Naturforsch. B.* 1987, **37**, 395.
3. See, for example, T. L. Brown, *Acc. Chem. Res.* 1968, **1**, 23.

Polyhedron Vol. 7, No. 1, pp. 79–81, 1988
Printed in Great Britain

0277–5387/88 $3.00+.00
© 1988 Pergamon Journals Ltd

COMMUNICATION

HETEROLEPTIC POLYPYRAZOLYLBORATE DERIVATIVES OF THE LANTHANIDE IONS. THE SYNTHESIS OF ACETYLACETONATE DERIVATIVES AND THE MOLECULAR STRUCTURES OF $[Ln\{HB(C_3N_2H_3)_3\}_2\{MeC(O)CHC(O)Me\}]$ (Ln = Ce, Yb)

MICHAEL A. J. MOSS, CHRISTOPHER J. JONES† and ANTHONY J. EDWARDS

Department of Chemistry, University of Birmingham, PO Box 363, Birmingham B15 2TT, U.K.

(*Received* 6 *July* 1987; *accepted* 24 *August* 1987)

Abstract—The air and moisture stable complexes $[Ln\{HB(C_3N_2H_3)_3\}_2\{MeC(O)CHC(O)Me\}]$ (Ln = La, Ce, Pr, Nd, Sm, Eu, Gd, Tb, Dy, Ho, Yb, Lu, Y), have been prepared and characterized. The molecular structures of the compounds with Ln = Ce and Yb reveal that a substantial distortion of the coordination geometry found for Ce^{3+} is necessary to allow the ligand set to accommodate the smaller Yb^{3+} ion.

The tripodal ligand hydrotris(pyrazol-1-yl)borate, L^-, is sterically bulky and can occupy three facial coordination sites on a metal ion.[1] In the case of trivalent lanthanide ions, homoleptic neutral complexes of formula $[LnL_3]$ may be prepared.[2–4] The molecular structure of the complex $[YbL_3]$ has been determined by X-ray methods and the geometry about the eight coordinate Yb^{3+} ion was found to be approximately bicapped trigonal prismatic (BCTP), having one bidentate and two tridentate polypyrazolylborate ligands.[3] This observation prompted us to investigate whether a new series of stable heteroleptic complexes containing the $\{LnL_2\}^+$ moiety could be prepared using bidentate uninegative coligands to complete the coordination shell of the Ln^{3+} ion. Preliminary reports of heteroleptic complexes containing the $\{LnL^*\}^{2+}$ (L^* = hydrotris(3,5-dimethylpyrazol-1-yl)borate) moiety have appeared[5] but to our knowledge this is the first report of a structure of a heteroleptic lanthanide complex containing L.

The reaction of Ln^{3+} salts with L^- and acetylacetone (acacH), in water at pH > 7 proceeded smoothly to give $[LnL_2(acac)]$ (Ln = La, Ce, Pr, Nd, Sm, Eu, Gd, Tb, Dy, Ho, Yb, Lu, Y), in high yield, even in the presence of excess acacH or L^-. All the derivatives were air and moisture stable.‡ Unlike the tris derivatives, $[LnL_3]$, for which insoluble products formed with Ln = La to Gd, all of these heteroleptic complexes were freely soluble in CH_2Cl_2 and other polar organic solvents. Again unlike the tris derivative $[YbL_3]$, which was found to be solution rigid on the NMR time-scale,[4] the heteroleptic complexes were non-rigid. Even in the case of the more sterically saturated complexes of the smaller ions the ^1H NMR spectra showed only three pyrazolyl proton environments indicating that ligand rotation was occurring on the NMR time-scale.

Powder X-ray diffraction studies revealed that the complexes with Ln = La to Dy were isostructural but different in structure from the complexes with Ln = Y and Ho to Lu. In order to structurally characterize representatives of the two structural types, single crystal X-ray diffraction

†Author to whom correspondence should be addressed.

‡All the new compounds have been characterized by ^1H NMR, IR and mass spectroscopy. All gave satisfactory elemental analyses for C, H and N.

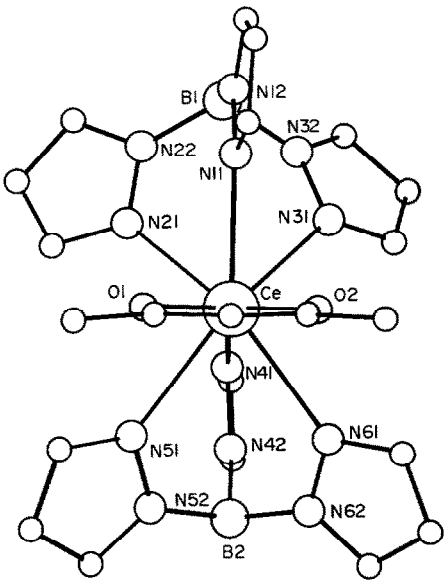

Fig. 1. The molecular structure of $[Ce\{HB(C_3N_2H_3)_3\}_2\{MeC(O)CHC(O)Me\}]$ showing the numbering of atoms other than C and H. Selected bond distances (Å) and angle(°): Ce—O(1), 2.397; Ce—O(2), 2.406(2); Ce—N(11), 2.664(3); Ce—N(21), 2.583(3); Ce—N(31), 2.617(3); Ce—N(41), 2.659(3); Ce—N(51), 2.634(3); Ce—N(61), 2.633(3); O(1)—Ce—O(2), 71.4(1).

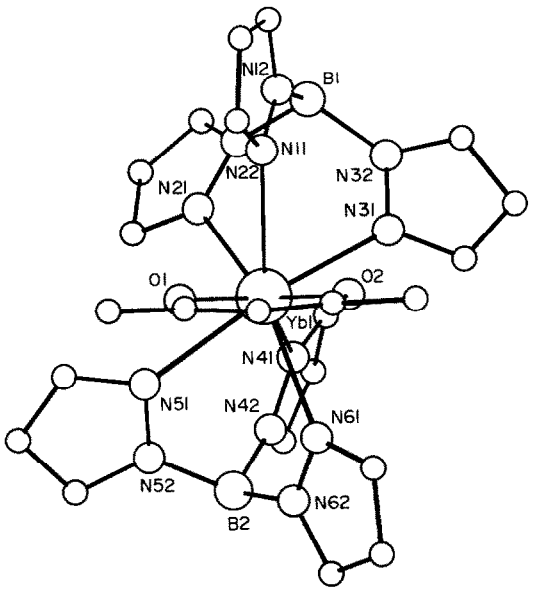

Fig. 2. The molecular structure of $[Yb\{HB(C_3N_2H_3)_3\}_2\{MeC(O)CHC(O)Me\}]$ (molecule 1) showing the numbering of atoms other than C and H. Selected bond distances (Å) and angle (°): Yb—O(1), 2.258(9); Yb—O(2), 2.199(11); Yb—N(11), 2.489(12); Yb—N(21), 2.576(11); Yb—N(31), 2.472(11); Yb—N(41), 2.489(13); Yb—N(51), 2.444(10); Yb—N(61), 2.528(10); O(1)—Yb—O(2), 75.8(4).

studies of the complexes with Ln = Ce and Yb have been carried out.† The complex $[CeL_2(acac)]$ is an eight coordinate monomer. It has a distorted bicapped trigonal prismatic geometry where the two hydrotris(pyrazol-l-yl)borate ligands each span one rectangular edge and cap one rectangular face of the trigonal prism as shown in Fig. 1. The third rectangular edge is spanned by the acetylacetonate ligand. The BCTP is an unusual geometry for eight coordination, the dodecahedron (Dod) and the square antiprism (SAP) usually being preferred.

The structure of $[YbL_2(acac)]$ is illustrated in Fig. 2 and may be considered to be derived from the cerium structure by a concerted rotation of the hydrotris(pyrazol-1-yl)borate ligands, thus destroying the approximate plane of symmetry originally present. There are two molecules in the asymmetric unit, both have coordination geometries which may be considered to be derived from square antiprismatic but shortening of one of the cross square diagonal distances, coupled with loss of planarity in the squares, puts both of the coordination geometries along a geometric pathway towards Dod or BCTP.

The structural studies clearly demonstrate the need for a bidentate coligand to coordinatively saturate the lanthanide ion of the $\{LnL_2\}^+$ moiety. The ambidentate nature of the trispyrazolylborate ligand and dynamic nature of these complexes indicate that any unidentate ligand, X, in a complex of formula $[LnL_2X]$ would need sterically to block two

† *Crystal Data.*—$CeL_2(acac)$: $C_{23}H_{27}B_2CeN_{12}O_2$, M = 665.3. Monoclinic, a = 14.943(2) Å, b = 12.981(2) Å, c = 15.178(2) Å, β = 102.02(1)°, U = 2879 Å^3, Z = 4, D_c = 1.53 g cm^{-3}, space group $P2_1/c$ (No. 14), Mo-K_α radiation (λ = 0.7107 Å, μ = 15 cm^{-1}). $YbL_2(acac)$: $C_{23}H_{27}B_2N_{12}O_2Yb$, M = 698.2. Triclinic, a = 11.422(4) Å, b = 16.361(5) Å, c = 18.237(6) Å. α = 75.92(3)°, β = 74.58(3)°, γ = 75.74(3)°, U = 3126 Å^3, Z = 4, D_c = 1.48 g cm^{-3}, space group $P\bar{1}$ (No. 2), Mo-K_α radiation (λ = 0.7107 Å, μ = 28 cm^{-1}). Data were collected on a CAD4 diffractometer at the Crystallography Unit, Universities of Aston and Birmingham. Both structures were solved by routine heavy atom methods. $CeL_2(acac)$, refined to R = 0.0261, R_w = 0.0264, using 4607 unique reflections with $I > 2.5\sigma I$. $YbL_2(acac)$, refined to R = 0.068, R_w = 0.069 using 7661 unique reflections which were corrected for absorption effects using the program difabs (N. Walker and D. Stuart, *Acta. Cryst.* 1983, **A39**, 158). Atomic coordinates, bond lengths and angles, and thermal parameters have been deposited at the Cambridge Crystallographic Data Centre. See Notice to Authors, Issue No. 1, 1987.

coordination sites. Otherwise disproportionation reactions might be expected to lead to more stable complexes of different ligand : metal stoichiometry. Indeed the resistance of these heteroleptic complexes to disproportionation is remarkable in view of their dynamic character.

Acknowledgements—We are grateful to Prof. W. J. Evans for helpful discussions, to the SERC and BP Chemicals, Hull Division, for support (to M. A. J. Moss) and to NATO for the provision of travel grant no. 175/84.

REFERENCES

1. S. Trofimenko, *Prog. Inorg. Chem.* 1986, **34**, 115.
2. K. W. Bagnall, A. C. Tempest, J. Takats and A. P. Masino, *Inorg. Nucl. Chem. Letts.* 1976, **12**, 555.
3. M. V. R. Stainer and J. Takats, *Inorg. Chem.* 1982, **21**, 4050.
4. M. V. R. Stainer and J. Takats, *J. Am. Chem. Soc.* 1983, **105**, 410.
5. R. Ball, J. G. Matisons and J. Takats, *Am. Chem. Soc. Meeting*, Chicago (1985).

Polyhedron Vol. 7, No. 2, pp. 83–86, 1988
Printed in Great Britain

0277–5387/88 $3.00+.00
© 1988 Pergamon Journals Ltd

SYNTHESIS AND MOLECULAR STRUCTURE OF THE FIRST DISCRETE RHENIUM POLYSULPHIDE COMPLEX, (n-Bu_4N)[ReS_9]

F. ALBERT COTTON,* PIOTR A. KIBALA and MAREK MATUSZ

Department of Chemistry and Laboratory for Molecular Structure and Bonding, Texas A&M University, College Station, TX 77843, U.S.A.

(*Received* 15 *June* 1987; *accepted* 24 *August* 1987)

Abstract—(n-Bu_4N)[$Re(S_4)_2S$] has been prepared by reacting (n-Bu_4N_2)[Re_2Cl_8] with Li_2S_5 in THF. It crystallizes in the monoclinic space group $P2_1/n$ with the following unit cell constants: $a = 11.215(3)$ Å, $b = 14.910(7)$ Å, $c = 16.654(4)$ Å, $\beta = 91.47\ (2)°$, $V = 2783(3)$ Å^3, $Z = 4$. The anion is the first mononuclear rhenium complex containing ReS_x chelate rings that has been isolated and structurally characterized. The $[ReS_9]^-$ anion consists of two chelating S_4^{2-} chains and a Re═S unit. The geometry around the Re atom is best described as a tetragonal pyramid with the metal atom displaced towards the centre of the pyramid. The Re═S bond length is 2.075(4) Å and the average Re—S bond length is 2.30[2] Å.

The chemistry of transition metal complexes with ligands containing only sulphur atoms has been intensively but rather selectively investigated in recent years.[1,2] While some metals, especially molybdenum, have been rather thoroughly studied, others such as rhenium, have been virtually ignored. In the case of rhenium, only two perthio complexes, the simple $[ReS_4]^-$ ion[3] and the complicated $[Re_4S_{22}]^{4-}$ ion[4] have been described. We have found that the $[Re_2Cl_8]^{2-}$ ion reacts at room temperature with polysulphide ions and report here the isolation and structural characterization of the first rhenium complex that contains ReS_4 chelate rings.

EXPERIMENTAL

Solvents were dried over appropriate drying agents and freshly distilled before use. (n-$Bu_4N)_2[Re_2Cl_8]$ was prepared according to a literature procedure.[5] The solutions of Li_2S_5[6] were prepared *in situ* from sulphur powder and $LiEt_3BH$ (1 M solution in THF, ALDRICH) in THF and used immediately.

Preparation of (n-Bu_4N)[ReS_9]

Li_2S_5 was prepared from 0.174 g of S powder, 2.2 cm^3 of a 1 M solution of $LiEt_3BH$ in THF and 5 cm^3 of THF, and (n-$Bu_4N)_2[Re_2Cl_8]$ (0.308 g, 0.272 mmol) was added in a counterstream of nitrogen. The reaction mixture was stirred for two days at room temperature. It was then filtered through Celite and layered with hexane. After a few days a brown–black oily layer was deposited at the bottom of the Schlenk tube. The supernatant liquid was decanted, the oil redissolved in THF and this solution layered with ether. The dark brown crystalline product deposited was filtered, washed with ether and vacuum dried. The yield was 0.22 g (58% based on Re).

X-ray crystallography

The general procedures were routine and have been described previously.[7]† Lorentz, polarization and empirical absorption corrections were applied to the data.

A small crystal was affixed to the end of a glass fiber and the fiber then mounted on the goniometer head of a CAD-4 diffractometer. Preliminary examination showed the space group to be $P2_1/n$ and data collection was carried out as indicated in Table 1. The solution and refinement of the structure pro-

*Author to whom correspondence should be addressed.

†All calculations were performed with the Enraf–Nonius Structure Determination Package on a VAX 11/780 computer at the Department of Chemistry, Texas A&M University, College Station, Texas 77843.

Table 1. Crystal data for $(n\text{-}Bu_4N)[ReS_9]$

Formula	$ReS_9NC_{16}H_{36}$
Formula weight	717.25
Space group	$P2_1/n$
Systematic absences	$h0l: h+l = 2n+1$, $0k0: k = 2n+1$
a, Å	11.215(3)
b, Å	14.910(7)
c, Å	16.654(4)
α, deg	90.0
β, deg	91.47
γ, deg	90.0
V, Å^3	2784(3)
Z	4
d_{calc}, g/cm^3	1.713
Crystal size, mm	$0.20 \times 0.12 \times 0.10$
$\mu(MoK_\alpha)$, cm^{-1}	50.86
Data collection instrument	CAD-4
Radiation (monochromated in incident beam)	$MoK_\alpha(\lambda_{\bar{\alpha}} = 0.71073Å)$
Orientation reflections, number, range (2θ)	24, $5 < 2\theta < 20$
Temperature, °C	22
Scan method	ω-2θ
Data col. range, 2θ. deg	4–45
No. unique data, total	3128
with $F_o^2 > 3\sigma(F_o^2)$	2196
Number of parameters refined	164
Trans. factors, max., min.	1.00, 0.95
R^a	0.049
R_w^b	0.058
Quality-of-fit indicator^c	1.403
Largest shift/esd, final cycle	0.17
Largest peak, e/Å^3	0.84

$^a R = \Sigma||F_o|-|F_c||/\Sigma|F_o|$.
$^b R_w = [\Sigma w(|F_o|-|F_c|)^2/\Sigma w|F_o|^2]^{1/2}$; $w = 1/\sigma^2(|F_o|)$.
^{c} Quality-of-fit $= [\Sigma w(|F_o|-|F_c|)^2/(N_{obs}-N_{parameters})]^{1/2}$.

ceeded straightforwardly. The coordinates of the Re atom were obtained from a Patterson map and an alternating series of least squares refinements and difference electron density maps progressively revealed all the remaining atoms. The carbon atoms of the cation were refined isotropically and hydrogen atoms were omitted. All other atoms were refined anisotropically to the satisfactorily low R values listed in Table 1. No disorder or other non-routine problem arose.*

RESULTS

The reaction of $(n\text{-}Bu_4N)_2[Re_2Cl_8]$ with Li_2S_5 affords the novel rhenium(V) polysulphide, $[Re(S_4)_2S]^-$ which has been crystallized as a tetrabutyl–ammonium salt. While the disruption of the quadruple bond in $[Re_2Cl_8]^{2-}$ is not wholly surprising, the oxidation of Re(III) to Re(V) was rather unexpected and without clear precedent.† The yield of the product is only 58% and we have not determined the fate of the remaining rhenium.

The structure of the $[N(n\text{-}C_4H_9)_4]^+$ cation

*Tables of atomic coordinates, structure factors, anisotropic thermal parameters and a complete list of bond distances and angles have been deposited with the Editor at Queen Mary College and at the Cambridge Crystallographic Data Centre.

†We thank a referee for suggesting that the following balanced equation could be written:

$$(NBu^n_4)_2Re_2Cl_8 + 4Li_2S_5 \rightarrow 2NBu^n_4ReS(S_4)_2 + 8LiCl + 1/4S_8$$

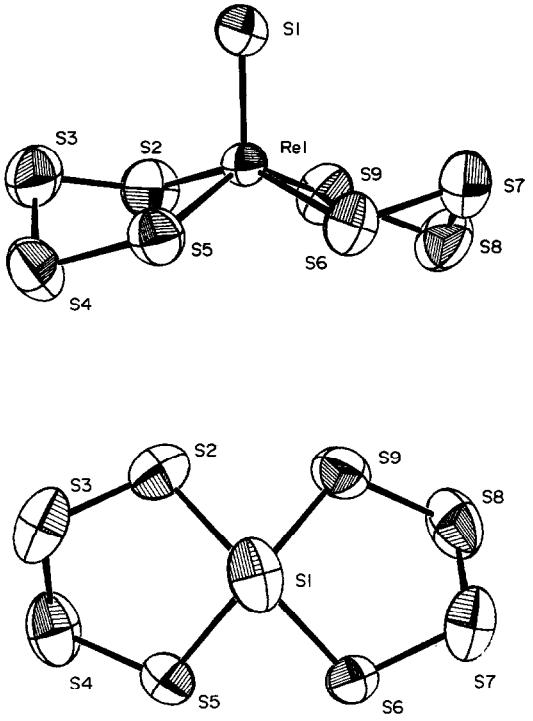

Fig. 1. Two ORTEP views of the $[ReS(S_4)_2]^-$ ion. Each atom is represented by its ellipsoid of thermal displacement (40%) level and labelled as in Tables 2 and 3. The lower view is directly down the Re=S bond so that the Re atom is totally hidden.

requires no comment. The $[ReS(S_4)_2]^-$ anion has the structure depicted in Fig. 1 and the distances and angles listed in Tables 2 and 3. The anion can be approximately described as a tetragonal pyramid with the basal plane formed by four sulphur atoms from the S_4^{2-} ligands and the apex formed by a sulphur atom doubly-bonded to the rhenium atom. The mean S=Re—S angle is 108[1]°, so that the Re atom clearly lies well above (0.726 Å) the basal plane. It is actually not quite accurate to describe the pyramid as tetragonal, since the two S—Re—S angles within the chelate rings have a mean value of 89.8[1]° while the other two have a mean value of 78.8[3]°. The Re—S distances also vary from 2.259(4) to 2.342(4) Å, with a mean value of 2.30[2]Å.

Table 2. Selected bond distances in angstroms

Atom 1	Atom 2	Distance
Rel	S1	2.075(4)
Rel	S2	2.320(4)
Rel	S5	2.275(4)
Rel	S6	2.342(4)
Rel	S9	2.259(4)
S2	S3	2.057(7)
S3	S4	1.987(8)
S4	S5	2.124(6)
S6	S7	2.082(7)
S7	S8	1.975(8)
S8	S9	2.135(7)

Numbers in parentheses are estimated standard deviations in the least significant digits.

Table 3. Selected bond angles in degrees

Atom 1	Atom 2	Atom 3	Angle
S1	Rel	S2	106.6(2)
S1	Rel	S5	109.8(2)
S1	Rel	S6	106.2(2)
S1	Rel	S9	111.2(2)
S2	Rel	S5	89.7(2)
S2	Rel	S6	147.2(2)
S2	Rel	S9	78.6(2)
S5	Rel	S6	79.1(2)
S5	Rel	S9	139.0(2)
S6	Rel	S9	89.8(2)
Rel	S2	S3	104.0(2)
S2	S3	S4	100.4(3)
S3	S4	S5	99.5(3)
Rel	S5	S4	112.5(2)
Rel	S6	S7	103.4(2)
S6	S7	S8	99.4(3)
S7	S8	S9	99.8(3)
Rel	S9	S8	112.4(3)

Numbers in parentheses are estimated standard deviations in the least significant digits.

DISCUSSION

The $[ReS_9]^-$ ion is of a structure type that can be compared with an exactly analogous molybdenum species, the $[MoS_9]^{2-}$ ion[8] and also with the $[ReS(SCH_2CH_2S)_2]^-$ ion.[9] The dimensions of the molybdenum species, including the deviations from four-fold symmetry, are very similar to those for the $[ReS_9]^-$ ion despite the differences in oxidation state and atomic number of the metal atoms. The more important common feature is evidently the d^2 electron configuration of Mo(IV) and Re(V). The resemblance of the $[ReS(S_4)_2]^-$ ion to the $[ReS(SCH_2CH_2S)_2]^-$ ion is also close. The Re=S distances of 2.075(4) Å in the present case and 2.101(4) Å in the thiolate complex, as well as the mean Re—S distances of 2.30[2] and 2.300[4] Å,

respectively, are not significantly different. The only notable difference is that the $[ReS(SCH_2CH_2S)_2]^-$ ion has a more nearly tetragonal base, with the mean internal and external S—Re—S angles being 84.9[1] and 84[1]°. This is a result of the shorter S—C and C—C distances (compared to S—S distances) within the chelate rings.

The IR spectrum of $[n\text{-}Bu_4N]$ $[ReS_9]$ in a mineral oil mull shows a sharp band of medium intensity at 528 cm^{-1} which we assign to the Re=S stretching mode. The $[ReS(SCH_2CH_2S)_2]^-$ ion, with a slightly longer Re=S distance has a strong, sharp band at a slightly lower frequency (517 cm^{-1}) which has been similarly assigned.[9] These assignments are consistent with a number of others for M=S vibrations.[10]

In conclusion we mention that chelating S_4^{2-} ligands (as well as S_n^{2-} with $n = 3$, 5) are not uncommon.[1,2,11] The existence of the $[ReS_9]^-$ ion and its structure, are not surprising and it seems likely that, as with molybdenum, there will be a fairly extensive series of polysulphido rhenium complexes.

Acknowledgement—We thank the National Science Foundation for support.

REFERENCES

1. M. Draganjac and T. B. Rauchfuss, *Angew.Chem. Int. Ed. Engl.* 1985, **24**, 742.
2. A. Müller, *Polyhedron* 1986, **5**, 323.
3. Y. Do, E. D. Simhon and R. H. Holm, *Inorg. Chem.* 1985, **24**, 4635.
4. A. Müller, E. Krickemeyer and H. Bögge, *Angew. Chem. Int. Ed. Engl.* 1986, **25**, 272.
5. T. Barder and R. A. Walton, *Inorg. Chem.* 1982, **21**, 2511.
6. A. Shaver and M. McCall, *Organometallics* 1984, **3**, 1823.
7. (a) A. Bino, F. A. Cotton and P. E. Fanwick, *Inorg. Chem.* 1979, **18**, 3558; (b) F. A. Cotton, B. A. Frenz, G. Deganello and A. J. Shaver, *J. Organomet. Chem.* 1973, **50**, 227.
8. M. Draganjac, E. Simhon, L. T. Chan, M. Kanatzidis, N. C. Baenziger and D. Coucouvanis, *Inorg. Chem.* 1982, **21**, 3321.
9. P. J. Blower, J. R. Dilworth, J. P. Hutchinson, T. Nicholson and J. Zubieta, *J. Chem. Soc., Dalton Trans.* 1986, 1339.
10. W.-H. Pan, M. E. Leonowicz and E. I. Stiefel, *Inorg. Chem.* 1983, **22**, 672.
11. D. Coucouvanis, P. R. Patel, M. G. Kanatzidis, B. Detering and N. C. Baenziger, *Inorg. Chem.* 1985, **24**, 24.

Polyhedron Vol. 7, No. 2, pp. 87–96, 1988
Printed in Great Britain

0277–5387/88 $3.00+.00
© 1988 Pergamon Journals Ltd

C—Br INSERTION REACTIONS IN RHODIUM AND IRIDIUM COMPOUNDS CONTAINING AN *ORTHO*-HALOARYLPHOSPHINE. X-RAY STRUCTURES OF TWO *ORTHO*-METALLATED COMPOUNDS OF FORMULA $IrX_2[P(C_6F_4)Ph_2][P(o\text{-}BrC_6F_4)Ph_2]$, (X = Cl, Br)

J. CARLOS BESTEIRO, PASCUAL LAHUERTA,* MERCEDES SANAÚ and ISABEL SOLANA

Departamento de Quimica Inorgánica, Facultad de Químicas, Universidad de Valencia, Burjasot, Valencia, Spain

and

F. ALBERT COTTON,* ROSA LLUSAR and WILLI SCHWOTZER

Department of Chemistry and Laboratory for Molecular Structure and Bonding, Texas A&M University, College Station, Texas 77843, U.S.A.

(*Received* 15 *May* 1987; *accepted after revision* 24 *August* 1987)

Abstract—A comparative study of the reaction of Rh and Ir complexes with the *ortho*-bromo-arylphosphine PCBr [PCBr = $P(o\text{-}BrC_6F_4)(C_6H_5)_2$], is presented. Various PCBr complexes of Ir(I) and Rh(I) undergo rapid insertion of the metal atom into a C—Br bond provided the phosphine is coordinated in a η^2-mode (P—Br). If the Br coordination is substituted by a superior ligand such as CO or an olefin, no reaction occurs under normal conditions. PCBr complexes of the tervalent metals require a two-electron reduction step prior to the *ortho*-metallation reaction. Most intermediates were characterized by chemical and spectroscopic analysis. Two intermediates of general formula $IrX_2(\eta^2\text{-PC})(\eta^2\text{-PCBr})$, [PC = $P(C_6F_4)(C_6H_5)_2$] (X = Cl, **5**, X = Br, **6**), were characterized by a single crystal analysis. **5** crystallizes in the monoclinic space group $P2_1/n$ with cell dimensions a = 14.741(5) Å, b = 13.558(5) Å, c = 18.303(7) Å, β = 112.35(2)°, Z = 4. **6** crystallizes in the same space group $P2_1/n$ and has cell dimensions a = 19.05(1) Å, b = 19.554(6) Å, c = 20.337(5) Å, β = 93.63(5)°, Z = 8. Both compounds have distorted octahedral coordination around the metal centre.

Reactions of coordinated phosphine ligands to give cyclometallated products have received considerable attention.[1] In particular, cyclometallated rhodium or iridium compounds obtained by C—H bond activation in triarylphosphites[2] or triarylphosphines[3] have been reported. Activation of C—H bonds in alkyl phosphines[4] is less common.

We have observed that rhodium(I) compounds containing PCBr can undergo thermal *ortho*-metallation by metal insertion into the C—Br bond. Mononuclear rhodium(III) compounds[5] containing a four atom metallocycle and binuclear compounds with an *ortho*-metallated PCBr phosphine bridging a dirhodium(+4) unit have been isolated.[6] Examples of *ortho*-metallation of this phosphine with activation of a C—H aryl bond are also known.[7]

We report here the results of a comparative study of the *ortho*-metallation reaction in rhodium and iridium compounds with PCBr. Included are the

*Authors to whom correspondence should be addressed.

X-ray structures of two metallated iridium(III) compounds **5** and **6**.

EXPERIMENTAL

$RhCl_3 \cdot 3H_2O$ was purchased from Johnson Matthey Ltd and $IrCl_3 \cdot 3H_2O$ was purchased from Englehard Industries. Chemical reactions were carried out in a dry argon or nitrogen atmosphere using standard Schlenck-type procedures. All the solvents were of reagent grade and were dried and distilled prior to use. The starting materials were prepared by literature methods.[8–15] ^1H NMR spectra were recorded on a BRUKER AC200 (200.132 MHz) spectrometer, using TMS as internal reference. The ^{31}P NMR spectra were recorded on a BRUKER AC200 (81.015 MHz) spectrometer, with H_3PO_4 85% as external reference. IR spectra were recorded on a PYE-UNICAM SP8-100 spectrophotometer.

X-ray crystallography

The crystallographic work followed the general procedures which were described previously.[16] The crystal parameters and basic information corresponding to data collection and structure refinement for compounds **5** and **6** are given in Table 1. The structure of compound **6** contains two independent molecules per asymmetric unit. Important bond distances and angles are given in Table 2. In both structures the positions of the iridium atoms

Table 1. Crystallographic data for $IrX_2[P(C_6F_4)Ph_2][P(o\text{-}BrC_6F_4)Ph_2]$

	X = Cl	X = Br
Formula	$IrBrCl_2P_2F_8C_{36}H_{20}$	$IrBr_3Cl_2P_2F_8C_{42}H_{34}$
Formula weight	1008.5	1144.35
Space group	$P2_1/n$	
Systematic absences	$0k0,\ k \neq 2n$; $h0l,\ h+l \neq 2n$	
a, Å	14.741(5)	19.05(1)
b, Å	13.558(5)	19.554(6)
c, Å	18.303(7)	20.337(5)
α, deg	90.0	90.0
β, deg	112.35(2)	93.63(6)
γ, deg	90.0	90.0
V, Å^3	3383(4)	7562(7)
Z	4	8
d_{calc}, g/cm^3	1.98	2.01
Crystal size, mm	$0.30 \times 0.30 \times 0.20$	$0.30 \times 0.30 \times 0.30$
μ(Mo-K_α), cm^{-1}	54.24	69.41
Data collection instrument	Syntex $P\bar{1}$	
Radiation (monochromated in incident beam)	Mo-K_α ($\lambda_\alpha = 0.71073$ Å)	
Orientation reflections, number, range (2θ)	15, 20–31	15, 20–32
Temperature, °C	10	10
Scan method	ω-2θ	ω-2θ
Data col. range, 2θ, deg	$4 < 2\theta < 45$	$4 < 2\theta < 45$
No. unique data, total	3831	7351
with $F_o^2 > 3\sigma(F_o^2)$	2659	5483
Number of parameters refined	451	925
R^a	0.0397	0.0430
$R_w{}^b$	0.0518	0.0530
Quality-of-fit indicator^c	0.996	1.040
Largest shift/esd, final cycle	0.00	0.22
Largest peak, e/Å^3	1.30	1.13

[a] $R = \Sigma \| |F_o| - |F_c| \| / \Sigma |F_o|$.

[b] $R_w = [\Sigma w(|F_o| - |F_c|)^2 / \Sigma w|F_o|^2]^{1/2}$; $w = 1/\sigma^2(|F_o|)$.

[c] Quality-of-fit = $[\Sigma w(|F_o| - |F_c|)^2 / (N_{obs} - N_{parameters})]^{1/2}$.

Table 2. Selected bond distances (Å) and angles (degrees) for compounds **5** and **6**

Compound **5**

Ir(1)—Br(1)	2.550(2)	Br(1)—Ir(1)—P(1)	168.71(8)
Ir(1)—P(1)	2.253(4)	Br(1)—Ir(1)—P(2)	86.2(1)
Ir(1)—P(2)	2.274(3)	Br(1)—Ir(1)—Cl(1)	85.1(1)
Ir(1)—Cl(1)	2.418(3)	Br(1)—Ir(1)—Cl(2)	83.10(9)
Ir(1)—Cl(2)	2.403(3)	Br(1)—Ir(1)—C(16)	101.8(4)
Ir(1)—C(16)	2.03(1)	P(1)—Ir(1)—P(2)	100.8(1)
P(1)—C(11)	1.80(1)	P(1)—Ir(1)—Cl(1)	103.3(1)
P(1)—C(21)	1.83(1)	P(1)—Ir(1)—Cl(2)	89.4(1)
P(1)—C(31)	1.81(2)	P(1)—Ir(1)—C(16)	69.2(4)
C(11)—C(16)	1.43(2)	P(2)—Ir(1)—Cl(1)	92.0(1)
P(2)—C(41)	1.82(1)	P(2)—Ir(1)—Cl(2)	169.1(1)
P(2)—C(51)	1.83(1)	P(2)—Ir(1)—C(16)	93.4(3)
P(2)—C(61)	1.83(1)	Cl(1)—Ir(1)—Cl(2)	89.3(1)
Br(1)—C(46)	1.90(1)	Cl(1)—Ir(1)—C(16)	171.5(4)
C(41)—C(46)	1.37(2)	Cl(2)—Ir(1)—C(16)	86.6(3)
		Ir(1)—P(1)—C(11)	86.3(5)
		Ir(1)—P(1)—C(21)	119.9(5)
		Ir(1)—P(1)—C(31)	123.6(5)
		Ir(2)—P(1)—C(41)	106.0(4)
		Ir(2)—P(1)—C(51)	112.3(4)
		Ir(2)—P(1)—C(61)	122.0(4)
		Ir—C(16)—C(11)	106.6(5)

Molecule A		Compound **6**	Molecule B
Ir(1)—Br(11)	2.549(2)	Ir(2)—Br(2)	2.561(2)
Ir(1)—P(11)	2.262(4)	Ir(2)—P(22)	2.251(4)
Ir(1)—P(12)	2.283(4)	Ir(2)—P(21)	2.274(4)
Ir(1)—Br(12)	2.568(2)	Ir(2)—Br(22)	2.550(2)
Ir(1)—Br(1)	2.542(2)	Ir(2)—Br(21)	2.517(2)
Ir(1)—C(26)	2.06(1)	Ir(2)—C(106)	2.05(2)
P(11)—C(21)	1.79(2)	P(22)—C(111)	1.79(2)
P(11)—C(11)	1.81(1)	P(22)—C(121)	1.82(2)
P(11)—C(31)	1.79(1)	P(22)—C(101)	1.79(2)
C(21)—C(26)	1.40(2)	C(101)—C(106)	1.41(2)
P(12)—C(41)	1.86(1)	P(21)—C(91)	1.86(1)
P(12)—C(51)	1.84(1)	P(21)—C(71)	1.85(1)
P(12)—C(61)	1.80(2)	P(21)—C(81)	1.81(2)
Br(11)—C(46)	1.88(1)	Br(2)—C(96)	1.89(2)
C(41)—C(46)	1.41(2)	C(91)—C(96)	1.41(2)
Br(11)—Ir(1)—P(11)	168.9(1)	Br(2)—Ir(2)—P(22)	169.7(1)
Br(11)—Ir(1)—P(12)	86.4(1)	Br(2)—Ir(2)—P(21)	85.9(1)
Br(11)—Ir(1)—Br(12)	86.63(6)	Br(2)—Ir(2)—Br(22)	86.16(6)
Br(11)—Ir(1)—Br(1)	82.21(6)	Br(2)—Ir(2)—Br(21)	82.93(6)
Br(11)—Ir(1)—C(26)	102.9(4)	Br(2)—Ir(2)—C(106)	103.0(5)
P(11)—(1)—P(12)	99.5(1)	P(22)—Ir(2)—P(21)	100.5(2)
P(11)—Ir(1)—Br(12)	102.3(1)	P(22)—Ir(2)—Br(22)	101.5(1)
P(11)—Ir(1)—Br(1)	91.1(1)	P(22)—Ir(2)—Br(21)	90.1(1)
P(11)—Ir(1)—C(26)	67.6(4)	P(22)—Ir(2)—C(106)	68.7(5)
P(12)—Ir(1)—Br(12)	93.5(1)	P(21)—Ir(2)—Br(22)	92.6(1)
P(12)—Ir(1)—Br(1)	167.7(1)	P(21)—Ir(2)—Br(21)	168.3(1)
P(12)—Ir(1)—C(26)	92.3(4)	P(21)—Ir(2)—C(106)	94.2(4)
Br(12)—Ir(1)—Br(1)	90.40(6)	Br(22)—Ir(2)—Br(21)	90.22(6)
Br(12)—Ir(1)—C(26)	169.2(4)	Br(22)—Ir(2)—C(106)	169.0(4)
Br(1)—Ir(1)—C(26)	85.9(4)	Br(21)—Ir(2)—C(106)	84.9(4)
Ir(1)—P(11)—C(21)	87.5(6)	Ir(2)—P(22)—C(101)	86.7(5)
Ir(1)—P(11)—C(11)	118.5(5)	Ir(2)—P(22)—C(121)	119.4(6)
Ir(1)—P(11)—C(31)	123.0(5)	Ir(2)—P(22)—C(111)	121.1(5)
Ir(1)—P(12)—C(41)	107.4(5)	Ir(2)—P(21)—C(91)	107.7(5)
Ir(1)—P(12)—C(51)	123.7(5)	Ir(2)—P(21)—C(81)	123.5(5)
Ir(1)—P(12)—C(61)	112.6(5)	Ir(2)—P(21)—C(71)	112.5(5)
Ir(1)—C(26)—C(21)	107(1)	Ir(2)—C(106)—C(101)	106(1)

were obtained from the three-dimensional Patterson map. The remaining atoms were located by using successive least-squares refinement and difference Fourier maps. The refinement converged at residuals of $R = 0.040$, $R_w = 0.052$ for **5** and $R = 0.043$, $R_w = 0.053$ for **6**.*

Preparation of $RhClBr(PC)(PCBr)$ (**1**)

(a) *From* $RhCl_3 \cdot 3H_2O$. $RhCl_3 \cdot 3H_2O$ (52.7 mg, 0.2 mmol) and PCBr (330 mg, 0.8 mmol) were refluxed in 10 cm^3 of ethanol. After 1 h the solution became lighter yellow and a yellow precipitate was obtained. It was then filtered off, washed with ethanol and air dried. Yield: 70–80%.

(b) *From* $[RhCl(C_8H_{14})_2]_2$. A weighted amount (100 mg, 0.14 mmol) of $[RhCl(C_8H_{14})_2]_2$ was added to a solution of 230.4 mg (0.56 mmol) of PCBr in 15 cm^3 of ethanol. The solution became red and then orange and a yellow product precipitated. This product was filtered off, washed with ethanol/ether and air dried. Yield: 70%.

(c) *From* RhCl(COD)PCBr. A solution of 100 mg (0.15 mmol) of RhCl(COD)(PCBr) and 62.5 mg (0.15 mmol) of PCBr were refluxed in 10 cm^3 of xylene. The reaction was followed by TLC and after 30 min no free phosphine was observed. The solvent was then evaporated to dryness and the product recrystallized from dichloromethane/ethanol. Yield: 80%. Molecular weight measurement by osmometry in benzene: Found: 980 (average of three determinations). Calc. for RhClBr(PC)(PCBr): 964. Found: C, 45.1; H, 2.2%. Calc. for $C_{36}H_{20}F_8P_2ClBr_2Rh$: C, 44.8; H, 2.1%.

Preparation of $RhBr_2(PC)(PCBr)$

$RhCl_3 \cdot 3H_2O$ (52.7 mg, 0.2 mmol) and NaBr (206 mg, 2.0 mmol) were refluxed in 20 cm^3 of ethanol for 1 h. Then PCBr (330 mg, 0.8 mmol) was added and the mixture was refluxed again for 1 h. The resulting yellow precipitate was separated and washed with a 1 : 1 mixture of water : ethanol and later with ethanol. The compound was crystallized from dichloromethane/hexane. Found: C, 43.0; H, 2.0%. Calc. for $C_{36}H_{20}F_8P_2Br_3Rh$: C, 42.9; H, 2.0%.

Preparation of IrXY(PC)(PCBr). (XY = Cl_2, **5**; Br_2, **6**; ClBr, **7a**, **7b**)

(a) *From* $[IrCl(C_8H_{14})_2]_2$. A weighted amount (90 mg, 0.1 mmol) of $[IrCl(C_8H_{14})_2]_2$ was dissolved in 10 cm^3 of dichloromethane on an ice-bath and 166 mg (0.4 mmol) of PCBr were added with stirring. The initially orange solution turned red rapidly. After 15 min the solution was slowly warmed to room temperature, and the stirring continued for 6 h, the colour becoming yellow. The solution was concentrated to *ca.* 2 ml and transferred to a chromatography column (30 × 2 cm) packed with silica-gel in hexane. Elution with dichloromethane/hexane 1 : 1 separated two yellow bands, which contained compounds **6** (fraction 1) and **7a** and **b** (fraction 2). Further elution with dichloromethane yielded a new yellow band, which contained compound **5**. All the fractions were evaporated to dryness and recrystallized from dichloromethane/hexane. Yields: **6**, 18; **7a** and **b**, 40; **5**, 25%. Found: C, 40.1; H, 2.1%. Calc. for $C_{36}H_{20}F_8P_2Br_3IrH$(**6**): C, 39.4; H, 1.8%. Found: C, 41.5; H, 1.9. Calc. for $C_{36}H_{20}F_8P_2ClBr_2Ir$ (**7**): C, 41.0; H, 1.9%. Found: C, 43.2; H, 2.0%. Calc. for $C_{36}H_{20}F_8P_2Cl_2BrIr$ (**5**): C, 42.8; H, 2.0%. When the reaction was carried out in the presence of a large excess of NEt_4X (X = Cl, Br) the compounds **5** and **6** were isolated in high yield (70–75%), respectively.

(b) *From* IrCl(COD)PCBr. A weighted amount of IrCl(COD)(PCBr) (150 mg, 0.2 mmol) and 83 mg (0.2 mmol) of PCBr were refluxed in 12 cm^3 of xylene for 10 h. During this time, the solution, initially orange, changed to yellow. The completeness of reaction was followed by TLC and ^{31}P NMR. The solvent was then evaporated to dryness, the resulting oil dissolved in dichloromethane and chromatographed on a column (30 × 2 cm) packed with silica-gel in hexane. The chromatographic separation was as described for method (a). Yields: **5**, 20; **6**, 15; **7**, 35%.

(c) *From* $IrCl(CO)(PCBr)_2$. A solution of $IrCl(CO)(PCBr)_2$ (112 mg, 0.1 mmol) in 8 cm^3 of xylene was boiled under reflux until IR and TLC showed no traces of starting material in solution. After 13 h the solution was cooled and evaporated to dryness. The isomers were separated as above. Yield: **5**, 18; **6**, 16; **7**, 30%.

Preparation of $IrBr_2(PC)(PCBr)$, (**6**)

A solution of IrBr(COD)(PCBr) (80 mg, 0.1 mmol) and PCBr (41 mg, 0.1 mmol) in 8 cm^3 of xylene was refluxed for 6 h, until the TLC and ^{31}P NMR showed no starting material in solution. The solvent was evaporated under vacuum, and the

* Supplementary material available: Fractional coordinates have been deposited with the Director, Cambridge Crystallographic Centre. Complete listings of bond distances and angles are available from the Editor.

crude product was recrystallized from dichloromethane/hexane. Yield 85%. Found: C, 39.8; H, 1.9%. Calc. for $C_{36}H_{20}F_8P_2Br_3Ir$: C, 39.4; H, 1.8%.

Preparation of $RhCl(CO)(PCBr)_2$, (8)

$[RhCl(C_8H_{14})_2]_2$ (143 mg, 0.2 mmol) and PCBr (165 mg, 0.4 mmol) were dissolved in 12 cm^3 of dichloromethane at −10°C. CO was bubbled through the solution until TLC showed no free phosphine in the reaction medium. The pale yellow solution was concentrated to *ca.* 2 ml and transferred to a column (25 × 1.5 cm) packed with silica-gel in hexane. Elution with dichloromethane/hexane 1:1 yielded a pale yellow band, which was collected and evaporated to dryness. Recrystallization from dichloromethane/hexane gave the pure product. Yield: 65%. Found: C, 44.7; H, 2.0%. Calc. for $C_{37}H_{20}OF_8P_2ClBr_2$: C, 45.0; H, 2.1%. IR ν(CO) = 1970 cm^{-1} (in $CHCl_3$).

Preparation of $IrCl(CO)(PCBr)_2$, (9)

This compound was made using an equivalent procedure to that for the rhodium analogue. Yield: 60%. Found: C, 40.9; H, 2.0. Calc. for $C_{37}H_{20}OF_8P_2ClBr_2$. C, 41.1; H, 1.8%. IR ν(CO) = 1965 cm^{-1} (in $CHCl_3$).

RESULTS AND DISCUSSION

An overview of the various chemical interconversions for the Rh and Ir phosphine compounds is given in Scheme 1. Most structures were derived by a combination of chemical methods and NMR spectroscopy. Additionally, compounds **5** and **6** were subjected to an X-ray structure analysis and thus served as structural anchors.

We have shown before that the ^{31}P spectroscopic parameters are of direct diagnostic value with respect to the various modes of ligation of the PCBr

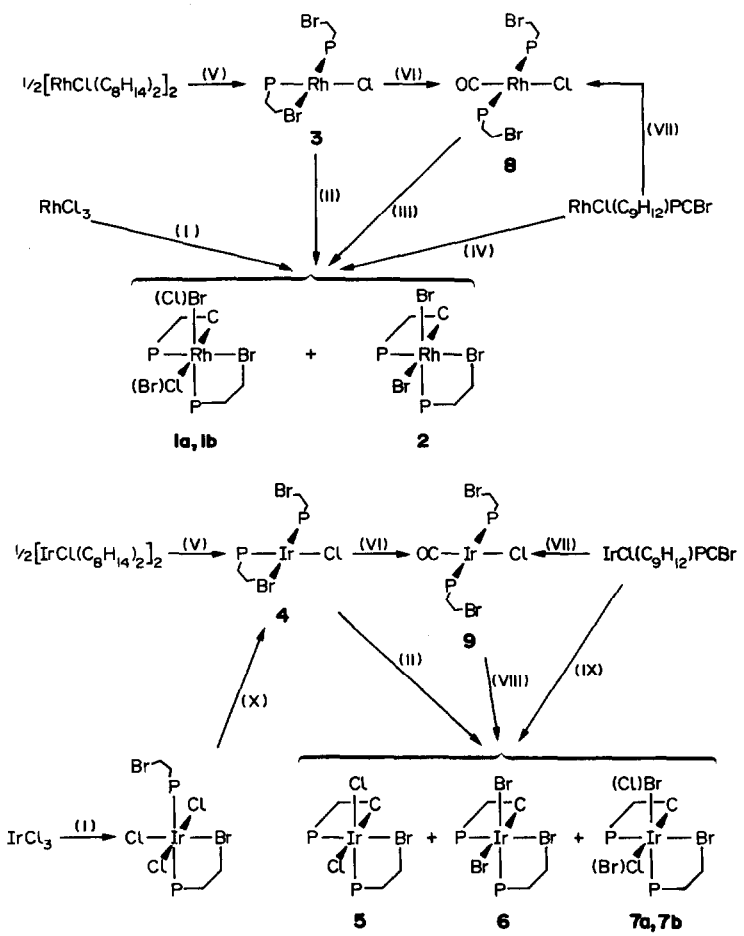

Scheme 1. Reactivity pattern for Rh and Ir compounds; (I) +4 PCBr, refluxing in EtOH; (II) CH_2Cl_2, R.T.; (III) refluxing in toluene; (IV) +PCBr, refluxing in toluene; (V) +PCBr, CH_2Cl_2, R.T.; (VI) +CO, CH_2Cl_2, R.T.; (VII) +PCBr, +CO, CH_2Cl_2, R.T.; (VIII) refluxing in xylene; (IX) +PCBr, refluxing in xylene; (X) electrochemical reduction ($2e^-$).

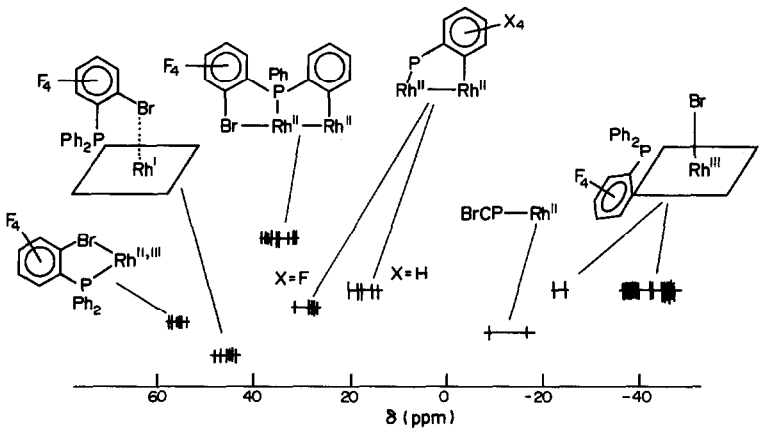

Scheme 2. ^{31}P chemical shifts vs coordination mode of the phosphine PCBr.

ligand in dirhodium systems.[6] This is equally true for mononuclear complexes.[5] The expected chemical shift ranges for various rhodium compounds are given in Scheme 2.[17] Although there are fewer examples of Ir(PCBr) complexes, the respective chemical shifts are systematically observed at lower frequencies (20–40 ppm).

Starting with the rhodium system we find that upon reaction of $RhCl_3 \cdot 3H_2O$ and PCBr in a 1 : 4 molar ratio in refluxing ethanol a yellow precipitate is obtained in high yield. It is soluble in most solvents but insoluble in hexane or ethyl ether. The elemental analysis is consistent with a composition "$RhCl(PCBr)_2$", **1**. Molecular weight measurements, by osmometry in benzene, confirm the mononuclear formulation.

The ^{31}P NMR spectrum shows two blocks of signals centred at 45–50 ppm and at about −27 ppm. The low field region shows two well resolved doublets: δ_{Pa} 51.9 ppm ($^1J_{Rh-Pa}$ 122 Hz) and δ_{Pb} 47.0 ppm ($^1J_{Rh-Pb}$ 123 Hz). THe high field region can be interpreted as the result of two partially overlapping doublets P'_a and P'_b centred at about −24 ppm.

The relative intensities of these signals assigned to P_a and P_b and consequently to P'_a and P'_b were observed to vary with the experimental conditions so as to indicate that compound **1** is in fact a mixture of two isomers **a** and **b**. The observed chemical shifts together with the analysis and molecular weight are consistent with the formulation $RhClBr(\eta^2\text{-PC})(\eta^2\text{-PCBr})$. The signals at higher field are thereby assigned to P atoms of the four-membered metallocycle.[5,18] The signals at lower field are in the chemical shift range which is typical for the chelating (P—Br) bonding mode.[6,7] All signals exhibit additional splitting due to intramolecular J_{F-P} long range coupling and possibly also due to $^2J_{PP'}$. The magnitudes of these couplings are small (< 20 Hz) in all cases, indicating that the phosphorus atoms in all the isomers are mutually in *cis*-configurations.

The above formulation of **1** is further corroborated by a comparison with the structurally characterized Ir analogues **5** and **6** (see below). Furthermore, two crystalline derivatives of **1** were isolated after prolonged exposure to air. They were structurally characterized by X-ray crystallography[19] and turned out to be isomers of $RhClBr[\eta^2\text{-OP}(C_6F_4)(C_6H_5)_2](\eta^2\text{-PCBr})$ formed by air oxidation of the metallocycle. Concomitantly the ^{31}P spectrum lacks the high field signal characteristic for the metallocycle and shows a singlet at 70.2 ppm instead, without a resolved Rh—O—P splitting.

If the reaction of $RhCl_3 \cdot 3H_2O$ and PCBr is performed in the presence of a 10 molar excess of NaBr, only one major product which analyses as $RhBr_2(\eta^2\text{-PC})(\eta^2\text{-PCBr})$, **2**, is obtained. It shows signals at δP 51.6 ppm, $^1J_{Rh-P}$ 121 Hz, and δP′ 24.7 ppm ($^1J_{Rh-P}$ 107 Hz).[17] Small amounts of **1a** and **1b** are also observed in solution.

A comparison of products **1a, b** and **2*** with the starting material $RhCl_3$ suggests a complex reaction mechanism involving a redox process. Whether or not this redox reaction precedes the *ortho*-metallation step was proved by the following experiment: $[RhCl(C_8H_{14})_2]_2$ was reacted with PCBr in a 1 : 4 molar ratio at room temperature to give a yellow product with analytical and spectroscopic results

*There is indication that **2** is a minor component (< 5%) of the reaction mixture containing **1a, b**, as peaks approximately corresponding to those of **2** are detected in high quality ^{31}P spectra.

Table 3. ^{31}P NMR data

Compound	Σ(PCBr)	J(Rh—P)	Σ(PC)	J(Rh—P)
RhCl(COD)(PCBr)	31.6	148		
IrCl(COD)(PCBr)	23.8			
RhCl(CO)(PCBr)	36.4	135		
IrCl(CO)(PCBr)$_2$	28.4			
RhCl(PCBr)$_2$	52.3	213		
	81.7	182		
IrCl(PCBr)$_2$	15.5			
	44.6			
RhBr$_2$(PC)(PCBr)	51.6	121	−24	107
IrBr$_2$(PC)(PCBr)	14.6		−68.6	
IrCl$_2$(PC)(PCBr)	10.2		−66.8	
RhClBr(PC)(PCBr)	51.9	122	−25[a]	90[a]
	47.4	123	−24[a]	90[a]
IrClBr(PC)[PCBr)	9.7		−67.8	
	15.2		−67.8	

Σ in ppm. J in Hz.
[a] estimated values.

similar to 1, albeit with a different ratio of the two isomers a and b. If the reaction is carried out at 0°C an intermediate red compound is obtained. In agreement with the elemental analysis and the ^{31}P NMR spectrum ($CDCl_3$, −40°C) we formulate this new compound as RhCl(η^2-PCBr)(η^1-PCBr) 3. The bidentate phosphine shows a resonance at δP 81.76 ppm ($^1J_{Rh—P}$182 Hz), and the monodentate one at δP 53.02 ppm ($^1J_{Rh—P}$ 213 Hz). The $^2J_{P—P'}$ coupling constant is 41 Hz indicative of a cis disposition of the two P nuclei in a square planar environment.

Compound 3 in dichloromethane undergoes intramolecular *ortho*-metallation yielding 1. If this reaction is monitored by ^{31}P NMR, new signals (δP −41.1 ppm; $^1J_{Rh—P}$ 525 Hz) corresponding to a new intermediate *ortho*-metallated compound with the two P atoms in a mutually *trans* disposition can be observed. If 3 is exposed to 1 atm of CO

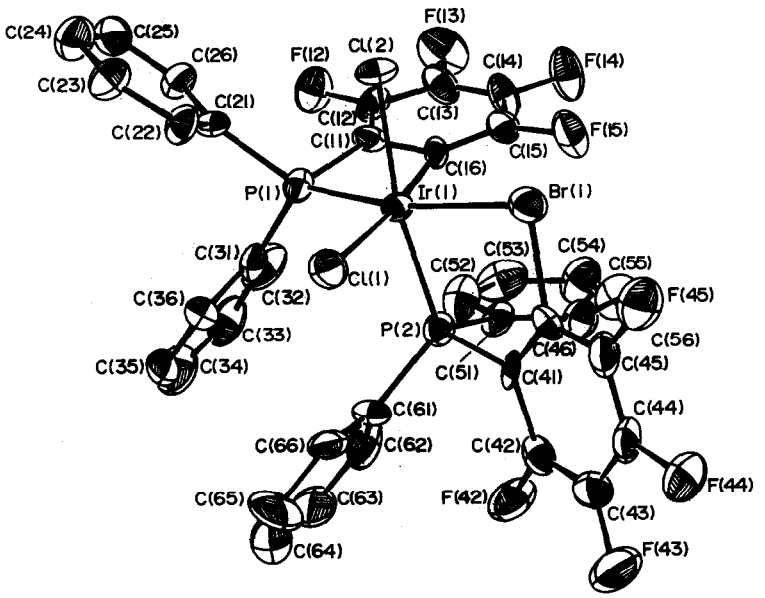

Fig. 1. ORTEP representation (thermal ellipsoid 50% probability) and labelling scheme of compound 5.

at $-10°C$ a carbonyl containing product **8** is obtained which analyses as $RhCl(CO)(PCBr)_2$. It shows only one signal in the ^{31}P spectrum (36.4 ppm; $^1J_{Rh-P}$ 135 Hz) and is therefore proposed to be a square planar $RhCl(CO)(\eta^1\text{-}PCBr)_2$ complex with a *trans* arrangement of the phosphines. This compound does not undergo *ortho*-metallation at room temperature and reacts only sluggishly in refluxing toluene to yield **1**.

Focusing our attention now on the Ir system we find an analogous reaction pattern for the Ir(I) starting material $IrCl(\eta^2\text{-}PCBr)(\eta^1\text{-}PCBr)$, **4**. Compound **4** shows ^{31}P resonances at 44.6 ppm (chelating phosphine, P—Br) and 15.5 ppm (monodentate, PCBr). The coupling constant $J_{PP'}$ 25 Hz is indicative of a *cis*-configuration. Compound **4** undergoes rapid *ortho*-metallation at room temperature in CH_2Cl_2 solution. The reaction is completed within 30–40 min analogously to the Rh system. CO substitution yields a carbonyl con-

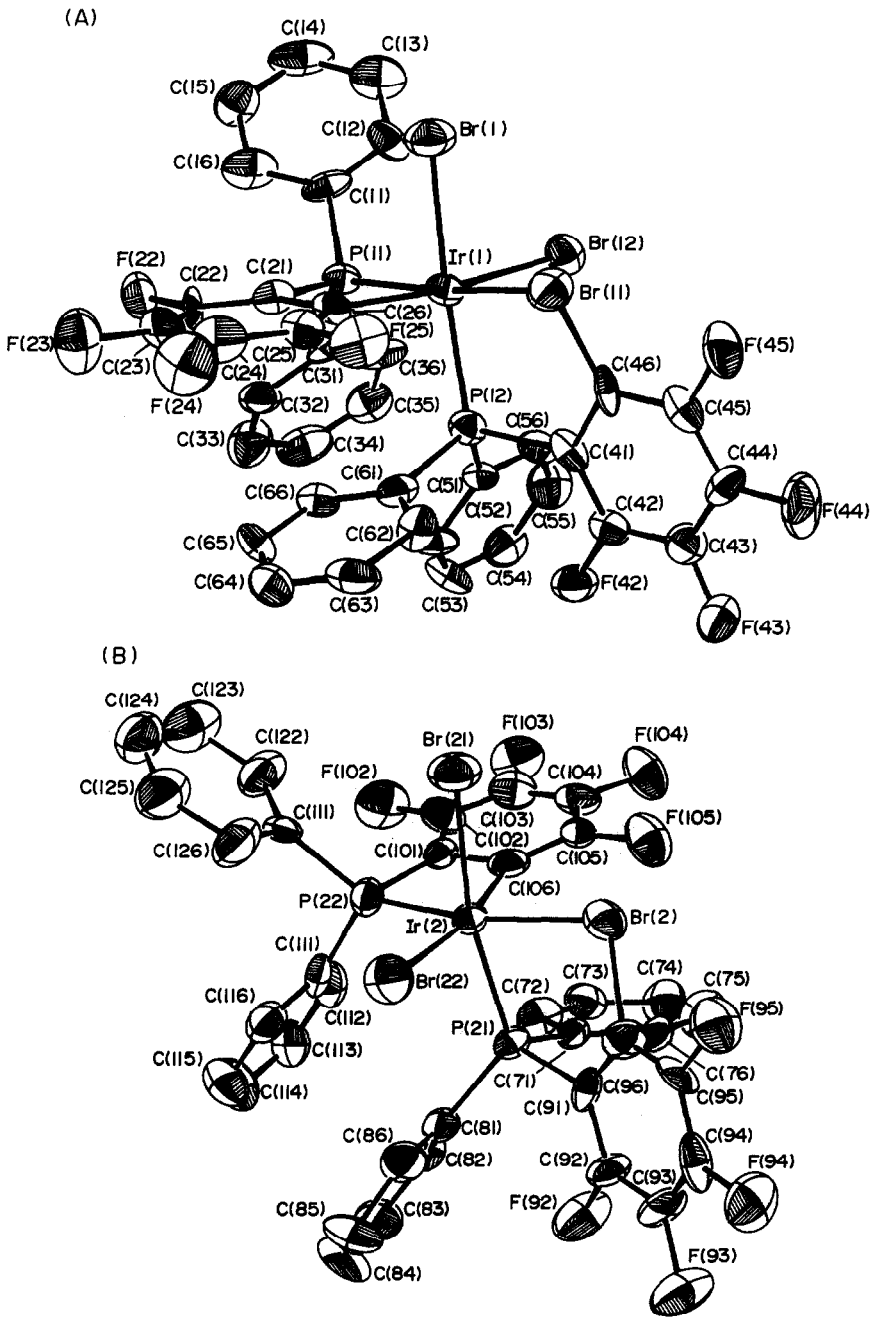

Fig. 2. (A and B). ORTEP representations (thermal ellipsoid 50% probability) and labelling scheme for the two independent molecules of compound **6**.

taining product $IrCl(CO)(PCBr)_2$, **9**, which is deactivated with respect to the *ortho*-metallation reaction. The single ^{31}P resonance at 28.4 ppm is consistent with the proposed *trans* arrangement.

The intramolecular *ortho*-metallation reaction of compound **4** yields three products **5**, **6** and **7** of general stoichiometry IrXX(PC)(PCBr) which differ in their halogen content. The following analyses were found: compound **5**: XY = Cl_2; compound **6**: XY = Br_2; compound **7**: XY = ClBr (isomeric mixture). For compound **7** which is the mixed Cl, Br species two isomers are detected by ^{31}P NMR. All the ^{31}P NMR data are given in Table 3.

The crystal structures of **5** and **6** have been determined. The compounds are isostructural though not crystallographically isomorphous because **6** crystallizes with two independent molecules per asymmetric unit and a molecule of solvent. Perspective views of the molecular complexes are shown in Figs 1 and 2 for **5** and **6**, respectively. Important bond lengths and angles are given in Table 3.

The coordination geometries of the iridium centres are based on the octahedron with distortions imposed by the geometrical constraints of the bidentate ligands. One of the phosphines is bonded through the phosphorus atom and the *ortho*-carbon atom of the perfluorinated phenyl ring such as to form a four-membered metallocycle. Consequently the Ir—P—C bond angles are compressed with respect to the octahedral geometry, *viz.* 69.2(4) and 68.1(8) for **5** and **6**, respectively. The second phosphine exhibits an η^2-mode of coordination through the phosphorus and the *o*-Br atoms, resulting in a five-membered metallocyle with P—Ir—Br bond angles of 86.2(1) and 86.1(3) for **5** and **6**, respectively. The average Ir—X distances are 2.41[1] — and 2.54[2] Å for Cl and Br. In light of the octahedral coordination and diamagnetic NMR behaviour a t_{2g}^6 electron configuration is postulated.

That the η^2-PCBr coordination mode is a precondition for the *ortho*-metallation step can be shown in an experiment other than the CO substitution reaction. Reaction of $[IrCl(COD)]_2$ (COD = *cis*-1,5-cyclooctadiene) with 1 equivalent of PCBr leads to the known mononuclear complex IrCl(COD)PCBr.[15] Because of the bidentate nature of the COD ligand the phosphine acts as a monodendate ligand. *Ortho*-metallation occurs in this compound only under vigorous conditions such as 10 h reflux in xylene to afford a mixture of **5**, **6** and **7**. The homologous Rh compound RhCl(COD)(PCBr) also gives **1a**, **b** after 3 h reflux in toluene.

Finally when $IrCl_3 \cdot 3H_2O$ is reacted with PCBr (1 : 4) in refluxing ethanol a complex of Ir(III) of composition $IrCl_3(\eta^2\text{-PCBr})(\eta^1\text{-PCBr})$ is obtained in near-quantitative yield.[8] This compound can be chemically or electrochemically reduced to yield a very reactive Ir(I) species assumed to be **4**.[9]

In conclusion we propose that the *ortho*-metallation reactions of mononuclear Rh and Ir compounds with PCBr occur from the univalent oxidation state of the metals. While this can be achieved, starting from the M(III) halides, by *in situ* reduction of the Rh(III) by the excess of phosphine, the Ir(III) has to be reduced chemically or electrochemically. The resulting square planar complexes $MCl(\eta^2\text{-PCBr})(\eta^1\text{-PCBr})$ undergo *ortho*-metallation at room temperature provided that one of the phosphines assumes the η^2-PCBr mode of ligation. If the *o*-halogen ligation is competitively substituted by a superior ligand such as CO or olefin, no *ortho*-metallated products are formed under normal reaction conditions. Finally, the Ir compounds are subject to halogen exchange while such reactions are only of marginal importance in the case of the Rh system.

Acknowledgements—We thank the National Science Foundation and the C.A.I.C.Y.T. (Spain) for financial support (Project 3275/83).

REFERENCES

1. I. Omae, *Coord. Chem. Rev.* 1980, **32**, 235.
2. (a) J. Dehand and M. Pfeffer, *Coord. Chem. Rev.* 1976, **18**, 327; (b) M. Laing, M. J. Nolte, E. Singleton and E. Van der Stok, *J. Organomet. Chem.* 1978, **146**, 77; (c) J. M. Guss and R. Mason, *J. Chem. Soc., Chem. Commun.* 1971, 58.
3. (a) W. Keim, *J. Organomet. Chem.* 1968, **14**, 179; (b) S. Bresadola, B. Longato and F. Morandini, *Inorg. Chim. Acta.* 1977, **25**, L135; (c) G. R. Clark, W. R. Roper and A. H. Wright, *J. Organomet. Chem.* 1984, **C17**, 273.
4. (a) R. J. Errington, W. S. McDonald and B. L. Shaw, *J. Chem. Soc., Dalton Trans.* 1982, 1829 and references therein; (b) S. Hietkamp, D. J. Stufkens and H. Vrieze, *J. Organomet. Chem.* 1977, 189.
5. F. Barceló, J. C. Besteiro, P. Lahuerta, C. Foces-Foces, F. H. Cano and M. Martinez-Ripoll, *J. Organomet. Chem.* 1984, **270**, 343.
6. F. Barceló, F. A. Cotton, P. Lahuerta, R. Llusar, M. Sanaú, W. Schwotzer and M. A. Ubeda, *Organometallics* 1986, **5**, 808.
7. F. Barceló, P. Lahuerta, M. A. Ubeda, C. Foces-Foces, F. H. Cano and M. Martinez-Ripoll, *J. Chem. Soc., Chem. Commun.* 1985, 43.
8. F. A. Cotton, P. Lahuerta, M. Sanaú, W. Schwotzer and I. Solana, *Inorg. Chem.* 1986, **25**, 3526.

9. P. Lahuerta, J. Latorre and I. Solana, *J. Organomet. Chem.* (in press).
10. G. Giordano and R. H. Crabtree, *Inorg. Synth.* 1979, **19**, 218.
11. A. Van der Ent and A. L. Onderdelinden, *Inorg. Synth.* 1973, **14**, 93.
12. J. L. Herde, J. C. Lambert and C. V. Senoff, *Inorg. Synth.* 1974, **15**, 18.
13. R. H. Crabtree, J. M. Quirk, H. Felkin and T. Fillebeen-Khan, *Synth. React. Met-Org. Chem.* 1982, **12**, 407.
14. P. G. Eller and D. W. Meek, *J. Organomet. Chem.* 1970, **22**, 631.
15. P. Lahuerta, I. Solana, X. Solans and M. Font-Altaba, *J. Chem. Res.* (in press).
16. (a) A. Bino, F. A. Cotton and P. E. Fanwick, *Inorg. Chem.* 1979, **18**, 3558; (b) F. A. Cotton, B. A. Frenz, G. Deganello and A. Shaver, *J. Organomet. Chem.* 1973, **50**, 227; (c) A. C. T. North, D. C. Phillips and F. S. Mathews, *Acta Cryst.* 1968, **A24**, 351.
17. F. L. Barceló, Ph.D. Thesis. Universidad de Valencia (1986).
18. P. Garrou, *Chem. Rev.* 1981, **81**, 229.
19. X. Solans, M. Font-Altaba, M. Aguiló, C. Miratvilles, J. C. Bestéiro and P. Lahuerta, *Acta. Cryst.* 1985, **C41**, 841.

Polyhedron Vol. 7, No. 2, pp. 97–101, 1988
Printed in Great Britain

0277–5387/88 $3.00+.00
© 1988 Pergamon Journals Ltd

CHARGE-TRANSFER COMPLEXES OF NITRIC OXIDE, TRI OR TETRAVALENT HALIDES AND AROMATIC HYDROCARBONS*

SYDNEY BROWNSTEIN† and BRIDGET IRISH

Division of Chemistry, National Research Council of Canada, Ottawa, Canada K1A 0R9

(*Received* 4 *May* 1987; *accepted* 24 *August* 1987)

Abstract—Complexes of nitric oxide, some aromatic hydrocarbons and the halides BF_3, BCl_3, $AlCl_3$, $FeCl_3$, $SiCl_4$, GeF_4, $SnCl_4$ and $TiCl_4$ have been identified and characterized by spectroscopic measurements.

Ternary charge transfer complexes of $NO^+MX_n^-$, X = Cl or F, with single ring aromatic hydrocarbons are well established, although oxidation of condensed aromatic ring compounds by NO^+ or MX_n^- occurs readily for polycyclic aromatic hydrocarbons.[1–3] It seemed worthwhile to investigate whether similar interactions would occur with NO itself, a suitable Lewis acid and an aromatic hydrocarbon and, if such interactions occur, whether the products would be more stable to oxidation. There is interaction between BF_3 and NO to give a molecular aggregate which cannot be isolated, but which has been studied by molecular beam electric deflection.[4] The reaction of $AlCl_3$ and $FeCl_3$ with NO has been known for a long time.[5] The IR spectrum of the $NO \cdot SnCl_4$ complex has been published.[6] There are no reports of interaction between NO and BCl_3, $SiCl_4$, GeF_4 and $TiCl_4$. There has been a thorough investigation of the reactions of phosphorus, arsenic and antimony pentafluorides with NO.[7]

Within these systems a second binary grouping whose interaction has been reported is that of NO with an aromatic hydrocarbon. The singlet–triplet bands of benzene are perturbed by nitric oxide, presumably because it is paramagnetic.[8] Anthracene is oxidized to anthraquinone by nitric oxide.[9] There are also interactions between another pair of reactants in the systems to be described. No significant interaction has been reported between BF_3 or BCl_3 and benzene. The system BF_3 in liquid SO_2 produces and stabilizes positive radical ions from polycyclic aromatic hydrocarbons.[10] In nonpolar solvents such as 1,2-dichloroethane both a covalent complex and the monopositive radical ion may be found with aromatic hydrocarbons and BF_3.[11] There is no evidence for the interaction of pure $AlCl_3$ and aromatic hydrocarbons.[12] Chlorination is the principal reaction between $FeCl_3$ and aromatic hydrocarbons.[13] Weak charge-transfer complexes were reported between $GeCl_4$, $SnCl_4$ or $TiCl_4$ and aromatic hydrocarbons.[14] For the case of $TiCl_4$ and hexamethylbenzene in CCl_4 a yellow precipitate was obtained rather than the charge-transfer complex.[15]

Since sulphur dioxide is used as the solvent in some of our studies its behaviour in simpler systems is also described. There is no apparent reaction between NO and SO_2 at pressures up to 50 atm but at 500 atm there is some reaction to yield SO_3 and nitrogen.[16] Aromatic species interact with sulphur dioxide to give 1 : 1 complexes which are largely dissociated.[17]

EXPERIMENTAL

Magnetic resonance spectra were obtained on a Bruker AM-400 spectrometer operating at 400 MHz for protons. All chemical shifts, except for ^{19}F, were measured with respect to neopentane as internal reference since it is inert in the solutions studied. A correction of 0.92 ppm was applied for protons and 31.4 ppm for ^{13}C, to refer these chemical shifts to tetramethylsilane. The ^{27}Al chemical shifts are reported relative to $Al(H_2O)_6^{3+}$ using the Ξ value of 26,056,780 for this species.[18] Fluorine chemical shifts are reported with respect to internal

* Issued as NRCC No. 28254.

†Author to whom correspondence should be addressed.

$CFCl_3$ as zero. UV spectra were obtained on a Cary 210 Spectrometer in CH_2Cl_2 as solvent, with concentrations expressed as moles per kg of solvent. Equilibrium constants have also been calculated using the same unit.

Chemicals. Boron, phosphorus arsenic and antimony trichlorides and trifluorides, ferric, lanthanum and vanadium trichlorides, germanium tetrafluoride, silicon, tin and titanium tetrachlorides, hexamethylbenzene, naphthalene, and 9,10-dimethylanthracene were used without further purification. Mesitylene, sulphur dioxide, neopentane, methylene chloride and aluminium chloride were purified and used as previously described.[2] Antimony, niobium and tantalum pentafluorides and pentachlorides were vacuum sublimed before use. Nitric oxide was purified by removal of NO_2 with silica gel.[19]

Sample preparation was always done in the absence of air using vacuum line and dry box techniques.[2]

RESULTS AND DISCUSSION

The ternary complex $NO \cdot BF_3 \cdot$ hexamethylbenzene has absorption bands at 2710 and 3360 Å. The one at 2710 Å is the same as for hexamethylbenzene itself, but is much more intense. If we assume that the extinction coefficients are the same for both of the absorption bands of the charge-transfer complex it is possible to calculate the concentrations, equilibrium constant and extinction coefficient for the charge-transfer complex. The optical density for the band at 2710 Å should increase since some of this absorption arises from hexamethylbenzene, whose concentration is decreasing. From the measured extinction coefficient for hexamethylbenzene itself, 370, and the change in relative intensities of the bands at 2710 and 3360 Å the calculations of Table 1 give an equilibrium constant of 2.9 ± 0.3 assuming all the BF_3 and NO are in solution. In fact the solubility of these gases at room temperature is such that their concentrations in the liquid and vapour phases are about the same. Applying this factor to the known optical cell volume gives an equilibrium constant of 850. The extinction coefficient of 6,800, which is not changed by this correction, since only the concentrations of volatile species are altered, is in good agreement with those observed for the corresponding NO^+ complexes.[2]

Results are also presented in Table 1 for mesitylene as the aromatic hydrocarbon. Significant overlap of the long wavelength absorption band of mesitylene at 2670 Å and that of its charge-transfer complex at 3440 Å prevent a simple calculation as with hexamethylbenzene. The concentrations and equilibrium constants for the mesitylene case, also listed in Table 1, were calculated with the assumption that the extinction coefficient for its charge-transfer band is the same as that determined for the hexamethylbenzene complex. Formation of the ternary charge-transfer complex of naphthalene, BF_3 and NO is very slight with a weak broad absorption between 3200 and 3600 Å. This is consistent with the fact that the equilibrium constant for charge-transfer complex formation between tetracyanoethylene and naphthalene is much less than that for hexamethylbenzene.[20] With anthracene, BF_3 and NO there is a reaction which destroys the anthracene,

Table 1. UV spectral results and equilibrium constants for complex formation in BF_3–NO–aromatic solutions

Initial concentration			Optical density		Final concentration				K
Hexamethylbenzene	BF_3	NO	2710 Å	3360 Å	Hexamethylbenzene	BF_3	NO	Complex	
0.0929	0	0	1.72	0.15	0.0929	0	0	0	—
0.0929	0.0844	0.104	2.39	0.87	0.0902	0.0817	0.101	0.0027	3.6
0.0929	0.0844	0.186	2.66	1.16	0.0891	0.0806	0.182	0.0038	2.9
0.0929	0.0844	0.287	2.85	1.37	0.0880	0.0795	0.282	0.0049	2.5
0.0929	0.0844	0.393	2.94	1.50	0.0859	0.0774	0.386	0.0070	2.7
Mesitylene	BF_3	NO	2670 Å	3440 Å	Mesitylene	BF_3	NO	Complex	
0.141	0	0	2.37	0.08	0.141	0	0	0	—
0.141	0.140	0.155	2.56	0.45	0.140	0.139	0.154	0.0013	0.4
0.141	0.140	0.301	3.39	1.95	0.135	0.134	0.295	0.0057	1.1
0.141	0.140	0.457	3.68	2.33	0.134	0.133	0.450	0.0069	0.9
0.058	0.073	0.134	2.07	1.34	0.054	0.130	2.03	0.0039	0.3
0.058	0.117	0.134	2.30	1.41	0.054	0.130	2.26	0.0041	0.3

presumably producing anthraquinone.[9] 9,10-Dimethylanthracene (DMA), BF_3 and NO immediately yield a blue solution with a broad absorption band centred at 6780 Å. This absorption quickly fades and is replaced by bands at 5200, 4900 and 4450 Å. A broad signal was found for the reference material in the proton resonance spectrum but no other signals could be observed. These results are consistent with the initial formation of the DMA radical cation,[21] which was confirmed by its electron spin resonance spectrum when using GeF_4 as the Lewis acid. DMA is rapidly oxidized by NO in the absence of BF_3, and also by $NOBF_4$. Presumably the fading of the initially formed long wavelength band arises from reaction of unaffected DMA and NO since formation of the radical cation does not go to completion. Spectral results are listed in Table 2.

The proton, carbon-13 and fluorine resonance shifts observed for solutions containing differing quantities of BF_3, NO and hexamethylbenzene in CH_3Cl_2 and SO_2 as solvents are listed in Table 3. From changes in chemical shift with change in concentration, it is clear that there is at least partial formation of the ternary charge complex. The chemical shift of the fluorines is displaced to higher field and the proton and carbon-13 signals to lower field upon complex formation. It is interesting to note that SO_2 in the absence of BF_3 also forms a ternary charge-transfer complex with NO and hexamethylbenzene. This formation was observed visually but could not be quantified by UV spectroscopy because of the strong absorption by SO_2 itself, nor by NMR since complex formation is slight.

Although complex formation appears to increase regularly with NO concentration this does not necessarily imply a reversible equilibrium. There could perhaps be a reaction which yields a small amount of $NOBF_4$ whose complex with hexamethylbenzene has similar absorption maxima. However it was found that removal of the NO and BF_3 by brief pumping under vacuum caused the disappearance of the charge-transfer absorption band, and removal of all readily volatile species under vacuum resulted in negligible weight gain. Therefore the assumption of a readily reversible complex formation is probably correct.

Boron trichloride, nitric oxide and aromatic molecules form charge-transfer complexes similar to those observed with boron trifluoride. The absorption spectra of the hexamethylbenzene, naphthalene and DMA complexes are similar in both cases but the complexes with BCl_3 and the polycyclic hydrocarbons appear more stable to oxidation by the nitric oxide. It was noted that the very weak charge-transfer band at 3600 Å for the system $BCl_3 \cdot NO \cdot$ naphthalene became more intense at 5° than at 25° indicating greater complex formation at lower temperature. The chemical shifts for the system containing $NO \cdot BCl_3 \cdot$ hexamethylbenzene, listed in Table 3, are at lower field than for the analogous BF_3 system also suggesting a greater degree of complex formation. Spectral results are listed in Table 2.

The reaction of $AlCl_3$ and NO in SO_2 as solvent produces a compound which is not $NOAlCl_4$ since $\delta^{27}Al$ for the $NO \cdot AlCl_3$ product is 102.7 ppm compared with 105.7 ppm for $NOAlCl_4$ and 95.6 ppm for tetramethylammonium $AlCl_4$.[18] Aluminium trichloride, NO and hexamethylbenzene react almost completely to form the ternary charge complex since the chemical shifts, listed in Table 3, are almost the same as with the nitrosyl salts.[2] The extinction coefficient, measured assuming complete formation, is the same as that calculated for the BF_3 congener and is listed in Table 2.

From the weight gain, after exposure to NO followed by pumping under vacuum, it appears that $FeCl_3$ forms a complex with one equivalent of NO. Ternary complexes of NO, $FeCl_3$ and hexamethylbenzene were prepared and characterized by the spectroscopic values listed in Table 2. It was found that the broad ESR signal from $FeCl_3$ dissolved in SO_2 became considerably more intense upon additions of NO but underwent no further change upon addition of hexamethylbenzene.

No complex formation was found between $SiCl_4$

Table 2. Absorption peaks for some ternary charge-transfer complexes

System	Absorption Å	
$BF_3 \cdot NO \cdot$ mesitylene	2660	3400
$BF_3 \cdot NO \cdot$ hexamethylbenzene	2710	3360 (6,800)[a]
$BCl_3 \cdot NO \cdot$ hexamethylbenzene	2720	3360
$AlCl_3 \cdot NO \cdot$ hexamethylbenzene		3340 (6,900)
$FeCl_3 \cdot NO \cdot$ hexamethylbenzene	3190 (29,000)	3610 (31,000)
$TiCl_4 \cdot NO \cdot$ mesitylene	3110	

[a] Extinction coefficients are listed in brackets.

and aromatic hydrocarbons.[14] In the system $SiCl_4$, NO and hexamethylbenzene there was no evidence of complex formation at room temperature but as the temperature was lowered the characteristic colour of the charge-transfer complex appeared. Chemical shifts, listed in Table 3, show that there is some complex formation in this system at −75°C.

There is nearly complete complex formation at room temperature between GeF_4, NO and hexamethylbenzene as evidenced by the magnetic resonance shifts listed in Table 3. Complex formation is not quite complete since upon removal of all volatiles under vacuum, hexamethylbenzene is recovered unchanged. There is reversible formation of the 9,10-dimethylanthracene radical cation by reaction of the parent hydrocarbon with GeF_4 in SO_2 or CH_2Cl_2 solution. Upon addition of NO the ESR signal of the radical disappears due to oxidation of the free 9,10-dimethylanthracene.

Tin tetrafluoride is insoluble in SO_2 and CH_2Cl_2 and is not brought into solution by NO and hexamethylbenzene. $SnCl_4$, NO and hexamethylbenzene react partially at room temperature to form the charge-transfer complex as evidenced by the chemical shifts listed in Table 3. With 9,10-dimethylanthracene and $SnCl_4$ the radical cation is produced.

There is no evidence for charge-transfer complex formation in the system NO–$TiCl_4$–benzene. With mesitylene and hexamethylbenzene as the aromatic species there was extensive charge-transfer complex formation according to the magnetic resonance and UV spectral results listed in Table 2 and 3. It was noted that addition of an equivalent amount of $TiCl_4$ to CH_2Cl_2 solutions of both hydrocarbons gave a yellow solid which redissolved upon addition of excess $TiCl_4$ to about 20% by weight of solvent. These results explain the differing previous reports.[14,15]

There is no evidence for reaction in the ternary systems nitric oxide, hexamethylbenzene and either PF_3, PCl_3, AsF_3, $AsCl_3$, SbF_3, VCl_3 or $LaCl_3$. In the

Table 3. Chemical shifts of some solutions containing ternary charge-transfer complexes and their precursors

System	Solvent	$\delta^{19}F$	$\delta^{1}H$	$\delta^{13}C$
BF_3	SO_2	−123.4 (−40)[a] −125.6		
BF_3+NO	SO_2	−123.6 (−40) −125.8		
Hexamethylbenzene (HMB)+NO (1 : 1)	SO_2		2.14 (−30)	16.40, 133.5 (−30)
HMB+NO (1 : 2)	SO_2		2.16 (−30)	16.4, 133.1 (−30)
HMB+NO (1 : 4.5)	SO_2		2.20 (−30)	16.5, 132.7 (−30)
HMB+BF_3	SO_2	−124.2 (−40)	2.13 (−30)	16.4, 134.1 (−30)
HMB+BF_3+NO (1 : 1 : 1)	SO_2	−130.7	2.24	16.7, 133.7
HMB+BF_3+NO (1 : 1 : 2)	SO_2	−140.2	2.20 (−30) 2.34	16.6, 136.7 (−30)
HMB+BF_3+NO (1 : 1 : 3)	SO_2	−138.4	2.32 (−30)	16.8, 142.4
BF_3	CH_2Cl_2	−122.3 (−40) −124.6		
HMB+NO (1 : 1)	CH_2Cl_2		2.19	16.6, 131.8
HMB+NO (1 : 2)	CH_2Cl_2		2.20	16.7, 131.5
HMB+NO (1 : 3)	CH_2Cl_2		2.20	16.6, 131.4
HMB+BF_3+NO (1 : 1 : 1)	CH_2Cl_2	−130.7	2.24	16.7, 133.7
HMB+SO_2+NO (1 : 1 : 1)	CH_2Cl_2		2.20 (−30) 2.19	16.9, 132.5 (−30) 16.7, 132.1
HMB+BCl_3+NO (1 : 4 : 3)	CH_2Cl_2		2.32 (0)	17.1, 140.5 (0)
HMB+$AlCl_3$+NO	CH_2Cl_2		2.44 (−60)	18.3, 147.4 (−60)
HMB+$SiCl_4$+NO	SO_2		2.22 (−80)	16.7, 136.5 (−75)
GeF_4	SO_2	−168.1		
GeF_4+NO	SO_2	−167.1		
HMB+GeF_4+NO	SO_2	−152.5	2.51	17.3, 149.7
HMB+$SnCl_4$+NO	SO_2		2.30	16.7, 139.5
Mesitylene+$TiCl_4$+NO	CH_2Cl_2		2.34, 6.96	20.5, 127.7 139.0
HMB+$TiCl_4$+NO	CH_2Cl_2		2.41	17.0, 142.7

[a] Temperatures other than room temperature are specified in brackets..

systems NbF_5, TaF_5 and PF_5 with NO and hexamethylbenzene, the colour of the solutions and the shift to low field of the proton and carbon resonances of the arene indicate that charge-transfer complex formation has occurred. However, in these cases the characteristic fluorine resonance spectra of the hexafluoroanions are observed. This is interpreted to indicate formation of $NO^+MF_6^-$ (M = P, Nb, or Ta), followed by reaction to give the previously reported complexes.[3,7] Although charge-transfer complex formation has also been observed with $SbCl_3$, SbF_5, $SbCl_5$, $NbCl_5$ and $TaCl_5$, it was not possible to determine in these systems whether the complexing agent was $NOMX_5$ or $NO^+MX_6^-$.

The data provided in this study show that reversible charge transfer complex formation is common in the systems NO, arene MX_n where X is F or Cl and $n = 3$ or 4, without intermediate formation of a nitrosonium salt. It is significant that the behaviour of the potential electron acceptor, NO in the present case, is modified by the presence of a Lewis acid with which it does not normally interact to a significant extent, when an arene is also present. Further electron acceptors will be studied to establish the generality of this reaction. Unfortunately, it was not possible to isolate pure materials for analytical or structural studies since partial or complete dissociation into the components appears to occur upon removal of the solvent.

REFERENCES

1. S. Brownstein, E. Gabe, F. Lee and L. Tan, *J. Chem. Soc., Chem. Comm.* 1984, 1566.
2. S. Brownstein, A. Morrison and L. Tan, *Can. J. Chem.* 1986, **64**, 265.
3. S. Brownstein, E. Gabe, F. Lee amd A. Piotrowski, *Can. J. Chem.* 1986, **64**, 1661.
4. S. E. Novick, P. B. Davies, T. R. Dyke and W. Klemperer, *J. Am. Chem. Soc.* 1973, **95**, 8547.
5. V. Thomas, *Compt. Rend.* 1895, **121**, 128.
6. V. N. Filimonov, D. S. Bystrov and A. N. Terenin, *Optika Spektrosk.* 1957, **3**, 480.
7. R. D. Peacock and I. L. Wilson, *J. Chem. Soc.* (*A*) 1969, 2030.
8. D. F. Evans, *J. Chem. Soc.* 1957, 3885.
9. M. Ilinskii and B. Maksorov, *Z. Farbenind.* 1929, **20**, 210.
10. J. P. Colpa and E. de Boer, *Mol. Phys.* 1963, **7**, 333.
11. W. I. Aalbersberg, G. J. Hoijtink, E. L. Mackor and W. P. Weijland, *J. Chem. Soc.* 1959, 3055.
12. H. C. Brown, H. W. Pearsall, L. P. Eddy, W. J. Wallace, M. Grayson and K. LeRoi Nelson, *Ind. Eng. Chem.* 1953, **45**, 1462.
13. P. Kovacic and N. O. Brace, *J. Am. Chem. Soc.* 1954, **76**, 5491.
14. L. A. Burkardt, P. R. Hammond, R. H. Knife and R. R. Lake, *J. Chem. Soc. A* 1971, 3789.
15. H. L. Krauss and H. Huettmann, *Z. Naturforsch.* 1963, **18b**, 976.
16. E. Briner and A. Wroczynski, *Z. anorg. Chem.* 1909, **63**, 49.
17. L. J. Andrews and R. M. Keefer, *J. Am. Chem. Soc.* 1951, **73**, 4169.
18. B. Glavincevski and S. K. Brownstein, *Can. J. Chem.* 1981, **59**, 3012.
19. E. E. Hughes, *J. Chem. Phys.* 1961, **35**, 1531.
20. R. E. Merrifield and W. D. Phillips, *J. Am. Chem. Soc.* 1958, **80**, 2778.
21. I. C. Lewis and L. S. Singer, *J. Chem. Phys.* 1965, **43**, 2712.

Polyhedron Vol. 7, No. 2, pp. 103–115, 1988
Printed in Great Britain

0277–5387/88 $3.00+.00
© 1988 Pergamon Journals Ltd

ALKOXY, THIOPHENOLATO AND AMIDO COMPLEXES OF MOLYBDENUM TRIS-(3,5-DIMETHYLPYRAZOLYL)BORATO NITROSYL ACETATE AND BENZOATE, AND THE X-RAY CRYSTAL STRUCTURE OF Mo{HB(3,5-$Me_2C_3HN_2)_3$}(NO)(NHPh)(OCOMe)·2$CHCl_3$

ANDRZEJ WLODARCZYK, ANTHONY J. EDWARDS† and JON A. McCLEVERTY†

Department of Chemistry, The University, P.O. Box 363, Birmingham B15 2TT, U.K.

(*Received* 11 *May* 1987; *accepted* 29 *June* 1987)

Abstract—The complexes MoL*(NO)(OR)(OCOR′) (L* = $HB(3,5\text{-}Me_2C_3HN_2)_3$; R = Me, Et, Pr^n, Pr^i; R′ = Me, Ph: R = CH_2CH_2OH, OH; R′ = Ph: R = Ph, C_6H_4OMe-*p*; R′ = Me, Ph: R = C_6H_4Me-p; R′ = Me), MoL*(NO)(SPh)(OCOR′) (R = Me or Ph) and MoL*(NO)(NHR)(OCOR′) (R = Me, Et, Ph; R′ = Me, Ph) were prepared by reaction of MoL*(NO)I(OR), MoL*(NO)I(SPh) and MoL*(NO)I(NHR) with AgOCOMe or AgOCOPh. The IR spectra of these complexes indicated that the carboxylate groups are monodentate and this was confirmed by a single crystal X-ray structural determination of MoL*(NO)(NHPh)(OCOMe).

Earlier we reported[1] the preparation of bis-alkoxides MoL*(NO)(OR)(OR′) (L* = tris(3,5-dimethylpyrazolyl)borate, $HB(Me_2C_3HN_2)_3$; R = R′ = Me, Et, Pr^i, Bu^i; R = Et, R′ = Pr′; R = Pr^i, R′ = Bu^i) and alkoxy-amides MoL*(NO)(OR)(NHR′) (R = Me, R′ = H, Me, Et; R = Et, R′ = H, Me, Et, Pr^n, CH_2Ph, C_6H_{11}, etc.) by treatment of MoL*(NO)I(OR) with AgOCOMe in the presence of R′OH or R′NH_2. We supposed that an intermediate in this reaction could be the acetate MoL*(NO)(OR)(OCOMe), but our attempts then to isolate this species were unsuccessful.

In this paper we report a more thorough examination of the reaction between MoL*(NO)I(OR) and silver acetate and benzoate, and report on the isolation of carboxylato species. We also describe the characterization of the related complexes MoL*(NO)(SPh)(OCOR) (R = Me or Ph) and MoL*(NO)(NHR)(OCOR′) (R = alkyl or aryl; R′ = Me or Ph) and the full X-ray structural determination of MoL*(NO)(NHPh)(OCOMe).

† Authors to whom correspondence should be addressed.

EXPERIMENTAL

All reactions were carried out under dry nitrogen and dichloromethane was purified to remove carabonyl-containing and alcoholic impurities. The molybdenum precursors [MoL*(NO)I(OR)] (R = Me, Et, Pr^n, Pr^i, CH_2CH_2OH,OC_6H_4Me-*p*, OC_6H_4OMe-*p*),[1-3] [MoL*(NO)I(SPh)][4] and [MoL*(NO)I(NHR)] (R = Me, Et, Ph)[2,5] were prepared as described in the literature. All yields are quoted relative to the molybdenum precursor and elemental analyses were determined by the Microanalytical Laboratory of this Department.

IR spectra were obtained as KBr discs using a PE 237 spectrophotometer and mass spectra using a Kratos MS80 instrument under normal E1 conditions. ^1H NMR spectra were obtained at 100 and 270 MHz using Varian XL 100 and Jeol GX 270 spectrometers.

[Mo{HB(3,5-$Me_2C_3HN_2)_3$}(NO)(OR)Y], R = Me, Et, Pr^i, Pr; Y = OCOMe; *and* R = Me, Et *and* Y = OCOPh. A solution of freshly prepared [Mo{HB(3,5-$Me_2C_3HN_2)_3$}(NO)(OR)I][1] (0.5 g) and a suspension of AgOCOMe or AgOCOPh (0.75–1 g) in dichloromethane (70 cm^3) was refluxed together with stirring for 2–3 h after which time it

had become a deep purple colour. The reaction mixture was cooled and on addition of pentane (10 cm^3) complete precipitation of silver salts and products of decomposition occurred. The precipitate was filtered off, and the filtrate was evaporated *in vacuo*. The residue was dissolved in dichloromethane and filtered, the blue solution being partially evaporated *in vacuo* and then treated with an equal volume of petroleum ether (b.p. 60–80°C) or hexane. The volume of the mixture was reduced until rapid precipitation of the purple product began. The purple powder was filtered off, washed with pentane, dried at *ca.* 120°C for 2 h and then *in vacuo* for 3 h.

Yields of pure products were higher than 70% when AgOCOMe was used and more than 50% for reactions with AgOCOPh.

$[Mo\{HB(3,5\text{-}Me_2C_3HN_2)_3\}(NO)(OH)(OCOPh)]$. A mixture of $[Mo\{HB(3,5\text{-}Me_2C_3HN_2)_3\}(NO)I_2]$[1] (0.5 g) and AgOCOPh (0.75 g) in dichloromethane (50 cm^3) was refluxed with stirring for 1 h. After cooling, filtration and evaporation *in vacuo*, a brown solid was formed which was then dissolved in thf to which *n*-pentane was added. After 2 h the colour of the solution had changed to purple and on partial evaporation, the complex was obtained as a purple powder insoluble in and washed with diethylether (0.31 g, 76%).

$[Mo\{HB(3,5\text{-}Me_2C_3HN_2)_3\}(NO)(OR)(OCOPh)]$; R = OPr^n, OPr^i. These complexes were prepared as described above, but the products were isolated from diethyl ether/petroleum ether/pentane mixtures. Yields of the pure purple products were more than 50%.

$[Mo\{HB(3,5\text{-}Me_2C_3HN_2)_3\}(NO)(OCH_2CH_2OH)(OCOPh)]$.

Method 1. $[Mo\{HB(3,5\text{-}Me_2C_3HN_2)_3\}(NO)I_2]$ (0.5 g) was dissolved in dry dichloromethane (100 cm^3) and an excess of ethylene glycol and silver benzoate (0.75 g) were added. The mixture was refluxed with stirring for 1 h after which time it had changed to a deep blue colour. The precipitate of AgI and of the excess of AgOCOPh were filtered off and the solvent evaporated *in vacuo*. The residue was dissolved in diethyl ether, filtered and hexane was added. The solution was evaporated slowly until precipitation commenced. The blue product was collected by filtration. Purification was effected by crystallization from diethyl ether–hexane (0.25 g, 55%).

Method 2. The complex was prepared in the same way as $[Mo\{HB(3,5\text{-}Me_2C_3HN_2)_3\}(NO)(OPr^n)(OCOPh)]$, using $[Mo\{HB(3,5\text{-}Me_2C_3HN_2)_3\}(NO)(OCH_2CH_2OH)I]$[2] as a starting material (> 50%).

$[Mo\{HB(3,5\text{-}Me_2C_3HN_2)_3\}(NO)(OR')(OCOMe)]$, R' = Ph, OC_6H_4OMe-*p*, OC_6H_4Me-*p*. $[Mo\{HB(3,5\text{-}Me_2C_3HN_2)_3\}(NO)(OR')I]$[3] (0.3 g), freshly prepared and purified chromatographically on silica gel using dichloromethane (90%)–hexane (10%) as eluant, was dissolved in dichloromethane (100 cm^3), containing AgOCOMe (0.4 g). The mixture was refluxed with stirring for 4 h and a brown solution was formed. This was filtered and petroleum-ether was added. The solution was evaporated slowly until precipitation began and the mixture was cooled to *ca.* −10°C. The brown solid which formed was filtered off and dried *in vacuo*.

The compounds where R' = OPh or OC_6H_4OMe-*p* could be recrystallized from $CHCl_3$–hexane and the compound with R' = OC_6H_4Me-*p* from methylcyclohexane–pentane. (Yields: R' = OPh; 0.14 g, 56%; R' = OC_6H_4OMe-*p*, 0.21 g, 78%; R' = OC_6H_4Me-*p*; 0.22 g, 85%).

$[Mo\{HB(3,5\text{-}Me_2C_3HN_2)_3\}(NO)(OC_6H_4OMe\text{-}p)(OCOPh)]$. This compound was prepared as described above but the reaction was finished after 2 h. The complex crystallized from dichloromethane–petroleum ether as a dark brown solid (2.57 g, 86%).

$[Mo\{HB(3,5\text{-}Me_2C_3HN_2)_3\}(NO)(SPh)Y]$; Y = OCOMe, OCPh. $[Mo\{HB(3,5\text{-}Mepyz)_3\}(NO)I(SPh)]$[4] (0.2 g), freshly prepared and purified chromatographically on silica gel using dichloromethane as eluant, was dissolved in dichloromethane (70 cm^3), mixed with AgOCOMe (0.35 g) or AgOCOPh (0.35 g) and refluxed with stirring for 1 h after which time the solution had changed from vermilion to brown. The mixture was filtered and hexane was added. After partial evaporation *in vacuo* and cooling to *ca.* 10°C the complexes were obtained as brown microcrystalline solids (Y = OCOMe; 0.07 g, 40%; Y = OCOPh; 0.14 g, 74%).

$[Mo\{HB(3,5\text{-}Me_2C_3HN_2)_3\}(NO)(NHR)Y]$, R = Me, Et *and* Y = OCOMe, OCOPh. A solution of freshly prepared, very dry $[Mo\{HB(3,5\text{-}Me_2C_3HN_2)_3\}(NO)I(NHR)]$[5] (0.5 g) and a suspension of AgOCOMe or AgOCOPh (0.75 g) in dichloromethane (100 cm^3) was stirred for 3–4 h, during which time the solution became yellow. After cooling, filtration, addition of petroleum ether or hexane and partial evaporation, a yellow powder precipitated. This was collected by filtration and the product could be recrystallized from dichloromethane–hexane giving a yellow microcrystalline solid (*ca.* 50%).

$[Mo\{HB(3,5\text{-}Me_2C_3HN_2)_3\}(NO)(NHPh)(OCOMe)]$. This complex was prepared as described

above being obtained as an orange–brown powder. The product was recrystallized from CH_2Cl_2–hexane or $CHCl_3$–hexane giving black crystals (0.32 g, 74%).

[Mo{HB(3,5-$Me_2C_3HN_2)_3$}(O)(NHPh)(OCOPh)]. The complex was prepared in the same way as [Mo{HB($Me_2C_3HN_2)_3$}(NO)I(HNR)] giving a maroon solution when the reaction was complete. The products were obtained as fine maroon crystals (0.38 g, 80%).

Crystallographic determination of [Mo{HB(3,5-$Me_2C_3HN_2)_3$} (NO)(NHPh)(OCOMe)]·$2CHCl_3$. Crystals were obtained from chloroform/*n*-hexane mixtures as black blocks. Unit cell and space group were originally investigated photographically and intensity data and accurate cell dimensions subsequently measured with a diffractometer.

Crystal data. $C_{23}H_{31}BN_8O_3Mo \cdot 2CHCl_3$, M = 813.0 (excluding solvent, 574.3). Monoclinic, a = 17.188(4), b = 10.573(3), c = 19.908(18) Å, β = 101.60(4)°, U = 3544 Å^3, Z = 4, Dc = 1.52 g cm^{-3}, $F(000)$ = 1648, space group $P2_1/n$ (non-standard setting of $P2_1/c$ No. 14, C_{2h}^5) Mo-K_α radiation (λ = 0.7107 Å, μ = 7.8 cm^{-1}).

Intensity data. After the preliminary photographic investigations the crystal was mounted on an Enraf-Nonius CAD-4 diffractometer at the Crystallography Unit, Universities of Aston and Birmingham. Accurate cell dimensions and intensity data were obtained by the standard methods described previously.[6] Within the range $2° < 2\theta < 50°$, 3765 independent reflections having $I > 2.5\sigma(I)$ were observed. Two standard reflections, measured every hour, showed no variation with time. Data were corrected for Lorentz and polarization factors but not for absorption.

Structure determination. The structure was solved by conventional Patterson–Fourier techniques. Scattering factors used were those for neutral atoms.[7] The chlorine atoms of the solvent molecules were obvious from the first Fourier map. Refinement by full-matrix least squares methods was performed initially with all atoms vibrating isotropically. After the initial refinement was complete (R = 0.098), anisotropic thermal parameters were introduced for all non-hydrogen atoms and hydrogen atoms in calculated positions included in the structure factor calculations, without refinement, and with two common, isotropic thermal parameters for the methyl and non-methyl hydrogen atoms. The B—H and N—H distances were fixed at 1.11±0.02 Å.

In the final stages, weights derived from counting statistics were employed, with $w = 1.5/\sigma^2(F) + 0.001(F)^2$. This gave a satisfactory analysis of the variation of $w\Delta^2$ with increasing $\sin\theta/\lambda$ and with increasing fractions of $|F_o|$. Final parameter shifts were $< 0.1\sigma$ and the final values of R and R' $\{= [\Sigma w(|F_o| - |F_c|)^2/\Sigma w|F_o|^2]^{1/2}$ were 0.045 and 0.049. The calculations were carried out using the Honeywell Multics system at Birmingham University Computer Centre and a CDC 7600 computer at the University of Manchester Regional Computer Centre, with the program[8] SHELX-76. Final positional parameters, displacement factor coefficients, full lists of bond lengths and angles, and F_o/F_c values have been deposited as supplementary data with the Editor, from whom copies are available on request. Atomic coordinates have also been deposited with the Cambridge Crystallographic Data Centre.

RESULTS AND DISCUSSION

Synthetic studies

The mixed alkoxy carboxylates MoL*(NO)(OR)(OCOR′) (R = Me, Et, Pr^n, Pr^i; R′ = Me; R = Me, Et, Pr^n, Pr^i, CH_2CH_2OH; R′ = Ph) were prepared by refluxing a mixture of MoL*(NO)I(OR) with AgOCOR′ in dichloromethane. The hydroxide MoL*(NO)(OH)(OCOPh) was obtained adventitiously by reaction of MoL*(NO)I_2 with AgOCOPh in an attempt to prepare the bis-benzoate MoL*(NO)$(OCOPh)_2$. It is possible that MoL*(NO)$(OCOPh)_2$ is formed transiently but is hydrolyzed by traces of moisture. In an earlier paper on bis-alkoxides[1] we noted that reactions of MoL*(NO)I_2 with an excess of AgOCOMe and water gave the bis-hydroxide MoL*(NO)$(OH)_2$, although this is a difficult reaction to repeat. These alkoxycarboxylates were purple in solution and as solids, although MoL*(NO)(OCH_2CH_2OH)(OCOMe) was blue.

The yellow aryloxy derivatives MoL*(NO)(OAr)(OCOR) (Ar = Ph, C_6H_4Me-*p*, C_6H_4OMe-*p*; R = Me, Ph) were prepared in the same way as their alkoxy analogues while MoL*(NO)(SPh)(OCOR) (R = Me or Ph) was obtained from MoL*(NO)I(SPh) and were isolated as brown solids.

The amido complexes MoL*(NO)(NHR)(OCOR′) (R = Me, Et; R′ = Me, Ph) were formed by stirring MoL*(NO)I(NHR) with AgOCOR′ in dichloromethane, and were isolated as yellow (R = Me, Ph), orange–brown (R = Ph, R′ = Me) or maroon (R = R′ = Ph) solids.

All complexes were obtained as air-stable crystalline or microcrystalline solids whose analytical data are listed in Table 1.

Table 1. Analytical (%) data obtained from [Mo{HB(Me$_2$pyz)$_3$}(NO)XY]

	X	Y	Calc. C	Calc. H	Calc. N	Found C	Found H	Found N
(1)	OH	OCOPh	47.1	5.0	17.5	46.8	5.0	17.2
(2)	OMe	OCOMe	42.1	5.5	19.1	42.3	5.5	19.4
(3)	OEt	OCOMe	43.3	5.7	18.6	43.5	5.7	18.8
(4)	OPr^i	OCOMe	44.4	5.9	18.1	44.5	5.9	17.8
(5)	OPr^n	OCOMe	44.4	5.9	18.1	44.4	6.2	18.1
(6)	OMe	OCOPh	48.0	5.2	17.0	47.8	5.5	17.0
(7)	OEt	OCOPh	48.9	5.4	16.4	48.8	5.7	16.5
(8)	OPr^i	OCOPh	49.8	5.6	16.2	48.9	5.4	16.3
(9)	OPr^n	OCOPh	49.8	5.6	16.2	49.6	5.4	16.1
(10)	OCH_2CH_2OH	OCOPh	45.6	5.3	16.2	46.0	4.8	16.7
(11)	OPh	OCOMe	48.0	5.2	17.0	47.7	5.3	17.2
(12)	OC_6H_4OMe-*p*	OCOMe	47.6	5.3	16.2	47.7	5.1	15.9
(13)	OC_6H_4Me-*p*	OCOMe	48.9	5.5	16.6	48.6	5.7	16.3
(14)	OC_6H_4OMe-*p*	OCOPh	52.2	5.1	14.7	52.1	4.8	14.5
(15)	SPh	OCOMe	46.7	5.1	16.6	46.5 46.4	5.4 5.3	16.3 16.4
(16)	SPh	OCOPh	51.5	4.9	15.0	51.5	4.8	15.3
(17)	NHMe	OCOMe	42.2	5.7	21.9	42.0	5.9	21.7
(18)	NHEt	OCOMe	43.3	5.7	21.3	43.6	6.0	21.0
(19)	NHMe	OCOPh	48.1	5.4	19.5	48.4	5.7	19.8
(20)	NHEt	OCOPh	49.0	5.6	19.0	48.9	5.7	19.0
(21)	NHPh	OCOMe	48.1	5.4	19.5	48.3	5.7	19.5
(22)	NHPh	OCOPh	52.8	5.2	17.6	52.6	5.3	17.9

Spectroscopic studies

The IR spectra (KBr discs, Table 2) of the new complexes exhibited absorptions typical of tris-(3,5-dimethylpyrazolyl)borates and a strong band due to the NO group. The position of ν(NO) was dependent on the donor atom set X and Y in MoL* (NO)XY. Thus, for the species where X = OR (R = alkyl or aryl) and Y = OCOR′ ν(NO) occurred in the range 1675–1690 cm^{-1}, when X = SPh and Y = OCOR′, ν(NO) = 1690–1692 cm^{-1} and when X = NHR (R = alkyl or Ph), Y = OCOR′ (R′ = Me or Ph) ν(NO) was in the range 1656–1668 cm^{-1}, although MoL*(NO)(NHPh)(OCOMe) had ν(NO) = 1680 cm^{-1}.

In the IR spectrum of MoL*(NO)(OH)(OCOPh), ν(OH) was detected at 3350 cm^{-1} and those complexes containing NHR exhibited ν(NH) in the range 3200–3290 cm^{-1}. The absorptions associated with the carboxylato group in the range 1626–1670 cm^{-1} suggest[6] that the ligand is monodentate and so not chelating. The IR spectra in the range 1000–1200 cm^{-1} were complex due to ligand bands associated with HB(Me$_2$C$_3$HN$_2$)$_3$ and OR, OAr, SPh, NHR or NHAr, and so it was not possible to confirm the nature of the OCOR ligand.

The ^{1}H NMR spectra (Table 3) of the complexes are unexceptional, but serve to confirm our formulation of these complexes. In general, for complexes containing OCH_2R or $NHCH_2R$, the chemical shifts of the protons on the α-C atom resonate at low fields. This effect has been noted many times in this class of compound,[7] and is due to the strongly electron-withdrawing effect of the "electron-poor" MoL*(NO) unit. In those species containing NHR, δ(NH) was detected in the range 12.00–12.36 ppm.

The mass spectra of the new compounds (EI mode, Table 4) in general failed to exhibit a molecular ion, the highest observed *m/e* peaks being either due to [MoL*(OR)(OCOR′)]$^+$ or [MoL*(NO)(OCOR′)]$^+$.

Structure of [Mo{HB(Me$_2$CHN$_2$)$_3$}(NO)(NHPh)(OCOMe)]·2CHCl$_3$. The monodenticity of the acetate group has been confirmed by the structure determination. The asymmetric unit consists of the complex and two solvent molecules (Fig. 1). Selected bond lengths and bond angles are given in Table 4.

The coordination geometry of the molybdenum atom is essentially octahedral with the tripodal pyrazolylborate ligand producing some distortion. The geometries of this ligand and of the phenylamide are unremarkable. The Mo(1)—N(41)—

Table 2. Selected IR spectral data for [M{HB(Me$_2$pyz)$_3$}(NO)XY]

Complex			IR data				
M	X	Y	$\nu_{(NO)}$ cm^{-1}	$\nu_{(CO)}$ cm^{-1}	$\nu_{(Mo-OC)}$ cm^{-1}	$\nu_{(OH)}$ cm^{-1}	$\nu_{(NH)}$ cm^{-1}
Mo	OH	OCOPh	1688	1640	1300, 1315	3350	
W	OH	OCOPh	1670	1628	1300, 1318	3370	
Mo	OMe	OCOMe	1688	1658	1250		
Mo	OEt	OCOMe	1688	1658	1260		
Mo	OPr^i	OCOMe	1688	1658	1250		
Mo	OPr	OCOMe	1688	1658	1260		
W	OMe	OCOMe	1688	1630	1250		
W	OEt	OCOMe	1688	1630	1250		
W	OPr^i	OCOMe	1688	1632	1250		
Me	OMe	OCOPh	1675	1642	1286, 1308		
Mo	OEt	OCOPh	1678	1642	1282, 1308		
Mo	OPr^i	OCOPh	1690	1660	1282, 1308		
Mo	OPr	OCOPh	1680	1650	1280, 1308		
Mo	OCH_2CH_2OH	OCOPh	1680	1646	1280, 1308		
W	OMe	OCOPh	1670	1620	1282, 1318		
W	$OCHMe_2$	OCOPh	1680	1640	1280, 1308		
Mo	OPh	OCOMe	1698	1670	1246		
Mo	OC_6H_4OMep	OCOMe	1688	1660	1248		
Mo	OC_6H_4Mep	OCOMe	1688	1670	1250		
Mo	OC_6H_4OMep	OCOPh	1675	1650	1248, 1282		
Mo	SPh	OCOMe	1632	1660	1250		
Mo	SPh	OCOPh	1690	1650	1252, 1276		
Mo	NHMe	OCOMe	1656	1632	1300		3250
Mo	NHEt	OCOMe	1656	1626	1296		3200
Mo	NHMe	OCOPh	1656	1635	1300, 1325		3255
Mo	NHEt	OCOPh	1668	1640	1300, 1315		3265
Mo	NHPh	OCOMe	1680	1650	1262		3245
Mo	NHPh	OCOPh	1665	1640	1290, 1310		3290
Mo	OCOMe	OCOMe					
Mo	OCOPh	OCOPh					

Spectra measured as KBr discs on PE 297 spectrometer.

C(41) angle of 138.3° and the Mo(1)—N(41) distance of 1.951 Å for this latter ligand are very similar to the corresponding angle of 137.5° and Mo—N distance of 1.945 Å for the *p*-methoxyphenylamide ligand in a closely related complex.[2] The molybdenum-nitrosyl system is linear, with bond lengths very similar to those found previously in bis-alkoxo-complexes.[1]

Table 3. ^{1}H NMR spectral data for [M{HB(Me$_2$pyz)$_3$}(NO)XY]

Complex			^{1}H NMR data				
M	X	Y	δ^a/ppm	A^b			Assignment
Mo	OH	OCOPh	2.14	3	18	(s)	$C_3H(\underline{CH}_3)_2N_2$
			2.26	3		(s)	
			2.38	6		(s)	
			2.41	3		(s)	
			2.44	3		(s)	
			5.71	1	3	(s)	$C_3N_2\underline{H}Me_2$
			5.89	2		(s)	
			7.34	3	5	(m)	$OCOC_6H_5$ (*m*, *p*-H)
			8.00	2		(m)	(O-H)

Table 3—*continued.*

Complex			^{1}H NMR data			
M	X	Y	δ^a/ppm	A^b		Assignment
W	OH	OCOPh	2.19	3	(s)	
			2.31	3	(s)	
			2.37	6 (18)	(s)	$C_3H(\underline{CH}_3)_2N_2$
			2.39	3	(s)	
			2.54	3	(s)	
			5.76	1	(s)	
			5.85	1 (3)	(s)	$C_3\underline{H}Me_2N_2$
			5.88	1	(s)	
			7.31	3 (5)	(m)	$OCOC_6H_5$ (*m*, *p*-H)
			7.96	2	(m)	(O-H)
Mo	OMe	OCOMe	2.14	3	(s)	
			2.18	3	(s)	
			2.34	3 (18)	(s)	$C_3H\underline{Me}_2N_2$
			2.40	6	(s)	
			2.43	3	(s)	
			2.51	3	(s)	$OCO\underline{Me}$
			5.80	3	(s)	$O\underline{Me}$
			5.73	1	(s)	$C_3N_2\underline{H}Me_2$
			5.90	2	(s)	
Mo	OEt	OCOMe	1.54	3	(t)	$OCH_2\underline{CH}_3$, $J = 6.8$ Hz
			2.17	3	(s)	
			2.20	3	(s)	
			2.35	3 (18)	(s)	$C_3H(\underline{CH}_3)_2N_2$
			2.40	6	(s)	
			2.44	3	(s)	
			2.51	3	(s)	$OCO\underline{CH}_3$
			5.74	1	(s)	$C_3N_2\underline{N}Me_2$
			5.30	2	(s)	
			6.14	2	(m)	*AB* pair, OCH_2Me, $J_{AB} = 11$ Hz, $A = 5.87$, $B = 6.42$ ($J_{HH} = 6.8$ Hz)
Mo	OPr^i	OCOMe	1.38	3	(d)	$OCH(\underline{CH}_3)_2$, $J_{HH} = 6$ Hz
			1.61	3	(d)	
			2.11	3	(s)	
			2.22	3	(s)	
			2.37	3 (18)	(s)	$C_3H(\underline{CH}_3)_2N_2$
			2.38	6	(s)	
			2.42	3	(s)	
			2.50	3	(s)	
			5.73	1	(s)	$OCO\underline{CH}_3$
			5.85	1	(s)	$C_3N_2\underline{H}Me_2$
			5.88	1	(s)	
			6.55	1	(m)	$OCHMe_2$, $J_{HH} = 6$ Hz
Mo	OPr	OCOMe	1.02	3	(t)	$OCH_2CH_2\underline{CH}_3$, $J_{HH} = 7.6$ Hz
			ca. 1.91	2	(m)	$OCH_2\underline{CH}_2CH_3$
			2.15	3	(s)	
			2.18	3	(s)	
			2.34	3	(s)	$C_3H(CH_3)_2N_2$
			2.39	6	(s)	
			2.42	3	(s)	
			2.51	3	(s)	$OCO\underline{CH}_3$

Table 3—*continued.*

Complex			^{1}H NMR data			
M	X	Y	δ^a/ppm	A^b		Assignment
			6.02	2	(m)	*AB* pair, O<u>CH</u>$_2$CH, $\delta_A = 5.76$, $\delta_B = 6.26$
			5.72	1 } 3	(s) }	$C_3N_2\underline{H}Me_2$
			5.88	2 }	(s) }	
W	OMe	OCOMe	2.17	3	(s)	$C_3H(\underline{CH}_3)_2N_2$
			2.19	3	(s)	
			2.32	3	(s)	
			2.36	6	(s)	
			2.62	3	(s)	
			2.50	3	(s)	$OCOCH_3$
			5.66	3	(s)	OCH_3
			5.76	1 }	(s) }	$C_3\underline{H}Me_2N_2$
			5.88	2 }	(s) }	
W	OEt	OCOMe	1.42	3	(t)	$OCH_2\underline{CH}_3$, $J_{HH} = 6.8$ Hz
			2.12	3	(s)	$C_3H(\underline{CH}_3)_2N_2$
			2.23	3 } 18	(s)	
			2.35	9 }	(s)	
			2.61	3	(s)	
			2.49	3	(s)	$OCO\underline{CH}_3$
			5.76	1 } 3	(s) }	$C_3HMe_2N_2$
			5.88	2 }	(s) }	
			6.1	2	(br. m)	OCH_2Me
W	OPr^i	OCOMe	1.29	3	(d)	$OCH(\underline{CH}_3)_2$, $J_{HH} = 6$ Hz
			1.55	3	(d)	
			2.10	3	(s)	$C_3H(\underline{CH}_3)_2Ne$
			2.29	3 } 18	(s)	
			2.39	9 }	(s)	
			2.63	3	(s)	
			2.50	3	(s)	$OCO\underline{CH}_3$
			5.79	1	(s)	$C_3\underline{H}Me_2N_2$
			5.86	1 } 3	(s)	
			5.90	1	(s)	
			6.38	1	(m)	$O\underline{CH}Me_2$, $J_{HH} = 6$ Hz
Mo	OMe	OCOPh	2.08	3	(s)	$C_3H(\underline{CH}_3)_2N_2$
			2.24	3	(s)	
			2.40	6 } 18	(s)	
			2.42	3	(s)	
			2.55	3	(s)	
			5.72	1	(s)	$C_3N_2\underline{H}Me_2$
			5.84	1 } 3	(s)	
			5.92	1	(s)	
			5.89	3	(s)	$O\underline{CH}_3$
			7.32	3 } 5	(m) }	$OCOC_6\underline{H}_5$ (*m*, *p*-H)
			8.01	2 }	(m) }	(O-H)
Mo	OEt	OCOPh	1.55	3	(t)	$OCH_2\underline{CH}_3$, $J_{HH} = 7$ Hz
			2.11	3	(s)	$C_3H(CH_3)_2N_2$
			2.22	3 } 18	(s)	
			2.40	9 }	(s)	
			2.53	3	(s)	
			5.73	1	(s)	$C_3N_2\underline{H}Me_2$
			5.80	1 } 3	(s)	
			5.90	1	(s)	
			6.23	2	(m)	*AB* pair, $J_{AB} = 11$ Hz, $\delta_A = 5.94$, $\delta_B = 5.62$

Table 3—*continued.*

Complex			^{1}H NMR data			
M	X	Y	δ^a/ppm	A^b		Assignment
			7.32	3	(m)	$OCOC_6\underline{H}_5$ (*m, p*-H)
			8.00	2	(m)	$OCOC_6\underline{H}_5$ (O-H)
Mo	OPr^i	OCOPh	1.39	3	(d)	$OCH(\underline{CH}_3)_2$
			1.63	3	(d)	$OCH(\underline{CH}_3)_2$
			2.15	3	(s)	$C_3H(\underline{CH}_3)_2N_2$
			2.22	3	(s)	$C_3H(\underline{CH}_3)_2N_2$
			2.38	3	(s)	$C_3H(\underline{CH}_3)_2N_2$
			2.41	6	(s)	$C_3H(\underline{CH}_3)_2N_2$
			2.53	3	(s)	$C_3H(\underline{CH}_3)_2N_2$
			5.74	2	(s)	$C_3N_2\underline{H}Me_2$
			5.88	1	(s)	$C_3N_2\underline{H}Me_2$
			6.63	1	(m)	$O\underline{CH}(CH_3)_2$
			7.30	3	(m)	$OCOC_6\underline{H}_5$ (*m, p*-H)
			7.95	2	(m)	$OCOC_6\underline{H}_5$ (O-H)
Mo	OPr	OCOPh	1.02	3	(t)	$OCH_2CH_2\underline{CH}_3$, J_{HH} = 7.8 Hz
			ca. 1.93	2	(m)	$OCH_2\underline{CH}_2CH_3$
			2.12	3	(s)	$C_3H(\underline{CH}_3)_2N$
			2.22	3	(s)	$C_3H(\underline{CH}_3)_2N$
			2.41	9	(s)	$C_3H(\underline{CH}_3)_2N$
			2.55	3	(s)	$C_3H(\underline{CH}_3)_2N$
			5.74	1	(s)	$C_3N_2\underline{H}Me_2$
			5.81	1	(s)	$C_3N_2\underline{H}Me_2$
			5.91	1	(s)	$C_3N_2\underline{H}Me_2$
			6.11	2		*AB* pair, $O\underline{CH}_2CH_2Me$ δ_A = 5.86, δ_B = 6.38
			7.30	3	(m)	$OCOC_6\underline{H}_6$ (*m, p*-H)
			7.95	2	(m)	$OCOC_6\underline{H}_6$ (O-H)
Mo	OCH_2CH_2OH	OCOPh	2.402	6	(s)	$C_3H(\underline{CH}_3)_2N$
			2.380	3	(s)	$C_3H(\underline{CH}_3)_2N$
			2.349	3	(s)	$C_3H(\underline{CH}_3)_2N$
			2.183	3	(s)	$C_3H(\underline{CH}_3)_2N$
			2.176	3	(s)	$C_3H(\underline{CH}_3)_2N$
			5.786	1	(s)	$C_3N_2\underline{H}Me_2$
			5.619	1	(s)	$C_3N_2\underline{H}Me_2$
			5.459	1	(s)	$C_3N_2\underline{H}Me_2$
			ca. 6.16	2		*AB* pair, $O\underline{CH}_2CH_2OH$ δ_A = 5.80, δ_B = 6.52
			ca. 2.45—2.15	*ca.* 2		OCH_2CH_2OH, lying under protons
					(m)	$OCOC_6\underline{H}_5$ (*m, p*-H)
					(m)	$OCOC_6\underline{H}_5$ (O-H)
W	OMe	OCOPh	2.12	3	(s)	$C_3H(\underline{CH}_3)_2N_2$
			2.20	3	(s)	$C_3H(\underline{CH}_3)_2N_2$
			2.29	3	(s)	$C_3H(\underline{CH}_3)_2N_2$
			2.31	3	(s)	$C_3H(\underline{CH}_3)_2N_2$
			2.54	3	(s)	$C_3H(\underline{CH}_3)_2N_2$
			2.65	3	(s)	$C_3H(\underline{CH}_3)_2N_2$
			5.76	3	(s)	OMe
			5.80	1	(s)	$C_3HMe_2\underline{N}_2$
			5.85	1	(s)	$C_3HMe_2\underline{N}_2$
			5.90	1	(s)	$C_3HMe_2\underline{N}_2$
			7.30	3	(m)	$OCOC_6\underline{H}_5$ (*m, p*-H)
			7.96	2	(m)	$OCOC_6\underline{H}_5$ (O-H)

Table 3—*continued.*

Complex			^{1}H NMR data			
M	X	Y	δ^a/ppm	A^b		Assignment
W	OPr^i	OCOPh	1.29	3	(d)	$OCH(\underline{CH_3})_2$, J_{HH} = 6 Hz
			1.59	3	(d)	
			2.21	3	(s)	$C_3H(\underline{CH_3})_2N_2$
			2.30	3	(s)	
			2.36	3	(s)	
			2.38	3	(s)	
			2.40	3	(s)	
			2.66	3	(s)	
			5.74	1	(s)	$C_3HMe_2N_2$
			5.79	1	(s)	
			5.90	1	(s)	
			6.47	1	(m)	$O\underline{C}HMe_2$, J_{HH} = 6 Hz
			7.30	3	(m)	$OCOC_6H_5$ (*m*, *p*-H)
			7.96	2	(m)	(O-H)
Mo	OPh	OCOMe	2.04	3	(s)	$C_3H(\underline{CH}_3)_2N_2$
			2.13	3	(s)	
			2.19	3	(s)	
			2.42	9	(s)	
			2.49	3	(s)	$OCO\underline{CH}_3$
			5.74	1	(s)	$C_3N_2\underline{H}Me_2$
			5.83	1	(s)	
			5.93	1	(s)	
			7.25	5	(m)	$O\underline{C_6H_5}$
Mo	OC_6H_4OMep	OCOMe	2.04	3	(s)	$C_3H(\underline{CH}_3)_2N_2$
			2.11	3	(s)	
			2.16	3	(s)	
			2.40	9	(s)	
			2.48	3	(s)	$OCO\underline{CH}_3$
			3.80	3	(s)	*p*-$\underline{CH}_3OC_6H_4O$
			5.72	1	(s)	$C_3N_2\underline{H}Me_2$
			5.80	1	(s)	
			5.91	1	(s)	
			7.14	4	(m)	*p*-$MeOC_6H_4O$, A_2B_2 pair, δ_A = 6.87, δ_B = 7.41, J_{AB} = 9 Hz
Mo	OC_6H_4Me-*p*	OCOMe	2.06	3	(s)	$C_3H(\underline{CH}_3)_2N_2$ and *p*-$\underline{CH}_3C_6H_4O$
			2.12	3	(s)	
			2.17	3	(s)	
			2.42	12	(s)	
			2.50	3	(s)	$OCO\underline{CH}_3$
			5.74	1	(s)	$C_3N_2HMe_2$
			5.83	1	(s)	
			5.93	1	(s)	
			7.26	4	(m)	OC_6H_4Mep, A_2B_2 pair, δ_A = 7.427, δ_B = 7.093 J_{AB} = 9 Hz
Mo	OC_6H_4OMep	OCOPh	2.06	3	(s)	$C_3H(\underline{CH}_3)_2N_2$
			2.09	3	(s)	
			2.30	3	(s)	
			2.43	9	(s)	
			3.81	3	(s)	*p*-$CH_3OC_6H_4O$
			5.74	1	(s)	$C_3N_2\underline{H}Me_2$
			5.83	2	(s)	

Table 3—*continued.*

Complex			^{1}H NMR data			
M	X	Y	δ^a/ppm	A^b		Assignment
			7.26	4	(m)	*p*-MeOC$_6$H$_4$O, A_2B_2 pair, $\delta_A = 6.94$, $\delta_B = 7.58$, $J_{AB} = 9$ Hz
			7.37	3	(m)	OCOC$_6$H$_5$ (*p*, *m*-H)
			8.02	2	(m)	OCOC$_6$H$_5$ (O-H)
Mo	SPh	OCOMe	2.07	3	(s)	$C_3H(\underline{CH}_3)_2N_2$
			2.12	3	(s)	
			2.29	3	(s)	
			2.38	6	(s)	
			2.42	3	(s)	
			2.44	3	(s)	$OCO\underline{CH}_3$
			5.76	1	(s)	$C_3N_2\underline{H}Me_2$
			5.86	2	(s)	
			7.36	3	(m)	$S\underline{C}_6\underline{H}_5$ (*m*, *p*-H)
			7.91	2	(m)	SC_6H_5 (O-H)
Mo	SPh	OCOPh	2.11	3	(s)	$C_3H(\underline{CH}_3)_2N_2$
			2.21	3	(s)	
			2.24	3	(s)	
			2.40	6	(s)	
			2.49	3	(s)	
			5.78	2	(s)	$C_3N_2\underline{H}Me_2$
			5.86	1	(s)	
			7.40	6	(m)	$S\underline{C}_6\underline{H}_5$, $OCO\underline{C}_6\underline{H}_5$ (*m*, *p*-H)
			8.04	4	(m)	$S\underline{C}_6\underline{H}_5$, $OCO\underline{C}_6\underline{H}_5$ (O-H)
Mo	NHMe	OCOMe	2.06	3	(s)	$C_3H(\underline{CH}_3)_2N_2$
			2.19	3	(s)	
			2.32	3	(s)	
			2.36	6	(s)	
			2.43	3	(s)	
			2.45	3	(s)	$OCO\underline{CH}_3$
			4.66	3	(d)	$NH\underline{CH}_3$, $J_{HH} = 8$ Hz
			5.80	3	(s)	$C_3N_2\underline{H}Me_2$
			12.14	(1)	(br)	$N\underline{H}CH_3$
Mo	NHEt	OCOMe	1.32	(3)	(t)	$NHCH_2\underline{CH}_3$, $J_{HH} = 7$ Hz
			2.05	3	(s)	$C_3H(\underline{CH}_3)_2N_2$
			2.21	3	(s)	
			2.32	3	(s)	
			2.36	6	(s)	
			2.44	3	(s)	
			2.45	3	(s)	$OCOCH_3$
			4.73	1	(m)	*AX* pair $NH\underline{CH}_2CH_3$, $J_{HH} = 7$ Hz
			5.48	1	(m)	
			5.81	3	(s)	$C_3N_2\underline{H}Me_2$
			12.01	1	(br)	$N\underline{H}CH_2CH_3$
Mo	NHMe	OCOPh	2.09	3	(s)	$C_3H(\underline{CH}_3)_2N_2$
			2.29	3	(s)	
			2.38	6	(s)	
			2.40	3	(s)	
			2.48	3	(s)	
			4.74	3	(d)	$NH\underline{CH}_3$, $J_{HH} = 7, 8$ Hz
			5.78	2	(s)	$C_3N_2\underline{H}Me_2$
			5.82	1	(s)	

Table 3—*continued.*

Complex			^{1}H NMR data			
M	X	Y	δ^a/ppm	A^b		Assignment
			7.28	3 } 5	(m) }	$OCOC_6\underline{H}_5$ (p, m-H)
			7.93	2 }	(m) }	$OCOC_6\underline{H}_5$ (O-H)
			12.18	1	(br)	$N\underline{H}Me$
Mo	NHEt	OCOPh	1.35	3	(t)	$NHCH_2\underline{CH}_3$, $J_{HH} = 7$ Hz
			2.16	3	(s)	
			2.27	3	(s)	
			2.38	6 } 18	(s)	$C_3H(\underline{CH}_3)_2N_2$
			2.41	3	(s)	
			2.47	3	(s)	
			4.73	1 } 2	(m) }	*AB* pair $NH\underline{CH}_2CH_3$
			5.55	1 }	(m) }	complex multiplets
			5.75	1	(s)	
			5.80	1 } 3	(s)	$C_3N_2\underline{H}Me_2$
			5.82	1	(s)	
			7.25	(3)	(m)	$OCOC_6H_5$ (m, p-H)
			7.92	(2)	(m)	$OCOC_6H_5$ (O-H)
			12.03	(1)	(br)	$N\underline{H}Et$
Mo	NHPh	OCOMe	1.99	3	(s)	
			2.08	3	(s)	
			2.22	3 } 18	(s)	$C_3H(\underline{CH}_3)_2N_2$
			2.37	6	(s)	
			2.41	3	(s)	
			2.54	3	(s)	$OCO\underline{CH}_3$
			5.73	1 } 3	(s) }	$C_3N_2\underline{H}Me_2$
			5.86	2 }	(s) }	
			7.22	3 } 5	(m) }	$NHC_6\underline{H}_5$ (m, p-H)
			7.70	2 }	(m) }	$NHC_6\underline{H}_5$ (O-H)
			12.36	1	(br)	$N\underline{H}Ph$
Mo	NHPh	OCOPh	2.05	3	(s)	
			2.17	3	(s)	
			2.41	9 } 18	(s)	$C_3H(\underline{CH}_3)_2N_2$
			2.48	3	(s)	
			2.78	1	(s)	
			2.81	1 } 3	(s)	$C_3N_2\underline{H}Me_2$
			2.88	1	(s)	
			7.32	6	(m)	$NHC_6\underline{H}_5$, $OCOC_6\underline{H}_5$
			7.82	2	(m)	$NHC_6\underline{H}_5$ (O-H)
			7.97	2	(m)	$OCOC_6\underline{H}_6$ (O-H)

The acetate ligand is monodentate, with no possible interaction for the terminal oxygen, for which the Mo(1)—O(2) distance is 3.284 Å compared with Mo(1)—O(3) of 2.044 Å for the bonded oxygen atom. The acetate ligand shows the expected lengthening of the coordinated C—O bond to 1.295 Å compared with the terminal C—O bond of 1.193 Å. The Mo—O—C angle of 128.8° is similar to the corresponding angles in the bis-alkoxo complexes[1] (129–133°). In these complexes the average Mo—O and O—C distances are 1.902 and 1.417 Å, compared with 2.044 and 1.295 Å in the acetate complex. This can be rationalized by considering more multiple bond character between the molybdenum and oxygen atoms in the former, and between the carbon and oxygen atoms in the latter case, with a corresponding balance in the other bond.

Table 4. Selected bond distances (Å) and angles (°) with estimated standard deviations in parentheses

(a) Coordination sphere and nitrosyl ligand			
Mo(1)—O(3)	2.044(5)	Mo(1)—N(11)	2.181(5)
Mo(1)—N(1)	1.763(6)	Mo(1)—N(21)	2.205(4)
Mo(1)—N(41)	1.951(5)	Mo(1)—N(31)	2.231(5)
N(1)—O(1)	1.201(8)		
O(3)—Mo(1)—N(1)	96.8(2)	N(11)—Mo(1)—N(21)	79.6(2)
O(3)—Mo(1)—N(41)	101.6(2)	N(11)—Mo(1)—N(31)	86.6(2)
N(1)—Mo(1)—N(41)	96.4(2)	N(21)—Mo(1)—N(31)	83.6(2)
O(3)—Mo(1)—N(21)	85.6(2)	N(1)—Mo(1)—N(21)	96.6(2)
O(3)—Mo(1)—N(31)	82.4(2)	N(41)—Mo(1)—N(11)	96.4(2)
N(1)—Mo(1)—N(11)	94.1(2)	N(4)—Mo(1)—N(31)	83.6(2)
Mo(1)—N(1)—O(1)	178.8(5)		
(b) Tris(3,5-dimethylpyrazolyl)borate ligand			
N(11)—N(12)	1.371(7)	B(1)—N(12)	1.543(9)
N(21)—N(22)	1.389(7)	B(1)—N(22)	1.552(9)
N(31)—N(32)	1.379(7)	B(1)—N(32)	1.547(10)
min. C—N	1.336(8)	max. C—N	1.355(9)
mean C—N	1.347(8)	min. C—C (ring)	1.366(11)
max. C—C (ring)	1.398(10)	mean C—C (ring)	1.379(10)
min. C—C (subst.)	1.484(10)	max. C—C (subst.)	1.502(10)
mean C—C (subst.)	1.493(10)		
Mo(1)—N(11)—N(12)	120.1(4)	Mo(1)—N(21)—N(22)	119.5(4)
Mo(1)—N(31)—N(32)	119.3(4)	N(12)—B(1)—N(22)	108.3(5)
N(12)—B(1)—N(32)	109.1(5)	N(22)—B(1)—N(32)	109.4(6)
N(12)—N(11)—C(12)	106.3(5)	N(22)—N(21)—C(22)	106.2(4)
N(32)—N(31)—C(32)	106.7(5)	N(11)—N(12)—C(14)	109.9(5)
N(21)—N(22)—C(24)	109.6(5)	N(31)—N(32)—C(34)	109.8(5)
C(12)—C(13)—C(14)	107.3(7)	C(22)—C(23)—C(24)	106.5(6)
C(32)—C(33)—C(34)	106.8(7)	min. C (subst.)—C—C	127.9(7)
max. C (subst.)—C—C	129.7(7)	mean C (subst.)—C—C	128.8(7)
(c) Phenylamide ligand			
N(41)—C(41)	1.410(7)	min. C—C	1.373(12)
Max. C—C	1.388(11)	mean C—C	1.379(11)
Mo(1)—N(41)—C(41)	138.3(4)	N(41)—C(41)—C(42)	119.6(6)
N(41)—C(41)—C(46)	121.2(5)	min. C—C—C	119.2(5)
max. C—C—C	120.6(7)	mean C—C—C	120.0(7)
(d) Acetate ligand			
C(1)—C(2)	1.476(13)	C(2)—O(2)	1.193(10)
C(2)—O(3)	1.295(8)		
Mo(1)—O(3)—C(2)	128.8(5)	O(3)—C(2)—C(1)	115.3(7)
O(3)—C(2)—O(2)	123.7(8)	C(1)—C(2)—O(2)	120.9(8)
(e) Chloroform molecules			
min. C—Cl	1.686(8)	max. C—Cl	1.749(9)
mean C—Cl	1.723(9)		
min. Cl—C—Cl	109.5(5)	max. Cl—C—Cl	111.5(5)
mean Cl—C—Cl	110.4(5)		

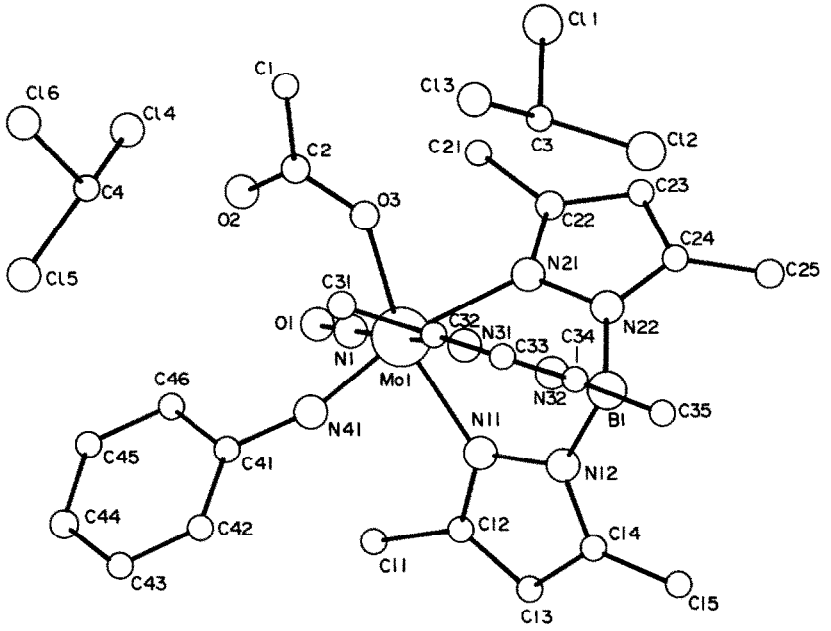

Fig. 1. The molecular structure of $Mo\{HB(3,5\text{-}Me_2C_3HN_2)_3\}(NO)(NHPh)(OCOMe)\cdot 2CHCl_3$ showing the atom numbering.

The geometry of the two independent chloroform solvent molecules is normal and they have no short contacts to the complex.

Acknowledgements—We are grateful to Messrs M. Tolley, A. Pemberton and T. Green for technical assistance, to the SERC for financial support and to the Institute of Physical Chemistry and Chemical Engineering, Politechnika Krakowska, Poland, for leave of absence (A.W.). We thank the staff of the University of Birmingham Computer Center for their assistance.

REFERENCES

1. J. A. McCleverty, A. E. Rae, I. Wolochowicz, N. A. Bailey and J. M. A. Smith, *J. Chem. Soc., Dalton Trans.* 1982, 951.
2. J. A. McCleverty, G. Denti, S. J. Reynolds, A. S. Drane, N. El Murr, A. E. Rae, N. A. Bailey, H. Adams and J. M. A. Smith, *J. Chem. Soc., Dalton Trans.* 1983, 81.
3. G. Denti, J. A. McCleverty and A. Wlodarczyk, *J. Chem. Soc., Dalton Trans.* 1981, 2021.
4. J. A. McCleverty, A. S. Drane, N. A. Bailey and J. M. A. Smith, *J. Chem. Soc., Dalton Trans.* 1983, 91.
5. J. A. McCleverty, A. E. Rae, I. Wolochowicz, N. A. Bailey and J. M. A. Smith, *J. Chem. Soc., Dalton Trans.* 1982, 429.
6. A. J. Edwards and K. I. Khallow, *J. Chem. Soc., Dalton Trans.* 1981, 1898.
7. *International Tables for X-ray Crystallography*, Vol. 4. Kynoch Press, Birmingham (1974).
8. SHELX 76, Program for crystal structure determination. G. M. Sheldrick, Cambridge University (1976).

Polyhedron Vol. 7, No. 2, pp. 117–128, 1988
Printed in Great Britain

0277–5387/88 $3.00+.00
© 1988 Pergamon Journals Ltd

ORGANOIMIDO COMPLEXES OF TUNGSTEN AND RHENIUM: OXO-IMIDO AND BIS-IMIDO COMPLEXES OF TUNGSTEN(VI), AND PHENYLIMIDO COMPLEXES OF RHENIUM(VI) AND (V). THE X-RAY CRYSTAL STRUCTURES OF $[W(NCMe_3)(NPh)Cl_2(bipy)]$ AND $[Re(NPh)Cl_3(NH_2CMe_3)_2]$

GEORGE R. CLARK, ALASTAIR J. NIELSON* and CLIFTON E. F. RICKARD

Department of Chemistry, University of Auckland, Private Bag, Auckland, New Zealand

(*Received* 28 *April* 1987; *accepted* 24 *August* 1987)

Abstract—Reaction of Me_3CNH_2 or $Me_3SiNHCMe_3$ with $WOCl_4$ gives a mixture containing $[W(O)(NCMe_3)Cl_2(NH_2CMe_3)]_x$ which on further reaction with 2,2′-bipyridyl (bipy) gives $[W(NCMe_3)_2Cl_2(bipy)]$ and insoluble oxo complexes. Reaction of $WOCl_4$ with *p*-$MeC_6H_4N(SiMe_3)_2$ and then bipy gives $[W(NC_6H_4Me\text{-}p)_2Cl_2(bipy)]$ and $[W(O)(NC_6H_4Me\text{-}p)Cl_2(bipy)]$; $[W(NPh)Cl_4]_2$ reacts with *p*-$MeC_6H_4N(SiMe_3)_2$ and then bipy to give $[W(NPh)(NC_6H_4Me\text{-}p)Cl_2(bipy)]$. $[W(NCMe_3)(\mu\text{-}NPh)Cl_2(NH_2CMe_3)]_2$ and bipy give $[W(NCMe_3)(NPh)Cl_2(bipy)]$ (**6**). $ReOCl_4$ reacts with PhNCO to give $[Re(NPh)Cl_4]_x$ which in tetrahydrofuran (THF) or MeCN give the adducts $[Re(NPh)Cl_4(THF)]$ and $[Re(NPh)Cl_4(MeCN)]$. $[Re(NPh)Cl_4]_x$ reacts with Me_4NCl to give $[Me_4N][Re(NPh)Cl_5]$, with PPh_3 to give $[Re(NPh)Cl_3(PPh_3)_2]$ and with $Me_3SiNHCMe_3$ gives $[Re(NPh)Cl_3(NH_2CMe_3)_2]$ (**12**). The complexes were characterized by elemental analysis, IR, ^1H and ^{13}C NMR spectroscopy. The structures of $[W(NCMe_3)(NPh)Cl_2(bipy)]$ (**6**) and $[Re(NPh)Cl_3(NH_2CMe_3)_2]$ (**12**) were determined by single-crystal X-ray diffraction methods. Crystals of (**6**) are orthorhombic, space group $P2_12_12_1$, with $a = 8.879(3)$ Å, $b = 13.036(3)$ Å, $c = 18.837(4)$ Å; crystals of (**12**) are orthorhombic, space group *Pbcn* with $a = 14.140(1)$ Å, $b = 11.806(1)$, Å, $c = 11.936(3)$ Å. Both structures were solved by Patterson and Fourier methods and refined to *R* values of 0.053 for the 2138 observed data for (**6**) and 0.035 for the 1108 observed data for (**12**). In complex (**6**) the tungsten atom is in a distorted octahedral environment comprising *cis*-*t*-butylimido and phenylimido groups, *trans* chlorides and bidentate bipy. The bipy nitrogens lie *trans* to the imido functions. Observed distances are: $W—N_{phenylimido}$ 1.774(8) Å, $W—N_{t\text{-}butylimido}$ 1.754(10) Å, W—Cl 2.412(3) and 2.390(3) Å and $W—N_{bipy}$ 2.312(10) Å and 2.333(9) Å. Interaction between the *t*-butylimido methyl groups and bipy is relieved by lengthening of one $W—N_{bipy}$ bond. In complex (**12**) the rhenium atom is in a distorted octahedral environment comprising three chloride ligands, two *trans*-*t*-butylamine ligands and a phenylimido ligand. Observed distances are: $Re—N_{phenylimido}$ 1.709(11) Å, $Re—N_{t\text{-}butylamine}$ 2.187(7) Å, and Re—Cl 2.404(2) and 2.411(5) Å. The complex attains an 18-electron count without π-bonding from the chloro ligands.

Recent interest in organoimido transition-metal chemistry has focussed on those complexes which contain a second multiple-bonded ligand.[1] Variations in the bonding mode of the imido ligand can occur in these complexes when an 18-electron count is exceeded and this is expected to increase the reactivity at the nitrogen atom.[2] We have recently shown that a variety of tungsten bis-organoimido complexes can be prepared from $[W(NR)Cl_4]_2$ (R = Ph, $CHMe_2$, Me) and the silylamines Me_3SiNHR' (R′ = Ph, CMe_3, $CHMe_2$, CH_2Me)[3,4] and that bis-*t*-butylimido complexes result when WCl_6 is reacted with $Me_3SiNHCMe_3$.[3,5] Routes to complexes con-

*Author to whom correspondence should be addressed.

taining terminal oxo and organoimido ligands are however not well developed. Apart from the osmium series $[Os(O)_x(NR)_{4-x}]$,[6] only $[Mo(O)(NH)Cl_2(OPPhEt_2)_2]$[7] and $[Mo(O)(NPh)(S_2CNEt_2)_2]$[8] have been reported. However, several complexes which contain a terminal organoimido ligand and a bridging oxo ligand are known.[9–12] We report here the preparation of oxo-imido and bis-imido complexes of tungsten(VI) and some mono-imido rhenium complexes prepared during attempts to establish a route to bis-imido complexes of this metal.

RESULTS AND DISCUSSION

Tungsten complexes

When $WOCl_4$ was reacted with *t*-butylamine in benzene a yellow non-crystalline solid was formed which analysed as $[W(O)(NCMe_3)Cl_2(NH_2CMe_3)] \cdot \frac{1}{4}C_6H_6$ (**1**) (Table 1). However, the ^{13}C NMR spectrum (Table 2) showed resonances characteristic of *t*-butylamido ligands as well as *t*-butylimido and *t*-butylamine ligands while the IR spectrum showed bands in the 100–700 cm^{-1} region attributable to oxo bridges.[13] Thus the product isolated appeared to be a mixture of the polymeric species $[W(O)(NCMe_3)Cl_2(NH_2CMe_3)]_x$ and $[W(O)(NHCMe_3)_2Cl_2]_x$. When the mixture was reacted with 2,2′-bipyridyl (bipy) in benzene, the known *bis-t*-butylimido complex $[W(NCMe_3)_2Cl_2(bipy)]$ (**2**)[5] was formed, together with a yellow insoluble oxo species which we have been unable as yet to obtain in a pure state.

Addition of two equivalents of $Me_3SiNHCMe_3$ to $WOCl_4$ in benzene again led to a yellow non-crystalline solid (**1a**) for which analytical figures were inconclusive. However, the spectral characteristics of the complex were similar to (**1**) and, on reaction with bipy an insoluble oxo species and $[W(NCMe_3)_2Cl_2(bipy)]$ (**2**) were formed. The reactions thus suggest that oxo-imido exchange occurs when bipy is reacted with the polymeric mixture formed from $WOCl_4$ and the amine or silylamine reagents, but as yet we have not been able to determine the complete nature of the reaction. IR spectra of the crude soluble products in the bipy reaction indicated further oxo products are formed along

Table 1. Physical data

Complex	Colour	m.p. (°)[a]	Analytical data[b] C	H	N	IR data[c] M—Cl (cm^{-1})
$[\{W(O)(NCMe_3)Cl_2(NH_2CMe_3)\} \cdot \frac{1}{4}C_6H_6]_x$ (**1**)[d]	yellow	—	26.6 (26.3)	5.4 (5.0)	6.6 (6.5)	370, 342 318, 290
$[W(NCMe_3)_2Cl_2(bipy)]$ (**2**)	yellow	245	39.2 (39.1)	4.7 (4.7)	10.2 (10.1)	305
$[W(O)(NC_6H_4Me\text{-}p)Cl_2(bipy)]$ (**3**)	yellow	> 265d	38.1 (38.4)	3.5 (2.8)	7.4 (7.9)	318
$[W(NPh)(NC_6H_4Me\text{-}p)Cl_2(bipy)]$ (**5**)	dark red	210–213	41.6 (41.9)	3.9 (3.9)	9.4 (9.8)	312, 304
$[W(NCMe_3)(NPh)Cl_2(bipy)]$ (**6**)	dark red	218–220	45.8 (45.5)	3.9 (3.3)	9.5 (9.2)	322, 303
$[Re(NPh)Cl_4]_2 \cdot \frac{1}{3}C_6H_6$ (**7**)	dark brown	d[e]	18.7 (18.3)	1.5 (1.3)	3.5 (3.3)	375, 352 340, 275
$[Re(NPh)Cl_4(THF)]$ (**8**)	green–brown	d[e]	24.2 (24.5)	3.1 (2.7)	3.2 (2.9)	330
$[Re(NPh)Cl_4(NCMe)]$ (**9**)	yellow–brown	> 165d	21.3 (20.9)	2.3 (1.8)	6.2 (6.1)	335
$[Re(NPh)Cl_5][NMe_4]1.5MeCN$ (**10**)	brown	> 160d	26.0 (26.4)	3.5 (3.7)	8.2 (8.3)	330, 275
$[Re(NPh)Cl_3(PPh_3)_2]$ (**11**)	green	215–218	56.1 (55.5)	4.3 (3.9)	1.6 (1.5)	300, 280

[a] d = decomposition point.
[b] Calculated figures in parentheses.
[c] Spectra obtained as nujol mulls between caesium iodide plates.
[d] Benzene solvate supported by ^1H and ^{13}C NMR spectra.
[e] Decomposition point not determined due to colour.

Table 2. NMR spectra

Complex	^{13}C NMR[a,b]	^{1}H NMR[a,b,c]
$[\{W(O)(NCMe_3)Cl_2(NH_2CMe_3)\}\cdot\frac{1}{4}C_6H_6]_x$ (**1**)[d]	27.9, 30.0, 31.3 and 32.3 (Me_3); 53.5 (NH_2C); 61.7 and 62.8 (NHC); 72.5 (NC); 128.4 (C_6H_6).	1.33–1.84 (several s, Me_3); 7.32 (s, C_6H_6).
$[W(NCMe_3)_2Cl_2(bipy)]$ (**2**)	32.0 (Me_3); 67.8 (N—C), ^{183}W satellites at 66.8 and 68.8, $^2J_{WC}$ = 14.4 Hz; 122.0 and 125.9 (β-CHs, bipy); 139.4 (γ-CHs, bipy); 150.6 (α-Cs, bipy); 152.5 (α-CHs, bipy).	1.58 (s, 18H, $2CMe_3$); 7.08–7.65 (m, 2H, γ-Hs, bipy); 7.64–8.04 (m, 4H, β-Hs, bipy); 9.75 (d, 2H, α-Hs, bipy).
$[W(O)(NCMe_3)Cl_2(NH_2CMe_3)]\cdot\frac{1}{3}C_6H_6$ (**1a**)	28.2, 29.8 and 32.2 (Me_3); 54.4 (NH_2C); 62.6 (NH_2C); 72.5 (NC); 128.5 (C_6H_6).	1.34–1.75 (bs, Me_3); 7.1–7.5 (b, NH); 7.35 (s, C_6H_6).
$[W(NC_6H_4Me\text{-}p)_2Cl_2(bipy)]$ (**4**)	21.0 (Me); 122.0 and 126.7 (β-CH, bipy); 123.8 (*ortho*-CHs, NC_6H_4Me-*p*); 128.7 (*meta*-CHs, NC_6H_4Me-*p*); 134.6 (*para*-C, NC_6H_4Me-*p*); 140.0 (γ-CHs, bipy); 151.0 (α-Cs, bipy); 153.1 (α-CHs, bipy); 154.2 (*ipso*-C, NC_6H_4Me-*p*).	2.38 (s, 6H, 2Me); 6.95–7.30 (m, 8H, *ortho*- and *meta*-CHs, NC_6H_4Me-*p*); 7.35–7.58 (m, 2H, γ-Hs, bipy); 7.80–8.08 (m, 4H, β-HS, bipy); 9.40 (d, 2H, α-HS, bipy).
$[W(NPh)(NC_6H_4Me\text{-}p)Cl_2(bipy)]$ (**5**)	21.0 (Me); 122.6 (*ortho*-CHs, NPh); 123.3 and 126.8 (β-CHs, bipy); 123.8 (*ortho*-CHs, NC_6H_4Me-*p*); 125.3 (*para*-CH, NPh); 128.2 (*meta*-CHs, NPh); 128.7 (*meta*-CHs, NC_6H_4Me-*p*); 129.0 (β-CHs, bipy); 134.7 and 134.9 (*para*-C, NC_6H_4Me-*p*); 140.1 (γ-CHs, bipy); 150.9 (α-Cs, bipy); 153.0 (α-CHs, bipy); 154.2 (*ipso*-C, NC_6H_4Me-*p*); 156.5 (*ipso*-C, NPh).	2.40 (s, 3H, Me); 6.80–7.64 (several m, 11H, aromatic Hs, NPh, NC_6H_4Me-*p*, and γ-Hs, bipy); 7.80–8.15 (m, 4H, β-Hs, bipy); 9.38 (d, 2H, α-Hs, bipy).
$[W(NCMe_3)(NPh)Cl_2(bipy)]$ (**6**)	31.8 (Me_3); 70.1 (N—C), ^{183}W satellites at 69.2 and 71.0, $^2J_{WC}$ = 12.6 Hz; 121.2 (*ortho*-CHs, NPh); 122.3, 122.5 and 122.8 (β-CHs, bipy); 126.5 (*para*-CH, NPh); 128.1 (*meta*-CHs, NPh); 139.7 and 139.9 (γ-CHs, bipy); 150.6 and 151.6 (α-Cs, bipy); 152.5 and 154.2 (α-CHs, bipy); 158.0 (*ipso*-C, NPh).	1.50 (s, 9H, CMe_3); 6.92–7.80 (m, 7H, aromatic Hs, NPh and γ-Hs, bipy); 7.90–8.20 (m, 4H, β-Hs, bipy); 9.40 and 9.80 (2d, 2H, α-Hs, bipy).
$[Re(NPh)Cl_3(NH_2CMe_3)_2]$ (**12**)	30.1 (Me_3); 59.8 (NH_2—C); 116.7 (*ortho*-CHs, NPh); 126.7 (*para*-CH, NPh); 130.9 (*meta*-CHs, NPh); 168.0 (*ipso*-C, NPh).	1.28 (s, 18H, $2CMe_3$); 6.85–7.25 (b, 4H, $2NH_2$); 7.23–8.00 (m, 5H, aromatic Hs).

[a] Spectra obtained in $CDCl_3$.
[b] Assignments for bipy made by comparison with the free ligand.
[c] b = broad, d = doublet, m = multiplet, s = singlet.
[d] Also contains $[\{W(O)(NHCMe_3)_2Cl_2\}\cdot\frac{1}{4}C_6H_6]_x$.

with (**2**) but they have not been obtained in a pure state.

Reaction between $WOCl_4$ and one equivalent of p-$MeC_6H_4N(SiMe_3)_2$ resulted in a further non-crystalline solid for which the IR spectrum again indicated the presence of oxo bridges. Reaction of this material with bipy in benzene led to an insoluble oxo species and an orange solution containing several components. After extensive recrystallization of the solubles, yellow microcrystals were obtained for which analytical and spectral data indicated the oxo-imido complex $[W(O)(NC_6H_4Me\text{-}p)Cl_2(bipy)]$ (**3**). The IR spectrum contained a strong absorption at 918 cm^{-1} characteristic of a terminal oxo ligand[14] and a single band at 318 cm^{-1} indicative of *trans* metal chloro ligands,[15] but the complex was insufficiently soluble in organic solvents to obtain an NMR spectrum. A small quantity of the dark red complex $[W(NC_6H_4Me\text{-}p)_2Cl_2(bipy)]$ (**4**) was also obtained which was characterized by NMR spectroscopy. The ^1H NMR spectrum showed the presence of two p-tolylimido ligands and one bipyridyl ligand for which the α-proton appeared as a doublet shifted downfield from that in the free ligand. In the ^{13}C NMR spectrum the tolylimido *ipso* carbon appeared at 154.2 ppm, which is in the region characteristic of *bis*-arylimido complexes,[4] and there was a single set of resonances for the carbons of the bipyridyl ligand.

In a study of the reactions between *bis*-silylamines and mono-organoimido complexes, $[W(NPh)Cl_4]_2$[16] was reacted with p-$MeC_6H_4N(SiMe_3)_2$. The red non-crystalline product obtained was then treated with bipy to give the dark red *bis*-organoimido complex $[W(NPh)(NC_6H_4Me\text{-}p)Cl_2(bipy)]$ (**5**). The ^1H NMR spectrum showed the correct ratio of protons with the α-protons of bipy appearing as a single doublet. The ^{13}C NMR spectrum contained phenyl ring *ipso* carbon resonances at 156.5 and 154.2 ppm which are similar in position to the respective resonances in $[W(NPh)_2Cl_2(bipy)]$[17] and $[W(NC_6H_4Me\text{-}p)_2Cl_2(bipy)]$ (**4**), and one set of resonances for the bipy ligand. In the far IR, there were W—Cl stretches at 312 and 304 cm^{-1} which suggested that for the expected *trans* chloro structure some small differences in the W—Cl bonds might occur related to distortion from octahedral symmetry. Comparison of the W—Cl stretches in other bis-organoimido complexes we have prepared indicated that the observed splitting was more pronounced when two different organoimido ligands were present in the complex.

To study further this aspect, $[W(NCMe_3)(\mu\text{-}NPh)Cl_2(NH_2CMe_3)]_2$[3,4] was reacted with bipy and pure crystals of $[W(NCMe_3)(NPh)Cl_2(bipy)]$ (**6**) were obtained. In this case the IR spectrum showed two well-separated W—Cl stretches at 322 and 303 cm^{-1}. Additionally, the NMR spectrum showed significant differences to other bis-organoimido bipyridyl complexes. Table 3 shows that $[W(NCMe_3)(NPh)Cl_2(bipy)]$ (**6**) has two sets of resonances for the α-protons and α-carbons of bipy and the remainder of the complexes have a single set. In the ^1H NMR spectra one α-proton resonates further downfield than the other more typical α-proton, while in the ^{13}C NMR the resonances are at higher and lower field compared to the others. In order to rationalize these spectral anomalies the structure of (**6**) was determined by X-ray crystallography.

Crystal structure of $[W(NCMe_3)(NPh)Cl_2(bipy)]$ (**6**)

The complex is monomeric. The tungsten atom adopts a distorted octahedral geometry comprising *cis*-orientated *t*-butylimido and phenylimido groups, *trans* chloro ligands and with the nitrogen

Table 3. Selected NMR data for the bipy ligand in bis-organoimido complexes of tungsten(VI)

Complex	^1H NMR[a] α-CHs	^{13}C NMR[a] α-CH	^{13}C NMR[a] α-C	Ref.
$[W(NCHMe_2)_2Cl_2(bipy)]$	9.5	153.6	150.8	17
$[W(NMe)(NCMe_3)Cl_2(bipy)]$	9.4	152.9	150.9	17
$[W(NCMe_3)_2Cl_2(bipy)]$ (**2**)	9.8	152.5	150.6	5
$[W(NPh)(NEt)Cl_2(bipy)]$	9.5	153.6	151.7	17
$[W(NCM_3)(NPh)Cl_2(bipy)]$ (**6**)	9.4, 9.8	152.5, 154.2	150.6, 151.6	present work
$[W(NPh)_2Cl_2(bipy)]$	9.4	153.0	150.9	17
$[W(NPh)(NC_6H_4Me\text{-}p)Cl_2(bipy)]$ (**5**)	9.4	153.0	150.9	present work
$[W(NC_6H_4Me\text{-}p)_2Cl_2(bipy)]$ (**4**)	9.4	153.1	151.0	present work

[a] Values in ppm from internal TMS standard.

atoms of the bipyridyl ring coordinated *trans* to the imido functions. The overall geometry of the molecule is shown in Fig. 1 and selected bond lengths and bond angles are listed in Table 4 where the values are compared with those for the structurally similar complex $[W(NPh)_2Cl_2(bipy)]$.[17]

The W—N(1) and W—N(2) bond lengths of 1.774(8) and 1.754(10) Å do not differ significantly from one another but are longer than predicted for a W—N triple bond involving a four-electron donor (1.71 Å).[8] The phenylimido W—N bond length (1.774(8) Å) lies outside the range observed (1.67(3) –1.757(12) Å) for terminal mono-organoimido complexes of tungsten[8,16–21] but is not significantly different from that found in the bis-imido complex $[W(NPh)_2Cl_2(bipy)]$.[3,17] The *t*-butylimido bond length (1.754(10) Å) is longer than those observed for the terminal *t*-butylimido ligands in $[W(NCMe_3)(\mu\text{-}NPh)Cl_2(NH_2CMe_3)]_2$ and $[W(NCMe_3)(\mu\text{-}NC_6H_4Me\text{-}p)Cl_2(NH_2CMe_3)]_2$ (1.736(7) and 1.729(10) Å, respectively)[4] but is slightly shorter than the phenylimido W—N bond lengths in $[W(NPh)_2$

Table 4. Comparison of selected bond lengths and angles for $[W(NPh)_2Cl_2(bipy)]$[a] and $[W(NCMe_3)(NPh)Cl_2(bipy)]$[b]

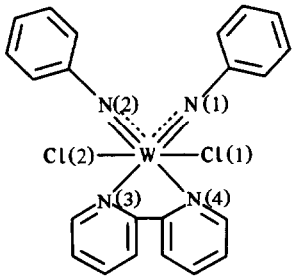

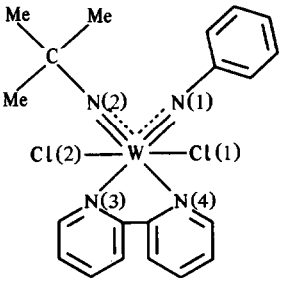

	Bond lengths (Å)		
W—N(1)	1.782(9)	1.774(8)	
W—N(2)	1.775(9)	1.754(10)	[−0.021]
W—N(3)	2.319(8)	2.333(9)	
W—N(4)	2.315(9)	2.312(10)	
W—Cl(1)	2.390(4)	2.412(3)	[+0.022]
W—Cl(2)	2.385(4)	2.390(3)	
N(1)—C(11)	1.36(2)	1.39(1)	
N(2)—C(21)	1.37(1)	1.44(2)	
	Bond angles (°)		
W—N(1)—C(11)	165.3(9)	160.8(8)	[−4.5]
W—N(2)—C(21)	166.3(8)	165.1(9)	
N(1)—W—N(2)	104.3(4)	104.2(5)	
N(1)—W—N(3)	163.3(4)	161.4(4)	
N(1)—W—N(4)	94.0(4)	92.9(4)	
N(2)—W—N(3)	91.9(4)	93.2(4)	
N(2)—W—N(4)	161.7(4)	162.4(4)	
N(3)—W—N(4)	69.8(4)	69.3(3)	
Cl(1)—W—Cl(2)	159.3(1)	158.2(1)	
Cl(1)—W—N(1)	97.1(3)	91.3(4)	[−5.8]
Cl(1)—W—N(2)	96.5(3)	95.4(4)	
Cl(1)—W—N(3)	82.3(3)	79.7(2)	[−2.6]
Cl(1)—W—N(4)	82.1(3)	79.5(3)	[−2.6]
Cl(2)—W—N(1)	94.9(3)	100.8(3)	[+5.9]
Cl(2)—W—N(2)	96.9(4)	99.1(4)	[+2.2]
Cl(2)—W—N(3)	81.3(2)	83.3(2)	[+2.0]
Cl(2)—W—N(4)	80.7(3)	81.8(8)	

[a] Data taken from reference 17.

[b] Values in square parentheses show significant changes in bond lengths or bond angles of $[W(NCMe_3)(NPh)Cl_2(bipy)]$ compared with those in $[W(NPh)_2Cl_2(bipy)]$. Positive values indicate length increases,angle opens; negative values indicate length decreases, angle closes.

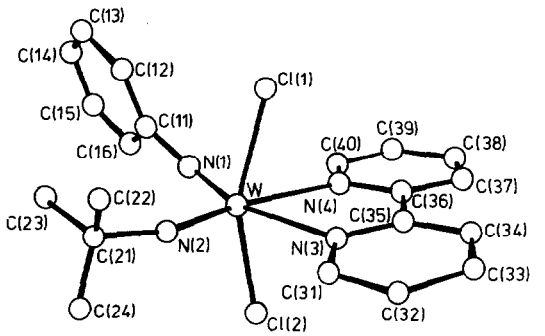

Fig. 1. Molecular geometry and atomic numbering of $[W(NCMe_3)(NPh)Cl_2(bipy)]$ (**6**).

$Cl_2(bipy)]$.[17] The phenylimido W—N(1)—C(11) bond angle (160.8(8)°) is smaller than the *t*-butylimido W—N(2)—C(21) bond angle (165.1(9)°) the latter being similar to both W—N—C bond angles in $[W(NPh)_2Cl_2(bipy)]$. Thus, as the W—N bond lengths and W—N—C bond angles in complex (**6**) are not significantly different, the six electrons required from the two imido ligands to give the complex an 18-electron count are essentially delocalized over the two W—N bonds, rather than existing as the separate four- and two-electron donor systems R—N≡W and R—N̈=W as observed in $[Mo(NPh)_2(S_2CNEt)_2]$ (Mo—N—C bond angles respectively 169.4(4)° and 139.4(3)°, Mo—N bond lengths respectively 1.754(4) and 1.789(4) Å).[22]

The W—Cl(1) bond (2.412(3) Å) is longer than the W—Cl(2) bond (2.390(3) Å) the latter being similar to those observed in $[W(NPh)_2Cl_2(bipy)]$. For the bipyridyl ligand W—N(3) is 0.02 longer than W—N(4), the latter being of similar length to those in $[W(NPh)_2Cl_2(bipy)]$. The extent of distortion from regular octahedral geometry in the molecule is shown by the wide N(1)—W—N(2) bond angle (104.2(5)°) and the non-linearity of the Cl(1)—W—Cl(2) bond angles (158.2(1)°), whereby the chloro ligands are bent away from the *cis*-imido ligands.

Comparison shows that the corresponding bond angles in $[W(NCMe_3)(NPh)Cl_2(bipy)]$ (**6**) and $[W(NPh)_2Cl_2(bipy)]$ (Table 4) are similar, apart from those associated with the nitrogen atom of the phenylimido ligand in (**6**) which is bent towards Cl(1), the Cl(1)—W—N(1) and Cl(2)—W—N(1) bond angles being 91.3(4)° and 100.8(3)° which compares with 97.1(3) and 94.9(3)° for the equivalent angles in the bis-phenylimido complex. Although one bipy ligand W—N bond is considerably longer in complex (**6**), the bite angle made by the bipy nitrogens (69.3(3)°) is no different to that found in the bis-phenylimido complex or in other bipy complexes.[20,21,23]

In complex (**6**) the imido nitrogen atoms are bent away from each other but the sense of the W—N—C bond angles are such that C(21) (*t*-butylimido ligand) bends slightly towards the region between N(3) and Cl(1) (W—N(2)—C(21) 165.1(9)°) and C(11) (phenylimido ligand) bends slightly towards the region between Cl(1) and N(2) (W—N(1)—C(11) 160.8(8)°). The phenyl ring is twisted from the N(1), N(2), N(3), N(4) plane to minimize interaction between *ortho* and α-hydrogens on the phenyl and bipy rings, respectively, while the orientation of the *t*-butyl methyl groups and the sense of the W—N(2)—C(21) angle are such as to minimize methyl group and bipy α-hydrogen interactions.

The overall features shown by the structural determination thus indicate that steric interaction between the bipy α-hydrogen and *t*-butylimido methyl groups is relieved by lengthening of one W—N_{bipy} bond. As to why the W—Cl(2) bond is lengthened is not immediately clear. The observed features do however explain the two W—Cl stretches in the IR spectrum and the two sets of resonances for the α-hydrogens in the ^{1}NMR spectrum. The difference in the two W—N_{bipy} bonds is reflected in the ^{13}C NMR spectrum by a set of resonances for the carbons of each bipy ligand ring.

Rhenium complexes

Rhenium oxytetrachloride reacts with phenylisocyanate in benzene solution to give $[Re(NPh)Cl_4]_2 \cdot \frac{1}{3}C_6H_6$ (**7**). The reaction proceeds according to eq. 1.

$$ReOCl_4 + PhNCO \rightarrow [Re(NPh)Cl_4] + CO_2. \quad (1)$$

The dark brown complex is sparingly soluble in chlorinated hydrocarbons and practically insoluble in benzene. The IR spectrum contains a strong absorbance at 1330 cm^{-1} characteristic of ν_s(Re—N—C) and weaker intensity bands at 990 and 682 cm^{-1} representative of ν_{as}(Re—N—C) and δ(M—N—C) respectively.[24] In the far IR the M—Cl stretches are represented by three strong intensity bands at 375, 352 and 340 cm^{-1} and a medium intensity absorption at 275 cm^{-1}. A dimeric structure involving bridging chloro ligands is therefore proposed for the complex similar to that found for $[W(NCHMe_2)Cl_4]_2$.[2]

$[Re(NPh)Cl_4]_2$ shows a similar chemistry to $[W(NPh)Cl_4]_2$.[16] The complex dissolves in THF (tetrahydrofuran) to give the adduct $[Re(NPh)Cl_4(THF)]$ (**8**) [strong IR absorptions at 1352 $\{\nu_s$(Re—N—C)$\}$, 832 (THF) and 330 cm^{-1} (Re—Cl)] and in MeCN to give $[Re(NPh)Cl_4(NCMe)]$ (**9**) [IR absorptions at 2280 (MeCN), 1445 $\{\nu_s$(Re—N—C)$\}$ and 335 cm^{-1} (Re—Cl)]. Being

d^1 systems the complexes give very broad NMR signals. The structure of the THF adduct (**8**) is expected to be similar to that found for $[W(NC_6H_4Me\text{-}p)Cl_4(THF)]$[17] in which the four chlorine atoms are equitorial and the THF ligand lies *trans* to the imido function with the W—O (THF) bond being lengthened due to the *trans* influence of the imido ligand (four-electron donor).

When reacted with two equivalents of Me_4NCl, $[Re(NPh)Cl_4]_2$ formed a brown solid which on recrystallization from MeCN gave the solvate $[Re(NPh)Cl_5][NMe_4]\cdot 1\cdot 5MeCN$ (**10**). The complex is a 1 : 1 conductor in nitromethane and its IR spectrum shows bands at 1350 {ν(Re—N—C)}, 330 and 275 cm^{-1} {ν(Re—Cl)}. The structure is expected to be similar to that of the anionic tungsten complexes $[W(NCHMe_2)Cl_5][NEt_4]$[2] and $[W(NC_6H_4Me\text{-}p)Cl_5][PPh_3(CH_2Ph)]$[17] in which the M—Cl bonds *trans* to the imido functions are lengthened due to the *trans* influence of the imido ligand.

On addition of triphenylphosphine to $[Re(NPh)Cl_4]_2$ in THF the yellow–brown solution of $[Re(NPh)Cl_4(THF)]$ (**8**) rapidly turns green and $[Re(NPh)Cl_3(PPh_3)_2]$ (**11**) precipitates. However, when PMe_3 is added to $[Re(NPh)Cl_4(THF)]$ in THF the solution colour does not change appreciably and there is no apparent reduction to $[Re(NPh)Cl_3(PMe_3)_2]$ which is green.[25] This chemistry contrasts with that of W(VI), where $[W(NPh)Cl_4]_2$ is reduced faster by PMe_3 than by PPh_3.[16,26]

Reaction of $[Re(NPh)Cl_4]_2$ with four equivalents of $Me_3SiNHCMe_3$ in benzene did not give the expected bis-organoimido complex $[Re(NCMe_3)(NPh)Cl_2(NH_2CMe_3)]_2$. Instead, the rhenium(V) complex $[Re(NPh)Cl_3(NH_2CMe_3)_2]$ (**12**) was obtained for which analytical data were inconclusive and thus the final characterization was made by X-ray crystallography (see later). In the IR spectrum the *t*-butylamine ligands showed NH absorptions at 3250 and 3180 cm^{-1} while in the ^1H NMR spectrum the NH protons appeared as a broad resonance at 7.00 ppm. In the ^{13}C NMR spectrum the *t*-butylamine quaternary resonance appeared at 59.8 ppm which is at lower field than those observed for organoimido complexes of groups V and VI containing this ligand (range 50.6–54.9 ppm). For the phenylimido ligand the *ortho* carbons are considerably more shielded and the *ipso* carbon deshielded compared with a range of tungsten(VI) complexes.[27]

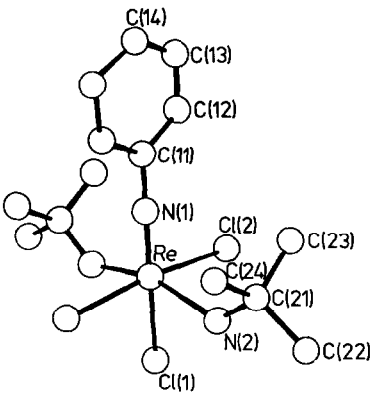

Fig. 2. Molecular geometry and atomic numbering of $[Re(NPh)Cl_3(NH_2CMe_3)_2]$ (**12**).

Crystal structure of $[Re(NPh)Cl_3(NH_2CMe_3)_2]$ (**12**)

The complex is monomeric with a distorted octahedral geometry consisting of *trans* chloro and *trans* *t*-butylamine ligands and a phenylimido ligand situated *trans* to a third chloro ligand (see Fig. 2). Bond distances and angles for the molecule are given in Table 5.

The Re—N(1) bond length 1.709(11) is not significantly different from those found in other arylimido complexes of rhenium(V) (range 1.685(11)–1.709(4) Å)[28–30] and is close to that predicted for an Re—N triple bond (1.69 Å).[8] The Re—Cl(1) bond length (2.411(5) Å) is slightly longer than the two *trans*-Re—Cl bond lengths (2.404(2) Å) and this

Table 5. Selected bond lengths and angles for $[Re(NPh)Cl_3(NH_2CMe_3)_2]$ (**12**)[a]

	Bond lengths (Å)		
Re—N(1)	1.709(11)	Re—Cl(2)	2.404(2)
Re—N(2)	2.187(7)	N(1)—C(11)	1.43(2)
Re—Cl(1)	2.411(5)	N(2)—C(21)	1.46(1)
	Bond angles (°)		
Cl(1)—Re—Cl(2)	86.1(1)	Cl(2)—Re—N(2)	87.6(2)
Cl(1)—Re—N(2)	79.6(2)	N(1)—Re—N(2)	100.4(2)
Cl(2)—Re—N(1)	93.9(1)	N(2)—Re—N(2′)	159.2(3)
Cl(2)—Re—Cl(2′)	172.2(2)	Re—N(2)—C(21)	128.6(6)

[a]Two-fold axis passes through Cl(1), Re, N(1), C(11).

is also found to be the case in $[Re(NC_6H_4OMe\text{-}p)Cl_3(PEt_2Ph)_2]$.[28] The reverse situation is however found for $[Re(NC_6H_4OMe\text{-}p)Cl_3(PEt_2Ph)_2]$ in which the phenylimido ligand contains an electron withdrawing substituent.[28] In comparison, the chloro ligand *trans* to the imido function in $[W(NPh)Cl_3(PPh_3)_2]$ shows a lengthening of 0.08 Å over the *trans* dichloro ligands.[26] For the *t*-butylamine ligands in $[Re(NPh)Cl_3(NH_2CMe_3)_2]$ the Re—N bond lengths (2.187(7) Å) are not significantly different from those in $[Re(NMe)Cl(NH_2Me)_4][ClO_4]_2$ (average value 2.18(1) Å)[29] but are shorter than those found in tungsten organoimido complexes where a *t*-butylamine ligand lies *trans* to the imido function.

The N(1)—Re—Cl, Cl—Re—Cl and Re—N(1)—C(11) bond angles are not significantly different from those found in other rhenium(V) organoimido complexes. The N(2)—Re—N(2′) bond angle (159.2(2)°) is smaller than the Cl(2)—Re—Cl(2′) bond angle (172.2(2)°), and is significantly different from the equivalent N—Re—N bond angles in $[Re(NMe)Cl(NH_2Me)_4][ClO_4]_2$ (169.9(8) and 168.2(7)°).[29] The Re—N—C_{amine} bond angles are however similar in the two complexes. The sense of the Re—N—C angles are such as to position the *t*-butyl methyl groups above the equatorial plane and slightly towards one of the chloro ligands. The *t*-butylamine NH protons are positioned below the equatorial plane but do not make close contacts with any of the chlorine atoms.

The structural features exhibited by the complex are consistent with the 18 electron configuration for the metal. If the imido, amine and chloro ligands act as four-, two- and one-electron donors respectively, the complex then attains an 18-electron count without invoking chloro ligand π-bonding to the metal. This contrasts with the tungsten(V) complex $[W(NPh)Cl_3(PPh_3)_2]$[26] (17 electron species) in which the shortened W—Cl bonds in the equatorial plane indicate a measure of π-bonding. In both complexes the M—Cl bonds *trans* to the phenylimido ligand are lengthened due to the strong *trans* influence of the imido ligand.

EXPERIMENTAL

$[WOCl_4]_n$ was prepared by prolonged reaction of WO_3 (BDH) with thionyl chloride[14] and $[W(NPh)Cl_4]_2$ by reaction of $[WOCl_4]_n$ with phenylisocyanate.[16] $[ReOCl_4]_2$ was prepared by heating rhenium pentachloride in the presence of oxygen and distilling the product.[31] *t*-Butylamine was dried over and distilled from calcium hydride. N(trimethylsilyl)-*t*-butylamine was prepared by treating trimethylsilyl chloride with two equivalents of *t*-butylamine and bis(trimethylsilyl)N-*p*-toluidine by treating trimethylsilyl chloride with four equivalents of *p*-toluidine.[32] Tetramethyl ammonium chloride was dried at 80°C *in vacuo* for 24 h and stored in a Schlenk tube. Petroleum ether (b.p. 40–60°C), benzene, toluene and tetrahydrofuran, were distilled over sodium wire and dichloromethane and acetonitrile over calcium hydride. Distillations and manipulations using bench-top air-sensitive techniques were carried out under N_2 treated to remove oxygen and water.[33] IR spectra were recorded on a Perkin–Elmer 597 spectrometer, ^1H NMR spectra on a Varian T60 Model spectrometer and ^{13}C NMR spectra on a Jeol FX60 spectrometer. Analytical data were obtained by Prof. A. D. Campbell and associates, University of Otago, New Zealand. Melting points were determined in sealed tubes under N_2 on an electro-thermal melting-point apparatus and are uncorrected.

$[W(O)(NCMe_3)Cl_2(NH_2CMe_3)\cdot\frac{1}{4}C_6H_6]_x$ (1)

t-Butylamine (3.1 cm^3, 30.0 mmol) in benzene (30 cm^3) was added slowly to a suspension of tungsten oxytetrachloride (2.5 g, 7.3 mmol) in benzene (60 cm^3) chilled to ice-water temperature and the mixture was stirred for 2 h with the ice bath removed. The solution was filtered and the solvent removed to give a non-crystalline yellow solid which was washed with petroleum ether (25 cm^3) and dried *in vacuo*.

IR (Nujol) bands at 3150m, 1600w, 1560w, 1510w, 1395m, 1360s, 1290m, 1245s, 1210s, 1022w, 960w, 815s, 780s, 720s, 540w, 442w, 370w, 342w, 318m and 290m cm^{-1}.

(2,2′-*Bipyridyl*)*bis*-*t*-*butylimidodichlorotungsten*(VI) (2)

(a) N(trimethylsilyl)-*t*-butylamine (2.4 cm^3, 12.4 mmol) in benzene (40 cm^3) was added slowly to a suspension of tungsten oxytetrachloride (2.1 g, 6.2 mmol) in benzene (60 cm^3) cooled to ice-water temperature. The ice-bath was removed and the mixture was stirred for 18 h. The solution was filtered and the solvent removed to give a light yellow non-crystalline solid which was washed with petroleum ether (20cm^3) and dried *in vacuo*. Found: C, 26.9; H, 5.9; N, 7.3%. $C_{10}H_{22}Cl_2N_2OW$ (i.e. $[W(O)(NCMe_3)Cl_2(NH_2CMe_3)]\cdot\frac{1}{3}C_6H_6$ (**1a**) requires C, 27.2; H, 5.0; N, 6.4%.

IR (Nujol) bands at 3175w, 3130m, 1600w, 1580w, 1400w, 1360s, 1340w, 1290w, 1250s, 1210m, 1195m, 1022w, 965w, 930w, 918w, 840w, 800w,

790w, 720w, 635w, 590w, 580w, 440w, 345w, 324m and 298s cm^{-1}

The complex (1.3 g) was dissolved in benzene (80 cm^3), 2,2′-bipyridyl (0.5 g) in benzene (30 cm^3) added and the mixture refluxed for 2 h. The cooled solution was filtered, the solvent removed and the residue washed several times with warm petroleum ether and dried *in vacuo*.

IR (Nujol) bands at 1598m, 1564w, 1350s, 1308m, 1270s, 1238s, 1208s, 1175w, 1150w, 1135w, 1100w, 1058w, 1018m, 910s, 835s, 800m, 770s, 736s, 705w, 650w, 630w, 595w, 564w, 474w, 418w, 358w and 305s cm^{-1}.

The solid was dissolved in boiling toluene (30 cm^3), filtered while still hot and the volume reduced. On standing at room temperature yellow crystals of (2,2′-bipyridyl)bis-*t*-butylimidodichlorotungsten(VI) (**2**) were deposited which were washed with petroleum ether (30 cm^3) and dried *in vacuo*.

IR (Nujol) bands at 1595s, 1560w, 1490w, 1350s, 1308m, 1272s, 1235s, 1210s, 1170w, 1155w, 1135w, 1104w, 1055w, 1042w, 1020m, 970w, 902w, 890w, 800w, 764s, 730s, 650m, 626m, 590m, 564w, 470w, 412w, 355w and 305s cm^{-1}.

(b) 2,2′-Bipyridyl (0.34 g, 2.2 mmol) in benzene (30 cm^3) was added to a solution of $[W(O)(NCMe_3)Cl_2(NH_2CMe_3)\cdot\frac{1}{4}C_6H_6]_x$ (0.9 g, 2.1 mmol) in benzene (60 cm^3) and the mixture was refluxed for 2 h. The solution was cooled, and the solid filtered, washed with petroleum ether and dried *in vacuo*.

IR (Nujol) bands at 1600m, 1560w, 1300w, 1265s, 1215w, 1158w, 1104w, 1060w, 1022m, 950m, 900s, 860s, 800s, 780s, 735s, 660m, 640w, 554w, 445w, 420w, 350w and 300w cm^{-1}.

The solvent was removed from the filtrate to give yellow crystals of complex (**2**) [identical IR, ^1H and ^{13}C NMR spectra to the sample prepared under (a)].

(2,2′ - Bipyridyl)dichloro(oxo)p - tolylimidotungsten (VI) (**3**)

N-bis(Trimethylsilyl)-*p*-toluidine (1.2 cm^3, 4.3 mmol) in benzene (50 cm^3) was added slowly to a solution of tungsten oxytetrachloride (1.4 g, 4.1 mmol) in benzene (80 cm^3) and the mixture was stirred for 4 h. The deep red solution was filtered and the solvent removed to give a red non-crystalline solid.

IR (Nujol) bands at 1585m, 1560m, 1500w, 1480s, 1350m, 1242s, 1210w, 1168m, 1108w, 1100w, 1018m, 925s, 820s, 750s, 720s, 680s, 640s, 520w, 485m, 432m, 320s and 280m cm^{-1}.

2,2′-Bipyridyl (0.55 g, 3.5 mmol) in benzene (30 cm^3) was added to the red solid dissolved in benzene (60 cm^3) and the mixture was refluxed for 1.5 h. The solution was filtered, the volume reduced to *ca.* 3 cm^3 and on standing, yellow microcrystals were deposited. The product was repeatedly recrystallized from benzene solution to give the complex as a yellow microcrystalline solid which was washed with petroleum ether (40 cm^3) and dried *in vacuo*.

IR (Nujol) bands at 1595m, 1562m, 1490m, 1445m, 1315m, 1280w, 1245w, 1208w, 1170w, 1158w, 1102w, 1060w, 1022m, 1015w, 980m, 960w, 918s, 822s, 768s, 745w, 730s, 720w, 680m, 625w, 592w, 542w, 530w, 500w, 475w, 445w, 430m, 390w, 362w and 318s cm^{-1}.

(2,2′ - Bipyridyl)dichlorobis(p - tolylimido)tungsten (VI) (**4**)

Further crystallization of the reaction mixture containing complex (**3**) led to formation of a small quantity of complex (**4**). Characterization was made by NMR spectroscopy.

Ir (Nujol) bands at 1595s, 1560m, 1442m, 1412s, 1290w, 1245w, 1210w, 1172w, 1168w, 1102w, 1060w, 1025w, 1018w, 980w, 822s, 768s, 730s, 680m, 595w, 544w, 530w, 500w, 475w, 430m, 390w, 364w and 318s cm^{-1}.

(2,2′ - Bipyridyl)dichlorophenylimido - p - tolylimido-tungsten (VI) (**5**)

N(bis-Trimethylsilyl)-*p*-toluidine (0.8 cm^3, 2.9 mmol) in benzene (50 cm^3) was added to the phenylimido tungstentetrachloride dimer (1.2 g, 1.4 mmol) in benzene (100 cm^3) and the mixture was stirred for 18 h. The solution was filtered and the solvent removed to give a red solid which was washed with petroleum ether (50 cm^3) and dried *in vacuo*. The solid (0.65 g) was dissolved in benzene (80 cm^3), 2,2′-bipyridyl (0.25 g) in benzene (30 cm^3) added and the mixture refluxed for 3 h. The cooled solution was filtered and the solvent removed to give a dark red crystalline solid which was washed with petroleum ether (50 cm^3) and dried *in vacuo*. Recrystallization from toluene at 0°C gave the complex as large dark red crystals.

IR (Nujol) bands at 1595w, 1560w, 1320s, 1295s, 1268w, 1240w, 1218w, 1160w, 1144w, 1098w, 1055w, 1040w, 1020w, 1012w, 980m, 970m, 935w, 920w, 900w, 818s, 765s, 730s, 685m, 650m, 595w, 550w, 528w, 475m, 442w, 412m, 375w, 360w, 335w, 312s and 304s cm^{-1}.

(2,2′ - Bipyridyl) - t - butylimidodichloro(phenylimido) tungsten(VI) (**6**)

2,2′-Bipyridyl (0.3 g, 1.9 mmol) in benzene (30 cm^3) was added to a solution of bis(*t*-butyl-

amine)bis(*t* - butylimido)tetrachlorobis(μ - phenylimido)ditungsten(VI) (0.9 g, 0.92 mmol) in benzene (60 cm^3) and the mixture was refluxed for 1 h. The solution was filtered and the solvent removed to give a red crystalline solid which was washed with warm petroleum ether (2 × 50 cm^3) to remove excess 2,2′-bipyridyl and dried *in vacuo* (crude yield 1.0g, 95%). The solid was dissolved in hot toluene (60 cm^3) and the volume reduced until crystallization of the complex commenced (*ca.* 25 cm^3). On standing at −20°C large dark red crystals of the complex were deposited.

IR (Nujol) bands at 1595m, 1575m, 1345s, 1308s, 1278m, 1255s, 1212m, 1175m, 1165m, 1160m, 1108w, 1068w, 1058m, 1018m, 996m, 970m, 912w, 900w, 895w, 835w, 802w, 770s, 734m, 695m, 675w, 652m, 634m, 620w, 590m, 578m, 550w, 535w, 498m, 465w, 442w, 422w, 385w, 364w, 342m, 322s, 303s and 278w cm^{-1}.

Tetrachloro(phenylimido)rhenium(VI) (**7**)

Rhenium oxytetrachloride (3 g, 8.7 mmol) and phenyl isocyanate (1 cm^3, 9.2 mmol) in benzene (60 cm^3) were refluxed for 24 h. The cooled solution was filtered and the solid washed several times with benzene (5 cm^3) and dried *in vacuo* giving the complex as a dark brown crystalline solid. Yield 3.2 g, 88%.

Ir (Nujol) bands at 1582w, 1550w, 1330s, 1158m, 1085w, 1018w, 990w, 975w, 935w, 762s, 725m, 680m, 665s, 560w, 555w, 398w, 375s, 352s, 340s and 275m cm^{-1}.

Tetrachloro (phenylimido) (tetrahydrofuran) rhenium(VI) (**8**)

Tetrachloro(phenylimido)rhenium(VI) (0.75 g, 1.8 mmol) was dissolved in tetrahydrofuran (50 cm^3). The solution was filtered and the solvent removed *in vacuo* to give a quantitative yield of the adduct. The complex was recrystallized by dissolving in tetrahydrofuran and cooling the solution to −20°C.

IR (Nujol) bands at 1588w, 1572m, 1355s, 1300w, 1255w, 1212w, 1165w, 1155w, 1087w, 1062w, 1042w, 995m, 990m, 925m, 838s, 764s, 725m, 672s, 625w, 562w, 555w, 395w and 330s cm^{-1}.

Acetonitriletetrachloro (phenylimido) rhenium(VI) (**9**)

Acetonitrile (30 cm^3) was added to tetrachloro(phenylimido)rhenium(VI) (0.5 g, 1.2 mmol) and the mixture heated to just below the boiling point of the solvent. The solution was filtered and the volume reduced until crystallization commenced. On standing at −20°C the complex formed as yellow–brown needles.

IR (Nujol) bands at 2280m, 1570m, 1445s, 1295m, 1165w, 1090w, 1024w, 995w, 975w, 950w, 935w, 903w, 842w, 768s, 670s, 625w, 604w, 564w, 558w, 425w, 400w and 335s cm^{-1}.

Tetramethylammonium pentachloro (phenylimido) rhenate(VI) (**10**)

Dichloromethane (80 cm^3) was added to phenylimido rhenium tetrachloride (0.5 g, 1.2 mmol) and tetramethyl ammonium chloride (0.15 g, 1.4 mmol) and the mixture was stirred for 18 h. The solution was decanted and the solid washed several times with dichloromethane (20 cm^3) and dried *in vacuo* (0.45 g, 71%) $\Lambda_m(MeNO_2) = 102.8\ \Omega^{-1}\ cm^2\ mol^{-1}$. The complex was dissolved in acetonitrile (30 cm^3), the volume reduced to *ca.* 10 cm^3, and the solution allowed to stand at −20°C whereupon large yellow crystals of the complex (acetonitrile solvate) were formed. On drying *in vacuo* for several hours, crystallinity was lost.

IR (Nujol) bands at 1582m, 1570w, 1495s, 1380m, 1350m, 1340w, 1298w, 1170w, 1102w, 1030w, 1005m, 965s, 780s, 735w, 685m, 678m, 630w, 575w, 570w, 465w, 358m, 330s, 294w and 275w cm^{-1}.

Trichloro (phenylimido) bis (triphenylphosphine) rhenium(V) (**11**)

Triphenylphosphine (1 g, 3.8 mmol) in tetrahydrofuran (30 cm^3) was added to tetrachloro (phenylimido)rhenium(VI) (0.5 g, 1.2 mmol) in tetrahydrofuran (50 cm^3) and the mixture was stirred for 5 h. The solution was filtered and the green product washed with tetrahydrofuran (50 cm^3) followed by benzene (50 cm^3) and dried *in vacuo*.

IR (Nujol) bands at 1570w, 1425s, 1376s, 1310w, 1184w, 1150w, 1118w, 1090m, 1060m, 1022w, 995w, 944w, 912w, 900w, 778m, 750s, 730w, 710s, 698s, 690s, 618w, 562w, 525m, 520s, 510s, 495s, 460m, 438w, 418w, 315w, 300s, 280w and 265w cm^{-1}.

Bis (t - butylamine) trichloro (phenylimido) rhenium(V) (**12**)

A solution of N(trimethylsilyl)-*t*-butylamine (0.6 cm^3, 3.1 mmol) in benzene (20 cm^3) was added to the phenylimido rhenium tetrachloride dimer (0.6 g, 0.72 mmol) in benzene (40 cm^3) and the mixture was stirred for 16 h. The yellow–brown solution was filtered, the solvent removed and the residue

extracted with toluene, leaving the complex as a light green solid which was dried *in vacuo*.

IR (Nujol) bands at 3252w, 3170m, 3100w, 2800m, 2700w, 2595w, 2495w, 2075w, 1605w, 1565m, 1560m, 1505w, 1398m, 1350w, 1330w, 1300w, 1280s, 1205s, 1170s, 1145m, 1065w, 1035w, 1025w, 990w, 935w, 895w, 765s, 720w, 685m, 615m, 550w, 460w, 448w, 420w, 385w, 325w, 315m, 298s and 265w cm^{-1}.

Crystallographic studies

Single crystals of $[W(NCMe_3)(NPh)Cl_2(bipy)]$ (**6**), grown from toluene solution, were sealed under nitrogen in glass capillaries. Crystals of $[Re(NPh)Cl_3(NH_2CMe_3)_2]$ (**12**), grown from dichloromethane solution, were stable enough to permit examination in air. All data were collected using an Enraf–Nonius CAD-4 diffractometer.

Crystal data. Compound (**6**): $C_{20}H_{22}Cl_2N_4W$, $M = 572.75$, orthorhombic, $a = 8.879(3)$, $b = 13.036(3)$, $c = 18.837(4)$ Å, $U = 2180.3$ Å^3, space group $P2_12_12_1$, $Z = 4$, $D_c = 1.745$ g cm^{-3}, $F(000) = 1112$, μ(Mo-K_α) = 58.6 cm^{-1}, λ(Mo-K_α) = 0.71069 Å.

Crystal data. Compound (**12**): $C_{14}H_{23}Cl_3N_2Re$, $M = 511.55$, orthorhombic, $a = 14.140(1)$, $b = 11.806(1)$, $c = 11.936(3)$ Å, $U = 1992$ Å^3, space group *Pbcn*, $Z = 4$, $D_c = 1.706$ g cm^{-3}, $F(000) = 988$, μ(Mo-K_α) = 114.3 cm^{-1}, λ(Mo-K_α) = 0.71069 Å.

Data collection. Accurate unit cell parameters were determined by least squares fits to the observed setting angles of 25 reflections using Mo-K_α radiation at −130°C for (**6**) and 21°C for (**12**).

Intensity data collection [−130°C for (**6**) and 21°C for (**12**)] employed the $2\theta/\omega$ scan technique with a total background/peak count time ratio of 1:2. Reflections were counted for either 60 s or until $\sigma(I)/I$ was 0.022. Measured data: compound (**6**) 2497 reflections ($2\theta_{max} = 48°$), compound (**12**) 1538 reflections ($2\theta_{max} = 50°$). The intensities of three standard reflections were monitored regularly throughout the data collection, no significant variation in intensity being observed. For (**12**), data with $h+k = 2n+1$ were systematically weak, consistent with the molecule lying on a two-fold axis. The data were corrected for Lorentz, polarization and absorption.[34]

Structure solution and refinements. Both structures were solved by conventional Patterson and Fourier techniques and refined by full matrix least squares.[2] The function minimized was $\Sigma w(|F_o|-|F_c|)^2$ using weights $1.00/[\sigma^2(F)+gF^2]$ with g being 0.00054 for (**6**) and 0.0056 for (**12**). Atomic scattering factors and dispersion corrections were for neutral atoms. Anisotropic thermal parameters were refined for the heavier atoms in (**6**) and all atoms in (**12**). Final residuals R and R_w were 0.053 and 0.055 for the 2138 observed data for (**6**) and 0.035 and 0.040 for the 1108 observed data for (**12**).

Final atomic coordinates for both complexes, tables of thermal parameters, and listings of observed and calculated structure factors have been deposited with the Editor as supplementary material.*

*Atomic coordinates have also been deposited with the Cambridge Crystallographic Data Centre for inclusion in their data base. Copies are available on request from the Editor at Queen Mary College, London.

REFERENCES

1. D. M. T. Chan, W. C. Fultz, W. A. Nugent, D. C. Roe and T. N. Tulip, *J. Am. Chem. Soc.* 1985, **107**, 251.
2. B. R. Ashcroft, G. R. Clark, A. J. Nielson and C. E. F. Rickard, *Polyhedron* 1986, **5**, 2081.
3. B. R. Ashcroft, D. C. Bradley, G. R. Clark, R. J. Errington, A. J. Nielson and C. E. F. Rickard, *J. Chem. Soc., Chem. Commun.* 1987, 170.
4. B. R. Ashcroft, A. J. Nielson, D. C. Bradley, R. J. Errington, M. B. Hursthouse and R. L. Short, *J. Chem. Soc., Dalton Trans.* 1987, 2059.
5. A. J. Nielson, *Polyhedron* 1987, **6**, 1657.
6. A. O. Chong, K. Oshima and K. B. Sharpless, *J. Am. Chem. Soc.* 1977, **99**, 3420.
7. J. Chatt, R. Choukroun, J. R. Dilworth, J. Hyde, P. Vella and J. Zubieta, *Transition Met. Chem.* 1979, **4**, 59.
8. W. A. Nugent and B. L. Haymore, *Coord. Chem. Rev.* 1980, **31**, 123.
9. D. C. Bradley, M. B. Hursthouse, K. M. A. Malik and A. J. Nielson, *J. Chem. Soc., Chem. Commun.* 1981, 103.
10. P. A. Bates, A. J. Nielson and J. M. Waters, *Polyhedron* 1985, **4**, 999.
11. A. A. Kuznetsova, Yu. G. Podzollko and Yu. A. Buslaev, *Russ. J. Inorg. Chem.* 1969, **14**, 393.
12. F. A. Cotton and E. S. Shamshoum, *J. Am. Chem. Soc.* 1984, **106**, 3222.
13. C. G. Barraclough and J. Stals, *Aust. J. Chem.* 1966, **19**, 741.
14. A. J. Nielson and R. A. Anderson, *Inorg. Synth.* 1985, **23**, 195.
15. K. Nakamoto, *Infrared and Raman Spectra of Inorganic and Coordination Compounds*, 3rd Edn, p317. John Wiley, New York (1978).
16. D. C. Bradley, M. B. Hursthouse, K. M. A. Malik, A. J. Nielson and R. L. Short, *J. Chem. Soc., Dalton Trans.* 1983, 2651.
17. D. C. Bradley, R. J. Errington, M. B. Hursthouse,

R. L. Short, B. R. Ashcroft, G. R. Clark, A. J. Nielson and C. E. F. Rickard, *J. Chem. Soc., Dalton Trans.* 1987, 2067.
18. D. C. Bradley, R. J. Errington, M. B. Hursthouse, A. J. Nielson and R. L. Short, *Polyhedron* 1983, **2**, 843.
19. W. A. Nugent, *Inorg. Chem.* 1983, **22**, 965.
20. R. H. Fenn, *J. Chem. Soc.* (*A*) 1969, 1764.
21. G. A. Barclay, B. F. Hoskins and C. H. L. Kennard, *J. Chem. Soc.* 1963, 5691.
22. E. A. Maatta, B. L. Haymore and R. A. D. Wentworth, *J. Am. Chem. Soc.* 1976, **101**, 2063.
23. G. N. Schauzer, L. A. Hughes, N. Strampach, P. R. Robinson and E. O. Schliuper, *Organometallics* 1982, **1**, 44.
24. J. H. Osborne and W. C. Trogler, *Inorg. Chem.* 1985, **24**, 3098; W. P. Griffith, A. J. Nielson and M. J. Taylor, *J. Chem. Soc., Dalton Trans.* 1987 (in press).
25. K. W. Chiu, W. Wong, G. Wilkinson, A. M. R. Galas and M. B. Hursthouse, *Polyhedron* 1982, **1**, 37.
26. A. J. Nielson and J. M. Waters, Aust. J. Chem. 1983, **36**, 243.
27. A. J. Nielson, *Inorg. Chim. Acta* 1987, **133**, 305.
28. D. Bright and J. A. Ibers, *Inorg. Chem.* 1968, **7**, 1099.
29. R. S. Shandles, R. K. Murmann and E. O. Schlemper, *Inorg. Chem.* 1974, **13**, 1373.
30. D. Bright and J. A. Ibers, *Inorg. Chem.* 1969, **8**, 703.
31. P. G. Edwards, G. Wilkinson, M. B. Hursthouse and K. M. A. Malik, *J. Chem. Soc., Dalton Trans.* 1980, 2467.
32. R. M. Pike, *J. Org. Chem.* 1961, **26**, 232.
33. A. J. Nielson, *Chem. In N.Z.* 1986, **49**, 11.
34. A. C. T. North, D. C. Phillips and F. S. Mathews, *Acta Cryst.* 1968, **A24**, 351.

Polyhedron Vol. 7, No. 2, pp. 129–135, 1988
Printed in Great Britain

0277–5387/88 $3.00+.00
Pergamon Journals Ltd

POLYPHOSPHORUS LIGANDS—II.* THE NEW PENTAPHOSPHORUS LIGAND BIS(2,2-BIS (DIPHENYLPHOSPHINO)ETHYL)PHENYLPHOSPHINE AND ITS SULPHIDES

JONATHAN L. BOOKHAM and WILLIAM McFARLANE†

Department of Chemistry, City of London Polytechnic, 31 Jewry Street, London EC3N 2EY, U.K.

(*Received* 8 *May* 1987; *accepted* 24 *August* 1987)

Abstract—The preparation of the title compound and its progressive reaction with elemental sulphur to give nine from a possible total of 19 different phosphine sulphides are described. One- and two-dimensional ^{31}P NMR experiments are used to disentangle the complicated spectra given by the unseparated reaction mixtures, and the ^{31}P NMR parameters are found to be strongly dependent on conformational influences.

Ligands having two or more phosphorus atoms capable of stabilizing transition metals in low formal oxidation states are of substantial and still growing importance in coordination chemistry, typical well-known examples being $Ph_2P(CH_2)_nPPh_2$ [n = 1–6],[1] $(Ph_2P)_3CH$[2] and $(Ph_2PCH_2)_3CMe$.[3] In this context we have recently used[4] the addition of species with a P—H bond to the double bond of 1,1-bis(diphenylphosphino) ethene, **1**, to prepare several new ligands containing up to seven phosphorus atoms as indicated below. Each of these ligands **2**–**4** has the potential to coordinate one or more metal atoms in many different modes, and for **3** and **4** there is the opportunity for the formation of diastereomers in several of these modes. In the case of **4** the number of possibilities is extremely large, but with **3** it is reasonably limited.

There is a formal analogy between the addition of sulphur or other chalcogens to phosphorus(III) and its coordination to a metal atom, both in terms of the change in phosphorus hybridization which occurs and in the ^{31}P NMR parameters. Hence the reaction between sulphur and **3** or **4** can provide models for the range of isomeric non-chelated products that might be produced by metal complex formation. With this in mind we have used ^{31}P NMR to study in detail the reaction of elemental sulphur with **3** and have identified nine out of a possible total of 19 products with one or more P=S bonds. It appears that the remaining ten potential products are not produced by this reaction to any appreciable

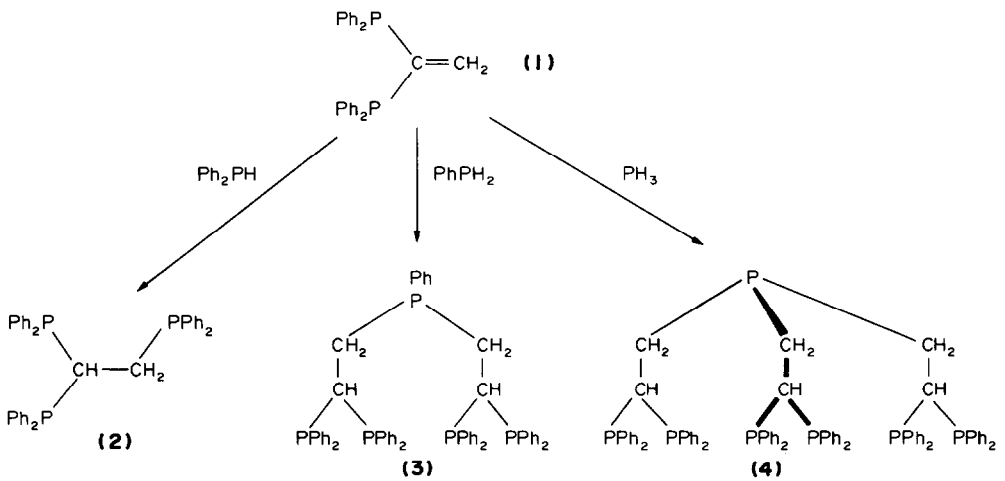

* See ref. 4 for part I.

† Author to whom correspondence should be addressed.

extent and we discuss the reasons for this. Although the sulphides of monophosphines are well studied,[5] comparatively little work has been done on those derived from polyphosphines, notable exceptions being the mono- and disulphides of diphosphines $R_2P(CH_2)_nPR_2$ [$n = 0$–6],[6,7] and derivatives of $(R_2P)_3CH$.[8] However, it is known from the foregoing work that on sulphurization the ^{31}P chemical shift increases by *ca.* 50 ppm and this is an important diagnostic aid. The reaction between **2** and selenium has also been studied, and 2D NMR experiments have been used[9] to identify the mixture of products.

RESULTS AND DISCUSSION

The reaction between elemental sulphur and **3** in benzene at room temperature yields species with one to five P=S bonds, there being no evidence of reactions that involve P—C bond cleavage. Structures **5**–**23** show schematically (phenyl groups omitted for clarity) the 19 chemically distinct (including diastereomers) sulphides that can in principle result from this reaction. In what follows the individual phosphorus atoms are lettered as in the parent **3**. Note that both P(III) and P(V) are configurationally stable so that P_X is chiral in **5, 6, 11**–**16, 21** and **22**. In addition, **5, 6, 11, 12, 14, 15, 21** and **22** have one asymmetric carbon, and **8**–**10** and **17**–**19** have two asymmetric carbon atoms, and hence P_X is pseudochiral in **8, 10, 17** and **19**. Overall, this leads to the range of diastereomers indicated: for example **5** and **6** are diastereomers and have different NMR parameters, while **8** and **10** are different *meso* forms and **9** is a racemate.

In the parent phosphine **3**, P_X is prochiral thus leading to inequivalence of P_A and P_B, and of $P_{A'}$ and $P_{B'}$. The phosphorus NMR spin system is therefore $AA'BB'X$, but in practice ^6J(PP) [i.e. $J(P_{AA'})$, $J(P_{BB'})$ or $J(P_{AB'})$] is zero and the system can be regarded as $(AB)_2X$ with negligible direct NMR interaction between the two $(Ph_2P)_2CH$ groups. Spectral analysis yielded $\delta(^{31}P_{A,A'}) = -2.9$, $\delta(^{31}P_{B,B'}) = -4.8$, $\delta(^{31}P_X) = -29.7$ ppm, and $^2J(P_AP_B) = {}^2J(P_{A'B'}) = 100.7$, $^3J(P_{A,A'}P_X) = 28.6$, $^3J(P_{B,B'}P_X) = 17.0$ Hz, no stereochemical assignment being implied.

Figure 1 shows the ^{31}P spectrum resulting from the reaction of one mole of **3** with one atomic equivalent of sulphur. The resonances are in three main regions: *ca.* −30, −10, and +50 ppm and can be assigned to $P(III)_X$, $P(III)_{A,B'}$, and $P(V)_{A,B}$ respectively. In the P(III) regions the characteristic patterns of peaks due to the unreacted starting phosphine **3** can still be identified in *ca.* 25% amount,

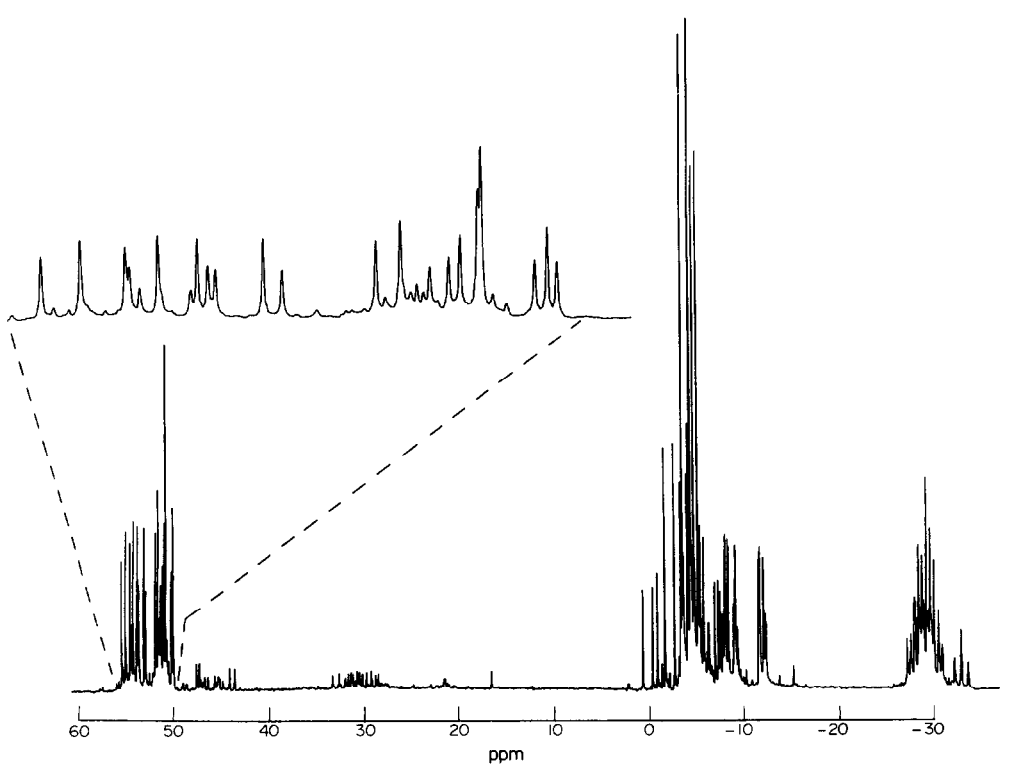

Fig. 1. ^{31}P NMR spectrum of the mixture resulting from the reaction between **3** and one atomic equivalent of sulphur. The upper trace shows a 10× expansion of part of the P(V) region.

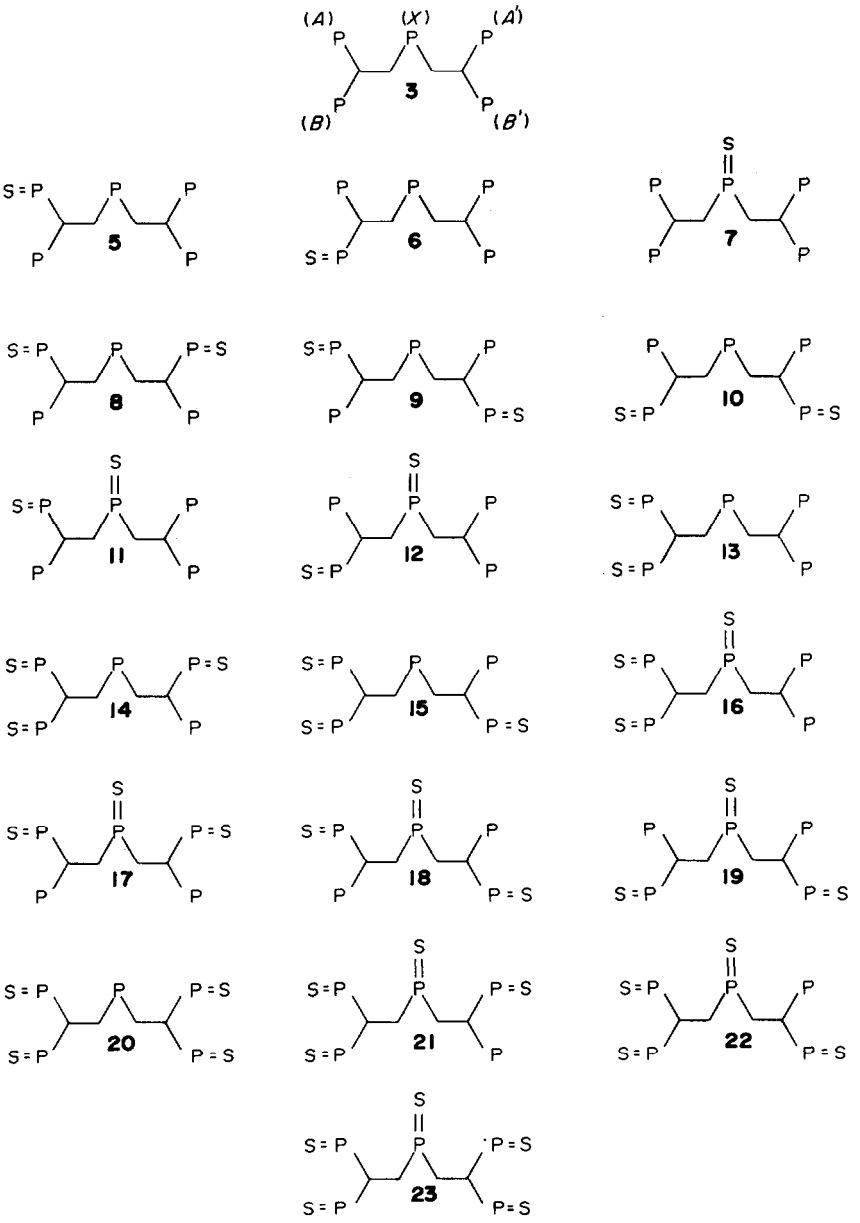

and it therefore follows that in addition to monosulphides there must also be some di- (and possibly tri-) sulphides present. The analysis of the P(V) region was facilitated by the homonuclear two-dimensional[10] (2D) ^{31}P *J*-spectrum shown in Fig. 2. Figure 3 shows an expansion of the P(V) part of the 1D spectrum together with appropriate 45° cross-sections from Fig. 2. There are thus six types of P(V) nucleus, each arising from a $Ph_2P(S)CHPPh_2$ fragment with an internal $^2J(P_AP_B)$ of 100–130 Hz and further coupled to P_X by 20–30 Hz. $Ph_2P(S)CHP(S)Ph_2$ fragments would be expected to have much smaller values of $^2J(P_AP_B)$ and might further display some second-order characteristics owing to the proximity of the two P(V) chemical shifts. These conclusions were supported by detailed analysis of the P(III) regions of the spectrum, and it was further confirmed that there were no lines attributable to species containing $P(V)_X$.

Addition of a second atomic equivalent of sulphur (see Fig. 4) reduced the intensities of the peaks corresponding to cross-sections a and b, and the associated P(III) resonances also diminished; these resonances are therefore assigned to the pair of diastereomeric monosulphides **5** and **6**. They are present in slightly unequal proportions, indicating a degree of steric control over the sulphurization reaction, but it is not possible to make a stereochemical assignment. The remaining four cross-sections c–f are attributed to the disulphides **8–10**, the pair of equal intensity (d and f) being assigned

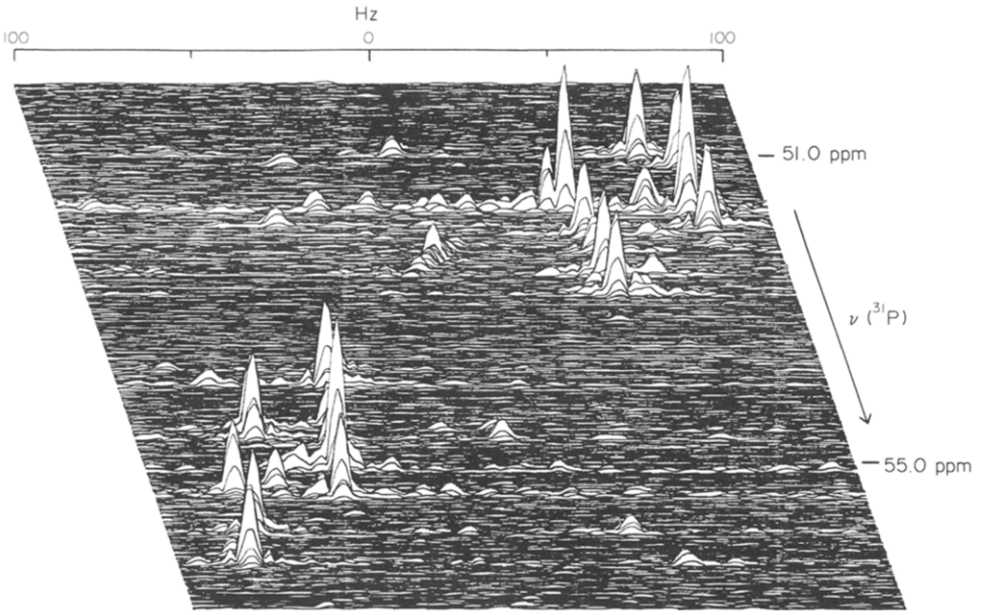

Fig. 2. Homonuclear two-dimensional ^{31}P *J*-spectrum at 36.2 MHz of the mixture resulting from the reaction between **3** and one atomic equivalent of sulphur. The horizontal axis shows separations due to spin coupling interactions only, and the back/front axis also includes dispersion due to chemical shift differences.

to **9** in which pseudo-chirality at P_X leads to inequivalence of the two $Ph_2P(S)$ moieties, although these have to be present in equal proportions. By contrast the lines due to **8** and **10** (i.e. cross-sections c and e or *vice versa*) are of markedly unequal intensities, again indicating steric effects upon the reaction, and this was confirmed by detailed scrutiny of the P(III) regions of the spectrum.

It was also found that the addition of the second equivalent of sulphur and then of further amounts, generated resonances in the region 45–50 ppm which are only vestigially present in Fig. 1. These are assigned to $[Ph_2P(S)]_2CH$ fragments in which prochirality at P_X generates the inequivalence of the two phosphorus nuclei. Again, this was confirmed by the appearance of the P(III) spectral regions, and the stepwise addition of sulphur was continued until the spectrum showed that essentially all of the material was present in the form of the pentasulphide **23** which was then isolated as a stable

Table 1. Phosphorus-31 NMR parameters of $[(Ph_2P)_2CHCH_2]_2PPh$ and its sulphides[a]

Species	$\delta(P_A)$	$\delta(P_B)$	$\delta(P_{A'})$	$\delta(P_{B'})$	$\delta(P_X)$	$^2J(P_AP_B)$	$^2J(P_{A'}P_{B'})$	$^3J(P_AP_X)$	$^3J(P_BP_X)$	$^3J(P_{A'}P_X)$	$^3J(P_{B'}P_X)$
3	−2.9	−4.8	−2.9	−4.8	−29.7	100.7	100.7	28.6	17.0	28.6	17.0
5, **6**[b]	54.1	−9.4	−0.6	−6.6	−30.0	(128.5)	85.9	(32.2)	1.7	38.6	13.2
	−9.6	53.8	−2.7	−4.1	−28.6	(122.8)	74.6	2.4	(29.8)	35.0	8.5
8, **10**[b]	53.5	−7.4	53.5	−7.4	−29.0	(111.7)	(111.7)	(19.6)	3.9	(19.6)	3.9
	−10.2	52.9	−10.2	52.9	−32.1	(108.9)	(108.9)	1.9	(25.6)	1.9	(25.6)
9	53.3	−10.2	−5.2	52.8	−29.1	(122.6)	(105.3)	(32.9)	2.0	12.7	(28.7)
14, **15**[b]	48.4	44.6	54.0	−13.1	−31.1	[1.4]	(127.7)	(11.2)	(20.5)	(41.3)	0.0
	47.5	46.3	−7.6	53.4	−26.9	[1.3]	(113.6)	(12.5)	(12.7)	0.7	(20.1)
20	49.7	46.2	49.7	46.2	−27.6	[2.7]	[2.7]	(14.9)	(10.5)	(14.9)	(10.5)
23	48.9	48.7	48.9	48.7	51.6	[0.0]	[0.0]	[6.8]	[27.1]	[6.8]	[27.1]

[a] Chemical shifts in ppm to high frequency of 85% H_3PO_4, ±0.1 ppm; coupling constants in Hz, ±0.2 Hz. Round brackets indicate P(III)—P(V) couplings, square brackets indicate P(V)—P(V) couplings. P(III)—P(III) couplings are not placed in brackets.

[b] Diastereomeric pair, assignments may need to be interchanged.

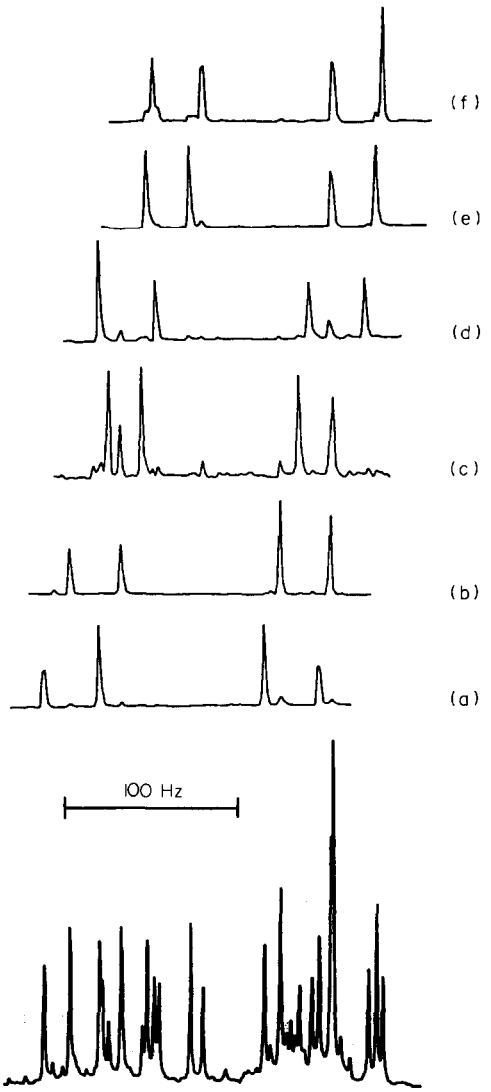

Fig. 3. ^{31}P spectra at 36.2 MHz of the mixture resulting from the reaction between **3** and one atomic equivalent of sulphur. Bottom trace: expansion of P(V) region of normal one-dimensional spectrum (see Fig. 1). Upper traces: 45° cross-sections from the two-dimensional spectrum shown in Fig. 2 corresponding to the six different P(V) environments in the mixture. The same horizontal scale has been used for all traces, but reliable intensities can only be derived from the one-dimensional spectrum. Phosphorus–phosphorus coupling constants can be obtained directly from the line positions in the cross-sections, and in each case the phosphorus chemical shift is given by the mean of the four frequencies.

white solid. Overall, nine different species were detected in the progressive reaction of **3** with elemental sulphur, and their ^{31}P NMR parameters are given in Table 1. It is particularly noteworthy that with the exception of **23**, no species was formed as a result of attack on P_X.

The products resulting from the sulphurization of **3** appear to be governed by the following rules, the first taking precedence over the second: (a) addition to P_X is avoided until all four other phosphorus atoms have been attacked; (b) the formation of species with geminally related $Ph_2P(S)$ groups is disfavoured. These two rules acting in concert reduce the number of actual reaction products from a possible 19 to just nine and it is interesting to reflect that they might also substantially limit the range of products obtained in the sulphurization of the heptaphosphine **4**.

As noted earlier, the ^{31}P chemical shift of a Ph_2P-group increases by *ca.* 50 ppm on addition of sulphur, and a specially valuable feature is that the P(V) resonances from $Ph_2P(S)CHPPh_2$ and $[Ph_2P(S)]_2CH$ groups lie in the mutually exclusive ranges of 53.5 ± 0.7 and 47.2 ± 2.6 ppm respectively. The variation within these ranges is clearly due to stereochemical effects but is so narrow that it cannot usefully be discussed further. Fortuitously, the chemical shift of $P(V)_X$ lies between these two ranges, and although it overlaps with neither range, the actual peaks themselves could overlap owing to the spread produced by large coupling constants.

The phosphorus–phosphorus coupling constants display substantial conformational dependences, and in the case of the geminal ones lie in the following non-overlapping ranges: ^2J(P(III)—P(III)), 88 ± 13 Hz; ^2J(P(III)—P(V)), 117 ± 12 Hz; ^2J(P(V)—P(V)), 1.5 ± 1.5 Hz. It is of interest that the coupling ^2J(P(III)—P(III)) can vary substantially with the degree of sulphurization of the other pair of geminal phosphorus atoms, even though there is a separation of six bonds, so that it is unlikely that the effect is an electronic one transmitted through the chemical bonds. Indeed, comparison of the diastereomeric pair **5** and **6** shows that this geminal coupling is markedly sensitive to the conformational relationships in these species. It is known[11] that electron lone-pair interactions can affect ^2J(P(III)—P(III)) very significantly, and we therefore suggest that the relative orientation of the lone pairs on $P_{A'}$ and $P_{B'}$ [which will determine $^2J(P_{A'}P_{B'})$] is affected by their interaction with the lone pair of P_X, and that the extent of this interaction is in turn affected by the P_X/P_A and P_X/P_B lone pair interactions. This then would provide a mechanism for the apparent transmission of the effect over as many as six single bonds.

In conformity with the above, the vicinal couplings ^3J(P(III)—P(III)) also show very large differences (ranging from 0.0–38.6 Hz) which are also clearly due to conformational effects. ^3J(P(III)—P(V)) and ^3J(P(V)—P(V)) are also conformationally dependent, but to a lesser extent.

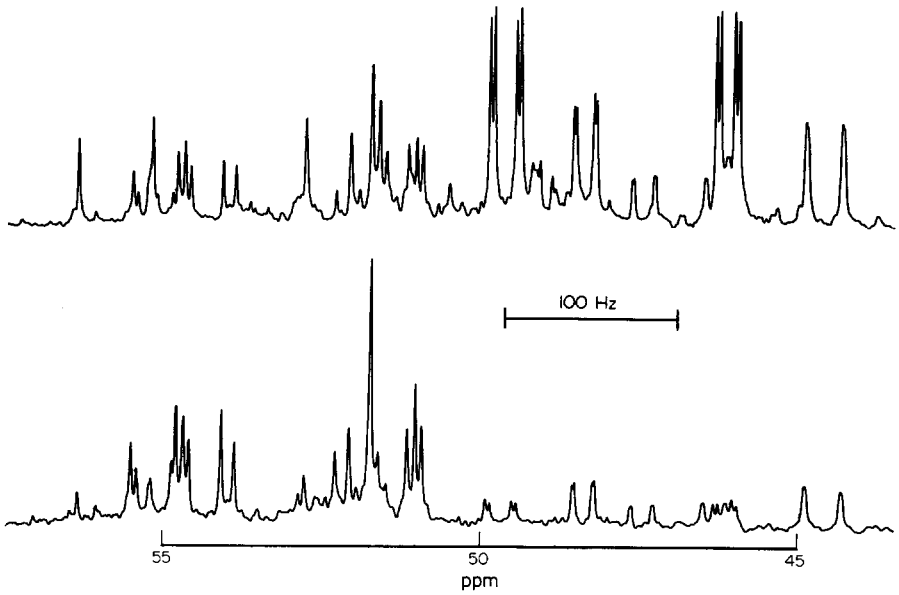

Fig. 4. Expansions of the P(V) region of the ^{31}P spectrum at 36.2 MHz of the mixtures obtained by the reaction between **3** and elemental sulphur. Lower trace: 2.0 atomic equivalents of sulphur added. Upper trace: 3.5 atomic equivalents of sulphur added.

EXPERIMENTAL

^{31}P NMR spectra were obtained from solutions in C_6H_6/C_6D_6 at room temperature on a JEOL FX 90Q multinuclear spectrometer operating at 36.2 MHz under conditions of broadband proton decoupling. Spectra displaying second-order effects were analysed using a computer program based upon LAOCOON. 2D homonuclear ^{31}P *J*-spectra were obtained using a standard 90°-t_1/2-180°-t_1/2-Acq.(t_2) pulse sequence[10] with appropriate cycling of the transmitter and receiver phases to minimize artefacts, and the resulting data matrices were transformed and manipulated using JEOL software. All materials were handled under an atmosphere of dry oxygen-free dinitrogen.

Bis(2,2 - *bis*(*diphenylphosphino*)*ethyl*)*phenylphosphine*

A solution of phenylphosphine (1 g, 9.1 mmol) and 1,1-bis(diphenylphosphino)ethene[11] (7.2 g, 18.2 mmol) containing a catalytic amount of KOBu^t in dry thf (100 cm^3) was refluxed for 0.3 h. Removal of solvent under vacuum yielded an oily residue which gave a powdery white precipitate on addition of methanol (50 cm^3). This was recrystallized from CH_2Cl_2/MeOH to give the product as white crystals, m.p. 154°. (yield 7.0 g, 85%.) Found: C 77.0, H 5.8, P 17.2%; $C_{58}H_{51}P_5$ requires: C 77.2, H 5.7, P 17.2%.

Bis(2,2 - *bis*(*diphenylphosphino*)*ethyl*)*phenylphosphinepentasulphide*

The room temperature reaction between **3** and elemental sulphur in benzene was followed by ^{31}P NMR as described in the main text. After the addition of five atomic equivalents of sulphur and warming to 50° the spectrum indicated that only pentasulphide **23** was present and this was precipitated by addition of methanol and was recrystallized from CH_2Cl_2/MeOH as white crystals, m.p. 201°C. Found: C 65.5, H 4.7, P 14.2%; $C_{58}H_{51}P_5S_5$ requires C 65.5, H 4.8, P 14.6%.

Acknowledgements—We thank the SERC for support and Mr B. Saunderson for microanalyses.

REFERENCES

1. R. J. Puddephatt, *Chem. Soc. Rev.* 1983, **12**, 99; J. Chatt and H. R. Watson, *J. Chem. Soc.* 1961, 4980; J. A. Connor, J. P. Day, E. M. Jones and G. K. McEwen, *J. Chem. Soc., Dalton Trans.* 1973, 347; S. O. Grim, W. L. Briggs, R. C. Barth, C. A. Tolman and J. P. Jesson, *Inorg. Chem.* 1974, **13**, 1095; P. F. Crossing and M. R. Snow, *J. Chem. Soc., A* 1971, 610; S. S. Sandhu and A. K. Mehta, *J. Organomet. Chem.* 1974, **77**, 45; G. J. Palenik, W. L. Steffen, M. Mathew, M. Li and D. W. Meek, *Inorg. Nucl. Chem. Lett.* 1974, **10**, 125; G. J. Palenik, M. Mathew, W. L. Steffen and G. Beran, *J. Am. Chem. Soc.* 1975, **97**, 1059.

2. K. Issleib and H. P. Abicht, *J. Prakt. Chem.* 1970, **312**, 456; H. H. Karsch, *Z. Naturforsch.* 1979, **34b**, 1171.
3. J. Chatt and F. A. Hart, *J. Chem. Soc.* 1960, 1378; J. Chatt, G. J. Leigh and N. Thankarajan, *J. Organomet. Chem.* 1971, **29**, 105.
4. J. L. Bookham, W. McFarlane and I. J. Colquhoun, *J. Chem. Soc., Chem. Commun.* 1986, 1041.
5. L. Almasi, *Sulfur in Org. Inorg. Chem.* 1982, **4**, 47.
6. R. J. Angelici and C. M. Ingemanson, *Inorg. Chem.* 1969, **8**, 83; G. E. Coates, C. Kowala and J. M. Swan, *Aust. J. Chem.* 1966, **19**, 539.
7. S. O. Grim and J. D. Mitchell, *Inorg. Chem.* 1977, **16**, 1763; S. O. Grim and E. D. Walton, *Inorg. Chem.* 1980, **19**, 1982.
8. S. O. Grim, L. C. Satek and J. O. Mitchell, *Z. Naturforsch.* 1980, **35b**, 832; S. O. Grim and E. D. Walton, *Phosphorus and Sulphur*, 1980, **a**, 123.
9. I. J. Colquhoun and W. McFarlane, *J. Chem. Soc., Chem. Commun.* 1982, 484.
10. W. P. Aue, J. Karhan and R. R. Ernst, *J. Chem. Phys.* 1976, **64**, 4226.
11. R. Keat, L. Manojlovic-Muir, K. W. Muir and D. S. Rycroft, *J. Chem. Soc., Dalton Trans.* 1981, 2192.

Polyhedron Vol. 7, No. 2, pp. 137–142, 1988
Printed in Great Britain

0277–5387/88 $3.00+.00
Pergamon Journals Ltd

A NEW ALLOSTERIC BIS CROWN ETHER LIGAND CONTAINING A 2,2′-BIPYRIDYL FRAGMENT

PAUL D. BEER* and ANNE S. ROTHIN

Department of Chemistry, University of Birmingham, P.O. Box 363, Birmingham B15 2TT, U.K.

(*Received* 3 *July* 1987; *accepted* 24 *August* 1987)

Abstract—The synthesis of a new allosteric bis crown ether ligand incorporating a 2,2′-bipyridyl function and two benzo-15-crown-5 subunits is described. Chelation of Ru(II) at the bipyridyl nitrogens forces the bipyridyl function towards coplanarity, restricting the conformational freedom of the two benzo-15-crown-5 binding units in such a way as to favour the formation of an intramolecular sandwich complex with sodium. A variety of bimetallic complexes have been isolated resulting from the simultaneous coordination of transition metals at the bipyridyl fragment and alkali metals at the crown ether moieties.

The construction of multisite molecular receptor molecules capable of binding sequentially two or more guest metal cations in close proximity to one another is of considerable current interest in the chemical literature.[1–4] Such molecular systems may exhibit allosteric behaviour,[5–7] resulting from the transmission of binding information from one coordinating site to another and hence serve as models of relevance to biological systems. Here we describe the synthesis and binding properties of a new bis crown ether ligand (L) designed to exhibit allosteric behaviour by the chelation of a transition metal at the bipyridyl function restricting the conformational freedom of the two benzo-crown ether binding sites.

RESULTS AND DISCUSSION

The ligand (L) was prepared in good yields by the condensation of 3,3′-dimethylol-2,2′-bipyridine[8] (**1**) with two moles of 4-chloromethylbenzo-15-crown-5[9] (**2**). (Scheme 1.) Its structure was verified by elemental analysis, mass spectrometry and ^{1}H and ^{13}C NMR spectroscopy (Tables 1 and 2).

Refluxing (L) with an excess of sodium hexafluorophosphate in methanol led to the successful isolation of a crystalline complex $L \cdot 2Na^+PF_6^-$.

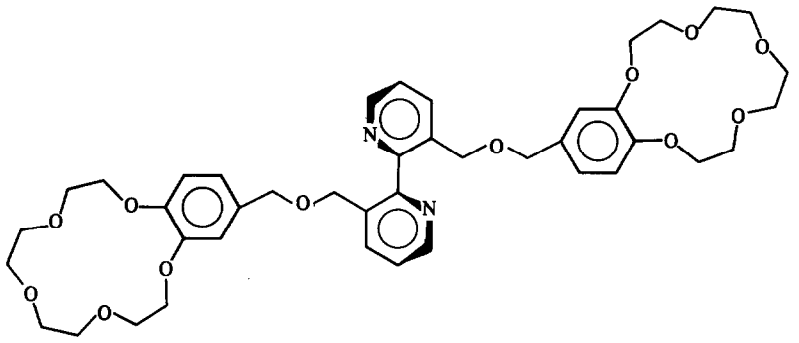

(L)

This result was confirmed by conductivity measurements (Λ = 244 ohm^{-1} cm^2 mol^{-1}) and suggests that the two benzo-15-crown-5 moieties of (L) are acting independently of one another, each complexing a sodium cation (**3**).

Molecular models (C.P.K.) suggested that chelation of a transition metal at the bipyridyl nitrogens

*Author to whom correspondence should be addressed.

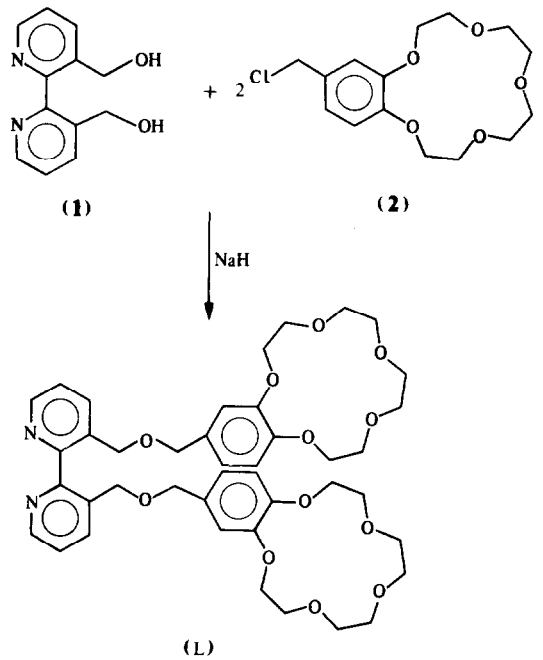

Scheme 1.

would force the bipyridyl function towards coplanarity resulting in the restriction of conformational freedom of the two benzo-crown ether groups in such a way as to favour the formation of an intramolecular sandwich complex with an alkali metal cation. (Scheme 2.)

The reaction of (L) with $(bipy)_2RuCl_2 \cdot 2H_2O$[10] followed by an excess of sodium hexafluorophosphate gave $[(bipy)_2RuLNa]^{3+}(PF_6^-)_3$ as an orange crystalline solid ($\lambda_{max} = 456$ nm $\varepsilon = 1.57 \times 10^4$ mol^{-1} cm^{-1}).

This observed stoichiometry, again confirmed by conductivity measurements ($\Lambda = 384$ ohm^{-1} cm^2 mol^{-1}), suggests that the sodium guest cation now forms an intramolecular sandwich complex with the two benzo-crown ether groups, aided by this allosteric effect of the chelation of Ru(II) at the bipyridyl function (**4**).

The results of cyclic voltammetry measurements in acetonitrile of the monometallic $[(bipy)_2RuL]^{2+}(PF_6^-)_2$ complex are reported in Table 3. Addition of one equivalent of sodium hexafluorophosphate to the electrochemical acetonitrile solutions of $[(bipy)_2RuL]^{2+}(PF_6^-)_2$ had little effect ($\Delta E_{1/2} \leqslant 20$ mV) on the respective oxidation and reduction waves of the complex, the sodium cation being bound too far away to influence the electron density at Ru(II).

The results of analogous complexing experiments with potassium, ruthenium and platinum are reported in Table 4. It is interesting to note that potassium forms a 1 : 1 complex with the free ligand

Table 1. ^{1}H NMR data (CD_3COCD_3) of L

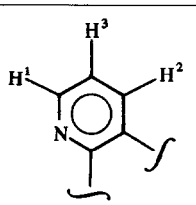

$J_{12} = 2$ Hz
$J_{13} = 5$ Hz
$J_{23} = 8$ Hz

Proton	δ ppm	Integration
H^1	8.51(d of d)	2
H^3	7.43(d of d)	2
H^2	8.03(d of d)	2
Aromatics	6.82–6.71(m)	6
bipy-CH_2-O	4.54(s)	4
Ar-CH_2-O	4.29(s)	4
Crown-OCH_2	4.05–3.65(m)	32

Table 2. ^{13}C NMR data ($CDCl_3$) of L

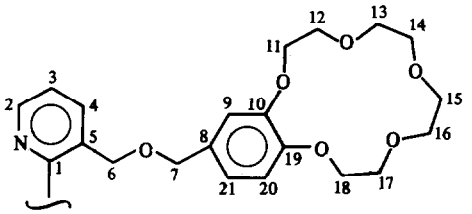

δ (ppm)	Assignment
68.4 69.1 69.5 (2)[a] 70.5 (2)[a] 71.0 (2)[a]	Crown OCH_2 (C^{11}–C^{18})
72.6	C^7
75.8	C^6
113.9 (2)[a]	C^9, C^{20}
120.9	C^{21}
123.1	C^4
131.0	C^8
133.3	C^5
136.4	C^3
147.4	C^2
148.7	C^{19}
149.1	C^{10}
155.7	C^1

[a] Relative integration.

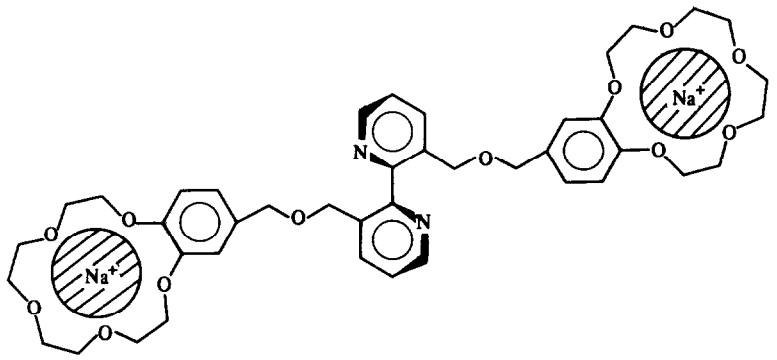
Na+
Na+

(3)

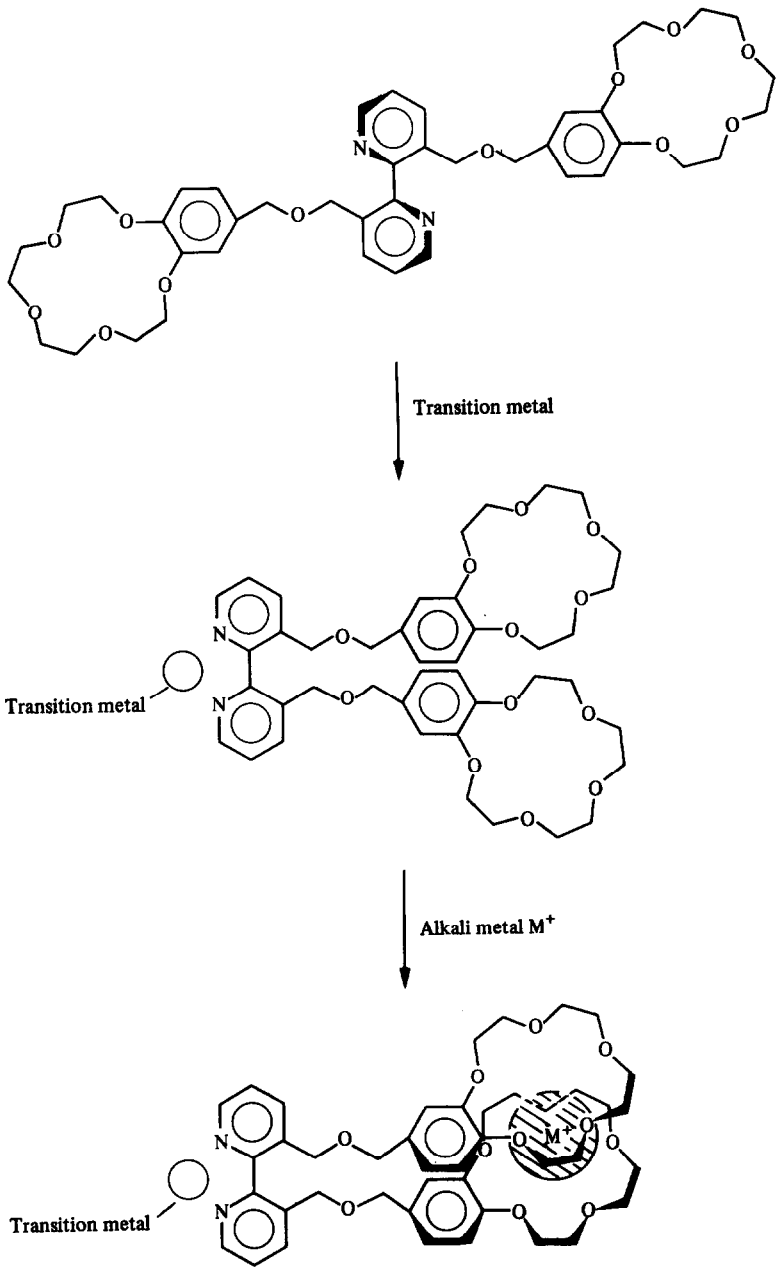
Transition metal
Transition metal
Alkali metal M+
Transition metal
M+

Scheme 2.

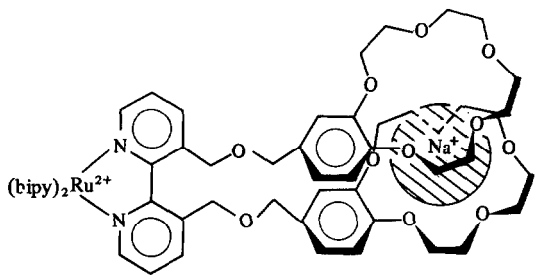

(4)

(L) in spite of the absence of chelation of a transition metal at the bipyridyl allosteric site.

We are currently extending our studies to preparing related L-transition metal–alkali metal bi- and poly-metallic complexes of catalytic interest.

EXPERIMENTAL

General

^{1}H NMR spectra were recorded at 400 MHz and ^{13}C NMR spectra at 67.8 and 100 MHz using TMS as internal standard: 3,3′-Dimethylol-2,2′-bipyridine,[8] 4-chloromethylbenzo-15-crown-5[9] and $RuCl_2(bipy)_2 \cdot 2H_2O$[10] were prepared according to literature methods. Tetrahydrofuran was dried by distillation from sodium, methanol by distillation from magnesium methoxide and acetonitrile from calcium hydride.

Syntheses

Preparation of (L)

Sodium hydride oil dispersion (0.30 g) was added to a solution of 3,3′-dimethylol-2,2′-bipyridine (0.10 g, 0.46 mmol) in dry THF (30 cm^3) under nitrogen. The solution was heated to reflux for 24 h and then cooled to room temperature. A solution of 4′-chloromethylbenzo-15-crown-5 (0.29 g, 0.92 mmol) in dry THF (20 cm^3) was added dropwise with stirring. The resulting mixture was stirred at room temperature for 2 h and then refluxed overnight. After cooling to room temperature, water (2 cm^3) was added dropwise to destroy excess NaH and the solution was evaporated to dryness. The residue was taken up in water (25 cm^3) and extracted with $CHCl_3$ (4×25 cm^3). The chloroform extracts were dried with $MgSO_4$ and evaporated to give the crude product as a yellow oil. This was purified by column chromatography on alumina using CH_2Cl_2/MeOH (99 : 1% v/v) as eluant. The appropriate fraction was collected and evaporated to dryness to give the product as a pale yellow oil. Yield 0.24 g, 67%. On repeat preparations yields in the range 56–77% were obtained. Found: C, 64.6; H, 6.5; N, 3.8. $C_{42}H_{52}N_2O_{12}$. Calc: C, 64.9; H, 6.8; N, 3.6, $m/z = 776$.

Preparation of $L \cdot 2NaPF_6$

The ligand (50.1 mg, 0.064 mmol) was dissolved in methanol (3 cm^3) and a solution of sodium hexafluorophosphate (32.5 mg, 0.19 mmol) in methanol (2 cm^3) added. The solution was heated to reflux under nitrogen for 1 h, cooled to room temperature and evaporated to dryness. The residue was extracted with chloroform, filtered and the volume of the filtrate reduced to *ca.* 5 cm^3. *n*-Hexane and diethylether were added to precipitate the product as a white powder. The solid was recrystallized twice from chloroform/ether/*n*-hexane and dried *in vacuo*. Yield 17.2 mg, 24%.

Preparation of $[(bipy)_2Ru(L)](PF_6)_2 \cdot 2H_2O$

$[(bipy)_2RuCl_2] \cdot 2H_2O$ (0.0594 g, 0.11 mmol) and the ligand (0.0882 g, 0.11 mmol) in methanol (10

Table 3. Electrochemical data

	$Ru^{2+/1+}$		$Ru^{1+/0}$		$Ru^{0/-1}$		$Ru^{2+/3+}$	
Complex	$E_{1/2}{}^a$ (V)	$\Delta E_p{}^b$ (mV)	$E_{1/2}{}^a$	$\Delta e_p{}^b$	$E_{1/2}{}^a$	$\Delta E_p{}^b$	$E_{1/2}{}^a$	$\Delta E_p{}^b$
$[(bipy)_2RuL]^{2+}(PF_6^-)_2$	−1.29	90	−1.47	100	−1.71	100	+1.30	80
$[(bipy)_2RuL]^{2+}(PF_6^-)_2 + Na^+$	−1.29	80	−1.48	90	−1.70	100	+1.31	80

[a] Obtained from cyclic voltammetry studies in dry acetonitrile solvent containg 0.2 M $[Bu^n{}_4N]BF_4$ as supporting electrolyte. Solutions were *ca.* 2×10^{-3} M in complex and measurements were made at 21 ± 1°C at 0.2 Vs^{-1} scan rate, with reference to ferrocene as internal standard but are quoted relative to the saturated calomel reference electrode.

[b] Separation between anodic and cathodic peak potentials, ΔE_p for ferrocene under the same conditions was 90 mV. No compensation was made for internal cell resistance.

Table 4. Conductivity and microanalytical data[a]

Complex	Analysis[a] % C	H	N	Λ (ohm^{-1} cm^2 mol^{-1})
L·2NaPF$_6$	45.3(45.3)	4.9(4.7)	2.7(2.5)	244
[(bipy)$_2$RuL]$^{2+}$(PF$_6^-$)$_2$·2H$_2$O	48.9(49.1)	4.6(4.8)	5.9(5.5)	243
[(bipy)$_2$RuLNa]$^{3+}$(PF$_6^-$)$_3$	45.3(45.2)	4.5(4.2)	5.4(6.0)	384
L·KPF$_6$	52.2(52.5)	5.7(5.5)	2.8(2.9)	125
[(bipy)$_2$RuLK]$^{3+}$(PF$_6^-$)$_3$	45.0(44.7)	4.3(4.1)	5.3(5.1)	376
[Cl$_2$PtLK]$^+$(PF$_6^-$)	40.6(41.1)	4.5(4.3)	2.8(2.3)	136

[a] Calculated values given in parentheses.

cm^3) and water (15 cm^3) were refluxed together overnight under nitrogen. The solution was cooled and the methanol removed on the rotary evaporator. NH_4PF_6 (0.2 g, excess) in water (1 cm^3) was added to give an orange precipitate. The solid was recovered by filtration and dissolved in acetone. The solution was dried with $MgSO_4$, filtered and treated with diethylether to precipitate the product. The solid was recrystallized from acetone/ethanol and dried *in vacuo* at 50°C. Yield 86 mg, 51%.

Preparation of [Ru(L)(bipy)$_2$Na](PF$_6$)$_3$

[Ru(bipy)$_2$L](PF$_6$)$_2$ (51.5 mg, 0.035 mmol) and NaSCN (12.1 mg, 0.15 mmol) in methanol (10 cm^3) were heated to reflux for 1.5 h. The solution was cooled and NH_4PF_6 (30 mg, excess) added. The volume of the solution was reduced to half and the solid filtered off. The product was recrystallized from acetone/diethylether. Yield 14.7 mg, 26%.

Prepatation of LKPF$_6$

The ligand (0.1041 g, 0.13 mmol) was dissolved in dry methanol (3 cm^3) and a solution of potassium hexafluorophosphate (0.0597 g, 0.32 mmol) in dry methanol (2 cm^3) added. The mixture was heated to reflux under nitrogen for 1 h, cooled and filtered. The solvent was removed on a rotary evaporator and the oily residue treated with several portions of ether and ethanol which were removed on the rotary evaporator. A cream powder was obtained. This was dissolved in chloroform and the solution filtered. The filtrate was evaporated to dryness and the residue recrystallized from methanol/ether/*n*-hexane to give the product as a white powder. Dried *in vacuo*. Yield 0.074 g, 57%.

Preparation of [(bipy)$_2$Ru(L)K](PF$_6$)$_3$

[(bipy)$_2$Ru(L)](PF$_6$)$_2$ (0.0504 g, 0.034 mmol) and KSCN (9 mg, 0.093 mol) in methanol (10 cm^3) were heated to reflux under nitrogen for 1.5 h. The solution was cooled to room temperature and NH_4PF_6 (30 mg, excess) in methanol (1 cm^3) was added. An orange solid precipitated immediately. The volume of the solution was reduced to half and the solid filtered off. Yield of crude product 44.2 mg. Recrystallized from acetone/ethanol/ether. Yield 29.2 mg, 51%.

Preparation of [Cl$_2$PtL(K)](PF$_6$)

The ligand (0.089 g, 0.115 mmol) was dissolved in dry methanol (20 cm^3) and a solution of K_2PtCl_4 (0.048 g, 0.115 mmol) in water (3 cm^3) added. The solution was stirred at room temperature for 3 h. Ammonium hexafluorophosphate (0.11 g, 0.67 mmol) was added and the mixture warmed to 50–60°C for 30 min, cooled, the volume reduced by half and the pale yellow precipitate filtered off. The solid was washed with ethanol (20 cm^3) and dissolved in acetone. The solution was filtered and the filtrate was treated with ethanol to give the product as a pale yellow powder. Dried *in vacuo*. Yield 0.0813 g, 58%.

Conductivity studies[11]

Conductivity measurements were carried out using a PT1–58 digital conductivity meter at concentrations of 10^{-3}–10^{-4} M in dry acetonitrile and temperature 20–22°C.

Electrochemistry

Cyclic voltammetry studies were carried out using a PAR 174A polarographic analyser and a Pt bead working electrode.

Acknowledgement—We thank the SERC for a post-doctoral research fellowship to A.S.R and for use of the high field NMR service at the University of Warwick.

REFERENCES

1. J. M. Lehn, *Pure and Applied Chem.* 1980, **52**, 2441.
2. A. Carroy and J. M. Lehn, *J. Chem. Soc., Chem. Commun.* 1986, 1232.
3. J. C. Chambron and J. P. Sauvage, *Tetrahedron Lett.* 1986, **27**, 865.
4. P. D. Beer, *J. Chem. Soc., Chem. Commun.* 1986, 1678.
5. J. Rebek, Jr. *Acc. Chem. Res.* 1984, **17**, 258.
6. I. Tabushi, S. Kugimiya and T. Sasaki, *J. Am. Chem. Soc.* 1985, **107**, 5159.
7. J. Rebek, Jr., T. Costello, L. Marshall, R. Wattley, R. C. Gadwood and K. Oman, *J. Am. Chem. Soc.* 1985, **107**, 7481.
8. J. Rebek, Jr., J. E. Trend, R. V. Wattley and S. Chakravorti, *J. Am. Chem. Soc.* 1979, **101**, 4333.
9. A. H. Haines, I. Hodgkisson and C. Smith, *J. Chem. Soc. Perkin Trans. I* 1983, 311.
10. P. A. Lay, A. M. Sargeson and H. Taube, *Inorg. Synth.* 1986, **24**, 291.
11. R. J. Angelici, *Synthesis and Techniques in Inorganic Chemistry*, 2nd Edn. W. B. Saunders, Philadelphia, U.S.A. (1977).

Polyhedron Vol. 7, No. 2, pp. 143–146, 1988
Printed in Great Britain

0277–5387/88 $3.00+.00
© 1988 Pergamon Journals Ltd

THORIUM(IV) NITRATE COMPLEXES WITH SOME SCHIFF BASES OF 4-AMINOANTIPYRINE AND CERTAIN CARBONYL COMPOUNDS

BABU KUNCHERIA and P. INDRASENAN*

Department of Chemistry, University of Kerala, Trivandrum 695 034, India

(*Received* 28 *January* 1987; *accepted after revision* 26 *August* 1987)

Abstract—Ten new complexes of thorium(IV) nitrate with some Schiff bases derived from 4-aminoantipyrine and certain carbonyl compounds such as benzaldehyde, 2-nitrobenzaldehyde, 3-nitrobenzaldehyde, 4-methylbenzaldehyde, 4-N,N-dimethylaminobenzaldehyde, 2-hydroxybenzaldehyde, 2-hydroxyacetophenone, acetylacetone, benzoylacetone and 2-hydroxy-1-naphthaldehyde have been synthesized and characterized by elemental analysis, molecular weight determination, and spectral and conductance studies.

As part of our programme for the synthesis and characterization of actinide complexes,[1] we report on some Schiff base complexes of thorium. Thorium forms complexes with acetylacetonate, 8-quinolinol[2–4] and with bi, tri and tetradentate Schiff bases,[5–9] and with antipyrine, 4-aminoantipyrine and 4-dimethylaminoantipyrine.[10,11] In this paper we report the synthesis and characterization of a series of ten new complexes of thorium(IV) nitrate with some Schiff bases derived from 4-aminoantipyrine and ten carbonyl compounds such as benzaldehyde, 2-nitrobenzaldehyde, 3-nitrobenzaldehyde, 4-methylbenzaldehyde, 4-N,N-dimethylaminobenzaldehyde, 2-hydroxybenzaldehyde, 2-hydroxyacetophenone, acetylacetone, benzoylacetone and 2-hydroxy-1-naphthaldehyde.

EXPERIMENTAL

Reagents

Thorium nitrate was obtained commercially (BDH, 99.9% pure) and used without further purification. The following ten Schiff bases were prepared by condensing equimolar amounts of 4-aminoantipyrine and the appropriate carbonyl compounds in ethanol under reflux conditions for 2–3 h. On cooling, yellow coloured Schiff bases were crystallized out and these were recrystallized from hot ethanol. The Schiff bases so prepared are 4N-(benzylidene)-aminoantipyrine (BAAP), 4N-(2′-nitrobenzylidene)-aminoantipyrine (*o*-NBAAP), 4N-(3′-nitrobenzylidene)-aminoantipyrine (*m*-NBAAP), 4N-(4′-methylbenzylidene)-aminoantipyrine (*p*-MBAAP), 4N-(4′-N,N-dimethylaminobenzylidene)-aminoantipyrine (ABAAP), 4N-(2′-hydroxybenzylidene)-aminoantipyrine (HBAAP), 4N-(2′-hydroxyacetophenylidene) - aminoantipyrine (HAPAAP), 4N-(acetylisopropylidene)-aminoantipyrine (AIPAAP), 4N-(benzoylisopropylidene)-aminoantipyrine (BIPAAP) and 4N-(2 - hydroxy - 1′ - naphthylidene) - aminoantipyrine (HNAAP). The purities of these Schiff bases were checked by TLC and IR spectral analysis.

Preparation and analysis of the complexes

The complexes were prepared by the following general method. Solutions of thorium nitrate (2 mmol) and the Schiff base (6.5 mmol) in minimum quantities of hot dry acetone were mixed and the resulting solution was kept under reflux for 2–3 h. The reaction mixture was concentrated to a viscous dark brown mass which on washing several times with hot benzene to remove excess ligand gave a brownish–yellow solid mass. This solid mass was dissolved in a minimum quantity of dry acetone and the solution was stirred vigorously with the addition of dry diethylether and the complex crystallized out,

*Author to whom correspondence should be addressed.

Table 1. Analytical,[a] molecular weight[a] and conductance[b] data of thorium(IV) nitrate complexes with some Schiff bases

Compound	% Metal	% Carbon	% Hydrogen	% Nitrogen	Molecular weight	Molar conductance[b]	
						Acetonitrile	Nitrobenzene
$[Th(BAAP)_3(NO_3)_3]NO_3$	16.9	47.6	3.4	13.6	1308	132.0	20.6
	(17.2)	(47.9)	(3.8)	(13.5)	(1353)		
$[Th(o\text{-}NBAAP)_3(NO_3)_3]NO_3$	15.5	43.9	3.6	15.4	1535	168.9	21.6
	(15.6)	(43.6)	(3.2)	(15.0)	(1488)		
$[Th(m\text{-}NBAAP)_3(NO_3)_3]NO_3$	15.4	43.9	3.5	15.5	1540	173.6	22.1
	(15.6)	(43.6)	(3.2)	(15.9)	(1488)		
$[Th(p\text{-}MBAAP)_3(NO_3)_2]NO_3$	16.3	49.5	3.8	12.9	1438	131.8	20.2
	(16.6)	(49.0)	(4.1)	(13.0)	(1395)		
$[Th(ABAAP)_3(NO_3)_3]NO_3$	15.5	48.7	4.6	15.3	1520	214.6	22.0
	(15.7)	(48.6)	(4.5)	(15.1)	(1482)		
$[Th(HBAAP)_2(NO_3)_3]NO_3$	21.2	38.2	3.7	11.5	1050	126.5	16.5
	(21.3)	(39.5)	(3.1)	(12.0)	(1094)		
$[Th(HAPAAP)_2(NO_3)_3]NO_3$	20.3	40.9	3.7	12.8	1250	128.5	16.9
	(20.7)	(40.6)	(3.4)	(12.5)	(1122)		
$[Th(AIPAAP)_2(NO_3)_3]NO_3$	30.2	36.3	3.7	12.8	1095	1067	16.8
	(30.3)	(36.6)	(3.6)	(13.3)	(1050)		
$[Th(BIPAAP)_2(NO_3)_3]NO_3$	19.5	43.2	3.8	12.2	1221	144.8	16.9
	(19.8)	(42.9)	(3.6)	(11.9)	(1174)		
$[Th(HNAAP)_2(NO_3)]NO_3$	21.3	49.2	3.6	11.1	1100	127.8	17.0
	(21.7)	(49.4)	(3.4)	(10.5)	(1068)		

[a] Calculated values in parentheses.

[b] $Ohm^{-1}\ cm^2\ mol^{-1}$; the concentration $\upsilon 10^{-3}$ M.

Table 2. Important IR spectral bands of thorium(IV) nitrate with some Schiff bases

Compound	Important IR spectral bands (in cm^{-1})							
	ν_{O-H}	$\nu C{=}O$ (side chain)	$\nu C{=}O$ (ring)	$\nu C{=}N$	$\nu 4(NO_3)$	$\nu 3(NO_3)$	$\nu 1(NO_3)$	$n2(NO_3)$
BAAP			1640s	1590m				
$[Th(BAAP)_3(NO_3)_3]NO_3$			1610m	1560m	1510s	1380s	1280s	1020m
***o*-NBAAP**			1640s	1590m				
$[Th(o\text{-}NBAAP)_3(NO_3)_3]NO_3$			1610m	1560m	1510s	1385s	1285s	1020m
***m*-NBAAP**			1640s	1590m				
$[Th(m\text{-}NBAAP)_3(NO_3)_3]NO_3$			1610m	1560sh	1510s	1380s	1280s	1020m
***p*-MBAAP**			1640s	1590s				
$[Th(p\text{-}MBAAP)_3(NO_3)_3]NO_3$			1610s	1560s	1510s	1385s	1285s	1020s
ABAAP			1640s	1590s				
$[Th(ABAAP)_3(NO_3)_3]NO_3$			1610m	1560m	1510s	1380s	1280s	1020m
HBAAP	3440br		1640s	1580s				
$[Th(HBAAP)_2(NO_3)_3]NO_3$	3400br		1610m	1540s	1505s	1380s	1280s	1020m
HAPAAP	3440br		1640s	1580s				
$[Th(HAPAAP)_2(NO_3)_3]NO_3$	3400br		1610s	1540s	1510s	1380s	1290s	1020m
AIPAAP		1680s	1620s	1580s				
$[Th(AIPAAP)_2(NO_3)_3]NO_3$		1610m	1610m	1540s	1510s	1380s	1280s	1020w
BIPAAP		1670s	1620s	1580s				
$[Th(BIPAAP)_2(NO_3)_3]NO_3$		1610m	1610m	1540s	1505s	1380s	1290s	1020m
HNAAP	3440br		1640s	1580s				
$[Th(HNAAP)_2(NO_3)]NO_3$	Absent		1600s	1540s	1510s	1380s	1280s	1020m

Abbreviations: s = strong; m = medium; w = weak; sh = shoulder; br = broad.

which was dried *in vacuo* over phosphorus(V) oxide.

The complexes were analysed for the thorium content by the oxalate–oxide method.[12] The carbon, hydrogen and nitrogen contents of the complexes were determined by microanalysis. (Carried out by the Central Drug Research Institute, Lucknow, India on a payment basis.)

Physical measurements

Molar conductivities of the complexes in acetonitrile and nitrobenzene ($\sim 10^{-3}$ M solutions) were measured at room temperature ($28 \pm 2°C$) using an ELICO conductivity bridge type Cm 82 with a dip-type cell (type CC-03) having platinum electrodes (cell constant, 1.33 cm^{-1}). The IR spectra of the ligands (Schiff bases) and the complexes were recorded in the 400–4000 cm^{-1} range on a Perkin–Elmer 397 IR spectrophotometer using KBr disc techniques. The molecular weights of the complexes ($\sim 10^{-3}$ M solutions) were determined by the cryscopic method using nitrobenzene as the solvent.[13]

RESULTS AND DISCUSSION

All the complexes are non-hygroscopic brownish–yellow crystalline solids which are soluble in acetone, acetonitrile, methanol, ethanol, chloroform and dimethylformamide and are insoluble in benzene, carbon tetrachloride, petroleum ether and diethyl ether. Analytical and molecular weight data (Table 1) show that five of the complexes have the general formula $ThL_3(NO_3)_4$ (where L = BAAP, *o*-NBAAP, *m*-NBAAP, *p*-MBAAP and ABAAP), the next four have the general formula $ThL_2(NO_3)_4$ (where L = HBAAP, HAPAAP, AIPAAP and BIPAAP) and the last one has the formula $Th(HNAAP)_2(NO_3)_2$.

From the conductance data (Table 1) it is seen that all the complexes behave as 1 : 1 electrolytes.[14,15] However, in acetonitrile slightly higher conductance values than those expected for 1 : 1 electrolytes, are observed for most of the complexes. These discrepancies are probably due to partial replacement of the coordinated nitrate groups by the solvent molecules (acetonitrile).

The important IR spectral bands of the free ligands and those of the complexes are presented in Table 2. The shifts in the frequencies of υC=O(ring) and υC=N for all the ten complexes indicate that both these groups are coordinated to the metal ion. For the complexes of AIPAAP and BIPAAP, the side chain C=O group is also coordinated. The hydroxy groups of HBAAP, HAPAAP and HNAAP are also coordinated to the metal ion in addition to the ring C=O and C=N groups. In the case of HNAAP, deprotonation is indicated by the absence of υ_{OH} in the spectrum of the complex. The IR spectra of the complexes also suggest that all the nitrate groups except one are coordinated to the metal ion in a bidentate fashion.[16] The following three sets of formulae are suggested for the present complexes: $[ThL_3(NO_3)_3]NO_3$ (where L = BAAP, *o*-NBAAP, *m*-NBAAP, *p*-MBAAP and ABAAP), $[ThL_2(NO_3)_3]NO_3$ (where L = HBAAP, HAPAAP, AIPAAP and BIPAAP) and $[Th(HNAAP)_2NO_3]NO_3$. The exact geometries of these complexes require single crystal X-ray analysis which is not available.

Acknowledgements—The authors are grateful to the Central Drug Research Institute (Lucknow, India) for doing the CHN analysis of the complexes and also to the University Grants Commission (India) for awarding a Teacher-fellowship to B.K. under the Faculty Improvement Programme.

REFERENCES

1. G. Sobhanadevi and P. Indrasenan, *Inorg. Chim. Acta* 1987, **133**, 157.
2. R. G. Young and J. J. Kovitz, *Inorg. Synth.* 1946, **2**, 123.
3. M. M. Jones, *J. Am. Chem. Soc.* 1959, **81**, 3188.
4. T. Moeller and M. V. Ramaniah, *J. Am. Chem. Soc.* 1954, **76**, 2022.
5. H. N. Mohanta and K. C. Dash, *J. Indian Chem. Soc.* 1977, **54**, 166.
6. K. C. Dash and H. H. Mohanta, *Transition Metal Chem.* 1977, **2**, 229.
7. R. J. Mill and C. E. F. Rickard, *J. Inorg. Nucl. Chem.* 1978, **40**, 793.
8. M. T. El-Haty and F. A. Adam, *Bull. Soc. Chim. Fr.* 1983, **11–12**, 253; *Chem. Abstr.* 1984, **100**, 64887f.
9. M. R. Mahmoud, M. A. Hamed, M. S. Kamel and S. A. El-Gyar, *Monatsh. Chem.* 1985, **116**, 1291.
10. V. V. Savant, P. Ramamurthy and C. C. Patel, *J. Less Common Metals* 1970, **22**, 479.
11. Jacob Chacko, *Synth. React. Inorg. Met.-Org. Chem.* 1982, **12**, 361.
12. A. I. Vogel, *A Textbook of Quantitative Inorganic Analysis*, p.541. Longmans, London (1961).
13. W. G. Palmer, *Experimental Physical Chemistry*, p.119. University Press, Cambridge (1954).
14. G. B. Deacon, J. H. S. Green and R. S. Nyholm, *J. Chem. Soc.* 1965, 3411.
15. D. N. Sathyanarayana and C. C. Patel, *Indian. J. Chem.* 1967, **5**, 360.
16. N. F. Curtis and Y. M. Curtis, *Inorg. Chem.* 1965, **4**, 804.

Polyhedron Vol. 7, No. 2, pp. 147–150, 1988
Printed in Great Britain

0277–5387/88 $3.00+.00
© 1988 Pergamon Journals Ltd

POTENTIOMETRIC STUDIES ON THE COMPLEXATION EQUILIBRIA BETWEEN La(III), Pr(III), Nd(III), Gd(III), Sm(III), Tb(III), Dy(III), Ho(III) AND 2-ACETYLPYRIDINETHIOSEMICARBAZONE (2-APT)

B. S. GARG,* S. R. SINGH, R. B. BASNET and R. P. SINGH

Department of Chemistry, University of Delhi, Delhi 110007, India

(*Received* 19 *February* 1987; *accepted after revision* 26 *August* 1987)

Abstract—Complex formation between trivalent La, Pr, Nd, Gd, Sm, Tb, Dy, Ho and 2-acetylpyridinethiosemicarbazone has been investigated by potentiometric measurements at 25°C and in 0.02 M, 0.05 M, 0.1 M and 0.2 M ($NaClO_4$) ionic strengths. The stability constants of the complexes formed have been determined and correlated to the size and ionic potentials of the metal ions.

Thiosemicarbazones are compounds which act as complexing agents for various metal ions. They have many analytical applications and they are also of interest in various biological systems. 2-Acetylpyridinethiosemicarbazone has been used earlier for the spectrophotometric determination of Cu(II), Ni(II),[1] Fe(II)[2] and Au(III).[3]

We have determined potentiometrically the stability constants of 2-APT with trivalent lanthanons, La, Pr, Nd, Gd, Sm, Tb, Dy, and Ho in 75% (v/v) ethanol–water at various ionic strengths.

EXPERIMENTAL

Reagents and solutions

2-Acetylpyridinethiosemicarbazone (2-APT) was prepared[4] by reacting requisite amounts of thiosemicarbazide (Fluka A. R.) dissolved in ethanol and equimolar amounts of 2-acetylpyridine (Fluka A. R.). A small amount of acetic acid was also added to the reaction mixture. The reaction mixture was boiled under reflux for 6–8 h on a water bath and then cooled overnight in a freezer. The light brown solid was separated by filtration. After crystallization from ethanol, the purity of the compound was checked by m.p., TLC, NMR, IR and UV. Its solution was prepared in ethanol. Me_4NOH (TMAH) (E. Merck, A. G. darmstadt) in 75% ethanol (v/v) was used as titrant. $HClO_4$ was standardized and diluted to the required molarity (0.1 M) with doubly distilled water. $NaClO_4$ (Riedel) was used to maintain that the ionic strength was constant.

The solutions of lanthanon(III) metal ions *viz.* La(III), Pr(III), Nd(III), Gd(III), Sm(III), Tb(III), Dy(III) and Ho(III) were prepared and standardized by conventional methods.

Apparatus

A digital pH meter ECIL, model pH 5651 in conjunction with a glass electrode was used for pH measurements. The pH meter was standardized with potassium hydrogen phthalate and phosphate buffers before performing the titration.

All measurements were made at a definite temperature, maintained constant by using a MLW (NBE type) thermostat. A VAX-11/750 computer was used for computation of equilibrium constants.

Procedure

Investigations have been carried out at four different ionic strengths *viz.* 0.02 M, 0.05 M, 0.1 M and 0.2 M $NaClO_4$ at 25°C. For each set of experiments, the final volume was made up to 20 cm^3 maintaining the 75% (v/v) ethanol medium.

*Author to whom correspondence should be addressed.

The concentrations of $HClO_4$, 2-APT and metal ions in the aforesaid volumes were 0.01, 0.00515 and 0.00051 M respectively. Each set was titrated against 0.1 M TMAH in 75% ethanol.

The titrations were carried out in a covered double walled glass cell in an atmosphere of nitrogen which was presaturated with the solvent (75% ethanol–water), before being passed into the reaction solution. The following sets of solutions have been titrated:

(i) 2.0 cm^3 $HClO_4$ (0.1 M) + 1.0 cm^3 $NaClO_4$ (2.0 M) + 15 cm^3 ethanol + 2.0 cm^3 water.
(ii) 2.0 cm^3 $HClO_4$ (0.1 M) + 1.0 cm^3 $NaClO_4$ (2.0 M) + 10.0 cm^3 ligand (0.01 M) in ethanol + 5.0 cm^3 ethanol + 2.0 cm^3 water.
(iii) 2.0 cm^3 $HClO_4$ (0.1 M) + 1.0 cm^3 $NaClO_4$ (2.0 M) + 10.0 cm^3 ligand (0.01 M) in ethanol + 0.5 cm^3 metal (0.02 M) + 5.0 cm^3 ethanol + 1.5 cm^3 water.

During complexation the acidic proton is replaced by an equivalent amount of metal(III).

From the titration curves of the above sets of solutions (i), (ii) and (iii) the values of $\bar{n}$ and pL have been calculated using the VAX-11/750 computer. The corresponding values of stability constants have been calculated using the weighted least squares method of Sullivan *et al.*[5] The weighted least squares treatment determines the set of β_n values which makes the function:

$$U\left[U = \sum_{n=0}^{N} (y - x - nx)\beta_n x^x\right]$$

nearest to zero, by minimizing

$$S\left[S = \sum_{i=1}^{I} U^2(x_i y_i z_i)\right]$$

with respect to the variation in β_n. We report the S_{min} values for different metal complexes. S_{min} has the same statistical distribution as χ^2 with K degrees of freedom and with weights defined in accordance with Sullivan *et al.*[6] S_{min} can be equated to χ^2. The stability constants thus calculated are given in Table 1.

Table 1. Stability constants of lanthanon(III) chelates of 2-APT at different ionic strengths at temperatures = 25 ± 0.5°C

Stability constant and S_{min} value	Weighted least squares method							
	La	Pr	Nd	Gd	Sm	Tb	Dy	Ho
1	2	3	4	5	6	7	8	9
				(μ = 0.2 M $NaClO_4$, pK_1 = 10.16)				
log K_1	6.82	7.05	7.38	7.51	7.60	7.86	7.88	7.95
log K_2	6.76	6.78	6.80	6.98	7.15	7.25	7.31	7.59
log β_2	13.58	13.83	14.18	14.49	14.75	15.11	15.19	15.54
S_{min}	0.1186	0.1780	0.0864	0.1369	0.0298	0.0067	0.1392	0.1586
				(μ = 0.1 M $NaClO_4$, pK_1 = 10.39)				
log K_1	6.91	7.12	7.54	7.57	7.66	7.81	7.93	8.02
log K_2	6.59	6.86	6.69	7.01	7.25	7.39	7.43	7.68
log β_2	13.50	13.98	14.23	14.58	14.91	15.20	15.36	15.70
S_{min}	0.0679	0.1235	0.0493	0.1176	0.0687	0.1897	0.1496	0.0298
				(μ = 0.05 M $NaClO_4$, pK_1 = 10.56)				
log K_1	7.02	7.33	7.59	7.63	7.79	8.06	8.08	8.15
log K_2	6.73	6.79	6.90	7.10	3.34	7.43	7.52	7.79
log β_2	13.75	14.12	14.49	14.73	15.13	15.49	15.60	15.94
S_{min}	0.1640	0.1589	0.0160	0.0376	0.1206	0.0273	0.1782	0.0918
				(μ = 0.02 M $NaClO_4$, pK_1 = 10.80)				
log K_1	7.14	7.40	7.74	7.84	7.95	8.06	8.24	8.26
log K_2	6.90	7.13	7.25	7.26	7.50	7.67	7.77	7.94
log β_2	14.04	14.53	14.99	15.10	14.45	15.73	16.10	16.20
S_{min}	0.1384	0.0246	0.0648	0.0419	0.0116	0.1780	0.0108	0.1683

RESULTS AND DISCUSSION

For calculation of $\bar{n}$ and pL values we have taken the volume of 19.40 instead of 20 cm^3 due to the volume contraction in the ethanol–water medium. pH correction factors have also been used. The values of $\bar{n}_H$ were calculated at various pH values from the titration curves. The pK_1 of the ligand was obtained by plotting $\log(\bar{n}_H/1\text{-}\bar{n}_H)$ *vs* pH and the values thus obtained were 10.80, 10.56, 10.39 and 10.16 at $\mu = 0.02$ M, 0.05 M, 0.1 M and 0.2 M $NaClO_4$ respectively at 25°C. In these studies the values of dissociation constants were found to decrease with increasing ionic strength of the medium, in agreement with the Debye–Huckel equation.[7]

$$pK_a^c[-A\sqrt{\mu}/1+\alpha\sqrt{\mu}]+C = pK_a.$$

It has been observed that stability from La to Ho follows the same order as increasing acidity. The order of log K values for 2-APT complexes is found to be:

$$La < Pr < Nd < Gd < Sm < Tb < Dy < Ho.$$

The same trend has also been reported by several workers. The log K_1, log K_2, log β_2 and S_{min} values at 25±0.5°C for the trivalent metal ion chelates at different ionic strengths are summarized in Table 1. For these chelates, $\bar{n}$ values greater than 2.0 have not been obtained. We have therefore concluded that not more than two chelates i.e. 1 : 1 and 1 : 2 (M : L) are formed in each system. In view of the fact that very low concentration of metal ions has been used in the titration, it has been assumed that the possibility of poly-nuclear complex formation is negligible. Thermodynamic stability constants obtained by extrapolation of a straight line plot of log K *vs* $\sqrt{\mu}$ to zero ionic strength (Fig. 1) are given in Table 2.

Table 2. Values of thermodynamic stability constants (log K_1^T) of lanthanon(III) complexes of 2-APT at 25±0.5°C

Metal ions	log K_1^T
La	7.60
Pr	7.76
Nd	7.95
Gd	8.16
Sm	8.26
Tb	8.34
Dy	8.49
Ho	8.64

The values of stability constants of lanthanon(III) complexes increase as the ionic radii of the ions decrease. Only two bidentate 2-APT molecules enter into the coordination sphere of lanthanon(III) ions. The remaining coordination protons are apparently occupied by water molecules.

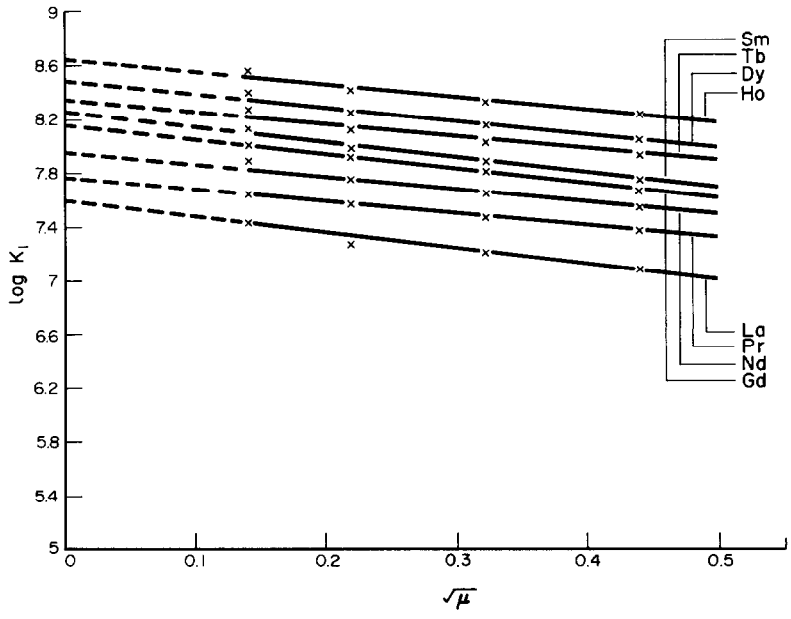

Fig. 1.

REFERENCES

1. H. G. Sanke, S, M. Ahmed and K. N. Thimmaih, *Curr. Sci.* 1983, **52**, 360.
2. H. G. Sanke, K. N. Thimmiah and S. M. Ahmed, *Indian J. Chem.* 1983, **22**, 551.
3. C. K. Bhaskare and S. Devi, *Indian J. Chem.* 1985, **24**, 901.
4. M. P. Martinez, M. Valcarcel and F. Pino, *Anal. Chim. Acta* 1976, **81**, 157.
5. J. C. Sullivan, J. Rydberg and W. F. Miller, *Acta Chem. Scand.* 1959, **13**, 2059.
6. J. Rydberg and J. C. Cullivan, *Acta Chem. Scand.* 1959, **13**, 2023.
7. R. Nasanen and A. Ekman, *Acta Chem. Scand.* 1952, **6**, 1939.

Polyhedron Vol. 7, No. 2, pp. 151–154, 1988
Printed in Great Britain

0277–5387/88 $3.00+.00
© 1988 Pergamon Journals Ltd

SYNTHESIS AND STRUCTURAL FEATURES OF ORGANO Si(IV) IMINE COMPLEXES

KIRAN SINGH, R. V. SINGH and J. P. TANDON*

Department of Chemistry, University of Rajasthan, Jaipur 302004, India

(*Received* 20 *March*, 1987; *accepted after revision* 26 *August* 1987)

Abstract—Complexes of the general formula, Me_2SiL_2 (where, LH = semi- and thiosemicarbazones) have been prepared by reacting dimethylsilicondichloride with the ligand in a 1 : 2 (metalloid : ligand) molar ratio. These complexes have been characterized by elemental analysis, molecular weight determinations and conductivity measurements, and structures have been proposed using electronic, IR, ^1H NMR and ^{13}C NMR spectral studies. The data suggest that the ligands function as monobasic bidentate towards the metalloid atom.

During the past few years, a plethora of references describing the transition metal complexes of semicarbazone and thiosemicarbazone ligands have appeared in the literature.[1–7] However, little is known about the complexing behaviour of non-transition elements with these ligands.[8] Mehrotra and coworkers[9,10] reported the preparation and characterization of organosilicon complexes of O, N donor ligands. Semicarbazones and thiosemicarbazones are amongst the most important nitrogen oxygen/sulphur donor ligands.[11] The sulphur containing ligands are well known for their biocidal activities,[12,13] which are probably due to their ability to chelate with trace metals. It has, however, been reported that the activity of sulphur containing ligands is increased on complexation.[14,15] Our continuing interest in the synthesis of biologically active complexes have led us to prepare and study the structural as well as other features of silicon(IV) complexes of semi- and thiosemicarbazones.

EXPERIMENTAL

Chemicals and solvents used were dried and purified by standard methods and moisture was excluded from the glass apparatus using $CaCl_2$ drying tubes. All the ligands were prepared according to the literature methods[16] and recrystallized before use.

Preparation of the complexes

To a weighed amount of dimethylsilicondichloride in ~ 30 cm^3 of dry methanol was added the calculated amount of sodium salt of the ligand (prepared by treating the ligand with the sodium metal in dry methanol, ~ 20 cm^3). The reactants were refluxed for 10–11 h, filtered to remove sodium chloride and the excess solvent removed under reduced pressure and the complexes were dried for 3–4 h.

The complexes were analysed by the methods reported in our earlier publications[17] (details are given in Table 1). Conductivity was measured at 34 ± 1°C with a conductivity bridge, type 305 Systronics model and the molecular weights were determined by the Rast–Camphor method. IR spectra were recorded on a Perkin–Elmer 577 grating spectrophotometer as Nujol mulls using KBr optics. The electronic spectra of the ligand and its silicon compound were obtained on a Perkin 202 spectrophotometer in dry methanol. PMR spectra were recorded on a Jeol FX 90Q spectrometer in DMSO-d_6 using TMS as the internal standard at 89.55 MHz. ^{13}C NMR spectra were recorded in methanol at 22.49 MHz.

* Author to whom correspondence should be addressed.

RESULTS AND DISCUSSION

The reactions of dimethylsilicondichloride with the sodium salt of monobasic bidentate ligands in a 1 : 2 molar ratio in a methanol medium result in the precipitation of sodium chloride as shown by the following equations:

$$Me_2SiCl_2 + 2\widehat{NO}Na \rightarrow Me_2Si(\widehat{NO})_2 + 2NaCl$$

$$Me_2SiCl_2 + 2\widehat{NS}Na \rightarrow Me_2Si(\widehat{NS})_2 + 2NaCl$$

(where $\widehat{ON}$ and $\widehat{SN}$ represent the donor sets of ligands).

The resulting complexes have been obtained as coloured solids which are soluble in most of the common organic solvents. The molar conductance values of 10^{-3} M solutions (10–15 ohm^{-1} cm^2 mol^{-1}) in DMF show them to be non-electrolytes. The monomeric nature of these complexes was confirmed by the molecular weight determinations.

Attempts to distil some of these complexes under reduced pressure as well as recrystallization from different solvents were unsuccessful. The complexes were purified by repeated washing with cyclohexane and their purity was further checked by TLC using silica gel-G in methanol.

The electronic spectra of furfuraldehyde semi- and thiosemicarbazones and their corresponding silicon complexes were recorded. The spectra of ligands show broad bands at 350 and 340 nm which can be assigned to the n–π^* transition of the azomethine groups. These bands show a blue shift in the silicon complexes and appear at 338 and 334 nm respectively. This clearly indicates the coordination of the azomethine nitrogen to the silicon atom. The two maxima at ~ 315 and ~ 264 nm of weak intensity due to a π–π^* electronic transition in the ligands remain almost unchanged in the spectra of the silicon complexes.

In the IR spectra of ligands, a broad band in the region 3150–3250 cm^{-1} may be assigned to νNH vibrations. In the solution spectra of ligands, an additional band due to νSH also appear at ~ 2550 cm^{-1} due to tautomerization.[18] These νNH or νSH bands do not appear in the complexes showing the chelation of ligands.

A sharp strong band at ~ 1620 cm^{-1} due to the νC=N frequency of the free azomethine group in

Table 1. Physical characteristics and elemental analyses of silicon complexes

Complex	Colour	M.p. (°C)	Analysis (%) C Found (Calc.)	H Found (Calc.)	N Found (Calc.)	S Found (Calc.)	Si Found (Calc.)
$Me_2Si(L_1)_2$	Yellowish–brown	130	42.6 (42.2)	4.6 (4.5)	21.3 (21.1)	16.2 (16.4)	7.1 (7.1)
$Me_2Si(L_2)_2$	Brown	205	38.9 (39.4)	4.1 (4.2)	19.5 (19.7)	15.2 (15.0)	6.3 (6.5)
$Me_2Si(L_3)_2$	Dark brown	188	53.2 (53.6)	4.5 (4.8)	22.9 (22.7)	13.1 (13.0)	5.5 (5.7)
$Me_2Si(L_4)_2$	Light brown	195d	46.6 (46.1)	5.0 (4.8)	27.0 (26.9)	15.2 (15.3)	6.3 (6.7)
$Me_2Si(L_5)_2$	Dark yellow	125	57.1 (56.6)	5.2 (5.5)	17.8 (18.0)	13.8 (13.7)	6.4 (6.0)
$Me_2Si(L_6)_2$	Dark brown	164	46.2 (46.4)	5.3 (4.9)	23.2 (23.2)	—	7.9 (7.7)
$Me_2Si(L_7)_2$	Yellow	220	43.0 (42.6)	4.8 (4.5)	21.1 (21.2)	15.9 (16.2)	7.0 (7.1)
$Me_2Si(L_8)_2$	Dark yellow	85	57.8 (57.3)	5.5 (5.2)	24.5 (24.3)	—	6.3 (6.1)
$Me_2Si(L_9)_2$	Cream	174	49.4 (49.9)	5.0 (5.2)	29.0 (29.1)	—	7.2 (7.3)
$Me_2Si(L_{10})_2$	Light yellow	205d	60.4 (60.8)	5.4 (5.9)	19.3 (19.3)	—	6.2 (6.4)

L_1–L_5 and L_6–L_{10} are the anions of the thiosemicarbazones and semicarbazones of furfuraldehyde, thiophene-2-aldehyde, indole-3-carbaldehyde, pyridine-2-aldehyde and cinnamaldehyde, respectively.

Table 2. ^{1}H NMR data (δ ppm) of ligands and their silicon complexes

No.	Compound	Aromatic	—NH	Azomethine	—NH_2	—CH_3
(i)	L_1H[a]	7.68–6.60m	11.40bs	8.00s	2.40bs	—
(ii)	$Me_2Si(L_1)_2$[b]	8.00–6.72m	—	8.32s	2.72bs	0.40
(iii)	L_2H	6.85–6.38m	10.90bs	7.93s	2.44bs	—
(iv)	$Me_2Si(L_2)_2$	7.49–6.40m	—	8.64s	2.45bs	0.43
(v)	L_3H	8.00–7.28m	11.28bs	8.40s	2.56bs	—
(vi)	$Me_2Si(L_3)_2$	8.12–7.48m	—	8.60s	2.68bs	0.44
(vii)	L_4H	8.48–7.52m	11.76bs	8.64s	2.94bs	—
(viii)	$Me_2Si(L_4)_2$	8.80–7.84m	—	8.88s	2.96bs	0.49
(ix)	L_5H	8.00–7.37m	11.96bs	8.15s	2.50bs	—
(x)	$Me_2Si(L_5)_2$	8.76–7.56m	—	8.68s	2.56bs	0.43
(xi)	L_6H	6.80–6.32m	10.68bs	7.75s	2.55bs	—
(xii)	$Me_2Si(L_6)_2$	7.44–6.36m	—	8.44s	2.58bs	0.36
(xiii)	L_7H	6.89–6.42m	10.88bs	7.96s	2.52bs	—
(xiv)	$Me_2Si(L_7)_2$	7.00–6.56m	—	8.36s	2.50bs	0.36
(xv)	L_8H	7.76–6.32m	11.52bs	8.16s	2.56bs	—
(xvi)	$Me_2Si(L_8)_2$	8.10–7.20m	—	8.70s	2.56bs	0.40
(xvii)	L_9H	7.48–6.20m	10.87bs	7.92s	2.44bs	—
(xviii)	$Me_2Si(L_9)_2$	7.56–7.12m	—	8.64s	2.48bs	0.32
(xix)	$L_{10}H$	8.08–7.45m	11.86bs	8.16s	2.48bs	—
(xx)	$Me_2Si(L_{10})_2$	8.38–7.72m	—	8.96s	2.85bs	0.39

s = singlet, bs = broad singlet and m = complex multiplet.

[a] ^{13}C spectrum: C_1 179.48; C_2 150.79; C_3 134.77; C_4 114.75; C_5 146.14; $C_6$199.97.

[b] ^{13}C spectrum: C_1 159.22; C_2 151.42; C_3 131.59; C_4 112.41; C_5 145.57; C_6 182.42; Si—CH_3 9.0.

ligands shifts to lower frequency ($\sim$ 10) in the silicon complexes and thus indicates the coordination of the azomethine nitrogen to the metalloid atom. In the literature, a shift of this frequency to the higher[19] as well as lower[20] wave number side has been reported and in some cases even, no change has been noted.[21]

Several new bands in the complexes at $\sim$ 620, 580 and 540 cm^{-1} are due to νSi—O,[22] νSi←N[23] and νSi—S[24] respectively, which are absent in the spectra of ligands. It is known that the *cis* form of such types of complexes give rise to two νM—N bands, whereas the *trans* complexes give rise to only one IR active νM—N band.[25] The presence of only one ν(Si—N) band in the present case, suggests that the complexes exist in the *trans* form.

The proton magnetic resonance spectral data of furfuraldehyde thiosemicarbazone (L_1H), furfuraldehyde semicarbazone (L_6H) and their corresponding silicon complexes have been recorded in Table 2. The broad signals due to NH protons at δ 11.40 (L_1H) and 10.68 ppm (L_6H) in the ligands disappear in the case of silicon complexes indicating the coordination of silicon with nitrogen and oxygen/sulphur. The azomethine proton signals (—C=N) appear at δ 8.00 (L_1H) and 7.75 ppm
H
(L_6H) in the ligands undergoing deshielding and appear at δ 8.32 and 8.44 ppm in the silicon complexes $Me_2Si(L_1)_2$ and $Me_2Si(L_6)_2$ respectively, which again confirms the coordination of the azomethine nitrogen to the silicon atom. The protons of the methyl groups appear at δ 0.40 and 0.36 ppm in the complexes $Me_2Si(L_1)_2$ and $Me_2Si(L_6)_2$ respectively. The results for other ligands and their silicon complexes have been given in Table 2.

^{13}C NMR spectra of furfuraldehyde thiosemicarbazone and its silicon complex were also recorded. The ^{13}C chemical shifts in the spectra of the complex compared to the ligand clearly show the coordination of the azomethine nitrogen to the silicon atom.

On the basis of the above evidence, it is suggested that the silicon is octahedrally coordinated.

Acknowledgement—Mrs Kiran Singh is thankful to the C.S.I.R. New Delhi for financial assistance.

REFERENCES

1. M. Akber Ali, S. E. Livingstone and D. J. Phillips, *Inorg. Chim. Acta* 1973, 7, 179.
2. M. Akber Ali, S. E. Livingstone and D. J. Phillips, *Inorg. Chim. Acta* 1973, 7, 531.

3. M. J. Campbell and R. Grzeskowiak, *J. Chem. Soc. A* 1967, 396.
4. S. K. Sahni, P. C. Jain and V. B. Rana, *Indian J. Chem.* 1978, **16A**, 699.
5. Michel J. M. Campbell, *Coord. Chem. Rev.* 1975, **15**, 279.
6. V. K. Arora, K. B. Pandeya and R. P. Singh, *J. Indian Chem. Soc.* 1979, **LVI**, 656.
7. P. L. Maurya, B. V. Agrawala and A. K. Dey, *J. Indian Chem. Soc.* 1980, **LV11**, 275.
8. A. K. Saxena, J. K. Koacher and J. P. Tandon, *J. Inorg. Nucl. Chem.* 1981, **43**, 3091.
9. P. Rupani, A. Singh, A. K. Rai and R. C. Mehrotra, *J. Organometal Chem.* 1978, **162**, 17.
10. P. Bajaj and R. C. Mehrotra, *J. Organometal Chem.* 1970, **25**, 359.
11. B. A. Gingras, R. W. Hornal and C. H. Baylay, *Can. J. Chem.* 1960, **38**, 712.
12. B. L. Feedlander and A. Fraust, *J. Am. Chem. Soc.* 1952, **81**, 638.
13. N. P. Buee-Hoi, T. B. Voc and N. D. Xuong, *Bull. Soc. Chim. France* 1955, 694.
14. P. Jain and K. K. Chaturvedi, *J. Inorg. Nucl. Chem.* 1977, **39**, 901.
15. D. R. Williams, *Chem. Rev.* 1972, **72**, 203.
16. A. I. Vogel, *A Text Book of Practical Organic Chemistry*, p. 722. Longmans, London (1963).
17. K. Singh, R. V. Singh and J. P. Tandon, *Synth. React. Inorg. Met-Org. Chem.* 1986, **16**, 1341.
18. M. A. Ali and R. Bose, *J. Inorg. Nucl. Chem.* 1977, **39**, 265.
19. D. H. Busch and J. C. Bailar, Jr, *J. Am. Chem. Soc.* 1956, **78**, 1137.
20. J. E. Kovacic, *Spectrochim. Acta* 1967, **23A**, 183.
21. B. D. Sharma and J. C. Bailar, *J. Am. Chem. Soc.* 1955, **77**, 5476.
22. R. V. Singh and J. P. Tandon, *Annal. de Sco Sci Brux*, 1979, **93**, 143.
23. E. A. V. Ebsworth and M. J. Mays, *J. Chem. Soc.* 1964, 3450.
24. R. Dashora, R. V. Singh and J. P. Tandon, *Synth. React. Inorg. Metal-Org. Chem.* 1983, **13**, 209.
25. N. S. Biradar, V. B. Mahale and V. H. Kulkarni, *Inorg. Chim. Acta* 1973, **7**, 267.

Polyhedron Vol. 7, No. 2, pp. 155–159, 1988
Printed in Great Britain

0277–5387/88 $3.00+.00
Pergamon Journals Ltd

SYNERGIC EXTRACTION OF LANTHANIDE(III) IONS WITH 2-THENOYLTRIFLUOROACETONE IN THE PRESENCE OF 2,2′-BIPYRIDINE OR PYRIDINE

SHIGETO NAKAMURA and NOBUO SUZUKI*

Department of Chemistry, Faculty of Science, Tohoku University, Sendai 980, Japan

(*Received* 15 *July* 1987; *accepted* 1 *September* 1987)

Abstract—The synergic extraction of various tervalent lanthanides (Ln), La, Ce, Nd, Sm, Gd, Tb, Yb and Lu, with 2-thenoyltrifluoroacetone (Htta) in the presence of a bidentate heterocyclic amine, 2,2′-bipyridine (bipy), in benzene was investigated. The synergic enhancement was attributed to the formation of the adducts, $Ln(tta)_3(bipy)$. The synergic extraction of La(III), Sm(III) and Lu(III) with Htta and a unidentate amine, pyridine (py), was also studied and the formation of the adducts, $Ln(tta)_3py$ and $Ln(tta)_3(py)_2$, was observed. The adduct formation constants, $\beta_{s,1}$ and $\beta_{s,2}$, were determined. The $\beta_{s,2}$ values for py decrease with increasing atomic number of Ln(III), but $\beta_{s,1}$ values for bipy increase with increasing atomic number of Ln(III). The synergic extraction constants and the separation factors in the bipy system were also determined.

The synergic enhancement of the extraction of tervalent lanthanides Ln(III) with an acidic chelating agent in the presence of a neutral ligand has been widely investigated. In most of these investigations unidentate organophosphorus compounds such as tributylphosphate (tbp) and trioctylphosphine oxide (topo) have been used as neutral ligands. Relatively little use has been made of bidentate neutral ligands. Recently we have investigated the synergic extraction of Tm(III) with β-diketones and neutral bidentate heterocyclic amines, such as 1,10-phenanthroline (phen) and 2,2′-bipyridine (bipy), and a large synergic enhancement was observed.[1] Furthermore, the effect of nonpolar diluents on the synergism in Ln(III)–acetylacetone(Hacac)–phen systems was discussed.[2–4] A very interesting dependence of synegrism on the atomic number of Ln with different combinations of β-diketones and bidentate heterocyclic amines was observed;[5,6] that is, in Hacac and benzoylacetone (Hba) systems, the synergic enhancement by phen as well as bipy decreases with increasing atomic number of Ln, but in pivaloyltrifluoroacetone (Hpta) and hexafluoroacetylacetone (Hhfa) systems, the dependence is inverse.

In the present work, the synergic extraction of various Ln(III) ions with 2-thenoyltrifluoroacetone (Htta) and bipy in benzene was investigated. Htta is a well established extracting reagent and has often been used in the synergic extraction of Ln(III) in combination with a unidentate organophosphorus compound containing oxygen as a donor atom.[7] On the other hand, unidentate neutral ligands containing nitrogen as a donor atom have been little used, so that the synergic extraction of Ln with Htta in the presence of a unidentate heterocyclic amine, pyridine (py), was also investigated to compare with that of Ln with Htta in the presence of a bidentate heterocyclic amine such as bipy.

EXPERIMENTAL

Materials and apparatus

Radioisotopes, ^{140}La, ^{141}Ce, ^{147}Nd, ^{153}Sm, ^{153}Gd, ^{160}Tb, ^{169}Yb and ^{177}Lu, used as tracers, were produced by the neutron irradiation of 0.5–5 mg of each oxide or nitrate in the nucleur reactor (JRR-4) of the Japan Atomic Research Institute at a thermal neutron flux of 5.5×10^{13} n cm^{-2} s^{-1} for 6 h. The radioactive solution of Ln(III) was prepared by dissolving a known amount of the irradiated sample in hydrochloric acid, evaporating to dryness and

*Author to whom correspondence should be addressed.

redissolving in 10^{-3} M perchloric acid solution before use.

Htta was purified by vacuum sublimation. Bipy was recrystallized in cyclohexane followed by drying under reduced pressure. Py was distilled twice. Benzene was purified by ordinary methods. Unless otherwise stated, reagents used were of guaranteed reagent grade.

The γ-radioactivity of each radioisotope was measured with a NaI(Tl) well-type scintillation detector connected with a single channel analyser. The extraction vial was shaken with a mechanical shaker at 330 strokes per min. The pH value of the equilibrated aqueous phase was measured with a glass electrode.

Procedure

An aqueous solution (6 cm^3) containing 10^{-7}–10^{-5} M Ln labelled with its radioisotope was placed in a 30 cm^3 extraction vial with a ground glass stopper. In the extraction of Ce(III), 10^{-3} M sodium ascorbate was also present. To the aqueous solution was added an equal volume of a benzene solution containing 10^{-4}–10^{-2} M Htta and 10^{-5}–10^{-1} M neutral ligand, and the vial was shaken for 1–3 h at 25°C and then centrifuged. An aliquot was taken from each phase and the γ-radioactivity was measured. The distribution ratio (D) of Ln was obtained as the radioactivity ratio. The pH of the aqueous phase was adjusted with 10^{-3}–10^{-2} M piperazine-N,N′-bis-(2-ethanesulphonic acid) and sodium hydroxide solution, and the equilibrium pH value of the aqueous phase was measured immediately after shaking. Ion strength was adjusted to 0.1 with sodium perchlorate in bipy systems and with sodium chloride in py systems.

Theoretical

The distribution ratio (D_0) of a tervalent cation, M^{3+}, with a chelating extractant, HA, can be expressed as follows;

$$D_0 = \frac{[\overline{MA_3}]}{[M^{3+}]+\sum[MA_n^{3-n}]} = \frac{P_{MA_3}\beta_3[A^-]^3}{1+\sum\beta_n[A^-]^n} \quad (1)$$

where the bar over the species denotes the organic phase, β_n the overall chelate formation constant of MA_n^{3-n} in the aqueous phase, P_M the partition coefficient of MA_3 and A^- the chelating anion in the aqueous phase. In the very low concentration of A^-, the formation of MA_n^{3-n} will be negligible, thus D_0 depends simply on the third power of the concentration of A^-. The extraction equilibrium with HA is given as:

$$M^{3+}+3\overline{HA} \rightleftharpoons \overline{MA_3}+3H^+ : K_{ex} \quad (2)$$

When MA_n^{3-n} chelates other than MA_3 can be neglected, the extraction constant, K_{ex}, can be expressed as follows:[1]

$$K_{ex} = \frac{[\overline{MA_3}][H^+]^3}{[M^{3+}][\overline{HA}]^3} = \left(\frac{K_{HA}}{P_{HA}}\right)^3 \frac{D_0}{[A^-]^3} \quad (3)$$

where K_{HA} and P_{HA} denote the acid dissociation constant and the partition coefficient of HA, respectively.

In the synergic extraction of M^{3+} with HA and a neutral ligand, S, the distribution ratio (D) can be expressed as follows:

$$D = \frac{[\overline{MA_3}]+\sum[\overline{MA_3S_m}]}{[M^{3+}]+\sum[MA_n^{3-n}]} = \frac{P_{MA_3}\beta_3[A^-]^3(1+\sum\beta_{s,m}[\bar{S}]^m)}{1+\sum\beta_n[A^-]^n} \quad (4)$$

where $\beta_{s,m}$ is the adduct formation constant in the organic phase corresponding to the following equilibrium:

$$\overline{MA_3}+m\bar{S} \rightleftharpoons \overline{MA_3S_m} : \beta_{s,m}. \quad (5)$$

From eqs (1) and (4), the following equation is obtained:

$$D/D_0 = 1+\sum\beta_{s,m}[\bar{S}]^m. \quad (6)$$

If MA_3S_m is the only dominant species in the organic phase, D/D_0 will depend on the mth power of the concentration of S in the organic phase.

The overall extraction reaction of the synergic extraction and its equilibrium constant, $K_{exs,m}$, are shown as eqs (7) and (8) respectively, and the latter is called the synergic extraction constant.

$$M^{3+}+3\overline{HA}+m\bar{S} \rightleftharpoons \overline{MA_3S_m}+3H^+ \quad (7)$$

$$K_{exs,m} = \frac{[\overline{MA_3S_m}][H^+]^3}{[M^{3+}][\overline{HA}]^3[\bar{S}]^m} = \left(\frac{K_{HA}}{P_{HA}}\right)^3 P_{MA_3}\beta_3\beta_{s,m}. \quad (8)$$

$K_{exs,m}$ can be related with K_{ex} and $\beta_{s,m}$ from eqs (3) and (8) as

$$K_{exs,m} = K_{ex}\beta_{s,m}. \quad (9)$$

RESULTS AND DISCUSSION

Extraction of Ln(III) *with* Htta

The extraction of La(III), Nd(III), Sm(III), Gd(III), Tb(III), Yb(III) and Lu(III) with Htta in benzene was carried out and the logarithmic distribution ratio was plotted against the logarithmic

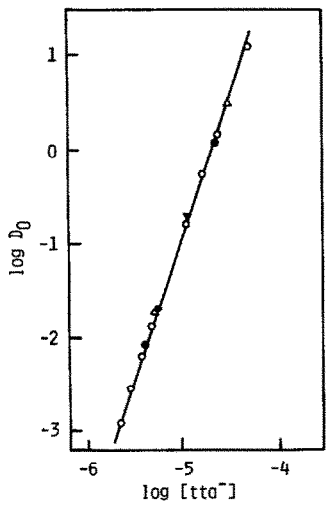

Fig. 1. Distribution ratio of Ce(III) in the extraction and back-extraction with Htta in benzene. ○: 10^{-2} M Htta, ●: 10^{-3} M Htta, ▼: back-extraction in the presence of 10^{-3} M ascorbate, △: 10^{-2} M in the absence of ascorbate.

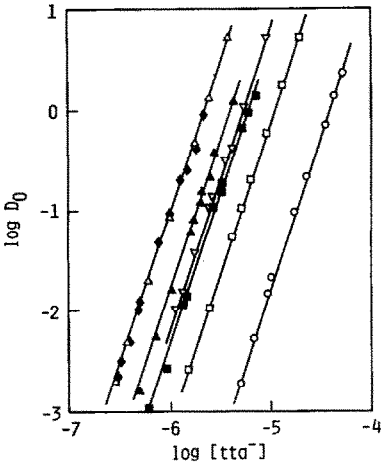

Fig. 2. Extraction of various Ln(III) with Htta in benzene. ○: La, □: Nd, ■: Sm, ▽: Gd, ▲: Tb, △: Yb, ◆: Lu.

concentration of tta$^-$. The equilibrium concentration of tta$^-$ in the aqueous phase was calculated from the following equation;

$$[A^-] = \frac{C_{HA}}{(P_{HA}+1)[H^+]/K_{HA}+1} \qquad (10)$$

where C_{HA} denotes the initial concentration of Htta. The literature values of K_{HA} and P_{HA} were adopted, i.e. log $K_{HA} = -6.23$[8] and log $P_{HA} = 1.62$.[9] It is known that the cerium ion takes two relatively stable oxidation states in an aqueous solution, tervalent and quadrivalent cerium. To make sure of the extraction of Ce(III) with Htta, the distribution ratio of cerium was determined in the presence or absence of ascorbate which behaves as a reducing agent. The plots of log D_0 vs log [tta$^-$] are shown in Fig. 1, together with that of the back extraction of the extracted organic phase. All the plots give straight lines with a slope of 2.96, and this indicates that the extraction equilibrium is attained at the present extraction condition, and the extraced chelate is Ce(tta)$_3$ of tervalent state even in the absence of ascorbate. To make sure, ascorbate was added in all the synergic extraction systems. The plots in Fig. 2 for La, Nd, Sm, Gd, Tb, Yb and Lu give straight lines with the slopes of 2.97, 2.95, 3.01, 2.93, 3.00, 2.92 and 2.95, respectively. These demonstrate that the extracted chelate for Ln is Ln(tta)$_3$, as is expected. From these plots in Figs 1 and 2, the extraction constants were calculated by eq. (3) and are listed in Table 1, together with that for Tm(III).[1]

Synergic extraction of Ln(III)

The synergic extraction of Ln with 10^{-3} M Htta and various concentrations of bipy in benzene was

Table 1. Extraction constants (K_{ex}), adduct formation constants (β_s) and synergic extraction constants (K_{exs}) in Ln(III)–Htta–bipy, py systems

Ln	log K_{ex}	bipy log $\beta_{s,1}$	bipy log $K_{exs,1}$	py log $\beta_{s,1}$	py log $\beta_{s,2}$	py log $K_{exs,2}$
La	−10.35	5.36	−4.99	2.60	4.68	−5.67
Ce	−9.47	5.66	−3.81			
Nd	−8.70	5.95	−2.75			
Sm	−7.93	6.14	−1.79	2.95	4.70	−3.23
Gd	−7.76	6.38	−1.38			
Tb	−7.38	6.46	−0.92			
Tm[a]	−6.84	6.58	−0.26	3.02	4.32	−2.52
Yb	−6.62	6.54	−0.08			
Lu	−6.65	6.51	−0.14	2.81	3.71	−2.94

[a] Ref. 1.

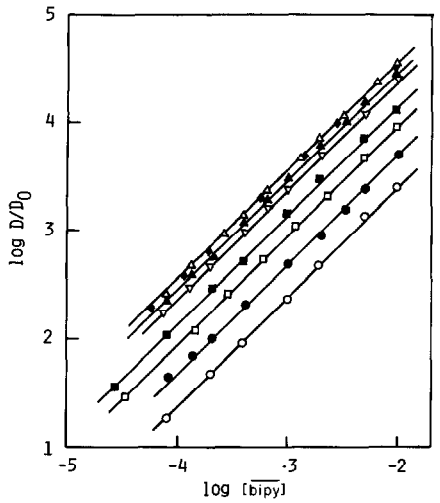

Fig. 3. Effect of the concentration of bipy in benzene on the synergic extraction of Ln(III) with Htta. ○ : La, ● : Ce, □ : Nd, ■ : Sm, ▽ : Gd, ▲ : Tb, △ : Yb, ◆ : Lu.

carried out and the plots of $\log D$ against $\log[\overline{\text{bipy}}]$ are given in Fig. 3. The equilibrium concentration of bipy in the organic phase was calculated by the following equation;

$$[\bar{S}] = \frac{C_S}{1+(1+[H^+]/K_{HS})/P_S} \qquad (11)$$

where C_S denotes the initial concentration of bipy, and K_{HS} and P_S are the acid dissociation constant of the protonated bipy and the partition coefficient of bipy, respectively. The values of K_{HS} and P_S have been obtained experimentally,[1] i.e. $\log K_{HS} = -4.50$ and $\log P_S = 2.05$.

The plots for La, Ce, Nd, Sm, Gd, Tb, Yb and Lu give straight lines with the slopes of 1.03, 0.97, 1.02, 1.00, 1.00, 1.00, 1.01 and 1.00, respectively. This indicates that the mole ratio of the neutral chelate and bipy in the adduct is 1 : 1, and no evidence for the formation of a higher adduct as $M(tta)_3(bipy)_2$ was obtained. The formation of the higher adducts was suggested in the synergic extraction of La, Nd, Gd and Lu with Htta and bipy,[10] but this conclusion is dubious because they did not pay any attention to the equilibrium concentrations of tta^- and phen. Therefore for example the slope analysis of the plots is ambiguous, and the adduct formation constants $\beta_{s,1}$ and $\beta_{s,2}$ reported in the literature[10] are also not plausible.

The $\beta_{s,1}$ are calculated from eq. (6) as listed in Table 1, and plotted in the order of the atomic number of Ln in Fig. 4. The larger atomic number of Ln has the larger value of $\beta_{s,1}$. This tendency is different from that in the general synergic extraction systems involving a unidentate organophosphorus

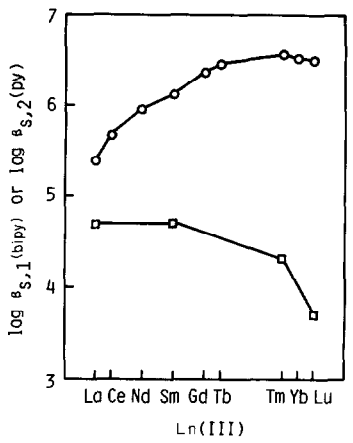

Fig. 4. Plots of $\beta_{s,1}$ in Ln(III)–Htta–bipy systems and $\beta_{s,2}$ in Ln(III)–Htta–py systems in the order of the atomic number of Ln. ○ : bipy, □ : py.

compound as a neutral ligand, such as Ln–Htta–tbp systems,[11,12] in which $\beta_{s,2}$ values decrease with increasing atomic number of Ln. The different tendency between commonly used tbp and the present bipy may be attributed to the different donor atoms such as oxygen of tbp and nitrogen of bipy. Here, the synergic extraction of Ln with Htta and py, which are unidentate neutral ligands and have a nitrogen as a donor atom, was carried out. The plots of $\log D/D_0$ against $\log[\overline{\text{py}}]$ are shown in Fig. 5. The equilibrium concentration of py in benzene was calculated from eq. (11) using K_{HS} and P_S values for py, i.e. $\log K_{HS} = -5.36$ and $\log P_s = 0.51$.[1] These plots show a curved line for each Ln(III), and in the higher concentration range of py, these plots for La and Sm are asymptotic to a straight line with a slope of two. The plots for Lu(III) do not reach

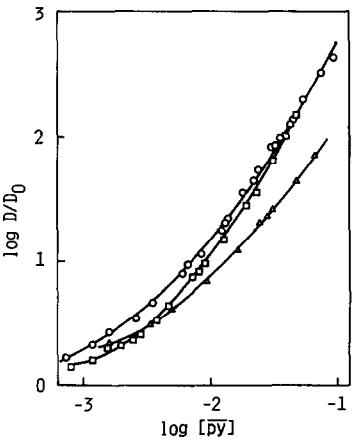

Fig. 5. Effect of the concentration of py in benzene on the synergic extraction of Ln(III) with Htta. □ : La, ○ : Sm, △ : Lu.

a limiting slope even at the higher concentration of py but seem to be getting close to the slope of two. Thus, it may be concluded that two adducts, $M(tta)_3py$ and $M(tta)_3(py)_2$, are formed. The adduct formation constants in the py system are calculated from eq. (6) using the least squares fitting method, and are listed in Table 1. The $\beta_{s,1}$ values of bipy, which seems to be a quasi dimer type compound of py, for every Ln is larger than the corresponding $\beta_{s,2}$ of py, and this suggests that bipy coordinates directly to the central metal of the chelate as a bidentate ligand. The plots of the $\beta_{s,2}$ values of py in the order of the atomic number of Ln are shown in Fig. 4. The values of $\beta_{s,2}$ for Ln with the higher atomic number is smaller than those for Ln with the lower atomic number. This tendency is the same as that of the general unidentate organophosphorus compound, and is inverse to that of bipy. Thus, the peculiar tendency of the synergism observed for bipy seems to be not only attributed to the donor nitrogen atom of the ligand, but also to its bidentate mode of coordination.

The peculiar tendency in the adduct formation with bipy is entirely favourable to the separation efficiency of Ln ions in the synergic extraction. The separation factors between two Ln's, M and M′, in the extraction system with Htta in the absence or presence of bipy are calculated simply by the following relations.

$$\Delta K_{ex}(M'/M) = K_{ex}(M')/K_{ex}(M) \quad (12)$$

$$\Delta K_{exs}(M'/M) = K_{exs}(M')/K_{exs}(M). \quad (13)$$

These values are summarized in Table 2. It has been generally believed that the separation of metals by the synergic extraction system is worse than that by the extraction system involving only the acidic chelating agent. However, the value of ΔK_{exs} in the present bipy system is larger than the value of ΔK_{ex} for each Ln pair. Thus the addition of a neutral bidentate ligand, bipy, can improve both the extraction efficiency of Ln and the separation factor of Ln's. The ΔK_{exs} values for Ln pairs of the lower atomic number are larger than those for the higher atomic number. The separation factors especially for the La—Ce pair and the Ce—Nd pair in the present system are larger than those in di-(2-ethylhexyl)-phosphoric acid (dehpa) systems, which is known as the extraction system for Ln's with a large separation factor, i.e. the separation factors for La—Ce pair and Ce—Nd pair in the dehpa system are 3.0 and 2.94 respectively.[13] This must be compared with the present system of 15.15 and 11.48 respectively. The synergic extraction system involving bipy seems to be favourable for the separation of light Ln's. Further investigation of the synergic extraction involving bidentate neutral ligands is very promising for the separation science of rare metals.

Table 2. Separation factors of Ln(III) in the extraction system with Htta in the absence and presence of bipy

M′/M	$\Delta K_{ex}(M'/M)^a$	$\Delta K_{exs}(M'/M)^b$
Ce/La	7.58	15.15
Nd/Ce	5.89	11.48
Sm/Nd	5.89	9.12
Gd/Sm	1.48	2.57
Tb/Gd	2.40	2.88
Tm/Tb	3.47	4.57
Yb/Tm	1.66	1.51
Lu/Yb	0.93	0.87

[a] Htta–benzene.
[b] Htta–bipy–benzene.

REFERENCES

1. S. Nakamura, H. Imura and N. Suzuki, *Inorg. Chim. Acta* 1985, **110**, 101.
2. S. Nakamura, H. Imura and N. Suzuki, *Inorg. Chim. Acta* 1985, **109**, 157.
3. N. Suzuki and S. Nakamura, *Inorg. Chim. Acta* 1985, **110**, 243.
4. S. Nakamura and N. Suzuki, *J. Radioanal. Nucl. Chem.* 1986, **99**, 145.
5. S. Nakamura and N. Suzuki, *Inorg. Chim. Acta* 1986, **114**, 101.
6. S. Nakamura and N. Suzuki, *Polyhedron* 1986, **5**, 1805.
7. Y. Marcus and A. S. Kertes, *Ion Exchange and Solvent Extraction of Metal Complexes*, Vol. 6, p. 815. Wiley-Interscience, London (1969).
8. J. C. Reid and M. Calvine, *J. Am. Chem. Soc.* 1950, **72**, 2948.
9. T. Wakahayashi, S. Oki, T. Omori and N. Suzuki, *J. Inorg. Nucl. Chem.* 1964, **26**, 2255.
10. E. F. Kassierer and A. S. Kertes, *J. Inorg. Nucl. Chem.* 1972, **34**, 3221.
11. L. Farbu, J. Alstad and J. H. Augstson, *J. Inorg. Nucl. Chem.* 1974, **36**, 2091.
12. T. Sekine and D. Dyrssen, *J. Inorg. Nucl. Chem.* 1967, **29**, 1481.
13. T. B. Pierce, P. F. Peck and R. S. Hobbs, *J. Chromatog.* 1968, **12**, 621.

Polyhedron Vol. 7, No. 2, pp. 161–162, 1988
Printed in Great Britain

0277–5387/88 $3.00+.00
© 1988 Pergamon Journals Ltd

COMMUNICATION

COPPER-63 NMR STUDIES OF INTERACTION BETWEEN COPPER(I) IONS AND DIARYLAZO COMPOUNDS

JOSEPH A. CONNOR* and RICHARD J. KENNEDY

Chemical Laboratory, University of Kent, Canterbury, Kent CT2 7NH, U.K.

(*Received* 4 *June* 1987; *accepted* 29 *June* 1987)

Abstract—The use of ^{63}Cu NMR to investigate the interaction between copper(I) in $[Cu(NCMe)_4][BF_4]$ and various organic molecules in acetonitrile solution is demonstrated.

Reactions of various organic molecules can be activated by the presence of copper metal or copper ions.[1] The precise function of copper in these reactions is unclear. The metal may act as an electron transfer or redox agent, it may function by polarizing the organic substrate as a result of a weak association between them, or it may form a specific coordination complex with the organic molecule as a ligand which then undergoes further reaction.

We have investigated the copper-assisted nucleophilic substitution of various aryl halides by cyanide and dialkylphosphonate. In these reactions, the nucleophile is formed from a precursor (formamide or formaldehyde oxime in the case of cyanide; a trialkyl phosphite in the case of dialkylphosphonate) which is coordinated to copper(I) during the reaction.[2] Experiments designed to identify or to isolate coordination complexes of copper(I) containing both the aryl halide and the nucleophile have been uniformly unsuccessful. Consequently, we have investigated the use of ^{63}Cu NMR as a means of detecting interaction between copper(I) and various organic substrates. For this purpose tetrakis(acetonitrile)copper(I) tetrafluoroborate is a convenient reagent.

EXPERIMENTAL

The NMR measurements were made with a Bruker WM200-SWB spectrometer using a broadband tuneable VSP probe. ^{63}Cu resonances were observed using a carrier frequency of 53.0422 MHz, a pulse width of 20 μs and with a sweep width of 100 KHz. A saturated solution of $[Cu(NCMe)_4][BF_4]$ in acetonitrile (*ca* 0.1 M) was used as an external reference at a constant temperature of 300 K. In order to circumvent the known concentration dependence of ^{63}Cu resonances,[3] spectra of saturated solutions of $[Cu(NCMe)_4][BF_4]$ (10 mg) in acetonitrile (2 cm^3) were recorded both before and after addition of the potential ligand. The results obtained are accurate to ± 1 ppm. The copper(I) salt, $[Cu(NCMe)_4][BF_4]$ was prepared by a standard method.[4] All reagents and solvents were purified and handled in an atmosphere of deaerated, dry dinitrogen using standard Schlenk-type apparatus and cannulae for solution transfers. The aryl bromides were prepared by standard methods and characterized by microanalysis and spectroscopy (IR, NMR, mass).

RESULTS

The addition of either benzene (0.6 mmol) or N,N-diethylaniline (0.3 mmol) to a standard solution of $[Cu(NCMe)_4][BF_4]$ in acetonitrile did not cause any significant change in the ^{63}Cu chemical shift and the width (8570 Hz) of the signal did not change. These observations indicate that the tetrahedral environment of the copper(I) has not been disturbed either by a σ-donor interaction with the tertiary nitrogen of the amine or by a π-type of interaction with the aromatic rings. That such an interaction can be recognized easily was established by the observation that the addition of triethyl

* Author to whom correspondence should be addressed.

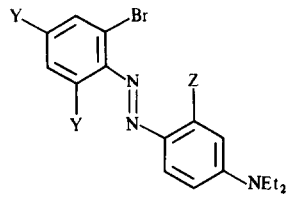

(1) Y = Me ; Z = H
(2) Y = H ; Z = NHCOMe
(3) Y = Me; Z = NHCOMe

Fig. 1.

phosphite to $[Cu(NCMe)_4][BF_4]$ in acetonitrile solution at room temperature, rapidly produces the quintet signal characteristic[5] of $[Cu(P(OEt)_3)_4][BF_4]$ ($J(^{63}Cu—^{31}P)$ 1208 Hz) at δ −86 ppm relative to the acetonitrile complex.

The 2-azoaryl bromide (**1**) is typical of substrates for which we have previously studied nucleophilic substitution of the halogen. When (**1**) is added to $[Cu(NCMe)_4][BF_4]$ in acetonitrile a shift of the ^{63}Cu resonance upfield δ +12 ppm is observed and the width of the signal increases (9650 Hz). Compound (**2**) contains an acetylamino substituent which is capable of interacting with copper(I) so that (**2**) is a potential bidentate ligand. When (**2**) is added to $[Cu(NCMe)_4][BF_4]$ in acetonitrile solution, the ^{63}Cu resonance is shifted further upfield, δ +17 ppm. The importance of the second potential donor site is reinforced by the observation that (**3**), which incorporates the essential features of both (**1**) and (**2**), causes a shift δ +18 ppm in the ^{63}Cu resonance of $[Cu(NCMe)_4][BF_4]$. In the presence of both (**2**) and (**3**) the ^{63}Cu resonance is significantly broader (average, 10150 Hz) than in $[Cu(NCMe)_4][BF_4]$. Addition of 2′-bromo-(2-acetylaminophenylmethylidene)benzeneamine, which comprises both of the potential donor sites but lacks the polarizing diethylamino substituent which would increase the electron density on the azomethine nitrogen, does not cause any shift in the ^{63}Cu resonance of $[Cu(NCMe)_4][BF_4]$.

CONCLUSION

The exchange equilibria between coordinated and bulk solvent in $[Cu(NCMe)_4]^+$ are sufficiently rapid on the NMR time scale that the ^{63}Cu signal is broadened both by exchange contributions to the relaxation rate and by the presence of species of low point symmetry. The presence of another potential ligand is expected to cause a shift in the resonance and an increase in the width of the signal. The results of the experiments reported here provide evidence for a weak interaction between copper(I) and various 2-haloarylazo compounds. The azo compounds appear to coordinate the copper(I) through the nitrogen atom of the azo group which is adjacent to the halogen-bearing benzene ring. The interaction between the metal and the organic substrate may be increased by the presence of a second donor atom in the substrate. The weakness of these metal–ligand interactions is emphasized by the fact that stable chelate complexes of these ligands with copper(I) could not be isolated.

Acknowledgement—We thank SERC and ICI Organics Division for a CASE studentship (RJK) and Dr D. O. Smith for recording the NMR spectra.

REFERENCES

1. A. E. Jukes, *Adv. Organomet. Chem.* 1974, **12**, 215; J. A. Lindley, *Tetrahedron* 1984, **40**, 1433.
2. J. A. Connor, D. Dubowski, A. C. Jones and R. Price, *J. Chem. Soc., Perkin Trans 1* 1982, 1143; J. A. Connor, D. Gibson and R. Price, *J. Chem. Soc., Perkin Trans. 1* 1987, 619.
3. V. Ochsenbein and C. W. Schlapfer, *Helv. Chim. Acta* 1980, **63**, 1926.
4. G. J. Kubas, *Inorg. Synth.* 1979, **19**, 90.
5. O. Lutz, A. Nolle and H. Oehler, *Z. Naturforsch. TeilA* 1980, **35**, 221.

Polyhedron Vol. 7, No. 2, pp. 163–165, 1988
Printed in Great Britain

0277–5387/88 $3.00+.00
Pergamon Journals Ltd

COMMUNICATION

DIHAPTO-ACYL VERSUS ALKYL(CARBONYL) COORDINATION. INFLUENCE OF ELECTRONIC AND STERIC EFFECTS

E. CARMONA* and L. SÁNCHEZ

Departamento de Química Inorgánica, Facultad de Química, Universidad de Sevilla, e Instituto de Ciencias de Materiales de Sevilla, CSIC., Aptdo. 553, Sevilla, Spain

(*Received* 16 *July* 1987; *accepted* 8 *September* 1987)

Abstract—The synthesis and characterization of a series of seven-coordinate methyl(carbonyl)- and the related six-coordinated η^2-acyl complexes of tungsten [e.g. $W(CH_3)Cl(CO)_2(PMe_3)_3$, $W(\eta^2\text{-}COR)(S_2CNMe_2)(CO)(PMe_3)_2$, etc.] were carried out to explore the influence of electronic and steric effects. By changing the nature of the R group and/or of the ancillary ligands, it is shown that a decrease in the electron density at the metal centre and an increase in the steric requirements of the R group, favour the η^2-acyl structure over the alkyl(carbonyl) formulation.

Recent work from several laboratories has allowed characterization of a growing number of formally six-coordinate η^2-acyl complexes of molybdenum[1–3] and tungsten,[4–5] e.g. $Mo(\eta^2\text{-}COR)X(CO)(PMe_3)_3$,[3] $TpMo(\eta^2\text{-}COR)(CO)_2$[1b,2] but the corresponding seven-coordinate alkyl(carbonyl) derivatives have not been found to occur. Since the interconversion of formulations **A** and **B** does not change the number of electrons at the metal centre, it was reasoned that in a series of analogous complexes, structure **B** should be favoured with respect to **A** for sterically demanding R groups, while an increase in the electron density at the metal centre, i.e. of the metal basicity, would favour formulation **A**, because of the strong acceptor properties of the carbonyl ligand. In this communication we present preliminary results which clearly show the influence of the steric and electronic effects on the relative stability of structures **A** and **B**, and report, for the first time, the controlled formation of both types of complexes and of an equilibrium mixture of the above structures.

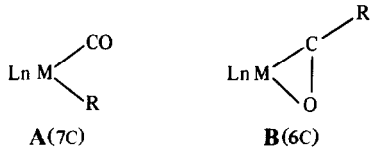

A(7C) **B**(6C)

The alkylation of complexes $MCl_2(CO)_2(PMe_3)_3$[6] yields the η^2-acyls $M(\eta^2\text{-}COR)Cl(CO)(PMe_3)_3$, or the alkyl(carbonyl), $W(Me)Cl(CO)_2(PMe_3)_3$, **1a**, as shown in eqs (1) and (2).

$$MCl_2(CO)_2(PMe_3)_3 + Mg(R)Cl \rightarrow M(\eta^2\text{-}COR)Cl(CO)(PMe_3)_3 + MgCl_2 \quad (1)$$

(M = Mo, ref. 3; M = W, R = CH_2SiMe_3, **1b**; CH_2CMe_3, **1c**; CH_2CMe_2Ph, **1d**)

$$WCl_2(CO)_2(PMe_3)_3 + LiMe \rightarrow W(Me)Cl(CO)_2(PMe_3)_3 + LiCl. \quad (2)$$

The new compounds have been fully characterized by analytical and spectroscopic studies,† which show the η^2-acyls have structures of type **C**,

* Author to whom correspondence should be addressed.

† Compounds **1a–1d** were prepared by a route similar to that reported for the molybdenum analogs (ref. 3). Selected spectroscopic data for **1a** and **1b** are as follows: **1a**, IR (Nujol): νCO 1890, 1790 cm^{-1}. ^1H NMR (C_6D_6): δ 1.3 (broad, PMe_3), 0.4 (pseudoquartet, W-CH_3). ^{31}P NMR (C_6D_6): δ −27.2 (t, $^2J_{P_AP_X}$ = 28.6 Hz), −22.15(d). Although stable as a solid when kept under N_2, **1a** decomposes in solution with the formation of $WCl_2(CO)_2(PMe_3)_3$ and other unidentified species. **1b**, IR(KBr): νCO 1800 cm^{-1}, νCOR 1460 cm^{-1}. ^1H NMR (C_6D_6): δ 2.9 (s, CH_2SiMe_3), 1.34 (d, $^2J_{HPA}$ = 7.8 Hz, P_AMe_3), 1.15 (t, $^2J_{ap(HPB)}$ = 3.1 Hz, P_BMe_3), 0.17 (s, CH_2SiMe_3); ^{31}P NMR (C_6D_6): AB_2 system, δ_A = −14.4, δ_B = −14.8 ppm, $^2J_{P_AP_B}$ = 10.4 Hz.

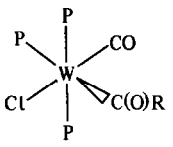

C

similar to those found for the molybdenum analogs.[3] The structure of **1b** (as well as that of **2a**, see below) has been determined by X-ray crystallography and will be reported elsewhere. Complexes **1a–1d** do not rearrange into their corresponding isomeric forms, i.e. **A** ⇌ **B**, upon thermal or photochemical activation. Since on the other hand no exchange between the CO groups of the acyl and carbonyl ligands is detected by ^{13}C NMR studies, these compounds are assumed to be the thermodynamic products of the above reactions. Therefore, the η^2-acyl structure is favoured for the above complexes with the only exception being the W—CH_3 derivative for which the alkyl–carbonyl formulation is preferred. We propose that this difference is due to a combination of electronic and steric effects. The former would make the alkyl(carbonyl) structure, **A**, more stable* in the order Mo < W because of the higher basicity of the tungsten derivatives,[8] while the latter are obviously responsible for the stabilization of the η^2-acyl structure for the bulkier CH_2SiMe_3, CH_2CMe_3 and CH_2CMe_2Ph alkyl groups.†

The reaction of $Mo(\eta^2\text{-}COR)Cl(CO)(PMe_3)_3$ complexes with the sodium salt of the strongly electron releasing $Me_2NCS_2^-$ ligand proceeds with formation of the η^2-acyls $Mo(\eta^2\text{-}COR)(S_2CNMe_2)(CO)(PMe_3)_2$ and of the unusual acetyl $Mo(COCH_3)(S_2CNMe_2)(CO)(PMe_3)_2$.[3] To determine the effect of this substitution reaction, which is accompanied by an increase in the electron density at the metal centre (ν(C=O) decreases by *ca* 60 cm^{-1}), in the relative stability of structures **A** and **B**, the reaction of complexes **1a–1d** with NaS_2CNMe_2 has been investigated,[10] with the results shown in eqs (3) and (4).

$$W(CH_3)Cl(CO)_2P_3 + NaS_2CNMe_2 \rightarrow \underset{\mathbf{2a}}{W(CH_3)(S_2CNMe_2)(CO)_2P_2} + NaCl \quad (3)$$

$$W(\eta^2\text{-}COR)Cl(CO)P_3 + NaS_2CNMe_2 \rightarrow W(\eta^2\text{-}COR)(S_2CNMe_2)(CO)P_2 + P + NaCl \quad (4)$$

(R = CH_2SiMe_3, **2b**; CH_2CMe_3, **2c**; CH_2CMe_2Ph, **2d**, P = PMe_3).

Two aspects of this process deserve further comments. First, in light of the results reported in this paper, the unusual structure displayed by the molyb denum–acetyl complex[3] can be thought of as "mid-way" between the η^2-acyl and the methyl-(carbonyl) structures. This further supports our initial proposal[3] of structure **D** as a model for the

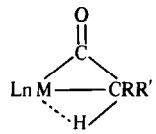

D

transition state (or intermediate) of the CO insertion into M—C bonds. (A similar structure has been proposed as a model for the formation of ketene and a metal hydride by β-elimination from a metal acetyl compound.)[11] The second point concerns the behaviour of complex **2b**, for which an equilibrium between the η^2-acyl and the alkyl-(carbonyl) formulation is quickly attained in solution [eq. (5)] as revealed by IR and NMR studies.‡ Observation of

$$W(\eta^2\text{-}COCH_2SiMe_3)(S_2CNMe_2)(CO)(PMe_3)_2 \overset{C_6H_6}{\rightleftharpoons} W(CH_2SiMe_3)(S_2CNMe_2)(CO)_2(PMe_3)_2 \quad (5)$$

both structures for **2b** and exclusively of the η^2-acyl isomer for **1b** is clearly electronic in origin and can be ascribed to the increase in the electron density at the metal centre which accompanies the transformation, of **1b** into **2b**. Note that the steric demands of the alkyl groups investigated in this work increase in the order $CH_3 < CH_2SiMe_3 < CH_2CMe_3 < CH_2CMe_2Ph$.

* Both the strength of the M—C bond (*5d* > *4d*) and the migratory aptitude of the alkyl group also favour structure **A** for the W—CH_3 complex.[7] However, a decrease in the electron density at the metal centre, caused by substitution of one PMe_3 ligand by CO (see Text), makes structure **B** the more favourable.

† A similar situation, although related to the steric effects of the ancillary ligands, has been found for the ruthenium complexes $Ru(\eta^2\text{-}COC_6H_4\text{-}p\text{-}CH_3)X(CO)(PPh_3)_2$. For these compounds,[9] which exist in solution in equilibrium with the corresponding aryldicarbonyls, the tendency towards formation of the dihapto linkage increases in the order Cl < Br < I.

‡ Only the η^2-acyl structure exists in the solid state: IR (Nujol): νCO 1725 cm^{-1}, νCOR is not observed, possibly due to overlapping with ν(C—N) of the S_2CNR_2 ligand, 1490 cm^{-1}. IR (C_6D_6): νCO 1900, 1810 and 1760 cm^{-1}. ^1H NMR (C_6D_6): (a) $W(R)(CO)_2(S_2CNMe_2)(PMe_3)_2$: δ 2.57 (s, S_2CNMe_2), 1.43 (d, PMe_3), 0.14 (s, CH_2SiMe_3), −0.06 (t, $^3J_{HP}$ = 5.4 Hz, W-CH_2SiMe_3). (b) W(COR) $CO(S_2CNMe_2)(PMe_3)_2$: 2.96 (s, $COCH_2SiMe_3$), 2.73 (s, S_2CNMe_2), 2.67 (s, S_2CNMe_2). 1.59 (t, PMe_3), 0.47 (s, $COCH_2SiMe_3$).

Confirmation of the above hypothesis, concerning the influence of electronic effects on the relative stability of structures **A** and **B**, requires that a sufficient decrease in the metal basicity causes transformation of the alkyl(carbonyl) species into the η^2-acyl. This decrease can be induced by substituting one of the strong σ-donor PMe_3 ligands[12] (cone angle[13] $\theta = 118°$), for the strongly π-acid and less steric demanding CO ligand ($\theta = 95°$). Indeed, the reaction of the methyl(carbonyl) complexes, $W(CH_3)Cl(CO)_2(PMe_3)_3$ and $W(CH_3)(S_2CNMe_2)(CO)_2(PMe_3)_2$, with carbon monoxide proceeds under mild conditions, with formation of the η^2-acetyls $W(\eta^2\text{-}COCH_3)Cl(CO)_2(PMe_3)_2$, **3a** and $W(\eta^2\text{-}COCH_3)(S_2CNMe_2)(CO)_2(PMe_3)$, **4a**, respectively. Furthermore, action of CO upon an equilibrium mixture of $W(\eta^2\text{-}COCH_2SiMe_3)(S_2CNMe_2)(CO)(PMe_3)_2$ and $W(CH_2SiMe_3)(S_2CNMe_2)(CO)_2(PMe_3)_2$, produces only the η^2-acyl complex $W(\eta^2\text{-}COCH_2SiMe_3)(S_2CNMe_2)(CO)_2(PMe_3)$, **4b**. In the absence of steric constraints which could favour rearrangement of the alkyl(carbonyl) into the η^2-acyl, the transformation observed must be entirely ascribed to electronic factors.

The results described in this paper indicate that: (i) the relative stability of seven-coordinated alkyl(carbonyl) complexes and their six-coordinated η^2-acyl isomers is greatly influenced by steric and electronic effects; (ii) an increase in the metal basicity preferentially stabilizes the alkyl(carbonyl) isomer, while a decrease in the electron density at the metal centre favours formation of the η^2-acyl linkage;[14] (iii) as it could reasonably be expected, an increase in the steric demands of the alkyl group favours the η^2-acyl structure, while the less steric demanding alkyl groups prefer the alkyl(carbonyl) formulation.

Acknowledgements—Useful discussions with Dr M. L. Poveda and the generous support of this work by the Comisión Asesora de Investigación Científica y Técnica (CAICYT) are very gratefully acknowledged.

REFERENCES

1. (a) E. Carmona, G. Wilkinson, R. D. Rogers, W. D. Hunter, M. J. Zaworotko and J. L. Atwood, *J. Chem. Soc., Dalton Trans.* 1980, 229; (b) T. Desmond, F. J. Lalor, G. Ferguson, B. Ruhl and M. Parvez, *J. Chem. Soc., Chem. Commun.* 1983, 55.
2. (a) C. A. Rusik, T. L. Tonker and J. L. Templeton, *J. Am. Chem. Soc.* 1986, **108**, 4652; (b) M. D. Curtis, K. B. Shiu and W. B. Butler, *J. Am. Chem. Soc.* 1986, **108**, 1550.
3. E. Carmona, L. Sánchez, J. M. Marín, M. L. Poveda, J. L. Atwood, R. D. Priester and R. D. Rogers, *J. Am. Chem. Soc.* 1984, **106**, 3214.
4. (a) E. Carmona, J. M. Marín, M. L. Poveda, L. Sánchez, R. D. Rogers and J. L. Atwood, *J. Chem. Soc., Dalton Trans.* 1983, 1003; (b) H. G. Alt, *J. Organomet. Chem.* 1977, **129**, 349.
5. F. R. Kreissl, W. J. Sieber, M. Wolfgruber and J. Riede, *Angew. Chem. Int. Ed. Engl.* 1984, **23**, 640.
6. E. Carmona, K. Doppert, J. M. Marín, M. L. Poveda, L. Sánchez and R. Sánchez-Delgado, *Inorg. Chem.* 1984, **23**, 530.
7. H. Berke and R. Hoffmann, *J. Am. Chem. Soc.* 1978, **100**, 7224.
8. D. F. Shriver, *Acc. Chem. Res.* 1970, 231.
9. W. R. Roper and L. J. Wright, *J. Organomet. Chem.* 1977, **142**, C1.
10. (The molecular structures of complexes **1b** and **2a** have been determined by X-ray crystallography.) R. D. Rogers and J. L. Atwood (to be submitted).
11. S. I. Hommeltoft and M. C. Baird, *Organometallics* 1986, **5**, 190.
12. M. N. Golovin, M. M. Rahman, J. E. Belmonte and W. P. Giering, *Organometallics* 1985, **4**, 1981.
13. C. A. Tolman, *Chem. Rev.* 1977, **77**, 313.
14. J. L. Templeton, P. B. Winston and B. C. Ward, *J. Am. Chem. Soc.* 1981, **103**, 7713.

Polyhedron Vol. 7, No. 2, pp. 167–168, 1988
Printed in Great Britain

0277–5387/88 $3.00+.00
Pergamon Journals Ltd

COMMUNICATION

PREPARATION OF URANIUM TRICHLORIDE BY THERMAL VACUUM DECOMPOSITION OF AMMONIUM TETRACHLOROURANATE(III) TETRAHYDRATE

J. DROŻDŻYNSKI

Institute of Chemistry, University of Wrocław, 50-383 Wrocław, Poland

(*Received* 27 *August* 1987, *accepted* 25 *September* 1987)

Abstract—Ammonium tetrachlorouranate(III) tetrahydrate may easily be converted into uranium trichloride at a non-static high-vacuum of 10^{-5}–10^{-6} Pa and temperatures ranging from 20–400°C.

The chemical literature reports several methods of preparation of uranium trichloride,[1] however this compound has been found to be difficult to obtain in a state of high purity. The most successful large scale synthesis involves the reaction of finely divided uranium metal or uranium hydride with gaseous hydrogen chloride at 250–300°C,[2,3] as well as the reduction of UCl_4 with hydrogen[3,4] or metallic zinc[5] at 450–650°C. The product obtained by any of these methods usually needs purification by chemical transport with iodine vapour.[3] Since uranium trichloride at higher temperatures is very sensitive to oxidation and hydrolysis, the preparative procedures need to be carried out under strict moisture- and oxygen-free conditions. Hence, the synthesis of UCl_3 requires a more or less complex apparatus as well as some experience and pure starting materials.

This paper presents a relatively simple method for the preparation of uranium trichloride by thermal decomposition of tetrachlorouranate(III) tetrahydrate. The method seems to be the most convenient in cases where only gram amounts of the compound are needed.

For the preparation of ammonium tetrachlorouranate(III) tetrahydrate, 1–5 g of uranium tetrachloride with a large excess of ammonium chloride was added to a solution consisting of 80 cm^3 methyl cyanide, 2.5 cm^3 water and 3.5 cm^3 propionic acid.[6] The mixture was shaken until all the tetrachloride dissolved, and was left standing for a couple of hours. Next, the solution was filtered off from the undissolved ammonium chloride and reduced in an inert atmosphere by gentle shaking with a 2.4% liquid zinc amalgam. The reduction resulted in the immediate formation of a well defined crystalline, violet–red precipitate of $NH_4UCl_4 \cdot 4H_2O$. An excess of water may result in the formation of a separate, oily phase consisting probably of a different, hydrated uranium(III) complex chloride. The precipitate was filtered off and washed under an inert atmosphere with degassed methylcyanide and freshly distilled ether, dried under reduced pressure at 25–35°C for about 20 min, and stored in sealed tubes at temperatures below 15°C. The yield of the reaction is *ca.* 80%.

The synthesis was carried out in a relatively simple all-glass apparatus as previously described.[7] The inert atmosphere glove box as well as by using a set necting the apparatus with a vacuum pump and evacuating the solutions and wash liquids for *ca.* 3 min. The synthesis may also be performed in an inert atmosphere glove box as well as by using a set of Schlenk tubes.

The compound crystallizes much easier and seems also to be much more resistant to oxidation by air, compared with the earlier obtained hydrated and anhydrous complex chlorides.[8–10] The physical and chemical properties of $NH_4UCl_4 \cdot 4H_2O$ along with its potassium and rubidium analogues will be given elsewhere.[11]

The ammonium tetrachlorouranate(III) tetra-

hydrate obtained in the above manner was converted into UCl_3 by a thermal high vacuum decomposition. For this purpose 1–3 g of $NH_4UCl_4 \cdot 4H_2O$ together with an excess (*ca.* 1.5 times) of NH_4Cl were placed in the bottom of the sealed off end of a quartz tube, 40 cm long and 2 cm in diameter. About 10 cm from the bottom, the tube narrowed and therefore the section of the tube with the product could be easily sealed off. The other end of the tube was fitted with a joint and vacuum stopcock. A furnace was slipped over the tube and the system was pumped off to *ca.* 10^{-6} Pa. Decomposition proceeds first between 25–80°C for at least 7 h. The temperature was never raised at a pressure higher than 10^{-4} Pa. At the end of the process the temperature was slowly rasied to 400°C. Samples of UCl_3 prepared in this manner are olive green in colour. The pyknometrically determined density of the compound is 5.46 g cm^{-3}. From X-ray data[11] a value of 5.51 g cm^{-3} was obtained. Found: U, 69.6; Cl, 31.1. Calc. for UCl_3: U, 69.1; Cl, 30.9%.

REFERENCES

1. *Gmelin—Handbuch der Anorganischen Chemie*, System 55, U Suppl., Vol. C9, Chap. 6. Springer, Berlin (1979).
2. O. Johnson, T. Buttler and A. S. Newton, TID-5290, pp. 1–28 (1958).
3. N. W. Gregory, TID-5290, pp. 465–510 (1958).
4. J. F. Suttle, *Inorg. Synth.* 1957, **5**, 145.
5. H. S. Young, TID-5290, pp. 757–758 (1958).
6. J. Drożdżyński, *16èmes Journées des Actinides*, Eibsee, F.R.G. (28–30 April 1986); Abstracts (Edited by G. M. Kalvius). p. VI5. Technische Universität München, F.R.G.
7. J. Drożdżyński, *Inorg. Chim. Acta*, 1979, **32**, L83.
8. R. Barnard, J. I. Bullock, B. J. Gellatly and L. F. Larkworthy, *J. Chem. Soc., Dalton Trans* 1972, **18**, 1932.
9. J. Drożdżyński and D. Miernik, *Inorg. Chim. Acta* 1986, **30**, L85.
10. E. Zych and J. Drożdżyński, *Inorg. Chim. Acta*, 1986, **115**, 219.
11. J. Drożdżyński, *J. Less-common Met.* (in press).

Polyhedron Vol. 7, No. 2, pp. 169–170, 1988
Pergamon Journals Ltd. Printed in Great Britain

BOOK REVIEW

Fluorine. The First Hundred Years (1886–1986). Edited by R. E. Banks, D. W. A. Sharp and J. C. Tatlow. Elsevier, Amsterdam, 1986. ISBN 0-444-75039-8.

Serendipity and persistence are both attributes of the successful research chemist and both find their place in the history of fluorine. This volume comprises a number of essays covering a wide range of fluorine chemistry, first published in the *Journal of Fluorine Chemistry*.

In Chapter 1, R. E. Banks gives a useful account of the properties of fluorine, including a summary of pre-Moissan work on anhydrous hydrogen fluoride and on the attempts to isolate fluorine, which ultimately hinged upon the preparation by Frémy of KHF_2. Unlike the other halogens, fluorine received its name before it was isolated; a name coined by Ampère that was followed by most chemists—fortunately, in view of alternatives such as phthorine and the Russian ftor. The early experimenters experienced the noxious and toxic nature of both hydrogen fluoride and fluorine—who would now emulate Bohuslav Brauner (1894) in testing for fluorine in the gases evolved from hot K_3HPbF_8 by inhaling a sample and noting whether "fumes of hydrofluoric acid issued from the nose" when he exhaled?

Chapter 2 is a biographical sketch of Moissan by J. Flahaut and C. Viel. He spent most of his youth in Meaux, home of the great Bossuet, where he seemed destined for a career as a clockmaker; following the Franco–Prussian war, he decided to attempt a scientific career. Because of his humble background, he had not taken the baccalauréat and therefore had to spend three years catching up. He is one of many scientists who has achieved success through persistence in following a non-traditional route. He obtained the diploma of pharmacist, first class, in 1879 for a thesis entitled "On the Amount of Oxygen absorbed and Carbonic acid emitted during Plant Respiration", but was already moving into Inorganic Chemistry and obtained his Doctor of Science in 1880 for studies on "Metallic Oxides from the Iron Family". His researches on fluorine began in 1884 and two years later he succeeded in preparing for the first time significant quantities of fluorine. (In 1890, he diversified into the preparation of artificial diamonds.)

The development of inorganic fluorine chemistry in the period until 1945 is the subject of O. Glemser's third chapter; it covers the synthesis of a whole range of binary compounds and early developments in the chemistry of both fluorinating agents and of liquid hydrogen fluoride as a solvent. A parallel chapter by Banks and Tatlow treats organic fluorine chemistry up to 1940, commencing with work on aryl fluorides—a one-pot synthesis of fluorobenzene from aniline was submitted one month before Moissan first isolated fluorine. Whilst the Balz–Schiemann reaction opened up a more general route in 1927, and in the 1930s elemental fluorine became a practical reagent. Aliphatic fluorine chemistry was harder, until Swarts used SbF_3Br_2 as a fluorinating agent. In the late 1920s Fridgidaire developed CF_2Cl_2 as a refrigerant followed in the ensuing decade by Freons, as well as by the quite fortuitous discovery of PTFE.

The role of fluorine in the Manhattan project is traced by H. Goldwhite. Much of the research was directed to producing substances suitable for use with UF_6 that would be totally inert to it, for use as coolants, lubricants, and gasket, packing and tubing materials.

Chapter 6 (J. F. Ellis and G. F. May) considers the current methods of fluorine generation, all based on electrolysis of $KF \cdot 2HF$. This covers extremely recent work; a photograph of the fluorine cell room in the UF_6 plant at Springfields is a reminder of the scale of fluorine production needed as well as the need for scrupulous care in operation and maintenance.

The most glamorous and far reaching developments in fluorine chemistry since the War have surely been the synthesis of the Noble Gas Fluorides, reviewed by J. H. Holloway in Chapter 7; Chapter 8, by J. M. Winfield, covers developments in transition metal fluorides over the last decade, covering uses (current interest in UF_6 and PuF_6 in laser isotope separation for example), synthetic routes, structural studies and reactions. J. M. Shreeve treats recent developments in Main Group Fluorides, with many references to N—F, O—F and S—F bonds, interhalogen compounds, and fluoroalkyl organometallics.

Chapter 11, by D. T. Meshri, is a review of the important compounds in the inorganic fluorochemical industry. It covers CaF_2, HF, UF_6, SF_6, AlF_3, Na_3AlF_6, HSO_3F, SnF_2, H_2SiF_6, Na_2PO_3F, BF_3, HBF_4, fluoroborates, and fluorides of the alkali and transition metals and halogens. Synthetic routes are given as well as important physical properties of the compounds together with an indication of their uses.

The longest chapter in the book (120 pp.) is a guide by Banks and Tatlow to the current organofluorine field. It covers areas such as new fluorinating agents and reactants, mechanistic aspects and a wide study of fluorinating routes. Lengthy appendices cover areas such as nomenclature, ^{19}F NMR, fluoroalkyl iodides, perfluoropolyether fluids, fluorocarbons in the electronics industry and in "artificial blood", all by experts in the field.

Chapter 12 (C. Wakselman and C. Kaziz) reviews recent advances in the chemistry of halogenofluorocarbons, beginning with comments about their effect on stratospheric ozone. Most of the chapter reviews their reactions—with nucleophilic reactions

predominating over radical additions and electrophilic reactions. R. Filler reviews biologically-active fluorochemicals—examples include 5-fluorouracil in cancer chemotherapy, fluothane anaesthetics, fluorine-containing anti-inflammatory drugs, diuretics and hypertensives, and perfluoro based artificial blood substitutes.

The final chapter (G. A. Olah, J. G. Shih and G. K. S, Prakash) is devoted to fluorine-containing reagents in organic synthesis, featuring stars like pyridinium poly(hydrogen fluoride), Olah's reagent, SO_2ClF, and SF_4.

Stanground School **SIMON COTTON**
Peterborough
Cambs, U.K.

Polyhedron Vol. 7, No. 3, pp. 171–185, 1988
Printed in Great Britain

0277–5387/88 $3.00+.00
© 1988 Pergamon Journals Ltd

COMPLEXES OF RHENIUM WITH BENZOYLAZO AND RELATED LIGANDS. CRYSTAL AND MOLECULAR STRUCTURES OF THE "GREEN CHELATE" BENZOYLAZO COMPLEX $[ReCl_2(PPh_3)_2(NNCOC_6H_4\text{-}p\text{-}Cl)](N_\alpha,O)$, OF THE ANALOGOUS 1-AZOPHTHALAZINE CHELATE COMPLEX $[ReCl_2(PPh_3)_2(NNC_8H_5N_2)](N_\alpha,N_1)$, AND OF THE *CIS*-DICHLORO ORGANODIAZENIDO COMPLEXES OF THE TYPE $[ReCl_2(PPh_3)_2(NNR)L]$ ($L = NCCH_3$, NH_3 AND C_5H_5N). A COMPARISON TO THE STRUCTURE OF THE *TRANS*-DICHLORO DIMETHYLFORMAMIDE DERIVATIVE $[ReCl_2(PPh_3)_2(NNCO_2CH_3)(Me_2NCHO)]$. THE STRUCTURAL CHARACTERIZATION OF THE MIXED HYDRAZIDO(1-) HYDRAZIDO(2-) COMPLEXES $[ReCl_2(PPh_3)_2(NNHR)(NHNHR')]$, ($R = R' = -COC_6H_5$; $R = -COC_6H_5$, $R' = -CO_2CH_3$)

TERENCE NICHOLSON and JON ZUBIETA*

Department of Chemistry, State University of New York at Albany,
1400 Washington Avenue, Albany, New York 12222, U.S.A.

(*Received* 12 *April* 1987; *accepted after revision* 24 *August* 1987)

Abstract—Reaction of $[ReOCl_3(PPh_3)_2]$ with potentially chelating organohydrazines in ethanol–HCl solutions gives six coordinate chelate complexes of the general formulation $[ReCl_2(PPh_3)_2(NNR)]$; [R = COC_6H_4-*p*-Cl, (**1**); R = $C_8H_5N_2$, (phthalazine), (**2**)]. Complexes (**1**) and (**2**) display octahedral geometries with mutually *trans* phosphine groups minimizing steric congestion and *cis*-chloride ligands. The chelated hydrazido(3−) ligand occupies the remaining two coordination sites. The weakly coordinated carbonyl group in complex (**1**) can be displaced by two ligand types. Neutral two electron donating ligands give organodiazenido adducts such as $[ReCl_2(PPh_3)_2(NCCH_3)(NNCOC_6H_5)]$, (**3**). Ligands with exchangable protons such as organohydrazines give the mixed hydrazido(2−), hydrazido(1−) complexes $[ReCl_2(PPh_3)_2(NNHR)(NHNHR')]$, [$R = R' = -COC_6H_5$, (**7**); $R = -COC_6H_5$, $R' = -CO_2Me$, (**8**)]. Reaction of $[ReOCl_3(PPh_3)_2]$ with orthobromophenylhydrazine hydrochloride gives the ammonia diazenido complex $[ReCl_2(PPh_3)(NNC_6H_4$-*o*-Br)], (**4**), with the ammonia generated from decomposition of excess hydrazine. Methylhydrazinocarboxylate fails to give the chelate complex analogous to (**1**) and (**2**). When dimethylformamide is added to the reaction medium, two products are isolated. The insoluble, *cis*-chloro N-bonded DMF adduct, $[ReCl_2(PPh_3)_2(Me_2NCHO)(NNCO_2Me)]$, (**5a**), which readily substitutes neutral donor ligands for the weakly coordinated dimethylformamide giving complexes such as $[ReCl_2(PPh_3)_2(C_5H_5N)(NNCO_2Me)]$, (**5**). From the filtrate, the *trans*-chloro, O-bonded dimethylformamide isomer $[ReCl_2(PPh_3)_2(Me_2NCHO)(NNCO_2Me)]$, (**6**) is isolated. Complexes (**3**), (**4**) and (**5**) each display *cis*-chloro, *trans*-phosphine coordination, with the diazenido unit —NNR and neutral donor ligand (NH_3, C_5H_5N and $NCCH_3$) occupying the remaining two sites. Complexes (**7**) and (**8**) are geometrically similar to (**3**)–(**5**) with hydrazido(2−) and hydrazido(1−) ligands in a *cis*-arrangement. The UV-Visible spectra appear to distinguish between the metal–organodiazenido and metal–hydrazido(2−) coordination modes.

*Author to whom correspondence should be addressed.

Crystal data (**1**): Monoclinic space group $P2_1/c$, $a = 14.863(2)$, $b = 10.614(3)$, $c = 24.636(4)$ Å, $\beta = 94.57(1)°$, $V = 3874.1(8)$ Å^3 to give $Z = 4$; structure solution and refinement based on 3751 reflections converged at $R = 0.0461$. (**2**): triclinic space group $P\bar{1}$, $a = 12.480(2)$, $b = 12.392(2)$, $c = 29.603(4)$ Å, $\alpha = 96.30(1)°$, $\beta = 97.30(1)°$, $\gamma = 114.06(1)°$, $V = 4080.0(8)$ Å^3 to give $Z = 4$; structure solution and refinement based on 6528 reflections converged at $R = 0.0620$. (**3**): monoclinic space group $P2_1/n$, $a = 14.004(3)$, $b = 14.329(3)$, $c = 20.019(4)$ Å, $\beta = 94.02(1)°$, $V = 4007.2(10)$ Å^3 to give $Z = 4$; structure solution and refinement based on 4314 reflections converged at 0.0432. (**4**): triclinic space group $P\bar{1}$, $a = 10.535(2)$, $b = 14.393(3)$, $c = 16.585(3)$ Å, $\alpha = 66.14(1)°$, $\beta = 78.93(1)°$, $\gamma = 84.93(1)°$, $V = 2342.5(8)$ Å^3 to give $Z = 2$; structure solution and refinement based on 5513 reflections converged at $R = 0.0506$. (**5**): monoclinic space group $P2_1/n$, $a = 15.105(3)$, $b = 15.619(3)$, $c = 19.449(4)$ Å, $\beta = 112.47(1)°$, $V = 4240.1(9)$ Å^3 to give $Z = 4$; structure solution and refinement based on 3478 reflections converged at 0.0726. (**6**): monoclinic space group $P2_1$, $a = 10.240(2)$, $b = 16.051(3)$, $c = 12.801(2)$ Å, $\beta = 110.94(1)°$, $V = 1965.0(5)$ Å^3 to give $Z = 2$; structure solution and refinment based on 3174 reflections converged at $R = 0.0410$. (**7**): triclinic space group $P\bar{1}$, $a = 12.276(2)$, $b = 14.147(2)$, $c = 15.284(2)$ Å, $\alpha = 86.33(1)°$, $\beta = 72.04(1)°$, $\gamma = 83.10(1)°$, $V = 2505.7(9)$ Å^3 to give $Z = 2$; structure solution and refinement based on 4995 reflections converged at $R = 0.0420$. (**8**): triclinic space group $P\bar{1}$, $a = 11.843(2)$, $b = 12.015(2)$, $c = 16.216(3)$ Å, $\alpha = 96.40(1)°$, $\beta = 100.40(1)°$, $\gamma = 103.56(1)°$, $V = 2177.5(8)$ Å^3 to give $Z = 2$; structure solution and refinement based on 4309 reflections converged at $R = 0.0409$.

Monosubstituted organohydrazine ligands display a rich coordination chemistry, presenting a variety of skeletal geometries and often reacting to give complexes containing other nitrogen ligands, including dinitrogen.[1] The most common structural form is the organodiazenido ligand, —NNR, a species isoelectronic with the nitrosyl ligand and chemically related to the diazenide unit, —NNH, a potential intermediate in the reduction of dinitrogen to ammonia. Structural studies have confirmed that the organodiazenido ligand may display a variety of geometries: "singly bent" (**I**),[2] "doubly bent" (**II**)[3] and bridging (**III**).[4]

Monosubstituted organohydrazines may also function as hydrazido(2−) ligands, —NNHR, which arise formally and often in practice from the protonation of the terminal nitrogen of the organodiazenido ligand. Once again linear (**IV**)[5] and bent (**V**)[6] M—N—N frameworks have been observed. Protonation may also occur at the metal bound nitrogen to give the bent organodiazene group (**VI**), examples of which have been prepared by direct protonation of type (**II**) organodiazenido complexes or by insertion of an organodiazonium group into a metal–hydride bond.[7] Subsequent protonation yields the organohydrazido(1−) ligand,

(**I**)

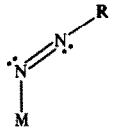

(**II**)

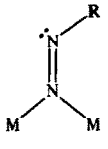

(**III**)

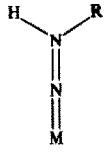

(**IV**)

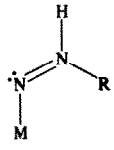

(**V**)

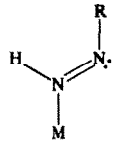

(**VI**)

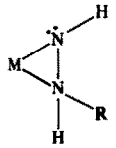

(**VII**)

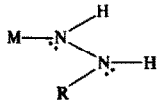

(**VIII**)

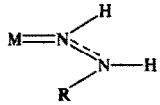

(**IX**)

—NHNHR, for which the side-on configuration (**VII**)[8] and the end-on geometries, (**VIII**) and (**IX**),[9] have been established. Furthermore, the organohydrazine group may function as a neutral two electron donor, H_2NNHR (**X**).[10]

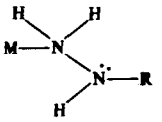

(**X**)

Functional substituents, such as $—COC_6H_5$ and $—CSNH_2$, result in the potential to form chelate complexes with transition metal ions and to further complicate the structural chemistry.[11] Thus, benzoylhydrazine reacts with a number of transition metal precursors to give N-benzoylhydrazine(3−)—O,N complexes, such as $[ReCl_2(PPh_3)_2(NNCOPh)]$.[12] This complex reacts with a number of nucleophiles via chelate ring opening to give species of the general type $[ReCl_2(PPh_3)_2(NNCOPh)L]$.[13]

In this paper, we present the synthesis and characterization of a series of chelating organohydrazido(3−) rhenium complexes of general formula $[ReCl_2(PPh_3)_2(NNR)]$, where R = $—COC_6H_4X$ and phthalazine, and the structural investigation of the products of a simple chelate ring opening, $[ReCl_2(PPh_3)_2(NNR)L]$, L = $NCCH_3$ and C_5H_5N. Furthermore, reaction of the chelate precursors with monosubstituted hydrazines is shown to yield complexes possessing both hydrazido(1−) and hydrazido(2−) ligands, $[ReCl_2(PPh_3)_2(NNHR)(NHNHR')]$. The series of complexes is thus seen to exhibit a range of coordination types for the monosubstituted organohydrazine precursor: metal–hydrazido(1−) (M—NHNHR), metal–hydrazido(2−) (M—NNHR), metal–diazenido (1+) (M—NNR) and chelating organohydrazido (3−) (M—NNCX).

RESULTS AND DISCUSSION

Synthetic and spectroscopic properties

Oxotrichlorobis(triphenylphosphine)rhenium(V) reacts with potentially chelating organohydrazines to give complexes of the type $[ReCl_2(PPh_3)_2(NNX)]$, where X = —COPh or phthalazine. The complexes are emerald green, air stable crystalline solids. The IR spectra exhibit no bands assignable to ν(N—H). The *p*-chlorobenzoylhydrazido complex (**1**), shows no IR bands assignable to ν(C=O) or to ν(N=N), suggesting that these species are best formulated as organohydrazido(3−) complexes of rhenium(V), as previously suggested by Chatt and coworkers.[13] The diamagnetism of the complexes is also consistent with this formulation. The IR spectrum of the phthalazinehydrazido(3−) derivative, $[ReCl_2(PPh_3)_2(NNC_8H_5N_2)]$, (**2**), exhibits IR bands associated with the coordinated phthalazine group, but no bands assignable to ν(C=N) or ν(N=N). The structures of (**1**) and (**2**) have been confirmed by X-ray crystallography.

The UV-Visible spectra of (**1**) and (**2**) in dichloromethane solution show intense charge transfer transitions in the 500–200 nm region and a medium intensity band at 660–690 nm associated with the chelate ring.

Reactions of (**1**) with neutral donor ligands, such as acetonitrile and pyridine in benzene, result in the opening of the chelate ring through displacement of the coordinated carbonyl group by the neutral donor ligands to give a organodiazenido species of the type $[ReCl_2(PPh_3)_2(NCMe)(NNCOPh)]$, (**3**). These bright red or orange species are best formulated as rhenium(I) complexes with linear terminally coordinated three electron donating organodiazenido ligands $(—NNCOPh)^{1+}$, a description consistent with the X-ray structural results discussed in the following section.

The appearance of IR bands in the 1500–1700 cm^{-1} range assigned to ν(N=N) and ν(C=O) confirm the opening of the chelate and the presence of the delocalized terminal organodiazenido group. The UV-Visible spectra of these derivatives exhibit intense charge transfer transitions in the 400–200 nm region and weak transition at *ca* 500 nm, which appears to be characteristic of metal–organodiazenido interactions.[14,15]

The phthalazine derivative (**2**) is unreactive towards donor ligands under similar conditions, reflecting the increased basicity of the chelating aromatic amine compared to the carbonyl group in (**1**). The phthalazine chelate can be displaced by warming (**2**) in pyridine giving a deep red solution, indicative of the organodiazenido species.

Reaction of the benzoyl chelate complex (**1**) with donor ligands with exchangable protons, such as organohydrazines, also proceeds via chelate ring opening. We suspect the initial step of these reactions is the protonation of the coordinated carbonyl group giving an enol intermediate which subsequently rearranges to the hydrazido(2−) species in the product. This reaction is not solvent assisted since it occurs in aprotic solvents.

In contrast to the reactions with aprotic donor ligands discussed earlier, these products are grey–green microcrystals and are best formulated as mixed hydrazido(1−) hydrazido(2−) species,

$[ReCl_2(PPh_3)_2(NHNHR)(NNHR')]$. The appearance of IR bands in the 1500–1700 cm^{-1} range confirms the opening of the chelate and the presence of hydrazido type ligands.

The UV-Visible spectra display not only the ubiquitous 400–200 nm charge transfer bands but a medium intensity band at 565 nm which may be characteristic of the metal–hydrazido(2−) functionality.[16]

The electronic spectra appear to distinguish the two types of coordination modes, thus the presence of the metal–organodiazenido unit (**XI**) in the red and orange species gives rise to the 500 nm transition, while the metal–hydrazido(2−) linkage (**XII**) of the grey–green derivatives is associated with the medium intensity band at 565 nm.

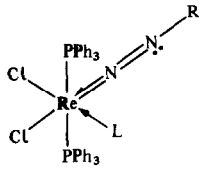

(XI)

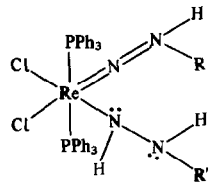

(XII)

The protons on the hydrazido ligands are capable of a variety of hydrogen bonding combinations, which greatly complicate the NMR spectra, and make them exceedingly solvent dependent. In CD_2Cl_2, 2-dimensional NMR of (7) shows a pair of coupled peaks at 6.2 and 9.8 ppm from the hydrazido(1−) ligand and a third broad but uncoupled signal at 1.3 ppm from the hydrazido(2−) ligand. In benzene-d_6, it appears that the hydrazido(1−) ligand is displaced as neutral hydrazine with the original chelate complex reforming. A doublet, triplet combination at 4.2 and 10.1 ppm confirms the presence of the uncoordinated benzoylhydrazine.

In an effort to exploit the tendency of the $[ReCl_2(PPh_3)_2]$ core to adopt a *trans*-phosphine, *cis*-dichloro geometry in complex formation, benzoylhydrazine was replaced by 2-bromophenylhydrazine in the synthetic procedure. It was anticipated that the *ortho*-bromo substituent would provide sufficient steric bulk to block the sixth coordination site at the rhenium centre, allowing isolation of the five coordinate 16 electron complex, $[ReCl_2(PPh_3)_2(NNC_6H_4Br)]$. Five coordinate species of this type have been demonstrated to be relatively common in the chemistry of rhenium and molybdenum with sterically bulky ligands.[17,18] However, the acidic conditions under which these complexes form causes decomposition of the excess hydrazine to ammonia, which subsequently occupies the vacant sixth coordination site, giving $[ReCl_2(PPh_3)_2(NH_3)(NNC_6H_4Br)]$, (**4**).

Methylhydrazinocarboxylate, $H_2NNHCOOCH_3$, fails to react with $[ReOCl_3(PPh_3)_2]$ under the conditions that afford complexes (**1**), (**2**) and (**4**), as the organohydrazine is only sparingly soluble in the reaction medium. With dimethylformamide as a solvent the solution colour gradually changes to red–brown with the formation of a maroon precipitate, (**5a**) which analyses for $[ReCl_2(PPh_3)_2(Me_2NCHO)(NNCOOCH_3)]$.

The IR spectrum of (**5a**) shows a broad band at 1750 cm^{-1}, assigned to ν(C=O) from both N-bonded DMF and the α-N coordinated carboxymethyldiazenido unit. The inductive effect of the methoxy-group on the carbonyl unit of the hydrazine diminishes the basicity of the carbonyl oxygen, and accordingly its tendency to chelate. The insolubility of this material in non-coordinating solvents precluded the isolation of X-ray quality crystals. However, the dimethylformamide ligand is readily displaced by a variety of ligands, including pyridine and acetonitrile. The pyridine adduct, $[ReCl_2(PPh_3)_2(C_5H_5N)(NNCOOCH_3)]$, (**5**), exhibits a single band at 1710 cm^{-1} in the IR spectrum, assigned to ν(C=O). A weak band at 1600 cm^{-1} is assigned to ν(N=N).

The filtrate from which (**5a**) is isolated, upon slow evaporation, yields a red crystalline material, (**6**), which also analyses for $[ReCl_2(PPh_3)_2(Me_2NCHO)(NNCOOMe)]$. The IR spectrum of this material shows a complex series of bands and shoulders between 1740 and 1620 cm^{-1}. The X-ray structure establishes this material as a coordination isomer of (**5a**), with mutually *trans* chlorine ligands and an O-bonded dimethyl formamide ligand *trans* to the diazenido unit. The free and coordinated carbonyl groups of these two ligands, in addition to the bands assigned to ν(N=N), account for the bands in the 1700 cm^{-1} region of the IR spectrum.

Structural studies

The structure of the "green chelate" prototype $[ReCl_2(PPh_3)_2(NNCOC_6H_4\text{-}p\text{-}Cl)]$ (**1**) consists of discrete mononuclear species with the rhenium atom coordinated to *trans* phosphine ligands and chloride ligands disposed *trans* to the nitrogen and carbonyl oxygen donors of the chelating *p*-chlorobenzoylhydrazido(3−) ligand, as shown in Fig. 1. The bonding parameters, presented in Table 1, are similar to those of the analogous 1-azophthalazine chelate complex, discussed at length below.

The structure of the chelate complex [N-phthalazinehydrazido(3−) — N'', N') dichlorobis(tri-

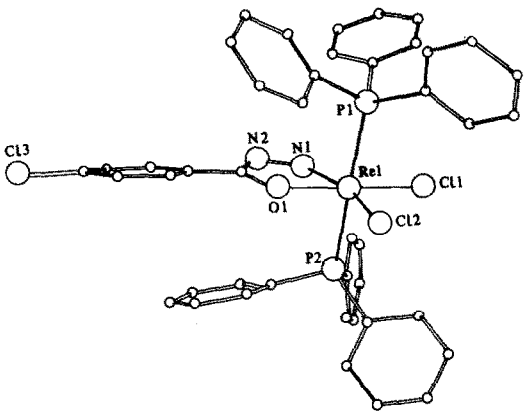

Fig. 1. ORTEP view of the structure of complex (**1**), $[ReCl_2(PPh_3)_2(NNOC_6H_4\text{-}p\text{-}Cl)]$, showing relevant atoms labelled.

phenylphosphine)rhenium(V), (**2**), is found to contain two discrete molecules in each asymmetric unit with the rhenium atoms displaying essentially equivalent, distorted octahedral geometries, as illustrated in Fig. 2 for one of the complexes independent molecules.

The coordination geometry about the rhenium centre exhibits mutually *trans* phosphine groups, minimizing steric congestion, and chloride ligands disposed *trans* to the nitrogen donors of the phthalazine hydrazido(3−) ligand which form a five-membered chelate ring with the metal. As indicated by the metrical parameters given in Table 1, there is considerable delocalization throughout the Re—N1—N2 unit. The short Re1—N1 distance of 1.79(2) Å suggests significant multiple bonding, in contrast to the Re1—N3 distance of 2.14(2) Å,

Table 1. Selected bond lengths (Å) and angles (°) for $[ReCl_2(PPh_3)_2(NNCOC_6H_4Cl)]$ (**1**) and $[ReCl_2(PPh_3)_2(NNC_8H_5N_2)]$ (**2**)

(**1**)		(**2**) Molecule 1		(**2**) Molecule 2	
Re1—Cl1	2.361(2)	Re1—Cl1	2.388(5)	Re2—Cl3	2.364(4)
Re1—Cl2	2.357(2)	Re1—Cl2	2.367(5)	Re2—Cl4	2.386(5)
Re1—P1	2.466(2)	Re1—P1	2.465(5)	Re2—P3	2.438(6)
Re1—P2	2.463(2)	Re1—P2	2.480(5)	Re2—P4	2.459(6)
Re—N1	1.769(8)	Re1—N1	1.79(2)	Re2—N1′	1.75(1)
Re—O1	2.119(6)	Re1—N3	2.14(2)	Re2—N3′	2.14(2)
N1—N2	1.30(2)	N1—N2	1.29(2)	N1′—N2′	1.30(2)
N2—C1	1.37(2)	N2—C1	1.36(2)	N2′—C1′	1.37(2)
C1—O1	1.27(2)	C1—N3	1.37(2)	C1′—N3′	1.34(2)
		N3—N4	1.38(2)	N3′—N4′	1.36(2)
Cl1—Re1—Cl2	98.9(1)	N4—C8	1.30(2)	N4′—C8′	1.34(3)
Cl1—Re1—P1	88.8(1)				
Cl1—Re1—P2	90.0(1)	Cl1—Re1—Cl2	93.7(2)	Cl3—Re2—Cl4	97.6(20)
Cl1—Re1—N1	107.6(3)	Cl1—Re1—P1	91.4(2)	Cl3—Re2—P3	87.4(2)
Cl1—Re1—O1	178.2(2)	Cl1—Re1—P2	88.0(2)	Cl3—Re2—P4	89.4(2)
Cl2—Re1—P1	88.7(1)	Cl1—Re1—N1	110.2(4)	Cl3—Re2—N1′	156.5(5)
Cl2—Re1—P2	89.5(1)	Cl1—Re1—N3	178.5(4)	Cl3—Re2—N3′	86.2(4)
Cl2—Re1—N1	153.5(3)	Cl2—Re1—P1	91.1(2)	Cl4—Re2—P3	87.3(2)
Cl2—Re1—O1	82.5(2)	Cl2—Re1—P2	92.8(2)	Cl4—Re2—P4	88.1(2)
P1—Re1—P2	177.7(1)	Cl2—Re1—N1	156.1(4)	Cl4—Re2—N1′	105.8(5)
P1—Re1—N1	92.1(3)	Cl2—Re1—N3	85.8(4)	Cl4—Re2—N3′	176.0(4)
P1—Re1—O1	90.1(2)	P1—Re1—P2	176.0(1)	P3—Re2—P4	174.0(2)
P2—Re1—N1	90.1(2)	P1—Re1—N1	89.0(5)	P3—Re2—N1′	92.8(6)
P2—Re1—O1	91.1(2)	P1—Re1—N3	90.0(4)	P3—Re2—N3′	93.8(5)
N1—Re1—O1	71.0(3)	P2—Re1—N1	87.5(4)	P4—Re2—N1′	92.2(6)
Re1—N1—N2	133.8(7)	P2—Re1—N3	90.7(4)	P4—Re2—N3′	91.0(5)
N1—N2—C1	104.8(7)	N1—Re1—N3	90.3(5)	N1′—Re2—N3′	70.3(6)
N2—C1—O1	116.9(8)	Re1—N1—N2	136.4(9)	Re2—N1′—N2′	137.1(11)
C1—O1—Re1	113.5(5)	N1—N2—C1	106.0(14)	N1′—N2′—C1′	104.7(12)
		N2—C1—N3	114.2(16)	N2′—C1′—N3′	115.0(16)
		N2—C1—C2	123.0(17)	N2′—C1′—C2′	120.9(14)
		C1—N3—N4	121.0(15)	C1′—N3′—N4′	119.5(15)
		C1—N3—Re1	113.1(9)	C1′—N3′—Re2	113.9(11)
		N4—N3—Re1	125.9(12)	N4′—N3′—Re2	127.6(11)

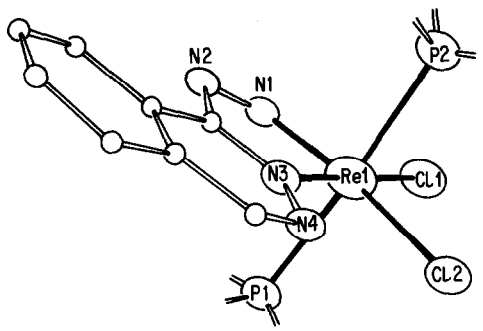

Fig. 2. ORTEP view of the structure of the complex $[ReCl_2(PPh_3)_2(NNC_8H_5N_2)]$ (**2**).

which approaches the limit for a rhenium–sp^2–nitrogen single bond. Similarly, the N1—N2 distance of 1.29(2) Å is marginally shorter than the N3—N4 distance, suggesting a bond order approaching 2 for N1—N2 in contrast to a bond order of 1.5 for N3—N4. The C1—N3 bond distance is consistent with negligible multiple bond character, suggesting major contributions of canonical forms (**XIII**) and (**XIV**) to the metallocycle structure. Although the α-hydrazido-nitrogen rhenium interaction displays a strong π interaction, this is not reflected in a significant *trans* influence in the Re1—Cl2 bond distance, which is equivalent to the Re1—Cl1 distance. A direct consequence of the representation of the hydrazido ligand as phthalazine-hydrazido(3−) is the assignment of the +5 oxidation state to the metal. Metal-ligand bond lengths confirm this formalism. Thus, the Re—Cl distances are within the range observed for $[ReCl_3(NCH_3)(PPh_2Et)_2]$[19] and $[ReCl_3(NC_6H_5COMe)(PEt_2Ph)_2]$[20] (2.399–2.433 Å), as are the Re—P distances. The major distortions from octahedral symmetry are consequences of chelate ring formation, resulting in a severely acute N1—Re1—N3 angle of 70.3(5)°, and of the strong Re1—N1 π-interaction which results in the short Re1—N1 bond distance.

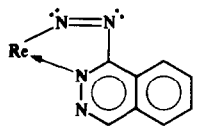

(**XIII**)

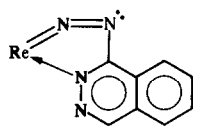

(**XIV**)

The structural consequences of chelate ring opening through displacement of the ligated hydrazine substituent donor group by a neutral "innocent" donor ligand are illustrated by the structures of $[ReCl_2(PPh_3)_2(NNCOPh)(NCCH_3)]$ (**3**) and $[ReCl_2(PPh_3)_2(NNCO_2CH_3)(C_5H_5N)]$ (**5**), illustrated in Figs 3 and 5. The structures of the discrete monomeric complexes reveal distorted octahedral geometries about the rhenium centres, with mutually *trans* phosphine ligands, and chloride donors *trans* to the monodentate organodiazenido ligand (—NNR) and to the donor ligand which has dis-

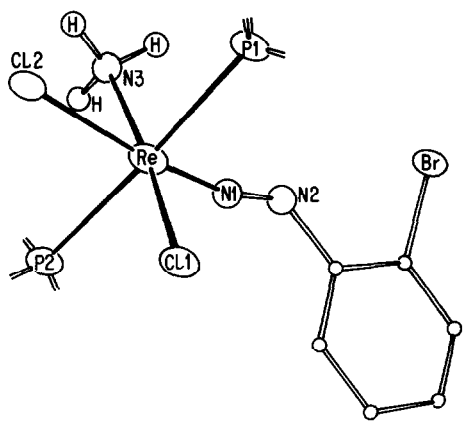

Fig. 4. ORTEP view of the structure of complex $[ReCl_2(PPh_3)_2(NNC_6OH_4\text{-}o\text{-}Br)(NH_3)]$ (**4**), showing relevant atoms labelled.

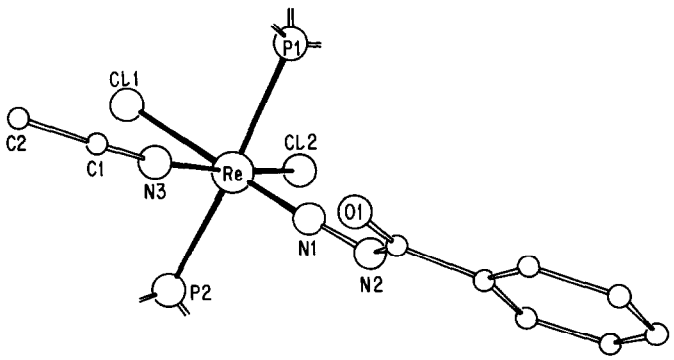

Fig. 3. ORTEP view of the structure of complex (**3**), $[ReCl_2(PPh_3)_2(NNOCPh)(MCMe)]$.

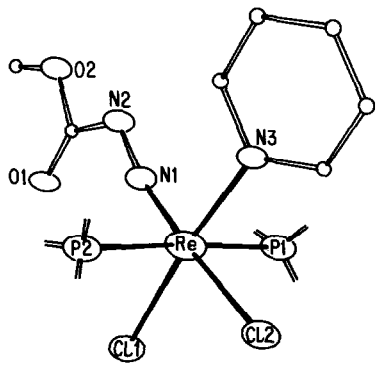

Fig. 5. ORTEP view of the structure of complex (**5**), $[ReCl_2(PPh_3)_2(NNCO_2Me)(C_5H_5N)]$.

placed the carbonyl oxygen of the diazenido substituent. The Re—NNR moiety is best described as a metal–diazenido linkage (**I**) with the ligand functioning as the three-electron donor $(—NNR)^{1+}$ unit in a linear end-on coordination mode.[2] With the donor ligand $NCCH_3$ in (**3**) and C_5H_5N (**5**) serving as a two electron donor, the formalism is consistent with an 18 electron configuration for the metal. Comparison to the structure of $[ReCl_2(PPh_3)_2(NNC_6H_4Br)(NH_3)]$, (**4**) shown in Fig. 4, a rhenium–diazenido complex with a hydrazine ligand bearing a non-coordinating substituent, reveals the persistence of this general structural type. The bonding parameters presented in Table 2 are similar for the three structures and support the description of the (—NNR) ligand by the organo–diazenido formalism. The extensive delocalization throughout the Re—N—N moiety is confirmed by the short Re—N1 and N1—N2 bond distances and by the linear valence angle at N1. The bonding parameters for the three structures are essentially equivalent, but for two significant exceptions. The Re—N3 distance of (**3**) is considerably shorter than the corresponding distances to the nitrogen donors in (**4**)

Table 2. Selected bond lengths (Å) and angles (°) for $[ReCl_2(PPh_3)_2(NNCOPh)(NCCH_3)]$ (**3**), $[ReCl_2(PPh_3)_2(NNCO_2CH_3)(C_5H_5N)]$ (**5**) and $[ReCl_2(PPh_3)_2(NNC_6H_4Br)(NH_3)]$ (**4**)

(3)		(5)		(4)	
Re—Cl1	2.425(2)	Re—Cl1	2.432(4)	Re—Cl1	2.426(2)
Re—Cl2	2.437(2)	Re—Cl2	2.420(5)	Re—Cl2	2.439(3)
Re—P1	2.472(2)	Re—P1	2.458(6)	Re—P1	2.447(2)
Re—P2	2.475(2)	Re—P2	2.479(6)	Re—P2	2.458(2)
Re—N1	1.756(7)	Re—N1	1.72(2)	Re—N1	1.755(7)
Re—N3	2.048(7)	Re—N3	2.20(1)	Re—N3	2.178(6)
N1—N2	1.25(1)	N1—N2	1.28(2)	N1—N2	1.25(1)
N2—C70	1.40(1)	N2—C1	1.44(2)	N2—C1	1.40(1)
C70—O	1.21(1)	C1—O1	1.20(2)	C1—C2	1.38(2)
C70—C71	1.49(1)	C1—O2	1.35(2)	C1—C6	1.37(1)
N3—C1	1.15(1)	N3—C4	1.33(2)	—	
C1—C2	1.44(1)	N3—C8	1.37(2)	—	
Cl1—Re—Cl2	90.5(1)	Cl1—Re—Cl2	87.6(2)	Cl1—Re—C12	92.2(1)
Cl1—Re—P1	90.9(1)	Cl1—Re—P1	90.2(2)	Cl1—Re—P1	90.6(2)
Cl1—Re—P2	90.1(1)	Cl1—Re—P2	88.3(2)	Cl1—Re—P2	90.1(1)
Cl1—Re—N1	93.9(2)	Cl1—Re—N1	98.4(4)	Cl1—Re—N1	97.4(2)
Cl1—Re—N3	169.9(2)	Cl2—Re—N3	172.5(4)	Cl1—Re—N3	171.8(2)
Cl2—Re—P1	88.5(1)	Cl2—Re—P1	91.4(2)	Cl2—Re—P1	88.4(1)
Cl2—Re—P2	88.1(1)	Cl2—Re—P2	86.6(2)	Cl2—Re—P2	89.1(1)
Cl2—Re—N1	175.4(2)	Cl2—Re—N1	174.0(4)	Cl2—Re—N1	170.2(2)
Cl2—Re—N3	79.3(2)	Cl2—Re—N3	84.9(4)	Cl2—Re—N3	79.5(2)
P1—Re—P2	176.4(1)	P1—Re—P2	177.6(2)	P1—Re—P2	177.4(1)
P1—Re—N1	89.9(2)	P1—Re—N1	88.8(6)	P1—Re—N1	89.5(2)
P1—Re—N3	88.8(2)	P1—Re—N3	90.1(5)	P1—Re—N	89.5(2)
P2—Re—N1	93.5(2)	P2—Re—N1	93.3(6)	P2—Re—N1	92.9(2)
P2—Re—N3	89.6(2)	P2—Re—N3	91.1(5)	P2—Re—N	89.4(2)
N1—Re—N3	96.3(3)	N1—Re—N3	89.1(5)	N1—Re—N	89.4(2)
Re—N1—N2	172.1(6)	Re—N1—N2	166.9(12)	Re—N1—N2	167.1(4)
Re—N3—C1	162.2(7)	R—N3—C4	123.8(11)	—	
N3—C1—C2	176.1(10)	Re—N3—C8	119.1(12)	—	
N1—N2—C7	120.5(7)	C4—N3—C8	117.2(14)	N1—N2—C1	119.9(6)

and (**5**), 2.048(7) Å vs 2.178(6) Å and 2.20(1) Å. This observation is consistent with the shorter bond length anticipated for the *sp* hybridized nitrogen of $NCCH_3$ as compared to the sp^2 and sp^3 hybridized N-donors of pyridine and NH_3, respectively. Although we might anticipate the Re—N (pyridine) distance to be somewhat shorter than the Re—N(amine) distance, this trend is not observed, possibly as a result of the relatively poorer quality of the structure of (**5**). The structures of (**3**) and (**4**) also reveal the anticipated *trans* influence of the strongly π-bonding diazenido ligand. Thus, in (**3**) and (**4**), the Re—Cl2 distances are marginally longer than the Re—Cl1 distances, although in absolute terms the effect is small, a 0.012–0.013 Å difference, whereas $3\sigma(\text{Re—Cl}) \simeq$ 0.009 Å. On the other hand, structure (**5**) exhibits equivalent Re—Cl distances. This may again be a consequence of the poorer quality of the structure making a small but real effect. In fact, the diazenido ligand has been demonstrated to exert a significant *trans* influence upon sulphur donor ligands.[21] In contrast to the strongly π-releasing nature of thiolate sulphur donors, chloride ligands exhibit poor π-bonding tendencies. This may suggest that the organodiazenido group, a strong π-acceptor, is relatively ineffective in transmitting a *trans* influence in the absence of significant π-interaction throughout the L_t—Re—NNR linkage (where L_t is the ligand *trans* to the diazenido group).

The structure of the dimethylformamide derivative $[ReCl_2(PPh_3)_2(Me_2NCHO)(NNCO_2Me)]$, (**6**), is shown in Fig. 6 and selected bond lengths and

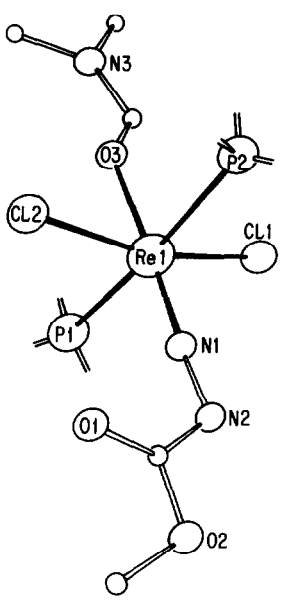

Fig. 6. ORTEP view of the structure of *trans*-chloro complex $[ReCl_2(PPh_3)_2(Me_2NCHO)(NNCO_2Me)]$ (**6**), showing relevant atoms labelled.

Table 3. Selected bond lengths (Å) and angles (°) for $[ReCl_2(PPh_3)_2(Me_2NCHO)(NNCOOCH_3)]$ (**6**)

Re1—P1	2.469(3)	P1—Re1—P2	171.4(1)
Re1—P2	2.446(3)	P1—Re1—N1	93.5(3)
Re1—Cl1	2.431(4)	P2—Re1—N1	94.8(3)
Re1—Cl2	2.408(4)	P1—Re1—O3	84.3(2)
Re1—N1	1.75(2)	P2—Re1—O3	87.5(2)
Re1—O3	2.10(2)	N1—Re1—O3	177.2(4)
N1—N2	1.28(2)	P1—Re1—Cl1	88.0(1)
N2—C1	1.37(3)	P2—Re1—Cl1	88.5(1)
C1—O1	1.21(3)	N1—Re1—Cl1	97.3(4)
O3—C3	1.23(2)	O3—Re1—Cl1	84.3(3)
C3—N3	1.33(2)	P1—Re1—Cl2	93.9(1)
		P2—Re1—Cl2	87.3(1)
		N1—Re1—Cl2	98.4(4)
		O3—Re1—Cl2	80.1(3)
		Cl1—Re1—Cl2	164.0(1)
		Re1—N1—N2	172.7(10)
		N1—N2—C1	114.1(13)
		Re1—O3—C3	139.1(9)
		O3—C3—N3	122.0(14)

angles are presented in Table 3. The structure is unusual in displaying a *trans* chloro geometry in contrast to the exclusively *cis* chloro geometry of other simple derivatives of the $[ReCl_2(PPh_3)_2]$ core. The bonding parameters are otherwise unexceptional with the relatively long Re—O3 (dimethylformamide) bond distances of 2.10 (2) Å consistent with the facile loss of dimethylformamide associated with this species.

Figures 7 and 8 illustrate the structures of products isolated from the reactions of the chelate complex (**1**) with organonitrogen ligands with exchangable protons. The gross features of the structures of $[ReCl_2(PPh_3)_2(NNHCOPh)(NHNHCOPh)]$ (**7**) and $[ReCl_2(PPh_3)_2(NNHCOPh)(NHNHCO_2CH_3)]$ (**8**) are similar to those of complexes (**3**), (**4**) and (**5**). Thus, the rhenium atom of each structure displays distorted octahedral geometry, coordinating to two mutually *trans* phosphine ligands and to two chloride donors occupying positions *trans* to the organohydrazine ligands which complete the coordination sphere. As illustrated in Table 4, the Re—P and Re—Cl distances are unexceptional. The observation of peaks consistent with N-bound hydrogen atoms in the final electron density maps of the structural studies confirms the identity of the nitrogen ligands as hydrazido(1−) and hydrazido(2−) units. In (**7**), the Re-hydrazido(2−) unit, Re—N3—N4(H)(COPh), assumes the linear end-on geometry most commonly encountered for this grouping. The short Re—N3 and N3—N4 distance and the linear valence angle at N3, listed in Table 4,

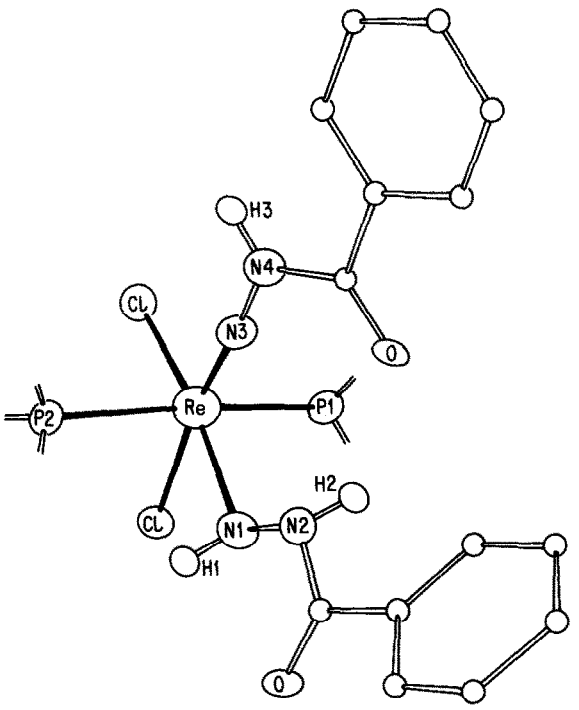

Fig. 7. ORTEP view of the structure of complex (**7**), $[ReCl_2(PPh_3)_2(NNHCOPh)(NHNHCOPh)]$.

are consistent with extensive multiple bonding throughout the Re—N3—N4 unit. On the other hand, the Re—N1 bond distance is significantly longer, 2.212(8) Å, suggesting a rhenium–nitrogen single bond. Likewise, the N1—N2 distance of 1.44(1) Å approaches the idealized value for a N—N single bond. This evidence, together with the valence angle of 119.5(4)° at N1, the appearance of two peaks on the final electron density map attributable to H(N1) and H(N2), and the spectroscopic data cited previously, supports that the unit is present as the hydrazido(1−) functionality, —NHNHR. A comparison of the structural parameters for this unit with those for bent isodiazene ligands[22] and for other end-on hydrazido(1−) fragments[9,23] is presented in Table 5. The bent isodiazene unit functions as a two-electron donor, consistent with valence structure (**IX**), whereas the hydrazido(1−) ligands of (**7**) and (**8**), also formally two-electron donors, are best described by structure (**VIII**). In contrast, the structural parameters reported for other examples of end-on coordinated hydrazido(1−) ligands (Table 5) are suggestive of a formalism based on a protonated form of the isodiazene structure (**IX**). Thus, while the —NHNHR units of (**7**) and (**8**) represent the hydrazido(1−) limit, valence form (**VIII**), with structural parameters consistent with sp^3 hybridization at N1 and N2, the $—NHNR_2$ units of structures (**9**)–(**14**) are best described by (**IX**), structural types more closely related to the isodiazenes and retaining sp^2 hybridization at the nitrogen atom.

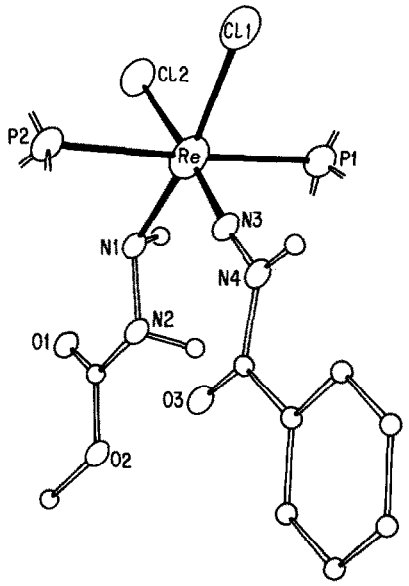

Fig. 8. ORTEP view of the structure of complex (**8**), $[ReCl_2(PPh_3)_2(NNHCOPh)(NHNHCO_2Me)]$, showing relevant atoms labelled.

Conclusions

Organohydrazines H_2NNHR with potentially coordinating substituents R, form six coordinate chelate complexes of the type $[ReCl_2(PPh_3)_2(NNR)]$, for R = —COPh and phthalazine, when reacted with $[ReOCl_3(PPh_3)_2]$. The subsequent reaction chemistry is governed both by the nature of donor group R responsible for chelate closure and by the type of donor ligand introduced. Thus, when R = phthalazine, no simple substitution products are isolated. On the other hand, for R = —COPh introduction of donor ligands L results in the opening of the chelate via displacement of the coordinated carbonyl oxygen by the donor ligand. The identity of the metal–hydrazine linkage in these species depends on the nature of L. When L is an "innocent" ligand with no exchangeable protons, simple displacement of the carbonyl oxygen by L yields organodiazenido complexes of the type $[ReCl_2(PPh_3)_2(NNR)L]$. In contrast, for organohydrazido ligands L, substitution and proton transfer occur to yield mixed hydrazido(1−)—hydrazido(2−) species of the general type $[ReCl_2(PPh_3)_2(NNHR)(NHNHR')]$. Thus, a series of related species has been isolated and structurally identified, presenting end-on coordinated organodiazenido, organohydrazido(1−) and or-

Table 4. Selected bond lengths (Å) and angles (°) for $[ReCl_2(PPh_3)_2(NNHCOPh)(NHNHCOPh)]$ (7) and $[ReCl_2(PPh_3)_2(NNHCOPh)(NHNHCO_2CH_3)]$ (8)

(7)		(8)	
Re—Cl1	2.416(3)	Re—Cl1	2.421(2)
Re—Cl2	2.427(2)	Re—Cl2	2.418(2)
Re—P1	2.479(2)	Re—P1	2.466(3)
Re—P2	2.470(2)	Re—P2	2.465(2)
Re—N1	2.212(8)	Re—N1	2.206(8)
Re—N3	1.730(7)	Re—N3	1.712(7)
N1—N2	1.44(1)	N1—N2	1.441(9)
N2—C10	1.35(1)	N2—C1	1.39(1)
O2—C10	1.23(1)	O1—C1	1.16(1)
N3—N4	1.275(9)	N3—N4	1.27(1)
N4—C20	1.38(1)	N4—C70	1.38(1)
O1—C20	1.23(1)	C70—O3	1.20(1)
Cl1—Re—Cl2	94.4(1)	Cl1—Re—Cl2	91.6(1)
Cl1—Re—P1	89.6(1)	Cl1—Re—P1	89.3(1)
Cl1—Re—P2	88.5(1)	Cl1—Re—P3	89.3(1)
Cl1—Re—N1	169.4(2)	Cl1—Re—N1	167.1(2)
Cl1—Re—N3	93.7(2)	Cl1—Re—N3	94.6(3)
Cl2—Re—P1	83.8(1)	Cl2—Re—P1	86.8(1)
Cl2—Re—P2	89.5(1)	Cl2—Re—P2	90.4(1)
Cl2—Re—N1	75.2(2)	Cl2—Re—N1	75.5(2)
Cl2—Re—N3	171.5(2)	Cl2—Re—N3	173.8(3)
P1—Re—P2	172.9(1)	P1—Re—P2	176.9(1)
P1—Re—N1	89.3(2)	P1—Re—N1	91.1(2)
P1—Re—N3	933.2(2)	P1—Re—N3	92.8(2)
P2—Re—N1	91.3(2)	P2—Re—N1	89.6(2)
P2—Re—N3	93.8(2)	P2—Re—N3	90.0(2)
N1—Re—N3	96.8(3)	N1—Re—N3	98.3(3)
Re—N1—N2	119.5(4)	Re—N1—N2	121.3(5)
Re—N3—N4	174.3(6)	Re—N3—N4	172.2(7)
N1—N2—C10	116.1(7)	N1—N2—C1	113.5(7)
N3—N4—C20	117.9(7)	N3—N4—C70	120.3(8)

ganohydrazido(2−) linkages and the chelating organohydrazido(3−) unit.

EXPERIMENTAL

Materials and methods

All reactions were performed in freshly dried and distilled solvents. Dichloromethane was technical grade and was redistilled from $CaCl_2$ and P_4O_{10}. All other solvents were reagent grade. All other reagents were obtained from standard commercial sources without further purification. $[ReOCl_3(PPh_3)_2]$ was prepared according to the published method.[1]

The following instruments were used in this work: IR, Perkin–Elmer 283B IR spectrophotometer; ^1H NMR, Bruker T-90 spectrometer; UV-Visible spectra, Varian DMS 90 UV-Visible spectrophotometer; X-ray crystallography, Nicolet R3m diffractometer.

Preparation of compounds

$[ReCl_2(PPh_3)_2(NNCOC_6H_4Cl)]$ (1). Complex (1) was prepared by a literature method.[1]

$[ReCl_2(PPh_3)_2(NNC_8N_2H_5)]$ (2). Oxotrichlorobis(triphenylphosphine)rhenium (1.0 g), hydralazine hydrochloride (0.6 g) and triphenylphosphine (1.0 g) were heated under reflux with stirring for 90 min in 200 cm^3 ethanol. The resultant red–brown precipitate was washed with methanol and air-dried, and suspended in a solution of 100 cm^3 benzene with 1 cm^3 triethylamine, which was warmed to dissolve the material. After filtration, solvent was removed by rotary evaporation. The resultant grey–green oil was dissolved in dichloromethane and layered with methanol/diethylether. Large green crystals formed after 3 days. Yield: 65%. Found: C, 56.0; H, 3.6; N, 5.8. Calc. for $ReC_{44}H_{35}N_4$: C, 55.9; H, 3.6; N, 5.87%.

$[ReCl_2(PPh_3)_2(CH_3CN)(NNCOC_6H_5)]$ (3). Oxo-

Table 5. Comparison of structural features of coordinated isodiazene and hydrazido(1 −) units[a]

Complex		Nitrogenous unit	M—N, Å	N—N, Å	<M—N—N,°	Ref.
$[ReBr_2(NNPh)(NNHPh)(PPh_3)_2]$	(9)	—NNHPh, isodiazene	1.922(11)	1.287(15)	131.2(10)	22
$[(cp)_2WH(NNHC_6H_4F\text{-}p)]^+$	(10)	—NNHR, isodiazene	1.837(7)	1.315(9)	146.4(5)	6
$[Mo\{HB(Me_2pz)_3\}(NO)(NHNMe_2)]$[b]	(11)	—$NHNR_2$, hydrazido(1 −)	1.98(2)	1.34(3)	140.3(15)	9b
$[(cp)Re(CO)_2\{p\text{-}NHN(CH_3)C_6H_4CH_3\}]^+$	(12)	—NHNHR, hydrazido(1 −)	1.949(9)	1.32(1)	139.1(7)	9c
$[IrF(PPh_3)_2(CO)(NHNHC_6H_3NO_2)]^+$[c]	(13)	—NHNHR, hydrazido(1 −)	1.912(10)	1.388(13)	119.1(8)	23
$[Mo(N_2COPh)(NHNHCOPh)\{PhCSN(Me)O\}_2]$	(14)	—NHNHR, hydrazido(1 −)	1.938(4)	1.361(7)	131.9(3)	9a
$[ReCl_2(PPh_3)_2(NNHCOPh)(NHNHCOPh)]$	(7)	—NHNHR, hydrazido(1 −)	2.212(8)	1.44(1)	119.5(40)	9d, this work
$[ReCl_2(PPh_3)_2(NNHCOPh)(NHNHCO_2Me)]$	(8)	—NHNHR, hydrazido(1 −)	2.206(8)	1.441(9)	121.3(5)	this work

[a] cp = cyclopentadienyl.
[b] Me_2pz = 3,5-dimethylpyrazol-1-yl.
[c] Orthometallated structure.

trichlorobis(triphenylphosphine)rhenium (2.0 g), benzoylhydrazine (2.0 g), and triphenylphosphine (2.0 g) were heated under reflux with stirring in 15 cm^3 1MHCl in ethanol and 50 cm^3 dichloromethane for 30 min. The emerald green precipitate was washed with methanol and air-dried. The green powder was dissolved in benzene and acetonitrile was added dropwise with gentle warming until a red–brown solution resulted. Solvents were removed by rotary evaporation to produce an oil which was dissolved in dichloromethane and layered with ether. Large red–brown crystals formed over a 2 day period. Yield: 85%. Found: C, 54.9; H, 4.0; N, 4.4. Calc. for $ReC_{45}H_{38}N_3O_1P_2Cl_2$: C, 55.2; H, 4.0; N, 4.4%.

$[ReCl_2(PPh_3)_2(NH_3)(NNC_6H_4Br)]$ (**4**). Oxotrichlorobis(triphenylphosphine)rhenium (2.0 g), 2-bromophenylhydrazine hydrochloride (2.0 g) and triphenylphosphine (2.0 g) were heated under reflux for 1 h with stirring in a solution of 100 cm^3 ethanol and 100 cm^3 benzene. An orange precipitate was removed by filtration. The dark red filtrate is evaporated to a red oil. Trituration of the red oil with ether caused precipitation of a tan coloured solid which was washed with dichloromethane which dissolved the bright red ammonia complex. Crystals formed from dichloromethane–diethylether crystallization. Yield: 20%. Found: C, 50.8; H, 3.62. Calc. for $ReC_{42}H_{37}N_3P_2Cl_2Br$: C, 51.3; H, 3.76%.

$[ReCl_2(PPh_3)_2(Me_2NCHO)(NNCOOCH_3)]$ (**5a**). Oxotrichlorobis(triphenylphosphine)rhenium (2.0 g), methylhydrazinocarboxylate (1.35 g) and triphenylphosphine (2.0 g) were heated under reflux with stirring in a solution of 15 cm^3 1M HCl in ethanol, 150 cm^3 ethanol, 50 cm^3 dimethylformamide and 20 cm^3 dichloromethane for 2 h. The resultant red–purple precipitate was washed with methanol and air dried. Yield: 65%. Found: C, 52.3; H, 4.3; N, 4.4. Calc. for $ReC_{41}H_{40}N_3O_3P_2Cl_2$: C, 52.2; H, 4.3; N, 4.5%.

$[ReCl_2(PPh_3)_2(C_5H_5N)(NNCOOCH_3)]$ (**5**). To a warmed suspension of $[ReCl_2(PCh_3)_2(Me_2NCOH)(NNCOOCH_3)]$ (**5a**) in dichloromethane, pyridine was added dropwise until the material dissolved. The solution was layered with methanol and diethylether. Bright red crystals formed over a period of 2 days. Yield 85%.

trans-$[ReCl_2(PPh_3)(Me_2NCHO)(NNCOOCH_3)]$ (**6**). The red filtrate from the work-up of (**5a**) is allowed to evaporate under air, yielding red crystals of (**6**) after 10 days. Yield: 10%, reproducible to ±2%.

$[ReCl_2(PPh_3)_2(NHNHCOC_6H_5)(NNHCOC_6H_5)]$ (**7**). $[ReCl_2(PPh_3)_2(NNCOC_6H_5)]$ ("green chelate"), (1.2 g) and benzoylhydrazine (0.25 g) were dissolved in 200 cm^3 benzene and stirred at room temperature

Table 6. Summary of crystal data and experimental details for the structural studies of $[ReCl_2(PPh_3)_2(NNCOC_6H_4$-*p*-Cl)] (**1**), $[ReCl_2(PPh_3)_2(NNC_8H_5N_2)]$ (**2**), $[ReCl_2(PPh_3)_2(NCMe)(NNCOPh)]$ (**3**) and $[ReCl_2(PPh_3)_2(NNC_6H_4$-*o*-Br)$(NH_3)]$ (**4**)

	(1)	(2)	(3)	(4)
(a) Crystal parameters at 23°C[a]				
a	14.863(2) Å	12.480(2) Å	14.004(3) Å	10.535(2) Å
b	10.614(2) Å	12.392(2) Å	14.329(3) Å	14.939(3) Å
c	24.636(2) Å	29.603(4) Å	20.019(4) Å	16.585(3) Å
α	90.00°	96.30(1)°	90.00°	66.14(1)°
β	94.57(1)°	97.30(1)°	94.02(1)°	78.93(1)°
γ	90.00°	114.06(1)°	90.00°	84.93(1)°
V	3874.1(8) Å^3	4080.0(8) Å^3	4007.2(10) Å^3	2342.5(8) Å
Space group	$P2_1/c$	$P\bar{1}$	$P2_1/c$	$P\bar{1}$
Z	4	4	4	2
D_{calc}	1.63	1.53	1.58	1.39
(b) Measurement of intensity data				
Crystal dimensions (mm):	0.18 × 0.22 × 0.16	0.16 × 0.20 × 0.14	0.12 × 0.20 × 0.16	0.18 × 0.20 × 0.12.
Instrument:	Nicolet R3m.			
Radiation:	MoK_α(γ = 0.71069 Å).			
Scan mode:	Coupled θ(crystal)−2θ(counter).			
Scan rate:	7° min^{-1}–30° min^{-1}.			
Scan range:	$2.0° < 2\theta \leqslant 45°$.			
Scan length:	$[2\theta(K\alpha_1-1.0)]°-[2\theta(K\alpha_2+1.0)]°$.			
Background measurement:	Stationary crystal, stationary counter, at the beginning and end of each 2θ scan, each for the time taken for the scan.			
Standards:	3 collected every 197.			
Number of reflections collected:	5710	9302	6591	6678
Number of independent reflections used in solution:	3751 ($I_o \geqslant 3\sigma(I_o)$)	6528 ($I_o \geqslant 3\sigma(I_o)$)	4314 ($I_o \geqslant 3\sigma(I_o)$)	5513 ($I_o \geqslant 3\sigma(I_o)$)
(c) Reduction of intensity data and summary of structure solution and refinement[b]				
Data corrected for background, attenuators, Lorentz and polarization effects in the usual fashion.				
Absorption coefficient (cm^{-1}):	60.43	34.00	57.87	57.85
Absorption corrections: Based on Ψ scans for five reflections with χ near 90° or 270°.				
T max/*T* min	1.15	1.09	1.23	1.06
Structure solution: Patterson synthesis yielded the Re position, all remaining non-hydrogen atom were located via standard Fourier techniques.				
Atom scattering factors:[c] Neutral atomic scattering factors were used throughout the analysis.				
Anomalous dispersion:[d] Applied to all non-hydrogen atoms.				
Final discrepancy factor:[e]				
R =	0.0461	0.0618	0.0432	0.0504
R_w =	0.0481	0.0643	0.0473	0.0505
Goodness of fit:[f]	1.067	1.525	1.049	1.433

[a] From a least squares fitting of the setting angle of 25 reflections.

[b] All calculations were performed on a Data General Nova 3 computer with 32K of 16-bit words using local versions of the Nicolet SHELXTL interactive crystallographic software package as described in G. M. Sheldrid *Nicolet SHELXTL Operations Manual*, Nicolet XRD Corp. Cupertino, California (1979).

[c] D. T. Cromer and J. B. Mann, *Acta Cryst. A* 1968, **24**, 321.

[d] *International Tables for X-ray crystallography*, Vol. III. Kynoch Press, Birmingham, U.K.

[e] $R = \Sigma[|F_o|-|F_c|/\Sigma|F_o|]$ $R_w = [\Sigma w(|F_o|-|F_c|)^2/\Sigma w|F_o|^2]^{1/2}$ $w = 1/\delta^2(F_o)+g^*(F_o)$ $g = 0.005$.

[f] $GOF = [\Sigma w(|F_o|-|F_c|)^2/(NO-NV)]^{1/2}$ where *NO* is the number of observations and *NV* is the number of variables.

Table 7. Summary of crystal data and experimental details for the structural studies of $[ReCl_2(PPh_3)_2(C_5H_5N)(NNCO_2CH_3)]$ (**5**), $[ReCl_2(PPh_3)_2(Me_2NCHO)(NNCO_2Me)]$ (**6**), $[ReCl_2(PPh_3)_2(NNHCOPh)(NHNHCOPh)]$ (**7**) and $[ReCl_2(PPh_3)_2(NNHCOPh)(NHNHCO_2Me)]$ (**8**)

	(5)	(6)	(7)	(8)
(a) Crystal parameters at 23°C[a]				
a	15.105(3) Å	10.240(3) Å	12.276(2) Å	11.843(2) Å
b	15.619(3) Å	16.051(3) Å	14.147(2) Å	12.015(2) Å
c	19.449(4) Å	12.80(2) Å	15.284(2) Å	16.216(3) Å
α	90.00°	90.00°	86.33(1)°	96.40(1)
β	112.47(1)°	110.94(1)°	72.04(1)°	100.40(1)°
γ	90.00°	90.00°	83.10(1)°	103.56(1)°
V	4240.1(9) Å^3	1965.0(5) Å^3	2505.7(9) Å^3	2177.5(8) Å
Space group	$P2_1/n$	$P2_1$	$P\bar{1}$	$P\bar{1}$
D_{calc}	1.48	1.59	1.39	1.59
Z	4	2	2	2
(b) Measurement of intensity data				
Crystal dimensions (mm):	0.18 × 0.20 × 0.22	0.16 × 0.14 × 0.22	0.20 × 0.17 × 0.14	0.15 × 0.15 × 0.15.
Instrument:	Nicolet R3m.			
Radiation:	MoK_α(γ = 0.71069 Å).			
Scan mode:	Coupled θ(crystal) − 2θ(counter).			
Scan rate:	7° min^{-1}–30° min^{-1}.			
Scan range:	$2.0° < 2\theta \leqslant 45°$.			
Scan length:	$[2\theta(K\alpha_1 - 1.0)]°$–$[2\theta(K\alpha_2 + 1.0)]°$.			
Background measurement:	Stationary crystal, stationary counter, at the beginning and end of each 2θ scan, each for the time taken for the scan.			
Standards:	3 collected every 197.			
Number of reflections collected:	6055	3875	6891	6917
Number of independent reflections used in solution:	3487 ($I_o \geqslant 3\sigma(I_o)$)	3174 ($I_o \geqslant 3\sigma(I_o)$)	4995 ($I_o \geqslant 3\sigma(I_o)$)	4309 ($I_o \geqslant 3\sigma(I_o)$)
(c) Reduction of intensity data and summary of structure solution and refinement[b]				
Data corrected for background, attenuators, Lorentz and polarization effects in the usual fashion.				
Absorption coefficient (cm^{-1}):	32.66	58.94	46.34	53.25
Absorption corrections: Based on Ψ scans for five reflections with χ near 90° or 270°.				
T max/T min	1.09	1.13	1.06	1.07
Structure solution: Patterson synthesis yielded the Re position, all remaining non-hydrogen atom were located via standard Fourier techniques.				
Atom scattering factors:[c] Neutral atomic scattering factors were used throughout the analysis.				
Anomalous dispersion:[d] Applied to all non-hydrogen atoms.				
Final discrepancy factor:[e]				
R =	0.0726	0.073	0.0420	0.0405
R_w =	0.0737	0.0417	0.0433	0.0405
Goodness of fit:[f]	1.528	1.219	1.169	1.238

[a] From a least squares fitting of the setting angle of 25 reflections.

[b] All calculations were performed on a Data General Nova 3 computer with 32K of 16-bit words using local versions of the Nicolet SHELXTL interactive crystallographic software package as described in G. M. Sheldrid *Nicolet SHELXTL Operations Manual*, Nicolet XRD Corp. Cupertino, California (1979).

[c] D. T. Cromer and J. B. Mann, *Acta Cryst. A* 1968, **24**, 321.

[d] *International Tables for X-ray crystallography*, Vol. III. Kynoch Press, Birmingham, U.K.

[e] $R = \Sigma[|F_o| - |F_c|/\Sigma|F_o|]$ $R_w = [\Sigma w(|F_o| - |F_c|)^2/\Sigma w|F_o|^2]^{1/2}$ $w = 1/\delta^2(F_o) + g^*(F_o)$ $g = 0.005$.

[f] $GOF = [\Sigma w(|F_o| - |F_c|)^2/(NO - NV)]^{1/2}$ where NO is the number of observations and NV is the number of variables.

overnight. The resulting green–brown solution was filtered and then the benzene was removed by rotary evaporation. The resulting oil was dissolved in dichloromethane and layered with methanol/diethylether. Green–brown dichroic crystals formed after 48 h. Yield: 80%. Found: C, 53.3; H, 4.5; N, 5.1. Calc. for $ReC_{50}H_{43}N_4O_2P_2Cl_2$: C, 53.3; H, 4.0; N, 5.2%.

$[ReCl_2(PPh_3)_2(NHNHCOOCH_3)(NNHCOC_6H_5)]$ (**8**). "Green chelate" (2.0 g) and methylhydrazinocarboxylate (0.5 g) were stirred in 200 cm^3 benzene overnight. The resulting green–brown solution was filtered, and the benzene was removed by rotary evaporation. The resulting oil was dissolved in dichloromethane and layered with methanol/diethylether. Green–brown dichroic crystals appeared after 3 days. Yield: 80%. Found: C, 53.1; H, 3.70. Calc. for $ReC_{44}H_{38}N_4O_3P_2Cl_2$: C, 53.4; H, 3.84%.

X-ray crystallography

The details of the crystal data, data collection methods and refinement procedures are given in Tables 6 and 7. (Supplementary Tables A–H1 provide atomic positional parameters for the structures reported. Tables of bond lengths and angles, anisotropic thermal parameters and calculated and observed structure factors for all complexes are available.*) Full details of the crystallographic methodologies may be found in ref. 24.

In no instance was an extinction correction applied for the data. Idealized hydrogen atom positions were used throughout the analyses, with the C—H and N—H distances set at 0.96 and 0.94 Å, respectively.

Since complex (**7**) crystallizes in the polar space group $P2_1$, both enantiomorphs were refined. The atomic coordinates reported are for the proper enantiomorph based on the residuals for both settings.

REFERENCES

1. J. Chatt, J. R. Dilworth and G. J. Leigh, *J. Chem. Soc., Dalton Trans.* 1973, 612.
2. D. Sutton, *Chem. Soc. Rev.* 1975, **4**, 443; G. Avitable, P. Ganis and M. Nemiroff, *Acta Cryst.* 1971, **B27**, 725; U. F. Duckworth, P. G. Douglas, R. Mason and B. L. Shaw, *J. Chem. Soc., Chem. Commun.* 1970, 1083; W. E. Carroll and F. J. Lalor, *J. Chem. Soc., Dalton Trans.* 1973, 1754; J. A. Ibers and B. L. Haymore, *Inorg. Chem.* 1975, **14**, 1369; J. V. McArdle, A. J. Schultz, B. J. Corden and R. Eisenberg, *Inorg. Chem.* 1973, **12**, 1676; M. Cowie, B. L. Haymore and J. A. Ibers, *Inorg. Chem.* 1975, **14**, 2617; B. L. Haymore and J. A. Ibers, *Inorg. Chem.* 1975, **14**, 1369.
3. A. P. Gaughan and J. A. Ibers, *Inorg. Chem.* 1975, **14**, 352.
4. E. W. Abel, C. A. Burton, M. R. Churchill and K.-K. G. Lin, *J. Chem. Soc., Chem. Commun.* 1974, 268.
5. P. G. Douglas, A. R. Galbraith and B. L. Shaw, *Trans. Met. Chem.* 1975, **1**, 17; R. Mason, K. M. Thomas, J. A. Zubieta, P. G. Douglas, A. R. Galbraith and B. L. Shaw, *J. Am. Chem. Soc.* 1974, **96**, 265; J. Chatt, M. E. Fakley, P. B. Hitchcock, R. L. Richards, N. T. Luong-Thi and D. L. Hughes, *J. Organomet. Chem.* 1979, **172**, C55 (see also ref. 8 for reformulation); V. W. Day, T. A. George, S. D. A. Iske and S. D. Wagner, *J. Organomet. Chem.* 1976, **112**, C55; F. C. March, R. Mason and K. M. Thomas, *J. Organomet. Chem.* 1975, **96**, C43.
6. F. W. B. Einstein, T. Jones, A. J. L. Hanlan and D. Sutton, *Inorg. Chem.* 1982, **21**, 2585.
7. S. D. Ittel and J. A. Ibers, *J. Am. Chem. Soc.* 1974, **96**, 4804.
8. P. D. Frisch, M. M. Hunt, W. G. Kita, J. A. McCleverty, G. E. Rae, D. Siddon, D. Swann and J. Williams, *J. Chem. Soc., Dalton Trans.* 1979, 1819; A. B. Gilchrist and D. Sutton, *Inorg. Chem.* 1977, **16**, 677; A. J. Carroll and D. Sutton, *ibid.* 1980, **19**, 3142; I. Chatt, J. R. Dilworth, P. L. Dahlstrom and J. Zubieta, *J. Chem. Soc., Chem. Commun.* 1980, 786; J. R. Dilworth and J. A. Zubieta, *Trans. Met. Chem.* 1984, **9**, 39; J. Chatt, M. Fakley, P. B. Hitchcock, R. L. Richards and N. T. Luong-Thi, *J. Chem. Soc., Dalton Trans.* 1982, 345; N. A. Bailey, P. D. Frisch, J. A. McCleverty, N. W. Walker and J. Williams, *J. Chem. Soc., Chem. Commun.* 1975, 350; J. R. Dilworth, I. A. Latham, G. J. Leigh, G. Huttner and I. Jibril, *J. Chem. Soc., Chem. Commun.* 1983, 1360.
9. (a) M. D. FitzRoy, J. M. Frederiksen, K. S. Murray and M. R. Snow, *Inorg. Chem.* 1985, **24**, 3265; (b) J. A. McCleverty, A. E. Rae, I. Wolochowicz, N. A. Bailey and J. M. A. Smith, *J. Chem. Soc., Dalton Trans.* 1983, 71; (c) C. F. Barrientos-Penna, C. F. Campana, F. W. B. Einstein, T. Jones, D. Sutton and A. S. Tracey, *Inorg. Chem.* 1984, **23**, 363; (d) T. Nicholson and J. A. Zubieta, *J. Chem. Soc., Chem. Commun.* 1985, 367.
10. J. R. Dilworth, *Coord. Chem. Rev.* 1976., **21**, 29.
11. R. Mattes and H. Scholand, *Angewandte Chem. Int. Ed.* 1983, **22**, 245; M. W. Bishop, G. Butler, J. Chatt, J. R. Dilworth and G. J. Leigh, *J. Chem. Soc., Dalton Trans.* 1979, 1843; J. R. Dilworth, P. L. Dahlstrom, J. R. Hyde, K. Kustyn, P. A. Vella and J. Zubieta, *Inorg. Chem.* 1980, **19**, 3562; M. W. Bishop, J. Chatt,

* *Supplementary materials available*: Fractional coordinates have been deposited with the Director, Cambridge Crystallographic Centre. Complete listings of bond distances and angles are available from the Editor, Queen Mary College, London.

J. R. Dilworth, J. R. Hyde, S. Kim, K. Venkatasubramanian and J. Zubieta, *Inorg. Chem.* 1978, **17**, 2917; J. R. Dilworth, J. R. Hyde, P. Lyford, P. Vella, K. Venkatasubramanian and J. Zubieta, *Inorg. Chem.* 1979, **18**, 268.
12. J. Chatt, J. R. Dilworth and G. J. Leigh, *J. Chem. Soc.* (*A*) 1970, 2239.
13. J. Chatt, J. R. Dilworth, G. J. Leigh and V. Gupta, *J. Chem. Soc.* (*A*) 1971, 2631.
14. G. W. Parshall, *J. Am. Chem. Soc.* 1965, **87**, 2133; C. D. Cook and C. S. Jaubal, *J. Am. Chem. Soc.* 1968, **90**, 1464.
15. T.-C. Hsieh and J. Zubieta, *Polyhedron* 1986, **5**, 305.
16. S. N. Shaikh and J. Zubieta (unpublished results).
17. T. Nicholson and J. Zubieta, *Polyhedron* 1987, to be published.
18. P. T. Bishop, P. J. Blower, J. R. Dilworth and J. A. Zubieta, *Polyhedron* 1986, **5**, 363.
19. D. Bright and J. A. Ibers, *Inorg. Chem.* 1969, **8**, 703.
20. D. Bright and J. A. Ibers, *Inorg. Chem.* 1968, **7**, 1099.
21. T.-C. Hsieh, K. Gebreyes and J. Zubieta, *J. Chem. Soc., Chem. Commun.* 1984, 1172; T.-C. Hsieh and J. Zubieta, *Inorg. Chim. Acta*, 1985, **99**, L47; T. Nicholson and J. Zubieta, *Inorg. Chim. Acta* 1985, **100**, L35.
22. J. R. Dilworth, S. A. Harrison, D. R. M. Walton and E. Schweda, *Inorg. Chem.* 1985, **17**, 2595.
23. J. A. Carroll, R. E. Cobbledick, F. W. B. Einstein, N. Farrell, D. Sutton and P. L. Vogel, *Inorg. Chem.* 1977, **16**, 2462.
24. A. Bruce, J. L. Corbin, P. L. Dahlstrom, J. R. Hyde, M. Minelli, E. I. Stiefel, J. T. Spence and J. Zubieta, *Inorg. Chem.* 1982, **21**, 917.

Polyhedron Vol. 7, No. 3, pp. 187–193, 1988
Printed in Great Britain

0277–5387/88 $3.00+.00
© 1988 Pergamon Journals Ltd

METALLAHETEROBORANE CHEMISTRY—II.* SYNTHESIS AND CHARACTERIZATION OF $[Ir(dppe)_2(X)_2][SeB_{10}H_{11}]$ {X = O(I) or H(II)} COMPLEXES. CRYSTAL AND MOLECULAR STRUCTURE OF *CIS*-BIS[1,2-BIS(DIPHENYLPHOSPHINO)ETHANE]DIHYDROIRIDIUM(III) SELENAUNDECAHYDRODECABORATE(1−), (II)

GEORGE FERGUSON† and MARK J. HAMPDEN-SMITH

Chemistry Department, University of Guelph, Guelph, Ontario, Canada N1G 2W1

and

ORLA NI DHUBHGHAILL and TREVOR R. SPALDING†

Chemistry Department, University College, Cork, Ireland

(*Received* 24 *June* 1987; *accepted* 8 *September* 1987)

Abstract—The reaction of $[Ir(dppe)_2]Cl$ with $[Et_4N][SeB_{10}H_{11}]$ in THF followed by work up in air gave $[Ir(dppe)_2O_2][SeB_{10}H_{11}]$ (**I**) in 46% yield. Heating (**I**) at 120°C for 7 h under reduced pressure gave $[Ir(dppe)_2H_2][SeB_{10}H_{11}]$ (**II**) as the major product. Compounds (**I**) and (**II**) were characterized spectroscopically (IR, ^1H, ^{11}B, ^{31}P NMR). Crystals of (**II**) are triclinic, space group $P\bar{1}$ with two formula units and a molecule of dichloromethane in the asymmetric unit. Cell data are $a = 18.308(4)$, $b = 27.580(4)$, $c = 12.017(2)$ Å, $\alpha = 98.33(1)$, $\beta = 95.94(2)$, $\gamma = 105.29(1)°$. The structure was refined with 7025 observed reflections to $R = 0.069$ by full matrix least-squares calculations. The $[Ir(dppe)_2H_2]^+$ cations have distorted octahedral coordination with *cis* H atoms and Ir—P(*trans* to H) (2.359 Å) larger than Ir—P(*trans* to P) (2.314 Å). The cations differ in their orientation of $—CH_2—CH_2—$ moieties in the dppe ligands. The anions have their unique Se atoms scrambled over several sites in the $[SeB_{10}H_{11}]^-$ cages with one cage being more disordered than the other.

In recent years a number of metallaborane and metallacarbaborane clusters containing Ir have been synthesized.[1] The majority have contained monophosphine ligands (L = PR_3) bonded to the Ir atom and compounds with the following units have been characterized: $\{L_2IrH\}$,[2] $\{L_2Ir(H)_2\}$,[3] $\{L_2Ir(CO)\}$[4] and $\{L_3IrH\}$ or $\{L_2(CO)IrH\}$.[5] In compounds containing these units the metal is part of the cage, e.g. *nido*-$[2,2\text{-}(PPh_3)_2\text{-}2\text{-}(CO)\text{-}2\text{-}IrB_5H_8]$[4] and *closo*-$[3,3\text{-}(PPh_3)_2\text{-}3\text{-}H\text{-}3,1,2\text{-}IrC_2B_9H_{11}]$.[3] In other cases ionic systems such as $[Ir(dppe)_2(Cl)H][B_{10}H_{12}X]$ (X = H, Cl),[6] $[Ir(dppe)_2(H)_2][B_3H_8]$ and $[Ir(dppe)_2CO][B_3H_8]$[7] have been isolated where Ir is not inserted into the cluster but is retained in a separate octahedrally coordinated cationic species. In one unusual case the $\{L_2Ir(H)_2\}^+$-unit was bonded *exo*polyhedrally via two Ir—H—B bonds to a $[C_2B_9H_{10}]^-$ cage in an *exo-nido* compound.[8]

Apart from the carbaborane derivatives, no iridaheteroboranes are known. In continuing our studies of metallaheteroborane chemistry we have investigated the reaction of the heteroborane anion, *nido*-$[B_{10}H_{11}Se]^-$, (isoelectronic with the carbaborane $[C_2B_9H_{12}]^-$) with $[Ir(dppe)_2]Cl$ in THF. It was hoped that the solvent chosen would favour the formation of an insertion rather than an ionic product. However no metal inserted product was isolated from the present work, instead two Ir(III) complexes containing the $[B_{10}H_{11}Se]^-$ anion were characterized.

* For Part I see ref. 11.

†Author to whom correspondence should be addressed.

RESULTS AND DISCUSSION

Reaction of the Ir(I) complex $[Ir(dppe)_2]Cl$ with $[Et_4N][B_{10}H_{11}Se]$ in THF followed by work up in air gave a 46% yield of an ionic Ir(III) product which was characterized spectroscopically as $[Ir(dppe)_2O_2][B_{10}H_{11}Se]$ (**I**). The cation was probably formed through air oxidation of the more reactive Ir(I) species $[Ir(dppe)_2]^+$. When (**I**) was heated as a solid at 120°C for 7 h under reduced pressure (0.3 mm Hg) the complex $[Ir(dppe)_2(H)_2][SeB_{10}H_{11}]$ (**II**) was produced and isolated in 19% yield. Compound (**II**) was characterized by spectroscopic and X-ray diffraction techniques.

The IR spectrum of (**I**) showed the characteristic η^2—O_2 absorption at 845 cm^{-1}[9] and the B—H terminal stretching absorption appeared as a single strong band at 2510 cm^{-1} as in the reagent $[B_{10}H_{11}Se]^-$ anion.[10,11] No band which could be associated with Ir—H was observed. The main features of the IR spectrum of (**II**) were a band of medium intensity at 2070 cm^{-1} and a strong band at 2510 cm^{-1}, due to Ir—H stretching[6] and B—H terminal stretching respectively. Again, the B—H stretching frequency is the same as that reported for $[SeB_{10}H_{11}]^-$.[10,11]

The 128 MHz $^{11}B\{^1H\}$ NMR spectra of both (**I**) and (**II**) are similar and clearly confirm the presence of $[B_{10}H_{11}Se]^-$ in both these compounds.[10,11] The 162 MHz $^{31}P\{^1H\}$ NMR spectrum of the $[Ir(dppe)_2O_2]^+$ cation consisted of two singlets at $\delta = 18.5$ and 13.6 ppm of equal areas. These values are close to those previously reported for the cation in the complexes $[Ir(dppe)_2O_2][X]$ (X = Cl,[12] PF_6[13]), namely 16.5 and 13.4, and 20.2 and 12.9 ppm respectively. Surprisingly, the $^{31}P\{^1H\}$ spectrum obtained for $[Ir(dppe)_2(H)_2][B_{10}H_{11}Se]$ comprised three singlets at $\delta = 40.3$, 33.9 and 22.4 ppm. The latter two signals were of equal area and are shifted downfield by 3 ppm from those reported previously for the cation (31.0 and 19.5 ppm)[12] however their relative positions are the same and we assign them to *cis*-$[Ir(dppe)_2(H)_2]^+$. On partial proton decoupling the signal at 22.4 ppm becomes a doublet due to *trans* ^{31}P—^1H coupling ($^2J_{PH}$ = 110 Hz). *cis* coupling was not resolved. The third signal ($\delta = 40.3$ ppm) is tentatively assigned to *trans*-$[Ir(dppe)_2(H)_2]^+$. The ^{31}P NMR spectrum of this isomer has not previously been reported but other *trans*-$[Ir(dppe)_2(X)Y]^+$ systems (X = Y = Cl, I, X = H, Y = CO, PF_6)[13,14] are reported to show unique singlets in their ^{31}P NMR spectra. In the present work further evidence for the presence of the *trans* isomer was obtained from the ^1H NMR spectrum, *vide infra*.

The 400 MHz ^1H spectrum of (**II**) initially shows two hydride resonances at $\delta = -11.63$ ppm (d of q) due to *cis* $[Ir(dppe)_2(H)_2]^+$ ($^2J_{HP_{trans}} = 110$ Hz and $^2J_{HP_{cis}} = 12$ Hz) and $\delta = -10.47$ ppm (quintet) possibly due to *trans*-$[Ir(dppe)_2(H)_2]^+$ ($^2J_{HP_{cis}} = 15$ Hz). The presence of a quintet in the ^1H NMR and the corresponding singlet in the ^{31}P NMR may be interpreted as indicating *trans* stereochemistry but these features may also occur as a consequence of stereochemical non-rigidity.[6,13,14] However in the present case the *cis* isomer is concurrently observed and so it is probable that the other signals are due to the *trans* system. On leaving the solution to stand for a day, the ratio of *trans* to *cis* changes from 1:6 to 1:2, thus *cis–trans* isomerization is apparently taking place. This reaction does not appear to have been reported for any previous $[Ir(dppe)_2(H)_2]^+$ complex. However stereochemical non-rigidity has been established for several complexes of the type $[Ir(dppe)_2(H)Cl]X$[13] and the related compound $[Ir(PPh_3)_2(nbd)(H)_2]^+$ has been the subject of a detailed isomerization study by ^1H and ^{31}P NMR.[15]

The mechanism of formation of $[Ir(dppe)_2(H)_2][B_{10}H_{11}Se]$ from $[Ir(dppe)_2O_2][B_{10}H_{11}Se]$ is clearly complicated but probably proceeds via initial loss of oxygen. Deoxygenation of the cation has previously been postulated to occur at 150°C *in vacuo*.[9] For the subsequent formation of the $Ir(H_2)$ entity there are three possible sources of the hydride ligands. Perhaps the most obvious is the borane anion, but alternatively the hydride could come from the dppe ligand or from an entrapped solvent molecule. If hydrogen was transferred from a dppe ligand intramolecularly, the resultant cation would be *cyclo*-metalated. Although several examples of this type of reaction are known e.g. the compound *closo*-[3,3,3-(PPh_3)(Ph_2P-*ortho*-C_6H_4)-3,1,2-$RhC_2B_9H_{11}$],[16] this possibility can be ruled out in the present case from the evidence of ^1H NMR and the X-ray crystallographic study. In some previously reported reactions involving the formation of $[Ir(dppe)_2(H)_2]^+$ from the reaction between $[Ir(dppe)_2]Cl$ and either $B_{10}H_{13}X$ (X = 6-Cl, H) or $[B_3H_8]^-$ in methanol,[6,7] it was thought most likely that the hydride came from the solvent,[6] however the ^1H NMR of (**I**) precluded the solvent as a source in the present work since there are no signals for either of the two solvents used in its preparation (THF or CH_2Cl_2). Although the reaction of metal reagents with $[BH_4]^-$ to give metal hydrides is common and well documented,[1,17] three dimensional cluster borane anions are in general notably less effective in the production of metal hydrides. However some oxidative addition reactions of iridium complexes with borane clusters are known which

involve both terminal B—H and bridging B—H—B bonds. Examples involving terminal B—H bonds include reactions of the neutral species *closo*-1-SB_9H_9 or 1,2-$C_2B_{10}H_{12}$ with $[IrCl(PPh_3)_2]$ yielding [2-*exo*{$(PPh_3)_2Ir(H)Cl$}-1-SB_9H_8][18] and [3-*exo*-{$(PPh_3)_2Ir(H)Cl$}-1,2-$C_2B_{10}H_{11}$].[19] Abstraction of a bridging hydrogen from $[C_2B_9H_{12}]^-$ by iridium has been reported in the formation of [3,3-$(PPh_3)_2$-3-H-3,1,2-$IrC_2B_9H_{11}$].[2] The formation of ionic rather than insertion products is a major feature of the present work. Similar results were observed for reactions of both $[Ir(dppe)_2]Cl$ and $[Ir(dppe)_2(CO)]Cl$ with $B_{10}H_{13}X$ (X = 6-Cl, H) and $[B_3H_8]^-$.[6,7] In the case of a monodentate ligand Ir complex such as $[IrCl(PPh_3)_3]$, insertion requires loss of only one PPh_3 ligand whereas for the bidentate (dppe)–Ir complex, the reaction would involve two Ir—P bonds being broken. The only known (dppe)M-cage bonded metallaborane clusters are those formed either from a metal complex with only one dppe ligand e.g. by reaction of $(dppe)NiX_2$ (X = Cl, Br) with $C_2B_4H_7^-$,[20] or where the free dppe ligand is added, together with the metal chloride, to the borane or carbaborane based anion e.g. the reaction of dppe and MCl_2 (M = Fe, Co) with *nido*-2,3-$Et_2C_2B_4H_5^-$.[21] In neither of these cases does insertion require the loss of a dppe unit. In the reaction of $[Ir(dppe)_2]Cl$ with $[B_{10}H_{11}Se]^-$ the metal displayed a clear preference to retain the dppe ligands and later, to increase its coordination number by reaction with O_2 rather than to become part of a metallaheteroborane cage.

The compound $[Ir(dppe)_2(H)_2][B_{10}H_{11}Se]$ (**II**) was the subject of an X-ray crystallographic study to confirm the nature of the cation and anion and to determine their structures. The system (space group $P\bar{1}$) contains four formula units per unit cell; two types of cation and two types of anion, and one molecule of CH_2Cl_2 are present in the asymmetric unit (Fig. 1). The cations A and B exist with different conformations of one of the $—CH_2—CH_2—$ portions of the dppe ligands, Fig. 2. Both the anions are disordered though one, A, is less disordered than the other, B, and the *nido* type 11-atom structure can clearly be seen in the case of A. In the less disordered cage the selenium is found at only four of the five open-face positions. The other seven sites are occupied only by boron atoms. In this system the bond distances involving the seven sites occupied wholly by boron atoms lie in the range 1.76(2)–1.91(2) Å, i.e. within the rather large range found in borane clusters. They may also be compared with B—B bond distances in other selena- and metallaselenaborane structures e.g. *closo*-$[B_{11}H_9Se_3]^{2-}$,[22] *closo*-[2,2-$(PPh_3)_2$-1,2-$SePtB_{10}H_{10}$][11] and *nido*-[(η-C_5H_5)-7,8,12-$CoSe_2B_9H_9$].[23] In the dianion and the

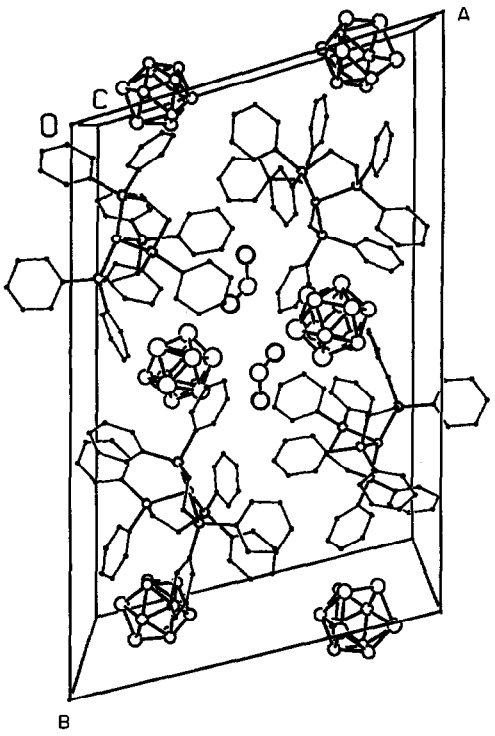

Fig. 1. A view of the crystal packing.

platinaselenaborane, the B—B bond distances lie in the ranges 1.738(20)–2.091(21) Å and 1.813(10)–1.919(10) Å, respectively, whereas those in the *nido* structure lie between 1.708(7)–2.007(7) Å. In the more disordered anion, bond distances lie within the range 1.71(3)–2.16(2) Å with a mean value of 1.93 Å. These may be compared with data from the wholly disordered system *closo*-$B_{11}H_{11}Se$ in which the distances were between 1.87 and 2.12 Å with a mean value of 2.00 Å.[11]

Both cations A and B have distorted octahedral *cis*-$[IrP_4H_2]$ structures. The important interatomic distances and bond angles are given in Table 1. The Ir—P bond lengths (2.308(2)–2.369(3) Å) fall within the expected range (2.277(1)–2.371(7) Å) for $[Ir(dppe)_2X]Y$ systems (Table 2).[6,24–26] The *trans* influence of the hydride ligands has been noted previously[6] and is also apparent in complex (**II**) with the Ir—P bonds *trans* to the hydride ligands being on average 0.045 Å longer than those *trans* to phosphorus atoms. The mean Ir—P bond length is 2.359 Å for those bonds *trans* to the hydrides while that for the bonds *trans* to phosphorus atoms is 2.314 Å. The *cis*-hydride ligands were identified spectroscopically and maxima corresponding to their expected location were observed in the final difference map. The extent of distortion from a purely

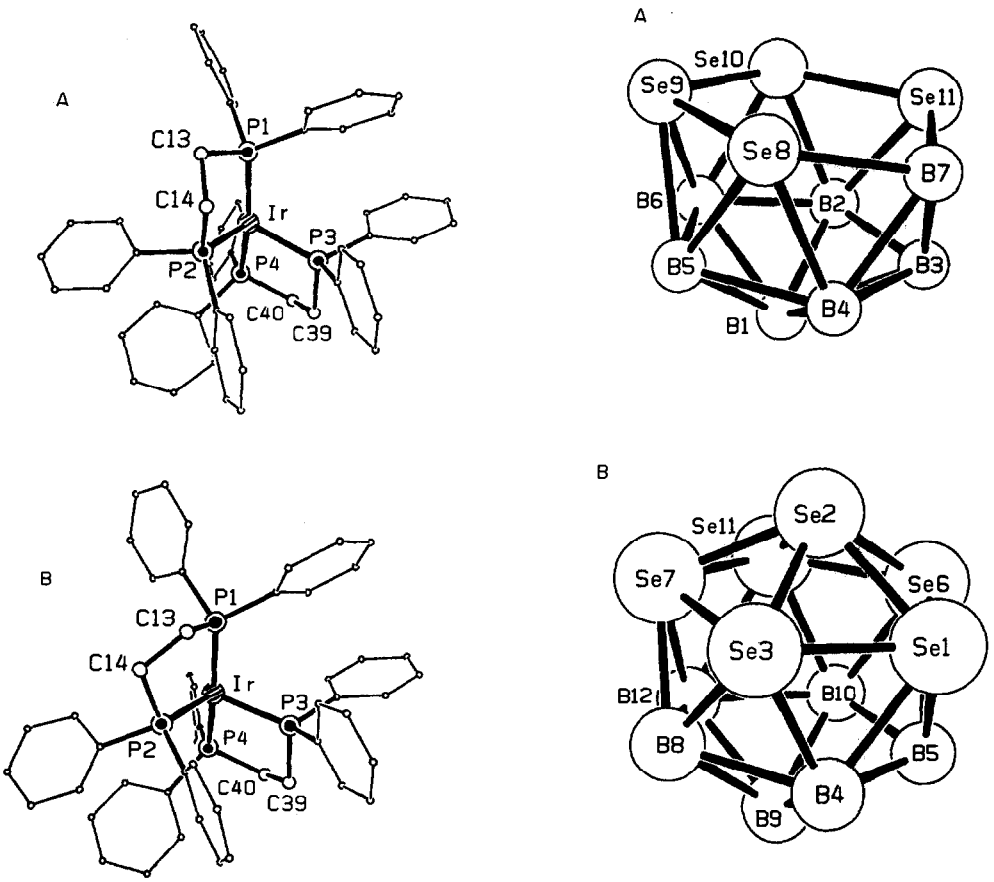

Fig. 2. Views of the A and B cations and anions. For clarity, in the cations, the various atoms are shown as spheres with different radii. In the disordered anions the spheres are at the 50% probability levels. A has the Se atoms scrambled over four sites and B over six sites. Labelling of atoms as Se or B is a function of the occupancy factor.

octahedral structure can be seen by comparison of the P—Ir—P angles between the two equatorial phosphorus atoms (α) and the two axial phosphorus atoms (β) (Table 2) with those in an idealized octahedral structure ($\alpha = 90°$, $\beta = 180°$). For cation A, $\alpha = 98.2(1)°$, $\beta = 163.4(1)°$, while for cation B, $\alpha = 104.05(9)°$ and $\beta = 168.75(9)°$. These distortions are comparable to those reported for the similar systems in Table 2. The chelate P—Ir—P "bite" angles (γ) are 84.49(9) and 85.41(9)° for cation A and 85.25(9) and 85.21(9)° for cation B which are similar to the values found in other $[Ir(dppe)_2X]Y$ systems (e.g. $X = H_2$, $Y = B_9H_{14}^-$, $(\gamma) = 86.2(2)°$,[6] $X = H_2$, $Y = PF_6^-$, $(\gamma) = 86.3°$,[24] $X = O_2$, $Y = PF_6^-$, $(\gamma) = 83.7(1)°$).[25]

EXPERIMENTAL

IR spectra were recorded as KBr discs on Perkin–Elmer 257 and 1310 spectrometers. The NMR spectra were recorded on a Bruker WH400 spectrometer. Chemical shifts δ are reported relative to $SiMe_4$ (^1H), BF_3OEt_2 (external) (^{11}B) and H_3PO_4 (external) (^{31}P); positive values represent shifts to high frequency ("low field") of the standards. Reactions and recrystallizations were carried out under dry, oxygen-free nitrogen, although manipulations and separatory procedures were carried out in air. THF was purified by distillation from potassium benzophenone ketyl under nitrogen. The compound $[Ir(dppe)_2]Cl$ was prepared by the literature method[9] as was $[Et_4N][B_{10}H_{11}Se]$.[10] The latter was purified by recrystallization from CH_2Cl_2 and identified spectroscopically; IR ν_{max} at 3050 w, 2980 m, 2950 vw, 2520 brs (BH), 1485 s, 1475 w, 1455 w, 1438 m, 1415 w, 1395 m, 1362 m, 1295 brw, 1070 vw, 1055 m, 1015 vw, 1002 s, 910 m, 880 w, 815 w, 790 vs, 755 w, 742 w, 695 w cm^{-1}. $^{11}B\{^1H\}$ NMR (CD_2Cl_2, 128 MHz, 25°C) −5.6 (s, 2B), −9.2 (s, 2B), −14.6 (s, 1B), −16.3 (s, 2B), −17.6 (s, 2B), −35.6 (s,1B) ppm.[10,11]

Reaction of nido-$[Et_4N][B_{10}H_{11}Se]$ *with*

Table 1. (i) Principal interatomic distances[a] in Å and (ii) selected angles (°) with e.s.d.s in parentheses

(i)	Atom 1	Atom 2	Distance	Atom 1	Atom 2	Distance
	IrA	P1A	2.317(2)	IrB	P1B	2.311(2)
	IrA	P2A	2.369(3)	IrB	P2B	2.340(3)
	IrA	P3A	2.366(3)	IrB	P3B	2.361(2)
	IrA	P4A	2.321(3)	IrB	P4B	2.308(2)
	P1A	C1A	1.790(9)	P1B	C1B	1.831(10)
	P1A	C7A	1.845(10)	P1B	C7B	1.860(9)
	P1A	C13A	1.860(10)	P1B	C13B	1.851(10)
	P2A	C14A	1.852(10)	P2B	C14B	1.834(10)
	P2A	C15A	1.854(11)	P2B	C15B	1.806(9)
	P2A	C21A	1.860(10)	P2B	C21B	1.860(10)
	P3A	C27A	1.816(11)	P3B	C27B	1.794(10)
	P3A	C33A	1.823(10)	P3B	C33B	1.823(10)
	P3A	C39A	1.854(10)	P3B	C39B	1.830(10)
	P4A	C40A	1.855(10)	P4B	C40B	1.855(10)
	P4A	C41A	1.823(10)	P4B	C41B	1.868(10)
	P4A	C47A	1.868(10)	P4B	C47B	1.795(9)

(ii) Cation A:	Atom 1	Atom 2	Atom 3	Angle
	P1A	IrA	P2A	84.49(9)
	P1A	IrA	P3A	107.21(9)
	P1A	IrA	P4A	163.4(1)
	P2A	IrA	P3A	98.2(1)
	P2A	IrA	P4A	104.78(9)
	P3A	IrA	P4A	85.41(9)
Cation B:	P1B	IrB	P2B	85.29(9)
	P1B	IrB	P3B	101.22(9)
	P1B	IrB	P4B	168.75(9)
	P2B	IrB	P3B	104.05(9)
	P2B	IrB	P4B	102.27(9)
	P3B	IrB	P4B	85.21(9)

[a] In the cations, C—C distances in aromatic rings and within the phosphine ligands are as follows: (a) aromatic C—C distances range from 1.31–1.48 Å, with a mean of 1.40 Å and (b) sp^3 C—C distances range from 1.56–1.61 Å, with a mean of 1.58 Å. In the disordered Se—B anion cages, the intramolecular bond distances are in the range of 1.71–2.16 Å with a mean of 1.93 Å.

Table 2. Ir—P bond lengths and P—Ir—P angles in $[Ir(dppe)_2X]Y$ complexes

X	Y	Ir—P range (Å)	α[a]	β[b]	Ref.
H_2	PF_6	2.277(1) to 2.345(1)	100.4	160.7	25
H_2	B_9H_{14}	2.315(8) to 2.371(7)	97.32(2)	161.0(2)	6
H_2	$B_{10}H_{11}Se$	2.308(2) to 2.369(2)	98.2(1) and 104.05(9)	163.4(1) and 168.75(9)	present work
O_2	PF_6	2.308(3) to 2.366(3)	97.01(1)	175.3(3)	26
S_2	Cl	2.331(4) to 2.371(5)	98.5(2)	171.6(2)	27

[a] α is the angle between the two equatorial phosphorus atoms.
[b] β is the angle between the two axial phosphorus atoms.

$[Ir(dppe)_2]Cl$. A solution of $[Et_4N][B_{10}H_{11}Se]$ (0.28 g, 0.853 mmol) in THF (75 cm^3) was added to a stirred suspension of $[Ir(dppe)_2]Cl$ (0.82 g, 0.8 mmol) in THF (75 cm^3) at ambient temperature. After sitrring for 45 h, the solution was filtered and concentrated under reduced pressure (rotary evaporator, 25°C). Preparative tlc of this mixture (solvent: CH_2Cl_2) yielded six bands of which the major one was characterized spectroscopically as $[Ir(dppe)_2O_2][B_{10}H_{11}Se]$ (I) (0.45 g, 46.2%); IR ν_{max} at 3050 m, 2950 w, 2910 w, 2510 vs (BH), 1715 w, 1700 w, 1685 vw, 1670 vw, 1480 s, 1435 s, 1330 vw, 1310 vw, 1278 vw, 1255 w, 1188 w, 1155 w, 1090 s, 1015 w, 995 w, 905 vw, 875 w, 845 m (O_2), 813 m, 690 vs cm^{-1}. NMR spectra: $^{11}B\{^1H\}$ (CD_2Cl_2, 128 MHz, 25°C) δ −5.6 (s, 2B), −9.2 (s, 2B), −14.6 (s, 1B), −16.3 (s, 2B), −17.6 (s, 2B), −35.6 (s, 1B)[10,11]; $^{31}P\{^1H\}$ (CH_2Cl_2, 162 MHz, 25°C) δ 18.5 (s, 1P), 13.6 (s, 1P) ppm.[12,13]

Thermolysis of $[Ir(dppe)_2O_2][B_{10}H_{11}Se]$. $[Ir(dppe)_2O_2][B_{10}H_{11}Se]$ (0.44 g, 0.361 mmol) was heated at 120°C for 7 h under reduced pressure (0.3 mm Hg). The resultant red–orange solid mixture was separated by preparative tlc (solvent: CH_2Cl_2) to give as the major product, a pale beige solid. Recrystallization from CH_2Cl_2/C_6H_{14} afforded $[Ir(dppe)_2H_2][B_{10}H_{11}Se]$. 1/2 CH_2Cl_2 (II) (0.08 g, 18.7%) which was identified spectroscopically and by X-ray crystallography; IR ν_{max} at 3050 w, 2955 s, 2925 s, 2850 s, 2510 vs (BH), 2070 m (IrH), 1725 vs, 1595 vw, 1575 w, 1460 s, 1435 s, 1380 m, 1280 vs, 1185 w, 1125 s, 1100 w, 1070 m, 1038 w, 998 w, 965 w, 880 m, 824 m, 770 w, 745 s, 695 cm^{-1}. NMR spectra, ^1H (CD_2Cl_2, 400 MHz, 25°C) δ 8.15–6.92 (complex m, 36 H, p-C_6H_5), 6.00 (t, 4H, *ortho* P-C_6H_5), 3.26 to 0.50 (complex m, 20 H, B*H* and CH_2), −4.13 (brs, 1H, B*H*B), −11.63 (d of q, 2H, IrH_2 *cis* ($^2J_{HP_{trans}}$ = 110 Hz, $^2J_{HP_{cis}}$ = 12 Hz); $^{11}B\{^1H\}$ (CH_2Cl_2/CD_2Cl_2, 128 MHz, 25°C) δ −5.7 (s, 2B), −9.1 (s, 2B), −14.7 (s, 1B), −16.2 (s, 2B), −17.4 (s, 2B), −35.4 (s, 1B); $^{31}P\{^1H$(broad band)$\}$ (CH_2Cl_2/CD_2Cl_2, 162 MHz, 25°C) δ 33.9 (s, 1P, P *cis* to H ligands), 22.4 (s, 1P, P *trans* to H ligands) ppm.

X-ray analysis of $[Ir(dppe)_2H_2][B_{10}H_{11}Se]$ 1/2 CH_2Cl_2 (II)—*Crystal data* $C_{105}H_{124}Cl_2Ir_2Se_2B_{20}P_8$. FW = 2463.37, triclinic, a = 18.308(4), b = 27.580(4), c = 12.017(2) Å, α = 98.33(1), β = 95.94(2), γ = 105.29(1)°, U = 5727 Å^3, Z = 4, D_c = 1.42 g cm^{-3}, $F(000)$ = 2448, λ(Mo-K_α) = 0.71073 Å, μ(Mo-K_α) = 31.4 cm^{-1}. Space group $P\bar{1}$ (No. 2). A crystal measuring approximately 0.04 × 0.09 × 0.02 mm was grown from CH_2Cl_2 solution which was suitable for X-ray data collection with an Enraf–Nonius CAD4 diffractometer. Following machine location and centering of 24 reflections with θ in the range $9 < \theta < 13°$; cell constants and an orientation matrix were determined by least squares refinement. A total of 11,846 reflections were collected of which 10,085 were unique ($R_{(int)}$ = 0.015), and the 7925 which had $I \geqslant 3\sigma(I)$ were used in structure solution and refinement. Data were corrected for Lorentz and polarization factors and for absorption. Maximum and minimum values of transmission coefficients are 0.673 and 0.297 respectively.

There are two independent formulae units in the asymmetric unit. The coordinates of the two independent Ir atoms were determined from an analysis of the three-dimensional Patterson synthesis and the remaining atoms located by the heavy atom method. The Se and B atoms in the two $[B_{10}H_{11}Se]^-$ cages are scrambled to different extents. This was allowed for by appropriate occupancy factor refinement. A loosely held dichloromethane of solvation was also located in the asymmetric unit. Initial refinement was by full-matrix least-squares calculations with isotropic thermal parameters and Se/B occupancy factors. Final refinement with anisotropic thermal parameters for Ir and P atoms (isotropic for remainder), 611 variables, 7025 observations, converged with R = 0.069, wR = 0.096. A final difference map showed maxima adjacent to the Ir atoms consistent with the anticipated sites of the two Ir bonded hydrogen atoms.

Table 1 lists selected dimensions. Figure 1 is the packing diagram and Fig. 2 shows views of the cations and anions. A complete list of final fractional coordinates, occupancy factors, dimensions, structure factors and thermal parameters has been deposited as Supplementary Material with the Editor, from whom copies are available on request.*

Acknowledgements—G. F. thanks NSERC Canada for Grants in Aid of Research. The loan of Ir salts by Johnson Matthey Ltd is gratefully acknowledged. O. Ni. D. thanks the Department of Education of the Republic of Ireland for a Research Studentship.

REFERENCES

1. J. D. Kennedy, *Prog. Inorg. Chem.* 1984, **32**, 579; *Metal Interactions with Boron Clusters* (Edited by R. N. Grimes). Plenum Press, New York (1982).
2. T. E. Paxson and M. F. Hawthorne, *J. Am. Chem. Soc.* 1974, **96**, 4674.

*Atomic coordinates have also been deposited with the Cambridge Crystallographic Data Centre.

3. J. Bould, N. N. Greenwood and J. D. Kennedy, *J. Organomet. Chem.* 1983, **249**, 11.
4. N. N. Greenwood, J. J. Kennedy, W. S. McDonald, D. Reed and J. Staves, *J. Chem. Soc., Dalton Trans.* 1979, 117.
5. J. Bould, J. E. Crook, N. N. Greenwood and J. D. Kennedy, *J. Chem. Soc., Dalton Trans.* 1984, 1903.
6. N. N. Greenwood, W. S. McDonald, D. Reed and J. Staves, *J. Chem. Soc., Dalton Trans.* 1979, 1339.
7. N. N. Greenwood, J. D. Kennedy and D. Reed, *J. Chem. Soc., Dalton Trans.* 1980, 196.
8. J. A. Doi, R. G. Teller and M. F. Hawthorne, *J. Chem. Soc., Chem. Commun.* 1980, 80.
9. L. Vaska and D. L. Catone, *J. Am. Chem. Soc.* 1986, **88**, 5324; A. Sacco, M. Rossi and C. F. Nobile, *J. Chem. Soc., Chem. Commun.* 1966, 589.
10. J. L. Little, G. D. Friesen and L. J. Todd, *Inorg. Chem.* 1977, **16**, 869.
11. G. Ferguson, M. Parvez, J. A. MacCurtain, O. Ni Dhubhghaill, T. R. Spalding and D. Reed, *J. Chem. Soc., Dalton Trans.* 1987, 699.
12. A. F. Williams, G. C. H. Jones and A. G. Maddock, *J. Chem. Soc., Dalton Trans.* 1975, 1952.
13. J. S. Miller and K. G. Caulton, *J. Am. Chem. Soc.* 1975, **97**, 1067.
14. M. J. Hopkinson and J. F. Nixon, *J. Organomet. Chem.* 1978, **148**, 201.
15. O. W. Howarth, C. H. McAteer, P. Moore and G. E. Morris, *J. Chem. Soc., Dalton Trans.* 1984, 1171.
16. R. E. King, D. C. Busby, and M. F. Hawthorne, *J. Organomet. Chem.* 1985, **279**, 103; C. B. Knobler, R. E. King and M. F. Hawthorne, *Acta Cryst.* 1986, **C42**, 159.
17. *Boron Hydride Chemistry* (Edited by E. L. Muetterties). Academic Press, New York (1975).
18. D. A. Thompson and R. W. Rudolph, *J. Chem. Soc., Chem. Commun.* 1976, 770.
19. E. L. Hoel and M. F. Hawthorne, *J. Am. Chem. Soc.* 1975, **97**, 6388.
20. L. Barton and P. K. Rush, *Inorg. Chem.* 1986, **25**, 91.
21. H. A. Boyter, R. G. Swisher, E. Sinn and R. N. Grimes, *Inorg. Chem.* 1985, **24**, 3810.
22. G. D. Friesen, J. L. Little, J. C. Huffman and L. J. Todd, *Inorg. Chem.* 1979, **18**, 755.
23. G. D. Friesen, A. Barriola, P. Daluga, P. Ragatz, J. C. Huffman and L. J. Todd, *Inorg. Chem.* 1980, **19**, 458.
24. T. Debaerdemaeker, *Cryst. Struct. Commun.* 1977, **6**, 11.
25. M. J. Nolte, E. Singleton and M. Laing, *J. Am. Chem. Soc.* 1975, **97**, 6396.
26. W. D. Bonds and J. A. Ibers, *J. Am. Chem. Soc.* 1972, **94**, 3413.

Polyhedron Vol. 7, No. 3, pp. 195–201, 1988
Printed in Great Britain

0277–5387/88 $3.00+.00
© 1988 Pergamon Journals Ltd

REDOX PROPERTIES OF A SERIES OF PSEUDOALLYL RHENIUM(I) COMPLEXES

P. ZANELLO,* A. CINQUANTINI and F. LASCHI

Dipartimento di Chimica dell'Università di Siena, Pian dei Mantellini, 44, 53100 Siena, Italy

and

R. ROSSI, A. DUATTI, A. MARCHI and L. MAGON

Dipartimento di Chimica dell'Università di Ferrara, Via L. Borsari, 46, 44100 Ferrara, Italy

(*Received* 19 *May* 1987; *accepted* 26 *August* 1987)

Abstract—The electrochemistry of a series of rhenium(I) complexes, namely $[Re(CO)_2(Ph_3)_2\{(ArN)_2X\}]$ (X = N, CH; Ar = C_6H_5, C_6H_4Me-*p*, C_6H_4Cl-*p*, C_6H_4F-*p*), has been studied in different nonaqueous solvents (CH_2Cl_2, MeCN, Me_2CO). The rhenium(I)/rhenium(II) redox change occurs at potentials varying from +0.60 V to +0.90 V (vs S.C.E.), depending upon the electron donating ability of the aryl groups. At room temperature this oxidation is complicated by slow following chemical reactions (proposed as the competing photochemical–thermal self-reduction and intramolecular oxidation processes), but below 0°C the electrogenerated rhenium(II) complexes, which are isostructural with their rhenium(I) precursors, are sufficiently stable to be characterized by UV-Visible, IR and ESR spectroscopy.

While both the 18-electron rhenium(I) and the 16-electron rhenium(III) derivatives are stable, the 17-electron rhenium(II) complexes are often kinetically labile and in some cases only electrochemical evidence can testify to their existence.[1–9] In this regard it is not surprising that only a few mononuclear rhenium(II) complexes have been up-to-now characterized.[10–14]

In recent years the electrochemistry of some mononuclear rhenium(I) carbonyl–phosphine derivatives has been investigated.[1,2,4–6,8] Previously we have characterized a series of isostructural rhenium(I) pseudoallyl complexes as $[Re(CO)_2(PPh_3)_2(L)]$ (L = $(RN_3R)^-$, $\{(RN)_2CH\}^-$, $(RNCHO)^-$ and $(amt)^-$ = anion of 2-aminothiazole derivatives).[15–18] We report here the redox behaviour of the mixed carbonyl–phosphine derivatives **1–8**, containing the triazenido and formamidinato ligands with different substituents,[15,16] which have been shown to give characterizable rhenium(II) derivatives. (See Structure 1.)

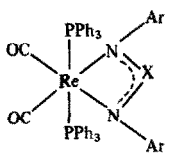

Structure 1.

X = N, Ar = C_6H_5(1)
X = N, Ar = C_6H_4Cl–*p*(2)
X = N, Ar = C_6H_4Me–*p* (3)
X = N, Ar = C_6H_4F–*p*(4)
X = CH, Ar = C_6H_5(5)
X = CH, Ar = C_6H_4Cl–*p*(6)
X = CH, Ar = C_6H_4Me–*p*(7)
X = CH, Ar = C_6H_4F–*p* (8)

RESULTS AND DISCUSSION

Electrochemistry

The electrochemistry of the formamidinato and triazenido rhenium(I) complexes under study has been preliminarily investigated by cyclic voltammetry. A typical response is reported in Fig. 1(a), which refers to **1** in dichloromethane solvent. In Figs 1(b) and (c) the responses of both free triazene and triphenylphosphine ligands are also reported.

As can be seen, **1** gives rise to two anodic charge transfers occurring at peaks A and B, respectively.

Controlled potential coulometric tests at +1.0 V, in correspondence to the first anodic process, showed that the anodic current abruptly falls after

*Author to whom correspondence should be addressed.

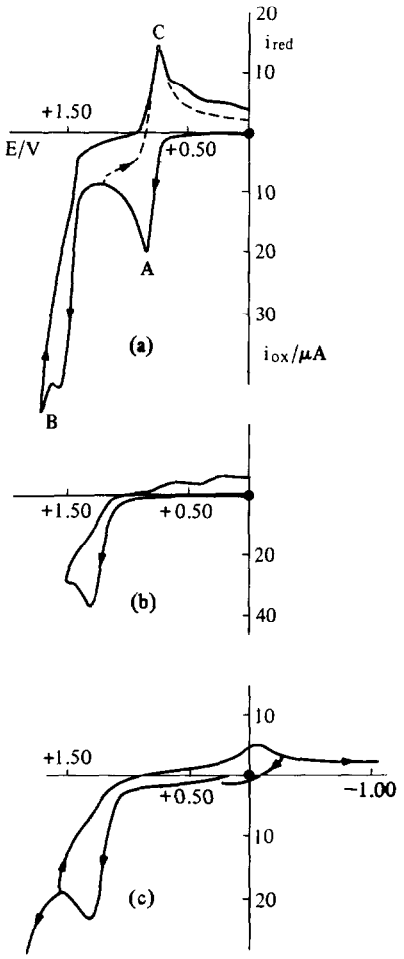

Fig. 1. Cyclic voltammograms recorded on a CH_2Cl_2 solution containing $[NBu_4](ClO_4)$ (0.1 mol dm^{-3}) and (a) **1** (1.37×10^{-3} mol dm^{-3}); (b) Ph—NH—N=N—Ph (2.1×10^{-3} mol dm^{-3}); (c) PPh_3 (1.3×10^{-3} mol dm^{-3}). Platinum working electrode. Scan rate: 0.2 V s^{-1}. (●) Starting potential.

the consumption of one electron per molecule of starting compound, but it remains significantly higher than the background current, up to the overall consumption of a number of electrons ranging from 1.6 to 1.8 per molecule of starting Re(I) complex. On the other hand, the comparison of the cyclic voltammetric response of **1** with that of an equimolar solution of ferrocene, which is known to involve a one-electron oxidation process, seems to indicate at first approximation* that, in the short time of the cyclic voltammetric experiment, only one electron is involved in the first anodic step.

The analysis of the cyclic voltammograms with scan rates[19] ranging from 0.02 to 50 V s^{-1} reveals the following features: the cathodic to anodic peak current ratio, $i_{p(C)}/i_{p(A)}$, is 0.84 at 0.02 V s^{-1}, 0.96 at 0.05 V s^{-1}, 1.0 at 0.1 V s^{-1} and then it remains constant; the current function $i_{p(A)}/v^{1/2}$ decreases by approx. 30%; the difference between the peak potential value of the anodic response A and that of its directly associated one *C*, ΔE_p, gradually increases from 80 to 450 mV, probably also because of some uncompensated solution resistance. In addition, chronoamperometric tests showed that the $(i \times t^{1/2})$ parameter remains practically constant in the time range 0.002–3 s.

All these electrochemical data indicate that the anodic process occurring at peak A is complicated by following chemical reactions, in part giving products oxidizable at the potentials of peak A. In electrochemical terms it can be thought that an e.c. mechanism is concomitant with an e.c.e. type mechanism (we shall discuss it in Additional Remarks). However, these following reactions are rather slow so that in cyclic voltammetry at sufficiently high scan rates only the first charge-transfer, quasi-reversible in character, is substantially operative.

The average value between the peak potential value of peak A and that of peak C, at scan rates where $i_{p(C)}/i_{p(A)} = 1$ (i.e. when the chemical complications following the first charge-transfer are prevented), can be assumed as a good approximation of the thermodynamic formal electrode potential, $E^{\ominus}$, for the first one-electron transfer involved in the less anodic oxidation of the Re(I) complex, i.e. the Re(I/II) charge-transfer.

As regards the second anodic process occurring at peak B, at least in principle it can be attributed either to the oxidation of the ligands (triazene or triphenylphosphine), or to the subsequent Re(II/III) anodic process. However both the closeness to the solvent discharge and its irreversibility convinced us to neglect its deeper examination.

The above reported electrochemical behaviour is typical for all studied Re(I) complexes, not only in the triazenido form, but also for the formamidinato complexes. In this connection it must be considered that in CH_2Cl_2 free formamidine ligands oxidize at about +1.1 V.

In order to test if the solvent may play some role in the stabilization of the electrogenerated rhenium(II) complexes, the electrode behaviour was also examined in acetonitrile and acetone solvents. In these media the chemical complications following the first anodic process are even more rapid. Table 1 summarizes the standard potentials for the Re(I/II) redox couple of the complexes studied here, together with those of other carbonyl/phosphino complexes reported in literature.

* Strictly speaking the comparison would require the knowledge of the diffusion coefficients of the two species.

Table 1. Formal electrode potentials (in Volts, vs S.C.E.) for the Re(I/II) redox couple in some Re(I) carbonyl–phosphino complexes.

Re(I) complex	CH_2Cl_2	MeCN	Me_2CO	Refs
$[Re(CO)_2(PPh_3)_2\{N(NC_6H_5)_2\}]$ (1)	+0.80	+0.78	+0.78	present work
$[Re(CO)_2(PPh_3)_2\{N(NC_6H_4Cl\text{-}p)_2\}]$ (2)	+0.90	not soluble	not soluble	present work
$[Re(CO)_2(PPh_3)_2\{N(NC_6H_4Me\text{-}p)_2\}]$ (3)	+0.67	+0.66	+0.71	present work
$[Re(CO)_2(PPh_3)_2\{N(NC_6H_4F\text{-}p)_2\}]$ (4)	+0.84	not soluble	not soluble	present work
$[Re(CO)_2(PPh_3)_2\{CH(NC_6H_5)_2\}]$ (5)	+0.70	+0.64	+0.68	present work
$[Re(CO)_2(PPh_3)_2\{CH(NC_6H_4Cl\text{-}p)_2\}]$)6)	+0.76	not soluble	not soluble	present work
$[Re(CO)_2(PPh_3)_2\{CH(NC_6H_4Me\text{-}p)_2\}]$ (7)	+0.60	+0.56	+0.60	present work
$[Re(CO)_2(PPh_3)_2\{CH(NC_6H_4F\text{-}p)_2\}]$ (8)	+0.71	not soluble	not soluble	present work
$[Re(CO)_2(PPh_3)_2(bpy)]^{+a}$	—	+1.37[b]	—	ref. 7
$[Re(CO)_2(PMe_2Ph)_2(bpy)]^{+a}$	—	+1.10	—	ref. 7
$[Re(CO)(PMe_2Ph)_4Cl]$	+0.20[c]	—	—	ref. 2
$[Re(CO)_2(PMe_2Ph)_3Cl]$	+0.82[d]	+0.82[e]	—	ref. 9; ref. 6
$[Re(CO)_3(PMe_3)_3(bpy)]^{+a}$	—	+1.84[b]	—	ref. 5
mer-$[Re(CO)_3(PMe_2Ph)_2Cl]$	+1.18[d]	+1.15[e]	—	ref. 9; ref. 6
fac-$[Re(CO)_3(PMe_2Ph)_2Cl]$	+1.46[d]	+1.38[e]	—	ref. 9; ref. 6
mer-$[Re(CO)_3(PPh_3)_2Cl]$	+1.44	—	—	ref. 3
mer-$[Re(CO)_3\{P(C_6H_4Me\text{-}p)_3\}_2Cl]$	+1.44	—	—	ref. 3
mer-$[Re(CO)_3\{P(C_6H_4Me\text{-}m)_3\}_2Br]$	+1.39	—	—	ref. 3
$[Re(CO)_4(PMe_2Ph)Cl]$	>1.7	—	—	ref. 9

[a] bpy = 2,2′-pyridine.
[b] Peak potential values at 0.2 Vs^{-1} for irreversible processes.
[c] 10% methanol present.
[d] Refer to ref. 9.
[e] Refer to ref. 6.

As it can be seen, starting from Re(I) complexes, the thermodynamic access to the Re(II) complexes is basically favoured by: (i) replacing the π-accepting carbon monoxide ligand with σ-donating phosphine ligands[9] and (ii) the possibility to substitute the halide or bipyridine ligands with ligands, such as pseudoallyl triazenides or formamidinates, containing electron-donating substituents. In addition, as expected on the basis of their electronegativity, the substitution of the nitrogen atom of triazene with the CH group of formamidine favours the anodic Re(I/II) charge-transfer.

A plot of the formal electrode potentials for the Re(I/II) couple vs Hammett's substituent constants[20] is shown in Fig. 2.

A linear correlation holds for both triazenido (correlation coeff. = 0.98) and formamidinato (correlation coeff. = 0.97) substituents, suggesting that the HOMO of the present complexes is conjugated to the phenyl moieties of the pseudoallyl ligands, as has been quoted for other Re(I) compounds with different ligands.[4]

Characterization of rhenium(II) complexes

In order to slow down the chemical complications following the Re(I/II) charge-transfer also in the longer time scale of macroelectrolysis, we performed electrolysis tests at 0°C in dichloromethane solvent.

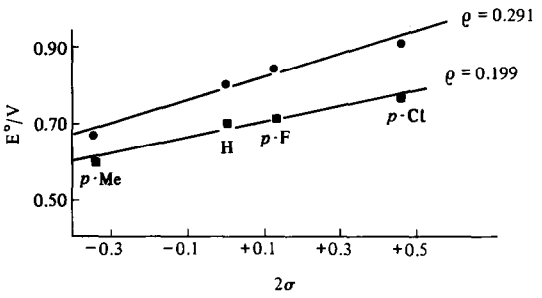

Fig. 2. Plot of the formal electrode potentials for the Re(I/II) redox couple in CH_2Cl_2 vs Hammett's constants. (●) Re(I)-triazenido derivatives; (■) formamidinato derivatives.

As an example of the behaviour of formamidinato complexes, controlled potential electrolysis in correspondence with the first anodic process of **7**, at 0°C, showed that after consumption of one electron/molecule the current fell to quite negligible values. The colour of the solution changed from yellow to deep green. Figure 3 shows the cyclic voltammogram recorded on the exhaustively electrolysed solution.

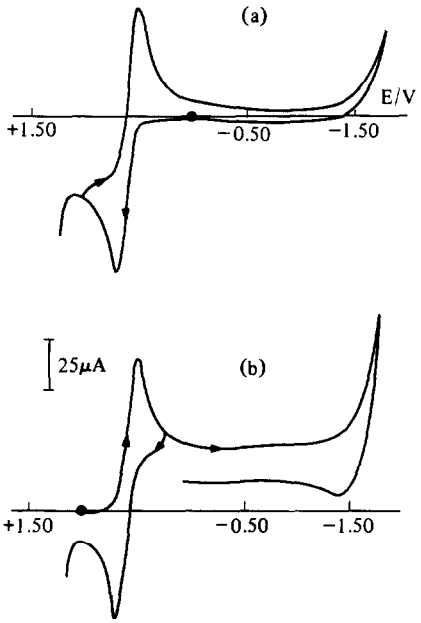

Fig. 3. Cyclic voltammetric responses recorded at a platinum electrode on a CH_2Cl_2 solution containing **7** (0.106 mmol) and $[NBu_4](ClO_4)$ (0.1 mol dm^{-3}) under the following conditions: (a) initial; (b) after the consumption of 1 e^-/molecule in controlled potential coulometry at +0.75 V. Temperature 0°C. Scan rate, 0.2 V s^{-1}.

The features of the cyclic voltammogram clearly indicate that no significant structural change occurs as a consequence of the Re(I/II) charge-transfer. The green rhenium(II) complex was characterized by ESR, IR and UV-Visible spectroscopy (Table 2), since any attempt to separate it from the $[NBu_4](ClO_4)$ supporting electrolyte failed.

In frozen solution (liquid nitrogen temperature) the rhenium(II) derivative exhibits a broad structured X-band ESR signal centred at $g_{\Delta H/2} = 2.040$ ($\Delta H = 365$ G). On the contrary at room temperature the green solution does not display detectable ESR signals.

Just the same behaviour holds when the electrogeneration of triazenido rhenium(II) complexes is concerned. In this case the rhenium(II) solutions are deep red–violet coloured. Their ESR spectra in frozen solution are very similar to those of the formamidinato complexes. However the solid–liquid transition of CH_2Cl_2 (~180 K) does not cause the complete disappearance of the signal, but a notable decrease (~75%) of its intensity, also accompanied by a change in line shape occurs. As an example Fig. 4 illustrates the ESR spectra recorded on **3**, after its one-electron oxidation, at both liquid nitrogen and room temperature.

The linewidth of the spectrum in frozen solution is quite reminiscent of the ESR features of the rhenium(II) (t_{2g}^5) complex $[ReCl_2(CO)_2(P(n\text{-}Pr)_3)_2]$.[12] In our case, it is also evidence of a partial resolution of the hyperfine structure due to the coupling of the unpaired electron with the $I = 5/2$ rhenium nucleus.

The noticeable dependence of both the intensity and line shape of ESR spectra on the temperature is likely to be related to a drastic increase of the intramolecular motional dynamics involved in the glassy–liquid phase transition, since the per-

Table 2. Comparison between the spectroscopic data of rhenium(I) complexes and their rhenium (II) congeners. CH_2Cl_2-$[NBu_4](ClO_4)$ (0.1 mol dm^{-3}) solution

Complexes	IR $\nu_{(C\equiv O)}(cm^{-1})$		UV absorption maximum $\lambda(m\mu)$	ESR(100 K) $g_{\Delta H/2}$	$\Delta H(G)$
$[Re(CO)_2(PPh_3)_2\{N(NC_6H_5)_2\}]$	1847(vs)	1922(vs)	442	—	
$[Re(CO)_2(PPh_3)_2\{N(NC_6H_5)_2\}]^+$	1912(s)	1960(vs)	527 728	2.075	485
$[Re(CO)_2(PPh_3)_2\{N(NC_6H_4Me\text{-}p)_2\}]$	1848(vs)	1921(vs)	445	—	
$[Re(CO)_2(PPh_3)_2\{N(NC_6H_4Me\text{-}p)_2\}]^+$	1901(s)	1951(vs)	538 757	2.044	370
$[Re(CO)_2(PPh_3)_2\{N(NC_6H_4Cl\text{-}p)_2\}]$	1850(vs)	1926(vs)	450	—	
$[Re(CO)_2(PPh_3)_2\{N(NC_6H_4Cl\text{-}p)_2\}]^+$	1914(s)	1962(vs)	550 759	2.090	525
$[Re(CO)_2(PPh_3)_2\{N(NC_6H_4F\text{-}p)_2\}]$	1848(vs)	1923(vs)	440	—	
$[Re(CO)_2(PPh_3)_2\{N(NC_6H_4F\text{-}p)_2\}]^+$	1910(s)	1957(vs)	533 731	2.067	465
$[Re(CO)_2(PPh_3)_2\{CH(NC_6H_5)_2\}]$	1837(vs)	1915(vs)	385	—	
$[Re(CO)_2(PPh_3)_2\{CH(NC_6H_5)_2\}]^+$	1912(s)	1940(s)	411 695	2.080	490
$[Re(CO)_2(PPh_3)_2\{CH(NC_6H_4Me\text{-}p)_2\}]$	1837(vs)	1916(vs)	386	—	
$[Re(CO)_2(PPh_3)_2\{CH(NC_6H_4Me\text{-}p)_2\}]^+$	1880(s)	1936(vs)	421 722	2.040	365
$[Re(CO)_2(PPh_3)_2\{CH(NC_6H_4Cl\text{-}p)_2\}]$	1840(vs)	1917(vs)	394	—	
$[Re(CO)_2(PPh_3)_2\{CH(NC_6H_4Cl\text{-}p)_2\}]^+$	1890(s)	1945(s)	409 723	2.085	520
$[Re(CO)_2(PPh_3)_2\{CH(NC_6H_4F\text{-}p)_2\}]$	1837(vs)	1915(vs)	379	—	
$[Re(CO)_2(PPh_3)_2\{CH(NC_6H_4F\text{-}p)_2\}]^+$	1886(vs)	1940(s)	415 698	2.063	450

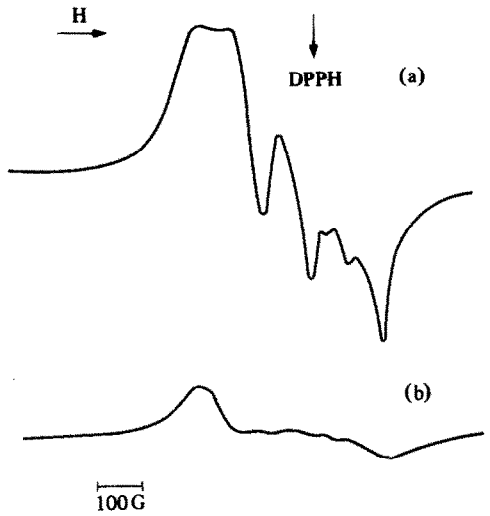

Fig. 4. ESR spectra recorded in CH_2Cl_2 solution containing $[NBu_4](ClO_4)$ (0.1 mol dm^{-3}) and **3** (0.153 mmol) after the exhaustive one-electron oxidation at +0.85 V. (a) 100 K; (b) room temperature.

manence at room temperature of the paramagnetism of the rhenium(II) species has been representatively tested in some cases by the Evans Method[21] ($\mu_{eff} = 2.0\ \mu_B$ for $|\mathbf{3}|^+$ and $1.9\ \mu_B$ for $|\mathbf{7}|^+$, consistent with the presence of one unpaired electron).

The bulk of the IR, UV-Visible and ESR data, characteristic for the rhenium(II) complexes, are reported in Table 2.

As expected, the $\nu_{(CO)}$ stretching vibrations of the rhenium(II) species are shifted towards higher frequencies in respect to the parent rhenium(I) compounds as a consequence of the increased positive charge on the metal centre.

ADDITIONAL REMARKS

The electrogenerated rhenium(II) complexes are appreciably stable only at temperatures lower than 0°C. At higher temperatures two parallel reactions appear to take place: (i) a photochemically[3] and/or thermally induced self-reduction to the starting rhenium(I) complex and (ii) an intramolecular oxidation of the non-innocent formamidine, or triazenide ligands by the rhenium(II) centre, followed by partial decomplexation of both CO and oxidized pseudoallyl ligands.

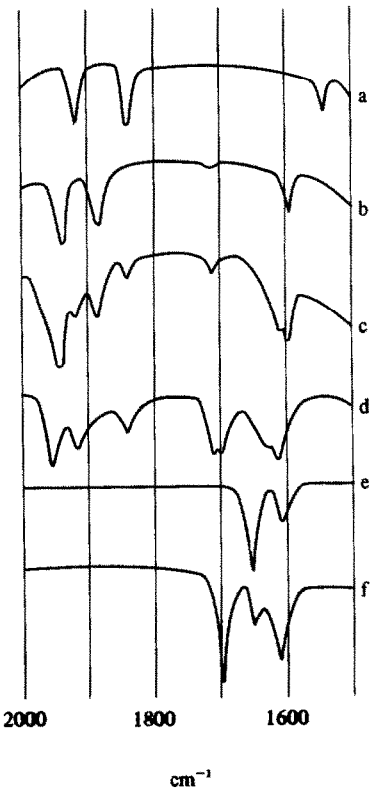

Fig. 5. IR spectra recorded in CH_2Cl_2 solution containing $[NBu_4](ClO_4)$ (0.1 mol dm^{-3}) under the following experimental conditions: (a) $[Re(CO)_2(PPh_3)_2\{CH(NC_6H_4Me\text{-}p)_2\}]$ starting derivative; (b) after exhaustive 1 e^-/molecule electrolysis at +0.75 V at 0°C in the sunlight; (c) leaving the solution resulting from (b) at 0°C in the sunlight for 2 h; (d) after 150 h at +5°C in the dark; (e) free-*p*-tolylformamidine; (f) after anodic oxidation (0.65 e^-/molecule formamidine) at +1.2 V.

$[Re(CO)_2(PPh_3)_2\{CH(NC_6H_4Me\text{-}p)_2\}]^+$ and $[Re(CO)_2(PPh_3)_2\{N(NC_6H_4Me\text{-}p)_2\}]^+$ were chosen to search for the instability of the rhenium(II) complexes presented here.

Figure 5 shows the IR spectra recorded on the electrogenerated rhenium(II)-*p*-tolyl-formamidinato complex under different experimental conditions. At the bottom of the figure the spectrum of the electro-oxidized ($E_W = +1.3$ V) free formamidine ligand is also reported.*

On standing at 0°C in the sunlight, or at +5°C in the dark, a slow regeneration of the starting rhenium(II) complex occurs (CO bands at 1837 and 1916 cm^{-1}), accompanied by restoration of a golden yellow colour. In addition the oxidation of the formamidine ligand following the intramolecular process is shown by the band centred at 1700 cm^{-1}. Cyclic voltammetry on the electrolysed solution,

* The anodic oxidation in CH_2Cl_2–$[NBu_4](ClO_4)$ (0.1 mol dm^{-3}) of free formamidine or free triazenido ligands is an elecrode poisoning process, and very frequent rinsing of the platinum macroelectrode with H_2SO_4 (conc.) is needed. During the electrolysis, the colourless formamidine turns to yellow, whereas the yellow triazene turns to red–amaranth.

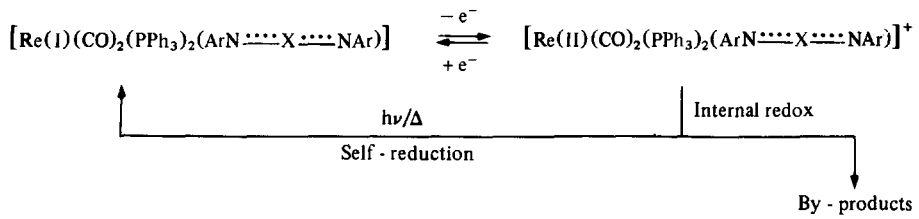

Scheme 1.

maintained for 150 h at +5°C in the dark, demonstrated the regeneration of about 15% of the starting rhenium(II) complex. A predominant cathodic process, due to a totally irreversible process, is also present at $E_p = -0.9$ V, which, if compared to the similar process for oxidized free formamidine (occurring at −0.8 V), is attributable to the reduction of oxidized pseudoallyl ligand in the rhenium by-product.

A qualitatively similar behaviour has been observed in the decomposition of the *p*-tolyl triazenido rhenium(II) complex, followed again at +5°C. In this case the slow intramolecular oxidation of the triazene ligand is demonstrated by the appearance of an IR band at 1586 cm^{-1}, comparable with the absorption at 1582 cm^{-1} typical for the anodically oxidized ($E_W = +1.4$ V) free *p*-tolyltriazene.* Also in this case the internal oxidation is concomitant with the gradual reappearance of the two bands at 1921 and 1848 cm^{-1} from the self-reduction process leading to the starting rhenium(II) complex.

It must however be noted that the triazenido–rhenium(II) complex is less kinetically labile than the corresponding formamidinato complex. In fact after 200 h at +5°C, about 20% of starting rhenium(I) complex is regnerated, but with variance of the formamidinato derivative, about 15% of the rhenium(II) complex is still present.

In conclusion, two competing processes appear to be responsible for the instability of the herein presented rhenium(II) complexes; they account for the electrode mechanism operative at room temperature and are shown in Scheme 1.

It can be observed that the increase in temperature notably favours the framework-destroying intramolecular oxidation in respect to the self-reduction process (which would maintain a catalytic current), if only 1.6–1.8 e^-/molecule are spent at room temperature in the electrolysis at the first anodic process. We underline that self-reduction processes, photochemically and/or thermally induced, are not unknown.[22] Unfortunately, we did not succeed in a more detailed identification of the products from the internal redox process, because of the failure in separating them from the supporting electrolyte.

EXPERIMENTAL

Materials

The starting formamidinato and triazenido rhenium(I) complexes have been prepared according to literature methods.[15] Dichloromethane, acetonitrile and acetone solvents (Burdick and Jackson, distilled in glass, UV grade) were used as received.

Tetrabuthylammonium perchlorate (Fluka) and tetraethylammonium perchlorate (Carlo Erba) supporting electrolytes were dried and stored in a vacuum oven at 50°C. Bis(η^5-cyclopentadienyl) iron(II)(ferrocene) (Alfa-Products) was used as an internal standard.

Nitrogen (99.99%) was employed to remove oxygen from the tested solutions.

Apparatus

The electrochemical apparatus has been described elsewhere.[23] The formal electrode potentials reported here are believed to be accurate to ±0.02 V. Potential values refer to an aqueous calomel electrode (SCE). Under the present experimental conditions the ferrocene/ferrocenium couple occurs at: +0.49 V in dichloromethane, +0.38 V in acetonitrile and +0.51 V in acetone. The room temperature was controlled at 20±0.1°C.

The IR absorption spectra were recorded on a Model 782 Perkin–Elmer grating spectrophotometer. UV-Visible absorption spectra were recorded with a Model 200 Perkin–Elmer spectrophotometer. ESR experiments were performed with an X-band ER 200D-SRC Bruker spectrometer, and the temperature was controlled (±1°K) with a Bruker Variable Temperature Unit ER 4111 VT. The NMR susceptibility shift method was employed to test the paramagnetism of some rhenium(II) solutions (see text), immediately after

* See footnote on p. 199.

their electrogeneration by bulk electrolysis, using Me_4Si as the reference signal.

Acknowledgement—We are indebted to Dr Claudio Rossi (University of Siena) for assistance with the NMR spectra.

REFERENCES

1. J. Chatt, C. M. Elson, N. E. Hooper and G. J. Leigh, *J. Chem. Soc., Dalton Trans.* 1975, 2392.
2. P. M. Treichel and J. P. Williams, *J. Organomet. Chem.* 1977, **135**, 39.
3. A. M. Bond, A. R. Colton and M. E. McDonald, *Inorg. Chem.* 1978, **17**, 2842.
4. A. J. L. Pombeiro, C. J. Pickett and R. L. Richards, *J. Organomet. Chem.* 1982, **224**, 285.
5. J. V. Caspar and T. J. Meyer, *J. Phys. Chem.* 1983, **87**, 952.
6. R. Seeber, G. A. Mazzocchin, U. Mazzi, E. Roncari and F. Refosco, *Transition Met. Chem.* 1984, **9**, 315 and refs therein.
7. J. V. Caspar, B. P. Sullivan and T. J. Meyer, *Inorg. Chem.* 1984, **23**, 2104.
8. C. J. Cameron, S. M. Tetrik and R. Walton, *Organometallics* 1984, **3**, 240.
9. K. R. Dumbar and R. A. Walton, *Inorg. Chim. Acta* 1984, **87**, 185.
10. J. Chatt, J. R. Dilworth and G. J. Leigh, *J. Chem. Soc., Dalton Trans.* 1973, 612.
11. J. Chatt, J. R. Dilworth, H. P. Gunz and G. J. Leigh, *J. Organomet. Chem.* 1974, **64**, 245.
12. C. A. Hertzer, R. E. Myers, P. Brant and R. A. Walton, *Inorg. Chem.* 1978, **17**, 2383.
13. J. D. Allison, P. E. Fanwick and R. A. Walton, *Organometallics* 1984, **3**, 1515.
14. S. Bucknor, F. A. Cotton, L. R. Falvello, A. H. Reid, Jr and C. D. Schmulbach, *Inorg. Chem.* 1986, **25**, 1021.
15. R. Rossi, A. Duatti, L. Magon and L. Toniolo, *Inorg. Chim. Acta* 1981, **48**, 243.
16. R. Graziani, L. Toniolo, U. Casellato, R. Rossi and L. Magon, *Inorg. Chim. Acta* 1981, **52**, 119.
17. R. Rossi, A. Duatti, L. Magon, U. Casellato, R. Graziani and L. Toniolo, *Inorg. Chim. Acta* 1983, **75**, 77.
18. R. Rossi, A. Duatti, L. Magon, A. Marchi, A. Medici, M. Fogagnolo, U. Casellato and R. Graziani, *Transition Met. Chem.* 1985, **10**, 413.
19. E. R. Brown and R. F. Large, *Physical Methods of Chemistry, Part IIA, Electrochemical Methods*, Vol. 1. Wiley-Interscience, New York (1971).
20. H. B. Mark Jr, L. J. Papa and C. N. Reilley, *Advances in Analytical Chemistry and Instrumentation*, Vol. 2, p. 318. Wiley-Interscience, New York (1963).
21. D. F. Evans, *J. Chem. Soc.* 1959, 2003.
22. P. Zanello, C. Bartocci, A. Maldotti and O. Traverso, *Polyhedron* 1983, **2**, 791.
23. D. Osella, R. Gobetto, P. Montangero, P. Zanello and A. Cinquantini, *Organometallics* 1986, **5**, 1247.

Polyhedron Vol. 7, No. 3, pp. 203–206, 1988
Printed in Great Britain

0277–5387/88 $3.00+.00
© 1988 Pergamon Journals Ltd

THE KINETICS OF COBALT(II) COMPLEXATION WITH *o*-PHTHALATE IN AQUEOUS SOLUTION

SOCK SUNG YUN,* KI YOUNG CHOI† and CHONG HOE PARK

Department of Chemistry, Chungnam National University, Daejon 300-31, Korea

(*Received* 9 *April* 1987; *accepted after revision* 26 *August* 1987)

Abstract—The rate constants for the formation and dissociation of cobalt(II) complexes with *o*-phthalate in aqueous solution have been determined by a pressure-jump technique. The forward and reverse rate constants obtained are $k_f = 1.1 \times 10^6$ M^{-1} s^{-1} and $k_r = 1.6 \times 10^3$ s^{-1} at 25°C, respectively. The activation parameters of the reaction were also obtained from the temperature variation study. The results indicate that chelate ring closure and rupture are affected by the rigidity of the benzene ring of the ligand, and thus the rate determining step of the reaction is the chelate ring closure process.

The kinetics of fast metal complex formation reactions have been extensively studied.[1–7] However, the studies have been concentrated mostly on the complexation reactions of the nickel(II) ion with a variety of ligands. The results have indicated that the multiple step mechanism is operative for the complexation reactions of the nickel(II) ion. In this mechanism the release of a water molecule from the inner coordination sphere of the cation is usually considered as the rate determining step. It has been generally known that the rates of complex formation reactions of the cobalt(II) ion are about one order faster than those of the nickel(II) ion.[1]

In the series of kinetic studies on the complex formation reactions of nickel(II) and cobalt(II) ions with aminocarboxylic acids, Kustin *et al.*[7–9] have observed that the dependence of the rate constants of the complex formations on the nature of the ligand is more significant for the cobalt(II) ion compared to those for the nickel(II) ion. Kinetic data[2,3,10,11] of the complexation reactions of nickel(II) and cobalt(II) ions with various kinds of dicarboxylates have also shown a similar trend with the aminocarboxylate systems. It is likely that cobalt(II) substitution reactions are sterically controlled by chelate ring closing, while the rate determining step for the nickel(II) ion is the solvent exchange process.

To confirm the sterically controlled reaction mechanism for the cobalt(II) ion complex formation reaction, we have carried out a kinetic study for the cobalt(II) *o*-phthalate system using a pressure-jump method. The *o*-phthalate ligand is particularly interesting since the rigidity of the aromatic ring is expected to influence the rate of chelate ring formation.

EXPERIMENTAL

All of the chemicals used were of reagent grade. A stock solution of cobalt(II) *o*-phthalate was prepared by mixing stoichiometric amounts of cobalt sulphate with the acid. The sulphate ion was precipitated out as insoluble barium sulphate by titrating the solution with a standard solution of barium hydroxide. The solid barium sulphate was removed by filtration. The concentration of cobalt(II) ion in the stock solution was determined by an I.C.P Atomic Emission Spectrometer. The working solutions were prepared by diluting the stock solution to desired concentrations. The pH's of the solutions were in the range 6.4–6.5, in which most of the ligand dissociates to the anionic form.

The pressure-jump apparatus constructed is similar to that described elsewhere.[12] The rise time of the apparatus measured by a 0.2 M nickel sulphate solution was found to be 50 μs. The relaxation time for the cobalt(II) *o*-phthalate system was deter-

* Author to whom correspondence should be addressed.
† Present address: Department of Chemistry, Mokwon College, Daejon 300-00, Korea.

mined at 20, 25 and 30°C for four different concentrations. The concentration of the species in each solution was calculated from stability constant data which had been obtained at $\mu \rightarrow 0$.[13]

RESULTS AND DISCUSSION

A relaxation time characterized by a single relaxation step was observed for all of the solutions. The complex formation reaction of the cobalt(II) ion with *o*-phthalate may be expressed as

$$M^{2+} + L^{2-} \underset{k_r}{\overset{k_f}{\rightleftharpoons}} ML \qquad (1)$$

where M^{2+} and L^{2-} represent the cobalt(II) cation and *o*-phthalate anion, respectively. The forward and reverse rate constants (k_f and k_r) are related to the relaxation time (τ) by eq. (2),

$$\frac{1}{\tau} = k_f f_{\pm}^2 (\bar{C}_{M^{2+}} + \bar{C}_{L^{2-}}) + k_r \qquad (2)$$

where $\bar{C}$ indicates the equilibrium concentrations of the species and $f_{\pm}$ is the mean activity coefficient of the free ions. The activity coefficients of the ions are estimated from the Davies equation.[14] Since equilibrium concentrations of ionic species in the solution are less than 10^{-2} M, the following Davies equation could be safely applied.

$$\log f_i = -0.5 Z_i^2 \left(\frac{\sqrt{\mu}}{1+\sqrt{\mu}} - 0.2\mu \right) \qquad (3)$$

where Z_i is the charge of the ith ion and μ is the ionic strength of the solution. Introducing the thermodynamic formation constant K_{eq}, eq. (2) can be written as

$$\frac{1}{\tau} = k_f f_{\pm}^2 (\bar{C}_{M^{2+}} + \bar{C}_{L^{2-}}) + \frac{k_f}{K_{eq}} \qquad (4)$$

where $K_{eq} = k_f/k_r$.

The forward and reverse rate constants for the cobalt(II) *o*-phthalate reaction were calculated using eq. (4). The literature value of K_{eq}[13] was used for the calculation of k_f and k_r. A typical set of the relaxation data is given in Table 1. Table 2 shows the average values of the experimentally determined forward and reverse rate constants for the reaction at three different temperatures.

The activation parameters were obtained from the Arrhenius plot of the rate constants against $1/\tau$ and general kinetic equations. They are given in Table 3.

The multiple step mechanism for the metal complexation reaction with the polydentate ligand is described by

$$M^{2+}_{(aq)} + L^{2-}_{(aq)} \underset{k_{21}}{\overset{k_{12}}{\rightleftharpoons}} W_2MW_1L \qquad (5)$$

(I)

$$\underset{k_{32}}{\overset{k_{23}}{\rightleftharpoons}} W_2M\text{-}L \underset{k_{43}}{\overset{k_{34}}{\rightleftharpoons}} ML_{(aq)}$$

(II) (III)

where W_1 and W_2 are the cation-coordinated water molecules. The first step is the diffusion controlled approach of two hydrated ions to form the outer sphere complex. The second step involves the loss of a water molecule from the inner hydration sphere of the metal ions and the formation of the mono-substituted metal complex. The third step is the formation of the fully chelated complex. With a

Table 1. Relaxation times and k_f for cobalt(II) *o*-phthalate at $\mu \rightarrow 0$

Temperature (°C)	$(\bar{C}_{M^{2+}} = \bar{C}_{L^{2-}}) \times 10^3$ (M)	$\mu \times 10^3$	$f_{\pm}$	$1/\tau \times 10^{-3}$ (s^{-1})	$k_f \times 10^{-6}$ ($M^{-1}\,s^{-1}$)
20	1.56	6.25	0.72	2.22	0.70
20	1.35	5.39	0.74	2.15	0.71
20	1.23	4.91	0.75	2.11	0.72
20	0.97	3.86	0.77	2.03	0.76
25	1.54	6.16	0.72	3.33	1.08
25	1.33	5.30	0.74	3.18	1.09
25	1.21	4.84	0.75	3.08	1.09
25	0.96	3.82	0.77	2.94	1.13
30	1.51	6.03	0.72	4.88	1.64
30	1.30	5.21	0.74	4.65	1.65
30	1.19	4.75	0.75	4.55	1.67
30	0.94	3.75	0.77	4.35	1.73

Table 2. Rate constants and stability constants of cobalt(II) *o*-phthalate complexation at $\mu \to 0$

Temperature (°C)	$k_f \times 10^{-6}$ ($M^{-1}\,s^{-1}$)	$k_r \times 10^{-3}$ (s^{-1})	$K_{eq} \times 10^{-2}$[13] (M^{-1})
20	0.72±0.04	1.12±0.06	6.47
25	1.10±0.04	1.62±0.06	6.77
30	1.67±0.08	2.33±0.12	7.17

Errors indicated are two standard deviations.

steady state assumption on the species W_2MW_1L and W_2M-L, the overall rate constants are related to individual rate constants as

$$k_f = K_o k_{23}\left(\frac{k_{34}}{k_{32}+k_{34}}\right) \text{ and } k_r = k_{32}\left(\frac{k_{43}}{k_{32}+k_{34}}\right) \quad (6)$$

where $K_o = k_{12}/k_{21}$.

If $k_{34} \gg k_{32}$, eq. (6) is reduced to $k_f = K_o k_{23}$ and $k_r = k_{32}/K_3$ with $K_3 = k_{34}/k_{43}$. If K_o is known, k_{23} can be estimated. The ion pair formation constant K_o at $\mu \to 0$ was estimated theoretically by the Fuoss equation.[15] The Fuoss equation derived on statistical grounds is,

$$K_o = \frac{4\pi N a^3}{3000} e^b \quad (7)$$

where N is Avogadro's number, a is the distance of the closest approach of two ions, and b is the Bjerrum ratio between potential and kinetic energy;

$$b = \frac{|Z_M Z_L| e_o^2}{aDkT} \quad (8)$$

where Z_M and Z_L are the ionic charges, D is the dielectric constant, and k is the Boltzmann constant. K_o at $\mu \to 0$ was calculated to be 46 M^{-1}. In the calculation, a was assumed to be 8 Å which had been obtained semi-empirically by Kustin *et al.*[7] The value of k_{23} calculated for the cobalt(II) *o*-phthalate system is about two orders smaller than the water exchange rate constant[16] ($k_w = 2.6 \times 10^6$ s^{-1}) of cobalt(II) ion. This fact would suggest that the rate determining step of the reaction is not the loss of the first water molecule from the inner coordination sphere of the cobalt(II) ion. When $k_{32} \gg k_{34}$, eq. (6) becomes $k_f = K_o K_2 k_{34}$ and $k_r = k_{43}$ with $K_2 = k_{23}/k_{32}$. Since K_o is constant for the ligand systems with the same negative charge, the values of k_f would be the relative rates of the chelate formation if K_2 does not significantly vary with the variation of the nature of ligands. The value of k_r becomes an exclusive function of the first bond breaking of the chelate ring. If these assumptions are correct, the value of k_f for cobalt(II) *p*-phthalate is about one order smaller than those of the malonate and malate.[10] The overall forward rate constants (k_f)[10] for cobalt(II) malonate and cobalt(II) malate have been reported to be 2.7×10^7 M^{-1} s^{-1} and 2.1×10^7 M^{-1} s^{-1}, respectively. This fact means that chelate ring formation of the *o*-phthalate is the most sterically hindred.

Table 3. Kinetic data for the cobalt(II) *o*-phthalate complex formation at 25°C and $\mu \to 0$

k_f, $M^{-1}\,s^{-1}$	$(1.10\pm0.04)\times10^6$
k_r, s^{-1}	$(1.62\pm0.06)\times10^3$
E_f^*, Kcal mol^{-1}	14.84±0.33
ΔH_f^*, Kcal mol^{-1}	14.25±0.53
ΔS_f^*, cal K^{-1} mol^{-1}	16.90±1.70
ΔG_f^*, Kcal mol^{-1}	9.20±1.04

In order to make a direct comparison of the kinetic data between the dicarboxylate systems, we evaluated the equilibrium and kinetic parameters of each individual step of the cobalt(II) *o*-phthalate complexation reaction. Yasunaga *et al.*[10] have derived the semi-empirical relationship between k_{32} and pK_a for the cobalt(II) dicarboxylate system as

$$\log(k_{32}/1.7\times10^6) = -0.22(pK_a - 4.75). \quad (9)$$

Using the eqs (6) and (9), the values of k_{32}, k_{34} and k_{43} were calculated. The solvent exchange rate constant for the cobalt(II) ion, $k_w = 2.6 \times 10^6$ s^{-1} was assumed as k_{23}.

The equilibrium and kinetic data of each individual step of cobalt(II) *o*-phthalate are given in Table 4 along with those of the malonate, malate and glycolate for comparison. The value of k_{34} is about two orders smaller than that of k_{23} for the *o*-phthalate system. This is evidence that the chelate ring formation process is the rate determining step for the cobalt(II) *o*-phthalate complexation reaction also. Similar analysis of kinetic data of the nickel(II) *o*-phthalate system showed that the solvent exchange step is the rate determining step for the complexation.[3] This difference in the mechanism between the nickel(II) and cobalt(II) ion systems would be due to the rate of the solvent exchange step in the cobalt(II) ion is much faster than that in the nickel(II) ion. $k_w = 2.7 \times 10^4$ s^{-1} for nickel(II) ion has been reported.[1] Both rate constants (k_{34} and k_{43}) for the chelate ring closure and rupture of cobalt(II) *o*-phthalate are the smallest among the carboxylate systems given in Table 4. The slowest rate of chelate ring formation of the *o*-phthalate may be due to the larger ring size of the seven-

Table 4. Rate and equilibrium constants of each individual step of the multiple step complex formation of cobalt(II) *o*-phthalate at 25°C and $\mu \rightarrow 0$

Ligand	K_0 (M^{-1})	K_2	K_3	k_{32} (s^{-1})	k_{34} (s^{-1})	k_{43} (s^{-1})	Reference
Malonate	46	2.4	4.0×10^1	1.1×10^6	3.2×10^5	7.9×10^3	8
Malate	46	1.8	2.7×10^1	1.4×10^6	3.0×10^5	1.1×10^4	8
Glycolate	7.7	1.0	1.8×10^1	2.7×10^6	1.2×10^6	6.6×10^4	8
o-Phthalate	46	2.2	6.9	1.2×10^6	1.1×10^4	1.6×10^3	This work

membered chelate. Once the chelate ring is formed in the case of *o*-phthalate, the ring is extraordinary stabilized since the two carboxylate groups are oriented nearer to each other in a planar structure by the rigidity of the benzene ring of the ligand. Thus, the rate of the chelate ring rupture of the *o*-phthalate is slower than those of other carboxylates. A similar argument has been applied to explain the general trend that the stability of the transition metal(II) *o*-phthalate is greater than that of the corresponding succinate.[13] In the case of the malate system in which the rate of the chelate ring formation is relatively faster, the hydroxyl group of the ligand may play a vital role in the complex formation.

Acknowledgement—This work was supported by a grant from Korea Science and Engineering Foundation.

REFERENCES

1. K. Kustin and J. Swinehart, *Prog. Inorg. Chem.* 1970, **13**, 107.
2. S. Harada, K. Amidaiji and T. Yasunaga, *Bull. Chem. Soc. Jap.* 1972, **45**, 1752.
3. S. Harada, H. Tanabe and T. Yasunaga, *ibid* 1973, **46**, 2450.
4. S. Harada, Y. Okuue, H. Kan and T. Yasunaga, *ibid* 1974, **47**, 769.
5. K. Tamura, S. Harada and T. Yasunaga, *ibid* 1977, **50**, 2317.
6. S. S. Yun and J. L. Bear, *J. Inorg. Nucl. Chem.* 1976, **38**, 1041.
7. K. Kustin and J. L. McClean, *J. Phys. Chem.* 1978, **82**, 2549.
8. K. Kustin, R. F. Pasternack and E. M. Weinstock, *J. Am. Chem. Soc.* 1966, **88**, 4610.
9. A. Kowalak, K. Kustin, R. F. Pasternack and S. Petrucci, *J. Am. Chem. Soc.* 1967, **89**, 3126.
10. S. Harada, M. Kawasawa and T. Yasunaga, *Bull. Chem. Soc. Jap.* 1980, **53**, 2074.
11. J. L. Bear and C. T. Lin, *J. Phys. Chem.* 1968, **72**, 2026.
12. G. Macri and S. Petrucci, *Inorg. Chem.* 1970, **9**, 1009.
13. I. R. Desai and V. S. K. Nair, *J. Chem. Soc.* 1962, 2360.
14. C. W. Davies, *Ion Association*. Butterworths, London (1962).
15. R. M. Fuoss, *J. Am. Chem. Soc.* 1958, **80**, 5059.
16. A. H. Zeltmann, N. A. Matwiyoff and L. O. Morgan, *J. Phys. Chem.* 1969, **73**, 2689.

Polyhedron Vol. 7, No. 3, pp. 207–211, 1988
Printed in Great Britain

0277–5387/88 $3.00+.00
© 1988 Pergamon Journals Ltd

PHOTOCHEMISTRY OF PLANAR FOUR-COORDINATE PALLADIUM(II) COMPLEXES—IV. PHOTOCHEMICAL BEHAVIOUR OF *TRANS*-[Pd(PPr^n_3)(PYRIDINE-4-ALDEHYDE-4-NITROPHENYLHYDRAZONE)Cl_2] IN VARIOUS SOLVENTS

S. CAMPAGNA, M. CUSUMANO, A. GIUFFRIDA, G. GUGLIELMO† and V. RICEVUTO

Dipartimento di Chimica Inorganica e Struttura Molecolare, Università di Messina, via dei Verdi, 98100 Messina, Italy

(*Received* 24 *April* 1987; *accepted after revision* 26 *August* 1987)

Abstract—The photochemical and photophysical behaviour of the complex *trans*-[Pd(PPr^n_3)(4-PAP-NO_2)Cl_2] (4-PAP-NO_2 = pyridine-4-aldehyde-4-nitrophenylhydrazone) has been investigated in various solvents. Under irradiations of different wavelengths, in the region of the lowest intraligand transition, photoisomerization of the coordinated ligand from a *syn* to an *anti* configuration occurs, and for each excitation wavelength a photoequilibrium is gained. Quantum yields for the process depend both on the energy of irradiation and on the solvent used; in all cases the quantum yields are lower than those corresponding to the free ligand. The complex emits at room temperature in acetonitrile solution, and emission spectra (also at 77K), excitation spectra and emission lifetime have been studied. The emission can probably be ascribed to a π–π^* fluorescence.

We have previously studied some isomerization processes on square planar palladium(II) complexes of the type $[Pd(AAA)NO_2]^+$ (AAA = dien, Et_4dien, $MeEt_4$dien) and *trans*-[Pd(PPr^n_3)$_2X_2$] (X = Cl, Br, I, NO_2, NCS).[1–4]

We have now extended our research to the complexes containing *n*-PAP ligands (*n*-PAP = pyridine-*n*-aldehyde-phenylhydrazone; *n* = 2, 3, 4) in order to study the effect of the coordination to metal on the *syn–anti* photoisomerization of the ligand. It is known, in fact, that *syn*-(*n*-PAP) ligands isomerize to the *anti* forms when irradiated with suitable energy light[5] (see Scheme 1). One more aim of this study is to scan the potential ability of these complexes as intramolecular photosensitizers for intraligand reactions. Moreover, we have observed luminescence for some of these complexes in fluid solution at room temperature. This circumstance could make them useful for photophysical studies of d^8 square planar complexes, less explored from this point of view[6–10] with respect to the octahedral complexes, in spite of the recent growing interest on the photophysical properties of coordination compounds, for both theoretical reasons[11–20] and potential applications.[21–26]

In this paper we report a photochemical and photophysical investigation of *trans*-[Pd(PPr^n_3)(4-PAP-NO_2)Cl_2] (4-PAP-NO_2 = pyridine-4-aldehyde-4-nitro-phenylhydrazone), in which the ligand 4-PAP-NO_2, in contrast to the generally preferred N-imine site,[27,28] is coordinated to the transition metal atom through the pyridinic nitrogen.

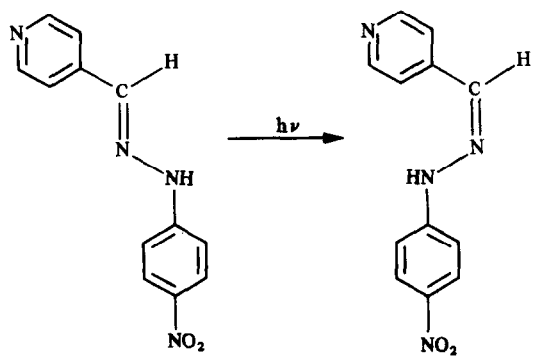

Scheme 1.

† Author to whom correspondence should be addressed.

EXPERIMENTAL

Preparation of syn-(4-PAP-NO_2) *and of its complex*

The ligand *syn*-(4-PAP-NO_2) was prepared by the classical condensation between 4-nitro-phenylhydrazine and pyridine-4-aldehyde in methanol solution and in the presence of acetic acid. A brown solid was immediately obtained and recrystallized from ethanol. The complex was prepared by cleavage of the halide bridge complex $[Pd(PPr^n_3)_2Cl_2]_2$ with the ligand (molecular ratio 1 : 2) in an acetone–chloroform mixture, under magnetic stirring for 24 h. The solvent was removed under reduced pressure and the yellow–orange residue was recrystallized from methanol–acetone solution. Elemental analysis was in agreement with expected percentage values.

Preparation of anti-(4-PAP-NO_2) *and of its complex*

The *anti* isomers both of ligand and complex were prepared by irradiation of methanol solutions of the respective *syn* isomers with non-filtered light and successive separation by alumina column chromatography, using chloroform as eluent. All the compounds were characterized by spectroscopic data.

Spectrophotometric measurements in the UV-Visible region were performed with a Perkin–Elmer Lambda 5 spectrophotometer, equipped with a thermostatted cell compartment. Monochromatic light of 333, 365 and 405 nm was obtained from a high pressure Hanau Q 400 mercury lamp and appropriate Bausch and Lomb filters. Solutions of the complexes in the range of concentrations 10^{-4}–10^{-5} mol dm^{-3} were irradiated at 25°C in standard spectrophotometric cells and periodically taken to the spectrophotometer for recording. The quantum yield measurements were based on a ferric oxalate actinometer.[29] In determining quantum yields, the isomerizations were carried to very low conversion (1–6%) to prevent the necessity of a back correction. The determinations were done in triplicate. A Perkin–Elmer LS-5 spectrofluorimeter was used to obtain uncorrected emission and corrected excitation spectra. Excitation was performed in the high intensity band at 395 nm. Emission was monitored at the emission spectra maximum, 490 nm. Emission lifetime measurements were carried out with JK System 2000 neodymium DLPY lasers (estimated errors $\pm 10\%$).

All the solvents used were commercial products of reagent grade, dried and freshly distilled, except for luminescence measurements, in which acetonitrile of the best commercial grade was used. For the low temperature experiments the solvent chosen was a propionitrile–butyronitrile (4 : 5 v/v) mixture because of the transparency of the matrix.

RESULTS AND DISCUSSION

It is known that the photoisomerization studies of most of the compounds containing the C=N group are complicated by the extremely low energy barrier between the *syn* and *anti* isomers, that rapidly leads the reaction products back to the reagents by thermal return. Hydrazone derivatives of aromatic aldehydes and ketones, for which thermal conversion is hampered, are therefore preferred for this purpose.

In the *trans*-$[Pd(PPr^n_3)(4\text{-PAP-}NO_2)Cl_2]$ complex the presence of a heteroatom in the aldehyde skeleton means the coordination to the metal occurs at the N pyridine site, as already shown by X-ray investigation performed on the closely related *trans*-$[Pd(PPr^n_3)(4\text{-PAP})Cl_2]$,[27] in contrast to the imine coordination typical for hydrazone ligands.[28] This type of coordination preserves the isomerization process, and offers the possibility of studying the effect of coordination to palladium on the photochemical process.

The absorption spectrum of the complex shows an intense absorption band centred at 382 nm, in benzene, assigned to the lowest π–π^* transition, red-shifted relative to the corresponding band for the uncoordinated ligand, as expected for the LC transitions (LC = ligand centred) in coordination compounds.[30] The weaker absorptions in the region 280–310 nm are probably due to overlaps of ligand field and spin allowed n–π^* transitions from the imine nitrogen fragment. The absorption spectrum of the complex shows a solvent dependence: the absorption maximum shifts to lower energy when the solvent polarity increases, ranging from 382 nm in benzene to 395 nm in acetonitrile. This suggests that a different polarity exists between ground and excited states.[31] The spectral changes of the complex under irradiation (Fig. 1) are characteristic of intraligand isomerization.[5] In addition the complex with the ligand coordinated in the *anti* configuration was the only species isolated in preparative experiments. The absorption of the π–π^* transition shows a blue-shift and a decreased intensity for the *anti* isomer relative to the *syn* isomer according to the lower planarity of the *anti* complex.[5] This is probably the consequence of the steric hindrance between the hydrogen atom in the *ortho* position with respect to the amide group in the pyridine ring, and the hydrogen atom of the phenylhydrazone fragment.

The comparison between the photoisomerization

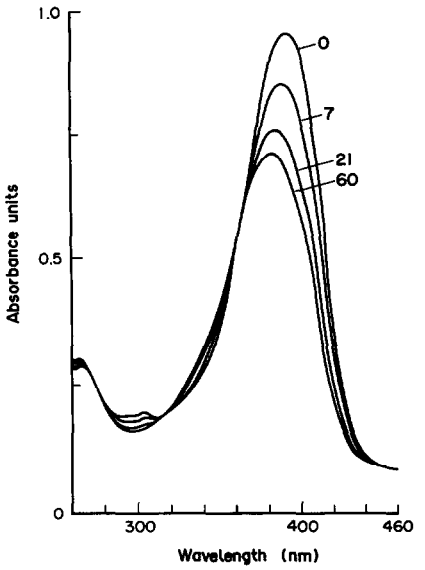

Fig. 1. Spectral changes of the complex with the *syn* ligand coordinated under irradiation (405 nm) in chloroform. The irradiation times (in seconds) are depicted in the figure. Times of irradiation longer than 60 s have caused no further significant variations.

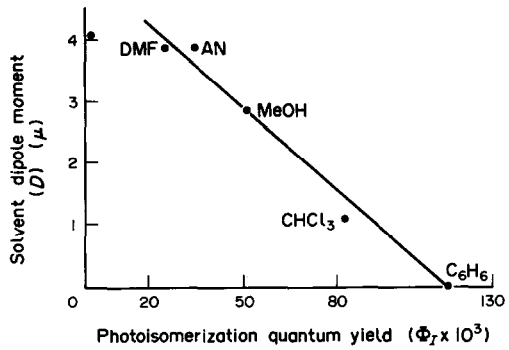

Fig. 2. Quantum yields for the photoisomerization process vs dipole moment of the solvents.

quantum yields in methanol of the complex and of the free ligand (Table 1) shows that the coordination of 4-PAP-NO_2 to palladium causes a decrease in the isomerization process. Furthermore, the quantum yields are clearly dependent on the solvent nature (Table 2); the trend in quantum yields makes clear that the polarity of the solvent is an inhibiting factor for the *syn–anti* isomerization pathway. On plotting these values against the solvents' dipole moments μ, a linear relationship is obtained (Fig. 2).

This solvent dependence can be accounted for by taking into account that the radiationless deactivation pathway of the excited state can be affected in a significant way by the nature of the solvent and, in our case, by the influence of the solvent on the energy gap between the states involved in the process. In fact, since in our case the polarity of the excited state is larger than the polarity of the ground state, as the solvent dependence of the absorption maximum seems to indicate, the excited state is preferentially stabilized with respect to the ground state by surrounding solvent dipoles,[9,31] and the radiationless rate constant increases as the solvent polarity increases (energy gap law[32,33]). So, the decrease of the experimental quantum yields with the solvent dipole moment would arise from the increase of alternative deactivation paths, rather than from a direct lowered efficiency of the isomerization process.

On performing excitation with different wavelengths, the photoequilibrium ratio varies, and the quantum yields increase on increasing the irradiation energy, the nature of the corresponding electronic transition remaining the same (see Tables 1 and 2).

It is interesting to note that the presence in solution of a triplet quencher such as oxygen does not

Table 1. Quantum yields for the photoisomerization processes and photoequilibrium compositions at different wavelengths in methanol. *a* and *s* are respectively the *anti* and *syn* isomers; data for the free ligand are reported for comparison

	Free ligand		Complex		Photoequilibrium composition (%)	
λ_{ex} (nm)	*s*—*a*	*a*—*s*	*s*—*a*	*a*—*s*	free ligand	complex
333	0.173	0.305	0.080	0.210	*a*: 53.20 *s*: 46.80	*a*: 38.20 *s*: 61.80
365	0.088	0.080	0.051	0.065	*a*: 52.60 *s*: 47.40	*a*: 34.68 *s*: 65.32
405	0.057	0.010	0.037	0.015	*a*: 74.90 *s*: 25.10	*a*: 52.10 *s*: 47.90

Table 2. Quantum yields of the *syn–anti* photoisomerization for the complex *trans*-[Pd(PPr^n_3)(4-PAP-NO_2)Cl_2] at different energy irradiations in various solvents

Solvent	λ_{ex} = 405 nm	λ_{ex} = 365 nm	λ_{ex} = 333 nm
DMSO	0.005	0.020	0.035
N,N′-DMF	0.007	0.025	0.038
CH_3CN	0.0015	0.034	0.048
CH_3OH	0.0037	0.051	0.081
$CHCl_3$	0.065	0.082	0.102
C_6H_6	0.094	0.116	0.130

affect the quantum yields; this circumstance rules out a triplet state as a state involved in the photoisomerization pathway.

In the light of the experimental results, a vibrationally upper excited state of the lowest singlet ligand centred excited state could be responsible for the photoisomerization process.

The palladium(II) investigated in this study emits at room temperature in acetonitrile solution, with λ_{max} for the emission at 490 nm (uncorrected spectrum, Fig. 3). The corrected excitation spectrum closely matches its absorption spectrum in the region 230–460 nm. The emission spectrum at 77K shows a single, intense band with a maximum at 460 nm.

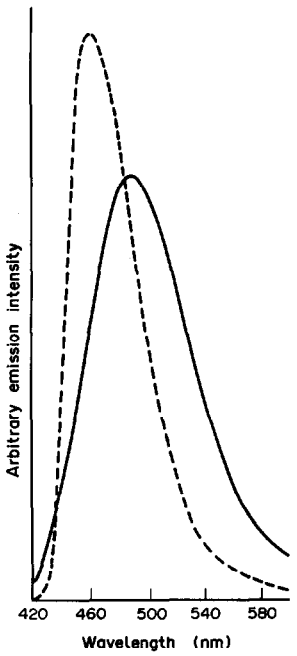

Fig. 3. Emission spectra of the complex in acetonitrile at room temperature (solid line) and in butyronitrile/propionitrile 5 : 4 v/v mixture at 77K (dashed line). λ_{ex} = 395 nm.

Based upon the low temperature emission spectrum, we estimate a O—O energy of about 22,000 cm^{-1} for the emitting state. Given the short emission lifetime at room temperature (330 ns in acetonitrile aerated solution) and the modest shift from the position of the π–π^* fluorescence of the free ligand, the emission can be assigned to a ligand centred fluorescence.

Work is in progress to clarify the relations between fluorescence and photochemical properties. Studies on closely related complexes in which the NO_2 group is replaced by other substituents with different electronic withdrawing ability, or others in which the position of the nitrogen atom in the pyridine ring is changed, could be useful to give more information on the factors that control photophysical and photochemical properties in these types of d^8 transition metal complexes. They can also be used to investigate their possible ability as intramolecular or intermolecular photosensitizers.

Acknowledgement—The authors thank the photochemistry group of the Dipartimento Chimico "G. Ciamician" of Bologna University for provision of luminescence equipment.

REFERENCES

1. L. Costanzo, A. Giuffrida, G. Guglielmo and V. Ricevuto, *Inorg. Chim. Acta* 1978, **33**, 29.
2. M. Cusumano, G. Guglielmo, V. Ricevuto, S. Sostero, O. Traverso and T. J. Kemp, *J. Chem. Soc., Dalton Trans.* 1981, 302.
3. G. Bombieri, G. Bruno, M. Cusumano, G. Guglielmo and V. Ricevuto, *Polyhedron* 1985, **4**, 1365.
4. G. Guglielmo, V. Ricevuto, P. Bergamini, S. Sostero and O. Traverso, *J. Organomet. Chem.* 1984, **276**, 281.
5. G. Condorelli, L. Costanzo, L. Alicata and A. Giuffrida, *Chem. Lett.* 1975, 227 and refs therein.
6. A. Vogler, H. Hunkely and B. Ratwisch, *Inorg. Chim. Acta* 1980, **46**, 101.

7. D. Eastwood and M. Gouterman, *J. Mol. Spectros.* 1970, **35**, 359.
8. T. Kobayashi, K. D. Staub and P. M. Rentzepis, *Photochem. Photobiol.* 1979, **29**, 925.
9. M. Maestri, D. Sandrini, V. Balzani, L. Chassot, P. Jolliet and A. von Zelewsky, *Chem. Phys. Lett.* 1985, **122**, 375.
10. Y. Wakatsuki, H. Yamakazi, P. A. Grutsch, M. Santhanam and C. Kutal, *J. Am. Chem. Soc.* 1985, **107**, 8153.
11. J. N. Demas, *J. Chem. Educ.* 1983, **60**, 803.
12. G. A. Crosby, *Acc. Chem. Res.* 1975, **8**, 321.
13. M. K. De Armond and C. M. Carlin, *Coord. Chem. Rev.* 1981, **36**, 325.
14. T. J. Meyer, *Pure Applied Chem.* 1986, **58**, 1193.
15. T. J. Kemp, *Progr. React. Kinet.* 1980, **10**, 301.
16. R. J. Watts, *J. Chem. Educ.* 1983, **60**, 834.
17. F. Scandola and V. Balzani, *J. Chem. Educ.* 1983, **60**, 814.
18. M. K. De Armond, K. W. Hanck and D. W. Wertz, *Coord. Chem. Rev.* 1985, **64**, 65.
19. G. A. Crosby, R. J. Watts and D. H. W. Carstens, *Science* 1970, **170**, 1195.
20. J. E. Baggot, G. K. Gregory, M. J. Pilling, S. Anderson, K. R. Seddon and J. E. Turp, *J. Chem. Soc., Faraday Trans. II* 1983, **79**, 195.
21. M. Graetzel (Ed.), *Energy Resources through Photochemistry and Catalysis*. Academic Press, New York (1983).
22. J. S. Connolly (Ed.), *Photochemical Conversion and Storage of Solar Energy*. Academic Press, London (1981).
23. V. Balzani, F. Bolletta, M. Ciano and M. Maestri, *J. Chem. Educ.* 1983, **60**, 447.
24. V. Balzani, F. Bolletta, M. T. Gandolfi and M. Maestri, *Top. Curr. Chem.* 1978, **75**, 1.
25. K. Kalianasundaram, *Coord. Chem. Rev.* 1982, **46**, 149.
26. V. Balzani, A. Juris, F. Barigelletti, P. Belser and A. von Zelewsky, *Riken Q* 1984, 78.
27. G. Bruno (unpublished work).
28. B. Galli, F. Gasparrini, L. Maresca, G. Natile and G. Palmieri, *J. Chem. Soc., Dalton Trans.* 1983, 1483 and refs therein.
29. G. C. Hatchard and C. A. Parker, *Proc. Roy. Soc., Sect. A* 1956, **235**, 518.
30. A. P. B. Lever, *Inorganic Electronic Spectroscopy*, 2nd Edn. Elsevier, Amsterdam (1984).
31. E. M. Kober, B. P. Sullivan and T. Meyer, *Inorg. Chem.* 1984, **24**, 2098 and refs therein.
32. N. J. Turro, *Modern Molecular Photochemistry*. Benjamin Cummings, Menlo Park, California (1978).
33. S. H. Lin, *Radiationless Transition*. Academic Press, New York (1980).

Polyhedron Vol. 7, No. 3, pp. 213–217, 1988
Printed in Great Britain

0277–5387/88 $3.00+.00
© 1988 Pergamon Journals Ltd

EQUILIBRIUM STUDIES ON THE FORMATION OF NITRITE COMPLEXES OF THE DIVALENT d^{10} ACCEPTORS

F. BEDIA ERIM and EFRAIM AVŞAR*

Department of Chemistry, Technical University of Istanbul, Maslak, 80626 Istanbul, Turkey

(*Received* 7 *April* 1987; *accepted after revision* 1 *September* 1987)

Abstract—The results of equilibria studies on the step-wise formation of complexes in an aqueous solution of unit ionic strength between sodium nitrite and Zn(II), Cd(II) and Hg(II) perchlorates are reported. The formation constants have been determined potentiometrically at 298K. Mononuclear complexes are formed in all cases. Values of the overall constants for the formation of $Zn(NO_2)^+$, $Zn(NO_2)_2$, $Cd(NO_2)^+$, $Cd(NO_2)_2$, $Hg(NO_2)^+$, $Hg(NO_2)_2$, $Hg(NO_2)_3^-$ and $Hg(NO_2)_4^{2-}$ are found to be 2.37 ± 0.03 M^{-1}, 3.1 ± 0.1 M^{-2}; 35 ± 1 M^{-1} $(6.8\pm0.1)\times10^2$ M^{-2}; $(8.76\pm0.15)\times10^5$ M^{-1} $(8.22\pm0.09)\times10^9$ M^{-2} $(2.85\pm0.02)\times10^{11}$ M^{-3} and $(7.31\pm0.03)\times10^{11}$ M^{-4} respectively.

The most striking feature of the nitrite anion as a ligand is that it shows linkage isomerism. It can be bonded to a metal ion via either the oxygen or the nitrogen atom. Thus, the metal ions can display their selective affinities to different donor atoms. Consequently, nitrito and/or nitro complexes can be formed. An interesting group to study in this connection is the divalent ions of electron configuration d^{10}, viz. Zn(II), Cd(II) and Hg(II), as their coordination behaviour varies very much within the group. Besides, since all of them contain completed *d*-shells no ligand field stabilization effects are to be considered. Within this group the softness rapidly decreases from the very soft Hg(II) to the intermediate Cd(II) and to the distinctly hard Zn(II).

The formation of nitrite complexes of Hg(II) and Zn(II) seems to have not been studied, while the data available for the Cd(II) system are rather few.[1]

Like the previous work in this series,[2] the present one was performed in an aqueous medium of unit ionic strength with sodium perchlorate as supporting electrolyte at 298.15K.

* Author to whom correspondence should be addressed.

EXPERIMENTAL

Chemicals

Zn(II) perchlorate, zinc amalgam, sodium perchlorate and the Ag, AgCl electrodes were prepared, and analysed as before.[3] Cd(II) perchlorate was prepared by dissolving cadmium carbonate (Merck, p.a.) in perchloric acid (Merck, p.a.). In order to avoid hydrolysis a small excess of the acid was added.[4] The cadmium concentration was determined by titration with EDTA using Erio-T as an indicator. A standard stock Hg(II) perchlorate solution was prepared by dissolving a weighed amount of red HgO (Merck, p.a.) in a standard perchloric acid solution. Sodium nitrite was prepared and analysed as described previously.[2]

Measurements

The procedure and the measurement technique have been described elsewhere.[2,3,5] The e.m.fs of the following cell were measured.

−Pt, Zn(Hg) or Cd-specific electrodes	C_M M $Me(ClO_4)_2$ C_L M $NaNO_2$ $NaClO_4$ to $I = 1.0$ M	1.0 M $NaClO_4$	0.025 M NaCl 0.975 M $NaClO_4$	Ag,AgCl+

where Me denotes Zn or Cd.

For the Hg(II)–nitrite system, on the other hand, the galvanic cell was of the following type:

−Ag,AgCl	0.025 M NaCl 0.975 M $NaClO_4$	1.0 M $NaClO_4$	C_M M $Hg(ClO_4)_2$ C_H M $HClO_4$ C_L M $NaNO_2$ $NaClO_4$ to $I = 1$ M	glass electrode+.

A Metrohm E580 ion-activity meter and/or E500 digital pH meter were used for the potentiometric measurements. The glass electrode was a Metrohm EA109 with a slope of 59.2 ± 0.2 mV. It has been checked and found that Cd-specific (Metrohm EA306-Cd) and zinc amalgam electrodes obey Nernst's law.

During the titrations of Zn(II) and Cd(II) systems, all the solutions were deaerated and mixed by a stream of oxygen-free nitrogen, which was first bubbled through 1.0 M $NaClO_4$ solutions in order to obtain the correct vapour pressure. The potentials reached their equilibrium values very quickly and the reproducibility was in general within ± 1 mV for Zn(II) and much better, i.e. ± 0.2 mV, for Cd(II) measurements. In the case of Hg(II), on the other hand, a magnetic stirrer was used for mixing. Stable e.m.fs were attained in a few minutes with a reproducibility of ± 0.2 mV.

Calculation

The consecutive formation constants have been evaluated both graphically and numerically. The graphical method has been described elsehwere.[2,5,6] For the numerical calculations Sandell's least squares program "UNINUX"[7] has been used.

RESULTS

Zn(II)–nitrite system

For this system the most favourable method for the determination of the constants of weak complexes, i.e. measurement of the free metal ion concentrations by means of the zinc amalgam electrodes can be applied. Since the zinc amalgam electrode is very sensitive to oxidation, any trace of oxygen has to be excluded.

The measurements were arranged as titrations where the solutions in the left-hand half-cell (*vide supra*) were obtained by adding a known volume v(ml) of a ligand solution to V_0 ml of Zn(II) perchlorate solution. Five different titrations series with values of C_M varying from 10 to 40 mM were used. In order to avoid the initial hydrolysis of the zinc ions the pH of the solutions was kept between 4 and 5.

The calculations indicated the formation of two mononuclear complexes of fairly weak strength. Evaluation of the overall constants gave $\beta_1 = 2.37 \pm 0.03$ M^{-1} and $\beta_2 = 3.1 \pm 0.1$ M^{-2}. The complex formation function and the distribution of two complexes, computed from this set of constants, are shown in Figs 1 and 2(a). The values of the average ligand number $\bar{n}$ obtained from the slopes of the C_L *vs* C_M lines[6] deviate at higher ligand concentrations. This deviation is probably due to changes in the activity coefficients caused by complex formation and by the progressive exchange of ClO_4^- for NO_2^- during the titrations.

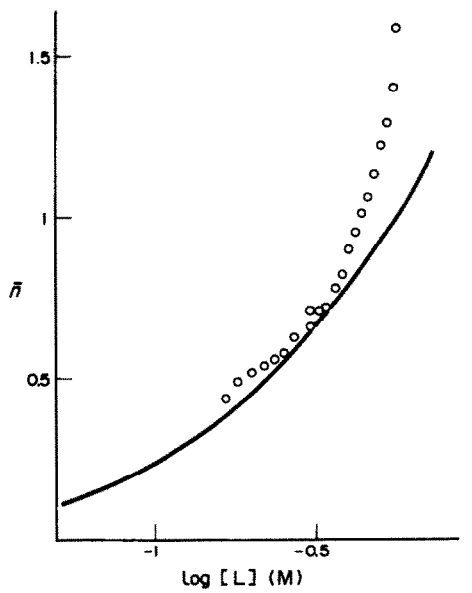

Fig. 1. Complex formation function of the Zn(II)–nitrite system. Values of $\bar{n}$ obtained from the slopes of the (C_L, C_M)-lines denoted by (○).

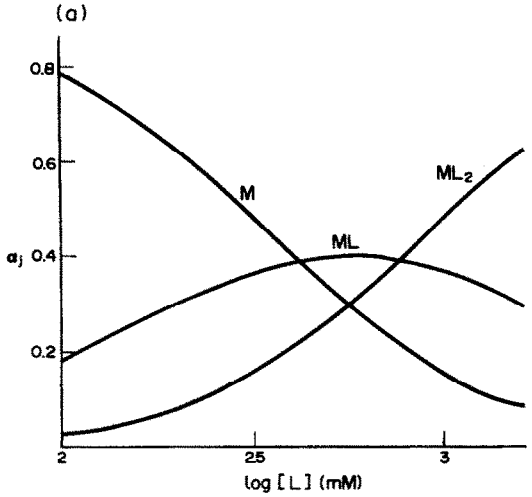

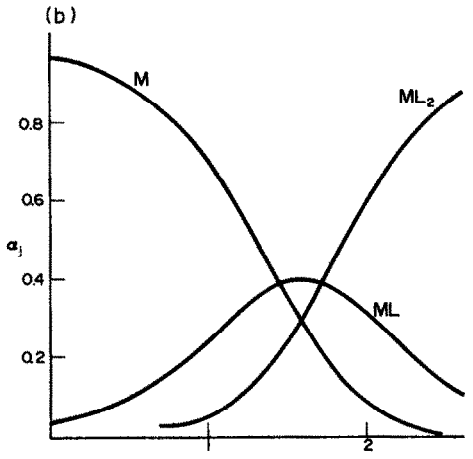

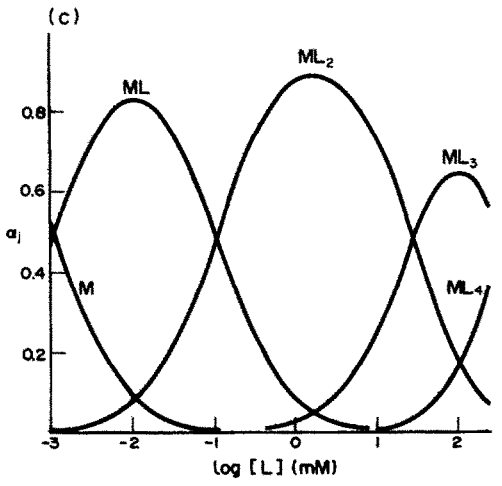

Fig. 2. Distribution of Zinc(II). (a) cadmium(II); (b) and mercury(II); (c) between the different ML_j complexes with varying nitrite ion concentration ([L] in mM).

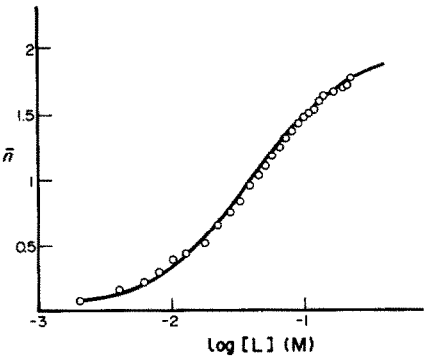

Fig. 3. Complex formation function of the Cd(II)–nitrite system.

Cd(II)–nitrite system

Four different cadmium solutions with values of C_M varying from 5 to 30 mM were employed. Values of the pH of these solutions were *ca.* 5. Higher values of pH can be applied since the Cd(II) ion is a weaker acid than the Zn(II) ion. Besides, stronger complexes are formed in this case.

The graphical evaluation of the formation constants indicates three mononuclear complexes. In the numerical calculation, however, a good fit to the potentiometric data required only two complexes. In the range of [L] studied, a third complex ML_3 will form to a rather small extent. The potentiometric data are best described if only two mononuclear complexes, with $\beta_1 = 35 \pm 1$ and $\beta_2 = (6.8 \pm 0.1) \times 10^2\ M^{-2}$, are considered. In spite of differences of medium and/or technique, these results are very compatible with those reported in the literature.[1]

The complex formation curve, calculated from the constants, and the values of $\bar{n}$ obtained from the slopes of the (C_L, C_M)-lines[5] are shown in Fig. 3. The distribution of cadmium between the different complexes, computed from this set of constants, is given in Fig. 2(b).

Hg(II)–nitrite system

Potentiometric measurements by means of a glass electrode were carried out on ten different titrations series with C_M varying from 2 to 15 mM. The acid concentrations, constant during the titrations, were kept high in order to prevent the hydrolysis of Hg(II); C_H/C_M ratios were varied from 2 to 5. A free ligand ion concentration up to $\simeq$ 170 mM could be reached in the measurements.

The constants were evaluated both graphically and numerically. Both methods gave concordant estimates. In the range of [L] studied, no evidence

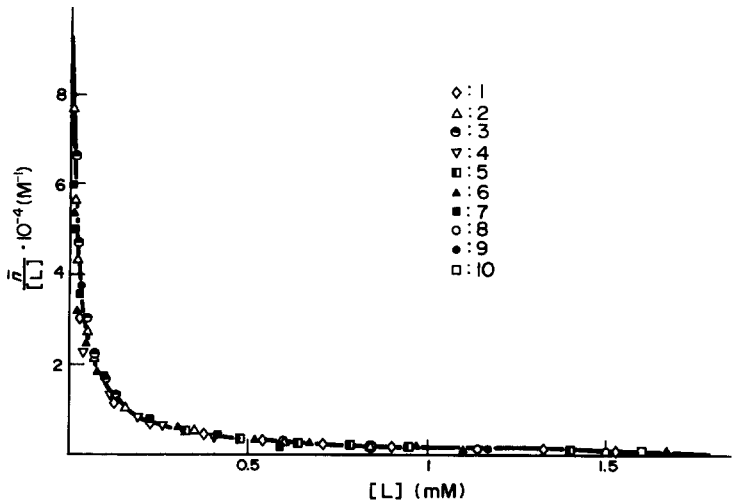

Fig. 4. Plot of $\bar{n}/[L]$ vs [L] for the Hg(II)–nitrite system. 1: $C_M = 2.072$ mM, $C_H = 6.708$ mM; 2: $C_M = 5.015$ mM, $C_H = 16.445$ mM; 3: $C_M = 10.32$ mM, $C_H = 34.116$ mM; 4: $C_M = 14.754$ mM, $C_H = 49.302$ mM; 5: $C_M = 10.30$ mM, $C_H = 24.516$ mM; 6: $C_M = 5.015$ mM, $C_H = 11.748$ mM; 7: $C_M = 5.18$ mM, $C_H = 22.804$ mM; 8: $C_M = 10.30$ mM, $C_H = 33.277$ mM; 9: $C_M = 5.09$ mM, $C_H = 22.531$ mM; 10: $C_M = 10.30$ mM, $C_H = 33.55$ mM. Only half of the experimental points, chosen at random, have been plotted.

has been found for the formation of polynuclear or acid complexes. The $\bar{n}/[L]$ vs [L] plot is shown in Fig. 4 and the complex formation function, i.e. $\bar{n}$ vs log [L], is plotted in Fig. 5. The full-drawn curves in both figures have been computed from the sets of constants found for this system (see Table 1).

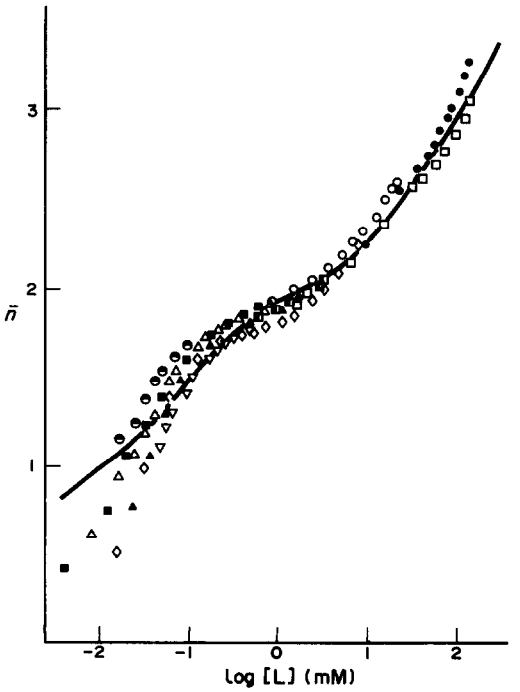

Fig. 5. Complex formation function of the Hg(II)–nitrite system. For symbols refer to Fig. 3 ([L] in mM).

Both evaluation methods gave four mononuclear complexes. The distribution of these complexes between the different ML_j species are drawn in Fig. 2(c).

It has to be pointed out that the experimental uncertainties in the determination of the value of β_1 for $Hg(NO_2)^+$ is large due to relatively weak formation of the competitive reaction $H^+ + NO_2^- \rightleftharpoons HNO_2$. The formation constant for this reaction has been found[2] to be $9.71 \times 10^2\ M^{-1}$. Comparing this value with $\beta_1 = 8.76 \times 10^5\ M^{-1}$ for the formation of $Hg(NO_2)^+$, one easily sees that practically only the formation of the strong $Hg(NO_2)^+$ complex takes place during the titrations. The change in the free acid concentration is not large enough to allow a better evaluation of both [L] and $\bar{n}$ in this range. As a result of this, a usually higher value of β_1 results from the measurements (*cf.* Fig. 5). The results of the present work are collected in Table 1.

DISCUSSION

For the divalent d^{10} acceptors the order of increasing softness is Zn(II) < Cd(II) ≪ Hg(II). Along this series of acceptors the covalency increases and the tendency for ionic bond formation decreases. The nitrite anion is ambidentate. It can coordinate an acceptor either via N or O. As a very soft acceptor one might expect that Hg(II) would prefer coordination through the N-atoms, while

Table 1. Overall formation constants and values of $\Delta G_j^{\ominus}$ for the consecutive steps of the Zn(II)–, Cd(II)– and Hg(II)–nitrite systems at 298.15 K and $I = 1.0$ M: errors given correspond to confidence limits at the 99.9% level of significance

System	j	β_j (M^{-j})	$-\Delta G_j^{\ominus}$ (kJ mol^{-1})
Zn(II)–nitrite	1	2.37 ± 0.03	2.14 ± 0.03
	2	3.1 ± 0.1	0.67 ± 0.09
Cd(II)–nitrite	1	35 ± 1	8.81 ± 0.07
	2	$(6.8 \pm 0.1) \times 10^2$	7.36 ± 0.08
Hg(II)–nitrite	1	$(8.76 \pm 0.15) \times 10^5$	33.92 ± 0.04
	2	$(8.22 \pm 0.09) \times 10^9$	22.67 ± 0.05
	3	$(2.85 \pm 0.02) \times 10^{11}$	8.79 ± 0.04
	4	$(7.31 \pm 0.03) \times 10^{11}$	2.34 ± 0.02

the hard Zn(II) prefers the harder O-atoms. The borderline acceptor Cd(II) is expected to have much the same affinity for both donor atoms. Neutron diffraction and X-ray studies on the tetranitrite $M(NO_2)_4^{2-}$ anionic complexes show that these divalent acceptors are bonded through both O-atoms in the solid state.[8,9,10]

The strong increase of stability in the order Hg(II) $\gg$ Cd(II) > Zn(II) is presumably due to the strong covalent bond formation. This is especially the case for the Hg(II) system. During the formation of the first two nitrite complexes, mercury(II) becomes virtually dehydrated. For ligands forming strongly covalent bonds a switch of the original aqua octahedral coordination to the final tetrahedral complex probably takes place when the first ligand has entered the coordination sphere of Hg(II).[11]

Acknowledgement—We are much indebted to Dr Arvid Sandell from the University of Lund, Lund, Sweden, for helpful comments and the most valuable help with computer calculations.

REFERENCES

1. R. M. Smith and A. E. Martell, *Critical Stability Constants*, Vol. 4. Plenum, New York (1976).
2. E. Avşar and F. B. Erim, *Polyhedron* 1986, **5**, 1335.
3. S. Ahrland and E. Avşar, *Acta Chem. Scand.* 1975, **A29**, 890.
4. G. Biedermann and L. Ciavatta, *ibid.* 1962, **16**, 2221.
5. S. Ahrland, E. Avşar and L. Kullberg, *ibid.* 1974, **A28**, 855.
6. S. Fronaeus, in H. B. Jonassen and A. Weisberger, *Techniques of Inorganic Chemistry*, Vol. 1, Chap. 1. Interscience, New York (1963).
7. A. Sandell (personal communication).
8. L. F. Power, J. A. King and F. H. Moore, *J. Chem. Soc., Dalton Trans.* 1976, 93.
9. D. Hall and R. V. Holland, *Inorg. Chim. Acta* 1969, **3**, 235.
10. M. A. Hitchman and G. L. Rowbottom, *Coord. Chem. Rev.* 1982, **42**, 55.
11. S. Ahrland, *Struct. Bonding* 1973, **15**, 167.

Polyhedron Vol. 7, No. 3, pp. 219–221, 1988
Printed in Great Britain

0277–5387/88 $3.00 + .00
Pergamon Journals Ltd

SYNTHESIS AND CHARACTERIZATION OF DICHLORODICARBONYLRUTHENIUM(II) COMPLEXES OF NAPHTHISOXAZOLE AND OTHER DONOR LIGANDS

A. O. BAGHLAF,* M. ISHAQ, S. A. RAHMAN, A. B. AL-TAHIR, A. ZAIDAN and R. A. KABLI

King Abdulaziz University, College of Science, Department of Chemistry, P.O. Box 9028, Jeddah 21413, Saudi Arabia

(*Received* 26 *June* 1987; *accepted* 1 *September* 1987)

Abstract—Complexes of dichlorodicarbonylruthenium(II) of the formula $[RuCl_2(CO)_2L_2]$ where L = naphthisoxazole (NISOX), 2-aminobenzthiazole (ABTZ), allylthiourea (ATU), thioacetamide (TAM) and triphenylphosphite (TPT) have been prepared and characterized by IR, NMR and elemental analysis. All the complexes were fairly stable solids and can be handled in air for a short time.

The preparation of dichlorodicarbonylruthenium (II) were reported by Manchot and Konig[1] and it was in the early 1960's when the importance of ruthenium and its derivatives was realized by a number of research groups. Wilkinson and co-workers[2,3] have reported compounds of the type $[RuCl_2(CO)_2L_2]$ where L = triphenylphosphine and other monodentate ligands. Some of the catalytic applications of this complex for hydrogenation has also been reported.[4] This is due to the fact that dihalodicarbonylruthenium(II) has proved to be a very useful precursor for the synthesis of a variety of complexes.

We have recently reported such complexes containing oxygen, sulphur and nitrogen donor ligands.[5] In our continued research in this area we now report the preparation of complexes with naphthisoxazole and other neutral ligands as shown in Table 1.

The metal atom Ru in the compound $[RuCl_2(CO)_2]_n$ acts as an electron acceptor. This enhances its ability to coordinate with electron donor ligands to yield stable and electron rich compounds of low ionization energy.

RESULTS AND DISCUSSION

All the ligands used in this work act as monodentate and react with the complex $[RuCl_2(CO)_2]_n$ in a 1 : 2 mole ratio respectively.

The ligand naphthisoxazole on treatment with $[RuCl_2(CO)_2]_n$ in THF deposited a small quantity of yellow crystals which showed identical IR spectrum and m.p. (163–164°C) with the product obtained from the main reaction mixture although it was a pale yellow powder.

The IR spectra of all the complexes (**2**)–(**6**) show only two strong bands in the region of 2000 cm^{-1} indicating that the terminal metal carbonyls M—CO are *cis*.[6] The decrease in the νM—CO stretching frequency in all the complexes is due to metal–ligand complexation. The IR spectrum of complex (**2**) shows that there is a small decrease (~ 5 cm^{-1}) in the ν-C=N-stretching frequency compared with the free ligand. Therefore, it is suggested that the coordination of the ligand naphthisoxazole to Ru may be through the N atom. Further, the NMR spectrum of the complex shows that the methine proton (H—C=N—) appeared at δ 9.9, compared to the free ligand which was at (δ 9.8), see Table 3. This shift may be attributed to the deshielding effect due to the coordination through N to the metal as shown in Fig. 1. The IR spectrum of complex (**3**) showed a decrease of ~ 100 cm^{-1} in the region of the νN—H stretching frequency indicating that it is coordinated to the metal through the N atom of the ($—NH_2$) group of the ligand 2-aminobenzthiazole. Similarly the IR spectrum of complex (**4**) shows that the ligand allylthiourea is coordinated to the metal through N, as the complex shows a decrease of more than (100 cm^{-1}) in νN—H stretching frequency compared

* Author to whom correspondence should be addressed.

Table 1. Analytical data (%)

No.	Compound	Expected C	Expected H	Expected N	Found C	Found H	Found N	Colour
1	$[RuCl_2(CO)_2]_n$	10.5	—	—	10.8	—	—	Yellow
2	$RuCl_2(CO)_2(NISOX)_2$	50.8	2.4	4.9	50.3	2.5	4.7	Yellow
3	$RuCl_2(CO)_2(ABTZ)_2$	39.9	3.0	10.6	41.0	3.2	10.0	Grey
4	$RuCl_2(CO)_2(ATU)_2$	26.1	3.5	12.1	26.6	3.8	12.0	Yellow
5	$RuCl_2(CO)_2(TAM)_2$	20.3	2.6	7.4	21.1	2.9	7.5	Yellow
6	$RuCl_2(CO)_2P(OPh)_3$	53.8	4.5	—	54.7	4.4	—	Yellow

Table 2. IR spectra[a]

No.	Compound	νM—CO	νC=N	νN—H	Other bands
1	$[RuCl_2(CO)_2]_n$	2145, 2075, 2020, 2080, 2020[b]	—	—	
2	$RuCl_2(CO)_2(NISOX)_2$	2060, 2000	1622 (1627)[F]	—	3050, 1575, 1527, 1428, 1245, 1173, 895, 805, 772, 750
3	$RuCl_2(CO)_2(ABTZ)_2$	2062, 1990	1608 (1632)[F]	3282, (3385)[F] 3180, (3260)[F]	3060, 1535, 1513, 1450, 1340, 1030, 750, 720
4	$RuCl_2(CO)_2(ATU)_2$	2040, 1980	—	3280, 3185, (3430)[F], (3220)[F] (3170)[F]	1610, 1555, 1040, (1055)[F] 985, 880, (920)[F], 717
5	$RuCl_2(CO)_2(TAM)_2$	2063, 1996	—	3300, (3300)[F] 3170, (3080)[F]	1640, 1470, 1370, 1160, 970, (1025)[F], 700, (710)[F]
6	$RuCl_2(CO)_2P(OPh)_3$	2070, 1990	—	—	3060, 1210, 1185, 1155, 920, 760, 685

[a] = KBr pellets.
[b] = Chloroform solution.
[F] = Free ligand.

with the free ligand. On the other hand complex (5) does not show a significant change in the νN—H stretching frequency. Thus the possibility of its coordination through the S atom cannot be ruled out.[7] See Table 2. The elemental analysis of all the complexes are given in Table 1 and are consistent with the proposed formulations.

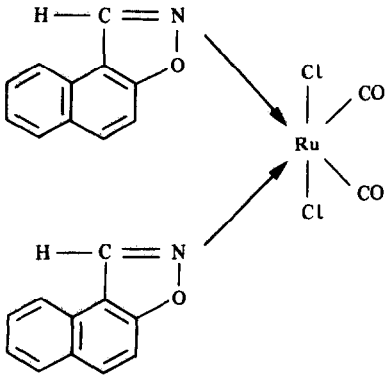

Fig. 1. L = naphthisoxazole, 2-aminobenzthiazole, N-allylthiourea, thioacetamide or triphenylphosphite.

EXPERIMENTAL

The salt $RuCl_3 \cdot xH_2O$ and all the ligands used in this work were purchased from Fluka Inc. The ligand naphthisoxazole was prepared as reported in the literature.[8] All the IR spectra were measured as KBr pellets using Pye–Unicam Spectrophotometer Model SP-1100. Proton magnetic resonance spectra were recorded on a Varian EM-390-90MHz NMR spectrometer. Elemental analyses were carried out by the Microanalysis Laboratory of King Abdulaziz University, Jeddah. The complex $[RuCl_2(CO)_2]_n$ was prepared by the procedure reported elsewhere.[9]

Table 3. Proton magnetic resonance spectra[a]

No.	Compound	Chemical shift (δ)	Relative intensity	Multiplicity	Assignment
1	$RuCl_2(CO)_2(NISOX)_2$ (in $CDCl_3$)	9.9	1	1	HC=N
		8.1	2	Multiplet	Naphthalene ring
		7.7	4	Multiplet	
2	$RuCl_2(CO)_2(ABTZ)_2$ (in $CDCl_3$)	7.45	—	Broad	NH_2+benzthiazole ring
3	$RuCl_2(CO)_2(ATU)_2$ (in $CDCl_3$)	8.1	3	Broad	NH_2+NH
		5.8	1	Multiplet	—CH=
		5.3	2	Multiplet	CH_2
		4.1	2	Multiplet	$=CH_2$
4	$RuCl_2(CO)_2(TAM)_2$ (in $CDCl_3$)	9.5	2	Broad	$-NH_2$
		2.7	3	S	$-CH_3$
5	$RuCl_2(CO)_2P(OPh)_3$ (in $CDCl_3$)	7.3		S	$P(OC_6H_5)_3$

[a] Using TMS as internal reference.

Preparation of dichlorodicarbonyl-bis-naphthisoxazole ruthenium (**11**)

A typical reaction is described. In a small two neck round bottom flask fitted with a water condenser and magnetic stirrer was added 200 mg (1.2 mmol) $[RuCl_2(CO)_2]_n$ dissolved in 20 cm^3 THF. To this was added 360 mg (2.2 mmol) of naphthisoxazole. The mixture was gently refluxed for 1 h. During this period some bright yellow crystals were deposited in the flask. These crystals were filtered and washed with pet. ether and dried *in vacuo*. The main THF solution was reduced to a small volume and the addition of pet. ether (b.p. 30–40°C) caused the separation of a pale yellow solid. This was washed with pet. ether and dried *in vacuo*. The IR spectra of both the solids were identical and they have the same m.p. (163–164°C). In another attempt the THF solution was passed through an alumina column and on elution with chloroform gave a yellow band. This was collected and addition of pet. ether gave a pale yellow powder. This powder showed identical IR spectrum and m.p. as the above samples.

All the complexes were prepared as described above giving yellow or pale yellow solids except complex (**3**) which was a grey solid and was sensitive to light.

Acknowledgement—A.B.T. and A.Z. thank KAU for financial support.

REFERENCES

1. W. Manchot and J. Konig, *Chem. Ber.* 1924, **57B**, 2130.
2. T. A. Stephenson and G. Wilkinson, *J. Inorg. Nucl. Chem.* 1966, **28**, 945.
3. J. V. Kingston, T. W. S. Jamieson and G. Wilkinson, *J. Inorg. Nucl. Chem.* 1967, **29**, 133.
4. D. R. Fahey, *J. Org. Chem.* 1973, **38**, 3343.
5. A. O. Baghlaf, M. Ishaq and A. K. A. Rashed, *Polyhedron* 1986, **6**, 837.
6. J. M. Jenkins, M. S. Lupin and B. L. Shaw, *J. Chem. Soc. A.* 1966, 1787.
7. L. J. Bellamy, *The Infrared Spectra of Complex Molecules*. Chapman and Hall, London (1975).
8. R. A. Kabli, S. Abdul Rahman and A. B. El-Tahir, *Bull. Fac. Sci. KAU*, 1983, **7**, 151.
9. M. J. Cleare and W. P. Griffith, *J. Chem. Soc. A* 1969, 372.

Polyhedron Vol. 7, No. 3, pp. 223–227, 1988
Printed in Great Britain

0277–5387/88 $3.00+.00
© 1988 Pergamon Journals Ltd

INTERMEDIACY OF NITRENE IN THE CURTIUS-TYPE REARRANGEMENT OF PHOSPHINIC AZIDES. INSIGHTS FROM *AB INITIO* STUDY OF THE $H_2P(=O)—N \rightleftharpoons HP(=O)=NH$ INTERCONVERSION

MINH THO NGUYEN†

Research School of Chemistry, Australian National University, Canberra, ACT 2601, Australia

and

N. J. FITZPATRICK‡

Department of Chemistry, University College, Belfield, Dublin 4, Ireland

(*Received* 23 *July* 1987; *accepted* 1 *September* 1987)

Abstract—*Ab initio* calculations on the model phosphinic nitrene $H_2P(=O)—N \rightleftharpoons$ oxoiminophosphorane $HP(=O)=NH$ interconversion in both lower-lying singlet and triplet states at the UMP4SDQ/6-31++G* level using the HF/3-21G*-optimized geometries are reported. The results support the proposition that the Curtius-type rearrangement of phosphinic azide (azidophosphine oxide) occurs via a non-nitrene mechanism in its singlet ground state. However, if the starting material could be sensitized photochemically into its triplet excited state, then the nitrene could be formed and the Curtius-type rearrangement would not be observed.

The Curtius rearrangement has been known since 1890[1] when the formation of isocyanates from acyl azides was reported (eqn (1)).

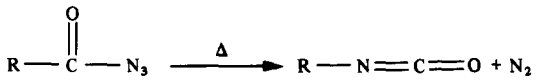

(1)

Subsequently, this reaction has been established as an efficient route for the preparation of imines (eqn (2)).[2]

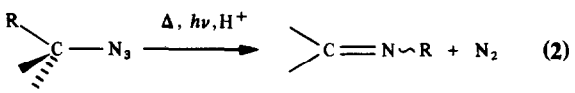

(2)

More recently, the rearrangement has been further generalized involving azides of heavier main group elements[3] (eqn (3)).

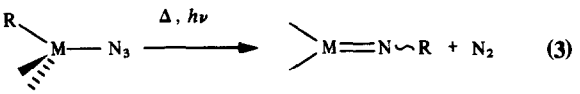

(3)

M = B, Si, Ge, P, As

In the phosphorus series, the photolysis of phosphinic azides **1** (azidophosphine oxides) has been recognized as a general method for the synthesis of transient oxoiminophosphoranes **2** (eqn (4)).[3–7]

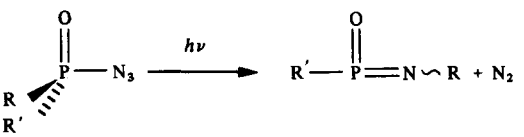

(4)

1 **2**

In their recent mechanistic study using different nitrene trapping agents, Harger and Westlake[6f–g] discussed whether the product is formed via a

†Present Address: Department of Organic Chemistry, University of Gronigen, 9747 AG Groningen, The Netherlands.

‡Author to whom correspondence should be addressed.

nitrene **3** or directly from the azide with concerted substituent migration and nitrogen loss. Their conclusion was not unequivocal: the results for the photolysis of *t*-butyl-phenyl phosphinic azide point to an exclusively concerted mechanism whereas those for the diphenyl derivative leave open the possibility that some may proceed through the *singlet* nitrene.

3 **4**

On the other hand, no substituent migration occurred during the decomposition of dialkoxy-substituted phosphinic azides **4** and only typical nitrene-insertion products were observed.[5] Under these circumstances, the key-process in the photochemical behaviour of each type of phosphinic azide appears to be transformation of phosphinic nitrene **3** to oxoiminophosphorane **2**. Indeed, similar considerations have recently contributed to the understanding of the decomposition of azides in the series of boron,[8] carbon,[9] silicon,[10] tricoordinated phosphorus[11] and cationic phosphorus.[12]

With regard to eqn (4), the present study aims to outline some insights into the role of nitrene, based on *ab initio* MO calculations on the interconversion of the simplest model species **5** ⇌ **6** (eqn (5)) in their lowest-lying singlet and triplet electronic states.

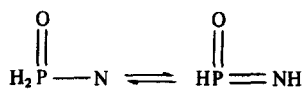

(5)

5 **6**

Geometrical parameters of the stationary points considered were determined from analytically computed energy first and second derivatives and the 3-21G* basis set[13] (split-valence plus *d*-functions on P only). Harmonic vibrational frequencies were calculated at the HF/3-21G* level in order to characterize stationary points as minima or transition structures and to calculate zero-point vibrational contributions to relative energies. The latter were obtained from single-point calculations with 3-21G*-geometries at the SCF and Møller–Plesset perturbation theory (second- through fourth-order neglecting the triple substitutions)[14] level employing the 6-31 + + G* basis set[15] (a 6-31G basis plus a set of diffuse *s* and *p*-functions on P, O and N, a set of diffuse *s*-functions on H and a set of polarization

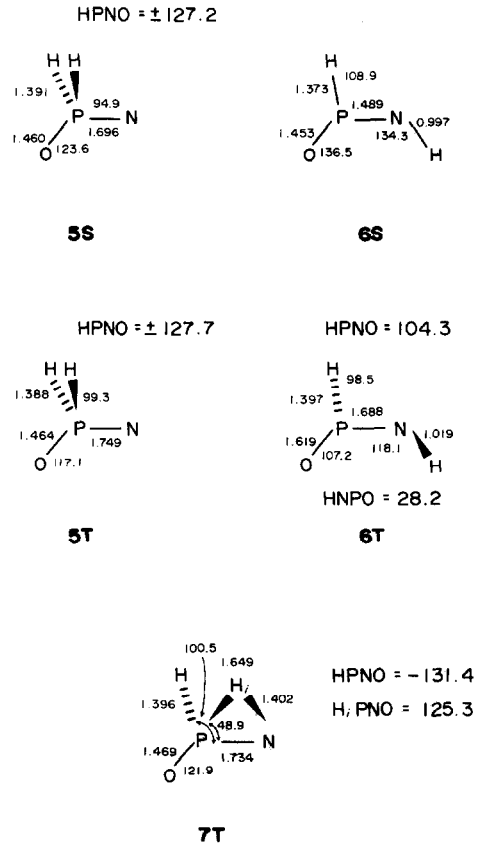

Fig. 1. HF/3-21G*-optimized geometries of stationary points considered: the singlets **5S** and **6S** and the triplets **5T**, **6T** and **7T**. Bond lengths in Å and bond angles in degrees.

d-functions on P, O and N). The unrestricted formalism (UHF; UMP) was used for the triplet states. Calculations were carried out using the Gaussian 82 program.[16]

The optimized geometries are shown in Fig. 1. The total, zero-point vibrational (ZPE) and relative energies of the five species considered are listed in Table 1.

The phosphinic nitrene has a triplet electronic ground state with a C_s-structure **5T**. The P—N bond length of 1.749 Å and stretching frequency of 776 cm^{-1} in **5T** indicate that this bond, due to some interaction with the oxygen atom, is somewhat stronger than that of the triplet phosphinonitrene H_2P—N (1.776 Å and 680 cm^{-1} respectively, at the UHF/3-21G* level of calculations).[11] Similarly, the P—N bond in the triplet oxoiminophosphorane **6T** (1.688 Å and 780 cm^{-1}) is also slightly stronger than that in the triplet iminophosphane HP—NH (1.7505 Å and 780 cm^{-1}).[11] With respect to the singlet iminophosphorane **6S**, both the P—N and P—O bonds in **6T** are appreciably stretched (0.17–

Table 1. Calculated total (hartrees), zero-point vibrational (ZPE, kcal mol^{-1}) and relative (kcal mol^{-1}) energies of species considered

	5S	6S	5T	7T	6T
			Total and ZP energies[a]		
HF/3–21G*	−468.70363	−468.82711	−468.79725	−468.70032	−468.79566
HF/6-31++G*	−471.03788	−471.17010	−471.13178	−471.03993	−471.12707
MP2/6-31++G*	−471.44983	−471.63398	−471.52057	−471.45717	−471.51034
MP3/6-31++G*	−471.46871	−471.63288	−471.53799	−471.47064	−471.53826
MP4SDQ/6-31++G*	−471.48298	−471.64609	−471.55007	−471.48578	−471.54970
ZPE[b]	14.4	17.2	15.6	11.7	14.5
$\langle s^2 \rangle$[c]			2.01	2.12	2.03
			Relative energies		
HF/3-21G*	77.5	0.0	18.7	79.6	19.7
HF/6-31++G*	83.0	0.0	24.0	81.7	27.0
MP2/6-31++G*	115.6	0.0	71.2	111.0	77.6
MP3/6-31++G*	103.0	0.0	59.5	101.8	59.4
MP4SDQ/6-31++G*	102.4	0.0	60.3	100.6	60.5
Estimated[d]	99.6	0.0	58.7	95.1	57.8

[a] Using HF/3-21G*-optimized geometries given in Fig. 1.
[b] At HF/3-21G* and scaled by 0.9.
[c] Expectation values for UHF-wavefunctions.
[d] Including ΔE(MP4SDQ)+Δ(ZPE).

0.20 Å). The two unpaired electrons in the latter are essentially localized on the oxygen atom. The transition structure **7T** for the 1,2-hydrogen shift linking both triplet minima **5T** and **6T** has no symmetry. The ratio of distances PH_i/NH_i in **7T** is comparable to that in the transition structure connecting the triplets $H_2P—N \rightleftharpoons HP—NH$.[11]

In the closed-shell singlet states, the phosphinic nitrene **5S** (C_s) is calculated to be a saddle point on the energy surface having one imaginary frequency. When the C_s-symmetry constraint is relaxed, this species collapses in fact to the planar oxoiminophosphorane **6S**. This situation differs from the phosphinonitrene $H_2P—N$ which is quite stable in its singlet ground state[11] but is in accord with the cases of $H_2B—N$,[8] $H_3C—N$,[9] $H_3Si—N$,[10] $H_3\overset{+}{P}—N$,[12] in which no barrier was found for the conversion to the more stable singlet dicoordinated nitrogen compounds $H_2X{=}N—H$. Such a difference has been accounted for by the availability of lone pair electrons in the phosphino group.[3] A more detailed comparison on this particular feature will be reported elsewhere.[17]

Structure and bonding in compounds similar to **6S** have been examined in some detail in previous papers.[18] We only note that the P—N bond in **6S** is quite short (1.489 Å), by far the shortest distance in the series under consideration. It lies between the values of 1.553 and 1.453 Å previously reported for the typical P=N double bond in HP=NH[11] and quasi-triple P≡N bond in $H_2P{\equiv}\overset{+}{N}H$[12], respectively (at the HF/3-21G* level).

The energy profile of the interconversion is given schematically in Fig. 2. It is seen that both triplet minima **5T** and **6T** are almost energetically

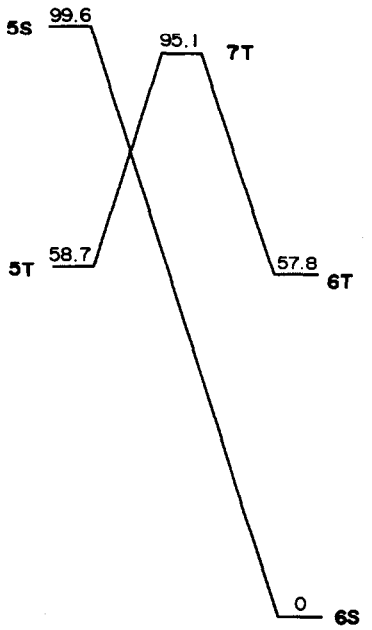

Fig. 2. Schematic energy profile for the $H_2P(=O)N \rightleftharpoons HP(=O)=NH$ interconversion. Relative energies (ΔH(OK)) are given in kcal mol^{-1}.

equivalent and there is, in addition, a sizeable energy barrier (36 kcal mol^{-1}) separating them from each other. The spin-contamination of UHF-wavefunctions obtained for all three triplet species appears to be reasonable (*cf.* $\langle s^2 \rangle$ values, Table 1). Accordingly, both triplet minima may be stable with respect to unimolecular rearrangement. When the H-atom is substituted by a poorer migrating group (such as alkoxy ...), the isomerization becomes even more unlikely. The singlet **6S** is calculated to be the global minimum among the species being considered. The triplet–singlet separation **6T–6S** amounts to about 58 kcal mol^{-1} whereas the energy gap between the two singlets **5S–6S** is extremely large (100 kcal mol^{-1}). Because the singlet states are being treated by methods considering only a single configuration as reference, their total energies are probably underestimated with respect to the triplets (which are treated by UHF-based methods). Therefore, the singlet states may be even more stable than expected from the present values (Fig. 2). However, the singlet nitrene **5S** appears, in any case, to be a high energy species. In this context, the obtained relative energies (Fig. 2) suggest the following points:

(a) Starting from a phosphinic azide **1** in its singlet ground state, the formation of the corresponding oxoiminophosphorane **2** (eqn (4)) is likely to occur *without the intermediacy of any singlet nitrene*. In other words, a non-nitrene process may prevail in this decomposition.

(b) On the contrary, under experimental conditions as reported in ref. 5, the dialkoxy-substituted phosphinic azide **4** appeared to be fragmented in its lowest-lying triplet excited state. This state correlates in fact with the triplet ground state of the phosphinic nitrene **3**. As mentioned above, the latter, if formed, does not rearrange to its triplet isomer but instead undergoes typical nitrene reactions. We note that the dialkoxy-phosphinic carbene **8** has recently been shown to be a reaction

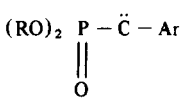

8

intermediate which further undergoes an intramolecular insertion reaction rather than a Wolff-type rearrangement.[19] In this regard, the small amount of nitrene-insertion product observed by Harger and coworkers[6] following photolysis of diphenylphosphinic azide should arise from a triplet nitrene intermediate rather than from a singlet nitrene as suggested by these authors.[6f] Thus, this photochemical process seems to involve both singlet and triplet electronic states of azide: the former which is the major proportion gives rise to oxoiminophosphorane **2** through a non-nitrene pathway whereas the latter state produces a minor quantity of phosphinic nitrene which subsequently reacts with trapping agents. The reason why the triplet state is not significantly involved in the decomposition of *t*-butyl-phenyl phosphinic azide is not clear. Explicit calculations on molecular and electronic structures of starting azides might provide information on this point. On the other hand, the participation of an excited state of azide is also possible and deserves consideration in future works.

In summary, the present theoretical study supports the proposition that the Curtius-type rearrangement of phosphinic azide **1** takes place via a *non-nitrene mechanism*[4–6] in its singlet ground state. However, if the starting material could be sensitized photochemically into its triplet excited state, then, the triplet nitrene could be formed and intervene in the process and the Curtius-type rearrangement would not be observed.

Acknowledgements—The authors thank University College Dublin Computer Centre for computer facilities and Mrs L. M. Phuong for friendly assistance.

REFERENCES

1. T. Curtius, *Ber.* 1890, **23**, 3023.
2. (a) S. Patai, *The Chemistry of the Azido Group*. Wiley-Interscience, New York (1971); (b) W. Lwowski, *Nitrenes*. Wiley-Interscience, New York (1970); (c) E. F. V. Scriven, *Azides and Nitrenes: Reactivity and Utility*. Academic Press, New York (1984).
3. For leading refs see: G. Bertrand, J. P. Majoral and A. Baceiredo, *Acc. Chem. Res.* 1986, **19**, 17.
4. (a) G. Bertrand, J. P. Majoral and A. Baceiredo, *Tetrahedron Lett.* 1980, **21**, 5015; (b) A. Baceiredo, G. Bertrand, J. P. Majoral, F. El Anba and G. Manuel, *J. Am. Chem. Soc.* 1985, **107**, 3945; (c) A. Baceiredo, G. Bertrand and J. P. Majoral, *Nouv. J. Chim.* 1983, **7**, 255.
5. (a) R. Breslow, A. Feiring and F. Herman, *J. Am. Chem. Soc.* 1974, **96**, 5937; (b) R. Breslow, F. Herman and A. W. Schwabacher, *J. Am. Chem. Soc.* 1984, **106**, 5359.
6. (a) M. J. P. Harger, *J. Chem. Soc., Chem. Commun.* 1971, 442; (b) M. J. P. Harger, *J. Chem. Soc., Perkin Trans. 1* 1974, 2604; (c) M. J. P. Harger and M. A. Stephen, *J. Chem. Soc., Perkin Trans. 1* 1981, 736; (d) M. J. P. Harger and S. Westlake, *Tetrahedron* 1982, **38**, 3073; (e) M. J. P. Harger and S. Westlake, *Tetrahedron* 1982, **38**, 1511; (f) M. J. P. Harger and S. Westlake, *J. Chem. Soc., Perkin Trans. 1* 1984, 2351.

7. J. Wiseman and F. H. Westheimer, *J. Am. Chem. Soc.* 1974, **96**, 4262.
8. M. T. Nguyen, *J. Chem. Soc., Chem. Commun*, 1987, 342.
9. M. T. Nguyen, *Chem. Phys. Lett.* 1985, **117**, 290.
10. M. T. Nguyen, M. Faul and N. J. Fitzpatrick, *J. Chem. Soc., Perkin Trans. 2* 1987, 1289.
11. M. T. Nguyen, M. A. McGinn and A. F. Hegarty, *J. Am. Chem. Soc.* 1985, **107**, 8029.
12. M. T. Nguyen, M. B. O'Regan and N. J. Fitzpatrick, *J. Chem. Soc., Perkin Trans. 2* 1987, 2003.
13. M. S. Gordon, J. S. Binkley, J. A. Pople, W. J. Pietro and W. J. Hehre, *J. Am. Chem. Soc.* 1982, **104**, 2792.
14. (a) J. A. Pople, H. A. Binkley and R. Seeger, *Int. J. Quant. Chem. Symp.* 1978, **14**, 91.
15. M. J. Frisch, J. A. Pople and J. S. Binkley, *J. Chem. Phys.* 1984, **80**, 3265.
16. J. S. Binkley, M. J. Frisch, R. A. Whiteside, K. Raghavachari, R. Seeger, D. J. DeFrees, H. B. Schlegel, E. M. Fluder and J. A. Pople, Gaussian 82, Carnegie–Mellon University (1983).
17. M. T. Nguyen (to be published).
18. (a) W. W. Schoeller and C. Lerch, *Inorg. Chem.* 1986, **25**, 576; (b) W. W. Schoeller and J. Niemann, *J. Am. Chem. Soc.* 1986, **108**, 22; (c) R. Alrichs, C. Ehrhardt, M. Lakenbrink, S. Schunk and H. Schnöckel, *J. Am. Chem. Soc.* 1986, **108**, 3596.
19. D. V. Griffiths and J. C. Tebby, *J. Chem. Soc., Chem. Commun.* 1986, 871.

Polyhedron Vol. 7, No. 3, pp. 229–234, 1988
Printed in Great Britain

0277–5387/88 $3.00+.00
© 1988 Pergamon Journals Ltd

ELECTRONIC PROPERTIES AND CRYSTAL STRUCTURE OF AQUA (MEPIRIZOLE-OXALATO)COPPER(II)MONOHYDRATE: $[Cu(C_{11}H_{14}N_4O_2)C_2O_4 \cdot H_2O]H_2O$

J. SUAREZ-VARELA,* L. SOTO† and J. P. LEGROS‡

Laboratoire de Chimie de Coordination du CNRS, Unité n° 8241 liée par convention à l'Université Paul Sabatier, 205 route de Narbonne, 31400 Toulouse Cedex, France

and

C. ESTEVE and J. GARCIA

Departamento de Quimica Inorganica, Facultad de Farmacia, Universidad de Valencia, Blasco Ibañez 13, 46010 Valencia, Spain

(*Received* 23 *June* 1987; *accepted* 8 *September* 1987)

Abstract—A Cu(II) complex with mepirizole: 4-methoxy-2-(5-methoxy-3-methyl-pyrazol-1-yl)-6-methylpyrimidine (L) and oxalate as ligands with the formula $[CuL(C_2O_4)(H_2O)] \cdot H_2O$ has been synthesized. The crystal structure has been determined by X-ray diffraction analysis: monoclinic, space group $P2_1/n$, $Z = 4$, $a = 7.707(1)$, $b = 14.951(3)$, $c = 14.986(2)$ Å, $\beta = 92.40(2)°$, $V = 1725.2(8)$ Å^3, $D_m = 1.61(1)$ g cm^{-3}, $D_c = 1.62$ g cm^{-3}, $R = 0.032$ and $R_w = 0.035$ for 2016 observed reflections. The CuN_2O_2O' chromophore can be described as square pyramidal strongly distorted towards trigonal bipyramidal. The basal coordination positions are occupied by the two oxygen atoms of the bidentate oxalate group, the coordinated water molecule and one nitrogen atom of the bidentate mepirizole group; the other coordinated nitrogen atom occupies the apical position. Magnetic moment, IR, electronic reflectance and ESR spectra are interpreted in accordance with the proposed stereochemistry.

The preparation of a number of 3*d* transition metal complexes with a biologically active pyrimidyl-pyrazole ligand: mepirizole, 4-methoxy-2-(5-methoxy-3-methyl-pyrazol-1-yl)-6-methylpyrimidine (L) has been previously reported.[1,2,3]

The existence of a strictly square planar coordination of the metal atom in copper(II) complexes is unusual: either, the chromophore is tetrahedrally distorted or additional ligands are involved to give a five-coordinate stereochemistry. The crystal structures of $CuL_2(ClO_4)_2$ and $CuLCl_2$ are described in previous papers.[4,5] Both exhibit a distorted tetrahedral coordination of the copper atom with a different distortion. In addition, we have isolated stable complexes with various metal atoms and the same mepirizole ligand which display electronic properties suggesting pentacoordination of the metal atom with a geometry intermediate between square pyramidal and trigonal bipyramidal.[1,3] The crystal structure and electronic properties of the new complex $[CuL(C_2O_4)(H_2O)] \cdot H_2O$ offer a possibility of studying a facet of pentacoordinated copper(II) chemistry.

EXPERIMENTAL

Preparation of the complex

A solution of $Cu(NO_3)_2 \cdot 3H_2O$ (4 mmol) in water (100 cm^3) and L (4 mmol) in ethanol (50 cm^3) was

*Permanent address: Departamento de Quimica General. Facultad de Ciencias, Universidad de Granada, 18071 Granada, Spain.

†Permanent address: Departamento de Quimica Inorganica. Facultad de Farmacia, Universidad de Valencia, Blasco Ibañez n° 13, 46010 Valencia, Spain.

‡Author to whom correspondence should be addressed.

Table 1. Crystallographic data

Formula	$CuC_{13}H_{18}N_4O_8$
M_r	421.85
Space group	monoclinic, $P2_1/n$
a (Å)	7.707(1)
b (Å)	14.951(3)
c (Å)	14.986(2)
β(°)	92.40(2)
V (Å^3)	1725.2(8)
Z	4
D_c (g cm^{-3})	1.62
D_m (g cm^{-3})	1.61(1) (flotation)
μ (cm^{-1})	13.2
Temperature (K)	293
Radiation	λ(Mo-K_α) = 0.71079 Å
Max. Bragg angle	$\theta_{max} = 22°$
Number of independent reflections	3403
Number of observed reflections	2016 for $I > 2\sigma(I)$
Number of refined parameters	244
R and R_w	0.032 and 0.035
Weighting scheme	Unit weights
e.s.d. of an observation of unit weight (S)	1.32

added to a solution of $K_2C_2O_4$ (4 mmol) in water (50 cm^3). Blue crystals were obtained and washed with a mixture of ethanol and water (20%). They were found to be stable to air and light and decomposed under heating at 220°C. Found: C, 37.0; N, 13.3; H, 4.0; Cu, 14.9. Calc. for $CuC_{13}H_{18}N_4O_8$: C, 37.0; N, 13.3; H, 4.3; Cu, 15.0%.

Crystallographic analysis

Crystal data are given in Table 1. The crystal used (0.2 × 0.2 × 0.3 mm) was stuck on the end of a glass fibre. Unit cell and intensity data were obtained using a CAD4 diffractometer and graphite-monochromatized Mo-K_α radiation following standard procedures.[5] The structure was solved by the Patterson method; least-squares refinement was conducted using the block-diagonal approximation in the first stages and full matrix in the final stages. Non-hydrogen atoms were assigned anisotropic thermal parameters. The water molecule of crystallization is statistically distributed over two different sites; the occupation factors (0.63 and 0.37 respectively) were first adjusted by making equal the isotropic temperature factors for both positions and then were kept fixed in subsequent refinements.

All hydrogen atoms except those belonging to the water molecule of crystallization were located on the difference Fourier map; idealized unrefined positions and an arbitrary isotropic temperature factor (B = 5 Å^2) were used in the final calculations. No absorption corrections were made because of the low absorption coefficient and block-like shape of the crystal.

Atomic scattering factors and anomalous dispersion corrections for all non-hydrogen atoms were taken from *International Tables for X-Ray Crystallography*.[6] Final atomic positional and thermal parameters and lists of F_o/F_c values have been deposited as supplementary material with the Editor from whom copies are available on request.*

Electronic properties

Magnetic susceptibility measurements were carried out in the solid state at room temperature (20°C) using a Gouy Balance with $[Ni(en)_3]S_2O_3$ as calibrant. Electronic spectra were recorded at room temperature on a Perkin–Elmer Hitachi 200 spectrophotometer with reflectance attachment fitted. IR spectra were obtained on a Perkin–Elmer 577 instrument, using Nujol mulls supported between CsI windows for the range 4000–200 cm^{-1}. X-band ESR spectra of a powder sample were recorded at room temperature on a Bruker ER 200 spectrometer. The microwave frequency was measured

* Atomic coordinates have also been deposited with the Cambridge Crystallographic Data Centre.

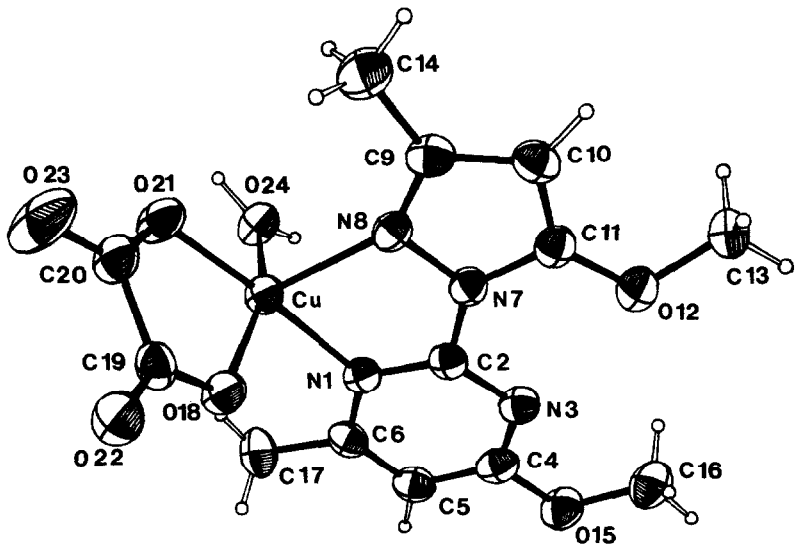

Fig. 1.

with a Racal-Dana frequency meter and the magnetic field with a Bruker NMR gaussmeter.

RESULTS AND DISCUSSION

Crystal structure

The asymmetric unit consists of one isolated neutral $[CuL(C_2O_4)(H_2O)]$ molecule and one non-coordinated water molecule. The structure of the CuL $(C_2O_4)(H_2O)$ unit is shown in Fig. 1 together with the atomic numbering scheme. Figure 2 is a view of the unit cell contents illustrating the molecular packing. The two statistically occupied sites for the non-coordinated water molecule are denoted by O(25) and O(26), O(25) only is drawn on Fig. 2; the distance O(25)... O(26) is 0.70 Å. Selected bond lengths and angles are given in Table 2.

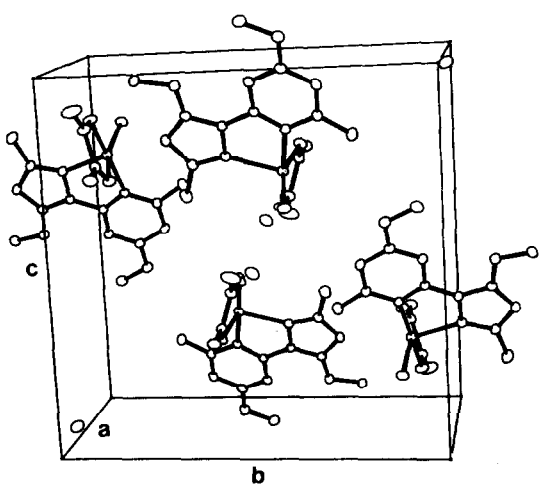

Fig. 2.

As a first approximation, the geometry of the pentacoordinated copper atom can be described as distorted square pyramidal. The basal coordination positions are occupied by the two oxygen atoms O(18) and O(21) of the bidentate oxalate group, the coordinated water molecule O(24) and one nitrogen atom N(1) of the bidentate mepirizole group; the other coordinated nitrogen atom N(8) occupies the apical position.

As usual the copper atom is situated 0.2 Å out of the basal plane towards the N(8) apical atom. The Cu—N and Cu—O distances fall within the normal range and compare well with the bond lengths in other Cu(II)–mepirizole[4,5] and Cu(II)–oxalato complexes[7] respectively. The axial Cu—N(8) bond is significantly longer (2.17 Å) than the equatorial Cu—N(1) bond (2.034 Å), both distances are similar to those previously reported for this type of geometry.[8] However it is important to point out that the coordination site of water is unusual for a regular square pyramidal geometry; from several examples[7,8,9] the water molecule would have been expected to prefer to occupy the apical position. This unusual feature may be attributed to steric hindrance due to the methyl groups of the ligand; this can also be related to the distortion of the coordination polyhedron. This distortion was quantified using the Muetterties and Guggenberger method[10] (Table 3). The value obtained indicates that the coordination polyhedron is intermediate between the tetragonal pyramid and the trigonal bipyramid.

Table 2. Selected bond lengths (Å) and angles (°)

Cu—N(1)	2.035(3)	N(1)—Cu—N(8)	77.3(1)
Cu—N(8)	2.174(3)	N(1)—Cu—O(18)	91.6(1)
Cu—O(18)	1.938(3)	N(1)—Cu—O(21)	175.4(1)
Cu—O(21)	1.941(3)	N(1)—Cu—O(24)	94.0(1)
Cu—O(24)	1.966(3)	N(8)—Cu—O(18)	105.1(1)
N(1)—C(2)	1.327(5)	N(8)—Cu—O(21)	103.8(1)
N(1)—C(6)	1.353(5)	N(8)—Cu—O(24)	97.8(1)
C(2)—N(3)	1.329(5)	O(18)—Cu—O(21)	83.8(1)
C(2)—N(7)	1.389(5)	O(18)—Cu—O(24)	157.1(1)
N(3)—C(4)	1.319(6)	O(21)—Cu—O(24)	90.3(1)
C(4)—C(5)	1.385(6)	C(2)—N(1)—C(6)	116.4(3)
C(4)—O(15)	1.343(5)	N(1)—C(2)—N(3)	127.6(4)
C(5)—C(6)	1.368(6)	N(1)—C(2)—N(7)	116.6(3)
C(6)—C(17)	1.476(6)	N(3)—C(2)—N(7)	115.8(4)
N(7)—N(8)	1.383(4)	C(2)—N(3)—C(4)	114.7(4)
N(7)—C(11)	1.373(5)	N(3)—C(4)—C(5)	123.5(4)
N(8)—C(9)	1.312(6)	N(3)—C(4)—O(15)	118.0(4)
C(9)—C(10)	1.410(6)	C(5)—C(4)—O(15)	118.5(4)
C(9)—C(14)	1.485(7)	C(4)—C(5)—C(6)	117.3(4)
C(10)—C(11)	1.361(6)	N(1)—C(6)—C(5)	120.6(4)
C(11)—O(12)	1.322(5)	N(1)—C(6)—C(17)	116.8(4)
O(12)—C(13)	1.443(6)	C(5)—C(6)—C(17)	122.6(4)
O(15)—C(16)	1.435(6)	C(2)—N(7)—N(8)	117.9(3)
O(18)—C(19)	1.264(5)	C(2)—N(7)—C(11)	132.0(3)
C(19)—C(20)	1.542(6)	N(8)—N(7)—C(11)	110.0(3)
C(19)—O(22)	1.227(5)	N(7)—N(8)—C(9)	105.5(3)
C(20)—O(21)	1.280(5)	N(8)—C(9)—C(10)	111.5(4)
C(20)—O(23)	1.210(5)	N(8)—C(9)—C(14)	120.3(4)
		C(10)—C(9)—C(14)	128.2(4)
		C(9)—C(10)—C(11)	105.5(4)
		N(7)—C(11)—C(10)	107.5(3)
		N(7)—C(11)—O(12)	120.3(4)
		C(10)—C(11)—O(12)	132.2(4)
		C(11)—O(12)—C(13)	144.4(3)
		C(4)—O(15)—C(16)	116.6(3)
		O(18)—C(19)—C(20)	114.6(3)
		O(18)—C(19)—O(22)	125.4(4)
		C(20)—C(19)—O(22)	120.0(4)
		C(19)—C(20)—O(21)	114.0(3)
		C(19)—C(20)—O(23)	120.9(4)
		O(21)—C(20)—O(23)	125.2(4)

As for the complexes $CuLCl_2$[5] and $CuL_2(ClO_4)_2$[4] the pyrazole and pyrimidine rings are planar: deviations (Å) of atoms from their least-square plane for $[CuL(C_2O_4)(H_2O)]\cdot H_2O$ are N(7): −0.002, N(8): 0.003, C(9): −0.002, C(10): 0.001, C(11): 0.001 and N(1): −0.003, C(2): 0.002, N(3): 0.001, C(4): −0.004, C(5): 0.004, C(6): 0.000. The dihedral angle between the two planes is 3.9° indicating a large degree of overall electronic delocalization. The bond angles and bond lengths are consistent with those of the other mepirizole complexes.

The oxalate group does not deviate strongly from planarity: the dihedral angle between the two

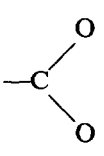

planes is 3.3°. As usual, the C—O bonds interacting with the metal are longer than the non-interacting ones. Furthermore the C—O bond lengths are also affected by H-bonding.

Short non-bonding O ... O contacts (< 2.8 Å) involving water molecules and non-coordinated oxygen atoms of the oxalate group suggest intermolecular hydrogen bonding. Adjacent molecules

Table 3. Coordination polyhedron about the copper atom: experimental vs theoretical dihedral angles (°) calculated for trigonal bipyramidal (TBP) and square pyramidal (SP) geometry; distortion estimated according to Muetterties and Guggenberger[10]

Dihedral angles	TBP	Experimental	SP
O(24)—N(8)—O(21)—O(18)	101.5	74.0	75.7
O(24)—O(21)—O(18)—N(8)	101.5	123.5	119.8
O(24)—N(8)—N(1)—O(18)	101.5	87.7	75.7
O(24)—O(18)—N(1)—N(8)	101.5	112.7	119.8
O(21)—N(8)—O(24)—N(1)	53.1	70.1	75.7
O(21)—N(8)—O(18)—N(1)	53.1	61.2	75.7
O(18)—O(24)—O(21)—N(8)	101.5	118.9	119.8
O(18)—O(24)—N(1)—N(8)	101.5	107.3	119.8
N(1)—O(18)—O(24)—O(21)	53.1	21.0	0
Distortion Δ	0	0.55	1

are linked through O(24)—H ... O(22) interactions: d[O(24) ... O(22)] = 2.66 Å, d[H ... O(22)] = 1.74 Å. Other intermolecular links are also suggested via the non-coordinated disordered water molecules: O(24)—H ... O(26), d[(O(24) ... O(26)] = 2.64 Å, d[H ... O(26)] = 1.87 Å and O(25)—H ... O(24), d[O(25) ... O(24)] = 2.77 Å, in this later case the position of the H atom of the water of crystallization molecule O(25) is unknown.

Electronic properties

The corrected magnetic moment of polycrystalline samples at 298K are 1.84 MB and is representative of magnetically dilute Cu(II) complexes, compatible with the proposed stereochemistry. The reflectance electronic spectrum of the compound studied exhibits one broad unresolved band in the visible region centred at 13.1 kK, consistent with other pentacoordinated copper chromophores.[3,11,12] Lever has pointed out that the band intensity maxima generally shift to lower energy as distortion proceeds from a regular square pyramidal to a regular bipyramidal structure.[13] The maximum observed agrees with the intermediate geometry deduced from the X-ray analysis.

The IR spectrum shows a very broad band at 3300–3500 cm^{-1} assigned to ν(OH) of water. The bidentate oxalate in the title compound exhibits four bands due to antisymmetric and symmetric (O—C—O) stretching modes at 1710, 1660 and 1410, 1270 cm^{-1} respectively. According to the literature[14,15,16] the positions of these bands are assignable to an oxalate group in a C_{2v} symmetry. At lower frequencies bands appear which can be assigned to M—O and M—N vibrations. The two bands at 300 and 280 cm^{-1} correspond to the Cu—N vibrations involving the nitrogen atoms of the pyrazole and pyrimidine rings respectively.[17,18,19] The bands at 460 and 380 cm^{-1} are assigned to Cu—O vibrations.[15,17]

The ESR line shapes leading to $g_{\parallel} = 2.21$, $g_{\perp} = 2.07$ $g_{\parallel} > g_{\perp} > 2.03$ point towards a mainly copper(II) $d_{x^2-y^2}$ orbital ground state, this result is indicative of a tendency of the coordination polyhedron to achieve a square pyramidal geometry.

Acknowledgements—The authors wish to thank Drs J. Galy and J. M. Savariault for their constant interest in this work and for fruitful discussions. L. S. acknowledges the CNRS for allowance to work in the Laboratoire de Chimie de Coordination (Toulouse, France) and the Generalitat Valenciana Conselleria de Cultura, Educacio i Ciencia of Valencia (Spain) for financial assistance.

REFERENCES

1. J. Garcia, M. C. Molla and J. Borras, *Polyhedron* 1985, **4**, 757.
2. M. C. Molla, J. Garcia and J. Borras, *Synth. React. Inorg. Met.-Org. Chem.* 1985, **15**, 553.
3. J. G. Tormos, M. C. Molla and J. Garcia, *Synth. React. Inorg. Met.-Org. Chem.* 1986, **16**, 821.
4. M. C. Molla, J. Garcia, J. Borras, C. Foces-Foces, F. H. Cano and M. Martinez Ripoll, *Transition Met. Chem.* 1985, **10**, 460.
5. L. Soto, J. P. Legros, M. C. Molla and J. Garcia, *Acta Cryst.* 1987, **C43**, 834.
6. *International Tables for X-Ray Crystallography*, Vol. 4. Kynoch Press, Birmingham (1974).
7. W. Fitzgerald, J. Foley, D. McSweeney, N. Ray, D. Sheahan, S. Tyagi, B. Hathaway and P. O'Brien, *J. Chem. Soc., Dalton Trans.* 1982, 1117.
8. B. J. Hathaway, *Coord. Chem. Rev.* 1983, **52**, 87.

9. J. Sletten, *Acta Chem. Scand.* 1983, **A37**, 569.
10. E. L. Muetterties and L. J. Guggenberger, *J. Am. Chem. Soc.* 1974, **96**, 1748.
11. S. Tyagi and B. J. Hathaway, *J. Chem. Soc., Dalton Trans.* 1983, 199.
12. N. F. Curtis, F. R. N. MacCormick and T. N. Waters, *J. Chem. Soc., Dalton Trans.* 1973, **15**, 37.
13. A. B. P. Lever, *Inorganic Electronic Spectroscopy* (2nd Edn). Elsevier, Amsterdam (1986).
14. N. F. Curtis, *J. Chem. Soc.* 1968, 1584.
15. K. Nakamoto, *Infrared and Raman Spectra of Inorganic and Coordination Compounds* (3rd Edn). Wiley, New York (1978).
16. K. L. Scott, R. Wieghardt and A. G. Sykes, *Inorg. Chem.* 1973, **12**, 655.
17. J. R. Ferraro, *Low Frequency Vibrations of Inorganic and Coordination Compounds*. Plenum Press, New York (1971).
18. N. Saha and D. Mukherjee, *Polyhedron* 1983, **2**, 47.
19. J. B. Lambert, H. F. Shurvell, L. Verbit, R. G. Cooks and G. H. Stout, *Organic Structural Analysis*. McMillan, New York (1976).

Polyhedron Vol. 7, No. 3, pp. 235–237, 1988
Printed in Great Britain

0277–5387/88 $3.00+.00
© 1988 Pergamon Journals Ltd

COMMUNICATION

STERIC CONTROL IN THE FORMATION OF AMINE OR AMIDE COMPLEXES FROM [Mo(NO){HB(3,5-$Me_2C_3N_2H)_3$}I_2]

NAJAT ALOBAIDI, CHRISTOPHER J. JONES* and JON A. McCLEVERTY

Department of Chemistry, University of Birmingham, PO Box 363, Birmingham, B15 2TT, U.K.

and

ANDREW J. HOWES and MICHAEL B. HURSTHOUSE

Department of Chemistry, Queen Mary College, University of London, Mile End Road, London E1 4NS, U.K.

(*Received* 28 *September* 1987; *accepted* 5 *October* 1987)

Abstract—The reaction between [Mo(NO){HB(3,5-$Me_2C_3N_2H)_3$}I_2] and pyrrolidine or piperidine produces both the amine complexes [Mo(NO){HB(3,5-$Me_2C_3N_2H)_3$}$I(NHC_nH_{2n})$] ($n = 4$ or 5) and the amide complexes [Mo(NO){HB(3,5-$Me_2C_3N_2H)_3$}$I(NC_nH_{2n})$]. The role of steric factors in the formation of these compounds is discussed.

The coordinatively unsaturated complex [Mo(NO)LI_2] (L = HB(3,5-$Me_2C_3N_2H)_3$) undergoes facile substitution reactions with primary amines[1–3] to give the amide derivatives [Mo(NO)LI(NHR)] (R = alkyl or aryl) according to eq. (1).

$$[Mo(NO)LI_2] + 2RNH_2 \rightarrow [Mo(NO)LI(NHR)] + RNH_3^+ + I^- \quad (1)$$

Magnetic resonance studies have shown[4,5] that paramagnetic intermediates are present during such reactions. The finding that [Mo(NO)LI_2] could be readily reduced and that the resulting anion could readily dissociate iodide[4,5] provides an explanation of this phenomenon. A sequence of reactions involving the labilization of iodide by reduction of [Mo(NO)LI_2] may thus be proposed to account for the facile formation of the amide derivatives. A slow initiation step involving the reaction of [Mo(NO)LI_2] with traces of moisture or a direct reaction with the amine would lead to the formation of free I^- as indicated in eqs (2) and (3).

$$[Mo(NO)LI_2] + OH_2 \rightarrow [Mo(NO)LI(OH_2)]^+ + I^- \quad (2)$$

$$[Mo(NO)LI_2] + RNH_2 \rightarrow [Mo(NO)LI(RNH_2)]^+ + I^- \quad (3)$$

The free I^- would then rapidly reduce [Mo(NO)LI_2] according to eq. (4).

$$[Mo(NO)LI_2] + I^- \rightarrow [Mo(NO)LI_2]^- + \tfrac{1}{2}I_2. \quad (4)$$

Solvolysis of the resulting anion followed by reaction with the amine, or direct reaction with the amine could then rapidly produce a 17-electron amine complex according to eqs (5)–(7).

$$[Mo(NO)LI_2]^- + Solvent \rightarrow [Mo(NO)LI(Solvent)] + I^- \quad (5)$$

$$[Mo(NO)LI(Solvent)] + RNH_2 \rightarrow [Mo(NO)LI(RNH_2)] + Solvent \quad (6)$$

$$[Mo(NO)LI_2]^- + RNH_2 \rightarrow [Mo(NO)LI(RNH_2)] + I^- \quad (7)$$

* Author to whom correspondence should be addressed.

An alternative more direct reaction pathway to this complex is also possible via the iodide reduction of the cationic amine complex formed in eq. (3). This is shown in eq. (8).

$$[Mo(NO)LI(RNH_2)]^+ + I^- \rightarrow [Mo(NO)LI(RNH_2)] + \tfrac{1}{2}I_2. \quad (8)$$

The amine complex might then be oxidized by the iodine produced in eqs (4) and (8) to give the amide complex according to eq. (9).

$$[Mo(NO)LI(RNH_2)] + \tfrac{1}{2}I_2 \rightarrow [Mo(NO)LI(RNH)] + HI. \quad (9)$$

This reaction might involve the prior deprotonation of $[Mo(NO)LI(RNH_2)]$ to give the amide anion which, by analogy with $[Mo(NO)LCl\{NC_nH_{2n}\}]^-$, would be powerfully reducing and readily oxidized as shown in eqs (10) and (11).

$$[Mo(NO)LI(RNH_2)] + RNH_2 \rightarrow [Mo(NO)LI(RNH)]^- + RNH_3^+ \quad (10)$$

$$[Mo(NO)LI(RNH)]^- + \tfrac{1}{2}I_2 \rightarrow [Mo(NO)LI(RNH)] + I^-. \quad (11)$$

An alternative route to the amide complex would involve direct deprotonation of the amine cation as shown in eq. (12).

$$[Mo(NO)LI(RNH_2)]^+ + RNH_2 \rightarrow [Mo(NO)LI(RNH)] + RNH_3^+. \quad (12)$$

Among the intermediates involved in this sequence of reactions $[Mo(NO)LI_2]^-$ has been isolated and characterized[5] in the form of $[Mo(NO)LI_2Li(OEt_2)_2]$ but no example of an amine complex of the type $[Mo(NO)LI(RNH_2)]$ or $[Mo(NO)LI(RNH_2)]^+$ has been characterized, so that no comment on its chemical properties was possible. Use of the sterically more bulky secondary amines, pyrrolidine and piperidine has allowed the isolation of examples of this previously uncharacterized amine complex.

The diiodide $[Mo(NO)LI_2]$ reacted with excess pyrrolidine or piperidine to produce mixtures of red and green compounds which could be separated by column chromatography. The red compounds were diamagnetic and shown to be the amide complexes $[Mo(NO)LI\{NC_nH_{2n}\}]$ on the basis of elemental analyses and IR, ^1H NMR and mass spectral data. In the case where $n = 4$ this formulation was confirmed by a single crystal X-ray diffraction study.[6] These compounds are analogues of the previously reported[7] species $[Mo(NO)LCl\{NC_nH_{2n}\}]$. The green compounds were paramagnetic and exhibited low nitrosyl stretching frequencies (ν_{NO} 1625 ($n = 4$) and 1620 ($n = 5$) cm^{-1}) suggesting that they were 17-electron species. A single crystal X-ray diffraction study of the compound in which $n = 5$ showed that it was the amine complex $[Mo(NO)LI\{HN(CH_2)_5\}]$.[8] Elemental analyses, ESR and mass spectral data were in accord with the formulation of both of these green compounds being amine complexes having the general formula $[Mo(NO)LI\{HNC_nH_{2n}\}]$ ($n = 4$ or 5).

Further synthetic studies have shown that the addition of NaH increases the proportion of the green amine complexes formed in the reaction. Thus hydride appears to act as a reducing agent in this reaction, rather than a base which would effect the deprotonation of the amine ligand. In addition the amine complexes $[Mo(NO)LI\{NHC_nH_{2n}\}]$ could be oxidized with iodine to give red amide derivatives in accordance with eq. (9). It is notable that the reactions of HNC_nH_{2n} with $[Mo(NO)LCl_2]$ alone do not afford green complexes, presumably because Cl^- is insufficiently reducing to produce 17-electron complexes.[7] However, the addition of NaH to the reaction mixtures led to the formation of the green chloro- complexes $[Mo(NO)LCl\{HNC_nH_{2n}\}]$. Again it would appear that NaH acts as a reducing agent rather than a base in this reaction.

The isolation of amine complexes with these cyclic secondary amine reagents warrants some comment in view of our failure to observe such species in the products obtained from reactions involving primary amines. The sterically demanding nature of L suggested that steric factors were responsible for these differences in behaviour.Accordingly we have carried out steric energy calculations on $[Mo(NO)LI\{HNC_5H_{10}\}]$ to investigate this point. These calculations show that the piperidine ligand in this complex is not free to rotate about the Mo—N(piperidine) bond. Furthermore the structural study establishes that the amine proton is surrounded by atoms in close non-bonded contact (iodide at 3.125 Å and two pyrazolyl-3-methyl protons at 2.184 and 2.696 Å). The hypothetical amino-bonded $EtNH_2$ complex was also modelled and there was found to be little restriction to the rotation of this ligand about the Mo—N(ethylamine) bond. Thus, in the case of this primary amine, there is no substantial steric energy barrier to the positioning of an amine hydrogen in a location accessible to approaching nucleophiles. This would facilitate the removal of a proton during the oxidation to give the amide complex. However, in the case of piperidine this will not be the case and kinetic control of the oxidation will arise because of the steric inaccessibility of the amine proton.

There may also be an energy barrier associated with the structural reorganization of the ligand.

The nitrogen of the piperidine ligand is effectively tetrahedral but in the piperidine ligand it is planar. Steric energy calculations were carried out in which the M—N—(pyrrolidine ring centroid) angle in a model $[Mo(NO)LCl\{NC_4H_8\}]$ structure was driven in 10° steps from 240° through the energy minimum at 170° to 120°. These showed that large energy barriers were encountered when the angle deviated by more than *ca* 10° from the minimum of 170°. This suggests that a change in the geometry of the pyrrolidine ring would have to precede the formation of the shortened Mo—N(amide) bond during oxidation. In the case of the sterically less demanding primary amines, only a rotation about the Mo—N(amide) bond would be necessary.

It may be concluded that $[Mo(NO)LX_2]$ (X = Cl or I) can react with HNC_nH_{2n} (n = 4 or 5) to produce amine complexes. A first step in this process could be the simple substitution of halide to give $[Mo(NO)LX\{HNC_nH_{2n}\}]^+$. This complex may then undergo a kinetically controlled deprotonation to a 16-electron amide complex or be reduced to a 17-electron amine complex. When X = Cl, amide complexes are normally formed by deprotonation but if a reducing agent is added in the form of NaH the neutral 17-electron amine complexes $[Mo(NO)LCl\{HNC_nH_{2n}\}]$ may be isolated. In the case where X = I, the iodide liberated in the substitution may function as the reducing agent so that a mixture of amide and amine complexes arises even without an added reductant. However, the nature of the reaction is more complicated in this case. An alternative reaction pathway involving labilization of I^- by reduction of $[Mo(NO)LI_2]$ becomes possible and redox reactions involving the iodine/iodide couple and amine/amide 17-electron/16-electron complex equilibria also become possible.

Acknowledgement—We are grateful to the S.E.R.C. for support (to A.J.H.).

REFERENCES

1. J. A. McCleverty, *Chem. Soc. Rev.* 1983, **12**, 331.
2. J. A. McCleverty, A. E. Rae, I. Wolochowicz, N. A. Bailey and J. M. A. Smith, *J. Chem. Soc., Dalton Trans.* 1982, 429.
3. J. A. McCleverty, G. Denti, S. J. Reynolds, A. S. Drane, N. El Murr, A. E. Rae, N. A. Bailey, H. Adams and J. M. A. Smith, *J. Chem. Soc., Dalton Trans.* 1983, 81.
4. J. A. McCleverty and N. El Murr, *J. Chem. Soc., Chem. Comm.* 1981, 960.
5. T. N. Briggs, C. J. Jones, J. A. McCleverty, B. D. Neaves, N. El Murr and H. M. Colquhoun, *J. Chem. Soc., Dalton Trans.* 1985, 1249.
6. A. J. Howes and M. B. Hursthouse, unpublished results.
7. N. AlObaidi, T. A. Hamor, C. J. Jones, J. A. McCleverty and K. Paxton, *J. Chem. Soc., Dalton Trans.*, in press, paper 6/2273.
8. T. A. Hamor and K. Paxton, personal communication.

Polyhedron Vol. 7, No. 3, pp. 239–241, 1988
Printed in Great Britain

0277-5387/88 $3.00+.00
© 1988 Pergamon Journals Ltd

COMMUNICATION

POLYPHOSPHORUS LIGANDS—IV.* THE ASYMMETRIC UNSATURATED BIPHOSPHINE 1,1-BIS(DIPHENYLPHOSPHINO)PROP-1-ENE

JONATHAN L. BOOKHAM and WILLIAM McFARLANE†

Department of Chemistry, City of London Polytechnic, Jewry Street, London EC3N 2EY, U.K.

(*Received* 28 *September* 1987; *accepted* 5 *October* 1987)

Abstract—The new ligand 1,1-bis(diphenylphosphino)prop-1-ene is valuable as a precursor of other polyphosphorus ligands and metal complexes in which the lowered symmetry induced by the methyl group can introduce diastereoisomerism and can facilitate the measurement of $^2J_{PP}$.

Phosphorus–phosphorus nuclear spin coupling constants are an important parameter in the study of phosphine complexes of transition metals, but are often difficult to measure in symmetrical species, and for this reason unsymmetric bi- and polydentate ligands are of considerable value. Following its original preparation[1] in 1982 1,1-bis(diphenylphosphino)ethene, **I**, has been valuable as (a) a precursor of a range of polyphosphorus ligands formed by addition to the double bond by species with P—H bonds,[2,3] and (b) as a ligand in its own right similar to dppm but with a rather different bite and able to form complexes that can themselves undergo addition to the double bond.[4,5] We now report the preparation, characterization, NMR and some reactions of the title homologue

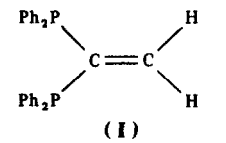

(I)

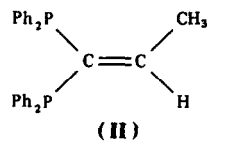

(II)

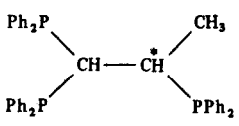

(III)

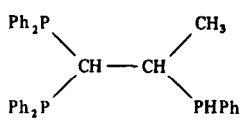

(IV)

II, which is potentially more valuable because its asymmetry facilitates the measurement of more NMR parameters (notably $^2J_{PP}$) than in **I**, and because in reactions with chiral substrates it can yield diastereomeric products.

II was obtained in *ca* 10% yield from the reaction between Ph_2PLi and 1,1-dichloroprop-1-ene in THF solution as white crystals, m.p. 133°C, for which satisfactory elemental analysis (C, H, P) figures have been obtained. Its structure was confirmed by its NMR spectra. ^1H: δ 1.94 ppm, doublet (J_{HH} 6.8 Hz, J_{PH} 0 Hz) CH_3 group; δ 6.18 ppm, multiplet (J_{HH} 6.8 Hz, J_{PH} 8.8, 21.8 Hz) CH group; δ 7.0–7.3 ppm, complex, C_6H_5 groups. ^{13}C: δ 18.4 ppm, double doublet (J_{PC} 27.8, 0.9 Hz), CH_3; δ 135.2 ppm, double doublet (J_{PC} 10.4, 4.9 Hz) CH; δ 149.1 ppm doublet (J_{PC} 25.9 Hz), ipso C. ^{31}P: δ_A −4.6 ppm, δ_B −14.0 ppm, $^2J_{PP}$ 7.0 Hz. In particular the value of 6.8 Hz for $^3J_{HH}$ confirms that no rearrangement of the alkene skeleton has occurred.

The geminal P—P coupling of only 7 Hz is remarkably small compared with a value of 98 Hz measured indirectly[1] in **I** and appears to be due to constraints imposed by the methyl group upon the rotation of the Ph_2P group to which it is *cis*. There is evidence[6,7] that large geminal P^{III}–P^{III} couplings occur when the electron lone pairs of the phosphorus atoms are directed approximately towards one another, and molecular models indicate that

* For part III see ref. 3.

† Author to whom correspondence should be addressed.

this is feasible in **I** (and in dppm in which $^2J_{PP}$ = 125 Hz[1]). However, such a conformation is strongly disfavoured in **II** by steric interaction between the methyl group and the phenyls of the Ph_2P group *cis* to it, and a small coupling results as, for example, in $(Ph_2P)_2NBu^t$. This interpretation is supported by a significant temperature dependence of $^2J_{PP}$ in **II** and by a similarly small value of the corresponding coupling constant in 1,1,2-tris(diphenylphosphino)ethene.[8]

Typical addition reactions to the double bond of **II** are with Ph_2PH, to yield **III** in which chirality at C* renders the geminal phosphorus atoms inequivalent and which has a characteristic ABC ^{31}P NMR spectrum; and with $PhPH_2$ to yield **IV** in which the presence of two asymmetric centres (at carbon and at phosphorus) leads to the formation of diastereomers in approximately equal proportions. In contrast to the behaviour of **I** this reaction stops at this stage and a further equivalent of **II** will not attack the remaining P—H bond, although an equivalent of **I** will. This is further evidence of the substantial steric effect of even the relatively small methyl group in this environment.

II also reacts with metal substrates in a manner similar to that of **I**, but again the lower symmetry of the products often permits the measurement of NMR parameters not accessible in the former case. As an example Fig. 1 shows the ^{31}P NMR spectrum from a mixture of **V** and **VI** which are obtained in

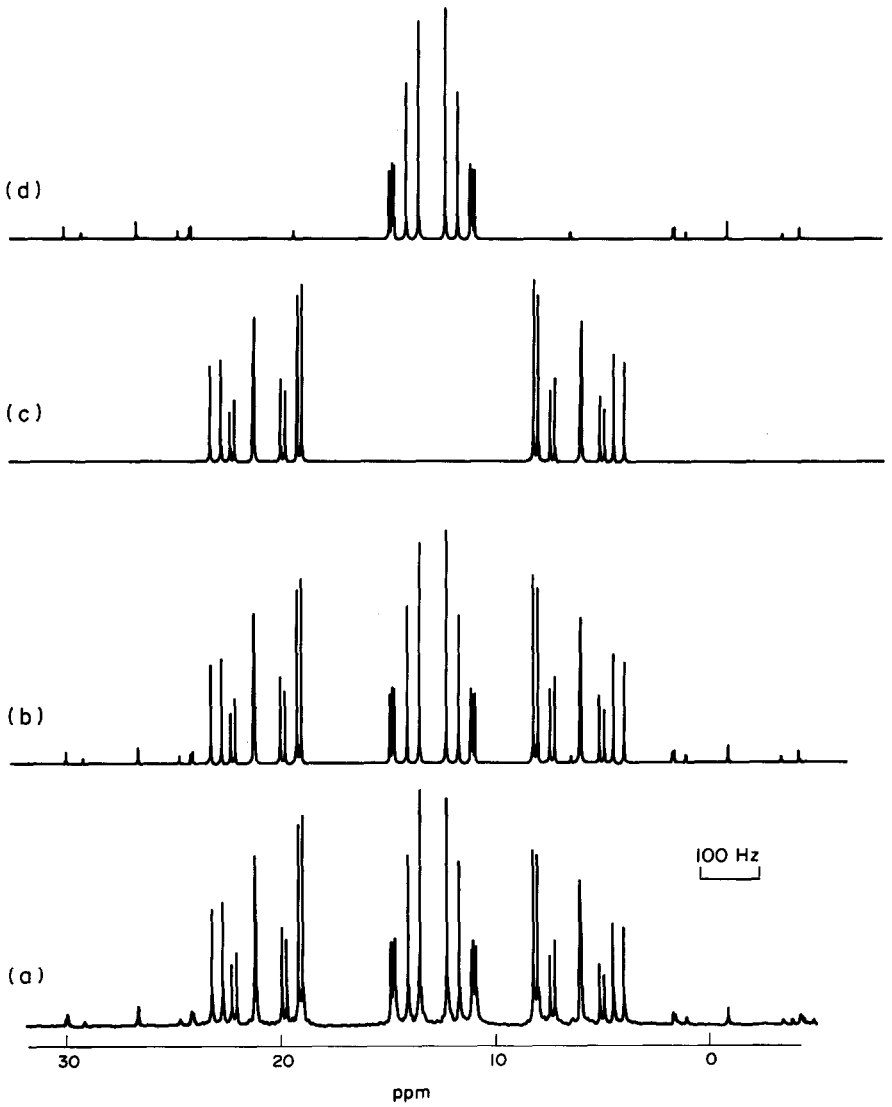

Fig. 1. ^{31}P NMR spectra at 36.2 MHz (JEOL FX90 Q) of **V** and **VI**. (a) Experimental spectrum of a mixture of the two isomers. (b) Computer simulation obtained by summing (c) and (d). (c) Calculated spectrum of **V** using $\delta_A = 21.1$, $\delta_B = 6.3$ ppm; $J_{AB} = 116.5$, $J_{AB'} = 31.2$, $J_{AA'} = 466.1$, $J_{BB'} = 457.7$ Hz. (d) Calculated spectrum of **VI** using $\delta_A = 17.5$, $\delta_B = 8.4$ ppm; $J_{AB} = 117.4$, $J_{AB'} = 461.6$, $J_{AA'} = 33.9$, $J_{BB'} = 29.0$ Hz.

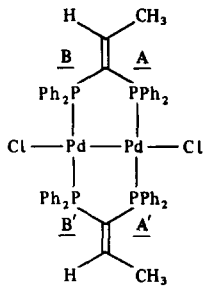

(V)

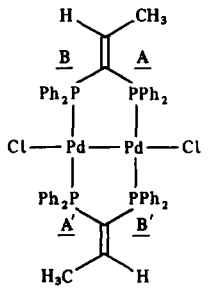

(VI)

equal proportions from the reaction between $Pd_2(dba)_3 \cdot CHCl_3$ and $Pd(PhCN)_2Cl_2$ and the free ligand **II**. In each case an AA′BB′ spectrum arises, but for **V** the largest coupling is $J_{AA'}$ (or $J_{BB'}$) = 466.1 Hz, whereas in **VI** it is $J_{AB'}$ that is the largest at 461.6 Hz, and this accounts for the different appearance of the two systems and permits their assignment.

Acknowledgement—We thank the SERC for support.

REFERENCES

1. I. J. Colquhoun and W. McFarlane, *J. Chem. Soc., Dalton Trans.* 1982, 1915.
2. J. L. Bookham, W. McFarlane and I. J. Colquhoun, *J. Chem. Soc., Chem. Commun.* 1986, 1041.
3. J. L. Bookham, W. McFarlane and I. J. Colquhoun, *J. Chem. Soc., Dalton Trans.*, in press.
4. G. R. Cooper, F. Hassan, B. L. Shaw and M. Thornton-Pett, *J. Chem. Soc., Chem. Commun.* 1985, 614.
5. X. L. R. Fontaine, F. S. M. Hassan, S. J. Higgins, G. B. Jacobsen, B. L. Shaw and M. Thornton-Pett, *J. Chem. Soc., Chem. Commun.* 1985, 1635.
6. R. J. Cross, T. H. Green and R. Keat, *J. Chem. Soc., Dalton Trans.* 1976, 1424.
7. R. Keat, L. Manojlovic-Muir, K. W. Muir and D. S. Rycroft, *J. Chem. Soc., Dalton Trans.* 1981, 2192.
8. J. L. Bookham, W. McFarlane and I. J. Colquhoun, to be published.

Polyhedron Vol. 7, No. 3, pp. 243–244, 1988
Printed in Great Britain

0277–5387/88 $3.00+.00
© 1988 Pergamon Journals Ltd

COMMUNICATION

THE STRUCTURE OF δ-UO_3

M. T. WELLER,* P. G. DICKENS and D. J. PENNY

Inorganic Chemistry Laboratory, South Parks Road, Oxford OX1 3QR, U.K.

(*Received* 11 *June* 1987; *accepted after revision* 13 *October* 1987)

Abstract—The proposed structure for δ-UO_3 has been confirmed by powder neutron diffraction. Data collected from a sample of good crystallinity, by time of flight neutron diffraction techniques, are consistent with the previous description of δ-UO_3 as having the ReO_3 structure, with an unusual regular octahedral environment for U(VI).

The uranium(VI)–oxygen system is one of great complexity; at least six polymorphs of the stoichiometry UO_3 have been described.[1] This structural diversity of uranium(VI) reflects its ability to exist in a variety of low symmetry, high coordination environments with similar energies. The majority of these materials have been studied using powder or single crystal X-ray diffraction with subsequent powder neutron diffraction studies for the accurate determination of the oxygen atom positions. However, the structure proposed for δ-UO_3 by Wait[2] is based solely on powder X-ray diffraction data with visual estimation of the reflection intensity. The technique is very insensitive to oxygen positions and relatively large distortions of the structure could be accommodated within the accuracy of this refinement. For example tilting of the octahedra with displacement of oxygen off the U—O—U direction would be very difficult to observe using X-ray techniques. However neutron diffraction techniques are ideally suited to the observation of any such distortion. As part of an investigation of uranium oxides and their insertion compounds we have recently completed a structural study of δ-UO_3 using powder neutron diffraction.

EXPERIMENTAL

δ-UO_3 was prepared by the method described by Wait[2] using AnalaR grade $UO_2(NO_3)_2 \cdot 6H_2O$ as the starting material. Uranyl nitrate was converted to γ-UO_3 by controlled thermal decomposition in a flowing oxygen atmosphere. Hydrothermal reaction of γ-UO_3 at 190°C in a sealed apparatus led to the formation of crystalline β-$UO_2(OH)_2$,[3] frequently described in the literature as β-$UO_3 \cdot H_2O$.

Thermogravimetric studies of β-$UO_2(OH)_2$ in association with powder X-ray diffraction have shown that decomposition occurs at 375°C with the formation of δ-UO_3: above 410°C δ-UO_3 undergoes a transformation to other polymorphs of UO_3.[4] In this work β-$UO_2(OH)_2$ was heated at 375°C for 24 h, resulting in decomposition to brick-red δ-UO_3. The products from decomposition at higher temperatures or longer heating times were of slightly higher crystallinity but had a considerable degree of contamination with other polymorphs of UO_3.

Powder X-ray diffraction data showed an almost pure material, which could be indexed on a cubic cell of dimensions 4.146(12). Two very weak lines (with intensity ~2% that of the δ-$UO_3\langle 100\rangle$ reflection) were assigned to the strongest peaks from the powder X-ray pattern of α-UO_3. It was found impossible to prepare a sample of δ-UO_3 totally free from this contaminating polymorph.

Neutron diffraction studies were carried out using the instrument GPPD at the IPNS, Argonne, Chicago; a full description of the diffractometer is given elsewhere.[5] The sample, 10 g, was contained in a vanadium can and data were collected over a period of 20 h. Neutron pulses scattered from the sample were collected in the four time-focussed detector arrays. The higher resolution back scat-

* Author to whom correspondence should be addressed. †Present address: Department of Chemistry, The University, Southampton SO9 5NH, U.K.

Table 1. Calculated and observed intensities for δ-UO_3

h	k	l	I_{obs}	I_{calc}
1	0	0	150.8	157.3
1	1	0	10.0	12.2
1	1	1	41.0	71.22
2	0	0	468.2	479.6
2	1	0	631.2	588.2
2	1	1	34.2	27.6
2	2	0	849.2	878.9
3	0	0	664.0	687.2
2	2	1		
2	2	2	385.0	359

tered data (150°) and that from the 90° and 60° banks were considered for the refinement. Although the higher angle data is generally better resolved and is used in profile refinements, for this material the line widths were such that an increase in resolution at the higher scattering angle was only weakly apparent. As a result it was decided to use the higher intensity 60° data for the refinement. This also had the advantage of allowing the ⟨100⟩ reflection to be included in the refinement; peaks with large d-spacings are beyond the maximum time of flight for the higher angle detector banks. The data were corrected for the distribution of wavelength intensities, and instrumental and geometrical factors controlled the scattered intensities by comparison with a spectrum obtained from a standard vanadium sample. The resultant diffraction profile showed nine well resolved peaks and some additional incompletely resolved low d-spacing peaks which could be indexed on the cubic unit cell of δ-UO_3. A refined lattice parameter of 4.165(8), in good agreement with the powder X-ray data, was determined. Three additional very weak features in the diffraction profile were assigned to reflections from α-UO_3, but these were sufficiently resolved from the δ-UO_3 peaks and could be ignored. No peak that would indicate a larger unit cell for δ-UO_3 was observed.

The background under the peaks was determined by linear extrapolation of that on either side and the intensity of the nine well resolved peaks determined by summing the counts under each. Calculated intensities based on the perfect ReO_3 structure were generated for the peaks observed in the experimental pattern and scaled to give the best fit to the experimental data. Reasonable temperature factors of 0.3 and 1.0 were assigned to uranium and oxygen, respectively taken from previous neutron diffraction work on uranium oxides.[6] The results are shown in Table 1 and the atomic coordinates summarized in Table 2. A reliability index of 5.3%

Table 2. Atomic coordinates for δ-UO_3
(Space group $Pm\bar{3}m$ No. 221 *International Tables*)

Atom	Scattering length[a]	Wyckoff symbol	x	y	z	B
U	0.850	1a	0	0	0	0.3[b]
O	0.5807	3d	$\frac{1}{2}$	0	0	1.0[b]

[a] 10^{-12} cm.
[b] Not refined.

was calculated using the expression

$$R = 100 \times \sum_i (I_{obs} - I_{calc}) \Big/ \sum_i I_{obs} \%.$$

Weak features apparent in the profile at the positions expected for the 310 and 311 reflections were of an intensity consistent with that calculated for these peaks.

DISCUSSION

The experimental neutron diffraction data are consistent with a description of δ-UO_3 with the ReO_3 structure. The agreement of the calculated and experimental intensity data coupled with the ability to index all the observed reflections on the simple unit cell suggests that there is no deviation from the perfect cubic structure. The sensitivity of neutron diffraction to scattering from oxygen, supports the model suggested by Wait with an unusual regular six-fold coordination for uranium. The derived uranium–oxygen single bond length of 2.08 Å is in good agreement with that found in other uranium(VI) oxides with low uranium coordination numbers such as α-UO_3.[6]

Acknowledgements—The authors wish to thank the Argonne National Laboratory for the provision of neutron beam facilities and R. L. Hitterman for help in analysing the data. We also wish to thank the S.E.R.C. for a travel grant for P.G.D. and M.T.W. and a research studentship for M.T.W., and the U.S.A.F. Office of Scientific Research for financial support (Grant AFOSR-83-0052).

REFERENCES

1. Gmelin, *Handbook of Inorganic Chemistry*, Chap. 2: Uranium. Springer (1978).
2. E. Wait, *J. Inorg. Nucl. Chem.* 1955, **1**, 309.
3. V. J. Wheeler, R. M. Dell and E. Wait, *J. Inorg. Nucl. Chem.* 1964, **26**, 1829.
4. H. R. Hoekstra and S. Siegel, *J. Inorg. Nucl. Chem.* **18**, 154.
5. J. D. Jorgensen and F. J. Rotella, *J. Appl. Cryst.* 1982, **15**, 27.
6. C. Greaves and B. E. F. Fender, *Acta Cryst.* 1972, **B28**, 3609.

Polyhedron Vol. 7, No. 3, pp. 245–247, 1988
Printed in Great Britain

0277–5387/88 $3.00+.00
Pergamon Journals Ltd

COMMUNICATION

X-RAY CRYSTAL STRUCTURE AND ^{13}C NMR SPECTRA OF $[WI_2(CO)_3(NCMe)_2]$

MICHAEL G. B. DREW*

Department of Chemistry, University of Reading, Whiteknights, Reading RG6 2AD, U.K.

and

PAUL K. BAKER,* ELAINE M. ARMSTRONG and STUART G. FRASER

Department of Chemistry, University College of North Wales, Bangor, Gwynedd LL57 2UW, U.K.

(*Received* 11 *August* 1987; *accepted* 13 *October* 1987)

Abstract—The X-ray crystal structure of $[WI_2(CO)_3(NCMe)_2]$ (**1**) was determined and the crystals are orthorhombic with $a = 12.405(8)$, $b = 7.590(8)$, $c = 13.844(12)$ Å. X-ray data for 911 independent reflections above background were collected on a diffractometer and the structure determined by Fourier methods and refined to $R = 0.074$. The tungsten geometry is capped octahedral with a carbonyl ligand in the unique capping position. The iodide ligands are *trans* to each other with the two acetonitrile and octahedral carbonyl ligands *cis* to each other. The low temperature (−70°C, CD_2Cl_2) ^{13}C NMR spectrum of (**1**) showed carbonyl resonances at $\delta = 202.36$ and 228.48 ppm with an intensity ratio of 2:1. The resonance at lower field can be ascribed to the carbonyl ligand in the unique capping position. However, the room temperature ^{13}C NMR spectrum of (**1**) shows a single carbonyl resonance at $\delta = 219.65$ ppm.

The structures of seven-coordinate complexes have been found to have (a) pentagonal bipyramidal, (b) capped octahedral or (c) capped trigonal prismatic type geometries.[1] The predominant geometry for complexes of the type $[MX_2(CO)_3L_2]$ (M = Mo or W; X = halide; L = neutral donor ligand) is capped octahedral. Recently Colton and Kevecordes[2] have shown how ^{13}C NMR spectroscopy can be used to indicate if there is a carbonyl ligand in the unique capping position in this type of complex. In this communication we wish to describe the X-ray crystal structure and ^{13}C NMR spectra of the highly versatile seven-coordinate complex $[WI_2(CO)_3(NCMe)_2]$.

EXPERIMENTAL

The complex $[WI_2(CO)_3(NCMe)_2]$ (**1**) was prepared[3] by reacting the zero-valent compound $[W(CO)_3(NCMe)_3]$ with an equimolar amount of I_2 *in situ* at 0°C. Crystals suitable for X-ray crystallography were obtained by cooling an acetonitrile solution of (**1**). Found: C, 13.9; H, 1.0; N, 4.7%. Calc. for $C_7H_6N_2O_3I_2W$: C, 13.9; H, 1.0; N, 4.6%.

The ^{13}C NMR spectra of $[WI_2(CO)_3(NCMe)_2]$ were recorded on a Bruker WH-400 MHz NMR spectrometer at the University of Warwick (both spectra were calibrated against tetramethylsilane).

Crystal data (**1**)

$[WI_2(CO)_3(NCMe)_2]$, $C_7H_6N_2O_3I_2W$, $M = 603.8$, orthorhombic, $a = 12.405(8)$, $b = 7.590(8)$, $c = 13.844(12)$ Å, $U = 1303.5$ Å, $d_c = 3.04$ g cm^{-3}, $d_m = 3.02$ g cm^{-3}, $F(000) = 1064$, $Z = 4$, $\lambda = 0.7107$ Å, $\mu = 139.8$ cm^{-1}, spacegroup *Pmnb* (No. 62).

A crystal of approximate size 0.25 × 0.3 × 0.3 mm was set up to rotate about the *a* axis on a Stoe Stadi2 diffractometer and data were collected via variable width *w* scan. Background counts were for 20 s and a scan rate of 0.0333° s^{-1} was applied to a width of $(1.5+\sin\mu/\tan\theta)$. 1264 independent

* Authors to whom correspondence should be addressed.

reflections were measured of which 911 with $I > 3\sigma(I)$ were used in subsequent refinement. An empirical absorption correction was applied.[4] The structure was determined by the heavy atom method. All non-hydrogen atoms were refined anisotropically. Hydrogen atoms were refined as a rigid group.

The structure was given a weighting scheme in the form $w = 1/[\sigma^2(F)+0.003F^2]$. The final R value was 0.074 ($R_w = 0.081$). Calculations were carried out using Shelx76[5] and some of our own programs on the Amdahl V7 at the University of Reading. Molecular dimensions are given in Table 1. Atomic parameters, thermal parameters and a list of structure factors have been deposited with the Editor as Supplementary Material; copies are available on request. Atomic coordinates have also been deposited with the Cambridge Crystallographic Data Centre.

RESULTS AND DISCUSSION

The structure consists of discrete molecules of $[WI_2(CO)_3(NCMe)_2]$ with imposed crystallographic mirror symmetry and these are illustrated in Fig. 1 together with the atomic numbering scheme. The geometry of the tungsten atom is a distorted capped octahedron with one carbonyl in the unique capping position [W—C(1) 1.991(26) Å]. The capped face contains one iodine atom [W—I(1) 2.846(2) Å], and two carbonyl groups [W—C(2) 2.030(26) Å]. The remaining iodine atom [W—I(2) 2.797(2) Å] together with the two acetonitrile groups [W—N 2.167(16) Å] make up the uncapped face.

Table 1. Molecular dimensions for (1)

Distances, Å, angles degrees	
W(1)—I(1)	2.846(2)
W(1)—I(2)	2.797(2)
W(1)—C(1)	1.991(26)
W(1)—C(2)	2.030(26)
W(1)—N(3)	2.167(16)
C(1)—O(1)	1.118(43)
C(2)—O(2)	1.054(27)
N(3)—C(3)	1.197(25)
C(3)—C(4)	1.418(31)
I(1)—W(1)—I(2)	160.3(9)
I(1)—W(1)—C(1)	69.0(7)
I(2)—W(1)—C(1)	130.7(7)
I(1)—W(1)—C(2)	114.2(6)
I(2)—W(1)—C(2)	76.5(7)
C(1)—W(1)—C(2)	74.0(8)
I(1)—W(1)—N(3)	81.2(4)
I(2)—W(1)—N(3)	83.9(4)
C(1)—W(1)—N(3)	129.8(6)
C(2)—W(1)—N(3)	156.1(9)
C(2)—W(1)—C(2[a])	104.5(10)
C(2)—W(1)—N(3[a])	83.6(9)
N(3)—W(1)—N(3[a])	80.9(6)
W(1)—C(1)—O(1)	171(2)
W(1)—C(2)—O(2)	176(2)
W(1)—N(3)—C(3)	168(2)
N(3)—C(3)—C(4)	180(2)

[a] Symmetry element $(1/2-x, y, z)$.

Using our method[1] for the calculation of r.m.s. deviations from ideal geometries, we find that after normalization of bond lengths the present geometry has a r.m.s. deviation of 0.042 Å from the ideal capped octahedron. This is a surprisingly low figure in view of the distortions in the capped and uncapped faces caused by the large iodine atoms.

These atoms are mutually *trans* and it is noteworthy that the W—I bond to the iodine in the capped face is longer by 0.049 Å than the bond to the uncapped face. This is presumably due to the greater crowding in the capped face. Remaining dimensions are as expected.

The low temperature (−70°C, CD_2Cl_2) ^{13}C NMR spectrum of (1) showed two carbonyl resonances at $\delta = 202.36$ and 228.48 ppm with an intensity ratio of 2 : 1. In view of the work of Colton and Kevecordes[2] the low field resonance at $\delta = 228.48$ ppm is highly likely to be due to a carbonyl ligand in the unique capping position. The resonance at $\delta = 202.36$ ppm can be ascribed to the two equivalent octahedral carbonyl ligands. It is

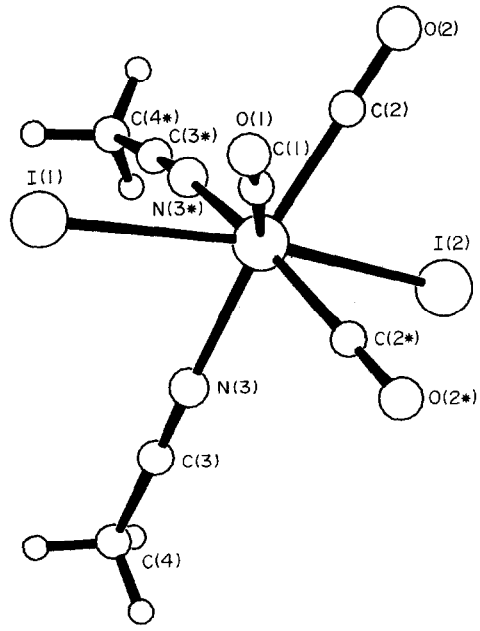

Fig. 1. X-ray crystal structure of $[WI_2(CO)_3(NCMe)_2]$ showing the atom numbering scheme.

interesting to note that the room temperature (+25°C, CD_2Cl_2) ^{13}C NMR spectrum of (**1**) shows only one carbonyl resonance at $\delta = 219.65$ ppm. Hence there must be a fluxional process occurring whereby the three carbonyl ligands are appearing in the same environment at room temperature. Variable temperature ^{13}C NMR studies are in progress in order to investigate the nature of this fluxional process.

Acknowledgements—We wish to thank Dr O. W. Howarth for measuring the ^{13}C NMR spectra of $[WI_2(CO)_3(NCMe)_2]$ at the University of Warwick and we thank the SERC for support.

REFERENCES

1. M. G. B. Drew, *Prog. Inorg. Chem.* 1977, **23**, 67.
2. R. Colton and J. Kevecordes, *Aust. J. Chem.* 1982, **35**, 895.
3. P. K. Baker, S. G. Fraser and E. M. Keys, *J. Organomet. Chem.* 1986, **309**, 319.
4. N. Walker and D. Stuart, *Acta. Cryst.* 1983, **A39**, 158.
5. G. M. Sheldrick, Shelx76, *Package for Crystal Structure Determination*, University of Cambridge (1976).

Polyhedron Vol. 7, No. 3, pp. 249–250, 1988
Printed in Great Britain

0277–5387/88 $3.00+.00
Pergamon Journals Ltd

COMMUNICATION

A SIMPLE REDOX TRANSMETALLATION SYNTHESIS OF URANIUM TETRACHLORIDE AND RELATED PREPARATIONS OF URANIUM TRIIODIDE AND CHLOROTRIS(CYCLOPENTADIENYL)URANIUM(IV)

G. B. DEACON* and T. D. TUONG

Chemistry Department, Monash University, Clayton, Victoria, 3168, Australia

(*Received* 5 *October* 1987; *accepted* 13 *October* 1987)

Abstract—Reaction of mercuric chloride with an excess of uranium metal in tetrahydrofuran (THF) yields $UCl_4(THF)_3$, whilst $UI_3(THF)_4$ is obtained from a similar reaction with mercuric iodide. Chlorotris(cyclopentadienyl)uranium(IV) has been obtained by treatment of either $(C_5H_5)_2Hg$ and mercuric chloride, or mercuric chloride and $Tl(C_5H_5)$ with an excess of uranium in tetrahydrofuran.

Anhydrous uranium tetrachloride is the reagent of choice for the synthesis of a wide range of uranium(IV) organometallics.[1,2] Although several preparations of UCl_4 are available,[3,4] they generally involve use of elevated temperatures and relatively complex procedures. We have introduced redox transmetallation reactions between mercuric halides and lanthanide metals in tetrahydrofuran as a route to anhydrous lanthanide trihalides,[5,6] and we now describe a facile synthesis of anhydrous uranium tetrachloride by a related method. Analogous syntheses of aqueous uranium tetrachloride, uranium triiodide and $(C_5H_5)_3UCl$ are also reported.

Reaction of mercuric chloride with an excess of uranium metal in boiling tetrahydrofuran (THF) yielded a suspension of mercury metal and a green solution from which $UCl_4(THF)_3$ (yield, 68%) was crystallized.

$$U + 2HgCl_2 \rightarrow Hg + UCl_4. \qquad (1)$$

The visible/near infrared spectrum of the filtered reaction mixture and of the isolated solid dissolved in tetrahydrofuran was identical with that of authentic (CERAC Chemicals) UCl_4 in the same solvent, and no UO_2Cl_2 could be detected by this technique. The composition of the complex from UCl_4 and THF has previously been established[7,8] and was confirmed in the present case by a chloride determination. Infrared absorption bands (1001s, 837s cm^{-1}) indicative[9] of coordinated tetrahydrofuran were observed. An analogous reaction in degassed water gave a green solution with a visible/near infrared spectrum identical with those of $UCl_4(THF)_3$ and commercial UCl_4 in water, and very similar to that of uranium(IV) in aqueous $DClO_4$.[10] Quantitative visible spectroscopy indicated the yield of U(IV) (based on $HgCl_2$) was *ca* 100%.

Reaction of an excess of uranium with mercuric iodide in tetrahydrofuran gave a violently air-sensitive green–black solid with the composition (uranium and iodine analyses) $UI_3(THF)_4$ (72% yield).

$$2U + 3HgI_2 \rightarrow 2UI_3 + 3Hg\downarrow. \qquad (2)$$

Absorption due to coordinated THF[9] was observed at 1011 and 841 cm^{-1}. The visible/near infrared spectrum in THF was markedly different from those of UCl_4 and UBr_4 in this solvent, consistent with a different oxidation state. Formation of UI_3, especially in the presence of an excess of uranium metal, accords with reports of easy loss of iodine from tetraiodouranium(IV) complexes.[11]

When uranium metal was reacted with bis(cyclo-

* Author to whom correspondence should be addressed.

pentadienyl)mercury (generated *in situ* from $HgCl_2$ and $Tl(C_5H_5)$[12]) in tetrahydrofuran, the visible/near infrared spectrum of the product corresponded to that[13,14] of $(C_5H_5)_3UCl$, the presence of chloride presumably deriving from unreacted mercuric chloride. It was then established that the reaction of uranium with bis(cyclopentadienyl)-mercury and mercuric chloride (mole ratio 2:4:1) yielded mercury metal and chlorotris(cyclopentadienyl)uranium(IV).

$$2U + 3(C_5H_5)_2Hg + HgCl_2 \rightarrow 2(C_5H_5)_3UCl + 4Hg\downarrow. \quad (3)$$

The product, obtained in *ca* 60% yield, was identified by visible/near infrared and mass spectroscopy. In a simpler synthesis, uranium metal was reacted with thallous cyclopentadienide and mercuric chloride (mole ratio, 2:6:1) in THF to give $(C_5H_5)_3UCl$, though a lower yield (36%) was obtained by this route.

$$2U + 6Tl(C_5H_5) + HgCl_2 \rightarrow 2(C_5H_5)_3UCl + Hg\downarrow + 6Tl\downarrow. \quad (4)$$

Although uranium metal does not react directly with $Tl(C_5H_5)$ in THF, transmetallation may occur with uranium activated *in situ* by reaction with mercuric chloride. Activation of lanthanide metals by mercuric chloride is known.[15] Alternatively, UCl_4 may be formed by reaction (1) and converted (see ref. 1) by $Tl(C_5H_5)$ into $(C_5H_5)_3UCl$, and/or some $(C_5H_5)_2Hg$ may be formed from mercuric chloride and $Tl(C_5H_5)$[12] and converted into $(C_5H_5)_3UCl$ by reaction (3).

Reactions (3) and (4) are the first examples of the use of redox transmetallation in the systhesis of organoactinides.

Acknowledgements—We are grateful to the Australian Research Grants Scheme and Monash University S.R.G. for support, Dr P. I. MacKinnon for exploratory studies, to the Australian Institute of Nuclear Science and Engineering for uranium metal and to Dr J. C. Taylor, Division of Energy Chemistry, CSIRO, for a sample of UBr_4.

REFERENCES

1. T. J. Marks and R. D. Ernst, Scandium, yttrium, and the lanthanides and actinides, in *Comprehensive Organometallic Chemistry* (Edited by G. Wilkinson, F. G. A. Stone and E. W. Abel) Chap. 31, Vol. 3. Pergamon Press, Oxford (1982).
2. B. Kanellakopulos and F. Baumgartner, Metallorganische Verbindungen in *Gmelin's Handbook of Inorganic Chemistry, Uranium Supplement E2*, pp. 113–253. Springer, Berlin (1980).
3. D. Brown, Compounds of uranium with chlorine, bromine and iodine in *Gmelin's Handbook of Inorganic Chemistry, Uranium Supplement C9*, pp. 13–15. Springer, Berlin (1979).
4. I. A. Khan and H. S. Ahuja, *Inorg. Synth.* 1982, **21**, 187.
5. G. B. Deacon and A. J. Koplick, *Inorg. Nucl. Chem. Lett.* 1979, **15**, 263.
6. G. B. Deacon, T. D. Tuong and D. L. Wilkinson, *Inorg. Synth.*, in press.
7. J. D. Ortega and D. L. Perry, *J. Inorg. Nucl. Chem.* 1974, **36**, 1179.
8. S. Herzog, K. Gustav, E. Krüger, H. Oberender and R. Schuster, *Z. Chem.* 1963, **3**, 428.
9. J. Lewis, J. R. Miller, R. L. Richards and A. Thompson, *J. Chem. Soc.* 1965, 5850; R. J. H. Clark, J. Lewis, D. J. Machin and R. S. Nyholm, *J. Chem. Soc.* 1963, 379.
10. D. Cohen and W. T. Carnall, *J. Phys. Chem.* 1960, **64**, 1933.
11. J. G. H. du Preez and B. Zeelie, *J. Chem. Soc., Chem. Commun.* 1986, 743.
12. A. N. Nesmeyanov, R. B. Materikova and N. S. Kochetkova, *Bull. Akad. Sci., USSR* 1963, 1211.
13. L. T. Reynolds and G. Wilkinson, *J. Inorg. Nucl. Chem.* 1956, **2**, 246.
14. M. L. Anderson and L. R. Crisler, *J. Organomet. Chem.* 1969, **17**, 345.
15. G. Z. Suleimanov, L. F. Rybakova, Ya. A. Nuriev, T. Kh. Kurbanov and I. P. Beletskaya, *J. Organomet. Chem.* 1982, **235**, C19; G. Z. Suleimanov, T. Kh. Kurbanov, Ya. A. Nuriev, L. F. Rybakova and I. P. Beletskaya, *Dokl. Chem.* 1982, **265**, 254.

Polyhedron Vol. 7, No. 3, p. 251, 1988
Pergamon Journals Ltd. Printed in Great Britain

ANNOUNCEMENT

RELATIONS BETWEEN HOMOGENEOUS AND HETEROGENEOUS CATALYSIS

VI INTERNATIONAL SYMPOSIUM

25–29 SEPTEMBER 1989
PISA, ITALY

ORGANIZATION

The Symposium is organized by: Department of Chemistry and Industrial Chemistry, University of Pisa, under the sponsorship of: Division of Industrial Chemistry and Catalysis Group of the Italian Chemical Society (S.C.I), Consiglio Nazionale delle Ricerche.

SCIENTIFIC PROGRAMME

The Symposium follows the previous meetings in Brussels (1974), Lyons (1977), Groningen (1980), Asilomar (1983) and Novosibirsk (1986).

The aim of the Symposium is to discuss problems at the interface between homogeneous and heterogeneous catalysis and to present results dealing with the catalytic mechanisms of heterogeneous, homogeneous and modelled enzymes catalysis, covering the following topics:

—Organometallic intermediates in heterogeneous catalysis.
—Catalysis by metal complexes attached to various interfaces.
—Surface models and catalytic activity.
—Homo and hetero-polymetallic catalysts (on surface and in solution).
—Stereospecific polymerization by supported catalysts.
—Asymmetric synthesis in heterogeneous phase.
—Relations between enzymes and synthetic catalysts.
—Electrocatalysis and photocatalysis.

The Symposium will include Plenary and Invited Lectures as well as a considerable number of contributed papers as oral or poster presentation.

Proceedings of the Symposium are planned to be published according to the tradition of the Symposium in a special issue of an International Journal, available at the registration in Pisa. Contributions will be reviewed before the publication, in accordance with the standard of the International Journal. Deadline for submission of papers: January 1989.

LOCATION

The Symposium will be held in Pisa, Palazzo dei Congressi.

ACCOMODATION AND TRAVEL

Pisa together with Tirrenia (seaside) is well provided for visitors. The International Airport "G. Gatilei" links with Frankfurt, Paris, London; one hour flights from Rome or Milano.

CORRESPONDENCE

For further information contact: **Prof. Glauco Sbrana, Secretary of the Symposium, Dipartimento di Chimica e Chimica Industriale, Università di Pisa, Via Risorgimento 35, 56100 Pisa, Italy.** Phone: 050-587226/587290. Telex: 590035 UNIV PI I.

Polyhedron Vol. 7, No. 4, pp. 253–283, 1988
Printed in Great Britain.

0277–5387/88 $5.00+.00
Pergamon Journals Ltd.

POLYHEDRON REPORT NUMBER 23

ELECTRON COUNTING IN CLUSTERS: A VIEW OF THE CONCEPTS

STEVEN M. OWEN

University Chemical Laboratory, Lensfield Road, Cambridge CB2 1EW, U.K.

CONTENTS

1. INTRODUCTION 253
1.1. Counting electrons 254
2. THE EFFECTIVE ATOMIC NUMBER (EAN) RULE 254
2.1. Breaking bonds and the EAN rule 257
3. THE POLYHEDRAL SKELETAL ELECTRON PAIR THEORY (PSEPT) 258
3.1. *Closo*-clusters 259
3.2. *Nido*- and *arachno*-structures and the capping principle 260
3.3. Condensed polyhedra 262
3.4. Extension of PSEPT to non-conical $M(CO)_4$ fragments 264
3.5. Gold clusters 265
3.6. Platinum clusters 269
3.7. The transition from molecular cluster to bulk metal 272
3.8. PSEPT and the EAN rule 274
3.9. Deviations from the PSEPT 275
4. OTHER ELECTRON COUNTING SCHEMES 276
5. CONCLUSION 277
ACKNOWLEDGEMENTS 277
APPENDIX I: STONE'S NOTATION 282
APPENDIX II: LIST OF ABBREVIATIONS 283

1. INTRODUCTION

There are few areas of chemistry where the elegance and simplicity inherent in nature manifest themselves more clearly than in the structures and electron counting rules for transition metal clusters.* The structures adopted range from the simple tri-metal triangular, arrays, through tetrahedra, octahedra, "rafts",[1] octa-metal "star clusters",[2] up to structures best described as fragments of a bulk metallic close-packed array. Added to these are capped and fused polyhedra, making the variety almost overwhelming.

By far the most important technique for determining the structure of cluster compounds is single crystal X-ray diffraction. This technique does have its limitations for some compounds containing "heavy atoms" but is generally regarded as the final determinant of a structure. The advantage of

* For the purpose of this article a "cluster" is defined as a compound containing at least three metal atoms and at least two formal metal–metal bonds. A "formal metal–metal bond" refers to a line drawn between two metal atoms in the structure. As will be seen below this need not imply anything about the bonding in the system.

X-ray crystallography is that atomic positional parameters can be obtained to a good level of accuracy. Problems of X-ray crystallography as applied to clusters are as follows:

(a) Absorption of X-rays when second or third row transition metals are present.

(b) Small atoms such as hydrogen are difficult to locate when heavy atoms are present. This is due to the small amount of electron density associated with the H atom and, therefore poor scattering of the X-rays. This problem can, however, be overcome by the use of indirect techniques such as potential energy calculations,[3] examination of the ligand polyhedral shell[4] and lengthening of metal–metal edges,[4,5] or by direct techniques such as neutron diffraction[6] and possibly by maximum entropy analysis.[7]

Once the structure has been determined, one of the most satisfying achievements is to be able to rationalize the structure in terms of the number of valence electrons available in the cluster, the "electron count". The electron count provides the vital link between structure and bonding which will allow us to understand cluster structures more fully.† Various electron counting schemes have been developed, which, although they do not pretend to provide a full explanation of bonding, do point us in the right direction. When these simple, general theories are coupled with specific molecular orbital (MO) calculations a more complete picture is obtained which can help us to understand the majority of cluster structures so far synthesized. This will be discussed in more detail below.

1.1. *Counting electrons*

Before proceeding any further it is necessary to understand how to count electrons in clusters. Probably the easiest method is to consider all metal atoms and ligands to be in the zero oxidation state. The total number of electrons is then calculated by adding together the valence electrons of the metal atoms and the electrons donated by the ligands. Any charge on the cluster is taken into account by adding (negative charge) or subtracting (positive charge) the appropriate number of electrons. A list of the number of electrons donated by various commonly encountered ligands is given in Table 1. It should be possible to work out most of these values fairly easily utilizing a simple valence bond approach. For instance a Cl atom exhibiting a μ_1-bonding mode is a one electron donor, using its singly filled p or sp hybrid orbital in a covalent bond to the cluster. However, when Cl adopts a μ_2-bonding mode it acts as a three electron donor since now it can be considered to use its singly filled orbital in a simple covalent bond and also one of its lone pairs in a dative covalent bond. Of course this is only a guide and nothing about the bonding is implied.

2. THE EFFECTIVE ATOMIC NUMBER (EAN) RULE

The simplest electron counting scheme involves the well known "18-electron", or Effective Atomic Number rule. Most of the clusters with which we shall be concerned here are composed of metals which are expected to obey the 18-electron rule in low oxidation state/organometallic mononuclear complexes i.e. the elements of Groups VIII and IX.

The 18-electron rule for mononuclear complexes derives from the fact that transition metals have nine valence atomic orbitals (AO's) [$5 \times nd$, $(n+1)s$, $3 \times (n+1)p$] which can be used, either for metal–ligand bonding or for accommodating non-bonding electron density.[56]

The "rule" can be extended to deal with transition metal (TM) cluster complexes. The assumptions of the EAN, as applied to TM clusters are as follows:[57]

(a) The metal uses all of its nine available AO's for metal–metal (M—M) bonding, metal–ligand (M—L) bonding or for the accommodation of non-bonding electrons.

(b) The edges of the metal polyhedron correspond to two centre–two electron (2c–2e) bonds.

On this basis the number of M—M bonds radiating from an ML_x unit in a cluster can be related to the number, v, of electrons in the valence shell of the metal (including those donated by ligands).

† In some respects "electron counting" is a slight misnomer since, as will be seen below, it is the nature of the orbitals, involved in bonding, which is more fundamental, so perhaps "orbital counting" would be a better name.

Table 1

Ligand	Bonding mode	Electrons donated	Example	Ref.
H	μ_1	1e	$Os_3(CO)_{11}(H)(AsMe_2)$	8
H	μ_2	1e	$[Os_4(CO)_{12}H_3]^-$	9
H	μ_3	1e	$HFeCo_3(CO)_9(P(OCH_3)_3)_3$	10
$AuPR_3$	μ_2	1e	$FeRu_3N(CO)_{12}(AuPPh_3)$	11
$AuPR_3$	μ_3	1e	$[Re_7C(CO)_{21}(AuPPh_3)]^{2-}$	12
Au	μ_4	1e	$[Os_6Au(CO)_{20}H_2]^-$	13
I	μ_1	1e	$[H_2Os_4(CO)_{12}I]^-$	14
SiR_3	μ_1	1e	$HOs_3(CO)_{10}(H)_2(SiHPh_2)$	15
$SnMe_3$	μ_1	1e	$Os_3(CO)_{10}(H)_2(SnMe_3)_2$	15
$HOs(CO)_5$	μ_1	1e	$Os_6H_2(CO)_{19}$	16
$W(CO)_3Cp$	μ_1	1e	$(Cp)WOs_3(CO)_{12}(CC_6H_4CH_3)(H)_2$	17
PR_3	μ_1	2e	$H_2Ru_2Rh_2(CO)_{11}(PPh_3)$	18
CO	μ_1	2e	$[Rh_{10}As(CO)_{22}]^{3-}$	19
CO	μ_2	2e	$Fe_3(COCH_3)(\mu_2\text{-}CO)_2(CO)_6(Cp)$	20
CO	μ_3	2e	$[Os_6O(CO)_{18}PPh_3]$	21
CS	μ_2	2e	$H_2Os_3(CO)_7(CS)S_2$	22
CR_2	μ_2	2e	$Os_3(SnCl_2)(CO)_{11}(CH_2)$	23
NR_3	μ_1	2e	$Fe_3(CO)_8(NHMe_2)(S)_2$	24
R_2CCR_2	μ_1–η^2	2e	$Os_3(CO)_{11}\{CF_3(H)CC(H)CF_3\}$	25
SO_2	μ_2	2e	$H_2Os_3(CO)_{10}(SO_2)$	26
NCMe	μ_1	2e	$Os_6H_2(CO)_{20}(MeCN)(PH)$	27
$SnCl_2$	μ_3	2e	$Os_3(SnCl_2)(CO)_{11}(CH_2)$	23
Hg	μ_4	2e	$Hg\{Fe_2Co(COMe)(CO)_7(Cp)\}_2$	28
PR_2	μ_2	3e	$H_2Rh_6(CO)_8(P^tBu_2)$	29
SR	μ_2	3e	$Os_3(CO)_{10}(CHCH_2)(SPh)$	30
CR	μ_3	3e	$[Fe_3(CO)_{10}(CH)]^-$	31
CR	μ_4	3e	$HRu_2Pt_2(CO)_3(P^iPr_3)(Cp)_2(CH)$	32
OR	μ_2	3e	$Ru_3(CO)_8(OC_6H_4OMe\text{-}2)$	33
NO	μ_1	3e	$[Fe_3(CO)_8(NO)(NH)]^-$	34
CCR	μ_2–η^1	3e	$Os_3(C_2Ph)(C_2Ph)(CO)_9$	35
$CRCR_2$	μ_1–η^1, μ_1–η^2	3e	$HOs_3(CO)_{10}(CPhCHPh)$	36
Br	μ_2	3e	$Os_4H_3Br(CO)_{13}$	37
I	μ_2	3e	$Os_5C(CO)_{14}(CO_2Me)I$	38
BCO	μ_3	3e	$H_3Os_3(CO)_9BCO$	39
Bi	μ_3	3e	$Fe_3(CO)_9(COCH_3)(Bi)$	40
$AsMe_2$	μ_2	3e	$Co_2MoFe(CO)_8(Cp)(S)(AsMe)_2$	41
RC:O	μ_2–η^2	3e	$Ru_3(C(O)(Ph))(P(Ph)(C_5H_4N))(CO)_9$	42
NO	μ_2	3e	$[Fe_2W(CO)_7(NO)(C_6H_4Me\text{-}4)(Cp)]$	43
CO	μ_3–η^1, μ_1–η^1	4e	$Os_6(CO)_{17}(NC_5H_5)_2$	44
PR	μ_3	4e	$Os_6H_3(CO)_{19}(CO_2Me)(PH)$	27
S	μ_3	4e	$[Pt_3H(S)(\mu_2\text{-dppm})_3]^+$	45
O	μ_2	4e	$(Cp)WOs_3(CO)_9(O)(Cl)(CHCH_2Tol)$	46
CCRR′	μ_2–η^1, μ_1–η^2	4e	$Os_5(CO)_{15}(CCHPh)$	47
C	Interstitial	4e	$[Re_7C(CO)_{21}(AuPPh_3)]^{2-}$	12
RCCR	μ_3–η^2	4e	$H_2Os_3(CO)_9(MeCCMe)$	48
Te	μ_3	4e	$(Cp)_2Mo_2FeTe_2(CO)_3(C_2H_2)$	49
C_2R_2	μ_2–η^2	4e	$(Cp)_2Mo_2FeTe_2(CO)_3(C_2H_2)$	49
Se	μ_3	4e	$[Ir_3Se_2(CO)_6]^-$	50
P	Interstitial	5e	$[Os_6(CO)_{18}P]^-$	51
Cp	η^5	5e	$Ru_5(CO)_{13}(Cp)(AuPPh_3)$	52
CCR	μ_3–η^2	5e	$Os_3(C_2Ph)(C_2Ph)(CO)_9$	35
N	Interstitial	5e	$[Co_6N(CO)_{13}]^-$	53
Arene	η^6	6e	$Ru_3(CO)_7(NPh)(C_6H_6)$	54
CS	μ_4–η^2	6e	$Co_3Fe(Cp)(CO)_9(CS)$	55

The number of M—M bonds is equal to $18-v$. This is just another way of saying that the metal must form $(18-v)$ 2c–2e bonds in order to bring its electron count up to the "magic number" of 18.

Consider the $Os(CO)_4$ unit. This has 16 valence electrons (eight from Os and two from each of the carbonyls) and it will therefore need to form 18 – 16, i.e. 2 M—M bonds to reach 18. This is seen in, for example,

$Os_3(CO)_{12}$[58]

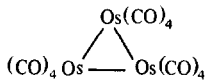

Rather than considering each ML_x fragment in turn, a simple counting rule which gives the number of 2c–2e bonds can be derived. Consider a cluster M_nL_x, in which all the metals or ligands need not be the same. The number of M—M 2c–2e bonds, m, is given by,

$$m = (18n-k)/2$$

where k is the total electron count. Consider some examples of this:

(a) $Ir_4(CO)_{12}$[59]

$$k = \underset{\text{metals}}{4\times 9} + \underset{\text{ligands}}{12\times 2} = 60$$

$$m = (18x-k)/2 = (18\times 4-60)/2$$

$$m = 6.$$

Therefore six M—M 2c–2e bonds are predicted for $Ir_4(CO)_{12}$ and indeed, the structure is a tetrahedron.

(b) $[Os_6(CO)_{18}P]^-$ [51]

$$k = \underset{\text{metals}}{6\times 8} + \underset{\text{carbonyls}}{18\times 2} + \underset{\text{P}}{5} + \underset{\text{charge}}{1} = 90$$

$$m = (18\times 6-90)/2$$

$$m = 9$$

(Note: P donates 5e to the valence shell of the metals, which is consistent with it occupying an interstitial site—Table 1).

Therefore nine 2c–2e bonds are predicted and the structure is a trigonal prism of Os atoms.

(c) $[Ni_8(PPh)_6(CO)_8]^{2-}$ [60]

$$k = 8\times 10+6\times 2+8\times 2+2 = 120$$

$$m = (8\times 18-120)/2$$

$$m = 12.$$

Therefore 12 2c–2e M—M bonds are predicted which is consistent with the observed cubic structure.

Note that, here the observed structure is not the only one which could have been predicted on the basis of the number of 2c–2e bonds. For instance, the cuneane structure (Fig. 1) is also possible and has been found for the 120 electron complex $Co_8S_2(N^tBu)(NO)_8$.[61]

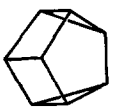

Fig. 1. The cuneane structure.

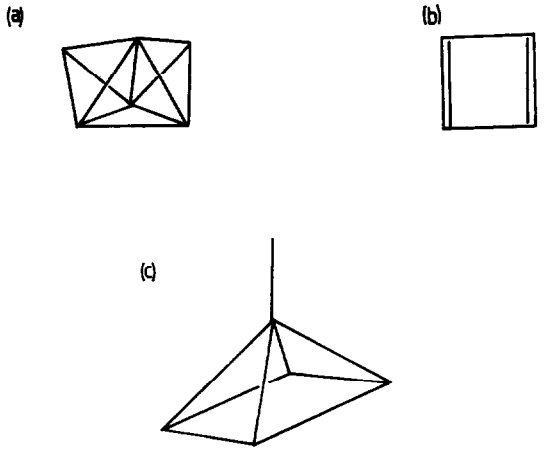

Fig. 2. (a) Bicapped tetrahedron. (b) Alternative four vertex structure with six M—M 2c–2e bonds. (c) Alternative six vertex structure with nine M—M 2c–2e bonds.

(d) Another example where more than one structure is possible is $Os_6(CO)_{18}$,[62]

$$k = 84$$

$$m = (108-84)/2 = 12.$$

Therefore 12 M—M bonds are predicted. The most obvious and most symmetrical polyhedron with 12 edges is the regular octahedron, however the actual structure of $Os_6(CO)_{18}$ is a bicapped tetrahedron [Fig. 2(a)]. This structure, although it does have 12 M—M bonds, could not reasonably have been predicted. Similarly, for (a) and (b), above, alternative structures could be envisaged [Fig. 2(b) and (c)]. This illustrates one failing of the EAN rule; others will now be discussed.

Consider $[Os_6(CO)_{18}]^{2-}$,

$$k = 86$$

$$m = (108-86)/2 = 11.$$

Therefore a polyhedron with 11 M—M 2c–2e bonds i.e. 11 edges would be predicted. The actual structure is an O_h octahedron.[63] This electron count is characteristic of octahedra and, in general, they show no tendency to undergo facile 2e oxidation reactions.[57] One possible explanation for 11 electron pairs shared between 12 edges of a polyhedron could be in terms of resonance, i.e. a resonance hybrid of 12 canonical forms, each involving an octahedron with one edge broken. This is not really a satisfying explanation and a better one will be discussed in the next section.

For all clusters of the Co and Fe subgroups so far synthesized the number of polyhedral edges is always greater than or equal to the number of 2c–2e bonds predicted by the EAN rule (see Table 2). For most clusters with six or more metal atoms the general tendency is to have more edges than predicted (Table 2). Indeed, Ciani and Sironi[85] have performed extended Hückel molecular orbital (EHMO) calculations on more than 100 hypothetical geometries for high nuclearity rhodium clusters, and have found that the "limit" imposed by the EAN rule is never violated. Clusters which obey the EAN rule are termed "electron precise".

No gold or platinum clusters are included in Table 2. This is because gold and platinum cluster compounds usually exhibit electron counts less than their Group VIII and Group IX counterparts. As the *s–p* separation increases from left to right across the TM series and down a group there is less tendency for *p* orbitals to be fully involved in skeletal bonding.[86] This is discussed in greater detail below.

2.1. *Breaking bonds and the EAN rule*

Examination of Table 2 will show that cluster geometries such as the "butterfly" and open triangle are related to the electron precise clusters by the removal of one, or more, edges. It is a

Table 2

Structure	E^a	k^b	m	Example	Ref.
Triangle	3	48	3	$[Os_3H(CO)_{10}(MeCN)_2]^+$	64
Linear/open triangle	2	50	2	$Os_3(CO)_{12}(SiCl_3)_2$	65
Tetrahedron	6	60	6	$CpMoIr_3(CO)_{11}$	66
Butterfly	5	62	5	$[HFe_4(CO)_{13}]^-$	67
Spiked triangle	4	64	4	$(Me_3P)(CO)_4OsOs_3(CO)_{11}$	68
Trigonal bipyramid	9	72	9	$Os_5(CO)_{16}$	69
Square pyramid	8	74	8	$Ru_5C(CO)_{15}$	70
Edge-bridged tetrahedron	8	74	8	$H_2Os_5(CO)_{16}$	71
Open square pyramid	7	76	7	$Ni_2Ru_3(\eta^5\text{-}Cp)_2(CO)_9(\mu_5\text{-}PPh)$	72
Bicapped tetrahedron	12	84	12	$Os_6(CO)_{16}(CNBu^t)_2$	73
Octahedron	12	86	11	$Rh_6(CO)_{16}$	74
Capped square pyramid	11	86	11	$H_2Os_6(CO)_{18}$	75
Spiked TBP	10	88	10	$[Fe_3Rh_3(CO)_{10}(\mu_2\text{-}CO)_7]^{3-}$	76
Trigonal prism	9	90	9	$[Os_6(CO)_{18}P]^-$	51
Edge broken trigonal prism	8	92	8	$Os_6(CO)_{18}PCl$	77
Linked butterfly[c]	7	94	7	$[Fe_4Ru_2(CO)_{22}]^{2-}$	78
Monocapped octahedron	15	98	14	$Ir_7(CO)_{12}(C_8H_{12})(C_8H_{11})(C_8H_{10})$	79
Bicapped octahedron	18	110	17	$[Os_8(CO)_{21}]^{2-}$	80
Square antiprism	16	114	15	$Ru_8(\mu_8\text{-}P)(\mu_2\text{-}\eta^1,\eta^6\text{-}CH_2C_6H_5)(CO)_{19}$	81
Tetracapped octahedron	24	134	23	$[Os_{10}(CO)_{24}]^{2-}$	82
Icosahedron	30	170	23	$[Rh_{12}Sb(CO)_{27}]^{3-}$	83
Twinned cuboctahedron	24	170	23	$[Rh_{13}(CO)_{24}H_{5-n}]^{n-}$	84

[a] E is the number of polyhedral edges.
[b] k and m are defined above.
[c] Linked butterfly = two triangles joined by a bond.

general rule that an edge is broken for every electron pair added to these clusters.[87] This is often put forward as evidence for the localized (i.e. "edge = 2c–2e bond") nature of the bonding in these systems, that is, donation of 2e into a M—M antibonding orbital causes the bond to break. A similar argument can, however, be used within a delocalized bonding scheme; placing 2e in an orbital which has M—M antibonding character along an edge causes the edge to lengthen in order to reduce the antibonding character, thereby stabilizing the orbital.[88] This distortion is accompanied by some reorganization of the orbitals.

Addition of 2e to a cluster not obeying the EAN rule does not tend to cause a bond to break but can result in a more fundamental structural reorganization.

The main problem with the EAN rule arises from the assumption that the edges of a metal polyhedron correspond to "normal" 2c–2e bonds. Although this tends to work for the planar ring compounds, three-connected polyhedra (tetrahedron, trigonal prism, cube, cuneane etc.) and some other low nuclearity geometries, it does not work at all well for most of the higher nuclearity clusters ($n \geqslant 6$). For these, a delocalized bonding picture, in which edges no longer correspond to bonds, *has* to be used. Even for the clusters where the EAN rule does work it is often better to accept it as a guide to the number of polyhedral edges rather than a description of the bonding within the system. A delocalized scheme usually provides a more satisfying picture of the bonding.

3. THE POLYHEDRAL SKELETAL ELECTRON PAIR THEORY (PSEPT)

The polyhedral skeletal electron pair theory (PSEPT) developed chiefly by Wade[89] and Mingos[87] is probably the most widely used electron counting scheme. It has the advantage that, in its simplest form it is easily remembered and applied, and when various extensions and modifications are included, it tends to work for the vast majority of TM cluster systems. It also works very well for main group compounds (which will not be discussed here but see, for example ref. 89). By "work" it is meant that PSEPT can provide a rationalization of the structures of cluster compounds and

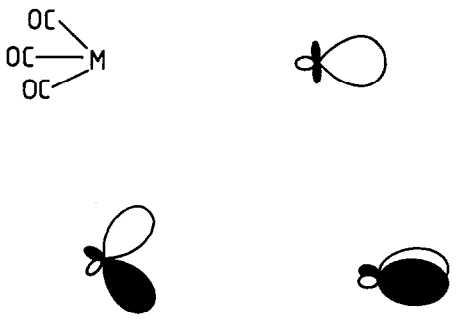

Fig. 3. Frontier orbitals of the $M(CO)_3$ unit.

also some insight into the bonding. It has also been used to predict electron counts for cluster geometries before they have been prepared and the presence of H atoms.

The PSEPT relies on the fact that the various polyhedra adopted by TM's tend to have characteristic numbers of valence electrons available for skeletal bonding (Table 2).

3.1. Closo-*clusters*

The PSEPT, as originally formulated, states that any *closo*-deltahedral* structure will have $(n+1)$ electron pairs involved in skeletal bonding.[57,89] It assumes that each skeletal M atom uses 6 AO's for M—L bonding and occupation by non-bonding electrons leaving three available for skeletal bonding.[57,89] These three orbitals are *dsp* hybrids and are shown in Fig. 3. Thus, there is one "radial" orbital (pointing towards the centre of the polyhedron) and two "tangential" orbitals. The symmetry of these orbitals is such that, in a deltahedral structure $(n+1)$ bonding or weakly antibonding MO's are produced.[90] This was originally shown for $[B_6H_6]^{2-}$ by Longuet-Higgins[91]† and has since been shown by Stone[92] using his Tensor Surface Harmonic (TSH) technique. Although, in the calculations on TM compounds it has not proved possible to identify the set of $(n+1)$ MO's involved solely in strong M—M skeletal bonding, $(2n-1)$ high-lying antibonding orbitals composed mainly of *s* and *p* character can usually be identified.[88,93] This is entirely equivalent from an electron counting point of view.

Consider the octahedral case; Lauher[88] has shown that the general features of the MO diagram for a bare M_6 cluster are as follows. There are 43 CVMO's (Cluster Valence Molecular Orbitals i.e. MO's involved in holding valence electrons) and 11 HLAO's (High Lying Antibonding Orbitals) with a large energy gap between the HCVMO (Highest CVMO) and the LHLAO (Lowest HLAO). When this "bare" cluster interacts with CO ligands to form a metal carbonyl cluster the symmetries of the possible combinations of CO orbitals are such that they match the existing CVMO's, and therefore a bonding and high-lying antibonding orbital are produced, only the lower of which will be occupied for each symmetry group. Thus the number of CVMO's in the octahedral TM cluster will be 43.[88] This result is confirmed by Mingos' calculations on $[Co_6(CO)_{14}]^{4-}$[93] and Mingos and Forsyth's work on M_6H_6 (M = Co, Ir).[94] For the octahedral case the PSEPT would predict (6×6) MO's involved in M—L bonding or holding non-bonding electron density and $(n+1) = 7$ MO's involved in skeletal bonding; thus the number of occupied MO's predicted by the PSEPT is also 43. It is reassuring that an electron count of 86 is observed for the majority of octahedral clusters. The predictions of the PSEPT for other systems are given in Table 3. Lauher[88] has performed EHMO calculations on several geometries and has produced results in general agreement with these predictions. This gives us the "rule" that a transition metal carbonyl cluster with a *closo*-deltahedral geometry will have $(7n+1)$ CVMO's.[96] This number has, in fact, been found for those deltahedral

* A deltahedral structure is one which has all triangular faces.

† B—H is isolobal with an $M(CO)_3$ unit in that the symmetry, energy and extent in space of the frontier orbitals of the two fragments are similar. This means that arguments based mainly on symmetry, as in the MO calculations will apply equally well to an $(M(CO)_3)_n$ cluster as to a $[B_nH_n]^{2-}$ cluster. See, for example Hoffmann in ref. 129.

Table 3

Structure	CVMO[a]	$CVMO_{obs}$	$7n+1$	Example	Ref.
TBP	36	36	36	$Os_5(CO)_{16}$	69
Octahedron	43	43	43	$[Os_6(CO)_{18}]^{2-}$	63
Pentagonal bipyramid	49	—	50	—	
Dodecahedron	56	—	57	—	
Tricapped trigonal prism	64	—	64	—	
Bicapped square antiprism	71	71	71	$[Rh_{10}S(CO)_{22}]^{2-}$	95
Icosahedron	85	85	85	$[Rh_{12}Sb(CO)_{27}]^{3-}$	83

[a] EHMO calculations by Lauher.[88]

Table 4

Structure	CVMO[90]	$CVMO_{obs.}$	$7n+1$	Example	Ref.
Square antiprism	57	57	57	$[Co_8(CO)_{18}C]^{2-}$	97
Bicapped cube	71	—	71	—	
Cube octahedron	85	85	85	$[Rh_{13}(CO)_{24}H_3]^{2-}$	84

geometries which have so far been synthesized (Table 3). For several non-deltahedral geometries the $(7n+1)$ CVMO count is also observed (Table 4).

Thus from PSEPT the 86e count for an octahedron is no longer anomalous. However, although the "$(2n+1)$ rule" works quite well for deltahedral and some other structures, there are a great many geometries for which it does not work. These structures will be discussed below.

3.2. Nido- *and* arachno-*structures and the capping principle*

(a) Nido-*clusters*. There is a family of clusters which have $(7n+2)$ CVMO's and structures based upon the polyhedron with $(n+1)$ vertices.[90,96] These polyhedra are called *nido-* (nest-like). Their structures can be derived by removing a vertex (not necessarily the one of highest connectivity) from the polyhedron with $(n+1)$ vertices. Examples of *nido*-clusters are given in Table 5.

It is perhaps slightly artificial to regard the tetrahedron as a "*nido*-trigonal bipyramid" and this structure will be discussed in more detail below.

(b) Arachno-*clusters*. *Arachno*-(web-like) clusters have $(7n+3)$ CVMO's and structures obtained by removing two vertices from $(n+2)$ vertex parent polyhedra.[90,96] Examples of *arachno*-clusters are in Table 6.

For both the *nido-* and *arachno*-clusters the number of skeletal bonding electron pairs is the same as that of the parent polyhedron. The number of CVMO's decreases by six for each vertex removed; consistent with the removal of the M—L bonding and non-bonding orbitals of the vertex unit (*vide infra*).

Table 5

Structure	Based on	Y^a	Z^b	$7n+2$	Example	Ref.
Tetrahedron	TBP	36	30	30	$Ir_4(CO)_{12}$	59
Square pyramid	Octahedron	43	37	37	$Fe_5(CO)_{15}C$	98
Capped square antiprism	Bicapped square antiprism	71	65	65	$[Rh_9P(CO)_{21}]^{2-}$	99

[a] Y is the no. of CVMO's of the parent, *closo*-polyhedron.
[b] Z is the observed number of CVMO's.

Table 6

Structure	Based on	Y^a	Z^b	$7n+2$	Example	Ref.
Triangle	TBP	36	24	24	$Os_3(CO)_{12}$	58
Butterfly	Octahedron	43	31	31	$[Fe_4H(CO)_{13}]^-$	67
Square antiprism	Bicapped square antiprism	71	59	59	$[Ni_8C(CO)_{16}]^{2-}$	100

[a] Y is the number of CVMO's of the parent, *closo*-polyhedron.
[b] Z is the observed number of CVMO's.

The *arachno*- and *nido*-clusters do not represent a very important class of cluster compounds and generally their description in terms of the PSEPT, although perfectly correct, is not really useful. For example, describing $Os_3(CO)_{12}$ as an "*arachno*-trigonal bipyramid" does not provide any further insights into the bonding in the system.

(c) *Capped clusters and the capping principle.* The capping principle was first introduced by Mingos.[87] It states that a capped polyhedral cluster has the same number of bonding skeletal MO's as the parent, uncapped polyhedron.[94] The capping principle does not just apply to capping of *closo*-polyhedra but also works for capping *nido*- and *arachno*-polyhedra and those structures which do not obey the PSEPT. The electron count for a capped polyhedron will generally be $12x$ greater than that for the parent polyhedron, where x is the number of capping atoms. The value 12 comes from the six MO's involved in M—L bonding or holding "non-bonding" electron density, which the capping group supplies. Table 7 gives some examples of capped structures.

MO justification of the capping principle. The capping principle is obeyed because the frontier orbitals of an $M(CO)_3$ capping group are of the correct symmetry to interact with CVMO's of the parent cluster.[94] The strongest interaction will be between the A_1 and E (referred to an axis through the centroid of the face to be capped) orbitals of the $M(CO)_3$ fragment and skeletal bonding orbitals of the same symmetry on the parent polyhedron. This interaction will, in each case, produce a bonding and an antibonding MO.[94] The antibonding MO will be high in energy (strong interaction) and therefore empty whereas the bonding orbital will be filled. The other six orbitals of the $M(CO)_3$ unit (those used for M—L bonding and holding non-bonding electron density) will not interact very strongly with the orbitals of the parent polyhedron and will remain relatively unperturbed. The number of M—M bonding MO's has thus remained the same and the number of CVMO's has increased by six. Figure 4 shows a schematic diagram of the capping process, after the one by Mingos and Forsyth,[94] which illustrates this point. The general features of the diagram are supported by EHMO calculations on Co_4H_4 and Co_5H_5.[94]

The capping principle is obviously related to the formation of *nido*- and *arachno*-clusters.[94]

Table 7

Structure[a]	n	Y	Z	x	$Y+6x$	Example	Ref.
M.C. TBP	6	36	42	1	42	$Os_6(CO)_{18}$	62
B.C.tetrahedron	6	30	42	2	42	$HOs_6(CO)_{16}(PPh_2Me)(AuPEt_3)$	101
M.C. square pyramid	6	37	43	1	43	$H_2Os_6(CO)_{18}$	75
M.C. octahedron	7	43	49	1	49	$[Rh_7(CO)_{16}]^{3-}$	102
B.C. octahedron	8	43	55	2	55	$[Re_8C(CO)_{24}]^{2-}$	103
B.C. trigonal prism	8	45	57	2	57	$Cu_2Rh_6(CO)_{15}(NCCH_3)_2$	104
M.C. square antiprism	9	57/59[b]	65	1	63/65	$[Rh_9P(CO)_{21}]^{2-}$	99
B.C. square antiprism	10	57/59	71	2	69/71	$[Rh_{10}S(CO)_{22}]^{2-}$	95
TETRA C. octahedron	10	43	67	4	67	$[Os_{10}C(CO)_{24}]^{2-}$	82
HEXA C. octahedron	12	43	80	6	79	$[Fe_6Pd_6(CO)_{24}H]^{3-}$	105
PENTA C. cube	13	60	90	5	90	$[Rh_{14}(CO)_{25}]^{4-}$	106

[a] M.C. = "monocapped"; B.C. = "bicapped"; C. = "capped".
[b] Both have been observed.[67,97]

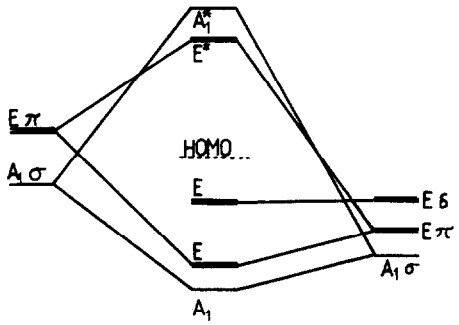

Fig. 4. Schematic diagram showing the effect of a capping group on the MO energy levels of a cluster.

When a vertex group is removed a strongly bonding and antibonding set of MO's will be replaced by just a bonding set. Also, six non-bonding/M—L bonding orbitals will be removed, therefore no extra skeletal bonding MO's have been produced and the number of CVMO's has decreased by six, as is seen for the clusters in Tables 5 and 6.

Mingos *et al.* have shown that "problems" can arise with multiple capping of polyhedra in that symmetry orbitals of the capping groups can be generated which are of the correct symmetry to interact with antibonding orbitals of the parent polyhedron and therefore produce "extra" occupied orbitals.[94,107,108] Indeed Mingos and Johnston[108] have predicted that capped three-connected polyhedra where the capping atoms form a ring will be characterized by $N+12x+2$ or $N+12x+4$ electrons, where x is the number of capping groups and N is the electron count characteristic of the parent polyhedron. Thus, one or two "extra" CVMO's are produced. Tricapped trigonal prismatic geometries have been observed for the post transition metals and $[Ge_9]^{2-}$ has an electron count of 128e ($N+12x+2$) and $[Bi_9]^{5+}$ has 130e ($N+12x+4$).[109,110] A similar argument is likely to apply to the hexacapped octahedron, $[Fe_6Pd_6(CO)_{24}H]^{3-}$ (Table 7) which has one more CVMO than "expected".

3.3 *Condensed polyhedra*

It has been noticed[97,111] that many higher nuclearity transition metal carbonyl compounds have structures derived by the condensation of smaller polyhedra; that is, they are fused *closo*-polyhedra sharing a common vertex, edge or face. Mingos[96,112,113] has derived a simple electron counting scheme for these clusters which can be stated,

The total electron count in a condensed polyhedron is equal to the sum of the electron counts for the parent polyhedra minus the electron count characteristic of the atom, pair of atoms, or face of atoms common to both polyhedra.

The characteristic electron counts[96,112,113] are shown in Table 8. They correspond to the electron counts for the shared unit when it exists as an isolated cluster e.g. 18e is characteristic of mononuclear compounds such as $Fe(CO)_5$,[114] 34e, a binuclear unit e.g. $Mn_2(CO)_{10}$[115] etc. Examples of condensed polyhedra with their electron counts are given in Table 9.

As well as viewing condensation as a fusion process between two *closo*-polyhedra it can be regarded as an interaction between a *closo*-unit and a *nido*-, *arachno*-unit etc.[96] This leads to a theoretical justification of the electron counts for condensed polyhedra. MO calculations have shown[94,124] that a *nido*-polyhedron has three frontier orbitals of a_1 and e symmetry, capable of interacting with suitable orbitals of a *closo*-polyhedron. These orbitals on the *closo*-polyhedron are the frontier orbitals which would have interacted with ligands had they been present and so are included in the number of available CVMO's for the *closo*-polyhedron. When the two units interact, three bonding and three antibonding orbitals are produced. The total number of orbitals available for occupation by electrons in the condensed polyhedron is, therefore, three less than the number in the separate *nido*- and *closo*-units.[96] Now, a *nido*-unit has six less CVMO's than the *closo*-unit from which it was derived and therefore, if the condensation process is viewed in terms of a *closo*–*closo*-interaction, the total number of CVMO's in the resultant molecule is nine less than the total for the two *closo*-units. A vertex sharing condensed polyhedron, thus, has 18e less than the sum of the electron counts for the two *closo*-polyhedra from which it was derived.

Table 8.

Shared unit	Subtract
Vertex	18e
Edge	34e
Triangular face	48e
Triangular face	50e[a]
Square face	62e[b]
Square face	64e[c]
"Butterfly face"	62e

[a] When both parent polyhedra are deltahedra and have nuclearity of six or greater.
[b] When either of the parent polyhedra is a deltahedron.
[c] When both parent polyhedra are three-connected polyhedra.

An edge sharing condensed polyhedron can be envisaged as being formed from a *closo*-fragment and an *arachno*-fragment. It has been shown[124–126] that an *arachno*-unit has five frontier orbitals (a_1, e_1, e_2) suitable for interaction with a *closo*-unit. This time, five bonding and five antibonding MO's are produced. An *arachno*-fragment has $(2 \times 6) = 12$ CVMO's less than a *closo*-unit and therefore, the total number of CVMO's for the condensed polyhedron is the sum of that for the *closo*-units minus $(12 + 5) = 17$. Seventeen being the number of CVMO's characteristic of a binuclear unit.

Following the above arguments, a *hypho*- (3 vertices missing) fragment could interact with a *closo*-polyhedron to give a triangular face sharing unit. A *hypho*-fragment would thus be expected to have six FO's available for interaction with the *closo*-unit in order to give a total of 24 CVMO's less than in the isolated *closo*-units. Of course, the situation is made more complicated by the possibility of two electron counts for the shared facial unit (48e and 50e) and a full MO approach would be desirable.

The capping principle (*vide supra*) is just a special case of the condensation principle in that addition of a capping atom to a triangular face can also be viewed as the condensation of a tetrahedron and a *closo*-polyhedron.

Table 9

Compound	Parent polyhedra	Shared unit	$Z_{obs.}$[a]	$Z_{predict}$[b]	Ref.
$H_2Os_5(CO)_{14}(S)_2$	2 triangles	1 vertex	78e	$48+48-18=78$	116
$[Os_5C(CO)_{15}I]^-$	Butterfly, open triangle	2 vertices	76e	$62+50-2\times18=76$	117
$[Re_4(CO)_{16}]^{2-}$	2 triangles	1 edge	62e	$48+48-34=62$	118
$Os_5H_2(CO)_{16}$	Tetrahedron, triangle	1 edge	74e	$60+48-34=74$	71
$[Ru_{10}C_2(CO)_{24}]^{2-}$	2 octahedra	1 edge	138e	$86+86-34=138$	119
$[Os_8H(CO)_{22}]^-$	Bicapped tetrahedron, tetrahedron	1 edge	110e	$84+60-34=110$	120
$Os_7(CO)_{19}(S)$	Square pyramid, TBP	1 face	98e	$74+72-48=98$	121
$[Rh_9(CO)_{19}]^{3-}$	2 octahedra	1 face	122e	$86+86-50=122$	122
$[Rh_{11}(CO)_{23}]^{3-}$	3 octahedra	1 face 1 butterfly	148e	$86\times3-50-62=146$[c]	123

[a] $Z_{obs.}$ is the observed electron count for the cluster.
[b] $Z_{predict}$ is the electron count predicted on the grounds of the condensation principle, above.
[c] One of the few clusters for which the condensation principle does not work. The count of 50e is subtracted for the triangle since the parent *closo*-polyhedra are deltahedra of nuclearity six.

The condensation principle holds quite generally for a wide range of clusters including those in which the individual *closo*-units do not obey the PSEPT. It must however be modified for dealing with gold and platinum clusters.[126]

3.4. *Extension of PSEPT to non-conical* $M(CO)_4$ *fragments*

Cluster compounds containing $M(CO)_4$ units often adopt "unusual" geometries e.g. the edge bridged tetrahedron of $H_2Os_5(CO)_{16}$;[71] the "bowtie" of $Os_5(CO)_{19}$;[127] the "raft" of $Os_6(CO)_{17}(POMe_3)_4$.[1] This can be attributed to the different bonding characteristics of an $Os(CO)_4$ as compared to an $Os(CO)_3$ unit.[128]

The PSEPT, as originally derived, assumed that a polyhedral vertex unit (e.g. $M(CO)_3$, BH) supplies three orbitals for cluster skeletal bonding. A comparison of the FO's of an $M(CO)_3$ and a C_{2v} $M(CO)_4$ unit shows that the arrangement is quite different, with one of the orbitals of the *e* set being substantially lowered in energy (Fig. 5). In spite of this difference Mingos and Evans[128] have shown that one $M(CO)_4$ fragment can replace an $M(CO)_3$ unit in an electron precise or deltahedral cluster without changing the electron count. There is, however, a decrease in the M—M bond strength within the cluster due to the different bonding characteristics of the two units.

The differences between the FO's of $M(CO)_3$ and $M(CO)_4$ does lead to differences in the bonding modes adopted by the units. The C_{2v} $Os(CO)_4$ group often adopts an edge bridging mode (see Table 10). In these cases the electron count can be rationalized by viewing it as a 2e donor ligand,[128] using its two high-lying frontier orbitals to bond to the cluster. In this way $Os(CO)_4$ is regarded as being isolobal with CH_2.[132]

Consider $H_2Os_5(CO)_{16}$ i.e. $[H_2Os_4(CO)_{12}][Os(CO)_4]$; the $H_2Os_4(CO)_{12}$ unit has 58 valence electrons and the extra two, required for the tetrahedral structure are provided by the $Os(CO)_4$ bridging ligand. If the $Os(CO)_4$ unit is included in the electron count for this cluster then the electron count is 74e rather than 60e. This increase of 14e in the electron count upon addition of an edge bridging group is a general feature and has lead Mingos and Evans[128] to the conclusion that the electron count for edge bridged polyhedra is $N+14x$; where N is the electron count characteristic of the unbridged polyhedron and x is the number of bridging groups (Table 10). The theoretical justification of this rule is the same as that for the capping principle and in fact this could be regarded as the "2-D capping principle".

Just as problems can occur with multiple capping of structures, Mingos and Evans[128] have shown that in the 90e M_6 raft systems (M_3 triangles with three edge bridging groups forming a ring) a low lying unoccupied a_2' MO is generated which gives the possibility of facile 2e reduction to the

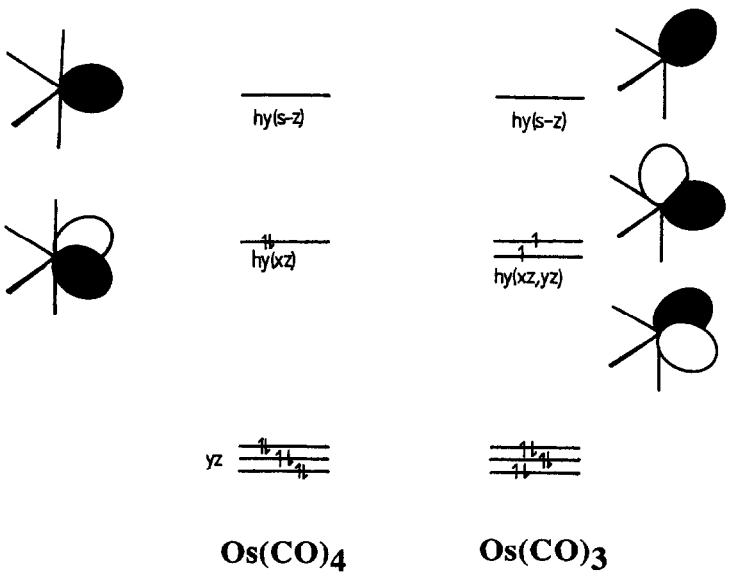

Fig. 5. Comparison of the frontier orbitals of an $M(CO)_3$ and $M(CO)_4$ unit.

Table 10

Structure	Basic unit	N^b	x	$N+14x$	$Z_{obs.}{}^a$	Example	Ref.
Triangle	Linear binuc.	34	1	48	48	$Os_3(CO)_{12}$	58
Butterfly	Linear binuc.	34	2	62	62	$HOs_3Re(CO)_{15}$	129
Edge bridged capped square pyramid		72	1	100	100	$H_2Os_7(CO)_{21}$	130
Edge bridged square pyramid		74[c]	1	88	88	$PtOs_5(CO)_{15}(PPh_3)_2S$	131

[a] $Z_{obs.}$ is the observed electron count.
[b] N is the electron count of the parent polyhedron.
[c] Based on $PtOs_4(CO)_{13}(PPh_3)_2S$.[131]

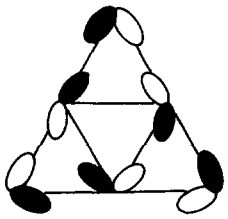

Fig. 6. The a_2' MO of a planar Os_6 raft system.

92e cluster. This MO is shown in Fig. 6. A 92e cluster with a structure based on a raft has been reported. $[Ru_6H(\mu_2\text{-}O{=}CNMe_2)_2(CO)_{18}]^-$ [133] is a 92e compound consisting of a puckered ring of six Ru atoms which can be viewed as being derived from the raft by breaking the internal edges i.e. adding two electrons to the a_2' orbital.

3.5 *Gold clusters*

So far no mention has been made of gold clusters; an examination of Table 11 shows why.

(a) *Homonuclear gold compounds.* All the clusters in Table 11 have electron counts lower than would be expected by the PSEPT as already discussed. The reason for this is the differences in the FO's between an $M(CO)_3$ group and an $AuPR_3$ group (Fig. 8).[142]

In $AuPR_3$ there is one low-lying radial sp_σ hybrid orbital and two high-lying p_π tangential orbitals.[142] In gold cluster compounds these tangential orbitals play very little part in cluster bonding, this being dominated by the radial interactions.[142–144] The reasons are the high-lying nature of the p_π orbitals (i.e. the high s–p promotion energy for gold) and the small $6p_\pi$–$6p_\pi$ overlap integrals.[143,144] MO calculations have confirmed the predominance of the radial interactions.[143,144]

An MO diagram for $[Au_6(PPh_3)_6]^{2+}$ is shown in Fig. 9.[144] The diagram shows the four fairly low-lying orbitals (of A_{1g} and T_{1u} symmetry) which are most important in skeletal bonding. Analysis

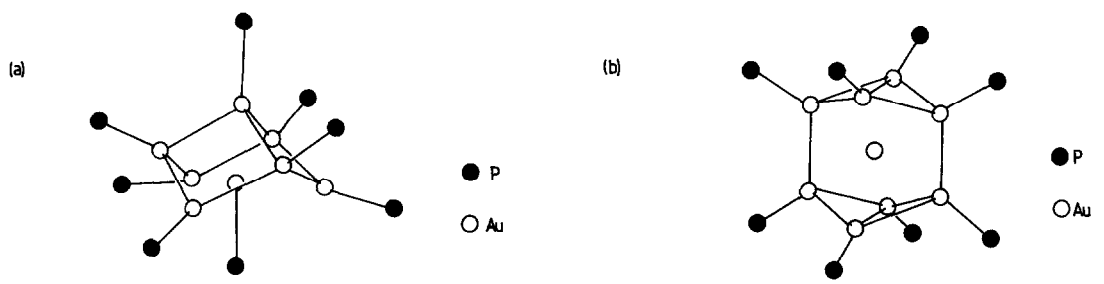

Fig. 7. (a) $[Au_8(PPh_3)_8]^{2+}$. (b) $[Au_9\{P(C_6H_4\text{-}p\text{Me})\}_8]^{3+}$.

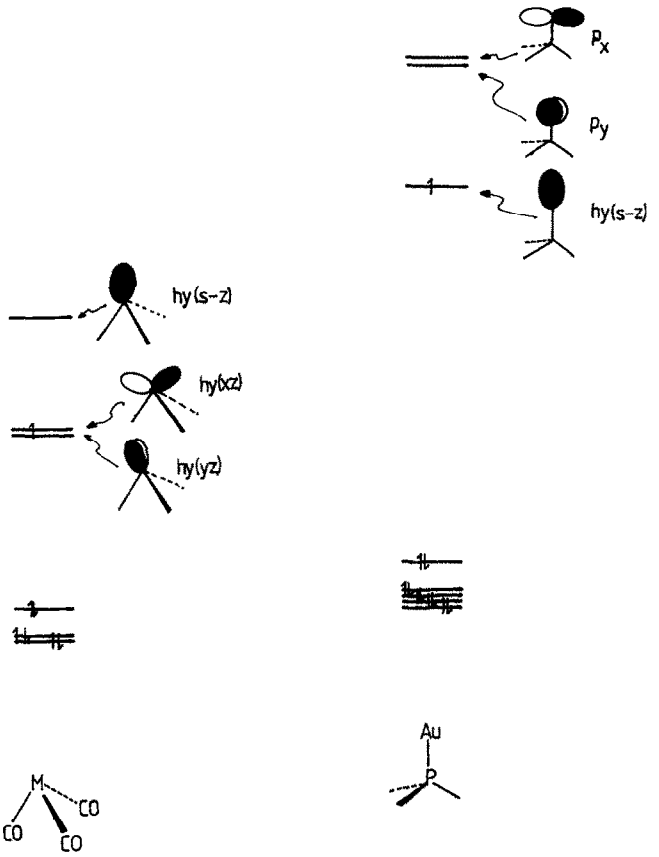

Fig. 8. Comparison of the frontier orbitals of an $M(CO)_3$ and an $AuPR_3$ unit.

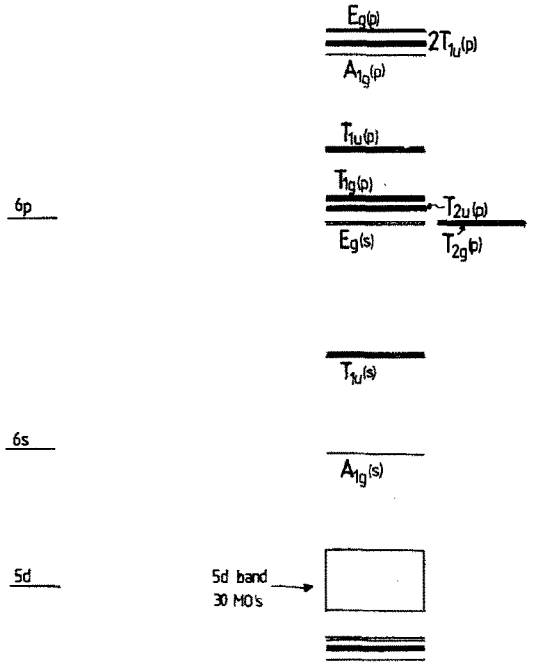

Fig. 9. MO energy level diagram for $[Au_6(PPh_3)_6]^{2+}$.

Table 11. Homonuclear gold clusters

Compound	Structure	$Z_{obs.}$[a]	PSEPT[b]	Diff.[c]	Ref.
$Au_4(\mu_2\text{-}I)_2(PPh_3)_2$	Distorted tetrahedron	54	60	−6	135
$Au_4(S_2CCH_3)_4$	Planar rhombus	52	62/64	−10/12	136
$[Au_6\{P(p\text{-}C_6H_4CH_3)_3\}_6]^{2+}$	Distorted octahedron	76	86	−10	137
$[Au_6(PPh_3)_6]^{2+}$	Edge sharing tetrahedron	76	86	−10	138
$[Au_7(PPh_3)_7]^{+}$	Pentagonal bipyramid	90	100	−10	139
$[Au_8(PPh_3)_8]^{2+}$	Fig. 7(a)	100	104?	−4	140
$[Au_9(P(p\text{-}C_6H_4CH_3)_3)_8]^{3+}$	Fig. 7(b)	112	122?	−10	141

[a] $Z_{obs.}$ is the observed electron count.

[b] Note—adoption of unusual geometries and distortions make predictions based on the PSEPT only approximate.[134]

[c] "Diff." refers to the difference between the electron count predicted on the basis of the PSEPT and that observed.

based upon Stone's Tensor Surface Harmonic (TSH) theory[92] reveals that for $Au(PR_3)_n$, with $n = 4$, the T_{1u} set is strongly antibonding but that it becomes less antibonding as the nuclearity is increased. For $n \leqslant 6$, TSH analysis thus predicts one stable low-lying MO but four stable radial MO's for $n > 6$.[144] Electron counts of $12n+2$ for $n \leqslant 6$[142] and $12n+8$ for $n > 6$[144] would therefore be expected. For low nuclearity clusters, although the electron counts are close to $12n+2$ they do not follow the rule exactly. This is because the situation can be further complicated by distortions of the metal framework and by the presence of bridging ligands, both of which can cause stabilization of some components of the T_{1u} set and therefore influence the electron count.[142]

The pentagonal bipyramid $[Au_7(PPh_3)_7]^+$ has a distorted geometry with a very short $Au_{ax.}$—$Au_{ax.}$ distance. This tends to destabilize one component of the T_{1u} set (P_z^a, using Stone's notation—see Appendix I) to give the $12n+6$ electron count observed.[134]

Mingos *et al.*[144,145] have proposed a simple electron counting scheme for high nuclearity clusters of general formula $[Au(AuPR_3)_n]^{x+}$, that is, clusters containing an interstitial or partially encapsulated Au atom. If the polyhedron is approximately spherical then the electron count is given by $12n+18$ whereas if the polyhedron has the general form of a ring or torus then the electron count is $12n+16$ (Table 12). The basis of the rule is quite simple. For the basic spherical cluster, without the interstitial atom, the MO diagram is shown in Fig. 9, with four radial bonding MO's. When the interstitial atom is added the s and three p orbitals match the A_{1g} and T_{1u} set of the spherical cluster[144] and produce a bonding and an antibonding set of four orbitals of which only the former is available for holding electron density. The five filled d orbitals of the interstitial atom will be virtually unperturbed,[143] therefore the number of bonding MO's does not change but the electron count is increased by ten. The total electron count is, thus

$$\underset{\text{parent polyhedron}}{12n} + \underset{\text{interstitial atom } d \text{ orbital}}{8} + 10 \qquad i.e. \quad 12n+18.$$

Table 12

Compound	$Z_{obs.}$[a]	n	Type	Prediction	Ref.
$[Au_{13}Cl_2(PMe_2Ph)_{10}]^{3+}$	162	12	Spherical	$12n+18 = 162$	146
$[Au_{11}I_3(PPh_3)_7]$	138	10	Spherical	$12n+18 = 138$	147
$[Au_9\{P(p\text{-Tol})_3\}_8]^{3+}$	112	8	Non-spherical	$12n+16 = 112$	148
$[Au_9\{P(p\text{-}C_6H_4OMe)_3\}_8]^{3+}$	112	8	Non-spherical	$12n+16 = 112$	141
$[Au_9(SCN)_3(PCy_3)_5]$	112	8	Non-spherical	$12n+16 = 112$	149
$[Au_8(PPh_3)_7]^{2+}$	100	7	Non-spherical	$12n+16 = 100$	140

[a] $Z_{obs.}$ is the observed electron count. n is the number of "surface" metal atoms.

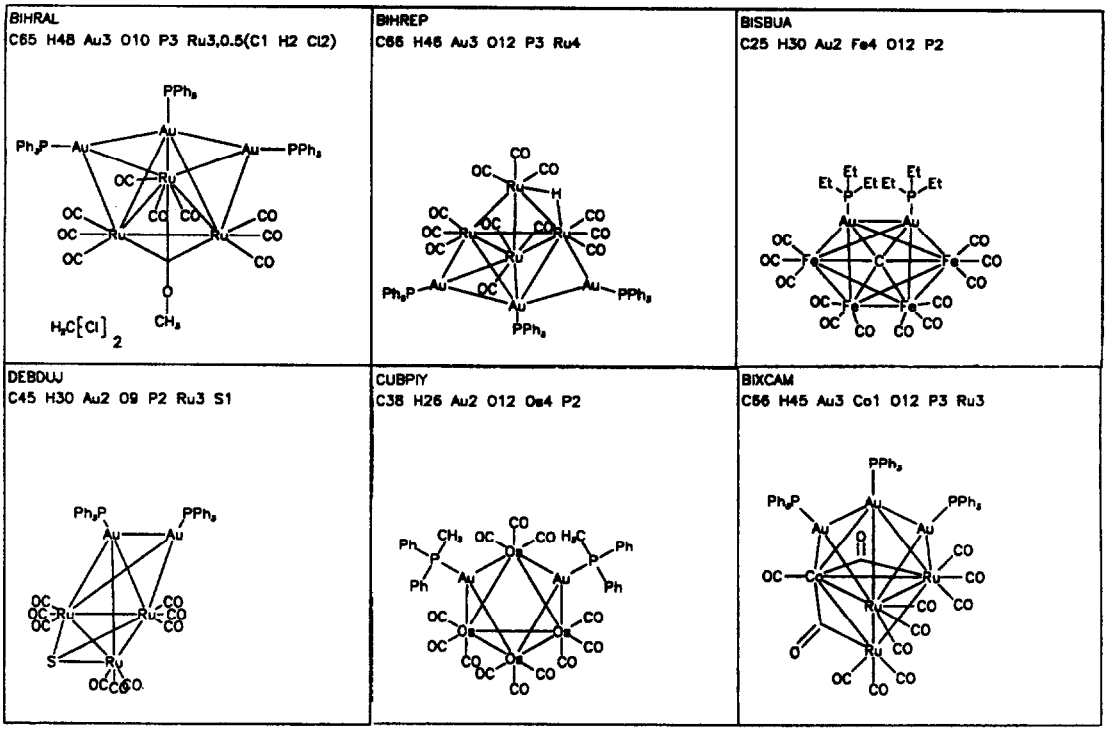

Fig. 10. Heteronuclear clusters containing gold atoms.

The difference for the non-spherical clusters arises because of the destabilization of the P_z^{σ} component of the T_{1u} set so that it becomes non-bonding or antibonding and unavailable for occupation.[134,143,144] Only two of the three p orbitals of the Au will interact with the T_{1u} set, the third remaining approximately non-bonding and unavailable. The electron count is, therefore $12n+16$. By interacting with the A_{1g} and T_{1u} set the interstitial atom causes a stabilization of these orbitals and, therefore enhances the skeletal bonding.[143]

Another consequence of the radial bonding in the gold clusters is the tendency to adopt structures with the maximum number of triangular faces. This maximizes the nearest neighbour bonding interactions and therefore stabilizes the structure.[142–144] The predominance of radial bonding has also been used as an explanation of the stereochemical non-rigidity of the Au framework in solution.[134,144]

(b) *Heteronuclear gold complexes*. The electron counts for heteronuclear gold compounds can generally be rationalized, either by: (i) regarding the $AuPR_3$ unit as a one electron donor ligand or (ii) by including the Au atom in the polyhedral skeleton.

(i) This approach relies on the well documented isolobal analogy between H and $AuPR_3$, whereby H and $AuPR_3$ are seen to adopt similar bonding modes in a wide variety of cluster compounds (see refs in Table 13). So, the electron count in $Ru_3(CO)_{10}(\mu_2\text{-Cl})(\mu_2\text{-AuPPh}_3)$[154] can be rationalized as 47e from the $Ru_3(CO)_{10}(\mu_2\text{-Cl})$ unit and 1e from $AuPPh_3$ giving the 48e characteristic of a trian-

Table 13. Gold compounds in which the isolobal analogy with H can be applied.

Compound	Structure	Electron count Obs.	Predict	Ref.
$FeCo_3(CO)_{12}AuPPh_3$	Tetrahedron	60e	60e	150
$Ru_3(COMe)(CO)_{10}AuPPh_3$	Triangle	48e	48e	151
$Ru_3(COMe)(CO)_9H_2AuPPh_3$	Triangle	48e	48e	151
$Ru_6(CO)_{15}C(NO)AuPPh_3$	Octahedron	86e	86e	152
$Os_6(CO)_{18}PAuPPh_3$	Trigonal prism	90e	90e	21
$Ru_5(CO)_{13}C(PPh_3)IAuPPh_3$	Open square pyramid	76e	76e	153

Table 14. Gold compounds with short Au---Au contacts or unusual electron counts

Compound	Struct. ref.[a]	Electron count Z_{obs}	Predict	Ref.
$Os_4(CO)_{12}(Au(PMePh_2))_2$	CUPBIY	82e	86?	156
$Ru_3(CO)_9S(AuPPh_3)_2$	DEBDUJ	72e	72e	157
$HRu_4(CO)_{12}(AuPPh_3)_3$	BIHREP	96e	96e	158
$Fe_4(CO)_{12}C(AuPEt_3)_2$	BISBUA	86e	86e	159
$Ru_3Co(CO)_{11}(AuPPh_3)_3$	BIXCAM	96e	96e	160
$Ru_3(CO)_9(OCH_3)(AuPPh_3)_3$	BIHRAL	86e	84e	161

[a] See Fig. 10.

gular framework. Similarly, for $Ni(Cp)Os_3(CO)_9(\mu_2\text{-}H)_2(\mu_2\text{-}AuPPh_3)$[155] there are 59e from the $Ni(Cp)Os_3(CO)_9(\mu_2\text{-}H)_2$ and 1e from $AuPPh_3$ giving the 60e required by a *closo*-tetrahedron.

(ii) Table 14 shows that bonding modes adopted by $AuPR_3$ are often quite different from those of H. The compounds in Table 14 all have Au---Au distances suggestive of an Au—Au bond. For these compounds it is more realistic to treat the Au atom as part of the polyhedral framework and utilize the condensation and capping principles (*vide supra*).

The single radial FO of the $AuPR_3$ unit can interact with a suitable orbital on the main cluster framework to produce a bonding and a high-lying antibonding orbital, of which only the former will be filled (Fig. 11). The tangential orbitals of the $AuPR_3$ unit are too high in energy to overlap effectively with cluster FO's and will remain empty. Thus, as in the capping principle for $M(CO)_3$ clusters, no extra cluster bonding orbitals are produced and the electron count for the capped cluster is 12e greater than for the parent polyhedron due to the six low-lying orbitals of $AuPR_3$ (5 *d* and 1 Au—P bonding) which remain relatively unperturbed.[134] When the $AuPR_3$ adopts an edge-bridging mode it also causes an increase of 12e in the total electron count.[134] This can be understood using the same reasoning.

This approach to bonding works well in the majority of clusters in Tables 13 and 14. The 60e count (now including $AuPPh_3$) for $Ru_3(CO)_{10}(\mu_2\text{-}Cl)(\mu_2\text{-}AuPPh_3)$ is that expected for an edge-bridged planar triangle. $H_2Os_4(CO)_{12}(AuPPh_3)_2$ can be regarded as a basic tetrahedron (60e) edge-bridged by one $AuPPh_3$ (+12e) then capped by another (+12e) to give the observed 84e count.

It is interesting to note that the heteronuclear gold containing tetrahedra and trigonal bipyramids will be expected to have the same electron counts as their Group VIII and Group IX metal carbonyl counterparts. Also $Fe_4(CO)_{12}C(AuPEt_3)_2$ has the 86e expected (on the basis of the "$(n+1)$ rule") for a *closo*-octahedron or "bicapped butterfly" (*vide supra*).

For some of the compounds in Table 14 the electron counts cannot be rationalized using PSEPT and in these cases the only recourse is to a full MO calculation.[162]

3.6. *Platinum clusters*

Homonuclear cluster complexes of platinum have electron counts intermediate between those for gold clusters and clusters based on the $M(CO)_3$ (M = Fe, Ru, Os) unit (Table 15). For the higher

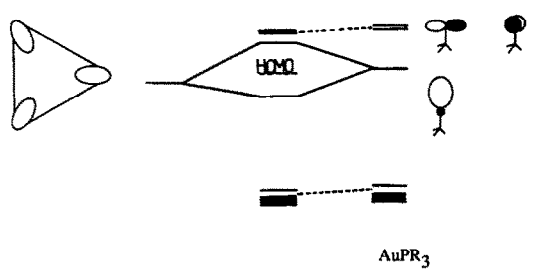

Fig. 11. Schematic diagram showing the effect of an AuL group on the frontier orbitals of a metal cluster unit.

Table 15. Electron counts for platinum clusters

Compound	Geometry	Z^a	Ref.
$Pt_3(\mu_2\text{-}CO)_3(PPh_3)_3$	Triangle	42e	166
$[Pt_3(CO)_3\{\mu_2\text{-}Fe(CO)_4\}_3]^-$	Triangle	43e	167
$Pt_3(\mu_2\text{-}SO_2)_3(PCy_3)_2(dppp)$	Triangle	44e	168
$Pt_3(\mu_2\text{-}PPh_2)_3(Ph)(PPh_3)_2$[b]	Open triangle	44e	169, 170
$[Pt_4(\mu_2\text{-}H)_2(P^tBu_3)_4]^-$	Tetrahedron	48e	171
$Pt_4(\mu_2\text{-}H)_2(P^tBu_3)_4$	Tetrahedron	50e	172
$[Pt_4(\mu_2\text{-}H)_4H_3(P^tBu_3)_4]^+$	Butterfly	54e	171
$Pt_4(\mu_3\text{-}H)_4H_4(P^iPr_2Ph)_4$	Tetrahedron	56e	172
$Pt_4(\mu_2\text{-}CO)_2(dppm)_3(dppm{=}O)$	Butterfly	58e	173
$[Pt_4(NH_3)_8(C_4H_6NO)_4]^{6+}$	Linear	62e	174
$Pt_4(S_2CHCHMe_2)_8$	Linear	64e	175
$Pt_5(\mu_2\text{-}H)_6H_2(PBu_2Ph)_5$	Edge broken TBP	68e	176
$Pt_5(\mu_2\text{-}SO_2)_3(\mu_2\text{-}CO)_2(CO)(PPh_3)_4$	Edge bridged tetrahedron	70e	177
$[Pt_6(\mu_2\text{-}CO)_6(CO)_6]^{2-}$	Trigonal prism	86e	178

[a] Z is the electron count for the cluster.
[b] Recrystallized from toluene/pentane[169] or benzene/diethyl ether.[170]

nuclearity clusters the bonding is dominated by the radial interactions but tangential orbitals become more important as the nuclearity is reduced.[86] As for gold complexes, the lower electron counts are the result of the high lying nature of the *p* orbitals on the metal making their full involvement in bonding energetically unfavourable.

Much theoretical work in this area has focussed on the compounds of general formula $Pt_3(\mu_2\text{-}X)_3(Y)_3$ (where all X and all Y need not necessarily be the same).[163–165] These compounds are characterized by electron counts of 42e or 44e, with 42e being more common (Tables 15 and 16). There is also one 43e complex which has been characterized by X-ray crystallography

Table 16. Pt_3 clusters

Compound	Z	Av. Pt—Pt dist./Å	Ref.
$[Pt_3(\mu_2\text{-}PPh_2)_2(\mu_2\text{-}H)(PPh_3)_3]^+$	42e	2.74	179
$Pt_3\{\mu_2\text{-}C(OMe)(p\text{-}C_6H_4Me)\}_3(CO)_3$	42e	2.62	180
$[Pt_3(\mu_2\text{-}CO)_3(PCy_3)_3(AuPCy_3)]^+$	42e	2.70	181
$Pt_3(\mu_2\text{-}CO)(\mu_2\text{-}CNC_8H_9)_2(CNC_8H_9)(PCy_3)_2$	42e	2.63	182
$Pt_3(\mu_2\text{-}CNC_8H_9)_3(CNC_8H_9)_2(PCy_3)$	42e	2.63	182
$[Pt_3(\mu_2\text{-}CO)_2(\mu_2\text{-}SO_2)(PCy_3)_3(AuPCy_3)]^+$	42e	2.70	183
$Pt_3\{\mu_2\text{-}SnN(SiMe_3)_2\}_3(CO)_3$	42e	2.76	184
$Pt_3(\mu_2\text{-}CO)_3(PPh_3)_3$	42e	2.66	166
$[Pt_3(\mu_3\text{-}CO)(dppm)_3]^+$	42e	2.63	185
$Pt_3(\mu_2\text{-}Ph)(\mu_2\text{-}PPh_2)(\mu_2\text{-}SO_2)(PPh_3)_3$	42e	2.76	165
$Pt_3(\mu_2\text{-}SO_2)_3(PPh_3)_3$	42e	2.70	186
$Pt_3(\mu_2\text{-}H)_3H_3(P^tBu_3)_3$	42e	2.82	172
$[Pt_3(CO)_3\{\mu_2\text{-}Fe(CO)_4\}_3]^-$	43e	2.66	167
$Pt_3(\mu_2\text{-}SO_2)_3(PCy_3)_2(dppp)$	44e	2.80	168
$Pt_3(\mu_2\text{-}Cl)(\mu_2\text{-}SO_2)_2(PCy_3)_3\{AuP(p\text{-}C_6H_4F)_3\}$	44e	2.86	183
$[Pt_3(CO)_3\{\mu_2\text{-}Fe(CO)_4\}_3]^{2-}$	44e	2.75	167
$Pt_3(\mu_2\text{-}PPh_2)_3(Ph)(PPh_3)_2$	44e	3.03[a]	169
$Pt_3(\mu_2\text{-}PPh_2)_3(Ph)(PPh_3)_2$	44e	3.00[b]	169
$Pt_3(\mu_2\text{-}PPh_2)_3(Ph)(PPh_3)_2$	44e	3.07[c]	170

[a] Recrystallized from toluene/pentane, Pt—Pt distances of 2.757(1), 2.757(1) and 3.586(1) Å.
[b] Recrystallized from CH_2Cl_2/pentane, Pt—Pt distances of 2.956(1), 2.956(1) and 3.037(1) Å.
[c] Recrystallized from benzene/diethyl ether, Pt—Pt distances of 2.785(1), 2.785(1) and 3.630(1) Å.

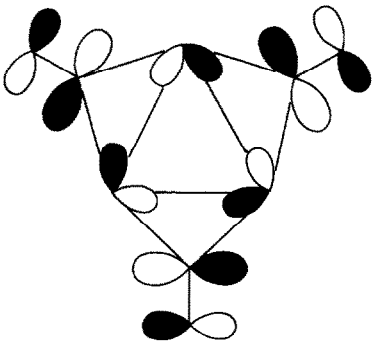

Fig. 12. The a_2'' MO of $Pt_3(\mu_2\text{-}CO)_3(CO)_3$.

(Table 15). The 42e count can be compared with the 48e found for $M_3(CO)_{12}$ (M = Fe, Ru, Os) clusters. The difference is due to *p* orbitals on the metals perpendicular to the M_3 triangle not being involved in bonding in the platinum clusters.[187] The bonding within the M_3 triangle is of a similar form for the two cases.

Several workers[163–165] have commented on the critical rôle played by the bridging ligands in determining the stable electron counts for the triangular clusters. Hoffmann *et al.*[163] have come to the conclusion, based on MO calculations, that complexes with π-donor bridging ligands (i.e. low lying tangential orbitals) such as PH_2^- or the halogens should be characterized by 44 valence electrons due to the stabilization of an a_2' MO (Fig. 12). This orbital is the HOMO in the 44e complexes but is empty in 42e systems. The 42e complexes will be formed by bridging ligands, such as CO, with π-acceptor properties (i.e. high lying tangential orbitals) which do not stabilize the a_2' orbital sufficiently for it to be occupied. The a_2' MO is antibonding between the metal atoms and its occupation would be expected to cause an increase in the Pt—Pt distance for the 44e complexes relative to the 42e ones.[163] It is indeed found that, in general, the 44e Pt complexes have longer M—M bonds than the 42e (Table 16). Occupation of the a_2' orbital can also lead to distortion away from D_{3h} symmetry although calculations have shown that this is probably the results of steric rather than electronic effects.[163,164] The presence of π-orbitals, on the bridging ligands, perpendicular to the M_3 plane can also influence the electron count and Mingos *et al.*[165] have attributed the formation of the 44e cluster $[Pt_3(\mu_2\text{-}CO)_3(CO)_3]^{2-}$[188] to the stabilization of an a_2'' orbital by CO π^*, as shown in Fig. 13. The X-ray crystal structure of this complex has not been determined but it would not be expected to show the longer bond lengths characteristic of the 44e clusters since the a_2'' orbital is not antibonding between the metals.

Thus, it is seen that the electronic properties of the bridging ligands are very important in determining the electron count in the Pt_3 systems. The variety of ligands found in these systems and the subtle differences between them, however, makes predictions of electron counts difficult.

Higher nuclearity platinum clusters. Evans and Mingos[189] have made some studies on higher nuclearity neutral Pt clusters, building them up from PtL_2 fragments and showing that the electron count depends on the orientation of these units. For larger clusters a modification of the condensation principle taking into account the incomplete use of *p* orbitals can be employed to rationalize the electron counts.[126] Characteristic electron counts are shown in Table 17 with examples of applications in Table 18. Uncertainties about electron counts for the parent polyhedra introduces some degree of arbitrariness into this approach, however it does provide a useful guide to electron counts. When condensation occurs through a Group VIII or IX atom (i.e. one that usually obeys the 18 electron rule in mononuclear complexes) then the usual condensation principle, discussed above is used.[126]

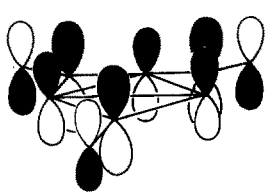

Fig. 13. The a_2' MO of $Pt_3(\mu_2\text{-}CO)_3(CO)_3$.

Table 17. Characteristic electron counts for platinum clusters[a]

Geometry	Electron count
Mononuclear	16e
Binuclear	30e
Triangular	42e, 44e
Tetrahedral	56e
Trigonal bipyramid	68e
Trigonal prism	86e

[a] Electron counts are based on observation of known cluster geometries and on MO calculations on clusters $(PtL_2)_n$.[126,187]

Table 18. Examples of condensed platinum clusters

Compound	Parent polyhedra	Shared unit	$Z_{obs.}$	$Z_{predict}$	Ref.
$[Pt_4(\mu_2\text{-}H)_4H_3(P^tBu_3)_4]^+$	2 triangles	1 edge	54e	$42+42-30=54$	171
$Pt_4(\mu_2\text{-}CO)_2(dppm)_3(dppm{=}O)$	2 triangles	1 edge	58e	$44+44-30=58$	173
$Pt_5(SO_2)_3(CO)_2(CO)(PPh_3)_4$	Tetrahedron □triangle	1 edge	70e	$56+44-30=70$	177
$Pt_7(CNR)_{11}(\mu_2,\eta^2\text{-}CNR)$	Trigonal bipyramid 2 triangles	2 edges	96e	$68+2\times44-2\times30=96$	190

3.7. *The transition from molecular cluster to bulk metal*

Here we will discuss the various theories which have been put forward in an attempt to rationalize the electron counts of high nuclearity close packed clusters with structures often based on fragments of a metallic lattice. Three main approaches for electron counting will be considered:

(a) Mingos[187] has divided the high nuclearity clusters into three classes:

(i) Clusters where radial bonding predominates: L:M ratio less than ~ 1.3.

(ii) Clusters where tangential bonding interactions make a partial contribution: L:M 1.3–2.0.

(iii) Clusters where radial and tangential bonding are both important: L:M $\geqslant 2$.

Type (i) resembles the situation for gold clusters already discussed. These clusters are characterized by an electron count of $12n_s+\Delta_i$,[144,145] where n_s is the number of surface metal atoms and Δ_i is the electron count characteristic of the interstitial group of metal atoms.[187] (Table 19.)

Thus, with a single interstitial atom we have an electron count of $12n_s+18$ i.e. the situation already noted for the spherical gold clusters. Clusters which conform to this rule are shown in Table 20(a).

For type (ii) the presence of a larger number of bridging ligands causes some of the tangential orbitals of the cluster to be sufficiently lowered in energy to be occupied.[187] Calculations on known clusters have suggested the electron counts $12n_s+24$, based on one interstitial atom and occupation of 3 F^π surface MO's[187]—Table 20(b).

When there are more bridging ligands present, i.e. type (iii), calculations have suggested that $(n_s-8)L^\pi$ (L = 3, 4) surface orbitals are occupied, giving an electron count of $12n_s+(2n_s+2)$ for clusters with one interstitial atom[187]—Table 20(c).

(b) Ciani and Sironi[85] have performed EHMO calculations on a large number of high nuclearity hypothetical bare (no ligands) close packed clusters of Rh, using the method of Lauher[88] to determine the number of CVMO's. Their results lead to the conclusion that these clusters are characterized by

Table 19

n_i[a]	Arrangement	Δ_i
1		18e
2	Binuclear	34e
3	Triangular	48e (50e)[b]
3	Linear	50e
4	Tetrahedral	60e
6	Octahedral	86e

[a] n_i is the number of interstitial metal atoms.

[b] The Δ_i value of 50e comes about from the stabilization of an a'_2 orbital of the triangular fragment c.f. the tricapped trigonal prism and raft clusters discussed above.

$6n+X$ CVMO's, where X is a variable depending on the geometry. They found that X lies in the range 6–11 and is very often equal to seven. This of course leads to electron counts in the range $12n+12$ to $12n+22$—Table 20.

(c) Teo[188] has developed an electron counting rule utilizing the relationship between these large clusters and bulk metals. He has proposed that the total number of electrons, N is given by,

$$N = (n_b + rn_s)m$$

where n_b is the number of bulk atoms, n_s is the number of surface atoms, m is the number of electrons

Table 20(a). L : M ratio less than ~ 1.3

Compound	n_b	n_s	Structure	$Z_{obs.}$[a]	$12n_2+\Delta_i$	Teo	X	Ref.
$[Au_{13}Cl_2(PMePh_2)_{10}]^{3+}$	1	12	i.c.p.	162e	162	162	3	146
$[Pt_{26}(CO)_{32}]^{2-}$	3	23	h.c.p.	326e	324/326[b]	339/324[c]	7	188
$[Pt_{19}(CO)_{22}]^{4-}$	2	17	Pentag.	238e	238	236	5	191
$[Ni_{38}Pt_6(CO)_{48}H_{6-n}]^{n-}$	6	38	f.c.c.	542e	542	548	7	192

[a] $Z_{obs.}$ is the observed electron count.

[b] Due to stabilization of a'_2 orbital; see above.

[c] $n = 11.25$ is also possible for relatively small h.c.p. structures (with one bulk atom).[188]

Table 20(b). L : M ratio 1.3–2

Compound	n_b	n_s	Structure	$Z_{obs.}$[a]	$12n_s+24$	Teo	X	Ref.
$[Rh_{14}(CO)_{25}]^{4-}$	1	13	b.c.c.	180e	180	180	6	193
$[Rh_{22}(CO)_{37}]^{4-}$	1	21	f.c.c./h.c.p.	276e	276	277	6	194
$[Pt_{24}(CO)_{30}]^{2-}$	1	23	f.c.c.	302e	300	302	7	188

[a] $Z_{obs.}$ is the observed electron count.

Table 20(c). L : M ratio $\geqslant 2$

Compound	n_b	n_s	Structure	$Z_{obs.}$[a]	$12n_s+2n_s+2$	Teo	X	Ref.
$[Rh_{13}(CO)_{24}H_5]$	1	12	h.c.p.	170e	170	170	7	84
$[Rh_{15}(CO)_{30}]^{3-}$	1	14	b.c.c.	198e	198	193	9	195

[a] $Z_{obs.}$ is the observed electron count.

Table 21

Structure	m
Pentagonal	11.17
f.c.c.	11.24
b.c.c.	11.50
γ (complicated cubic)	11.62
h.c.p.	11.75

per bulk atom and $r = (m/m_s)$, m_s being the number of electrons per surface atom. r and m are determined from the Hume–Rothery rule.[188] The calculated values of m are given in Table 21.[188] A value of r was derived from calculations on known compounds and this was found to be approximately equal to 1.125.[188] Table 20 shows the electron counts, utilizing this rule, for some clusters.

The basis for the scheme is the similarity between the density of states for these high nuclearity clusters and that found in bulk metals.[188]

3.8. *PSEPT and the EAN rule*

The clusters which obey the EAN rule belong to the general class of rings and three-connected polyhedra and their capped derivatives. The electron counts for the rings can be expressed within the PSEPT as $16n$ i.e. with $2n$ skeletal electron pairs and that for the three-connected structures as $15n$ i.e. $3n/2$ skeletal electron pairs. The normal capping rule still applies, with a capping group adding 12e. The electron counts for both these systems have been rationalized by using MO calculations.

Lauher[88] has discussed the bonding in M_3 triangular systems and shown the necessity for 48 cluster valence electrons to fill up all the strongly bonding MO's. The MO diagram for $Os_3(CO)_{12}$ is shown in Fig. 14.

Mingos and Johnston[107,108] have performed MO calculations using Stone's TSH aproach and have concluded that three-connected polyhedra are characterized by four (S^σ and P^σ) radial bonding MO's, $(n-4)/2$ bonding L^π ($L > 1$) surface MO's and $(n-2)$ L^π and $\overline{L^\pi}$ matched non-bonding

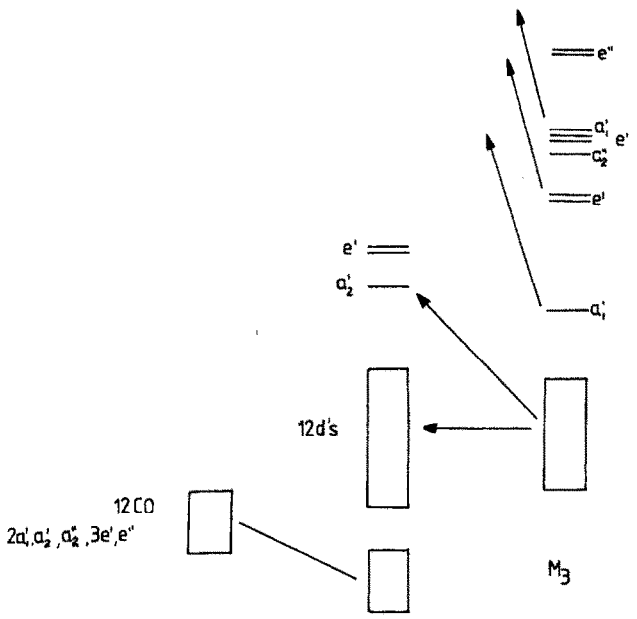

Fig. 14. Schematic MO energy level diagram for $Os_3(CO)_{12}$.

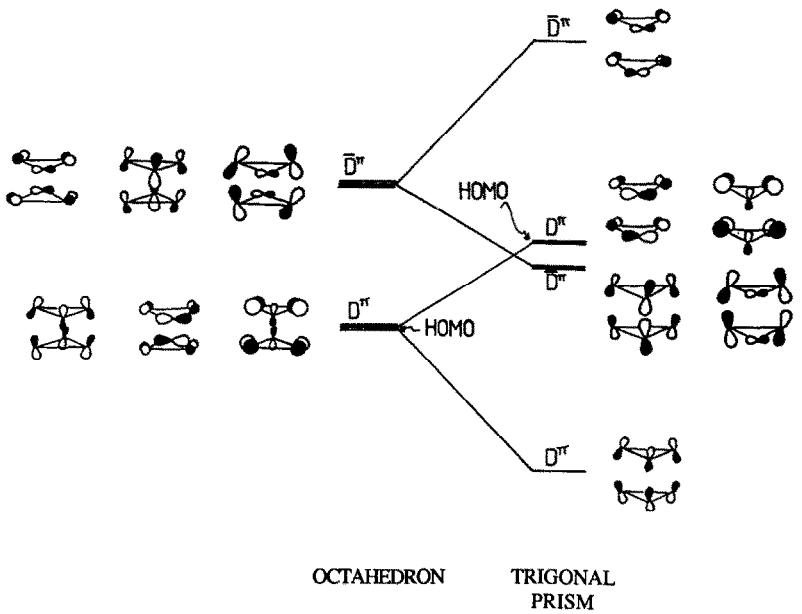

Fig. 15. Comparison of the frontier orbitals of a trigonal prism and an octahedron.

MO's.[107,108] This gives an explanation of the seemingly anomalous six skeletal bonding pairs for the tetrahedron which cannot be explained by the simple PSEPT. The difference between the three-connected polyhedra and the deltahedra arises because in the deltahedra the $(n-2)$ L^{π} MO's are more strongly bonding and the $(n-2)$ $\overline{L^{\pi}}$ more strongly antibonding, so that only the L^{π} orbitals are occupied.[107,108] This can be seen fairly easily by comparing the MO diagrams for an octahedron and a trigonal prism (Fig. 15). The differences arise because the triangles are staggered in the octahedron but eclipsed in the trigonal prism.[107]

3.9. *Deviations from the PSEPT*

Within the framework of PSEPT the electron counts for most cluster geometries can be rationalized. Deviations do occur from the "expected" electron counts when the polyhedra are distorted. An example is the elongated trigonal bipyramid, $[Ni_5(CO)_{12}]^{2-}$,[196] which has 76e. In these cases the electron counts can be rationalized by MO calculations. For instance MO calculations on the trigonal bipyramid[107] suggest that an elongation results in stabilization of a low lying antibonding orbital so that it becomes available for occupation. Thus, in Fig. 16, elongation parallel to the C_3 axis results in stabilization of $\overline{D^{\pi}}$ and destabilization of D^{π}; where D^{π} is the HOMO in the undistorted structure. Other bipyramids can be similarly treated and a general rule for these systems is that they will have $(N-1)$, $(N+1)$ or $(N+3)$ electron pairs.[107] This rule should hold for relatively small distortions from the ideal symmetry.[107]

For systems in which the electron count cannot be easily rationalized, the only recourse is to a

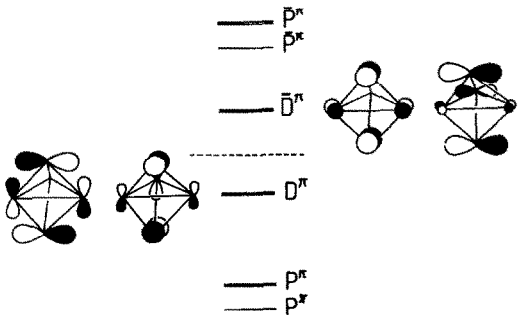

Fig. 16. Part of the MO energy level diagram for a trigonal bipyramid.

Table 22. Summary of electron counts within the PSEPT

Polyhedral type	Electron count
Deltahedron *closo-*	$14n+2$
niido-	$14n+4$
arachno-	$14n+6$
Three-connected	$15n$
Ring compounds	$16n$
Capped structures	$N+12x$
Edge bridged structures	$N+14x$
Condensed polyhedra:	
vertex shared	$A+B-18$
edge shared	$A+B-34$
Δ-face shared	$A+B-48$ or $A+B-50^a$
□-face shared	$A+B-62$ or $A+B-64^a$

[a] See appropriate section above.

Where: n is the nuclearity of the cluster. N is the electron count of the uncapped or unbridged parent polyhedron. x is the number of capping or edge-bridging groups. A and B are the electron counts of the parent polyhedra.

full MO calculation. This should always give the "right answer" but of course it offers no predictive power, the real beauty of the PSEPT! A summary of electron counts within the PSEPT is given in Table 22.

4. OTHER ELECTRON COUNTING SCHEMES

The most commonly used electron counting scheme outside the PSEPT and EAN rule is the Topological Electron Counting (TEC) scheme developed by Teo.[197-200] This approach is based on Euler's Theorem,

$$E = V+F-2 \quad \text{where} \quad \begin{array}{l} E \text{ is the number of edges of a polyhedron,} \\ V \text{ is the number of vertices of a polyhedron,} \\ F \text{ is the number of faces of a polyhedron.} \end{array}$$

and the EAN rule.

The result is,

$$\text{number of CVMO's} = T = 8V-F+2+X$$

where X is an "adjustment factor" i.e. the number of electron pairs in excess of the EAN rule prediction.[197] In other words X is the number of "missing" M—M antibonding orbitals if each edge is considered as a 2c–2e bond.[197]

Teo developed a set of rules for estimating the value of X. These were originally based largely on empirical observations but have since been justified on the basis of MO calculations.[197,200] Rules for estimating X are:[197]

(i) $X = 0$ for three-connected polyhedra.
(ii) Capping an n-gonal face of a polyhedron gives an increase in X of $n-3$.
(iii) $X = 0$ for all pyramids.
(iv) $X = 0$ for trigonal bipyramids.
$X = 1, 3$ for tetragonal bipyramids.
$X = 2$ for pentagonal bipyramids.

Higher values should be considered "exceptions" and are usually associated with distortions of the polyhedral framework.

(v) $X = 1$ for trigonal antiprism (octahedron).
$X = 1, 3$ for square antiprism.
$X = 3$ for pentagonal antiprism.

(vi) $X = S$ for vertex or edge sharing condensed polyhedra, where S is the number of shared edges or vertices.
$X = H$ for face sharing condensed polyhedra, where H is the number of "hidden edges".

The electrons are counted in the same way as for the PSEPT.

Examples

(a) $[Os_6(CO)_{18}]^{2-}$ [93] octahedron 86e
$T = 8V - F + 2 + X$
$V = 6 \quad F = 8$
$43 = 48 - 8 + 2 + X.$
Therefore $X = 1$ as expected for a tetragonal bipyramid.

(b) $Os_6(CO)_{18}$ [62] bicapped tetrahedron 84e
$T = 8V - F + 2 + X$
$V = 6 \quad F = 8$
$42 = 48 - 8 + 2 + X.$
Therefore $X = 0$.

The $X = 0$ value can be regarded as being derived from rule (i), since the tetrahedron is a three-connected polyhedron, and rule (ii) where $n = 3$, therefore $(n-3) = 0$.

The similarities and differences between TEC and PSEPT have been discussed by Mingos[201] and Teo[202] independently. Mingos has shown how the TEC can be related to the PSEPT simply by some simple algebraic manipulation using Euler's rule.[201] TEC and PSEPT are very similar and represent the same situation but from slightly different viewpoints. The main advantage of the TEC, however, is in its prediction of multiple electron counts for certain structures—rules (iv) and (v).

5. CONCLUSION

It is hoped that this article has furnished the reader with enough knowledge to be able to work out and rationalize the electron counts for the majority of transition metal cluster compounds encountered in the current literature. Of course there are always clusters for which the rules do not work, clusters which become more interesting simply because of this, clusters seemingly designed just to keep the theoretical inorganic chemist happy!

Acknowledgements—I am greatly indebted to Drs P. R. Raithby and C. E. Housecroft for all their help in the preparation of this work. I should also like to thank the Cambridge Crystallographic Data Centre for the use of their files and the S.E.R.C. for financial support.

REFERENCES

1. R. J. Goudsmit, B. F. G. Johnson, J. Lewis, P. R. Raithby and K. H. Whitmire, *J. Chem. Soc., Chem. Commun.* 1982, 640.
2. G. P. Elliott, J. A. K. Howard, T. Mise, C. M. Nunn and F. G. A. Stone, *Angew. Chem. Int. Ed.* 1986, **25**, 190; G. P. Elliott, J. A. K. Howard, C. M. Nunn and F. G. A. Stone, *J. Chem. Soc., Chem. Commun.* 1986, 431.
3. A. G. Orpen, *J. Chem. Soc., Dalton Trans.* 1980, 2509.
4. M. R. Churchill, *Advances in Chemistry Series*, 1978, No. 167, 36–60.
5. M. R. Churchill and R. A. Lashewycz, *Inorg. Chem.* 1979, **18**, 326 and refs therein.
6. See, for example: A. G. Orpen, D. Pippard, G. M. Sheldrick and K. D. Rouse, *Acta. Cryst.* 1978, **B34**, 2466; Z. Dawoodi, M. J. Mays and A. G. Orpen, *J. Organomet. Chem.* 1981, **219**, 251.
7. S. F. Gull and G. J. Daniell, *Nature* 1978, **272**, 686; S. F. Gull, A. K. Livesey and D. S. Sivia, *Acta Cryst.* 1987, **A43**, 112; M. J. Doyle, personal communication.
8. K. Guldner, J. Lewis, B. F. G. Johnson, S. M. Owen and P. R. Raithby, *J. Organomet. Chem.*, in press.

9. M. McPartlin and W. J. H. Nelson, *J. Chem. Soc., Dalton Trans.* 1986, 1557.
10. R. G. Teller, R. D. Wilson, R. K. McMullan, T. F. Koetzle and R. Bau, *J. Am. Chem. Soc.* 1978, **100**, 3071.
11. M. L. Blohm and W. L. Gladfelter, *Inorg. Chem.* 1987, **26**, 459.
12. T. J. Henly, J. R. Shapley and A. L. Rheingold, *J. Organomet. Chem.* 1986, **310**, 55.
13. B. F. G. Johnson, D. A. Kaner, J. Lewis and P. R. Raithby, *J. Chem. Soc., Chem. Commun.* 1981, 753.
14. J. Puga, R. Sanchez-Delgado, A. Andmallo, J. Ascamio and D. Braga, *Organometallics* 1985, **4**, 2064.
15. F. W. B. Einstein, R. K. Pomeroy and A. C. Willis, *J. Organomet. Chem.* 1986, **311**, 257.
16. B. F. G. Johnson, R. Khattar, J. Lewis, M. McPartlin, J. Morris and G. L. Powell, *J. Chem. Soc., Chem. Commun.* 1987, 507.
17. Y. Chi, J. R. Shapley, M. R. Churchill and Y-J. Li, *Inorg. Chem.* 1986, **25**, 4165.
18. J. Pursiainen and T. A. Pakkanen, *J. Organomet. Chem.* 1986, **315**, 353.
19. J. L. Vidal, *Inorg. Chem.* 1981, **20**, 243.
20. A. A. Aitchison and L. J. Farrugia, *Organometallics* 1987, **6**, 819.
21. C. M. Hay, Ph.D Thesis, Cambridge (1987).
22. P. V. Broadhurst, B. F. G. Johnson, J. Lewis, A. G. Orpen, P. R. Raithby and J. R. Thornback, *J. Organomet. Chem.* 1980, **187**, 141.
23. N. Viswanathan, E. D. Morrison, G. L. Geoffroy, S. J. Geib and A. L. Rheingold, *Inorg. Chem.* 1986, **25**, 3100.
24. R. D. Adams and J. E. Babin, *Inorg. Chem.* 1986, **25**, 3418.
25. Z. Dawoodi, K. Henrick and M. J. Mays, *J. Chem. Soc., Chem. Commun.* 1982, 696.
26. G. D. Jarvinen and R. R. Ryan, *Organometallics* 1984, **3**, 1434.
27. C. J. Cardin, S. B. Colbran, B. F. G. Johnson, J. Lewis and P. R. Raithby, *J. Chem. Soc., Chem. Commun.* 1986, 1288.
28. L. J. Farrugia, *J. Chem. Soc., Chem. Commun.* 1987, 147.
29. A. M. Arif, D. E. Heaton and R. A. Jones, *J. Chem. Soc., Chem. Commun.* 1986, 1506.
30. E. Boyar, A. J. Deeming, K. Henrick, M. McPartlin and A. Scott, *J. Chem. Soc., Dalton Trans.* 1986, 1431.
31. J. W. Kalis, E. M. Holt and D. F. Shriver, *J. Am. Chem. Soc.* 1983, **105**, 7307.
32. D. L. Davies, J. C. Jeffery, D. Miguel, P. Sherwood and F. G. A. Stone, *J. Chem. Soc., Chem. Commun.* 1987, 454.
33. C. C. Santini, J-M. Basset, B. Fontal, J. Krause, S. G. Shore and C. Charrier, *J. Chem. Soc., Chem. Commun.* 1987, 512.
34. A. Gourdon and Y. Jeanin, *Organometallics* 1986, **5**, 2406.
35. A. J. Deeming, M. S. B. Felix, P. A. Bates and M. B. Hursthouse, *J. Chem. Soc., Chem. Commun.* 1987, 461.
36. A. D. Clauss, M. Tachikawa, J. R. Shapley and C. G. Pierpont, *Inorg. Chem.* 1981, **20**, 1528.
37. E. J. Ditzel, B. F. G. Johnson, J. Lewis, P. R. Raithby and M. J. Taylor, *J. Chem. Soc., Dalton Trans.* 1985, 555.
38. B. F. G. Johnson, J. Lewis, W. J. H. Nelson, J. N. Nicholls, M. D. Vargas, D. Braga, K. Henrick and M. McPartlin, *J. Chem. Soc., Dalton Trans.* 1984, 1809.
39. S. G. Shore, D-Y. Jan, L.-Y. Hsu and W. L. Hsu, *J. Am. Chem. Soc.* 1983, **105**, 5923.
40. K. H. Whitmire, C. B. Lagrone and A. L. Rheingold, *Inorg. Chem.* 1986, **25**, 2472.
41. M. Müller, H-T. Schacht, K. Fischer, J. Ensling, P. Gütlich and H. Vahrenkamp, *Inorg. Chem.* 1986, **25**, 4032.
42. N. Lugan, G. Lavigne and J. J. Bonnet, *Inorg. Chem.* 1987, **26**, 585.
43. E. Delgado, J. C. Jeffery, N. D. Simmons and F. G. A. Stone, *J. Chem. Soc., Dalton Trans.* 1986, 869.
44. B. F. G. Johnson, J. Lewis, M. McPartlin, M. A. Pearsall and A. Sironi, *J. Chem. Soc., Chem. Commun.* 1984, 1089.
45. M. C. Jennings, N. C. Payne and R. J. Puddephatt, *J. Chem. Soc., Chem. Commun.* 1986, 1809.
46. Y. Chi, J. R. Shapley, J. W. Ziller and M. R. Churchill, *Organometallics* 1987, **6**, 301.
47. J. G. Jeffrey, B. F. G. Johnson, J. Lewis, P. R. Raithby and D. A. Welch, *J. Chem. Soc., Chem. Commun.* 1986, 318.
48. S. Aime, R. Bertoncello, V. Busetti, R. Gobetto, G. Granozzi and D. Osella, *Inorg. Chem.* 1986, **25**, 4004.
49. L. E. Bogan, Jr., G. R. Clark and T. B. Rauchfuss, *Inorg. Chem.* 1986, **25**, 4050.
50. R. Della Pergola, L. Garlaschelli, S. Martinengo, F. Demartin, M. Manassero and M. Sansoni, *J. Chem. Soc., Dalton Trans.* 1986, 2463.
51. S. B. Colbran, C. M. Hay, B. F. G. Johnson, F. J. Lahoz, J. Lewis and P. R. Raithby, *J. Chem. Soc., Chem. Commun.* 1986, 1766.
52. A. G. Cowie, B. F. G. Johnson, J. Lewis, J. N. Nicholls, P. R. Raithby and A. G. Swanson, *J. Chem. Soc., Chem. Commun.* 1984, 637.

53. G. Ciani and S. Martinengo, *J. Organomet. Chem.* 1986, **306**, C49.
54. A. Basu, S. Bhaduri, H. Khwaja, P. G. Jones, K. Meyer-Bäse and G. M. Sheldrick, *J. Chem. Soc., Dalton Trans.* 1986, 2501.
55. L. Busetto, V. Zanotti, V. G. Albano, D. Braga and M. Monari, *J. Chem. Soc., Dalton Trans.* 1986, 1791.
56. See, for example, J. E. Huheey, *Inorganic Chemistry*, 3rd Edn, p. 590. Harpper International, New York (1983).
57. K. Wade in *Transition Metal Clusters* (Edited by B. F. G. Johnson), Chap. 3. Wiley Interscience, Chichester (1980).
58. M. R. Churchill and B. G. DeBoer, *Inorg. Chem.* 1977, **16**, 878.
59. M. R. Churchill and J. P. Hutchinson, *Inorg. Chem.* 1978, **17**, 3528.
60. L. D. Lower and L. F. Dahl, *J. Am. Chem. Soc.* 1976, **98**, 5046.
61. C. T. W. Chu, Ph.D. Thesis, University of Wisconsin, Madison (1977).
62. R. Mason, K. M. Thomas and D. M. P. Mingos, *J. Am. Chem. Soc.* 1973, **95**, 3802.
63. M. McPartlin, C. R. Eady, B. F. G. Johnson and J. Lewis, *J. Chem. Soc., Chem. Commun.* 1976, 833.
64. C. E. Anson, E. J. Ditzel, M. Fajardo, D. H. Holden, B. F. G. Johnson, J. Lewis, J. Puga and P. R. Raithby, *J. Chem. Soc., Dalton Trans.* 1984, 2723.
65. A. C. Willis, G. N. van Buuren, R. K. Pomeroy and F. W. B. Einstein, *Inorg. Chem.* 1983, **22**, 1162.
66. M. R. Churchill, Y.-J. Li, J. R. Shapley, D. S. Foose and W. S. Uchiyama, *J. Organomet. Chem.* 1986, **312**, 121.
67. M. Manassero, M. Sansoni and G. Longoni, *J. Chem. Soc., Dalton Trans.* 1976, 919.
68. F. W. B. Einstein, L. R. Martin, R. K. Pomeroy and P. Rushman, *J. Chem. Soc., Chem. Commun.* 1985, 345.
69. C. R. Eady, B. F. G. Johnson, J. Lewis, B. E. Reichert and G. M. Sheldrick, *J. Chem. Soc., Chem. Commun.* 1976, 271.
70. D. H. Farrar, P. F. Jackson, B. F. G. Johnson, J. Lewis, J. N. Nicholls and M. McPartlin, *J. Chem. Soc., Chem. Commun.* 1981, 415.
71. J. J. Guy and G. M. Sheldrick, *Acta Cryst.* 1978, **B34**, 1725.
72. M. Lanfranchi, A. Tiripicchio, E. Sappa and A. J. Carty, *J. Chem. Soc., Dalton Trans.* 1986, 2737.
73. A. G. Orpen and G. M. Sheldrick, *Acta Cryst.* 1978, **B34**, 1989.
74. E. R. Corey, L. F. Dahl and W. Beck, *J. Am. Chem. Soc.* 1963, **85**, 1202.
75. M. McPartlin, C. R. Eady, B. F. G. Johnson and J. Lewis, *J. Chem. Soc., Chem. Commun.* 1976, 883.
76. A. Ceriotti, R. Della Pergola, G. Longoni, B. T. Heaton, F. Demartin and M. Manassero, *J. Organomet. Chem.* 1986, **311**, C31.
77. S. B. Colbran, C. E. Housecroft, J. Lewis, B. F. G. Johnson, S. M. Owen and P. R. Raithby, in preparation.
78. F. R. Furuya and W. L. Gladfelter, *J. Chem. Soc., Chem. Commun.* 1986, 129.
79. C. G. Pierpont, G. F. Stuntz and J. R. Shapley, *J. Am. Chem. Soc.* 1978, **100**, 616.
80. P. F. Jackson, B. F. G. Johnson, J. Lewis and P. R. Raithby, *J. Chem. Soc., Chem. Commun.* 1980, 60.
81. L. M. Bullock, J. S. Field, R. J. Haines, E. Minshall, D. N. Smit and G. M. Sheldrick, *J. Organomet. Chem.* 1986, **310**, C47.
82. P. F. Jackson, B. F. G. Johnson, J. Lewis, W. J. H. Nelson and M. McPartlin, *J. Chem. Soc., Dalton Trans.* 1982, 2099.
83. J. L. Vidal and J. M. Troup, *J. Organomet. Chem.* 1981, **213**, 351.
84. V. G. Albano, A. Ceriotti, P. Chini, S. Martinengo and W. M. Anker, *J. Chem. Soc., Chem. Commun.* 1975, 859.
85. G. Ciani and A. Sironi, *J. Organomet. Chem.* 1980, **197**, 233.
86. D. M. P. Mingos and R. W. M. Wardle, *Transition Met. Chem.* 1985, **10**, 441.
87. D. M. P. Mingos, *Nature Phys. Sci. (London)*, 1972, **236**, 99.
88. J. W. Lauher, *J. Am. Chem. Soc.* 1978, **100**, 5305.
89. K. Wade, *Adv. Inorg. Chem. Radiochem.* 1976, **18**, 1.
90. K. Wade, *Inorg. Nucl. Chem. Lett.* 1972, **8**, 559; K. Wade, *Inorg. Nucl. Chem. Lett.* 1972, **8**, 567.
91. H. C. Longuet-Higgins and M. de V. Roberts, *Proc. R. Soc. Ser. A*, 1954, **224**, 339.
92. A. J. Stone, *Mol. Phys.* 1980, **41**, 1339; A. J. Stone, *Inorg. Chem.* 1981, **20**, 563; A. J. Stone, *Polyhedron* 1984, **3**, 1299.
93. D. M. P. Mingos, *J. Chem. Soc., Dalton Trans.* 1974, 133.
94. D. M. P. Mingos and M. I. Forsyth, *J. Chem. Soc., Dalton Trans* 1977, 610.
95. G. Ciani, L. Garlaschelli, A. Sironi and S. Martinengo, *J. Chem. Soc., Chem. Commun.* 1981, 563.
96. D. M. P. Mingos, *Acc. Chem. Res.* 1984, **17**, 311.
97. V. G. Albano, P. Chini, S. Martinengo and M. Sansoni, *J. Chem. Soc., Dalton Trans.* 1978, 463.
98. E. H. Braye, L. F. Dahl, W. Hübel and D. L. Wampler, *J. Am. Chem. Soc.* 1962, **84**, 4633.

99. J. L. Vidal, W. E. Walker, R. L. Pruett and R. C. Schoening, *Inorg. Chem.* 1979, **18**, 129.
100. G. Longoni, A. Ceriotti, R. Della Pergola, M. Manassero, M. Perego, G. Piro and M. Sansoni, *Philos. Trans. R. Soc. London Ser. A*, 1982, **308**, 47.
101. L. G. Scott and D. N. Smit, personal communication.
102. V. G. Albano, P. L. Bellon and G. Ciani, *J. Chem. Soc., Chem. Commun.* 1969, 1024.
103. P. F. Jackson, B. F. G. Johnson, J. Lewis and P. R. Raithby, *J. Chem. Soc., Chem. Commun.* 1980, 60.
104. V. G. Albano, D. Braga, S. Martinengo, P. Chini, M. Sansoni and D. Strumolo, *J. Chem. Soc., Dalton Trans.* 1980, 52.
105. G. Longoni, M. Manassero and M. Sansoni, *J. Am. Chem. Soc.* 1980, **102**, 3242.
106. S. Martinengo, G. Ciani, A. Sironi and P. Chini, *J. Am. Chem. Soc.* 1978, **100**, 7096.
107. R. L. Johnston and D. M. P. Mingos, *J. Chem. Soc., Dalton Trans.* 1987, 647.
108. R. L. Johnston and D. M. P. Mingos, *J. Organomet. Chem.* 1985, **280**, 407.
109. C. H. E. Belin, J. D. Corbett and A. Cisar, *J. Am. Chem. Soc.* 1977, **99**, 7163.
110. R. M. Friedman and J. D. Corbett, *Inorg. Chem.* 1973, **12**, 1134.
111. B. F. G. Johnson and J. Lewis, *Proc. R. Soc. London, Ser. A* 1982, **5**, 308.
112. D. M. P. Mingos, *J. Chem. Soc., Chem. Commun.* 1983, 106.
113. D. M. P. Mingos and R. L. Johnston, *J. Organomet. Chem.* 1985, **280**, 419.
114. B. Beagley and D. G. Schmidling, *J. Mol. Struct.* 1974, **22**, 466.
115. L. F. Dahl, E. Ishisti and R. E. Rundle, *J. Chem. Phys.* 1957, **26**, 1750.
116. R. D. Adams, I. T. Horvath and L-W. Yang, *Organometallics* 1983, **2**, 1257.
117. P. F. Jackson, B. F. G. Johnson, J. Lewis, J. N. Nicholls, M. McPartlin and W. J. H. Nelson, *J. Chem. Soc., Chem. Commun.* 1980, 564.
118. M. R. Churchill and R. Bau, *Inorg. Chem.* 1968, **7**, 2606.
119. C-M. T. Hayward, J. R. Shapley, M. R. Churchill, C. Bueno and A. L. Rheingold, *J. Am. Chem. Soc.* 1982, **104**, 7347.
120. D. Braga, K. Henrick, B. F. G. Johnson, J. Lewis, M. McPartlin, W. J. H. Nelson and M. D. Vargas, *J. Chem. Soc., Chem. Commun.* 1982, 419.
121. R. D. Adams, D. T. Foust and P. Mather, *Organometallics* 1983, **2**, 990.
122. S. Martinengo, A. Fumagalli, R. Bonfichi, G. Ciani and A. Sironi, *J. Chem. Soc., Chem. Commun.* 1982, 825.
123. S. Martinengo, A. Fumagalli, G. Ciani and A. Sironi, *J. Chem. Soc., Chem. Commun.* 1983, 453.
124. A. J. Stone and M. J. Alderton, *Inorg. Chem.* 1982, **21**, 2297.
125. D. M. P. Mingos, *J. Chem. Soc., Dalton Trans.* 1977, 602.
126. D. M. P. Mingos and D. G. Evans, *J. Organomet. Chem.* 1983, **251**, C13.
127. D. H. Farrar, B. F. G. Johnson, J. Lewis, P. R. Raithby and M. J. Rosales, *J. Chem. Soc., Dalton Trans.* 1982, 2051.
128. D. M. P. Mingos and D. G. Evans, *Organometallics* 1983, **2**, 435.
129. M. R. Churchill and F. J. Hollander, *Inorg. Chem.* 1977, **16**, 2493.
130. B. F. G. Johnson, J. Lewis, M. McPartlin, J. Morris, G. L. Powell, P. R. Raithby and M. D. Vargas, *J. Chem. Soc., Chem. Commun.* 1986, 429.
131. R. D. Adams, J. E. Babin, R. Mahtab and S. Wang, *Inorg. Chem.* 1986, **25**, 1623.
132. R. Hoffmann, *Angew. Chem. Int. Ed.* 1982, **21**, 71.
133. N. M. Boag, C. B. Knobler and H. D. Kaesz, *Angew. Chem. Suppl.* 1983, 198.
134. D. M. P. Mingos, *Polyhedron* 1984, **3**, 1289.
135. F. Demartin, M. Manssero, L. Naldini, R. Ruggeri and M. Sansoni, *J. Chem. Soc., Chem. Commun.* 1981, 22.
136. O. Piovesena and P. F. Zanazzi, *Angew. Chem. Int. Ed.* 1980, **19**, 561.
137. P. Bellon, M. Manssero and M. Sansoni, *J. Chem. Soc., Dalton Trans.* 1973, 2423.
138. K. P. Hall, C. E. Briant and D. M. P. Mingos, *J. Organomet. Chem.* 1983, **254**, C18.
139. J. W. A. van der Velden, P. T. Beurskens, J. J. Bour, W. P. Bosman, J. H. Noordik, M. Kolenbrander and J. A. K. M. Buskes, *Inorg. Chem.* 1984, **23**, 146.
140. M. Manassero, L. Naldini and M. Sansoni, *J. Chem. Soc., Chem. Commun.* 1979, 385; F. A. Vollenbroek, W. P. Bosman, J. J. Bour, J. H. Noordik and P. T. Beurskens, *J. Chem. Soc., Chem. Commun.* 1979, 387.
141. P. L. Bellon, F. Cariati, M. Manassero, L. Naldini and M. Sansoni, *J. Chem. Soc., Chem. Commun.* 1971, 1423.
142. D. G. Evans and D. M. P. Mingos, *J. Organomet. Chem.* 1982, **232**, 171.
143. D. M. P. Mingos, *J. Chem. Soc., Dalton Trans.* 1976, 1163.
144. K. P. Hall and D. M. P. Mingos, *Prog. Inorg. Chem.* 1984, **32**, 237.
145. K. P. Hall, D. I. Gilmour and D. M. P. Mingos, *J. Organomet. Chem.* 1984, **268**, 275.
146. C. E. Briant, B. R. C. Theobald, J. W. White, L. K. Bell and D. M. P. Mingos, *J. Chem. Soc., Chem. Commun.* 1981, 201.

147. V. G. Albano, B. L. Bellon, M. Manassero and M. Sansoni, *J. Chem. Soc., Chem. Commun.* 1970, 1210.
148. K. P. Hall, B. R. C. Theobald, D. I. Gilmour, A. J. Welch and D. M. P. Mingos, *J. Chem. Soc., Chem. Commun.* 1982, 528.
149. M. K. Cooper, G. R. Dennis, K. Henrick and M. McPartlin, *Inorg. Chim. Acta* 1980, **45**, L151.
150. J. W. Lauher and K. Wald, *J. Am. Chem. Soc.* 1981, **103**, 7648.
151. L. W. Bateman, M. Green, K. A. Mead, R. M. Mills, I. D. Salter, F. G. A. Stone and P. Woodward, *J. Chem. Soc., Dalton Trans.* 1983, 2599.
152. B. F. G. Johnson, J. Lewis, W. J. H. Nelson, J. Puga, P. R. Raithby, D. Braga, M.McPartlin and W. Clegg, *J. Organomet. Chem.* 1983, **243**, C13.
153. A. G. Cowie, B. F. G. Johnson, J. Lewis, J. N. Nicholls, P. R. Raithby and M. J. Rosales, *J. Chem. Soc., Dalton Trans.* 1983, 2311.
154. G. Lavigne, F. Papageorgiou and J-J. Bonnet, *Inorg. Chem.* 1984, **23**, 609.
155. M. Castaglioni, E. Sappa, M. Valle, M. Lanfranchi and A. Tiripicchio, *J. Organomet. Chem.* 1983, **241**, 99.
156. C. M. Hay, B. F. G. Johnson, J. Lewis, R. C. S. McQueen, P. R. Raithby, R. M. Sorrell and M. J. Taylor, *Organomtallics* 1985, **4**, 202.
157. M. I. Bruce, O. B. Shawkataly and B. K. Nicholson, *J. Organomet. Chem.* 1985, **286**, 427.
158. J. A. K. Howard, I. D. Salter and F. G. A. Stone, *Polyhedron* 1984, **3**, 567.
159. B. F. G. Johnson, D. A. Kaner, J. Lewis, P. R. Raithby and M. J. Rosales, *J. Organomet. Chem.* 1982, **231**, C59.
160. M. I. Bruce and B. K. Nicholson, *J. Chem. Soc., Chem. Commun.* 1982, 1141.
161. L. W. Bateman, M. Green, J. A. K. Howard, K. A. Mead, R. M. Mills, I. D. Salter, F. G. A. Stone and P. Woodward, *J. Chem. Soc., Dalton Trans.* 1983, 2599.
162. C. E. Housecroft and A. L. Rheingold, *Organometallics* 1987, **6**, 1332.
163. D. J. Underwood, R. Hoffmann, K. Tatsumi, A. Nakamura and Y. Yamamoto, *J. Am. Chem. Soc.* 1985, **107**, 5968.
164. C. Mealli, *J. Am. Chem. Soc.* 1985, **107**, 2245.
165. D. G. Evans, G. R. Hughes, D. M. P. Mingos, J-M. Bassett and A. J. Welch, *J. Chem. Soc., Chem. Commun.* 1980, 1255.
166. Jiang Anbei and Cong Qiuzi, *J. Struct. Chem.* 1985, **4**, 96.
167. G. Longoni, M. Manassero and M. Sansoni, *J. Am. Chem. Soc.* 1980, **102**, 7973.
168. M. F. Hallam, N. D. Howells, D. M. P. Mingos and R. W. M. Wardle, *J. Chem. Soc., Dalton Trans.* 1985, 845.
169. R. Bender, P. Braunstein, A. Tiripicchio and M. T. Camellini, *Angew. Chem. Int. Ed.* 1985, **24**, 861.
170. N. J. Taylor, P. C. Chieh and A. J. Carty, *J. Chem. Soc., Chem. Commun.* 1975, 449.
171. R. G. Goodfellow, E. M. Hamon, J. A. K. Howard, J. L. Spencer and D. G. Turner, *J. Chem. Soc., Chem. Commun.* 1984, 1604.
172. P. W. Frost, J. A. K. Howard, J. L. Spencer, D. G. Turner and D. Gregson, *J. Chem. Soc., Chem. Commun.* 1981, 1104.
173. A. A. Frew, R. H. Hill, L. Manojlovic-Muir, K. W. Muir and R. J. Puddephat, *J. Chem. Soc., Chem. Commun.* 1982, 198.
174. K. Matsumoto and K. Fuwa, *J. Am. Chem. Soc.* 1982, **104**, 897.
175. C. Bellitto, G. Dessy, V. Fares and A. Flamini, *J. Chem. Soc., Chem. Commun.* 1981, 409.
176. D. Gregson, J. A. K. Howard, M. Murray and J. L. Spencer, *J. Chem. Soc., Chem. Commun.* 1981, 716.
177. C. E. Briant, D. G. Evans and D. M. P. Mingos, *J. Chem. Soc., Dalton Trans.* 1986, 1535.
178. J. C. Calabrese, L. F. Dahl, P. Chini, G. Longoni and S. Martinengo, *J. Am. Chem. Soc.* 1974, **96**, 2614.
179. P. L. Bellon, A. Ceriotti, F. Demartin, G. Longoni and B. T. Heaton, *J. Chem. Soc., Dalton Trans.* 1982, 1671.
180. J. C. Jeffery, I. Moore, M. Murray and F. G. A. Stone, *J. Chem. Soc., Dalton Trans.* 1982, 1741.
181. C. E. Briant, D. G. Evans and D. M. P. Mingos, *J. Organomet. Chem.* 1984, **267**, C49.
182. C. E. Briant, D. I. Gilmour, D. M. P. Mingos and R. W. M. Wardle, *J. Chem. Soc., Dalton Trans.* 1985, 1693.
183. D. M. P. Mingos and R. W. M. Wardle, *J. Chem. Soc., Dalton Trans.* 1986, 73.
184. G. K. Campbell, P. B. Hitchcock, M. F. Lappert and M. C. Misra, *J. Organomet. Chem.* 1985, **289**, C1.
185. G. Ferguson, B. R. Lloyd and R. J. Puddephatt, *Organometallics* 1986, **5**, 344.
186. D. C. Moody and R. R. Ryan, *Inorg. Chem.* 1977, **16**, 1052.
187. D. M. P. Mingos, *J. Chem. Soc., Chem. Commun.* 1985, 1353.
188. B. K. Teo, *J. Chem. Soc., Chem. Commun.* 1985, 1362 and refs therein.
189. D. G. Evans and D. M. P. Mingos, *J. Organomet. Chem.* 1982, **240**, 321.
190. Y. Yamamoto, K. Aoki and H. Yamazaki, *Organometallics* 1983, **2**, 1377.

191. D. M. Washecheck, E. J. Wuchener, L. F. Dahl, A. Ceriotti, G. Longoni, M. Manassero, M. Sansoni and P. Chini, *J. Am. Chem. Soc.* 1979, **101**, 6110.
192. A. Ceriotti, F. Demartin, G. Longoni, M. Manassero, M. Marchionna, G. Piva and M. Sansoni, *Angew. Chem. Int. Ed.* 1985, **24**, 697.
193. G. Ciani, A. Sironi and S. Martinengo, *J. Organomet. Chem.* 1980, **192**, C42.
194. G. Ciani, A. Sironi and S. Martinengo, *J. Am. Chem. Soc.* 1980, **102**, 7564.
195. J. L. Vidal, L. A. Kapieak and J. M. Troup, *J. Organomet. Chem.* 1981, **215**, C11.
196. G. Longoni, P. Chini, L. D. Lower and L. F. Dahl, *J. Am. Chem. Soc.* 1975, **97**, 5034.
197. B. K. Teo, *Inorg. Chem.* 1984, **23**, 1251.
198. B. K. Teo, G. Longoni and F. R. K. Chung, *Inorg. Chem.* 1984, **23**, 1257.
199. B. K. Teo, *Inorg. Chem.* 1985, **24**, 4209.
200. B. K. Teo, *Inorg. Chem.* 1984, **23**, 1627.
201. D. M. P. Mingos, *Inorg. Chem.* 1985, **24**, 114.
202. B. K. Teo, *Inorg. Chem.* 1985, **24**, 115.

APPENDIX I: STONE'S NOTATION

Here we shall give a brief account of the notation developed by Stone[92] to describe the MO's in cluster compounds. The theoretical details of the Tensor Surface Harmonic technique of molecular orbital analysis will not be discussed, this being adequately covered elsewhere.[92]

The approach considers the M atoms of the cluster to be arranged on the surface of a sphere. The MO's are then described by a label L_i^c (Fig. A1).

L can take values 0, 1, 2, 3, . . . , which are given the labels S, P, D, F, ... The value of L indicates the number of radial nodes in the MO, referred to axes through the centre of the sphere. Nodes inherent in the atomic orbitals are not included in this. Thus, an S orbital is considered to have no radial nodes, even if it is

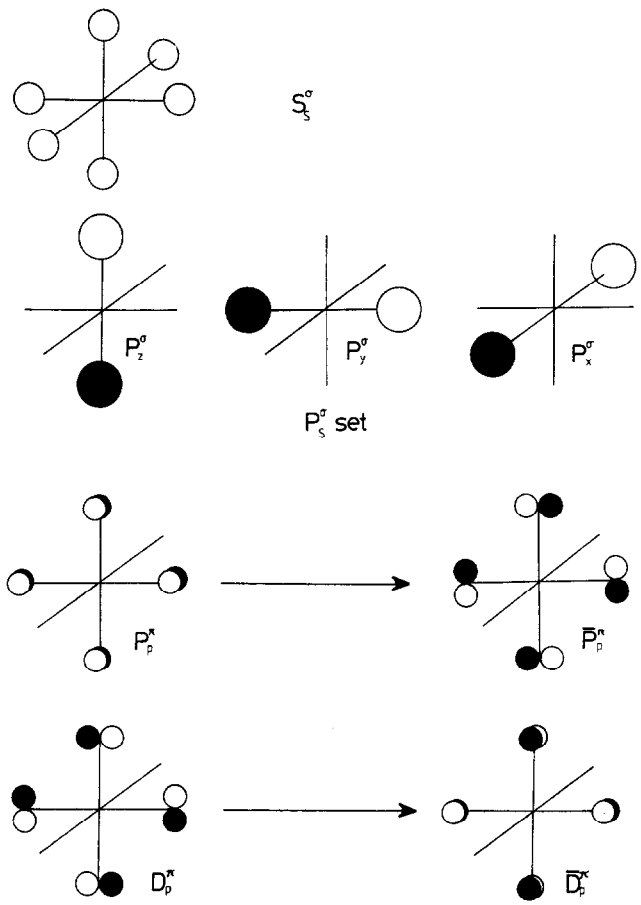

Fig. A1. Examples of the application of Stone's notation to the labelling of MO's of an octahedral cluster. The arrows refer to parity operations.

made up of p atomic orbitals. The labelling is analogous to that used to describe the atomic orbitals of the hydrogen atom.

c is used to differentiate between "radial" and "surface" MO's. Radial MO's have the label σ and are constructed from AO's which are directed along a radius of the sphere. Surface MO's are denoted π or δ, depending on the number of nodes of the constituent AO's parallel to the radius of the sphere passing through the atom. π refers to one nodal plane and δ to two.

The l label refers to the AO parentage of the MO.

L^{π} and $\overline{L^{\pi}}$ MO's are related by a parity operation, where a 90° rotation of the AO's will convert a bonding MO into one which is antibonding.[92]

APPENDIX II: LIST OF ABBREVIATIONS

Ph	Phenyl, C_6H_5
Me	Methyl, CH_3
Et	Ethyl, C_2H_5
Pr	Propyl, C_3H_7
^{i}Pr	*iso*-propyl, $C(H)(CH_3)_2$
^{t}Bu	Tertiary butyl, $C(CH_3)_3$
Cp	C_5H_5, in an η^5-bonding mode unless otherwise stated
Tol	Tolyl, $C_6H_4CH_3$
Cy	Cyclohexyl, C_6H_{11}
dppm	$P(C_6H_5)_2$-CH_2-$P(C_6H_5)_2$
TM	Transition metal
L	Ligand
M	Metal
AO	Atomic Orbital
MO	Molecular Orbital
HOMO	Highest Occupied Molecular Orbital
LUMO	Lowest Unoccupied Molecular Orbital
CVMO	Cluster Valence Molecular Orbital i.e. occupied molecular orbitals in a cluster
HLAO	High Lying Antibonding Orbital
LHLAO	Lowest High Lying Antibonding Orbital
HCVMO	Highest Cluster Valence Molecular Orbital
EHMO	Extended Hückel Molecular Orbital
EAN	Effective Atomic Number
PSEPT	Polyhedral Skeletal Electron Pair Theory
TEC	Topological Electron Counting

Polyhedron Vol. 7, No. 4, pp. 285–289, 1988
Printed in Great Britain

0277–5387/88 $3.00+.00
© 1988 Pergamon Journals Ltd

NITRIDO COMPLEXES OF TECHNETIUM WITH TERTIARY PHOSPHINES AND ARSINES

ULRICH ABRAM*

Central Institute of Nuclear Research Rossendorf, PF 19, Dresden, DDR-8051, G.D.R.

BERND LORENZ and LENZI KADEN

Central Institute of Isotopes and Radiation Research Leipzig, Permoserstr. 15, Leipzig, DDR-7050, G.D.R.

and

DIETER SCHELLER

Dresden University of Technology, Department of Chemistry, Mommsenstr. 13, Dresden, DDR-8027, G.D.R.

(*Received* 5 *May* 1987: *accepted after revision* 26 *August* 1987)

Abstract—Diamagnetic technetium(V) complexes of general formulae $[TcNX_2(Ph_3Y)_2]$ and $[TcNX_3(Me_2PhP)_3]$ (X = Cl, Br; Y = P, As) were prepared starting from $TcNCl_4^-$ and $TcNBr_4^-$, respectively and were characterized. Ligand exchange rates with diethyldithiocarbamate, et_2dtc^- and N-(N″-morpholinylthiocarbonyl)benzamidinate, morphtcb$^-$, were determined.

Nitrido complexes of technetium which can be prepared easily from TcO_4^- by reduction with hydrazine[1,2] and sodium azide,[3] respectively, have attracted a growing interest in view of their relevance to nuclear pharmacological research.[4,5] In recent years a large number of TcN compounds have been prepared and characterized using the long-lived isotope ^{99}Tc (weak β^--emitter with $E_{max} = 0.29$ MeV, half-life $t_{1/2} = 2.13 \times 10^5$ yr).[1,6,7] Convenient starting materials are the Tc(VI) complex $TcNCl_4^-$ [3] and $[Tc(V)NCl_2(Ph_3P)_2]$.[1]

Here we report on the synthesis and characterization of Tc(V) nitrido complexes of general formulae $[TcNX_2(Ph_3P)_2]$ and $[TcNX_2(Me_2PhP)_3]$ (X = Cl, Br; Y = P, As). The new compounds were tested for ligand exchange starting materials to prepare Tc(V) chelate complexes.

EXPERIMENTAL

The Tc(VI) starting materials $(Bu_4N)TcNCl_4$ and $(Bu_4N)TcNBr_4$ were prepared by literature methods.[3] NMR spectra ($CDCl_3$ solutions) were obtained using a WX 90 DS spectrometer (Bruker). UV–Visible and IR–spectra were recorded on a M 40 and on a UR 40 spectrometer (Carl–Zeiss Jena), respectively.

Preparation of the phosphine (arsine) complexes

In typical preparations, 50 mg of $(Bu_4N)TcNCl_4$ (or 64 mg of $(Bu_4N)TcNBr_4$) (0.1 mmol) dissolved in 10 cm^3 acetone were refluxed with a 10-fold excess of phosphine (arsine) ligand for 10 min followed by stirring for 1 h at room temperature. The volume was halved *in vacuo*. After adding 5 cm^3 of methanol and allowing to stand at 5°C, the crystalline products can be separated by suction filtration and washed by water, methanol and diethylether.

Ligand exchange studies

0.02 mmol of the title complexes were put into a vial equipped with a stir bar. After adding 0.1 mmol sodium diethyldithiocarbamate, $Naet_2dtc$,

* Author to whom correspondence should be addressed.

or N-(N″-morpholinylthiocarbonyl)benzamidine, Hmorphtcb, in 3 cm^3 acetone, the mixture was stirred for 1 h at an ambient temperature. The reaction with the Hmorphtcb ligand was initiated by addition of one drop of triethylamine. Diethylether (2 cm^3) was added and after allowing to stand overnight in a refrigerator, the yellow products were separated, methanol and diethylether washed and dried over P_4O_{10}.

The resulting complexes were characterized by their melting points and IR spectra.

Health precautions

Due to the radioactivity of ^{99}Tc some health precautions were taken. All operations were carried out in a fume cupboard with gloves. NMR spectra were measured in sealed glass tubes to avoid contaminations.

^{99}Tc is only a weak β^--emitter, consequently, no further precautions are required provided some elementary ones are taken. Normal glassware gives adequate protection against the weak β-emission. Secondary X-rays (bremsstrahlung) become important if ^{99}Tc is handled on a larger scale only.

RESULTS AND DISCUSSION

The reaction of the Tc(VI) complexes $TcNX_4^-$ (X = Cl, Br) with triphenylphosphine, triphenylarsine and dimethylphenylphosphine results in the formation of Tc(V) nitrido compounds. The brick-red to red–brown coloured $[TcNX_2(Ph_3Y)_2]$ (**I**) complexes are poorly soluble in all organic solvents, whereas $[TcNCl_2(Me_2PhP)_3]$ and $[TcNBr_2(Me_2PhP)_3]$ (**II**) are easily soluble in dichloromethane, benzene and acetonitrile. Yields and analytical data are summarized in Table 1. Tc≡N stretches in the IR spectra are in the range between 1020 and 1100 cm^{-1} comparable to Re≡N frequencies in Re(V) nitrido complexes.[8,9] The yields are always high and it can be suggested that these ligand exchange reactions are a proper way to prepare such complexes. Principally, the same products can be obtained starting from $[TcNCl_2(Ph_3P)_2]$. However, the yields are lower and by the small differences in physical properties of the $[TcNX_2(Ph_3Y)_2]$ complexes (melting points, solubility, UV–Visible and IR spectral parameters) the evaluation of the completed ligand exchange is rendered more difficult.[1]

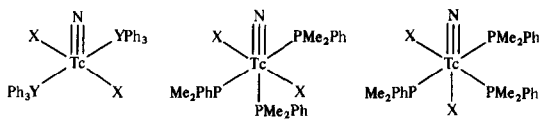

I **IIa** **IIb**

Whereas the **mer**-configuration for the $[TcNX_2$

Table 1. Yields and analytical data of $[TcNX_2(Ph_3Y)_2]$ and $[TcNX_2(Me_2PhP)_3]$ complexes (X = Cl, Br; Y = P, As)

Complex	Yield (%)	Colour	M.p. (°C)	Elemental analysis[a] C	H	N	X	Tc	IR (cm^{-1}) Tc≡N	UV–Visible (nm(lgε))
$[TcNCl_2(Ph_3P)_2]$[b]	95	brick-red	225–7	61.0	4.3	2.0	10.0	14.0	1095[c]	276(3.6)
				61.7	4.5	2.0	10.8	13.6		485(2.1)
$[TcNBr_2(Ph_3P)_2]$	90	red–brown	237–43	54.2	3.8	1.8	20.1	12.7	1090[c]	276(4.0)
				54.2	4.1	1.8	17.3	12.0		289(3.9)
										494(2.3)
$[TcNCl_2(Ph_3As)_2]$	85	yellow–brown	232–4	54.3	3.8	1.8	8.9	12.4	1091	273(4.1)
				53.6	4.1	1.7	10.0	10.9		374(2.3)
										495(2.1)
$[TcNBr_2(Ph_3As)_2]$	90	red–brown	236–7	48.8	3.4	1.6	18.0	11.2	1091	250(4.3)
				48.1	3.4	1.6	18.0	10.3		299(3.7)
										532(2.4)
$[TcNCl_2(Me_2PhP)_3]$[d]	80	yellow	170–1	48.7	5.6	2.3	11.8	16.5	1048	255(4.4)
				48.8	5.3	2.1	11.0	16.0		365(2.4)
$[TcNBr_2(Me_2PhP)_3]$	85	orange	168–70	41.9	4.8	2.0	23.3	14.4	1028	261(4.4)
				43.3	5.5	2.1	20.9	13.4		370(2.4)
										422(2.2)

[a] Calc./found (%).
[b] See also refs 1 and 3.
[c] Superposition with ligand bands.
[d] See also ref. 1.

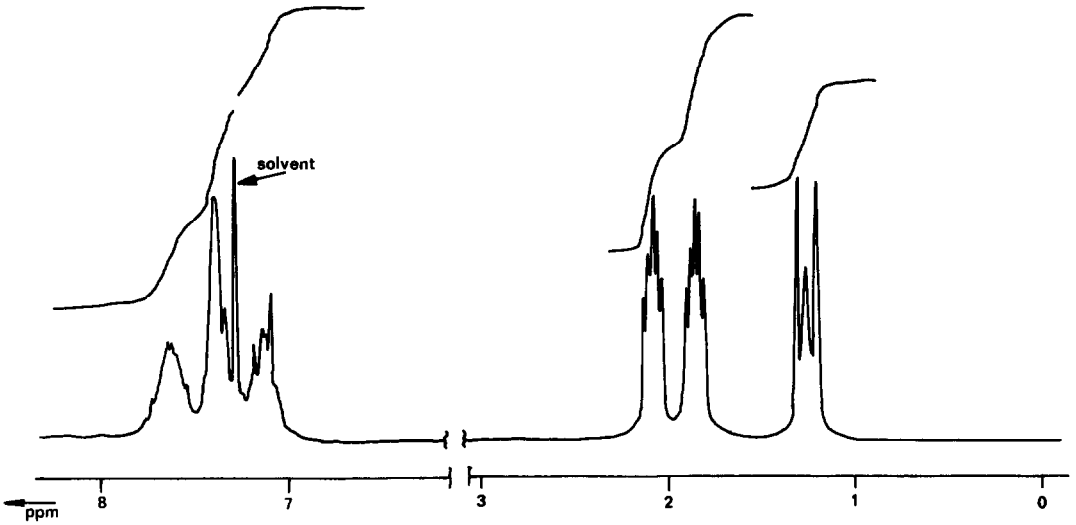

Fig. 1. ^{31}P coupled proton NMR spectrum of $[TcNCl_2(Me_2PhP)_3]$ in $CDCl_3$ ($T = 295$ K; chemical shift relative to TMS).

$(Me_2PhP)_3]$ complexes is strongly suggested by IR spectral results, an assignment to structure **IIa** or **IIb** cannot be derived from those.

The ^1H-NMR spectra of the $[TcNX_2(Me_2PhP)_3]$ complexes (Fig. 1 shows that of the chloro complex) consist of the typical high order pattern in the aromatic region between 6.91 and 7.91 ppm and of three well-separated signals due to the methyl protons (see Table 2). The high order splitting patterns of the two downfield methyl signals caused by ^{31}P couplings are identical, but differ from those of the high field signal. With ^{31}P decoupling, all signal groups in the aliphatic region become sharp singlets with an intensity ratio of 1 : 1 : 1.

Therefore, a complex structure with a low degree of symmetry has been assumed. Each of the structures **IIa** and **IIb** includes two equivalent and one different Me_2PhP ligands. Due to the symmetry of **IIa**, the two methyl groups of each substituent are enantiotopic, e.g. equal chemical shifts result, and the methyl part of the **IIa** complex ^1H-NMR spectrum consists of two signals with a 2 : 1 intensity ratio. In **IIb**, however, the two methyl groups of the two equivalent ligands are diastereotopic, and different chemical shifts are expected. Therefore, structure **IIb** is established for both the complexes with X = Cl and Br. This result comes close to the structure found for the corresponding Re(V) complex $[ReNCl_2(Me_2PhP)_3]$ by an X-ray study.[10] The ^{31}P coupled ^1H-NMR spectra of the methyl

Table 2. NMR chemical shifts of $[TcNCl_2(Me_2PhP)_3]$ and $[TcNBr_2(Me_2PhP)_3]$ in ppm from TMS and H_3PO_4, respectively

Complex	Nucleus	Chemical shift, multiplet, intensity
$[TcNCl_2(Me_2PhP)_3]$	^1H	phenyl: 6.91–7.91 m (15H)
		CH_3: 2.08 m (6H)
		1.85 m (6H)
		1.27 m (6H)
	^{31}P	broadened peak 2.1 ppm at 220 K
$[TcNBr_2(Me_2PhP)_3]$	^1H	phenyl: 6.91–7.91 m (15H)
		CH_3: 2.19 m (6H)
		2.00 m (6H)
		1.30 m (6H)
	^{31}P	broadened peaks at −0.3 and −4.4 ppm at 220 K

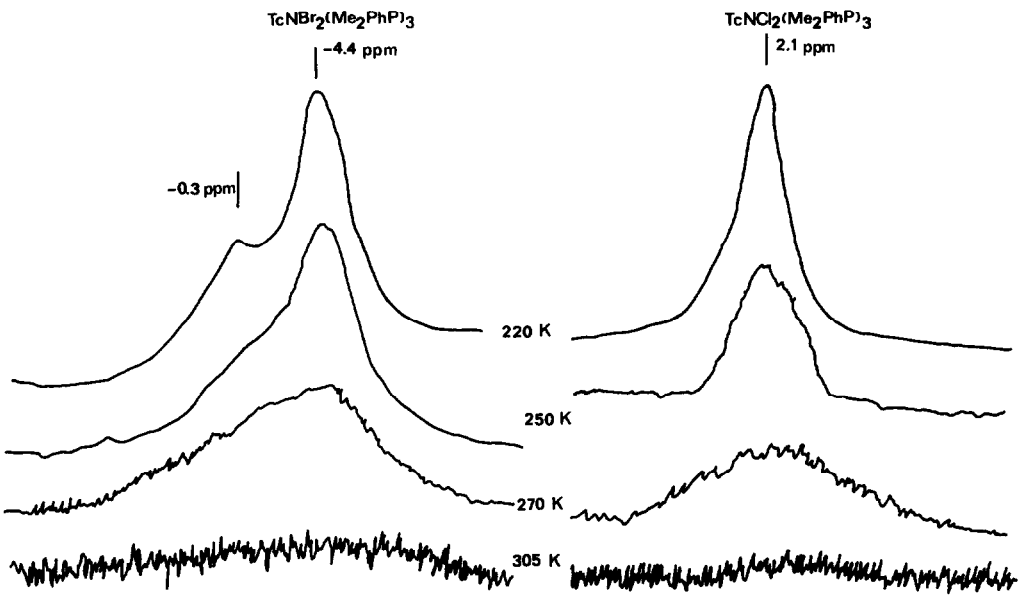

Fig. 2. ^{31}P-NMR spectra of $[TcNCl_2(Me_2PhP)_3]$ and $[TcNBr_2(Me_2PhP)_3]$ (Solvent: $CDCl_3$).

groups show a typical high order pattern, which varies with the ligand X, caused by small geometry differences of the complexes.

In contrast to the ^{1}H-spectra, the ^{31}P-NMR lines at room temperature are strongly broadened. By lowering the temperature the signals become much narrower, and for the Br complex two maxima appear as can be seen in Fig. 2. The expected spectra type with ^{1}H-decoupling is A_2B. Because of residual line broadening, the nine peaks are not resolved, and the coupling constants between the ^{31}P nuclei may not be calculated. The chemical shift difference of these nuclei decrease if X changes from Br to Cl, and a slightly nonsymmetric signal is observed. Attempts to considerably increase the chemical shift differences by adding paramagnetic shift reagents failed.

The line broadening in the ^{31}P spectra cannot be discussed in terms of dynamic effects (see also ^{1}H-NMR results). It most probably arises from a scalar coupling of the ^{31}P nuclei with the quadrupole nucleus ^{99}Tc ($Q = 0.3 \times 10^{-28}$ m^2). With decreasing temperature, the relaxation time T_2 for the ^{31}P nuclei increases. This results in the narrower lines found in the experiment (Fig. 2).

The reaction of the title complexes with the chelating ligands et_2dtc^- (**III**) and morphtcb$^-$ (**IV**)

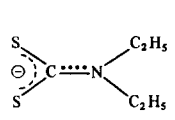

III

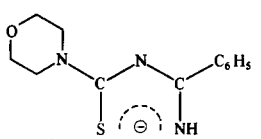

IV

Table 3. Yields of ligand exchange reactions with et_2dtc^- and morphtcb$^-$

Starting material	Yield (%) et_2dtc^-	Yield (%) morphtcb$^-$
$[TcNCl_2(Ph_3P)_2]$	85[a]	95
$[TcNBr_2(Ph_3P)_2]$	80	90
$[TcNCl_2(Ph_3As)_2]$	82	87
$[TcNBr_2(Ph_3As)_2]$	90	92
$[TcNCl_2(Me_2PhP)_3]$	87	85
$[TcNBr_3(Me_2PhP)_3]$	90	89

[a] See also ref. 1.

results in the formation of the well-known Tc(V) complexes $[TcN(et_2dtc)_2]$[1,3] and $[TcN(morphtcb)_2]$.[11] The yields obtained are summarized in Table 3. Significant differences cannot be found, indicating the title complexes to be good starting materials for the synthesis of further Tc(V) nitrido compounds in the same way. The yields of the reactions with the more lipophilic tcb$^-$ ligand are much higher than those obtained starting from $TcNCl_4^-$ (about 50%).[11] So, the synthetic route stated above should be preferred for special purposes.

REFERENCES

1. L. Kaden, B. Lorenz, K. Schmidt, H. Sprinz and M. Wahren, *Isotopenpraxis* 1981, **17**, 174.
2. J. Baldas, J. Bonnyman, P. M. Pojer, G. A. Williams and M. F. Mackay, *J. Chem. Soc., Dalton Trans.* 1981, 1798.
3. J. Baldas, J. F. Boas, J. Bonnyman and G. A. Williams, *J. Chem. Soc., Dalton Trans.* 1984, 2394.

4. J. Baldas and J. Bonnyman, *Int. J. Appl. Radiat. Isot.* 1985, **36**, 133.
5. S. Abram, U. Abram, H. Spies and R. Münze, *J. Radioanal. Nucl. Chem.* 1986, **102**, 309.
6. J. Baldas, J. Bonnyman and G. A. Williams, *Inorg. Chem.* 1986, **25**, 150.
7. U. Abram, S. Abram, H. Spies, R. Kirmse and K. Köhler, *Z. anorg. allg. Chem.* 1987, **544**, 106.
8. J. Chatt, J. D. Garforth, N. P. Johnson and G. A. Rowe, *J. Chem. Soc.* 1964, 1012.
9. J. Chatt, C. D. Falk, G. J. Leigh and R. J. Paske, *J. Chem. Soc.* (*A*) 1969, 2288.
10. E. Forsellini, U. Casellato, R. Graziani and L. Magon, *Acta Cryst.* 1982, **B38**, 3081.
11. U. Abram, J. Hartung, L. Beyer, R. Kirmse and K. Köhler, *Z. Chem.* 1987, **27**, 101.

Polyhedron Vol. 7, No. 4, pp. 291–295, 1988
Printed in Great Britain

0277–5387/88 $3.00+.00
© 1988 Pergamon Journals Ltd

EVALUATION OF ABSOLUTE STABILITY CONSTANTS OF COMPLEXES—I. THEORY AND APPLICATIONS TO THE INORGANIC ONE-TO-ONE COMPLEXES OF IRON(III) IN PERCHLORATE MEDIA

QI FENG and HIROHIKO WAKI*

Department of Chemistry, Faculty of Science, Kyushu University,
Hakozaki, Higashiku, Fukuoka, Japan

(*Received* 7 *April* 1987; *accepted after revision* 26 *August* 1987)

Abstract—A method for evaluating a true stability constant termed the "absolute stability constant" is presented and the absolute stability constants for some first complexes of iron(III) with inorganic anionic ligands, are evaluated by spectrophotometric measurement and mathematical treatment. The K_1 values obtained are: 2.1 for $Fe(ClO_4)^{2+}$, 7.6 for $FeCl^{2+}$, 3.6 for $FeBr^{2+}$, 383 for $Fe(SO_4)^{+}$ and 3.2 for $Fe(NO_3)^{2+}$ at $I = 0.4$ M and 20°C. These values are much larger than the apparent constants, that is, than the values which have conventionally been reported as "stability constants".

In experimentally determining stability constants of complexes, an inert medium electrolyte has been added to maintain the activity coefficients of all ions involved constant within a series of solutions to be measured. In all cases no participation of the supporting medium ions in complex formation has been assumed. Nevertheless, it seems undeniable that poly-valent ions can form ion-pairs to some degree with medium ions of opposite charge, though these ion-pairs are in general not very stable. This side reaction should affect the complex formation to be investigated, giving an erroneous stability constant. The conventional treatment has only been that perchlorate anion or tetramethylammonium cation is employed as an "inert medium ion" and the stability constants with these medium ions are assumed to be zero.[1–4] However, the relative error produced by ignoring complex formation with the medium ion may be very pronounced in investigating an especially weak complex whose stability is of comparative magnitude to that of the medium ion complex. This erroneous stability constant should not only lead to a false recognition of the species distribution in a practical solution but also to an incorrect evaluation for physical quantities such as molar absorptivity.

Johanson[5] discussed these problems with perchlorate as a typical medium electrolyte in his review and concluded that the estimation of such a medium ion contribution may be impossible by means of an equilibrium calculation only, unless more than one method directly distinguishing the species involved can be applied simultaneously. However, it may not be easy to find out such an effective direct method. The authors thought that the medium ion effect could be estimated by suitable mathematical treatment of the experimental equilibrium data. We use the term "absolute stability constant" for the pure stability constant obtained by estimating the ion-pair formation with the weakest medium ion, which has been thought so far to be undeterminable. In this paper a theoretical background to obtain such an absolute stability constant and the application to practical simple complex systems are presented.

THEORY

We restrict the determination of absolute stability constants by absorption spectrophotometry, to the simplest case of a M^{m+}—L^{-} complex system containing a monovalent medium anion B^{-} where only one-to-one complexes $ML^{(m-1)-}$ and $MB^{(m-1)-}$ are formed, as is often observed in weak inorganic ligand complexes. Assuming that the MB complex

*Author to whom correspondence should be addressed.

has no absorptivity at a wavelength of the measurement for ML, the apparent molar absorptivity ε is expressed by

$$\varepsilon \equiv \frac{A}{C_M l} = \frac{\varepsilon_1[\mathrm{ML}]}{[\mathrm{M}]+[\mathrm{ML}]+[\mathrm{MB}]} \tag{1}$$

where A is the absorbance, C_M the total concentration of the sample metal, l the light path and ε_1 is the molar absorptivity of the ML complex. If the medium anion is added to the system in such a way that the ionic strength of a series of solutions is kept constant, i.e. $I = [\mathrm{L}^-]+[\mathrm{B}^-] = \text{const.}$, eq. (1) can be transformed to

$$\frac{\varepsilon}{[\mathrm{L}^-]} = \frac{\varepsilon_1 K_1}{1+K_B I} - \frac{K_1 - K_B}{1+K_B I}\cdot\varepsilon \tag{2}$$

where K_1 and K_B are the absolute stability constants of ML and MB at ionic strength I, respectively.

In a conventional treatment, K_B for the weakest medium anion such as the perchlorate ion is assumed to be zero and a simpler equation has been adopted,

$$\frac{\varepsilon}{[\mathrm{L}^-]} = K_1\varepsilon_1 - K_1\varepsilon \tag{3}$$

obtaining K_1 from the slope of $\varepsilon/[\mathrm{L}^-]$ vs ε plot. However, the assumption of $K_B = 0$ cannot be considered as a generally acceptable one. Thus

$$\frac{\varepsilon}{[\mathrm{L}^-]} = \text{const.} - K_1^{\mathrm{ap}}\varepsilon \tag{4}$$

$$K_1^{\mathrm{ap}} = \frac{K_1 - K_B}{1+K_B I} \tag{5}$$

and the slope of the $\varepsilon/[\mathrm{L}^-]$ vs ε plot gives only an apparent constant K_1^{ap} which is smaller than the absolute stability constant. Since K_B for the weakest medium ion cannot be determined experimentally, K_1 is also undeterminable. An extrapolation of K_1^{ap} to zero ionic strength only gives a stability constant difference of $K_1 - K_B$, not K_1. Neither could simultaneous standing of eq. (5) at arbitrarily different ionic strengths produce the absolute constants through the alteration of K_1 and/or K_B values due to the activity coefficient change.

The best and only possible treatment in such a case may be by a reasonable extrapolation of the approximate absolute stability constant derived from simultaneous equations at two selected ionic strengths, to the midpoint of these two ionic strengths.

Let these ionic strengths be $I-\Delta I$ and $I+\Delta I$ for simplification, I being the ionic strength where the stability constants are to be investigated, then eq. (5) is written as

$$K^{\mathrm{ap}}_{1(I-\Delta I)} = \frac{K_{1(I-\Delta I)} - K_{B(I-\Delta I)}}{1+K_{B(I-\Delta I)}(I-\Delta I)} \tag{6}$$

or

$$K^{\mathrm{ap}}_{1(I+\Delta I)} = \frac{K_{1(I+\Delta I)} - K_{B(I+\Delta I)}}{1+K_{B(I+\Delta I)}(I+\Delta I)}. \tag{7}$$

If a relationship

$$\frac{K_{1(I-\Delta I)}}{K_{1(I)}} = \frac{K_{1(I)}}{K_{1(I+\Delta I)}} = f \tag{8}$$

is assumed and the ratio f is assumed to be the same for a ligand ion and medium ion of similar types when ΔI is not very large, then

$$K^{\mathrm{ap}}_{1(I-\Delta I)} = \frac{fK_{1(I)} - fK_{B(I)}}{1+fK_{B(I)}(I-\Delta I)} \tag{9}$$

$$K^{\mathrm{ap}}_{1(I+\Delta I)} = \frac{K_{1(I)} - K_{B(I)}}{f+K_{B(I)}(I+\Delta I)}. \tag{10}$$

Using eqs (9) and (10), the absolute stability constants $K_{1(I)}$ and $K_{B(I)}$ can be written as

$$K_{1(I)} = \frac{\frac{1}{f}K^{\mathrm{ap}}_{1(I-\Delta I)} - fK^{\mathrm{ap}}_{1(I+\Delta I)} + K^{\mathrm{ap}}_{1(I-\Delta I)}K^{\mathrm{ap}}_{1(I+\Delta I)}\left[\frac{1}{f}(I+\Delta I) - f(I-\Delta I)\right]}{K^{\mathrm{ap}}_{1(I+\Delta I)}(I+\Delta I) - K^{\mathrm{ap}}_{1(I-\Delta I)}(I-\Delta I)} \tag{11}$$

$$K_{B(I)} = \frac{\frac{1}{f}K^{\mathrm{ap}}_{1(I-\Delta I)} - fK^{\mathrm{ap}}_{1(I+\Delta I)}}{K^{\mathrm{ap}}_{1(I+\Delta I)}(I+\Delta I) - K^{\mathrm{ap}}_{1(I-\Delta I)}(I-\Delta I)}. \tag{12}$$

Although $K_{1(I)}$ and $K_{B(I)}$ cannot be solved from these equations, these absolute stability constants may be determined by an extrapolating treatment described below.

If f is set to be unity, approximate absolute stability constants K_1^* and K_B^* at ionic strengths $I+\Delta I$ and $I-\Delta I$ can be calculated by

$$K^*_{1(I\pm\Delta I)} = \frac{K^{\mathrm{ap}}_{1(I-\Delta I)} - K^{\mathrm{ap}}_{1(I+\Delta I)} + K^{\mathrm{ap}}_{1(I-\Delta I)}K^{\mathrm{ap}}_{1(I+\Delta I)}(2\Delta I)}{K^{\mathrm{ap}}_{1(I+\Delta I)}(I+\Delta I) - K^{\mathrm{ap}}_{1(I-\Delta I)}(I-\Delta I)} \tag{13}$$

$$K^*_{B(I\pm\Delta I)} = \frac{K^{\mathrm{ap}}_{1(I-\Delta I)} - K^{\mathrm{ap}}_{1(I+\Delta I)}}{K^{\mathrm{ap}}_{1(I+\Delta I)}(I+\Delta I) - K^{\mathrm{ap}}_{1(I-\Delta I)}(I-\Delta I)}. \tag{14}$$

The differences between K_1^* and K_1 and between K_B^* and K_B

$$K^*_{B(I\pm\Delta I)} - K_{B(I)} = \frac{\left(1-\frac{1}{f}\right)K^{ap}_{1(I-\Delta I)} - (1-f)K^{ap}_{1(I+\Delta I)}}{K^{ap}_{1(I+\Delta I)}(I+\Delta I) - K^{ap}_{1(I-\Delta I)}(I-\Delta I)} \quad (15)$$

$$K^*_{1(I\pm\Delta I)} - K_{1(I)} = \frac{\left(1-\frac{1}{f}\right)K^{ap}_{1(I-\Delta I)} - (1-f)K^{ap}_{1(I+\Delta I)}}{K^{ap}_{1(I+\Delta I)}(I+\Delta I) - K^{ap}_{1(I-\Delta I)}(I-\Delta I)} + \frac{K^{ap}_{1(I-\Delta I)}K^{ap}_{1(I+\Delta I)}\left[2\Delta I - \frac{1}{f}(I+\Delta I) + f(I-\Delta I)\right]}{K^{ap}_{1(I+\Delta I)}(I+\Delta I) - K^{ap}_{1(I-\Delta I)}(I-\Delta I)} \quad (16)$$

approach zero with decreasing ΔI

$$\lim_{\Delta I\to 0}(K^*_{B(I\pm\Delta I)} - K_{B(I)}) = \left(\frac{df}{d\Delta I}\right)_{\Delta I=0} = 0 \quad (17)$$

$$\lim_{\Delta I\to 0}(K^*_{1(I\pm\Delta I)} - K_{1(I)}) = (1+K^{ap}_{1(I)}I)\left(\frac{df}{d\Delta I}\right)_{\Delta I=0} = 0. \quad (18)$$

Therefore, the absolute stability constants K_1 and K_B at ionic strength I can be determined by extrapolating $K^*_{1(I\pm\Delta I)}$ and $K^*_{B(I\pm\Delta I)}$ from ionic strength $I+\Delta I$ to I. Once the absolute stability constant K_B of the medium anion becomes clear, the absolute stability constant of any other ligand anion at the same ionic strength can easily be obtained using eq. (5) through the experimental measurement of K_1^{ap} in the binary system with B^-.

EXPERIMENTAL

Apparatus and chemicals

A Hitachi Recording Spectrophotometer EPS-3T was employed with a 1 cm quartz cell for absorbance measurements. All chemicals used were of commercially available reagent grade.

Spectrophotometric measurement for determination of apparent stability constants

In an iron(III)–chloride complex system, the absorbance for a series of solutions containing 8.0×10^{-4} M iron(III) perchlorate, and hydrochloric acid and perchloric acid of different concentrations at different ionic strengths was measured at 336 nm. In an iron(III)–bromide complex system, the absorbance of solutions containing 7.7×10^{-3} M iron(III) perchlorate, and hydrobromic acid and perchloric acid of different concentrations at ionic strength of 0.4 M was measured at 403 nm. In an iron(III)–sulphate complex system, the absorbance of solutions containing 4.0×10^{-4} M ferric perchlorate, and sulphuric acid and perchloric acid of different concentrations at ionic strength of 0.4 M was measured at 330 nm. In an iron(III)–nitrate complex system, the absorbance of solutions containing 8.0×10^{-4} M ferric perchlorate, and hydrochloric acid and nitric acid of different concentrations at ionic strength of 0.4 M was measured at 355 nm.

All measurements were carried out at room temperature 20 ± 1°C, with a reference cell containing water.

RESULTS AND DISCUSSION

Evaluation of absolute stability constants for $FeCl^{2+}$ *and* $Fe(ClO_4)^{2+}$ *complexes*

The first step for evaluating absolute stability constants is to determine the conventional stability constants according to an ordinary method. The iron(III)–chloride–perchlorate system seemed to be convenient for our purpose, since aquated ferric iron and the perchlorate complex are non-absorptive at the wavelength of 336 nm, with the maximal absorption by the chloro complexes. The $\varepsilon_{Fe}^{336}/[Cl^-]$ vs ε_{Fe}^{336} plot based on eq. (4) gave a straight line in all ionic strengths studied, indicating that the chloride or perchlorate complexes higher than one to one are negligible. The presence of hydroxo complexes of iron can also be neglected under this condition (pH < 1), as log β_1 for $FeOH^{2+}$ is less than 3.0.[1] The plot with an ionic strength of 0.4 M is shown in Fig. 1 as an example. The apparent stability constants obtained in this way at different ionic strengths are given in Fig. 2. The constant first decreased, then seemed to pass through a minimum with increasing ionic strength. This change is caused by an increased formation of the iron–perchlorate complex and the variation in ionic activity coefficients.

The second step for evaluating the absolute stability constants is to remove the effect of the activity coefficient change from these apparent constants by an appropriate extrapolation treatment. The ionic strength region around $I = 0.4$ M seems to be convenient for analysis, since the activity coefficients of at least the chloride ion and perchlorate ion may be sufficiently constant.[6] Also, the ratios $\gamma_{Fe^{3+}}/\gamma_{FeCl^{2+}}$

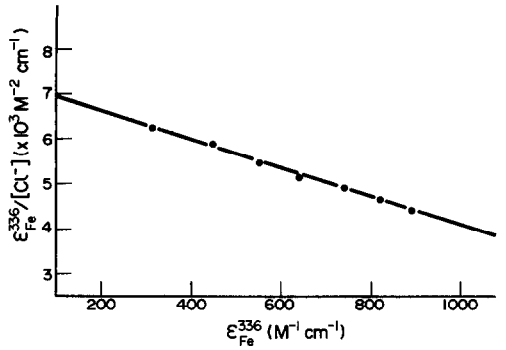

Fig. 1. Determination of the apparent stability constant for the $FeCl^{2+}$ complex by spectrophotometry at $I = 0.4$ ($HCl + HClO_4$).

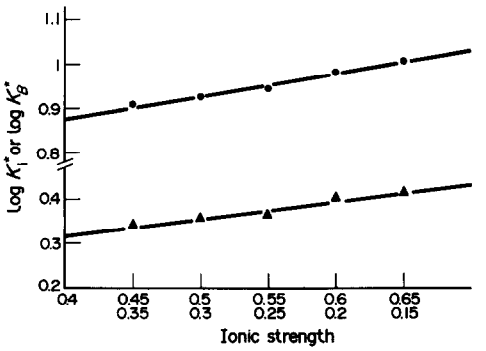

Fig. 3. Determination of the absolute stability constants for $FeCl^{2+}$ and $FeClO_4^{2+}$ complexes at $I = 0.4$ by extrapolation of log K_1^* and log K_B^*. ●: log K_1^*; ▲: log K_B^*.

and $\gamma_{Fe^{3+}}/\gamma_{Fe(ClO_4)^{2+}}$ may be similar to each other and both change only gradually with ionic strength. For extrapolation, pairs of ionic strengths of equal difference from the central ionic strength $I = 0.4$ M, i.e. $I = 0.35$ and 0.45, $I = 0.30$ and 0.50, $I = 0.25$ and 0.55 M and so on, were taken and the corrected apparent stability constants of $FeCl^{2+}$ with these pairs of ionic strengths were taken from the smooth curve which best fits experimental points, as shown in Fig. 2. By inserting these values into eqs (13) and (14), the approximate absolute stability constants of the $FeCl^{2+}$ complex and also of the $Fe(ClO_4)^{2+}$ complex were calculated, respectively. These values were extrapolated to $I = 0.4$ M as indicated in Fig. 3. A good linearity from the extrapolation was obtained, from which the true absolute stability constants were evaluated to be $K_1 = 7.6$ for $FeCl^{2+}$ and $K_B = 2.1$ for $Fe(ClO_4)^{2+}$. Almost the same value, i.e. 2.0 for $Fe(ClO_4)^{2+}$ can be obtained by substituting $K_1 = 7.6$ and the experimental value $K_1^{ap} = 3.05$ into eq. (5).

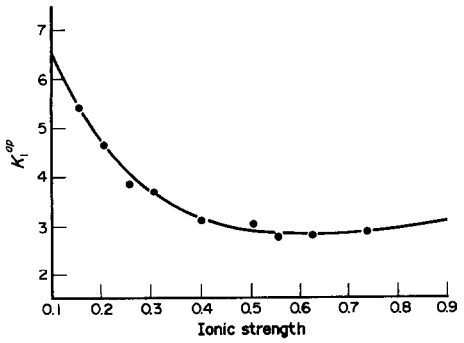

Fig. 2. Ionic strength dependence of the apparent stability constant for the $FeCl^{2+}$ complex.

Evaluation of absolute stability constants for other complex systems from the stability constant with medium anion determined

Since the stability constant of the iron(III) complex with perchlorate ion in a medium electrolyte, together with that of the $FeCl^{2+}$ complex, is known, other iron(III) complex systems could easily be analysed using the same perchlorate medium.

The iron(III)–bromide–perchlorate system was analysed in order to evaluate the absolute stability constant of $FeBr^{2+}$ at $I = 0.4$ M. The $\varepsilon_{Fe}^{403}/[Br^-]$ was plotted against ε_{Fe}^{403} to determine the apparent stability constant (Fig. 4a). A straight line was drawn by an error-weighted least square technique, from whose slope K_1^{ap} was obtained. The absolute stability constant of $FeBr^{2+}$ was calculated from the equation

$$K_1^{ap} = \frac{K_{FeBr^{2+}} - K_{Fe(ClO_4)^{2+}}}{1 + K_{Fe(ClO_4)^{2+}} \times I} \qquad (19)$$

using the $K_{Fe(ClO_4)^{2+}}$ value determined in the foregoing section.

In a similar way, the iron(III)–sulphate–perchlorate system was analysed to evaluate the absolute stability constant of $Fe(SO_4)^+$ at $I = 0.4$ M. In this case the free sulphate concentration as the ordinate of Fig. 4b was calculated from the first protonation constant $[HSO_4^-]/[SO_4^{2-}][H^+] = 18.8$ at $I = 0.4$ M*. With the apparent stability constant obtained from the $\varepsilon_{Fe}^{330}/[SO_4^{2-}]$ vs ε_{Fe}^{330} plot (Fig. 4b), the absolute stability constant was calculated using

* This value was determined by the present authors using a separate experiment whose details are omitted in this paper.

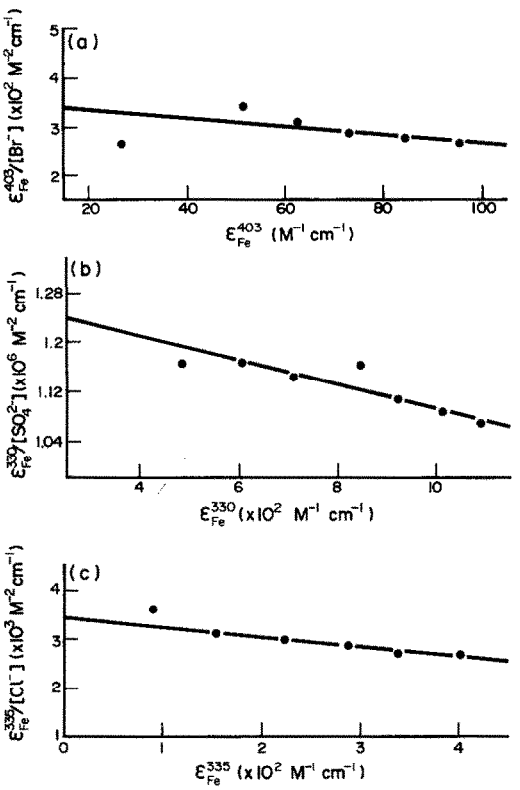

Fig. 4. Determination of the apparent stability constants of some other iron(III) complexes. (a) $FeCl^{2+}$(HBr–$HClO_4$); (b) $FeSO_4^+$(H_2SO_4–$HClO_4$); (c) $FeNO_3^{2+}$(HCl–HNO_3).

the equation

$$K_1^{ap} = \frac{K_{Fe(SO_4)^+} - 3K_{Fe(ClO_4)^{2+}} - K_{Fe(ClO_4)^{2+}}K_{HSO_4^-}[H^+]}{1 + K_{Fe(ClO_4)^{2+}} \times I}. \quad (20)$$

Generally speaking, if the absolute stability constant with one ligand in a binary ligand system is known, the constant with another ligand can be determined. The absolute stability constant of the $Fe(NO_3)^{2+}$ complex cannot be determined spectrophotometrically in a perchlorate medium, because of non-absorptivity of the complex. Instead the iron(III)–chloride–nitrate system could be utilized for the analysis. First the apparent stability constant of $FeCl^{2+}$ in a nitric acid media was determined (Fig. 4c), then the absolute stability constant of $Fe(NO_3)^{2+}$ at $I = 0.4$ M was calculated from the equation

$$K_1^{ap} = \frac{K_{FeCl^{2+}} - K_{Fe(NO_3)^{2+}}}{1 + K_{Fe(NO_3)^{2+}} \times I} \quad (21)$$

by inserting the known absolute stability constant $K_{FeCl^{2+}}$.

The absolute stability constants evaluated are tabulated in Table 1, as well as the apparent constants. Some of these apparent constants were in good agreement with "stability constants" reported by other investigators,[7–9] considering the difference in ionic strength. It can be seen from the table that the error produced by taking the apparent stability constant as the true constant may become significant when the value of the stability constant is small.

The extension of the present method for evaluating the absolute stability constant using ionic strengths other than $I = 0.4$ M in HCl–$HClO_4$ media, for other metal complex systems, and for the evaluation of other constants such as K_2 or K_3, will be tried and reported elsewhere.

REFERENCES

1. R. M. Smith and A. E. Martell (Eds), *Critical Stability Constants*, Inorganic Complexes, Vol. 4. Plenum Press, New York (1976).
2. E. Hogfeldt (Ed.), *Stability Constants of Metal–Ion Complexes*, Part A: Inorganic Ligands. Pergamon Press, Oxford (1982).
3. L. G. Sillen and A. E. Martell (Eds), *Stability Constants of Metal–Ion Complexes*, Special Publication No. 17, London (1964).
4. L. G. Sillen and A. E. Martell (Eds.), *Stability Constants of Metal–Ion Complexes*, Special Publication No. 25, London (1971).
5. L. Johansson, *Coord. Chem. Rev.* 1974, **12**, 241.
6. W. J. Hamer and Yung-Chi Wu, *J. Phys. Chem* (Ref. Data), 1972, **1**, 1047.
7. E. Rabinowitch and W. H. Stockmayer, *J. Am. Chem. Soc.* 1942, **64**, 335.
8. D. F. C. Morris and A. R. Wilson, *J. Inorg. Nucl. Chem.* 1969, **31**, 1532.
9. D. F. C. Morris and P. J. Sturgess, *Electrochim. Acta.* 1969, **14**, 629.

Table 1. Absolute and apparent stability constants for some iron(III) complexes at $I = 0.4$ M, 20°C

Complex	Absolute ($I = 0.4$ M)	Apparent ($I = 0.4$ M) = conventional	Relative error of conventional constant (%)
$Fe(ClO_4)^{2+}$	2.1	0	−100
$FeCl^{2+}$	7.6	3.1	−59
$FeBr^{2+}$	3.6	0.81	−78
$Fe(SO_4)^+$	383	196	−49
$Fe(NO_3)^{2+}$	3.2	(0.60)	−81

Polyhedron Vol. 7, No. 4, pp. 297 301, 1988
Printed in Great Britain

0277-5387/88 $3.00+.00
© 1988 Pergamon Journals Ltd

STRUCTURAL EVIDENCE FOR NON-REACTIVITY TOWARDS DEHYDROHALOGENATION IN A BIS-*t*-BUTYLAMINE-*t*-BUTYLIMIDO COMPLEX OF TUNGSTEN(V). THE PREPARATION AND X-RAY CRYSTAL STRUCTURE OF $[W(NCMe_3)Cl_3(NH_2CMe_3)_2]$

GEORGE R. CLARK, ALASTAIR J. NIELSON* and CLIFTON E. F. RICKARD

Department of Chemistry, University of Auckland, Private Bag, Auckland, New Zealand

(*Received* 9 *June* 1987; *accepted* 8 *September* 1987)

Abstract—Reaction of WCl_6 with four equivalents of $Me_3SiNHCMe_3$ in benzene gives a low yield of $[W(NCMe_3)Cl_3(NH_2CMe_3)_2]$ for which the IR spectrum indicates a *mer* arrangement of metal trichlorides. Further dehydrohalogenation to give an amido ligand does not take place. The structure of the complex was determined by single-crystal X-ray diffraction methods. The crystals are monoclinic, space group $C2/c$ with four molecules in a unit cell of dimensions $a = 19.701(3)$, $b = 9.674(2)$, $c = 11.430(2)$ Å and $\beta = 116.40(1)°$. The structure was solved by Patterson and Fourier methods and refined to an R value of 0.030. The tungsten atom is in a distorted octahedral environment comprising three *mer* chloro ligands, two *trans* *t*-butylamine ligands and a *t*-butylimido ligand. A crystallographic two-fold axis passes through Cl(1), W and $N_{t\text{-butylimido}}$. Observed distances are $W—N_{t\text{-butylimido}} = 1.728(5)$, $W—N_{t\text{-butylamine}} = 2.230(4)$, W—Cl(2) = 2.407(1) and W—Cl(1) = 2.473(2) Å. The Cl(2)—W—$N_{t\text{-butylamine}}$ bond angle is 99.0(1)°. The *t*-butylamine quaternary carbon, C(21), lies close to the equatorial plane thereby reducing methyl group contact with the *t*-butylimido methyls. Rotation about the N(2)—C(21) bond positions the methyl groups C(22) and C(24) above and below the equatorial plane. The hydrogens on N(2) also lie above and below the plane. As a consequence of this arrangement the NH and Cl atoms are unfavourably placed for further dehydrohalogenation to occur.

We have recently shown that the interaction of primary amines and in particular *t*-butylamine, with the higher oxidation state metal chlorides of the group 5 and 6 transition metals, can lead to bis-imido complexes[1,2] (eq. 1) or complexes containing both imido and amido ligands[3–5] (eq. 2).

$$2WCl_6 + 16Me_3CNH_2 \rightarrow [W(NCMe_3)_2Cl_2(NH_2CMe_3)]_2 + 8Me_3CNH_3Cl \quad (1)$$

$$MCl_5 + 6Me_3CNH_2 \rightarrow [W(NCMe_3)(NHCMe_3)Cl_2(NH_2CMe_3)] + 2Me_3CNH_3Cl \quad (2)$$

(M = Nb, Ta, Mo).

Of particular interest in these reactions is the manner in which the amine coordinates to the metal and subsequently deprotonates. By using the silylamine $Me_3SiNHCMe_3$ we have shown that where two amido ligands are formed, the coordination geometry is likely to be *cis* and that interligand proton transfer occurs readily resulting in an imido and an amine ligand.[2,4–6] With *t*-butylamine, deprotonation could also conceivably take place by dehydrohalogenation to produce two *cis* amido ligands which could then react further by interligand proton transfer or by a series of dehydrohalogenation reactions.[2] When complexes containing an imido and an amine ligand are reacted with *t*-butylamine, further amine deprotonation takes place[2,4] (eqs 3 and 4).

$$[W(NCMe_3)Cl_4(NH_2CMe_3)] + 4Me_3CNH_2 \rightarrow [W(NCMe_3)_2Cl_2(NH_2CMe_3)] + 2Me_3CNH_3Cl + Me_3CNH_2 \quad (3)$$

$$[M(NCMe_3)Cl_3(NH_2CMe_3)]_2 + 4Me_3CNH_2 \rightarrow [M(NCMe_3)(NHCMe_3)Cl_2(NH_2CMe_3)]_2 + 2Me_3CNH_3Cl. \quad (4)$$

*Author to whom correspondence should be addressed.

A feature of these reactions is the absence of intermediary complexes, particularly those containing bis-amine ligands which are expected to be extremely reactive towards further deprotonation. We report here the synthesis and structure of a bis-*t*-butylamine-*t*-butylimido complex of tungsten(V) that is stable and does not deprotonate further to form a *t*-butylamido ligand.

RESULTS AND DISCUSSION

Reaction of WCl_6 with four equivalents of $Me_3SiNHCMe_3$ in benzene affords a yellow solution containing $[W(NCMe_3)_2Cl_2(NH_2CMe_3)]_2$.[2] When the solvent is removed and the crude reaction mixture extracted with petroleum ether, the extracts are orange coloured. On crystallization, some $[W(NCMe_3)_2Cl_2(NH_2CMe_3)]_2$ is obtained along with a small quantity of dark red crystals which have been characterized by X-ray crystallography (see later) as the tungsten(V) complex $[W(NCMe_3)Cl_3(NH_2CMe_3)_2]$.

In the IR spectrum the complex exhibited a series of coordinated primary amine NH stretches at 3275, 3220, 2800, 2720, 2660, 2500 and 2075 cm^{-1}, there was a strong band at 1360 cm^{-1} characteristic of ν_s(M—N—C)[7] and in the far IR there were W—Cl stretches at 310, 298 and 260 cm^{-1} which are characteristic of a *mer* arrangement of metal trichlorides.[8] By analogy with oxo complexes containing a single chloro ligand *trans* to an oxo function which gives rise to one M—Cl stretching band near 280 cm^{-1},[9] the absorption at 260 cm^{-1} most likely arises from the metal chloride *trans* to the *t*-butylimido function.

$[W(NCMe_3)Cl_3(NH_2CMe_3)_2]$ is stable in air for periods of up to 24 h and for extended periods in petroleum ether under an inert atmosphere. Addition of *t*-butylamine to solutions of the complex causes no change indicating that further deprotonation of the *t*-butylamine ligands to give an amido complex (eq. 5) does not take place.

$$[W(NCMe_3)Cl_3(NH_2CMe_3)_2] + 2Me_3CNH_2 \not\rightarrow [W(NCMe_3)(NHCMe_3)Cl_2(NH_2CMe_3)] + Me_3CNH_3Cl. \quad (5)$$

The non-reactivity of this bis-*t*-butylamine complex contrasts with that of the mono-*t*-butylamine complexes $[M(NCMe_3)Cl_3(NH_2CMe_3)]_2$ (M = Nb, Ta, Mo) which react rapidly with *t*-butylamine to give the amido complexes $[M(NCMe_3)(NHCMe_3)Cl_2(NH_2CMe_3)]_2$.[4,5] To examine the structural features associated with the observed non-reactivity of $[W(NCMe_3)Cl_3(NH_2CMe_3)_2]$ an X-ray crystal structure determination was undertaken.

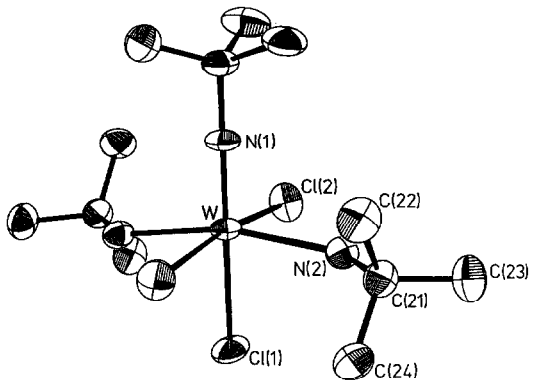

Fig. 1. The $[W(NCMe_3)Cl_3(NH_2CMe_3)_2]$ molecule. One orientation of the *t*-butylimido group is shown. Thermal ellipsoids have been drawn at the 50% probability level.

X-ray crystal structure of $[W(NCMe_3)Cl_3(NH_2CMe_3)_2]$

The complex is monomeric with a distorted octahedral geometry consisting of *trans* chloro and *trans* *t*-butylamine ligands and with a *t*-butylimido ligand situated *trans* to a third chloro ligand (see Fig. 1). Bond distances and angles for the molecule are given in Table 1.

The W—N(1) bond length (1.728(5) Å) is not significantly different from the W—N_{imido} bond lengths observed in the d^1 tungsten complexes $[W(NPh)Cl_3(PMe_3)_2]$ (1.731(6) Å)[10] and $[W(NPh)Cl_3(PPh_3)_2]$ (1.742(8) Å),[11] and is close to that predicted for a W—N triple bond (1.71 Å).[12] It is also not significantly different from the Re—N_{imido} distance of 1.709(11) Å observed in the structurally similar d^2 rhenium complex $[Re(NPh)Cl_3(NH_2CMe_3)_2]$.[13] The W—Cl(1) bond length (2.473(2) Å) is considerably longer than the two *trans* W—Cl bond lengths (both 2.407(1) Å) which is also a feature of the phenylimido tungsten complexes $[W(NPh)Cl_3(L)_2]$ (L = PMe_3, PPh_3).[10,11] By comparison, the chloro ligand *trans* to the imido function in the d^2 tungsten complex $[W(NPh)Cl_2(PMe_3)_3]$ shows only a small lengthening (W—Cl bond lengths 2.491(1), 2.483(1) and 2.501(1) Å)[11] and this is also a feature of the rhenium complex $[Re(NPh)Cl_3(NH_2CMe_3)_2]$.

The two W—N_{amine} bond lengths (2.230(4) Å) are longer than those observed in $[Re(NPh)Cl_3(NH_2CMe_3)_2]$ (2.187(7) Å)[13] but are shorter than that in $[W(NPh)(OCMe_3)_3Cl(NH_2CMe_3)]$ (2.40(2) Å) where the *t*-butylamine ligand lies *trans* to the four-electron donor phenylimido ligand.[14]

The N(1)—W—Cl, Cl—W—Cl and W—N(1)—C(11) bond angles are not significantly dif-

Table 1. Selected bond lengths and angles for $[W(NCMe_3)Cl_3(NH_2CMe_3)_2]$

	Bond length (Å)		
N(1)—W	1.728(5)	Cl(2)—W	2.407(1)
N(2)—W	2.230(4)	N(1)—C(11)	1.500(6)
Cl(1)—W	2.473(2)	N(2)—C(22)	1.438(10)
	Bond angle (°)		
N(1)—W—Cl(1)	180.0(0)	N(2)—W—Cl(2)	99.0(1)
N(1)—W—Cl(2)	94.1(1)	Cl(1)—W—Cl(2)	85.9(1)
N(1)—W—N(2)	97.3(1)	W—N(1)—C(11)	179.9(0)
N(2)—W—Cl(1)	82.7(1)	W—N(2)—C(21)	130.8(3)

ferent to those found in other tungsten(V) complexes[10,11] or the structurally similar rhenium complex.[13] However $[W(NCMe_3)Cl_3(NH_2CMe_3)_2]$ does show differences to $[Re(NPh)Cl_3(NH_2CMe_3)_2]$ in the bond angles incorporating the *t*-butylamine ligand nitrogen atom N(2). The major variation occurs in the N(2)—W—Cl(2) bond angle which at 99.0(1)° is nearly 12° larger than the comparable bond angle in the rhenium complex (N(2)—Re—Cl(2), bond angle 87.6°).[13] The N(2)—W—Cl(1) bond angle (82.7(1)°) is larger than that in the rhenium complex (79.6(1)°) with the respective N(2)—M—N(2′) bond angles in the complexes being 165.4 and 159.2°. In comparison, the Cl—M—Cl bond angles in the two complexes are similar, at 171.8 and 172.2°, respectively.

The structural differences observed between the tungsten and rhenium complexes arise from steric factors associated with the imido and amine ligands. In both complexes these ligands lie in a *mer* configuration but the bulky *t*-butylimido ligand forces the *t*-butylamine ligands to adopt a different orientation in the tungsten complex than that observed in the phenylimido rhenium complex.

In both complexes the M—N(2)—C(21) bond angles are similar (130.8(3)°, M = W; 128.6(6)°, M = Re) but while the sense of this angle is such as to position C(21) (*t*-butylamine quaternary carbon) close to the equatorial plane N(2), Cl(2), N(2′) and Cl(2′) in the tungsten complex, C(21) is close to the longitudinal plane N(2), N(1), N(2′) and Cl(1) in the rhenium complex.[13] For the phenylimido complex, interaction between the *t*-butylamine ligand methyl groups and the phenyl group is relieved by a decrease in the N(2)—Re—N(2′) bond angle (159.2(1)°) while in the tungsten complex this angle (165.4(1)°) opens out somewhat when the interaction is not present. The increase in the N(2)—W—Cl(2) bond angle (*ca* 12°) apparently arises from a compatible mesh of the *t*-butylamine methyl groups with both Cl(2′) and the imido ligand methyl groups. As a consequence the W—N(2) bond length (2.230(4) Å) is slightly longer than in the rhenium complex (2.187(7) Å).[13]

The *t*-butylamine ligand's NH protons in $[W(NCMe_3)Cl_3(NH_2CMe_3)_2]$ lie above and below the equatorial plane and are staggered with respect to the pair on the opposite side of the molecule. This compares with $[Re(NPh)Cl_3(NH_2CMe_3)_2]$ where the protons point to either side of the longitudinal Cl(1) ligand with the two pairs being more nearly eclipsed.[13] The W—N—H, H—N—H′ and C—N—H angles are not significantly different to the ideal tetrahedral angle and the NH protons do not make close contacts with any of the chlorine atoms. The closest approach of an amine ligand proton is made by H(1′) with the central tungsten atom at a distance of 2.45 Å.

The structure of the complex gives an indication of why further dehydrohalogenation fails to take place. Since the *t*-butylamine ligands occupy *trans* sites, coordination takes place without severe steric strain being generated in the molecule. Although X-ray crystallographic studies have not been carried out on the $[M(NR)Cl_3(NH_2R)]_2$ complexes which do undergo further dehydrohalogenation,[4,5] their coordination chemistry suggests that a second amine ligand would bind *cis* to the first.[5] If close approach between a coordinated amine proton and a chloro ligand is a necessary prerequisite for dehydrohalogenation, this process might be facilitated by steric congestion arising from *cis*-oriented amine ligands. The NH protons in $[W(NCMe_3)Cl_3(NH_2CMe_3)_2]$ do not preferentially project towards any of the chloro ligands and no close contacts are made. Even though Cl(1) is significantly lengthened by the *trans* influence of the imido function,[11,15] no further reaction occurs. Coordination of a chloro ligand *trans* to the imido function in the complex, is apparently a result of the reductive process involved and is observed to occur when other tungsten (VI) complexes are reduced to tungsten(V).[10,11] Reaction of MCl_5 (M = Nb, Ta, Mo) with *t*-butylamine or

$Me_3SiNHCMe_3$ gives rise to complexes in which a neutral two-electron donor (*t*-butylamine or bridging chlorine) coordinates *trans* to the imido function.[4,5]

EXPERIMENTAL

N(trimethylsilyl)*t*-butylamine was prepared by treating chlorotrimethylsilane with two equivalents of *t*-butylamine and distilling the product.[16] *t*-Butylamine was dried over and distilled from calcium hydride. Tungsten hexachloride was sublimed prior to use. Petroleum ether (b.p. range 40–60°) and benzene were distilled from sodium wire. IR spectra were recorded on a Perkin–Elmer 597 spectrometer as Nujol mulls between CsI plates. The preparations and manipulations were carried out under dry oxygen-free nitrogen using standard bench-top air-sensitive techniques.[17]

Bis-t-butylamine-t-butylimidotrichlorotungsten(V)

N(trimethylsilyl)*t*-butylamine (2 cm^3, 10.4 mmol) in benzene (40 cm^3) was added to tungsten hexachloride (1 g, 2.5 mmol) in benzene (80 cm^3) and the mixture was stirred for 18 h. The solution was filtered and the solvent removed to give an impure sample of bis-*t*-butylaminebis-*t*-butylimidobis(μ-*t*-butylimido)tetrachloroditungsten(VI) which was washed with warm petroleum ether (100 cm^3). The solution was filtered, the volume reduced to *ca* 40 cm^3 and on standing a small quantity of yellow and red crystals formed which were filtered off, washed with cold petroleum ether (2 × 10 cm^3) and dried *in vacuo*. The red crystals of bis-*t*-butylamine-*t*-butylimidotrichlorotungsten(V) were separated manually. M.p.: decomposes above 155°C.

IR (Nujol) bands at 3275w, 3220w, 2800w, 2720w, 2660w, 2500w, 2075w, 1610w, 1550w, 1505w, 1400m, 1360s, 1325w, 1300w, 1282m, 1256s, 1210m, 1165s, 1098w, 1030w, 995w, 950w, 930w, 910w, 890m, 808w, 745w, 725w, 665w, 655w, 578w, 565w, 480w, 450m, 418w, 370w, 345m, 310m, 298s and 260m cm^{-1}.

Crystallographic studies

A single crystal of $[W(NCMe_3)Cl_3(NH_2CMe_3)_2]$ from the petroleum ether extracts of the $[W(NCMe_3)_2Cl_2(NH_2CMe_3)]_2$ preparation was mounted on a glass fibre and coated with polyurethane to prevent contact with oxygen and moisture. Data were collected using an Enraf–Nonius CAD-4 diffractometer.

Crystal data. $C_{12}H_{31}Cl_3N_3W$, $M = 507.6$, monoclinic, $a = 19.701(3)$, $b = 9.674(2)$, $c = 11.430(2)$ Å, $\beta = 116.40(1)°$, $U = 1951.1$ Å^3, space group $C2/c$, $Z = 4$, $D_c = 1.726$ g cm^{-3}, $F(000) = 996$, μ(Mo-K_α) = 66.6 cm^{-1}, λ(Mo-K_α) = 0.71069 Å.

Data collection. Accurate unit cell parameters were determined by least-squares fit to the observed setting angles of 25 reflections at 294K. Intensity data collection employed the $2\theta/\omega$ scan technique with total peak : background count time ratio 2 : 1. Reflections were counted for either 60 s or until $\sigma(I)/I$ was 0.02. Measured data : 3078 reflections to 2θ limit of 60°. The intensity of three reflections was monitored throughout the data collection, a slow decrease which was linear with time being observed. The data were corrected for Lorentz, polarization, absorption[18] and decomposition.

Structure solution and refinement. The structure was solved by conventional Patterson and Fourier techniques and refined by full-matrix least-squares.* The function minimized was $\Sigma w(|F_o|-|F_c|)^2$ using weights $1.0/[\sigma^2(F)+gF^2]$ with $g = 0.005$. Atomic scattering factors and dispersion corrections were for neutral atoms, anisotropic thermal parameters being refined for all non-hydrogen atoms. The molecule lies on a crystallographic two-fold axis passing through tungsten, chlorine (1) and the *t*-butylimido group. As a consequence the *t*-butylimido methyl groups occupy alternate positions with each being half-weighted. Attempts to refine the structure in space group *Cc* were unsuccessful as the refinement diverged. Hydrogen atoms for the *t*-butylamine group were located in a final difference map whereas hydrogen coordinates for the *t*-butylimido group were calculated. Final residuals R and R_w were 0.030 and 0.033, respectively, for the 2295 unique observed reflections.

Final atomic coordinates, thermal parameters and observed and calculated structure factors have been deposited with the Editor as supplementary material.†

* Computing was carried out using the SDP suite of programs on a PDP-11 computer for data processing and SHELX-76 on an IBM 4341 computer for structure solution and refinement.

† Atomic coordinates have also been deposited with the Cambridge Crystallographic Data Centre for inclusion in their data base. Copies are available on request from the Editor at Queen Mary College.

REFERENCES

1. B. R. Ashcroft, D. C. Bradley, G. R. Clark, R. J. Errington, A. J. Nielson and C. E. F. Rickard, *J. Chem. Soc., Chem. Commun.* 1987, 170.
2. A. J. Nielson, *Polyhedron* 1987, **6**, 1657.
3. T. C. Jones, A. J. Nielson and C. E. F. Rickard, *J. Chem. Soc., Chem. Commun.* 1984, 206.

4. P. A. Bates, A. J. Nielson and J. M. Waters, *Polyhedron* 1985, **4**, 1391.
5. A. J. Nielson, *Polyhedron* 1987, **7**, 67.
6. B. R. Ashcroft, A. J. Nielson, D. C. Bradley, R. J. Errington, M. B. Hursthouse and R. L. Short, *J. Chem. Soc., Dalton Trans.* 1987, 2059.
7. W. P. Griffith, A. J. Nielson and M. J. Taylor, *J. Chem. Soc., Dalton Trans.* 1987 (in press).
8. J. Chatt, G. J. Leigh and D. M. P. Mingos, *J. Chem. Soc. A.* 1969, 1674.
9. W. Levason, C. A. McAuliffe and F. P. McCullough, *Inorg. Chem.* 1977, **16**, 2911.
10. A. J. Nielson and J. M. Waters, *Aust. J. Chem.* 1983, **36**, 243.
11. D. C. Bradley, M. B. Hursthouse, K. M. A. Malik, A. J. Nielson and R. L. Short, *J. Chem. Soc., Dalton Trans.* 1983, 2651.
12. W. A. Nugent and B. L. Haymore, *Coord. Chem. Rev.* 1980, **31**, 123.
13. G. R. Clark, A. J. Nielson and C. E. F. Rickard, *Polyhedron* 1987, **7**, 117.
14. A. J. Nielson, J. M. Waters and D. C. Bradley, *Polyhedron* 1985, **2**, 285.
15. P. A. Bates, A. J. Nielson and J. M. Waters, *Polyhedron* 1985, **4**, 999.
16. R. M. Pike, *J. Org. Chem.* 1961, **26**, 232.
17. A. J. Nielson, *Chem. N.Z.* 1985, **49**, 11.
18. A. C. T. North, D. C. Phillips and F. S. Mathews, *Acta Cryst.* 1968, **A24**, 351.

Polyhedron Vol. 7, No. 4, pp. 303–306, 1988
Printed in Great Britain

0277–5387/88 $3.00+.00
© 1988 Pergamon Journals Ltd

CRYSTAL STRUCTURE OF COPPER(II) 2-THENOYLTRIFLUOROACETONATE

C. LECOMTE* and D. BAYEUL

Laboratoire de Minéralogie et Cristallographie (UA 809), Faculté des Sciences, Centre de 2ème Cycle, Boite Postale n° 239, 54506 Vandouevre les Nancy Cedex, France

and

N. SENGLET and R. GUILARD

Laboratoire de Synthèse et d'Electrosynthèse Organométallique, associé au C.N.R.S (UA 33), Faculté des Sciences "Gabriel", 6 Bd Gabriel, 21100 Dijon, France

(*Received* 15 *July* 1987; *accepted* 8 *September* 1987)

Abstract—$Mw = 505.9$, triclinic, $P\bar{1}$, $a = 4.573(2)$, $b = 9.2673(3)$, $c = 11.0765(3)$ Å, $\alpha = 80.98(2)$, $\beta = 76.95(2)$, $\gamma = 79.42(2)°$, $V = 446.3$ Å^3, $Z = 1$, $D_x = 1.88$ Mg m^{-3}, Mo-K_α, $\lambda = 0.70928$ Å, $\mu = 15.81$ cm^{-1}, room temperature, $F(0,0,0) = 251$ e. Final $R(F) = 0.046$, $Rw(F) = 0.049$. G.O.F. = 1.86 for 2176 reflections [$I > 3\sigma(I)$]. The copper atom lies on the (0,0,0) inversion centre and its coordination polyhedron is square planar (Cu—O = 1.908(3) Å, O—Cu—O = 86.7, 93.3(1)°. The molecules are stacked approximately along the [110] direction with an intermolecular distance of 3.25 Å.

The metal chelates of thenoyltrifluoroacetone have been the subject of much research.[1–6] The majority of reports relate their role as synergists in the solvent extraction of metal ions by phosphorus esters.[7–10] Moreover, the presence of such complexes in heavy oils have been postulated by many authors.[11,12] The same complexes could also be good candidates for the preparation of highly conducting molecular materials with $M(TTA)_2$ as the fundamental unit. Although many papers focussed on the characteristics and spectroscopic properties of these chelates, X-ray structure determinations are very scarce. Here, we report on the X-ray structure determination of the copper(II)2-thenoyltrifluoroacetonate, $Cu(TTA)_2$.

$Cu(TTA)_2$ was prepared by the standard method.[1,13,14] To 22.5 mmol of TTA was added a solution of 12.5 mmol of copper acetate in a mixed solvent of acetone/water (8/2). The mixture was refluxed for 2 h. The filtered complex was washed with an alcoholic ammonia solution in water. After purification by extraction in a Soxhlet apparatus with chloroform, 4.85 g (9.05 mmol, 80% yield) of dark green crystals of $Cu(TTA)_2$ was obtained. The spectroscopic data are given in Table 1.

A suitable crystal of $Cu(TTA)_2$ recrystallized from $CHCl_3$ was mounted on a glass fibre in random orientation. Preliminary Weissenberg photographs did not reveal any symmetry leading to the possible space groups $P1$ or $P\bar{1}$. Experimental details of the data collection are given in Table 2. The crystal structure was solved in the $P\bar{1}$ space group by the heavy atom method. At the end of the refinement, difference-Fourier syntheses revealed rotational disorders of the CF_3 and of the thienyl groups. Any attempts to solve this problem in the $P1$ group failed. Finally it was possible to refine three positions of the CF_3 group [(F_1, F_2, F_3), (F_4, F_5, F_6), (F_7, F_8, F_9)] together with two positions of the thienyl group [(S_{11}, C_{31}, C_{41}, C_{51}), (S_{12}, C_{32}, C_{42}, C_{52})].† The final occupation factors are given in supplementary material. The scattering factors were taken from refs 20 and 21; a summary of the convergence results is given in Table 2. Fractional coordinates, anisotropic thermal parameters, bond lengths and angles in the disordered parts of the molecule, least squares planes, and a list of structure factors have been deposited as supplementary material with the Editor from whom copies are available on request.‡

*Author to whom correspondence should be addressed.

† This disorder seems to be usual in this type of complexes (see for example ref. 23).

‡ Atomic coordinates have also been deposited with the Cambridge Crystallographic Data Centre.

Table 1. Spectroscopic data of the copper(II) 2-thenoyltrifluoroacetonate

					Ref.
UV-visible					
$\lambda max(\varepsilon 10^{-3})^a$	273 (25.9)			336.5(47.5)	4, 7, 15
IR $\nu(cm^{-1})$	1325.3	1541		1599.8	4, 5, 6, 7, 9, 16
RPE	g			A(G)	17, 18, 19
	2.1479			61.33	
RMN	H_1	H_2	H_3	H_4	19
$\delta_{ppm(m/i)}{}^b$	−16.53	15.23	7.31	10.66	
	(s/2)	(s/2)	(s/2)	(s/2)	

[a] λ_{nm}; $\varepsilon(M^{-1}\,cm^{-1})$.
[b] m = multiplicity; i = intensity; s = singlet.

Table 2. Experimental conditions and refinement

Formula, formula weight	$C_{16}H_8CuF_6O_4S_2$, 506
Space group	Triclinic $P\bar{1}$
Crystal dimensions	$0.2 \times 0.3 \times 0.15$ mm^3
Lattice parameters	See abstract
Diffractometer	CAD 4F, Mo-K_α graphite monochromatized
$\theta_{min}-\theta_{max}$, sin θ/λ max	$1-30°$, 0.70 Å^{-1}
Scan speed (° mm^{-1})	$1 < v < 3$
Scan range (°)	$1+0.40 \tan(\theta)$
Take-off angle (°)	3
Aperture (mm)	$4+\tan(\theta)$
Number of reflections measured	3247
Number of unique reflections used	$N = 2176$ ($\sigma(I)/I < 0.3$)
Number of parameters, N/N_p	176, 12.4
Programs	SDP,[22] SHELX 76,[20] ORTEP
$R(F)$, $Rw(F)$, G.O.F.	0.0456; 0.0490; 1.86
w	$[\sigma^2(F)+0.0007\,F^2]^{-1}$
$(\Delta/\sigma)_{max}$	−0.58 for $z(S_{12})$
Max residual density	0.74 e Å^{-3} at 0.8 Å from Cu

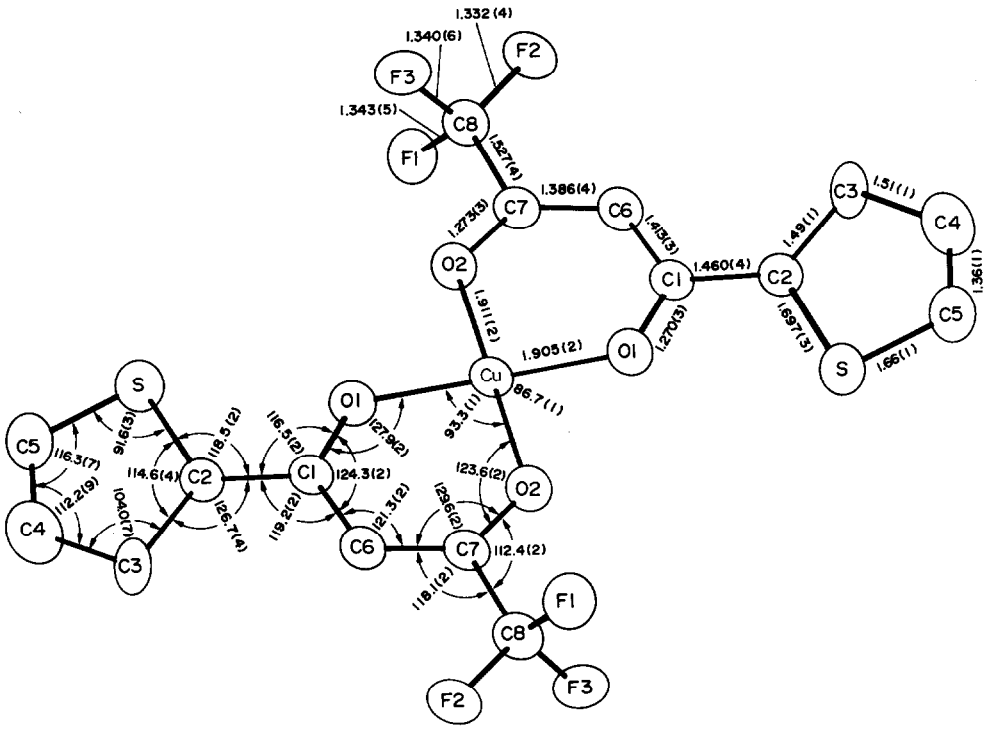

Fig. 1. ORTEP view of $Cu(TTA)_2$; bond lengths and angles.

Figure 1 gives the ORTEP view of the molecule with the main bond distances and angles. The copper atom which lies on the (0,0,0) inversion centre of the triclinic cell has a square planar coordination (Cu—O(1) = 1.905(2), Cu—O(2) = 1.911(2) Å, O(1)—Cu—O(2) = 93.3(1) and 86.7(1)°). Furthermore, the whole molecule, except the F_1 and F_3 atoms has a planar conformation and all the molecules in the crystal are stacked approximately along the [110] axis with an intermolecular distance of 3.25 Å (Fig. 2). This structure is very close to that of bis[(thienyl-2)-2-glyoxylato]copper(II).[23]

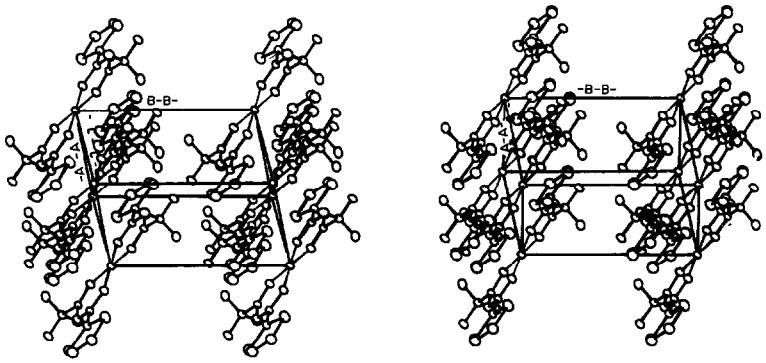

Fig. 2. ORTEP view of the molecular packing.

REFERENCES

1. E. W. Berg and J. T. Truemper, *J. Am. Chem. Soc.* 1960, **64**, 487.
2. E. W. Berg and J. T. Truemper, *Anal. Chim. Acta* 1965, **32**, 245.
3. E. W. Berg and K. P. Reed, *Anal. Chim. Acta* 1968, **42**, 207.
4. K. S. Patel, *J. Inorg. Nucl. Chem.* 1980, **42**, 1235.
5. G. S. Shephard and D. A. Thornton, *J. Mol. Struct.* 1976, **34**, 83.
6. K. Ohwada, *J. Inorg. Nucl. Chem.* 1967, **29**, 833.
7. W. R. Walker and N. C. Li, *J. Inorg. Nucl. Chem.* 1965, **27**, 411.
8. T. Sekine and D. Dryssen, *J. Inorg. Nucl. Chem.* 1964, **26**, 1727.
9. H. Akaiwa, H. Kawamoto and M. Abe, *J. Inorg. Nucl. Chem.* 1972, **34**, 1763.
10. E. F. Kassierer and A. S. Kertes, *J. Inorg. Nucl. Chem.* 1972, **34**, 778.
11. T. F. Yen, L. J. Boucher, J. P. Dickie, and E. C. Tynan and G. B. Vaughan, *J. Inst. Petrol.* 1969, **55**, 87.
12. J. G. Reynolds, E. J. Gallegos, R. H. Fish and J. J. Komlenic, *Energy and Fuels* 1987, **1**, 36.
13. S. Z. Haider, M. S. Khan, *J. Bangladesh Acad. Sci.* 1977, **1**, 53.
14. H. F. Holtzclaw and J. P. Collman, *J. Am. Chem. Soc.* 1957, **79**, 3318.
15. P. R. Johnson and D. A. Thornton, *J. Mol. Struct.* 1975, **29**, 97.
16. G. S. Shephard and D. A. Thornton, *Helv. Chim. Acta* 1971, **54**, 2212.
17. S. Antonsik, N. M. D. Brown, A. A. McConnell and A. L. Porte, *Inorg. Phys. Theor.* 1969, 545.
18. H. A. Kuska, M. T. Rogers and R. E. Drullinger, *J. Phys. Chem.* 1967, **71**, 109.
19. H. A. Kuska and M. T. Rogers, *J. Chem. Phys.* 1965, **43**, 1744.
20. G. M. Sheldrick, SHELX 76 Crystallographic Calculation Programme, University of Göttingen, West Germany (1976).
21. *International Tables for X-Ray Crystallography*, Vol. IV. Kynoch Press, Birmingham (1974).
22. Structure Determination Package (SDP), Enraf–Nonius, Delft, Netherlands (1977).
23. C. Arnaud, R. Faure and H. Loiseleur, *Acta Cryst.* 1986, **C42**, 814.

Polyhedron Vol. 7, No. 4, pp. 307–314, 1988
Printed in Great Britain

0277–5387/88 $3.00+.00
© 1988 Pergamon Journals Ltd

CRYSTAL STRUCTURE OF COPPER(II) CIMETIDINE SULPHATE NONAHYDRATE. CATION DISTORTION AND STRUCTURE ISOMERISM IN THREE COPPER(II) CIMETIDINE COMPLEXES

L. SOTO* and J. P. LEGROS†

Laboratoire de Chimie de Coordination du CNRS, Unité n° 8241 liée par convention à l'Université Paul Sabatier, 205 Route de Narbonne, 31400 Toulouse Cédex, France

and

A. SANCHO

Departamento de Quimica Inorganica, Facultad de Farmacia, Universidad de Valencia, Blasco Ibañez n°13, 46010 Valencia, Spain

(*Received* 24 *July* 1987; *accepted* 8 *September* 1987)

Abstract—In the crystalline state, the complex $[Cu(CM)_2]SO_4 \cdot 9H_2O$ (CM = cimetidine) is constituted of two-dimensional cations $[Cu(CM)_2^{2+}]_n$ separated by SO_4^{2-} anions and water molecules. As in the related complexes $[Cu(CM)_2](ClO_4)_2$ and $[Cu(CM)_2](NO_3)_2$, the copper atom lies in a strongly distorted octahedral CuN_4S_2 environment. The distortion is quite different from one complex to another (cation distortion isomerism). In the title compound the Cu—S bond is unusually long (2.91 Å). Unlike the title compound, the $[Cu(CM)_2^{2+}]_n$ cations in the perchlorate and nitrate salts are one-dimensional infinite chains characterized by different conformations of the cimetidine molecules (cation structure isomerism).

For years the "plasticity effect"[1] of the copper(II) ion has been invoked to account for its ability to accommodate, within a given set of ligands, a range of different geometries and, within a given geometry, a range of different degrees of distortion. The term "cation or anion distortion isomerism" has been introduced to classify complexes where the copper(II) ion, coordinated to the same ligands, possess the same environment with some changes in the geometry, usually depending on the counter-ion.[1–5]

Cimetidine(CM): N-cyano-N′-methyl-N″-[2-{(5-methyl-1H-imidazol-4-yl)-methylthio}ethyl]guanidine (Structure 1) is a biologically active molecule liable to coordinate to transition metal ions. In the complexes $[Cu(CM)_2](ClO_4)_2$ **(I)**[6] and $[Cu(CM)_2](NO_3)_2$ **(II)**[7] the ligand is coordinated through S(thioether), N(imidazole) and N(cyano) atoms. In both compounds the copper(II) ion is octahedrally surrounded but with a significantly different distortion, thus providing another example of cation distortion isomerism. Furthermore, both crystal structures are built of one-dimensional $[Cu(CM)_2^{2+}]_n$ cationic infinite chains but with different conformations. This can be referred to as "cation structure isomerism".

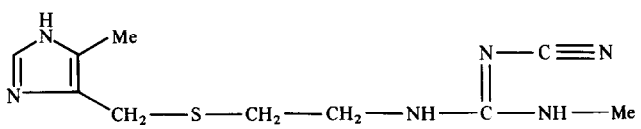

Structure 1.

* Permanent address: Departamento de Quimica Inorganica, Facultad de Farmacia, Universidad de Valencia, Blasco Ibañez n°13, 46010 Valencia, Spain.

†Author to whom correspondence should be addressed.

In this paper we report the structure of a third "cation distortion and structure isomer": $[Cu(CM)_2]SO_4 \cdot 9H_2O$ **(III)**. Another hydrate $[Cu(CM)_2]SO_4 \cdot 4H_2O$ **(IV)** has been previously prepared as a microcrystalline powder and characterized by spectroscopic methods,[8] but has not yet been obtained as single crystal suitable for X-ray structure determination.

This work gives more insight into the chelating properties of cimetidine and reveals the influence of the coordination on the conformation of this ligand in connection with the nature of the counter-ion.

EXPERIMENTAL

An EtOH solution (100 cm^3) of CM (2.5 mmol) was slowly added to an aqueous solution (50 cm^3) of $CuSO_4 \cdot 5H_2O$ (1 mmol). Green hexagonal crystalline plates were obtained by slow evaporation of the solvent. The crystals were washed with EtOH and water and dried in air. They were found to be stable to air, light and X-ray exposure. Found: Cu, 7.6; C, 29.0; N, 20.5; H, 6.3; SO_4^{2-}, 11.7. Calc. for $CuS_3C_{20}N_{12}O_{13}H_{50}$: Cu, 7.7; C, 29.1; N, 20.3; H, 6.1; SO_4^{2-}, 11.6%.

Thermogravimetric analysis were performed on a Mettler TG 50 thermobalance using samples of *ca* 15 mg and a heating rate of 10° min^{-1} with ignited α-Al_2O_3 as a reference. The DSC measurements were performed with a Mettler DSC 20 differential scanning calorimeter, using samples of *ca* 5 mg and a heating rate of 5° min^{-1}. Both TG and DSC studies were carried out in a dynamic atmosphere of air (100 ml min^{-1}). Magnetic moment, IR, ESR and solid state electronic spectra were recorded as described in a previous paper.[8]

Crystal data and relevant parameters of the crystallographic study are given in Table 1. General operating procedures have been described previously.[9] Systematic absences indicate space groups *Cc* or *C2/c*, the non-centrosymmetric space group was discarded on the basis of convincing intensity statistics. The structure was determined by the Patterson method[10] and refined using standard full-matrix least-squares and Fourier procedures.[11] Structure factors were corrected for absorption and anomalous dispersion. The sulphate ion is disordered over two positions which were assigned the same occupancy factor (50%) on the basis of the similarity of the temperature factors of the oxygen atoms. All hydrogen atoms were located on difference Fourier maps, idealized, unrefined positions and arbitrary isotropic temperature factors were used in the final calculations. Final atomic positional and thermal parameters and lists of F_o/F_c values have been deposited as supplementary

Table 1. Crystallographic data

Formula	$CuS_3C_{20}N_{12}O_{13}H_{50}$
M_r	826.43
Diffractometer	CAD4 Enraf–Nonius
Radiation	Mo-K_α
Wavelength (Å)	0.71069
Space group	Monoclinic, *C2/c*
a (Å)	25.417(4)
b (Å)	13.905(2)
c (Å)	10.677(2)
β(°)	97.61(1)
V (Å^3)	3740(2)
Z	4
Dc (g cm^{-3})	1.47
Dm (g cm^3)	1.47(1) (flotation)
μ (cm^{-1})	7.7
Temperature (K)	293
Crystal size (mm)	0.55 × 0.28 × 0.08
Max. Bragg angle	$\theta_{max} = 25°$
Number of independent reflections	3299
Number of observed reflections ($I > 3\sigma$)	2206
Number of refined parameters	242
R and R_w	0.034 and 0.036
Weighting scheme	Unit weights

material with the Editor from whom copies are available on request. Atomic coordinates have also been deposited with the Cambridge Crystallographic Data Centre.

RESULTS AND DISCUSSION

Thermogravimetric analysis

Two differentiated processes occur in the thermal decomposition of the compound studied: a dehydration followed by the pyrolitic decomposition of the anhydrous complex. Under the experimental conditions used, the nine water molecules are lost in one step in the temperature range 50–110°C (weight loss 19.4%). The low value of the dehydration enthalpy (30 kJ mol^{-1}) indicates water of crystallization.

The pyrolitic decomposition of the anhydrous complex takes place in two steps: a weight loss of 32% in the range 200–380°C followed by another weight loss of 39% in the range 420–600°C. The final black solid residue (9.7% of the initial sample) corresponds to the CuO oxide as confirmed by X-ray powder pattern.

Magnetic and spectroscopic properties

Magnetic and spectroscopic properties of **(III)** are very similar to those previously reported for **(IV)**,[8] only small changes can be noticed in the 3140–3400 cm^{-1} range of the IR spectrum for bands assigned to N—H stretching vibrations: these modifications may be attributed to differences in the hydrogen bond network of the two hydrates.[12] In both cases the pattern of vibrations of the SO_4 group (1110, 980, 615 cm^{-1}) is indicative of an uncoordinated SO_4^{2-} anion.

Table 2. Bond lengths (Å) and angles (°) with e.s.d.'s in parentheses

Cu—S(1)	2.910(1)	C(9)—C(8)	1.519(5)
Cu—N(2)	1.981(3)	N(10)—C(9)	1.447(5)
Cu—N(14)[a]	2.001(3)	C(11)—N(10)	1.335(5)
N(2)—C(1)	1.383(5)	N(12)—C(11)	1.342(4)
C(5)—C(1)	1.353(6)	N(15)—C(11)	1.323(5)
C(7)—C(1)	1.493(5)	C(13)—N(12)	1.293(5)
C(3)—N(2)	1.323(5)	N(14)—C(13)	1.155(4)
N(4)—C(3)	1.326(6)	C(16)—N(15)	1.442(5)
C(5)—N(4)	1.369(6)	S(2)—O(1)	1.446(9)
C(6)—C(5)	1.482(6)	S(2)—O(2)	1.443(8)
C(7)—S(1)	1.813(4)	S(2)—O(3)	1.415(8)
C(8)—S(1)	1.807(3)	S(2)—O(4)	1.468(9)
N(2)—Cu—S(1)	77.4(1)	C(9)—C(8)—S(1)	113.7(2)
N(14)[b]—Cu—S(1)	87.3(1)	N(10)—C(9)—C(8)	112.1(3)
N(14)[a]—Cu—N(2)	89.0(1)	C(11)—N(10)—C(9)	123.7(3)
C(7)—S(1)—Cu	84.3(1)	N(12)—C(11)—N(10)	117.4(3)
C(8)—S(1)—Cu	104.8(1)	N(15)—C(11)—N(12)	123.3(3)
C(5)—C(1)—N(2)	109.4(3)	C(13)—N(12)—C(11)	120.7(3)
C(7)—C(1)—N(2)	120.8(3)	N(14)—C(13)—N(12)	173.8(4)
C(7)—C(1)—C(5)	129.8(4)	C(13)—N(14)—Cu[c]	155.7(3)
C(1)—N(2)—Cu	123.6(2)	C(16)—N(15)—C(11)	124.1(3)
C(3)—N(2)—Cu	129.9(3)	O(1)—S(2)—O(2)	106.7(5)
C(3)—N(2)—C(1)	105.9(3)	O(1)[d]—S(2)—O(2)	111.1(5)
N(4)—C(3)—N(2)	110.4(4)	O(4)—S(2)—O(3)	106.8(5)
C(5)—N(4)—C(3)	108.9(4)	O(4)[d]—S(2)—O(3)	110.6(5)
N(4)—C(5)—C(1)	105.4(4)		
C(6)—C(5)—C(1)	131.9(4)		
C(6)—C(5)—N(4)	122.7(4)		
C(1)—C(7)—S(1)	112.6(3)		
C(8)—S(1)—C(7)	100.4(2)		

Symmetry codes: [a] x, $1-y$, $z-1/2$. [b] $1/2-x$, $y-1/2$, $1/2-z$. [c] x, $1-y$, $1/2+z$. [d] $1-x$, $1+y$, $3/2+z$.

The solid state reflectance spectrum of (**III**) and the X-band ESR spectrum ($g_{\parallel} = 2.32$, $g_{\perp} = 2.06$ and $A_{\parallel} = 204$ G) are consistent with an essentially elongated octahedral geometry of the copper(II) coordination polyhedron[8,13,14] and with a $d_{x^2-y^2}$ ground state.[15]

Coordination of the copper(II) *atom*

Bond lengths and angles are listed in Table 2. The coordination scheme of the copper atom is shown in Fig. 1. The copper atom lies on a centre of symmetry and possesses a strongly elongated octahedral CuN_4S_2 environment: two centrosymmetrically related CM molecules are chelated through imidazole N(2) and thioether S(1) atoms and two other centrosymmetrically related CM molecules are coordinated through the cyano N(14) atom. The SO_4^{2-} groups and the lattice water molecules are far removed from the Cu(II) centres (all Cu—O distances are larger than 4.14 Å).

The N(2) and N(14) donors occupy the equatorial positions while the S(1) atoms are apical. The CuN_4 equatorial group is strictly planar by symmetry, with Cu—N(2) and Cu—N(14) distances equal to 1.982 and 2.001 Å, respectively, similar to those observed in related compounds.[7,16–19] However the apical Cu—S bond length of 2.910 Å is strikingly long and falls in the very far end of the range of thioether-containing copper(II) complexes.[16–18,20,21] This long distance can be compared with Cu—S distances in blue proteins of copper(II) such as plastocyanin and azurin[22,23] where a methionine thioether sulphur atom is weakly bonded to the metal. Such Cu—S distances are so long that the question may arise whether they can still be regarded as coordination bonds; the Cu—S—C angles, close to the expected value of 90–100°, indicate that the lone pairs of the sulphur atoms are directed towards the copper atom and argue for a weakly coordinating Cu—S interaction.

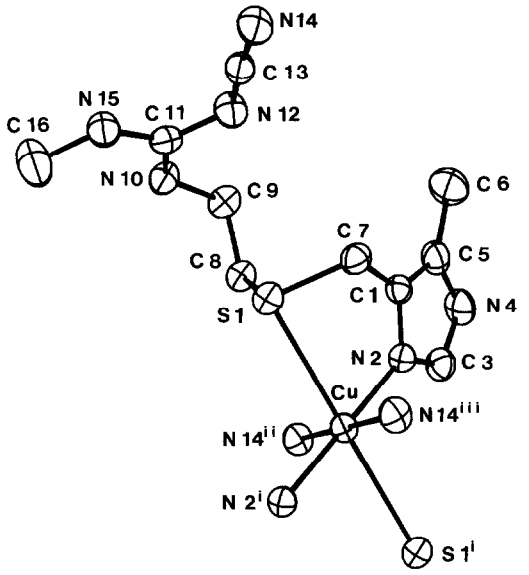

Fig. 1. $[Cu(CM)_2]SO_4 \cdot 9H_2O$. Cu(II) environment and numbering scheme in the cimetidine molecule. Symmetry codes: (i) $1/2-x, 1/2-y, -z$; (ii) $x, 1-y, z-1/2$; (iii) $1/2-x, y-1/2, 1/2-z$.

Table 3 compares the geometries of the copper environment in the three copper(II)–cimetidine cation distortion isomers (**I**), (**II**) and (**III**). Although no strong interaction exists between the metal atom and the counter-ions, the latter induce changes in the sterochemistry of the former. So, in both (**I**) and (**III**), the thioether S(1) sulphur atom is weakly bonded and the imidazole N(2) and cyano N(14) nitrogen atoms give usual Cu—N bonds *ca* 2 Å long, resulting in an elongated tetragonally distorted octahedral geometry. On the contrary, the coordination polyhedron in (**II**) can be considered as rhombically distorted octahedral, elongated along the Cu—N(14) bond which is unusually long (2.558 Å).

Metal centre linkage

The cimetidine molecules link copper atoms to form two-dimensional infinite cations $[Cu(CM)_2^{2+}]_n$ parallel to (100) (Fig. 2). These cationic planes lie at the levels $x = 1/4$ and $x = 3/4$ and are separated by SO_4^{2-} anions and lattice water molecules (Fig. 3). It is worthwhile to compare the linkage of the copper atoms in the title compound (**III**) and in complexes (**I**) and (**II**). Although the coordination of cimetidine takes place through the same S(1), N(2) and N(14) atoms in the three complexes, in the two latter cases the structure is built of one-dimensional $[Cu(CM)_2^{2+}]_n$ parallel chains where two cimetidine molecules link two copper atoms. Such chains are shown in ref. 7 for (**II**) and are drawn on Fig. 4 for (**I**). The linkage distances between two copper atoms are 8.56, 10.56 and 8.77 Å (along [011]) for (**I**), (**II**) and (**III**) respectively. Such a difference can easily be explained by the well-known flexibility of the cimetidine molecule.

This comparison supports the idea of "cation structure isomerism": complexes (**I**), (**II**) and (**III**) contain polymeric cations of the same empirical formula $[Cu(CM)_2^{2+}]_n$, the CM ligands are coordinated via the same atoms, but the linkage of the metal atoms is quite different.

Table 3. Geometries around Cu(II) in cimetidine complexes

Compound	Cu—N(2) (Å)	Cu—S(1) (Å)	Cu—N(14) (Å)	N(2)—Cu—N(14)[a] (°)	N(2)—Cu—S(1) (°)	S(1)—Cu—N(14)[b] (°)
$[Cu(CM)_2](ClO_4)_2$ (I)	1.980(6)	2.790(2)	2.042(7)	88.6(3)	78.9(2)	86.5(2)
$[Cu(CM)_2](NO_3)_2$ (II)	1.942(2)	2.419(1)	2.558(2)	88.7(1)	84.9(1)	79.3(1)
$[Cu(CM)_2]SO_4 \cdot 9H_2O$ (III)	1.981(3)	2.910(2)	2.001(3)	89.0(1)	77.4(1)	87.3(1)

Symmetry codes: [a] $x, 1-y, z-1/2$. [b] $1/2-x, y-1/2, 1/2-z$.

Geometry of cimetidine

Again it is suitable to present the results as a comparison between the title compound (**III**) and the related complexes (**I**) and (**II**). The uncoordinated ligand should be included in this discussion, however several conformers of the free molecule are known owing to its flexibility; for clarity conformers *A*[24] and *Z*[25] only will be considered.

Several features, common to all cimetidine forms and derivatives have been discussed in previous papers:[6,7,24,25] (i) the imidazole ring is planar with the methyl group in the plane (Table 4), bond lengths indicate electronic delocalization; (ii) the C(11)—N(10), C(11)—N(12) and C(11)—N(15) bond lengths in the guanidine residue do not show significant differences, these almost equivalent values and the planarity of the guanidine moiety (Table 4) can be explained by a delocalized bonding system; (iii) coordination bonds being excluded, the bond lengths listed in Table 2, namely the C—S bond lengths, have similar values in free cimetidine and Cu–cimetidine complexes.

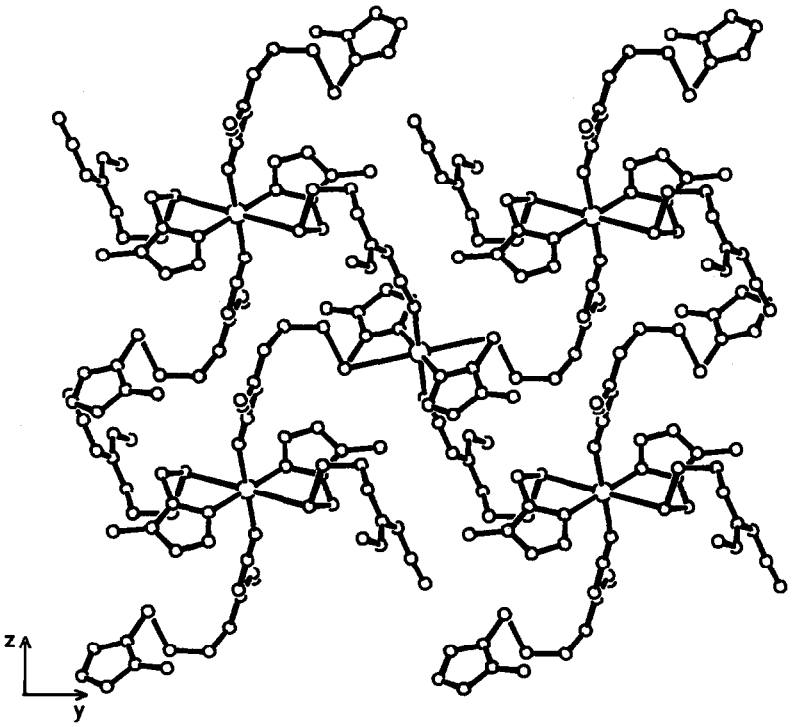

Fig. 2. $[Cu(CM)_2]SO_4 \cdot 9H_2O$. Structure of the two dimensional $[Cu(CM)_2^{2+}]_n$ cation. Projection onto (100), tilted by 10° around *y* and −15° around *z* axis for clarity.

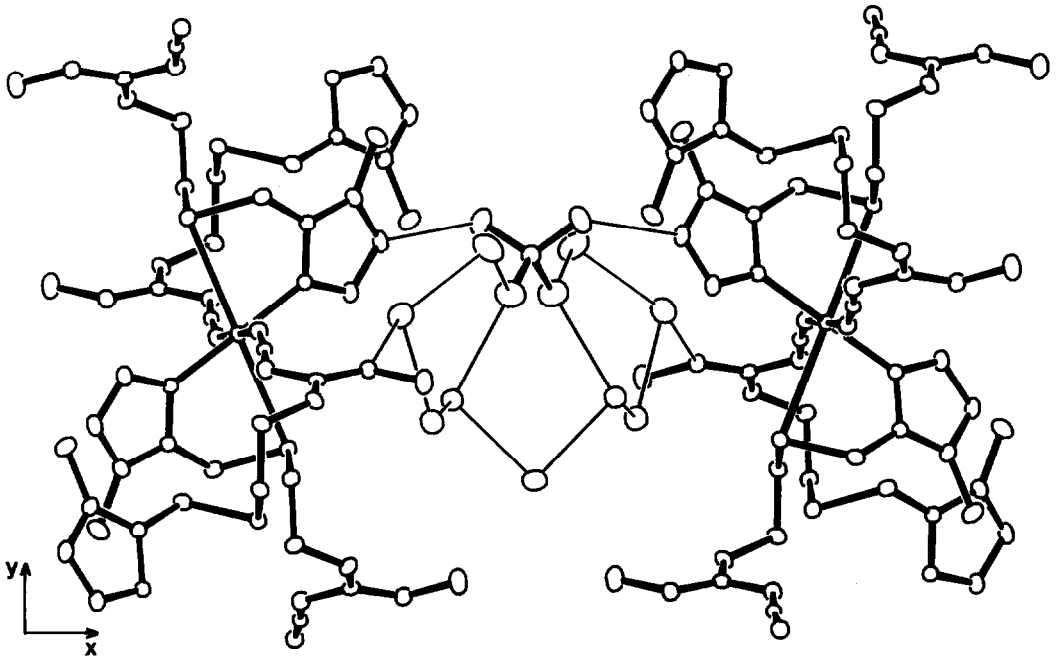

Fig. 3. Hydrogen bonding in $[Cu(CM)_2]SO_4 \cdot 9H_2O$; thin lines represent hydrogen bonds. Only one of the two disordered positions of the SO_4^{2-} anion have been drawn. Projection onto (001).

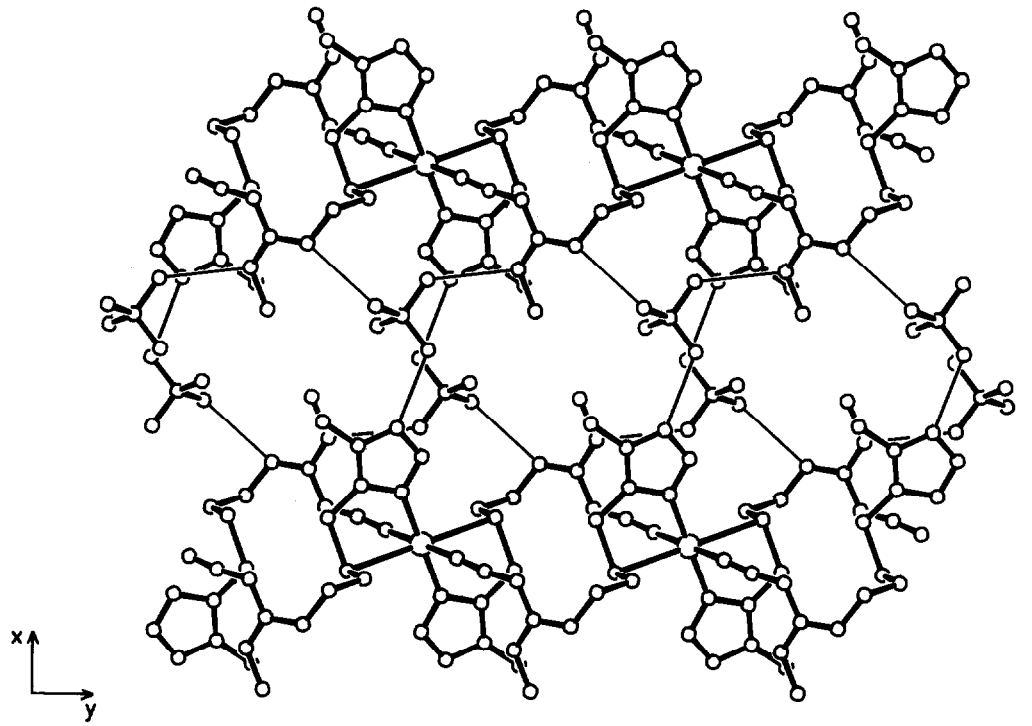

Fig. 4. $[Cu(CM)_2](ClO_4)_2$. Two one-dimensional $[Cu(CM)_2^{2+}]_n$ cations connected by ClO_4^- anions. Thin lines represent hydrogen bonds. Projection onto (001).

Table 4. Displacements (Å) from least-squares planes through the imidazole ring and guanidine residue. Atoms used to calculate the equations of planes are denoted by asterisks

Imidazole ring		Guanidine residue	
C(1)*	−0.002(3)	C(11)*	−0.008(3)
N(2)*	0.002(3)	N(10)*	0.002(3)
C(3)*	−0.005(4)	N(12)*	0.002(3)
N(4)*	0.003(3)	N(15)*	0.002(3)
C(5)*	−0.001(4)	C(16)	−0.043(5)
C(6)*	−0.001(5)	C(13)	−0.033(3)
		N(14)	−0.032(4)

In the title compound the methyl and cyano groups C(16), C(13) and N(14) lie close to the guanidine mean plane. Changes in the conformation of the ligand derive from bond angles and torsion angles listed in Table 5: (i) in the guanidine part of the molecule the two bond angles N(10)—C(11)—N(12) and N(12)—C(11)—N(15) of (**I**) and (**III**) show values close to those found in conformer Z[25] while the same angles in (**II**) correspond to conformer A[24]; (ii) the same analogy between (**II**) and conformer A on the one hand, and (**I**) and (**III**) and conformer Z on the other hand is observed for torsion angles around the

Table 5. Comparison of selected bond angles, torsion angles and dihedral angles (°) in the copper–cimetidine complexes and in forms A and Z of the cimetidine molecule

Angle	(III)	(I)	(II)	CM(A)	CM(Z)
N(10)—C(11)—N(12)	117.4	117.5	123.2	123.1	117.5
N(12)—C(11)—N(15)	123.3	122.9	116.9	117.0	123.3
N(10)—C(11)—N(15)—C(16)	3.1	4.4	−179.0	171.1	−7.6
N(10)—C(11)—N(12)—C(13)	−178.6	−168.3	4.6	−12.5	167.6
C(9)—N(10)—C(11)—N(15)	−167.3	−169.6	−1.0	−8.9	179.2
C(9)—N(10)—C(11)—N(12)	14.0	11.6	179.8	172.5	−0.1
C(8)—C(9)—N(10)—C(11)	99.6	100.5	79.1	90.6	110.1
S(1)—C(8)—C(9)—N(10)	−64.0	−49.4	−179.9	−175.7	−60.1
C(7)—S(1)—C(8)—C(1)	−72.3	−81.8	−86.2	62.7	−69.8
C(8)—S(1)—C(7)—C(1)	−60.8	−74.4	−74.3	61.8	−45.2
N(2)—C(1)—C(7)—S(1)	−46.5	−25.0	−33.8	−69.8	−49.4
C(5)—C(1)—C(7)—S(1)	132.9	160.7	150.7	111.6	129.8
Dihedral angles between imidazole ring and guanidine residue	59.1	44.2	89.6	28.2	54.2

Table 6. Hydrogen bonds with e.s.d.'s in parentheses

X—H ... Y	X ... Y (Å)	X—H (Å)	H ... Y (Å)	< X—H ...Y (°)	Symmetry code for atom Y
N(4)—H(4) ... O(2)	2.867(9)	0.97	1.90	175	$x, y, z-1$
N(4)—H(4) ... O(3)	2.947(9)	0.97	2.14	140	$x, y, z-1$
N(15)—H(15) ... Ow(3)	2.853(5)	0.97	1.93	159	x, y, z
Ow(1)—Hw(11) ... O(1)	2.804(9)	0.97	1.86	165	$x, 1/2-y, 3/2+z$
Ow(1)—Hw(11) ... O(3)	2.742(10)	0.97	1.90	144	$x, 1/2-y, 3/2+z$
Ow(1)—Hw(12) ... Ow(2)	2.758(5)	0.97	1.79	175	$-x, 1-y, -z$
Ow(2)—Hw(2) ... Ow(4)	2.781(4)	0.97	1.87	156	$x, -y, 1/2+z$
Ow(3)—Hw(31) ... Ow(5)	2.629(6)	0.97	1.92	128	$1/2-x, 3/2+y, 3/2-z$
Ow(4)—Hw(41) ... Ow(3)	2.752(5)	0.98	1.85	153	$1/2+x, y-1/2, z$
Ow(4)—Hw(42) ... Ow(1)	2.865(5)	1.00	1.87	174	$1/2+x, y-1/2, z$
Ow(5)—Hw(51) ... O(4)	2.721(10)	0.97	1.88	142	$-x, 1-y, -z$
Ow(5)—Hw(51) ... O(1)	2.878(9)	0.97	1.94	163	$-x, 1-y, -z$
Ow(5)—Hw(52) ... O(4)	2.698(9)	0.97	1.73	174	$3/2+x, 1/2+y, 1+z$

C(11)—N(12), C(11)—N(15), N(10)—C(11), C(9)—N(10) and C(8)—C(9) bonds, (iii) the other torsion angles about bonds close to the metal centre do not show the same relationship.

To sum up, cimetidine takes form *A* in (**II**) and form *Z* in (**I**) and (**III**), both forms being perturbed by the coordination through the sulphur atom. The perurbation arises from the flexibility of the four atom chain, binding the imidazole ring and the guanidine residue. The resulting dihedral angles between the imidazole and guanidine least-squares planes are given in Table 5.

Hydrogen bonding

Hydrogen bonding (between N—H groups of the cimetidine ligand, oxygen atoms of the sulphate ion and oxygen atoms of water molecules) appears to be important for the stabilization of the crystal lattice. The characteristics of the hydrogen bond network are given in Table 6. Note that the water molecule Ow(2) lies on a two-fold axis. The two-dimensional parallel cationic layers are connected by two kinds of hydrogen bonds. The first one is between the N(4) imidazole nitrogen atom and the disordered oxygen atoms of the sulphate group. The second one links water molecule Ow(2) with the N(15) nitrogen atom. Furthermore hydrogen bonds exist between the water molecules and between the sulphate ion and the water molecules (Fig. 3).

The hydrogen bond network of the anhydrous complexes (**I**) and (**II**) is much more simple: each anion connects three cationic chains in (**II**) and two cationic chains in (**I**) (Fig. 4).

Sulphate ion

The sulphur atom lies on a two-fold axis and the oxygen atoms are disordered over two positions (50% occupancy). The temperature factors of the oxygen atoms are rather high indicating the presence of a dynamical component or a bad resolution of the disorder. Thus the geometry of the sulphate ion will not be discussed further.

Acknowledgements—The authors wish to thank Dr J. Galy for his constant interest in this work. They are grateful to Dr F. Dahan and I. Luneau for their friendly help and fruitful discussions. L. S. acknowledges the CNRS for the allowance to work in the Laboratoire de Chimie de Coordination (Toulouse, France) and the Generalitat Valenciana Conselleria de Cultura, Educacio i Ciencia of Valencia (Spain) and CAICYT (932/84) for financial assistance.

REFERENCES

1. B. J. Hathaway, *Structure and bonding* 1984, **57**, 55.
2. B. Morosin and E. C. Lingafelter, *J. Phys. Chem.* 1961, **65**, 50.
3. J. A. McGinnety, *J. Am. Chem. Soc.* 1972, **94**, 8406.
4. R. L. Harlow, W. J. Wells, G. W. Watt and S. H. Simonsen, *Inorg. Chem.* 1975, **14**, 1468.
5. F. S. Stephens, *J. Chem. Soc.* 1969, **A**, 883; 1969, **A**, 2233.
6. A. Sancho, J. Borras, L. Soto-Tuero, C. Esteban-Calderon, C. Martinez-Rippol and M. Garcia-Blanco, *Polyhedron* 1985, **4**, 539.
7. L. Soto, J. Borras, A. Sancho, A. Fuertes and C. Miravitlles, *Acta Cryst.* 1985, **C41**, 1431.
8. A. Sancho, L. Soto, J. Borras, *Transition Met. Chem.* 1985, **10**, 214.
9. L. Soto, J. P. Legros, M. C. Molla and J. Garcia, *Acta Cryst.* 1987, **C43**, 834.
10. G. M. Sheldrick, SHELXS-86, Program for crystal structure solution, University of Göttingen, Göttingen (1986).
11. G. M. Sheldrick, SHELX: A program for crystal structure determination, University Chemical Laboratory, Cambridge (1976).
12. A. Abadia, A. Sancho, L. Soto and J. Borras, *Transition Met. Chem.* 1986, **11**, 8.
13. I. Bertini and R. S. Drago, *ESR and NMR of Paramagnetic Species in Biological and Related Systems. Nato Advan. Study Institute Ser.*, Vol 52. D. Reidel, Dordrecht (1979).
14. A. B. P. Lever, *Inorganic Electronic Spectroscopy*, 2nd Edn. Elsevier, Amsterdam (1986).
15. B. J. Hathaway and D. E. Billing, *Coord. Chem. Rev.* 1970, **5**, 143.
16. J. V. Rijn, W. L. Driessen, J. Reedijk and J. M. Lehn, *Inorg. Chem.* 1984, **23**, 3584.
17. J. V. Dagdigan, V. McKee and C. A. Reed, *Inorg. Chem.* 1982, **21**, 1332.
18. A. W. Addison, T. N. Rao, J. Reedijk, J. V. Rijn and G. C. Vershoor, *J. Chem. Soc., Dalton Trans.* 1984, 1349.
19. S. J. Brown, X. Tao, D. W. Stephan and P. K. Mascharak, *Inorg. Chem.* 1986, **25**, 3377.
20. H. J. Prochaska, W. F. Schwindinger, M. Schwartz, E. Bernaducci, M. J. Burk, R. A. Lalancette, J. A. Potenza and H. J. Schugar, *J. Am. Chem. Soc.* 1981, **103**, 3446.
21. M. B. Ferrari, L. C. Capacchi, G. G. Fava, A. Montenero and M. Nardelli, *Kristallografiya* 1972, **17**, 22.
22. P. M. Colman, H. C. Freeman, J. M. Guss, M. Murata, V. A. Norris, J. A. M. Ramshaw and M. P. Ventkappa, *Nature* 1978, **272**, 319.
23. E. J. Solomon, J. W. Hare, D. M. Dooley, J. H. Dawson, P. J. Stephens and H. B. Gray, *J. Am. Chem. Soc.* 1980, **102**, 168.
24. E. Hädicke, F. Frickel and A. Franke, *Chem. Ber.* 1978, 3222.
25. L. Parkanyi, A. Kalman, B. Hegedüs, K. Harsanyi and J. Kreidl, *Acta Cryst.* 1984, **C40**, 676.

Polyhedron Vol. 7, No. 4, pp. 315–322, 1988
Printed in Great Britain

0277–5387/88 $3.00+.00
© 1988 Pergamon Journals Ltd

ELECTROCHEMICAL OXIDATIVE ADDITION OF CHLORIDE TO $Rh_2(\mu\text{-dppm})_2(CO)_2Cl_2$

LOUIS J. TORTORELLI, PETER W. TINSLEY, CLIFTON WOODS* and CHRISTOPHER J. JANKE

Department of Chemistry, University of Tennessee, Knoxville, Tennessee 37996, U.S.A.

(*Received* 19 *May* 1987; *accepted after revision* 2 *September* 1987)

Abstract—The electrochemical oxidation of *trans*-$Rh_2(\mu\text{-dppm})_2(CO)_2Cl_2$ (dppm = bis (diphenylphosphino)methane) in the presence of chloride has afforded the new dirhodium(II) unsymmetrical complex $Rh_2(\mu\text{-dppm})_2(\mu\text{-Cl})(CO)Cl_3$ which is readily converted to the complex $[Rh_2(\mu\text{-dppm})_2(\mu\text{-CO})(\mu\text{-Cl})Cl_2]PF_6$. This species has been shown to undergo addition reactions with chloride to regenerate $[Rh_2(\mu\text{-dppm})_2(\mu\text{-Cl})Cl_3(CO)]$, and with carbon monoxide and *t*-butylisocyanide to give the additional new dirhodium(II) complexes $[Rh_2(\mu\text{-dppm})_2(\mu\text{-Cl})Cl_2(CO)_2]PF_6$ and $[Rh_2(\mu\text{-dppm})_2(\mu\text{-Cl})(CNC(CH_3)_3)_2Cl_2]PF_6$, respectively. During prolonged exposure to carbon monoxide $[Rh_2(\mu\text{-dppm})_2(\mu\text{-CO})(\mu\text{-Cl})Cl_2]PF_6$ undergoes reduction with the loss of chloride to give $[Rh_2(\mu\text{-dppm})_2(\mu\text{-Cl})(CO)_2]PF_6$.

Since the compound *trans*-$Rh(\mu\text{-dppm})_2(CO)_2Cl_2$, **1**, (dppm = bis(diphenylphosphino)methane) was first reported,[1] it has served as a precursor to numerous other dinuclear rhodium complexes. In some cases, oxidative addition of various reagents to **1** or some of its Rh(I) derivatives has clearly produced dimers with formal oxidation states of two.[2–5] In other cases, such as with *cis* dimetallated olefins,[6] there is some uncertainty as to the oxidation state of the metal atoms.

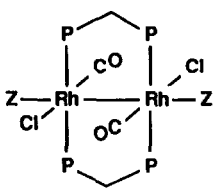

Z = Br, I

I

The oxidative addition of bromine or iodine to **1**, has led to Rh(II) complexes with structure **I**. However, the analogous chlorine oxidation product with structure **I** has not been reported, and our attempts to prepare this derivative have led to what appears to be a mixture of products that has so far defied separation and characterization. Our initial thought was that chlorine might be too strong an oxidizing agent, thus giving a mixture of rhodium containing products.

Some of our previous studies[7,8] involving electrochemistry of dinuclear Rh(I) complexes in the presence of coordinating species suggest that electrochemical oxidation of complexes such as **1** in the presence of halide ions might generate $Rh_2(\mu\text{-dppm})_2(CO)_2Cl_4$ with structure **I**. This seemed to be a viable approach since electrochemical oxidation allows one to "tune" the oxidation potential, thus possibly avoiding undesirable oxidation of the rhodium atoms or even the ligands. We report here the results of the electrochemical oxidation of **1** in the presence of Cl^- and some reactions involving the oxidation product as the precursor. The compounds involved in this study are given in Table 1.

EXPERIMENTAL

Materials

Procedures described in the literature were used to prepare **1**[9] and $[Rh_2(\mu\text{-dppm})(\mu\text{-CO})(\mu\text{-Cl})(CNC(CH_3)_3)_2]PF_6$.[10] Spectroanalysed dichloromethane and reagent grade acetone were used without further purification. Tetra-*n*-butylammonium chloride (TBAC) and tetra-*n*-butylammonium tetrafluoroborate (TBAT) were pur-

*Author to whom correspondence should be addressed.

Table 1

Compound No.	Compound formula[a]
1	$Rh_2(\mu\text{-dppm})_2(CO)_2Cl_2$
2	$[Rh_2(\mu\text{-dppm})_2(\mu\text{-CO})(\mu\text{-Cl})Cl_2]PF_6$
3	$Rh_2(\mu\text{-dppm})_2(\mu\text{-Cl})Cl_3(CO)$
4	$[Rh_2(\mu\text{-dppm})_2(\mu\text{-Cl})Cl_2(CO)_2]PF_6$
5	$[Rh_2(\mu\text{-dppm})_2(\mu\text{-Cl})(CO)_2]PF_6$
6	$Rh_2(\mu\text{-dppm})_2(CO)_2Cl_4$
7	$Rh_2(\mu\text{-dppm})_2(\mu\text{-CO})Cl_2$
8	$[Rh_2(\mu\text{-dppm})_2(\mu\text{-Cl})(\mu\text{-CO})(CO)_2]PF_6$
9	$[Rh_2(\mu\text{-dppm})_2(\mu\text{-Cl})(CNC(CH_3)_3)_2Cl_2]PF_6$
10	$[Rh_2(\mu\text{-dppm})(\mu\text{-CO})(\mu\text{-Cl})(CNC(CH_3)_3)_2]PF_6$

[a] dppm = bis(diphenylphosphino)methane.

chased from Aldrich and recrystallized several times from acetone–ether and methanol–water, respectively, and dried *in vacuo*. Tetra-*n*-butylammonium nitrate (TBAN) was purchased from Fluka and recrystallized from chloroform–ligroin. Tetra-*n*-butylammonium hexafluorophosphate (TBAH) was prepared from the metathesis reaction of tetra-*n*-butylammonium iodide and KPF_6, and was recrystallized three times from acetone–water and dried *in vacuo* at 50°C.

Physical measurements

UV-vis spectra were recorded with a Cary Model 219 spectrophotometer. Infrared (IR) spectra were recorded with a Digilab FTS-20 Fourier transform spectrometer. All IR samples were run as Nujol mulls. All NMR spectra were obtained using a JEOL FX90Q Fourier transform spectrometer. All ^{31}P spectra were proton decoupled and obtained at 36.21 MHz with 85% H_3PO_4 as the external reference, and ^1H spectra were obtained at 90 MHz using tetramethylsilane (TMS) as the internal reference. An Orion Research chloride-ion electrode (Model No. 94-17) was used in conjunction with an Orion Research double junction reference electrode (Model No. 90-02) to test for chloride ion. All elemental analyses were performed by Galbraith Laboratories Inc., Knoxville, TN.

Electrochemical procedures

Cyclic voltammetry was performed using either a BAS-100 electrochemical analyser (Bioanalytical) or a PAR (Princeton Applied Research) Model 364 polarographic analyser in conjunction with a function generator of the design of Woodward and coworkers[11] and a 2000 Omigraphic X-Y recorder (Houston Instruments). The working electrode was a platinum inlay electrode (Beckman No. 19021) with a surface area of 0.24 cm^2. The surface of the working electrode was polished with polishing alumina prior to each run. A 2.76 cm^2 platinum grid was used as the auxiliary electrode. The reference electrode was a saturated calomel electrode (SCE) and was located in the cell compartment in a glass capillary with a glass frit on one end to separate the reference electrode from the bulk solution. Coulometry and bulk electrolysis experiments were performed either with the BAS-100 electrochemical analyser or a PAR model 173 potentiostat/galvanostat equipped with a PAR 179 digital coulometer. The electrolysis cell was a conventional H-shaped three compartment cell in which the compartments were separated by glass frits of medium porosity. The working electrode, a 25 cm^2 platinum grid, and the auxiliary electrode, a carbon rod, were placed in separate outer compartments of the H-cell. The reference electrode for all electrolyses was the saturated calomel electrode (SCE). All solutions for electrochemical experiments were degassed with argon unless otherwise stated.

Preparation of $[Rh_2(\mu\text{-dppm})_2(\mu\text{-CO})(\mu\text{-Cl})Cl_2]PF_6$

50 cm^3 of a CH_2Cl_2 solution of **1** (141 mg, 0.128 mmol) containing 0.10 M TBAH and TBAC (356 mg, 1.28 mmol) was oxidized at +0.60 V via controlled potential electrolysis. The volume of the reddish–brown oxidized solution was reduced to *ca.* 5 cm^3, to which 50 cm^3 of CH_3OH was added. The resulting suspension was stirred for 24 h, during which time it turned from brown to green. The solid was filtered and stirred overnight in 10 cm^3 of CH_2Cl_2. The green solid was filtered and dried *in vacuo*. The product was recrystallized from CH_2Cl_2. Yield: 70%. IR(Nujol mull): ν(CO), 1794 cm^{-1}(s); $\nu(PF_6^-)$, 839 cm^{-1}(s), 557 cm^{-1}(m). UV-vis (CH_2Cl_2): [λ_{max}, nm (ε)]: 346 (16,000), 310 (32,000). ^{31}P NMR data: δ, 9.80 ppm; [^1J(Rh—P)+ ^xJ(Rh—P)], 97.7 Hz. Found: C, 47.8; H, 3.8; Cl, 8.8; P, 11.7. Calc. for $C_{51}H_{44}Cl_3F_6OP_5Rh_2$: C, 48.8; H, 3.5; Cl, 8.5; P, 12.3%.

Preparation of $[Rh_2(\mu\text{-dppm})_2(\mu\text{-Cl})Cl_3(CO)]$

Method 1. 50 cm^3 of a CH_2Cl_2 solution of **1** (121 mg, 0.110 mmol) containing 0.10 M TBAN and TBAC (167 mg, 0.55 mmol) was oxidized at +0.75 V via controlled potential electrolysis. The volume of the brown oxidized solution was reduced to 30 cm^3 and the solution was washed with three 100 cm^3

portions of water. The CH_2Cl_2 layer was reduced in volume and a brown product was obtained upon addition of ether. The product was recrystallized from CH_2Cl_2–ether in 75% yield.

Method 2. Excess TBAC was added to 30 cm^3 of a CH_2Cl_2 solution of **2** (105 mg, 0.087 mmol). The resulting brown solution was stirred for 1 h and reduced in volume to *ca.* 10 cm^3, after which 50 cm^3 of ether was added. The brown product was collected by filtration, washed with copious amounts of water and ether, and dried *in vacuo*. IR (Nujol mull): ν(CO) 2025 cm^{-1}(s). UV-vis (CH_2Cl_2): [λ_{max}, nm (ε)]: 383 (11,500), 303 (23,600). Found: Cl, 11.2. Calc. for $C_{51}H_{44}Cl_4OP_4$: Cl, 12.4%.

Preparation of $[Rh_2(\mu\text{-dppm})_2(\mu\text{-Cl})Cl_2(CO)_2]PF_6$

CO was passed over an acetone solution of **2** (80 mg, 0.064 mmol) until the solution turned bright orange. The resulting solution was reduced to 15 cm^3 via a rotary evaporator. A 1 : 1 ether–hexanes solution was added to precipitate an orange product. The product was recrystallized from CH_2Cl_2–ether–hexanes. The yield is quantitative. IR (Nujol mull): ν(CO), 2058 cm^{-1}(s), 2025 cm^{-1}(sh); $\nu(PF_6^-)$, 839 cm^{-1}(s), 560 cm^{-1}(m). UV-vis (CH_2Cl_2): [λ_{max}, nm (ε)]: 444 (2,200), 362 (31,000), 317 (41,000). ^{31}P NMR: δ, 11.3 ppm; [$^1J_{Rh-P}+{}^xJ_{Rh-P}$], 75.7 Hz. Found: C, 46.7; H, 3.4; Cl, 12.3. Calc. for $C_{52}H_{44}F_6O_2P_5Rh_2 \cdot CH_2Cl_2$: C, 46.6; H, 3.4; Cl, 13.0%.

Preparation of $[Rh_2(\mu\text{-dppm})_2(CO)_2Cl_4]$

A CH_2Cl_2 solution of **3** (50 mg, 0.044 mmol) was bubbled with CO for 5 min, during which the solution turned from brown to orange. The product precipitated upon addition of a 1 : 1 mixture of ether–hexanes. The yield is quantitative. IR (Nujol mull): ν(CO), 2041 cm^{-1}(s). UV-vis (CH_2Cl_2): [λ_{max}, nm (ε)]: 454 (4,800), 383 (20,000), 304 (37,000). ^{31}P NMR: δ, 8.76 ppm; [$^1J_{Rh-P}+{}^xJ_{Rh-P}$], 87.9 Hz.

Preparation of $[Rh_2(\mu\text{-dppm})_2(CNC(CH_3)_3)_2Cl_3]PF_6$

Method 1. To 0.173 mmol of **2** or **4** in 150 cm^3 of acetone, two equivalents (0.346 mmol) of $CNC(CH_3)_3$ were added. After stirring for *ca.* 0.5 h, the solution was reduced in volume on a rotary evaporator. The product precipitated when a 1 : 1 mixture of ether–ligroin was slowly added. The product was recrystallized from an acetone–ether–ligroin mixture.

Method 2. 50 cm^3 of a CH_2Cl_2 solution of 0.20 M TBAH, 48.7 mg (0.0361 mmol) of **10**, and a five-fold molar excess of TBAC was oxidized at +0.55 V. After the volume of the oxidized solution was reduced to *ca.* 10 cm^3, approximately 100 cm^3 of methanol was added and the resulting suspension was stirred overnight. Compound **9** precipitated from the solution and was recrystallized from CH_2Cl_2–ether–ligroin. Yield, 81%. IR (Nujol mull): ν(CN), 2172 cm^{-1}(s) 2153 cm^{-1}(sh); $\nu(PF_6^-)$, 839 cm^{-1}(s), 557 cm^{-1}(m). ^{31}P NMR: δ, 2.84 ppm; [$^1J_{Rh-P}+{}^xJ_{Rh-P}$], 85.4 Hz. UV-vis (CH_2Cl_2): [λ_{max}, nm (ε)], 499 (1,300), 371 (26,000), 309 (25,000), 269 (23,000). Found: C, 49.8; H, 4.7; N, 1.9; Cl, 7.6. Calc. for $C_{60}H_{62}Cl_3F_6P_5Rh_2$: C, 51.8; H, 4.5; N, 2.0; Cl, 7.6%.

RESULTS AND DISCUSSION

Electrochemical oxidation of $Rh_2(\mu\text{-dppm})_2Cl_2(CO)_2$ *in excess chloride*

The cyclic voltammetric behaviour of **1** in the presence of excess Cl^- is illustrated in Fig. 1. When the initial scan is in the positive direction, the cyclic voltammogram exhibits several oxidation waves between +0.40 and +1.30 V (Fig. 1a). When the initial scan is in the negative direction, a reduction wave appears at −1.39 V with an associated oxidation wave occurring at −0.25 V on the reverse scan. Oxidation waves with E_{pa} values more positive than +0.70 V are associated with or overlapped by the Cl^- waves and will not be discussed. Likewise

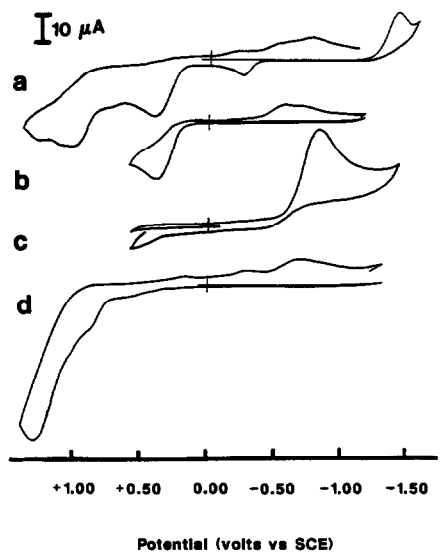

Fig. 1. Cyclic voltammogram of **1** in CH_2Cl_2/TBAH/Cl^-, (a) and (b) before oxidation, (c) after oxidation at +0.60 V, (d) after oxidation at +0.60 V followed by reduction at −1.30 V.

the reduction wave at −1.39 V and its associated oxidation wave will not be discussed at this time. The wave associated with the oxidation of **1** that is of current interest is the irreversible wave at +0.40 V. The oxidation products formed on the cyclic voltammetric time scale exhibit two reduction waves at −0.55 and −0.70 V. Controlled potential coulometry at +0.60 V indicates that **1** undergoes a two electron oxidation in the presence of Cl^-. The HOMO of face-to-face dppm-bridged dirhodium(I) compounds such as **1** has been described as a doubly occupied $\sigma^*(d_z2)$ molecular orbital.[12] Therefore, the oxidation of **1** represented by the wave at +0.40 V leads to the removal of these electrons, resulting in a transformation from a Rh(I)—Rh(I) to a Rh(II)—Rh(II) species. The electrolysis product exhibits an irreversible reduction wave at −0.82 V (Fig. 1c). After the oxidized solution is reduced at −1.30 V, the cyclic voltammogram does not exhibit the oxidation wave of the original Rh(I)—Rh(I) species (Fig. 1d), even though controlled potential coulometry at −1.30 V indicates that the reduction is a two electron process.

When a yellow CH_2Cl_2 solution of **1** is oxidized at +0.60 V and the solvent is removed from the resulting orange–brown solution, an orange–brown residue containing the Rh(II)—Rh(II) product, the excess TBAC and the TBAH is obtained. An IR spectrum of a Nujol mull of the solid orange–brown residue exhibits a CO stretching frequency at 2024 cm^{-1} which is assigned to a terminal CO. Upon treating the orange–brown residue with CH_3OH to remove the tetra-*n*-butylammonium salts, the mixture turns green and a green solid is isolated. After recrystallization from CH_2Cl_2 the product exhibits an IR band at 1794 cm^{-1}, consistent with the presence of a bridging CO. The ^{31}P NMR spectrum of this product is shown in Fig. 2a and exhibits the typical AA′A″A‴XX′ pattern observed for symmetrical dimers containing two *trans* bridging dppm ligands. The spectroscopic and analytical data are consistent with the formulation of the green solid as **2**.

Two different structural formulations of **2** are possible. One has the bridging CO symmetrically bound to the two Rh atoms. This formulation requires that CO be a two electron donor, resulting in no formal Rh—Rh bond as indicated by structure **II**. The other possible formulation is one in which the CO acts as a four electron donor and thus is unsymmetrically bound to the two Rh atoms as shown by structure **III**. Structure **III** requires the formation of a metal–metal bond. It has been suggested that complexes with structures such as **II** are likely to be unstable due to non-bonded contacts of the bridging CO and the bridging ligand opposite the CO created by the large metal–metal separation.[6e]

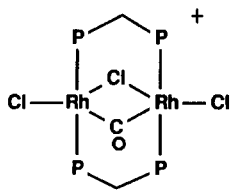

II

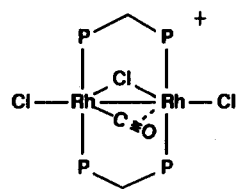

III

The general trend for the values of the coupling constant $[^1J_{Rh-P}+{}^xJ_{Rh-P}]$ in dppm dirhodium complexes is that for complexes with a Rh—Rh bond the values of the coupling constant are usually in the range of 90–115 Hz and those for complexes with no Rh—Rh bond are in the range of 125–140 Hz.[6e,13,14] The observed value of 97.7 Hz for **2** is in the range of values generally observed for dppm-bridged dirhodium complexes that contain a formal Rh—Rh bond; hence, structure **III** is consistent

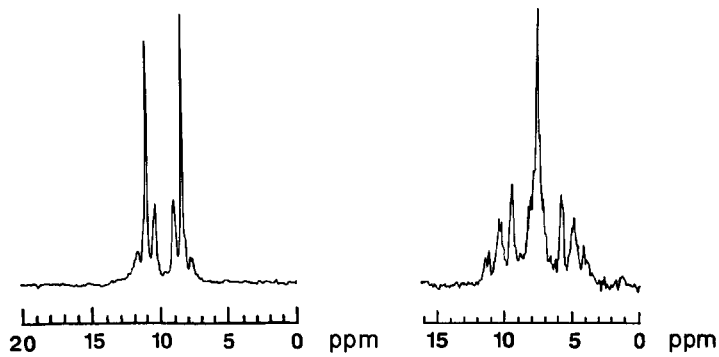

(a) (b)

Fig. 2. ^{31}P NMR spectrum of (a) **2** and (b) **3**.

with the general trend for the coupling constants in dppm-bridged dirhodium complexes that contain a Rh—Rh bond. Structure **III** however, is not consistent with the symmetrical AA'A''A'''XX' ^{31}P NMR pattern unless the complex is fluxional, thus leading to equivalent time-averaged environments for the four phosphorus atoms. The ^{31}P NMR spectrum has been measured over the temperature range +25 to −90°C. There was no observable change in the spectrum over this range; thus, if interconversion is occurring, it is still rapid at −90°C. Though we are attempting to obtain crystals suitable for an X-ray structure determination, we have not yet been successful.

We postulate that during the conversion of **1** to **2** the complex **3** is formed as the initial oxidation product and is converted to **2** during isolation procedures. This behaviour is summarized in Scheme 1 (the dppm bridging ligands have been omitted from all complexes for clarity). At least one of the chloro ligands on **3** is apparently labile enough, such that the ionizing power of methanol facilitates its removal during attempts to isolate **3** from a solution containing a non-coordinating anion such as PF_6^-. We have been unable to identify any proton resonances in the ^1H NMR spectrum of **2** that can be attributed to methanol, indicating that though methanol facilitates the removal of Cl^- it does not appear to coordinate to the complex or crystallize as solvent of crystallization.

Though many dirhodium carbonyl complexes containing two bridging dppm ligands in a *trans* disposition are fluxional,[13,15] the ^{31}P NMR spectrum of **3** shown in Fig. 2b remains essentially unchanged over the temperature range +35 to −85°C. This indicates that exchange is either not occurring or is still very rapid at −85°C.

Reaction of $[Rh_2(\mu\text{-dppm})_2(\mu\text{-Cl})(\mu\text{-CO})Cl_2]PF_6$ *with carbon monoxide*

When CO is passed over an open acetone solution of **2** the solution turns orange instantly. Upon addition of 1 : 1 ether–hexanes an orange product precipitates. The IR spectrum reveals the presence of terminal CO ligands and PF_6^- counter ions. The analytical data indicate the presence of three chloride ligands and 1 mole of dichloromethane. These data are consistent with the formulation of the product as **4** (Scheme 1). The bridging Cl^- is postulated on the basis of the electron count of 18 for each Rh and the symmetrical AA'A''A'''XX' ^{31}P NMR pattern.

When a solution of **2** or **4** is bubbled with CO for several minutes or is allowed to stand under a CO atmosphere overnight, the solution turns orange–yellow. The ^{31}P NMR and IR data of the product isolated from this solution are identical to that of a freshly prepared sample of **5**. On the other hand, if a solution of **2** or **4** is kept under an atmosphere of CO and the product is not isolated, the ^{31}P NMR spectrum of the solution indicates that the complex present is **8**. These observations are consistent with previous results that show that **8** is formed when a solution of **5** is saturated with CO.[15]

The conversion of **2** or **4** to **5** involves the reduction of a Rh(II) dimer to a Rh(I) dimer. Though we have not been able to identify any CO oxidation products, we have demonstrated, using a chloride-ion selective electrode, that a stoichiometric amount of chloride ions is produced as **2** or **4** is converted to **5**. These results suggest that the conversion is not a simple reductive elimination of elemental chlorine but is a reduction by CO accompanied by the loss of Cl^-.

The cyclic voltammogram of **2** in CH_2Cl_2/TBAH reveals irreversible cathodic waves at −0.21 and −0.79 V and an associated anodic wave at +0.82 V. Reduction of the dimer at −0.90 V is a two electron process. The reduction product contains a bridging CO with an IR stretching frequency of 1745 cm^{-1}. The AA'A''A'''XX' ^{31}P NMR pattern with a $[^1J_{Rh-P} + {}^xJ_{Rh-P}]$ value of 117.2 HZ suggests a symmetrical species. The NMR spectrum also indicates the absence of PF_6^- ions. These data are consistent with those reported for **7**[13b] and thus the electrochemical reduction product of **2** is formulated as **7**.

The difference between the electrochemical reduction product of **2** and the CO reduction product of **2** is the presence of excess CO during the process. For the CO reduction, the excess CO is available to coordinate to the metal and stabilize the low oxidation state. It has been previously shown that **7** readily adds CO to form **8**. In the electrochemical reduction there is no CO available, thus **7** is the isolated product.

Reaction of $[Rh_2(\mu\text{-dppm})_2(\mu\text{-Cl})(CO)Cl_3]$ *with carbon monoxide*

When CO is bubbled through a CH_2Cl_2 solution of **3** the solution turns orange. Upon the addition of 1 : 1 ether–hexanes a dark orange product is obtained. The ^{31}P NMR spectrum of this product exhibits the AA'A''A'''XX' pattern with a $[^1J_{Rh-P} + {}^xJ_{Rh-P}]$ value of 87.9 Hz. These data indicate that the complex is a symmetrical Rh(II) dimer containing four equivalent phosphorus atoms and suggest that it contains a metal–metal bond. The

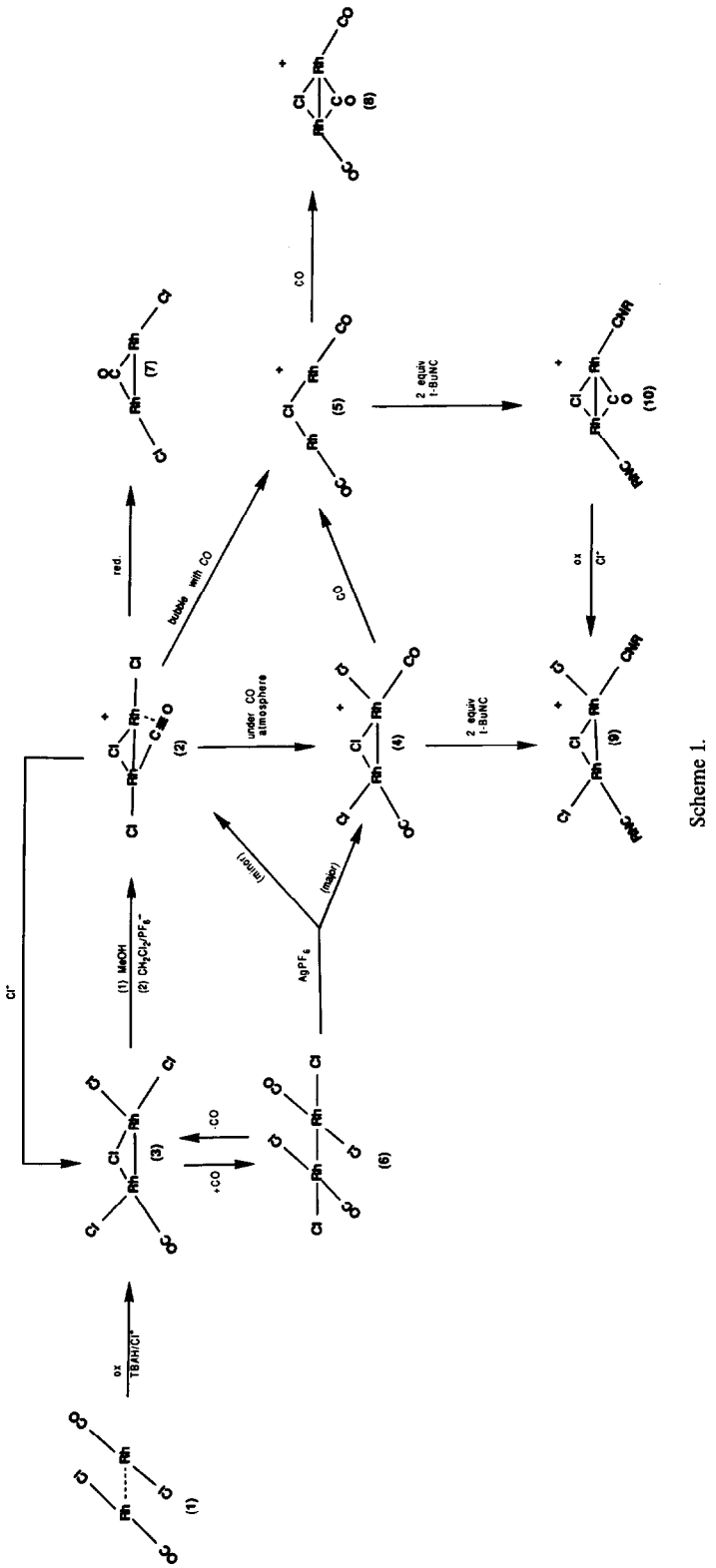
ox
TBAH/Cl⁻
(1)
Cl⁻
(1) MeOH
(2) CH₂Cl₂/PF₆⁻
AgPF₆
(minor)
(major)
(3)
-CO
+CO
(6)
(2)
under CO atmosphere
(4)
2 equiv t-BuNC
(9)
ox
Cl⁻
bubble with CO
red.
CO
(5)
2 equiv t-BuNC
(10)
CO
(8)
(7)

Scheme 1.

solid state IR spectrum reveals the presence of terminal CO ligands. This conversion is illustrated in Scheme 1 and the product is formulated as **6**.

The ^{31}P NMR spectrum of a CH_2Cl_2 solution of **6** indicates that the complex is stable under an atmosphere of CO; however, it reverts to **3** in the absence of a CO atmosphere. Even under a CO atmosphere, **6** decomposes in acetone solution to give products that we have been unable to characterize. Complex **6** appears to be the chlorine oxidative addition product analogous to those obtained by treating **1** with Br_2 and I_2.[2,4] The fact that **6** is unstable explains why we have been unable to isolate the product after treating a solution of **1** with Cl_2.

When **6** is treated with one equivalent of $AgPF_6$ two products are obtained. The major product is **4** and the minor product is **2** (Scheme 1). The most likely explanation for this observation is that a small amount of **6** loses CO to form **3** and the reaction with $AgPF_6$ removes a Cl^- from both **3** and **6** to form **2** and **4**, respectively.

The cyclic voltammogram of **6** in CH_2Cl_2 containing TBAH and CO exhibits two irreversible reduction waves at -0.15 and -0.62 V. Reduction at -0.70 V is a two-electron process that leads to an irreversible oxidation wave at $+0.86$ V. The isolated reduction product exhibits CO stretching frequencies at 1976 and 2000 cm^{-1}. The ^{31}P NMR spectrum exhibits an AA'A''A'''XX' pattern with a chemical shift of 18.98 ppm and a $[^1J_{Rh-P}+{}^xJ_{Rh-P}]$ value of 114.8 Hz and indicates the presence of PF_6^-. These data are identical to those of a freshly prepared sample of **5** and thus the reduction product of **6** was characterized as complex **5**.

Reaction of $[Rh_2(\mu\text{-dppm})_2(\mu\text{-Cl})(\mu\text{-CO})Cl_2]PF_6$ *and* $[Rh_2(\mu\text{-dppm})_2(\mu\text{-Cl})Cl_2(CO)_2]PF_6$ *with* $CNC(CH_3)_3$

When **2** or **4** is treated with two equivalents of $CNC(CH_3)_3$, a new complex is obtained which, on the basis of analytical data, has been formulated as **9**. The IR spectrum of **9** exhibits two bands at frequencies about 60 cm^{-1} higher than those found in **10**. The higher ν(NC) in **9** compared to that of **10** is consistent with a higher oxidation state in **9** since a higher oxidation state means less π backbonding and thus a higher NC stretching frequency. The lack of an IR band in either the terminal or the bridging CO stretching region confirms the absence of CO in **9**. The presence of a PF_6^- counterion is confirmed by both IR and ^{31}P NMR. The chemical equivalence of the phosphorus atoms is demonstrated by the AA'A''A'''XX' pattern observed in the ^{31}P NMR spectrum. The $[^1J_{Rh-P}+{}^xJ_{Rh-P}]$ value of 85.4 Hz suggests the presence of a metal–metal bond. A bridging chloride is postulated on the basis of analytical data that show that there are three chloride ions per dimer, the chemical equivalence of the phosphorus atoms, and the fact that a bridging chloride gives the two rhodium centres electron counts of 18. The two isomers **9a** and **9b**

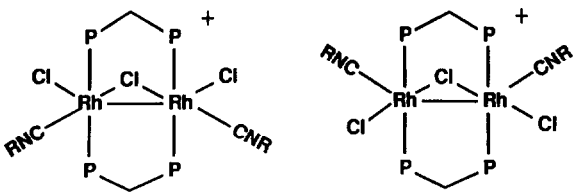

9a

9b

(R = $(CH_3)_3C$) are potentially possible. The spectroscopic data do not permit an unequivocal identification of the isomer obtained. However, it has been shown by several structural analyses of *trans*-bis(dppm)-bridged dirhodium A-frame complexes, that the methylene groups of the dppm ligands are folded in a *cis* position towards the bridging apex ligand.[16] This configuration allows the more bulky phenyl groups to occupy more open sites and thus minimize unfavourable intramolecular contacts of the dppm ligands and the apex ligand. This folding of the dppm ligands also creates more open sites opposite the apex ligand and would therefore minimize steric interactions between the phenyl

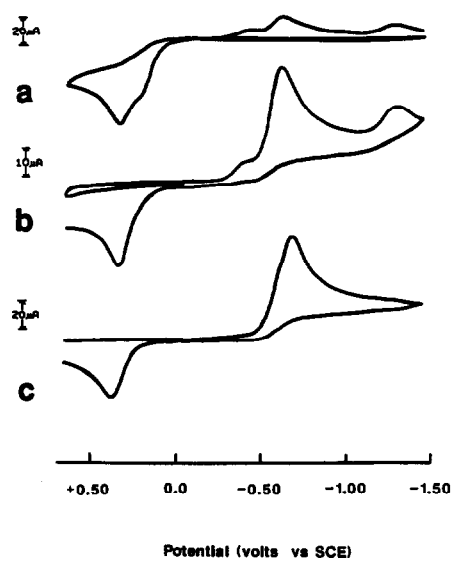

Fig. 3. Cyclic voltammogram of (a) **10** in CH_2Cl_2/TBAH/Cl^- before oxidation, (b) **10** in CH_2Cl_2/TBAH/Cl^- after oxidation at $+0.55$ V, (c) **9** after being isolated from an oxidized solution of **10**.

groups and the isocyanide groups occupying positions *trans* to the apex ligand. This would thus favour **9a**.

Complex **9** has also been prepared by electrochemical techniques. The cyclic voltammogram of **10** in the medium CH_2Cl_2/TBAH/Cl^- exhibits overlapping irreversible oxidation waves at +0.25 and +0.39 V and associated reduction waves at −0.36, −0.55 and −1.19 V (Fig. 3a). The overlapping oxidation waves are due to two one-electron processes. Controlled potential electrolysis at +0.55 V leads to a colour change from red to orange. The reduction waves at −0.39 and −1.31 V (Fig. 3b) are apparently due to minor products since the complex isolated from the oxidized solution exhibits only an irreversible reduction wave at −0.64 V. The corresponding oxidation wave of the isolated product occurs at +0.42 V. The differences in peak potentials of the major oxidation and reduction waves for the isolated product (Fig. 3c) and the corresponding waves of the initially oxidized solution (Fig. 3b) might be ascribed to the presence of some minor products and the excess Cl^- in the oxidized solution that are not present in the solution of the isolated product.

Acknowledgements—The authors wish to thank the National Science Foundation for support of this work and Johnson Matthey, Inc for a generous loan of rhodium trichloride.

REFERENCES

1. J. T. Mague, *Inorg. Chem.* 1969, **8**, 1975.
2. A. L. Balch and B. Tulyathan, *Inorg. Chem.* 1977, **16**, 2840.
3. A. L. Balch, J. W. Labadie and G. Delker, *Inorg. Chem.* 1979, **18**, 1224.
4. A. L. Balch, *J. Am. Chem. Soc.* 1976, **98**, 8049.
5. L. A. Oro, D. Carmona, P. L. Perez, M. Esteban, A. Tiripicchio and M. Tiripicchio-Camellini, *J. Chem. Soc., Dalton Trans.* 1985, 973.
6. (a) M. Cowie and T. G. Southern, *Inorg. Chem.* 1982, **21**, 246; (b) M. Cowie and R. S. Dickson, *Inorg. Chem.* 1981, **20**, 2682; (c) J. T. Mague and S. H. DeVries, *Inorg. Chem.* 1982, **21**, 1632; (d) M. Cowie and T. G. Southern, *J. Organometal. Chem.* 1980, **193**, C46; (e) M. Cowie, R. S. Dickson and B. W. Hames, *Organometallics* 1984, **3**, 1879.
7. D. R. Womack, P. D. Enlow and C. Woods, *Inorg. Chem.* 1982, **22**, 2653.
8. P. D. Enlow and C. Woods, *Inorg. Chem.* 1985, **24**, 1273.
9. J. T. Mague and J. P. Mitchner, *Inorg. Chem.* 1969, **8**, 119.
10. J. T. Mague and S. H. DeVries, *Inorg. Chem.* 1980, **19**, 3743.
11. W. S. Woodward, R. D. Rocklin and R. W. Murray, *Chem. Biomed. Environ. Instrum.* 1979, **9**, 95.
12. W. A. Fordyce and G. A. Crosby, *J. Am. Chem. Soc.* 1982, **104**, 95.
13. (a) M. Cowie and S. K. Dwight, *Inorg. Chem.* 1980, **19**, 209; (b) M. Cowie and S. K. Dwight, *ibid.* 1980, **19**, 2500.
14. A. L. Balch, *Homogeneous Catalysis with Metal Phosphine Complexes* (Edited by L. G. Pignolet), Chap. 5. Plenum Press, New York (1984).
15. M. Cowie, J. T. Mague and A. R. Sanger, *J. Am. Chem. Soc.* 1978, **100**, 3628.
16. C. P. Kubiak and R. Eisenberg, *J. Am. Chem. Soc.* 1977, **99**, 6129.

Polyhedron Vol. 7, No. 4, pp. 323–327, 1988
Printed in Great Britain

0277–5387/88 $3.00+.00
Pergamon Journals Ltd

THE X-RAY CRYSTAL STRUCTURE AND MAGNETIC PROPERTIES OF A BINUCLEAR COPPER(II) COMPLEX OF 2-α-HYDROXYBENZYLBENZIMIDAZOLE AND ITS ANION $\{[Cu_2(C_{14}H_{12}N_2O)_2(C_{14}H_{11}N_2O)_2](ClO_4)_2 \cdot 5C_2H_5OH\}$

BRIAN PIGGOTT*

Inorganic Chemistry Research Laboratory, School of Natural Sciences, Hatfield Polytechnic, Hatfield, Hertfordshire AL10 9AB, U.K.

and

MICHAEL B. HURSTHOUSE,* PETER THORNTON and NIGEL P. C. WALKER

Department of Chemistry, Queen Mary College, University of London, Mile End Road, London E1 4NS, U.K.

(*Received* 28 *July* 1987; *accepted* 8 *September* 1987)

Abstract—The preparation, crystal structure and diamagnetism of $Cu_2(HOBB)_2(OBB)_2(ClO_4)_2 \cdot 5C_2H_5OH$ where HOBB is 2-α-hydroxybenzylbenzimidazole and OBB its deprotonated form are reported. The crystals are triclinic $P\bar{1}$ with $a = 19.380(4)$, $b = 21.345(6)$, $c = 9.484(3)$ Å, $\alpha = 102.52(2)$, $\beta = 103.93(2)$, $\gamma = 105.76(2)°$, $Z = 2$. The structure was refined with 6593 reflections [$I \geqslant 2\sigma(I)$] to $R = 0.059$. The molecule contains bridging OBB and non-bridging HOBB resulting in a geometry around each copper ion that is distorted square pyramidal with apical hydroxyl groups. An interesting feature of the molecule is that both of the apical hydroxyl groups lie on the same side of the plane defined by the Cu_2O_2 core.

With $Cu(NO_3)_2 \cdot 3H_2O$, 2-α-hydroxybenzylbenzimidazole forms the deep blue diamagnetic solid $Cu(HOBB)_3(NO_3)_2$ and with $Cu(ClO_4)_2 \cdot 6H_2O$ a deep blue diamagnetic crystalline solvate $Cu_2(HOBB)_2(OBB)_2(ClO_4)_2 \cdot 5(C_2H_5OH)$ (the title complex). The room temperature magnetic measurements of both complexes indicate the presence of magnetically coupled copper ions and yet their structures, as far as can be deduced from stoichiometry, are different. In order to elucidate these structural differences and try to rationalize their magnetic behaviour, attempts were made to obtain crystals of both complexes for an X-ray crystallographic study. For $Cu_2(HOBB)_2(OBB)_2(ClO_4)_2 \cdot 5(C_2H_5OH)$ this was possible but repeated attempts using a variety of solvents produced only "powders" for $Cu(HOBB)_3(NO_3)_2$. Failure to get crystals of the nitrate complex was unfortunate but it was thought that by solving the structure of the perchlorate complex sufficient information on the coordination properties of HOBB (and OBB) could be obtained to provide insight into the structure of $Cu(HOBB)_3(NO_3)_2$ and hence its magnetic properties.

EXPERIMENTAL

2-α-hydroxybenzylbenzimidazole (HOBB) was synthesized as described previously.[1]

$Cu_2(HOBB)_2(OBB)_2(ClO_4)_2 \cdot 5(C_2H_5OH)$

3.7 g of $Cu(ClO_4)_2 \cdot 6H_2O$ and 4.5 g of HOBB were dissolved in 10 cm^3 of ethanol and the resulting blue solution was filtered. The filtrate on standing for approx. two weeks produced large blue crystals. Analysis of these crystals was not attempted because of rapid solvent loss. Instead the desolvated

*Authors to whom correspondence should be addressed.

product formed by vacuum drying was analysed. Found: C, 53.9; H, 4.4; N, 8.4; O, 18.7. Calc. for $Cu(C_{14}H_{11}N_2O)(C_{14}H_{12}N_2O)(ClO_4)$: C, 55.1; H, 3.8; N, 9.2; O, 15.7%.

$Cu(HOBB)_3(NO_3)_2$

1.2 g of $Cu(NO_3)_2 \cdot 3H_2O$ were dissolved in about 25 cm^3 of acetone and shaken vigorously with about 5 g of anhydrous Na_2SO_4. This solution was then filtered into 3.4 g of HOBB dissolved in about 15 cm^3 of acetone and the resulting blue solution concentrated to approx. 100 cm^3. On standing for several days a blue solid was deposited which was filtered off and dried *in vacuo*. Found: C, 58.2; H, 4.2; N, 12.8; O, 14.8. Calc. for $Cu(C_{14}H_{12}N_2O)_3(NO_3)_2$: C, 58.6; H, 4.2; N, 13.0; O, 14.9%.

Magnetic susceptibility measurements were made by the Faraday method using apparatus described previously.[2]

$Cu_2(HOBB)_2(OBB)_2(ClO_4)_2 \cdot 5(C_2H_5OH)$ produces blue crystals which are very sensitive to loss of solvent and consequently were mounted in Lindemann tubes in the presence of mother liquor. The crystal data are: $[Cu_2C_{56}H_{46}N_8O_4] \cdot (ClO_4)_2 \cdot 5C_2H_5OH$, $M_r = 1447.3$ triclinic, $a = 19.380(4)$. $b = 21.345(6)$, $c = 9.484(3)$ Å, $\alpha = 102.52(2)$, $\beta = 103.93(2)$, $\gamma = 105.76(2)°$, $V = 3493.6$ $Å^3$, space group $P\bar{1}$, $Z = 2$, $D_c = 1.38$ g cm^{-3}, $\lambda = 0.71069$, μ (Mo-K_α) = 7 cm^{-1}. Refined unit cell parameters were obtained by centering 25 reflections ($15.7° \leqslant \theta \leqslant 16°$) on an Enraf–Nonius CAD4 diffractometer. 12,267 unique reflections ($1.5° \leqslant \theta \leqslant 25°$) were measured with graphite monochromated Mo-K_α radiation using an $\omega/2\theta$ scan procedure.[3] Of these, 7155 were considered observed [$I \geqslant 1.5\ \sigma(I)$]. Lorentz, polarization and a semi-empirical absorption correction[4] using normalized and averaged transmission curves measured from three reflections (minimum transmission = 98.1%) were applied to the data. Measurement of three strong reflections every hour during data collection showed no decrease in intensity.

The positions of the two Cu atoms were determined from a sharpened Patterson map and the rest of the non-hydrogen atoms were found from difference–Fourier syntheses following isotropic refinement of the Cu positions. Both perchlorate anions were found to have disordered oxygen atoms in which eight positions with half occupancy could be assigned to each anion, however, for neither anion site could the arrangement of peaks be interpreted in terms of two intersecting tetrahedra. In addition to the cations and anions, five molecules of ethanol were located in the asymmetric unit although one did not possess an ordered hydroxyl group and hence only the two carbon atoms could be seen. Following refinement with anisotropic thermal parameters for all atoms, all hydrogen atoms attached to carbon atoms were included and refined with geometric constraints and a single isotropic temperature factor for the hydrogen atoms on each benzene ring. A subsequent difference–Fourier revealed the positions of the four imidazole hydrogens and the two hydroxyl hydrogens on the protonated OBB ligands, and these were included in the structure refinement with restraint imposed on the bond lengths. Final refinement was with blocked full-matrix least-squares with unit weighting of the 6593 reflections with $I \geqslant 2\sigma(I)$ and the omission of ten low-angle reflections. The final R factors were, $R = \Sigma|\Delta F|/\Sigma|F_o| = 0.059$, and $R_w = [\Sigma w|\Delta F|^2/\Sigma w|F_o|^2]^{1/2} = 0.064$. All calculations were performed on a DEC VAX-11/750 using SHELX 76.[5] Table 1 contains selected bond lengths and angles. Tables of atomic positional and thermal parameters, full lists of bond lengths and angles and F_o/F_c values have been deposited as supplementary data with the Editor, from whom copies are available on request. Atomic coordinates have also been deposited with the Cambridge Crystallographic Data Centre.

RESULTS AND DISCUSSION

The structure of the title complex which is shown in Fig. 1 contains some interesting features. The molecule has two HOBB ligands that are each coordinated to a single Cu atom through their imino nitrogen atom and the oxygen atom of their hydroxyl group. The other two OBB ligands each coordinate to a Cu ion through their imino nitrogen atom and form a bridge between the two Cu ions with their alkoxy oxygen atoms. The resulting geometry around each Cu ion is distorted square pyramidal with the hydroxyl groups at the apex. A novel feature of this arrangement is that both of the apical hydroxyl groups lie on the same side of the plane defined by the Cu_2O_2 core. The reason for this unusual conformation could be due to another interesting structural feature of this complex *viz* the presence of hydrogen bonded perchlorate. Only one perchlorate is hydrogen bonded to the cation but both are disordered. The disorder in the hydrogen bonded perchlorate gives rise to two bonding schemes. In one the perchlorate bridges the two apical hydroxyl groups by forming hydrogen bonds through two of its oxygens, specifically O(22) ... H(2) and O(21) ... H(1). Note that these two oxygens do seem to belong to the same ClO_4 orientation, since O(21)—Cl(2)—O(22) = 114.(1)°. The

Table 1. Selected bond lengths and bond angles

O(1)—Cu(1)	2.453(8)	N(11)—Cu(1)	1.960(8)
O(3)—Cu(1)	1.925(6)	O(4)—Cu(1)	1.926(7)
N(41)—Cu(1)	1.972(6)	O(2)—Cu(2)	2.451(8)
N(21)—Cu(2)	1.963(8)	O(3)—Cu(2)	1.926(7)
N(31)—Cu(2)	1.965(7)	O(4)—Cu(2)	1.930(6)
H(1)—O(1)	1.074(85)	H(2)—O(2)	1.077(118)
Cu(2)—O(3)—Cu(1)	102.7(3)	Cu(2)—O(4)—Cu(1)	102.5(3)
N(11)—Cu(1)—O(1)	74.2(3)	O(3)—Cu(1)—O(1)	98.6(3)
O(3)—Cu(1)—N(11)	96.5(3)	O(4)—Cu(1)—O(1)	101.0(3)
O(4)—Cu(1)—N(11)	171.2(2)	O(4)—Cu(1)—O(3)	76.7(3)
N(41)—Cu(1)—O(1)	93.9(3)	N(41)—Cu(1)—N(11)	105.4(3)
N(41)—Cu(1)—O(3)	157.0(2)	N(41)—Cu(1)—O(4)	82.1(3)
N(21)—Cu(2)—O(2)	74.5(3)	O(3)—Cu(2)—O(2)	99.4(3)
O(3)—Cu(2)—N(21)	170.3(3)	N(31)—Cu(2)—O(2)	93.9(3)
N(31)—Cu(2)—N(21)	105.1(3)	N(31)—Cu(2)—O(3)	82.6(3)
O(4)—Cu(2)—O(2)	98.6(3)	O(4)—Cu(2)—N(21)	96.6(3)
O(4)—Cu(2)—O(3)	76.6(3)	O(4)—Cu(2)—N(31)	157.2(3)
H(2)—O(2)—Cu(2)	122.1(64)	H(1)—O(1)—Cu(1)	111.5(45)
O(1)—Cu(1)—Cu(2)	108.3(2)	N(11)—Cu(1)—Cu(2)	135.1(1)
O(3)—Cu(1)—Cu(2)	38.7(1)	O(4)—Cu(1)—Cu(2)	38.8(1)
N(41)—Cu(1)—Cu(2)	118.8(3)	O(2)—Cu(2)—Cu(1)	107.3(3)
N(21)—Cu(2)—Cu(1)	135.3(1)	O(3)—Cu(2)—Cu(1)	38.6(1)
N(31)—Cu(2)—Cu(1)	119.1(3)	O(4)—Cu(2)—Cu(1)	38.7(1)

Selected non-bonded distances. Intramolecular: Cu(2)—Cu(1) 3.008(4).

second bonding scheme, again involves bridging perchlorate but in this case only one of its oxygens is used *viz* H(1) .. O(21′) ... H(2), Fig. 2.

The four ordered ethanol molecules each hydrogen bond through their hydroxyl oxygen atoms to the amino nitrogen of the imidazole moiety of the HOBB and OBB ligands. The fifth ethanol molecule is disordered. Hydrogen bond lengths are given in Table 2.

Both $[Cu(HOBB)(OBB)(ClO_4)]_2$ and its ethanol

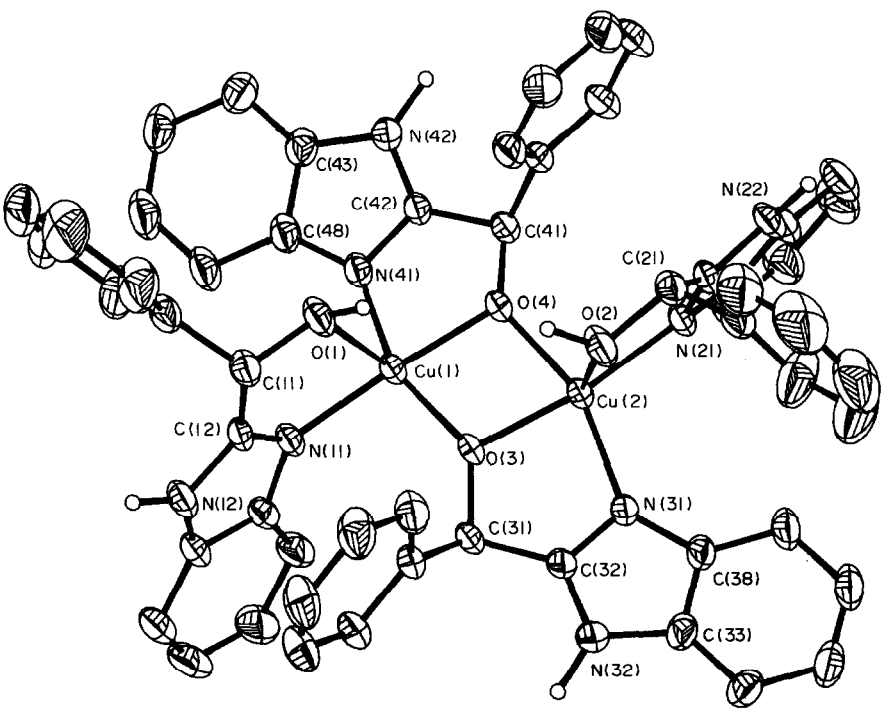

Fig. 1.

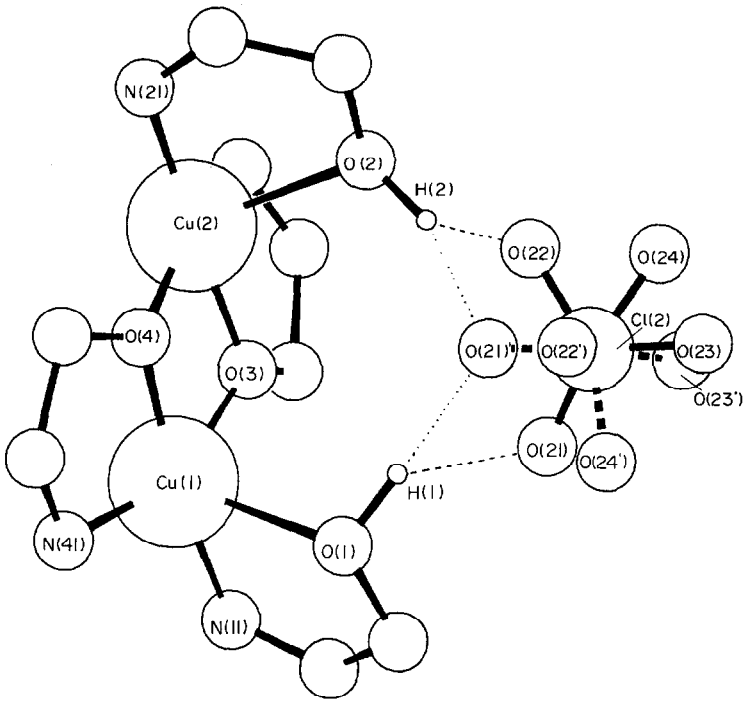

Fig. 2.

Table 2. Hydrogen bond lengths (Å)

O(21)—H(1)	1.847	O(22)—H(2)	1.766
O(21')—H(1)	1.846	O(21')—H(2)	1.832
O(51)—H(12)	1.678	O(52)—H(22)	1.701
O(53)—H(32)	1.737	O(54)—H(42)	1.789

solvate are strongly antiferromagnetic. The solvated complex is effectively diamagnetic throughout the temperature range down to liquid nitrogen. The magnetic moment of the desolvated complex is 0.99 BM per copper atom at 286.4K and 0.78 BM at 76.1K. It is possible that heating the complex to remove solvent introduced some paramagnetic impurity by a side reaction. The small variation in moment with temperature is barely outside experimental error and detailed analysis is inappropriate.

There have been a number of reports of diamagnetic binuclear copper(II) complexes, and some of these have been reviewed.[6] In the majority, the copper(II) atoms are in regular square planar geometry and it has been noted[7,8] that significant tetrahedral distortion from planarity of the CuL_4 unit reduces the complexes' antiferromagnetism. Examples from five coordination are much rarer and the data do not at present permit such easy rationalization. Many of these complexes involve triketonate ligands[9] with square pyramidal geometry at the copper atoms. However, much more irregular geometry is found in the other instances, which involve carbonate,[10] hydroxide[11] or in the present case, alkoxide bridging. Until more examples of closely related compounds are available it is impossible to correlate magnetic interactions with structure in five-coordinate copper(II) dimers.

REFERENCES

1. M. A. Phillips, *J. Chem. Soc.* 1928, 2395.
2. M. A. Laffey and P. Thornton, *J. Chem. Soc., Dalton Trans.* 1982, 313.
3. M. B. Hursthouse, R. A. Jones, K. M. A. Malik and G. Wilkinson, *J. Am. Chem. Soc.* 1979, **101**, 4128.
4. A. C. T. North, D. C. Phillips and F. S. Mathews, *Acta Cryst. A* 1968, **24**, 351.
5. G. M. Sheldrick, SHELX 76, Program for crystal structure determination. University of Cambridge (1976).
6. M. Melnik, *Coord. Chem. Rev.* 1982, **42**, 259.
7. J. A. Davis and E. Sinn, *J. Chem. Soc., Dalton Trans.* 1976, 165; E. Sinn, *Inorg. Chem.* 1976, **15**, 358.
8. L. Walz, H. Paulus and W. Haase, *J. Chem. Soc., Dalton Trans.* 1985, 913.
9. M. D. Glick and R. L. Lintvedt, *Prog. Inorg. Chem.* 1976, **21**, 233; J. W. Guthrie, R. L. Lintvedt and M. D. Glick, *Inorg. Chem.* 1980, **19**, 2949; M. J. Heeg, J. L. Mack, M. D. Glick and R. L. Lintvedt,

Inorg. Chem. 1981, **20**, 833; J. F. Wishart, C. Ceccarelli, R. L. Lintvedt, J. M. Berg, D. P. Foley, T. Frey, J. E. Hahn, K. O. Hodgson and R. Weis, *Inorg. Chem.* 1983, **22**, 1667.

10. M. R. Churchill, G. Davis, M. A. El-Sayed, M. F. El-Shazly, J. P. Hutchinson and M. W. Rupich, *Inorg. Chem.* 1980, **19**, 201; A. R. Davis and F. W. B. Einstein, *Inorg. Chem.* 1980, **19**, 1203.
11. P. K. Coughlin and S. J. Lippard, *J. Am. Chem. Soc.* 1981, **103**, 3228.

Polyhedron Vol. 7, No. 4, pp. 329–330, 1988
Printed in Great Britain

0277-5387/88 $3.00+.00
© 1988 Pergamon Journals Ltd

COMMUNICATION

THE FIRST CHELATING IMIDO COMPLEX: THE REACTION OF $ReOCl_3(PPh_3)_2$ WITH ANTHRANILIC ACID

OLIVIER D. SLOAN and PETER THORNTON*

Department of Chemistry, Queen Mary College, Mile End Road, London E1 4NS, U.K.

(*Received* 21 *August* 1987; *accepted* 5 *November* 1987)

Abstract—Anthranilic acid ($NH_2C_6H_4CO_2H$) reacts with $[ReOCl_3(PPh_3)_2]$ in ethanol to give $[ReCl(OEt)(PPh_3)_2(NC_6H_4CO_2)]$, containing the new imidobenzoate ligand. IR and NMR (^1H, ^{13}C, ^{14}N, ^{31}P) spectra establish the structure, which must have a bent ReNC framework, making this one of the few bent organoimido complexes, as well as the first which is a chelate.

Most of the organoimido complexes which have been crystallographically characterized have linear M=N—C groupings.[1] The exceptions are $[Mo(NPh)_2(S_2CNEt_2)_2]$[2] and $[OsO_2(NBu^t)_2]$.[3] In both of these, one of the organoimido ligands is bent at the nitrogen atom and the other is linear. For the bent linkage the bond angles at nitrogen are 139.4 and 155.1°, respectively. If the organoimido group was part of a five- or six-membered chelate ring it would be constrained to be bent. We report the first such complex.

Following the pioneering work of Chatt and Rowe,[4] who prepared phenylimido complexes by reacting $[ReOCl_3(PEt_2Ph)_2]$ with aniline, we studied the reaction of $NH_2C_6H_4CO_2H$ (anthranilic acid) with the triphenylphosphine analogue of the rhenium complex in ethanol. Schematically, water and HCl are lost and the complex $[ReCl(OEt)(PPh_3)_2(NC_6H_4CO_2)]$ is isolated in 59% yield.

Infrared and NMR spectra are consistent with the chelating imidobenzoate structure (I). There are no N—H or O—H stretching vibrations in the IR spectrum and the antisymmetric CO_2 stretch at 1619 cm^{-1} is appropriate for a monodentate carboxylate.[5] We can also identify an Re—Cl stretch at 310 cm^{-1} and Re=N vibrations at 1186 and 778 cm^{-1}.[1] The absence of NH_2 and CO_2H moieties is confirmed by their absence in the ^1H NMR spectrum, which has only ethoxide resonances at δ 0.35 (triplet) and 3.6 ppm (quartet), and a complicated aromatic region (δ 6.5–7.5 ppm) with appropriate integration. The *trans*- disposition of the PPh_3 ligands is shown by the singlet in the ^{31}P spectrum at δ −5.97 ppm (v H_3PO_4). In the ^{13}C spectrum we see the ethoxide group at δ 17.00 (CH_3) and 64.43 (CH_2), the PPh_3 carbons at δ 128.34 (*m*), 130.49 (*p*), 134.64 (*o*) and 131.62 (quaternary), the carboxyl carbon at 150.35 ppm and four signals from the imidobenzoate aromatic carbons at δ 113.53, 125.12, 129.55 and 133.95 ppm, with the quaternary carbon signals probably remaining undetected.

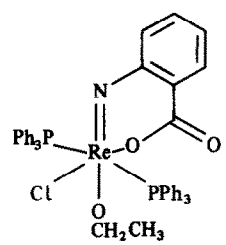

(I)

We had hoped to use the ^{14}N NMR spectrum to establish the bent character of the organoimido group with more certainty, and we did indeed observe a signal, at δ 289.51 ppm (v NH_4^+), but this resonance, although at an appropriate chemical shift, is more likely[6] to be due to dissolved N_2, with the signal from the imido-nitrogen broadened too much to be detected.

An alternative interpretation of our reaction, sug-

* Author to whom correspondence should be addressed.

gested by a thoughtful referee, is that the anthranilic acid has been esterified to give the five-coordinate rhenium(III) complex $[ReCl(NC_6H_4CO_2Et)(PPh_3)_2]$. However the elemental analysis is more in accord with the rhenium(V) complex and a carbonyl stretching frequency of 1619 cm^{-1} is unusually low for an ester complex.[7] Moreover there is no obvious reducing agent in the system to account for reduction in the rhenium oxidation state from (V) to (III).

We therefore conclude that our compound has indeed the Structure (**I**) shown, though we are unable to settle the minor question of whether the Cl or OEt ligand lies *trans-* to the Re═N unit. This is the first chelating organoimido complex and must have a bent configuration. Perhaps an additional incentive for its formation is the establishment of conjugation through the Re═N, C═C and C═O bonds.

EXPERIMENTAL

Infrared spectra were obtained using a Perkin–Elmer 577 spectrophotometer and NMR spectra on Bruker 80 MHz (^1H) and 400 MHz (^{14}N) spectrometers at QMC and a 250 MHz spectrometer (^{13}C, ^{31}P) at KQC, London. Microanalyses were by the microanalytical laboratory, University College, London.

Synthesis

$[ReOCl_3(PPh_3)_2]$ (0.40 g, 0.5 mmol)[8] was refluxed with anthranilic acid (1.00 g, 7.5 mmol) in ethanol (150 cm^3) for 4 h. The hot solution was filtered and left to cool, when fine green needles were deposited. These were filtered off after 48 h further cooling at −20°C. Yield 0.27 g (59%). Found: C, 57.4; H, 4.1; Cl, 4.0; N, 1.2; P, 6.7; $C_{45}H_{39}ClNO_3P_2Re$ requires C, 58.4; H, 4.2; Cl, 3.8; N, 1.2; P, 6.7%.

Acknowledgements—We thank SERC for a CASE studentship to ODS with the valued collaboration of ICI Petrochemicals and Plastics Division. We are also grateful to Prof. D. C. Bradley for helpful discussions.

REFERENCES

1. W. A. Nugent and B. L. Haymore, *Coord. Chem. Rev.* 1980, **30**, 123.
2. B. L. Haymore, E. A. Maata and R. A. D. Wentworth, *J. Am. Chem. Soc.* 1979, **101**, 2063.
3. W. A. Nugent, R. L. Harlow and R. J. McKinney, *J. Am. Chem. Soc.* 1979, **101**, 7265.
4. J. Chatt and G. A. Rowe, *J. Chem. Soc.* 1962, 4019.
5. G. B. Deacon and R. J. Phillips, *Coord. Chem. Rev.* 1980, **33**, 227.
6. J. D. Runnacles, Ph.D Thesis, Queen Mary College, London (1987).
7. W. L. Driessen, W. L. Groeneveld and F. W. van der Wey, *Rec. Trav. Chim.* 1970, **89**, 353.
8. G. W. Parshall, *Inorg. Synth.* 1978, **17**, 110.

Polyhedron Vol. 7, No. 4, pp. 331–334, 1988
Printed in Great Britain

0277–5387/88 $3.00+.00
Pergamon Journals Ltd

COMMUNICATION

A POTENTIOMETRIC STUDY OF THE COMPLEXATION OF MANGANESE(II) BY 2-MERCAPTO-3-PHENYLPROPENOATE IN SOLUTION

MONTSERRAT FILELLA, NÚRIA GARRIGA and ALVARO IZQUIERDO*

Departament de Química Analítica, Universitat de Barcelona, Diagonal 647, 08028 Barcelona, Spain

(*Received* 12 *October* 1987; *accepted* 30 *October* 1987)

Abstract—Complex formation between manganese(II) and 2-mercapto-3-phenylpropenoate (MPP) has been studied at 25°C and 100 mmol dm^{-3} NO_3^- in 30% (v/v) ethanol–water using glass electrode potentiometry. The titration data can be explained by the formation of the complex MnMPP, $\log \beta_{110} = 5.407$.

Although manganese is ubiquitous in nature, generally occurring at levels comparable to copper, the chemistry of bivalent manganese is only beginning to be understood. At present, studies on the coordination chemistry of manganese can provide a useful insight into the functional role of this transition metal in biological systems. Thus, models for the superoxide dismutase reaction have evolved in recent years as a result of the work done on manganese complexes. Furthermore, the similarity of the coordination chemistry for iron and manganese ions indicate that the properties of manganese model complexes can be usefully extrapolated to iron-containing biological systems.[1]

The chemistry of manganese complexes with sulphur containing ligands is even less known than that for oxygen and nitrogen donor ligand complexes, probably due to the easy oxidation of sulphur. Nevertheless, although there is no evidence for manganese binding to sulphur groups in metalloproteins, the chemistry of these kinds of complex is interesting, particularly if one considers the mentioned chemical similarity between iron and manganese, and the biological importance of iron–sulphur proteins.

The study of the complexation of manganese(II) by 2-mercapto-3-phenylpropenoate has been performed as part of a research project on equilibria involving metal ions and biologically interesting ligands which contain bivalent sulphur. 2-Mercaptoacids have two donor groups in their molecule; one carboxylate and one thiol group, that account for their high metal-binding ability. In fact, 2-mercapto-3-phenylpropenoate has already shown a great complexing ability with zinc[2,3] which seems to be related to the biological activity displayed by this ligand.[4]

EXPERIMENTAL

2-Mercapto-3-phenylpropenoic acid was obtained as described by Campaigne and Cline,[5] and recrystallized from benzene (m.p. 134–135°C). *Analysis*. Found: C, 60.3; H, 4.5; S, 17.6. Calc. for $C_9H_8O_2S$: C, 59.98; H, 4.47; S, 17.79%. Freshly prepared solutions were used for each titration. Manganese nitrate (Merck) solution was analysed for metal ion concentration by EDTA titration and for hydrogen ion concentration by Gran's plots. Other solutions were prepared and analysed as in refs 2 and 6. It was observed that it is extremely important to maintain a totally oxygen-free atmosphere in the vessel in order to obtain reproducible titrations.

Formation constants were determined by potentiometric titrations at 25°C and $I = 100$ mmol dm^{-3}

*Author to whom correspondence should be addressed.

Table 1. Summary of the titration data used for calculating formation constants. Number of titration points, initial concentrations of manganese (C_{Mn}) and ligand (C_{MPP}) and approximate $-\log[H]$ ranges. Concentrations are expressed in mmol dm^{-3}

Titration	Number of points	C_{Mn}	C_{MPP}	$-\log[H]$ ranges
1	51	0.619	2.505	2.2–6.0
2	49	0.799	3.881	2.3–6.6
3	39	0.999	3.102	2.3–5.9
4	33	0.999	3.795	2.3–6.3
5	33	0.999	4.823	2.3–6.0
6	53	1.237	4.786	2.3–6.2
7	41	1.598	6.464	2.4–6.4
8	47	1.998	8.012	1.9–6.1

nitrate in 30% (v/v) ethanol–water due to the insolubility of the ligand in water. The equipment and procedures used are described in refs 2 and 6. Values of manganese and ligand concentrations as well as $-\log[H]$ ranges used in calculating the formation constants are summarized in Table 1.

The autoprotolysis constant of the medium ($10^{-14.20}$) and the 2-mercapto-3-phenylpropenoate protonation constants ($\log \beta_{011} = 8.989$, $\log \beta_{012} = 12.773$) have been previously determined.

Following our usual approach,[7] the computer program library ESTA[8] was used to analyse the potentiometric data, to develop the equilibrium model and to optimize the formation constant values. Formation constant refinement was performed using the ESTA optimization module with a weighted least-square objective function based on emf residuals. The weight at each titration point was based on a standard deviation in titre of 0.005 cm^3 and in emf of 0.1 mV. The computer program MINIQUAD[9] was also used for comparison purposes.

All calculations were performed on a VAX 11/750 computer.

RESULTS AND DISCUSSION

The system Mn^{2+}–MPP–H^+ (MPP = L^{2-} = deprotonated 2-mercapto-3-phenylpropenoate) was studied by doing eight titrations with initial metal concentrations between 0.6 and 2 mmol dm^{-3} (Table 1). The upper concentrations used were limited by the insolubility of the ligand and the lower ones by the lack of reproducibility of the titrations. The upper limits of the $-\log[H]$ ranges were determined by a sudden drop in the rate at which equilibrium was attained as evidenced by a steady drift in the potentiometric readings.

The formation curves obtained show maximum $\bar{Z}_M$ values[7] ranging from 0.4 to 0.8. The analysis of the curves suggests that mononuclear species are predominant, since all points tend to fall on a single curve. This was confirmed by the fact that the neutral species, 110, was found to be the only one formed. No evidence was found for the formation of the following species, which were also tested in the search for the best model: 111, 112, 121, 122, 11-1, 11-2, 12-1, 12-2. Although the computer programs used are able to calculate a value for the formation constant of the 120 complex, its inclusion in the model causes no improvement of the fit and its formation extent ranges from 1 to 4% in the last 2–3 points of some titrations. Therefore, the species was considered to be close to the limit of detectability and was not included in the final "best

Table 2. Formation constants determined in this study at 25°C and $I = 100$ mmol dm^{-3} NO_3^- (30% (v/v) ethanol–water). Number of points = 346; number of titrations = 8.

Program	$\log \beta_{110}$[a]	d[b]	Complementary information[c]
ESTA	5.407	0.007	$U = 16.4$ $R = 0.004$ (R-lim = 0.001)
MINIQUAD	5.412	0.009	$u = 2.19E\text{-}07$ $R = 0.003$

[a] $\beta_{pqr} = [M_pL_qH_r]/[M]^p[L]^q[H]^r$.

[b] Standard deviations given by the programs.

[c] U, in ESTA output: $[\Sigma w(\text{emf}^o - \text{emf}^c)^2]/(N\text{-}n_p)$ where N = number of points, n_p = number of refined parameters; in MINIQUAD output: $\Sigma(T_i^o - T_i^c)^2$ where T_i = total concentrations. R = Hamilton R factor; R-lim = Hamilton R-limit.

Table 3. Literature potentiometric formation constants of manganese(II) complexes of similar ligands

Ligand	p	q	r	$\log \beta_{pqr}$	Conditions	Ref.
Mercaptoacetate	1	1	0	4.38	25°C	12
	1	2	0	7.56	100 mmol dm^{-3} KCl	
	1	1	0	4.48	35°C	13
	1	2	0	7.70	100 mmol dm^{-3} KCl	
Mercaptosuccinate	1	1	0	4.92	35°C	14
					200 mmol dm^{-3} $NaClO_4$	
	1	1	0	5.91	31°C	15
					100 mmol dm^{-3} $NaClO_4$	
L-cysteinate	1	1	0	4.1	20°C	16
					10 mmol dm^{-3}	
	1	1	0	4.56	25°C	17
					100 mmol dm^{-3} KNO_3	

model". As expected,[10] no metal hydrolysis was detected at the working pH.

Values for the formation constant of the 110 complex formed in the system Mn^{2+}–MPP–H^+ are found in Table 2. Its low value as compared with the ones previously determined for the 110 nickel and zinc complexes (8.69 and 9.668 respectively[2]) is in agreement with the Pearson's HSAB theory.[11] The scarce values reported in literature for the formation constants for complexes of similar ligands with manganese(II) are also given in Table 3 for purposes of comparison.

Figure 1 shows the species distribution for the Mn^{2+}–MPP–H^+ system computed from the values reported in Table 2 for total concentrations of 2-mercapto-3-phenylpropenoate = 4 mmol dm^{-3} and manganese(II) = 1 mmol dm^{-3}.

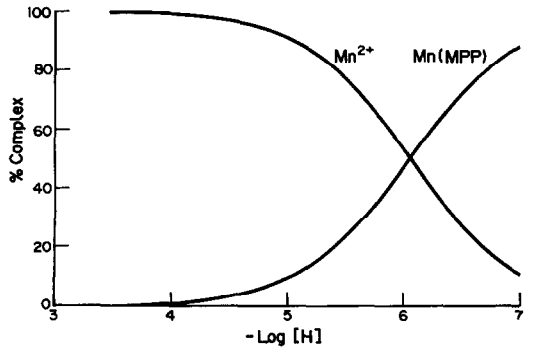

Fig. 1. Species distribution as a function of −log[H] in the system Mn^{2+}–MPP–H^+. Ligand concentration = 4 mmol dm^{-3}; metal concentration = 1 mmol dm^{-3}.

Acknowledgement—This research was supported by CAYCIT grant 657/81.

REFERENCES

1. G. D. Lawrence and D. T. Sawyer, *Coord. Chem. Rev.* 1978, **27**, 173.
2. M. Filella, N. Garriga and A. Izquierdo, *J. Chim. Phys.* 1987, **84**, 93.
3. M. Filella, N. Garriga, A. Izquierdo and D. R. Williams, *Plzen. Lek. Sb.*, in press.
4. W. O. Foye and J. R. Lo, *J. Pharm. Sci.* 1972, **61**, 1209; J. Wagner. P. Vitali, J. Schoun and E. Giroux, *Can. J. Chem.* 1977, **55**, 4028; N. J. Prakash, P. J. Schechter, E. Giroux and A. Sjoerdsma, *Clin. Exp. Pharmacol. Physiol.* 1977, **4**, 17; E. Giroux and P. J. Lachmann, *Toxicon* 1981, **19**, 481; E. Giroux, P. J. Lachmann, H. G. Petering, N. J. Prakash and P. J. Schechter, *Biol. Trace Elem. Res.* 1983, **5**, 115.
5. E. Campaigne and R. E. Cline, *J. Org. Chem.* 1956, **21**, 32.
6. M. Filella, N. Garriga and A. Izquierdo, *Talanta*, in press.
7. M. Filella and D. R. Williams, *Inorg. Chim. Acta* 1985, **106**, 49.
8. K. Murray and P. M. May, *ESTA. Equilibrium Simulation for Titration Analysis.* UWIST, Cardiff (1984).
9. A. Sabatini, A. Vacca and P. Gans, *Talanta* 1974, **21**, 53.
10. C. F. Baes and R. E. Mesmer, *The Hydrolysis of Cations.* John Wiley, New York (1976).
11. R. G. Pearson, *J. Am. Chem. Soc.* 1963, **85**, 3533.
12. D. L. Leussing, *J. Am. Chem. Soc.* 1958, **80**, 4180.
13. Unpublished results quoted in L. G. Sillén and A. E.

Martell, *Stability Constants of Metal–Ion Complexes*. Special Publication No. 17, The Chemical Society, London (1964).
14. M. V. Reddy and P. K. Bhattacharya, *J. Indian Chem. Soc.* 1969, **46**, 1058.
15. N. K. Mohanty and R. K. Patnaik, *J. Indian Chem. Soc.* 1980, **57**, 224.
16. A. Albert, *Biochem. J.* 1952, **50**, 690.
17. G. R. Lenz and A. E. Martell, *Biochemistry* 1964, **3**, 745.

Polyhedron Vol. 7, No. 4, p. 335 1988
Pergamon Journals Ltd. Printed in Great Britain

ANNOUNCEMENTS

XXVII INTERNATIONAL CONFERENCE ON COORDINATION CHEMISTRY

2–7 JULY 1989
GOLD COAST (NR BRISBANE), QUEENSLAND, AUSTRALIA

Persons wishing to receive the First Circular should contact: **The XXVII ICCC Conference Secretariat, UniQuest Ltd, University of Queensland, QLD 4067, Australia.**

XIV INTERNATIONAL SYMPOSIUM ON MACROCYCLIC CHEMISTRY

25–28 JUNE 1989
TOWNSVILLE, NORTH QUEENSLAND, AUSTRALIA

For further details contact: **The Conference Chairman, Dr L. F. Lindoy, Department of Chemistry and Biochemistry, Townsville, QLD 4811, Australia.**

Polyhedron Vol. 7, No. 5, pp. 337–343, 1988
Printed in Great Britain

0277–5387/88 $3.00+.00
Pergamon Press plc

SYNTHESIS AND CHARACTERIZATION OF Fe(III), Co(II), Ni(II), Cu(II) AND Zn(II) COMPLEXES WITH N-SALICYDENE-*o*-HYDROXYMETHYLENEANILINE

B. JEZOWSKA-TRZEBIATOWSKA, J. LISOWSKI, A. VOGT and P. CHMIELEWSKI*

Institute of Chemistry, University of Wrocław, Wrocław, Poland

(*Received* 10 *December* 1986; *accepted after revision* 26 *August* 1987)

Abstract—The new Fe(III), Co(II), Ni(II), Cu(II) and Zn(II) complexes with tridentate Schiff base, the product of condensation of *o*-aminobenzyl alcohol with salicylaldehyde have been synthesized and characterized by elemental analysis, IR, electronic, EPR and Mössbauer spectra, thermal analysis, magnetic susceptibility and molecular weight measurements. Dimeric or polymeric structures for the investigated complexes were proposed. The interaction of the cobalt complex with dioxygen is also described.

The complexes of Cu(II), Fe(III), Ni(II) and other transition metals with potentially tridentate Schiff bases (Fig. 1) have attracted much attention. Most of them are dimers, although monomeric, trimeric or tetrameric forms are also known. The ligand can act both as dibasic tridentate or monobasic bidentate.[1] The interest has been focused mainly on magnetic properties of these compounds. In particular antiferro- and ferromagnetic coupling in Cu(II) complexes have been thoroughly investigated.[2]

We have undertaken the present study of the Schiff base complex derived from salicylaldehyde and *o*-aminobenzyl alcohol H_2HMPS (R = *o*-CH_2Ph), as a part of our efforts to synthesize the Co(II) complexes with attached free —OH groups being able to form an H-bond with a coordinated O_2 molecule. We have found that cobalt(II) complexes with HMPS react reversibly with dioxygen in the presence of amine, and for better understanding of coordinating properties of the ligand we have extended our study to complexes with other metals.

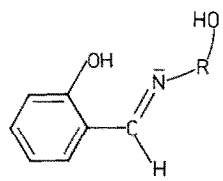

Fig. 1. General formula of potentially tridentate Schiff bases derived from salicylaldehyde and aminoalcohols.

EXPERIMENTAL

Reagents

Salicylaldehyde was obtained from LOBA-Chemie, anthranilic acid from POCH-Gliwice and triethylamine from LABORCHEMIE-Apolda. Metal salts and solvents for synthesis were reagent grade. *o*-Aminobenzyl alcohol was obtained from anthranilic acid by electrochemical reduction.[3] Solvents for spectroscopic measurements were purified before use.

Physical measurements

Electronic spectra in solution and diffuse reflectance spectra were recorded on a Beckman UV 5240 spectrophotometer, ESR spectra on a Jeol JES-Me 3× spectrometer (X-band). IR spectra were taken on a Perkin–Elmer 180 IR spectrometer using KBr pellets and Nujol mulls. Magnetic susceptibilities (80–300K) were measured by the Gouy method using $HgCo(SCN)_4$ as calibrant. Diamagnetic corrections were calculated using Pascal constants. Thermal analyses were done on a MOM Derivatograph Q 1500 D. Molecular weight measurements were performed in benzene by cryoscopic

*Author to whom correspondence should be addressed.

methods. Mössbauer spectra were recorded at room and liquid nitrogen temperatures as described in ref. 4. ^{1}H NMR spectra were recorded on a 100 MHz Tesla BS 567A spectrometer.

Preparation of ligand

Solutions of salicylaldehyde (0.05 mol) in 20 cm^3 of methanol and *o*-aminobenzyl alcohol (0.05 mol) in 30 cm^3 of methanol were mixed together and refluxed for 30 min. After cooling the yellow crystalline precipitate was filtered off and recrystallized from methanol. Yield *ca.* 80%. M.p. 124°C (literature data[5] 126–128°C). Analytical data are given in Table 1.

Preparation of complexes

[FeLCl]$_2$. Solutions of $FeCl_3$ (0.005 mol) in methanol (15 cm^3) and H_2L (0.005 mol) in methanol (15 cm^3) were mixed together and triethylamine (0.01 mol) was added. The black crystalline complex precipitated immediately. It was separated, washed with methanol and dried over calcium chloride. Yield 90%. The compound is practically insoluble in non-coordinating solvents and sparingly soluble in DMF and pyridine.

[CoL(H_2O)$_2$]$_2$. A solution of cobalt acetate tetrahydrate (0.005 mol) in methanol (20 cm^3) was added to the hot solution of H_2L (0.005 mol) in methanol (20 cm^3). The solution turned deep red, then triethylamine (0.01 mol) was added. The orange–red precipitate settled down. This was separated, washed with methanol and dissolved in a minimum amount of hot $CHCl_3$. The solution was filtered off and the complex was reprecipitated by addition of methanol, washed with methanol and dried in a stream of nitrogen. Yield 75%.

All operations were carried out under a nitrogen atmosphere in Schlenk apparatus. The same product was obtained with a 2 : 1 ligand to metal ratio.

The orange–red complex is easily soluble in non-coordinating solvents such as $CHCl_3$, toluene and benzene as well as in deoxygenated pyridine and DMF.

[CoL]$_n$. Bissalicylaldehydato cobalt(II) dihydrate (0.005 mol) was suspended in boiling toluene (200 cm^3). Addition of *o*-aminobenzyl alcohol (0.01 mol) caused the suspension to dissolve. The red–brown solution was refluxed for 2 h and then the solvent was slowly evaporated for 3 h until the volume reduced to 30 cm^3. The brown–red crystalline product that gradually formed was filtered off, washed with toluene and methanol, and dried in a stream of nitrogen. Yield 40%. All operations were carried out under nitrogen.

The compound is insoluble in non-coordinating solvents, but it dissolves slowly in deoxygenated DMF and pyridine.

[NiL(H_2O)$_2$]$_2$. (a) H_2HMPS (0.005 mol) and nickel acetate tetrahydrate (0.005 mol) were dissolved in boiling methanol (30 cm^3) and then triethylamine (0.01 mol) was added. A green precipitate formed which was separated and recrystallized from $CHCl_3$/CH_3OH mixture. The product was dried in a stream of air. The same product was obtained with a 1 : 2 metal to ligand ratio.

(b) Bissalicylaldehydato nickel(II) dihydrate (0.005 mol) was suspended in boiling toluene. *o*-Aminobenzyl alcohol (0.01 mol) was added and the mixture was refluxed for 2 h. The complex was precipitated from the olive solution by the addition of *n*-heptane. Yield 75%.

[CuL]$_n$. Copper(II) acetate hydrate (0.005 mol) was dissolved in boiling methanol (50 cm^3) and a hot solution of H_2L (0.005 mol) in methanol (30 cm^3) was added. The green complex precipitated almost immediately. This was then filtered off, washed with hot methanol and dried over calcium chloride in a desiccator. Yield 70%.

[Zn—L]. The compound was obtained in a similar way to the Ni(II) complex according to method (a). Yield 60%.

RESULTS AND DISCUSSION

[FeLCl]$_2$

Analytical data gave a 1 : 1 : 1 metal to ligand to chlorine ratio (Table 1). As shown by thermal analysis, there is no loss of weight until 260°C. Diffuse reflectance spectrum of [FeLCl]$_2$ gave no information about the geometry of the Fe(III) environment because the weak, spin-forbidden *d–d* transitions are completely covered by the tail of the very intensive CT band reaching nearly into the IR. A similar situation is observed for the complex solution in DMF with a CT band at 35,100 cm^{-1} and a shoulder at *ca.* 27,800 cm^{-1}.

Magnetic susceptibility corresponds to a high-spin Fe(III) ion with magnetic moment equal to 4.52 BM at room temperature, and clearly indicates the antiferromagnetic coupling with the exchange integral $-2J = 33$ cm^{-1}, calculated for a binuclear model.

The well resolved IR spectrum of [FeLCl]$_2$ shows absorption at 1607 cm^{-1}, characteristic of the coordinated —C=N— group. This indicates that the ligand is present in the Schiff base form, while investigations of the free ligand in solution suggested that it exists mainly in the benzoxazine form in

Table 1. Elemental analysis and IR data (in cm^{-1}) of investigated compounds

Compound	%C	%H	%N	%M	%Cl	νC=N	νCO_{ph}	νCO_{alk}
$[FeLCl]_2$	53.2	3.6	4.2	16.5	10.9	1607	1540	1019
	(53.1)	(3.5)	(4.4)	(17.6)	(11.2)			
[FeL]	56.2	3.9	4.6	19.0	—	1607	1535	1029
$[CoL(H_2O)_2]_2$	52.5	4.3	4.4	19.0	—	1607	1533	1031
	(52.5)	(4.7)	(4.4)	(18.4)	—			
$[CoL]_n$	59.0	3.5	4.6	19.9	—	1608	1528	1029
	(59.2)	(3.9)	(4.6)	(20.7)	—			
$[NiL(H_2O)_2]_2$	52.7	4.4	4.4	18.8	—	1607	1532	1041
	(52.6)	(4.7)	(4.4)	(18.4)	—			
$[CuL]_n$	59.1	4.1	5.0	21.7	—	1608	1528	1020
	(58.2)	(3.9)	(4.9)	(22.0)	—			
[ZnL]	44.9	3.4	3.2	21.6	—	1611	1531	1028
H_2L	73.9	5.8	66.1	—	—	1620	1506	1034
	(74.0)	(5.7)	(6.2)	—	—			

tautomeric equilibrium with the Schiff base.[5] The band at 1540 cm^{-1} is connected with the phenolic C—O stretching vibration and appears in the region characteristic for a coordinated phenolic group. The position of this band indicates that phenolic oxygen is not the bridging atom, because in phenoxo bridged compounds the C—O stretching vibration is shifted to a higher frequency.[6] Some of the other bands may be tentatively assigned as follows: 3050, 760 cm^{-1}—aromatic C—H, 2850, 2930 cm^{-1}—CH_2 stretching, 1490 cm^{-1}—CH_2 scissors, 1580, 1467 cm^{-1}—C=C aromatic, 1019 cm^{-1}—alkoxy C—O stretching.

The Mössbauer spectrum of the complex measured at room temperature shows well resolved quadrupole splitting with $QS = 0.832$ mm s^{-1} and $IS = 0.598$ mm s^{-1} {relative to $Na_2[Fe(CN)_5NO] \cdot 2H_2O$} confirms the presence of high-spin Fe(III). The intensity of the two lines are not equal, with the peak-height ratio $I-/I+ = 1.38$ and $\Gamma- = 0.341$, $\Gamma+ = 0.466$ mm s^{-1}, while the integral intensities of both lines are the same. At 80K the spectrum is much more symmetrical with $QS = 0.848$ mm s^{-1}, $IS = 0.697$ mm s^{-1}, $\Gamma- = 0.343$, $\Gamma+ = 0.365$ mm s^{-1} and $I-/I+ = 1.03$. The observed asymmetry of the spectrum at room temperature probably arises from spin relaxation effects observed for penta-coordinated Fe(III)[7] or for Fe(III) complexes with the strong antiferromagnetic coupling. Increasing the thermal population of the higher electronic states (which have longer relaxation times than the ground state) increases the overall relaxation time and causes the broadening of one line.

The magnetic properties and stoichiometry of the compound indicate a dimeric structure with alkoxo bridges.[8] The Mössbauer parameters and J value are similar to those of the complex $[Fe(SALPA)Cl]_2$ (R = —$(CH_2)_3$—), which has a dimeric structure with two alkoxy bridges and two Cl atoms axially coordinated to the Fe ion.[9] The analogous structure is proposed for the present complex $[FeLCl]_2$ (Fig. 2).

We were also successful in preparing presumably the Fe(II) complex using a similar method as for $[CoL(H_2O)_2]_2$, starting from $FeCl_2$. This compound, isolated as a black precipitate, turned into a red-brown one (assigned as FeL in Table 1) within less than 1 min when exposed to air. A Mössbauer spectrum for the latter compound with $IS = 0{,}622$ and $QS = 0.971$ mm s^{-1} indicates the presence of only one high-spin Fe(III) complex. The magnetic properties of this complex show an antiferromagnetic interaction ($\mu_{eff} = 2.81$ BM at 82K and 3.64 BM at 298K), however the plot of magnetic susceptibility vs temperature does not fit to any curve calculated from the dimeric model, so more than one kind of magnetic interaction between the Fe(III) centres could be predicted.

$[CoL(H_2O)_2]_2$

The analytical data (Table 1) and the 10.3% weight loss (theoretically 11.2%) at about 110°C

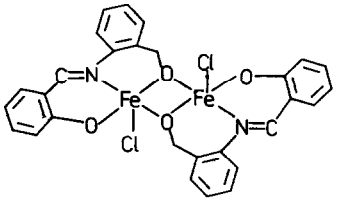

Fig. 2. Proposed structure for $[FeLCl]_2$.

indicates a 1 : 1 : 2 metal to ligand to H_2O ratio. The experimental molecular weight of 560 ± 30 daltons (mean value of three independent measurements) suggests the presence of the dimeric form.

The IR spectrum of $[CoL(H_2O)_2]_2$ is similar to that of $[FeLCl]_2$ in the region 700–1700 cm^{-1} (Table 1) and similar assignments may be made. Again the position of the phenolic C—O stretching band i.e. 1533 cm^{-1} indicates the lack of phenoxy bridges. The weak and broad band at *ca.* 3260 cm^{-1} may be attributed to a ν-OH vibration of a coordinated water molecule. The broadening of this band may be caused by strong intermolecular H-bonds.

The electronic spectrum of $[CoL(H_2O)_2]_2$ in toluene exhibits two CT bands at 34,480 and 25,640 cm^{-1} and a *d–d* band at 10,150 cm^{-1} with a shoulder at *ca.* 7810 cm^{-1} (Fig. 3) which may be assigned to the $^4T_{1g}(F) \rightarrow {}^4T_{2g}(F)$ transition in pseudo-octahedral Co(II).[10] The $^4T_{1g}(F) \rightarrow {}^4T_{1g}(P)$ transition is probably masked by an intensive CT band at 25,640 cm^{-1}. The spectra of $[CoL(H_2O)_2]_2$ in the solid state and $CHCl_3$ solution with bands at 10,050 and 10,200 cm^{-1} respectively are similar to that of toluene solution. The magnetic moment of 4.9 BM (over the temperature range 82–298K) is typical for the high-spin Co(II) in a pseudo-octahedral environment.[10]

On the basis of the above results and elemental analysis the dimeric structure with two alkoxy bridges and two water molecules coordinated to each Co atom is proposed. The similar dimeric structure for the Co(II) complex with HMPS was postulated by Syamal,[11] although he suggested two phenolic, not alkoxy bridges.

The electronic spectra of $[CoL(H_2O)_2]_2$ in DMF (13,700 and 5430 cm^{-1}) (Fig. 3) do not resemble the simple spectra of octahedral, tetrahedral or square-planar Co(II) complexes. The low-energy bands in the 5260–7150 cm^{-1} region, as well as the higher molar extinction coefficients indicate that penta-coordinated complexes are present in pyridine and DMF solutions. However, electronic spectra of square pyramidal or trigonal bipyramidal Co(II) complexes are not diagnostic enough to enable prediction of the exact geometry of the complex.[12]

When the oxygen is passed through the deoxygenated pyridine solution of $[CoL(H_2O)_2]_2$, the solution darkens, the band at 25,640 cm^{-1} shifts to 25,000 cm^{-1} and its intensity declines. A new shoulder appears at *ca.* 21,280 cm^{-1} which is characteristic for dioxygen complexes of Co(II).[13] These changes may be reversed by prolonged passage of inert gas through the solution. Complex solutions in non-coordinating solvents, such as toluene, also bind dioxygen reversibly after addition of amines such as pyridine or piperidine.

The characteristic EPR spectra of these systems (Fig. 4) obtained for the frozen solution indicate the existence of end-on superoxo complexes of Co(II)

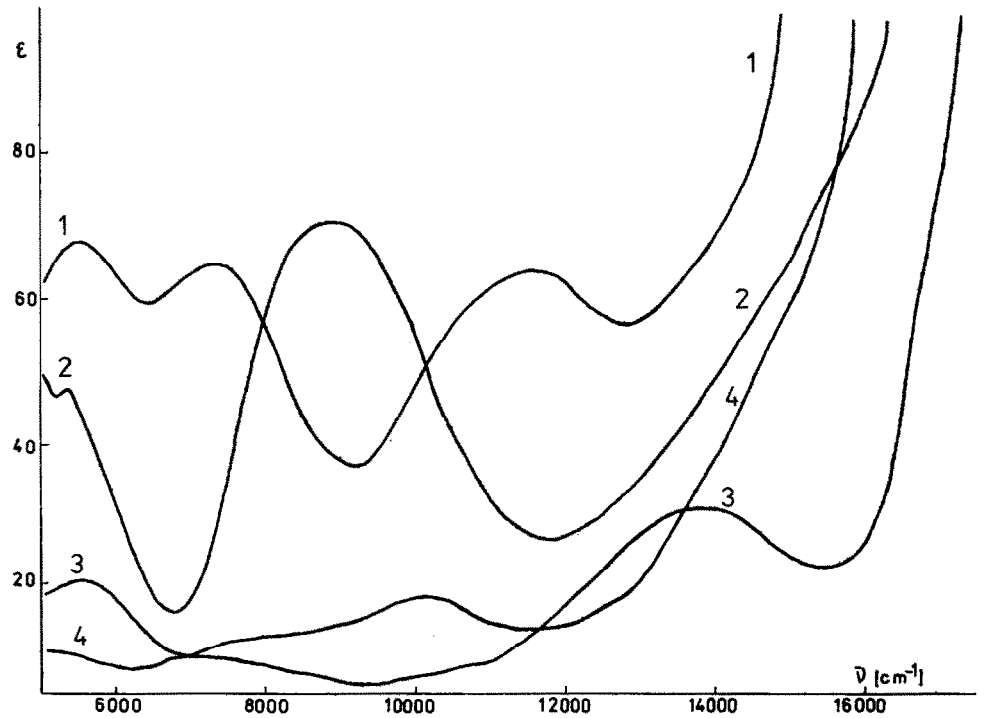

Fig. 3. Electronic spectra of Co(II) complexes: $[CoL(H_2O)_2]_2$ in pyridine (1), DMF (3) and toluene (4); $[CoL]_n$ reflectance spectrum (2).

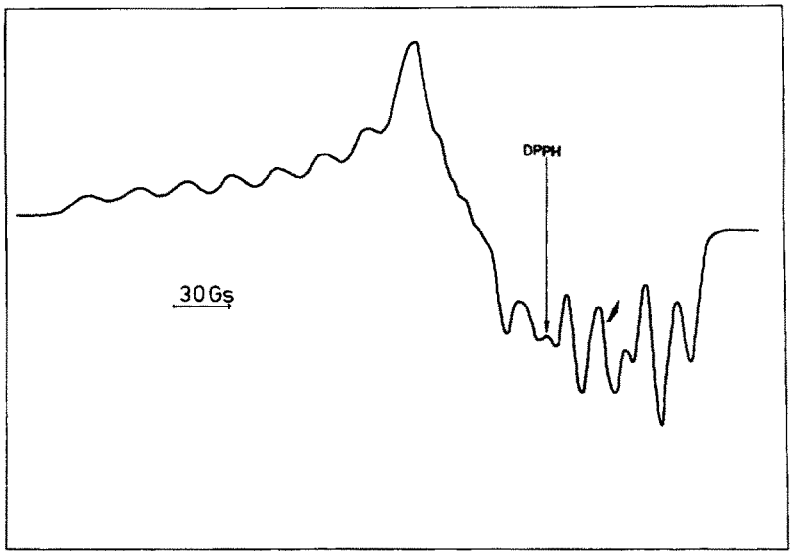

Fig. 4. EPR spectrum of the $[CoL(H_2O)_2]_2$–piperdine–O_2 system in frozen toluene/dichloromethane mixture at 77K.

in low temperatures,[14] although μ-peroxo complexes may also be present. There is indirect confirmation of the existence of such binuclear diamagnetic species in liquid solutions. At room temperature there is no EPR signal for the complex solution containing the nitrogen base admixture. However after addition of I_2 or other oxidants, a well resolved 15-line EPR signal appears ($g = 2.03$, $A = 13.0$ G) which is characteristic for dimeric μ-superoxo complexes, products of oxidation of μ-peroxo complexes.

The experimental anisotropic EPR parameters for a monomeric dioxygen adduct (Fig. 4) ($g_1 = 2.098$, $g_2 = 2.01$, $g_3 = 1.99$, $A_1 = 25.0$, $A_2 = 13.5$, $A_3 = 16.5$ G) are significantly different from those obtained for cobalt complexes with tetra- and bidentate Schiff bases[15] or with porphyrins.[16] They are rather similar to the EPR parameters of dioxygen adducts derived from Co(II) complexes with pentadentate Schiff bases.[17] In the latter group of complexes dioxygen is coordinated in the *trans* position to the phenolic oxygen of the salicydene residue. The experimental EPR parameters are however not the spin-Hamiltonian ones because of the low symmetry of the dioxygen adducts, so computer simulation is necessary.[18] This is why we do not present here a detailed interpretation of EPR data.

$[CoL]_n$

Thermal analysis revealed no loss of weight until 270°C. Diffuse reflectance spectrum of $[CoL]_n$ exhibits two bands at 8850 and 4950 cm^{-1} with a shoulder at 5320 cm^{-1} (Fig. 3), as well as an intensive CT band at *ca.* 25,000 cm^{-1} with a weak shoulder at *ca.* 17,400 cm^{-1}. The band at 8850 cm^{-1} occurs in the range typical for $^4T_{1g}(F) \rightarrow {}^4T_{2g}$ transitions of octahedral Co(II) complexes . On the other hand, the low-energy band at 4950 cm^{-1} is indicative of the presence of penta-coordinated Co(II).[12] Magnetic moments equal to 5.1 BM at room temperature and 5.6 BM at 82K indicate a weak ferromagnetic interaction between Co(II) centres.

The complex dissolves slowly in DMF and pyridine giving the same electronic spectra as $[CoL(H_2O)_2]_2$ solutions in the same solvents. Similarly, when $[CoL]_n$ solutions in coordinating solvents are exposed to oxygen, one can observe the same EPR spectra as for $[CoL(H_2O)_2]_2$. These data suggest that the $[CoL]_n$ structure is broken upon solvolysis.

The band positions in the IR spectrum of $[CoL]_n$ are generally similar to that of $[CoL(H_2O)_2]_2$ (Table 1), except it is lacking the ν-OH absorption, although the striking feature of the $[CoL]_n$ spectrum is the splitting of some bands. The alcoholic C—O absorption consists of two bands at 1029 and 1040 cm^{-1}, and the phenolic C—O absorption is split into two equal peaks at 1528 and 1544 cm^{-1}. The shift of the latter is commonly assigned to the bridging group.[6] This splitting of some IR bands may arise from the fact that the ligand exists in two different forms in this compound. A tetrameric structure, consistent with the above data is proposed (Fig. 5), although the higher polymeric structures cannot be excluded.

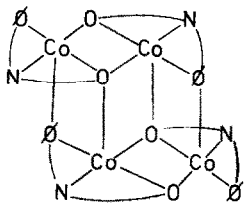

Fig. 5. The proposed structure for $[CoL]_n$.

$[NiL(H_2O)_2]_2$

The bright green complex turns red–brown on heating at *ca.* 115°C, which is accompanied with the loss of 10.8% in weight. This is close to 11.2% calculated for the loss of two water molecules per one Ni atom.

The electronic spectrum of $[NiL(H_2O)_2]_2$ in $CHCl_3$ exhibits the CT bands at 33,300 and 24,400 cm^{-1}. The bands at 16,390 and 10,750 cm^{-1} with a shoulder at 8510 cm^{-1} (Fig. 6) occur in the range typical for distorted octahedral Ni(II) complexes and may be assigned to the spin-allowed transitions $^3A_{2g}(F) \rightarrow {}^3T_{2g}(F)$ and $^3A_{2g}(F) \rightarrow {}^3T_{1g}(F)$. The third spin-allowed transition $^3A_{2g}(F) \rightarrow {}^3T_{1g}(P)$, expected in the region near 25,000 cm^{-1} is not observed due to the very intensive charge-transfer band. Apart from spin allowed transitions there is a much weaker band at 13,160 cm^{-1} which may be assigned to the spin-forbidden transition $^3A_{2g} \rightarrow {}^1E_{2g}$. The magnetic moment of the complex equal to 3.23 BM is typical for octahedral Ni(II) complexes.[10]

The electronic spectra of $[NiL(H_2O)_2]_2$ in $CHCl_3$, toluene or in solid state are essentially the same, while the spectra in DMF (16,400 and 11,360 cm^{-1}) and pyridine (*ca.* 16,000 and 10,500 cm^{-1}) solutions, although still typical for octahedral Ni(II) complexes, vary in band positions (Fig. 6). The IR spectrum of $[NiL(H_2O)_2]_2$ is almost identical with that of $[CoL(H_2O)_2]_2$, even in the "fingerprint" region, so the same assignments were made.

The above data are in accordance with the dimeric structure analogous to that proposed for $[CoL(H_2O)_2]_2$. The electronic spectra of pyridine and DMF solutions indicate that solvent molecules coordinate to the Ni(II) ion, replacing water molecules and/or breaking the alkoxy bridges.

$[CuL]_n$

Thermal analysis for this complex demonstrates no loss of weight until 235°C and elemental analysis agrees with a 1 : 1 metal to ligand ratio (Table 1). The IR spectrum shows no ν-OH band and is very similar to that of Fe and Co complexes in the region 700–1800 cm^{-1}. Magnetic moments of 1.62 BM at 82K and 1.85 BM at 298K indicates some extent of antiferromagnetic interaction between Cu centres.

$[CuL]_n$ gives no EPR signal in the solid state or in DMF and toluene solutions, neither at room nor at liquid nitrogen temperature, while pyridine and 1-methylimidazole solutions give spectra typical for monomeric Cu(II) (for frozen pyridine solutions $A_{11} = 166$ G, $g_{11} = 2.257$). We explain this behaviour by assuming the polymeric structure of the complex with interaction between Cu(II) centres causes a very short spin–spin relaxation time, and hence the absence of the EPR signal. The polymeric

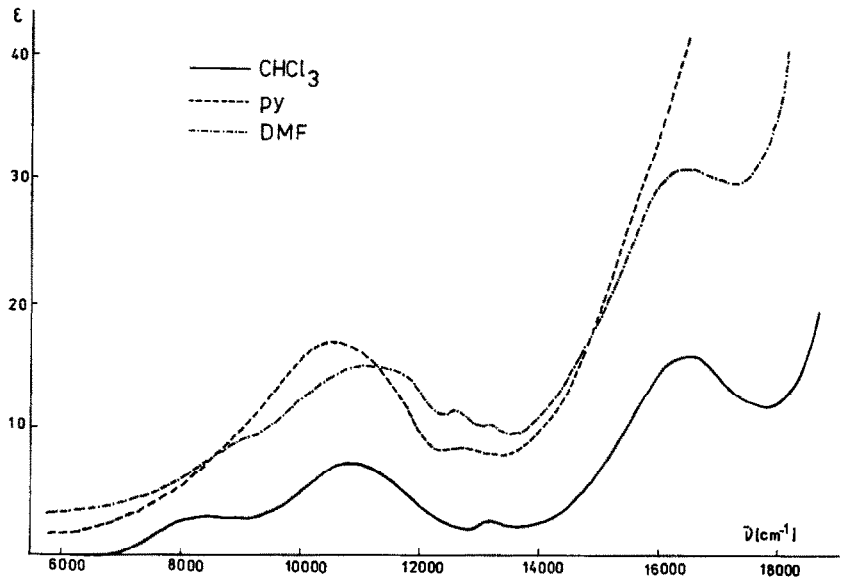

Fig. 6. Electronic spectra of $[NiL(H_2O)_2]_2$.

structure is destroyed when the complex is dissolved in coordinating amines and monomeric species form.

All the above results suggest non-monomeric nature of the complex, however we are not able to state how many Cu(II) centres it contains.

[Zn—L]

The complex lost 5% in weight at *ca.* 100°C. The IR spectrum exhibits broad, weak *v*-OH absorption at *ca.* 3340 cm^{-1} and the other band positions are almost identical with that of cobalt or nickel complexes, except for small changes in the "fingerprint" region.

The ^1H NMR spectrum of [Zn—L] in DMSO-d_6 with azomethine produces a proton resonance at 8.5 ppm (s, 1H), an aromatic proton multiple peak centred at 7.25 ppm (m, 8H), and a CH_2 peak at 4.4 ppm (s, 2H). This clearly indicates the existence of the Schiff base form. It should be noted that the NMR spectrum of the free ligand in DMSO-d_6 [8.85 (s, 1H), 7.35 (m, 8H), 5.05 (m, 1H), 4.65 (d, 2H), 3.2 ppm (m, 1H)] or $CDCl_3$ [8.6 (s, 1H), 7.3 (m, 8H), 4.85 ppm (s, 1H)] does not confirm the existence of the postulated benzoxazine form.[5]

The NMR spectrum of [Zn—L] in $CDCl_3$ [8.1 (s, 1H), 7.0 (m, 8H), 4.85 (s, 2H) ppm] differs from that of the DMSO-d_6 solution; apart from the shift of the resonances, the peaks are much broader and less accurately resolved. The broadening of the peaks probably arises from the polymeric structure of the complex dissolved in $CDCl_3$. In DMSO solution the polymeric structure of the complex is destroyed and a new complex with coordinated DMSO is formed.

Although it seems that the type of coordination of the ligand in [Zn—L] is the same as in Co, Ni or Cu complexes, we are not able to propose any definite formulation consistent with the analytical data.

CONCLUSIONS

The similarity of IR spectra indicates the same coordination mode for the ligand in all investigated complexes. Under the synthesis conditions applied for the complexes under study, the H_2HMPS has a strong tendency to act as a dibasic tridentate ligand and forms non-monomeric complexes. This tendency is reflected by the fact that the alcoholic OH group is deprotonated and coordinates to the metal even when the only base in the system is the salicylaldehyde anion derived from the starting $M(sal)_2 \cdot 2H_2O$.

It is noteworthy, that $[FeLCl]_2$ has magnetic properties similar to $[Fe(SALPA)Cl]_2$,[9] while magnetic, the properties of the Cu complex of our ligand and SALPA are quite different. The reason for this may be the greater sensitivity of the magnetic properties to geometrical factors for bridged Cu(II) complexes than for those of Fe(III).[2,8]

The studies on colbalt(II) complexes with HMPS and their interaction with dioxygen are being continued.

REFERENCES

1. U. Casellato and P. A. Vigato, *Coord. Chem. Rev.* 1977, **23**, 31.
2. M. Melnik, *Coord. Chem. Rev.* 1982, **42**, 259.
3. G. H. Coleman and H. L. Johnson, *Org. Synth.* 1941, **XXI**, 10.
4. S. Wajda, K. Drabent and A. Ozarowski, *Inorg. Chim. Acta* 1980, **45**, L201.
5. A. A. H. Saeed and E. K. Ebraheem, *Can. J. Spec.* 1983, **6**, 28.
6. J. O. Miners and E. Siun, *Bull. Chem. Soc. Jpn.* 1973, **46**, 1457.
7. M. Blume, *Phys. Rev. Lett.* 1965, **14**, 96.
8. B. Chiari, O. Piovesana, T. Tarantelli and P. F. Zanazzi, *Inorg. Chem.* 1982, **21**, 1396.
9. J. A. Bertrand, J. L. Breece, A. R. Kalyanaraman, G. J. Long and W. A. Baker Jr., *J. Am. Chem. Soc.* 1970, **92**, 17.
10. A. B. P. Lever, *Inorganic Electronic Spectroscopy*, pp. 317–348. Elsevier, Amsterdam (1968).
11. A. Syamal and B. K. Gupta, *Rev. Roum. Chim.* 1983, **28**, 805.
12. M. A. Hitchman, *Inorg. Chim. Acta* 1977, **26**, 237.
13. G. McLendon and A. E. Martell, *Coord. Chem. Rev.* 1976, **19**, 1.
14. R. D. Jones, D. A. Summerville and F. Basolo, *Chem. Rev.* 1979, **79**, 139.
15. (a) E.-I. Ochiai, *J. Inorg. Nucl. Chem.* 1973, **34**, 1727; (b) B. Jezowska-Trzebiatowska, P. Chmielewski and A. Vogt, *Inorg. Chim. Acta* 1984, **83**, 129.
16. F. A. Walker, *J. Magn. Res.* 1974, **15**, 201.
17. R. H. Niswander and L. T. Taylor, *J. Magn. Res.* 1977, **26**, 491.
18. T. D. Smith and J. R. Pilbrow, *Coord. Chem. Rev.* 1981, **39**, 295.

Polyhedron Vol. 7, No. 5, pp. 345–348, 1988
Printed in Great Britain

0277–5387/88 $3.00+.00
Pergamon Press plc

FRAGMENTATION OF ZIRCONIUM AND HAFNIUM TETRAPERCHLORATES AND COPPER PERCHLORATE UNDER ELECTRON IMPACT

V. A. SIPACHEV,* YU. S. NEKRASOV, N. I. TUSEEV, D. V. GROMOV and V. P. BABAEVA

Department of Chemistry, Moscow State University, Moscow 117234, U.S.S.R.

(*Received* 7 *July* 1987; *accepted* 8 *September* 1987)

Abstract—The mass spectra of $Zr(ClO_4)_4$, $Hf(ClO_4)_4$ and $Cu(ClO_4)_2$ are reported. The major fragmentation path for Zr and Hf compounds involves the loss of $ClO_4\cdot$ followed by the elimination of Cl_2O_7 (Cl_2O_6) and, eventually $ClO_3\cdot$ ($ClO_2\cdot$). The copper perchlorate molecular ion dissociates to Cu^+ by sequentially splitting off $ClO_4\cdot$ radicals. Transformations of coordination polyhedra during fragmentation are predetermined by metal redox properties. The mass spectra were employed to roughly estimate the extent of thermal dissociation of initial molecules under mass-spectrometric experiment conditions.

This work is an extension to our earlier studies on molecular ion stabilization paths in mass spectra of inorganic coordination compounds containing variable valence elements in the inorganic core and/or the ligands such as Ti, Zr, Hf, and Sn nitrates and oxovanadium nitrate[1] and μ_4-oxohexa-μ-nitratotetraberyllium.[2] The destruction of the coordination polyhedra was found to be highly characteristic of the set of stable metal valence states (see also refs 3 and 4), while the behaviour of ligands under electron impact did not change appreciably from one compound to another even though the series studied included metals of quite different nature. This is probably explained by the slowness of intramolecular V—V relaxation processes caused by a substantial difference in vibrational transition energies between ligands and coordination polyhedra, which therefore behave as comparatively independent units in an elementary fragmentation event. The results described below lend further support to this conclusion.

EXPERIMENTAL

The preparation of the zirconium, hafnium and copper perchlorates was as previously reported.[5–7] All the samples studied had satisfactory analyses. The mass spectra were obtained on an AEI MS-30 instrument using a DS-50 data processing system. The experimental conditions were: ionizing chamber temperature 250°C, ionizing electron energy 70 eV, emission current 100 mcA. The direct inlet system temperature was varied from 60 to 180°C for Zr, 50 to 180°C for Hf and 160 to 200°C for Cu perchlorates. No definite trends were observed in ion intensity variations with temperature. The spectra were reduced to the monoisotopic form using the AELITA program.[8] The detected metal-containing ions are listed in Tables 1 and 2.

RESULTS AND DISCUSSION

Zirconium, hafnium and copper perchlorates are highly reactive, and the presence of certain ions in their mass spectra can only be explained by hydrolysis and thermolysis of the compounds during the preparation and evaporation of samples. Thus appreciable amounts of $[HClO_4]^+$ and $[HCl]^+$ were always observed (alongside the ions $[Cl_2]^+$, $[Cl]^+$ and a number of chlorooxygen ions including $[ClO_2]^+$ which dominated all the spectra).

No molecular ions were detected in the mass spectra of zirconium and hafnium nitrates.[1] The percentages of $[Zr(ClO_4)_4]^+$ and $[Hf(ClO_4)_4]^+$ were also only small (Table 1). On the contrary, $[Cu(NO_3)_2]^+$ and $[Cu(ClO_4)_2]^+$ were among the most intense ions in the mass spectra of copper nitrate[9] and per-

*Author to whom correspondence should be addressed.

Table 1. Relative intensities of metal-containing ions in the mass spectra of zirconium and hafnium tetraperchlorates (in % of the summed intensity of metal-containing ions)

No.	Ion Type[a]	Ion Composition	Intensity $Zr(ClO_4)_4$	Intensity $Hf(ClO_4)_4$	No.	Ion Type	Ion Composition	Intensity $Zr(ClO_4)_4$	Intensity $Hf(ClO_4)_4$
1	a	MCl_4O_{16}	1.4	1.3	13	c	MCl_2O_6	1.0	0.9
2	a	MCl_4O_{14}	0.4	0.6	14	e	$MClO_5$[b]	11.9	5.0
3	a	MCl_4O_{10}	2.6	4.1	15	c	MCl_2O_2	1.0	0.9
4	j	MCl_3O_{13}	0.3	0.7	16	f	$MClO_4$	0.8	1.2
5	b	MCl_3O_{12}[b]	55.7	51.2	17	f	$MClO_3$[b]	1.0	0.9
6	b	MCl_3O_{11}	1.3	2.0	18	k	$MClO_2$	2.6	4.2
7	j	MCl_3O_9	1.2	3.0	19	e	MClO	2.8	5.7
8	b	MCl_3O_8[b]	0.9	1.1	20	g	MO_3	3.3	2.2
9	c	MCl_2O_{10}[b]	3.1	5.0	21	f	MCl	0.9	0.6
10	b	MCl_3O_7	0.6	0.6	22	h	MO_2	4.4	4.9
11	d	MCl_2O_9	0.6	1.1	23	i	MO	1.5	1.7
12	d	MCl_2O_7[b]	1.1	0.8					

[a] The same letter is used to denote ions of different compositions with the same structure of the coordination polyhedron. See text and Table 3.

[b] Also observed in the mass spectrum of titanium tetraperchlorate (V. P. Babaeva and V. Ya. Rosolovskii, *Izv. Akad. Nauk SSSR. Ser. Khim* 1974, 2414).

chlorate (Table 2). Note also that unlike alkali metal nitrates[10] and perchlorates[11] transition metal derivatives[1] did not form polynuclear ions (binuclear ions were however, reported for copper nitrate[12]).

A detailed comparison of the mass spectra of Zr and Hf nitrates and perchlorates is given in Table 3, which illustrates a close correspondence in the directions and relative intensities of various fragmentation processes for complexes of both types.

We have shown earlier that the most important fragmentation path for Group IV metal nitrates includes the loss of $NO_3\cdot$ (a→b) to produce the most abundant metal-containing ions, $[M(NO_3)_3]^+$, followed by the elimination of N_2O_5 or N_2O_4 (e.g. b→e, d→h), and eventually, the $NO_2\cdot$ and $NO\cdot$ radicals from ions containing a single NO_3 group (e→h, f→i). A similar sequence [the loss of $ClO_4\cdot$, Cl_2O_7 (Cl_2O_6), and then $ClO_3\cdot$ ($ClO_2\cdot$)] dominates the electron impact induced dissociation of Zr and Hf perchlorates. The splitting off of acid anhydrides from ML_3^+ (M = Zr, Hf; L = NO_3, ClO_4) leads to oxo-ions where the metals are formally tetravalent as in parent particles. The summed intensity of the ions containing Zr and Hf in the oxidation state +4 far exceeds that of all the other metal-containing ions produced in the fragmentation of $[ML_4]^+$ (more details are given in ref. 1).

A substantial intensity of molecular ions as in the mass spectra of CuL_2 [L = NO_3,[9] ClO_4 (Table 2)] is typical for complexes where the central atom can be promoted to a higher oxidation state (+3). The parent particle fragments by sequentially loosing L·, and the ions $[CuL]^+$ and $[Cu]^+$ have comparable intensities, which is in harmony with comparable

Table 2. Relative intensities of metal-containing ions in the mass spectrum of copper perchlorate (in % of the summed intensity of metal-containing ions)

No.	Ion Type[a]	Ion Composition	Intensity	No.	Ion Type	Ion Composition	Intensity
1	a	$CuCl_2O_8$	18.7	6	d	CuClO	4.0
2	a	$CuCl_2O_6$	2.1	7	e	CuCl	3.3
3	b	$CuClO_4$	45.1	8	f	CuO	7.2
4	b	$CuClO_3$	3.2	9	g	Cu	11.8
5	c	$CuClO_2$	4.6				

[a] The same letter is used to denote ions of different compositions with the same structure of the coordination polyhedron. See text and Table 3.

Table 3. A comparison of the mass spectra of zirconium and hafnium tetranitrates and tetraperchlorates. The numbering of ions corresponds to Table 1. The relative intensities are given in % of the total intensity of metal-containing ions less molecular and mixed-ligand ions

No.	Type	Ion	L = NO_3		L = ClO_4		No.	Type	Ion	L = NO_3		L = ClO_4	
			Zr	Hf	Zr	Hf				Zr	Hf	Zr	Hf
5	b	$[ML_3]^+$	75.7	82.8	68.5	70.5	16	f	$[ML]^+$	2.0	2.9	1.0	1.7
9	c	$[MO_2L_2]^+$	—	2.3	3.8	6.9	20	g	$[MO_3]^+$	3.2	2.7	4.1	3.1
11	d	$[MOL_2]^+$	2.4	1.0	0.7	1.5	22	h	$[MO_2]^+$	8.3	4.1	5.4	6.6
14	e	$[MOL]^+$	7.5	2.9	14.6	6.9	23	i	$[MO]^+$	0.9	1.2	1.8	2.8

stabilities of intermediate copper oxidation states (cf. the mass spectrum of tin nitrate[1] where $[Sn(NO_3)_3]^+$ splits off two $NO_3\cdot$ radicals at a time to produce $[Sn(NO_3)]^+$, also in agreement with the metal redox properties).

These results show that coordination polyhedra transformations in the course of electron impact induced dissociation are fully determined by the ability of metals to undergo oxidation (reduction) being independent of the ligands involved. A comparison of the mass spectra of tetranuclear beryllium nitrato and acetato complexes[2] allows this conclusion to be extended to compounds containing quite dissimilar ligands.

There are however, certain differences in the behaviour of metal nitrates and perchlorates under mass spectrometric experiment conditions that are worth mentioning.

First, the spectra of perchlorato complexes contain detectable although small amounts of ions with ClO_3 or Cl as ligands, e.g. ions 2 and 3 in Table 1 and 2 in Table 2. It was shown convincingly that the appearance of like species in the mass spectra of alkali metal perchlorates resulted from thermal decomposition of the initial compounds rather than electron impact induced fragmentation.[11] Therefore these ions should probably be interpreted as the thermolysis product molecular ions $[M(ClO_4)_2(ClO_3)_2]^+$, $[M(ClO_4)(ClO_3)_2Cl]^+$ (M = Zr, Hf) and $[Cu(ClO_3)_2]^+$, respectively. Note that the products only contain ClO_3 groups in pairs, which is indicative of the detachment of molecular oxygen from isolated molecules. The relative intensity of mixed-ligand ions decreases substantially at the first fragmentation stage (ions b, Tables 1 and 2), and this also points to thermolysis of neutral molecules as the major source of such particles.

Thermal dissociation leads to a complex molecular composition of the gas phase and the appearance of "parallel" fragmentation chains. As a result the mass spectra contain several fragment ions of the same type, e.g. ions $[ML_3]^+$ marked "b" in Table 1 are observed as $[M(ClO_4)_3]^+$ (No. 5) and minor features at m/z corresponding to $M(ClO_3)(ClO_4)_2^+$, $MCl(ClO_4)_2^+$, and $[MCl(ClO_3)(ClO_4)]^+$ (Nos 6, 8 and 10, respectively). The "structural assignments" suggested in Table 1 are not ambiguous. Thus the ion $[MCl_2O_6]^+$ (No. 13) can be written as $[M(ClO_3)_2]^+$ (i.e. $[ML_2]^+$) or $[M(O_2)(Cl)(ClO_4)]^+$ ($= [M(O_2)L_2]^+$). The former interpretation is difficult to reconcile with the absence of the ions $[M(ClO_4)_2]^+$ and $[M(NO_3)_2]^+$ (see ref. 1), whereas the latter is favoured by appreciable concentration of $[M(O_2)(ClO_4)_2]^+$ and $[Hf(O_2)(NO_3)_2]^+$ (Table 3). Similar considerations were applied with other ambiguous ions.

One more feature distinguishing zirconium and hafnium perchlorates from their nitrato analogues is detectability of their molecular ions (ion 1, Table 1). It is also likely that molecular ion stabilities increase from $[M(ClO_4)_4]^+$ to mixed-ligand species (ions 2 and 3), because the percentages of mixed-ligand neutral molecules in the gas phase are certainly far below that of the major component. We therefore have the following stability series: $[M(NO_3)_4]^+$ (0,0) < $[M(ClO_4)_4]^+$ (1.4, 1.3) < $[M(ClO_4)_2(ClO_3)_2]^+$ (0.4, 0.6) < $[M(ClO_4)(ClO_3)_2Cl]^+$ (2.6, 4.1). (Parenthesized values are the relative peak intensities for zirconium and hafnium compounds, respectively.)

This observation makes it easy to conform to the idea[1] that metal complex ionization consequences can for a period of time be localized within a certain complex fragment, because V—V exchange between the ligand and the coordination polyhedron is probably decelerated because of a substantial difference in their vibrational transition energies. States resulting from vertical ionization can therefore relax to different molecular ion "CT isomers". Stability of a charged ligand must depend on (i) the number of degrees of freedom participating in the distribution of initial excitation (ClO_4 > NO_3) and (ii) the ease of promoting ligand atoms to a higher oxidation state (Cl ≫ ClO_3 > ClO_4). The dissoci-

ative stabilization of charged ligands can be responsible for the appearance of ions j

$$[ML_4]^+ - ClO_{x \leqslant 3} \rightarrow [MOL_3]^+$$

and c

$$c\,[ML_4]^+ - Cl_2O_{x \leqslant 6} \rightarrow [M(O_2)L_2]^+.$$

As with molecular ions the intensities of these species increase noticeably from metal nitrates to their perchlorato analogues. Possible mechanisms of the elimination of various neutral oxides from metal-containing ions with the formation of oxo- or peroxo-structures are considered in detail in ref. 1.

Mixed-ligand and molecular ions, however, make only an insignificant contribution to the total ion current in the mass spectra of Zr and Hf perchlorates. So far as the predominant fragmentation processes are concerned these spectra are practically identical to those of the nitrato complexes, as is clearly seen from Table 3. Such processes involve transformations of the metal coordination polyhedra, and the relative intensities of the corresponding ions do not change significantly from one ligand to another. We can therefore use mass spectral data to estimate (of course only very roughly) the gas phase molecular composition under mass spectrometric experimental conditions. Thus the percentages of thermolysis products based on $[ML_3]^+$ ion intensities were found to be *ca* 5% for $Zr(ClO_4)_4$ and *ca* 7% for $Hf(ClO_4)_4$ and $Cu(ClO_4)_2$.

The data on the behaviour of inorganic complexes under electron impact collected in this study and in the works on metal nitrates,[1,2] carboxylates[13,14] and alkoxocarboxylates[13] show that there are three major paths for fragmentation stabilization of their molecular ions.

(1) The promotion of the central atom to the higher oxidation state followed by consecutive elimination of ligand radicals to realize intermediate metal valences. Copper complexes can serve as examples: $[CuL_2]^+ \rightarrow [CuL]^+ \rightarrow [Cu]^+$ (L = NO_3, ClO_4).

(2) If a polyvalent atom is in its highest oxidation state and has stable intermediate valences, the molecular ions are usually undetectable. The major fragmentation path is then the splitting off of ligand radicals as in tin nitrate:[1]

$[Sn(NO_3)_4]^+$ (unobserved)

$$\rightarrow [Sn(NO_3)_3]^+ (68.2) \rightarrow [Sn(NO_3)]^+ (21.2)$$

(parenthesized values are relative ion intensities). Note that two ligand radicals are eliminated from $[Sn(NO_3)_3]^+$ in one step, which correlates with the absence of stable tin oxidation state +3.

(3) Lastly, in the absence of stable intermediate valences we observe stabilization processes involving fragmentation of ligands and reorganization of the metal environment. The major processes are the loss of anhydride fragments at early fragmentation stages and simple oxides at later ones to produce substantial amounts of ions with oxo- structures where the metal preserves its characteristic oxidation state. The examples are titanium, zirconium and hafnium, nitrates[1] and perchlorates, tetranuclear zinc and beryllium complexes M_4OL_5L' (M = Zn, L = L′ = CH_3CO_2[14]; M = Be, L = L′ = NO_3,[2] L = L′ = RCO_2, and L = RCO_2, L′ = R′O[13]).

This type of complex fragmentation is highly characteristic for a given metal and independent of ligands, therefore mass spectral data can be used to estimate the molecular composition of products formed by vaporization of initial compounds under the mass spectrometric experimental conditions.

REFERENCES

1. Yu. S. Nekrasov, V. A. Sipachev and N. I. Tuseev, *J. Inorg. Nucl. Chem.* 1980, **42**, 1677.
2. V. A. Sipachev, N. I. Tuseev and Yu. S. Nekrasov, *Polyhedron* 1982, **1**, 820.
3. J. S. Shannon and J. M. Swan, *J. Chem. Soc., Chem. Commun.* 1965, 33.
4. M. J. Lacey and J. S. Shannon, *Org. Mass Spect.* 1972, **6**, 931.
5. V. P. Babaeva and V. Ya. Rosolovskii, *Izv. Akad. Nauk SSSR. Ser. Khim.* 1977, 495.
6. A. V. Dudin, V. P. Babaeva and V. Ya. Rosolovskii, *Zh. neorg. Khim.* 1981, **26**, 2933.
7. Z. K. Nikitina and V. Ya. Rosolovskii, *Zh. neorg. Khim.* 1980, **25**, 1285.
8. Yu. N. Sukharev and Yu. S. Nekrasov, *Org. Mass Spect.* 1976, **11**, 1232.
9. L. Dauerman and G. E. Salser. *J. Inorg. Nucl. Chem.* 1973, **35**, 304.
10. I. Lauder, C. Tawler and T. Wuth, *Adv. Mass Spect.* 1971, **5**, 379.
11. E. N. Nikolaev, K. V. Ovchinnikov and G. A. Semenov, *Zh. obshch. Khim.* 1981, **51**, 1710.
12. P. F. Porter, R. C. Schoonmaker and C. C. Addison, *Proc. Chem. Soc.* 1959, 11.
13. Yu. S. Nekrasov, S. Yu. Sil'vestrova, A. I. Grigor'ev, L. N. Reshetova and V. A. Sipachev, *Org. Mass Spect.* 1978, **13**, 491.
14. V. A. Sipachev. L. N. Reshetova, Yu. S. Nekrasov and S. Yu. Sil'vestrova, *Org. Mass Spect.* 1980, **15**, 192.

Polyhedron Vol. 7, No. 5, pp. 349–352, 1988
Printed in Great Britain

0277–5387/88 $3.00+.00
Pergamon Press plc

MIXED NEUTRAL COMPOUNDS OF PALLADIUM(II) AND PLATINUM(II) CHELATED BY DIOLATO(2−) AND DI-IMINE LIGANDS

S. G. FOX and R. D. GILLARD*

Department of Chemistry, University College, P.O. Box 78, Cardiff CF1 1XL, U.K.

(*Received* 11 *March* 1986; *accepted after revision* 16 *September* 1987)

Abstract—The synthesis and characterization are described for compounds abbreviated (a) **1–5**: [Pd(phen)(OO)], where OO = the dianion from 1,2-ethanediol (**1**), (+)-1,2-propanediol (**2**), (±)-2,3-butanediol (**3**), (−)-1,2-butanediol (**4**), catechol (**5**); (b) the sulphur analogue (**6**) [Pd(phen)(SCH_2CH_2S)], from ethane-1,2-dithiol; (c) the platinum analogue (**7**) [Pt(phen)(OCH_2CH_2O)]; (d) the 2,2′-bipyridyl analogue (**8**), [Pd(bipy)(OCH_2CH_2O)] (phen = 1,10-phenanthroline and bipy = 2,2′-bipyridyl).

A recent report[1] of compounds [Pd(malonate)(en)] (en = 1,2-diaminoethane) and [Pd(malonate)$(N)_2$], where N = unidentate N-heterocycles like N-methylimidazole prompts us to describe briefly our work[2] on the related compounds **1–8** shown in Scheme 1. Since the advent[3] of treatment of tumours by "*cis* platin", *cis*-[$Pt(NH_3)_2Cl_2$], efforts have been made both to synthesize other anti-tumour agents of analogous structure [Pt(NN)XY] and to understand the mode of action of such species.

Under the first heading are such compounds as *cis*-dichloro-2,2′-bipyridylplatinum(II), [Pt(bipy)Cl_2], which shows[4] no anti-tumour activity and complexes containing the [$Pt(bipy)^{2+}$] fragment with amino acids (alanine and methionine) which turn out to have[5] lower inhibitory doses than [$Pt(NH_3)_2Cl_2$], and under the second heading are studies of the binding between platinum-containing drugs and the DNA helix.[6]

The suggestion was made[7] that the presence of a chiral diamine element, NN, say (+)-1,2-diaminocyclohexane rather than its enantiomer in a potential anti-tumour agent might have a beneficial effect on specificity. Experiment suggests[8] that there is in fact an absence of chiral recognition. However, there seem to be no studies in which the potential drug had "leaving group"[6] chirality in the XY moiety of [Pt(NN)XY], a property of obvious potential relevance to the transport of drugs to, into and within the cell. We therefore made a few compounds containing racemic and optically active chelated diols, as their dianions, giving neutral complex compounds, as in the equation:

$$[Pd(NN)(OH)_3]^- + {}^-OCHRCHR'O^- \rightarrow [Pd(NN)(OCHRCHR'O)] + 3OH^-.$$

Stable crystalline products were produced by reacting strongly alkaline solutions of ML_{aq}^{2+} (M = palladium or platinum, L = 1,10-phenanthroline or 2,2′-bipyridyl, forming $ML(OH)_3^-$) with the appropriate diol.

As an example of the present syntheses, shaking a dilute aqueous solution of [Pd(phen)$(OH)_3]^-$ with a few drops of ethane-1,2-diol leads to an immediate colour change to a paler yellow, followed by formation of pale lemon–yellow, needle-shaped crystals over a few minutes. All the compounds described below were prepared by such combination of diimine complex and diol. The compounds synthesized are listed in Scheme 1. All were characterized by nuclear resonance spectroscopy, elemental and thermogravimetric analysis, IR spectroscopy and where applicable, circular dichroism (C.D.) spectroscopy.

Compounds **1, 2, 3** and **4** show an interesting solubility in water: 1—insoluble, 2—soluble, 3—insoluble, 4—soluble, possibly due to differences in lattice energies of the four solids.

Compounds **2** and **4** were prepared using resolved

*Author to whom correspondence should be addressed.

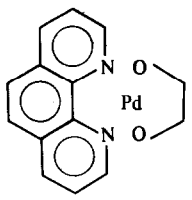

1

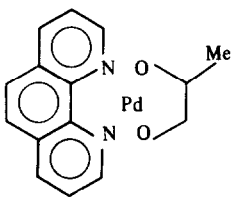

2

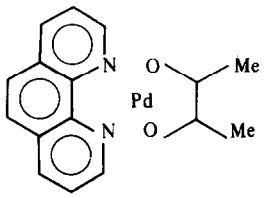

3

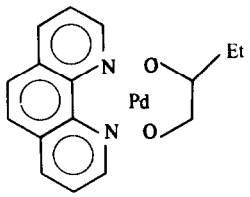

4

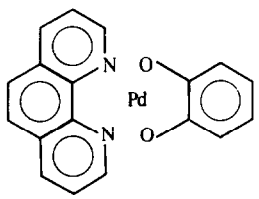

5

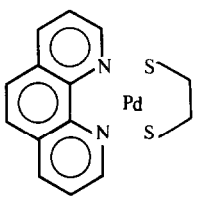

6

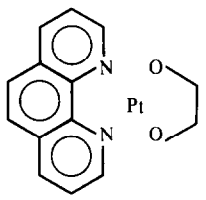

7

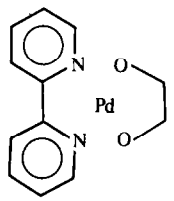

8

Scheme 1. Structures of the compounds **1–8**.

chiral diols and circular dichroism spectra are shown in Table 1. It is quite clear from the essentially enantiomeric circular dichroism spectra of the two complex compounds in Table 1 [Pd(phen)(diolate)], that the (−)1,2-diolata-butane ion generates in the $[Pd(phen)]^{2+}$ chromophore of **4** chirality opposite to that generated in **2** by (+)-1,2-diolatopropane. These two diolate di-imines (and hence their parent diols) have opposite configurations. The present method of deducing relative configurations by coupling the diol chirality to the remarkably stable $[Pd(phen)]^{2+}$ chromophore should be general for optically active 1,2-diols, for which satisfactory chromophores are lacking. (Although the recent examples[9] of the use of dimeric carboxylates of dimolybdenum, dirhodium and diruthenium as "Cottonogenic derivatives" for 1,2-diols by Snatzke and his colleagues seem very promising.)

Table 1. Circular dichroism spectra of [Pd(phen)(OCHRCHRO)] **2** and **4**

2		**4**	
λ	$\Delta\varepsilon^a$	$\Delta\varepsilon^a$	λ
530	0	0	530
455	−13	+24	450
410	0	0	412
360	+51	−98	357
312	0	0	312
308	−85	+160	310
299	0	0	299

[a] The $\Delta\varepsilon$ values are estimates, because both powdered products contained a small amount (<5%) of unreacted diol: the diols are colourless and hence have no visible or near UV C.D. spectra before complexation.

In the context of stereoselective effects in drugs containing chiral ligands, the recent work[10] of Totani at the Shionogi laboratories is noteworthy. Compounds containing α-hydroxyacidates [e.g. (glycolato-O,O′)diammineplatinum(II)] have been made and evaluated in chemotherapy.

Compound **5**, a deep red microcrystalline powder, is insoluble in water, but dissolved in dimethylsulphoxide to give a deep violet solution. Its red colour is probably produced by intramolecular conjugation of the π-systems of the heterocycle with those of the benzene ring, since the DMSO solution is violet, whereas the isolated unconjugated N_2PdO_2 chromophore should be yellow. In the $Pt(bipy)Cl_2$ case, the red solid dimorph gives a yellow solution, where the non-conjugated N_2PtCl_2 chromophore is present.

Compound **6** (in which the oxygen atoms are replaced by sulphur) was formed by adding drops of ethane-1,2-dithiol to a dilute alkaline solution of $Pd(phen)(OH)_2 \cdot 3H_2O$. The reaction was rapid, with formation of an orange–yellow water-insoluble powder.

EXPERIMENTAL

$Pd(phen)Cl_2$ and the analogous compounds $Pt(bipy)Cl_2$ etc. were made by dissolving

Table 2. Elemental analyses for $[M(LL)X]nH_2O$

Serial number		LL[a]	X	n	Formula	Found (%) C	H	N	Required (%) C	H	N
—	Pd	P	Cl_2		$C_{12}H_8Cl_2N_2Pd$	39.9	2.2	9.0	40.3	2.2	7.9
—	Pd	P	$(OH)_2$	3	$C_{12}H_{16}N_2O_5Pd$	38.6	3.7	6.9	38.5	4.3	7.4
1	Pd	P	eg		$C_{14}H_{12}N_2O_2Pd$	48.3	4.3	8.4	48.6	3.5	8.1
2	Pd	P	pn[b]		$C_{15}H_{14}N_2O_2Pd$	50.0	4.1	7.4	50.0	4.0	7.8
3	Pd	P	2,3-bn		$C_{16}H_{16}N_2O_2Pd$	50.8	4.7	7.4	51.3	4.3	7.5
4	Pd	P	1,2-bn[b]		$C_{16}H_{16}N_2O_2Pd$	51.6	4.6	7.3	51.3	4.3	7.5
5	Pd	P	cat	3[c]	$C_{18}H_{18}N_2O_5Pd$	48.9	5.7	6.2	48.2	5.6	6.3
6	Pd	P	dithiol		$C_{14}H_{12}N_2PdS_2$	43.1	3.9	7.1	44.4	3.2	7.7
—	Pd	B	Cl_2		$C_{10}H_8Cl_2N_2Pd$	36.4	2.5	7.9	36.0	2.4	8.4
—	Pd	B	$(OH)_2$	4	$C_{10}H_{18}N_2O_6Pd$	32.4	4.2	7.6	32.6	4.8	7.6
8	Pd	B	eg		$C_{12}H_{12}N_2O_2Pd$	45.2	4.1	9.0	44.7	3.7	8.7
—	Pt	P	Cl_2		$C_{12}H_8Cl_2N_2Pt$	33.8	2.1	6.1	32.3	1.8	6.3
—	Pt	P	$(OH)_2$	3	$C_{12}H_{16}N_2O_5Pt$	31.1	2.2	6.0	30.9	2.5	6.0
7	Pt	P	eg		$C_{14}H_{12}N_2O_2Pt$	35.7	3.0	6.4	36.2	2.7	6.4
—	Pt	B	Cl_2[d]		$C_{10}H_8Cl_2N_2Pt$	28.6	1.6	7.0	28.4	1.9	6.6

[a] B = 2,2′-bipyridyl, P = 1,10-phenanthroline.

[b] Elemental analysis in these cases does not reveal that the powders contain a little unreacted diol: this can be seen microscopically as colourless crystals and from proton magnetic resonance, where its amount is estimated as less than 5%: an assumed 5% has however been used to calculate the values of molar circular dichroism for 2 and 4 in Table 1.

[c] The deep red trihydrate became black on dehydration (over warm silica gel); the anhydrous black crystals reverted to the red trihydrate under hot water.

[d] This well-known compound (yellow dimorph) was used to check analytical procedures.

K_2MCl_4(M = palladium or platinum) in 2 M HCl and adding an ethanolic solution of the ligand with rapid stirring. After digesting the precipitate by boiling for 1–2 h, the pale yellow or pale tan-coloured finely divided product was collected at the pump, washed with water, then ethanol (thoroughly to remove any unreacted ligand), acetone and diethyl ether, and dried at 100°C. Yields were all quantitative within experimental error.

$Pd(phen)(OH)_2 \cdot 3H_2O$ was prepared by suspending $Pd(phen)Cl_2$ (0.182 g) in distilled water (100 cm^3) containing NaOH (0.1 g). The mixture was heated (hot plate stirrer) until the solid dissolved, giving a lemon–yellow colour. The solution was cooled and poured through an Amberlite resin IRA 400 anion exchange column prepared in the OH^- form by washing with 0.05 M NaOH solution. The eluate solution was reduced in volume (rotary evaporator) until a yellow powder began to precipitate, after which the flask was removed and allowed to cool. $Pt(phen)(OH)_2 \cdot 3H_2O$, $Pd(bipy)(OH)_2 \cdot 3H_2O$ and $Pt(bipy)(OH)_2 \cdot 3H_2O$ were prepared by (*mutatis mutandis*) the above procedure.

Yields for the step $MLCl_2 \rightarrow ML(OH)_2$ were low in all cases. We assume that the presence of some ML^{2+}_{aq} as $ML(OH)_3^-$ in the very alkaline conditions led to some interaction with the anion exchange resin.

1,2 - *ethanediolato* - 1,10 - *phenanthrolinepalladium* (*II*), **1**

This was prepared by dissolving $Pd(phen)(OH)_2 \cdot 3H_2O$ (0.2 g) in water (50 cm^3) containing NaOH (0.1 g) and adding dropwise ethane-1,2-diol (0.2 g). Crystals of the desired product formed in a few minutes and were collected and washed carefully with ice-cold distilled water. (Compounds **3** and **8** were made in the same way.)

Compound **1** had IR adsorption at : 230, 260, 370, 445, 615, 720, 855, 880, 890, 1050, 1110, 1150, 1230, 1360s, 1430, 1515, 1660, 2820, 3400b. Compound **1** had ^1H resonance at: δ2.62, 8.13m, 8.31, 8.96.

S(+)1,2 - *propanediolato* - 1,10 - *phenanthroline-palladium*(II), **2**

This was prepared by dissolving $Pd(phen)(OH)_2 \cdot 3H_2O$ (0.2 g) in water (50 cm^3) containing NaOH (0.1 g) and adding S(+)1,2-propanediol (0.2 g) with rapid shaking and stirring. The solution was warmed on a steam bath for several hours and allowed to cool. Reduction of volume of the resultant pale yellow solution to approximately 1/10th of the original led to precipitation of a finely divided pale yellow product which was

evidently contaminated with small amounts of the diol. Compound **4** was made by an adaptation of this method.

Compound **2** had IR absorption (measurements were made from 625 cm^{-1}) at: 640b, 680s, 710s, 840s, 850s, 865s, 920, 990, 1050, 1080, 1150, 1220, 1280, 1350, 3400b. Compound **2** had ^1H resonance at: δ1.07d, 3.49m, 3.87q, 7.63, 7.82m, 8.22d, 8.47m.

Catecholato-1,10-*phenanthrolinepalladium*(II), **5**

This was prepared by dissolving Pd(phen)$(OH)_2 \cdot 3H_2O$ (0.2 g) in distilled water containing NaOH (0.1 g) and adding a solution of catechol in distilled water (0.25 g in 5 cm^3). An immediate precipitation of deep red product occurred. This was collected on a fine sintered glass crucible (Grade 4) and washed with large quantities of water to remove NaOH and excess diol.

Compound **5** had IR absorption at: 230, 340s, 390, 440, 460, 535, 560, 580, 605, 635, 665, 715, 730, 755, 800, 845, 860, 885, 905, 965, 990, 1020s, 1040, 1095s, 1120, 1155, 1200, 1260s, 1355, 1415, 1435, 1480, 1530, 1570, 1585, 1805, 1635, 1660, 3060, 3305b. Compound **5** had ^1H resonance at: δ6.22q, 6.38q, 8.10q, 8.28, 8.95.

1,2 - *ethanedithiolato* - 1,10 - *phenanthrolinepalladium*(II), **6**

This was produced immediately on adding 1,2-ethanedithiol (0. 1g) dropwise to a solution of Pd(phen)$(OH)_2 \cdot 3H_2O$ (0.2 g) in distilled water (50 cm^3) containing NaOH (0.1 g). The orange–yellow finely divided precipitate was collected at the pump and washed with large amounts of cold distilled water to remove the unreacted thiol (smell!).

Compound **6** had IR absorption at: 230, 250, 350, 360, 430, 455, 500, 620, 650, 660, 715s, 735, 765, 840s, 875, 1100, 1140, 1220, 1240, 1275s, 1355s, 1410, 1415s, 1500, 1510s, 2600, 1625, 1660, 2720, 2880s, 2900, 3040, 3380b. Compound **6** had ^1H resonance at: δ2.63, 8.05q, 8.23, 8.57d, 8.90d, 9.07.

1,2 - *ethanediolate* - 1,10 - *phenanthrolineplatinum* (II), **7**

This was made by the same method as the palladium analogue, **1** above, modified by heating the reacting solution on the steam bath for 24 h. Acicular yellow crystals were produced on cooling to room temperature.

Compound 8 had IR bands at: 280, 420, 480, 490, 545, 610, 725, 770, 895s, 1025, 1060s, 1110, 1160, 1225, 1255, 1360, 1450, 1470, 1495, 1565, 1600, 1665, 2350b, 2820, 3360b. Compound **8** had ^1H resonance at: δ2.52, 8.36t, 8.66m.

IR spectra were measured using Nujol mulls: the numbers appended to each compound are in order of frequency (cm^{-1}), s, strong; b, broad. Proton magnetic resonance spectra (δ-values relative to TMS) were obtained in DMSO solution, with TMS reference, except for compound **2**, measured in D_2O, with TSS reference.

Acknowledgements—We wish to thank Dr E. R. J. Sillanpaa (University of Turku) for helpful comments and Miss R. Dhoot for technical assistance.

REFERENCES

1. M. Massacesi, R. Pinna, G. Ponticelli, G. Devoto and I. A. Zakharova, *Polyhedron* 1985, **4**, 1989.
2. S. G. Fox, Di-imine complexes of nickel, palladium and platinum, M.Sc. Thesis, University of Wales at U.C. Cardiff (1985).
3. (a) B. Rosenberg, L. Van Camp and T. Krigers, *Nature* 1965, **205**, 698; (b) B. Rosenberg, L. Van Camp, J. E. Trosko and V. H. Mansour, *Nature* 1969, **222**, 385.
4. S. J. Meischen, G. R. Gale, L. M. Lake, C. J. Frangakis, M. G. Rosenblum, E. M. Walker, L. M. Atkins and A. B. Smith, *J. Nat. Cancer Inst.* 1976, **57**, 841.
5. L. Kumar, N. R. Kandasamy, T. S. Srivastava, A. J. Amonkar, M. K. Adwanker and M. P. Chitnis, *J. Inorg. Biochem.* 1985, **23**, 1.
6. *Chemistry in Britain*, p. 610 (1985).
7. R. D. Gillard, *New Trends in Bio-inorganic Chemistry* (Edited by R. J. P. Williams and J. J. R. F. da Silva), p. 355. Academic Press, London (1978). (Note especially pp. 380–381.)
8. M. Gullotti, A. Pasini, R. Ugo, S. Filippeschi, L. Marmonti and F. Spreafico, *Inorg. Chim. Acta* 1984, **91**, 223 and refs therein.
9. W. Diener, J. Freick, M. Gerards, Z. Majer, A. Perkowska, G. Snatzke and U. Warner, *Int. Conf. CD, FECS Sofia*, Vol. 6, p. 10 (1985). (Note especially Figs 3–7.)
10. T. Totani, *Chem. Lett.* 1986, 429.

Polyhedron Vol. 7, No. 5, pp. 353–361, 1988
Printed in Great Britain

0277–5387/88 $3.00+.00
Pergamon Press plc

BRIDGE-SPLITTING REACTION OF A DINUCLEAR PLATINUM(II) COMPLEX CROSS-LINKED BY TETRA-ACETYLETHANE DIANION $[Pt_2(L_2)_2(dahd\text{-}O_2,O_2')][BF_4]_2$ (dahd = TETRA-ACETYLETHANE; L = SEt_2, PMe_2Ph; L_2 = 1,5-CYCLOOCTADIENE); METAL–CARBON BONDED PLATINUM(II) COMPLEX OF TETRA-ACETYLETHANE WITH (C^3,O′)-CHELATE

SHINSAKU YAMAZAKI*

Chemistry Laboratory, Gakuen College Kochi, 292 Asahi Tenjin-cho, Kochi 780, Japan

TOMOHARU AMA

Department of Chemistry, Faculty of Science, Kochi University, 2-5-1 Akebono-cho, Kochi 780, Japan

and

ZENEI TAIRA

Department of Pharmaceutical Sciences, Tokushima Bunnri University, 180 Boji Yamashiro-cho, Tokushima 770, Japan

(*Received* 10 *April* 1987; *accepted after revision* 16 *September* 1987)

Abstract—A Pt(II) complex of tetra-acetylethane (dahd = 3,4-diacetyl-2,4-hexadiene-2,5-diol) dianion bonding with (C^3,O′)-chelate, Pt(L)(L′)(dahd-C^3,O′){L = L′ = SEt_2; L = L′ = PMe_2Ph; L = SEt_2, L′ = PPh_3; L = L′ = 2,9-R_2-1,10-phen(R = H, Me) where L′ is *trans* to C^3} has been prepared. *cis*-$PtCl_2L_2$(L = SEt_2, PMe_2Ph) reacts with K_2-dahd in CH_3OH to produce a dinuclear cationic complex $[Pt_2L_4(dahd\text{-}O_2,O_2')]^{2+}$ in which dahd is cross-linked with symmetrical bifunctional chelation. An analogous COD (1,5-cyclo-octadiene) complex $[Pt_2(COD)_2(dahd\text{-}O_2,O_2')][BF_4]_2$ has been prepared by treating $PtCl_2$(COD) with $AgBF_4$ and H_2-dahd. $[Pt_2L_4(dahd\text{-}O_2O_2')][BF_4]_2$, by treating with K_2-dahd, readily transforms into $PtL_2(dahd\text{-}C^3,O')$ (L = SEt_2, PMe_2Ph). This $PtL_2(dahd\text{-}C^3,O')$(L = SEt_2, PMe_2Ph) in HBF_4/acetone solution converts to the dinuclear complex $[Pt_2L_4(dahd\text{-}O_2,O_2')][BF_4]_2$, liberating H_2-dahd in a stoichiometric yield.

These anomalous Pt(II) complexes linked by the dahd dianion are characterized using IR, ^1H, ^{13}C-NMR and fast atom bombardment mass spectroscopy, conductance and molecular weight measurements.

Dinuclear Pd(II) and Rh(I) complexes of tetra-acetylethane (dahd = 3,4-diacetyl-2,4-hexadiene-2,5-diol) cross-linking two metal nuclei as bifunctional O_2-chelates have been described before.[1] In them, a reaction of $[Pt_2(PPh_3)_4(dahd\text{-}O_2,O_2')][BF_4]_2$ with the bidentate azaheterocyclic ligand phen have been seen to undergo an anomalous bridge-splitting between the two metal nuclei giving a five-coordinate complex $[Pd(PPh_3)(phen)_2][BF_4]_2$,[2] and concurrently an insoluble complex containing dahd cross-linking of the metal nuclei as an O_1-uni, O_1'-unidentate ligand $[Pd(phen)(dahd\text{-}O_1,O_1')]_n$. The latter product readily transforms into its linkage isomer with a metal–carbon bond Pd(phen)(dahd-

*Author to whom correspondence should be addressed.

C^3,O'). Knowing that H_2-dahd itself is stabilized in a dienolate form as a γ,γ'-bis(acetylacetone),[1] the activation of its C(3) to form a M–C bond has been an unexpected result. Some evidence for catena-[Pd(phen)(dahd-O_1,O_1')]$_n$ which somewhat surprisingly accompanies a trace amount of paramagnetic species may indicate that this novel linkage isomerization of the dahd from (O_2,O_2')-chelate to (C_3,O')-chelate proceeds via a two electron transfer from the dahd ligand to the metal or to the other ligand.

One problem in these Pd(II) complexes is that the reaction products were obtained in low yields as the stoichiometry indicates, in addition to their low solubilities. From these previous findings, we have thus attempted the syntheses and characterizations of dinuclear and mononuclear Pt(II) complexes in which the dahd dianion links Pt(II) as a bidentate O_2-chelate and (C^3,O')-chelate, using a monodentate SEt_2 or PMe_2Ph and bidentate 1,5-COD as ligands.

EXPERIMENTAL

Preparation of complexes—[$Pt_2(SEt_2)_4$(dahd-O_2,O_2')][BF_4]$_2$

cis-$PtCl_2(SEt_2)_2$[3] (3.0 g) in acetone containing 1.4 g of H_2-dahd was added with $AgBF_4$ (2.8 g) and the solution after stirring for 2 h, was filtered (2 g of AgCl ppt. 200% per Pt atom). The solution was then evaporated forming a yellow oil. The oil product was washed with water to remove liberated HBF_4. The residue was dried *in vacuo* and crystallized from acetone–diethylether to give white crystals (2.7 g; 71%). Found: C, 27.7; H, 4.6. Calc. for $C_{18}H_{16}O_4B_2F_8$: C, 27.9; H, 4.7%. Conductance (acetone): Λ_M, 224 Ω^{-1} cm^2 mol^{-1}.

[$Pt_2(PMe_2Ph)_4$(dahd-O_2,O_2')][BF_4]$_2$

cis-$PtCL_2(PMe_2Ph)_2$[4] (0.7 g) was dissolved in mixed solvents of CH_2Cl_2–CH_3OH containing 0.16 g of H_2-dahd. To the solution, 0.52 g of $AgBF_4$ was added. The solution, after stirring for 2 h, was filtered (0.34 g of AgCl ppt. 181% per Pt atom), reduced in volume to ~ 5 cm^3 and addition of diethylether to the residual solution gave pale brown crystals (0.74 g; 87% per Pt atom). Found: C, 37.2; H, 4.3. Calc. for $C_{21}H_{30}O_3BF_4P_2Pt$ (with one water of solvation): C, 37.4; H, 4.5%. ^{1}H NMR{$CDCl_3$-$(CD_3)_2CO$}: δ_H (water of solvate ion), 5.2 ~ 5.3 ppm(vb). The signal due to the hydrogen from water which is always concomitant with the solvent $(CD_3)_2CO$ is observed at ~ 3.00 ppm and is relatively sharp. Conductance (acetone): Λ_M, 236 Ω^{-1} cm^2 mol^{-1}.

[Pt_2(COD)$_2$(dahd-O_2,O_2')][BF_4]$_2$

$PtCl_2$(COD)[5] (1.3 g) was dissolved in CH_2Cl_2 containing 0.4 g of H_2-dahd. To this solution, an acetone solution of $AgBF_4$ (1.3 g) was added. The solution, after stirring overnight, was filtered (0.9 g of AgCl ppt. 185% per Pt atom). The filtrate was then added to silica gel and filtered. The solution was reduced in volume to ~ 5 cm^3 under pressure, and addition of diethylether to the residual solution gave pale brown crystals (1.1 g; 63% per Pt atom). Found: C, 31.3; H, 3.7. Calc. for $C_{13}H_{20}O_3BF_4Pt$ (with one water of solvation): C, 30.9; H, 4.0%. ^{1}H NMR{$(CD_3)_2CO$}: δ_H(H_2O of solvation), 3.0 ppm(vb). Conductance (acetone): Λ_M, 226 Ω^{-1} cm^2 mol^{-1}.

Pt(SEt_2)$_2$(dahd-C^3,O')

cis-$PtCl_2(SEt_2)_2$ (0.3 g) in CH_3OH was mixed with 0.2 g of K_2-dahd[1] and a few drops of NEt_3. The solution was stirred for 16 h and then filtered. The filtrate was evaporated. The residue was dissolved in about 20 cm^3 of CH_2Cl_2 and the solution was transferred to a separating funnel. After addition of an equi-volume of H_2O, the solution was vigorously shaken to mix. The CH_2Cl_2 phase was transferred to a round bottom flask and the solvent was removed under reduced pressure to give a yellow oil. After drying *in vacuo*, the product was crystallized from CH_2Cl_2–diethylether to give pale brown micro-crystals (0.13 g; 34%). When the reaction oily product is not washed with H_2O, the yield of crystal product is raised to 78%. Found: C, 37.8; H, 5.6. M.W. (cryoscopic method in $C_6H_5NO_2$), 381. Calc. for $C_{18}H_{32}O_4S_2Pt$: C, 37.8; H, 5.6%. M = 572. ^{1}H, ^{13}C NMR are in *vide infra*. The low molecular weight measurement in nitrobenzene suggests that one SEt_2 of the complex is displaced in solution by the nitrobenzene solvent. FABMS: M^+ = 572 (*vide infra*).

Pt(SEt_2)$_2$(dahd-C^3,O') was also obtained by treating [$Pt_2(SEt_2)_4$(dahd-O_2,O_2')][BF_4]$_2$ with K_2-dahd in CH_3OH. When [$Pt_2(SEt_2)_4$(dahd-O_2,O_2')][BF_4]$_2$ (0.75 g) was added to K_2-dahd (0.2 g) in CH_3OH the pale yellow solution turned dark yellow. The solution, after stirring for a day, was filtered to separate a small amount of dark white ppt. The solvent was then removed under reduced pressure to give a pale brown oil, which was washed with water and decanted. The oily residue, after being dried *in vacuo*, was crystallized from CH_2Cl_2–diethylether to give white crystals (0.64 g; 84% per Pt atom).

Pt(PPh$_3$)(SEt$_2$)(dahd-C^3,O′)

Pt(SEt$_2$)$_2$(dahd-C^3,O′) (0.24 g) in CH_2Cl_2 was added to 0.22 g of PPh_3. The solution was stirred for 1 day and reduced in volume under pressure to about 5 cm^3. Addition of diethylether and *n*-hexane to the residual solution gave a pale yellow solid, which was recrystallized from CH_2Cl_2 and diethylether (0.24 g; 79%). Found: C, 51.3; H, 5.0. M.W. (vapour pressure osmometry in CH_2Cl_2) 680. Calc. for $C_{32}H_{37}O_4PSPt$: C, 51.7; H, 5.0. M = 744.

Pt(phen)(dahd-C^3,O′)

Pt(SEt$_2$)$_2$(dahd-C^3,O′) (0.11 g) was dissolved in CH_2Cl_2 and to the solution 0.05 g of phen · H_2O was added. The solution was stirred for about a week giving a pale orange precipitate. The product was crystallized from CH_2Cl_2 using isothermal vaporization (0.09 g; 82%). Found: C, 47.0; H, 3.6; N, 5.0. M.W. (vapour pressure osmometry in CH_2Cl_2) 532. Calc. for $C_{20}H_{24}N_2O_4Pt$: C, 46.2; H, 3.5; N, 4.9%. M = 574.

Pt(2,9-Me$_2$-phen)(dahd-C^3,O′)

Pt(SEt$_2$)$_2$(dahd-C^3,O′) (0.12 g) in CH_2Cl_2–acetone was added with 2,9-Me$_2$-phen · 0.5H_2O (0.06 g). The solution was refluxed for about a week and then diethylether and *n*-hexane were added. On allowing the solution to stand in a refrigerator overnight an orange solid with CH_2Cl_2 of solvate (0.08 g; 55%) was produced. Found: C, 44.0; H, 3.9; N, 4.1. Calc. for $C_{25}H_{26}Cl_2N_2O_4Pt$: C, 43.9; H, 3.8; N, 4.1%. ^{1}H NMR ($CDCL_3$): δ_{CH_2}(CH_2Cl_2 of solvate) 5.23 ppm.

Pt(PMe$_2$Ph)$_2$(dahd-C^3,O′)

cis-PtCl$_2$(PMe$_2$Ph)$_2$ (0.63 g) was suspended in CH_3OH and 0.3 g of Na$_2$-dahd-$(CH_3OH)_x$ and NEt_3 (0.25 g) was added, giving a homogeneous solution. The solution, after stirring for 5 days (the time required to produce a small amount of dark white solid) was filtered. The solvent was removed under reduced pressure to give a pale green oil, which was added to water and allowed to stand for a day to give pale green crystals with one water of solvation (0.4 g; 50%). Found: C, 45.6; H, 5.1. Calc. for $C_{26}H_{36}O_5P_2Pt$: C, 45.6; H, 5.3%.

IR spectra were recorded on a Hitachi 260-10 infrared spectrophotometer. Spectrometers used for NMR studied were: ^{1}H NMR, JEOL JNM-MH-100, Hitachi R-90H FT-NMR spectrometers; ^{13}C NMR: Hitachi R-90H FT-NMR (22.66 MHz). Molecular weights were obtained using a Corona Molecular Weight Apparatus M-117 (vapour pressure osmometry) in CH_2Cl_2 at 30°C. Electroconductivity was measured in a dried acetone solution (*ca* 1×10^{-3} M) using a DKK AO-6 instrument. FABMS spectra was produced using a JEOL HX-100. Elemental analyses were performed by the Micro-Analytical Centre, Department of Pharmaceutical Sciences, Kyoto University.

RESULTS AND DISCUSSION

Dinuclear Pt(II) complex cross-linked by the dahd(3,4-diacetyl-2,4-hexadiene-2,5-diol) dianion [Pt$_2$(L$_2$)$_2$(dahd-O$_2$,O′$_2$)][BF$_4$]$_2$ {L = SEt$_2$, PMe$_2$Ph, or L$_2$ = 1,5-cyclooctadiene(COD)} is formed by treating *cis*-PtCl$_2$L$_2$ (L = SEt$_2$, PMe$_2$Ph) and PtCl$_2$(COD) with $AgBF_4$ in the presence of H_2-dahd in acetone or CH_3OH. IR and ^{1}H NMR data of [Pt$_2$(L$_2$)$_2$(dahd-O$_2$,O′$_2$)][BF$_4$]$_2$, is given in Table 1 and shows that dahd bonds the Pt(II) nuclei by symmetrical O-bonding bifunctional chelation. These spectral data agree well with those of the corresponding Pd(II) and Rh(I) complexes [M$_2$(L$_2$)$_2$(dahd-O$_2$,O′$_2$)][BF$_4$]$_n$ (M = Pd, L = PPh$_3$, L$_2$ = bdpe{1,2 - bis(diphenylphosphino)ethane}, *n* = 2; M = Rh, L = CO, *n* = 0).[1]

[Pt$_2$L$_4$(dahd-O$_2$,O′$_2$)][BF$_4$]$_2$ (L = SEt$_2$,PMe$_2$Ph), by treating with K$_2$-dahd or Na$_2$-dahd in CH_3OH, readily transforms into PtL$_2$(dahd). PtL$_2$(dahd) was directly obtained in a moderate yield by reacting *cis*-PtCl$_2$L$_2$ with K$_2$-dahd or Na$_2$-dahd in the presence of NEt_3.

IR, ^{1}H and ^{13}C NMR spectra of PtL$_2$(dahd) {L = SEt$_2$, PMe$_2$Ph, PPh$_3$; L$_2$ = 2,9-R$_2$-phen (R = H, Me)} are shown in Fig. 2 (L = SEt$_2$) and Tables 1 and 2. ^{1}H NMR spectrum of Pt(SEt$_2$)$_2$(dahd) shows that two Me groups of the dahd are equivalent, while the other two are non-equivalent. A resonance occurs at 2.51 in the lower field region close to that proposed for an acetyl group of, for example, γ-carbon-bonded β-diketonate Pt(II) complexes,[6] while the resonance at 2.10 is consistent with one carbonyl bound to Pt(II) in the enol form. This indicates that one acetylacetonate group of the dahd contains a localized (C=C) group. Characteristic IR absorption bands are consistent with those, in which 1502 cm^{-1} is due to ν(C—O), 1636 cm^{-1} to ν(C=C), and two bands at 1728 and 1670 cm^{-1} are due to ν(C=O). The ^{1}H NMR also exhibits magnetically non-equivalency of the two sulphur atoms. A ^{13}C{^{1}H} NMR spectrum of Pt(SEt$_2$)$_2$(dahd) obtained when operating in the Fourier Transform Mode (with 30,000 of pulse acquisition and 4 s of pulse intervals) agrees well with these observations. The satellites due to the ^{195}Pt splitting at 73.1 is due to the 3-carbon nucleus

Table 1. IR and ^1H NMR data

Complex	Characteristic bands (IR)[a]				^1H[b]		
	ν(C=O)		ν(C=C)	ν(C···C)+ν(C···O) or ν(C—O)	δ_{Me}		
$[Pt_2(SEt_2)_4(dahd)][BF_4]_2$[c]				1562(vs)			2.10
$[Pt_2(PMe_2Ph)_4(dahd)][BF_4]_2$[d]				1556(vs)			2.13
$[Pt_2(COD)_2(dahd)][BF_4]_2$[e]				1542(vs)			2.15
$Pt(SEt_2)_2(dahd)$[f]	1728(w)	1670(vs)	1636(m)	1502(vs)	2.51(1)	2.15(2)	2.10(1)
$Pt(PPh_3)(SEt_2)(dahd)$[g]	1719(w)	1673(vs)	1632(m)	1501(vs)	2.18(2)	2.08(1)	1.99(1)
$Pt(PMe_2Ph)_2(dahd)$[h]		1673(vs)	1627(s)	1515(s)	2.40(1)	2.14(2)	1.96(1)
Pt(phen)(dahd)[i]	1735(w)	1680(vs)	1632(m)	1547(vs)	2.47(1)	2.14(2)	2.07(1)
Pt(2.9-Me_2-phen)(dahd)[j]		1680(vs)	1632(m)	1503(vs)	2.26(1)	2.10(2)	1.95(1)

[a] Measured in nujol mulls.

[b] Measured in $CDCl_3$ unless otherwise indicated. Chemical shifts are relative to Me_4Si at 0.00.

[c] $\delta_{Me}(SEt_2)$ 1.47(t), $\delta_{CH_2}(SEt_2)$ 3.04 with $[J(^{195}Pt—H)] = 35$ Hz, $J_{H,H'} = 7$ Hz.

[d] $\delta_{Me}(PMe_2Ph)$ 1.71 with $[J(^{195}Pt—H)] = 34$ Hz, $J_{P,H} = 13$ Hz. Measured in $(CD_3)_2CO$-$CDCl_3$.

[e] Measured in $(CD_3)_2CO$. $\delta_{CH}(COD)$ 5.93 with $[J(^{195}Pt—H)] = 74$ Hz. $\delta_{CH_2}(COD)$ 2.5 ~ 2.9 (multiplet).

[f] $\delta_{Me}(SEt_2)$ 1.44(t) 1.33(t), $\delta_{CH_2}(SEt_2)$ 3.05 (q, $J_{H,H'} = 7$ H, $J_{Pt,H} = 28$ Hz) 2.67(q); $[^4J(^{195}Pt—H)]$ (Me-protons at 1,8-positions of $dahd^2$) = 5 Hz.

[g] $\delta_{Me}(SEt_2)$ 0.91(t), $\delta_{CH_2}(SEt_2)$ 2.56(q, $J_{H,H} = 8$ Hz) where $J_{Pt,H} = \sim 35$ Hz. $[^4J(^{195}Pt—H)]$ (Me-protons at 6-position of dahd) = 6 Hz.

[h] $\delta_{Me}(PMe_2Ph)$ 1.60(d) with $J_{P,H} = 12$ Hz, $J_{Pt,H} = 37$ Hz. 1.44(d) with $J_{P,H} = 11$ Hz, $J_{Pt,H} = 24$ Hz. $[^4J(^{195}P—H)]$ (Me-protons at 1,8-positions of dahd) = 7 Hz.

[i] δ of the azaheterocyclic ligand: 2,9-H 10.18(d) 9.40(d), 4,7-H 8.60(d) 8.41(d), 5,6-H 7.90(s) where ^{195}Pt satellites could not be discerned.

[j] δ of the azaheterocyclic ligand: 4,7-H 8.38(d), 5.6-H 7.74(s) 3,8-H 7.64(d) 7.52(d), 2,9-Me 3.10(s), 3.03(s).

Table 2. $^{13}C\{^1H\}$ NMR data[a]

Complex	dahd								SEt_2		PMe_2PH	
	$C^{2,7}$	C^5	C^9	C^4	C^3	$C^{1,8}$	C^{10}	C^6	C^1	C^2		
$Pt(SEt_2)_2(dahd)$	201.8	194.3	188.5	120.1	73.1	30.3	28.6	24.3	31.4	13.1		
	[51.1]	[41.5]	[28.3]	[40.1]	[489.2]			[42.2]	[22.1]	[15.2]		
									30.6	12.5		
$Pt(PPh_3)(SEt_2)(dahd)$	201.8	195.5	191.1	118.3	81.5	30.5	28.7	24.2	27.9	12.9		
									[15.2]			
	(6.2)	(4.5)			(60.0)							
$Pt(PMe_2Ph)_2(dahd)$	202.4	196.0	190.7	117.8	80.7	30.4	28.8	25.7			12.6	11.8
	[34.2]							[64.8]				
	(6.2)	(4.8)	(9.7)	(4.8)	(56.0)			(5.5)			(34.6)	(40.8)
Pt(phen)(dahd)[b]	205.4	195.4	—	—	—	30.2	28.5	23.9				
Pt(2,9-Me_2-phen)(dahd)[c]	207.0	193.7	189.7	118.9	60.2	29.6	28.7	23.8				
	[49.9]				[313.5]			[75.3]				

[a] Chemical shifts are relative to Me_4Si at 0.00. The solvent used is $CDCl_3$. [$J(^{195}Pt—H)$] are in braces; J(P—C) in parentheses; the other resonances and their coupling constants which are not described in the table were not discernible owing to the low solubilities or insufficient S/N ratio.

[b] Resonances due to azaheterocyclic ligand are as the following: C^2, C^9 153.3 149.0; C^3, C^8 128.0 125.0; C^4, C^7 138.3 137.0; $C^{5,6}$ 126.6; C^{13}, C^{14} 130.2 130.0; C^{11}, C^{12} 147.6 145.1.

[c] Resonances due to azaheterocyclic ligand are as the following; C^2, C^9 167.5 162.5; C^3, C^8 125.8 125.5; C^4, C^7 127.0 126.7; C^5, C^6 137.1 136.9; C^{13}, C^{14} 127.6 127.3; C^{11}, C^{12} 149.2 147.4; *Me*-C^2, *Me*-C^9 28.5 24.3.

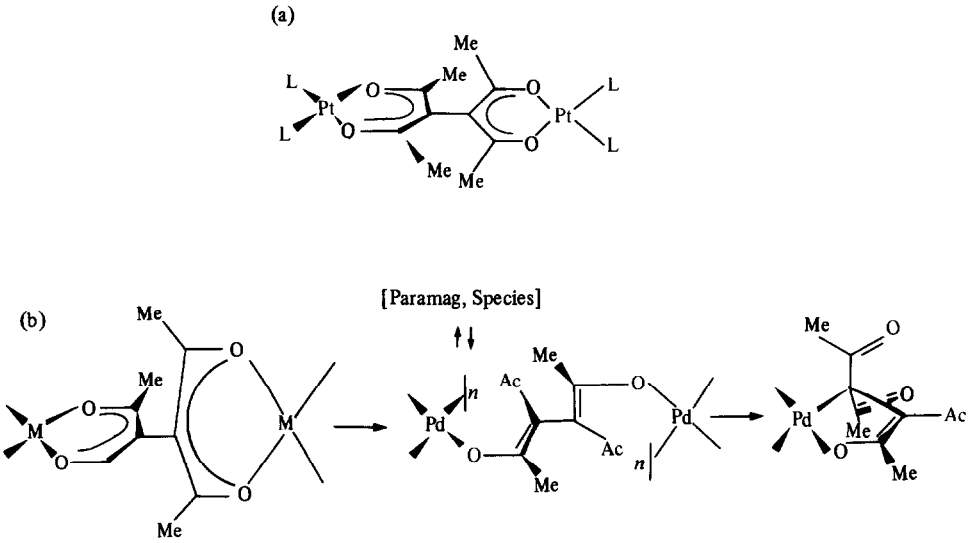

Fig. 1. (a) Proposed structure of $[Pt_2(L_2)_2(dahd\text{-}O_2,O_2')]^{2+}$. (b) Linkage modes of tetra-acetylethane dianion given by a bridge splitting reaction of $[M_2(L_2)_2(dahd\text{-}O_2,O_2')][BF_4]_n$ (M = Pd, L = PPh_3, $n = 2$; M = Rh, L = CO, $n = 0$); Ac = CH_3CO-.

of the dahd and the large coupling constant $[^1J(^{195}Pt—^{13}C)] = 489.2$ Hz is consistent with C-3 atom directly bonding to Pt(II),[7] while $[^2J(^{195}Pt—C^4)]$ was obtained as 40.1 Hz at 120.1.

These spectral data of $Pt(SEt_2)_2(dahd)$ agree with a structure having low symmetry in which dahd bonds to Pt(II) with a (C^3,O')-chelate as proposed in Fig. 3. Interestingly, ^{13}C NMR resonances due to one SEt_2 could be observed with ^{195}Pt satellites, while the other has no ^{195}Pt satellites.

It has been reported from variable temperature ^1H NMR evidence that *cis*-$PtCl_2\{S(CH_2C_6H_5)_2\}_2$[8] undergoes dynamic inversion motion at the pyramidal sulphur. In the present case, one sulphide in $Pt(SEt_2)_2(dahd\text{-}C_3,O')$ is assumed likely to be undergoing analogous dynamic behaviour at an ambient temperature, but lower temperature NMR spectra have not been obtained. However, ^{13}C NMR data of the analogous central carbon-bonded Pt(II) complexes of acetylacetone, $Pt(acac\text{-}O)(acac\text{-}C^3)(py)$ and $Pt(acac\text{-}C^3)_2(py)_2$[9] may be useful for the arrangement of sulphides in $Pt(SEt_2)_2(dahd\text{-}C^3,O')$. From the magnitude of the coupling constant $^{195}Pt—C^3$, observed for the acetylacetonate complexes, where $J(^{195}Pt—C^3)$ for $Pt(acac\text{-}O)(acac\text{-}C_3)(py)$ is 619 Hz and for $Pt(acac\text{-}C^3)_2(py)_2$ is 369 Hz, *s*-bonding character of C-3 is apparently correlated with a *trans* labilizing effect:[10] O(acac) < C(3)(acac). Thus, the sulphur being stereochemically nonrigid in $Pt(SEt_2)_2(dahd\text{-}C^3,O')$ can be explained by an arrangement which is *trans* to C(3) (a resonance in the higher field region) and not to O. FABMS of $Pt(SEt_2)_2(dahd\text{-}C^3,O')$ is given in Fig. 4 as an explicit pattern, in which the basal peak is $M^+(m/z = 572)$ and the isotopic ion distribution patterns agree well with the calculated ones.

A sulphide of $Pt(SEt_2)_2(dahd\text{-}C^3,O')$ is readily displaced by PPh_3 to give $Pt(PPh_3)(SEt_2)(dahd\text{-}C^3,O')$. ^{13}C NMR spectrum of the complex with a relatively large $[^2J(P—C)] = 60.0$ Hz is as expected, consistent with PPh_3 being arranged at the *trans* position to C^3. In addition, NMR resonances due to the CH_2 group of SEt_2 with ^{195}Pt satellites may be due to the stereochemical rigidity being arranged *trans* to O.

^1H and ^{13}C NMR of $Pt(PMe_2Ph)_2(dahd)$ is comparable with $Pt(SEt_2)_2(dahd\text{-}C^3,O')$, and they exhibit non-equivalency of the two phosphorus atoms. The chemical shifts due to the dahd carbons of $Pt(PMe_2Ph)_2(dahd)$ agree with those obtained for $Pt(SEt_2)_2(dahd\text{-}C^3,O')$. The weak resonances at 81.8 and 79.4 Hz, the latter of which was partially overlapped with that of the solvent $CDCl_3$ are tentatively assigned to the C^3 nucleus coupled to the *trans* phosphorus nucleus. Its chemical shift and two bond coupling constant $[^2J(^{31}P—C^3)] = 56.7$ Hz are however comparable with those obtained for $Pt(PPh_3)(SEt_2)(dahd\text{-}C^3,O')$.

$Pt(SEt_2)_2(dahd\text{-}C^3,O')$ reacts with the bidentate azaheterocyclic ligand phen to give $Pt(phen)(dahd\text{-}C^3,O')$. IR, ^1H and ^{13}C NMR spectral data of this complex agree very closely with those of $PtL_2(dahd\text{-}C^3,O')$(L = SEt_2, PMe_2Ph) and also with $Pd(phen)(dahd\text{-}C^3,O')$.[1] ^{13}C NMR of an analogous 2,9-Me_2-phen complex was more informative than the phen complex, because we could raise its solubility, and the data are compatible with the proposed structure (Fig. 3).

The bridge-splitting reaction of the dinuclear

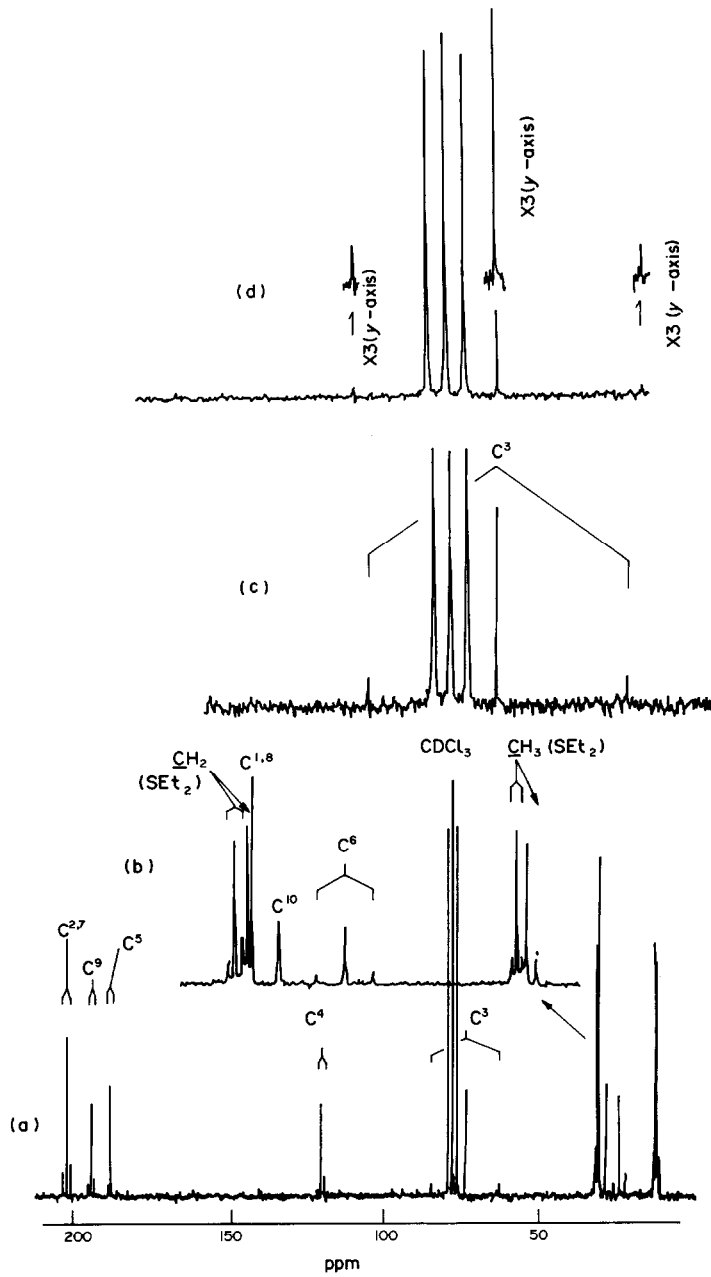

Fig. 2. (a) $^{13}C\{^1H\}$ NMR spectrum of $Pt(SEt_2)_2$(dahd-C^3,O′) in $CDCl_3$; (b) expanded in the range of 0 ~ 50 ppm; (c) expanded (× 3) in the range 50 ~ 100 ppm; (c) expanded in the range 50 ~ 100 ppm; (d) expanded (× 3) through y-axis. *Due to impurity included.

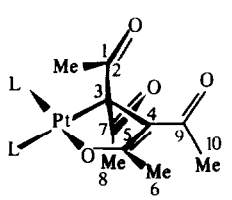

Fig. 3. Proposed structure of PtL_2(dahd-C^3,O′){L = SEt_2, PMe_2Ph, L_2 = 2,9-R_2-phen(R = H, Me)}.

Pt(II) complex cross-linked by the dahd dianion as an (O_2,O'_2)-chelate by the attack of basic K_2-dahd, may firstly proceed via an uptake of the counter anion (KBF_4) and concurrent insertion of the dahd dianion into the inner sphere (Scheme 1). On the other hand, by treating PtL_2(dahd-C3,O′) (L = SEt_2, PMe_2Ph) with an equivalent amount of HBF_4 in aqueous acetone, $[Pt_2L_4(dahd)][BF_4]_2$ (L = PMe_2Ph, yield 73%) and H_2-dahd (46%) were obtained.

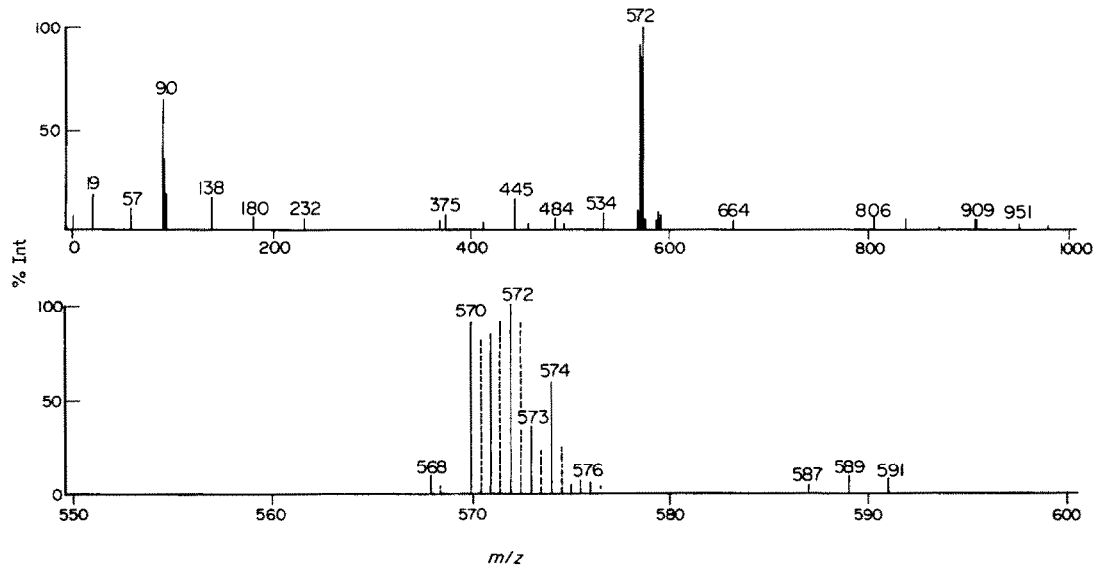

Fig. 4. FABMS of $Pt(SEt_2)_2$(dahd-C^3,O′).

These indicate that linkage modes of the dahd dianion to Pt(II) in acidic conditions favour the bifunctional (O_2,O'_2)-chelate, while in basic conditions it prefers the (C^3,O′)-chelate. It has so far been known that deprotonation of β-diketonate Pt(II) complexes, $Pt(tfac)_2(PPh_3)$ (tfac = 1,1,1- trifluoroacetylacetone),[11] PtCl(acac-O)(π-val) (val = vynylalcohol)[12] and PtCl(acac-O)(acac)[12] favours carbon-bonded complexes of the β-diketone at C-3 and up to C-1. Considering that dahd itself is γ,γ′-bis(acetylacetonate) and stabilized in the dienol–dienolate form both in H_2-dahd[13] and $[M_2(L_2)_2(dahd)][BF_4]_n$ (M = Pd, L = PPh_3, L_2 = bdpe, $n = 2$; M = Rh, L = CO, $n = 0$; M = Pt, L = SEt_2, PMe_2Ph, L_2 = COD, $n = 2$), an activation of C-3 of the dahd forming metallation should still be noteworthy. Unfortunately, an intermediate, such as $[PtL_2(dahd\text{-}O_1,O'_1)]_n$ or any paramagnetic species as found for catena-[Pd(phen)(dahd-O_1,O'_1)]$_n$, have not been isolated.

Interestingly, the linkage mode of the dahd dianion to Pt(II) as a (C^3,O′)-chelate is comparable with the Pt(II) complex of Vitamin C Pt(*cis*-dach) (ascorbate) (dach = diaminocyclohexane),[14] having antitumor properties which Hollis *et al.* established by X-ray analysis, in addition to their similar frameworks.

Acknowledgement—An author (S. Y.) is grateful to Y. Tanaka (Hitachi Ltd, Naka Engineering Centre, Ibaragi) for obtaining ^{13}C NMR spectra.

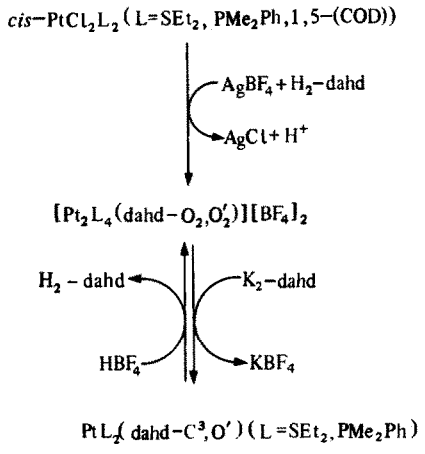

Scheme 1.

REFERENCES

1. S. Yamazaki, *Polyhedron* 1986, **5**, 1183.
2. S. Yamazaki, *Polyhedron* 1985, **4**, 1915; S. Yamazaki, *Bull. Chem. Soc. Jpn.* 1987, **60**, 1155.
3. G. B. Kauffman and D. O. Cowan, *Inorg. Synth.* 1960, **6**, 211.
4. J. M. Jenkins and B. L. Shaw, *J. Chem. Soc.* (A) 1966, 770.
5. J. X. McDermott, J. F. White and G. M. Whitesides, *J. Am. Chem. Soc.* 1976, **98**, 6521.
6. J. Lewis and C. Oldham, *J. Chem. Soc.* (A). 1966, 1456; S. Kawaguchi, *Coord. Chem. Rev.* 1986, **70**, 51.
7. B. E. Mann and B. F. Taylor, *^{13}C NMR Data for Organometallic Compounds*. Academic Press, London (1981).

8. P. Haake and P. C. Turley, *Inorg. Nucl. Chem. Lett.* 1966, **2**, 173; P. Haake and P. C. Turley, *J. Am. Chem. Soc.* 1967, **89**, 4611.
9. T. Ito. T. Kiriyama, Y. Nakamura and A. Yamamoto, *Bull. Chem. Soc. Jpn.* 1976, **49**, 3257.
10. A. Yamamoto, *Organometallic Chemistry*. Syokabo, Tokyo (1986); F. Basolo and R. G. Pearson, *Mechanism of Inorganic Reactions* 2nd edn. John Wiley, New York (1967).
11. S. Okeya, Y. Nakamura and S. Kawaguchi, *Bull. Chem. Soc. Jpn.* 1981, **54**, 3396.
12. J. Hills, J. Francis, M. Mori and M. Tsutsui, *J. Am. Chem. Soc.* 1974, **96**, 4800.
13. L. F. Power and K. E. Turner, *Inorg. Nucl. Chem. Lett.* 1972, **8**, 313; J. P. Schaefer and P. J. Wheatley, *J. Chem. Soc.* 1966, 528.
14. L. S. Hollis, A. R. Amundsen and E. W. Stern, *J. Am. Chem. Soc.* 1985, **107**, 274.

Polyhedron Vol. 7, No. 5, pp. 363–368, 1988
Printed in Great Britain

0277–5387/88 $3.00+.00
Pergamon Press plc

A SYSTEMATIC SEARCH FOR THE VALENCE STRUCTURES OF THE TETRADECAHYDROTETRADECABORATE DIANION

MARCEL GIELEN

Free University of Brussels V.U.B., Faculty of Engineering, Pleinlaan 2,
B-1050 Brussels, Belgium

(*Received* 12 *June* 1987; *accepted* 16 *September* 1987)

Abstract—A systematic search has been used to find all the allowed valence structures of the D_{6d} bicapped hexagonal antiprismatic $B_{14}H_{14}^{2-}$ *closo*-boron hydride dianion. From the number of allowed valence structures (72), a valence state index (VSI) equal to 0.0773 can be deduced for the tetradecahydrotetradecaborate dianion, that is compared to those of the parent $B_nH_n^{2-}$ derivatives (n = 6–12).

The topological rules defined by Lipscomb[1a] allow one to find[1] all the possible valence structures for boron hydrides. The number of allowed valence structures (NVS) has been determined for the *closo*-boron hydrides $B_nH_n^{2-}$ (n = 1–12)[2] and have been used[3] to determine the valence state index (VSI), defined as the ratio of the logarithm of the NVS over the number of triangular faces of the polyhedron, and have been correlated with the stability of these cage compounds.

We describe in the present paper the systematic search for the allowed valence structures of the D_{6d} tetradecahydrotetradecaborate dianion making use of the framework symmetry. It has indeed been shown that a bicapped hexagonal antiprismatic arrangement of the boron atoms is the most stable one found for $B_{14}H_{14}^{2-}$.[4] Jemmis[5] has made calculations on 14-vertex boranes and carboranes, and concludes that the orbitals of BH are not diffuse enough to overlap favourably with the orbitals of a six-membered ring as in a bicapped hexagonal antiprism, and states that caps with more diffuse orbitals, like transition metal fragments, should stabilize such polyhedra. No $B_nH_n^{2-}$ ions are indeed known for $n > 12$, but two *closo* 14 vertex metallacarboranes that are cage-isoelectronic with $B_{14}H_{14}^{2-}$, i.e. having 30 valence electrons in the cage skeleton, as from Wade's rules, have been described. A differacarborane, 1,14,2,5,9,12-(η^5-$C_5H_5Fe)_2(CH_3C)_4B_8H_8$, with the bicapped hexagonal antiprism structure has been prepared[6] and structurally proved[7] by Grimes. Hawthorne has reported a cobaltacarborane, 1,14,2,10-(η^5-$C_5H_5Co)_2C_2B_{10}H_{12}$, with this structure,[8] although it was not crystallographically confirmed. We determined the number of valence structures for $B_{14}H_{14}^{2-}$ in order to have an idea about the estimation of its stability we would get using this very crude approach and to compare the results with Jemmis' conclusions.

TOPOLOGICAL RULES AND NUMBERING CONVENTION

Lipscomb's topological rules[1] applied to the $B_nH_n^{2-}$ case can be summarized as follows:

(1) Every pair of boron atoms that are neighbours (see Fig. 1) must be connected by at least one bond (either a covalent bond, or one or two three-centre bonds).

(2) No boron framework bond may include a pair of non-neighbour boron atoms.

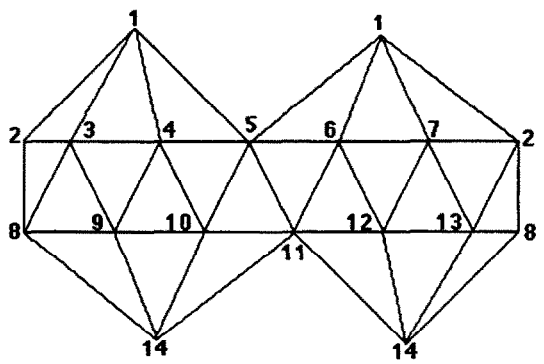

Fig. 1. "Opened" representation of, and numbering convention used for $B_{14}H_{14}^{2-}$.

(3) Each boron, since it has four valence atomic orbitals, must participate in three boron framework bonds, because it has one terminal hydrogen covalently bonded to it.

(4) Since each boron atom contributes three valence electrons and four valence orbitals, $B_nH_n^{2-}$ must have three covalent B—B bonds and (n-2) closed three-centre bonds.

(5) No two boron atoms may be bonded simultaneously to both a covalent and a three-centre bond.

We will use the "opened" representation of the polyhedron,[9] showing more clearly the 24 triangular faces of the D_{6d} bicapped hexagonal antiprism, using the numbering proposed earlier for this polyhedron[10] (see Fig. 1).

SYSTEMATIC SEARCH OF THE POSSIBLE VALENCE STRUCTURES OF $B_{14}H_{14}^{2-}$

Vertical apical covalent bonds are not allowed

First of all, it is quite obvious that the covalent bonds may not be placed on one of the vertical edges of the apical triangles of the upper or lower pyramids. Indeed, the two adjacent triangles must be discarded* (because a three-centre bond may not connect two boron atoms already bonded by a covalent bond, rule 5). Because two adjacent triangles cannot be discarded (rule 1), we must place a three-centre bond in both triangles adjacent to the discarded ones. This saturates boron atom 1 (see Fig. 2) and does not allow us any longer to place another three-centre bond in one of the two remaining adjacent apical triangles. Both of these should therefore be discarded, which is forbidden by rule 1.

The apical three-centre bonds

The covalent bonds must therefore all be placed in equatorial triangles, and both the upper and lower apical boron atoms (1 and 14) must be saturated by three three-centre bonds. These may not be placed in adjacent triangles, otherwise other adjacent triangles would have to be discarded.

Therefore, six horizontal equatorial locations (2–3, 4–5, 6–7, 8–9, 10–11, 8–13, if the six apical three-centre bonds are placed as in Fig. 3) are not allowed for the covalent bonds (rule 5), which means that only six remain possible.

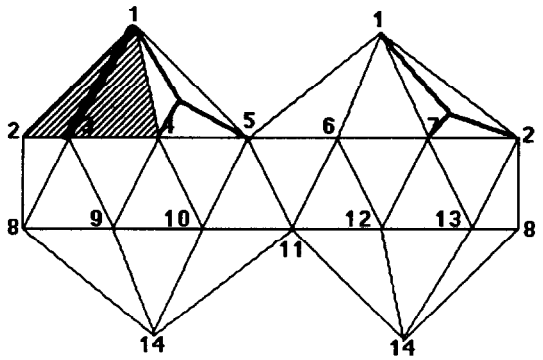

Fig. 2. A covalent bond may not be placed on one of the vertical edges of the apical triangles of the upper (or lower) pyramids, because two adjacent triangles (here 1 5 6 and 1 6 7) must then be discarded.

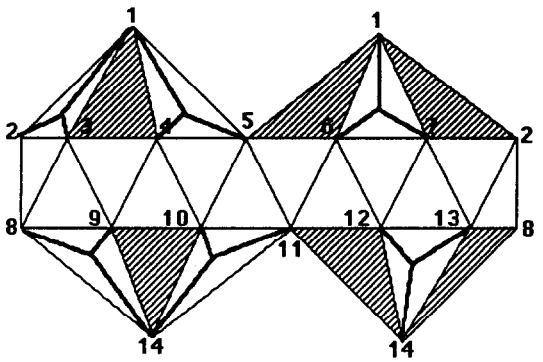

Fig. 3. One of the four allowed positions of the six apical three-centre bonds.

The three covalent bonds are placed horizontally

If two covalent bonds are put horizontally as the adjacent edges of apical and equatorial triangles of *the same pyramid* (for instance in 3–4 and 5–6, cf. Fig. 4), then the third one cannot be put on one of the horizontal equatorial edges of the *other* pyramid, because in this case, it is impossible to saturate all the boron atoms using rules 1–5,

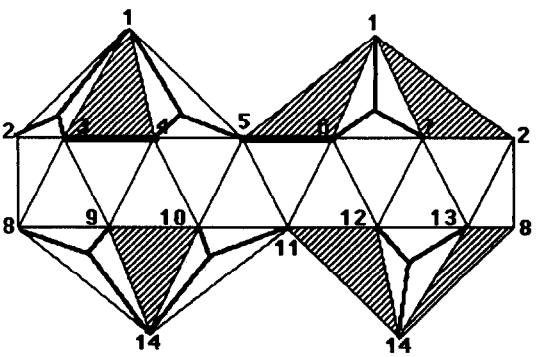

Fig. 4. Possible position of the first two covalent bonds on horizontal equatorial edges of the same pyramid.

*Shaded triangles are triangles in which no three-centre bond may be placed because of constraints due to the presence of already placed covalent and/or three-centre bonds, and to Lipscomb's rules 1–5.

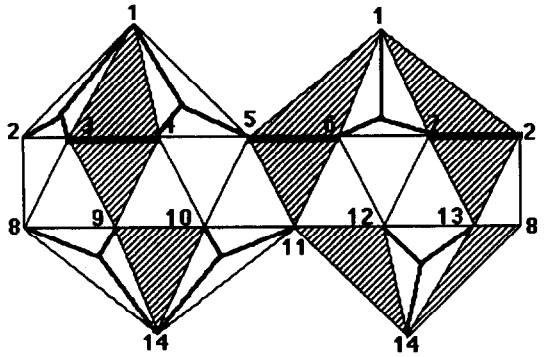

Fig. 5. Allowed positions of the three covalent bonds on three horizontal edges of the same pyramid (3–4, 5–6, 2–7).

whereas it can be put on the third allowed equatorial edge (2–7) of the *same* pyramid (see Fig. 5), which gives an allowed resonance structure.

If the three covalent bonds are all placed on these three allowed horizontal equatorial edges (3–4, 5–6 and 2–7), then it is quite obvious that there is only one way to saturate atoms 9, 11 and 13: indeed, only two triangles are available for each of them and each of them must get two more three-centre bonds, because they must participate in three boron framework bonds. If we do this, then all the other boron atoms are saturated because we have then placed the 12 (i.e. $n-2$ for $n = 14$) three-centre bonds (see Fig. 6). There are eight possible resonance structures of this type, because the three covalent bonds can be placed either on the upper or lower pyramid, and because there are four ways to place the first six three-centre bonds in the apical triangles (see Fig. 7).

Two horizontal and one vertical equatorial covalent bond

If the first six three-centre bonds are placed as in Fig. 3, and if the first two covalent bonds are placed

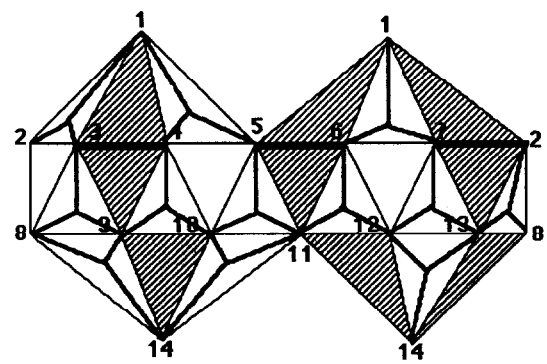

Fig. 6. Allowed resonance structures with the three covalent bonds on the three horizontal edges of the upper pyramid.

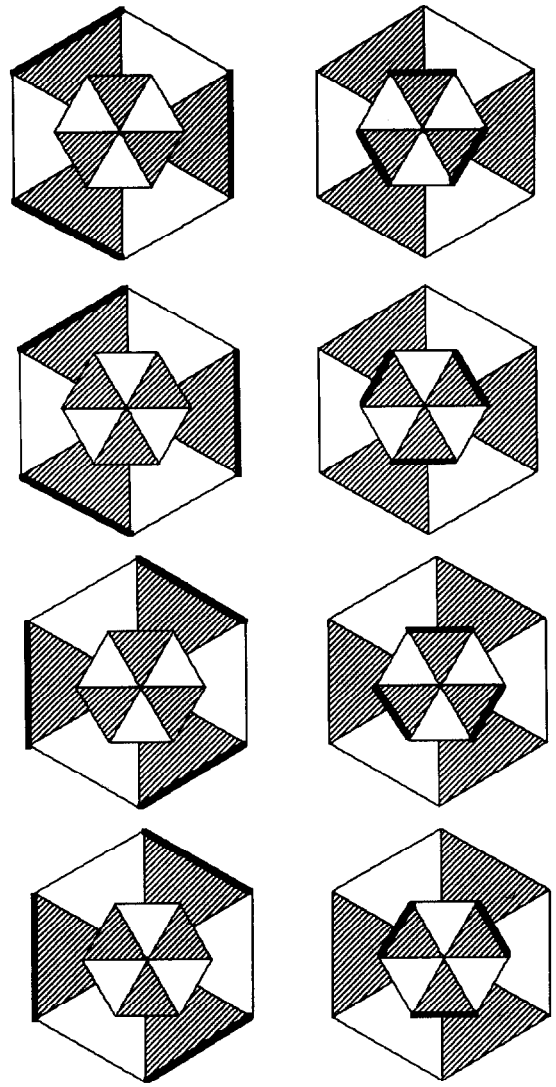

Fig. 7. The eight possible ways to put the three covalent bonds on horizontal edges of the same pyramid, either the upper or the lower one; the equatorial triangles and the six apical three-centre bonds are not shown. The D_{6d} polyhedron is viewed from vertex 1 along the 1–14 C_3 axis.

horizontally in the same pyramid as in Fig. 4, then, for nine of the 12 vertical equatorial positions, we would get two adjacent discarded triangles, which is forbidden by rule 1. If the third covalent bond is placed in two other positions, 3–9 (or 5–11), then atoms 3 (or 5) would be saturated and two adjacent triangles are again to be discarded, which is not allowed. Therefore, only one vertical equatorial position of the third covalent bond is allowed, i.e. in 7–11 (cf. Fig. 8). For this case, there is obviously only one way to saturate atoms 9, 11, 12 and 13 (see Fig. 9) by using six more three-centre bonds. These saturate the remaining boron atoms. If the first two covalent bonds are placed horizontally,

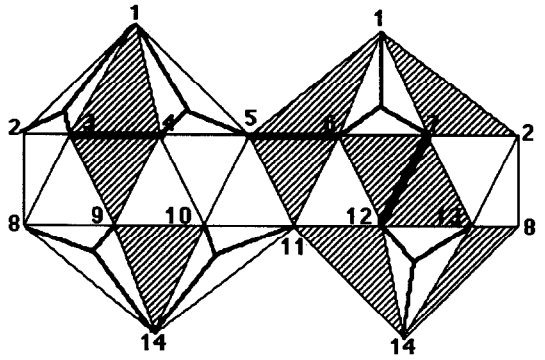

Fig. 8. Allowed position of the three covalent bonds on two horizontal edges of the same pyramid (3–4 and 5–6), and on the only allowed vertical equatorial edge, 7–11.

one in each pyramid, then there is only one acceptable way to do this, i.e. in 3–4 and 11–12, that allows one to place the third covalent bond on the only available vertical equatorial edge so that rule 1 is followed (edge 5–10) (see Fig. 10). It can be easily shown that if the two covalent bonds are put in 3–4 and 8–13, then it is impossible to put the third

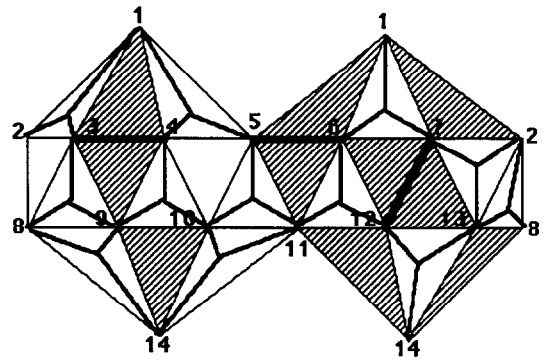

Fig. 9. Allowed resonance structure with two horizontal covalent bonds in the same pyramid, and one vertical equatorial bond.

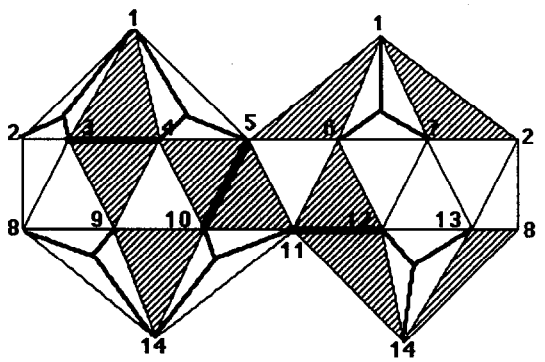

Fig. 10. Allowed position of the three covalent bonds on two horizontal edges of different pyramids (3–4 and 11–12), and on the only allowed vertical equatorial edge, 5–10.

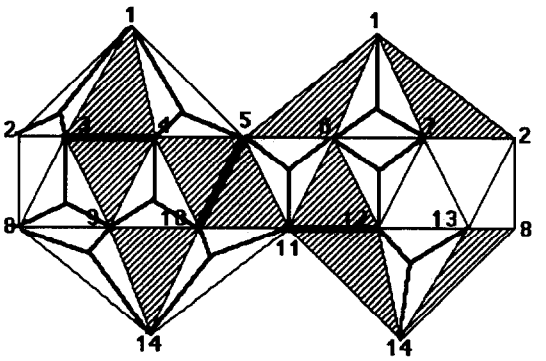

Fig. 11. The only way to saturate atoms 4, 5, 6, 9, 10 and 11 for the allowed position of the three covalent bonds on two horizontal edges of different pyramids (3–4 and 11–12), and on the only allowed vertical equatorial edge, 5–10.

covalent bond on a vertical equatorial edge: when trying to place the other three-centre bonds, rule 1 cannot be followed.

Clearly, there is only one way to saturate atoms 4, 5, 6, 9, 10 and 11, by using four three-centre bonds (see Fig. 11). This saturates atoms 3 and 12, so that the two triangles 2 3 8 and 7 12 13 have to be discarded. The last two three-centre bonds must therefore be put in the two still available triangles, as shown in Fig. 12. There are 12 different resonance structures of this type, because the vertical equatorial covalent bond can be placed on any of the 12 vertical equatorial edges (these resonance structures indeed belong to the C_2 symmetry point group).

One horizontal and two vertical equatorial covalent bonds

If the first covalent bond is put horizontally, for instance in 3–4, then only two vertical equatorial positions are compatible with rule 1 for another covalent bond (5–10 and 7–12), so that there is only one way to place the two next vertical covalent

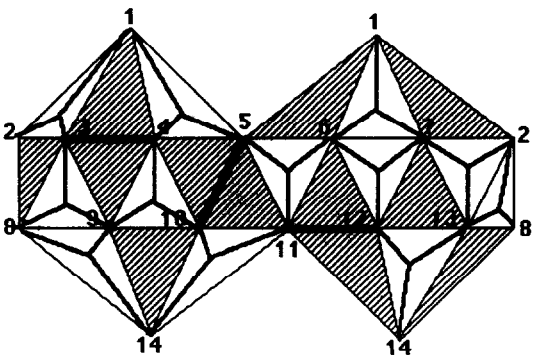

Fig. 12. Allowed resonance structure for the relative position of the three covalent bonds in 3–4, 5–10 and 11–12.

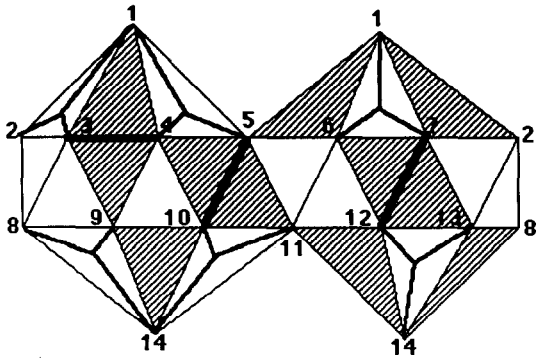

Fig. 13. Allowed position of the three covalent bonds on one horizontal edge (3–4), and on the only two allowed vertical equatorial edges (5–10 and 7–12).

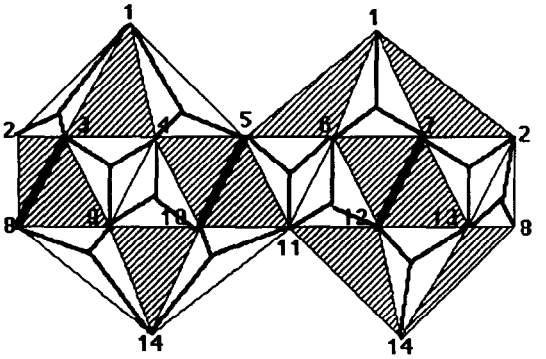

Fig. 16. One of the four equivalent allowed resonance structures for the relative position of the three covalent bonds in 3–8, 5–10 and 7–12.

bonds if the first one is placed in 3–4 (see Fig. 13). Here again, there is only one way to saturate atoms 4, 5, 6, 7, 9, 10, 11, 12 and 13 by placing the last six three-centre bonds that saturate atom 2 (see Fig. 14). There are 24 equivalent resonance structures of this type, belonging to the C_1 symmetry point group, because there are six ways to place the horizontal covalent bond for each of the four possible positions of the six apical three-centre bonds.

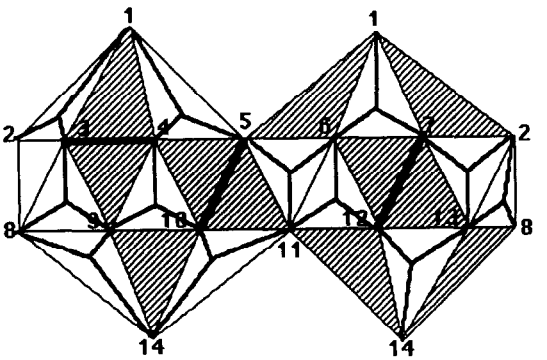

Fig. 14. Allowed resonance structure for the relative position of the three covalent bonds in 3–4, 5–10 and 7–12.

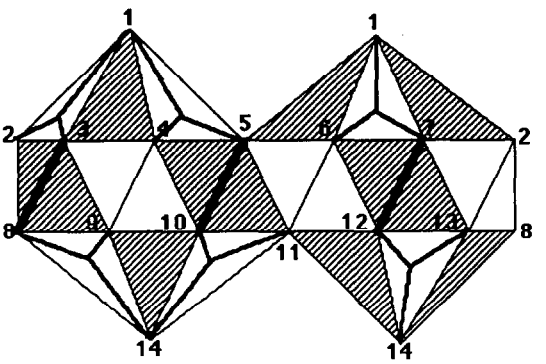

Fig. 15. Only allowed relative position of the three covalent bonds on three vertical equatorial edges, 3–8, 5–10 and 7–12.

Three vertical equatorial covalent bonds

Finally, the three covalent bonds can be placed on three vertical equatorial edges in only four (because of their C_{3v} symmetry) equivalent acceptable ways compatible with rule 1 (e.g. 3–8, 5–10 and 7–12, see Fig. 15), because nine of the 12 vertical positions are indeed excluded. Only six triangles are available in which the last six three-centre bonds have to be placed to saturate the remaining boron atoms (see Fig. 16).

CONCLUSION

The NVS can now be easily determined for $B_{14}H_{14}^{2-}$: it is equal to $8+24+12+24+4=72$. The VSI is therefore equal to $\log 72/24 = 0.0773$, which is more than for $B_{11}H_{11}^{2-}$ (0.0669), but less than for the other $B_nH_n^{2-}$ structures (see Table 1 of ref. (3); note that, for $B_{12}X_{12}$, the NVS is five and not 20 as mentioned in that paper, because the allowed valence structures belong to the T_h symmetry point group and not to the C_3 one; the VSI for $B_{12}X_{12}$ is therefore 0.0349 instead of 0.0651 mentioned in that paper). This seems to confirm Jemmis' assumption.[7] Table 1 gives the number of valence structures (NVS) and valence structure index (VSI), compared to the resonance energies per face[3] and estimated PRDDO-SCF energies per BH unit[4] for some *closo*-boron hydrides $B_nH_n^{2-}$.

When these theoretical stabilities are compared with the sequence of valence state indexes given in Table 1 ($6 > 7 > 12 > 10 > 8 > 9 > 11$), important discrepancies can be noticed: for instance, $B_{12}H_{12}^{2-}$ is exceptionally stable and $B_{14}H_{14}^{2-}$ is quite stable too in comparison with the lower analogs,[4] whereas they are characterized by lower VSI values than $B_6H_6^{2-}$ and $B_7H_7^{2-}$. The question about the validity of the VSI values to estimate the stability of these *closo* cages remains open.

Table 1.

n	NVS	VSI	Resonance energy per face	Energy per BH unit
6	32	0.1881	0.1055	−25.215
7	20	0.1301	0.0938	−25.232
8	14	0.0955	0.0665	−25.238
9	16	0.0860	0.0580	−25.249
10	72	0.1161	0.0716	−25.259
11	16	0.0669	0.0555	−25.257
12	240	0.1191	0.0881	−25.276
14	72	0.0773 (this work)		−25.266

Acknowledgements—I am thanking Prof. Veith who invited me to be an associate Professor at the Universität des Saarlandes in Saarbrücken in May 1987, which allowed me to write this paper. I am thanking the referees for their pertinent remarks and suggestions that improved this manuscript considerably.

REFERENCES

1. (a) I. R. Epstein and W. N. Lipscomb, *Inorg. Chem.* 1971, **10**, 1921; (b) M. E. O'Neill and K. Wade, *Inorg. Chem.* 1982, **21**, 461; M. E. O'Neill and K. Wade, *Polyhedron* 1983, **2**, 963; M. E. O'Neill and K. Wade, *Polyhedron* 1984, **3**, 199; M. A. Cavanaugh, T. P. Fehlner, M. E. O'Neill and K. Wade, *Polyhedron* 1985, **4**, 687.
2. W. N. Lipscomb and I. R. Epstein, *Inorg. Chem.* 1982, **21**, 846.
3. M. Gielen, *Theoret. Chim. Acta* 1982, **61**, 21; J. I. Aihara, *J. Am. Chem. Soc.* 1978, **100**, 3339.
4. L. D. Brown and W. N. Lipscomb, *Inorg. Chem.* 1977, **16**, 2989; J. Bicerano, D. S. Marynick and W. N. Lipscomb, *Inorg. Chem.* 1978, **17**, 3443; J. Bicerano, D. S. Marynick and W. N. Lipscomb, *Inorg. Chem.* 1978, **17**, 2041.
5. E. D. Jemmis, *J. Am. Chem. Soc.* 1982, **104**, 7017.
6. W. M. Maxwell, R. Weiss, E. Sinn and R. N. Grimes, *J. Am. Chem. Soc.* 1977, **99**, 4016.
7. J. R. Pipal and R. N. Grimes, *Inorg. Chem.* 1978, **17**, 6.
8. W. J. Evans and M. F. Hawthorne, *J. Chem. Soc., Chem. Comm.* 1974, 38.
9. M. Gielen, *Bull. Soc. Chim. Belg.* 1981, **90**, 501.
10. J. B. Casey, W. J. Evans and W. H. Powell, *Inorg. Chem.* 1981, **20**, 1333.

Polyhedron Vol. 7, No. 5, pp. 369–377, 1988
Printed in Great Britain

0277-5387/88 $3.00 + .00
Pergamon Press plc

PHYSICOCHEMICAL STUDIES OF *FAC–MER* ISOMERISM OF ALUMINIUM BETA-DIKETONATES BY HIGH PERFORMANCE LIQUID CHROMATOGRAPHY AT LOW TEMPERATURE

DAVID E. HENDERSON* and STEVEN J. SALTZMAN

Department of Chemistry, Trinity College, Hartford, CT 06106, U.S.A.

and

PETER C. UDEN and ZUBEN CHENG†

Department of Chemistry, University of Massachusetts, Amherst, MA 01003, U.S.A.

(*Received* 23 *February* 1987; *accepted after revision* 21 *September* 1987)

Abstract—The kinetics of interconversion of *fac* and *mer* isomers of Al(III) beta-diketonates both in free solution and during chromatographic elution are reported using low temperature high performance liquid chromatography to prepare and analyse pure isomeric complexes. Studies of retention and separation mechanisms of these complexes are also conducted using variation in column temperature to elucidate the contributions of enthalpy and entropy effects.

Low temperature high performance liquid chromatography (LT-HPLC) has been used to study the interconversion of *fac* and *mer* isomers of Al(III) beta-diketonate complexes with asymmetric ligands. Specifically the rate of isomer interchange is determined in free solution using pure samples of the *mer* isomer of $Al(tfa)_3$. The effect of various types of HPLC column material on the rate of isomer interconversion during chromatographic elution is also estimated. The thermodynamics of the separation process for the two isomers is evaluated for a homologous series of ligands shown in Table 1.

The *fac* and *mer* isomers of beta-diketonate complexes have been widely studied.[1] In many cases, the stable complexes are separable by gas chromatography[2] (GC) or by high-performance liquid chromatography[3] (HPLC). Several studies have reported the determination of physicochemical properties of specific complexes, most notably the interchange of the *fac* and *mer* isomers in the gas phase for the chromium(III) complex of 1,1,1-trifluoro-2,4-pentanedione[4] ($Cr(tfa)_3$).

The separation of labile beta-diketonates such as those of iron(III), aluminium(III) and gallium(III) has proved more difficult than that of the stable complexes due to ligand exchange with subsequent complex decomposition.[5] There are two cases of chromatographic behaviour which are expected for these species depending on the nature of the ligand exchange process. If the exchange of ligands in solution leads to the replacement of one or more ligand donor atoms by solvent molecules or by active sites on the stationary phase, the peaks if observed at all, are expected to be broad with severe tailing. This type of behaviour has been demonstrated for the diketonates of the above mentioned metals when they are separated on silica gel columns in normal phase HPLC.[5]

On the other hand, if the isomerization reaction is strictly intramolecular, either due to stronger ligand metal bonds or the absence of suitable competiton for the metal coordination sites by solvent and stationary phase donor ligands, then the chromatographic profiles observed depend only on the

*Author to whom correspondence should be addressed.

† Present address: Institute of the Salt Lake, Academia Sinica, Xining, Qinghai, People's Republic of China.

Table 1. Nomenclature of beta-diketone ligands

Abbreviation	IUPAC name
tfa	1,1,1-trifluoro-2,4-pentanedionate
thd	1,1,1-trifluoro-2,4-hexanedionate
tmhd	1,1,1-trifluoro-5-methyl-2,4-hexanedionate
tmhpd	1,1,1-trifluoro-6-methyl-2,4-heptanedionate
tmod	1,1,1-trifluoro-7-methyl-2,4-octanedionate
tpm	1,1,1-trifluoro-5,5-dimethyl-2,4-hexanedionate

degree of separation of the isomeric forms of the complex and the rate of isomerization between the forms. Melander and co-workers[6] have recently explored the theoretical relationship between peak shape and these factors. The results reported here for Al(III) diketonates using a phenyl bonded stationary phase appear to fall into the latter case, in that the peaks are distorted by isomerization on the column but the total sample appears to elute in the chromatographic envelope. It has recently been shown that if the HPLC column is maintained at a low temperature, both ligand exchange and isomerization can be slowed sufficiently to allow quantitative elution of labile complexes with good chromatographic peak shape. With judicious selection of column type and mobile phase it is possible to separate the *fac* and *mer* isomers of these labile complexes using low temperature HPLC (LT-HPLC).[7] The general principles and methods of LT-HPLC have been reviewed recently[8] and will not be discussed in detail here.

Traditionally, variable temperature nuclear magnetic resonance spectroscopy has been the primary method available for the study of the labile isomers of metal complexes.[1] The temperature at which distinct peaks for the different isomers are observed and the time scale of the NMR measurement allowed reaction rates and thermodynamic constants to be obtained. While this is a very powerful technique, the precision obtained in the measurement of physicochemical values is normally poor.

HPLC provides an alternative technique for the measurement of physicochemical constants for metal complex reactions. Melander *et. al.* have demonstrated[6] that a detailed analysis of HPLC peak profiles for species undergoing equilibrium during chromatographic elution can provide a powerful tool for measurement of reaction rates which is directly analogous to the NMR technique although the mathematical treatments are different. Their technique requires that the various equilibria be reversible and that the solute does not undergo decomposition to a form which is not eluted or detected by the chromatograph. They demonstrated the application of this technique using several dipeptides.[9] Unfortunately, reversible behaviour is not always the case for labile metal complex species and their technique is thus not applicable to these systems.

The third alternative for making such measurements is the use of LT-HPLC to allow direct analytical determinations of kinetic and thermodynamic properties of the normally labile metal complex species. The application of LT-HPLC to the separation of several labile metal beta-diketonate complexes has been demonstrated using both normal[5] and reversed phase HPLC.[7] This approach was recently demonstrated for the study of the kinetics and thermodynamics of the rotation about the peptide bond for dipeptides containing proline at the C-terminus.[10] The principal advantage of LT-HPLC, which is not possible in NMR studies, is the ability to prepare pure samples of labile isomers for further study. This could include spectral studies of individual isomeric forms of labile metal complexes and the use of pure samples for kinetic and thermodynamic measurements.

EXPERIMENTAL

Instrumentation

Two different chromatographic systems were used for this study.

System I consisted of a Model LC/9533 high performance liquid chromatograph (IBM Instruments, Danbury, CT, U.S.A.) with a fixed wavelength detector at 254 nm. Chromatograms were recorded on a Omniscribe strip chart recorder (Houston Instruments, Austin, TX, U.S.A.). In addition, data was recorded using an Apple IIe microcomputer (Apple Computer Inc.) equipped with a Model 42A Chemical Module Interface (Cyborg).

System II consisted of a Constametric III pump and Spectromonitor II variable wavelength detector (Laboratory Data Control, Riveria Beach, FL, U.S.A.) equipped with a 10 μl injection valve (Rheodyne). Chromatograms were obtained as in system I except that the computer used was a Rainbow 100PC (Digital Equipment Corp., May-

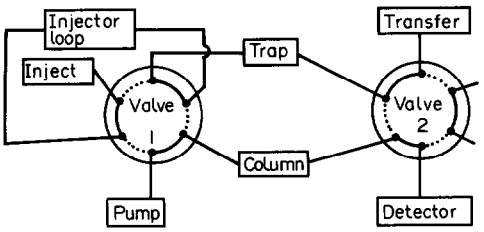

Fig. 1. Valve diagram for collection and reinjection of HPLC peaks.

nard, MA, U.S.A.) equipped with a LDT-2801 interface board (Data Translations, Marlboro, MA, U.S.A.).

Chromatographic columns were 250 × 4.6 mm ID stainless steel packed with 5.0 μ phenyl bonded silica (IBM Instruments). The column temperature for System I was maintained using a water bath while that for System II was controlled using an ethanol bath to allow operation at sub-zero temperatures.

A valve system was constructed to facilitate the collection of pure isomers and allow their reinjection for purity and kinetic determinations. The system consisted of a 7126 pneumatic injection valve with a 10 μl loop and a six port switching valve (Rheodyne). The valves were connected as shown in Fig. 1. The switching valve allowed the column effluent to be directed either to the detector or into a holding coil with a total volume of 2 ml (0.030 in ID × 0.0625 in OD stainless steel tubing). Samples could be transferred from the holding coil back to the sample loop of the injection valve for reinjection into the chromatographic column. The entire valve system was immersed in the temperature controlled bath. To use for kinetic measurements, an air bubble was injected into the holding coil to prevent mixing of the collected sample with the solvent used to transfer the sample to the injection valve loop.

Synthesis and characterization of complexes

All complexes were prepared by the method of Fay and Piper.[1] Authenticity of the complexes was confirmed by elemental analysis. The elution of the complexes was confirmed by the use of a three-electrode Spectraspan IV Direct Current Argon Plasma Emission Spectrometer as an element specific detector to verify the eluted peak metal content.

RESULTS AND DISCUSSION

On-column isomerization of Al(III) *beta-diketonates*

The elution of labile complexes such as those of Al(III) and Ga(III) has been shown to be possible using HPLC at low temperatures. The precise temperatures required depend on several factors; the rate of isomerization of the complex in the HPLC mobile phase, the chromatographic retention for the mobile phase and the mobile phase flow rate. These factors can be evaluated quantitatively using the Dahmkoler number D_a as shown by Melander.[6] The Dahmkoler number is defined by the equation

$$D_a = Lk_1(1+1/K_{eq})/\mu$$

where L is the column length, k_1 the forward rate constant for the reaction, K_{eq} the equilibrium constant for the reaction, and μ the retention time of an unretained solute on the column. While a careful analysis of the exact elution profile can be used to determine approximate reaction kinetics, this study depended on the fact that baseline resolution of two forms of a complex can only be obtained under conditions where the value of D_a is less than 1×10^{-3}. While the Dahmkoler number defines the kinetic parameters necessary for separation of species undergoing secondary equilibria on the column, it does not address factors which lead to separation of the various forms of the labile species. Obviously the column and mobile phase selected must provide for full separation of the various forms. In cases where the various forms cannot be separated, only a single peak will be observed independent of the value of the Dahmkoler number. In fact, this behaviour has been observed for several Al(III) and Ga(III) diketonates using octadecylsilica columns where the only effect of reduced temperature was to prevent complex decomposition.[11]

Figure 2 shows chromatograms obtained at several temperatures for the complex $Al(tmhd)_3$ using a mobile phase of 7% CH_2Cl_2–93% hexane. The increase in retention which results from reducing the temperature works against the effort to elute the complex without isomerization and could be mitigated by increasing the CH_2Cl_2 concentration in the mobile phase. In spite of this, at 0°C the resolution of the isomers is complete. The unchromatographic profile at the higher temperatures is characteristic of the isomerization of the two isomers during the elution process. At 0°C the interaction zone is no longer evident, indicating that the reaction is now sufficiently slowed to allow each isomer to pass through the column unchanged. Figure 3 shows chromatograms of $Al(tfa)_3$ obtained on a silica column under conditions of temperature and mobile phase where both isomerization and ligand exchange are negligible. This chromatogram can be compared with those obtained using the phenyl silica column in Fig. 4. These were obtained using a mobile phase of 10% CH_2Cl_2–90% hexane (v/v) at 0°C while that on the silica column was

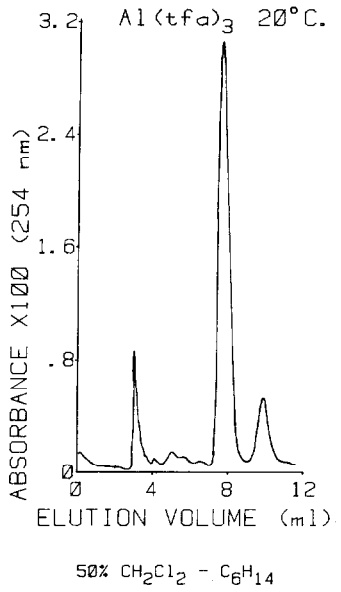

Fig. 2. Chromatograms of $Al(tmhd)_3$ at various temperatures. Column 250 × 46 mm stainless steel packed with 5μ phenyl silica; mobile phase 7:93 (v/v) CH_2Cl_2 : hexane; flow rate 1.0 ml min^{-1}; detection at 254 nm. The *mer* isomer elutes first.

obtained with a 50% CH_2Cl_2–50% hexane mobile phase at 20°C. When a more polar mobile phase is employed with the phenyl column, the resolution is reduced and a chromatogram very similar to that in Fig. 3 is observed. In each case the value of D_a is approximately 1×10^{-3}. From this and the equilibrium constant calculated from the peak areas, it is possible to esimate the relative rates of the complex isomerization during passage through the two columns. The rates of reaction calculated are 3.4×10^{-4} and 8.8×10^{-4} s^{-1} for the silica and phenyl columns respectively. These values are not for the complexes in free solution but include all effects produced by passage through the column.

The rate of isomer interconversion for $Al(tfa)_3$ has been shown by Fay and Piper to vary with the dielectric constant of the solvent[1] and with temperature. From this fact one would qualitatively predict a larger rate constant for the conditions employed with the silica column where both the dielectric constant of the solvent and the temperature are greater. In spite of the 20°C higher temperature of the silica column, the rate constant for isomerization on the phenyl column is greater.

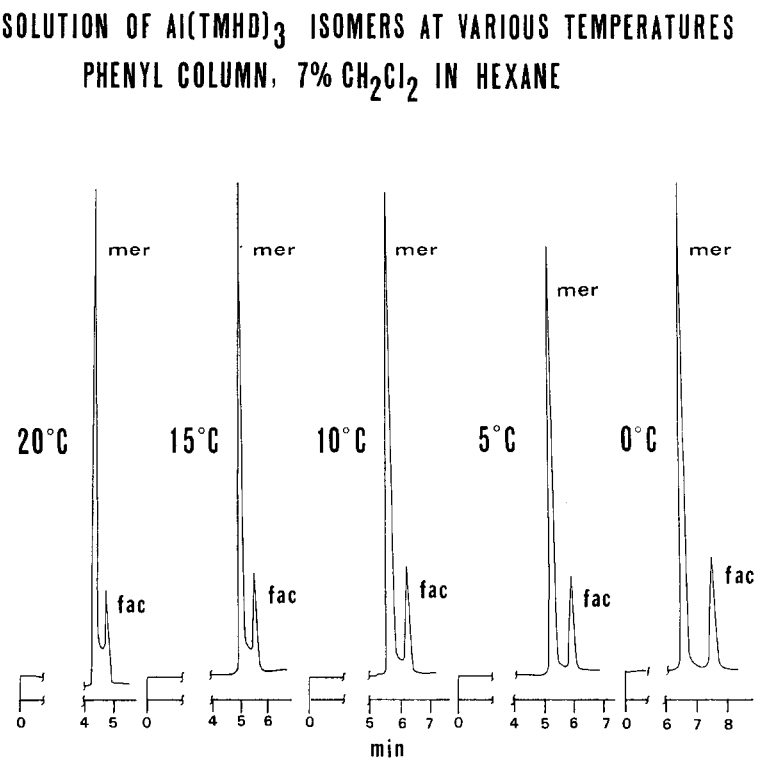

Fig. 3. Chromatograms of $Al(tfa)_3$ on silica. Column 250 × 46 mm stainless steel packed with 10μ Spherosorb silica; mobile phase 1:1 (v/v) hexane: CH_2Cl_2; column temperature 20°C; detection at 254 nm. The *mer* isomer elutes first.

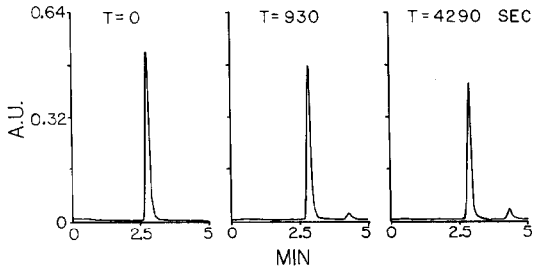

Fig. 4. Chromatograms of $Al(tfa)_3$ during free solution kinetics analysis. Column as in Fig. 2; mobile phase 10:90 (v/v) CH_2Cl_2:hexane; column temperature 0°C; flow rate 1.0 ml min^{-1}; detection at 254 nm. The *mer* isomer elutes first.

Thus the reaction on the column support proceeds significantly faster for the phenyl column than for the silica column. Clearly the interaction between the complex and the stationary phase plays a large role in the isomerization process during elution. This result is consistent with data for *cis–trans* isomerization of dipeptides containing proline as shown by Jacobson and coworkers.[9]

The situation is somewhat more complicated than the above discussion would indicate. This is demonstrated by the effect of increasing hexane concentration in the mobile phase on the elution of $Al(tfa)_3$ on silica. While it is possible to obtain complete resolution of the *mer* and *fac* isomers of this complex at room temperature in a mobile phase of 50% CH_2Cl_2–50% hexane,[11] increased retention leads to substantial isomerization and a resultant non-Gausian peak shape using 40% CH_2Cl_2–60% hexane. This trend continues until, at 30% CH_2Cl_2, no evidence is observed for complex elution at room temperature. The result is not simply the loss of resolution of the isomers which would be observed for a simple reversible reaction, but a complete decomposition of the complex. At a reduced temperature of 0°C the complex is successfully eluted in the 40% CH_2Cl_2 mobile phase without decomposition or significant isomerization. It is apparent that any efforts to alter the chromatographic retention through changes in the mobile phase polarity must also change the reaction kinetics. It is clear from the studies on silica that the increased decomposition is not due to the free solution reaction kinetics of the complex but rather to the interplay of forces while the complex is resident in the stationary phase. While the kinetics in the mobile phase are measurable, those in the stationary phase are not readily amenable to determination except through evaluation of the observed chromatographic profiles.

Studies of the thermodynamics of separation

The enthalpy and entropy changes associated with the retention process for any solute in a chromatographic system can be determined by evaluating the change in the capacity factor, k', for solutes as the temperature is varied. The value of k' is defined as

$$k' = \frac{t_r - t_0}{t_0}$$

where t_r is the retention time of the solute and t_0 is the retention time of an unretained solute. The capacity factor is useful in that it is a direct measure of the equilibrium between the mobile and stationary phases for the solute. The capacity factor varies with temperature according to the equation

$$\ln k' = -\Delta H/RT + \Delta S/R + \ln \Phi$$

where Φ is the phase ratio for the column which normally has a value of approximately 0.001 for chemically bonded column materials. Graphs of $\ln k'$ vs $1/T$ should yield linear relationships for which the slope is $-\Delta H/R$ and the intercept is $\Delta S/R + \ln \Phi$. These graphs are commonly referred to as Van't Hoff plots. Linearity is expected in the absence of temperature dependent conformational changes or other intramolecular changes which effect the retention of the species.

Van't Hoff plots were prepared over the temperature range 0–25°C for all of the complexes listed in Table 1. These plots are shown in Figs 5–8. Figure 5 shows the data obtained for the *fac* and *mer* isomers of $Al(tfa)_3$ and $Al(thd)_3$. The greater separation obtained for the isomers of $Al(tfa)_3$ is shown by the fact that the lines for these isomers lie outside those for $Al(thd)_3$. The data indicates similar slopes, indicative of similar enthalpy for the retention process for each complex. The observed differences in retention and the ability to separate the various isomers thus depends on the variation in the entropy for the retention of the respective complexes and isomers. Similar observations can be made in Fig. 6 which shows data for $Al(tpm)_3$ and $Al(tmhpd)_3$, the *tert*-butyl and *iso*-butyl substituted diketonates respectively. Again, the retention enthalpies of each complex and isomer are similar and separation depends on the variation in the entropy of solute–column interaction.

Results for a homologous series of substituted complexes yields a somewhat different picture. Specifically, in Fig. 7, the slope of the Van't Hoff plot for the *mer* isomers of $Al(tmhd)_3$, $Al(tmhpd)_3$ and $Al(tmod)_3$, which are the *iso*-propyl, *iso*-butyl, and *iso*-amyl substituted diketonates respectively, indicates a substantial difference in the retention

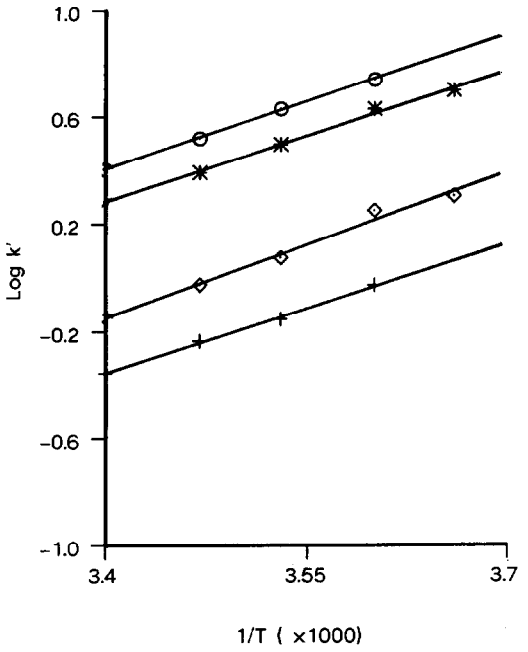

Fig. 5. Van't Hoff plots for Al(III) diketonates. Chromatographic conditions as in Fig. 2. +—*mer*-Al(tfa)$_3$, ⊙—*fac*-Al(tfa)$_3$, ◇—*mer*-Al(thd)$_3$, ∗—*fac*-Al(thd)$_3$.

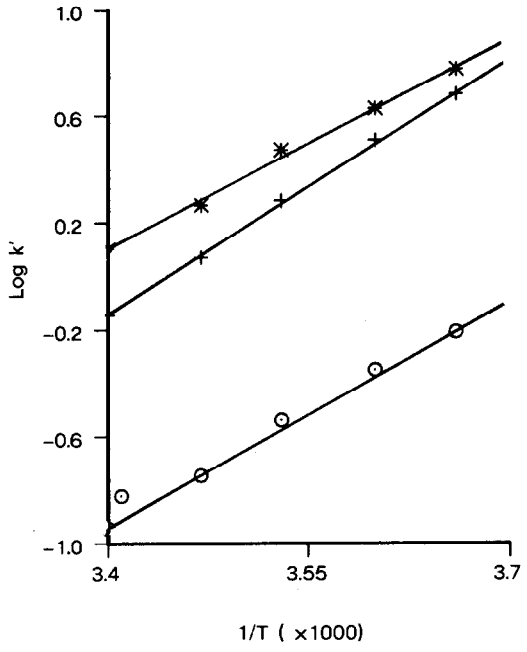

Fig. 7. Van't Hoff plots for Al(III) diketonates. Chromatographic conditions as in Fig. 2. ⊙—*mer*-Al(tmhd)$_3$, +—*mer*-Al(tmhpd)$_3$, ∗—*mer*-Al(tmod)$_3$.

enthalpy of Al(tmhpd)$_3$ relative to the other two complexes. The results for the *fac* isomers of these complexes, not shown, demonstrate the same effect.

Finally, Fig. 8 shows the results for the *mer* isomers of the complexes Al(tfa)$_3$, Al(thd)$_3$, Al(tmhpd)$_3$ and Al(tmod)$_3$ plotted together. Again, the anomalous behaviour of the butyl substituted diketonate is seen in the greater slope of the Van't Hoff plot for this complex. There is no clear explanation available for this behaviour which is seen for

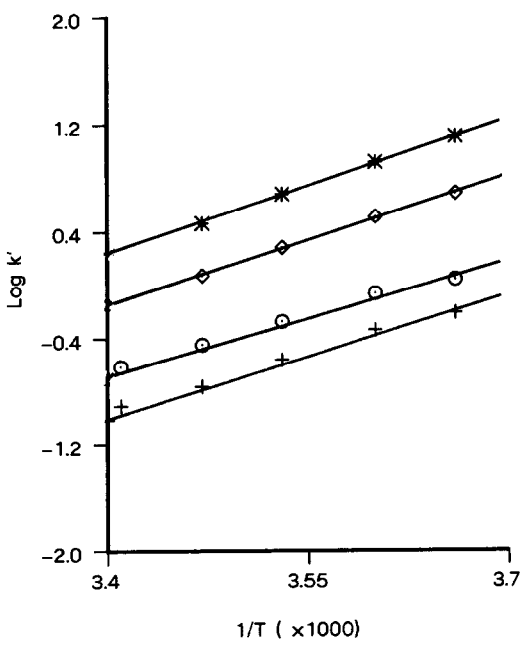

Fig. 6. Van't Hoff plots for Al(III) diketonates. Chromatographic conditions as in Fig. 2. +—*mer*-Al(tpm)$_3$, ⊙—*fac*-Al(tpm)$_3$, ◇—*mer*-Al(tmhpd)$_3$, ∗—*fac*-Al(tmhpd)$_3$.

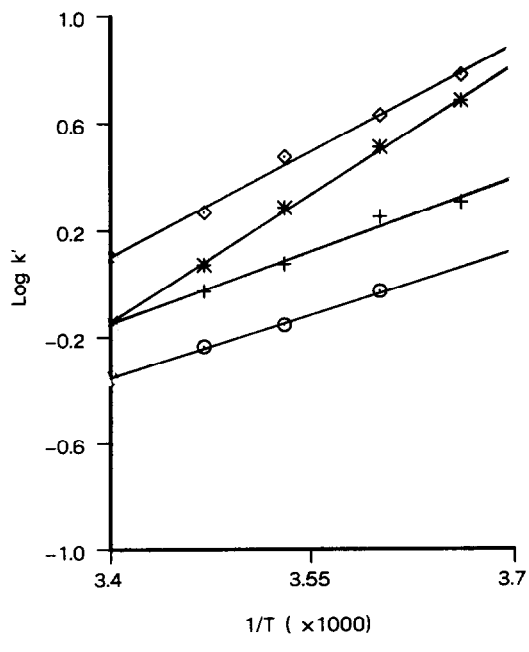

Fig. 8. Van't Hoff plots for Al(III) diketonates. Chromatographic conditions as in Fig. 2. ⊙—*mer*-Al(tfa)$_3$, +—*mer*-Al(thd)$_3$, ◇—*mer*-Al(tmhpd)$_3$, ∗—*mer*-Al(tmod)$_3$.

Table 2. Linear regression data for Van't Hoff plots for Al(III) beta-diketonates over the range 0–25°C

Complex	*mer* isomer Slope	*mer* isomer Intercept	*fac* isomer Slope	*fac* isomer Intercept	*N*
$Al(tfa)_3$	1.6	−5.8	1.7	−5.4	3
$Al(thd)_3$	1.8	−6.4	1.7	−5.3	4
$Al(tmhd)_3$	2.9	−10.7	2.9	−10.6	5
$Al(tmhpd)_3$	3.2	−11.1	3.4	−11.3	4
$Al(tmod)_3$	2.6	−8.8	2.8	−9.2	4
$Al(tpm)_3$	3.2	−11.8	3.0	−10.7	5

the *fac* isomers as well. Similar anomalous behaviour is noted for the *tert*-butyl complexes which exhibit slopes similar to those of the *iso*-butyl complexes as shown in Fig. 6.

The values of the slope and intercept determined by least squares regression analysis is indicated in Table 2. A fairly consistent trend is observed towards increases in both the enthalpy and entropy terms of the retention process with increasing length of the hydrocarbon substituent of the ligand. This is reasonable in light of the expected greater affinity of these increasingly hydrocarbonaceous species with the phenyl bonded silica. Only minor differences are observed between the *iso*-butyl and *tert*-butyl substituted diketonates. However, the values observed for these complexes are remarkable, especially in light of the disparity in retention between the two butyl isomers. A number of studies have found anomalous behaviour for the *tert*-butyl substituted diketonates which frequently exhibit substantially less retention. This data indicates that for these complexes, this retention difference is due to a dramatic decrease in the entropy change associated with the retention of the *tert*-butyl isomer which is less by approximately one order of magnitude. In many instances, linear free energy relationships have been observed for entropy and enthalpy of retention in studies of homologous series. In this case no such simple behaviour is observed.

Several additional observations can be made regarding the retention of the Al(III) diketonates on this and other types of columns. In all cases where resolution of the *fac* and *mer* isomers has been observed, the less polar *mer* isomer eluted first. This is the expected elution order for normal phase separations using silica and is not unexpected using phenyl silica with non-polar solvents as in this study. However, similar studies of other Al(III) beta-diketonates in reversed phase HPLC have observed the same elution order with methanol as solvent on octadecyl–silica.[7] In this case the less polar *mer* isomer should be retained more according to conventional models of the retention process. To date, only by using acetone as the mobile phase with octadecyl silica as the stationary phase has there been any evidence for the reversal of this elution order.

Studies of isomerization kinetics of $Al(tfa)_3$ *in free solution*

The technique of low temperature HPLC was also employed to isolate *mer* and *fac* forms of $Al(tfa)_3$ for subsequent determination of the rate of the isomerization in free solution. Effluent fractions containing the *fac* and *mer* isomers were collected at −10.0, 0.0 and 5.0°C using the apparatus shown in Fig. 1. Immediate rechromatography of the fractions at −10°C showed only a single peak of the particular isomer while at 0°C less than 1% of the isomer had converted to the other form in the time required to reinject the collected material.

The kinetics of *mer* $Al(tfa)_3$ isomerization in the mobile phase, 10% CH_2Cl_2–90% hexane, was investigated at these temperatures using the fractions collected. The kinetics of the reaction

$$mer \underset{k_{-1}}{\overset{k_1}{\rightleftharpoons}} fac$$

was assumed to be first order and reversible and gives rise to the following relationship:

$$\ln \frac{C - C_{eq}}{C_o - C_{eq}} = -\frac{K_{eq}+1}{K_{eq}} k_1 t. \qquad (1)$$

Where C is the concentration of the *mer* isomer at time t, C_o is the initial concentration of *mer* isomer, C_{eq} is the equilibrium concentration of the *mer* isomer.

The procedure described above was then employed to collect a pure fraction of the *mer* isomer which was rechromatographed over a period of 24

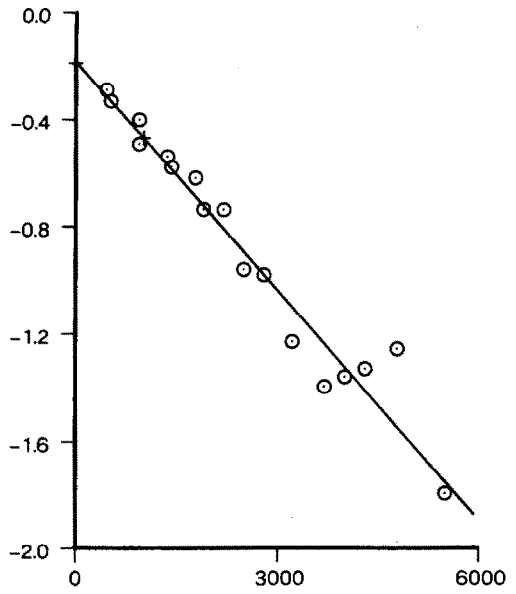

Fig. 9. Kinetics plot of $\log(C-C_{eq})/(C_o-C_{eq})$ vs time (s) for $Al(tfa)_3$ at 0°C.

h to observe the return to equilibrium. The concentrations of *mer* and *fac* isomers at each time were determined from peak areas using the microcomputer of System II. Figure 4 shows the chromatograms obtained at three times during the analysis. The first chromatogram shows essentially pure *mer* isomer immediately after trapping. The subsequent chromatograms show the gradual return to the equilibrium mixture. The value of C_{eq} was taken as the average of the values from all runs after the system had clearly returned to equilibrium. Values for C_{eq} of the *mer* isomer were 90.30, 90.15 and 92.96% determined for temperatures of −10, 0 and 5°C respectively. The value at 5°C is somewhat suspect due to the occurrence of noticeable geometric isomerization during the elution of the complex at this temperature.

The plot of data according to eq. 1 is shown in Fig. 9 for data obtained at 0°C. The data is a composite of two separate experiments with a total of 17 analyses. The slope is -2.84×10^{-4} with a relative standard deviation of 6%. From eq. 4, the rate constant for the *mer* to *fac* conversion, k_1, is $2.63 \times 10^{-3} \pm 0.16 \times 10^{-3}$ s^{-1} and the reverse rate constant k_{-1} is 2.87×10^{-4} s^{-1} at 0°C. Values for these constants at all three temperatures are shown in Table 3. An Arrhenius plot was constructed and the value of the activation energy for the *mer–fac* isomerization was determined to be 19 ± 2 kcal. The large error in this determination is believed to be due in large part to the inclusion of the rate data at 5°C for which the error is relatively large.

CONCLUSIONS

Low temperature HPLC is a powerful technique for the analysis and study of labile metal complexes. Reduced column temperature can facilitate the measurement of physicochemical quantities such as kinetic and equilibrium constants for labile species by HPLC. Furthermore, it is a useful tool to prepare conformational isomers in pure form for subsequent study by other techniques. In this regard, displacement chromatography[12] at subambient temperatures may offer particular advantages. It is believed that for a significant number of metal complexes low temperature HPLC may represent the method of choice to study conformational changes due to the ability to determine rate constants directly and to isolate pure conformers for further analysis.

Acknowledgements—Acknowledgement is made to the Donors of the Petroleum Research Fund, administered by the American Chemical Society, for support of this research (Grant 15527-B3). Acknowledgement is also made to E.I. duPont de Nemours and Co. which made possible the purchase of some equipment used in this study through a college science grant. The work of Wendy Sherman and John Muntean who conducted preliminary studies of the kinetics of $Al(tfa)_3$ is acknowledged.

Table 3. Isomerization rates of $Al(tfa)_3$ in free solution of 10% CH_2Cl_2–90% hexane (v/v) at 0°C by low temperature HPLC

Temperature	C_{eq}	k_1	k_{-1}	CV^a
−10	90.30	8.22×10^{-4}	8.84×10^{-5}	0.2
0	90.15	2.69×10^{-3}	2.87×10^{-4}	0.5
5	92.3	6.6×10^{-3}	5.0×10^{-4}	21.0

[a] Coefficient of variation or per cent relative standard deviation.

REFERENCES

1. R. C. Fay and T. S. Piper, *Inorg. Chem.* 1964, **3**, 348.
2. R. E. Seivers, B. W. Ponder, M. L. Morris and R. W. Moshier, *Inorg. Chem.* 1963, **2**, 693.
3. P. C. Uden, I. E. Bigley and F. H. Walters, *Anal. Chim. Acta* 1978, **100**, 555.
4. C. Kutal and R. E. Sievers, *Inorg. Chem.* 1974, **13**, 897.
5. D. E. Henderson and F. P. Novak, *J. Chromatogr. Sci.* 1982, **20**, 256.
6. W. R. Melander, H.-J. Lin, J. Jacobson and Cs. Horváth, *J. Phys. Chem.* 1984, **88**, 4527.
7. D. E. Henderson, D. J. O'Conner, J. F. Kirby and C. P. Sears III, *J. Chromatogr. Sci.* 1985, **23**, 477.
8. D. E. Henderson and D. J. O'Conner, *Advances in Chromatography* (Edited by J. C. Giddings, E. Grushka, J. Cazes and P. R. Brown), Vol. 23, pp. 65–96. Marcel Dekker, New York (1984).
9. J. Jacobson, W. R. Melander, G. Vaisnys and Cs. Horváth, *J. Phys. Chem.* 1984, **88**, 4536.
10. D. E. Henderson and Cs. Horváth, *J. Chromatogr.* 1986, **368**, 203.
11. D. E. Henderson, P. M. Scola and F. P. Novak, 1982 Pittsburgh Conf. Analytical Chemistry and Applied Spectroscopy, Paper No. 179, March (1982).
12. Cs. Horváth, J. Frenz and Z. El Rassi, *J. Chromatogr.* 1983, **255**, 273.

Polyhedron Vol. 7, No. 5, pp. 379–383, 1988
Printed in Great Britain

0277–5387/88 $3.00+.00
Pergamon Press plc

ELECTRICAL CONDUCTIVITIES OF BIS(1,3-DITHIOLE-2-THIONE-4,5-DITHIOLATO)RHODATE ANION SALTS

KENJI YOKOYAMA, GEN-ETSU MATSUBAYASHI* and TOSHIO TANAKA

Department of Applied Chemistry, Faculty of Engineering, Osaka University, Yamadaoka, Suita, Osaka 565, Japan

(*Received* 10 *August* 1987; *accepted* 25 *September* 1987)

Abstract—$RhCl_3 \cdot 3H_2O$ reacted with Na_2dmit ($dmit^{2-}$; 1,3-dithiole-2-thione-4,5-dithiolate anion) and $[NBu^n_4]OH$ in methanol to afford $[NBu^n_4][Rh(dmit)_2]$ (**1**) and $[NBu^n_4]_{1.5}[Rh(dmit)_2]$ (**2**). Salt **1** was oxidized electrochemically in acetonitrile to afford $[NBu^n_4]_{0.4}[Rh(dmit)_2]$ (**3**). Suspended powders of **1** or **2** reacted with iodine in hexane to afford $[NBu^n_4][Rh(dmit)_2][I_3]_{1.3}$ (**4**) or $[NBu^n_4]_{1.5}[Rh(dmit)_2][I_3]_{0.4}$ (**5**). On the other hand, **1** dissolved in acetonitrile, reacted with bromine and iodine to yield $[NBu^n_4]_{0.25}[Rh(dmit)_2Br]$ (**6**) and $[NBu^n_4]_{0.35}[Rh(dmit)_2I]$ (**7**), respectively. All the salts behave as semi-conductors with electrical conductivities of $1 \times (10^{-5} \sim 10^{-8})$ S cm^{-1} at 25°C measured for compacted pellets. Electronic absorption, ESR and X-ray photoelectron spectra of the salts are discussed.

Many planar bis(dithiolene)metal complexes have been prepared and their electrical properties investigated,[1,2] where the electrical conductivities arise from metal–metal, metal–sulphur and/or sulphur–sulphur interactions. Recently, several planar metal (Ni, Pd, and Pt) complexes containing the 1,3-dithiole-2-thione-4,5-dithiolate ligand ($dmit^{2-}$) have attracted much interest because two-dimensional molecular interactions through sulphur–sulphur contacts of the dmit ligands lead to high conductivities.[3] In particular, it is noteworthy that TTF[Ni(dmit)$_2$]$_2$ (TTF = tetrathiafulvalene) becomes a superconductor at low temperatures and under pressure.[3d]

Rhodium–dmit complexes, if partially oxidized, are expected to exhibit high electrical conductivities through possible rhodium–rhodium, rhodium–sulphur, and/or sulphur–sulphur interactions. To date, however, little has been reported on rhodium–dithiolate complexes[4,5] and their electrical properties are unknown.

This paper reports the preparation of some dmit–rhodium salts as well as their spectroscopic and electrical properties.

*Author to whom correspondence should be addressed.

EXPERIMENTAL

Materials

4,5 - Bis(benzoylthio) - 1,3 - dithiole - 2 - thione,[6] $Rh_2(CH_3COO)_4 \cdot 2CH_3OH$[7] and $[NBu^n_4]_m[Rh(mnt)_2]$ ($m = 1$ and 2; mnt^{2-} = the maleonitriledithiolate anion)[5] were prepared according to literature methods.

*Preparations of rhodium–*dmit *salts*

Sodium metal (18 mg, 780 μmol) and 4,5-bis(benzoylthio)-1,3-dithiole-2-thione (160 mg, 390 μmol) were dissolved in methanol (5 cm^3). To the dark red solution was added a methanol (10 cm^3) solution of $RhCl_3 \cdot 3H_2O$ (50 mg, 190 μmol), followed by addition of a methanol (1 cm^3) solution of $[NBu^n_4]OH$ (65 mg, 250 μmol). The solution was allowed to stand overnight in a refrigerator. The originally dark violet solution turned dark brown and dark brown microcrystals of $[NBu^n_4][Rh(dmit)_2]$ (**1**) precipitated, which were collected by filtration, washed with methanol, and dried *in vacuo* (40% yield based on $RhCl_3 \cdot 3H_2O$). To a methanol (30 cm^3) solution of $Rh_2(CH_3COO)_4 \cdot 2CH_3OH$ (30 mg, 59 μmol) was added a methanol (150 cm^3) solution of Na_2dmit (250 μmol) prepared as mentioned above, followed

by addition of a methanol (1 cm^3) solution of $[NBu^n_4]OH$ (65 mg, 250 μmol) and black microcrystals of **1** were formed (31% yield based on $Rh_2(CH_3COO)_4 \cdot 2CH_3OH$).

To a stirred methanol (15 cm^3) solution containing Na_2dmit (390 μmol)) prepared as mentioned above and $RhCl_3 \cdot 3H_2O$ (50 mg, 190 μmol), an aqueous (10 cm^3) solution of $[NBu^n_4]OH$ (100 mg, 390 μmol) was added. Immediately black microcrystals of $[NBu^n_4]_{1.5}[Rh(dmit)_2]$ (**2**) precipitated, which were collected by filtration, washed with water and methanol, and dried *in vacuo* (51% yield based on $RhCl_3 \cdot 3H_2O$). Salt **2** was gradually converted to **1** in solution, although it was stable in the solid state.

Oxidation of salts **1** *and* **2**

Using a conventional electrochemical cell consisting of a platinum wire as a working electrode and a carbon rod as a counter electrode, salt **1** (30 mg, 41 μmol) was electrochemically oxidized in an acetonitrile (10 cm^3) solution containing $[NBu^n_4]ClO_4$ (0.1 mol dm^{-3}) as a supporting electrolyte under a constant current (10 μ A) for a week, to afford microcrystals of $[NBu^n_4]_{0.4}[Rh(dmit)_2]$ (**3**) on the platinum wire (21% yield).

Finely powdered salt **1** (30 mg, 41 μmol) was suspended in a hexane (30 cm^3) solution containing iodine (27 mg, 105 μmol) and the system was stirred for 24 h at room temperature. The solid of $[NBu^n_4][Rh(dmit)_2][I_3]_{1.3}$ (**4**) was collected by filtration and dried *in vacuo* (60% yield). Similarly, the iodine-doped solid of **2** was obtained as $[NBu^n_4]_{1.5}[Rh(dmit)_2][I_3]_{0.4}$ (**5**) by the reaction of the suspended powders of **2** with a small excess of iodine in hexane (40% yield). The presence of the I_3^- anion in these salts was confirmed by Raman spectra, as described later.

To an acetonitrile (20 cm^3) solution of **1** (810 mg, 1.0 mmol) was added an equimolar amount of bromine dissolved in acetonitrile (2 cm^3), and the solution was allowed to stand overnight in a refrigerator. A black solid of $[NBu^n_4]_{0.25}[Rh(dmit)_2Br]$ (**6**) was obtained, collected by centrifugation, washed with acetonitrile and dried *in vacuo* (37% yield). Salt **1** dissolved in acetonitrile, reacted similarly with iodine to give a black solid of $[NBu^n_4]_{0.35}[Rh(dmit)_2I]$ (**7**) (48% yield).

Elemental analyses as well as properties of the salts obtained are listed in Table 1.

Physical measurements

Electronic absorption,[8] powder electronic reflectance,[8] ESR[8] and X-ray photoelectron spectra[9] were recorded as described elsewhere. Raman spectra of powder samples were recorded on a Nippon Bunko JASCO R-500 spectrometer with KBr pellets set on a rotating holder to suppress thermal decomposition by the laser beam (an NEC GLG-3200 argon ion laser, $\lambda = 514.5$ nm). Cyclic voltammetry was performed in acetonitrile containing $[NBu^n_4]ClO_4$ as a supporting electrolyte, using a conventional cell consisting of platinum plates as working and counter electrodes and a saturated calomel electrode (SCE) as a reference.

Electrical conductivities were measured for compacted pellets by the conventional two-probe method.[10]

Table 1. Analyses and colours of the salts[a]

No.	Salt	Colour	Found (Calc.) % C	H	N
1	$[NBu^n_4][Rh(dmit)_2]$	Dark brown	36.1 (35.8)	5.3 (4.9)	1.9 (1.9)
2	$[NBu^n_4]_{1.5}[Rh(dmit)_2]$	Black	42.1 (41.9)	6.5 (6.3)	2.3 (2.4)
3	$[NBu^n_4]_{0.4}[Rh(dmit)_2]$	Black	24.7 (25.1)	2.6 (2.4)	1.1 (0.9)
4	$[NBu^n_4][Rh(dmit)_2] \cdot [I_3]_{1.3}$	Dark brown	21.0 (21.2)	3.0 (2.9)	1.1 (1.1)
5	$[NBu^n_4]_{1.5}[Rh(dmit)_2] \cdot [I_3]_{0.4}$	Black	35.5 (35.6)	5.5 (5.4)	2.0 (2.1)
6	$[NBu^n_4]_{0.25}[Rh(dmit)_2Br]$	Black	18.1 (18.9)	1.2 (1.4)	0.9 (0.5)
7	$[NBu^n_4]_{0.35}[Rh(dmit)_2I]$	Black	19.2 (19.7)	1.8 (1.8)	1.1 (0.7)

[a] Melting points (decomp.) > 300°C.

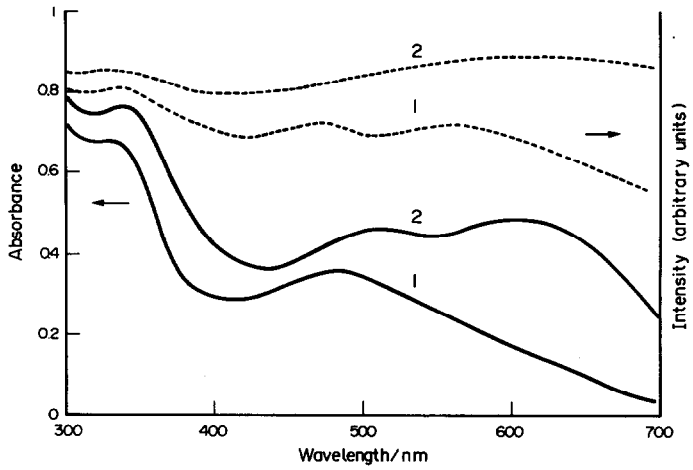

Fig. 1. The absorption spectra (——) of **1** (1.1×10^{-4} mol dm^{-3}) and **2** (1.3×10^{-4} mol dm^{-3}) in N,N-dimethylformamide and their reflectance spectra (---).

RESULTS AND DISCUSSION

Figure 1 shows the absorption spectra of salts **1** and **2** in N,N-dimethylformamide and their powder reflectance spectra. The absorption band of **1** observed at 488 nm is ascribed to the local excitation of the dmit ligand. Similar bands were also observed for Na_2dmit (514 nm in methanol) and $[NBu^n_4]_2[Zn(dmit)_2]$ (530 nm in acetonitrile).[11] The spectrum of **2** exhibits another broad band at 600 nm together with a band at 510 nm due to the dmit ligand transition. This lower energy band is somewhat sensitive to the solvent used; 570 nm in acetone and 560 nm in dichloromethane. Salt **2** is possibly an associated species of the $[Rh(II)(dmit)_2]$ moieties through a rhodium–rhodium linkage, as was suggested in $[NBu^n_4]_n[Rh(mnt)_2]_n$ ($n > 1$) (mnt^{2-} = the maleonitriledithiolate anion).[5] In addition, the salt is paramagnetic owing to one-electron oxidation centred at a dmit ligand, as described below. Thus, the low energy band is tentatively ascribed to a charge-transfer transition between the $[Rh(dmit)_2]$ moieties within the associated species. In the reflectance spectrum of **1** a broad band is observed at 570 nm together with a band at 460 nm due to the dmit transition, although the spectrum of **2** is too broad to distinguish bands in the lower energy region. This may suggest an interanionic interaction in the solid state of **1**, as reported for $[N\text{-ethylpyridinium}]_2[Cu(dmit)_2]$.[11]

Salt **1** exhibits no ESR signal and is considered to be formally a rhodium(III) complex. On the other hand, **2** shows a strong ESR signal as illustrated in Fig. 2, which also illustrates signals of other rhodium–dmit salts. The signal appearance of **2**, although it may have a rhodium(II)–rhodium(II) bond, is considerably different from that ($g_1 = 1.950$, $g_2 = 2.015$ and $g_3 = 2.35$) of $[NBu^n_4]_2[Rh(mnt)_2]$ containing a rhodium(II) atom.[4] The partially oxidized salts **3, 4, 6** and **7** also exhibit appreciable ESR signals. These signals resemble those of Pt(dmit)(bpy)$I_{2.2}$ and Pt(dmit)(phen)$I_{1.9}$,[12] which may indicate a dmit-centred oxidation in these salts.

A cyclic voltammogram of salt **1** in acetonitrile has shown an irreversible oxidation peak at 0.15 V vs SCE. Such a low oxidation potential is close to those of $[M(dmit)_2]^{2-}$ salts (M = Ni, −0.03 V; Pt, −0.08 V;[3c] Cu, 0.02 V vs SCE[11]). Thus, **1** can be easily oxidized electrochemically and chemically to give partially oxidized salts **3, 4, 6** and **7**.

Binding energies of Rh $3d_{3/2}$ and $3d_{5/2}$ electrons

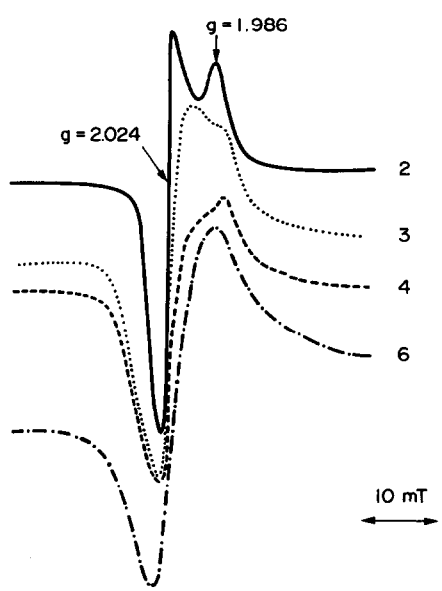

Fig. 2. Powder ESR spectra of **2, 3, 4** and **6** at 77 K.

Table 2. Binding energies (eV) of the Rh 3*d* electrons of the salts determined from the X-ray photoelectron spectra

Salt	Rh $3d_{3/2}$	Rh $3d_{5/2}$
1	312.2	307.6
2	311.9	307.6
3	311.8	307.3
4	312.8	308.1
5	313.2	308.2
6	311.3	306.9
7	311.3	306.6
$[NBu^n_4]_2[Rh(mnt)_2]$	311.6	307.0
$[NBu^n_4][Rh(mnt)_2]$	312.5	307.8

of the rhodium–dmit and rhodium–mnt salts which have been determined from the X-ray photoelectron spectra are summarized in Table 2.

The binding energies of the rhodium–dmit salts **1** and **2** fall between those of $[NBu^n_4]_2[Rh(mnt)_2]$ and $[NBu^n_4][Rh(mnt)_2]$. The energies of the partially oxidized salt **3** are rather close to those of **1**, supporting that the oxidation occurs essentially on the dmit ligands, as was reported for partially oxidized $[M(dmit)_2]^{m-}$ (M = Ni, Pd and Pt; m = 1–0.6) salts.[3c] Iodine-doped salts **4** and **5** contain the I_3^- ion, which has been confirmed from the appearance of a Raman scattering peak at 106 cm^{-1} due to the totally symmetric stretching pattern of the I_3^- ion.[13] The binding energies of Rh 3*d* electrons of these salts are somewhat higher than those of **1** and **2**, indicating that in **4** and **5** the metal is also somewhat oxidized besides the dmit ligands. On the other hand, the binding energies of **6** and **7** are lower than those of **1**, which suggests the formation of a rhodium–halogen bond in these salts. The Raman spectra of **6** and **7** exhibited peaks at 150 and 94 cm^{-1}, respectively. They are presumably assigned to stretching frequencies of Rh—Br and Rh—I bonds, and halogen atoms seem to interact further with another rhodium atom to form a —Rh—X—Rh—X—Rh— linkage (X = Br and I). These findings are similar to the cases of $K_2[Pt(NH_3)X_3][Pt(NH_3)X_5]$ containing the —Pt—X—Pt—X— bonds; ν(Pt—Br), 162 cm^{-1} and ν(Pt—I), 115 cm^{-1}.[14]

Electrical conductivities (σ) at 25°C and activation energies (E_a) for electrical conduction of the rhodium–dmit salts are listed in Table 3. All the salts behave as typical semiconductors in the temperature range −30 to +30°C. Salts **1** and **2** exhibit low conductivities. Even the partially oxidized salts **3**, **4**, and **5** have low conductivities, presumably because of unsuitable molecular packings. These findings are in great contrast to the high conductivities of partially oxidized planar $[M(dmit)_2]^{n-}$ salts (M = Ni, Pd, and Pt; $0 < n < 1$).[3c] Salts **6** and **7** behave as considerably better electrical conductors. This may be partially caused by the electrical conduction through the above-mentioned —Rh—X—Rh—X— bond, which seems to be rather close to cases of linear chain halogen-bridged platinum complexes $[Pt_2(L—L)_4X]$ (L—L = diphosphonate or dithioacetate, X = Cl, Br or I) with somewhat high conductivities ($10^{-3} \sim 10^{-4}$ S cm^{-1}).[15,16]

Table 3. Electrical conductivities (σ) and activation energies (E_a) of the rhodium–dmit salts

Salt	$\sigma_{25°C}$/S cm^{-1}	E_a/eV
1	3.2×10^{-8}	0.19
2	9.1×10^{-11}	0.77
3	1.6×10^{-7}	0.22
4	5.0×10^{-7}	0.52
5	4.2×10^{-7}	0.72
6	2.0×10^{-5}	0.28
7	2.0×10^{-5}	0.27

REFERENCES

1. L. Alcacer and H. Novais, in *Extended Linear Chain Compounds* (Edited by J. S. Miller), Vol. 3, pp. 319–351. Plenum Press, New York (1983).
2. J. S. Miller and A. J. Epstein, in *Progress Inorganic Chemistry* (Edited by S. J. Lippard), Vol. 20, pp. 1–151. Interscience, New York (1976).
3. (a) L. Valade, J.-P. Legros, M. Bousseau, P. Cassoux, M. Garbauskas and L. V. Interrante, *J. Chem. Soc., Dalton Trans.* 1985, 783; (b) H. Kobayashi, R. Kato, A. Kobayashi and Y. Sasaki, *Chem. Lett.* 1985, 191;

(c) Y. Sakamoto, G. Matsubayashi and T. Tanaka, *Inorg. Chim. Acta* 1986, **113**, 137; (d) M. Bosseau, L. Valade, J. Legros, P. Cassoux, G. Garbouskas and L. V. Interrante, *J. Am. Chem. Soc.* 1986, **108**, 1908 and refs therein.

4. E. Billig, S. I. Shupack, J. H. Waters, R. Williams and H. B. Gray, *J. Am. Chem. Soc.* 1964, **84**, 926.
5. N. G. Connelly and J. A. McCleverty, *J. Chem. Soc.*, (*A*) 1970, 1621.
6. G. Steimecke, H. J. Sieler, R. Kirmse and E. Hoyer, *Phosphorus and Sulfur*, 1979, **7**, 49.
7. G. A. Rempel, P. Legzdins, H. Smith and G. Wilkinson, *Inorg. Synth.* 1972, **13**, 90.
8. K. Ueyama, G. Matsubayashi and T. Tanaka, *Inorg. Chim. Acta*, 1984, **87**, 143.
9. G. Matsubayashi, K. Kondo and T. Tanaka, *Inorg. Chim. Acta* 1983, **69**, 167.
10. S. Araki, H. Ishida and T. Tanaka, *Bull. Chem. Soc. Jpn.* 1978, **51**, 407.
11. G. Matsubayashi, K. Takahashi and T. Tanaka, *J. Chem. Soc., Dalton Trans.* (in press).
12. G. Matsubayashi, M. Hirao and T. Tanaka, *Inorg. Chim. Acta* (in press).
13. B. N. Diel, T. Inabe, J. W. Iyding, K. F. Schoch, Jr., C. R. Kannewurf and T. J. Marks, *J. Am. Chem. Soc.* 1983, **105**, 1551.
14. G. C. Papavassiliou and D. Layek, *Z. Naturforsch.* 1980, **35b**, 676.
15. Che Chi-Ming, F. H. Herbstein, W. P. Schaefer, R. E. Marsh and H. B. Gray, *J. Am. Chem. Soc.* 1983, **105**, 4604.
16. C. Bellito, A. Flamini, L. Gastaldi and L. Scaramizza, *Inorg. Chem.* 1983, **22**, 444.

Polyhedron Vol. 7, No. 5, pp. 385–391, 1988
Printed in Great Britain

0277–5387/88 $3.00+.00
Pergamon Press plc

THE INFLUENCE OF COPPER ON THE TRANSFORMATION OF FERRIHYDRITE ($5Fe_2O_3 \cdot 9H_2O$) INTO CRYSTALLINE PRODUCTS IN ALKALINE MEDIA

R. M. CORNELL*

Laboratorium für anorg. Chemie, ETH-Zentrum, CH-8092 Zürich, Switzerland

and

R. GIOVANOLI

Universität Bern, Laboratorium für Elektronenmikroskopie, Freiestrasse 3, CH-3000 Bern 9, Switzerland

(*Received* 27 *August* 1987; *accepted* 25 *September* 1987)

Abstract—The presence of Cu retards the transformation of ferrihydrite ($5Fe_2O_3 \cdot 9H_2O$) into crystalline products. Low levels of Cu (9 mol%) suppress formation of goethite [(α-FeO(OH)] and lead to a product consisting entirely of haematite (α-Fe_2O_3). Cu prevents formation of goethite by hindering dissolution of ferrihydrite rather than by interfering with nucleation and growth of goethite in solution.

Chemical analysis showed that as much as 9 mol% of Cu replaces Fe in the haematite structure. The a_0 value of the unit cell of haematite increases from 0.5040 nm for unsubstituted haematite to 0.5048 nm for haematite with 9 mol% Cu incorporation. Transmission electron microscopy showed that Cu–haematite grows as rhombohedral crystals instead of the hexagonal plates typically obtained from ferrihydrite.

As the level of Cu in the system increases above 9 mol%, Cu–magnetite (Fe_3O_4) forms together with Cu–haematite. At 33 mol% Cu, tenorite (CuO) as well as Cu–magnetite is obtained.

In alkaline media, ferrihydrite ($5Fe_2O_3 \cdot 9H_2O$) transforms with time, into goethite [α-FeO(OH)] and haematite (α-Fe_2O_3). The transformation into crystalline products proceeds via two competing mechanisms.[1,2,3] Haematite nucleates and grows within the solid precursor by an internal dehydration and rearrangement process. Formation of goethite involves dissolution of ferrihydrite followed by reprecipitation of the crystalline oxide in solution. Which mechanism predominates depends on a number of factors including pH, temperature and the presence of foreign ions.

The broad outlines of the transformation mechanisms were established over 20 years ago, but little is known about the details of these processes. Useful information concerning various aspects of the transformation is being supplied, however, by examination of the effects of foreign ions on the reaction. Ions studied recently include Al^{3+}, Si^{4+} and Mn^{2+}.[4,5,6,7,8,9] Al and Mn both replace a proportion of Fe in the goethite and haematite structures, but whereas Al increases the level of haematite in the reaction product, Mn suppresses haematite formation.

Another ion that might be expected to show some interesting effects and to provide further details of the transformation process is Cu^{2+}. Earlier studies showed that Cu stabilized ferrihydrite against transformation into goethite and haematite.[10,11] How Cu influences the formation of crystalline oxides from ferrihydrite does not appear to have been investigated. The effect of Cu might be expected to differ from that of other ions considered previously both because the radius of Cu^{2+} is greater than that of Fe^{3+} and because, in an octahedral environment

*Author to whom correspondence should be addressed.

such as that found in iron oxides, Cu exhibits a distorted coordination. Cu is also of interest because it is a constituent of anti-weathering steels.[12] Addition of small amounts (< 5%) of Cu to these steels promotes the formation of protective rusts, but how this is achieved is not fully understood.

The present investigation is concerned with the effect of Cu on the kinetics and products of the transformation of ferrihydrite in alkaline media. Earlier workers restricted the concentration of Cu added to the system to less than 6 mol%.[10,11] In this study attention was focussed on the effect of 9.09 mol% Cu in order to facilitate comparison with the effects of the same levels of other ions considered in previous investigations.[8,9] However, the influence of both lower and higher concentrations of Cu was considered briefly.

Besides investigating the kinetics and products of the transformation in the presence of Cu, it was of interest to determine whether any isomorphous replacement of Fe in the oxide structure took place and finally, whether the presence of Cu induced any changes in the morphology of the reaction product.

EXPERIMENTAL

Preparation and characterization of samples

Ferrihydrite was precipitated with 1 M KOH from solutions of $Fe(NO_3)_3 \cdot 9H_2O$ and $Cu(NO_3)_3 \cdot 6H_2O$ having Cu/(Cu+Fe) mol ratios between 0.01 and 1.0. Most experiments were carried out with Cu/(Cu+Fe) = 0.09 (i.e. 10^{-3} M Cu). The pH of the suspensions ranged from 11 to 12.8. The suspensions (1.0 g ferrihydrite/l) were held in closed polypropylene bottles at 70°C for up to 168 h. Although in most experiments Cu^{2+} and Fe^{3+} were coprecipitated, experiments were also carried out in which Cu^{2+} was added after precipitation of ferrihydrite: where necessary the pH was readjusted with KOH after addition of Cu^{2+}. Subsequent results refer to coprecipitated systems unless otherwise stated. In some experiments, Cu^{2+} was replaced by $Mn(NO_3)_3 \cdot 4H_2O$ or $Al(NO_3)_3 \cdot 9H_2O$. In other experiments both Cu^{2+} and Mn^{2+} were present in the system. All chemicals were AR (Merck).

The kinetics of the transformation to goethite and/or haematite was followed by taking subsamples during the reaction and dissolving the unconverted ferrihydrite by a 2 h acid/oxalate (pH 3) extraction in the absence of light.[13] The extent of the transformation was expressed as the ratio Fe_o/Fe_t where Fe_o is the oxalate soluble material (i.e. unconverted ferrihydrite) and Fe_t is the total Fe in the system. Fe and Cu were measured by atomic absorption spectroscopy.

The crystalline product of the transformation was dried at 50°C and X-ray powder diffraction (XRD) patterns were obtained using a Guinier–Enraf camera (MK IV) with $FeK\alpha_1$ radiation. The proportions of goethite and haematite in the product were estimated by comparison with a series of standards made by mixing known amounts of synthetic goethite and haematite. The 110 and 111 peaks of goethite and the 10.2 peak of haematite were used for comparison.

The total amount of Fe and Cu in the crystalline product was found by dissolving the oxide in 4 M HCl. Where the product consisted of only one compound, the level of Cu incorporation was taken as the difference between oxalate soluble Cu (Cu_o) and the total Cu (Cu_t) in the oxide. The degree of Cu substitution was expressed as the ratio $(Cu_t - Cu_o)/[(Cu_t - Cu_o) + (Fe_t - Fe_o)]$.

Transmission electron micrographs were obtained with a Hitachi H-600-2 (100 kV) electron microscope equipped with a tracor TN 5400 energy-dispersive X-ray spectrometer. For TEM examination, the samples were dispersed in twice-distilled water using an ultrasonic treatment and a drop of suspension was dried on a carbon coated bronze grid. For EDSX spectra the sample was dried on a graphitized nylon grid.

RESULTS AND DISCUSSION

Reaction products

As the level of Cu in the system increased from 1 to 23 mol%, ferrihydrite transformed successively into goethite, Cu–haematite and finally into Cu–magnetite (Fe_3O_4) (Table 1).

Even low levels of Cu (10^{-4} M) led to an increase in the amount of haematite in the product up to pH 12; in the absence of Cu, haematite did not form above pH 11. With an order of magnitude increase in the concentration of Cu, goethite was almost entirely suppressed and replaced by Cu–haematite, at least up to pH 12.8. According to the XRD data the product consisted only of haematite. TEM however, showed a few per cent of small crystals of goethite to be present.

Increasing the concentration of Cu above 10^{-3} M led to the formation of mixtures of Cu–haematite and Cu–magnetite, until, when the concentration of Cu reached 3×10^{-3} M (23 mol%), all haematite formation was suppressed (Table 1). When more than 33 mol% Cu was present in the system, tenorite (CuO) formed as well as magnetite. Tenorite

Table 1. Effect of Cu concentration on the transformation products of ferrihydrite. pH 12.2, 70°C

Cu [M]	Initial mol% Cu	Product
0	0	Goethite
1×10^{-4}	0.9	Geothite
2.5×10^{-4}	2.43	Goethite + haematite (30%)
5×10^{-4}	4.5	Goethite + haematite (85%)
1×10^{-3}	9.09	Haematite
2×10^{-3}	16.6	Haematite + magnetite
3×10^{-3}	23.0	Magnetite
5×10^{-3}	33.0	Magnetite + tenorite
1×10^{-2}	100.0	Tenorite
1×10^{-3} [a]	9.09	Haematite (60%) + goethite
1×10^{-3} [b]	9.09	Haematite (55%) + goethite
$1 \times 10^{-3} + 1 \times 10^{-3}$ Mn[c]	9.09	Haematite (95%) + goethite

[a] 6% goethite seeds added.
[b] Cu added to ferrihydrite.
[c] Cu–Mn–ferrihydrite coprecipitate.

was also the end product when the pH of a solution of copper nitrate was raised to pH 12.

Seeding a coprecipitated Cu–ferrihydrite suspension (9.09 mol% Cu) with 6% (by weight) goethite increased the amount of goethite in the product (Table 1). Less haematite also formed if Cu (10^{-3} M) was added to already formed ferrihydrite instead of being coprecipitated with it; for example, the product at pH 12 contained 45% goethite. Addition of higher levels of Cu (3×10^{-3} M) to ferrihydrite led to some suppression of magnetite in favour of tenorite.

Cu haematite gave XRD patterns with sharp lines, whereas the XRD lines for Cu–magnetite and for tenorite were broad and diffuse.

When both Cu and Mn (10^{-3} M) were present in the system, the haematite suppressing effect of Mn was overcome (Table 1). Mn–Cu–ferrihydrite coprecipitates transformed into $\simeq 95\%$ haematite. Addition of Cu to Mn–ferrihydrite led to a product containing 40–50% goethite: however, a similar result was obtained in the absence of Mn.

Substitution of Cu *in* Fe–*oxides*

No Cu could be detected in the supernatant liquid, either during or after the transformation of ferrihydrite. Hence all Cu added to the system must have been associated with the solid Fe phase.

EDXS indicated that Cu was associated with haematite grown from Cu–ferrihydrite (Fig. 1). Chemical analysis of this haematite showed that at Cu : Fe < 0.1, the bulk of the Cu added was incorporated in haematite. The maximum level of incorporation was around 9 mol%. Additional Cu led to formation of Cu–magnetite as well as Cu–haematite.

All the XRD lines of Cu–haematite showed a consistent and regular increase in their corresponding d spacings. The a_0 values (calculated from the 110 line) increased from 0.5040 nm for unsubstituted haematite to 0.5048 nm for haematite with 9 mol% Cu substitution. The increase in unit cell size can be attributed to the larger radius of the Cu^{2+} ion (0.073 nm) compared to that of the Fe^{3+} ion (0.065 nm)[14] that it replaces. The difference of 15% between the radii of the two ions is within the tolerated limits for isomorphous substitution. However, its larger size and distorted coordination may make incorporation of additional Cu into the haematite structure difficult and thus, 9 mol% may be the maximum level of substitution that can be achieved.

Cu–haematites show the opposite trend to Al substituted haematites. Al^{3+} has a smaller radius (0.051 nm) than Fe^{3+} and as a result, the unit cell of Al–haematite decreases with increasing replacement of Fe by Al.[6]

Chemical analysis of goethite formed at pH 12.2 in the presence of 10^{-4} M Cu indicated that no incorporation of Cu into the crystal structure had taken place. With 10^{-3} M Cu in the system and under conditions where goethite formed as well as haematite (Table 1), XRD line shifts suggested that some Cu may have replaced Fe in the goethite structure. The degree of substitution could not be estimated by chemical methods because Cu–haematite

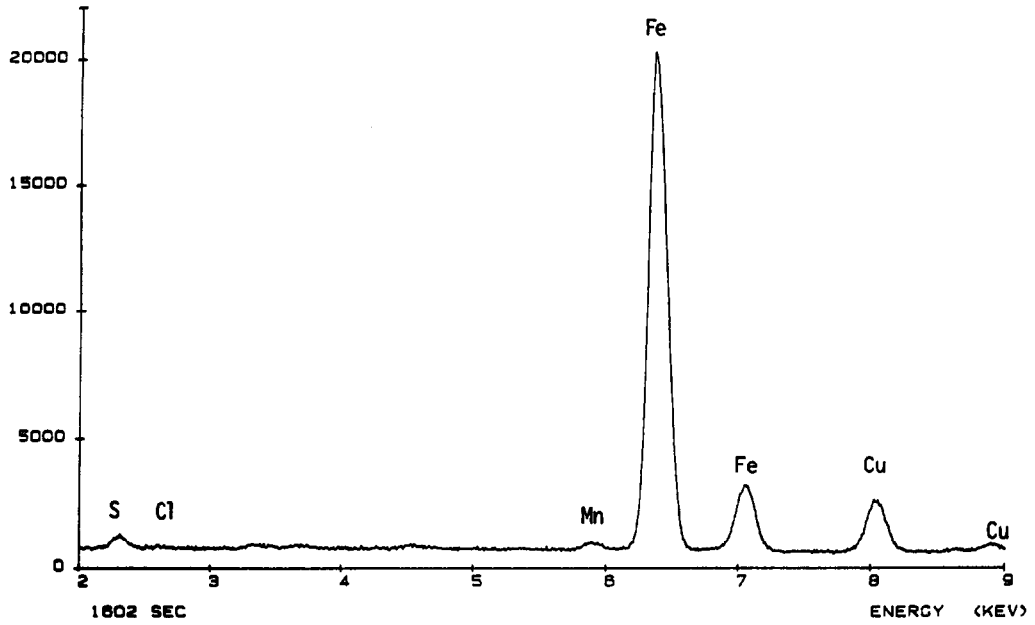

Fig. 1. Energy dispersive X-ray spectrum of Cu–haematite showing the presence of Cu.

was associated with the goethite. As the haematite in the mixture appeared to be fully substituted, it is probable that any incorporation of Cu in the goethite structure was less than 5 mol%.

Chemical analysis showed that magnetite also contained Cu in the structure. The maximum possible level of Cu substitution was 23 mol%: higher levels of Cu in the system led to formation of CuO rather than $CuFe_2O_4$. Accurate a_0 values for Cu–magnetites could not be measured owing to the diffuseness of the XRD lines.

Kinetics

A plot of the extent of conversion of ferrihydrite vs time consists of an initial period corresponding to the time required for nucleation of the products followed by a faster transformation stage.[15] For systems both with and without Cu (10^{-3} M), a plot of ln (Fe_o/Fe_t) against time was linear over the main part of the reaction indicating a first order reaction.

At pH 12.2 the reaction kinetics for a system containing 10^{-4} M Cu were the same as for the control system without Cu. With 10^{-3} M Cu, however, the induction time lengthened and the subsequent reaction was strongly retarded (Fig. 2). The induction time was reduced from 6 to 3 h (and at the same time the amount of goethite in the product increased) by seeding the system with 6% goethite. Seeding did not accelerate the main reaction. These observations suggest that Cu stabilizes ferrihydrite both against dissolution (which leads to goethite) and against internal rearrangement leading to haematite. Uptake of Cu and Fe by haematite was congruent over the bulk of the transformation.

The rate of transformation increased if Cu was added to already formed ferrihydrite instead of being coprecipitated with it.

Coprecipitated Cu–ferrihydrite transformed to Cu–haematite more rapidly if the ionic strength was raised from 10^{-2} to 1.0 (with KNO_3). An essential prerequisite for haematite formation is the aggregation of the particles (diameter 0.2–0.4 nm) of ferrihydrite;[3] this facilitates nucleation of haematite. Increasing the ionic strength compresses the electrical double layer around the particles of ferrihydrite, thus promoting their aggregation and, in

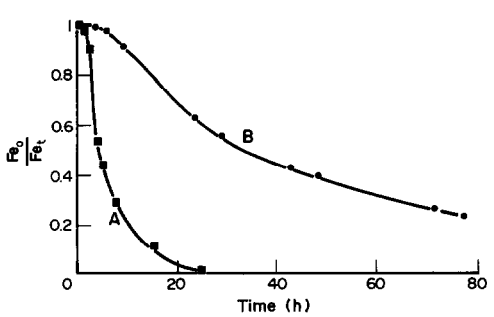

Fig. 2. Fe_o/Fe_t as a measure of the degree of transformation of ferrihydrite into crystalline oxides vs time. (A) Cu absent, product goethite. (B) 10^{-3} M Cu coprecipitated with ferrihydrite, product Cu–haematite. pH 12.2, 70°C.

Table 2. Effect of different ions on the kinetics and products of the transformation of ferrihydrite. pH 12.2, 70°C

Ion	[Ion] M	Induction time (h)	Rate (min^{-1})	Product
Control	0	0.5	0.002	Goethite
Al	10^{-3}	1.0	0.002	Goethite
Al	2×10^{-3}	2.5	0.0035	Goethite + haematite (10%)
Mn	10^{-3}	0.5	0.002	Goethite
Si	4×10^{-4}	50.0	0.00016	Goethite + haematite (15%)
Cu	10^{-3}	6.0	0.00030	Haematite + goethite (3–5%)

turn, formation of nuclei. No haematite promoting effect or acceleration of the reaction was noted if ferrihydrite was not stabilized by Cu. In the absence of Cu, dissolution of ferrihydrite to form goethite was far more rapid than the formation of haematite.

The retarding effect of 10^{-3} M Cu on the transformation of ferrihydrite was greater than that of equivalent concentrations of Al or Mn, but far less than that of Si (Table 2).

Electron microscopy

The presence of Cu led to the formation of rhombohedral crystals of Cu–haematite bounded by {10.2} faces (Fig. 3(a), arrow 1). The rhombohedral crystals had a fairly narrow size distribution with diameters of between 150 and 200 nm. Unlike the flat, hexagonal haematite crystals that grow from ferrihydrite in the absence of Cu[15], the Cu–

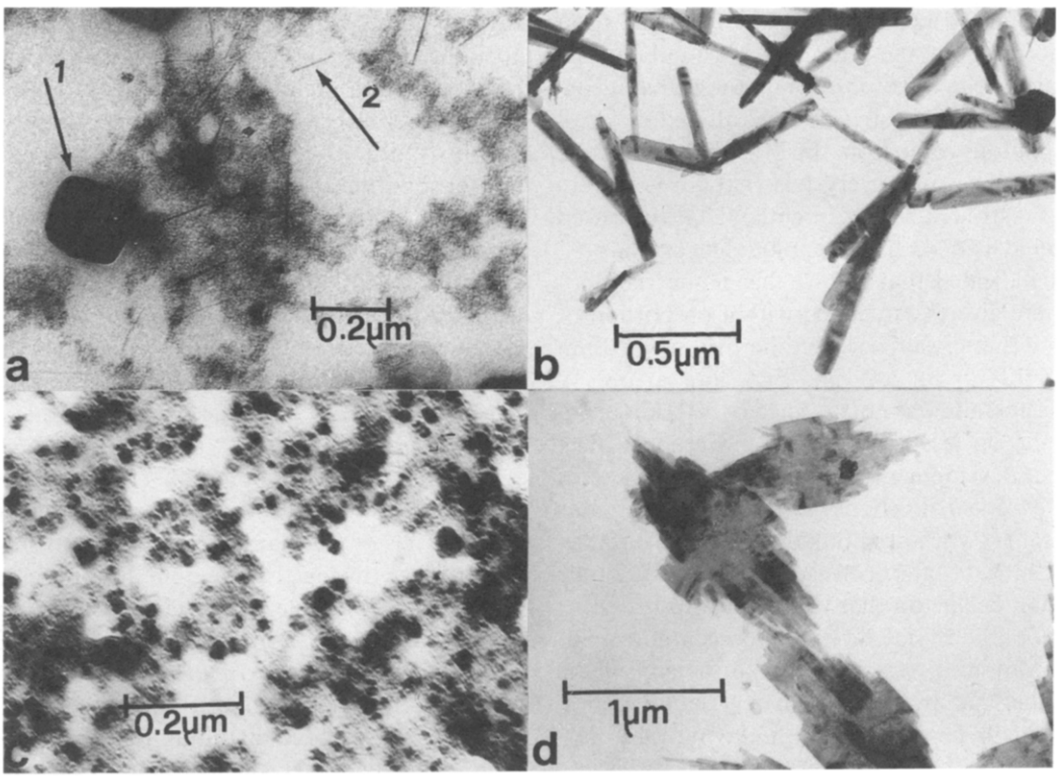

Fig. 3. Transmission electron micrographs of oxides formed in presence of Cu. pH 12.2, 70°C. (a) Rhombohedral crystal of Cu–haematite (arrow 1) and thin crystals of goethite (arrow 2). The amorphous background material is Cu–ferrihydrite (10^{-3} M Cu). (b) Goethite formed upon addition of 10^{-3} M Cu to ferrihydrite. (c) Cu–magnetite and ferrihydrite, 3×10^{-3} M Cu. (d) Multi-domainic crystals of CuO.

haematite crystals were well developed in all three crystallographic directions. Owing to their larger dimensions, these crystals were a deeper, crimson red than the hexagonal platelets.

Haematite usually grows from ferrihydrite as hexagonal plates. It can also form round plates, rods or ellipsoids depending on the pH of synthesis and on whether foreign, adsorbing species are present.[8,15,16] Modifications of morphology frequently arise as a result of preferential adsorption of a foreign species on specific crystal planes. Such adsorption can retard growth of these planes, thus increasing their development and so altering crystal morphology.

Rhombohedral crystals of haematite have not been produced from the ferrihydrite system before. Although this morphology may have arisen as a result of preferential adsorption of Cu species on the {10.2} faces of the growing crystals, it is equally probable that it maybe due to incorporation of Cu in the crystal structure. In an octahedral lattice site, the Cu octahedron is distorted with the four ligands in the *ab* plane being closer to the central atom than the two along the *c* axis (Jahn Teller effect). Ions exhibiting the Jahn Taller effect cause an elongation of the octahedral sites along a trigonal axis for compounds like haematite, where the octahedra are partly connected by sharing faces. This distortion could account for the adoption of rhombohedral morphology. Support for the hypothesis that incorporation of Cu in the structure has altered the crystal morphology came from the Mn–Cu–ferrihydrite system. The haematite crystals that formed were not Cu substituted to any extent and TEM showed them to have grown as large, plate-like crystals.

TEM indicated that the Cu–haematite rhombohedra were always associated with a proportion of extremely thin crystals of goethite (width < 20 nm and lengths up to 200 nm, Fig. 3(a), arrow 2). Since the goethite was not detected by XRD, it probably made up less than 5% of the product. The restricted development of these goethite crystals along the *a* and *b* directions indicates that conditions for crystal growth were not particularly favourable. The goethite structure consists of chains of double $Fe(O,OH)_6$ octahedra that run parallel to the *c* (i.e. long) axis of the crystal. Growth proceeds more readily by addition of a growth unit to the end of the chain rather than by initiation of new chains. Hence, when growth conditions are unfavourable, particularly when the supersaturation with respect to goethite is low, long, thin crystals result.[15]

Well-developed crystals of goethite formed in systems in which Cu was added to already formed ferrihydrite [Fig. 3(b)]. These crystals were usually single domain[17] and often terminated in well formed 021 faces. Occasionally the crystals contained etch pits. Twinned crystals were rare and when present were the dendritic type.[15] Such twinned crystals have been observed for goethites grown in the presence of high levels of Mn;[9] their formation was attributed to adsorption of foreign species on the growing crystals. Epitaxial outgrowths of goethite on the rhombohedral crystals of haematite were seen occasionally.

Cu-magnetite formed very small cubic crystals with diameters of around 20 nm [Fig. 3(c)]. These crystals were much smaller than those obtained by air oxidation of $Fe(OH)_2$ suspensions.[18] The small size of the crystals accounts for the diffuse XRD lines obtained for this material.

CuO grew at pH 12 as spindle shaped crystals up to 600 nm in length [Fig. 3(d)]. These crystals were composed of narrow intergrowths arising from a central point within the crystals. These intergrowths are responsible for the broad XRD lines of the sample.

Formation of crystalline compounds from Cu–*ferrihydrite*

Goethite forms from ferrihydrite by dissolution of the amorphous phase followed by reprecipitation of goethite in solution. Kinetic and TEM evidence suggests that Cu prevents or retards formation of goethite principally by hindering dissolution of ferrihydrite and release of soluble ferric species. Regardless of how it was introduced into the system, all the Cu added initially was taken up by the ferrihydrite and then gradually released into solution, together with ferric species, as the ferrihydrite dissolved. Cu stabilized ferrihydrite against dissolution far more if it was coprecipitated with ferrihydrite, than if it was added to ferrihydrite. In the latter case, Cu was probably mainly adsorbed on the surface of the ferrihydrite, whereas in a coprecipitated system it was incorporated into the structure.

Goethite formed comparatively readily from ferrihydrite to which Cu had been added despite the higher levels of Cu that were released into solution at any stage during the reaction. This observation indicates that soluble Cu species do not interfere in nucleation of goethite to any extent. Seeding a coprecipitated Cu–ferrihydrite system with goethite promoted goethite formation, because in this case, Cu retarded dissolution of ferrihydrite to such an extent that the critical level of supersaturation for nucleation of goethite was not readily achieved. The development of goethite crystals in all three crystallographic directions (when Cu was added to ferrihydrite) indicates that there is little interference by Cu in crystal growth. Some Cu may

have been incorporated into the crystal structure. Only low levels of Cu substitution would be expected because at pH 12, the predominant Cu species is $Cu(OH)_4^{2-}$,[19] and this would not be competitive with the monovalent $Fe(OH)_4^-$ which is the favoured growth unit for goethite in alkaline media.[20] Comparison with the effects of other substituents suggests that much higher levels of substitution are needed to produce any noticeable changes in goethite morphology.[7,9]

At pH 12–12.5, haematite usually forms so much more slowly than goethite that it does not appear in the reaction product.[15] Since goethite and haematite form by competing mechanisms, haematite is indirectly favoured by conditions that suppress goethite formation. Of the ions studied previously, Al does not retard dissolution of ferrihydrite, but hinders nucleation and growth of goethite in solution, and in this way leads to an increase in the amount of haematite in the product. Si, on the other hand, stabilizes ferrihydrite for many months but the end product is mainly goethite because formation of haematite is more strongly retarded.[8] Cu differs from these two ions, in that although the overall transformation is retarded, ferrihydrite is stabilized more against dissolution than against internal rearrangement to form haematite.

Earlier workers reported that concentrations of Cu above 2.5 mol% prevented transformation of ferrihydrite into crystalline oxides.[10,11] However, their experiments were carried out at much lower temperatures (30°C) than used here, and sufficient time was not allowed for the transformation to go to completion. The mechanism by which Cu stabilizes ferrihydrite is not clear. It is not a question of differences in the ionic radii of Cu and Fe since Mn^{2+} which has an even larger radius (0.083 nm) does not retard the dissolution of ferrihydrite.[9] There is no unequivocal evidence that Cu induces haematite to form. However, the ability of Cu to overcome the haematite suppressing effect of Mn in Mn–Cu–ferrihydrite coprecipitates suggests that Cu may facilitate haematite formation.

The magnetite promoting effect of Cu in ferrous systems is well known[21] and the present results show that high enough levels of Cu have a similar effect in ferric systems.

Tamuara *et al.*[22] showed that formation of magnetite from γ-FeOOH in alkaline media involved adsorption of Fe^{2+} on the oxide surface leading to formation of ferric ferrous hydroxo complexes. These complexes then dissolved from the surface and reprecipitated as magnetite. Other studies showed that Mn^{2+} also interacts with ferrihydrite to form a spinel phase (jacobsite, $MnFe_2O_4$) that precipitates in solution.[9] A similar mechanism, therefore, may operate with Cu–ferrihydrite. In this case, dissolution of ferrihydrite could release cupric ferric hydroxo complexes which then precipitate as Cu–magnetite.

It is of interest to note that the magnetite which makes up the teeth of chitons is formed from ferrihydrite.[23] The mechanism by which it forms is not fully understood, but it may involve interaction with a divalent ion.

Acknowledgements—Thanks are due to Miss E. Ettinger for carrying out the electron microscopy and to Mr M. Faller for the X-ray powder diffraction measurements. We are grateful to the Swiss National Foundation for financial support.

REFERENCES

1. W. Feitknecht and W. Michaelis, *Helv. Chim. Acta* 1962, **26**, 212.
2. U. Schwertmann and W. R. Fischer, *Z. anorg. allg. Chem.* 1966, **346**, 137.
3. W. R. Fischer and U. Schwertmann, *Clays Clay Miner.* 1975, **23**, 33.
4. U. Schwertmann, R. W. Fitzpatrick, R. M. Taylor and D. G. Lewis, *Clays Clay Miner.* 1979, **27**, 105.
5. D. G. Lewis and U. Schwertmann, *Clay Miner.* 1979, **14**, 115.
6. D. G. Schulze, *Clays Clay Miner.* 1984, **32**, 36.
7. D. G. Schulze and U. Schwertmann, *Clay Miner.* 1984, **19**, 521.
8. R. M. Cornell, R. Giovanoli and P. W. Schindler, *Clays Clay Miner.* 1987, **35**, 21.
9. R. M. Cornell and R. Giovanoli, *Clays Clay Miner.* 1987, **35**, 11.
10. K. Inouye, S. Ishii, K. Kaneko and T. Ishikawa, *Z. anorg. allg. Chem.* 1972, **391**, 86.
11. R. Furuichi, N. Sato and G. Okamoto, *Chimia* 1969, **23**, 455.
12. U. R. Evans, *Corrosion and Oxidation of Metals*, Chap. 13. Edward Arnold, London (1960).
13. U. Schwertmann, *Z. Pflanzenernähr. Düng Bodenkd.* 1964, **105**, 194.
14. R. D. Shannon and C. T. Prewitt, *Acta Cryst.* 1969, **B25**, 925.
15. R. M. Cornell and R. Giovanoli, *Clays Clay Miner.* 1985, **33**, 424.
16. R. M. Cornell, *Clays Clay Miner.* 1985, **33**, 219.
17. R. M. Cornell, S. Mann and A. J. Skarnulis, *J. Chem. Soc., Faraday Trans 1*, 1983, **79**, 2679.
18. A. E. Regazzoni, G. A. Urrutia, M. A. Blesa and J. G. Maroto, *J. Inorg. Nucl. Chem.* 1981, **43**, 1489.
19. C. F. Baes Jr. and R. E. Mesmer, *The Hydrolysis of Cations*. John Wiley, New York (1976).
20. H. Lengweiler, W. Buser and W. Feitknecht, *Helv. Chim. Acta* 1961, **91**, 796.
21. K. Inouye, K. Murata and T. Ishikawa, *Z. anorg. allg. Chem.* 1971, **383**, 340.
22. Y. Tamuara, K. Ito and T. Katsura, *J. Chem. Soc., Dalton Trans*, 1983, 189.
23. H. A. Lowenstamm, *Science*, 1981, **211**, 1126.

Polyhedron Vol. 7, No. 5, pp. 393–398, 1988
Printed in Great Britain

0277–5387/88 $3.00+.00
Pergamon Press plc

BIS[(1-METHYL-1-BENZOYLHYDRAZONOETHYL)CYCLOPENTADIENYL]IRON AND ITS COMPLEXES WITH TRANSITION METALS

ZHAO GANG, LI FENG, XIE JISHAN and MA YONGXIANG*

Department of Chemistry, Lanzhou University, China

(*Received* 4 *September* 1987; *accepted* 25 *September* 1987)

Abstract—The organometallic ligand derived from ferrocene(H_2L), bis(1-methyl-1-benzoylhydrazonoethyl)cyclopentadienyl] iron has been prepared. A series of transition metal complexes: ML [M = Co(II), Ni(II), Zn(II), Cd(II), Cu(II) and Mn(II)] and $M(H_2L)Cl_2$ [M = Co(II), Ni(II), Cd(II) and Mn(II)] were obtained by reaction of the ligand with metal(II) acetates and chlorides respectively. The data of elemental analyses, IR, UV, NMR, molar conductance, TG and DTA show that the ligand coordinates in the enolic form with $M(OAc)_2$ and in the keto form with MCl_2, and that the C—N bond in complexes became very strong and much more thermostable than in the ligand due to forming the chelate ring.

In recent years, organometallic ligands including ferrocene and its coordination compounds have been extensively investigated.[1–7] Due to formation of stable chelates with transition metals present in the cell, aroyl hydrazones are reported to possess tuberculostatic activity.[8,9] When aromatic groups in the penicilins and cephalosporins are replaced by ferrocene, their activities are improved,[10] but 1,1′-diaroylhydrazonoferrocene and its complexes with transition metals have not been reported as yet. In the present work, bis[(1-methyl-1-benzoylhydrazonoethyl)cyclopentadienyl]iron(H_2L) and its complexes with some transition metal(II) ions are studied. The structure and properties of these complexes were elucidated by IR, UV, NMR, molar conductance, thermogravimetry (TG) and differential thermal analysis (DTA).

EXPERIMENTAL

Transition metal(II) acetates and chlorides, and benzoylhydrazine of analytic reagent grade were used. 1,1′-diacetylferrocene was prepared by the method described in the literature.[11]

Preparation of the ligand (**1**, H_2L)

A mixture of 1,1′-diacetylferrocene and benzoylhydrazine with a molar ratio of 1:2 was reacted in benzene under reflux. The red fine crystals which separated out on cooling were filtered and washed with warm benzene. The crude product was recrystallized in 95% ethanol to obtain deep red crystals as shown in formula (**1**). Yield 81.5%, m.p. 199–200°C. Found: C, 66.7; H, 5.1; N, 11.0. Calc. for $C_{28}H_{26}FeN_4O_2$: C, 66.7; H, 5.2; N, 11.1%.

Preparation of complexes ML(**2**)

A hot solution of H_2L (0.25 mmol) in anhydrous ethanol (20 cm^3) was added dropwise with stirring to a solution of $M(OAc)_2 \cdot 2H_2O$ (0.25 mmol) (M = Co, Ni, Zn, Cd, Cu and Mn) in warm anhydrous ethanol (10 cm^3) and immediately a red precipitate was produced. The reaction mixture was heated under reflux for 30 min. The solid that separated out was collected on a filter, washed several times with warm ethanol and dried under vacuum. The complexes prepared are listed with their decomposition temperature and elemental analyses in Table 1.

Preparation of complexes $M(H_2L)Cl_2$(**3**)

A hot solution of H_2L (0.25 mmol) in anhydrous ethanol (20 cm^3) was added to $MCl_2 \cdot 2H_2O$ (0.25 mmol) (M = Co, Ni, Cd and Mn) in warm anhydrous ethanol (10 cm^3). The mixture was heated under reflux with stirring until the precipitates separated. The isolated complexes were filtered,

*Author to whom correspondence should be addressed.

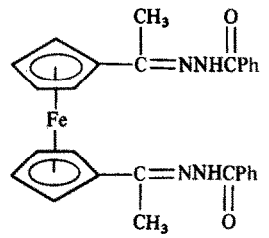

(1, H_2L)

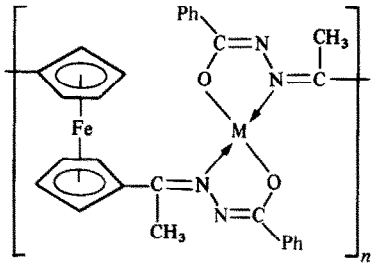

(2)

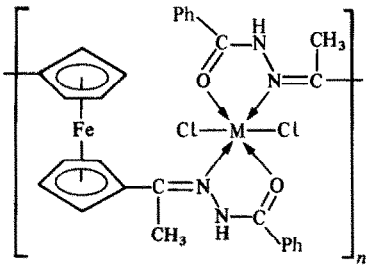

(3)

washed with hot ethanol and dried under vacuum. The complexes thus prepared are given in Table 1.

Spectral measurements

IR spectra were obtained using KBr discs with a NIC-5DX spectrophotometer using sodium chloride optics. UV spectra were recorded on a DJ-240 spectrophotometer in the 200–500 nm region using a solution in N,N-dimethylformamide (DMF). NMR spectra were measured with a PMX-60 spectrophotometer using deuterodimethyl sulphoxide (DMSO) as solvent and tetramethylsilane as an internal standard.

Table 1. Decomposition temperature and elemental analysis of complex

Complex	Formula	D.t. (°C)	Elemental analysis (%)[a] C	H	N	Cl
I	$C_{28}H_{24}N_4O_2FeCo$	300	60.0 (59.7)	4.4 (4.3)	10.0 (9.8)	
II	$C_{28}H_{24}N_4O_2FeNi$	300	59.5 (59.5)	4.2 (4.3)	9.8 (9.9)	
III	$C_{28}H_{24}N_4O_2FeZn$	300	58.3 (58.9)	4.1 (4.2)	9.6 (9.8)	
IV	$C_{28}H_{24}N_4O_2FeCd$	300	54.5 (54.5)	3.9 (3.9)	9.0 (9.1)	
V	$C_{28}H_{24}N_4O_2FeMn$	300	60.0 (60.1)	4.2 (4.3)	9.3 (10.1)	
VI	$C_{28}H_{24}N_4O_2FeCu$	300	58.5 (59.1)	3.9 (4.2)	9.6 (9.8)	
VII	$C_{28}H_{26}Cl_2N_4O_2FeCo$	250	52.7 (52.8)	4.0 (4.1)	8.7 (8.8)	11.1 (11.2)
VIII	$C_{28}H_{26}Cl_2N_4O_2FeNi$	250	52.7 (52.8)	4.0 (4.1)	8.6 (8.8)	11.2 (11.1)
IX	$C_{28}H_{26}Cl_2N_4O_2FeCd$	250	48.5 (48.8)	3.6 (3.8)	7.9 (8.1)	10.8 (10.3)
X	$C_{28}H_{26}Cl_2N_4O_2FeMn$	250	53.7 (53.2)	4.1 (4.1)	8.8 (8.9)	11.3 (11.2)

D.t. = decomposition temperature.

[a] Calculated values are given in parentheses.

Electrolytic conductance measurements

Molar conductances of complexes were obtained using a DDS-IIA conductometer in DMF and DMSO solvents at 25°C.

Thermal property measurements

TG and DTA were determined using a thermobalance Thermoflex model.

RESULTS AND DISCUSSION

The ligand dissolves in polar solvents such as methanol, ethanol and acetonitrile, but is insoluble in weak polar or nonpolar solvents such as ether, benzene and alkanes. All complexes dissolve only in DMF and DMSO. The ligand is tetradentate in nature having two carbonyl and two azomethine groups. The elemental analyses given in Table 1 show that the ligand can coordinate either in the enolic form as ML described in type (**2**) with $M(OAc)_2$ accompanied by the loss of acetate ions, or in the keto form as $M(H_2L)Cl_2$ described in type (**3**) without loss of chloride ions.

IR spectra

The IR frequencies along with their relative assignments are given in Table 2. The bands due to ν(N—H), ν(C=O)(amide I), δ(N—H)(amide II), ν(C—N)(amide III) and ν(C=N) are observed in the ligand spectra at 3318, 1670, 1529, 1300 and 1651 cm^{-1} respectively.[12] The band observed at 915 cm^{-1} is attributed to ν(N—N).[13] The characteristic bands of the ferrocene group appear at 3051, 1472, 1132, 814 and 482 cm^{-1}.[14] The band observed at 1372 cm^{-1} arises from δCH_3.

The IR spectra of complexes ML show significant changes as compared with those of the parent ligand. The bands due to N—H and C=O(amide I) stretching vibrations disappeared, but two new bands are observed around 1590 and 1275 cm^{-1} which can be attributed to the stretching vibrational modes of conjugate —C=N—N=C— and C—O groups.[15,16] It is shown that the ligand undergoes enolization in solution and then reacts with metal ions to form the metal complexes, accompanied by the release of acetate ions. It is also observed that one ν(C=N) band was shifted to a lower frequency by 45–64 cm^{-1}, while the ν(N—N) band was shifted to a higher frequency by about 5 cm^{-1}. The frequency changes of ν(C=N) and ν(N—N) support the coordination through the azomethine nitrogen atom.[7]

The IR spectra of the complexes $M(H_2L)Cl_2$ are similar to that of the ligand. The bands due to ν(N—H) and ν(C=O)(amide I) do not disappear, and the bands arising from ν(C=O) and ν(C=N) are shifted to a lower frequency by 30–45 and 50–70 cm^{-1} respectively, while the band given by ν(N—N) was shifted to a higher frequency by 1–7 cm^{-1}. These changes show that the ligand coordinates with transition metal ions in the keto form when using their chlorides. The oxygen atom in the carbonyl and the nitrogen atom in the azomethine participate in coordination.[16]

All characteristic bands attributed to the benzene ring and cyclopentadienyl in both complexes are observed.

UV spectra

The UV spectra of the ligand and its complexes $M(H_2L)Cl_2$ in DMF are shown in Fig. 1. It can be seen that the UV spectra of all complexes are

Table 2. Important IR absorption bands (in cm^{-1}) of the ligand and its complexes

Complex	ν(N—H)	Amide I, ν(C=O)	ν(C=N)	ν(C···C), phenyl	Amide II	ν(C···C), ferrocene	δ(C—H), methyl	ν(C—O)	ν(N—N)
H_2L	3318br,m[a]	1669sh	1651vs	1578w	1529vs	1442m	1371m		914s
I			1589s	1573sh	1529vs	1440m	1366vs	1277m	920m
II			1593vs	1565vs	1539vs	1441m	1372vs	1274m	917m
III			1587vs		1503vs	1435s	1369vs	1299m	919m
IV			1587vs		1510vs	1435s	1346vs	1273m	915m
V			1588s	1560s	1529vs	1441m	1367vs	1272m	919m
VI			1589s	1576vs	1527vs	1440m	1369vs	1276m	923m
VII	3234br,m	1624vs	1564sh	1540vs	1491m	1436w	1316s		919m
VIII	3381br,m	1639vs	1568vs	1606vs	1539s	1444m	1325m		921w
IX	3240br,m	1626vs	1574s	1605sh	1529vs	1436w	1301s		915m
X	3170br,m	1628vs	1569s	1606sh	1538vs	1436w	1311s		916m

[a] vs = very strong, s = strong, m = medium, w = weak, sh = shoulder, br = broad.

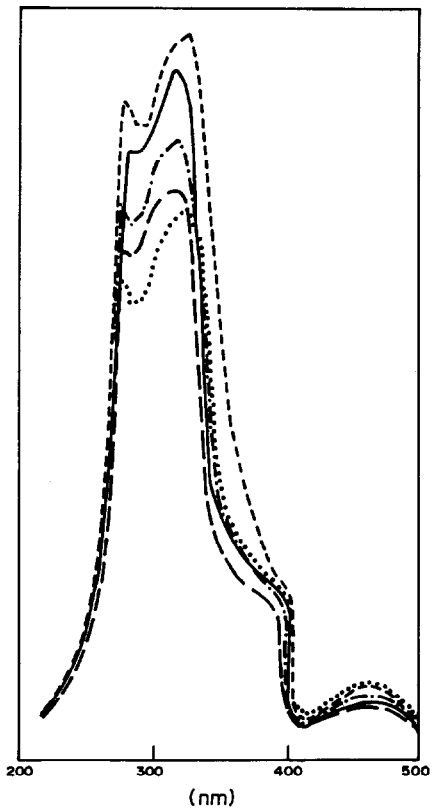

Fig. 1. The UV spectra of the ligand and its complexes $M(H_2L)Cl_2$. ——H_2L, ----$Ni(H_2L)Cl_2$, -·-·-· $Cd(H_2L)Cl_2$, ———$Mn(H_2L)Cl_2$, ····$Co(H_2L)Cl_2$.

similar, but they are different from that of the ligand. The K band (π–π^* transition) of the ligand is observed at 302 nm, but in its complexes, $M(H_2L)Cl_2$, a bathochromic shift of 2–8 nm occurred resulting from the chelation of the ligand with transition metal ions, and the band appears at 304–310 nm. The shoulder peak at 272 nm arising from the B band of the cyclopentadienyl ring in the ligand changes into a single peak at about 262–265 nm which is due to a bathochromic shift of the K band and hypsochromic shift of the B band. The broad band near 460 nm was attributed to charge-transfer in the ferrocene group (transition of the 3*d* electrons on iron to either the nonbonding or antibonding orbitals of the cyclopentadienyl ring).[17] The position of this band in complexes as compared with that of the ligand hardly changes. In the complexes ML, the above mentioned three bands exist too, but the K band occurs bathochromic shifted by 10–11 nm, which is more than that of $M(H_2L)Cl_2$. The 460 nm band also undergoes a slight bathochromic shift (about 2 nm). In addition, two new bands near 328 and 352 nm appeared and suggested that the whole molecule changed into a large conjugate system due to chelation in the enolic form.

NMR spectra

The ^{1}HNMR spectra of the ligand shows the eight protons on the two cyclopentadienyl rings split into two groups of peaks with equal height at 4.3 and 4.7 ppm. The protons on the aromatic ring, the methyl and the nitrogen atom appeared at 7.2–7.6 (multiplet), 2.2 (singlet) and 10.7 ppm (singlet) respectively. The integral ratio of these protons on the cyclopentadienyl ring, the aromatic ring and methyl was 4 : 5 : 3.

The ^{1}H NMR spectra of the complexes $M(H_2L)Cl_2$ exhibit the chemical shift of the protons on the cyclopentadienyl ring, the aromatic ring, methyl and the nitrogen atom at 4.5 and 4.7 (doublet), 7.4–7.8 (multiplet), 2.3 (singlet) and 10.6 ppm (singlet) respectively. All of them shifted downfield resulting from the deshielding effect after forming complexes. It was also indicated that the ligand coordinated in the keto form in these complexes.

The ^{1}H NMR spectra of the complexes ML shows that the signal arising from the proton on the nitrogen atom disappeared. It is clearly indicated that the ligand coordinates in the enolic form with metal ions. Aromatic proton signals shifted downfield and appeared at 7.5–7.9 ppm (multiplet), whereas the cyclopentadienyl ring and methyl signals shifted upfield and appeared at 3.9–4.3 (doublet) and 2.1 ppm (singlet).

Electrolytic conductance

Deep brown solutions were obtained on dissolving the complexes $M(H_2L)Cl_2$ in DMF and DMSO separately. The molar conductances (Table 3) of the complexes of Co, Ni and Mn approached those reported for 1 : 1 electrolytes.[18] A lower molar conductance for the Cd(II) complex indicated that the ionization ability of the complex in DMF and DMSO was weak due to the greater ionic radius of cadmium and a stronger complexing ability.

TG and DTA

The results of TG and DTA for H_2L, CdL and $Cd(H_2L)Cl_2$ are shown in Fig. 2 (a–c). It can be seen from Fig. 2(a) that the ligand melted endothermally at 200°C, then decomposed exothermally at 211–250°C and weight-loss was about 21% which suggests that the $PhCO^+$ group breaks away from the molecule (Calc. 21%). Between 250–343°C it is continuously broken down exothermally and again

Table 3. Molar conductance of the complexes $M(H_2L)Cl_2$, at 25°C

Complex	In DMF		In DMSO	
	Conc. (10^{-3} mol)	λm (Ω^{-1} cm^2 mol^{-1})	Conc. (10^{-3} mol)	λm (Ω^{-1} cm^2 mol^{-1})
VII	0.99	39.7	1.12	53.1
VIII	1.20	73.0	1.03	53.5
IX	1.05	26.3	1.00	15.2
X	1.06	46.1	1.04	48.9

loses about 21% of its weight (perhaps the other $PhCO^+$ was removed). The exothermal peak at 420°C was attributed to the loss of two molecules of nitrogen (Found: 10%; Calc. 11%). The decomposition was complete at 697°C and the weight of the residue was 13% (Calc. for Fe 11%).

The complex CdL [Fig. 2(b)] decomposed at 332°C, accompanied by the release of a great amount of heat and lost 24.5% of its weight (Calc. for $C_{12}H_{10}$25.0%). The complex then resolved continuously at 364–440° and the weight loss was about 24.5% due to the remaining parts of two substituents on the cyclopentadienyl ring (Calc. for $C_6H_6N_4O_2$ 26.9%). It broke down at 710°C releasing intense heat and the weight loss of 23% was attributed to the release of two cyclopentadienyl rings (Calc. for $C_{10}H_8$21%). The weight of the remainder was about 28%, therefore perhaps it is a mixture of iron and cadmium (Calc. for FeCd 27%).

The complex $Cd(H_2L)Cl_2$ [Fig. (2c)] decomposed exothermally at 236°C to lose 12% of its weight arising from the release of two molecules of HCl (Calc. for 2HCl 11%). It broke down slowly between 252 and 365°C and maybe loses two aromatic rings, accompanied by a weight-loss of about 26% (Calc. for $C_{12}H_{10}$ 23%). The decomposition continued at 561 and 610°C, and was finally complete at 720°C. (Found: 40%; Calc. for $C_{16}H_{14}N_4O_2$ 42%).

It can be seen from the above-mentioned results that the thermostability of complexes is increased much more than that of the ligand after chelation with transition metal ions, but the thermostability of the complexes ML is greater than for $M(H_2L)Cl_2$. It is clear that the C—N bond in complexes becomes much stronger than in the ligand.

REFERENCES

1. C. R. Hauser and J. O. K. Lindsay, *J. Org. Chem.* 1957, **22**, 482.
2. S. S. Crawford, C. B. Knobler and H. D. Kaesz, *Inorg. Chem.* 1977, **16**, 3201.
3. H. Alper, *J. Organomet. Chem.* 1974, **80**, C29.
4. A. Kasahara, T. Izumi and H. Watabe, *Bull. Chem. Soc. Jpn.* 1979, **52**, 957.
5. A. W. Rudie, D. W. Lichtenberg, M. L. Katcher and A. Davison, *Inorg. Chem.* 1978, **17**, 2859.
6. D. M. Wiles and T. Suprunchuk, *Can. J. Chem.* 1968, **46**, 1865.
7. S. R. Patil, U. H. Kantak and D. N. Sen, *Inorg. Chim. Acta* 1982, **63**, 261.
8. Ng. Ph. Buu-Hoi, Ng. D. Xuong, Ng. H. Ham, F. Binon and R. Roger, *J. Chem. Soc.* 1953, 1358.
9. L. El. Sayed and M. F. Iskander, *J. Inorg. Nucl. Chem.* 1971, **33**, 435.
10. E. I. Edwards, R. Epton and G. Marr, *J. Am. Chem. Soc.* 1975, **85**, C23.
11. M. Rosenblum and R. B. Woodward, *J. Organomet. Chem.* 1958, **80**, 5443.
12. M. Mashima, *Bull. Chem. Soc. Jpn.* 1962, **35**, 1882; 1963, **36**, 210.
13. R. C. Aggakval and K. K. Narang, *Ind. J. Chem.* 1971, **9**, 1413.

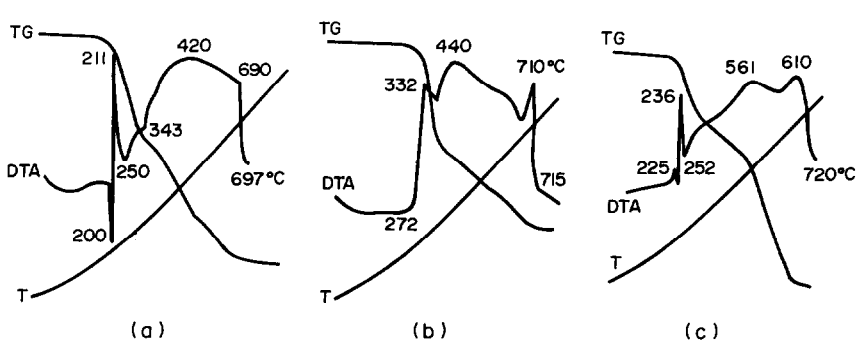

Fig. 2. The TG-DTA diagram of (a) the ligand, (b) complexes CdL and (c) $Cd(H_2L)Cl_2$.

14. K. Nakamoto, *Infrared Spectra of Inorganic and Coordination Compounds*, 2nd edn. Wiley-Interscience, New York (1970).
15. R. G. R. Bacon and W. S. Lindsay, *J. Chem. Soc.* 1958, 1382.
16. M. F. Iskander and L. El. Sayed, *Inorg. Chim. Acta* 1976, **16**, 147.
17. M. Rosenblum, J. O. Santer and W. G. Jowells, *J. Am. Chem. Soc.* 1963, **85**, 1450.
18. W. J. Geary, *Coord. Chem. Rev.* 1971, **7**, 81.

Polyhedron Vol. 7, No. 5, pp. 399–400, 1988
Printed in Great Britain

0277-5387/88 $3.00+.00
Pergamon Press plc

COMMUNICATION

$Mo(NMe_2)_6Li_2(THF)_2$

MALCOLM H. CHISHOLM,* CHARLES E. HAMMOND and JOHN C. HUFFMAN

Department of Chemistry and Molecular Structure Center, Indiana University, Bloomington, IN 47405, U.S.A.

(*Received* 23 *October* 1987; *accepted* 23 *October* 1987)

Abstract—Addition of $LiNMe_2$ to $Mo(NMe_2)_4$ in tetrahydrofuran establishes the equilibrium: $Mo(NMe_2)_4+2LiNMe_2 \overset{THF}{\rightleftharpoons} Mo(NMe_2)_6Li_2$. Red crystals of the THF adduct $Mo(NMe_2)_6Li_2(THF)_2$ have been shown to involve an octahedral MoN_6 moiety, Mo—N = 2.12 Å (averaged). The lithium atoms cap opposite faces, LiN_3MoN_3Li, and are ligated by one THF molecule to complete the pseudo tetrahedral coordination of lithium.

Organometallic chemistry evolved with π-acceptor ligands, and only within the last decade have π-donor ligands attracted general attention.[1,2] Historically $Mo(NMe_2)_4$ provided the first example of a low spin four-coordinate complex and Bradley and Chisholm[3] in their initial report noted that this could be understood as a consequence of ligand-to-metal π-bonding. In D_{2d} symmetry it is possible to formulate the complex as an 18 electron valence shell complex: Mo(IV), d^2+8e(4Mo—N σ) +8e(4Mo—N π).[2,4] However, in contrast to typical organometallic complexes which satisfy the 18 electron rule[5] and are thus coordinatively and electronically saturated, $Mo(NMe_2)_4$ should be viewed, like most other π-donor stabilized 18 electron complexes, as unsaturated. The reason for this unsaturation is that while π-donation from ligands such as NR, NR_2 and OR may lead to a formal 18 electron count, the π-electrons are ligand centred. Thus the metal d_π orbitals represent low lying antibonding M—L π bonds and are easily attacked by nucleophiles. Furthermore, the ligand based π-electrons are susceptible to attack by electrophiles. Consequently we should anticipate that the ligand π-donor stabilized complexes should be substitutionally labile providing that stertic factors allow for associative reaction pathways. We describe here our discovery of the equilibrium shown in eq. (1) which provides a prototypical example of the above considerations.

$$Mo(NMe_2)_4+2LiNMe_2 \rightleftharpoons Mo(NMe_2)_6Li_2. \quad (1)$$

Addition of $LiNMe_2$ (> 2 equivs) to a purple solution of $Mo(NMe_2)_4$ leads to the formation of $Mo(NMe_2)_6Li_2(THF)_2$ which can be isolated as red crystals. A view of the molecular structure found† in the solid state is given in Fig. 1. The central MoN_6 octahedral moiety, Mo—N = 2.12 Å (av.), is supported by two lithium atoms which are coordinated to opposite MoN_3 faces. Thus each nitrogen is coordinated in a distorted tetrahedral manner to two carbon atoms, a lithium and a molybdenum atom. The Mo—N distances of 2.12, 2.03 and 1.93 Å seen in $Mo(NMe_2)_6Li_2(THF)_2$, $Mo(NMe_2)_6$[6] and $Mo(NMe_2)_4$[4] reflect, at least in part, the relative π-

* Author to whom correspondence should be addressed.

† Crystal data for $Mo(NMe_2)_6Li_2(THF)_2$ at −155°C: a = 8.568(3), b = 10.303(5), c = 15.586(7) Å, β = 95.69(2)°, Z = 2, d_{calcd} = 1.258 g cm^{-3} in the space group $A2/m$. Using Mo-K_α, 6° < 2θ < 55°, 2693 reflections were collected. Of these, the number of unique intensities was 1595 and these were used in the final least squares refinement leading to residuals $R(F)$ = 0.0689 and $Rw(F)$ = 0.0660.

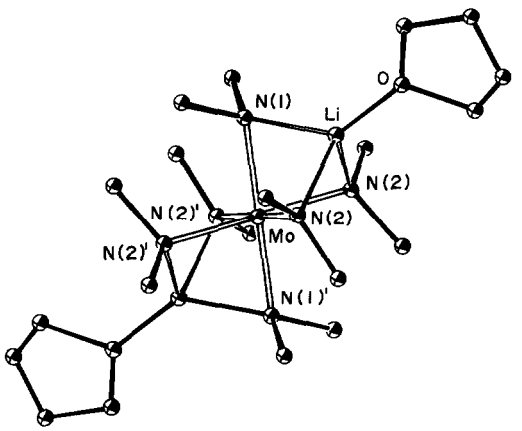

Fig. 1. Ball-and-stick drawing of the $Mo(NMe_2)_6Li_2(THF)_2$ molecule without hydrogen atoms, showing the atom number scheme. Pertinent distances (Å) and angles (°) are:

Mo—N(1) = 2.132(7),	N(1)—Mo—N(1)′ = 180.0(3),
Mo—N(2) = 2.119(5),	N(1)—Mo—N(2) = 84.55(18),
N(1)—Li = 2.090(14),	N(1)—Mo—N(2)′ = 95.5(3),
N(2)—Li = 2.075(12),	N(2)—Mo—N(2) = 84.9(3),
Li—O = 1.897(14),	N(2)—Mo—N(2)′ = 95.1(3).

bond character in the Mo—N bonds, which for this series are formally 0, 1/2 and 1, respectively, i.e. in $Mo(NMe_2)_4$ the Mo—N bonds are double bonds ($\sigma^2+\pi^2$) but in $Mo(NMe_2)_6Li_2(THF)_2$ they are single bonds.

The compound $Mo(NMe_2)_6Li_2(THF)_2$ readily dissociates to $LiNMe_2$ in solution and, in benzene or toluene, purple solutions of $Mo(NMe_2)_4$ and white precipitates of $LiNMe_2$ are obtained.

It seems likely that other early transition metal elements form related complexes, e.g. $M(NMe_2)_6Li_2(THF)_2$, where M = Zr[7] and Hf,[8] and given that the related equilibria may lie further to the right for M = Zr and Hf relative to M = Mo, this may well account for the occasional low yields of the group IV dimethylamides in reactions involving MCl_4 and $LiNMe_2$ (4 equivs).

Further studies are in progress.

Acknowledgement—We thank the National Science Foundation for support.

REFERENCES

1. W. E. Buhro and M. H. Chisholm, *Adv. Organomet. Chem.* 1987, in press.
2. M. H. Chisholm and D. L. Clark, *Comments Inorg. Chem.* 1987, **6**, 23.
3. D. C. Bradley and M. H. Chisholm, *J. Chem. Soc. (A)* 1971, 2741.
4. M. H. Chisholm, F. A. Cotton and M. W. Extine, *Inorg. Chem.* 1978, **17**, 1329.
5. C. A. Tolman, *Chem. Soc. Rev.* 1972, **1**, 337.
6. M. H. Chisholm, C. E. Hammond and J. C. Huffman, *J. Chem. Soc., Chem. Commun.* 1987, 1423.
7. D. C. Bradley and I. M. Thomas, *J. Chem. Soc., Chem. Commun.* 1960, 3857.
8. D. C. Bradley and M. H. Gitlitz, *J. Chem. Soc. (A)* 1969, 980.

Polyhedron Vol. 7, No. 5, pp. 401–404, 1988
Printed in Great Britain

0277–5387/88 $3.00+.00
Pergamon Press plc

COMMUNICATION

SYNTHESIS AND STRUCTURAL CHARACTERIZATION OF A DIPHENYLCARBAZONE COMPLEX OF MOLYBDENUM(VI), (n-Bu_4N)[$MoO_2(C_6H_5NNC(O)NNC_6H_5)(C_6H_5NNC(O)NHNC_6H_5)$], A SPECIES CONTAINING ORGANOHYDRAZIDO(2−) AND ORGANOHYDRAZIDO(1−) LIGANDS AND FUNCTIONING AS A SYNTHETIC PRECURSOR IN THE PREPARATION OF THE TETRANUCLEAR DIAZENIDO COMPLEX, (n-Bu_4N)$_2$[$Mo_4O_6(OCH_3)_2(OC_6H_4NH)_2(NNC_6H_5)_4$]

SHUNCHENG LIU and JON ZUBIETA*

Department of Chemistry, State University of New York at Albany, Albany, NY 12222, U.S.A.

(*Received* 14 *July* 1987; *accepted after revision* 7 *October* 1987)

Abstract—Reaction of α-(Bu_4N)$_4$[Mo_8O_{26}] with diphenylcarbazone in CH_2Cl_2 yields the hydrazido(1−), hydrazido(2−) species (Bu_4N)[$MoO_2(C_6H_5NNCONHNC_6H_5)(C_6H_5NNCONNC_6H_5)$] (**I**). Treatment of (**I**) with phenylhydrazine in MeOH yields the unexpected product, (Bu_4N)$_2$[$Mo_4O_6(OMe)_2(OC_6H_4NH)_2(NNC_6H_5)_4$] (**II**), a tetranuclear polyoxomolybdate with the $[Mo_2(OMe)_2(NNC_6H_5)_4]^{2+}$ core. Crystal Data: (**I**), space group $P2_1/n$, $a = 11.026(2)$, $b = 21.600(3)$, $c = 18.851(3)$ Å, $\beta = 98.04(1)°$; (**II**), space group $P2_1/a$, $a = 24.675(4)$, $b = 19.937(4)$, $c = 17.295(3)$ Å, $\beta = 112.62(1)°$.

Our recent investigations of the chemistry of Mo(VI) with substituted organohydrazines have revealed a varied structural chemistry, based upon polynuclear oxomolybdate cores.[1] In an effort to extend these studies to potentially multidentate or ambidentate organonitrogen ligands, investigations of the chemistry of Mo(VI) with organocarbazone and organocarbazide ligands were initiated. Although diphenylcarbazone, $C_6H_5NNC(O)NHNHC_6H_5$, has long been employed in the photometric determination of molybdenum,[2] the intensely coloured molybdenum–organohydrazido complexes which are formed have remained uncharacterized.

Reaction of α-(n-Bu_4N)$_4$[Mo_8O_{26}][3] with an excess of diphenylcarbazone in refluxing CH_2Cl_2 results in a bright violet solution, from which lustrous dark irregular crystals are isolated in 30% yield upon addition of diethylether and standing at room temperature for three days. The elemental analysis and the observed diamagnetism are consistent with the formulation (n-Bu_4N)[$MoO_2(C_6H_5NNCONHNC_6H_5)(C_6H_5NNCONNC_6H_5)$] (**I**). The IR spectrum exhibits strong absorbances at 1660 and 1593 cm^{-1} assigned to ν(C=O) and ν(N=N) of the coordinated diphenylcarbazone ligands, respectively, and bands at 870 and 899 cm^{-1}, characteristic of ν(Mo=O) for the *cis*-dioxomolybdenum(VI) unit. Crystal data:† $C_{42}H_{57}N_9O_4Mo$, monoclinic space group, $P2_1/n$ with $a = 11.026(2)$, $b = 21.600(3)$, $c = 18.851(3)$ Å, $\beta = 98.04(1)°$, $V = 4445.1(12)$ Å^3, $Z = 4$, $D_{calc} = 1.27$ g cm^{-1}. Structure solution and refinement based on 3002 reflections with $I_o \geq 3\sigma(I_o)$ (Mo-K_α, 0.71073 Å) converged at a conventional discrepancy factor of 0.0655.

As illustrated by Fig. 1, the structure of (**I**) consists of discrete (n-Bu_4N)$^+$ cations and mononuclear anionic units [$MoO_2(C_6H_5NNC(O)NNC_6H_5)$

* Author to whom correspondence should be addressed.

† Tables of fractional coordinates have been deposited with the Editor and also with Cambridge Crystallographic Data Centre.

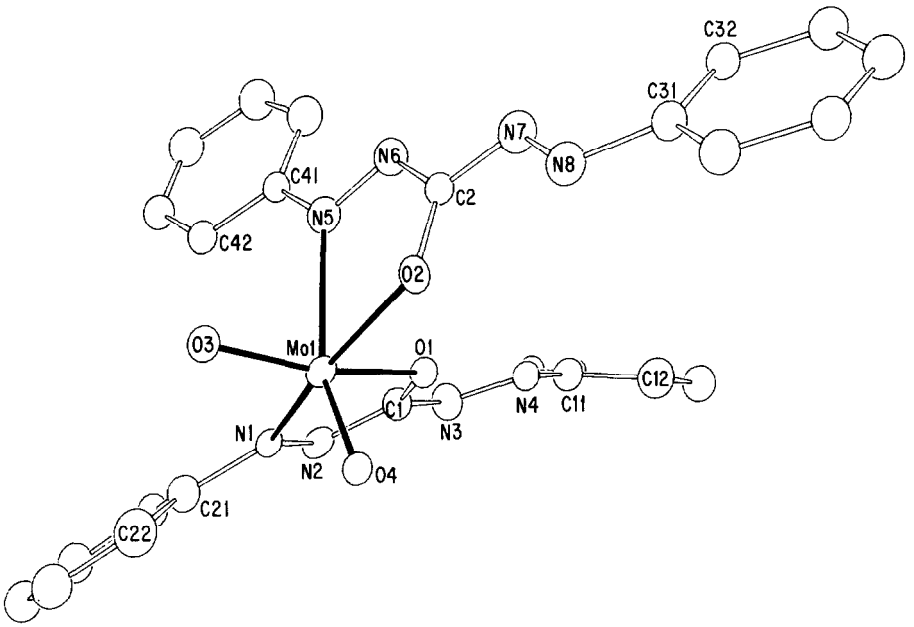

Fig. 1. ORTEP view of the structure of the molecular anion $[MoO_2(C_6H_5NNCONHNC_6H_5)(C_6H_5NNCONNC_6H_5)]^{1-}$, showing the atom labelling scheme. Selected bond lengths (Å) and angles (°): Mo—O1, 2.059(6); Mo—O2, 2.030(8); Mo—O3, 1.704(7); Mo—O4, 1.701(7); Mo—N1, 2.068(8); Mo—N5, 2.432(8); N1—N2, 1.39(1); N2—C1, 1.31(1); C1—N3, 1.39(1); N3—N4, 1.29(1); C1—O1, 1.31(1); N5—N6, 1.29(1); N6—C2, 1.36(1); C2—N7, 1.33(1); N7—N8, 1.35(1); C2—O2, 1.32(1); N3—N4, 1.27(1); N7—N8, 1.35(1); O1—Mo—O2, 85.2(3); O1—Mo—O3, 149.4(3); O1—Mo—O4, 102.5(3); O1—Mo—N1, 72.4(3); O1—Mo—N5, 72.4(2); O2—Mo—O3, 106.7(3); O2—Mo—O4, 91.5(3); O2—Mo1—N1, 156.1(3); O2—Mo1—N5, 67.7(3); O3—Mo—O4, 105.1(3); O3—Mo—N1, 89.6(3); O3—Mo—N5, 86.0(3); O4—Mo—N1, 101.2(3); O4—Mo—N5, 158.7(3); N1—Mo—N5, 96.9(3); Mo1—N1—N2, 120.1(6); N1—N2—C1, 108.7(7); Mo1—N5—N6, 115.2(6); N5—N6—C2, 110.5(9).

$(C_6H_5NNC(O)NHNC_6H_5)]^{-1}$. The Mo(VI) centre displays the ubiquitous *cis*-dioxo geometry, with the remaining pseudo-octahedral positions occupied by nitrogen donors and the carbonyl oxygen groups of the chelating organohydrazido ligands. The chelate ring parameters confirm that the organohydrazide ligands are inequivalent, the MoO1C1N2N1 ring functioning as a doubly deprotonated organohydrazido(2−) unit, while the MoO2C2N4N5 ring retains the proton at the N4 site to assume the hydrazido(1−) formalism. The ring parameters associated with the organohydrazido(2−) moiety are similar to those observed for the MoOCNN chelate rings of $[Mo_2O(S_2CNEt_2)_2(C_6H_5CON_2)_2]$,[4] where the organohydrazide ligand assumes the chelating deprotonated structure. The major distortions from octahedral geometry are consequences of the acute angles at the Mo(VI) centre generated by chelate ring formation and of the usual expansion of the *cis*-dioxomolydenum angle, necessary to accommodate the strongly π-bonded oxo-groups.

The oxo-groups of (**I**) appear to be substitution labile in the common condensation type reactions, exploited in the synthesis of *cis*-diazenidomolybdenum complexes.[1] Reaction of (**I**) with a stoichiometric amount of phenylhydrazine in methanol yielded a dark purple solution, from which dark prismatic crystals of a material, analysing for $(n\text{-}Bu_4N)_2[Mo_4O_6(OCH_3)_2(OC_6H_4NH)_2(NNC_6H_5)_4]$ (**II**), were isolated in 10% yield upon standing for several days. It was subsequently confirmed that (**II**) could also be synthesized directly from the reaction of $(n\text{-}Bu_4N)_2[Mo_4O_8(OCH_3)_2(NNC_6H_5)_4]$ with diphenylcarbazone. Crystal data:† $C_{70}H_{108}N_{12}O_{10}Mo_4$, monoclinic space group, $P2_1/a$ with $a = 24.675(4)$, $b = 19.937(4)$, $c = 17.295(3)$ Å, $\beta = 112.62(1)°$, $V = 7853.7(14)$ Å, $Z = 4$, $D_{calc} = 1.40$ g cm^{-3}. Structure solution and refinement based on 4014 reflections with $I_o \geqslant 3\sigma(I_o)$ (Mo-K_α, 0.71073 Å) converged at a conventional discrepancy factor of 0.0783.

† See footnote † on previous page.

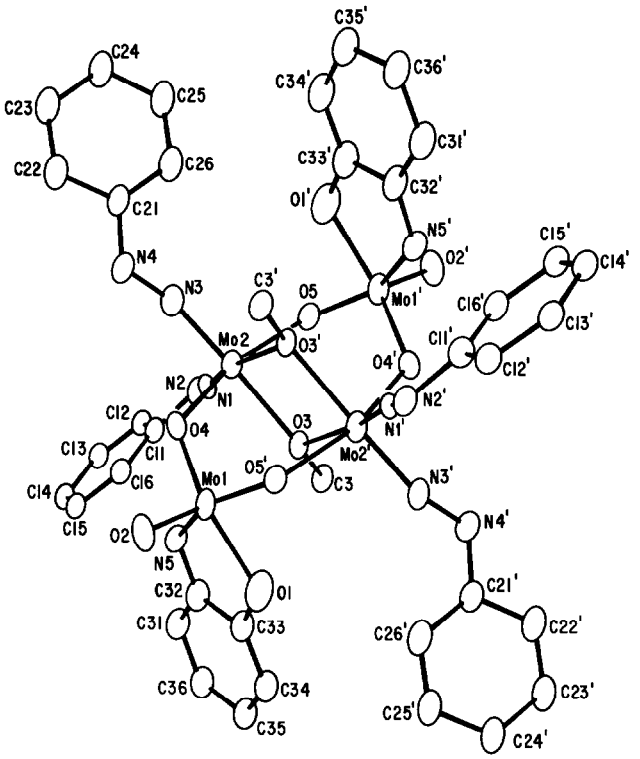

Fig. 2. ORTEP view of the structure of the tetranuclear dianion $[Mo_4O_6(OC_6H_4NH)_2(OCH_3)_2(NNC_6H_5)_4]^{2-}$, showing the atom labelling scheme. Selected bond lengths (Å) and angles (°): Mo1—N5, 1.99(1); Mo1—O1, 2.05(2); Mo1—O2, 1.70(1); Mo1—O4, 1.81(1); Mo1—O5, 1.78(1); Mo2—N1, 1.76(2); Mo2—N3, 1.84(2); Mo2—O3, 2.17(1); Mo2—O4, 2.03(1); Mo2—O5, 2.05(1); Mo2—O3′, 2.14(1); O1—Mo1—N5, 75.6(7); O1—Mo1—O4, 150.4(6); O5—Mo1—N5, 147.0(5); O2—Mo1—N5, 103.8(7); O2—Mo1—O1, 101.1(7); O2—Mo1—O4, 104.9(6); O2—Mo1—O5, 105.6(6); N1—Mo2—O3′, 166.7(5); N3—Mo2—O3, 167.7(6); O4—Mo2—O5, 160.9(5); Mo2—N1—N2, 167.2(15); Mo2—N3—N4, 163.4(15).

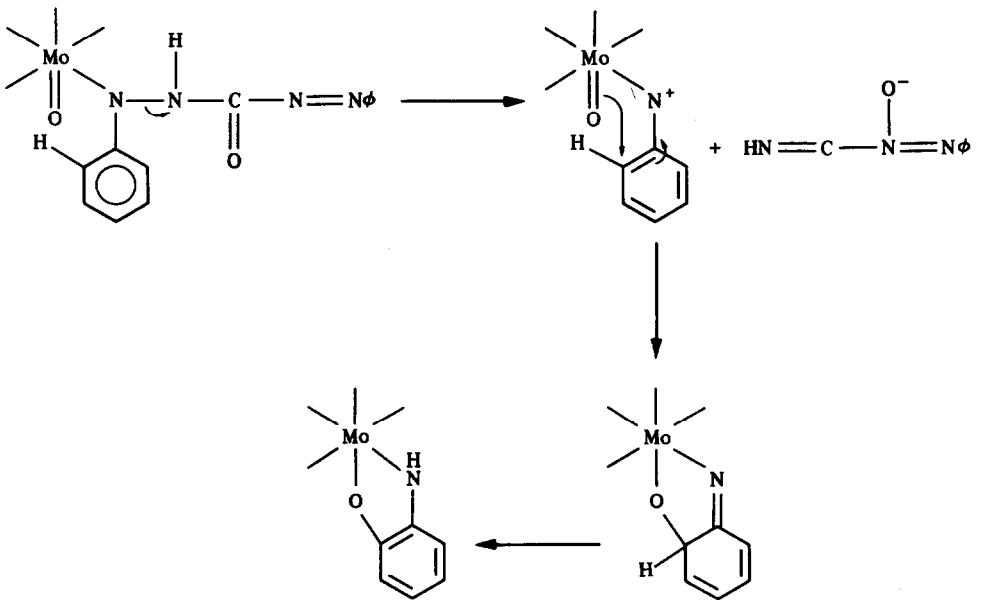

Scheme 1.

The anion of (**II**) is seen to be structurally related to the tetranuclear clusters of the general types $[Mo_4O_8(OR)_2(NNR)_4]^{2-}$ and $[Mo_4O_{10}(OR)_2(NNR_2)_2]^{2-}$.[1] Thus, the structure of (**II**) may be described in terms of a planar $[Mo_2(OCH_3)_2(NNC_6H_5)_4]^{2+}$ unit, bridged through axially doubly bridging oxo-units to the bidentate $[MoO_3(OC_6H_4NH)]^{2-}$ groups (see Fig. 2). The planar core, $[Mo_2(OCH_3)_2(NNC_6H_5)_4]^{2+}$, exhibits the usual geometry, with short Mo—N and N—N distances and linear Mo=N=N linkages characteristic of the *cis*-bisdiazenidomolybdenum unit.[1,5,6] The bridging bidentate groups $[MoO_3(OC_6H_4NH)]^{2-}$ exhibit distorted square pyramidal geometry with the terminal oxo-group occupying the apical position and the vertices of the square plane defined by the two bridging oxo-groups and the oxygen and nitrogen donors of the coordinated *o*-amidophenolato ligand. The structure of (**II**) is thus formally derived from that previously reported for $[Mo_4O_8(OCH_3)_2(NNC_6H_5)_4]^{2-}$ by replacement of a terminal oxo-group on each of the bridging bidentate $[MoO_4]^{2-}$ units by the *o*-amidophenolato unit $(OC_6H_4NH)^{2-}$. Although the mechanism of complex formation has yet to be elucidated, the chemistry may proceed through coordination of the terminal hydrazido nitrogen of the diphenylcarbazone ligand to a molybdenum-oxo-unit, followed by oxo-group attack on the *ortho* position of the phenyl substituent, in a reaction reminiscent of quinone–methide chemistry as shown in Scheme 1. The isolation of complex (**II**) suggests that the fundamental structural type $[Mo_4O_8(OR)_2(NNR)_4]^{2-}$ is capable of considerable modification and may serve as a precursor for a variety of substitution reactions and as a building block for further aggregation. Mechanistic studies are in progress to confirm the nature of the putative *ortho*-oxo insertion reaction, as are chemical and structural studies of related ligand and substrate molecules.

Acknowledgement—This work was supported by a grant from the National Science Foundation to J.Z. (CHE8514634).

REFERENCES

1. T.-C. Hsieh and J. Zubieta, *Inorg. Chem.* 1985, **24**, 1287; T.-C. Hsieh and J. Zubieta, *J. Chem. Soc., Chem. Comm.* 1985, 1749; T.-C. Hsieh and J. Zubieta, *Polyhedron* 1986, **5**, 305; S. N. Shaikh and J. Zubieta, *Inorg. Chem.* 1986, **25**, 4613; T.-C. Hsieh and J. Zubieta, *Inorg. Chim. Acta* 1987, **127**, L31; T.-C. Hsieh and J. Zubieta, *Polyhedron* 1986, **5**, 1655.
2. A. K. Babko and T. E. Get'man, *Ukr. Khim. Zh.* 1961, **27**, 807.
3. M. Filowitz, R. K. C. Ho, W. G. Klemperer and W. Shum, *Inorg. Chem.* 1979, **18**, 93.
4. M. W. Bishop, J. Chatt, J. R. Dilworth, J. R. Hyde, S. Kim, K. Venkatasubramanian and J. Zubieta, *Inorg. Chem.* 1978, **17**, 2917.
5. D. Attanasio, V. Fares and P. Imperatori, *J. Chem. Soc., Chem. Comm.* 1986, 1476.
6. D. Carillo, P. Gouzerh and Y. Jeannin, *Nouv. J. Chim.* 1985, **9**, 749.

Polyhedron Vol. 7, No. 5, pp. 405–407, 1988
Printed in Great Britain

0277–5387/88 $3.00 + .00
Pergamon Press plc

COMMUNICATION

LIGAND DEPENDENT NATURE OF THREE POSSIBLE SHAPES FOR A d^6 PENTACOORDINATED COMPLEX

YVES JEAN and ODILE EISENSTEIN*

Laboratoire de Chimie Théorique (UA 506), Bâtiment 490, Centre de Paris-Sud, 91405 Orsay, France

(*Received* 17 *September* 1987; *accepted* 7 *October* 1987)

Abstract—The distortion of model XMH_4 d^6 complexes (X-equatorial ligand) away from their unstable trigonal bipyramidal (TBP) structure is studied by means of Extended Hückel calculations. The distortion is represented by the angle α between the two equatorial M—H bonds ($\alpha = 120°$ in the TBP geometry). Departure from $\alpha = 120°$ leads to two minima, one for $\alpha = 180°$ (square pyramid geometry) and one for $\alpha = 70°$, the origin of both being traced to a first order Jahn–Teller effect and not to a favourable ligand–ligand interaction ($\alpha = 70°$). The relative energies of these two minima are strongly dependent on the nature of the equatorial ligand X opposite to the α angle. In particular it is shown that a π donor X ligand favours $\alpha = 70°$ while a π acceptor favours $\alpha = 180°$. Finally a third minima is found for $\alpha = 30°$. In this case, there is a strong interaction between the equatorial hydrides and this structure is better viewed as a d^8 square planar complex with a molecular H_2 ligand side-bonded to the metal.

There is a current interest in synthesizing electron deficient organometallic complexes since they may present interesting chemical properties and may also give insight on the mechanisms of organometallic reactions.

Werner has recently isolated and structurally characterized an Ir(III) d^6 pentacoordinated complex **1**.[1] The striking structural property of the complex is the small (77.9°) C—Ir—H α angle in place of the expected 120° angle usually found for a d^8 trigonal bipyramid. As pointed out by the authors, this distortion does not permit the formation of a significant carbon ··· hydrogen bond but hinders the rotation of the phenyl ring lying in the equatorial plane.

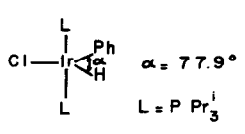

1

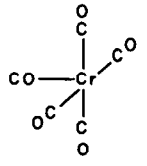

2

It is well known that a trigonal bipyramid is structurally unstable for 6 *d* electrons. The *d* splitting in a trigonal bipyramid is well known.[2] Since there are only six electrons to be hosted by the *d* block, four of them go into the fully non-bonding *xz* and *yz* orbitals and only two need to be put in either x^2-y^2 or *xy* (*e'* set). This is a typical first order Jahn–Teller[3] situation where either x^2-y^2 (**3**) or *xy* (**4**) is stabilized by a structural distortion. Closing α stabilizes x^2-y^2, since the hydrogen orbitals enter its nodal planes, and destabilizes *xy*, because the hydrogen orbitals are more directed towards its lobes. The reverse consequences arise from the opening of α. The interesting point is that these two distortions, the one which increases α and the one which decreases α, are in principle permitted. An example of the first distortion is the Werner compound and one example of the second distortion is the square pyramidal structure of $Cr(CO)_5$ **2**.[4]

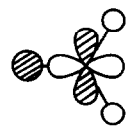

3

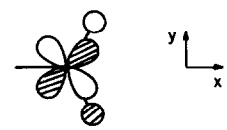

4

*Author to whom correspondence should be addressed.

In this preliminary report, we show that three structures can be expected for these complexes and that their relative energies are highly dependent on the nature of the equatorial ligand opposite the α angle. Three model complexes have been used for this purpose: $XIrH_4^-$ (X = H^-, Cl^-, CO) in which the ligand opposite to α is either π neutral (H^-), π donor (Cl^-) or π acceptor (CO) (see Fig. 1). For each complex, α has been varied from 180° to 30°. The total energies obtained by extended Hückel calculations[5] are shown in Fig. 1.

The least stable structure of IrH_5^{2-} is obtained for $\alpha = 120°$. Closing or opening α to 70° or 180° stabilizes the complex by approximately the same amount of energy. It should be noted that there is still no H ··· H bond at $\alpha = 70°$ in agreement with the fact that Werner did not observe any C ··· H bond in his structure. Greater closing of α leads to the occurrence of a third minimum ($\alpha = 30°$) which is better viewed as a d^8 square planar complex with a molecular H_2 ligand side-bonded to the metal perpendicularly to the molecular frame, reminiscent of the Zeise' salt.

For $ClIrH_4^{2-}$, the energy maximum is shifted towards α larger than 120° and the more stable structure occurs for $\alpha = 70°$. The minimum at $\alpha = 180°$ is considerably destabilized. The molecular complex is still present as a minimum. Opposite results are obtained for $COIrH_4^-$. The energy maximum is shifted to a value of α less than 120° and the primary minimum occurs for $\alpha = 180°$. Also in this case the molecular complex is present as a possible structure. The above results are in agreement with the presence of a Cl atom in the Werner compound ($\alpha = 80°$) and with that of a CO group in the square pyramid $Cr(CO)_5$.

The examination of the evolution of the *d* orbitals

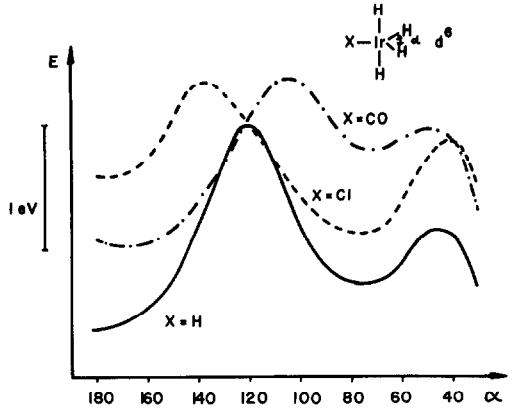

Fig. 1. Variation of the total energy (kcal mol^{-1}) for IrH_5^{2-} (solid line), $ClIrH_4^{2-}$ (dashed line), $COIrH_4^-$ (dashed dotted line) as a function of the angle α between the two equatorial hydrogen atoms.

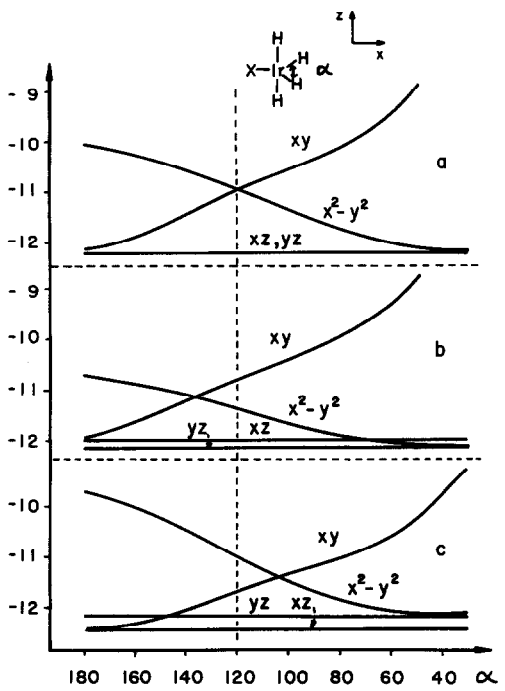

Fig. 2. Partial Walsh diagram showing only the *d* block for $XIrH_4^-$ (a: X = H^-; b: X = Cl^-; c: X = CO) as a function of α.

energy upon distortion (shown schematically in Fig. 2) reveals the reasons for the above behaviour. We focus here on the comparison between the two minima when $\alpha = 70°$ and $\alpha = 180°$.

Since the x^2-y^2 and xy orbitals are degenerate in IrH_5^{2-}, by first approximation, and as long as α does not depart too much from 120°, closing or opening α has the same energetical consequences.

Substituting Cl^- for H^- removes the degeneracy for the two orbitals for $\alpha = 120°$.[6] xy becomes higher in energy than x^2-y^2 since it is destabilized by the Cl lone pair lying in the equatorial plane as shown in **5**. This has two consequences: (i) the point

5 6

of maximum energy is shifted to a value of α larger than 120° where the energies of x^2-y^2 and xy meet, (ii) better stabilization is obtained by closing α, since this takes advantage of the lower energy of x^2-y^2. The analysis is analogous but with reverse conclusions when CO is substituted for H^- since xy is now stabilized by π^*_{CO} (**6**). The complex should therefore gain more energy by further stabilization of xy by the opening of α.

The possible existence of a molecular H_2 complex will not be discussed in this preliminary calculation since the interaction of H_2 with a T shaped ML_3 is essentially similar to the interactions that are at work[7] in the many molecular H_2 complexes presently known. It is however of interest to notice that such complexes have an electronic structure reminiscent of a square planar d^8 olefin complex and might be of some stability.

The structure of d^6 pentacoordinated complexes is thus highly sensitive to the nature of the ligands. Fryzuk[8] has suggested a square pyramid structure for Ir(III) complexes which have two *trans* π donor groups at the equatorial sites ($\alpha = 180°$) and a neutral alkyl ligand at the apical site of the square pyramid. Preliminary calculations on model $H_3IrCl_2^{-2}$ varying the α angle between the equatorial Ir—Cl bonds reproduce this tendency. A complete understanding of the structural preference of d^6 pentacoordinated complexes clearly requires to take explicitly into account the nature of each ligand. This study is presently under way in our laboratory.

Acknowledgement—This work was completed during the stay of O.E. at Indiana University which is thanked for its hospitality.

REFERENCES

1. H. Werner, A. Höhn and M. Dziallas, *Angew. Chem. Int. Ed. Engl.* 1986, **25**, 1090.
2. A. R. Rossi and R. Hoffmann, *Inorg. Chem.* 1975, **14**, 365.
3. M. Elian and R. Hoffmann, *Inorg. Chem.* 1975, **14**, 1058; J. K: Burdett, *J. Chem. Soc., Faraday Trans. II* 1974, **70**, 1599.
4. R. N. Perutz and J. J. Turner, *Inorg. Chem.* 1975, **14**, 262; R. N. Perutz and J. J. Turner, *J. Am. Chem. Soc.* 1975, **97**, 4791; T. A. Seder, S. P. Church, A. J. Ouderkirk and E. Weitz, *J. Am. Chem. Soc.* 1985, **107**, 1432. A review on the subject can be found in M. Poliakoff and E. Weitz, *Adv. Organomet. Chem.* 1986, **25**, 277.
5. The weighted H_{ij} formula was used: J. H. Ammeter, H.-B. Bürgi, J. C. Thibeault and R. Hoffmann, *J. Am. Chem. Soc.* 1978, **100**, 3686; The parameters for Iridium were taken from D. L. Dubois and R. Hoffmann, *Nouv. J. Chem.* 1977, **1**, 479.
6. D. L. Thorn and R. Hoffmann, *Nouv. J. Chim.* 1979, **3**, 39.
7. J. Y. Saillard and R. Hoffmann, *J. Am. Chem. Soc.* 1984, **106**, 2006; Y. Jean, O. Eisenstein, F. Volatron, B. Maouche and F. Sefta, *J. Am. Chem. Soc.* 1986, **108**, 6587.
8. M. D. Fryzuk, P. A. MacNeil and S. J. Rettig, *Organometallics* 1986, **5**, 2469.

Polyhedron Vol. 7, No. 5, pp. 409–415, 1988
Printed in Great Britain

0277–5387/88 $3.00+.00
Pergamon Press plc

COMMUNICATION

EFFECT OF A SERIES OF PHOSPHINE AND PHOSPHITE LIGANDS ON THE TAFT SUBSTITUENT CONSTANTS OF ARENECHROMIUMCARBONYL AND CYCLOPENTADIENYLMANGANESECARBONYL COMPLEXES

THOMAS E. BITTERWOLF

Department of Chemistry, U.S. Naval Academy, Annapolis, MD 21402, U.S.A.

(*Received* 5 *March* 1987; *accepted after revision* 28 *October* 1987)

Abstract—A series of *m*- and *p*-fluorophenylarenechromiumcarbonyl and *m*- and *p*-fluorophenylcyclopentadienylmanganesecarbonyl complexes of phosphines and phosphites have been prepared and characterized by IR and NMR spectroscopy. Taft substituent constants were calculated from the ^{19}F chemical shifts and carbonyl stretching force constants were calculated from the carbonyl stretching frequencies of the compounds. It has been found that the phosphine and phosphite groups exert parallel effects on the Taft constants and stretching force constants and, furthermore, that the trends in the chromium and manganese series are strongly related.

The physical and chemical properties of organometallic compounds are known to be sensitive to the nature of the ligands bound to the metal atom. For example, variations of carbonyl stretching frequencies of metal carbonyl complexes of the type $LM(CO)_n$ were used to establish the order of π acidities for a broad series of phosphine and phosphite ligands.[1] Similarly, Bodner *et al.*[2] have related the carbonyl ^{13}C NMR chemical shifts of a variety of $LM(CO)_n$ complexes to the σ and π acidity of the ligands. Work in this laboratory on dihydrogen evolution from dinuclear organometallic complexes has demonstrated that the rates of these reactions are affected by the electron donor properties of phosphine groups bound to the metal atom.[3]

As much of our research concerns the manipulation of the electron density, or basicity, at a reactive metal atom, we have sought methods which can provide a quantitative measure of the electronic changes brought about by varying the ligands on a metal atom. One technique which is well suited to organometallic chemistry is the measurement of Taft substituent constants by examination of the ^{19}F NMR chemical shifts of substituted *m*- and *p*-fluorobenzenes.[4] This technique is broadly applicable to organometallic compounds, including those which are too air or water sensitive to survive other methods. Parshall has reported Taft substituent constants for a series of σ-bonded aryl compounds of Ni, Pd and Pt.[5] Stewart and Treichel have examined a large number of σ-bonded complexes of metal carbonyls and mixed carbonyl, phosphine compounds as well as cyclopentadienyl compounds.[6] Nesmeyanov *et al.* have reported substituent constants for σ-bonded aryl derivatives of cyclopentadienylmetalcarbonyl compounds, where the metals were iron, molybdenum and tungsten.[7] These workers also reported the substituent constants for cyclopentadienyliron metallated arene rings.[8] Gubin *et al.* have been concerned with the effect of metallation on the cyclopentadienyl ring and have reported substituent constants for the iron group metallocenes,[9] cymantrene and its rhenium analog,[10] and for alkali metal complexed cyclopentadienide anions.[11] This group also reported substituent constants for the arenechromiumtricarbonyl moiety.[12]

We have reported the Taft substituents of a set of $[(arene)Cr(CO)_2L]$ complexes (where L = CO, PPh_3 and $AsPh_3$).[13] It was shown that both the inductive, σ_I and resonance, σ_R^0, substituent constants of the metallated arene are sensitive to the identity of L.

In order to gain a better understanding of the relationship between the Taft constants and the metal ligands, we have prepared an extended series of *m*- and [(*p*-fluorophenylarene)$Cr(CO)_2L$] (**I**) and $CpMn(CO)_2L$ (**II**) complexes and determined the Taft substituent constants of these compounds.

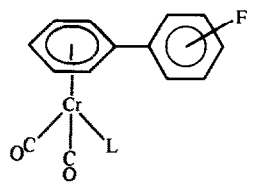

I

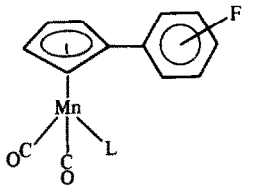

II

As an expansion of these studies, we have calculated the stretching force constants of these compounds using the approximations developed by Cotton and Kraihanzel.[14] Linear regression analysis has been used to examine the correlations between stretching force constants and Taft constants within and between the sets of compounds.

RESULTS AND DISCUSSION

m- and *p*-Fluorobiphenylchromiumtricarbonyl can be prepared in good yield by reaction of the appropriate biphenyl with chromium hexacarbonyl in refluxing butyl ether–THF according to the procedures of Top and Jaouen.[15] Photolysis of these complexes in benzene in the presence of phosphines or phosphites gives the corresponding [(arene)$Cr(CO)_2L$] complexes in good yield.[16]

Substituted $CpMn(CO)_3$ derivatives were prepared by reaction of *m*- or *p*-fluorophenylcyclopentadienylthallium with $BrMn(CO)_5$. Gubin *et al.* have prepared these compounds from the analogous cyclopentadienyl sodium salts.[10] As in the chromium series, photolysis of the manganese carbonyl compounds in benzene gave the phosphine and phosphite complexes in good yield.[17]

Analyses and physical data on the new compounds are presented in Table 1. In several cases it was not possible to obtain elemental analyses because of the instability of the complexes. For those materials the spectral data were taken to be sufficient proof of identity.

Spectra of all compounds were recorded in deuterobenzene. In the cases of the trimethylphosphine derivatives of manganese the air-sensitivity of the compounds precluded rigorous purification, so ^1H NMR spectra were not recorded. ^{19}F NMR chemical shifts were measured relative to both C_6F_6 and C_6H_5F to insure reproducibility. ^{19}F chemical shifts are reported relative to C_6F_6. ^{31}P NMR chemical shifts were measured relative to 85% H_3PO_4. The

Table 1. Analytical data and physical properties of new compounds

Compound [(Arene)$Cr(CO)_2L$] L (*m*/*p*-F)	Theory %C	Theory %H	Found %C	Found %H	M.p.
$P(OCH_2CF_3)_3$ (*m*-F)	—	—	—	—	Yellow-orange oil
$P(OCH_2CF_3)_3$ (*p*-F)	—	—	—	—	Yellow-orange oil
$P(OC_6H_5)_3$ (*m*-F)	65.1	4.1	64.8	4.2	112–114°C
$P(OC_6H_5)_3$ (*p*-F)	65.1	4.1	65.2	4.3	128–130°C
$P(OCH_3)_3$ (*m*-F)	50.5	4.5	50.5	4.4	96.98°C
$P(OCH_3)_3$ (*p*-F)	50.5	4.5	50.4	4.5	121–123°C
$P(CH_3)_3$ (*m*-F)	57.3	5.1	55.4	5.2	42–43°C
$P(CH_3)_3$ (*p*-F)	57.3	5.1	57.0	5.1	Yellow oil
$P(C_4H_9)_3$ (*m*-F)	—	—	—	—	Orange oil
$P(C_4H_9)_3$ (*p*-F)	—	—	—	—	Orange oil
$CpMn(CO)_2L$ L (*m*/*p*-F)					
$P(OC_6H_5)_3$ (*m*-F)	64.1	4.0	64.2	4.4	99–100°C
$P(OC_6H_5)_3$ (*p*-F)	64.1	4.0	63.6	4.2	115–117°C
$P(C_6H_5)_3$ (*m*-F)	69.9	4.3	71.2	4.6	96–97°C
$P(C_6H_5)_3$ (*p*-F)	69.9	4.3	69.6	4.3	111–112°C
$P(CH_3)_3$ (*m*-F)	—	—	—	—	Yellow oil
$P(CH_3)_3$ (*p*-F)	—	—	—	—	Yellow oil

phosphorus resonances of the chromium compounds were all sharp singlets, while those of the manganese series were broadened. Presumably coupling between the phosphorus and the 5/2 spin manganese atom is responsible for the broadening. All NMR spectral parameters are presented in Table 2.

IR spectra of all compounds were recorded in chloroform and the carbonyl stretching frequencies are presented in Table 3. Force constants for the chromium and manganese series were calculated by use of the approximations developed by Cotton and Kraihanzel and are also presented in Table 3.

The Taft substituent constants were computed using the relationships developed byTaft *et al.*[4] and are presented in Table 4. In principle, the σ_I value is a relative measure of the ability of a substituent to inductively contribute or withdraw electron density from the fluorophenyl ring, while the σ_R^0 is a measure of the resonance contributions from the substituent.

Linear regression analysis was used to determine correlations between selected sets of data and the slopes, intercepts and correlation coefficients for these sets of data are presented in Table 5. Several broad observations can be made on the basis of these correlations. (1) In general, the correlation between stretching force constants and σ_R^0 are better than those between the force constants and σ_I substituent constants. (2) There is a good correlation between σ_R^0 and σ_I within a metal series. It is interesting that these sets of data seem to fall on the same line indicating that the relationship between inductive and resonance contributions are the same for the two series despite the fact that two different metals and quite different aromatic rings are being compared. (3) This last observation is reinforced by comparison of the σ_I and σ_R^0 constants between the two series for which the correlations are excellent.

These data indicate that electron density at the metal atoms increases in the order:

$$P(OCH_2CF_3)_3 \approx CO < P(OPh)_3 < P(OMe)_3 < AsPh_3 \approx PPh_3 < PMe_3 \approx PBu_3.$$

Parallel trends have been reported by Tolman[1] for carbonyl stretching frequencies and by Bodner *et al.*[2] for ^{13}C chemical shifts of carbonyl carbons.

Of particular interest is the similarity between $P(OCH_2CF_3)_3$ and CO. Shreeve and Williamson have recently reported the first synthesis of metal complexes containing this interesting, strongly electron withdrawing ligand.[18] As no complete multinuclear NMR analysis of this compound has previously been reported, we have included the ^1H, ^{19}F and ^{31}P NMR chemical shift and coupling constants in Table 2. Spectral data presented by Shreeve and Williamson and our own observations indicate that the spin–spin coupling between the phosphorus atom and the fluorine atoms is damped by complexation to metals.

EXPERIMENTAL

Infrared spectra were recorded on a Perkin–Elmer Model 1750 FT/IR Spectrophotometer. NMR spectra were recorded on a Varian Associates FT80A NMR Spectrometer. Thallium ethoxide,[19] cyclopentenone[20] and *m*- and *p*-fluorobiphenyl[21] were prepared by literature procedures. Chromium hexacarbonyl and bromomanganesepentacarbonyl were purchased from Strem, and *m*- and *p*-bromofluorobenzene were purchased from Aldrich. Purchased materials were used as received. Photolysis reactions were conducted in dry, air-free benzene which was distilled from sodium under N_2 immediately before use. Photolyses were conducted in an Ace doubly-jacketed photolysis vessel with a quartz inner vessel using a medium pressure mercury lamp. Phosphine and phosphite derivatives of arenechromiumtricarbonyl and cyclopentadienylmanganesecarbonyl complexes were prepared by photochemical exchange of phosphine for carbonyl in benzene solution as has been previously reported.[13] Microanalysis was conducted by Micro-Analysis Inc. of Wilmington, DE.

Synthesis of m- *and* p-*fluorophenylcyclopentadiene*

Cyclopentenone (10.0 g, 0.12 mol), was placed in a 250 cm^3 three neck flask outfitted with an addition funnel, reflux condenser and nitrogen inlet. About 100 cm^3 of ethyl ether was added to the flask and the contents were cooled to -5 to $-10°C$ in a salt-ice bath.

m-Fluorophenylmagnesiumbromide in ethyl ether (prepared from *m*-bromofluorobenzene (20.8 g, 0.12 mol), and 4.9 g of magnesium turnings over a 3 h period) was added over 90 min to the cyclopentenone solution. (Note: *m*- and *p*-bromofluorobenzenes are severe skin irritants and have been found to cause chloracne in this laboratory. They should both be handled with appropriate protective equipment.) A pink precipitate formed immediately. After addition was complete the suspension was stirred for an additional 90 min at $-5°C$.

The pink suspension was poured into 300 cm^3 of ice-cold concentrated aqueous ammonia saturated with ammonium chloride in a 1 l separatory funnel and shaken vigorously. The organic layer separated and the aqueous layer was extracted with three, 100

Table 2. NMR spectral data for [(Arene)$Cr(CO)_2L$] and $CpMn(CO)_2L$ complexes in C_6D_6

Compound [(Arene)$Cr(CO)_2L$] L (*m*/*p*-F)	^1H	$^{19}F^1$	^{31}P
$P(OCH_2CF_3)_2$ (*m*-F)	6.96 (4H, s) 4.92 (2H, m) 4.54 (3H, m) 3.97 (6H, m)	50.75 (F—Ph) 88.05 (t, J_{F-H} = 8.28 Hz)	215.13
$P(OCH_2CF_3O)_3$ (*p*-F)	7.15 (4H, m) 4.39–4.01 (5H, m) 3.92 (6H, m)	50.49 (F—Ph) 88.12 (t, J_{F-H} = 8.01 Hz)	212.40
$P(OC_6H_5)_3$ (*m*-F)	7.16 (m) 4.55 (broad s)	50.08	185.62
$P(OC_6H_5)_3$ (*p*-F)	7.15 (m) 4.54 (broad s)	49.42	185.57
$P(OCH_3)_3$ (*m*-F)	7.16 (4H, m) 4.97 (2H, m) 4.66 (3H, m) 3.32 (9H, d, J_{P-H} = 11.1 Hz)	50.01	215.22
$P(OCH_3)_3$ (*p*-F)	6.98 (4H, AB quartet) 4.94 (2H, m) 4.69 (3H, m) 3.34 (9H, d, J_{P-H} = 11.1 Hz)	48.83	215.63
$P(CH_3)_3$ (*m*-F)	7.00 (4H, m) 4.81 (2H, m) 4.40 (3H, m) 0.93 (9H, d, J_{P-H} = 7.3 Hz)	49.74	38.61
$P(CH_3)_3$ (*p*-F)	7.02 (4H, m) 4.78 (2H, m) 4.43 (3H, m) 0.95 (9H, d, J_{P-H} = 7.7 Hz)	48.05	39.08
$P(C_4H_9)_3$ (*m*-F)	7.30–6.90 (4H, m) 5.19 (2H, s) 4.89 (3H, s) 1.37 (18H, m) 0.87 (9H, m)	46.63	60.22
$P(C_4H_9)_3$ (*p*-F)	7.30–6.90 (4H, m) 5.13 (2H, s) 4.87 (3H, s) 1.37 (18H, m) 0.87 (9H, m)	48.87	60.75
$CpMn(CO)_2L$ L (*m*/*p*-F)			
$P(OC_6H_5)_3$ (*m*-F)	7.33–6.78 (4H, m) 4.26 (2H, broad s) 3.88 (2H, broad s)	49.78	Not observed
$P(OC_6H_5)_3$ (*p*-F)	7.26–6.76 (4H, m) 4.25 (2H, m) 3.94 (2H, m)	48.56	Not observed
$P(C_6H_5)_3$ (*m*-F)	7.50–6.97 (15H, s) 4.52 (2H, broad s) 4.02 (2H, broad s)	49.54	91.42

Table 2—*continued*

Compound $CpMn(CO)_2L$ L (*m*/*p*-F)	^1H	$^{19}F^1$	^{31}P
$P(C_6H_5)_3$ (*p*-F)	7.51–6.98 (15H, s) 4.51 (2H, broad s) 4.04 (2H, broad s)	47.86	91.94
$P(CH_3)_3$ (*m*-F)	—	50.36	Not observed
$P(CH_3)_3$ (*p*-F)	—	47.35	45.60 (broad)
$P(OCH_2CF_3)_3$			
	3.56 (d of t) $J_{F-H} = 8.20$ Hz $J_{P-H} = 8.14$ Hz	87.60 (d of t) $J_{F-H} = 8.20$ Hz $J_{P-F} = 4.60$ Hz	138.30 (m) $J_{F-P} = 4.60$ Hz

C_6H_5F is 49.98 ppm relative to C_6F_6.

Table 3. Carbonyl stetching frequencies and stretching force constants

Compound [(Arene)Cr(CO)$_2$L] L (*m*/*p*-F)	CO (cm^{-1}) Sym	CO (cm^{-1}) Antisym	k(CO) (10^5 dyn cm^{-1})
CO (*m*-F)	1978	1902	15.00
CO (*p*-F)	1980	1900	15.02
$P(OCH_2CF_3)_3$ (*m*-F)	1920	1860	14.46
$P(OCH_2CF_3)_3$ (*p*-F)	1921	1863	14.43
$P(OPh)_3$ (*m*-F)	1917	1860	14.40
$P(OPh)_3$ (*p*-F)	1918	1860	14.41
$P(OMe)_3$ (*m*-F)	1903	1846	14.20
$P(OMe)_3$ (*p*-F)	1903	1844	14.18
$AsPh_3$ (*m*-F)	1902	1850	14.22
$AsPh_3$ (*p*-F)	1897	1837	14.08
PPh_3 (*m*-F)	1895	1837	14.06
PPh_3 (*p*-F)	1890	1836	14.02
PMe_3 (*m*-F)	1888	1828	13.94
PMe_3 (*p*-F)	1885	1828	13.92
PBu_3 (*m*-F)	1883	1835	13.96
PBu_3 (*p*-F)	1885	1826	13.91
$CpMn(CO)_2L$ L (*m*/*p*-F)			
CO (*m*-F)	2010	1926	15.43
CO (*p*-F)	2010	1930	15.47
$P(OPh)_3$ (*m*-F)	1960	1895	15.01
$P(OPh)_3$ (*p*-F)	1960	1895	15.01
PPh_3 (*m*-F)	1930	1865	14.52
PPh_3 (*p*-F)	1933	1862	14.54
PMe_3 (*m*-F)	1938	1860	14.57
PMe_3 (*p*-F)	1924	1852	14.40

cm^3 portions of ethyl ether. The combined ether extracts were dried over magnesium sulphate. After removal of ethyl ether by rotary evaporator, the remaining yellow oil was distilled under high vacuum to give a mixture of *m*-fluorophenylcyclopentadiene isomers. The portion between 160–210°C was recovered. The fluorophenylcyclopentadiene prepared in this way was used immediately without further purification.

Table 4. Taft substituent constants for [(Arene)Cr(CO)$_2$L] and $CpMn(CO)_2L$

Compound [(Arene)Cr(CO)$_2$L]	σ_I	$-\sigma_R^0$
CO	0.173	0.004
$P(CH_2CF_3)_3$	0.193	0.009
$P(OPh)_3$	0.099	0.022
$P(OMe)_3$	0.089	0.043
$AsPh_3$	0.065	0.047
PPh_3	0.062	0.042
PMe_3	0.051	0.057
PBu_3	0.037	0.057
$CpMn(CO)_2L$		
CO	0.141	0.024
$P(OPh)_3$	0.056	0.041
PPh_3	0.023	0.057
PMe_3	0.014	0.072

Table 5. Linear regression analysis of [(Arene)Cr(CO)$_2$L] and CpMn(CO)$_2$L spectral data[a]

x	y	m	b	r
k(CO) (Cr)	σ_I (Cr)	0.135	−1.834	0.845
k(CO) (Cr)	σ_R^0 (Cr)	0.0532	−0.795	0.916
k(CO) (Mn)	σ_I (Mn)	0.125	−1.823	0.855
k(CO) (Mn)	σ_R^0 (Mn)	0.0489	−0.781	0.934
k(CO) (Cr)	k(CO) (Mn)	0.707	4.843	0.870
σ_I (Cr)	σ_R^0 (Cr)	0.344	−0.0681	0.947
σ_I (Mn)	σ_R^0 (Mn)	0.333	−0.0680	0.934
σ_I (Cr)	σ_I (Mn)	1.048	−0.0423	0.998
σ_R^0 (Cr)	σ_R^0 (Mn)	0.892	−0.0206	0.999
σ_I (all)	σ_R^0 (all)	0.342	−0.0682	0.949

[a] Data are presented for the relationship: $y = mx + b$.

Linear regression calculations were performed using standard statistical methods. The correlation coefficient R is reflective of "goodness of fit" where $R = 1.0$ for a perfect straight line.

p-Fluorophenylcyclopentadiene can be prepared similarly. Typical yields are 50–80%.

Synthesis of thallium m- *and* p-*fluorophenylcyclopentadienide*

m- or *p*-Fluorophenylcyclopentadiene (8.5 g, 22 mmol), were taken up in 100 cm^3 of ethanol in a 250 cm^3 round bottom flask. A septum was fitted onto the flask and the contents were flushed with nitrogen using a syringe for 5 min. Thallium ethoxide (7.0 g, 29 mmol), was added slowly by syringe to give a yellow precipitate which formed immediately. After all of the thallium ethoxide had been added, the suspension was allowed to stir for 1 h and then filtered on a medium glass frit funnel. The yellow solid was washed once with 10 cm^3 of ethanol, 10 cm^3 of ethyl ether and then with hexane. Yield: 80–90%.

Thallium cyclopentadienyl compounds are stable in air for short periods but darken on long exposure to air or light. They should be stored under nitrogen in the cold. Under these conditions they are stable for several months. (Note: Thallium compounds are highly toxic and should be handled with gloves.)

Synthesis of m- *and* p-*fluorophenylcymantrene*

Thallium fluorophenylcyclopentadienide (5.0 g, 14 mmol), were placed in a 250 cm^3 round bottom flask and the flask was flushed with nitrogen. About 100 ml of dry, air-free benzene was added to the flask followed by bromomanganesepentacarbonyl (3.8 g, 14 mmol). The reaction flask was outfitted with a reflux condenser and the mixture was refluxed overnight. The reaction mixture was filtered hot through Celite and the solvent removed by rotary evaporator. The resulting orange–yellow solid was chromatographed on alumina using 10% methylene chloride in petroleum ether as an eluant. *m*- and *p*-Fluorophenylcymantrene were recovered as orange–yellow crystalline solids after solvent removal.

Acknowledgements—We wish to thank the Naval Academy Research Council and the Research Corporation for their generous support of this research.

REFERENCES

1. C. A. Tolman, *J. Am. Chem. Soc.* 1970, **92**, 2953.
2. G. M. Bodner, M. P. May and L. E. McKinney, *Inorg. Chem.* 1980, **19**, 1951.
3. (a) T. E. Bitterwolf, *J. Organometal. Chem.* 1983, **252**, 301; (b) T. E. Bitterwolf and K. S. Raghuveerr, unpublished results, 1986.
4. R. W. Taft, E. Price, I. R. Fox, I. C. Lewis, K. K. Andersen and G. T. Davis, *J. Am. Chem. Soc.* 1963, **85**, 709, 3146.
5. G. W. Parshall, *J. Am. Chem. Soc.* 1966, **88**, 704; *Ibid.* 1974, **96**, 2360.
6. R. P. Stewart and P. M. Treichel, *J. Am. Chem. Soc.* 1970, **92**, 2710.
7. (a) A. N. Nesmeyanov, L. G. Makarova, N. A. Ustynyuk, B. A. Kvasov and L. V. Bogatyreva, *J. Organomet. Chem.* 1972, **34**, 185; (b) A. N. Nesmeyanov, I. F. Leshcheva, I. V. Polovyanyuk, Yu. A. Ustynyuk and L. G. Makarova, *J. Organomet. Chem.* 1972, **37**, 159.

8. A. N. Nesmeyanov, I. F. Leshchova, Yu. A. Ustynyuk, Ye. I. Sirotkina, I. N. Bolesova, L. S. Isayeva and Vol'kenau, *J. Organomet. Chem.* 1970, **22**, 689.
9. S. P. Gubin, A. A. Koridze, N. A. Ogorodnikova, A. A. Bezrukova and B. A. Kvasov, *Izv. Akad. Nauk SSSR, Ser. Khim.* (*English trans.*) 1981, 929.
10. S. P. Gubin, A. A. Koridze, N. A. Ogorodnikova and B. A. Kvasov, *Doklady Akad. Nauk SSSR* (*English trans.*) 1972, **205**, 571.
11. N. A. Ogorodnikova, A. A. Koridze and S. P. Gubin, *J. Organomet. Chem.* 1981, **215**, 293.
12. (a) S. P. Gubin and V. S. Khandkarova, *J. Organomet. Chem.* 1970, **22**, 449; (b) V. S. Khandkarova, S. P. Gubin and B. A. Kvasov, *J. Organomet. Chem.* 1970, **23**, 509.
13. T. E. Bitterwolf, *Polyhedron* 1983, **2**, 675.
14. F. A. Cotton and C. S. Kraihanzel, *J. Am. Chem. Soc.* 1962, **84**, 4432.
15. S. Top and G. Jaouen, *J. Organometal. Chem.* 1979, **182**, 381.
16. W. Strohmeier and H. Hellmann, *Chem. Ber.* 1963, **96**, 2859.
17. W. Strohmeier and H. Hellmann, *Chem. Ber.* 1965, **98**, 1598.
18. (a) J. M. Shreeve and S. M. Williamson, *J. Organomet. Chem.* 1983, **249**, C13; (b) *Ibid, Organometallics* 1984, **3**, 1104.
19. M. Fieser and L. F. Fieser, *Reagents for Organic Synthesis*, Vol. 2, p. 407. Wiley-Intersciences, New York (1969).
20. A. Vogel, *Practical Organic Chemistry*, 3rd Edn, p. 870. Longman Group Limited, New York (1978).
21. A. Roe, *Org. React.* 1949, **5**, 103.

Polyhedron Vol. 7, No. 5, pp. 417–418, 1988
Printed in Great Britain

0277–5387/88 $3.00+.00
Pergamon Press plc

COMMUNICATION

1,3-DIARYLTRIAZENIDO COMPLEXES OF RUTHENIUM(I), (II) AND (III), AND OF OSMIUM(III), RHODIUM(III) AND IRIDIUM(III)

STEPHEN F. COLSON and STEPHEN D. ROBINSON†

Department of Chemistry, King's College, Strand, London WC2R 2LS, U.K.

(*Received* 28 *July* 1987; *accepted* 10 *November* 1987)

Abstract—The synthesis and characterization of the platinum metal–1,3-diaryltriazenido complexes $[Ru(ArNNNAr)(CO)_3]_2$, $[Ru(ArNNNAr)_2]_2$, *cis*-$Ru(ArNNNAr)_2(CO)_2$, $MX_2(ArNNNAr)(PPh_3)_2$ (M = Ru, Os; X = Cl, Br) and $M'(ArNNNAr)_3$ (M′ = Ru, Os, Rh and Ir) are reported. Axial ligand substitution in $[Ru(ArNNNAr)(CO)_3]_2$ and adduct formation by $[Ru(ArNNNAr)_2]_2$ are described. In contrast to other known Ru(II)/Ru(II) "lantern" molecules, the species $[Ru(ArNNNAr)_2]_2$ have measured magnetic moments equivalent to *ca* one unpaired electron per dimer, which are presumably due to population of the spin states $\sigma^2\pi^4\delta^2\pi^{*4}$ and $\sigma^2\pi^4\delta^2\pi^{*3}\sigma^{*1}$.

Since the discovery of 1,3-diaryltriazenes in the mid 19th century[1] their conjugate bases, $ArN\cdots N\cdots NAr^-$ have been extensively used as terminal, chelate or bridging ligands and examples of triazenido complexes are known for most of the *d*-block transition metals.[2] However, homoleptic tris 1,3-diaryltriazenido complexes of ruthenium, osmium, rhodium and iridium do not appear to have been described in the literature.[3] We now report the synthesis of these and some related 1,3-diaryltriazenido complexes including binuclear triazenido-bridged derivatives of ruthenium(I) and (II).

Treatment of $Ru_3(CO)_{12}$ with 1,3-diaryltriazenes (ArNNNHAr, Ar = *p*-C_6H_4X, X = H, Cl, Me) in boiling benzene under a CO atmosphere generates the diamagnetic, orange binuclear triazenido-bridged species $[Ru(ArNNNAr)(CO)_3]_2$ analogous to the well-known ruthenium(I) carboxylates $[Ru(O_2CR)(CO)_3]_2$.[4] These triazenido complexes may also be obtained from the carboxylates by ligand metathesis reactions performed in MeCN solution in the presence of NEt_3 and a carbon monoxide atmosphere. If these reactions are performed in the absence of carbon monoxide, substitution of the axial CO ligand occurs. For Ar = C_6H_4Cl-*p*, the product appears to be a simple bis adduct of the form $[Ru(ArNNNAr)(CO)_2(ArNNNHAr)]_2$ analogous to the known carboxylate adduct $[Ru(O_2CPh)(CO)_2(PhCO_2H)]_2$.[5] However the species obtained when Ar = C_6H_4Me-*p* has been shown by X-ray diffraction methods[6] to be a *p*-toluidine adduct $[Ru(ArNNNAr)(CO)_2(H_2NAr)]_2$, formed by cleavage of excess triazene. Like their carboxylate analogues the ruthenium(I) triazenido complexes readily undergo axial carbonyl ligand substitution reactions to give a series of products $[Ru(ArNNNAr)(CO)_2L]_2$ (L = PPh_3 or $P(OMe)_3$).

The binuclear ruthenium(II/III) carboxylate $Ru_2(O_2CMe)_4Cl$ reacts cleanly with excess 1,3-diaryltriazene in boiling toluene in the presence of NEt_3 to yield binuclear homoleptic 1,3-diaryltriazenido complexes $[Ru(ArNNNAr)_2]_2$ as air stable purple microcrystals. In the absence of triethylamine, mixed carboxylate/triazenide products are formed. The binuclear complexes $[Ru(ArNNNAr)_2]_2$ form bis adducts with carbon monoxide but not with the more bulky triphenylphosphine ligand. This difference in behaviour presumably reflects some hindrance of the axial sites by the aryl groups of the triazenide ligands. In contrast to the recently reported paramagnetic carboxylate

†Author to whom correspondence should be addressed.

$[Ru(O_2CMe)_2(THF)]_2$ for which the electronic structure $\sigma^2\pi^4\delta^2\delta^{*1}\pi^{*3}$ has been proposed,[7] the Ru(II/II) triazenido complexes have magnetic moments equivalent to only one unpaired electron per dimer which can be rationalized in terms of the mixed spin states $\sigma^2\pi^4\delta^2\pi^{*4}$ and $\sigma^2\pi^4\delta^2\delta^{*1}\pi^{*3}$.[8]

Carbonylation of $RuCl_3 \cdot 3H_2O$ in boiling ethanol and subsequent treatment of the refluxing red solution with triethylamine and 1,3-diaryltriazene under a CO atmosphere, affords the mononuclear ruthenium(II) products *cis*-$Ru(ArNNNAr)_2(CO)_2$ as air stable orange–red crystals (ν(CO) *ca* 2065 and 2000 cm^{-1}, $CHCl_3$ solution).

In a reaction similar to one previously devised in this laboratory to produce the corresponding carboxylates,[9] the green paramagnetic ruthenium(III) species $RuX_2(ArNNNAr)(PPh_3)_2$ (X = Cl, Br) and their osmium(III) analogues $OsCl_2(ArNNNAr)(PPh_3)_2$ have been obtained by treatment of the halides $MX_2(PPh_3)_3$ with 1,3-diaryltriazenes in warm (*ca* 70°C) benzene under *aerobic* conditions. Two complexes of this type, $OsX_2(PhNNNPh)(PPh_3)_2$ (X = Cl, Br), have previously been prepared by an alternative route.[10]

Finally, 1,3-diaryltriazenes react with $RuCl_3 \cdot 3H_2O$ in the presence of NEt_3 in refluxing ethanol to afford modest yields of the homoleptic, low spin d^5, ruthenium(III) complexes $Ru(ArNNNAr)_3$, as dark green paramagnetic needles. Similar reactions using the reagent/solvent combinations Na_2OsCl_6/2-methoxyethanol, $RhCl_3 \cdot 3H_2O$/ethanol and Na_3IrCl_6/2-methoxyethanol afford the tris(1,3-diaryltriazenido) derivatives of osmium, rhodium and iridium, respectively. The tris(chelate) nature of these complexes has been established by an X-ray diffraction study on $Ru(ArNNNAr)_3$ (Ar = Ph)[6] and by comparison of vibrational spectra. Satisfactory analytical and spectroscopic data have been obtained for the new complexes described.

REFERENCES

1. P. Griess, *Proc. R. Soc. London*, 1859, **9**, 594.
2. D. S. Moore and S. D. Robinson, *Adv. Inorg. Chem. Radiochem.* 1986, **30**, 1.
3. A synthesis of $Rh(ArNNNAr)_3$ was mentioned in an earlier report from this laboratory, K. R. Laing, S. D. Robinson and M. F. Uttley, *J. Chem. Soc., Dalton Trans.* 1974, 1205.
4. (a) G. R. Crooks, B. F. G. Johnson, J. Lewis, I. G. Williams and G. Gamlen, *J. Chem. Soc. A* 1969, 2761; (b) H. Schumann, J. Opitz and J. Pickardt, *J. Organometal. Chem.* 1977, **128**, 253; (c) H. Schumann and J. Opitz, *Chem. Ber.* 1980, **113**, 989.
5. M. Rotem, Y. Shvo, I. Goldberg and U. Shmuell, *Organometallics* 1984, **3**, 1758.
6. M. B. Hursthouse, personal communication.
7. A. J. Lindsay, R. P. Tooze, M. Motevalli, M. B. Hursthouse and G. Wilkinson, *J. Chem. Soc., Chem. Commun.* 1984, 1383.
8. J. G. Norman, G. E. Renzoni and D. A. Case, *J. Am. Chem. Soc.* 1979, **101**, 5256.
9. D. S. Moore and S. D. Robinson, *Inorg. Chem.* 1979, **18**, 2307.
10. J. E. Armstrong and R. A. Walton, *Inorg. Chem.* 1983, **22**, 1545.

Polyhedron Vol. 7, No. 5, pp. 419–420, 1988
Printed in Great Britain

0277–5387/88 $3.00+.00
Pergamon Press plc

COMMUNICATION

PREPARATION OF $Pd(S_2N_2H)(Br)(PMe_2Ph)$ VIA A FACILE BROMINE–PHOSPHINE EXCHANGE REACTION

PAUL F. KELLY and J. DEREK WOOLLINS*

Department of Chemistry, Imperial College of Science and Technology, South Kensington, London SW7 2AY, U.K.

(*Received* 9 *October* 1987; *accepted* 27 *November* 1987)

Abstract—$Pt(S_2N_2H)(Br)(PMe_2Ph)$ (**1**) reacts with $Pd(S_2N_2)(PMe_2Ph)_2$ (**2**), with proton, transfer and halogen and phosphine exchange to give the novel palladium complex $Pd(S_2N_2H)(Br)(PMe_2Ph)$ (**3**) together with $Pt(S_2N_2)(PMe_2Ph)_2$ (**4**). The ^{31}P NMR and IR spectra of (**3**) suggest that it has an analogous structure to that of (**1**).

As part of a continuing investigation into metalla–sulphur–nitrogen chemistry we have recently reported on the preparation of complexes of the type $Pt(S_2N_2)(PR_3)_2$[1,2] and $[Pt(S_2N_2H)(PR_3)_2]X$,[3,4] in which the $S_2N_2^{2-}$ ligand forms part of a five membered metallocycle which can be protonated on the nitrogen-bound metal. The latter complexes are especially interesting and we have reported on their ability to form 1D stacking structures,[5,6] their solution equilibria[7] and their reaction with bromine to give complexes of the type $[Pt(S_2N_2H)(Br)_2(PR_3)_2]BF_4$ and $[Pt(S_2N_2H)(Br)(PR_3)]$.[8]

Here we report on the reaction of $[Pt(S_2N_2H)(Br)(PMe_2Ph)]$ (**1**) with $Pd(S_2N_2)(PMe_2Ph)_2$ (**2**) which proceeds via a protonation, and an exchange of a bromine for a phosphine group to give $[Pd(S_2N_2H)(Br)(PMe_2Ph)]$ (**3**), the first example of a palladium complex of this class.

EXPERIMENTAL

General reaction conditions, drying of solvents and spectroscopic measurements were as described previously.[2] $[Pt(S_2N_2H)(Br)(PMe_2Ph)]$[8] and $Pd(S_2N_2)(PMe_2Ph)_2$[4] were prepared as in previous work, the latter being crystallized by slow hexane diffusion into a CH_2Cl_2 solution to ensure maximum purity.

$[Pd(S_2N_2H)(Br)(PMe_2Ph)]$ (3)

Solid samples of (**1**) (22 mg, 0.043 mmol) and (**2**) (20 mg, 0.042 mmol) were mixed in CH_2Cl_2 (20 cm^3) and the resulting solution was allowed to stand overnight. Measurement of the ^{31}P NMR spectrum of the products revealed the presence of $Pt(S_2N_2)(PMe_2Ph)_2$ (δ −8.3 {^1J (^{195}Pt–^{31}P) 2763}, −24.7 {^1J (^{195}Pt–^{31}P) 2828}; lit. δ −7.9 {^1J (^{195}Pt–^{31}P) 2731}, −24.9 ppm {^1J (^{195}Pt–^{31}P) 2799 Hz}) and a new complex shown by a singlet at $\delta = 0.4$ ppm. The solvent was removed *in vacuo* and the residue extracted into warm Et_2O (30 cm^3). After filtration, the Et_2O was removed and the residue taken into a small volume of $CHCl_3$; the final product was obtained as a small crop of orange crystals by slow hexane diffusion. Found C 23.3, H 2.9, N 6.5; Calc. C 23.0, H 2.9, N 6.7%. IR 3280(s) ν(N—H), 1055(m) ν(N—S), 360(w) ν(Pt—S), 330(m) cm^{-1} δ(N—S).

RESULTS AND DISCUSSION

In previous work we noted that ^{31}P NMR investigations into the solution properties of $M(S_2N_2)(PR_3)_2$ (M = Pt/Pd) revealed the palladium complexes to be the stronger bases, i.e. $Pd(S_2N_2)(PR_3)_2$ can almost completely deprotonate

*Author to whom correspondence should be addressed.

$[Pt(S_2N_2H)(PR_3)_2]X$ [eq. (1)]. In view of this we investigated the reaction of (**1**) with (**2**) in the hope that this would lead to the preparation of a salt of the type $[Pd(S_2N_2H)(PMe_2Ph)_2]^+$ $[Pt(S_2N_2)(Br)(PMe_2Ph)]$. Such a salt would be of interest since both the cations and anions have the potential to form stacking structures.

$$[Pt(S_2N_2H)(PMe_2Ph)_2]BF_4 + Pd(S_2N_2)(PMe_2Ph)_2 \rightleftharpoons Pt(S_2N_2)(PMe_2Ph)_2 + [Pd(S_2N_2H)(PMe_2Ph)_2]BF_4. \quad K \approx 80. \quad (1)$$

However, measurement of the ^{31}P NMR spectrum of the products reveals the presence of (**4**) and so indicates that the reaction is much more complicated than a simple proton transfer. The other component of this spectrum is a singlet at $\delta = 0.4$ ppm. The lack of satellites associated with this singlet indicates that it is due to a palladium complex, and this can be separated from (**4**) by extraction into warm ether, in which the latter (along with other complexes of the type $Pt(S_2N_2)(PR_3)_2$) is insoluble. Crystallization of this new complex by slow hexane diffusion into a concentrated $CHCl_3$ solution yields orange crystals, which analyse correctly for $Pd(S_2N_2H)(Br)(PMe_2Ph)$ (**3**). Thus the overall reaction involves the transfer of a proton, together with the exchange of a bromine and a phosphine ligand [eq. (2)].

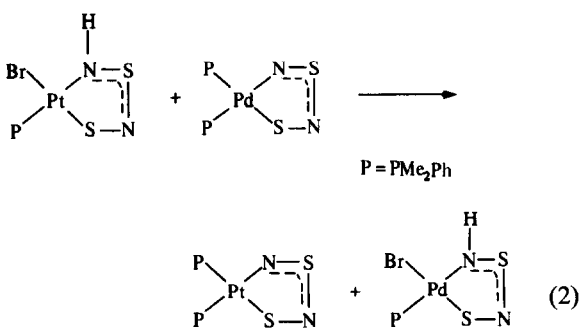

(2)

We have recently reported the crystal structure of the platinum analogue of (**3**) which revealed the bromine to be *trans* to sulphur; although we have yet to perform an X-ray analysis of (**3**) it is reasonable to assume that it has a similar structure. The only other reasonable structure which could fit the above observations would be one in which the bromine was *trans* to nitrogen rather than sulphur. However, this would be contrary to the results obtained for platinum complexes such as $[Pt(S_2N_2H)(Br)_2(PMe_2Ph)_2]BF_4$, $Pt(S_2N_2H)(I)(PMe_2Ph)_8$ and $[Pt(S_2N_2)(PPh_3)]_2$,[9] which indicate that it is the phosphine *trans* to sulphur which is the most labile.

We have yet to establish a mechanism for the reaction, although it should be noted that if the reaction is performed in an NMR tube, and the ^{31}P NMR spectrum measured as it proceeds, only the starting materials and the products can be observed, indicating that there are no particularly long lived intermediates. A speculative mechanism would involve (1) the close approach of (**1**) and (**2**) in a similar fashion to that in $[Pt(S_2N_2H)(PR_3)_2]X$, (2) transfer of the proton from (**1**) to (**2**), (3) formation of a binuclear Br bridged complex, (4) transfer of the phosphine with bridge cleavage and formation of (**3**) and (**4**). Although this mechanism is speculative, the reaction shown in eq. (2) further underlines the strong *trans* labilizing influence of the sulphur in the $S_2N_2^{2-}$. Previous evidence for this includes the formation of a binuclear complex,[9] the elimination of phosphine and halide from complexes of the type $[Pt(S_2N_2H)(Br)_2(PR_3)_2][BF_4]$,[8] and the preparation of $[Pt(S_2N_2H)(S_2O_3)(PPh_3)][Ph_3PNH_2]$.[10]

Acknowledgement—We are grateful to Johnson Matthey for loans of precious metals.

REFERENCES

1. R. Jones, P. F. Kelly, D. J. Williams and J. D. Woollins, *Polyhedron* 1985, **4**, 1947.
2. P. A. Bates, M. B. Hursthouse, P. F. Kelly and J. D. Woollins, *J. Chem. Soc., Dalton Trans.* 1986, 2367.
3. R. Jones, C. P. Warrens, D. J. Williams and J. D. Woollins, *J. Chem. Soc., Dalton Trans.* 1987, 907.
4. R. Jones, P. F. Kelly, D. J. Williams and J. D. Woollins, *Polyhedron* 1987, **6**, 1541.
5. R. Jones, P. F. Kelly, C. P. Warrens, D. J. Williams and J. D. Woollins, *J. Chem. Soc., Chem. Commun.* 1986, 711.
6. R. Jones, P. F. Kelly, D. J. Williams and J. D. Woollins, *J. Chem. Soc., Dalton Trans.*, in press.
7. P. F. Kelly and J. D. Woollins, *J. Chem. Soc., Dalton Trans.*, in press.
8. R. Jones, P. F. Kelly, D. J. Williams and J. D. Woollins, *J. Chem. Soc., Dalton Trans.*, in press.
9. R. Jones, P. F. Kelly, D. J. Williams and J. D. Woollins, *J. Chem. Soc., Chem. Commun.* 1985, 1325.
10. P. F. Kelly, Ph.D. Thesis, Sulphur–Nitrogen Compounds of Platinum and Palladium. Imperial College (1987).

Polyhedron Vol. 7, No. 6, pp. 421–424, 1988
Printed in Great Britain

0277–5387/88 $3.00+.00
Pergamon Press plc

STANDARD ENTHALPIES OF FORMATION OF BIS(β-DIKETONATE)COBALT(II) COMPLEXES: THE MEAN (Co—O) BOND-DISSOCIATION ENTHALPIES

MANUEL A. V. RIBEIRO DA SILVA* and M. LUISA C. C. H. FERRÃO

Departamento de Química, Faculdade de Ciências, Universidade do Porto, 4000 Porto, Portugal

(*Received* 15 *July* 1987; *accepted* 1 *September* 1987)

Abstract—The standard enthalpies of formation, at 298 K, of the 1-phenyl-1,3-butanedione (HBZAC) and 1,1,1-trifluoro-2,4-pentanedione (HTFAC) crystalline complexes of cobalt(II) were determined by precise solution–reaction calorimetry:

$$\Delta H_f^0\{Co(BZAC)_2,cr\} = -632 \pm 6.0 \text{ kJ mol}^{-1}$$

$$\Delta H_f^0\{Co(TFAC)_2,cr\} = -2140 \pm 10 \text{ kJ mol}^{-1}.$$

The average molar bond-dissociation enthalpies, $\langle D \rangle$(Co—O) were derived.

Previous determinations of the standard enthalpies of formation of cobalt(II) β-diketonates are limited to the complexes of 2,4-pentanedione (HACAC) and 2,2,6,6-tetramethyl-3,5-heptanedione (HDPM). For $Co(ACAC)_2$ the published values differ widely, Kakolowicz and Giera[1] give -884.1 ± 2.1 kJ mol^{-1}, whilst Irving and Ribeiro da Silva[2] give -864 ± 3 kJ mol^{-1}. Kakolowicz measured the enthalpy of hydrolysis in aqueous hydrochloric and the derived enthalpy of formation was related to that of $CoCl_2 \cdot 6H_2O$(s), using $\Delta H_f^0(CoCl_2 \cdot 6H_2O, s) = -2129.2$ kJ mol^{-1} taken from the NBS Circular 500:[3] the revision of this compilation[4] gives $\Delta H_f^0(CoCl_2 \cdot 6H_2O, s) = -2115.4$ kJ mol^{-1}; recalculating the Kakolowicz and Giera value from data in their paper, one obtains $\Delta H_f^0(Co(ACAC)_2, s) = -871.4$ kJ mol^{-1}, closer to the Irving and Ribeiro da Silva value. For $Co(DPM)_2$, Giera and Kakolowicz[5] used in their calculations the old value for the enthalpy of formation of $CoCl_2 \cdot 6H_2O$(s) and so, by making the same revision, their calculated standard enthalpy of formation of $Co(DPM)_2$ should be -1212.3 ± 7.6 kJ mol^{-1}.

This paper reports the determination of the standard enthalpies of formation of two cobalt(II) β-diketonates to investigate the effect of structural changes in the ligand upon the mean molar (Co—O) bond-dissociation enthalpy.

EXPERIMENTAL

The solution calorimeter. The isoperibol LKB 8700 reaction and solution precision calorimeter was used. The operation and calculation methods have been described.[6,7] The accuracy of the calorimeter was checked by measuring the molar enthalpy of a solution of tris(hydroxymethyl)aminomethane (THAM) in aqueous 0.100 mol dm^{-3} HCl at 298.15 K: $\Delta H_{sol}^0 = -29.7 \pm 0.02$ kJ mol^{-1}, in agreement with the value of Kilday and Prosen,[8] $\Delta H_{sol}^0 = -29.77 \pm 0.03$ kJ mol^{-1}.

1-*Phenylbutane*-1,3-*dione*. HBZAC (Koch–Light Laboratories Ltd) was purified by repeated crystallization from ethanol and water; m.p. = 54°C (lit. 56°C[9]). Found: C, 73.9; H, 6.2. Calc. for $C_{10}H_{10}O_2$: C, 74.1; H, 6.2%.

1,1,1-*Trifluoropentane*-2,4-*dione*. HTFAC (Koch–Light Laboratories Ltd) was purified by fractional distillation in a vacuum and the purity was assessed as greater than 99.9 mol% by g.l.c. using two different columns. The purified β-diketone was stored under nitrogen in the dark and was freshly distilled prior to use.

Bis(1 - *phenylbutane* - 1,3 - *dionato*)*cobalt*(*II*). $Co(BZAC)_2$ was prepared as described by Cotton

* Author to whom correspondence should be addressed.

and Holm,[10] purified by crystallization from ethanol and dehydrated by heating *in vacuo*, at 353 K, for 24 h. Found: C, 62.2; H, 4.7; Co, 15.4. Calc. for $C_{20}H_{18}O_4Co$: C, 63.0; H, 4.8; Co, 15.4%.

Bis(1,1,1-*trifluoropentane*-2,4-*dionato*)*cobalt*(*II*). $Co(TFAC)_2$ was prepared as described by Holm and Cotton,[11] purified by crystallization from ethanol and water and dehydrated by heating *in vacuo*, at 333 K, for 24 h. Found: C, 32.9; H, 2.2; Co, 16.2. Calc. for $C_{10}H_8O_4F_6Co$: C, 32.9; H, 2.2; Co, 16.1 %.

Cobalt(*II*) *sulphate hexahydrate*. This was obtained from the corresponding heptahydrate (B.D.H., AnalaR) by dehydration in a vacuum desiccator until the composition was found to be $CoSO_4 \cdot 6.00H_2O$, exactly.

Sulphuric acid. 1 mol dm^{-3} H_2SO_4 was made from a B.D.H. concentrated volumetric solution; the concentration was checked by acid–base titration against $Na_2B_4O_7 \cdot 10H_2O$ and found to be (by a series of six titrations) 1.000 ± 0.002 mol dm^{-3}, which corresponds[9] to the composition $H_2SO_4 \cdot 53.54H_2O$.

Hydrochloric acid. Concentrated HCl (B.D.H., AnalaR) was diluted with distilled water; the concentration was determined by titration against $Na_2B_4O_7 \cdot 10H_2O$ and found to be (by a series of six titrations) 4.213 ± 0.003 mol dm^{-3}.

1,4-*Dioxan*. 1,4-Dioxan (Carl Erba) was purified according to ref. 12.

Analyses. Carbon and hydrogen analyses were carried out by the Microanalytical Service of the University of Surrey; cobalt was analysed by the ethylenediaminetetra-acid method.[13] The relative atomic masses used were those recommended by the IUPAC Commission.[14]

RESULTS AND DISCUSSION

Preliminary tests of solubility showed that rapid hydrolyses of the cobalt(II) β-diketonates complexes occurred using 0.75 (1,4-dioxan) and 0.25 HCl(aq, 4.2 mol dm^{-3}) by volume as the initial calorimetric solvent.

The standard molar enthalpies of formation of $Co(BZAC)_2$ and $Co(TFAC)_2$ were determined, at 298.15 K, from the thermochemical reaction:

$$CoL_2(s) + H_2SO_4 \cdot 53.54H_2O(l) \rightarrow$$

$$47.54H_2O(l) + CoSO_4 \cdot 6.00H_2O(s) + 2HL(s \text{ or } l).$$

The same batch of solvent was used for both complexes. The enthalpies of the thermochemical reactions were determined by measuring the enthalpies of solution of the reactants and products successively in the initial calorimetric solvent so that the final solution resulting from dissolution of all reactants was of the same composition as that from dissolution of all products. The difference between the molar enthalpies of solution of products and reactants, in the correct stoichiometric ratio, gives the enthalpy of the thermochemical reaction (ΔH_r^0), provided equilibrium is reached from either side, within the period of the experiment. This was checked by mixing the final solution of reactants into the final solution of products, with no heat detected.

The experimental results are summarized in Table 1, where, in accordance with normal thermochemical practice, the errors given are uncertainty intervals, i.e. twice the standard deviation of the mean. The enthalpies of the thermochemical reactions were derived from the values in Table 1 according to

$$\begin{aligned}\Delta H_r^0[Co(BZAC)_2] &= \Delta H_1 + \Delta H_2 - 47.54\Delta H_4 \\ &\quad - \Delta H_5 - 2\Delta H_6 \\ &= -119.9 \pm 0.8 \text{ kJ mol}^{-1},\end{aligned}$$

$$\begin{aligned}\Delta H_r^0[Co(TFAC)_2] &= \Delta H_1 + \Delta H_3 - 47.54\Delta H_4 \\ &\quad - \Delta H_5 - 2\Delta H_7 \\ &= 46.0 \pm 0.8 \text{ kJ mol}^{-1}.\end{aligned}$$

With the following auxiliary data, $\Delta H_f^0(H_2O, l) = -285.83 \pm 0.04$ kJ mol^{-1},[15] $\Delta H_f^0(H_2SO_4$ in 53.54 H_2O, l) $= -886.9 \pm 0.3$ kJ mol^{-1},[4] $\Delta H_f^0(CoSO_4 \cdot 6.00H_2O$, s) $= -2684.0 \pm 2$ kJ mol^{-1},[4] and from the standard enthalpies of formation of the different ligands (Table 2), the standard molar enthalpies of formation of the crystalline cobalt(II) complexes were derived.

To derive the enthalpies of formation of these complexes in the gaseous state, the enthalpies of sublimation are needed. Measurements of these enthalpies of sublimation, using the "vacuum sublimation" drop calorimetric method,[21] were unsuccessful because for temperatures at which the vapour pressure was sufficiently high to permit vacuum sublimation, partial thermal decomposition occurred. So, the standard enthalpies of sublimation of the crystalline cobalt(II) complexes were estimated on the basis of their structure, molecular weight and other known values for similar complexes, using an estimation scheme.[22]

Table 3 lists the estimated enthalpies of sublimation and the standard enthalpies of formation, in the crystalline and gaseous states of the complexes studied, together with the corresponding values for the bis(pentane-2,4-dionato)cobalt(II), recalculated from the value of Irving and Ribeiro da Silva[2] using the most recent auxiliary data.

The mean cobalt–oxygen bond-dissociation enthalpies, $\langle D \rangle$(Co—O), may be defined as 1/4 of

Table 1. Molar enthalpies of solution and reaction at 298.15 K

1	Reactant	Solvent	Solution	No. of expts	ΔH_i (kJ mol^{-1})
1	$H_2SO_4 \cdot 53.54H_2O$(l)	initial	A_1	6	-57.93 ± 0.27
2	$Co(BZAC)_2$(s)	A_1	B_1	5	-16.34 ± 0.27
3	$Co(TFAC)_2$(s)	A_1	B_2	5	-39.55 ± 0.31
4	H_2O(l)	initial	A_2	5	-0.999 ± 0.004
5	$CoSO_4 \cdot 6.00H_2O$(s)	A_2	A_3	6	$+41.25 \pm 0.60$
6	HBZAC(s)	A_3	B'_1	5	$+25.93 \pm 0.15$
7	HTFAC(l)	A_3	B'_2	5	-22.64 ± 0.19
8	Solution B_1	B'_1	$B_1 = B'_1$	5	0.00 ± 0.05
9	Solution B_2	B'_2	$B_2 = B'_2$	5	0.00 ± 0.06

Table 2. Standard molar enthalpies of formation and vaporization of the ligands at 298.15 K

Ligand	ΔH_f^0(s *or* l) (kJ mol^{-1})	$\Delta H^0_{vap/sub}$ (kJ mol^{-1})	ΔH_f^0(enol, g) (kJ mol^{-1})
HCAC(l)	-425 ± 1.0[a]	$+41.8 \pm 0.2$[b]	-384 ± 1.0
HBZAC(s)	-335 ± 2.8[c]	$+83.8 \pm 0.4$[d]	-251 ± 2.9
HTFAC(l)	-1051 ± 5.0	$+37.2 \pm 0.2$[e]	-1014 ± 5.0[f]
HDPM(l)	-588 ± 3.8[c]	$+59.5 \pm 0.1$[e]	-528 ± 3.8

[a] Ref. 16.
[b] Ref. 17.
[c] Ref. 18.
[d] Ref. 19.
[e] Ref. 20.
[f] Estimated by using a Group Scheme.

the enthalpy of the disruption reaction:

$$CoL_2(g) \rightarrow Co(g) + 2L(g)$$

$$\Delta H^0_{disr} = \Delta H_f^0(Co, g) + 2\Delta H_f^0(HL, enol, g) - 2\Delta H_f^0(H, g) - \Delta H_f^0(CoL_2, g) + 2D(O\text{—}H, HL, enol)$$

where D(O—H, HL, enol) is the molar enthalpy of dissociation of the enolic hydrogen in the parent ligand

$$HL(g) \rightarrow L(g) + H(g).$$

Table 3. Standard molar enthalpies of formation and sublimation at 298.15 K

Complex	ΔH_f^0(s) (kJ mol^{-1})	ΔH^0_{sub} (kJ mol^{-1})	ΔH_f^0(g) (kJ mol^{-1})
$Co(ACAC)_2$	-868 ± 3[a]	117 ± 16[b]	-751 ± 16
$Co(BZAC)_2$	-632 ± 6	150 ± 10[b]	-482 ± 12
$Co(TFAC)_2$	-2140 ± 10	110 ± 10[b]	-2030 ± 14

[a] Ref. 2.
[b] Estimated values.

There are no measured values for the molar enthalpy of dissociation of the enolic hydrogen from β-diketones. Different values have been estimated for this parameter, and the situation has recently been reviewed.[22] In this work, for comparison reasons the value D(O—H, HL, enol) = 420 ± 20 kJ mol^{-1},[22] is used.

With ΔH_f^0(H, g) = 218.00 ± 0.01 kJ mol^{-1},[5] ΔH_f^0(Co, g) = 425 ± 4 kJ mol^{-1},[5] the mean cobalt(II)–oxygen bond-dissociation enthalpies, $\langle D \rangle$(Co^{II}—O) for the complexes studied here, and also for $Co(ACAC)_2$ and $Co(DPM)_2$, were derived and are listed in Table 4. Values of $\langle D \rangle$(Co^{III}—O) in some cobalt(III) β-diketonates are also listed in Table 4.

Within the uncertainties associated with the mean cobalt(II)–oxygen bond-dissociation enthalpies, there are no significant differences on $\langle D \rangle$(Co^{II}—O) for the various cobalt(II) β-diketonates. Inductive effects due to $-CF_3$ or $-C_6H_5$ substitution in the ligand appear to have no influence, or only a very small one, on the donor properties of oxygen. This effect has already been observed for complexes of β-diketones with Be(II),[24] Al(III),[24] Cu(II),[25] Cr(III),[26] Fe(III)[27] and Co(III).[23]

Table 4. Mean cobalt–oxygen bond-dissociation enthalpies

Ligand	$\langle D \rangle$(Co^{II}—O) (kJ mol^{-1})	$\langle D \rangle$$Co^{III}$—O) (kJ mol^{-1})
HACAC	202 ± 11[a]	
HBZAC	201 ± 10	164 ± 10[b]
HTFAC	206 ± 11	177 ± 11[b]
HDPM	209 ± 11[c]	171 ± 10[b]

[a] Ref. 2.
[b] Ref. 23.
[c] Derived from Ref. 4.

It has been pointed out[28] that, in general, for a series of MX_n molecules, the trends in $\langle D \rangle$ (M—X) are primarily dependent on the number of X ligands and not on the oxidation number of M: $\langle D \rangle$(M—X) decreases as n increases and normally n increases as the oxidation number of M increases. The data of Table 4 show that for the cobalt β-diketonates $\langle D \rangle$(Co—O) is greater in the Co(II) complexes, CoL_2, than for the Co(III) complexes, CoL_3. The larger values for $\langle D \rangle$ (Co^{II}—O) in comparison to $\langle D \rangle$(Co^{III}—O), for the same complexes, can also be assigned[29] to the increase in electronic density of the metal atom.

Acknowledgements—We thank NATO, Research Grant 1709, for partial support and the Instituto Nacional de Investigação Cientifica, Lisboa, for support given to a research project (L.5) of the Centro de Investigação em Química, Universidade do Porto. Thanks are also due to Junta Nacional de Investigação Cientifica e Tecnológica, Lisboa, for partial support under research contract no. 220–80.32.

REFERENCES

1. W. Kakolowicz and E. Giera, *J. Chem. Thermodynamics* 1983, **15**, 203.
2. R. J. Irving and M. A. V. Ribeiro da Silva, *J. Chem. Soc., Dalton Trans.* 1981, 99.
3. *Selected Values of Chemical Thermodynamics Properties*, N.B.S., Circular 500, Washington DC (1952).
4. The N.B.S. Tables of Chemical Thermodynamic Properties, *J. Phys. Chem. Ref. Data* 1982, **11**, Supplement No. 2.
5. E. Giera and W. Kakolowicz, *Thermochim. Acta* 1985, **90**, 71.
6. R. J. Irving and M. A. V. Ribeiro da Silva, *J. Chem. Soc., Dalton Trans.* 1978, 399.
7. M. A. V. Ribeiro da Silva and R. J. Irving, *Bull. Chem. Soc. Jpn* 1977, **50**, 734.
8. M. V. Kilday and E. J. Prosen, *J. Res. Nat. Bur. Stand.* 1973, **A77**, 581, 589.
9. R. C. Weast (Ed.), *Handbook of Chemistry and Physics*, 55 edn. The Chemical Rubber Co., Cleveland, Ohio (1974).
10. F. A. Cotton and R. H. Holm, *J. Am. Chem. Soc.* 1960, **82**, 2979.
11. R. H. Holm and F. A. Cotton, *J. Inorg. Nucl. Chem.* 960, **15**, 63.
12. D. D. Perrin, W. L. Armarego and R. D. Perrin, *Purification of Laboratory Chemicals*. Pergamon Press, Oxford (1966).
13. A. I. Vogel, *Quantitative Inorganic Analysis*, 4th edn. Longmans, London (1978).
14. Atomic weights of the elements, *Pure Appl. Chem.* 1979, **51**, 409.
15. CODATA, *J. Chem. Thermodynamics* 1978, **10**, 903.
16. J. M. Hacking and G. Pilcher, *J. Chem. Thermodynamics* 1979, **11**, 1015.
17. R. J. Irving and I. Wadsö, *Acta Chem. Scand.* 1970, **24**, 589.
18. M. L. C. C. H. Ferrão, M. A. V. Ribeiro da Silva, S. Suradi, G. Pilcher and H. A. Skinner, *J. Chem. Thermodynamics* 1981, **13**, 567.
19. A. Aihara, *Bull. Chem. Soc. Jpn* 1959, **32**, 1242.
20. R. J. Irving and M. A. V. Ribeiro da Silva, *J. Chem. Soc., Dalton Trans.* 1975, 798.
21. F. A. Adedeji, D. L. S. Brown, J. A. Connor, M. Leung, M. I. Paz-Andrade and H. A. Skinner, *J. Organometallic Chem.* 1975, **97**, 221.
22. M. A. V. Ribeiro da Silva (Ed.), *Thermochemistry and Its Applications to Chemical and Biochemical Systems*, p. 331. NATO ASI series, Reidel, Dordrecht (1984).
23. M. A. V. Ribeiro da Silva and M. L. C. C. H. Ferrão, *Bull. Chem. Soc. Jpn* (accepted 1987).
24. M. A. V. Ribeiro da Silva and A. M. M. V. Reis, *J. Chem. Thermodynamics* 1983, **15**, 957.
25. M. A. V. Ribeiro da Silva, M. D. M. C. Ribeiro da Silva, A. P. S. M. Carvalho, M. J. Akello and G. Pilcher, *J. Chem. Thermodynamics* 1984, **16**, 137.
26. M. A. V. Ribeiro da Silva and M. L. C. C. H. Ferrão, *J. Chem. Thermodynamics* 1987, **19**, 645.
27. M. A. V. Ribeiro da Silva and M. L. C. C. H. Ferrão, *J. Chem. Thermodynamics* (accepted 1987).
28. E. H. Jamea and G. Pilcher, *Thermochim. Acta* 1986, **97**, 77.
29. J. O. Connor, *Topics in Current Chemistry* 1977, **71**, 71.

Polyhedron Vol. 7, No. 6, pp. 425–438, 1988
Printed in Great Britain

0277–5387/88 $3.00+.00
© 1988 Pergamon Press plc

A STUDY OF THE MECHANISM OF ALKANE HYDROXYLATION USING THE $Fepy_4Cl_2$–PhNHNHPh–O_2 SYSTEM

REG DAVIS,* JIM L. A. DURRANT and MOHAMMED A. KHAN

School of Inorganic and Physical Chemistry, Kingston Polytechnic, Penrhyn Road, Kingston Upon Thames, KT1 2EE, U.K.

(*Received* 7 *September* 1987; *accepted* 5 *October* 1987)

Abstract—Selective alkane hydroxylation has been investigated employing O_2 in the presence of PhNHNHPh, $PhCO_2H$ and the catalyst, $[Fepy_4Cl_2]$. The conversion of cyclohexane to cyclohexanol and the direct reaction between PhNHNHPh and O_2 were studied kinetically in the presence of the catalyst. These studies, together with an examination of a range of potential reaction intermediates, suggest that the active species for alkane hydroxylation is an iron–hydroperoxide complex. Hydrazobenzene plays an essential role in the formation of this intermediate. However, a competitive reaction of the hydroperoxide complex leads to the formation of a $[Fe(II)(H_2O_2)]$–complex which reacts further with PhNHNHPh. A comparison of the efficiency of a range of iron complexes and a range of substituted hydrazobenzenes in promoting alkane hydroxylation is reported. This oxidation system cannot be viewed as a model for cytochrome P_{450}.

Selective oxidation of hydrocarbons has been the subject of many studies in recent years. In particular, the action of the mono-oxygenase, cytochrome P_{450} and systems believed to model its behaviour have been extensively investigated.[1] There is now a substantial body of evidence that the crucial intermediate in such reactions contains the ferryl unit, which may be considered as consisting of [L(Por)Fe(V)=O] or [L(Por$^+$)Fe(IV)=O] (Por = porphyrinato dianion).[2] There also exists a large group of iron-based "model" oxidation systems which are not so well characterized,[3–7] in many cases the veracity of the model depending on isolated criteria such as overall stoichiometry or product distribution. A further group of oxidation systems that do not contain iron-based complexes have also been reported.[8–11] By employing kinetic isotope effect studies of the oxidative demethylation of anisole, Lindsay Smith and Sleath have shown that the majority of the iron-based systems do not model the behaviour of cytochrome P_{450} and probably function through oxidation by the hydroxyl radical.[12]

The system, Fe(II)–complex/PhNHNHPh/carboxylic acid/O_2 reported by Mimoun and Seree de Roch has been shown to lead to selective hydroxylation of alkanes, alkenes and arenes,[7] but was not amongst those studied by Lindsay Smith and Sleath.[12] The overall stoichiometry of this reaction [eq. (1)] parallels that of cytochrome P_{450} [eq. (2)].

$$RH + PhNHNHPh + O_2 \xrightarrow{Fe(II)} ROH + PhN{:}NPh + H_2O \quad (1)$$

$$RH + O_2 + 2e^- + 2H^+ \xrightarrow{P_{450}} ROH + H_2O. \quad (2)$$

There is also considerable product selectivity. Thus, oxidation of cyclohexane gives cyclohexanol and cyclohexanone in a ratio varying between 7 : 1 and 50 : 1 depending upon the reaction conditions. The efficiency of the reaction is limited (turnover = 1.6 h^{-1} at 20°C, employing $[Fe(py)_4Cl_2]$ and $PhCO_2H$ in acetone), but this appears to largely arise by virtue of the direct oxidation of hydrazobenzene, thereby consuming the essential source of "hydrogen" in an unproductive side reaction. (Cytochrome P_{450} receives the hydrogen required for hydroxylation in the form of two protons and two electrons; the Mimoun system receives hydrogen from hydrazobenzene.) In a typical hydroxylation reaction, between four and five moles of hydra-

*Author to whom correspondence should be addressed.

zobenzene are consumed in producing one mole of cyclohexanol, the exact figure depending on the conditions and catalyst used. Nevertheless, this system is of considerable interest, since hydrazobenzene can be regenerated from azobenzene in a separate step by hydrogenation, thereby giving the overall stoichiometry shown in eq. (3).

$$RH + O_2 + H_2 \rightarrow ROH + H_2O. \qquad (3)$$

More recently, Sawyer *et al.* have developed an analogous system and have applied this to the oxidation of a range of compounds, but not to alkanes.[13] They have provided evidence that such reactions proceed by a mechanism involving: (i) an O_2-activation segment, leading to production of H_2O_2 from O_2 and PhNHNHPh, and (ii) an H_2O_2-activation segment which leads to oxidation. This group have also developed a related system using anhydrous H_2O_2.[14] Others have used related $Fe(II)/H_2O_2$ systems in mixed aqueous solvents. Although such reactions were originally thought to involve the $[FeO]^{2+}$ intermediate in the oxidation of both aliphatic and aromatic C—H bonds,[15,16] it has now been shown that the hydroxyl radical is the active oxidant.[17] Thus, these systems have been termed "non-aqueous Fenton reagents".

Herein we report our studies of the Mimoun system utilizing $[Fe(py)_4Cl_2]$/PhNHNHPh/benzoic acid/O_2 in acetone for the oxidation of cyclohexane. We also report a separate study of the oxidation of PhNHNHPh by O_2 in the presence of $[Fe(py)_4Cl_2]$ and $PhCO_2H$. Previous mechanistic studies of hydrazobenzene oxidation have been confined to an examination of the reaction in aqueous solvents.[18,19]

RESULTS

(i) *The catalysed oxidation of hydrazobenzene*

The reaction between hydrazobenzene and O_2 in the presence of $[Fe(py)_4Cl_2]$ and $PhCO_2H$ in acetone has been studied. The only product was found to be azobenzene. The stoichiometry of the reaction was strictly 2:1 (PhNHNHPh : O_2) when benzoic acid was present. However, in the absence of the acid it was not possible to obtain reproducible results for this determination.

A kinetic study has been carried out on the reaction. Examination of the dependence of the rate upon the concentration of benzoic acid gave rise to the plot shown in Fig. 1 (PhNHNHPh concentration 2.6×10^{-2} M, $[Fe(py)_4Cl_2]$ concentration 1.3×10^{-2} M). At concentrations of $PhCO_2H$ below 4×10^{-2} M, the reaction was not well behaved and the solution was heterogenous,

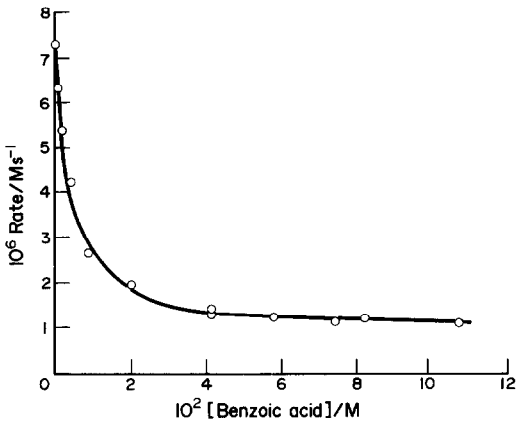

Fig. 1. Variation in the rate of azobenzene formation with benzoic acid concentration.

containing a flocculent precipitate. Thus, all other aspects of this study were carried out in the presence of a $PhCO_2H$ concentration at least equal to that of PhNHNHPh. Under these conditions, the reaction was found to show a first order dependence on the concentration of PhNHNHPh (Fig. 2). The dependence on the concentration of $[Fe(py)_4Cl_2]$ (Fig. 3) was also found to be first order, but the plot showed a positive intercept indicating an accompanying uncatalysed oxidation process. Further evidence for this behaviour was obtained from examination of the variation in the rate of reaction with O_2 partial pressure (Fig. 4). Line (a) in Fig. 4 shows the variation in the presence of $[Fe(py)_4Cl_2]$ and line (b) shows the variation in the absence of the catalyst. It is clear that the positive slope in line (a) arises from the uncatalysed process and thus the catalysed reaction is independant of oxygen concentration. The overall rate law for PhN : NPh formation in the presence of $[Fe(py)_4Cl_2]$ is thus of the form shown in eq. (3), with the catalysed component exhibiting

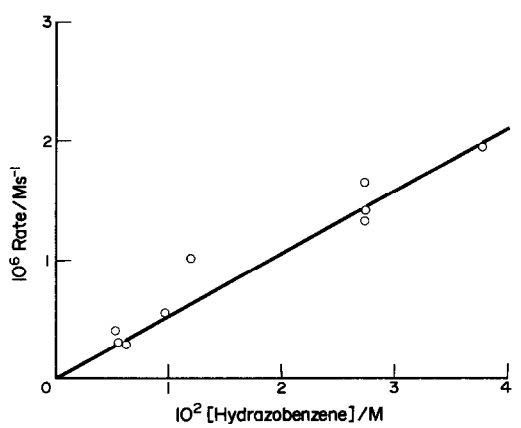

Fig. 2. Variation in the rate of azobenzene formation with hydrazobenzene concentration.

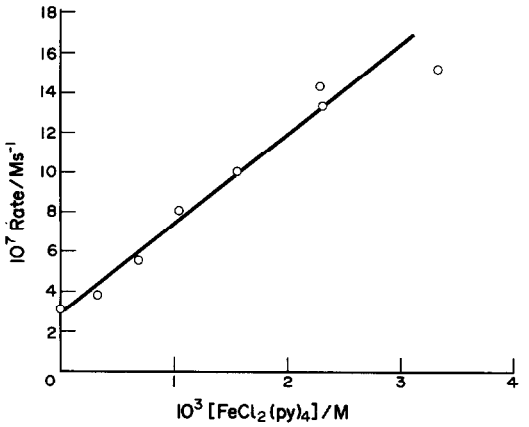

Fig. 3. Variation in the rate of azobenzene formation with $[FeCl_2(py)_4]$ concentration.

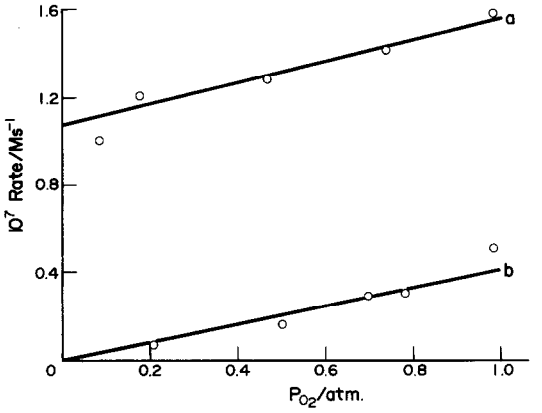

Fig. 4. Variation in the rate of azobenzene with oxygen partial pressure, (a) in the presence of $[FeCl_2(py)_4]$ and (b) in the absence of $[FeCl_2(py)_4]$.

the rate law shown in eq. (4).

$$\frac{d(PhN:NPh)}{dt} = \{k'_{obs}[Fe(py)_4Cl_2]_o + k''_{obs}P_{O_2}\}[PhNHNHPh] \quad (3)$$

$$\frac{d(PhN:NPh)}{dt} = k'_{obs}[Fe(py)_4Cl_2]_o[PhNHNHPh]. \quad (4)$$

In view of the fact that this reaction shows simultaneous catalysed and uncatalysed components it is not possible to calculate meaningful activation parameters.[20]

Variation in the relative rate of the catalysed reaction of PhNHNHPh for complexes of the type $[Fe(4\text{-}RC_5H_4N)_4Cl_2]$ (R = H, Me, Et, Bu^t) is shown in Table 1. Also included in this table are relative rates of reaction of some substituted hydrazobenzenes in the presence of $[Fe(py)_4Cl_2]$.

(ii) *The catalysed oxidation of cyclohexane in the presence of* $[Fe(py)_4Cl_2]$ *and hydrazobenzene*

Oxidation of cyclohexane by the $[Fe(py)_4Cl_2]$/PhNHNHPh/$PhCO_2H/O_2$ system in acetone yielded only azobenzene, cyclohexanol and cyclohexanone, as previously reported by Mimoun and Seree de Roch.[6] A rigorous search was made (g.c. and g.c.–m.s.) for other products, but none was found. There is therefore no further oxidation of cyclohexanol or cyclohexanone, or oxidation of the solvent, acetone or the ligand, pyridine. Use of cyclohexanol as the substrate in place of cyclohexane gave only trace quantities of cyclohexane-1,3- and -1,4-diols, and no cyclohexanone was detected.

A kinetic study of the formation of cyclohexanol revealed the reaction rate to be independant of the partial pressure of oxygen and to display a first order dependence on $[Fe(py)_4Cl_2]_o$ (Fig. 5). A first order dependence of the rate on cyclohexane concentration was also observed (Fig. 6), although

Table 1. Dependence of the rate of hydrazobenzene oxidation upon the nature of the catalyst and the substrate

Catalyst	Reagent	Relative rate
$Fe(py)_4Cl_2$	PhNHNHPh	1.0
$Fe(4\text{-}MeC_5H_4N)_4Cl_2$	PhNHNHPh	0.8
$Fe(4\text{-}EtC_5H_4N)_4Cl_2$	PhNHNHPh	0.79
$Fe(4\text{-}Bu^tC_5H_4N)_4Cl_2$	PhNHNHPh	0.84
$Fe(py)_4Cl_2$	$2\text{-}MeC_6H_4NHNHPh$	0.85
$Fe(py)_4Cl_2$	$2\text{-}EtC_6H_4NHNHPh$	0.75
$Fe(py)_4Cl_2$	$(2\text{-}MeC_6H_4NH)_2$	0.75
$Fe(py)_4Cl_2$	$(2\text{-}EtC_6H_4NH)_2$	0.45
$Fe(py)_4Cl_2$	$2\text{-}MeOC_6H_4NHNHPh$	1.30
$Fe(py)_4Cl_2$	$4\text{-}MeC_6H_4NHNHPh$	1.65

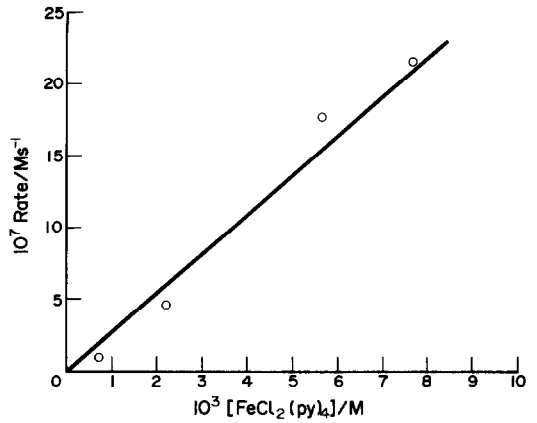

Fig. 5. Variation in the rate of cyclohexanol formation with $[FeCl_2(py)_4]$ concentration.

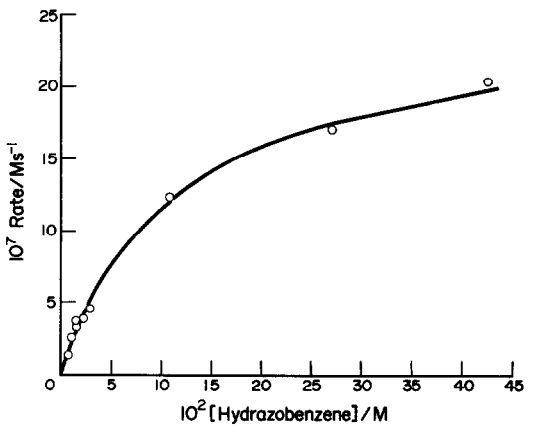

Fig. 7. Variation in the rate of cyclohexanol formation with hydrazobenzene concentration.

some deviation occurred at higher concentrations. Unfortunately, lack of miscibility between the alkane and the water generated during the reaction, limited the investigation to the range of concentrations shown and may have affected the quality of the data at the higher end of this range. The dependence of the rate of reaction upon PhNHNHPh concentration was found to be of the Michelis–Menten type (Fig. 7) and the corresponding Lineweaver–Burke plot[21] is shown in Fig. 8. The rate equation for this reaction is, therefore, of the form shown in eq. (5).

$$\frac{d[C_6H_{11}OH]}{dt} = \frac{k[Fe(py)_4Cl_2]_o[C_6H_{12}][PhNHNHPh]}{(k' + k''[PhNHNHPh])} \quad (5)$$

Oxidation of C_6H_{12} and C_6D_{12} by the above system gave rise to a k_H/k_D ratio of 1:61. Oxidation of cyclohexane by $[Fe(py)_4Cl_2]$/PhNHNHPh/$PhCO_2H/H_2O_2$ was previously reported to give poor yields of cyclohexanol and cyclohexanone compared to reactions in the presence of O_2. Such reactions also show a marked alteration in selectivity [-ol/-one ratio = 56 in the presence of $FeCl_2$/PhNHNHPh/$PhCO_2H/O_2$; -ol/-one ratio = 0.29 in the presence of $FeCl_2$/PhNHNHPh/$PhCO_2H/H_2O_2$ (-ol/-one ratio = ratio of the yields of cyclohexanol to cyclohexanone)].[6] We have confirmed these findings and have also observed low yields and low -ol/-one ratios by employing either aqueous H_2O_2 or anhydrous H_2O_2 in the absence of PhNHNHPh. Reactions employing either iodosylbenzene or *para*-cyano-dimethyl-aniline-N-oxide (*p*-CDMANO) in both the presence and absence of hydrazobenzene gave negligible yields of oxidation products. Furthermore, no reaction was observed between styrene and either PhIO or PhIO and PhNHNHPh in the presence of $[Fe(py)_4Cl_2]$, whereas a similar reaction between PhIO and styrene in the presence

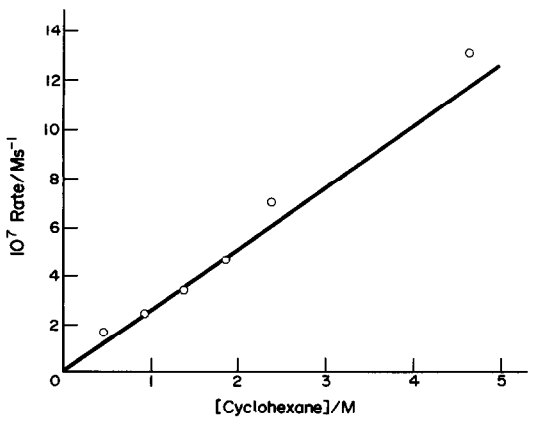

Fig. 6. Variation in the rate of cyclohexanol formation with cyclohexane concentration.

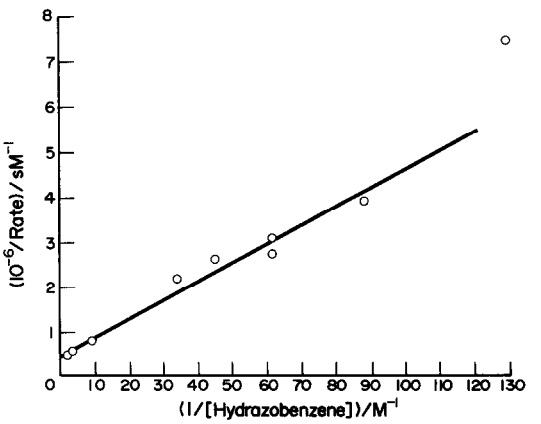

Fig. 8. Plot of the reciprocal of the rate of cyclohexanol formation with the reciprocal of the hydrazobenzene concentration.

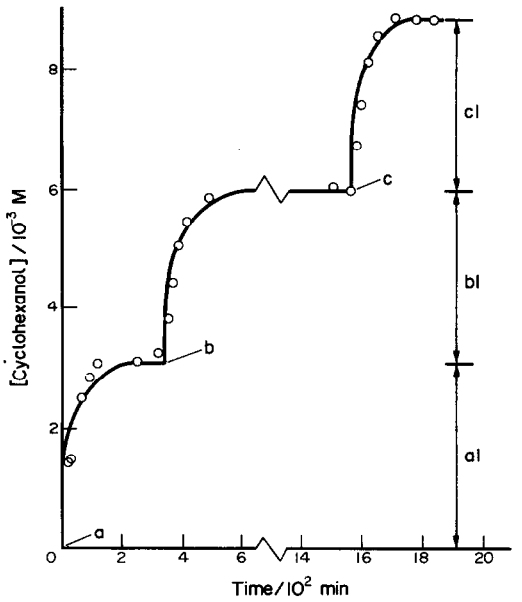

Fig. 9. Plot of the formation of cyclohexanol with sequential additions of hydrazobenzene [at points (a), (b) and (c)].

of [Fe(TPP)Cl] (TPP = tetraphenylporphyrinate) yielded styrene oxide and phenylacetaldehyde (9.92 and 2.82% respectively based on PhIO).

When a reaction between cyclohexane and O_2 in the presence of $[Fe(py)_4Cl_2]$ and $PhCO_2H$ was carried out with sequential addition of PhNHNHPh, the behaviour shown in Fig. 9 was observed. Thus, with consecutive additions of PhNHNHPh, the reaction was sustained and this behaviour was observed for 15 consecutive additions.

Reactions of adamantane with O_2 in the presence of $[Fe(py)_4Cl_2]$/PhNHNHPh/CH_3CO_2H yielded the results shown in Table 2. Similar reactions carried out in the presence of CCl_4 produced reduced amounts of adamantanols and adamantanone, but gave amounts of chloroadamantanes such that the total conversion of adamantane was maintained at a level approximately equal to that in the absence of CCl_4 (Table 3). Similar results were obtained for analogous comparisons of the conversion of cyclohexane in the presence and absence of CCl_4.

An examination has been carried out on the effect of variations in the nature of the catalyst and the hydrazobenzene derivative used for oxidation of cyclohexane. These results are contained in Tables 4–6, and comparisons have been made of the -ol/-one ratio and the ratio of number of moles of hydrazobenzene derivative consumed per mole of oxidized products formed (n).

(iii) *Nature of the catalyst in solution*

$[Fe(py)_4Cl_2]$ was found to be unstable in acetone solution under nitrogen in the absence of benzoic acid, forming a flocculent percipitate. However, the complex formed a stable homogeneous solution in acetone in the presence of $PhCO_2H$ or in dimethylformamide in the absence of acid. Infrared spectroscopic studies of such solutions showed bands attributable to both coordinated and free pyridine. However, we were unable to obtain direct evidence for the formation of complexes involving coordinated DMF, $PhCO_2H$ or $PhCO_2^-$.

Measurements of the magnetic moment of $[Fe(py)_4Cl_2]$ in DMF solution using the NMR method were obtained.[22] Such data could not be obtained for $[Fe(py)_4Cl_2]$ in acetone/$PhCO_2H$ due to limited solubility, however, the improved solubility of $[Fe(4\text{-}Bu^tC_5H_4N)_4Cl_2]$ in this solvent system allowed such measurements to be obtained for this complex. The data for these two complexes is contained in Table 7. Values of approximately 5.0 μ_B were obtained for both complexes under nitrogen. More accurate values could not be obtained since the accurate molecular weights of the complexes could not be estimated due to pyridine dissociation.

Table 2. Oxidation of adamantane[a]

$Fe(py)_4Cl_2$ × (10^2 M)	PhNHNHPh × (10 M)	Yield of adamantan-1-ol (%)	Yield of adamantan-2-ol (%)	Yield of adamantanone (%)	-ol/-one	C^2/C^3
0.05596	0.5440	2.57	2.13	—	—	0.83
0.3159	1.095	3.39	3.32	—	—	0.98
0.6860	1.089	4.25	4.35	0.03	265.4	1.03
1.540	1.101	3.64	4.06	0.09	84.1	1.14
1.738	1.087	4.26	4.21	0.16	52.3	1.02
3.645	1.090	3.72	3.85	0.17	45.0	1.08
—	1.094	0.98	0.86	—	—	0.87

[a] Concentrations of other components were: acetone, 13.60 M; CH_3CO_2H, 1.06 M.

Table 3. Oxidation of adamantane in the presence of CCl_4[a]

Acetone [M]	CCl_4 [M]	Yield of adamantan-1-ol (%)	Yield of adamantan-2-ol (%)	Yield of adamantanone	Yield of 1-chloroadamantane	Yield of 2-chloroadamantane	-ol/-one	C^2/C^3	Total 1-subst. products	Total 2-subst. products
13.60	0	4.26	4.21	0.16	—	—	52.3	1.03	4.26	4.37
10.88	2.07	0.30	3.30	0.16	3.85	0.61	22.1	0.98	4.15	4.07
10.88	2.07	0.23	2.95	0.15	3.99	1.03	20.7	0.98	4.22	4.14
8.16	4.15	0.09	1.88	0.11	3.67	1.84	17.38	1.02	3.76	3.84
5.44	6.22	0.04	1.70	0.11	3.19	1.56	15.46	1.04	3.24	3.38
13.60[b]	0	0.98	0.86	—	—	—	—	0.87	0.98	0.86
10.88[b]	2.07	0.14	0.81	—	0.83	—	—	0.83	0.97	0.81

[a] Concentrations of other components were: CH_3CO_2H, 1.06 M; $[Fe(py)_4Cl_2]$, 1.68×10^{-2} M; PhNHNHPh, 1.09×10^{-1} M.
[b] In the absence of $[Fe(py)_4Cl_2]$.

Attempts to carry out molecular weight determinations by vapour phase osmometry were unsuccessful. When oxygen was admitted to the solutions, the magnetic moments fell to approximately 2.0 μ_B per iron. Again, more accurate values could not be obtained, since the precise nature of the product from the reaction between the complexes and oxygen is unknown. Addition of hydrazobenzene to the oxygenated solutions led to the magnetic moments being restored to values close to those observed under nitrogen.

Infrared spectroscopic studies of the above solutions showed the growth of a new band at 870 cm^{-1} when oxygen was admitted to a DMF solution of $[Fe(py)_4Cl_2]$. This band was considerably reduced in intensity when PhNHNHPh was added to the oxygenated solution.

DISCUSSION

Mimoun and Seree de Roch proposed the mechanism shown in Scheme 1 for the hydroxylation of alkanes in the presence of $[Fe(py)_4Cl_2]$ and PhNHNHPh. The mechanism must be more complex than that proposed by these workers, since it must also account for the over-consumption of PhNHNHPh as demonstrated by the value of n in Table 6. There is clearly competition between PhNHNHPh and C_6H_{12} at some stage in the reaction cycle. However, PhNHNHPh is essential for alkane hydroxylation since the selectivities observed, as shown by the observed -ol/-one ratios, are not obtained obtained in absence of this reagent.

In order to gain information on the mechanisms of these processes we have carried out a wide ranging study. On this basis we propose that the mechanism of the reaction is that shown in Scheme 2. In this scheme, the active metal catalyst is simply represented as Fe(II).

There has been only one previous study on the oxidation of hydrazobenzene to azobenzene in the presence of metal catalysts. This involved reactions in the presence of Cu(II) ions in aqueous solution.[19] The mechanism shown in Scheme 3 was postulated but this reaction shows a different stoichiometry and different kinetic behaviour from that observed in the present study.

In the presence of $[Fe(py)_4Cl_2]$ and $PhCO_2H$ in acetone, the reaction stoichiometry is strictly 2 : 1 ($PhNHNHPh : O_2$) and the overall kinetic behaviour is that shown in eq. (3). This rate equation is a composite arising from concurrent catalysed and uncatalysed oxidations, and the expression relating to the catalysed reaction is shown in eq. (4). Oxidation of PhNHNHPh in the absence of cyclohex-

Table 4. Oxidation of cyclohexane in the presence of a range of catalysts

Complex	*n*	-ol/-one	Complex	*n*	-ol/-one
$Fe(py)_4Cl_2$	4.1	16.8	$Fe(py)_4Cl_3$	4.9	15.6
$Fe(dipy)_2Cl_2$	9.2	15.5	Fe(salen)	8.6	1.5
$Fe(dipy)_3Cl_2$	11.1	16.0	$FeBr(CO)_3(\eta^3\text{-allyl})$	4.8	25.0
$FeCl_2$(anhyd.)	5.0	20.4	$[Fe(CO)_3(\eta^3\text{-allyl})_2$	9.3	3.0
$FeCl_3$(anhyd.)	5.9	18.5			

Table 5. Oxidation of cyclohexane in the presence of the catalysts, $[Fe(4\text{-}XC_5H_4N)_4Cl_2]$

X	*n*	-ol/-one
H	4.1	16.8
Me	4.6	13.2
Et	4.7	12.2
Bu^t	4.3	16.2

ane proceeding according to Scheme 2, gives rise to the rate expression shown in eq. (6) under conditions where the reaction of the species represented by $[Fe(H_2O_2)]$ with PhNHNHPh is the rate determining step and the equilibrium defined by K_1 lies well to the right.

Table 6. Oxidation of cyclohexane in the presence of a range of hydrazobenzene derivatives

Substituents	*n*	-ol/-one
H	4.1	16.8
2-Me	3.9	16.3
2-Et	3.6	20.4
2,2′-Me_2	3.7	15.7
2,2′-Et_2	3.3	28.2
2-MeO	4.6	12.8
2-Ph	3.3	20.7
2,2′-Ph_2	2.8	10.9
4-Me	4.6	16.7
4,4′-Cl_2	4.5	17.5
4,4′-Et_2	7.0	9.5
4-COOH	8.9	4.0
4-COOBu	5.2	18.0
4-OCONHBu	5.1	23.5

Table 7. Magnetic moment values of $[Fe(py)_4Cl_2]$ and $[Fe(4\text{-}Bu^t\text{-}C_5H_4N)_4Cl_2]$

Complex	Magnetic moment (μ_B) per iron atom		
	under N_2	under O_2	PhNHNHPh added
$Fe(py)_4Cl_2$	5.12[a]	1.96[b]	5.10[a]
$Fe(4\text{-}Bu^t\text{-}C_5H_4N)_4Cl_2$	5.16[a]	1.92[b]	5.20[a]

[a] Based on the formula $[FeL_4Cl_2]$.
[b] Based on the formula $[L_4Fe\text{-}O\text{-}FeL_4]Cl_4$.

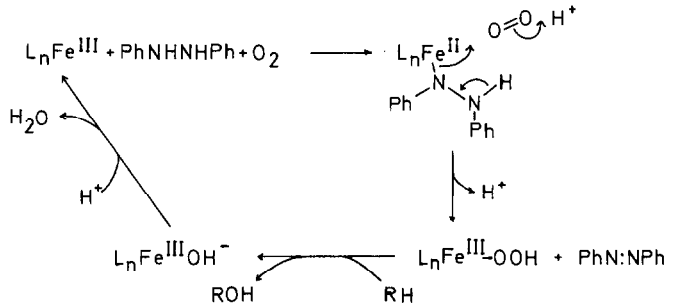

Scheme 1.

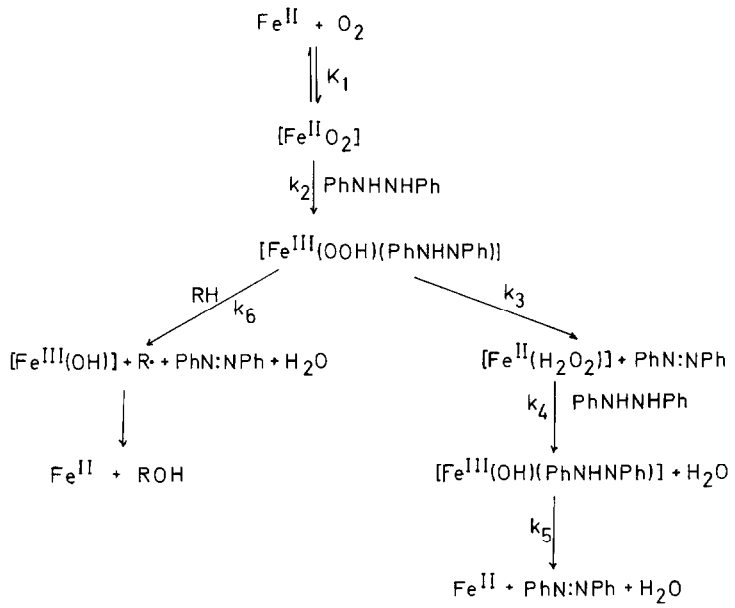

Scheme 2.

$$PhNHNHPh \rightleftharpoons PhNNHPh^- + H^+$$

$$PhNNHPh^- + Cu^{2+} \longrightarrow Ph\dot{N}NHPh + Cu^+$$

$$Ph\dot{N}NHPh + Cu^{2+} \longrightarrow PhN{:}NPh + H^+ + Cu^+$$

$$Cu^+ + O_2 \longrightarrow Cu^{2+} + O_2^-$$

Scheme 3.

$$\frac{d(PhN:NPh)}{dt} = 2k_4[Fe(py)_4Cl_2]_n[PhNHNHPh]. \quad (6)$$

Employing the rate expressions given in eqs (3) and (6), it is possible to calculate a set of values for k''_{obs} [eq. (3)], associated with the uncatalysed reaction, and for k_4 [eq. (6)], associated with the catalysed reaction. [k_4 is equivalent to k'_{obs} in eq. (3).] This data is shown in Table 8 and it may be seen that the values for these rate constants obtained using the variations in concentration of $[Fe(py)_4Cl_2]$, O_2 and PhNHNHPh, respectively, give an acceptable agreement considering the data was obtained by the initial rate method.

In an effort to gain some insight into the nature of the active catalyst and of the interaction between PhNHNHPh and this species, the following studies were performed. An IR spectroscopic study demonstrated the presence of both free and coordinated pyridine in solutions consisting of either $[Fe(py)_4Cl_2]$ and $PhCO_2H$ in acetone, or $[Fe(py)_4Cl_2]$ in DMF. It is demonstrated by the relative rate data shown in Table 1 that pyridine dissociation is an important step of the reaction. Use of 4-substituted pyridine ligands containing alkyl groups gave rise to reduced rate of reaction, as would be expected, because electron donating substituents increase the strength of the pyridine–Fe bond.

We were unable to obtain direct spectroscopic evidence for the interaction of PhNHNHPh with the catalyst. However, the relative rate data for substituted hydrazobenzenes (Table 2) suggest this

Table 8. Rate constants for the oxidation of hydrazobenzene

Determination	$k'(\times 10^{-5}\ s^{-1}\ atm^{-1})$	$k_4(\times 10^{-3}\ M^{-1}\ s^{-1})$
Variation in $[Fe(py)_4Cl_2]$	1.17	7.99
Variation in $[O_2]$ [line (a)]	1.60	8.53
Variation in $[O_2]$ [line (b)]	1.44	—
Variation in [PhNHNHPh][a]	—	9.21
Mean	1.40 ± 0.22	8.58 ± 0.61

[a] k_4 calculated using the man value of k'.

may be occurring. Thus hydrazobenzenes containing electron donating substituents in the 4-position show enhanced reaction rates, in line with a stronger interaction between the substrate and the metal. 2- and 2,2′-substituted hydrazobenzenes show reduced rates, as might be expected from steric considerations. 2-$MeOC_6H_4NHNHPh$ is an exception to this trend presumably since here electronic effects outweigh steric effects. Since k_4 is rate determining, these results strictly apply to the reaction of the second PhNHNHPh molecule with the $[Fe(H_2O_2)]$ intermediate, however such a finding also suggests that the interaction of the $[FeO_2]$ complex with PhNHNHPh is a reasonable possibility.

Interaction between the catalyst and O_2 is clearly illustrated by the magnetic measurements in solution shown in Table 7. The values of approximately 5.0 μ_B obtained for both complexes under nitrogen are consistent with the presence of high spin Fe(II).[23] When oxygen is admitted to the solutions the magnetic moments drop to approximately 2.0 μ_B per iron. This value is not consistent with either high spin or low spin Fe(III) and we ascribe it to the formation of a μ-oxo dimer of the type $[py_nCl_2Fe\text{-}O\text{-}FeCl_2py_n]$.[24] In accord with this, the IR spectrum of such a solution shows a strong band at 870 cm^{-1}, which is not present in the spectra of $[Fe(py)_4Cl_2]$ under nitrogen. This absorption is in the region associated with the Fe(III)—O—Fe(III) unit.[24] Presumably the μ-oxo dimer arises via a sequence beginning with formation of an iron–dioxygen complex in a manner similar to that observed for iron(II) prophyrin complexes.[25] In the presence of PhNHNHPh there is no evidence for formation of the μ-oxo dimer and indeed, addition of PhNHNHPh to a preformed solution of the μ-oxo dimer leads to diminution of the 870 cm^{-1} band in the IR spectrum and to the magnetic moment being restored to the original value of approximately 5.0 μ_B. On the basis of these results we suggest that the active catalytic species is an $[Fe(II)(O_2)]$ complex rather than the dimer. In support of this we find that $[(FePc)_2(\mu\text{-}O)]$ does not display the same behaviour as $[Fe(py)_4Cl_2]$ in both PhNHNHPh and cyclohexane oxidation reactions. Furthermore, when $[Fe_3(\mu_3\text{-}O)(OAc)_6(H_2O)]$, is used in these reactions, the behaviour also differs from that of $[Fe(py)_4Cl_2]$. Barton *et al.* have previously suggested that such trimers are active catalysts in related alkane oxidation reactions.[26]

We propose that the $[Fe(O_2)]$ intermediate reacts with coordinated hydrazobenzene to yield an $[Fe(H_2O_2)]$ complex, the reaction proceeding via an iron–hydroperoxide intermediate. Sawyer *et al.* have provided good evidence for this mode of reaction.[13] In the present system the $[Fe(H_2O_2)]$ intermediate subsequently reacts with a second PhNHNHPh molecule as shown in Scheme 2. We do not, however, favour this second step involving formation of a ferryl intermediate, $[FeO^{2+}]$, as previously proposed.[13] This aspect will be further discussed later in this section.

The role of the benzoic acid which is necessary in reactions performed in acetone has not been completely resolved. In the absence of the acid, $[Fe(py)_4Cl_2]$ is unstable in acetone, although it is stable in DMF. It may be that DMF and either $PhCO_2H$ or $PhCO_2^-$ are better able to stabilize the coordinatively unsaturated complex formed by pyridine dissociation, than is acetone. We have not been able to obtain spectroscopic evidence concerning the nature of any interaction between the iron complex and either the acid or the benzoate anion. Furthermore, removal of the solvent from an acetone solution of $[Fe(py)_4Cl_2]$ and $PhCO_2H$ yields only a physical mixture of the reactants.

Benzoic acid may well play a further role. Although it is a weak acid in aprotic solvents,[27] it may inhibit any tendancy of hydrazobenzene to undergo dissociation to $PhNHNPh^-$, thereby inhibiting oxidation by a mechanism similar to that observed in aqueous solution (Scheme 3).

A kinetic study of the oxidation of cyclohexane in the presence of $[Fe(py)_4Cl_2]$/PhNHNHPh/$PhCO_2H/O_2$ yielded a rate expression for cyclohexanol formation of the type shown in eq. (5). This is in accord with the mechanism shown in Scheme 2 which gives rise to the rate expression shown in eq. (7).

$$\frac{d(C_6H_{11}OH)}{dt} = \frac{k_2k_4k_5k_6[Fe(py)_4Cl_2]_o[PhNHNHPh][C_6H_{12}]}{[k_2k_4(k_3+k_5)[PhNHNHPh]+k_3k_5(k_2+k_4)]} \quad (7)$$

Examination of the data of the variation in concentrations of $[Fe(py)_4Cl_2]$ and C_6H_{12}, allows the calculation of values for the term $k_2k_4k_5k_6/[k_2k_4(k_3+k_5)[PhNHNHPh]+k_3k_5(k_2+K_4)]$. Values of 5.98×10^{-3} and 4.37×10^{-3} M^{-2} s^{-1}, respectively, were obtained. These are in reasonable agreement in view of the fact that the data were obtained using the initial rate method. Variation in the concentration of PhNHNHPh gave values of $(k_2+k_4)k_3/k_2k_4k_6$ and $(k_3+k_5)/k_5k_6$ of 214.5 M^2 and 547 M s respectively. Use of these values and a value for the concentration of PhNHNHPh identical to that used in obtaining data for the variation in the concentrations of $[Fe(py)_4Cl_2]$ and $[C_6H_{12}]$ gives a further value for $k_2k_4k_5k_6/[k_{2k}(k_3+k_5)[PhNHNHPh]+k_3k_5(k_2+k_4)]$ of 4.37×10^{-3} M^{-2} s^{-1}. Thus, there is excellent agreement of the

data obtained for the production of cyclohexanol.

Kinetic behaviour of this type can only be obtained if the alkane and the second molecule of PhNHNHPh each react with different intermediates, as shown in Scheme 2. Competing reactions for the same intermediate, for example, the $[Fe(H_2O_2)]$ complex, produce a rate expression of the type given in eq. (8).

$$\frac{d(C_6H_{11}OH)}{dt} = \frac{k[Fe(py)_4Cl_2]_o[PhNHNHPh][C_6H_{12}]}{k'[PhNHNHPh]+k''[C_6H_{12}]}. \quad (8)$$

This is clearly not in accord with the observed behaviour. Further evidence against the reaction of the alkane with an $[Fe(H_2O_2)]$ intermediate is provided by the observations that reactions involving replacement of O_2 by either aqueous or anhydrous H_2O_2, both in the presence and absence of PhNHNHPh, do not exhibit the same selectivity or yields as are observed when employing O_2.

Sawyer *et al.*[13,14] have suggested that reactions involving $[Fe(H_2O_2)]$ intermediates proceed by formation of the $[FeO]^{2+}$ ion as the active intermediate. Others have suggested that such reactions can be viewed as "non-aqueous Fenton's reagents" on the basis of kinetic isotope effects, product distributions and other evidence, and thus involve reactions of $OH^{\cdot}$.[12,17] In the present system we have found no evidence for the reactions involving the $[FeO]^{2+}$ intermediate. Thus, reactions of cyclohexane involving $[Fe(py)_4Cl_2]$, $PhCO_2H$ and either iodosylbenzene or *para*-cyanodimethylaniline-N-oxide, both in the presence and absence of PhNHNHPh, which might be expected to yield $[FeO]^{2+}$, give negligible yields of oxidation products.

Furthermore, the kinetic isotope effect for the present system was found to be 1.61 for cyclohexane oxidation. This value is slightly larger than the value reported by Groves and van der Puy for cyclohexanol hydroxylation by Fe(II)–H_2O_2(k_H/k_D = 1.18)[16] and those reported by Smith and Sleath for oxidative demethylation of anisole by "non-aqueous Fenton's reagents".[12] It is not, however in the range expected ($k_H/k_D > 6.0$) for systems that model the behaviour of cytochrome P_{450}.[12,28] The value obtained in this work is also smaller than that shown by reactions employing $[VO(O_2)L_3]$, which are believed to involve the [V(IV)—O—Ȯ] species.[29] Further evidence that the present system differs from that of Groves and van der Puy comes from the fact that, in a separate reaction, we observe only trace amounts of hydroxylation, and no dehydrogenation of cyclohexanol. Neither does this system appear to be acting as a "non-aqueous Fenton reagent", since it is unreactive towards the solvent, acetone, whereas $OH^{\cdot}$ radicals induce the production of $Me^{\cdot}$ radicals.[14,28] It is also noteworthy that unlike the "non-aqueous Fenton's reagents", which convert anisole into phenol (2.4%) and a mixture of methoxyphenols (3.4%; *o*:*m*:*p* ratio = 87:1:12), the present system yields only phenol (4.3%) and *o*-methoxyphenol (trace amount; could not be quantified by g.c.). We are thus driven to the conclusion that in the $[Fe(py)_4Cl_2]$/PhNHNHPh system, the alkane undergoes reaction with a metal hydroperoxide intermediate.

Mimoun and Seree de Roch examined the efficiency of the $[Fe(py)_4Cl_2]$/PhNHNHPh/$PhCO_2H/O_2$ system for oxidation of a range of hydrocarbons. In the present study we have confined our interest to cyclohexane and adamantane. The latter has been used as a model substrate by Barton *et al.* in a study of the so-called Gif oxidation systems. These systems give predominant attack at the secondary positions and produce a ketone as the major product. It has been proposed that the major process in these reactions involves an $[FeO]^{2+}$ intermediate, formed via [Fe(OOH)], which undergoes insertion into a C—H bond giving $[Fe(OH)(CHR_2)]$. Subsequent dehydration leads to a carbene, $[Fe(CR_2)]$, which reacts further with oxygen to give the ketone.[31]

The results of the oxidation of adamantane by the present system are contained in Table 2. Typical conditions produce adamantan-1-ol (4.26%), adamantan-2-ol (4.21%) and adamantanone (0.16%). The selectivity for hydroxylation is thus, large (-ol/-one ratio = 52.3) and the ratio of reaction at the secondary to tertiary carbon (C^2/C^3) is 1.18. The C^2/C^3 is much larger than that observed for reactions of [FeCl(Por)]/PhIO (0.02–0.09),[28] but is lower than that reported for the Gif system.[31] The present system does not appear to follow a mechanism similar to that proposed for the Gif systems.

Table 3 contains data for the oxidation of adamantane in the presence of CCl_4. Under these conditions, the yields of both isomers of adamantanol are reduced, while that of adamantanone remains constant. 1- and 2-chloroadamantane are formed in amounts that lead to an approximate mass balance for the conversion of adamantane in the presence and absence of CCl_4. The formation of chloroadamantanes suggests that CCl_4 is intercepting the alkyl free radicals. The production of such radicals is part of the proposed mechanism (Scheme 2).

Data for the oxidation of cyclohexane by O_2/PhNHNHPh/$PhCO_2H$ in the presence of a range of iron complexes is given in Table 4, where relative efficiencies are compared in terms of the *n*

value (the ratio of the number of moles of PhNHNHPh consumed per mole of oxidized products formed) and the -ol/-one ratio—a number of points emerge. Thus, iron(II) complexes containing chelating ligands (dipy, salen and η^3-allyl) are less efficient than $[Fe(py)_4Cl_2]$, presumably due to decreased ligand lability among the chelates. However, the efficiency of anhydrous $[FeCl_2]$, which presumably forms the labile complex $[FeCl_2(acetone)_n]$, is also slightly lower than that of $[Fe(py)_4Cl_2]$. This may, perhaps, reflect an increased rate of PhNHNHPh oxidation by the complex. The efficiency of iron(III) complexes is only slightly less than that of those of iron(II), the decrease probably arising as a consequence of the necessity to effect an initial reduction to iron(II) by PhNHNHPh. The complex, $(Fe(CO)_3(\eta^3\text{-allyl})]_2$ is known to readily form metal-centred radicals.[32] This gives a low n value and a drastically different -ol/-one ratio, probably reflecting preferential oxidation to a ketone by a different mechanism.

Substituent effects of the pyridine ligands in complexes of the type $[Fe(4\text{-}XC_5H_4N)_4Cl_2]$ are demonstrated in Table 5. Presumably, these trends also reflect a reduced propensity for ligand dissociation among complexes of alkyl-substituted pyridines, as noted earlier. The relative efficiencies of a range of substituted hydrazobenzenes are illustrated in Table 7. Apparently, steric effects are over-riding in reducing the over-consumption of hydrazobenzene, since the n value increases both for compounds containing electron donating and electron withdrawing groups at the 4-position. The lowest n values are obtained for compounds with bulky substituents at the 2- and 2′- positions.

In summary, we believe that the $[Fe(py)_4Cl_2]$/PhNHNHPh/$PhCO_2H/O_2$ system produces an iron–hydroperoxide intermediate which is capable of inducing alkane hydroxylation. The PhNHNHPh molecule plays an essential role in the formation of this intermediate. However a competitive reaction including the hydroperoxide complex leading to an $[Fe(H_2O_2)]$ species allows a further reaction with PhNHNHPh. Possible routes for these competing reactions are shown in Scheme 4. The system shows great selectivity in alkane hydroxylation.

The source of the small amounts of ketone formed could not be investigated in detail since the low yields of cyclohexanone precluded an accurate kinetic investigation. Evidence has been presented showing that alcohol dehydrogenation is not occurring. It is also relevant that reactions in the presence of CCl_4 do not reduce the ketone yield, although the alcohol is markedly affected. Although of lower accuracy than that for the alcohol, the kinetic isotope effect for cyclohexanone formation was found to be approximately 5.9, close to the value observed by Barton *et al.* for the Gif system.[31] It is, thus, possible that ketone formation arises by a

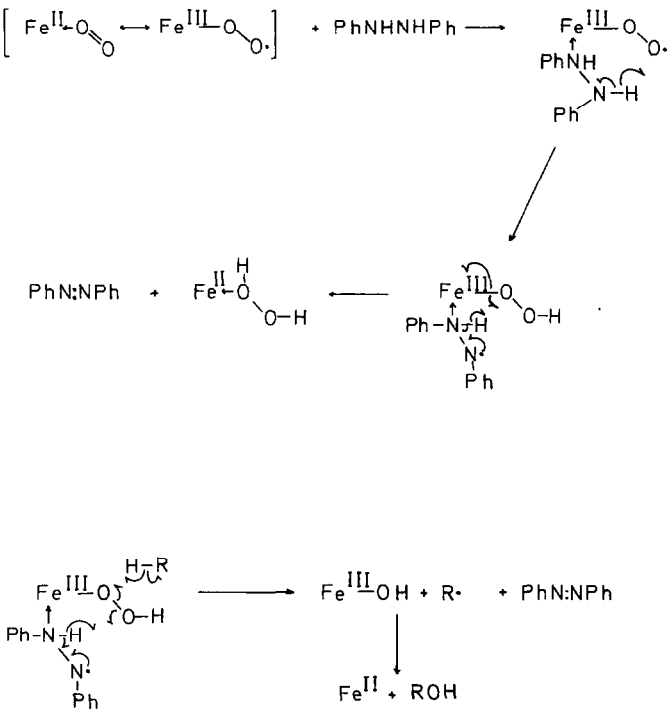

Scheme 4.

non-radical carbene route, as proposed by Barton. However, the selectivity of the present system is markedly different to the Gif oxidations.

EXPERIMENTAL

$[Fe(py)_4Cl_2]$,[33] $[Fe(bipy)_2Cl_2]$,[34] $[Fe(bipy)_3Cl_2]$,[35] $[Fe(CO)_3(\eta^3\text{-}C_3H_5)]_2$,[32] $[FeBr(CO)_3(\eta^3\text{-}C_3H_5)]$[36] were prepared by literature methods. $[Fe(4\text{-}XC_5H_4N)_4Cl_2]$ (X = Me, Et, But) were prepared by the method reported for $[Fe(py)_4Cl_2]$.[33] Hydrazobenzene was prepared by direct hydrogenation of commercial (impure) hydrazobenzene or azobenzene using H_2/Pd (10% on charcoal), yielding a white product which was stored under vacuum at −15°C. Substituted hydrazobenzenes were prepared according to standard methods.[37] $FeCl_2 \cdot 4H_2O$ was purified by standing a deoxygenated aqueous solution of the salt over iron powder for 24 h under N_2. Filtration, followed by evaporation of water under reduced pressure, and drying gave a pure product. $FeCl_3$(anhyd.) was used as received. Iodosylbenzene,[38] *para*-cyanodimethylaniline-N-oxide (*p*-CDMANO)[39] and anhydrous H_2O_2[14] were prepared by literature methods. Solvents and liquid reagents were purified by standard techniques and distilled under N_2 immediately prior to use. All solid reagents were used as received. Solvents and liquid reagents were degassed by three freeze–pump–thaw cycles prior to use. Gas chromatographic analyses were carried out on either a Pye-Unicam 204 instrument (2 m column; Carbowax 20M on Chromasorb W), equipped with an FID and a Pye–Unicam DP88 integrator or a Perkin–Elmer Sigma 3B (25 mm capillary column; *I.D.* 0.22 mm, 0.25 μm film, B.P.1) equipped with an FID and a Perkin–Elmer 3600 data station. The internal standard used throughout was *o*-dichlorobenzene. Ultraviolet spectra were recorded on a Pye–Unicam SP7-500, which was used in single wavelength mode when necessary. Infrared spectra were recorded either on a Perkin–Elmer 457 spectrometer, or a Perkin–Elmer 782 spectrometer, equipped with a 3600 data station. ^{1}H NMR spectra were obtained using either a Perkin–Elmer R32, 90 MHz instrument or a Brucker WP80, 80 MHz, F.T. instrument.

The oxidation of hydrazobenzene using $[Fe(py)_4Cl_2]$

(i) *The stoichiometry of the reaction.* $[Fe(py)_4Cl_2]$ (0.6983 g, $2.1.7 \times 10^{-4}$ mol) and $PhCO_2H$ (0.4887 g, 4.00×10^{-3} mol) were placed in a round-bottomed jacketted reactor fitted with rotatable spoon containing PhNHNHPh (0.7365 g, 4.00×10^{-3} mol). The vessel contained a sampling port closed by a rubber septum. The vessel was evacuated and previously degassed acetone (100 cm^3) was introduced via the septum. Oxygen was admitted to the system using a gas burette and the reaction mixture was stirred vigorously. The reaction vessel was maintained at a temperature of 21.6±0.2°C. PhNHNHPh was added to the reaction mixture by inverting the spoon and samples were then taken from the solution at regular intervals. Each sample was analysed by UV spectrometry for azobenzene (λ = 447 nm, $\varepsilon = 4.401 \times 10^3$ mol^{-1} dm^2). Absorption of oxygen was measured at the time when each sample was removed, using the gas burette which was also thermostated to maintain it at the same sample temperature as the reactor. Measurements were made until there was no further change in the findings. At this point the stoichiometry of the reaction was found to be 2 : 1 (PhNHNHPh : O_2).

(ii) *The kinetics of the reaction.* The apparatus described in (i) was used for the kinetic study. Typically, acetone (20 cm^3), $PhCO_2H$ (0.1069 g, 8.76×10^{-4} mol) and $[Fe(py)_4Cl_2]$ (0.0229 g, 5.19×10^{-5} mol) were placed in the vessel and allowed to equilibrate with the oxygen atmosphere. (For determination of the order with respect to oxygen, gas mixtures consisting of appropriate amounts of oxygen and nitrogen were used). At least 15 min were allowed for equilibration to the reaction temperature of 21.6±0.2°C, before PhNHNHPh (0.1564 g, 8.50×10^{-4} mol) was added and the reaction was started. Samples were removed at intervals and analysed by UV spectrometry as above. Plots of the concentration of azobenzene vs time were used to determine the initial rate of reaction.

This method was used to determine the initial rates of reaction for varying concentrations of $PhCO_2H$, PhNHNHPh $[Fe(py)_4Cl_2]$ and oxygen partial pressure, keeping all other factors constant for each series of runs. These results are shown in Figs 1–4. Data for a range of metal complexes and a range of substituted hydrazobenzenes is shown in Table 1.

The oxidation of cyclohexane using $[Fe(py)_4Cl_2]$/PhNHNHPh/$PhCO_2H/O_2$

(i) *General.* In a typical reaction, PhNHNHPh (0.7370 g, 4.00×10^{-3} mol), $PhCO_2H$ (0.4887 g, 4.00×10^{-3} mol) and $[Fe(py)_4Cl_2]$ (0.0886 g, 2.00×10^{-4} mol) were added to a mixture of acetone (75 cm^3) and cyclohexane (75 cm^3). The resulting solution was stirred under oxygen for 24 h. Yields of cyclohexanol and cyclohexanone were determined by g.c. Similar reactions were performed using a range of metal complexes and a range of

substituted hydrazobenzenes. Results are given in the text and in Tables 4, 5 and 6. Oxidation of admantane, in the presence and absence of CCl_4 was carried out under similar conditions, but using CH_3CO_2H. The results are contained in Tables 2 and 3.

(ii) *The attempted oxidation of cyclohexanol.* The conditions described in (i) were used for the reaction of cyclohexanol. G.c. analyses showed only traces of cyclohexan-1,3-diol and cyclohexane-1,4-diol (0.09% and 0.07% respectively based on cyclohexanol).

(iii) *The use of oxygen substitutes.* Reactions were performed as described in (i), but carried out under N_2 using vigorously deoxygenated materials and gave no discernible oxidation products in the presence of PhIO or *p*-CDMANO.

(iv) *Determination of the kinetic isotope effect.* Parallel reactions were carried out under identical conditions using cyclohexane and cyclohexane–D_{12} respectively. Values of k_h/k_D were found to be 1.61, 5.90 and 1.63 for cyclohexanol, cyclohexanone, and cyclohexanol + cyclohexanone respectively.

(v) *The kinetics of the reaction.* The kinetics of the oxidation of cyclohexane were investigated using a method exactly analogous to that used for the study of PhNHNHPh. Typical conditions were: $[Fe(py)_4Cl_2]$ (0.0230 g, 5.19×10^{-5} mol), PhNHNHPh (0.1027 g, 5.57×10^{-4} mol), $PhCO_2H$ (0.1069 g, 8.75×10^{-4} mol), cyclohexane (5.0 cm^3, 0.046 mol) and acetone (15 cm^3), temperature, 21.6 ± 0.2°C. The effect of varying the concentration of $[Fe(py)_4Cl_2]$, PhNHNHPh, C_6H_{12} and oxygen partial pressure upon the initial rate of reaction were each determined. The total volume of mixture was kept constant by varying the amount of acetone. The results are shown in Figs 5–8.

Acknowledgements—We thank the SERC and B.P. Research Centre for provision of a CASE studentship (to M.A.K.) and Kingston Polytechnic for the award of a post-doctoral fellowship (to J.L.A.D.). We also thank Dr J. Betts (of Kingston Polytechnic) and Dr D. J. H. Smith, Dr G. Morris, Mr R. Hancock and Mr P. J. Robinson (all of B.P. Research Centre) for helpful discussions.

REFERENCES

1. V. Ullrich, *Top. Curr. Chem.* 1979, **83**, 68; J. T. Groves, *Adv. Inorg. Biochem.* 1979, 1119; F. P. Guengerich and T. L. Macdonald, *Acc. Chem. Res.* 1984, **17**, 9.
2. J. T. Groves and D. V. Subramanion, *J. Am. Chem. Soc.* 1984, **106**, 2177; J. T. Groves, *J. Chem. Ed.* 1985, **62**, 928.
3. G. A. Hamilton, J. W. Hanifia and J. R. Friedman, *J. Am. Chem. Soc.* 1986, **88**, 5269.
4. S. Udenfriend, C. T. Clark, J. Axelrod and B. B. Brodie, *J. Biol. Chem.* 1954, **208**, 731.
5. V. Ullrich, *Z. Naturforsch.* 1969, **24b**, 699.
6. H. Mimoun and I. Seree de Roch, *Tetrahedron* 1975, **31**, 777.
7. M. B. Dearden, C. R. Jefcoate and J. R. Lindsay Smith, *Adv. Chem. Ser.* 1968, **77**, 260.
8. G. A. Hamilton and J. R. Giacin, *J. Am. Chem. Soc.* 1966, **88**, 1584.
9. V. Ullrich and H. Staudinger, *Z. Naturforsch.* 1969, **24b**, 583.
10. R. Higgins, K. M. Kitson and J. R. Lindsay Smith, *J. Chem. Soc. B.* 1971, 430.
11. J. R. Lindsay Smith, D. M. Jerina, S. Kaufman and S. Milstein, *J. Chem. Soc., Chem. Commun.* 1975, 881.
12. J. R. Lindsay Smith and P. R. Sleath, *J. Chem. Soc., Perkin Trans. II* 1983, 621.
13. D. T. Sawyer, H. Sugimoto and T. S. Calderwood, *Proc. Natl. Acad. Sci. U.S.A.* 1984, **81**, 8025; T. S. Calderwood, C. L. Johlmann, J. L. Roberts, C. L. Wilkins and D. T. Sawyer, *J. Am. Chem. Soc.* 1984, **106**, 4683.
14. H. Sugimoto and D. T. Sawyer, *J. Am. Chem. Soc.* 1985, **107**, 5712.
15. T. Yamamoto and M. Kimura, *J. Chem. Soc., Chem. Commun.* 1977, 948.
16. J. T. Groves and M. van der Puy, *J. Am. Chem. Soc.* 1978, **98**, 5290.
17. M. A. Brook, L. Castle, J. R. Lindsay Smith, R. Higgins and K. P. Morris, *J. Chem. Soc., Perkin Trans. II* 1982, 687.
18. D. A. Blackadder and C. Hinshelwood, *J. Chem. Soc.* 1957, 2898.
19. D. A. Blackadder and C. Hinshelwood, *J. Chem. Soc.* 1957, 2904.
20. G. A. Moelwyn-Hughes, *Chemical Statics and Kinetics of Solutions*, p. 340. Academic Press, New York (1971).
21. H. Lineweaver and D. Burke, *J. Am. Chem. Soc.* 1934, **56**, 658.
22. D. F. Evans, *J. Chem. Soc.* 1959, 1003.
23. R. M. Golding, K. F. Mok and J. F. Duncan, *Inorg. Chem.* 1966, **5**, 774.
24. J. Lewis, F. E. Mabbs and A. Richards, *J. Chem. Soc. (A)*, 1967, 1014; A. B. Hoffman, D. M. Collins, V. W. Day, E. B. Fleischer, T. S. Srivastava and J. L. Hoard, *J. Am. Chem. Soc.* 1972, **94**, 3620.
25. F. A. Cotton and G. Wilkinson, *Advanced Inorganic Chemistry*, p. 1320. Wiley-Interscience, Chichester (1980).
26. D. H. R. Barton, M. J. Grastiger and W. B. Motherwell, *J. Chem. Soc., Chem. Commun.* 1983, 731.
27. H. S. Dunsmore and J. C. Speakman, *Trans. Farad. Soc.* 1954, 236.
28. J. T. Groves and T. E. Nemo, *J. Am. Chem. Soc.* 1983, **105**, 6243.
29. H. Mimoun. L. Sanssine, E. Daise, M. Postel, J.

Fischer and R. Weiss, *J. Am. Chem. Soc.* 1983, **105**, 3101.
30. B. C. Gilbert, R. O. C. Norman and R. C. Sealey, *J. Chem. Soc., Perkin Trans. II* 1975, 303.
31. D. H. R. Barton, J. Boivin, W. B. Motherwell, N. Ozbalik and K. M. Schwattzentruber, *Nouv. J. Chim.* 1986, **10**, 387.
32. E. L. Muetterties, B. A. Sosinsky and K. I. Zamaraev, *J. Am. Chem. Soc.* 1975, **97**, 5299.
33. G. J. Long, D. L. Whitney and J. E. Kennedy, *Inorg. Chem.* 1971, **10**, 1406.
34. F. Basolo and F. P. Dwyer, *J. Am. Chem. Soc.* 1954, **76**, 1454.
35. J. E. Fergusson and G. M. Harris, *J. Chem. Soc.* (*A*) 1966, 1293.
36. R. F. Heck and C. R. Boss, *J. Am. Chem. Soc.* 1964, **86**, 2580.
37. A. I. Vogel, *A Textbook of Practical Organic Chemistry*, 3rd Edn, p. 632. Longmans, London (1956).
38. A. I. Vogel, *A Textbook of Practical Organic Chemistry*, 3rd Edn, p. 541. Longmans, London (1956).
39. J. C. Craig and K. K. Purushothaman, *J. Org. Chem.* 1970, **35**, 1721.

Polyhedron Vol. 7, No. 6, pp. 439–442, 1988
Printed in Great Britain

0277–5387/88 $3.00+.00
© 1988 Pergamon Press plc

COORDINATION COMPOUNDS OF 2,6-DIACETYLPYRIDINEDIHYDRAZONE—II. PREPARATION AND CHARACTERIZATION OF THE COMPLEXES WITH HEAVIER LANTHANIDE CHLORIDES, PERCHLORATES AND NITRATES*

WANDA RADECKA-PARYZEK,† EWA JANKOWSKA and EMILIA LUKS

Faculty of Chemistry, Adam Mickiewicz University, 60780, Poznań, Poland

(*Received* 11 *September* 1987; *accepted* 5 *October* 1987)

Abstract—The Tb, Dy, Ho, Er, Tm, Yb and Lu (Ln) complexes of 2,6-diacetylpyridinedihydrazone (L) with chlorides, perchlorates and nitrates as counterions have been prepared and characterized by spectral data, thermal and elemental analysis. They are formulated as $[LnL_2(H_2O)_2]Cl_3 \cdot 2H_2O$, $[LnL_2(H_2O)_2] \cdot (ClO_4)_3 \cdot 2H_2O$ and $[LnL(NO_3)_3(H_2O)_2] \cdot 2H_2O$. The hydrazone acts as a terdentate NNN donor ligand and the nitrates appear to coordinate in the monodentate fashion.

Due to the physiological activity, chelating capability and analytical application of hydrazones, and continuing our studies on the complexes of lanthanides with acyclic and macrocyclic nitrogen donor ligands, we describe here the preparation and characterization of the complexes of heavier lanthanide (Tb–Lu) chlorides, perchlorates and nitrates with 2,6-diacetylpyridinedihydrazone. In Part I in the series we reported the synthesis and properties of the lighter lanthanide (La–Gd) complexes of this ligand.[1]

EXPERIMENTAL

The preparation of the lanthanide salts and 2,6-diacetylpyridinehydrazone (L) was described earlier.[1,2]

The Tb, Dy, Ho, Er, Tm, Yb and Lu complexes of L were synthesized by direct reaction of the metal chlorides, perchlorates or nitrates with the ligand in ethanol, in the M : L ratios 1 : 1, 1 : 2, 1 : 3 or 1 : 4 according to the procedure of a previous paper.[1]

The IR spectra were recorded using CsI pellets in the range 4000–200 cm^{-1} on a Perkin–Elmer 580 IR spectrophotometer. The electronic spectra were measured on a Beckman 25 spectrophotometer. The NMR spectra were run on a Varian EM-360 60 MHz spectrometer for solutions in DMSO–d_6 using TMS as an internal standard. Thermogravimetric measurements were performed using the Derivatograph OD-102, MOM.

RESULTS AND DISCUSSION

From the reaction of chlorides and perchlorates of Tb, Dy, Ho, Er, Tm, Yb and Lu with 2,6-diacetylpyridinedihydrazone, the yellow air stable complexes with the metal to ligand stoichiometries of 1 : 2 were isolated irrespective of the molar proportions of starting materials. With the small but strongly coordinating nitrates as counterions all heavier lanthanides form 1 : 1 complexes. All the complexes are appreciably soluble in DMSO and slightly soluble in acetonitrile.

The stoichiometry and the mode of coordination in the complexes were deduced by means of elemental and thermal analysis and spectral data (IR, UV-vis and ^1H NMR). Table 1 reports the results of elemental analysis of the complexes.

The IR spectra of the complexes (Tables 2 and 3) in the region 4000–200 cm^{-1} are analysed in comparison with that of the free ligand. This data gives evidence for the coordination of 2,6-diacetyl-

* Presented in part at the 2nd International Conference on the Basic and Applied Chemistry of *f*-Transition (Lanthanide and Actinide) and Related Elements, Lisboa, Portugal, 6–10 April, 1987. For Part I see ref. 1.

† Author to whom correspondence should be addressed.

Table 1. Analytical data for the lanthanide complexes of 2,6-diacetylpyridinedihydrazone (L)

Compound	Calculated %C	%H	%N	Found %C	%H	%N
$[TbL_2(H_2O)_2]Cl_3 \cdot 2H_2O$	30.0	4.8	19.5	30.1	4.7	19.6
$[TbL_2(H_2O)_2](ClO_4)_3 \cdot 2H_2O$	23.7	3.8	15.4	23.9	3.7	15.3
$[TbL(NO_3)_3(H_2O)_2] \cdot 2H_2O$	17.8	3.5	18.4	17.5	3.5	18.3
$[DyL_2(H_2O)_2]Cl_3 \cdot 2H_2O$	29.9	4.7	19.4	29.8	4.7	19.3
$[DyL_2(H_2O)_2](ClO_4)_3 \cdot 2H_2O$	23.6	3.7	15.3	23.8	3.8	15.4
$[DyL(NO_3)_3(H_2O)_2] \cdot 2H_2O$	17.7	3.5	18.3	17.8	3.5	18.4
$[HoL_2(H_2O)_2]Cl_3 \cdot 2H_2O$	29.8	4.7	19.3	30.0	4.7	19.5
$[HoL_2(H_2O)_2](ClO_4)_3 \cdot 2H_2O$	23.6	3.7	15.3	23.4	3.7	15.3
$[HoL(NO_3)_3(H_2O)_2] \cdot 2H_2O$	17.6	3.4	18.2	17.6	3.4	18.3
$[ErL_2(H_2O)_2]Cl_3 \cdot 2H_2O$	29.7	4.7	19.2	29.8	4.6	19.2
$[ErL_2(H_2O)_2](ClO_4)_3 \cdot 2H_2O$	23.5	3.7	15.2	23.4	3.6	15.2
$[ErL(NO_3)_3(H_2O)_2] \cdot 2H_2O$	17.5	3.4	18.2	17.4	3.8	18.1
$[TmL_2(H_2O)_2]Cl_3 \cdot 2H_2O$	29.6	4.7	19.2	29.5	4.6	19.1
$[TmL_2(H_2O)_2](ClO_4)_3 \cdot 2H_2O$	23.4	3.7	15.2	23.3	3.6	15.1
$[TmL(NO_3)_3(H_2O)_2] \cdot 2H_2O$	17.5	3.4	18.1	17.4	3.3	18.0
$[YbL_2(H_2O)_2]Cl_3 \cdot 2H_2O$	29.5	4.7	19.1	29.3	4.5	19.0
$[YbL_2(H_2O)_2](ClO_4)_3 \cdot 2H_2O$	23.3	3.7	15.1	23.3	3.6	15.2
$[YbL(NO_3)_3(H_2O)_2] \cdot 2H_2O$	17.4	3.4	18.0	17.4	3.5	18.1
$[LuL_2(H_2O)_2]Cl_3 \cdot 2H_2O$	29.4	4.7	19.0	29.3	4.5	18.9
$[LuL_2(H_2O)_2](ClO_4)_3 \cdot 2H_2O$	23.3	3.7	15.1	23.4	3.8	15.2
$[LuL(NO_3)_3(H_2O)_2] \cdot 2H_2O$	17.3	3.4	17.9	17.3	3.4	17.9

pyridinedihydrazone to the metal ion via three nitrogen donor atoms. The $\nu C{=}N$ absorption band observed in the spectrum of the ligand at 1600 cm^{-1} is shifted by 40–60 cm^{-1} to lower wavenumbers resulting from a decrease in the C=N double bond strength owing to coordination by the nitrogen atom. Bonding of the pyridine nitrogen is shown by the increase in frequency of the higher and lower energy pyridine ring vibrations by about 20–65 cm^{-1} in the complexes, relative to the ligand. The significant change in the ligand bands upon coordination is the increase in N—N frequency. The band at 1150 cm^{-1} assigned to the νN—N of the ligand is shifted by about 50 cm^{-1} to higher values in the spectra of all the complexes. Such movements of this band are observed in the complexes of other N—N bonded ligands and may be explained by the coordination of one of the nitrogen atoms from each N—N bond to the metal ion. This causes the reduction of the lone pair–lone pair repulsive forces in the adjacent nitrogen atoms.[3–6]

The shift of the bands at 3360 and 3200 cm^{-1} assignable to antisymmetric and symmetric stretching vibrations of the NH_2 groups in the free ligand, to a higher frequency region in metal complexes, and the unchanged position of the band observed at 1635 cm^{-1}, further confirms the nonbonding of the NH_2 nitrogen atoms.

Comparison of the far-IR spectra of all the complexes with the spectrum of the uncoordinated ligand and of the lighter lanthanide complexes[1] allows a tentative assignment of the weak absorption band in the region 375–392 cm^{-1} to the metal–nitrogen stretching vibration.

The IR spectra of all the complexes exhibit a broad band of medium intensity in the 3600–3500 cm^{-1} region which is usually assigned to OH stretching modes for lattice water. In addition, the absorption bands observed at *ca* 3380 and at 915–850 cm^{-1} indicate that the water coordinated to the metal ion is also present.[7] This is confirmed by the results of the thermogravimetric analysis. All the complexes were found to lose two lattice water molecules below 100°C and two molecules at 160–180°C.

Information about the bonding mode of the anions in these complexes may also be obtained from IR spectra. The Ln—Cl frequency usually occurs around 240–220 cm^{-1}.[8,9] The spectra of the chloride complexes do not show any additional absorption bands in this region indicating the absence of coordinated chloride anions. Infrared absorption attributable to the ClO_4^- anions occurs as unsplit bands at *ca* 1100 and 625 cm^{-1} in the spectra of the perchlorate complexes, as expected for these anions in the ionic state. Perchlorate anions are known to coordinate under special conditions, but such an interaction normally manifests

Table 2. Infrared (cm^{-1}) and electronic (nm) spectral data for 2,6-diacetylpyridinedihydrazone (L) and its complexes with lanthanide chlorides and perchlorates

Compound	OH	NH_2	C=N	py	N—N	ClO_4^-	M—N	λ
L		3360, 3200, 1635	1600	1570, 950, 640, 400	1150			275
$[TbL_2(H_2O)_2]Cl_3 \cdot 2H_2O$	3500, 890	3410, 3300, 3210, 1640	1550	1590, 975, 670, 445	1195		375	288, 360
$[TbL_2(H_2O)_2](ClO_4)_3 \cdot 2H_2O$	3510, 870	3400, 3330, 3200, 1638	1550	1590, 980, 675, 450	1195	1100, 620	375	287, 357
$[DyL_2(H_2O)_2]Cl_3 \cdot 2H_2O$	3510, 870	3410, 3300, 3205, 1638	1545	1595, 985, 675, 450	1195		380	286, 359
$[DyL_2(H_2O)_2](ClO_4)_3 \cdot 2H_2O$	3510, 870	3390, 3330, 3200, 1635	1545	1598, 980, 675, 455	1200	1100, 620	380	287, 360
$[HoL_2(H_2O)_2]Cl_3 \cdot 2H_2O$	3500, 915	3420, 3290, 3200, 1635	1540	1590, 970, 675, 450	1200		380	287, 360
$[HoL_2(H_2O)_2](ClO_4)_3 \cdot 2H_2O$	3510, 890	3420, 3295, 3210, 1640	1540	1590, 980, 640, 450	1200	1100, 625	375	287, 360
$[ErL_2(H_2O)_2]Cl_3 \cdot 2H_2O$	3500, 890	3405, 3300, 3205, 1635	1545	1595, 985, 675, 455	1205		375	285, 357
$[ErL_2(H_2O)_2](ClO_4)_3 \cdot 2H_2O$	3500, 890	3420, 3290, 3205, 1635	1545	1595, 980, 670, 450	1205	1095, 620	375	287, 360
$[TmL_2(H_2O)_2]Cl_3 \cdot 2H_2O$	3520, 870	3400, 3320, 3210, 1635	1550	1595, 980, 670, 460	1205		380	288, 360
$[TmL_2(H_2O)_2](ClO_4)_3 \cdot 2H_2O$	3520, 870	3380, 3300, 3200, 1640	1550	1590, 990, 675, 460	1205	1095, 625	385	287, 360
$[YbL_2(H_2O)_2]Cl_3 \cdot 2H_2O$	3510, 910	3360, 3300, 3200, 1640	1560	1590, 990, 670, 465	1200		375	287, 358
$[YbL_2(H_2O)_2](ClO_4)_3 \cdot 2H_2O$	3520, 890	3380, 3320, 3200, 1640	1550	1595, 990, 675, 460	1205	1100, 620	377	287, 358
$[LuL_2(H_2O)_2]Cl_3 \cdot 2H_2O$	3520, 870	3390, 3330, 3205, 1635	1550	1595, 985, 675, 455	1205		385	287, 360
$[LuL_2(H_2O)_2](ClO_4)_3 \cdot 2H_2O$	3520, 870	3400, 3305, 3210, 1635	1545	1590, 985, 675, 455	1200	1100, 625	385	287, 360

itself by a splitting of the antisymmetric Cl—O stretching mode due to the reduced symmetry of the coordinated species.[10] No such splitting of the ClO_4 absorption band at 1100 cm^{-1} was observed.

The IR spectra of all the nitrate complexes demonstrates the presence of coordinated nitrates. The bands characteristic of ionic nitrates at 1390 and 830 cm^{-1} are absent. The splitting and magnitude of separation of the vibrational modes in the 1800–1700 cm^{-1} and 1500–1280 cm^{-1} regions has been used as a criterion to distinguish between monodentate and bidentate coordination of nitrates.[1,10-12] In the Tb–Lu complexes of 2,6-diacetylpyridinedihydrazone, the separation of the combination frequencies in the 1800–1700 cm^{-1} region is about 20 cm^{-1}. The two bands associated with the asymmetric stretch appear near 1455 and 1310 cm^{-1}. The magnitude of these separations along with the appearance of the bands at 1035 and 815 cm^{-1} is indicative of the interaction of the oxygen atom from the nitrates with the lanthanide ions, and gives evidence for chelating monodentate behaviour of the nitrate groups in these complexes.

The electronic spectra of the lanthanide complexes of 2,6-diacetylpyridinedihydrazone (Tables 2 and 3) taken in the range 220–700 nm for a solution in acetonitrile consist of two bands at 277–288 and 342–360 nm, respectively. The differences in the spectra of the complexes and free ligand can be attributed to the metal–ligand interaction.

Further evidence for the coordination of the azomethine and pyridine nitrogen atoms arises from comparison of the ^1H NMR spectra of 2,6-diacetylpyridinedihydrazone and its diamagnetic complex of luthetium nitrate. A small downfield shift of the methyl and pyridine proton resonances from δ 2.25 and 7.82, respectively, in the free ligand to δ 2.32 and 8.05 in the complex indicates the bonding mode discussed above.

On the basis of available evidence it seems reasonable to conclude that in the lanthanide complexes the 2,6-diacetylpyridinedihydrazone coordinates in the terdentate NNN donor fashion. The tentative coordination number of eight is assigned to all heavier lanthanide complexes, but the stoichiometry and filling of the coordination sphere depends on the type of counterions.

The Tb–Lu chlorides and perchlorates form the 2,6-diacetylpyridinedihydrazone complexes with metal to ligand stoichiometry equal to 1:2 and incorporating two water molecules in the coordination sphere. There is no evidence for the coordination of chloride and perchlorate ions with lanthanides in these complexes. For lighter lanthanide (La–Gd) chlorides and perchlorates, the tentative

Table 3. Infrared (cm^{-1}) and electronic (nm) spectral data for complexes of L with lanthanide nitrates

Complexes	OH	NH_2	C=N	py	N—N	NO_3^-	M—N	λ
$[TbL(NO_3)_3(H_2O)_2]\cdot 2H_2O$	3560, 3380, 850	3422, 3310, 3240, 1635	1550	1595, 1010, 678, 430	1205	1765, 1740, 1450, 1305, 1030, 817	380	277, 342
$[DyL(NO_3)_3(H_2O)_2]\cdot 2H_2O$	3560, 3380, 850	3420, 3310, 3240, 1635	1550	1595, 1010, 675, 430	1205	1765, 1740, 1450, 1310, 1030, 815	380	277, 346
$[HoL(NO_3)_3(H_2O)_2]\cdot 2H_2O$	3560, 3380, 850	3415, 3310, 3243, 1635	1545	1595, 1010, 675, 435	1200	1760, 1740, 1455, 1315, 1030, 815	385	277, 346
$[ErL(NO_3)_3(H_2O)_2]\cdot 2H_2O$	3565, 3380, 845	3415, 3310, 3240, 1635	1545	1595, 1008, 675, 430	1190	1765, 1740, 1455, 1310, 1030, 813	387	277, 351
$[TmL(NO_3)_3(H_2O)_2]\cdot 2H_2O$	3570, 3385, 855	3420, 3310, 3240, 1635	1550	1595, 1005, 680, 435	1200	1765, 1745, 1450, 1310, 1030, 818	390	277, 350
$[YbL(NO_3)_3(H_2O)_2]\cdot 2H_2O$	3570, 3385, 855	3422, 3310, 3238, 1635	1555	1590, 1010, 680, 440	1210	1765, 1745, 1450, 1315, 1035, 815	390	277, 348
$[LuL(NO_3)_3(H_2O)_2]\cdot 2H_2O$	3570, 3385, 860	3420, 3310, 3340, 1635	1550	1595, 1010, 675, 445	1200	1765, 1745, 1455, 1310, 1035, 815	392	277, 350

coordination number of nine was assigned assuming the coordination sphere was filled by two molecules of hydrazone and three water molecules (La–Gd), and by one ligand and six water molecules (La).[1]

With nitrates as counterions the heavier lanthanides yield complexes with a 1 : 1 metal to ligand ratio. The coordination sphere of the trivalent lanthanide ions in these complexes is filled by three nitrate groups coordinating in the monodentate fashion and two water molecules. These findings contrast with those reported earlier for lighter (La–Gd) lanthanide nitrate complexes of 2,6-diacetylpyridinedihydrazone, which appeared to have a metal to hydrazone stoichiometry of 1 : 2 and the tentative coordination number of twelve (La, Ce, Pr, Nd) or ten (Sm, Eu, Gd) depending on the nitrate mode of binding (bidentate or monodentate).[1]

The decrease in coordination number through the series of La–Lu complexes is clearly a consequence of the decrease in ionic radii due to the lanthanide contraction.

The results discussed in this paper along with our earlier findings lead to the conclusion that the final geometry around the lanthanide ions depends not only on the chelating behaviour of the organic ligand involved in the coordination, but also on the complexing properties of the counterions.

Acknowledgement—Financial support from the Polish Academy of Sciences (Project CPBP No. 01.12.4.18) is gratefully acknowledged.

REFERENCES

1. W. Radecka-Paryzek and Ewa Jankowska, *Inorg. Chim. Acta* 1987, **134**, 179.
2. W. Radecka-Paryzek, *Inorg. Chim. Acta* 1981, **52**, 261.
3. D. N. Sathyanarayana and D. Nicholls, *Spectrochim. Acta* 1978, **34A**, 263.
4. D. Demertzi and D. Nicholls, *Inorg. Chim. Acta* 1983, **73**, 37.
5. M. R. Harrison and D. Nicholls, *Transition Met. Chem.* 1984, **9**, 144.
6. S. P. Perlepes, D. Nicholls and M. R. Harrison, *Inorg. Chim. Acta* 1985, **102**, 137.
7. L. S. Gelfand, F. J. Iaconianni, L. L. Pytlewski, A. N. Speca, C. M. Mikulski and N. M. Karayannis, *J. Inorg. Nucl. Chem.* 1980, **42**, 377.
8. J.-C. G. Bünzli and D. Wessner, *Inorg. Chim. Acta* 1980, **44**, L55.
9. S. P. Perlepes and A. G. Galinos, *J. Less-Common Met.* 1984, **96**, 69.
10. J.-C. G. Bünzli, D. Wessner and Huynh Thi Tham Oanh, *Inorg. Chim. Acta* 1979, **32**, L33.
11. W. Radecka-Paryzek, *Inorg. Chim. Acta* 1985, **109**, L21.
12. J.-C. G. Bünzli, G. A. Leonard, D. Plancherel and G. Chapuis, *Helv. Chim. Acta* 1986, **60**, 288.

Polyhedron Vol. 7, No. 6, pp. 443–448, 1988
Printed in Great Britain

0277–5387/88 $3.00+.00
© 1988 Pergamon Press plc

SYNTHESIS OF THE COMPOUNDS $[Re(\equiv CR)(CO)_2(\eta^5\text{-}C_9H_7)][BF_4]$ ($R = C_6H_4Me\text{-}4$ OR $C_6H_3Me_2\text{-}2,6$) AND THE PREPARATION OF COMPLEXES WITH Fe—Re BONDS

DANIEL MIGUEL, UWE STEFFAN and F. GORDON A. STONE*

Department of Inorganic Chemistry, The University of Bristol, Bristol BS8 1TS, U.K.

(*Received* 21 *September* 1987; *accepted* 5 *October* 1987)

Abstract—The salts $[Re(\equiv CR)CO)_2(\eta^5\text{-}C_9H_7)][BF_4]$ [R = C_6H_4Me-4 or C_6H_3Me-2,6; η^5-C_9H_7 = indenyl] have been prepared and used to synthesize the dimetal compounds $[FeRe(\mu\text{-}CR)(\mu\text{-}NO)(CO)_4(\eta^5\text{-}C_9H_7)]$. The iron–rhenium species containing a bridging *p*-tolylmethylidyne ligands react with $[Fe_2(CO)_9]$ or with $[Ru(CO)_4(\eta\text{-}C_2H_4)]$, respectively, to yield the trimetal compounds $([FeMRe(\mu_3\text{-}CC_6H_4Me\text{-}4)(\mu\text{-}CO)(\mu\text{-}NO)(CO)_6(\eta^5\text{-}C_9H_7)]$ (M = Fe or Ru).

Certain compounds containing carbon-to-metal triple bonds readily add low-valent metal fragments to form stable complexes in which alkylidyne groups span linkages between dissimilar transition elements (see Scheme 1).[1] Using this synthetic methodology we have earlier shown[2] that the rhenium salt $[Re(\equiv CC_6H_4Me\text{-}4)(CO)_2(\eta\text{-}C_5H_5)][BF_4]$ (**1a**) reacts with $[Pt(PMe_2Ph)_2(\eta\text{-}C_2H_4)]$ to give

$[(L)(OC)_2R \equiv CR][BF_4]$

	R	L
(**1a**)	C_6H_4Me-4	η-C_5H_5
(**1b**)	C_6H_4Me-4	η^5-C_9H_7
(**1c**)	$C_6H_3Me_2$-2,6	η^5-C_9H_7

the dimetal complex $[RePt(\mu\text{-}CC_6H_4Me\text{-}4)(CO)_2(PMe_2Ph)_2(\eta\text{-}C_5H_5)][BF_4]$ (**2**). In other studies[3] the

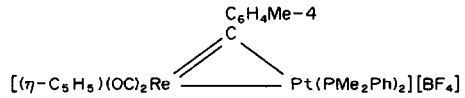

(**2**)

μ-ketenyl complex $[MnRe\{\mu\text{-}C(C_6H_4Me\text{-}4)CO\}(CO)_6(\eta\text{-}C_5H_5)]$ (**3a**) was obtained from the reaction between (**1a**) and $[N(PPh_3)_2][Mn(CO)_5]$, while

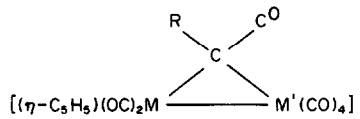

	R	M	M'
(**3a**)	C_6H_4Me-4	Re	Mn
(**3b**)	Ph	Mn	Re

independently E. O. Fischer and coworkers[4] prepared the related compound (**3b**) from $[Mn(\equiv CPh)(CO)_2(\eta\text{-}C_5H_5)][BCl_4]$ and $Na[Re(CO)_5]$. These results prompted us to to prepare the salts $[Re(\equiv CR)(CO)_2(\eta^5\text{-}C_9H_7)][BF_4]$ (R = C_6H_4Me-4 (**1b**) or $C_6H_3Me_2$-2,6 (**1c**); η^5-C_9H_7 = indenyl], and to investigate some reactions of these species with anionic carbonyl–metal complexes. The ability of the idenyl ligand to influence substitution reactions at metal centres is well established,[5] and it was thought that the presence of the η^5-C_9H_7 group in the salts (**1b**) and (**1c**) would lead to different results from those previously obtained with (**1a**).

RESULTS AND DISCUSSION

In order to prepare (**1b**) and (**1c**), the compound $[Re(CO)_3(\eta^5\text{-}C_9H_7)]$ was required as a precursor. Indenyl (tricarbonyl)rhenium was first reported by Fischer and Fellmann,[6] who obtained the complex

*Author to whom correspondence should be addressed.

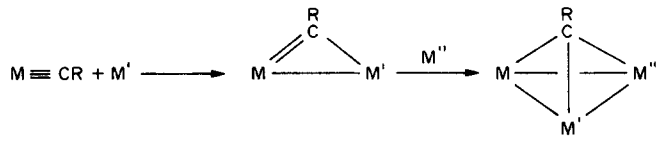

Scheme 1. Ligands on metal atoms have been omitted for clarity. M = Cr, Mo, W, Mn, or Re, while M′ and M″ can be a transition element, or Cu or Au.

by treating $[ReCl(CO)_5]$ with NaC_9H_7. We prepared the desired compound in virtually quantitative yield by refluxing $[Re_2(CO)_{10}]$ in indene, as described in the Experimental Section. Indenyl(tricarbonyl) rhenium was then used to prepare the new alkylidene–rhenium complexes $[Re\{=C(OR')R\}(CO)_2(\eta^5\text{-}C_9H_7)]$ (R = C_6H_4Me-4, R′ = Me (**4a**) or $SiMe_3$

$[(\eta^5\text{-}C_9H_7)(OC)_2Re{=}C(OR')R]$

	R	R′
(4a)	C_6H_4Me-4	Me
(4b)	C_6H_4Me-4	$SiMe_3$
(4c)	$C_6H_3Me_2$-2,6	$SiMe_3$

(**4b**); R = $C_6H_3Me_2$-2,6, R′ = $SiMe_3$ (**4c**)], employing standard procedures, and the latter were subsequently converted into the salts (**1b**) or (**1c**). Thus treatment of (**4a**) with an excess of $BF_3 \cdot OEt_2$, or (**4b**) with $HBF_4 \cdot OEt_2$ gave (**1b**) in *ca* 80–90% yield. Similarly, (**1c**) was obtained by treating (**4c**) with $HBF_4 \cdot OEt_2$. The alkylidene–rhenium compound (**4c**) is thermally unstable, and it is best if it is immediately converted to (**1c**).

The salts (**1b**) and (**1c**) each show in their IR spectra two strong CO stretching bands [2086 and 2034 cm^{-1} (**1b**); 2083 and 2033 cm^{-1} (**1c**)]. In the $^{13}C\text{-}\{^1H\}$ NMR spectra the two compounds show characteristic signals for the ligated alkylidyne carbon nuclei at δ 319.2 ppm for (**1b**) and at δ 312.0 ppm for (**1c**).

Treatment of (**1b**) with $[N(PPh_3)_2][Mn(CO)_5]$ in tetrahydrofuran failed to yield a complex analogous to (**3a**). Moreover, reaction between $[N(PPh_3)_2][Co(CO)_4]$ and (**1b**) afforded an unstable product which could not be characterized. This contrasts with the reaction between $Na[Co(CO)_4]$ and $[Mn(\equiv CPh)(CO)_2(\eta\text{-}C_5H_4Me)][BCl_4]$ which affords the complex $[CoMn(\mu\text{-}CPh)(CO)_6(\eta\text{-}C_5H_4Me)]$[4] in which the CPh group forms a bridge between the Co and Mn centres, but there is no metal–metal bond. In spite of our inability to isolate stable products from reactions of (**1b**) with the anionic complexes $[Mn(CO)_5]^-$ or $[Co(CO)_4]^-$, we have found that reactions readily occur between (**1b**) or (**1c**) and $[N(PPh_3)_2][Fe(CO)_3(NO)]$ in tetrahydrofuran, affording the dark green dimetal compounds $[FeRe(\mu\text{-}CR)(\mu\text{-}NO)(CO)_4(\eta^5\text{-}C_9H_7)]$ [R = C_6H_4Me-4 (**5a**) or $C_6H_3Me_2$-2,6 (**5b**)].

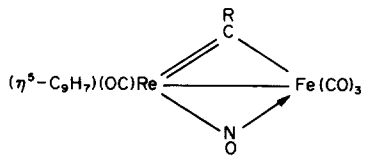

	R
(5a)	C_6H_4Me-4
(5b)	$C_6H_3Me_2$-2,6

Compound (**5a**) decomposes slowly at room temperature, especially in chlorinated solvents. The product (**5b**) is more stable and both complexes were fully characterized spectroscopically. In the IR spectrum of each compound there are four absorptions due to terminal CO groups (see Experimental Section) and a band [1723 cm^{-1} (**5a**), 1706 cm^{-1} (**5b**)] which can be attributed to a bridging NO ligand. The $^{13}C\text{-}\{^1H\}$ NMR data revealed the expected resonances for alkylidyne–carbon groups bridging two metal centres,[7] with signals appearing in the spectra of (**5a**) and (**5b**) at δ 400.7 and 391.8 ppm, respectively.

The compounds (**5**) are examples of a rapidly growing family of dimetal compounds containing dimetallacyclopropene rings, some members of which add metal–ligand fragments to afford trimetal complexes (see Scheme 1). Accordingly, (**5a**) was treated with $[Fe_2(CO)_9]$ in Et_2O, and in this manner the complex $[Fe_2Re(\mu_3\text{-}CC_6H_4Me\text{-}4)(\mu\text{-}CO)(\mu\text{-}NO)(CO)_6(\eta^5\text{-}C_9H_7)]$ (**6a**) was obtained.

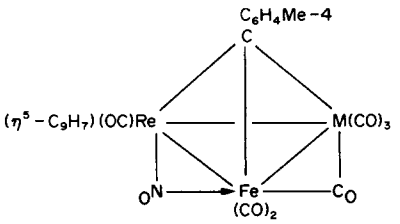

	M
(6a)	Fe
(6b)	Ru

and characterized by microanalysis and by spectroscopic data. Bands in the IR spectrum (see Experimental Section) at 1867 and 1760 cm^{-1} are assigned to bridging or semi-bridging CO, and bridging NO groups, respectively. The $^{13}C\text{-}\{^1H\}$ NMR spectrum shows a characteristic resonance (δ 274.9 ppm) for the μ_3-C nucleus.[8] Compound (**6a**) is related to the previously characterized complexes $[Fe_2M(\mu_3\text{-}CR)(\mu\text{-}CO)(CO)_8(L)]$ (L = $\eta\text{-}C_5H_5$, M = W, R = C_6H_4Me-4 or Me; M = Mo, R = C_6H_4Me-4; L = $\eta\text{-}C_5Me_5$, M = W, R = C_6H_4Me-4)[9,10] and $[N(PPh_3)_2][Fe_2W(\mu_3\text{-}CR)(\mu\text{-}NO)(\mu\text{-}CO)(CO)_6(\eta\text{-}C_5H_5)]$ (R = C_6H_4Me-4 or Me).[11] In their IR spectra these species show CO stretching bands indicative of the presence in solution of more than one diastereoisomer. It is probable that (**6a**) also displays this phenomenon since seven rather than six CO absorptions are observed in the terminal carbonyl region of the spectrum. Interestingly, (**5b**) did not react with $[Fe_2(CO)_9]$ to give a trimetal complex, a result which is probably due to the steric bulk of the $CC_6H_3Me_2$-2,6 ligand preventing addition of an $Fe(CO)_3$ fragment.[12]

The synthesis of (**6a**) suggested that it might be possible to add an $Ru(CO)_3$ fragment to (**5a**) to produce the trimetallatetrahedrane complex $[FeReRu(\mu_3\text{-}CC_6H_4Me\text{-}4)(\mu\text{-}CO)(\mu\text{-}NO)(CO)_6(\eta^5\text{-}C_9H_7)]$ (**6b**). This was successfully accomplished by treating (**5a**) with $[Ru(CO)_4(\eta\text{-}C_2H_4)]$. Compound (**6b**) was fully characterized by microanalysis and spectroscopic data (Experimental Section). It belongs to the interesting class of trimetal complexes in which an alkylidyne group triply bridges three different transition elements. Other examples with R = C_6H_4Me-4 include $[FeCoW(\mu_3\text{-}CR)(\mu\text{-}CO)(CO)_5(\eta\text{-}C_5H_5)(\eta\text{-}C_5Me_5)]$,[13] $[FeRhW(\mu_3\text{-}CR)(\mu\text{-}CO)(CO)_5(\eta\text{-}C_5H_5)(\eta^5\text{-}C_9H_7)]$,[13] $[FePtW(\mu_3\text{-}CR)(CO)_5(PMePh_2)_2(\eta\text{-}C_5H_5)]$,[14] $[CuPtW(\mu_3\text{-}CR)(CO)_2(PMe_3)_2(\eta\text{-}C_5H_5)(\eta\text{-}C_5Me_5)]$,[15] $[AuPtW(\mu_3\text{-}CR)(CO)_2(PMe_3)_3(\eta\text{-}C_5H_5)][PF_6]$,[15] $[FeRhW(\mu_3\text{-}CR)(\mu\text{-}CO)(CO)_5(\eta^5\text{-}C_9H_7)\{HB(pz)_3\}]$ [$HB(pz)_3$ = hydrotris(pyrazol-1-yl)borate][16] and $[MReFe(\mu_3\text{-}CR)(\mu\text{-}CO)(CO)_{11}]$ (M = Cr, Mo or W).[17] Some compounds of this type have also been reported by Vahrenkamp.[18]

EXPERIMENTAL

All experiments were carried out under nitrogen, using Schlenk tube techniques. Solvents were rigorously dried befopre use. Light petroleum refers to that fraction of b.p. 40–60°C. IR spectra were measured with Nicolet MX10 and MX5 FT spectrophotometers, and NMR spectra were recorded with JNM FX 90Q, FX 270 and GX 400 instruments. For NMR data all chemical shifts listed are in ppm and coupling constants are given in Hz. The salt $[N(PPh_3)_2][Fe(CO)_3(NO)]$ was prepared as previously described.[19]

Synthesis of the complex $[Re(CO)_3(\eta^5\text{-}C_9H_7)]$

A mixture of indene (5 cm^3, excess) and $[Re_2(CO)_{10}]$ (5.4 g, 8.28 mmol) was heated under reflux for 4 h. Volatile material was removed *in vacuo*, affording a brown oily residue, which was dissolved in CH_2Cl_2 (20 cm^3) and chomatographed on an alumina column (*ca* 4 × 20 cm). Elution with CH_2Cl_2–light petroleum (1 : 1) gave a yellow eluate. Removal of the solvent *in vacuo* afforded pale yellow *microcrystals* of $[Re(CO)_3(\eta^5\text{-}C_9H_7)]$ (5.73 g, 90%). (Found: C, 37.9; H, 2.0. $C_{12}H_7O_3Re$ requires C, 37.4; H, 1.8%). IR, ν_{max} (CO) at 2030s, 1942vs and 1936vs cm^{-1} (in light petroleum). NMR: ^1H (in $CDCl_3$), δ 5.54 [t, 1 H, C_9H_7, J(HH) 3], 6.97 [d, 2 H, C_9H_7, J(HH) 3] and 7.02–7.47 (m, 4 H, C_9H_7); $^{13}C\text{-}\{^1H\}$ (in CD_2Cl_2–CH_2Cl_2), δ 193.6 (3 × CO), 126.3, 123.7, 108.0, 91.4 and 71.3 (C_9H_7).

Synthesis of alkylidene–rhenium complexes

(i) The compound $[Re(CO)_3(\eta^5\text{-}C_9H_7)]$ (2.0 g, 5.2 mmol) in Et_2O (200 cm^3) was treated dropwise with LiC_4H_4Me-4 (5.2 mmol, 0.7 molar solution in Et_2O), yielding a dark solution of the acyl complex $Li[Re\{C(O)C_6H_4Me\text{-}4\}(CO)_2(\eta^5\text{-}C_9H_7)]$. When all of the $[Re(CO)_3(\eta^5\text{-}C_9H_7)]$ had been consumed (monitored by IR), the solvent was removed *in vacuo* and the residue was washed with light petroleum and dried *in vacuo*. Degassed distilled water (70 cm^3), Et_2O (100 cm^3) and solid $[Me_3O][BF_4]$ (0.88 g, 5.96 mmol) were then added and the mixture stirred for 15 min. The organic layer was decanted and the aqueous layer was extracted with Et_2O (6 × 50 cm^3). The combined extracts and the organic layer were filtered through an anhydrous Na_2SO_4 pad and the solvent was removed *in vacuo*. The brown residue was dissolved in CH_2Cl_2–light petroleum (20 cm^3, 1 : 3) and chromatographed on an alumina column (2 × 20 cm). Elution with the same solvent mixture gave a pale yellow eluate. Removal of the solvent *in vacuo* afforded pale yellow *microcrystals* of $[Re\{C(OMe)C_6H_4Me\text{-}4\}(CO)_2(\eta^5\text{-}C_9H_7)]$ (**4a**) (1.58 g, 62%). (Found: C, 48.8; H, 3.6. $C_{20}H_{17}O_3Re$ requires C, 48.9; H, 3.5%). IR, ν_{max} (CO) at 1964s and 1895s cm^{-1} (in light petroleum). NMR: ^1H (in $CDCl_3$), δ 2.34 (s, 3 H, Me-4), 4.05 (s, 3 H, OMe), 4.77 [t, 1 H, C_9H_7, J(HH) 3], 5.79 [d, 2 H, C_9H_7, J(HH) 3] and 6.87–7.32 (m, 8 H, C_6H_4 and C_9H_7); $^{13}C\text{-}\{^1H\}$ (in CD_2Cl_2–CH_2Cl_2), δ 285.9 [*C*(OMe)

C_6H_4Me-4], 202.7 (2 × CO), 154.9–75.5 (C_6H_4 and C_9H_7), 65.1 (OMe) and 21.3 (Me-4).

(ii) A CH_2Cl_2 (40 cm^3) solution of Li[Re{C(O)C_6H_4Me-4}(CO)$_2(\eta^5$-$C_9H_7)$] (3.1 mmol) was cooled to −78°C and $SiClMe_3$ (0.40 cm^3, 3.2 mmol) at 0°C was added slowly with stirring. The mixture was allowed to warm slowly to room temperature and the solvent was removed *in vacuo*. The orange residue was extracted with Et_2O (3 × 20 cm^3) and the extracts combined and filtered through a Celite pad (2 × 2 cm). Removal of solvent *in vacuo* afforded bright yellow *microcrystals* of [Re{C(OSiMe_3)C_6H_4Me-4}(CO)$_2(\eta^5$-$C_9H_7)$] (**4b**) (1.2 g, 73%). (Found: C, 49.0; H, 4.5. $C_{22}H_{23}O_3$ReSi requires C, 48.1; H, 4.2%). IR, ν_{max} (CO) at 1958s and 1883 cm^{-1} (in CH_2Cl_2). NMR: ^1H (in CD_2Cl_2), δ 0.06 (s, 9 H, $SiMe_3$), 2.27 (s, 3 H, Me-4), 5.38 [t, 1 H, C_9H_7, J(HH) 3], 5.99 [d, 2 H, C_9H_7, J(HH) 3] and 6.96–7.40 (m, 8 H, C_6H_4 and C_9H_7); ^{13}C-{^1H} (in CD_2Cl_2–CH_2Cl_2), δ 284.9 [*C*(OSiMe_3)C_6H_4Me-4], 202.7 (2 × CO), 157.6 [C^1(C_6H_4)], 138.7–75.5 (C_6H_4 and C_9H_7), 21.3 (Me-4) and 1.0 ($SiMe_3$). Complex (**4b**) is thermally unstable and should be stored at *ca* −20°C.

(iii) The compound [Re(CO)$_3(\eta^5$-$C_9H_7)$] (2.0 g, 5.2 mmol) in Et_2O (200 cm^3) was treated dropwise with Li$C_6H_3Me_2$-2,6 (5.2 cm^3 of a 1 molar solution in Et_2O). The solution was stirred (15 min), slowly turning dark red. The solvent was removed *in vacuo* and the residue was washed with light petroleum (3 × 50 cm^3), and then dried *in vacuo* affording yellow *microcrystals* of Li[Re{C(O)$C_6H_3Me_2$-2,6}(CO)$_2(\eta^5$-$C_9H_7)$] (2.2 g, 85%). [ν_{max} (CO) at 1909s and 1812s cm^{-1} (in Et_2O)]. The latter (4.0 mmol) was dissolved in CH_2Cl_2 (40 cm^3), and the solution was cooled to −78°C and $SiClMe_3$ (0.52 cm^3, 4.1 mmol) at 0°C was added. The reactants were slowly warmed to room temperature with stirring. The solvent was removed *in vacuo*, and the dark red residue was extracted with Et_2O (3 × 20 cm^3). The extracts were filtered through a Celite pad (2 × 3 cm). Removal of the solvent afforded orange *microcrystals* of [Re{C(OSiMe_3)$C_6H_3Me_2$-2,6}(CO)$_2(\eta^5$-$C_9H_7)$] (**4c**) (1.7 g, 75%). This complex is very air and temperature sensitive. If storage is necessary it should be kept at low temperatures. It is best used immediately to prepare the salt (**1c**).

Preparation of the salts [Re(≡CR)(CO)$_2(\eta^5$-$C_9H_7)$][BF_4] (R = C_6H_4Me-4 *or* $C_6H_3Me_2$-2,6)

(i) Compound (**4a**) (1.0 g, 2.0 mmol) was dissolved in Et_2O (50 cm^3) and excess of $BF_3 \cdot OEt_2$ (1 cm^3) was slowly added with stirring. After 15 min, the solvent was decanted from the residue, which was then pumped *in vacuo* (30 min) and washed with Et_2O (3 × 50 cm^3) to afford bright yellow *crystals* of [Re(≡CC_6H_4Me-4)(CO)$_2(\eta^5$-$C_9H_7)$][BF_4] (**1b**) (0.97 g, 87%). (Found: C, 41.1; H, 2.8. $C_{19}H_{14}BF_4O_2Re$ requires C, 41.7; H, 2.6%). IR, ν_{max} (CO) at 2086s and 2034s cm^{-1} (in CH_2Cl_2). NMR: ^1H (in $CDCl_3$), δ 2.39 (s, 3 H, Me-4), 6.32 [t, 1 H, C_9H_7, J(HH) 3], 6.94 [d, 2 H, C_9H_7, J(HH) 3] and 7.21–7.85 (m, 8 H, C_6H_4 and C_9H_7); ^{13}C-{^1H} (in CD_2Cl_2–CH_2Cl_2), δ 319.2 (*C*C_6H_4Me-4), 186.4 (2 × CO), 150.3–78.1 (C_6H_4 and C_9H_7) and 23.0 (Me-4).

(ii) Compound (**4c**) (1.0 g, 1.8 mmol) in Et_2O (15 cm^3) was treated with $HBF_4 \cdot OEt_2$ (0.33 cm^3 of a 54% solution in Et_2O) and the mixture was stirred (15 min). The solvent was removed with a syringe and the yellow precipitate was washed with Et_2O (3 × 30 cm^3) and crystallized from CH_2Cl_2–Et_2O (*ca* 20 cm^3, 1:4) to give yellow crystals of [Re(≡$CC_6H_3Me_2$-2,6)(CO)$_2(\eta^5$-$C_9H_7)$][BF_4] (**1c**) (0.86 g, 85%). (Found: C, 41.6; H, 2.9. $C_{20}H_{16}BF_4O_2Re$ requires C, 42.8; H, 2.9%). IR, ν_{max} (CO) at 2083s and 2033s cm^{-1} (in CH_2Cl_2). NMR: ^1H (in CD_2Cl_2), δ 2.64 (s, 6 H, Me-2,6), 6.38 [t, 1 H, C_9H_7, J(HH) 3], 6.94 [d, 2 H, C_9H_7, J(HH) 3], 7.16 [d, 2 H, C_6H_3, J(HH) 8], 7.47–7.53 (m, 2 H, C_9H_7), 7.60 [t, 1 H, C_6H_3, J(HH) 8] and 7.70–7.84 (m, 2 H, C_9H_7); ^{13}C-{^1H} (in CD_2Cl_2–CH_2Cl_2), δ 312.0 (*C*$C_6H_3Me_2$-2,6), 186.5 (CO), 146.2–77.7 (C_6H_3 nd C_9H_7) and 21.0 (Me-2,6).

Compound (**1b**) may be prepared in a similar manner from the alkylidene–rhenium complex (**4b**).

Preparation of iron–rhenium compounds

(i) A mixture of the salts [$N(PPh_3)_2$][Fe(CO)$_3$(NO)] (0.22 g, 0.31 mmol) and (**1b**) (0.12 g, 0.31 mmol) in tetrahydrofuran (10 cm^3) afforded a dark green product. After stirring for 15 min the solvent was removed *in vacuo* and the residue was extracted with Et_2O (3 × 30 cm^3). The extracts were filtered through Celite (2 × 10 cm). Removal of the solvent *in vacuo* gave dark green *microcrystals* of [FeRe(μ-CC_6H_4Me-4)(μ-NO)(CO)$_4$ η^5-$C_9H_7)$] (**5a**) (0.16 g, 85%). The compound was characterized spectroscopically: IR, ν_{max} at 2025s, 1961s, 1949vs, 1904w (CO) and 1723m (NO) cm^{-1} (in Et_2O). NMR: ^1H ($CDCl_3$), δ 2.33 (s, 3 H, Me-4) and 5.93–7.69 (m, 11 H, C_6H_4 and C_9H_7); ^{13}C-{^1H} (CD_2Cl_2–CH_2Cl_2), δ 400.7 (μ-*C*C_6H_4Me-4), 216.8, 200.5, (CO), 156.8–76.6 (C_6H_4 and C_9H_7) and 22.1 (Me-4).

(ii) Similarly, (**1c**) (0.26 g, 0.46 mmol) was treated with [$N(PPh_3)_2$][Fe(CO)$_3$(NO)] (0.35 g, 0.49 mmol) in tetrahydrofuran (10 cm^3) with stirring for 2 h. After removing solvent *in vacuo*, the brown residue was treated with Et_2O (5 cm^3) and chromatographed on a Kieselgel column (2 × 20 cm),

eluting with Et_2O–light petroleum (1 : 5). The first dark eluate was evaporated *in vacuo* and the residue was crystallized from Et_2O–light petroleum (*ca* 10 cm^3, 1 : 10) to give dark green *crystals* of $[FeRe(\mu\text{-}CC_6H_3Me_2\text{-}2,6)(\mu\text{-}NO)(CO_4(\eta^5\text{-}C_9H_7)]$ (**5b**) (0.11 g, 40%). (Found: C,. 43.3; H, 2.9; N, 2.0. $C_{21}H_{16}FeNO_5Re$ requires C, 42.9; H, 2.6; N, 2.3%). IR, ν_{max} at 2025s, 1974s, 1960s, 1891m (CO) and 1706m (NO) cm^{-1} (in Et_2O). NMR: ^1H (in C_6D_6). δ 2.18 (s, 3 H, Me-4), 5.29 (s br, 1 H, C_9H_7), 5.30 (s br, 2 H, C_9H_7) and 6.40–7.30 (m, 11 H, C_6H_4 and C_9H_7); $^{13}C\text{-}\{^1H\}$ (in CD_2Cl_2–CH_2Cl_2), δ 391.8 (μ-CC_6H_4Me-4), 217.8, 201.3 (CO), 154.6 [$C^1(C_6H_3)$], 132.5–101.1 (C_6H_3 and C_9H_7) and 20.4 (Me-2,6).

(iii) Compound (**5a**) (0.50 g, 0.79 mmol) in Et_2O (30 cm^3) was treated with $[Fe_2(CO)_9]$ (0.16 g, 0.44 mmol) and the mixture was stirred. After 15 min, more $[Fe_2(CO)_9]$ (0.30 g, 0.83 mmol) was added and the mixture was stirred for a further 2 h. If after this period the IR spectrum shows peaks due to (**5a**), more $[Fe_2(CO)_9]$ should be added and stirring continued. The solvent was removed *in vacuo* and the residue was dissolved in Et_2O–light petroleum (8 cm^3, 1 : 1) and chromatographed on an alumina column (2 × 10 cm), eluting with the same solvent mixture. The first dark eluate was recovered and the solvent was removed *in vacuo* to give black *microcrystals* of $[Fe_2Re(\mu_3\text{-}CC_6H_4Me\text{-}4)(\mu\text{-}CO)(\mu\text{-}NO)(CO)_6(\eta^5\text{-}C_9H_7)]$ (**6a**) (0.28 g, 47%). (Found: C, 39.0; H, 2.1; N, 1.9. $C_{24}H_{14}Fe_2NO_8Re$ requires C, 38.8; H, 1.9; N, 1.9%). IR, ν_{max} at 2061s, 2055s, 2022vs, 2000s, 1979m, 1957m, 1926m, 1867m (CO) and 1760m (NO) cm^{-1} (in Et_2O). NMR: ^1H (in CD_2Cl_2), δ 2.49 (s, 3 H, Me-4), 5.53 [t, 1 H, C_9H_7, J(HH) 3], 5.77 [d, 2 H, C_9H_7, J(HH) 3], 6.95–7.30 (m, 4 H, C_9H_7) and 7.45–7.55 (m, 4 H, C_6H_4); $^{13}C\text{-}\{^1H\}$ (in CD_2Cl_2–CH_2Cl_2), δ 274.9 (μ_3-C), 214.3, 212.3, 210.9, 209.9, 202.7 (CO), 159.9 [$C^1(C_6H_4)$], 138.0–77.5 (C_6H_4 and C_9H_7) and 21.2 (Me-4).

(iv) The compound $[Ru_3(CO)_{12}]$ (0.07 g, 0.11 mmol) dissolved in light petroleum (150 cm^3) in a water cooled Schlenk tube (*ca* 10°C), was treated with a slow stream of C_2H_4, while the reaction vessel was exposed for 12 h to light from two 250 watt light bulbs. This procedure affords a colourless solution of $[Ru(CO)_4(\eta\text{-}C_2H_4)]$. The Schlenk tube was then cooled to *ca* −78°C and (**5b**) (0.20 g, 0.32 mmol) dissolved in toluene (20 cm^3) was slowly added. The mixture was allowed to warm to *ca* −30°C and stirred for 5 h. The dissolved C_2H_4 was removed by pumping and stirring was continued until all the $[Ru(CO)_4(\eta\text{-}C_2H_4)]$ had been consumed (monitored by IR). The Schlenk tube was then warmed to *ca* 15°C and all the volatile material was removed *in vacuo*. The dark residue in Et_2O (10 cm^3) was chromatographed on a Kieselgel column (3 × 30 cm, cooled to *ca* 10°C). Elution of the column with Et_2O–light petroleum (1 : 5) removed initially some $[Ru_3(CO)_{12}]$ followed by a brown eluate. The solvent was removed *in vacuo* from the latter and the residue crystallized from Et_2O–light petroleum (*ca* 10 cm^3, 1 : 6) at −78°C to give black *crystals* of $[FeReRu(\mu_3\text{-}C_6H_4Me\text{-}4)(\mu\text{-}CO)(\mu\text{-}NO)(CO)_6(\eta^5\text{-}C_9H_7)]$ (**6b**) (0.09 g, 34%). (Found: C, 38.0; H, 2.0; N, 1.8. $C_{24}H_{14}FeNO_8ReRu$ requires C, 36.6; H, 1.8; N, 1.8%). IR, ν_{max} at 2071s, 2025s, 2009s, 1973m, 1928m, 1911m, 1854m (CO) and 1756m (NO) cm^{-1} (in Et_2O). NMR: ^1H (in CD_2Cl_2), δ 2.47 (s, 3 H, Me-4), 5.42 (s br, 1 H, C_9H_7), 5.82 (s br, 2 H, C_9H_7) and 6.80–7.52 (m br, C_6H_4 and C_9H_7); $^{13}C\text{-}\{^1H\}$, (in CD_2Cl_2–CH_2Cl_2), δ 257.8 (μ_3-C), 217.8, 211.8, 208.5, 204.4, 195.9 (CO), 160.3 [$C^1(C_6H_4)$], 137.5–77.3 (C_6H_4 and C_9H_7) and 21.2 (Me-4).

REFERENCES

1. F. G. A. Stone, *Pure Appl. Chem.* 1986, **58**, 529; Inorganic Chemistry: Toward the 21st Century (Edited by M. H. Chisholm) *ACS Symp. Ser.* 1983, **211**, 383.
2. J. A. K. Howard, J. C. Jeffery, M. Laguna, R, Navarro and F. G. A. Stone, *J. Chem. Soc., Dalton Trans.* 1981, 751.
3. J. Martin-Gil, J. A. K. Howard, R. Navarro and F. G. A. Stone, *J. Chem. Soc., Chem. Commun.* 1979, 1168.
4. O. Orama, U. Schubert, F. R. Kreissl and E. O. Fischer, *Z. Naturforsch., Teil B* 1980, **35**, 82; E. O. Fischer, J. K. R. Wanner, G. Müller and J. Riede, *Chem. Ber.* 1985, **118**, 3311.
5. J. M. O'Connor and C. P. Casey, *Chem. Rev.* 1987, **87**, 307.
6. E. O. Fischer and W. Fellmann, *J. Organomet. Chem.* 1963, **1**, 191.
7. J. A. Abad, L. W. Bateman, J. C. Jeffery, K. A. Mead, H. Razay, F. G. A. Stone and P. Woodward, *J. Chem. Soc., Dalton Trans.* 1983, 2075.
8. J. A. Abad, E. Delgado, M. E. Garcia, M. J. Grosse-Ophoff, I. J. Hart, J. C. Jeffery, M. S. Simmons and F. G. A. Stone, *J. Chem. Soc., Dalton Trans.* 1987, 41.
9. L. Busetto, J. C. Jeffery, R. M. Mills, F. G. A. Stone, M. J. Went and P. Woodward. *J. Chem. Soc., Dalton Trans.* 1983, 101; E. Delgado, A. T. Emo, J. C. Jeffery, N. D. Simmons and F. G. A. Stone, *ibid* 1985, 1323; E. Delgado, J. Hein, J. C. Jeffery, A. L. Ratermann, F. G. A. Stone and L. J. Farrugia, *ibid* 1987, 1191.
10. M. E. Garcia, J. C. Jeffery, P. Sherwood and F. G. A. Stone, *J. Chem. Soc., Dalton Trans.* 1987, 1209.
11. E. Delgado, J. C. Jeffery, N. D. Simmons and F. G. A. Stone, *J. Chem. Soc., Dalton Trans.* 1986, 869.
12. F.-E. Baumann, J. A. K. Howard, R. J. Musgrove,

P. Sherwood and F. G. A. Stone, *J. Chem. Soc., Dalton Trans.* in press.
13. M. Green, J. C. Jeffery, S. J. Porter, H. Razay and F. G. A. Stone, *J. Chem. Soc., Dalton Trans.* 1982, 2475.
14. M. J. Chetcuti, J. A. K. Howard, R. M. Mills, F. G. A. Stone and P. Woodward, *J. Chem. Soc., Dalton Trans.* 1982, 1757.
15. G. A. Carriedo, J. C. Jeffery and F. G. A. Stone, *J. Chem. Soc., Dalton Trans.* 1984, 1555; *ibid* 2545.
16. M. Green, J. A. K. Howard, A. P. James, C. M. Nunn and F. G. A. Stone, *J. Chem. Soc., Dalton Trans.* 1986, 187.
17. D. G. Evans, J. A. K. Howard, J. C. Jeffery, D. B. Lewis, G. E. Lewis, M. J. Grosse-Ophoff, M. J. Parrott and F. G. A. Stone, *J. Chem. Soc., Dalton Trans.* 1986, 1723.
18. H. Vahrenkamp, *Adv. Organomet. Chem.* 1983, **22**, 169; D. Mani and H. Vahrenkamp, *Chem. Ber.* 1986, **119**, 3639 and refs cited therein.
19. R. E. Stevens, T. J. Yanta and W. L. Gladfelter, *Inorg. Synth.* 1983, **22**, 163.

Polyhedron Vol. 7, No. 6, pp. 449–462, 1988
Printed in Great Britain

0277–5387/88 $3.00+.00
Pergamon Press plc

MONO- AND BIS-ALKOXIDES OF TRIS(3,5-DIMETHYLPYRAZOLYL)BORATO MOLYBDENUM AND TUNGSTEN NITROSYLS

JON A. McCLEVERTY† and ANDRZEJ WLODARCZYK

Department of Chemistry, University of Birmingham, PO Box 363, Birmingham B15 2TT, U.K.

(*Received* 24 *September* 1987; *accepted* 5 *October* 1987)

Abstract—The complexes [ML*(NO)Cl(OR)] {L* = $HB(3,5\text{-}Me_2C_3HN_2)_3$; M = Mo, R = CH_2CH_2X, X = Cl, OMe or OEt; $(CH_2)_nOH$, n = 2, 5, 6; M = W, R = CH_2CH_2X, X = Cl, OMe or OEt; $(CH_2)_nOH$, n = 2–6; $CH_2(CF_2)_3CH_2OH$; $CHMeCH_2CMe_2OH$} and [ML*(NO)$(OR)_2$] {M = Mo, R = CH_2CH_2X, X = Cl, OMe or OEt; $(CH_2)_nOH$, n = 2–6; M = W, R = CH_2CH_2X, X = Cl, OMe or OEt; $(CH_2)_nOH$, n = 2, 4–6; $CH_2(CF_2)_3CH_2OH$} have been prepared from [ML*(NO)Cl_2] and the appropriate alcohol in the presence of NEt_3 or $NaCO_3$, and have been characterized by IR, ^1H NMR and mass spectroscopy.

In our development of the chemistry of alkoxide complexes of the tris(3,5-dimethylpyrazolyl)borato molybdenum and tungsten nitrosyls ([ML*(NO)X(OR)] and [ML*(NO)$(OR)_2$]; L* = HB$(3,5\text{-}Me_2C_3HN_2)_3$) we have established certain facts. These are that (i) the complexes are generally air and moisture stable,[1,2] in contrast to many other alkoxides of these metals, (ii) that the central metal atoms in these complexes are formally coordinatively unsaturated, containing $\{M(NO)\}^4$ or $\{L^*M(NO)\}^{3+}$ cores (the metal having a formal 16-electron configuration), this "unsaturation" being maintained probably by the steric bulk of the L* group,[1,2,3] (iii) that this "unsaturation" is to some extent relieved by p_π–d_π bonding from O to the metal and (iv) that the complexes undergo one-electron reductions, $[ML^*(NO)X(OR)]+e^- \rightarrow [ML^*(NO)X(OR)]^-$, which may be reversible, depending on X.[3]

We have also demonstrated that it is possible to prepare mono- and bimetallic redox-active complexes of type A and B.[4] The former is a polycyclic ether in which a redox-active metal fragment is included within the framework of the ring. The latter, derived from an appropriately functionalized dibenzo-18-crown-6, contains two redox-active fragments which do not interact with each other, an observation entirely consistent with our studies of closely related redox-active bimetallic species containing diphenolato and dianilido bridging ligands.[5] Our goal is to synthesize redox-active bimetallic species similar to B but containing two bridging polyether linkages, e.g. L*(NO)$M\{O(CH_2CH_2O)_nCH_2CH_2O\}_2$M(NO)L*, where n = 1–4 and also to prepare related complexes containing hydrocarbon-only bridges, e.g. L*(NO)$M\{O(CH_2CH_2)_nO\}_2$M(NO)L* or L*(NO)M{O$(CH_2CH_2)_nC_6H_4(CH_2CH_2)_nO\}_2$M(NO)L*. To this end, it is important to extend the "simple" alkoxide chemistry of the molybdenum and tungsten species [ML*(NO)X(OR)] and [ML*(NO)$(OR)_2$], since a number of these complexes have not been reported. In this paper, we describe mono- and bis-alkoxides derived from some other simple alcohols, $HOCH_2CH_2X$ (X = Cl, OMe and OEt) and more importantly, from a range of α,ω-diols, $HO(CH_2)_nOH$, where n = 2–6. Some related compounds have been reported earlier, e.g. [ML*(NO)Cl(OR)] (M = Mo, R = Me, Et, Pr^i, Bu^t and $(CH_2)_3Br$;[1,3] M = W, R = $(CH_2)_3Br$[3]), [ML*(NO)$(OR)_2$] (M = Mo, R = Me, Et, Pr^i, Bu^i;[1,2] M = W, R = Et[2]), [MoL*(NO)I(OCH_2CH_2X)] (X = Cl, OMe, OH, $(CH_2)_nOH$, n = 1–4)[5] and [MoL*(NO)$(OCH_2CH_2OH)_2$].[6] In a subsequent paper, we will describe the formation of "chelated" compounds, [ML*(NO)O$(CH_2)_nO$] and "doubly bridged" species, [ML*(NO){O$(CH_2)_nO\}_2$

†Author to whom correspondence should be addressed.

ML*(NO)]. A preliminary report of some of this work has been briefly presented.[7]

RESULTS AND DISCUSSION

The mono-alkoxides, [ML*(NO)Cl(OR)], M = Mo or W, were conveniently prepared in good yields by refluxing the parent dichloride, [ML*(NO)Cl_2], with the appropriate alcohol in toluene containing triethylamine or sodium carbonate. Dichloromethane could also be used as the solvent and the amine or carbonate was necessary to absorb HCl liberated during the reactions. The list of compounds prepared is given in Table 1, which contains elemental analytical data. The molybdenum complexes were bright blue, whereas the tungsten compounds were either a mauve–blue shade or purple. It was necessary in most cases to purify the compounds by column chromatography followed by crystallization/precipitation. This is especially important in the reactions involving α,ω-diols, since bimetallic, "chelated" or "doubly-bridged" compounds may also be formed during the reactions.

The bis-alkoxides, [ML*(NO)$(OR)_2$], M = Mo or W, were obtained by refluxing either [MoL*(NO)I_2] or [WL*(NO)Cl_2] with the appropriate alcohol, in the molar ratio 1 : 2 or greater, again in the presence of sodium carbonate. Chromatographic separation was essential and the complexes (Table 1) were obtained as pink (Mo) or orange (W) microcrystals.

All of the complexes are air and moisture stable, as expected, and all dissolve well in chloroform, dichloromethane, acetonitrile and tetrahydrofuran. In general, they are not soluble in hydrocarbons, although they will dissolve in warm toluene.

The IR spectra (Table 2) of the compounds

Table 1. Analytical data obtained from [M{$HB(Me_2C_3HN_2)_3$}(NO)XY]

			Calculated			Found		
M	X	Y	C	H	N	C	H	N
Mo	Cl	OCH_2CH_2Cl	37.9	4.9	18.2	38.2	5.0	18.1
Mo	Cl	OCH_2CH_2OMe	40.5	5.5	18.4	40.3	5.8	18.3
Mo	Cl	OCH_2CH_2OEt	41.7	5.7	17.9	42.0	5.9	17.9
Mo	Cl	OCH_2CH_2OH	39.3	5.2	18.9	40.0	5.3	18.7
Mo	Cl	$O(CH_2)_5OH$	42.8	5.9	17.4	42.9	6.0	17.3
Mo	Cl	$O(CH_2)_6OH$	43.8	6.1	17.0	43.5	6.1	17.3
W	Cl	OCH_2CH_2Cl	32.6	4.0	15.7	32.9	4.1	15.8
W	Cl	OCH_2CH_2OMe	34.8	4.7	15.8	34.7	4.5	15.5
W	Cl	OCH_2CH_2OEt	35.9	4.9	15.4	35.9	4.8	15.1
W	Cl	OCH_2CH_2OH	33.6	4.5	16.1	33.6	4.4	15.9
W	Cl	$O(CH_2)_3OH$	34.8	4.7	15.8	35.1	5.0	16.0
W	Cl	$O(CH_2)_4OH$	35.9	4.9	15.4	35.7	4.9	15.7
W	Cl	$O(CH_2)_5OH$	37.0	5.1	15.1	37.2	5.1	15.4
W	Cl	$O(CH_2)_6OH$	38.0	5.3	14.8	38.0	5.4	15.0
W	Cl	$OCH_2(CF_2)_3CH_2OH$	31.7	3.6	12.9	31.7	3.7	13.2
W	Cl	$OCHMeCH_2CMe_2OH$	38.0	5.3	14.8	38.3	5.6	14.5
Mo	OCH_2CH_2Cl	OCH_2CH_2Cl	39.2	5.2	16.8	39.5	5.5	16.5
Mo	OCH_2CH_2OMe	OCH_2CH_2OMe	44.0	6.3	17.1	44.3	6.5	17.2
Mo	OCH_2CH_2OEt	OCH_2CH_2OEt	45.9	6.7	16.3	45.6	6.4	16.5
Mo	OCH_2CH_2OH	OCH_2CH_2OH	41.8	5.9	18.0	42.1	5.6	18.3
Mo	$O(CH_2)_3OH$	$O(CH_2)_3OH$	44.0	6.3	17.1	44.0	6.5	17.0
Mo	$O(CH_2)_4OH$	$O(CH_2)_4OH$	45.9	6.7	16.3	46.2	6.7	16.5
Mo	$O(CH_2)_5OH$	$O(CH_2)_5OH$	47.7	7.0	15.6	48.6	6.8	15.5
Mo	$O(CH_2)_6OH$	$O(CH_2)_6OH$	49.3	7.3	14.9	49.3	7.5	14.7
W	OCH_2CH_2Cl	OCH_2CH_2Cl	34.0	4.5	14.6	34.3	4.7	14.9
W	OCH_2CH_2OMe	OCH_2CH_2OMe	38.1	5.5	14.8	38.9	5.5	14.9
W	OCH_2CH_2OEt	OCH_2CH_2OEt	40.1	5.8	14.2	40.2	5.7	14.5
W	OCH_2CH_2OH	OCH_2CH_2OH	36.0	5.1	15.5	35.7	5.3	15.8
W	$O(CH_2)_4OH$	$O(CH_2)_4OH$	40.1	5.8	14.2	39.9	5.9	14.5
W	$O(CH_2)_5OH$	$O(CH_2)_5OH$	41.9	6.2	13.7	42.2	6.4	14.0
W	$O(CH_2)_6OH$	$O(CH_2)_6OH$	43.5	6.5	13.1	43.5	6.2	13.3
W	$OCH_2(CF_2)_3CH_2OH$	$OCH_2(CF_2)_3CH_2OH$	32.2	3.5	10.5	32.5	3.5	10.5

Table 2. Selected IR and ^{1}H NMR spectral data for [ML*(NO)XY]

M	X	Y	ν_{NO}[a]	δ[b]	A[c]	Assignment
Mo	Cl	OCH_2CH_2Cl	1672	2.34	3	(s)
				2.23	3	(s)
				2.37	3	18 (s)
				2.38	3	(s) $(CH_3)_2C_3HN_2$
				2.41	3	(s)
				2.50	3	(s)
				3.92	2	(m) OCH_2CH_2Cl
				5.76	1	(s)
				5.87	1	(s) $Me_2C_3HN_2$
				5.93	1	(s)
				6.00	2	*AB* pair; OCH_2CH_2Cl, $J_{AB} = 12.1$ Hz; $\delta_A = 6.05$; $\delta_B = 5.95$
Mo	Cl	OCH_2CH_2OMe	1665	2.34	3	(s)
				2.35	3	(s)
				2.37	6	18 (s) $(CH_3)_2C_3HN_2$
				2.41	3	(s)
				2.51	3	(s)
				3.38	3	(s) $OCH_2CH_2CH_3$
				3.85	2	(m) OCH_2CH_2OMe
				5.74	1	(s)
				5.87	2	3 (s) $Me_2C_3HN_2$
				6.02	2	*AB* pair; OCH_2CH_2OMe; poorly resolved
Mo	Cl	OCH_2CH_2OEt	1662	1.19	3	(t) $OCH_2CH_2OCH_2CH_3$
				2.34	3	(s)
				2.35	3	(s)
				2.37	6	18 (s) $(CH_3)_2C_3HN_2$
				2.42	3	(s)
				2.52	3	(s)
				2.54	2	(q) $OCH_2CH_2OCH_2Me$
				3.89	2	(m) OCH_2CH_2OEt
				5.74	1	(s)
				5.86	1	3 (s) $Me_2C_3HN_2$
				5.90	1	(s)
				6.00	2	*AB* pair; OCH_2CH_2OEt; poorly resolved
Mo	Cl	OCH_2CH_2OH	1678	2.36	3	(s)
				2.37	3	(s)
				2.38	6	18 (s) $(CH_3)_2C_3HN_2$
				2.42	3	(s)
				2.51	3	(s)
				4.15	2	(m) OCH_2CH_2OH
				5.77	1	(s)
				5.89	1	3 (s) $Me_2C_3HN_2$
				5.93	1	(s)
				6.00	2	*AB* pair; OCH_2CH_2OH; $J_{AB} = 11.1$ Hz; $\delta_A = 6.15$; $\delta_B = 5.85$
Mo	Cl	$O(CH_2)_5OH$	1670	1.58	4	(m) $O(CH_2)_2CH_2CH_2CH_2OH$
				2.03	2	(m) $OCH_2CH_2(CH_2)_3OH$

Table 2—*continued*

M	X	Y	ν_{NO}[a]	δ[b]	A[c]	Assignment
Mo	Cl	$O(CH_2)_5OH$	1670	2.35	3	(s)
				2.36	6	(s)
				2.37	3	18 (s) $(CH_3)_2C_3HN_2$
				2.43	3	(s)
				2.52	3	(s)
				3.68	2	(m) $O(CH_2)_4CH_2OH$
				5.76	1	(s)
				5.86	2	3 (s) $Me_2C_3HN_2$
				5.91	2	*AB* pair; $OCH_2(CH_2)_4OH$; poorly resolved
Mo	Cl	$O(CH_2)_6OH$	1670	1.55	6	(m) $OCH_2CH_2(CH_2)_3CH_2OH$
				1.99	2	(m) $OCH_2CH_2(CH_2)_4OH$
				2.34	3	(s)
				2.35	3	(s)
				2.36	3	18 (s)
				2.37	3	(s) $(CH_3)_2C_3HN_2$
				2.43	3	(s)
				2.52	3	(s)
				3.66	3	(t) $O(CH_2)_5CH_2OH$
				5.58	1	(s)
				5.76	1	3 (s) $Me_2C_3HN_2$
				5.90	1	(s)
				5.94	2	*AB* pair; $OCH_2(CH_2)_5OH$; poorly resolved
W	Cl	OCH_2CH_2Cl	1630	2.35	3	(s)
				2.36	3	(s)
				2.37	3	18 (s)
				2.43	3	(s) $(CH_3)_2C_3HN_2$
				2.55	3	(s)
				2.58	3	(s)
				3.87	2	(m) OCH_2CH_2OH
				5.92	2	*AB* pair; OCH_2CH_2OH; poorly resolved
				5.83	1	(s)
				5.88	1	3 (s) $Me_2C_3HN_2$
				5.95	1	(s)
W	Cl	OCH_2CH_2OMe	1630	2.34	3	(s)
				2.35	6	(s)
				2.43	3	18 (s) $(CH_3)_2C_3HN_2$
				2.56	3	(s)
				2.59	3	(s)
				3.37	3	(s) $OCH_2CH_2OCH_3$
				3.77	2	(m) OCH_2CH_2OMe
				5.81	1	(s)
				5.87	1	3 (s) $Me_2C_3HN_2$
				5.92	1	(s)
				5.92	2	*AB* pair; OCH_2CH_2OMe; poorly resolved
W	Cl	OCH_2CH_2OEt	1628	1.19	3	(t) $OCH_2CH_2OCH_2CH_3$
				2.34	3	(s)
				2.35	6	(s)
				2.44	3	18 (s) $(CH_3)_2C_3HN_2$
				2.56	3	(s)
				2.59	3	(s)

Table 2—*continued*

M	X	Y	ν_{NO}[a]	δ[b]	A[c]	Assignment
W	Cl	OCH_2CH_2OEt	1628	3.52	2	(q) $OCH_2CH_2OCH_2Me$
				3.82	2	(m) OCH_2CH_2OMe
				5.81	1	(s)
				5.87	1	3 (s) $Me_2C_3HN_2$
				5.92	1	(s)
				5.93	2	*AB* pair; OCH_2CH_2OEt; poorly resolved
W	Cl	OCH_2CH_2OH	1630	2.36	6	(s)
				2.34	3	(s)
				2.37	3	18 (s) $(CH_3)_2C_3HN_2$
				2.55	3	(s)
				2.59	3	(s)
				4.08	2	(m) OCH_2CH_2OH
				5.88	2	*AB* pair; OCH_2CH_2OH; poorly resolved
				5.82	1	(s)
				5.87	1	3 (s) $Me_2C_3HN_2$
				5.94	1	(s)
W	Cl	$O(CH_2)_3OH$	1630	2.11	2	(m) $OCH_2CH_2CH_2OH$
				2.35	6	(s)
				2.37	3	18 (s)
				2.41	3	(s) $(CH_3)_2C_3HN_2$
				2.58	6	(s)
				3.86	2	(m) $OCH_2CH_2CH_2OH$
				5.93	2	*AB* pair; $OCH_2CH_2CH_2OH$; poorly resolved
				5.82	1	(s)
				5.87	1	3 (s) $Me_2C_3HN_2$
				5.94	1	(s)
W	Cl	$O(CH_2)_4OH$	1630	1.97	4	(m) $OCH_2(CH_2)_2CH_2OH$
				2.35	6	(s)
				2.37	6	18 (s)
				2.57	3	(s) $(CH_3)_2C_3HN_2$
				2.60	3	(s)
				3.71	2	(m) $O(CH_2)_3CH_2OH$
				5.87	2	*AB* pair; $OCH_2(CH_2)_3OH$; poorly resolved
				5.79	1	(s)
				5.87	1	3 (s) $Me_2C_3HN_2$
				5.93	1	(s)
W	Cl	$O(CH_2)_5OH$	1626	1.74	6	(m) $O(CH_2)_4CH_2OH$
				2.34	6	(s)
				2.36	3	(s)
				2.40	3	18 (s) $(CH_3)_2C_3HN_2$
				2.56	3	(s)
				2.59	3	(s)
				3.68	2	(m) $O(CH_2)_4CH_2OH$
				5.81	2	(broad m); $OCH_2(CH_2)_4OH$
				5.80	1	(s)
				5.83	1	3 (s) $Me_2C_3HN_2$
				5.86	1	(s)
W	Cl	$O(CH_2)_6OH$	1624	1.49	6	(m) $O(CH_2)_2(CH_2)_3CH_2OH$
				1.89	2	(m) $OCH_2CH_2(CH_2)_4OH$

Table 2—*continued*

M	X	Y	ν_{NO}[a]	δ[b]	A[c]	Assignment
W	Cl	$O(CH_2)_6OH$	1624	2.34	6	(s)
				2.36	3	(s)
				2.41	3	18 (s) $(CH_3)_2C_3HN_2$
				2.57	3	(s)
				2.60	3	(s)
				3.65	2	(m) $O(CH_2)_5CH_2OH$
				5.82	2	*AB* pair; $OCH_2(CH_2)_5OH$; poorly resolved
				5.82	1	(s)
				5.86	1	3 (s) $Me_2C_3HN_2$
				5.92	1	(s)
W	Cl	$OCH_2(CF_2)_3CH_2OH$	1640	2.35	3	(s)
				2.36	6	(s)
				2.38	3	18 (s) $(CH_3)_2C_3HN_2$
				2.50	3	(s)
				2.56	3	(s)
				4.07	2	(m) $OCH_2(CF_2)_3CH_2OH$
				5.86	2	*AB* pair; $OCH_2(CF_2)_3CH_2OH$; poorly resolved
				5.82	1	(s)
				5.89	1	3 (s) $Me_2C_3HN_2$
				5.96	1	(s)
W	Cl	$OCHMeCH_2CMe_2OH$	1630	1.03	3	(s) $OCHMeCH_2C(CH_3)_2OH$
				1.08	3	(s) $OCHMeCH_2C(CH_3)_2OH$
				1.80	2	(m) $OCHMeCH_2CMe_2OH$
				1.83	3	(d) $OCH(CH_3)CH_2CMe_2OH$
				2.32	3	(s)
				2.33	3	(s)
				2.35	3	18 (s)
				2.48	3	(s) $(CH_3)_2C_3HN_2$
				2.57	3	(s)
				2.65	3	(s)
				5.84	2	3 (s) $Me_2C_3HN_2$
				5.92	1	(s) $Me_2C_3HN_2$
				6.02	1	$OCHMeCH_2CMe_2OH$
Mo	OCH_2CH_2Cl	OCH_2CH_2Cl	1658	2.31	3	(s)
				2.33	9	18 (s) $(CH_3)_2C_3HN_2$
				2.52	6	(s)
				3.76	4	(m) OCH_2CH_2Cl
				5.57	4	*AB* pair; OCH_2CH_2Cl; $J_{AB} = 11.5$ Hz; $\delta_A = 5.64$, $\delta_B = 5.50$
				5.75	1	3 (s) $Me_2C_3HN_2$
				5.84	2	(s)
Mo	OCH_2CH_2OMe	OCH_2CH_2OMe	1635	2.29	3	(s)
				2.31	9	18 (s) $(CH_3)_2C_3HN_2$
				2.54	6	(s)
				3.38	6	(s) $OCH_2CH_2OCH_3$
				3.68	4	(m) OCH_2CH_2OMe
				5.54	4	*AB* pair; OCH_2CH_2OMe; $J_{AB} = 11.3$ Hz; $\delta_A = 5.66$, $\delta_B = 5.42$
				5.72	1	3 (s) $Me_2C_3HN_2$
				5.81	2	(s)
Mo	OCH_2CH_2OEt	OCH_2CH_2OEt	1635	1.21	6	(t) $OCH_2CH_2OCH_2CH_3$

Table 2—*continued*

M	X	Y	ν_{NO}[a]	δ[b]	A[c]	Assignment
Mo	OCH_2CH_2OEt	OCH_2CH_2OEt	1635	2.29	3	(s)
				2.31	9	18 (s) $(CH_3)_2C_3HN_2$
				2.54	6	(s)
				3.53	4	(q) $OCH_2CH_2OCH_2Me$
				3.72	4	(m) OCH_2CH_2OEt
				5.55	4	*AB* pair; OCH_2CH_2OEt; $J_{AB} = 11.2$ Hz; $\delta_A = 5.66$, $\delta_B = 5.44$
				5.71	1	3 (s) $Me_2C_3HN_2$
				5.80	2	(s)
Mo	$O(CH_2)_3OH$	$O(CH_2)_3OH$	1640	1.90	4	(m) $OCH_2CH_2CH_2OH$
				2.30	3	(s)
				2.32	9	18 (s) $(CH_3)_2C_3HN_2$
				2.54	6	(s)
				3.82	4	(m) $OCH_2CH_2CH_2OH$
				5.51	4	(broad m); $OCH_2CH_2CH_2OH$
				5.81	1	3 (s) $Me_2C_3HN_2$
				5.82	2	(s)
Mo	$O(CH_2)_4OH$	$O(CH_2)_4OH$	1640	1.70	4	(m) $OCH_2CH_2CH_2CH_2OH$
				1.88	4	(m) $OCH_2CH_2CH_2CH_2OH$
				2.30	3	(s)
				2.32	9	18 (s) $(CH_3)_2C_3HN_2$
				2.55	6	(s)
				3.66	4	(m) $O(CH_2)_3CH_2OH$
				5.35	4	*AB* pair; $OCH_2(CH_2)_3OH$; poorly resolved
				5.74	1	3 (s) $Me_2C_3HN_2$
				5.81	2	(s)
Mo	$O(CH_2)_5OH$	$O(CH_2)_5OH$	1640	1.53	4	(m), $O(CH_2)_2CH_2(CH_2)_2OH$
				1.63	4	(m) $O(CH_2)_3CH_2CH_2OH$
				1.82	4	(m) $OCH_2CH_2(CH_2)_3OH$
				2.30	3	(s)
				2.31	9	(s) $(CH_3)_2C_3HN_2$
				2.54	6	(s)
				3.66	4	(m) $O(CH_2)_4CH_2OH$
				5.59	4	*AB* pair; $OCH_2(CH_2)_4OH$; poorly resolved
				5.73	1	3 (s) $Me_2C_3HN_2$
				5.80	2	(s)
Mo	$O(CH_2)_6OH$	$O(CH_2)_6OH$	1640	1.62	16	(m) $OCH_2(CH_2)_4CH_2OH$
				2.30	3	(s)
				2.31	9	(s) $(CH_3)_2C_3HN_2$
				2.55	9	(s)
				3.64	4	(t) $O(CH_2)_5CH_2OH$
				5.40	4	*AB* pair; $OCH_2(CH_2)_5OH$; poorly resolved
				5.73	1	3 (s) $Me_2C_3HN_2$
				5.80	2	(s)
W	OCH_2CH_2Cl	OCH_2CH_2Cl	1605	2.32	6	(s)
				2.33	3	18 (s)
				2.38	3	(s) $(CH_3)_2C_3HN_2$
				2.62	6	(s)
				5.59	4	*AB* pair; OCH_2CH_2Cl; $J_{AB} = 11.4$ Hz; $\delta_A = 5.69$, $\delta_B = 5.49$
				5.73	4	(t) OCH_2CH_2Cl

Table 2—*continued*

M	X	Y	ν_{NO}[a]	δ[b]	A[c]	Assignment
W	OCH_2CH_2Cl	OCH_2CH_2Cl	1605	5.81	1	3 (s) $Me_2C_3HN_2$
				5.86	2	(s)
W	OCH_2CH_2OMe	OCH_2CH_2OMe	1590	2.30	9	(s)
				2.37	3	18 (s) $(CH_3)_2C_3HN_2$
				2.64	6	(s)
				3.38	6	(s) $OCH_2CH_2OCH_3$
				3.66	4	(t) OCH_2CH_2OMe
				5.56	4	*AB* pair; OCH_2CH_2OMe; $J_{AB} = 11.5$ Hz; $\delta_A = 5.71$, $\delta_B = 5.41$
				5.77	1	3 (s) $Me_2C_3HN_2$
				5.83	2	(s)
W	OCH_2CH_2OEt	OCH_2CH_2OEt	1598	1.99	3	(t) $OCH_2CH_2CH_2CH_3$
				2.30	9	(s)
				2.37	3	18 (s) $(CH_3)_2C_3HN_2$
				2.64	6	(s)
				3.52	4	(d) $OCH_2CH_2POCH_2Me$
				3.70	4	(t) OCH_2CH_2OEt
				5.57	4	*AB* pair; OCH_2CH_2OEt; $J_{AB} = 11.2$ Hz; $\delta_A = 5.70$, $\delta_B = 5.44$
				5.76	1	3 (s) $Me_2C_3HN_2$
				5.82	2	(s)
W	OCH_2CH_2OH	OCH_2CH_2OH	1610	2.32	6	(s)
				2.36	3	18 (s)
				2.41	3	(s) $(CH_3)_2C_3HN_2$
				2.64	6	(s)
				3.86	4	(m) OCH_2CH_2OH
				5.46	4	*AB* pair; OCH_2CH_2OH; poorly resolved
				5.87	3	(s) $Me_2C_3HN_2$
W	$O(CH_2)_4OH$	$O(CH_2)_4OH$	1600	1.68	4	(m) $O(CH_2)_2CH_2CH_2OH$
				1.86	4	(m) $OCH_2CH_2(CH_2)_2OH$
				2.31	6	(s)
				2.32	3	18 (s)
				2.37	3	(s) $(CH_3)_2C_3HN_2$
				2.64	6	(s)
				3.67	4	(m) $O(CH_2)_3CH_2OH$
				5.41	4	*AB* pair; $OCH_2(CH_2)_3OH$; poorly resolved
				5.79	1	3 (s) $Me_2C_3HN_2$
				5.83	2	(s)
W	$O(CH_2)_5OH$	$O(CH_2)_5OH$	1600	1.50	4	(m) $O(CH_2)_2CH_2(CH_2)_2OH$
				1.71	8	(m) $OCH_2CH_2CH_2CH_2CH_2OH$
				2.30	6	(s)
				2.31	3	18 (s)
				2.36	3	(s) $(CH_3)_2C_3HN_2$
				2.64	6	(s)
				3.66	4	(t) $O(CH_2)_4CH_2OH$
				5.43	4	*AB* pair; $OCH_2(CH_2)_4OH$; poorly resolved
				5.78	1	3 (s) $Me_2C_3HN_2$
				5.83	2	(s)

Table 2—*continued*

M	X	Y	ν_{NO}[a]	δ[b]	A[c]	Assignment
W	$O(CH_2)_6OH$	$O(CH_2)_6OH$	1600	1.44	8	(m) $O(CH_2)_2CH_2CH_2(CH_2)_2OH$
				1.60	4	(m) $O(CH_2)_4CH_2CH_2OH$
				2.30	6	(s)
				2.31	3	18 (s)
				2.36	3	(s) $(CH_3)_2C_3HN_2$
				2.64	6	(s)
				3.64	4	(t) $O(CH_2)_5CH_2OH$
				5.43	4	*AB* pair; $OCH_2(CH_2)_5OH$; poorly resolved
				5.78	1	3 (s) $Me_2C_3HN_2$
				5.83	2	(s)
W	$OCH_2(CF_2)_3CH_2OH$	$OCH_2(CF_2)_3CH_2OH$	1618	2.30	3	(s)
				2.31	3	18 (s)
				2.33	6	(s) $(CH_3)_2C_3HN_2$
				2.57	6	(s)
				4.05	4	(m) $OCH_2(CF_2)_3CH_2OH$
				5.70	4	(broad m); $OCH_2(CF_2)_3CH_2OH$
				5.88	1	3 (s) $Me_2C_3HN_2$
				5.90	2	(s)

[a] In KBr discs (cm^{-1}).
[b] In $CDCl_3$ solution.
[c] Relative areas.

revealed the expected features due to the L* ligand (e.g. ν_{BH} at *ca* 2220 cm^{-1}) and ν_{NO} which varied according to M and X, but not R. Thus the molybdenum mono-alkoxides exhibited an NO stretching frequency at *ca* 1670 cm^{-1} while their tungsten analogues showed ν_{NO} at *ca* 1630 cm^{-1}. The spectra of $[ML^*(NO)(OR)_2]$ revealed ν_{NO} (Mo) at *ca* 1641 cm^{-1} and ν_{NO}(W) at *ca* 1603 cm^{-1}. These values are in general consistent with trends observed earlier.[1-5]

The ^1H NMR spectra (Table 2) substantiated our formulations of these compounds. For the molybdenum mono-alkoxides, a group of five or six resonances (total integrated area equivalent to 18 protons) appeared in the range $\delta = 2.34$–2.54, due to the six methyl groups of L*. In the tungsten complexes, these protons frequently gave rise to five such signals, although occasionally six or four resonances were detected, again in the region $\delta = 2.34$–2.65. The 4-H proton on the pyrazolyl rings gave rise to three resonances, consistent with the lack of a plane of symmetry in these complexes. These signals were observed in the range $\delta = 5.58$–5.93 (Mo) and 5.79–5.96 (W). As had been reported and discussed earlier,[1] the protons attached to the α-carbon atom of the alkoxide resonate at an unusually low field. This is probably due to deshielding of the C and H atoms caused by being bound to the extremely electronegative {ML*(NO)Cl} group. Thus, the α-protons in the Mo complexes appeared, usually as poorly resolved *AB* pairs, in the range $\delta = 5.91$–6.02 (av. 5.98), whereas the comparable signals in the W complexes appeared in the range $\delta = 5.81$–5.93 (av. 5.88). In the complex [WL*(NO)Cl(OCHMeCH$_2$CMe$_2$OH)], the α-proton appeared as an ill-defined multiplet at $\delta = 6.02$.

The bis-alkoxides $[ML^*(NO)(OR)_2]$ contain a plane of symmetry and this is reflected in the ^1H NMR spectra. Thus, the methyl protons of L* appeared as a group of three (Mo) or usually four (W) signals (the latter species occasionally gave rise to a set of three resonances) in the ranges δ(Mo) = 2.29–2.55 and δ(W) = 2.30–2.64. The 4-H protons occurred as two signals (relative areas 1 : 2 usually), in the regions δ(Mo) = 5.71–5.82 and δ(W) = 5.76–5.90, although occasionally, these resonances might appear as a singlet, probably due to accidental degeneracy. Once again, the protons on the α-carbon atom of the alkoxides resonated at low fields, although at a chemical shift less positive than those of their mono-alkoxide analogues. This presumably reflects a subtle alteration in the effective electronegativity of {ML*(NO)Cl} vs that of {ML*(NO)(OR)}. Thus in the molybdenum com-

plexes these *AB* pairs usually occurred in the range $\delta = 5.35$–5.40 (av. 5.50). In the tungsten complexes, $\delta = 5.41$–5.70 (av. 5.52).

The differences between the chemical shifts of the α-protons in the mono- and bis-alkoxides is very useful in determining the presence of either type of species in solution and in estimating the relative amount of each in mixtures.

The mass spectra of the new compounds (Table 3) usually provided parent molecular ions ([M^+]) and revealed fragmentation patterns consistent with loss of NO, R, O and/or OR.

CONCLUSION

Mono- and bis-alkoxide complexes of the type [ML*(NO)Cl(OR)] and [ML*(NO)$(OR)_2$] (M = Mo or W) can be simply and reliably prepared by treatment of [ML*(NO)Cl_2] with the appropriate alcohol, ROH, in the presence of triethylamine or better, sodium carbonate. They have distinct ^{1}H NMR spectral properties, and the chloro complex will be useful in electrochemical studies, since related iodo-complexes undergo voltammetric reduction with loss of I^- which complicates the study of this process.[3,5]

EXPERIMENTAL

All reagents were used as supplied. [M{(3,5-$Me_2C_3HN_2)_3$}(NO)Cl_2] was synthesized as described previously.[8] For column chromatography silica gel (70–230 mesh) was used under nitrogen. All reactions were carried out under N_2 and elemental analyses were determined by the Microanalytical Laboratory of this Department. All yields are quoted relative to the metal-containing starting material.

IR spectral data were obtained using a PE297 spectrophotometer and ^{1}H NMR spectra were measured using a Jeol GX270 instrument. Mass spectra were performed with a Kratos MS80 instrument in the EI mode.

[Mo{(3,5-$Me_2C_3HN_2)_3$}(NO)Cl(OCH_2CH_2Cl)]

Mo{HB(3,5-$Me_2C_3HN_2)_3$}(NO)Cl_2] (0.3 g) and $HOCH_2CH_2Cl$ (0.5 cm^3) were dissolved in toluene (50 cm^3) and triethylamine (0.2 cm^3) was added. The solution was refluxed for 4 h during which time the colour had changed to blue. The mixture was then cooled to R.T., *n*-pentane added and further cooled to −10°C. [$NHEt_3$]Cl which had precipitated was filtered off and the filtrate was evaporated *in vacuo*. The crude product was extracted from the residue in diethylether and then reprecipitated by addition of *n*-hexane. The solid was collected by filtration and purified by chromatography on silica gel using dichloromethane/*n*-hexane (2 : 1 v/v) as eluant. The second blue fraction was collected, the solvent evaporated *in vacuo* and the complex recrystallized from diethylether/*n*-hexane giving blue crystals (0.19 g, 57%).

[Mo{HB(3,5-$Me_2C_3HN_2)_3$}(NO)Cl(OCH_2CH_2OMe)]

This compound was prepared in the same way as the one above, using $HOCH_2CH_2OMe$ (0.5 cm^3) and was obtained as blue crystals (0.21 g, 66%).

[Mo{HB(3,5-$Me_2C_3HN_2)_3$}(NO)Cl(OCH_2CH_2OEt)]

[Mo{HB(3,5-$Me_2C_3HN_2)_3$}(NO)Cl_2] (0.3 g) and $HOCH_2CH_2OEt$ (0.5 cm^3), dissolved in dichloromethane (50 cm^3), were treated with Na_2CO_3 (0.5 g) and the mixture was refluxed for 16 h during which time it became blue. The mixture was then cooled to R.T., *n*-pentane added and further cooled to −10°C. After filtration, the filtrate was evaporated *in vacuo*, the residue dissolved in the minimum volume of dichloromethane and chromatographed on silica gel using dichloromethane/*n*-hexane (2 : 1 v/v) as eluant. The blue fraction was collected, the solvent evaporated and the complex obtained by recrystallization from dichloromethane/*n*-hexane as blue crystals (0.28 g, 85%).

[Mo{HB(3,5 - $Me_2C_3HN_2)_3$}(NO)Cl{$O(CH_2)_nOH$}], ($n = 2, 5, 6$)

[Mo{HB(3,5 - $Me_2C_3HN_2)_3$}(NO)Cl_2] (0.3 g) and an excess of the appropriate dialcohol were stirred and refluxed in toluene (100 cm^3) for 5–8 h, during which time the colour of the solution changed through green to deep blue. The reaction mixture was cooled to R.T., *n*-hexane added and cooled further to −10°C. An oily deposit formed and the supernatant solution was decanted and evaporated to dryness. The desired complexes were worked up by chromatography as described above and were isolated as blue powders ($n = 2$, 0.13 g, 41% ; $n = 5$, 0.20 g, 59% ; $n = 6$, 0.18 g, 51%).

When $n = 3$ or 4, this method afforded predominantly bimetallic products [Mo{HB(3,5-$Me_2C_3HN_2)_3$}(NO)Cl_2{$O(CH_2)_nO$}]. These species are described elsewhere.

Table 3. Mass spectral data obtained from [ML*(NO)XY]

M	X	Y	m/e	Tentative assignment
Mo	Cl	OCH_2CH_2Cl	539	$[M]^+$
			509	$[M—NO]^+$
			446	$[M—NO—CH_2CH_2Cl]^+$
			430	$[M—NO—Y]^+$
Mo	Cl	OCH_2CH_2OMe	535	$[M]^+$
			505	$[M—NO]^+$
			460	$[M—Y]^+$
			446	$[M—NO—CH_2CH_2OMe]^+$
			430	$[M—NO—Y]^+$
			395	$[M—NO—Y—Cl]^+$
Mo	Cl	OCH_2CH_2OEt	549	$[M]^+$
			519	$[M—NO]^+$
			460	$[M—Y]^+$
			446	$[M—NO—CH_2CH_2OEt]^+$
			430	$[M—NO—Y]^+$
Mo	Cl	OCH_2CH_2OH	521	$[M]^+$
			491	$[M—NO]^+$
			446	$[M—NO—CH_2CH_2OH]^+$
			430	$[M—NO—Y]^+$
			426	$[M—Cl—Y]^+$
			395	$[M—NO—Y—Cl]^+$
Mo	Cl	$O(CH_2)_5OH$	563	$[M]^+$
			527	$[M—Cl]^+$
			497	$[M—Cl—NO]^+$
			460	$[M—Y]^+$
			446	$[M—NO—(CH_2)_5OH]^+$
			395	$[M—Cl—NO—Y]^+$
Mo	Cl	$O(CH_2)_6OH$	577	$[M]^+$
			541	$[M—Cl]^+$
			511	$[M—Cl—NO]^+$
			446	$[M—NO—(CH_2)_6OH]^+$
			430	$[M—NO—Y]^+$
			425	$[M—Cl—Y]^+$
W	Cl	OCH_2CH_2Cl	625	$[M]^+$
			546	$[M—Y]^+$
			527	$[M—Cl—CH_2CH_2Cl]^+$
			532	$[M—NO—CH_2CH_2Cl]^+$
			516	$[M—NO—Y]^+$
W	Cl	OCH_2CH_2OMe	621	$[M]^+$
			546	$[M—Y]^+$
			527	$[M—Cl—CH_2CH_2OMe]^+$
			516	$[M—NO—Y]^+$
W	Cl	OCH_2CH_2OEt	635	$[M]^+$
			600	$[M—Cl]^+$
			546	$[M—Cl—Y]^+$
			527	$[M—Cl—CH_2CH_2OEt]^+$
			516	$[M—NO—Y]^+$

Table 3—*continued*

M	X	Y	m/e	Tentative assignment
W	Cl	OCH_2CH_2OH	607	$[M]^+$
			532	$[M—NO—CH_2CH_2OH]^+$
			512	$[M—Cl—Y]^+$
W	Cl	$O(CH_2)_3OH$	621	$[M]^+$
			585	$[M—Cl]^+$
			555	$[M—NO—Cl]^+$
			527	$[M—Cl—(CH_2)_3OH]^+$
			512	$[M—Cl—Y]^+$
			481	$[M—Cl—NO—Y]^+$
W	Cl	$O(CH_2)_4OH$	635	$[M]^+$
			599	$[M—Cl]^+$
			569	$[M—Cl—NO]^+$
			527	$[M—Cl—(CH_2)_4OH]^+$
			512	$[M—Cl—Y]^+$
W	Cl	$O(CH_2)_5OH$	649	$[M]^+$
			613	$[M—Cl]^+$
			583	$[M—Cl—NO]^+$
W	Cl	$O(CH_2)_6OH$	663	$[M]^+$
			627	$[M—Cl]^+$
			527	$[M—Cl—(CH_2)_6OH]^+$
Mo	OCH_2CH_2Cl	OCH_2CH_2Cl	583	$[M]^+$
			504	$[M—CH_2CH_2Cl]^+$
Mo	OCH_2CH_2OMe	OCH_2CH_2OMe	575	$[M]^+$
			545	$[M—NO]^+$
			500	$[M—OCH_2CH_2OMe]^+$
			425	$[M—(OCH_2CH_2OMe)_2]^+$
Mo	OCH_2CH_2OEt	OCH_2CH_2OEt	603	$[M]^+$
			573	$[M—NO]^+$
			514	$[M—OCH_2CH_2OEt]^+$
			484	$[M—OCH_2CH_2OEt—NO]^+$
			425	$[M—(OCH_2CH_2OEt)_2]^+$
Mo	$O(CH_2)_5OH$	$O(CH_2)_5OH$	528	$[M—\{O(CH_2)_5OH\}]^+$
			498	$[M—\{O(CH_2)_5OH\}—NO]^+$
			425	$[M—\{O(CH_2)_5OH\}_2]^+$
			395	$[M—\{O(CH_2)_5OH\}_2—NO]^+$
W	OCH_2CH_2Cl	OCH_2CH_2Cl	669	$[M]^+$
			590	$[M—OCH_2CH_2Cl]^+$
W	OCH_2C_2OMe	OCH_2CH_2OMe	661	$[M]^+$
			586	$[M—OCH_2CH_2OMe]^+$
			527	$[M—OCH_2CH_2Cl—CH_2CH_2OMe]^+$
W	OCH_2CH_2OEt	OCH_2CH_2OEt	689	$[M]^+$
			600	$[M—OCH_2CH_2OEt]^+$
			527	$[M—OCH_2CH_2OEt—CH_2CH_2OEt]^+$
W	OCH_2CH_2OH	OCH_2CH_2OH	633	$[M]^+$
			603	$[M—NO]^+$

Table 3—*continued*

M	X	Y	m/e	Tentative assignment
W	$O(CH_2)_4OH$	$O(CH_2)_4OH$	689	$[M]^+$
			599	$[M—\{O(CH_2)_4OH\}]^+$
			569	$[M—\{O(CH_2)_4OH\}—NO]^+$
			527	$[M—\{O(CH_2)_4OH\}—\{(CH_2)_4OH\}]^+$
W	$O(CH_2)_5OH$	$O(CH_2)_5OH$	717	$[M]^+$
			613	$[M—\{O(CH_2)_5OH\}]^+$
			527	$[M—\{O(CH_2)_5OH\}—\{(CH_2)_5OH\}]^+$
W	$O(CH_2)_6OH$	$O(CH_2)_6OH$	745	$[M]^+$
			627	$[M—\{O(CH_2)_6OH\}]^+$
			598	$[M—\{O(CH_2)_6OH\}—NO]^+$
			527	$[M—\{O(CH_2)_6OH\}—\{(CH_2)_6OH\}]^+$
			512	$[M—\{O(CH_2)_6OH\}_2]^+$
			481	$[M—\{O(CH_2)_5OH\}_2—NO]^+$
W	$OCH_2(CF_2)_3CH_2OH$	$OCH_2(CF_2)_3CH_2OH$	721	$[M—\{OCH_2(CF_2)_3CH_2OH\}]^+$
			691	$[M—\{OCH_2(CF_2)_3CH_2OH\}—NO]^+$
			512	$[M—\{OCH_2[(CF_2)_3CH_2OH\}_2]^+$

$[W\{(3,5\text{-}Me_2C_3HN_2)_3\}(NO)Cl(OCH_2CH_2X)]$, X = Cl, OMe *or* OEt

A mixture of $[W\{(3,5\text{-}Me_2C_3HN_2)_3\}(NO)Cl_2]$ (0.3 g), the appropriate alcohol $HOCH_2CH_2X$ (1 cm^3) and NEt_3 (0.5 cm^3) in toluene (100 cm^3) was stirred and refluxed for 2 h during which time the solution became blue. After cooling to R.T., *n*-hexane was added and the mixture further cooled to −10°C. An oil formed and the supernatant liquid which contained the desired product was collected, filtered and evaporated *in vacuo* to one third of its volume. Hexane was again added, the mixture filtered and the filtrate reduced partially *in vacuo*. The residue was purified by column chromatography using $CHCl_3$ as eluant. The second fraction was collected, evaporated *in vacuo* and recrystallized from diethylether/*n*-hexane mixture to afford the complex as blue crystals (yield 55–65%).

$[W\{(3,5\text{-}Me_2C_3HN_2)_3\}(NO)ClY]$, *where* Y = $O(CH_2)_nOH$ (n = 2–6), $O(CH_2(CF_2)_3CH_2OH$ *or* $OCHMeCH_2CMe_2OH$

A mixture of $[W\{(3,5\text{-}Me_2C_3HN_2)_3\}(NO)Cl_2]$ (0.5 g) and the appropriate dialcohol (1.0 cm^3) in toluene (100 cm^3) was stirred and refluxed for 4–8 h. During this time the solution became purple. On cooling to R.T., *n*-pentane was added and the mixture further cooled to −10°C. An oil formed and the purple supernatant liquid was decanted and filtered, being worked up in the same way as the compounds described immediately above. Dichloromethane was used as eluant and in a second chromatographic purification, $CHCl_3$ was used. Two purple bands were observed on the column, the first of which is bimetallic and is described elsewhere. The second fraction contains the desired complex which was finally recrystallized from a CH_2Cl_2/*n*-hexane mixture (when Y = $O(CH_2)_nOH$) or diethylether/*n*-hexane affording the complexes as purple powders (yields 35–55%).

$[Mo\{3,5\text{-}Me_2C_3HN_2)_3\}(NO)X_2]$, *where* X = OCH_2CH_2Y (Y = Cl, OMe, OEt) *or* $O(CH_2)_nOH$ (n = 3 *or* 4)

A mixture of $[Mo\{(3,5\text{-}Me_2C_3HN_2)_3\}(NO)I_2]$ (0.5 g), the appropriate alcohol (1.0 cm^3) and Na_2CO_3 (1.0 g) in toluene (100 cm^3) was stirred and refluxed for between 5 and 15 h. The length of reflux depended on the time taken to fully develop the pink solution characteristic of the final product. The reaction mixture was then cooled, *n*-pentane added and the mixture further cooled to −10°C. The oil which formed was discarded and the supernatant liquid evaporated *in vacuo*. The residue was dissolved in diethylether, and mixtures of *n*-hexane and *n*-pentane added. The solvent volume was then slowly reduced *in vacuo* until a pink precipitate formed. This was collected by filtration and dried *in vacuo*, affording a pure complex except for the species derived from $O(CH_2)_3OH$. This last compound was further purified by column chromatography using CH_2Cl_2/diethylether as eluant, affording yields greater than 75%.

$[Mo\{HB(3,5\text{-}Me_2C_3HN_2)_3\}(NO)\{O(CH_2)_nOH\}_2]$, $n = 4$, 5 *or* 6

To $[Mo\{HB(3,5\text{-}Me_2C_3HN_2)_3\}(NO)I_2]$ (0.5 g) dissolved in toluene (100 cm^3) was added the appropriate alcohol (1 cm^3) and Na_2CO_3 (1.0 g), and the mixture was refluxed for 15 h during which time the colour changed from green to pink. Purification was effected in the same way as for propanediolate described above. Further recrystallization from CH_2Cl_2/*n*-pentane/*n*-hexane gave a pink powder (yields 60–70%).

$[W\{HB(3,5\text{-}Me_2C_3HN_2)_3\}(NO)X_2]$ *where* X = OCH_2CH_2Cl, OCH_2CH_2OMe *and* OCH_2CH_2OEt

These complexes were prepared similarly to their Mo-containing analogues described above, using $[W\{HB(3,5\text{-}Me_2C_3HN_2)_3\}(NO)Cl_2]$ (0.5 g). After 15 h refluxing, the colour of the solutions had become orange. The complexes were purified by chromatography using CH_2Cl_2/acetone as eluant and precipitated from diethylether/*n*-pentane as an orange powder (yield 45–55%).

$[W\{HB(3,5\text{-}Me_2C_3HN_2)_3\}(NO)(OCH_2CH_2OH)_2]$

This compound was prepared in the same way as its analogues described immediately above, but using acetone as the reaction solvent (yield *ca* 60%).

$[W\{HB(3,5\text{-}Me_2C_3HN_2)_3\}(NO)X_2]$ *where* X = $O(CH_2)_nOH$ ($n = 4$, 5 *or* 6) *and* $OCH_2(CF_2)_3CH_2OH$

To $[W\{HB(3,5\text{-}Me_2C_3HN_2)_3\}(NO)Cl(OR)]$ (0.2 g), where R = Me or Et, dissolved in toluene (100 cm^3) was added Na_2CO_3 (0.5 g) and the appropriate dialcohol (0.5 cm^3). The mixture was stirred and refluxed for 10–15 h during which time the colour changed from blue to orange. Separation and purification of the complexes was the same as that described for the tungsten complexes X = OCH_2 CH_2Cl, etc. (yields 45–55%).

Acknowledgements—We are grateful to the SERC for support of part of this work and to the Politechnika Krakowska, Krakow, Poland for leave of absence of AW. We thank Messrs Malcolm Tolley and Tony Pemberton for assistance with NMR and mass spectroscopy respectively, and Mr Terry Green for technical help.

REFERENCES

1. J. A. McCleverty, D. Seddon, N. A. Bailey and N. W. Walker, *J. Chem. Soc., Dalton Trans.* 1976, 898.
2. J. A. McCleverty, A. E. Rae, I. Wolochowicz, N. A. Bailey and J. M. A. Smith, *J. Chem. Soc., Dalton Trans.* 1982, 951.
3. C. J. Jones, J. A. McCleverty, B. D. Neaves, S. J. Reynolds, H. Adams, N. A. Bailey and G. Denti, *J. Chem. Soc., Dalton Trans.* 1986, 733.
4. N. Al-Obaidi, P. D. Beer, J. P. Bright, C. J. Jones, J. A. McCleverty and S. S. Salam, *J. Chem. Soc., Chem. Comm.* 1986, 239.
5. S. M. Charsley, C. J. Jones, J. A. McCleverty, B. D. Neaves, S. J. Reynolds and G. Denti, *J. Chem. Soc., Dalton Trans.* 1988, in press.
6. G. Denti, J. A. McCleverty and A. Wlodarczyk, *J. Chem. Soc., Dalton Trans.* 1981, 2021.
7. J. A. McCleverty and A. Wlodarczyk, *24th Int. Conf. on Coordination Chemistry*, Athens, Greece; *Chimika Chronika New Series*, 1986, 404; A. Wlodarczyk, *Proc. 11th Summer School on Coordination Chemistry*, Karpacz, Poland, 1987, 48.
8. J. Trofimenko, *J. Am. Chem. Soc.* 1967, **89**, 3904; *ibid.* 1969, **91**, 588.

Polyhedron Vol. 7, No. 6, pp. 463–470, 1988
Printed in Great Britain

0277–5387/88 $3.00+.00
© 1988 Pergamon Press plc

DIRECT EVIDENCE FAVOURING AN INTERNAL FLIP OF DIMETAL UNITS IN CUBOIDAL LIGAND CAGES

F. ALBERT COTTON* and SUSUMU KITAGAWA

Department of Chemistry and Laboratory for Molecular Structure and Bonding, Texas A&M University, College Station, TX 77843, U.S.A.

(*Received* 3 *August* 1987; *accepted* 7 *October* 1987)

Abstract—Four isomeric compounds, $Mo_2Cl_4(dpdbp)_2$, have been synthesized: **1**, α-anti; **2**, α-syn; **3**, β-anti; **4**, β-syn. When the α isomers are synthesized from a $K_4Mo_2Cl_8$/1-diphenylphosphino-2-di(*p*-tert-butylphenyl)phosphinoethane (dpdbp)/CH_3OH reaction mixture, the ratio **1/2** obtained is ~ 97/3. The β isomers are obtained in an 85/15 mole ratio (**3/4**) from the reaction mixture $Mo_2(O_2CCF_3)_4$/Me_3SiCl/dpdbp/THF. **1** has been crystallized and structurally characterized by X-ray diffraction. The space group is $P\bar{1}$ and the unit cell constants are $a = 13.309(2)$, $b = 18.641(8)$, $c = 9.452(2)$ Å, $\alpha = 104.70(4)°$, $\beta = 106.77(2)°$, $\gamma = 83.14(2)°$, $V = 2169(2)$ Å^3 and $Z = 1$. The α-anti configuration is rigorously centrosymmetric with Mo—Mo = 2.149(1) Å, mean Mo—P = 2.551(3) Å and mean Mo—Cl = 2.424(4) Å. The **1/2** ratio can be altered by column chromatography. It is found by TLC that when a mixture of the α isomers is isomerized to a mixture of the β isomers the **3/4** ratio is the same as the initial **1/2** ratio. The α → β isomerization reaction, therefore, is stereospecific. An internal flip is the only process that necessarily has this essential character, and its occurrence is thus corroborated.

It has long been known that compounds of the type $M_2X_4(dppe)_2$, exist in both α (chelated) and β (bridged) forms,[1] and that generally the α form is thermodynamically less stable than the β form. The rates and activation parameters for several α → β rearrangements have been reported.[2–4] Several suggestions have been made as to the detailed course of these rearrangements (which are, incidently, reversible[4,5]), of which the most explicit and intriguing, is that they occur by a flip of the M_2 dumb-bell within the quasi-cubic set of coordinated ligand atoms.[2] Some persuasive evidence for this is provided by the fact that the rate is unaffected by the presence of a large excess of dppe and that the isomerization can occur cleanly in the solid state.[4] In spite of this evidence, we have been endeavouring to obtain independent and more direct evidence to support the internal flip proposal. In this paper we report results concerning stereospecificity in the α → β process that can be explained by the internal flip process but probably not by other pathways in which ligand dissociation and recombination occur.

* Author to whom correspondence should be addressed.

EXPERIMENTAL

All operations were carried out under an atmosphere of purified argon. Solvents were dried by conventional methods and distilled under nitrogen. $K_4Mo_2Cl_8$ and $Mo_2(O_2CCF_3)_4$ were prepared as described elsewhere.[6,7]

p-tert-butylbromobenzene was purchased from Alfa Products. Phosphorus trichloride, diphenylvinylphosphine and 1,2-bis(dichlorophosphino) ethane were purchased from Aldrich Chemicals. Silica gel powders (60–200 mesh, 140 Å) for chromatography and silica gel plates for thin layer chromatography (TLC) were purchased from Aldrich Chemicals and Sigma Chemical Company, respectively.

Preparation of 1-diphenylphosphino-2-di(p-tert-butylphenyl)-phosphinoethane (Dpdbp)

Dry *p*-tert-butylbromobenzene (50 g, 0.23 mol) in THF was treated with Mg (5.6 g, 0.23 mol) to give *p*-tert-butylphenyl magnesium bromide. To this solution was added PCl_3 (9.57 g, 0.069 mol)

in THF. The resultant solution was treated with aqueous saturated NH_4Cl solution, dried over Na_2SO_4 and evaporated to dryness, giving yellow crude powder. This powder was recrystallized from ethanol–$CHCl_3$ to provide tris(*p*-tert-butyl)phosphine as a white crystalline solid. Yield, 25.8 g (85%), m.p. 235.1–235.9°C. Found: C, 83.4; P, 6.8; H, 9.1. Calc. for $C_{30}H_{39}P$: C, 83.7; P, 6.8; H, 9.1%.

For the synthesis of bis(*p*-tert-butyl)phosphine the usual synthetic method[8,9] was modified because lithium metal did not react with tris(*p*-tert-butyl) phosphine. A mixture of potassium metal (3.0 g, 0.077 mol) and tris(*p*-tert-butyl)phosphine (5.1 g, 0.012 mol) in 160 cm^3 THF was refluxed for 3 h. After removal of the unreacted K, the resultant dark red solution was hydrolysed, extracted with ether and the ether extract was washed with dilute acid and water. Evaporation of the solvent gave a yellow residue, which was washed with methanol and the crude white solid was separated by filtration. This solid was recrystallized from benzene/methanol to give a white crystalline solid; yield 1.8 g (50%); ν_{P-H}(Nujol), 2300 cm^{-1}.

A mixture of 1.2 g (0.0057 mol) of diphenylvinylphosphine, 1.7 g (0.0057 mol) of bis(tert-butyl)phosphine, and 0.14 g potassium tert-butoxide in THF was refluxed for 6 h, followed by evaporation of the solvent. The resultant orange–yellow residue was washed with methanol and filtered. The crude white solid was recrystallized from benzene/methanol to give a white crystalline solid. Yield, 1.4 g (48%). M.p. 118.5–119.2°C. Found: C, 78.4; P, 11.6; H, 7.9. Calc. for $C_{34}H_{40}P_2$: C, 80.0; P, 12.1; H, 7.9%. 400 MHz NMR (CD_2Cl_2, 25°C): δ 1.295 (s, 18H), 2.078 (m, 4H), 7.25–7.36 (m, 18H).

Preparation of 1,2-*bis*(*di*(p-*tert-butylphenyl*)*phosphino*)*ethane* (*Dbppe*)

A THF solution of *p*-tert-butylphenylmagnesium bromide was prepared from *p*-tert-butylbromobenzene (4.23 g, 0.020 mol), by the method described above. To this solution, 1,2-bis(dichlorophosphino)ethane (1.15 g, 0.0050 mol) in 10 cm^3 THF was added dropwise with vigorous stirring. Heat was evolved and the solution refluxed spontaneously. When cool, the reaction mixture was poured slowly with stirring into a saturated solution of NH_4Cl. The aqueous layer was separated and extracted with ether. The combined ether and THF portions were evaporated and a white solid remained behind. This solid was recrystallized from benzene/CH_3OH to give the pure product. Yield, 1.6 g (50%). M.p. 238.5–239.5°C. Found: C, 79.8; P, 9.8; H, 9.0. Calc. for $C_{42}H_{56}P_2$: C, 81.0; P, 9.9; H, 9.1%. 200 MHz NMR (CD_2Cl_2, 25°C): δ 1.30 (s, 36H), 2.09 (m, 4H), 7.2–7.5 (m, 16H).

Preparation of α-$Mo_2Cl_4(dpdbp)_2$

A mixture of $K_4Mo_2Cl_8$ (0.21 g, 0.34 mmol) and dpdbp (0.34 g, 0.68 mmol) in 25 cm^3 of methanol was refluxed for 2 h. A green powder precipitated and was separated by filtration, washed once with methanol and diethylether and dried in vacuum. Yield, 0.23 g (50%). This powder contained small amounts of the β form and $K_4Mo_2Cl_8$; the pure α form was obtained from the second main CH_2Cl_2 fraction by silica gel column chromatography.[5] IR: ν_{M-Cl}(Nujol), 308, 295 cm^{-1}. UV-Vis: λ_{max} nm (ε_{max} M^{-1} cm^{-1}), 341 (6780), 385 sh, 470 (381), 669 (3030). The ^1H NMR spectrum of α-$Mo_2Cl_4(dpdbp)_2$ showed the two isomers, *anti* (**1**) and *syn* (**2**). 400 MHz NMR (CD_2Cl_2, −80°C): the full spectrum together with the assignments is shown in Fig. 1. Signals of **1**; δ (ppm), 0.926 (s, 18H), 1.211 (s, 18H), 3.33 (br, 1H), 3.49 (br, 1H), 4.58 (br, 1H), 4.74 (br, 1H), 6.32 (t, 2H), 6.52 (t, 2H), 6.55 (d, 2H), 6.65 (d, 2H), 6.69 (t, 1H), 7.00 (d, 2H), 7.23 (t, 2H), 7.44 (m, 3H), 7.67 (br, 1H). Most of the signals for **2** are partially or wholly overlapped by the intense signals of **1**. A tert-butyl methyl signal at 1.245 ppm of the "parallel"[5] aryl group is well-separated from that of **1**. The ratio **1**/**2** is approximately 97/3, as inferred from the ratio of the two tert-butyl methyl signals of the "parallel" aryl groups. With the use of CH_2Cl_2/*n*-hexane (11/2, v/v) as an eluting solvent, **1** was separated from the mixture by silica gel column chromatography.

Preparation of β-$Mo_2Cl_4(dpdbp)_2$

$Mo_2(O_2CCF_3)_4$ (0.23 g, 0.40 mmol) was dissolved in 10 cm^3 THF and Me_3SiCl (0.3 cm^3) was added.[10] This solution was stirred for 12 h and then 0.40 g of dpdbp (0.79 mmol) was added. The solution was refluxed for 10 h and a brown precipitate was separated from the reaction mixture by filtration. This brown powder was washed once with methanol and cold ether, and dried *in vacuo*. Yield, 0.22 g (40%). IR: ν_{M-Cl}(Nujol), 335, 298 cm^{-1}. UV-Vis: λ_{max} nm (ε_{max} M^{-1} cm^{-1}), 343 (2550), 456 (560), 542 sh, 758 (730). 400 MHz NMR (CD_2Cl_2): at 20°C, δ 1.300 (s, 18H), 3.40 (s, 4H), 7.25–7.80 (br, 18H); at −90°C, there are four broad signals, shown in Fig. 3 (part 4), which are ascribed to tert-butyl methyl protons, *viz.* δ 1.01, 1.09, 1.27, 1.33. Other signals, 2.52 (br, 4H), 6.55–8.10 (br, 18H).

We were unable to identify the *anti* (**3**) and *syn* (**4**)

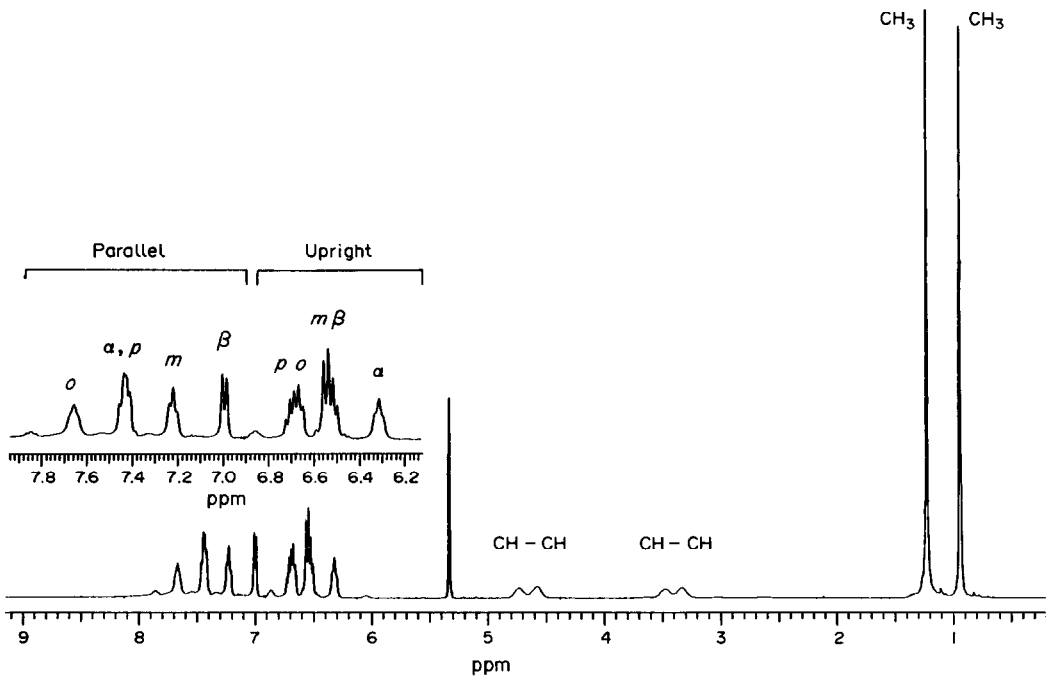

Fig. 1. ^{1}H NMR spectrum at −80°C of α-$Mo_2Cl_4(dpdbp)_2$ obtained in CD_2Cl_2 at 400 MHz. An enlargement of the aryl region is also shown. The assignments of the α-*anti* isomer are made and indicated above each signal. "Upright" and "parallel" denote the orientation of the aryl ring in the molecule of α-$Mo_2Cl_4(dpdbp)_2$, as discussed in the text.

isomers of β-$Mo_2Cl_4(dpdbp)_2$ by ^{1}H NMR spectra because a low-energy fluxional process broadens the signals. The molar ratio **3/4** was checked by TLC. By use of the mixture of CH_2Cl_2/*n*-hexane (11/2, v/v) as an eluting solvent, two spots were obtained, which correspond to the *anti* and the *syn* isomers. The spot area of the *anti* isomer at $Rf = 0.65$,[11] was much bigger than that of the *syn* isomer at $Rf = 0.58$; we can estimate the **3/4** ratio as 6 ± 1. Since the ratio **1/2** is about five times greater than the ratio **3/4**, the β-*syn* isomer is clearly preferred to the α-*syn* one.

Preparation of β-$Mo_2Cl_4(dbppe)_2$

β-$Mo_2Cl_4(dbppe)_2$ was prepared from $Mo_2(O_2CCF_3)_4$/Me_3SiCl/dbppe/THF in a way similar to that described above. The α form could not be synthesized from $K_4Mo_2Cl_8$/dbppe/CH_3OH, which also gave the brown β form. IR: ν_{M-Cl}(Nujol) 345, 293 cm^{-1}. UV-Vis: λ_{max} (ε_{max} M^{-1} cm^{-1}), 341 (3010), 456 (654), 540 sh, 760 (850). 400 MHz NMR (CD_2Cl_2, −110°C): δ 1.201 and 1.235 (s, 18H), 2.47 (br, 4H), 6.943 (br, 4H), 7.233 (br, 4H), 7.41 (br, 4H), 7.80 (br, 4H).

Isomerization of α-$Mo_2Cl_4(dpdbp)_2$ *to the* β *form*

The purity of the α form and its *anti* to *syn* isomer ratio for each fraction were checked by ^{1}H NMR measurements and TLC. In each of the chromatographic fractions of the α form the solvent was completely evaporated. The residue of each fraction was then dissolved in THF and the solution was refluxed for 1 h. The green colour turned brown, indicating the formation of the β form. Complete conversion to the β form was confirmed by the ^{1}H NMR measurements and TLC, and it was further shown that no detectable decomposition occurred during the conversion experiment.

In the case of TLC experiments, the α and β isomers gave green and brown spots, respectively. To confirm the stained spot area, iodine vapour[11] was applied to a developed TLC plate, which yielded a brown colour. Quantitative estimation of the areas of the two spots on each TLC plate was done by visual comparison of the stained spots.[11]

* *Rf* is the retardation factor.[11] In the case of the α-form, the *anti*- and the *syn*-isomers gave spots at $Rf = 0.24$ and 0.13, respectively, when the same silica gel plate and eluting solvent were used.

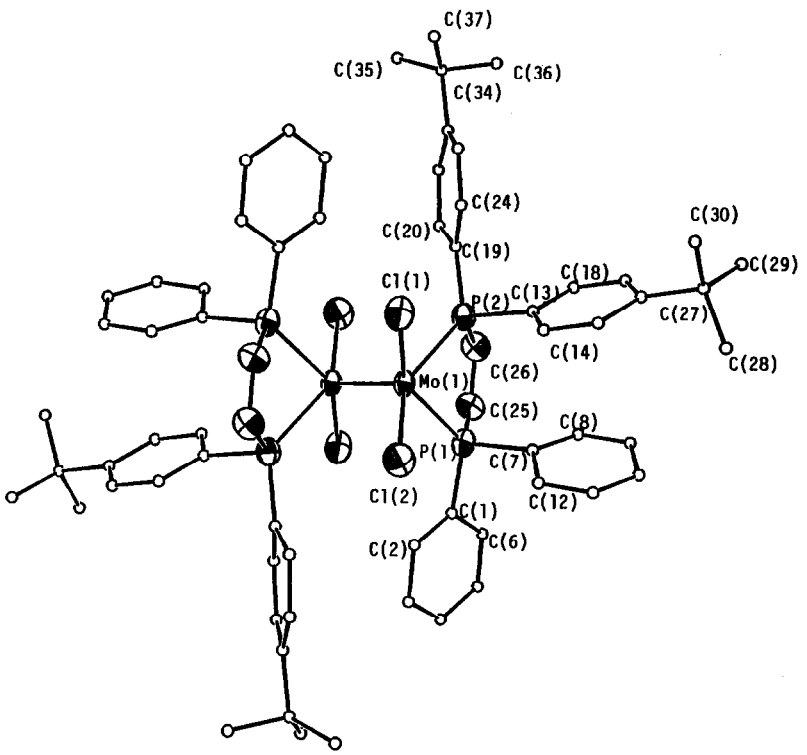

Fig. 2. An ORTEP drawing of the entire molecule of *anti*-α-$Mo_2Cl_4(dpdbp)_2$ with thermal ellipsoids at the 50% level for Mo, Cl and P atoms as well as C(25) and C(26). Those of atoms in the phenyl rings and tert-butyl groups have been arbitrarily reduced. The numbers of unlabelled phenyl carbon atoms follow from those given. Only half the atoms are labelled since the others are related by a centre of inversion at the midpoint of the Mo—Mo bond.

Physical measurements

Electronic absorption spectra were measured on dichloromethane solutions with a Cary 17D spectrophotometer. Infrared spectra were recorded as Nujol mulls using a Perkin–Elmer 783 spectrophotometer. ^1H NMR spectra were obtained on Varian XL 200 and 400 NMR spectrometers, operating in the Fourier transform mode at −115, −90 and 25°C.

Preparation of crystals

α-$Mo_2Cl_4(dpdbp)_2$ (in a **1/2** ratio of 97/3) was dissolved in dichloromethane and a layer of methanol was gently introduced over the green solution. The two layers were kept below 0°C for several days and plate shaped crystals were obtained.

X-ray diffraction procedures. Data collection

The crystal was placed in a thin-walled glass capillary, surrounded by mother liquor and was examined on an Enraf–Nonius CAD-4 automated diffractometer. Unit cell constants were determined from the geometric parameters of 25 well-centred reflections with 2θ values in the range $18 \leqslant 2\theta \leqslant 29°$ and are listed in Table 1. The crystal was extremely unstable under the conditions of measurement and decomposed completely within 48 h. We tried many times to collect an entire set of data from one crystal but did not succeed. Consequently, the data employed were obtained from two crystals of similar size. For both crystals, significant decay of intensity was observed for three standards monitored throughout 30 h of data collection, and the corrections were made in each case. Each data set was also corrected for Lorenz and polarization effects, and an empirical absorption correction was applied on the basis of azimuthal scans of selected reflections with the χ angle near 90°. These two data sets were finally merged by using the SHELX-76 program. The agreement (R) factor was 0.0509.

Structure solution and refinement

The position of the unique Mo atom was determined from a three-dimensional Patterson map. With the midpoint of the dinuclear unit residing on

Table 1. Crystal data for α-*anti*-$Mo_2Cl_4(dpdbp)_2 \cdot 4CH_2Cl_2$

Formula	$Mo_2Cl_{12}P_4C_{72}H_{88}$
Formula weight	1694.58
Space group	$P\bar{1}$
a, Å	13.309(2)
b, Å	18.641(8)
c, Å	9.452(2)
α, deg	104.70(4)
β, deg	106.77(2)
γ, deg	83.14(2)
V, Å^3	2169(2)
Z	1
d_{calc}, g cm^{-3}	1.29
Crystal size, mm	$0.3 \times 0.25 \times 0.3$
μ(Mo-K_α), cm^{-1}	6.68
Data collection instrument	CAD-4S
Radiation (monochromated in incident beam)	Mo-K_α ($\lambda_\alpha^- = 0.71073$ Å)
Orientation reflections, number, range (2θ)	25, $18 \leqslant 2\theta \leqslant 29$
Temperature, °C	22 ± 3
Scan method	ω-scan
Data col. range, 2θ, deg	4–45
No. unique data, total with $F_o^2 > 3\sigma(F_o^2)$	3959
Numbers of parameters refined	393
Trans. factors, max., min.	0.951, 0.754
R^a	0.0796
R_w^b	0.105
Quality-of-fit indicator[c]	1.11
Largest shift/esd, final cycle	0.18
Largest peak, e Å^{-3}	1.05

[a] $R = \Sigma ||F_o| - |F_c|| / \Sigma |F_o|$.
[b] $R_w = [\Sigma w(|F_o| - |F_c|)^2 / \Sigma w|F_o|^2]^{1/2}$; $w = 1/\sigma^2(|F_o|)$.
[c] Quality-of-fit = $[\Sigma w(|F_o| - |F_c|)^2 / (N_{obs} - N_{parameters})]^{1/2}$.

a crystallographic inversion centre, the asymmetric unit is defined by half of a molecule of $Mo_2Cl_4(dpdbp)_2$. A series of alternating least-squares refinements and difference Fourier maps led to satisfactory development of the atoms in the coordination sphere of the molybdenum atom. Full matrix least-squares refinement followed by a difference Fourier map revealed the positions of all the other non-hydrogen atoms, including atoms of the CH_2Cl_2 molecules. A subsequent Fourier map revealed disorder in the two tert-butyl groups. The refinement of alternative orientations was made with constraints on the bond distances and angles of the tert-butyl groups by use of the SHELX-76 program, leading finally to two orientations, with site occupancies of 0.54/0.46 and 0.76/0.24 for C_{28}–C_{33} and C_{35}–C_{40}. At this stage, the R value was 0.095. One of two CH_2Cl_2 showed large isotropic thermal factors. Several peaks with heights of 1.3–1.1 eÅ^{-3} were still present in the difference Fourier map. There are three positions for CH_2Cl_2 molecules in the asymmetric unit, of which one is fully occupied but with two-fold orientational disorder. The other two positions are each half occupied and one of these also showed some orientational disorder. These occupancies are in accord with the overall composition $Mo_2Cl_4(dpdbp)_2 \cdot 4CH_2Cl_2$. After site occupancies had been determined with fixed isotropic thermal factors, the positions and the isotropic thermal factors were refined with the site occupancies fixed. The final full matrix least-squares refinement gave $R = 0.079$.*

* *Supplementary material available*: Atomic coordinates, full listing of bond angles, bond distances and anisotropic displacement parameters (six pages); tables of observed and calculated structure factors (twenty-two pages). Copies are available from the Editor. Atomic coordinates have also been deposited with the Cambridge Crystallographic Data Centre.

RESULTS AND DISCUSSION

Structure of anti-α-$Mo_2Cl_4(dpdbp)_2$

Anti-α-$Mo_2Cl_4(dpdbp)_2$ shows a molecular structure very similar to that of *anti-α-*$Mo_2Cl_4(dpdt)_2$.[5] A dpdbp ligand chelates to each of the Mo atoms of the dimer. The principal bond distances and angles are listed in Table 2. As in the case of the dpdt complex, the aryl groups of each phosphorus atom are differentiated into parallel and upright types in terms of their relationship to the mean plane of the $MoCl_2P_2$ ring. This can be clearly seen in Fig. 2. The distance between the centres of nearest neighbour parallel phenyl groups is 3.56 Å.* In the case of *syn-α-*$Mo_2Cl_4(dpdbp)_2$, it is expected that there is steric repulsion involving the tert-butyl groups on two of the parallel phenyl groups, thus accounting for the observation that the *syn* form is a minor product of the reaction of $K_4Mo_2Cl_8$/dpdbp/CH_3OH. This hypothesis is corroborated by the fact that with the symmetrical dbppe ligand no α form could be prepared at all. In the case of dbppe, these steric repulsions would be much more severe than in the case of dpdbp, because there would be four sterically interacting parallel tert-butyl groups in α-$Mo_2Cl_4(dbppe)_2$. This large amount of repulsive interaction evidently prevents the formation of any of the α form, and all preparative reactions give exclusively the β form, in which very little repulsion involving the tert-butyl groups would be expected.

Fortunately, unsymmetrical dpdbp still provides the α-*syn* isomer, but at the same time the perturbation by the tert-butyl group is large enough to make it possible to separate the *anti* and *syn* isomers by chromatography.

Characterization of α-$Mo_2Cl_4(dpdbp)_2$

The ^1H NMR spectrum of α-$Mo_2Cl_4(dpdbp)_2$ is shown in Fig. 1, which gives a pattern similar to that of α-$Mo_2Cl_4(dpdt)_2$.[5] The ring current effect of "parallel" aryl groups characteristic of the α form allows a definitive assignment of these signals. This was done by referring to the assignment of the ^1H NMR spectrum of the analogous dpdt system.[5] In α-$Mo_2Cl_4(dpdt)_2$, it was hard to separate the two isomers and the recorded spectrum afforded the signals of both isomers with equal intensities. On the other hand, the spectrum of α-$Mo_2Cl_4(dpdbp)_2$ shows a large difference in signal intensities between the *anti* and *syn* isomers. The methyl signals of the "parallel" tert-butyl groups can be used to infer that the ratio **1**/**2** is 97/3 (Fig. 3). Because the yield of the *syn* isomer is so very small and most of the aryl signals of **2** are obscured by those of **1**, only a partial assignment was made in the case of the *syn* isomer.

The ^1H NMR spectrum of β-$Mo_2Cl_4(dpdbp)_2$ gives broad, averaged signals even at −90°C, indicative of a low-energy fluxional process similar to those in β-$Mo_2Cl_4(dpdt)_2$[5] and β-$Mo_2I_4(dppe)_2$.[13] The most probable process is an interconversion between the two rotational isomers, which have different conformations for the six-membered rings of the $Mo_2P_2C_2$ moiety.[10] The −90°C spectrum in the region of the tert-butyl groups is shown in Fig. 3 (part 4). The four broad signals (line-width at half height: 11 Hz) can be assigned to the two slowly interconverting rotomers, and the intensity ratio of the weak outer

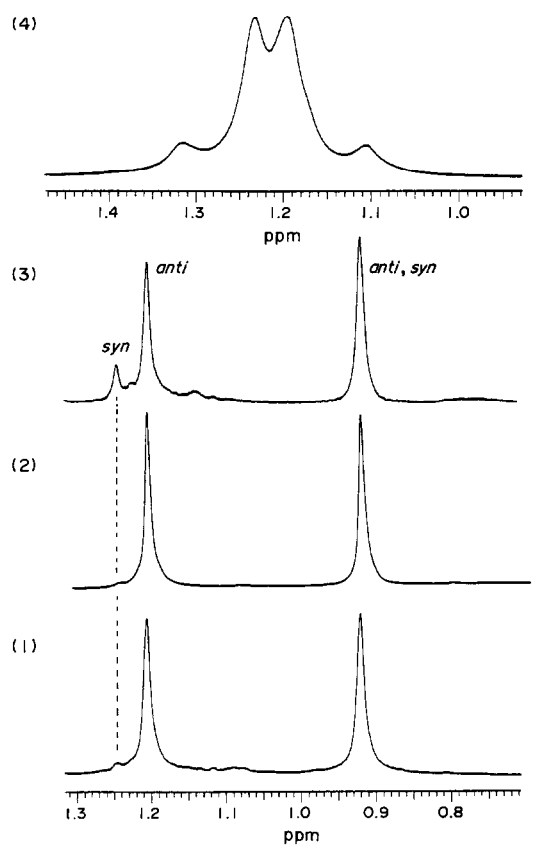

Fig. 3. (1)–(3) the ^1H NMR methyl signals of α-$Mo_2Cl_4(dpdbp)_2$ at −80°C. (1) the reaction mixture, (2) the chromatographic first fraction and (3) the chromatographic third fraction. (4) The ^1H NMR methyl signals of β-$Mo_2Cl_4(dpdbp)_2$ at −90°C.

* By use of the structure of Fig. 2, an assumed pivot carbon atom (C*) of a tert-butyl group is placed on C(10), with the C(10)—C* distance = 1.52 Å. The distance between C* and C(27) atoms is 4.64 Å.

Table 2. Bond distances (Å) and bond angles (deg)

Bond distances			
Mo(1)—Mo(1)′	2.149(1)	Mo(1)—P(1)	2.550(3)
Mo(1)—Cl(1)	2.436(4)	Mo(1)—P(2)	2.551(3)
Mo(1)—Cl(2)	2.412(3)		
Bond angles			
Mo(1)′—Mo(1)—Cl(1)	111.32(7)	Cl(1)—Mo(1)—P(1)	147.1(1)
Mo(1)′—Mo(1)—Cl(2)	109.45(8)	Cl(1)—Mo(1)—P(2)	88.6(1)
Mo(1)′—Mo(1)—P(1)	99.85(8)	Cl(1)—Mo(1)—Cl(2)	88.7(1)
Mo(1)′—Mo(1)—P(2)	101.72(7)	Cl(2)—Mo(1)—P(1)	90.5(1)
P(1)—Mo(1)—P(2)	74.74(9)	Cl(2)—Mo(1)—P(2)	147.43(9)

pair to the strong inner pair is 0.22. This ratio may be compared with the ratio of the minor and major rotamers for β-Mo_2Cl_4(dppe)$_2$ in the solid state[10] which was 0.15. An attempt to sharpen the spectrum by further cooling to −115°C (below which the solution froze) was ineffective.

Chromatographic separation of **1** *and* **2**

In our previous study[5] of the *p*-tolyl analogs of the Mo_2Cl_4(dpdbp)$_2$ isomers, we were unable to separate the *syn* and *anti* forms of the α isomer (the counterparts of **1** and **2**). Evidently the difference between the *p*-tolyl and phenyl substituents on the phosphorus atoms is too slight to alter the chromatographic properties of the two geometric isomers sufficiently. With the use of the dpdbp ligand we have surmounted this problem. From the preparative reaction we obtained an equilibrated mixture of **1** and **2** in the ratio of about 97/3 as shown in Fig. 3, spectrum (1). Upon chromatographing this mixture, the *anti*(**1**) and *syn*(**2**) isomers are separated. The first fraction off the column (Fig. 3, spectrum 2) is essentially pure (⩾ 99%) *anti*-α while the third fraction (Fig. 3, spectrum 3) is enriched in the *syn* isomer (*ca* 17%).

Chromatographic separation of **3** *and* **4**

By TLC the β-Mo_2Cl_4(dpdbp)$_2$ synthesized from $Mo_2(O_2CCF_3)_4$ was separated into two fractions with *Rf* values of 0.65 and 0.58,* which correspond to **3** and **4**, respectively. The *anti*/*syn*(**3**/**4**) ratio here is much smaller (by a factor of about five) than that for **1**/**2**. This is clearly in accord with the fact that the steric effects of the *p*-tert-butyl groups are much less important in the β isomers. Column chromatography was found to be effective for separating **3** and **4** in larger quantities.

Stereospecific α → β isomerization

The first and third fractions of the chromatographed α isomer were each thermally isomerized to the β form. The sample of β form obtained from the first fraction (the pure α-*anti* isomer) gave only one spot at 0.65 when subjected to TLC, which corresponds to the *anti* isomer of the β form. The third fraction (**1**/**2** = 83/17) of the α form gave a sample of the β form which TLC showed to consist of both **3** and **4** in the same (83/17) ratio within the errors of estimation. In the conversion of α to β isomers, the *syn*/*anti* ratio remains unchanged.

CONCLUSION

In Fig. 4 we show schematic representations of the four isomeric molecules, **1**–**4**, and indicate all possible interconversions that might be considered prior to any experimental study. In the present system we have not actually observed any β → α conversions, i.e. (2), (4), (6), (8), but in general they are as possible as their respective α → β conversions (1), (3), (5), (7), respectively, except that they are generally slower. In our previous study of Mo_2Cl_4(dpdt)$_2$, β → α conversion was directly observed. Our observation that the **1**/**2** ratio in an α sample is maintained in the resulting β product tells us that only the processes (1), (2), (3) and (4) can occur appreciably over the periods of time we allowed for the α → β transformations. All remaining processes, (5)–(12) must be enormously slower.

* *Rf* is the retardation factor.[11] In the case of the α-form, the *anti*- and the *syn*-isomers gave spots at *Rf* = 0.24 and 0.13, respectively, when the same silica gel plate and eluting solvent were used.

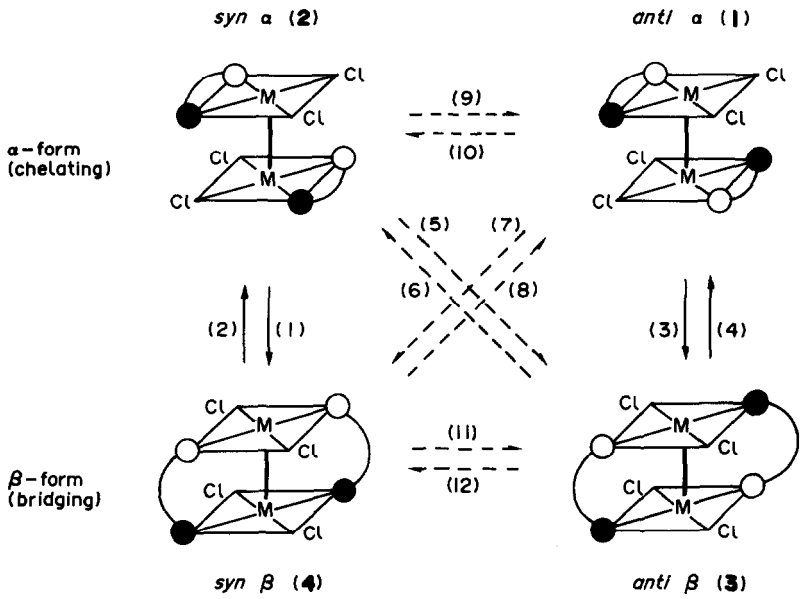

Fig. 4. A diagram depicting the four isomeric $Mo_2Cl_4(dpdbp)_2$ molecules in a schematic way and showing the six reversible interconversions that can be considered. The experimental observations indicate that only those with full arrows [i.e. (1)(2) and (3)(4)] occur.

This situation is naturally and rigorously accounted for if the only readily accessible pathway for interconverting α and β isomers is by an internal rotation of the Mo_2 unit within the ligand cage.

Acknowledgement—We are grateful to Dr L. Falvello for advice relating to the structure of refinement 1.

REFERENCES

1. S. A. Best, T. J. Smith and R. A. Walton, *Inorg. Chem.* 1978, **17**, 99.
2. P. A. Agaskar, F. A. Cotton, D. R. Derringer, G. L. Powell, D. R. Root and T. J. Smith, *Inorg. Chem.* 1985, **24**, 2786.
3. I. F. Fraser, A. McVitie and R. D. Peacock, *J. Chem. Res.* 1984, 420.
4. P. A. Agaskar and F. A. Cotton, *Inorg. Chem.* 1986, **25**, 15.
5. F. A. Cotton and S. Kitagawa, *Inorg. Chem.* 1987, **26**, 3464.
6. F. A. Cotton and J. G. Norman, Jr., *Coord. Chem.* 1972, **1**, 161.
7. F. A. Cotton and J. V. Brencic, *Inorg. Chem.* 1970, **9**, 351.
8. D. Wittenberg and H. Gilman, *J. Org. Chem.* 1958, **23**, 1063.
9. S. O. Grim and R. P. Molenda, *Phosphorus* 1974, **4**, 189.
10. P. A. Agaskar and F. A. Cotton, *Inorg. Chem.* 1984, **23**, 3383.
11. E. Stahl (Ed.), *Thin-Layer Chromatography. A Laboratory Handbook*. Springer, New York (1965).
12. F. A. Cotton, K. R. Dunbar and M. Matusz, *Inorg. Chem.* 1986, **25**, 3641.

Polyhedron Vol. 7, No. 6, pp. 471–476, 1988
Printed in Great Britain

0277–5387/88 $3.00 + .00
© 1988 Pergamon Press plc

SULPHUR MEDIATED INDUCED ELECTRON TRANSFER REACTIONS IN W—S SYSTEMS: SYNTHESIS AND REACTIVITY OF $(Et_4N)_2[W_2(V)O_2(\mu\text{-}S)_2(S_2)_2]$

MOHD. ASIM ANSARI, JAYANTHI CHANDRASEKARAN and SABYASACHI SARKAR*

Department of Chemistry, Indian Institute of Technology, Kanpur 208 016, India

(*Received* 26 *May* 1987; *accepted after revision* 13 *October* 1987)

Abstract—Reaction of $[W(VI)OS_3]^{2-}$ with I_2, $S_2O_4^{2-}$, peroxide or disulphide leads to the formation of $[W_2(V)O_2(\mu\text{-}S)_2(S_2)_2]^{2-}$ which goes back to $[W(VI)OS_3]^{2-}$ on treatment with S_x^{2-} via an induced electron transfer process. $[W_2(V)O_2(\mu\text{-}S)_2(S_2)_2]^{2-}$ reacts with activated acetylene and KCN to give $[W_2(V)O_2(\mu\text{-}S)_2(S_2C_2(COPh)_2)_2]^{2-}$, a dithiolene complex and $[W_2(V)O_2(\mu\text{-}S)_2(CN)_6]^{4-}$, a simple substitution product respectively. The synthesized complexes have been characterized by a variety of spectroscopic techniques. CV and XPS results are also discussed.

The sulphur mediated induced electron transfer reaction, a process relevant to several biological systems[1,2] was first reported in cobalt chemistry.[3] Recently Coucouvanis and coworkers have reported the novel reaction between $[Mo(VI)S_4]^{2-}$ and elemental sulphur to yield $[Mo(IV)S(S_4)_2]^{2-}$.[4] Subsequently, Stiefel and coworkers reported the complementary reaction i.e. the conversion of $[Mo(IV)S(S_4)_2]^{2-}$ to $[Mo(VI)S_4]^{2-}$ using dithiol as an external reductant.[5] In all such reactions, use of an external oxidant/reductant resulted in desired changes at the coordinated ligands and the metal centre. Following this strategy some difficult synthetic goals in Mo—S chemistry have been achieved.[5,6] Until very recently, application of this strategy to W—S systems was not known.[6,7] We report here the synthesis, characterization and reactivity of our preliminarily communicated title compound, $[W_2O_2(\mu\text{-}S)_2(S_2)_2]^{2-}$ (**2**).†[8]

EXPERIMENTAL

H_2MoO_4 was used as received. $(NH_4)_2WOS_3$[9] and dibenzoyl acetylene (DBA)[10] were prepared by literature methods. Solvents and other reagents were of analytical grade and distilled before use.

C, H and N were analysed at the microanalytical laboratory, I.I.T. Kanpur, India and sulphur was estimated gravimetrically as $BaSO_4$. Infrared spectra using CsI pellets were recorded on a Perkin–Elmer model 580 spectrophotometer. Electronic spectra were recorded on a Shimadzu (UV-190) double beam spectrophotometer. ^1H NMR and ^{13}C NMR spectra were taken on Varian EM-390, 90 MHz and Varian CFT-20, 400 MHz spectrometers, respectively in DMSO-d_6. An X-ray diffractogram was obtained on an ISO-BEBYFLEX X-200 diffractometer using a Cu-K_α radiation source. XPS measurements were carried out on an ESCALAB 510 photoelectron spectrometer using the Al-K_α line (1486.6 eV) radiation, taking the carbon ($1s_{1/2}$) binding energy (285.0 eV) as a standard. CV was recorded on a PAR model 370-4 electrochemistry system, a 174 A polarographic analyser, a 175 universal programmer and a RE-0074 X-Y recorder. All the experiments were done under a nitrogen atmosphere in a three electrode configuration using platinum and glassy-carbon working electrodes in positive and negative potential regions.

Synthesis of $(Et_4N)_2[W_2O_2(\mu\text{-}S)_2(S_2)_2]$ (2)

Method A. To a solution of $(NH_4)_2WOS_3$ (**1**) (664 mg, 2 mmol) and Et_4NBr (630 mg, 3 mmol) in H_2O

* Author to whom correspondence should be addressed.

† It is interesting to note that the molybdenum analogue of **2** i.e. $[MoO_2(\mu\text{-}S)_2(S_2)_2]^{2-}$ was synthesized as early as 1980 by Müller and coworkers,[11] but the role of oxygen as the external oxidant was not recognized at that time.

(20 cm^3), iodine (253.8 mg, 2 mmol) dissolved in EtOH (5 cm^3) was added. The resulting mixture was warmed on a water bath for 20 min and then KOH (100 mg, 2.56 mmol) dissolved in a minimum amount of H_2O was added to it and again warmed for 5 min. The solution was filtered and the precipitate was washed with H_2O, EtOH and ether, and recrystallized from CH_3CN/2-PrOH. Found: C, 22.5; H, 4.5; N, 3.1; S, 22.6. $C_{16}H_{40}N_2O_2S_6W_2$ requires: C, 22.5; H, 4.7; N, 3.3; S, 22.5%. Yield: 180 mg (~ 21%).

Method B. **1** (664 mg, 2 mmol) was dissolved in H_2O (30 cm^3) and solid $(NH_4)_2S_2O_8$ (228.20 mg, 1 mmol) was added to it. The solution was stirred vigorously for 4 h, then Et_4NBr (630 mg, 3 mmol) was added. After 10 min a 25% ammonia solution (5 cm^3) was added to it. After 5 min this was filtered and the precipitate was recrystallized as mentioned above. Yield: 205 mg (24%).

Method C. **1** (664 mg, 2 mmol) and Et_4NBr (630, 3 mmol) were dissolved in DMF (20 cm^3) by warming at 110°C for 5 min. PhSSPh (218.34 mg, 1 mmol) or *t*-butyl hydroperoxide (0.1 cm^3, 1 mmol) or PhOOPh (186.21 mg, 1 mmol) was added to it. The resulting red solution was left at 110°C for $\frac{1}{2}$ h and then cooled to R.T. Addition of 2-PrOH (15 cm^3) and ether (20 cm^3) yielded a red crystalline product which was washed with H_2O, EtOH and ether, and recrystallized from CH_3CN/2-PrOH. Yield: 60–70%.

Analysis was found to be satisfactory in both methods B and C.

Reaction of **2** *with* DBA *or synthesis of* $(Et_4N)_2[W_2O_2(\mu\text{-}S)_2(S_2C_2(COPh)_2)_2]$ **(3)**

Dibenzoyl acetylene (DBA) (234 mg, 1 mmol) was dissolved in CH_3CN (10 cm^3) and stirred for 5 min at R.T. When the colour of the solution changed from orange to green, absolute EtOH was added dropwise until the solution became hazy. This was filtered and the solution was kept at room temperature for 2 days. The needle shaped brown crystals which separated out were washed with EtOH and ether, and dried under vacuum. Found: C, 43.6; H, 4.5; N, 2.0. $C_{48}H_{60}N_2S_6W_2$ requires: C, 43.6; H, 4.5; N, 2.1%. Yield: 130 mg (~ 20%).

Reactivity of **2** *with* KCN *or synthesis of* $(Et_4N)_2[W_2O_2(\mu\text{-}S)_2(CN)_6]\cdot 3H_2O$ **(4)**

A suspension of $(Et_4N)_2[W_2O_2(\mu\text{-}S)_2(S_2)_2]$ **(2)** (852 mg, 1 mmol), KCN (2 g, 31 mmol) in H_2O (10 cm^3) was stirred for 10 min. The colour of the solution changed from green to brown and finally to bright yellow. Addition of 2-PrOH (20 cm^3) gave an oily mass which was recrystallized from H_2O and EtOH. The yellow crystalline product thus obtained was filtered and washed with EtOH and ether, and dried under vacuum. Found: C, 9.2; H, 0.8; N, 10.0. $C_6H_6N_6O_5S_2K_4W_2$ requires: C, 8.7; H, 0.7; N, 10.1%. Yield: 600 mg (~ 74%).

RESULTS AND DISCUSSION

Conversion of $[W(VI)OS_3]^{2-}$ to $[W_2(V)O_2(\mu\text{-}S)_2(S_2)_2]^{2-}$ using elemental iodine is reminiscent of the reaction of iodine with RS^- to form RSSR. The process can be viewed as in eq. (1).

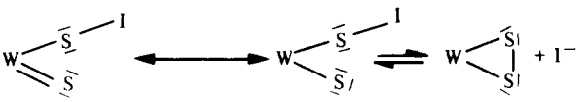

(1)

The W(V) intermediate species* might dimerize to give the desired product as shown in eq. (2).

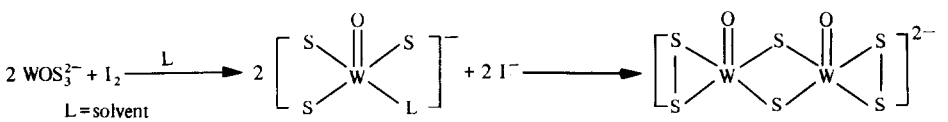

(2)

The other possible electron transfer pathway, similar to that of the scheme proposed by Müller and coworkers in the synthesis of $[Mo_2O_2(\mu\text{-}S)_2(S_2)_2]^{2-}$ [11] **(5)** as shown below, cannot be ruled out.

$$W(VI) \xrightarrow{2e^-} W(IV)$$

$$W(VI) + W(IV) \longrightarrow 2W(V)$$

$$2W(V) \longrightarrow \{W(V)\text{—}W(V)\}\ \text{core.} \qquad (3)$$

* In a similar study of $MoOS_3^{2-}$ we could identify the Mo(V) ESR active ($\langle g \rangle = 1.976$) intermediate species. But we could not identify any W(V) intermediate species in the present study. However in the isolation of a similar core containing complex, $[W_2O_2(\mu\text{-}S)_2(Dtc)_2]$ where $(R_2NH_2)_2WOS_3$ was treated with CS_2 in the presence of air, an ESR active W(V) species ($\langle g \rangle = 1.876$) has been identified.

Other oxidants PhSSPh, $(CH_3)_2COOH$, and $S_2O_8^{2-}$ also behave similarly except that $S_2O_8^{2-}$ reacts even at room temperature.

Interestingly, the reaction of $[W_2(V)O_2(\mu\text{-}S)_2(S_2)_2]^{2-}$ with a methanolic polysulphide solution at ambient conditions produces $[W(VI)OS_3]^{2-}$, which suggests the involvement of a complementary reaction. Here the induced electron transfer process takes place in a reverse direction. Polysulphide, S_x^{2-} functions as an external reductant and causes the electron transfer from W(V) to coordinated S_2^{2-}. Conversion of two S_2^{2-} to four S^{2-} requires four electrons which are supplied by the internal reductant W(V) and external reductant S_x^{2-}. The reaction can be shown as in eq. (4).

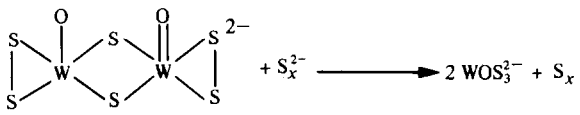

2 **1**

(4)

The complementary reaction, mentioned above, has also been observed by Stiefel and coworkers in the synthesis of $[W_2S_2(\mu\text{-}S)_2(S_4)_2]^{2-}$[12] (**6**). The following reaction proceeds only under a strong jet of argon on the surface of the reaction mixture. If the reaction conditions are not standardized, W(VI) species are also obtained along with the desired product **6**.

$$2(NH_4)_2W(VI)S_4 + 5/8S \xrightarrow[Et_4NBr]{DMF,\ 110^\circ C,\ Ar} \underset{\mathbf{6}}{(Et_4N)_2[W_2S_2(\mu\text{-}S)_2(S_4)_2]} + 2NH_4Br + (NH_4)_2S. \quad (5)$$

Here, one of the by-products $(NH_4)_2S$ might combine with elemental sulphur to form ammonium polysulphide which in turn might react with **6** in a complementary fashion, pushing the equilibrium in the reverse direction, thereby forming WS_4^{2-}.

2 has a persulphido group attached to tungsten in a side-on fashion i.e. $\left\{W\begin{smallmatrix}S\\|\\S\end{smallmatrix}\right\}$ (C_{2v}) for which the expected normal mode of vibrations are ν(S—S) (A_1), ν_s(W—S) (A_1) of the $\left\{W\begin{smallmatrix}S\\|\\S\end{smallmatrix}\right\}$ moiety and ν_{as}(W—S) (B_1) of the $\left\{W\begin{smallmatrix}S\\|\\S\end{smallmatrix}\right\}$ moiety, respectively.[13,14] All these vibrations are IR active. Results are summarized in Table 1. Identification of $\nu_{(S—S)}$ which appears at 520 cm^{-1} is not a problem since there is no other functional group showing an absorption in this region. The exact identification of the ν_s and ν_{as} vibrations are difficult because of the possible coupling of the A_1 mode with that of $\nu_{(S—S)}$. Excluding $\nu_{(W—S_b)}$ which appears at 450 cm^{-1}, the other two vibrations at 335 and 310 cm^{-1} in the lower region can be assigned to ν_s and ν_{as}

Table 1. Infrared and electronic spectral data

Compound	IR (cm^{-1}) ν(M=O)	ν(S—S)	ν(M—S_b)	Other important frequencies	Electronic (nm) (ε)
$[W_2O_2(\mu\text{-}S)_2(S_2)_2]^{2-}$ **2**	960s 950sh	520m	450m	335w, 310w ($\nu_{W—S_2}$)	430 (2.3×10^3) 380(sh) 260 (41.3×10^3)
$[Mo_2O_2(\mu\text{-}S)_2(S_2)_2]^{2-}$ **6**	925s	516m	467m	357w, 321w ($\nu_{Mo—S_2}$)	463 (2×10^3) 377(sh) 305 (10.6×10^3) 278 (11.3×10^3)
$[W_2O_2(\mu\text{-}S)_2(S_2C_2(COPh)_2)_2]^{2-}$ **3**	960s 955sh	—	440m	1660s ($\nu_{C=O}$) 1453m ($\nu_{C=C}$)	382 (11.5×10^3) 315 (31.8×10^3)
$[W_2O_2(\mu\text{-}S)_2(CN)_6]^{4-}$ **4**	920s	—	470m	2160s, 2080w ($\nu_{C=N}$)	425 (0.15×10^3) 325 (1.4×10^3) 268 (5.1×10^3) 238 (5.5×10^3) 210 (6.3×10^3)

respectively. An important point worth noting is the appearance of $\nu_{(W=O)}$ at a higher wave number than in its molybdenum analogue $[Mo_2O_2(\mu\text{-}S)_2(S_2)_2]^{2-}$. Although tungsten is heavier than molybdenum, the appearance of $\nu_{(W=O)}$ at a higher wave number is suggestive of greater multiple bonding between tungsten and oxygen than molybdenum and oxygen.

Electronic spectral results are summarized in Table 1. Following the assignments made in the case of the other side-on bound persulphido complexes[13,14] the assignments can be made in the case of **2**. The longest wavelength band at 430 nm can be assigned to LMCT ($\pi(S) \rightarrow d(W)$). The second band appearing as a shoulder at 380 nm may be due to a $\sigma \rightarrow \sigma^*$ transition originating from W—W bonding. The high energy band at 260 nm may be due to the charge transfer from the bridging sulphur to tungsten and/or a $\pi \rightarrow \pi^*$ transition in the moiety. Comparison of an X-ray powder pattern of **2** with its molybdenum analogue **5**, suggests that both are isostructural.

The reactivity of binuclear molybdenum compounds with different nucleophiles have been studied in detail.[15-18] Depending upon the strength of the nucleophile, products with different oxidation states are formed.[7,19] We have found that with **2** no reduction of the metal centre takes place (eqs 6 and 7). Reaction of **2** with KCN gives a cyanide substituted product $[W_2O_2(\mu\text{-}S)_2(CN)_6]^{4-}$, (4) as shown below:

$$[W_2O_2(\mu\text{-}S)_2(S_2)_2]^{2-} + CN^- \text{ (excess)} \xrightarrow{H_2O} [W_2O_2(\mu\text{-}S)_2(CN)_6]^{4-} + XSCN^- + \cdots \quad (6)$$

Retention of the formal oxidation state by tungsten suggests that the 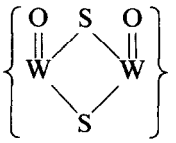 core is very sluggish and does not undergo any change under ambient conditions.

Recently an interesting reaction between $[Mo_2O_2(\mu\text{-}S)_2(S_2)_2]^{2-}$ (**5**) and dimethyl acetylene dicarboxylate has been shown to yield the vinyl disulphide complex.[20] In this reaction, insertion of an acetylene across a Mo—S bond rather than a S—S bond, against the symmetry considerations, has been explained on the basis of the lower energy difference between the 4*d* orbitals of Mo and the 3*p* orbitals of sulphur.[21-23] Coucouvanis and coworkers in a series of reactions have shown that there is a distinct difference in the reactivity of S_2^{2-} and S_4^{2-} ligands coordinated to molybdenum.[21] To testify the generalization made with Mo—S systems in W—S systems, we carried out the reaction between dibenzoyl acetylene (DBA) and **2** at room temperature and found that it gives a dithiolene complex.

Formation of **3** has been established by spectral studies. Reaction of **2** with DBA yields a product which does not show any absorption assignable to the $\nu_{(S-S)}$ mode of vibration in the IR spectrum, suggesting the formation of **3** instead of **3'** (eq. 7).

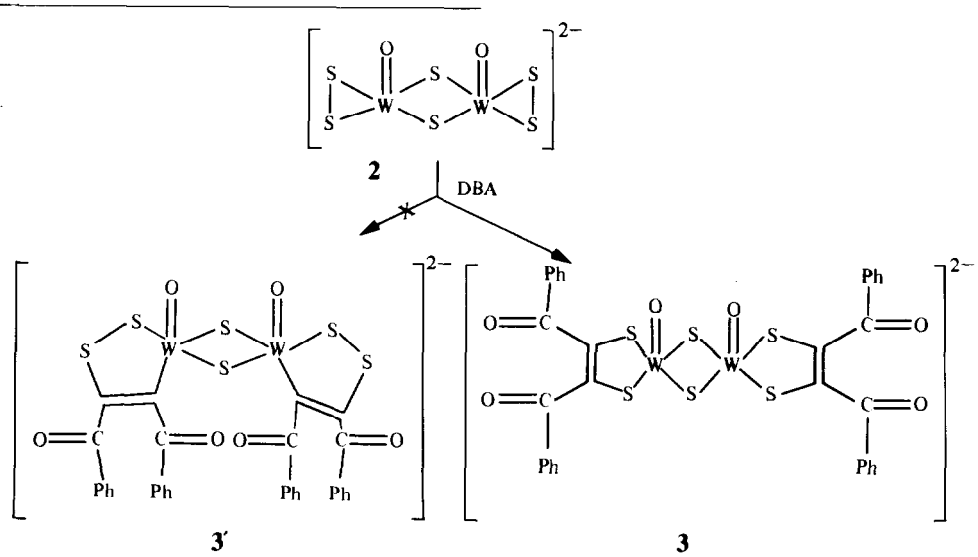

2 DBA (7)

3' **3**

^1H and ^{13}C NMR results are presented in Table 2. On the basis of ^{13}C NMR data which do not show any signals representing a carbon directly attached to tungsten,[24,25] the formation of **3** instead of **3'** is proposed. This is also confirmed when the ^{13}C NMR data of $(Et_4N)_2[MoO(S_2C_2(COPh)_2)_2]$[26] was compared with that of **3** (Table 2). Both spectra are almost identical, suggesting the presence of simi-

Table 2. NMR spectral data

Compound	Solvent	^{1}H NMR Chemical shift δ (ppm)	Assignment	^{13}C NMR Chemical shift δ (ppm)	Assignment	Ref.
$[W_2O_2(\mu\text{-}S)_2(S_2C_2(COPh)_2)_2]^{2-}$	DMSO-d_6	1.10	t, 24H, CH_3 (cation)	51.41	$-CH_3$ (cation)	This
		3.20	q, 16H, CH_2 (cation)	6.96	$-CH_2-$ (cation	work
		7.2–8.0	m, 20H, Ph	137.56, 132.11 129.02, 127.85	—Ph	
				148.53	—C=C—	
				193.92	CO	
$[MoO(S_2C_2(COPh)_2)_2]^{2-}$	DMSO-d_6	1.08	t, 24H, CH_3 (cation)	51.40	$-CH_3$ (cation)	
		3.14	q, 16H, CH_2 (cation)	6.96	$-CH_2-$ (cation)	26
		7.3–7.9	m, 20H, Ph	137.56, 132.11 129.02, 127.85	—Ph	
				148.53	—C=C	
				193.92	CO	

Table 3. XPS data, binding energy (eV)

Compound	W($4f_{7/2}$)	W($4f_{5/2}$)	s(2p) (FWHM)	S($2s_{1/2}$)	W($4d_{5/2}$)	W($4d_{3/2}$)	Ref.
$[Mo_2O_2(\mu\text{-}S)_2(S_2)_2]^{2-}$ **6**	—	—	163.2 (2.92)	—	—	—	23
$[W_2O_2(\mu\text{-}S)_2(S_2)_2]^{2-}$ **2**	33.9	36.1	162.6 (2.92)	226.7	246.7	260.6	This work
$[W_2O_2(\mu\text{-}S)_2(S_2C_2(COPh)_2)_2]^{2-}$ **3**	33.4	35.6	162.7 (2.60)	226.8	246.7	259.0	-do-

lar ligands (eq. 7). Further support to this proposition comes from XPS (Table 3). Compound **3** shows a narrow symmetrical peak for S(2*p*) at 162.6 eV (FWHM 2.6 eV) suggesting an effective mixing and complete loss of individual identity of the different types of sulphur present in the compound. If **3′** was the product, at least S^3 which is not directly attached to tungsten, would have given rise to some asymmetry in the S(2*p*) peak (Fig. 1). In the case of $(Et_4N)_2[W_2O_2(\mu\text{-}S)_2(S_2)_2]$ **2**, deconvolution of the broad band for S(2*p*) is possible. Following the method adopted by Siegbahn, the two sets of binding energies in the ratio 1:2 at 163.3 (±0.2) and

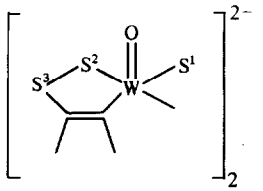

3′

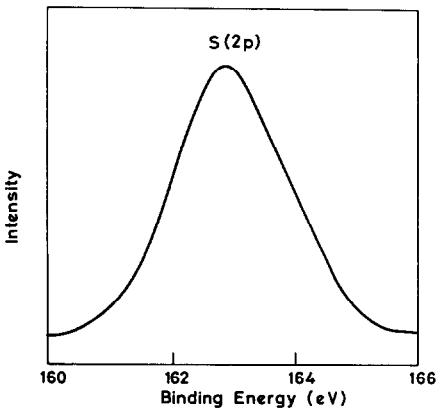

Fig. 1. XPS spectrum of $[W_2O_2(\mu\text{-}S)_2(S_2C_2(COPh)_2)_2]^{2-}$.

162.0 (±0.2) eV have been resolved.[27] Insertion of acetylene across the S—S bond rather than the W—S bond may be due to the larger energy difference of the 5*d* orbitals of W and the 3*p* orbitals of S.[28]

Cyclic voltammograms of complexes **2** and **3** taken in CH_3CN solution at concentrations of 1.11 and 1.59 mM show one electron irreversible oxidation at +0.12 and +0.97 V (SCE) respectively. A negative scan shows a one electron reduction of an irreversible nature at −0.72 V in the case of **2** but **3** undergoes decomposition on reduction.

Acknowledgements—The authors wish to thank Prof. Achim Müller, University of Bielefeld, FRG, for XPS measurements and Prof. A. Chakravorty, IACS, Calcutta, for recording the CV. This project has been supported by the Department of Science and Technology, Government of India.

REFERENCES

1. E. I. Stiefel, *Molybdenum and Molybdenum Containing Enzymes* (Edited by M. P. Coughlan). Pergamon Press, Oxford (1980).
2. A. L. F. Luharly, *The Chemistry of the Thiol Group* (Edited by S. Patai) Part 2. Wiley, London (1974).
3. M. Woods, J. C. Sullivan and E. Deutsch, *J. Chem. Soc., Chem. Commun.* 1975, 749.
4. M. Draganjac, E. Simhon, L. T. Chan, M. Kanatzidis, N. C. Baenziger and D. Coucouvanis, *Inorg. Chem.* 1982, **21**, 3321.
5. W.-H. Pan, M. A. Harmer, T. R. Halbert and E. I. Stiefel, *J. Am. Chem. Soc.* 1984, **106**, 459 and refs therein.
6. W.-H. Pan, T. R. Halbert, L. L. Hutching and E. I. Stiefel, *J. Chem. Soc., Chem. Commun.* 1985, 927.
7. A. Müller, *Polyhedron* 1986, **3**, 323.
8. S. Sarkar and M. A. Ansari, *J. Chem. Soc., Chem. Commun.* 1986, 324.
9. J. W. McDonald, G. D. Friesen, L. D. Rosenhein and W. E. Newton, *Inorg. Chim. Acta* 1983, **72**, 205.
10. E. R. Lutz and W. R. Smithey, Jr, *J. Org. Chem.* 1951, **16**, 51.
11. W. Clegg, M. Mohan, A. Müller, A. Neumann, W. Rittner and G. M. Sheldrick, *Inorg. Chem.* 1980, **19**, 2066.
12. S. A. Cohen and E. I. Stiefel, *Inorg. Chem.* 1985, **24**, 4657.
13. W. Jaegermann, Ph.D. Thesis, University of Bielefeld (1981).
14. J. Dirand, L. Ricard and R. Weiss, *Inorg. Nucl. Chem. Lett.* 1975, **11**, 661.
15. P. J. Vergmini and G. J. Kuhas, *Prog. Inorg. Chem.* 1970, **21**, 216.
16. A. Müller, W. Eltzner, W. Clegg and G. M. Sheldrick, *Angew. Chem. Int. Ed. Engl.* 1982, **21**, 536.
17. A. Müller, R. G. Bhattacharyya, N. Mohan and B. Pfefferkorn, *Z. Anorg. Allg. Chem.* 1979, **454**, 118.
18. K. F. Miller, A. E. Bruce, J. L. Corbui, S. Wherland and E. I. Stiefel, *J. Am. Chem. Soc.* 1980, **102**, 5102.
19. A. Müller, R. Jostes, W. Eltzner, C. H. Nie, E. Diemann, H. Bögge, M. Zimmermann, M. Dartmann, V. Reinsch-Vogell, S. Che, S. J. Cyvin and B. N. Cyvin, *Inorg. Chem.* 1985, **24**, 2872.
20. T. R. Halbert, W.-H. Pan and E. I. Stiefel, *J. Am. Chem. Soc.* 1983, **105**, 5476.
21. D. Coucouvanis, A. Hajikyriacou, M. Draganjac, M. G. Kanatzidis and O. Ileperuma, *Polyhedron* 1986, **5**, 349.
22. J. Bernholc and N. A. W. Holzwarth, *J. Chem. Phys.* 1984, **81**, 3984.
23. J. Bernholc and E. I. Stiefel, *Inorg. Chem.* 1986, **25**, 3876.
24. E. O. Fischer, T. Selmayr, F. R. Kreißl and U. Schubert, *Chem. Ber.* 1977, **110**, 2574.
25. E. O. Fischer, T. Lother, G. Huttner, P. Friedrich, F. R. Kreißl and J. O. Besenhard, *Chem. Ber.* 1977, **110**, 3397.
26. M. A. Ansari, J. Chandrasekaran and S. Sarkar, *Inorg. Chim. Acta* 1987, **133**, 133.
27. K. Siegbahn, C. Nordling, G. Johansson, J. Hedman, P. F. Heden, K. Hamrin, U. Gelius, T. Bergmark, L. D. Werme, R. Manne and Y. Baer (Eds), *ESCA Applied to Free Molecules*. North-Holland, Amsterdam (1969).
28. E. Clementi and C. Roetti, *At. Data Nucl. Data Tables* 1974, **14**, 3.

Polyhedron Vol. 7, No. 6, pp. 477–481, 1988
Printed in Great Britain

0277–5387/88 $3.00+.00
© 1988 Pergamon Press plc

SELECTIVE PHOTOCATALYTIC OXIDATION OF ALCOHOLS BY HETEROPOLYTUNGSTATES

A. HISKIA and E. PAPACONSTANTINOU*

Chemistry Department, N.R.C. Demokritos, Athens, Greece

(*Received* 29 *May*, 1987; *accepted after revision* 13 *October* 1987)

Abstract—A series of primary, secondary, saturated and unsaturated alcohols have been selectively oxidized photocatalytically to the corresponding aldehydes and ketones by a series of heteropolytungstates using near visible and UV light. Stoichiometrically, one photon adds two electrons onto the heteropolytungstates and produces one molecule of aldehyde or ketone. Using oxygen-saturated solutions, the photocatalytic cycle is obtained at the early stage of the photoredox reaction, with optimization of the quantum yield for the oxidized organic product being ~ 0.1. After at least 20 photocatalytic cycles, when the production of the organic oxidation product was 20 times the amount of catalyst, there was no sign of decomposition of the catalyst.

In the process of converting solar energy into chemical fuel homogeneously, several systems have been used that are based on a photosensitizer (S) for the absorption of light, and a relay (R) which carries the electrons of the photoredox reactions and delivers them for the production of fuel, for instance reduction of H^+ into H_2, in the presence of a Pt catalyst, according to the scheme

$$S + R \xrightarrow{h\nu} S^+ + R^-$$

$$R^- + H^+ \xrightarrow{Pt} R + 1/2\ H_2$$

$$S^+ + EDTA \rightarrow S + EDTA(ox.).$$

The process involves, as is well known, an organic compound (mainly EDTA and/or TEA) which is consumed (oxidized) during the process (sacrificial reagent) to revert the sensitizer to its original form.[2]

The system that has produced the most satisfactory results and has been the focus of many prominent laboratories is based on $Ru(bpy)_3^{2+}$ as the sensitizer and MV^{2+} as the relay, using the above mentioned sacrificial reagents.

Polyoxometalates especially of the keggin type, i.e. $[XW_{12}O_{40}]^{n-}$ (XW_{12}^{n-}), (in this paper X = P, Si, Fe, H_2)[3], and Dawson structures i.e. $[P_2W_{18}O_{62}]^{6-}$ ($P_2W_{18}^{6-}$),[4] have been shown to be effective in an analogous process for H_2 production[5] and conversion of sun light into electricity (photogalvanic cells).[6] As has been mentioned elsewhere, they present the advantage that, unlike other systems, the polyoxometal acts as a sensitizer, relay and catalyst, with the main drawback being the limited effective absorption of the visible light (< 400 nm). In the process, they also use organic species that are oxidized during the process. Another advantage is that the organic species are not sacrificial reagents, in the sense that the oxidized products are useful reagents, so that the process of hydrogen production can be converted to an effective photocatalytic oxidation of certain organic compounds.

A previous communication has outlined the basic principles of the process.[7] During the course of this investigation other works have been published on the subject. Generally their results, whenever there is an overlap in the investigation, are in good agreement with ours.[8]

EXPERIMENTAL

Polyoxometalates were prepared according to well established methods.[9] Aqueous solutions of polyoxometalates in the presence of organic compounds were photolyzed with a high pressure Hg arc and a 150 W Xe lamp using filters, in the pres-

*Author to whom correspondence should be addressed.

ence and absence of oxygen. Deaeration was performed with Ar scrubbed with V^{2+}. In photocatalysis experiments about 3 cm^3 solutions were saturated with oxygen in spectrophotometric cells to which ~ 35 cm^3 ampules had been attached to secure the excess of oxygen. Samples from the photolysed solution were withdrawn and analysed for products. A packard 427 FID G.C was used with a 10% Carbowax 20 M on Chromosorb W NAW, 60/80 mesh, 2 m column. The early stage of the photoreaction was monitored spectrophotometrically at 700 nm, which is a characteristic absorption of the reduced polyoxometalates in question.

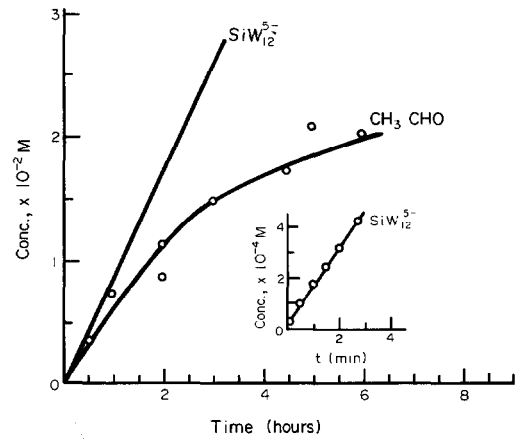

RESULTS AND DISCUSSION

(a) *Saturated alcohols*

It has been stated before that photolysis of polyoxometalates with near visible and UV light, in the presence of alcohols, results in the reduction of the polyoxometalate with concomitant oxidation of the alcohols. Thus, methyl, ethyl and propyl alcohols give the corresponding aldehydes.[7] Stoichiometrically one photon adds two electrons on the heteropolytungstates and produces one molecule of oxidized organic compound. This is deduced from the following facts as indicated in the mechanism below: (a) Photoreduction of the polyoxometalates is mainly due to hydrogen transfer rather than electron transfer. This conclusion is drawn from the fact that only species that have easily removable hydrogen atoms, for instance, primary and secondary alcohols, act as photoreducing reagents, whereas, the tertiary alcohol has only minor reducing ability. Ward's work[10] supports this statement, which shows a deuterium isotope effect in the acetone production, $k_H/k_D = 3.7$ when deuterated Me_2CDOH is photolysed with $Mo_7O_{24}^{6-}$, thus establishing reaction (3) of the scheme below as the rate determining step. (b) Hydroxyalkyl radicals are known to react with polyoxometalates with diffusion controlled rates;[12] reaction (4a, b) of the scheme below.

Figure 1 shows the formation of reduced heteropolytungstate (heteropoly blue, HPB) followed spectrophotometrically, and oxidized alcohols followed by gas chromatography. Some experiments were carried out in deaerated solutions at the initial stages of the photoreaction to test the stoichiometry. The linear variation of concentrations of HPB and the organic oxidation product is zero order as is generally the case. At higher photolysis times, in solutions saturated initially with oxygen, the yield curves off because of the depletion of oxygen.

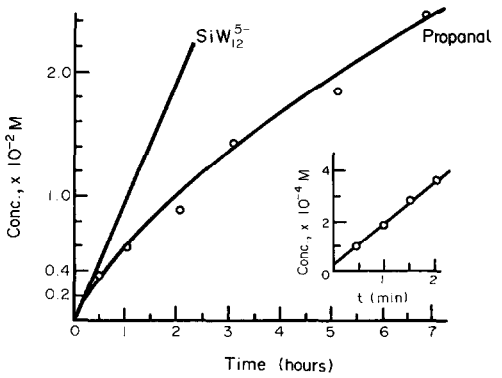

Fig. 1. Variation of concentration of ethanol, propanol and SiW_{12}^{5-} with photolysis time in the presence of O_2. Si W_{12}^{4-} 5×10^{-3} M, ethanol and propanol 2 M, $HClO_4$ 10^{-4} M. High pressure Hg-lamp with Pyrex filter. The variation of SiW_{12}^{5-} concentration with time was calculated by extrapolation of the corresponding curve in deaerated solutions at the initial stages of photolysis (inset) followed spectrophotometrically ($\lambda \sim 700$ nm).

Secondary alcohols, i.e. Me_2CHOH under the same conditions give ketones. Figure 2 shows a corresponding diagram where the same 2 : 1 ratio (two-electrons per molecule of oxidized alcohol) is observed, as is generally the case for redox reactions involving organic compounds.

(b) *Unsaturated alcohols*

Figure 3 shows the formation of the HPB and organic oxidation product with time when the heteropolytungstate was photolysed in the presence of allyl, $CH_2{=}CHCH_2OH$ and 2-propynyl (propargyl), $CH{\equiv}CCH_2OH$, alcohols. Only the alcoholic moieties were oxidized, whereas the double and the

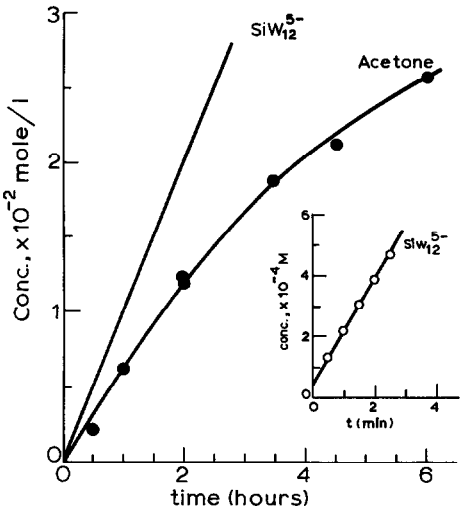

Fig. 2. Variation of concentration of acetone and Si W_{12}^{5-} with photolysis time. Conditions as in Fig. 1.

triple carbon–carbon bonds remained intact. Thus, the allyl alcohol gave acrolein, and propargyl alcohol the corresponding aldehyde. The method can be considered useful for the selective oxidation of the above organic compounds.

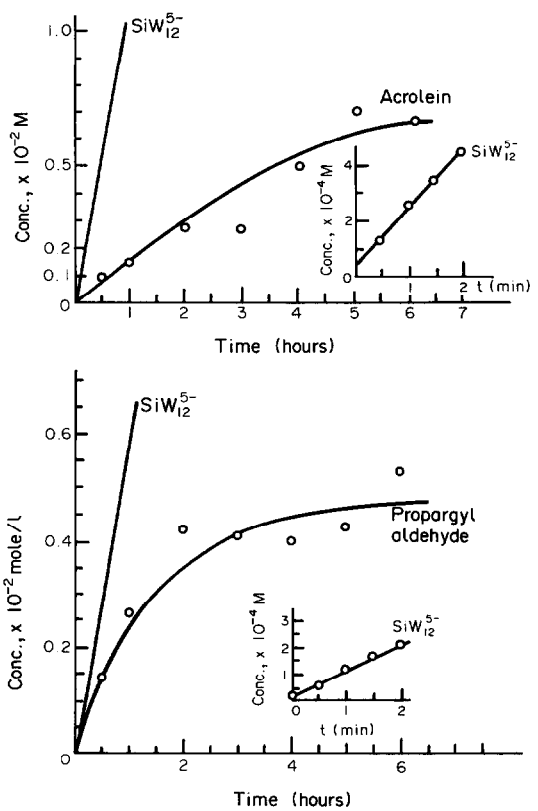

Fig. 3. Variation of concentration of acrolein propargyl aldehyde and SiW_{12}^{5-} with photolysis time. Conditions as in Fig. 1.

Designating the heteropolytungstates generally, as W^{n-}, the photochemical reaction mechanism which has been proposed earlier[7,11] is as follows:

$$W^{n-} \xrightarrow{h\nu} {}^*W^{n-} \quad (1)$$

$${}^*W^{n-} \rightarrow W^{n-} \quad (2)$$

$${}^*W^{n-} + Me_2CHOH \rightarrow W^{(n+1)-} + Me_2COH + H^+ \quad (3)$$

$$W^{n-} + Me_2COH \rightarrow W^{(n+1)-} + Me_2CO + H^+ \quad (4a)$$

$$W^{(n+1)-} + Me_2COH \rightarrow W^{(n+2)-} + Me_2CO + H^+ \quad (4b)$$

$$W^{(n+2)-} + W^{n-} \rightarrow 2W^{(n+1)-}. \quad (4c)$$

Reactions (4a–c) are known to take place.[12] They proceed until all W^{n-} has been converted to $W^{(n+1)-}$. The photochemical reaction proceeds in an analogous manner to the higher reduction steps, i.e. $W^{(n+2)-}$, $W^{(n+3)-}$ depending on the conditions.

The quantum yields for the first reduction step, i.e. ($W^{n-} \rightarrow W^{(n+1)-}$) in 5.0 M Me_2CHOH and 0.1 M $HClO_4$ are ~ 0.12, ~ 0.09, ~ 0.02 and $\lesssim 0.01$ for PW_{12}^{3-}, SiW_{12}^{4-}, FeW_{12}^{5-} and $H_2W_{12}^{6-}$ respectively.[13] However, it has been stated before that the q.y. for the second reduction step, i.e. ($W^{(n+1)} \rightarrow W^{(n+2)-}$) drops to $\sim 10\%$ of the q.y. of the first.

The above mentioned reactions (1)–(4c) refer to the basic photochemistry of the system. The system becomes photocatalytic from the moment we have regeneration of the photosensitizer and relay, i.e. reoxidation of tungstate. In the presence of H^+ the above reactions are followed by, for instance,

$$2W^{(n+2)-} + 2H^+ \rightarrow 2W^{n-} + H_2. \quad (5)$$

(The reaction, for simplicity reasons, refers to the two-electron reduced product, $W^{(n+2)-}$. Actually it should be written as $W_{12}^{(n+m)-} + H^+ \rightarrow W^{(n+m-1)-} + 1/2H_2$.) The system serves for generation of H_2.[5] It has been stated before that photoreduction of the polyoxometalates proceeds until the reduction product is sufficient to reduce H^+, from the thermodynamic point of view. At this point a steady state evolution of hydrogen is obtained, in which the rate of photoreduction [reactions (1)–(4c)] is matched by the rate of reoxidation, reaction (5). The q.y. of hydrogen production at the steady state is $\sim 1\%$.[5b] The corresponding yield of the oxidized organic compounds is the same, as can be seen from the sequence of reactions (1)–(5).

Oxygen, on the other hand, is a more efficient oxidizing reagent than H^+. The overall reaction is

presented as follows:

$$W^{(n+1)-} + 1/4O_2 + H^+ \rightarrow W^{n-} + 1/2H_2O. \quad (6)$$

This reaction is pH dependent and has been reported to be first order in H^+, $W^{(n+1)-}$ and oxygen.[5c] Using laser flash photolysis to generate the reduced tungstates, the second order rate constant for the reaction

$$PW_{12}^{4-} + 1/4O_2 + H^+ \rightarrow PW_{12}^{3-} + 1/2H_2O$$

at pH = 1, was 88 M^{-1} s^{-1},[7] assuming $[O_2] \sim 2.5 \times 10^{-4}$ M. The work was expanded by Darwent to other heteropolytungstates for which the following rate constants were obtained at pH = 1, 75, 6.5×10^3, 2.8×10^5 and 1.75×10^5 M^{-1} s^{-1} for PW_{12}^{4-}, SiW_{12}^{5-}, FeW_{12}^{6-} and $H_2W_{12}^{7-}$ respectively.[5c] We have pursued similar work with $P_2W_{18}^{6-}$. The rate constant for the reoxidation of $P_2W_{18}^{7}$, at pH = 1, was $k \sim 250$ M^{-1} s^{-1}. This reaction was followed by conventional methods. It should be noted that the rate constant for the reoxidation of PW_{12}^{4-} by conventional methods was ~ 150 M^{-1} s^{-1} and agrees reasonably well with the laser flash photolysis results. The rate was found to diminish with ionic strength and increasing pH. Actually the rate varied with $[H^+]^n$, where $0 \lesssim n \lesssim 1$. This is investigated further.

These rates closely follow the one-electron reduction potentials of the 12-tungstates, namely, −0.023, −0.187, −0.349 and −0.581 V vs SCE, respectively; the corresponding potential for $P_2W_{18}^{-6}$ is 0.10 V.

The upper limit of the q.y. for the photocatalytic oxidation of organic compounds will be the q.y. of formation of the first reduction product. In other words optimization of results would be obtained by forcing the photocatalytic cycle at the initial stage of the photoreaction. This is obtained by saturating the solution with oxygen and using either PW_{12}^{3-} or SiW_{12}^{4-}, in this order, which presents the highest q.y. for the first reduction step. (PW_{12}^{3} is unstable to hydrolytic degradation at pH $\gtrsim$ 1.5 and therefore makes the use of SiW_{12}^{4-} which is stable up to pH $\sim$ 6 more attractive.)

We can simply treat the problem mathematically as a steady state that involves the oxidized W^{n-} species which is consumed and regenerated through reactions (1)–(4c) and (6). Using, for simplicity, only the first reduction step, we obtain:

$$\frac{d[W^{n-}]}{dt} = k[H^+][O_2][W^{(n+1)-}] - \Phi_1 I_o = O$$

and

$$[W^{(n+1)-}] = \frac{\Phi_1 I_o}{k[H^+][O_2]} = \frac{\Phi_1 I_o}{k'}$$

where Φ_1 is the q.y. of the first reduction step [sequence of reactions (1)–(4c)], I_o is the intensity of radiation assuming 100% absorption and $k' = k[H^+][O_2]$. From reaction (6) and using the previous expression for $[W^{(n+1)-}]$ we obtain

$$\frac{dW^{(n+1)}}{dt} = k[H^+][O_2][W^{(n+1)-}] = \Phi_1 I_o.$$

Stoichiometrically, the rate of production of the first reduction step is twice the rate of production of the organic oxidation product. Using SiW_{12}^{4-} in oxygen saturated solutions, thus establishing the photocatalytic cycle at the initial stage of the photoreaction, we were able to obtain with a Pyrex filter, quantum yields for the oxidized organic products of the saturated alcohols, at the steady state, of the order of 0.1. Notice that the q.y. of H_2 production and therefore alcohol oxidation, at the steady state, was 10 times less, i.e. 0.01, than has been mentioned earlier.[5b]

After at least 20 photocatalytic cycles, i.e. when the production of the organic oxidation product was at least 20 times the amount of catalyst, there was no sign of decomposition of the catalyst.

Acknowledgements—We thank M. Z. Hoffman for useful discussions and comments, and D. Arapoglou for helping with the experimental work, and P. Daniel for instrumentation. E. P. and M. Z. H. acknowledge partial financial support from NATO.

REFERENCES

1. Taken in part from: A. Hiskia, Ph.D. Thesis, to be submitted.
2. See for instance: *Energy Resources through Photochemistry and Catalysis* (Edited by M. Gratzel). Academic Press, New York (1983).
3. J. F. Keggin, *Nature*. 1983, **131**, 908; *idem.*, *Proc. Roy. Soc. A*, 1934, **144**, 75.
4. B. Dawson, *Acta Cryst.* 1953, **6**, 113.
5. (a) S. S. Saidkhanov, A. I. Kokorin, E. N. Saninov, A. I. Vokov and V. N. Parmon, *J. Mol. Catal.* 1983, **31**, 365; (b) A. Ioannidis and E. Papaconstantinou, *Inorg. Chem.* 1985, **24**, 349; (c) R. Akid and J. R. Darwent, *J. Chem. Soc., Dalton Trans.* 1985, 395; (d) T. Yamase, *Inorg. Chim. Acta* 1982, **64**, L155; (e) P. Argitis and E. Papaconstantinou, *J. Photochem.* 1985, **30**, 445.
6. E. Papaconstantinou and A, Ioannidis, *Inorg. Chim. Acta* 1983, **75**, 235.
7. E. Papaconstantinou, *J. Chem. Soc., Chem. Commun.* 1982, 12.
8. (a) C. L. Hill and D. A. Bouchard, *J. Am. Chem.*

Soc. 1985, **107**, 5148; (b) K. Nomiya, Y. Sugie, T. Miyazaki and M. Miwa, *Polyhedron* 1986, **5**, 1267.
9. (a) M. T. Pope and G. M. Varga, Jr., *Inorg. Chem.* 1966, **5**, 1249. (b) M. T. Pope and E. Papaconstantinou, *ibid.*, 1967, **6**, 1147.
10. M. D. Ward, J. F. Bradjil and R. K. Grasselli, *J. Phys. Chem.* 1984, **88**, 4210.
11. E. Papaconstantinou, P. Argitis, D. Dimotikali, A. Hiskia and A. Ioannidis in *Homogeneous and Heterogeneous Photocatalysis* (Edited by E. Pelizzetti and N. Serpone), pp. 415. D. Reidel (1986).
12. E. Papaconstantinou, *J. Chem. Soc., Faraday I* 1982, **78**, 2769.
13. D. Dimotikali and E. Papaconstantinou, *Inorg. Chim. Acta* 1984, **87**, 177.

Polyhedron Vol. 7, No. 6, pp. 483–487, 1988
Printed in Great Britain

0277–5387/88 $3.00+.00
© 1988 Pergamon Press plc

SYNTHESIS AND CHARACTERIZATION OF MONOTHIOCARBAMATES AND MONOTHIOACETYLACETONATES OF BISMUTH(III) AND ANTIMONY(III)

D. K. SRIVASTAVA, R. P. SINGH and V. D. GUPTA*

Department of Chemistry, Faculty of Science, Banaras Hindu University, Varanasi-221 005, India

(*Received* 10 *July* 1987; *accepted* 13 *October* 1987)

Abstract—Bismuth(III) and antimony(III) tris(monothiocarbamate), $M(SOCNR_2)_3$ (where $—NR_2 = —N(CH_2CH_3)_2$ or $—NC_4H_4$), and bismuth(III) tris(monothioacetylacetonate), $Bi(CH_3CSCHCOCH_3)_3$, have been synthesized and studied. These have been characterized by elemental analyses, molecular weight measurement and, IR and NMR spectral analyses. PMR spectra of bismuth(III) tris(diethylthiocarbamate), $Bi[SOCN(CH_2CH_3)_2]_3$, suggests a high temperature process that involves the rotation about the C—N bond in the $OSCN(CH_2CH_3)_2$ ligand.

Stereochemistry and configurational rearrangements of the metal tris-chelate complexes[1] containing symmetrical ligands like β-diketones and dithiocarbamates have been examined in detail. Metal chelates derived from unsymmetrical sulphur ligands like monothio-β-diketones and monothiocarbamates provide excellent systems to probe the origin of novel properties observed in the sulphur complexes. With this aim, we have undertaken a systematic investigation on these, and have recently reported the crystal and molecular structure of indium(III) tris(monothiodibenzoylmethanate),[2] and tin(IV) monothio-β-diketonates[3] and pyrrolylthiocarbamates.[4] The indium(III) tris-chelate interestingly displays clustering of the sulphur atoms on the distorted octahedron. We report here the syntheses and characterization of a few tris complexes of bismuth and antimony, and variable temperature PMR spectra of $Bi[SOCN(CH_2CH_3)_2]_3$.

EXPERIMENTAL

Reactions were carried out under anhydrous conditions under a nitrogen atmosphere. Solvents were purified and dried by the standard methods. Diethylthiocarbamate[5] and pyrrolylthiocarbamate[6,7] were obtained as ammonium and potassium salts, respectively, by the literature procedures. Monothioacetylacetone[8] was synthesized by the H_2S method and converted into the sodium salt.[9] Bismuth trichloride (H.P.C.) and antimony trichloride (B.D.H.) were purified by sublimation and distillation, respectively, before use.

Bismuth was analysed gravimetrically as Bi_2O_3 and antimony volumetrically by using potassium bromate. Sulphur was estimated by Messenger's method and nitrogen by Kjeldahl's method. Molecular weights of the complexes were determined cryoscopically in benzene. Infrared spectra were recorded as Nujol mulls using CsI plates in the range 4000–200 cm^{-1} on a Perkin–Elmer model 621. ^1H and ^{13}C NMR spectra were recorded on a JEOL FX90Q spectrometer in $CDCl_3$ using TMS as an internal standard.

Preparation of bismuth(III) *tris*(*diethylthiocarbamate*), $Bi[SOCN(CH_2CH_3)_2]_3$ *and bismuth*(III) *tris* (*pyrrolylthiocarbamate*), $Bi(SOCNC_4H_4)_3$ (*Table* 1)

Bismuth trichloride (0.99 g, 3.1×10^{-3} mol in the case of diethyl- and 0.44 g, 1.3×10^{-3} mol in the case of pyrrolylthiocarbamate) in methanol (~ 15 cm^3) was added dropwise with stirring to a methanol (~ 30 cm^3) solution of the salts of thiocarbamate (1.95 g, 9.3×10^{-3} mol diethyl- and

*Author to whom correspondence should be addressed.

Table 1. Analytical and physical data for bismuth(III), antimony(III) tris complexes of monothiocarbamates and monothioacetylacetone

No.	Complex	Colour	M.p. (°C)	Analyses (%)[a] M	S	N	Molecular[a] weight
1	$Bi[SOCN(CH_2CH_3)_2]_3$	Yellow	90	33.3 (33.4)	15.4 (15.8)	6.6 (6.9)	587 (607)
2	$Bi(SOCNC_4H_4)_3$	Yellow	165–166[b]	34.7 (35.6)	15.9 (16.3)	7.0 (7.2)	571 (587)
3	$Sb[SOCN(CH_2CH_3)_2]_3$	Yellow	94	23.2 (23.5)	18.3 (18.5)	7.9 (8.1)	496 (518)
4	$Sb(SOCNC_4H_4)_3$	Yellow	145–147	23.8 (24.4)	18.8 (19.2)	8.4 (8.5)	488 (500)
5	$Bi(CH_3CSCHCOCH_3)_3$	Yellow	125–127	37.5 (37.7)	17.3 (17.9)	—	559 (544)

[a] Calculated values in parentheses.
[b] Decomposed.

0.70 g, 3.9×10^{-3} mol pyrrolylthiocarbamate) maintained at 0°C under a nitrogen atmosphere. The reaction mixture was stirred for ~ 12 h at room temperature (28°C). From the mixture, volatile materials were removed and the products obtained were extracted with benzene. Removal of the solvent and crystallization from a dichloromethane/*n*-hexane (1 : 1) mixture produced yellow crystalline solids. The products were dried at 0.1 mm Hg/~ 30°C/5 h.

Preparation of antimony(III) *tris(diethylthiocarbamate)*, $Sb[SOCN(CH_2CH_3)_2]_3$ (*Table* 1)

Into a stirred benzene solution (~ 25 cm^3) of the diethylammonium salt of diethylthiocarbamate (1.0 g, 7.2×10^{-3} mol) maintained at ~ 10°C, antimony trichloride (0.55 g, 2.4×10^{-3} mol) dissolved in benzene (~ 15 ml) was added dropwise. The stirring was continued for ~ 12 h. The separated diethylammonium chloride was filtered out. The solvent was removed from the filtrate under reduced pressure and the product thus obtained was dried at 0.1 mm Hg/~ 30°C/~ 6 h.

Preparation of antimony(III) *tris(pyrrolylthiocarbamate)*, $Sb(SOCNC_4H_4)_3$ (*Table* 1)

A solution of antimony trichloride (0.50 g, 2.1×10^{-3} mol) in dichloromethane (~ 15 cm^3) was added dropwise into a suspension of the potassium salt of pyrrolylthiocarbamate (1.09 g, 6.3×10^{-3} mol) in dichloromethane (~ 30 cm^3) with stirring under a nitrogen atmosphere. The reaction mixture was stirred for 12 h at ambient temperature. It was filtered to remove the separated potassium chloride and volatile materials were evaporated from the filtrate to obtain the solid product, which was dried at 0.1 mm Hg/30°C/5 h and finally crystallized from dichloromethane solution.

Preparation of bismuth(III) *tris(monothioacetylacetonate)*, $Bi(CH_3CSCHCOCH_3)_3$ (*Table* 1)

To a stirred solution of bismuth trichloride (0.50 g, 1.5×10^{-3} mol) in methanol, the sodium salt of monothioacetylacetone (0.66 g, 4.5×10^{-3} mol) dissolved in ~ 15 cm^3 of methanol was added dropwise at 0°C. The reaction mixture was stirred at room temperature for 2 h. After complete removal of methanol the reaction product was treated with dichloromethane (~ 20 cm^3). Insoluble sodium chloride was filtered out and the solvent was removed from the filtrate under reduced pressure. The products were dried at 0.1 mm Hg/~ 30°C/~ 4 h and finally crystallized from chloroform and ethanol.

RESULTS AND DISCUSSION

Tris-complexes of bismuth(III) and antimony(III) with monothiocarbamates and monothioacetylacetone have been synthesized in good yields by the following reaction routes

$$MCl_3 + \begin{cases} 3[(CH_3CH_2)_2NH_2]^+ [SOCN(CH_2CH_3)_2]^- \rightarrow M[SOCN(CH_2CH_3)_2]_3 + 3(CH_3CH_2)_2NH_2Cl \\ 3KSOCNC_4H_4 \rightarrow M(SOCNC_4H_4)_3 + 3KCl \\ 3NaCH_3CSCHCOCH_3 \rightarrow M(CH_3CSCHCOCH_3)_3 + 3NaCl \end{cases}$$

(where M = Sb or Bi).

Monothiocarbamates and monothioacetylacetonates of bismuth(III) and antimony(III) are crystalline soluble in common organic solvents and monomeric in benzene.

Sodium salts of dialkylthiocarbamates exhibit a very strong but broad band at 1507–1520 cm^{-1} assignable to highly coupled $\nu(C\cdots O)$ and $\nu(C\cdots N)$ vibrations.[5,10] Bismuth(III) and antimony(III) tris(diethylthiocarbamate) show strong broad bands at 1545 and 1580 cm^{-1}, respectively (Table 2), assignable to these coupled vibrations. The absorption at a comparatively higher frequency in the antimony derivative probably suggests a weaker Sb ··· O interaction in comparison to the bismuth analogue, this may be a consequence of the lone pair of electrons over antimony being more effective. The oxygens are perhaps strongly coordinated to bismuth or the marked change may arise due to the size effect. The point can only be settled after single crystal X-ray structure analysis. Notably in $Fe[SOCN(CH_3)_2]_3$[11] whose crystal structure[12] shows that the Fe—O and Fe—S bond lengths are equivalent to covalent bond distances, the $\nu(C\cdots O)$ absorption appears at 1540 cm^{-1}.

In distinction to dialkylthiocarbamate, the potassium salt of aromatic thiocarbamates displays a sharp band at a higher frequency (1525–1550 cm^{-1}) due to the $\nu(C\cdots O)$ vibrations.[6,7] This is consistent with the increased mercaptide character arising from the greater contribution by the canonical form 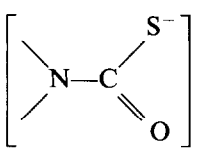 . The IR spectra of the tris-pyrrolylthiocarbamates of bismuth(III) and antimony(III) display a sharp $\nu(C\cdots O)$ absorption at 1582–85 cm^{-1} (Table 2). This absorption is at a somewhat higher frequency than that which has been found for the nickel complex, $Ni_2(SOCNC_4H_4)_4 \cdot 3THF$ (1568 cm^{-1})[6] where the ligands are acting as bidentate. In a sulphur bonded unidentate pyrrolylthiocarbamate such as $Ph_3Sn(SOCNC_4H_4)$ whose crystal structure[4] is known, the free $\nu(C{=}O)$ is observed at a considerably higher frequency (1640 cm^{-1}). Another significant band is $\nu(C\cdots N)$ at ~ 1286 cm^{-1}. $\nu(M—O)$[13] (480–500 cm^{-1}) and $\nu(M—S)$[14] (380–390 cm^{-1}) vibrations can be seen in both diethyl- and pyrrolylthiocarbamate derivatives.

^1H NMR spectra of bismuth and antimony tris-(diethylthiocarbamate) exhibit overlapping quartets and triplets respectively, due to methylene and methyl protons (Table 3), perhaps arising from the magnetic non-equivalence of the ethyl groups, due to partial double bond character in the C—N bond.[10] In order to get more insight, variable temperature PMR spectra of $Bi[SOCN(CH_2CH_3)_2]_3$ have been studied.

Variable temperature PMR spectra of $Bi[SOCN(CH_2CH_3)_2]_3$ afford evidence for the distinct kinetic process involving hindered rotation around the C—N partial double bond in the diethylthiocarbamate ligand. Since the multiplet observed at 25°C is symmetrical in nature, it can be considered to arise due to the two overlapping triplets from the methyl protons of the same ligand moiety. Any non-equivalence of the spanning and equatorial ligands would amount to non-symmetrical multiplets. In this process by using the time averaged resonance of a simple triplet owing to the onset of rapid C—N bond rotation, the coalescence temperature was found to be 49°C (Fig. 1). Rotation about the C—N bond would exchange the ethyl groups between the sites adjacent to sulphur and the sites adjacent to oxygen. This non-equivalence is further reflected in its ^{13}C NMR spectrum. At ambient temperature, the spectrum displays one signal for COS carbons and two resonances for methylene as well as methyl carbons. Thus on the basis of available evidence, a distorted

Table 2. Important IR bands[a] (cm^{-1}) of bismuth(III) and antimony(III) tris complexes of monothiocarbamates and monothioacetylacetonate

Sl. No.	Complex	$\nu(C\cdots O)$ $\nu(C\cdots N)$	$\nu(C\cdots N)$	$\nu(C\cdots C)$	$\nu(C\cdots S)$	$\delta(COS)$	$\nu(M—O)$	$\nu(M—S)$
1	$Bi[SOCN(CH_2CH_3)_2]_3$	1545v	—	—	942m	667m	508s	380s
2	$Sb(SOCN(CH_2CH_3)_2]_3$	1580vs	—	—	943m	663m	508s	385m
3	$Bi(SOCNC_4H_4)_3$	1582s[b]	1292s	—	982m	664m	489m	384m
4	$Sb(SOCNC_4H_4)_3$	1585s[b]	1280s	—	975m	660m	480m	380m
5	$Bi(CH_3CSCHCOCH_3)_3$	1600[b]	—	1500s	1210s	—	490s	348s

[a] Spectra were recorded in the range 4000–200 cm^{-1} as Nujol mulls on CsI plates.
[b] Bands due to purely the $\nu(C\cdots O)$ vibration.

Table 3. ^{1}H and ^{13}C NMR chemical shifts[a] of bismuth(III) and antimony(III) tris complexes of monothiocarbamates and monothioacetylacetonate

^{1}H NMR(δ)[b]					
$Bi[SOCN(CH_2CH_3)_2]_3$	$Bi(SOCNC_4H_4)_3$	$Sb[SOCN(CH_2CH_3)_2]_3$	$Sb(SOCNC_4H_4)_3$	$Bi(CH_3CSCHCOCH_3)_3$	Assignments
3.41[c]	—	3.19[c]	—	—	(N)—CH_2
1.25[d]	—	0.99[d]	—	—	(C)—CH_3
—	7.34[e]	—	7.25[e]	—	α-H
—	6.26[e]	—	6.23[e]	—	β-H—NC_4H_4
—	—	—	—	3.39	(S)—CH_3
—	—	—	—	2.18	(O)—CH_3
—	—	—	—	6.33	>CH—

^{13}C NMR (ppm)[b]			
$Bi[SOCN(CH_2CH_3)_2]_3$	Assignments	$Bi(CH_3CSCHCOCH_3)_3$	Assignments
173.1	(COS)	195.6	C—(S)
46.4	(N)—CH_2	167.2	C—(O)
41.6	(N)—CH_2	123.3	>CH—
13.8	CH_3 of (N)—CH_2CH_3	35.3	CH_3—(S)
13.5	CH_3 of (N)—CH_2CH_3	29.6	CH_3—(O)

[a] At 90 MHz.
[b] Spectra were recorded in $CDCl_3$ with TMS as internal reference.
[c] Centre of overlapping quartets.
[d] Centre of overlapping triplets.
[e] Centre of triplet.

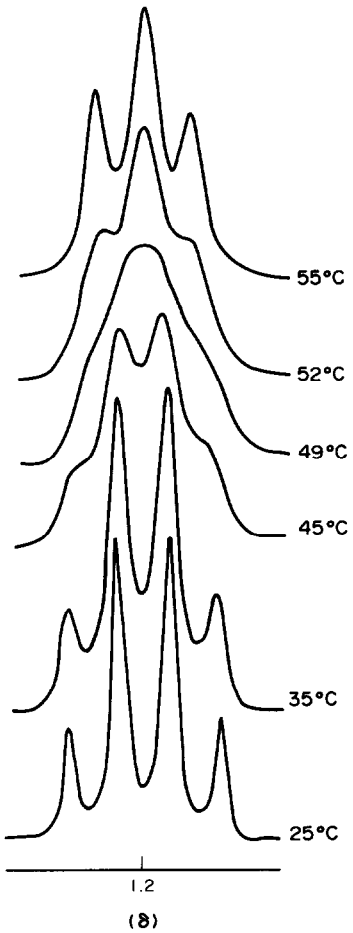

Fig. 1. Variable temperature PMR spectrum of $Bi[SOCN(CH_2CH_2)_2]_3$ (for simplicity only methyl signals have been shown).

cis(facial) octahedral structure may be proposed for tris-thiocarbamates of bismuth and antimony. However, PMR spectra of metal tris(pyrrolylthiocarbamate) at ambient temperature give only two sets of triplets (Table 3) due to α- and β-protons of the ligand.

The IR spectrum of bismuth(III) tris-(monothioacetylacetonate), shows a lowering in the frequencies of $\nu(C{\cdots}O)$ (1600 cm^{-1}) and $\nu(C{\cdots}C)$ (1500 cm^{-1}) vibrations[15,16] (Table 2) in comparison to the free ligand. This is consistent with the conjugated chelate ring structure having a higher degree of π-delocalization in the monothioacetylacetone moiety. In the far IR region two bands appearing at 490 and 390 cm^{-1} are considered to be due to (Bi—O)[13] and (Bi—S)[14] stretching vibrations, respectively.

The PMR spectrum of $Bi(CH_3CSCHCOCH_3)_3$ shows only a single resonance each for S—CH_3, O—CH_3 and methine protons (Table 3). The presence of only five resonances in the ^{13}C NMR spectrum, furthermore suggests fairly high symmetry of the complex. With the available spectral evidence, bismuth(III) tris(monothioacetylacetonate) may be considered to possess symmetrical *cis*(facial) octahedral geometry. However, the presence of a lone pair of electrons on bismuth may bring about some distortion of the octahedron. It may be mentioned that in the ^{13}C NMR spectrum, substantial downfield positions of CS (195.6 ppm) and CO (167.2 ppm) carbons (Table 3) are very indicative of the bidentate mode of the ligand.

Attempts to prepare antimony(III) tris(monothioacetylacetonate) were not successful due to the thermal instability of the complex. Repeated efforts to grow single crystals of all of the above described tris-chelate complexes by using various solvent combinations have been unsuccessful.

Acknowledgement—We are thankful to CSIR, New Delhi for financial assistance.

REFERENCES

1. L. M. Jackman and F. A. Cotton, *Dynamic Nuclear Magnetic Resonance*, p. 317. Academic Press, New York (1975).
2. Ch. Sreelatha, V. D. Gupta, C. K. Narula and H. Nöth, *J. Chem. Soc., Dalton Trans.* 1985, 2623.
3. Ch. Sreelatha, D. K. Srivastava, V. D. Gupta and H. Nöth, *J. Chem. Soc., Dalton Trans.* 1987, in press.
4. D. K. Srivastava, V. D. Gupta, H. Nöth and W. Rattay, *J. Chem. Soc., Dalton Trans.* 1987, in press.
5. S. L. Hawthorne, A. H. Bruder and R. C. Fay, *Inorg. Chem.* 1978, **17**, 2114 and refs therein.
6. R. D. Bereman, D. N. Baird and W. E. Hatfield, *J. Inorg. Nucl. Chem.* 1981, **43**, 2729.
7. R. D. Bereman, D. N. Baird, J. Bordner and J. R. Dorfman, *Polyhedron* 1983, **2**, 25.
8. F. Duss and J. W. Anthonsen, *Acta Chem. Scand.* 1977, **B31**, 40.
9. O. Siiman and J. Fresco, *J. Chem. Phys.* 1971, **54**, 734.
10. S. L. Hawthorne and R. C. Fay, *J. Am. Chem. Soc.* 1979, **101**, 5268.
11. H. Nakajema, T. Tanaka, H. Kobayashi and I. Tsujibawa, *Inorg. Nucl. Chem. Lett.* 1976, **12**, 689.
12. J. Ahmed and J. A. Ibers, *Inorg. Chem.* 1977, **16**, 935.
13. S. T. Yuan and S. K. Madan, *Spectrochim. Acta* 1972, **6**, 463.
14. T. B. Brill and N. C. Campbell, *Inorg. Chem.* 1973, **12**, 1884.
15. S. E. Livingstone, *Coord. Chem. Rev.* 1971, **7**, 29.
16. M. Cox and J. Darken, *Coord. Chem. Rev.* 1971, **7**, 729.

Polyhedron Vol. 7, No. 6, pp. 489–494, 1988
Printed in Great Britain

0277–5387/88 $3.00+.00
© 1988 Pergamon Press plc

COORDINATION OF A POLYFUNCTIONAL CYCLIC LIGAND CONTAINING A P—P BOND TO THE FRAGMENT $[Mo(CO)_3(NN)]$ (NN = 2,2′-BIPYRIDINE, 1,10-PHENANTHROLINE). SPECTROSCOPIC AND ELECTROCHEMICAL CHARACTERIZATION

J. GRANIFO* and M. E. VARGAS*

Departamento de Ciencias Químicas, Facultad de Ingeniería y Administración, Universidad de La Frontera, Casilla 54-D, Temuco, Chile

J. COSTAMAGNA*

Departamento de Química, Facultad de Ciencia, Universidad de Santiago de Chile, Santiago 2, Chile

and

M. A. FRANCOIS

Departamento de Ciencias Naturales, Area de Química, Pontificia Universidad Católica, M.Montt 56, Temuco, Chile

(*Received* 29 *July* 1987; *accepted* 13 *October* 1987)

Abstract—The reaction of 1,3,4,6-tetramethyl-1H,4H-1,3,4,6-tetraaza-3a, 6a-diphosphapentalen-2,5(3H,6H)-dithion-3a-sulphide (TDP) with the derivatives of metal carbonyls $[Mo(CO)_3(NN)(CH_3CN)]$ (NN = 2,2′-bipyridine, 1,10-phenanthroline) leads to *fac*-$Mo(CO)_3(NN)(TDP)$ complexes with the ligand coordinated through the trivalent phosphorus atom. The IR and visible spectra of the new complexes as well as their electrochemical and general properties are discussed.

In a recent paper Kleeman *et al.*[1] have reported that the reaction product from N,N′-dimethylthiourea and phosphortrichloride is the compound tetraazadiphosphapentalene (TDP) containing a cyclic system involving a P—P bond. (See Structure 1.)

As can be seen, TDP is a potential multiple ligand with possible donor positions at the N, S and tervalent P atoms. Hitherto, there are no works described in the literature dealing with the coordination form of this interesting polyfunctional ligand uniting the characteristics of thioureas, phosphines and sulphur phosphines.

Mixed derivatives of the formula *fac*-$[Mo(CO)_3(NN)L]$ [NN = 2,2′-bipyridine (bipy) or 1,10-phenanthroline (phen)], L being a wide range of monodentate Lewis bases are well known.[2–9] These trisubstituted complexes are usually obtained through thermal displacement of one carbonyl group by direct reaction of $Mo(CO)_4(NN)$ with an excess of L in high boiling solvents.[7] Nevertheless, in order to protect the sensitive ligand TDP from thermal decomposition, a less drastic procedure has

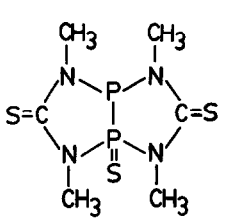

Structure 1.

* Authors to whom correspondence should be addressed.

Table 1. Analytical and IR spectra for the complexes $[Mo(CO)_3(NN)(TDP)]$

Compound	Analysis (%)[a] C	H	N	Mo	$\nu(CO)$[b] A_1	E
$[Mo(CO)_3(bipy)(TDP)]$	35.8 (36.0)	3.2 (3.2)	12.9 (13.2)	15.2 (15.1)	1955	1860, 1810
$[Mo(CO)_3(phen)(TDP)]$	38.3 (38.3)	3.1 (3.1)	12.6 (12.8)	14.3 (14.6)	1930	1840, 1805

[a] Required values are given in parentheses.
[b] Nujol mulls, in cm^{-1}, all bands are strong.

been employed in the present work for obtaining tricarbonyl derivatives by substitution of acetonitrile in the complexes *fac*-$[Mo(CO)_3(NN)(CH_3CN)]$.[9]

RESULTS AND DISCUSSION

The reaction of $[Mo(CO)_3(NN)(CH_3CN)]$ with TDP in dichloromethane at room temperature, gave the new complexes of the formula $[Mo(CO)_3(NN)(TDP)]$. These red coloured crystalline solids are air stable and soluble in organic solvents such as benzene, methylene chloride and chloroform; slightly soluble in alcohols and unsoluble in light petroleum. However, their solutions are unstable in air.

IR spectra

IR spectra of the complexes $[Mo(CO)_3(NN)(TDP)]$ present two intense bands in the CO stretching region. The one of lower frequency is split into two (Table 1) producing a pattern similar to that from the complexes *fac*-$[Mo(CO)_3(NN)L]$, L being a phosphorus donor ligand (specifically some phosphites).[7] The behaviour of the vibrational modes A_1 and E of these complex *fac*-tricarbonyls have been interpreted through considerations of the differences in the bond properties of the ligand groups NN and L.[6] If the π-acceptor capacity of L is superior to that of NN, then the E mode is split. This effect increases with the π-acidity of L and, simultaneously, the CO bands are shifted to higher frequencies. The results obtained for the complexes $[Mo(CO)_3(NN)(TDP)]$ suggest the existence of a considerable difference in π-acceptor capacity between the substituent groups (TDP > NN). Furthermore, if the reported magnitudes for the phosphites[7] are compared with those found for TDP, this shows a slightly greater π-acidity. Accordingly, this conclusion permits us to discard the fact that TDP coordination occurs through their thiocarbonyl or thiophosphoryl groups, since they are weaker π-acceptors than phosphites or phosphines.[7,10]

The other regions of the IR spectra show the presence of the bands assigned to TDP (v.g.: 1420(s), 1105(s) and 855(s) cm^{-1}), in some cases superimposed on those of the bipy or phen.

Electronic spectra in the visible region

(a) *Band assignments.* The visible spectra in solution of the complexes $Mo(CO)_3(NN)(TDP)$ are dominated by a broad and intense band ($\varepsilon > 4000$ M^{-1} cm^{-1}). The position of this absorption is strongly sensitive to the used solvent. The more polar the medium, the more the band is shifted to the blue (Table 2). Bands with similar characteristics have been assigned to metal to ligand charge-

Table 2. Visible absorption maxima (cm^{-1}) of the complexes $[Mo(CO)_3(NN)(TDP)]$ and $[Mo(CO)_4(NN)]$ in several solvents

Compound	Solvent (E^*_{MLCT})[a] Benzene (0.34)	$CHCl_3$ (0.42)	Butanol (0.55)	CH_2Cl_2 (0.67)	Acetone (0.82)	CH_3CN (0.98)
$[Mo(CO)_3(bipy)(TDP)]$	20 000	20 200	20 490	20 750	21 370	21 650
$[Mo(CO)_3(phen)(TDP)]$	20 040	20 120	20 620	20 750	—[b]	21 600
$[Mo(CO)_4(bipy)]$[c]	20 310	20 520	20 780	21 260	22 010	22 520
$[Mo(CO)_4(phen)]$	20 390	20 790	20 830	21 390	22 170	22 830

[a] Solvent parameters E^*_{MLCT} from ref. 11.
[b] Complex too unstable in this solvent.
[c] Data from ref. 11.

transfer transitions (MLCT) $NN(\pi^*) \leftarrow Mo(4d)$ in the complexes $[Mo(CO)_3(diimine)(PR_3)]$.[12,13]

The solvatochromic behaviour of the related complexes $Mo(CO)_4(diimine)$ (M = Cr, Mo, W; diimine = bipy, phen or derivatives) has been employed by Manuta and Lees[11] in order to derive a scale of solvent polarity. They have defined the parameter E^*_{MLCT} and correlated it with the absorption energies $NN(\pi^*) \leftarrow M(d)$ of these complexes. The values of E^*_{MLCT} are displayed in the interval given by the isooctane ($E^*_{MLCT} = 0.00$) and DMSO ($E^*_{MLCT} = 1.00$). The application of this solvent polarity scale to the complexes $[Mo(CO)_3(NN)(TDP)]$ by plotting their absorption maxima ($\bar{\nu}_{MLCT}$) vs E^*_{MLCT} leads to a linear relationship similar to that observed for the parent complexes $Mo(CO)_4(NN)$ (Fig. 1 and Table 2) and given by the equation $\bar{\nu}_{MLCT} = A + B \cdot E^*_{MLCT}$.

When the parameters of the corresponding straight lines of the complexes $Mo(CO)_4(NN)$ (bipy: $A = 18983$, $B = 3571$ cm^{-1}, $r = 0.991$; phen: $A = 19021$, $B = 3775$ cm^{-1}, $r = 0.982$) and $Mo(CO)_3(NN)(TDP)$ (bipy: $A = 19062$, $B = 2668$ cm^{-1}, $r = 0.993$; phen: $A = 19160$, $B = 2476$ cm^{-1}, $r = 0.993$) are compared, a good correlation is observed in all cases, evidencing that these transitions are of the same nature.

On the other hand, the values of the slope indicate that the tetracarbonyl complexes are more sensitive to the solvent changes than the tricarbonyls. This fact can be explained by considering that solvatochromism occurs if the solute–solvent interactions in the ground state differ from that in the excited state of the substrate. In particular, the strongest absorption in the visible region of the complexes $Mo(CO)_4(NN)$ (C_{2v} symmetry) comes

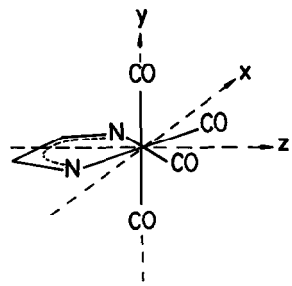

Structure 2.

from the transition $b_2(\pi^*) \leftarrow b_2(dyz)$.[12,13] (See Structure 2.) This MLCT transition induces a dipole moment in the excited state opposed to that of the ground state (z direction). Hence, a less polar situation occurs for the complexes in the excited state reducing the solute–solvent interactions. The expected stabilization of the ground state by polar solvents appears evident from the extensive blue shift of this transition in such media, i.e. negative solvatochromism.[12,13] The substitution of one carbonyl group by a phosphorus-donor ligand destabilizes the metal orbitals; consequently, the electronic transition from the metal to the ligands diminishes its CT character and hence its negative solvatochromism is less intense. The effect of the destabilization of the metal orbitals can be clearly appreciated in Fig. 1, where the wavenumbers of the tetracarbonyl absorptions are always higher than those of the corresponding tricarbonyls.

(b) *Ligand exchange reactions in acetonitrile.* The dissolution of the complexes $[Mo(CO)_3(NN)(TDP)]$ in acetonitrile produce slow colour changes

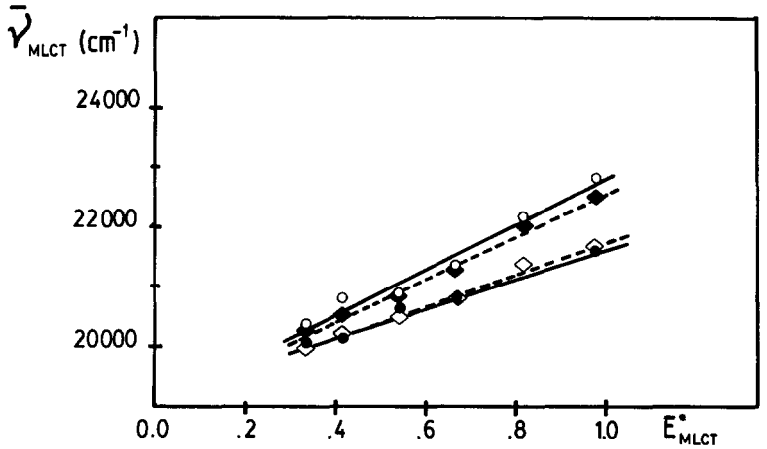

Fig. 1. Wavenumbers of maxima MLCT absorptions ($\bar{\nu}_{MLCT}$) of $[Mo(CO)_4(NN)]$ and $[Mo(CO)_3(NN)(TDP)]$ complexes plotted against E^*_{MLCT} values: ◆ (– – –) $[Mo(CO)_4(bipy)]$, ○ (——) $[Mo(CO)_4(phen)]$, ◇ (– – –) $[Mo(CO)_3(bipy)(TDP)]$ and ● (——) $[Mo(CO)_3(phen)(TDP)]$.

of the solution from yellow to violet. The position of the maximum in the visible region is shifted to lower energy with an isosbestic point in the intermediate region. The spectrum of the final solution is superposed on that of a sample of the complex $[Mo(CO)_3(NN)(CH_3CN)]$. Therefore, it is concluded that there is competition between TDP and the solvent for the same coordination site.

$$[Mo(CO)_3(NN)(TDP)] + CH_3CN = [Mo(CO)_3(NN)(CH_3CN)] + TDP. \quad (1)$$

The ligand exchange reactions in the metal carbonyl complexes of the 6B group are usual and the mechanisms of such reactions have been suggested.[14] Under the experimental conditions used (CH_3CN as solvent), the reaction should have first-order or pseudo-first-order kinetics. The rate was measured by following the absorbance at 500 nm; the plots of $\ln(A - A_\infty)$ vs time lead to straight lines and the corresponding rate constants were extracted from the slopes (k_{obs}(bipy) = 5.4×10^{-3} s^{-1}; k_{obs}(phen) = 1.8×10^{-2} s^{-1}) confirming the predictions of the mechanism proposed for these reactions.[14]

Electrochemistry

The cyclic voltammograms of $[Mo(CO)_3(NN)(TDP)]$ complexes in CH_2Cl_2 show an irreversible oxidation peak which depends on the scan rate; a shift towards a more anodic direction is observed when the scan rate is increased (Fig. 2). The coulometry in the same solvent through an exhaustive oxidation (0.99 V vs SCE) results in the loss of 0.5 electrons per Mo, giving a species with an electronic spectrum that resembles the initial

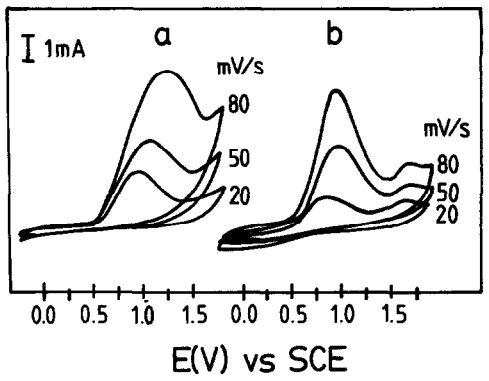

Fig. 2. Cyclic voltammograms of (a) $[Mo(CO)_3(phen)(TDP)]$ and (b) $[Mo(CO)_3(bipy)(TDP)]$ in dichloromethane. The values indicate the scan rates (mV s^{-1}).

compound except for the presence of a broad and weak band at long wavelengths and slight displacement of the others (Fig. 3).

It has been reported that the $Mo(CO)_4(bipy)$ complex in CH_2Cl_2 suffers an oxidation by a quasi-reversible process giving the cation $[Mo(CO)_4(bipy)]^+$ ($E_{1/2}$ = 0.62 V vs SCE).[15] However, we have observed that the complexes $Mo(CO)_4(NN)$ in CH_3CN present the oxidation in an irreversible way (E_p(bipy) = 0.68 V, E_p(phen) = 0.67 V at 200 mV s^{-1}). This can be understood assuming that the molybdenum atom has the possibility to obtain heptacoordination by reacting the monocation with a molecule of the donor solvent to yield species of the formula $[(Mo(CO)_4(NN)(CH_3CN)]^+$. Similar behaviour in the same solvent has been observed in the related complexes $[Mo(CO)_4$ (bidentate phos-

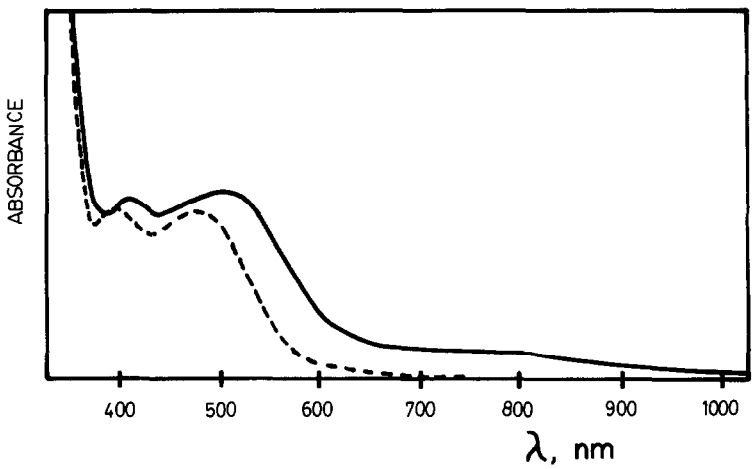

Fig. 3. Electronic spectra of $[Mo(CO)_3(phen)(TDP)]$ solutions before (---) and after (——) controlled-potential electrolysis in dichloromethane (0.99 V vs SCE).

phine)].[16] Furthermore, the oxidized electrogenerated species derived from $Mo(CO)_6$ may also react with CH_3CN.[16,17]

Accordingly, these anticedents suggest that the cations produced from the molybdenum carbonyl derivatives have a great tendency to increase their coordination number if the medium proportionates some adequate donor species. Under this premise it is possible to make clear the electrochemical behaviour of the complexes $[Mo(CO)_3(NN)(TDP)]$ in CH_2Cl_2 through the following reaction mechanism:

$$[Mo(CO)_3(NN)(TDP)] \rightarrow [Mo(CO)_3(NN)(TDP)]^+ + e \quad (2)$$

$$[Mo(CO)_3(NN)(TDP)] + [Mo(CO)_3(NN)(TDP)]^+ \rightarrow [Mo(CO)_3(NN)(TDP) - Mo(CO)_3(NN)(TDP)]^+. \quad (3)$$

The first step should be the electrochemical generation of the monocation, which in a second fast step, is coordinated by a molecule of the neutral complex through the ligand TDP. Therefore, this acts as a bridge by way of one of its sulphur atoms producing a binuclear species. Then, the net result of the oxidation must be the elimination of 0.5 electrons per Mo.

The electronic spectra of the oxidation products seem to confirm the above hypotheses (Fig. 3). If the final spectrum results from the superposition of both; that of the oxidized species with that of the neutral one, this might explain the great similarity with the spectrum of the non-electrolyzed substance.

EXPERIMENTAL

The solvents were purified by standard methods and all operations were carried out under a nitrogen atmosphere. The complexes $Mo(CO)_4(NN)$, $Mo(CO)_3(NN)(CH_3CN)$[7] and the ligand TDP[1] were prepared by methods described in the literature. The IR spectra were obtained in a Perkin–Elmer 577 spectrophotometer. The electronic spectra were recorded on a Carl-Zeiss DMR 22 instrument.

Synthesis of $[Mo(CO)_3(NN)(TDP)]$ (NN = *bipy, phen*; TDP = *tetraazadiphosphapentalene*)

An example of the general procedure is the following. $Mo(CO)_3$(phen)(TDP): Into a solution of 225 mg (0.635 mmol) of just prepared $Mo(CO)_3$(phen)(CH_3CN) in 10 cm^3 dichloromethane were added 190 mg (0.637 mmol) of TDP and was stirred for 30 min. The dark red coloured solution was then filtered. To this filtrate 10 cm^3 methanol were added, followed by vacuum evaporation to eliminate the major part of the dichloromethane. The red crystals were separated by filtration and washed with three portions of methanol (10 cm^3) and dried in vacuum (yield: 327 mg, 78%). The elemental analysis of these compounds are given in Table 1.

Electrochemical measurements

All voltammograms were recorded in CH_2Cl_2 or CH_3CN (0.1 M Bu_4NClO_4) on a Model 173/175 PAR electrochemistry system. A three-electrode cell consisting of a platinum-disc working electrode, a platinum wire counterelectrode and an Ag/AgCl (in Me_4NCl, ±0.01 vs SCE) reference electrode was used. Controlled-potential electrolysis experiments were performed with a PAR 179 coulometer.

Acknowledgements—Financial support given by the Dirección de Investigación de la Universidad de La Frontera (Project N° 1032126), the Comisión Nacional de Investigación Científica y Tecnológica (Project N° 5007/85) and the Dirección de Investigaciones Científicas y Tecnológicas de la Universidad de Santiago to carry out this work is gratefully acknowledged. A gift of some metal hexacarbonyls from Dr H. Müller of Merck Química, Chile is also gratefully acknowledged.

REFERENCES

1. S. Kleemann, E. Fluck and W. Schwarz, *Z. anorg. Chem.* 1981, **475**, 137.
2. W. Hieber and Mühlbauer, *Z. anorg. Chem.* 1935, **221**, 337.
3. W. Hieber and E. Romberg, *Z. anorg. Chem.* 1935, **221**, 349.
4. M. H. B. Stiddard, *J. Chem. Soc.* 1963, 756.
5. H. Behrens and N. Harder, *Chem. Ber.* 1964, **97**, 433.
6. L. W. Houk and G. R. Dobson, *J. Chem. Soc.* 1966, 317.
7. L. W. Houk and G. R. Dobson, *Inorg. Chem.* 1966, **5**, 2119.
8. H. Behrens, E. Lindner and G. Lehnert, *J. Organomet. Chem.* 1970, **22**, 439.
9. P. Correa, M. E. Vargas and J. Granifo, *Polyhedron.* 1987, **6**, 1781.
10. E. W. Ainscough, A. M. Brodie and A. R. Furness, *J. Chem. Soc., Dalton Trans.* 1973, 2360.
11. D. M. Manuta and A. J. Lees, *Inorg. Chem.* 1983, **22**, 3825.
12. H. tom Dieck and I. W. Renk, *Angew. Chem. Int. Edn* 1970, **9**, 793.
13. R. W. Balk, D. J. Stufkens and A. Oskam, *Inorg. Chim. Acta* 1978, **28**, 133.

14. G. R. Dobson, *Acc. Chem. Res.* 1976, **9**, 300.
15. M. K. Lloyd, J. A. McCleverty, D. G. Orchard, J. A. Connor, M. B. Hall, I. H. Hillier, E. M. Jones and G. K. M. Ewen, *J. Chem. Soc., Dalton Trans.* 1973, 1743.
16. R. I. Cook and J. G. Morse, *Inorg. Chem.* 1984, **23**, 2332.
17. C. J. Pickett and D. Pletcher, *J. Chem. Soc., Dalton Trans.* 1975, 879.

Polyhedron Vol. 7, No. 6, pp. 495–499, 1988
Printed in Great Britain

0277–5387/88 $3.00+.00
Pergamon Press plc

COMPLEXATION EQUILIBRIA BETWEEN PALLADIUM(II) AND 3-(4′,5′-DIMETHYL-2′-THIAZOLYLAZO)-2,6-DIAMINOPYRIDINE. SPECTROPHOTOMETRIC DETERMINATION OF PALLADIUM

Mª J. SÁNCHEZ, B. SANTANA, Mª L. PÉREZ PONT, V. GONZÁLEZ and F. GARCÍA MONTELONGO*

Department of Analytical Chemistry, University of La Laguna, 38204-La Laguna, Spain

(*Received* 12 *October* 1987; *accepted* 30 *October* 1987)

Abstract—The complexation equilibria between palladium(II) and 3-(4′,5′-dimethyl-2′-thiazolylazo)-2,6-diaminopyridine have been spectrophotometrically studied in aqueous medium, and the species PdHR ($\log\beta_{111} = 16.36 \pm 0.18$), PdH_3R_2 ($\log\beta_{132} = 31.47 \pm 0.20$) and PdH_4R_2 ($\log\beta_{142} = 27.36 \pm 0.18$) are established by graphical and numerical calculation methods. A method is developed for the determination of 0.43–3.40 ppm Pd ($\varepsilon = 1.42 \times 10^4$ l mol^{-1} cm^{-1} at 690 nm) which can be applied to its determination in small samples of hydrogenation catalysts.

Palladium(II) forms soluble green, blue or violet complexes with *o*-amino heterocyclic azo-dyes in strongly acidic media. The high sensitivity and selectivity of these reactions make them very useful for the spectrophotometric determination of palladium even though the complexation equilibria have seldom been studied.[1–4]

This paper reports on the complexation equilibria between palladium(II) and 3-(4′,5′-dimethyl-2′-thiazolylazo)-2,6-diaminopyridine(DMTADAP)[5] studied spectrophotometrically. Complex species in solution were established by graphical as well as numerical analysis of the absorbance–[H^+] curves.[6–8] The distribution diagrams established using the HALTAFALL program,[9] enable the accurate assessment of the distribution of the individual complexes in solution and their identification by visible absorption spectra.

A method is developed for the spectrophotometric determination of palladium and is applied to its determination in small samples of hydrogenation catalysts.

EXPERIMENTAL

A 10^{-3} M solution of 3-(4′,5′-dimethyl-2′-thiazolylazo)-2,6-diaminopyridine (DMTADAP) in 1 M perchloric acid. Standard 10^{-2} M $Pd(ClO_4)_2$ prepared from the chloride by perchloric acid treatment and standardized gravimetrically. Analytical reagent grade chemicals and de-ionized water were used throughout with no further purification.

Absorption measurements were performed on Beckman 25 and Perkin–Elmer 550S recording spectrophotometers provided with 1 cm matched quartz cells. The pH measurements were made with a Radiometer PHM64 digital pH-meter provided with a glass-calomel combination electrode. Measurements were performed at 25 ± 0.1°C. Calculations were carried out on a Digital VAS/VMX 11/780 (V.4.0) computer.

Spectrophotometric determination of palladium

To a solution of 21.3–74.5 μg of palladium as the perchlorate, in a 25-cm^3 calibrated flask, was added 2 cm^3 of 10^3 M DMTADAP perchloric solution. After 20 min 3 cm^3 of 70% $HClO_4$ was added and diluted to volume with de-ionized water. The absorbance was measured at 690 nm against a reagent blank.

Spectrophotometric determination of palladium in hydrogenation catalysts

10 mg of the catalyst were weighed accurately and dissolved in perchloric acid, nitric acid, aqua

* Author to whom correspondence should be addressed.

Table 1. Optical characteristics of 3-(4′,5′-dimethyl-2′-thiazolylazo)-2,6-diaminopyridine (8% *v/v* ethanol–water, $I = 0.25$ M $NaClO_4$)

Species	λ_{max} (nm)	ε (l mol^{-1} cm^{-1})	pK_a
H_3R^{3+}	495	2,200	-4.16 ± 0.07
H_2R^{2+}	510	21,500	2.75 ± 0.05
HR^+	520	13,500	4.83 ± 0.04
R	495	17,000	

regia or EDTA according to the support, and heated in a water bath if necessary. The cooled solution was diluted with 1 M $HClO_4$ to 100 cm^3 in a calibrated flask. Suitable aliquots (2–5 cm^3) were analysed for palladium as described above.

RESULTS AND DISCUSSION

3-(4′,5′-dimethyl-2′-thiazolylazo)-2,6-diaminopyridine (DMTADAP), whose acid-base and optical characteristics are shown in Table 1, reacts with palladium(II) to form green coloured solutions. However, species formed at pH $\geqslant 0$ precipitate, thus spectrophotometric studies have to be carried out at higher acidities.

Absorption spectra for solutions with palladium ion excess at $H_0 \leqslant 0$ show an absorption maximum at 390 nm and an absorption band at 680–760 nm. In order to obtain maximum and stable absorbances it is necessary to mix the Pd(II) and DMTADAP first and leave them to stand for at least 20 min before adding the other reagents. Absorption–H_0 curves at 690 nm for several C_{Pd}/C_R.

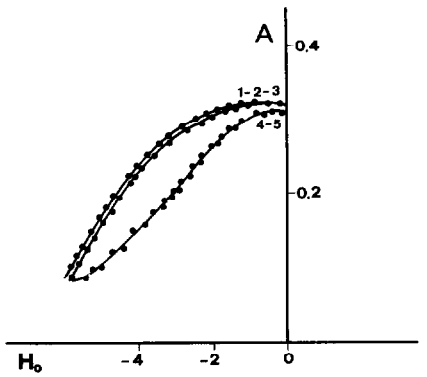

Fig. 1. Absorbance–H_0 curves for the system Pd(II)–DMTADAP at 690 nm. $C_R = 4 \times 10^{-5}$ M, C_{Pd} = (1) 2×10^{-3} M, (2) 8×10^{-4} M, (3) 4×10^{-4} M, (4) 4×10^{-5} M, (5) $C_R = 2 \times 10^{-4}$ M, $C_{Pd} = 2 \times 10^{-5}$ M.

Fig. 1, show constant absorbances in the range $-1 \leqslant H_0 \leqslant 0$; the difference in absorbance of the curves with metal ion excess and reagent excess suggests the presence of several complex species in solution.

The stoichiometry determined by the continuous variations and mole ratio methods at $H_0 = -0.7$ and 690 nm shows the formation of 1:2 Pd:R complex species.

In order to ascertain the complex species in solution and to calculate the corresponding stability constant, a method of graphical analysis of the $A = f([H^+])$ curves derived from that of Sommer *et al.*[6,7] was used. Upon applying the set of equations previously deduced[10] the formation of species PdHR ($\log \beta_{111} = 16.40$), PdH_3R_2 ($\log \beta_{132} = 9.04$) and PdH_4R_2 ($\log \beta_{142} = 9.66$) was established.

Next the experimental data were analysed by applying the LETAGROP-SPEFO program,[8] using the complex species and their stability constants calculated by the graphical method as starting values, and then the species model was modified by introducing new species in order to ascertain which one of the proposed models could fit the experimental data with the minimum sum of squares of the residuals, U, and of the standard deviation of absorbances, $\sigma(A)$.

As can be seen in Table 2 the model containing the species PdHR, PdH_3R_2 and PdH_4R_2 simultaneously, is the best to fit the experimental data. The introduction of other species such as hydroxylated, polynuclear and/or mixed ligand complexes, did not improve the results. Values calculated for the stability constants as well as the respective molar absorptivities are included in Table 2.

With a view to confirm the results obtained and to identify the absorption maxima of the different species in solution, the distribution diagrams for several metal-to-ligand ratios were established using the HALTAFALL program,[9] Fig. 2, and absorption spectra of such solutions were recorded. As can be seen in Figs 3 and 4 the species PdH_3R_2 is responsible for the absorption maximum at 550 nm at $H_0 < -1$ in solutions with $C_{Pd}/C_R \gg 1$, and the species PdH_4R_2 produces the absorption band at 680–760 nm. The species PdHR is responsible for the shoulder at 610 nm.

On comparing the results obtained for the system Pd(II)–DMTADAP with those for the complexes of palladium(II) with 3-(2′-thiazolylazo)-2,6-diaminopyridine[11,12] and its 4′-methyl derivative[13] in Table 3, one can see that the PdHR complex of DMTADAP is the most stable but it does not form the PdH_2R complex. Besides, DMTADAP is the only one out of these three reagents which forms PdH_3R_2 and PdH_4R_2 complexes.

Table 2. Values of U, $\sigma(A)$, $\log\beta_{pqr}$ and ε_{pqr} for the different species model tested by the LETAGROP-SPEFO method

Species model	U	$\sigma(A)$	$\log\beta_{pqr}$	ε_{pqr}
PdHR	0.88×10^{-1}	0.04	14.14±0.21	6,000±75
PdH_2R_2			29.38 Max 33.90	—
PdHR	0.473×10^{-2}	0.010	16.68 Max 16.93	7,400±100
PdH_4R_2			27.15 Max 27.40	9,300±250
PdHR	0.437×10^{-2}	0.010	16.67 Max 16.88	7,500±93
PdH_4R_2			27.15 Max 23.39	9,300±200
PdH_2R_2			32.58 Max 33.10	—
PdHR	0.193	0.007	16.36±0.18	7,693±50
PdH_4R_2			27.26±0.11	8,384±161
PdH_3R_2			31.47±0.20	13,249±162

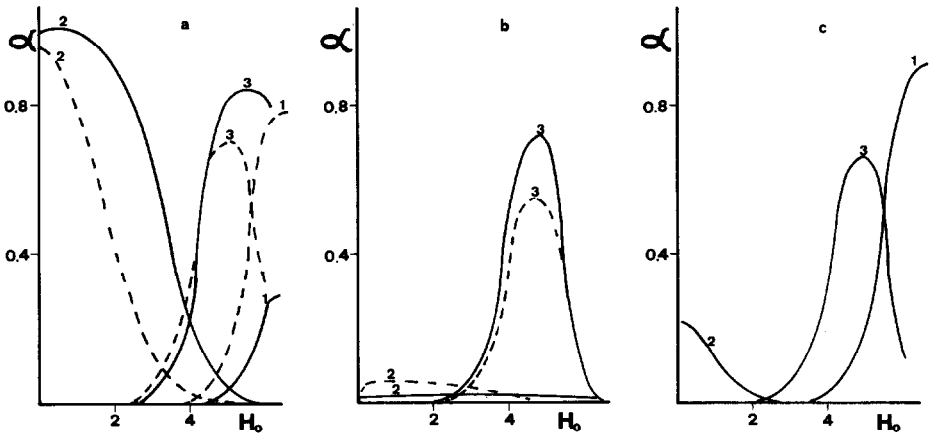

Fig. 2. Distribution diagrams for the system Pd(II)–DMTADAP. Species: (1) PdHR, (2) PdH_4R_2, (3) PdH_3R_2. (a) C_{Pd}/C_R = 50/1 (——), 2/1 (---); (b) = 1/5 (——), 1/2 (---); (c) $C_{Pd} = C_R$. ($C_R = 4\times10^{-5}$ M.)

Spectrophotometric determination of palladium with DMTADAP

In solutions where $H_0 = -0.7$ (1.5 M $HClO_4$) and palladium is present as the perchlorate, the system Pd(II)–DMTADAP conforms to Beer's law between 0.43–3.40 ppm of palladium. The molar absorptivity is 1.42×10^4 at 690 nm. The optimum range for the determination is 0.85–2.98 ppm as evaluated by Ringbom's method.

The statistical study carried out on ten samples each containing 2.56 ppm Pd, gives 2.56 ppm as the mean value, 3.63×10^{-3} as the standard deviation and 0.30% relative error (P = 0.05).

A study of the effect of several ions on the determination of 2.56 ppm of palladium was carried out

Table 3. Comparison between the palladium complexes of TADAP, MTADAP and DMTADAP

Reagent	$\log\beta_{111}$	$\log\beta_{121}$	$\log\beta_{132}$	$\log\beta_{142}$	λ_{max}	H_0[a]	$\varepsilon\times10^{-4}$	Ref.
TADAP	8.98	6.30			665	−0.7	1.37	11, 12
MTADAP	8.05	4.20			675	−0.57	1.60	13
DMTADAP	16.36		31.47	27.26	690	−0.57	1.42	This work

[a] $HClO_4$.

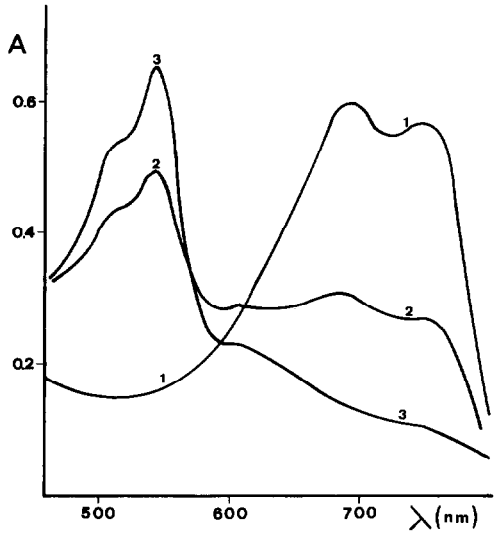

Fig. 3. Absorption spectra for the system Pd(II)–DMTADAP at different H_0 values ($C_{Pd} = 2 \times 10^{-3}$ M, $C_R = 4 \times 10^{-5}$ M).

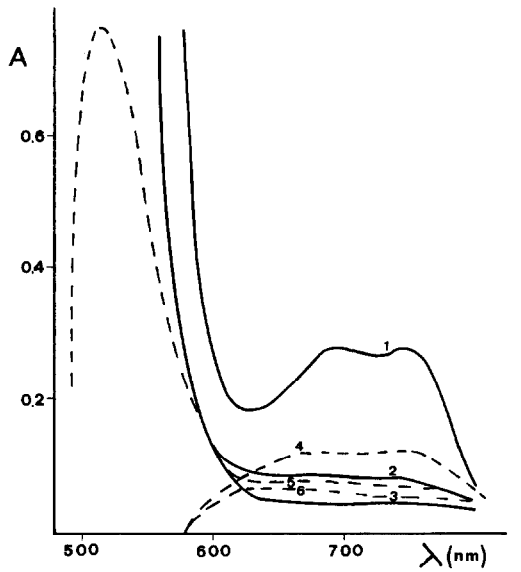

Fig. 4. Absorption spectra for the system Pd(II)–DMTADAP ($C_{Pd} = 4 \times 10^{-5}$ M, $C_R = 2 \times 10^{-4}$ M) at different H_0 values (– – –), and at $H_0 = -5.14$ as a time function (——): (1) 5 min, (2) 10 min, (3) < 20 min. (Water as the blank.)

firstly by applying the recommended procedure to solutions containing a 200-fold (*m/m*) ratio of interferent to palladium and if interference occurred, the ratio was reduced until interference ceased. Higher ratios were not tested. The criterion for an interference was a variation in the concentration of palladium found, of more than ±2% from the value taken. The results are shown in Table 4.

Table 4. Spectrophotometric determination of palladium with DMTADAP in the presence of foreign ions, [Pd^{2+}] taken = 2.56 ppm

[Interferent]/[Pd^{2+}]	Interference
200/1	NO_3^-, SO_4^{2-}, Ni, Ca, Sr, Ba.
100/1	As(V), Zn, $C_2O_4^{2-}$.
60/1	F^-, HPO_4^{2-}.
50/1	Co(II), Cu, Cd, Fe(II,III), Ag(I), U(VI)
5/1	Bi, Cr(III)
1/1	Hg(II), Pt(II), Ru(III), Au(III), Os(IV), the halides (high interference)

As can be seen from Table 3 the introduction of the methyl groups in the TADAP molecule causes a displacement of the absorption maximum towards longer wavelengths, while molar absorptivities remain very similar. However, the method based on DMTADAP has less interference from the fluoride ion but more interference from Fe(II,III) and Hg(II), than the TADAP method.

The method developed was applied to the determination of palladium in small samples (≃ 10 mg) of hydrogenation catalysts. Results are shown in Table 5 where they are compared with those obtained by A.A.S.

Table 5. Spectrophotometric determination of palladium with DMTADAP in hydrogenation catalysts

Catalysts (Fluka)	Found (%)[a] A.A.S.	DMTADAP
Pd/asbestos	4.41	4.45
Pd/active charcoal	9.40	9.38
$Pd/CaCO_3$	5.60	5.94
$Pd/BaSO_4$	9.80	9.98

[a] Mean of three determinations.

Acknowledgement—The authors wish to acknowledge the financial support of this work by CAICYT (Spain) grant No. 4133/79.

REFERENCES

1. A. I. Busev, V. M. Ivanov and U. ElDvick, *Vestn. Mosk. Univ., Ser. Khim.* 1969, **2**, 92.
2. S. Shibata, Y. Ishiguro and R. Nakashima, *Anal. Chim. Acta* 1973, **64**, 325.
3. F. García Montelongo, V. González and C. R. Tallo, *Analusis*, 1981, **9**, 353.

4. F. Kai and Y. Sakanashi, *Anal. Lett.* 1983, **16**(A13), 1013.
5. B. Gallo, M. Aguilar and F. García Montelongo, *An. Quim.* 1985, **81B**, 240.
6. L. Sommer and S. P. Mushran, *Coll. Czech. Chem. Commun.* 1969, **31**, 3695.
7. L. Sommer, M. Langova and V. Kuvan, *Coll. Czech. Chem. Commun.* 1976, **41**, 1317.
8. L. G. Sillén and B. Warnqvist, *Arkiv Kemi* 1969, **31**, 377.
9. N. Ingri, W. Kakolowicz, L. G. Sillén and B. Warnqvist, *Talanta* 1967, **14**, 1261.
10. J. J. Arias, F. Jiménez, A. I. Jiménez and F. García Montelongo, *An. Quim.* 1983, **79B**, 248.
11. F. García Montelongo, V. González and C. R. Tallo, *Microchem. J.* 1982, **27**, 194.
12. V. González, C. R. Tallo and F. García Montelongo, *An. Quim.* 1983, **79B**, 83.
13. M^{a}L. Pérez Pont, Ph.D. Dissertation, University of La Laguna (1983).

Polyhedron Vol. 7, No. 6, p. 501, 1988
Pergamon Press plc. Printed in Great Britain

BOOK REVIEW

Gmelin Handbook of Inorganic Chemistry, Mn—Manganese D_6 Coordination Compounds 5. Published by Gmelin Institute for Inorganic Chemistry of the Max Planck Society for the Advancement of Science, 8th Auflage, Main Series System-Nr. 56. Springer, Berlin, 1987. ISBN 3-540-93550-9, 25 Figs, xix, 349 pp., 950 g. Hard cover, DM 1541.

There are 17 volumes on manganese of which this is the most modern. Although earlier volumes were in German, this volume is in English and is one of five volumes concerning the coordination compounds of manganese in particular with the ligands amine-N-polycarboxylic acids, hydrazinecarboxylic acids, amides, hydrazides, derivatives of hydroxylamine, oximes and nitroso compounds, and triazenes.

The stabilities of the complexes formed between these agents and manganese are reviewed. Solution chemistry formation constants and X-ray investigations are referenced. The analytical chemistry arising from hydroxamic acids and the biochemistry of isonicotinohydrazide–manganese(II) and (III) complexes are covered. Literature references up until 1985 are included.

This is another very useful reference book in the mega-series. It is a well-founded and forward-looking library that stocks this series and this volume is up to the high standards of its predecessors.

DAVID R. WILLIAMS
Department of Applied Chemistry
UWIST
PO Box 13
*Cardiff, CF*1 3*XF, U.K.*

Polyhedron Vol. 7, No. 6, p. 503, 1988
Pergamon Press plc. Printed in Great Britain

ANNOUNCEMENT

XIII INTERNATIONAL CONFERENCE ON ORGANOMETALLIC CHEMISTRY

4–9 SEPTEMBER 1988 TORINO, ITALY

The Conference, which is sponsored by The International Union of Pure and Applied Chemistry and by The Federation of the European Chemical Societies, will take place at Torino Esposizioni/Teatro Nuovo from Monday 5 September to Friday 9 September 1988, with participants foregathering on Sunday 4 September.

The aim of the Conference is to cover several aspects of Organometallic Chemistry, including solution, solid state and catalytic properties. The XIII ICOMC will be organized in plenary and main session lectures, communications and posters.

The deadline for Scientific Contributions is 31 March 1988.

Further information and copies of the second circular with details about accommodation are available from the **Congress Secretariat: Notes S.n.c., Via Romani 25, I 10131 Torino, Italy. Telephone: (011) 877580.**

Polyhedron Vol. 7, No. 7, pp. 505–512, 1988
Printed in Great Britain

0277–5387/88 $3.00+.00
© 1988 Pergamon Press plc

THE REACTION OF A ZWITTERIONIC DIPHOSPHORUS COMPOUND WITH THE PLATINUM(0) COMPLEX, $(C_2H_4)Pt(PPh_3)_2$

PETRA LOOK and REINHARD SCHMUTZLER*

Institut für Anorganische und Analytische Chemie der Technischen Universität, Hagenring 30, 3300 Braunschweig, F.R.G.

ROBIN GOODFELLOW and MARTIN MURRAY

School of Chemistry, The University, Cantock's Close, Bristol BS8 1TS, U.K.

and

DIETMAR SCHOMBURG

Gesellschaft für Biotechnologische Forschung mbH, Mascheroder Weg 1, 3300 Braunschweig/Stöckheim, F.R.G.

(*Received* 16 *September* 1987; *accepted* 13 *October* 1987)

Abstract—The oxidation–reduction reaction between a zwitterionic diphosphorus compound, involving the grouping $Cl—P^{(-)}—P^{(+)}—NEt_2$ with the platinum(0) complex, $(C_2H_4)Pt(PPh_3)_2$, has furnished a novel platinum(II) complex with a Pt—P four-membered ring as the central feature. The identity and structure of this platinum complex has been established by NMR spectroscopy and by a single-crystal X-ray structure determination.

The reaction between N,N′-dimethyl-N,N′-(trimethylsilyl)-urea with diorganoaminodichlorophosphines, R_2NPCl_2, has been shown to furnish a number of representatives of a new class of diphosphorus compounds of type **1**, with a phosphorus–phosphorus bond.[1,2,3]

A single-crystal X-ray structure determination has been conducted for **1** (R = Et), and the presence of a zwitterionic system involving negatively charged (phosphoranide) phosphorus and positively charged (phosphonium) phosphorus directly bonded has been suggested.[3] The two dimethylurea groupings apparently serve to stabilize the phosphorus-phosphorus system in this and numerous related diphosphorus compounds. Molecules of type **1** are expected to display several sites of reactivity, *vis.* the lower-valent and the higher-valent phosphorus atom, and the phosphorus–phosphorus bond.

Numerous experiments have been conducted with a view of establishing to what extent the typical properties of pentavalent phosphorus are affected by the proximity of lower-valent phosphorus, as

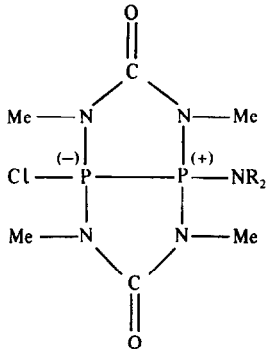

1

* Author to whom correspondence should be addressed.

well as to ascertain how pentavalent phosphorus directly bonded to tri-coordinate phosphorus will alter the typical reactivity of the latter. Experiments have been performed, to this end, on compounds of type **1**, as well as on related, mixed-valence diphosphorus compounds, involving the groupings $\lambda^3P\lambda^5P$, and a large number of new and novel diphosphorus compounds were created in which the reactivity of both the lower- or higher-valent phosphorus atom was not abnormal.[1,2,3] As a rule, the phosphorus–phosphorus bond in the diphosphorus compounds was left intact in these reactions. The same observation was also made during the reaction of the lower-valent phosphorus atom of the mixed valence diphosphorus compounds involving the system $\lambda^3P\lambda^5P$ with $Fe_2(CO)_9$, which produced P—P bonded $\lambda^5P\lambda^4P$-$Fe(CO)_4$ compounds.[2,4,5] The course of the reaction between a zwitterionic diphosphorus compound of type **1** (R = Et) with a platinum(0) complex, $(C_2H_4)Pt(PPh_3)_2$, **2**, proved dissimilar from previous experience in that, in an oxidation–reduction reaction, a novel type of binuclear platinum(II) complex, **3**, was formed. See eq. 1.

The reaction between **1** (R = Et), as a suspension in benzene and **2** (as a benzene solution) was complete overnight at room temperature. The product, **3**, was recovered after removal of the benzene *in vacuo*. The other products, formed according to eq. (1) were ethylene and triphenylphosphine, i.e. the ligands of the starting platinum complex, **2**, were completely stripped off, so as to form what may be termed "naked" platinum.[6]

The characterization of the novel complex, **3**, rests on its elemental analysis, ^1H, ^{31}P and ^{195}Pt NMR data (*vide infra*), on its IR spectrum [$\nu_{C=O}$ for the N,N′-dimethylurea grouping, 1665 cm^{-1}; for the five-membered rings a shift of $\nu_{C=O}$ to higher wavenumbers (*ca* 1700–1730 cm^{-1} would be expected), and on the mass spectrum (found, M^+ 1073; calc. for $C_{20}H_{44}Cl_2N_{10}O_4P_4Pt_2$, M = 1073.61 g mol^{-1}); the isotopic distribution observed and calculated for **3** were in good agreement].

NMR spectroscopy

The ^{31}P and ^{195}Pt NMR spectra of compound **3** are complicated by the presence of various isotopomers (0, 1, and 2 spin active ^{195}Pt nuclei in the molecule), and even the molecules with no ^{195}Pt nuclei show second order ^{31}P spectra because the spin system is $[AX]_2$ (or $AA'XX'$). Analysis of the $[AX]_2$ spectrum which is the strongest feature of the ^{31}P spectrum gave values of the P—P coupling constants and the two ^{31}P chemical shifts. Values of the P—Pt coupling constants were then obtained from the ^{31}P and ^{195}Pt spectra of the isotopomer containing one ^{195}Pt nucleus. At this stage of the analysis some difficulty was experienced in getting a good fit between simulated and observed spectra, which was found to be due to the assignments of the two P—Pt coupling constants in the ring, which is opposite to that expected; i.e. the P—Pt coupling for the bond *trans* to the chlorine ligand is in fact smaller than the coupling for the bond *trans* to the exocyclic phosphine ligand.

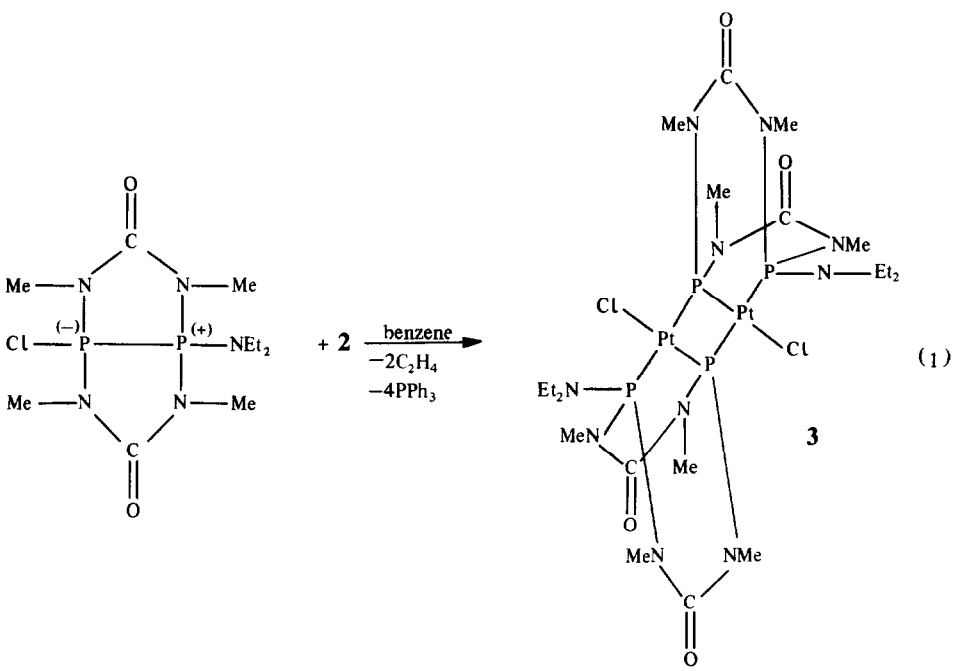

(1)

Table 1. Chemical shifts[a] and coupling constants[b] for **3**

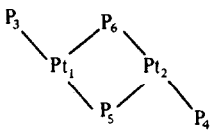

Pt—Pt couplings:	1–2	1077.3
Pt—P couplings:	1–3, 2–4	3488.9
	1–6, 2–5	2103.8
	1–5, 2–6	2535.7
	1–4, 2–3	−4.4
P—P couplings:	3–5, 4–6	728.0
	3–6, 4–5	−11.5
	3–4	0.1
	5–6	−126.6
Chemical shifts:	Pt_1, Pt_2	555
	P_3, P_4	69.2
	P_5, P_6	−51.7

[a] In ppm.
[b] In Hz.

This assignment was confirmed by simulation of the spectra of the isotopomer with two ^{195}Pt nuclei, which also yielded the value of the Pt—Pt coupling constant. A final refinement of the coupling constants and chemical shifts was achieved by an iterative fitting to a total of 111 observed transitions of the two Pt isotopomers in both ^{31}P and ^{195}Pt spectra. The r.m.s. deviation between the observed and simulated spectra was 1.5 Hz, less than the spot resolution of the spectrometer, and the standard deviations of the iterated values of the chemical shifts and coupling constants were all less than 0.6 Hz. The final values are presented in Table 1 and the observed spectra are shown in Figs 1 and 2 along with the simulated spectra. These values may be compared to the values obtained by Glaser *et al.*[7] for the related compound, **4**.

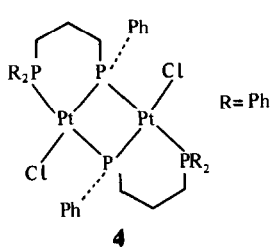

4

In general the larger values found for most of the couplings in our system reflect the increased electronegativity of the groups attached to phosphorus (nitrogen as opposed to carbon), but the greatest difference is in the assignments of the two couplings for the P—Pt bonds in the ring. In Glaser's compound the two values (2228.4 and 1820.2 Hz) are assigned so that the larger value corresponds to the bond *trans* to chlorine, the smaller value to the bond *trans* to the phosphine ligand.

As the authors mention in their paper, this is in agreement with the normal behaviour pattern of the P—Pt couplings, and reflects the *trans*-effect of the ligands at the square-planar platinum. There is no doubt that in our system the assignment is the opposite one, the larger coupling (2535.7 Hz) corresponding to the bond *trans* to phosphorus, the smaller coupling (2103.8 Hz) corresponding to the bond *trans* to chlorine. When we first noticed this discrepancy we wondered whether the assignment given by Glaser *et al.* was unambiguous, since their spectra were observed at higher field, and the second order effects which distinguished between the two assignments should be less noticeable in their systems. We therefore checked the assignments for their compounds by simulating theoretical spectra using their reported NMR parameters. This showed that the two assignments were indeed not distinguishable in the spectra of the isotopomer containing one ^{195}Pt nucleus, but simulation of the spectra of the isotopomer with two ^{195}Pt nuclei showed sufficient significant differences between the two assignments to indicate that Glaser's assignment was indeed correct and therefore the opposite of that required for our compound.

On the basis of this single example of divergence from the normal effect of the *trans* ligand on P—Pt couplings we are unable to offer any conclusive explanation for this behaviour, especially when normal behaviour is observed for the closely related ring system of Glaser *et al.* One possibility is that the explanation lies in the two chelating ring systems (—N—CO—N—) between the two *cis* phosphorus ligands at each platinum, whereas Glaser *et al.*'s compounds have only one such chelating ring system (and therefore display a measure of isomerism which our compound does not display). While this may affect the amount of distortion from idealized square-planar geometry at platinum, it is worth noting that the bond lengths (see below) are as predicted by the normal *trans* effect considerations, i.e. the longer ring P—Pt bond is *trans* to phosphorus, although it has the larger P—Pt coupling constant.

X-ray structure of **3**

The structure of **3**, involving the cleavage of the phosphorus–phosphorus bond in **1** and the formation of two eight-membered rings, was established unambiguously by a single crystal X-ray

structure determination. In recent years the structures of several phosphido-bridged diplatinum complexes have been described in the literature. In several, but not in all cases the central four-membered, Pt—P—Pt—P ring is planar.[7,8,9] Compound **3** displays crystallographic C_i symmetry which means that it has a crystallographically imposed planar central four-membered ring. (See Fig. 3.)

The bond lengths in the ring are 222.5(2) pm (*trans* to chlorine) and 232.9(2) pm (*trans* to phosphorus). This significant difference in bond lengths of 10.4 pm (50 times the standard deviation) clearly reflects the expected *trans* influence of the chlorine and phosphine ligands on the bonding at platinum. (See Table 2.) The length of the exocyclic Pt—P bond is 224.6(2) pm. The bonding geometry around platinum is essentially planar (sum of *cis* bond angles 359.9°) with strong distortions from a square. As is generally observed the P—Pt—P bond angles (77.3(1)° for the endocyclic and 81.2(1)° for the exocyclic angle) are around 20° smaller than the Cl—Pt—P angles [100.9(1)° and 100.5(1)°]. The platinum–chlorine bond length (236.4(2) pm) is in the range typical of this bond.

The two tetra-coordinated phosphorus atoms are in rather different bonding states, one being formally a phosphine phosphorus with an additional

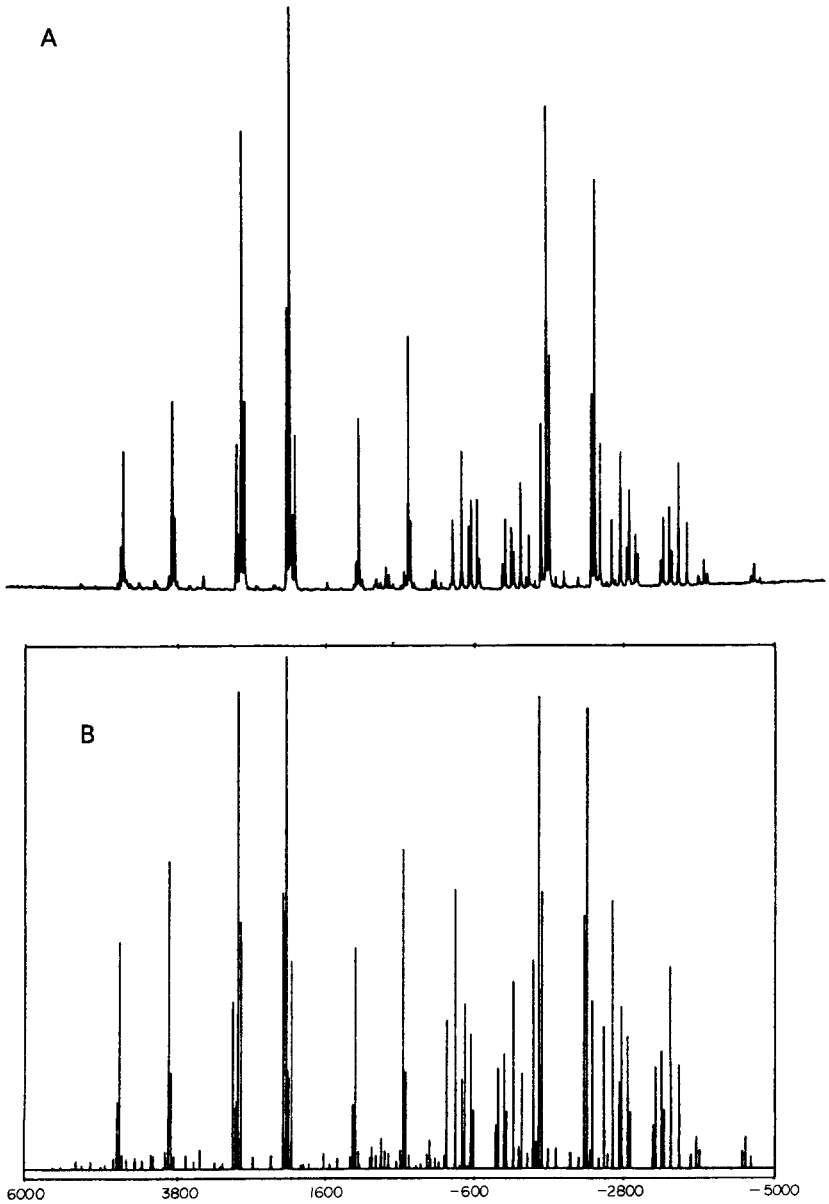

Fig. 1. Observed (A) and simulated (B) ^{31}P NMR spectra of **3** (scale in Hz).

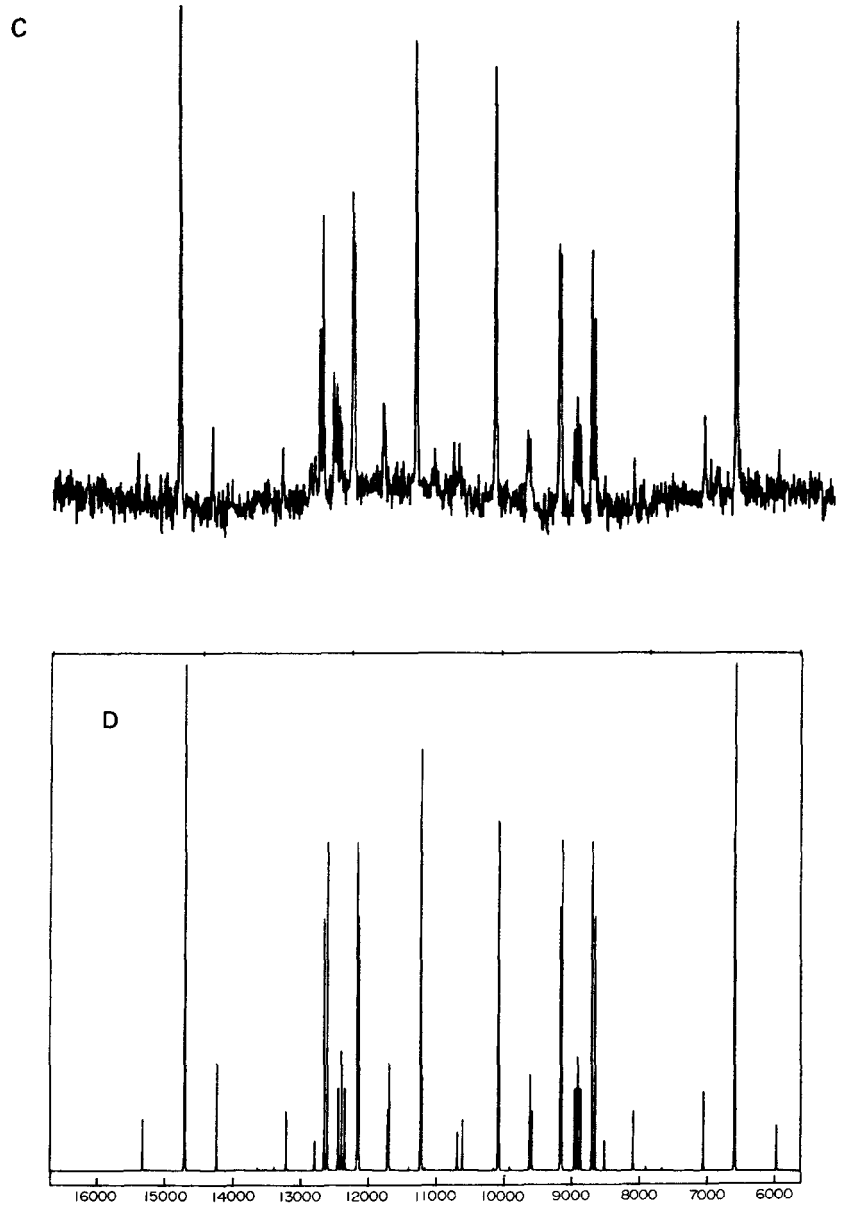

Fig. 2. Observed (C) and simulated (D) ^{195}Pt NMR spectra of **3** (scale in Hz).

coordinative bond and the other displaying two normal covalent bonds and two additional coordinative bonds to platinum. This difference is clearly reflected in the bonding geometry. Whereas both phosphorus atoms are in a strongly distorted tetrahedral environment, this distortion is larger for the exocyclic (bond angles between 101.3(2)° for N(1)—P(1)—Pt and 123.0(2)° for N(7)—P(1)—Pt) than for the endocyclic phosphorus [bond angles between 102.7(1)° for Pt—P(2)—Pt and 112.2(2)° for Pt—P(2)—N(3)]. The difference also becomes obvious in the different P—N bond lengths, which are 171.2(6) and 171.9(6) pm at the phosphido phosphorus atom and 169.5(6) and 169.6(6) pm at P(1). The bond to the diethylamino nitrogen atom (162.9(6) pm) is still *ca* 7 pm shorter.*

EXPERIMENTAL

All operations were conducted with exclusion of air and moisture, using standard techniques. The IR spectrum of **3** was recorded on a Beckman 4260

* This difference in the bond distances between phosphorus and the amino-nitrogen vs the bond to the urea-nitrogen is generally observed in this class of phosphorus compounds (see refs 1–3).

Table 2. Bond lengths (pm) and angles (°) in **3**

P(1)—Pt	224.6(2)	P(2)—Pt	222.5(2)
Cl—Pt	236.4(2)	N(1)—P(1)	169.5(6)
N(4)—P(1)	169.7(6)	N(7)—P(1)	162.9(6)
N(3)—P(2)	171.2(6)	N(6)—P(2)	171.9(6)
C(11)—N(1)	147.2(10)	C(2)—N(1)	139.3(9)
O(2)—C(2)	120.6(9)	N(3)—C(2)	139.4(9)
C(31)—N(3)	147.0(9)	C(41)—N(4)	149.6(9)
C(5)—N(4)	140.6(10)	O(5)—C(5)	118.4(9)
N(6)—C(5)	138.1(9)	C(61)—N(6)	148.5(9)
C(7)—N(7)	149.9(10)	C(9)—N(7)	149.7(10)
C(8)—C(7)	149.2(14)	C(10)—C(9)	149.5(15)
P(2)—Pt—P(1)	81.2(1)	Cl—Pt—P(1)	100.9(1)
Cl—Pt—P(2)	177.8(1)	N(1)—P(1)—Pt	101.3(2)
N(4)—P(1)—Pt	113.4(2)	N(4)—P(1)—N(1)	101.7(3)
N(7)—P(1)—Pt	123.0(3)	N(7)—P(1)—N(1)	104.6(3)
N(7)—P(1)—N(4)	109.6(3)	N(3)—P(2)—Pt	112.2(2)
N(6)—P(2)—Pt	106.2(2)	N(6)—P(2)—N(3)	102.8(3)
C(11)—N(1)—P(1)	119.6(5)	C(2)—N(1)—P(1)	120.8(5)
C(2)—N(1)—C(11)	115.2(6)	O(2)—C(2)—N(1)	120.4(7)
N(3)—C(2)—N(1)	119.7(6)	N(3)—C(2)—O(2)	119.9(7)
C(2)—N(3)—P(2)	128.6(5)	C(31)—N(3)—P(2)	116.1(5)
C(31)—N(3)—C(2)	115.2(6)	C(41)—N(4)—P(1)	116.8(5)
C(5)—N(4)—P(1)	129.8(5)	C(5)—N(4)—C(41)	112.7(6)
O(5)—C(5)—N(4)	122.2(7)	N(6)—C(5)—N(4)	115.3(6)
N(6)—C(5)—O(5)	122.4(8)	C(5)—N(6)—P(2)	122.4(5)
C(61)—N(6)—P(2)	121.0(5)	C(61)—N(6)—C(5)	116.2(6)
C(7)—N(7)—P(1)	114.4(5)	C(9)—N(7)—P(1)	125.6(6)
C(9)—N(7)—C(7)	115.7(6)	C(8)—C(7)—N(7)	114.0(7)
C(10)—C(9)—N(7)	111.8(10)	C(74)—C(71)—C(73)	59.2(17)

instrument. The mass spectrum of **3** was recorded at 70 eV on a Varian MAT 8222 instrument at 300°C. The melting point of **3** was determined in a sealed tube. The elemental analyses were conducted at Mikroanalytisches Laboratorium Beller, Göttingen.

NMR spectra

Spectra were recorded on a JEOL FX90Q spectrometer with ^{2}D internal lock and ^{1}H broad-band decoupling on samples dissolved in CD_2Cl_2 in 10 mm tubes. ^{31}P spectra at 36.4 MHz are referenced to external H_3PO_4 (85%) and ^{195}Pt spectra at 19.16 MHz are referenced to 21.4 MHz (TMS at 100 MHz).

X-ray analysis

Crystals of **3** obtained by slow evaporation of the solvent from a solution in acetone/toluene have monoclinic symmetry, space group $P2_1/n$. The unit cell which has the parameters $a = 985.3(2)$, $b = 1141.7(2)$, $c = 1860.9(3)$ pm, $\beta = 102.24(3)°$ contains two molecules yielding a calculated density of 1.742 g cm^{-3}. The data were collected at 293 K on a Syntex $P2_1$ diffractometer using graphite-monochromated Cu-K_α radiation ($\lambda = 154.178$ pm) in the θ-2θ mode in the range $3° \leqslant 2\theta \leqslant 135°$ at a scan speed between 2.93 and 29.30°/min, depending on the intensity of the reflection.

The data were corrected for Lorentz, polarization and absorption effects ($\mu = 15.743$ mm^{-1}). The structure was solved by direct methods and difference-Fourier synthesis. The compound was found to display crystallographic C_i symmetry. Rigid methyl groups of idealized geometry were employed. Near the centre of symmetry at 0.5/0.0/0.5 a molecule of acetone was contained in the unit cell. The molecule is strongly disordered. The refinement using 3266 out of 3530 measured independent reflections ($F \geqslant 1.25\sigma(F)$) converged at $R = 0.043$. A final difference map displayed no electron density higher than 0.795×10^6 e/pm^3. The program SHELX-76[10] and our own programs were used. Complex atom scattering factors[11] were employed.

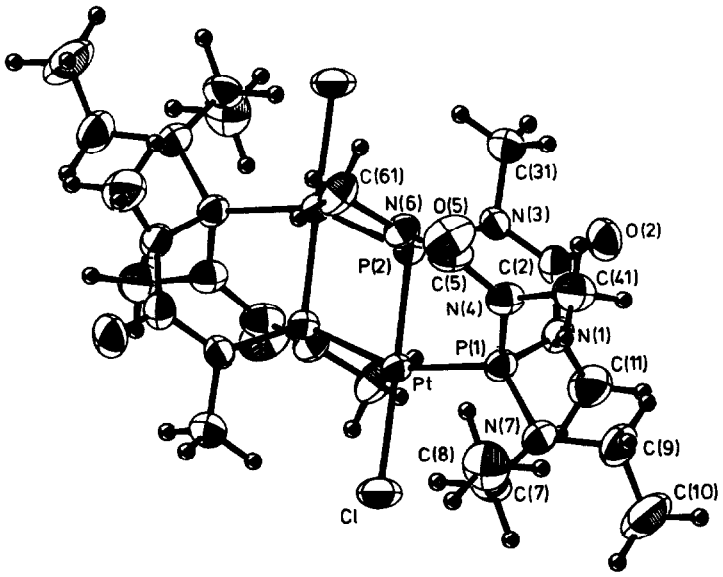

Fig. 3. X-ray crystal structure of **3**.

Preparation of compound **3**

The reaction between **1** (R = Et) and **2** was conducted in a glass tube, fitted with a Teflon stopcock. To a suspension of 0.46 g (1.3 mmol) of **1** in 5 cm^3 of benzene, a solution of 1 g (1.3 mmol) of the platinum complex, **2**,[12] in 10 cm^3 of benzene was added dropwise during 5 min. The glass tube was sealed and the reaction mixture was stirred for 12 h at room temperature. The colour of the reaction mixture was found to change from orange–yellow to light yellow. The residue left after removal of the benzene solvent *in vacuo* (0.1 mm) was washed with 10 cm^3 portions of benzene (*ca* three times) until the solvent remained colourless. The product was recrystallized from dichloromethane/methylcyclohexane (3/1) or small amounts (for the X-ray study) from acetone/toluene (5/1). Yield of **3**, 0.52 g (75%); m.p. 260° (dec.). The analytical sample of **3** was recrystallized from dichloromethane/methylcyclohexane and was found to crystallize as $3 \cdot 0.5CH_2Cl_2$. Found: C, 21.7; H, 4.0; Cl, 15.1; P, 10.7. Calc. for $C_{20}H_{44}Cl_2N_{10}O_4P_4Pt_2 \cdot 0.5CH_2Cl_2$: C, 21.5; H, 3.9; Cl, 14.8; P, 10.2%.

Acknowledgements—BASF AG, Bayer AG, Degussa and Hoechst AG are thanked for gifts of chemicals. The support of Fonds der Chemischen Industrie is gratefully acknowledged. We are grateful to Dr H. M. Schiebel, Institut für organische Chemie der Technischen Universität, Braunschweig, for the mass spectrum of compound **3**.

REFERENCES

1. G. Bettermann, H. Buhl, R. Schmutzler, D. Schomburg and U. Wermuth, *Phosphorus and Sulphur* 1983, **18**, 77.
2. G. Bettermann, Ph.D. Thesis, Technische Universität, Braunschweig (1986).
3. G. Bettermann, D. Schomburg and R. Schmutzler, *Chem. Ber.*, in preparation.
4. J. W. Gilje, W. S. Sheldrick, N. Weferling and R. Schmutzler, *Angew. Chem.* 1982, **94**, 393; *idem.*, *Int. Edit. Engl.* 1982, **21**, 379.
5. H. Buhl, Diplomarbeit, Technische Universität, Braunschweig (1983).
6. For an account of "ligand-free" platinum compounds, see F. G. A. Stone, *Acc. Chem. Res.* 1981, **14**, 318.
7. R. Glaser, D. J. Kountz, R. D. Waid, J. C. Galluci and D. W. Meek, *J. Am. Chem. Soc.* 1984, **106**, 6324.
8. P. Braunstein, D. Matt, J. Fischer and A. Mitschler, *J. Organometal. Chem.* 1981, **213**, 79.
9. A. J. Carty, F. Hartstock and N. J. Taylor, *Inorg. Chem.* 1982, **21**, 1349.
10. G. M. Sheldrick, unpublished.
11. D. T. Cromer and J. T. Waber, in *International Tables for Crystallography*, Vol. IV, pp. 99, 149. Kynoch Press, Birmingham (1974).
12. (a) L. Malatesta and S. Cenini, *Zerovalent Compounds of Metals*, p. 70. Academic Press, London (1974). (b) F. R. Hartley, *The Chemistry of Platinum and Palladium*, p. 398. Applied Science Publishers, London (1973). (c) U. Nagel, *Chem. Ber.* 1982, **115**, 1998.

Polyhedron Vol. 7, No. 7, pp. 513–521, 1988
Printed in Great Britain

0277–5387/88 $3.00+.00
© 1988 Pergamon Press plc

EFFECT OF AN ALKYL CHAIN SUBSTITUENT ON THE KINETICS AND THERMODYNAMICS OF COMPLEXATION OF 8-HYDROXYQUINOLINES WITH Ni^{2+} AND Co^{2+} IN METHANOLIC SOLUTIONS

M. BOUMEZIOUD and C. TONDRE*

Laboratoire d'Etude des Solutions Organiques et Colloïdales (L.E.S.O.C.) U.A. C.N.R.S. 406, Université de Nancy I, B.P. 239, 54506 Vandoeuvre les Nancy, France

and

P. LAGRANGE

Laboratoire de Chimie Physique et Electrochimie, U.A. C.N.R.S. 405, Ecole Nationale Supérieure de Chimie de Strasbourg, 1 rue Blaise Pascal, 67000 Strasbourg, France

(*Received* 7 *September* 1987; *accepted* 13 *October* 1987)

Abstract—7-(4-ethyl-1-methyloctyl)-8-hydroxyquinoline (C_{11}—HQ) is the active component of the industrial extractant Kelex 100. The thermodynamic as well as the kinetic parameters for the complexation of this ligand molecule with Ni^{2+} and Co^{2+} are compared with that of 8-hydroxyquinoline (HQ) in identical conditions (methanolic solutions with up to 0.4% of water, 0.1 M $NaClO_4$, 0.1 M triethanolamine buffer). From stopped-flow experiments, the alkyl-chain substituent is shown to be responsible for a seven-fold decrease of the rate constant for the 1 : 1 complex formation between the neutral form of the ligands and the Ni^{2+} ion. A similar behaviour is observed for the Co^{2+} ion, for which quantitative data have only been obtained with the alkylated ligand. Two different mechanisms are considered to explain the pH-dependence of the observed rate constant, which is attributed to the metal hydrolysis rather than to the ligand deprotonation.

The complexation reactions of metal ions with all sorts of ligands have been extensively studied during the last 20 years both from a thermodynamic and a kinetic point of view. The fast kinetic methods introduced by Eigen and his coworkers have been largely involved in the numerous studies from which a clear mechanistic picture has emerged.[1–4]

Although alkylated extractants have been used for a long time in hydrometallurgy, there is presently a growing need for ligand molecules having a highly lipophilic nature, not only for industrial applications in the field of liquid–liquid extraction,[5] but also for chemical studies related to the use of organized assemblies.[6] In many instances an alkyl chain has thus been grafted on an extractant molecule whose properties are known, just to confer on it a hydrophobic character.[7–9]

The effect of such an alkyl chain substituent on the complexing and kinetic properties of the new ligand is generally not known. The main reason for this comes from the fact that the former ligand is often used in homogeneous conditions whereas the alkylated one is used most of the time in heterogeneous conditions. In the first case the reaction takes place in the bulk, but in the latter case it may occur at a liquid–liquid interface.

A comparison between the homogeneous kinetics and the interfacial kinetics in terms of reaction mechanism is difficult to make without a prior knowledge of the effect due to the alkyl chain substituent by itself.

In this work we have compared the kinetics and thermodynamics of complexation of 8-hydroxyqui-

*Author to whom correspondence should be addressed.

noline (HQ) and of 7-(4-ethyl-1-methyloctyl)-8-hydroxyquinoline(C_{11}—HQ) with Ni^{2+} and Co^{2+} ions in methanol, in which both ligands can be solubilized. The alkylated ligand investigated here constitutes the active species of the industrial extractant Kelex 100. Note that according to Demopoulos and Distin,[10] the main active component of the commercial product sold under this trade name before 1976 had a slightly different chemical structure.

These lipophilic extractants are commonly used for the liquid–liquid extraction of galium,[11a] whose kinetics can be improved using micro-emulsions as the organic phase.[11b]

Although rate constants characterizing the reactions of complex formation can in principle be obtained from extraction experiments provided that a "kinetic regime" is set up (plateau region in the rate of extraction vs stirring speed), the values obtained may be altered by other contributions.[12] The stopped-flow technique was used in the present investigation where homogeneous conditions guarantee that only the complexation step is observed.

EXPERIMENTAL

Chemicals

8-quinolinol (puriss) was obtained from Fluka and used without further purification. Kelex 100 was from Schering (R.F.A.) which was thoroughly purified to obtain the active component 7-(4-ethyl-1-methyloctyl)-8-hydroxyquinoline. The crude product was supposed to be a mixture of at least eight different components. A good separation procedure was perfected using column chromatography and thin layer chromatography. The most efficient separation was obtained with a column of 120–130 cm filled with Kieselgel 60 (70–230 mesh ASTM) Merck using hexane–ethylacetate 80/20 (v/v) as the eluent. The desired product was identified by mass spectrometry and its purity was checked by ^1H NMR (400 MHz) and elemental analysis: Found (theor.) C 80.3 (80.3), H 9.8 (9.7), N 4.6 (4.7)%.

Methanol was freshly distilled over magnesium before use. Nickel(II) and cobalt(II) nitrates were analytical grade products from Prolabo and their exact water contents were deduced from complexometry with EDTA. Note that we were interested in the comparison of two ligands under identical conditions but not necessarily in totally water-free solutions. Up to 0.4% of water could then be present in the solutions. Small variations in the water contents below this value have been found not to affect the results. Triethanolamine Fluka was used with perchloric acid to buffer the solutions.

Equilibrium measurements

The stoichiometry of the complexes and the equilibrium constants for complex formation have been obtained with a Varian DMS-100 UV–vis spectrometer on-line with a DS-15 data station. The LETAGROP program[13] (Spefo version) was used to deduce the best equilibrium values from the spectrophotometric data and the assumed model.

Potentiometric measurements in methanolic solutions have been carried out to obtain the ionization constants of HQ and C_{11}—HQ, and the hydrolysis constants of Ni(II) and Co(II). The glass electrode has been shown to furnish reliable data in methanol provided that appropriate standard solutions are used.[14] A combined glass electrode Metrohm was employed for the present determinations with the following standards: $HClO_4$ 10^{-2} M (pH2), salicylic acid 10^{-2} M/sodium salicylate 10^{-2} M (pH7.53)[14] and sodium methylate 10^{-2} M (pH14.7). Low concentrations of either the ligands or the metals have been used so that the activity coefficients could be neglected.

The ionization constants of HQ and C_{11}—HQ have been determined from the titration curves of these ligands using methanolic solutions of perchloric acid (for the basic nitrogen function) and of sodium hydroxide (for the hydroxylic function) respectively. Theoretical simulations of the former titration curves have been performed using the PKB1F FORTRAN program.[15] The pK values obtained were in excellent agreement with the values of the pH at half neutralization ($pK_1 = 5.77$ and 5.01 respectively for HQ and C_{11}—HQ). The titration of the hydroxyl group could not be simulated with the preceding program and the pH at half-neutralization was considered to provide a good enough estimation for the purpose of the present work ($pK_2 \simeq 14.0$ and 14.4 respectively for HQ and C_{11}—HQ with an uncertainty of ± 0.2).

The hydrolysis constants K_h of Ni(II) and Co(II) have been evaluated from the titration curves of these metals by sodium methylate. The analysis of the curves was done according to the procedure described by Baes and Mesmer.[16] The values obtained for the formation of the $M(OH)^+$ species were not very different from those in water:[16] for Ni(II), $pK_h = 10.65$ (± 0.2) (water: 9.86–10.5 depending on the medium) and for Co(II), $pK_h = 11$ (± 0.2) (water: 9.8–10.82).

Kinetic measurements

The stopped-flow technique with optical detection was used for the kinetic measurements. The apparatus was a Durrum D-110 on-line with a data

acquisition system (Biomation 805 transient recorder interfaced with a NM 4/30 Computer Automation set up (Yrel, France). Pseudo first-order conditions were ensured by keeping the metal ion concentration at least ten times larger than the ligand concentration, provided that the pH was buffered. The solutions that were mixed were of the same composition, except that one contained the metal ion and the other the ligand. The concentrations given refer to the overall stoichiometry after mixing. The observed rate constants (or reciprocal relaxation times) were obtained from a non-linear least-squares analysis of the exponential change of the optical density proportional to the complex concentration. The analysis, performed on a sampling of a 100 points equally distributed on the kinetic curve, involved the optimization of three adjustable parameters (relaxation amplitude, relaxation time and asymptote). The experiments were carried out at 20°C and the ionic strength was adjusted to 0.1 M with $NaClO_4$. For safety reasons the perchlorate was not dried and used in its monohydrated form.

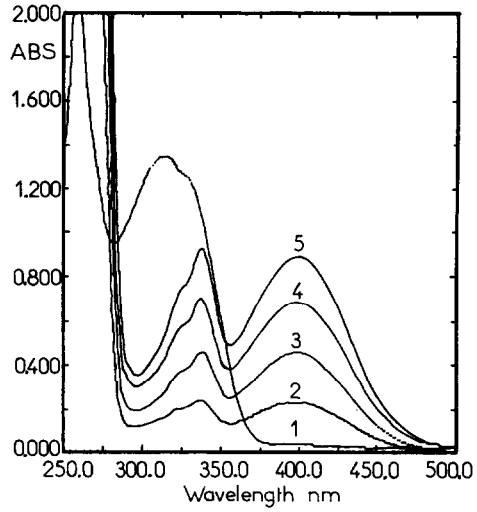

Fig. 1. UV–vis spectra showing the absorption peak at 400 nm for the C_{11}—HQ/Ni^{2+} complex in 0.1 M $NaClO_4$, pH 9. (1) free C_{11}—HQ 6×10^{-4} M; (2)–(5) variable [C_{11}—HQ]/[Ni^{2+}]: (2) 10^{-4} M/9×10^{-4} M; (3) 2×10^{-4} M/8×10^{-4} M; (4) 3×10^{-4} M/7×10^{-4} M; (5) 4×10^{-4} M/6×10^{-4} M.

RESULTS

For each ligand–metal couple a series of UV-vis spectra at different concentrations, have been recorded for the free ligand, the free metal ion and their mixtures, respectively. An example is given in Fig. 1 for the C_{11}—HQ/Ni^{2+} couple. The stoichiometry of the complexes has been determined from the change in absorption at 400 nm. The method of continuous variations and a method varying the molar ratio have both been used. In the first case, the plots of the optical density measured on the complex absorption band vs the mole fraction of the metal ion showed a maximum at 0.33. With the second method, a break at 0.5 was found when plotting the optical density vs the [Metal]/[Ligand] molar ratio. These values indicate that a 2:1 (ligand:metal) complex forms in all cases in the presence of an excess of ligand.

On the basis of these results, the following equilibria were introduced in the LETAGROP program to calculate the more probable binding constants from the spectrophotometric data obtained at neutral pH:

$$M^{2+} + LH \rightleftarrows LM^{+} + H^{+} \quad K_{b1} \qquad (1)$$

$$M^{2+} + 2LH \rightleftarrows L_2M + 2H^{+} \quad K_{b2} \qquad (2)$$

in addition to the ionic product of methanol (16.82)[14] and to the ionization constants of the ligands (see Experimental section). The hydrolyzed species of M^{2+} were assumed to be in sufficiently low concentration in the experimental conditions to be neglected in this treatment.

The results obtained for K_{b1} and K_{b2} are given in Table 1, in which β_1 and β_2 are the corresponding

Table 1. Thermodynamic data for the ligand:metal complex formation of HQ and C_{11}—HQ with Ni^{2+} and Co^{2+} at 20°C, pH 9.0 (±0.1), 0.1 M $NaClO_4$

Ligand	Metal	Log K_{b1}[a] (1:1 complex)	Log K_{b2}[a] (2:1 complex)	Log β_1	Log β_2	Log β_2/β_1
HQ	Ni^{2+}	−3.5 (±0.5)	−7.8 (±0.3)	10.5 (±0.7)	20.2 (±0.7)	9.7 (±1.4)
	Ni^{2+} (buffer TEA)	−2.9 (±0.2)	−7.53 (±0.05)	—	—	—
C_{11}—HQ	Ni^{2+}	−2.8 (±0.4)	−7.0 (±0.4)	11.6 (±0.6)	21.8 (±0.8)	10.2 (±1.4)
HQ	Co^{2+}	−3.6 (±0.4)	−7.0 (±0.2)	10.4 (±0.6)	21.0 (±0.6)	10.6 (±1.2)
C_{11}—HQ	Co^{2+}	−2.0 (±0.3)	−7.1 (±0.1)	12.4 (±0.5)	21.7 (±0.5)	8.7 (±1.0)

[a] K_{b1} = [complex 1:1][H^+]/[ligand][metal]; K_{b2} = [complex 2:1][H^+]^2/[ligand]^2[metal].

complex formation constants:

$$K_{b1} = \beta_1 K_2; \quad K_{b2} = \beta_2 K_2^2. \qquad (3)$$

It is clear from these data that the alkyl chain increases the stability of the 1 : 1 complexes as indicated by the log β_1 values for Ni^{2+} and Co^{2+}. The alkyl arm can probably interact with the metal ion through a coordinated methanol molecule of the first solvation shell, leading to a tridentate chelate. In all the cases, the second stepwise formation constant given by log β_1/β_2 is smaller than the first one, as expected. Within the experimental accuracies indicated in Table 1, (i) the binding constants of Ni^{2+} are about equal or slightly less than that of Co^{2+} and (ii) the addition of TEA buffer does not drastically change the K_b values obtained.

The variations in the observed rate constant k_{obs} with the metal ion concentration at different pHs and for different ligand–metal couples are represented in Figs 2–4. A linear dependence of k_{obs} vs the metal ion concentration has been observed in all the cases.

The observed rate constant for the Ni^{2+} ion is decreased by a factor of 4–6 when going from HQ to C_{11}—HQ. On the other hand, the reaction becomes much faster with the Co^{2+} ion, as expected from the solvent exchange kinetics characteristic of these cations.[17] In fact the reaction is so fast with HQ/Co^{2+} that it cannot be measured using the stopped-flow technique, which requires a mixing time of at least 1–2 ms, but the kinetics are again slower for C_{11}—HQ for which some experiments could be performed. In all these experiments only the 1 : 1 complex is expected to be formed because of the

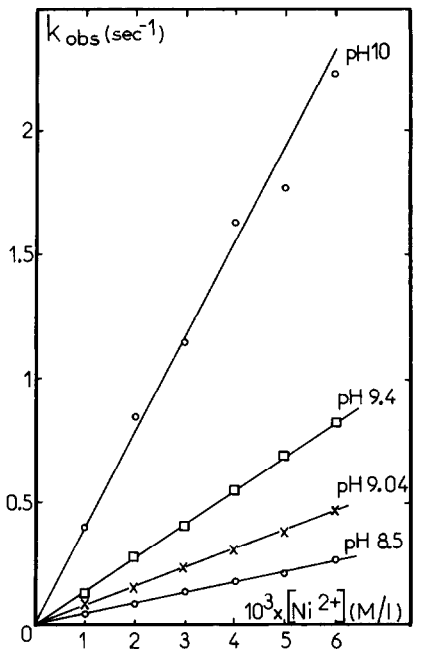

Fig. 3. System C_{11}—HQ/Ni^{2+}, 0.1 M $NaClO_4$, 0.1 M TEA/$HClO_4$ buffer: variation of k_{obs} vs the metal ion concentration at different pHs. [C_{11}—HQ] = 10^{-4} M; λ = 400 nm; T = 20°C.

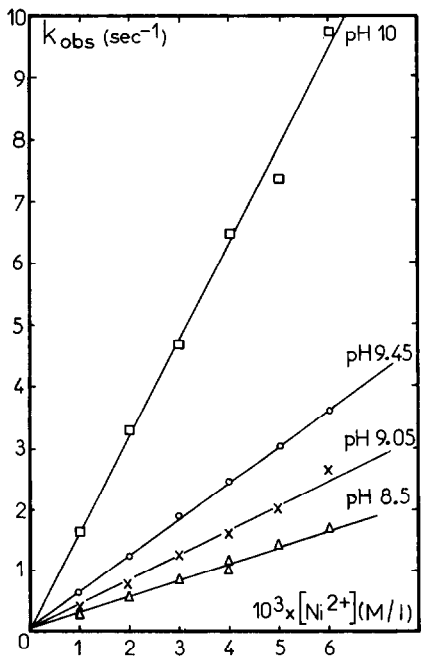

Fig. 2. System HQ/Ni^{2+}, 0.1 M $NaClO_4$, 0.1 M TEA/$HClO_4$ buffer: variation of k_{obs} vs the metal ion concentration at different pHs. [HQ] = 10^{-4} M; λ = 400 nm; T = 20°C.

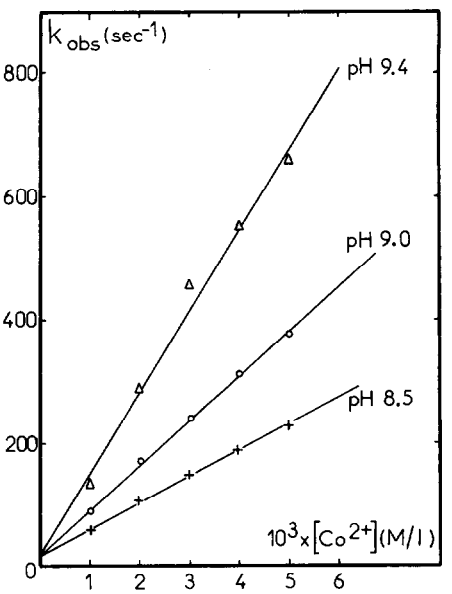

Fig. 4. System C_{11}—HQ/Co^{2+}, 0.1 M $NaClO_4$, 0.1 M TEA/$HClO_4$ buffer: variation of k_{obs} vs the metal ion concentration at different pHs. [C_{11}—HQ] = 10^{-4} M, λ = 400 nm, T = 20°C.

very small concentration of the ligand (10^{-4} M) in comparison to the metal ion concentration. We would have preferred to avoid the use of a pH buffer, but when the medium was not buffered the kinetics were not first-order and, due to the departure of a proton when reaction(1) proceeds, the final pH was much lower than the initial one. A triethanolamine buffer, previously used by Hague and Eigen[18] for similar studies in water, was thus added to the solutions.

Two different mechanisms have been considered to explain the increase of k_{obs} with increasing pH.

Mechanism I.

$$LH + M^{2+} \underset{k_{\overline{LH}}}{\overset{k_{LH}}{\rightleftharpoons}} LM^{+} + H^{+} \quad (4)$$

$$L^{-} + M^{2+} \underset{k_{\overline{L}}}{\overset{k_{L}}{\rightleftharpoons}} LM^{+} \quad (5)$$

$$LH \overset{\text{fast}}{\rightleftharpoons} H^{+} + L^{-} \quad (6)$$

$$K_2 = \frac{1}{K_2'} = \frac{[H^+][L^-]}{[LH]}. \quad (7)$$

Mechanism II.

$$LH + M^{2+} \underset{k_{\overline{LH}}}{\overset{k_{LH}}{\rightleftharpoons}} LM^{+} + H^{+} \quad (8)$$

$$LH + M(OH)^{+} \underset{k'_{\overline{LH}}}{\overset{k'_{LH}}{\rightleftharpoons}} LM^{+} + H_2O \quad (9)$$

$$M^{2+} + OH^{-} \overset{\text{fast}}{\rightleftharpoons} M(OH)^{+} \quad (10)$$

$$K_{OH} = \frac{[M(OH)^+]}{[M^{2+}][OH^-]}. \quad (11)$$

The first mechanism is analogous to the kinetic model postulated by Hague and Eigen[18] to account for the reaction of HQ with Mg^{2+} ions in water. The first equation could have been split into two steps with an intermediate form (LHM^{2+}), not represented here, to which the steady-state approximation can be applied.[18] The rate constants k_{LH} and $k_{\overline{LH}}$ should thus be considered as overall rate constants. On the other hand, the diprotonated form of the ligand has not been considered because it was previously shown to be of very low reactivity in water[19] and its concentration is assumed to be negligible under the experimental conditions.

Due to the fast equilibrium between the neutral form and the anionic form of the ligand, the system involving the three reactions is characterized by only two relaxation times. The slowest relaxation time which can be identified with the observed rate constant can be easily calculated using relaxation kinetic methods,[20] from the rate equation (see Appendix):

$$\frac{d[LM^+]}{dt} = k_{LH}[LH][M^{2+}] - k_{\overline{LH}}[LM^+][H^+] + k_L[L^-][M^{2+}] - k_{\overline{L}}[LM^+]. \quad (12)$$

Taking into account the facts that (i) the metal ion concentration was always much larger than the ligand concentration and (ii) $K_2'[H^+] \gg 1$, the relaxation time can be expressed in the following simplified form:

$$\frac{1}{\tau_{slow}} = k_{obs} = \left\{\frac{k_L}{K_2'[H^+]} + k_{LH}\right\}[M^{2+}] + k_{\overline{LH}}[H^+] + k_{\overline{L}}. \quad (13)$$

In this expression, the concentrations are equilibrium concentrations and under the experimental conditions used $[M^{2+}]$ can be taken as the total concentration of metal ions. From the linear variations of k_{obs} with $[M^{2+}]$ at constant pH (see Fig. 2), the overall formation (k_f) and dissociation (k_d) rate constants can be obtained:

$$k_f = k_L/K_2'[H^+] + k_{LH} \quad (14)$$

and

$$k_d = k_{\overline{LH}}[H^+] + k_{\overline{L}}. \quad (15)$$

Equation (14) provides the values of k_L and k_{LH} from a simple linear plot of k_f vs $1/K_2'[H^+]$.

The second mechanism is assuming that the pH dependence is related to the presence of a hydrolyzed form of the metal ion, which can react with the ligand. Owing to the very large excess of water (around 0.2 M) compared to metal ion concentration, the existence of such hydrolyzed species cannot be ruled out. The fast equilibrium is now involving the metal ion, instead of the ligand in mechanism I. The equilibrium constant K_{OH} could in principle be obtained from:

$$K_{OH} = \frac{K_h}{K_\omega'[H_2O]} \quad (16)$$

with

$$K_h = \frac{[M(OH)^+][H^+]}{[M^{2+}]} \quad (17)$$

(hydrolysis constant)

$$K_\omega' = \frac{[H^+][OH^-]}{[H_2O]} \quad (18)$$

(ionization product of water in methanol).

The rate equation is in this case:

$$\frac{d[LM]}{dt} = k_{LH}[LH][M^{2+}] - k_{LH}^{-}[LM^{+}][H^{+}] + k'_{LH}[LH][M(OH)^{+}] - k_{LH}^{-}[LM^{+}][H_2O] \quad (19)$$

and the corresponding observed rate constant, assuming the same approximations as for mechanism I is:

$$\frac{1}{\tau_{slow}} = k_{obs} = \{k'_{LH}K_{OH}[OH^{-}] + k_{LH}\}[M^{2+}] + k_{LH}^{-}[H^{+}] + k_{LH}^{-}[H_2O] \quad (20)$$

where, according to eqs (16)–(18):

$$K_{OH}[OH^{-}] = \frac{K_h}{[H^{+}]}. \quad (21a)$$

In contrast to mechanism I, $[M^{2+}]$ can no longer be taken as the total concentration of metal ions:

$$[M^{2+}] = [M^{2+}]_{tot}\frac{[H^{+}]}{K_h + [H^{+}]}. \quad (21b)$$

The overall rate constants are:

$$k_f = k'_{LH}\frac{K_h}{[H^{+}]} + k_{LH} \quad (22)$$

and

$$k_d = k_{LH}^{-}[H^{+}] + k_{LH}^{-}[H_2O]. \quad (23)$$

The concentration of water can be considered as roughly constant under our experimental conditions. A comparison of eqs (13) and (20) shows that the two postulated mechanisms cannot be kinetically distinguished because the constant K_h plays the same part as $1/K'_2$. This type of situation has been described earlier as suffering from formal "proton ambiguity".[21] This difficulty arises in many systems involving ligands with dissociable protons and in some cases the uncertainty can be removed by an examination of whether the values obtained for the rate constants are reasonable.

The values for both mechanisms are given in Table 2. Figure 5 shows the linear plots, expected from eq. (14), from which k_L and k_{LH} have been determined for mechanism I. Similarly k_{LH} and k'_{LH} can be obtained for mechanism II from an appropriate linear plot.

Some indications concerning the reverse rate constants k_{LH}^{-}, k_L^{-} and k_{LH}^{-} are also given in Table 2. The former was obtained from the combination of k_{LH} with the equilibrium constant K_{bl}, but for mechanism I only a higher estimation of k_L^{-} can be given. Indeed, the very small value of k_d which does not show a pH-dependence, suggests that $k_{LH}^{-}[H^{+}] \ll k_L^{-}$ so that $k_L^{-} \simeq k_d$. Similarly for mechanism II, $k_{LH}^{-}[H_2O] \simeq k_d$.

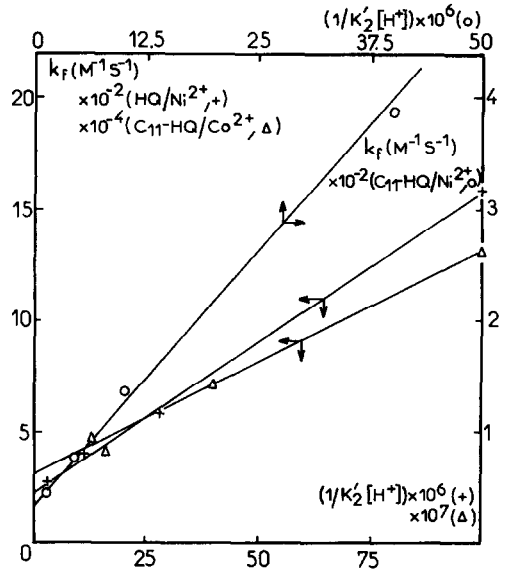

Fig. 5. Plots of k_f vs $1/K'_2[H^{+}]$ according to mechanism I and eq. (14).

Table 2. Kinetic data for the reactions of complexation of HQ and C_{11}—HQ with Ni^{2+} and Co^{2+} at 20°C, 0.1 M $NaClO_4$, 0.1 M TEA-$HClO_4$ buffer

		Mechanism I[a]		Mechanism II[a]			
Ligand	Metal	k_L ($M^{-1}s^{-1}$)	k_L^{-} (s^{-1})	k_{LH} ($M^{-1}s^{-1}$)	k_{LH}^{-} ($M^{-1}s^{-1}$)	k'_{LH} ($M^{-1}s^{-1}$)	$k_{LH}^{-}\cdot[H_2O]$ (s^{-1})
HQ	Ni^{2+}	1.4×10^{7}	$\leqslant 5 \times 10^{-2}$	2.4×10^{2}	$\sim 7.5 \times 10^{5}$	7.4×10^{3}	$\leqslant 5 \times 10^{-2}$
C_{11}—HQ	Ni^{2+}	9.8×10^{6}	$\leqslant 10^{-2}$	3.3×10^{1}	$\sim 2.0 \times 10^{4}$	1.9×10^{3}	$\leqslant 10^{-2}$
C_{11}—HQ	Co^{2+}	1.0×10^{10}	~ 16	3.1×10^{4}	$\sim 3.1 \times 10^{6}$	4.3×10^{6}	~ 16

[a] Note that the couple of values k_L, k_L^{-} and k'_{LH}, k_{LH}^{-} cannot be simultaneously correct (see Results and Discussion).

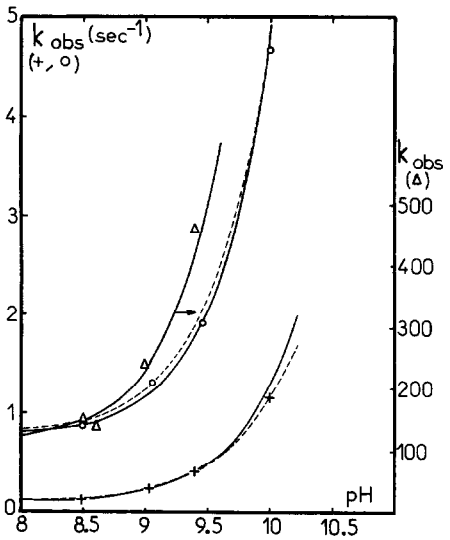

Fig. 6. Plots of k_{obs} vs pH: $[M^{2+}] = 3 \times 10^{-3}$ M; [ligand] = 10^{-4} M, TEA/$HClO_4$ buffer 0.1 M, $NaClO_4$ 0.1 M, $T = 20°C$. (o) HQ/Ni^{2+}; (+) C_{11}—HQ/Ni^{2+}; (Δ) C_{11}—HQ/Co^{2+}. The lines show the theoretical predictions calculated from eq. (13) (—) or (20) (---) with the values given in Table 2 (for C_{11}—HQ/Co^{2+} they are indistinguishable).

The observed rate constants calculated from eqs (13) or (20) and the values given in Table 2 furnish a theoretical prediction almost independent of the mechanism chosen and in excellent agreement with the experimental results as shown in Fig. 6.

DISCUSSION

We will mainly discuss the values of k_{LH}, k_L and k'_{LH} and not the values of the reverse rate constants which are only indicative.

The values of k_{LH} (Table 2) are the only ones which are unambiguously determined because they do not depend on the chosen mechanism. A comparison of the values obtained respectively for Ni^{2+} and Co^{2+} for the reaction with the same ligand, C_{11}—HQ, shows a large acceleration of the observed kinetics in favour of the Co^{2+} ion. This was expected because the reaction is assumed to depend on the rate of exchange between ligand molecules and coordinated solvent molecules, which is often comparable to the solvent exchange rate k_{ex}.[4] From previously published values in methanol,[4,17] an accelerating factor of 10–100 was expected when going from Ni^{2+} to Co^{2+} whereas a three order of magnitude change has been obtained. This unusually high factor is hard to explain. As k_{LH} is the product of an outer-sphere equilibrium constant K_{os} and the ligand/solvent exchange rate,[3,4,22] an unusual value of either one of these constants could be invoked. The ligand/solvent exchange rate constant may be affected by the presence of a small amount of water in the methanol as observed in earlier studies.[23] Another explanation might be found with the use of the TEA buffer. The oxidation of Co^{2+} or its complexes in the presence of amines may be a complicating factor, but for this reason, particular care was taken when preparing solutions of this ion to avoid oxidation in the presence of the TEA buffer. On the other hand, a weak interaction of TEA with Co^{2+} (and to a lesser extent with Ni^{2+} ions) cannot be completely ruled out as small changes have been observed in the UV–vis spectrum. Such a solvent substitution in the inner sphere of the metal ion is known to result in an acceleration of the rate of reaction with an incoming ligand.[22] This should not affect the conclusions of this work as regards the effect of an alkyl chain substituent as long as the conditions are identical for the two ligands.

For the reasons given above, the comparison between the two ligands was unfortunately not possible for Co^{2+}.

Turning to the case of the Ni^{2+} ion, we notice that the value of k_{LH} obtained with HQ is lower than the value obtained in water by Johnson and Wilkins[19] (1.3×10^3 M^{-1} s^{-1} at 25°C), in agreement with the known difference in the solvent exchange rate.[4] Comparing now the values obtained for HQ and C_{11}—HQ, a noticeable effect of the alkyl chain on the value of k_{LH} is observed. The rate of formation of the ligand–metal complex from the neutral ligand is decreased by a factor of around seven by the alkyl substituent, probably because of a steric hindrance limiting the accessibility of the coordination site. On the other hand, the dissociation constant deduced from the equilibrium binding constant appears to be lower for the alkylated ligand, suggesting that the chain can retain the complexed metal ion.

The rate constants k_L and k'_{LH} listed in Table 2 cannot be simultaneously correct and we will now discuss the soundness of the two mechanisms which are both consistent with our kinetic data.

Mechanism I assumes a very high reactivity of the deprotonated oxines as compared to the neutral ligands since $pK_2 = 14$–14.4, whereas the range of pH in these experiments was from 8.5–10. The very low concentration of the anionic form at these pH's should be neglected in the kinetic treatment, unless this species is extremely reactive. This observation is in line with the large values obtained for k_L. The k_L/k_{LH} ratio varies from 5.8×10^4 for HQ to 3×10^5 for C_{11}—HQ. A ratio of the order 10^5 has been previously obtained for the reaction of Ni^{2+} with 2-methyl-8-hydroxyquinoline-5-sulphonic acid in water at 20°C,[24] whereas a ratio of only 40 has been

found for the reaction of HQ with Mg^{2+} at 16°C.[18]

In spite of some similarity with previous observations, our confidence in mechanism I is seriously affected by the k_L value obtained for the Co^{2+}/C_{11}—HQ system, which is close to the diffusion-controlled limit. On the basis of this unreasonable value, we tend to reject the first proposed mechanism.

Mechanism II is assuming the existence of a hydrolyzed form of the metal ions in the pH range investigated, due to the presence of water molecules in the solvation shell of these cations. In the case of pure water, it is well known[16] that hydrolyzed species of general formula $M_x(OH)_y^{(xz-y)+}$ exist in significant concentration, both for Ni(II) and Co(II), at above pH 8. Much less is known concerning the solvolysis in pure organic solvents, but owing to the fact that the basicity of methanol is less than that of water, the methanolysis is expected to be negligible in the pH conditions employed in the present experiments. For this reason we have not felt it necessary to consider species of the form $M(CH_3O)^+$ or $M(CH_3O)_2$. On the other hand, the potentiometric measurements that we have performed in order to determine the hydrolysis constants (see Experimental section) could be fitted fairly well to an equation taking into account two mononuclear species, $M(OH)^+$ and $M(OH)_2$, with essentially the first one being present at pH lower than 10.

The values of k'_{LH} given in Table 2 have been obtained from eq. (22) by using the K_h values potentiometrically determined. They are much larger than the values obtained for the unhydrolyzed metal ions, which is consistent with earlier observations.[21] This is also in agreement with the fact that an incoming ligand (here OH^-) in the solvation sphere of a metal ion is known to labilize the remaining coordinated solvent molecules.

The reactivity of the neutral form of the ligands, with the hydrolyzed metal ions appears to decrease by a lesser extent in the presence of the alkyl chain than with the unhydrolyzed species. On the other hand, the rate constant is 2000 times larger for Co^{2+} than for Ni^{2+}. This factor, which is unusually large for unhydrolyzed metal ions in methanol (see discussion above) is also in favour of mechanism II.

In conclusion, the present data have shown a difference in behaviour between the neutral forms of 8-hydroxyquinoline and its alkylated derivative (Kelex 100) towards the complexation of Ni^{2+} and Co^{2+} ions in methanolic solutions. The alkyl chain was found to increase the stability of the 1 : 1 complexes. It is also responsible for a seven-fold decrease of the rate constant for the complexation with Ni^{2+}. The same trend has been observed with the Co^{2+} ion for which the complexation with 8-hydroxyquinoline was too fast to be measured using the same technique.

The pH-dependence of the complexation kinetics has been explained by metal hydrolysis, due to the presence of a small concentration of water molecules.

Experiments are now in progress in micro-emulsion systems in order to compare the mechanisms of the bulk and interfacial reactions. A full report of this study will be given in a forthcoming publication.[25]

Acknowledgements—We thank Prof. J. Bessière for helpful discussions concerning the hydrolysis problem. We also acknowledge the technical assistance of J. L. Fringant and we are grateful to Mr Ziegler for the use of the mass spectrometry facilities at the University of Nancy I.

REFERENCES

1. M. Eigen, *Pure Appl. Chem.* 1963, **6**, 97.
2. M. Eigen and R. G. Wilkins, in mechanism of inorganic reactions, *Adv. Chem. Ser.* 1965, **49**, 55.
3. D. N. Hague, in *Molecular Biology, Biochemistry and Biophysics*, Vol. 24. (Edited by I. Pecht and R. Rigler.) Springer, Heidelberg (1977).
4. J. Burgess, *Metal Ions in Solution.* John Wiley, New York (1978).
5. G. M. Ritcey and A. W. Ashbrook, *Solvent Extraction, Principles and Applications to Process Metallurgy*, Part I. Elsevier, Amsterdam (1984).
6. P. L. Kuo, I. Ikeda and M. Okahara, *Tenside Detergents* 1982, **19**, 204.
7. S. Kitazawa, K. Kimura, H. Yano and T. Shono, *J. Am. Chem. Soc.* 1984, **106**, 6978.
8. P. Geneste, A. Guida, C. Reminiac, G. Amblard and C. Gavach, *Tetrahedron Lett.* 1981, **22**, 1397.
9. G. Doucet-Ladeveze, Y. Jabbari-Azad, L. Rodehüser, P. Rubini, C. Selve and J. J. Delpuech, *Tetrahedron Lett.* 1986, **42**, 371.
10. G. P. Demopoulos and P. A. Distin, *Hydrometallurgy* 1983, **11**, 389.
11. (a) A. Leveque and J. Helgorsky, *ISEC* 77, *CIM Special* Vol. 21, p. 439; (b) D. Bauer, P. Fourre and J. Lemerle, *C. R. Acad. Sci., Paris* 1981, **292**, 1019; P. Fourre and D. Bauer, *ibid.* 1981, **292**, 1077; D. Bauer and J. Komornicki, *ISEC* 83, p. 315, Denver.
12. P. R. Danesi and R. Chiarizia, The kinetics of metal solvent extraction, CRC critical review in *Anal. Chem.* 1980, **10**, 1.
13. L. G. Sillen and B. Warnqvist, *Arkiv. Chem.* 1968, **31**, 377.
14. J. Juillard and M. L. Dondon, *Soc. Chim.* (*France*) *5° série—Mémoires*, 1963, 2535.
15. J. J. Delpuech, M. N. Deschamps and Y. Martinet, *J. Chim. Phys.* 1969, **66**, 232.

16. C. F. Baes and R. E. Mesmer, *The Hydrolysis of Cations*. Wiley, New York (1976).
17. H. P. Bennetto and E. F. Caldin, *J. Chem. Soc. A*, 1971, 2198; R. G. Wilkins, *The Study of Kinetics and Mechanism of Reactions of Transition Metal Complexes*, p. 219. Allyn and Bacon (1974).
18. D. N. Hague and M. Eigen, *Trans. Faraday Soc.* 1966, **62**, 1236.
19. W. A. Johnson and R. G. Wilkins, *Inorg. Chem.* 1970, **9**, 1917.
20. C. F. Bernasconi, *Relaxation Kinetics*. Academic Press, New York (1976).
21. S. Gouger and J. Stuehr, *Inorg. Chem.* 1974, **13**, 379.
22. J. F. Coetzee, D. Frollini, C. G. Karakatsanis, E. J. Subak and K. Umemoto, in *Characterization of Solutes in Nonaqueous Solvents* (Edited by G. Mamantov), Plenum Press, New York (1978).
23. W. J. MacKellar and D. B. Rorabacher, *J. Am. Chem. Soc.* 1971, **93**, 4379.
24. K. Saito, Y. Masuda and E. Sekido, *Inorg. Chim. Acta*, 1986, **111**, 113.
25. M. Boumezioud and C. Tondre, to be published.

APPENDIX

For mechanism I, the rate equation in the neighbourhood of equilibrium for the slowest relaxation process is:

$$\frac{d\delta[LM^+]}{dt} = k_{LH}[LH]\delta[M^{2+}]+k_{LH}[M^{2+}]\delta[LH]$$
$$-k_{LH}^{-}[LM^+]\delta[H^+]-k_{LH}^{-}[H^+]\delta[LM^+]$$
$$+k_L[L^-]\delta[M^{2+}]+k_L[M^{2+}]\delta[L^-]-k_L^{-}\delta[LM^+] \quad (A1)$$

where δ designates the deviations from equilibrium of the concentrations. As the pH was buffered, $\delta[H^+] = 0$.

The other δ quantities must be evaluated from the mass conservation equations:

$$\delta[M^{2+}]+\delta[LM^+] = 0 \quad (A2)$$

$$\delta[L^-]+\delta[LH]+\delta[LM^+] = 0 \quad (A3)$$

and the derivative of the equilibrium relationship (the fast equilibrium is assumed to be always established)

$$K'_1[H^+]\delta[L^-]-\delta[LH] = 0 \quad (A4)$$

so as to obtain the rate equation in the form:

$$\frac{d\delta[LM^+]}{dt} = -\frac{1}{\tau}\delta[LM^+] \quad (A5)$$

where $1/\tau = k_{obs}$ defines the reciprocal relaxation time. A similar treatment applies to mechanism II.

Polyhedron Vol. 7, No. 7, pp. 523–527, 1988
Printed in Great Britain

0277–5387/88 $3.00+.00
© 1988 Pergamon Press plc

STRUCTURAL AND SPECTROSCOPIC PROPERTIES OF POTASSIUM BIS(GLYCYLGLYCINATO(2−)-O,N,N′)CHROMATE(III) PIPERAZINE-2,5-DIONE

VASEETHA SUBRAMANIAM, KYU-WANG LEE, ROY G. GARVEY* and PATRICK E. HOGGARD*

Department of Chemistry, North Dakota State University, Fargo, ND 58105, U.S.A.

(*Received* 13 *August* 1987; *accepted* 23 *October* 1987)

Abstract—$K[Cr(C_4H_6N_2O_3)_2 \cdot C_4H_6N_2O_2 \cdot 2H_2O$, $M_r = 501.44$, crystallizes in the monoclinic space group $P2_1/c$, with $a = 11.364(4)$, $b = 12.333(6)$, $c = 14.630(7)$ Å, $\beta = 107.39(4)°$, $V = 1956.6$ Å^3 and $Z = 4$. The structure was solved by direct methods and converged to a final R value of 0.062 ($R_w = 0.072$). The incorporation of piperazine-2,5-dione, formed by self-condensation of glycylglycine, in the crystal structure results in some changes in bond lengths and bond angles and a many-fold increase in the luminescence lifetime of the chromium complex, relative to the structure without piperazinedione.

Meridional coordination by tridentate ligands is rare, but 2,6-pyridinedicarboxylate(2−) (= PDC), in which the coordinating atoms are constrained to approximate planarity, is probably always meridional.[1] The visible spectrum of the chromium(III) complex, $[Cr(PDC)_2]^-$, exhibits a very intense first band and a weak second band.[2] This is sufficiently unusual to probe the possibility that it might be diagnostic for meridional coordination.

Dipeptides are also constrained to relative planarity and many are known to adopt meridional coordination as tridentate ligands, with the peptide nitrogen coordinated.[3] We therefore sought to prepare bis(glycylglycinato-O,N,N′)chromate(III). Before we succeeded in crystallizing it, the visible spectrum confirmed our predictions for a *mer*-bis(tridentate) complex, but elemental analysis of the finally crystallized potassium salt showed there to be *three* glycylglycines per chromium. While diffraction data were being collected Freeman *et al.* (C. M. Murdoch, M. K. Cooper, T. W. Hambley, W. N. Hunter and H. C. Freeman, *J. Chem. Soc., Chem. Comm.* 1986, 1329), published the crystal structure of $Na[Cr(glygly)_2]$,[4] with the expected two ligands in the formula unit, and a visible spectrum identical to ours.

RESULTS AND DISCUSSION

Solution of the X-ray crystal structure revealed that the third glycylglycine was actually 2,5-piperazinedione (glycine anhydride), as shown in Fig. 1. This raises two questions: why and how does the piperazinedione form, and why is it so readily incorporated in the crystal structure?

The self-condensation of H_2glygly to form piperazinedione is negligible in aqueous solution, but both self-condensation and hydrolysis are known to be catalyzed by metal ions.[5,6] Cr(III) does catalyze hydrolysis, as is confirmed by our isolation of $[Cr(gly)_3]$ when the synthesis was carried out in water. In methanol the solvolysis should be greatly retarded, but catalytic self-condensation may even be enhanced.

We were unable to co-crystallize the title compound from a solution made by dissolving $K[Cr(glygly)_2]$ and piperazinedione. The latter was not sufficiently soluble in methanol, and the co-crystallite did not form in water or water/methanol mixtures.

The key factor in this preparation that leads to co-crystallization with piperazinedione appears to be a longer heating time before neutralization than that used by Freeman *et al.*[4] The choice of cation is unimportant and we were able to repeat Freeman's synthesis using KOH, crystallizing $K[Cr(glygly)_2]$. The native and co-crystallized solids can be readily

* Authors to whom correspondence should be addressed.

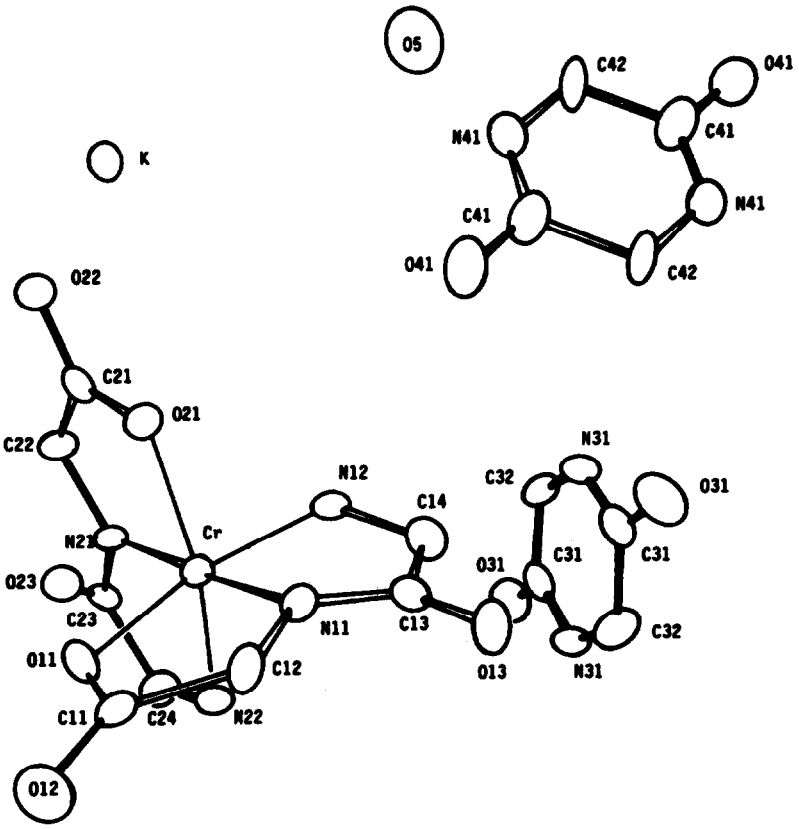

Fig. 1. ORTEP view of $K[Cr(glygly)_2] \cdot C_4H_6N_2O_2 \cdot 2H_2O$. Atoms are numbered so that the first digit identifies the glycylglycinate or piperazinedione molecule of origin.

distinguished by IR spectroscopy. The piperazinedione carbonyl stretching frequency at 1664 cm^{-1} is prominent in the co-crystallite and the glycylglycinate carboxylate stretching frequency shifts from 1602 cm^{-1} in $K[Cr(glygly)_2]$ to 1589 cm^{-1} in the co-crystallite.

The absorption spectrum of $K[Cr(glygly)_2]$ in water is shown in Fig. 2. The $^4A_{2g} \rightarrow {}^4T_{2g}$ transition at 548 nm has an extinction coefficient of 216, much larger than is usual in Cr(III) spectra. The $^4A_{2g} \rightarrow {}^4T_{1g}$ transitions are somewhat less intense than average. The same behavior is exhibited by the analogous cobalt(III) complex.[7] This may indeed be characteristic of meridional coordination, probably resulting from the severe distortion from octahedral ligand positions.

$K[Cr(glygly)_2]$ exhibits a sharp line phosphorescence based on an electronic transition at 13,608 cm^{-1} (735 nm), with considerable vibronic structure. At 14 K the emission lifetime of the crystals without anhydride is 20 ns. With co-crystallized piperazinedione it is 25 μs. The quantum yield of the latter phase is also larger by an equivalent factor.

Since quenching by neighboring chromophores is a dominant deactivation mechanism for crystalline transition metal complexes,[8] one might suppose that the higher lifetime is due to a larger Cr—Cr separation caused by insertion of the piperazinediones. This is only partly true. In fact, the closest Cr—Cr distances are 6.72 Å, compared to

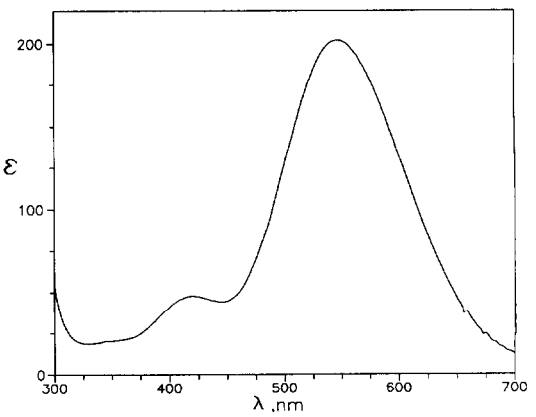

Fig. 2. Absorption spectrum of $K[Cr(glygly)_2]$ in H_2O.

5.95 Å in Na[Cr(glygly)$_2$]. It is unlikely that this difference can account for the thousand-fold increase in lifetime.

The co-crystallized phase may be described in terms of a layer structure. The $P2_1/c$ space group is the same as that of Na[Cr(glygly)$_2$]. The co-crystallite may be approximately described in terms of the removal of alternate layers of [Cr(glygly)$_2$]$^-$ from the native structure and their replacement with layers containing piperazinedione. The [Cr(glygly)$_2$]$^-$ units are distributed near the $x = 0$ plane, as are the counterions. The piperazinedione rings are situated near the $x = 0.5$ plane. The center of each ring occupies an inversion center exactly in the $x = 0.5$ plane. Waters of hydration are found between the planes. The layering can indeed account for the longer lifetime, since in one direction the Cr—Cr distance is 11 Å or more.

That both native K[Cr(glygly)$_2$] and 2,5-piperazinedione[9] crystallize in the same monoclinic space group may contribute to the ease with which they co-crystallize. Specific interactions are distinctly long range. Each ring carbonyl points towards an open face of a chromium complex, a distance of 5.08 Å away. The Cr—O interaction, though slight at that distance, appears to be sufficient for the piperazinedione to anchor layers of [Cr(glygly)$_2$]$^-$ together. Under appropriate conditions this provides a reason for the two to crystallize together rather than separately.

Table 1. Bond lengths and bond angles in K[CrL$_2$]·C$_4$H$_6$N$_2$O$_2$·2H$_2$O and Na[CrL$_2$]·4.5H$_2$O (H$_2$L = glycylglycine)

	K[CrL$_2$]·C$_4$H$_6$N$_2$O$_2$	Na[CrL$_2$][a]
Bond lengths (Å)		
Cr—O11	2.004(3)	1.993(5)
Cr—N11	1.969(3)	1.956(5)
Cr—N12	2.097(3)	2.079(5)
Cr—O21	1.997(3)	1.989(7)
Cr—N21	1.976(4)	1.957(7)
Cr—N22	2.072(4)	2.078(7)
Bond angles (deg)		
O11—Cr—N11	81.5(1)	81.0(2)
O11—Cr—N12	161.6(1)	160.5(2)
O11—Cr—O21	93.9(1)	89.3(2)
O11—Cr—N21	99.7(1)	100.5(2)
O11—Cr—N22	87.9(1)	90.7(2)
N11—Cr—N12	80.3(1)	79.8(3)
N11—Cr—O21	97.4(1)	101.6(3)
N11—Cr—N21	178.0(2)	177.2(3)
N11—Cr—N22	100.3(2)	97.8(3)
N12—Cr—O21	90.7(1)	91.5(2)
N12—Cr—N21	98.6(2)	98.9(2)
N12—Cr—N22	93.1(2)	95.0(3)
O21—Cr—N21	81.0(1)	81.0(2)
O21—Cr—N22	162.2(1)	160.4(2)
N21—Cr—N22	81.3(2)	79.8(3)

[a] Ref. 4.

Table 2. Metal–ligand stretching frequencies from the 13 K luminescence spectrum of K[CrL$_2$]·C$_4$H$_6$N$_2$O$_2$ (0–0 line at 13608 cm^{-1}) and Na[CrL$_2$] (0–0 line at 13631 cm^{-1}). (H$_2$L = glycylglycine)

Mode descriptor	K[CrL$_2$]·C$_4$H$_6$N$_2$O$_2$	Na[CrL$_2$]
ν(Cr—O)	391 cm^{-1}	388 cm^{-1}
ν(Cr—N$_{amine}$)	454 cm^{-1}	449 cm^{-1}
ν(Cr—N$_{amide}$)	326 cm^{-1}	328 cm^{-1}

Table 1 shows that all metal–ligand bond lengths are slightly longer in the co-crystallite than in the native complex. In addition there is a 3–4° difference in the tilt of one glygly^{2-} ring relative to the other, and minor differences in other bond angles. The frequencies of some modes that may be assigned primarily to metal–ligand stretching, taken from luminescence vibronic intervals, are displayed in Table 2. Differences in bond lengths cannot be correlated with frequency shifts and it appears that electronic factors, as perhaps influenced by bond angle changes or the cation environment, are responsible. The assignment for the Cr–peptide nitrogen stretching frequency is tentative. It was reasoned that, in spite of the negative charge on the nitrogen, the CR—N bond would be weakened, relative to that with the amine nitrogen, by electron withdrawal into the adjacent carbonyl oxygen.

EXPERIMENTAL

K[Cr(glygly)$_2$]·C$_4$H$_6$N$_2$O$_2$·2H$_2$O

H$_2$glygly (glycylglycine) (3.96 g, 0.030 mol) and Cr(NO$_3$)$_3$·9H$_2$O (4.0 g, 0.010 mol) were dissolved in methanol (100 cm^3). The solution was refluxed for 5 h and KOH (3.4 g, 0.052 mol) then added in small portions. After refluxing for another 4 h the purple solution was cooled and the KNO$_3$ that had settled out was removed by filtration. After standing for several days a water-soluble purple crystalline product was collected, washed with methanol and air dried. Found: C, 28.7; H, 4.5; N, 16.5; Cr, 10.5. Calc. for KCrC$_{12}$H$_{18}$N$_6$O$_8$·2H$_2$O: C, 28.7; H, 4.4; N, 16.8; Cr, 10.4%.

Table 3. Experimental and data processing parameters

A. Crystal data	
Bis(glycylglycinato)chromate(III) potassium salt $C_{12}H_{22}CrKN_6O_{10}$ F.W. 501.44 $F(000) = 518$	
Crystal dimensions, mm	$0.20 \times 0.15 \times 0.05$
Peak width at half height	0.25°
Radiation	Mo-K_α ($\lambda = 0.71073$ Å)
Temperature	$23 \pm 1°$
Space group	monoclinic $P2_1/c$ (#14)
a, b, c (Å)	11.364(4), 12.333(6), 14.630(7)
β	107.39(4)°
V	1956.6 Å^3
Z	8
d	1.70 g cm^{-3}
Linear absorption coefficient	8.5 cm^{-1}
B. Intensity measurements	
Diffractometer	Enraf–Nonius CAD4
Monochromator	graphite crystal, incident beam
Attenuator	Zr foil, factor 20.7
Take-off angle	2.8°
Detector aperture	2.0–2.5 mm horizontal 2.0 mm vertical
Crystal detector distance	21 cm
Scan type	$\omega - 2\theta$
Scan rate	4°/min (in omega)
Scan width (degrees)	$0.7 + 0.350 \tan\theta$
Maximum 2θ	55.0°
No. of reflection measured	4874 total, 4693 unique
Corrections	Lorentz polarization
C. Structure solution and refinement	
Solution	direct methods
Minimization function	$\Sigma w(\|F_o\| - \|F_c\|)^2$
Least squares weight	$4F_o^2/\sigma^2(F_o^2)$
Anomalous dispersion	all non-hydrogen atoms
Reflections included	2257 with $F_o^2 > 3.0 \cdot \sigma(F_o^2)$
Parameters refined	271
Unweighted agreement factor	0.062
Weighted agreement factor	0.074
Esd of observation of unit wt	1.45
Highest peak in final diff. map	0.61 e Å^{-3}

Infrared spectra were recorded on a Mattson Cygnus-25 FT-IR spectrometer in KBr discs. UV–vis absorption spectra were measured in aqueous solution with a Hewlett Packard 8451A diode array spectrometer. Luminescence spectra were recorded with an apparatus using a PAR Dyescan nitrogen laser-pumped dye laser source and an SRS boxcar averager detector system. The microcrystalline samples were mounted with conductive grease on the cold head of an Air Products Displex cryostat.

Structure solution and refinement

X-ray diffraction data were collected by the Molecular Structure Corporation on an Enraf-Nonius CAD4 diffractometer.* The structure was refined using direct methods[10] and full-matrix least

* *Supplementary material.* Tables of refined atomic coordinates, complete bond lengths and angles, and anisotropic thermal parameters have been deposited at the Cambridge Crystallographic Data Centre. See Notice to Authors, Issue No. 1, 1987.

squares optimization[11] for 2257 reflections to a final R value of 0.061 ($R_w = 0.072$). Details are given in Table 3.

Acknowledgements—The TexRay 230 computer system used to refine the diffraction data was purchased with the assistance of the National Science Foundation through Grant CHE-8311371. One of us (P.E.H.) acknowledges support from the National Science Foundation under Grant RII8610675 and from the donors of the Petroleum Research Fund, administered by the ACS.

REFERENCES

1. W. Fuerst, P. Gouzerh and Y. Jeannin, *J. Coord. Chem.* 1979, **8**, 237.
2. P. E. Hoggard and H.-H. Schmidtke, *Inorg. Chem.* 1973, **12**, 1986.
3. M. Sekizaki, *Bull. Chem. Soc. Japan* 1978, **51**, 1991.
4. C. M. Murdoch, M. K. Cooper, T. W. Hambley, W. N. Hunter and H. C. Freeman, *J. Chem. Soc., Chem. Comm.* 1986, 1329.
5. D. A. Long, T. G. Truscott, J. R. Cronin and R. G. Lee, *Trans. Faraday Soc.* 1971, **67**, 1094.
6. S. K. Oh and C. B. Storm, *Biochem.* 1974, **13**, 3250.
7. L. V. Boas, C. A. Evans, R. D. Gillard, P. R. Mitchell and D. A. Phipps, *J. Chem. Soc., Dalton Trans.* 1979, 582.
8. B. Di Bartolo, *Optical Interactions in Solids*. Wiley, New York (1968).
9. R. Degeilh and R. E. Marsh, *Acta Cryst.* 1959, **12**, 1007.
10. P. Main, S. E. Fiske, G. Germain, J. P. Declerq and M. M. Woolfson, *MULTAN, a System of Computer Programs for Crystal Structure Determination from X-ray Diffraction Data*. Universities of York (England) and Louvain (Belgium) (1980).
11. B. A. Frenz, *SDP-PLUS Structure Determination Package*. Enraf–Nonius, Delft, Netherlands (1982).

Polyhedron Vol. 7, No. 7, pp. 529–534, 1988
Printed in Great Britain

0277–5387/88 $3.00+.00
© 1988 Pergamon Press plc

COBALT(III) COMPLEXES OF N,N′-DIMETHYLETHYLENE-DIAMINE-N,N′-DI-α-BUTYRIC ACID

MOO-JIN JUN* and CHANG HWAN KIM

Department of Chemistry, Yonsei University, Seoul, Korea

and

JIN-SEUNG JUNG

Department of Chemistry, Kangreung National University, Kangreung, Korea

(*Received* 14 *July* 1987; *accepted* 30 *October* 1987)

Abstract—A new ONNO-system tetradentate ligand, N,N′-dimethylethylenediamine-N,N′-di-α-butyric acid (dmedba), has been synthesized and the cobalt(III) complexes of dmedba, $[Co(dmedba)L]^+$ (L = en, $2NH_3$, trimethylenediamine), have been prepared. Only s-*cis* isomers were obtained and the IR, UV–VIS and ^1H NMR spectral data along with the elemental analyses were used to characterize the ligand and complexes obtained in this work.

The octahedral cobalt(III) complexes of the tetradentate ligand, ethylenediamine-N,N′-diacetate (edda) and its analogues can exist in three geometrical isomers (Fig. 1). Mori *et al.*[1] have prepared the cobalt(III) complexes of edda, $[Co(edda)L]^{n+}$, (L = CO_3^{2-}, $2H_2O$, $2NO_2^-$), in which the s-*cis* configuration has been postulated. Legg and other workers[2–7] have prepared and characterized the uns-*cis* isomers of $[Co(edda)L]^{n+}$ (L = en, S-alanine, $2NH_3$, R-propylenediamine). Schoenberg *et al.*[8] have synthesized the C-alkyl substituted analogue of edda, ethylenediamine-N,N′-di-S-α-Propionic acid (SS-eddp). Both s-*cis* and uns-*cis* isomers of $[Co(SS\text{-}eddp)L]^{n+}$ (L = en, R–Pn) have been isolated. The dichloro cobalt(III) complex of SS-eddp has, however, been found to exist as the s-*cis* isomer only.[9]

The N-alkyl substituted analogues of edda which are N,N′-dimethylethylenediamine-N,N′-diacetic acid (dmedda) and N,N′-diethylethylenediamine-N,N′-diacetic acid (deedda) have been prepared by Legg and Cooke.[2] The cobalt(III) complexes of both dmedda and deedda have yielded the s-*cis* isomer only.[10,11] The dichloro rhodium(III) complexes of dmedda in which both the s-*cis* and uns-*cis* isomers are found to exist have been prepared.[12] Recently, two other C-alkyl substituted edda ligands have been reported. One is S-stilbenediamine-N,N′-diacetate (S-sdda)[13] whose cobalt(III) complexes, $[Co(S\text{-}sdda)L]^{n+}$, (L = en, S-stilbenediamine), have yielded the s-*cis* isomer only, and the other ethylenediamine-N,N′-di-S-α-isovalerate (ven).[14,15] The $[Co(ven)(H_2O)NO_2]$ complex exists as the s-*cis* isomer only, while in the case of $[Co(ven)(H_2O)_2]^+$ and $[Co(ven)(en)]^+$ both the s-*cis* and uns-*cis* configurations have been found to exist. Woon and O'Connor,[16] and Strasak and Bachraty[17] have prepared 2S, 2′S-1,1′-(ethane-1,2-diyl-bis(pyrrolidine-2-carboxylate) (pren), in which the nitrogen atom and the α-carbon atom are connected by a pyrrolidine ring. The $[Co(pren)L_2]^{n+}$ complexes yielded the s-*cis* isomers only when

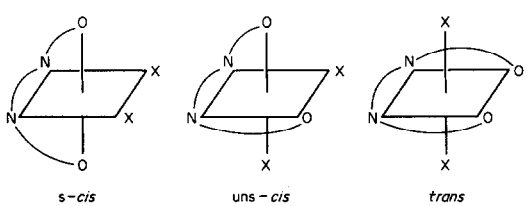

Fig. 1. The possible geometric isomers of the $[Co(edda)X_2]^{n+}$ complexes.

*Author to whom correspondence should be addressed.

L = Cl or H_2O, while both the s-*cis* and uns-*cis* isomers have been isolated when L_2 = en. A ligand, N,N′-dimethylethylenediamine-N,N′-di-α-propionic acid (dmedpa), containing methyl groups at both the α-carbon and nitrogen donor atoms, has been prepared in this laboratory.[18] The [Co(dmedpa)(en)]$^+$ and [Co(dmedpa)$(NH_3)_2$]$^+$ complexes exist as the s-*cis* isomer only, while only the uns-*cis* isomer is found to exist in the case of [Co(dmedpa)Cl_2]$^-$.

In the present work the synthesis of a new ONNO-system quadridentate ligand, N,N′-dimethylenediamine-N,N′-di-α-butyric acid (dmedba), containing both the C-ethyl and N-methyl sustitutions, and the cobalt(III) complexes of dmedba, [Co(dmedba)L]$^+$ (L = en, $2NH_3$, trimethylenediamine), are described. It is of interest to see which isomers will be obtained from the preparation of the cobalt(III) complexes of dmedba. It will be shown that only the s-*cis* isomer is formed in the cobalt(III) complexes of dmedba prepared in this work.

EXPERIMENTAL

Chemical reagents

N,N′-dimethylethylenediamine was purchased from Aldrich Chemical Co. and α-chlorobutyric acid was obtained from Tokyo Kasei Tokyo Co., both of which were used without further purification.

Physical measurements

Electronic absorption spectra were obtained with a Hitachi U-3200 spectrophotometer. ^{1}H NMR spectra were recorded on a Varian EM 360 L spectrometer. IR spectra were obtained using a Hitachi 270-30 Spectrophotometer. Elemental analyses were performed by Micro-Tech Analytical Laboratories, Skokie, Illinois, U.S.A.

Preparation of barium N,N′-dimethylethylenediamine-N,N′-di-α-butyrate (dmedba)

A cold solution of 10.0 g of sodium hydroxide in 20 cm^3 of water was carefully added to a cold solution of 31 g of α-chlorobutyric acid in 20 cm^3 of water with stirring, at a rate so that the temperature did not rise above 20°C. To this solution 11.0 g of N,N′-dimethylethylenediamine were added dropwise over a period of 90 min while stirring. Then 10.0 g of sodium hydroxide in 20 cm^3 of water were added. The temperature was kept between 90–100°C during this addition. After standing for 90 min, 32.0 g of barium chloride dihydrate dissolved in 60 cm^3 of boiling water were added rapidly and the solution was shaken. The cloudy suspension of Ba(dmedba) formed was heated at 60°C for 30 min with occasional stirring, filtered from the hot solution, and washed. The product was purified by stirring in 50 cm^3 of water at about 90°C for 10 min, and filtered while hot. The product was washed with hot water and dried for 5 h at 50°C. Yield: 8.5 g (17.2%). Found: C, 36.4; H, 5.6; N, 7.1. Calc. for $BaC_{12}H_{22}N_2O_4$: C, 36.4; H, 5.7; N, 7.1%.

Preparation of s-cis-(N,N′-dimethylethylenediamine-N,N′-di-α-butyrato)(ethylenediamine)cobalt(III) perchlorate, s-*cis*-[Co(dmedba)(en)]ClO_4

To a rapidly stirred suspension of Ba(dmedba) (3.96 g, 0.01 mol) dissolved in 20 cm^3 of water at about 60°C, 2.81 g of cobalt sulphate heptahydrate dissolved in 20 cm^3 of water were added over a period of 20 min. After heating at 60°C for 30 min, the solution was filtered. The precipitate was washed with 20 cm^3 of hot water. To the combined filtrate and washings were added successively 5 cm^3 of 2.0 N nitric acid, 1.0 g of activated charcoal and 0.61 g of ethylenediamine in 4 cm^3 of water. The oxidation reaction was carried out using 2 cm^3 of 30% hydrogen peroxide. After stirring for several more minutes, air was bubbled through the solution for 8 h. The resulting wine-red solution was filtered from the charcoal. It was then added to an ion-exchange column containing 200–400 mesh Dowex 50W-X4 cation exchange resin in the H^+ form. The complexes formed a compact band at the top. Only one fraction was obtained by elution with 0.2 N $HClO_4$ at a rate of about 1 cm^3 min^{-1}. The red product was obtained by evaporating the solution to dryness on a water bath. Yield: 0.90 g (19%). Found: C, 35.4; H, 5.9; N, 11.8. Calc. for $CoC_{14}H_{28}N_4O_8Cl$: C, 35.3; H, 5.9; N, 11.75%.

Preparation of s-cis-(N,N′-dimethylethylenediamine-N,N′-di-α-butyrato)(diammine) cobalt(III) perchlorate, s-*cis*[Co(dmedba)$(NH_3)_2$]ClO_4

A mixture of 3.96 g of Ba(dmedba) and 2.81 g (0.01 mol) of $CoSO_4 \cdot 7H_2O$ in 20 cm^3 of water was stirred for 20 min at 60°C and filtered to remove $BaSO_4$, which was then washed on the filter with 20 cm^3 of hot water. To the combined filtrate and washings were added 1.1 g of NH_4Cl and then 2 cm^3 of 30% H_2O_2 dropwise. After stirring for a few minutes, air was bubbled through the solution for 8 h. It was then added to an ion-exchange column containing 200–400 mesh Dowex 50W-X4 cation

exchange resin in the H^+ form. Only one fraction was obtained by elution with 0.2 N $HClO_4$ using a flow rate of about 0.5 cm^3 min^{-1}. The red product was obtained by evaporating the solution to dryness on a water bath. Yield: 0.55 g (12%). Found: C, 32.1; H, 6.2; N, 12.4. Calc. for $CoC_{12}H_{28}N_4O_8Cl$: C, 32.0; H, 6.3; N, 12.4%.

Preparation of s-*cis*-(*N,N′-dimethylethylenediamine-N,N′-di-α-butyrato*) (*trimethylenediamine*) *cobalt (III) perchlorate*, s-*cis*-[Co(dmedba)(tn)]ClO_4

A mixture of 3.96 g (0.01 mol) of Ba (dmedba) and 2.81 g (0.01 mol) of $CoSO_4 \cdot 7H_2O$ in 20 cm^3 of water was stirred for 20 min at 60°C and filtered to remove $BaSO_4$, which was then washed on the filter with 20 cm^3 of hot water. To the combined filtrate and washings were added 5 cm^3 of 2 N nitric acid, 0.8 g of trimethylenediamine, and 1.0 g of activated charcoal. This mixture was vigorously stirred while adding 20 cm^3 of 30% H_2O_2 dropwise, and then air was bubbled through the solution for 10 h. The charcoal was removed by filtration and the filtrate was reduced in volume on a rotary evaporator. It was then added to an ion-exchange column containing 200–400 mesh Dowex 50W-X4 cation exchange resin in the H^+ form. Only one fraction was obtained by elution with 0.2 N $HClO_4$ using a flow rate of about 0.5 cm^3 min^{-1}. The dark red product was obtained by evaporating the solution to dryness on a water bath. Yield: 0.53 g (11%). Found: C, 36.8; H, 6.2; N, 11.4. Calc. for $CoC_{15}H_{30}N_4O_8Cl$: C, 36.7; H, 6.2; N, 11.4%.

RESULTS AND DISCUSSION

The dmedba ligand, N,N′-dimethylethylenediamine-N,N′-di-α-butyric acid, has been prepared as a barium salt from the reaction between N,N′-dimethylethylenediamine and α-chlorobutyric acid. The ^1H NMR spectrum of the dmedba ligand is shown in Fig. 2. The α-ethyl protons resonate at 0.9 ppm as a triplet and at 1.65 ppm as a quintet, the N-methyl protons at 2.3 ppm as a singlet, and the α-carbon proton at 2.95 ppm as a triplet.

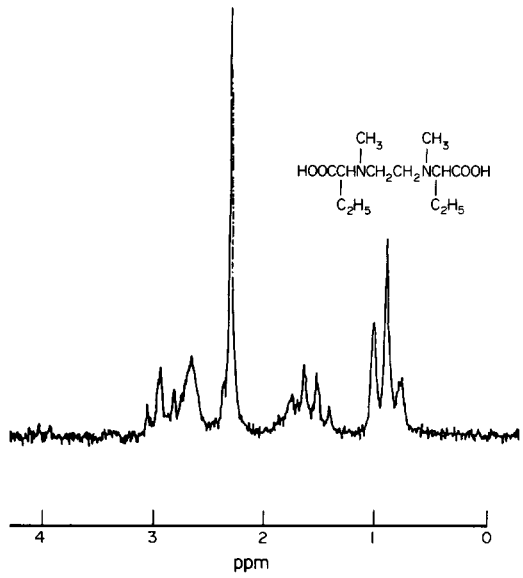

Fig. 2. Pmr spectrum of N,N′-dimethylethylenediamine-N,N′-α-butyric acid.

The cobalt(III) complexes of the dmedba ligand, $[Co(dmedba)L]^+$, have been prepared in this work, where L is ethylenediamine, trimethylenediamine or two ammine ligands. Only one isomer, the s-*cis* isomer, has been obtained during the course of our preparation. Table 1 shows the IR spectral data for the dmedba ligand as well as for the Co(III) complexes of dmedba. Although IR spectroscopy is not the most reliable method for the differentiation between the s-*cis* and uns-*cis* isomers, it gives valuable information on the order of strength of the coordinate bands, by observing the magnitudes of the band shifts.[14,17] The magnitude of separation ($\Delta\nu$) between the frequencies due to $\nu_{as}OCO$ and ν_sOCO in the different butyrato arms has been found helpful in distinguishing all the main types of the carboxylate binding. From the data in Table 1 it may be observed that in all of the complexes, the shifts in the frequencies due to $\nu_{as}OCO$ and ν_sOCO are higher and lower, respectively, relative to those for the dmedba ligand. The separation of the two CO bands is proportional to the strength of the cobalt–oxygen bond. The higher stability of

Table 1. COO stretching frequencies of the cobalt(III) complexes (in cm^{-1})

Compound	$\nu_{as}OCO$	ν_sOCO	$\Delta\nu = (\nu_{as}-\nu_s)$
dmedba	1600	1410	190
s-*cis*-$[Co(dmedba)(en)]^+$	1633	1397	236
s-*cis*-$[Co(dmedba)(tn)]^+$	1625	1398	227
s-*cis*-$[Co(dmedba)(NH_3)_2]^+$	1620	1398	222

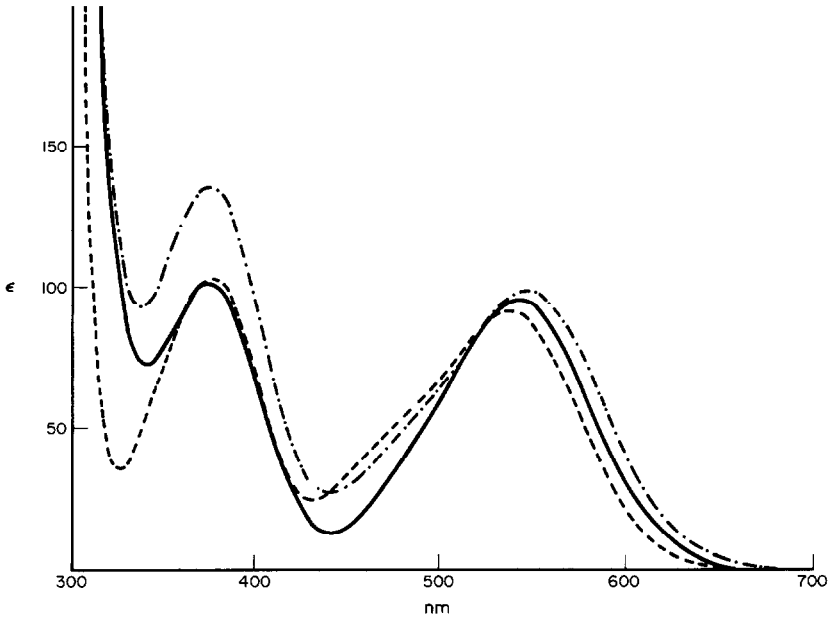

Fig. 3. Electronic absorption spectra of cis-α-[Co(dmedba)(en)]ClO_4 (– – –), *cis*-α-[Co(dmedba)(tn)]ClO_4 (– · – · –) and *cis*-α-[Co(dmedba)$(NH_3)_2$]ClO_4 (——).

$[Co(dmedba)(en)]^+$ complexes could be due to the chelate effect of en.

The electronic absorption spectra of the complexes prepared in this work are shown in Fig. 3 and all of the spectral data are summarized in Table 2. The bands I and II, which are due to the *d-d* transitions in the octahedral CoN_4O_2 crystal field, appear between 350–550 nm. For the diamine Co(III) complexes of dmedba, the frequencies of the absorption maxima decrease in the order en > diammine > tn, corresponding to the decreasing ligand field strength. This is in keeping with the expected greater stability due to the chelate effect of ethylenediamine when compared to two ammines. The shape of the first band consists of a shoulder superimposed upon a symmetrical trace of the major peak from the observed spectrum.[19]

The fact that the Co(III) complexes of dmedba prepared in this work has the s-*cis* configuration is clearly shown in the PMR spectra of these complexes shown in Figs 4 and 5. Figure 4 shows the PMR spectrum of $[Co(dmedba)(en)]^+$. The ethyl protons at the α-carbon atom are shown as a triplet at 1.4 ppm and as a quintet at 2.1 ppm. The ethylenediamine functioning as a bidentate ligand and the ethylenediamine backbone ring protons of the dmedba ligand are shown between 2.7–3.2 ppm. In Fig. 5, which shows the PMR spectrum of $[Co(dmedba)(tn)]^+$, the ethyl protons at the α-carbon atom are shown as a triplet at 1.35 ppm and as a quintet at 2.25 ppm, while the protons at the α-carbon atom are shown as a triplet at 3.8 ppm. If the complexes have the uns-*cis* configuration, the same ethyl protons would have shown two triplets

Table 2. Electronic spectral data for aqueous solutions of the cobalt(III) complexes

Compound	Absorption			
	Band I		Band II	
	λ (nm)	ε	λ (nm)	ε
s-*cis*-$[Co(dmedba)(en)]^+$	540	91	375	102
	485	sh		
s-*cis*-$[Co(dmedba)(NH_3)_2]^+$	545	97	373	101
	490	sh		
s-*cis*-$[Co(dmedba)(tn)]^+$	550	99	370	136
	500	sh		

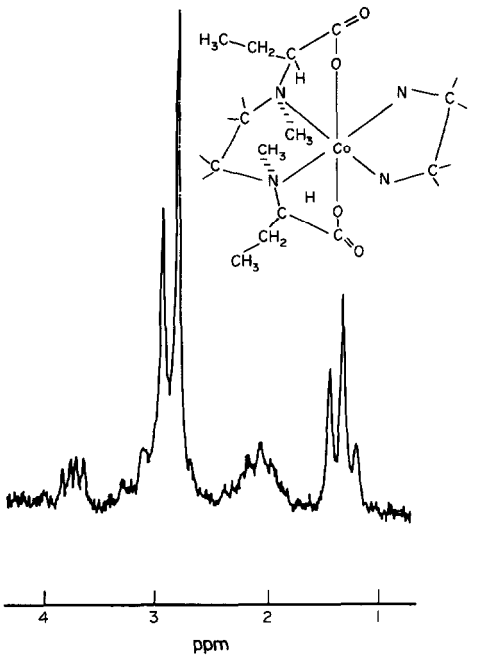

Fig. 4. Spectrum of *cis*-α-[Co(dmedba)(en)]$^+$ in D_2O.

and two quintets. The uns-*cis* isomer has only C_1 symmetry and the two butyrato arms are no longer equivalent in the uns-*cis* geometry. The methyl protons as well as the CH proton in the planar carboxylate arm in the uns-*cis* geometry, no longer lie in the same shielding area of the C—N bond, and such loss of shielding would cause the ethyl protons at the α-carbon atom to resonate at lower fields with two triplets and two quintets. The s-*cis* configuration is, therefore, assigned to each of the two complexes obtained in this work on the basis of the ^{1}H NMR spectra.

Although the s-*cis* isomer appears to have been mostly formed, in the CoN_4O_2 system so far reported,[1,11,20–24] it is quite interesting to observe that the Co(III) complexes of our new ligand dmedba have yielded only the s-*cis* isomer. Severe ring strain totally prevents the formation of the *trans* isomer. Due to the tetrahedral nature of the nitrogen atom, the puckered chelate ring in the uns-*cis* isomer are somewhat strained and slightly distorted from the plane containing the nitrogen atoms, so that the uns-*cis* isomer is expected to be less stable than the s-*cis* isomer. The dmedba ligand has an ethyl substituent at each of the two α-carbon atoms as well as a methyl substituent at each of the two nitrogen donor atoms. Because of such alkyl groups, the steric interaction would be greater for the in-plane chelate rings if an uns-*cis* isomer were to be formed. Therefore, in our experimental observation the dmedba ligand appears to favour an s-*cis* configuration due to such increased steric interactions for the uns-*cis* isomer.

Acknowledgement—We thank the Korea Science and Engineering Foundation for financial support for this work.

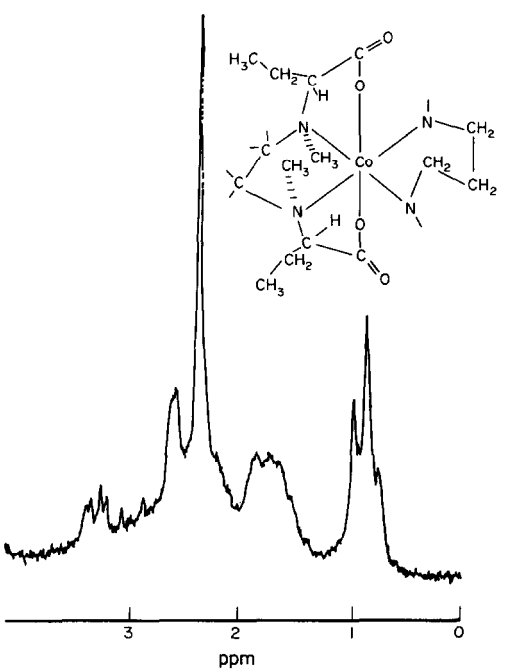

Fig. 5. Spectrum of *cis*-α-[Co(dmedba)(tn)]$^+$ in D_2O.

REFERENCES

1. M. Mori, M. Shibata, E. Kyuno and F. Maruyama, *Bull. chem. Soc. Japan* 1962, **35**, 75.
2. J. Legg and D. Cooke, *Inorg. Chem.* 1965, **4**, 1576.
3. K. Kuroda and K. Watanabe, *Bull. chem. Soc. Japan* 1971, **44**, 1034, 2520.
4. K. Kuroda and K. Watanabe, *Bull. chem. Soc. Japan* 1974, **45**, 2176.
5. L. Halloran and J. Legg, *Inorg. Chem.* 1974, **13**, 2193.
6. J. Dabrowski and D. Cooke, *J. Am. Chem. Soc.* 1970, **92**, 1097.
7. W. Jordan and J. Legg, *Inorg. Chem.* 1974, **13**, 955.
8. L. Schoenberg, D. Cooke and C. Liu, *Inorg. Chem.* 1968, **7**, 2386.
9. M. J. Jun, Y. Park, C. Han and S. R. Choi, *J. Korean chem. Soc.* 1985, **29**, 247.
10. C. Maricondi and B. Douglas, *Inorg. Chem.* 1972, **11**, 688.
11. W. Jordan and B. Douglas, *Inorg. Chem.* 1973, **12**, 403.
12. J. S. Jung, C. H. Kim and M. J. Jun, *Bull. Korean chem. Soc.* 1986, **7**, 145.
13. G. Hawn, C. Maricondi and B. E. Douglas, *Inorg. Chem.* 1973, **18**, 2542.

14. M. Strasak and J. Majer, *Inorg. Chim. Acta* 1983, **70**, 231.
15. M. Strasak, F. Bachraty and J. Majer, *Coll. Czech Chem. Comm.* 1982, **47**, 210.
16. T. Woon and M. O'Connor, *Aust. J. Chem.* 1979, **32**, 166.
17. M. Strasak and F. Bachraty, *J. Coord. Chem.* 1984, **13**, 105.
18. J. S. Jung, C. H. Kim and M. J. Jun, *Bull. Korean chem. Soc.* 1985, **6**, 369.
19. G. R. Brubaker, D. P. Schaefer, J. H. Worrell and J. Legg, *Coord. Chem. Rev.* 1971, **7**, 161.
20. H. Yamatera, *Bull. chem. Soc. Japan* 1968, **31**, 95.
21. F. Basolo, C. Ballhausen and J. Bjerrum, *Acta Chem. Scand.* 1955, **9**, 810.
22. J. Legg, D. Cooke and B. Douglas, *Inorg. Chem.* 1967, **6**, 700.
23. D. Radanovic, *Coord. Chem. Rev.* 1984, **54**, 159.
24. P. Harrington, S. Linke and M. Alexander, *Inorg. Chem.* 1973, **12**, 168.

Polyhedron Vol. 7, No. 7, pp. 535–542, 1988
Printed in Great Britain

0277–5387/88 $3.00+.00
© 1988 Pergamon Press plc

STABILITY, SPECTRA AND STRUCTURE OF THE COBALT(II) CHLORIDE COMPLEXES IN HEXAMETHYLPHOSPHORAMIDE SOLUTION AT 25°C

MICHAŁ PILARCZYK,* WACŁAW GRZYBKOWSKI and LUCYNA KLINSZPORN

Department of Physical Chemistry, Technical University of Gdańsk, Majakowskiego 11/12. 80-952 Gdańsk, Poland

(*Received* 17 *July* 1987; *accepted after revision* 30 *October* 1987)

Abstract—Cobalt(II) chloride complexes were investigated spectrophotometrically in hexamethylphosphoramide (HMPA) solutions. It has been established that four consecutive tetrahedral chloro complexes of cobalt(II) are formed in the $Co(ClO_4)_2$–$CoCl_2$ and $CoCl_2$–LiCl–HMPA solutions. The formation constants of the complexes have been calculated: $\log K_1 = 9.0$ (± 0.5), $\log K_2 = 6.5$ (± 0.5), $\log K_3 = 3.05$ (± 0.05) and $\log K_4 = -1.42$ (± 0.03). The high stability of the dichloro-complex results in the fact that this species is the only complex of cobalt(II) existing in HMPA solutions of $CoCl_2$.

In previous papers from this laboratory, the coordination state of $CoCl_2$ in the strongly polar, coordinating solvents such as N,N-dimethylformamide,[1] N-methylformamide,[2] N,N-dimethylacetamide,[3] dimethylsulphoxide[4] and acetonitrile[5] was reported. It seems that the electrolytic properties of these systems can be discussed in terms of a coordination disproportionation equilibria

$$3CoCl_2L_2 + 2L \rightleftharpoons CoL_6^{2+} + 2CoCl_3L^-$$

where L denotes a solvent molecule. It is obvious that the position is determined by the stability of the complexes involved in the above scheme. Very high stability of the trichloro-complex in DMF results in the formation of the $[Co(DMF)_6^{2+}][CoCl_3(DMF)^-]_2$ complex electrolytes. The most stable chloro-complex of cobalt (II) in DMA is the $CoCl_2(DMA)_2$ neutral species. Thus, $CoCl_2$ in DMA may be considered as a non-electrolyte. The high stability of the dichloro-complex is a consequence of a low stability of the octahedral cationic species arising from steric crowding close to the metal centre. In the DMA solution the equilibrium between $Co(DMA)_4^{2+}$ and $Co(DMA)_6^{2+}$ has been shown to exist,[6,7] while $Co(DMF)_6^{2+}$ is the only detectable species in the DMF solution of $Co(ClO_4)_2$.[8] Thus, the differences among the $CoCl_2$–solvent systems arise from differences in the donicities and the molecular size of the solvent.

The effect of shape and size of the solvent molecules is the most important factor in determining the solvating properties of HMPA. Numerous metal ions, which are known to exist as the hexakis-solvent cationic species when the coordinatively anions are absent, exist as the tetrakis–HMPA complex cations in HMPA solution.[9] The high donicity of HMPA (donor number, DN = 38.8) suggests that this solvent will be a highly ionizing medium. However, our preliminary conductometric data indicate that the solutions of $CoCl_2$ in HMPA exhibit very low conductivity. Thus, the solute exists as an electrically neutral species. The solid $CoCl_2(HMPA)_2$ complex was obtained by Donoghue and Drago, and it is well established that the pseudotetrahedral $CoCl_2(HMPA)_2$ complex is stable in the solvents having low donor numbers.[10]

The Co^{2+}–Cl^-–HMPA system was studied by Gutmann and Weisz but in a rather qualitative way.[11] They studied the electronic absorption spectra and demonstrated the formation of consecutive chloro-complexes of cobalt(II).

In the present work we report a detailed description of the Co^{2+}–Cl^-–HMPA systems and the formation constants for all complexes formed. The results obtained seem to be very interesting in light of the fact that the stepwise complex formation is not accompanied by a stereochemical trans-

* Author to whom correspondence should be addressed.

formation, i.e. the coordination number of the central metal ion is always the same.

EXPERIMENTAL

Hexamethylphosphoramide was dried over CaH_2 and distilled under reduced pressure at 70–80°C. The specific conductivity of the final product was (1.0–2.5) 10^{-8} S cm^{-1} at 25°C.

Solid $CoCl_2(HMPA)_2$ was obtained from anhydrous $CoCl_2$ according to a procedure described by Donoghue and Drago.[10] Solid $Co(ClO_4)_2 \cdot 4HMPA$ was prepared from the corresponding hydrate using the method reported by the same authors. The solid solvates were used to prepare the stock solutions. Lithium chloride was dried at 120°C under reduced pressure and used without further purification. Use of LiCl enables the preparation of high chloride concentration solutions and consequently a large Cl^-/Co^{2+} molecular ratio, up to 1000.

The stock solutions of the cobalt(II) salts were analysed by standards EDTA titrations. Solutions for measurements were prepared by weighed dilutions, and the concentrations were calculated using densities determined independently. Preparation of the solution and other manipulations were carried out in dry-boxes. Absorption spectra were recorded using a Beckman UV 5270 spectrophotometer equipped with a thermostated cell compartment.

RESULTS AND DISCUSSION

Figure 1 shows the visible absorption spectrum of $CoCl_2$ in HMPA solution at 25°C. The spectrum consists of a broad band with maxima located at 596, 610, and 664 nm and shoulders at *ca* 580 and 630 nm. The spectrum is close to those reported by Donoghue and Drago for a 0.002 mol dm^{-3} solution of $CoCl_2(HMPA)_2$ in nitromethane. However, they observed only one maximum at 650 nm, and some shoulders at 515, 590 and 605 nm.[10] The spectrum obtained by Gutmann and Weisz for the $Co(ClO_4)_2$–Et_4NCl–HMPA system at a Cl^-/Co^{2+} ratio of 2.0 exhibits maxima at 597, 610, and 663 nm and shoulders at 580 and 630 nm.[11] The band position, contour and high intensity are typical of the complexes of the CoX_2L_2 type. The most characteristic feature of the $CoCl_2$–HMPA is "optical constancy". It means that the band position and the intensity are independent of the salt concentration within the studied concentration range, i.e. from 0.0001 to 0.01 mol dm^{-3}.

In Fig. 1 the molar conductance curve of $CoCl_2$ in HMPA at 25°C is also presented. As is seen, the values do not exceed 0.5 S cm^2 mol^{-1} and are

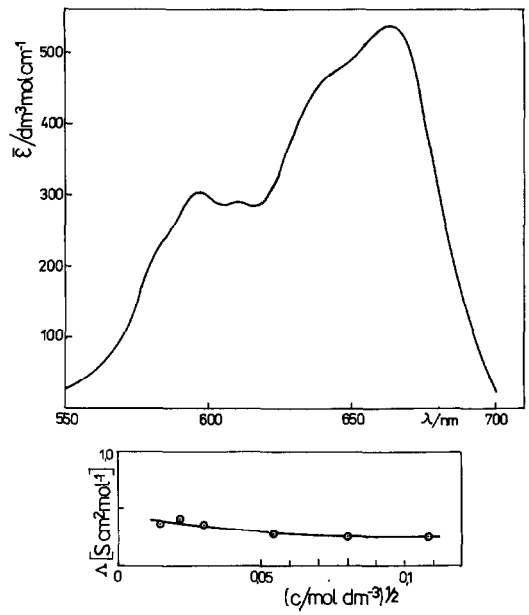

Fig. 1. Visible absorption spectrum of cobalt(II) and plot of the molar conductance against the square root of the concentration for $CoCl_2$ in HMPA solution at 25°C.

drastically lower than the corresponding values for $Co(ClO_4)_2$ reported previously. The latter salt is known to exist in HMPA solution as the $Co(HMPA)_4^{2+} \cdot 2ClO_4^-$ type complex electrolyte, and its molar conductance changes from *ca* 49 to 32 S cm^2 mol^{-1}, within the same concentration range.[12] Thus, the obvious conclusion follows, that $CoCl_2$ exists as the pseudotetrahedral $CoCl_2(HMPA)_2$ complex in HMPA solution. This fact is an indication of the unusually high stability of the mixed complex related to the shape and size of the HMPA molecule. Gutmann and Weisz reported that in the $CoCl_2(HMPA)_2$ complex, the bond energies of Co–HMPA are higher than those in the $Co(HMPA)_4^{2+}$ solvocation.[11] A proton resonance study has shown that owing to the high space requirements of HMPA, even the four donor atoms in the tetrasolvate cannot approach the central metal ion close enough to be strongly bounded by it. Thus, two of the four HMPA molecules can be replaced by a chloride anion, and even by an iodide ion, a ligand of comparatively low donicity.[10,11]

In order to check the possibility of the formation of lower chloro-complexes of cobalt(II) in the Co^{2+}–Cl^-–HMPA system we have studied the visible absorption spectra of cobalt(II) for a series of equimolar mixtures of $Co(ClO_4)_2$ with $CoCl_2$. Figure 2 shows the spectra of cobalt(II) from the series of the equimolar mixtures covering the 0–1 range of the Cl^-/Co^{2+} ratio, with the total concentration of cobalt(II) being constant, *ca* 0.001 mol

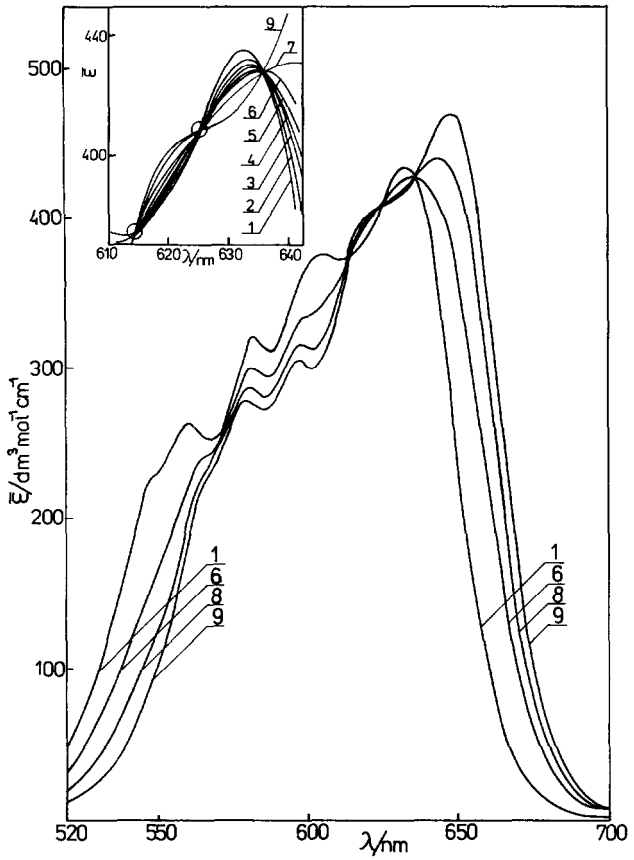

Fig. 2. Absorption spectra of cobalt(II) for a series of equimolar mixtures of $Co(ClO_4)_2$ with $CoCl_2$ at 25°C. The total metal concentration is constant (*ca* 0.001 mol dm^{-3}), while the Cl^-/Co^{2+} ratios are: 1—0.0, 2—0.107, 3—0.203, 4—0.300, 5—0.398, 6—0.497, 7—0.720, 8—0.794, 9—0.997.

dm^{-3}. The spectrum of cobalt(II) for pure $Co(ClO_4)_2$ is indicated by curve 1. As is seen, substitution of $CoCl_2$ for $Co(ClO_4)_2$ brings about distinct changes in the spectrum of cobalt(II). The maxima at 560, 582, 605, and 633 nm characteristic of the $Co(HMPA)_4^{2+}$ solvate[12] disappear gradually and a new spectrum of cobalt(II) with the maxima shifted towards longer wavelenghths is developed. However, the spectrum of cobalt(II) is not identical with the spectrum of the $CoCl_2(HMPA)_2$ complex presented in Fig. 1. The spectral changes are accompanied by the appearance of three well-defined isosbestic points at 614, 625, and 636 nm. Their presence on the spectra indicate a two-species equilibrium within the 0–1 range of the Cl^-/Co^{2+} ratio. The obvious conclusion that the second of the complexes is the pseudotetrahedral C_{3v} monochloro-complex of cobalt(II), $CoCl(HMPA)_3^+$, does not need additional support.

In Fig. 3 the spectra of cobalt(II) for the range 1–2 of the Cl^-/Co^{2+} ratio, are presented. The spectrum of cobalt(II) obtained for pure $CoCl_2$ is indicated by curve 15, while curve 9 shows the spectrum of cobalt(II) determined at the Cl^-/Co^{2+} ratio amounting to 1.0. Inspection of the spectral lines shows that the spectrum due to the presence of the $CoCl(HMPA)_3^+$ complex is transformed into the spectrum of $CoCl_2(HMPA)_2$. Subsequently, one isosbestic point located at 632.5 nm can be observed on the spectra, once again indicating a two-species equilibrium, now between the monochloro- and dichloro-complexes of cobalt(II). The spectrum obtained at the Cl^-/Co^{2+} ratio amounting to 1.0 passes through the isosbestic points at 614, 625, and 636 nm, as well as through the isosbestic point at 632.5 nm. Thus, the spectrum of cobalt(II) may be considered as the spectrum of the $CoCl(HMPA)_3^+$ complex. Moreover, it means that in the mixed solution containing $Co(ClO_4)_2$ and $CoCl_2$ at the molar ratio amounting to 1.0, cobalt(II) exists exclusively as the $CoCl(HMPA)_3^+$ complex. It indicates that replacement of even one HMPA molecule by a chloride anion results in high stability of the complex of cobalt(II).

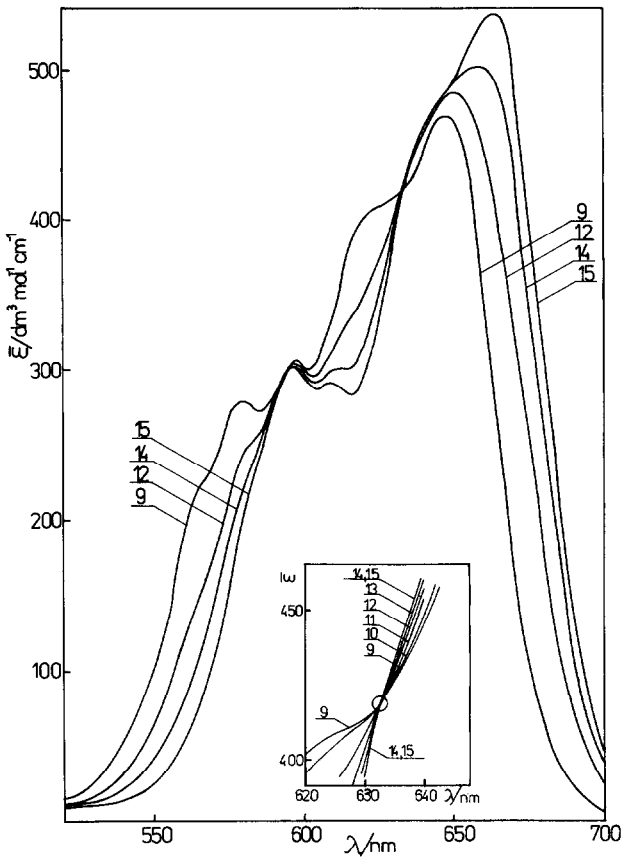

Fig. 3. Absorption spectra of cobalt(II) for a series of equimolar mixtures of $Co(ClO_4)_2$ with $CoCl_2$ at 25°C. The total metal concentration is constant (*ca* 0.001 mol dm^{-3}), while the Cl^2/Co^{2+} ratios are: 9—0.997, 10—1.091, 11—1.283, 12—1.503, 13—1.697, 14—1.794, 15—2.00.

Further changes in the spectrum of cobalt(II) induced by an increase in the Cl^-/Co^{2+} ratio are presented in Figs 4 and 5, showing the spectra of a series of solutions containing $CoCl_2$ at an approximately constant concentration of 0.001 mol dm^{-3} and LiCl at a number of different concentrations. Figure 4 shows the spectra obtained at Cl^-/Co^{2+} ratios from 2.0 (pure $CoCl_2$ solution) to *ca* 53. As is seen, an increase in LiCl concentration results in the gradual growth of the observed band accompanied by a further shift of the maximum towards longer wavelengths. Subsequently, the maxima at 596 and 610 nm characteristic of the $CoCl_2(HMPA)_2$ complex disappear and the new local maximum at 614 nm is observed. Simultaneously, the next set of isosbestic points at 606, 624, and 650 nm appears on the spectra. Further increase in the LiCl concentrations, now corresponding to the Cl^-/Co^{2+} ratios from 53 to 1017, causes the changes presented in Fig. 5. As is seen, the maximum at 614 nm vanishes and the band with a maximum at 634 nm is developed, while the highest maximum at *ca* 680 nm is split into two bands with maxima at *ca* 668 and 690 nm. The latter spectrum of cobalt(II) shows the characteristics of the tetrachloro-complexes. At the same time, a new set of isosbestic points located at 622, 642 and 657 nm appears on the spectra. The appearance of the two sets of isosbestic points indicates that the two consecutive two-species equilibria is established within the 2–53 and 53–1017 ranges of the Cl^-/Co^{2+} ratio, respectively. It seems obvious that the first of them is related to the formation of the trichlorocomplex, while the second equilibrium is related to the formation of the highest chloro-complex of cobalt(II), i.e. the tetrahedral $CoCl_4^{2-}$ anion. The spectrum obtained at the Cl^-/Co^{2+} ratio amounting to 53.5 pass through two sets of isosbestic points. We infer that this spectrum of cobalt (II) is the spectrum of the $CoCl_3(HMPA)^-$ complex. The spectra obtained at the highest Cl^-/Co^{2+} ratios show the characteristics of the tetrachloro-complex. However, this spectrum is not the limiting one. The molecular ratios of Cl^-/Co^{2+}

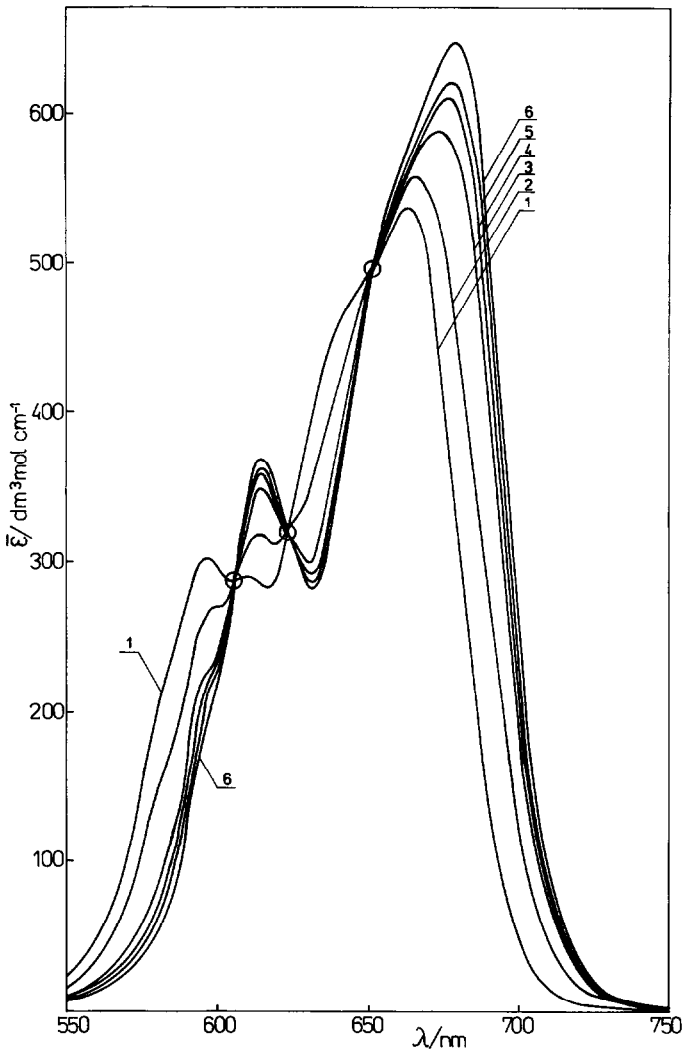

Fig. 4. Absorption spectra of cobalt(II) for a series of $CoCl_2$–LiCl solutions at 25°C. The concentration of $CoCl_2$ is constant (*ca* 0.001 mol dm^{-3}), while the Cl^-/Co^{2+} ratios are: 1—2.00, 2—2.977, 3—5.54, 4—7.94, 5—10.68, 6—53.43.

exceeding 1000 are not sufficient to transform the $CoCl_3(HMPA)^-$ complex into the tetrachloro-species.

The most characteristic feature of the Co^{2+}–Cl^-–HMPA system arrives from the fact that only two chloro-complexes are formed simultaneously. This made it possible to derive the spectra of the individual chloro-complexes of cobalt(II), except for that of $CoCl_4^{2-}$. The spectra are presented in Fig. 6 along with the spectrum of the $Co(HMPA)_4^{2+}$ solvate.

Inspection of Fig. 6 shows that a shift towards longer wavelengths is observed on going from $Co(HMPA)_4^{2+}$ to $CoCl_3(HMPA)^-$, i.e. on replacing HMPA molecules by chlorides. This trend was observed for numerous cobalt(II)–halide–donor systems, and was predicted theoretically by Flamini *et al.* on the basis of ligand field theory.[13] It seems to be of interest to compare the spectra of cobalt(II) obtained for different ligands. The visible spectrum of the $CoCl_3L^-$ complex is characterized by an asymmetric band with two maxima. The wavelengths corresponding to the absorption maxima are listed in Table 1. Inspection of the table shows that the position of the maxima, to a small extent, depends on the nature of the solvent indicating the identity of the nearest neighbour. The differences are reflected only in the intensities of the bands.

It should be noted that the contour of the spectrum of cobalt(II) obtained for $Co(HMPA)_4^{2+}$ differs essentially from those of tetrachloro- and tetrabromo-complexes of cobalt(II) of the same

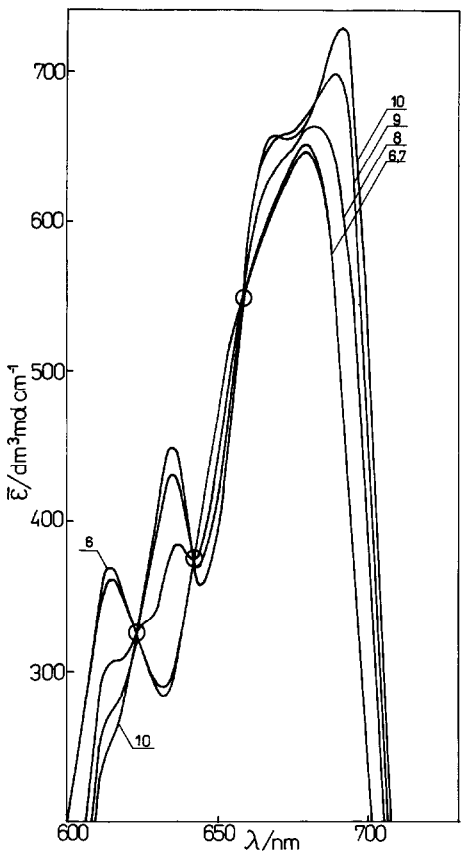

Fig. 5. Absorption spectra of cobalt(II) for a series of $CoCl_2$–LiCl solutions at 25°C. The concentration of $CoCl_2$ is constant (*ca* 0.001 mol dm^{-3}), while the Cl^-/Co^{2+} ratios are: 6—5.53, 7—106.3, 8—432.9, 9—703.5, 10—1017.2.

symmetry.[1,3,4,14] It seems that the difference arises from the space requirements of the HMPA molecules.

The above presented spectra of the individual chloro-complexes permit direct calculation of the equilibrium concentrations of the $CoCl(HMPA)_3^+$ and $CoCl_2(HMPA)_2$ complexes in the $Co(ClO_4)_2$–$CoCl_2$ mixed solutions, as well as the concentrations of the $CoCl_2(HMPA)_2$ and $CoCl_3(HMPA)^-$ complexes in the $CoCl_2$–LiCl solutions in which the $CoCl_4^{2-}$ complex is absent, i.e. for Cl^-/Co^{2+} ratios lower than 53. The results show that the abundance of the $CoCl(HMPA)_3^+$ and $CoCl_2(HMPA)_2$ complexes in the $Co(ClO_4)_2$–$CoCl_2$ system are immediately determined by the composition of the mixture. It means that all the chloride ions are consumed for the formation of the $CoCl(HMPA)_3^+$ and $CoCl_2(HMPA)_2$ complexes. The equilibrium concentrations of the single complexes have been used for preparing the distribution diagram shown in Fig. 7.

Table 1. The position of the band maxima for the visible spectrum of the $CoCl_3L^-$ complexes

L =	HMPA	DMF[1]	DMA[3]	DMSO[4]
λ	614	610	614	615
(nm)	678	680	680	675

The results obtained provide the possibility to calculate the formation constants of all the complexes which are formed in the Co^{2+}–Cl^-–HMPA system. The corresponding constants are defined as

$$K_n = \frac{c_n}{c_{n-1}[Cl^-]} Y_n \qquad (1)$$

where $n = 1$, 2 or 3 and Y_n is the quotient of the respective activity coefficients. Variations in the activity coefficients were assumed to follow the Debye–Hückel equation involving the ion size parameter, å, the latter being estimated as 6.4 Å from the conductometric data.[12] The resulting values of the logarithms of the formation constants of mono-, di- and trichloro-complexes are 9.0 (±0.5), 6.5 (±0.5) and 3.05 (±0.05). The high uncertainty in the values derived for the mono- and dichloro-complexes is related to their very high stability. The solid lines in the distribution diagram are calculated using the formation constants reported above.

The attempt to derive the formation constant of the tetrachloro-complex, made use of the assumption that its molar absorption coefficient is an adjustable parameter. Moreover, spectrophotometric data were obtained for the $CoCl_2$–LiCl solutions of high ionic strength, up to 1.00 mol dm^{-3}, and the Davies equation for the activity coefficients was used. The corresponding relation between the formation constant and ionic strength, I, has the form

$$\log K_4 = \log \frac{c_4}{c_3[Cl^-]} - 2A\left(\frac{I^{1/2}}{1+I^{1/2}} - CI\right) \qquad (2)$$

where A is the theoretical slope arising from the Debye–Hückel equation.

The numerical procedure resulted in the best values for the formation constant and the molar absorption coefficient of the tetrachloro-complex. The best fit was obtained when the value of 0.06 was used for parameter C in eq. (2). The calculations yielded the value of -1.42 (±0.03) for the logarithm of the formation constant, K_4. The values of the molar absorption coefficient of the $CoCl_4^{2-}$ complex compare well with those for the same complex in different media, in which the limit-

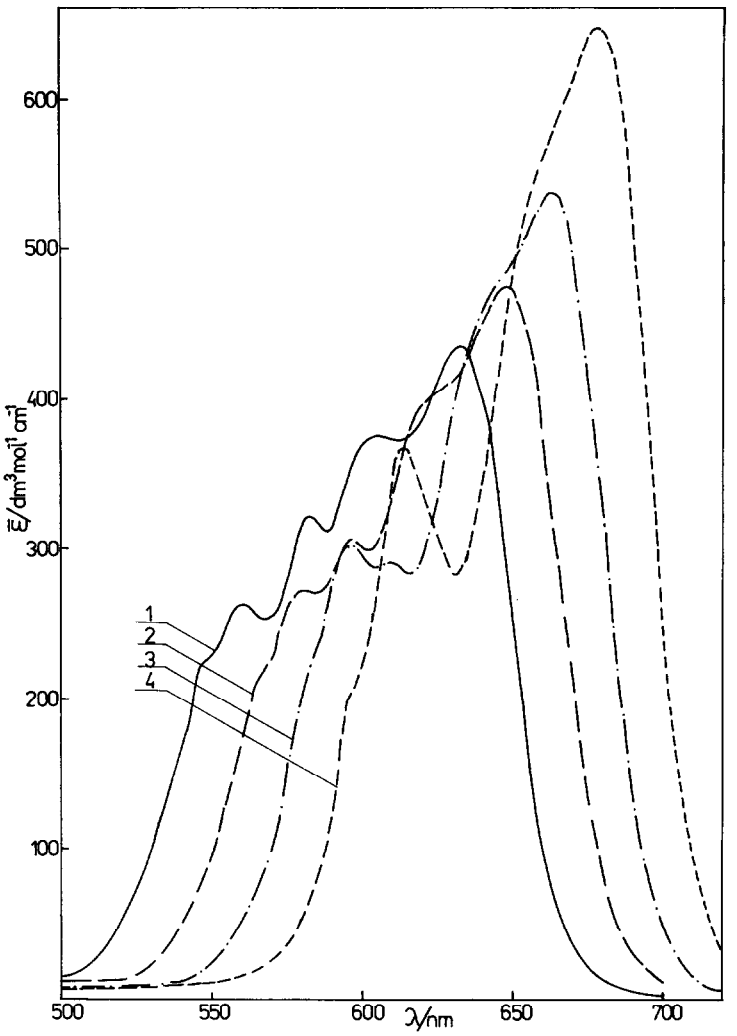

Fig. 6. Absorption spectra of the individual complexes of cobalt(II) in the Co^{2+}–Cl^-–HMPA system. 1—$Co(HMPA)_4^{2+}$, 2—$CoCl(HMPA)_3^+$, 3—$CoCl_2(HMPA)_2$, 4–$CoCl_3(HMPA)^-$.

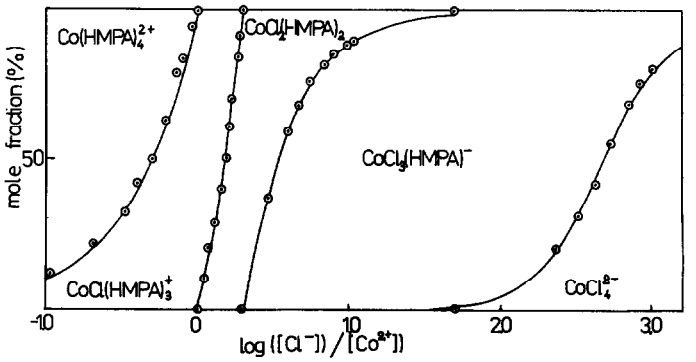

Fig. 7. Formation diagram for the chloro-complexes of cobalt(II) in the Co^{2+}–Cl^-–HMPA system at 25°C.

ing spectrum was determined spectrophotometrically. The value of 780 dm^3 mol^{-1} cm^{-1} was found for the molar absorption coefficient at 690 nm, while values of 773 and 790 dm^3 mol^{-1} cm^{-1} were obtained for $CoCl_4^{2-}$ in DMSO[4] and DMA[3] solutions at the same wavelengths, respectively. The equilibrium concentrations of the $CoCl_4^{2-}$ and $CoCl_3(HMPA)^-$ complexes found for different concentrations of LiCl at the same time have been used to extend the distribution diagram. The formation curve for $CoCl_4^{2-}$ was calculated using this formation constant.

The most striking feature of the Co^{2+}–Cl^-–HMPA systems is the very high stability of the mono- and dichloro-complexes of cobalt(II). Yet, it is obvious that the $CoCl_2(HMPA)_2$ complex is the only form of $CoCl_2$ in HMPA solution.

The high stability of the mono- and dichloro-complexes arises from an enthalpy factor related to the spatial requirements of the HMPA molecule. However, a substitution of the Cl^- anions for the solvent molecules in the first coordination sphere of a metal ion results in a substantial entropy gain on desolvation and from the loss of order in the bulk solvent. The latter effect should be especially distinct when the second solvent molecule is replaced with the Cl^- ion. The negative entropy factor seems to be responsible for the lower stability of the higher chloro-complex of cobalt(II) in HMPA.

Acknowledgement—This work was supported by C.P.B.P.-05.12.

REFERENCES

1. W. Grzybkowski and M. Pilarczyk, *J. Chem. Soc., Faraday Trans. I* 1986, **82**, 1703.
2. M. Pilarczyk and L. Klinszporn, *Bull. Pol. Ac. Chem.* 1985, **33**, 67.
3. E. Kamieńska and I. Uruska, *Bull. Pol. Ac. Chem.* 1976, **24**, 576.
4. W. Libuś, M. Pilarczyk, R. Pastewski and T. Szuchnicka, *Electrochim. Acta* 1982, **27**, 573.
5. W. Libuś, W. Grzybkowski and M. Walczak, *Bull. Pol. Ac. Chem.* 1970, **18**, 141.
6. V. Gutmann, R. Beran and W. Kerber, *Monatsh. Chem.* 1972, **103**, 764.
7. S. F. Lincoln, A. M. Houslow and A. N. Boffa, *Inorg. Chem.* 1986, **25**, 1038.
8. W. Grzybkowski and M. Pilarczyk, *J. Chem. Soc., Faraday Trans. I* 1983, **79**, 2319.
9. Y. Abe and G. Wada, *Bull. Chem. Soc. Japan* 1980, **53**, 3547.
10. J. T. Donoghue and R. S. Drago, *Inorg. Chem.* 1963, **2**, 572.
11. V. Gutmann and A. Weisz, *Monatsh. Chem.* 1969, **100**, 2104.
12. W. Grzybkowski, M. Pilarczyk and L. Klinszporn, *J. Chem. Soc.*, in press.
13. A. Flamini, L. Sestilli and C. Furlani, *Inorg. Chim. Acta* 1971, **5**, 241.
14. W. Libuś and W. Grzybkowski, *Bull. Pol. Acad. Chem.* 1970, **18**, 501.

Polyhedron Vol. 7, No. 7, pp. 543–545, 1988
Printed in Great Britain

0277–5387/88 $3.00 + .00
© 1988 Pergamon Press plc

MAGNETIC AND ESR STUDY OF A DIMERIC COPPER(II) COMPLEX WITH A SCHIFF BASE LIGAND DERIVED FROM SALICYLHYDRAZIDE AND *o*-HYDROXYPROPIOPHENONE

M. S. PALACIOS

Departamento de Química Inorgánica, Facultad de Ciencias, Universidad de la Laguna, Tenerife (Islas Canarias), España

and

J. M. DANCE*

Laboratoire de Chimie du Solide du CNRS, Université de Bordeaux I, 351, cours de la Libération, 33405 Talence Cedex, France

(*Received* 23 *June* 1987; *accepted after revision* 30 *October* 1987)

Abstract—The ESR spectra and temperature dependence of the magnetic susceptibility of a Cu(II) complex with a Schiff-base ligand derived from salicylhydrazide and *o*-hydroxypropiophenone suggest a dimeric structure with strong antiferromagnetic interactions within the pairs. A superexchange pathway via the oxygen atom is proposed.

Magnetic exchange interactions within pairs of transition metal ions have been widely investigated especially for divalent copper dimers.[1,2] In most cases, in a first step, the crystal structure has been determined and then spectroscopic and magnetic investigations were carried out. For other compounds the impossibility of growing suitable single crystals did not allow an X-ray diffraction study and only the magnetic and ESR studies permitted the assumption of a dimeric structure. This is the case for the copper(II) compound studied in this paper where the ligand is a Schiff base derived from salicylhydrazide and *o*-hydroxypropiophenone. Magnetic and ESR studies have given evidence for a dimeric structure with strong antiferromagnetic coupling.

EXPERIMENTAL

Salicylhydrazide was prepared by the usual method.[3] Copper(II) and Zn(II) acetate monohydrates, and *o*-hydroxypropriophenone were reagent grade and used as received. The Schiff base ligand was prepared by a standard method.[4] The copper(II) compound was obtained by mixing hot ethanolic solutions of the metal salt and the ligand in a 1 : 1 molar ratio and refluxing for 4 h. The green precipitate was recrystallized in DMF and dried under vacuum. The compound did not decompose up to 330°C and was insoluble in common organic solvents. Chemical analysis of H, N and C was carried out on a Carlo Erba 1106 Elemental Analyser. Cu titration was performed on a Perkin–Elmer 305 apparatus.

The analytical data found for $CuC_{16}H_{14}N_2O_3$ were: C, 55.3; H, 4.1; N, 9.0 and Cu, 18.3. Calc. C, 55.6; H, 4.0; N, 8.1 and Cu, 18.3%.

A copper doped zinc compound was identically prepared using a 95 : 5 molar ratio of Zn(II) and Cu(II) acetates. Its X-ray pattern is identical to the pure copper one without considering the shift of the diffraction lines due to the different parameters. The magnetic susceptibility was measured on a Faraday type microbalance and the ESR spectra were recorded on a X-band Bruker spectrometer.

MAGNETIC PROPERTIES

Magnetic susceptibility data were corrected from the diamagnetism of the ligand system ($-150 \cdot 10^{-6}$

*Author to whom correspondence should be addressed.

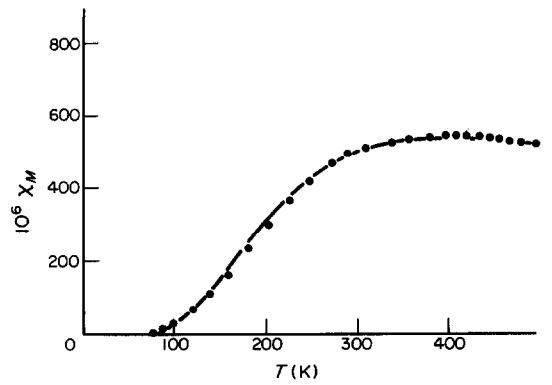

Fig. 1. Thermal variation of the molar susceptibility (● experimental points, full curve: susceptibility calculated with eq. (1) and $J/k = -444$ cm^{-1}).

emu mole^{-1}) and from the temperature independent paramagnetism, N_α (60.10^{-6} emu mole^{-1}). A mononuclear impurity was only detected at very low temperature and was calculated to represent about 1.4% of the amount (assuming a $\chi_{imp} = C/T$ law). The variation of the resulting magnetic molar susceptibility with temperature is given in Fig. 1. It exhibits a large maximum near 400 K. The best fit was obtained using the expression:

$$\chi_m = \frac{Ng^2\beta^2}{3kT}\left[1+\frac{1}{3}e^{-J/kT}\right]^{-1} \qquad (1)$$

where N, β, k have their usual meanings and $g = 2.141$ is given by the ESR data. It corresponds to a singlet–triplet separation of 444 cm^{-1} indicating a strong antiferromagnetic interaction between the two copper ions of the unit.

ESR SPECTRA

The ESR experiments were performed either on the non-diluted compound or the homologous zinc material doped with 5% Cu. The ESR spectra are quite different and both give evidence of the presence of dimeric units in the structure.

The spectrum corresponding to the non-diluted compound exhibits, even at room temperature, the features of a triplet state spectrum. Around $g \simeq 2.2$, resonance lines corresponding to monomeric units (already evidenced by susceptibility measurements) are observed. The triplet state spectrum is governed by the usual $S = 1$ hamiltonian:

$$\mathcal{H} = \beta H.g.S + D(S_z^2 - 2/3) + E(S_x^{2'} - S_y^2),$$

where D and E are the zero-field splitting parameters. The determination of the ESR parameters was done by the so-called Wasserman method[6] applied to previous copper dimer compounds.[7,8] The observed and calculated ESR transitions are given in Table 1.

Table 1. Experimental and calculated ESR transitions for the dimeric compound with $g_\parallel = 2.36$, $g\perp = 2.04$, $D = 0.36$ cm^{-1}. Numbering of the transitions corresponds to that of ref. 5

	$H_{\parallel 1}$	$\Delta M_s = 2$	$H_{\perp 2}$	$H_{\parallel 2}$
Obs.	225 ± 50	1710 ± 20	5000 ± 50	not obs.
Calc.	250	1680	4955	690

The width of the resonance lines prevents the determination of E, which must hence be smaller than 0.003 cm^{-1}. The other values obtained are: $g_\parallel = 2.36$, $g_\perp = 2.04$ and $D = 0.36 \pm 0.01$ cm^{-1}. The intensity of the triplet spectrum diminishes with decreasing temperature, following the same variation as the susceptibility. The spectrum is hardly seen below 100 K. The monomer spectrum increases, down to helium temperatures. The spectrum of the doped compound at room temperature is somewhat different and is given in Fig. 2(a) and

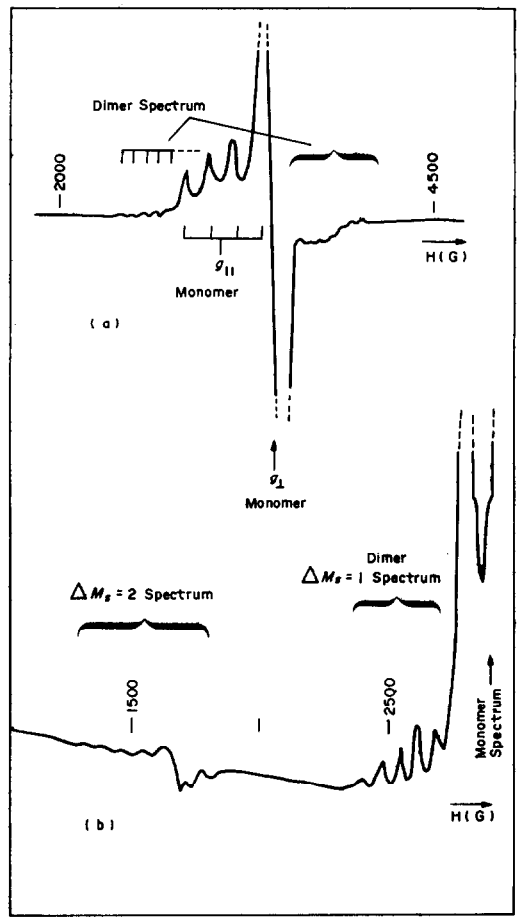

Fig. 2. Room temperature ESR spectra of the Cu-doped Zn compound. (a) The $\Delta M_s = 1$ spectrum. (b) The low field part of the spectrum.

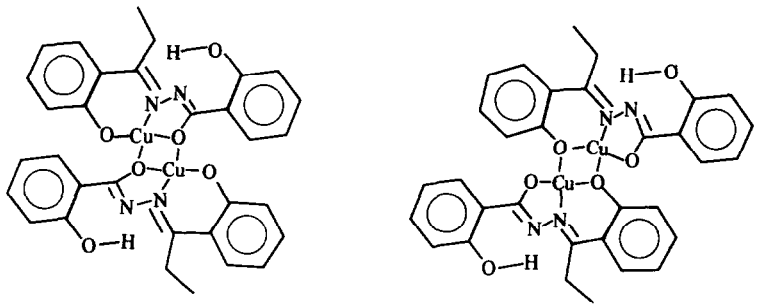

Fig. 3. Possible Cu—Cu bridgings in the dimeric unit.

(b). Fig. 2(a) shows the $\Delta M_s = 1$ part: a strong monomer spectrum characterized by $g_\parallel = 2.357$, $g_\perp = 2.033$, $A_\parallel = 171$ G and $A_\perp = 30$ G is surrounded on each side by some hyperfine lines. On the low field side of the monomer spectrum they are equally separated by 85 G (parallel components). This seems to correspond to a $\Delta M_s = 1$ dimer spectrum. It is indeed not surprising that with a diluted composition of 5% copper, the probability of finding monomers is far higher than that of dimers. The $\Delta M_s = 2$ dimer spectrum is given in Fig. 2(b), it is also characterized in its low field portion by equally spaced (85 G) hyperfine lines (parallel contribution). The $\Delta M_s = 1$ and $\Delta M_s = 2$ spectra have been fitted by various authors for other copper(II) dimers.[8] Here, as the structure is unknown, such a fitting would be hazardous, but the various ESR data besides the magnetic results are nevertheless consistent with the presence of strongly interacting copper(II) pairs:

—Triplet state spectrum observable at room temperature.

—Equally spaced hyperfine lines of $A_\parallel$dimer = $1/2(A_\parallel$ monomer) observable at 295 K for the diluted compound.

—Intensity of the EPR spectra following the same variation as the susceptibility.

In conclusion, by using those results, a possible superexchange pathway for our compound would be given by the two cases of Fig. 3. Such an assumption most probably involves bridging via the phenolic or hydrazine oxygen atoms if the dimeric structure is really of this type.

Acknowledgement—Dr M. S. Palacios wishes to thank Prof. P. Hagenmuller for welcoming him at the Laboratoire de Chimie du Solide du CNRS in Bordeaux.

REFERENCES

1. A. P. Ginsberg, *Inorg. Chem. Acta* 1971, **5**, 45.
2. G. F. Kokoszka and R. W. Duerst, *Coord. Chem. Rev.* 1970, **5**, 209.
3. M. S. Kadihawata and A. K. Bhattacharya, *J. Inorg. Nucl. Chem.* 1963, **25**, 361.
4. A. Syamal and K. S. Kale, *Indian J. Chem.* 1978, **16A**, 46.
5. Melnik Milan, *Coord. Chem. Rev.* 1982, **42**, 259.
6. E. Wasserman, L. C. Snyder and W. A. Yager, *J. Chem. Phys.* 1964, **41**, 6.
7. N. D. Chasteen, *Inorg. Chem.* 1971, **10**, 2339.
8. J. A. Barnes, D. J. Hodgson and W. E. Hatfield, *Inorg. Chem.* 1972, **11**, 144.
9. P. Boyd, A. D. Toy, T. D. Smith and J. Pilbrow, *J. Chem. Soc., Dalton Trans.* 1973, 1549.

Polyhedron Vol. 7, No. 7, pp. 547–556, 1988
Printed in Great Britain

0277–5387/88 $3.00+.00
© 1988 Pergamon Press plc

EQUILIBRIUM STUDY OF THE ADSORPTION OF MOLYBDENUM(VI) ON ACTIVATED CARBON

J. J. CRUYWAGEN* and H. F. DE WET

Department of Chemistry, University of Stellenbosch, Stellenbosch 7600, South Africa

(*Received* 18 *June* 1987; *accepted* 30 *October* 1987)

Abstract—The adsorption of molybdenum(VI) onto activated carbon from aqueous solution has been investigated in the pH_c range 1.0–6.5 at 25° in 1.0 mol dm^{-3} sodium chloride. The molybdenum concentration was varied from 5×10^{-4} to 2×10^{-2} mol dm^{-3}. Computer treatment of the distribution data in which all the relevant protonation and condensation equilibria of molybdate were taken into account, led to an adsorption model comprising the three species $[HMo_2O_7]^-$, $Mo(OH)_6$ and $[HMoO_4]^-$, of which $[HMo_2O_7]^-$ predominates by far. The very strong adsorption of $[HMo_2O_7]^-$ is attributed to its small hydration energy and an increase in the coordination number of molybdenum(VI) by bonding to basic surface oxygen atoms analogous to complex formation with e.g. oxalate.

Strong adsorption of molybdenum(VI) from acid solution by activated carbon has been reported by several workers.[1–6] These investigations, which have been aimed mainly at practical applications involving the separation and concentration of molybdenum, have shown that adsorption is strongly dependent on pH. The best adsorption occurs at pH ~ 2 (initial value) but both the type of carbon and acid used can affect the pH value of optimum adsorption.[2,3,5] The loading capacity of activated carbon for molybdenum(VI) is also markedly dependent on the type of carbon used.[5] Very little adsorption occurs at pH < 0.5 and also at pH > 4.5. Since various polyanions occur in acidified molybdate solution these results have been explained qualitatively in terms of the adsorption of polynuclear species.[3,4,5] This apparent logical explanation however, does not lead to a clear understanding of the molybdenum(VI) adsorption system. Thus, it is by no means clear why polyanions should be strongly adsorbed while bimolybdate, for example, is not adsorbed at all. Equilibrium analysis in which all relevant protonation and condensation reactions of molybdate are taken into account is essential before an unambiguous interpretation of the adsorption behaviour of molybdenum(VI) can be attempted.

This paper reports the results of a systematic investigation of the adsorption of molybdenum(VI) onto activated carbon as a function of both molybdenum concentration and pH under carefully controlled equilibrium conditions. The adsorption model proposed, is based on an analysis of the data in terms of the equilibrium concentrations of the various molybdenum(VI) species in the aqueous phase. According to this model the species predominantly adsorbed is dimeric in nature rather than polymeric.

EXPERIMENTAL

Materials and solutions

All reagents were of analytical grade and solutions were prepared with water obtained from a Milli-Q system. Sodium molybdate and sodium chloride solutions were prepared from the recrystallized salts and standardized gravimetrically as described previously.[7] Hydrochloric acid was standardized indirectly against potassium hydrogen phthalate by titration with sodium hydroxide. Granular peat based activated carbon (Chemviron, type BPL) of particle size 0.5–2.0 mm was used in all adsorption experiments. The carbon was soaked for a week in a concentrated acid solution (10 M HCl; 1 M HF) to remove soluble ash components, iron and other metal ions.[8] It was washed, first with excess 1 M HCl and then with distilled water to remove the acid. The carbon was dried at 110°C.

* Author to whom correspondence should be addressed.

pH measurements

The free hydrogen concentration, h, was determined by measuring the potential (to ± 0.2 mV) with a Radiometer PHM64 research pH meter. A Ross combination electrode (suplied by Orion Research) with a 3 M KCl internal filling solution was used. The relationship between the measured potential E (in mV) and the hydrogen ion concentration at 25°C is given by eq. (1):

$$E = E^0 + 59.16 \log h + E_j. \quad (1)$$

Values for E^0 and E_j were determined from titrations of 1.0 M NaCl with hydrochloric acid as described by Rossotti.[9] The value of E_j was found to be $-17h$ and has been taken into account for solutions with $h > 0.01$ M. A value for E^0 was determined before each series of measurements. For brevity, $-\log h$ is denoted by pH_c.

Adsorption experiments

A known mass of carbon (usually *ca* 0.25 g) was equilibrated with 50 cm^3 sodium molybdate solution in a well stoppered polythene tube by slow mechanical shaking for 7–8 days in a constant temperature room at 25 ± 1°C. The solution was 1 M with respect to NaCl and for each series of experiments at a given molybdenum(VI) concentration the hydrochloric acid concentration was varied to obtain pH_c values in the range 1–6 after equilibration. The initial molybdate concentrations for the various adsorption experiments were 0.5075, 1.00, 15.00 (1 g activated carbon), 5.075, 10.00 and 20.15 mM. An experiment carried out at a concentration of 100 mM failed because molybdenum trioxide started to precipitate in some of the solutions before adsorption equilibrium had been established. After equilibration the molybdenum concentration in the aqueous phase was determined spectrophotometrically by the Tiron method.[10] Because of the very strong adsorption, the amount of molybdenum adsorbed on the carbon was obtained from the difference between the initial and equilibrium molybdenum concentration of the solution. One experiment was carried out in which the total molybdenum concentration was varied from 0.50–69.3 mM for a nearly constant initial $pH_c = 2.30 \pm 0.01$. The equilibrium pH_c values were 2.54 ± 0.10.

Equilibration time and reversibility of adsorption process

Preliminary adsorption experiments carried out with a 1.0 mM molybdate solution at different pH_c values namely 1.98, 2.49 and 3.58 showed that about 75–95% of the adsorption takes place within 24 h but that at least 6–7 days are necessary for the adsorption equilibrium to be established. Although the total equilibration time is not affected by pH_c a slightly faster rate of adsorption is observed at the lower pH_c values during the first half hour of equilibration. The reversibility of the adsorption reaction was verified by a number of "desorption" experiments at various pH_c values in the range 2–4. Samples of activated carbon loaded with various amounts of molybdenum (190–330 mg Mo per g activated carbon) were equilibrated with 1 M Na(H)Cl solutions containing no molybdate but to which different amounts of "clean" activated carbon (0.25–0.65 g) had been added. The mass of clean carbon added, was calculated to give equilibrium loadings comparable to those of some adsorption experiments, and in all cases the amount of molybdenum adsorbed was within 1–2% of the expected value.

RESULTS AND DISCUSSION

Adsorption isotherms

The results of adsorption experiments at various molybdenum(VI) concentrations are shown in Fig. 1 as plots of adsorption (mg Mo(VI) per g activated

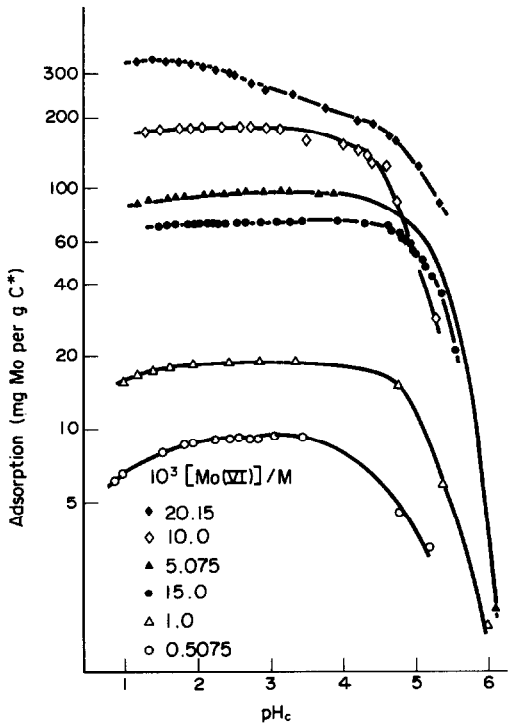

Fig. 1. Adsorption of molybdenum(VI) by activated carbon from a 1.0 M Na(H)Cl solution as a function of pH_c at various molybdenum concentrations.

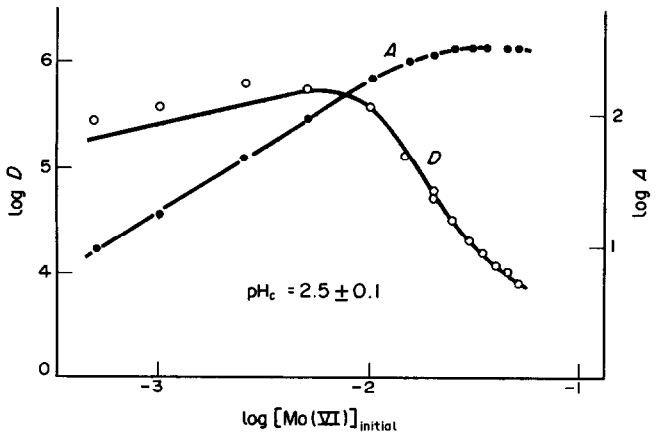

Fig. 2. Distribution (curve *D*) and adsorption (curve *A*) of molybdenum(VI) as a function of initial molybdenum concentration at nearly constant pH$_c$.

carbon) against equilibrium pH$_c$. It is seen that the adsorption increases with increases in the initial molybdenum concentration. At first sight it may appear as if the curve pertaining to molybdenum concentration 15.0 mM does not fit in with the others, but since 1 g of activated carbon was used in this experiment compared to 0.25 g in the others, the "normalized" molybdenum concentration for this experiment is 3.75 mM, in which case the curve lies perfectly in place. At a given pH$_c$ in the range 2–4 the adsorption is proportional to the initial molybdenum concentration up to a value of ~ 10.0 mM (Figs 1 and 2). At pH$_c$ 2.5 about 96% of the molybdenum in the aqueous phase is adsorbed for molybdenum concentrations < 10.0 mM, but this percentage begins to decrease above 10.0 mM, until at a concentration of 50.0 mM only ~ 30% is adsorbed which then amounts to a loading of ~ 320 mg Mo per g activated carbon.

Although the relatively weaker adsorption at concentrations greater than 10 mM could be indicative of a shortage of adsorption sites, it may also reflect poor adsorption of polynuclear species. The percentage concentration of polynuclear species in the aqueous phase increases with an increase in molybdenum concentration which would impair adsorption, if for example a monomeric species is predominantly adsorbed. In fact, calculations show that for the straight line part of curve A in Fig. 2 (initial Mo concentration < 10 mM and pH$_c$ ~ 2.5) $Mo(OH)_6$ and $[HMo_2O_7]^-$ are the major species in the aqueous phase after adsorption equilibrium has been established. It is therefore clear that an unambiguous interpretation of the adsorption behaviour of molybdenum will only be possible if it is based on a quantitative treatment of the data in which all the relevant equilibria in the aqueous phase are taken into account.

Equilibria

The equilibria for the various protonation and condensation reactions can be represented by the general equation

$$pMoO_4^{2-} + qH^+ \rightleftharpoons (MoO_4^{2-})_pH_q^+. \qquad (2)$$

For brevity a species with overall formation constant β_{pq} will occasionally be denoted by the stoichiometric coefficients defining its composition, for example (1,1), and (7,8), for $[HMoO_4]^-$ and $[Mo_7O_{24}]^{6-}$, respectively. Also, for the six-coordinated monomeric molybdic acid the shorter formula $Mo(OH)_6$ is used instead of the structurally more acceptable $[MoO_2(OH)_2(H_2O)_2]$ or $MoO_3(H_2O)_3$, while the (2,3) species is represented by the simplest formula i.e. $[HMo_2O_7]^-$. The total molybdenum concentration, *B*, in solution is given by

$$B = b + \sum p\beta_{pq}b^p h^q \qquad (3)$$

where *b* and *h* are the equilibrium concentrations of MoO_4^{2-} and H^+ respectively. The following species have to be taken into account for the quantitative treatment of the data in the pH$_c$ and concentration ranges investigated: (1,0), (1,1), (1,2), (1,3), (2,3), (2,5), (7,8), (7,10) and (8,12); the large polyanion (36,64) could be neglected at the relatively low equilibrium molybdenum concentrations of the experiments.[11,12] Formation constants for these species in 1 M NaCl medium are known from previous work.[11-14]

For the adsorption by activated carbon (C*) of a given molybdenum species, say X, the adsorption equilibrium can be represented by the equation

$$X(aq) + C^* \rightleftharpoons X(ads). \qquad (4)$$

If the concentration of X(ads) is expressed in terms

of mg molybdenum adsorbed per g of activated carbon and the equilibrium concentration of carbon is set equal to $M-[X(ads)]$, the adsorption equilibrium constant is given by

$$K = [X(ads)]/[X(aq)](M-[X(ads)]\ dm^3/mol \quad (5)$$

where M is the initial carbon concentration also expressed in mg Mo(VI) adsorbed per g activated carbon; M therefore represents the maximum amount of species X(aq) that can be adsorbed by 1 g of activated carbon. If eq. (5) is recast in the form

$$[X(ads)]/M = K[X(aq)]/(1+K[X(aq)]) = \theta \quad (6)$$

the classical Langmuir adsorption isotherm[15] is obtained where θ represents the fraction of the total available adsorption sites occupied. In the present treatment it is assumed that the carbon concentration is directly proportional to the available adsorption sites.

Species adsorbed

The adsorption curves in Fig. 1 show that (except for the highest concentration) the amount of molybdenum adsorbed is practically constant in the pH_c range 1.5–4.5. It is therefore a good approximation to assume a constant concentration for the activated carbon in this pH_c range. The mathematical expression for the adsorption equilibrium then takes the form

$$[X(ads)] = K'[X(aq)] \quad (7)$$

where K' is a conditional constant having a different value (depending on the loading) for each of the adsorption curves. For the experiments at the lowest molybdenum concentrations where the activated carbon is present in a relatively large excess, the approximation of constant concentration is valid for the whole pH_c range.

The distribution of molybdenum(VI) between the solid and liquid phase is given by

$$D = [X(ads)]/B \quad (8)$$

and substitution from eq. (7) gives the expression

$$D = K'[X(aq)]/B. \quad (9)$$

The variation in distribution with pH_c for the different experiments (Fig. 3) should therefore give an indication as to the identity of the species that is predominantly adsorbed. The species distribution curves in Figs 4–8 represent the variation of $[X(aq)]/B$ with pH_c for the various mononuclear and polynuclear molybdenum species in the aqueous phase after equilibration. It is seen that for each of the experiments a very good correspondence exists between the D/pH_c curve and the distribution curve for the dimeric anion $[HMo_2O_7]^-$. For the

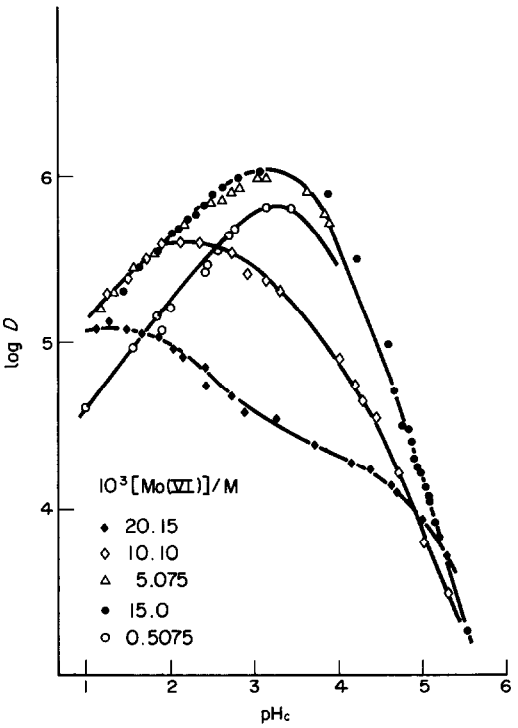

Fig. 3. Distribution of molybdenum(VI) between activated carbon and 1.0 M Na(H)Cl medium as a function of pH_c are various molybdenum concentrations.

experiments at the lowest molybdenum concentrations the pH_c at which the maxima of the D curves occur namely 3.2, tallies with the pH_c for which $[HMo_2O_7]^-$ attains its highest percentage. For the two experiments at the highest molybdenum concentrations (i.e. 10.0 and 20.15 mM) the percentages of polyanions increase considerably so that the pH_c where $[HMo_2O_7]^-$ attains its highest share shifts to lower values namely 2.3 and 1.8, respectively. A similar shift in the pH_c for maximum distribution is observed in Fig. 3. Also noteworthy, is the qualitative agreement between the relative concentration of the dimeric anion, in the aqueous phase and the maximum value of D for the different experiments. These observations clearly show that the dimeric anion, $[HMo_2O_7]^-$, is the main adsorbing species. In view of this finding a computer treatment of the data in terms of the adsorption of the dimeric anion and some minor species seemed worthwhile.

Computer treatment of data

If $[HMo_2O_7]^-$ is the only absorbing species, eq. (9) takes the form

$$D = K'_{2,3}[HMo_2O_7]^-/B$$
$$= K'_{2,3}\beta_{2,3}b^2h^3/(b+\sum p\beta_{pq}b^ph^q) \quad (10)$$

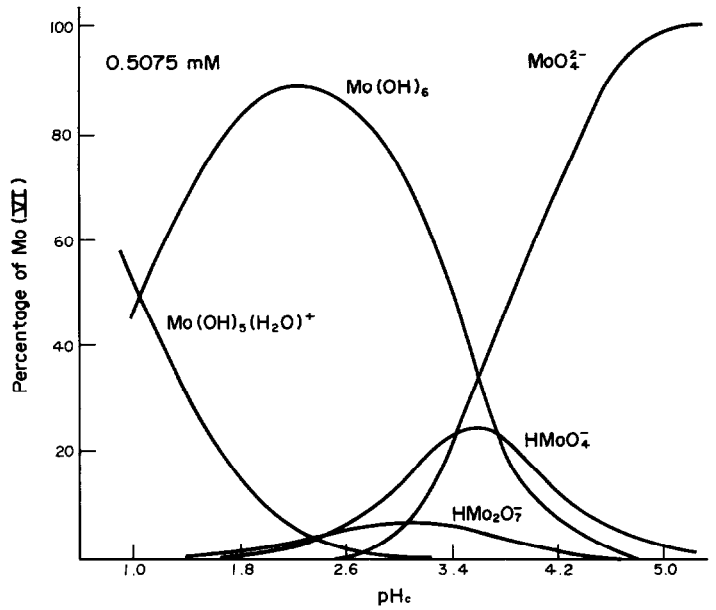

Fig. 4. Concentration of various species, expressed as a percentage of the total molybdenum(VI) concentration in the aqueous phase after equilibration, as a function of pH_c. Initial molybdenum concentration 0.5075 mM.

where $K'_{2,3}$ denotes the conditional adsorption constant for the dimeric anion assuming constant concentration for the activated carbon. The distribution data of the experiment at molybdenum concentration 15.0 mM are the most suitable for quantitative treatment; a relatively large number of data points are available over the very wide pH range 1.6–5.5 and $[HMo_2O_7]^-$ occurs in relatively high concentration (max ~ 20%) in the aqueous phase after equilibration (Fig. 6). The experimental points on the distribution curve (log values) were fitted to eq. (10) using the non-linear least squares program BMDPAR.[16] The free MoO_4^{2-} concentration, b, at each point was calculated from the

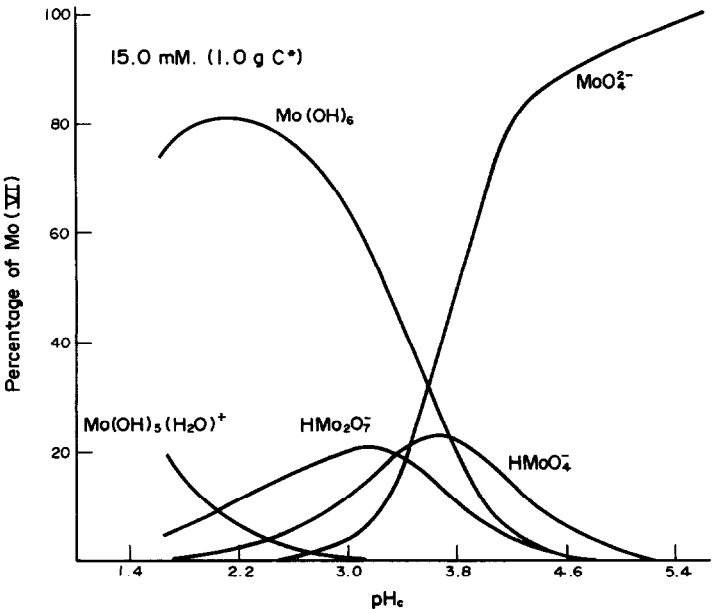

Fig. 5. Concentration of various species, expressed as a percentage of the total molybdenum(VI) concentration in the aqueous phase after equilibration, as a function of pH_c. Initial molybdenum concentration 15.0 mM. (1.0 g C*).

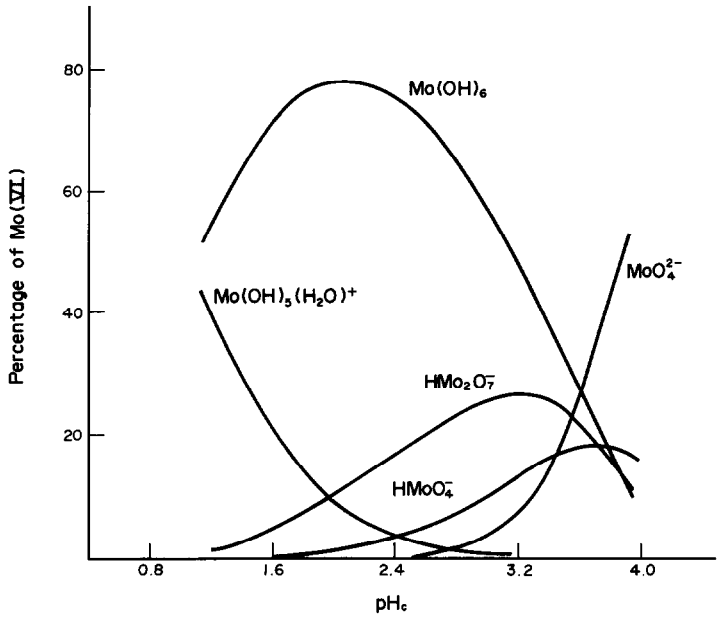

Fig. 6. Concentration of various species, expressed as a percentage of the total molybdenum(VI) concentration in the aqueous phase after equilibration, as a function of pH_c. Initial molybdenum concentration 5.075 mM.

total molybdenum concentration in a subroutine by iteration according to Newton's method. Previously determined β_{pq} values,[11-14] pertaining to an ionic medium of 1 M NaCl, were introduced and eq. (10) therefore contained only $K'_{2,3}$ as the unknown parameter for which the value $\log K'_{2,3} = 6.99 \pm 0.06$ was obtained. A very good fit of the theoretical curve for the experimental points was obtained over the whole pH range (Fig. 3). A similar calculation based on the assumption that $[HMoO_4]^-$ is the adsorbing species resulted in a very poor fit; the sum of squares increased by a factor of ~ 50.

The species distribution curves in Fig. 5 show that among the protonated species, $Mo(OH)_6$

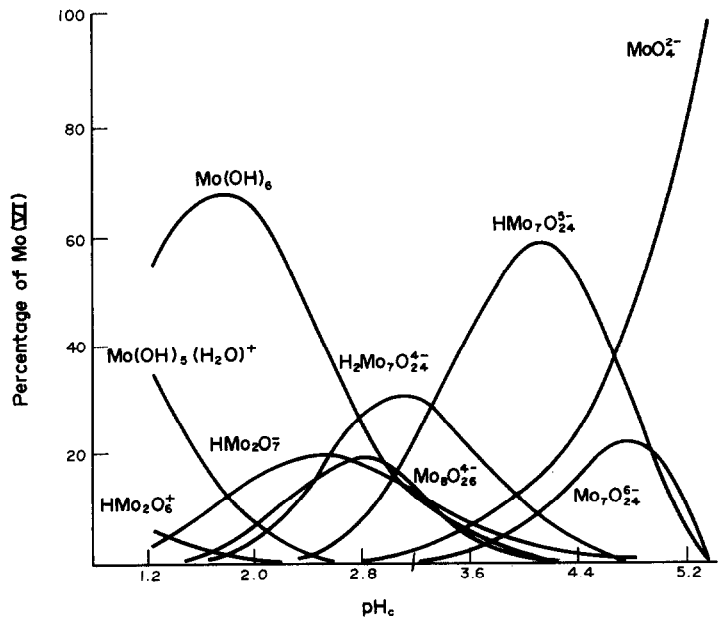

Fig. 7. Concentration of various species, expressed as a percentage of the total molybdenum(VI) concentration in the aqueous phase after equilibration, as a function of pH_c. Initial molybdenum concentration 10.0 mM.

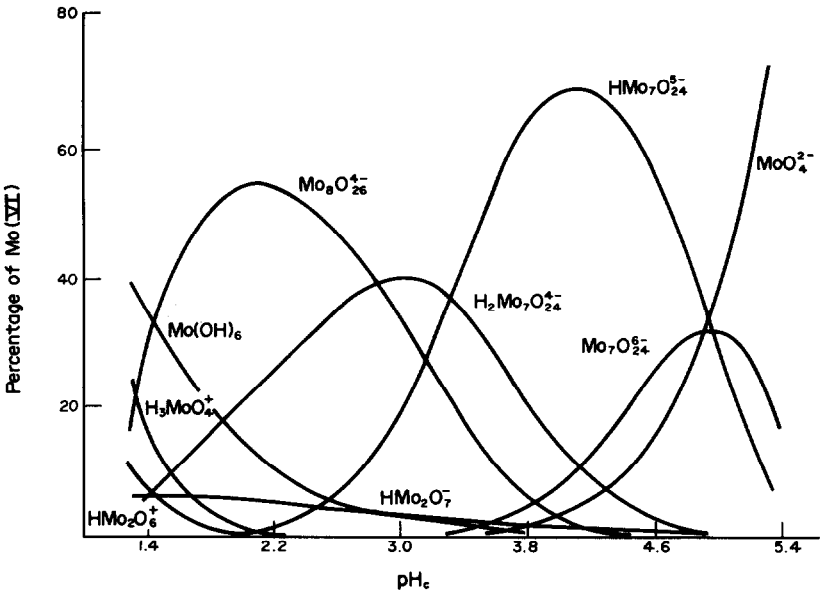

Fig. 8. Concentration of various species, expressed as a percentage of the total molybdenum(VI) concentration in the aqueous phase after equilibration, as a function of pH_c. Initial molybdenum concentration 20.15 mM.

attains the highest concentration, reaching a maximum share of 80% of the total molybdenum concentration in the aqueous phase at pH ~ 2.2. It therefore seemed feasible to attempt the calculation of its formation constant from the adsorption data. It was also felt that such a calculation could serve as a further check on the acceptability of the adsorption model. So, treating both $K'_{2,3}$ and $\beta_{1,2}$ as unknowns the computations were repeated. The following values were obtained: $\log K'_{2,3} = 6.99 \pm 0.08$ and $\log \beta_{1,2} = 7.12 \pm 0.10$, the latter value being in good agreement with those previously determined spectrophotometrically[17] ($\log \beta_{1,2} = 7.21$) and potentiometrically[11,18] ($\log \beta_{1,2} = 7.16$ and 7.20). To the best of our knowledge this is the first time that an equilibrium constant has been calculated from adsorption data. In a subsequent run, $\log \beta_{2,3} = 14.6 \pm 0.9$ was obtained (together with $K'_{2,3}$), again in satisfactory agreement with a value ($\log \beta_{2,3} = 14.84$) previously reported.[11]

In view of these results computer treatment of the data of some of the other experiments seemed justified. For the experiments at total Mo(VI) concentrations of 5.075 and 10.0 mM, the percentage of the adsorbing dimer is high enough (25 and 19% respectively) to warrant such calculations. Although a limited number of data points were collected for the curve pertaining to 5.075 mM especialy in the pH range > 3.0, a satisfactory fit was obtained with the above model. The value of the adsorption constant $\log K'_{2,3} = 7.15 \pm 0.04$ agreed reasonably well with that obtained in the previous calculations. It was found, however, that the fit could be improved significantly if the calculations were done on the assumption that the monomeric species $[HMoO_4]^-$ and $Mo(OH)_6$ also adsorb. The adsorption constants calculated for these species ($\log K'_{1,1} = 5.03$ and $\log K'_{1,2} = 5.17$) were an order of magnitude smaller than that of the dimeric anion. Although there is good reason to believe that these species will also adsorb (cf. discussion below) the relatively small adsorption constants show that their share of the total amount of molybdenum adsorbed is relatively small.

Treatment of the 10.0 mM data assuming $[HMo_2O_7]^-$ to be the only adsorbing species again, resulted in a good fit, except at the maximum of the curve where the experimental points were slightly displaced towards lower pH_c values relative to the calculated curve. The species distribution curves (Fig. 7) show considerable overlapping of equilibria and that several polyions occur in comparable concentrations at pH_c values corresponding to the maximum of the D/pH_c curve. Uncertainties in the values of the formation constants of these species (the dimer included) will inevitably have a greater effect on the "goodness" of fit of the data of this experiment, compared to that of the two discussed above. Attempts to treat all these formation constants simultaneously as unknowns failed because of convergence problems. With only $\beta_{7,9}$ and $\beta_{7,10}$ as unknowns in addition to $K'_{2,3}$, convergence and a very good fit of the theoretical curve on the experimental points were obtained. The values

Table 1. Results of computer treatment of distribution data; error limits are 3σ

10^3[Mo(VI)]/M	$\log K'_{2,3}$	$\log K'_{1,1}$	$\log K'_{1,2}$	$\log \beta'_{1,2}$	$\log \beta'_{2,3}$	$\sigma(\log D)$
5.075	7.15±0.40	—	—	[a]	[a]	0.34
	6.82±0.09	5.03±0.13	5.17±0.26	[a]	[a]	0.05
15.0	6.99±0.06	—	—	[a]	[a]	0.079
	6.99±0.08	—	—	7.12±0.10	[a]	0.076
	7.22±0.6	—	—	[a]	14.6±0.9	0.079
10.0	6.58±0.07	—	—	[a]	[a]	0.134
	6.50±0.08	5.04±0.40	5.30±0.29	[a]	[a]	0.084
	6.50±0.09	5.04±0.40	5.30±0.38	7.12±0.60	[a]	0.087

[a] Values of constants were fixed at previously determined values (see text).

$\log \beta_{7,9} = 58.6 \pm 0.7$ and $\log \beta_{7,10} = 62.4 \pm 0.7$, however, differed from the potentiometric values ($\log \beta_{7,9} = 57.5$ and $\log \beta_{7,10} = 60.8$) by too great a margin to take uncertainties in the constants as the sole explanation for the relatively small deviation between experimental points and the theoretical curve in the vicinity of the maximum. Again, if for this experiment, adsorption of the monomeric species $[HMoO_4]^-$ and $Mo(OH)_6$ are taken into account, the fit is practically just as good as that with the adjusted $\beta_{7,9}$ and $\beta_{7,10}$ values and the adsorption constants agree satisfactorily with those calculated from the data of the experiment at a molybdenum concentration of 5.075 mM (Table 1).

Finally, the data of the experiment at constant pH_c (Fig. 2) were used to estimate a value for M, the maximum loading capacity of activated carbon for molybdenum(VI). Assuming $[HMo_2O_7]^-$ to be the only absorbing species, eq. (10) was used in its extended form

$$D = K_{2,3}M[X(aq)]/(1 + K_{2,3}[X(aq)])\,(b + \sum p\beta_{pq}b^p h^q)$$

to calculate $K_{2,3}$ and M from the distribution data: $\log K_{2,3} = 3.85 \pm 0.06$ and $M = 1108 \pm 54$ mg Mo per g C*. A quite acceptable fit of the theoretical curve on the experimental points was obtained with a deviation only at a molybdenum concentration less than 3.2 mM. The large value for M indicates that even at the highest loadings obtained in this investigation namely ~ 330 mg, only about 30% of the available active sites had been occupied.

Adsorption model

These results show that the adsorption data can be satisfactorily described in terms of a model comprising the three adsorbing species $[HMo_2O_7]^-$, $[HMoO_4]^-$ and $Mo(OH)_6$ of which the dimeric anion is by far the predominant one. The very strong adsorption of molybdenum(VI) can be ascribed to chemical bonding with basic oxygen atoms available at the surface of the activated carbon. A variety of oxygen containing groups, e.g. carboxylic acid, phenolic hydroxyl, quinone-type carbonyl groups, lactones etc. are believed to exist in the structure of activated carbon.[19] Coordination of molybdenum(VI) by some of these groups is well known, for example in complex formation with oxalate,[7,20-22] malate,[23] citrate[24] and several catechol derivatives.[25] Adsorption of the dimeric and monomeric molybdenum(VI) species onto the activated carbon can therefore be interpreted in terms of surface "complex" formation. Possible structures for such complexes analogous to that of the X-ray characterized oxalate complexes[20,22] $[MoO_3C_2O_4H_2O]^{2-}$ and $[Mo_2O_5(C_2O_4)_2(H_2O)_2]^{2-}$ are shown in Fig. 9. The structures as represented in the diagram each carries an extra negative charge relative to the absorbed species. This implies bonding of a negatively charged oxygen atom to molybdenum, with simultaneous protonation of a basic group (not depicted) which belongs to the activated carbon.

The important feature of the structures shown in Fig. 9 is the octahedral coordination of molybdenum. The gain in bond energy, when the coordination sphere of molybdenum(VI) is expanded from four to six, is the major driving force for complexation of molybdate with oxalate[7] and citrate,[26] and this should also apply to the adsorption reactions. Working in the opposite direction, however, is the hydration energy of the absorbing species; activated carbon has, in general, only a small affinity for ions because of their strong hydration.[19]

Therefore, although adsorption of $[HMoO_4]^-$ should be favourable because of an increase in coor-

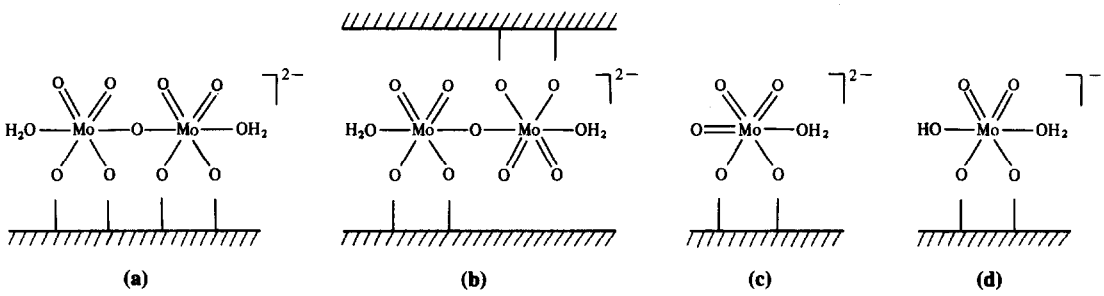

Fig. 9. Proposed structures for adsorbed species: (a) dimer, (b) dimer in a micropore, (c) $[HMoO_4]^-$, (d) $Mo(OH)_6$.

dination number of molybdenum from four to six, it must take place at the expense of hydration energy. Adsorption of the uncharged acid $Mo(OH)_6$, on the other hand, will not be hampered so much by hydration energy, but the gain in bond energy by expansion of the molybdenum coordination sphere is absent. These two mononuclear species are therefore weakly adsorbed compared to the dimeric anion. The dimer can be expected to have a smaller hydration energy than $[HMoO_4]^-$ and will also benefit from an increase in the coordination number of one molybdenum atom. The structure of $[HMo_2O_7]^-$ is not known, but is assumed to consist of a MoO_4 tetrahedron linked to an octahedron by sharing a common vertex.[27] Further, the polyanions $[Mo_7O_{26}]^{6-}$, $[Mo_8O_{26}]^{4-}$, etc. will not chemisorb because all the molybdenum atoms in these ions are already octahedrally coordinated.

Adsorption of the dimeric species is expected to be limited to some extent (compared to monomers) by the availability of surface groups having just the right dimensions to allow coordination of two adjacent molybdenum atoms. This implies a lower concentration of the activated carbon for the dimer than for the monomers. The dynamic process of equilibrium establishment by adsorption and desorption could therefore take longer for the dimer than for the monomers. This can result in an increase in the concentration of dimers relative to monomers adsorbed with time, while the total amount of molybdenum adsorbed remains nearly constant. This possibility has not been verified experimentally, but it could be the explanation for the finding that the best fit of the data for the experiment at a molybdenum concentration of 15.0 mM was obtained with $[HMo_2O_7]^-$ as the only absorbing species. By coincidence 10 days were allowed for equilibration for this experiment instead of the usual 7–8 days for the other experiments.

CONCLUSION

The results of this investigation show that molybdenum(VI) is strongly adsorbed by activated carbon in the pH_c range 1.0–5.0. Quantitative treatment of the distribution data have shown that the adsorption behaviour of molybdenum(VI) can be adequately described in terms of the adsorption of the dimeric anion $[HMo_2O_7]^-$ in addition to small amounts of the monomeric species $[HMoO_4]^-$ and $Mo(OH)_6$. This quantitative interpretation is consistent with current knowledge about molybdenum(VI) equilibria in aqueous solution and differs from previous qualitative explanations where adsorption of only polynuclear species have been considered.

Acknowledgements—We thank MINTEK and the University of Stellenbosch for financial support.

REFERENCES

1. G. B. Alexander, *J. Am. Chem. Soc.* 1949, **71**, 3043.
2. E. A. Sigworth, *Proc. Ontario Industrial Waste Conf.* 1963, **10**, 177.
3. R. B. Bhappu, D. H. Reynolds, R. J. Roman and D. Schwab, *Bur Mines Mineral Resources* 1965, (Circ) **81**.
4. A. Sai, A. Onuki, K. Ohashi, K. Motojima and K. Yamamato, *Bunseki Kagako* 1981, **30**, 804.
5. G. J. McDougall, D. L. Wellington and R. D. Hancock, PIN Report No. 499, MINTEK, Randburg, 1980.
6. S. El-Bayoumy and M. El-Kolaly, *J. Radioanal. Chem.* 1982, **68**, 7.
7. J. J. Cruywagen, J. B. B. Heyns and R. F. van de Water, *J. Chem. Soc., Dalton Trans.* 1986, 1857.
8. K. A. Kraus and F. Nelson, *12th Biennial Conf. Carbon*, Pittsburg, Pennsylvania, 1975.
9. H. S. Rossotti, *Talanta* 1974, **21**, 809.
10. F. Will and J. H. Yoe, *Anal. Chim. Acta* 1953, **8**, 596.
11. J. J. Cruywagen, *Inorg. Chem.* 1980, **19**, 552.
12. K. H. Tytko, G. Baethe and J. J. Cruywagen, *Inorg. Chem.* 1985, **24**, 3132.
13. J. J. Cruywagen, J. B. B. Heyns and E. F. C. H. Rohwer, *J. Inorg. Nucl. Chem.* 1976, **38**, 2033.
14. J. J. Cruywagen, J. B. B. Heyns and E. F. C. H. Rohwer, *J. Inorg. Nucl. Chem.* 1978, **40**, 53.

15. D. Freifelder, *Physical Chemistry for Students of Biology and Chemistry*. Science Books International, Boston, Massachusetts (1982).
16. W. J. Dixon (Ed.), *BMDP Statistical Software*. University of California Press, Berkeley, California (1981).
17. J. J. Cruywagen and E. F. C. H. Rohwer, *Inorg. Chem.* 1975, **14**, 3137.
18. J. Aveston, E. W. Anacker and J. S. Johnson, *Inorg. Chem.* 1964, **3**, 735.
19. G. J. McDougall and R. D. Hancock, *Minerals Sci. Engng* 1980, **12**, 85.
20. F. A. Cotton, S. M. Morehouse and J. S. Wood, *Inorg. Chem.* 1963, **3**, 1603.
21. E. S. Johansen and O. Jøns, *Talanta* 1984, **31**, 743.
22. L. R. Nassimbeni, M. L. Niven, J. J. Cruywagen and J. B. B. Heyns, *J. Cryst. Spec. Res.* 1987, **17**, 99.
23. C. B. Knobler, A. J. Wilson, R. N. Hider, I. W. Jenson, B. R. Penfold, W. T. Robinson and C. J. Wilkins, *J. Chem. Soc., Dalton Trans.* 1983, 1299.
24. L. R. Nassimbeni, M. L. Niven, J. J. Cruywagen and J. B. B. Heyns, *J. Cryst. Spec. Res.* 1987, **17**, 373.
25. K. Gilbert and K. Kustin, *J. Am. Chem. Soc.* 1976, **98**, 5502.
26. J. J. Cruywagen and R. F. van de Water, *Polyhedron* 1986, **5**, 521.
27. J. J. Cruywagen and J. B. B. Heyns, *Inorg. Chem.* 1987, **26**, 2569.

Polyhedron Vol. 7, No. 7, pp. 557–560, 1988
Printed in Great Britain

0277–5387/88 $3.00+.00
© 1988 Pergamon Press plc

SYNTHESIS AND STUDY OF SOME NOVEL METAL COMPLEXES OF PHOSPHORAMIDOTHIOIC AND PHOSPHORODIAMIDOTHIOIC LIGANDS

A. S. SYNGOLLITOU-KOURAKOU* and I. A. TOSSIDIS

Department of General & Inorganic Chemistry, Aristotelian University of Thessaloniki, Thessaloniki, Greece

(*Received* 27 *January* 1987: *accepted* 30 *October* 1987)

Abstract—A new series of metal complexes of V(III), Cr(III), Pb(II), Sn(II) and Ag(I) with the phosphoramidothioic (PAT) and phosphorodiamidothioic (PDAT) ligands has been synthesized and characterized on the basis of elemental analyses, magnetic susceptibility measurements and spectral (electronic and infrared) data. Apart from the Ag(I) complexes, all the other ones are found to have a six-coordinate pseudooctahedral structure.

The biologically important[1–3] phosphoramidothioic (PAT) and phosphorodiamidothioic (PDAT) ions have been known for many years,[4–6] as well as the crystal structures of their ammonium salts. In regard to the nucleophilic reactivity of phosphoramidothioates very little has been reported up to now. Only phosphorodiamidate[7–9] and dithiophosphate[10–13] complexes have been reported. It was therefore, of interest to synthesize complexes of some transition or non-transition metals with the (PAT) and (PDAT) ligands. In an attempt to understand the bonding capacity of the studied ligands CNDO/2 calculations were employed.[14] In order to complete our work on these ligands we also prepared complexes with metals of the IIB group and we investigated their thermal behaviour by applying TG and DTA techniques.[15]

In continuation of our previous work on the phosphoramidothioates we describe in the present paper the preparation of ten new complexes which have been isolated in the solid state and their structures have been assigned on the basis of their elemental analyses, spectral and magnetic properties.

EXPERIMENTAL

(a) *Physical measurements*

Infrared spectra were recorded in the region 4000–250 cm^{-1} on a Perkin–Elmer 467 spectrophotometer using KBr disks. Electronic absorption spectra were obtained on a Perkin–Elmer Hitachi 200 spectrophotometer in the solid state with Nujol mulls. The hydrogen and nitrogen analyses were performed on a Perkin–Elmer 240 Elemental Analyser. The metal determinations were carried out by published methods.[16] Magnetic susceptibility measurements in the solid state were carried out by the Faraday technique using $Hg[Co(SCN)_4]$ as the calibrant. Diamagnetic corrections were made using Pascal's constants.[17] The thermogravimetric curves were obtained on a Mettler TA 2000 system in a dynamic atmosphere of nitrogen; sample sizes of 20–40 mg were used at a heating rate of 6° min^{-1}. The chart speed was maintained at 5 mm min^{-1}.

(b) *Preparation of the complexes*

The ligands were prepared by published methods.[4] The complexes were prepared and isolated as described elsewhere.[14]

RESULTS AND DISCUSSION

The elemental analysis (Table 1) reveals complexes of the types $ML^1X(H_2O)$, $M_2L^1_3X(H_2O)$ and $ML^2_2X(H_2O)$, $ML^2_3X(H_2O)$ where L^1 = (PAT) and L^2 = (PDAT) ions. The complexes are coloured or white, hydrated, insoluble in water and common organic solvents, the latter suggesting polymeric structures. The V(III) and Cr(III) com-

*Author to whom correspondence should be addressed.

Table 1. Analytical data and relevant IR frequencies (cm^{-1}) for the new (PAT) and (PDAT) complexes of V(III), Cr(III), Pb(II), Sn(II) and Ag(I)

Compound		%H	%N	%S	%M	ν(OH)	ν(P—O)	ν(P—S)	ν(M—O)	ν(M—S)
I	$V_2[PO_2SNH_2]_3 6H_2O$	3.1	7.7	17.6	18.0	3380 br[a]	1040 vs	640 m	510 m	320 w
		(3.3)[b]	(7.7)	(17.7)	(18.7)					
II	$V[POS(NH_2)_2]_3$	3.1	21.7	24.8	12.9	—	1020 vs	600 m	540 m	330 w
		(3.1)	(21.8)	(25.3)	(13.2)					
III	$Cr_2[PO_2SNH_2]_3 6H_2O$	3.3	7.7	17.6	18.9	3360 br	1010 vs	615 m	500 m	280 m
		(3.3)	(7.7)	(17.6)	(19.7)					
IV	$Cr[POS(NH_2)_2]_3 6H_2O$	4.6	17.6	18.7	9.6	3400 br	1010 vs	630 m	525 m	300 m
		(4.9)	(17.0)	(19.4)	(10.5)					
V	$Pb_2[PO_2SNH_2]_2 2H_2O$	0.6	4.4	9.8	64.6	3470 br	1055 s	585 s	520 m	300 m
		(0.6)	(4.3)	(10.0)	(65.1)					
VI	$Pb[POS(NH_2)_2]_2 4H_2O$	3.0	11.0	11.9	40.8	3420 br	1000 s	580 s	460 m	300 w
		(3.2)	(11.16)	(12.7)	(41.4)					
VIII	$Sn[PO_2SNH_2]2H_2O$	2.2	5.0	11.9	44.0	3480 br	1000 s	580 s	480 m	330 s
		(2.2)	(5.2)	(12.0)	(44.6)					
VIII	$Sn[POS(NH_2)_2]_2 2H_2O$	2.9	14.2	16.8	30.8	3480 br	1000 s	575 s	470 m	330 s
		(3.2)	(14.8)	(17.0)	(31.4)					
IX	$Ag_2[PO_2SNH_2]$	0.6	4.0	9.2	65.7	—	1050 s	580 s	480 m	315 s
		(0.6)	(4.2)	(9.8)	(66.0)					
X	$Ag[POS(NH_2)_2]$	1.7	12.6	13.9	48.6	—	1050 s	570 s	480 w	310 s
		(1.8)	(12.7)	(14.6)	(49.2)					

[a] vs = very strong, s = strong, m = medium, w = weak, br = broad.

[b] Figures in parentheses are the calculated values.

plexes are soluble in concentrated aqueous solutions of (PAT) and (PDAT) ammonium salts indicating formation of anionic complexes, which unfortunately we have not been able to study with the known methods.[18-19] All these complexes were characterized by elemental analysis (Table 1), spectroscopic methods (IR, UV–vis) and magnetic measurements. The thermoanalytical analysis data for complexes **III** and **V** are also discussed. The assignments of the main IR bands of the new compounds (Table 1) were based on the data reported previously.[4] The IR spectra of the studied compounds show broad bands in the 3500–3200 cm^{-1} region which, with those at 840 and near 330 cm^{-1} may be assigned to ν(OH) of the water.[20-22] The bands in the 1050–1000 and in the 640–570 cm^{-1} regions are attributed to ν(P—O) and ν(P—S) stretching vibrations, respectively.[4,20] The latter vibrations are shifted by 40–50 cm^{-1} from those of the free ligands to lower wave numbers.[4] Their positions are an indication that the oxygen and sulphur atoms of the ligands act as the donor atoms, and the coordination occurs via these atoms which are more potential coordinate sites than the nitrogen atoms.[23-24] Support for this argument is provided by the appearance of new bands at 520–480 and 330–300 cm^{-1} assignable to ν(M—O) and ν(M—S) vibrations,[25] respectively. The quantum chemical CNDO/2 calculations also show[14] that strong coordination may take place via the sulphur and oxygen atoms although coordination through the nitrogen atoms cannot be excluded in the case of dimeric or polymeric structures.

The electronic spectral data and the solid state magnetic moments of the investigated compounds are given in Table 2. All the electronic spectra of the studied compounds show an intense band in the UV region, attributable to an intraligand $\pi^* \leftarrow \pi$ transition located on the ligand. The electronic spectra of compounds **I** and **II** show bands at 15.8–16.0 and 22.2–22.7 kK due to spin allowed transitions $^3T_{2g}(F) \leftarrow {}^3T_{1g}(F)$ and $^3T_{1g}(P) \leftarrow {}^3T_{1g}(F)$, respectively. Compounds **III** and **IV** show bands at 16.2–17.0, 22.6–23.2 and 37.5–40.0 kK regions which can be assigned to $^4T_{2g}(F) \leftarrow {}^4A_{2g}(F)$, $^4T_{1g}(F) \leftarrow {}^4A_{2g}(F)$ and $^4T_{1g}(P) \leftarrow {}^4A_{2g}(F)$ transitions in increasing order of energy. The two transitions ν_1 and ν_2 for the complexes **I–IV** have been used to evaluate[26] the ligand field (10 Dq) and nephelauxetic (B) parameters in the same way as employed for other complexes having *Oh* symmetry. The values of these parameters along with that of β (covalency parameter) (Table 2) are comparable to those reported for other V(III) and Cr(III) complexes of *Oh* symmetry involving similar donors.[11,27] The B values are about 63–80% of

Table 2. Solid state magnetic moments and electronic spectra of the new complexes of the (PAT) and (PDAT) ligands

Compound		μ_{eff} (BM)[a]	Electronic spectra (kK)		Other bands	10 Dq (cm^{-1})	B (cm^{-1})	β
I	$V_2[PO_2SNH_2]_3 6H_2O$	2.8	$^3T_{2g}(F) \leftarrow {}^3T_{1g}(F)$ 16.1	$^3T_{1g}(P) \leftarrow {}^3T_{1g}(F)$ 22.2	44.5	16,100	0.599	0.695
II	$V[POS(NH_2)_2]_3$	2.7	$^3T_{2g}(F) \leftarrow {}^3T_{1g}(F)$ 15.8	$^3T_{1g}(P) \leftarrow {}^3T_{1g}(F)$ 22.7	44.2	15,800	0.713	0.826
III	$Cr_2[PO_2SNH_2]_3 6H_2O$	3.6	$^4T_{2g}(F) \leftarrow {}^4A_{2g}(F)$ 17.0	$^4T_{1g}(F) \leftarrow {}^4A_{2g}(F)$ 23.2	40.0	17,000	0.603	0.656
IV	$Cr[POS(NH_2)_2]_3 6H_2O$	3.8	$^4T_{2g}(F) \leftarrow {}^4A_{2g}(F)$ 16.2	$^4T_{1g}(F) \leftarrow {}^4A_{2g}(F)$ 22.6	37.5	16,200	0.637	0.693
V	$Pb_2[PO_2SNH_2]_2 2H_2O$	—			42.0, 43.6 sh			
VI	$Pb[POS(NH_2)_2]_2 4H_2O$	—			40.2, 41.0 sh			
VII	$Sn[PO_2SNH_2]2H_2O$	—			44.8			
VIII	$Sn[POS(NH_2)_2]_2 2H_2O$	—			43.2			
IX	$Ag_2[PO_2SNH_2]_2$	—			43.0, 40.0 sh			
X	$Ag[POS(NH_2)_2]$	—			42.1, 39.0 sh			

[a] = measured at room temperature.

the free ion values [861 for V(III) and 918 for Cr(III)], and suggest that medium covalent bonding occurs between the ligands and the metal ions. The room temperature magnetic moments of compounds **I, II, III** and **IV** lie at 2.7–2.8 and 3.6–3.8 BM, respectively, and they consist of an octahedral arrangement of the donor atoms around the metal ions. The electronic spectra of compounds **V–X** show bands only in the UV region and are all diamagnetic as expected.

The thermogravimetric study of both complexes **III** and **V** shows that these complexes show three decomposition stages, with loss of their water molecules in the first stage. The TG thermogram of complex **III** displays three steps at 190, 795 and 960°C, all of them endothermic which correspond to the loss of $[5H_2O]$ (Found: 16.0%; calc: 16.4%), $[H_2O+SO(NH_2)_3]$ (Found: 21.5%; calc: 20.8%), [PO] (Found: 8.5%; calc: 8.6%), respectively.

The thermogram of complex **V** has two endothermic peaks at 185 and 800°C. The weight losses occurring at all the three stages can be attributed to the loss of $[2H_2O]$ (Found: 5.6%; calc: 5.3%), $[2NH_2]$ (Found: 4.9%; calc: 4.7%), $[PO_2S]$ (Found: 15.0%; calc: 14.1%) which finally give a residue consisting of Pb_2PO_2S.

Thus on the basis of the available experimental data and the above discussion, it appears that the studied compounds are polymeric in nature, which is also supported by their insolubility in organic solvents, and each unit of polymeric structure possesses a pseudo-octahedral stereochemistry for the compounds **I–IV**. For complexes **V–VIII** we suggest that each unit forms infinite chains in the solid state in which the Pb(II) or the Sn(II) atoms are six-coordinate, as we can assume from the evaluation of the crystal structure of their analogues of dithiophosphate ligands.[28-29] Finally, for compounds **IX** and **X** the more plausible structure is that in which one silver atom is coordinated to oxygen and the other to sulphur.

Acknowledgement—We wish to thank Asst. Prof. A. Christofides for his help during this work.

REFERENCES

1. C. Steffer and M. Fluegel, *Strahlentherapie* 1973, **146**, 450; *Chem. Abs.* 1974, **80**, 104070r.
2. I. Hammann, *Pfbanzenschutz–Nachr.* 1970, **23**, 133.
3. S. Akerfeldt, C. Ronnbach, M. Hellstrom and A. Nelson, *Radiat. Res.* 1968, **35**, 61; *Chem. Abs.* 1968, **69**, 33389m.
4. H. Falius, *Chem. Ber.* 1965, **98**, 3270.
5. V. D. Mootz, W. Look and G. Sassmannshausen, *Z. Anorg. Allgem. Chem.* 1968, **358**, 282.
6. V. D. Mootz and J. Goldmann, *Acta Cryst.* 1969, **B25**, 1256.
7. R. Klement and O. Koch, *Chem. Ber.* 1954, **87**, 333.
8. Y. N. Sadana, *Can. J. Chem.* 1969, **47**, 2613.
9. R. Klement and G. Biberacher, *Z. Anorg. Allgem. Chem.* 1956, **285**, 75.
10. J. J. Dickert and C. N. Rowe, *J. Org. Chem.* 1967, **32**, 647.
11. A. Müller, V. Krishna Rao and E. Diemann, *Chem. Ber.* 1971, **104**, 461.
12. J. Fackler Jr. and L. Thompson, *Inorg. Chim. Acta* 1981, **48**, 45.
13. A. Tomlinson and L. Mattogno, *Inorg. Chim. Acta* 1978, **26**, L11.
14. A. S. Syngollitou-Kourakou, I. A. Tossidis and M. P. Sigalas, *Inorg. Chim. Acta* 1986, **118**, 141.
15. I. A. Tossidis and A. S. Syngollitou-Kourakou, *J. Therm. Anal.* 1987, **32**, 491.
16. A. I. Vogel, *Quantitative Inorganic Analysis*, pp. 362, 378, 450, 522, 538. Longmans Green, London (1961).
17. B. N. Figgis and J. Lewis, *Modern Coordination Chemistry* (Edited by J. Lewis and R. G. Wilkins), p. 403. Interscience, New York (1960).
18. J. H. Yoe and A. L. Jones, *Ind. Eng. Chem. Anal. Edn.* 1944, **16**, 111.
19. P. Job, *Ann. Chim.* 1928, **9**, 113.
20. G. Sartri, C. Furlani and A. Damiani, *J. Inorg. Nucl. Chem.* 1959, **8**, 119.
21. M. Goodgame and A. Hayao, *J. Chem. Soc. A.* 1968, 1108.
22. J. Frei and E. Steger, *Z. Anorg. Allgem. Chem.* 1966, **344**, 194.
23. J. I. G. Cadogan, *J. Chem. Soc. A.* 1957, 1079.
24. W. F. Slinkard and D. W. Meek, *Inorg. Chem.* 1969, **8**, 1811.
25. P. M. Adams, *Metal-ligand and Related Vibrations*, p. 319. Edward Arnold, London (1967).
26. Y. Tanabe and S. Sugano, *J. Phys. Soc. Japan* 1954, **9**, 753.
27. J. R. Wasson and S. J. Wasson, *Inorg. Chem.* 1970, **9**, 1576.
28. C. Glidewell, *Inorg. Chim. Acta* 1977, **24**, 255.
29. S. L. Lawton and G. T. Kokotailo. *Inorg. Chem.* 1972, **11**, 363.

Polyhedron Vol. 7, No. 7, pp. 561–572, 1988
Printed in Great Britain

0277–5387/88 $3.00+.00
© 1988 Pergamon Press plc

TRINUCLEAR HYDRIDOBIS-μ_3-SULPHIDO COMPLEXES OF Rh(I); SYNTHESIS AND STRUCTURES OF $Rh_3(COD)_3(\mu_3\text{-}S)_2(\mu\text{-}H)$, $Rh_3(COD)_2(t\text{-}Bu_2PH)_2(\mu_3\text{-}S)_2(\mu\text{-}H)$, (COD = 1,5-CYCLOOCTADIENE) AND $Rh_3(CO)_4(t\text{-}Bu_2PH)_2(\mu\text{-}S)_2(\mu\text{-}H)$

ATTA M. ARIF, JOHN G. HEFNER, RICHARD A. JONES* and STEFAN U. KOSCHMIEDER

Department of Chemistry, The University of Texas at Austin, Austin, Texas 78712, U.S.A.

(*Received* 12 *August* 1987; *accepted* 3 *November* 1987)

Abstract—Reaction of $[Rh(COD)Cl]_2$ (COD = 1,5-cyclooctadiene) with two equivalents of NaSH in methanol at −78°C gives bright red crystalline $Rh_3(COD)_3(\mu_3\text{-}S)_2(\mu\text{-}H)$ (**1**) (83%), H_2S is also formed. The overall molecular geometry of (**1**) consists of a Rh_3 triangle capped on each face by a μ_3-S atom. Each Rh atom bears a COD ligand in the boat configuration. The centroids of the carbon–carbon double bonds of each COD and the μ_3-S atoms give each Rh a roughly planar coordination geometry. One Rh—Rh bond is notably longer than the other two: (2.814(1), 2.962(1) and 3.210(3) Å). The overall molecular geometry suggests that the μ-H atom bridges the longest Rh—Rh bond, although this could not be confirmed by X-ray data. Reaction of (**1**) with excess t-Bu_2PH in THF gives $Rh_3(COD)_2(t\text{-}Bu_2PH)_2(\mu_3\text{-}S)_2(\mu\text{-}H)$, (**2**), in which the unique COD ligand bonded to the Rh atom opposite the long Rh(μ-H)Rh bond is replaced by two *cis* t-Bu_2PH ligands. (**2**) reacts with CO (1 atm., 25°C) in toluene to give $Rh_3(CO)_4(t\text{-}Bu_2PH)_2(\mu_3\text{-}S)_2(\mu\text{-}H)$, (**3**). Both (**2**) and (**3**) are formed quantitatively. In (**3**), two terminal CO ligands replace each of the COD ligands. Crystal data for (**1**): $C_{24}H_{37}Rh_3S_2$, $M = 698.40$, monoclinic, $C2/c$ (No. 15), $a = 27.808(5)$, $b = 9.060(1)$, $c = 19.248(3)$ Å, $\beta = 97.52(2)°$, $U = 4807.6(5)$ Å^3, $D_c = 1.930$ g cm^{-3}, $Z = 8$, λ(Mo-K_α) = 0.71073 Å (graphite monochromator), μ(Mo-K_α) = 21.83 cm^{-1}. Methods: MULTAN, difference Fourier, full matrix least-squares. Refinement of 2432 reflections ($I > 3\sigma(I)$) out of 4123 unique observed reflections ($3° < 2\theta < 50°$) gave R and R_w values of 0.048 and 0.062, respectively. Data/parameter ratio = 9.28, highest peak in final difference Fourier = 1.051 e Å^{-3}. Crystal data (**2**): $C_{39}H_{69}P_2Rh_3S_2$, $M = 972.78$, triclinic, $P\bar{1}$, (No. 2), $a = 10.738(1)$, $b = 19.503(2)$, $c = 20.353(4)$ Å, $\alpha = 90.36(1)$, $\beta = 105.47(2)$, $\gamma = 92.77(1)°$, $U = 4102.3(5)$ Å^3, $D_c = 1.58$ g cm^{-3}, $Z = 4$, μ(Mo-K_α) = 13.76 cm^{-1}. Refinement of 4205 reflections ($I > 3\sigma(I)$) out of 5674 unique observed ($3° < 2\theta < 48°$) gave R and R_w values of 0.0559 and 0.0632, respectively. Data/parameter ratio = 10.23, highest peak in final difference Fourier = 0.751 e Å^{-3}. Crystal data (**3**): $C_{20}H_{38}P_2O_4Rh_3S_2$, $M = 777.31$, monoclinic, $C2/c$ (No. 15), $a = 21.727(1)$, $b = 19.457(2)$, $c = 17.809(2)$ Å, $\beta = 116.87(2)°$, $U = 6716.4(5)$ Å^3, $D_c = 1.537$ g cm^{-3}, $Z = 8$, μ(Mo-K_α) = 16.69 cm^{-1}. Refinement of 1084 reflections ($I > 3\sigma > (I)$) out of 4649 unique observed ($3° < 2\theta < 46°$) gave R and R_w values of 0.0750 and 0.0870, respectively. Data/parameter ratio = 6.302, highest peak in the difference Fourier = 1.023 e Å^{-3}.

As part of a broad study of *d* block transition metal-SH^- or sulphido (S^{2-}) complexes bearing weakly bound ligands such as PR_3 or alkenes, we recently reported the synthesis of the unusual Cr_3 sulphido cluster $Cr_3(\mu_3\text{-}S)_2(\mu_2\text{-}S)_3(dmpe)_3$, (dmpe = bis-1,2-dimethylphosphino ethane) from the reaction of NaSH with $CrCl_2$ and dmpe.[1] We have extended our studies to the late transition metals, in particular those bearing olefin or di-olefin ligands. The reaction of NaSH in methanol with $[Rh(COD)Cl]_2$ (COD = 1,5-cyclooctadiene) gives red crystalline

* Author to whom correspondence should be addressed.

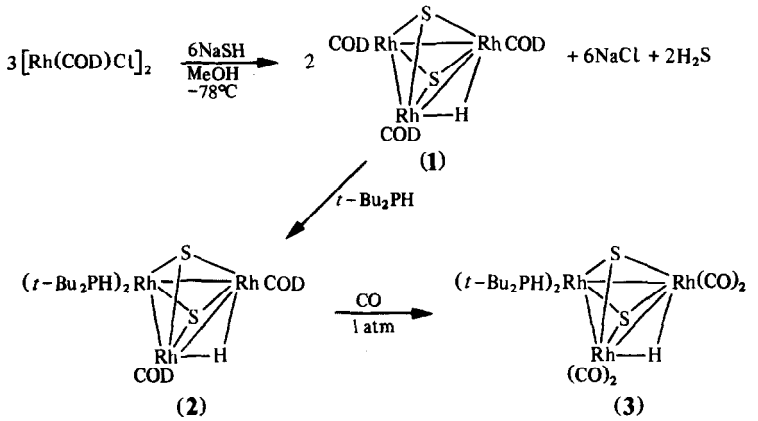

Scheme 1.

$Rh_3(COD)_3(\mu_3\text{-}S)_2(\mu\text{-}H)$ (**1**), cleanly and in high yield (Scheme 1). Both phosphine and CO derivatives of (**1**) may be obtained in high yields: $Rh_3(COD)_2(t\text{-}Bu_2PH)_2(\mu_3\text{-}S)_2(\mu\text{-}H)$ (**2**) and $Rh_3(CO)_4(t\text{-}Bu_2PH)_2(\mu_3\text{-}S)_2(\mu\text{-}H)$ (**3**). We describe here the synthesis, characterization and X-ray crystal structures of (**1**), (**2**), and (**3**).

Although numerous μ_3-S bridged sulphido clusters of the transition metals are known,[1,2] relatively few based on Rh_3 have been described. Of particular relevance here are the carbonylate anions $[Rh_3(CO)_6(\mu_3\text{-}S)_2]^-$ and $[Ir_3(\mu_3\text{-}S)_2(CO)_6]^-$ recently reported by Garlaschelli *et al.*[3] Also of related interest is the recent report by Cotton *et al.* of the Ir_3 complex $Ir_3(COD)_3(\mu_3\text{-}O)_2(\mu_2\text{-}I)$ which is essentially isoelectronic and isostructural with (**1**).[4] In addition, a number of heterobimetallic sulphido bridged Rh complexes are known. For example, Howard *et al.* recently described complexes of the type $MS_4[Rh(COD)]_2$ (M = Mo, W).[5]

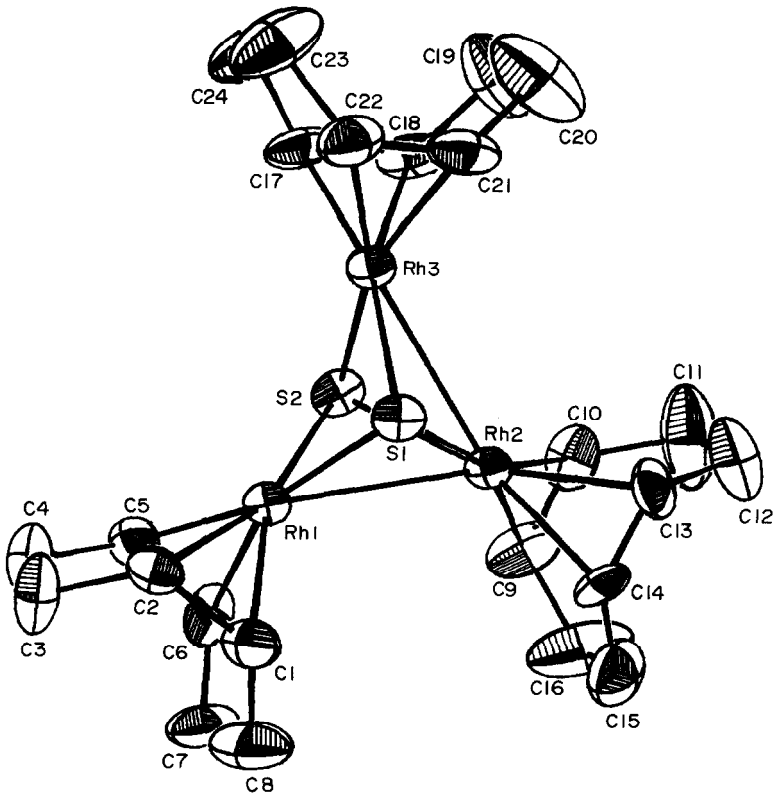

Fig. 1. ORTEP view of (**1**) showing the atom numbering scheme.

Table 1. Crystal structure parameters for complexes (1), (2) and (3)

Description of crystal	(1)	(2)	(3)
Colour	Red	Bright red	Yellow
Habit	Prism	Plate	Plate
Max. crystal dimension (mm)	$0.25 \times 0.15 \times 0.10$	$0.32 \times 0.28 \times 0.20$	$0.35 \times 0.15 \times 0.08$
Unit cell			
Crystal system	Monoclinic	Triclinic	Monoclinic
Space group	$C2/c$	$P\bar{1}$ (No. 2)	$C2/c$ (No. 15)
Unit cell parameters:			
a (Å)	27.808(5)	10.738(1)	21.727(1)
b (Å)	9.060(1)	19.503(2)	19.457(2)
c (Å)	19.248(3)	20.353(4)	17.809(2)
α (deg)	90	90.364(1)	90
β (deg)	97.52(2)	105.471(2)	116.865(2)
γ (deg)	90	92.765(1)	90
U (Å^3)	4807.6(5)	4102.3(5)	6716.4(5)
Molecules per unit cell	8	4	8
Formula	$C_{24}H_{37}Rh_3S_2$	$C_{39}H_{69}P_2Rh_3S_2$	$C_{20}H_{38}O_4P_2Rh_3S_2$
Molecular weight (g mol^{-1})	698.40	972.78	777.31
Calculated density (g cm^{-3})	1.930	1.575	1.537
μ-calc. (cm^{-1})	21.83	13.76	16.69
Data collection			
Radiation (Å)	Mo-K_α (0.71073)	Mo-K_α (0.71073)	Mo-K_α (0.71073)
Scan technique	$\theta/2\theta$	$\theta/2\theta$	$\theta/2\theta$
Scan width (deg)	$0.8+0.35 \tan\theta$	$0.8+0.35 \tan\theta$	$0.8+0.35 \tan\theta$
Range of indices h, h, l	0 30, 0 10, −22 20	0 12, −20 20, −20 20	0 23, 0 21, −19 19
2θ range (deg)	3.0–46.0	3.0–48.0	3.0–48.0
No. reflections measured	4123	5674	4649
Standard reflections:			
intensity	13 3 1, 16 2 1	5 1 8, 5 3 6	5 7 3, 2 10 2
orientation	16 0 2, 11 3 7	3 3 7, 6 6 2	1 7 6, 2 8 5
Decay of standards	2.1%	8.5%	38%
Min. % transmission	82.13	—	—
Max. % transmission	99.78	—	—
Average % transmission	92.26	—	—
Agreement factor for average reflections			
F (obs)	0.033	0.03	0.043
intensity	0.028	—	0.036
Structure determination			
No. reflections used ($I > 3\sigma(I)$)	2432	4205	1084
No. parameters varied	262	411	172
Data/parameter ratio	9.282	10.231	6.302
Shift to error ratio	1.637	0.484	0.560
E.s.d. of an observation of unit weight	1.83	2.93	2.97
R	0.0480	0.0559	0.0750
R_w	0.0620	0.0632	0.0870

Table 2. Selected bond lengths (Å) for (**1**)[a]

Atom 1	Atom 2	Distance	Atom 1	Atom 2	Distance
Rh1	Rh2	2.814(1)	Rh3	S2	2.299(4)
Rh1	S1	2.327(3)	Rh3	C17	2.160(14)
Rh1	S2	2.318(3)	Rh3	C18	2.128(14)
Rh1	C1	2.191(14)	Rh3	C21	2.14(2)
Rh1	C2	2.192(13)	Rh3	C22	2.167(15)
Rh1	C5	2.165(11)	C1	C2	1.43(2)
Rh1	C6	2.189(15)	C1	C8	1.54(2)
Rh2	Rh3	2.962(1)	Rh3	Rh1	3.210(3)
Rh2	S1	2.326(3)			
Rh2	S2	2.328(3)			
Rh2	C9	2.189(14)			
Rh2	C10	2.175(13)			
Rh2	C13	2.159(14)			
Rh2	C14	2.175(13)			
Rh3	S1	2.299(3)			

[a] A complete listing is available in the supplementary material. Numbers in parentheses are estimated standard deviations in the least significant digits.

Synthesis of $Rh_3(COD)_3(\mu_3\text{-}S)_2(\mu\text{-}H)$ (**1**)

The reaction of $[Rh(COD)Cl]_2$ with NaSH in methanol at −78°C gives an orange solution which gradually turns bright red on warming to room temperature. From this solution, bright red $Rh_3(COD)_3(\mu_3\text{-}S)_2(\mu\text{-}H)$ (**1**) may be obtained in high yield from toluene. The reaction appears to be quite clean and H_2S is also produced in the reaction indicating the fate of the hydrogen in the starting material NaSH. The ^1H NMR spectrum of (**1**) has resonances attributable to the COD ligands in addition to a high field triplet assigned to a $(\mu_2\text{-}H)$ atom (δ −11.73, *t*, $^1J_{Rh-H}$ = 24 Hz). Integration of the spectrum is consistent with the ratio of three COD ligand groups to one hydride.

X-ray structure of (**1**)

The complex crystallizes in the monoclinic space group *C*2/*c* with eight molecules in the unit cell. A view of the molecule is shown in Fig. 1. Crystallographic data is collected in Table 1 and bond lengths and angles are in Tables 2 and 3, respectively.

The molecular structure consists of a Rh_3 triangle which is capped on each face by a μ_3-S atom. Two Rh—Rh bonds are significantly shorter than the third. Thus Rh(1)—Rh(2) = 2.814(1), Rh(2)—Rh(3) = 2.962(1) and Rh(1)—Rh(3) = 3.210(3) Å. It seems likely that the single hydride ligand bridges the longest Rh—Rh interaction although it could not be located in the X-ray structure. This suggestion is supported by the simple triplet observed for the μ-H ligand in the ^1H NMR spectrum. The Rh—S distances range from 2.299(3) to 2.328(3) Å and are slightly shorter on average than those found in the rhodium carbonyl trimer $[Rh_3(CO)_6(\mu_3\text{-}S)_2]^-$ which range from 2.344(4) to 2.356(4) Å. The COD ligands are bound in the familiar boat or tub configuration.[6] The midpoints of the C—C double bonds of these alkene units and the μ_3-S atoms give each Rh atom a roughly planar coordination geometry.*

* Deviations (Å) from the least squares planes are as follows. *For* (**1**): Around Rh(1), Plane (1): Rh(1) −0.029(1), S(1) 0.052(3), S(2) −0.037(3), CT(1) −0.040(3), CT(2) 0.055(3). Around Rh(2), Plane (2): Rh(2) 0.001(1), S(1) −0.007(3), S(2) 0.007(3), CT(3) −0.008(3), CT(4) 0.007(3). Around Rh(3), Plane (3): Rh(3) −0.033(1), S(1) 0.029(3), S(2) −0.015(3), CT(5) 0.033(3), CT(6) −0.015(3). Where CT(1), CT(2) are the centroids of C(1)—C(2), C(5)—C(6), etc. Angles (deg.) between planes: (1)–(2) 105.7, (1)–(3) 41.5, (2)–(3) 64.2. *For* (**2**): around Rh(1), Plane (1): Rh(1) −0.020(2), S(1) 0.045(6), S(2) −0.036(6), CT(1) 0.049(6), CT(2) −0.039(6). Around Rh(2), Plane (2): Rh(2) 0.048(2), S(1) 0.015(5), S(2) −0.037(5), CT(3) 0.015(6), CT(4) −0.041(6). Around Rh(3), Plane (3): Rh(3) −0.009(2), P(1) −0.023(6), P(2) 0.028(6), S(1) 0.030(6), S(2) −0.025(6). Where CT(1), CT(2) are the centroids of C(1)—C(2), C(5)—C(6), etc. Angles between planes: (1)–(2) 117.1, (1)–(3) 59.0, (2)–(3) 58.1. *For* (**3**): Around Rh(1), Plane (1): Rh(1) 0.019(5), S(1) 0.02(2), S(2) −0.03, C(1) 0.03(5), C(2) −0.04(7). Around Rh(2), Plane (2): Rh(2) 0.008(4), S(1) 0.01(2), S(2) −0.01(2), C(3) −0.01(6), C(4) 0.01(5). Around Rh(3), Plane (3): Rh(3) −0.006(4), S(1) −0.02(2), S(2) 0.02(2), P(1) 0.02(2), P(2) −0.02(2). Angles between planes (1)–(2) 54.3, (1)–(3) 117.1, (2)–(3) 62.8.

Table 3. Selected bond angles (deg) for (1)[a]

Atom 1	Atom 2	Atom 3	Angle	Atom 1	Atom 2	Atom 3	Angle
Rh2	Rh1	S1	52.77(8)	S2	Rh2	C14	161.9(4)
Rh2	Rh1	S2	52.88(9)	C9	Rh2	C10	37.7(6)
Rh2	Rh1	C1	108.9(4)	C9	Rh2	C13	93.7(6)
Rh2	Rh1	C2	139.6(4)	C9	Rh2	C14	83.1(6)
Rh2	Rh1	C5	134.6(3)	C10	Rh2	C13	82.5(6)
Rh2	Rh1	C6	109.2(3)	C10	Rh2	C14	95.1(6)
S1	Rh1	S2	82.3(1)	C13	Rh2	C14	36.6(6)
S1	Rh1	C1	90.9(4)	Rh2	Rh3	S1	50.59(8)
S1	Rh1	C2	96.6(4)	Rh2	Rh3	S2	50.65(9)
S1	Rh1	C5	165.5(4)	Rh2	Rh3	C17	136.3(4)
S1	Rh1	C6	157.4(4)	Rh2	Rh3	C18	110.5(4)
S2	Rh1	C1	160.7(3)	Rh2	Rh3	C21	113.2(4)
S2	Rh1	C2	160.5(4)	Rh2	Rh3	C22	139.0(4)
S2	Rh1	C5	94.3(4)	S1	Rh3	S2	83.4(1)
S2	Rh1	C6	97.2(4)	S1	Rh3	C17	163.6(4)
C1	Rh1	C2	38.2(5)	S1	Rh3	C18	156.8(4)
C1	Rh1	C5	96.5(5)	S1	Rh3	C21	93.1(4)
C1	Rh1	C6	82.2(6)	S1	Rh3	C22	95.7(4)
C2	Rh1	C5	81.9(5)	S2	Rh3	C17	93.1(5)
C2	Rh1	C6	91.2(5)	S2	Rh3	C18	93.4(5)
C5	Rh1	C6	36.9(5)	S2	Rh3	C21	160.6(4)
Rh1	Rh2	Rh3	67.55(3)	S2	Rh3	C22	162.9(4)
Rh1	Rh2	S1	52.79(8)	C17	Rh3	C18	39.1(6)
Rh1	Rh2	S2	52.56(8)	C17	Rh3	C21	95.3(6)
Rh1	Rh2	C9	109.7(4)	C17	Rh3	C22	83.0(6)
Rh1	Rh2	C10	135.8(5)	C18	Rh3	C21	82.4(6)
Rh1	Rh2	C13	139.2(4)	C18	Rh3	C22	93.9(6)
Rh1	Rh2	C14	111.9(4)	C21	Rh3	C22	36.2(5)
Rh3	Rh2	S1	49.78(8)	Rh1	S1	Rh2	74.4(1)
Rh3	Rh2	S2	49.77(9)	Rh1	S1	Rh3	88.0(1)
Rh3	Rh2	C9	137.7(4)	Rh2	S1	Rh3	79.6(1)
Rh3	Rh2	C10	113.7(4)	Rh1	S2	Rh2	74.6(1)
Rh3	Rh2	C13	115.9(4)	Rh1	S2	Rh3	88.2(1)
Rh3	Rh2	C14	138.5(4)	Rh2	S2	Rh3	79.6(1)
S1	Rh2	S2	82.1(1)	Rh1	C1	C2	71.0(8)
S1	Rh2	C9	160.3(5)	Rh1	C1	C8	109(1)
S1	Rh2	C10	161.0(5)	C2	C1	C8	127(1)
S1	Rh2	C13	96.4(4)	Rh1	C2	C1	70.9(8)
S1	Rh2	C14	95.1(4)	Rh1	C2	C3	112(1)
S2	Rh2	C9	93.5(5)				
S2	Rh2	C10	92.9(5)				
S2	Rh2	C13	161.3(4)				

[a] A complete listing is available in the supplementary material.

Numbers in parentheses are estimated standard deviations in the least significant digits.

Reaction of (1) *with* t-Bu_2PH: *synthesis and structure of* $Rh_3(COD)_2(t\text{-}Bu_2PH)_2(\mu_3\text{-}S)_2(\mu\text{-}H)$ (2)

(1) reacts with t-Bu_2PH in THF to give a dark red–purple solution from which $Rh_3(COD)_2(t\text{-}Bu_2PH)_2(\mu_3\text{-}S)_2(\mu\text{-}H)$ may be isolated in high yield. Spectroscopic data for (2) again confirm the presence of one hydride ligand as well as COD and t-Bu_2PH ligands. The IR spectrum contains a weak P—H stretch at 2280 cm^{-1} and the $^{31}P\{^1H\}$ NMR spectrum is a simple doublet at δ 78.26, (d, $^1J_{Rh-P} = 134.7$ Hz). The ^1H NMR signal for the hydride is now at δ −20.05 (m). This resonance is more complicated than that observed for (3). We have simulated this signal as well as the similar one observed for (3) (Fig. 2). Interestingly, in both cases

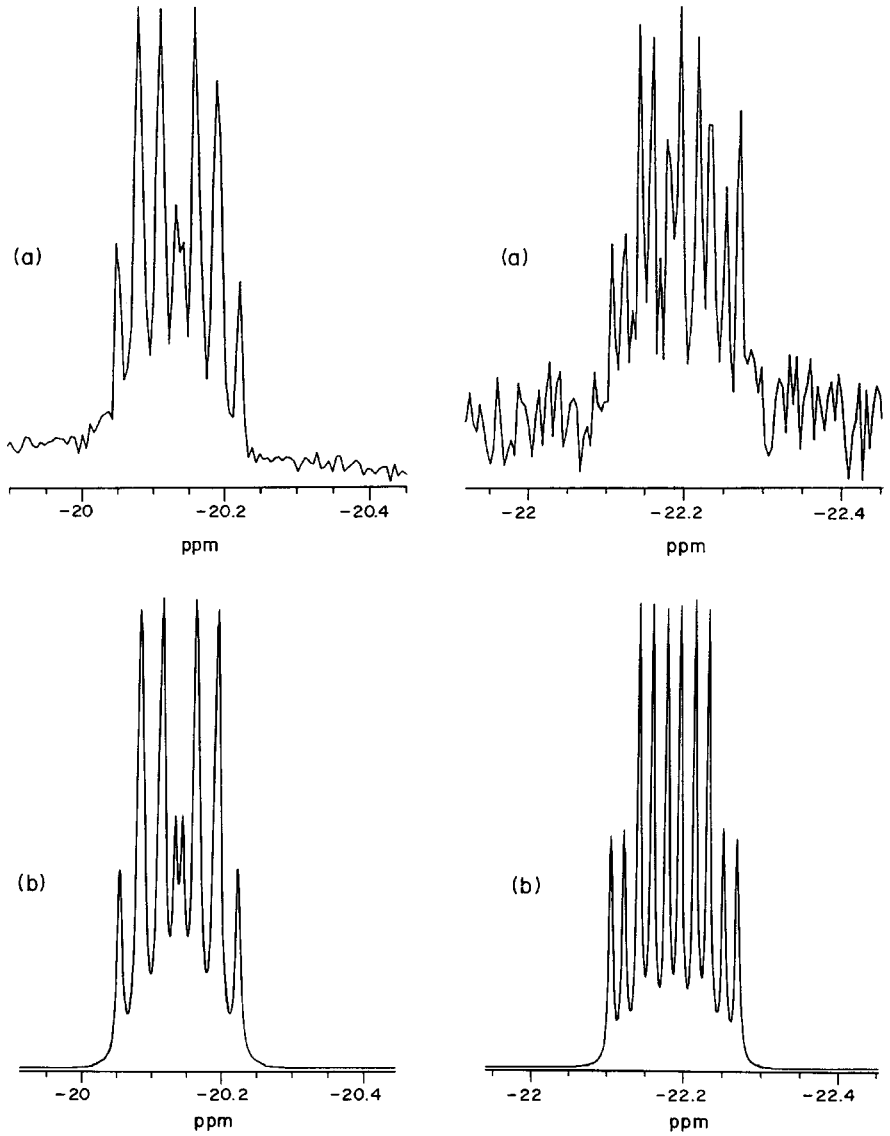

Fig. 2. Observed (a) and calculated (b) ^{1}H NMR spectra for the μ-H resonance in (**2**) and (**3**). Coupling constants (Hz) used in the simulations are for (**2**) (360 MHz), δ −20.13; $J_{H—Rh(1)} = J_{H—Rh(2)} = 10.17$, $J_{H—Th(3)} = 0.05$, $J_{H—P(1)} = 12.09$, $J_{H—P(2)} = 28.70$ Hz. For (**3**), (360 MHz), δ −22.18; $J_{H—Rh(1)} = J_{H—Rh(2)} = 13.31$, $J_{H—Rh(3)} = 0.05$, $J_{H—P(1)} = 6.25$, $J_{H—P(2)} = 26.35$. The atom numbering is as in Figs 2 and 4; in both cases, P(1) and P(2) may be reversed.

seemingly reasonable simulations could only be achieved when the couplings between the μ-H atom and P(1) and P(2) were quite different [(**2**) 10.09, 28.70 Hz, and (**3**) 6.25, 26.35 Hz]. This suggests that the hydride ligand in these complexes is no longer located in a symmetrical position but lies out of the Rh_3 plane. However, this would also make the phosphorus nucleii inequivalent, which is inconsistent with the $^{31}P\{^1H\}$ NMR data. Both ^{1}H and ^{31}NMR spectra are unchanged down to −80°C (d_8-toluene) and at present we have no simple explanation for this apparent dichotomy. Unfortunately, the μ-H ligands could not be located in any of the X-ray structures and the structural parameters (see below) give little clue as to where the hydride is located. There are no significant differences in Rh—Rh or Rh—S bond lengths.

Molecules of (**2**) crystallize in the triclinic space group $P\bar{1}$ with two independent molecules in the asymmetric unit (four per cell). A view of one molecule of (**2**) is shown in Fig. 3. Key bond lengths and angles for this molecule are given in Tables 4 and 5 respectively. The structural parameters of both molecules are similar and their Rh_3S_2 cores

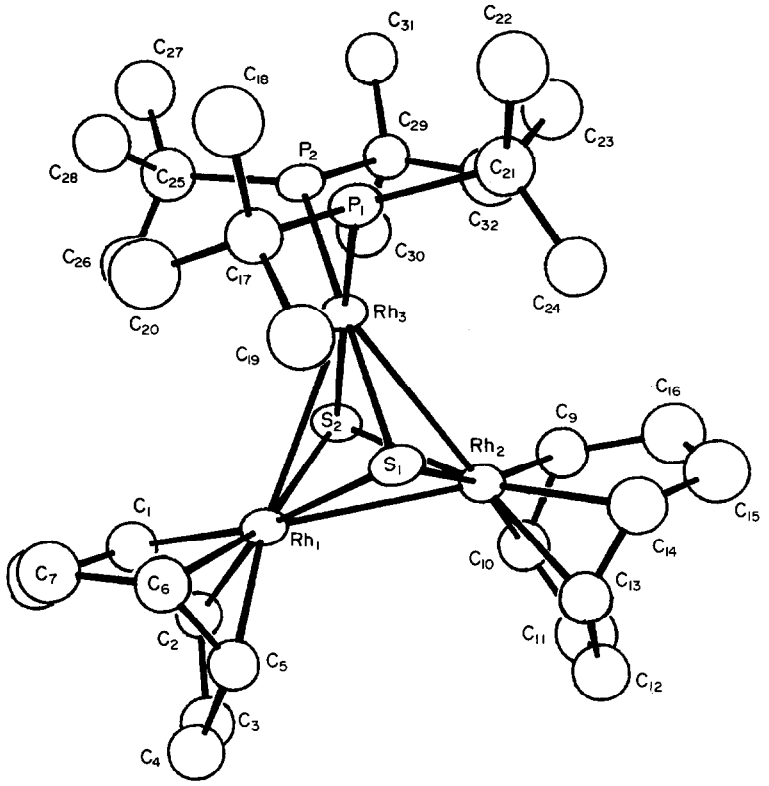

Fig. 3. ORTEP view of one independent molecule of (**2**) showing the atom numbering scheme.

Table 4. Selected bond distances (Å) for one molecule of (**2**)[a]

Atom 1	Atom 2	Distance	Atom 1	Atom 2	Distance
Rh1	Rh2	2.992(2)	Rh2	C10	2.19(2)
Rh1	Rh3	3.029(1)	Rh2	C13	2.150(14)
Rh1	S1	2.307(4)	Rh2	C14	2.17(2)
Rh1	S2	2.313(3)	Rh3	P1	2.295(4)
Rh2	Rh3	3.039(1)	P1	C17	1.875(15)
Rh2	S1	2.320(4)	P1	C21	1.902(15)
Rh2	S2	2.306(3)	P2	C25	1.88(2)
Rh3	S1	2.348(3)	P2	C29	1.928(14)
Rh3	S2	2.347(3)	C1	C2	1.38(2)
Rh3	P1	2.295(4)	C1	C8	1.56(2)
Rh3	P2	2.301(3)			
Rh1	C1	2.131(15)			
Rh1	C2	2.187(14)			
Rh1	C5	2.159(14)			
Rh1	C6	2.189(15)			
Rh2	C9	2.16(2)			

[a] A complete listing is available in the supplementary material.

Numbers in parentheses are estimated standard deviations in the least significant digits.

Table 5. Selected bond angles (deg.) for one molecule of (2)[a]

Atom 1	Atom 2	Atom 3	Angle	Atom 1	Atom 2	Atom 3	Angle
Rh2	Rh1	Rh3	60.64(3)	S1	Rh3	S2	81.7(1)
Rh2	Rh1	S1	49.91(9)	S1	Rh3	P1	92.6(1)
Rh2	Rh1	S2	49.53(9)	S1	Rh3	P2	174.0(1)
Rh3	Rh1	S1	50.01(8)	S2	Rh3	P1	174.3(1)
Rh3	Rh1	S2	49.95(8)	S2	Rh3	P2	92.6(1)
S1	Rh1	S2	83.3(1)	C1	Rh1	C2	37.4(5)
Rh1	Rh2	Rh3	60.28(3)	C1	Rh1	C5	92.0(5)
Rh1	Rh2	S1	49.52(9)	C1	Rh1	C6	82.4(6)
Rh1	Rh2	S2	49.73(9)	C2	Rh1	C5	82.2(5)
Rh3	Rh2	S1	49.78(8)	C2	Rh1	C6	96.6(5)
Rh3	Rh2	S2	49.80(8)	C5	Rh1	C6	38.1(5)
S1	Rh2	S2	83.2(1)	C9	Rh2	C10	38.7(5)
Rh1	Rh3	Rh2	59.08(3)	C9	Rh2	C13	96.9(6)
Rh1	Rh3	S1	48.82(9)	C9	Rh2	C14	82.0(6)
Rh1	Rh3	S2	48.97(8)	C10	Rh2	C13	82.4(6)
Rh1	Rh3	P1	126.1(1)	C10	Rh2	C14	91.7(6)
Rh1	Rh3	P2	128.0(1)	C13	Rh2	C14	37.3(5)
Rh2	Rh3	S1	48.97(9)	P1	Rh3	P2	93.1(1)
Rh2	Rh3	S2	48.63(9)	C17	P1	C21	112.0(7)
Rh2	Rh3	P1	127.5(1)	C25	P2	C29	109.7(7)
Rh2	Rh3	P2	125.4(1)				

[a] A complete listing is available in the supplementary material.

Numbers in parentheses are estimated standard deviations in the least significant digits.

are similar to that of (**1**). Interestingly, compared to (**1**), the Rh—Rh distances for (**2**) are all approximately equal (Rh(1)—Rh(3) = 3.029(1), Rh(2)—Rh(3) = 3.039(1) and Rh(1)—Rh(2) = 2.992(2) Å).

Reaction of (**2**) *with* CO: *synthesis and structure of* $Rh_3(CO)_4(t\text{-}Bu_2PH)_2(\mu_3\text{-}S)_2(\mu\text{-}H)$ (**3**)

(**2**) reacts rapidly with CO (1 atm.) in toluene displacing both COD ligands and forming the tetracarbonyl derivative $Rh_3(CO)_4(t\text{-}Bu_2PH)_2(\mu_3\text{-}S)_2(\mu\text{-}H)$ (**3**) quantitatively. Spectroscopic data is again in accord with the X-ray crystal structure. Thus the IR spectrum contains terminal CO bands (ν_{CO} = 2050 m, 2030 m and 1980 s cm^{-1}) and a weak ν_{P-H} stretch at 2300 cm^{-1}. The $^{31}P\{^1H\}$ NMR spectrum is a simple doublet (δ 73.24, $^1J_{Rh-P}$ = 122.24 Hz). Again, as for (**2**), this is inconsistent with our best attempts to simulate the ^1H NMR hydride signal. A view of the molecule is shown in Fig. 4. Important bond lengths and angles are given in Tables 6 and 7. The main structural features of the molecule are similar to those of (**1**) and (**2**) with two CO molecules replacing each of the remaining COD groups.

The present study leaves several questions unanswered. One of the key issues is the location of the hydrides in (**2**) and (**3**). At present, neither spectroscopic data nor X-ray structures provide unambiguous answers. Why is only one COD ligand displaced from the cluster by excess PR_3? Why does CO only replace the COD ligands in (**2**)? Further studies on this system and related Ir_3 complexes are in progress.

EXPERIMENTAL

All compounds were prepared under dry nitrogen using standard vacuum line techniques. Methanol was dried over magnesium turnings then refluxed and distilled from Mg turnings under nitrogen before use. Toluene was distilled from sodium metal under nitrogen. Hexane was distilled from sodium benzophenone ketyl under nitrogen. CO used was cp grade. Microanalytical data were obtained from the Schwarzkopf Microanalytical Laboratory, Woodside, New York. $[Rh(COD)Cl]_2$[7] and NaSH[8] were prepared by the literature methods.

Instruments

IR: Perkin–Elmer 1330; NMR: Varian EM-390 (^1H, 90 MHz) FT-80 (^{31}P, 32.384 MHz) Bruker

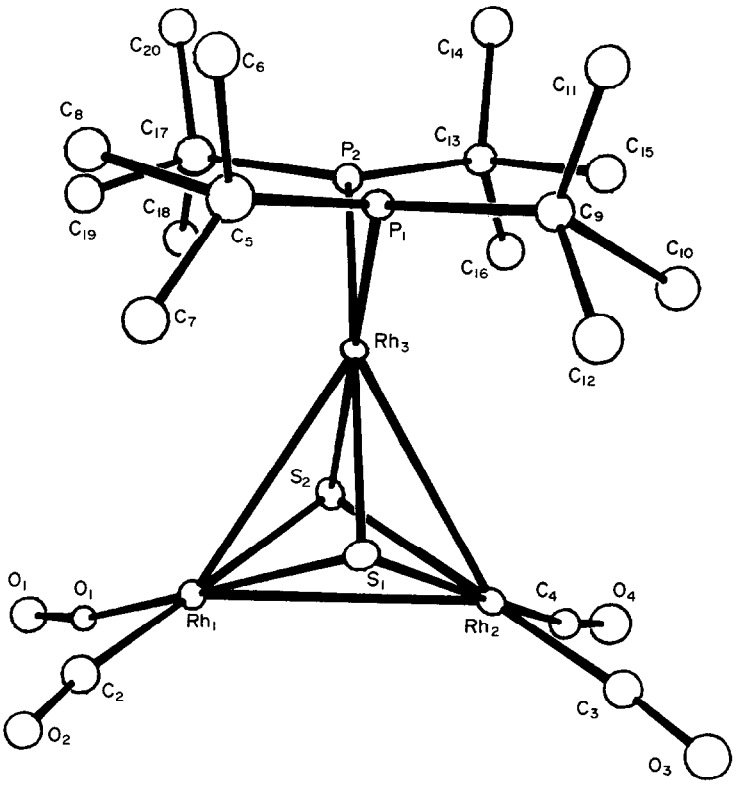

Fig. 4. ORTEP view of (3) showing the atom numbering scheme.

Table 6. Selected bond lengths (Å) for (3)[a]

Atom 1	Atom 2	Distance	Atom 1	Atom 2	Distance
Rh1	Rh2	3.079(3)	P1	C5	1.68(4)
Rh1	Rh3	3.010(3)	P1	C9	1.77(3)
Rh2	Rh3	3.024(3)	P2	C13	1.90(3)
Rh1	S1	2.333(8)	P2	C17	1.92(4)
Rh1	S2	2.306(7)	O1	C1	1.15(3)
Rh1	C1	1.79(2)	O2	C2	1.08(3)
Rh1	C2	1.85(3)	O3	C3	1.18(3)
Rh2	S1	2.368(7)	O4	C4	1.05(3)
Rh2	S2	2.318(8)	C5	C6	1.53(4)
Rh2	C3	1.81(3)	C5	C7	1.32(4)
Rh2	C4	1.82(3)			
Rh3	S1	2.372(7)			
Rh3	S2	2.361(7)			
Rh3	P1	2.303(7)			
Rh3	P2	2.287(6)			

[a] A complete listing is provided in the supplementary material.
Numbers in parentheses are estimated standard deviations in the least significant digits.

Table 7. Selected bond angles (deg.) for (3)[a]

Atom 1	Atom 2	Atom 3	Angle	Atom 1	Atom 2	Atom 3	Angle
Rh2	Rh1	Rh3	59.55(7)	Rh1	S1	Rh2	81.8(2)
Rh1	Rh2	Rh3	59.09(7)	Rh1	S1	Rh3	79.5(2)
Rh1	Rh3	Rh2	61.36(7)	Rh2	S1	Rh3	79.3(2)
S1	Rh1	S2	84.0(2)	Rh1	S2	Rh2	83.5(2)
S1	Rh1	C1	176.5(7)	Rh1	S2	Rh3	80.3(2)
S1	Rh1	C2	88.5(9)	Rh2	S2	Rh3	80.5(2)
S2	Rh1	C1	92.5(7)	Rh3	P1	C5	117(1)
S2	Rh1	C2	172.0(9)	Rh3	P1	C9	117(1)
C1	Rh1	C2	95(1)	C5	P1	C9	109(2)
S1	Rh2	S2	83.0(2)	Rh3	P2	C13	119.3(9)
S1	Rh2	C3	91.6(9)	Rh3	P2	C17	117(1)
S1	Rh2	C4	173.9(9)	C13	P2	C17	109(2)
S2	Rh2	C3	174.5(9)	Rh1	C1	O1	168(2)
S2	Rh2	C4	90.9(9)	Rh1	C2	O2	172(3)
C3	Rh2	C4	94(1)	Rh2	C3	O3	175(3)
S1	Rh3	S2	82.0(3)	Rh2	C4	O4	172(3)
S1	Rh3	P1	91.2(2)				
S1	Rh3	P2	175.1(3)				
S2	Rh3	P1	173.0(2)				
S2	Rh3	P2	93.2(3)				
P1	Rh3	P2	93.7(3)				

[a] A complete listing is provided in the supplementary material.

Numbers in parentheses are estimated standard deviations in the least significant digits.

WM-90 (^{31}P, 36.43 MHz), Nicolet NT-200 (^{1}H and ^{31}P) or NT 360 (^{1}H and ^{31}P). IR spectra were as KBr disks, Nujol mulls (KBr plates) or in solution (matched KBr or CaF_2 cells). NMR spectra were recorded in C_6D_6 at ambient temperature and are referenced to Me_4Si (δ 0.0, ^{1}H) and 85% H_3PO_4 (aq.) (δ 0.0, ^{31}P).

Synthesis of $Rh_3(COD)_3(\mu_3\text{-}S)_2(\mu\text{-}H)$ (1)

A solution of $[Rh(COD)Cl]_2$ (0.20 g, 0.41 mmol) in methanol (40 cm^3) was cooled (−78°C) and a solution of NaSH (0.50 cm^3 of a 1.71 M MeOH solution, 2 equiv.) was added. An orange colour was produced immediately. The solution was stirred magnetically and became bright red while warming to room temperature. It was stirred an additional 8 h. Volatile materials were removed under reduced pressure, and the bright orange residue was washed with hexane (10 cm^3). The residue was then extracted into toluene (40 cm^3), the solution filtered and reduced in volume (10 cm^3). Cooling (−20°C) gave bright red prisms of (1). They were collected and dried *in vacuo*. Yield 0.08 g, 83%. M.p. 148–150°C, (dec.), IR (Nujol mull), 2972 s, 2890 m, 2848 s, 2800 s, 1471 m, 1418 s, 1315 s, 1290 m, 1250 w, 1229 m, 1205 w, 1168 m, 1140 m, 1061 m, 981 br.m, 942 br.s, 836 s, 806 m, 782 m, 753 w, 684 w, 650 w, 562 w, 461 m, 421 s, 391 w, 368 w, 310 m (cm^{-1}). ^{1}H NMR: δ 5.03, [br.s, 4H, -C<u>H</u>-C<u>H</u>-(COD)], δ 4.68 [br.s, 4H, -C<u>H</u>-C<u>H</u>-(COD)], δ 4.53 [br.s, 4H, -C<u>H</u>-C<u>H</u>(COD)], δ 2.14, [s, 24H, -C<u>H</u>$_2$(COD)], δ −11.73 (dd, 1H, $^{1}J_{Rh-H}$ = 24 Hz, μ-<u>H</u>). Found: C, 41.2; H, 5.3; S, 8.7. Calc. for $C_{24}H_{37}Rh_3S_2$: C, 41.3; H, 5.3; S, 9.2%.

$Rh_3(COD)_2(t\text{-}Bu_2PH)_2(\mu_3\text{-}S)_2(\mu\text{-}H)$ (2)

Di-*tert*-butylphosphine (*t*-Bu_2PH, 0.33 cm^3, 2.42 mmol) was added to a solution of (1) (0.28 g, 0.40 mmol) in THF (40 cm^3) at −70°C. The solution was allowed to warm to room temperature and stirred for an additional 10 h to give a dark red–purple solution. Volatile materials were removed under reduced pressure and the residue washed with hexane (2 × 15 cm^3). The residue was then extracted into toluene (40 cm^3), the solution filtered and evaporated to *ca* 15 cm^3 under reduced pressure. Cooling (−20°C) gave bright red plates of (2) which were collected and dried *in vacuo*. The compound is stable in air for short periods. Yield: quantitative, m.p. 140–142°C (dec.), IR (KBr disc), 3000 w, 2980 w, 2940 s.br, 2900 s.br, 2860 s.sh, 2810 s.sh, 2280 w.sh, 1475 s, 1430 w, 1390 w, 1360 m.sh, 1325 w,

1300 w, 1235 w, 1200 w.br, 1175 m.br, 1150 w, 1070 w, 1020 m, 945 w, 930 w.br, 860 s, 845 m, 810 s, 685 w, 730 m, 690 w, 600 m, 575 w, 470 m, 450 w, 350 w.br (cm^{-1}). ^1H NMR, δ 2.20 (m, 16H, COD), δ 1.30 (m, 18H, *t*-Bu), δ −20.05 [m, 1H, (μ-H)], $^{31}P\{^1H\}$ NMR: δ 78.26 (d, $^1J_{Rh-P}$ = 134.7 Hz) (unchanged at −80°C, d_8-toluene). Found: C, 48.0; H, 7.0. Calc. for $C_{39}H_{69}P_2Rh_3S_2$: C, 48.1; H, 7.1%.

$Rh_3(CO)_4(t\text{-}Bu_2PH)_2(\mu_3\text{-}S)_2(\mu\text{-}H)$ (3)

Carbon monoxide (1 atm.) was passed through a solution of (2) (0.28 g, 0.32 mmol) in toluene (40 cm^3) at room temperature for 1 h. The solution became bright yellow during this time. Volatile materials were removed under reduced pressure and the yellow residue was extracted into toluene (35 cm^3). Cooling (−20°C) gave yellow prisms of (3) after *ca* 18 h. They were collected and dried *in vacuo*. The crystals are stable in air for periods of several hours. Yield: quantitative, m.p. 186–188°C (dec.); IR (KBr disc.): 2300 w, 2050 m.sh, 2030 m.sh, 1980 s.sh, 1770 w.br, 1370 w, 1260 w, 1175 w, 1085 w, 1025 w, 560 w, 470 w (cm^{-1}); NMR: ^1H (360 MHz, C_6D_6, ambient temp): δ 3.716 (d, 1H, $^1J_{P-H}$ = 337 Hz, *t*-Bu_2PH); δ 3.719 (d, 1H, $^1J_{P-H}$ = 15 Hz, *t*-Bu_2PH); δ 1.28 (d, 18H, $^1J_{P-H}$ = 15 Hz, *t*-Bu_2PH); δ 1.12 (d, 18H, $^1J_{P-H}$ = 13 Hz, *t*-Bu_2PH); δ −22.15 [m, 1H, (μ-H)]. $^{31}P\{^1H\}$: δ 73.24 (d, $^1J_{Rh-P}$ = 122.24 Hz) (the spectrum remains essentially unchanged at −80°C in d_8-toluene). Found: C, 29.9; H, 4.5. Calc. for $C_{20}H_{38}O_4P_2Rh_3S_2$: C, 30.9; H, 4.9%.

X-ray experimental

General. Data were collected on an Enraf–Nonius CAD-4 diffractometer using graphite monochromated Mo-K_α radiation. Data for the unit cell determinations were collected by the $\theta/2\theta$ scan technique at 23 ± 2°C. Details of the standard collection methods were similar to those outlined in ref. 9. All calculations were performed on a PDP 11/44 computer using the Enraf–Nonius software package "SDP PLUS".[10] Crystal structure and refinement parameters for all three compounds are collected in Table 1 and supplementary material is available.* Scattering factors were taken from ref. 11.

For (1). A single crystal was mounted under nitrogen in a Lindemann glass capillary. Unit cell parameters were obtained by carefully centering 25 reflections having 2θ values between 22 and 24°. Examination of the diffraction symmetry and the systematic absences hkl, $h+k = 2n = 1$; $hk0$, $h+k = 2n+1$; $hk0$, $l = 2n+1$, and $00l$, $l = 2n+1$ indicated a choice of the space groups *Cc* or *C*2/*c*. The space group *C*2/*c* (No. 15) was chosen to be the correct one on the basis of successful refinement of the structure. Data were collected in the $+h+k\pm l$ quadrant between 2θ values of 3.0 and 48.0°. The data were then corrected for Lorentz and polarization effects. The check reflections showed a 2.1% decrease in intensity over the course of data collection. Reflections having χ values between 80–90° showed a minimum percent transmission of 82.13 and a maximum percent transmission of 99.78. An empirical absorption correction was applied (program EAC). The observed structure factors of the equivalent reflections were averaged with agreement factors of 0.028 for intensity and 0.033 for F_{obs}. The positions of heavy atoms were obtained by direct methods (MULTAN)[12] and the remaining non-hydrogen atoms were located by successive cycles of difference Fourier maps followed by least squares refinement. Hydrogen atoms were not located. Data with intensities of less then $3\sigma(I)$ and $\sin\theta/\lambda$ less than 0.05 were excluded, and a non-Poisson contribution weighting scheme with an experimental instability factor, P of 0.04 was used in the final stages of refinement.† The structure was refined to final values of 0.0483 and 0.062 for R and R_w. The maximum peak in the final difference Fourier map had a height of 0.918 e $Å^{-3}$ and was located 1.051 Å from C(17).

For (2). Unit cell parameters were obtained from 25 reflections ($22° < 2\theta < 26°$). Unit cell dimensions indicated a triclinic space group and $P\bar{1}$ was chosen on the basis of successful refinement of the structure. Data were collected in the $(+h, \pm k, \pm l)$ hemisphere between 2θ values of 3.0 and 48° in the $\theta/2\theta$ mode. Data were then corrected for Lorentz and polarization effects and also for decay (anisotropic correction). No absorption correction was applied since none was deemed necessary. The

* Tables of atomic positional and thermal parameters, complete tables of bond lengths, angles and thermal parameters for (1)–(3) and observed and calculated structure factors for (1)–(3) have been deposited as supplementary material with the Editor, from whom copies are available on request. Atomic coordinates have also been submitted to the Cambridge Crystallographic Data Centre.

† P is used in the calculation of $\sigma(I)$ to downweight intense reflections in the least squares refinement. The function minimized was $\Sigma w(|F_o|-|F_c|)^2$ where $w = 4(F_o)^2/[\Sigma(F_o)^2]^2$, where $[\Sigma(F_o)^2]^2 = [S^2(C+R^2B)+\{P(F_o)^2\}^2]/Lp^2$, where S is the scan rate, C is the total integrated peak count, R is the ration of scan time to background counting time, B is the total background count and Lp is the Lorentz–polarization factor.

observed structure factors of equivalent reflections were averaged. The structure was solved by direct methods (MULTAN)[12] followed by successive cycles of difference Fourier maps, followed by least squares refinement. The non-Poisson contribution weighting scheme with an experimental instability factor $P = 0.07$ was used in the final stages of refinement.* Hydrogen atoms were not located. The Rh, S, and P atoms were refined anisotropically and the carbon atoms isotropically. The maximum peak in the final difference Fourier map had a height of 0.751 e $Å^{-3}$ and was located 0.85 Å from Rh(1).

For (**3**). Unit cell parameters were obtained from 25 reflections ($20° < 2\theta < 26°$). Systematic absences indicated a choice of $C2/c$ or Cc. $C2/c$ was chosen on the basis of successful refinement of the structure. Data were collected in the $(+h, \pm k, \pm l)$ quadrant ($3° < 2\theta < 46°$) in the $\theta/2\theta$ mode. Data were then corrected for Lorentz and polarization effects but not for absorption since the absorption coefficient was low. A decay correction was also applied. Equivalent reflections were averaged and the structure was solved by direct methods (MULTAN) followed by successive cycles of difference Fourier maps, followed by least squares refinement. The non-Poisson contribution weighting scheme with an experimental instability factor $P = 0.07$ was used. Hydrogen atoms were not located. The Rh, S, and P atoms were refined anisotropically and the remaining non-hydrogen atoms were refined isotropically. The maximum peak in the final difference Fourier map had a height of 1.023 e $Å^{-3}$ and was located 1.219 Å from C(8).

* See footnote † on previous page.

Acknowledgements—We thank the Robert A. Welch Foundation (Grant F-816), the National Science Foundation (CHE-8517759) and the Texas Advanced Technology Research Program for support. We also thank Johnson Matthey Inc. for a generous loan of $RhCl_3 \cdot x(H_2O)$. R.A.J. thanks the Alfred P. Sloan Foundation for a fellowship (1985–1987).

REFERENCES

1. A. M. Arif, J. G. Hefner and R. A. Jones, *J. Am. Chem. Soc.* 1986, **108**, 1701.
2. See for example: H. Vaharenkamp, *Angew. Chem. Int. Ed. Engl.* 1975, **14**, 322, and refs therein.
3. D. Galli, L. Garlaschelli, G. Ciani, A. Fumagalli, S. Martinengo and A. Sironi, *J. Chem. Soc., Dalton Trans.* 1984, 55; R. D. Pergola, L. Garaschelli, S. Martinengo, F. Demartin, M. Manassero and M. Sansoni, *J. Chem. Soc., Dalton Trans.* 1986, 2463.
4. F. A. Cotton, P. Lahuerta, M. Sanau and W. Schwotzer, *J. Am. Chem. Soc.* 1985, **107**, 8284.
5. K. E. Howard, T. B. Rauchfuss and A. L. Rheingold, *J. Am. Chem. Soc.* 1986, **108**, 297.
6. I. Omae, *Coord. Chem. Rev.* 1983, **51**, 1.
7. G. Giordano and R. H. Crabtree, *Inorg. Synth.* 1979, **19**, 218.
8. J. Keinber (Ed.) *Inorganic Synth.* 1963, **7**, 128.
9. R. A. Jones and T. C. Wright, *Organometallics* 1983, **2**, 1842.
10. *SDP Plus* (4th edn). B. A. Frenz and Associates, College Station, Texas 77840 (1981).
11. *International Tables for X-ray Crystallography*, Vol. 4. Kynoch Press, Birmingham, U.K. (1974).
12. G. Germain, P. Main and M. M. Wolfson, *Acta. Cryst. Sect. A Cryst. Phys. Diffr. Theor. Gen. Cryst.* 1971, **A27**, 368.

Polyhedron Vol. 7, No. 7, pp. 573–574, 1988
Printed in Great Britain

0277–5387/88 $3.00+.00
© 1988 Pergamon Press plc

COMMUNICATION

ACTINIDE(III) CARBONATE COMPLEXATION

KIRK J. CANTRELL

School of Geophysical Sciences, Georgia Institute of Technology, Atlanta, GA 30332, U.S.A.

(*Received* 27 *August* 1987; *accepted* 11 *December* 1987)

Abstract—The following equations have been developed to estimate trivalent actinide and lanthanide carbonate stability constants: $\log B_1^0 = -6.128+35.206R-21.557R^2$; $\log B_2^0 = 14.797+7.945R-10.304R^2$, where $B_1^0 = a\mathrm{MCO_3^+}/(a\mathrm{M^{3+}}a\mathrm{CO_3^{2-}})$, $B_2^0 = a\mathrm{M(CO_3)_2^-}$ $(a\mathrm{M^{3+}}(a\mathrm{CO_3^{2-}})^2)$, aX is the activity of ion X, M indicates a metal ion and R is the effective ionic radius of the metal ion in six-fold coordination. These equations describe carbonate stability constants for cerium, europium and ytterbium at zero ionic strength. Constants at zero ionic strength were estimated from experimental determinations made in 0.68 molal $NaClO_4$ by accounting for medium effects.

The fate of radioactive material accidentally released or entering the environment from waste disposal sites is controlled principally by solution chemistry and solution–surface interactions. Some of the processes involved are complexation, precipitation–dissolution, surface adsorption, colloid formation and redox reactions.[1,2] Quantitative modelling of these processes is severely constrained by a dearth of appropriate chemical data, or in some cases by widely varying results among researchers.

Trivalent actinide and lanthanide elements are known to form stable complexes with carbonate ions.[1,3,4,5] It has been suggested that complexation by carbonate may have been responsible for the migration of ^{242}Cm and ^{244}Cm out of a radioactive waste disposal site previously used by the Oak Ridge National Laboratory.[6] Subsequent decay of ^{242}Cm and ^{244}Cm to ^{238}Pu and ^{240}Pu resulted in plutonium contamination near the trench.

In spite of the potential importance of trivalent actinide complexation by carbonate, few experimental stability constant determinations have been undertaken.

LANTHANIDE AND ACTINIDE STABILITY CONSTANTS

Actinide elements are major components of radioactive waste. Carbonate complexation is of particular importance to actinide solution chemistry. Allard[7] has estimated carbonate stability constants ($\log B_1^0$) for trivalent actinides to be 6.5; where

$$B_1^0 = a\mathrm{MCO_3^+}/(a\mathrm{M^{3+}}a\mathrm{CO_3^{2-}}). \quad (1)$$

aX is the activity of ion X and M indicates a metal ion. This value was estimated from literature values of lanthanide carbonate stability constants ($\log B_1'$) which range from 4.6 to 6.3, measured at ionic strengths of 1–3 M. $B_1' = [\mathrm{MCO_3^+}]/([\mathrm{M^{3+}}][\mathrm{CO_3^{2-}}]_T)$, where brackets indicate molar concentrations and T denotes total carbonate concentrations. Spahiu[8] has shown that differences in yttrium carbonate stability constants between 1–3 M ionic strength are relatively small (0.43 log units). Therefore, it is concluded that the large variation in lanthanide carbonate stability constant results is not due to ionic strength effects. This degree of uncertainty in stability constants is undesirable for quantitative modelling of solution chemical behaviour.

Recently, we have presented carbonate stability constants for cerium, europium and ytterbium measured in 0.68 molal $NACIO_4$.[4,5] Additionally, equations were developed for estimating carbonate stability constants for all lanthanide elements as a function of atomic number for various ionic media. In these works we have critically reviewed a number of lanthanide carbonate stability constants

obtained by other workers. It was found that substantial agreement exists between our results and those of other authors after taking into account certain inconsistencies. Since the lanthanide atomic radii are nearly linear with atomic number, similar equations may be derived to describe lanthanide carbonate stability constants as a function of ionic radius:

$$\log B_1^0 = -6.128 + 35.206R - 21.557R^2 \quad (2)$$

$$\log B_2^0 = 14.797 + 7.945R - 10.304R^2. \quad (3)$$

R is the effective ionic radius in six-fold coordination[9] and $B_2^0 = a\mathrm{M(CO_3)_2^-}/(a\mathrm{M^{3+}}(a\mathrm{CO_3^{2-}})^2)$.

It has been recognized that trivalent lanthanide elements are useful chemical analogs to the trivalent actinides.[7,10] This is due to similarity in electronic structure and ionic radius. Using eqs (2) and (3) and ionic radii, carbonate stability constants for a number of trivalent actinides have been estimated. Apparently, the only experimental trivalent actinide carbonate stability constants available for comparison, are the americium carbonate constants determined by Lundqvist[3] in 1.0 M $NaClO_4$. Lundqvist's americium carbonate results appropriate to zero ionic strength are $\log B_1^0 = 8.1$ and $\log B_2^0 = 13.1$. These values were determined by accounting for sodium carbonate ion pairing[11] and adjusting to zero ionic strength using the methods of Millero and Schreiber.[12] The methods of Millero and Schreiber do not provide activity coefficients for complexes such as $AmCO_3^+$ and $Am(CO_3)_2^-$. Activity coefficient estimation for these species is not straightforward. The following estimates appropriate to 1.0 M ionic strength were used, $\gamma AmCO_3^+ = \gamma Am(CO_3)_2^- = 0.5$, where X is the activity coefficient of ion X. This value is somewhat smaller than estimates appropriate to singly charged non-polar ions, but larger than estimates appropriate to divalent ions. As noted previously,[4,5] the carbonic acid ionization constants used by Lundqvist are slightly low. An adjustment for this discrepancy would put Lundqvist's values at about $\log B_1^0 = 8.0$ and $\log B_2^0 = 12.9$. Table 1 shows our actinide carbonate stability constant estimates along with our experimental lanthanide data, appropriate to zero ionic strength. Also included in Table 1 are the ionic radii for each metal ion.[9] It can be seen that our estimated americium results and those of Lundqvist, agree reasonably well. In order to adjust our experimental lanthanide carbonate stability constants, determined at 0.68 molal ionic strength, to zero ionic strength, it was necessary to account for activity coefficient changes and sodium carbonate ion pairing. In view of the uncertainties involved in these calculations, error limits for the actinide stability constants in Table 1 are estimated to be 0.2 log units. The temperature dependence of europium carbonate stability constants has been found to be quite small.[4,13] Therefore, the constants in Table 1 should be appropriate to most aqueous low temperature conditions encountered (0–35°C).

Table 1. Estimated trivalent actinide and lanthanide carbonate stability constants appropriate to zero ionic strength and 25°C, and effective ionic radii

Trivalent metal ion	$\log B_1^0$	$\log B_2^0$	Radius
Np	7.4	12.3	1.01
Pu	7.5	12.4	1.00
Am	7.7	12.8	0.975
Cm	7.7	12.8	0.97
Bk	7.8	12.9	0.96
Cf	7.9	13.1	0.95
Ce	7.44	12.31	1.01
Eu	7.88	13.08	0.947
Yb	8.19	13.93	0.868

REFERENCES

1. B. Allard, U. Olofsson and B. Torstenfelt, *Inorg. Chim. Acta* 1984, **94**, 205.
2. G. R. Choppin, *Radiochim. Acta* 1983, **32**, 43.
3. R. Lundqvist, *Acta Chem. Scand.* 1982, **A36**, 741.
4. K. J. Cantrell, Rare earth element speciation in seawater, Thesis, University of South Florida, St. Petersburg (1986).
5. K. J. Cantrell and R. H. Byrne, *Geochim. Cosmochim. Acta* 1987, **51**, 597.
6. C. R. Olsen, P. D. Lowry, S. Y. Lee, I. L. Larsen and N. H. Cutshall, *Geochim. Cosmochim. Acta* 1986, **50**, 593.
7. B. Allard, *Actinides in Perspective* (Edited by N. M. Edenlstein), pp. 553–580. Pergamon Press, Oxford (1982).
8. K. Spahiu, *Acta Chem. Scand.* 1985, **A39**, 33.
9. R. D. Shannon, *Acta Cryst.* 1976, **A32**, 751.
10. K. B. Krauskopf, *Chem. Geology* 1986, **55**, 323.
11. R. H. Byrne and W. L. Miller, *Geochim. Cosmochim. Acta* 1985, **49**, 1837.
12. F. J. Millero and D. R. Schreiber, *Am. J. Sci.* 1982, **282**, 1508.
13. K. J. Cantrell and R. H. Byrne, *J. Sol. Chem.* 1987, **16**, 555.

Polyhedron Vol. 7, No. 7, pp. 575–577, 1988
Printed in Great Britain

0277–5387/88 $3.00+.00
Pergamon Press plc

COMMUNICATION

PREPARATION AND CHARACTERIZATION OF RUTHENIUM COMPLEXES WITH THE NEW 4,4′,4″-TRI-*TERT*-BUTYL-TERPYRIDINE LIGAND AND WITH 4,4′-DI-*TERT*-BUTYL-BIPYRIDINE

T. BEN HADDA and H. LE BOZEC†

Laboratoire de Chimie de Coordination Organique, U.A. 415, Campus de Beaulieu, Université de Rennes, 35042 Rennes Cedex, France

(*Received* 19 *November* 1987; *accepted* 16 *December* 1987)

Abstract—An efficient procedure for the preparation of 4,4′,4″-tri-*tert*-butylterpyridine (trpy*) which is formed together with 4,4′-di-*tert*-butylbipyridine (bipy*) is described, and the preparation of the complexes (trpy*)$RuCl_3$, [(trpy*)L_2Ru—Cl]PF_6 (L_2 = bipy, bipy*), and (bipy*)$_2RuCl_2$ and their characterization by cyclic-voltametry, UV–vis and ^1H NMR spectroscopy are reported. It is shown that introduction of *tert*-butyl substituents increases the solubility of the resultant complexes and enhances the electron donating influence of the trpy ligand.

Polypyridines such as 2,2′-bipyridine (bipy) or 2,2′,2″-terpyridine (trpy) have been widely used as chelating agents. In particular, since the use of $Ru(bipy)_3^{2+}$ as a photosensitizer,[1] there has been an upsurge of interest in d^6 polypyridine metal complexes[2,3] because of their exceptional electrochemical and photochemical properties and their potential use in the conversion of light energy into chemical energy.[3] Moreover, high-valent polypyridyl ruthenium–oxo complexes have been found to be stoichiometric or catalytic oxidants.[4] Solution chemistry of bipy and trpy complexes is often limited to highly polar aprotic and/or protic solvents. For example, (bipy)$_2RuCl_2$ is insoluble in toluene and ether and [(trpy)(bipy)Ru—Cl]PF_6 has limited solubility in polar organic solvents such as CH_2Cl_2 and THF. Use of alkyl-substituted bipy and trpy should enhance solubilities in non-polar solvents. Although the chemistry of complexes containing 4,4′ disubstituted bipyridines is established,[5] the chemistry of complexes containing 4,4′,4″-trisubstituted-2,2′,2″-terpyridines is unexplored probably because the substituted ligands have not been readily available.‡

We wish to report here an efficient and convenient preparation of the new ligand 4,4′,4″-di-*tert*-butyl-2,2′,2″-terpyridine (trpy*) formed together with 4,4′-di-*tert*-butyl-2,2′-bipyridine (bipy*). The potential utility of these ligands is demonstrated by preparation and characterization of several Ru(II) complexes which exhibit increased solubility in non-polar solvents and modified redox properties relative to their bipy and trpy analogs.

Trpy* (**2**) was prepared by using an adaptation of the procedure of Rosevear and Sasse.[6] Freshly distilled 4-*tert*-butylpyridine was refluxed with 10% palladium on a carbon catalyst for 3 days. Extraction of the mixture with dichloromethane followed by filtration to remove the catalyst, and distillation of the unreacted pyridine (5–8%) gave a mixture of (**1**) and (**2**). Their separation using column chromatography proved to be tedious, but we found

† Author to whom correspondence should be addressed.

‡ Only one preliminary report of the preparation of 4,4′,4″-trialkyl-terpyridines (R = Me, Et, *i*-Pr, *n*-Bu, *n*-pent) has appeared and yields were unattractive for large scale preparations (1–15%).[6]

Table 1. Spectral and reduction potential values

Complex	$E_{1/2}$[a] (V) [ΔEp (mV)]	λ max[b] (nm)	ε max (L mol^{-1} cm^{-1})
[(trpy)(bipy)Ru—Cl]PF_6	0.81	504[11]	—
[(trpy*)(bipy)Ru—Cl]PF_6	0.73(70)	507	11500
[(trpy*)(bipy*)Ru—Cl]PF_6	0.69(70)	510	11000
[bipy]$_2RuCl_2$	0.32(65)[12]	553[12]	9100
[bipy*]$_2RuCl_2$	0.22(70)	555	9850

[a] Determined by cyclic voltammetry at a scan rate of 200 mV s^{-1} in 0.1 M Bu_4NPF_6—CH_3CN *vs* SCE.

[b] ε max in CH_3CN for the lowest energy absorption band only.

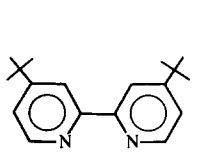

1: bipy*

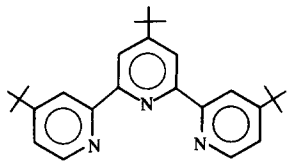

2: trpy*

that bipy* (**1**) could be efficiently separated by sublimation† (45–60%). This derivative has been previously prepared in 64% yield by Belser and Von Zelewsky[7] using Raney nickel as catalyst. Extraction of the unsublimed residue with dichloromethane afforded pure trpy* (**2**) in 37–50% yield.† To our knowledge this procedure represents the first large-scale preparation of a 4,4′,4″-trialkyl-2,2′,2″-terpyridine (15–25 g).

(trpy*)$RuCl_3$,‡ was easily synthesized by treatment of trpy* (**2**) with $RuCl_3$,$3H_2O$ in ethanol under reflux, a method earlier described to make the corresponding complex (trpy)$RuCl_3$.[8] Reaction of (**3**) with bipy or bipy* (**1**) in the presence of the reductant Et_3N in a 2/1 mixture of ethanol/water under reflux gave, after treatment with NH_4PF_6, high yields of [(trpy*)(bipy)Ru—Cl]PF_6 (**4**) (95%) and [(trpy*)(bipy*)Ru—Cl]PF_6 (**5**) (95%), respectively‡ (Scheme 1). Unlike [(trpy)(bipy)RuCl]PF_6,[9] complexes (**4**) and (**5**) are very soluble in dichloromethane, chloroform and the tetrahydrofuran. Moreover, their slight solubility in *toluene* allowed their purification by soxhlet extraction. As for the free ligand (**2**), complex (**4**) shows in the ^{1}H NMR spectrum two signals for the *tert*-butyl groups in the ratio $\frac{1}{2}$ [δ ($CDCl_3$) 1.63(9H); 1.33(18H)]. In the case of complex (**5**), the ^{1}H NMR data supports the structure represented in Fig. 1. The *tert*-butyl groups give rise to two additional signals characteristic of a disymmetric bipy* ligand [δ ($CDCl_3$) 1.63(9H); 1.58(9H); 1.30(18H); 1.23(9H)].

The black violet (bipy*)$_2RuCl_2$ (**6**)‡ was obtained in 15% yield only by using the procedure reported for the preparation of (bipy)$_2RuCl_2$,[10] i.e. by heating $RuCl_3$,$3H_2O$ with LiCl and bipy* in DMF at reflux. The yield increased markedly (63%) simply by using ethylene glycol as solvent instead of DMF. In DMF, the formation of a carbonylated complex (bipy*)$_2$Ru(CO)Cl$^+$ was also observed§ whereas in ethylene glycol the luminescent complex (bipy*)$_3Ru^{2+}$ was isolated in low yield.[7] Compound (**6**) was easily separated from these salts and purified by soxhlet extraction in toluene. In contrast to the insolubility of (bipy)$_2RuCl_2$, complex (**6**) can be dissolved in toluene or ether. Complex (**6**) shows in

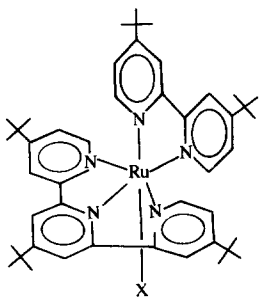

Fig. 1. Structure of complex (**5**) in solution.

† Compounds (**1**) and (**2**) gave satisfactory elemental analyses and/or mass spectral measurements. ^{1}H NMR data (δ, $CDCl_3$) (**1**): 8.59 (dd, J = 5.3 and 0.6 Hz, 2H); 8.42 (dd, J = 2.0 and 0.6 Hz, 2H); 7.29 (dd, J = 5.3 Hz and 2.0 Hz, 2H); 1.37 (s, 18H). [(δ, $CDCl_3$) (**1**):[7] 8.64 (d, J = 5.4 Hz, 2H); 8.48 (s, 2H); 7.3 (d, J = 5.2, 2H); 1.38 (s, 18H)]. (**2**): 8.74 (dd, J = 1.9 and 0.7 Hz, 2H); 8.62 (dd, J = 5.1 and 0.7 Hz, 2H); 8.48 (s, 2H); 7.32 (dd, J = 5.1 and 1.9 Hz, 2H); 1.46 (s, 9H, ^{t}Bu); 1.42 (s, 18H, ^{t}Bu).

‡ New complexes (**3**)–(**6**) have all given satisfactory elemental analyses.

§ (bipy*)$_2$Ru(CO)Cl](PF$_6$): IR(Nujol) ν(CO) 1955 cm^{-1}; cyclic voltammetry (0.1 M Bu_4NPF_6 in CH_3CN *vs* SCE) $E_{1/2}$(Ru(III)/Ru(II)) = 1.42 V; ΔEp = 80 mV.

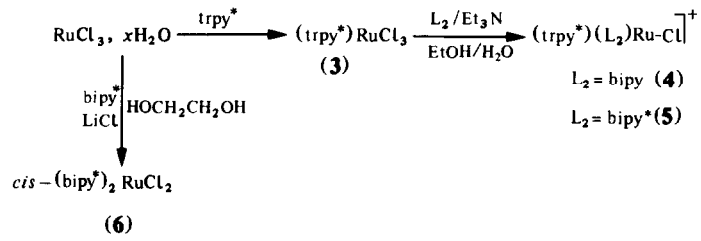

Scheme 1.

the ^{1}H NMR spectrum two signals for the *tert*-butyl groups [δ($CDCl_3$) 1.48(9H); 1.44(9H)] in agreement with the *cis* position of the chloro groups.

Relevant electrochemical and spectroscopic data for (**4**), (**5**) and (**6**) are listed in Table 1. Their lowest energy absorption band can be assigned to MLCT transitions of the type Ru(dπ) → trpy* or bipy*/bipy(π*). Comparison with the MLCT absorption maxima of the related bipy and trpy ruthenium complexes shows a small but progressive bathochromic shift as *tert*-butyl groups are introduced. $E_{1/2}$ values for the reversible Ru(III)/Ru(II) couples were determined by cyclic voltammetry (Table 1). These values show that progressive introduction of *tert*-butyl groups on bipy and trpy ligands results in a substantial decrease of the half-wave potential and makes the complexes easier to oxidize by *ca* 25 mV per *t*-Bu.

Acknowledgement—We wish to thank Prof. P. H. Dixneuf for many helpful discussions.

REFERENCES

1. (a) J. N. Demas and A. W. Adamson, *J. Am. Chem. Soc.* 1971, **93**, 1800; (b) H. Gafney and A. W. Adamson, *J. Am. Chem. Soc.* 1972, **94**, 8238.
2. (a) G. L. Geoffroy and M. S. Wrighton, *Organometallic Photochemistry*. Academic Press, New York (1979); (b) J. V. Caspar, B. P. Sullivan and T. J. Meyer, *Inorg. Chem.* 1984, **23**, 2104; (c) E. M. Kober, B. P. Sullivan, W. J. Dressick, J. V. Caspar and T. J. Meyer, *J. Am. Chem. Soc.* 1980, **102**, 7383; (d) C. Creutz, M. Chou, T. L. Netzel, M. Okumura and N. J. Sutin, *J. Am. Chem. Soc.* 1980, **102**, 1309; (e) G. A. Allen, B. P. Sullivan and T. J. Meyer, *J. Chem. Soc., Chem. Commun.* 1981, 793.
3. K. Kalyanasundaram, *Coord. Chem. Rev.* 1982, **46**, 159 and refs therein.
4. (a) B. A. Moyer, M. S. Thompson and T. J. Meyer, *J. Am. Chem. Soc.* 1980, **102**, 2310; (b) M. S. Thompson and T. J. Meyer, *J. Am. Chem. Soc.* 1982, **104**, 4106; (c) M. S. Thompson, W. F. De Giovani, B. A. Moyer and T. J. Meyer, *J. Org. Chem.* 1984, **25**, 4972; (d) M. E. Marmion and K. J. Takeuchi, *J. Am. Chem. Soc.* 1986, **108**, 510; (e) J. C. Dobson, W. K. Seok and T. J. Meyer, *Inorg. Chem.* 1986, **25**, 1513.
5. (a) G. Sprintschnik, H. W. Sprintschnik, P. P. Kirsch and D. G. Whitten, *J. Am. Chem. Soc.* 1977, **99**, 4947; (b) P. J. Delaive, J. T. Lee, H. W. Sprintschnik, H. Abruna, T. J. Meyer and D. G. Whitten, *J. Am. Chem. Soc.* 1977, **99**, 7094; (c) A. Juris, V. Balzani, P. Belser and A. Von Zelewski, *Helv. Chim. Acta* 1981, **64**, 2175; (d) A. Basu, M. A. Weiner, T. C. Strekas and H. D. Gafney, *Inorg. Chem.* 1982, **21**, 1085; (e) C. M. Elliot and E. J. Hershenhart, *J. Am. Chem. Soc.* 1982, **104**, 7519; (f) A. A. Del. Paggio and D. R. McMillin, *Inorg. Chem.* 1983, **22**, 691; (g) J. A. Connor and C. Overton, *J. Organometal. Chem.* 1983, **249**, 165; (h) J. A. Connor, C. Overton and N. El Murr, *J. Organometal. Chem.* 1984, **277**, 277; (i) W. F. Wacholtz, R. A. Auerbach and R. H. Schmehl, *Inorg. Chem.* 1986, **25**, 227.
6. P. E. Rosevear and W. H. F. Sasse, *J. Heterocycl. Chem.* 1971, **8**, 483.
7. P. Belser and A. Von Zelewsky, *Helv. Chim. Acta* 1980, **63**, 1675.
8. B. P. Sullivan, J. M. Calvert and T. J. Meyer, *Inorg. Chem.* 1980, **19**, 1404.
9. (a) F. P. Dwyer, H. A. Goodwin and E. C. Gyarfas, *Aust. J. Chem.* 1963, **16**, 42; (b) K. J. Takeuchi, M. S. Thompson, D. W. Pipes and T. J. Meyer, *Inorg. Chem.* 1984, **23**, 1845.
10. B. P. Sullivan, D. J. Salmon and T. J. Meyer, *Inorg. Chem.* 1978, **17**, 3334.
11. M. J. Root and E. Deutsch, *Inorg. Chem.* 1985, **24**, 1464.
12. J. N. Braddock and T. J. Meyer, *Inorg. Chem.* 1973, **12**, 723.

Polyhedron Vol. 7, No. 7, pp. 579–580, 1988
Printed in Great Britain

0277–5387/88 $3.00+.00
Pergamon Press plc

COMMUNICATION

NEW, IMPROVED SYNTHESES OF THE GROUP 6 OXYHALIDES, $W(O)Cl_4$, $W(O)_2Cl_2$ AND $Mo(O)_2Cl_2$

VERNON C. GIBSON,* TERENCE P. KEE and ALAN SHAW

Department of Chemistry, University Science Laboratories, South Road, Durham DH1 3LE, U.K.

(*Received* 2 *December* 1987; *accepted* 18 *December* 1987)

Abstract—Hexamethyldisiloxane is a useful reagent for the convenient, high yield preparation of oxyhalide derivatives of molybdenum and tungsten.

Oxo complexes of the group 6 elements play a central role in a variety of industrial and biological oxidation processes.[1] Progress towards understanding the reactivity of the metal–oxo moiety in these systems is largely dependent upon the availability of convenient and generally applicable routes to complexes through which the properties of the oxo ligand can be addressed. However, useful starting materials such as oxyhalides have not generally been available via mild synthetic procedures. For example, $W(O)Cl_4$ is most commonly accessed by prolonged reflux of the hydrated metal oxide with $SOCl_2$,[2,3]† while $Mo(O)_2Cl_2$ and $W(O)_2Cl_2$ are prepared by a pyrolysis of $Mo(O)Cl_3$ resulting in a mixture of $Mo(O)_2Cl_2$ and $Mo(O)Cl_4$,[4] and by heating a 2 : 1 mixture of WO_3 and WCl_6 in a sealed tube,[5] respectively.

As part of a programme of research directed towards the study of metal-bound oxygen atoms, we have searched for a method of introducing oxygen atoms into the metal coordination sphere under controlled, mild conditions. Here, we wish to describe the use of hexamethyldisiloxane, $(Me_3Si)_2O$ for the convenient preparation of oxyhalide compounds of the group 6 metals.

EXPERIMENTAL

All manipulations of air and/or moisture sensitive materials were carried out on a conventional vacuum line using standard Schlenk or cannula techniques, or in a dry-box under an atmosphere of nitrogen. Solvents were dried, distilled and degassed prior to use. Metal and halide analyses were provided by the microanalytical service at Durham. IR spectra (Nujol mulls between KBr plates) were recorded using Perkin–Elmer 577 and 457 spectrophotometers. WCl_6, $Mo(O)Cl_4$ (Alfa) and $(Me_3Si)_2O$ (Aldrich) were used as received.

All oxyhalide products were obtained in analytically pure form.

Synthesis of $W(O)Cl_4$

A dichloromethane solution of $(Me_3Si)_2O$ (2.05 g, 12.6 mmol in 15 cm^3 CH_2Cl_2) was added dropwise to a suspension of WCl_6 (5.0 g, 12.6 mmol) in dichloromethane (20 cm^3) at room temperature over a period of 15 min. An immediate reaction ensued leading to deposition of $W(O)Cl_4$ in the form of red crystals. The mixture was stirred for a further 60 min. The supernatant liquor was then removed by filtration and the solid was collected, washed with petroleum ether (b.p. 40–60°C, 2 × 20 cm^3) and dried *in vacuo*. Yield 4.28 g, 99%. Found: W, 53.9; Cl, 41.2. Calc. for Cl_4OW: W, 53.8; Cl, 41.5%. IR: ν(W—O—W), 880–900 cm^{-1} (broad, strong). For synthesis purposes, further purification by sublimation is unnecessary.

* Author to whom correspondence should be addressed.

† $W(O)Cl_4$ may also be prepared by the treatment of WCl_6 with Me_3SiOMe at room temperature in dichloromethane (R. R. Schrock, personal communication).

Synthesis of $W(O)_2Cl_2$

A petroleum ether (b.p. 100–120°C) solution of $(Me_3Si)_2O$ (2.38 g, 14.7 mmol in 15 cm^3 petroleum ether) was added to a suspension of $W(O)Cl_4$ (5.0 g, 14.6 mmol) in high boiling petroleum ether (b.p. 100–120°C, 40 cm^3). The mixture was heated overnight at 100°C to give a yellow solid and a colourless solution. After cooling to room temperature, the supernatant solution was decanted from the solid, which was collected, washed with light petroleum ether (b.p. 40–60°C, 2×20 cm^3) and dried *in vacuo*. Yield 3.99 g, 95%. Found: W, 63.7; Cl, 24.4. Calc. for Cl_2O_2W: W, 64.1; Cl, 24.7% IR: ν(W—O—W), 800–830 cm^{-1} (broad, strong).

Synthesis of $Mo(O)_2Cl_2$

A dichloromethane solution of $(Me_3Si)_2O$ (3.2 g, 19.7 mmol in 15 cm^3 CH_2Cl_2) was added to a suspension of $Mo(O)Cl_4$ (5.0 g, 19.7 mmol) in dichloromethane (20 cm^3). The mixture was stirred at room temperature overnight to give a yellow solid and a colourless solution. The supernatant solution was decanted from the solid, which was collected, washed with light petroleum ether (b.p. 40–60°C, 2×20 cm^3) and dried *in vacuo*. Yield 3.78 g, 97%. Found: Cl, 35.7. Calc. for Cl_2O_2Mo: Cl, 35.7%. IR: ν(Mo—O—Mo), 800–830 cm^{-1} (broad, strong).

CONCLUSION

Treatment of the halides (or oxyhalides) of the group 6 metals with commercially available hexamethyldisiloxane facilitates the introduction of oxygen atoms into the metal coordination sphere in a controlled, mild fashion, with minimal risk of product contamination as the sole by-product, Me_3SiCl, is volatile and hence readily removed. The pertinent features of this transformation are shown in eq. (1).

$$[M]Cl_2 + (Me_3Si)_2O \rightarrow [M]{=}O + 2Me_3SiCl. \quad (1)$$

Thus, the preparations described here offer improved, high yield routes to excellent purity oxyhalide products, which should have general use in the synthesis of new oxo complexes of these metals. The use of $(TMS)_2O$ for the introduction of oxygen atoms into the coordination sphere of other metals and well-defined organotransition metal environments will form subjects of future reports.

Acknowledgements—We would like to thank the S.E.R.C. for a grant and studentships (to T.P.K. and A.S.), and Prof. R. R. Schrock for helpful discussions.

REFERENCES

1. See, for example (a) Proc. Climax Fifth Int. Conf. The chemistry and uses of molybdenum compounds, *Polyhedron* 1986, **5**, 1; (b) R. A. Sheldon and J. K. Kochi, *Metal Catalysed Oxidations of Organic Compounds*. Academic Press, New York (1981); (c) C. D. Garner and S. Bristow, *Molybdenum Enzymes* (Edited by T. G. Spiro), pp. 343–410. John Wiley, New York (1985).
2. R. Colton, I. B. Tompkins and P. W. Wilson, *Aust. J. Chem.* 1964, **17**, 496.
3. R. H. Crabtree and G. G. Hlatky, *Polyhedron* 1985, **4**, 521.
4. I. A. Glukhov and S. S. Eliseev, *Russ. J. Inorg. Chem.* 1963, **8**, 50.
5. P. C. Crouch, G. W. A. Fowles and R. A. Walton, *J. Inorg. Nucl. Chem.* 1970, **32**, 329.

Polyhedron Vol. 7, No. 7, pp. 581–583, 1988
Printed in Great Britain

0277–5387/88 $3.00+.00
Pergamon Press plc

COMMUNICATION

^{77}Se NMR SPECTRA OF Se_7 AND Se_5S_2 PREPARED FROM TITANOCENE PENTASELENIDE; EVIDENCE FOR PSEUDOROTATION†

RALF STEUDEL‡ and MARIA PAPAVASSILIOU

Institut für Anorganische und Analytische Chemie, Technische Universität Berlin, Sekr. C 2, D-1000 Berlin 12, F.R.G.

and

WILLI KRAMPE

Institut für Anorganische Chemie, Universität zu Köln, D-5000 Köln 41, F.R.G.

(*Received* 10 *December* 1987; *accepted* 4 *January* 1988)

Abstract—The natural abundance ^{77}Se NMR spectra of Se_7 (singlet at 996 ppm *vs* Me_2Se) and of Se_5S_2 (singlets at 976, 1023 and 1085 ppm) show that these puckered seven-membered ring molecules undergo pseudorotation at 20°C in CS_2 solution. This internal puckering motion makes all atoms of Se_7 equivalent on the NMR time scale, and results in only three sets of non-equivalent Se atoms in Se_5S_2. The chemical shift of seven-membered Se-containing ring molecules is much larger than that of comparable six- or eight-membered homo- or heterocycles, reflecting the unique bonding situation.

Titanocene pentachalcogenides $(C_5H_5)_2TiE_5$ (E = S, Se) react with the sulphur and selenium chlorides S_2Cl_2 and Se_2Cl_2 to give the seven-membered ring molecules S_7,[2] 1,2-Se_2S_5,[3] 1,2,3,4,5-Se_5S_2[4] and Se_7,[4] respectively.

$$(C_5H_5)_2TiE_5 + E'_2Cl_2 \rightarrow E_5E'_2 + (C_5H_5)_2TiCl_2 \qquad (E, E' = S, Se).$$

According to solid state Raman spectra, single crystal X-ray diffraction results and theoretical calculations, all four Se_nS_{7-n} compounds mentioned above form chair-like puckered rings.[3–7] However, there is evidence that at least S_7 and Se_2S_5 undergo pseudorotation in the vapour phase (S_7)[5,8] and in CS_2 solution (S_7, Se_2S_5),[8] respectively. This ring puckering motion known from cycloheptane averages the different atomic positions in these low symmetry molecules, and consequently Se_2S_5 exhibits only one ^{77}Se NMR signal (in CS_2: 1077 ppm *vs* Me_2S)[6] although in solid Se_2S_5 the Se atoms occupy non-equivalent sites.[3] Se_7 has four and Se_5S_2 five non-equivalent Se atoms in the solid state.[4] However, we now report evidence that these Se-rich seven-membered ring molecules also undergo pseudorotation.

All selenium allotropes dissolve in CS_2 at 20°C to give a solution of mainly Se_8 with a few per cent each of both Se_6 and Se_7 which are in equilibrium with each other.[9] ^{77}Se NMR spectra of such solutions show the signals of Se_8 (615 ppm) and Se_6 (685 ppm) only.[10] We have prepared solutions of higher Se_7 concentrations by reacting $(C_5H_5)_2TiSe_5$ with Se_2Cl_2 at 20°C in CS_2[4] and recorded the ^{77}Se NMR spectra immediately after the mixing of the components and filtering off the titanocene dichloride (natural abundance of ^{77}Se: 7.6%). The spectra [see Fig. 1(a)] showed in addition to the signals of Se_8 (614 ppm) and Se_6 (684 ppm) a small peak at 996 ppm which we assign to Se_7 since Se_2S_5[8] and

† Part 116 of the series sulfur and selenium compounds. For Part 115 see ref. 1.

‡ Author to whom correspondence should be addressed.

Se_5S_2 (see below) also exhibit their NMR signals near 1000 ppm. During the measurement which took 61.5 h, Se_7 decomposed partly to give the above mentioned equilibrium mixture of the three homocycles.[4,9] The average concentration of Se_7 therefore cannot be estimated. No other signals were observed in the range 542–1512 ppm and all peaks were reproduced with an independent sample.

In an analogous experiment $(C_5H_5)_2TiSe_5$ was reacted with S_2Cl_2 in CS_2 at 20°C and the ^{77}Se spectrum of Se_5S_2 recorded immediately after mixing and filtration (recording time: *ca* 17 h). The result shown in Fig. 1(b) demonstrates that there are three sets of Se atoms in an approximate ratio of 2 : 1 : 2. From the synthesis, the X-ray and Raman spectroscopic results it is obvious that the Se atoms are all neighbouring and we therefore assign the 1023 ppm signal to the central and the 1085 ppm signal to the two terminal atoms of the Se_5 unit, leaving the 976 ppm signal for the other two Se atoms. On this basis, typical ranges for the chemical shift of the structural units of seven-membered Se—S heterocycles can be defined as follows (the shift applies to the starred atoms):

—Se—Se—Se*—Se—Se— : *ca* 1010 ppm

(e.g. Se_7, Se_5S_2)

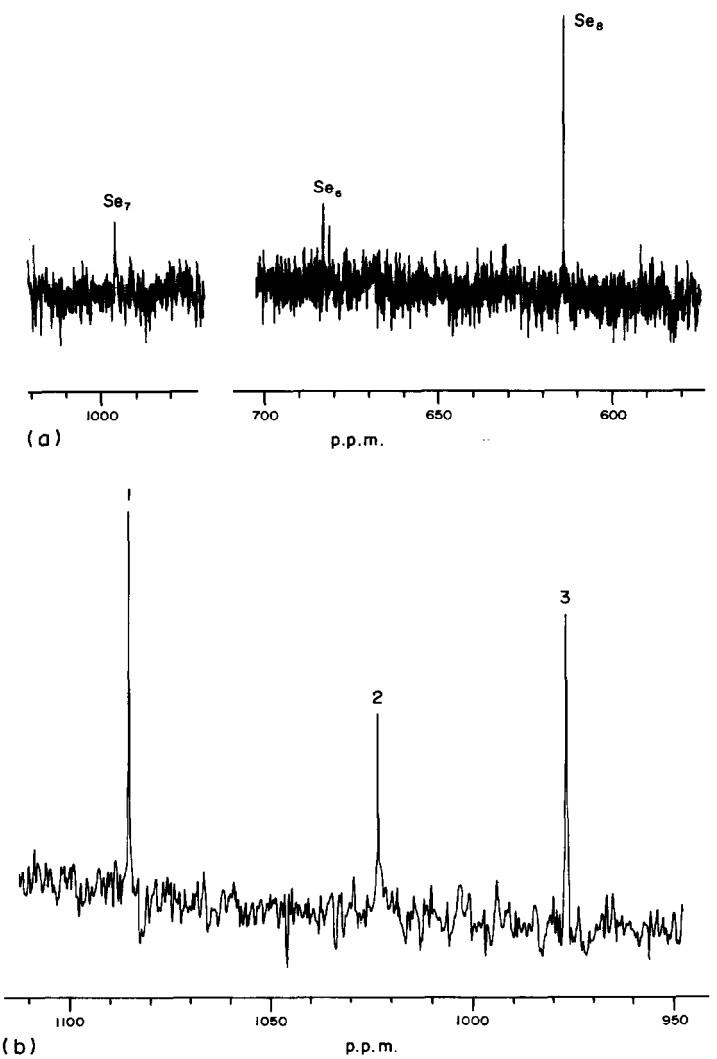

Fig. 1. 300 MHz ^{77}Se NMR spectra of (a) Se_7 (996 ppm), Se_6 (614 ppm) and Se_8 (684 ppm) in CS_2 solution, prepared from 74 mg $(C_5H_5)_2TiSe_5$ and 30 mg Se_2Cl_2 in 11 cm^3 CS_2 (21516 pulses; range: 542–1512 ppm). (b) 1,2,3,4,5-Se_5S_2 (1: 1085, 2: 1023, 3: 976 ppm) in CS_2, prepared from 57 mg $(C_5H_5)_2TiSe_5$ and 13 mg S_2Cl_2 in 11 cm^3 CS_2 (6070 pulses; range: −90–1655 ppm). (Spectrometer: Bruker WM 300 (operating at 57.315 MHz), ext. lock: d_6-acetone, ext. standard: SeO_2(aq) [$\delta(Me_2Se) = \delta(SeO_2(aq)) + 1303$[11]], pulse width: 25 μs, relaxation delay: 10 s, temperature: 296 ± 1 K.)

—Se—Se—Se*—Se—S—: *ca* 980 ppm (e.g. Se_5S_2)

—S—S—Se*—Se—: *ca* 1080 ppm (e.g. Se_5S_2, Se_2S_5)

—S—Se*—S—: > 1100 ppm (not observed yet).

These trends are in agreement with the observations made with eight-membered rings of type Se_nS_{8-n}[10] and with six-membered rings of type Se_nS_{6-n},[8] the ^{77}Se signals of which are found in the range 560–730 ppm.[11] The considerably higher chemical shift of the seven-membered rings must be due to the unique bonding situation in these molecules which is characterized by an alternation of bond orders of the neighbouring bonds.[3–7]

Our results indicate that the barrier to rotation about SeS and SeSe bonds in chalcogen ring molecules is similarly low as the one for SS bonds which has been estimated as $\leqslant 24\ kJ\ mol^{-1}$.[12] An accurate determination of this barrier height from low temperature NMR spectra was not possible due to the low solubility of Se_7 and Se_5S_2.

Se_6 and Se_7 are important components of saturated selenium vapour and must consequently also be present in liquid selenium.[13] The ^{77}Se NMR spectrum of liquid Se[14] will therefore be influenced by the variation of the ratios $Se_6:Se_7:Se_8$ with varying temperature; due to rapid interconversion of these and other Se_n species at temperatures above the melting point of metallic (trigonal) Se (217°C), an average signal only is of course observed.[15]

Acknowledgements—Support by the Deutsche Forschungsgemeinshaft and the Verband der Chemischen Industrie is gratefully acknowledged.

REFERENCES

1. G. Holdt, T. Göbel and R. Steudel, *Königsteiner Chromatograhie-Tage*, Proc., p. 437. Waters-Millipore, Eschborn (1987).
2. M. Schmidt, B. Block, H. D. Block, H. Köpf and W. Wilhelm, *Angew. Chem.* 1968, **80**, 660; M. Schmidt, B. Block, H. D. Block, H. Köpf and E. Wilhelm, *Angew. Chem. Int. Ed. Engl.* 1968, 7, 632.
3. R. Steudel and E.-M. Strauss, *Angew. Chem.* 1984, **96**, 356; R. Steudel and E.-M. Strauss, *Angew. Chem. Int. Ed. Engl.* 1984, **23**, 362.
4. R. Steudel, M. Papavassiliou, E.-M. Strauss and R. Laitinen, *Angew. Chem.* 1986, **98**, 81; R. Steudel, M. Papavassiliou, E.-M. Strauss and R. Laitinen, *Angew. Chem. Int. Ed. Engl.* 1986, **25**, 99.
5. R. Steudel and F. Schuster, *J. Mol. Struct.* 1978, **44**, 143.
6. R. Steudel, J. Steidel, J. Pickardt, F. Schuster and R. Reinhardt, *Z. Naturforsch.* 1980, **35b**, 1378.
7. D. Hohl, R. O. Jones, R. Car and M. Parrinello, *Chem. Phys. Lett.* 1987, **139**, 540.
8. R. Steudel, M. Papavassiliou, D. Jensen and K. Seppelt, *Z. Naturforsch.* 1988, **42b**, 245.
9. R. Steudel and E.-M. Strauss, *Z. Naturforsch.* 1981, **36b**, 1085.
10. R. S. Laitinen and T. A. Pakkanen, *Inorg. Chem.* 1987, **26**, 2598.
11. R. S. Laitinen and T. A. Pakkanen, *J. Chem. Soc., Chem. Commun.* 1986, 1381.
12. R. Steudel, *Z. Naturforsch.* 1983, **38b**, 543.
13. For a recent review on elemental selenium see R. Steudel and E.-M. Strauss, *Adv. Inorg. Chem. Radiochem.* 1984, **28**, 135.
14. W. W. Warren and R. Dupree, *Phys. Rev. B* 1980, **22**, 2257.
15. S. G. Bishop and P. C. Taylor, *Solid State Commun.* 1972, **11**, 1323.

Polyhedron Vol. 7, No. 7, pp. 585–586, 1988
Printed in Great Britain

0277-5387/88 $3.00+.00
© 1988 Pergamon Press plc

COMMUNICATION

PREPARATION OF CRYSTALLINE TIN(IV) MOLYBDATE HAVING AN UNEXPECTEDLY LOW DENSITY

J. BUITEN

DSM Central Laboratory, P.O. Box 18, 6160 MD Geleen, The Netherlands

(*Received* 4 *August* 1987; *accepted after revision* 13 *January* 1988)

Abstract—Crystalline tin(IV) molybdate ($Sn(MoO_4)_2$) which is stable at temperatures below 500°C is not known in the literature. It has been found that this compound is formed when MoO_3 is exposed at 430–500°C to the action of $SnCl_4$ in the presence of O_2. The reaction involves the formation of MoO_2Cl_2. Characteristic *d*-values of the X-ray diffraction lines of the new compound are given. Its density (4.1 g cm^{-3}) is very low compared with the densities of MoO_3 and SnO_2 (4.7 and 7.0 g cm^{-3}). The compound decomposes when heated at 700°C.

In the past 20 years numerous papers have been published on the system SnO_2–MoO_3 as a catalyst for the partial oxidation of propylene in the gas phase. It appears from general experience that SnO_2–MoO_3 catalysts do not contain a compound of the two oxides which can be identified by X-rays, although the formation of a compound could be expected from the mode of preparation of these catalysts. The absence of a compound is confirmed by recent investigations of Berry *et al.*[1–3] However, some years ago Safonov *et al.*[4] reported a phase equilibrium diagram of the system SnO_2–MoO_3 in which a compound $SnO_2 \cdot 2MoO_3$ melting at 903°C appears (presumably evaporation of MoO_3 was prevented in the experiments). Its X-ray diffraction lines were determined at 750°C. The compound is stable only at high temperatures; Safonov *et al.* observed that it decomposes into SnO_2 and MoO_3 at temperatures below 500°C. As is shown by the present communication, a compound $SnO_2 \cdot 2MoO_3$ or $Sn(MoO_4)_2$ which is *stable at temperatures below 500°C* and shows X-ray diffraction lines which are quite different from those of Safonov's compound also exists.

THE REACTION BETWEEN $SnCl_4$ AND MoO_3

Oxygen saturated with $SnCl_4$ at 60°C was led through a fluidized bed of 20 g of MoO_3 for 7 h; the temperature of the bed was 430°C.* A SEM photo of a specimen of the resulting mass showed that rods of MoO_3, while retaining their overall shape, had changed into conglomerates comprising rounded crystals of 10–20 μm. As appears from the X-ray diffraction lines of the reaction product, an unknown compound had been formed. This compound is not a chloride or oxychloride, as only a small trace of Cl could be detected. Moreover experiments were performed using a reactor, the central part of which was an open cylindrical vessel (internal diameter 20 mm) with a flat bottom. 1 g of MoO_3 powder was introduced into the vessel and a stream of oxygen or air carrying $SnCl_4$ was supplied from above to the layer of MoO_3, for 3–6 h and at a temperature of 500°C. Observations of some vessel reactor masses with a light or a scanning electron microscope showed the presence of octahedric crystals, the size of which was about 0.1 mm. The same characteristic X-ray diffraction lines were found as with the fluid bed.

Diffraction lines of MoO_3 and SnO_2 were observed in addition to those of the new compound.

* The combination of $SnCl_4$ and MoO_3 was proposed by Dr H. Bruins Slot of the DSM Central Laboratory.

The contents of these oxides could be estimated by means of the ratios of the intensities of suitable lines. By variation of the reaction conditions it was found that as long as MoO_3 has not been used up, the compound is formed and only a little SnO_2 is deposited as such. However, once the free MoO_3 is exhausted, the compound itself is attacked, resulting in the formation of SnO_2. The atomic Sn/Mo ratio of the compound was calculated from the Sn content of some fluid bed and vessel reactor preparations containing little amounts of free SnO_2 and MoO_3 (which were taken into account). Values varying from 0.47 to 0.50 were obtained, so it can be concluded that the compound is a 1 : 2 compound of SnO_2 and MoO_3. This can be considered as tin molybdate with the formula $Sn(MoO_4)_2$.

Molecular oxygen strongly favours the formation of tin molybdate, for it appears that from the beginning more tin is deposited as SnO_2 than as $Sn(MoO_4)_2$ if nitrogen is used as the carrier gas for $SnCl_4$. MoO_3 is not only consumed for the formation of $Sn(MoO_4)_2$ but also for the formation of MoO_2Cl_2 which, being a sublimable substance, is deposited on cooler parts of the reactor. The weight loss of the vessel combined with the Sn percentage always agreed with the reaction:

$$SnCl_4 + 2MoO_3 \rightarrow SnO_2\,(\text{bound plus free}) + 2MoO_2Cl_2\uparrow$$

PROPERTIES OF TIN MOLYBDATE

If $Sn(MoO_4)_2$ is heated in air or argon at 750°C for 2 h, it decomposes completely and MoO_3 is deposited on a cooler part. There is partial decomposition at 700°C (in argon to a higher degree than in air). The compound is fairly stable at 600°C.

X-ray diffraction gave the following characteristic *d*-values (in Å; relative intensities in parentheses): 5.16 (25), 4.47 (30), 4.00 (100), 3.65 (74), 3.16 (53), 2.70 (78), 2.48 (15), 2.39 (27), 2.00 (41), 1.95 (24). These are clearly different from those of the phase $SnO_2 \cdot 2MoO_3$ noted by Safonov *et al.*[4]

A 0.1 mm crystal was used for making Weissenberg X-ray exposures, which showed the crystal to belong to the primitive cubic space group *Pa*3. This complies with the presence of four $Sn(MoO_4)_2$ "molecules" per unit cell, with Sn atoms at the corners and at the centres of the side faces. Debije–Scherrer exposures of powdered single crystals yielded a lattice constant of 8.939 Å. The density of the compound following from this value and the presence of $4 \times Sn(MoO_4)_2$ in the cubic unit cell is 4.078 g cm^{-3}. The density of 12 g of a fluid bed preparation was determined by the helium method. A value of 4.11 g cm^{-3} was found, which is in sufficient agreement with the X-ray value. It follows from the density value of 4.078 that the volume of 1 mole of $Sn(MoO_4)_2 (= SnO_2 \cdot 2MoO_3)$ is 30% larger than the volume of 1 mole of SnO_2 plus the volume of 2 moles of MoO_3 (densities used for SnO_2 and MoO_3 7.0 and 4.7 g cm^{-3}, respectively). It is believed that an expansion of this magnitude is quite uncommon for compounds based on two metal oxides.

REFERENCES

1. F. J. Berry and C. Hallett, *Inorg. Chim. Acta* 1985, **98**, 135.
2. F. J. Berry, C. Hallett and M. H. Loretto, *J. Solid State Chem.* 1985, **58**, 176.
3. D. J. Smith, L. A. Freeman, F. J. Berry and C. Hallett, *J. Solid State Chem.* 1985, **58**, 342.
4. V. V. Safonov, N. V. Porotnikov and N. G. Chaban, *Russ. J. Inorg. Chem.* 1983, **28**, 462.

Polyhedron Vol. 7, No. 7, p. 587, 1988
Pergamon Press plc. Printed in Great Britain

BOOK REVIEW

Gmelin Handbook of Inorganic Chemistry, Ga—Organogallium Compounds, Part 1. Published by Gmelin Institute for Inorganic Chemistry of the Max Planck Society for the Advancement of Science. Springer, Berlin, 1987. ISBN 3-540-93545-2, xiv + 514 pp., 105 illus. Hard cover DM 1998.

This volume contains a comprehensive treatment of the literature of compounds containing at least one gallium–carbon bond, up to 1984, and a selective treatment up to the end of 1985. As is to be expected from Gmelin, the presentation is highly systematic and includes liberal tabulation of data; between the Table of Contents and the indices of empirical formulae and ligand formulae (which also contain references to tabular data) the location of information is fairly effortless. As is indicated by the absence of a subject index, this volume has not been intended as a text for general background reading but as its title implies, a handbook primarily for those with some familiarity with the field. The presentation contains 105 illustrations, principally of X-ray crystal structures.

The first chapter deals with the triorganyls and their adducts. Besides the usual physical and chemical properties (once again largely in tables), there is some emphasis on thermolysis/photolysis as well as an attempt to compare purity for the different preparative routes. This obviously alludes to the principal use of these compounds, namely for Metal–organic Chemical Vapour Deposition (MOCVD) of semi-conducting materials, which was dismissed in one paragraph (albeit with 126 refs for further reading).

Subsequent chapters deal with organogallium halides, pseudohalides, chalcogenides and pnictides, plus brief but comprehensive accounts of compounds of organogallium with both main group- and transition metal-containing moieties. The remaining chapters deal with the considerable number of ionic compounds and finally with the gallium(I)–η^6-arene complexes.

In summary, besides the isolated blot e.g. reproduction of literature data such as 8.0761 ± 0.66 (p. 10, line 10), this book can be recommended as an extremely useful reference work for those in this field of chemistry, and particularly for those involved in MOCVD of gallium-containing materials.

Department of Chemistry
Queen Mary College
Mile End Road
Lond, E1 4NS, U.K.

DARIO M. FRIGO

Polyhedron Vol. 7, No. 8, pp. 589–596, 1988
Printed in Great Britain

0277–5387/88 $3.00+.00
Pergamon Press plc

THE ELECTROCHEMISTRY OF THIOCARBONYL AND SELENOCARBONYL IRON OCTAETHYLPORPHYRINS

LAWRENCE A. BOTTOMLEY* and JEAN-NOEL GORCE

School of Chemistry, Georgia Institute of Technology, Atlanta, GA 30332-0400, U.S.A.

(*Received* 3 *October* 1987; *accepted* 11 *November* 1987)

Abstract—The redox reactivity of thiocarbonyl(2,3,7,8,12,13,17,18-octaethylporphinato) iron(II) and selenocarbonyl(2,3,7,8,12,13,17,18-octaethylporphinato)iron(II) was investigated in both non-coordinating and coordinating media at a Pt electrode. Electro-oxidation of both complexes occurred in three discrete, single electron transfer steps with complete retention of the diatomic ligands. Reaction of each porphyrin with a series of nitrogenous bases produced exceptionally stable six-coordinate complexes which could also be oxidized or reduced without loss of the diatomic ligand. Based on the results of detailed spectral (both infrared and electronic), voltammetric and spectroelectrochemical experiments, an electron transfer pathway is proposed.

The discovery[1] of an organometallic intermediate in the metabolic reduction pathway of polyhalogenated hydrocarbons by cytochrome P-450 has spawned considerable interest in the synthesis and properties of model compounds possessing an Fe—C bond.[2] Recent work has focused on two main classes of synthetic models for the cytochrome P-450 intermediate: sigma bonded alkyl or aryl Fe porphyrins and Fe–carbene porphyrin complexes.[3–10] The redox reactivity of compounds from both classes has been of special interest.[11–17] Noteworthy accomplishments include the elucidation of the redox pathway operative in the reversible aryl migration from the Fe centre to the N core of the porphyrin.[12] This work exemplifies the relevance of electrochemical and spectroelectrochemical investigations in providing insights into the metabolic pathway(s) operative *in vivo*.

Our recent efforts have focused on thiocarbonyl[13,14] and selenocarbonyl[15,16] iron porphyrins, structural analogs of carboxy hemoproteins. The electrochemistry of five- and six-coordinate carbonyl iron porphyrin complexes, (Por)FeCO† and (Por)FeCO(L), has been studied by various authors.[18] Without exception, the oxidation of carbonyl ferrous porphyrins is chemically irreversible whereas the reduction of carbonyl ferrous porphyrins yields a unique Fe(I)CO complex.[18e] In contrast, both (TPP)FeCS and (TPP)FeCSe as well as their six-coordinate counterparts can undergo two chemically reversible one-electron-transfer oxidations and a chemically complicated reduction with full retention of the diatomic axial ligand. This work was initiated to assess how changes in the electron donating properties of the porphyrin‡ would affect the lability of the diatomic ligand. Our results are discussed in the context of *cis–trans* effects operative in Fe porphyrins possessing Fe—C bonds.

*Author to whom correspondence should be addressed.

† Abbreviations used: porphinato dianion = POR, 2,3,7,8,12,13,17,18-octaethylporphinato dianion = OEP; 5,10,15,20-tetraphenylporphinato dianion = TPP; tetra-*n*-butylammonium perchlorate = TBAP; nitrogenous base ligand = L; pyridine = py; 1,2-dichloroethane = $EtCl_2$; dimethylformamide = DMF; saturated calomel electrode = SCE; 1,4-diazabicyclo[2,2,2]octane = dabco; Z = S or Se.

‡ We chose the more basic porphyrin OEP (as compared to TPP) rather than the many phenyl or pyrrole substituted TPP porphyrins available, because of the extensive work previously published on this Fe porphyrin. See, for example the following reviews: (a) K. M. Kadish, in *Iron Porphyrins*: *Part II* (Edited by A. B. P. Lever and H. B. Gray), Chap. 4 and refs therein. Addison Wesley, Reading, Massachusetts (1983); (b) R. H. Felton, in *The Porphyrins* (Edited by D. Dolphin), Vol. V, Chap. 3 and refs therein. Academic Press, New York (1979).

EXPERIMENTAL

The syntheses of (OEP)FeCS and (OEP)FeCSe were accomplished in an analogous fashion to that previously reported for the preparation of (TPP)FeCS and (TPP)FeCSe.[6a,b,14,15,18d] Product purity was verified by ^{1}H NMR, both infrared and visible spectroscopy and by satisfactory elemental analyses. All nitrogenous bases were purchased and used as received from the Aldrich Chemical Company. TBAP and $EtCl_2$ were purified in the manner previously described.[14,15]

Infrared spectra were obtained with a Nicolet 5DXB FT-IR spectrometer. Variable temperature ^{1}H NMR spectra were obtained on a Bruker WM-300 spectrometer. A full description of the apparatus and methods of analysis for the spectroelectrochemical and voltammetric experiments has been previously reported.[14,15]

RESULTS AND DISCUSSION

Steady state voltammograms typical of those obtained for (OEP)FeCS are depicted in Fig. 1. Four chemically reversible electron transfer reactions were observed within the accessible potential range of $EtCl_2$ (0.1 M TBAP). Analysis of the current–voltage curves obtained for each process over the potential sweep rate range of 20 mV s^{-1} to 10 V s^{-1} yielded trends consistent with the assignment of the first two oxidation processes (at 0.72 and 1.01 V) as quasireversible one-electron-transfer reactions,* and the first reduction process (at −1.38 V) as a quasireversible one-electron-transfer with a slow following chemical reaction.† A third oxidation process was observed near the anodic limit of the solvent supporting electrolyte system. Due to the overlap with the solvent discharge, a detailed analysis of the current–voltage dependence on potential sweep rate was not possible. However, analysis of the differential pulse voltammetry data by the method of Birke[19] indicated that this was also a one-electron process. A second reduction process, chemically coupled to the first, occurred at an E_p of −1.73 V (measured at a sweep rate of 200 mV s^{-1}). The product of this charge transfer was irreversibly oxidized back to the parent complex at a potential of −0.65 V (measured at 200 mV s^{-1}). Similar results were obtained for (OEP)FeCSe. The midpoint potentials of all charge transfer processes observed for the chalcocarbonyl iron porphyrins are listed in Table 1.

Addition of L to solutions of either (OEP)FeCS or (OEP)FeCSe produced substantial red shifts in the electronic spectrum; for (OEP)FeCS the Soret

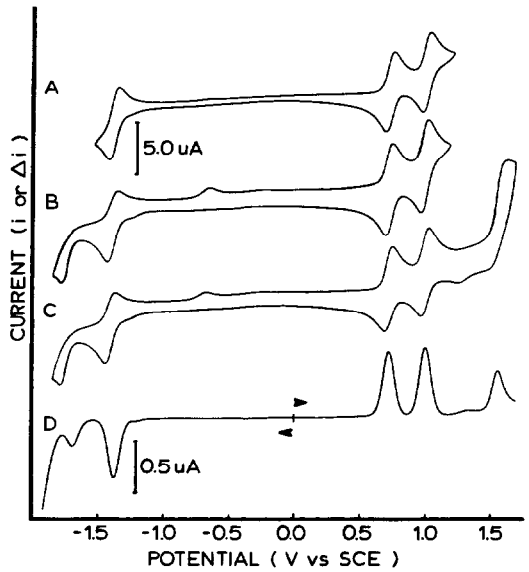

Fig. 1. Steady state cyclic and differential pulse voltammograms of 0.74 mM (OEP)FeCS in $EtCl_2$. Traces A–C are cyclic voltammograms obtained at a potential sweep rate of 200 mV s^{-1}. Trace D is the differential pulse voltammogram taken at a potential sweep rate of 10 mV s^{-1}, a pulse amplitude of 25 mV and a pulse frequency of 0.1 s.

* Spectroelectrochemical experiments confirmed the stability and chemical reversibility of each of the oxidation products. When the applied potential was stepped from 0.20 to 0.85 V in 10 mV increments, the spectrum characteristic of (OEP)FeCS (Soret band at 390 nm and two visible bands at 516 and 551 nm) was transformed into a new spectrum with a diminished Soret band at 383 nm and no dominant visible features. The transition occurred reversibly with isosbestic points at 381, 411, 506 and 568 nm. Similarly, when the applied potential was incrementally increased to 1.20 V, the Soret band at 383 nm shifted to 425 nm and two very low intensity visible bands appeared at 566 and 615 nm. This transition occurred reversibly with isosbestic points at 349, 398, 460, 560 and 579 nm. Nernst plots confirmed the passage of one electron per porphyrin for each charge transfer reaction.

† The presence of the following chemical reaction was confirmed by spectroelectrochemical experiments. When the potential of the optically transparent electrode was stepped from −1.00 to −1.50 V, the Soret band of the parent species was replaced by a new band at 422 nm. The visible bands (at 516 and 551 nm) lost intensity and shifted to 525 and 570 nm, respectively. This transition occurred with isosbestic points at 405, 503 and 560 nm. This spectrum is that characteristic of the thioformyl Fe(II) porphyrin anion. Only when the potential was reset to values positive of −0.65 V, were spectral changes observed. The spectrum obtained was that of the parent compound. Similar results were obtained with (OEP)FeCSe.

Table 1. Mid-Point potentials[a] of (Por)FeCZ complexes in $EtCl_2$

Complex	Charge on redox couple +3/+2	+2/+1	+1/0	0/−1	−1/−2
(OEP)FeCO			+0.49[b]		
(OEP)FeCS	+1.75	+1.01	+0.72	−1.38	−1.73
(OEP)FeCSe	+1.73	+0.98	+0.71	−1.39	−1.73
(TPP)FeCO			+0.56[b]	−1.22[c]	
(TPP)FeCS		+1.16	+0.85	−1.29[d]	−1.62[e]
(TPP)FeCSe		+1.11	+0.83	−1.31	−1.63

[a] Potentials are in Volts vs SCE.
[b] $E_{p,a}$ at 200 mV s^{-1}.
[c] Taken from ref. 18a.
[d] $E_{1/2} = 1.31$ in DMF, ref. 13d.
[e] $E_{1/2} = -1.69$ in DMF, ref. 13d.

band shifted from 390 to 408 ± 2 nm, the alpha band at 516 shifted to 528 ± 2 nm and the beta band at 551 shifted to 559 ± 2 nm, depending upon the identity of L. Analysis of the absorbance changes as a function of [L] indicated that the complexation reaction involved one molecule of porphyrin per molecule of L. The spectra acquired during titrations of (OEP)FeCSe possessed maxima at wavelengths within 1 nm of those listed for (OEP) FeCS.

The observation of C═S and C═Se stretching vibrations in the IR spectrum of all complexes investigated provided verification that the reaction with L did not displace the CS or CSe groups. Addition of L to a benzene solution of (OEP)FeCS shifted the C═S stretch from 1297 to 1285 ± 6 cm^{-1}, depending upon the identity of L. Similarly, addition of L to benzene solutions of (OEP) FeCSe shifted the C═Se stretch from 1134 to 1115 ± 10 cm^{-1}. This is illustrated in Fig. 2 for both (OEP) FeCS and (OEP)FeCSe when L = pyridine. Analysis of the absorbance changes as a function of [L] confirmed the reaction stoichiometry observed in the electronic spectral experiments.

To identify the number of L molecules bound to the oxidized and reduced forms of (OEP)FeCS and (OEP)FeCSe, titrations were monitored by both cyclic and differential pulse voltammetry in the manner previously described.[14,15] A typical data set is shown in Fig. 3 for the titration of (OEP)FeCS with pyridine. Trace A is the cyclic voltammogram recorded in the absence of the ligand and depicts only the three chemically reversible charge transfer processes. Each of the following voltammograms (traces B–E), were taken after the molar ratio of pyridine to (OEP)FeCS was incremented by 0.25. Note that the redox couple corresponding to the first oxidation of the uncomplexed material

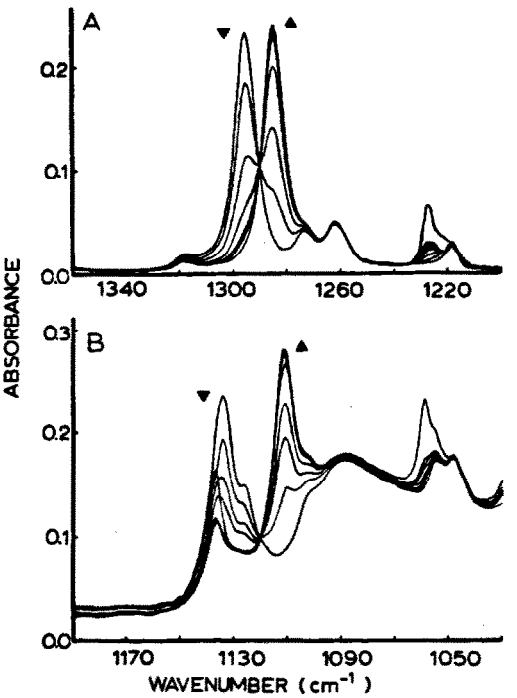

Fig. 2. Infrared spectral data obtained during titrations of 1.2 mM (OEP)FeCS (upper portion) and (OEP)FeCSe (lower portion) with pyridine. Spectra were recorded after the molar ratio of pyridine/(OEP)FeCS or (OEP) FeCSe was incremented by 0.25 (up to a value of 1.50). The last spectrum displayed was taken after a molar ratio of 10.0 was achieved. The new bands growing at 1228 cm^{-1} (part A), and 1059 and 1137 cm^{-1} (part B), are due to ligand vibrations.

decreased in current, with the generation of a new process at 0.68 V. In contrast to the behaviour observed for (TPP)FeCS(L) or (TPP)FeCSe(L), both the second oxidation process and the first reduction process for OEPFeCS(Py) and (OEP)

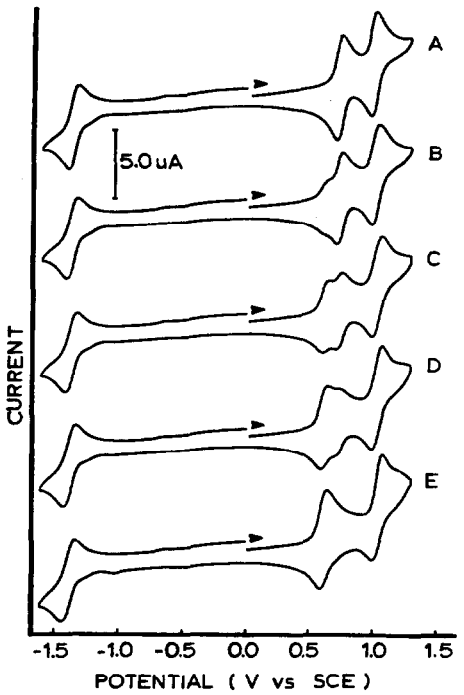

Fig. 3. Cyclic voltammetric data obtained during the titration of 0.70 mM (OEP)FeCS in $EtCl_2$ solution with pyridine. All voltammograms were taken at a potential sweep rate of 200 mV s^{-1}. The voltammograms depicted were obtained at the following molar ratios of pyridine/(OEP)FeCS (A) 0.00; (B) 0.25; (C) 0.50; (D) 0.75 and (E) 1.00.

FeCS are too similar in potential to permit their resolution by cyclic voltammetry or differential pulse voltammetry (not shown in Fig. 3). In the presence of a molar ratio of pyridine/(OEP)FeCS of 1.0 (trace E), three chemically reversible charge transfer reactions were observed at $E_{1/2} = -1.43$, 0.68 and 1.05 V, respectively, and correspond to the oxidation and reduction of the six-coordinate complex (OEP)FeCS(Py). Similar results were obtained for all the (OEP)FeCS(L) and (OEP) FeCSe(L) complexes investigated. Mid-point potentials for all reactions are tabulated in Table 2. From the spectral and electrochemical data, formation constants for all forms of complexed chalcocarbonyl iron porphyrins were computed and are listed in Table 3. The chemical reversibility and long term stability of the oxidized complexes were confirmed spectroelectrochemically.*

* For example, the peak maxima and molar absorptivities of the oxidized pyridine complex were: {(OEP) FeCS(pyridine)}$^{+1}$ = 397 (0.88), 553 (0.10); and {(OEP)FeCS(pyridine)}$^{+2}$ = 404 (1.08), 537 (0.10). Peak maxima are given in nm and the molar absorptivities are given in parentheses as $e \times 10^5$.

The following electron transfer pathway is proposed for the five-coordinate (OEP)FeCS and (OEP)FeCSe.

Scheme 1. *Electron transfer pathway for* (OEP) FeCZ *complexes* (*where* Z = S or Se)

$$\{(OEP)Fe(III)CZ\}^{3+} + e^- \leftrightarrow \{(OEP)Fe(III)CZ\}^{2+} \quad (1)$$

$$\{(OEP)Fe(III)CZ\}^{2+} + e^- \leftrightarrow \{(OEP)Fe(III)CZ\}^{+} \quad (2)$$

$$\{(OEP)Fe(III)CZ\}^{+} + e^- \leftrightarrow (OEP)Fe(II)CZ \quad (3)$$

$$(OEP)Fe(II)CZ + e^- \leftrightarrow \{(OEP)Fe(II)CZ\}^-. \quad (4)$$

The fate of the anion radical depends upon the applied potential and the [H^+], from the residual water in the solvent-supporting electrolyte system. On the cyclic voltammetric timescale and at more negative potentials, the anion radical is further reduced and the chalcocarbonyl group is subject to proton attack.

$$\{(OEP)Fe(II)CZ\}^- + e^- \leftrightarrow \{(OEP)Fe(II)CZ\}^{2-} \quad (5)$$

$$\{(OEP)Fe(II)CZ\}^{2-} + H^+ \rightarrow \{(OEP)Fe(II)CHZ\}^-. \quad (6)$$

At higher [H^+] or longer electrolysis times (the spectroelectrochemical timescale) at potentials within the range -1.35 to -1.70 V, the chalcocarbonyl group on the anion radical species is attacked by adventitious protons and further reduced.

$$\{(OEP)Fe(II)CZ\}^- + H^+ \rightarrow (OEP)Fe(II)CHZ \quad (7)$$

$$(OEP)Fe(II)CHZ + e^- \rightarrow \{(OEP)Fe(II)CHZ\}^-. \quad (8)$$

In either case, the thioformyl or selenoformyl anion radical species is converted back to the corresponding chalcocarbonyl Fe(II) species at potentials positive of -0.65 V.

$$\{(OEP)Fe(II)CHZ\}^- \rightarrow (OEP)Fe(II)CZ + 2e^- + H^+. \quad (9)$$

This scheme is similar to that previously proposed by Lexa *et al.*[13] for the reduction of (TPP)FeCS, and by ourselves[14,15] for the oxidation of the TPP complexes.

The following electron transfer pathway is proposed for the six-coordinate (OEP)FeCS(L) and (OEP)FeCSe(L) complexes.

Table 2. Mid-point potentials[a] for electrode reactions of (OEP)FeCZ(L) complexes in $EtCl_2$

Ligand	Redox reaction[b] (OEP)FeCS +2/+1	+1/0	0/−1	(OEP)FeCSe +2/+1	+1/0	0/−1
None	1.01	0.72	−1.38	0.98	0.71	−1.39
3,5-Dichloropyridine	1.05	0.71	−1.42	1.02	0.70	−1.41
3-Cyanopyridine	1.04	0.70	−1.41	1.03	0.69	−1.42
3-Bromopyridine	1.05	0.68	−1.43	1.02	0.66	−1.42
4,4′-Bipyridine	1.04	0.60	−1.42			
1,2-Bis-(4-pyridyl)ethane	1.03	0.60	−1.41	1.01	0.61	−1.42
Pyridine	1.04	0.60	−1.41	1.02	0.59	−1.41
4-Picoline	1.03	0.59	−1.43			
3,4-Lutidine	1.03	0.58	−1.42	1.04	0.56	−1.43
Imidazole	1.04	0.55				
Dabco			−1.40			−1.42
Quinuclidine			−1.41			−1.40

[a] Potentials are in Volts vs SCE.
[b] Denotes the charge on the electrode reactant and electrode product.

Table 3. Formation constants[a] for (OEP)FeCZ(L) adducts

Porphyrin	Ligand	pK_{BH^+}[b]	Charge on complex 0[c]	+1[d]	+2[e]	−1[e]
(OEP)FeCS	3,5-Dichloropyridine	0.67	2.08	2.5	1.6	1.4
	3-Cyanopyridine	1.45	2.29	2.7	2.1	1.8
	3-Bromopyridine	2.84	2.46	3.3	2.6	1.7
	4-Acetylpyridine	3.51	2.72			
	4,4′-Bipyridine	4.82, 3.17[f]	2.86	5.0	4.6	2.2
	1,2-Bis-(4-pyridyl)ethane		2.92	5.0	4.9	2.5
	Pyridine	5.28	2.83	5.0	4.5	2.3
	3-Picoline	5.77	2.94			
	4-Picoline	5.98	2.99	5.3	5.0	2.2
	3,4-Lutidine	6.46	3.08	5.5	5.2	2.4
	Imidazole	6.65	3.47	6.4	5.8	
	1-Methylimidazole	7.33	3.67			
	Dabco	8.19, 4.18[g]	2.43			2.1
	Quinuclidine	10.95	2.45			2.0
(OEP)FeCSe	3,5-Dichloropyridine	0.67	1.80	2.0	1.3	1.5
	3-Bromopyridine	2.84	2.22	3.0	2.3	1.7
	1,2-Bis-(4-pyridyl)ethane		2.56			
	Pyridine	5.28	2.52	4.6	3.9	1.9
	3,4-Lutidine	6.46	2.81	5.4	4.6	2.2
	Imidazole	6.65	3.29			
	Dabco	8.19, 4.18[g]	2.29			
	Quinuclidine	10.95[h]	2.26			

[a] Measured at 25.0±2.0°C in 0.10 M TBAP/$EtCl_2$.
[b] Values taken from K. S. Schoefield, *Hetero-Aromatic Nitrogen Compounds*, p. 146. Plenum Press, New York (1967).
[c] Uncertainties are ±0.05 in the log unit.
[d] Uncertainties are ±0.2 in the log unit.
[e] Uncertainties are ±0.3 in the log unit.
[f] Value taken from P. Krumholz, *J. Am. Chem. Soc.* 1951, **73**, 3483.
[g] Value taken from G. Schwarzenbach, H. Maissen and H. Ackermann, *Helv. Chim. Acta* 1952, **35**, 2333.
[h] Value taken from C. A. Grob, A. Kaiser and E. Renk, *Chem. Ind. (London)*, 1957, 598.

Scheme 2. *Electron transfer pathway for* (OEP)FeCZ(L) *complexes* (*where* Z = S or Se)

$$\{(OEP)Fe(III)CZ(L)\}^{2+} + e^- \leftrightarrow \{(OEP)Fe(III)CZ(L)\}^+ \quad (10)$$

$$\{(OEP)Fe(III)CZ(L)\}^+ + e^- \leftrightarrow (OEP)Fe(II)CZ(L) \quad (11)$$

$$(OEP)Fe(II)CZ(L) + e^- \leftrightarrow \{(OEP)Fe(II)CZ(L)\}^-. \quad (12)$$

As in the case of the five-coordinate chalcocarbonyl Fe porphyrins, the fate of the anion radical species depends upon the $[H^+]$, the applied potential and the timescale of the experiment. Under cyclic voltammetric conditions, the following sequence ensues.

$$\{(OEP)Fe(II)CZ(L)\}^- + e^- \leftrightarrow \{(OEP)Fe(II)CZ(L)\}^{2-} \quad (13)$$

$$\{(OEP)Fe(II)CZ(L)\}^{2-} + H^+ \rightarrow \{(OEP)Fe(II)CHZ(L)\}^-. \quad (14)$$

Under spectroelectrochemical conditions, the chalcocarbonyl group of the anion radical species undergoes attack by adventitious protons prior to reduction.

$$\{(OEP)Fe(II)CZ(L)\}^- + H^+ \rightarrow (OEP)Fe(II)CHZ(L) \quad (15)$$

$$(OEP)Fe(II)CHZ(L) + e^- \rightarrow \{(OEP)Fe(II)CHZ(L)\}^-. \quad (16)$$

The six-coordinate thioformyl or selenoformyl anion radical species is converted back to the corresponding six-coordinate chalcocarbonyl Fe(II) species at potentials positive of -0.65 V.

$$\{(OEP)Fe(II)CHZ(L)\}^- \rightarrow (OEP)Fe(II)CZ(L) + 2e^- + H^+. \quad (17)$$

For both schemes, EPR evidence confirmed that the first oxidation is metal centred, whereas the second oxidation and first reduction are porphyrin ring centred reactions. Battioni has proven that proton attack on the chalcocarbonyl group can occur following either the first or second reduction of the parent complex, producing a chalcoformyl ferrous porphyrin anion radical species.[13d] In this work, we have shown that the potential for the oxidation of the six-coordinate chalcoformyl anion radical species is shifted from that observed for the corresponding five-coordinate species *and* is independent of the identity of L. This suggests that the site of electron transfer for the chalcoformyl complex is also not metal centred.

The potential data collected in Tables 1 and 2 contain several interesting trends. First, the mid-point potentials for metal-centred reactions of (POR)FeCZ(L) were linearly related to the pK_{BH^+} of the N donor atom, whereas the mid-point potentials for non-metal-centred reactions were independent of pK_{BH^+}. This trend mirrored that observed previously with other axial ligands (e.g. NO,[20] C_6H_5[5a,12,13] and anionic ligands[21]). Secondly, the redox reactions of thiocarbonyl porphyrins occurred at slightly more positive potentials (typically 20 mV) compared to the corresponding redox reaction of the selenocarbonyl porphyrin. This reflects the marginal difference in the sigma donor and pi acceptor abilities between the two diatomic ligands. Thirdly, the potential of the redox reactions of the TPP derivatives were consistently positive compared to the OEP derivatives, in accord with the relative basicities of each porphyrin. The magnitude was typically 90 ± 10 mV for reductions and 120 ± 10 mV for oxidations, and also compared favourably with previous work using other axial ligands.[11,21] However, the potential difference for the ring centred oxidation was nearly twice that observed for the metal-centred oxidation, inferring a significant change in the energy of the HOMO of OEP vs TPP. The magnitude of the potential difference between the two oxidation processes for both porphyrins was consistently 290 ± 20 mV. Fourthly, the potential difference $E_{1/2\,\text{ring oxidn}} - E_{1/2\,\text{ring redn}}$ was 2.43 ± 0.02 for (TPP)FeCZ vs 2.38 ± 0.01 for (OEP)FeCZ, and 2.63 ± 0.02 for (TPP)FeCZ(L) vs 2.45 ± 0.01 for (OEP)FeCZ(L). Thus, coordination of the chalcocarbonyl TPP derivatives caused a 200 mV increase in this potential separation, compared to only a 70 mV increase for the OEP derivatives.

The formation constant data collected in Table 3 also contains several trends. Formation constants for the thiocarbonyl porphyrins were consistently greater than the corresponding selenocarbonyl porphyrins (in accord with the relative basicities of the porphyrins), with one exception. The formation constants for $\{(OEP)FeCS(L)\}^{2+}$ were greater than those of the corresponding TPP complex, and formation constants for $\{(OEP)FeCSe(L)\}^{2+}$ were equal to those observed for the TPP complexes. The log of the formation of each complex investigated was linearly related to the pK_{BH^+} of the N donor atom. For the (OEP)FeCS(L) complexes, slopes of 0.16, 0.55 and 0.64 were obtained for B^0, B^+ and B^{2+}, respectively. Similar values were obtained for the selenocarbonyl derivatives. The B^+ and B^{2+} values compared favourably with those previously

obtained for the TPP complexes. The B^0 value, however, is significantly less than that of the TPP complexes where values of 0.27 and 0.21 were measured for (TPP)FeCS(L) and (TPP)FeCSe(L) complexes, respectively. This phenomenon can be explained from consideration of a simple charge attraction model.[22] The more basic porphyrin donates more electron density to the Fe(II) atom and thus decreasing its charge attraction for the sigma donating axial ligands.

In summary, we have shown that the Fe—C bond in chalcocarbonyl Fe porphyrins is exceptionally stable when compared to the bond strength found in carboxy or carbenoid Fe porphyrins. This bond is not broken in the presence of a large excess of aromatic amines, or by successive charge transfer reactions (up to three oxidative steps and two reductive steps for the OEP derivatives). Changes in the basicity of the porphyrin N core (indirectly measured via redox potential and formation constants for the addition of substituted aromatic amines *trans* to the chalcocarbonyl group), modified the total electron density on the Fe atom, but did not alter the stability of the Fe—C bond.

Acknowledgements—The authors are grateful to Mr Chris Gaylor, formerly with Nicolet Instruments, for the generous loan of the FTIR spectrometer. The Financial support of this research by DHHS (Grant No. HL33734–02) is also acknowledged.

REFERENCES

1. (a) C. R. Wolf, D. Mansuy, N. Nastainczyk, G. Deutschmann and V. Ullrich, *Mol Pharmacol.* 1977, **13**, 698; (b) H. J. Ahr, L. J. King, W. Nastainczyk and V. Ullrich, *Biochem. Pharmacol.* 1982, **31**, 383; (c) W. Nastainczyk, H. J. Ahr and V. Ullrich, *Biochem. Pharmacol.* 1982, **31**, 391.
2. P. J. Brothers and J. P. Collman, *Acc. Chem. Res.* 1986, **19**, 209.
3. (a) D. Brault, C. Bizet, P. Morliere, M. Rougee, E. J. Land, R. Santus and A. J. Swallow, *J. Am. Chem. Soc.* 1980, **102**, 1015; (b) D. Brault and P. Neta, *J. Am. Chem. Soc.* 1981, **103**, 2705; (c) D. Brault and P. Neta, *J. Phys. Chem.* 1982, **86**, 3405.
4. (a) P. R. Ortiz de Montellano, K. L. Kunze and O. Augusto, *J. Am. Chem. Soc.* 1982, **104**, 3545; (b) K. L. Kunze and P. R. Ortiz de Montellano, *J. Am. Chem. Soc.* 1983, **105**, 1380.
5. (a) P. Cocolios, E. Laviron and R. Guilard, *J. Organomet. Chem.* 1982, **228**, C39; (b) P. Cocolios, G. Lagrange and R. Guilard, *J. Organomet. Chem.* 1983, **253**, 65; (c) G. Lagrange, P. Cocolios and R. Guilard, *J. Organomet. Chem.* 1984, **260**, C16.
6. (a) J. P. Battioni, J. C. Chottard and D. Mansuy, *Inorg. Chem.* 1982, **21**, 2056; (b) J. P. Battioni, D. Mansuy and J. C. Chottard, *Inorg. Chem.* 1980, **19**, 791; (c) D. Mansuy, M. Lange, J. C. Chottard, P. Guerin, P. Morliere, D. Brault and M. Rougee, *J. Chem. Soc., Chem. Commun.* 1977, 648; (d) D. Mansuy, M. Lange, J. C. Chottard, J. F. Bartolia, B. Chevrier and R. Weiss, *Angew. Chem. Int. Ed. Engl.* 1978, **17**, 781; (e) D. Mansuy, *Pure Appl. Chem.* 1980, **7**, 215 and refs therein; (f) D. Mansuy, P. Guerin and J. C. Chottard, *J. Organomet. Chem.* 1979, **171**, 195; (g) P. Guerin, J. P. Battioni and J. C. Chottard, *J. Organomet. Chem.* 1981, **218**, 201; (h) D. Mansuy, J. P. Battioni, J. C. Chottard and V. Ullrich, *J. Am. Chem. Soc.* 1979, **101**, 3971; (i) D. Mansuy, J. P. Lecomte, J. C. Chottard and J. F. Bartoli, *Inorg. Chem.* 1981, **20**, 3119; (j) D. Mansuy and J. P. Battioni, *J. Chem. Soc., Chem. Commun.* 1982, 638; (k) D. Mansuy, M. Fontecave and J. P. Battioni, *J. Chem. Soc., Chem. Commun.* 1982, 317; (l) D. Mansuy, J. P. Battioni, D. Dupre and E. Sartori, *J. Am. Chem. Soc.* 1982, **104**, 6159; (m) J. P. Battioni, P. Mahy, G. Gillet and D. Mansuy, *J. Am. Chem. Soc.* 1983, **103**, 1399.
7. R. S. Wade and C. E. Castro, *J. Am. Chem. Soc.* 1973, **95**, 231.
8. C. M. Elliot and C. A. Marrese, *J. Electroanal. Chem.* 1981, **19**, 395.
9. (a) D. A. Clarke, D. Dolphin, R. Grigg, A. W. Johnson and H. A. Pinnock, *J. Chem. Soc. C* 1968, 881; (b) D. A. Clarke, R. Grigg and A. W. Johnson, *J. Chem. Soc., Chem. Commun.* 1966, 208.
10. (a) H. Ogoshi, H. Sugimoto, Z. Yoshida, H. Kobayashi, H. Sakai and Y. Maeda, *J. Organomet. Chem.* 1982, **234**, 185; (b) L. Latos-Grazynski, R.-J. Cheng, G. N. LaMar and A. L. Balch, *J. Am. Chem. Soc.* 1981, **103**, 4270.
11. K. M. Kadish, *Prog. Inorg. Chem.* 1986, **34**, 435.
12. (a) D. Lancon, P. Cocolios, R. Guilard and K. M. Kadish, *J. Am. Chem. Soc.* 1984, **106**, 4472; (b) D. Lancon, P. Cocolios, R. Guilard and K. M. Kadish, *Organometallics* 1984, **3**, 1164; (c) R. Guilard, B. Boisselier-Cocolios, A. Tabard, P. Cocolios, B. Simonet and K. M. Kadish, *Inorg. Chem.* 1985, **24**, 2509; (d) R. Guilard, G. Lagrange, A. Tabard, D. Lancon and K. M. Kadish, *Inorg. Chem.* 1985, **24**, 3649.
13. (a) D. Lexa, J. M. Saveant, J. P. Battioni, M. Lange and D. Mansuy, *Angew. Chem. Int. Ed. Engl.* 1981, **20**, 578; (b) D. Lexa, J. Mispelter and J. M. Saveant, *J. Am. Chem. Soc.* 1981, **103**, 6806; (c) D. Lexa and J. M. Saveant, *J. Am. Chem. Soc.* 1982, **104**, 3503; (d) J. P. Battioni, D. Lexa, D. Mansuy and J. M. Saveant, *J. Am. Chem. Soc.* 1983, **105**, 207.
14. L. A. Bottomley, M. R. Deakin and J.-N. Gorce, *Inorg. Chem.* 1984, **23**, 3563.
15. J.-N. Gorce and L. A. Bottomley, *Inorg. Chem.* 1985, **24**, 1431.
16. J.-N. Gorce, *J. Electrochem. Soc.* 1984, **131**, 35C.
17. L. A. Bottomley and J.-N. Gorce, submitted for publication in *J. Am. Chem. Soc.*
18. (a) L. Olson, D. Schaeper, D. Lancon and K. M. Kadish, *J. Am. Chem. Soc.* 1982, **104**, 2042; (b) G. M.

Brown, F. R. Hopf, T. J. Meyer and D. G. Whitten, *J. Am. Chem. Soc.* 1975, **97**, 5385; (c) R. C. Gurira and J. Jordan, *Anal. Chem.* 1981, **34**, 864; (d) J. W. Buchler, W. Kokish, P. D. Smith and B. Tonn, *Z. Naturforsch. B. Anorg. Chem., Org. Chem.* 1978, **33B**, 1371; (e) A. Croisy, D. Lexa, M. Momenteau and J.-M. Saveant, *Organometallics* 1985, **4**, 1574.

19. R. L. Birke, M.-H. Kim and M. Strassfeld, *Anal. Chem.* 1981, **53**, 852.
20. (a) D. Lancon and K. M. Kadish, *J. Am. Chem. Soc.* 1983, **105**, 5610; (b) E. Fujita and J. Fajer, *J. Am. Chem. Soc.* 1983, **105**, 6743; (c) K. M. Kadish, D. Lancon, P. Cocolios and R. Guilard, *Inorg. Chem.* 1984, **23**, 2372; (d) J. W. Buchler and K. L. Lay, *Z. Naturforsch. B. Anorg. Chem., Org. Chem.* 1975, **30**, 985.
21. L. A. Bottomley, L. Olson and K. M. Kadish, in *Electrochemical and Spectrochemical Studies of Biological Redox Components* (Edited by K. M. Kadish), Chap. 13 and refs therein. American Chemical Society, Washington, D.C. (1982).
22. (a) D. K. Geiger and W. R. Scheidt, *Inorg. Chem.* 1984, **23**, 1970; (b) W. R. Scheidt and D. K. Geiger, *Inorg. Chem.* 1982, **21**, 1208.

Polyhedron Vol. 7, No. 8, pp. 597–600, 1988
Printed in Great Britain

0277–5387/88 $3.00+.00
© 1988 Pergamon Press plc

THERMOLYSIS AND MASS SPECTRA OF POLYMERIC GERMANIUM HYDRIDE PRODUCED BY γ-RADIOLYSIS

P. BENZI, M. CASTIGLIONI* and P. VOLPE

Istituto di Chimica Generale ed Inorganica, Facoltà di Scienze M.F.N., Università di Torino, Corso Massimo d'Azeglio 48, 10125 Torino, Italy

L. BATTEZZATI

Istituto di Chimica Generale ed Inorganica, Facoltà di Farmacia, Università di Torino, Via Pietro Giuria 9, Torino, Italy

and

M. VENTURI

Dipartimento di Chimica "G. Ciamician", Università di Bologna, Italy

(*Received* 23 *June* 1987; *accepted after revision* 10 *November* 1987)

Abstract—TGA, MS and DSC of a solid polymeric Ge hydride, obtained by γ-radiolysis of GeH_4, are reported. Upon heating, it undergoes two successive weight losses at 463 and 1173 K. At 948 K two crystal phases are formed, one of them is pure germanium. Some comparisons with a-Ge : H produced via RF sputtering or glow discharge are reported.

The preparation and the elemental analysis of the solid polymeric hydride obtained by gas phase radiolysis of GeH_4 have been reported already.[1]

This paper will give more insight on the properties and thermal behaviour of the hydride in view of its possible use for the preparation of a-Ge : H.

EXPERIMENTAL

GeH_4 was produced and purified as previously reported.[1] The purity of the compound was, from time to time, checked by mass spectrometry. The samples, at a pressure ranging from 80 to 90 KPa, were sealed in cylindrical Pyrex vials 21.0 cm high and 3.5 cm i.d., and were then irradiated in a Gammacell (Atomic Energy of Canada Ltd) for a total dose of 8.0×10^5 Gy ($T \sim 315$ K), as previously described.[1] After irradiation, the ampoules were evacuated and the dark brown solid product was recovered from the bottom of the ampoule. The product was carefully outgassed for at least 8 h, before any further treatment, to free it from any short chain volatile hydrides.

The IR spectra were collected from KBr discs using a Perkin–Elmer 580B IR spectrophotometer. Mass spectra were recorded on a Kratos MS 80 using both electron impact and chemical ionization. Thermogravimetric analysis (TGA) was performed with a Du Pont 1090 instrument and differential scanning calorimetry (DSC) using a 910 cell. X-ray analysis was performed with a wide angle Philips diffractometer using Co-K_α radiation.

For purpose of comparison, some samples of solid polymeric hydrides were obtained by wet methods using both acetic and sulphuric acid.[2,3]

RESULTS AND DISCUSSION

A typical radiolysis run yields about 10 mg of a dark brown waxy powder: the solid germanium hydride. According to the previously reported data[1] the composition of the solid is $GeH_{1.15}$. The hydride is not soluble in ordinary solvents, is stable and does not show an appreciable change in properties

* Author to whom correspondence should be addressed.

after three months of exposure to the atmosphere. Due to the apparent stability of the compound, and the invariability of the IR and mass spectra, after months of exposure to the laboratory atmosphere, it was decided not to investigate the possibility of the formation of a transparent thin film of oxide on the surface of the material.

Samples of polygermane obtained by wet chemistry[2,3] and by radiolysis of GeH_4+O_2 mixtures show wide IR absorption bands in the regions 3300–2800, 1380–1030 and 800–500 cm^{-1}, which have been attributed to OH and Ge—O (Ge—O—Ge) groups.[4,5,6]

The IR spectra of oxygen free radiolytic germanium hydride show absorptions at 2065, 2045, 810 and 780 cm^{-1}, which have been attributed to Ge—H bonds.[2,6,7,8] As the sample is annealed under an inert atmosphere (argon) at 463 K, the intensities of the Ge—H bond absorptions decrease.

The mass spectra of the hydride are complicated due to the presence of five germanium isotopes and to its low degree of hydrogenation. Nevertheless, the mass spectrum shows, for the unannealed material, a mass distribution corresponding to units ranging from one to eleven Ge atoms, as the temperature of the ion source is raised from that of the room up to 580 K.

Figure 1 shows the average hydrogen content, per Ge atom, of the fragments observed in the mass spectrometer. When the sample is annealed at 773 K for 1 h (under argon), the fragment of the lowest *m/e* value observed in the mass spectrum corresponds to a cluster of seven germanium atoms with an average Ge/H ratio of 1/0.17.

TGA of the solid hydride indicates that in the 323–1173 K range, the sample undergoes a total loss of weight corresponding to 23.4% (Fig. 2). There is a 6% weight loss during an exothermic transformation (see below) at 463 K; a second mass loss occurs at 1148 K, somewhat before the melting point of germanium (1210.4 K).

The change in both the IR and the mass spectra after annealing above 463 K indicates that some Ge—H bonds have been destroyed and that hydrogen is lost by the hydride. The loss of 6% in weight upon annealing is too high to be accounted for by only hydrogen loss; in fact not even GeH_4 could lose 6% of its weight as hydrogen only. To identify the material released by the sample at 463 K, it has been collected and analysed by GC–MS: it consists of a mixture of GeH_4, Ge_2H_6, and Ge_3H_8, in the 1 : 1.4 : 1.7 ratio, plus trace amounts of both isomeric tetragermanes. The average composition of the released material, calculated from the mass abundance of the fragments and the ionization potentials[9,10] is GeH_3, as the composition could be roughly calculated from a 6% mass loss from a substance having the $GeH_{1.15}$ composition. After annealing at 463 K the compound has the same aspect as the original hydride and undergoes a further weight loss of 17.8% (as referred to the weight after the annealing at 463 K) at 1148 K. The material released at the above temperature has been analysed by mass spectrometery and has been shown to consist of only GeH_4.

DSC analysis (Fig. 2) shows a first exothermal effect around 463 K, corresponding to the loss of 6% in weight as evidenced by TGA. A second very

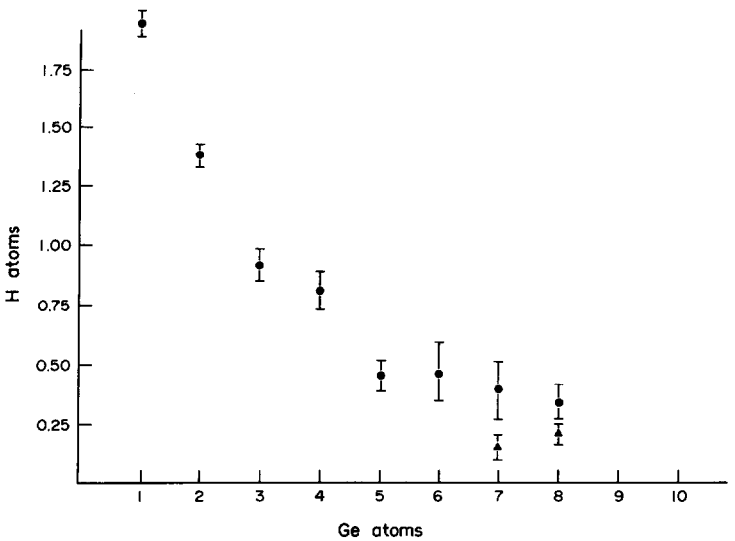

Fig. 1. Average hydrogen content of the fragments observed in the mass spectrum: ● unannealed samples; ▲ samples annealed at 773 K.

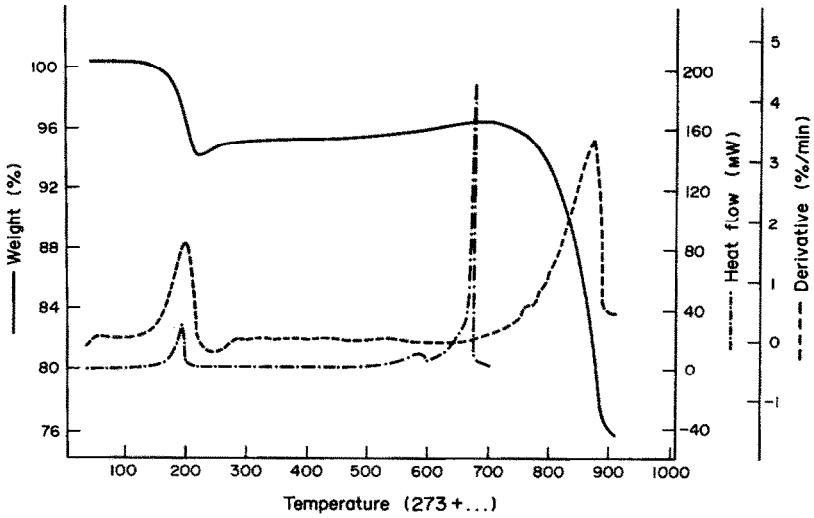

Fig. 2. TGA of the polymeric hydride: —— weight loss (%); – – – – weight loss derivative (%/min). DSC of the polymeric hydride: ·—·—· heat flow.

sharp exothermal transition occurs at 948 K, which is not associated with any mass change. X-ray analysis has shown the solid to be amorphous both before and after the thermal effect at 463 K. However, the sample appears polyphasic after the transition at 948 K. The presence of two crystalline phases is evidenced in its X-ray spectrum: (a) pure germanium, diamond type structure[11] and (b) a second phase, giving a number of reflections, which has not yet been identified. Therefore, we conclude that the sharp exotherm at 948 K is due to crystallization of the amorphous sample involving a phase change. Two small thermal effects are also manifested in the DSC trace, as shown in Fig. 2, occurring at temperatures immediately lower than the main crystallization peak. No detailed structural analysis of their origin has been performed, but it is not unreasonable to assume that they correspond to an early crystallization of a small fraction of the sample.

The second phase present in the sample disappears after the thermal treatment at 1148 K involving the loss of GeH_4, as shown by the X-ray spectrum where only reflections due to pure Ge are present.

The absence of any IR absorption at about 1880 cm^{-1}[6] and the presence of bands at 2065 and 2045 cm^{-1} indicates that the compound is a kind of unsaturated, crosslinked polygermane, rather than an amorphous hydrogenated germanium.

The properties of the polygermane obtained by γ-radiolysis appear similar to that of the material prepared by glow discharge,[12] but are quite different from the properties of the compound prepared by RF sputtering.[6]

The bonded hydrogen atom concentration in the radiolytic polygermane, prepared at about 315 K and 80–90 KPa, is 53.5 atom %, whilst in the compound obtained by glow discharge, at the same temperature, but at a pressure three orders of magnitude lower,[6] is 35 atom %. As already reported,[1] also with γ-radiolysis, as the pressure of the reactant gas is lowered, the percentage of the hydrogen atoms in the solid decreases. Moreover, with the glow discharge method, the hydrogen concentration seems to be correlated to the temperature of the substrate during the deposition; when the temperature is kept under 498 K the hydrogen concentration is in the 35–25 atom % range, but when it is raised to about 498 K the hydrogen concentration rapidly drops to 10–12 atom %.[6] A similar trend is observed on annealing the radiolysis product: at 463 K a rapid loss of H (as germanium hydrides) is observed. The 35 K temperature difference for the two phenomena does not seem to be of relevance, taking into account the rather different preparation conditions. It should be pointed out that A.A.[6b] observed, in plasma deposited materials, a sharp change in the hydrogen status of the a-Ge: H vs the substrate temperature at about 473 K (which is in the 463–498 K temperature range).

Connel and Pawlich,[12] from the IR analysis of the material prepared at room temperature by RF sputtering, inferred that the material annealed up to 523 K does not lose hydrogen by breakage of Ge—H bonds, but rather undergoes a network reorganization. Probably, such material is more cross-linked than the radiolytic (and glow discharge) one, which indeed loses hydrogen (through Ge–hydrides) in the 463–498 K range, probably by

rupture of the more hydrogenated boundary chains of the network.

Finally, in the radiolytic material a further exothermic transformation occurs at 948 K which is very rapid (see the very narrow DSC signal) and is not likely to correspond to the proposed network reorganization at 523 K occurring on the RF sputtered material.[12]

The last hydrogen loss (at 1148 K) by the elimination of GeH_4, appears to be associated with a process, the rate of which increases with the temperature but falls abruptly as the supply of the reactant falls; this behaviour is observed in reactions where diffusion and/or evaporation are implicated. GeH_4 is released instead of molecular or atomic hydrogen, because the bond dissociation energy for Ge—H[13] is higher than for Ge—Ge.[13,14]

The similarity of the compounds prepared by glow discharge and γ-radiolysis is not surprising because in both methods highly excited states of atoms, molecules, radicals and ions could be involved even though the temperature of the gas is quite low[15] and of course is lower in γ-radiolysis than in glow discharge.

Acknowledgements—This work has been supported by the Italian Ministry of Education. The authors wish to acknowledge the cooperation of the staff of the FRAE Institute of the CNR for sample irradiations and absorbed dose measurements.

REFERENCES

1. R. Belluati, M. Castiglioni, P. Volpe and M. C. Gennaro, *Polyhedron* 1987, **6**, 441.
2. W. L. Jolly and J. E. Drake, *Inorg. Synth.* 1963, **7**, 36.
3. W. L. Jolly and J. E. Drake, *Inorg. Synth.* 1963, **7**, 37.
4. T. D. Goldfarb and S. Sujishi, *J. Am. Chem. Soc.* 1964, **86**, 1679.
5. S. Cradock, *J. Chem. Soc.* (*A*) 1968, 1426.
6. (a) G. Lucovsky, S. S. Chao, J. Yaug, J. E. Tyler, R. C. Ross and W. Czubatyj, *Phys. Rev. B* 1985, **31**, 2190; (b) J. S. Rayson and R. C. Ross, *J. Non-Cryst. Solids* 1985, **77–78**, 579.
7. D. A. Dows and R. M. Hexter, *J. Chem. Phys.* 1956, **24**, 1029.
8. J. E. Drake and W. L. Jolly, *J. Chem. Soc.* 1962, 2807.
9. F. E. Saalfeld and H. J. Svec, *Inorg. Chem.* 1963, **2**, 46.
10. F. E. Saalfeld and H. J. Svec, *Inorg. Chem.* 1963, **2**, 50.
11. *X-ray Powder Data File.* A.S.T.M., Philadelphia (1962).
12. G. A. N. Connell and J. R. Pawlik, *Phys. Rev. B* 1985, **31**, 2190.
13. M. J. Almond, A. M. Doncaster, P. N. Noble and R. Walsh, *J. Am. Chem. Soc.* 1982, **104**, 5717.
14. R. A. Jackson, *J. Organomet. Chem.* 1979, **166**, 17.
15. F. Cramarossa and P. Capezzuto, *Material Chem. Phys.* 1983, **9**, 213.

Polyhedron Vol. 7, No. 8, pp. 601–604, 1988
Printed in Great Britain

0277–5387/88 $3.00+.00
© 1988 Pergamon Press plc

SPECTRAL STUDIES ON SILVER CHROMATE AND NITRATE COMPLEXES WITH HETEROCYCLIC AMINES

MARIA CIEŚLAK-GOLONKA,* ADAM BARTECKI* and MARIA RACZKO

Institute of Inorganic Chemistry and Metallurgy of Rare Elements, Technical University of Wrocław, 50-370 Wrocław, Poland

(*Received* 9 *July* 1987; *accepted after revision* 10 *November* 1987)

Abstract—Silver chromate and nitrate complexes of the general formulae $[Ag_2(L)_x(CrO_4)]$ and $[Ag(L)_x(NO_3)]$ (L—heterocyclic amine) were synthesized and spectrally investigated. The coordination of the anion in $[Ag_2(4,4'bipy)(CrO_4)]$ and $[Ag_2(HMTA)(CrO_4)]$ was proposed from the IR data. A prominent matrix effect on the electronic spectra has been observed.

The reason for the "anomalous" dark colour of silver chromate, Ag_2CrO_4, in comparison to alkali metal salts, is most probably the silver–oxygen (CrO_4^{2-}) excited state(s) interaction, resulting in a large bathochromic shift of the 360 nm "yellow" CT Cr ← O band down to 450–550 nm.[1] In this paper we have prepared and spectrally investigated a series of Ag_2CrO_4 complexes with heterocyclic bases: 2,2′-bipyridine (2,2′bipy), 4,4′-bipyridine (4,4′bipy), 1,10-phenanthroline (phen), 4,7-diphenylphenanthroline (DPP) and hexamethylenetetramine (HMTA), with the following goals in mind:

(i) from the spectral data, we intended to attempt to elucidate the ligand influence on the cation–anion interaction in the parent Ag_2CrO_4.

(ii) $[M(HB)_xA]$ types of compound (HB—heterocyclic base, A—oxidizing anion) have caused special attention due to being milder and more efficient reagents in organic reactions than the "classical" $KMnO_4$ and $K_2Cr_2O_7$ oxidizers.[2]

To our knowledge Ag_2CrO_4 complexes with the exception of $Ag_2(NH_3)_4(CrO_4)$[3] are not known in the literature.

EXPERIMENTAL

All the reagents used were of analytical grade. Stoichiometries of the solid compounds were established by microanalytical techniques. Satisfactory analytical results were obtained. The complexes of the following formulae were prepared: yellow $[Ag_2(4,4'bipy)_3(CrO_4)]$, $[Ag_2(HMTA)(CrO_4)]$ and red $[Ag_2(4,4'bipy)(CrO_4)]$, $[Ag_2(2,2'bipy)_2(CrO_4)]$, $[Ag_2(phen)_2(CrO_4)]$ and $[Ag_2(DPP)(CrO_4)]$. Additionally, for comparison purposes, $AgNO_3$ complexes with the same ligands were obtained. Generally, the complexes were formed during the reaction of the ligand previously dissolved in K_2CrO_4, with 0.1 M solution of $AgNO_3$. The precipitates were washed with water and dried over P_4O_{10}. Chromate complexes do not appear to dissolve in common solvents.

(1) Silver chromate, Ag_2CrO_4

The compound was prepared metathetically by the reaction of $AgNO_3$ (0.01 M) and K_2CrO_4 (0.01 M).

(2) Yellow $[Ag_2(4,4'bipy)_3(CrO_4)]$

A solution of 1 g 4,4′bipy dissolved in 50 cm^3 of acetone, was added dropwise to a stirred solution of 0.5 g K_2CrO_4 in 50 cm^3 of water. Eight cm^3 of 0.1 M $AgNO_3$ was slowly added. The precipitate formed immediately.

(3) Red $[Ag_2(4,4'bipy)(CrO_4)]$

This compound was prepared during washing of the respective tris complex with methanol.

(4) Red $[Ag_2(2,2'bipy)_2(CrO_4)]$

A solution of 0.5 g bipy in 20 cm^3 of methanol was slowly added to 0.5 g of K_2CrO_4 dissolved in

† Authors to whom correspondence should be addressed.

50 cm^3 of H_2O. A red precipitate was formed during the addition of 10 cm^3 of 0.1 M $AgNO_3$.

(5) Red $[Ag_2(phen)_2(CrO_4)]$

This compound was obtained as described in procedure (4).

(6) Red $[Ag_2(DPP)(CrO_4)]$

A saturated methanolic solution of the ligand was added to 0.5 g of K_2CrO_4 dissolved in 50 cm^3 of a 1 : 1 H_2O : methanol solution. The complex precipitates immediately upon addition of 5 cm^3 0.1 M $AgNO_3$.

(7) Orange $[Ag_2(HMTA)(CrO_4)]$

A solution of 0.3 g HMTA in a 1 : 1 H_2O : acetone solution was slowly added to 0.1 g K_2CrO_4 dissolved in 30 cm^3 of water. Finally, 10 cm^3 of 0.1 M $AgNO_3$ was added.

(8) White $[Ag(4,4'bipy)(NO_3)$

To a solution of 0.5 g of 4,4'bipy in 5 cm^3 of acetone, 15 cm^3 of 0.1 M $AgNO_3$ was slowly added.

(9) Pale yellow $[Ag(DPP)_2(NO_3)]$

To a solution of saturated DPP in acetone (15 cm^3), 0.1 M $AgNO_3$ was added.

(10) $[Ag(2,2'bipy)_2(NO_3)]$, $[Ag(phen)_2(NO_3)]$ and $[Ag(HMTA)(NO_3)]$ were prepared as in procedure (8).

Infrared spectra were obtained on a Perkin–Elmer 180 (50–3500 cm^{-1}) spectrophotometer in Nujol mulls and hexachlorobutadiene(1,3) sandwiched between AgBr plates. FIR spectra were recorded in Nujol mulls sandwiched between polyethylene plates.

UV–vis spectra were obtained on a double beam Hitachi 356 spectrophotometer in the 200–850 nm spectral range. As the studied compounds appeared not to dissolve in common solvents, we have measured their diffuse reflectance spectra as Li_2CO_3, BaO and Ag_2SO_4 pellets.

RESULTS AND DISCUSSION

Infrared spectra

The vibrations associated with the CrO_4^{2-} ion in its ground state are: $\nu_1(a_1) = 846$ cm^{-1} (R), $\nu_2(e) = 349$ cm^{-1} (R), $\nu_3(t_2) = 884$ cm^{-1} (IR, R) and $\nu_4(t_2) = 378$ cm^{-1} (IR, R).[5] In the spectra of Ag_2CrO_4, we were able to observe the following vibrations: 801 cm^{-1} ν_1, 345–350 cm^{-1} ν_2, 845 cm^{-1} ν_3 and 375 cm^{-1} ν_4. The appearance of ν_1 and splitting of ν_4 in the IR spectra is due to the presence of both site group and factor group perturbations operating in Ag_2CrO_4.[6] Moreover, a strong cation–anion influence is seen by a substantial red shift (in comparison to alkali metal salts) of the bands ascribed to the Cr—O stretching vibrations. Although all complexes studied here show splitting of the bands in the 770–1000 cm^{-1} absorption region (region of the Cr—O stretching mode vibrations in the chromate ion), only in $[Ag_2(4,4'bipy)(CrO_4)]$ and $[Ag(HMTA)(CrO_4)]$ is the splitting so large that is seems to be explicable only in terms of a coordinated CrO_4 group. A detailed analysis shows that the chromate ion here is most probably acting as a bidentate ligand with C_{2v} symmetry (Table 1).

This is a rare case when the CrO_4^{2-} ion appears to be coordinated.[7] In the literature the arguments for coordination of the chromate ion taken from the IR data are well established, and additionally supported by Raman, conductometric and kinetic studies.[8] Moreover, the application of IR spectroscopy for studying the predicted variation in the spectra when the ligand acts as a mono or bidentate molecule, was presented by taking the CrO_4^{2-} ion as an example.[9]

The metal–ligand vibrational region is expected between 300–175 cm^{-1}. Tentative assignment of the

Table 1. Splitting of the bands due to Cr—O vibrations upon $T_d \rightarrow C_{2v}$ symmetry lowering (in cm^{-1})

Compound	ν_3 A_1, B_1, B_2	ν_4 A_1, B_1, B_2	ν_1 A_1	ν_2 A_1	Bridge B_1 Ag—O—Cr
$[Ag_2(HMTA)(CrO_4)]$	930 vs 900 vs 865 vs	395 s 385 s 368 s	825 s	358 ms	790 vs
$[Ag_2(4,4'bipy)(CrO_4)]$	950 vs 930 vs 860 vs	385 ms 378 ms	830 s	360 ms	801 s

Table 2. Important bands in FIR spectra of silver chromate and nitrate complexes (in cm^{-1})

$[Ag_2(2,2'bipy)_2(CrO_4)]$	$[Ag_2(4,4'bipy)(CrO_4)]$	$[Ag_2(4,4'bipy)_3(CrO_4)]$	$[Ag(4,4'bipy)(NO_3)]$	Assignment
402 vs	462 s	462 ms	458 s	Ligand
385 w	385 ms			ν_{Cr-O} ligand
	378 ms	368 s		
	360 ms	240 w,b		
208 s	224 ms,b	230 w,b	228 s	ν_{Ag-N}
160 s	160 s	180 ms,b	145 s	Ligand
135 ms	145 s	130 ms,b	135 s	
125 ms	145 s	130 ms,b	125 s	
$[Ag_2(phen)_2(CrO_4)]$	$[Ag_2(DPP)(CrO_4)]$	$[Ag(DPP)_2(NO_3)]$	$[Ag_2(HMTA)(CrO_4)]$	Assignment
420 ms	495 ms	490 s	515 s	Ligand
	458 ms	458 ms	510 s	
	445 ms		495 m	
			460 ms,b	
268 s	378 ms	335 vw	395 s	ν_{Cr-O}, ligand
	360 ms		385 s	
			368 s	
			358 ms	
			338 ms	
235 s	240 ms	241 ms,b	265 vw	ν_{Ag-N}
135 ms		235 sh		Ligand
		155 w		

bands for the complexes are made and recorded in Table 2. It is not inferred that these are pure vibrations because of the possible coupling with the ligand and M—L bending vibrations.

Electronic spectra

Two types of silver chromate complexes were obtained: (i) red $[Ag_2(HB)_x(CrO_4)]$ with a strong 500 nm "Ag_2CrO_4" band. (ii) yellow $[Ag_2(HMTA)(CrO_4)]$ and $[Ag_2(4,4'bipy)_3(CrO_4)]$ with a 360 nm "K_2CrO_4" band slightly bathochromically shifted (Fig. 1).

Similar to $Ag_2Cr_2O_7$ complexes, for the same ligand, one may obtain red and yellow compounds, which is evidence that the colour depends upon the amount of coordinated ligand molecule, i.e. the formal number of N atoms per one silver atom.[4] The 500 nm "red" band is most probably evidence of the Ag—O (CrO_4) interaction still present in the complexes. On the other hand, since in some

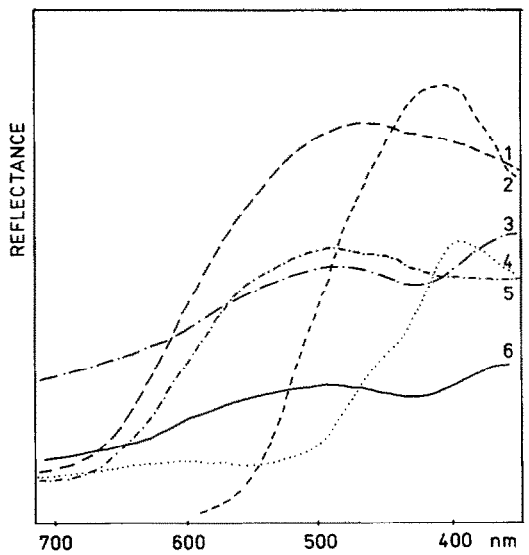

Fig. 1. Diffuse reflectance spectra of red and yellow silver chromate complexes in Li_2CO_3 matrix. 1—mono 4,4'bipy; 2—HMTA; 3—DPP; 4—tris 4,4'bipy; 5—2,2'bipy; 6—phen.

red compounds both bands are observed (i.e. red and yellow), we can not exclude a hypothesis that red complexes should be written as $[Ag_2(HB)_{2x}(CrO_4)\cdot Ag_2CrO_4]$. Thermal analysis, which probably could be helpful in this respect, is in progress. The results of this paper also confirmed the observation that the electronic spectra do not depend upon anion coordination.[10] A significant matrix influence both in the spectra of silver chromate and nitrate complexes has been observed. In comparison to the Ag_2CrO_4 spectrum, the hypochromic shift due to the matrix effect in complexes for various matrices is $BaO > Li_2CO_3 > Ag_2SO_4$.

Finally, the comparison of ligand influence in Ag_2CrO_4 and $Ag_2Cr_2O_7$ complexes[4] shows that the former is more resistant towards the HB ligand than the latter. Ag_2CrO_4 in its complexes retains, to a great degree, its own spectral characteristics. On the other hand, the coordination of the anion has been observed only in silver chromate complexes, which is in accordance with the observation that $Cr_2O_7^{2-}$ has less tendency for coordination than the CrO_4^{2-} ion.[10] The matrix effect was found to be more prominent in Ag_2CrO_4 than in $Ag_2Cr_2O_7$ complexes.

REFERENCES

1. D. J. Robins and P. Day, *Mol. Phys.* 1977, **34**, 893.
2. H. Firouzabadi, A. Sardarian, M. Naderi and B. Vessal, *Tetrahedron* 1984, **40**, 5001.
3. *Nouv. Traite de Chimie Minerale*, Vol. XIV. Nasson et Cie, Paris (1959).
4. M. Cieślak-Golonka, submitted for publication to *Pol. J. Chem.*
5. K. Nakamoto, *Infrared and Raman Spectra of Inorganic and Coordination Compounds*, Wiley, New York (1978).
6. R. J. H. Clark and T. J. Dines, *Inorg. Chem.* 1982, **21**, 3585.
7. G. M. Godziela, L. A. Ridnour and H. M. Goff, *Inorg. Chem.* 1985, **24**, 1609 and refs therein.
8. R. Coomber and W. P. Griffith, *J. Chem. Soc.* 1968, **5**, 1128.
9. J. Ribas, J. Casabo and J. M. Coronas, *J. Chem. Educ.* 1977, **54**, 321.
10. C. J. Puglisi, *J. Inorg. Nucl. Chem.* 1970, **32**, 692.

Polyhedron Vol. 7, No. 8, pp. 605–608, 1988
Printed in Great Britain

0277–5387/88 $3.00+.00
© 1988 Pergamon Press plc

LARGE TRANSITION METAL CLUSTERS—VI.* LIGAND EXCHANGE REACTIONS ON $Au_{55}(PPh_3)_{12}Cl_6$—THE FORMATION OF A WATER SOLUBLE Au_{55} CLUSTER

GÜNTER SCHMID,† NORBERT KLEIN and LUDGER KORSTE

Institut für Anorganische Chemie der Universität Essen, D-4300 Essen 1, F.R.G.

and

UWE KREIBIG and DETLEV SCHÖNAUER

Fachbereich 11 -Physik- der Universität des Saarlandes, D-6600 Saarbrücken, F.R.G.

(*Received* 3 *November* 1987; *accepted* 10 *November* 1987)

Abstract—The cluster compound $Au_{55}(PPh_3)_{12}Cl_6$ is soluble in organic solvents like pyridine or dichloromethane but decomposes rapidly thus precluding crystal growth and other investigations. Exchange of PPh_3 in $Au_{55}(PPh_3)_{12}Cl_6$ by $Ph_2PC_6H_4SO_3Na$ takes place quantitatively and yields the stable water soluble cluster $Au_{55}(Ph_2PC_6H_4SO_3Na \cdot 2H_2O)_{12}Cl_6$. Molecular weight determinations and conductivity measurements in H_2O show that the cluster is completely dissociated into $12Na^+$ and $[Au_{55}(Ph_2PC_6H_4SO_3)_{12}]^{12-}$. From such aqueous solutions very small, probably crystalline particles are obtained which can, in the dried state, be observed in the transmission electron microscope using a 100 kV electron beam. Here we present images that show columns or layers of cluster molecules with a distance of 2.1 ± 0.1 nm. The diameters of a cluster molecule including the ligand shell and of the naked cluster are calculated as 2.2 ± 0.1 and 1.3–1.4 nm, respectively. It is concluded that the cluster molecules, forming the layered structures, are intact. This is the first time that M_{55} clusters could be imaged with an intact ligand shell by means of TEM. Earlier microscopic investigations with a 400 kV beam gave high resolution images of the cluster nuclei only.

Since the discovery of the first M_{55} cluster in 1981[2] a series of other clusters of this type has been prepared and investigated by different methods.[3,4] The NMR spectroscopy especially, has shown some of the very novel properties of these large clusters. One important piece of information was that the ligands in all the different M_{55} clusters (M = Rh, Ru, Pt and Au) are extremely fluxional. For example in $Rh_{55}[P(t\text{-}Bu)_3]_{12}Cl_{20}$ the mobility of the phosphane ligands is so high that the expected ^{31}P—^{103}Rh coupling is completely averaged, leading to only one sharp singlet in the ^{31}P NMR spectrum.[4] On adding PPh_3 to a solution of $Au_{55}(PPh_3)_{12}Cl_6$, the original ^{31}P NMR signal of the complex at 34 ppm is shifted stepwise up to 12 ppm finally, when 24 moles of PPh_3 have been added to 1 mole of the cluster.[5] This behaviour is caused by a very fast exchange between coordinated and free phosphanes.

The contact time between a PPh_3 molecule and the cluster surface is calculated to be 3.0 ± 0.5 μs.[5] ^{103}Rh NMR investigations indicate even faster rearrangement of the cluster nucleus in solution.[4] These results stimulated us to some preparative experiments. As the most attractive exchange reaction, we regarded the one between the air stable $Au_{55}(PPh_3)_{12}Cl_6$ and the water soluble monosulphonated triphenylphosphane ($Ph_2PC_6H_4SO_3Na$).[6] Though the ligand size in our type of M_{55} clusters is mainly responsible for their stability, the change from PPh_3 to the monosulphonated derivative appeared justifiable.

* For Part V, see ref. 1.

† Author to whom correspondence should be addressed.

RESULTS AND DISCUSSION

If a solution of $Au_{55}(PPh_3)_{12}Cl_6$ in CH_2Cl_2 is stirred with an aqueous solution of $Ph_2PC_6H_4SO_3Na$ in a molar ratio of 1:12, the ligand exchange occurs quantitatively within one day.

$$\underset{\text{in } CH_2Cl_2}{Au_{55}(PPh_3)_{12}Cl_6} + 12\underset{\text{in } H_2O}{Ph_2PC_6H_4SO_3Na} \rightarrow \underset{\text{in } H_2O}{Au_{55}[Ph_2PC_6H_4SO_3Na]_{12}Cl_6} + 12\underset{\text{in } CH_2Cl_2}{PPh_3}.$$

The organic phase becomes almost colourless, containing mainly PPh_3, and the water phase turns to red–brown, the typical cluster colour. The isolation of $Au_{55}[Ph_2PC_6H_4SO_3Na]_{12}Cl_6$ takes place very easily by evaporation of the water. The black solid compound is air stable like the PPH_3 containing starting material, but its aqueous solution is much more stable compared with solutions of the PPh_3 containing cluster in organic solvents. It is probably the high ionic charge on the cluster surface which stabilizes the particles by repulsion, as is known from colloids. In aqueous solution, $Au_{55}[Ph_2PC_6H_4SO_3Na]_{12}Cl_6$ is completely dissociated into $12Na^+$ and the 12-fold negative charged anion $[Au_{55}(Ph_2PC_6H_4SO_3Na)_{12}Cl_6]^{12-}$. This can be evidenced by molecular weight determinations and conductivity measurements. The molecular weight in water is 1185 ± 2. This is almost exactly the thirteenth part of the value for the undissociated molecule of 15.418, namely 1186. The conductivity of a 6.48×10^{-6} M aqueous cluster solution was found to be 9.6 μS. Comparison with a 4.21×10^{-5} M NaCl solution (6.5 fold molar amount to give the same number of ions) results in a conductivity of 9.2 μS, and also proves the complete dissociation of the ionic cluster.

The ^{31}P NMR spectrum of $Au_{55}[Ph_2PC_6H_4SO_3Na]_{12}Cl_6$ shows only one singlet at 44.6 ppm for the coordinated phosphanes. Compared with the signal of $Au_{55}(PPh_3)_{12}Cl_6$ at 34 ppm there is a remarkable low field shift, although the free ligands have almost identical ^{31}P NMR shifts of -6 ± 1 ppm. This means that the sulphonated phosphane ligands are more strongly bonded to the cluster surface, leading to a higher electron deficiency at the phosphorus atoms. This result agrees completely with the higher stability of the water soluble cluster compared with that of the starting cluster. A further indication for the greater stability is that the technique to generate naked Au_{13} clusters from $Au_{55}(PPh_3)_{12}Cl_6$ using platinum electrodes and 10–20 V d.c.[1] fails here, probably because the ligands cannot be removed from the cluster surface. The sodium cations can be exchanged completely e.g. by Ba^{2+} or Ag^+ ions, leading to water insoluble red precipitates.

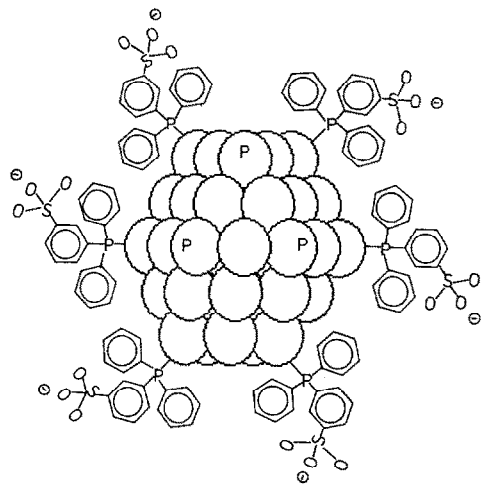

Fig. 1. Model of the cluster anion $[Au_{55}(Ph_2PC_6H_4SO_3)_{12}]^{12-}$ (P symbolizes positions where the other phosphane ligands are coordinated).

Figure 1 shows a model of the cluster ion $[Au_{55}(Ph_2PC_6H_4SO_3)_{12}]^{12-}$. Though we are not yet successful in preparing crystals of $Au_{55}[Ph_2PC_6H_4SO_3Na]_{12}Cl_6$ of directly visible size, small crystalline areas can be prepared by drying the aqueous solution on thin carbon films, which were then observed by means of transmission electron microscopy.

Figure 2 shows, as an example, several cluster aggregates, where rows or layers of clusters with preferential parallel arrangement, i.e. crystalline structure, are indicated. The observed distances between the imaged rows is 2.1 ± 0.1 nm. The diameters of cluster molecules including and excluding the sphere of the ligands are about 2.2 ± 0.1 and 1.3–1.4 nm, respectively. Using a 100 kV beam, the cluster molecules seem to hold their ligand shell during irradiation, in contrast to many HRTEM investigations where a voltage of 400 kV was applied.[7–9] These TEM images probably show the arrangements of intact cluster molecules for the first time.

EXPERIMENTAL

$Au_{55}(PPh_3)_{12}Cl_6$[2] was prepared as described elsewhere. Different sulphonated derivatives of PPh_3 are described in a patent.[6] For the synthesis of $Ph_2PC_6H_4SO_3Na$, some important changes have been necessary. Therefore its preparation is described here in detail. The ^{31}P NMR spectra were recorded with a Bruker AC 80 spectrometer. The determination of molecular weights was carried out with a Knauer Osmometer Nr. 11.00 and the con-

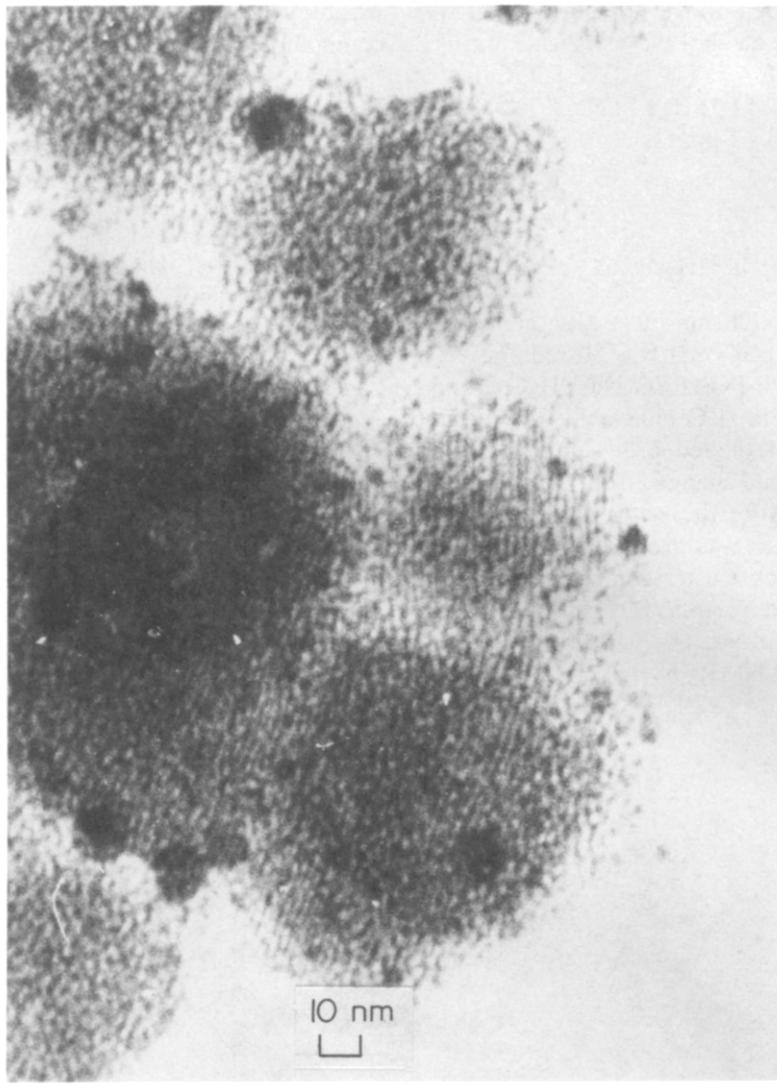

Fig. 2. TEM images of cluster aggregates with a preferential parallel arrangement. The distance between rows: 2.1±0.1 nm. The diameter of a cluster molecule including the ligand: 2.2±0.1 nm; without the ligand sphere: 1.3–1.4 nm.

ductivity measurement with an Orion Research Conductivity Meter, Model 101.

$Ph_2PC_6H_4SO_3Na \cdot 2H_2O$

A three-necked flask (250 cm^3) equipped with a stirrer, thermometer, dropping funnel and a reflux condenser was charged in an atmosphere of pure nitrogen with fuming sulphuric acid (100 g, 25%). In the course of 2 h and with stirring, PPh_3 (20.4 g, 78 mmol) was added at room temperature. The stirring was continued for another 2 h. After that, the reaction mixture was carefully added to H_2O (301 g) at 10–15°C under the exclusion of oxygen. Still using the N_2 atmosphere, a mixture of triisooctylamine (55.2 g, 67.6 cm^3, 156 mmol) and toluene (25 cm^3) are added to the aqueous solution. The mixture was then stirred for about 30 min. Thirty minutes later the two phases had separated. The organic phase (~ 308 g) was poured into a three-necked flask (500 cm^3), equipped with a pH glass electrode and a dropping funnel. Using 8% NaOH, the water containing toluene solution was titrated stepwise to pH = 6. At pH = 1.5 the aqueous phase was separated, and again at pH = 2.5. Both samples were disposed of. At pH = 6, 3% NaOH was used to titrate to pH = 7. The aqueous solution was again separated and the solvent evaporated under reduced pressure to dryness. For purification the following procedure is advisable: the crude product (e.g. 50 g from some experiments) was dissolved under nitrogen in H_2O (250 cm^3) in a 2 l flask. 10% H_2SO_4 (710 g) was added, followed by triisooctylamine (44.2 g) in toluene (176 cm^3). After 30 min stirring under nitrogen, the organic phase was separated and titration with NaOH was

repeated as described above. Finally the salt was recrystallized from alcohol (95%). Yield: ~ 50%. Found: C, 53.9; H, 4.5; Na, 5.8; S, 8.0. Calc. for $C_{18}H_{18}NaO_5PS$: C, 54.0; H, 4.5; Na, 5.7; S, 8.0%. ^{31}P NMR: $\delta = -6 \pm 1$ ppm (s).

$Au_{55}[Ph_2PC_6H_4SO_3Na \cdot 2H_2O]_{12}Cl_6$

$Au_{55}[PPh_3]_{12}Cl_6$ (100 mg, 7.04×10^{-3} mmol) dissolved in CH_2Cl_2 (50 cm^3) was stirred for 24 h with a solution of $Ph_2PC_6H_4SO_3Na \cdot 2H_2O$ (34 mg, 8.45×10^{-2} mmol) in H_2O (50 cm^3) at room temperature. After that, the red–brown colour, indicative of the cluster, had changed from the organic to the water phase. After the water phase had been separated, the water was evaporated completely, leading to the black cluster compound in quantitative yield. Found: C, 16.8; H, 1.5; Na, 2.1. Calc. for $C_{216}H_{216}Au_{55}Cl_6Na_{12}O_{60}P_{12}S_{12}$: C, 16.4; H, 1.4; Na, 1.7%. ^{31}P NMR: $\delta = 44.6$ ppm (s). Mol. weight: found: 1185 ± 2, calc. for the dissociated compound: 1186.

REFERENCES

1. G. Schmid and N. Klein, *Angew. Chem.* 1986, **98**, 910; *Angew. Chem. Int. Ed. Engl.* 1986, **25**, 922.
2. G. Schmid, R. Pfeil, R. Boese, F. Bandermann, S. Mayer, G. H. M. Calis and J. W. A. van der Velden, *Chem. Ber.* 1981, **114**, 3634.
3. G. Schmid and W. Huster, *Z. Naturforsch.* 1986, **41b**, 1028.
4. G. Schmid, U. Giebel, W. Huster and A. Schwenk, *Inorg. Chim. Acta* 1984, **85**, 97.
5. G. Schmid, *Structure and Bonding*, Vol. 62, p. 51. Springer, Berlin (1985).
6. Ruhrchemie AG, Oberhausen, European Patent No. 0163233 (1985).
7. L. R. Wallenberg, J.-O. Bovin and G. Schmid, *Surface Sci.* 1985, **156**, 256.
8. L. R. Wallenberg, J.-O. Bovin, A. K. Petford-Long and D. J. Smith, *Ultramicroscopy* 1986, **20**, 71.
9. A. K. Petford-Long, D. J. Smith, L. R. Wallenberg and J.-O. Bovin, *J. Cryst. Growth* 1987, **80**, 218.

Polyhedron Vol. 7, No. 8, pp. 609–614, 1988
Printed in Great Britain

0277–5387/88 $3.00+.00
© 1988 Pergamon Press plc

SYNTHESIS AND STRUCTURE OF A TETRANUCLEAR COPPER(II) 3,5-DI-*TERT*-BUTYLCATECHOLATE PYRIDINE COMPLEX, $[Cu(DTBC)Py]_4 \cdot 2CH_3CN$

M. M. OLMSTEAD* and P. P. POWER

Department of Chemistry, University of California, Davis, California 95616, U.S.A.

and

G. SPEIER* and Z. TYEKLÁR

Institute of Organic Chemistry, Veszprém University of Chemical Engineering, 8201 Veszprém, Hungary

(*Received* 14 *July* 1987; *accepted* 20 *November* 1987)

Abstract—The tetranuclear copper(II)-catecholate complex, [Cu(3,5-di-*tert*-butylcatecholate)(pyridine)]$_4 \cdot 2CH_3CN$ has been isolated from the reaction between Cu(0), pyridine and 3,5-di-*tert*-butyl-*o*-benzoquinone in acetonitrile solution in nearly quantitative yield. Brown crystals of $C_{80}H_{106}N_6O_8Cu_4$ are orthorhombic, space group $P2_12_12_1$, with $a = 13.395(5)$, $b = 24.287(11)$, $c = 24.918(11)$ Å, $Z = 4$. The crystal structure determination allows for the cluster to be formulated as four square planar Cu(II) ions, each bonded to two oxygens of chelating catecholate, a pyridine nitrogen and a bridging oxygen from a neighbouring catecholate. The Cu···Cu distances range from 3.152(1) to 3.572(1) Å. The tetranuclear complex exhibits an approximate parallel stacking of two pairs of coordination planes that is suggestive of a through-space pathway for antiferromagnetic interaction. It may also have a bearing on the observed catalytic oxidation by O_2 in solution.

In recent years, a limited number of structures of copper(II) complexes of 3,5-di-*tert*-butyl-*o*-semiquinone (DTBSQ)[1,2] and 3,5-di-*tert*-butylcatecholate (DTBC)[3] have been characterized. These show both monomeric and dimeric species in the solid state. In solution these derivatives display a complicated redox chemistry involving both the metal and the ligand.[4–10] The structural type found is dependent on the presence or absence of counterligands and on molecules of solvent which may be incorporated into the crystal structure. These effects are just beginning to be understood. In so far as they lend an insight into the range of possible species, the determination of new crystal structures aids the understanding of models for biological[9,11–15] or synthetic[9,11,16] oxidation catalysts.

We wish to report the synthesis and X-ray structural characterization of a new structural type for copper(II), namely, a cluster containing four catecholate ligands and four pyridine ligands coordinated to four copper(II) ions. The compound has been synthesized by the reaction of 3,5-di-*tert*-butyl-*o*-benzoquinone (DTBQ) with Cu(0) in the presence of pyridine, with the net reaction as shown in Scheme 1. This reaction differs from the usual methods[1,4,17] of preparation of copper catecholate complexes in that it uses elemental copper as a starting material.

It has often been observed that, in the presence of pyridine, copper(II) complexes containing semiquinone and catecholate ligands are unstable with respect to oxidation of the ligand by molecular oxygen.[1–3] Oxidation is not limited to the formation of benzoquinone, but also involves scission of the chelating C—C bond.[11,16,18] Somewhat surprisingly, the products of the latter decomposition do

* Authors to whom correspondence should be addressed.

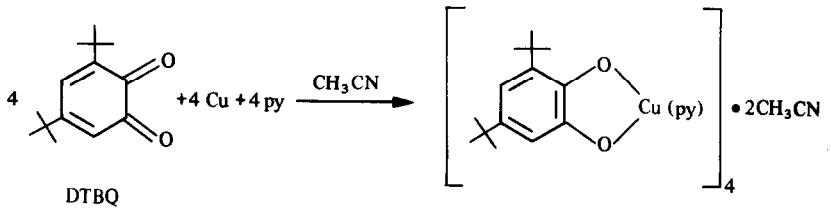

DTBQ

1

Scheme 1.

not contain copper(I), but rather copper(II). (In the presence of phosphines or other soft donors, the copper(I) state is stabilized and copper(I) complexes can be isolated.)[3] In the present case, even the use of excess Cu(0) does not lead to ready disproportionation to a copper(I) species. The crystal structure of **1** is the first structure of a pyridine-containing copper(II)-catecholate species, from which the possibility of an efficient two-electron oxidation can be appreciated.

EXPERIMENTAL

Preparation of $[Cu(DTBC)py]_4 \cdot 2CH_3CN$ (**1**)

Method A. Copper turnings (5 g, 79 mmol) were added to a solution of acetonitrile (30 cm^3), DTBQ (3.30 g, 15 mmol) and pyridine (3.6 cm^3, 45 mmol), and the mixture stirred under Ar for 25 h. The originally red solution turned to brown and a dark brown product precipitated. The mixture was heated until the products dissolved and was filtered to remove unreacted copper turnings. On cooling to room temperature the product crystallized as brown plates. It was filtered, washed with acetonitrile and ether, and dried under vacuum, yielding 4.7 g (82%) of the product $[Cu(DTBC)py]_4 \cdot 2CH_3CN$, **1**. M.p. 162–166°C(dec). Found: C, 62.5; H, 6.9; N, 5.4; Cu, 16.6. Calc. for $C_{80}H_{106}N_6O_8Cu_4$: C, 62.6; H, 7.0; N, 5.5; Cu, 16.6%.

Method B. Copper powder (1.0 g, 15 mmol) was added to a solution of acetonitrile (50 cm^3), DTBQ (2.20 g, 10 mmol) and pyridine (3.6 cm^3, 45 mmol), and the mixture refluxed under Ar for 1 h. The colour of the solution turned to brown. The hot solution was filtered to remove unreacted copper and from the filtrate on slow cooling to room temperature, a dark brown crystalline product deposited. The solution was washed and dried as above, yielding 3.3 g (86%) of **1**. Found: C, 61.5; H, 7.0; N, 5.4; Cu, 16.4%. Compound **1** possesses a room temperature magnetic moment of 1.75 μ_B/Cu determined by the Faraday method. Crystals suitable for X-ray diffraction studies were grown from acetonitrile.

X-ray crystallography

$C_{80}H_{106}N_6O_8Cu_4$, $M = 1533.94$, orthorhombic, space group $P2_12_12_1$ (No. 19), $a = 13.395(5)$, $b = 24.287(11)$, $c = 24.918(11)$ Å, $Z = 4$, $D_c = 1.26$ g cm^{-3}, $\lambda = 0.71069$ Å, $\mu = 10.8$ cm^{-1}, $F(000) = 202$. Data were collected at 130 K using a locally modified LT-1 apparatus and a fast scan method.[19] The intensities of two standard reflections showed no decay during data collection. Solution of the structure was accomplished by Patterson and Fourier techniques. Of the 7809 unique data, 5120 with $I > 3\sigma(I)$ were used in the refinement. Three reflections which suffered from large extinction were also omitted from the data set. The data were corrected for absorption using the program XABS.* Final refinement was carried out using isotropic thermal parameters for all non-hydrogen atoms and a riding model for the inclusion of hydrogen atoms. Methyl hydrogen atoms were not included. In the riding model, idealized C—H vectors of 0.96 Å length are recalculated with each cycle of refinement, and the hydrogen isotropic thermal parameters are set at 1.2 times those for the bonded carbon. At convergence, R was 0.069, R_w [$w = 1/\sigma^2$] = 0.074. Crystallographic programs used were those of SHELXTL, version 4.[20] Scattering factors and corrections for anomalous dispersion were taken from the *International Tables.*[21] No significant features were present on a final difference map. The largest was 0.84 e $Å^{-3}$, 0.72 Å from Cu(3).†

* XABS: the method obtains an empirical absorption tensor from an expression relating F_o and F_c: H. Hope and B. Moezzi, Department of Chemistry, University of California, Davis, California.

† Supplementary materials. Atomic positional parameters have been deposited with the Director, Cambridge Crystallographic Data Centre.

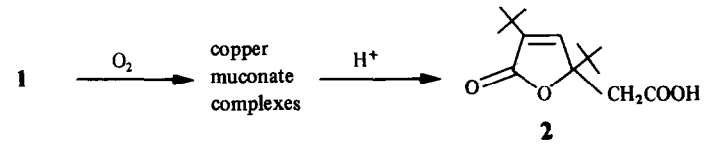

Scheme 2.

RESULTS

Complex **1** is air-stable in the solid form but undergoes oxygenolysis in pyridine. The dioxygen uptake is significantly more than the 4 : 1 per complex that would be required for the formation of copper(II) muconate complexes. Acidic hydrolysis of the oxygenated products gives 5-(carboxymethyl)-3,5-di-*tert*-butylfuran-2-one (**2**) in yields up to 23% (see Scheme 2).* Similar yields have been obtained by reactions of 1,10-phenanthroline and 2,2′-bipyridine derivatives of Cu(II)(DTBC) with molecular oxygen.[11]

Description of the structure of $[Cu(DTBC)py]_4 \cdot 2CH_3CN$

A drawing of the structure is given in Fig. 1. Table 1 summarizes the important bond distances and angles. Two acetonitrile molecules of crystallization are present in the lattice and have no significant interaction with the tetrameric species shown. The four copper ions are at the corners of a distorted tetrahedron with copper–copper distances ranging from 3.152 to 3.572 Å. The coordination geometry around each copper is best described as square planar. However there are tetrahedral distortions in three of the four copper coordination spheres. These can be seen from the twist angles of 15.9, 11.4, 0.8 and 15.0° for Cu(1) through to Cu(4), respectively. There is no apparent reason for the greater planarity at Cu(3). Each copper has the same set of ligands. These are comprised of a chelating DTBC, a pyridine and an oxygen that is bridging from another DTBC. From the standpoint of the DTBC group itself, one oxygen is involved in bridging between two coppers, while one is terminal. It is always the bridging oxygen which is *trans* to the pyridine. The copper–oxygen bond lengths are different for bridging and terminal coordination. The bridging Cu—O bond lengths are between 1.921–1.963 Å while the terminal ones range from 1.862 to 1.897 Å. The same trend appears in the C—O bond lengths, which average 1.39 Å for a bridging oxygen and 1.34 Å for a terminal oxygen. The C—C bond lengths within the chelate ring average to 1.39 Å.

An interesting feature of the structure is the near parallel stacking of pairs of coordination planes within the tetrameric unit. For example, the coordination planes of Cu(1) and Cu(4) are within 7° of perpendicular to those of Cu(2) and Cu(3). Also, the CuO_3N planes of Cu(1) and Cu(4) and those of Cu(2) and Cu(3) are 21.3 and 22.0° with respect to each other, respectively. This can be seen in the stereoview, Fig. 2. The shortest distances between copper atoms are those between coppers in the parallel stacks: 3.152 and 3.205 Å. The disposition of two parallel planes is such that a pairwise interaction appears to be present between the copper atom in one plane and a Cu—O bond in the other plane. The perpendicular distances from one Cu to the opposite Cu—O bond range from 2.874 to 3.175 Å. There are four such contacts in the tetramer. One set of two is portrayed in Fig. 3.

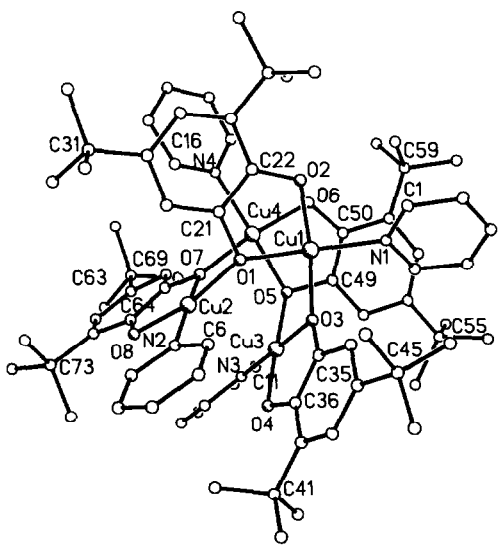

Fig. 1. A computer-generated drawing of $[Cu(DTBC)py]_4$ showing the atom numbering scheme. Atoms are given an arbitrary size.

* M.p. 132–134°C (ref. 22, 133–136°C); structure also confirmed by IR and NMR spectroscopy.

Table 1. Selected bond distances (Å) and angles (deg) for $[Cu(DTBC)py]_4 \cdot 2CH_3CN$

Cu(1)···Cu(2)	3.538(1)	Cu(2)···Cu(3)	3.205(1)
Cu(1)···Cu(3)	3.486(1)	Cu(2)···Cu(4)	3.572(1)
Cu(1)···Cu(4)	3.152(1)	Cu(3)···Cu(4)	3.311(1)
Cu(1)—O(1)	1.943(8)	Cu(3)—O(3)	1.933(8)
Cu(1)—O(2)	1.886(9)	Cu(3)—O(4)	1.897(9)
Cu(1)—O(3)	1.948(8)	Cu(3)—O(5)	1.921(8)
Cu(1)—N(1)	2.010(9)	Cu(3)—N(3)	1.997(11)
Cu(2)—O(1)	1.951(8)	Cu(4)—O(5)	1.927(8)
Cu(2)—O(7)	1.940(8)	Cu(4)—O(6)	1.881(8)
Cu(2)—O(8)	1.862(8)	Cu(4)—O(7)	1.963(8)
Cu(2)—N(2)	1.997(10)	Cu(4)—N(4)	2.024(10)
	C—O, terminal O		C—O, bridging O
C(22)—O(2)	1.335(14)	C(21)—O(1)	1.393(15)
C(64)—O(8)	1.343(15)	C(63)—O(7)	1.400(14)
C(36)—O(4)	1.365(14)	C(35)—O(3)	1.372(15)
C(50)—O(6)	1.315(15)	C(49)—O(5)	1.402(15)
	C—C lengths within chelate ring		
C(21)—C(22)	1.40(2)	C(49)—C(50)	1.38(2)
C(35)—C(36)	1.39(2)	C(63)—C(64)	1.39(2)
O(1)—Cu(1)—O(2)	86.2(3)	O(3)—Cu(3)—O(4)	85.6(3)
O(1)—Cu(1)—O(3)	88.8(3)	O(3)—Cu(3)—O(5)	89.7(3)
O(1)—Cu(1)—N(1)	164.8(4)	O(3)—Cu(3)—N(3)	179.1(4)
O(2)—Cu(1)—O(3)	172.0(3)	O(4)—Cu(3)—O(5)	175.4(3)
O(2)—Cu(1)—N(1)	91.6(4)	O(4)—Cu(3)—N(3)	94.7(4)
O(3)—Cu(1)—N(1)	94.8(4)	O(5)—Cu(3)—N(3)	90.0(4)
O(1)—Cu(2)—O(7)	89.8(3)	O(5)—Cu(4)—O(6)	85.8(4)
O(1)—Cu(2)—O(8)	168.2(4)	O(5)—Cu(4)—O(7)	87.9(3)
O(1)—Cu(2)—N(2)	95.0(4)	O(5)—Cu(4)—N(4)	167.6(4)
O(7)—Cu(2)—O(8)	85.1(4)	O(6)—Cu(4)—O(7)	168.2(4)
O(7)—Cu(2)—N(2)	173.6(4)	O(6)—Cu(4)—N(4)	91.3(4)
O(8)—Cu(2)—N(2)	90.9(4)	O(7)—Cu(4)—N(4)	96.8(4)

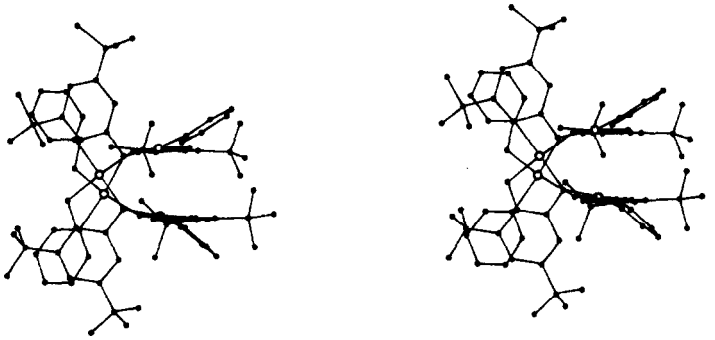

Fig. 2. A stereoview of the tetrameric species emphasizing the perpendicular orientation of two sets of parallel coordination planes.

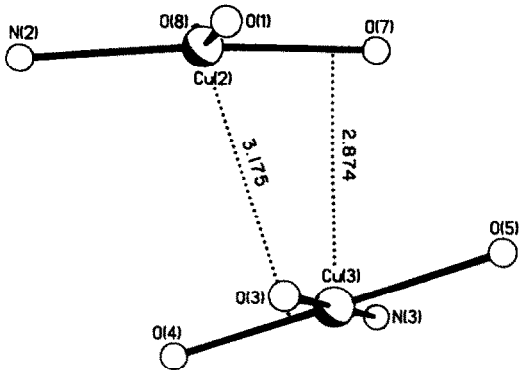

Fig. 3. A drawing of the stacked coordination planes of Cu(2) and Cu(3) indicating the pairwise Cu···Cu—O interactions.

Spectroscopy

The UV–vis absorption spectrum of **1** in CH_2Cl_2 shows bands with λ_{max}(nm), (ε, M^{-1} cm^{-1}) 295 (15,000), 390(sh), 498(1580) and 698(750). Upon standing and with exposure to O_2, the shoulder at 390 nm is resolved into a large peak at 387 nm and the two peaks at 498 and 698 nm diminish in intensity. Assignment of the peaks in the solution spectrum is difficult and still a matter of some controversy.[6a,16b,17] The IR spectrum (KBr pellets) exhibits the following absorptions (cm^{-1}): 2950s, 3904s, 2864m, 1604m, 1550m, 1470s, 1450s(sh), 1441s, 1417s, 1384w, 1350m, 1317s, 1277s(sh), 1262s, 1330m, 1217m, 1197w, 1170w, 1066m, 1037m, 1077w, 965s, 830m, 807m, 750s, 691s, 641w, 620w and 586w. A single crystal, powder and benzene solution of **1** were found to be EPR-silent at room temperature and at 175 K.

DISCUSSION

The two-electron oxidation–reduction reaction reported here differs from the one-electron processes reported[1,2] previously, in which a semiquinone complex is formed, e.g.

$$2[Cu(py)_4]ClO_4 + 2DTBC \rightarrow Cu(DTBSQ)_2 + [Cu(py)_4](ClO_4)_2.$$

The two reactions employ different conditions: in the two-electron reaction, Cu(0) is present in excess, acetonitrile is the solvent and brief heating is used to dissolve the products; in the one-electron reaction, the reactants are present in stoichiometric amounts and the solvent is methanol. In each case, O_2 is excluded from the reaction. Whether the two-electron process involves two one-electron steps cannot be stated; however, it is clear that the excess Cu(0) would allow any DTBSQ formed to be further reduced to DTBC, while the extra Cu^{2+} formed would remain in solution. The existence of the one- and two-electron processes raises the interesting possibility of the formation of a mixed valence species by careful control of reaction conditions. Formation of the tetramer is understandable in terms of charge balance and satisfaction of the coordination requirements for copper(II): with $DTBC^{2-}$ as one ligand, the two remaining coordination sites are filled by pyridine and a bridging oxygen from a neighbouring Cu(DTBC)py group. Association could stop at the dimer, but the three electronegative oxygens from the catecholate ligands render the copper somewhat electropositive; further association to the tetramer (with two bridging and one terminal oxygen) is therefore favoured.

The determination of the crystal structure of **1** establishes the formulation copper(II)–DTBC for each of the four copper centres. Characteristic changes in the C—O and C—C bond distances would be expected for oxidation of the ligand to the semiquinone or quinone forms.[1-4] In addition, larger tetrahedral distortions in the coordination planes would be expected if any copper(I) was present. The Cu—O distances themselves are not as sensitive to these changes and are more commonly related to changes in coordination number.[1-3] Thus, the Cu—O and Cu—N distances found, are close to those seen in the monomeric, four-coordinate (bipy)Cu(DTBC) complex.[3]

The observation of weak interactions between ligand planes in catecholato complexes is not new and has been observed in Fe, Cr and Mo complexes.[4] The Cu···Cu—O distances are probably short enough to provide a through-space pathway for antiferromagnetic interaction. The lack of an EPR signal is in agreement with the coupling of d^9 metal centres. Variable temperature magnetic measurements would be valuable in assessing the extent of this interaction. The role played by the stacking in oxygen binding is not known and perhaps it plays no role. Clearly, solution molecular weight experiments would aid the understanding of mechanistic phenomena. A large body of electrochemistry has been reported, which fails to consider the possibility of oligomeric species in solution. In this context, it is worth pointing out that the cobalt(II) catalysed oxidation of DTBC in ethanol has the stoichiometry[23]

$$2DTBC + O_2 \rightarrow 2DTBQ + 2H_2O.$$

Further, a tetrameric cobalt(II) complex, $[Co_4(DTBC)_4(THF)_{4.5}]$ has a structure very similar to that of the tetrameric copper complex reported

here.[24] Other, somewhat different, tetranuclear species are known.[4,7] It therefore seems reasonable to consider these tetranuclear complexes as structural models for potential intermediates in copper catalysed oxidation reactions.

Acknowledgements—We thank Dr A. Rockenbauer (Budapest) and Mr Paul Bruins (Davis) for the EPR measurements.

REFERENCES

1. J. S. Thompson and J. C. Calabrese, *Inorg. Chem.* 1985, **24**, 3167.
2. J. S. Thompson and J. C. Calabrese, *J. Am. Chem. Soc.* 1986, **108**, 1903.
3. R. M. Buchanan, C. Wilson-Blumenberg, C. Trapp, S. K. Larson, D. L. Greene and C. G. Pierpont, *Inorg. Chem.* 1986, **25**, 3070.
4. C. G. Pierpont and R. M. Buchanan, *Coord. Chem. Rev.* 1981, **38**, 45.
5. M. D. Stallings, M. M. Morrison and D. T. Sawyer, *Inorg. Chem.* 1981, **20**, 2655.
6. (a) S. Harmalker, S. E. Jones and D. T. Sawyer, *Inorg. Chem.* 1983, **22**, 2790; (b) M. E. Bodnini, G. Copia, R. Robinson and D. T. Sawyer, *Inorg. Chem.* 1983, **22**, 126.
7. M. W. Lynch, D. N. Hendrickson, B. J. Fitzgerald and C. G. Pierpont, *J. Am. Chem. Soc.* 1984, **106**, 2041.
8. K. D. Karlin, Y. Gultneh, T. Nicholson and J. Zubieta, *Inorg. Chem.* 1985, **24**, 3725.
9. (a) T. R. Demmin, M. D. Swerdloff and M. M. Rogic, *J. Am. Chem. Soc.* 1981, **103**, 5795; (b) M. M. Rogic, M. D. Swerdloff and T. R. Demmin, in *Copper Coordination Chemistry: Biochemical and Inorganic Perspectives* (Edited by K. D. Karlin and J. Zubieta), pp. 259–280. Adenine Press, New York (1983).
10. M. D. Stallings, M. M. Morrison and D. T. Sawyer, *Inorg. Chem.* 1981, **20**, 2655.
11. (a) D. G. Brown, L. Beckman, C. H. Ashby, G. C. Vogel and J. T. Reinprecht, *Tetrahedron Lett.* 1977, **16**, 1363; (b) D. T. Brown and W. J. Hughes, *Z. Naturforsch., B: Anorg. Chem., Org. Chem.* 1981, **36B**, 1324.
12. (a) G. Speier and Z. Tyeklár, *J. Mol. Catal.* 1980, **9**, 233; (b) G. Speier and Z. Tyeklár, *J. Chem. Soc., Dalton Trans.* 1983, 1995; (c) G. Speier and Z. Tyeklár, *React. Kinet. Catal. Lett.* 1980, **15**, 91; (d) G. Speier, *J. Mol. Catal.* 1986, **37**, 258; (e) É. Balogh-Hergovich and G. Speier, *J. Mol. Catal.* 1986, **37**, 309.
13. J. Tsuji and H. Takayanagi, *J. Am. Chem. Soc.* 1974, **96**, 7349.
14. E. I. Solomon, *Metal Ions Biol.* 1981, **3**, 41.
15. D. E. Wilcox, A. G. Porras, Y. T. Hwang, K. Lerch, M. E. Winkler and E. I. Solomon, *J. Am. Chem. Soc.* 1985, **107**, 4015.
16. (a) D. G. Brown, W. J. Hughes and G. Knerr, *Inorg. Chim. Acta* 1980, **46**, 123; (b) D. G. Brown and W. J. Hughes, *Z. Naturforsch., B: Anorg. Chem., Org. Chem.* 1979, **34B**, 1408.
17. D. G. Brown, J. T. Reinprecht and G. C. Vogel, *Inorg. Nucl. Chem. Lett.* 1976, **12**, 399.
18. R. D. Willett and G. L. Breneman, *Inorg. Chem.* 1983, **22**, 326.
19. H. Hope and B. G. Nichols, *Acta Cryst.* 1981, **B37**, 158.
20. G. Sheldrick, SHELXTL; Nicolet Analytical Instruments, Madison, WI.
21. *International Tables for X-ray Crystallography*, Vol. IV. Kynoch Press, Birmingham (1974).
22. T. Matsuura, H. Matsushima, S. Kato and I. Saito, *Tetrahedron* 1972, **28**, 5119.
23. S. Tsuruya, S. Yanai and M. Masai, *Inorg. Chem.* 1986, **25**, 141.
24. M. Olmstead, P. Power and G. Sigel, *Inorg. Chem.*, in press.

Polyhedron Vol. 7, No. 8, pp. 615–621, 1988
Printed in Great Britain

0277–5387/88 $3.00+.00
© 1988 Pergamon Press plc

SYNTHESIS AND CHARACTERIZATION OF TRINUCLEAR PALLADIUM CARBOXYLATE COMPLEXES

DANIEL P. BANCROFT, F. ALBERT COTTON,* LARRY R. FALVELLO and WILLI SCHWOTZER

Department of Chemistry and Laboratory for Molecular Structure and Bonding, Texas A&M University, College Station, TX 77843, U.S.A.

(*Received* 10 *October* 1987; *accepted* 20 *November* 1987)

Abstract—The structures of three trinuclear palladium(II) carboxylates, $Pd_3(O_2CR)_6$, with $R = C_2H_5$ (**1**), $C(CH_3)_3$ (**2**) and 2,4,6-$C_6H_2(CH_3)_3$ (**3**), have been determined in order to determine whether the Pd_3 triangle in such compounds deviates from equilateral to isosceles because of packing forces or for other reasons. The results lead us to conclude that these molecules are inherently of three-fold symmetry but become easily deformed by intermolecular contacts. In **1** the Pd—Pd distances (Å) are 3.135(1), 3.191(1) and 3.191(1); in **2** they are 3.131(1), 3.132(1) and 3.132(1); in **3** they are 3.137(3), 3.140(3) and 3.116(3). The crystallographic properties of the three compounds are as follows. (**1**) Space group $C2/c$, $a = 17.280(2)$, $b = 8.802(1)$, $c = 16.452(3)$ Å, $\beta = 92.75(1)°$, $Z = 4$. (**2**) Space group $Pnma$, $a = 23.066(3)$, $b = 17.578(2)$, $c = 10.465(1)$ Å, $Z = 4$. (**3**) Space group $P2_1/n$, $a = 19.951(11)$, $b = 12.738(5)$, $c = 27.618(7)$ Å, $\beta = 102.26(6)°$, $Z = 4$.

Palladium(II) acetate has previously been shown to have a trinuclear molecular structure with unequal Pd—Pd distances.[1,2] Early crystallographic studies showed a distinct pattern to the distortion of the Pd_3 triangle.[2,3] In all cases, the triangle was exactly (by crystal symmetry) or effectively isosceles. More recently, a second study by Cotton and Han[4] has suggested that the apparent predisposition of the molecule to form an isosceles triangle of Pd atoms is due to intermolecular crystal packing forces. We have further investigated this hypothesis by preparing and studying the crystal structures of several other trinuclear palladium carboxylates. By varying the nature of the bridging ligand it should be possible to ascertain whether or not the observed structural anomaly present in the acetate case is primarily due to crystal packing effects, or whether it is due to some other factor. We have chosen three different carboxylate ligands of differing steric bulk in order to provide variation in the crystal packing of the complexes. Two of the complexes, the propionate and the pivalate, contain relatively non-bulky carboxylate ligands, while the third complex contains fairly large 2,4,6-trimethylbenzoate bridging ligands. The palladium carboxylate complexes are readily prepared by substitution of palladium acetate with either the sodium salt or the acid form of the carboxylate. The compounds are similar to palladium acetate in that they contain a Pd_3 triangle with each pair of palladium atoms bridged by two carboxylate ligands. The details of the synthesis and the results of the crystallographic studies are reported.

EXPERIMENTAL

Palladium acetate was purchased from Johnson Matthey Company and was used without further purification.

Preparation of $Pd_3(O_2CC_2H_5)_6$ **1**

A mixture of $Pd_3(O_2CCH_3)_6$ (0.25 g, 0.37 mmol), propionic acid (8.0 cm^3) and propionic anhydride (1.0 cm^3) was refluxed for 3 h. The resulting red–orange solution was filtered to remove some elemental palladium. The excess propionic acid was then removed at room temperature *in vacuo*. The remaining red–orange microcrystalline solid was

* Author to whom correspondence should be addressed.

dissolved in a 1 : 1 mixture of benzene and propionic acid and slowly evaporated in air to give crystals of $Pd_3(O_2CC_2H_5)_6$, compound **1**, suitable for X-ray diffraction. The complex is soluble in most organic solvents. The overall isolated yield of $Pd_3(O_2CC_2H_5)_6$ was 0.19 g (68% with respect to Pd).

Preparation of $Pd_3(O_2CC_4H_9)_6$ **2**

An excess of pivalic acid (≈ 10 cm^3) was added to a solution of $Pd_3(O_2CCH_3)_6$ (0.20 g, 0.30 mmol) in 20 cm^3 of dry benzene. The solution was refluxed for 3 h during which time the colour changed from orange–red to dark red. After filtration through Celite to remove some insoluble material the solvent was removed *in vacuo*. The excess pivalic acid was removed by carefully washing the red solid with small portions of ice cold diethylether. Plate-like crystals of $Pd_3(O_2CC_4H_9)_6$, compound **2**, were grown by slow evaporation of a benzene solution in air. The compound is soluble in most organic solvents. The yield of $Pd_3(O_2CC_4H_9)_6$ was 0.22 g (81% with respect to Pd).

Preparation of $Pd_3(O_2CC_9H_{11})_6$ **3**

A chloroform solution (30.0 cm^3) consisting of $Pd_3(O_2CCH_3)_6$ (0.20 g, 0.30 mmol) and 2,4,6-trimethylbenzoic acid (0.29 g, 1.8 mmol) was stirred at room temperature for 24 h. The red solution was filtered through Celite and evaporated to dryness *in vacuo*. Large red crystals of composition $Pd_3(O_2CC_9H_{11})_6 \cdot 2C_6H_6$, were grown by slow evaporation of a benzene solution in air. The compound is very soluble in most organic solvents. The yield of $Pd_3(O_2CC_9H_{11})_6 \cdot 2C_6H_6$ was 0.30 g (78% with respect to Pd).

*X-ray crystallography**

$Pd_3(O_2CC_2H_5)_6$ **1**. A crystal with dimensions $0.5 \times 0.5 \times 0.5$ mm was coated with epoxy cement and mounted on top of a glass fibre. A Syntex $P\bar{1}$ four-circle diffractometer equipped with graphite-monochromated Mo-K_α ($\lambda = 0.71073$ Å) radiation was used to collect 2300 unique reflections of which 2089 had $I > 3\sigma(I)$. Lorentz, polarization and absorption corrections (by the ψ-scan method) were applied. Relevant crystal parameters and data are given in Table 1.

Preliminary examination of the crystal showed it to have monoclinic symmetry. The systematic absences, hkl: $h+k = 2n+1$ and $h0l$: $l = 2n+1$ were consistent with the space groups Cc or $C2/c$. The space group $C2/c$ was confirmed by successful refinement of the structure. The heavy atom positions were obtained by the direct methods program Multan 11/82. Alternating difference Fourier maps and least-squares cycles revealed the remaining non-hydrogen atoms. No attempt was made to find the hydrogen atoms. Full matrix least-squares refinement converged to final residuals of $R = 0.029$ and $R_w = 0.036$. Expressions for R and R_w are included in Table 1. The largest peaks in the final difference map were *ca* 0.6 e Å^{-3} and were located approximately where the hydrogen atoms would be; however, refinement of these peaks as hydrogen atoms was not attempted.

$Pd_3(O_2CC_4H_9)_6$ **2**. A plate-like crystal with dimensions $0.4 \times 0.3 \times 0.5$ mm was coated with epoxy cement and mounted on top of a glass fibre. A Nicolet $P3/F$ four-circle diffractometer equipped with graphite-monochromated Mo-K_α ($\lambda = 0.71073$ Å) radiation was used to collect 2639 unique reflections of which 2058 had $I > 3\sigma(I)$. Lorentz, polarization and absorption corrections (by the ψ-scan method) were applied. Relevant crystal parameters and data are included in Table 1.

Preliminary examination of the crystal showed it to have orthorhombic symmetry. The orthorhombic space group was determined to be *Pnma* by successful refinement. The systematic absences were $0kl$: $k+l = 2n+1$ and $hk0$: $h = 2n+1$. The heavy atom positions were obtained by the direct methods program Multan 11/82. Alternating difference Fourier and least-squares cycles revealed the remaining non-hydrogen atoms. No attempt was made to find the hydrogen atoms. Two of the pivalate groups contained rotationally disordered terminal methyl groups. The methyl groups on C(7) were refined with partial occupancies for two preferred orientations. In addition, the terminal methyl groups of C(6) were refined similarly. Both orientations have one methyl group located on a crystallographic mirror plane. There was evidence of disorder for the terminal methyl groups of C(5); however, a reasonable disorder model could not be found. In all cases, the terminal methyl groups were refined isotropically. All of the other atoms were refined with anisotropic thermal parameters. Full matrix least-squares refinement converged to final residuals of $R = 0.049$ and $R_w = 0.069$. The largest peaks in the final difference map were *ca* 1.0 e Å^{-3} and were located near disordered pivalate methyl groups. Attempts to incorporate these peaks into a disorder model were unsuccessful.

* Calculations were done with the VAX-SDP software package on the Vax 11/780 computer in the Department of Chemistry, Texas A&M University.

Table 1. Crystal data

Crystal data	Compound **1**	Compound **2**	Compound **3**
Formula	$Pd_3(O_2CC_2H_5)_6$	$Pd_3(O_2CC_4H_9)_6$	$Pd_3(O_2C_9H_{11})_6 \cdot 2C_6H_6$
Formula weight	757.63	925.96	1454.62
Space group	*C2/c*	*Pnma*	$P2_1/n$
Systematic absences	$hkl: h+k = 2n+1$	$0kl: k+l = 2n+1$	$0k0: k = 2n+1$
	$h0l: l = 2n+1$	$hk0: h = 2n+1$	$h0l: h+l = 2n+1$
a, Å	17.280(2)	23.066(3)	19.951(11)
b, Å	8.802(1)	17.578(2)	12.738(5)
c, Å	16.452(3)	10.465(1)	27.618(7)
α, deg	90.00	90.00	90.00
β, deg	92.75(1)	90.00	102.26(6)
γ, deg	90.00	90.00	90.00
V, Å^3	2499.4(6)	4243.1(9)	6589(5)
Z	4	4	4
d_{calc}, g cm^{-3}	2.013	1.449	1.409
Crystal size, mm	$0.05 \times 0.5 \times 0.5$	$0.4 \times 0.3 \times 0.5$	$0.5 \times 0.4 \times 0.4$
μ(Mo-K_α), cm^{-1}	21.63	12.88	8.24
Data collection instrument	Syntex $P\bar{1}$	*P*3	*P*-1
Radiation (monochromated in incident beam)		Mo-K_α ($\bar{\lambda} = 0.71073$Å)	
Orientation reflections,	15	25	15
number, range (2θ)	20–29	20–30	20–30
Temperature, °C	25	25	5
Scan method	*θ–2θ*	*θ–2θ*	*θ–2θ*
Data col. range, 2θ, deg	4.0–50.0	4.0–45.0	4.0–45.0
No. of unique data, total	2300	2639	3186
with $F_o^2 > 3\sigma(F_o^2)$	2089	2058	2550
Number of parameters refined	150	191	439
Trans. factors, max., min.	99.90, 73.09%	99.97, 86.84%	99.79, 92.21%
R^a	0.029	0.049	0.068
$R_w{}^b$	0.036	0.069	0.079
Quality-of-fit indicator^c	3.795^d	1.583	1.308
Largest shift/esd, final cycle	0.04	0.26	0.02
Largest peak, e Å^{-3}	0.646	1.040	0.642

[a] $R = \Sigma ||F_o| - |F_c|| / \Sigma |F_o|$.
[b] $R_w = [\Sigma w(|F_o| - |F_c|)^2 / \Sigma w|F_o|^2]^{1/2}$; $w = 1/\sigma^2(|F_o|)$.
[c] Quality-of-fit = $[\Sigma w(|F_o| - |F_c|)^2 / (N_{obs} - N_{parameters})]^{1/2}$.
[d] Unit weights used for Compound **1**.

$Pd_3(O_2CC_9H_{11})_6 \cdot 2C_6H_6$ **3**. A hexagonal shaped crystal with dimensions $0.5 \times 0.4 \times 0.4$ mm was coated with epoxy cement and mounted on top of a glass fibre. A Syntex $P\bar{1}$ four-circle diffractometer equipped with graphite-monochromated Mo-K_α ($\lambda = 0.71073$ Å) radiation was used to collect 3186 unique reflections of which 2550 had $I > 3\sigma(I)$. Lorentz, polarization and absorption corrections were applied. Relevant crystal parameters and data are included in Table 1.

Preliminary examination of the crystal showed it to have a primitive monoclinic lattice. The monoclinic space group, $P2_1/n$, was determined by the systematic absences $0k0$: $k = 2n+1$ and $h0l$: $h+l = 2n+1$. The heavy atom positions were obtained by the direct methods program Multan 11/82. Alternating difference Fourier maps and least-squares cycles revealed the remaining non-hydrogen atoms. No attempt was made to locate the hydrogen atoms. With a few exceptions the carbon atoms of the 2,4,6-trimethylbenzoate bridging ligands were refined isotropically. In addition, the oxygen atom O(2), which could not be refined successfully with anisotropic thermal parameters, was refined isotropically. Full matrix least-squares refinement converged to final residuals of $R = 0.068$ and $R_w = 0.079$. The largest peaks in the final difference map were *ca* 0.6 e Å^{-3}.

Table 2. Table of selected bond distances and their esds in angstroms

	$Pd_3(O_2CC_2H_5)_6$	$Pd_3(O_2CC_4H_9)_6$	$Pd_3(O_2CC_9H_{11})_6$
Pd(1)—Pd(1)	3.135(1)	—	—
Pd(1)—Pd(2)	3.191(1)	3.132(1)	3.137(3)
Pd(2)—Pd(2)	—	3.131(1)	—
Pd(1)—Pd(3)	—	—	3.140(3)
Pd(2)—Pd(3)	—	—	3.116(3)
Pd—Pd (av)	3.172[32]	3.131[1]	3.131[13]
Pd—O (av)	1.995[7]	1.980[11]	2.00[2]
O—C (av)	1.246[10]	1.226[18]	1.26[7]

Table 3. Selected bond angles

	$Pd_3(O_2CC_2H_5)_6$	$Pd_3(O_2CC_4H_9)_6$	$Pd_3(O_2CC_6H_{11})_6$
Pd(1)—Pd(2)—Pd(1)′	60.58(1)	—	—
Pd(1)′—Pd(1)—Pd(2)	58.85(1)	—	—
Pd(2)—Pd(1)—Pd(2)′	—	59.99(3)	—
Pd(1)—Pd(2)—Pd(2)′	—	60.01(3)	—
Pd(1)—Pd(2)—Pd(3)	—	—	60.29(6)
Pd(1)—Pd(3)—Pd(2)	—	—	60.20(6)
Pd(2)—Pd(1)—Pd(3)	—	—	59.52(6)
cis O—Pd—O	89.2[29]	88.8[35]	89.7[34]
trans O—Pd—O	166.1[23]	166.9[3]	166.6[46]
Pd—O—C	130.3[21]	131.8[7]	126[4]
O—C—O	126.6[7]	125[1]	128[3]

RESULTS*

Structure of $Pd_3(O_2CC_2H_5)_6$ 1

Figure 1 shows an ORTEP view of the $Pd_3(O_2C_3H_5)_6$ unit. Tables 2 and 3 list selected bond lengths and angles, respectively.

The structure consists of a cyclic trinuclear molecule with one of the Pd atoms residing on a crystallographic two-fold axis. The molecule is similar to the acetate analogue in that the palladium atoms form an isosceles triangle with two carboxylate groups bridging each pair of Pd atoms. The metal–metal distances are 3.135(1) and 3.191(1) Å. As in the acetate case, two of the Pd—Pd distances are significantly longer than the third. Each Pd atom

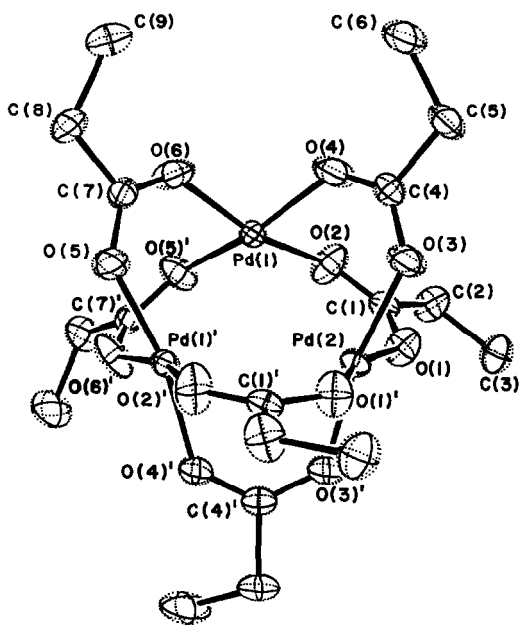

Fig. 1. An ORTEP drawing of the $Pd_3(O_2CC_2H_5)_6$ molecule. All atoms are represented by their thermal displacement ellipsoids at the 40% probability level.

* Supplementary Material Available. For each structure, atomic positional parameters, observed and calculated structure factors, a listing of all bond distances, a listing of all bond angles, and a table of general temperature factors (B's), (54 pp.). Copies are available from the Editor. Atomic coordinates have also been deposited with the Cambridge Crystallographic Data Centre.

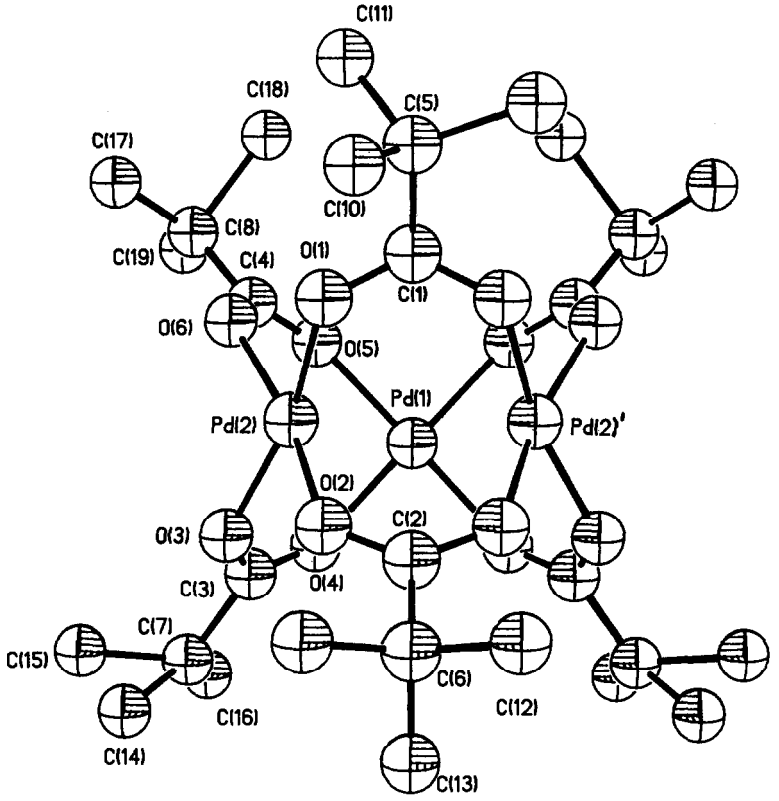

Fig. 2. The structure of the $Pd_3(O_2CC_4H_9)_6$ molecule. All atoms are represented by spheres of arbitrary radius.

exists in approximately a square-planar environment with only slight deviations from planarity. The average Pd—O bond distance is 1.995[7] Å. In addition, most of the important bond angles are similar to those in the acetate compound.

Structure of $Pd_3(O_2CC_4H_9)_6$ **2**

Figure 2 shows an ORTEP view of the molecule. Tables 2 and 3 list selected bond lengths and angles, respectively.

The structure consists of a cyclic trinuclear molecule with one Pd atom residing on a crystallographic mirror plane. In contrast to the other trinuclear Pd complexes, however, the pivalate complex forms an equilateral triangle of Pd atoms. The metal–metal distances are 3.132[1]. The complex, which is similar to the other palladium compounds, contains two pivalate ligands bridging each pair of palladium atoms. Each Pd atom is in a square-planar environment and is coordinated to oxygen atoms from four different carboxylate groups. The Pd–ligand bond distances and angles are very similar to those in the propionate compound, with only minor, chemically insignificant differences.

Structure of $Pd_3(O_2CC_9H_{11})_6 \cdot 2C_6H_6$ **3**

Figure 3 shows an ORTEP view of the molecule. Some selected bond lengths and angles are included in Tables 2 and 3, respectively.

The structure consists of a cyclic trinuclear molecule with the palladium atoms residing on general lattice positions. In addition to the trinuclear Pd complex, the structure contains two benzene solvent molecules. The palladium atoms form a nearly isosceles triangle with two sides [3.140(3) and 3.137(3) Å] longer than the third side, which has a Pd—Pd separation of 3.116(3) Å. The average Pd—Pd separation, 3.131[13] Å is identical to that in the pivalate analogue. As before, each Pd atom is in an approximate square-planar arrangement with each Pd atom coordinated to four oxygen atoms from four different carboxylate groups. The Pd—O bond distance, 2.00[2] Å, is slightly longer than in the other two compounds; however, this is clearly of no chemical importance.

DISCUSSION

The structures of the trinuclear palladium carboxylate complexes prepared in this study are very

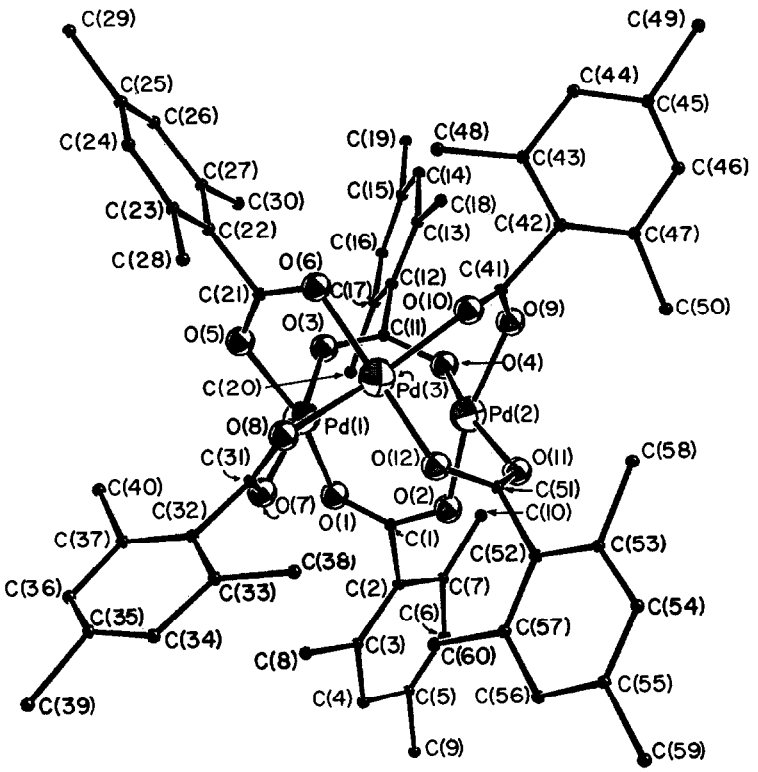

Fig. 3. An ORTEP drawing of the $Pd_3(O_2CC_9H_{11})_6$ molecule. Only Pd and O atoms are represented by thermal displacement ellipsoids at the 40% level; all other atoms are represented by arbitrarily small spheres for the sake of clarity.

similar to those of the previously investigated palladium acetate complex. All three compounds consist of cyclic trinuclear molecules with each pair of palladium atoms bridged by two carboxylate ligands. The Pd—Pd distances range from 3.191(1) to 3.116(1) Å in compounds **1**–**3**. The Pd—Pd distances in the three previously characterized acetate compounds are similar, ranging from 3.171(1) to 3.081(1) Å. In addition, the Pd—O distances are similar, ranging from 1.980[11] to 2.00[2] Å in compounds **1**–**3**, and from 1.972[12] to 1.996[20] Å in the acetate compounds. As expected, the important bond angles are also very close to those in the acetate compounds as well.

The palladium carboxylate compounds crystallize in a wide variety of space groups, some that impose crystallographic symmetry on the molecule and some that do not. Two of the compounds, **1** and **3**, have an isosceles triangle of metal atoms. In compound **1** there is a crystallographic two-fold axis which necessarily requires two of the Pd—Pd distances to be equal, while in compound **3** there is no crystallographically imposed symmetry on the molecule. Compound **2** differs from compounds **1** and **3** and the acetate analogues in that the Pd_3 triangle is equilateral. This occurs in spite of a crystallographically imposed mirror plane that requires that only two of the distances be equal. In the acetate case there was a question of whether or not the imposition of crystallographic symmetry forced the molecule to adopt an isosceles configuration of metal atoms. The presence of compound **2** clearly indicates that the imposition of crystallographic symmetry does not require the molecules to adopt an isosceles configuration. In addition, there is now ample evidence showing that there is no predisposition for the molecules to form isosceles triangles of metal atoms. The appearance of isosceles type distortions in these molecules must be considered to be a chance occurrence, caused by interaction of the molecules with their surroundings.

The results of this study, as well as the results of the previous studies, suggest that the formation of isosceles triangles of palladium atoms in several of the structures is solely due to intermolecular packing forces. The palladium carboxylate compounds are inherently more susceptible to this type of distortion than other types of trinuclear compounds. The palladium carboxylate compounds do not

possess metal–metal bonds, oxygen atoms in their centres, or μ_3-O atoms above and below the Pd_3 planes, features which would tend to add rigidity to the structures. Thus, they are relatively "soft" and therefore more susceptible to distortions from environmental effects.

Acknowledgement—We thank the National Science Foundation for support.

REFERENCES

1. T. A. Stephenson, S. M. Morehouse, A. R. Powell, J. P. Heffer and G. Wilkinson, *J. Chem. Soc.* 1965, 3632.
2. A. C. Skapski and M. L. Smart, *J. Chem. Soc., Chem. Comm.* 1970, 658.
3. F. A. Cotton and S. Han, *Revue de Chim. Min.* 1983, **20**, 496.
4. F. A. Cotton and S. Han, *Revue de Chim. Min.* 1985, **22**, 277.

Polyhedron Vol. 7, No. 8, pp. 623–628, 1988
Printed in Great Britain

0277–5387/88 $3.00+.00
© 1988 Pergamon Press plc

CYCLOPENTADIENYLRUTHENIUM(II) COMPLEXES: REACTIONS OF $[(\eta^5\text{-}C_5H_5)RuCl(AsPh_3)_2]$ WITH SOME AROMATIC THIOAMIDES

VEENA CHAUHAN, H. K. GUPTA and S. K. DIKSHIT*

Department of Chemistry, Indian Institute of Technology, Kanpur 208 016, U.P., India

(*Received* 20 *July* 1987; *accepted after revision* 20 *November* 1987)

Abstract—Reactions of $[(\eta^5\text{-}C_5H_5)RuCl(AsPh_3)_2]$ with the ligands of the type $RCSNHCOOC_2H_5$ (R = 4-toluene, 2-pyrrole, 1-pyrrole, 2-thiophene), $R_1CSNHCOOR_2$ (R_1 = 2-pyrrole, $R_2 = NH_2$, NHPh) and 2-thiopyrrole-1,2-dicarboximide, lead to the formation of diamagnetic compounds of the formula $[(\eta^5\text{-}C_5H_5)RuCl(AsPh_3)(LH)] \cdot xCH_2Cl_2$ ($x = 0$ or 1/2). These compounds and spectroscopic (UV, Vis, IR, and ^1H NMR) data are reported. A distorted octahedral geometry is proposed for the complexes.

It is recognised that the properties of the metal complexes of phosphorus donor ligands[1–3] are markedly affected by the electronic and steric[3] effects of the substituents on phosphorus. However, investigations on the electronic and/or steric effects in metal complexes of arsenic donor ligands have been lacking. Recently, we reported reactions of $[Ru(\eta^5\text{-}C_5H_5)(PPh_3)_2Cl]$ with some aromatic thioamides ($R_1CSNHCOR_2$).[4] We now report the reaction of $[RuCl(\eta^5\text{-}C_5H_5)(AsPh_3)_2]$ with thioamides and the characterization of the reaction products. The names and abbreviations of the ligands reported here are as shown in Fig. 1.

EXPERIMENTAL

All the reagents were Analar or of chemically pure grade. All the solvents were dried and distilled before use. The reactions were carried out under a dry and pure nitrogen atmosphere. $[(\eta^5\text{-}C_5H_5)RuCl(AsPh_3)_2]$ and all the ligands were prepared by literature methods.[5–8]

Preparation of complexes

Preparation of the complexes $[(\eta^5\text{-}C_5H_5)RuCl(LH)(AsPh_3)] \cdot 1/2CH_2Cl_2$ (LH = Hctt, Hcept, Hcpt, Hcett, Hcapt, Hcppt, Htp).

A solution of $(\eta^5\text{-}C_5H_5)RuCl(AsPh_3)_2$ (0.105 g, 0.25 mmol) and the appropriate ligand (0.35 mmol) in 40 cm^3 methanol was stirred for 2–3 h under a dry N_2 atmosphere. (In case of Hcapt and Hcppt, the compound was separated during stirring.) The resulting solution was evaporated to near dryness, the residue extracted by CH_2Cl_2 and the complex precipitated from the extract using petroleum ether. It was centrifuged and purified by recrystallization from CH_2Cl_2–petroleum ether. It was filtered, washed with petroleum ether and dried *in vacuo*.

In the case of the ligands (Hcapt and Hcppt), orange complexes of the formula $(\eta^5\text{-}C_5H_5)RuCl(AsPh_3)(LH)$ were precipitated during stirring, isolated by centrifugation and washed with petroleum ether. The filtrate was evaporated to dryness under reduced pressure. The residue was dissolved in the minimum quantity of dichloromethane followed by addition of petroleum ether. On scratching the walls of the beaker and allowing to stand for 1–2 h, the precipitate $[(\eta^5\text{-}C_5H_5)RuCl(AsPh_3)(LH)] \cdot 1/2CH_2Cl_2$ appeared, which was centrifuged, washed several times with petroleum ether and dried *in vacuo*.

Physical measurements

Carbon, hydrogen and nitrogen analyses were carried out by the Microanalytical Laboratory of I.I.T., Kanpur, India. The percentage of halide and sulphur in the filtrate obtained, was determined by the standard method after fusing the sample with a fusion mixture, extracting it with distilled water and filtering it. IR, UV–vis, ^1H NMR and magnetic

*Author to whom correspondence should be addressed.

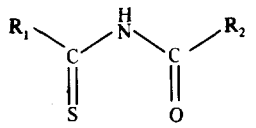

R_1=4–toluene, R_2=OC_2H_5, *N*–carboethoxy–4–toluenethioamide (Hctt);
R_1=2–pyrrole, R_2=OC_2H_5, *N*–carboethoxy–2–pyrrolethioamide (Hcept);
R_1=1–pyrrole, R_2=OC_2H_5, *N*–carboethoxy–1–pyrrolethioamide (Hcpt),
R_1=2–thiophene, R_2=OC_2H_5, *N*–carboethoxy–2–thiophenethioamide (Hcett);
R_1=2–pyrrole, R_2=NH_2, *N*–carboamido–2–pyrrolethioamide (Hcapt);
R_1=2–pyrrole, R_2=NHC_6H_5, *N*–carbophenylamido–2–pyrrolethioamide (Hcppt),

and 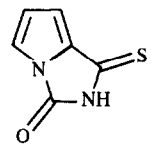 , 2–thiopyrrole–1, 2–dicarboximide (Htp).

Fig. 1.

measurements were determined by the methods described elsewhere. The results are given in Tables 1–3. All the complexes were found to be diamagnetic.

RESULTS AND DISCUSSION

Analytical data are in good agreement with the stoichiometry proposed for the complexes (Table 1). All compounds were found to be diamagnetic and non-ionic in nature. The compounds are in general, air stable and soluble in most organic solvents. The donor ability of this class of ligand can perhaps be best understood in terms of the resonance structures given in Fig. 2.

Ordinarily, only structure **I** is considered but **II** and **III** may predominate under certain situations. In the case of coordination of the ligand through its carbonyl oxygen atom the ν(C=O) should shift to a lower wavenumber and the thioamide band I [δ(N—H)+ν(C=N)][9,10] should shift to a higher wavenumber, whereas if coordination is through the N atom, the thioamide band I will shift to a lower wavenumber. Based on the above criterion a bonding mode has been arrived at (Table 2). In all the complexes except those with the ligands Hcpt and Hcett, ν(C=O) of the ligands shifts to a lower wavenumber after complexation, hence coordination through oxygen is likely. Coordination through the ring nitrogen or sulphur of the pyrrole or thiophene is unlikely as they are weakly basic. The thioamide band II [ν(C=N)+ν(C=S)+δ(C—H)] and III [ν(C—N)+ν(C—S)][11] do not shift systematically after complexation, hence they could not be reliably used for deciding a bonding site. The ν(N—H) in the complexes could not be observed and a new strong band at 2360 cm^{-1} (2340 cm^{-1} in the cases of [(η^5-C_5H_5)RuCl(Hcppt)($AsPh_3$)] and [(η^5-C_5H_5)RuCl(Hcapt)($AsPh_3$)]·$1/2CH_2Cl_2$, 2350 cm^{-1} in case of [(η^5-C_5H_5)RuCl(Htp)($AsPh_3$)]·$1/2CH_2Cl_2$ appears, indicating the presence of the ligand in the thiol form in the final product. The value for ν(SH) is relatively smaller, possibly because of the stronger intermolecular hydrogen bonding. The ν(C=S) of the ligands are not discernible and one could conclude from the above shifts that there is coordination through the carbonyl oxygen in all the cases. The band at 1585 cm^{-1} ($\nu_{C=N}$) in the case of [(η^5-C_5H_5)RuCl(Hctt)($AsPh_3$)]·$1/2CH_2Cl_2$ shifts to a higher value of 1600 cm^{-1}. In the case of [(η^5-C_5H_5)RuCl(Hcapt)($AsPh_3$)], the band at 1730 cm^{-1} ($\nu_{C=O}$) shifts to 1665 cm^{-1} indicating that the ligand is monodentate through the carbonyl oxygen, but

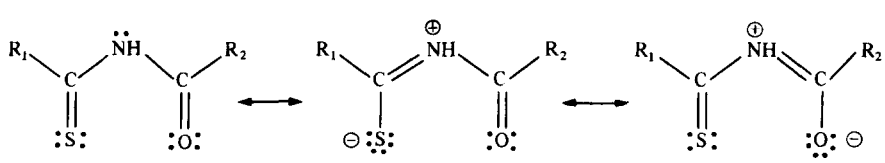

I **II** **III**

Fig. 2.

Table 1. Analytical data

Compounds	Colour	M.p. (°C)	Yield (%)	Analyses, found (calc.) C	H	N	Cl	S
$[(\eta^5\text{-}C_5H_5)RuCl(Hctt)(AsPh_3)]\cdot 1/2\ CH_2Cl_2$	Yellow–brown	105–110	25	53.8 (53.6)	4.6 (4.4)	1.6 (1.8)	9.2 (9.5)	4.4 (4.1)
$[(\eta^5\text{-}C_5H_5)RuCl(Hcept)(AsPh_3)]\cdot 1/2CH_2Cl_2$	Maroon	85	34	50.6 (50.5)	4.3 (4.1)	3.7 (3.7)	9.7 (9.5)	4.4 (4.3)
$[(\eta^5\text{-}C_5H_5)RuCl(Hcpt)(AsPh_3)]\cdot 1/2CH_2Cl_2$	Grey	155	67	50.7 (50.5)	4.2 (4.1)	3.6 (3.7)	9.6 (9.5)	4.5 (4.3)
$[(\eta^5\text{-}C_5H_5)RuCl(Hcett)(AsPh_3)]\cdot 1/2CH_2Cl_2$	Violet	92–95	60	49.5 (49.4)	3.8 (3.9)	1.9 (1.8)	9.5 (9.3)	8.6 (8.4)
$[(\eta^5\text{-}C_5H_5)RuCl(Hcapt)(AsPh_3)]\cdot 1/2CH_2Cl_2$	Reddish violet	170	20	49.4 (49.2)	4.0 (3.9)	5.9 (5.8)	10.1 (9.9)	4.6 (4.4)
$[(\eta^5\text{-}C_5H_5)RuCl(Hcapt)(AsPh_3)]$	Orange	180	67	51.6 (51.4)	4.2 (4.0)	6.5 (6.2)	5.4 (5.2)	4.9 (4.7)
$[(\eta^5\text{-}C_5H_5)RuCl(Hcppt)(AsPh_3)]\cdot 1/2CH_2Cl_2$	Dark violet	115–120	47	53.7 (53.6)	4.1 (4.0)	5.5 (5.3)	8.8 (8.9)	4.2 (4.0)
$[(\eta^5\text{-}C_5H_5)RuCl(Hcppt)(AsPh_3)]$	Orange	172–175	26	56.1 (55.9)	4.3 (4.1)	5.8 (5.6)	4.8 (4.7)	4.3 (4.2)
$[(\eta^5\text{-}C_5H_5)RuCl(Htp)(AsPh_3)]\cdot 1/2CH_2Cl_2$	Violet	82–85	45	50.6 (50.4)	3.8 (3.6)	4.2 (4.0)	10.3 (10.1)	4.8 (4.6)

Table 2. Major IR bands

Compounds	ν(NH)	ν(C═O)	ν(C═S)	Thioamide bands I	II	III	IV	Possible coordination
[Hctt]	3220	1765s	1130s	1540s	1360s	1075s	850m	
$[(\eta^5\text{-}C_5H_5)RuCl(Hctt)(AsPh_3)]\cdot 1/2CH_2Cl_2$	—	1750s	1150m	1550s	1350s	1080s	860m	O
[Hcept]	3350m, 3325m	1765s	1120s	1540s	1340s	1070s	870m	
$[(\eta^5\text{-}C_5H_5)RuCl(Hcept)(AsPh_3)]\cdot 1/2CH_2Cl_2$	—	1740s	1130s	1530s	1350s	1050s	880m	O
[Hcpt]	3210	1730s	1125s	1500s	1320s	1015s	880s	
$[(\eta^5\text{-}C_5H_5)RuCl(Hcpt)(AsPh_3)]\cdot 1/2CH_2Cl_2$	—	1740s	1125s	1520s	1310s	1010s	880s	N
[Hcett]	3240s, br	1730s	1180s, br	1510s	1360s	1020s	770s	
$[(\eta^5\text{-}C_5H_5)RuCl(Hcett)(AsPh_3)]\cdot 1/2CH_2Cl_2$	—	1735s	1180s	1510s	1355s	1035s	770s	N
[Hcapt]	3400, 3370, 3250	1730s	1120s	1580s	1330s	1060s	845s	
$[(\eta^5\text{-}C_5H_5)RuCl(Hcapt)(AsPh_3)]\cdot 1/2CH_2Cl_2$	—	1700s	1130s	1560s	1350s	1080s	850s	O
$[(\eta^5\text{-}C_5H_5)RuCl(Hcapt)(AsPh_3)]$	—	1685s	1135s	1540s	1330s	1080s	850s	O
[Hcppt]	3410m, 3260m, 3160m	1720s	1125s	1520s	1350s	1000m	860m	
$[(\eta^5\text{-}C_5H_5)RuCl(Hcppt)(AsPh_3)]\cdot 1/2CH_2Cl_2$	—	1700s	1130s	1540s	1380s	1000m	870s	O
$[(\eta^5\text{-}C_5H_5)RuCl(Hcppt)(AsPh_3)]$	—	1680s	1135s	1525s	1370s	1000m	870s	O
[Htp]	3200m	1765s	1145s	1555s	1305s	1000m	850	
$[(\eta^5\text{-}C_5H_5)RuCl(Htp)(AsPh_3)]\cdot 1/2CH_2Cl_2$	—	1760s	1140s	1540s	1300s	1020s	855	O

Table 3. Electronic spectra of the ligands and the complexes in CH_2Cl_2, and ^1H NMR spectra of the complexes in $CDCl_3$

Compound	Band position (nm) λ_{max}	Assignment	NMR signals with assignments (δ)
[Hctt]	450	$n \rightarrow \pi^*$	
		$\pi \rightarrow \pi^*$	
$[(\eta^5\text{-}C_5H_5)RuCl(Hctt)(AsPh_3)] \cdot 1/2CH_2Cl_2$	376br, sh	IL	1.3 (t, 3 H, —CH_3);
	238 (2.59×10^4)	CT	2.4 (s, —CH_3 ring), 4.1 (s, 5 H, η^5-C_5H_5), 4.4 (q, 2 H, —OCH_2), 5.3 (s, 1 H, —CH_2—Cl_2), 7.3 (m, 22 H, aromatic)
[Hcept]	440	$n \rightarrow \pi^*$	
	365	$\pi \rightarrow \pi^*$	
$[(\eta^5\text{-}C_5H_5)RuCl(Hcept)(AsPh_3)] \cdot 1/2CH_2Cl_2$	483sh	$^1A_{1g} \rightarrow {}^1T_{2g}$	1.3 (t, 3 H, —CH_3), 4.2 (m, 7 H, OCH_2, coupled with η^5-C_5H_5), 5.3 (s, 1 H, —CH_2Cl_2), 7.4 (m, 21 H, aromatic)
	360 (2.95×10^4)	IL	
	266sh	IL	
	240 (4.11×10^4)	CT	
[Hcpt]	300	$n \rightarrow \pi^*$	
	262	$\pi \rightarrow \pi^*$	
$[(\eta^5\text{-}C_5H_5)RuCl(Hcpt)(AsPh_3)] \cdot 1/2CH_2Cl_2$	364 (5.39×10^3)	IL	
	236 (6.58×10^3)	CT	
[Hcett]	350	$n \rightarrow \pi^*$	
	292	$\pi \rightarrow \pi^*$	
$[(\eta^5\text{-}C_5H_5)RuCl(Hcett)(AsPh_3)] \cdot 1/2CH_2Cl_2$	460br, sh	$^1A_{1g} \rightarrow {}^1T_{2g}$IL	1.3 (t, 3 H, —CH_3), 4.2 (m, 7 H, OCH_2, coupled with η^5-C_5H_5), 5.3 (s, 1 H, —CH_2Cl_2), 6.9–7.7 (m, 21 H, aromatic)
	344sh	IL	
	236 (3.22×10^4)	CT	
[Hcapt]	350	$\pi \rightarrow \pi^*$	
	290	CT	
$[(\eta^5\text{-}C_5H_5)RuCl(Hcapt)(AsPh_3)] \cdot 1/2CH_2Cl_2$	496 (3.14×10^3)	$^1A_{1g} \rightarrow {}^1T_{2g}$	4.2 (s, 5 H, η^5-C_5H_5), 5.3 (s, 1 H, —CH_2Cl_2) 7.3–7.7 (m, 21 H, aromatic)
	352 (9.83×10^3)	IL	
	272 (4.24×10^3)	IL	
	236 (1.42×10^4)	CT	
$[(\eta^5\text{-}C_5H_5)RuCl(Hcapt)(AsPh_3)]$	472 (3.50×10^3)	$^1A_{1g} \rightarrow {}^1T_{2g}$	4.2 (s, 5 H, η^5-C_5H_5), 7.3–7.7 (m, 21 H, aromatic)
	358 (1.09×10^4)	IL	
	238 (1.98×10^4)	CT	
[Hcppt]	415	$n \rightarrow \pi^*$	
	390	$\pi \rightarrow \pi^*$	
$[(\eta^5\text{-}C_5H_5)RuCl(Hcppt)(AsPh_3)] \cdot 1/2CH_2Cl_2$	460sh	$^1A_{1g} \rightarrow {}^1T_{2g}$	4.1 (s, 5 H, η^5-C_5H_5), 5.3 (s, 1 H, CH_2Cl_2), 7.4 (m, 26 H aromatic)
	364 (1.07×10^4)	IL	
	240 (2.80×10^4)	CT	
$[(\eta^5\text{-}C_5H_5)RuCl(Hcppt)(AsPh_3)]$	480br (4.54×10^3)	$^1A_{1g} \rightarrow {}^1T_{2g}$	4.1 (s, 5 H, η^5-C_5H_5), 7.3 (m, 26 H, aromatic)
	364 (1.81×10^4)	IL	
	234 (3.27×10^4)	CT	
[Htp]	370	$n \rightarrow \pi^*$	
	330	$\pi \rightarrow \pi^*$	
$[(\eta^5\text{-}C_5H_5)RuCl[Htp)(AsPh_3)] \cdot 1/2CH_2Cl_2$	560br	$^1A_{1g} \rightarrow {}^1T_{1g}$	4.2 (s, 5 H, η^5-C_5H_5), 5.4 (s, 1 H, CH_2Cl_2), 7.3–7.9 (m, 21 H, aromatic)
	368sh	IL	
	256sh	CT	
	230 (1.89×10^4)	CT	

surprisingly only in this case, does the ligand seem to be present in the thione form rather than in the thiol form, after complexation.

In the case of complexes containing Hcpt and Hcett ligands, coordination is through the nitrogen atom. A new strong band appears at 2360 cm^{-1}, indicating the presence of the ligand in the thiol form and not the thione form. All the characteristic bands of $AsPh_3$ and η^5-C_5H_5 (820–850 cm^{-1})[12] were present in the IR spectra of the complexes. The new bands of medium intensity in the region 350–480 cm^{-1} may be attributed to the coupled vibration of ν(Ru—Cl) + ν(Ru—S) or ν(Ru—N).[13]

The proton NMR spectra (Table 3) of the complexes display a sharp singlet δ 4.1–4.3 (for η^5-C_5H_5) apart from all characteristic signals of the concerned ligands and $AsPh_3$. However, the NH proton resonance could not be detected in the NMR spectra of the complexes.

The electronic spectra of the complexes as well as the ligands were taken in chloroform. The band positions and their assignments are given in Table 3. The ground state of ruthenium(II) in an octahedral environment is $^1A_{1g}$ and only two spin allowed transitions, $^1A_{1g} \rightarrow {}^1T_{1g}$ or $^1T_{2g}$, are expected. The band in the region 465–485 nm may be assigned to $^1A_{1g} \rightarrow {}^1T_{2g}$ and a shoulder at 525 nm in the Hctt complex may be due to $^1A_{1g} \rightarrow {}^1T_{1g}$. Some of the intraligand (IL) bands with small shifts were present in the electronic spectra of the respective complexes. The intense bands at 240–245 and 270–280 nm are assigned to charge-transfer (CT) transitions.

REFERENCES

1. C. A. McAuliffe and W. Levasan, *Phosphine Arsine and Stibine Compounds of the Transition Elements*. Elsevier, Amsterdam (1979).
2. C. A. McAuliffe (Ed.), *Transition Metal Complexes of Phosphine, Arsine Antimony Ligands*. Wiley, New York (1973).
3. C. A. Tolman, *Chem. Rev.* 1977, **77**, 313.
4. H. K. Gupta, Veena Chauhan and S. K. Dikshit, *Inorg. Chim. Acta*, 1987, **128**, 175.
5. M. I. Bruce, M. G. Humphrey, A. G. Swincer and R. C. Wallis, *Aust. J. Chem.* 1984, **37**, 1747.
6. E. P. Papadopolous, *J. Org. Chem.* 1976, **41**, 962.
7. E. P. Papadopolous, *J. Org. Chem.* 1973, **38**, 667.
8. E. P. Papadopolous, *J. Org. Chem.* 1974, **39**, 2540.
9. C. N. R. Rao, R. Venkataraghvan and T. Kasturi, *Can. J. Chem.* 1964, **42**, 36.
10. A. C. Fabretti, M. Ferrari, G. C. Franchim, C. Preti, L. Tasri and G. Tosi, *Transition Met. Chem.* 1982, **7**, 279.
11. B. Singh, M. M. P. Rukhaiyar and R. J. Sinha, *J. Inorg. Nucl. Chem.* 1977, **39**, 29.
12. K. A. Jensen and P. H. Nidsen, *Acta Chem. Scand.* 1963, **17**, 1875.
13. D. M. Adams, *Metal Ligand and Related Vibrations*, pp. 316, 284. St. Martins Press, NewYork (1968).

Polyhedron Vol. 7, No. 8, pp. 629–634, 1988
Printed in Great Britain

0277–5387/88 $3.00+.00
© 1988 Pergamon Press plc

A MATRIX-ISOLATION STUDY OF GASEOUS INTERMEDIATES IN THE DIRECT FORMATION OF POLY(SULPHUR NITRIDE) FROM TETRASULPHUR TETRANITRIDE USING A SILVER SELENIDE CATALYST: EVIDENCE FOR THE INVOLVEMENT OF HNSO

MATTHEW J. ALMOND,* ANTHONY J. DOWNS and TREVOR L. JEFFERY

Department of Inorganic Chemistry, University of Oxford, South Parks Road, Oxford OX1 3QR, U.K.

(*Received* 19 *October* 1987; *accepted* 20 *November* 1987)

Abstract—Matrix isolation of the vapour species produced by the passage of S_4N_4 vapour over silver selenide heated to *ca* 160°C produces unequivocal IR evidence (including the results of experiments with ^{15}N-enriched samples) not of the thiazyl monomer, NS$^{\cdot}$, but of thionylimide, HNSO, in addition to disulphur dinitride, S_2N_2. The significance of these findings is considered in relation to possible synthetic routes to poly(sulphur nitride).

Within the past 15 years polymeric sulphur nitride, $[SN]_x$, or "polythiazyl", has attracted intense interest. In 1973 Labes *et al.*[1] suggested that "polythiazyl" is metallic, and subsequent studies showed that it remains metallic down to very low temperatures, becoming superconducting near 0.3 K.[2,3] Vacuum deposition permits, moreover, the production of oriented epitaxial films of $[SN]_x$ on a wide range of polymer substrates;[4] such films have a high optical anisotropy throughout the near-IR and low-frequency portion of the visible spectrum suggesting possible applications in optical devices.

The original method of synthesis was via disulphur dinitride, S_2N_2, crystals which polymerize at room temperature to "polythiazyl".[5] More recent methods have sought to exploit the direct formation of "polythiazyl" from tetrasulphur tetranitride, which is an altogether more convenient, but by no means 100% risk-free, precursor. Thus, thin films of $[SN]_x$ have been prepared by four different methods: (i) the pyrolysis of tetrasulphur tetranitride vapour over silver wool;[2,6,7] (ii) the pyrolysis of tetrasulphur tetranitride vapour over Pyrex or quartz wool at *ca* 275°C;[8] (iii) sublimation *in vacuo* of "polythiazyl" itself and (iv) polymerization of a volatile red material produced by the pyrolysis of tetrasulphur tetranitride vapour over silver wool.[9]

The nature of the volatile red material which is the key intermediate in method (iv) has been the subject of some discussion. On the basis of elemental analysis and ESR and mass spectrometric measurements, Labes *et al.* have claimed[9] that it consists almost entirely of the thiazyl monomer, NS$^{\cdot}$. In practice, however, the red material was always accompanied by a second volatile product characterized by its brown colour and the elemental analysis of which could not be reconciled with the composition NS. The red and brown materials proved to be difficult to separate; conditions of fractionation varied from preparation to preparation and in several cases multiple fractionation was necessary in order to achieve effective separation.

More recently Banister and Hauptman have reported to us that the red material can be generated in a much improved yield if tetrasulphur tetranitride vapour is passed over solid silver selenide heated to *ca* 160°C.[10] Hence, for example, they have been able to produce films of $[SN]_x$ by condensation of the vapour. The aim of the experiments reported here was to trap the vapour of this red material in an inert matrix at *ca* 20 K and hence to characterize it by its IR spectrum. In this way we sought to determine whether or not the red material is indeed composed largely of the thiazyl monomer, NS$^{\cdot}$ and, if this species could be trapped in reasonable con-

* Author to whom correspondence should be addressed. Present address: Department of Chemistry, University of Reading, Whiteknights, P.O. Box 224, Reading RG6 2AD, U.K.

centrations, to investigate its chemistry, as represented for example, by matrix reactions such as

$$n\mathrm{NS}^{\cdot} \xrightarrow{\text{anneal}} [\mathrm{NS}]_n \quad (n = 2, 3 \ldots) \qquad (1)$$

$$\mathrm{NS}^{\cdot} + \mathrm{X}^{\cdot} \longrightarrow \mathrm{XNS} (\mathrm{X} = \mathrm{O} \text{ or } \mathrm{S} \text{ atoms}). \qquad (2)$$

EXPERIMENTAL

The matrix-isolation apparatus used at Oxford has been described elsewhere.[11] An Air Products CSW 202B "Displex" closed-cycle helium refrigerator gave window temperatures of 15–35 K inside a shroud maintained at a pressure below 10^{-7} torr (1 torr $\approx 13.6 \times 9.8$ Pa). IR spectra were recorded on a Perkin–Elmer Model 580A spectrophotometer. The internal calibration available on the instrument was supplemented by superimposing on the measured spectra, sharp vibration-rotation or rotation lines due to ammonia, atmospheric water vapour or carbon dioxide.[12] Such measurements were reproducible within 0.4 cm^{-1} for sharp absorptions and the resolution was invariably better than 0.5 cm^{-1} in measurements involving precise wavenumber measurements.

Tetrasulphur tetranitride was prepared via thiotrithiazyl chloride, S_4N_3Cl[13] and was recrystallized from either chloroform or liquid sulphur dioxide. Samples of tetrasulphur tetranitride enriched in ^{15}N were prepared by the passage of disulphur dichloride vapour over heated ammonium chloride—^{15}N (Merck, Sharp and Dohme, 99 atom % ^{15}N) by an adaptation of the flow method described by Jolly and Becke-Goehring;[14] purification involved recrystallization from chloroform. Silver selenide was prepared by the direct reaction of the elements in an evacuated quartz vessel at 600°C over a period of 24 h.[10] To prepare the catalyst, the silver selenide was ground with powdered silica under methanol in a ball mill and the dried, finely powdered mixture was supported on quartz wool.[10] All matrix gases—Ar, Kr and N_2—were of grade "X" quality and were used as supplied by B.O.C.

In the matrix-isolation experiments which we report, samples of tetrasulphur tetranitride contained in all-glass apparatus were vaporized at 85–100°C. The vapour passed through a short Pyrex column containing the silver selenide catalyst maintained at 160°C. The volatile pyrolysis products issuing from the column were delivered via a trap, the temperature of which could be regulated to remove disulphur dinitride and other less volatile components, admixed with an excess of the matrix gas and condensed on the cold CsI window of the matrix assembly. The rate of deposition of the matrix gas was typically 3 mmol h^{-1}, and deposition times in the order of 1–5 h were needed to build up to a reasonable level, the absorptions due to the pyrolysis products. Baking out the apparatus was an essential preliminary to any experiment, and as part of this exercise the catalyst was "outgassed" by heating to *ca* 200°C for up to 48 h under continuous pumping.

RESULTS

When tetrasulphur tetranitride vapour was passed over the silver selenide catalyst heated to *ca* 160°C, condensation of the resulting vapour with an excess of argon, krypton or nitrogen at 15–20 K gave a deposit whose IR spectrum showed the presence of disulphur dinitride, S_2N_2[15] as a major pyrolysis product. The disulphur dinitride could be removed, however, by passing the vapour through a trap cooled to −45°C prior to admixture with the matrix gas and deposition on the CsI window. When this procedure was followed, the matrix exhibited typically the IR spectrum illustrated in Fig. 1. It included, conspicuously, bands due to the solvent ($CHCl_3$[16] or SO_2[17]) used to recrystallize the tetrasulphur tetranitride. That this occurred irrespective of the precautions taken to "outgas" the sample testifies to the capacity of solid tetrasulphur tetranitride to occlude solvent molecules. The spectrum of the matrix contained, in addition to these solvent absorptions, a number of other features, the most prominent occurring at *ca* 1250 cm^{-1}. Such a transition is close in energy to the fundamental frequency of the thiazyl monomer, $NS^{\cdot}$, in the gas phase, viz. 1204 cm^{-1}.[18] The intensity of the band near 1250 cm^{-1} could be optimized either by reducing the flux of pyrolysis products through the use of a narrow-bore (*ca* 0.5 mm) nozzle for deposition, or by employing a more rigid host material and the lowest deposition temperature which could be achieved, e.g. condensation with krypton at *ca* 15 K.

The performance of numerous experiments established, however, that the band near 1250 cm^{-1} belongs not to the diatomic $NS^{\cdot}$ molecule but to the thionylimide molecule, HNSO. Thus, the growth of the absorption near 1250 cm^{-1} paralleled that of other absorptions at 3310, 1095, 925, 775 and 455 cm^{-1} (in an argon matrix). The wavenumbers of the relevant features are listed in Table 1, where they are compared with the results of previous experiments involving matrix-isolated HNSO.[19]

The assignment of the absorption at *ca* 1250 cm^{-1} to the ν_2 mode of the matrix-isolated HNSO molecule was confirmed beyond doubt by repeating the experiment with a sample of tetrasulphur tetranitride, 50% enriched in ^{15}N. The spectrum of a nitro-

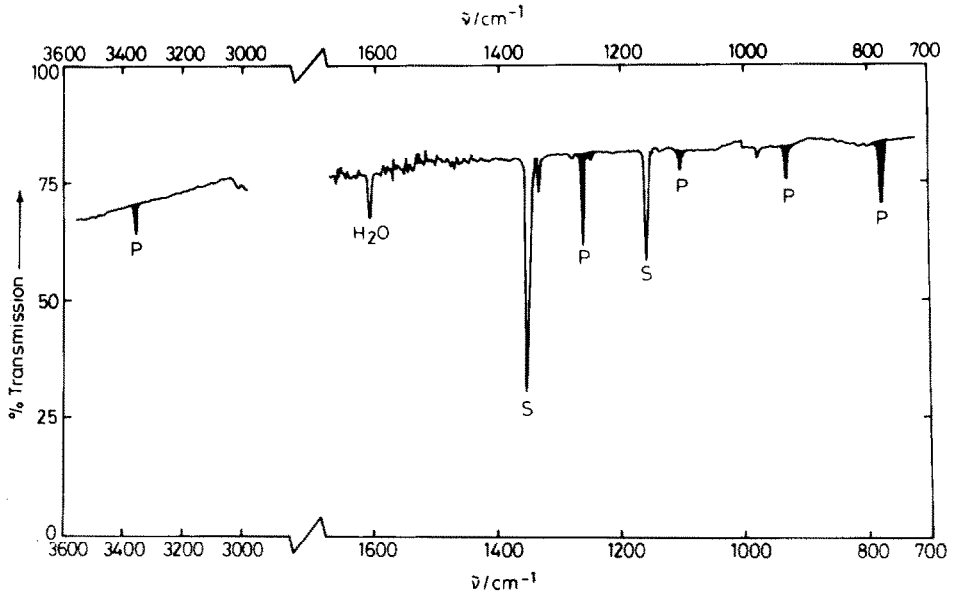

Fig. 1. IR spectrum of an N_2 matrix formed at 15 K after 4 h deposition of the vapour, produced by passage of S_4N_4 vapour over Ag_2Se heated to 160°C. A trap held at −45°C was used to remove S_2N_2. Bands marked P are due to HNSO, and bands marked S are due to SO_2, the solvent used to recrystallize the S_4N_4.

gen matrix, displayed in the region 1220–1270 cm^{-1} not a singlet but a doublet with clearly discernible satellites associated with molecules containing the ^{34}S isotope (4.22% natural abundance), as illustrated in Fig. 2. The wavenumbers of the relevant bands are listed in Table 2, where they are compared with the results of the earlier matrix study of HNSO[19] and also with the wavenumbers calculated for the corresponding vibrational transition of the monomeric NS' radical. The pattern of the isotopic splitting certainly testifies to the presence of an oscillator containing a single nitrogen and a single sulphur atom. However, the isotopic *shifts* are quite incompatible with an isolated diatomic NS unit, the ^{14}N—^{15}N shift being only one-quarter of that, and the ^{32}S—^{34}S shift 33% *greater* than that, calculated for the NS' molecule. These results clearly imply some form of coordination of the NS oscillator but could not be reconciled satisfactorily with any model involving only aggregates of NS', e.g. NS···NS.

When the matrix was annealed at temperatures up to 30 K, the region of the IR spectrum between 1220 and 1270 cm^{-1} was observed to change sig-

Table 1. Wavenumbers and ^{14}N—^{15}N isotopic shifts of the IR absorptions associated with matrix-isolated HNSO

Fundamental	$\tilde{\nu}$ (cm^{-1}) This work[a,b,c]	$\tilde{\nu}$ (cm^{-1}) Previous work[a,b,d]	$\Delta\tilde{\nu}(^{14}N—^{15}N)$ (cm^{-1}) This work[a,b]	$\Delta\tilde{\nu}(^{14}N—^{15}N)$ (cm^{-1}) Previous work[d,e,f]
ν_1	3310 w	3303	8	7.1
ν_2	1253 m	1252	6.7	5.4
ν_3	1095 w	1094	12	10.3
ν_4	925 w	923	11	11.2
ν_5	775 wm	774	3	3.8
ν_6	455 vw	455	[g]	3.0

[a] Error limits ±1 cm^{-1}. [b] N_2 matrix. [c] Intensities: w weak; m medium; v very. [d] Ref. 19. [e] Error limits ±0.1 cm^{-1}. [f] Ar matrix. [g] ν_6 of $H^{15}NSO$ was too weak to be detected in our experiments.

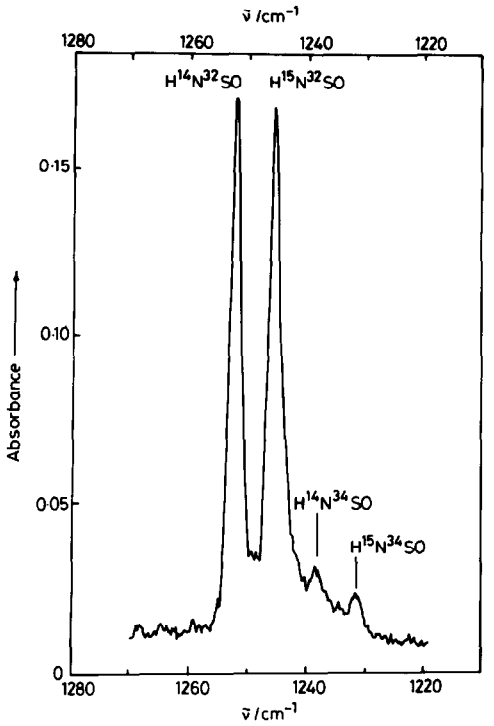

Fig. 2. The region 1220–1270 cm^{-1} of the IR spectrum displayed by an N_2 matrix formed after 2.75 h deposition of the vapour, produced by passage of S_4N_4 vapour 50% enriched in ^{15}N over Ag_2Se heated to 160°C.

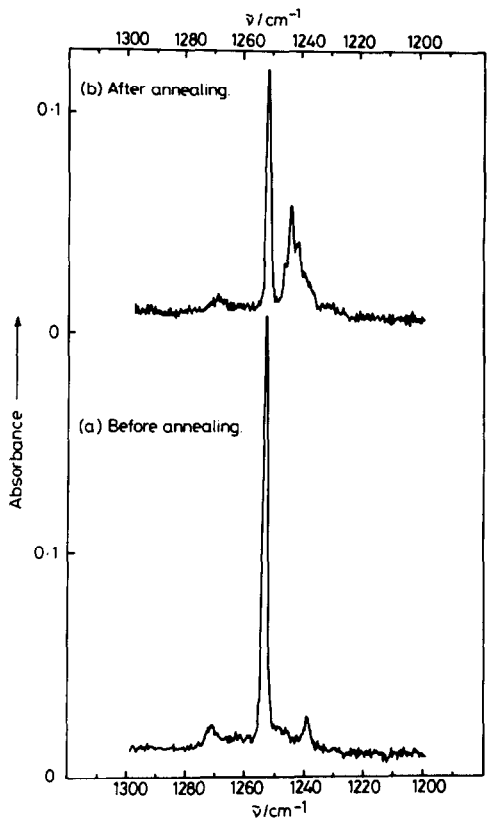

Fig. 3. The region 1200–1290 cm^{-1} in the IR spectrum of an N_2 matrix: (a) after 4 h deposition at 15 K, of the vapour produced by passage of S_4N_4 vapour over Ag_2Se heated to 160°C and (b) after annealing the same matrix at 30 K for 20 min.

nificantly. Under these conditions the intensity of the band near 1250 cm^{-1} decayed while a new broad band centred at *ca* 1245 cm^{-1} appeared and grew. These changes are illustrated for a nitrogen matrix in Fig. 3. Tchir and Spratley observed a band at 1245 cm^{-1} which they ascribed to the dimer of HNSO isolated in a nitrogen matrix.[19] It follows that the changes observed in our spectrum are consistent with diffusion of the molecules in the matrix to form the hydrogen-bonded dimer $[HNSO]_2$ [see eq. (3)] representing the first stage in the polymerization of thionylimide.

In a further series of experiments we condensed in a trap at liquid nitrogen temperature, the volatile

Table 2. Observed wavenumbers and isotopic shifts for ν_2 of HNSO isolated in an Ar matrix and isotopic shifts calculated for NS˙

	HNSO (observed)				NS˙		
	This work[a,b]		Previous work[c,d]			Calculated[e]	
Isotopomer	$\tilde{\nu}$ (cm^{-1})	Isotopic shift $\Delta\tilde{\nu}$ (cm^{-1})	$\tilde{\nu}$ (cm^{-1})	Isotopic shift $\Delta\tilde{\nu}$ (cm^{-1})	Isotopomer	$\tilde{\nu}$ (cm^{-1})	Isotopic shift $\Delta\tilde{\nu}$ (cm^{-1})
$H^{14}N^{32}SO$	1253.0	0.0	1248.7	0.0	$^{14}N^{32}S$	1253.0	0.0
$H^{15}N^{32}SO$	1246.3	6.7	1243.3	5.4	$^{15}N^{32}S$	1223.6	29.4
$H^{14}N^{34}SO$	1238.0	15.0	1233.4	15.3	$^{14}N^{34}S$	1241.7	11.3
$H^{15}N^{34}SO$	1231.5	21.5	1228.4	20.3	$^{15}N^{34}S$	1212.1	40.9

[a] Error limits ±0.4 cm^{-1}. [b] N_2 matrix. [c] Ref. 19. [d] Ar matrix. [e] Calculated on the assumption that the molecule behaves as a harmonic oscillator.

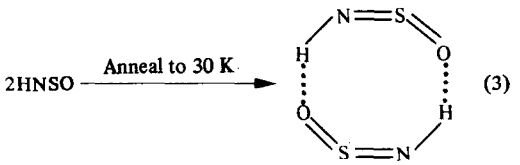

(3)

products formed by passing the vapour of tetrasulphur tetranitride over silver selenide heated to 160°C. Hence we were able to trap a red volatile material with properties similar to those described by Labes *et al.*[9] and by Banister and Hauptman.[10] The contents of the trap were then allowed to warm up and the resulting vapour was co-condensed with an excess of argon on a CsI window at *ca* 20 K. The major component of the matrix formed in this way was disulphur dinitride, S_2N_2,[15] together with small amounts of thionylimide, HNSO.

DISCUSSION

Our results do not discount the proposal that the red volatile material produced by passing the vapour of tetrasulphur tetranitride over heated silver wool[9] or heated silver selenide[10] contains the thiazyl monomer, NS˙. Although we obtained no direct spectroscopic evidence pointing to this radical, it may be too reactive to be trapped under the experimental conditions described here. Thus, the familiar dimer S_2N_2 was always detected in relatively high concentration on condensation of the matrix, unless steps were deliberately taken to remove it by means of a cold trap interposed between the silver selenide catalyst and the nozzle giving access to the matrix assembly. It is pertinent to note, in this context, that the NO˙ monomer is relatively difficult to trap cleanly under matrix conditions as a result of its facile dimerization to give $[NO]_2$.[11b,20]

The most positive and striking inference to be drawn from our experiments is that thionylimide is one of the components of the vapour. This may arise from the reaction of one or more sulphur–nitrogen molecules, e.g. S_4N_4, S_2N_2 or NS˙, with adventitious water vapour present in the apparatus, but this explanation seems improbable in view of the almost total absence of matrix-isolated water[21] in our experiments. More likely is that HNSO is produced by a reaction of one or more sulphur–nitrogen molecules with water or some other hydroxylic agent adsorbed on the catalyst. Since the silver selenide catalyst was prepared by milling under methanol,[10] adsorbed methanol may well be responsible for the formation of the HNSO.

In the light of our experiments, the involvement of HNSO in some preparations of "polythiazyl" may well account for the observation of hydride impurity (typically 1–4%) in the samples of the polymer. Of particular significance in this respect are the observations of Smith *et al.*[22] that the hydride impurity of a sample of $[SN]_x$ could be increased to about 8% when it was prepared from disulphur dinitride in the presence of water vapour. Furthermore, these workers have also reported a MS peak, *inter alia*, at $m/e = 63$ for the vapour derived from a sample of $[SN]_x$ prepared in this way, which they assigned tentatively to the molecule HNSO. It is also interesting to note that May and Vallet report that the polymerization of S_2N_2 to $(SN)_x$ occurs by two distinct processes depending on whether moisture is present or absent.[23]

We consider that the possibility of the active intermediacy of thionylimide in some "polythiazyl" preparations warrants fuller investigation. Of potential significance is the knowledge that thionylimide is itself susceptible to polymerization yielding both red and brown volatile materials.[24] In particular the existence of the tetramer $(HNSO)_4$[24] and a polymer $(HNSO)_x$[23] have been reported; the latter material, itself, showing interesting electrical properties. It behaves as a *p*-type semiconductor and shows a resistivity which varies with water content.[23] It is possible that HNSO has the capacity to act as an initiator in the polymerization of disulphur dinitride or even tetrasulphur tetranitride to "polythiazyl", perhaps in a manner analogous to the action of dibromine vapour on tetrasulphur tetranitride.[6,25] It is clear, however, that matrix-isolation experiments are capable of yielding significant information about the vapour species affording these polymers.

CONCLUSIONS

Our experiments reveal that thionylimide, HNSO, is formed in the vapour phase when the vapour of tetrasulphur tetranitride is passed over heated silver selenide. It is quite feasible that thionylimide is formed in other preparations which have been devised for the synthesis of "polythiazyl",[6,7] e.g. from disulphur dinitride, particularly when water vapour or other hydroxylic impurities are present.[22] Although we were unable to obtain direct spectroscopic evidence for the formation of the thiazyl monomer, NS˙, in the vapour phase, our results do not rule out its involvement in the production of "polythiazyl". Experiments now under way are designed to see whether monomeric NS˙ can be generated within a matrix by UV photolysis of a precursor like ClSN, if necessary

with the assistance of a relatively reactive matrix like solid CO.[26]

Acknowledgements—We are indebted to the S.E.R.C. for financial support. To Drs A. J. Banister and Z. V. Hauptman, we are most grateful for helpful discussions and practical advice, as well as for supplying a sample of the silver selenide catalyst. We acknowledge too with gratitude, the work of Mr J. M. C. Ockenden who carried out some of the preliminary experiments.

REFERENCES

1. V. V. Walatka Jr, M. M. Labes and J. H. Perlstein, *Phys. Rev. Lett.* 1973, **31**, 1139.
2. R. L. Greene, G. B. Street and L. J. Suter, *Phys. Rev. Lett.* 1975, **34**, 577.
3. A. A. Bright, M. J. Cohen, A. F. Garito, A. J. Heeger, C. M. Mikulski and A. G. MacDiarmid, *Appl. Phys. Lett.* 1975, **26**, 612.
4. A. A. Bright, M. J. Cohen, A. F. Garito, A. J. Heeger, C. M. Mikulski, P. J. Russo and A. G. MacDiarmid, *Phys. Rev. Lett.* 1975, **34**, 206.
5. M. Goehring and D. Voigt, *Z. Anorg. Allg. Chem.* 1956, **285**, 181.
6. See for example, M. M. Labes, P. Love and L. F. Nichols, *Chem. Rev.* 1979, **79**, 1.
7. C. M. Mikulski, P. J. Russo, M. S. Saran, A. G. MacDiarmid, A. F. Garito and A. J. Heeger, *J. Am. Chem. Soc.* 1975, **97**, 6358; R. L. Patton, Ph.D. thesis, University of California, Berkeley (1969); F. A. Kennett, G. K. MacLean, J. Passmore and M. N. Sudheendra Rao, *J. Chem. Soc., Dalton Trans.* 1982, 851 (for other synthetic methods).
8. E. J. Louis, A. G. MacDiarmid, A. F. Garito and A. J. Heeger, *J. Chem. Soc., Chem. Commun.* 1976, 426.
9. P. Love, G. Myer, H. I. Kao, M. M. Labes, W. R. Junker and C. Elbaum, *Ann. New York Acad. Sci.* 1978, **313**, 745.
10. A. J. Banister and Z. V. Hauptman, private communication.
11. See for example (a) A. J. Downs, G. P. Gaskill and S. B. Saville, *Inorg. Chem.* 1982, **21**, 3385; (b) M. Hawkins and A. J. Downs, *J. Phys. Chem.* 1984, **88**, 1527, 3042; (c) M. J. Almond, D.Phil. thesis, University of Oxford (1984).
12. *IUPAC Commission on Molecular Structure and Spectroscopy, Tables of Wavenumbers for the Calibration of Infrared Spectrometers*, (Compiled by A. R. H. Cole) 2nd Edn. Pergamon Press, Oxford (1977).
13. W. L. Jolly, K. D. Maguire and D. Rabinovich, *Inorg. Chem.* 1963, **2**, 1304; M. Becke-Goehring and H. P. Latscha, *Z. Anorg. Allg. Chem.* 1964, **333**, 181.
14. W. L. Jolly and M. Becke-Goehring, *Inorg. Chem.* 1962, **1**, 76.
15. R. Evans, D.Phil. thesis, University of Oxford (1980).
16. E. L. Varetti and A. Müller, *Can. J. Spectrosc.* 1977, **22**, 77.
17. M. Allavena, R. Rysnik, D. White, V. Calder and D. E. Mann, *J. Chem. Phys.* 1969, **50**, 3399; D. Maillard, M. Allavena and J. P. Perchard, *Spectrochim. Acta, A* 1975, **31A**, 1523.
18. K. Matsumura, K. Kawaguchi, K. Nagai, C. Yamada and E. Hirota, *J. Mol. Spectrosc.* 1980, **84**, 68.
19. P. O. Tchir and R. D. Spratley, *Can. J. Chem.* 1975, **53**, 2311.
20. J. Laane and J. R. Ohlsen, in *Progress in Inorganic Chemistry* (Edited by S. J. Lippard), Vol. 27, p. 465. Interscience, New York (1980).
21. R. L. Redington and D. E. Milligan, *J. Chem. Phys.* 1962, **37**, 2162; A. J. Tursi and E. R. Nixon, *J. Chem. Phys.* 1970, **52**, 1521; G. P. Ayers and A. D. E. Pullin, *Spectrochim. Acta, A* 1976, **32A**, 1629; L. Fredin, B. Nelander and G. Ribbergård, *J. Chem. Phys.* 1977, **66**, 4065.
22. R. D. Smith, J. R. Wyatt, D. C. Weber, J. J. DeCorpo and F. E. Saalfeld, *Inorg. Chem.* 1978, **17**, 1639.
23. J. F. May and G. Vallet, *Rev. Gen. Elec.* 1972, **81**, 255.
24. M. Becke-Goehring, R. Schwarz and W. Spiess, *Z. Anorg. Allg. Chem.* 1958, **293**, 294.
25. N. N. Greenwood and A. Earnshaw, *Chemistry of the Elements*, p. 861. Pergamon Press, Oxford (1984).
26. A. J. Downs and M. J. Almond, unpublished results.

Polyhedron Vol. 7, No. 8, pp. 635–639, 1988
Printed in Great Britain

0277–5387/88 $3.00+.00
© 1988 Pergamon Press plc

THE LIGATIONAL BEHAVIOUR OF THIOSEMICARBAZONES AND SEMICARBAZONES WITH TELLURIUM(IV)—REACTIONS WITH $TeCl_4$

J. K. BASUMATARY, A. K. SINGH and B. L. KHANDELWAL

Department of Chemistry, Indian Institute of Technology, New Delhi 110 016, India

and

W. R. McWHINNIE*

Department of Molecular Sciences, Aston University, Birmingham B4 7ET, U.K.

(*Received* 19 *October* 1987; *accepted* 20 *November* 1987)

Abstract—The reactions of thiosemicarbazones and semicarbazones of benzaldehyde, salicylaldehyde, acetophenone and 2-hydroxyacetophenone with $TeCl_4$ give the complexes $LTeCl_4$, $(L—H)TeCl_3$ or $(L—H)Te_2Cl_7$ (L = semicarbazone or thiosemicarbazone). The structural features of these tellurium derivatives are explored by IR, ^1H and ^{13}C NMR, and conductance (in acetonitrile) measurements, and structures based on an octahedral arrangement of ligands around tellurium are proposed. The presence of facial and meridian isomers in equilibrium is indicated in some cases. The complexation occurs through S/O, the nitrogen of the > C=N— group and O^- (if present on benzene ring). The $(L—H)Te_2Cl_7$ species seem to have chlorine bridged and octahedrally coordinated tellurium.

The complexes of tellurium(II or IV) with sulphur donors have been investigated more than the complexes with other ligands. Probably some of their applications such as the utility of the dithiocarbamates of tellurium(IV) as rubber vulcanizers[1–3] and, more recently, their promise as antioxidants for polypropylene[4] are in part responsible for the greater attention. Thiosemicarbazones[5,6] have emerged as an important class of sulphur ligands particularly for transition metals in the last two decades. The real impetus towards developing their coordination chemistry[6] was: (i) the remarkable antitumor, antiviral and antimalarial activity observed for some of the derivatives was found to be related to their complexation with metal ions and, (ii) the unique combination of N, O and S present in some of such compounds was an attractive model for understanding the complexation in biological systems. Their complexation[7,8] with main group metals and metalloids is the subject of very few papers in the literature and on tellurium complexes there are no reported studies. In view of this fact, we are investigating thiosemicarbazone complexes of tellurium(II and IV) with a hope that some of the resulting complexes may be evaluated in rubber or polymer technology. In the present paper, the results of reactions of tellurium tetrachloride with the thiosemicarbazones of benzaldehyde (L_1), salicylaldehyde (L_2), acetophenone (L_3) and 2-hydroxyacetophenone (L_4) are reported (see Structure 1). For comparison, the reactions of the corresponding semicarbazones are also studied.

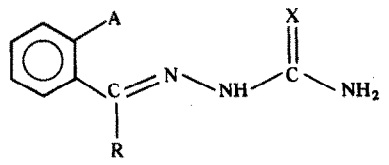

L_1: A=H, R=H, X=S; L_2: A=OH, R=H, X=S;
L_3: A=H, R=Me, X=S; L_4: A=OH, R=Me, X=S;
L_5: A=OH, R=H, X=O; L_6: A=OH, R=Me, X=O.

Structure 1.

* Author to whom correspondence should be addressed.

Not unexpectedly, the latter complex only when an OH group is present at a position *ortho* to the azomethine group, results in (L—H)$TeCl_3$ type species. The isolated complexes are characterized by elemental analyses, conductance and spectral (IR, ^1H and ^{13}C NMR) measurements.

EXPERIMENTAL

General procedure for the reaction with $TeCl_4$

Tellurium tetrachloride (2.69 g, 10 mmol) dissolved in dry benzene was deaerated with dry and oxygen free nitrogen for 0.5 h. A slurry of an equimolar amount of the ligand (half for (L—H)Te_2Cl_7) in deaerated benzene was slowly added to the solution of $TeCl_4$ and refluxed for 24–36 h with constant stirring on an oil bath. In the cases of L_2, L_4, L_5 and L_6, HCl was liberated. The resulting precipitate was filtered, washed 3–4 times with dry benzene, recrystallized with acetonitrile, and dried under vacuum over anhydrous calcium chloride.

The carbon, hydrogen and nitrogen analyses were carried out on a Perkin–Elmer elemental analyzer 240C. The tellurium[9] and chlorine[10] were estimated volumetrically. The conductance measurements were made on a WG Pye conductivity bridge. The IR spectra on a KBr/CsI disc were recorded on a Nicolet 5 DX FTIR spectrometer in the range 200–4000 cm^{-1}. The ^1H and ^{13}C NMR were recorded on Jeol FX-100 FT-NMR spectrometer.

RESULTS AND DISCUSSION

Tellurium tetrachloride reacts with thiosemicarbazones according to the following equations. In the absence of any phenolic group the reactions of type (1) occur, but the ligands having an OH group react according to eqs (2) or (3) depending on the molar ratio of the reactants. Tellurium tetrabromide reacts in an analogous manner. The results of elemental analyses (Table 1) authenticate the proposed stoichiometries of the compounds.

$$TeCl_4 + L \rightarrow TeCl_4(L) \quad (1)$$

$$TeCl_4 + L \rightarrow TeCl_3(L—H) + HCl \quad (2)$$

$$2TeCl_4 + L \rightarrow Te_2Cl_7(L—H) + HCl. \quad (3)$$

The molar conductance values (Table 1) have been found to be lower than those expected for a 1 : 1 electrolyte, except for (L$_2$—H)Te_2Cl_7 and (L$_4$—H)Te_2Cl_7 which exhibit values very close to those expected. All the compounds are only soluble in polar solvents, but after setting the solutions aside for 2–3 days the deposition of tellurium metal is observed. The (L—H)Te_2Cl_7 type derivatives are relatively less stable.

The ^1H NMR data are recorded in Table 2 along with the possible assignments. Contrary to earlier reports[7] on thiosemicarbazones, the NH_2 protons have been found to resonate downfield at δ, 6.0 ppm. Our assignment seems to be reasonable in view of the literature reports on substituted semi- and thiosemicarbazides[11], and the observation of an

Table 1. Analytical data and physical properties of Te(IV)–thiosemicarbazone/semicarbazone complexes

Compound	Colour	M.p. (°C)	Analysis: Found (calc.) % C	H	N	Te	Cl	Λ_M[a] (ohm^{-1} cm^2 mol^{-1})
L_1TeCl_4	Greenish yellow	138–140	23.1 (21.4)	2.5 (2.0)	9.3 (9.0)	26.8 (28.6)	29.9 (31.6)	64.72–73.78
(L$_2$—H)$TeCl_3$	Yellow	95–97	21.2 (22.4)	1.6 (1.9)	9.1 (10.0)	30.4 (29.9)	24.2 (24.7)	58.64–64.66
(L$_2$—H)Te_2Cl_7	Orange–yellow	88–90	15.0 (13.7)	1.2 (1.1)	6.9 (6.0)	36.1 (36.7)	33.7 (35.7)	107.51–116.23
L_3TeCl_4	Brown	95–97(d)	22.5 (23.3)	1.4 (2.0)	8.0 (9.0)	26.8 (27.6)	28.8 (30.7)	51.99–56.61
(L$_4$—H)$TeCl_3$	Dark brown	86–88(d)	24.5 (24.4)	2.3 (2.4)	8.7 (9.0)	30.4 (29.8)	24.1 (24.9)	53.47–56.24
(L$_4$—H)Te_2Cl_7	Dark brown	86–88(d)	17.1 (15.4)	1.8 (1.5)	5.3 (6.0)	34.6 (35.8)	33.6 (34.9)	98.53–108.30
(L$_5$—H)$TeCl_3$	Dark brown	140–142(d)	23.0 (23.3)	2.3 (1.9)	8.9 (10.2)	30.4 (31.0)	25.6 (25.8)	—
(L$_6$—H)$TeCl_3$	Dark	100–102(d)	25.8 (25.3)	3.0 (2.3)	9.0 (9.8)	28.5 (29.9)	25.0 (25.0)	—

[a] Solvent: acetonitrile; concentration: 0.40–1.0 mM.

Table 2. Chemical shifts in ^{1}H NMR spectra of ligands and their Te(IV) complexes in DMSO–d^6 at 25°C

Compound	Chemical shift (δ, ppm)					
	CH_3	NH_2	Phenyl	CH	NH	OH
L_1	—	8.21	8.08–7.40	8.21	11.45	—
L_1TeCl_4	—	3.54	7.84–7.40	8.05	11.43	—
L_2	—	8.08	7.93–6.75	8.38	9.92	11.36
$(L_2—H)TeCl_3$	—	3.89	7.70–6.96	8.58	10.20	—
$(L_2—H)Te_2Cl_7$	—	4.25	7.03–6.97	8.58	10.10	—
L_3	2.31	8.28	7.97–7.30	—	10.19	—
L_3TeCl_4	2.53	4.25	7.94–7.37	—	9.41	—
L_4	2.31	7.86	7.57–6.79	—	10.64	12.03
$(L_4—H)TeCl_3$	2.61	3.79	7.89–6.89	—	9.07	—
$(L_4—H)Te_2Cl_7$	2.68	3.48	7.89–6.89	—	9.07	—
L_5	—	6.43	7.79–6.74	8.15	9.99	10.22
$(L_5—H)TeCl_3$	—	4.70	7.78–6.61	8.14	10.20	—
L_6	2.24	6.24	7.54–6.76	—	9.71	12.79
$(L_6—H)TeCl_3$	2.24	4.72	7.64–6.78	—	9.75	—

NH_2 signal at δ, 7.03 ppm in the case of thiourea. The intramolecular hydrogen bonding in these ligands, as shown in structure **A**, is indicated by the

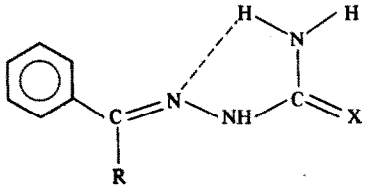

(A)

fact that on complexation, the NH_2 protons are shielded, probably due to the breaking of this strong hydrogen bond. The recently reported single crystal X-ray structure of pyridoxal thiosemicarbazone[12] also suggests that the conformation shown in structure **A** is preferred, supporting the concept of intramolecular hydrogen bonding. In the Te(II)–thiosemicarbazone complexes of the type TeL_2Cl_2 and TeL_4Cl_2, where the ligands are invariably bonded through sulphur alone, the shielding of the NH_2 protons was found to be nearly unaffected[13] on complexation, thus further supporting structure **A**. The OH signal observed in the case of L_2, L_4, L_5 and L_6 vanishes on complexation, indicating its deprotonation and participation of the resulting —C—O$^-$ in the formation of the complex as rep-

Table 3. Chemical shifts in ^{13}C NMR spectra of ligands and their Te(IV) complexes in DMSO–d^6 at 25°C

Compound	Chemical shift (δ, ppm)			
	CH_3	Phenyl	C=N	C=S/S=O
L_1	—	127.59–134.52	142.62	178.37
L_1TeCl_4	—		150.27	178.48
L_2	—	110.04–140.57	150.86	178.11
$(L_2—H)TeCl_3$	—	117.30–137.01	161.20	198.09
$(L_2—H)Te_2Cl_7$	—	117.15–137.08	161.00	198.55
L_3	14.50	126.98–138.04	148.27	179.36
L_3TeCl_4	14.50	127.41–134.08	153.13	179.30
L_4	15.27	110.93–131.00	157.74	180.87
$(L_4—H)TeCl_3$	15.27	117.57–148.30	162.32	197.52
$(L_4—H)Te_2Cl_7$	15.27	116.82–149.25	161.53	198.45
L_5	—	116.44–138.10	150.24	157.00
$(L_5—H)TeCl_3$	—	116.38–138.28	156.18	—
L_6	13.59	117.31–149.14	155.71	158.18
$(L_6—H)TeCl_3$	13.70	116.96–149.43	155.31	158.18

resented by eq. (2). The minor shielding of the NH protons may be attributed to the secondary effect of coordination through sulphur and the azomethine nitrogen. The presence of an NH signal also indicates that coordination occurs through the thione form.

The ^{13}C NMR data (Table 3) support the coordination of thiosemicarbazones through the azomethine nitrogen and the sulphur of the >C=S group, as the carbons of both the groups get deshielded on complexation, except in the case of adducts, where the carbon of the >C=S group is little affected, probably due to weak coordination of sulphur. The ^{13}C NMR spectra of semicarbazone complexes are very similar to that of the ligand. Sometimes in the spectra of complexes of L_3, L_4 and L_6, weak signals around 26 and 60 ppm have been observed, probably due to oxidized ligands (Scheme 1). In the case of the $(L—H)TeCl_3$ species a greater number of aromatic signals has been observed than expected. Thus $(L_2—H)TeCl_3$ shows nine distinct resonances (117.3–137.0 ppm); $(L_4—H)TeCl_3$ shows eleven resolved resonances (117.6–148.3 ppm) and $(L_5—H)TeCl_3$ gives ten well resolved peaks (116.4–138.3 ppm). The appearance of the spectra is consistent with two overlapping phenyl sets (each ligand shows the expected six resonances). This is possibly due to an equilibrium of *fac* and *mer* isomers (Scheme 2).

The single crystal X-ray diffraction analysis would have been the obvious choice to assign the structure in such systems, but the failure to grow suitable crystals has restricted us. However, in view of the earlier reports regarding the sterically inactive lone pair of tellurium(IV), the assumption about an octahedral arrangement of ligands around the tellurium atom in all these complexes does not seem to be unreasonable. Of course, distortion is not ruled out. The most logical structures for $LTeCl_4$ and $(L—H)Te_2Cl_7$ type species are **B** and **C**, respectively. The existence of $TeCl_4$ in a tetrameric form[14] is a strong driving force for speculating the **C** type of structure for $(L—H)Te_2Cl_7$. The infrared spectra

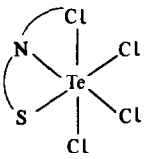

(B)

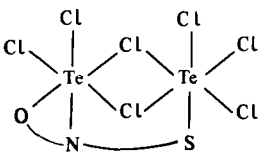

(C)

support coordination of the ligand via the azomethine nitrogen, >C=S/O and phenolic OH (if present).[15] Thus a red shift of ν(C=S) and ν(C=N) as well as the presence of ν(TeO) (390–425 cm^{-1}),

Table 4. Tellurium ligand vibrations (cm^{-1}) of the complexes

L_1TeCl_4	$(L_2—H)TeCl_3$	$(L_2—H)Te_2Cl_7$	L_3TeCl_4	$(L_4—H)TeCl_3$	$(L_4—H)Te_2Cl_7$	$(L_5—H)TeCl_3$	$(L_6—H)TeCl_3$	Assignments
—	418m	418m	—	418m	425m	420m	414m	$\nu_{Te—O}$
—	398m	392w	—	390m	—	397w	392m	
341w	353m	347w	356m	338m	354s	353m	354w	$\nu_{Te—N}$
—	324m	—	314m	308m	326m	328m	—	
290w	303m	300m	297m	293m	298s	302s	302m	$\nu_{Te—Cl}$
255w	280s	270s	277s	280s	287s	282s	279s	
247m	244m	244sh	250w	247w	249s	244m	247w	
228s	231sh	230s	228m	231m	231s	230s	—	$\nu_{Te—Cl/Te—S}$
213s	223m	220w	210m	211m	213m			

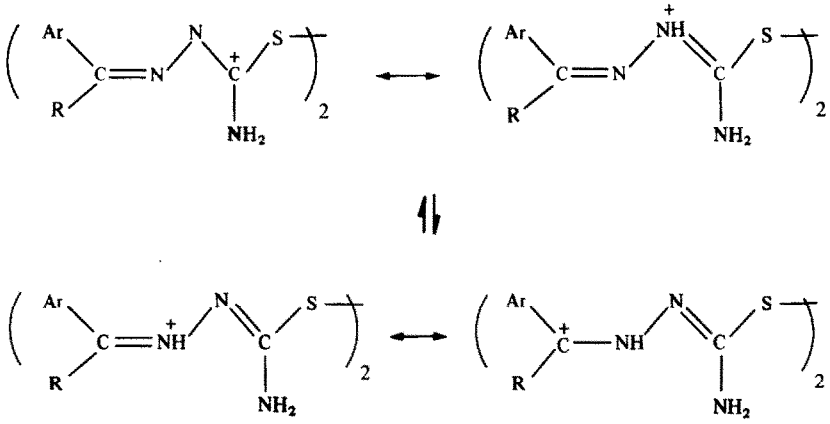

Scheme 1.

Scheme 2.

ν(TeN)(338–354 cm^{-1}) and ν(TeS)(210–230 cm^{-1}) suggest this mode of coordination.

Comparison of the spectra with those of the corresponding bromides enables some estimates of ν(TeCl) to be made (Table 4). For the (L—H)$TeCl_3$ complexes, three bands are seen (244–302 cm^{-1}). This is in accord with the low symmetry of these materials. For the (L—H)Te_2Cl_7 species, at least four bands are observed in the wider range 230–300 cm^{-1} and the lower frequency bands (230 cm^{-1}) could certainly be ascribed to bridging chlorine atoms.[16]

REFERENCES

1. P. I. Murrill, U.S. Patent 1,921,091 (1930).
2. P. I. Murrill, U.K. Patent, 359,328 (1931).
3. K. G. K. De Silva, J. E. Stuckey and W. R. McWhinnie, *Inorg. Chim. Acta* 1986, **122**, 153.
4. M. A. K. Ahmed, S. Abed Ali, W. R. McWhinnie and G. Scott, *J. Appl. Polymer Sci.* 1986, **32**, 4857.
5. M. J. M. Campbell, *Coord. Chem. Rev.* 1975, **37**, 463.
6. S. Padhye, *Coord. Chem. Rev.* 1985, **63**, 127.
7. A. Saxena and J. P. Tandon, *Polyhedron* 1984, **3**, 681.
8. A. Varshney, J. P. Tandon and A. J. Crowe, *Polyhedron* 1986, **5**, 739.
9. F. H. Kruse, R. E. Sanftner and J. F. Suttle, *Anal. Chem.* 1953, **25**, 500.
10. A. I. Vogel, *A Text Book of Quantitative Inorganic Analysis*, 3rd Edn, p. 266. Longmans, London (1961).
11. Asahi Research Centre, *Hand Book of Proton–NMR Spectra and Data*, Vol. 2, p. 340. Academic Press (1985).
12. M. Ferrai Belicchi, G. Fava Gasparri, E. Leporati, C. Pelizzi, P. Tarasconi and G. Tosi, *J. Chem. Soc.* 1986, 2455.
13. A. K. Singh, J. K. Basumatary and N. Mann, unpublished results.
14. B. Buss and B. Krebs, *Angew. Chem. (Int. Edn)* 1970, **9**, 463.
15. J. K. Basumatary, unpublished observation.
16. W. R. McWhinnie and P. Thavornyntikan, *J. Chem. Soc., Dalton Trans.* 1972, 551.

Polyhedron Vol. 7, No. 8, pp. 641–645, 1988
Printed in Great Britain

0277-5387/88 $3.00+.00
© 1988 Pergamon Press plc

SPECTROSCOPIC PROPERTIES AND STRUCTURE OF THE HOLMIUM PERCHLORATE-1,10 PHENANTHROLINE COMPLEXES IN NON-AQUEOUS SOLVENTS

KRYSTYNA BUKIETYŃSKA* and PHAM NGOC THUY†

Institute of Chemistry, University of Wrocław, 50-383 Wrocław, 14 Joliot-Curie, Poland

(*Received* 3 *August* 1987; *accepted after revision* 25 *November* 1987)

Abstract—Absorption spectroscopy studies of the anhydrous $Ho(ClO_4)_3$ in CH_3OH and CH_3CN solutions with different concentrations of 1,10-phenanthroline are reported. Analysis of the intensities of the *f–f* transitions (in terms of Judd–Ofelt parameters and oscillator strengths of the "hypersensitive" transition) indicates that stable complex species with the N-donor ligand are formed. The species with four molecules of 1,10-phenanthroline in acetonitrile solution is characterized by one of the highest known P_{hyp} values observed for the heavy lanthanide compounds in solution. Studies of this species mixed CH_3CN-solv. solutions (where solv.-H_2O and CH_3OH) showed the first coordination sphere of holmium as $[Ho(phen)_4 \cdot (CH_3CN)]^{3+}$. The spectral characteristics of these systems are particularly suitable for studies of the "hypersensitivity" mechanisms.

In our recent paper[1] we have studied the spectroscopic properties of anhydrous and hydrated neodymium perchlorates in methanol solutions with 2,2′-bipyridine (bipy) and 1,10-phenanthroline (phen). It was found, that in non-aqueous solutions, species with N-donor ligand molecules in the direct environment of the lanthanide ion can exist. It is interesting then, to compare the behaviours of heavy and light lanthanide ion complexes. Some structural differences between them can be expected—because the lanthanide contraction may be responsible for some difficulties in the packing of relatively large ligand molecules in the first coordination sphere of the smaller ($r_{Nd^{3+}} = 0.995$ Å, $r_{Ho^{3+}} = 0.894$ Å) holmium ion. The more interesting aspect of this paper, however, appeared in the influence of the solvents and N-donor ligand on the intensities of the *f–f* transitions of the heavy lanthanide ion. A particular role of CH_3CN is clearly seen from results presented in this paper. We have investigated anhydrous holmium perchlorates with 1,10-phenanthroline in CH_3OH and CH_3CN solutions. Solvates of some anhydrous lanthanide perchlorates in these solvents were studied recently by different methods, which were helpful in our studies.[2–5]

EXPERIMENTAL

Hydrated $Ho(ClO_4)_3$ was prepared from 99.9% Ho_2O_3 (Merck), by the method given by Forsberg.[6] Anhydrous $Ho(ClO_4)_3$ was prepared by the slow heating of the hydrated holmium perchlorate, for at least 120 h. All salts used were fully analysed. 1,10-phenanthroline was dehydrated *in vacuo* (1 mm Hg) for at least one week.

All anhydrous reagents were checked for water contamination. Only samples with no O—H stretching bands in their IR spectra, were used for spectral measurements. The solvents used were also dried carefully. CH_3OH was dried using molecular sieves (A-4). Acetonitrile was doubly distilled over P_4O_{10}, then dehydrated using CaH_2 and redistilled. In freshly prepared solvent, no O—H stretching bands were observed in the IR. The solutions in mixed solvents were prepared from an anhydrous solution of $Ho(ClO_4)_3$ in anhydrous acetonitrile with 1,10-phenanthroline (molar ratio Ho^{3+} : phen = 1 : 4), with CH_3CN diluted with an appropriate amount of water or methanol, respectively. All solutions for the spectroscopic measurements were stored under a dry nitrogen atmosphere.

*Author to whom correspondence should be addressed.
†Permanent address: University of Hanoi, Hanoi, Vietnam.

MEASUREMENTS AND CALCULATIONS

Spectral measurements were made on a Cary 14-spectrophotometer at 293 K, over the spectral range available (11,000–30,000 cm^{-1}). UV bands of the Ho^{3+} ion have not been used in the intensity parameter calculations, because basic lines of the absorption bands were not well determined due to the strong absorption of the ligand in this spectral region.

Experimental oscillator strengths of solution absorption bands were obtained by graphical integration of the area under the absorption curves after the appropriate correction of the base line.

Ω_λ parameters were calculated from the experimental oscillator strength values by applying the Judd–Ofelt equation in the form:

$$P = \frac{8\pi^2 mc}{3h}\frac{\sigma}{2J+1}\chi \times \sum_{\lambda=2,4,6}\Omega_\lambda(\psi_J\|U^{(\lambda)}\|\psi_J)^2$$

where: χ—refraction index $\chi = (n^2+2)^2/9n$;
$U^{(\lambda)}$—matrix elements of the unit tensor operator calculated by Carnall *et al.*[7] from the free ion state eigenvectors;
J—total quantum number.

Calculations were performed for the different sets of levels, however, sets of levels with minimal mean square error were the same for all the considered systems. Absorption spectra of Ho^{3+}—1,10-phenanthroline complexes in CH_3OH and CH_3CN were measured for different M:L ratios (from M:L = 1:0.5 to M:L = 1:5). The spectra with M:L = 1:0 are the spectra of pure holmium perchlorate dissolved in the appropriate solvent.

The spectra of anhydrous holmium perchlorate with phen (M:L = 1:4) in CH_3CN, with different molar ratios of H_2O and CH_3OH were also measured.

RESULTS AND DISCUSSION

As was proved previously for Nd^{3+} with phen,[1] the most significant differences for different Ho^{3+}:phen molar ratios are observed for the "hypersensitive" transition.

This is illustrated in Fig. 1(a), where the influence of the increasing 1,10-phenanthroline concentration on the $^5G_6 \leftarrow {}^5I_8$ Ho^{3+} transition is presented. The Judd–Ofelt parameter values Ω_λ of the $Ho(ClO_4)_3$–phen system in methanol solutions are collected in Table 1.

Among the three Ω_λ parameters (Table 1), as can be expected, Ω_2 exhibits the most significant changes, whereas Ω_4 and Ω_6 remain almost constant within the limit of experimental error. Detailed analysis of the influence of the increasing metal to ligand ratios on the oscillator strength values of the "hypersensitive" transition (P_{hyp}) and the Ω_λ parameter values, is presented in Figs 2(a) and 3(a),

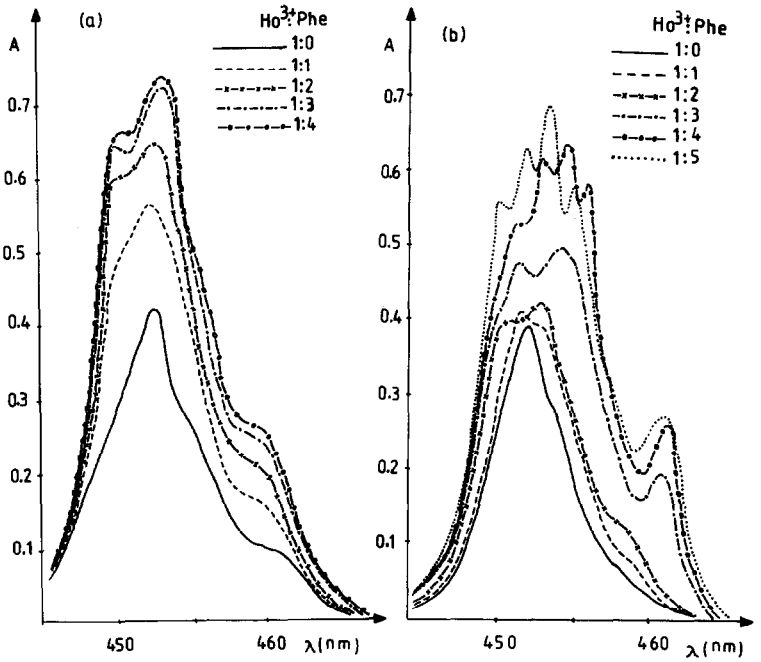

Fig. 1. Effect of the increasing phen concentration on the "hypersensitive" transition $^5G_6 \leftarrow {}^5I_8$ of the Ho^{3+} ion in the absorption spectrum of the anhydrous holmium perchlorate in: (a) CH_3OH ($c_{Ho^{3+}} = 1.60 \times 10^{-2}$ M, $d = 5$ cm), (b) CH_3CN ($c_{Ho^{3+}} = 1.75 \times 10^{-2}$ M, $d = 2$ cm).

Table 1. Judd–Ofelt parameter values (Ω_λ) for hydrated and anhydrous holmium perchlorate with phen in CH_3OH and for anhydrous holmium perchlorate with phen in CH_3CN

$\Omega_\lambda \times 10^{20}$	Ho^{3+}:phen 1:0	1:0.5	1:1	1:2	1:3	1:3.5	1:4	1:5
	$Ho(ClO_4)_3 \cdot (6H_2O)$ in CH_3OH				$c_{Ho^{3+}} = 2.68 \times 10^{-2}$ M			
Ω_2			1.82±0.20	3.32±0.21	4.14±0.26		4.24±0.25	4.61±0.22
Ω_4			3.55±0.31	3.51±0.32	3.55±0.39		3.61±0.39	3.62±0.34
Ω_6			3.06±0.21	3.09±0.21	3.07±0.26		2.97±0.27	3.11±0.23
	$Ho(ClO_4)_3$ in CH_3OH				$c_{Ho^{3+}} = 1.60 \times 10^{-2}$ M			
Ω_2			2.30±0.18	3.52±0.24	4.23±0.25	4.44±0.25	4.61±0.26	
Ω_4			3.62±0.28	3.67±0.36	3.83±0.37	3.82±0.38	4.05±0.42	
Ω_6			3.14±0.18	3.20±0.24	3.20±0.25	3.17±0.25	3.11±0.28	
	$Ho(ClO_4)_3$ in CH_3CN				$c_{Ho^{3+}} = 1.75 \times 10^{-2}$ M			
Ω_2	2.53±0.45	3.42±0.40	4.12±0.32	5.58±0.36	7.79±0.33		10.87±0.34	11.18±0.35
Ω_4	5.35±0.67	4.97±0.60	4.90±0.41	4.96±0.54	4.93±0.50		5.11±0.51	5.15±0.52
Ω_6	6.00±0.45	5.73±0.40	5.17±0.33	4.84±0.36	4.48±0.39		4.40±0.35	4.32±0.32

respectively. The results of spectral measurements on the anhydrous $Ho(ClO_4)_3$–phen system in acetonitrile solutions are also collected in Table 1 and in Figs 1(b), 2(b) and 3(b). In this case, generally, higher intensities are observed. P_{hyp} and Ω_2 parameter values again exhibit the strongest increase in their values with increasing 1,10-phenanthroline concentration. A more detailed inspection of these data provided us with the conclusion that ligand influence is even more distinct on the intensities of other *f–f* transitions. A small, but systematic decrease of the Ω_6 parameter values is also observed.

To make a comparison of the spectral properties of the $Ho(ClO_4)_3$–phen system in both solvents more realistic, we have expressed the intensity parameters in Ω_λ values.

It seems, however, that we should be very careful, when applying the unified formula of the refractive index function to all calculations. Taking into account the rather undoubtful fact that the spectroscopic mechanism of the "hypersensitive" transition is different from that for other *f–f* transitions,[8] we can not expect very good correspondence amongst the measurements in CH_3OH and CH_3CN solutions.

The general picture of the spectral changes, however, in CH_3OH and CH_3CN is rather different and presumably different complex species can form in solutions of these solvents. Moreover, it seems very probable that no species higher than $[Ho(phen)_2]^{3+}$can exist in significant amounts in CH_3OH solution. It is also very characteristic that for metal to ligand ratios higher than 1 : 4, a solid complex compound precipitates out from the solution. On the other hand, for the acetonitrile solutions, both the shape of the $P = f(M/L)$ and the very high intensity [Figs 1(b), 2(b)], together with the good solubilities of the solutions with high M : L ratios (up to 1 : 5), suggest that the highest stable species which exists in CH_3CN solution is the species containing four 1,10-phenanthroline molecules. A very high intensity of this species in the acetonitrile solution suggests that besides four phen molecules, some solvent molecules are present in the first coordination sphere of the lanthanide ion. Recently, however, Bunzli *et al.*[3–5] proved that in acetonitrile solution some perchlorate ions are preserved in the first coordination sphere of the lanthanide solvate. We decided to check the influence of other solvents (H_2O, CH_3OH) on the spectral intensity of the 1 : 4 species in CH_3CN solution. Results are presented in Fig. 4 and Table 2. In Fig. 4, relations between $P_{hyp} = f(c_{Ho^{3+}}/c_{solv})$ are presented and quite striking differences can be seen between the influence of H_2O and CH_3OH on the intensity of the "hypersensitive"

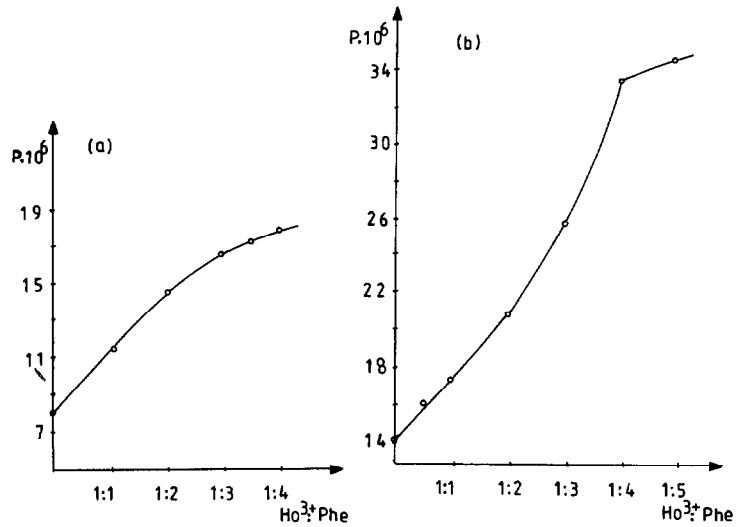

Fig. 2. Oscillator strength values (P) of the "hypersensitive" transition ${}^5G_6 \leftarrow {}^5I_8$ of the Ho^{3+} ion as a function of the molar ratio of Ho^{3+} : phen: (a) for the anhydrous holmium perchlorate in CH_3OH ($c_{Ho^{3+}} = 1.60 \times 10^{-2}$ M), (b) for the anhydrous holmium perchlorate in CH_3CN ($c_{Ho^{3+}} = 1.75 \times 10^{-2}$ M).

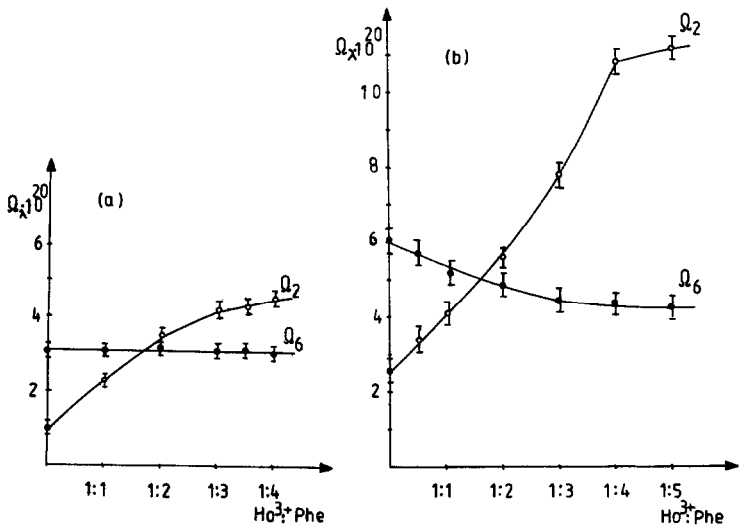

Fig. 3. Ω_λ parameter values of the anhydrous holmium perchlorate in: (a) CH_3OH ($c_{Ho^{3+}} = 1.60 \times 10^{-2}$ M), (b) CH_3CN ($c_{Ho^{3+}} = 1.75 \times 10^{-2}$ M) as a function of the molar ratio of Ho^{3+} : phen.

Table 2. Judd–Ofelt parameter values (Ω_λ) of $Ho(ClO_4)_3$ + four phen solutions in CH_3CN for different $c_{Ho^{3+}} : c_{solv.}$ ratios where solv.–H_2O and CH_3OH × $c_{Ho^{3+}} = 2.22 \times 10^{-2}$ M

Solv.	$\Omega_\lambda \times 10^{20}$	Ho^{3+} : solv. 1:0	1:1	1:2	1:4	1:8
H_2O	Ω_2	10.60±0.36	8.93±0.33	8.67±0.33	8.33±0.30	8.24±0.28
	Ω_4	5.34±0.57	4.45±0.50	4.62±0.50	4.50±0.46	4.48±0.41
	Ω_6	4.18±0.38	3.93±0.33	3.88±0.34	3.85±0.31	3.84±0.34
CH_3OH	Ω_2	10.63±0.46	10.52±0.42	10.67±0.42	10.60±0.43	10.41±0.42
	Ω_4	5.34±0.57	5.05±0.64	5.13±0.62	5.08±0.63	5.20±0.62
	Ω_6	4.18±0.38	4.45±0.43	4.28±0.42	4.23±0.42	4.25±0.43

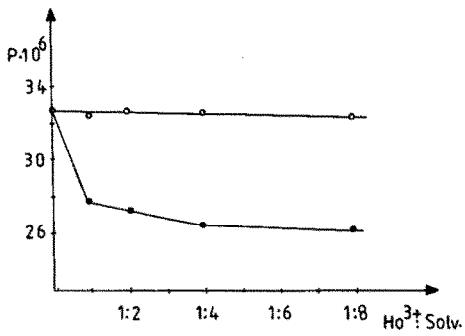

Fig. 4. Oscillator strength values of the "hypersensitive" transition ${}^5G_6 \leftarrow {}^5I_8$ of the Ho^{3+} ion as a function of the Ho^{3+} : solv. (where $Ho^{3+}:H_2O$ ●, $Ho^{3+}:CH_3OH$ ○) for $[Ho(phen)_4](ClO_4)_3$ phen solutions in CH_3CN ($c_{Ho^{3+}} = 1.75 \times 10^{-2}$ M).

transition of the $[Ho(phen)_4]^{3+}$ species in CH_3CN. In the case of H_2O—one water molecule added per one Ho^{3+} ion caused a significant decrease of the P_{hyp}. The addition of the next two water molecules caused only slight intensity changes, and practically no further changes in intensity were observed when an additional amount of water was added. In the case of CH_3OH, addition of this solvent up to a Ho^{3+} : Solv. molar ratio of 1 : 8 does not cause any change of the P_{hyp} value. These results can be explained in terms of differences between the solvation ability of the $[Ho(phen)_4]^{3+}$ species in CH_3CN by these two solvents. If we assume the $[Ho(phen)_4]^{3+}$ species in CH_3CN has a coordination number of nine, with eight of the coordination positions occupied by four 1,10-phenanthroline molecules and one position occupied by CH_3CN or ClO_4^-, a significant decrease in intensity should be observed when one H_2O molecule is exchanged for CH_3CN or ClO_4^- in the first coordination sphere of Ho^{3+}. CH_3OH has lower polarity and its size is significantly larger than H_2O.

It seems that the presence of a CH_3CN molecule is more probable in the first coordination sphere than a ClO_4^- ion, which should be exchanged by the large chelating 1,10-phenanthroline molecule, when a large excess of this ligand is added.

In our opinion, coordination numbers higher than nine seem to be rather doubtful for this system, in the case of such large ligands as 1,10-phenanthroline.

These data are particularly interesting from the point of view of the spectral properties of systems with Ln^{3+}—N bonding. The species $[Ho(phen)_4 \cdot (CH_3CN)]^{3+}$ gave higher values of all the parameters, even in comparison with the mixed Ln^{3+}—phen—CH_3OH species. It should be pointed out that Ω_6 parameter values [Fig. 3(b)] decrease slightly but systematically, when 1,10-phenanthroline exchanges with CH_3CN molecules in the first coordination sphere of the Ho^{3+} ion. It suggests that this solvent is more tightly bonded to the Ln^{3+} ion, and complexation with 1,10-phenanthroline is due mainly to the entropy effect.

Very high intensities of $[Ho(phen)_4 \cdot (CH_3CN)]^{3+}$ may be the result of the very significant anisotropy of this species.[8] Unfortunately, since we were unable to prepare crystals good enough for X-ray and spectroscopic analysis, studies of the luminescence and absorption spectroscopy of Ln^{3+}—phen systems with different anions and solvents should be very helpful in understanding their properties and will be the subject of forthcoming papers.

The Ln^{3+}—phen—CH_3CN system, however, seems to be particularly interesting from the point of view of the "hypersensitivity" mechanism.

REFERENCES

1. K. Bukietyńska and Pham Ngoc Thuy, *Inorg. Chim. Acta* 1987, **132**, 21.
2. B. Keller, J. Legendziewicz and G. Oczko, *Bull. Acad. Pol. Sci.* 1986, **34**, 257.
3. J. C. G. Bunzli and M. M. Vuckovic, *Inorg. Chim. Acta* 1983, **73**, 53.
4. J. C. G. Bunzli, J. R. Yersin and C. Mabillard, *Inorg. Chem.* 1982, **21**, 1471.
5. J. C. G. Bunzli and C. Mabillard, *Inorg. Chem.* 1986, **25**, 2750.
6. J. H. Forsbeg and T. Moeller, *Inorg. Chem.* 1969, **8**, 883.
7. W. T. Carnall, P. R. Field and K. Rajnak, *J. Chem. Phys.* 1968, **49**, 4437.
8. S. F. Mason, *Structure and Bonding* 1980, **39**, 43.

Polyhedron Vol. 7, No. 8, pp. 647–650, 1988
Printed in Great Britain

0277-5387/88 $3.00+.00
© 1988 Pergamon Press plc

PALLADIUM COMPLEXES WITH AZOBENZENE AND SULPHUR–NITROGEN LIGANDS. X-RAY CRYSTAL STRUCTURE OF [Pd(Tmaz)(S_2N_2H)]

RAY JONES, THOMAS G. PURCELL, DAVID J. WILLIAMS and J. DEREK WOOLLINS*

Department of Chemistry, Imperial College of Science and Technology, South Kensington, London SW7 2AY, U.K.

(*Received* 26 *October* 1987; *accepted* 4 *December* 1987)

Abstract—Reaction of $[(Azb)PdCl]_2$ (**1**) with $Me_2Sn(S_2N_2)$ (**2**) or $PhHgS_7N$ (**3**) gave $Pd(Azb)(S_2N_2H)$ (**4**) and $Pd(Azb)(S_3N)$ (**5**), respectively. (Azb = azobenzene or tetramethylazobenzene.) The new compounds were characterized by IR, microanalyses and, in the case of $Pd(Tmaz)(S_2N_2H)$ (Tmaz = tetramethylazobenzene) X-ray crystallography.

We have recently developed routes to a number of interesting metalla–sulphur–nitrogen compounds.[1] For example, binuclear complexes[2] such as $[Pt(PPh_3)(S_2N_2)]_2$, ionic stacking compounds[3,4] of the general type $[Pt(S_2N_2H)(PR_3)_2]X$ as well as complexes containing small ligands[5,6] are all now known. Currently, there are few examples of mixed ligand palladium sulphur–nitrogen complexes and there has been little work on the synthesis of SN complexes in which the other ligands are coplanar. These types of compounds are of interest from the point of view of their potential stacking properties. Clearly, one limitation with previous work is the bulk of the phosphine ligands which hinders very close approach of adjacent molecules in the solid state. Here we report on the preparation of palladium SN complexes with azobenzene ligands, together with the crystal structure of $Pd(Tmaz)(S_2N_2H)$.

EXPERIMENTAL

General reaction conditions, drying of solvents and spectroscopic measurements were as described previously.[4] Azobenzene was purchased from Aldrich and used without further purification. Tetramethylazobenzene was prepared from 5-nitro-*m*-xylene as described in the literature.[7] $[Pd(Azb)Cl]_2$ was prepared[8] by stirring a methanolic solution/suspension of $PdCl_2$ with the appropriate azobenzene overnight. The resulting precipitate was collected, washed with methanol and water and dried *in vacuo*. $PhHgS_7N$ and $Me_2SnS_2N_2$ were prepared as previously described.[9,10]

$Pd(Azb)(S_2N_2H)$

To a suspension of $[Pd(Az)Cl_2]$ (150 mg, 0.23 mmol) in dry CH_2Cl_2 (10 cm^3), was added solid $Me_2Sn(S_2N_2)$ (102 mg, 0.46 mmol); the reaction immediately gave a deep brick red solution. The reaction was stirred under argon for 2 h, filtered through celite and reduced in volume to *ca* 5 cm^3 before purification using a Biobeads SX-8 column with CH_2Cl_2 as the eluent. The product was obtained as the second (orange) band which eluted down the column. Evaporation of the solvent *in vacuo* gave analytically pure material, 104 mg, 60%. The complex may be further purified by recrystallization from hot toluene. Crystals of $Pd(Tmaz)(S_2N_2H)$ suitable for X-ray crystallography were obtained by slow evaporation of a CH_2Cl_2 solution.

$Pd(Azb)(S_3N)$

To a suspension of $[Pd(Azb)Cl]_2$ (173 mg, 0.27 mmol) in CH_2Cl_2 (10 cm^3) was added $PhHgS_7N$ (275 mg, 0.53 mmol). The reaction went dark red immediately and was stirred for 4 h under argon. After filtration through celite, the CH_2Cl_2 solution was reduced to *ca* 5 cm^3 and eluted down a Biobeads

*Author to whom correspondence should be addressed.

SX-8 column using CH_2Cl_2. The product was the second (red) band. Evaporation of the CH_2Cl_2 *in vacuo* gave a mauve solid which was recrystallized from toluene. Yield 45 mg, 22%. The Tmaz complex was obtained in a similar fashion.

X-ray structural analysis of Pd(Tmaz)(S_2N_2H)

Crystal data. $C_{16}H_{18}N_4S_2Pd$, $M = 436.86$, monoclinic, $a = 13.072(3)$, $b = 8.006(1)$, $c = 17.285(4)$ Å, $\beta = 102.27(2)°$, $U = 1768$ Å^3, space group $P2_1/c$, $Z = 4$, $D_c = 1.65$ g cm^{-3}. Orange, air stable prism, dimensions 0.1 × 0.2 × 0.15 mm, μ(Cu-K_α) = 108.8 cm^{-1}, $\lambda = 1.54178$ Å, $F(000) = 880$.

Data collection and processing. Refined unit cell parameters were obtained by centring 20 reflections on a Nicolet R3m diffractometer, ω-scan method, ($\theta \leqslant 58°$), graphite monochromated Cu-K_α radiation; 2381 independent measured reflections, 2128 observed [$|F_o| > 3\sigma(|F_o|)$], corrected for Lorentz and polarization factors; numerical absorption correction (face indexed crystal).

Structure analysis and refinement. The structure was solved by direct methods and all the non-hydrogen atoms refined anisotropically. The positions of all the hydrogen atoms were clearly revealed in a ΔF map. The position of the hydrogen attached to N(1) was idealized (N—H = 0.96 Å) and refined isotropically. Two orientations (each 50% occupancy) of the methyl group on C(7) were detected, and these and the other methyl groups were refined as rigid bodies. All other hydrogen atoms were idealized (C—H = 0.96 Å), assigned isotropic thermal parameters [$U(H) = 1.2U_{eq}(C)$] and allowed to ride on their parent carbon atoms. Refinement was by block-cascade full-matrix least-squares to $R = 0.051$, ($R = \Sigma[|F_o| - |F_c|]/\Sigma|F_o|$), $R_w = 0.056$ ($w^{-1} = \sigma^2(F) + 0.00161F^2$). The maximum residual electron density in the final ΔF map was 1.79 eÅ^{-3} and the mean and maximum shifts/error in the final refinement cycle were 0.006 and 0.069, respectively. Computations were carried out on an Eclipse S140 computer using the SHELXTL program system[11] and published scattering factors.[12] Tables of atomic coordinates, displacement factor coefficients, full lists of bond lengths and angles and F_o/F_c values have been deposited as supplementary material with the Editor, from whom copies can be obtained.*

RESULTS AND DISCUSSION

We have previously made use[4] of reactions of $Me_2Sn(S_2N_2)$ (**2**) with *cis*-$PtCl_2(PR_3)_2$ to form $Pt(S_2N_2H)(PR_3)_2$, with elimination of Me_2SnCl_2. With CH_2Cl_2 as solvent, we believe that the initially formed platinum–S_2N_2 complex and the Me_2SnCl_2 pick up HCl to give the overall reaction shown in eq. (1); the final product from this reaction has been characterized by X-ray crystallography.[4]

$$PtCl_2(PEt_3)_2 + Me_2Sn(S_2N_2) \rightarrow [Pt(S_2N_2H)(PEt_3)_2][Me_2SnCl_3]. \quad (1)$$

Clearly, if HCl from the solvent can be involved in the reation there is no absolute requirement for bis chloro complexes to be used. As an alternative strategy we have employed the dimeric compounds $[Pd(Azb)Cl]_2$ (**1**) (Azb = azobenzene, tetramethylazobenzene) assuming that the other chloride will be provided by the solvent. Reaction of (**1**) with (**2**) proceeds smoothly according to eq. (2).

$$[Pd(Azb)Cl_2] + 2Me_2Sn(S_2N_2) + HCl \rightarrow 2Pd(Azb)(S_2N_2H) + 2Me_2SnCl_2. \quad (2)$$

The products (**4**) are obtained in reasonable yield (Table 1).

We have recently[13] made use of reactions of $Hg(S_7N)_2$ with $PtCl_2(PR_3)_2$ to form complexes of the type $[Pt(S_3N)(PR_3)_2][PF_6]$. In these types of reactions it is believed that $Hg(S_7N)_2$ acts as a source of S_7N^- which disproportionates to give S_3N^- and sulphur. An alternative reagent is PhHg(S_7N) (**3**) which reacts[14] with $PtCl_2(PR_3)_2$ to give $PtCl(S_3N)(PR_3)$. As expected (**3**) reacts with (**1**) to give Pd(Azb)(S_3N) (**5**) (eq. 3).

$$[Pd(Azb)Cl]_2 + 2PhHg(S_7N) \rightarrow 2Pd(Azb)(S_3N) + 2PhHgCl + S_8. \quad (3)$$

Compounds (**4**) and (**5**) gave satisfactory analyses (Table 1). Their IR spectra are dominated by absorptions due to the azobenzene ligand, but some bands due to the SN ligands are observed. In the case of (**4**) the ν(NH) bands (3284 and 3257 cm^{-1} for Azb and Tmaz, respectively) together with ν(NS) bands (1074(m) and 1096(m) cm^{-1}), δ(NS) (515(m), 332(m) and 506(m), 338(m) cm^{-1}) are not obscured by azobenzene bands. In Pd(Azb)(S_3N) ν(NS) (986 cm^{-1}) and δ(NS) (343 cm^{-1}) bands are seen.

The X-ray structure of Pd(Tmaz)(S_2N_2H) (**4a**) is shown in Fig. 1 and selected bond distances and angles are in Table 2. The complex is square-planar with a maximum deviation from the Pd—N(1)—S(2)—C(10)—N(3) mean plane of 0.057 Å for C(10). A more detailed analysis of the coordination geometry reveals that the departure from planarity of the substituents on palladium is caused by a slight twisting of the Tmaz ligand relative to the *trans* $S_2N_2H^-$ unit. The dihedral angle

* Atomic coordinates have also been deposited with the Cambridge Crystallographic Data Centre.

Table 1. Yields and microanalytical data (calculated values in parentheses)

Compound	Colour	% Yield	Analyses[a] C%	H%	N%
$Pd(Azb)(S_2N_2H)$	Orange	60	37.9 (37.8)	2.6 (2.6)	14.2 (14.7)
$Pd(Tmaz)(S_2N_2H)$	Orange	42	44.1 (44.0)	4.1 (4.1)	12.6 (12.8)
$Pd(Azb)(S_3N)$	Mauve	22	36.9 (36.2)	2.3 (2.3)	10.1 (10.6)
$Pd(Tmaz)(S_3N)$	Red	36	42.7 (42.3)	3.9 (3.8)	9.1 (9.3)

[a] Calc. values in parentheses.

Table 2. Selected bond distances and angles in $Pd(Tmaz)(S_2N_2H)$

Pd—S(2)	2.253(2)	Pd—N(1)	2.049(6)
Pd—N(3)	2.048(6)	Pd—C(10)	2.013(6)
S(1)—N(1)	1.588(7)	S(1)—N(2)	1.536(8)
S(2)—N(2)	1.668(7)	N(3)—N(4)	1.277(7)
N(3)—C(1)	1.434(9)	N(4)—C(9)	1.395(9)
S(2)—Pd—N(1)	85.0(2)	S(2)—Pd—N(3)	179.2(1)
N(1)—Pd—N(3)	95.8(2)	S(2)—Pd—C(10)	99.6(2)
N(1)—Pd—C(10)	172.8(3)	N(3)—Pd—C(10)	79.6(3)
N(1)—S(1)—N(2)	108.8(4)	Pd—S(2)—N(2)	104.9(3)
Pd—N(1)—S(1)	120.1(4)	S(1)—N(2)—S(2)	121.0(5)
Pd—N(3)—N(4)	117.7(4)	Pd—N(3)—C(1)	126.7(4)
N(4)—N(3)—C(1)	115.4(6)	N(3)—N(4)—C(9)	113.5(6)
N(3)—C(1)—C(2)	118.2(7)	N(3)—C(1)—C(6)	119.6(6)
Pd—C(10)—C(11)	135.5(6)	Pd—C(10)—C(9)	109.9(5)
N(4)—C(9)—C(10)	119.0(6)	N(4)—C(9)—C(14)	116.3(7)

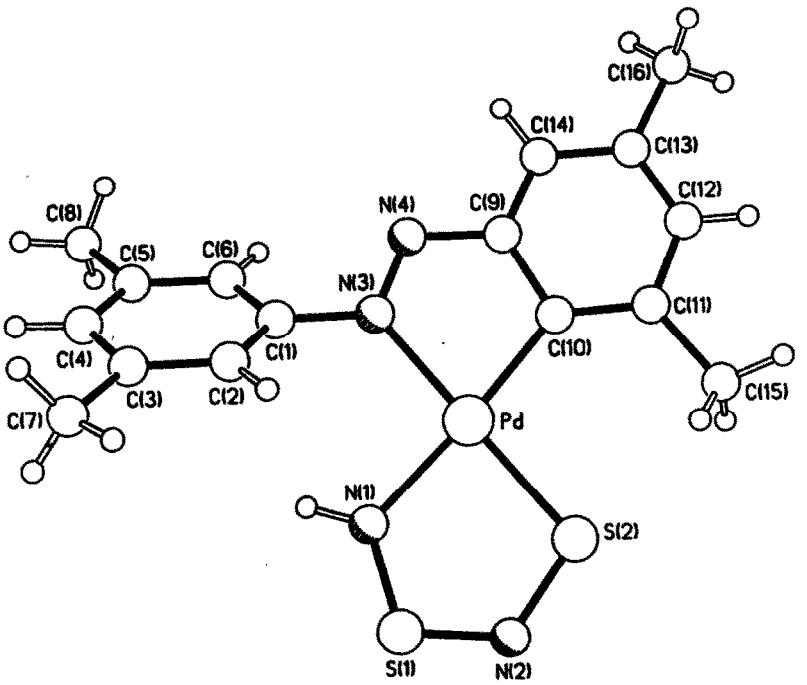

Fig. 1. The X-ray crystal structure of $Pd(Tmaz)(S_2N_2H)$.

between the Pd—N(1)—S(2) and Pd—N(3)—C(10) planes is 5.5°. This twist of the Tmaz ligand is almost certainly due to the steric interaction between the C(15) methyl and S(2) [the shortest intramolecular contact is 2.44 Å between H(15) and S(2)]. This results in deviations of 0.27 and 0.43 Å from the PdS_2N_2 plane for C(10) and C(9), respectively. The C(1)—C(6) xylyl ring is also rotated 45° out of the Pd—N(3)—N(4)—C(9)—C(10) plane due to the steric repulsion between N(1) and C(2) [N(1)···C(2) 3.08 Å]. The distances and angles within the PdS_2N_2H metallacycle are most readily compared with those in $[Pd(S_2N_2H)(PMe_2Ph)_2][BF_4]$ (**6**).[15] The only significant difference is the Pd—S(2) bond length which is shorter in (**4a**) than in (**6**) (2.253(2) cf. 2.290(2) Å, respectively) due to the difference in *trans* ligands (M—P vs M—C *trans* bonds). In contrast to (**6**), although there are no steric restrictions, (**4a**) does not stack in the solid state. Ionic structures appear to be preferred for this type of packing to occur.

Acknowledgements—We are grateful to the SERC for support and to Johnson Matthey for loans of precious metals.

REFERENCES

1. P. F. Kelly and J. D. Woollins, *Polyhedron* 1985, **5**, 607.
2. R. Jones, P. F. Kelly, D. J. Williams and J. D. Woollins, *J. Chem. Soc., Chem. Commun.* 1985, 1325.
3. R. Jones, P. F. Kelly, C. P. Warrens, D. J. Williams and J. D. Woollins, *J. Chem. Soc., Chem. Commun.* 1986, 711.
4. R. Jones, C. P. Warrens, D. J. Williams and J. D. Woollins, *J. Chem. Soc., Dalton Trans.* 1987, 907
5. N. P. C. Walker, M. B. Hursthouse, C. P. Warrens and J. D. Woollins, *J. Chem. Soc., Chem. Commun.* 1985, 227.
6. R. Short, M. B. Hursthouse, T. G. Purcell and J. D. Woollins, *J. Chem. Soc., Chem. Commun.* 1987, 407.
7. R. B. Carlin, *J. Am. Chem. Soc.* 1945, **67**, 928.
8. A. C. Cope and R. W. Siekman, *J. Am. Chem. Soc.* 1965, **87**, 3272.
9. H. W. Roesky and H. Weizer, *Angew. Chem. Int. Ed. Engl.* 197, **12**, 674.
10. H. G. Heal and R. J. Ramsay, *J. Inorg. Nucl. Chem.* 1974, **36**, 950.
11. G. M. Sheldrick, SHELXTL, *An Integrated System for Solving, Refining and Displaying Crystal Structures from Diffraction Data*, University of Gottingen, Gottingen, F.R.G. (1978). Revision 4.1 (1983).
12. *International Tables for X-Ray Crystallography*, Vol. IV. Kynoch Press, Birmingham (1974).
13. R. Jones, T. G. Purcell, D. J. Williams and J. D. Woollins, *Polyhedron* 1987, **6**, 2165.
14. J. D. Woollins, unpublished.
15. R. Jones, P. F. Kelly, D. J. Williams and J. D. Woollins, *J. Chem. Soc., Dalton Trans.* accepted for publication.

Polyhedron Vol. 7, No. 8, pp. 651–657, 1988
Printed in Great Britain

0277–5387/88 $3.00+.00
© 1988 Pergamon Press plc

SYNTHESIS, STRUCTURE AND SPECTROSCOPY OF HETEROMETALLIC COMPOUNDS CONTAINING LINEAR AuCNM, AuNCM AND MNCAuCNM CHAINS OF ATOMS (M = Rh OR Ir): CRYSTAL STRUCTURE OF $[\{PMe_2Ph)_3Cl_2Rh(\mu\text{-}NC)\}_2Au][ClO_4]\cdot 2CH_2Cl_2$

ANTONY J. DEEMING* and GRAEME P. PROUD

Department of Chemistry, University College London, 20 Gordon Street, London WC1H 0AJ, U.K.

and

HELEN M. DAWES and MICHAEL B. HURSTHOUSE*

Department of Chemistry, Queen Mary College, Mile End Road, London E1 4NS, U.K.

(*Received* 17 *November* 1987; *accepted* 4 *December* 1987)

Abstract—The aqua-complexes $[MCl_2(H_2O)(PMe_2Ph)_3][ClO_4]$ (M = Rh or Ir) react rapidly with $[Au(CN)(PPh_3)]$ to give the cyano-bridged compounds $[(PPh_3)Au(\mu\text{-}CN)MCl_2(PMe_2Ph)_3][ClO_4]$. These could not be isolated in a pure state because they readily disproportionate to a mixture also containing $[Au(PPh_3)_2]^+$ and $[\{(PMe_2Ph)_3Cl_2M(\mu\text{-}NC)\}_2Au][ClO_4]$. The disproportionation is much more rapid when $[Au(CN)(PPh_3)]$ is in slight excess. The complexes were characterized by ^1H, ^{13}C and ^{31}P NMR methods, and the single-crystal X-ray structure of $[\{(PMe_2Ph)_3Cl_2Rh(\mu\text{-}NC)\}_2Au][ClO_4]$ is reported.

The water ligands in the aqua-complexes *mer*, *trans*-$[MCl_2(H_2O)(PMe_2Ph)_3][ClO_4]$ (M = Rh or Ir) are labile. Phosphine site-exchange occurs rapidly by a water-dissociation pathway.[1,2] Addition of any ligand more strongly coordinating than H_2O to the aqua-complexes leads very rapidly to the substituted derivatives. This is in very marked contrast to the behaviour of $[Rh(H_2O)_6]^{3+}$ and $[Ir(H_2O)_6]^{3+}$ which are among the most inert aqua-complexes known.[3,4] For example, acetonitrile readily gives $[MCl_2(MeCN)(PMe_2Ph)_3][ClO_4]$ and we have used metal cyano-compounds instead of MeCN to form μ-cyano derivatives.[5] In this way we have formed $[(PMe_2Ph)_3Cl_2Ir(\mu\text{-}CN)IrCl_2(PMe_2Ph)_3][ClO_4]$ (X-ray structure) by adding $[IrCl_2(CN)(PMe_2Ph)_3]$ to $[IrCl_2(H_2O)(PMe_2Ph)_3][ClO_4]$.[5] Here we describe the use of $[Au(CN)(PPh_3)]$[6–8] as a ligand with $[MCl_2(H_2O)(PMe_2Ph)_3][ClO_4]$ but have found that, although the initially formed species with μ-CN can be observed spectroscopically, disproportionation leads to $[\{(PMe_2Ph)_3Cl_2M(\mu\text{-}CN)\}_2Au][ClO_4]$ and other products.

RESULTS AND DISCUSSION

Synthesis of cyano-bridged compounds

The ^1H and ^{31}P NMR spectra (Tables 1 and 2) of a dichloromethane solution of the complexes $[Au(CN)(PPh_3)]$ and $[IrCl_2(H_2O)L_3][ClO_4]$ (L = PMe_2Ph) in equimolar quantities showed that $[(PPh_3)Au(\mu\text{-}CN)IrCl_2(PMe_2Ph)_3][ClO_4]$ (**1a**) had formed rapidly and completely (Scheme 1). Over hours, however, ^{31}P NMR signals for $[Au(PPh_3)_2]^+$ and another species (**3a**), not containing PPh_3, appeared in the spectrum. Complexes (**1a**) and (**3a**) could not be isolated pure but have been characterized as $[(PPh_3)Au(\mu\text{-}CN)IrCl_2L_3][ClO_4]$ and $[\{L_3Cl_2Ir(\mu\text{-}NC)\}_2Au][ClO_4]$, respectively by the spectroscopic data in Tables 1 and 2 obtained for mixtures. At equilibrium, reached after several days, the solution contained approximately 60% (**1a**), 20% (**3a**) and 20% $[Au(PPh_3)_2][ClO_4]$

*Authors to whom correspondence should be addressed.

Table 1. ^{1}H (methyl) NMR and IR data for gold complexes

Compound	ν(CN)[a] (cm^{-1})	Doublets δ	Doublets ^2J(PH) (Hz)	Triplets δ	Triplets J(PH)[b] (Hz)
$[(PPh_3)Au(\mu\text{-}CN)IrCl_2(PMe_2Ph)_3][ClO_4]$[c] **(1a)**	2204	1.54	11.0	1.69	8.0
$[(PPh_3)Au(\mu\text{-}CN)RhCl_2(PMe_2Ph)_3][ClO_4]$[c] **(1b)**	2200	1.45	11.4	1.74	7.7
$[(PPh_3)Au(\mu\text{-}NC)IrCl_2(PMe_2Ph)_3][ClO_4]$[d] **(2a)**	2164	1.48	10.2	1.80	8.1
$[(PPh_3)Au(\mu\text{-}NC)RhCl_2(PMe_2Ph)_3][ClO_4]$[d] **(2b)**	2174	1.41	10.5	1.82	7.6
$[\{(PMe_2Ph)_3Cl_2Ir(\mu\text{-}NC)\}_2Au][ClO_4]$[c] **(3a)**	2188	1.40	11.1	1.74	8.1
$[\{(PMe_2Ph)_3Cl_2Rh(\mu\text{-}NC)\}_2Au][ClO_4]$[c] **(3b)**	2184	1.33	11.5	1.78	8.0
$[Au(CN)(PPh_3)]$	2146				

[a] In Nujol mull.
[b] $J(PH) = {}^2J(PH) + {}^4J(PH)$, separation of outer lines of triplet.
[c] NMR recorded in CD_2Cl_2 at 200 MHz.
[d] NMR recorded in $CDCl_3$ at 200 MHz.

(reported previously).[9] The attainment of equilibrium is accelerated if a 10% excess of $[Au(CN)(PPh_3)]$ is used; equilibrium then only takes a few minutes to be reached. Under these conditions a single broad ^{31}P NMR resonance for PPh_3 is observed at room temperature indicating PPh_3 exchange between $[(PPh_3)Au(\mu\text{-}CN)IrCl_2L_3]^+$ and $[Au(PPh_3)_2]^+$. At -80°C separate sharp signals are obtained. Likewise when PPh_3 (1 mol/mol Ir) is added to a solution of **(1a)**, a single broad ^{31}P NMR signal is observed for free and coordinated PPh_3, which are rapidly exchanging.

We do not know the mechanism of the slow equilibrium shown in Scheme 1. It could be that dissociation of $[Au(CN)(PPh_3)]$ from **(1a)** occurs and that this gold compound is in equilibrium with low concentrations of $[Au(CN)_2]^-$ and $[Au(PPh_3)_2]^+$. Coordination of $[Au(CN)_2]^-$ to Ir would then give complex **(3a)**. The catalysis by $[Au(CN)(PPh_3)]$ could be explained by the higher concentrations of $[Au(CN)_2]^-$ which are then present. Alternatively, exchange could occur with Au still linked to Ir, in which case the equilibrium in Scheme 1 corresponds with:

$$2[Au(CN)(PPh_3)] \rightleftharpoons [Au(PPh_3)_2]^+ + [Au(CN)_2]^-$$

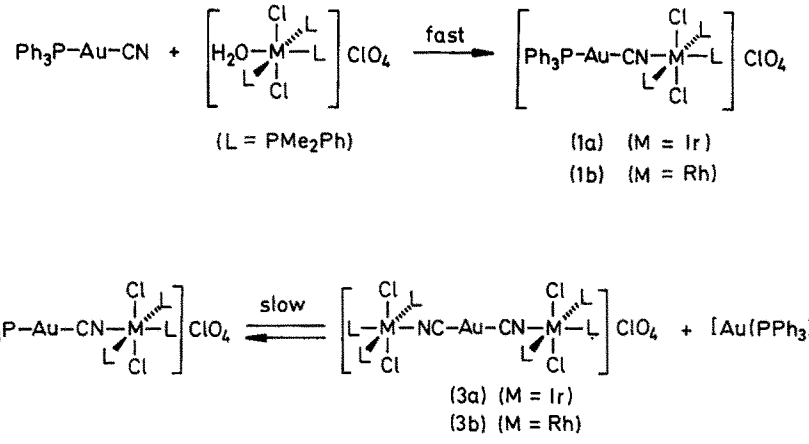

Scheme 1.

Table 2. ^{31}P and ^{13}C NMR data[a] for the gold complexes

Compound[b,c]	$\delta(P_t)$[d]	$J(RhP_t)$	$\delta(P_c)$[e]	$J(RhP_c)$	$J(P_cP_t)$	$\delta(P_{Au})$[f]	$\delta(C)$[g]	$^2J(CP)$	$^3J(PC)$
$[(PPh_3)Au(\mu\text{-}CN)IrCl_2L_3][ClO_4]$ **(1a)**	−196.8		−181.3		20.1	−103.5	162.3	132.7	13.3
$[(PPh_3)Au(\mu\text{-}NC)IrCl_2L_3][ClO_4]$ **(2a)**	−196.4		−186.7		23.7	−111.8			
$[(PPh_3)Au(\mu\text{-}CN)RhCl_2L_3][ClO_4]$ **(1b)**	−138.3	106.6	−146.3	80.6	28.2	−103.4	166.0	131.5	13.4
$[(PPh_3)Au(\mu\text{-}NC)RhCl_2L_3][ClO_4]$ **(2b)**	−155.1	85.7	−149.2	77.2	29.7	−111.9			
$[\{L_3Cl_2Ir(\mu\text{-}NC)\}_2Au][ClO_4]$ **(3a)**	−196.5		−182.0		20.0		155.2		14.9[h]
$[\{L_3Cl_2Rh(\mu\text{-}NC)\}_2Au][ClO_4]$ **(3b)**	−139.0	107.1	−147.1	80.8	28.2		159.1		15.0[h]
$[Au(CN)(PPh_3)]$						−101.8	155.1		
$[Au(PPh_3)_2][ClO_4]$						−96.1			

[a] $P(OMe)_3$ in C_6D_6 and TMS as references, respectively.
[b] L = PMe_2Ph.
[c] In CH_2Cl_2 (^{31}P) or CD_2Cl_2 (^{13}C).
[d] PMe_2Ph *trans* to C or N.
[e] PMe_2Ph *cis* to C or N.
[f] PPh_3.
[g] ^{13}CN signal.
[h] Separation of outer lines of the virtual triplets; $|^3J(CP)+{}^5J(CP)|$.
[i] Not observed since the signal is a broad singlet.

except that the cyanide ligands remain bridged to iridium atoms. However, if free $[L_3Cl_2Ir—NC]$ were generated at any stage in this process, one would expect this to convert readily to the carbon-bonded form $[L_3Cl_2Ir—CN]$ and there is no evidence for this with iridium.

A reaction between $[Au(CN)(PPh_3)]$ and $[RhCl_2(H_2O)L_3][ClO_4]$ (L = PMe_2Ph) similarly gave the simple dinuclear species $[(PPh_3)Au(\mu\text{-}CN)RhCl_2L_3][ClO_4]$, (**1b**) but disproportionation was more rapid, being complete within minutes, to give a mixture containing $[\{L_3Cl_2Rh(\mu\text{-}NC)\}_2Au][ClO_4]$, (**3b**). In the rhodium case, another very slow reaction followed this disproportionation. Cleavage of the Au—CN bonds occurs to give after several days, a solution also containing $[L_3Cl_2Rh(\mu\text{-}CN)RhCl_2L_3][ClO_4]$[5] in addition to the other complexes shown in Scheme 1.

We have evidence also for the isomers (**1a**) and (**1b**) with the CN orientations reversed. Thus the compounds $[MCl_2(CN)L_3]$ (M = Rh or Ir; L = PMe_2Ph) react with $[Au(PPh_3)][ClO_4]$, formed *in situ* by reaction of $[AuCl(PPh_3)]$ with $AgClO_4$ in methanol (Scheme 2). Precipitation with diethyl ether gave white crystals of $[(PPh_3)Au(\mu\text{-}CN)MCl_2L_3][ClO_4]$ (**2a**: M = Ir) and (**2b**: M = Rh), but these were contaminated with $[L_3Cl_2M(\mu\text{-}CN)MCl_2L_3L_3][ClO_4]$ (*ca* 5%). On leaving a $CDCl_3$ solution of (**2b**) to stand for several days, the ^1H NMR spectrum indicated that approximately equal amounts of $[L_3Cl_2Rh(\mu\text{-}CN)RhCl_2L_3][ClO_4]$. $[(PPh_3)Au(\mu\text{-}CN)RhCl_2L_3][ClO_4]$ (**1b**), and its isomer $[(PPh_3)Au(\mu\text{-}NC)RhCl_2L_3][ClO_4]$, (**2b**) were present.

Spectroscopic characterization of compounds

In spite of our difficulties in isolating analytically pure samples of compounds (**1**)–(**3**), we have very good evidence for their formulations and structures from the data in Tables 1 and 2. The ^1H and ^{31}P NMR data clearly indicate that the *mer*-configurations at Rh and Ir are maintained and that, whereas PPh_3 remains coordinated at Rh and Ir in compounds (**1**) and (**2**), it is lost in the formation of compounds (**3**). Notice in Table 2 that $^1J(RhP_t)$ is larger for PMe_2Ph *trans* to N (106.6 Hz) than for PMe_2Ph *trans* to C (85.7 Hz), consistent with the carbon atom of the bridging cyanide having a greater *trans*-influence than the nitrogen atom. An exactly comparable effect was observed for $[L_3Cl_2Rh(\mu\text{-}CN)RhCl_2L_3][ClO_4]$ for which $^1J(RhP_t)$ is 107.7 Hz when the PMe_2Ph ligand is *trans* to N but only 86.7 Hz when the ligand is *trans* to C of the bridging cyanide.[5]

The syntheses of ^{13}CN-enriched cyanide derivatives (90% enriched) has given very useful NMR data. As an example, Fig. 1 shows the ^{13}C NMR spectrum of a mixture of compounds (**1b**) and (**3b**) (each 90% isotopically-enriched at cyanide). The ^{13}C NMR spectrum of $[Au(CN)(PPh_3)]$ is a single broad peak with no observable coupling to phosphorus. Almost certainly this indicates that there is a rapid intermolecular exchange of cyanide or PPh_3, or both (see discussion in the synthetic section above). However, Fig. 1 shows well-resolved ^{31}P-coupling in the μ-CN compounds showing that exchange of this kind is slow in the cyanide-bridged complexes. Compound (**1b**) shows $^2J(PC)$ to PPh_3

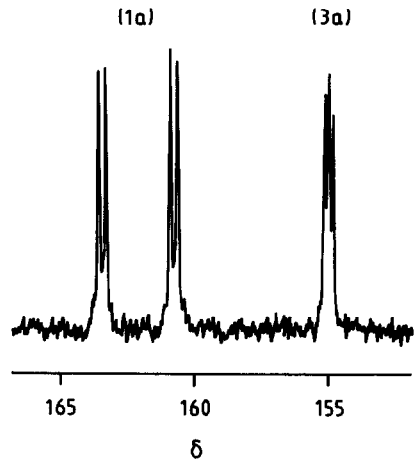

Fig. 1. $^{13}C\{^1H\}$ NMR spectrum of a dichloromethane solution containing $[(PPh_3)Au(\mu\text{-}^{13}CN)IrCl_2(PMe_2Ph)_3]^+$ (**1b**) and $[\{(PMe_2Ph)_3Cl_2Ir(\mu\text{-}N^{13}C)\}_2Au]^+$ (**3b**), each 90% isotopically enriched at the μ-cyanide ligand.

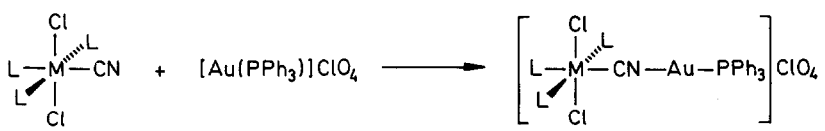

(M = Rh or Ir)

(2a) (M = Rh)
(2b) (M = Ir)

Scheme 2.

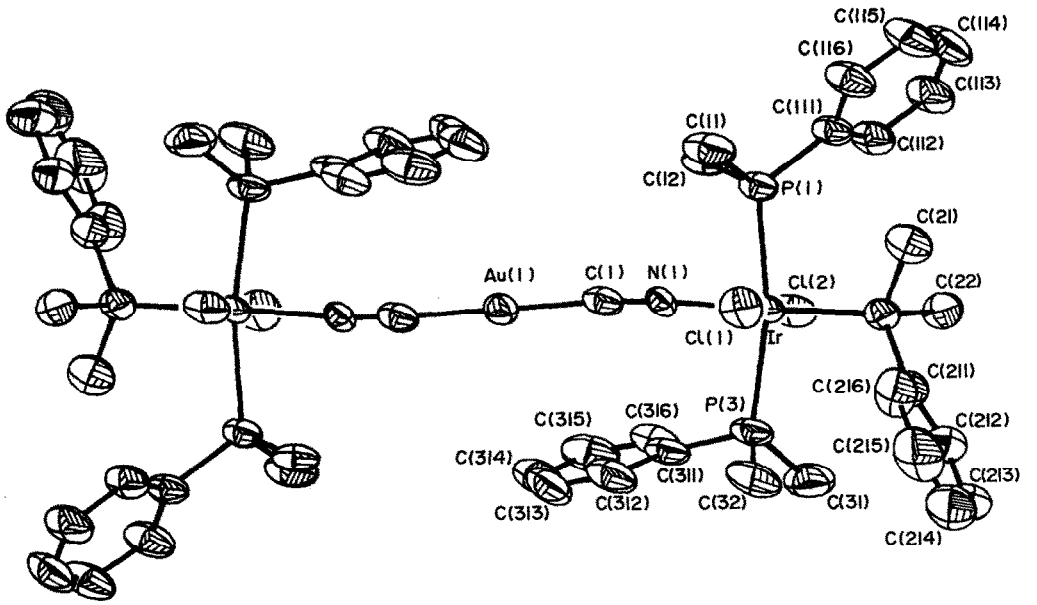

Fig. 2. Molecular structure of $[\{(PMe_2Ph)_3Cl_2(\mu\text{-}NC)\}_2Au]^+$. The gold atom lies at a centre of symmetry and only half of the atoms are labelled.

of 131.5 Hz and ^3J(PC) to PMe_2Ph (*trans*) of 13.4 Hz. In contrast, the large coupling between ^{13}C and PPh_3 is clearly absent from the ^{13}C signal for (**3b**). The triplet pattern for (**3b**) is an interesting case of *virtual coupling*. The magnitude of ^2J(CC′) is large enough to give a virtually coupled set of atoms (PCC′P′) where the P-atoms are those *trans* to the cyanide bridges.

Structure of compound (**3b**)

Conclusions from the above spectroscopic data were finally substantiated by a single-crystal X-ray structure determination for this compound. We had difficulties obtaining pure samples, but on one occasion the addition of diethyl ether to a dichloromethane solution of compounds (**1b**), (**3b**) and $[Au(PPh_3)_2][ClO_4]$, gave well-formed crystals of $[\{(PMe_2Ph)_3Cl_2Rh(\mu\text{-}NC)\}_2Au][ClO_4]\cdot 2CH_2Cl_2$ suitable for X-ray analysis. Selected bond lengths and angles are given in Table 3 and a view of the cation is shown in Fig. 2. The cation is centrosymmetric, with the Au atom at this centre. The two *mer*-arrangements are therefore eclipsed with the P—Rh—P directions parallel, which contrasts with the arrangement found for $[\{PMe_2Ph)_3$

Table 3. Selected bond lengths and angles for $[\{(PMe_2Ph)_3Cl_2Rh(\mu\text{-}NC)\}_2Au][ClO_4]\cdot 2CH_2Cl_2$, (**3b**)

	Bond lengths (Å)		
C(1)—Au(1)	2.000(8)	Cl(1)—Rh(1)	2.347(4)
Cl(2)—Rh(1)	2.348(4)	P(1)—Rh(1)	2.396(4)
P(2)—Rh(1)	2.301(4)	P(3)—Rh(1)	2.386(4)
N(1)—Rh(1)	2.080(7)	C(1)—N(1)	1.124(9)
	Bond angles (°)		
Cl(2)—Rh(1)—Cl(1)	179.7(1)	P(1)—Rh(1)—Cl(1)	92.3(2)
P(1)—Rh(1)—Cl(2)	88.0(2)	P(2)—Rh(1)—Cl(1)	87.2(2)
P(2)—Rh(1)—Cl(2)	92.7(2)	P(3)—Rh(1)—Cl(1)	91.5(2)
P(3)—Rh(1)—Cl(2)	88.2(2)	P(2)—Rh(1)—P(1)	97.4(2)
P(3)—Rh(1)—P(1)	166.9(1)	P(3)—Rh(1)—P(2)	95.3(2)
N(1)—Rh(1)—Cl(1)	88.3(3)	N(1)—Rh(1)—Cl(2)	91.8(3)
N(1)—Rh(1)—P(1)	81.2(3)	N(1)—Rh(1)—P(2)	175.2(2)
N(1)—Rh(1)—P(3)	86.5(3)	C(1)—N(1)—Rh(1)	174.3(7)
N(1)—C(1)—Au(1)	175.4(8)		

$Cl_2Ir\}_2(\mu\text{-}CN)][ClO_4]$ which is also eclipsed but with the P—Ir—P directions orthogonal.[5] The Rh—P bond *trans* to N [2.302(4) Å] is 0.09 Å shorter than the other two Rh—P bonds [2.396(4) and 2.386(4) Å]. The two cyanide bridges are approximately linear with angles of 175.4(8)° at carbon and 174.3(7)° at nitrogen. An unusual feature of the structure is that the phenyl ring on P(3) is oriented towards the centre of the cation and that on P(1) away from it. A more normal situation is found in $[IrCl_3(PMe_2Ph)_3]$[10] and in $[IrCl_2(H_2O)(PMe_2Ph)_3][ClO_4]$[2] for which there are conformations with the two mutually *trans* PMe_2Ph ligands having the phenyl groups *anti* as here but in a plane perpendicular to that in (**3a**).

Cation (**3a**) has a remarkably long linear chain of atoms (PRhNCAuCNRhP) but related chains have been proposed before. Reaction of $K[Cr(CN)(CO)_5]$ with $HgCl_2$ gives $(CO)_5Cr$—NC—Hg—CN—$Cr(CO)_5$ although the structure has not been established.[11] In this Cr/Hg example there is evidence for CN/NC orientation isomerism, whereas (**3a**) exists in only one isomeric form.

EXPERIMENTAL

CAUTION: We had no problem in the handling of the perchlorate complexes but **there is always a risk of explosion with such compounds.** $[Au(CN)(PPh_3)]$ has been prepared from gold cyanide and triphenylphosphine,[6] or from $[Au(MeCO_2)(PPh_3)]$ and HCN,[7] but we have used the method given below. Likewise we report a modified synthesis of $[Au(PPh_3)_2][ClO_4]$.[9] The syntheses of $[MCl_2(H_2O)(PMe_2Ph)_3][ClO_4]$ (M = Rh or Ir) have been reported earlier.[2,12] $K^{13}CN$ (90% ^{13}C) was obtained from Amersham International. ^1H, $^{31}P\{^1H\}$ and $^{13}C\{^1H\}$ NMR spectra were recorded on a Varian XL200 spectrometer, and IR spectra were of Nujol mulls of solid mixtures formed by removal of the solvent and were obtained on a Perkin–Elmer PE983 spectrometer.

Synthesis of $[Au(CN)(PPh_3)]$

A solution of $[AuCl(PPh_3)]$[13] (0.278 g) and KCN (0.037 g) in dichloromethane (15 cm^3) and methanol (30 cm^3) was refluxed for 20 min. The solution was filtered and reduced to 30 cm^3 to give the product as white needles (0.165 g). The ^{13}CN analogue (90% ^{13}C-enriched) was prepared similarly.

Synthesis of $[Au(PPh_3)_2][ClO_4]$

Silver perchlorate (0.052 g) in methanol (2 cm^3) was added to a solution of $[AuCl(PPh_3)]$ (0.121 g) in THF (25 cm^3). The AgCl was filtered off and PPh_3 (0.065 g) in THF (2 cm^3) added. Removal of the solvent and recrystallization of the residue from a CH_2Cl_2/Et_2O mixture gave the product as white needles (0.103 g).

Reaction of $[Au(CN)(PPh_3)]$ *with* $[MCl_2(H_2O)(PMe_2Ph)_3][ClO_4]$

Solutions were prepared containing accurate equimolar amounts of $[Au(CN)(PPh_3)]$ and $[MCl_2(H_2O)(PMe_2Ph)_3][ClO_4]$ (M = Rh or Ir) (*ca* 0.1 mmol each) in dichloromethane (0.5–2.0 cm^3) and the formation of $[(PPh_3)Au(\mu\text{-}CN)MCl_2(PMe_2Ph)_3][ClO_4]$ was followed by ^1H, ^{13}C and ^{31}P NMR spectroscopy. Spectra were recorded periodically over several days. Attempts to isolate products gave impure materials in general. IR spectra are of Nujol mulls of solids formed by removal of the solvent. In one case, addition of diethylether to a dichloromethane solution of $[RhCl_2(H_2O)(PMe_2Ph)_3][ClO_4]$ and $[Au(CN)(PPh_3)]$, after the NMR spectra had confirmed the formation of $[\{(PMe_2Ph)_3Cl_2Rh(\mu\text{-}NC)\}_2Au][ClO_4]$ (**3b**), gave well-formed crystals of this compound which were used in the single-crystal X-ray study and to determine the value of $\nu(CN)$ for (**3b**) which may be compared with that for (**1b**).

Reaction of $[RhCl_2(CN)(PMe_2Ph)_3]$ *with* $[Au(PPh_3)]^+$

Silver perchlorate (0.019 g) in methanol (2 cm^3) was added to a solution of $[AuCl(PPh_3)]$ (0.043 g) in THF (10 cm^3). The AgCl was filtered off and the filtrate added dropwise to a solution of $[RhCl(CN)(PMe_2Ph)_3]$ (0.053 g) in THF (10 cm^3). The solvent was removed to give a yellow solid which was recrystallized from CH_2Cl_2/diethylether mixtures. The ^1H NMR spectrum confirmed the presence of (**2b**), but this was not totally pure (see Discussion). The iridium compound was prepared similarly.

Single-crystal X-ray structure determination for $[\{(PMe_2Ph)_3Cl_2Rh(\mu\text{-}NC)\}_2Au][ClO_4]\cdot 2CH_2Cl_2$

The crystal used for the X-ray study was sealed in a thin-walled glass capillary. All crystallographic measurements were made at 293 ± 2 K using a CAD4 diffractometer operating in the ω-2θ scan mode with graphite monochromated Mo-K_α radiation ($\lambda = 0.71069$ Å) as previously described.[14] The structure was solved via the heavy atom method and refined using full-matrix least squares. Non-hydrogen atoms were refined anisotropically, phenyl hydrogen atoms freely isotropically, but

methyl hydrogen atoms were refined as components of rigid CH_3 fragments with group U_{iso} values. The perchlorate ion is sited on a centre of symmetry and is disordered, with two related orientations of the four oxygen atoms.

Crystal data

$C_{52}H_{70}AuCl_9N_2O_4P_6Rh_2$, $M_r = 1694.8$, triclinic, $a = 9.426(2)$, $b = 12.852(3)$, $c = 15.653(3)$ Å, $\alpha = 101.33(2)$, $\beta = 104.10(1)$, $\gamma = 103.42(2)°$, $U = 1690.47$ Å^3, space group $P\bar{1}$, $Z = 1$, $D_c = 1.66$ g cm^3, μ(Mo-K_α) = 30.14 cm^{-1}, F(000) = 840. Total data recorded 6161 ($1.5 \leqslant \theta \leqslant 25°$), unique 5924, observed [$I > 1.5\sigma(I)$] 4759. Corrected for absorption empirically. Final $R = 0.054$, $R_\omega = 0.074$, 448 parameters, $\omega = [\sigma^2(F_0) + 0.00035 F_0^2]^{-1}$. Final atomic coordinates, displacement factor coefficients, full lists of bond lengths and angles and F_0/F_c values have been deposited as supplementary material with the Editor, from whom copies can be obtained.*

Acknowledgements—We thank the S.E.R.C. for a studentship (for G.P.P.) and for support of the crystallographic work and Johnson Matthey plc for loans of rhodium trichloride and chloroiridic acid.

*Atomic coordinates have also been deposited with the Cambridge Crystallographic Data Base.

REFERENCES

1. A. J. Deeming and G. P. Proud, *Inorg. Chim. Acta*, 1985, **100**, 223.
2. A. J. Deeming, G. P. Proud, H. M. Dawes and M. B. Hursthouse, *J. Chem. Soc., Dalton Trans.* 1986, 2545.
3. K. Swaminathan and G. M. Harris, *J. Am. Chem. Soc.* 1966, **88**, 4411; W. Plumb and G. M. Harris, *Inorg. Chem.* 1964, **3**, 542.
4. S. E. Castillo-Blum and A. G. Sykes, *Polyhedron* 1987, **6**, 101.
5. A. J. Deeming, G. P. Proud, H. M. Dawes and M. B. Hursthouse, *J. Chem. Soc., Dalton Trans.*, in press.
6. F. Cariarti, D. Galizziolo and L. Naldini, *Chim. Inds (Milan)* 1970, **52**, 995.
7. D. I. Nichols and A. S. Charleston, *J. Chem. Soc. (A)* 1969, 2581.
8. P. L. Bellon, M. Manassero and M. Sansoni, *Ric. Sci.* 1969, **93**, 173.
9. L. Naldini, L. Malatesta, F. Cariati and G. Simonetta, *Coord. Chem. Rev.* 1966, **1**, 255.
10. G. B. Robertson and P. A. Tucker, *Acta Cryst. Sect. B* 1981, **37**, 814.
11. M. Höfler, W. Jung, M. Scobel and J. Rademacher, *Chem. Ber.* 1986, **119**, 3268.
12. H. C. Clark and K. J. Reimer, *Inorg. Chem.* 1975, **14**, 2133.
13. C. A. McAuliffe, R. V. Parish and P. D. Randall, *J. Chem. Soc., Dalton Trans.* 1972, 1730.
14. M. B. Hursthouse, R. A. Jones, K. M. A. Malik and G. Wilkinson, *J. Am. Chem. Soc.* 1979, **101**, 4128.

Polyhedron Vol. 7, No. 8, pp. 659–664, 1988
Printed in Great Britain

0277–5387/88 $3.00 + .00
© 1988 Pergamon Press plc

SPECTROCHEMICAL STUDIES ON THE 4,6-DIAMINE-2-METHYLTHIO-5-NITROSO PYRIMIDINE COMPLEXES OF Pd(II), Pt(II), Ag(I), Au(III), Cd(II) AND Hg(II)

M. A. ROMERO,* J. M. SALAS, R. LÓPEZ and M. D. GUTIÉRREZ

Departamento de Química Inorgánica, Universidad de Granada, 18071 Granada, Spain

(*Received* 25 *June* 1987; *accepted* 16 *December* 1987)

Abstract—The Pd(II), Pt(II), Ag(I), Au(III), Cd(II) and Hg(II) complexes of 4,6-diamine-2-methylthio-5-nitroso pyrimidine (H_2DAMTNP) have been prepared and investigated by IR, ^{1}H NMR and magnetic methods: $M(H_2DAMTNP)_2X_2$ (M = Hg, X = Cl; M = Pd, X = Br; M = Pt, X = Cl, Br), $Cd(H_2DAMTNP)Cl_2$, Pd(HDAMTNP)Cl, Au(DAMTNP)Cl and Ag(HDAMTNP)·H_2O. The ligand is S-coordinated to the metal in Cd(II) and Pt(II) complexes; for the remaining complexes IR spectra suggest coordination involving N,S-chelation of the ligand through the ring nitrogen atom and exocyclic sulphur atom. Metal halogen coordination has been assigned on the basis of the position of ν(M—X) in the far-IR spectra. From DSC and TG curves, the thermal behaviour of these complexes has been deduced.

The stimulus for much of the research into the coordination chemistry of heterocyclic thione donors stems from the wide range of applications of the complexes of such ligands, mainly those derived from their biological activity.[1] Medical-biological bacteriostatic activity has been related to coordination ability of some thione imidazoline and thiazoline derivatives,[2] and zinc pyridine thione has a bacteriostatic activity.[3] Other thione derivatives have thyrotoxic[4] or anticonvulsant activities or central nervous system depressant capacity.[5] Finally, carcinostatic activity of some of their heavy metal complexes has been reported[6] and a platinum pyridine thione complex has been patented for use in cancer treatment.[7]

Among the heterocyclic derivatives with sulphur in their molecules, the thiopyrimidine derivatives are very important because of their wide biological activity. Some of these derivatives can act as inhibitors[8–9] and antimetabolites.[10–11] 2-Thiopyrimidine shows a strong *in vitro* bacteriostatic activity on *E. Coli*.[12] Likewise 6-amino-2-thiouracile is well known because of its antiviral[13] and chemitherapeutic activities.[13–15] On the other hand, in many cases it seems probable that there is intervention of complex formation processes in the biological action mechanism of these pyrimidine derivatives.[16]

In the last few years we have published some papers concerning the study of metal complex formation of several 2-methylthiopyrimidine derivatives.[17–25] Most recently the X-ray study of a Cd(II) complex with 4,6-diamino-1,2-dihydro-2-thiopyrimidine has been published.[26] As a continuance of these works, in the present paper we report the synthesis and study of eight new complexes, formed by the reactions between Cd(II), Hg(II), Pd(II), Pt(II), Ag(I) and Au(III) and 4,6-diamino-2-methylthio-5-nitroso pyrimidine (H_2DAMTNP).

EXPERIMENTAL

Methods

The pyrimidine derivative, H_2DAMTNP, was prepared following a previously reported method[27] using analytical reagent grade chemicals.

The complexes were prepared as follows: 1.1 mmol of H_2DAMTNP was dissolved in the minimum amount of water (ethanol was used for the preparation of the Cd(II) complex) at 40°C. Then an aqueous solution of the corresponding metallic salt was added ($AgNO_3$, Cd(II) and Hg(II) chlor-

* Author to whom correspondence should be addressed.

ides and the sodium tetrachloride or tetrabromide complex salts in the cases of Pt(II), Pd(II) and Au(III) ions) in such a way that the metal/ligand ratios were 1/1 in all cases except for the Cd(II)/H_2DAMTNP and Hg(II)/H_2DAMTNP systems in which the former was equal to 3/1. The complexes precipitated almost immediately except for the Cd(II) complex which precipitated after evaporation at room temperature for three days.

The complexes were filtered off, washed consecutively with ethanol and diethylether and dried over P_4O_{10}.

Apparatus

Chemical analyses of C, H and N were made in the Instituto de Química Bioorgánica (C.S.I.C.), Barcelona.

The determination of metal ions in each complex was carried out as follows: Ag(I) by the Volhard method; Cd(II) and Hg(II) by atomic absorption spectrophotometry; Pd(II) using dimethylglyoxime as the titrating agent; Pt(II) and Au(III) were determined from the residues of the samples used for TG analyses.

Ir spectra were obtained from KBr (4000–180 cm^{-1} range) and polyethylene pellets (600–180 cm^{-1} range) using a Perkin–Elmer 983G spectrophotometer. ^{1}H NMR spectra were recorded on a Hitachi Perkin–Elmer R-600 FT-NMR using DMSO-d_6 and D_2O as solvents, and TMS as internal standard. The UV–vis. spectra were recorded in a Baush Lomb, Spectronic 2000 spectrophotometer from DMSO (visible) and water (UV) solutions. Magnetic susceptibilities at room temperature were determined using a Faraday Bruker Magnet B-E15 with a field intensity of 30.1 A and $HgCo(NCS)_4$ as the standard.

RESULTS AND DISCUSSION

The compound used as the ligand, H_2DAMTNP, can exist in aqueous solution either as nitroso–amino or imino–oxime in the main tautomeric forms (Scheme 1).

The UV–vis. spectrum of the thiopyrimidine derivative shows three bands; the first; at 632 nm, is assigned to the NO chromophore group and the remaining two, at 345 nm and 300 nm, correspond to $\pi \rightarrow \pi^*$ transitions.[28]

The pK_a and pK_b values are in the same range as those found by other authors for some salycylaldoxime derivatives[29] and some 5-nitroso-6-oxo-pyrimidine derivatives.[30–32] The very low K_a value for the compound studied here ($pK_a \simeq 12$), can be explained on the basis of the strong basic character of the N atoms of the NH_2 groups, which are in adjacent positions to the nitroso group.

The ^{1}H NMR spectrum of H_2DAMTNP shows five signals at 2.5; 8.0 (H_C); 8.4 (H_A); 9.0 (H_B) and 10.2 (H_D) ppm. The first (2.5 ppm) is assigned as the S—CH_3 group (three H) and the remaining four (one H each) to the four hydrogen NH_2 atoms. The difference in the chemical shift values corresponding to the signals of these four atoms point out the different magnetic environments. These can be explained by the hydrogen bridge intramolecular interaction shown in Scheme 2.

The analytical data and colours together with proposed formulae for the eight new complexes are given in Table 1. The ^{1}H NMR spectral data of the ligand and some of its complexes are summarized in Table 2. ^{1}H NMR spectra of Hg(II), Pd(II) and Au(III) complexes could not be obtained because of their insolubility in common organic solvents.

The signals corresponding to the NH_2 groups of the complexes are at values practically equal to those of the free ligand, which confirms that the hydrogen atoms of such groups are magnetically different.

In the ^{1}H NMR spectra of the DMSO soluble complexes, the signals corresponding to the NH_2 groups appear practically at the same chemical shifts as in ^{1}H NMR of the free ligand which also confirms the existence of hydrogen bonds between NH_2 and NO groups and the non-participation of these groups in metal coordination.

Concerning the S—CH_3 signals, these appeared slightly shifted to lower field values in the case of the $Pd(H_2DAMTNP)_2Br_2$ complex and were also split (a main signal and a satellite) in both Pt(II) complexes. These facts prove the intervention of the S atom in the coordination of the S—CH_3 group in the three former complexes. Finally, the ^{1}H NMR

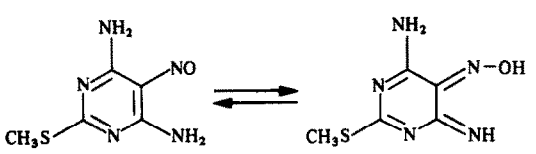

Scheme 1.

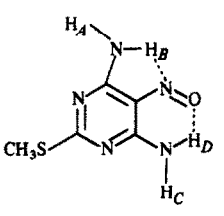

Scheme 2.

Table 1. Analytical data, found % (calc. %), of the isolated complexes

Compound	Colour	C(%)	H(%)	N(%)	X(%)	M(%)
$Cd(H_2DAMTNP)Cl_2$	Pink	16.3	1.8	18.3	19.8	31.2
		(16.3)	(1.9)	(19.0)	(19.3)	(30.5)
$Hg(H_2DAMTNP)_2Cl_2$	Green	18.7	1.6	20.0		33.0
		(18.7)	(2.2)	(21.8)	(11.1)	(31.3)
Pd(HDAMTNP)Cl	Brown	18.4	1.9	22.0		31.8
		(18.4)	(1.8)	(21.5)	(10.9)	(32.6)
$Pd(H_2DAMTNP)_2Br_2$	Brown	19.1	1.9	22.5		18.5
		(18.9)	(2.2)	(22.0)	(25.1)	(16.7)
$Pt(H_2DAMTNP)_2Cl_2$	Brown	18.3	2.1	19.7		31.3
		(18.9)	(2.2)	(22.0)	(11.2)	(30.7)
$Pt(H_2DAMTNP)_2Br_2$	Brown	15.6	1.9	18.5		28.4
		(16.6)	(1.9)	(19.3)	(22.0)	(26.9)
$Ag(HDAMTNP)\cdot H_2O$	Dark green	19.0	2.2	21.8		34.0
		(19.4)	(2.6)	(22.6)		(34.8)
Au(DAMTNP)Cl	Brown	14.2	1.2	15.8	8.8	48.7
		(14.4)	(1.2)	(16.8)	(8.5)	(47.4)

spectrum of the $Ag(HDAMTNP)\cdot H_2O$ exhibits a signal at 3.3 ppm due to the water of hydration of the complex.

The most significant IR data of the ligand and complexes are summarized in Table 3. The corresponding assignments have been made from literature data concerning both 2-thiopyrimidine derivatives[33–35] of their metal complexes.[36] Concerning the ν(N=O) band, this appears in all the complexes (except in the Au(DAMTNP)Cl complex) at the same or at a higher wavenumber value than in the IR spectrum of the free H_2DAMTNP. This fact points to the lack of participation of the nitroso group in coordination, which is in accordance with the ^{1}H NMR data. In the IR spectrum of Au(DAMTNP)Cl, this band disappears; nevertheless a new strong band at 1280 cm^{-1} assigned as the $\nu(=\overset{(-)}{N}-O)$ nitrone group[37–38] suggests that the said NO group is involved in coordination through its N atom.

On the other hand, the ν(C=C)+ν(C=N) double band which appears at 1540 cm^{-1} in the free ligand spectrum is strongly split into two in the IR spectra of the three complexes in which the ligand acts as monoanion or dianion, suggesting the participation of the cyclic N atom in coordination to the metal ions. The same feature is also observed in the IR spectra of $Hg(H_2DAMTNP)_2Cl_2$ and $Pd(H_2DAMTNP)_2Br_2$ complexes, suggesting that in both complexes the cyclic N atom is a coordination position. On the contrary to the above, the bands due to δ(N—H) and ν(C=C)+ν(C=N) in the IR spectra of the $Cd(H_2DAMTNP)Cl_2$, $Pt(H_2DAMTNP)_2Cl_2$ and $Pt(H_2DAMTNP)_2Br_2$ complexes appear at a position similar to that of the free ligand, suggesting the non-intervention of the cyclic N atoms in the coordination of such complexes.

Besides, the above IR data, in the low frequency range, Hg(II), Pt(II)–chlorine, Pt(II)–bromine and

Table 2. ^{1}H NMR data[a] (δ, ppm)[b]

Compound	H_2O	S—CH_3	—NH_2			
H_2DAMTNP	—	2.50	8.0	8.4	9.0	10.2
$Cd(H_2DAMTNP)Cl_2$	—	2.50	8.0	8.4	9.0	10.2
$Pd(H_2DAMTNP)_2Br_2$	—	2.65	8.7	9.1	9.3	9.9
$Pt(H_2DAMTNP)_2Cl_2$	—	2.50[c]	8.0	9.1	10.0	10.3
$Pt(H_2DAMTNP)_2Br_2$	—	2.60[c]	8.1	9.1	9.9	10.3
$Ag(HDAMTNP)\cdot H_2O$	3.3	2.50	7.9	8.4	8.8	—

[a] Solvent DMSO-d_6.
[b] Relative to TMS.
[c] Doublet.

Table 3. IR data for DAMTNP and its isolated complexes (cm^{-1})

Compound	ν(N—H)	δ(N—H)	ν(C=C)+ ν(C=N)	ν(N=O)	ν(=N—O)	ν(M—N)	ν(M—X)
H_2DAMTNP	3380 3310 3210 3040	1635	1540 d	1465	—	—	—
Cd(H_2DAMTNP)Cl_2	3380 3315 3210	1645	1545 d	1465	—	—	217 182
Hg(H_2DAMTNP)$_2Cl_2$	3400 b 3120	1620	1560 sh 1525 1500 sh	1470	—	—	345
Pd(HDAMTNP)Cl	3300 b	1620	1570 b 1520	1485	—	—	320 b
Pd(H_2DAMTNP)$_2Br_2$	3280 b	1611 sh	1569 1522	1488	—	—	—
Pt(H_2DAMTNP)$_2Cl_2$	3440 3370 3320	1615 sh	1545	1470	—	—	330
Pt(H_2DAMTNP)$_2Br_2$	3380 3280 3210	1609 sh	1547	1470	—	—	232
Ag(HDAMTNP)·H_2O	3290 b 3190b	1620	1540 b 1500	1470	—	345	—
Au(DAMTNP)Cl	3300 b	—	1610 sh 1570 1515	—	1280	—	327

d = double band; sh = shoulder; b = broad.

Au(III) complexes show a ν(M—X) (where X = Cl, Br), stretching vibration band. This proves that the halogen atoms are coordinated to the above cited metal ions. Likewise, the chloride ion is coordinated in the Pd(HDAMTNP)Cl complex, nevertheless the nature and position of the ν(Pd—Cl) band point out the existence of chlorine acting as a bridge between two Pd(II) ions.[39]

Finally, the Cd(H_2DAMTNP)Cl_2 complex shows two new bands at 217 and 182 cm^{-1}, very similar to those found in the IR spectrum of Cd(H_2DATP)Cl_2·H_2O[26] where there was one bridging chlorine and another terminal.

From the above considerations it is proposed that a distorted octahedral arrangement of two H_2DAMTNP molecules and two chloride ions in *trans* positions around the Hg(II) ions is probable in the case of the Hg(H_2DAMTNP)$_2Cl_2$ complex.

The five Pd(II), Pt(II) and Au(III) complexes are diamagnetic, suggesting square-planar four coordination of these metals. The two Pt(II) complexes show the halogen atoms coordinated in *trans* positions, whereas in the case of the Pd(H_2DAMTNP)$_2Br_2$ complex the bromide ions are probably uncoordinated. On the other hand, the Pd(HDAMTNP)Cl complex probably has a dimeric structure in which two chlorine ions act as bridging ligands between two Pd atoms.

The whole data concerning the Ag(HDAMTNP)·H_2O complex are compatible with a chain polymeric structure, where N(1) and N(3) atoms should be the coordination positions. Finally, it is suggested that the Au(III) complex probably has a chain structure (viz. Scheme 3).

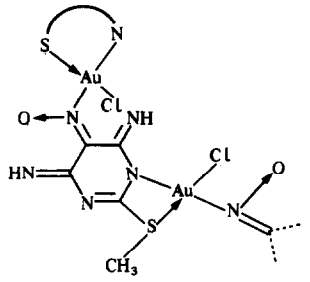

Scheme 3.

Table 4. Decomposition temperatures and DSC data for DAMTNP and its isolated complexes

	Temperature range of pyrolysis, TG (°C)	DSC peak temperatures (°C)	ΔH (kJ mol^{-1})	Wt loss (%) Found	Wt loss (%) Calc.	Residue
H_2DAMTNP	220–680	263(exo)	−122.0	—	—	—
		400(exo), 450(exo)	—	—	—	—
$Cd(H_2DAMTNP)Cl_2$	200–700	250(exo), 294(exo)	−84.9	82.3	66.5	CdO
		482(exo)	—			
$Hg(H_2DAMTNP)_2Cl_2$	220–625	280(exo), 370(exo)	—	—	—	—
Pd(HDAMTNP)Cl	220–420	340(exo), 422(exo)	−1829.6	62.4	62.4	PdO
$Pd(H_2DAMTNP)_2Br_2$	220–550	340(exo), > 420(exo)	—	78.7	80.8	PdO
$Pt(H_2DAMTNP)_2Cl_2$	220–800	320(exo), 480(exo)	—	68.7	69.3	Pt
$Pt(H_2DAMTNP)_2Br_2$	220–650	270(exo), 310(exo), > 440(exo)	—	71.6	73.1	Pt
Ag(HDAMTNP)·H_2O	40–150	88.0(endo)	23.2	6.1	5.8	Ag(HDAMTNP)
	150–750	197(exo), 220(exo)	−118.8	59.9	59.4	Ag
Au(DAMTNP)Cl	220–650	220(exo), 240(exo)	—	51.3	52.6	Au

In the $Cd(H_2DAMTNP)_2Cl_2$ complex the absence of Cd—N cyclic interactions is opposite to a probable tetrahedral monomeric structure with the H_2DAMTNP S,N(cyclic) coordinated. Thus a chain structure is suggested with a tetrahedral arrangement of the ligands; three chloride ions coordinated to the central ion with just two of them acting as a bridge between two Cd(II) ions, in a similar way to that found in the case of the $Cd(H_2DATP)Cl_2 \cdot H_2O$ complex[26] (where H_2DATP = 4,6-diamine-1,2-dihydre-2-thiopyrimidine).

Thermal data of the ligand and complexes obtained from the corresponding TG and DSC curves are summarized in Table 4. These data confirm the anhydrous character of all the complexes except for Ag(HDAMTNP)·H_2O which loses a water molecule in the 40–150°C temperature range; the low energy calculated from the corresponding area of the endothermic effect was 23.2 kJ mol^{-1}; this value is indicative of a weak interaction between the water molecule and the ligand.

TG curves of the complexes are very similar to that of H_2DAMTNP proving that pyrolytic decomposition starts with the organic ligand H_2DAMTNP, at the temperature values given in Table 4. These values are lower for Cd(II) and Ag(I) complexes than for the organic ligand (220°C) which indicates that the coordination of H_2DAMTNP to the said metal ions implies the weakness of some of the bonds in the H_2DAMTNP molecule. On the other hand, dehalogenation processes overlap with those corresponding to the pyrolysis of the ligand. Moreover, the absence of stable intermediate species also prevents us from proposing a tentative pyrolytic decomposition mechanism for the complexes.

The final residues of pyrolytic decomposition of the complexes were characterized by IR spectroscopy; they are summarized in Table 4. In the case of the $Cd(H_2DAMTNP)Cl_2$ complex the final residue (CdO) (17.7%) is much lower than that calculated (33.49%), due to the partial sublimation of $CdCl_2$ in the 575–725°C temperature range.[40] Likewise, the absence of a final residue in the pyrolysis of the $Hg(H_2DAMTNP)_2Cl_2$ complex is due to the sublimation of $HgCl_2$. In the remaining six complexes, the calculated and found residue values are in good agreement.

REFERENCES

1. E. S. Raper, *Coord. Chem. Rev.* 1985, **61**, 115.
2. W. O. Foye and J. R. Lo, *J. Pharm. Sci.* 1972, **61**, 1209.
3. United States Patent: US3590035 (710629), British

Patent: GB1202716 (700819), French Patent: FR1506349 (671222).
4. Martindate Extra Pharmacopoeia. 27th Edn. Pharmaceutical Press, London (1972).
5. H. Kohn, B. A. Kohn, M. L. Steenberg and J. P. Buckley, *J. Med. Chem.* 1977, **20**, 158.
6. J. Dehand, J. Jordanov and J. P. Beck, *Chem-Biol. Interactions* 1975, **11**, 605.
7. Japanese Patent: JP8061522 (800509).
8. E. B. Astwood, A. Bissell and A. M. Hughes, *Endocrinology* 1945, **37**, 456.
9. R. K. Robins, *J. Med. Chem.* 1964, **7**, 186.
10. R. Hamers and C. Hamer Casterman, *J. Mol. Biol.* 1972, **3**, 166.
11. W. R. Trotter, *Nature* 1949, **164**, 63.
12. A. Holy, I. Votruba and K. Jost, *Coll. Czech. Chem. Commun.* 1974, **39**, 634.
13. V. N. Krishna Murthy, K. V. Nageswara Rao, P. L. Narasimha Rao and B. Praphulla, *Br. J. Pharmacol. Chemother.* 1967, **31**, 1.
14. R. Truhaut and M. Declercq, *Rev. Ranc. Etudes Clin. Biol.* 1962, **7**, 68.
15. R. H. Lindsay, H. Nakagawa and P. Philipcohen, *Endocrinology* 1965, **76**, 728.
16. D. H. Petering, W. E. Autholine and L. A. Saryan, Metal complexes as antitumor agents in *Anticancer and Interferon Agents*, Vol. 24, Chap. 7. M. Dekker, New York (1984).
17. C. Valenzuela-Calahorro, J. D. López-González, R. López-Garzón and M. Melgarejo-Sampedro, *An. Quím.* 1981, **77B**, 143.
18. C. Valenzuela-Calahorro, J. D. López-González and R. López-Garzón, *An. Quím.* 1982, **78B**, 184; C. Valenzuela-Calahorro, J. D. López-González and R. López-Garzón, *Rev. Acad. Cien. Gran.* 1983, **2**, 123; C. Valenzuela-Calahorro, J. D. López-González and R. López-Garzón, *An. Quím.* 1983, **79B**, 467.
19. M. P. Sánchez-Sánchez, J. M. Salas-Peregrín, M. A. Romero-Molina and E. Colacio-Rodríguez, *Thermochim. Acta* 1985, **89**, 165.
20. M. P. Sánchez-Sánchez, J. M. Salas-Peregrín, M. A. Romero-Molina and J. Ruiz-Sánchez, *Thermal. Anal.* 1986, **31**, 573.
21. J. M. Salas-Peregrín, M. A. Romero-Molina, E. Colacio-Rodríguez and R. López-Garzón, *An. Quím.* 1984, **80B**, 465.
22. A. M. Martinez-Garzón, R. López-Garzón and M. N. Moreno-Carretero, *Thermochim. Acta* 1984, **80**, 143.
23. M. N. Moreno-Carretero, A. M. Martinez-Garzón, R. López-Garzón and J. M. Salas-Peregrín, *Rev. Chim. Minér.* 1985, **22**, 369.
24. R. López-Garzón, M. D. Gutiérrez-Valero, M. Nogueras-Montiel, A. Sánchez-Rodrigo and C. Valenzuela-Calahorro, *C. Monatsh. Chem.* 1986, **117**, 905.
25. R. López-Garzón, A. M. Martinez-Garzón, M. D. Gutiérrez-Valero and M. Domingo-Garcia, *Thermochim. Acta* 1986, **108**, 181.
26. M. A. Romero-Molina, M. D. Gutiérrez-Valero, R. López-Garzón and J. M. Salas-Peregrín, *Inorg. Chim. Acta* 1987, **136**, 87.
27. J. Baddiley, B. Lithgoe, D. McNeil and A. R. Todd, *J. Chem. Soc.* 1943, 383.
28. D. J. Pasto and C. R. Johnson, *Determinación de Estructuras Orgánicas*, p. 109. Reverté, Barcelona (1974).
29. K. Burger and I. Egyed, *J. Inorg. Nucl. Chem.* 1965, **27**, 2361.
30. C. Valenzuela, J. M. Salas and J. D. López González, *An. Quim.* 1980, **76B**, 197.
31. J. M. Salas-Peregrín, Tesis Doctoral Universidad de Granada (1979).
32. M. P. Sánchez-Sánchez, Tesis Doctoral Universidad de Granada (1984).
33. M. Gupta and M. N. Srivastova, *Polyhedron* 1985, **4**, 475.
34. E. Spinner, *J. Chem. Soc.* 1960, 1237.
35. Z. Shunmugan and D. N. Sathyanarayana, *Bull. Soc. Chim. Belg.* 1983, **92**, 11; Z. Shunmugan and D. N. Sathyanarayana, *Bull. Soc. Chim. Belg.* 1984, **93**, 2.
36. R. Battiztuzzi and G. Peyronel, *Spectrochim. Acta* 1980, **36A**, 113; R. Battiztuzzi and G. Peyronel, *Transition Met. Chem.* 1978, **3**, 345; R. Battiztuzzi and G. Peyronel, *Can. J. Chem.* 1981, **59**, 591.
37. C. Natarajan and A. N. Hussain, *Transition Met. Chem.* 1984, **9**, 18.
38. G. S. Sanyal and A. B. Modak, *Synth. React. Inorg. Met. Org. Chem.* 1986, **16**, 113.
39. J. R. Ferraro, *Low-Frequency Vibrations of Inorganic and Coordination Compounds*. Plenum Press, New York (1971).
40. F. A. Cotton and G. Wilkinson, *Química Inorgánica Avanzada*, 4ª Edn. Limusa, Mexico (1986).

Polyhedron Vol. 7, No. 8, pp. 665–668, 1988
Printed in Great Britain

0277–5387/88 $3.00+.00
© 1988 Pergamon Press plc

COMMUNICATION

CHARACTERIZATION OF THE BIS(PYRIDINE) COMPLEX OF THE BUTYLLITHIUM–PYRIDINE ADDUCT, 2-Bu^n(C_5H_5N)Li·(C_5H_5N)$_2$; ITS DECOMPOSITION TO 2-BUTYLPYRIDINE VIA A DIHYDROPYRIDINE

DONALD BARR and RONALD SNAITH*

University Chemical Laboratory, Lensfield Road, Cambridge CB2 1EW, U.K.

ROBERT E. MULVEY

Department of Pure & Applied Chemistry, University of Strathclyde, Glasgow G1 1XL, U.K.

and

DAVID REED

Department of Chemistry, University of Edinburgh, Edinburgh EH9 3JJ, U.K.

(*Received* 1 *December* 1987; *accepted* 18 *December* 1987)

Abstract—The complexed adduct, 2-Bu^n(C_5H_5N)Li·(C_5H_5N)$_2$, (**3**), synthesized by reaction of Bu^{n}Li with a three-fold excess of pyridine, has been characterized. ^{1}H NMR studies on solutions of (**3**) of various ages and histories (thermal and photochemical) have shown that the adduct deteriorates to the hydrolysis product 2-butylpyridine (**1**) via 1,2-dihydro-2-butylpyridine (**4**).

Since 1930 it has been known that reactions of organolithiums, e.g. Bu^{n}Li, with pyridine can lead ultimately to 2-substituted pyridines, e.g. (**1**),[1] with highly reactive adducts such as (**2**) assumed to be key intermediates in these processes.[2] More recently, solutions of such adducts have been synthesized in Lewis base media, e.g. Et_2O,[3,4] TMEDA,[4–6] then ^{1}H NMR spectra recorded; solution species so examined were presumably Lewis base complexes of adducts such as (**2**). Furthermore, deliberate methanolysis at −70°C of these highly moisture sensitive solutions gives 2-substituted pyridines such as (**1**) via, it has been proposed, dihydropyridines such as (**4**).[6] This note reports the first actual isolation and characterization of a crystalline complexed adduct of this type, viz. Bu^n(C_5H_5N)Li·(C_5H_5N)$_2$, (**3**). The room-temperature ^{1}H NMR spectra of (**3**) show that it decomposes to (**1**) on trace hydrolysis, possibly photochemically-assisted, via the dihydropyridine (**4**).

Addition of Bu^{n}Li in hexane to a chilled three-fold molar excess of pyridine in hexane gave a clear orange solution which, on refrigeration, afforded large yellow crystals of complex-adduct (**3**).† In this reaction, then, pyridine acts as the reactant in the usual sense, but also as a Lewis base which helps to stabilize, and certainly to crystallize and solubilize, the addition product. The crystals are exceedingly air- and moisture-sensitive, and seemingly heat and light sensitive also: they can be kept indefinitely at −10°C in nitrogen-filled, foil-wrapped flasks, but storage in daylight and/or at ambient temperature rapidly causes darkening, first to orange then to

* Author to whom correspondence should be addressed.

† Compound (**3**), yield 88%, m.p. 70–72°C. Elemental analysis: Found: C, 75.6; H, 8.2; Li, 2.5; N, 13.1. $C_{19}H_{24}LiN_3$ requires C, 75.8; H, 8.0; Li, 2.3; N, 14.0%. For further details of synthesis see ref. 7.

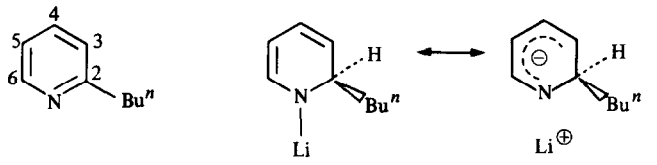

(1) (2)

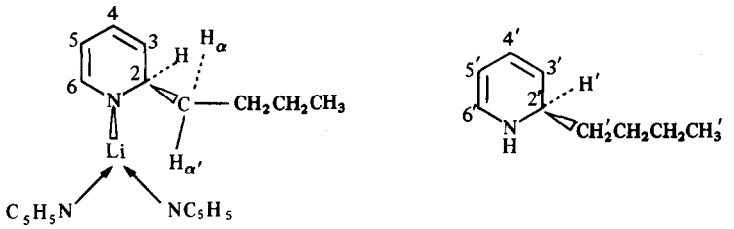

(3) (4)

deep brown. In this context, organo-N—Li complexes with monodentate donors almost always have 1:1 stoichiometry and are dimers e.g. $[Bu^t_2C{=}NLi \cdot O{=}P(NMe_2)_3]_2$,[8] $[(Me_3Si)_2NLi \cdot OEt_2]_2$,[9] but in this case molecular models for a 1:1 complex, $Bu^n(C_5H_5N)Li \cdot (C_5H_5N)$, show that dimerization would be impossible sterically; therein lies the preference for attachment of two C_5H_5N molecules to Li, this being an alternative way for each Li to attain 3-coordination.

The presumed monomeric nature of solid (3) largely persists in solutions, though with some dissociation of pyridine: cryoscopic measurements on benzene solutions give association state (n) values of 0.86 to 0.71 for 4.5×10^{-2} to 1.5×10^{-2} mol dm^{-3} solutions, respectively. The ^{1}H NMR spectrum of a solution of freshly-isolated (3) at 25°C is shown in Fig. 1; the solution was prepared in a glove-box, the tube sealed and the spectrum recorded forthwith. This spectrum proves conclusively the identity and purity of the sample, there being three typical signals (4H:2H:4H) representing two donor pyridine molecules, five separate signals for protons H(2)–H(6) of the reduced pyridine ring,*

* H6 δ 7.17 (d, J_{56}5.6), H4 δ 6.58 (dd, J_{34}8.4, J_{45}5.6), H5 δ 5.29 (td, J_{56}5.6, J_{45}5.6, J_{35}1.3), H3 δ 4.87 (dd, J_{34}8.4, J_{23}4.3), H2 δ 4.07 (ddd, $J_{2\alpha}$8.9, $J_{2\alpha'}$4.3, J_{23}4.1).

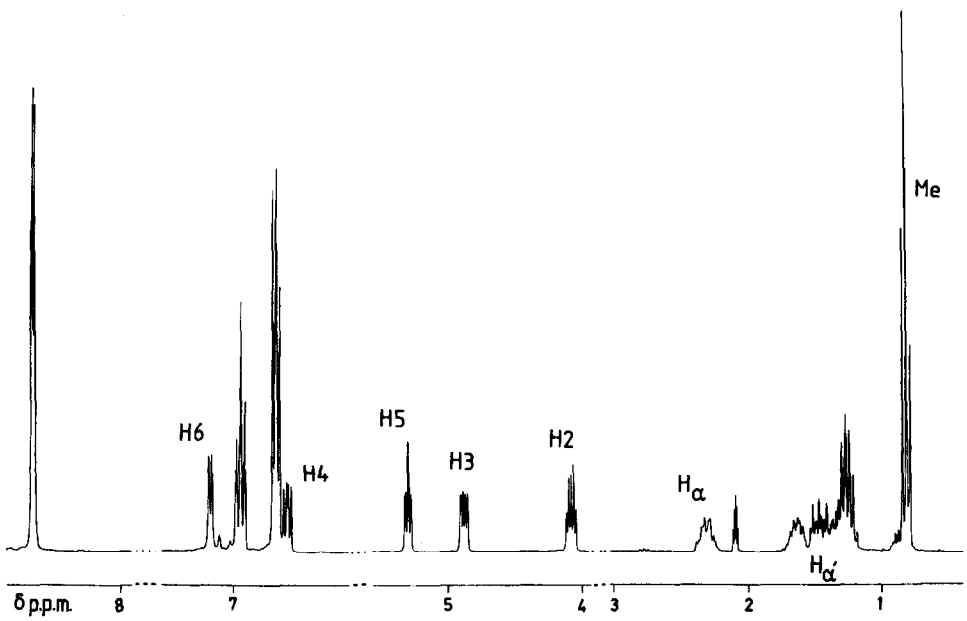

Fig. 1. ^{1}H NMR spectrum (250.13 MHz) of freshly isolated (3) in $\{^2H_8\}$-toluene, 1.0×10^{-1} mol dm^{-3}.

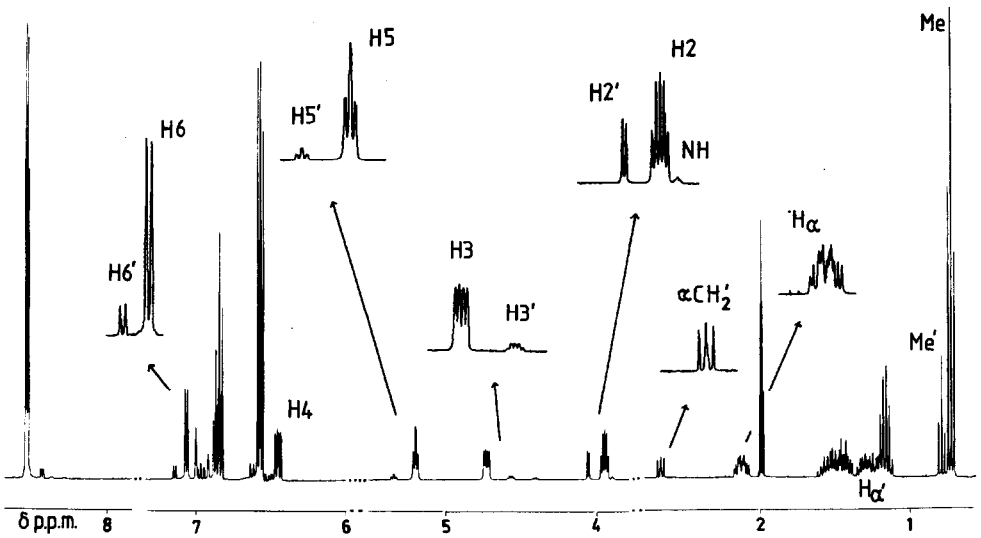

Fig. 2. ^{1}H NMR spectrum (360.13 MHz) of a one-week old sample of (3) in {$^2H_8$}-toluene, 1.0×10^{-1} mol dm^{-3}.

and a set of resonances due to the C_4H_9 group, one (H_α) being quite distinct since the diastereotopic α-methylene protons, ($CH_\alpha H_{\alpha'}$), are anisochronous; assignments were verified by specific proton decoupling of each resonance in turn.

Figure 2 depicts the ^{1}H NMR spectrum of a one week old solution of (3), stored in the dark but at room temperature. Signals due to the H(6), H(5), H(3) and Me now have nearby, but much smaller (*ca* 1 : 8) signals (primed) of the same multiplicity; the same is probably true for H(4), although H(4′) is partly obscured by a pyridine resonance. Further, signals for H(2) and H_α also have smaller signals in their vicinity, but these are, in contrast, of very different multiplicities, viz. near H(2), a doublet and a single resonance (both *ca* 1 : 8 with respect to H(2)'s integral), and near H_α a triplet (*ca* 1 : 4). With the aid of specific proton decoupling, all these additional (primed) resonances can be assigned to 1,2-dihydro-2-butylpyridine (4) as follows: H(6′)–H(3′) to the ring protons as shown; the doublet to H(2′) (now only coupled to H(3′) and not to the

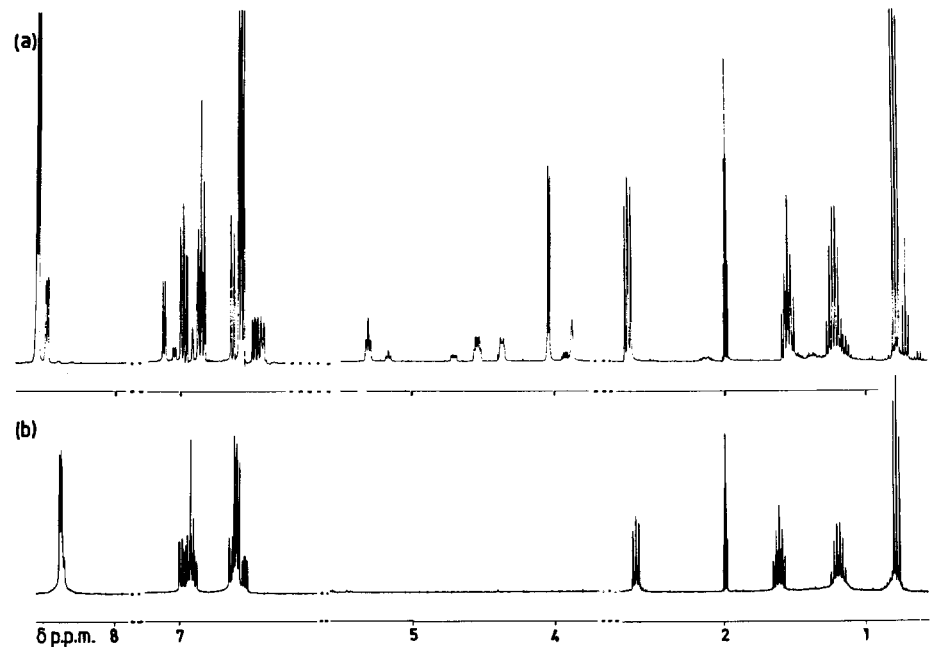

Fig. 3. (a) ^{1}H NMR spectrum (360.13 MHz) of the solution referred to in Fig. 2 after exposure to daylight for several hours. (b) Spectrum of the solution in (a) after brief exposure to the atmosphere.

butyl α-CH'_2) and the singlet to N*H*; and the triplet to the α-CH'_2 protons (still inequivalent, but now only observed to couple to the β-CH_2 unit). The triplet near Me is clearly due to Me′, and the outermost multiplets in the range δ 1.6–1.2 ppm are due to the β, γ-CH_2CH_2-units: the central multiplet here has, like H_α, diminished in intensity on appearance of α-CH'_2, and so can be assigned to $H_{\alpha'}$ in (**3**). It is noteworthy that the chemical shift nonequivalence of the diastereotopic butyl α-methylene protons, ($CH_\alpha H_{\alpha'}$), was enhanced in (**3**) by the presence of the $Li(NC_5H_5)_2$ unit, so giving observed couplings of H_α and $H_{\alpha'}$ to each other and, separately, to H(2).

After exposure of such a solution to daylight for several hours (when it darkens markedly), the rerecorded spectrum [Fig. 3(a)] shows that (**4**) has become the major solution component. After opening this NMR tube to the atmosphere for several minutes, the reaccumulated spectrum [Fig. 3(b)] has no signals due to (**3**) or (**4**): it is the spectrum of 2-butylpyridine, (**1**). The implications of these results are that conversion of (**2**), or its complexes such as (**3**), into (**1**) does not, or does not exclusively, occur in a single step via LiH elimination, but that slight hydrolysis, possibly photochemically encouraged, produces (**4**). This then formally eliminates dihydrogen, by a mechanism as yet unknown, to give (**1**).

Acknowledgements—We thank the SERC for financial support (D.B., R.E.M., R.S.) and for use of high-field NMR facilities, and the Royal Society for a Research Fellowship (to R.E.M.).

REFERENCES

1. K. Ziegler and H. Zeiser, *Chem. Ber.* 1930, **63**, 1847.
2. R. A. Abramovitch and G. A. Poulton, *J. Chem. Soc., Chem. Comm.* 1967, 274.
3. G. Fraenkel and J. W. Cooper, *Tetrahedron Lett.* 1968, 1825.
4. R. F. Francis, C. D. Crews and B. S. Scott, *J. Org. Chem.* 1978, **43**, 3227.
5. C. S. Giam and J. L. Stout, *J. Chem. Soc., Chem. Comm.* 1969, 142.
6. R. F. Francis, W. Davis and J. T. Wisener, *J. Org. Chem.* 1974, **39**, 59.
7. D. Reed, D. Barr, R. E. Mulvey and R. Snaith, *J. Chem. Soc., Dalton Trans.* 1986, 557.
8. D. Barr, W. Clegg, R. E. Mulvey, D. Reed and R. Snaith, *Angew. Chem. Int. Ed. Engl.* 1985, **24**, 328.
9. L. M. Engelhardt, A. S. May, C. L. Raston and A. H. White, *J. Chem. Soc., Dalton Trans.* 1983, 1671.

Polyhedron Vol. 7, No. 8, pp. 669–670, 1988
Printed in Great Britain

0277–5387/88 $3.00+.00
Pergamon Press plc

COMMUNICATION

A NEW FAMILY OF STABLE PARENT *NIDO*-TETRACARBABORANES 5,6,8,9-$C_4B_6H_{10}$, 2,7,8,11-$C_4B_7H_{11}$ AND 7,8,9,10-$C_4B_7H_{11}$

BOHUMIL ŠTÍBR,* TOMÁŠ JELÍNEK, EVA DRDÁKOVÁ, STANISLAV HEŘMÁNEK and JAROMÍR PLEŠEK

Institute of Inorganic Chemistry, Czechoslovak Academy of Sciences, 250 68 Řež near Prague, Czechoslovakia

(*Received* 3 *December* 1987; *accepted* 4 *January* 1988)

Abstract—The parent tetracarbaboranes, *nido*-5,6,8,9-$C_4B_8H_{11}$ and *nido*-2,7,8,11-$C_4B_7H_{11}$ were isolated via HPLC from the reaction of *arachno*-4,5-$C_2B_7H_{13}$ with acetylene in hexane (120°C, 8 h); thermal decomposition of the *arachno*-$[C_4B_7H_{12}]^-$ anion at 140°C produced the isomeric *nido*-7,8,9,10-$C_4B_7H_{11}$ species.

We have recently[1] reported a general reaction of alkynes R_2C_2 (R = H, Me) and *arachno*-4,5-$C_2B_7H_{13}$ (**1**)[2] leading to new tricarbaborane systems, *arachno*-μ-6,9-CHR-9-R-5,6,9-$C_3B_7H_{10}$ and *nido*-5,6,10-Me_3-5,6,10-$C_3B_7H_8$. We now report the isolation and characterization of further *nido* tetracarbaborane systems also arising from the reaction of (**1**) with acetylene.

Column chromatography of the product mixture from the reaction between (**1**) and acetylene (120°C, 8 h) in hexane produced two main fractions of R_f 0.10 and 0.40 (checked by TLC on silica gel in hexane). The first fraction comprised the previously reported[1] μ-6,9-CH_2-5,6,9-$C_3B_7H_{11}$ (**2**) species (*ca* 11%) on evaporation of the solvent and sublimation at 60°C/1.3 Pa. The second fraction, a mixture of products, was evaporated and subsequently separated via preparative HPLC in hexane to yield 5,6,8,9-$C_4B_6H_{10}$ (**3**) (*ca* 3%) and 2,7,8,11-$C_4B_7H_{11}$ (**4**) (*ca* 6%) *nido*-tetracarbaboranes as white crystals, which were further purified by sublimation at 40°C/1.3 Pa after removal of the solvent.

Deprotonation of (**2**) with sodium hydride in diethylether resulted in the formation of the $[C_4B_7H_{12}]^-$ anion (**5**) whose constitution has, as yet, not been determined. Nevertheless, thermal decomposition of the sodium salt of (**5**) yielded a 1:2 mixture of compound (**2**) (*ca* 15%) and *nido*-7,8,9,10-$C_4B_7H_{11}$ (**6**) (*ca* 30%) which were separated via preparative HPLC in hexane.

Mass spectra (high mass molecular cut-off, *m/z*, chemical ionization of positive ions): (**3**) 125; (**4**) 137; (**5**) 137, (P+1) peaks. FT NMR data ($CDCl_3$, 25°C): δ (^{1}H) (200 MHz)/ppm, with respect to Me_4Si, relative intensities other than 1 in parentheses; all signals assigned to the protons of skeletal {CH} groups; (**3**) 5.93, 4.68; (**4**) 2.74, 1.96(2), 1.35; (**6**) 2.57, 2.00. δ (^{11}B) (64.18 MHz)/ppm, with respect to $Et_2O \cdot BF_3$; tentative assignments based on [^{11}B–^{11}B]-COSY NMR experiments: (**3**) BH(1,3) −0.86, BH(7,10) −2.88, BH(2,4) −28.57; (**4**) BH(3) −13.65, BH(6) −15.68, BH(9 or 10) −17.50, BH(9 or 10) −17.98, BH(5) −24.96, BH(4) −25.59, BH(1) −51.66; (**6**) BH(11) −14.03, BH(3,5) −14.54, BH(2,6) −15.33, BH(4) −23.50, BH(1) −46.32.

The above NMR data are consistent with the proposed structures shown in Fig. 1. The [^{11}B–^{11}B]-COSY NMR experiments allowed all of the ^{11}B resonances to be assigned to specific boron nuclei. All cross peaks expected for structures (**3**), (**4**) and (**6**) were found in their 2D spectra.

Along with the earlier reported[3] 2,3,4,5-$C_4B_2H_6$ tetracarbaborane, compounds (**3**), (**4**) and (**6**) represent the first family of parent tetracarbaboranes.

* Author to whom correspondence should be addressed.

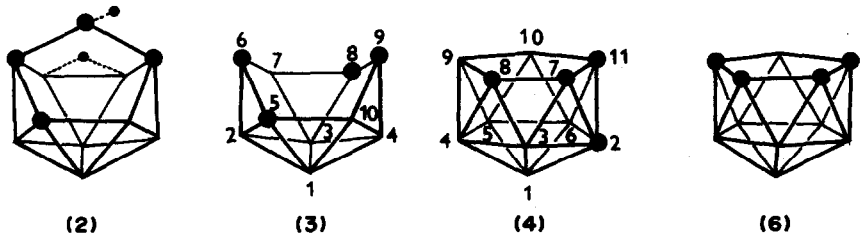

Fig. 1. Proposed structures of tetracarbaboranes (**2**)–(**4**) and (**6**); solid circles denote the positions of {CH} cluster units, the vertices of individual deltahedra identify cage {BH} groups.

Compounds (**4**) and (**6**) are the first known 11-vertex *nido*-tetracarbaboranes and carborane (**3**) is the parent-cage isomer of the recently reported[4,5] peralkylated $R_4C_4B_6R'_6$ fluxional tetracarbaborane systems.

REFERENCES

1. B. Štíbr, T. Jelínek, Z. Janoušek, S. Heřmánek, E. Drdáková, Z. Plzák and J. Plešek, *J. Chem. Soc., Chem. Commun.* 1987, 1107.
2. S. Heřmánek, T. Jelínek, J. Plešek, B. Štíbr and J. Fusek, *J. Chem. Soc., Chem. Commun.* 1987, 927.
3. T. P. Onak and G. T. Wong, *J. Am. Chem. Soc.* 1970, **92**, 5226.
4. R. Köster, G. Siedel and B. Wrackmeyer, *Angew. Chem. Int. Ed. Engl.* 1984, **23**, 512.
5. R. Köster, G. Siedel and B. Wrackmeyer, *Angew. Chem. Int. Ed. Engl.* 1985, **24**, 326.

Polyhedron Vol. 7, No. 8, p. 671, 1988
Pergamon Press plc. Printed in Great Britain

BOOK REVIEW

Radiothermoluminescence and Transitions in Polymers. Vol. 12 in the series **Polymers—Properties and Applications.** L. Zlatkevich. Springer, New York, U.S.A., 1987. ISBN 0-387-96407-X and 3-540-96407-X, pp. 200 + xi.

Radiothermoluminescence refers to the light emitted by a sample which has been irradiated with a massive dose of X- or gamma-rays (in excess of 1 MRad) at low temperature, as it warms up. The intensity of the light emitted varies during the warming-up period and this variation can be plotted as a function of temperature to give a "glow-curve". This book is concerned with the interpretation of such glow-curves from polymers and critically considers their physical and chemical significance.

It can be argued that "the easier the experiment, the worse the science". This is because easy experiments require little forethought and planning, with the unfortunate corrolary that the results are difficult (or impossible) to interpret, the conditions and parameters that might vary having been ill-controlled. Radiothermoluminescence experiments are very easy to carry out and the author is to be congratulated on producing some order out of chaotic and sometimes apparently conflicting results. By considering the probable processes that could most reasonably occur in a severely damaged polymeric solid on warming the bumps, lumps and peaks of the glow-curve are rationalized for many different samples. As proposed mechanisms can sometimes be supported by evidence from other types of experiment (e.g. NMR, dielectric spectroscopy) these techniques are also described. Other chapters show how radiothermoluminescence can be used to study molecular mobility in polymers and to analyse the different types of transition that can occur in solids, both crystalline and glassy, composed of long-chain molecules. The final chapter critically reviews the interpretation of radiothermoluminescence results from many different polymers.

The book is well produced, with a clear and well laid out text that is free from errors and complimented by excellent diagrams. The style is clear and succinct. A book that brings a glow of light to an obscure topic.

Department of Chemistry
Queen Mary College
Mile End Road
London, E1 4NS, U.K.

D. S. URCH

Polyhedron Vol. 7, No. 9, pp. 673–677, 1988
Printed in Great Britain

0277–5387/88 $3.00+.00
© 1988 Pergamon Press plc

COORDINATING PROPERTIES OF SOME SOLVENTS IN $Cr(CO)_5L$ COMPLEXES

C. DÍAZ* and N. YUTRONIC

Departamento de Química, Facultad de Ciencias, Universidad de Chile, Casilla 653, Santiago, Chile

(*Received* 8 *September* 1987; *accepted* 13 *October* 1987)

Abstract—The influence of the donor–acceptor properties of several solvents on the $Cr(CO)_5$ group in the solid [$Cr(CO)_5$ · solvent] complexes has been examined by spectroscopic methods. Relationships were found between the acceptor number of solvent with the π acceptor ability (Graham π parameter) and with the λ_{max} for the ligand field $^1A_1 \rightarrow {}^1E$ transition, in the carbonyl chromium complexes. These relations are discussed in terms of the dative metal–ligand π bonding. From these results, it is possible to demonstrate the π contribution in the acceptor number.

Although $M(CO)_5L$ complexes (L = neutral donor ligands) have been largely studied, very little work has been done with those where L is a solvent molecule. This has been due to instability of those complexes which are usually generated *in situ* by UV and irradiation of a metal hexacarbonyl solution.[1–3] It has been generally found that these irradiated solutions containing the [$M(CO)_5$ · solvent] complexes exhibit a marked tendency to revert to the original reactants after the irradiation is stopped.[1,3] Such properties render isolation of many complexes impractical and the characterization is limited mainly to the determination of the IR[1–3] and in some cases UV-vis. spectra.[4]

Furthermore numerous [$M(CO)_5$ · solvent] complexes (M = Cr, Mo and W) produced by photolysis of $M(CO)_6$ have been used as labile intermediates in the synthesis of stable $M(CO)_5L$ compounds; e.g. with tetrahydrofuran one of the most widely used,[5–9] several monosubstituted metal hexacarbonyls have been prepared.[9]

$$M(CO)_6 + THF \rightarrow [M(CO)_5(THF)] + CO$$

$$[M(CO)_5(THF)] + L \rightarrow M(CO)_5L + THF.$$

The [$M(CO)_5$(THF)] labile intermediate has been specially useful in the synthesis of complexes with sulphur donor ligands.[6–8] This synthetic method is based indeed on the lability of the intermediate [$M(CO)_5$ · solvent] complexes. Nevertheless some [$M(CO)_5$ · solvent] compounds (M = Cr) can be isolated as relatively stable solids.

On the other hand, the solvent effect on metal coordination compounds usually has been interpreted by the formation of substrate–solvent outer-sphere complexes.[10,11] However in some cases the solvent molecule acts directly on the coordination sphere producing a specific metal–solvent interaction.[12,13] Other systems with such a characteristic could be the complexes $Cr(CO)_5L$ where L is a solvent molecule. In this paper we have studied the IR, ^1H NMR and UV-vis. spectral properties of several solid [$Cr(CO)_5$ · solvent] complexes.

The possible effect of the solvent acting like a ligand on the $Cr(CO)_5$ fragment is discussed in terms of the donor and acceptor numbers proposed by Gutmann.[14,15]

For this study we have selected the compounds [$Cr(CO)_5$ · solvent], where the solvent is; acetonitrile [An), benzylcyanide, isobutyronitrile, *n*-butyronitrile, hexamethylphosphoramide (HMPA), benzonitrile (BN), dimethylsulphoxide (DMSO), ethylene sulphite (ES) and ammonia. The complexes were chosen according to two requirements; they must be isolated as solids and the solvent parameter (acceptor number *AN* or donor number *DN*) must be known.[14,15]

*Author to whom correspondence should be addressed.

RESULTS AND DISCUSSION

The carbonyl stretching frequencies of the complexes [Cr(CO)$_5$·solvent] are shown in Table 1. They are characteristic of octahedral M(CO)$_5$L compounds with C_{4v} symmetry.[16] We have assigned the modes using the procedure outlined by Cotton and Kraihanzel.[16] The k_1 and k_2 carbonyl force constants are shown in Table 1. For evaluating the π acceptor ability of the solvent as a ligand we have calculated the π parameter proposed by Graham.[17] These are given in Table 1. In order to determine some relation between π acceptor ability of the complexes with typical properties of the solvents, a plot between the π parameter and the acceptor number AN[14,15] was made for the solvent ligands (Fig. 1). In spite of the fact that the acceptor number is not known for all the solvent complexes given in Table 1, a satisfactory linear relationship is observed with the exception of acetonitrile. This relationship can be understood by considering the influence of the solvent nature on the limiting structures given below, usually applied to describe carbonyl compounds[10]

$$\overset{\delta+}{O}\equiv C-\overset{\delta-}{M}-\text{solvent} \leftrightarrow O=C=M-\text{solvent}.$$

(I) (II)

The contribution of structure (I) should increase with increasing solvent acceptivity if it is assumed that this property involves some π character. In fact, the acceptor number is based on the ^{31}P-NMR chemical shift in triethylphosphine oxide using the respective pure solvent.[14] The highest occupied molecular orbital (HOMO) of Et_3PO has considerable π P—O character,[19,20] therefore it is plausible that the Et_3PO–solvent interaction involve some π character. Consequently the acceptor number could have some π acceptor character.

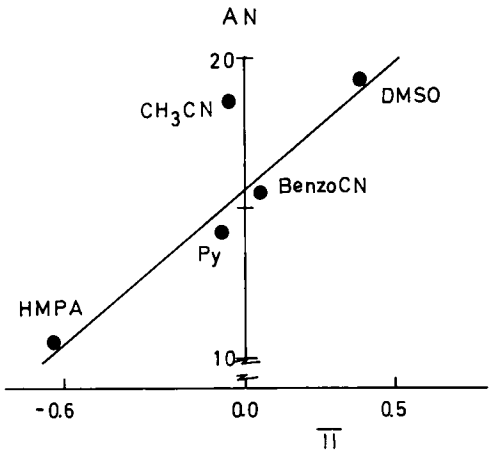

Fig. 1. Variation of the solvent acceptor number with the π parameter in Cr(CO)$_5$ solvent complexes.

The influence of the donicity solvent on the properties of the Cr(CO)$_5$ moiety was examined by comparing the solvent donor number D with the k_1 carbonyl stretching force constant. It is well known that k_1 is determined by a donor and π acceptor effect.[17] If the π contribution remains constant or is nil, a relationship between donicity and k_1 could be expected. The variation of the donor number with k_1 is exhibited in Fig. 2. A tendency appears to

Table 1. Carbonyl stretching frequencies,[a] force constants,[b] π parameters[c] and UV-vis. data for[d] Cr(CO)$_5$ solvent complexes

Complex	A_1^2	B_1	E	A_1^1	k_1	k_2	π	λ_{max}(nm)
[Cr(CO)$_5$(CH$_3$CN)]	2078	1991	1954	1930	15.20	16.00	−0.02	390
[Cr(CO)$_5$((CH$_3$)$_2$CHCN)]	2060	1985	1949	1924	15.10	15.91	−0.06	392
[Cr(CO)$_5$(C$_6$H$_5$CH$_2$CN)]	2070	—	1950	1929	15.17	15.89	0.03	390
[Cr(CO)$_5$(CH$_3$CH$_2$CH$_2$CN)]	2062	1990	1941	1920	15.11	15.99	−0.13	388
[Cr(CO)$_5$(C$_6$H$_5$CN)]	2065	1983	1952	1930	15.17	15.87	0.05	375
[Cr(CO)$_5$((CH$_3$)$_2$SO)]	2080	1990	1955	1955	15.62	15.99	0.38	372
[Cr(CO)$_5$(CH$_2$OSOCH$_2$)]	2010	1989	1955	1955	15.61	15.97	0.39	—
[Cr(CO)$_5$(C$_5$H$_4$N)]	2063	1993	1940	1922	15.17	16.00	0.01	394
[Cr(CO)$_5$[(CH$_3$)$_2$N]$_3$PO]	2068	2000	1929	1891	14.76	16.15	−0.64	448

[a] n-Hexane solution.
[b] Calculated according to Cotton and Kraihanzel, ref. 16.
[c] Calculated according to refs 17 and 18.
[d] λ_{max} for the $^1A_1 \rightarrow {}^1E$ transition, in n-hexane solution.

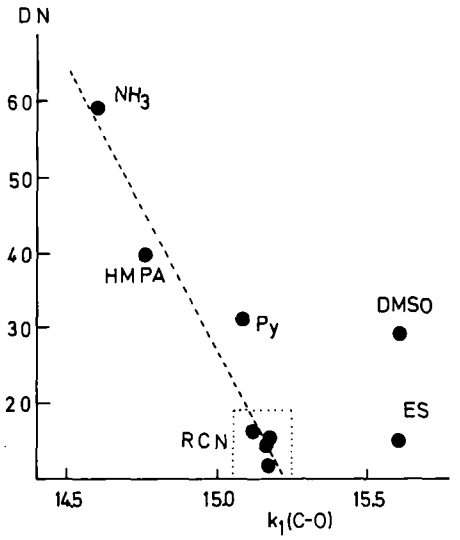

Fig. 2. Variation of the solvent donor number with the k_1 carbonyl force constant.

exist with solvents having a nil or weak π acceptor capacity. In this case the contribution from structure (**II**) could be enhanced with the increase of solvent donor number.

Dimethylsulphoxide and ethylene sulphite show a departure in behaviour from the system presented above. This can be attributed to the greater π acceptor capacity of these sulphoxide solvents than of the other solvents.*[18] It is apparent that the donor properties of the solvent are modified by π effects when it possesses a high π acceptor capacity. This behaviour may be similar to the σ-donor–π acceptor synergic interaction that occurs in metal carbonyl complexes.[23] The dependence of the $Cr(CO)_5$ moiety on the donicity as well as on the acceptivity of the solvent can be explained by the characteristic σ–π interaction of the $Cr(CO)_5$ group with a sixth ligand.[24] Consistent with this in the systems where the metal–ligand interaction is principally σ, the complexes Cu(tmen) (acac)ClO_4 and Ni(tmen)acac (tmen = N,N,N′,N′-tetramethylethylendiamine) dissolved in donor solvents[13] produce good correlations between the wave number of the maximum absorption band and the donor solvent number.

Regarding the UV-vis. spectral data, as we reported previously[21] the π acceptor capacity is related to λ_{max} for the d–d $^1A_1 \rightarrow {}^1E$ transition in the complexes $M(CO)_5L$. Hence a relationship between the acceptor number for the solvent and λ_{max} (Table 1) could be expected. As seen in Fig. 3 a relation does exist, except for CH_3CN. The π levels of $M(CO)_5$ can be modified by the acceptivity to solvent in the same fashion that these orbitals are modified by π acceptor ligands.[24]

The ^{1}H-NMR spectral data for the $Cr(CO)_5$ solvent complexes are shown in Table 2. From these values it is not possible to state a general conclusion due to the different nature of the protons near to the donor atoms of the solvent–ligand.

By comparison of chemical shift values of the free ligand protons with respect to the coordinated solvent molecules, a downfield shift is observed (see Table 2). In general, the magnitude of the shifts depend on two factors: the distance of the protons from the donor atom and the σ-donor and π-acceptor characteristics of the ligands. A large proton shift on complexation is exhibited by the ligand whose protons are near to the donor atom and which are weak π-acceptors (benzylcyanide, pyridine and acetonitrile). Despite dimethylsulphoxide being a moderate π-acceptor* the methyl groups protons produce a large shift on coordination probably due to the coordination of the ligand to the metal via the sulphur atom in pentacarbonyl (sulphoxides) complexes.*

On the other hand, solvent ligands with protons at a distance from the donor atom show small shifts upon coordination (hexamethylphosphoramide, ethylene sulphite and benzonitrile).

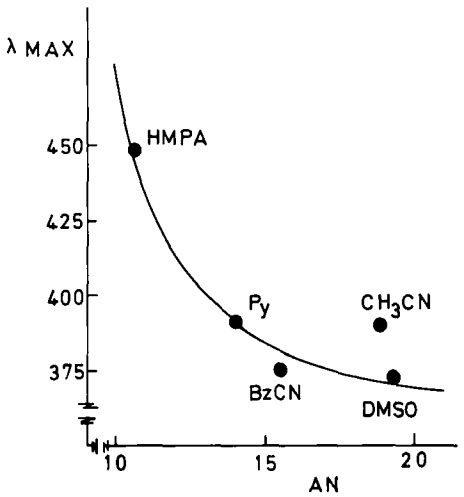

Fig. 3. Variation of λ_{max} for the $^1A_1 \rightarrow {}^1E$ transition in the $Cr(CO)_5$ solvent complexes with the solvent acceptor number.

*Using a relation between Cr—C(ax) and the π acceptor ability previously reported by us (see ref. 21) we estimate a value of $\pi = 0.48$ (with d(Cr—C_{ax}) = 1.86 Å for the complex $Cr(CO)_5C_4H_6SO$)[22] for the sulphoxide ligand. According to the π parameter scale for $Cr(CO)_5L$ complexes (see ref. 18) this value indicates that the sulphoxide ligand is a good π acceptor.

Table 2. Proton NMR data for $[Cr(CO)_5 \cdot (Solvent)]$ complexes

Solvent	δ (in ppm from TMS)[a]	$Cr(CO)_5$ solvent	Δ[b]
CH_3CN	1.96	2.20	0.24
$(CH_3)_2CHCN$	1.26 (CH_3)	1.33	0.07
$C_6H_5CH_2$—CN	3.38 (CH_2)	3.90	0.52
	7.06 (C_6H_5)	7.23	0.17
$(CH_3)_2SO$	2.53	3.05	0.52
$CH_3CH_2CH_2CN$	1.05 (CH_3)	1.13	0.08
	1.66 (CH_2)	1.76	0.10
	2.26 (CH_2CN)	2.46	0.20
C_6H_5CN	7.50	7.58	0.08
C_5H_4N	8.43[c]	8.65[c]	0.12
$[(CH_3)_2N]_3PO$	2.60	2.63	0.03
$CH_2OS(O)OCH_2$	4.40	4.53	0.13

[a] In CCl_4 solution except for ethylene sulphite, which is in $CDCl_3$.
[b] $\Delta = |\delta complex - \delta free|$.
[c] α protons of ring.

It is interesting to note that the deshielding effect by coordination is gradually transmitted throughout the ligand molecule. Ligands that possess protons at different distances from the donor atom as in *n*-butyronitrile, benzylcyanide and pyridine show a variation in chemical shift, Δ, depending on the distance of proton from the donor atom (see Table 2).

EXPERIMENTAL

Infrared, proton NMR and UV-vis. spectral data were obtained as described elsewhere.[6,21] Chromium hexacarbonyl was purchased from Fluka. Dimethylsulphoxide, acetonitrile, hexamethylphosphoramide and ethylene sulphite were obtained from Aldrich. Benzonitrile and benzylcyanide were purchased from Fluka.

Preparation of the complexes

Pentacarbonyl (hexamethylphosphoramide) chromium. A solution of 1 g of $Cr(CO)_6$ (4.6 mmol) in *ca* 60 cm^3 THF was irradiated (UV-lamp HANAU medium pressure 150 W) for 90 min at room temperature. A solution of 0.9 g (5 mmol) of hexamethylphosphoramide was then added and the mixture stirred for 60 min. The resulting yellow solution was concentrated under reduced pressure and then a yellow solid was precipitated and filtered. The product was washed with THF and dried under vacuum then stored under an argon atmosphere. The compound is highly unstable[25] and must be kept in the freezer.

Pentacarbonyl (ammonia) chromium. A stream of dry ammonia gas was bubbled through the solution of $[Cr(CO)_5(THF)]$ photochemically generated, until a colour change was observed. After removing the solvent under reduced pressure, the excess of hexacarbonyl and ammonia was eliminated from the residue under vacuum. The solid was then redissolved in a *n*-hexane/*n*-pentane mixture and filtered through Kieselguhr. The filtrate was then evaporated to give a yellow solid.[9]

The general procedure for the synthesis of the other complexes. A solution of 3.5 mmol of $Cr(CO)_6$ in *ca* 60 cm^3 THF was irradiated for 90 min. A solution of 3 mmol of the ligand solvent in *ca* 20 cm^3 THF was then added and the mixture stirred for 60 min. After removing the solvent under reduced pressure, the excess of hexacarbonyl was sublimed from the residue under vacuum at room temperature. The solid was then redissolved in a *n*-hexane/*n*-pentane mixture, filtered through Kieselguhr and recovered by evaporating the solvent. The complexes with acetonitrile,[9] benzonitrile,[9] ethylene sulphite[26] and dimethylsulphoxide[26] have been previously reported. The new complexes with *n*-butyronitrile and isobutyronitrile were fully characterized.

Found C, 40.3; H, 2.7; N, 4.9. Calc. for $C_{10}H_7O_5NCr$; C, 41.3; H, 2.7; N, 5.4%. Mp 89–90°C.

Found C, 40.1; H, 2.7; N, 5.2. Calc. for $C_{10}H_7O_5NCr$: C, 41.3; H, 2.7; N, 5.4%. Mp 68–70°C.

Acknowledgement—We thank the Departamento de Investigacion y Bibliotecas de la Universidad de Chile for financial support.

REFERENCES

1. I. W. Stolz, G. R. Dobson and R. K. Sheline, *Inorg. Chem.* 1963, **2**, 323.
2. I. W. Stolz, H. Hass and R. Sheline, *J. Am. Chem. Soc.* 1965, **87**, 716.
3. I. W. Stolz, G. R. Dobson and R. K. Sheline, *Inorg. Chem.* 1963, **2**, 1265.
4. M. Wrighton, G. S. Hammond and H. B. Gray, *J. Am. Chem. Soc.* 1971, **93**, 4336.
5. W. Strohmeier and F. J. Muller, *Chem. Ber.* 1969, **102**, 3608.
6. C. Díaz and G. González, *Inorg. Chim. Acta* 1984, **85**, 61.
7. E. W. Ainscough, F. J. Birch and A. M. Brodie, *Inorg. Chim. Acta* 1976, **20**, 187.
8. H. G. Raubenheimer, S. Lotz, H. W. Viljoen and A. A. Chalmers, *J. Organomet. Chem.* 1978, **152**, 73.
9. *Gmelin Handbuch der Anorganischen Chemie*, Band 3 chrom-organische Verbindungen. Springer (1974).
10. I. Chadwick, C. Díaz, G. González, M. A. Santa Ana and N. Yutronic, *J. Chem. Soc., Dalton Trans.* 1986, 1867.
11. W. O. Horrocks and R. H. Mann, *Spectrochim. Acta* 1965, **21**, 399.
12. J. Selbin and T. R. Ortolano, *J. Inorg. Nucl. Chem.* 1964, **26**, 37.
13. R. W. Soukop and R. Schmid, *J. Chem. Ed.* 1985, **62**, 459.
14. V. Gutmann. *The Donor–acceptor Approach to Molecular Interactions*. Plenum Press, New York (1978).
15. V. Gutmann, G. Resch and W. Linert, *Coord. Chem. Rev.* 1982, **43**, 133.
16. F. A. Cotton and C. S. Kraihanzel, *J. Am. Chem. Soc.* 1962, **83**, 4432.
17. W. A. Graham, *Inorg. Chem.* 1968, **7**, 315.
18. C. Díaz, *Rev. Chil. Educ. Quim.* 1985, **10**, 7.
19. R. M. Archibald and P. G. Perkins, *Rev. Roum. Chim.* 1971, **16**, 1137.
20. I. H. Hilier and V. R. Saunders, *J. Chem. Soc. A* 1970, 2475.
21. C. Díaz and N. Yutronic, *Polyhedron* 1987, **6**, 503.
22. J. H. Ekhof, H. Hogeveen and R. M. Kellog, *J. Organomet. Chem.* 1978, **161**, 361.
23. J. B. Johnson and W. G. Klemperer, *J. Am. Chem. Soc.* 1977, **99**, 7132.
24. T. A. Albright, R. Hoffmann, J. C. Thibeault and D. L. Thorn, *J. Am. Chem. Soc.* 1979, **101**, 3801.
25. D. Rogues and R. Poilblanc, *J. Organomet. Chem.* 1970, **24**, C47.
26. W. Strohmeier, J. D. Guttenberger and G. Popp, *Chem. Ber.* 1965, **98**, 2248.

Polyhedron Vol. 7, No. 9, pp. 679–684, 1988
Printed in Great Britain

0277–5387/88 $3.00+.00
© 1988 Pergamon Press plc

SYNTHESIS AND STRUCTURE OF PSEUDO ATRANE COMPOUNDS DERIVED FROM 2,2′,2″-NITRILOTRIPHENOL AND $BH_3 \cdot THF$, $P(NMe_2)_3$ AND $AlCl_3$

M. A. PAZ-SANDOVAL,* C. FERNÁNDEZ-VINCENT, G. URIBE and R. CONTRERAS

Centro de Investigación y de Estudios Avanzados del I.P.N., Departamento de Química, Apartado Postal 14-740, 07000-México, D.F.

and

A. KLAÉBÉ

E.R.A. au CNRS No. 926, Université Paul Sabatier, 31062 Toulouse, Cedex, France

(*Received* 21 *July* 1987; *accepted after revision* 16 *December* 1987)

Abstract—Synthesis of heterocyclic compounds of the type $M(OC_6H_4)_3N$ [M = B (**2**); M = B ← $NH_2CH_2C_6H_5$ (**4**); M = P (**5**); M = P → BH_3 (**6**); M = Al (**7**); M = Al ← $NH_2CH_2C_6H_5$ (**8**)] and $B(OC_6H_4)_3N \rightarrow BH_3$ (**3**) are reported. NMR parameters ^{11}B, ^{31}P, ^{27}Al, ^{13}C and ^{1}H are consistent with cyclic structures. There is no intramolecular bond in **2** and **5**, but **2** showed an acidic boron and basic nitrogen. Some amines (**4**, **8**) and borane (**3**, **6**) adducts support the study of inter- or intramolecular bonds. The NMR spectra (^{1}H, ^{13}C) for the reported complex $C_6H_5Si(OC_6H_4)_3N$ (**9**) are included.

We report the synthesis and structural studies of the heterocyclic compounds $M(OC_6H_4)_3N$ [M = B (**2**); M = B ← $NH_2CH_2C_6H_5$ (**4**); M = P (**5**); M = P → BH_3 (**6**); M = Al (**7**); M = Al ← $NH_2CH_2C_6H_5$ (**8**)] and $B(OC_6H_4)_3N \rightarrow BH_3$ (**3**). Previous studies of atranes have been of special interest because of their geometry and types of bonding. The description of the M ← N bond (M = P, Si) and the extent of the interaction between the two atoms, has been a subject of discussion.[1] In fact, evidence for these structures suggests that NMR data should be interpreted critically because the existence of a coordinate link from N to the different elements is not always evident.

EXPERIMENTAL

All manipulations were carried out under a dry nitrogen atmosphere using standard techniques. Solvents were dried and distilled before use. Published procedures were used to prepare 2,2′,2″-nitrilotriphenol **1**, $C_6H_5Si(OC_6H_4)_3N$ **9** and $Al(OC_6H_4)_3N$ **7**.[2]

Spectra

^{11}B, ^{27}Al, ^{13}C and ^{31}P NMR spectra were obtained using a Jeol FX-90Q spectrometer operating at 28.7, 23.29, 22.49 and 36.23 MHz, respectively. Chemical shifts are relative to $Et_2O \cdot BF_3$, $AlCl_3(H_2O)$, TMS and H_3PO_4 (80%). Proton NMR were obtained with a Varian EM 390 spectrometer. IR were obtained with a Nicolet MX-1-FT spectrophotometer. Mass spectra were obtained using a Hewlett–Packard 5985-A spectrometer operated by the Instituto de Química-UNAM.

Synthesis of 2,2′,2″-*nitrilotriphenylborate* **2**

A mixture of **1** (4 g, 13.6 mmol) and $BH_3 \cdot THF$ (7 cm^3, 15.4 mmol) in THF (50 cm^3) at room temperature gave after evaporation of the solvent under reduced pressure, a white powder (96%) which does not melt below 300°C. The resulting product is very

* Author to whom correspondence should be addressed.

insoluble in non-polar solvents and decomposes in the presence of moisture.

Reaction of **2** *with benzylamine. The preparation of* $C_6H_5CH_2H_2N \cdot B(OC_6H_4)_3N$ **4**

Addition of 0.2 cm^3 (1.84 mmol) of benzylamine to a solution of **2** (0.5 g, 1.66 mmol) in THF (25 cm^3) gave a yellow solid (75%) which decomposed at 200°C.

Reaction of **2** *with* $BH_3 \cdot THF$. *The preparation of* $B(OC_6H_4)_3N \cdot BH_3$ **3**

A solution of **2** (0.5 g, 1.66 mmol) in THF (25 cm^3) in the presence of one equivalent of $BH_3 \cdot THF$ gave the adduct **3**. The only spectroscopic evidence for structure **3** is its ^{11}B chemical shift ($^{11}B = -6.9$ ppm) which is in the range for amine–borane adducts. Its isolation was impossible because the borane was lost during evaporation of the solvent.

Synthesis of 2,2′,2″*-nitrilophenylaluminate* **7**

An equivalent mixture of **1** (1.34 g, 4.57 mmol) and $AlCl_3$ (0.61 g, 4.57 mmol) under refluxing THF (50 cm^3) for 4 h gave after evaporation of the solvent under reduced pressure, a brown powder (43%) which does not melt below 300°C and is soluble in most common solvents.

Reaction of **7** *with benzylamine. The preparation of* $C_6H_5CH_2H_2N \cdot Al(OC_6H_4)_3N$ **8**

A solution of **7** (0.62 g, 1.96 mmol) in THF (50 cm^3) in presence of an excess of benzylamine (1.65 cm^3, 15.1 mmol) gave after 4 h of reflux a white powder, insoluble in most common solvents and soluble in DMSO. It sublimes at 240°C.

Synthesis of 2,2′,2″*-nitrilotriphenylphosphite* **5**

It was prepared from an equivalent mixture of **1** (3.5 g, 12 mmol) and hexamethylphosphorustriamide (2.2 cm^3, 12 mmol) in refluxing benzene (25 cm^3) for 2 h, after evaporation of the solvent a white powder was obtained (78%) which decomposes at 115°C.

Reaction of **5** *with* $BH_3 \cdot THF$. *The preparation of* $H_3B \cdot P(OC_6H_4)_3N$ **6**

Addition of $BH_3 \cdot THF$ (0.8 cm^3, 1.76 mmol) to **5** (0.5 g, 1.55 mmol) gave a white solid (85%) which decomposes at 140°C.

RESULTS AND DISCUSSION

Figure 1 illustrates the reaction of 2,2′,2″-nitrilotriphenol **1** with $BH_3 \cdot THF$, $P(NMe_2)_3$ and $AlCl_3$ giving cyclic compounds of the type $M(OC_6H_4)_3N$ (M = B, **2**), (M = P, **5**) and (M = Al, **7**).

Direct reaction of these complexes with amines and borane afforded the species $RM(OC_6H_4)_3N$, M = B, R = $C_6H_5CH_2NH_2$ **4**; M = P, R = BH_3 **6**; M = Al, R = $C_6H_5CH_2NH_2$ **8** and $B(OC_6H_4)_3N \cdot BH_3$ **3**.

Boron compounds

Interesting studies have been carried out in boratran, **10**, where the X-ray structure reveals that the sum of the angles around nitrogen and boron are 342.8 and 346.4°, respectively, and that these atoms are connected by a 1.693 Å bond. The stabilization of the nitrogen lone pair on formation of the B—N bond is 2.4 eV according to the revised assignment on the photoelectron spectrum of **10**.[3] Considering the lone pair stabilization as roughly indicative of the "electronic" strength of the B—N bonds (with steric factors excluded) as suggested by Livant *et al.*,[3] they conclude that **10** possess a very weak B—N bond.

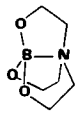

10

Compared with compound **10**, compound **2** showed absence of an intracyclic coordination. The structural determination of **2** was based on the ^{11}B NMR signal, which is characteristic of boric esters and suggests the absence of N—B coordination (see Tables 1 and 2). This lack of coordination could be attributed to the low basicity of nitrogen and to the intracyclic strain. In order to clarify this phenomenon, we decided to determine the acidity of the boron atom and to observe the ^{11}B NMR chemical shift of **2** in the presence of a Lewis base. Addition of one equivalent of benzylamine to a solution of **2** in THF, gave a single signal at +4.4 ppm, this clearly shows that the boron atom is very acidic, the adduct **4** was isolated and characterized (Tables 1 and 2). Conversely, the next experiment was to check the basic character of **2**; a solution of **2** in THF in the presence of one equivalent of $BH_3 \cdot THF$ gave a signal at −6.9 ppm that can be attributed to compound **3**; this fact gives information about the basicity of the nitrogen which is evidently low according to the easy loss of borane (see Experimental section). Our attempts to prepare a triphenylamine borane adduct were unsuccessful.[4]

Formation of adduct **3** is interesting because it

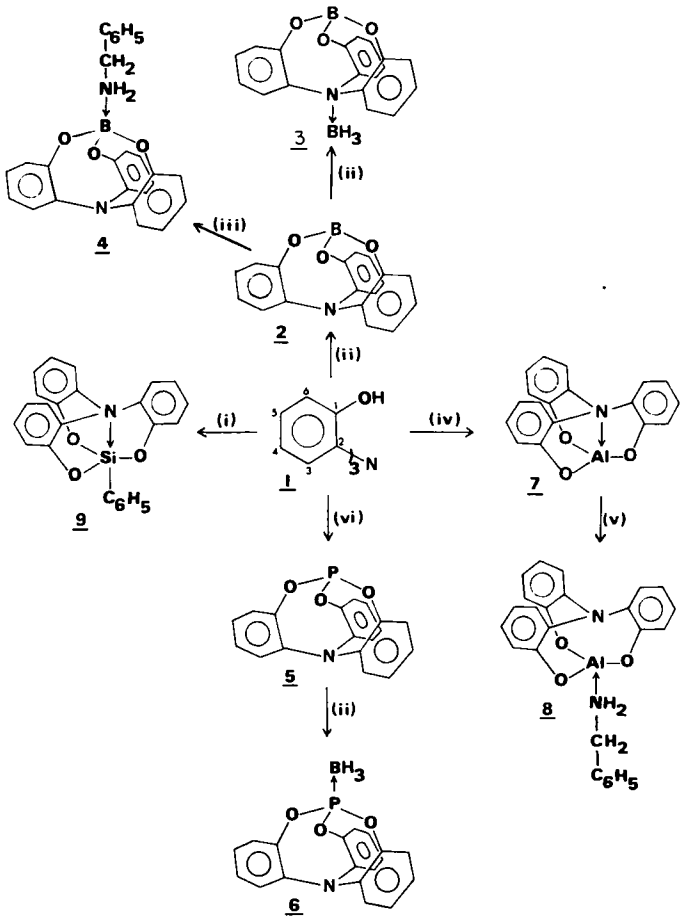

Fig. 1. Synthetic routes to heterocyclic molecules and some of its reactions: (i) $C_6H_5SiCl_3$ in buthylether[2]; (ii) BH_3THF (1 equiv) in THF at room temperature; (iii) $C_6H_5CH_2NH_2$ in THF at room temperature; (iv) $AlCl_3$ in refluxing THF 4 h or $Al(OPr^i)_3$ at 150–170°C[2]; (v) $C_6H_5CH_2NH_2$ in refluxing THF 4 h; (vi) $P(NMe_2)_3$ in refluxing benzene 2 h.

suggests that an intramolecular B—N bond is not present and it also shows that nitrogen is in a tetrahedral geometry with an *exo* lone pair strong enough to coordinate to borane.

Phosphorus compounds

The reaction of hexamethylphosphorustriamide with triol **1** afforded a white powder in 78% yield, which decomposed at 115°C. The stability of this aromatic phosphatrane **5** contrasts with the unisolated $P(OCH_2CH_2)_3N$, which apparently forms in a similar reaction, in which an uncharacterized polymer has been obtained as the major product.[5]

Addition of BH_3·THF showed that **5**, the same as many other aminophosphanes, behaves as P-donor only, giving adduct **6**. A second equivalent of the Lewis acid afforded a very insoluble precipitate, whose structure was not elucidated.

Compounds **5** and **6** were compared with other reported aminophosphanes and phosphatranes which were either coordinated or not coordinated to boron, finding that **5** showed the same δ $^{31}P = +115$ ppm as $P(OCH_2CH_2)_3N$.[5] This value is in the characteristic range for pyramidal phosphorus in phosphites and suggests a similar structure for both compounds.

Formation of adduct **6** suggest that the geometry assumed by the P atom is tetrahedral. The near identity of ^{11}B and ^{31}P chemical shifts of **6** (^{11}B $\delta = -40.6$ ppm, $J_{P-B} = 92.3$ Hz; ^{31}P $\delta = +107$ ppm) with **11** (^{11}B $\delta = -43.8$ ppm, $J_{P-B} = 96$ Hz; ^{31}P $\delta = +97$ ppm)[6] suggest that P—N is absent. The $J_{P-B} = 92.3$ Hz differs markedly from an unusually large P—B coupling reported for H_3B·$P(OCH_2CH_2)_3N$ ($J_{P-B} = 120$ Hz, $^{31}P = +98.3$)[5] which they were tempted to ascribe to a tricyclic structure.

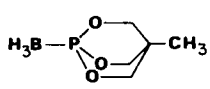

11

Table 1. Physical and infrared data

Compound	Melting point (°C)	Molecular weight[a]	IR (ν, cm^{-1})
1	170–171	293	3419(s,br)
2	200/0.1 mmHg (sublime)[b]	301	1321(s), 1190(m), 1065(s), 1045(s), 912(w), 888(s)
4	200 (decomp)	—	1301(s), 1056(m), 942(m)
5	115 (decomp)	321	1307(m), 1225(w), 1181(m), 1044(w), 910(w), 888(m), 848(s), 696(m)
6	140 (decomp)	335	1316(s), 1286(m), 1238(s), 1063(m), 961(vs), 946(vs), 935(vs), 908(vs), 850(m), 644(m)
7	[b]	—	1613(m), 1138(m), 937(vw), 913(w), 713(w), 569(vw), 425(w)
8	240 (sublime)	[c]	3000(s,br), 1613(m), 1375(w), 1063(w), 963(w), 913(vw), 875(w), 688(s), 556(w)
9	[d]	395	1625(m,br), 1292(vs), 1132(s), 934(vs), 901(vs), 894(vs), 850(m), 782(s), 719(m), 588(s), 475(w), 435(m)

[a] Determined from mass spectra; **2** based on ^{11}B isotope and **9** based on ^{28}Si isotope only.

[b] It does not melt below 300°C.

[c] Only the characteristic fragment patterns of benzylamine 107 (67.7%), 106 (100%) and 79 (62.8%) are observed without evidence of the rest of the molecule.

[d] As [b], but it sublimes when heated strongly.[2]

We believe that the extent of nitrogen–phosphorus bond for **6** is not reflected in the $^1J_{P-B}$ coupling constant, because the coupling data in the literature[7-10] of cyclic, acyclic compounds, P—N bond complexes, and especially, species without P—N interaction[11] are not significantly different. Furthermore, according to X-ray studies[12] the P—N distance in $H_3B \cdot P(OCH_2CH_2)_3N$ is 3.098 Å which does not support the tricyclic argument.

Aluminium compounds

The preparation of **7** can be carried out by refluxing **1** in THF with $AlCl_3$, or by condensation of **1** with aluminium isopropoxide.[2] In reference 2, **7** was characterized only by analysis and the statement that its IR spectrum showed the chelate cage structure.

The alatrane **7** contained coordinated solvents, such as THF, isopropyl alcohol and diethylether which were removed by heating under vacuum (*vide infra*). As might be expected from the above, addition of benzylamine to **7** gave the coordinated compound **8**. Interesting in this regard is the narrowing of ^1H, ^{13}C and ^{27}Al signals when the benzylamine is introduced in molecule **7** (see Table 2). This fact suggests a significant change in the corresponding symmetry of these species.

The addition of one equivalent of $BH_3 \cdot THF$ to a THF solution of **7** did not give amineborane adduct formation as evidenced by ^{11}B NMR. There is only a signal at +19 ppm, characteristic of boric esters, presumably formed from $BH_3 \cdot THF$ and the ring opening of THF and a similar fact was observed when $BH_3 \cdot THF$ was added to **9**. Formation of **2** is discarded according to IR spectroscopy.

The absence of reactivity of the nitrogen with borane suggests the presence of a tetracoordinated aluminium in **7** and pentacoordinated silicon in **9**, formed via a transannular dative bond between M (M = Al, Si) and N. Addition of $BH_3 \cdot DMS$ to a DMS solution of **8** did not show any reaction

Table 2. Nuclear magnetic resonance data

Compound	Solvent	^{1}H NMR	^{13}C NMR						Other nuclei δ (ppm)
			1	2	3	4	5	6	
1	$CDCl_3$	6.8–7.31(m) 7.32(s)	150.1	133.4	121.7	126.9	125.5	117.4	
	DMSO	6.6–7.05(m) 8.70(s)	151.6	135.6	119.3	125.6	124.7	116.2	
2	DMSO	8.10–7.80(d,br) 7.35–6.65(m)	156.7	136.1	120.6	129.0	126.3	117.0	δ ^{11}B = +14.2 (THF/DMSO)
4[a]	$CDCl_3$	7.4–7.1(s,br,10H) 7.1–6.9(d,3H) 3.22(s,CH_2) 6.9–6.5(m,4H)	156.2	137.7	121.7	131.3	126.8	119.6	δ ^{11}B = +4.4
5	$CDCl_3$	6.98–7.52(m)	151.3[b]	137.4	124.8	131.0	127.5	121.4[c]	δ ^{31}P = +115 (DMSO)
7[d]	$CDCl_3$	7.98–7.5(m,3H) 7.20–6.3(m,9H)	156	137	119	129	126	118	δ ^{27}Al = 68 ω = ~ 3000 Hz
8[e]	DMSO	8.20–7.90(d,3H) 7.70–7.30(m,5H) 7.20–6.90(m,3H) 6.88–6.55(m,6H) 4.18(s,2H)	159.7	138.8	117.2	127.9	126.9	116.6	δ ^{27}Al = 66 (ω = ~ 800 Hz) δ ^{27}Al = 3.9 (ω = 30 Hz)
9[f]	$CDCl_3$	8.23–8.03(m,2H) 7.94–7.78(d,3H) 7.63–7.41(m,3H) 7.30–6.87(m,9H)	153.7	136.7	122.2	129.1	126.2	118.1	

[a] Benzyl carbons δ ^{13}C = 45.4(CH_2), 134.5(*i*), 128.4(*o*), 128.9(*m*), 128.1(*p*). Free benzylamine 46.5, 143.4, 126.6, 128.4 and 127.0, respectively.
[b] (d, J = 12 Hz).
[c] (d, J = 3.7 Hz).
[d] δ ^{13}C broad signals ~ 4 Hz.
[e] δ ^{13}C broad signals ~ 0.7 Hz, benzyl carbons δ ^{13}C = 42.7(CH_2), 135.8(*i*), 128.3(*p*), 128.4, 128.6 (*o* or *m*).
[f] δ ^{13}C aromatic carbons 135.2(*i*), 134.9(*o*), 127.7(*m*), 129.7(*p*).

($^{11}B = -19.9$ ppm) after 24 h. It was impossible to study the reactivity of **8** in the presence of $BH_3 \cdot THF$ because **8** reacts with THF giving a red solution.

When a toluene solution of **1** was stirred with one equivalent of $Ph_3Al \cdot OEt$ at 60°C for 6 h, **7** was obtained with a half equivalent of toluene coordinated. Even after treatment of the sample *in vacuo*, at 100°C for 6 h the solvent remained. The ^1H NMR spectrum showed that DMSO-d_6 used as a solvent was also coordinated ($\delta = 3.33$ ppm). (This has been observed from traces of non-deuterated solvent.)

NMR spectroscopy

The shifts of the signals in the ^1H, ^{11}B, ^{13}C, ^{27}Al and ^{31}P NMR are shown in Table 2. ^1H NMR spectra of the complexes show a displacement to lower field and splitting of the aromatic signals due to complexation of **1**.

Carbon spectra of these compounds show a deshielding for C_1, C_2 and C_4, C_5, C_6 in major and minor extents, respectively. It can be observed that $\Delta\delta$, defined as $\Delta\delta = \delta$ complex $-\delta$ **1**, for C_2 and C_6 is almost the same in **2** and **5**, while in **7** and **9** $\Delta\delta$ is different. This suggests that the latter compounds, **7** and **9** should have an intramolecular bond, but the former compounds, **2** and **5** should not. A higher acidity of the metal is observed in **8** compared to **4** according to chemical shifts observed for C_1 and CH_2.

The aluminium compounds **7** and **8** were found in the same region on the ^{27}Al chemical shift scale, and accordingly, it is expected that in each case the metal has a similar coordination number. The linewidth is much larger for **7** and may be due to lower symmetry compared to **8**.

The determination of the structure of **9** has indicated that the geometry at silicon is a distorted trigonal bipyramid with the oxygen atoms bent away from the phenyl group and towards the nitrogen.[13] In order to complete the characterization of **9** we report here the NMR spectroscopy. ^{13}C NMR has been assigned based on the NOE decoupling mode and ^{13}C data for $C_6H_5Si(OEt)_3$ and $C_6H_5Si(OC_2H_4)_3N$.[14]

CONCLUSIONS

It is concluded that the utility of the ^1H and ^{13}C NMR spectroscopy, along with P—B coupling data in predicting the intramolecular bond of these pseudoatrane complexes is not reliable. However, addition reactions have been useful in the study of these structures, confirming that there is no internal coordination in these compounds, except for **7** and **9**.

REFERENCES

1. L. E. Carpenter II and J. G. Verkade, *J. Am. Chem. Soc.* 1985, **107**, 7084.
2. C. L. Frye, G. A. Vincent and G. L. Hauschildt, *J. Am. Chem. Soc.* 1966, **88**, 2727.
3. K. J. Lee, P. D. Livant, M. L. McKee and S. D. Worley, *J. Am. Chem. Soc.* 1985, **107**, 5901.
4. C. Camacho, M. A. Paz-Sandoval and R. Contreras, *Polyhedron* 1986, **5**, 1723.
5. D. S. Milbrath and J. G. Verkade, *J. Am. Chem. Soc.* 1977, **99**, 6607.
6. J. G. Verkade, R. W. King and C. W. Heitsch, *Inorg. Chem.* 1964, **3**, 884.
7. A. Murillo, R. Contreras, A. Klaébé and R. Wolf, *Heterocycles* 1983, **20**, 1487.
8. R. Contreras, D. Houalla, A. Klaébé and R. Wolf, *Tetrahedron Lett.* 1981, **22**, (40) 3953.
9. R. Contreras, A. Murillo, G. Uribe and A. Klaébé, *Heterocycles* 1985, **23**, 2187.
10. D. Grec, L. G. Hubert-Pfalzgraf, A. Grand and J. Riess, *Inorg. Chem.* 1985, **24**, 4642, and refs. therein.
11. R. Contreras, A. Murillo and A. Klaébé, *Heterocycles* 1984, **22**, 1307.
12. J. C. Clardy, D. S. Milbraith and J. G. Verkade, *Inorg. Chem.* 1977, **16**, 2135.
13. F. P. Boer, J. W. Turley and J. J. Flynn, *J. Am. Chem. Soc.* 1968, **90**, 5102.
14. R. K. Harris, J. Jones and S. Ng, *J. Mag. Res.* 1978, **30**, 521.

Polyhedron Vol. 7, No. 9, pp. 685–687, 1988
Printed in Great Britain

0277–5387/88 $3.00+.00
Pergamon Press plc

SYNTHESIS AND PHYSICO-CHEMICAL PROPERTIES OF DIRUTHENIUM(III, II) TETRA-ARYL CARBOXYLATO COMPOUNDS

BIRINCHI K. DAS and AKHIL R. CHAKRAVARTY*

Department of Inorganic and Physical Chemistry, Indian Institute of Science, Bangalore-560012, India

(*Received* 4 *November* 1987; *accepted* 16 *December* 1987)

Abstract—Monochloro-tetra-μ-aryl-carboxylatodiruthenium(III, II) compounds $Ru_2Cl(O_2CAr)_4$ (Ar = $-C_6H_5$; $-C_6H_4$-*p*-OCH_3), are prepared and characterized. The compounds have magnetic moments that correspond to three unpaired spins per dimer. The Ru—Ru bond order is 2.5 and the ground electronic configuration is $\sigma^2\pi^4\delta^2$ $(\delta^*\pi^*)^3$. The visible spectral band is observed at *ca* 450 nm along with a shoulder near 580 nm in DMF solution. The compounds undergo a one-electron Ru(III)Ru(II) → Ru(II)Ru(II) quasi-reversible reduction in DMF near 0.0 V *vs* sce.

Since the discovery[1] of diruthenium(III, II) compounds, several carboxylato species were prepared and characterized.[2,3] While the study is thorough on alkyl–carboxylato complexes, the chemistry of aryl–carboxylato compounds[4] has remained virtually unexplored, except in one case where only magnetic properties of $Ru_2Cl(O_2CC_6H_5)_4$ were reported.[4] We have previously shown[5] that $Ru_2Cl(O_2CAr)$ when reacted with $P(C_6H_5)_3$ in an alcoholic medium, $R'CH_2OH$, forms monomeric carbonyl compounds by a novel decarbonylation process. In this paper we report the synthesis and physico-chemical properties of two diruthenium (III, II) compounds. A comparison has been made between $Ru_2Cl(O_2CAr)_4$ and other known[2,3,6] structurally analogous diruthenium compounds.

EXPERIMENTAL

$Ru_2Cl(O_2CCH_3)_4$ was prepared using a literature procedure.[7] Solution electrical conductivity, electronic and IR spectra were recorded using a Digisun digital conductivity meter model D1-909, a Hitachi U-3400 spectrophotometer, and a Perkin–Elmer 597 infrared spectrophotometer, respectively. Magnetic measurements were carried out by the Faraday method using a Cahn R.G. electrobalance. Electrochemical studies were performed using a Princeton applied research (Par) 370-4 electrochemistry system. A planar Beckman model 39273 platinum inlaly working electrode, a platinum wire auxililary electrode and a standard calomel reference electrode (sce) were used in three-electrode measurements. All electrochemical data were obtained at 298 K and are uncorrected for junction potentials.

Preparation of monochlorotetra-μ-benzoato-diruthenium(III, II), $Ru_2Cl(O_2CC_6H_5)_4$

To a solution of 94 mg $Ru_2Cl(O_2CCH_3)_4$ (0.2 mmol) in 30 cm^3 of a 1:1 methanol–water (v/v) mixture, 146 mg of benzoic acid (1.2 mmol) were added. The mixture was heated to reflux for 4 h. It was then cooled and filtered. The brown product was washed several times with methanol and then with diethylether. The compound thus obtained was dried *in vacuo* over P_4O_{10} (Yield: 130 mg, *ca* 90%). (Found: C, 46.3; H, 2.7. Calc. for $C_{28}H_{20}O_8ClRu_2$: C, 46.6; H, 2.8). IR spectrum (KBr phase and Nujol mull): 3050(w), 1595(m), 1480(w), 1450(m), 1395(s), 1140(w), 1060(w), 1020(w), 840(m), 710(s), 685(s), 525(s), 385(m), cm^{-1} (s, strong; m, medium; w, weak).

*Author to whom correspondence should be addressed.

*Preparation of monochloro-tetra-μ-*p*-methoxybenzoatodiruthenium*(III, II), $Ru_2Cl(O_2CC_6H_4$-*p*-$OCH_3)_4$

This was prepared by using the method given above for the preparation of $Ru_2Cl(O_2CC_6H_5)_4$ (Yield: 150 mg, *ca* 90%) (Found C, 45.9; H, 3, 3. Calc. for $C_{32}H_{28}O_{12}ClRu_2$: C, 46.5; H, 3, 3). IR spectrum (KBr phase and Nujol mull): 3055(w), 2840(w), 1595(m), 1430(w), 1395(s), 1250(m), 1160(m), 840(m), 765(m), 710(w), 695(w), 635(s), 520(w), 450(m), 385(m) cm^{-1}.

RESULTS AND DISCUSSION

Brown coloured tetra-arylcarboxylato compounds, $Ru_2Cl(O_2CAr)_4$ are prepared in near quantitative yields by reacting $Ru_2Cl(O_2CCH_3)_4$ and $ArCO_2H$ in a boiling 1 : 1 (v/v) methanol–water mixture. $Ru_2Cl(O_2CC_6H_5)_4$ was earlier prepared[4] by using $Ru_2Cl(O_2CH)_4$ as the starting material and the reaction time was 7 days. Under refluxing conditions we have been able to isolate the product in 4 h. The compounds are sparingly soluble in water and in common organic solvents, but are appreciably soluble in dimethylformamide (DMF) and dimethylsulphoxide (DMSO). Physico-chemical data on $Ru_2Cl(O_2CAr)_4$ are presented in Table 1.

In DMF, $Ru_2Cl(O_2CAr)_4$ dissolves slowly and forms a brown solution. Conductivity measurements show the presence of a 1 : 1 electrolyte in solution. The species in the solution is believed to be $[Ru_2(O_2CAr)_4(DMF)_2]^+$. Structural studies[2,3,8,9] on $Ru_2Cl(O_2CR)_4$ (R, alkyl group) and $Ru_2Cl(ArCONH)_4$, show the presence of linear or zigzag $\{Ru_2—Cl—Ru_2\}_n$ chains and a relatively weak Ru—Cl bond. In polar solvents the polymer breaks into discrete dimeric units. The formation of the solvent adduct is well documented[2,6] in diruthenium(III, II) and diruthenium(II, II) systems.

IR spectra of $Ru_2Cl(O_2CAr)_4$ exhibit characteristic symmetric and antisymmetric vibrations of carboxylate ligands. The absence of a Ru—Cl stretch near 350 cm^{-1} indicates the involvement of Cl in a bridge to hold dimeric Ru_2 units together. Magnetic measurements show the presence of three unpaired spins per Ru_2 dimer in accordance[10,11] with the ground electronic configuration of $\sigma^2\pi^4\delta^2(\delta^*\pi^*)^3$, a characteristic feature of diruthenium(III, II) compounds having ruthenium in the non-integral oxidation state of +2.5 and an Ru—Ru bond order of 2.5. Electronic spectra of these compounds in DMF solution display a band near 450 nm along with a shoulder near 580 nm. While the low energy absorption could be assigned to an axial ligand $\rightarrow Ru_2$ (δ^* or π^*) transition, the higher energy band is most likely due to the $O(\pi) \rightarrow Ru_2(\pi^*)$ transition with the $O(\pi)$ primarily Ru—O bonding orbital having appreciable Ru_2–π bonding character.[10] The $O(\pi) \rightarrow Ru_2(\pi^*)$ transition is reported to occur[12] at 459 and 445 nm in $Ru_2Cl(CF_3CONH)_4$ and $Ru_2Cl(C_6H_5CONH)_4$, respectively, in DMSO solution. The diruthenium(II, II) benzoato compound, $Ru_2(O_2CC_6H_5)_4(THF)_2$ is known[6] to display a shoulder at 440 nm. The bands observed[13] in the diffuse reflectance spectrum of $Ru_2(O_2CCH_3)_4Cl$

Table 1. Physico-chemical data on $Ru_2Cl(O_2CAr)_4$ compounds

Physico-chemical measurements	Ar = -C_6H_5	Ar = -C_6H_4-*p*-OCH_3
Conductivity[a]		
Λ, $ohm^{-1}\,cm^2\,mol^{-1}$, 298 K	75.2	73.8
Electronic spectra[a,b]	451 (2200)	452 (2100)
λ_{nm}(ε, $dm^3\,mol^{-1}\,cm^{-1}$)	580(Sh)	580(Sh)
Magnetic Moment		
μ_{eff}, 298 K, (Per Ru) BM	2.74	2.67
μ_{eff}, 298 K, (per dimer) BM	3.88	3.77
Cyclic voltammetry[a,c]		
E^0_{298}, V (*vs* sce)	0.043	−0.048
ΔE_p, mV v = 50 m Vs^{-1}	240	210
= 100 m Vs^{-1}	250	230
= 200 m Vs^{-1}	270	260

[a] Solvent, dimethylformamide.
[b] Sh, shoulder.
[c] v, scan rate, ΔE_p, peak to peak separation.

at 568(Sh) and 462 nm are proposed[10] to be due to $Cl \rightarrow Ru_2(\pi^*)$ and $O(\pi) \rightarrow Ru_2(\pi^*)$ transitions, respecitvely.

Cyclic voltammetric studies in a 0.1 M tetrabutylammonium perchlorate–DMF solution of $Ru_2Cl(O_2CAr)_4$ show a single voltammogram near 0.0 V *vs* the sce reference electrode (Table 1). Both compounds undergo a quasi-reversible one-electron $Ru(III)Ru(II) + e^- \rightleftharpoons Ru(II)Ru(II)$ reduction to form a $Ru_2(O_2CAr)_4(DMF)_2$ species as is evidenced from the constant potential electrolysis carried out at a potential of 200 mV negative to the cathodic peak. The observed shift of the Ru(III)Ru(II)/Ru(II)Ru(II) couple in going from $Ar = C_6H_5$ to $Ar = C_6H_4$-*p*-OCH_3, is consistent with the inductive effect of the substituent on the phenyl ring. Addition of electron density to the antibonding $\delta^*\pi^*$ level is likely to make the system difficult for reduction. A similar effect is known[6] to occur in $Ru_2(O_2CR)_4$ complexes. A recent report[6] shows that $Ru_2(O_2CC_6H_5)_4(THF)_2$ undergoes a one-electron oxidation at 0.07 V (*vs* sce). The observed difference of 30 mV between THF and DMF adducts could be due to the difference in solvent donating capacity. A comparison among the reduction potentials of diruthenium(III, II) systems reveals[2,3,12,14–16] that E^0_{298} of the Ru(III)Ru(II)/Ru(II)Ru(II) couple follows the order O,O > O,N > N,N, where O,O; O,N and N,N are three atom anionic bridging ligands having O,O (e.g. carboxylates), O,N (e.g. amides, hydrooxypyridines) and N,N (e.g. aminopyridines) coordination at the equatorial positions. The potential is also dependent on the solvent medium. Highly polar solvents can easily remove axial Cl to form axial solvent adducts as is evidenced[12,14] from electrochemical experiments.

Acknowledgements—We thank Prof. A. Chakravorty, IACS, Calcutta, for obtaining elemental analytical and cyclic voltammetric results, and CSIR, New Delhi for financial support.

REFERENCES

1. T. A. Stephenson and G. Wilkinson, *J. Inorg. Nucl. Chem.* 1966, **28**, 2285.
2. F. A. Cotton and R. A. Walton, *Multiple Bonds Between Metal Atoms*. John Wiley (1982).
3. F. A. Cotton and R. A. Walton, *Structure and Bonding* 1986, **62**, 1.
4. M. Mukaida, T. Nomura and T. Ishimori, *Bull. Chem. Soc., Japan* 1972, **45**, 2143.
5. S. K. Mandal and A. R. Chakravarty, *Inorg. Chim. Acta*. 1987, **132**, 157.
6. A. J. Lindsay, G. Wilkinson, M. Motevalli and M. B. Hursthouse, *J. Chem. Soc., Dalton Trans.* 1985, 2321.
7. R. W. Mitchell, A. Spencer and G. Wilkinson, *J. Chem. Soc., Dalton Trans.* 1973, 846.
8. A. R. Chakravarty and F. A. Cotton, *Polyhedron* 1985, **4**, 1957.
9. A. R. Chakravarty, F. A. Cotton and D. A. Tocher, *Poplyhedron* 1985, **4**, 1097.
10. J. G. Norman, Jr., G. E. Renzoni and D. A. Case, *J. Am. Chem. Soc.* 1979, **101**, 5256.
11. V. M. Miskowski, T. M. Loehr and H. B. Gray, *Inorg. Chem.* 1987, **26**, 1098.
12. T. Malinsky, D. Chang, F. N. Feldmann, J. L. Bear and K. M. Kadish, *Inorg. Chem.* 1983, **22**, 3225.
13. R. J. H. Clark and M. R. Franks, *J. Chem. Soc., Dalton Trans.* 1976, 1825.
14. F. A. Cotton and E. Pederson, *Inorg. Chem.* 1975, **14**, 388.
15. A. R. Chakravarty, F. A. Cotton, D. A. Tocher and J. H. Tocher, *Polyhedron* 1985, **4**, 1475.
16. M. Y. Chavan, F. N. Feldmann, X. Q. Lin, J. L. Bear and K. M. Kadish, *Inorg. Chem.* 1984, **23**, 2373.

Polyhedron Vol. 7, No. 9, pp. 689–694, 1988
Printed in Great Britain

0277-5387/88 $3.00+.00
© 1988 Pergamon Press plc

POTENTIOMETRIC STUDY OF THE PROTONATION AND BINARY COMPLEXATION EQUILIBRIA BETWEEN THE HYDROGEN ION, COPPER(II) ION AND ZINC(II) ION AND THE PICOLINATE ION IN DIOXANE–WATER MIXTURES

E. CASASSAS* and G. FONRODONA

Department of Analytical Chemistry, Universitat de Barcelona, Diagonal 647, Barcelona 08028, Spain

(*Received* 27 *November* 1987; *accepted* 16 *December* 1987)

Abstract—Protonation constants of picolinic acid and stability constants of Cu(II) and Zn(II) picolinate complexes were determined potentiometrically in 50% (v/v) dioxane–water solution at 25°C and 0.2 M KNO_3. The values obtained for the constants were: protonation constants for picolinate ion: $\log\beta_1 = 5.36 \pm 0.01$ and $\log\beta_2 = 6.80 \pm 0.04$; stability constants for copper(II) complexes: $\log\beta_{1,1} = 7.766 \pm 0.001$ and $\log\beta_{1,2} = 16.826 \pm 0.007$; stability constants for the Zn(II) complexes: $\log\beta_{1,1} = 6.10 \pm 0.05$, $\log\beta_{1,2} = 11.47 \pm 0.03$ and $\log\beta_{1,3} = 15.77 \pm 0.08$. No protonated nor hydroxo-complex was detected in the metal ion-picolinate systems.

Picolinic acid (Hpic) shows two well-defined forms in the extreme zones of pH; it is wholly protonated in strong acid medium and wholly deprotonated in the basic medium: the neutral species is found in equilibrium with the predominating zwitterionic form[1–4] in the intermediate zone. It has been shown[4] that in aqueous solution the protonation of the nitrogen atom in the heteroatomic nucleus takes place in a more acidic range than the protonation of the carboxylate group, and that the macroscopic constants for the equilibria: $pic^- + 2H^+ \rightleftharpoons H_2pic^+$ and $pic^- + H^+ \rightleftharpoons Hpic$ are $\log\beta_2 = 6.22$ and $\log\beta_1 = 5.22$.

In the course of a general study of the solvent effects on complexation equilibria, extensive use has been made of dioxane–water mixtures.[5,6] Complexation equilibria in the Cu(II)–picolinate and the Zn(II)–picolinate systems are studied in this paper in the same mixed solvent. A prior study of protonation equilibria of the picolinate ion in the same solvent was needed. The evaluation of stability constants for the metal complexes only requires the knowledge of exact values of the overall protonation constants in the same medium and the microscopic constants are not needed. A knowledge of these constants would be useful in the determination of the exact atom where protonation takes place or the exact atom which acts as the donor in complex formation. This structural conclusion is out of the scope of this work which describes the evaluation from fem data of constants which have only a thermodynamic meaning.

Protonation equilibria of the picolinate ion (pic) have been studied mainly in aqueous solution and only scarcely in dioxane–water mixtures,[7] which, on the other hand, are frequently used in the studies of solution equilibria. The physiological activity of several pyridine carboxylic acid derivatives may be one of the main reasons for the interest shown on the behaviour of their aqueous solutions.

The complexes in the Cu–pic system were obtained in the very acidic zone, at pH < 2.0; and their formation constants in aqueous solution were determined using spectrophotometric[8] or polarographic[9] methods. Casassas and Tauler[4] evaluated the formation constants for the complexes obtained in this system in an aqueous medium using emf data obtained simultaneously from a glass electrode and from a copper(II) ion selective electrode; they observed a much better fit with the measurements performed with the copper(II) ion selective electrode. Only Holmes and Crimmin[7] reported a partial study on the equilibriums in this system in dioxane–water mixtures.

For the Zn–pic system in aqueous solution, up

* Author to whom correspondence should be addressed.

to three successive complexes (all of them already present in solutions of pH < 4.0) have been studied.[10] No reference is found for this system in dioxane–water solvents.

EXPERIMENTAL

(1) *Reagents and solutions*

Picolinic acid (Fluka, purum), nitric acid (Merck, analytical–reagent grade), copper(II) nitrate and zinc(II) nitrate (both Merck, analytical–reagent grade) were used without further purification. Potassium nitrate (Probus, analytical grade) was purified by recrystallization in water. Ligand solutions and metal ion solutions were prepared from these reagents in dioxane–water (1 : 1, v/v) mixtures, at 0.2 mol l^{-1} ionic strength, adjusted with potassium nitrate. Metal ion solutions were standardized by EDTA titration. CO_2-free potassium hydroxide (Merck, analytical reagent grade) solutions in dioxane–water (1 : 1, v/v) prepared and standardized as usual[11] were used as the titrant. The mixed solvent used was prepared from dioxane (Carlo Erba) purified by Eigenberger' method[12] and doubly distilled freshly boiled water.

(2) *Apparatus*

The potentiometric cell was

Ag/AgCl/KCl(sat)/test solution/working electrode.

Values of the emf of the potentiometric cell were taken with an Orion 701A potentiometer (accuracy ± 0.1 mV), using a reference Ag/AgCl electrode (Orion 9005 with a keramic type junction) and a different working electrode according to the nature of the test solution: a glass electrode (Orion 9101), a copper(II) ion selective electrode (Orion 94-29) or a zinc amalgam electrode. The cell was thermostated externally at 25 ± 0.1°C. The titrant was added with a Metrohm Multidosimat E415 burette cylinder 552 with an antidiffusion burette tip.

The potentiometric assembly was controlled by an HP9816 microcomputer via an HP3421A data acquisition control unit (for details see ref. 5).

(3) *Procedure*

(a) *Calibration.* The glass electrode was calibrated in the working medium (dioxane–water 1 : 1, (v/v), 0.2 M ionic strength) by Gran'titrations[13] and the calibration parameters were evaluated using a multiparametric data-fitting procedure, or Gran's plots. As the protonation of the nitrogen atom in picolinic acid takes place at rather low pH, the value of the liquid junction potential was determined between the pH range from 0.7 to 2.0 (from emf readings taken in a solution which was initially 0.2 M in mineral acid and which was successively diluted by addition of a solution 0.2 M in KNO_3 all in the same mixed solvent). Results were obtained for the simultaneous determination of the standard potential, E_0, and j_H (the slope in the classical expression for the liquid junction potential, $E_0 = j_H [H^+]$) for this electrode in strongly acidic solutions and are given in Table 1, where the technique used for the evaluation of these parameters is also shown. The values obtained for j_H in the working potentiometric cell showed a rather high degree of dispersion, probably due to the known behaviour of the keramic junction reference electrode[14] used. The mean value of j_H adopted for further work is 16.14 mV mol^{-1} l; which implies that the liquid junction potential must be taken into account, given the precision of the potentiometer used, in all readings taken in solutions below pH 2.1. In order to obtain precise values for the second protonation constant of picolinate ion, LETAGROP[15] and MINIGLASS[16] programs were used because both accept as input the j_H values previously known for the treatment of the emf data. (LETAGROP can also perform the simultaneous refining of j_H, E_0 and log K).

The copper(II) ion selective electrode was calibrated from readings taken in a solution which was initially 0.2 M HNO_3 in dioxane–water (1 : 1, v/v) and into which successive known amounts of copper(II) ion were added, and also from readings taken from the titration of a copper(II) ion solution with EDTA (both in the same solvent and at the same ionic strength). In the copper(II) ion concentration range of 6.3×10^{-7}–3.98×10^{-2} M, a Nernstian behaviour was observed for this electrode, with a g value of 29.8 ± 1.2 mV.

The zinc amalgam electrode was prepared by controlled electrolysis of a zinc(II) nitrate solution between a zinc anode and a mercury cathode,[17] up to a zinc concentration in the amalgam in the range 0.6–1.6%. The amalgam was kept under a nitrogen-saturated diluted nitric acid solution. The amalgam electrode used was similar in shape to the *J*-electrode described by Holloway and Reilley.[18] Calibration of this electrode was performed in the pH range from 5.0 to 6.0, where its response is pH-independent, as observed by Perrin and Sayce,[19] and the calibration procedure was like the one described for the Cu(II)–ISE. Nernstian behaviour was obtained in the Zn(II) concentration range from 6×10^{-5}–2×10^{-3} M, and the g value was 27.8 ± 1.7 mV.

(b) *Protonation of picolinic acid* (pic). A known

Table 1. Results from numerical treatment of data for the glass electrode calibration in strongly acidic medium

Curve No.	Number of points	E_0	j_H	Correlation coefficient	U	σ	Method
1	51	384.8	19.35	0.997	—	—	LR
		384.8	19.40	—	1.4E−5	5.4E−5	(16)
2	51	384.3	10.70	0.960	—	—	LR
		384.2	13.00	—	1.0E−3	1.0E−3	(16)
3	50	384.6	9.71	0.975	—	—	LR
		384.4	11.60	—	1.5E−5	5.6E−4	(16)
4	40	383.5	18.42	0.992	—	—	LR
		383.3	20.30	—	2.9E−5	9.0E−4	(16)
5	21	383.6	14.30	—	4.4E−6	6.6E−4	(16)
6	26	384.3	16.50	—	4.3E−5	1.3E−3	(16)
7	27	384.3	17.30	—	3.8E−5	1.3E−3	(16)
8	17	384.4	17.60	—	2.2E−5	1.3E−3	(16)
9	19	384.2	14.70	—	7.9E−6	7.5E−4	(16)
10	19	395.2	12.54	0.920	—	—	LR
		395.4	10.70	—	1.4E−4	2.7E−3	(16)
all curves		16.14±2		0.999988	—	—	LR
		16.27±0.2		—	8E−3	6E−3	(16)

U: minimization function of MINIGLASS program (in pH).
σ: standard deviation of the residuals.
LR: linear regression.
(16): MINIGLASS program.

amount of picolinic acid was added to a solution with a known concentration of mineral acid in the titration cell. Five solutions containing HNO_3 concentrations in the range 0.18–0.19 M and pic concentrations in the range 0.029–0.060 M were titrated with 0.02 M potassium hydroxide. After each titrant addition the emf was read using a previously calibrated glass electrode. The stabilization time for the readings was always less than 3 min.

(c) *Complexation in the* Cu(II)–pic *system.* A glass electrode in a solution of known mineral acid concentration was calibrated according to Gran[13] from a few readings in a rather strong acidic medium. At a given acidity, the glass electrode is switched off and a copper(II)–ISE is switched on and the latter is calibrated from readings taken after several copper(II) nitrate additions. The solution is titrated using a pic solution as titrant and emf readings are taken with each of the electrodes after each titrant addition. Ten different solutions initially containing Cu(II) ion concentrations in the range 0.002–0.020 M, and HNO_3 concentrations in the range 0.07–0.12 M were titrated with pic solutions. The titrant concentration was in the range 0.09–0.17 M. Different titrations were ended when the molar ratio pic : Cu(II) reached different prefixed values in the range 2.0–10.0. As Cu(II) complexation occurs at strongly acid pH, readings from the glass electrode showed small changes during the titration and the evaluation of the stability constants of the complexes formed must be carried out using readings obtained by the Cu(II) ion selective electrode.

(d) *Complexation in the* Zn(II)–pic *system.* The study was done using the glass and the zinc amalgam electrodes. The experimental procedure was similar to the one described for the copper ion system.

Using the zinc amalgam electrode, five different acid solutions containing Zn(II) concentrations in the range 0.0016–0.0032 M were titrated with 0.0597 M potassium picolinate until the final ligand-to-metal ratio was in the range 3.0–7.0.

Using the glass electrode to obtain more significant results for the predominant formation of the 1 : 1 complex, four different solutions containing the zinc(II) ion in the concentration range 0.003–0.012 M and pic in the range 0.0038–0.016 M (ligand-to-metal ratios from 3.6 to 1) were titrated with 0.1973 M potassium hydroxide. In the second series of experiments, planned to study the simultaneous formation of the 1 : 1, 1 : 2 and 1 : 3 species, seven solutions with Zn(II) in the range 0.0009–0.0017 M and pic in the range 0.0039–0.0125 M (ligand-to-metal ratio from 3.0 to 10.0) were titrated with the same titrant.

Table 2. Values of the protonation constants of picolinate ion in dioxane–water (1 : 1, v/v) at 0.2 M KNO_3 ionic strength and at 25°C, obtained from the treatment of emf data by LETAGROP or MINIGLASS programs

	LETAGROP		
	Val 1[a]	Val 4[b]	MINIGLASS
$\log \beta_1$	5.37±0.04	5.361±0.007	5.356±0.003
$\log \beta_2$	6.93±0.05	6.80±0.04	6.81±0.015
Standard deviation	1.351	1.585	0.030
U	0.513 10^3	0.706 10^3	0.270

Total number of curves: 5
Number of points: 307

[a] Val 1: minimization function of residuals in total acid concentration.
[b] Val 4: minimization function of residuals in potential.

RESULTS

The values of the protonation constants of the picolinate ion in the dioxane–water (1 : 1, v/v) solution at 0.2 M ionic strength and 25°C obtained from the numerical analysis of the experimental emf data using the computer programs LETAGROP[15] and MINIGLASS,[16] are shown in Table 2, together with resulting statistical parameters. From these values of the constants, the distribution of species of picolinic acid as a function of pH was evaluated (Fig. 1).

The values of the stability constants for the complexes detected in the copper(II) ion–picolinate ion system in the before mentioned solvent and ionic strength, obtained from the treatment of the emf data with the programs MINIQUAD[20] and SUPERQUAD,[21] are given in Table 3. The results for the complexes detected in the zinc(II) ion–picolinate ion system, where the numerical treatment was performed by means of the three mentioned programs, are given in Table 4. Figures 2 and 3 give

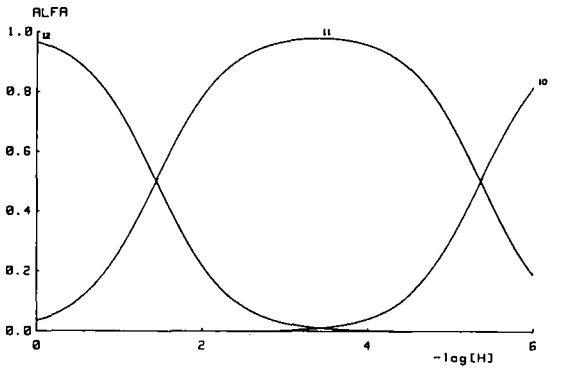

Fig. 1. Distribution plot of the species of picolinic acid. In the figure, 10, 11 and 12 refer respectively to the species pic^-, Hpic and H_2pic^+.

Table 3. Values of the formation constants of the complexes obtained in the binary system Cu(II)–pic in dioxane–water (1 : 1, v/v) at 0.2 M KNO_3 ionic strength and at 25°C, obtained from the treatment of emf data by MINIQUAD or SUPERQUAD programs

		SUPERQUAD	
	MINIQUAD	Mode 0	Mode 1
$\log \beta_1$	8.702±0.006	8.766±0.001	8.747±0.006
$\log \beta_2$	18.869±0.008	16.826±0.007	16.921±0.008
χ^2	268.5	37.52	21.2
Sigma		5.1	1.5
U	1.5×10^{-6}		
SK	−0.23		
K	12.40		
F	0.00086		

Total number of curves: 10
Number of points: 275

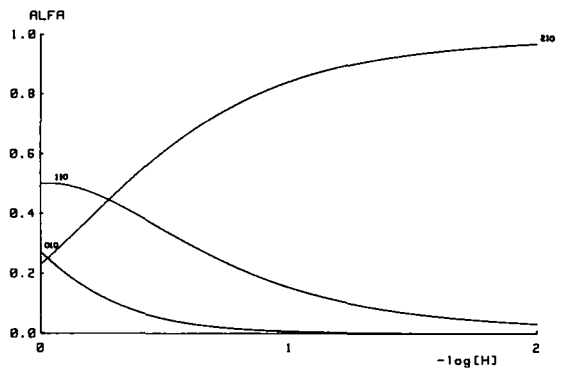

Fig. 2. Distribution plot of the species which contain copper(II) in the Cu(II)–pic system. In the figure, 010, 110 and 210 refer respectively to Cu(II), Cupic and $Cu(pic)_2$. ALFA is the ratio of each species concentration to total copper(II) concentration.

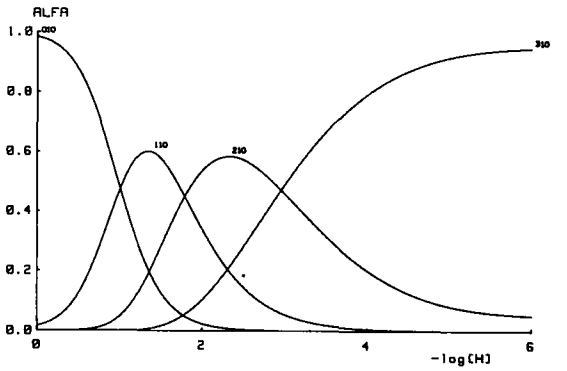

Fig. 3. Distribution plot of the species which contain zinc(II) in the Zn(II)–pic system. In the figure, 010, 110, 210 and 310 refer respectively to Zn(II), Znpic, $Zn(pic)_2$ and $Zn(pic)_3$. ALFA is the ratio of each species concentration to total zinc(II) concentration.

the distribution plots of the metal ion containing species, respectively, in the systems Cu–pic and Zn–pic, as a function of pH, evaluated from the obtained numerical values of the stability constants.

DISCUSSION

(a) *Protonation constants of picolinate ion*

Values given in Table 1 show for the first protonation constant of pic, a very narrow confidence range and quite good statistical parameters, which indicate a very good fit. For the second protonation constant the confidence range is wider, and the fit is not as good as the former, due to the very acidic range ($pH < 2.0$) in which this protonation equilibrium occurs. The values of $\log\beta$ obtained for both protonation steps in the dioxane–water mixture used as solvent are higher than those obtained in aqueous solution ($\log\beta_1 = 5.21$ and $\log\beta_2 = 6.21$ according to ref. 4), as usual in this mixed solvent. It is useful to note the very low value obtained for $\log K_2 = 1.56$, which can be explained by an extra stabilization of the zwitterionic form of the picolinic acid (in tautomeric equilibrium with the non-charged molecular form) due to the contributing effect of the aromatic system in the pyridine nucleus. Thus, aliphatic α-aminoacids in water have $\log K_2$ values in the neighbourhood of 2.3 (e.g. 2.36 for aminoacetic acid, 2.30 for L-2-amino-

Table 4. Values of the formation constants of the complexes obtained in the binary system Zn(II)–pic in dioxane–water (1 : 1, v/v) at 0.2 M KNO_3 ionic strength and at 25°C, obtained from the treatment of emf data by MINIGLASS, MINIQUAD or SUPERQUAD programs for every series of experiences

Series	1	2	3
Working electrode	Zn(Hg)	G.E	G.E
Number of curves	5	6	7
Number of points	129	221	326
Program	MINIQUAD	SUPERQUAD	MINIGLASS
$\log\beta_{1,1}$	6.3±0.2	6.23±0.02	6.23±0.04
$\log\beta_{1,2}$	11.2±0.4	—	11.49±0.03
$\log\beta_{1,3}$	16.9±0.5	—	15.84±0.03
Program			SUPERQUAD
$\log\beta_{1,1}$			6.10±0.05
$\log\beta_{1,2}$			11.47±0.03
$\log\beta_{1,3}$			15.77±0.08

propanoic acid), but when a heteroatomic N is involved, the value drops to 1.0 (for picolinic acid in water) or to 1.56 (for the same in dioxane–water).

(b) Cu(II)–pic *system*

The formation of the different complex species in the Cu(II)–pic system occurs in a very acidic range (pH < 2.0), but protonated complexes have not been detected. It must be accepted then, that the picolinate ion acts as a bidentate ligand. The model which contains the 1 : 1 and 1 : 2 species describes quite well this binary system, as shown by statistical parameters in Table 3. The values obtained for the formation constants are lower than those obtained in the water solution,[4] as usual.

(c) Zn(II)–pic *system*

In this binary system, as in the Cu(II)–pic system, the picolinate ion acts as a bidentate ligand and a model including the 1 : 1, 1 : 2 and 1 : 3 complexes describes the data fairly well. This same model was accepted by Anderegg[10] for his data in an aqueous solution. The formation of the complexes occurs at acidic pH (below 4.0), but, as before, protonated complexes are not formed.

As Table 4 shows, from emf data obtained with the zinc amalgam electrode, the evaluated formation constants are not very reliable, since their confidence intervals are rather high, as a result of the fact that at optimum working pH (5.0–6.0) for this electrode the highest complex is by far the predominating species (see the distribution plot in Fig. 3). In order to study the formation of the lower species, solutions at lower pH are needed and these solutions can be best studied with the glass electrode. As can be seen in Table 4, two series of experiments performed using different concentrations and different concentration ratios allowed the evaluation of $\log \beta$ for the first complex and for the three co-existent complexes with satisfactorily narrow confidence intervals. The quite low pH of the starting solution (pH < 2.0) required the liquid junction potential to be taken into account in the calibration process as well as in the complex forming experiments.

REFERENCES

1. M. Paris, Thesis, Lyon (1963).
2. H. Jaffé, *J. Am. Chem. Soc.* 1955, **77**, 4445.
3. R. F. Evans, E. F. G. Herington and W. Kynaston, *Trans. Faraday Soc.* 1953, **49**, 1284.
4. E. Casassas and R. Tauler, *J. Chim. Phys.* 1984, **81**, 557.
5. E. Casassas, G. Fonrodona and R. Tauler, *Polyhedron* 1987, **6**, 1517.
6. E. Casassas and G. Fonrodona, *J. Chim. Phys.*, submitted for publication.
7. F. Holmes and W. R. C. Crimmin, *J. Chem. Soc.* 1955, 1175 and 3467.
8. C. Petitfaux, J. P. Barbier and J. Faucherre, *Bull. Soc. Chim. France* 1970, 3441.
9. K. Susuki, M. Yasuda and K. Yamasari, *J. Phys. Chem.* 1957, **40**, 576.
10. G. Anderegg, *Helv. Chim. Acta* 1960, **43**, 414.
11. J. E. Powell and M. A. Hiller, *J. Chem. Ed.* 1957, **34**, 330.
12. A. I. Vogel, *Textbook of Practical Organic Chemistry*, p. 177. Longmans, London (1961).
13. G. Gran, *The Analyst* 1952, **77**, 661.
14. F. J. C. Rossotti, *Talanta* 1974, **21**, 809.
15. (a) N. Ingri and L. G. Sillén, *Arkiv. för Kemi* 1964, **23**, 97; (b) P. Brauner, L. G. Sillén and R. Whiteker, *Arkiv för Kemi* 1968, **31**, 365.
16. A. Izquierdo and J. L. Beltran, *Anal. Chim. Acta* 1986, **181**, 87.
17. G. Schorsch, *Bull. Soc. Chim. France* 1964, 1456.
18. J. H. Holloway and C. N. Reilley, *Anal. Chem.* 1960, **32**, 249.
19. D. D. Perrin and I. G. Sayce, *J. Chem. Soc. (A)* 1967, 82.
20. A. Sabatini, A. Vacca and P. Gans, *Talanta* 1974, **21**, 53; A. Sabatini, A. Vacca and P. Gans, *Inorg. Chim. Acta* 1976, **18**, 237.
21. P. Gans, A. Sabatini and A. Vacca, *J. Chem. Soc., Dalton Trans.* 1985, 1195.

Polyhedron Vol. 7, No. 9, pp. 695–703, 1988
Printed in Great Britain

0277-5387/88 $3.00+.00
© 1988 Pergamon Press plc

SYNTHESIS AND CHARACTERIZATION OF COPPER(II) AND ZINC(II) COMPLEXES OF CHELATING LIGANDS DERIVED FROM 2,6-DIACETYLPYRIDINE AND PHENYLALANINE/TYROSINE/HISTIDINE/HISTAMINE AND 2-(2-AMINOETHYL)-PYRIDINE

W. L. KWIK,* K. P. ANG and ALICE W. N. TAY

Department of Chemistry, National University of Singapore, Lower Kent Ridge, Singapore 0511

(*Received* 21 *July* 1987; *accepted after revision* 21 *December* 1987)

Abstract—The copper(II) and zinc(II) complexes of Schiff base ligands L^1 and L^2 derived from the condensation of 2,6-diacetylpyridine with 2 mol of phenylalanine methyl ester or tyrosine ethyl ester have been prepared. The IR spectral data indicate that the ester group undergoes hydrolysis in the formation of the Zn(II) complexes more readily than that of the Cu(II). The ^1H and ^{13}C NMR spectra of the Zn(II) complexes of L^1 and L^2 as well as those derived from condensation of 2,6-diacetylpyridine and histidine methyl ester (L^3), histamine (L^4) and 2-(2-aminoethyl)-pyridine (L^5) were examined. Differences in IR spectral properties as well as in chemical shifts of similar ^1H and ^{13}C nuclei in these five types of complexes have been attributed to significant Zn(II)–carboxylate oxygen interactions in complexes of L^1 and L^2.

Metal complexes of Schiff bases derived from the condensation of a dicarbonyl and various amines, have of late received considerable attention[1–8] in the design of synthetic models for O_2-transport metalloproteins. For example, Wilson *et al.*[4–6] synthesized the copper(I), copper(II) and zinc(II) complexes of the open-chain pentadentate ligands formed by condensation of 2,6-diacetylpyridine with 2 mol of histamine (imep) or 2-(2-aminoethyl)-pyridine (pyep). In the solid state, all five nitrogen atoms of the ligand system in $[Cu(imep)]^{2+}$ and $[Zn(imep)]^{2+}$ are shown by X-ray crystal studies[5,6] to be bonded to the metal, to yield a coordination geometry intermediate between a trigonal bipyramid and a square pyramid. The Cu(I), Cu(II) and Zn(II) complexes of a closely related ligand (bisp) derived from 2,6-diacetylpyridine and l-histidine methyl ester were subsequently prepared by Ibers *et al.*[7] via metal ion template condensation. X-ray crystallographic study shows that this ligand also serves as a pentadentate.

The constraint on the coordination geometry of the metal ions in complexes of all these five nitrogen Schiff bases is apparent. Thus, it has been presumed that the corresponding Cu(I) complexes also assume the rather uncommon pentacoordinate structure.[5,6] More recently, acyclic Schiff base ligands containing only three nitrogen donor atoms have been obtained by Nelson *et al.*[3] via condensation of 2,6-diacetylpyridine and 2 mol of aliphatic amines. In complexes of these ligands, four coordination could be achieved by the metal ion through interaction with the aliphatic side chain.

It is of considerable interest to note that there is significant difference in the chemical behaviour of the Cu(I) complexes of the 5N and those of the 3N Schiff bases. Whereas the former display reactivities towards dioxygen only, those of the 3N Schiff bases, in addition, bind carbon monoxide reversibly.

In the present investigation we set out to examine ligand systems that would allow for changes in coordination geometry as the metal ions are varied. The ligands L^1 and L^2 (Scheme 1) derived from condensation of 2,6-diacetylpyridine and phenylalanine methyl ester or tyrosine ethyl ester, respectively, contain three nitrogen donor atoms as well as ester carboxylate groups in the side chain, so

* Author to whom correspondence should be addressed.

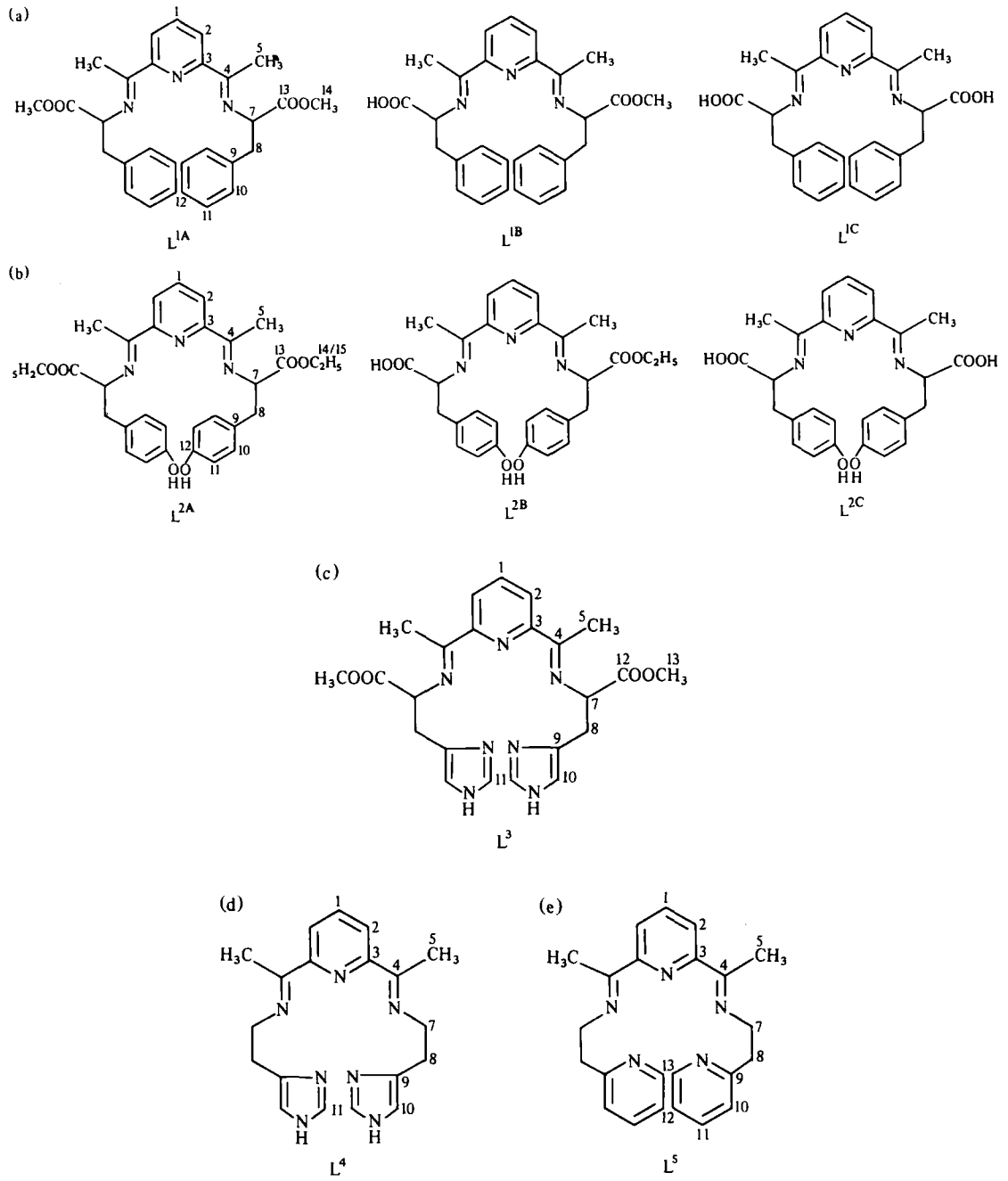

Scheme 1. Schiff bases derived from 2,6-diacetylpyridine and (a) phenylalanine methyl ester; (b) tyrosine ethyl ester; (c) histidine methyl ester; (d) histamine; (e) 2-(2-aminoethyl)-pyridine.

that an increase in coordination number may be achieved. For the purpose of probing the modes of interaction between L^1 or L^2 with the d^9 and d^{10} ions, the syntheses and various spectral studies of the Cu(II) and Zn(II) complexes of these Schiff base ligands have been undertaken. Furthermore, for comparison purposes, the spectral properties of the Cu(II) and Zn(II) complexes of bisp, imep and pyep* are examined under comparable experimental conditions.

EXPERIMENTAL

Synthesis

All solvents were deoxygenated and stored under nitrogen over molecular sieves (4 Å). Methanol,

* These have been labelled as L^3, L^4 and L^5 as shown in Scheme 1, in the following text.

acetonitrile and dichloromethane were treated according to published procedures prior to use. Spectrochemical grade dimethyl sulphoxide (Aldrich, Gold Label) was used for electronic, electrochemical and conductivity measurements. Deuterated dimethyl sulphoxide (Aldrich, Gold Label) for NMR spectral studies was stored under nitrogen in a dry-box.

2,6-diacetylpyridine and 2-(2-aminoethyl)-pyridine (Aldrich Chemical Co.) were used as received. Phenylalanine methyl ester hydrochloride, tyrosine ethyl ester hydrochloride, histidine methyl ester dihydrochloride and histamine dihydrochloride (Sigma Chemical Co.) were treated to remove the hydrochloride. Electrochemical grade tetraethylammonium perchlorate (Eastman Chemicals) was used without further purification.

In the syntheses of all the copper(II) and zinc(II) complexes in this study, the ligand solution was first prepared by allowing 2,6-diacetylpyridine and the base (amino acid esters/histamine/2-(2-aminoethyl)-pyridine) to reflux in dry, deoxygenated MeOH. Great care was taken to eliminate moisture from the solvents and glassware since the final products were hygroscopic. Phenylalanine methyl ester, tyrosine ethyl ester, histidine methyl ester and histamine were freed from their respective hydrochloride salts by the method described by Casella *et al.*[7] Tetra(acetonitrile)copper(I) tetrafluoroborate was prepared by the method of Hemmerich and Sigwart.[9]

Complex (**1A**), $[CuL^{1A}](BF_4)_2$. A ligand solution was prepared by refluxing a methanolic solution (100 cm^3) of 2,6-diacetylpyridine (2 mmol) and phenylalanine methyl ester (4 mmol) under nitrogen for about 20 h. The yellow solution was allowed to cool to room temperature before the addition of the BF_4^- salt of copper(II). Solvent removal from the orange solution yielded a hygroscopic, dark reddish–brown solid which was recrystallized from CH_3CN and then dried *in vacuo* at 80°C for 6 h.

Complex (**1B**), $[CuL^{1B}](BF_4)_2$. The method of preparation of this complex differed from that of complex (**1A**) in the recrystallization steps: the dark reddish–brown solid was washed with isopropanol and then recrystallized from CH_3CN.

Complex (**2A**), $[CuL^{2B}](BF_4)_2$ *and complex* (**2B**), $[CuL^{2C}](BF_4)_2$. The method employed was similar to that for the synthesis of complex (**1A**), with tyrosine ethyl ester substituting for phenylalanine methyl ester. After solvent removal, the yellowish–brown solid obtained was recrystallized from MeOH to give a dark brown product, complex (**2A**). A portion of complex (**2A**) was further crystallized from CH_3CN to yield complex (**2B**).

Complex (**3**), $[CuL^{2C}](NO_3)_2$ *and complex* (**4**), $[CuL^{2B}](OAc)_2$. These two complexes were prepared in a manner similar to that for complex (**2A**) except that $Cu(NO_3)_2 \cdot 3H_2O$ and $Cu(OAc)_2 \cdot H_2O$ were used as the respective sources of copper(II).

Complexes (**5A**)–(**10**). In the syntheses of these complexes, the ligand solution was first prepared by refluxing 2,6-diacetylpyridine (2 mmol) and histidine methyl ester (4 mmol) in MeOH (50 cm^3) under nitrogen for about 6 h to produce an intense yellow colouration. To this was added a methanolic solution (50 cm^3) of the copper(II) salt (2 mmol).* Solvent removal from the dark green solution gave a hygroscopic product which was washed with CH_2Cl_2 then recrystallized from MeOH.

Complex (**11**), $[CuL^4](BF_4)_2$ *and complex* (**12**), $[CuL^5](NO_3)_2$. The method of preparation for complex (**1A**) was applied with histamine and 2-(2-aminoethyl)-pyridine substituting for phenylalanine methyl ester.

Complexes (**13A**)–(**17B**). The ligand solution was prepared in the same manner as for the copper(II) complexes. After the yellow solution had cooled to room temperature, a methanolic solution of the ClO_4^- or NO_3^- salt of zinc(II) was added to produce an orange solution which was stirred for $\frac{1}{2}$ h. Upon solvent removal, isopropanol was added to the extremely hygroscopic, yellow product. This extraction was repeated with fresh portions of isopropanol in the case of complexes (**13A**) and (**14A**). The resulting hygroscopic, yellow solid was washed with CH_2Cl_2 then dried *in vacuo* at 60°C for 4 h.

Measurements

Infrared spectra in the region 4000–400 cm^{-1} were recorded on a Perkin–Elmer Model 1710 Fourier Transform Infrared spectrometer. Spectra extending into the far-IR region of 200 cm^{-1} were recorded on a Perkin–Elmer Model 567 spectrometer calibrated with polystyrene film. CsI and KBr pellets were employed throughout. Electronic spectra were recorded on a Perkin–Elmer Lambda 9 UV/vis/near IR spectrophotometer. Conductivities of 10^{-3} M solutions of the complexes were measured at 30°C using a CM-115 conductivity meter (Kyoto Electronics). Magnetic susceptibilities for the complexes in the solid state were determined by the Faraday technique at 25°C on a Cahn Model RTL #7050 magnetic susceptibility system. Corrections for ligand and anion diamagnetism were estimated by measurements on zinc(II) complexes with the use of appropriate Pascal constants. Cyclic voltammograms were obtained in DMSO solutions

* In the case of complex (**5B**), approximately 10% excess of the BF_4^- salt was added.

at room temperature under a constant flow of N_2 using a Pine Instrument RDE 4 potentiostat. A three-electrode system was employed with a glassy carbon ring-disc electrode (disc radius = 0.382 cm) serving as the working electrode, a platinum foil as the counter electrode and a saturated calomel electrode (SCE) as the reference electrode. All solutions were 0.1 mol dm^{-3} in tetraethylammonium perchlorate and 10^{-3} moll dm^{-3} in the complex.

RESULTS AND DISCUSSION

Synthesis

The ligand solutions of L^1 and L^2 were prepared by prolonged refluxing under N_2 of 2,6-diacetylpyridine and 2 mol of phenylalanine methyl ester or tyrosine ethyl ester in carefully dried MeOH. When an intensely yellow colour developed, a methanolic solution of Cu(II) or Zn(II) salt was added. The desired complex was isolated after the resultant solution had been stirred for about $\frac{1}{2}$ h. Those of L^3, L^4 and L^5 were prepared by methods adapted from the literature.

All the Cu(II) and Zn(II) complexes were characterized by microanalysis, IR spectral and electrical conductance measurements (Table 1). Magnetic susceptibility measurements were also performed on the less hygroscopic Cu(II) complexes (Table 1). In general the molar conductance values in MeOH, DMSO and MeCN fall into the range for 1 : 2 electrolytes. The somewhat low values for complexes (**4**) and (**8**) suggest a possible bridging effect due to OAc^- and SO_4^{2-}, respectively. That OAc^- is likely to bridge between Cu(II) centres may account for the observed low value of the magnetic moment for complex (**10**).

Table 1. Microanalysis (%), conductivity data and magnetic moment

Complex	Microanalysis (%) Found C	H	N	Cu/Zn	Calculated C	H	N	Cu/Zn	Conductivity data and magnetic moment at 30°C Δ_M (mho cm^2 mol^{-1}) MeOH	DMSO	CH_3CN	μ(BM)
(**1A**) $[CuL^{1A}](BF_4)_2$	47.0	4.4	5.7	8.8	47.0	4.5	5.7	8.6	167	79	177	
(**1B**) $[CuL^{1B}](BF_4)_2$	47.2	4.0	6.1	8.9	47.5	4.0	5.9	9.0	—	—	—	
(**2A**) $[CuL^{2B}](BF_4)_2$	45.9	4.3	5.6	8.8	46.2	4.0	5.6	8.4	128	82	220	
(**2B**) $[CuL^{2C}](BF_4)_2$	43.7	4.1	5.4	8.9	43.6	3.9	5.7	8.6	132	79	202	
(**3**) $[CuL^{2C}](NO_3)_2$	43.4	4.6	9.7	8.8	43.4	4.4	9.4	8.5	130	76	—[a]	
(**4**) $[CuL^{2B}](OAc)_2$	54.1	5.7	5.9	8.5	54.0	5.4	5.7	8.7	47	10	—	
(**5A**) $[CuL^3](BF_4)_2$	37.6	4.4	13.1	8.9	37.4	4.2	13.3	8.6	200	72	—	
(**5B**) $[CuL^3](BF_4)_2 \cdot \frac{1}{2}[Cu(CH_3CN)_4]BF_4$	37.7	3.8	14.1	11.5	37.7	3.8	14.6	11.1	149	60	222	1.99
(**6**) $[CuL^3](NO_3)_2$	37.4	4.3	16.9	8.1	37.2	4.9	17.0	8.6	220	83	182	
(**7**) $[CuL^3](BPh_4)_2 \cdot Cu(NO_3)_2$	62.7	4.9	9.3	8.9	62.9	5.0	9.3	9.4	121	—	—	1.92
(**8**) $[CuL^3]SO_4$	38.8	4.6	13.9	8.5	38.6	5.1	13.7	8.9	63	15	—	2.08
(**9**) $[CuL^3]Cl_2 \cdot 2HCl$	36.4	5.1	13.3	9.0	36.6	5.0	13.0	8.4	207	76	190	1.96
(**10**) $[CuL^3](OAc)_2$	50.2	5.2	15.7	9.4	50.1	5.1	15.2	9.8	137	40	—	1.55
(**11**) $[CuL^4](BF_4)_2$	34.8	4.9	15.1	9.4	34.6	4.7	14.9	9.6	222	80	—	
(**12**) $[CuL^5](NO_3)_2$	46.3	4.8	18.5	10.9	45.7	5.0	16.2	10.5	150	67	238	
(**13A**) $[ZnL^{1C}](ClO_4)_2$	43.0	3.7	5.5	8.5	42.9	3.8	5.6	8.7	—	—	—	
(**13B**) $[ZnL^{1A}](ClO_4)_2$	46.3	4.4	6.0	8.8	46.4	4.1	5.6	8.7	137	44	—	
(**13C**) $[ZnL^{1A}](NO_3)_2$	—[b]	—	—	—	—	—	—	—	—	—	—	
(**14A**) $[ZnL^{2C}](ClO_4)_2$	41.8	3.6	5.5	8.2	41.6	3.6	5.4	8.4	—	—	—	
(**14B**) $[ZnL^{2B}](NO_3)_2$	46.0	4.5	9.1	8.2	45.8	4.7	9.2	8.6	141	70	—	
(**15A**) $[ZnL^3](ClO_4)_2 \cdot 2HCl$	31.5	4.3	11.1	7.5	31.6	4.2	11.2	7.5	240	80	—	
(**15B**) $[ZnL^3](NO_3)_2$	37.3	4.8	17.0	8.4	37.1	5.0	16.9	8.8	179	75	—	
(**16**) $[ZnL^4](NO_3)_2$	35.3	5.2	19.5	9.3	35.3	5.4	19.5	10.0	—	66	259	
(**17A**) $[ZnL^5](ClO_4)_2$	43.5	4.0	10.8	10.5	43.4	3.9	11.0	10.3	146	76	309	
(**17B**) $[ZnL^5](NO_3)_2$	47.1	4.7	16.8	11.5	47.0	4.8	16.7	11.1	229	80	—	

[a] Limited solubility.

[b] Too hygroscopic to be accurately analysed.

Table 2. Selected IR absorptions (cm^{-1})

Complex	$\nu_{C=N}$	Amino acid ester	
		$\nu_{C=O}$ stretching vibration	ν_{C-OR} stretching vibration
(1A)	1632(m,b), 1593(s,s)	1742(s,s)	1279(m,b)
(1B)	1654(m,b), 1595(s,s)	1742(s,s), 1640(m,b)	1280(s,b)
(2A)	1614(s,s), 1595(s,s)	1738(m,b), 1623(s,b)	1265(s,s)
(2B)	1638(s,s), 1614(s,s), 1594(s,s)	1737(w,sb), 1638(s,sb)	—
(3)	1640(sh), 1613(s,s), 1593(s,s)	1744(m,s), 1638(s,sb)	1265(m,sb)
(4)	1614(s,s), 1595(s,s)	1741(s,s), 1614(s,sb)	part of OAc^- absorption
(5A)	1624(s,s), 1587(s,s)	1740(vs,s)	1273(s,s)
(5B)	1623(m,s), 1588(s,s)	1740(vs,s)	1275(s,s)
(6)	1624(m,s), 1587(s,s)	1737(vs,s)	1274(s,s)
(7)	1621(m,s), 1589(s,s)	1740(vs,s)	1270(s,s)
(8)	1620(m,sb), 1588(s,s)	1737(vs,s)	1273(s,s)
(9)	1625(m,s), 1590(s,s)	1735(vs,s)	1275(m,s)
(10)	1624(m,s), 1595(vs,s)	1738(vs,s)	1274(s,s)
(11)	1622(s,s), 1588(s,s)	—	—
(12)	1605(s,sb), 1593(s,sb)	—	—
(13A)	1630(s,b), 1595(sh)	1743(w,s), 1630(vs,s)	—
(13B)	1622(s,s), 1588(s,s)	1741(vs,s)	1260(s,s)
(13C)	1623(s,sb), 1585(s,sb)	1740(vs,s)	1280(m,b)
(14A)	1620(s,b), 1595(s,s)	1734(w,s), 1620(vs,b)	—
(14B)	1620(s,s), 1595(s,s)	1739(m,s), 1614(m,b)	1270(sh)
(15A)	1620(m,s), 1588(s,s)	1741(vs,s)	1276(m,s)
(15B)	1638(m,sb), 1590(m,s)	1740(vs,s)	1273(m,s)
(16)	1600(s,s), 1580(s,s)	—	—
(17A)	1649(s,s), 1611(s,s), 1592(s,s)	—	—

IR spectral study

The IR spectra of the Cu(II) and Zn(II) complexes are similar in important aspects (Table 2). All are characterized by the strong absorption at 1605–1650 cm^{-1} due to the imino $\nu_{C=N}$.[10] For the complexed Schiff base ligands L^1 and L^2, the absorptions due to the amino acid ester fall into three groups: those displayed a sharp band at *ca* 1740 cm^{-1} of much higher intensity than that at 1620 cm^{-1}, those with a band at 1740 cm^{-1} of intensity much reduced relative to that at 1620 cm^{-1} and finally those displaying only strong absorption at 1620 cm^{-1} with that at 1740 cm^{-1} reduced to a mere shoulder.[11,12] These results together with microanalytical data are consistent with formulations of amino acid components containing, respectively, two, one or no intact carboxylate ester groups [Table 3(a)]. It would appear that the carboxylate group of TEE* undergoes hydrolysis more readily than that of PME. For the latter, there appears to be some discriminations by the metal ions towards the ease of hydrolysis: thus Zn^{2+} apparently catalyses hydrolysis more efficiently than Cu^{2+}.

The presence of intact ester groups is further evident from the absorption at 1260 cm^{-1}; those containing two such groups display strong absorption relative to that with only one ester group.[13] Furthermore, this band is apparently sensitive to the type of metal ion in contrast to a corresponding band in L^3 which is insensitive to metal ions (Table 2).

In complexes **(1B)**, **(2A)**, **(2B)**, **(3)**, **(4)**, **(13A)**, **(14A)** and **(14B)** the carboxylate absorptions appear as a broad band at 1540–1615 cm^{-1} which is intermediate between those reported for the coordinated ionic COO^- (1610–1590 cm^{-1})[13] and those for intramolecular hydrogen bonded carboxyl groups (1680–1650 cm^{-1}).[11,12] It is then tentatively proposed that the carboxylate oxygen atoms probably interact with both a Zn(II) ion and a proton as depicted in Fig. 1 for L^{1C} and L^{2C}. Increased interaction between the central metal ion and the ionic COO^- groups was further suggested from the generally larger value of $(\nu_{as} - \nu_s)$ found among the complexes [Table 3(b)]. Although a similar structure has

* Abbreviations: DAP = 2,6-diacetylpyridine; PME = phenylalanine methyl ester; TEE = tyrosine ethyl ester; HME = histidine methyl ester, HMN = Histamine; AEP = 2-(2-aminoethyl)pyridine.

Table 3(a). Summary of the types of complexes

Amino acid precursor of Schiff base	Metal ion	Number of ester groups in complex
Phenylalanine methyl ester	Cu^{2+}	Two in complex (**1A**), one in complex (**1B**)
Phenylalanine methyl ester	Zn^{2+}	Two in complex (**13B**) and complex (**13C**), none in complex (**13A**)
Tyrosine ethyl ester	Cu^{2+}	One in complex (**2A**), and complex (**4**), none in complex (**2B**) and complex (**3**)
Tyrosine ethyl ester	Zn^{2+}	One in complex (**14B**), none in complex (**14A**)

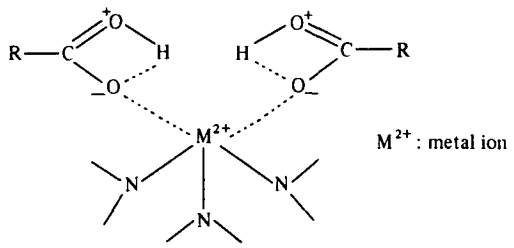

Fig. 1.

been proposed,[14] further hydrogen bonding between the H^+ ion on the RCOOH unit and the corresponding anion (BF_4^-, NO_3^-, OAc^- or ClO_4^-) remains a strong possibility. Efforts are currently being made to obtain crystals of suitable size for an X-ray structural elucidation of some of these complexes.

Table 3(b). Symmetric and antisymmetric carboxylation stretching (cm^{-1})

Complex	$\nu_{as(COO^-)}$	$\nu_{s(COO^-)}$	$\nu_{as}-\nu_s$
(**1A**)	1630	1363	267
(**1B**)	1635	1363	272
(**2A**)	1635	1363	272
(**2B**)	1638	1364	274
(**3**)	1638	Masked by NO_3^- absorption	—
(**13A**)	1630	1364	266
(**13B**)	1622	1360	262
(**14A**)	1638	1364	272
(**14B**)	1614	Masked by NO_3^- absorption	—
(**15A**)	1620	1374	246
(**15B**)	1620	Masked by NO_3^- absorption	—

^1H *NMR spectral study*

The ^1H NMR spectra in DMSO-d_6 of the ligands L^1 and L^2 as well as those of the Zn(II) complexes of L^1–L^5 are given in Table 4.

In general, the protons of the DAP moiety in comparison to those of the imidazole or pyridine ring are not significantly affected upon condensation and complexation. Thus, the change in chemical shifts in going from the precursor to the complex was only 0.1 ppm for the pyridine proton while corresponding values of 0.10–0.47 ppm were observed for the imidazole or pyridine rings of HME, HMN and AEP (Table 4). It has been shown from the X-ray structural study of Zn(II) complex of L^3 and L^5 that the Cu—N(imidazole) bond is shorter by about 0.036 Å than the Cu—N(pyridine) bond.[5] In addition it was pointed out that there is no evidence from observed bond lengths for conjugation from N(imino) through C(4) to the pyridine ring (DAP)[7] for both complexes of L^3 and L^5. These may be contributing factors to the observed magnitudes of change in chemical shifts of pyridine or imidazole ring protons in the present study. Thus, it is not unexpected to find that the methyl protons of the DAP moiety in the complexes are hardly affected.

Relatively larger changes in chemical shifts of 1.1 ppm and 0.6 ppm are observed for H(7) in the 5N and 3N coordinate systems, respectively. A comparison with the values for the chemical shifts of H(7) in L^1 and L^2 strongly indicates that the large change results primarily from the effect of condensation, as would be expected from the proximity of H(7) to the imino nitrogen. The effect of complexation ensues in a change of *ca* 0.2 ppm similar to those reported by Nelson *et al.*[3] As it is likely that the effect of condensation would result in similar changes in chemical shifts, it appears then that the

Table 4. Chemical shifts (ppm) of ^{1}H NMR signals

Compound/complex	H(1), H(2)	H(7)	H(10)	H(11)	H(12)	H(13)	H(14)	H(15)
2,6-Diacetylpyridine	8.16							
Phenylalanine methyl ester		3.58	7.21	7.21	7.21	—	3.58	—
Tyrosine ethyl ester		3.4	6.65	6.95	—	—	4.0	1.04, 1.12, 1.20
Histidine methyl ester		3.14	6.99	7.71	—	3.69	—	—
Histamine		2.88	6.90	7.58	—	—	—	—
2-(2-Aminoethyl)-pyridine		2.93	7.22	7.22	7.70	8.55	—	—
(13A)	8.18	4.15	7.3	7.3	7.3	—	—	—
(13B)	8.2	4.13	7.28	7.28	7.28	—	3.66	—
(13C)	8.2	4.10	7.3	7.3	7.3	—	3.67	—
(14A)	8.19	4.0	6.76	7.04	—	—	—	—
(14B)	8.1	4.0	6.70	7.00	—	—	4.3	1.7
(15A)	8.20	4.28	7.08	7.90	—	3.73	—	—
(15B)	8.18	4.30	7.13	8.03	—	3.72	—	—
(16)	8.23	4.04	7.13	8.04	—	—	—	—
(17A)	8.2	4.25	7.56–7.82	7.56–7.82	8.18	8.57	—	—
L^1	8.15	3.2	7.25	7.25	7.25	—	3.6	—
L^2	8.15	3.2	6.7	7.0	—	—	—	—

Zn—N(imido) interaction is stronger in the 5N coordinate systems.

The apparently weaker Zn—N(imino) interaction in the 3N systems may be partially due to the interaction of the carboxylate oxygen in L^1/L^2 with Zn(II). Such interaction is quite clearly indicated from the observed chemical shifts of alkyl protons (Table 4) of the ester group in complexes of L^1, L^2 and L^3, respectively. In going from the precursors to the complexes, those of the histidine moiety H(13) are almost unaffected while definite effects are detected for those in PME/TEE viz. H(14)/H(15).

Finally, it is interesting to note that the phenyl ring protons of TEE appear as a non-symmetrical A_2X_2 structure.[15] This is similar to that of AEP in L^5, suggesting possible interaction of the phenolic oxygen with a Zn(II) ion.

^{13}C *NMR spectral study*

All the ^{13}C NMR spectra of the Zn(II) complexes were recorded in DMSO-d_6 using broad-band proton decoupling. Tentative assignments are made with the aid of "off resonance" technique[16] (Table 5). The changes in chemical shifts in going from the precursors to the Schiff base complexes are examined, with reference also being made to values reported for similar systems.[3]

The largest changes are found for C(4) and C(7) (Table 5). Furthermore, while the magnitude of such changes in C(4) of L^1/L^2 (23.5–27.3 ppm) are somewhat lower than those for $L^3/L^4/L^5$ (29.3–31.7 ppm), those of C(7) are higher for L^1/L^2 (11.7–22.3 ppm) than for $L^3/L^4/L^5$ (6.6–11.5 ppm). Correlation of these two sets of values suggests a larger coordination effect of the Zn—N(imino) bond on C(4) in the five nitrogen coordinate system $L^3/L^4/L^5$, while combined bonding effects of Zn—N(imino) and Zn—O(carboxylate) are greater for C(7) in L^1 and L^2. This rationalization is consistent with the observed trend of changes in chemical shifts for the carboxylate carbon of $L^1/L^2/L^3$. Thus, relatively large values of 21.5–24.2 ppm are observed for C(13) in the Zn(II) complexes of L^1/L^2, as compared to a lower value of 2 ppm for C(12) of L^3, strongly indicative of interaction of the carboxyl oxygen with Zn(II) in the case of L^1 and L^2 only. Furthermore the corresponding value for C(13) is higher by about 2 ppm for L^{1C} and L^{2C}, then for L^{1A}, L^{1B} and L^{2B} (Scheme 1) in their respective complexes, as would be expected from the more effective interaction of the carboxyl oxygen in comparison to the carboxylate oxygen.

Thus, it would appear that the magnitude of changes in chemical shifts for the different protons as well as for the carbon atoms are consistent with the modes of bonding proposed on the basis of IR spectral analysis. It is, however, to be noted that such use of the ^{13}C chemical shifts is only tentative

Table 5. Chemical shifts (ppm) of ^{13}C NMR signals

Compound/complex	C(1)	C(2)	C(3)	C(4)	C(7)	C(12)/C(13)
2,6-Diacetylpyridine	138.8	124.4	152.1	198.5	—	—
Phenylalanine methyl ester	—	—	—	—	41.0	175.5
Tyrosine ethyl ester	—	—	—	—	40.0	174.9
Histidine methyl ester	—	—	—	—	40.3	166.7
Histamine	—	—	—	—	40.3	—
2-(2-Aminoethyl)pyridine	—	—	—	—	42.0	—
(13A)	139.1	124.7	152.3	172	52.7	198.9
(13B)	139.2	124.8	152.5	171.5	54.3	175
(13C)	139	124.5	152	171.3	54.3	175
(14A)	138.8	124.5	152.1	175	52.3	198.7
(14B)	139.2	124.8	152.5	171.5	62.3	199.0
(15A)	139.1	124.6	152	169.2	51.7	169.0
(15B)	139.2	124.6	152.3	169.0	51.9	169.2
(16)	139.0	124.5	148	167	51	—
(17A)	141.5	124.0	159.1	168.3	35.4	—
(17B)	141.1	123.8	159.3	168.0	35.5	—

in view of the number of different factors that control the position of a ^{13}C resonance line.

Electronic and ESR spectral studies

The electronic spectra of the Cu(II) and Zn(II) complexes were determined in MeOH and DMSO. The Cu(II) complexes of L^1 and L^2 display only one broad *d–d* absorption band in the region 600–700 nm, whereas those of L^3, L^4 and L^5 contain an additional shoulder at 570 nm due to a second *d–d* transition. These different electronic absorption patterns indicate a significant different in the coordination symmetry around the Cu(II) ion in going from the three nitrogen to the five nitrogen Schiff base ligands. The coordination geometry of the latter is intermediate between trigonal bipyramid and a square pyramid, while that of the 3N system probably approaches the tetragonal symmetry.

The UV spectra of all the Cu(II) and Zn(II) complexes display bands at 290, 270 and 220 nm, characteristic of the Schiff base ligands. Of these, the lower energy band is attributable to a transition localized within the trimethine group.[7] It is interesting to note that the change in polarity in going from MeOH to DMSO results in a red shift of the UV bands in most cases, probably due to the differences in polarities of these two solvents.[17,18]

The solution and frozen-glass EPR spectra of the Cu(II) complexes in 5:1 methanol–water are generally well-resolved. The spin-Hamiltonian parameters [$g_\parallel$, $g_\perp$, $A_\parallel$ ($^{63/65}$Cu)] (Table 6) are close to those of tetragonal Cu(II) complexes. The $A_\parallel$ components are similar to those of [Cu(terpy)LC]Cl (terpy = 2,2,2″-terpyridine and L = phenolate).[19] However unlike the latter, the ^{14}N-superhyperfine although discernible, is not well defined. This could be due to the non-equivalence of the nitrogen donor atoms of the Schiff bases.

Electrochemical studies

The cyclic voltammetric behaviour of the complexes was examined within the potential range of +0.40 to −0.60 V (Table 7), as reduction of ligands was found to take place between −0.68 to −0.87 V.

Both the Cu(II) complexes of L^1 and L^2 display two reduction waves of mid-point potentials similar to those for Cu(II) → Cu(I) and Cu(I) → Cu(0) (Table 7).[20] However, only one oxidation wave corresponding to Cu(I) → Cu(II) could be detected. The absence of a Cu(0) → Cu(I) oxidation wave suggests that the electrode reduction of Cu(I) species in the forward cathodic scan is accompanied by a chemical reaction yielding an unstable product within the time frame of the experiment.[21]

The Cu(II) complex of L^3 displays two cathodic

Table 6. ESR parameters for selected copper(II) complexes

Complex	$g_\perp$	$g_\parallel$	$A_\parallel$ (cm^{-1})
(1B)	2.11	2.22	0.0184
(2B)	2.14	2.25	0.0187
(5A)	2.10	2.26	0.0166
(9)	2.10	2.26	0.0170
(11)	2.08	2.26	0.0164

Table 7. Mid-point redox potential (mV) vs SCE

Complex	First wave E^a	Second wave E^b
(1A)	+225	—
(2A)	+140	—
(5A)	—	−130
(5B)	+280	−130
(6)	+200	−100
(8)	+135	−190
(9)	—	−115
(10)	—	—

waves at +0.180 and −0.120 V and corresponding anodic waves at +0.350 and −0.100 V. These have been assigned to electrode processes of Cu(II) → Cu(I) and Cu(I) → Cu(0), respectively. In contrast to those of L^1 and L^2, the reduction of Cu(I) → Cu(0) is reversible with ΔEp being 60 mV.

REFERENCES

1. M. G. Simmons and L. J. Wilson, *J. Chem. Soc., Chem. Commun.* 1978, 634.
2. S. M. Nelson, in *Copper Coordinating Chemistry* (Edited by K. D. Karlin and J. Zubieta), p. 332. Adenine Press, New York (1983).
3. S. M. Nelson, A. Lavery and M. G. B. Drew, *J. Chem. Soc., Dalton Trans.* 1986, 911.
4. M. G. Simmons, C. L. Merrill, L. J. Wilson, L. A. Bottomley and K. M. Kadish, *J. Chem. Soc., Dalton Trans.* 1980, 1827.
5. J. D. Korp, I. Bernal, C. L. Merrill and L. J. Wilson, *J. Chem. Soc., Dalton Trans.* 1981, 1951.
6. C. L. Merrill, L. J. Wilson, T. J. Thamann, T. N. Loehr, N. S. Ferres and W. H. Woodruff, *J. Chem. Soc., Dalton Trans.* 1984, 2207.
7. L. Casella, M. E. Silver and J. A. Ibers, *Inorg. Chem.* 1984, **23**, 1409.
8. L. Casella and L. Rogini, *J. Chem. Soc., Chem. Commun.* 1985, 1668.
9. P. Hemmerich and C. Sigwart, *Experientia* 1963, **19**, 488.
10. L. Casella and M. Gullotti, *Inorg. Chem.* 1981, **20**, 1306.
11. A. D. Cross and R. A. Jones, *An. Introduction to Practical Infrared Spectroscopy*. Butterworth, London (1969).
12. L. J. Bellamy, *The Infrared Spectra of Complex Molecules*. Chapman and Hall, London (1975).
13. K. Nakamoto, *Infrared and Raman Spectra of Inorganic and Coordination Compounds*. John Wiley, New York (1978).
14. R. M. Silverstein and G. C. Bassler, *Spectrometric Identification of Organic Compounds*, 2nd Edn, pp. 99, 236. John Wiley, New York.
15. R. H. Bible, *Interpretation of N.M.R. Spectra*, pp. 17, 97. Plenum Press, New York (1966).
16. R. J. Abraham and P. Loftus, *Proton and* C-13 *NMR Spectroscopy*. Heyden, London (1978).
17. R. Stolarski, M. Remin and D. Schugar, *Z. Naturforsch, C. Biosci.* 1977, **32C**, 898.
18. *Handbook of Chemistry and Physics* (Edited by R. C. Weast), 52nd Edn, p.E-52. The Chemical Rubber Co., Ohio.
19. W. L. Kwik and K. P. Ang, *Transition Met. Chem.*, in press.
20. W. L. Kwik, K. P. Ang and G. Chen, *J. Inorg. Nucl. Chem., Bioinorg. Sec.* 1980, **42**, 312.
21. A. J. Bard and L. R. Faulkner, *Electrochemical Methods*, pp. 223, 229, 452. John Wiley, New York (1980).

Polyhedron Vol. 7, No. 9, pp. 705–707, 1988
Printed in Great Britain

0277–5387/88 $3.00+.00
© 1988 Pergamon Press plc

SOLVOLYSIS OF THE ReO_4^- ANION IN THE HSO_3Cl SOLVENT SYSTEM; SYNTHESIS AND CHARACTERIZATION OF AN OXOBRIDGED BINUCLEAR Re(VII) CHLOROSULPHATE

S. A. A. ZAIDI,* LUTFULLAH and Z. A. SIDDIQI

Division of Inorganic Chemistry, Chemistry Department, Aligarh Muslim University, Aligarh-202002, India

(*Received* 28 *September* 1987; *accepted after revision* 21 *December* 1987)

Abstract—Solvolytic reactions of perrhenates $MReO_4$ (M = Na and NH_4) in chlorosulphuric acid yielded ReO_3SO_3Cl in solution. A lemon–yellow coloured solid has been isolated and characterized by elemental analyses, and magnetic and spectroscopic studies as an oxobridged dimeric rhenium(VII) species formulated as $Re_2O_6(SO_3Cl)_2$.

Stable compounds of rhenium in the oxidation states from zero to seven are well known.[1,2] Mallela *et al.*[3] have recently shown that a solution of rhenium metal in HSO_3F comprising of a rhenium(II) species, is oxidized to rhenium(VII) characterized as $ReO_2(SO_3F)_3$ in the form of a stable pale yellow oil. A similar species has also been isolated[3] from the reaction of Re_2O_7 with $S_2O_6F_2$. A large number of metal, non-metal and oxo-metal chlorosulphates containing manganese in the +3 oxidation state have been reported.[4–10] During recent years investigations on trivalent rhenium have been made by several workers. It was of interest to study the reaction of the perrhenate anion with chlorosulphuric acid, with a view to isolating a stable Re(III) species similar to that obtained from MnO_4^- and MnO_4^{2-} anions.[4] In this paper we report the formation of a stable lemon–yellow coloured solid compound characterized as an oxobridged dimeric rhenium(VII) i.e. $Re_2O_6(SO_3Cl)_2$.

EXPERIMENTAL

Pure chlorosulphuric acid (Riedel) was used. Sodium perrhenate and ammonium perrhenate (Koch light) were used as obtained. Thionyl chloride was distilled twice before use, other solvents used were anhydrous.

The conductance measurements were carried on an Elico type CMB-2T conductivity bridge, thermostated at 25±0.1°C. The shape of the conductivity cell used, the meaning and significance of notations Ψ and Ψ and their determination have been described elsewhere.[6,11,12]

The solid compound was isolated by taking a concentrated solution of perrhenates in 15 cm^3 of chlorosulphuric acid and when the colour of the solution became mustard–yellow it was treated with thionyl chloride. After this, an excess of dry chilled ether was added under ice cold conditions. Immediately a lemon–yellow solid settled to the bottom of the container. It was filtered in a closed system,[6] washed several times with thionyl chloride and finally dried at 59–60°C *in vacuo*, to a constant weight. The solid was extremely hygroscopic and dissolved in water with a hissing sound. It was soluble only in dimethyl sulphoxide in which the conductivity and UV visible spectrum has been measured.

The IR spectra of the solids were taken on a Perkin–Elmer Model 621 spectrometer using a potassium bromide pellet. Elemental analysis of chlorine, sulphur and rhenium were carried out gravimetrically according to established methods.[13,14] Magnetic susceptibilities were measured using a vibrating sample magnetometer model 155 at 298 K. All manipulations on the solid materials were carried out in a dry nitrogen atmosphere.

RESULTS AND DISCUSSION

Sodium perrhenate and ammonium perrhenate have been found to be fairly soluble in chlorosulphuric acid producing a similar bright yellow coloured, highly conducting solution (Fig. 1). The

* Author to whom correspondence should be addressed.

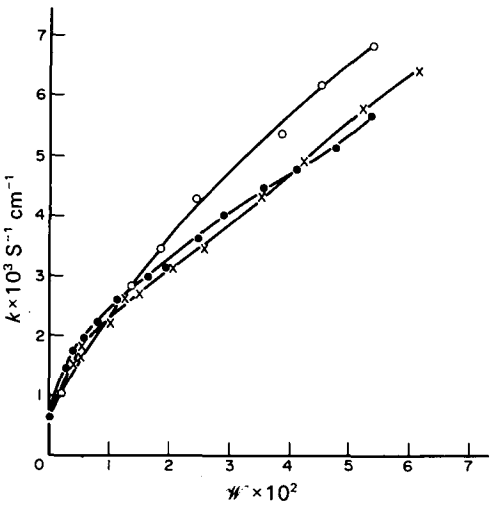

Fig. 1. Specific conductance—concentration curves of the compounds at 25±0.1°C. ○, KCl; ×, $NaReO_4$; ●, NH_4ReO_4.

conductance of the solution remained constant for a fairly long time but its colour became mustard–yellow after 3 days. The average γ-value is 0.88 and it is evident from the specific conductance concentration curves that at higher concentration (above 1.5×10^{-2} M) the curve is much depressed in comparison to that of KCl, suggesting possible oligomerization of the species formed in solution, resulting in the separation of a similar lemon–yellow coloured solid from the solution.

The electronic spectra of the solutions of perrhenate in HSO_3Cl exhibited absorption bands at 430, 580 and 610 nm. This spectra is quite different from the spectra of ReO_4^- and TcO_4^- anions having T_d symmetry.[15,16] However, it is comparable to that reported[16] for ReO_3Cl and TeO_3Cl. This suggests that the solvolyzed species formed in HSO_3Cl is ReO_3SO_3Cl. The mode of reaction compatible with the observed γ-value of 0.88 may therefore be given as:

$$MReO_4 + 3HSO_3Cl = M^+ + SO_3Cl^- + H_2SO_4 + HCl + ReO_3SO_3Cl$$
$$M = Na^+ \text{ and } NH_4^+ \quad (1)$$

It is interesting that the mode of reaction of the ReO_4^- anion in HSO_3Cl is apparently different from that reported[4] for the oxanions MnO_4^- and MnO_4^{2-} in HSO_3Cl, where the MnO_3SO_3Cl species formed in dilute solutions is decomposed to the stable Mn(3+) species. $MnOSO_3Cl$, is a stable solid compound. However, perrhenate solutions separated to give a lemon–yellow coloured solid when treated with thionyl chloride. The solid has been isolated in the manner described in the Experimental.

The results of elemental analysis (Table 1) suggest the stoichiometry of the compound as $[(ReO_3(SO_3Cl)]_x$. The observed molar conductance of 32.80 $cm^2\ mol^{-1}\ ohm^{-1}$ in dimethyl sulphoxide suggests a non-electrolytic nature of the compound. The compound was further characterized by carrying out IR, magnetic and electronic spectral studies.

The IR spectrum shows the characteristic chlorosulphate group vibrations with all three degenerate modes well split, suggesting[6] C_s symmetry of the chlorosulphate group. The symmetric SO_3 stretching vibration ν_1(A) is sufficiently positively shifted compared to the free chlorosulphate ion. This indicates considerable covalent bonding of the chlorosulphate group with the metal ion. A strong band at 1000 cm^{-1} is characteristic of a Re=O bond which is about 30 cm^{-1} higher than that reported[17] for a terminal Re=O bond. A band of medium intensity at 780 cm^{-1} has been assigned[18,19] to the νRe—O—Re stretching mode. The position of the νRe—O—Re band is higher compared[17] to the *trans*-oxo arrangement of the Re=O bond. A weak band at 260 cm^{-1} may be

Table 1. Elemental analyses and IR frequencies (cm^{-1}) of oxobridged binuclear Re(VII) chlorosulphate. A—chlorosulphate obtained by $NaReO_4$. B—chlorosulphate obtained by NH_4ReO_4

		A	B
% S	c	9.2	9.2
	f	(9.1)	(9.1)
% Cl	c	10.2	10.2
	f	(10.1)	(10.0)
% Re	c	53.3	53.3
	f	(53.2)	(53.1)
Re=O stretch		1000 vs	1005 vs
S—Cl wag.		310 w	310 m
ν_6(E)		350 m	350 m
S—Cl stretch			
ν_2(A)		450 vs	450 s
Sym SO_3 deformation			
ν_3(A)		570 vs	570 vs
Asym SO_3 deformation			
ν_5(E)		610 s	610 s
		640 m	640 s
Sym SO_3 stretch			
ν_1(A)		1070 vs	1070 vs
Asym SO_3 stretch			
ν_4(E)		1240 w	1265 s
		1280 m	1300 s
ν(Re—O—Re)		790 m	790 m
ν(Re—OSO_2Cl)		260 w	260 w

vs = very strong, s = strong, m = medium, w = weak.
c = calculated.
f = found.

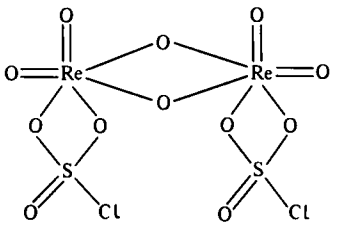

Fig. 2.

assigned to coordinate the Re—OSO_2Cl bond. In view of this, it is reasonable to suggest that the solid compound is a dimer presumably with the double oxobridge having molecular geometry other than the *trans*-oxo type, as shown in Fig. 2.

The electronic spectra of the solid compound in DMSO solution contains a strong bond at 290 nm with a shoulder at 350 nm in the UV region, along with three weak absorptions at 430, 475 and 620 nm. The positions of these bands are quite comparable to those reported[20] for the hexa-coordinated rhenium species characterized as mesoperrhenate, with a geometry analogous to that shown in Fig. 2. Furthermore, the compound is diamagnetic in nature supporting the +7 oxidation state of rhenium.

Acknowledgement—The Chairman, Department of Chemistry is thanked for providing research facilities. One of us (Lutfullah) is grateful to C.S.I.R. (New Delhi) for financial assistance.

REFERENCES

1. J. E. Fergusson, *Coord. Chem. Rev.* 1966, **1**, 459.
2. A. A. Woof, *Quart. Rev.* 1961, **15**, 372.
3. S. P. Mallela and F. Aubke, *Inorg. Chem.* 1985, **24**, 2969.
4. Z. A. Siddiqi, Lutfullah, S. A. A. Zaidi and K. S. Siddiqi, *Bull. Soc. Chim. France* 1980, **1**, 228.
5. Z. A. Siddiqi, Lutfullah and S. A. A. Zaidi, *Bull. Soc. Chim. France* 1980, **1**, 466.
6. E. A. Robinson and J. A. Ciruna, *Can. J. Chem.* 1968, **46**, 1716.
7. E. A. Robinson and J. A. Ciruna, *Can. J. Chem.* 1968, **46**, 3196.
8. S. A. A. Zaidi and Z. A. Siddiqi, *J. Inorg. Nucl. Chem.* 1975, **37**, 1806.
9. S. A. A. Zaidi and Z. A. Siddiqi, *J. Inorg. Nucl. Chem.* 1976, **38**, 1434.
10. Z. A. Siddiqi, M. Aslam, N. A. Ansari, M. Shakir and S. A. A. Zaidi, *Synth. React. Inorg. Met. Org. Chem.* 1981, **11**, 475.
11. R. J. Gillespie and C. Solomons, *J. Chem. Soc.* 1957, 1796.
12. R. H. Flowers, R. J. Gillespie, J. V. Oubridge and C. Solomons, *J. Chem. Soc.* 1958, 667.
13. I. Vogel, *A. Text Book of Quantitative Inorganic Analysis*, pp. 399–401. Longman Green (1958).
14. H. H. Willard and G. M. Smith, *Ind. Eng. Chem.* 1939, **11**, 305.
15. P. Mullen, K. Schwochow and C. K. Jorgenson, *Chem. Phys. Lett.* 1969, **3**, 49.
16. C. L. Rulfs, R. A. Pacer and R. F. Hirsch, *J. Inorg. Nucl. Chem.* 1967, **29**, 681.
17. B. J. Brisdon and D. A. Edwards, *Inorg. Chem.* 1968, **7**, 1898.
18. F. A. Cotton, W. R. Robinson and R. A. Walton, *Inorg. Chem.* 1967, **6**, 223.
19. K. Ulbricht and M. Kriegsmann, *Z. Chem.* 1967, **7**, 244.
20. S. K. Majumdar, R. A. Pacer and C. L. Rulfs, *J. Inorg. Nucl. Chem.* 1969, **31**, 33 and refs cited therein.

Polyhedron Vol. 7, No. 9, pp. 709–714, 1988
Printed in Great Britain

0277–5387/88 $3.00+.00
© 1988 Pergamon Press plc

SYNTHESIS AND REACTIONS OF OSMIUM NITROSYL COMPLEXES

KRISHNA KUMAR PANDEY,* DELEEP TOLU NEHETE, SHARAD KUMAR TEWARI, SUJATA REWARI and RAVINDRA BHARDWAJ†

Department of Chemistry, Devi Ahilya University Indore, Khandwa Road, Indore 452 001, India

(*Received* 19 *October* 1987; *accepted after revision* 21 *December* 1987)

Abstract—Nitrosyl halides NOX (X = Cl, Br) reacted with osmium carbonyl complexes $[OsH(CO)ClL_3]$, $[Os(CO)Cl_2L_3]$ and $[OsH_2(CO)L_3]$ (L = PPh_3, $AsPh_3$) to give osmium nitrosyl complexes $[Os(NO)X_3L_2]$, $[Os(NO)ClBr_2L_2]$ and $[Os(NO)Cl_2BrL_2]$ and osmium carbonyl complexes $[Os(CO)_2X_2L_2]$ (X = Cl, Br; L = PPh_3, $AsPh_3$). Low valent osmium nitrosyl complexes $[Os(NO)X(AsPh_3)_3]$ (X = Cl, Br) were prepared by refluxing $[Os(NO)X_3(AsPh_3)_2]$ with excess $AsPh_3$. Reaction of sulphur with $[Os(NO)X_3(PPh_3)_2]$ resulted in the formation of novel thionitro complexes $[Os(NSO)X_2(PPh_3)_2]$. $[Os(NO)Cl_3(PPh_3)_2]$ reacted with $[Na(S_2CNR_2)\cdot xH_2O]$ (R = Et. Me) under different reaction conditions to produce the complexes $[Os(NO)Cl_2(S_2CNR_2)(PPh_3)]$ and $[Os(S_2CNR_2)_3]$. The products have been characterized by elemental analyses, magnetic measurements, IR and electronic spectral studies.

The activation of nitrosyl halides in homogeneous systems by metal complexes, has received considerable attention because of the possible synthetic applications as well as interest in the catalytic processes.[1–15] Osmium nitrosyl complexes of the type $[Os(NO)X_3L_2]$ (L = PPh_3, $AsPh_3$, $SbPh_3$) have been prepared previously by (a) the reaction of $[OsX_6]^{2-}$ with NO or MNTS in the presence of ligand L (L = PPh_3, $AsPh_3$, $SbPh_3$),[16] (b) the reactions of $OsCl_3$ with NOX (X = Cl, Br, Br_3 or NO_2) in the presence of triphenylphosphine or triphenylarsine[17] and (c) the reactions of NOX (X = Cl, Br) with some osmium(II) complexes.[18] Synthesis of osmium(0) complexes $[Os(NO)X(PPh_3)_3]$ (X = Cl, Br) have also been reported.[18–19]

The formation of either nitrato or nitro/nitrito complexes in the reactions of nitrosyl complexes with O_2,[20–25] and the formation of the Fe—N(O)S moiety,[26] in the reaction of sodium nitroprusside with SH^- or S^{2-}, prompted us to undertake the reaction of osmium nitrosyl complexes with sulphur. Sulphur ligands stabilize several nitrosyl complexes, but to the best of our knowledge no sulphur derivative of the osmium nitrosyl complex has been reported. Herein we wish to report (i) the reactions of osmium carbonyl complexes with nitrosyl chloride and nitrosyl bromide, (ii) synthesis of $[Os(NO)X(AsPh_3)_2]$, (iii) the reactions of $[Os(NO)X_3L_2]$ (X = Cl, Br; L = PPh_3) with sulphur and (iv) the reactions of $[Os(NO)Cl_3(PPh_3)_2]$ with $[Na(S_2CNR_2)]$ (R = Et, Me).

EXPERIMENTAL

All the reagents used were AnalaR or of chemically pure grade. The solvents were dried and freshly distilled before use. Hydridochlorocarbonyltris(triphenylphosphine)osmium(II), dichlorocarbonyltris(triphenylphosphine)osmium(II), dihydridocarbonyltris (triphenylphosphine) osmium (II), hydridochlorocarbonyltris (triphenylarsine) osmium (II), dichlorocarbonyltris(triphenylarsine)osmium(II), dihydridocarbonyltris(triphenylarsine)osmium(II), nitrosyl chloride and nitrosyl bromide were prepared by literature methods.[27–31] A saturated solution of NOCl and *ca* a 2 M solution of NOBr in CH_2Cl_2 have been used in these reactions. $[Na(S_2CNR_2)\cdot xH_2O]$ (R = Et or Me) salts were used as purchased from Flucka.

The analyses for sulphur, chloride and bromide

* Author to whom correspondence should be addressed.
† Department of Biochemistry.

in the complexes were carried out using standard methods.[32,33] Carbon, hydrogen and nitrogen analyses were performed using a Carlo Erba 1106 Thomas CH-analyser 35 and Coleman N-analyser 29. For the estimation of phosphorus and arsenic, samples were decomposed with sodium peroxide, sugar and sodium nitrate in the ratio 20 : 1 : 3 in a Parr bomb crucible and extracted with water. The solution was neutralized with dilute H_2SO_4 and an excess of concentrated H_2SO_4 (0.5 cm^3) added. This was heated until the evolution of SO_3 fumes ceased, then cooled and diluted with water. From the filtrate of the solution, phosphorus and arsenic was estimated by standard methods.[34] The results are reported in Table 1.

The IR spectra have been recorded in the range 4000–250 cm^{-1} with a Perkin–Elmer 580 spectrophotometer at the R.S. Instrument Centre of the Indian Institute of Technology, Bombay. Samples were prepared as KBr pellets. Important IR frequencies are given in Table 2. The electronic spectra have been recorded using a Shimadzu 160 spectrophotometer. Magnetic measurements were carried out by Gouy's method at room temperature

Table 1. Colour and analytical data of osmium complexes

Compounds	Colour	Analysis % found (calc.) C	H	N	Cl/Br	S	P/As
$Os(NO)Cl_3(PPh_3)_2$	Red	50.6	3.4	1.5	12.7	—	7.4
	Brown	(50.8)	(3.5)	(1.6)	(12.5)		(7.3)
$Os(NO)Cl_2Br(PPh_3)_2$	Red	48.4	3.5	1.7	8.2	—	7.2
	Brown	(48.2)	(3.3)	(1.6)	(7.9)		(6.9)
$Os(NO)ClBr_2(PPh_3)_2$	Brown	45.9	3.0	1.6	3.9	—	6.8
		(46.0)	(3.2)	(1.4)	(3.8)		(6.6)
$Os(NO)Br_3(PPh_3)_2$	Brown	43.8	3.2	1.2	—	—	6.5
		(43.9)	(3.0)	(1.4)			(6.3)
$Os(CO)_2Cl_2(PPh_3)_2$	White	54.4	3.4	—	8.6	—	7.5
		(54.2)	(3.6)		(8.4)		(7.4)
$Os(CO)_2Br_2(PPh_3)_2$	White	49.1	3.1	—	17.5	—	6.8
		(49.0)	(3.2)		(17.2)		(6.7)
$Os(NO)Cl_3(AsPh_3)_2$	Red	46.2	3.4	1.6	11.5	—	16.2
	Brown	(46.0)	(3.2)	(1.5)	(11.3)		(16.0)
$Os(NO)Cl_2Br(AsPh_3)_2$	Brown	43.8	3.2	1.6	7.4	—	15.4
		(43.9)	(3.0)	(1.4)	(7.2)		(15.2)
$Os(NO)ClBr_2(AsPh_3)_2$	Brown	42.2	2.8	1.5	3.6	—	14.8
		(42.0)	(2.9)	(1.4)	(3.4)		(14.6)
$Os(NO)Br_3(AsPh_3)_2$	Brown	40.1	2.7	1.1	—	—	14.2
		(40.3)	(2.8)	(1.3)			(14.0)
$Os(CO)_2Cl_2(AsPh_3)_2$	White	49.2	3.4	—	7.8	—	16.3
		(49.1)	(3.2)		(7.6)		(16.1)
$Os(CO)_2Br_2(AsPh_3)_2$	White	44.6	2.7	—	—	—	14.9
		(44.8)	(2.9)				(14.7)
$Os(NO)Cl(AsPh_3)_3$	Green	55.4	3.7	1.3	3.2	—	19.3
		(55.2)	(3.8)	(1.2)	(3.0)		(19.2)
$Os(NO)Br(AsPh_3)_3$	Green	53.0	3.8	1.2			18.6
		(53.2)	(3.7)	(1.1)			(18.5)
$Os(NSO)Cl_2(PPh_3)_2$	Green	51.2	3.7	1.5	8.5	3.9	7.5
		(51.0)	(3.5)	(1.6)	(8.4)	(3.8)	(7.3)
$Os(NSO)Br_2(PPh_3)_2$	Green	46.3	3.1	1.6	—	3.6	6.8
		(46.1)	(3.2)	(1.5)		(3.4)	(6.6)
$Os(NO)Cl_2(S_2CNEt_2)(PPh_3)$	Brownish	39.1	3.4	3.7	10.3	9.3	4.6
	Yellow	(39.4)	(3.6)	(4.0)	(10.1)	(9.1)	(4.4)
$Os(S_2CNEt_2)_3$	Brown	28.5	4.9	6.5	—	30.4	—
		(28.4)	(4.7)	(6.6)		(30.3)	
$Os(NO)Cl_2(S_2CNMe_2)(PPh_3)$	Khakhi	37.3	3.0	4.3	10.7	9.7	4.8
		(37.4)	(3.1)	(4.2)	(10.5)	(9.5)	(4.6)
$Os(S_2CNMe_2)_3$	Brown	19.5	3.3	7.5	—	35.2	—
		(19.6)	(3.3)	(7.6)		(34.9)	

Table 2. Melting point and important IR frequencies (cm^{-1}) of osmium complexes

Compounds	ν(NO)	ν(CO)	ν(NSO)	ν(Os—Cl)	ν(CN)	M.p. (°C)
$Os(NO)Cl_3(PPh_3)_2$	1850	—	—	325, 310	—	260
$Os(NO)Cl_2Br(PPh_3)_2$	1860	—	—	320	—	> 280
$Os(NO)ClBr_2(PPh_3)_2$	1855	—	—	310	—	> 280
$Os(NO)Br_3(PPh_3)_2$	1860	—	—	—	—	> 280
$Os(CO)_2Cl_2(PPh_3)_2$	—	2040, 1973	—	329	—	> 280
$Os(CO)_2Br_2(PPh_3)_2$	—	2035, 1970	—	—	—	> 280
$Os(NO)Cl_3(AsPh_3)_2$	1847	—	—	322, 312	—	> 280
$Os(NO)Cl_2Br(AsPh_3)_2$	1858	—	—	318	—	> 280
$Os(NO(ClBr_2(AsPh_3)_2$	1852	—	—	312	—	> 280
$Os(NO)Br_3(AsPh_3)_2$	1856	—	—	—	—	> 280
$Os(CO)_2Cl_2(AsPh_3)_2$	—	2038, 1972	—	—	—	> 280
$Os(CO)_2Br_2(AsPh_3)_2$	—	2035, 1970	—	—	—	> 280
$Os(NO)Cl(AsPh_3)_3$	1635	—	—	310	—	140
$Os(NO)Br(AsPh_3)_3$	1630	—	—	—	—	130
$Os(NSO)Cl_2(PPh_3)_2$	—	—	1237, 1052	325	—	210
$Os(NSO)Br_2(PPh_3)_2$	—	—	1235, 1055	—	—	215
$Os(NO)Cl_2(S_2CNEt_2)(PPh_3)$	1810	—	—	330	1530	275
$Os(NO)Cl_2(S_2CNMe_2)(PPh_3)$	1800	—	—	330	1542	180
$Os(S_2CNEt_2)_3$	—	—	—	—	1540	225
$Os(S_2CNMe_2)_3$	—	—	—	—	1535	> 280

(25°C), using mercury tetrathiocyanato cobaltate(II) as calibrant. Melting points were determined by the capillary method and are uncorrected.

(a) *Reactions of* NOX (X = Cl *or* Br) *with* $[OsH(CO)ClL_3]$, $[Os(CO)Cl_2L_3]$ *or* $[OsH_2(CO)L_3]$ (L = PPh_3 *or* $AsPh_3$)

The experiments were performed similarly and the reaction of NOCl with $[OsH(CO)Cl(PPh_3)_3]$ is described as a representative example.

A saturated solution of NOCl (25 cm^3) in dichloromethane was added dropwise to a stirred solution of $[OsH(CO)Cl(PPh_3)_3]$ (0.2 g) in dichloromethane (20 cm^3). The reaction mixture was refluxed for 20 min. On addition of hot methanol (60 cm^3), the red brown crystals of $[Os(NO)Cl_3(PPh_3)_2]$ which separated out, were filtered, washed with methanol, diethylether and dried *in vacuo*.

On keeping the filtrate for 3 h, a white compound $[Os(CO)_2Cl_2(PPh_3)_2]$ separated out, which was filtered, washed with methanol, ether and dried *in vacuo*.

Similarly the complexes $[Os(NO)Cl_3L_2]$ and $[Os(CO)_2Cl_2L_2]$ (L = PPh_3 or $AsPh_3$) were isolated by the reactions of NOCl with $[OsH(CO)Cl(AsPh_3)_3]$, $[Os(CO)Cl_2L_3]$ or $[OsH_2(CO)L_3]$ and the complexes of the type $[Os(NO)ClBr_2L_2]$ and $[Os(CO)_2Br_2L_2]$; $[Os(NO)Cl_2BrL_2]$ and $[Os(CO)_2Br_2L_2]$; $[Os(NO)Br_3L_2]$ and $[Os(CO)_2Br_2L_2]$ were isolated by the reactions of NOBr with $[OsH(CO)ClL_3]$, $[Os(CO)Cl_2L_3]$ and $[OsH_2(CO)L_3]$, respectively.

(b) *Reactions of* $AsPh_3$ *with* $[Os(NO)X_3(AsPh_3)_2]$ (X = Cl *or* Br)

Triphenylarsine (1.0 g) was added to a solution of $[Os(NO)X_3(AsPh_3)_2]$ (0.2 g) in benzene (25 cm^3). The resulting solution was refluxed for 50 h and then concentrated to 5 cm^3 under reduced pressure. On addition of *n*-hexane, green complexes of $[Os(NO)X(AsPh_3)_3]$ precipitated out which were centrifuged, washed with *n*-hexane and dried *in vacuo* (yield 0.13 g, 52% for X = Cl; 0.10 g, 44% for X = Br).

(c) *Reactions of sulphur with* $[Os(NO)X_3(PPh_3)_2]$ (X = Cl *or* Br)

To a solution of $[Os(NO)Cl_3(PPh_3)_2]$ (0.85 g, 1 mmol) in benzene (100 cm^3), was added sulphur (0.064 g, 0.25 mmol). The reaction mixture was refluxed for 4 h, whereby its colour changed from orange to green. It was concentrated to 5 cm^3 under reduced pressure. On addition of *n*-hexane, the green complex $[Os(NSO)Cl_2(PPh_3)_2]$ precipitated and was centrifuged, washed with hexane and dried *in vacuo*. It was recrystallized with benzene–hexane (1 : 3) (yield 0.25 g, 30%).

The green complex $[Os(NSO)Br_2(PPh_3)_2]$ was isolated by a similar procedure using [Os(NO)

$Br_3(PPh_3)_2$] (0.98 g, 1 mmol) and sulphur (0.064 g, 0.25 mmol) (yield 0.22 g, 22%).

(d) *Reaction of* [$Na(S_2CNR_2)\cdot xH_2O$] *with* [$OsNOCl_3(PPh_3)_2$] (R = Et, Me)

(i) The compounds [$Os(NO)Cl_3(PPh_3)_2$] (0.2 g) and [$Na(S_2CNR_2)\cdot xH_2O$] (0.1 g) were stirred in benzene (25 cm^3) for 5 h. The resulting solution was filtered and reduced to 5 cm^3 under reduced pressure. On addition of *n*-hexane brownish–yellow complexes [$Os(NO)Cl_2(S_2CNR_2)(PPh_3)$] separated, filtered, washed with water and dried *in vacuo*.

(ii) Compounds [$Os(NO)Cl_3(PPh_3)_2$] (0.2 g) and [$Na(S_2CNR_2)\cdot xH_2O$] (0.5 g) were refluxed in benzene (25 cm^3) for 4 h. The resulting solution was filtered and reduced to about 5 cm^3 under reduced pressure. On addition of *n*-hexane, the brown complex [$Os(S_2CNR_2)_3$] separated, this was centrifuged, washed with water, cold ethanol and dried *in vacuo*.

RESULTS AND DISCUSSION

Reactions of nitrosyl halides NOX (X = Cl, Br) with [$OsH(CO)ClL_3$], [$Os(CO)Cl_2L_3$] and [$OsH_2(CO)L_3$] (L = PPh_3, $AsPh_3$) gave osmium nitrosyl complexes [$Os(NO)X_3L_2$], [$Os(NO)ClBr_2L_2$] and $Os(NO)Cl_2BrL_2$ in good yield (50–70%) and osmium carbonyl complexes [$Os(CO)_2X_2L_2$] (X = Cl, Br; L = PPh_3, $AsPh_3$) in low yield (8–10%).

The IR spectra of [$Os(NO)X_3L_2$], [$Os(NO)ClBr_2L_2$] and [$Os(NO)Cl_2BrL_2$] exhibited intense bands in the region 1840–1860 cm^{-1} due to the nitrosyl stretching frequency and in the region 340–300 cm^{-1} (in chloro complexes) due to ν(Os—Cl). The IR spectra of osmium dicarbonyl complexes [$Os(CO)_2X_2L_2$] (X = Cl, Br; L = PPh_3, $AsPh_3$) which agreed with those previously reported,[35–37] exhibit two strong ν(CO) vibrations (Table 2) consistent with a *cis*-configuration (**I**).

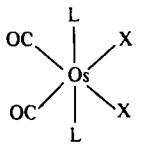

I

The complexes [$Os(NO)X_3(AsPh_3)_2$] (X = Cl, Br), on refluxing with triphenylarsine in benezene for 50 h afforded green complexes [$Os(NO)X(AsPh_3)_3$]:

$$Os(NO)X_3(AsPh_3)_2 + AsPh_3 \xrightarrow[\text{reflux}]{\text{benzene}} Os(NO)X(AsPh_3)_3 + \cdots \quad (1)$$

The complex [$Os(NO)Cl(AsPh_3)_3$] is a green coloured solid, a non-electrolyte and its solution is air sensitive. The IR spectrum of [$Os(NO)Cl(AsPh_3)_3$] shows a strong band at 1635 cm^{-1} due to ν(NO) and at 310 cm^{-1} due to ν(Os—Cl).

The electronic spectrum in benzene shows bands at 13400, 15750, 20200 and 25120 cm^{-1}. Complex [$Os(NO)Br(AsPh_3)_3$] is a green coloured solid, a non-electrolyte and its solution is air sensitive. The IR spectrum of [$Os(NO)Br(AsPh_3)_3$] shows a strong band at 1630 cm^{-1} due to ν(NO). The electronic spectrum in benzene shows bands at 13330, 15670, 19610 and 25000 cm^{-1}. The corrected nitrosyl stretching frequencies, ν(NO), calculated by Ibers empirical rules,[38] fall above 1610 cm^{-1}. This is evidence for the presence of a linear nitrosyl group in these complexes. Combining the rules which have been suggested by Ibers,[39] and Hoffmann *et al*,[40] for penta-coordinated nitrosyl complexes, with the empirical rules of stereochemistry, the geometry about the osmium atom can be described as distorted trigonal bipyramid with equatorial triphenylarsine ligands and the NO group *trans*axial to X (X = Cl, Br) and the molecule has C_{3v} symmetry (**II**).

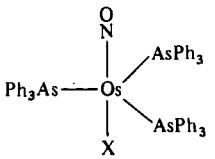

II

The reaction of sulphur with [$Os(NO)X_3(PPh_3)_2$] (X = Cl, Br) in benzene results in the formation of thionitro complexes, [$Os(NSO)X_2(PPh_3)$]

$$Os(NO)X_3(PPh_3)_2 + \tfrac{1}{4}S_8 \xrightarrow{\text{benzene}} Os(NSO)X_2(PPh_3)_2 + \cdots \quad (2)$$

These complexes are green coloured solids, stable under nitrogen atmosphere and paramagnetic compounds, with magnetic moments μ = 1.70, 1.72 BM, respectively. The IR spectra of [$Os(NSO)X_2(PPh_3)_2$] show absorption bands in the region 1230, 1050 and 575 cm^{-1} due to ν_{asym}(NSO), ν_{sym}(NSO) and δ(NSO), respectively.[41,42] The electronic spectrum of [$Os(NSO)Cl_2(PPh_3)_2$] shows bands at 19800, 21500, 25640 and 36360 cm^{-1}.

Stirring the benzene solution of [$Os(NO)Cl_3(PPh_3)_2$] with [$Na(S_2CNR_2)$] (R = Et, Me)

afforded the nitrosyl complexes [Os(NO)$Cl_2(S_2CNR_2)(PPh_3)$]

$$Os(NO)Cl_3(PPh_3)_2 + Na(S_2CNR_2) \xrightarrow[\text{stirring}]{\text{benzene}} Os(NO)Cl_2(S_2CNR_2)(PPh_3). \quad (3)$$

Refluxing the complex $[Os(NO)Cl_3(PPh_3)_2]$ with excess $[Na(S_2CNR_2)]$ gave osmium(II) complexes $[Os(S_2CNR_2)_3]$:

$$Os(NO)Cl_3(PPh_3)_2 + \text{excess } Na(S_2CNR_2) \xrightarrow[\text{reflux}]{\text{benzene}} Os(S_2CNR_2)_3. \quad (4)$$

The IR spectra of the complexes [Os(NO)$Cl_2(S_2CNR_2)(PPh_3)$] (R = Et, Me) show intense bands at 1810 and 1800 cm^{-1} due to ν(NO), respectively, in addition to the absorption bands due to S_2CNR_2 and (PPh_3) ligands. The ν(CN) frequency in these complexes appears at 1530 and 1542 cm^{-1}, respectively. It is shifted to higher energy compared with the free ligand, as a result of increased double bond character upon coordination to the metal centre.[43,44]

The electronic spectra of [Os(NO)Cl_2 $(S_2CNEt_2)(PPh_3)$] show absorption bands at 23690, 30300 and 34480 cm^{-1}. The electronic spectra of $[Os(S_2CNEt_2)_3]$ show bands at 35714 cm^{-1} and a very weak band at 20200 cm^{-1}. A study of dithiolic acids assigned the high energy absorption to π–π^* transitions.[45] The IR spectra of $[Os(S_2CNR_2)_3]$ (R = Et, Me) show no band due to ν(NO), indicating the absence of the NO group in the complexes. The complexes $[Os(S_2CNR_2)_3]$ are paramagnetic with magnetic moments $\mu = 1.80$, 1.83 BM, respectively.

Acknowledgement—This research was supported by the Council of Scientific and Industrial Research, New Delhi under the Research Project No. 1(998)/84-EMR-II.

REFERENCES

1. W. P. Griffiths, J. Lewis and G. Wilkinson, *J. Chem. Soc.* 1961, 775.
2. G. R. Crooks and B. F. G. Johnson, *J. Chem. Soc. A* 1968, 1236.
3. G. R. Crooks and B. F. G. Johnson, *J. Chem. Soc. A* 1970, 1662.
4. J. R. Fowler and J. Kleinberg, *Inorg. Chem.* 1970, **9**, 1005.
5. B. F. G. Johnson and R. Davis, *J. Chem. Soc., Dalton Trans.* 1976, 508.
6. K. D. Hodge and J. U. Rund, *Inorg. Chem.* 1975, **14**, 525.
7. W. L. Waters and P. G. March, *J. Organomet. Chem.* 1975, **40**, 3344.
8. P. Legzdins and J. T. Malito, *Inorg. Chem.* 1975, **14**, 1875.
9. K. E. Voss, S. D. Hudman and J. Kleinberg, *Inorg. Chim. Acta* 1976, **20**, 78.
10. N. G. Connelly and C. Gardner, *J. Chem. Soc., Dalton Trans.* 1976, 1525.
11. K. K. Pandey, S. Datta and U. C. Agarwala, *Transition Met. Chem.* 1979, **4**, 237.
12. K. K. Pandey and U. C. Agarwala, *Z. Anorg. Allg. Chem.* 1979, **457**, 235.
13. K. K. Pandey and U. C. Agarwala, *J. Inorg. Nucl. Chem.* 1980, **42**, 293.
14. R. F. N. Ashok, M. Gupta, K. S. Arulsamy and U. C. Agarwala, *Inorg. Chim. Acta* 1985, **98**, 169.
15. K. K. Pandey, S. R. Ahuja and V. Vijayavergiya, *Polyhedron* 1986, **5**, 767.
16. A. Araneo, V. Valenzio and F. Cariati, *J. Inorg. Nucl. Chem.* 1970, **32**, 1877.
17. K. K. Pandey, R. D. Tiwari and U. C. Agarwala, *Indian J. Chem.* 1981, **20A**, 370.
18. K. K. Pandey and S. R. Ahuja, *Inorg. Chem.* 1985, **24**, 2855.
19. A. F. Hill, W. R. Roper, J. M. Waters and A. H. Wright, *J. Am. Chem. Soc.* 1983, **105**, 5939.
20. M. Kubota and D. A. Phillips, *J. Am. Chem. Soc.* 1975, **97**, 5637.
21. J. A. McCleverty, *Chem. Revs* 1979, **79**, 53.
22. P. G. Ashmore, M. G. Burnett and B. J. Taylor, *Trans. Faraday Soc.* 1962, **80**, 685.
23. M. Tamaki, I. Masuda and K. Sinra, *Bull. Chem. Soc. Jpn.* 1975, **45**, 171.
24. S. G. Clarkson and F. Basolo, *Inorg. Chem.* 1973, **12**, 1528.
25. W. C. Trogler and L. G. Marzilli, *Inorg. Chem.* 1974, **13**, 1008.
26. P. A. Rock and J. H. Swinehart, *Inorg. Chem.* 1969, **5**, 1078.
27. N. Ahmad, S. D. Robinson and M. F. Uttley, *J. Chem. Soc., Dalton Trans.* 1972, 843.
28. N. Ahmad, J. J. Levison, S. D. Robinson and M. F. Uttley, *Inorg. Synth.* 1975, **15**, 45.
29. A. R. Harris and S. D. Robinson, *Inorg. Chim. Acta* 1980, **42**, 25.
30. Shell, Internat. Research Maatschappij, N.U. Neth. Appl. 61512661 (Cl. CO. 1b) 31.3 (1967).
31. W. G. Burns and H. J. Bernstein, *J. Chem. Phys.* 1950, **18**, 1669.
32. F. P. Treadwell and W. T. Hall, *Analytical Chemistry*, Vol. 2 9th Edn. John Wiley, New York (1958).
33. A. I. Vogel, *A Text-Book of Quantitative Inorganic Analysis*, 3rd Edn. Longmans Green, London (1961).
34. K. K. Pandey, *Spectrochim. Acta* 1983, **39A**, 925.
35. L. A. W. Hales and R. J. Irving, *J. Chem. Soc. A* 1962, 1669.
36. J. P. Collman and W. R. Roper, *J. Am. Chem. Soc.* 1966, **88**, 3504.
37. D. S. Moore and S. D. Robinson, unpublished results, taken from ref. 29.
38. B. L. Haymore and J. A. Ibers, *Inorg. Chem.* 1975, **14**, 3060.

39. B. L. Haymore and J. A. Ibers, *Inorg. Chem.* 1975, **14**, 2610.
40. R. Hoffmann, M. M. L. Chen, M. Elean, A. R. Rossi and D. M. P. Mingos, *Inorg. Chem.* 1974, **13**, 2666.
41. K. K. Pandey and U. C. Agarwala, *Ind. J. Chem.* 1980, **20A**, 1906.
42. H. W. Roesky, K. K. Pandey, B. Krebs and M. Dartmann, *J. Chem. Soc., Dalton Trans.* 1984, 2271.
43. C. O'Connor, J. D. Gilbert and G. Wilkinson, *J. Chem. Soc. A* 1969, 84.
44. J. Chatt, L. A. Dun, L. A. Ducanson and L. M. Vananzi, *Nature* 1966, **177**, 1042.
45. M. L. Shankaranaryana and C. C. Patel, *Acta Chim. Scand.* 1965, **19**, 1113.

Polyhedron Vol. 7, No. 9, pp. 715–719, 1988
Printed in Great Britain

0277-5387/88 $3.00 + .00
© 1988 Pergamon Press plc

THE INFLUENCE OF AQUEOUS CHLORIDE MEDIA ON THE SOLVENT EXTRACTION OF CADMIUM BY TRILAURYLAMMONIUM CHLORIDE IN TOLUENE

A. MASANA and LL. NADAL

Departamento de Química, Col. legi Universitari Girona, -U.A.B.- 17071 Girona, Spain

and

M. VALIENTE*

Departamento de Química, Química analítica, -U.A.B.- 08193 Bellaterra (Barcelona), Spain

(*Received* 9 *November* 1987; *accepted* 21 *December* 1987)

Abstract—The extraction of Cd(II) from chloride solutions by trilaurylammonium chloride, TLAHCl, dissolved in toluene has been studied by means of metal distribution measurements. The experimental data have been obtained at different chloride concentrations of the aqueous phase (ranging from 1.0 to 3.0 mol dm^{-3}) and applying the constant ionic medium method. The results show an enhancement of the cadmium extraction when the aqueous chloride concentration is increased. The extraction process is explained by assuming that the species $CdCl_2(TLAHCl)_2$ and $CdCl_2(TLAHCl)_3$ are formed in the organic phase, and the corresponding extraction reactions are:

$$Cd^{2+} + 2Cl^- + 2TLAHCl(org) \rightleftharpoons CdCl_2(TLAHCl)_2(org); K_2$$

$$Cd^{2+} + 2Cl^- + 3TLAHCl(org) \rightleftharpoons CdCl_2(TLAHCl)_3(org); K_3$$

This model has been found to be independent of the chloride concentration in the aqueous phase. However, the values of their extraction constants K_2 and K_3 are different for the various chloride concentrations used. The values of K_2 and K_3 at a different chloride concentration, I, have been correlated by using the specific-interaction theory (S.I.T.), and the interaction coefficient for the Cd^{2+}, Cl^- ions, as well as, the thermodynamic constants, K_n^0, have been determined.

Solvent extraction of divalent metals from aqueous chloride solutions has been investigated under different experimental conditions.[1] During the last decade, long-chain amines and quaternary ammonium salts have been extensively used as ion exchangers in the hydrometallurgy and production of metals.[2–4] Solvent extraction of Cd(II) has been scarcely studied in spite of the technological importance of this metal. Few works were reported and these generally used tertiary amines as extracting agents.[4–6]

In the present work a detailed analysis of the extraction equilibria taking place between solutions of aqueous cadmium chloride and trilaurylammonium chloride, TLAHCl, in toluene is performed in order to delve into the knowledge of some important aspects of this extraction process. Thus, this work has been undertaken to determine the influence of ionic media on the extraction of divalent metals and also to ascertain the metal organic species formed in the extraction process of Cd(II). Comparison of the results obtained with those already reported in the extraction of Cu(II), Pb(II) and Zn(II) under similar experimental conditions[7–9] is presented.

*Author to whom correspondence should be addressed.

EXPERIMENTAL

Reagents and solutions

All chemicals used were of analytical grade. Trilaurylammonium chloride, TLAHCl, was obtained from the corresponding amine (Merck) as described in the literature.[10] Toluene (Merck) was used without further purification. Cadmium chloride (Merck) was purified by recrystallization before use. Sodium chloride (Panreac) was carefully treated as previously described.[11] The total TLAHCl concentration in toluene solutions varied from 15 to 250 mmol dm^{-3}.

Aqueous Cd(II) solutions were prepared by dissolving cadmium chloride in NaCl solutions. The total chloride concentration of the aqueous phase, I, was set at 1.0, 2.0 and 3.0 mol dm^{-3} for the respective three different series of experiments. The Cd(II) total concentration varied from 10 to 90 mmol dm^{-3}. The H^+ concentration was kept constant in all experiments at 0.1 mol dm^{-3} to avoid hydrolysis of both Cd(II) and TLAHCl.

Distribution measurements

The experiments were carried out at 20°C. Equal volumes (10 cm^3) of the organic and aqueous solutions were shaken for 1 h in a continuous rotary mixer (these conditions were found to be sufficient to attain equilibrium). The total Cd(II) concentration in both phases was determined by titration with EDTA using xylenol orange as indicator.[12] Ethanol was used to homogenize the organic solution before titration.

RESULTS AND DISCUSSION

A series of experiments were performed at the ionic strengths, $I = 1.0$, 2.0 and 3.0 mol dm^{-3} to determine the metal distribution coefficient, D, defined by:

$$D = [\mathrm{Cd(II)}]_{org}/[\mathrm{Cd(II)}]_{aq}. \quad (1)$$

In each series, D was determined as a function of the total concentration of the amine salt at a given total Cd(II) concentration. In Figs 1 and 2, $\log D$ is plotted vs $\log[\mathrm{TLAHCl}]_{total}$. As seen, the increase of chloride concentration enhances the extraction of the metal (Fig. 1). It is also observed that the distribution coefficient depends on the Cd(II) concentration (Fig. 2).

The experimental data were treated assuming that the extraction of cadmium can be expressed by the equation:

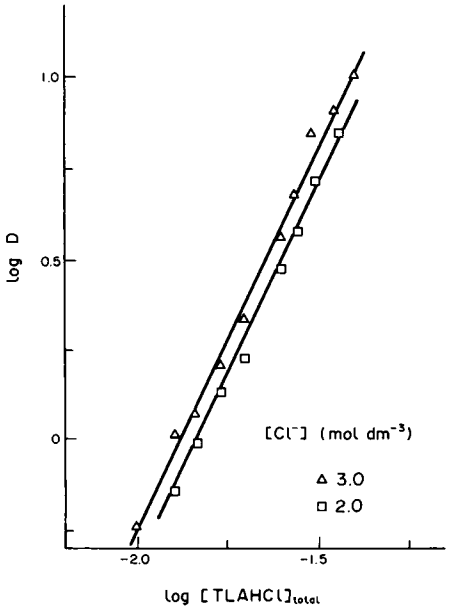

Fig. 1. Plot of $\log D$ vs $\log[\mathrm{TLAHCl}]_{total}$ at different ionic strengths and Cd(II) concentration 10.0 mmol dm^{-3}.

$$Cd^{2+} + 2Cl^- + n\mathrm{TLAHCl(org)} \rightleftharpoons CdCl_2(\mathrm{TLAHCl})_n(org). \quad (2)$$

For each ionic strength the data were treated separately.

Thus, considering ideal behaviour in the organic phase and assuming the activity coefficients of the aqueous species to be constant, the equilibrium con-

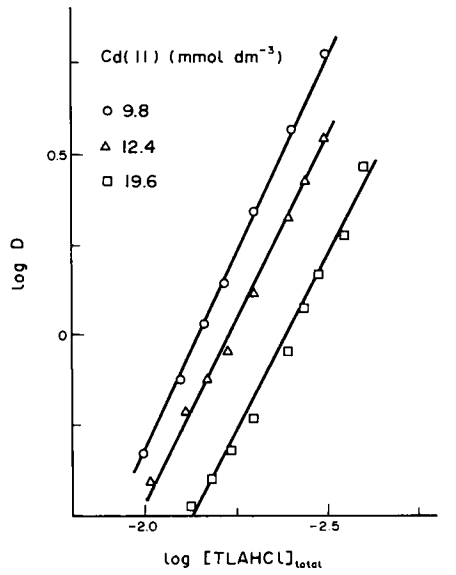

Fig. 2. Plot of $\log D$ vs $\log[\mathrm{TLAHCl}]_{total}$ at 1.0 mol dm^{-3} ionic strength for different Cd(II) total concentration.

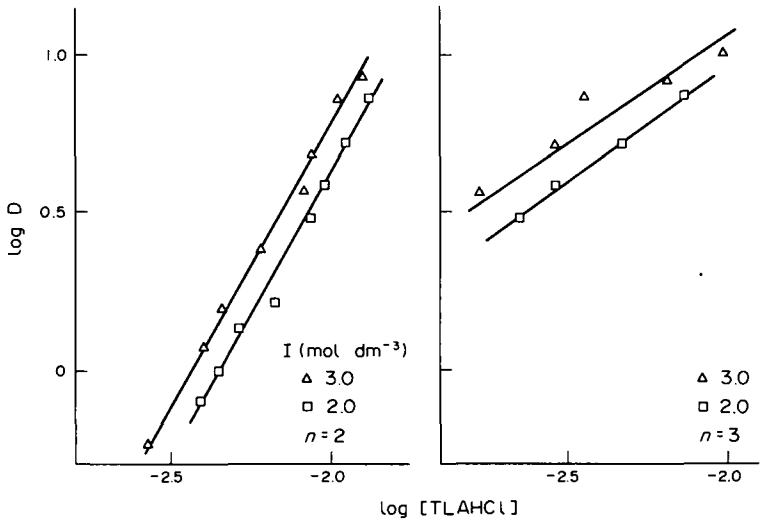

Fig. 3. Log D plotted as a function of free TLAHCl concentration at different ionic strengths for $n = 2$ and $n = 3$.

stant of reaction (2) can be expressed by

$$Kn = \frac{[(CdCl_2)(TLAHCl)_n]}{[Cd^{2+}][Cl^-]^2[TLAHCl]^n}, \quad (3)$$

where no polynuclear species have been considered.

To estimate the composition of extracted species, possible values for n were determined by applying mass balance equations as follows:

$$[Cd(II)]_{total} = [Cd(II)]_{org} + [Cd(II)]_{aq} \quad (4)$$

$$[Cd(II)]_{org} = Kn[Cd^{2+}][Cl^-]^2[TLAHCl]^n \quad (5)$$

$$[Cd(II)]_{aq} = [Cd^{2+}](1 + \Sigma\beta_i[Cl^-]^i) \quad (6)$$

$$D = K[TLAHCl]^n \quad (7)$$

$$K = \frac{K_n[Cl^-]^2}{1 + \Sigma\beta_i[Cl^-]^i} \quad (8)$$

being β_i the formation constants of the cadmium chlorocomplexes.[13]

$$\log D = \log K + n \log [TLAHCl]. \quad (9)$$

The equilibrium concentration of TLAHCl was calculated taking into account the formation of trimers in toluene[14] and the corresponding constant, Q, defined by:

$$Q = [(TLAHCl)_3]/[TLAHCl]^3;$$

$$Q = 5.01 \times 10^2 \quad (10)$$

$$[TLAHCl]_{total} = [TLAHCl] + 3Q[TLAHCl]^3 + n[CdCl_2(TLAHCl)_n] \quad (11)$$

$$[TLAHCl]_{total} - n[Cd(II)]_{org} = [TLAHCl] + 3Q[TLAHCl]^3. \quad (12)$$

Figure 3 shows the experimental values of log D as a function of the calculated log TLAHCl from eq. (12), for $n = 2$ and $n = 3$ at two different chloride concentrations. As seen, the plots can fit to straight lines with slopes 2.0 and 1.0 for $n = 2$ and $n = 3$, respectively, $n = 2$ having the best fit. These results give an indication of the possible stoichiometry for the metal species formed in the organic phase. From these indications, the data have been treated numerically to determine the stoichiometry as well as the stability constants of the species more exactly, by using the LETAGROP-DISTR computer program.[15] In this case the calculations were based on the minimization of the error square sum U defined by

$$U = \sum_{Np} (\log D_{calc} - \log D_{exp})^2, \quad (13)$$

where log D_{exp} represents the experimental values of the distribution coefficient, log D_{calc} is a corresponding quantity calculated by the program assuming a determined model of chemical species and formation constants in the two liquid phases, and Np is the total number of experimental points. The results of this treatment are given in Table 1, where the "best fit" to the experimental data is given by the model involving the following metal extraction reactions:

$$Cd^{2+} + 2Cl^- + 2TLAHCl \rightleftharpoons CdCl_2(TLAHCl)_2 \quad (14)$$

$$Cd^{2+} + 2Cl^- + 3TLAHCl \rightleftharpoons CdCl_2(TLAHCl)_3. \quad (15)$$

Table 1. Results of numerical calculations by the LETAGROP-DISTR program

Model Cd^{2+}, Cl^-, TLAHCl	I	$\log K_n$	σ	U
1,2,2	1.0	8.28±0.17	0.167	1.939
	2.0	8.41±0.11	0.104	0.400
	3.0	8.52±0.16	0.121	0.503
	1.0	8.43±0.07 10.40±0.19	0.055	0.117
1,2,2 1,2,3	2.0	8.58±0.08 10.36±0.20	0.046	0.076
	3.0	8.74±0.11 10.62±0.20	0.059	0.115
	1.0	8.66±0.20 14.5 max 14.9	0.083	0.260
1,2,2 1,2,5	2.0	8.59±0.12 13.5 max 13.8	0.061	0.136
	3.0	8.78±0.17 14.2 max 14.7	0.067	0.152

This model was obtained as a result of calculations where the chosen species (Cd(II), Cl^-, TLAHCl) 1,2,2, 1,2,3 and 1,2,5 were made to compete. The species 1,2,5 were rejected throughout this calculation process. This model has been found to be independent of the chloride concentration in the aqueous phase. However the values of the stability constants for reactions (14) and (15) are different for the different aqueous chloride concentrations considered. This fact has been explained in terms of the ionic strength effect and the different values have been correlated by using the specific-interaction theory (S.I.T.).[16,17] In this treatment, the relationship between the equilibrium constant, K^I, and the ionic strength, I, is given by the equation:

$$\log K^I = \log K^0 - \frac{\Delta z^2 A\sqrt{I}}{1+1.5\sqrt{I}} + b(i,k)I$$

$$\Delta z^2 = n_j z_j^2 - r_j z_j^2$$

where n_j are the stoichiometric coefficients of the ionic reacting species of charge z_j, and r_j are the corresponding coefficients of the ionic species formed in eq. (2), in this case $\Delta z^2 = 6$. K^I and K^0 are the extraction constants at I and 0 ionic strength, respectively. $b(i,k)$ is the sum of the specific interaction coefficients. $A = 0.1507$ and I is expressed in mol kg^{-1}.

The plot of $\log K^I + 6A\sqrt{I}/(1+1.5\sqrt{I})$ vs I, fits to a straight line (Fig. 4). From the intercept and the slope of these lines, the thermodynamic extraction constants are determined, as well as the sum of the specific interaction coefficients:

$$b = \varepsilon_{Cd^{2+},Cl^-} + 2\varepsilon_{Na^+,Cl}\ .$$

As ε_{Na^+,Cl^-} is known[18] the value of $\varepsilon_{Cd^{2+},Cl^-}$ can be determined. The results obtained correspond to the values: $\log K_2^0 = 9.41$; $\log K_3^0 = 11.4$; $\varepsilon_{Cd^{2+},Cl^-} = 0.197$.

CONCLUSIONS

The extraction of Cd(II) from the chloride solutions by trilaurylammonium chloride can be explained assuming the formation of two metal

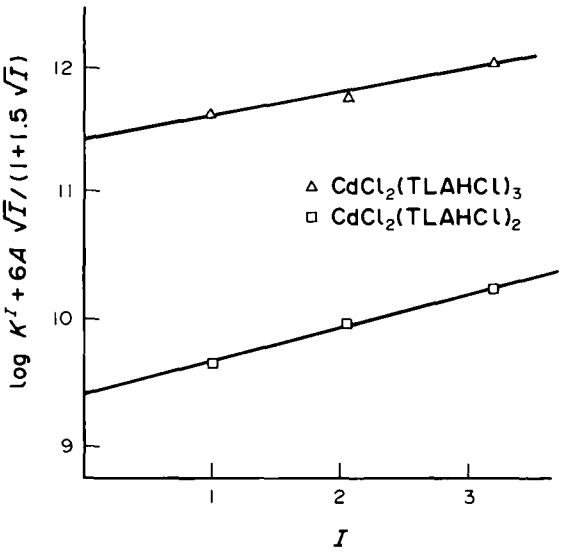

Fig. 4. Numerical values of the expression $\log K^I + 6A\sqrt{I}/(1+1.5\sqrt{I})$ plotted vs the ionic strength, I.

species in the organic phase : $CdCl_2(TLAHCl)_2$ and $CdCl_2(TLAHCl)_3$. The results collected in Table 1 indicate that the composition of extracted species is independent of the ionic strength, but the formation constants vary with I. This is in agreement with our previous finding in the extraction of the divalent metals Pb(II), Cu(II) and Zn(II)[7-9] under similar experimental conditions.

The fact that the extraction of Cd(II) increases with the aqueous chloride concentration can be explained by the nature of the extraction system which is assumed to behave as an anionic exchange process. Thus, the increase of chloride concentration enhances the formation of anionic Cd(II) chlorocomplexes.

Comparison of the results obtained for the studied divalent metals shows that the extracted species depend on the nature of the metal ion. In this concern, two different behaviours were observed. Thus, while Cd(II) and Zn(II) form species of stoichiometry 1:2 and 1:3 (metal(II):ammonium salt), Pb(II) and Cu(II) are found to give 1:2 and 1:5 as extracted species. M. Leszko *et al*[6] using octadecyldimethylbencylammonium chloride, ODBACl, as the extracting agent have also found a different behaviour of Cd(II) and Zn(II) with respect to Cu(II) and Pb(II) ions. They ascribed this fact to the polarity of the extracted complexes.

On the other hand diluents play an important role in the extraction process, the effect of the diluent on the distribution coefficient have been explained using properties such as the dielectric constant, the dipole moment and the solubility parameters. The distribution coefficient obtained under our experimental conditions, using toluene as a diluent, is smaller than the reported value[5] in benzene. A similar diluent effect has been observed previously when using ODBACl as the extractant for Zn(II) and Cd(II) ions[6] and also in the extraction of Zn(II) by trioctylmethylammonium chloride, TOMAC.[19] In both works the authors found this fact to be related to the Hildebrand solubility parameter of the diluent, δ,[20] which applies to our results in the sense that a higher δ value gives higher D values.

Acknowledgement—The Spanish Commission for Scientific development (CICYT), provided the facilities to carry out the present work (project PA 0564/84).

REFERENCES

1. I. Marcus and A. S. Kertes, *Ion Exchange and Solvent Extraction of Metal Complexes*. Wiley Interscience, New York (1969).
2. W. Boyed, *Solvent Extr. Ion Exch.* 1974, **6**, 189.
3. S. Lindenbaum and G. E. Boyd, *J. Phys. Chem.* 1963, **67**, 1238.
4. T. Sato, A. Katsuhiko, K. Toshikazu and N. Takato, *Sep. Sci. Technol.* 1982, **17**, 1565.
5. J. De Pablo and M. Aguilar, *Chem. Scr.* 1984, **24**, 147.
6. M. Leszko and W. Zaborska, *Roczniki Chemii Ann. Soc. Chim. Polonorum* 1977, **51**, 1961.
7. J. Coello, J. M. Madariaga, M. Muhammed, M. Valiente and H. Iturriaga, *Polyhedron*, 1986, **5**, 1845.
8. A. Masana and M. Valiente, *Solvent Extr. Ion Exch.* 1987, **5**, 667.
9. A. Masana and M. Valiente, *Analyt. Sci.* 1988, **4**, 21.
10. M. Muhammed, J. Szabon and E. Högfeldt, *Chem. Scr.* 1974, **6**, 61.
11. *Some Laboratory Methods*, Mimeograph, Dept. of Inorganic Chemistry, The Royal Institute of Technology, Stockholm (1959).
12. G. Schwarzenbach and H. Fleschka, *Complexometric Titrations*, p. 253. Methuen, London (1969).
13. E. Högfeldt, *Stability Constants of Metal Ion Complexes*, part A, IUPAC Chemical data series 2. Pergamon Press, Oxford (1982).
14. J. Coello, J. Aparicio, L. A. Fernandez and M. Muhammed, *Chem. Scr.* 1987, **27**, 377.
15. D. H. Liem, *Acta Chem. Scand.* 1971, **25**, 1421.
16. E. A. Guggenheim, *Application of Statistical Mechanics*. Clarendon Press, Oxford (1966).
17. G. Scatchard, *Equilibrium in Solution Surface and Colloid Chemistry*. Harvard University Press, Cambridge, Massachusetts (1976).
18. L. Ciavatta, *Annali Chim., Societá chim. Italiana*, 1980, 550.
19. T. Sato, T. Nakamura and M. Kuwahara, Proc. *ISEC 83*, Denver, Colorado, U.S.A., 1983, **1**, 274.
20. T. Sekine and Y. Hasegawa, *Solvent Extraction Chemistry*, M. Dekker, New York (1977).

Polyhedron Vol. 7, No. 9, pp. 721–724, 1988
Printed in Great Britain

0277-5387/88 $3.00+.00
Pergamon Press plc

THE FORMATION OF 1:1 AND 2:1 COMPLEXES OF CROWN ETHERS AND CRYPTANDS WITH K^+ IN ACETONITRILE AND PROPYLENE CARBONATE

HANS-JÜRGEN BUSCHMANN

Physikalische Chemie, Universität-GH Siegen, Postfach 101240, D-5900 Siegen, FRG

(*Received* 9 *November* 1987; *accepted* 4 *January* 1988)

Abstract—The formation of 1:1 and 2:1 complexes of crown ethers and cryptands with K^+ was studied by means of potentiometric and calorimetric titrations in acetonitrile and propylene carbonate solutions. With the exception of the diaza crown ether (21) all twelve- and fifteen-membered monocyclic ligands examined are able to form 2:1 complexes. Structural changes of the ligand (21) during complex formation are mainly responsible for this observation. The complexes formed with the cryptands (222) and (221) are more stable compared to the monocyclic ligands. The smallest cryptand (211) is not able to encapsulate the potassium ion completely. Therefore, the formation of 2:1 complexes in both solvents are measured. The reaction enthalpies indicate that the macrobicyclic structure of the ligand is important during the formation of the 1:1 complexes. During the formation of the 2:1 complexes the cryptand (211) behaves like the diaza crown ether (21). Therefore, the conclusion is that the formation of 2:1 complexes with cryptands is only observable in a given solvent if a reaction with the corresponding diaza crown ether is measured.

Many results for the complexation of ions by crown ethers and cryptands have been published during recent years. Most of them can be found in a compilation given by Izatt *et al.*[1] However, thermodynamic data for the formation of 2:1 complexes of crown ethers with cations (ratio of ligand to cation) are scarce. Meanwhile, more data are available about the formation of such complexes in methanol solutions.[2,3]

In contrast, no direct evidence of the existence of 2:1 complexes of cryptands has been reported up to now. The first hint of the existence of such a complex between the cryptand (221) and Cs^+ was given by Lehn *et al.*[4] From kinetic measurements of ligand-exchange reactions between cryptates and cryptands, 2:1 complexes were proposed as intermediates.[5]

We have already reported earlier unsuccessful attempts to study the formation of 2:1 complexes with cryptands in methanol solution.[6] In order to obtain more information as to whether or not the formation of such complexes is possible in principle, the complex formation of K^+ with macrocyclic and macrobicyclic ligands has been studied in several solvents.

EXPERIMENTAL

The salts used, potassium perchlorate (Ventron), silver tetrafluoroborate (Merck) and tetraethylammonium perchlorate (Fluka) are anhydrous and of the highest purity available. Potassium tetraphenylborate was prepared and purified according to published procedures.[7]

The macrocyclic and macrobicyclic ligands, see Figs 1 and 2 (all from Merck) were used without further purification. As solvents, acetonitrile (AN; Merck; H_2O content less than 0.3%) and propylene carbonate (PC; Merck; p.a.) were used.

In order to determine the stability constants, the ion activity of K^+ was directly measured by means of an ion-selective electrode (Ingold pK201-S7). During the potentiometric titrations the ionic strength was kept constant at $I = 0.05$ mol dm^{-3} using tetraethylammonium perchlorate as the supporting electrolyte.

The reaction observed can be shown by eq. (1):

$$M^+ + L \overset{K_1}{\rightleftharpoons} ML^+ + L \overset{K_2}{\rightleftharpoons} ML_2^+ \qquad (1)$$

with

$$K_1 = \frac{[ML^+]}{[M^+][L]} \quad \text{and} \quad K_2 = \frac{[ML_2^+]}{[ML^+][L]}.$$

The treatment of the experimental data has already been described in detail.[2] The response of the potassium electrode in both solvents was found to be almost ideal. Another possibility for obtaining the stability constants of the potassium complexes indirectly by means of potentiometric titrations is given by disproportionative reactions with Ag^+.[8]

All reaction enthalpies were measured using a Tronac Model 450 calorimeter. To ensure the formation of only 1 : 1 complexes in the reaction vessel, a solution of the ligand (0.02–0.04 M) was titrated continuously into a solution containing a potassium salt (4×10^{-3}–6×10^{-3} M). Under these conditions during the titration, the concentration of the salt in the reaction vessel was higher compared to that of the ligand concentration.

The sum of the reaction enthalpies for the formation of 1 : 1 and 2 : 1 complexes was determined by titrating a potassium salt solution (0.01–0.02 M) into a ligand solution (0.02–0.04 M). The ligand concentration in the reaction vessel was then much higher in comparison with the salt concentration. Thus, the formation of 2 : 1 complexes was expected to be almost complete. Using the separately estimated value of ΔH_1, the value of ΔH_2 was easily calculated.

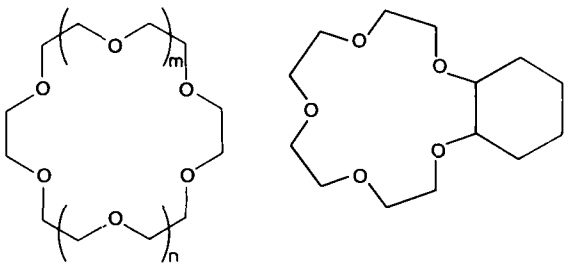

m = 0, n = 0 : 12C4
m = 0, n = 1 : 15C5
m = 1, n = 1 : 18C6

Fig. 1. Crown ethers.

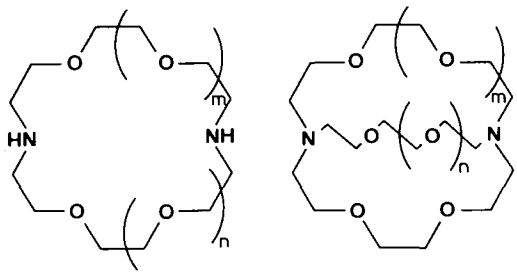

m = 1, n = 0 : 21
m = 1, n = 1 : 22

m = 0, n = 0 : 211
m = 1, n = 0 : 221
m = 1, n = 1 : 222

Fig. 2. Aza crown ethers and cryptands.

RESULTS AND DISCUSSION

The values of the stability constants, reaction enthalpies and reaction entropies for the formation of 1 : 1 and 2 : 1 complexes of K^+ with macrocyclic and macrobicyclic ligands in acetonitrile and propylene carbonate are given in Tables 1 and 2, respectively. No data are available from the literature for the formation of 2 : 1 complexes in both solvents. However, some stability constants for the formation of 1 : 1 complexes of K^+ with the ligands 18C6,[11,12] (22),[12] (211),[13,14] (221),[13,14] and (222),[8,13,15] in propylene carbonate have already been reported.

Table 1. Stability constants (log K; K in M^{-1}) and thermodynamic parameters (ΔH, $T\Delta S$ in kJ mol^{-1}) for the formation of 1 : 1 and 2 : 1 complexes of crown ethers and cryptands with K^+ in acetonitrile at 25°C.

	log K_1	$-\Delta H_1$	$T\Delta S_1$	log K_2	$-\Delta H_2$	$T\Delta S_2$
12C4	2.40	9.5	4.1	2.29	14.5	−1.5
15C5	4.29 (4.33)[a]	32.0[a]	−7.6	2.75	30.1	−14.5
C15C5	4.15	24.3	−0.7	2.50	13.0	1.2
(21)	2.11[b]	18.8[b]	1.2[b]			
18C6	5.72[b]	9.9[b]	29.1[b]			
(22)	4.13[b]	15.3[b]	8.2[b]			
(211)	3.50[b]	29.3[b]	−9.4[b]	2.42	4.2	9.6
(221)	9.10[b]	64.1[b]	−12.4[b]			
(222)	9.56[b]	74.0[b]	−19.7[b]			

[a] See ref. 9.
[b] See ref. 10.

Table 2. Stability constants (log K; K in M^{-1}) and thermodynamic parameters (ΔH, $T\Delta S$ in kJ mol^{-1}) for the formation of 1 : 1 and 2 : 1 complexes of crown ethers and cryptands with K^+ in propylene carbonate at 25°C.

	log K_1	$-\Delta H_1$	$T\Delta S_1$	log K_2	$-\Delta H_2$	$T\Delta S_2$
12C4	2.02	14.6	−3.1	2.65	8.7	6.4
15C5	3.78	30.5	−9.0	2.84	29.5	−13.4
C15C5	3.70	26.2	−5.2	3.20	20,1	−1.9
(21)	2.25	7.7	5.1			
18C6	6.08	45.4	−10.9			
(22)	4.43	21.9	3.3			
(211)	3.49	30.0	−10.1	2.43	5.0	8.8
(221)	9.15	66.0	−14.0			
(222)	11.00	72.8	−10.3			

They are in accordance with our data. Up to now, only values of the reaction enthalpy for the complexation of potassium with the cryptand (222) in propylene carbonate are known.[8,16] Within the margin of experimental error they are identical with the value measured in this work.

The crown ether 12C4 ($r = 0.6$ Å[15]) and the different 15C5 ligands ($r = 0.9$ Å[17]) examined, are too small to accommodate the potassium ion ($r = 1.38$ Å[18]). Therefore, in both solvents the formation of 2 : 1 complexes is expected and they are experimentally observed. The only exception is with the diaza crown ether (21). The values of the reaction enthalpy for the formation of the 1 : 1 complexes are higher or nearly equal to the values for the addition of the second ligand to the already formed complex. In this case, no strong repulsion between both ligand molecules takes place.

Although the crown ethers 15C5 and (21) possess similar dimensions to the ligand cavity, their complexation behaviour is quite different in both solvents. The potassium complexes with (21) are less stable compared to 15C5. This observation can be explained by the different conformational forms in which diaza crown ethers exist in solution.[19] The conformation of the uncomplexed ligand (21) with the lone electron pairs of both nitrogen atoms directed inside the cavity is less stable compared to other ones due to repulsion effects. However, during the complex formation the ligand has to adopt this unfavourable conformation. Thus, the values observed for the reaction enthalpy with the diaza crown ether (21) are much smaller than with the crown ether 15C5.

This conformational change of the ligand (21) may be mainly responsible for the absence of 2 : 1 complex formation. The reaction enthalpies measured with the ligands 18C6 and (22) in propylene carbonate support this interpretation. In acetonitrile the situation is different due to the strong interactions between 18C6 and the solvent molecules.[20]

The cavity dimensions of the macrocyclic cryptand (222) ($r = 1.4$ Å[21]) are exactly the same size as the potassium cation. Therefore, this cryptand forms the most stable complexes with K^+ in the solvents examined. The cryptand (221) is already too small ($r = 1.1$ Å[20]) to accommodate the potassium ion without any deformation. This means, the values of the reaction enthalpy decrease in both solvents compared to the ligand (222). The cavity of the cryptand (211) ($r = 0.8$ Å[21]) is too small to encapsulate this cation completely. As a result, the formation of 2 : 1 complexes (ratio of ligand to cation) is observed. Such a complex is schematically shown in Fig. 3.

To understand the reasons for the formation of 2 : 1 complexes with the cryptand (211) in these solvents it is necessary to discuss the experimental results in more detail, since in methanol solutions no evidence for the existence of such a complex was found.[6]

It is worthwhile to compare the results for the reaction with the ligands (211) with that for the ligands (21) and (221). All these ligands are too small to accommodate K^+ completely. However,

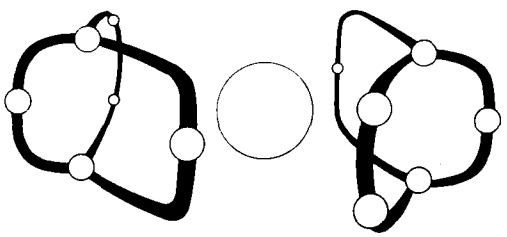

Fig. 3. Schematic representation of a 2 : 1 complex with the cryptand (211).

the values of the reaction enthalpies for the formation of 1 : 1 complexes between the cryptand (211) and K^+ are only half the value of the reaction of the ligand (221) but more than double that for the reaction of the monocyclic ligand (21). Also, the reaction entropies in the case of the cryptands are very similar. Obviously the macrobicyclic structure of the ligand is important for the reaction with the first ligand molecule.

The experimental data for the reaction of the second cryptand molecule (211) are comparable with that for the monocyclic ligand (21). During this reaction step, the cryptand (211) behaves like the diaza crown ether (21). The first bound ligand influences the interactions between the cation and the second cryptand molecule. As a result, the formation of 2 : 1 complexes between cryptands and cations is only expected in solvents in which the formation of the corresponding diaza crown ethers complexes can be observed.

REFERENCES

1. R. M. Izatt, J. S. Bradshaw, S. A. Nielsen, J. D. Lamb, J. J. Christensen and D. Sen, *Chem. Rev.* 1985, **85**, 271.
2. H.-J. Buschmann, *Chem. Ber.* 1985, **118**, 2746 and refs therein.
3. H.-J. Buschmann, *J. Sol. Chem.* 1987, **16**, 181.
4. J.-M. Lehn and J. P. Sauvage, *J. Am. Chem. Soc.* 1975, **97**, 6700.
5. B. G. Cox, N. van Truong and H. Schneider, *J. Chem. Soc., Faraday Trans. I* 1984, **80**, 3285.
6. H.-J. Buschmann, *Inorg. Chim. Acta* 1986, **125**, 31.
7. D. N. Bhattacharyya, C. L. Lee, J. Smid and M. Szwarc, *J. Phys. Chem.* 1965, **69**, 608.
8. J. Gutknecht, H. Schneider and J. Stroka, *Inorg. Chem.* 1978, **17**, 3326.
9. H.-J. Buschmann, *J. Sol. Chem.*, in press.
10. H.-J. Buschmann, *Inorg. Chim. Acta* 1986, **120**, 125.
11. I. M. Kolthoff and M. K. Chantooni, *Anal. Chem.* 1980, **52**, 1039.
12. R. D. Boss and A. I. Popov, *Inorg. Chem.* 1986, **25**, 1747.
13. B. G. Cox, J. Garcias-Rosas and H. Schneider, *J. Phys. Chem.* 1980, **84**, 3178.
14. M. K. Chantooni and I. M. Kolthoff, *J. Sol. Chem.* 1985, **14**, 1.
15. I. M. Kolthoff and M. K. Chantooni, *Proc. Natl. Acad. Sci. USA* 1980, **77**, 5040.
16. A. F. Danil de Namor and L. Ghousseini, *J. Chem. Soc., Faraday Trans. I* 1985, **81**, 781.
17. N. K. Dalley, *Synthetic and Multidentate Macrocyclic Compounds* (Edited by R. M. Izatt and J. J. Christensen). Academic Press, New York (1978).
18. R. D. Shannon and C. T. Prewitt, *Acta Cryst.* 1969, *B*25, 925.
19. H.-J. Buschmann, *Inorg. Chim. Acta* 1985, **102**, 95.
20. R. D. Boss and A. I. Popov, *Inorg. Chem.* 1986, **25**, 1747.
21. J.-M. Lehn, *Struct. Bonding (Berlin)* 1973, **16**, 1.

Polyhedron Vol. 7, No. 9, pp. 725–730, 1988
Printed in Great Britain

0277–5387/88 $3.00 + .00
© 1988 Pergamon Press plc

SOLUTION SYNTHESIS OF CALCIUM, STRONTIUM AND BARIUM METALLOCENES

M. J. McCORMICK, R. A. WILLIAMS, L. J. LEVINE and T. P. HANUSA*

Department of Chemistry, Vanderbilt University, Nashville, Tennessee 37235, U.S.A.

(*Received* 10 *October* 1987; *accepted* 5 *January* 1988)

Abstract—Bis(cyclopentadienyl)metal complexes of calcium, strontium and barium can be prepared in synthetically useful yields (> 65%) from the reaction of lithium or potassium cyclopentadienides and the appropriate metal dihalides in THF. The THF-soluble complexes $(C_5H_5)_2Ca(THF)_2$ and $(Me_5C_5)_2M(THF)_2$ (M = Ca, Sr, Ba) are extracted from the reaction of the appropriate potassium cyclopentadienide with a metal halide; the THF-insoluble $(C_5H_5)_2M(THF)_x$($x \approx 1$ for Sr; $x \approx 0.25$ for Ba) remain after the reaction of a lithium cyclopentadienide and the metal iodide.

Bis(cyclopentadienyl) complexes of the transition metals ("metallocenes") have played a prominent role in the chemistry of the *d*-block elements ever since the discovery of ferrocene in 1951,[1] and the investigation of their bonding and reactivity continues to be a subject of active interest.[2]

In contrast, the metallocenes of the heavy alkaline-earth (HAE = Ca, Sr and Ba) metals have received comparatively little study.[3] "Calciocene" $[(C_5H_5)_2Ca]$, "strontiocene" $[(C_5H_5)_2Sr]$ and "bariocene" $[(C_5H_5)_2Ba]$ have been known for over 25 years and are thermally stable, but they have remained difficult to obtain.[4,5] All three $(C_5H_5)_2M$ species have been prepared in yields of 90% or greater using metal–vapour synthesis techniques,[6] but solution syntheses for the Sr and Ba compounds provide extremely low yields.[4] Only the calcium complex has been investigated to any extent; some of its reactions with nitrogen and oxygen donors have been examined[7] and the oligomeric nature of the unsolvated complex has been established by X-ray crystallography.[8] The chemistry of the Sr and Ba analogues is virtually unknown.[2]

As part of our investigation of the organometallic chemistry of the HAE metals,[9] we sought a convenient, high yield solution route to all three metallocenes. In addition, in order that large-scale investigations of their chemistry would be practical, we hoped that solvated forms of strontiocene and bariocene might be obtained which would be synthetically more useful than the insoluble, unsolvated complexes.†

EXPERIMENTAL

All manipulations were performed with the rigid exclusion of air and moisture. Chemicals were handled with high-vacuum or Schlenk techniques, or in a Vacuum Atmospheres HE-143 drybox equipped with an MO-40-1 recirculating purifier. Proton NMR spectra (Table 1) were obtained at 200 MHz with a Bruker NR-200 spectrometer and were referenced to the residual proton resonances of C_4D_8O (δ 3.58), $(CD_3)_2SO$ (δ 2.49), or C_6D_6 (δ 7.15); carbon (^{13}C) NMR spectra (Table 2) were recorded at 50.3 MHz on a Bruker instrument and were referenced to the residual ^{13}C resonances of $(CD_3)_2SO$ (δ 39.5) or C_6D_6 (δ 128.0). Infrared spectra were obtained as Nujol mulls on a Perkin–Elmer 1430 spectrometer. Elemental analysis was performed by Analytiche Laboratorien, Engelskirchen, West Germany. Melting points were determined under nitrogen in sealed capillaries and are uncorrected.

Materials

The alkali metal cyclopentadienides were prepared from potassium hydride or *n*-butyl lithium and the monomeric cyclopentadienes. The anhy-

*Author to whom correspondence should be addressed.

† As the present work was being completed, reports appeared describing preparation of the $(Me_5C_5)_2ML_x$ metallocenes using essentially the synthetic route presented here.[10] The method was not applied to the parent metallocenes, however.

Table 1. ^{1}H NMR data for HAE metallocenes[a]

	C_5R_5 (R = H, Me)	Other
$(C_5H_5)_2Ca(THF)_2$	5.41 (s, C_5H_5)	1.76, 3.59 (THF)
	5.73 (s, C_5H_5)[b]	[c]
$(C_5H_5)_2Sr(THF)$	5.48 (s, C_5H_5)	1.76, 3.60 (THF)
$(C_5H_5)_2Ba(THF)_{0.25}$	5.51 (s, C_5H_5)	1.75, 3.59 (THF
$(Me_5C_5)_2Ca(THF)_2$	1.82 (br s, (Me_5C_5))	3.59,[c] (THF)
	2.06 (sh s, (Me_5C_5))[d]	1.32, 3.36 (THF)
$(Me_5C_5)_2Sr(THF)_2$	1.81 (br s, (Me_5C_5))	3.60,[c] (THF)
	2.14 (s, (Me_5C_5))[d]	1.32, 3.35 (THF)
$(Me_5C_5)_2Ba(THF)_2$	1.77 (br s, (Me_5C_5))	3.60,[c] (THF)
	2.12 (br s, (Me_5C_5))[d]	3.38, 1.35 (THF)

[a] In DMSO-d_6 unless otherwise noted.
[b] In THF-d_8.
[c] Obscured by other resonances.
[d] In C_6D_6.

Table 2. ^{13}C {^{1}H} NMR data for HAE metallocenes[a]

	C_5R_5 (R = H, Me)	Other
$(C_5H_5)_2Ca(THF)_2$	104.1 (C_5H_5)	25.2, 67.0 (THF)
$(C_5H_5)_2Sr(THF)$	104.7 (C_5H_5)	25.3, 67.0 (THF)
$(C_5H_5)_2Ba(THF)_{0.25}$	106.4 (C_5H_5)	[b]
$(Me_5C_5)_2Ca(THF)_2$	11.0 (Me_5C_5)[c]	25.5, 68.2 (THF)
	112.4 (Me_5C_5)[c]	
$(Me_5C_5)_2Sr(THF)_2$	11.4 (Me_5C_5)[c]	25.4, 68.5 (THF)
	111.6 (Me_5C_5)[c]	
$(Me_5C_5)_2Ba(THF)_2$	11.2 (Me_5C_5)[c]	25.5, 67.9 (THF)
	112.8 (Me_5C_5)[c]	

[a] In DMSO-d_6 unless otherwise noted.
[b] THF signal not detected.
[c] In C_6D_6.

drous metal halides were obtained from Strem Chemicals Inc. Solvents were distilled under nitrogen from sodium or potassium benzophenone ketyl.

$(C_5H_5)_2Ca(THF)_2$. *From* CaI_2

Anhydrous CaI_2 (4.669 g, 15.9 mmol) and $(C_5H_5)K$ (3.644 g, 35.0 mmol) were added to a 250 cm^3 Erlenmeyer flask containing 75 cm^3 of THF. The cloudy reaction mixture was stirred overnight, during which time it assumed a faint pink tinge.

The turbid solution was then filtered through a fine glass frit, which retained a white precipitate. The precipitate was washed with 3×30 cm^3 portions of THF, and the solvent was evaporated from the combined washings and filtrate, leaving crude $(C_5H_5)_2Ca(THF)_2$ (3.738 g, 75% yield). Elemental analysis on this material (10.5% Ca, 0.5% K) was not entirely satisfactory and a qualitative test for iodide using $AgNO_3$(aq) was positive; both its ^{1}H and ^{13}C NMR spectra were consistent with the presence of $(C_5H_5)_2Ca(THF)_2$, however.

From $CaCl_2$

Following the procedure used with CaI_2, anhydrous $CaCl_2$ (0.883 g, 7.96 mmol) and $(C_5H_5)K$ (1.740 g, 16.7 mmol) were allowed to react in 75 cm^3 of THF. Work-up was as given above: the yield of crude $(C_5H_5)_2Ca(THF)_2$ was 0.351 g, (14% yield, but see below). The solid was extracted into THF (*ca* 75 cm^3), filtered and the filtrate reduced to dryness. The extraction procedure was repeated once. Analysis of the product indicated that both potas-

sium and chloride were present in minor amounts and that some desolvation of the metallocene had evidently occurred. Found: Ca, 14.2; K, 1.3; Cl, 0.2. Calc. for the mixture $(C_5H_5)_2Ca(THF)_{1.5}$ (91%)/$(C_5H_5)K$ (7%)/KCl (2%): Ca, 13.9; K, 1.3; Cl, 0.2%. Major IR bands: 3087 m, 1033 s, 1013 s, 930 w, sh, 882 m, 797 m, 771 vs, 752 vs cm^{-1}. The product lost solvent near 100°C (ref. 7 for $(C_5H_5)_2Ca(THF)_2$, > 100°C, dec).

$(C_5H_5)_2Sr(THF)$

Using a procedure analogous to that for $(C_5H_5)_2Ca(THF)_2$, SrI_2 (4.711 g, 13.8 mmol) and $(C_5H_5)Li$ (2.191 g, 30.4 mmol) were stirred overnight in THF (75 cm^3). The turbid white solution was filtered through a fine glass frit and the fine white precipitate was washed with THF (3 × 30 cm^3). Drying the precipitate *in vacuo* left crude, white $(C_5H_5)_2Sr(THF)$ (3.95 g, 99% yield, but see below). The crude material was stirred vigorously with 2 × 75 cm^3 portions of THF before drying again *in vacuo*. Analysis suggested that both lithium and iodide were retained in the rewashed material. Found: Sr, 28.3; Li, 0.4; I, 3.4. Calc. for the mixture $(C_5H_5)_2Sr(THF)$ (86%)/$(C_5H_5)Li$ (7%)/LiI (7%): Sr, 28.5; Li, 0.4; I, 3.5%. Major IR bands: 3077 m, 1038 s, 1012 s, 930 w, sh, 885 m, 790 m, 767 vs, 744 vs cm^{-1}. The material did not melt below 400°C.

$(C_5H_5)_2Ba(THF)_{0.25}$

In a manner similar to that used for $(C_5H_5)_2Ca(THF)_2$, BaI_2 (4.694 g, 12.0 mmol) and $(C_5H_5)Li$ (1.902 g, 26.4 mmol) were stirred overnight in THF (75 cm^3). The resulting pale pink precipitate was collected by filtration, washed repeatedly with THF and dried *in vacuo*, yielding crude $(C_5H_5)_2Ba(THF)_{0.25}$ (4.23 g, quantitative, but see below). Re-extraction of the solid with THF (2 × 75 cm^3) left a material which retained both lithium and iodide. Found: Ba, 43.8; Li, 0.6; I, 7.8. Calc. for the mixture $(C_5H_5)_2Ba(THF)_{0.25}$ (79%)/$(C_5H_5)Li$ (6%)/LiI (15%): Ba, 43.4; Li, 0.6; I, 7.7%. Major IR bands: 3103 m, 1016 m, 750 br vs cm^{-1}. The material did not melt below 400°C.

$(Me_5C_5)_2Ca(THF)_2$

Anhydrous CaI_2 (4.672 g, 15.9 mmol) and $(Me_5C_5)K$ (6.137 g, 35.2 mmol) were added to a 250 cm^3 Erlenmeyer flask containing 75 cm^3 of THF. The cloudy reaction mixture was stirred vigorously overnight.

The turbid solution was then filtered through a fine glass frit, which retained a white precipitate. The solvent was evaporated from the filtrate leaving crude $(Me_5C_5)_2Ca(THF)_2$ (5.875 g, 81% yield). The solid was extracted into toluene (*ca* 75 cm^3), the solution filtered and the filtrate reduced to dryness. The material was then redissolved in THF and the solvent removed. The product lost solvent near 100°C, but the remainder did not melt until 208–210°C (ref. 10(b) for unsolvated $(Me_5C_5)_2Ca$, 207–210°C). Analysis indicated that some desolvation of the metallocene had occurred.* Found: Ca, 9.6. Calc. for $(Me_5C_5)_2Ca(THF)_{1.5}$: Ca, 9.6%. A qualitative test for iodide using $AgNO_3$(aq) was negative. Major IR bands: 2729 m, 1308 w, 1263 w, 1172 w, br, 1030 vs, 923 w, 878 s, 804 w, 727 m, 677 w cm^{-1}.

$(Me_5C_5)_2Sr(THF)_2$

The procedure used was analogous to that for the calcium derivative. Anhydrous SrI_2 (3.414 g, 10.0 mmol) and $(Me_5C_5)K$ (3.850 g, 22.1 mmol and THF (60 cm^3) were combined and the mixture stirred for 2 days. Work-up was as for the calcium derivative. The crude $(Me_5C_5)_2Sr(THF)_2$ (3.349 g, 67% yield) was extracted with toluene and resolvated in THF. The product decomposed with loss of solvent at 190–192°C. Analysis of the white product indicated that partial desolvation of the metallocene had occurred. Found: Sr, 18.6. Calc. for $(Me_5C_5)_2Sr(THF)_{1.6}$: Sr, 18.5%. A qualitative test for iodide using $AgNO_3$(aq) was negative. Major IR bands: 2729 m, 1263 w, 1249 w, 1216 w, 1037 vs, 905 vs, 803 m, br, 729 m, 648 w cm^{-1}.

$(Me_5C_5)_2Ba(THF)_2$.

The procedure was similar to that used for the calcium derivative. Anhydrous BaI_2 (4.694 g, 12.0 mmol) and $(Me_5C_5)K$ (4.602 g, 26.4 mmol) were suspended in THF (75 cm^3) and after stirring overnight, the reaction was worked up as for the calcium derivative. Yield of $(Me_5C_5)_2Ba(THF)_2$: 5.597 g (84%). The product began to decompose with loss of solvent at 185°C (ref. 10(a) m.p. for $(Me_5C_5)_2Ba(THF)_2$, 187–191°C). Analysis of the white product indicated that partial desolvation of the metallocene had occurred. Found: Ba, 26.3. Calc. for $(Me_5C_5)_2Ba(THF)_{1.6}$: Ba, 26.2%. A qualitative test for iodide using $AgNO_3$(aq) was negative. Major IR bands: 2728 m, 1262 m, 1216 w, 1089 w, br, 1039 vs, 905 vs, 804 m, br, 728 m, 647 w cm^{-1}.

* Loss of solvent from $(Me_5C_5)_2Sr(OEt_2)$ was suspected as the cause of its unsatisfactory analysis.[10(a)].

RESULTS AND DISCUSSION

Solution synthesis of metallocenes

The most commonly used synthesis of the alkaline-earth metallocenes involves the reaction of a metal or metal hydride with cyclopentadiene in solvents such as THF, DMF or liquid ammonia [eq. (1)].[5,7,11]

$$M + 2C_5H_6 \xrightarrow{THF,\,NH_3(l)} (C_5H_5)_2ML_x + 2H_2\uparrow. \quad (1)$$

The reaction is particularly unsatisfactory for strontium and barium complexes; $(C_5H_5)_2Sr$ is obtained in only 4% yield from Sr metal and C_5H_6, and $(C_5H_5)_2Ba$ is generated in a minuscule 0.2% yield from the reaction of BaH_2 with C_5H_6.[5]

The metathetical exchange of an alkali metal cyclopentadienide with an HAE dihalide could serve as an alternative route to the metallocenes, but the low solubility of $(C_5H_5)_2Sr$ and $(C_5H_5)_2Ba$ in all but extremely polar organic solvents suggests that they would be difficult to separate from the alkali halide by-products of the reaction.* Although this "salt problem" cannot be entirely eliminated (see below), with the proper choice of alkali cyclopentadienides, ionic metathesis can be a useful route to the HAE metallocenes.

The straightforward reaction of CaI_2 or $CaCl_2$ with two equivalents of $(C_5H_5)K$ in THF produces crude $(C_5H_5)_2Ca(THF)_2$ in 75%(CaI_2) or 14% ($CaCl_2$) yield, along with KX which is removed by filtration [eq. (2)].

$$2(C_5H_5)K + CaX_2 \xrightarrow{THF} (C_5H_5)_2Ca(THF)_2 + 2KX\downarrow. \quad (2)$$

The smaller yield from the chloride probably stems from the lesser solubility of $CaCl_2$ in THF. Potassium cyclopentadienide provides a more cleanly separated by-product than is the case if the more common $(C_5H_5)Na$ is used.† The use of $(C_5H_5)Tl$ as the cyclopentadienylating agent also produces high yields (*ca* 80%), although the extremely finely divided TlI which precipitates is difficult to remove completely by filtration.

The bis(cyclopentadienyl)calcium produced from $CaCl_2$ by this method constitutes *ca* 90% of the isolated product; the residue contains both potassium and chloride ions (see Experimental), even after repeated extraction with THF. The data can be interpreted as suggesting the presence of KCl (2%) and unreacted $(C_5H_5)K$ (7%),‡ although the existence of species such as $K^+[(C_5H_5)_3Ca]^-$ or $K^+[(C_5H_5)_2CaCl]^-$ cannot be excluded.§ The presence of the residual halide is a manifestation of the "salt problem" which complicates the synthesis of organolanthanide and -actinide complexes as well,‖[12(a)] and is an indication of the high reactivity of these materials. As the size of the metal cation increases, both the difficulty of achieving steric saturation of the metal centre and the likelihood of residual alkali salt complexation increase. Since the HAE cations are as large or larger than any of the common lanthanide and actinide ions,¶ the problem is particularly difficult to control. For many synthetic purposes, however, the level of salt contamination is not severe enough to interfere with further reactions.[9]

Strontiocene and bariocene are sufficiently insoluble in ethers that we sought to extract the alkali metal halide rather than the metallocene from the reaction mixture. This was accomplished by reacting lithium cyclopentadienide with the alkaline earth metal halide; the resulting LiI is then removed with THF, leaving the metallocenes as insoluble solids [eq. (3)].

$$2(C_5H_5)Li + MI_2 (M = Sr, Ba) \xrightarrow{THF} (C_5H_5)_2M(THF)_x\downarrow + 2LiI. \quad (3)$$

The "salt problem" observed with the calcium

---

* Sublimation of the metallocenes from the involatile by-products could be used to effect separation. Losses during such sublimations can be high,[5] however, limiting their use as a purification method.

† The THF-soluble portion from the reaction of $(C_5H_5)Na$ and CaI_2 weighs 89% of the sum of the starting materials. Simple stoichiometric considerations then suggest that even if complete conversion to $(C_5H_5)_2Ca(THF)_2$ occurs, the product contains at least 25% non-metallocene material, most of it probably NaI. As both the metallocene and NaI are reasonably soluble in THF and insoluble in hydrocarbons, their separation by solvent extraction is not efficient.

‡ Although a saturated solution of $(C_5H_5)K$ in THF-d_8 at ambient temperature displays an ^1H NMR signal at δ 5.61 (R. A. Williams and T. P. Hanusa, unpublished results), this peak was never observed in any spectrum of the calcium complex. Presumably cyclopentadienyl ring exchange is occurring between the potassium and calcium metal centres, as a sample of calciocene deliberately doped with potassium cyclopentadienide (*ca* 10%) contains only the resonance corresponding to calciocene.

§ This possibility is currently under investigation (R. A. Williams and T. P. Hanusa, research in progress).

‖ In some cases, alkali halides can be incorporated into the structure to form $(C_5H_5)_2M(\mu\text{-}X)_2M'L_x$ species.[12(b)]

¶ The HAE cations range in size from 1.00 (Ca^{2+}) to 1.35 Å (Ba^{2+});[13] these values should be compared to 1.03 Å for La^{3+}, the largest of the trivalent lanthanide ions, and to 0.94 Å for Th^{4+}, the largest of the tetravalent actinides.

system is more severe with Sr and Ba, to the extent that bariocene constitutes only *ca* 80% of the washed precipitate from $(C_5H_5)Li$ and BaI_2. In these cases, the possibility of "double salt" formation would probably be greater than in the case of calcium. Unlike the calcium complex, the strontium and barium derivatives are isolated from the reaction mixtures with considerably less than two equivalents of THF, although the precise degree of solvation is difficult to determine. Integration of their ^1H NMR spectra in DMSO-d_6 suggests that x in the formula $(C_5H_5)M(THF)_x$ is 0.54 for M = Sr and 0.25 for M = Ba; elemental analysis supports this value for Ba but indicates $x = 1.0$ for Sr.* It is clear in any case that considerable desolvation has occurred. The size of the strontium and barium ions may preclude the formation of stable monomeric disolvated complexes and the low solubility of the complexes may indicate that oligomerized structures have formed similar to those of $(C_5H_5)_2Ca$,[8] $(C_5H_5)_3Sc$,[14] or $[(CH_3C_5H_4)_3Nd]_4$.[15]

As the limited range of solubility of the HAE metallocenes evidently stems from coordinative unsaturation of the metal centre, we prepared derivatives from pentamethylcyclopentadiene, which frequently confers improved solubility on its complexes.[16] Bis(pentamethylcyclopentadienyl) metallocenes form from the reaction of potassium pentamethylcyclopentadienide and the metal diiodides in THF. The improvement in solubility over the unsubstituted metallocenes is dramatic; all three $(Me_5C_5)_2M(THF)_2$ complexes are readily soluble in THF and aromatic hydrocarbons, and are slightly soluble even in alkanes. The increase in solubility greatly eases their purification, since by extracting them into toluene, the decamethylmetallocenes can be obtained free of alkali halide by-products.†

Spectroscopic studies

All the alkaline-earth complexes exhibit well-resolved ^1H and ^{13}C NMR spectra (see Tables 1 and 2). Appreciable chemical shifts occur with a change in solvent; the methyl proton resonances of $(Me_5C_5)_2Sr(THF)_2$, for example, move from δ 2.14 in C_6D_6 to δ 1.81 in DMSO-d_6 (Table 1). Judging by the positions of the THF resonances, it appears that DMSO displaces THF from the coordination sphere of the metal. Similar displacement of THF has been noted when $(C_5H_5)_2Ca(THF)_2$ is dissolved in pyridine-d_5.[7]

CONCLUSIONS

Metathetical exchange between alkali metal cyclopentadienides and alkaline earth dihalides produces $(C_5R_5)_2M(THF)_x$ complexes in high yield. Although residual alkali halides are difficult to remove from the parent metallocenes, the hydrocarbon solubility of the decamethylmetallocenes permits their ready purification and extends the range of reaction media with which they are useful. They should serve as attractive starting materials for further studies of organoalkaline-earth chemistry.

Acknowledgement—Acknowledgement is made to the Donors of the Petroleum Research Fund, administered by the American Chemical Society, for partial support of this research.

REFERENCES

1. T. J. Kealy and P. L. Pauson, *Nature* 1951, **168**, 1039.
2. C. M. Lukehart, *Fundamental Transition Metal Organometallic Chemistry*, Chap. 4. Brooks/Cole, Monterey, California (1985).
3. For a recent review of HAE chemistry, see W. E. Lindsell in *Comprehensive Organometallic Chemistry* (Edited by G. Wilkinson, F. G. A. Stone and E. Abel), Vol. 1, Chaps. 2–4. Pergamon Press, Oxford (1982).
4. K. Ziegler, H. Froitzheim-Kühlhorn and H. Hafner, *Chem. Ber.* 1956, **89**, 434.
5. E. O. Fischer and G. Stölzle, *Chem. Ber.* 1961, **94**, 2187.
6. B. G. Gowenlock, W. E. Lindsell and B. J. Singh, *J. Chem. Soc., Dalton Trans.* 1978, 657.
7. K. A. Allen, B. G. Gowenlock and W. E. Lindsell, *J. Organomet. Chem.* 1973, **55**, 229.
8. R. Zerger and G. Stucky, *J. Organomet. Chem.* 1974, **80**, 7.
9. M. J. McCormick, R. A. Williams and T. P. Hanusa, manuscript in preparation.
10. (a) C. J. Burns and R. A. Andersen, *J. Organomet. Chem.* 1987, **325**, 31; (b) R. A. Andersen, R. Blom, J. M. Boncella, C. J. Burns and H. V. Volden, *Acta Chem. Scand.* 1987, **A41**, 24.
11. M. Kirilov, G. Petrov and C. Angelov, *J. Organomet. Chem.* 1976, **113**, 225.
12. (a) W. J. Evans, R. Dominguez and T. P. Hanusa,

*The limited solubilities of both strontiocene and bariocene even in DMSO makes accurate integration of their residual THF resonances difficult.

†By using procedures analogous to those for the unsubstituted metallocenes, we have produced bis(methylcyclopentadienyl) complexes from $(CH_3C_5H_4)(Li, K)$ and $(Ca, Sr, Ba)I_2$ (R. A. Williams and T. P. Hanusa, unpublished results). Their chemistry is similar to that of the parent metallocenes; in particular, the solubility differences are slight [$(CH_3C_5H_4)_2Ca(THF)_2$ is sparingly soluble in aromatic hydrocarbons, $(CH_3C_5H_4)_2Sr(THF)_x$ is slightly soluble in THF and $(CH_3C_5H_4)_2Ba(THF)_x$ is insoluble in THF].

Organometallics, 1986, **5**, 263; (b) H. Schumann, E. Palamidis, G. Schmid and R. Boese, *Angew. Chem.* 1986, **25**, 718 and refs. therein.
13. R. D. Shannon, *Acta Cryst.* 1976, **A32**, 751.
14. J. L. Atwood and K. D. Smith, *J. Am. Chem. Soc.* 1973, **95**, 1488.
15. J. H. Burns, W. H. Baldwin and F. H. Fink, *Inorg. Chem.* 1974, **13**, 1916.
16. (a) R. B. King, *Coord. Chem. Rev.* 1976, **20**, 155; (b) P. T. Wolczanski and J. E. Bercaw, *Acc. Chem. Res.* 1980, **13**, 121; (c) T. D. Tilley, R. A. Andersen, B. Spencer, H. Ruben, A. Zalkin and D. H. Templeton, *Inorg. Chem.* 1980, **19**, 2999; (d) P. J. Fagan, J. M. Manriguez, E. A. Maata, A. M. Seyam and T. J. Marks, *J. Am. Chem. Soc.* 1981, **103**, 6650.

Polyhedron Vol. 7, No. 9, pp. 731–735, 1988
Printed in Great Britain

0277–5387/88 $3.00+.00
© 1988 Pergamon Press plc

SYNTHESIS OF MONOMETALLIC AND BIMETALLIC 2,2′-BIPYRIMIDINE AND 2,3-BIS(2-PYRIDYL)PYRAZINE COMPLEXES OF RUTHENIUM, PLATINUM AND PALLADIUM

NICHOLAS C. THOMAS* and JERRY COX

Chemistry Department, Auburn University at Montgomery, Montgomery, AL 36193, U.S.A.

(*Received* 11 *December* 1987; *accepted* 5 *January* 1988)

Abstract—The reaction of 2,2′-bipyrimidine (bpym) or 2,3-bis(2-pyridyl)pyrazine (dpp) with $[Ru(CO)_2Cl_2]_n$ gives the monometallic $Ru(CO)_2Cl_2$(bidentate) (bidentate = bpym or dpp) complexes. The $Ru(CO)_2Cl_2$(bidentate) complexes react further with $[Ru(CO)_2Cl_2]_n$ or with $MCl_2(dmso)_2$ (M = Pt, Pd) to yield the homobimetallic $Cl_2(CO)_2Ru$(bidentate)$Ru(CO)_2Cl_2$ or heterobimetallic Cl_2M(bidentate)$Ru(CO)_2Cl_2$ complexes, respectively. The complexes have been characterized by microanalysis and electronic absorption and IR spectroscopy.

The chemistry of homo- and heterobimetallic complexes containing bridging ligands has significantly expanded in recent years. Of particular interest are bimetallic transition metal complexes linked via a common binucleating ligand, such as 2,2′-bipyrimidine (bpym) or 2,3-bis(2-pyridyl)pyrazine (dpp), and the electronic interaction that exists between the two metal centres.[1]

Recently, several examples of heterobimetallic complexes of bipyrimidine have been described,[2–9] but no analogous bis(pyridyl)pyrazine complexes appear to have been reported, and only a few homobimetallic complexes of this ligand are known.[10,11] These bimetallic complexes have a variety of potential applications, including use as models for biologically related systems[4,9] and as multi-electron transfer catalysts.[1,6] In the present study, the synthesis and spectroscopic properties of some new homo- and heterobimetallic ruthenium(II), platinum(II) and palladium(II) complexes of both bpym and dpp are described.

EXPERIMENTAL

General

Microanalyses were performed by Galbraith Laboratories, Tennessee. IR spectra (4000–600 cm^{-1}) were recorded as Nujol mulls between NaCl plates with a Perkin–Elmer 167 instrument. Far-IR spectra (500–200 cm^{-1}) were recorded as Nujol mulls between polyethylene plates with a Perkin–Elmer 457 instrument. Electronic absorption spectra were obtained in DMF solutions with a Perkin–Elmer lambda 3A spectrophotometer.

All reactions were shielded from light and carried out under an inert atmosphere of nitrogen. Methanol was HPLC grade (Aldrich) and degassed for 15 min prior to use. The compounds $[Ru(CO)_2Cl_2]_n$[12] and $MCl_2(dmso)_2$ (M = Pt, Pd)[13] were prepared by literature methods.

Preparation of complexes

(2,2′ - *Bipyrimidine)dicarbonyldichlororuthenium*(II). A solution of $[Ru(CO)_2Cl_2]_n$ (0.64 g) in methanol (60 cm^3) was boiled for 5 min and filtered into a solution of 2,2′-bipyrimidine (0.70 g) in methanol (50 cm^3). The mixture was heated under reflux for 10 min, cooled and the yellow product collected by filtration. The solid was washed with methanol (2 × 10 cm^3), ether (2 × 10 cm^3) and dried *in vacuo*. Yield 0.72 g (67%).

[2,3 - *Bis*(2 - *pyridyl)pyrazine]dicarbonyldichlororuthenium*(II). The complex was prepared by the above procedure from 2,3-bis(2-pyridyl)pyrazine (0.54 g) and $[Ru(CO)_2Cl_2]_n$ (0.41 g), and recrys-

* Author to whom correspondence should be addressed.

tallized from methanol to yield the yellow crystalline product. Yield 0.62 g (75%).

μ - (2,2′ - Bipyrimidine)tetracarbonyltetrachlorodiruthenium(II). A filtered solution of $[Ru(CO)_2Cl_2]_n$ (0.25 g) in methanol (25 cm^3) and $Ru(CO)_2Cl_2$(bpym) (0.10 g) were heated together under reflux for 1.5 h. The hot solution was filtered and the product washed with methanol, ether and dried *in vacuo*. Yield 0.12 g (75%).

μ - [2,3 - Bis(2 - pyridyl)pyrazine]tetracarbonyltetrachlorodiruthenium(II). The complex was prepared by the above procedure from $[Ru(CO)_2Cl_2]_n$ (0.16 g) and $Ru(CO)_2Cl_2$(dpp) (0.19 g). Yield 0.21 g (84%).

Dichloroplatinum(II) - *μ* - (2,2′ - *bipyrimidine*) *dicarbonyldichlororuthenium*(II). A mixture of $Ru(CO)_2Cl_2$(bpym) (0.073 g) and $PtCl_2(dmso)_2$ (0.083 g) in methanol (35 cm^3) was heated at reflux temperature for 3 h. The hot solution was filtered and the brown precipitate washed with methanol, ether and dried *in vacuo*. Yield 0.11 g (89%).

Using the above procedure, the following compounds were also obtained:

Dichloropalladium(II) - *μ* - (2,2′ - *bipyrimidine*)*dicarbonyldichlororuthenium*(II): from $Ru(CO)_2Cl_2$(bpym) (0.074 g) and $PdCl_2(dmso)_2$ (0.073 g), yield 0.089 g (82%);

Dichloroplatinum(II) - *μ* - [2,3 - *bis*(2 - *pyridyl*)-*pyrazine*]*dicarbonyldichlororuthenium*(II): from $Ru(CO)_2Cl_2$(dpp) (0.065 g) and $PtCl_2(dmso)_2$ (0.067 g), yield 0.090 g (88%);

Dichloropalladium(II) - *μ* - [2,3 - *bis*(2 - *pyridyl*) *pyrazine*]*dicarbonyldichlororuthenium*(II): from $Ru(CO)_2Cl_2$(dpp) (0.021 g) and $PdCl_2(dmso)_2$ (0.025 g), yield 0.024 g (83%).

RESULTS AND DISCUSSION

Syntheses

When an equimolar mixture of $[Ru(CO)_2Cl_2]_n$ and either 2,2′-bipyrimidine (bpym) or 2,3-bis(2-pyridyl)pyrazine (dpp) are refluxed together in methanol, the neutral monometallic $Ru(CO)_2Cl_2$ (bidentate) complexes (bidentate = bpym or dpp) precipitate from solution as yellow solids. By this procedure, pure $Ru(CO)_2Cl_2$(bpym) is obtained, whereas recrystallization from methanol yields pure $Ru(CO)_2Cl_2$(dpp).

Treatment of the $Ru(CO)_2Cl_2$(bidentate) complexes with an excess of $[Ru(CO)_2Cl_2]_n$ in methanol yields the diruthenium complexes $Cl_2(CO)_2Ru$(bidentate)$Ru(CO)_2Cl_2$ as insoluble solids. A similar reaction between $Ru(CO)_2Cl_2$(bidentate) and $MCl_2(dmso)_2$ (M = Pt or Pd) gives the neutral heterobimetallic derivatives Cl_2M(bidentate)$Ru(CO)_2Cl_2$ as brown solids in good yields (80–89%). Elemental analyses (Table 1) for the mono- and bimetallic complexes are consistent with the above formulations.

Table 1. Analytical data for complexes

Complex	% Found (calc.) C	H	N
$Ru(CO)_2Cl_2$(bpym)	31.3	1.6	14.5
	(31.3)	(1.6)	(14.5)
$Ru(CO)_2Cl_2$(dpp)	41.6	2.1	12.1
	(41.6)	(2.2)	(12.1)
$Cl_2(CO)_2Ru$(bpym)$Ru(CO)_2Cl_2$	23.4	1.0	9.1
	(24.2)	(1.2)	(9.3)
$Cl_2(CO)_2Ru$(dpp)$Ru(CO)_2Cl_2$	31.3	1.5	8.3
	(31.3)	(1.5)	(8.1)
Cl_2Pt(bpym)$Ru(CO)_2Cl_2$	18.2	0.9	8.5
	(18.4)	(0.9)	(8.6)
Cl_2Pt(dpp)$Ru(CO)_2Cl_2$	26.9	2.0	7.3
	(26.4)	(1.4)	(7.7)
Cl_2Pd(bpym)$Ru(CO)_2Cl_2$	20.9	1.2	9.8
	(21.3)	(1.1)	(9.9)
Cl_2Pd(dpp)$Ru(CO)_2Cl_2$	30.1	2.1	8.2
	(30.0)	(1.6)	(8.8)

Infrared spectra

The structures of all complexes may be determined from the IR data (Table 2). Spectra for the monometallic complexes show two strong bands in the *ν*(CO) region, consistent with *cis* CO groups and a single *ν*(Ru—Cl) band at *ca* 355 cm^{-1} indicating *trans* Cl ligands [Fig. 1(a)]. This stereochemistry is generally observed for $Ru(CO)_2Cl_2$(bidentate) complexes prepared from $[Ru(CO)_2Cl_2]_n$.[14–16] Similar IR data for the bimetallic complexes also indicate *cis* CO and *trans* Cl groups for the $Ru(CO)_2Cl_2$ fragment in $Cl_2(CO)_2Ru$(bidentate)$Ru(CO)_2Cl_2$ and Cl_2M(bidentate)$Ru(CO)_2Cl_2$ (M = Pt or Pd) complexes [Fig. 1(b) and (c)]. Spectra of the Cl_2M(bidentate)$Ru(CO)_2Cl_2$ compounds contain two additional bands between 300–350 cm^{-1} which may be assigned to *ν*(Pt—Cl) or *ν*(Pd—Cl) as expected for square-planar MCl_2(bidentate) complexes.[17]

Several characteristic vibrational bands are also observed for the aromatic diimine bridging ligands (Table 2) and provide further evidence to distinguish between monometallic and bimetallic coordination of bpym and dpp. A single absorption in the 1570–1580 cm^{-1} region, due to C—N and C—C ring stretching, is observed for the bimetallic com-

Table 2. IR absorptions for complexes

Complex	ν(CO)[a]	ν(M—Cl)	ν(C—C) ν(C—N)	π(C—H)
$Ru(CO)_2Cl_2(bpym)$	2050 1991	358m	1575m 1551m	748m
$Ru(CO)_2Cl_2(dpp)$	2058 1998	355m	1551w	779m 751m 738m
$Cl_2(CO)_2Ru(bpym)Ru(CO)_2Cl_2$	2060 2007	353m	1574m	729m
$Cl_2(CO)_2Ru(dpp)Ru(CO)_2Cl_2$	2046 1991	340m	1591w	772m
$Cl_2Pt(bpym)Ru(CO)_2Cl_2$	2065 2016	360m 340m 336sh	1580m	719m
$Cl_2Pt(dpp)Ru(CO)_2Cl_2$	2068 2010	352m 346m 335sh	1598w	775m
$Cl_2Pd(bpym)Ru(CO)_2Cl_2$	2082 2031	353m 347m 335sh	1578m	722m
$Cl_2Pd(dpp)Ru(CO)_2Cl_2$	2065 2008	345m 337m 334sh	1597w	779m

[a] All bands are strong.

plexes and is characteristic for bpym complexing to two metals.[18] By contrast, monometallic bpym complexes generally contain two bands in this region and accordingly two bands are observed for $Ru(CO)_2Cl_2(bpym)$. The C—H out-of-plane bending mode of bpym is also sensitive to mono- and bimetallic coordination[18] and we observe a corresponding 20–30 cm^{-1} reduction in the C—H vibration for the bimetallic complexes.

The IR spectrum of $Ru(CO)_2Cl_2(dpp)$ contains a weak ring stretching band at 1551 cm^{-1} which in the bimetallic dpp complexes shifts to about 45

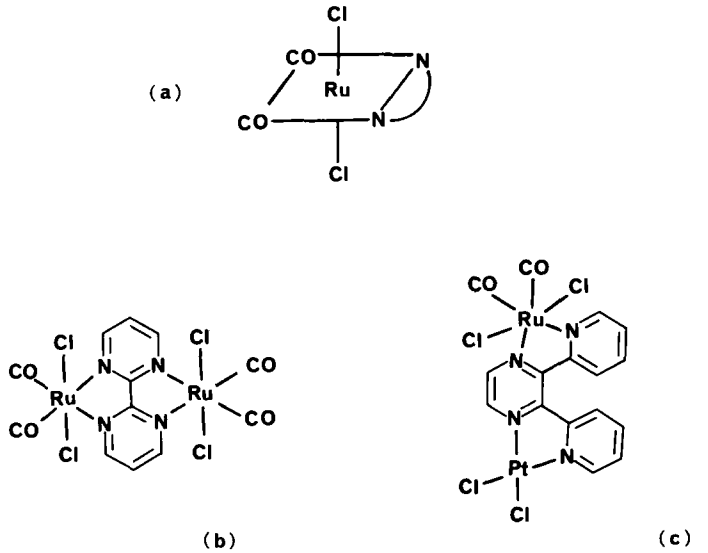

Fig. 1. Representative structures of (a) $Ru(CO)_2Cl_2(bidentate)$; (b) $Cl_2(CO)_2Ru(bidentate)$ $Ru(CO)_2Cl_2$ (bidentate = bpym) and (c) $Cl_2M(bidentate)Ru(CO)_2Cl_2$ (M = Pt, bidentate = dpp) complexes.

Table 3. Electronic absorption spectra for complexes

Complex	λ_{max} (nm) [ε (M^{-1} cm^{-1})][a]
$Ru(CO)_2Cl_2(bpym)$	365 [1500]
$Cl_2(CO)_2Ru(bpym)Ru(CO)_2Cl_2$	634 [1150] 424 [3330]
$Cl_2Pt(bpym)Ru(CO)_2Cl_2$	666 [350] 429 [2750]
$Cl_2Pd(bpym)Ru(CO)_2Cl_2$	627 [680] 478 [1535]
$Ru(CO)_2Cl_2(dpp)$	538 [1185]
$Cl_2(CO)_2Ru(dpp)Ru(CO)_2Cl_2$	596 [3590] 448 [3220]
$Cl_2Pt(dpp)Ru(CO)_2Cl_2$	598 [2310] 432 [2860]
$Cl_2Pd(dpp)Ru(CO)_2Cl_2$	603 [3650] 443 [1900]

[a] Recorded in DMF at 298 K.

cm^{-1} higher. In addition, three bands observed in the 700–800 cm^{-1} region for $Ru(CO)_2Cl_2(dpp)$ become a single band when a second metal is added.

Absorption spectra

Due to the low solubility of the bimetallic complexes in most common solvents, DMF was used to obtain absorption spectra (Table 3). Some complexes are very slightly soluble in dichloromethane and give similar, albeit weaker, spectra to those in DMF and therefore indicate the chemical stability of the complexes in DMF.

The spectrum of $Ru(CO)_2Cl_2(bpym)$ contains the longest wavelength band at $\lambda_{max} = 365$ nm ($\varepsilon = 1.5 \times 10^3$ M^{-1} cm^{-1}), similar to that observed for $Ru(CO)_2Cl_2$(bipyridyl) ($\lambda_{max} = 354$ nm, $\varepsilon = 1.2 \times 10^3$ M^{-1} cm^{-1}),[19] and can therefore be assigned to the metal-to-ligand charge-transfer transition (MLCT) from Ru(II) to bpym(π^*). Upon coordination to a second metal, the absorption maxima for the MLCT band shifts to longer wavelengths (> *ca* 420 nm) as previously observed for other related bpym complexes.[1,6,8] A second weaker absorption occurs in the spectra of the bimetallic complexes at > 620 nm and may also be attributed to MLCT transitions.[1] The absorption coefficient of the main band for the diruthenium bpym complex is about twice the value for $Ru(CO)_2Cl_2(bpym)$, with one ruthenium centre. The MLCT band for the monometallic dpp complex also shifts to higher wavelength in the bimetallic compounds. The additional band at higher energy for some of the bimetallic complexes may be assigned to the $^1A_1, ^1E_1 \leftarrow {}^1A_1$ LF transition.[5,20]

By contrast to other bimetallic bpym and dpp complexes, which absorb strongly in the visible region and therefore have potential for photon absorption and energy transfer reactions, the bimetallic ruthenium complexes prepared in this work absorb light to a lesser extent. However, in view of the numerous substitution reactions known for the monometallic MCl_2(bidentate) (M = Pt, Pd; bidentate = phenanthroline, bipyridyl)[21] and $Ru(CO)_2Cl_2$(bidentate)[16] complexes, we are currently investigating the substitution reactions of $Cl_2M(bpym)Ru(CO)_2Cl_2$ and $Cl_2M(dpp)Ru(CO)_2Cl_2$.

Acknowledgements—The authors are grateful to the AUM Grant-in-Aid program for supporting this work and to the Chemistry Department, Tusgekee University for the far-IR spectra.

REFERENCES

1. J. D. Petersen, W. R. Murphy, R. Sahai, K. J. Brewer and R. R. Ruminski, *Coord. Chem. Rev.* 1985, **64**, 261.
2. K. A. Goldsby and T. K. Meyer, *Inorg. Chem.* 1984, **23**, 3002.
3. M. P. Garcia, J. L. Millan, M. A. Esteruelas and L. A. Oro, *Polyhedron* 1987, **6**, 1427.
4. R. H. Petty, B. R. Welch, L. J. Wilson, L. A. Bottomley and K. M. Kadish, *J. Am. Chem. Soc.* 1980, **102**, 611.
5. C. Overton and J. A. Connor, *Polyhedron* 1982, **1**, 53.
6. R. Sahai and D. P. Rillema, *Inorg. Chim. Acta* 1986, **118**, L35.
7. S. Lanza, *Inorg. Chim. Acta* 1983, **75**, 131.
8. A. Vogler and J. Kisslinger, *Inorg. Chim. Acta* 1986, **115**, 193.
9. G. A. Brewer and E. Sinn, *Inorg. Chem.* 1984, **23**, 2532.
10. R. R. Ruminski and J. O. Johnson, *Inorg. Chem.* 1987, **26**, 210.
11. C. H. Braustein, A. D. Baker, T. C. Streaks and H. D. Gafney, *Inorg. Chem.* 1984, **23**, 857.
12. M. J. Cleare and W. P. Griffith, *J. Chem. Soc.* (*A*) 1969, 372.
13. J. H. Price, A. N. Williamson, R. F. Schramm and B. B. Wayland, *Inorg. Chem.* 1972, **11**, 1280.
14. N. C. Thomas and G. B. Deacon, *Synth. React. Inorg. Met.-Org. Chem.* 1986, **16**, 85.
15. D. St. C. Black, G. B. Deacon and N. C. Thomas, *Aust. J. Chem.* 1982, **35**, 2445.
16. N. C. Thomas, *Coord. Chem. Rev.* 1986, **70**, 121 and refs therein.

17. A. H. Norbury and A. I. P. Sinha, *J. Inorg. Nucl. Chem.* 1973, **35**, 1211.
18. V. F. Sutcliffe and G. B. Young, *Polyhedron* 1984, **3**, 87.
19. J. M. Kelly, C. M. O'Connell and J. G. Vos, *J. Chem. Soc., Dalton Trans.* 1986, 253.
20. K. J. Moore and J. D. Petersen, *Polyhedron* 1983, **2**, 279.
21. J. V. Marzik, A. D. Sabatelli, P. J. Fitzgerald and J. E. Sarneski, *J. Chem. Ed.* 1981, **58**, 589 and refs therein.

Polyhedron Vol. 7, No. 9, pp. 737–740, 1988
Printed in Great Britain

0277–5387/88 $3.00+.00
© 1988 Pergamon Press plc

BINUCLEAR CATIONIC μ-BROMO COMPLEXES OF VANADIUM(II)

JO ANN M. CANICH, F. ALBERT COTTON* and WIESLAW J. ROTH

Department of Chemistry and Laboratory for Molecular Structure and Bonding, Texas A&M University, College Station, TX 77843, U.S.A.

and

STAN A. DURAJ

Department of Chemistry, Cleveland State University, Cleveland, OH 44115, U.S.A.

(*Received* 10 *October* 1987; *accepted* 5 *January* 1988)

Abstract—The compounds $[V_2(\mu\text{-}Br)_3L_6]BPh_4$, with L = 3-methyltetrahydrofuran (**1**) and tetrahydrofuran (**2**), have been prepared. The crystal and molecular structures of **1** have been determined. The compound crystallizes in space group *Cc* with unit cell dimensions $a = 18.499(3)$, $b = 10.923(3)$, $c = 29.619(7)$ Å, $\beta = 103.18(2)^\circ$, $V = 5827(5)$ Å^3 and $Z = 4$. The $[V_2(\mu\text{-}Br)_3(CH_3C_4H_7O)_6]^+$ ion is analogous to the $[V_2(\mu\text{-}Cl)_3L_6]^+$ cations previously described, but has a longer V—V distance, viz. 3.146(4) Å. The UV-vis spectrum shows a double spin-flip transition but it is extremely weak compared to that in the chloro analog. Qualitatively, this was expected because of the *ca* 0.16 Å increase in the V—V distance, but the magnitude of the decrease (~ 5 fold) is of interest.

Vanadium(II), face-sharing bioctahedral complexes of the following general formula $[L_3V(\mu\text{-}Cl)_3VL_3]^+B^-$, where L = tetrahydrofuran[1–4] or 3-methyltetrahydrofuran[5] and B = 1/2 $Zn_2Cl_6^{2-}$, BPh_4^-, or $AlEt_2Cl_2^-$, constitute readily available starting materials[6–10] for entry into a wide range of interesting dinuclear and polynuclear low-valent vanadium chemistry.

All these starting materials contain the same structural core, namely $V(\mu\text{-}Cl)_3V$ in which the vanadium-to-vanadium distance is *ca* 2.98 Å; at this distance the two vanadium atoms show characteristic, intense, double spin-flip transitions in the electronic spectrum, previously observed only in some solid-state cases. These narrow bands appear at 405 and 395 nm for the tris(μ-chloro)hexakis(tetrahydrofuran)divanadium(II) cation in CH_2Cl_2/THF solution.[2]

As an extension of this interesting dinuclear vanadium(II) chemistry we wish to report here the preparation and X-ray crystallography of a new compound in this area: $[V_2(\mu\text{-}Br)_3$(3-methyltetrahydrofuran$)_6]^+BPh_4^-$. As anticipated, the V—V′ distance in the new complex is longer (*ca* 3.1 Å) compared to that in the chloro analog. The intensity of the characteristic double spin-flip transition in the UV-vis spectrum is greatly diminished for the bromo derivative in which the supporting ligand L = THF. This suggests, but does not prove that direct coupling of the V(II) centres is the predominant factor providing intensity for the transition.

EXPERIMENTAL

All operations were performed under an atmosphere of argon by using standard Schlenk techniques, a Vacuum Atmospheres Co. dry-box and a double manifold vacuum line. Tetrahydrofuran, 3-methyltetrahydrofuran and hexane were freshly distilled from benzophenone ketyl prior to use. Solutions were transferred via stainless steel cannulae and/or syringes. Anhydrous VBr_3 was purchased from Strem Chemicals Inc., and 3-methyltetrahydrofuran and $AlEt_2(OEt)$ (as a 25 wt % solution in toluene) were purchased from Aldrich Chemical Company. $NaBPh_4$ was deaerated under vacuum at room temperature. The UV-vis spectrum was

*Author to whom correspondence should be addressed.

measured on a Varian 2290 spectrophotometer at room temperature.

Preparation of $[V_2(\mu\text{-}Br)_3(3\text{-}methyltetrahydrofuran)_6]BPh_4$ (**1**)

A solution of VBr_3 (0.8 g, 2.76 mmol) in 10 cm^3 of freshly distilled 3-methyltetrahydrofuran was refluxed for 12 h under argon in a 50 cm^3 round-bottomed three-necked flask equipped with a magnetic stirrer and a reflux condenser. The solution became deep red in colour. The reflux was stopped and the reaction mixture cooled to room temperature. To this solution of VBr_3(3-methyltetrahydrofuran)$_3$ in 3-methyltetrahydrofuran was added 5.3 cm^3 of a 25 wt % solution of $AlEt_2(OEt)$ in toluene via a syringe. The solution was stirred for 10 days at room temperature during which time the colour of the reaction mixture changed from dark red–brown to bright green.

This solution of $[V_2(\mu\text{-}Br)_3$(3-methyltetrahydrofuran)$_6]AlBr_2Et_2$ (which we believe is formed essentially quantitatively[3]) was then filtered through Celite 545 (Fisher Scientific Company) onto 0.90 g, 2.64 mmol of $NaBPh_4$. The solution was stirred for 12 h at room temperature and filtered through Celite to a Schlenk tube. Freshly distilled hexane (25 cm^3) was carefully placed on top of this solution and the Schlenk tube was allowed to stand undisturbed for several days. Green X-ray quality crystals of $[V_2(\mu\text{-}Br)_3$(3-methyltetrahydrofuran$)_6]^+BPh_4^-$ were obtained, isolated by filtration, washed with hexane and dried *in vacuo* (yield: 1.24 g, 1.06 mmol, 76.5%).

Preparation of $[V_2(\mu\text{-}Br)_3(THF)_6]BPh_4$ (**2**)

This compound was prepared from VBr_3 (0.8 g, 2.76 mmol) following a procedure analogous to that described above for $[V_2(\mu\text{-}Br)_3$(3-methyltetrahydrofuran$)_6]BPh_4$ (**1**). The yield of the bright green, extremely air-sensitive product was 0.91 g (61%).

Visible spectrum (THF), λ, nm (ε given per mole of $[V_2Br_3(THF)_6]^+$): 650 (11), 490 (sh) (12), 405 (16), 395 (16.5).

X-ray crystallography

The unit cell determinations and collection of intensity data for $[V_2(\mu\text{-}Br)_3$(3-methyltetrahydrofuran$)_6]BPh_4$ (**1**) were carried out by following routine procedures which have been previously described elsewhere.[11] The intensity data were corrected for Lorentz and polarization effects, and an empirical absorption correction based upon azimuthal scans of nine reflections near $\chi = 90°$ was applied to the intensity data. Pertinent crystallographic data for **1** are given in Table 1. Inspection of the Patterson function led to the inference that the correct space group would be *Cc* rather than *C*2 or *C*2/*c*, and successful solution and refinement confirmed this choice.

The position of the vanadium atom in the unit cell of **1** was determined by direct methods using the program MULTAN 84. All non-hydrogen atoms were subsequently located by an alternating series of difference Fourier syntheses and least-square refinements. Since the 3-methyltetrahydrofuran compound crystallized in a non-centrosymmetric space group, both enantiomorphs were refined and the one giving lower residuals is reported here.

Tables of positional and isotropic equivalent displacement parameters, anisotropic displacement parameters, observed and calculated structure factors as well as full lists of bond distances and

Table 1. Crystallographic data

Formula	$V_2Br_3O_6C_{54}H_{80}B$
Formula weight	1177.66
Space group	*Cc*
Systematic absences	*hkl*, $h+k \neq 2n$
	*h*0*l*, $l \neq 2n$
a, Å	18.499(3)
b, Å	10.923(3)
c, Å	29.619(7)
β, degrees	103.18(2)
V, Å^3	5827(5)
Z	4
d_{calc} (g cm^{-3})	1.342
Crystal size (mm)	0.45 × 0.35 × 0.30
μ (Mo-K_α) (cm^{-1})	23.897
Data collection instrument	Enraf–Nonius CAD-4
Radiation (monochromated in incident beam)	Mo-K_α (λ = 0.71073 Å)
Orientation reflections, number, range (2θ)	25, 14.92–30.26
Temperature (°C)	22
Scan method	$\omega - 2\theta$
Data col. range, 2θ (deg)	$4 \leqslant 2\theta \leqslant 50$
No. unique data, total with $F_o^2 > 3\sigma(F_o^2)$	4483
	3258
Number of parameters refined	578
Trans. factors, max., min.	0.9990, 0.9086
R^a	0.0647
R_w^b	0.0789
Quality-of-fit indicator^c	1.639
Largest shift/esd, final cycle	0.02
Largest peak, e Å^3	0.72

^{a} $R = \Sigma\|F_o| - |F_c|/\Sigma|F_o|$.
^{b} $R_w = [\Sigma w(|F_o| - |F_c|)^2/\Sigma w|F_o|^2]^{1/2}$; $w = 1/\sigma^2(|F_o|)$.
^{c} Quality of fit $= [\Sigma w(|F_o| - |F_c|)^2/(N_{obs} - N_{parameters})]^{1/2}$.

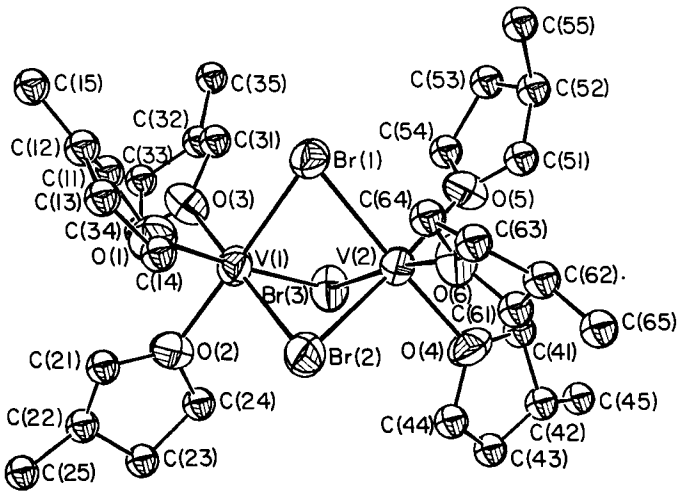

Fig. 1. An ORTEP drawing of the $[V_2Br_3(3\text{-methyltetrahydrofuran})_6]^+$ cation. Thermal ellipsoids are drawn at 40% probability level.

bond angles have been deposited as supplementary material with the Editor at Queen Mary College.

RESULTS AND DISCUSSION

An ORTEP drawing of the $[V_2(\mu\text{-Br})_3(3\text{-methyltetrahydrofuran})_6]^+$ cation is shown in Fig. 1, which also defines the numbering scheme. Important interatomic distances and angles are presented in Table 2. Clearly, the general structure is similar to that of $[V_2(\mu\text{-Cl})_3(\text{Me-THF})_6]BPh_4$ and other analogous compounds. Again, by using the methyl-substituted THF as the ligand, problems with disorder that usually plague structures with THF ligands are negligible. The key structural result—the antici-

Table 2. Important interatomic distances (Å) and angles (°) for $[V_2(\mu\text{-Br})_3(3\text{-methyltetrahydrofuran})_6]BPh_4$[a]

V(1)—V(2)	3.146(4)	V(2)—Br(1)	2.643(4)
V(1)—Br(1)	2.634(2)	V(2)—Br(2)	2.641(4)
V(1)—Br(2)	2.642(3)	V(2)—Br(3)	2.650(4)
V(1)—Br(3)	2.647(4)	V(2)—O(4)	2.16(1)
V(1)—O(1)	2.20(1)	V(2)—O(5)	2.15(1)
V(1)—O(2)	2.14(1)	V(2)—O(6)	2.16(1)
V(1)—O(3)	2.12(1)		
Br(1)—V(1)—Br(2)	88.11(7)	Br(1)—V(2)—Br(3)	89.2(1)
Br(1)—V(1)—Br(3)	89.48(9)	Br(1)—V(2)—O(4)	175.0(4)
Br(1)—V(1)—O(1)	87.1(3)	Br(1)—V(2)—O(5)	87.7(4)
Br(1)—V(1)—O(2)	175.3(4)	Br(1)—V(2)—O(6)	95.0(4)
Br(1)—V(1)—O(3)	93.9(3)	Br(2)—V(2)—Br(3)	87.2(1)
Br(2)—V(1)—Br(3)	87.22(9)	Br(2)—V(2)—O(4)	96.3(3)
Br(2)—V(1)—O(1)	93.7(4)	Br(2)—V(2)—O(5)	175.4(4)
Br(2)—V(1)—O(2)	90.1(4)	Br(2)—V(2)—O(6)	87.8(3)
Br(2)—V(1)—O(3)	174.6(4)	Br(3)—V(2)—O(4)	88.4(4)
Br(3)—V(1)—O(1)	176.4(3)	Br(3)—V(2)—O(5)	94.4(4)
Br(3)—V(1)—O(2)	94.8(4)	Br(3)—V(2)—O(6)	173.3(4)
Br(3)—V(1)—O(3)	87.8(4)	O(4)—V(2)—O(5)	88.1(5)
O(1)—V(1)—O(2)	88.7(5)	O(4)—V(2)—O(6)	87.8(5)
O(1)—V(1)—O(3)	91.4(5)	O(5)—V(2)—O(6)	91.0(5)
O(2)—V(1)—O(3)	88.3(5)	V(1)—Br(1)—V(2)	73.2(1)
Br(1)—V(2)—Br(2)	87.9(1)	V(1)—Br(2)—V(2)	73.1(1)
		V(1)—Br(3)—V(2)	72.89(9)

[a] Numbers in parentheses are estimated standard deviations in the least significant digits.

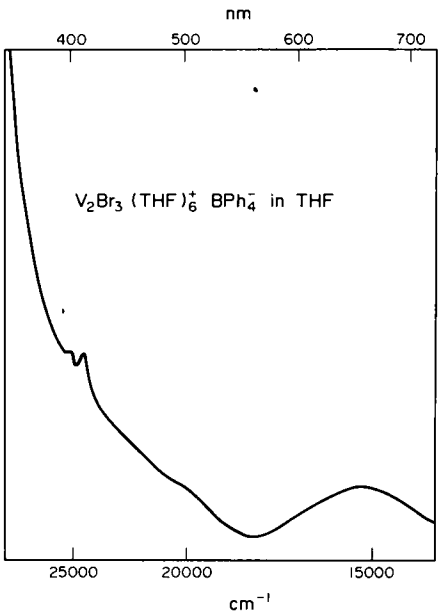

Fig. 2. Visible spectrum of the $[V_2Br_3(3\text{-methyltetrahydrofuran})_6]BPh_4$ molecule in the region 340–720 nm.

pation of which constituted the main reason for conducting this study—is that the V to V distance is appreciably greater than that in the previous μ-Cl compounds. For the latter, the distances were all 2.98–2.99 Å, whereas in the present case, because of the greater size of the bridging atoms, it is 3.146(4) Å.

All attempts to prepare $[V_2Br_3(THF)_6]_2Zn_2Br_6$, as an exact analog to the chloro compound that was the point of departure[1] for our work in this area, failed. Reduction of $VBr_3(THF)_3$ with Zn in refluxing THF gave only a brown–black amorphous solid that could not be characterized. The bromo compounds appear to be much more sensitive to oxygen than the chloro analogues. They become pink (V(III)?) immediately on exposure to air.

The main point of interest in studying the bromo cations, $[V_2Br_3L_6]^+$, with their longer V to V distances as compared with the chloro analogue, was to test our previous proposal[2] that a strong, sharp doublet at *ca* 25,000 cm^{-1} was due to a double spin-flip transition occurring in the coupled pair of the d^3 V(II) ions. Our reasoning was that an increase in the V to V distance would lessen the coupling if it were based on direct V(II)···V(II) interaction, and that this should have the effect of reducing the intensity of the transition while not affecting either its position or its breadth significantly. Of course, the two V(II) centres might be coupled indirectly through the bridging halide ions. In that case the effect of replacing Cl^- bridges by Br^- bridges would be hard to anticipate, since we know of no empirical or theoretical criterion for predicting which one would provide the more efficient coupling.

If the spectrum in Fig. 2 is compared with those in Fig. 2 of ref. 2 (for the $[V_2Cl_3(THF)_6]^+$ ion), it is clear that all observations are consistent with the assignment proposed and with the expectation that a larger V(II)···V(II) separation would lead to weaker coupling. Since we had no prior idea as to how sensitive the intensity might be to the distance, there was the dismaying possibility that the experiment might be fruitless as a result of the transition disappearing altogether. Fortunately, this did not happen; the decrease is by about a factor of five for the *ca* 0.16 Å increase in the V—V separation. As can be seen, however, the energy is essentially unchanged and the bands are still extremely narrow, as befits a transition in which electrons retain the same orbital quantum numbers.

Acknowledgements—We thank the Robert A. Welch Foundation (Grant No. A-494) for support. SAD thanks the Cleveland State University Research Challenge Program approved by the Ohio Board of Regents for partial support of this work.

REFERENCES

1. F. A. Cotton, S. A. Duraj, M. W. Extine, G. E. Lewis, W. J. Roth, C. D. Schmulbach and W. Schwotzer, *J. Chem. Soc., Chem. Commun.* 1983, 1377.
2. F. A. Cotton, S. A. Duraj and W. J. Roth, *Inorg. Chem.* 1985, **24**, 913.
3. F. A. Cotton, S. A. Duraj, L. E. Manzer and W. J. Roth, *J. Am. Chem. Soc.* 1985, **107**, 3850.
4. R. J. Bouma, J. H. Teuben, W. R. Beukema, R. L. Bansemer, J. C. Huffman and K. G. Caulton, *Inorg. Chem.* 1985, **24**, 2715.
5. J. A. Canich, F. A. Cotton, S. A. Duraj and W. J. Roth, *Polyhedron* 1987, **6**, 1433.
6. F. A. Cotton, G. E. Lewis and G. Mott, *Inorg. Chem.* 1982, **21**, 3316.
7. F. A. Cotton, S. A. Duraj and W. J. Roth, *Inorg. Chem.* 1984, **23**, 4113.
8. F. A. Cotton, S. A. Duraj and W. J. Roth, *Inorg. Chem.* 1984, **23**, 4042.
9. F. A. Cotton, S. A. Duraj, W. J. Roth and C. D. Schmulbach, *Inorg. Chem.* 1985, **24**, 525.
10. R. J. Bansemer, J. C. Huffman and K. G. Caulton, *J. Am. Chem. Soc.* 1983, **105**, 6163.
11. See, for example, A. Bino, F. A. Cotton and P. E. Fanwick, *Inorg. Chem.* 1979, **18**, 3558.

Polyhedron Vol. 7, No. 9, pp. 741–745, 1988
Printed in Great Britain

0277–5387/88 $3.00+.00
© 1988 Pergamon Press plc

NOVEL POLYMERIC COMPLEXES OF RHODIUM(I)–COBALT(II) AND 4,4′-DIISOCYANOBIPHENYL WITH GOOD ELECTRICAL CONDUCTIVITY

S. A. LAWRENCE* and K. A. K. LOTT

Department of Chemistry, Brunel University, Uxbridge, Middlesex UB8 3PH, U.K.

and

I. FEINSTEIN-JAFFE†

Department of Materials Science, The Weizmann Institute of Science, Rehovot, Israel 76000

(*Received* 24 *September* 1987; *accepted after revision* 13 *January* 1988)

Abstract—The synthesis, spectroscopic analysis and unit cell dimensions of a novel mixed metal cobalt(II)–rhodium(I) organometallic polymer containing 4,4′-diisocyanobiphenyl and thiocyanide ligands are reported. The electrical resistivity of the polymer was found to be dependent upon the percentage of Co(II) (by mass) incorporated into the product and reaches a limiting value of 200 Ω cm. Preliminary trials indicate that this type of material may be potentially useful as electrodes in glycol/air fuel cells.

Polymeric organometallic complexes of the stereorigid, bidentate ligand 4,4′-diisocyanobiphenyl have previously been prepared for rhodium,[1,2,3] iridium,[2] palladium and platinum,[4,5] copper[6] and chromium, molbdenum and tungsten.[7] All of these complexes are electrical semiconductors with electrical resistivities in the range 4×10^9 to 5×10^5 Ω cm (found for the complexes, copper(I) bis-4,4′-diisocyanobiphenyl hexafluorophosphate[6] and the hexagonal structural modification of rhodium(I) bis-4,4′-diisocyanobiphenyl chloride,[8] respectively). It is assumed that in the hexagonal and tetragonal structural modifications of the rhodium(I) complexes of diisocyanobiphenyl [see Figs 1(a) and 1(b)], electrical conductivity is facilitated through π-bonded, conjugated ligand bridges between metal centres, in addition to one-dimensional extended Rh—Rh interactions.[8] The rhodium ions contained in this complex have been shown to be well dis-

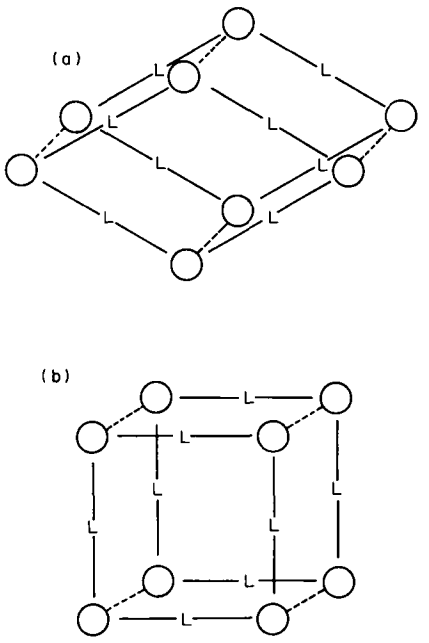

Fig. 1. Unit cells of (a) hexagonal and (b) tetragonal rhodium(I) bis-4,4′-diisocyanobiphenyl chloride polymers, ○ = rhodium(I) ions; —L— = bidentate bridging ligands (Cl^- ions not shown).

* Author to whom correspondence should be addressed. Present address: Development Dept, Johnson Matthey, Jeffreys Road, Enfield, Middlesex EN3 7PW, U.K.

† Present address: Radiopharmaceuticals, Soreq Nuclear Research Centre, Yavne, Israel 70600.

persed within the organic ligand matrix and to possess moderate catalytic activity.[9,10] However, to date, the relatively high resistivities of these complexes have precluded their application in electrocatalytic devices, where good conductivity is required in addition to proven catalytic activity. Initial attempts to prepare a more highly conductive material by doping the rhodium polymer with Pt(0) bis-4,4′-diisocyanobiphenyl in order to create mixed Rh—Pt—Rh—Pt chains have proved unsuccessful, because of incompatability of the two different polymer structures. However, it has been found possible to incorporate Co(II) ions into the rhodium polymer, and electrical resistivities as low as 200 Ω cm are reported here for the first time, in this type of compound.

EXPERIMENTAL

The addition of a solution of 4,4′-diisocyanobiphenyl[11] in tetrahydrofuran/diethyl ether (50/50 v/v) to a mixed solution of tetracarbonyl di-μ-chloro dirhodium[12] and dithiocyanato cobalt(II) in the same solvent, resulted in the precipitation of a black granular material that was found to contain Rh(I) and Co(II) in the exact ratio as which they had been added to the original solution. For example, addition of excess 4,4′-diisocyanobiphenyl, L, (1.6 g) to a well stirred solution of tetracarbonyl di-μ-chloro dirhodium (0.615 g) and dithiocyanato cobalt(II) (0.0977 g, BDH, 88% purity) in tetrahydrofuran/diethylether (50 cm^3, 50 : 50 v/v) resulted in the immediate precipitation of a black material (2 g). Found: C, 58.4; H, 3.1; N, 9.7; S, 1.8%. Calc. for $Rh_{17}Co_3L_{37}(SCN)_6Cl_{17}$: C, 58.6; N, 9.6; S, 1.8%. Analysis of this material by powder X-ray diffractometry (Phillips PW 1710) showed it to contain diffraction patterns corresponding to two different crystalline phases. The first set of lines was found to match exactly with the *d* spacings reported in the literature for the tetragonal structural modification of rhodium(I) bis-4,4′-diisocyanobiphenyl chloride[1] ($a = b = 15.15$, $c = 3.42$ Å, $\alpha = \beta = \gamma = 90°$); however, the second set of *d* spacings did not match with any of the standard patterns reported for 4,4′-diisocyanobiphenyl metal complexes and constituted a new phase. Analysis of the diffraction pattern by Ito's method[13] gave a triclinic unit cell with the best fit parameters; $a = 29.21$, $b = 27.80$, $c = 7.82$ Å, $\alpha = 81$, $\beta = 81.95$, $\gamma = 90°$. Lines corresponding to this new phase have been identified in powder X-ray diffraction patterns of all of the mixed Co/Rh polymers prepared, with the relative line intensities increasing with the proportion of cobalt(II) contained in the product. At a composition of 50% Co to 50% Rh in the complex, only lines corresponding to this new phase were observed in the powder X-ray diffractogram.

Comparison of the unit cell parameters for the new Co/Rh polymer phase with the previously reported tetragonal rhodium bis-4,4′-diisocyanobiphenyl chloride phase shows that only a small distortion from tetragonal symmetry is required to create the triclinic unit cell found for the mixed rhodium–cobalt polymer. Almost undoubtedly, it is the substitution of $Co(SCN)_2 \cdot \frac{1}{2}L_2$ units for RhL_4Cl units in the polymer that gives rise to this triclinic distortion.

RESULTS AND DISCUSSION

The relative ease of substitution of $Co(SCN)_2 \cdot \frac{1}{2}L_2$ into the solid state of the tetragonal rhodium polymer suggests that, like $[RhL_4]^+$, the Co(II) species formed in co-precipitation will have a square planar rather than a tetrahedral geometry. Evidence for the approximate square planar geometry of Co(II) in the novel polymer phase here, comes from the results of electron paramagnetic resonance spectroscopy (EPR) and diffuse reflectance UV-vis spectroscopy. Figure 2 shows the EPR spectra (Varian EPR3) of (a) $Co(SCN)_2 \cdot \frac{1}{2}L_2$ (prepared by the above method, but in the absence of tetracarbonyl di-μ-chloro dirhodium) and (b) freshly prepared $Rh_{17}Co_3L_{37}(SCN)_6Cl_{17} \cdot nH_2O$. The spectrum shown in Fig. 2(a) shows a single peak at $g = 2.0574$ (no hyperfine splitting), that is attributed to the presence of tetrahedral Co(II) d^7 ions in the solid state of $Co(SCN)_2 \cdot \frac{1}{2}L_2$. In contrast to Fig. 2(a), the spectrum in Fig. 2(b) shows a total of twelve lines that are attributed to the presence of two overlapping eight line multiplets (for ^{59}Co $I = 7/2$). Consideration of published EPR spectra for Co(II) phthalocyanines[14] and Co(II) carbonic anhydrase[15] led to the assignments; $g_\parallel \approx 2$, $A_\parallel = 67$ G, $g_\perp = 2.112$ and $A_\perp = 85$ G being given to the EPR spectrum in Fig. 2(b) ($g_\parallel$ and $g_\perp$ are the parallel and perpendicular *g* factors and $A_\parallel$ and $A_\perp$ are the parallel and perpendicular hyperfine coupling constants). These values are indicative of Co(II) in square planar or square pyramidal geometry with a $d_{z^2}^1$ electronic configuration[16] (i.e. $g_\perp > g \approx 2.0023$ and $A_\perp > A_\parallel$). The fact that ^{59}Co hyperfine splitting is detected at all in cobalt(II) complexes of this type at room temperature is interesting and shows that the Co^{2+} ions contained within the solid state of this material must be relatively well dispersed. Lastly, in connection with Fig. 2(b) it should be noted that the two EPR adsorption peaks of low intensity reported for the tetragonal form of rhodium bis-4,4′-diisocyanobiphenyl chloride[8] are not seen here and are

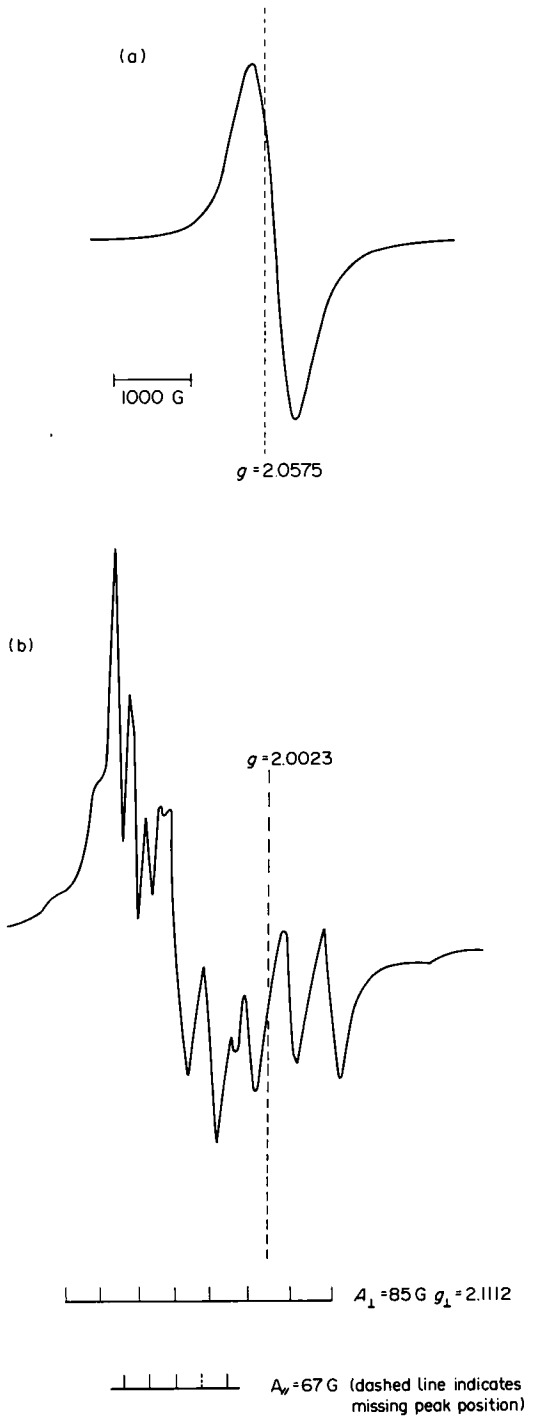

Fig. 2. EPR spectrum of (a) $Co(SCN)_2 \cdot \frac{1}{2}L_2$ at room temperature and (b) freshly prepared $Rh_{17}Co_3L_{37}(SCN)_6Cl_{17} \cdot nH_2O$ at room temperature.

most probably hidden beneath the strong Co(II) signal.

The presence of one-dimensional chains of rhodium(I) ions with extended Rh—Rh interactions have already been identified in this type of complex.[8] The observation that the Co(II) contained in the mixed metal complex here occupies sites of similar geometry to Rh(I) in the solid state is intriguing and the possibility arises that under certain conditions the unpaired electron spin on the Co(II) ions may delocalize along established Rh—Rh chains and/or along the π-conjugated ligand bridges. Results of electrical resistivity measurements carried out upon polycrystalline samples of these materials in a specially designed low-pressure measurement cell[17] are given in Fig. 3 and show the mixed rhodium/cobalt polymers to be semiconductors, with the overall electrical resistivity decreasing markedly with increasing cobalt content in the product (up to a maximum of 50% Co : 50% Rh for this type of phase). The low electrical resistivity of these materials was, however, found to be time dependant and was lost to an extent upon standing in air at room temperature. For example, the low resistivity of a sample of polymer containing 5% cobalt (to 95% rhodium) was found to be stable for several months, but the lowest resistivity of 200 Ω cm measured on a polymer containing 50% cobalt (to 50% rhodium) was lost after only 90 min.

The line intensities of the EPR spectra and powder X-ray diffraction patterns of these materials were also found to be time dependent and dropped in intensity on standing in air at room temperature. These results would seem to indicate that the good

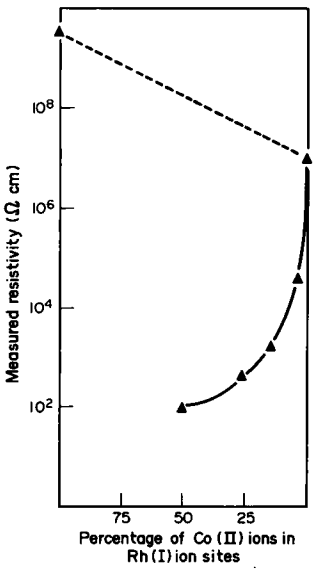

Fig. 3. Plot of resistivity against rhodium/cobalt polymer composition. The dotted line shows the resistivity that would be expected for a physical mixture of the component rhodium and cobalt polymers only, in the absence of the new phase.

electrical conductivity found in these complexes originates from the presence of a novel phase in the solid state of the polymers.

Diffuse reflectance UV-vis spectra recorded for samples of $Rh_{15}Co_5L_{35}(SCN)_{10}Cl_{15}\cdot nH_2O$ before and after loss of the metastable phase, are shown in Figs 4(a) and (b), respectively. The absorption peak at 900 nm in Fig. 4(a) arises from an $a_{1g}(d_{z^2}) \rightarrow a_{2u}(p_z, \pi^*)$ transition shifted from 520 nm because of the presence of extended rhodium–rhodium interactions.[18] In Fig. 4(b) this peak is shifted to a shorter wavelength and is of reduced intensity. The position and intensity of this peak are related to the extent of electronic conductivity of the diisocyanide complexes of this type.[2] The results here indicate that rhodium–rhodium extended interactions in the aged rhodium/cobalt polymer are far less extensive than in the freshly prepared material. The absorption peaks at 700 and 1230 nm in Figs 4(a) and (b) are attributed to electronic transitions originating from Co(II) ions in square planar symmetry,[19] present in the solid state of this material. The decrease in the intensity of these two peaks upon ageing, is accounted for in terms of a structural rearrangement occurring within the material that results in Co(II) ions moving out of square planar geometry. A new absorption band at 300 nm found in the spectrum of the aged polymer, is attributed to a $\sigma \rightarrow \sigma^*$ transition within a Co(III)—Co(III) ($d_{z^2}-d_{z^2}$) bond[20] and is consistent with the above proposal.

Fig. 4. Diffuse reflectance UV-vis spectra of (a) feshly prepared $Rh_{17}Co_3(SCN)_6L_{37}Cl_{17}\cdot nH_2O$ ($\rho = 600$ Ω cm) and (b) the same sample after standing in air for 6,000 h ($\rho = 50{,}000$ Ω cm).

Analysis of samples of the freshly prepared and aged polymer $Rh_{15}Co_5L_{35}(SCN)_{10}Cl_{15}\cdot nH_2O$ by ESCA. (Kratos ES300 spectrometer with radiation at 1468.6 eV) confirmed the appearance of Co(III) within solid samples of the aged polymer, but interestingly failed to detect the presence of Rh(II) (sensitivity limit *ca.* 1% by weight of the total sample mass), precluding the formation of Co(III)—Rh(II) bonds within this system.

Evidence obtained from powder X-ray diffraction studies carried out on samples of freshly prepared and aged samples of the novel Co/Rh polymer showed that the materials contained two distinct structural phases. As the polymer precipitates immediately on addition of the ligand solution to the metal solution, two possibilities exist:

(i) A uniform polymer is produced in which there is a random occupation of metal sites by Co(II), the occupancy varying as the proportion of cobalt in the original mixture.
(ii) A doped polymer of approximately constant composition is precipiated first, followed by an undoped polymer that removes all of the rhodium from solution.

In this instance it is thought that (ii) but not (i) would give rise to two sets of diffraction patterns. If this assumption is correct then the observed variation in conductivity can only be caused by particles of a conducting Co/Rh polymer embedded in a less-conductive matrix.

The experimental results of powder X-ray diffraction, electron paramagnetic resonance, diffuse reflectance UV-vis spectroscopy, ESCA and electrical conductivity measurements are thus best rationalized on the basis of adjacent Co(II) ions undergoing a kinetically slow dimerization to form Co(III)—Co(III) bonded species that result in the loss of the metastable paramagnetic phase (identified here as being responsible for the good conductivity found in the mixed rhodium/cobalt polymers). This type of dimerization by oxidative-addition of Co(II) has been reported for cobalt(II) tetramethyl isocyanide in solution,[21] but until now has not been reported to occur in the solid state. Obviously, the dimerization of $Co(SCN)_2\cdot\frac{1}{2}L_2$ here, becomes increasingly favourable with increasing cobalt(II) concentration in the solid state of the polymer, as the likelihood of finding two adjacent Co(II) sites increases.

In response to a recent report on the use of polynuclear metal complexes in the fabrication of battery electrodes,[22] it was decided to investigate the potential of the novel cobalt/rhodium polymers

Table 1. Performance of 4,4′-diisocyanobiphenyl complexes of cobalt and rhodium as fuel cell electrodes

Electrode material	Resistivity (ρ) (Ω cm)	Rest voltage E_0 (mV)	Current density[a] at 10 mV (μA cm^{-2})
$Co(SCN)_2 \cdot \frac{1}{2}L_2$	5×10^9	10.4	0.05
RhL_2Cl (tetragonal form)	1×10^7	41.3	1.60
$Rh_{17}Co_3L_{37}(SCN)_6Cl_{17} \cdot nH_2O$	2×10^3	168.2	2.51
$Rh_{15}Co_5L_{35}(SCN)_{10}Cl_{15} \cdot nH_2O$	6.5×10^2	465.2	3.58

[a] Measured over 90 min continuous operation.

described here as fuel cell electrodes. The ethylene glycol/air fuel cell was chosen for investigation here, because of its good operating performance at room temperature[23] and because of the good activity of rhodium(I) bis-4,4′-diisocyanobiphenyl in alcohol disproportionation reactions.[10] Here, the fuel cell used was constructed according to the design of Qiu[24] and used a disc of highly orientated pyrolytic graphite (H.O.P.G.) as an air electrode, and an electrolyte solution of 3.5 M ethylene glycol to 7.5 M potassium hydroxide (both in distilled water). It can be seen (Table 1) that the performance of the organometallic polymers of cobalt and/or rhodium as fuel cell electrodes is clearly related to their solid-state resistivity, with high cobalt, low resistive phases giving the best results (the low current densities are a reflection of the low surface porosity of the polymers in the form of compressed pellets). The results of the experimental trials conducted here are encouraging and indicate that it may be possible to prepare commercially viable fuel cell electrodes out of metal aryl diisocyanide systems provided that stable polymers with good conductivity and catalytic activity can be synthesized.

Further research work with the aim of achieving this objective is currently being undertaken.

Acknowledgements—I. F.-J. thanks the N.C.R.D. (Israel) for funding. Johnson Matthey are thanked for the loan of rhodium(III) chloride. Union Carbide (Dr A. W. Moore) are thanked for the gift of H.O.P.G. samples.

REFERENCES

1. A. Efraty, I. Feinstein, F. Frolow and L. Wackerle, *J. Am. Chem. Soc.* 1980, **102**, 6341.
2. A. Efraty, I. Feinstein and F. Frolow, *Inorg. Chem.* 1982, **21**, 485.
3. I. Feinstein-Jaffe and A. Efraty, in *Organometallic Synthesis*, (Edited by R. B. King and J. Eisch), Vol. 4, in press (1988).
4. I. Jaffe, M. Segal and A. Efraty, *J. Organometal. Chem.* 1985, **294**, C17.
5. I. Feinstein-Jaffe and A. Efraty, *J. Mol. Catal.* 1986, **35**, 285.
6. I. Feinstein-Jaffe, I. Biran, D. Mahalu, S. Cohen and S. A. Lawrence, *J. Chem. Soc., Dalton Trans.*, submitted.
7. I. Feinstein-Jaffe and S. E. Maisuls, *J. Organometal. Chem.* 1987, **326**, C97.
8. S. A. Lawrence, K. A. K. Lott, P. A. Sermon, E. L. Short and I. Feinstein-Jaffe, *Polyhedron* 1987, **6**, 2027.
9. I. Feinstein-Jaffe and A. Efraty, *J. Mol. Catal.* 1987, **40**, 1.
10. S. A. Lawrence, I. Feinstein-Jaffe and P. A. Sermon, *Proc. R. Soc. Lond. A*, submitted.
11. A. Efraty, I. Feinstein, L. Wackerle and A. Goldman, *J. Org. Chem.* 1980, **45**, 4059.
12. J. A. McCleverty and G. Wilkinson, *Inorg. Synth.* 1966, **8**, 211.
13. T. Ito, *Nature* 1949, **164**, 755.
14. J. M. Assour and W. K. Kahn, *J. Am. Chem. Soc.* 1965, **87**, 207.
15. S. A. Cockle, *J. Am. Chem. Soc.* 1965, **87**, 207.
16. A. Abragam and M. H. L. Price, *Proc. R. Soc. Lond. A* 1951, **206**, 905.
17. S. A. Lawrence, S. Stevenson, K. Mavadia and P. A. Sermon, *Proc. R. Soc. Lond. A* 1987, **411**, 95.
18. J. C. Gordon, R. Williams, C. H. Hsu, E. Cuellar, S. Samson, K. Mann, H. B. Gray, V. Hadek and R. R. Somoano, *R. Ann. N.Y. Acad. Sci.* 1978, **313**, 580.
19. F. L. Urbach, R. D. Bereman, J. A. Topich, M. Hariharan and B. J. Kalbacher, *J. Am. Chem. Soc.* 1974, **17**, 311.
20. Y. Yamamoto and H. Yamazaki, *Inorg. Chem.* 1978, **17**, 311.
21. F. A. Cotton, T. G. Dunne and J. S. Wood, *Inorg. Chem.* 1964, **3**, 1495.
22. M. Kanebo, *J. Polymer Sci.* 1986, **C24**, 435.
23. W. Vielstich, *Fuels Cells* (English Edn) p. 271. Wiley, U.K. (1970).
24. R. Qiu, *Int. J. Hydrogen Energy* 1986, **11**, 817.

Polyhedron Vol. 7, No. 9, pp. 747–752, 1988
Printed in Great Britain

0277-5387/88 $3.00+.00
© 1988 Pergamon Press plc

COMPLEXES OF HYDROXAMATES—IV.* THE AFFINITY OF SERINEHYDROXAMATE TO IRON(III); EQUILIBRIUM AND KINETIC STUDY

LAMYA J. HAYAT

Department of Biochemistry, Kuwait University, P.O. Box 5969, 13060 Safat, Kuwait

and

HAYAT M. MARAFIE, MANSOUR M. HASSAN and MOHAMED S. El-EZABY†

Department of Chemistry, Kuwait University, P.O. Box 5969, 13060 Safat, Kuwait

(*Received* 16 *October* 1987; *accepted* 13 *January* 1988)

Abstract—The SQUAD II program has been used to determine the formation constants of the serinehydroxamate (SX^-) complexes of iron(III) at $I = 0.15$ M NaCl and $T \simeq 25°C$. The data were obtained from a spectrophotometric study in the wavelength range 400–600 nm and pH range 2.24–9.00. Stopped-flow kinetic data were also obtained in the wavelength range 350–480 nm ($I = 0.15$, $T = 25°C$) and the pH range 1.2–4.2. The kinetic data conformed to the equation

$$k_{obs} = A + BT_{SX},$$

where T_{SX} is the analytical concentration of SX and the parameters A and B are pH dependent. A mechanism was proposed to account for the kinetic result in which the species ($SX^- : Fe^{3+} : H^+$) 1 : 1 : 0 and 1 : 1 : 1 are the sole complexes formed.

In recent years considerable attention has been given to hydroxamates and their metal complexes due to their chemical and biological importance.[2–6] The only hydroxamates which exist in nature are the di- and trihydroxamates. They have a high affinity to iron(III). These siderophores may help to carry iron through metabolic channels to the needed biological molecules such as porphyrins and enzymes. It has also been reported that some low molecular weight monohydroxamate complexes of iron(III) catalyse the iron exchange from its siderophores to another polydentate ligand such as EDTA.[7]

Although the equilibrium reactions of monohydroxamates with several metal ions have been the subject of many reports[4–8] in the last two decades, only a few have dealt with the kinetics of these reactions.[8–10] In this work we report the equilibria and reaction kinetics of the binary system Fe(III)–serinehydroxamic acid (SX).

* For part III, see ref. 1.

†Author to whom correspondence should be addressed.

EXPERIMENTAL

A stock solution of iron(III) chloride (Merck) was prepared with an equivalent concentration of HCl (not less than 0.5 M). It was freshly sub-diluted for kinetic runs and equilibrium studies. A stock solution of serinehydroxamic acid (≥ 99% Sigma) was freshly prepared by weighing the solid and dissolving in triply distilled water. The ionic strength was kept constant at 0.15 M NaCl. The concentration of Fe(III) was checked complexiметrically as previously described.[11]

Measurements of pH were carried out using a Radiometer pH-meter type-63 equipped with a combined glass electrode type GK-2311C. The pH-meter was calibrated by the two buffers procedure in the pH range used. The hydrogen ion concentration was taken to be 10^{-pH}.

Spectral measurements were made using a Shimadzu 160 spectrophotometer in the wavelength range 300–600 nm. The spectral and pH measurements were recorded at room temperature (25.0 ± 1°C).

Kinetic measurements were performed using a Union Giken stopped flow reaction analyser RA-401, interfaced with a RA-451 data processor and a RA-115 rapid scan attachment. The temperature in the mixing unit was controlled at 25°C by a Grant circulator. The kinetic data were processed by the Guggenheim method program. At least an average of ten kinetic runs (for a set of experimental conditions) were carried out in the wavelength range 350–480 nm. The calculated rate constants were fitted to the experimental kinetic data. The kinetic experimental procedure was to keep the pH of the iron(III) chloride low (1.5–2.0) to avoid iron(III) polymerization and hydrolysis at higher pHs, and only to change the pH of the SX solutions. It is assumed that in the stopped-flow mixing, the required pH was equilibrated in microseconds. The concentration of iron(III) was kept constant at 2.0×10^{-4} M for the kinetic study and in the range (1.0–4.0) 10^{-4} M for the equilibrium study. The ligand concentration was varied between 3.0×10^{-3} and 10×10^{-3} M for the kinetic study and between (3.0–8.0) 10^{-3} M for the equilibrium study.

RESULTS AND DISCUSSION

(i) *Equilibrium study*

The addition of serinehydroxamate to a solution of ferric ions gave a reddish–brownish colour showing as usual the effect of hydroxamates grouping as a ligating entity for Fe^{3+}. The spectra as function of pH for fresh solutions are shown in Fig. 1. They are similar to a large extent to spectra of other Fe(III)–aminohydroxamic acids systems.[1,8,11] The band at $\sim$ 490 nm shifts to a shorter wavelength with an increase in intensity as the pH increases, until pH 7. A decrease in intensity occurred at pH > 7. The spectra of fresh as well as overnight solutions are similar in pattern but slightly different in intensity especially in the pH range 2.5–6.0; being a little lower in the case of the overnight spectra. The SQUAD II program has been used to determine the formation constants of the species in fresh and overnight solutions. Table 1 lists their values under the experimental conditions used. It seems that the fresh and overnight solutions gave almost similar species with approximately equal formation constants. It is interesting, however, that in fresh solutions of the species 3:1:3 (SX^- : Fe^{3+} : H^+) was replaced by a dimeric species 1:2:1. This conclusion may indicate the slow formation of polymerized products with time. This has been observed in the Fe^{3+}–AX and Fe^{3+}–HX systems (AX = acetohydroxamic acid and HX = histidinehydroxamic acid).[1] It is also interesting to note that most of the species are protonated, designating the non-involvement of the amino group in ligation with Fe(III). The proton is presumed to be located on the amino group. Although the magnitude of the formation constants is comparable to those of other pertinent systems (Table 1), the species are not totally identical under the same experimental conditions. The distribution of the species for the fresh solution equilibria as function of pH for the Fe(III)–SX system is shown in Fig. 2.

(ii) *Kinetic study*

One rate step in the millisecond time range was observed in the kinetic study of the reaction of Fe(III) with SX in the pH range 2.0–4.2. It is comparable to that which occurred in the Fe(III)–GX[11] and Fe(III)–MX[8] systems (GX = glycinehydrox-

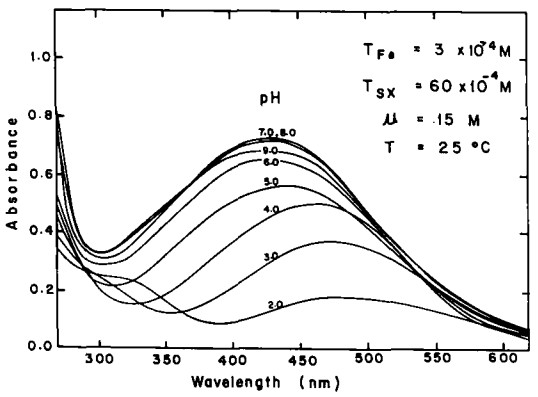

Fig. 1. The spectra of the Fe(III)–SX system at different pH for the fresh solutions.

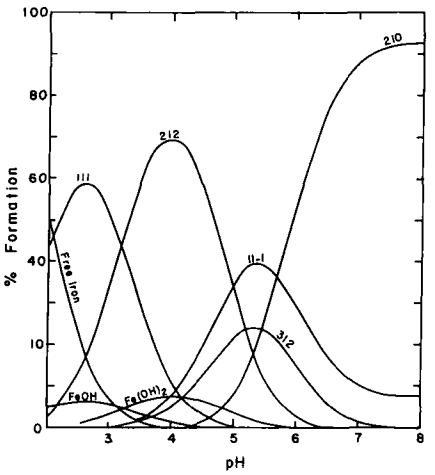

Fig. 2. The distribution diagam of the Fe(III)–SX system as a function of pH.

Table 1. Summary of the overall formation constants of Fe(III)–SX (GX or MX) $L_pM_qH_r$ [L = ligand, M = Fe(III)] at $I = 0.15$ and 25°C and other pertinent constants

L	Stoichiometric coefficients p	q	r	log β_{pqr} ($\pm\sigma$)[a] Fresh solution	Overnight solution	Wavelength range, No. of wavelengths, No. of solutions, pH range, ref.
SX^-	1	0	1	9.121(0.005)[b]		400–600 nm, 21
	1	0	2	15.930(0.005)[b]		.19, 2.24–9.00,
	1	1	1	16.26(0.02)	16.07(0.04)	This work
	2	1	2	31.43(0.05)	31.26(0.02)	
	3	1	3	44.62(0.17)		
	2	1	0	20.75(0.10)	19.59(0.18)	
	1	1	−1	8.06(0.08)	7.23(0.12)	
	1	2	1	—	19.76(0.07)	
GX^-	1	0	1		9.55	Ref. 11
	1	0	2		17.15	
	1	1	0		14.14	
	1	1	1		17.30	
	2	1	0		22.72	
	2	1	1		28.94	
MX^-	1	0	1		9.033	Ref. 8
	1	0	2		15.803	
	1	1	0		12.73	
	1	1	1		16.26	
	2	1	1		26.12	
	2	1	2		30.94	
	3	2	0		38.24	
OH^-	0	1	−1	−3.05		Ref. 8, 12
	0	1	−2	−6.31		
	0	0	−1	13.76		

[a] The standard deviation in absorbance data did not exceed the 5.50×10^{-3} absorbance unit.
[b] Obtained from potentiometric study using the SUPERQUAD program.

amic acid and MX = methioninehydroxamic acid). However, the slow steps observed in the latter systems were not observed in the current system. Similarly, this step may be attributed to the formation of metal chelates with the ligand.

Figure 3 shows the dependence of the observed pseudo-first-order rate constant, k_{obs}, on both pH and T_{SX} ($T_{SX} \gg T_{Fe}$). This system did not behave like the Fe(III)–GX and Fe(III)–MX systems. The rate increased as the pH, as well as T_{SX}, increased. At a given pH, the rate constant is a linear function of T_{SX}. Figure 4 shows this dependence at interpolated values of pH which were obtained from Fig. 3. Empirically the curves are represented by the following equation:

$$k_{obs} = A_i + B_i T_{SX} \quad (1)$$

where A_i and B_i are the intercepts and slopes of the linear plots shown in Fig. 4; their values are pH-

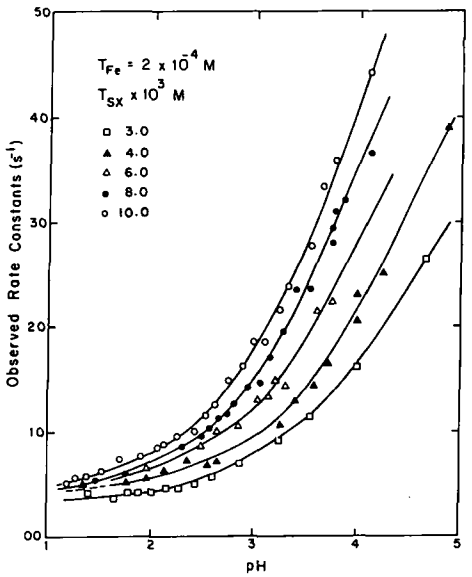

Fig. 3. The dependence of k_{obs} on T_{SX} and pH.

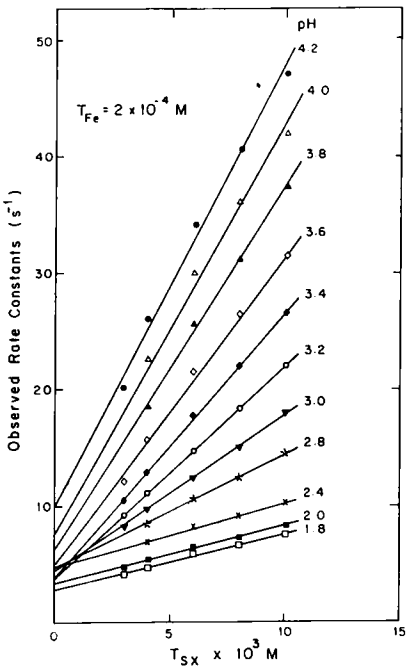

Fig. 4. The plot of k_{obs} as a function of T_{SX} at interpolated pH values.

dependent (Table 2). The dependence of A on pH is irregular while that of B is a monotonic increasing function.

The iron(III) solution exhibits several aquated chloro species imposed by the experimental conditions used in this study. They are of the form $Fe(OH)_iCl_{n-i}(H_2O)_{6-n-i}$. Dimeric forms are excluded since the pHs were usually in the range of 1.5–2.0 and also due to the presence of a high concentration of chloride ions (Table 1). The mixed equilibrated pH was in the range ~ 1.0–4.2. Due to the presence of a high concentration of the ligand, polymerization and/or hydrolysis of iron(III) were prohibited. One should expect that these processes are slow and may not be observed in the millisecond time range. Although this may be true, no slow processes have been observed. On the other hand, SX shows only one species, the diprotonated SXH_2^+, Table 1.

The interaction of the Fe(III) species with the SX species can be summarized in Scheme 1; where k_i and k_{-i} are the forward and backward rate constants and K_{1OH}, K_{2OH} and K_{HC} are the first and

Table 2. The dependence of A_i and B_i on pH and their pertinent quantities

pH	A_i (s^{-1})	$A_i \times (H^+) \times 10^3$	$B_i \times 10^{-2}$ ($s^{-1} M^{-1}$)	$(B_i \times Q_2/\alpha_0) \times 10^{-4}$
1.80	3.0	47.4	4.40	0.0470
2.00	3.8	38.0	4.40	0.0480
2.40	4.4	17.5	5.00	0.0630
2.60	4.0	10.0	8.60	0.123
2.80	4.6	7.27	10.0	0.776
3.00	4.6	4.60	13.2	0.314
3.20	4.0	2.52	18.0	0.655
3.40	4.0	1.75	22.4	1.42
3.60	5.0	1.26	26.5	3.27
3.80	6.4	1.01	30.9	7.80
4.00	7.6	0.860	35.4	20.8
4.20	10.4	0.656	37.6	51.9

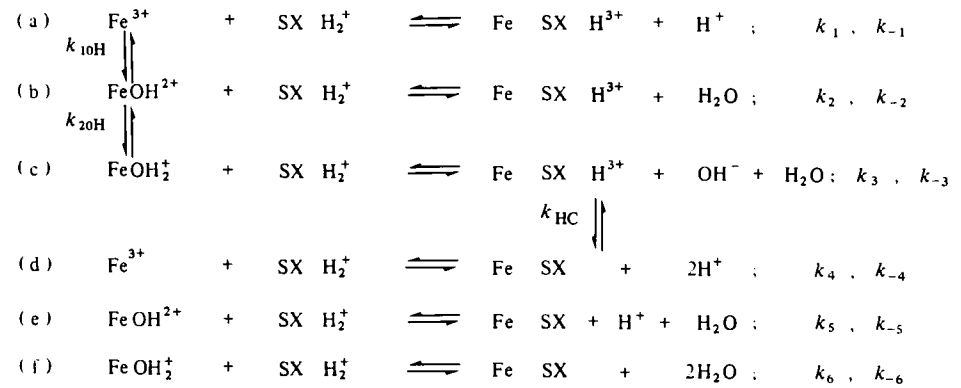

Scheme 1.

second hydrolysis constants of Fe^{3+} and the deprotonation constant of Fe SXH^{3+}, respectively.

At fixed pH, the rate equation is as follows:

$$Q_1 d(FeSX)/dt = [(T_{Fe}-(FeSX)Q_1)/Q_2] \times [T_{SX}Q_3\alpha_0]-[(FeSX)Q_4] \quad (2)$$

where

$$\alpha_0 = (H^+)^2/((H^+)^2+K_{1h}(H^+)+K_{1h}K_{2h})$$

(K_{1h} and K_{2h} are the stepwise deprotonation constants of the species SXH_2^+)

$$Q_1 = ((H^+)/K_{HC})+1,$$

$$K_{HC} = (FeSX^{2+})(H^+)/(FeSXH^{3+})$$

$$Q_2 = 1+K_{1OH}(/H^+)1K_{1OH}K_{2OH}/(H^+)^2$$

[where K_{1OH} and K_{2OH} are the first and second hydrolysis constant of iron(III)]

$$Q_3 = k_1+k_2K_{1OH}/(H^+)+k_3K_{1OH}K_{2OH}/(H^+)^2 +k_4+k_5K_{1OH}/(H^+)+k_6K_{1OH}K_{2OH}$$

and

$$Q_4 = (k_{-3}K_w/K_{HC})+k_{-6}+(H^+)(k_{-2}/K_{HC}+k_{-5}) +(H^+)^2(k_{-1}/K_{HC}+k_{-4}),$$

(K_w is the ionic product of water, Table 1).

The integrated form of eq. (2) is

$$\ln[(FeSX)_\infty/(FeSX)_\infty-(FeSX)_t] = kt \quad (3)$$

where $(FeSX)_\infty$ and $(FeSX)_t$ are the concentration of the species at infinite time and time t (both are directly proportional to the change in absorbance at a given wavelength), and k is identical to the observed rate constant

$$k_{obs} = Q_4/Q_1+Q_3T_{SX}\alpha_0/Q_2. \quad (4)$$

Now from eqs (1) and (4) one should expect that A_i is equal to Q_4/Q_1 and B_i is equal to $Q_3\alpha_0/Q_2$. If A_i is multiplied by Q_1, and B_i by α_0/Q_2, one gets the following equations:

$$A_i[((H^+)_i/K_{HC})+1] = (k_{-6}+k_{-3}K_w/K_{HC}) +(k_{-2}/H_{HC}+k_{-5})(H^+)_i+(k_{-1}/K_{HC}+k_{-4})(H^+)_i \quad (5)$$

and

$$B_iQ_2/\alpha_0 = (k_1+k_4)+K_{1OH}(k_2+k_5)/(H^+)_i +K_{1OH}K_{2OH}(k_3+k_6)/(H^+)_i^2. \quad (6)$$

The plot of $A(H^+)$ vs (H^+) was linear. This indicates that $(H^+)/K_{HC}$ should be much greater than one. The intercept and slope are $(5.97\pm2.59)\times10^{-4}$ and (3.81 ± 0.08), respectively. The intercept corresponds to $(k_{-6}K_{HC}+k_{-3}K_w)$ and the slope to $(k_{-2}+k_{-5}K_{HC})$. On the other hand, the plot of B_iQ_2/α_0 vs $(H^+)^{-1}$ is quadratic with the coefficients $(k_1+k_4) = (1.03\pm0.74)\times10^3$, $K_{1OH}(k_2+k_5)\cong0$ and $[K_{1OH}K_{2OH}(k_3+k_6)] = (2.10\pm0.02)\times10^{-3}$. Table 3 summarizes the micro-rate constants obtained in this work if some approximations are made, which are shown in footnote *a* of the table.

One may conclude that the reactions (a), (c), (d) and (f) in Scheme 1 are significant in the formation of the 1:1:1 and 1:1:0 species ($SX^-:Fe^{3+}:H^+$). However, this conclusion does not agree with that obtained from the equilibrium study. Other mechanisms have been tried, to include other species such as 1:1:−1 and 2:1:2. Unfortunately, they were not compatible with the kinetic data. This has been rationalized on the basis of the fact that the data is not quadratically dependent on T_{SX}. There is, however, a possibility that the formation of 2:1:2

Table 3. Summary of the rate constants and equilibrium constants and their magnitudes obtained in this work

Rate constant	Magnitude[a]	Equilibrium constant
k_1, k_{-1}	$\sim10^3, <1$	$\gg10^3$
k_2, k_{-2}	$<1, 3.8$	<1
k_3, k_{-3}	$4.3\times10^3, 3.4\times10^{10}$	1.3×10^{-7}
k_4, k_{-4}	$\sim10^3, <1$	$\gg10^3$
k_5, k_{-5}	$<1, 7.6\times10^3$	<1
k_6, k_{-6}[b]	$4.3\times10^3, 1.2$	3.6×10^3

[a] In evaluating the rate constants, the assumption was made that one term in the combined expression of the micro-rate constants extracted from eqs (5) and (6) is equal to zero with respect to the other and *vice versa*.

[b] pK_{HC} was estimated to be equal to 3.3.

species is much faster than 1:1:1 and 1:1:0 species, and the half-life period is out of the time range of the stopped-flow technique. In addition, the intercepts of the k_{obs} vs T_{SX} curves are not totally dependent on H^1 concentration as is shown from Fig. 4.

Acknowledgements—The authors acknowledge the provision of a Kuwait University Grant, No. SC036 and the Kuwait Foundation for the Advancement of Sciences (KFAS) Grant No. 86–07–09.

REFERENCES

1. N. M. Shuaib, H. M. Marafie, M. M. Hassan and M. S. El-Ezaby, *J. Inorg. Biochem.* 987, **31**, 171.
2. A. K. Madundar, *International Series of Monographs in Analytical Chemistry*, p. 50. Pergamon Press, New York (1971).
3. J. B. Neilands, *Science* 1967, **156**, 1443.
4. D. A. Brown, M. V. Chidambaram, J. J. Clarke and D. M. McAleese, *Bioinorg. Chem.* 1978, **9**, 255.
5. D. A. Brown, M. V. Chidambaram and J. D. Glennon, *Inorg. Chem.* 1980, **19**, 3260.
6. D. A. Brown and B. S. Sekhon, *Inorg. Chim. Acta* 1984, **91**, 103.
7. B. Monzyk and A. L. Crumbliss, *J. Inorg. Biochem.* 1983, **19**, 19.
8. M. S. El-Ezaby, H. M. Marafie, M. M. Hassan and H. M. Abu Soud, *Inorg. Chim. Acta* 1986, **123**, 53.
9. B. Mouzyk and A. L. Crumbliss, *J. Am. Chem. Soc.* 1979, **101**, 21, 6203.
10. N. Kujundzic and M. Probanic, *J. Inorg. Nucl. Chem.* 1978, **40**, 729.
11. M. S. El-Ezaby and N. M. Hassan, *Polyhedron* 1985, **4**, 429.
12. L. N. Mulay and P. W. Selwood, *J. Am. Chem. Soc.* 1954, **77**, 2693.

Polyhedron Vol. 7, No. 9, pp. 753–756, 1988
Printed in Great Britain

0277-5387/88 $3.00+.00
© 1988 Pergamon Press plc

COMMUNICATION

CYCLOTANTALATION OF 2,6-DIPHENYLPHENOXIDE; X-RAY CRYSTAL STRUCTURE OF $Ta(OC_6H_3PhC_6H_4)(OAr\text{-}2,6Ph_2)_2Me$

ROBERT W. CHESNUT, BRYAN D. STEFFEY and IAN P. ROTHWELL*

Chemistry Department, Purdue University, West Lafayette, IN 47907, U.S.A.

and

JOHN C. HUFFMAN

Molecular Structure Center, Indiana University, Bloomington, IN 47405, U.S.A.

(*Received* 10 *December* 1987; *accepted* 19 *January* 1988)

Abstract—Treatment of the mixed chloro, aryloxide compounds $Ta(OAr\text{-}2,6Ph_2)_2Cl_3$ and $Ta(OAr\text{-}2,6Ph_2)_3Cl_2$(OAr-2,6Ph$_2$ = 2,6-diphenylphenoxide) with $LiCH_3$ or $Mg(CH_2C_6H_4\text{-}4Me)_2$($CH_2$Ph-4Me = 4-methylbenzyl) allows isolation of the corresponding alkyls $Ta(OAr\text{-}2,6Ph_2)_2R_3$ (**1**) and $Ta(OAr\text{-}2,6Ph_2)_3R_2$ (**2**) (**a**, R = CH_3; **b**, R = CH_2Ph-4Me). Thermolysis of these compounds either in the melt (**1**) or toluene solution (**2**) results in the loss of one equivalent of methane or *para*-xylene and the formation of a series of mono-cyclometallated compounds (**3**) and (**4**). A solid state structural study of $Ta(OC_6H_3Ph\,C_6H_4)(OAr\text{-}2,6Ph_2)_2Me$ (**4a**) using X-ray diffraction techniques confirms the presence of the six-membered metallacycle formed by cyclometallation of the 2,6-diphenylphenoxide ligand. Spectroscopically, the new Ta—C(ipso) carbon atom is clearly visible at δ-200 ppm in the ^{13}C NMR spectra of (**3**) and (**4**). Attempts to thermally induce a second ring closure proved difficult, with considerable decomposition taking place. However, reduction of $Ta(OAr\text{-}2,6Ph_2)_3Cl_2$ with Na/Hg (2 equiv) generates the bis-metallated compound $Ta(OC_6H_3PhC_6H_4)_2(OAr\text{-}2,6Ph_2)$ (**5**) in good yield. The cyclometallation of 2,6-diphenyl-phenoxide ligands by tantalum has thus been achieved both by the use of alkyl leaving groups attached to Ta(V) metal centres as well as by intramolecular oxidative–addition of the aromatic CH bond to Ta(III).

The recognition that high valent, electron-deficient early *d*-block,[1,2] lanthanide[2] and actinide[4] metal compounds have the ability to activate normally inert carbon–hydrogen bonds under mild conditions has prompted considerable research interest. The absence of an available oxidative–addition pathway for this reactivity has led to the acceptance of heterolytic mechanisms proceeding via multi-centre transition states in order to account for the experimental data obtained.[5] Our studies of the early *d*-block metal chemistry associated with sterically demanding aryloxide ligation[6,7] have led us to characterize just such reactivity involving the mild cycometallation of 2,6-di-*tert*-butylphenoxide ligands at d^0-metal centres.[5,8] Given the electrophilic nature of the metal centres involved, we have recently focussed our attention on the ligand 2,6-diphenylphenoxide.[9,10] This group offers the potential for related reactivity only this time the metallacycle formation involves the activation of an aromatic carbon–hydrogen bond.[11] In this communication we wish to report our initial finding concerning the cyclometallation of this ligand by tantalum. In particular we have observed carbon–hydrogen activation by both heterolytic Ta(V), as well as oxidative–addition, Ta(III), pathways.

The mixed chloro-aryloxides Ta(OAr-

*Author to whom correspondence should be addressed.

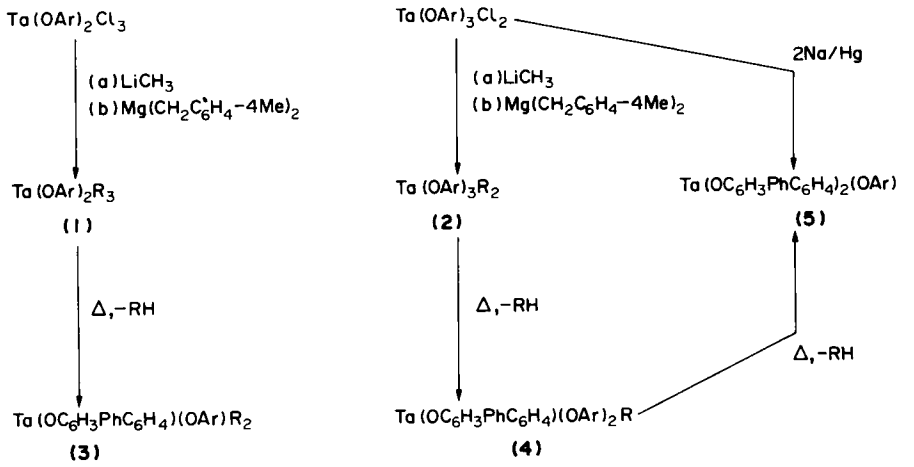

(a) R = CH_3 ; (b) R = $CH_2C_6H_4$-4Me

OAr = 2,6-diphenylphenoxide

Scheme 1.

$2,6Ph_2)_2Cl_3$ and $Ta(OAr\text{-}2,6Ph_2)_3Cl_2$[12] prove to be convenient substrates for the synthesis of organometallic compounds containing 2,6-diphenylphenoxide (OAr-2,6Ph_2) ligation. Hence, alkylation with LiMe or $Mg(CH_2Ph\text{-}4Me)_2$(CH_2Ph-4Me = 4-methylbenzyl) allows the isolation of a series of tris- and bis-alkyl derivatives as shown (Scheme 1).* All of these alkyl compounds exhibit thermal instability to various degrees. On thermolysis either in hydrocarbon solution or in the melt they undergo loss of alkane and formation of a series of cyclometallated compounds. The trisalkyls are significantly more stable than their bisalkyl analogues needing much more forcing conditions for reaction. The most stable compound, $Ta(OAr\text{-}2,6Ph_2)_2Me_3$ (**1a**) only very slowly eliminates methane on heating above 200°C for hours. However, a mixture of dark, so far uncharacterized products are formed from the thermolysis. The trisbenzyl derivative (**1b**) however, cleanly loses one equivalent of zylene on heating at 175°C in the melt. The product, mono-cyclometallated derivative (**3b**) is formed in essentially quantitative yield. The presence of the six-membered metallacycle is readily demonstrated by solution NMR spectra.* Particularly characteristic is the resonance for the new Ta—C(*ipso*) bond at $\approx \delta$ 200 ppm in the ^{13}C NMR spectrum, while the diastereotopic benzyl methylene protons appear as a well resolved *AB* pattern.

Thermal elimination of hydrocarbon occurs under much milder conditions for the bis-alkyls. In both cases, thermolysis in toluene solvent leads to the quantitative formation of the corresponding mono-cyclometallated derivatives (Scheme 1) with the generation of one equivalent of methane or xylene. A kinetic study shows these two ring closure reactions to be first order with the dependence of the rate of ring closure on the alkyl leaving group following the trend CH_2Ph-4Me > CH_3. The activation parameters obtained for thermolysis of the dimethyl (**2a**) show a moderately large, negative value for the entropy of activation, consistent with results found for other related ring closure reactions. Rate constants obtained at various temperatures 10^5 k/s^{-1}(T°C) are 4.15(120), 10.1(130),

* *Selected spectroscopic data*: due to its very nature, the ^1H and ^{13}C NMR spectra of unmetallated 2,6-diphenylphenoxide ligands are typically uninformative, giving rise to a set of resonances in the δ 6.8–7.2 and 115–160 ppm regions. However, cyclometallation results in not only a distinctive, new M—C(*ipso*) resonance, but also in the appearance of characteristic doublets in the ^1H NMR spectrum, slightly downfield of the normal aromatic region. Spectroscopic data on (**1a**) and (**2a**) has been reported. ^1H NMR (C_6D_6, 30°C): (**1b**): δ 1.33 (s, Ta—CH_2), 2.09 (s, 4*Me*), 6.53 (d, *meta*-C_6H_4-4Me), 6.38 (d, *ortho*-C_6H_4-4Me). (**2b**): δ 1.88 (s, Ta—CH_2), 2.22 (s, 4*Me*), 6.73 (d, *meta*-C_6H_4-4Me), 6.21 (d, *ortho*-C_6H_4-4Me). (**3b**): δ 1.92 (d), 1.80 (d, Ta—C_6H_2), 2.23 (s, 4*Me*), 6.87 (d, *meta*-C_6H_4-4Me), 6.35 (d, *ortho*-C_6H_4-4Me). (**4a**): δ −0.39 (s, Ta—CH_3)(**4b**): δ 2.19 (s, Ta—CH_2), 2.23 (s, 4Me), 6.42 (d, *meta*-C_6H_4-4Me), 5.57 (d, *ortho*-C_6H_4-4Me). ^{13}C NMR (C_6D_6, 30°C): (**1b**): δ 78.4 (Ta—CH_2), 20.9 (4*Me*). (**2b**): δ 88.3 (Ta—CH_2), 20.8 (4*Me*). (**3b**): δ 74.6 (Ta—CH_2), 21.0 (*Me*), 201.7 [Ta—C(*ipso*)]. (**4a**): δ 64.3 (Ta—CH_3), 199.9 [Ta—C(*ipso*)]. (**4b**): δ 86.6 (Ta—CH_2), 21.6 (4*Me*), 200.7 [Ta—C(*ipso*)]. (**5**): δ 202.2 [Ta—C(*ipso*)].

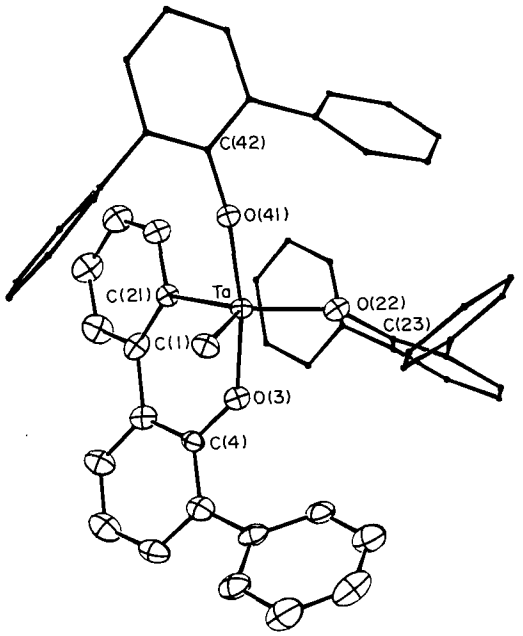

Fig. 1. ORTEP view of (**4a**) emphasizing the central coordination sphere and metallacycle ring. Selected bond distances (Å) and angles (°) are: Ta—O(3) 1.909(4), Ta—O(22) 1.883(4), Ta—O(41) 1.899(4), Ta—C(2) 2.125(7), Ta—C(21) 2.215(5), Ta—O(3)—C(4) 141.4(4), Ta—O(22)—C(23) 146.6(4), Ta—O(41)—C(42) 169.5(4), O(3)—Ta—C(21) 80.8(2).

9.75(130), 18.0(139), 50.0(151) yielding $\Delta H^{\ddagger} = 25.3 \pm 0.8$ kcal mol^{-1}; $\Delta S^{\ddagger} = -15 \pm 5$ cal mol^{-1} K^{-1}. Furthermore, use of the labelled compound Ta(OAr-2,6Ph$_2$)$_3$(CD$_3$)$_2$ shows conclusively the absence of a methylidene intermediate during the ring closure reaction, with only CD$_3$H being formed.

A single crystal X-ray diffraction study of the mono-methyl compound (**4a**) was undertaken* and an ORTEP view of the molecule is shown in Fig. 1. The metal environment is best described as trigonal bipyramidal with two axial oxygen atoms. The oxygen atom of the metallated 2,6-diphenylphenoxide occupies one of the axial sites with a bite at the metal of the metallacycle of only 80.8(2)°. This small angle is compensated by the characteristically large Ta—O—C angle of 141.4(4)°, resulting in an almost planar six-membered metallacycle ring.

Attempts to thermally induce a second ring closure in these compounds proved difficult. Extended thermolysis at high temperatures (200–275°C) does result in further loss of alkane, but a mixture of products results. However, it was found that reduction of the dichloride Ta(OAr-2,6Ph$_2$)$_3$Cl$_2$ with Na/Hg (2 equiv) in hydrocarbon solvents led to the bis-cyclometallated compound Ta(OC$_6$H$_3$PhC$_6$H$_4$)$_2$(OAr-2,6Ph$_2$) (**5**) in good yields. Analysis of the mixtures obtained by extended thermolysis of (**4**) did show the presence of (**5**) but only as a minor component. The room temperature formation of (**5**) by reduction of the dichloride presumably proceeds via the unisolated Ta(III) compound "Ta(OAr-2,6Ph$_2$)$_3$" which then undergoes intra-molecular oxidative–addition to produce an intermediate hydride compound.† A second cyclometallation with elimination of H_2 would then lead to (**5**).[2] Similarly we find that reduction of the trichloride Ta(OAr-2,6Bu$^t_2$)$_2$Cl$_3$ with sodium amalgam (2Na per Ta) results in the high yield formation of the bis-metallated compound Ta(OC$_6$H$_3$Bu^{t}CMe$_2$CH$_2$)$_2$Cl.[8] Presumably a similar pathway is present for the activation of these alphatic CH bonds as is operative in the reduction of Ta(OAr-2,6Ph$_2$)$_3$Cl$_2$.

Acknowledgements—We thank the National Science Foundation and Department of Energy for financial support of this research. I.P.R. gratefully acknowledges the Camille and Henry Dreyfus Foundation for the award of a Teacher–Scholar Grant and the Alfred P. Sloan Foundation for the award of a Fellowship.

* *Crystal data*: (**4a**), TaC$_{55}$H$_{41}$O$_3$·3/2C$_6$H$_6$, M = 1048.05, space group $P\bar{1}$, $a = 13.497(3)$, $b = 17.033(6)$, $c = 10.744(2)$ Å, $\alpha = 94.76(1)$, $\beta = 906.34(1)$, $\lambda = 79.80(1)°$, $U = 2411.01$ Å^3, $Z = 2$, $D_c = 1.444$ g cm^{-3}, λ(Mo-K_α) = 0.71069 Å. Of the 6354 unique intensities measured, 5659 with $F_o > 3\sigma(F_o)$ yielded $R(F) = 0.0355$, $R_w(F) = 0.0356$. All hydrogen atoms were refined isotropically. Atomic coordinates, bond lengths and angles, and thermal parameters have been deposited at the Cambridge Crystallographic Data Centre.

† The intramolecular oxidative-addition of an aliphatic CH bond to Ta(III) has been observed previously, see ref. 13.

REFERENCES

1. M. E. Thompson and J. E. Bercaw, *Pure Appl. Chem.* 1984, **56**, 1; M. E. Thompson, S. M. Baxter, A. R. Bulls, B. J. Burger, N. C. Nolan, B. D. Santasiero, W. R. Schaefer and J. E. Bercaw, *J. Am. Chem. Soc.* 1987, **109**, 203; A. R. Bulls, W. P. Schaefer, M. Serfas and J. E. Bercaw, *Organometallics* 1987, **6**, 1219.
2. R. P. Planalp and R. A. Andersen, *Organometallics* 1983, **2**, 16 and refs therein.
3. P. L. Watson and G. W. Parshall, *Acc. Chem. Res.* 1985, **18**, 51; P. L. Watson, *J. Am. Chem. Soc.* 1983, **105**, 6491.
4. J. W. Bruno, G. M. Smith, T. J. Marks, C. K. Fair, A. J. Schultz and J. M. Williams, *J. Am. Chem. Soc.* 1986, **108**, 40 and refs therein.

5. I. P. Rothwell, *Polyhedron* 1985, **4**, 177.
6. L. R. Chamberlain, L. D. Durfee, P. E. Fanwick, L. Kobriger, S. L. Latesky, A. K. McMullen, I. P. Rothwell, K. Folting, J. C. Huffman, W. E. Streib and R. Wang, *J. Am. Chem. Soc.* 1987, **109**, 390; L. R. Chamberlain, I. P. Rothwell, K. Folting and J. C. Huffman, *J. Chem. Soc., Dalton Trans.* 1987, 155; T. W. Coffindaffer, I. P. Rothwell, K. Folting and J. C. Huffman, *Organometallics* 1985, **4**, 902.
7. T. W. Coffindaffer, G. Niccolai, D. Powell, I. P. Rothwell and J. C. Huffman, *J. Am. Chem. Soc.* 1985, **107**, 3572; L. D. Durfee, I. P. Rothwell and J. C. Huffman, *Inorg. Chem.* 1985, **24**, 4569; L. D. Durfee, P. E. Fanwick, I. P. Rothwell, K. Folting and J. C. Huffman, *J. Am. Chem. Soc.* 1987, **109**, 4720.
8. L. R. Chamberlain, J. L. Kerschner, A. P. Rothwell, I. P. Rothwell and J. C. Huffman, *J. Am. Chem. Soc.* 1987, **109**, 6471; L. R. Chamberlain, I. P. Rothwell and J. C. Huffman, *J. Am. Chem. Soc.* 1986, **108**, 1502; S. L. Latesky, A. K. McMullen, I. P. Rothwell and J. C. Huffman, *J. Am. Chem. Soc.* 1985, **107**, 5981.
9. P. E. Fanwick, A. E. Ogilvy and I. P. Rothwell, *Organometallics* 1987, **6**, 73; T. W. Coffindaffer, W. M. Westler and I. P. Rothwell, *Inorg. Chem.* 1985, **24**, 4565.
10. J. R. Dilworth, J. Hanich, M. Krestel, J. Beuk and and J. Strahle, *J. Organomet. Chem.* 1986, **315**, C9.
11. J. L. Kerschner, P. E. Fanwick and I. P. Rothwell, *J. Am. Chem. Soc.* 1987, **109**, 5840.
12. R. W. Chesnut, L. D. Durfee, P. E. Fanwick, I. P. Rothwell, K. Folting and J. C. Huffman, *Polyhedron*, 1987, **6**, 2019.
13. R. L. Lapointe and P. T. Wolczanski, *J. Am. Chem. Soc.*, 1986, **108**, 3535.

ANNOUNCEMENT

ANNUAL POLYHEDRON PUBLICATION AWARD

Pergamon Press plc is pleased to announce the award annually of a cash prize of $1000 for the best paper published in *Polyhedron*.

The award will be made to the authors of the original research paper (not including *Polyhedron* Reports) judged to be the best on the basis of scientific originality, significance, clarity and style of presentation. The first award will be made for a paper published in Volume 6, 1987. Members of the Editorial Board will each be invited to nominate two papers for the award and the final selection will be made by an anonymous committee appointed by the Editors who themselves will not be eligible for the award.

The recipient of the first award will be notified later in 1988. The award for this year's volume will be announced in 1989.

Polyhedron Vol. 7, No. 10/11, pp. 759–766, 1988
Printed in Great Britain

0277–5387/88 $3.00+.00
© 1988 Pergamon Press plc

REVERSIBLE REDUCTION OF COORDINATED CARBON MONOXIDE BY PERMETHYLZIRCONOCENE HYDRIDES. SYNTHESIS AND REACTIVITY OF A BRIDGING DIRUTHENIUM ZIRCONOXY CARBENE COMPLEX§

DONALD H. BERRY¶ and JOHN E. BERCAW‖

Division of Chemistry and Chemical Engineering, California Institute of Technology, Pasadena, CA 91125, U.S.A.

(*Accepted* 5 *November* 1987)

Abstract—Reaction of the binuclear ruthenium complex $[CpRu(CO)_2]_2$, **2**, ($Cp = \eta^5$-C_5H_5) with $Cp^*_2ZrH_2$, **1**, ($Cp^* = \eta^5$-$C_5(CH_3)_5$) produces the carbene complex $Cp_2Ru_2(CO)_2(\mu$-$CO)(\mu$-$CHOZr(H)Cp^*_2)$, **3**, in which the zirconoxy carbene occupies a bridging position, and the ruthenium Cp ligands are mutually *trans*. The complex undergoes a fluxional process on the NMR time scale at room temperature whereby the inequivalent pairs of Cp and Cp* ligands are exchanged. A value of $\Delta G^{\ddagger} = 14.0(2)$ kcal mol^{-1} has been determined for this process from the coalescence temperature (−4°C at 90 MHz). The hafnium analogue exhibits a similar value (14.4(2) kcal mol^{-1} at +5°C). The Zr—H addition to the carbonyl is reversible at 25°C, regenerating **2** and the zirconium hydride, which can be trapped with reagents such as CO, CH_3I and CF_3CO_2H. Lewis acids, on the other hand, induce the transfer of a second hydride from zirconium with concurrent C—O cleavage, yielding the bridging methylene complex $Cp_2Ru_2(CO)_3(\mu$-$CH_2)$. A modified procedure for the conversion of $[CpRu(CO)_2]_2$ to $Cp_2Ru_2(CO)_3(CH_2)$ with $LiHBEt_3$ in non-polar solvents is also reported.

The reduction of carbon monoxide to alkoxide or enolate ligands by permethylzirconocene dihydride represents one of the early examples of homogeneous reduction of CO by a transition metal hydride complex.[1] A key finding from subsequent studies is that $Cp^*_2ZrH_2$ **1** ($Cp^* = \eta^5$-$C_5(CH_3)_5$) will transfer a hydride to terminal carbonyl ligands to produce "zirconoxy" carbene complexes [eq. (1)]. Zirconoxy carbenes have been observed in the reaction of zirconium hydride complexes with $Cp_2M(CO)$ (M = Cr, Mo, W),[2] $Cp_2NbR(CO)$ (R = H, alkyl, phenyl),[2,3] $Cp_2Zr(PMe_3)(CO)$[4] and $CpM(CO)_2$ (M = Co, Rh).[5]

$$L_nM{-}CO + Cp^*_2ZrH_2 \rightarrow L_nM{=}CHOZr(H)Cp^*_2. \quad (1)$$

We now report the reduction by **1** of coordinated carbon monoxide in a binuclear ruthenium complex, $[CpRu(CO)_2]_2$, **2**. The resulting complex, $Cp_2Ru_2(CO)_2(\mu$-$CO)(\mu$-$CHOZr(H)Cp^*_2)$, **3**, contains a zirconoxy carbene moiety which bridges the two metals. As found for many diruthenium complexes, **3** exhibits fluxional behaviour in solution. The reaction chemistry of **3**, however, differs significantly from most of the previously reported carbene complexes, in that the parent ruthenium carbonyl complex can be relatively easily regenerated by the reversible transfer of hydride back to zirconium. In addition, Lewis acids further activate the C—O bond of the carbene ligand, inducing C—O cleavage and transfer of a second zirconium hydride to produce the bridging methylene complex.

RESULTS AND DISCUSSION

1. *Formation and structure of a bridging zirconoxy carbene complex*

$Cp^*_2ZrH_2$, **1**, reacts with $[CpRu(CO)_2]_2$, **2**, rapidly at 25°C in hydrocarbon solvents to

§ Contribution No. 7626.

¶ Present address: Department of Chemistry, University of Pennsylvania, Philadelphia, PA 19104, U.S.A.

‖ Author to whom correspondence should be addressed.

yield $Cp_2Ru_2(CO)_2(\mu\text{-}CO)(\mu\text{-}CHOZr(H)Cp^*_2)$, **3**, in which a carbon monoxide ligand has been reduced to a zirconoxy carbene by addition of zirconium hydride across the C—O bond.

$$\underset{\mathbf{1}}{Cp^*_2ZrH_2} + \underset{\mathbf{2}}{[CpRu(CO)_2]_2} \rightarrow \underset{\mathbf{3}}{Cp_2Ru_2(CO)_3(CHOZr(H)Cp^*_2)} \quad (2)$$

At $-70°C$, the ^1H NMR spectrum for **3** exhibits resonances for the carbene (δ 12.67) and zirconium hydride (δ 5.90), and two resonances each for inequivalent Cp and Cp* ligands. These signals coalesce into single Cp and Cp* resonances at higher temperatures (*vida infra*). Assignment of the zirconoxy carbene to a bridging position is determined by the ^{13}C NMR spectrum ($-70°C$), in which resonances due to a single bridging (δ 248) and two terminal (δ 201 and 203) carbonyls are found. A doublet at δ 192 is assigned to the carbene carbon ($^1J_{C-H} = 153$ Hz). Interestingly, this coupling constant is somewhat larger than the 136 Hz reported for a terminal niobium zirconoxy carbene,[2] despite the formal sp^3 hybridization of the bridging carbene. The IR spectrum for **3** (Nujol mull) shows strong bands at 1929 and 1771 cm^{-1} attributed to terminal and bridging carbonyl stretching modes. The C—O stretch of the zirconoxy carbene is found as a strong band at 1108 cm^{-1}.

It is not possible to unequivocally assign the stereochemistry of the Cp rings on the diruthenium fragment solely on the basis of the NMR data. The Cp rings in a *trans* arrangement would clearly be inequivalent, leading to diastereotopic Cp* rings in agreement with the observed ^1H and ^{13}C spectra. In the *cis* arrangement, the Cp and Cp* rings should be equivalent, provided there is free rotation at the Zr—O—C linkage. Considering the steric bulk of permethylzirconocene and the diruthenium moieties, however, hindered rotation is a distinct possibility. The IR spectrum is more definitive in assessing the stereochemistry of **3**. The observation of a single band for the two terminal carbonyl stretching modes is most consistent with a *trans*, planar OC—Ru—Ru—CO structure (local C_{2h} symmetry), whereas two bands are expected for the *cis* isomer.[6] Thus **3** can be assigned as *trans*-$Cp_2Ru_2(CO)_2(\mu\text{-}CO)(\mu\text{-}CHOZr(H)Cp^*_2)$ (see Fig. 1).

Addition of a second equivalent of **1** to **3** yields $Cp_2Ru_2(CO)_2(\mu\text{-}CHOZ(H)Cp^*_2)_2$, **4**. NMR analysis of **4** is limited by the insolubility of this compound, but bands are found at 1913 and 1058 cm^{-1} in the IR, consistent with a *trans* structure containing two bridging carbenes and two terminal carbonyls. Other than elemental analysis, no further characterization of **4** has been attempted. As a result of this interfering reaction, preparation of **3** is best carried out by the slow addition of **1** to a solution of **2**. Alternatively, clean samples of **3** can be obtained by reaction of dihydrogen with $Cp^*_2Zr(O_2C_2)Ru_2Cp_2(CO)_2$, a complex in which the terminal carbonyls are reductively coupled.[7] As shown previously, this compound is in equilibrium with a small concentration of **2** and permethylzirconocene. The latter adds dihydrogen to form **1**, which rapidly reacts with **2** to produce **3**. In this manner **3** is cleanly formed without an excess of **1** present.

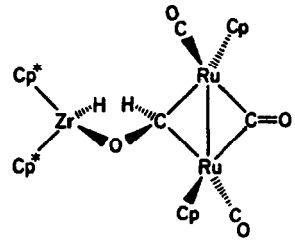

Fig. 1. *trans*-$Cp_2Ru_2(CO)_2(\mu\text{-}CO)(\mu\text{-}CHOZr(H)Cp^*_2)$.

2. *Reversibility of the hydride transfer*

An intriguing aspect underlying most of the reaction chemistry of **3** is the apparent reversibility of the carbonyl reduction. For example, **3** reacts under 4 atm of carbon monoxide at 25°C in 14 h to yield $Cp^*_2Zr(CO)_2$, $[CpRu(CO)_2]_2$ and presumably H_2.

$$Cp_2Ru_2(CO)_2(\mu\text{-}CO)(\mu\text{-}CHOZr(H)Cp^*_2) \xrightarrow{CO} Cp^*_2Zr(CO)_2 + [CpRu(CO)_2]_2. \quad (3)$$

It has been previously shown that dilute solutions of **1** react with carbon monoxide to eliminate H_2 and form the dicarbonyl complex.[8]

Treatment of a solution of **3** with D_2 at 25°C results in the disappearance of the ^1H NMR resonances for the hydride and carbene hydrogens with a half-life of *ca* 3 h.

$$Cp_2Ru_2(CO)_2(\mu\text{-}CO)(\mu\text{-}CHOZr(H)Cp^*_2) \xrightarrow{D_2} Cp_2Ru_2(CO)_2(\mu\text{-}CO)(\mu\text{-}CDOZr(D)Cp^*_2). \quad (4)$$

Although exchange of zirconium hydrides with D_2 is facile,[9] there is no precedent for direct H–D exchange between deuterium and a carbene C—H bond. Equilibrium conversion of **3** back to **1** and **2** is the most logical explanation for the deuteration and carbonylation reactions.

Treatment of **3** with CH_3I results in rapid formation of methane and the iodide analogue of **3**, which then reacts further with CH_3I to produce $Cp^*_2ZrI_2$ and **2** over a period of several days.

$$Cp_2Ru_2(CO)_3(CHOZr(H)Cp^*_2) \xrightarrow[-CH_4]{CH_3I} Cp_2Ru_2(CO)_3(CHOZr(I)Cp^*_2)$$

$$\xrightarrow[-CH_4]{CH_3I} Cp^*_2ZrI_2 + [CpRu(CO)_2]_2. \quad (5)$$

Protonation of **3** with CF_3CO_2H results in formation of $Cp^*_2Zr(O_2CCF_3)_2$, H_2 and **2** via $Cp_2Ru_2(CO)_3(CHOZr(O_2CCF_3)Cp^*_2)$. This intermediate is observed by ^1H NMR, although the subsequent reaction is complete within 15 min. These reactions are likely to proceed through the formation of Cp^*_2ZrHX (X = I, CF_3CO_2), generated by a hydrogen shift from the carbene to zirconium.

The initial product of protonation of **3** with HX has been isolated for X = OH. Compound **3** reacts with H_2O in benzene to yield H_2 and the hydroxy complex $Cp_2Ru_2(CO)_2(\mu\text{-}CO)(\mu CHOZr(OH)Cp^*_2)$, **5**, isolated in 70% yield.

$$Cp_2Ru_2(CO)_3(CHOZr(H)Cp^*_2) \xrightarrow[-H_2]{H_2O} Cp_2Ru_2(CO)_3(CHOZr(OH)Cp^*_2). \quad (6)$$

The ^1H NMR spectrum of **5** at 25°C shows resonances at δ 12.64 and 4.35 attributable to carbene and hydroxide hydrogens, as well as singlets for Cp and Cp* ligands. The O—H stretch is observed at 3675 cm^{-1}.

Reversion of the oxycarbene back to the respective carbonyl and hydride complexes under mild conditions is surprising in light of the strong bonds formed between Zr(IV) and oxygen ligands. Reversible hydride transfer is, however, also indicated for the terminal zirconoxy carbene complex, $Cp_2Nb(H)=CHOZr(H)Cp^*_2$, presumably due to unfavourable interactions between Cp and Cp* ligands, and for $Cp_2Mo=CHOZr(H)Cp^*_2$, under more forcing conditions.[2] The facile cleavage of the Zr—O bond in zirconoxy carbenes in all three cases is likely due in part to unfavourable steric interactions between permethylzirconocene and the second metal fragment.

3. *Fluxional behaviour of* $Cp_2Ru_2(CO)_2(\mu\text{-}CO)(\mu\text{-}CHOZr(H)Cp^*_2)$

Although inequivalent pairs of Cp and Cp* rings are observed in the low temperature ^1H and ^{13}C NMR spectra of **3**, these resonances collapse into singlets at higher temperatures as a result of a dynamic process which averages the ligand environments. A free energy of activation of 14.0(2) kcal mol^{-1} is calculated for this process from the coalescence temperature (−4°C at 90 MHz). The dynamic behaviour exhibited by **3** is not surprising in light of similar observations for bridging alkylidenes of iron,[10] ruthenium[11] and cobalt.[12] In a logical extension of studies on the parent carbonyl dimers,[13–15] Knox has explained the *cis* ⇄ *trans* isomerization of $Cp_2Ru_2(CO)_2(\mu\text{-}CO)(\mu\text{-}CMe_2)$ in terms of simultaneous opening of the bridging carbene and carbonyl to terminal ligands, followed by rotation about the Ru—Ru bond.[11] Such a mechanism is applicable to **3**, although a small distinction must be made. The dynamic process under consideration for **3** is the equilibration of the inequivalent Cp rings of the *trans* isomer, in which two bridge-openings and rotations are required (Scheme 1).

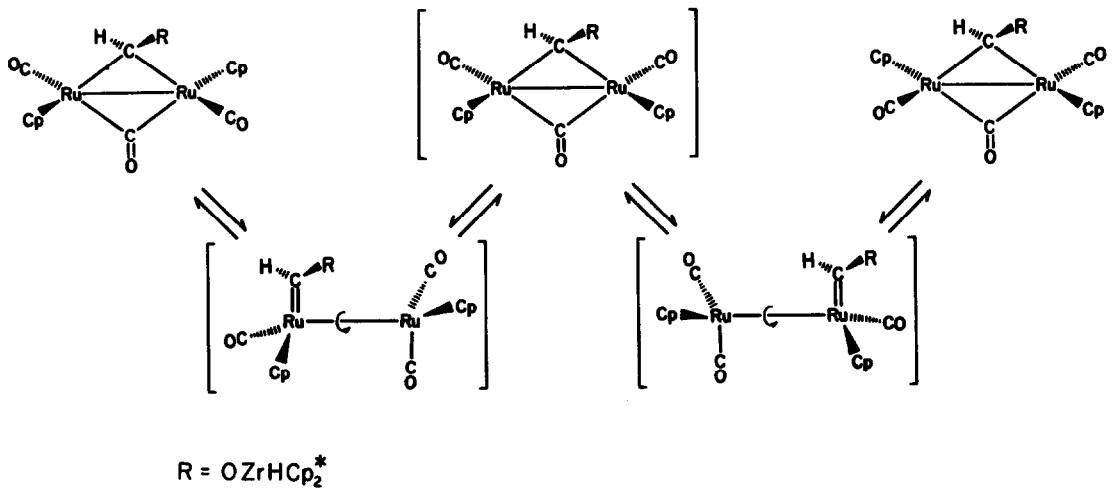

Scheme 1.

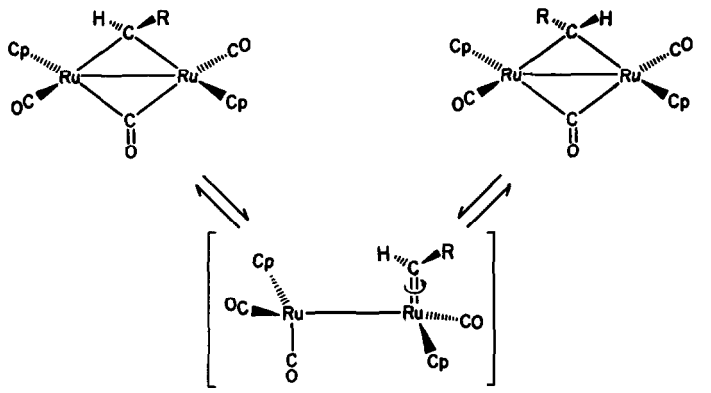

Scheme 2.

Alternatively, rotation about the M=C bond of the terminal carbene in the intermediate followed by closure, results in Cp equilibration with only a single bridge-opening step (Scheme 2). Carbene rotation in a related terminal carbene complex appears to be facile: Fischer and co-workers have reported that rotation of the isopropylidene ligand in $CpMn(CO)_2(=CMe_2)$ is rapid on the ^1H NMR time-scale at $-55°C$.[16,17] Rapid alkylidene rotation is also in agreement with theoretical studies published by Kostic and Fenske in which the rotational barrier in $CpMn(CO)_2(=CMe_2)$ was calculated to be *ca* 9 kcal mol^{-1}.[18]

It is not possible to distinguish between the two possibilities described above on the basis of the activation barrier for **3**. The 14.0 kcal mol^{-1} barrier does not differ sufficiently from those reported for *cis* ⇄ *trans* isomerization of $Cp_2Co(CO)_2(\mu\text{-}CH_2)$ (*ca* 17 kcal mol^{-1})[12] and $Cp_2Ru_2(CO)_2(\mu\text{-}CO)(\mu\text{-}CMe_2)$ (*ca* 20 kcal mol^{-1}),[11] given the range of metals and carbene substituents. Furthermore, there is another mechanism for Cp equilibration in **3** which is not accessible for most bridging alkylidene complexes. As described above, the addition of the zirconium hydride to the carbonyl is reversible. Thus, a hydride shift from carbene back to zirconium may produce a symmetrical intermediate as shown in Scheme 3. Transfer of the other hydride to the carbonyl would yield the carbene in which the environments of the Cp rings have been interchanged. Alternatively, uncomplexed **1** and **2** may be produced, which then recombine to give **3** with randomization of the rings. Although the reactivity of **3** (*vida supra*) indicates that the process in Scheme

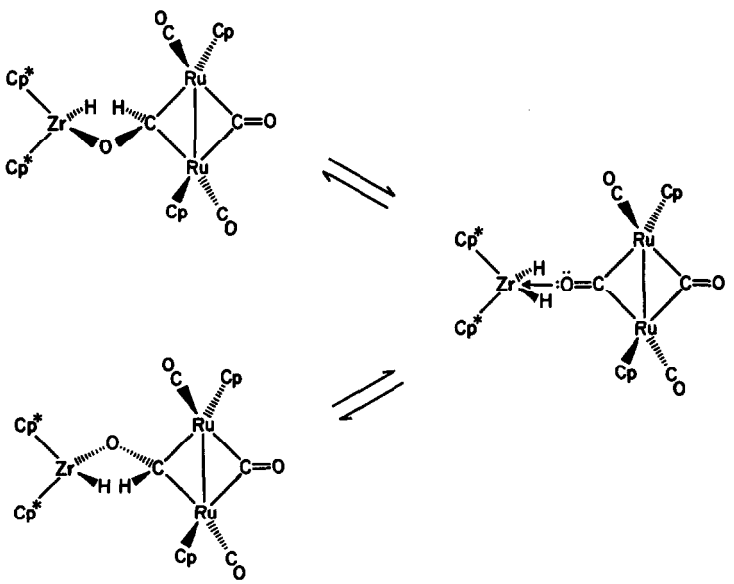

Scheme 3.

3 is indeed occurring, it is unlikely that it is the dominant mechanism for the dynamic behaviour of **3**. In the fast exchange limit the ^{13}C resonance for the carbene carbon is found as a doublet at δ 197 with $J_{C-H} = 154$ Hz, as compared with 153 Hz in the slow exchange limit. Rapid, reversible cleavage of the C—H bond during ring equilibration would be expected to result in a reduction or total loss of the observed C—H coupling in the spectrum for fast exchange. Moreover, at −4°C the rate for Cp ring equilibration as determined from coalescence is 26 s^{-1}, yet magnetization transfer between the carbene proton and the zirconium hydride positions is not observed at 28°C, setting an upper limit of *ca* 1 s^{-1} for the slow step of the mechanism shown in Scheme 3. Finally, the hafnium analogue of **3** has been prepared from $Cp_2^*HfH_2$ and **2**. Hydride transfer reactions are generally slower for hafnium as compared with zirconium analogues. The barrier to ring equilibration in the "hafnoxy" complex at coalescence (+5°C), however, is 14.4(2) kcal mol^{-1}, virtually the same as in **3**. The hydrogen shift mechanism, therefore, does not appear to be the primary fluxional process.

4. *Reaction of* $Cp_2Ru_2(CO)_3(CHOZr(H)Cp_2^*)$, **3**, *with Lewis acids*

Although reaction of CF_3CO_2H or H_2O with **3** results in protonation of the hydride position with formation of dihydrogen and substitution at zirconium, stronger acids react with **3** in a different manner. Compound **3** reacts with $HBF_4 \cdot Me_2O$ in benzene at 25°C to rapidly yield the known[19] bridging μ-methylene complex $Cp_2Ru_2(CO)_3(\mu\text{-}CH_2)$, **6** (mixture of *cis* and *trans* isomers, 54% by ^1H NMR). The fate of the zirconium fragment has not been determined.

$$Cp_2Ru_2(CO)_3(CHOZr(H)Cp_2^*) + HBF_4 \cdot Me_2O \rightarrow Cp_2Ru_2(CO)_3(\mu\text{-}CH_2). \quad (7)$$

Cleavage of oxygen-substituted bridging carbenes by Lewis acids has precedent in the reaction of the $Cp_2Fe_2(CO)_2(\mu\text{-}CO)(\mu\text{-}CHOCH_3)$ with electrophiles, in which the methoxy group is cleaved to yield $[Cp_2Fe_2(CO)_2(\mu\text{-}CO)(\mu\text{-}CH)]^+$ [eq. (8)]. Both Casey and Pettit have shown that this bridging methylidyne reacts with hydride sources to produce $Cp_2Fe_2(CO)_3(CH_2)$ [eq. (9)].[10]

$$Cp_2Fe_2(CO)_3(CHOCH_3) \xrightarrow{Ph_3C^+ \text{ or } H^+} [Cp_2Fe_2(CO)_3(CH)]^+ \quad (8)$$

$$[Cp_2Fe_2(CO)_3(CH)]^+ \xrightarrow{H^-} Cp_2Fe_2(CO)_3(CH_2). \quad (9)$$

The presence of an internal hydride source in **3** suggests a similar reaction sequence for the conversion of **3** to **6**.

The origin of the second methylene proton is demonstrated by the reaction of d_2-**3** with HBF_4, in which d_2-**6** is produced [eq. (10)].§ Thus both methylene protons are derived from zirconium hydrides, while protonation by HBF_4 facilitates the C—O cleavage. Consistent with this view, **6** (70% by ^1H NMR) is also formed in the reaction of **3** with BF_3, which functions solely as a Lewis acid.

$$Cp_2Ru_2(CO)_3(CDOZr(D)Cp_2^*) \xrightarrow{HBF_4 \cdot Me_2O} Cp_2Ru_2(CO)_3(CD_2). \quad (10)$$

5. *Reduction of* $[CpRu(CO)_2]_2$ *with* $LiHBEt_3$

The stepwise reduction of **2** to **6** by hydride transfer from **1**, treatment with Lewis acid, followed by a second hydride transfer suggested to us that **6** might be accessible from **2** with other hydride sources. Indeed, the borohydride reduction of coordinated carbon monoxide to formyl, hydroxymethyl, methyl and bridging methylene ligands is well established.[20–24] In particular, Geoffroy and Steinmetz have studied the reduction of $Os_3(CO)_{12}$ with $K[BH(O\text{-}i\text{-}Pr)_3]$ in THF. The reaction proceeds with initial formation of the formyl complex, $[Os_3(CO)_{11}(CHO)]^-$, which requires treatment with H_3PO_4 before conversion to $Os_3(CO)_{11}(CH_2)$ occurs.[20] The key step is the activation of the formyl C—O bond by protonation at oxygen.

In the present studies, we have examined the reaction of $[CpRu(CO)_2]_2$ with $LiBEt_3H$ ("Superhydride"). Treatment of a toluene solution of **2** with excess $LiBEt_3H$ results in conversion to **6** in moderate yield (57%).

$$[CpRu(CO)_2]_2 \xrightarrow[\text{toluene}]{LiBEt_3H} Cp_2Ru_2(CO)_3(CH_2). \quad (11)$$

This one-step synthesis of **6** from **2** is a substantial improvement over the previous preparation.[19]

In contrast to the reduction of $Os_3(CO)_{12}$, additional acid need not be introduced to effect the C—O cleavage and transfer of the second hydride. The clean reduction of **2** to **6** is, however, very dependent upon the choice of solvent and reducing agent. Compound **6** is only produced in hydrocarbon solvents such as toluene or benzene; reduction in tetrahydrofuran leads to extensive decomposition and no **6**. Similarly, reduction with excess $NaAl(OCH_2CH_2OCH_3)_3H$ ("Red-Al") in

§ Although d_2-**6** is initially produced, subsequent proton exchange occurs between d_2-**6** and excess HBF_4.

toluene solution does not yield the methylene complex.

Consistent with previous studies, these results suggest that a relatively strong Lewis acid is required to ensure C—O cleavage during reduction. Thus reduction to the methylene complex is not observed in THF where the lithium counter-ion is well solvated and hence is a poorer Lewis acid. In addition, the effectiveness of $LiBEt_3H$ *vis-a-vis* $NaAl(OCH_2CH_2OCH_3)_3H$ in preparing **6** may well be due to the greater acidity of Li^+.

Gladysz has reported that $LiBEt_3H$ is a convenient reagent for reducing THF solutions of binuclear metal carbonyl compounds to the corresponding anions, via the formyls.[21] It is interesting to note that clean reduction of $[CpFe(CO)_2]_2$ to $Li[CpFe(CO)_2]$ requires a more polar solvent system (50% THF/HMPA) than used for most dimers. Presumably carbonyl reduction is competitive with cleavage of the metal–metal bond in this instance. Unfortunately, our attempts to reduce $[CpFe(CO)_2]_2$ to $Cp_2Fe_2(CO)_3(CH_2)$ with $LiBEt_3H$ in non-polar solvents were not successful.

EXPERIMENTAL

General considerations

All manipulations were performed using either glove-box or high vacuum line techniques.[25] Hydrocarbon solvents were purified by vacuum transfer first from $LiAlH_4$ and then from "titanocene".[26] NMR solvents, toluene-d_8 and benzene-d_6 were also purified by transfer from "titanocene". Dihydrogen was passed through MnO on vermiculite and then over 4 Å molecular sieves.[27] Carbon monoxide (MCB) was used directly from the cylinder. $Cp_2^*ZrH_2$,[28] $Cp_2^*HfH_2$,[29] $[CpRu(CO)_2]_2$[30,31] and $Cp_2^*Zr(O_2C_2)Ru_2(CO)_2Cp$[7] were synthesized as described previously. Infrared spectra were measured on a Beckman 4240 spectrophotometer. NMR spectra were obtained using Varian EM-390 and JEOL FX-90Q spectrometers (90 MHz ^1H, 22.6 MHz ^{13}C). ^{13}C NMR experiments were generally prepared with ^{13}CO enriched $[CpRu(CO)_2]_2$[14] and *ca* 0.1 M $Cr(acac)_3$[32] added to facilitate observation of the carbonyl carbons. Coupling constants were measured either from gated coupled spectra or spectra obtained using the INEPT pulse sequence. The magnetization transfer experiments were run as described elsewhere.[33] Elemental analyses were performed by Bernhardt Microanalytical Laboratory, Dornis and Kolbe Microanalytical Laboratory or by Larry Henling at the CIT analytical service.

$Cp_2Ru_2(CO)_3(CHOZr(H)Cp_2^*)$, 3

(a) *From* **1** *and* **2**. A solution of **1** (330 mg, 0.909 mmol) and **2** (300 mg, 0.676 mmol) in 30 cm^3 toluene was stirred for 30 min at −80°C, warmed to 25°C and stirred for an additional 1 h. After filtration the solvent volume was reduced to 5 cm^3 and 5 cm^3 petroleum ether was added. Stirring for 30 min produced a bright yellow slurry, which upon filtration yielded 393 mg (73%) of yellow solid. ^1H NMR (toluene-d_8, 25°C): δ 12.75 (s, 1H, ZrOC*H*), 6.10 (s, 1H, Zr—*H*), 5.04 (s, 10H, (η^5-C_5H_5)), 2.01 (s, 30H, (η^5-C_5Me_5)); (toluene-d_8, −70°C): δ 12.67 (s, 1H, ZrOC*H*), 5.94 (s, 1H, Zr—*H*), 4.98 (s, 5H, (η^5-C_5H_5)), 4.85 (s, 5H, (η^5-C_5H_5)), 2.04 (s, 15H, (η^5-C_5Me_5)), 1.95 (s, 15H, (η^5-C_5Me_5)). $^{13}C\{^1H\}$ NMR (toluene-d_8, −70°C): δ 248 (μ-CO), 203, 201 (Ru—CO), 192 (CHOZr, J_{CH} = 153 Hz), 118, 117 (η^5-$C_5(CH_3)_5$), 95, 92 (η^5-C_5H_5), 12 (η^5-$C_5(CH_3)_5$). IR ν(CO) (Nujol mull): 1929(s), 1771(s), 1108(s) cm^{-1}. Anal. Found: C, 51.21; H, 5.40; Ru, 24.39; Zr, 10.93. Calc. for $C_{34}H_{42}O_4Ru_2Zr$: C, 50.54; H, 5.24; Ru, 25.02; Zr, 11.28%.

(b) *From* $Cp_2^*Zr(O_2C_2)Cp_2Ru_2(CO)_2$ *and* H_2. A slurry of $Cp_2^*Zr(O_2C_2)Cp_2Ru_2(CO)_2 \cdot 0.5C_7H_8$ (500 mg, 0.587 mmol) and 20 cm^3 petroleum ether was stirred under 1 atm H_2 for 14 h at 25°C. Filtration yielded 393 mg (83%) of yellow solid. Compound **3**-d_2 was prepared by method (b) using D_2. $Cp_2Ru_2(CO)_3(CHOHf(H)Cp_2^*)$ was prepared by method (a) using $Cp_2^*HfH_2$. Anal. Found: C, 45.85; H, 4.75. Calc. for $C_{34}H_{42}HfO_4Ru_2$: C, 45.61; H, 4.73%.

Reaction of **3** *under* CO

Compound **3** (10 mg, 0.012 mmol) and benzene-d_6 (0.3 cm^3) were added to an NMR tube, CO (0.33 mmol) was introduced at −196°C§ and the tube sealed. After 14 h at 25°C the ^1H NMR spectrum showed complete conversion to **2** and $Cp_2^*Zr(CO)_2$.

Reaction of **3** *with* CH_3I

Compound **3** (15 mg, 0.019 mmol) and benzene-d_6 (0.3 cm^3) were added to an NMR tube into which there was distilled CH_3I (0.036 mmol) at −196°C. The tube was sealed and the course of the reaction monitored by ^1H NMR spectroscopy. After 20 min at 25°C conversion of **3** to a new compound with resonances at δ 5.12 (s, 10H, (η^5-C_5H_5)), 2.00 (s, 30H, (η^5-C_5Me_5)) and 12.80 (s, 1H, C*H*) was *ca* 70% complete. A small quantity of **2** was also

§ Extreme care should be taken to assure liquid CO does not accumulate in the tube during this operation.

observed. After 15 h no **3** remained, and conversion to **2** was about 60% complete. $Cp^*_2ZrI_2$ and CH_4 were also observed.

Reaction of **3** *with* CF_3CO_2H

Compound **3** (17 mg, 0.020 mmol) and benzene-d_6 (0.3 cm^3) were added to an NMR tube and sealed with a latex septum. CF_3CO_2H (1 μl, 0.013 mmol) was injected via a syringe. A ^1H NMR spectrum measured after *ca* 30 s showed **2**, **3** and a new product [δ 5.10 (s, (η^5-C_5H_5)), 2.78 (s, (η^5-C_5Me_5))] in ratio of *ca* 2:6:3. After addition of a second 1 μl aliquot of CF_3CO_2H, the ratio was 6:2:5. A third aliquot was added, and after 15 min only **2** and $Cp^*_2Zr(O_2CCF_2)_2$ were observed.

Reaction of **3** *with* $BF_3 \cdot Me_2O$

Compound **3** (15 mg, 0.019 mmol) and benzene-d_6 were added to an NMR tube and sealed with a latex septum. $BF_3 \cdot Me_2O$ (2 μl, 0.011 mmol) was injected via a syringe. The brown solid formed was centrifuged to the top of the tube. A ^1H NMR spectrum showed signals for a mixture of *cis* and *trans* $Cp_2Ru_2(CO)_3(CH_2)$ (70% conversion based on integrated intensities relative to internal TMS).

Reaction of **3** *with* $HBF_4 \cdot Et_2O$

Treatment of **3** (15 mg, 0.019 mmol) with $HBF_4 \cdot Et_2O$ (4 μl, 0.030 mmol) as above, resulted in 54% conversion to $Cp_2Ru_2(CO)_3(CH_2)$. As in the reaction with $BF_3 \cdot Me_2O$, the only [CpRu] containing species remaining in solution besides $Cp_2Ru_2(CO)_3(CH_2)$ was a small amount of **2**.

$Cp_2Ru_2(CO)_2(CHOZr(H)Cp^*_2)_2$, **4**

A solution of **3** (111 mg, 0.14 mmol) and **1** (55 mg, 0.15 mmol) in 10 cm^3 toluene was stirred for 2 h at 25°C. The slurry was filtered and dried to yield 134 mg (82%) of the yellow solid. IR (Nujol mull) ν(CO): 1913(s), 1058(s) cm^{-1}. Anal. Found: C, 55.71; H, 6.31. Calc. for $C_{54}H_{74}O_4Ru_2Zr_2$: C, 55.35; H, 6.37%.

$Cp_2Ru_2(CO)_3(CHOZr(OH)Cp^*_2)$, **5**

Into a solution of **3** (142 mg, 0.176 mmol) in benzene (25 cm^3) was injected H_2O (3.5 μl, 0.194 mmol) at 25°C. The yellow solution was stirred for 4 h, filtered and then the solvent volume reduced to 5 cm^3. Petroleum ether (10 cm^3) was added and the slurry was stirred an additional 45 min followed by filtration to yield 100 mg (70%) of yellow solid. ^1H NMR (toluene-d_8, 25°C): δ 12.65 (s, 1H, ZrOC*H*), 5.15 (s, 10H, (η^5-C_5H_5)), 4.25 (s, 1H, Zr—O*H*), 1.86 (s, 30H, (η^5-C_5Me_5)). IR (Nujol mull) ν(CO): 1925(s), 1770(s), 1100(s,br) cm^{-1}; ν(OH): 3675(w) cm^{-1}. Anal. Found: C, 49.43; H, 5.15. Calc. for $C_{34}H_{42}O_5Ru_2Zr$: C, 49.55; H, 5.14%.

Synthesis of $Cp_2Ru_2(CO)_3(CH_2)$, **6**, *from* **2**

$LiBEt_3H$ (2.5 cm^3, 1 M in THF) was added to a solution of **2** (505 mg, 1.14 mmol) in 30 cm^3 toluene, and the reaction mixture was stirred for 2 h at 25°C. Solvent was removed to yield a dark oil which contained **2** and **6** in a 1:2 ratio (^1H NMR). The oil was dissolved in 30 cm^3 of toluene and an additional 1 cm^3 $LiBEt_3H$ added. After 2h at 25°C the reaction mixture was opened to the air and poured into 50 cm^3 H_2O. The organic phase was separated and washed twice with H_2O, dried over $MgSO_4$ and column chromatographed (SiO_2/C_6H_6). The single yellow band was collected and the solvent was flash evaporated. Recrystallization from toluene/petroleum ether yielded yellow crystals of **6** (280 mg, 57%).

Acknowledgements—This work was supported by the National Science Foundation (Grant No. CHE-83-03735). Use of the Southern California Regional NMR Facility (Grant No. CHE-79-16324A1) is gratefully acknowledged. D.H.B. also thanks the National Science Foundation for a pre-doctoral fellowship (1979–1982).

REFERENCES

1. P. T. Wolczanski and J. E. Bercaw, *Accts. Chem. Res.* 1980, **13**, 121.
2. P. T. Wolczanski, R. S. Threlkel and J. E. Bercaw, *J. Am. Chem. Soc.* 1979, **101**, 218.
3. R. S. Threlkel and J. E. Bercaw, *J. Am. Chem. Soc.* 1981, **103**, 2650.
4. P. T. Barger, B. D. Santarsiero, J. Armantrout and J. E. Bercaw, *J. Am. Chem. Soc.* 1984, **106**, 5178.
5. P. T. Barger and J. E. Bercaw, *Organometallics* 1984, **3**, 278.
6. A. F. Dyke, S. A. R. Knox, M. J. Morris and P. J. Naish, *J. Chem. Soc., Dalton Trans.* 1983, 1417.
7. (a) D. H. Berry, J. E. Bercaw, A. J. Jircitano and K. B. Mertes, *J. Am. Chem.* 1982, **104**, 4712; (b) D. H. Berry, Ph.D. Thesis, California Institute of Technology (1984).
8. J. A. Marsella, C. J. Curtis, J. E. Bercaw and K. G. Caulton, *J. Am. Chem. Soc.* 1980, **102**, 7244.
9. J. E. Bercaw, *Adv. Chem. Ser.* 1978, **167**, 136.
10. (a) C. P. Casey, P. J. Fagan and W. H. Miles, *J. Am. Chem. Soc.* 1982, **104**, 1134; (b) S. C. Rao, P. P. Y. Lu and R. Pettit, *Organometallics* 1982, **1**, 911.
11. A. F. Dyke, S. A. R. Knox, R. A. Mead and P. Woodward, *J. Chem. Soc., Chem. Commun.* 1982, 861.
12. K. H. Theopold and R. G. Bergman, *J. Am. Chem. Soc.* 1983, **105**, 464.

13. R. D. Adams and F. A. Cotton, in *Dynamic Nuclear Magnetic Resonance Spectroscopy*, Chap. 12 and refs therein. Academic Press, New York (1975).
14. J. D. Roberts, E. Rosenberg and D. C. Harris, *J. Chem. Soc., Dalton Trans.* 1974, 2398.
15. O. A. Gansow, A. R. Burke and W. D. Vernon, *J. Am. Chem. Soc.* 1976, **98**, 5817.
16. E. O. Fischer, R. L. Clough, G. Bessl and F. R. Kreissl, *Angew. Chem. Int. Ed., Engl.* 1976, **15**, 543.
17. P. Friedrich, G. Besl, E. O. Fischer and G. Huttner, *J. Organomet. Chem.* 1977, **139**, C68.
18. N. M. Kostic and R. F. Fenske, *J. Am. Chem. Soc.* 1982, **104**, 3879.
19. (a) D. L. Davies, A. F. Dyke, S. A. R. Knox and M. J. J. Morris, *J. Organomet. Chem.* 1981, **215**, C30; (b) D. L. Davies, S. A. R. Knox, K. A. Mead, M. J. Morris and P. J. Woodward, *J. Chem. Soc., Dalton Trans.* 1984, 2293.
20. (a) G. R. Steinmetz and G. L. Geoffroy, *J. Am. Chem. Soc.* 1981, **103**, 1278; (b) G. R. Steinmetz, E. O. Morrison and G. L. Geoffroy, *J. Am. Chem. Soc.* 1984, **106**, 2559.
21. J. A. Gladysz, G. M. Williams, W. Tam and D. L. Johnson, *J. Organomet. Chem.* 1972, **140**, C1.
22. W. A. G. Grahmn and J. R. Sweet, *J. Am. Chem. Soc.* 1982, **104**, 2811.
23. C. P. Casey, M. A. Andrews and D. R. McAlister, *J. Am. Chem. Soc.* 1980, **102**, 1927.
24. D. Astruc and C. Lapinty, *J. Chem. Soc., Chem. Commun.* 1983, 430.
25. B. J. Burger and J. E. Bercaw, in *New Developments in the Synthesis, Manipulation and Characterization of Organometallic Compounds*, (Edited by A. Wayda and M. Darensbourg), ACS Symposium Series, 1987, **357**, 79.
26. R. H. Marvich and H. H. Brintzinger, *J. Am. Chem. Soc.* 1971, **94**, 2046.
27. T. L. Brown, D. W. Dickerhoof, D. A. Bafus and G. L. Morgan, *Rev. Sci. Instrum.* 1962, **33**, 491.
28. J. M. Manriquez, D. R. McAlister, R. D. Sanner and J. E. Bercaw, *J. Am. Chem. Soc.* 1978, **100**, 2716.
29. D. M. Roddick, M. D. Frysuk, P. F. Seidler, G. L. Hillhouse and J. E. Bercaw, *Organometallics* 1985, **4**, 97.
30. A. P. Humphries and S. A. R. Knox, *J. Chem. Soc., Dalton Trans.* 1975, 1710.
31. D. H. Gibson, W. Hsu and A. L. Steinmetz, *J. Organomet. Chem.* 1981, **208**, 89.
32. O. A. Gansow, A. R. Burke and W. D. Vernon, *J. Am. Chem. Soc.* 1972, **94**, 2550.
33. T. Perkins, Ph.D. Thesis, California Institute of Technology (1981).

Polyhedron Vol. 7, No. 10/11, pp. 767–773, 1988
Printed in Great Britain

0277-5387/88 $3.00+.00
© 1988 Pergamon Press plc

μ-METHYLENE COMPLEXES WITHOUT METAL–METAL BONDS

R. J. PUDDEPHATT

Department of Chemistry, University of Western Ontario, London, Canada N6A 5B7

(*Accepted* 5 *November* 1987)

Abstract—A review is given of the chemistry of μ-methylene complexes of the transition elements in which there is no metal–metal bonding. The emphasis is on the synthetic routes, the structural and spectroscopic properties and the chemical reactivity of these complexes, particularly when compared to μ-methylene complexes with metal–metal bonds.

The synthesis and study of μ-methylene complexes have been subjects of great interest, especially with respect to the role of these compounds in catalytic reactions such as the Fischer–Tropsch synthesis.[1–7] This chemistry has been reviewed either alone or as part of wider reviews on μ-hydrocarbyl complexes.[1–4,8–11] Most μ-methylene groups bridge a metal–metal bond of order one or two, and the major reviews have focussed attention especially on these compounds.[1–4,11] Since there have been major advances recently in the synthesis and study of μ-methylene complexes without metal–metal bonds, a brief review of these compounds is now given. The emphasis is on the major synthetic pathways, the mechanisms involved in the syntheses and the reactivity of the products. Comprehensive coverage has not been attempted.

SYNTHETIC METHODS

1. *Synthesis using diazomethane*

The first μ-methylene complex without a metal–metal bond was prepared by this method (eq. (1), PP = $Ph_2PCH_2PPh_2$ = dppm).[12,13]

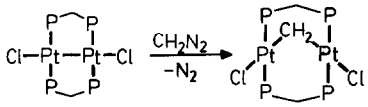

(1)

The structure has been confirmed crystallographically (Fig. 1),[14] and the absence of a metal–metal bond is shown by the non-bonding Pt—Pt distance of 3.151(1) Å and the relatively open PtCPt angle of 103.4(7)°. These values may be compared to typical MM distances and MCM angles in metal–metal bonded derivatives of 2.5–2.8 Å and 75–78°, respectively.[1] The absence of a metal–metal bond is expected from simple electron counting rules, and molecular orbital calculations on an isoelectronic species have supported this interpretation.[15]

The insertion of a CH_2 group from diazomethane into a Pt—Pt bond is general and further insertions into other Pt—L bonds may occur as shown in eq. (2), L = CO, C_5H_5N, NH_3,[16] eq. (3) L = CO, PMe_2Ph[14,17] or eq. (4), L = PPh_3.[14,17]

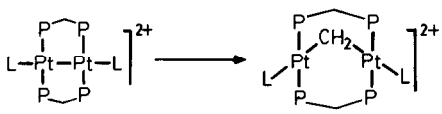

(2)

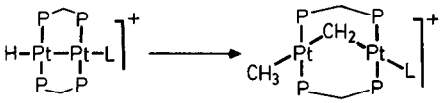

(3)

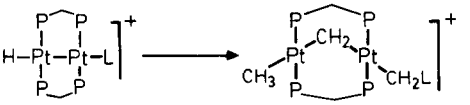

(4)

A one-step mechanism has been proposed for these reactions, involving donation of the Pt—Pt bonding electron pair to the CH_2 group of diazomethane and synchronous loss of N_2. Consistent with this hypothesis is the lower rate observed for

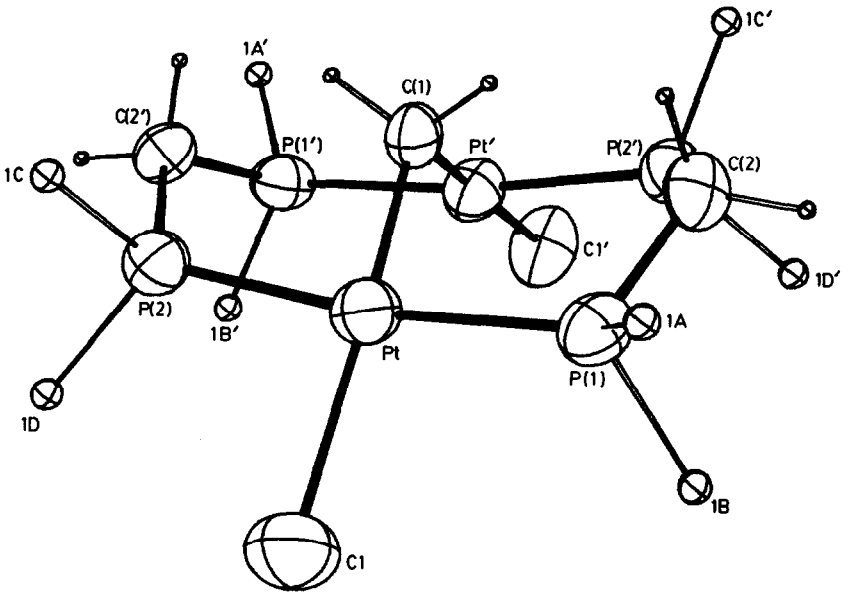

Fig. 1. The structure of $[Pt_2Cl_2(\mu\text{-}CH_2)(\mu\text{-dppm})_2]$.[14]

cationic complexes and the near-zero values of $\Delta S^{\ddagger}$ for the reactions.[16]

A related reaction is observed with a Rh—Rh bonded precursor $[Rh_2Cl_2(\mu\text{-}CF_3C{=}CCF_3)(\mu\text{-dppm})_2]$ to give $[Rh_2Cl_2(\mu\text{-}CH_2)(\mu\text{-}CF_3C{=}CF_3)(\mu\text{-dppm})_2]$. In this case a bridging alkyne is also present, but no coupling with the CH_2 group is observed.[18] Similarly the bis(ylide) derivative $[Au_2Cl_2(\mu\text{-}CH_2PR_2CH_2)_2]$ adds CH_2N_2 across the Au—Au bond to give $[Au_2Cl_2(\mu\text{-}CH_2)(\mu\text{-}CH_2PR_2CH_2)_2]$.[19]

Reaction of $[Mo_2(CO)_4(\eta\text{-}C_5Me_5)_2]$ with CH_2N_2 gave a complex, containing both $\mu\text{-}CH_2$ and $\mu\text{-}CH_2N_2$ ligands, formulated as $[Mo_2(\mu\text{-}CH_2)(\mu\text{-}CH_2N_2)(\eta\text{-}C_5Me_5)_2(CO)_4]$ without a MoMo bond.[20]

Finally, a remarkable CH_2 addition to a ruthenium cluster complex $[Ru_3(CO)_8(R{-}DAB)]$ to give $[Ru_3(\mu\text{-}CH_2)(CO)_8(R{-}DAB)]$ has been discovered (eq. (5), R—DAB = RN=CHCH=NR, R = *neo*-pentyl or *i*-butyl). The precursor complex is formally coordinatively saturated and addition occurs with cleavage of a Ru—Ru bond. This

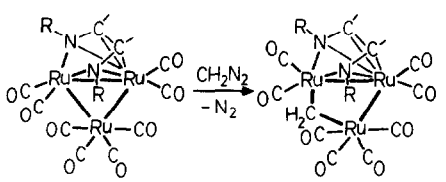

(5)

appears to be the only cluster complex with a $\mu\text{-}CH_2$ group unsupported by a metal–metal bond.[21]

2. *Synthesis using dihalogenoalkanes or halogenomethylmetal complexes*

The first μ-methylene complex without a metal–metal bond or other supporting ligands was prepared by reaction of $Na[Ru(\eta\text{-}C_5H_5)(CO)_2]$ with CH_2Cl_2 and characterized as $[\{(\eta\text{-}C_5H_5)(CO)_2Ru\}_2(\mu\text{-}CH_2)]$, whose structure is given in Fig. 2. The RuCRu angle is 123°, much larger than the tetrahedral angle, due to steric crowding about the μ-methylene group.[22]

The first synthesis by double oxidative addition of a dihalogenomethane involved the dipalladium(0) precursor $[Pd_2(\mu\text{-dppm})_3]$, which with $CHRX_2$ (X = Cl, Br, I; R = H, Me) gave $[Pd_2X_2(\mu\text{-}CHR)(\mu\text{-dppm})_2]$.[23] The reaction with CH_2Cl_2 has been shown to be photochemically initiated.[24] Recent studies have shown that similar reactions can give μ-vinylidene derivatives of palladium or nickel, starting from $CH_2{=}CCl_2$ and $[M_2(\mu\text{-dppm})_3]$ equivalents. For example, $[Pd(PPh_3)_4]$, dppm and $CH_2{=}CCl_2$ gave $[Pd_2Cl_2(\mu\text{-}C{=}CH_2)(\mu\text{-dppm})_2]$.[25,26]

The nature of the double oxidative additions has been elucidated by studies with digold and diiridium complexes. The digold reactions occur as shown in eq. (6), R = Me or Ph; X,Y = Cl, Br or I.[19,27,28]

The gold(II) intermediates have been identified when Y = I, X = Cl and when Y = Br, X = Cl,[19,28] but not when X = Y.[27] The X-ray structure of the

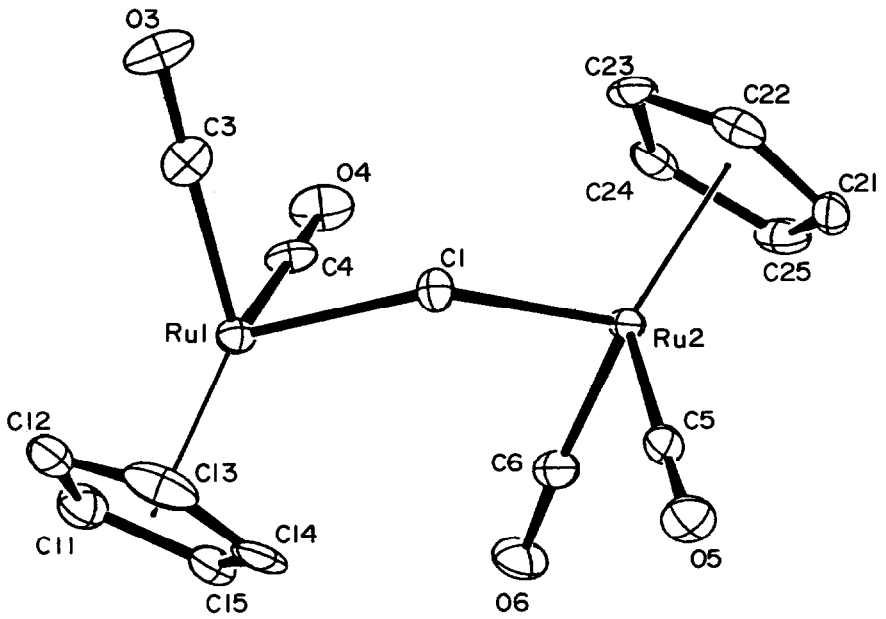

Fig. 2. The structure of $[Ru_2(\mu\text{-}CH_2)(\eta\text{-}C_5H_5)(CO)_4]$.[22]

intermediate when Y = Br, X = Cl shows a Au···Cl interaction, and it is thought that α-elimination gives a Au(=CH_2)Cl group followed by rearrangement to the stable μ-methylene product.[28]

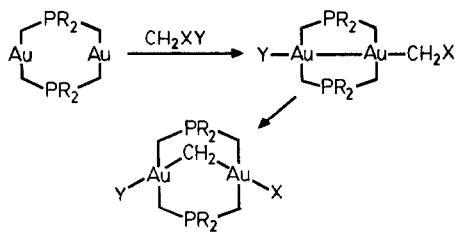

(6)

Similarly, oxidative addition of CH_2I_2 to $[Ir_2(CO)_4(\mu\text{-pz})_2]$, pzH = pyrazole, gives the diiridium(II) intermediate which then rearranges to the $Ir_2(\mu\text{-}CH_2)$complex,eq.(7),N⁀N = μ-pz.[29]

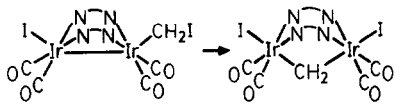

(7)

The first step of the double oxidative addition may be photochemically initiated and is thought to occur by initial electron transfer followed by free radical formation giving the successive intermediates $[Ir_2(CO)_4(\mu\text{-pz})_2]^{+}CH_2X_2^{-}$ and $[Ir_2X(CO)_4(\mu\text{-pz})_2]\cdot CH_2X^{\cdot}$, followed by radical recombination. This mechanism may be common to all the oxidative additions involving CH_2X_2.[30]

The nature of the reactions of dihalogenomethanes with diiridium(I) complexes appears to depend critically on the nature of the bridging ligands. For example, $[Ir_2(\mu\text{-S-}t\text{-Bu})_2(CO)_2L_2]$ reacts with CH_2I_2 by double oxidative addition to give $[Ir_2I_2(\mu\text{-}CH_2)(\mu\text{-S-}t\text{-Bu})_2(CO)_2L_2]$, L = CO, PMe_3, $P(OMe)_3$,[31] but reaction with $[Ir_2(CO)_4(\mu\text{-}SC_5H_4N)_2]$ reacts only to give the iodomethyl derivative $[Ir_2I(CH_2I)(CO)_4(\mu\text{-}SC_5H_4N)_2]$.[32] The iridium(III) μ-methylene complexes exist in isomeric forms and have an extensive chemistry.[31]

The first heteronuclear μ-methylene complexes without metal–metal bonds or other bridging ligands were prepared by oxidative addition of chloromethylgold or chloromethylmercury compounds to a platinum(II) precursor, eqs (8) and (9), NN = 2,2′-bipyridine; L = PPh_3, PEt_3; X = Cl, Me, CH_2Cl.

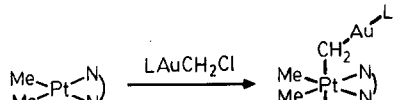

(8)

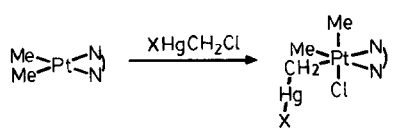

(9)

These reactions occur by the S_N2 mechanism and it has been estimated that the metal activates the C—Cl bond of the chloromethyl derivative, MCH_2Cl, by a factor of 4×10^3 when M = $AuPPh_3$

and 2×10^4 when M = $HgCH_2Cl$, compared to CH_3Cl. In these compounds, the presence of a linear d^{10} metal centre is important since steric hindrance about the μ-methylene group is minimized.[33]

3. *Synthesis by deprotonation of methylmetal groups and related methods*

The first complexes prepared in this way, such as the remarkable compound $[Ru_2(\mu\text{-}CH_2)_3(PMe_3)_6]$[34] formed from dimethylmagnesium and $[Ru_3O(OAc)_6(H_2O)_3]^+$, also contained a metal–metal bond. Other examples contained a μ-methylene group bridging between a transition element and a main group element, as in Tebbe's reagent $[(\eta\text{-}C_5H_5)_2Ti(\mu\text{-}CH_2)(\mu\text{-}Cl)AlMe_2]$ which is prepared from $(\eta\text{-}C_5H_5)_2TiCl_2$ and Me_6Al_2.[35] This reaction is thought to occur by loss of methane from an intermediate $Cp_2TiMeCl \cdot AlMe_3$, involving α-elimination.[36] Similarly, the ionic complex $[(\eta\text{-}C_5H_5)_2TaMe_2]^+[AlMe_4]^-$ slowly loses methane to give $[(\eta\text{-}C_5H_5)_2TaMe(CH_2AlMe_3)]$.[37] These compounds are regarded as complexes of metal–alkylidenes with organo-aluminum acceptors. If a transition metal acceptor is present, μ-methylene complexes may be formed.

Dimerization of a titanium–methylene derivative leads to a dimetallacyclobutane. The titanium–methylene is prepared *in situ* by loss of an alkene from a metallacyclobutane (eq. (10), Cp = η-C_5H_5).[38]

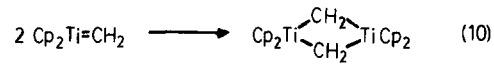

(10)

Reaction with other transition metal acceptors leads to thermally labile μ-methylene complexes (eq. (11), MCl = $(\eta\text{-}C_5Me_5)TiCl_3$; $(\eta\text{-}C_5Me_5)ZrCl_3$; (cod)RhCl or (cod)IrCl).[39]

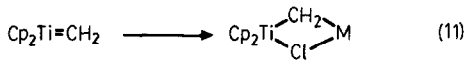

(11)

Similar methods have been used to prepare μ-alkylidene complexes of zirconium.[40,41] An unequivocal demonstration of μ-methylene, methyl exchange has been found in the $TiCH_2Rh$ system of eq. (12).[42] This complex has an agostic CHTi interaction, as shown in Fig. 3, and there is almost certainly a Ti—Rh bonding interaction also.

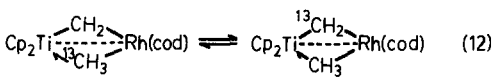

(12)

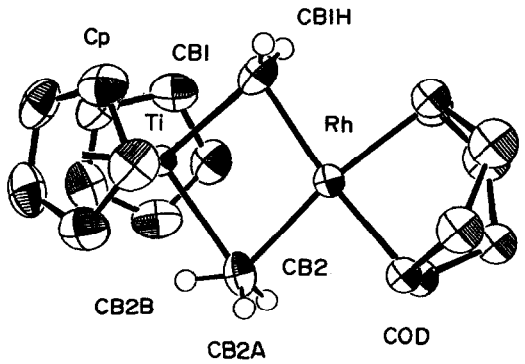

Fig. 3. The structure of $[(\eta\text{-}C_5H_5)_2Ti(\mu\text{-}CH_2)(\mu\text{-}CH_3)Rh(cod)]$, cod = 1,5-cyclooctadiene.[42]

An important example of this synthetic method is the reversible deprotonation of a $[Pt_2Me]^+$ complex to a $Pt_2(\mu\text{-}CH_2)$ group, eq. (13).[43]

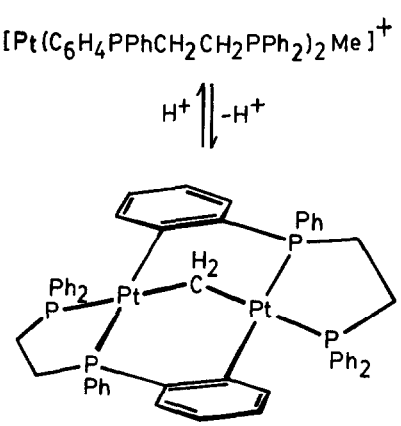

(13)

Finally, a digold complex containing an $Au_2(\mu\text{-}CHNO_2)$ group, $[Au_2(\mu\text{-}CHNO_2)(O_2CPh)_2(\mu\text{-}CH_2PPh_2CH_2)_2]$, has been prepared directly from nitromethane. This reaction involves double deprotonation of CH_3NO_2 to give the μ-$CHNO_2$ group.[44]

PROPERTIES OF μ-METHYLENE COMPLEXES

1. *Structural and spectroscopic properties*

Some structural and spectroscopic properties of μ-methylene complexes are given in Table 1. Of the complexes which clearly do not contain a metal–metal bond, the parameters r(MM), r(MC) and $\angle$(MCM) span the ranges 2.84–3.8, 1.80–2.18 Å and 89–123°, respectively. The $\angle$(MCM) appears to be the best distinguishing feature for complexes with metal–metal bonds, for which the range 73–88° has been given.[1] As expected, there are no clear distinctions between the two types of μ-methylene complexes when weak metal–metal interactions are

Table 1. Structural and spectroscopic properties of selected μ-methylene complexes

Complex	r(MM) (Å)	r(MC) (Å)	∠(MCM) (°)	δ(CH_2) (ppm)	δ(CH_2) (ppm)	Ref.
$\{MoCp(CO)_2\}_2(\mu\text{-}CH_2N_2)(\mu\text{-}CH_2)$	—	—	—	1.44 3.77	64.2	20
$\{RuCp(CO)_2\}_2(\mu\text{-}CH_2)$	3.8	2.18	123	2.30	−37.42[a]	22
$Ru_3(CO)_8(R\text{—}DAB)(\mu\text{-}CH_2)$	3.102	2.05 2.20	93.6	3.7	32.5	21
$\{RhCl(\mu\text{-dppm})\}_2(\mu\text{-}C_4F_6)(\mu\text{-}CH_2)$	3.464	2.06	114.5	6.07	—	18
$\{IrI(CO)_2(\mu\text{-pz})\}_2(\mu\text{-}CH_2)$	—	—	—	3.52	0.3	29
$\{IrI(\mu\text{-}t\text{-BuS})(CO)P(OMe)_3\}_2(\mu\text{-}CH_2)$	3.198	1.85	98.7	2.50	−28.9[b]	31
$\{PdCl(\mu\text{-dppm})\}_2(\mu\text{-}CH_2)$	—	—	—	1.64	—	23
$\{PtCl(\mu\text{-dppm})\}_2(\mu\text{-}CH_2)$	3.151	1.80	103.4	1.08	—	13, 14
$[Pt_2Cl(CH_2PPh_3)(\mu\text{-dppm})_2(\mu\text{-}CH_2)]^+$	3.120	1.82 2.13	94	1.57	—	14
$\{Pt(\mu\text{-}C_6H_4PPhCH_2CH_2PPh_2)\}_2(\mu\text{-}CH_2)$	2.915	2.08	88.9	3.46	46.0[c]	43
$\{AuCl(\mu\text{-}CH_2PMe_2CH_2)\}_2(\mu\text{-}CH_2)$	3.052	2.00	99	3.40	48.5	27
$\{AuMe(\mu\text{-}CH_2PMe_2CH_2)\}_2(\mu\text{-}CH_2)$	3.118	2.09	96.3	1.09	47.8	45
$\{AuCN(\mu\text{-}CH_2PPh_2CH_2)\}_2(\mu\text{-}CH_2)$	3.167	2.056	100.7	1.74	—	46
$\{Au(OCOPh)(\mu\text{-}CH_2PPh_2CH_2)\}_2(\mu\text{-}CHNO_2)$	3.073	2.03	—	—	—	44
$(Cp_2Ti)(codRh)(\mu\text{-}CH_3)(\mu\text{-}CH_2)$	2.835	2.09 2.15	83.9[d]	7.24[d]	185.4[d]	42
$\{NiNCS(\mu\text{-dppm})\}_2(\mu\text{-}C{=}CH_2)$	2.840	1.88	98.3	4.26	—	26

[a] ^1J(CH), 137.2 Hz.
[b] ^1J(CH), 149.
[c] ^1J(PtC), 467, ^1J(CH), 140.
[d] These data indicate a metal–metal bond is present.

present. For example, the complex $Cp_2Ti(\mu\text{-}CH_2)(\mu\text{-}CH_3)Rh(cod)$, Fig. 3, has ∠TiCRh 83.9° suggesting a metal–metal bond is present. This metal–metal interaction is presumably associated with the electron-deficient $Ti(\mu\text{-}CH_3)Rh$ bridge, and is also indicated by the NMR properties (see below).[42]

The ^1H chemical shifts from the NMR spectra of μ-methylene complexes without metal–metal bonds fall in the range δ 1–6 ppm (Table 1), a range which overlaps slightly with the range δ 5–11 ppm for μ-methylene complexes with metal–metal bonds.[1] In most cases, this criterion of structure will be useful since the majority of complexes without metal–metal bonds have δ 1–5 ppm. However, it would have given an incorrect structure for $[Rh_2Cl_2(\mu\text{-dppm})_2(\mu\text{-}C_4F_6)(\mu\text{-}CH_2)]$ with δ 6.07 ppm.[18]

The ^{13}C chemical shifts (Table 1) fall in the range δ 64.2 to −37.4 ppm, compared to the range δ = 100–210 ppm for complexes with metal–metal bonds.[1] This criterion of structure therefore appears to be a reliable one. There are relatively few examples of μ-methylene complexes without metal–metal bonds for which X-ray structures and ^{13}C chemical shifts have both been determined. However, the limited data (Table 1) suggest a strong correlation between δ($^{13}CH_2$) and r(MM). Thus, the extreme cases are $[Ru_2Cp_2(CO)_4(\mu\text{-}CH_2)]$ with δ −37.4 ppm and r(MM) 3.8 Å and $[Pt_2(\mu\text{-}C_6H_4PPhCH_2CH_2PPh_2)_2(\mu\text{-}CH_2)]$ with δ 46.0 and r(MM) 2.9 Å. Clearly, the correlation is not expected to be exact since the nature of the metal and its other ligands will also affect δ(^{13}C). The metal–metal bonded derivatives with δ 100–210 ppm and shorter metal–metal distances may also be considered as an extension of this correlation. A similar correlation of δ(^{31}P) for $\mu\text{-}PPh_2$ complexes is well-known and is very useful in structure determination.[47]

2. *Chemical properties*

The μ-methylene group has a reactivity which varies greatly from complex to complex, and it is often sufficiently inert that ligand substitutions can occur without disruption of the μ-methylene group.[45,46,48] Nevertheless, some typical organometallic reactions do occur and are described below.

2a. Insertion reactions

The complex $[Ru_2Cp_2(CO)_4(\mu\text{-}CH_2)]$ readily undergoes CO insertion to give a μ-ketene derivative and undergoes photolysis in the presence of methanol to give methyl acetate. These results are rationalized in terms of the mechanism of eq. (14), and the ease of reaction is attributed to the steric strain in the μ-methylene complex.[22]

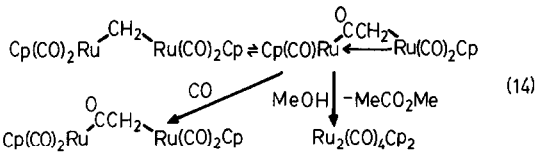

(14)

An isomeric form of the ketene complex is formed from a $Ti_2(\mu\text{-}CH_2)$ complex by CO insertion [eq. (15)].[39]

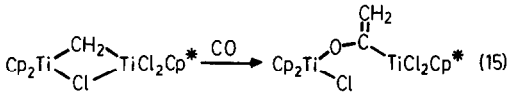

(15)

2b. Reductive elimination reactions

A remarkable reductive elimination involving coupling of two methyl groups with a μ-methylene group to give propane has been observed [eq. (16)].[45]

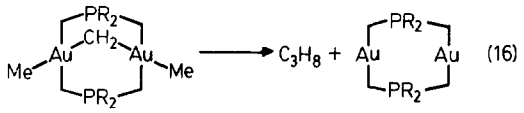

(16)

In contrast, pyrolysis of methyl(μ-methylene) diplatinum complexes gave only methane.[14] Pyrolysis of $[Cp_2Ti(\mu\text{-}CH_2)_2TiCp_2]$ also gave mostly methane, but reaction with iodine gave 78% ethylene by coupling of the two μ-methylene groups.[38]

2c. Cleavage by electrophiles

μ-Methylene groups can be cleaved by a proton to give methyl derivatives. The methyl group may remain bridging, as is probably considered in eq. (13),[42] or, if a better bridging group is present a rearrangement to give a terminal methyl group may occur, eq. (17), M = Pd or Pt, PP = dppm.[23,49]

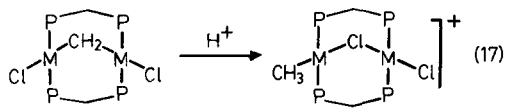

(17)

The basicity of the μ-methylene group in these dppm complexes increases as more electron-donating substituents occupy the *trans* coordination sites. For example, attempts to prepare neutral derivatives with hydride or methyl groups in *trans* positions led to spontaneous protonation of the μ-methylene groups [eq. (18)].

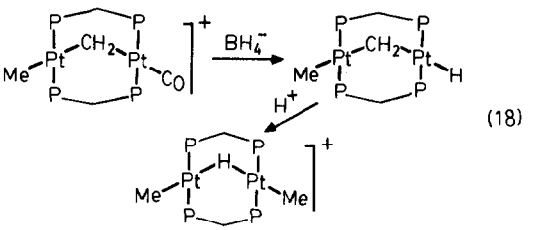

(18)

In heteronuclear μ-methylene derivatives, the more reactive metal–carbon bond is cleaved by the electrophile [eq. (19)].

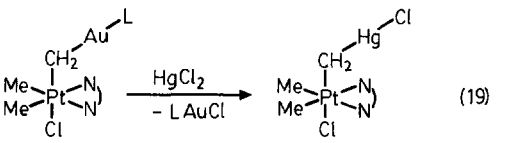

(19)

Similar cleavage with HCl gives [$PtMe_3Cl$(2,2′-bipyridine).[33]

CONCLUSIONS

μ-Methylene complexes without metal–metal bonds are now a well-established class of compounds. Synthetic methods, as well as the general mechanisms involved, are reasonably well understood. They can be distinguished from the better known complexes with metal–metal bonds[1] by X-ray structure determination, or by ^1H and ^{13}C NMR spectroscopy. Most examples of μ-methylene complexes without metal–metal bonds contain additional bridging ligands. The reason for this is that in complexes of the type $L_nMCH_2ML_n$ there are usually severe steric interactions between the ligands L, as seen in Fig. 2. If additional bridging ligands are present there is much less steric hindrance, as seen in Fig. 1. Clearly it helps to use metals with a low coordination number, such as gold(I) in eq. (8), if μ-methylene complexes without extra bridging ligands are required.

The reactivity of the complexes is that expected for σ-bonded alkyl derivatives of transition metals, which may be modified by steric or angle strain at the μ-methylene site. However, the chemical reactivity of the μ-methylene complexes, particularly as related to the Fischer–Tropsch synthesis, clearly requires further study.

Acknowledgements—The author's research in this area was funded by NSERC (Canada) and was carried out

by the able coworkers whose names are given in the references. The collaboration of Dr Lj. Manojlović-Muir in crystal structure determination is gratefully acknowledged.

REFERENCES

1. W. A. Herrmann, *Adv. Organomet. Chem.* 1982, **20**, 159.
2. W. A. Herrmann, *Angew. Chem.* 1982, **94**, 118.
3. W. A. Herrmann, *J. Organomet. Chem.* 1983, **250**, 319.
4. W. A. Herrmann, *Pure Appl. Chem.* 1982, **54**, 65.
5. R. C. Brady III and R. Pettit, *J. Am. Chem. Soc.* 1980, **102**, 6181.
6. K. Isobe, A. V. de Miguel, P. M. Bailey, S. Okeya and P. M. Maitlis, *J. Chem. Soc., Dalton Trans.* 1983, 1441.
7. G. R. Steinmetz and G. L. Geoffroy, *J. Am. Chem. Soc.* 1981, **103**, 1278.
8. J. Holton, M. F. Lappert, R. Pearce and P. I. W. Yarrow, *Chem. Rev.* 1983, **83**, 135.
9. J. R. Moss and L. G. Scott, *Coord. Chem. Rev.* 1984, **60**, 171.
10. C. P. Casey and J. D. Audett, *Chem. Rev.* 1986, **86**, 339.
11. J. E. Hahn, *Prog. Inorg. Chem.* 1984, **31**, 205.
12. M. P. Brown, J. R. Fisher, S. J. Franklin, R. J. Puddephatt and K. R. Seddon, *J. Chem. Soc., Chem. Commun.* 1978, 749.
13. M. P. Brown, J. R. Fisher, R. J. Puddephatt and K. R. Seddon, *Inorg. Chem.* 1979, **18**, 2808.
14. K. A. Azam, A. A. Frew, B. R. Lloyd, Lj. Manojlović-Muir, K. W. Muir and R. J. Puddephatt, *Organometallics* 1985, **4**, 1400.
15. D. M. Hoffman and R. Hoffmann, *Inorg. Chem.* 1981, **20**, 3543.
16. S. Muriladharan and J. H. Espenson, *Inorg. Chem.* 1983, **22**, 2786.
17. K. A. Azam, A. A. Frew, B. R. Lloyd, Lj. Manojlović-Muir, K. W. Muir and R. J. Puddephatt, *J. Chem. Soc., Chem. Commun.* 1982, 614.
18. I. R. McKeer and M. Cowie, *Inorg. Chim. Acta.* 1982, **65**, L107.
19. H. H. Murray, J. P. Fackler Jr and A. M. Mazany, *Organometallics* 1984, **3**, 1310.
20. W. A. Herrmann and L. K. Bell, *J. Organomet. Chem.* 1982, **239**, C4.
21. J. Keijsper, L. H. Polm, G. van Koten, K. Vrieze, K. Goubitz and C. H. Stam, *Organometallics* 1985, **4**, 1876.
22. Y. C. Lin, J. C. Calabrese and S. S. Wreford, *J. Am. Chem. Soc.* 1983, **105**, 1680.
23. A. L. Balch, C. T. Hunt, C.-L. Lee, M. M. Olmstead and J. P. Farr, *J. Am. Chem. Soc.* 1981, **103**, 3764.
24. J. V. Caspar, *J. Am. Chem. Soc.* 1985, **107**, 6718.
25. S. J. Higgins and B. L. Shaw, *J. Chem. Soc., Chem. Commun.* 1986, 1629.
26. X. L. R. Fontaine, S. J. Higgins, B. L. Shaw, M. Thornton-Pett and W. Yichang, *J. Chem. Soc., Dalton Trans.* 1987, 1501.
27. P. Jandik, U. Schubert and H. Schmidbaur, *Angew. Chem. Int. Ed. Engl.* 1982, **21**, 73.
28. H. H. Murray III, J. P. Fackler Jr and D. A. Tocher, *J. Chem. Soc., Chem. Commun.* 1985, 1278.
29. D. G. Harrison and S. R. Stobart, *J. Chem. Soc. Chem. Commun.* 1986, 285.
30. J. V. Caspar and H. B. Gray, *J. Am. Chem. Soc.* 1984, **106**, 3029.
31. M. El Amane, A. Maisonnat, F. Dahan, R. Pince and R. Poilblanc, *Organometallics* 1985, **4**, 773.
32. M. A. Ciriano, F. Viguri, L. A. Oro, A. Tiripicchio and M. Tiripicchio-Camellini, *Angew. Chem. Int. Ed. Engl.* 1987, **26**, 444.
33. G. J. Arsenault, M. Crespo and R. J. Puddephatt, *Orgarnometallics*, 1987, **6**, 2255.
34. M. B. Hursthouse, R. A. Jones, K. M. Abdul-Malik and G. Wilkinson, *J. Am. Chem. Soc.* 1979, **101**, 4128.
35. F. N. Tebbe, G. W. Parshall and G. S. Reddy, *J. Am. Chem. Soc.* 1978, **100**, 3611.
36. K. C. Ott, E. J. M. deBoer and R. H. Grubbs, *Organometallics* 1984, **3**, 223.
37. R. R. Schrock and P. R. Sharp, *J. Am. Chem. Soc.* 1978, **100**, 2389.
38. K. C. Ott and R. H. Grubbs, *J. Am. Chem. Soc.* 1981, **103**, 5922.
39. P. B. Mackenzie, K. C. Ott and R. H. Grubbs, *Pure Appl. Chem.* 1984, **56**, 59.
40. F. W. Hartner, J. Schwartz and S. M. Clift, *J. Am. Chem. Soc.* 1983, **105**, 640.
41. S. Sabo, B. Chaudret and D. Gervais, *Nouv. J. Chim.* 1983, **7**, 181.
42. J. W. Park, P. B. Mackenzie, W. P. Schaefer and R. H. Grubbs, *J. Am. Chem. Soc.* 1986, **108**, 6402.
43. D. P. Arnold, M. A. Bennett, G. M. McLaughlin and G. B. Robertson, *J. Chem. Soc., Chem. Commun.* 1983, 34.
44. H. C. Knachel, D. S. Dudis and J. P. Fackler Jr, *Organometallics* 1984, **3**, 1312.
45. H. Schmidbaur, C. Hartmann, J. Riede, B. Huber and G. Müller, *Organometallics* 1986, **5**, 1652.
46. H. H. Murray, A. M. Mazany and J. P. Fackler Jr, *Organometallics* 1985, **4**, 154.
47. A. J. Carty, *Catalytic Aspects of Metal Phosphine Complexes, ACS Adv. Chem. Ser.* 1982, **196**, 163.
48. H. Schmidbaur and C. Hartmann, *Angew. Chem. Int. Ed. Engl.* 1986, **25**, 575.
49. K. A. Azam and R. J. Puddephatt, *Organometallics* 1983, **2**, 1396.

Polyhedron Vol. 7, No. 10/11, pp. 775–790, 1988
Printed in Great Britain

0277–5387/88 $3.00+.00
© 1988 Pergamon Press plc

REACTIVITY OF BRIDGING HYDROCARBYL LIGANDS IN BINUCLEAR SYSTEMS

JOHN C. JEFFERY

Department of Inorganic Chemistry, The University, Bristol BS8 1TS, U.K.

and

MICHAEL J. WENT

University Chemical Laboratory, Canterbury, Kent CT2 7NH, U.K.

(*Accepted* 5 *November* 1987)

Abstract—Hydrocarbyl ligands bridging heteronuclear transition metal centres display a wide range of reactivity, especially with respect to the formation of carbon–hydrogen and carbon–carbon bonds. This article summarizes progress made in this area by Prof. F. G. A. Stone and coworkers at the University of Bristol.

The reactions of low-valent transition metal complexes containing metal–carbon multiple bonds with sources of metal–ligand fragments has led to the synthesis of a plethora of polynuclear systems containing bridging hydrocarbyl ligands.[1] This article reviews the chemistry of these hydrocarbyl moieties ligated simultaneously to two different transition metal centres, excluding systems of nuclearity greater than two and systems containing carborane ligands where cage transformations dominate the reactivity.[2] Particular emphasis is placed on reactions leading to carbon–hydrogen and carbon–carbon bond formation.*

CARBON–HYDROGEN BOND FORMATION

Alkylidyne carbon–hydrogen bond formation

The alkylidyne ligand, with only one organic substituent attached to the ligated carbon, is the least saturated hydrocarbyl fragment. Dinuclear alkylidyne bridged complexes can be considered as dimetallacyclopropene ring systems and display varying chemical reactivity depending on the nature of the metal ligand fragments and the alkylidyne substituent. Investigations at Bristol have concentrated on heteropolynuclear alkylidyne complexes bearing tolyl, methyl and, more recently, xylyl substituents. Two factors dominate the substituent effects, firstly the ability of aryl groups to coordinate to a transition metal centre via the π system and secondly the presence of active β-hydrogens in the methyl group.

Addition of a hydrogen atom to an alkylidyne carbon forms an alkylidene ligand. Such a transformation can be effected by reagents acting as proton or hydride sources, or by internal hydrogen migrations. Each of these three possibilities will be considered in turn.

(i) *Reactions with protic acids.* Formation of a carbon–hydrogen bond requires two electrons, therefore straightforward protonation of an alkylidyne carbon leads to an electron deficient system. A dimetallacyclopropene ring normally possesses 34 valence electrons (a count of 32 is possible if one of the metals prefers, like platinum, to adopt a 16 electron configuration). Protonation of the alkylidyne carbon decreases the number of valence electrons by two, but this initial electron deficiency is invariably satisfied by one of a variety of means. An incoming ligand, such as the conjugate base of the acid used for protonation, can coordinate to

* Throughout this paper R represents C_6H_4Me-4, unless otherwise stated, and Cp and Cp* represent η-C_5H_5 and η-C_5Me_5, respectively.

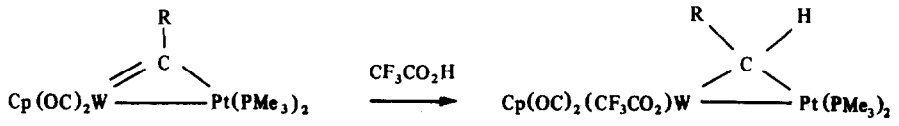

	R		R
(1a)	C_6H_4Me-4	(2a)	C_6H_4Me-4
(1b)	Me	(2b)	Me

(1)

Eq. (1)

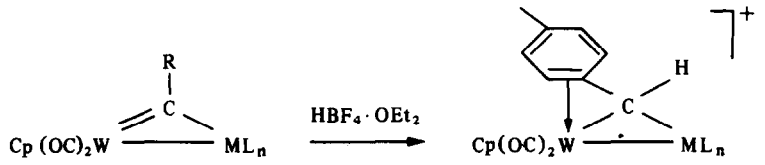

(3)	$Rh(PMe_3)(\eta-C_9H_7)$	(7)	
(4)	Cr (CO) (NO) Cp	(8)	
(5)	Co (CO) Cp^*	(9)	
(6a)	Pt $(PMe_3)_2$	(10a)	
(6b)	Pt $(PMe_2Ph)_2$	(10b)	

(2)

Eq. (2)

the system to re-establish the number of valence electrons [eq. (1)],[3] or it no external ligand is available a newly formed tolylmethylidene ligand can donate two additional valence electrons by adopting an η^3-bonding mode [eq. (2)].[4,5] The η^3-interaction is relatively weak and the greatest stability is observed when ML_n is an electron rich $Pt(PR'_3)_2$ fragment. The coordination of the tolyl ring to the tungsten centre can readily be displaced by other two electron donor ligands [eq. (3)].[6]

Protonation of the methyl substituted alkylidyne complexes (**1b**) does not result in alkylidene containing products (Scheme 1).[3] The unsaturated intermediate **A** cannot coordinate the BF_4^- ion and the possibility of stabilization via a β-agostic interaction in an analogous fashion to the η^3-tolyl ligation is not observed, although **B** may be an intermediate in hydrogen migration. Intermediate **C** is also not detected, although the vinyl complex (**13**) can be prepared by the methylation of (**1b**), and the isolated product is the ethene complex (**12**).

As yet, no stable products have been isolated from the protonation of anionic alkylidyne systems such as $[P(CH_2Ph)Ph_3][WPt(\mu\text{-}CR)(CO)_2(cod)(\eta\text{-}C_2B_9H_9Me_2)]$.[7]

(ii) *Reactions with potassium selectride.* The reagent $K[BH(CHMeEt)_3]$, known as potassium selectride, has proven to be a particularly useful source of the hydride ion, which possessing two electrons available for the formation of a carbon–hydrogen bond should in principle afford alkylidene complexes in a more straightforward manner than protonation. Surprisingly few examples of this form of reactivity have been observed. Reactions of dimetallacyclopropene complexes with anionic reagents are often complicated by product instability or nucleophilic attack at centres other than the alkylidyne carbon.[8] For example, treatment of

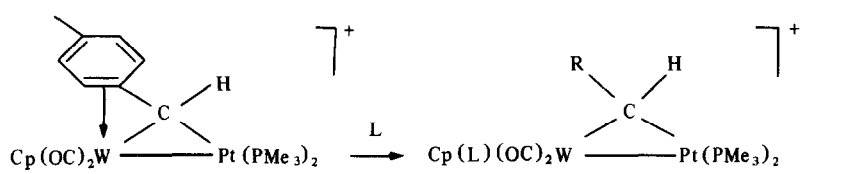

(10a)

	L
(11a)	CO
(11b)	PMe_3

(3)

Eq. (3)

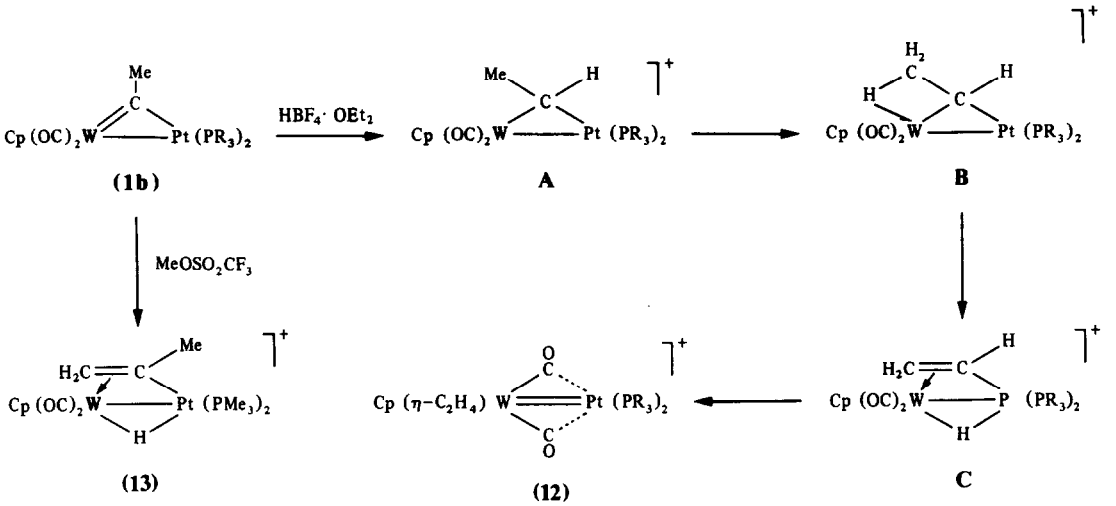

Scheme 1. $PR_3 = PMe_3$, PEt_3, PMe_2Ph or $PMePh_2$.

the salt $[WPt(\mu\text{-}CR)(CO)_5(PMe_3)_2][BF_4]$ with the nucleophilic reagents $Li(C_6H_4Me\text{-}4)$, NaOMe or NaOEt affords complexes with bridging alkylidene ligands in very poor yields, *ca* 5%.[8] The reason for this may be in part, the facile cleavage of the tungsten–platinum bond in these complexes. Stabilizing the metal–metal bond with a bidentate ligand such as bis(diphenylphosphino) methane can have a dramatic effect on the chemistry. For example eq. (4) proceeds in *ca* 70% yield.[9] Competing reactions are less easily circumvented. Two of the potential problems, illustrated by eqs (5) and (6), are deprotonation and nucleophilic attack at a site other than the alkylidyne carbon.[8,10]

Potassium selectride can also be used to form bridging alkylidene complexes by reaction with binuclear complexes containing terminal alkylidyne ligands [eq. (7)].[11] Related anionic alkylidene complexes can be synthesized by the reaction of anionic pentacarbonyl hydrides with $[W(\equiv CR)(CO)_2(Cp)]$

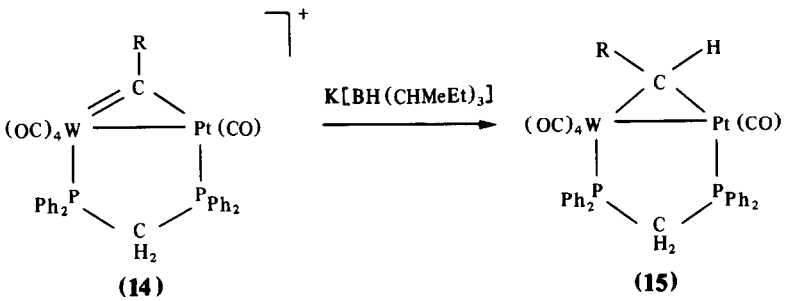

(4)

Eq. (4)

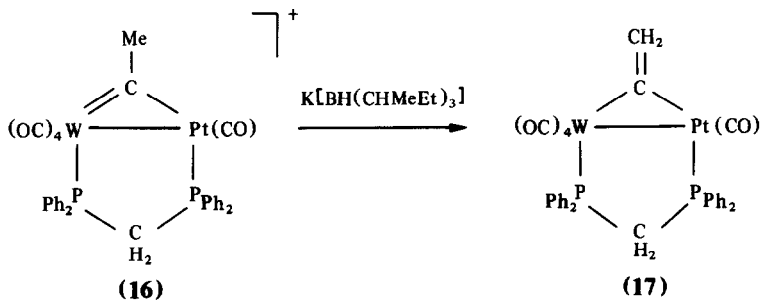

(5)

Eq. (5)

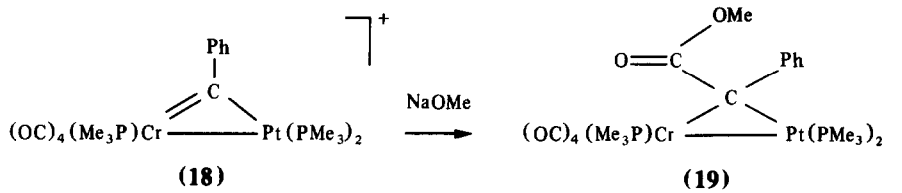

(18) (19) (6)

Eq. (6)

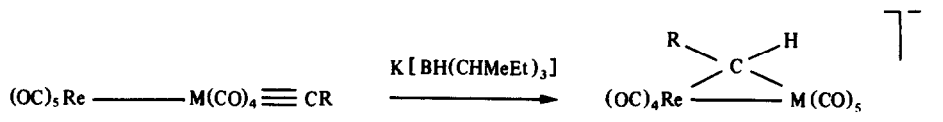

(7)

	M	R	
(20a)	W	Me	**(21a)**
(20b)	W	C_6H_4Me-4	**(21b)**
(20c)	Cr	C_6H_4Me-4	**(21c)**
(20d)	Mo	C_6H_4Me-4	**(21d)**

Eq. (7)

[eq. (8)] and in the case of the homonuclear tungsten complex (**22b**) either method can be employed, the hydride addition being reversible [eq. (9)].[12] The Cp containing complexes are less stable than the all carbonyl compounds (**21**) reflecting the lower ability of the cyclopentadienyl ligand to stabilize an anionic system. Hydride abstraction is not observed from compounds (**21**) although β-migrations are possible if coordinative unsaturation can be generated at one of the metal centres [eq. (10)].[11] Such rearrangements are familiar from the protonation chemistry illustrated in Scheme 1. A similar series

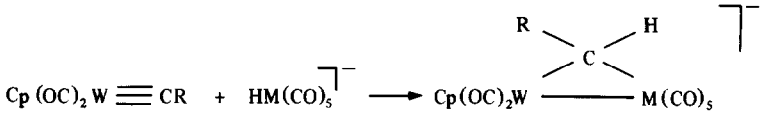

	M
(22a)	Cr
(22b)	W

(8)

Eq. (8)

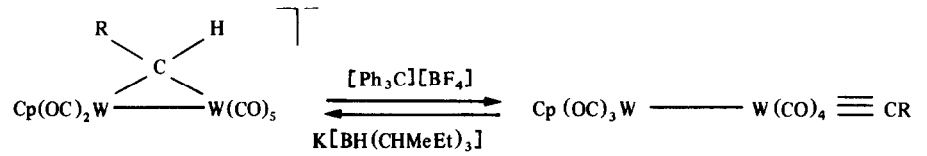

(22b) **(23)** (9)

Eq. (9)

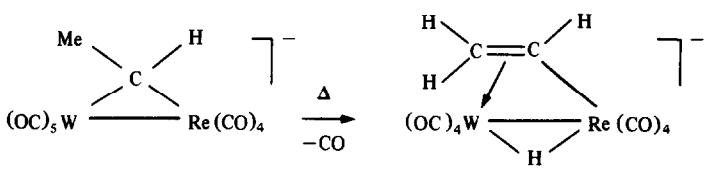

(21a) **(24)** (10)

Eq. (10)

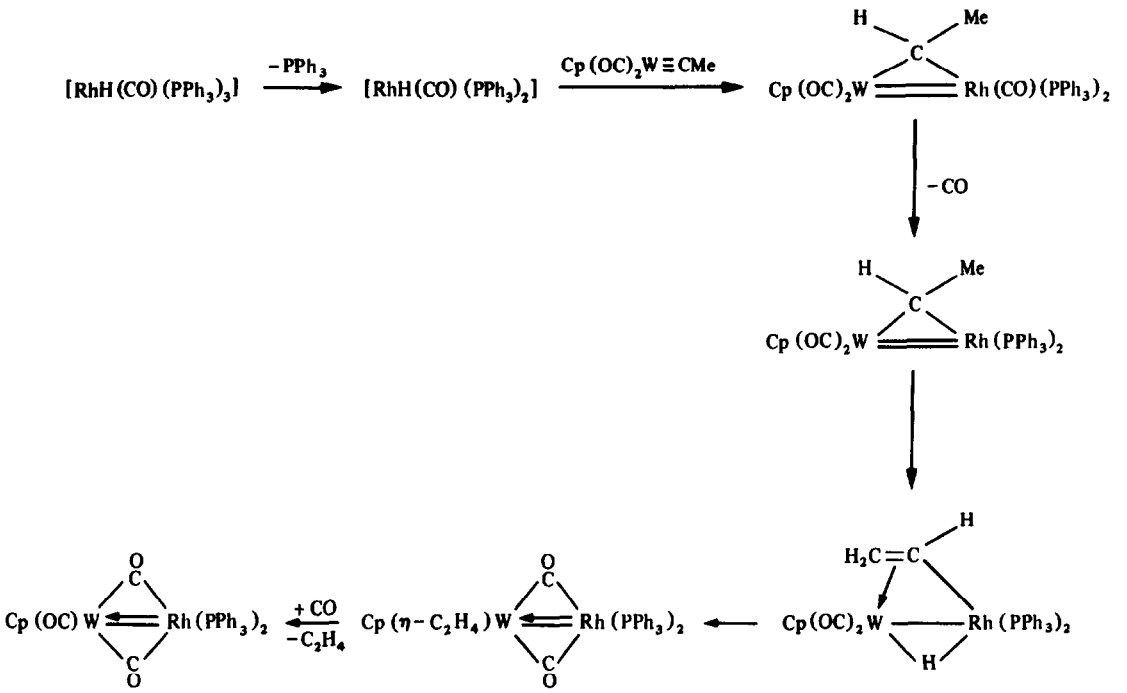

Scheme 2.

of rearrangements is postulated for the reaction of $[RhH(CO)(PPh_3)_3]$ with $[W(\equiv CMe)(CO)_2Cp]$ (Scheme 2).[13]

(iii) *Intramolecular hydrogen migration.* Rearrangement of a diphenylphosphine ligand to a bridging diphenylphosphido ligand with hydrogen migration to an alkylidyne carbon results in alkylidene formation [eqs (11) and (12)].[13,14] Again the η^3-tolyl coordination is observed due to the unsaturated nature of the iron–tungsten alkylidyne complexes (**25**) and (**27**). The preference for the tolyl ring in (**28**) to coordinate to the iron centre is probably a reflection of the steric bulk of the tris(pyrazolyl)borate ligand. If this chemistry is per-

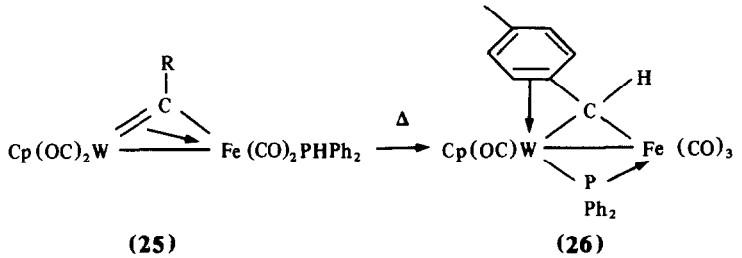

(11)

(**25**) (**26**)

Eq. (11)

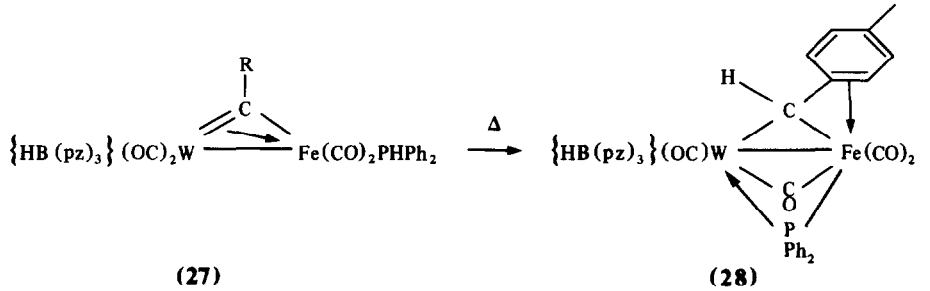

(12)

(**27**) (**28**)

Eq. (12)

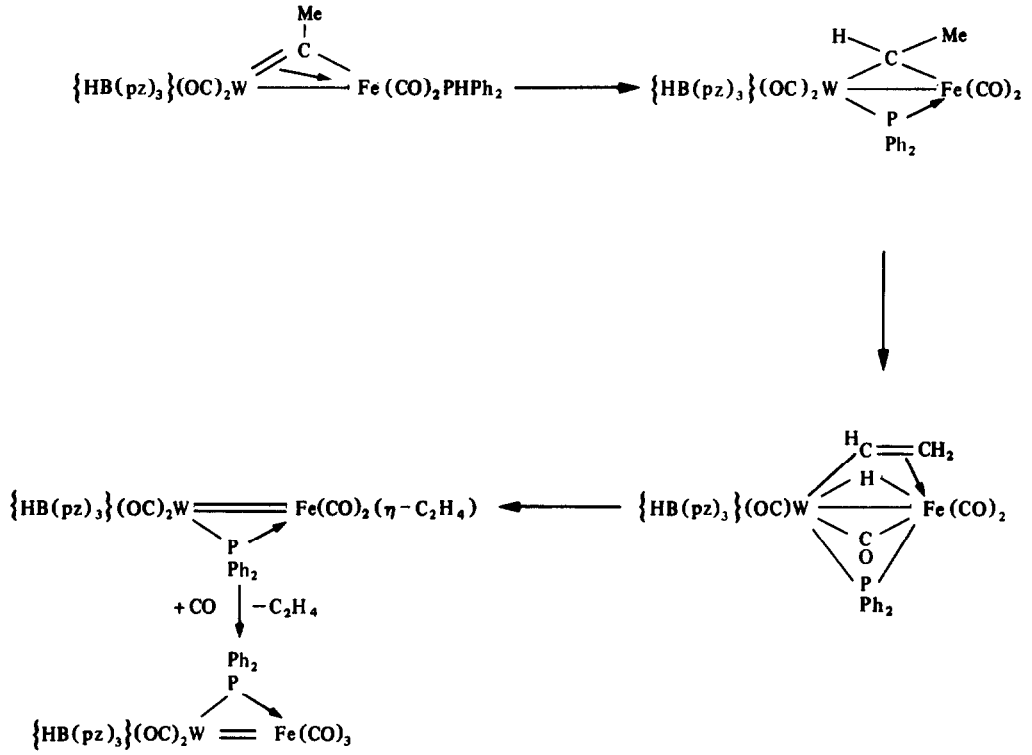

Scheme 3.

formed with a methyl substituent, the result is a non-alkylidene containing product due to migration of a β-hydrogen (Scheme 3).[13]

Alkylidene carbon–hydrogen bond formation

Binuclear complexes containing alkylidene ligands also react with proton and hydride sources. Protonation of alkoxide substituted alkylidenes results in removal of the alkoxide to form an alkylidyne as illustrated by the formation of (**14**) by the treatment of $[WPt\{\mu\text{-}C(OMe)R\}(\mu\text{-}Ph_2PCH_2PPh_2)(CO)_5]$ with $HBF_4 \cdot OEt_2$.[9] The anionic rhenium–tungsten system (**21b**) can be protonated to afford stable alkyl complexes if the tungsten–rhenium bond is first bridged by a bidentate phosphine ligand [eq. (13)]. The two electron agostic interaction compensates for the electrons required for carbon–hydrogen bond formation and can be displaced by additional two electron ligands.[11] In contrast, (**10a**) or (**11a**) reacts with potassium selectride to afford the alkylidene–hydride complex (**31**) [eq. (14)] and not the hypothetical isomeric alkyl complex $[WPt(\mu\text{-}CH_2R)(CO)_2(PMe_3)_2(Cp)]$.[6] Reaction of (**10a**) with other nucleophilic reagents such as NaH or NaCp results in deprotonation to reform

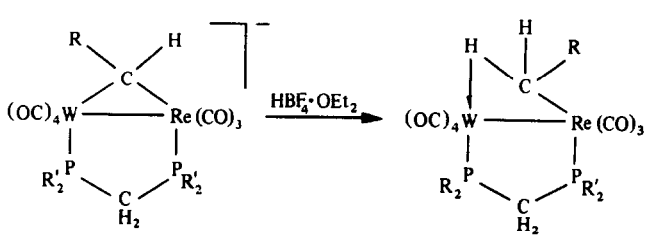

(13)

	R'	
(**29a**)	Ph	(**30a**)
(**29b**)	Me	(**30b**)

Eq. (13)

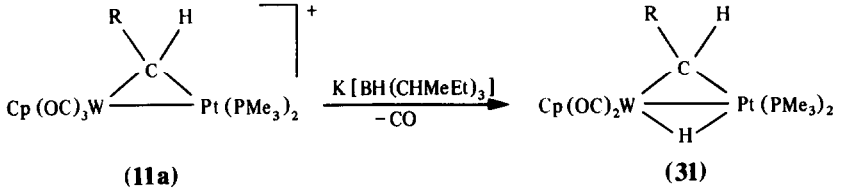

(11a) (31) (14)

Eq. (14)

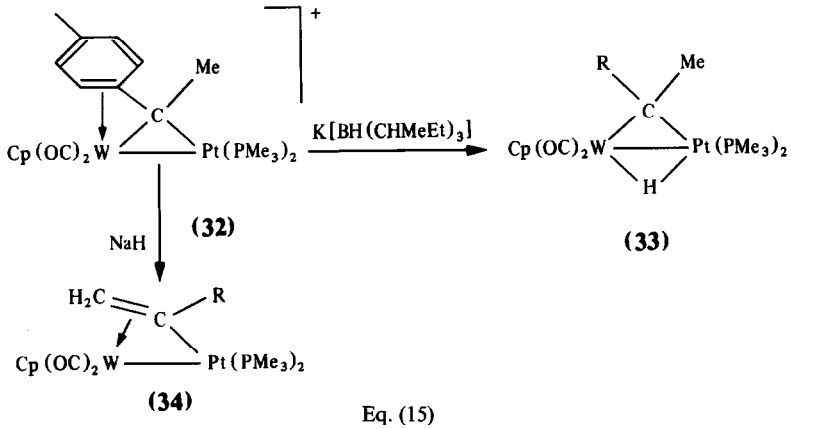

(32) (33) (34) (15)

Eq. (15)

the alkylidyne complexes (**1a**). Similarly complex (**32**) forms a bridging hydride (**33**) upon reaction with potassium selectride, and a bridging vinyl (**34**) with sodium hydride [eq. (15)].[6] The cobalt–tungsten complex (**9**) deprotonates to the parent alkylidene complex (**5**) even when treated with potassium selectride.[15]

CARBON–CARBON BOND FORMATION

Reactions of MM′μ-CR *complexes with sources of* "CH_2" *fragments*

The complex [WPt(μ-CR)(CO)$_2$(PMe$_3$)$_2$(Cp)] (**1a**) does not react with CH_2N_2 but will undergo a facile methylene addition reaction when treated with the reagent [Ti{Cl(AlMe$_2$)CH$_2$}(CH$_2$)(Cp)$_2$] giving the *gem*-CH_2 vinyl complex [WPt{μ-CR=CH$_2$}(CO)$_2$(PMe$_3$)$_2$(Cp)] (**34**).[16] This synthesis is akin to cyclopropanation of an alkene and was also successfully employed to obtain [TiW{μ-CR=CH$_2$}(μ-CO)(CO)(Cp)$_3$] (**35**) from [TiW(μ-CR)(μ-CO)(CO)(Cp)$_3$] (**36**).[16]

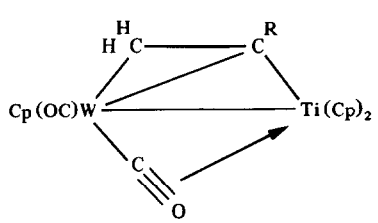

(35)

The exceptional reactivity of the complexes [WFe(μ-CR)(CO)$_5$(Cp*)] (**37**) and [MoFe(μ-CR)(CO)$_6$(Cp)] (**38**) leads to successful reactions with CH_2N_2 (Scheme 4).[17,18] The pentamethylcyclopentadienyl complex (**37**) with excess CH_2N_2 and a CuCl catalyst predominantly affords the kinetically favoured *gem*-CH_2 derivative [WFe(μ-CR=CH$_2$)(μ-CH$_2$)(CO)$_5$(Cp*)] (**39**), which arises from insertion of "CH_2" fragments into both the W—μ-CR and the metal–metal bonds. In contrast, slow addition of CH_2N_2 allows time for vinyl isomerization to occur and this leads to the formation of the thermodynamically favoured *trans-vicinal* complex [WFe(μ-CH=CHR)(μ-CH$_2$)(CO)$_5$(Cp*)] (**40**), together with traces of (**39**) and the μ-CO complex [WFe(μ-CH=CHR)(μ-CO)(CO)$_5$(Cp*)] (**41**). Interestingly, treatment of (**41**) with excess CH_2N_2 affords both (**40**) and (**39**). Formation of the latter *gem*-CH_2 species indicates that vinyl isomerization must be partially reversible as shown (Scheme 4).

The reaction of [MoFe(μ-CR)(CO)$_6$(Cp)] (**38**) with CH_2N_2 at ambient temperatures gives [MoFe(μ-CR=CH$_2$)(μ-CH$_2$)(CO)$_5$(Cp)] (**42**), and there is no evidence that vinyl isomerization can occur in this system to give analogues of the WFe complexes (**40**) and (**41**). In contrast, the reaction of (**38**) with CH_2N_2 at −40°C gives the allylic derivative [MoFe(μ-CR·COMe·CH)(CO)$_5$(Cp)] (**43**). Formation of (**43**) is complex, but appears to involve coupling of μ-CR·C(O) and CH_2, hydrogen migration and addition of a second molecule of

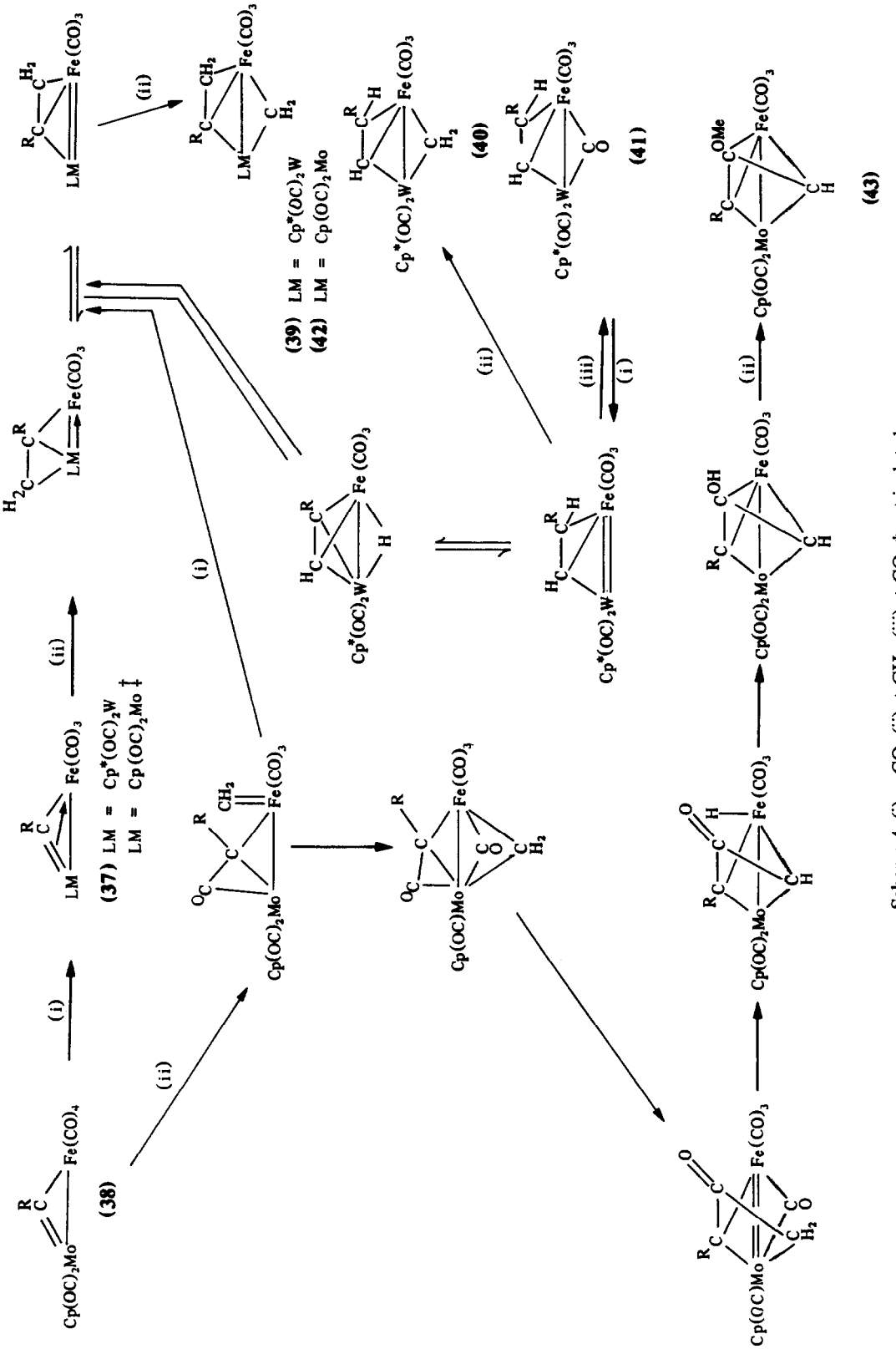

Scheme 4. (i) $-CO$, (ii) $+CH_2$, (iii) $+CO$, ‡ not isolated.

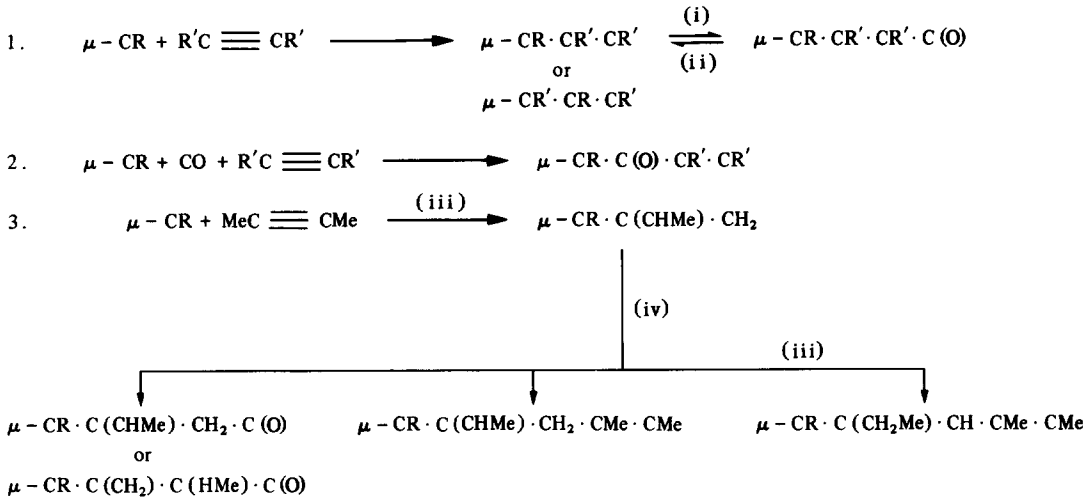

Scheme 5. Typical organic ligands obtained from coupling of μ-CR, alkynes and CO at dimetal centres. (i) +CO, (ii) −CO, (iii) requires alkyne isomerization, (iv) +MeC≡CMe or CO.

CH_2N_2 (Scheme 4). A closely related reaction occurs between the PMe_3 complex [MoFe(μ-CR)$(CO)_5(PMe_3)$(Cp)] (**44**) and CH_2N_2, but here a stable hydroxy derivative [MoFe(μ-CR·COH·CH)$(CO)_4(PMe_3)$(Cp)] (**45**) is obtained which does not react with further CH_2N_2 to give a phosphine analogue of (**43**).[18]

Reactions with alkynes

(i) *Alkylidyne complexes.* Heterometallic alkylidyne complexes react with alkynes at rates which reflect the availability of substitution labile CO ligands, or the presence of vacant coordination sites. Substitution inert complexes such as [WRh(μ-CR)$(CO)_3$(Cp)(Cp*)] (**46**) require prolonged reaction at high temperatures (2–3 days at 100°C) whilst [MoFe(μ-CR)$(CO)_6$(Cp)] (**38**) which is a source of the coordinatively unsaturated complex [MoFe(μ-CR)$(CO)_5$(Cp)] reacts rapidly with alkynes at or below ambient temperatures.

Scheme 5 shows the types of organic ligands which have been obtained via coupling of μ-CR, alkyne and CO ligands at mixed-metal centres, and specific examples of reactions which afford these ligands are discussed in more detail below.

Diphenylacetylene reacts with a wide variety of MM'μ-CR complexes to give products with allylic μ-σ, σ': η^3-CR·CPh·CPh ligands which arise from coupling of μ-CR and alkyne (Scheme 6). Related dimetal complexes are also formed when PhC≡CPh reacts with trimetal μ_3-alkylidyne clusters such as [$WFe_2(\mu_3$-CR)(μ-CO)$(CO)_8$(Cp)] (**47**).[19] Here, there is evidence that initial transverse coordination of the alkyne across a W—Fe bond precedes alkyne–μ-CR bond formation and cluster fragmentation.

Comparatively unreactive μ-CR complexes such as [WM(μ-CR)$(CO)_3$(Cp*)(Cp)] [M = Rh (**46**) or Co (**5**)] and [WRh(μ-CR)$(CO)_3(\eta^5$-$C_9H_7)$(Cp)] (**50**) with MeC≡CMe, give products analogous to those obtained with PhC≡CPh, and it has been shown that (**50**) reacts with asymmetrically substituted alkynes, $R^1C{\equiv}CR^2$, to give complexes with isomeric μ-CR·CR^1·CR^2 and μ-CR·CR^2·CR^1 ligands.[20]

Reactions of the terminal alkylidyne complexes [CoW(≡CR)$(CO)_8$] [R = C_6H_4Me-4 (**51a**), Ph (**51b**) or Me (**51c**)] with a wide range of alkynes have been studied in particular detail (Scheme 6). Treatment of (**51a**) with PhC≡CPh gives the allylic complex [WCo(μ-CR·CPh·CPh)$(CO)_7$] (**52**) and a minor by-product [WCo(μ-CPh·CR·CPh)$(CO)_7$] (**53**). Formation of the μ-CPh·CR·CPh ligand in (**53**) requires cleavage of the alkyne into its constituent CPh moieties during the course of the reaction. This behaviour has precedent in the reaction of [WFe_2(μ-CR)(μ-CO)$(CO)_8$(Cp)] with PhC≡CPh and also arises in reactions of (**51**) with EtC≡CEt. More nucleophilic alkynes, such as MeC≡CMe, give metalloketone complexes [WCo{μ-CR·CMe·CMe·C(O)}$(CO)_7$] (**54**) and these may be protonated at the C=O oxygen atom giving cationic hydroxyl derivatives [WCo(μ-CR·CMe·CMe·COH)$(CO)_7$][BF_4] (**55**).[23,24]

The alkylidyne complexes [MoFe(μ-CR)$(CO)_6$(Cp)] (**38**), [MoFe(μ-CR)$(CO)_5(PMe_3)$(Cp)] (**44**), [WFe(μ-CR)$(CO)_5$(Cp*)] (**37**), [$MoFe_2$(μ-CR)(μ-CO)

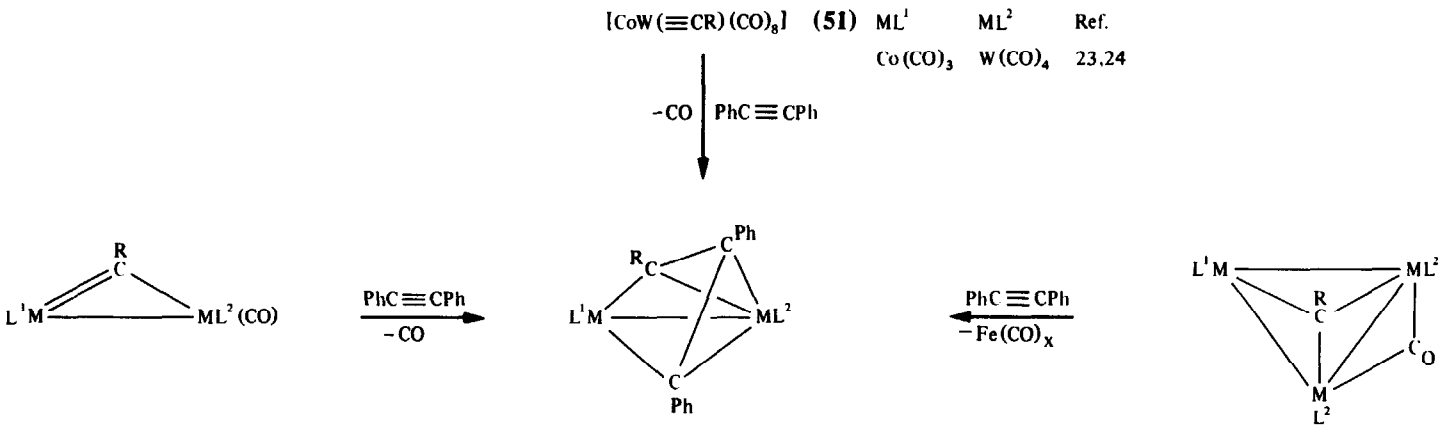

	ML^1	ML^2	Ref.
(5)	$W(CO)_2Cp$	$CoCp^*$	19
(46)	$W(CO)_2Cp$	$RhCp^*$	20
(50)	$W(CO)_2Cp$	$Rh(\eta^5-C_9H_7)$	20
(38)	$Mo(CO)_2Cp$	$Fe(CO)_3$	21

	ML^1	ML^2	Ref.
(47)	$W(CO)_2Cp$	$Fe(CO)_3$	19
(48)	$Mo(CO)_2Cp$	$Fe(CO)_3$	21
(49)	$W(CO)_2Cp^*$	$Fe(CO)_3$	22

Scheme 6. Principal products obtained from reactions of alkylidyne complexes with PhC≡CPh.

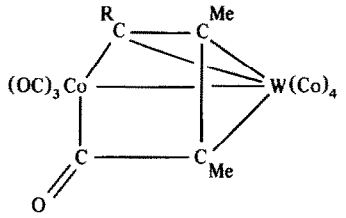

(54)

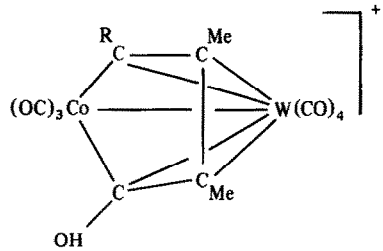

(55)

$(CO)_8(Cp)]$ (**48**) and $[MoW(\equiv CR)(CO)_7(Cp)]$ (**61**), are exceptionally reactive and with MeC≡CMe afford a fascinating series of products whose formation often requires isomerization of one molecule of MeC≡CMe and the insertion of additional alkyne or CO ligands into the growing organic chain (Scheme 7).[21,22] Compound (**38**) with MeC≡CMe gives two diastereoisomers of $[MoFe\{\mu\text{-}CR \cdot C(HMe) \cdot CH_2\}(CO)_5(Cp)]$ (**56a,b**), and (**56a**) was characterized by an X-ray diffraction study. The structure is particularly interesting since there is no metal–metal bond and the complex may be regarded as a molybdenum substituted "trimethylenemethane" $Fe(CO)_3$ compound.[21] Formation of (**56a,b**) results from coupling of the μ-CR group in (**38**) with a molecule of MeC≡CMe, together with a metal assisted 1,3 hydrogen shift from a CMe group to an *anti* site on an adjacent *C*Me carbon atom. Two such hydrogen shifts are required to account for the formation of the CEt·CH fragment found in $[WFe(\mu\text{-}CR \cdot CEt \cdot CH \cdot CMe \cdot CMe)(\mu\text{-}CO)(CO)_3(Cp^*)]$ (**59**),[22] and it is interesting that the insertion of additional alkyne or CO ligands required to form complexes (**57**), (**58**) and (**59**) occurs exclusively at the CH or CH_2 terminus of the carbon chain. In contrast, under mild conditions the terminal alkylidyne complex $[MoW(\equiv CR)(CO)_7(Cp)]$ (**61**) with MeC≡CMe gives $[MoW\{\mu\text{-}CR \cdot C(CH_2) \cdot C(HMe) \cdot C(O)\}(CO)_6(Cp)]$ (**62**) in which CO insertion has occurred at the CHMe end of the carbon chain. Remarkably, treatment of (**62**) with more MeC≡CMe in refluxing tetrahydrofuran gives $[MoW(\mu\text{-}CR \cdot CMe \cdot CMe)(CO)_3(\eta^2\text{-}MeC{\equiv}CMe)_2(Cp)]$ (**63**). Evidently retroisomerization of the $C(CH_2) \cdot C(HMe)$ moiety is also a facile process at a Mo—W dimetal centre.[25]

Related reactions of $[MoFe(\mu\text{-}CR)(CO)_6(Cp)]$ (**38**) with EtC≡CEt do not involve β-hydrogen migration. Instead, complexes with μ-CR·CEt·CEt (**64**), μ-CR·C(O)·CEt·CEt (**66**), or anomalous μ-CR·CEt·C{C(O)Me} (**67**) and μ-CR·C{C(O)Me}·CEt (**68**) ligands are obtained (Scheme 8).[26] The latter acyl complexes (**67**, **68**) arise from selective scavenging of EtC≡CC(O)Me, which was present as a trace impurity in the commercial sample of EtC≡CEt used, and we are grateful to Prof. Dixon for drawing our attention to the fact that he had previously encountered this problem.[27] Reversible insertion of CO into the Fe—CEt bond in (**64**), gives (**65**) which has a μ-CR·CEt·CEt·C(O) ligand. The isomeric μ-CR·C(O)·CEt·CEt group found in (**66**) does not lose CO and appears to arise from coupling of EtC≡CEt with a transient μ-CR·C(O) ketenyl precursor. Related ketenyl intermediates were also implicated in the low temperature reactions of (**38**) with CH_2N_2 noted in a previous section.

(ii) *Reaction of* $WM\{\mu\text{-}\sigma:\eta^3\text{-}CH(C_6H_4Me\text{-}4)\}$ *complexes with alkynes.* Heterodimetal complexes with μ-C(R)(OMe) ligands do not generally react readily with alkynes. In contrast, the weakly η^2-coordinated tolyl ligand in complexes having $\mu\text{-}\sigma:\eta^3$-CH(R) groups is readily displaced by a variety of nucleophiles (see earlier section) including alkynes (Scheme 9).

Reaction of $[PtW\{\mu\text{-}\sigma:\eta^3\text{-}CH(R)\}(CO)_2(PR_3)_2(Cp)][BF_4]$ (**10**) (PR_3 = PMe_3, PMe_2Ph or $PMePh_2$) with but-2-yne or diphenylacetylene gives the terminal alkyne complexes $[PtW\{\mu\text{-}CH(R)\}(\mu\text{-}CO)(PR_3)_2(\eta^2\text{-}R'C{\equiv}CR')(Cp)][BF_4]$ (R′ = Me or Ph). The alkyne is *anti* to the displaced tolyl ligand and none of the alternative *syn* diastereoisomer is obtained in these reactions.[15]

Initial attack of but-2-yne on the neutral phosphido bridged complex $[WFe\{\mu\text{-}\sigma:\eta^3\text{-}CH(C_6H_4Me\text{-}4)\}(\mu\text{-}PPh_2)(CO)_4(Cp)]$ (**26**) presumably affords a terminal alkyne intermediate analogous to (**69**), but rapid insertion of MeC≡CMe into a M—μ-CR bond leads to isolation of the delocalized vinylcarbene derivative $[WFe\{\mu\text{-}\sigma:\eta^3\text{-}C(Me)C(Me)C(R)H\}(\mu\text{-}PPh_2)(CO)_4(Cp)]$ (**70**).[28]

In contrast but-2-yne formally appears to insert into the μ-CH bond of $[WCo\{\mu\text{-}\sigma:\eta^3\text{-}CH(R)\}(CO)_3(Cp)(Cp^*)][BF_4]$ (**9**) giving the coordinatively unsaturated complex $[WCo\{\mu\text{-}\sigma:\eta^3\text{-}C(R)C(Me)C(Me)H\}(\mu\text{-}CO)(CO)(Cp)(Cp^*)][BF_4]$ (**71**). This difference may be readily understood if initial alkyne insertion into a M—μ-CR bond is followed by a rapid metal assisted 1,3 hydrogen

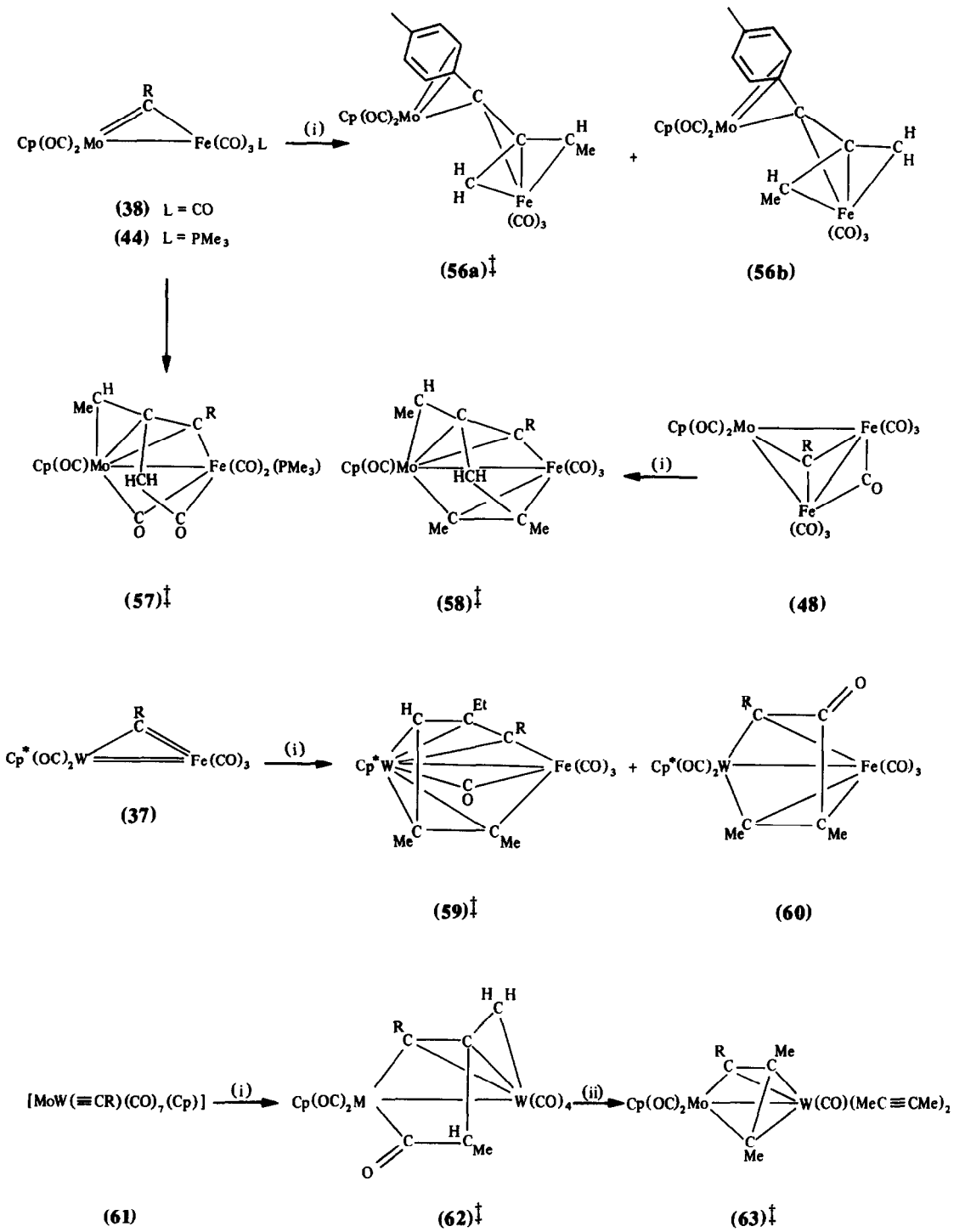

Scheme 7. Reactions involving isomerization of MeC≡CMe. (i) MeC≡CMe, (ii) MeC≡CMe in refluxing tetrahydrofuran. ‡ Characterized by X-ray diffractions.

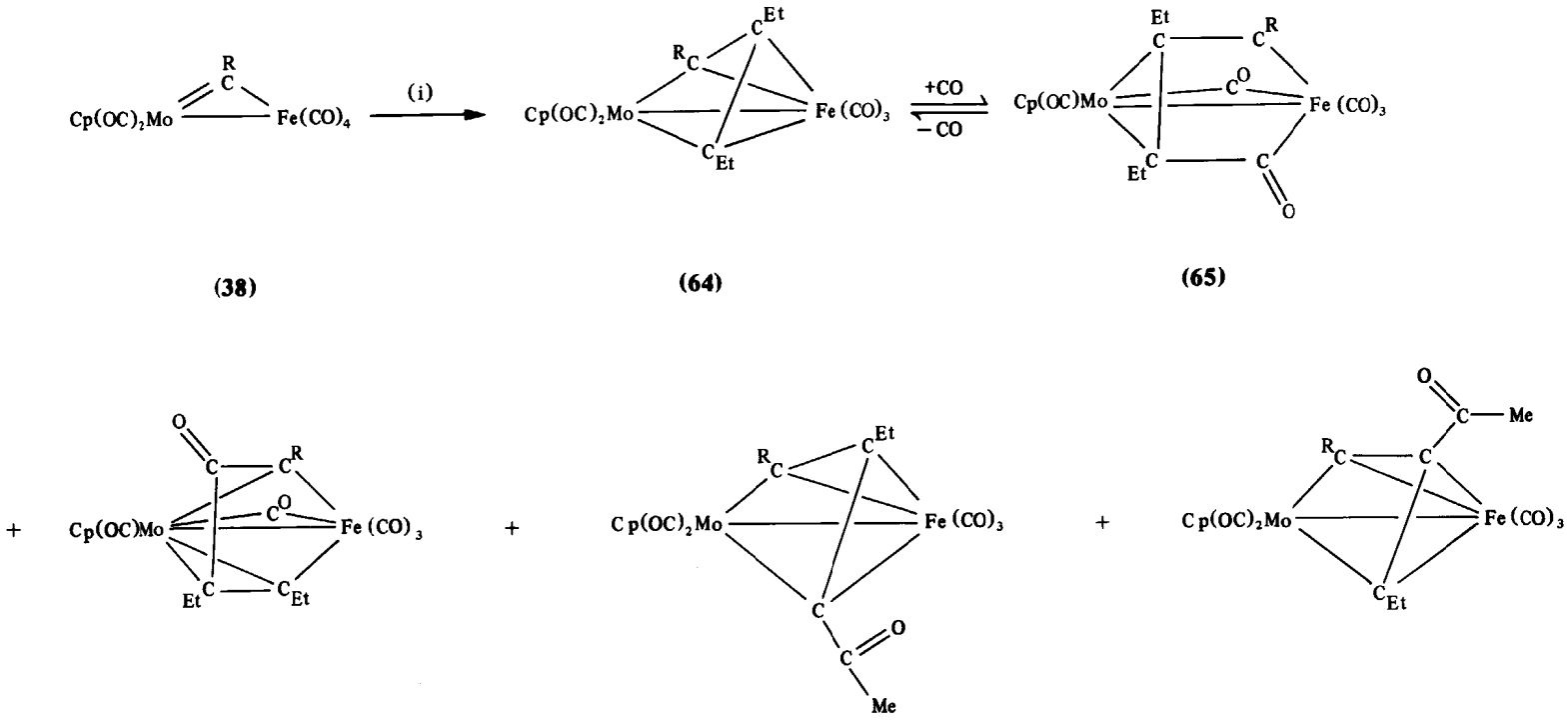

Scheme 8. (i) Hex-3-yne, R = C_6H_4Me-4. * Characterized by X-ray structure determination.

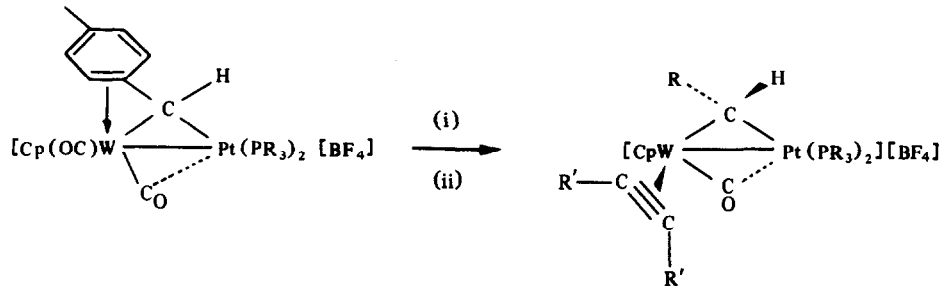

	PR_3
(10a)	PMe_3
(10b)	PMe_2Ph
(10c)	$PMePh_2$

	PR_3	R′
(69)‡	PMe_3	Me
	PMe_2Ph	Me
	PMe_2Ph	Ph
	$PMePh_2$	Ph

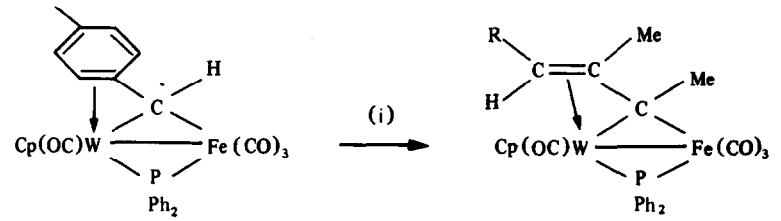

(26) **(70)**‡

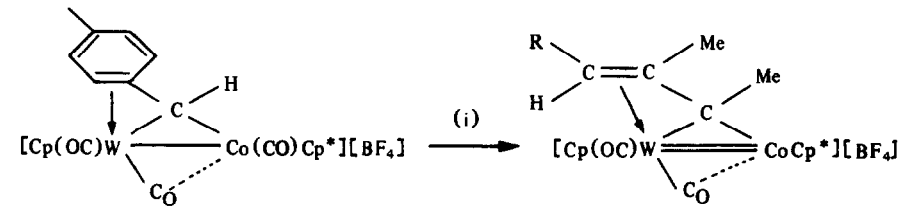

(9) **A**

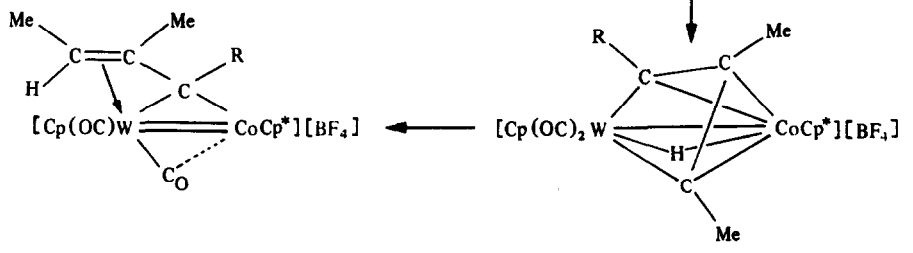

(71)‡ **B**

Scheme 9. (i) MeC≡CMe, (ii) PhC≡CPh, R = C_6H_4Me-4. ‡Characterized by X-ray structure diffraction.

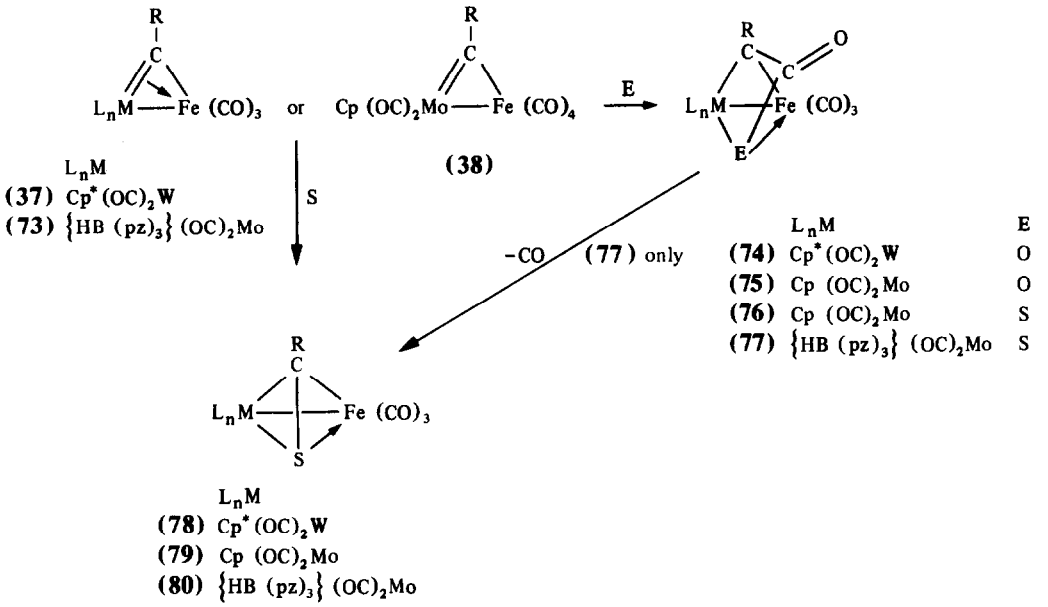

Scheme 10.

migration reaction as shown in Scheme 9. Complex (**71**) may also be obtained via protonation of the neutral complex [WCo{μ-C(R)C(Me)C(Me)}(CO)$_3$(Cp)(Cp*)] (**72**).[15]

REACTIONS WITH OXYGEN AND SULPHUR

Reaction of the bridging alkylidyne complexes (**37**) and (**38**) with oxygen, results in carbon–carbon and carbon–oxygen bond formation between alkylidyne, and carbonyl groups and an oxygen atom to form (**74**) and (**75**) in which the metal–metal bond is bridged by a CRC(O)O fragment (Scheme 10).[17,29] Reaction with elemental sulphur can follow two paths. Compound (**38**) forms a mixture of (**76**), the sulphur analogue of (**75**), and (**79**) in which the iron–molybdenum bond is bridged by a thioacyl ligand (Scheme 4).[29] Reaction of (**37**) with sulphur results in the thioacyl complex (**78**) as the sole product, whilst (**73**) affords both possibilities (**77**) and (**80**). Compound (**77**) decomposes into (**80**) with the loss of a carbonyl group.[30]

REFERENCES

1. F. G. A. Stone, *Angew. Chem. Int. Ed. Engl.* 1984, **23**, 89.
2. See for example, M. J. Attfield, J. A. K. Howard, A. N. de M. Jelfs, C. M. Nunn and F. G. A. Stone, *J. Chem. Soc., Chem. Commun.* 1986, 918.
3. M. R. Awang, J. C. Jeffery and F. G. A. Stone, *J. Chem. Soc., Dalton Trans.* 1986, 165.
4. J. C. Jeffery, C. Sambale, M. F. Schmidt and F. G. A. Stone, *Organometallics* 1982, **1**, 1597.
5. J. C. Jeffery, J. C. V. Laurie, I. Moore, H. Razay and F. G. A. Stone, *J. Chem. Soc., Dalton Trans.* 1984, 1563.
6. J. C. Jeffery, I. Moore and F. G. A. Stone, *J. Chem. Soc., Dalton Trans.* 1984, 1571.
7. F.-E. Baumann, J. A. K. Howard, O. Johnson and F. G. A. Stone, *J. Chem. Soc., Dalton Trans.* 1987, 2661
8. J. A. K. Howard, J. C. Jeffery, M. Laguna, R. Navarro and F. G. A. Stone, *J. Chem. Soc., Dalton Trans.* 1981, 751.
9. K. A. Mead, I. Moore, F. G. A. Stone and P. Woodward, *J. Chem. Soc., Dalton Trans.* 1983, 2083.
10. M. R. Awang, J. C. Jeffery and F. G. A. Stone, *J. Chem. Soc., Dalton Trans.* 1983, 2091.
11. J. C. Jeffery, A. G. Orpen, F. G. A. Stone and M. J. Went, *J. Chem. Soc., Dalton Trans.* 1986, 173.
12. D. Hodgson, J. A. K. Howard, F. G. A. Stone and M. J. Went, *J. Chem. Soc., Dalton Trans.* 1985, 1331.
13. S. V. Hoskins, A. P. James, J. C. Jeffery and F. G. A. Stone, *J. Chem. Soc., Dalton Trans.* 1986, 1709.
14. J. C. Jeffery, J. G. Lawrence-Smith and A. G. Webb, unpublished results.
15. J. C. Jeffery, I. Moore, H. Razay and F. G. A. Stone, *J. Chem. Soc., Dalton Trans.* 1984, 1581.
16. M. R. Awang, R. D. Barr, M. Green, J. A. K. Howard, T. B. Marder and F. G. A. Stone, *J. Chem. Soc., Dalton Trans.* 1985, 2009.
17. E. Delgado, L. J. Farrugia, J. Hein, J. C. Jeffery, A. L. Ratermann and F. G. A. Stone, *J. Chem. Soc., Dalton Trans.* 1987, 1191.
18. M. E. Garcia, J. C. Jeffery, P. Sherwood and F. G. A. Stone, *J. Chem. Soc., Chem. Commun.* 1986, 802; M. E. Garcia, N. H. Tran-Huy, J. C. Jeffery, P. Sherwood and F. G. A. Stone, *J. Chem. Soc., Dalton Trans.* 1987, 2201.

19. J. C. Jeffery, K. A. Mead, H. Razay, F. G. A. Stone, M. J. Went and P. Woodward, *J. Chem. Soc., Dalton Trans.* 1984, 1383.
20. M. Green, J. A. K. Howard, S. J. Porter, F. G. A. Stone and D. C. Tyler, *J. Chem. Soc., Dalton Trans.* 1984, 2553.
21. P. G. Byrne, M. E. Garcia, J. C. Jeffery, P. Sherwood and F. G. A. Stone, *J. Chem. Soc., Chem. Commun.* 1987, 53; P. G. Byrne, M. E. Garcia, J. C. Jeffery, P. Sherwood and F. G. A. Stone, *J. Chem. Soc., Dalton Trans.*, in press.
22. J. Hein, J. C. Jeffery, P. Sherwood and F. G. A. Stone, *J. Chem. Soc., Dalton Trans.* 1987, 2211.
23. I. J. Hart, J. C. Jeffery, M. J. Grosse-Ophoff and F. G. A. Stone, *J. Chem. Soc., Dalton Trans.*, in press.
24. I. J. Hart and F. G. A. Stone, *J. Chem. Soc., Dalton Trans.*, in press.
25. E. Delgado, M. E. Garcia, J. C. Jeffery, P. Sherwood and F. G. A. Stone, *J. Chem. Soc., Dalton Trans.* 1988, 207.
26. M. E. Garcia, J. C. Jeffery, P. Sherwood and F. G. A. Stone, *J. Chem. Soc., Dalton Trans.*, in press.
27. C. N. Bainbridge, R. S. Dickson, G. D. Fuller, I. Grayson, R. J. Nesbit and J. Weigold, *Aust. J. Chem.* 1986, **39**, 1187.
28. J. C. Jeffery, J. G. Lawrence-Smith and A. G. Webb, unpublished results.
29. P. G. Byrne, M. E. Garcia, J. C. Jeffery, P. Sherwood and F. G. A. Stone, *J. Chem. Soc., Dalton Trans.* 1987, 1215.
30. M. D. Bermudez, E. Delgado, G. P. Elliott, N. H. Tran-Huy, F. Mayor-Real, F. G. A. Stone and M. J. Winter, *J. Chem. Soc., Dalton Trans.* 1987, 1235.

Polyhedron Vol. 7, No. 10/11, pp. 791–805, 1988
Printed in Great Britain

0277–5387/88 $3.00+.00
© 1988 Pergamon Press plc

GENERATION AND REACTIVITY OF KETENE LIGANDS ON TRIOSMIUM CLUSTERS

SHERRI L. BASSNER and GREGORY L. GEOFFROY*

Department of Chemistry, The Pennsylvania State University, University Park, PA 16802, U.S.A.

and

ARNOLD L. RHEINGOLD

Department of Chemistry, The University of Delaware, Newark, Delaware 19716, U.S.A.

(*Accepted* 5 *November* 1987)

Abstract—A summary of the synthesis, spectroscopic properties, and reactivity characteristics of the triosmium μ-ketene clusters $Os_3(CO)_{12}(\mu\text{-}CH_2CO)$, **3**, and $[PPN][Os_3(CO)_{10}(\mu\text{-}X)(\mu\text{-}CH_2CO)]$, (**5a**, X = Cl; **5b**, X = Br; **5c**, X = I; **6c**, X = NCO) is presented. In addition, the preparation of the $Bu^tN{\equiv}C$ substituted ketene clusters $Os_3(CO)_{10}(Bu^tNC)_2(\mu\text{-}CH_2CO)$, **4**, and $[PPN][Os_3(CO)_9(Bu^tNC)(\mu\text{-}X)(\mu\text{-}CH_2CO)]$ (**7c**, X = I; **7d**, X = NCO) by reaction of the appropriate μ-CH_2 precursors with $Bu^tN{\equiv}C$ is described. Cluster **4** has been crystallographically characterized: $P2_1/c$, $a = 19.262(4)$, $b = 22.486(4)$, $c = 13.197(3)$ Å, $\beta = 97.73(2)°$, $V = 5790(2)$ Å^3, $Z = 2$, $R(F) = 0.0639$, $R(wF) = 0.0671$ for 4172 reflections with $I > 4\sigma(F_0)$. The three Os atoms and the μ-ketene ligand form a triosmacyclopentanone ring with the isocyanide ligands in equatorial positions on different Os atoms and *trans* to the ketene methylene and carbonyl carbons, respectively. A variable temperature ^1H NMR study has shown that cluster **4** undergoes a fluxional process involving an inversion of the triosmacyclopentanone ring conformation which causes exchange of the positions of the methylene protons of the μ-ketene ligand. The activation energy for this process is ~ 11 kcal mol^{-1}.

Ketenes are reactive organic molecules that have been extensively investigated since the early 1900s when Staudinger[1] and Wilsmore[2] conducted their pioneering studies. The characteristic organic chemistry of ketenes is now well defined, and excellent reviews on various aspects of the synthesis and properties of ketenes are available.[3] In contrast, the *organometallic* chemistry of ketenes is only now beginning to be seriously developed, although a number of interesting metal–ketene reactions were described in the early organometallic literature. We recently compiled a comprehensive review of the interaction of ketenes with organometallic complexes,[4] and one surprising finding was the diversity of bonding modes that this ligand adopts. If we take the generic view that any complex containing a "CR_2CO" ligand is a ketene complex regardless of the hybridization of the ligand, then the established ketene complexes can be grouped into the structural types shown on the next page.

Type **I** has an η^2-(C,C) ligand bound to a single metal centre typically found for low-valent middle to late transition metals. In Type **II**, a μ_2,η^2-(C,C) ligand bridges adjacent metals in binuclear and cluster compounds. In Type **III** the carbonyl oxygen also interacts with a third metal atom. Early transition metals generally give η^2-(C,O) ketene complexes with this ligand bound to a single metal as in **IV** or to two metals as in **V** and **VI**. A few metalla-enolate complexes of Type **VII** have been mentioned and there are several vinylketene complexes of Type **VIII**. Type **IX** complexes form when E is a potential ligand such as phosphorus and

* Author to whom correspondence should be addressed.

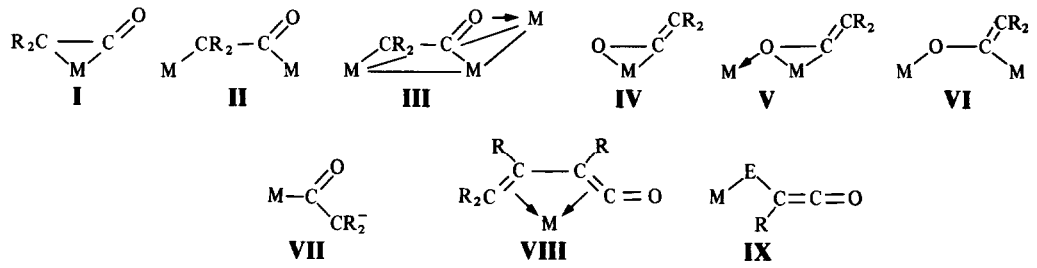

Structures I–IX.

arsenic. The above classification has excluded metalla ketene complexes in which a metal is one of the ketene substituents, although such "ketenyl" and "ketenylidene" complexes were included in the above-mentioned review.[4] Synthetic methods for ketene complexes vary, but the most useful have involved carbonylation of carbene ligands, addition of free ketenes to unsaturated complexes, and deprotonation of acyl ligands.[4]

Ketene complexes are important for a variety of reasons. One is to model reactions which have been suggested to occur during heterogeneous synthesis gas catalysis. For example, insertion of CO into metal–methylene and –carbene bonds to form surface bound ketenes has been suggested to be an important step in the production of hydrocarbons and C_2-oxygenates.[5] Similarly, ketene complexes generated by carbene–CO coupling or from the addition of ketenes to unsaturated metals have been used in several recent synthetic transformations of organic interest.[6]

Whereas much is known about the structure of ketene complexes, relatively little is understood about the reactivity of these ligands and particularly how the coordination mode influences its chemistry.[4] Such knowledge is vital if ketene complexes are to find extensive use in organic synthesis.[6] Especially important would be a comparison of the reactivity of free and coordinated ketenes. Much of the reactivity of *free* ketenes can be rationalized by the polarization of the molecule shown in eq. (1). The same conclusion is reached by frontier orbital analysis that shows the LUMO to be mainly localized on the β carbon and the HOMO on the α carbon and the oxygen atom.[7] Nucleophiles typically add to the β-carbon whereas electrophiles add to the terminal atoms, particularly the α-carbon, and a characteristic reaction is the addition of polar H—X bonds across the ketene C=C bond, eq. (1).[3] Free ketenes also undergo cycloaddition reactions with electron-rich olefins, alkynes, and other unsaturated organics, e.g., eq. (2).[3] These reactions are thought to proceed via an allowed antarafacial [π2s + π2a] concerted process.[7]

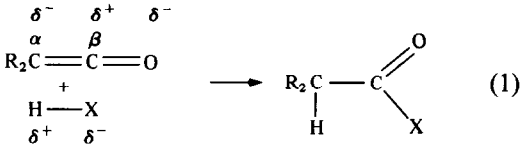

(1)

X = OR, NR_2, SR, etc.

Eq. (1)

Our interest in this area arose through our studies of the chemistry of the methylene cluster **1**[8] and its halide-substituted derivatives **2a–d** which are easily formed by the reaction of eq. (3).*[9] We found that both **1** and the anionic clusters **2** readily insert CO into the metal–methylene bonds to form ketene ligands,[10,11] and we then began a series of in-depth studies of the genesis and reactivity of ketenes coordinated to these Os_3 clusters. The purpose of this article is to collect and summarize the most important results from our several studies[10,12,13] in this area[10–13] so as to put all the data and observations in total perspective. We also present new results involving the reactions of **1** and **2** with $Bu^tN{\equiv}C$ which have led to the formation of novel isocyanide substituted ketene clusters.

SYNTHESIS OF TRIOSMIUM μ-KETENE CLUSTERS

Our initial result in this area was the discovery that methylene cluster **1** slowly reacts with CO under mild conditions to form in good yield the neutral ketene cluster **3**, eq. (4).[10] This species was isolated as extremely water sensitive yellow crystals, and it was both spectroscopically and structurally characterized (see below). The CO insertion reaction was not readily reversible as evidenced by the low yield (8%) recovery of **1** following heating **3** (64°C, 30 min) under reduced pressure. Of interest is the mechanism by which this reaction occurs, and

*$PPN^+ = (Ph_3P)_2N^+$. The isocyanate derivative **2d** was formed from the reaction of **1** with $[PPN]N_3$.

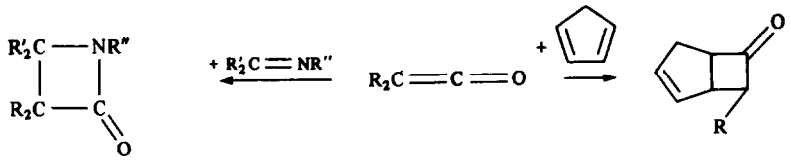

(2)

Eq. (2)

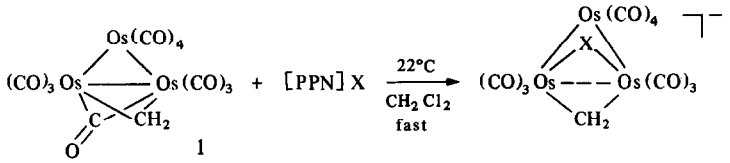

(3)

2a X = Cl **2c** X = I
2b X = Br **2d** X = NCO*

Eq. (3)

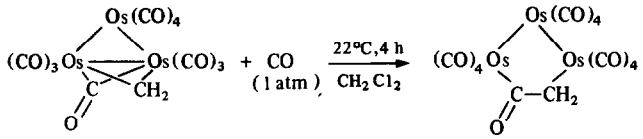

(4)

1 **3** (76%)

Eq. (4)

a key issue here is the source of the CO that was incorporated into the ketene ligand. ^{13}C-labelling studies clearly showed that this carbonyl was an original cluster CO ligand and that the two exogenous COs simply add as carbonyl ligands in the final product **3**. This leads to the mechanistic suggestion of eq. (5) involving reversible insertion of a cluster CO into the osmium–methylene bond.[10]

Consistent with the above mechanistic suggestion is the recent finding that tert-butylisocyanide also reacts with **1** to induce CO insertion to form the ketene cluster **4**, eq. (6), rather than to form a ketenimine derivative which could have arisen from isocyanide insertion into the metal–methylene bond. Cluster **4** was isolated in good yield as air and moisture stable orange microcrystals and was both spectroscopically and structurally characterized (see below). Also isolated from this reaction was $Os_3(CO)_{10}(Bu^tNC)_2$ (23%) which apparently forms from loss of ketene from **4**. Note that reaction (6) is complete within 10 min whereas the reaction of **1** with CO to give ketene cluster **3** required 4–6 h for completion. Although isocyanides induce the CO insertion to form a ketene ligand, phosphines have not been found to give similar chemistry but instead give a complex mixture of PR_3 substituted Os_3 clusters.[10]

The anionic halide-substituted methylene clusters **2a–d** also react with CO to form ketene derivatives, eq. (7).[11] Surprisingly, these reactions are totally reversible; removal of the CO atmosphere from the above solutions of **5a–d** causes instantaneous

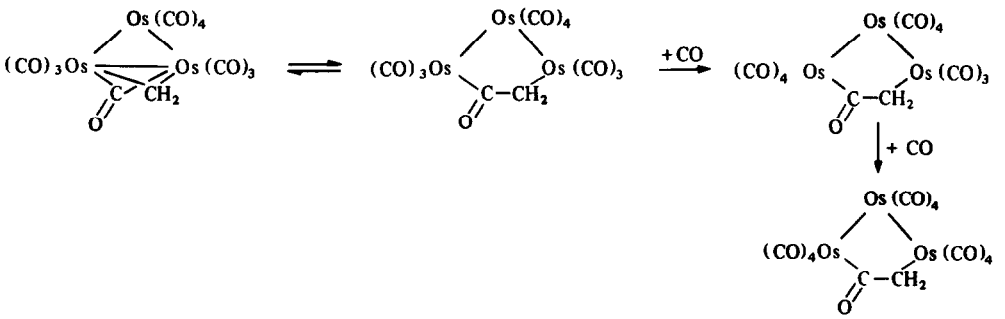

(5)

Eq. (5)

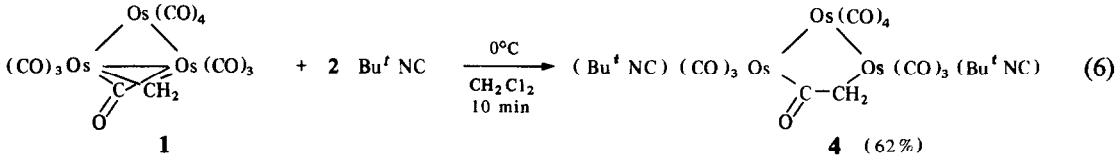

(6)

Eq. (6)

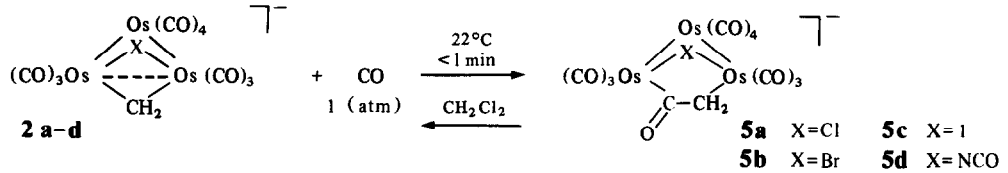

(7)

Eq. (7)

regeneration of the methylene clusters **2a–d**. Note that such a reaction does not occur for the neutral ketene cluster **3**. The anionic ketene clusters **5a–d** cannot be isolated because of their ready loss of CO, but when needed they can immediately and quantitatively be generated by exposure of **2a–d** to a CO atmosphere. As above, a ^{13}C-labelling study showed that the CO incorporated into the ketene ligand in **2c** was an original cluster CO and that the exogenous CO simply added as a cluster carbonyl.[11]

Prolonged exposure of ketene clusters **5a–c** to CO induces slow loss of halide with uptake of two COs to form the neutral ketene cluster **3**.[11] However, the isocyanate derivative **5d** *reversibly* adds just one CO to form a 1 : 1.3 mixture of the isomeric clusters **6a** and **6b** having terminal NCO ligands, eq. (8).[11] Note that **6a** and **6b** differ only in the osmium to which the isocyanate ligand is attached. These complexes are indefinitely stable under a CO atmosphere and show no tendency to lose the isocyanate ligand. However, upon removal of the CO atmosphere, they quantitatively regenerate the starting methylene cluster **2d**, a reaction which presumably proceeds via initial formation of the ketene cluster **5d** which then loses CO to form **2d**. It is likely that the CO induced slow conversion of the halide substituted clusters **5a–c** into **3** with loss of the halide proceeds via initial formation of analogues of **6** with terminal halide ligands which then undergo substitution of CO for the halide.

As reactions (4) and (7) illustrate, halides dramatically promote the rate of the methylene carbonylation to form ketenes. Note that the halide-substituted clusters **2a–d** undergo complete carbonylation in < 1 min whereas the neutral methylene cluster **1** requires ~ 4 h for total reaction. While the reasons for this kinetic acceleration are unknown, both spectroscopic and structural data indicate that reaction (7) with **2** is far more thermodynamically favoured than is reaction (4) with **1**. The clusters **2a–d** are 50 electron species and as such should have only two Os—Os bonds. However, X-ray structural studies of **2c** and **2d** showed the presence of two unbridged Os—Os bonds and an Os · · · Os separation of 3.112 (**2c**) and 3.053 Å (**2d**) for the edge which is simultaneously bridged by the methylene and X ligands.[9] The Os atoms on this edge should be non-bonded and much further apart, but the constraints imposed by the bridging ligands force the metals close together. This strain is apparently relieved by CO insertion to form the ketene species **5a–d**. Further support for the favourable thermodynamics of reaction (7) comes from IR data that indicate that the excess negative charge on the $[Os_3(\mu\text{-}X)(\mu\text{-}R)(CO)_{10}]^-$ ($R = CH_2$, CH_2CO) clusters is better accommodated in the ketene complexes than in the methylene species. This is mainly indicated by the 10–20 cm^{-1} shift to higher energy of the *metal carbonyl vibrations* when the ketene ligand is formed in the

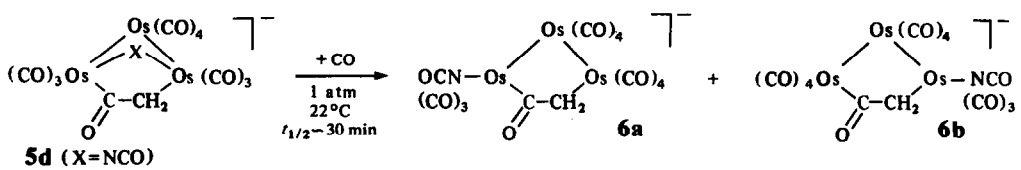

(8)

Eq. (8)

Table 1. Spectroscopic data for triosmium μ-ketene clusters[10,11]

Cluster	Ketene ν(CO)[a] (cm^{-1})	^{1}H NMR[b] $\delta(CH_2CO)$	^{1}H NMR[b] J_{HH} (Hz)	^{13}C NMR[b] $\delta(CH_2CO)$	^{13}C NMR[b] J_{HH} (Hz)	^{13}C NMR[b] $\delta(CH_2CO)$
3	1573w	2.77s,br	($\nu_{1/2}$ 11Hz)	32.8	136	210.4
4	1549w	2.81s,br	($\nu_{1/2}$ 7Hz)	30.5	132	226.0
5a	1556w	3.81d, 3.01d	13.1	35.3t	126	257.3
5b	1554w	3.95d, 3.40d	13.2	—	—	—
5c	1551w	4.04d, 3.89d	13.6	30.5t	125	256.4
5d	1561w	3.51d, 2.80d	13.2	—	—	—
6a	1550/1560[c]	3.10d, 2.46d	6.7	20.5t	136	240.7
6b	1550/1560[c]	4.14d, 2.52d	5.8	50.9t	132	219.4
7c	1539	4.02d, 3.72d	13.8	29.4t	124	259.8
7d	1547	3.44d, 2.75d	12.9	31.2t	125	259.7

[a] CH_2Cl_2.
[b] $CDCl_3$.
[c] The individual ketene ν(CO) stretches for **6a** and **b** were not assigned.

2 → **5** conversion and also by the relatively low vibrational frequency of the ketene carbonyls in the anionic ketene clusters **5a–d** (compare the IR data for **3** and **5a–d** in Table 1).

Isocyanides also induce the methylene to ketene transformation in the halide-substituted clusters **2c,d**, eq. (9).

$$[Os_3(CO)_{10}(\mu\text{-X})(\mu\text{-}CH_2)]^- + Bu^tNC \xrightarrow[<\,1\text{ min } CDCl_3]{-40^\circ C} [Os_3(CO)_9(Bu^tN{\equiv}C)(\mu\text{-X})(\mu\text{-}CH_2CO)]^- \quad (9)$$

2c,d → **7c**, X = I; **7d**, X = NCO

Eq. (9)

These reactions are fast even at −40°C, again illustrating the promoting effect of the presence of the anionic I^- and NCO^- ligands. Although clusters **7** are stable in solution at −40°C under an N_2 atmosphere, upon warming they deinsert CO to yield a complex but reproducible mixture of isocyanide substituted Os_3 methylene clusters. These apparently arise from multiple additions of $Bu^tN{\equiv}C$. Although not isolated, clusters **7** were spectroscopically characterized. The presence of the ketene ligand was indicated by IR vibrations in the 1540–1550 cm^{-1} region and by the ^{1}H and ^{13}C NMR data summarized in Table 1. The stoichiometry of the reaction involving incorporation of only one isocyanide was shown by ^{1}H NMR titration experiments. The spectroscopic data do not conclusively indicate to which Os atom the isocyanide is bound, although the very low ν(CO) stretch of the ketene ligand at 1539 and 1547 cm^{-1} for **7c** and **7d**, respectively, indicative of a strong σ-donor suggests the isocyanide is bound to the same Os atom as the ketene carbonyl and *trans* to it as in **4**.

Interestingly, the isocyanide substituted ketene clusters do not cleanly lose CO to form methylene clusters such as $[Os_3(CO)_9(Bu^tNC)(\mu\text{-}CH_2)(\mu\text{-X})]^-$, in contrast to the ready reversibility of the methylene/ketene transformations in the parent clusters without the isocyanide ligand, eq. (7). However, when placed under a CO atmosphere, clusters **7c,d** quickly undergo substitution of CO for the isocyanide ligand to form the μ-ketene clusters **5c,d**, eq. (10).

$$[Os_3(CO)_9(Bu^tNC)(\mu\text{-X})(\mu\text{-}CH_2CO)]^- + CO \rightarrow [Os_3(CO)_{10}(\mu\text{-X})(\mu\text{-}CH_2CO)]^- + Bu^tNC \quad (10)$$

7c,d → **5c,d**

Eq. (10)

If the CO atmosphere is then removed, clusters **7c,d** rapidly reform, probably via the sequence **5** → **2** → **7**.

SPECTROSCOPIC CHARACTERIZATION

Table 1 summarizes the important spectroscopic data for the μ-ketene clusters within the triosmium family. The ketene carbonyl IR stretch is in the 1535–1560 cm^{-1} region for all the anionic clusters, but the neutral ketene cluster **3** has a slightly higher energy ketene band at 1573 cm^{-1}. However, the

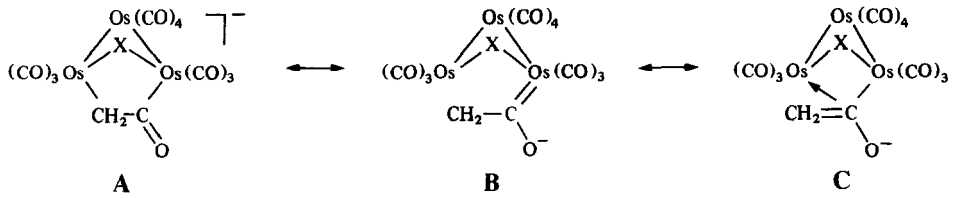

Structures **A**, **B** and **C**

corresponding band in the related μ-ketene complex $Cp(CO)_2Ru(\mu\text{-}CH_2CO)RuCp(CO)_2$[14] is far higher at 1622 cm^{-1}. The lower energy position of this band in the anionic clusters implies significant delocalization of electron density onto the ketene carbonyl and the importance of the oxycarbene and oxyvinyl resonance forms **B** and **C** drawn above. The importance of **B** and **C** are also indicated by the facile addition of electrophiles to the ketene carbonyl oxygen (see below). Similar oxycarbene resonance forms are important for anionic metal *acyl* complexes and contribute to the ease with which these are alkylated at the carbonyl oxygen to yield metal carbenes, but the oxyvinyl resonance form has no precedent in mononuclear chemistry.

The methylene protons of the ketene ligands in the *anionic* clusters are inequivalent and always appear as a pair of doublets in the δ 2.0–4.5 ^1H NMR range. However, the neutral ketene clusters **3** and **4** show only a broad singlet for the ketene protons at 22°C even though their crystal structures (see below) show the protons to be inequivalent.

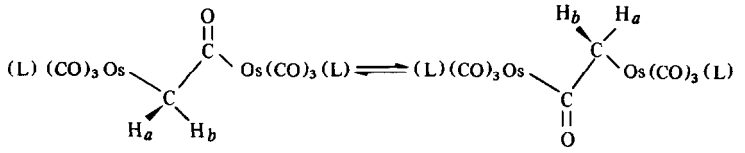

Scheme 1.

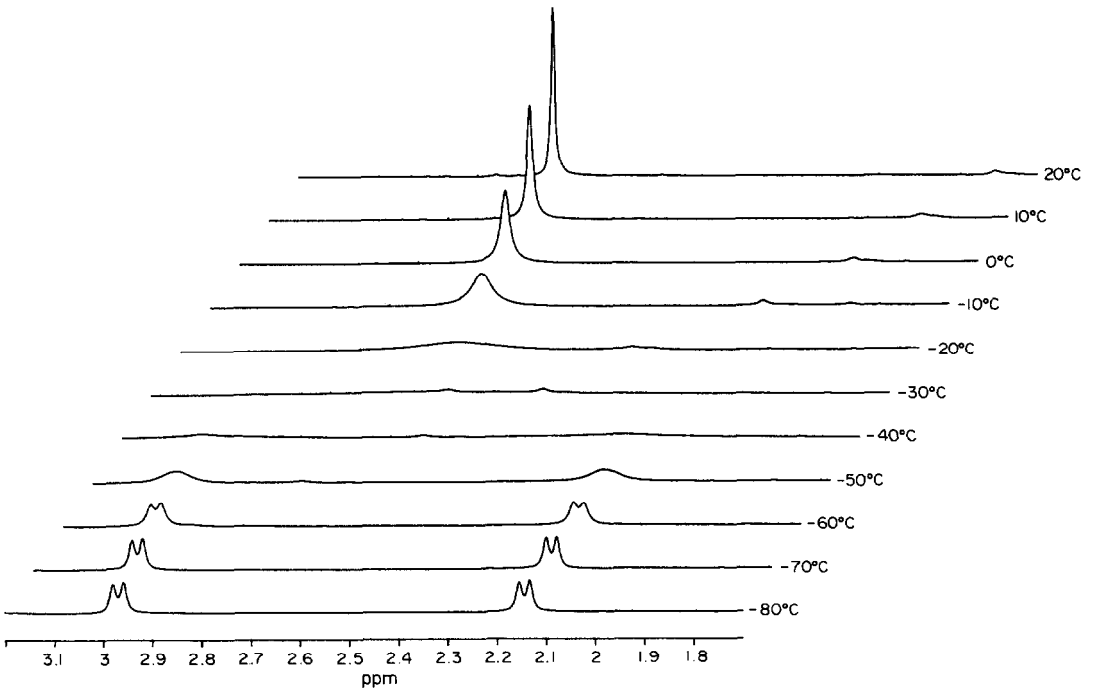

Fig. 1. Variable temperature ^1H NMR spectra for $Os_3(CO)_{10}(Bu^tNC)_2(\mu\text{-}CH_2CO)$, **4**, recorded in CD_2Cl_2 solution.

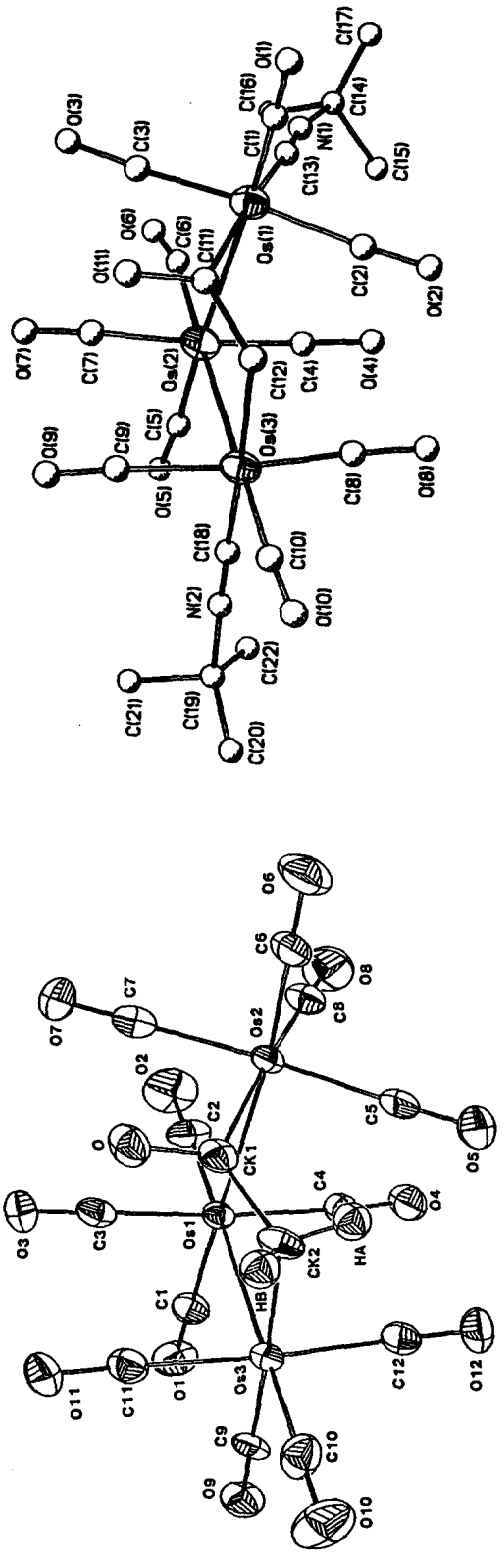

$Os_3(CO)_{12}(\mu\text{-}CH_2CO)$

3

$Os_3(CO)_{10}(Bu^tNC)_2(\mu\text{-}CH_2CO)$

4

Fig. 2. ORTEP drawings for $Os_3(CO)_{12}(\mu\text{-}CH_2CO)$, **3**, and $Os_3(CO)_{10}(Bu^tN{\equiv}C)_2(\mu\text{-}CH_2CO)$, **4**.

The single resonance implies rapid exchange of the methylene protons, presumably by inversion of the Os_3C_2 ring as illustrated in Scheme 1. This process has been probed by a variable temperature ^1H NMR experiment with **4**, the results of which are shown in Fig. 1. At $-80°C$, the CH_2CO resonances appear as two sharp doublets at δ 2.97 and 2.14 with $J_{HH} = 6.3$ Hz. These broaden upon warming, coalesce at $-30°C$, and then appear again at 20°C as a single resonance at δ 2.68. From the coalescence temperature and the chemical shifts in the static spectrum we calculate $\Delta G \approx 11$ kcal mol^{-1} for the exchange process which is presumably that depicted below.

The coordinated ketene ^{13}C NMR resonances are in typical positions for metal acyls and metal methylenes with the latter always appearing as a triplet with a 124–136 Hz coupling to the two hydrogens. This value is characteristic of an sp^3 hybridized carbon.[15]

CRYSTALLOGRAPHIC CHARACTERIZATION

Ketene clusters **3** and **4** have both been structurally characterized, with that of **3** reported in ref. 10 and that of **4** described for the first time herein. ORTEP drawings for both are shown in Fig. 2, and the pertinent crystallographic data for **4** are listed in Tables 2 and 3. Two molecules of complex **4** comprise the asymmetric unit, one of which was ordered and the other disordered (see Experimental). Bond distance and angle data are given in Table 3 only for the ordered molecule. A comparison of the structural parameters of the ketene ligand in **3** and **4** is given in Table 4. The clusters are remarkably similar with only minor variations in bond angles and distances caused by the substitution of the Bu^{t}NC ligands for CO. The two Bu^{t}NC ligands in **4** are coordinated to the two osmium atoms to which the ketene ligand is attached and are bound in equatorial positions with respect to the Os_3 plane. Each is *trans* to the ketene ligand.

Both molecules appear to be best described as triosmacyclopentanone derivatives, and an expanded view of the Os_3CH_2CO core of **3** which illustrates this point is shown in Fig. 3. The angles about the ketene carbonyl carbon closely approximate 120° as expected for an sp^2 hybridized carbon, and the 1.25–1.27 Å bond lengths of the ketene carbonyls are only slightly longer than the 1.23 Å bond length of typical organic carbonyls.[16] Likewise, the angles about the methylene carbons are close to the 109.5° value expected for a tetrahedral sp^3 carbon and the carbon–carbon distances within the ketene ligands

Table 2. Parameters for the crystallographic study of $Os_3(CO)_{10}(Bu^tN{\equiv}C)_2(\mu\text{-}CH_2CO)$, **4**

Formula	$C_{22}H_{20}N_2O_{11}Os_3$
Crystal system	monoclinic
Space group	$P2_1/c$
a, Å	19.692(4)
b, Å	22.486(4)
c, Å	13.197(3)
β	97.73(2)
V, Å^3	5790(2)
Z	9
D(calc), g cm^{-3}	2.430
T	293 K
Diffractometer	Nicolet R3m/μ
Radiation	Mo-K_α (graphite monochromated)
μ, cm^{-1}	155.8
Scan limits, deg	$4 \leqslant 2\theta \leqslant 45$
Scan method	omega
Rflns collected	8189
Indepdt rflns	7551
Obs. rflns ($4\sigma F_0$)	4172
R(int), %	3.55
$R(F)$, %	6.39
$R(wf)$, %	6.71
GOF	1.149
Δ/σ	0.11
$\Delta(\rho)$, e Å^{-3}	2.2 (near Os(3′))
N_0/N_v	8.6

of **3** and **4** are near the typical carbon–carbon single bond distance for carbons adjacent to carbonyls (1.52 Å[16]). It is thus somewhat inappropriate to refer to these compounds as ketene complexes, even though they contain the CH_2CO ligand, since the bond angles and the indicated carbon hybridizations are not those of free ketene.

The coordination at the osmium atoms in the two structures are essentially octahedral, and the Os—Os bond lengths fall within the range of typical Os—Os single bonds. The Os(1)···Os(3) distance of 4.277 Å in **4** clearly indicates that these two atoms are non-bonding as was also shown for **3**.

REACTIVITY OF THE μ-KETENE LIGANDS

Given the developing role of ketene complexes in synthetic transformations of organic interest[6] and the proposed involvement of surface bound ketenes during heterogeneous synthesis gas catalysis,[5] it is important to define as fully as possible the reactivity features of this ligand in its different coordination geometries. Thus we have tried to do this with the triosmium ketene complexes prepared in these laboratories, emphasizing the representative com-

Table 3. Selected bond distances and angles for $(Os_3(CO)_{10}(Bu^tN{\equiv}C)_2(\mu\text{-}CH_2CO)$, **4**[a]

	(a) Bond distances (Å)		
Os(1)—Os(2)	2.946(1)	Os(1)—C(11)	2.11(2)
Os(2)—Os(3)	3.023(1)	Os(3)—C(12)	2.23(2)
Os(1′)—Os(2′)	3.028(1)	C(11)—C(12)	1.44(2)
Os(2′)—Os(3′)	2.962(2)	C(11)—O(11)	1.27(2)
Os(1)—C(13)	2.05(2)	Os(1″)—Os(2″)	2.92(1)
Os(3)—C(18)	2.01(2)	Os(2″)—Os(3″)	2.86(1)
	(b) Bond angles (deg)		
Os(1)—Os(2)—Os(3)	90.2(1)	Os(3)—Os(2)—C(7)	84.3(4)
Os(1)—Os(2′)—Os(3′)	90.3(1)	C(4)—Os(2)—C(5)	92.3(8)
Os(1″)—Os(2″)—Os(3′)	93.4(4)	C(4)—Os(2)—C(6)	90.2(8)
C(1)—Os(1)—C(2)	92.7(7)	C(4)—Os(2)—C(7)	167.6(7)
C(1)—Os(1)—C(3)	92.4(7)	C(5)—Os(2)—C(6)	96.7(8)
C(1)—Os(1)—C(11)	87.6(7)	C(5)—Os(2)—C(7)	98.4(7)
C(1)—Os(1)—C(13)	103.5(7)	C(6)—Os(2)—C(7)	94.9(8)
C(1)—Os(1)—Os(2)	169.4(4)	Os(2)—Os(3)—C(8)	86.1(4)
C(2)—Os(1)—C(3)	174.7(7)	Os(2)—Os(3)—C(9)	90.4(4)
C(2)—Os(1)—C(11)	94.2(7)	Os(2)—Os(3)—C(10)	179.3(4)
C(2)—Os(1)—C(13)	84.1(7)	Os(2)—Os(3)—C(12)	89.1(3)
C(2)—Os(1)—Os(2)	89.3(6)	Os(2)—Os(3)—C(18)	87.5(3)
C(3)—Os(1)—C(11)	84.9(6)	C(8)—Os(3)—C(9)	173.9(6)
C(3)—Os(1)—C(13)	95.8(7)	C(8)—Os(3)—C(10)	93.7(7)
C(3)—Os(1)—Os(2)	85.4(5)	C(8)—Os(3)—C(12)	92.1(6)
C(11)—Os(1)—C(13)	168.C13	C(8)—Os(3)—C(18)	88.4(6)
C(11)—Os(1)—Os(2)	81.9(5)	C(9)—Os(3)—C(10)	89.9(7)
C(13)—Os(1)—Os(2)	87.0(5)	C(9)—Os(3)—C(12)	82.8(6)
Os(1)—Os(2)—C(4)	84.7(6)	C(9)—Os(3)—C(18)	96.5(6)
Os(1)—Os(2)—C(5)	176.3(6)	C(10)—Os(3)—C(12)	91.6(6)
Os(1)—Os(2)—C(6)	85.6(6)	C(10)—Os(3)—C(18)	91.9(6)
Os(1)—Os(2)—C(7)	84.3(4)	C(12)—Os(3)—C(18)	176.5(4)
Os(3)—Os(2)—C(4)	89.9(5)	Os(3)—C(12)—C(11)	115(1)
Os(3)—Os(2)—C(5)	87.6(4)	Os(1)—C(11)—C(12)	122(1)
Os(3)—Os(2)—C(6)	85.6(6)	Os(1)—C(11)—O(11)	124(1)
		C(12)—C(11)—O(11)	114(1)

[a] Except for the primed Os_3 framework parameters, all values are taken from the ordered molecule only.

Table 4. Comparison of bond lengths and angles for **3** and **4**

3		**4**	
Os(2)—CK(1)	2.162(10) Å	Os(1)—C(11)	2.11(2) Å
Os(3)—CK(2)	2.218(9) Å	Os(3)—C(12)	2.23(2) Å
CK(1)—CK(2)	1.470(14) Å	C(11)—C(12)	1.44(2) Å
CK(1)—O	1.256(11) Å	C(11)—O(11)	1.27(2) Å
Os(2)—CK(1)—CK(2)	121.4(6)°	Os(1)—C(11)—C(12)	122(1)°
Os(2)—CK(1)—O	120.6(7)°	Os(1)—C(11)—O(11)	124(1)°
CK(2)—CK(1)—O	117.9(9)°	C(12)—C(11)—O(11)	114(1)°
CK(1)—CK(2)—Os(3)	112.2(6)°	C(11)—C(12)—Os(3)	115(1)°

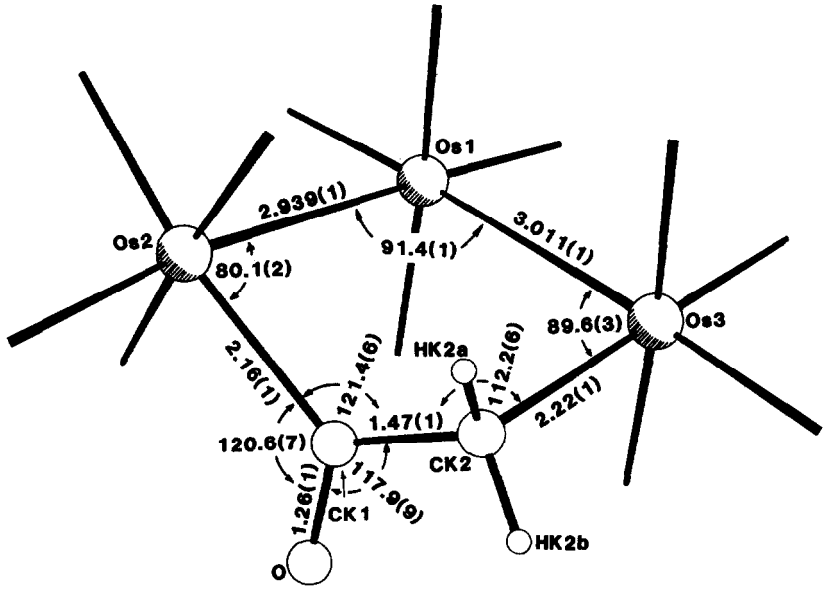

Fig. 3. A drawing showing the central metallacycle of $Os_3(CO)_{12}(\mu\text{-}CH_2CO)$, **3**, giving relevant bond angles and distances. Carbonyl positions are depicted as vectors to the carbon atoms.

pounds **3** and **5c**. Summarized below are the results of our various reactivity studies.[10,12,13] The ketene ligands in these triosmium clusters have been shown to be highly susceptible to both electrophilic and nucleophilic attack, and in particular, the observed reactivity pattern of **5c** shows that nucleophiles preferentially attack the ketene carbonyl carbon whereas electrophiles add to the ketene carbonyl oxygen.

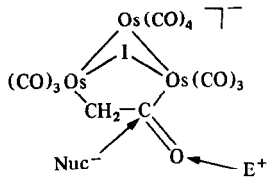

5

Structure 5

Addition of nucleophiles to the μ-ketene ligands of **3** *and* **5**

The neutral ketene complex **3** reacts with both H_2O and CH_3OH over a period of several hours to yield acetic acid and methyl acetate, respectively, eq. (11).[10]

$$Os_3(CO)_{12}(\mu\text{-}CH_2CO) + \underset{R = H,Me}{ROH} \xrightarrow{22°C} CH_3CO_2R + Os_3(CO)_{12}. \quad (11)$$

Both ^1H NMR and IR data imply these products form in > 95% yield. The reaction of **3** with H_2O accounts for the instability of the complex in air and the difficulty in purifying it by chromatography. A competitive experiment involving the reaction of **3** with a 1 : 1 mixture of H_2O and CH_3OH under a CO atmosphere gave a 2.46 : 1 ratio of CH_3CO_2H to $CH_3CO_2CH_3$, implying that **3** reacts faster with H_2O than with MeOH.

The above reactions were conducted with preformed **3**. Another way to conduct such studies is to add methanol and/or water to solutions of the methylene cluster $Os_3(CO)_{12}(\mu\text{-}CH_2)$, **1**, which does not readily react with these reagents, and then add CO to generate cluster **3** *in situ*. Under such conditions, methyl acetate and acetic acid form on the same time scale as the reaction of **1** with CO to form **3**. However, a competitive experiment conducted as above with a 1 : 1 mixture of H_2O–MeOH gave a 0.99 : 1 ratio of CH_3CO_2H to $CH_3CO_2CH_3$, significantly different from the ratio obtained beginning with pure **3**. This implies the formation of an intermediate ketene complex enroute to **3** such as that drawn in eq. (5) and which is much less selective in its reactions with these nucleophiles. The decreased selectivity of the intermediate ketene complex is likely due to it being coordinatively unsaturated. Similarly, Lin *et al.*[14] concluded that an open coordination site was necessary for $Cp(CO)_2Ru(\mu\text{-}CH_2CO)RuCp(CO)_2$ to undergo reaction with methanol. In addition, the isocyanide sub-

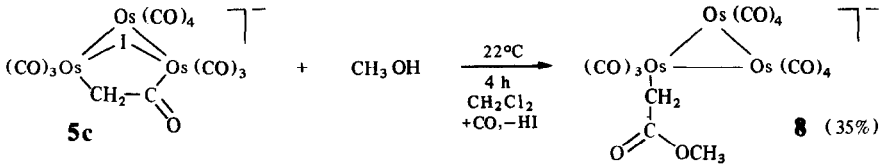

(12)

Eq. (12)

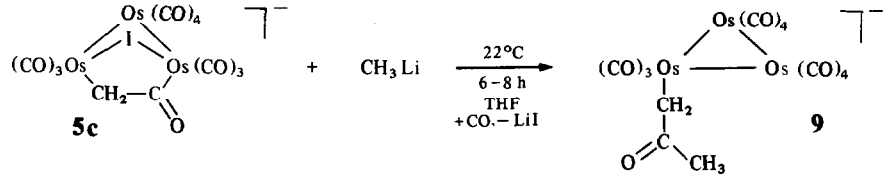

(13)

Eq. (13)

stituted ketene cluster **4** was found to slowly decompose upon addition of MeOH or H_2O. Presumably, the lack of an open coordination site also retards any reactions of nucleophiles with **4**.

The anionic ketene cluster **5c** also slowly reacts with methanol, but not to give methyl acetate as above. Instead the organic ligand stays attached to the cluster and the novel enolate species **8** is isolated, eq. (12).[12,13] Cluster **8** also forms when **5c** reacts with $NaOCH_3$. Cluster **8** was isolated as a microcrystalline solid and was spectroscopically and structurally characterized. The alkyl ligand in **8** is formally the enolate of methyl acetate, and this formalism is reflected in its spectroscopic data. The ester ν(CO) stretch at 1684 cm^{-1} is 51 cm^{-1} lower in energy than that of the free methyl acetate at 1735 cm^{-1}, implying significant delocalization of electron density onto the ligand carbonyl.* The δ 2.31 ^1H NMR resonance for the methylene protons is in the range found for mononuclear metal enolates,[17(b)] but downfield from the normal metal alkyl region (δ $-1.0 \rightarrow 0.5$). The CO which is taken up in the **5c**→**8** conversion comes from the CO atmosphere, which the reaction must be conducted under to keep **5c** from losing CO and reforming the methylene cluster **2c**, eq. (5).

Ketene cluster **5c** similarly reacts with MeLi to form the enolate cluster **9**, eq. (13).[12,13] This species was obtained as an orange oil, and the similarity of its spectroscopic data to those of **8** imply a structure similar to that of **8**. The alkyl ligand in **9** is formally the enolate of acetone, and it shows a ketonic ν(CO) stretch at 1676 cm^{-1}, 39 cm^{-1} lower in energy than that of free acetone.

* Free Li^+ enolates generally show ν(CO) bonds in the 1550–1600 cm^{-1} region (see Ref. 17a).

It is interesting to compare the reactions of the ketene clusters **3** and **5c** with methanol. Neutral cluster **3** reacts with CH_3OH to give acetic acid and $Os_3(CO)_{12}$.[10] In contrast, the anionic ketene cluster **5c** reacts with CH_3OH to form the alkyl cluster **8**. Presumably neutral **3** initially reacts with CH_3OH to give a similar alkyl cluster, but the alkyl ligand must be quickly removed by protonation by the H^+ released in the CH_3OH addition. The alkyl ligand in **8** is presumably retained because the released H^+ is taken up by the iodide ligand of **5c** to form HI which should not be extensively dissociated in the organic solvents used in these reactions.

Similar, but not as extensive, reactivity studies were conducted with amines.[13] In one series of experiments, reactions were conducted by adding the free amine (Bu^n_2NH, Bu^nNH_2) to the neutral methylene cluster $Os_3(CO)_{11}(\mu\text{-}CH_2)$, **1**, and then admitting CO to form the ketene cluster **3** *in situ*. Over the course of 2–4 h, the same time scale for formation of **3** from **1**, the IR bands of **1** were smoothly replaced by those of $Os_3(CO)_{12}$ and the corresponding free amide which forms by addition of the amine to a ketene ligand, eq. (14). However,

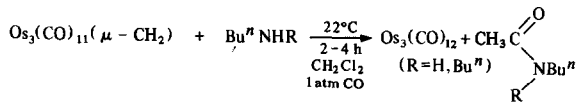

(14)

Eq. (14)

the IR bands of the ketene cluster **3** were never observed, implying that the amines either react with cluster **3** immediately as it forms, or that they intercept an intermediate in the $Os_3(CO)_{11}(\mu\text{-}CH_2)$ to $Os_3(CO)_{12}(\mu\text{-}CH_2CO)$ conversion, as proposed above for the similar reactions with methanol. That the latter is likely correct was indicated by the very

slow (4 days) reaction observed when free amine was added to solutions of *preformed* **3**.

The anionic ketene cluster **5c** also reacts with $(Bu^n)_2NH$ and Bu^nNH_2, but much more slowly than does **3**. The reaction of **5c** with $(Bu^n)_2NH$ gives $Os_3(CO)_{12}$ and $CH_3C(O)N(Bu^n)_2$ in near quantitative yield, although the reaction takes 5 h to reach completion. Reaction of **5c** with Bu^nNH_2 requires over 12 h for completion and gives the corresponding amide in 72% yield. However, we know that when maintained under a CO atmosphere for several hours as in these experiments, ketene cluster **5c** slowly loses I^- and adds CO to form the neutral ketene cluster **3**.[11] Given the time scale of the above reactions of **5c** with amines, it is possible that cluster **5c** may be unreactive with these amines and that reaction only occurs when cluster **3** is formed from **5c**.

Addition of electrophiles to the μ-ketene ligand of **5c**

Electrophilic $CH_3OSO_2CF_3$ adds to the ketene carbonyl oxygen of **5c** to form the σ,π-vinyl cluster **10**, eq. (15).[11] Complex **10** was spectroscopically and structurally characterized. A variable temperature ^{13}C NMR study showed that the cluster is fluxional and that the exchange process involves a movement of the vinyl ligand from one $Os(CO)_3$ unit to the other in a "windshield wiper" motion similar to that seen in other σ-π-vinyl compounds, eq. (16).[18]

Preliminary results indicate that similar addition of CH_3^+ occurs to the ketene oxygen of $[Os_3(CO)_9(Bu^tNC)(\mu\text{-}I)(\mu\text{-}CH_2CO)]^-$, **7c**, to give isomeric σ,π-vinyl clusters which apparently have the isocyanide coordinated to different Os atoms—the Os with the ligand σ-bond or the Os with the π-bond.

The simple electrophile H^+ also adds to the μ-ketene ligand of **5c** to give the known μ-acetyl cluster **11**,[19,20] eq. (17).[12,13] However, both IR and ^1H NMR data showed that this reaction proceeds via the formation of an unstable intermediate that slowly transforms into cluster **11**. Although this species could not be isolated, its spectroscopic data indicate a structure similar to that of the σ,π-vinyl cluster **10**, and we believe it to be the corresponding hydroxy-vinyl cluster **12** formed by pro-

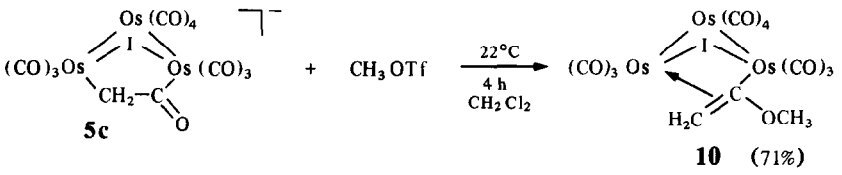

(15)

Eq. (15)

(16)

Eq. (16)

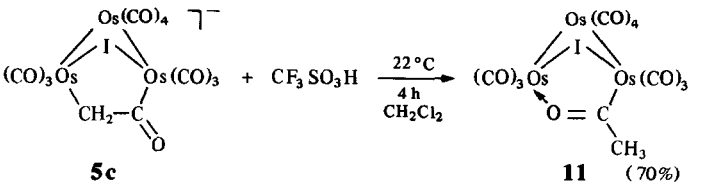

(17)

Eq. (17)

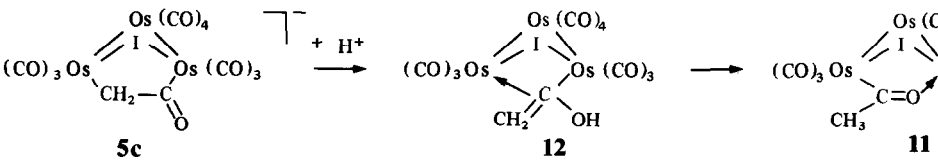

(18)

Eq. (18)

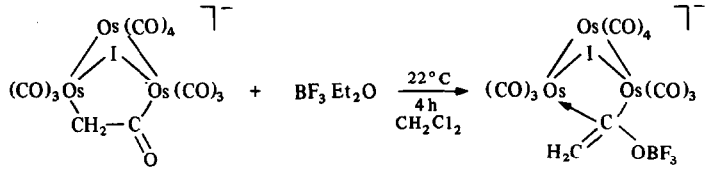

5c

Eq. (19)

tonation of the μ-ketene oxygen. This species then apparently tautomerizes to give the acetyl ligand in the observed product **11**, eq. (18). The latter is, of course, similar to organic keto–enol tautomerization.

Spectroscopic data also indicate that the Lewis acid BF_3 adds to the μ-ketene oxygen in **5c** to give an adduct which although spectroscopically characterized could not be isolated, eq. (19).[12,13]

SUMMARY

These studies have shown that μ-ketene ligands of structural type **II** readily form on triosmium carbonyl clusters upon carbonylation of the appropriate μ-methylene precursor. Structural data for the neutral μ-ketene clusters $Os_3(CO)_{12}(\mu\text{-}CH_2CO)$, **3**, and its $Bu^tN{\equiv}C$ substituted derivative **4** indicate that these complexes are best viewed as triosmacyclopentanones, or alternatively as metallated acetyl complexes. Similar descriptions may be appropriate for the anionic μ-ketene clusters **5**, although both spectroscopic and reactivity data indicate significant localization of the negative charge on the ketene oxygen atom. The μ-ketene ligands in all these clusters are reactive, undergoing attack by both electrophiles and nucleophiles. The reactivity data for **5c** show that nucleophiles add to the ketene carbonyl carbon whereas electrophiles add to the carbonyl oxygen.

EXPERIMENTAL

General

The methylene clusters $Os_3(CO)_{11}(\mu\text{-}CH_2)$, **1**,[8] and $[PPN][Os_3(CO)_{10}(\mu\text{-}I)(\mu\text{-}CH_2)]$[9] were prepared as described in the literature. Solvents were dried by standard methods and all reactions were conducted under prepurified N_2 atmospheres with use of standard Schlenk techniques. Methods of spectroscopic analysis have been previously described.[11,13] Elemental analyses were obtained by Schwarzkopf Microanalytical Laboratories, Woodside, NY.

Preparation of $Os_3(CO)_{10}(Bu^tNC)_2(\mu\text{-}CH_2CO)$, **4**

Cluster **1** (812.3 mg, 0.911 mmol) was dissolved in 10 cm^3 CH_2Cl_2 and cooled to 0°C. Bu^tNC (206 μl, 1.82 mmol) was then added dropwise by syringe. The solution changed colour from burgundy to yellow over the course of 5–10 min. The solution was then filtered through a pad of celite, the solvent was removed by rotary evaporation, and the residue was extracted with 3×2 cm^3 portions of pentane to yield pure **4** (596.5 mg, 0.564 mmol, 62%). The pentane extracts were combined and chromatographed on an SiO_2 TLC plate (Fischer) with 5% acetone–45% CH_2Cl_2–50% hexanes as eluant. The cluster $Os_3(CO)_{10}(Bu^tNC)_2$[21] was isolated from the leading yellow band (212.8 mg, 0.210 mmol, 23%). This was followed by several small bands of presently unidentified products.

4: *Anal.* Found: C, 24.92; H, 1.63. Calc. for $C_{22}H_{20}N_2O_{11}Os_3$: C, 24.94; H, 1.89%. MS(EI): 1058 $[M]^+$. IR (CH_2Cl_2) ν(CO): 2174m,br, 2095w, 2068w, 2045s, 2020s, 1987w, 1971w, 1549w,br cm^{-1}. ^1H NMR ($CDCl_3$): δ 2.81 (s,2H), 1.49 (s,6H), 1.47 (s,6H). $^{13}C\{^1H\}$ NMR ($CDCl_3$): δ 226.0 (CH_2CO), 185.1 (2CO), 185.0 (2CO), 182.9 (2CO), 173.7 (CO), 172.8 (CO), 169.9 (CO), 169.4 (CO), 58.2 ($\{CH_3\}_3C$), 58.1 ($\{CH_3\}_3C$), 30.1 (CH_2CO), 32.5–27.9 (CH_3).

Variable temperature ^1H *NMR study of* **4**

Cluster **4** (49.9 mg) was dissolved in ~ 1 cm^3 CD_2Cl_2 and filtered into a 5 mm NMR tube. The probe of a Bruker AM-300 300 MHz NMR spectrometer was cooled to −80°C (by MeOH standard) and the ^1H NMR spectrum of **4** was recorded at 10 or 5°C intervals as the probe was warmed. Coalescence occurred at −30°C corresponding to $\Delta G \approx 11$ kcal mol^{-1}.[22]

Preparation of $[PPN][Os_3(CO)_9(Bu^tNC)(\mu\text{-}X)(\mu\text{-}CH_2CO)]$

In a typical experiment, cluster **2c** (65.6 mg, 0.043 mmol) was dissolved in 10 cm^3 CH_2Cl_2 and cooled to −78°C. Bu^tNC (4.9 μl, 0.043 mmol) was added by syringe and the reaction monitored by IR spec-

troscopy. Alternatively, the starting methylene cluster was dissolved in ~ 1 g $CDCl_3$ in a dry box, filtered through celite into an NMR tube and capped with a septum. Addition of Bu^{t}NC was made through the septum into the cooled solution and the reaction was monitored by ^{1}H NMR spectroscopy with a probe temperature of −40°C. In both cases the characteristic features of **2c** disappeared and IR and ^{1}H NMR bands grew which are assigned to **7c**. However, upon warm-up to room temperature these bands disappeared and were replaced by a complex pattern attributed to a mixture of compounds. The stoichiometry of these reactions was determined by sequential addition of 0.5 equiv. of Bu^{t}NC to $CDCl_3$ solutions of the methylene clusters with ^{1}H NMR monitoring at −40°C which showed coordination of only one isocyanide per cluster. ^{1}H and ^{13}C NMR data for **7c** and **7d** are listed in Table 1. Infrared data are: **7c**, IR (CH_2Cl_2), ν(CO): 21517br, 2064w, 2024m, 1979s, 1917w, 1539w cm^{-1}. **7d**, IR (CH_2Cl_2), ν(CO): 2193s, 2155br, 2062r, 2023m, 1977s, 1943w, 1919w, 1546wbr cm^{-1}.

Reaction of **7c** *with* $CH_3OSO_2CF_3$

The methylene cluster **2c** (76.2 mg, 0.051 mmol) was dissolved in 10 cm^3 CH_2Cl_2 and cooled to −78°C. One equivalent of Bu^{t}NC (5.76 μl) was added by syringe to form **7c**. To this solution was added by syringe $CH_3OSO_2CF_3$ (5.79 μl, 0.051 mmol), and the reaction was maintained at −78°C for 4 h before slow warming to room temperature. The solvent was removed from the yellow–orange solution by rotary evaporation, and the oily residue was chromatographed on SiO_2 with 30% CH_2Cl_2–pentane as eluant. A single yellow band was collected, yielding a mixture of isomers of $Os_3(CO)_8$(Bu^{t}NC)(μ-I)(σ,π-CH_2=C(OMe)), **13a** and **13b** in 89% yield (49.4 mg). IR (pentane): 2180wbr, 2085w, 2076w, 2053vs, 2029m, 2011w, 2002w, 1995s, 1983w, 1970w, 1960w cm^{-1} ^{1}H NMR ($CDCl_3$): δ 5.09 (**13a**, 1.8H, CH_2, d, J_{HH} = 4.7 Hz), 5.03 (**13a**, 1.8H, CH_2, d, J_{HH} = 4.7 Hz), 5.00 (**13b**, 1H, CH_2, d, J_{HH} = 5.0 Hz), 4.91 (**13b**, 1H, CH_2, d), 3.77 (**13b**, 3H, OCH_3, s), 3.73 (**13a**, 5.4H, OCH_3, s), δ 1.52 (**13b**, 9H, Bu^t, s). 1.46 s (**13a**, 16.2H, Bu^t). ^{13}C{^{1}H} NMR ($CDCl_3$): **13a**, δ 193.8 (—*C*(OCH$_3$)=CH$_2$), 36.3 (—C(OCH$_3$)=*C*H$_2$); **13b**, δ 199.9 (—*C*(OCH$_3$)=CH$_2$), 29.9 (—C(OCH$_3$)=*C*H$_2$).

Crystallographic study of $Os_3(CO)_{10}$(Bu^{t}N≡C)$_2$(μ-CH_2CO), **4**

A yellow crystal, with a nearly cubic shape (0.33 mm),[3] diffracted only moderately well. The lattice parameters given in Table 2 were obtained from the least squares fit of the angular settings of 25 reflections ($21° \leqslant 2\theta \leqslant 26°$). The data were corrected for a ~ 11% linear decay in intensity of three standard reflections and for absorption (empirical, 216 data, T_{max}/T_{min} = 2.3). The six major (see below) Os atom positions were obtained by direct methods. A difference Fourier map phased by the six Os atoms showed that of the two molecules comprising the asymmetric unit, one was ordered (mol. A), and the other disordered (mol. B). Molecule B revealed two orientations for the bent Os_3 framework; Os(1′) and Os(2′) have alternative 5% occupancy locations labelled Os(1″) and Os(2″). Os(3′) is fully occupied. No contributions from the non-osmium atoms of the minor form were visible (or expected at 5% occupancy). Full modelling of molecule B was, therefore, impossible. All non-hydrogen atoms (except the carbon atoms) were refined anisotropically. Hydrogen atom contributions were idealized. SHELXTL (5.1) software was used for all computations (Nicolet Corp., Madison, WI). Selected bond distances and angles are given in Table 3. Fractional atomic coordinates, thermal parameters, full lists of bond lengths and angles, and lists of F_o/F_c values have been deposited as supplementary material with the Editor, from whom copies are available on request. Atomic coordinates have also been deposited with the Cambridge Crystallographic Data Centre.

Acknowledgements—We gratefully acknowledge the Department of Energy, Office of Basic Energy Sciences for support of this research and the National Science Foundation for contributing funds toward the purchase of the X-ray diffractometer at the University of Delaware.

REFERENCES

1. H. Staudinger, *Die Ketene*. Enke, Stuttgart (1912).
2. N. T. M. Wilsmore, *J. Chem. Soc.* 1907, 1938.
3. (a) S. Patai (Ed.), *The Chemistry of Ketenes, Allenes, and Related Compounds*. John Wiley, New York (1980); (b) H. Ulrich, *Cycloaddition Reactions of Heterocumulenes*. Academic Press, New York (1967); (c) H. R. Seikaly and T. T. Tidwell, *Tetrahedron* 1986, **42**, 2587; (d) W. E. Hanford and J. C. Sauer, *Org. Reactions* 1946, **3**, 108; (e) R. N. Lacy, in *The Chemistry of Alkenes* (Edited by S. Patai), pp. 1161–1227. Interscience, New York (1964); (f) D. Borrmann, *Methoden der Organische Chemie*, Vol. 7, Part 4. Georg Thieme Verlag, Stuttgart (1968); (g) W. T. Brady, *Tetrahedron* 1981, **37**, 2949; (h) D. P. N. Satchell and R. S. Satchell, *Chem. Soc. Rev.* 1975, **4**, 231.
4. S. L. Bassner and G. L. Geoffroy, *Adv. Organometal. Chem.* 1988, **28**, 1.

5. (a) A. Takeuchi and J. R. Katzer, *J. Phys. Chem.* 1982, **86**, 2438; (b) A. Takeuchi, J. R. Katzer and G. C. A. Schuit, *J. Catal.* 1983, **82**, 477; (c) A. Takeuchi, J. R. Katzer and R. W. Crecely, *J. Catal.* 1983, **82**, 474; (d) P. M. Loggenberg, L. Carlton, R. G. Copperthwaite and G. J. Hutchings, *J. Chem. Soc., Chem. Commun.* 1987, 541.
6. (a) A. Miyashita, T. Kihara, K. Nomura and H. Nohira, *Chem. Lett.* 1986, 1607; (b) T.-A. Mitsudo, M. Kadokura and Y. Watanabe, *J. Chem. Soc., Chem. Commun.* 1986, 1539; (c) T.-A. Mitsudo, M. Kadokura and Y. Watanabe, *Tetrahedron. Lett.* 1985, **26**, 3697.
7. I. Fleming, *Frontier Orbitals and Organic Chemical Reactions.* John Wiley, New York (1976).
8. G. R. Steinmetz, E. D. Morrison and G. L. Geoffroy, *J. Am. Chem. Soc.* 1984, **106**, 2559.
9. E. D. Morrison, R. R. Whittle, G. L. Geoffroy and A. L. Rheingold, *Organometallics* 1985, **4**, 1413.
10. E. D. Morrison, G. R. Steinmetz, G. L. Geoffroy, W. C. Fultz and A. L. Rheingold, *J. Am. Chem. Soc.* 1986, **106**, 4783.
11. E. D. Morrison and G. L. Geoffroy, *J. Am. Chem. Soc.* 1985, **107**, 3541.
12. S. L. Bassner, E. D. Morrison, G. L. Geoffroy and A. L. Rheingold, *J. Am. Chem. Soc.* 1986, **108**, 5358.
13. S. L. Bassner, E. D. Morrison, G. L. Geoffroy and A. L. Rheingold, *Organometallics* 1987, **6**, 2207.
14. Y. C. Lin, J. C. Calabrese and S. S. Wreford, *J. Am. Chem. Soc.* 1983, **105**, 1679.
15. R. M. Silverstein, B. C. Bassler and T. C. Morrill, *Spectrometric Identification of Organic Compounds.* John Wiley, New York (1981).
16. L. E. Sutton (Ed.), *Tables of Interatomic Distances and Configurations in Molecules and Ions*, Special Publication No. 11. The Chemical Society, London (1958).
17. (a) L. M. Jackman and B. C. Lange, *Tetrahedron* 1977, **33**, 2737; (b) J. J. Doney, R. G. Bergman and C. H. Heathcock, *J. Am. Chem. Soc.* 1985, **107**, 3724.
18. (a)J. B. Keister and J. R. Shapley, *J. Organomet. Chem.* 1975, **94**, C43; (b) K. W. Lee and T. L. Brown, *Organometallics* 1985, **4**, 1030, and references cited therein; (c) M. Mlekuz, P. Boureard, B. G. Sayer, S. Peng, M. J. McGlinchey, A. Marinetti, J. Saillard, J. B. Naceur, B. Mentzen and G. Jaouen, *Organometallics* 1985, **4**, 1123, and references cited therein.
19. C. M. Jensen, C. B. Knobler and H. D. Kaesz, *J. Am. Chem. Soc.* 1984, **106**, 5926.
20. E. D. Morrison, S. L. Bassner and G. L. Geoffroy, *Organometallics* 1986, **6**, 408.
21. M. J. Mays and P. D. Gavens, *J. Chem. Soc., Dalton Trans.* 1980, 911.
22. H. Gunther, *NMR Spektroskopie.* Verlag, Stuttgart (1973).

Polyhedron Vol. 7, No. 10/11, pp. 807–825, 1988
Printed in Great Britain

0277–5387/88 $3.00+.00
© 1988 Pergamon Press plc

MIXED METAL CLUSTERS CONTAINING CARBYNE OR KETENYLIDENE BRIDGES: HIGH FIELD NMR SPECTROSCOPY AS A PROBE FOR STRUCTURE AND MECHANISM

MICHAEL F. D'AGOSTINO and MICHAEL J. McGLINCHEY*

Department of Chemistry, McMaster University, Hamilton, Ontario, L8S 4M1, Canada

(*Accepted* 5 *November* 1987)

Abstract—High field NMR spectroscopy is shown to be exceedingly valuable as an aid to the determination of the structures of mixed metal clusters and also as a probe for molecular rearrangements. In particular, the incorporation of an isopropyl group into chiral organometallic clusters of the tetrahedral (M_2C_2) and square-pyramidal (M_3C_2) types allows the detection of "hidden processes" such as intramolecular racemization or ligand migrations. It is possible to slow, on the NMR time scale, local rotation of individual vertices (e.g., $CpMo(CO)_2$ or $Co(CO)_3$) in M_3CR clusters, when the capping carbynyl group is very bulky. The cation $[Co_3(CO)_9C{=}C{=}O]^+$ can be shown to adopt a C_S rather than a C_{3v} geometry. Finally, the mechanism of the decarbonylation of $Ar{-}CO{-}CCo_3(CO)_9$ clusters to the corresponding $Ar{-}CCo_3(CO)_9$ molecules proceeds via initial loss of a cobalt carbonyl ligand rather than by elimination of the ketonic carbonyl.

The chemistry of organometallic clusters may be viewed from a variety of perspectives. Over the last few years there have appeared many syntheses—both rational and serendipitous, X-ray structural determinations of picturesque symmetry, ingenious bonding theories which relate molecular geometries with skeletal electron counts, organic transformations of remarkable specificity and other elegant studies too numerous to mention. Our own particular interests have focussed on the use of Nuclear Magnetic Resonance spectroscopy as a tool to determine not only the structures but also the mechanisms of rearrangement of metal clusters containing carbynyl or alkyne moieties.

NMR spectroscopy has undergone an almost exponential growth over the last few years. This phenomenon is attributable partly to enormous advances in cryomagnet technology such that spectra are now routinely obtainable at a field of 11.7 T (500 MHz for ^1H, 125 MHz for ^{13}C, 202 MHz for ^{31}P, etc.) but also because of tremendously enhanced computational facilities which permit the ready manipulation of the large quantities of data produced in two-dimensional NMR experiments.[1] Perhaps the most useful recent innovation is the development of reverse 2D spectroscopy whereby polarization transfer from a high frequency nucleus (such as ^1H or ^{31}P) coupled to a low frequency nucleus of low abundance (such as ^{57}Fe) makes detection of the transition metal nuclei themselves a simple and viable endeavour.[2] Thus, the investigation of fluxional behaviour which was (with few exceptions[3]) restricted to studies of the peripheral ligands, such as hydrides, carbonyls or phosphines, can now be carried out via direct observation of the metal centres.[4,5] The full potentialities of these novel techniques will doubtless become apparent in the near future. For these reasons, NMR spectroscopy has been and remains an integral component of our research programme.[6]

1. THE ISOPROPYL GROUP AS AN EFFECTIVE NMR PROBE

Since much of the work we shall discuss involves molecules lacking an improper axis of symmetry, viz. chiral clusters, it is perhaps worthwhile to remind ourselves about the phenomenon of diastereotopic nuclei. As is well known, all magnetically

*Author to whom correspondence should be addressed.

active nuclei in a molecule of C_1 symmetry are in different environments and should thus resonate at different frequencies. However, if there exists a particular molecular rotation or rearrangement pathway which interconverts two or more nuclei then this magnetic non-equivalence will be lost at some appropriate temperature dependent upon the activation energy barrier which must be overcome. As a trivial example we note that the methyl protons in the chiral ethane **1** are in principle magnetically different. However, it is readily apparent that simple rotation about the carbon–carbon axis brings all three methyl protons successively into identical positions. In contrast, substitution of a single hydrogen by another atom or group as in **2** renders the two remaining protons permanently different irrespective of the rate of rotation about the carbon–carbon axis. In this particular molecule, these so-called diastereotopic nuclei can only be equilibrated by inverting the chirality at the other carbon centre to give **3**, as shown below:

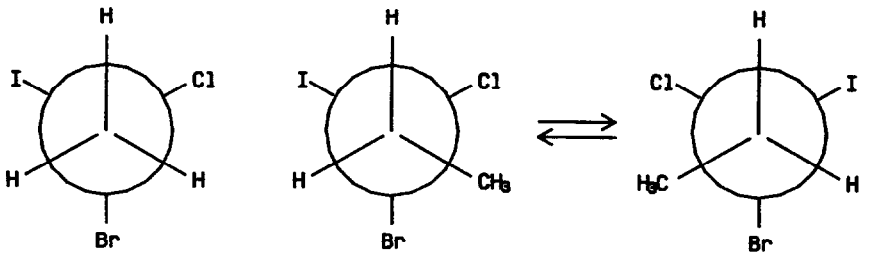

1 2 3

(a) *Alkyne-dimetallic tetrahedral clusters*

Over the last several years we have prepared numerous clusters, the chirality of which depended not merely on the use of mixed metal systems, as in **4** and **5**, but also by incorporating ligands which lowered the molecular symmetry. Nevertheless, it has become apparent that several classes of cluster which would appear to be chiral are in fact undergoing intramolecular rearrangements which bring about loss of stereochemical integrity even on the NMR time scale.[7]

It is thus necessary to build into the systems a probe with which one can ascertain the configurational stability of the molecule. In practice, a convenient probe is the isopropyl group which provides two potentially diastereotopic methyl resonances (in either ^1H or ^{13}C NMR spectroscopy) and we see this moiety used in the tetrahedral dimetal-alkyne clusters **6a** and **6b**. This system is made up of four chemically different fragments disposed in a tetrahedral array. The cluster fulfils all the classical criteria for chirality and so, in principle, should be resolved into enantiomers. Despite several attempts, these enantiomers have thus far resisted all efforts to resolve them. Subsequently however, it was shown that, although the two isopropyl methyls are indeed non-equivalent at room temperature, the NMR peaks coalesce at elevated temperatures suggesting that the molecule can racemize with a barrier which exceeds 20 kcal mol^{-1}.[8]

This particular system illustrates some of the potential problems which may arise in such investigations. First of all, one must be certain that the coalescence phenomenon observed is not merely attributable to a temperature-dependent change in chemical shift. (This is most easily accomplished by recording the spectrum at temperatures below that

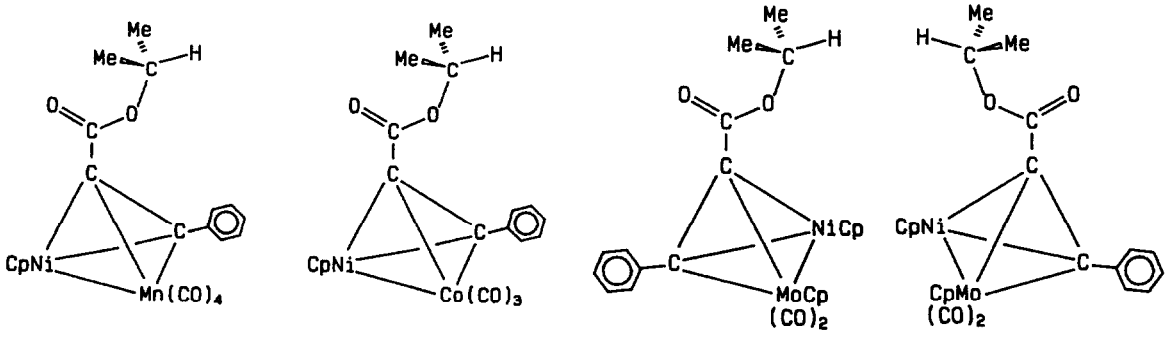

4 5 6a 6b

required to see the limiting spectrum and then extrapolating any observed temperature dependence to higher temperatures.) Secondly, the proton spectrum of **6** measured on a low field instrument shows only a single methyl environment at any temperature leading one to suppose that racemization was occurring rapidly on the NMR time scale. In fact, the chemical shift difference between the diastereotopic methyls is rather small in this system and only becomes apparent on a high field instrument (400 MHz). There is, however, a "Catch-22" in that use of a high field spectrometer to separate the methyl resonances has the consequence that the sample must be heated close to its decomposition point to bring about peak coalescence thus raising the possibility of alkyne dissociation as the racemization mechanism. In this particular case, no exchange with added free alkyne was observable under the reaction conditions but clearly one must take suitable precautions to test for other mechanisms. A possible intramolecular process could involve a tetrahedral ⇄ square-planar interconversion;[9] such a mechanism has been calculated[10] to have a very high activation energy barrier for the model system $(C_2H_2)Co_2(CO)_6$ but may be considerably lower for the mixed metal cluster (D. M. Hoffman and R. Hoffmann, personal communication). Subsequent calculations[11] involving a less symmetrical transition state have indicated that the symmetry restrictions may well be less severe than originally thought.

(b) *Alkyne-trimetallic square-pyramidal clusters*

Treatment of the tetrahedral $(RC{\equiv}CR)[(C_5H_5)Ni]M$ clusters, where M can be $Co(CO)_3$, $(C_5H_5)Mo(CO)_2$ or $(C_5H_5)Ni$ with $Fe_2(CO)_9$ leads to cluster expansion[12] as exemplified in eq. (2). When the alkyne is unsymmetrical as in $Ph{-}C{\equiv}C{-}CO_2CHMe_2$ the cluster is chiral even when the two original metal vertices are identical. The chiral nature of the system is readily detectable by use of the diastereotopic methyl groups of the isopropyl functionality. One should perhaps pause a moment to clarify a point which is commonly raised concerning such systems. It is of course true that we are dealing with a 50/50 mixture of enantiomers, that is, a racemic system in which each enantiomer gives rise to the same spectrum (assuming that one is using an achiral solvent). However, the NMR experiment detects the chirality of each molecule individually; this situation is quite different from chiroptical measurements which detect, for example, the rotation of a polarized light beam by the bulk sample. Since we do not have an excess of one enantiomer there is no rotation measurable using a polarimeter. However, each individual chiral molecule (in our case 100% of the sample) will exhibit different resonances for diastereotopic pairs of nuclei *unless there is a process which interconverts the enantiomers rapidly on the NMR time scale.* This phenomenon is well understood by the spectroscopic community[13,14] but is occasionally not

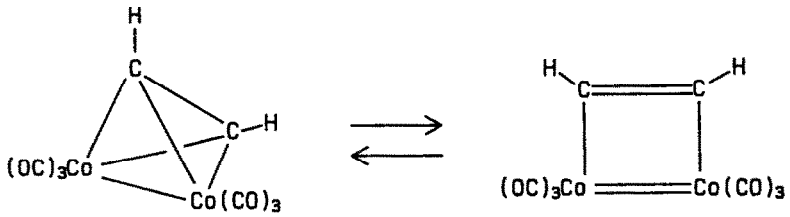

(1)

Eq. (1)

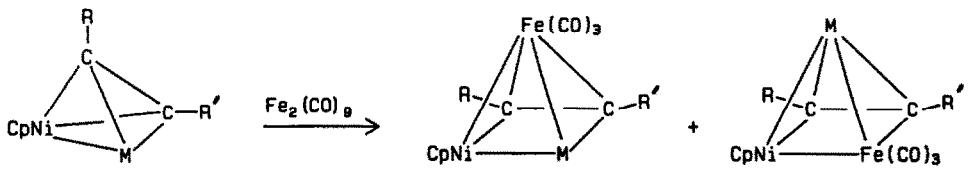

(2)

5 M = Co (CO) 3
6 M = CpMo (CO) 2
7 M = CpNi

8 M = Co (CO) 3
10 M = CpNi

9 M = CpMo (CO) 2

Eq. (2)

fully appreciated by those who specialize in other areas.

In the Ni_2Fe complex, **10**, the room temperature ^1H spectrum reveals a single cyclopentadienyl peak and a simple doublet for the isopropyl methyls. In contrast, at low temperature, one observes two equally intense cyclopentadienyl resonances and a pair of methyl peaks (each doublet split by the unique isopropyl hydrogen).[15] Clearly, there must be a racemization process occurring which brings about interconversion not only of the diastereotopic methyl groups but also of the $(C_5H_5)Ni$ environments. Analogous behaviour has been reported previously for triosmium-benzyne clusters, e.g. $HOs_3(C_6H_4)(PMe_2)(CO)_9$;[16] the problem is complicated by hydride and carbonyl migrations but, ignoring these interesting side issues, it was suggested that there might be a rotation of the benzyne moiety relative to the metal triangle. Now, applying these ideas to the Ni_2Fe cluster, **10**, one could certainly visualize a process whereby the acetylene ligand rotated so as to generate an intermediate possessing a molecular mirror plane which would equilibrate not only the methyls but also the cyclopentadienyl rings, as in Scheme 1.

However, one must also consider the possible intervention of another process, that is the independent rotation of the CpNi—NiCp unit relative to the FeC_2 triangular face, as illustrated in Scheme 2. As Hoffmann has shown,[17] the CpNi moiety is isolobal with a CH unit thus making the Cp_2Ni_2 fragment a pseudo-alkyne. If such a process were to occur then one could interconvert the nickel vertices *without racemizing the cluster*; in this case, the isopropyl methyls would retain their diastereotopic character.

The experimental data are unequivocal in that the activation energy barriers to methyl interconversion and to cyclopentadienyl exchange are the same within experimental error, i.e. ≈ 15 kcal mol^{-1}. Hence, only the single process shown in Scheme 1 need be invoked and the evidence thus favours a process involving formal alkyne rotation relative to the trimetallic plane.[15] We note also that such a rotation could not be a simple circumambulation of the alkyne around the periphery of the triangle (Scheme 3) since the net result of such a rearrangement would regenerate the same enantiomer; instead, as suggested by Schilling and Hoffmann,[18] the alkyne would have to execute a more intricate series of manoeuvres (Scheme 4) rather in the manner of a molecular windshield wiper.

The above mechanistic arguments all assume that the rearrangement pathway is entirely intramolecular, but one could easily imagine a process whereby the alkyne becomes detached from the metal triangle (with the latter perhaps being stabilized via coordination of solvent). To verify the intramolecular nature of the process, it was decided to construct clusters containing three different organometallic vertices since alkyne rotation in such molecules would merely interconvert diastereomers rather than enantiomers, as shown in Scheme 5. Thus, at the low temperature limit, each diastereomer should generate in the ^1H spectrum a pair of diastereotopic methyl doublets, but at high

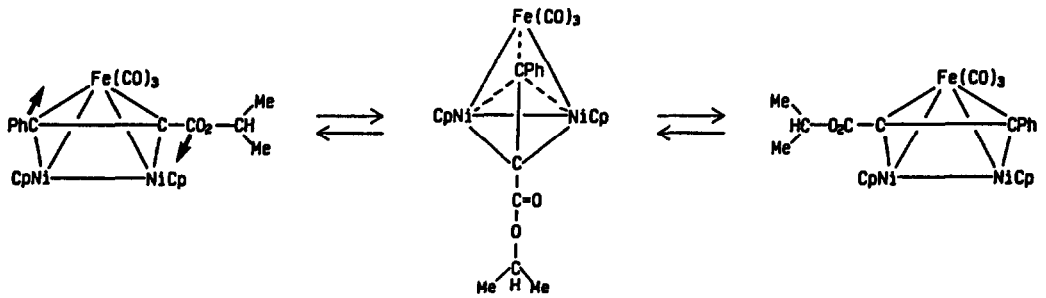

Scheme 1. Racemization via rotation of the alkyne R—C≡C—R.

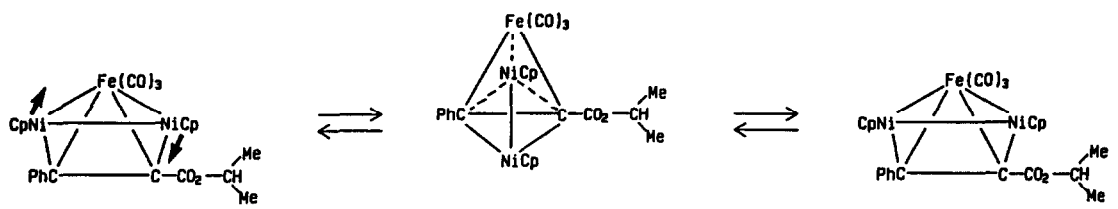

Scheme 2. Rotation of the pseudo-alkyne CpNi≡NiCp.

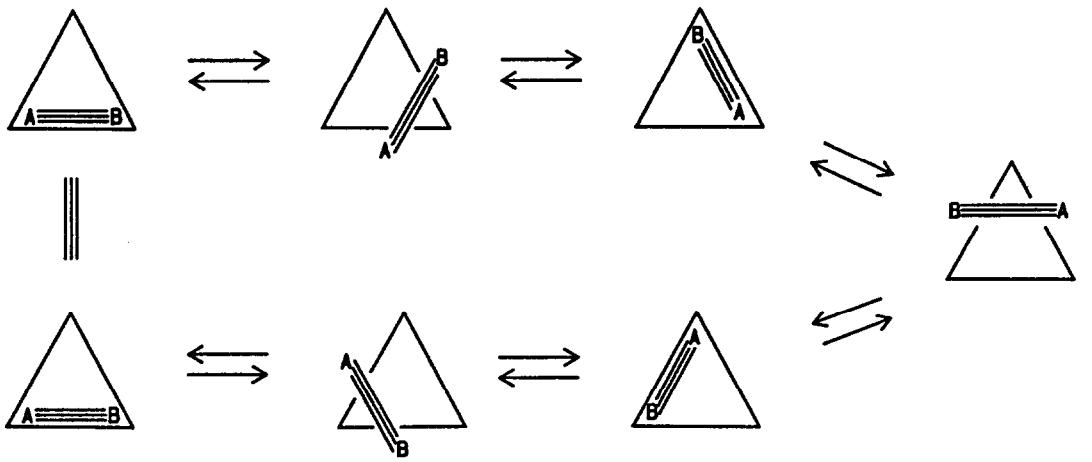

Scheme 3. Migration of an alkyne about the molecular periphery does not racemize the cluster.

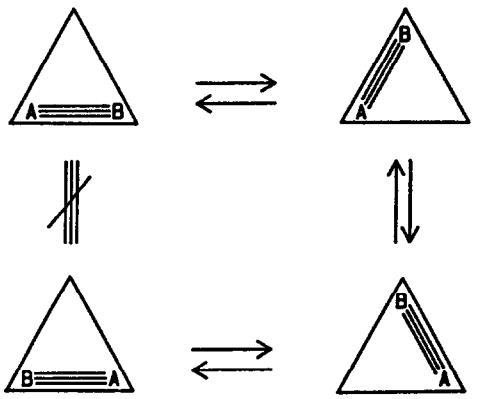

Scheme 4. "Windshield wiper" motion of an unsymmetrical alkyne leading to racemization of the cluster.

temperature one should observe only one pair of doublets attributable to a single isopropyl group still in a chiral environment.

In contrast, if the rearrangement were to proceed via an intermolecular decomposition pathway, then the alkyne would become free; such a process would not only equilibrate the CpNi vertices in **10** but also the isopropyl methyls in the liberated alkyne would become equivalent and hence exhibit one simple methyl doublet. The low temperature spectrum of **9** (Fig. 1) shows two pairs of methyl doublets (showing the existence of two diastereomers) while at high temperature these peaks coalesce to give a single pair of methyl doublets (proving that the chirality of the system is retained). These observations provide

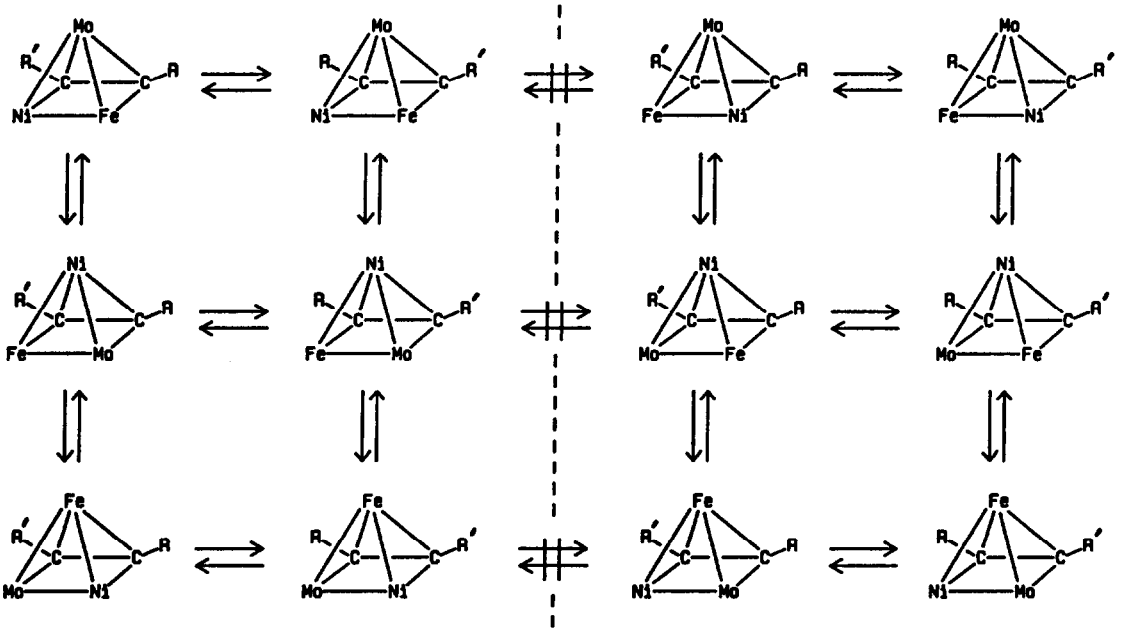

Scheme 5. Alkyne rotation on one face of a cluster showing interconversion of diastereomers but not of enantiomers.

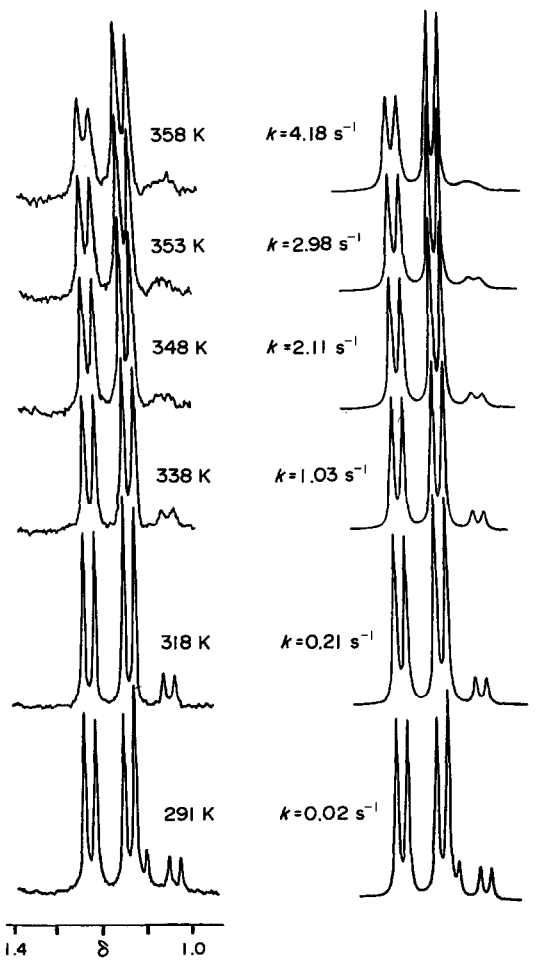

Fig. 1. Experimental and simulated 250 MHz variable-temperature ^{1}H NMR spectra of **9**.

convincing evidence of the intramolecular nature of the rearrangement pathway. Furthermore, since the barrier to the interconversion of the diastereomers of **9** is very similar to that for the racemization of **10** one can deduce that the same rearrangement mechanism is operative. These experiments demonstrate the importance of incorporating multiple and independent probes for rearrangement processes to see whether they yield mechanistic results which are in agreement or which are mutually exclusive. Fortunately, in the systems discussed above, the ^{1}H and ^{13}C data on both the isopropyl and (cyclopentadienyl)nickel moieties reinforce each other.

A comment is in order about the bonding in these five-vertex square-pyramidal clusters. They were originally classified as σ, π-acetylene complexes but are now more profitably viewed as *nido* octahedral clusters analogous to B_5H_9.[19] According to the Wade–Mingos formalism[20,21] these organometallic clusters can be regarded as coordinatively unsaturated systems even though they possess formal 18-electron configurations at each metal. Following the isolobal analogy to its logical conclusion, one can relate the square-pyramidal M_3C_2 clusters to the carbocationic cluster $C_5H_5^+$, the molecular dynamics of which have been the subject of a theoretical investigation at the extended Hückel level.[22] These calculations revealed that in the interconversion of the various C_{4v} isomers the intermediacy of a D_{3h} *closo* trigonal bipyramidal structure is strongly disfavoured. The proposed lowest energy pathway (Scheme 6) involves the sequence

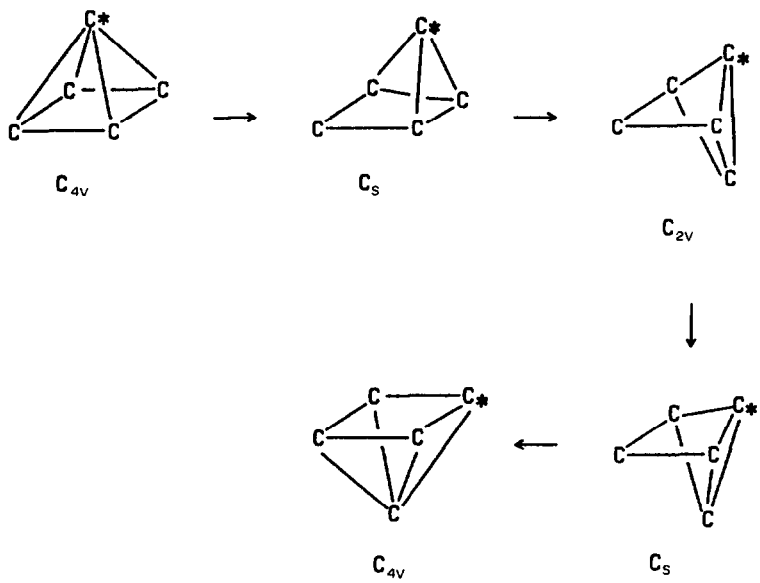

Scheme 6. Scrambling mechanism for $[C_5H_5]^+$.

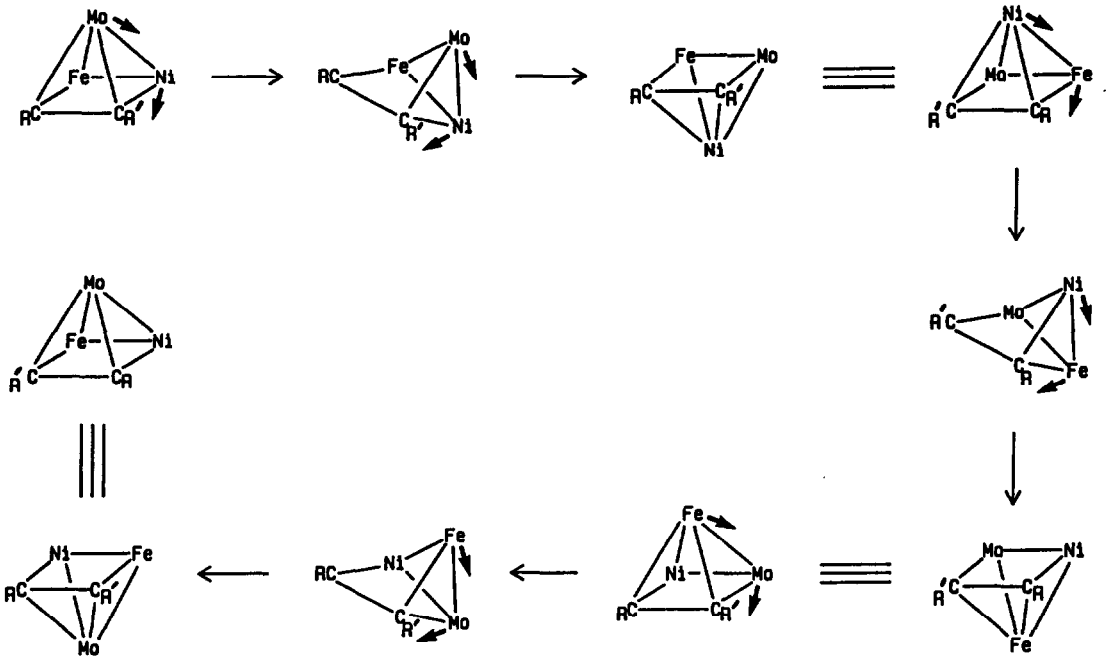

Scheme 7. Rearrangement mechanism for the M_3C_2 cluster analogous to that for the $[C_5H_5]^+$ system.

$C_{4v} \rightarrow C_{2v} \rightarrow C_{2v} \rightarrow C_{2v} \rightarrow C_{4v}$ and Scheme 7 shows how such a rearrangement pathway can be applied to the M_3C_2 system. The overall transformation is identical to that resulting from the "windshield wiper" mechanism described above; that is, there is interconversion of diastereomers of **9** but not of enantiomers. NMR data on other mixed-metal square-based pyramidal clusters have been published and are in complete accord with the mechanistic proposals we have outlined above.[23,24]

(c) *Tetrahedral clusters containing arphos*

Tetrahedral clusters can be rendered chiral by incorporating four chemically different vertices into the molecule. Another method would be to use an unsymmetrical bidentate ligand to destroy any molecular mirror planes. For this purpose, we selected $Ph_2P—CH_2—CH_2—AsPh_2$ (arphos), which readily displaces two carbonyls from adjacent metals and thus generates a chiral cluster.[8] The X-ray crystal structure of (arphos)$Co_3(CO)_7C—CO_2CHMe_2$, **11** (see Fig. 2) reveals that the arphos ligand occupies equatorial positions.[25]

However, the ^1H and ^{13}C NMR spectra of the isopropyl group measured at ambient temperature showed just a single methyl environment implying that the molecule was undergoing racemization on the NMR time scale. Indeed, at $-50°C$, the diastereotopic character of the methyl protons was clearly evident (see Fig. 3) and the barrier was evaluated as ≈ 13 kcal mol^{-1}.

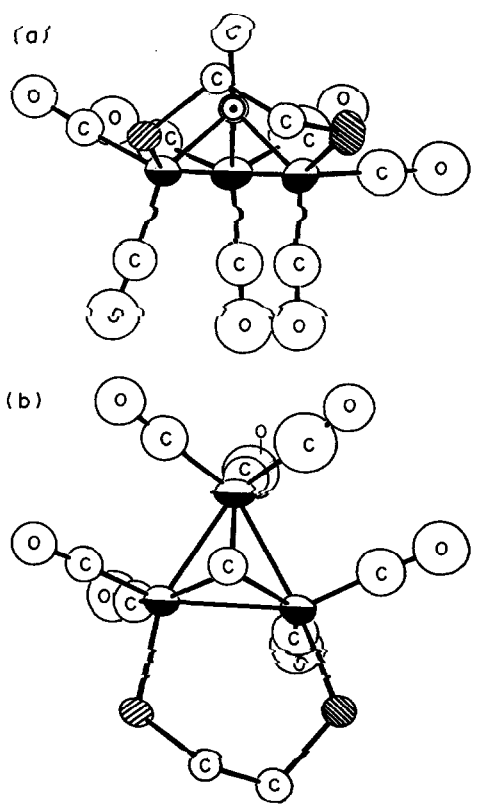

Fig. 2. X-ray crystal structure of $Co_3(CO)_7$(arphos)C—CO_2CHMe_2, **11**, with the phenyl rings and the ester functionality removed for clarity: (a) view in the tricobalt plane showing the half-chair conformation of the chelate ring; (b) view down the pseudo-three-fold axis showing the equatorial orientation of the arphos ligand.

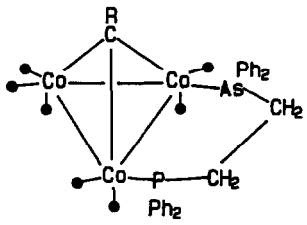

11

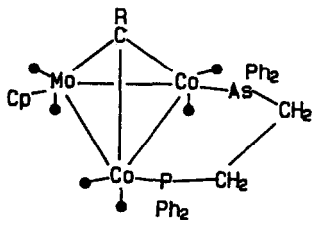

12

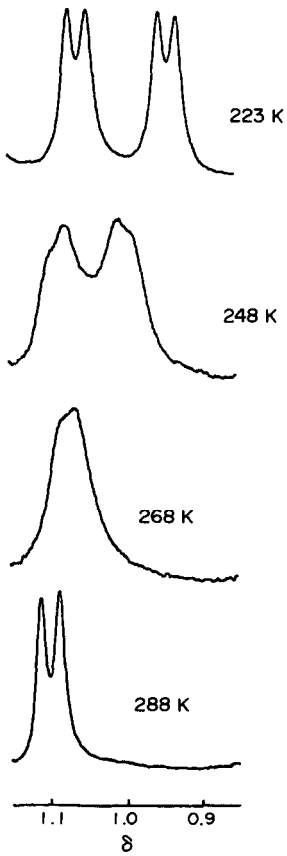

Fig. 3. Variable-temperature 250 MHz ^{1}H NMR spectra of the methyl region of $Co_3(CO)_7$(arphos) C—CO_2CHMe_2, **11**.

The racemization process is so much more facile in this case compared with that for the tetrahedral cluster **6** that a mechanism involving interconversion of the metal vertices themselves seems to be ruled out. The most likely process is that in which the diphenylarsenido terminus of the arphos ligand migrates from one cobalt vertex to another, as depicted in Scheme 8. In accordance with such a proposal, all four protons of the —CH_2—CH_2— chain are distinguishable at low temperature. They are differentiated not only by their proximity to either phosphorus or arsenic but also by their *exo or endo* orientation with respect to the cluster. Upon raising the temperature, however, the *exo* and *endo* positions are interconverted and the protons are differentiated solely by the identity of their neighbour, viz, P or As.

This view is reinforced by the observation that in the corresponding diphos complex ($Ph_2PCH_2CH_2PPh_2$)$Co_3(CO)_7$C—CO_2CHMe_2, one observes only two methylene resonances (attributable to *exo* and *endo* protons) at all temperatures; hence, the cobalt–phosphorus linkage apparently remains intact. A further point to make is that for migration of arsenic from one cobalt to another there must be concomitant carbonyl migration; in fact, interchange of the carbonyl ligands between the metal centres is much faster than cluster racemization so the rate-determining step is the cobalt–arsenic bond-breaking process.[25]

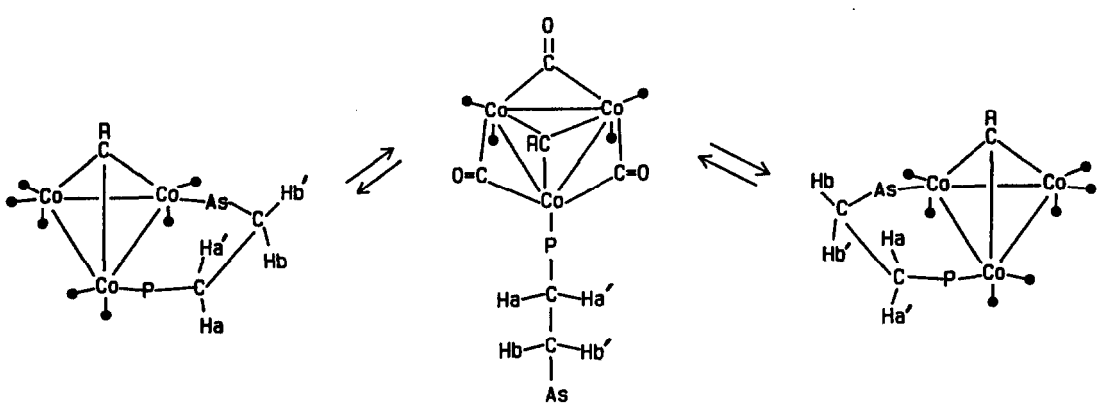

Scheme 8. Interconversion of the enantiomers of **11** via arsenic migration.

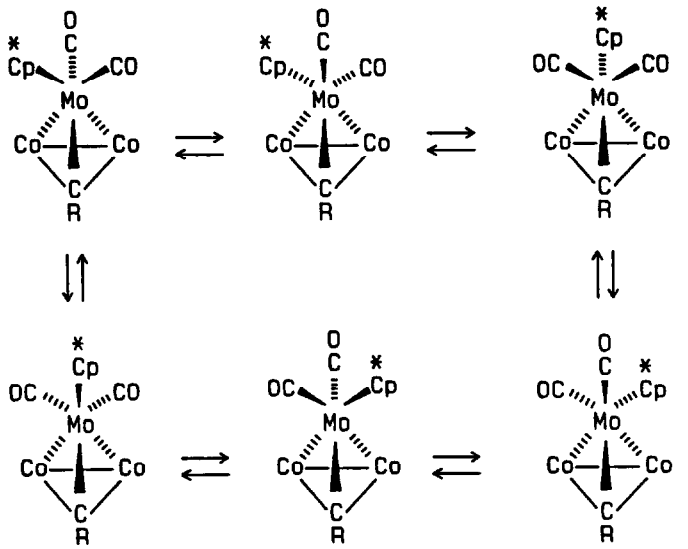

Scheme 9. Rotation of a Cp*Mo(CO)$_2$ vertex relative to a Co$_2$C triangular face. Other ligands have been omitted for simplicity.

Arphos complexes in which one of the Co(CO)$_3$ vertices has been replaced by a (C$_5$Me$_5$)Mo(CO)$_2$ unit, as in **12**, retain their stereochemical integrity. This is very clearly shown by the diastereotopic nature of the isopropyl methyls even at high temperature. Furthermore, there is a serendipitous bonus in that the isopropyl methyls are further split at low temperature demonstrating the presence of other diastereomers. Work currently in progress (K. A. Sutin, B. G. Sayer, B. H. Hunter and M. J. McGlinchey, in preparation) has shown that these other isomers arise because of restricted rotation of the (C$_5$Me$_5$)Mo(CO)$_2$ vertex relative to the dicobalt–carbynyl–carbon triangle, as shown in Scheme 9. We shall return to this point in Section 2(b).

2. ^{13}CO NMR SPECTRA AS STRUCTURAL PROBES

The availability of high field instrumentation, in conjunction with ^{13}CO isotopic enrichment, allows the use of carbonyl resonances not only to study rearrangement processes but also to determine molecular structures. Of course, metal carbonyl spectra have long been measurable[26] but, because of the enormous dispersion provided by high field instruments, it is nowadays feasible to follow the progress of ligand migrations occurring with very low activation energy barriers. In some cases, such processes have been investigated by IR or Raman spectroscopic techniques but these can be somewhat limited since not all vibrations are unequivocally assignable to a particular isomer in a complex mixture. NMR spectroscopy has a potentially enormous advantage in that the observation of direct coupling between the ^{13}CO and spin-active metal nuclei, such as ^{103}Rh, ^{183}W or ^{195}Pt, or with neighbouring ligands containing ^{11}B, ^{31}P, ^{77}Se, etc. can provide unambiguous evidence concerning the chemical and geometric environment of a particular carbonyl group.

(a) *Dimetalla-tetrahedranes containing molybdenum or tungsten vertices*

The reactions of alkynes with metal–metal triple-bonded species provide a good route to dimetallatetrahedranes.[27–31] Typically, a series of clusters of the general type [(C$_5$Me$_x$H$_{5-x}$)M(CO)$_2$]$_2$RC≡CR), where M = Mo or W, and x = 0, 1 or 5, have been prepared[32,33] and their variable-temperature NMR spectra recorded. Crystallographic data on [CpMo(CO)$_2$]$_2$(RC≡CR), where R = H or Ph, revealed the presence of a single semi-bridging carbonyl ligand;[32] in accordance with this structure, the low temperature ^{13}C NMR spectra displayed three terminal and one semi-bridging carbonyl environments. As befits a molecule of C_1 symmetry, the two cyclopentadienyl moieties are also magnetically non-equivalent. Upon raising the temperature, the semi-bridging carbonyl was observed to exchange with a terminal carbonyl and the CpMo(CO)$_2$ vertices underwent partial rotation, as depicted in Scheme 10.

This fluxional process generates a system of time-averaged C_s symmetry which exhibits only two carbonyl environments and a single cyclopentadienyl resonance. Analogous low temperature ^{13}C NMR studies were also carried out for the series of methyl-substituted (cyclopentadienyl)molybdenum molecules discussed above and all demonstrated the

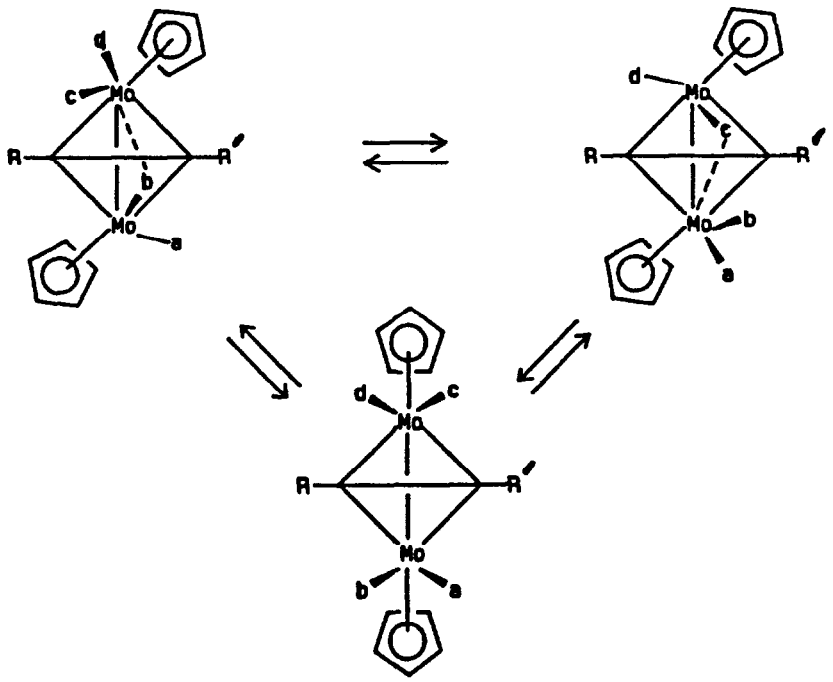

Scheme 10. Semi-bridging carbonyl exchange process.

same type of fluxional behaviour.[33] The barrier to carbonyl exchange was *ca* 8 kcal mol^{-1} but this increased in proportion to the steric bulk of the substituted cyclopentadienyl group. However, when the same studies were carried out on the analogous tungsten compounds only a single carbonyl environment and one cyclopentadienyl resonance were observed,[33] even when using a 400 MHz instrument at $-100°C$! It was clear from the IR data that semi-bridging carbonyls were also present in the tungsten systems but it was not possible to freeze out the exchange even at this low temperature on a high field machine. Apparently, the barrier to exchange must be considerably lower in the tungsten compounds than in the molybdenum clusters, but the factors controlling such behaviour remain unclear for the moment. Interestingly, carbonyl fluxionality in these molecules can be stopped on the NMR time scale when the cyclopentadienyl rings bear extremely bulky phenyl substituents.[34]

(b) *Trimetalla-tetrahedranes containing molybdenum or tungsten vertices*

There now exist many tetrahedral clusters containing three organometallic vertices and a capping carbynyl fragment. The two most widely used routes to such molecules are shown in Scheme 11 and involve either (i) the interaction of a metal–metal triple-bonded unit with a metal carbyne complex[35] or (ii) the isolobal substitution of one organometallic vertex for another in a readily available precursor.[36]

The first two X-ray crystal structures of such clusters, **13** and **14**, were almost identical and showed that the cyclopentadienyl ring was positioned below the trimetallic plane and distal with respect to the capping aryl-carbynyl unit. The ^{13}C NMR spectrum of these molecules at $-50°C$ showed a single averaged peak for all the CO ligands showing the rapid interchange of cobalt-

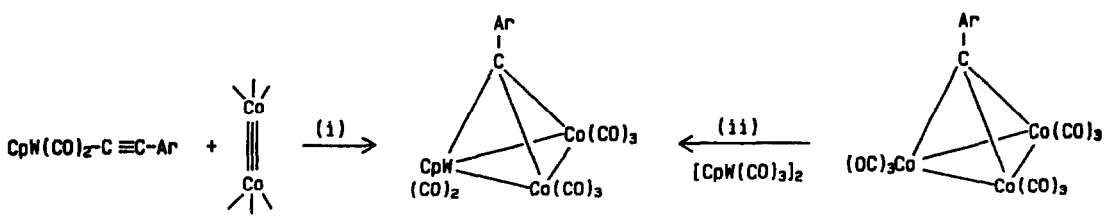

Scheme 11. Routes to mixed-metal M_3CR clusters.

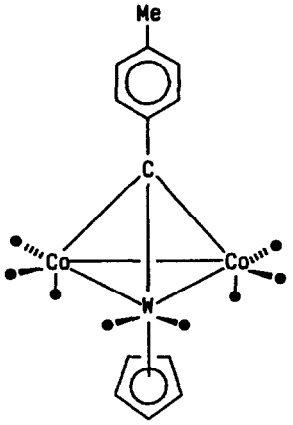

13

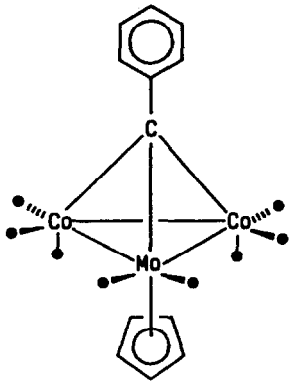

14

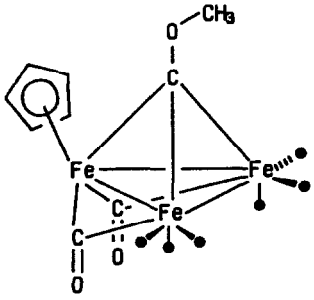

15

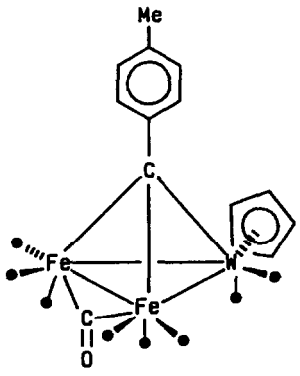

16

and tungsten-bound carbonyls. Nevertheless, both Stone[37] and Vahrenkamp[38] noted that there were too many IR bands in the carbonyl stretching region to be assigned to a single isomer, and it was proposed that the $CpM(CO)_2$ vertex might be able to adopt several rotameric conformations. Subsequent X-ray structural determinations[39,40] of related molecules revealed that the cyclopentadienyl ring could indeed adopt other orientations in the solid state, as in **15** and **16**.

The first indication that this facile rotation could be stopped on the NMR time scale came with the recent measurement of the ^{13}C spectrum of $(C_5Me_5)Mo(CO)_2Co_2(CO)_6C—CO_2CHMe_2$, **17**, at $-100°C$ on a 400 MHz instrument.[25] At this temperature, one observes not merely two carbonyl resonances at ≈ 200 and 230 ppm in the ratio 3 : 1 as anticipated for COs bound to cobalt and molybdenum, respectively, but also another less intense set of peaks (also in a 3 : 1 ratio) attributable to a different rotamer. The pentamethylcyclopentadienyl resonances are also no longer singlets and their intensities correspond to those of their carbonyl partners in the two rotamers. It is noteworthy that the iso-

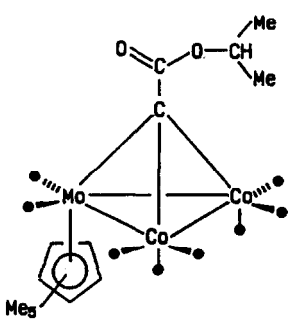

17a

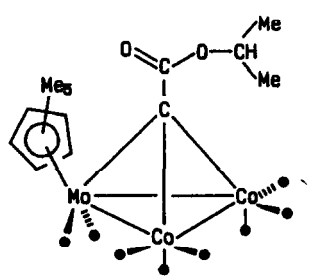

17b

propyl groups in each of the rotamers show no evidence of diastereotopic behaviour suggesting that both isomers are achiral. One can thus propose that the rotamers differ in the orientation of the five-membered ring; in the major isomer, the pentamethylcyclopentadienyl ring lies below the plane of the metals, **17a**, and vice versa in the minor isomer **17b**. This pattern of behaviour has now been extended to the complete set of clusters $[(C_5Me_xH_{5-x})MCo_2(CO)_8C{-}CO_2CHMe_2]$, where M = Mo or W, and $x = 0$, 1 or 5 (K. A. Sutin, B. G. Sayer, B. H. Hunter and M. J. McGlinchey, in preparation). Interestingly, for the clusters bearing C_5H_5 or C_5H_4Me rings, the predominant rotamer in solution is the one corresponding to **17b** whereby the Cp ring is proximal to the capping carbynyl moiety. This places the molybdenum (or tungsten) carbonyls in a better position for bridging and ultimately for transfer to the cobalt vertices. One can now see the parallel between these M_3C systems and the M_2C_2 clusters described in Section 2(a). There has merely been an isolobal substitution of an HC vertex by an organometallic fragment, but the ability of the $CpMo(CO)_2$ moiety to rotate with respect to the opposite triangular face of the tetrahedron—whether it be a C_2M face or an M_2C face—is maintained. Of course, it is particularly easy for vertex rotation to occur for a metal tricarbonyl fragment and this topic is discussed in the next section.

(c) *The question of axial–equatorial exchange in tetrahedral clusters*

Numerous X-ray crystallographic structural determinations[41] have shown that clusters of the type $RCCo_3(CO)_9$ or $RCCo_3(CO)_{9-x}L_x$ adopt one of two isomeric forms; all the carbonyl groups can be terminal, as in **18**, so that there are six equatorial and three axial ligands,[42] or the molecule can have three bridging, three radial and three axial ligands as in **19**.[43] All known $RCCo_3(CO)_9$ clusters show a single ^{13}CO resonance even at low temperature indicating that there is rapid exchange of axial and equatorial carbonyls. It is not possible to prove whether inter-cobalt exchange occurs since there is no suitable cobalt isotope with an observable cobalt–carbon coupling constant. (In $[Cp_3Rh_3(CO)_3]$, **20**, each carbonyl exhibits a triplet attributable to coupling to two ^{103}Rh nuclei; upon warming, the ^{13}CO resonance becomes a quartet since rapid migration allows each carbonyl carbon to interact with all three rhodium atoms.[44])

The slowing of intermetal migration of the carbonyls on the NMR time-scale is readily observable in clusters such as **21** which, upon cooling, yields a 3 : 6 peak pattern for the $Fe(CO)_3$ and $Co(CO)_3$ groups. The freezing out of the rotation of the tricarbonyl–iron fragment ultimately yields a 1 : 2 : 6 spectral pattern[45] but local rotation of a $Co(CO)_3$ vertex has never been stopped. However, in mol-

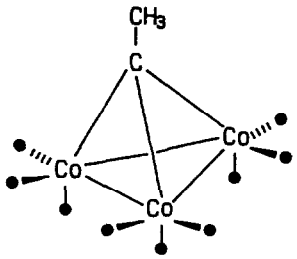

18

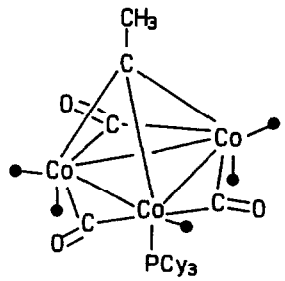

19

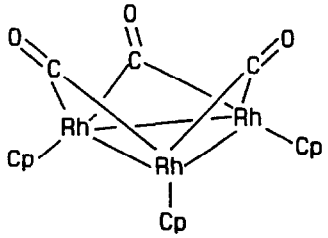

20

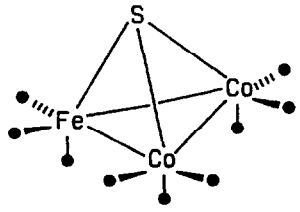

21

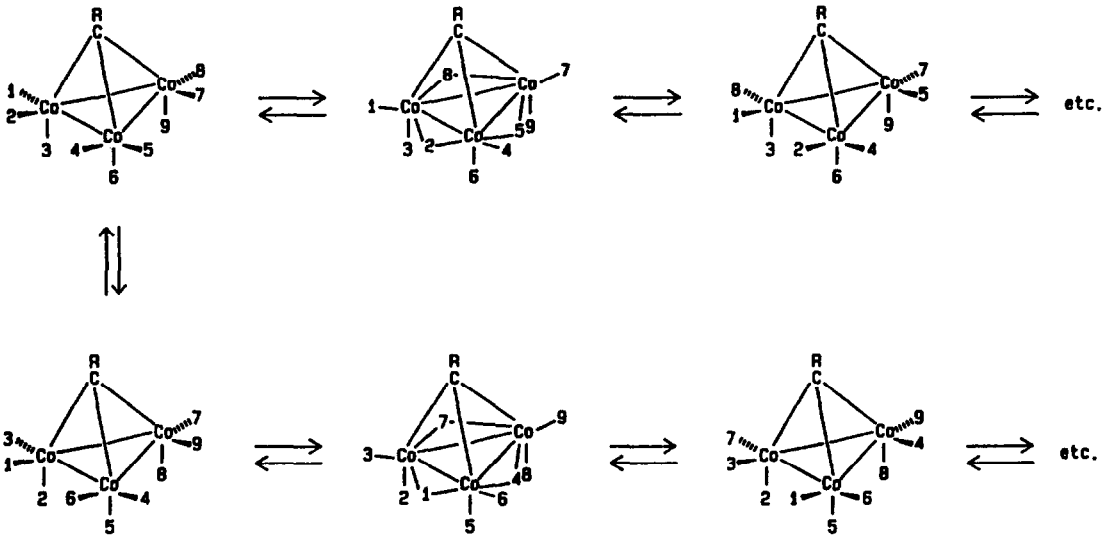

Scheme 12. Mechanisms for complete interconversion of carbonyl ligands in $Co_3(CO)_9CR$ clusters.

ecules bearing three bridging carbonyls, e.g. **19**, all the different carbonyl environments are detectable.[46] It is generally assumed that inter-metal exchange of the six equatorial environments can be accomplished via the "merry-go-round" process, while axial–equatorial interchange merely requires a local rotation.[47] Scheme 12 shows how a combination of these two mechanisms allows each carbonyl access to all nine sites.

In continuation of our studies of molecules containing potentially sterically demanding ligands, we treated $Co_2(CO)_8$ with a series of reagents each containing a trichloromethyl moiety (see Scheme 13).

In particular, the reaction of dicobalt octacarbonyl with the well-known insecticide DDT yielded the anticipated diarylmethylcarbynyl cluster **22**, the X-ray structure of which (see Fig. 4) shows a molecule of almost C_S symmetry (R. A. Gates, K. A. Sutin, M. F. D'Agostino, R. Faggiani, M. J. McGlinchey, T. S. Janik and M. R. Churchill, in preparation).

Our original goal was to stop rotation of the aryl groups on the NMR time-scale and, consequently, the ^{13}C spectrum was recorded on a high field spectrometer at $-120°C$. We saw no evidence of the cessation of phenyl ring rotation, but the ^{13}CO res-

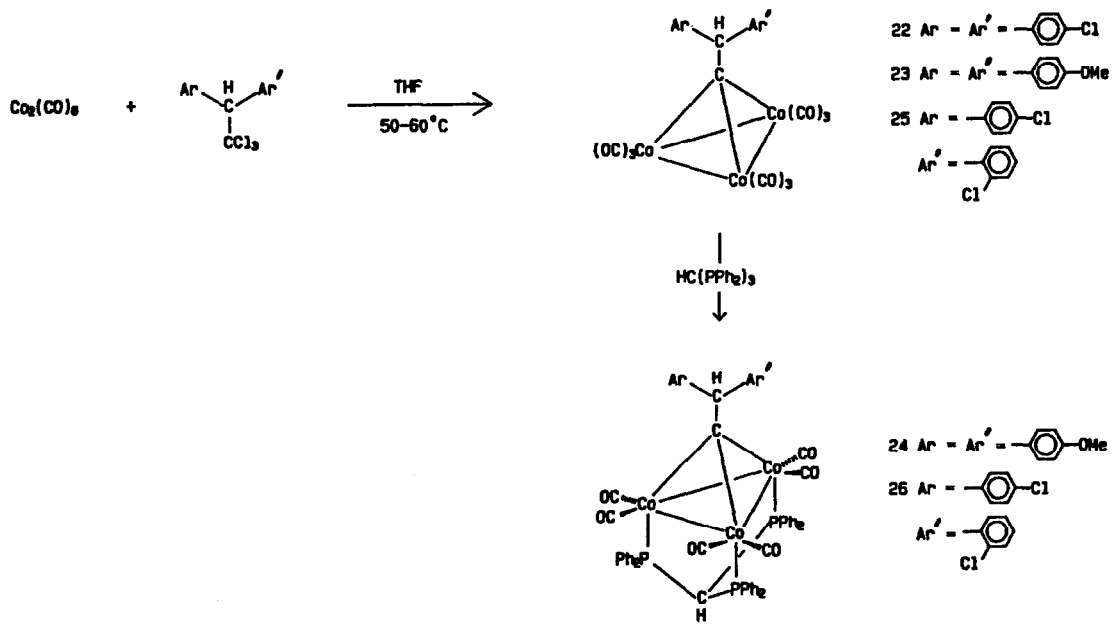

Scheme 13. Syntheses of DDT-related clusters.

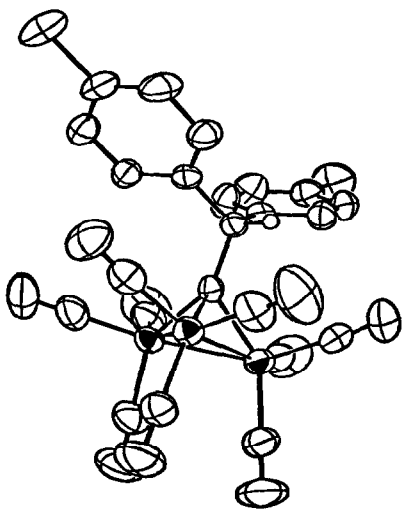

Fig. 4. X-ray crystal structure of $(Cl—C_6H_4)_2CH—CCo_3(CO)_9$, **22**.

onance appeared as a 3:6 peak pattern (R. A. Gates, K. A. Sutin, M. F. D'Agostino, R. Faggiani, M. J. McGlinchey, T. S. Janik and M. R. Churchill, in preparation). This observation is interpretable either (i) in terms of slowed rotation of the capping carbynyl unit to give a structure like that in the solid state (thus splitting the triple degeneracy of the $Co(CO)_3$ vertices), or (ii) by invoking the cessation of axial–equatorial exchange—a hitherto unprecedented phenomenon. Identical low temperature ^{13}C NMR results were obtained for the corresponding 4,4′-bis-methoxy cluster, **23**, prepared analogously from the commercially available insecticide "Methoxychlor". To investigate this further, we replaced the three axial carbonyls by a triphos ligand and recorded the ^{31}P NMR spectrum at −120°C. Cessation of rotation of the capping group in **24** would generate a molecule of C_S symmetry and so should split the single ^{31}P resonance into a 1:2 peak pattern. In contrast, if the capping group continues to spin freely, the molecule retains its three-fold symmetry and so the ^{31}P peak should remain a sharp singlet. In fact, the latter situation obtains (M. F. D'Agostino and M. J. McGlinchey, in preparation), clearly demonstrating that the carbynyl substituent can still spin freely. Assuming that the same situation prevails in the tricobalt nonacarbonyl clusters **22** and **23**, that is, rotation of the capping moiety continues unhindered, the only explanation for the 6:3 splitting of the carbonyls would necessarily involve a cessation of axial–equatorial exchange on the NMR time-scale. To obtain unequivocal evidence that rotation of the capping group continues in the non-acarbonyl systems, we prepared the chiral 2,4′-dichloro cluster **25** (derived from *o,p′*-DDT) and recorded its ^{13}C NMR spectrum at −120°C. As with **22** and **23**, a 6:3 ^{13}CO pattern was observed. If rotation of the capping group had been slowed on the NMR time-scale, the three $Co(CO)_3$ vertices would have been rendered non-equivalent; such a scenario is inconsistent with the observed 6:3 splitting. Furthermore, the corresponding triphos complex, **26**, shows a ^{31}P singlet even at −120°C, again supporting our contention that the apical group is free to rotate (M. F. D'Agostino and M. J. McGlinchey, in preparation).

Interestingly, at −120°C the ^{13}CO resonance in **24** (and in **26**) is split into two equally intense peaks at ≈ 203 and 205 ppm. These chemical shifts are clearly attributable to terminally bound carbonyl ligands and the situation is quite different from that previously reported[48] for $Rh_4(CO)_9$(triphos), **27** which has three bridging ligands, as in **19**. It is apparent that in the cobalt–triphos clusters **24** and **26** the molecular symmetry is not C_{3v} but rather C_3. This phenomenon presumably arises because at low temperature the six phenyls of the triphos ligand freeze out in a propeller conformation and thus lower the molecular symmetry to C_3, as shown in Fig. 5. X-ray crystallographic data show that this conformational preference is also exhibited in $Co_4(CO)_9$(triphos).[49]

The net result of these experiments is to show that, since the capping carbynyl moiety continues to rotate freely, the splitting of the carbonyls in **22**–**24** into a 3:6 pattern must arise from a freezing out of the axial–equatorial exchange presumably because of the bulk of the diarylmethyl carbynyl unit. Indeed, when the chlorophenyl groups in the DDT-derived cluster are replaced by even more

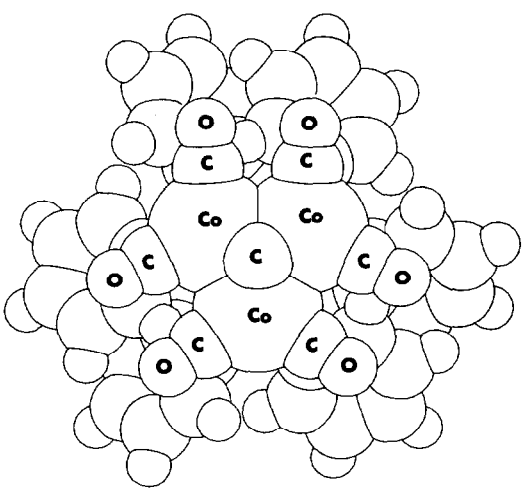

Fig. 5. CHEM-X plot showing the propellor type orientation of the phenyl rings of the triphos ligand in **24**. This reduces the effective symmetry to C_3 thus splitting the six-fold degeneracy of the carbonyls into a 3:3 pattern.

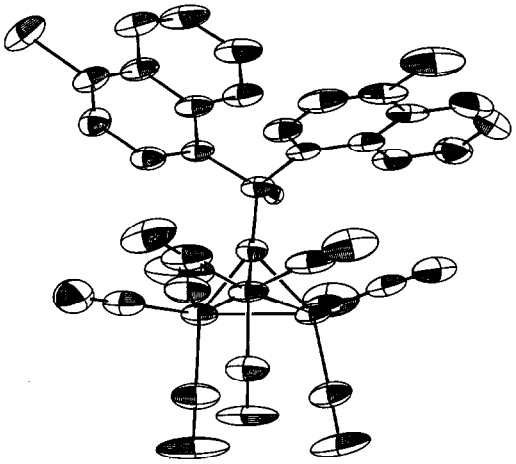

Fig. 6. X-ray crystal structure of $(Cl—C_{10}H_6)_2CH—CCo_3(CO)_9$.

bulky chloronaphthyl units (see Fig. 6) the X-ray crystal structure (R. A. Gates, K. A. Sutin, M. F. D'Agostino, R. Faggiani, M. J. McGlinchey, T. S. Janik and M. R. Churchill, in preparation) reveals that one of the cobalt carbonyl vertices twists and orients itself so as to avoid one of the naphthyl rings.

(d) *The structure of cluster cations*

These observations on axial–equatorial carbonyl exchange processes are relevant to those described in a recent publication from this laboratory in which it was reported that the cation $[Co_3(CO)_9C{=}C{=}O]^+$ also shows a 6:3 ^{13}CO NMR splitting at low temperature.[50] In the absence of a bulky capping group it seemed highly improbable that axial–equatorial carbonyl exchange could be slowed and so it was proposed that the cluster adopts a bent structure in which the ketenylidene moiety leans either towards a single vertex or towards the middle of a cobalt–cobalt vector. Although Extended Hückel Molecular Orbital calculations showed that either of these bent structures were favoured over the linear (C_{3v}) isomer, it is difficult to prove unambiguously which of the C_s conformations **28a** or **28b** is the predominant isomer in solution.

A more definitive conclusion could be drawn in the case of the vinylidene cation, $[Co_3(CO)_9C{=}CH_2]^+$, which had also been envisaged as being more stable in the bent configuration **29a** rather than the linear isomer **29b**.[51] In an ingenious experiment,[52] it was shown that one could substitute a vinylidene hydrogen by an isopropyl group and then detect the presence of diastereotopic methyl groups. Chirality can only arise if the alkylidene fragment is tilted towards one of the cobalt vertices, as in **30**; this result is in accord with EHMO calculations on the unsubstituted cluster.[53]

It is interesting to note here that the isolobal analogy would lead one to predict that the $[Co_2(CO)_6(RC{\equiv}C—CH_2)]^+$ cations produced in the Nicholas reaction[54] should adopt the bent configuration already demonstrated for their tricobalt analogues. Indeed, the viability of such a structure could be investigated by the use of alkynes bearing potentially diastereotopic functionalities, as in **31**.

(e) *The mechanism of decarbonylation of* $Ar—CO—CCo_3(CO)_9$ *to* $Ar—CCo_3(CO)_9$

In the course of his pioneering investigations on the $RCCo_3(CO)_9$ cluster system, Seyferth had reported that the aryl ketones **32** underwent ready decarbonylation to yield the aryl clusters **33** [see eq. (3)].[55] However, the identity of the CO which had been eliminated was unknown, and two mechanistically reasonable proposals were advanced. The first required homolytic cleavage of the carbynyl–carbon–ketonic–carbon bond with eventual loss of the originally ketonic CO; the second involved initial loss of a cobalt carbonyl ligand with subsequent migration of the ketonic carbonyl into the vacant site at the coordinatively unsaturated metal vertex. As is apparent in Scheme 14, these mechanistic possibilities can be distinguished by labelling the ketonic carbon and then locating the label in either the eliminated carbon monoxide or as a CO now bonded to cobalt.[56]

In fact, it turned out to be experimentally easier to enrich the cobalt carbonyls with ^{13}CO than to label exclusively the ketonic CO. Thus, if pathway (a) was operative, the ^{13}C enrichment factor for the metal carbonyls relative to the naturally

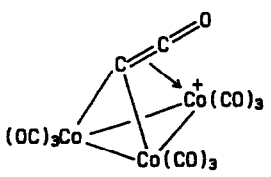

28a

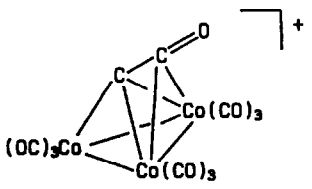

28b

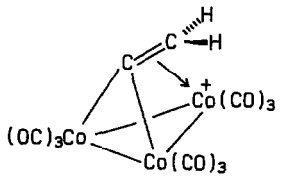

29a

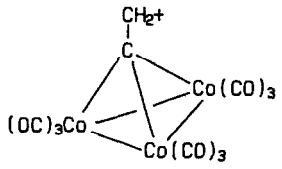

29b

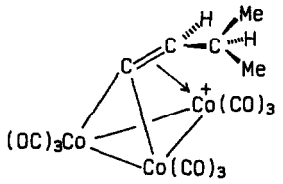

30

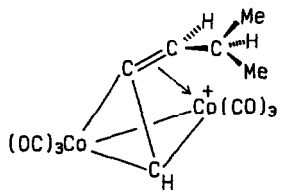

31

abundant ^{13}C nuclei in the aryl capping group should be unchanged; in contrast, if the CO which is lost is a cobalt carbonyl, as in pathway (b), then the vacant site so generated will be occupied by the naturally abundant CO from the ketonic position. The experimental result is unequivocal, the relative integrated intensity of the cobalt carbonyl ^{13}C resonance in the decarbonylated product decreases by $\approx 12\%$ with respect to the remaining carbon nuclei in the cluster. This is in complete accord with the

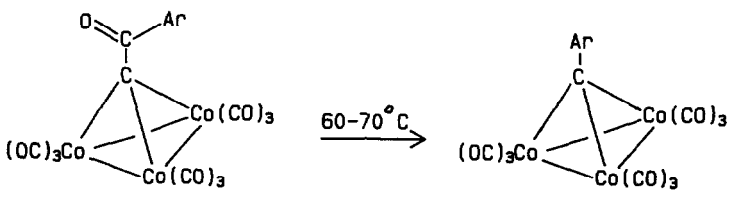

32 33 (3)

Eq. (3)

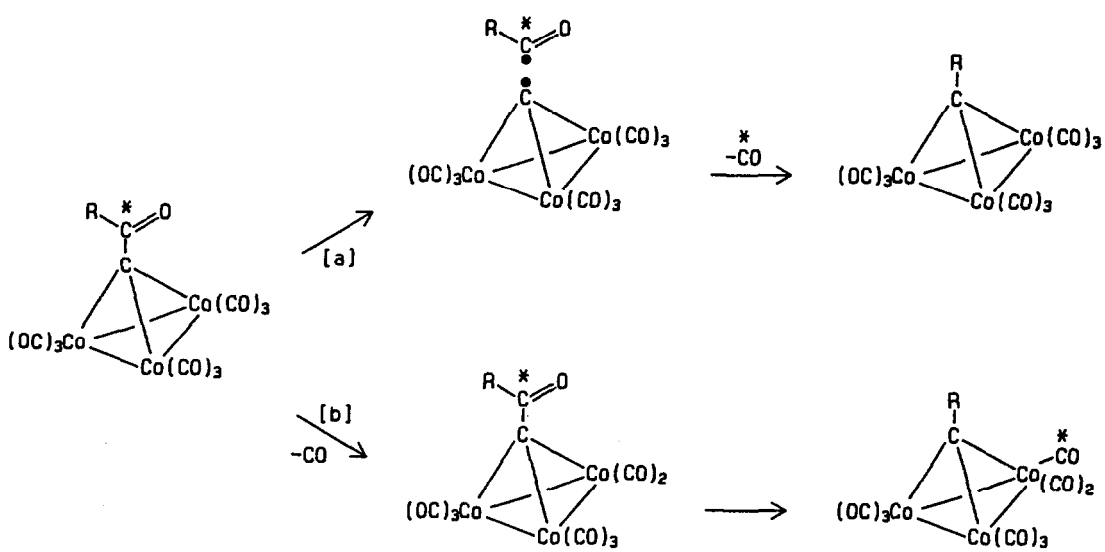

Scheme 14. Proposed pathways for loss of CO from aroyl tricobalt clusters.

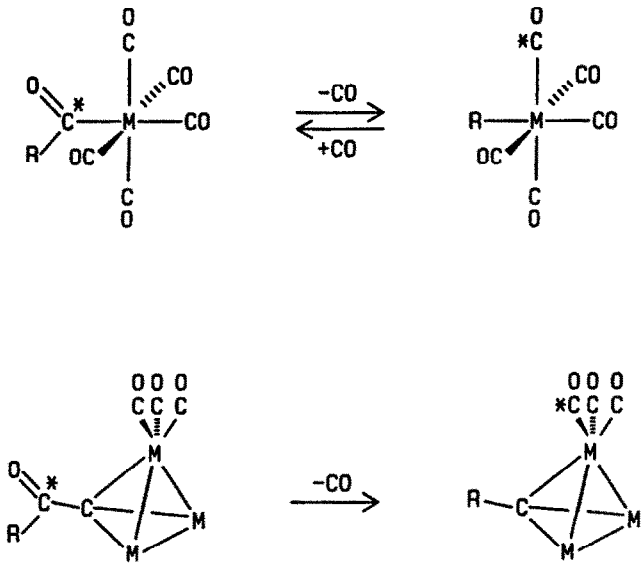

Scheme 15. Decarbonylation mechanisms for a monometallic system and for a trimetallic tetrahedral cluster.

second pathway, i.e. the CO which is eliminated was originally bonded to cobalt. Thus, only eight of the original nine enriched cobalt carbonyl ligands remain after decarbonylation and so the intensity of the metal carbonyl ^{13}CO resonance at 200 ppm is correspondingly diminished.[56]

The significance of this finding lies in the realization that the mechanism of decarbonylation (and presumably of carbonylation) of metal clusters parallels that established for monometallic complexes,[57] and the two generalized reactions are shown in Scheme 15.

3. CONCLUSIONS

It is apparent, not only from the examples presented here but also from the elegant studies which appear elsewhere, that NMR spectroscopy has become an exceedingly powerful technique for the determination of mechanisms of reaction and for the unravelling of molecular rearrangements which have appropriate activation energy barriers. The particular rôle of high field NMR spectroscopy is not merely to provide greater separation between peaks and so reduce overlap and hence simplify spectral assignment. Rather, the powerful and versatile hardware and software now available facilitate the use and development of multi-pulse sequences which readily yield information not only for structural assignments but also for molecular topology as well as for connectivity between interconverting sites.

For the organometallic cluster chemist this will provide a welcome opportunity to look directly at main group or transition metal vertices to probe their electronic environments. Of course, one is no longer restricted merely to acquiring data on molecules in solution. Solid state techniques are advancing by leaps and bounds and the correlation of X-ray crystallographic data with NMR parameters obtained from cross-polarization/magic angle spinning experiments[58] have shown that these are truly complementary approaches.

Acknowledgements—We thank the donors of the Petroleum Research Fund, administered by the American Chemical Society, and the Natural Sciences and Engineering Research Council of Canada for financial support. We also thank the trustees of the Harry Lyman Hooker Fund for contributing to the purchase of the 500 MHz NMR spectrometer. MFD is the recipient of an NSERC postgraduate scholarship. Finally, it is a particular pleasure to acknowledge Professor G. Jaouen (Ecole Nationale Supérieure de Chimie, Paris) for his many valuable and perspicacious comments over the last several years.

REFERENCES

1. R. Benn and H. Guenther, *Angew. Chem. Int. Ed. Engl.* 1983, **22**, 350.
2. R. Benn and C. Brevard, *J. Am. Chem. Soc.* 1986, **108**, 5622.
3. O. A. Gansow, D. S. Gill, F. J. Bennis, J. R. Hutchinson, J. L. Vidal and R. C. Shoening, *J. Am. Chem. Soc.* 1980, **102**, 2449.
4. P. Laszlo (Ed.), *NMR of Newly Accessible Nuclei.* Academic Press, New York (1983).
5. R. K. Harris and B. E. Mann (Eds), *NMR and the Periodic Table.* Academic Press, London (1978).

6. D. G. Bickley, M. J. McGlinchey and G. J. Schrobilgen, *Can. Chem. News* 1984, **36**, 19.
7. M. J. McGlinchey, M. Mlekuz, P. Bougeard, B. G. Sayer, A. Marinetti, J.-Y. Saillard and G. Jaouen, *Can. J. Chem.* 1983, **61**, 1319.
8. G. Jaouen, A. Marinetti, J.-Y. Saillard, B. G. Sayer and M. J. McGlinchey, *Organometallics* 1982, **1**, 225.
9. Y. Iwashita, F. Tamura and H. Wakmatsu, *Bull. Chem. Soc. Jpn.* 1970, **43**, 1520.
10. D. M. Hoffman, R. Hoffmann and C. R. Fisel, *J. Am. Chem. Soc.* 1982, **104**, 3858.
11. H. Pepermans, C. Hoogzand and P. Geerlings, *J. Organomet. Chem.* 1986, **306**, 395.
12. G. Jaouen, A. Marinetti, B. Mentzen, R. Mutin, J.-Y. Saillard, B. G. Sayer and M. J. McGlinchey, *Organometallics* 1982, **1**, 753.
13. K. Mislow, *Introduction to Stereochemistry*. W. A. Benjamin, Reading, MA (1965).
14. J. K. M. Sanders and B. H. Hunter, *Modern NMR Spectroscopy*, pp. 299–302. Oxford University Press, Oxford (1987).
15. M. Mlekuz, P. Bougeard, B. G. Sayer, S. Peng, M. J. McGlinchey, A. Marinetti, J.-Y. Saillard, J. Ben Naceur, B. Mentzen and G. Jaouen, *Organometallics* 1985, **4**, 1123.
16. A. J. Deeming, R. E. Kimber and M. Underhill, *J. Chem. Soc., Dalton Trans.* 1973, 2859.
17. R. Hoffmann, *Angew. Chem. Int. Ed. Engl.* 1982, **21**, 711.
18. B. E. R. Schilling and R. Hoffmann, *Acta Chem. Scand., Ser. B* 1979, **B33**, 231.
19. J.-F. Halet, J.-Y. Saillard, R. Lissillour, M. J. McGlinchey and G. Jaouen, *Inorg. Chem.* 1985, **24**, 218 and refs therein.
20. K. Wade, *Adv. Inorg. Chem. Radiochem.* 1976, **18**, 1.
21. D. M. P. Mingos, *Acc. Chem. Res.* 1984, **17**, 311.
22. W. D. Stohrer and R. Hoffman, *J. Am. Chem. Soc.* 1972, **94**, 1661.
23. L. Busetto, M. Green, B. Hessner, J. A. K. Howard, J. C. Jeffery and F. G. A. Stone, *J. Chem. Soc., Dalton Trans.* 1983, 519.
24. F. W. B. Einstein, K. G. Tyers, A. S. Tracey and D. Sutton, *Inorg. Chem.* 1986, **25**, 1631.
25. K. A. Sutin, J. W. Kolis, M. Mlekuz, P. Bougeard, B. G. Sayer, M. A. Quilliam, R. Faggiani, C. J. L. Lock, M. J. McGlinchey and G. Jaouen, *Organometallics* 1987, **6**, 439.
26. B. E. Mann and B. F. Taylor, ^{13}C *NMR Data for Organometallic Compounds*. Academic Press, London (1981).
27. D. S. Ginley, C. R. Brock and M. S. Wrighton, *Inorg. Chim. Acta* 1977, **23**, 85.
28. R. M. Laine and P. C. Ford, *J. Organomet. Chem.* 1977, **124**, 29.
29. F. Y. Petillon, F. LeFloch-Perennou, J. E. Guerchais, D. W. A. Sharp and L. Manojlovic-Muir, *J. Organomet. Chem.* 1978, **202**, 23.
30. S. R. Finnimore, S. A. R. Knox and G. E. Taylor, *J. Chem. Soc., Dalton Trans.* 1982, 1783.
31. M. Green, S. J. Porter and F. G. A. Stone, *J. Chem. Soc., Dalton Trans.* 1983, 513.
32. W. I. Bailey, Jr., M. H. Chisholm, F. A. Cotton and L. A. Rankel, *J. Am. Chem. Soc.* 1978, **100**, 5764.
33. P. Bougeard, S. Peng, M. Mlekuz and M. J. McGlinchey, *J. Organomet. Chem.* 1985, **296**, 383.
34. G. A. Carriedo, J. A. K. Howard, D. B. Lewis, G. E. Lewis and F. G. A. Stone, *J. Chem. Soc., Dalton Trans.* 1985, 905.
35. F. G. A. Stone. *Angew. Chem. Int. Ed. Engl.* 1984, **23**, 89.
36. H. Vahrenkamp, *Adv. Organomet. Chem.* 1983, **22**, 169.
37. M. J. Chetcuti, P. A. M. Chetcuti, J. C. Jeffery, R. M. Mills, P. Mitrprachachon, S. J. Pickering, F. G. A. Stone and P. Woodward, *J. Chem. Soc., Dalton Trans.* 1982, 699.
38. H. Beurich and H. Vahrenkamp, *Angew. Chem. Int. Ed. Engl.* 1978, **17**, 863.
39. L. Busetto, J. C. Jeffery, R. M. Mills, F. G. A. Stone, M. J. Went and P. Woodward, *J. Chem. Soc., Dalton Trans.* 1983, 101.
40. A. A. Aitchison and L. J. Farrugia, *Organometallics* 1987, **6**, 819.
41. B. R. Penfold and B. H. Robinson, *Acc. Chem. Res.* 1973, **6**, 73.
42. P. W. Sutton and L. F. Dahl, *J. Am. Chem. Soc.* 1967, **89**, 261.
43. T. W. Matheson and B. R. Penfold, *Acta Cryst.* 1977, **B33**, 1980.
44. R. J. Lawson and J. R. Shapley, *J. Am. Chem. Soc.* 1976, **98**, 7433.
45. S. Aime, L. Milone, R. Rossetti and P. L. Stanghellini, *Inorg. Chim. Acta* 1977, **25**, 103.
46. T. W. Matheson and B. H. Robinson, *J. Organomet. Chem.* 1975, **88**, 367.
47. E. Band and E. L. Muetterties, *Chem. Rev.* 1978, **78**, 639.
48. A. A. Bahsoun, J. A. Osborn, C. Voelken, J. J. Bonnet and G. Lavigne, *Organometallics* 1982, **1**, 1114.
49. D. J. Darensbourg, D. J. Zalewski and T. Delord, *Oraganometallics* 1984, **3**, 1210.
50. M. F. D'Agostino, M. Mlekuz, J. W. Kolis, B. G. Sayer, C. A. Rodger, J.-F. Halet, J.-Y. Saillard and M. J. McGlinchey, *Organometallics* 1986, **5**, 2345.
51. D. Seyferth, *Adv. Organomet. Chem.* 1976, **14**, 97.
52. R. T. Edidin, J. R. Norton and K. Mislow, *Organometallics* 1982, **1**, 561.
53. B. E. R. Schilling and R. Hoffmann, *J. Am. Chem. Soc.* 1979, **101**, 3456.
54. K. M. Nicholas, *Acc. Chem. Res.* 1987, **20**, 207.
55. D. Seyferth, M. O. Nestle and C. S. Eschbach, *J. Am. Chem. Soc.* 1976, **98**, 6724.
56. R. A. Gates, M. F. D'Agostino, R. E. Perrier, B. G. Sayer and M. J. McGlinchey, *Organometallics* 1987, **6**, 1181.
57. J. P. Collman and L. S. Hegedus, *Principles and Applications of Organotransition Metal Chemistry*, pp. 259–263. University Science Books, Mill Valley, CA (1980).

58. C. A. Fyfe, *Solid State NMR for Chemists*. CFC Press, Guelph, Canada (1983).
59. S. L. Schreiber, M. T. Klimas and T. Sammakia, *J. Am. Chem. Soc.* 1987, **109**, 5749.
60. S. F. T. Froom, M. Green, K. R. Nagle and D. J. Williams, *J. Chem. Soc. Chem. Commun.* 1987, 1305.
61. A. Meyer, D. J. McCabe and M. D. Curtis, *Organometallics* 1987, **6**, 1491.

Note added in proof. Refers to section 2(d) The structure of cluster cations. Very recent results have provided experimental verification of this idea.[59–61]

Polyhedron Vol. 7, No. 10/11, pp. 827–835, 1988
Printed in Great Britain

0277–5387/88 $3.00+.00
© 1988 Pergamon Press plc

C—C—C COUPLING REACTIONS ON THE DIRHODIUM COMPLEXES $[\{C_5Me_5Rh(\mu\text{-}CH_2)(R)\}_2]$ AND $[\{C_5Me_5Rh(\mu\text{-}CH_2)\}_2R(MeCN)]^+$ AS ANALOGUES OF THE POLYMERIZATION STEPS IN THE FISCHER–TROPSCH REACTION

ISABEL M. SAEZ, DAVID G. ANDREWS and PETER M. MAITLIS*

Department of Chemistry, The University, Sheffield S3 7HF, U.K.

(*Accepted* 5 *November* 1987)

Abstract—The normally stable dialkyl-di-μ-methylene dirhodium complexes, $[\{C_5Me_5Rh(\mu\text{-}CH_2)(R)\}_2]$ (**2**, R = Et), (**3**, R = *n*-Pr) and (**4**, R = *n*-Bu) are all decomposed easily by one-electron oxidants ($FeCl_3$, in aqueous dioxane or THF; Na_2IrCl_6 in moist MeCN) to give the C—C—C coupling product RC_2H_3 amongst others, analogous to the decomposition of $[\{C_5Me_5Rh(\mu\text{-}CH_2)(CH_3)\}_2]$ (**1**), to give propene, MeC_2H_3. Thus, (**2**) gave butene(s), (**3**) gave pentene(s) and (**4**) gave hexene(s). Products, RCH and RCH_2 [propene and propane from (**2**), butene(s) and butane from (**3**), and pentene(s) and pentane from (**4**)] arising from the coupling of R and one methylene, were also observed. The alkanes, RC_2H_5 (butane, pentane and hexane) were also formed, as were the chlorides, RCl; these were not observed in the decomposition of (**1**). The alkanes, RH and the olefins (R—H), were also formed from (**2**)–(**4**). Oxidative decomposition of $[\{C_5Me_5Rh(\mu\text{-}CH_2)\}_2(R)(MeCN)]^+$ (**5**, R = Me; **6**, R = Et) gave chiefly RC_2H_3 and some RCH. Complex (**5**, R = $^{13}CH_3$) gave largely $^{13}CH_2 = CHCH_3$, while (**5**, R = CD_3) gave largely $CD_2 = CHCDH_2$ with Na_2IrCl_6; the mechanism of the C—C—C coupling in this molecule therefore exactly parallels that in (**1**). The decomposition reactions were rather insensitive to the nature of the oxidant and the solvent; this supports the proposal that it is the positive charge on the complex which assists C—C—C coupling. Similar promotion may also be possible over a heterogeneous Fischer–Tropsch catalyst. Complexes (**2**) and (**6**) in the presence of $PdCl_2$ and Fe(III) or Ir(IV) and some water gave rise to acetone, butanone, (and acetaldehyde) by a type of Wacker-oxidation of the olefins initially produced; analogously complexes (**1**) and (**5**) gave acetone and acetaldehyde. This may be related to the process which gives oxygenates from syn-gas over mixed metal catalysts.

Reactions (usually reductive elimination) at metals which lead to organic products, in which carbon–carbon coupling has occurred, are common. With the exception of carbonylation processes, reactions in which three ligands grouped around a metal centre combine to give an organic product are much rarer.

Some time ago we reported that the dimethyl-di-μ-methylene dirhodium complex (**1**), $[\{C_5Me_5Rh(\mu\text{-}CH_2)(CH_3)\}_2]$, decomposed thermally ($\geq$ 300°C) to give largely methane and propene.[1] We later observed that an apparently similar reaction could be induced (at 20–50°C) by the addition of four equivalents of a one-electron oxidizer; initially we used hexachloroiridate(IV), but more recently we have found that the identical reaction occurs (and often more cleanly) with ferric salts. The other products are Rh(III) complexes, and one version of the overall process, in the presence of acetonitrile, can be described by eq. (1),[2]

$$[\{C_5Me_5Rh(\mu\text{-}CH_2)(CH_3)\}_2] \xrightarrow{-4e^- + 6MeCN} 2[C_5Me_5Rh(MeCN)_3]^{2+} \quad (2)$$

$$+ CH_2 = CHCH_3 + CH_4. \quad (1)$$

*Author to whom correspondence should be addressed.

Processes of this type accounted for some 70% of the overall reaction, the remainder being side-reactions leading to methane and ethene.

Very extensive labelling studies have recently been completed which show that the Ir(IV) or Fe(III) induced reactions are intramolecular, and that the C_5Me_5Rh rings do not break up under these conditions. All the gases arise only from the C_1 methyl and methylene ligands; the methane comes from the combination of one Rh—CH_3 and a hydrogen from a bridging methylene, the propene from one Rh—CH_3 and two μ-CH_2's, and the ethene from one Rh—CH_3 and one μ-CH_2.[2] An NMR (^1H, ^2H and ^{13}C) investigation showed that the propene from $[\{C_5Me_5Rh(\mu\text{-}^{12}CH_2)(^{13}CH_3)\}_2]$ was $> 85\%$ $^{13}CH_2 = CHCH_3$ (and *ca* 15% $CH_2 = CH^{13}CH_3$). Similarly, the propene was 75% $CD_2 = CHCDH_2$ (and 25% $CH_2 = CHCD_3$) from the analogous decomposition of $[\{C_5Me_5Rh(\mu\text{-}CH_2)(CD_3)\}_2]$.[13]

The thermal reactions were also examined with the aid of isotopomers of complex (**1**). Again, there was little evidence for the involvement of the C_5Me_5 ring in the C_1—C_3 products, but some tetramethylfulvene and pentamethylcyclopentadiene, arising from the complete break-up of the complex, were detected. The ethene and propene again arose chiefly from one Rh–methyl and one or two μ-methylenes, respectively, and crossover experiments showed that the thermal decomposition was largely intramolecular.[2] The only significant difference between these reactions and those with a one electron oxidizer were (i) that the methane from $[\{C_5Me_5Rh(\mu\text{-}CH_2)(^{13}CH_3)\}_2]$ contained about equal amounts of $^{12}CH_4$ and $^{13}CH_4$, and (ii) that owing to extensive H/D scrambling on heating, it was not possible to probe further into the intimate details of the thermal reaction. The general conclusion however, was that very similar processes must be occurring thermally at $\geqslant 300°C$ and under oxidizing conditions at 20–50°C.

The detailed labelling used to examine the propene from the Ir(IV) or Fe(III) reactions, has allowed an extremely detailed picture to be established, regarding the mode by which three C_1 units in a bimolecular complex come together.

It must be emphasized that two metal atoms appear to be needed for this process. Thus, while the iridium analogue, $[\{C_5Me_5Ir(\mu\text{-}CH_2)(CH_3)\}_2]$, also decomposed thermally [though with greater difficulty than (**1**)], to give *ca* 53% of methane and 30% of propene, the mononuclear $[C_5Me_5IrMe_4]$ gave 93% methane, a little ethane and ethene, and less than 1% of propene on decomposition under the same conditions.[2]

The significance of these data lies in their relation to the polymerization step in current models of the Fischer–Tropsch reaction.[2,4] It is therefore instructive to show how variations in the structure of the dinuclear complex affect the decomposition reactions. This paper describes the decomposition of higher homologues of (**1**), and of the dinuclear ionic species, $[\{C_5Me_5Rh(\mu\text{-}CH_2)\}_2R(MeCN)]^+$.

RESULTS AND DISCUSSION

The higher homologues of (**1**), the diethyl-, the di-*n*-propyl-, and the di-*n*-butyl- complexes (**2**), (**3**) and (**4**), respectively, were prepared from (**1**) by the sequence,[5]

$$[\{C_5Me_5Rh(\mu\text{-}CH_2)(Me)\}_2] + 2HCl \quad (\mathbf{1}) \rightarrow [\{C_5Me_5Rh(\mu\text{-}CH_2)(Cl)\}_2]$$

$$[\{C_5Me_5Rh(\mu\text{-}CH_2)(Cl)\}_2] + 2RMgX \rightarrow [\{C_5Me_5Rh(\mu\text{-}CH_2)(R)\}_2].$$

(**2**, R = Et)
(**3**, R = n-C_3H_7)
(**4**, R = n-C_4H_9)

The dinuclear cationic complexes were prepared by the route,[5]

$$[\{C_5Me_5Rh(\mu\text{-}CH_2)(R)\}_2] + HSO_3C_6H_4Me/KPF_6/MeCN \rightarrow [\{C_5Me_5Rh(\mu\text{-}CH_2)\}_2(R)(MeCN)]PF_6.$$

(**5**, R = Me)
(**6**, R = Et)

The oxidative decomposition of $[\{C_5Me_5Rh(\mu\text{-}CH_2)(R)\}_2]$

Decomposition of the diethyl complex (**2**), $[\{C_5Me_5Rh(\mu\text{-}CH_2)(Et)\}_2]$ occurred readily and efficiently with hexachloroiridate in acetonitrile (Table 1), the gases evolved accounting for some 89% of the ethyl and methylene ligands in the initial complex. Rather similar reactions occurred for the di-*n*-propyl and di-*n*-butyl complexes (**3**) and (**4**). In all cases, around 60% of the volatile products arose from R, i.e. RCl, RH and the olefin (R—H), corresponding to the loss of H from R; the chloride, RCl, was the main product. The amounts of olefin and alkane were comparable, except for (**2**) where ethene predominated over ethane.

The more interesting products were RCH and RC_2H_3, arising from the coupling of R with one or two methylenes. Thus the diethyl complex (**2**) gave a small amount of propene, while the di-*n*-propyl complex (**3**) gave butene(s) and the di-*n*-butyl com-

plex (**4**) gave pentene(s); in each case some of the alkane, RCH_3, propane, butane and pentane, respectively, were also formed. This was directly comparable to the formation of ethene and ethane from (**1**).

The olefins RC_2H_3, butene(s) from (**2**), pentene(s) from (**3**) and hexene(s) from (**4**), were also formed. A major product from all these reactions was the saturated alkane, RC_2H_5; this contrasted with the decomposition of (**1**) where propene was the main product and propane was only formed in trace amounts. We presume that the RC_2H_3 and RC_2H_5 products arise in a basically similar manner to that deduced for C_3 formation from (**1**), but that hydrogen transfer to give the alkane is easier for the higher alkyls.

The other contrast is that the RCH (and RCH_3) product is generally rather small for (**1**) and (**2**), but predominates over RC_2H_3 (and RC_2H_5) for (**3**) and (**4**). This indicates that chain extension even in these Fischer-Tropsch model complexes becomes progressively more difficult with longer alkyl groups, a conclusion broadly in agreement with the Flory–Schulz distribution commonly observed in Fischer–Tropsch reactions.[4]

Coupling of two μ-methylenes to give ethene is not an important process in the decomposition of (**1**) and so is also unlikely to be important in the higher homologues either. This is confirmed by the fact that while ethene is a major product (26%) from the diethyl complex (**2**), it is formed in only trace (1–2%) amounts from the di-*n*-propyl and di-*n*-butyl complexes (**3**) and (**4**) on decomposition.

Trace amounts of methane were observed in the decompositions of (**2**)–(**4**), presumably from a side reaction of the μ-CH_2. In the decomposition of the diethyl complex (**2**), the C_4 hydrocarbons could be formed either by the oxidative coupling of one ethyl and two methylenes, by analogy with the decomposition of (**1**), or by the coupling of two ethyls directly. The latter path is again unlikely since we observed negligible R—R coupling in (**1**). A further reason against this happening is that one would expect R—R coupling, i.e. the formation of C_8 hydrocarbons from the di-*n*-butyl complex (**5**), and C_6 hydrocarbons from the di-*n*-propyl complex, (**4**), neither of which are observed.

The production of RCl could occur either via transfer of alkyl from Rh to Ir followed by elimination of RCl or, much more likely, via formation of an R$^{\bullet}$ radical from the product of a one electron oxidation, $[\{C_5Me_5Rh(\mu\text{-}CH_2)R\}_2] + IrCl_6^{2-} \rightarrow [\{C_5Me_5Rh(\mu\text{-}CH_2)R\}_2]^{+\cdot} + IrCl_6^{3-}$. The last type of reaction is well-known in $IrCl_6^{2-}$ mediated oxidations of alkyl metal complexes.[6]

By contrast to the formation of RCl from decomposition of complexes (**2**)–(**4**), methyl chloride was only occasionally observed during the decomposition of (**1**). This could be because, as we have shown, the analogous one electron oxidation for (**1**) is reversible and because, when a second electron is then removed, the path leading to methane formation from the Rh—Me and an H from a μ-methylene, becomes more favourable.[2] It is likely that the Rh—R bond is less stable for the higher alkyls, possibly for steric reasons, which also precludes facile removal of an H from the μ-methylene, and thus different decomposition processes become predominant. Were H-transfer a favoured process, much more RH would be observed from the decomposition of complexes (**2**)–(**5**), corresponding to the formation of methane from (**1**).

Decompositions were carried out under a variety of conditions, using different oxidizers and differing solvents. Despite small variations, in some cases arising from overlapping peaks in the GC-analysis in the presence of certain solvents, the overall pattern from one to another was very similar. Table 1 also shows two sets of data for complex (**1**), to compare with those previously reported.[2]

On present evidence we favour a mechanism (Scheme 1) rather similar to the one we have established for the oxidative decomposition of (**1**). However, as has been indicated, the relative importance of some of the steps is rather different for (**2**)–(**4**) by comparison with (**1**). The greater tendency to form RCl and the formation of the olefin from R by loss of H have little parallel in (**1**). Labelling studies have not yet been carried out on the homologues of (**1**) and because of the greater scope for scrambling we anticipate that they will be much harder to interpret.

Thermal decomposition of complexes (**3**) and (**4**) was also investigated. GC–MS data showed that at 400°C the di-*n*-butyl complex (**4**) gave C_6H_{12} and C_5H_{10} in addition to C_4H_8; only small amounts of saturated hydrocarbons appeared to be present. Similar data were obtained from decomposition of the di-*n*-propyl complex (**3**). This reinforces the basic analogy between the oxidative and thermal decompositions.

Oxidative decomposition of $[\{C_5Me_5Rh(\mu\text{-}CH_2)\}_2R(MeCN)]^+$ *to give* RCH *and* RC_2H_3

The two cationic dirhodium complexes (**5**, R = Me) and (**6**, R = Et) were decomposed oxidatively in the same manner as above. The most remarkable feature of the reaction of (**5**), was that propene formed an even larger proportion of the gases than in the decomposition of (**1**) (Table 1); very little methane was formed, but some ethene

Table 1. Products from the decomposition of $[\{C_5Me_5Rh\}_2(\mu\text{-}CH_2)_2R_2]$ and of $[\{C_5Me_5Rh\}_2(\mu\text{-}CH_2)_2R(MeCN)]^+$ by Na_2IrCl_6 or $FeCl_3$, and by $PdCl_2$ plus Na_2IrCl_6 or $FeCl_3$

Complex	Products[a] C_1	C_2	C_3	C_4	C_5	C_6
$[\{C_5Me_5Rh\}_2(\mu\text{-}CH_2)_2Me_2]$, (1)						
$FeCl_3/C_6H_{12}$ (78%[b])	24, CH_4	5, C_2H_4 2, C_2H_6	70, C_3H_6			
Na_2IrCl_6/MeCN (77%[b])	26, CH_4	10, C_2H_4 5, C_2H_6	60, C_3H_6			
$[\{C_5Me_5Rh\}_2(\mu\text{-}CH_2)_2Et_2]$, (2)						
Na_2IrCL_6/MeCN (89%[b])	2, CH_4	26, C_2H_4 14, C_2H_6 26, EtCl	4, C_3H_6 3, C_3H_8	25, $(C_4H_8+C_4H_{10})$		
$[\{C_5Me_5Rh\}_2(\mu\text{-}CH_2)_2(n\text{-}Pr)_2]$, (3)						
$FeCl_3/C_6H_{12}$ (63%[b])	2, CH_4	1, C_2H_4 1, C_2H_6	16, C_3H_6 11, C_3H_8 35, C_3H_7Cl	12, C_4H_8 11, C_4H_{10}	2, 1-C_5H_{10} 7, 2-C_5H_{10} 2, n-C_5H_{12}	
$[\{C_5Me_5Rh\}_2(\mu\text{-}CH_2)_2(n\text{-}Bu)_2]$, (4)						
$FeCl_3/C_7H_{14}$ (92%[b])	1, CH_4	2, C_2H_4 tr, C_2H_6	tr, C_3H_6	18, C_4H_8 14, C_4H_{10} 26, C_4H_9Cl	17, C_5H_{10} 8, C_5H_{12}	3, C_6H_{12} 10, C_6H_{14}
$[\{C_5Me_5Rh\}_2(\mu\text{-}CH_2)_2Me(MeCN)]^+$ (5)						
Na_2IrCl_6/MeCN (60%[b])	2, CH_4	16, C_2H_4 tr, C_2, H_6	82, C_3H_6			

$[\{C_5Me_5Rh\}_2(\mu\text{-}CH_2)_2Et(MeCN)]^+$ (6)				
$FeCl_3$/dioxane–H_2O (47%[b])	tr, CH_4	29, C_2H_4	10, C_3H_6	38, ($C_4H_8+C_4H_{10}$)
		tr, C_2H_6		
		22, EtCl		
$[\{C_5Me_5Rh\}_2(\mu\text{-}CH_2)_2Me_2]$, (1)				
$FeCl_3+PdCl_2$/THF–H_2O[c] (78%[b])	18, CH_4	tr, C_2H_4	1, C_3H_6	
		2, C_2H_6	4, C_3H_8	
		2, MeCHO	74, Me_2CO	
$Na_2IrCl_6+PdCl_2$/THF–H_2O[c] (73%[b])	25, CH_4	4, C_2H_6	3, C_3H_6	
	4, MeCl	4, MeCHO	60, Me_2CO	
$[\{C_5Me_5Rh\}_2(\mu\text{-}CH_2)_2Et_2]$, (2)				
$FeCl_3+PdCl_2$/dioxane–H_2O[c] (64%[b])	2, CH_4	3, C_2H_4	tr, C_3H_6	3, ($C_4H_8+C_4H_{10}$)
		26, C_2H_6	4, C_3H_8	21, MeCOEt
		17, EtCl	7, Me_2CO	
		21, MeCHO		
$[\{C_5Me_5Rh\}_2(\mu\text{-}CH_2)_2Me(MeCN)]^+$ (5)				
$Na_2IrCl_6+PdCl_2$/THF–H_2O[c] (73%[b])	7, CH_4	tr, C_2H_4	1, C_3H_6	
	4, MeCl	4, C_2H_6	71, Me_2CO	
		12, MeCHO		
$[\{C_5Me_5Rh\}_2(\mu\text{-}CH_2)_2Et(MeCN)]^+$ (6)				
$FeCl_3+PdCl_2$/dioxane–H_2O[c] (79%[b])	1, CH_4	11, C_2H_4	7, C_3H_6	21, ($C_4H_8+C_4H_{10}$)
		tr, C_2H_6	7, Me_2CO	7, MeCOEt
		22, EtCl		
		22, MeCHO		

[a] Numbers quoted are the percentages of products, normalized to take account of the number of C_1 and R ligands present in the original complex, see text.
[b] Percentage of complex which has been decomposed, judged by the total amount of volatile organic products produced.
[c] Molar ratio, Rh_2 complex : $FeCl_3 \cdot 6H_2O$ or $Na_2IrCl_6 \cdot 6H_2O$: $PdCl_2$ = 1 : 6 : 6, for details see Experimental Section.

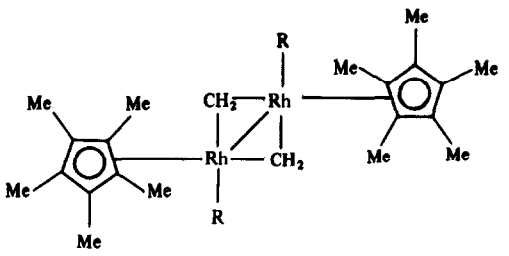

$$\xrightarrow{-e^-} [\{C_5Me_5Rh\}_2(\mu\text{-}CH_2)_2R_2]^+ \longrightarrow R^\bullet + [\{C_5Me_5Rh\}_2(\mu\text{-}CH_2)_2R]^+$$

$$R^\bullet + MCl_n \longrightarrow RCl + MCl_{n-1}$$

$$[\{C_5Me_5Rh\}_2(\mu\text{-}CH_2)_2R_2]^{2+} \longrightarrow RH + (R\text{—}H) + [\{C_5Me_5Rh\}_2(\mu\text{-}CH_2)_2]^{2+}$$

$$[\{C_5Me_5Rh\}_2(\mu\text{-}CH_2)_2R_2]^+ \xrightarrow{-e^-} RH + [\{C_5Me_5Rh\}_2(\mu\text{-}CH_2)(\mu\text{-}CH)R]^{2+}$$

$$[\{C_5Me_5Rh\}_2(\mu\text{-}CH_2)(\mu\text{-}CH)R]^{2+} \xrightarrow[solv.]{-2e^-} RC_2H_3 + 2\,[C_5Me_5Rh(solv.)_3]^{2+}$$

$$[\{C_5Me_5Rh\}_2(\mu\text{-}CH_2)_2R_2]^{2+} \longrightarrow RH + (R\text{—}H) + [\{C_5Me_5Rh\}_2(\mu\text{-}CH_2)_2]^{2+}$$

$$[\{C_5Me_5Rh\}_2(\mu\text{-}CH_2)_2]^{2+} \xrightarrow[solv.]{-2e^-} C_2H_4 + 2[C_5Me_5Rh(solv.)_3]^{2+}$$

Scheme 1.

was detected. By contrast, ethene was a major product from the decomposition of (**6**); this could again be a reflection of the greater lability of the longer R group and the lower tendency to homologate. Propene was formed [cf. ethene from (**5**)], and again, as in the decomposition of (**2**), butane as well as butene(s) are formed. It is noteworthy that more C_4 products were also formed from (**6**) than in the corresponding reaction of (**2**).

We have also prepared two labelled samples of (**5**) and have subjected them to decomposition. Thus, when a solution of $[\{C_5Me_5Rh\text{-}\mu\text{-}CH_2\}_2(^{13}CH_3)(MeCN)]PF_6$ was decomposed with Na_2IrCl_6 in CD_3CN/D_2O (50°C, 5 h) and the solution then analysed by ^{13}C NMR spectroscopy, the label was found at δ116.1 (CH_2=). Accurate estimation of intensities, by comparison with the natural abundance of ^{13}C in propene showed that > 70% was present as $^{13}CH_2{=}{}^{12}CH\text{—}{}^{12}CH_3$ and < 30% was present as $^{12}CH_2{=}CH\text{—}{}^{13}CH_3$; there was no significant amount of ^{13}C in the 2-position. Bearing in mind that the original sample of (**5**) contained 92% ^{13}C and 8% ^{12}C at the Rh—Me (from the MeI used to make it), this means that at least 77% of the reaction follows a path leading to $^{13}CH_2{=}CHCH_3$.

A similar study was carried out oxidizing a sample of $[\{C_5(CH_3)_5Rh\text{-}\mu\text{-}CH_2\}_2(CD_3)(MeCN)]PF_6$ with Na_2IrCl_6 in CD_3CN/D_2O. The $^2H\{^1H\}$ NMR spectrum showed three singlets of approximately equal intensity, at δ 1.69 (methyl), 4.94 (D^c) and 5.05 (D^b) indicating that the same number of deuteriums were in each site. There was no peak at δ 5.9, indicating insignificant D-labelling at H^a. The ^1H-coupled ^2H spectrum showed doublets for D^c [$J(D^c\text{—}H^a)$ 1.5 Hz] and D^b [$J(D^b\text{—}H^a)$ 2.5 Hz] and a triplet of doublets for the methyl [$J(D^d\text{—}H^d)$ 1.9 Hz; $J(D^d\text{—}H^a)$ 1 Hz], showing the presence of —CDH_2 there. The relative intensities of the peaks, estimated from both the ^2H, the $^2H\{^1H\}$ and the ^1H spectra, led to the conclusion that the two isotopomers $CD_2{=}CH\text{—}CH_2D$ and $CH_2{=}CH\text{—}CD_3$ were present in the ratio of 10 : 1.

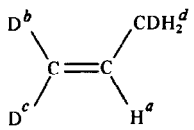

This result is virtually identical to that obtained for the propene from the oxidation of labelled $[\{C_5Me_5Rh\text{-}\mu\text{-}CH_2\}_2(^{13}CH_3)_2]$ and especially of $[\{C_5Me_5Rh\text{-}\mu\text{-}CH_2\}_2(CD_3)_2]$.[3] The overall process

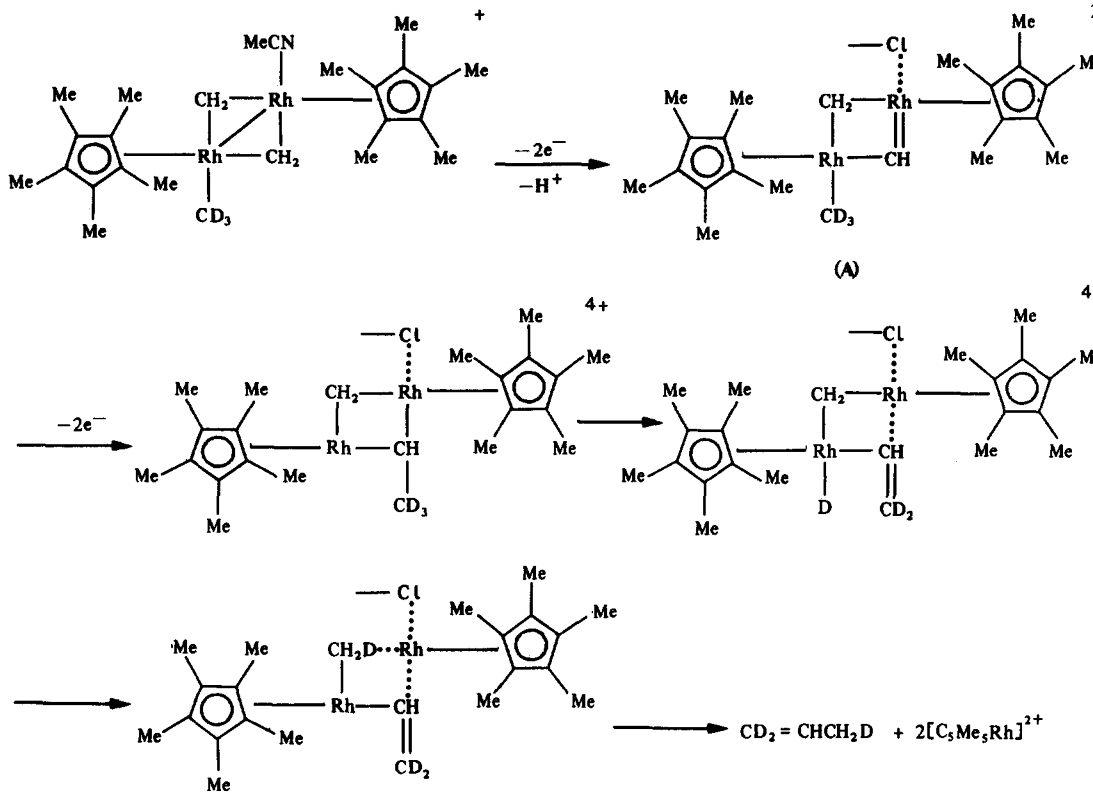

Scheme 2.

for the oxidation of (5) must therefore be

$$[\{C_5Me_5Rh\text{-}\mu\text{-}CH_2\}_2Me(MeCN)]^+ - 4e^- + MeCN \rightarrow C_3H_6 + H^+ + 2[C_5Me_5Rh(MeCN)_3]^{2+}.$$

Since the product from the oxidation of $[\{C_5Me_5Rh\text{-}\mu\text{-}CH_2\}_2(CD_3)(MeCN)]^+$ still contains three deuteriums (by NMR and mass-spectrometry, $C_3H_3D_3$, *m/e* 45), the proton lost must have come from a μ-CH_2. This is of course a similar process to that which occurred for (1). We are therefore able to define the decomposition path followed by (5) as shown in Scheme 2. The first step is loss of a proton consequent upon oxidation, probably a two-electron process, leaving the same skeleton (A) that we have discussed before,[3] which then decomposes in the same way with further oxidant. This occurs via the migration of a methyl onto the μ-CH, β-elimination of H(D) from the so-formed μ-ethylidene to give a Rh–vinyl hydride (deuteride); the H(D) is then transferred to the μ-CH_2 giving a Rh–methyl which reductively eliminates with the vinyl to give propene, with the labelling in the appropriate places.

In our previous studies of (5) we established that, even though the Rh–methyl migrates readily between the two rhodiums, the molecule is configurationally very stable; there is for example, no interchange between the hydrogens on the Rh–methyl with those on the μ-methylenes, even with the timescale of an NMR spin saturation transfer experiment. Thus we conclude that one effect of the oxidation is to substantially labilize the ion.

The first step of the decomposition of (5) (Scheme 2) is similar to the proton losses from bridging methylenes observed by Knox and collaborators.[7] It is however interesting to note that while many different types of C—C bond formation take place within di- or polynuclear clusters,[8] in some cases consequent on such oxidations, it seems very rare for organics to be released from the metal under quite such mild conditions as we have found here.

Oxidative decomposition of $[\{C_5Me_5Rh(\mu\text{-}CH_2)(R)\}_2]$ *and of* $[\{C_5Me_5Rh(\mu\text{-}CH_2)_2R(MeCN)]^+$ *to give ketones (and acetaldehyde)*

As we have disclosed previously,[9] (1) undergoes further reaction if $PdCl_2$ is added to the oxidant [Fe(III) or Ir(IV)], to give acetaldehyde (from ethene) and acetone (from the propene). This combination of a Wacker-type oxidation to the oxidative C—C—C coupling thus allows the

direct production of acetone from three C_1 units. We also noted that pentanones were obtained by an analogous reaction of the di-*n*-propyl complex (**3**).

As Table 1 shows, this reaction also occurs with the cationic methyl complex (**5**); curiously enough the actual yield of acetone is higher from the reaction of (**1**) with $FeCl_3 + PdCl_2$ than from (**5**), rather than the reverse, as might have been expected from the relative production of propene from the two complexes. This shows that the two components act in a concerted, synergistic manner, rather than separately. In both cases hardly any olefin remains.

More complications occur when either the diethyl complex (**2**) or the monoethyl cation (**6**), is oxidized with $PdCl_2$ and Ir(IV) or Fe(III). The ketone butanone, from C—C—C coupling, is formed, but other carbonyls, notably acetone and acetaldehyde, are formed too. A further major product is ethyl chloride and quite substantial amounts of olefins remain; presumably under more forceful conditions these could be oxidized too.

CONCLUSION

We have shown that the C—C—C coupling is quite general and leads to the formation of olefins RC_2H_3 from (**1**) and its homologues, and that the cationic complexes such as (**5**) react very similarly too. There are however many examples of other polynuclear metal complexes containing alkyl and alkylidene ligands, which couple, but which do not seem to eliminate in similar ways.[8] We also note that a reaction that contributes most minimally to the overall products in our dirhodium systems, the direct coupling of two μ-methylenes, appears by contrast to be a key decomposition for diruthenium complexes.[10] This highlights one of the contrasts and suggests an area for seeking better Fischer–Tropsch catalysts.

One of the most intriguing aspects of this work arises from its relation to that recently published, in patents, of Fischer–Tropsch type syntheses of C_2 oxygenates (ethanol, acetaldehyde and acetic acid) using two component catalysts, for example, Pd—Fe and either Rh—Mg—Li or Rh—Sc—Li on silica (H_2:CO 2.5:1; 275–285°C; 30 atm).[11] We feel that the analogy between those data and our own results, relating to the formation of oxygenates by C—C—C coupling on Rh promoted by Fe + Pd or Ir + Pd discussed here is too close to be accidental. It also confirms that (**1**) and its analogues are good models for part of the Fischer–Tropsch reaction and raises the possibility that oxygenates could be formed via the oxidation of the initially formed alkenes there too.

EXPERIMENTAL

Complexes (**1**)–(**6**) were synthesized by published methods.[1,5] All solvents were Analar grade and were dried and distilled under nitrogen before use. Reactions were carried out with rigorous exclusion of air; however in most cases no reaction occurred unless moisture was present.

The decomposition reactions were carried out as follows. A known weight of the complex (usually 19 μmol) was placed in a small flask of accurately known volume (4 cm^3), fitted with a tightly wired-on Suba-seal. The flask was evacuated and filled with nitrogen (using cannulae). The reagent of choice [for example, $Na_2IrCl_6 \cdot 6H_2O$ (53 mg, 112 μmol), dissolved in acetonitrile (0.5 cm^3)] was added by syringe and the contents of the flask were shaken well to ensure dissolution and good mixing. The reactions using ferric chloride hydrate in dioxane or THF were conducted in the same way. Those in which the oxidant was dispersed in cyclohexane or cycloheptane were prepared by mixing the rhodium complex and the ferric chloride as solids in the flask and then injecting the hydrocarbon medium (1.0 cm^3). The reaction usually proceded slowly (8 h at 20°C). The flask was briefly heated in a water bath (50–60°C) to ensure completion of the reaction; this was usually clearly denoted by a change in colour and/or deposition of metal. The flask was then cooled to room temperature and a sample of the gas (50 μl) was removed with a gas syringe, injected into the port of a Carlo–Erba gas chromatograph and the gases analysed. The solution was also analysed; this was extremely necessary with the higher hydrocarbons, where often only a small proportion was in the gas phase.

A variety of methods were used to obtain good GC resolution; these included capillary and Poropak Q packed columns. The identities of the gases were checked by GC–MS using a MS-25 spectrometer. Since the differences in product between the various conditions were rather small, the reactions were usually run in solvents where GC resolution was optimal. Even so, complete resolution was very hard to achieve; for example, the separation of butenes from each other and from butane.

The reactions in which carbonyl compounds were produced by the addition of palladium chloride were carried out in the same way, except that a mixture of the rhodium complex and solid $PdCl_2$ was placed in the flask initially and that a solution of THF (or dioxane) and water (1.5 cm^3 and 0.15 cm^3, respectively) was added to dissolve the reactants.

In each case the GC trace of the product, once

it had been identified by mass spectrometry, was integrated and the integral compared to that of an authentic sample of the material, in order to estimate how much of that component was present in the original mixture (gas or solution). The results are presented in Table 1; the numbers given are normalized percentages. These are calculated on the basis of the total amount of R and C_1 ligands present in each complex; thus (**1**) has $4 \times C_1$ ligands, (**2**) has $2 \times C_2$ and $2 \times C_1$ ligands, (**3**) has $2 \times C_3$ and $2 \times C_1$ ligands, and so forth (for further details see ref. 2). There is no evidence for the breakdown of either R or C_5Me_5 ligands; thus the di-*n*-butyl complex (**4**) gave only trace amounts of C_1, C_2 or C_3 products.

Decomposition of the labelled complexes (**5**, R = $^{13}CH_3$) *and* (**5**, R = CD_3)

The labelled complexes (**5**, R = $^{13}CH_3$ and CD_3) were prepared from the appropriately labelled precursors (**1**, R = $^{13}CH_3$ and CD_3)[2] by reaction with one equivalent of *p*-toluene sulphonic acid in the presence of KPF_6.[5] NMR analysis showed the presence of 92% ^{13}C and 8% ^{12}C in the rhodium methyl and normal abundances elsewhere in the first, and of Rh—CD_3, and essentially no Rh—CH_3, in the second. A sample of (**5**, R = $^{13}CH_3$; 20 mg, 28 μmol) was placed in a flask (3 cm^3), the flask was sealed by a Suba-seal, carefully flushed with nitrogen (via cannulae), and a solution of sodium hexachloroiridate (recrystallized from D_2O; 65 mg, 113 μmol) in CD_3CN (1 cm^3) was injected by syringe. The reaction was stirred (5 h, 50°C) to give a golden yellow solution and a yellow precipitate. The solution was transferred by syringe to a 5 mm NMR tube and the ^{13}C NMR spectrum recorded (Bruker AM-250 spectrometer). An exactly similar experiment was carried out on (**5**, R = CD_3). In this case, as well as measuring the $^2H\{^1H\}$ and the ^2H NMR spectra described above, a GC–MS analysis of the gases produced revealed that the propene is entirely $C_3H_3D_3$ (*m/e* 45), and the ethene *ca* 90% $C_2H_2D_2$ and 10% C_2HD_3.

Acknowledgements—We thank SERC for support, Johnson Matthey for the loan of rhodium chloride, Dr Paul Yarrow and Dr Neil Meanwell for preliminary experiments, Mr P. R. Ashton and Mr I. R. Johnstone for mass-spectrometric data, and Dr B. F. Taylor for Bruker AM-250 NMR measurements.

REFERENCES

1. K. Isobe, D. G. Andrews, B. E. Mann and P. M. Maitlis, *J. Chem. Soc., Chem. Commun.* 1981, 809; K. Isobe, A. Vazquez de Miguel, P. M. Bailey, S. Okeya and P. M. Maitlis, *J. Chem. Soc., Dalton Trans.* 1983, 1441.
2. I. M. Saez, N. J. Meanwell, A. Nutton, K. Isobe, A. Vazquez de Miguel, D. W. Bruce, S. Okeya, D. G. Andrews, P. R. Ashton, I. R. Johnstone and P. M. Maitlis, *J. Chem. Soc., Dalton Trans.* 1986, 1565.
3. I. M. Saez, N. J. Meanwell, B. F. Taylor, B. E. Mann and P. M. Maitlis, *J. Chem. Soc., Chem. Commun.* 1987, 361.
4. See, for example, R. A. Sheldon, *Chemicals from Synthesis Gas.* Reidel, Dordrecht (1983); R. B. Anderson, *Fischer–Tropsch Synthesis.* Wiley–Interscience, New York (1984); G. Henrici-Olive and S. Olive, *The Chemistry of the Catalysed Hydrogenation of Carbon Monoxide.* Springer, Berlin (1983).
5. S. Okeya, N. J. Meanwell, B. F. Taylor, K. Isobe, A. Vazquez de Miguel and P. M. Maitlis, *J. Chem. Soc., Dalton Trans.* 1984, 1453.
6. See, for example, J. K. Kochi, *Organometallic Mechanisms and Catalysis*, p. 466 et seq. Academic Press, New York (1978).
7. N. G. Connelly, N. J. Forrow, B. P. Gracey, S. A. R. Knox and A. G. Orpen, *J. Chem. Soc., Chem. Commun.* 1985, 14; N. G. Connelly, N. J. Forrow, S. A. R. Knox, K. A. Macpherson and A. G. Orpen, *J. Chem. Soc., Chem. Commun.* 1985, 16; N. M. Doherty, M. J. Fildes, S. A. R. Knox, K. A. Macpherson and A. G. Orpen, *J. Chem. Soc., Chem. Commun.* 1986, 1355; see also B. P. Gracey, S. A. R. Knox, K. A. Macpherson and A. G. Orpen, *J. Chem. Soc., Dalton Trans.* 1985, 1935 and refs. therein.
8. See for example, J. S. Holmgren, J. R. Shapley, S. R. Wilson and W. T. Pennington, *J. Am. Chem. Soc.* 1986, **108**, 508; C. P. Casey, M. W. Meszaros, P. J. Fagan, R. K. Bly, S. R. Marder and E. A. Austin, *J. Am. Chem. Soc.* 1986, **108**, 4043; C. P. Casey, M. W. Meszaros, P. J. Fagan, R. K. Bly, S. R. Marder and R. E. Colborn, *J. Am. Chem. Soc.* 1986, **108**, 4053; A. H. Liu, R. C. Murray, J. C. Dewan, B. D. Santarsiero and R. R. Schrock, *J. Am. Chem. Soc.* 1987, **109**, 4283.
9. I. M. Saez and P. M. Maitlis, *J. Organomet. Chem.* 1987, **334**, C17.
10. S. A. R. Knox, *Pure Appl. Chem.* 1984, **56**, 81.
11. T. Saito, N. Taniguchi, K. Mitarai, S. Arimitsu, K. Yanagi and K. Takada, *Japan Kokai Tokkyo Koho*, JP 61 178 938 and 61 178 942; *Chem. Abstr.* 1987, **106**, 17880s and 17881t.

Polyhedron Vol. 7, No. 10/11, pp. 837–845, 1988
Printed in Great Britain

0277-5387/88 $3.00+.00
© 1988 Pergamon Press plc

ORGANIC CHEMISTRY OF DINUCLEAR METAL CENTRES—X.* DIMERIZATION OF ALLENE AT A DIRUTHENIUM CENTRE; X-RAY CRYSTAL STRUCTURE OF $[Ru_2(CO)_2\{\mu\text{-}C(Me)CHCH_2CCH_2\}(\eta\text{-}C_5Me_5)_2]$

GLENN S. LEWANDOS, NANCY M. DOHERTY, SELBY A. R. KNOX,† KIRSTY A. MACPHERSON and A. GUY ORPEN

Department of Inorganic Chemistry, The University, Bristol BS8 1TS, U.K.

(*Accepted* 5 *November* 1987)

Abstract—Photolysis of $[Ru_2(CO)_4(\eta\text{-}C_5R_5)_2]$ (R = H or Me) in the presence of allene yields complexes $[(\eta\text{-}C_5R_5)(CO)_2RuCH_2C(CH_2)C(CH_2)CH_2Ru(CO)_2(\eta\text{-}C_5R_5)]$ and $[Ru_2(CO)_2\{\mu\text{-}C(Me)CHCH_2CCH_2\}(\eta\text{-}C_5Me_5)_2]$, containing dimers of allene derived by C(2)—C(2) and C(1)—C(1) coupling, respectively. The molecular structure of $[Ru_2(CO)_2\{\mu\text{-}C(Me)CHCH_2CCH_2\}(\eta\text{-}C_5Me_5)_2]$ has been determined by X-ray diffraction. The structure was solved by heavy-atom methods and refined by least-squares to give a final R 0.047 for 4678 unique, observed diffractometer data. Crystals are monoclinic, space group $P2_1/c$, with $Z = 8$ in a unit cell of dimensions $a = 10.403(8)$, $b = 28.804(27)$, $c = 19.882(18)$ Å, $\beta = 117.14(6)°$. The molecule is based on a *trans*-$(\eta\text{-}C_5Me_5)(CO)Ru$—$Ru(CO)(\eta\text{-}C_5Me_5)$ unit with one terminal and one semi-bridging carbonyl ligand. This unit is bridged by a linear $MeCCHCH_2CCH_2$ six-carbon chain which is η^2-bound to one ruthenium through two σ-bonds, making a metallacyclopentene ring, and to the other through an η^2-interaction of an exocyclic double bond. The formation of the allene dimer products is attributed to the attack of $Ru(CO)_2(\eta\text{-}C_5R_5)$ radicals upon the C(1) or C(2) carbon of allene, followed by dimerization of the radicals so formed. The μ-allene species $[Ru_2(CO)_2(\mu\text{-}CH_2CCH_2)(\eta\text{-}C_5H_5)_2]$ is obtained by photolysis of the μ-vinylidene complex $[Ru_2(CO)_3(\mu\text{-}CCH_2)(\eta\text{-}C_5H_5)_2]$ in acetonitrile, followed by the addition of diazomethane.

Complexes containing dimers of allene (propa-1,2-diene) as a ligand are of interest as models for species involved in the oligomerization and polymerization of the hydrocarbon at metal centres.[2] Coupling of the two central carbons of allene [C(2)—C(2)] is most commonly observed, exemplified by species of types (**1**),[3–6] (**4**)[7,8] and (**5**),[9–12] the latter arising with and without metal–metal bonding. Terminal–central carbon coupling [C(1)—C(2)] has been found in one complex of type (**2**),[13] but terminal–terminal carbon coupling [C(1)—C(1)], as in (**3**), is unknown for unsubstituted allene; it does, however, arise in the dimerization of 1,3-dimethylallene.[13] We describe here the reactions of allene with the diruthenium complexes $[Ru_2(CO)_4L_2]$ (**8**, L = C_5H_5; **9**, L = C_5Me_5), which provide the first examples of allene dimer species of types (**6**) and (**7**). The latter is, to our knowledge, the first transition metal complex evolving from C(1)—C(1) coupling of the unsubstituted allene.

RESULTS AND DISCUSSION

UV irradiation of $[Ru_2(CO)_4(\eta\text{-}C_5H_5)_2]$ (**8**) with a 15-fold excess of allene in tetrahydrofuran (THF) solution results in the consumption of the diruthenium complex within 5 h. IR spectra indicated that a variety of products was formed but these were inseparable by crystallization techniques. Chromatography, however, led to the isolation of the air-stable, white crystalline complex $[(\eta\text{-}C_5H_5)(CO)_2RuCH_2C(CH_2)C(CH_2)CH_2Ru(CO)_2(\eta\text{-}C_5H_5)]$ (**10**) in low yield.

* For Part IX, see ref. 1.

† Author to whom correspondence should be addressed.

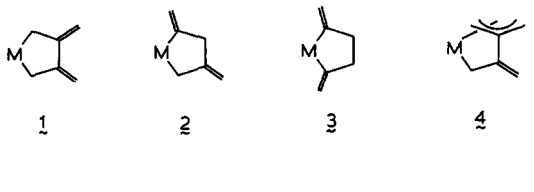

1 2 3 4

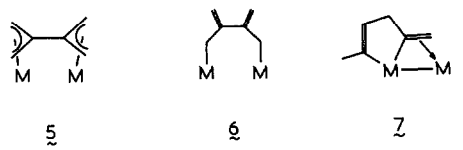

5 6 7

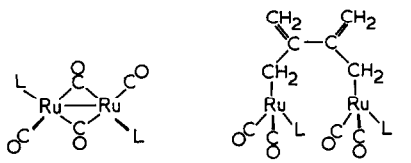

8 L=C_5H_5
9 L=C_5Me_5

10 L=C_5H_5
11 L=C_5Me_5

The mass spectrum of (**10**) shows a weak molecular ion and more intense ions corresponding to the sequential loss of four carbon monoxides. Ready cleavage of the Ru—CH_2 bond is apparent in the presence of very strong ions attributable to $[(\eta\text{-}C_5H_5)(CO)_nRuCH_2C(CH_2)C(CH_2)CH_2]^+$ ($n = 2$, 0) and $[(\eta\text{-}C_5H_5)(CO)_nRu]^+$ ($n = 2$, 1 and 0).

IR and NMR spectra clearly indicate that (**10**) has the illustrated structure based on C(2)—C(2) coupling of two allene units, with each unit carrying a σ-bound $Ru(CO)_2(\eta\text{-}C_5H_5)$ grouping; i.e. the complex is of form (**6**), an expanded variant of (**1**). Thus, the IR spectrum shows two bands typical of terminal carbonyl ligands, at 2025 and 1970 cm^{-1} (in cyclohexane), consistent with the presence of the $Ru(CO)_2(\eta\text{-}C_5H_5)$ group. By way of comparison, the carbonyl absorptions for structurally related $[(\eta\text{-}C_5H_5)(CO)_2Ru(CH_2)_4Ru(CO)_2(\eta\text{-}C_5H_5)_2]$ are at 2022 and 1958 cm^{-1} (in hexane).[14] The two-fold symmetry of (**10**) is reflected in the ^1H NMR spectrum, which has the equivalent cyclopentadienyls as a signal at δ 4.84 (10 H), and the allene "dimer" protons as three singlets at δ 5.91 (2 H), 5.01 (2 H) and 2.68 (4 H). Of the latter group, the signal at δ 2.68 is readily attributed to the two ruthenium-bound CH_2 groups and those at δ 5–6 to the inequivalent olefinic protons of each vinylidene CH_2 unit. For a platinum complex of type (**1**) [M = Pt(1,5-cyclo-octadiene)], containing the same hydrocarbon skeleton, the allene dimer proton resonances occur at very similar chemical shifts [δ 2.95 (4 H), 5.00 (2 H) and 5.45 (2 H)].[5] The ^{31}C NMR signals for this species are also similar to those observed for (**10**); whereas for the platinum complex the allene dimer carbons appear pairwise equivalent at δ 33.5 ($PtCH_2$), 101.2 ($C{=}CH_2$) and 162.0 ($C{=}CH_2$) ppm,[5] those of (**10**) are at δ 53.8 ($RuCH_2$), 123.4 ($C{=}CH_2$) and 148.4 ($C{=}CH_2$).

Treatment of $[Ru_2(CO)_4(\eta\text{-}C_5Me_5)_2]$ (**9**) with an excess of allene for *ca* 5 h under photolytic conditions gives, like $[Ru_2(CO)_4(\eta\text{-}C_5H_5)_2]$, a complex of type (**6**): white crystalline $[(\eta\text{-}C_5Me_5)(CO)_2RuCH_2C(CH_2)C(CH_2)CH_2Ru(CO)_2(\eta\text{-}C_5Me_5)]$ (**11**), isolated in 47% yield. This complex displays no molecular ion in the mass spectrum but has ions corresponding to $(M{-}nCO)^+$ ($n = 1$–4) and others to $[(\eta\text{-}C_5Me_5)(CO)_nRuCH_2C(CH_2)C(CH_2)CH_2]^+$ ($n = 2$, 1 and 0) and $[(\eta\text{-}C_5Me_5)(CO)_nRu]^+$ ($n = 2$, 1 and 0). The IR spectrum is similar in form to that of (**10**), but the two terminal carbonyl stretching bands are seen at lower frequencies (2006 and 1948 cm^{-1}), appropriate to the more strongly electron-donating $\eta\text{-}C_5Me_5$ ligand. The ^1H and ^{13}C NMR spectra (see Experimental Section) indicate that (**11**) is structurally identical to (**10**). In addition, a proton-coupled ^{13}C NMR spectrum of (**11**) confirms the assignments made earlier for (**10**). A singlet at δ 164.2 is clearly due to the vinylidene $C{=}CH_2$ carbons, while triplets at δ 52.7 (J_{CH} 127 Hz) and 119.0 (J_{CH} 149 Hz) can be attributed (both on the basis of chemical shifts and coupling constants[15]) to the sp^3 and sp^2 carbons of the $RuCH_2$ and $C{=}CH_2$ methylene groups.

A second product of the reaction of allene with $[Ru_2(CO)_4(\eta\text{-}C_5Me_5)_2]$ was isolated as air-stable red crystals in 11% yield and identified through an X-ray diffraction study as $[Ru_2(CO)_2\{\mu\text{-}C(Me)CHCH_2CCH_2\}(\eta\text{-}C_5Me_5)_2]$ (**12**).

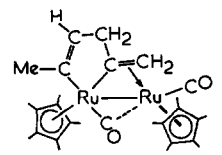

12

The structure determination revealed that the asymmetric unit contained two crystallographically independent molecules of the complex, which differ significantly only in the orientations of the $\eta\text{-}C_5Me_5$ ligands. The molecular structure of one of these two is shown in Fig. 1, which also gives the atomic numbering scheme; selected bond lengths and angles are presented in Table 1. The ruthenium atoms are at a single bond distance (2.823(2) Å) and each carries an $\eta\text{-}C_5Me_5$ ring, which adopts a *trans* orientation about the metal–metal bond. Each ruthenium atom also carries a carbonyl ligand; that on Ru(1) is terminal but that on Ru(2) is semi-bridging, as indicated by the Ru(2)—C(2) and Ru(1)—C(2) distances of 1.869(11) and 2.566(10) Å, respectively. The Ru(2)—C(2)—O(2) and Ru(1)—Ru(2)—C(2) angles of 162.0(7) and

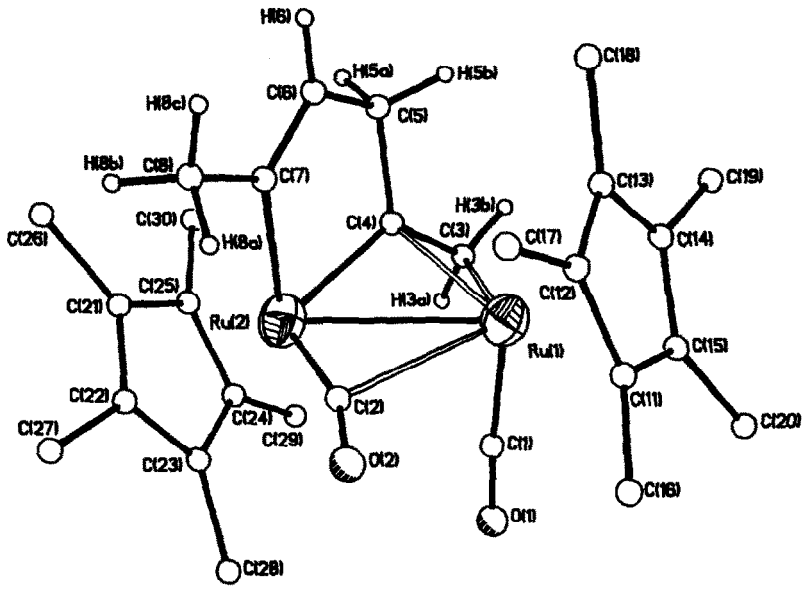

Fig. 1. Molecular structure and numbering scheme for $[Ru_2(CO)_2\{\mu\text{-}C(Me)CHCH_2CCH_2\}(\eta\text{-}C_5Me_5)_2]$ (**12**); pentamethylcyclopentadienyl hydrogens omitted for clarity.

62.4(3)°, respectively, are also typical of such an interaction.

The major interest in (**12**) attaches to the linear six-carbon bridging ligand, derived by an unprecedented C(1)—C(1) dimerization of allene and an associated 1,3-hydrogen shift [from C(6) to C(8)]. Carbons C(4), C(5), C(6) and C(7) make up, with Ru(2), a metallacyclopentene ring with an exocyclic double bond [C(3), C(4)] η^2-coordinated to Ru(1). The ruthenium atom Ru(2) and the six carbon atoms C(3)–C(8) of the allene dimer are approximately coplanar, none deviating more than 0.27 Å from the mean plane. This plane lies roughly parallel to the planes of the η-C_5Me_5 ligands, shown by angles of 12.6 and 21.4° made with the C(11)—C(15) and C(21)—C(25) planes, respectively. The angle between the C_6 mean plane and the Ru—Ru axis is 35.8°.

The bond lengths along the C_6 chain correspond to the localized bonding illustrated, with the C(3)—C(4) double bond longer (at 1.407(16) Å) than C(6)—C(7) (1.324(15) Å), as a result of its coordination to ruthenium.

The allene dimer can be viewed as an exotic variant of the μ-vinyl ligands found in $[Ru_2(\mu\text{-}H)(CO)_2\{\mu\text{-}C(Me)CH_2\}(\eta\text{-}C_5H_5)_2]$ (**13**)[16] and $[Ru_2(CO)(\mu\text{-}CHCH_2)\{\mu\text{-}C(Ph)CHPh\}(\eta\text{-}C_5H_5)_2]$ (**14**).[17] The Ru(2)—C(4), Ru(1)—C(4), Ru(1)—C(3) and C(3)—C(4) distances of 2.043(8), 2.162(8), 2.227(10) and 1.407(16) Å for (**12**) are similar to the corresponding distances for the μ-$CHCH_2$ ligand of (**14**), at 2.049(4), 2.089(4), 2.212(3) and 1.396(5) Å, respectively. The main discrepancy lies in the Ru(1)—C(4) bond length and probably arises from the greater Ru—Ru separation in (**12**) (2.823(2) Å) cf. (**14**) (2.720(1) Å).

A much related type of structure has been established for the di-iron complex $[Fe_2(CO)_2\{\mu$-

Table 1. Selected bond lengths (Å) and angles (°) for (**12**) (both molecules; atoms of the second molecule are distinguished by the suffix a); estimated standard deviations in the least significant digit are given in parentheses

Ru(1)—Ru(2)	2.823(2)	Ru(1)—C(1)	1.858(11)
Ru(1)—C(2)	2.566(10)	Ru(1)—C(3)	2.227(10)
Ru(1)—C(4)	2.162(8)	Ru(1)—C(11)	2.241(9)
Ru(1)—C(12)	2.321(10)	Ru(1)—C(13)	2.303(9)
Ru(1)—C(14)	2.206(7)	Ru(1)—C(15)	2.181(8)
Ru(2)—C(2)	1.869(11)	Ru(2)—C(4)	2.043(8)

Table 1—*continued*

Ru(2)—C(7)	2.108(13)	Ru(2)—C(21)	2.242(8)
Ru(2)—C(22)	2.246(8)	Ru(2)—C(23)	2.289(10)
Ru(2)—C(24)	2.298(11)	Ru(2)—C(25)	2.240(10)
C(1)—O(1)	1.145(14)	C(2)—O(2)	1.164(13)
C(3)—C(4)	1.407(16)	C(4)—C(5)	1.520(16)
C(5)—C(6)	1.481(20)	C(6)—C(7)	1.324(15)
C(7)—C(8)	1.501(20)	Ru(1a)—Ru(2a)	2.819(2)
Ru(1a)—C(1a)	1.832(12)	Ru(1a)—C(2a)	2.570(11)
Ru(1a)—C(3a)	2.231(9)	Ru(1a)—C(4a)	2.173(9)
Ru(1a)—C(11a)	2.213(9)	Ru(1a)—C(12a)	2.321(9)
Ru(1a)—C(13a)	2.331(9)	Ru(1a)—C(14a)	2.235(8)
Ru(1a)—C(15a)	2.185(8)	Ru(2a)—C(2a)	1.867(10)
Ru(2a)—C(4a)	2.053(9)	Ru(2a)—C(7a)	2.085(12)
Ru(2a)—C(21a)	2.237(8)	Ru(2a)—C(22a)	2.245(8)
Ru(2a)—C(23a)	2.274(9)	Ru(2a)—C(24a)	2.338(9)
Ru(2a)—C(25a)	2.270(8)	C(1a)—O(1a)	1.177(16)
C(2a)—O(2a)	1.178(13)	C(3a)—C(4a)	1.428(15)
C(4a)—C(5a)	1.509(17)	C(5a)—C(6a)	1.491(16)
C(6a)—C(7a)	1.334(15)	C(7a)—C(8a)	1.507(17)
Ru(2)—Ru(1)—C(1)	83.8(2)	Ru(2)—Ru(1)—C(2)	40.2(2)
C(1)—Ru(1)—C(2)	81.8(4)	Ru(2)—Ru(1)—C(3)	73.5(2)
C(1)—Ru(1)—C(3)	83.2(4)	C(2)—Ru(1)—C(3)	113.1(3)
Ru(2)—Ru(1)—C(4)	46.1(2)	C(1)—Ru(1)—C(4)	103.0(4)
C(2)—Ru(1)—C(4)	84.8(3)	C(3)—Ru(1)—C(4)	37.4(4)
Ru(2)—Ru(1)—C(11)	130.1(2)	C(1)—Ru(1)—C(11)	99.2(4)
C(2)—Ru(1)—C(11)	90.5(3)	C(3)—Ru(1)—C(11)	156.3(3)
C(4)—Ru(1)—C(11)	156.4(4)	Ru(2)—Ru(1)—C(12)	112.8(2)
C(1)—Ru(1)—C(12)	133.9(4)	C(2)—Ru(1)—C(12)	85.3(3)
C(3)—Ru(1)—C(12)	141.9(3)	C(4)—Ru(1)—C(12)	119.7(4)
C(11)—Ru(1)—C(12)	36.8(4)	Ru(2)—Ru(1)—C(13)	121.4(2)
C(1)—Ru(1)—C(13)	154.1(3)	C(2)—Ru(1)—C(13)	112.7(4)
C(3)—Ru(1)—C(13)	108.4(3)	C(4)—Ru(1)—C(13)	99.7(3)
C(11)—Ru(1)—C(13)	60.9(3)	C(12)—Ru(1)—C(13)	34.8(3)
Ru(2)—Ru(1)—C(14)	152.3(3)	C(1)—Ru(1)—C(14)	121.3(4)
C(2)—Ru(1)—C(14)	145.2(4)	C(3)—Ru(1)—C(14)	96.4(3)
C(4)—Ru(1)—C(14)	111.4(3)	C(11)—Ru(1)—C(14)	62.1(3)
C(12)—Ru(1)—C(14)	59.8(4)	C(13)—Ru(1)—C(14)	36.4(4)
Ru(2)—Ru(1)—C(15)	166.6(2)	C(1)—Ru(1)—C(15)	93.1(4)
C(2)—Ru(1)—C(15)	126.5(3)	C(3)—Ru(1)—C(15)	119.2(3)
C(4)—Ru(1)—C(15)	146.9(3)	C(11)—Ru(1)—C(15)	37.5(4)
C(12)—Ru(1)—C(15)	60.7(4)	C(13)—Ru(1)—C(15)	61.0(4)
C(14)—Ru(1)—C(15)	37.1(3)	Ru(1)—Ru(2)—C(2)	62.4(3)
Ru(1)—Ru(2)—C(4)	49.6(2)	C(2)—Ru(2)—C(4)	109.7(3)
Ru(1)—Ru(2)—C(7)	91.0(2)	C(2)—Ru(2)—C(7)	88.3(5)
C(4)—Ru(2)—C(7)	77.8(4)	Ru(1)—Ru(2)—C(21)	167.9(3)
C(2)—Ru(2)—C(21)	129.5(4)	C(4)—Ru(2)—C(21)	119.5(3)
C(7)—Ru(2)—C(21)	91.4(4)	Ru(1)—Ru(2)—C(22)	152.6(3)
C(2)—Ru(2)—C(22)	97.5(4)	C(4)—Ru(2)—C(22)	152.5(3)
C(7)—Ru(2)—C(22)	107.8(4)	C(21)—Ru(2)—C(22)	35.5(4)
Ru(1)—Ru(2)—C(23)	122.1(3)	C(2)—Ru(2)—C(23)	94.7(4)
C(4)—Ru(2)—C(23)	133.3(4)	C(7)—Ru(2)—C(23)	144.1(4)
C(21)—Ru(2)—C(23)	59.5(4)	C(22)—Ru(2)—C(23)	36.3(5)
Ru(1)—Ru(2)—C(24)	113.8(3)	C(2)—Ru(2)—C(24)	123.6(5)
C(4)—Ru(2)—C(24)	99.8(4)	C(7)—Ru(2)—C(24)	145.7(4)
C(21)—Ru(2)—C(24)	59.6(4)	C(22)—Ru(2)—C(24)	60.1(4)
C(23)—Ru(2)—C(24)	35.6(4)	Ru(1)—Ru(2)—C(25)	132.3(3)
C(2)—Ru(2)—C(25)	154.3(4)	C(4)—Ru(2)—C(25)	92.3(3)
C(7)—Ru(2)—C(25)	109.9(4)	C(21)—Ru(2)—C(25)	36.3(4)

Table 1—*continued*

C(22)—Ru(2)—C(25)	60.3(4)	C(23)—Ru(2)—C(25)	59.9(4)
C(24)—Ru(2)—C(25)	35.8(5)	Ru(1)—C(1)—O(1)	174.8(7)
Ru(1)—C(2)—Ru(2)	77.3(4)	Ru(1)—C(2)—O(2)	120.1(6)
Ru(2)—C(2)—O(2)	162.0(7)	Ru(1)—C(3)—C(4)	68.8(5)
Ru(1)—C(4)—Ru(2)	84.3(3)	Ru(1)—C(4)—C(3)	73.8(5)
Ru(2)—C(4)—C(3)	123.9(7)	Ru(1)—C(4)—C(5)	121.3(6)
Ru(2)—C(4)—C(5)	115.2(7)	C(3)—C(4)—C(5)	120.4(8)
C(4)—C(5)—C(6)	107.4(9)	C(5)—C(6)—C(7)	118.9(12)
Ru(2)—C(7)—C(6)	115.8(10)	Ru(2)—C(7)—C(8)	121.1(8)
C(6)—C(7)—C(8)	123.1(12)	Ru(2a)—Ru(1a)—C(1a)	85.0(3)
Ru(2a)—Ru(1a)—C(2a)	40.2(2)	C(1a)—Ru(1a)—C(2a)	83.0(4)
Ru(2a)—Ru(1a)—C(3a)	73.3(2)	C(1a)—Ru(1a)—C(3a)	84.2(5)
C(2a)—Ru(1a)—C(3a)	113.0(3)	Ru(2a)—Ru(1a)—C(4a)	46.2(5)
C(1a)—Ru(1a)—C(4a)	105.4(4)	C(2a)—Ru(1a)—C(4a)	84.6(3)
C(3a)—Ru(1a)—C(4a)	37.8(4)	Ru(2a)—Ru(1a)—C(11a)	132.8(3)
C(1a)—Ru(1a)—C(11a)	96.6(4)	C(2a)—Ru(1a)—C(11a)	93.0(3)
C(3a)—Ru(1a)—C(11a)	153.9(3)	C(4a)—Ru(1a)—C(11a)	157.4(4)
Ru(2a)—Ru(1a)—C(12a)	112.4(2)	C(1a)—Ru(1a)—C(12a)	130.6(4)
C(2a)—Ru(1a)—C(12a)	83.3(3)	C(3a)—Ru(1a)—C(12a)	144.2(4)
C(4a)—Ru(1a)—C(12a)	120.3(4)	C(11a)—Ru(1a)—C(12a)	37.3(4)
Ru(2a)—Ru(1a)—C(13a)	119.8(2)	C(1a)—Ru(1a)—C(13a)	153.6(4)
C(2a)—Ru(1a)—C(13a)	109.4(3)	C(3a)—Ru(1a)—C(13a)	110.4(3)
C(4a)—Ru(1a)—C(13a)	99.1(4)	C(11a)—Ru(1a)—C(13a)	60.5(4)
C(12a)—Ru(1a)—C(13a)	34.8(3)	Ru(2a)—Ru(1a)—C(14a)	148.9(3)
C(1a)—Ru(1a)—C(14a)	123.5(4)	C(2a)—Ru(1a)—C(14a)	143.5(3)
C(3a)—Ru(1a)—C(14a)	95.7(3)	C(4a)—Ru(1a)—C(14a)	108.1(3)
C(11a)—Ru(1a)—C(14a)	62.0(3)	C(12a)—Ru(1a)—C(14a)	60.5(3)
C(13a)—Ru(1a)—C(14a)	36.2(4)	Ru(2a)—Ru(1a)—C(15a)	169.5(2)
C(1a)—Ru(1a)—C(15a)	92.9(4)	C(2a)—Ru(1a)—C(15a)	129.4(3)
C(3a)—Ru(1a)—C(15a)	116.7(3)	C(4a)—Ru(1a)—C(15a)	143.6(3)
C(11a)—Ru(1a)—C(15a)	37.2(3)	C(12a)—Ru(1a)—C(15a)	61.6(4)
C(13a)—Ru(1a)—C(15a)	61.0(4)	C(14a)—Ru(1a)—C(15a)	37.7(4)
Ru(1a)—Ru(2a)—C(2a)	62.7(3)	Ru(1a)—Ru(2a)—C(4a)	50.0(3)
C(2a)—Ru(2a)—C(4a)	109.7(4)	Ru(1a)—Ru(2a)—C(7a)	92.1(2)
C(2a)—Ru(2a)—C(7a)	87.3(4)	C(4a)—Ru(2a)—C(7a)	77.9(4)
Ru(1a)—Ru(2a)—C(21a)	162.5(2)	C(2a)—Ru(2a)—C(21a)	134.7(4)
C(4a)—Ru(2a)—C(21a)	114.3(3)	C(7a)—Ru(2a)—C(21a)	91.3(4)
Ru(1a)—Ru(2a)—C(22a)	156.3(3)	C(2a)—Ru(2a)—C(22a)	100.1(4)
C(4a)—Ru(2a)—C(22a)	150.2(3)	C(7a)—Ru(2a)—C(22a)	103.8(4)
C(21a)—Ru(2a)—C(22a)	36.8(3)	Ru(1a)—Ru(2a)—C(23a)	123.0(3)
C(2a)—Ru(2a)—C(23a)	93.4(4)	C(4a)—Ru(2a)—C(23a)	137.2(4)
C(7a)—Ru(2a)—C(23a)	140.6(4)	C(21a)—Ru(2a)—C(24a)	61.0(4)
C(22a)—Ru(2a)—C(23a)	37.3(4)	Ru(1a)—Ru(2a)—C(24a)	111.8(2)
C(2a)—Ru(2a)—C(24a)	120.2(4)	C(4a)—Ru(2a)—C(24a)	102.5(3)
C(7a)—Ru(2a)—C(24a)	149.3(3)	C(21a)—Ru(2a)—C(24a)	60.2(4)
C(22a)—Ru(2a)—C(24a)	60.9(3)	C(23a)—Ru(2a)—C(24a)	35.8(3)
Ru(1a)—Ru(2a)—C(25a)	128.2(2)	C(2a)—Ru(2a)—C(25a)	153.3(4)
C(4a)—Ru(2a)—C(25a)	91.1(3)	C(7a)—Ru(2a)—C(25a)	114.2(4)
C(21a)—Ru(2a)—C(25a)	36.0(4)	C(22a)—Ru(2a)—C(25a)	60.7(3)
C(23a)—Ru(2a)—C(25a)	59.9(3)	C(24a)—Ru(2a)—C(25a)	35.7(4)
Ru(1a)—C(1a)—C(1a)	173.5(7)	Ru(1a)—C(2a)—Ru(2a)	77.1(4)
Ru(1a)—C(2a)—C(2a)	120.4(6)	Ru(2a)—C(2a)—O(2a)	161.6(7)
Ru(1a)—C(3a)—C(4a)	68.9(5)	Ru(1a)—C(4a)—Ru(2a)	83.6(3)
Ru(1a)—C(4a)—C(3a)	73.3(5)	Ru(2a)—C(4a)—C(3a)	121.5(8)
Ru(1a)—C(4a)—C(5a)	122.5(6)	Ru(2a)—C(4a)—C(5a)	115.4(7)
C(3a)—C(4a)—C(5a)	122.4(8)	C(4a)—C(5a)—C(6a)	106.9(9)
C(5a)—C(6a)—C(7a)	118.7(11)	Ru(2a)—C(7a)—C(6a)	116.2(8)
Ru(2a)—C(7a)—C(8a)	122.9(8)	C(6a)—C(7a)—C(8a)	120.9(11)

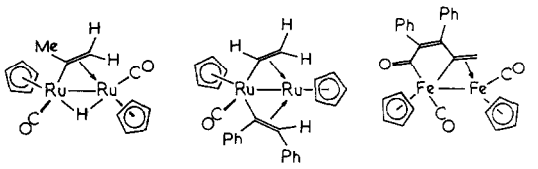

13 14 15

C(O)C(Ph)C(Ph)CCH$_2$}(η-C$_5$H$_5$)$_2$] (**15**), derived by reaction of a μ-vinylidene complex with diphenylacetylene.[18] The presence of four sp^2 hybridized carbons in the metallacyclopentenone ring of (**15**), compared with only three in (**12**), demands even greater planarity of the constituent atoms. The largest deviation from the mean plane of the ring is only 0.06 Å and the methylene carbon is 0.09 Å away.

The solid state structure of (**12**) is clearly retained in solution. Terminal and semi-bridging carbonyl absorptions are seen at 1941 and 1845 cm^{-1}, respectively, in the IR, while in the NMR spectra (see Experimental Section) the inequivalence of the η-C$_5$Me$_5$ ligands is apparent. Following the structural determination the assignment of the ^{1}H and ^{13}C NMR spectra is straightforward; in what follows the numbering system of Fig. 1 is employed to identify the nuclei.

In the ^{1}H NMR spectrum a singlet in the olefinic region at δ 5.91 is readily attributed to H(6), and a singlet of relative intensity three at δ 2.30 to the methyl group based on C(8). A pair of singlets at δ 3.07 and 3.35 is characteristic of the vinyl protons H(3a), H(3b), both in terms of the upfield shift brought about by coordination and the very low (effectively zero) geminal coupling.[16] In contrast, a large geminal coupling of 20.5 Hz is seen for the aliphatic methylene protons H(5a), H(5b), which appear at δ 3.63 and 2.61.

The partially-decoupled ^{13}C NMR spectrum of (**12**) clearly identifies the C(8) methyl group as a quartet at δ 31.9 and the C(6) methyne group as a doublet at δ 125.3. The two methylene carbons appear as triplets at δ 50.7 and 53.0; by analogy with complex (**13**),[16] which has μ-C(*Me*)CH$_2$ at δ 44.6 and μ-C(Me)*C*H$_2$ at δ 52.0, these signals are assigned to C(5) and C(3), respectively. The μ-carbon C(4) is seen as a singlet at δ 167.5, a shift betraying the μ-alkylidene character similar to that of the μ-*C*(Me)CH$_2$ carbon in (**13**), which resonates at δ 175.8. Of the three singlets between δ 200–225, that at δ 200.2 is typical of a terminal carbonyl C(1)O(1) and that at 220.3 of the semi-bridging carbonyl C(2)O(2). The remaining signal at δ 209.1 is in the range associated with the metal-bound vinyl carbons of metallacycles of types (**2**) and (**3**) (δ 205–210)[13,19] and is consequently attributed to the C(7) carbon.

We now turn to the question of how complexes (**10**), (**11**) and (**12**) are formed. There is evidence that the initial photoactivation of complexes of type (**8**) and (**9**) can involve either CO loss,[20,21] to give a species [Ru$_2$(CO)$_3$L$_2$], or homolytic metal–metal bond fission, generating Ru(CO)$_2$L radicals.[22,23] It is difficult to explain the formation of the products on the basis of the first process, but the radical pathway neatly accounts for (**10**), (**11**) and (**12**). The proposed mechanism is outlined in Scheme 1. We suggest that Ru(CO)$_2$L radicals attack allene predominantly at the terminal carbon, as expected,[24] to afford the radical (**16**) which dimerizes to give the observed C(2)—C(2) coupling products (**10**) and (**11**). Less favoured attack upon the central allene carbon will generate radical (**17**), which upon dimerization gives the C(1)—C(1) coupling product (**18**). The instability of Ru—C(sp^2) relative to Ru—C(sp^3) bonds probably results in (**18**) decomposing under the reaction conditions when L = η-C$_5$H$_5$ and transforming to (**12**) when L = η-C$_5$Me$_5$. A plausible pathway for the transformation, via intermediates (**19**) and (**20**), is included in Scheme 1.

In principle, photolysis of the σ-allyl complexes (**10**) and (**11**) could give bis-η^3-allyl species of type (**5**), following CO loss. No such products were isolated from the reactions of allene with (**8**) and (**9**), but photolysis of (**9**) in the presence of allene,

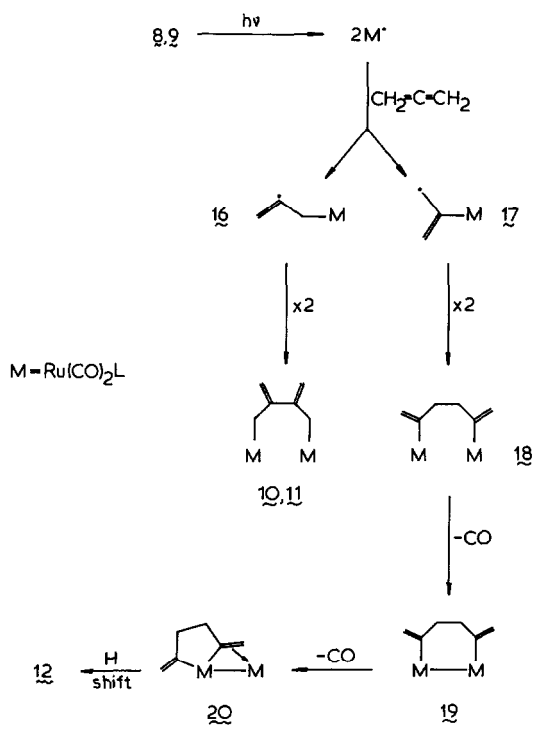

Scheme 1.

surprisingly gave a good yield (33%) of (**12**). The implied isomerization of the allene dimer skeleton is unlikely; it seems that (**11**) undergoes ready homolysis of the ruthenium–carbon σ-bonds to provide an allene dimer diradical, of unknown fate, and $Ru(CO)_2(\eta\text{-}C_5Me_5)$ radicals which react with allene to afford (**11**) and (**12**), as before.

It was expected that a μ-allene complex of the form $[Ru_2(CO)_2(\mu\text{-}CH_2CCH_2)(\eta\text{-}C_5H_5)_2]$ (**21**) might be produced in the reaction of allene with (**8**), especially as di-iron analogues are known.[25,26] No trace was found, but it has been possible to prepare the compound by another route, addition of methylene to a coordinated vinylidene ligand. We have previously shown that the μ-η^2-vinylidene ligand in the dimolybdenum complex (**22**) is transformed to the μ-allene species (**23**) upon treatment with diazomethane.[27] In a modification of this approach, the μ-vinylidene complex $[Ru_2(CO)_3(\mu\text{-}CCH_2)(\eta\text{-}C_5H_5)_2]$ (**24**)[28] was subjected to UV irradiation in acetonitrile, generating an IR-identified mono-acetonitrile substitution product (**25**) which, upon addition of diazomethane, yielded (**21**) in *ca* 10% yield as a red air-stable powder (see Scheme 2). Satisfactory analytical data could not be obtained for the complex because of the persistent presence of impurities, but the mass, IR and NMR spectra are definitive. In the mass spectrum a molecular ion is observed and intense ions corresponding to $(M—nCO)^+$ (n = 1 and 2) and $(M—allene)^+$. The IR spectrum shows one strong and one medium intensity terminal carbonyl stretching band, and the ^1H NMR spectrum, which displays one signal for the two η-C_5H_5 groups and pairwise equivalence of the μ-allene protons, seen at δ 3.61 and 2.70, demands the *trans* configuration illustrated. For the di-iron analogue of (**21**) the allene proton signals appear at δ 3.41 and 2.89.

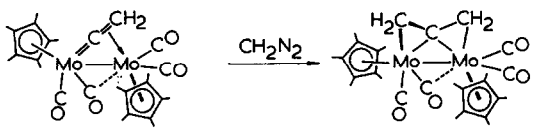

22 23

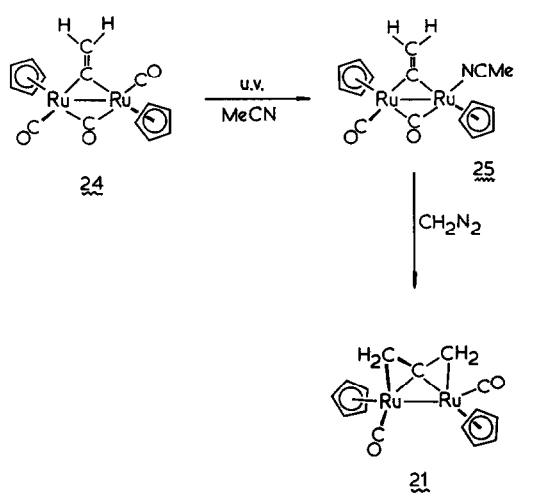

Scheme 2.

EXPERIMENTAL

Techniques and instrumentation were as described in Part IX[1] of this Series. The UV radiation source was a 500 W medium pressure HANOVIA mercury vapour lamp, held 20–40 cm from borosilicate glass reaction vessels. The complexes $[Ru_2(CO)_4(\eta\text{-}C_5H_5)_2]$[28,29] $[Ru_2(CO)_4(\eta\text{-}C_5Me_5)_2]$[30] and $[Ru_2(CO)_3(\mu\text{-}CCH_2)(\eta\text{-}C_5H_5)_2]$[31] were prepared by literature methods; allene was supplied by ARGO International Limited and Diazald (N-methyl-N-nitroso-*p*-toluenesulphonamide) by Aldrich.

Reaction of allene with $[Ru_2(CO)_4(\eta\text{-}C_5H_5)_2]$

Allene (0.60 g, 15.0 mmol) was condensed at −196°C into a Young's tube containing $[Ru_2(CO)_4(\eta\text{-}C_5H_5)_2]$ (0.47 g, 1.05 mmol) and THF (110 cm^3). After warming to room temperature the mixture was subjected to UV irradiation for 5 h. The solvent was then removed under reduced pressure and the residual red oil was chromatographed on an alumina column. Elution with pentane–ether (19 : 1) gave a red band which yielded a red oil on evaporation of the solvent. After washing with five 50 cm^3 portions of pentane, there remained 0.03 g (5%) of $[(\eta\text{-}C_5H_5)(CO)_2RuCH_2C(CH_2)C(CH_2)CH_2Ru(CO)_2(\eta\text{-}C_5H_5)]$ (**10**) as a light tan powder [ν(CO) (in cyclohexane) at 2025s and 1970m cm^{-1}; ^1H NMR (in d^8-toluene) δ 5.91 (s, 2H, C=CH_2), 5.01 (s, 2H, C=CH_2), 4.84 (s, 10H, $2C_5H_5$) and 2.68 (s, 4H, $2RuCH_2$); $^{13}C\{^1H\}$NMR (in C_6D_6), δ 53.8 ($2RuCH_2$), 88.7 ($2C_5H_5$), 123.4 (2C=CH_2), 148.4 (2*C*=CH_2) and 202.1 (4CO). Found: C, 45.7; H, 3.6%; M, 525. $C_{20}H_{18}O_4Ru_2$ requires: C, 45.8; H, 3.5%; M, 525]. Chromatography of the combined pentane washings yielded no identifiable products.

Reaction of allene with $[Ru_2(CO)_4(\eta\text{-}C_5Me_5)_2]$

Allene (0.60 g, 15.0 mmol) was condensed at −196°C into a Young's tube containing $[Ru_2(CO)_4(\eta\text{-}C_5Me_5)_2]$ (0.61 g, 1.05 mmol) in THF (100 cm^3). After warming to room temperature, UV irradiation of the reactants for 4.5 h resulted in a colour change from orange to red. Evaporation of

the solvent under reduced pressure gave a red oil which was extracted with three 50 cm^3 portions of pentane, to give a red solution, and leave 0.33 g (47%) of white, crystalline $[(\eta\text{-}C_5Me_5)(CO)_2RuCH_2C(CH_2)C(CH_2)CH_2Ru(CO)_2(\eta\text{-}C_5Me_5)]$ (**11**) [ν(CO) (in cyclohexane) at 2006s and 1948s cm^{-1}; ^1H NMR (in C_6D_6), δ 6.15 (m, br, 2H, C=CH_2), 5.16 (d, J_{gem} 2 Hz, 2H, C=CH_2), 2.91 (s, br, 4H, 2RuCH_2) and 1.63 (s, 30H, 2C_5Me_5); $^{13}C\{^1H\}$ NMR (in C_6D_6), δ 10.0 (2C_5Me_5), 52.7 (2RuCH_2), 100.1 (2C_5Me_5), 119.0 (2C=CH_2), 164.2 (2C=CH_2) and 204.3 (4CO). Found: C, 54.3; H, 5.6%; M, not observed. $C_{30}H_{38}O_4Ru_2$ requires: C, 54.2; H, 5.8%; M, 665].

Evaporation of the combined pentane extracts gave a red solid which was chromatographed on an alumina column. Elution with pentane gave a red band from which, after recrystallization from pentane, 0.07 g (11%) of red, crystalline $[Ru_2(CO)_2\{\mu\text{-}C(Me)CHCH_2CCH_2\}(\eta\text{-}C_5Me_5)_2]$ (**12**) was obtained [ν(CO) (in cyclohexane) at 1941s and 1854m cm^{-1}; ^1H NMR (in C_6D_6), δ 5.91 (s, 1H, CH), 3.63 (d, J_{gem} 20.5 Hz, CHCH_2), 3.35 (s, 1H, C=CH_2), 3.07 (s, 1H, C=CH_2), 2.61 (d, 1H, J_{gem} 20.5 Hz, CHCH_2), 2.30 (s, 3H, RuCMe), 1.74 (s, 15H, C_5Me_5) and 1.53 (s, 15H, C_5Me_5); $^{13}C\{^1H\}$ NMR (in C_6D_6), δ 220.3 (μ-CO), 209.1 (Ru*C*Me), 200.2 (CO), 167.5 (μ-*C*CH_2), 125.3 (CH), 97.4 (*C*$_5$Me$_5$), 96.8 (*C*$_5$Me$_5$), 53.0 (C=*C*H_2), 50.7 (CH*C*H_2), 31.9 (Ru*C*Me), 9.7 (C_5Me_5) and 9.2 (C_5Me_5). Found: 55.3; H, 6.5%; M, 610. $C_{28}H_{38}O_2Ru_2$ requires: C, 55.3; H, 6.3%; M, 610].

Reaction of allene with $[(\eta\text{-}C_5Me_5)(CO)_2RuCH_2C(CH_2)C(CH_2)CH_2Ru(CO)_2(\eta\text{-}C_5Me_5)]$ (**11**)

Allene (0.60 g, 15.0 mmol) was condensed at −196°C into a Young's tube containing (**11**) (0.21 g, 0.32 mmol) and THF (110 cm^3). After warming to room temperature and photolysis for 4 h, the now red–orange solution was evaporated and the residual red oil was extracted with three 50 cm^3 portions of pentane, leaving 0.03 g of white crystalline (**11**). Chromatography of the combined pentane extracts on alumina, eluting with pentane, gave a red band, from which 0.063 g (33%) of red crystalline $[Ru_2(CO)_2\{\mu\text{-}C(Me)CHCH_2CCH_2\}(\eta\text{-}C_5Me_5)_2]$ (**12**) was obtained after recrystallization from pentane. Further elution with acetone removed 0.05 g of (**11**).

Preparation of $[Ru_2(CO)_2(\mu\text{-}CH_2CCH_2)(\eta\text{-}C_5H_5)_2]$ (**21**)

A solution of $[Ru_2(CO)_3(\mu\text{-}CCH_2)(\eta\text{-}C_5H_5)_2]$ (**24**) (0.214 g, 0.484 mmol) in 100 cm^3 of acetonitrile was subjected to UV irradiation for 9 h while slowly purging with nitrogen. After this time, new carbonyl bands at 1935s and 1755m cm^{-1}, attributed to the formation of $[Ru_2(CO)_2(MeCN)(\mu\text{-}CCH_2)(\mu\text{-}C_5H_5)_2]$ (**25**), had replaced those of (**24**). THF (100 cm^3) was added to the reaction mixture, which was then cooled to 0°C, and a freshly prepared diethylether solution of diazomethane (excess, from treatment of 2.19 g (14 mmol) of Diazald with KOH) added. The mixture was stirred while warming to room temperature over 1 h. The solvent was removed at reduced pressure to leave an orange oil. Chromatography on alumina, eluting with dichloromethane–hexane (2 : 3), provided an orange band which yielded 21 mg (10%) of red crystalline $[Ru_2(CO)_2(\mu\text{-}CH_2CCH_2)(\eta\text{-}C_5H_5)_2]$ (**21**), and was further purified by sublimation (90°C, 10^{-1} torr) [ν(CO) (in CH_2Cl_2) at 1935 m,sh and 1914s cm^{-1}; ^1H NMR (in $CDCl_3$), δ 4.91 (s, 10H, 2C_5H_5), 3.61 (dd, J 2 and 3 Hz, CH_2) and 2.70 (dd, J 2 and 3 Hz, CH_2). Found: M, 429. $C_{15}H_{14}O_2Ru_2$ requires: M, 429].

X-ray data collection and structure determination

Crystals of (**12**) were grown from a hexane solution as orange prisms. A single crystal (approximate dimensions $0.2 \times 0.25 \times 0.4$ mm) was mounted under nitrogen in a thin-walled glass capillary. Diffracted intensities were recorded on a Nicolet P3m four-circle diffractometer at room temperature. Of the total of 5687 independent profile-fitted intensities recorded in the range $4 < 2\theta < 45°$, 4678 with $F^2 > 2.0\sigma(F^2)$ were used in the structure solution and refinement. The data were corrected for Lorentz, polarization and X-ray absorption effects, the latter by an empirical method based on 400 azimuthal scan data. Check reflections ($\bar{2}$, 0, 4 and $\bar{1}$, $\bar{6}$, 2) were measured every 50 reflections and showed no evidence of significant decay over the 204 h of data collection.

Crystal data. $C_{28}H_{38}O_2Ru_2$, $M = 608.4$, monoclinic, space group $P2_1/c$ (No. 14), $a = 10.403(8)$, $b = 28.804(27)$, $c = 19.882(18)$ Å, $\beta = 117.14(6)°$, $U = 5302(8)$ Å^3, $Z = 8$, $D_c = 1.52$ g cm^{-3}, $F(000) = 2480$, Mo-K_α X-radiation, graphite monochromator, $\bar{\lambda} = 0.71069$ Å, μ(Mo-K_α) = 11.39 cm^{-1}.

The structure was solved by conventional Fourier and Patterson heavy-atom methods and refined by full-matrix blocked-cascade least-squares. The asymmetric unit contains two crystallographically independent molecules of the complex. All non-hydrogen atoms and non-(η-C_5Me_5) carbons were allowed anisotropic thermal parameters. Hydrogen atoms were included at idealized positions (C—H

0.96 Å), methyl hydrogens being refined as part of rigid groups and the others as "riding" on the carbon to which they are attached. Isotropic thermal parameters for hydrogen atoms were fixed at values *ca* 1.2 times those of their parent carbons. Refinement converged at R 0.047 (R_w 0.046), $S = 1.46$,* with a weighting scheme of the form $w = [\sigma^2(F_o) + 0.0002|F_o|^2]^{-1}$. The final electron density difference synthesis showed no peaks > 1.66 e A^{-3}. Calculations were carried out on an Eclipse (Data General) computer in this laboratory using the SHELXTL system of programs.[32] Complex, neutral atom scattering factors for all atoms were from ref. 33. Final atom coordinates, tables of thermal parameters, and listings of observed and calculated structure factors have been deposited with the Editor as supplementary material. Atomic coordinates have also been deposited with the Cambridge Crystallographic Data Centre.

Acknowledgements—We are grateful to the S. E. R. C. for support and for the award of a Research Studentship (to K.A.M.), Johnson Matthey PLC for a loan of ruthenium trichloride, Central Michigan University for granting sabbatical leave (to G.S.L.), and the donors of the Petroleum Research Fund, administered by the American Chemical Society for travel funds (to G.S.L.).

REFERENCES

1. Part IX. G. S. Lewandos, S. A. R. Knox and A. G. Orpen, *J. Chem. Soc., Dalton Trans.* 1987, 2703.
2. For a review through 1975 see: F. L. Bowden and R. Giles, *Coord. Chem. Rev.* 1976, **20**, 81.
3. G. Ingrosso, L. Porri, G. Pantini and P. Racanelli, *J. Organomet. Chem.* 1975, **84**, 75 and refs therein.
4. P. Diversi, G. Ingrosso, A. Immirzi and M. Zocchi, *J. Organomet. Chem.* 1976, **104**, C1.
5. G. K. Barker, M. Green, J. A. K. Howard, J. L. Spencer and F. G. A. Stone, *J. Chem. Soc., Dalton Trans.* 1978, 1839.
6. P. W. Jolly, C. Krüger, R. Salz and J. C. Sekutowski, *J. Organomet. Chem.* 1979, **165**, C39.
7. A. van der Ent and A. L. Onderdelinde, *Inorg. Chim. Acta* 1973, **7**, 203.
8. A. Borrini and G. Ingrosso, *J. Organomet. Chem.* 1977, **132**, 275.
9. S. Otsuka, A. Nakamura and K. Tani, *J. Chem. Soc. (A)* 1968, 2248, and refs therein.
10. Y. Gaoni and S. Sadeh, *J. Org. Chem.* 1980, **45**, 870.
11. R. P. Hughes and J. Powell, *J. Organomet. Chem.* 1973, **54**, 345, and refs therein.
12. A. E. Smith, *Inorg. Chem.* 1972, **11**, 165.
13. J. R. Schmidt and D. M. Duggan, *Inorg. Chem.* 1981, **20**, 318.
14. M. Cooke, N. J. Forrow and S. A. R. Knox, *J. Chem. Soc., Dalton Trans.* 1983, 2435.
15. R. M. Silverstein, G. C. Bassler and T. C. Morrill, *Spectrometric Identification of Organic Compounds*, Edn 4, p. 273. Wiley, New York (1981).
16. R. E. Colborn, A. F. Dyke, S. A. R. Knox, K. A. Mead and P. Woodward, *J. Chem. Soc., Dalton Trans.* 1983, 2099.
17. R. E. Colborn, S. A. R. Knox and K. A. Mead, unpublished results.
18. C. P. Casey, W. H. Miles, P. J. Fagan and K. J. Hallen, *Organometallics* 1985, **4**, 559.
19. D. M. Duggan, *Inorg. Chem.* 1981, **20**, 1164.
20. B. P. Gracey, S. A. R. Knox, K. A. Macpherson, A. G. Orpen and S. R. Stobart, *J. Chem. Soc., Dalton Trans.* 1985, 1935.
21. B. D. Moore, M. B. Simpson, M. Poliakoff and J. J. Turner, *J. Chem. Soc., Chem. Commun.* 1984, 972.
22. H. B. Abrahamsen, M. C. Palazzotto, C. L. Reichel and M. S. Wrighton, *J. Am. Chem. Soc.* 1979, **101**, 4123.
23. N. D. Feasey, N. J. Forrow, G. Hogarth, S. A. R. Knox, K. A. Macpherson, M. J. Morris and A. G. Orpen, *J. Organomet. Chem.* 1984, **267**, C41.
24. M. C. Caserio, *Selective Organic Transformations* (Edited by B. S. Thyagarajan), Vol. 1, p. 239. Wiley-Interscience, New York (1970).
25. C. P. Casey and E. A. Austin, *Organometallics* 1986, **5**, 584.
26. E. L. Hoel, G. B. Ansell and S. Leta, *Organometallics* 1986, **5**, 585.
27. N. M. Doherty, C. Elschenbroich, H. J. Kneuper and S. A. R. Knox, *J. Chem. Soc., Chem. Commun.* 1985, 170.
28. N. M. Doherty and S. A. R. Knox, *Inorg. Synth.* in press.
29. A. P. Humphries and S. A. R. Knox, *J. Chem. Soc., Dalton Trans.* 1975, 1710.
30. R. B. King, M. Z. Iqbal and A. D. King, *J. Organomet. Chem.* 1979, **171**, 53.
31. R. E. Colborn, D. L. Davies, A. F. Dyke, A. Endesfelder, S. A. R. Knox, A. G. Orpen and D. Plaas, *J. Chem. Soc., Dalton Trans.* 1983, 2661.
32. G. M. Sheldrick, *SHELXTL, an Integrated System for Solving, Refining and Displaying Crystal Structures from Diffraction Data*, revision No. 4. Nicolet Instruments Ltd, Warwick (1983).
33. *International Tables for X-Ray Crystallography*, Vol. 4. Kynoch Press, Birmingham (1974).

* $R = \Sigma||F_o|-|F_c||/\Sigma|F_o|$; $R_w = \Sigma w^{1/2}||F_o|-|F_c||/\Sigma w^{1/2}|F_o|$; $S = [\Sigma w(|F_o|-|F_c|)^2/(N_o-N_v)]^{1/2}$, N_o and N_v = numbers of observations and variables.

Polyhedron Vol. 7, No. 10/11, pp. 847–858, 1988
Printed in Great Britain

0277–5387/88 $3.00+.00
© 1988 Pergamon Press plc

REACTIVITY OF METHYLIDYNE LIGANDS ON TRINUCLEAR CLUSTERS OF GROUP 8 METALS

JEROME B. KEISTER

Department of Chemistry, University at Buffalo, S.U.N.Y., Buffalo, NY 14214, U.S.A.

(*Accepted* 5 *November* 1987)

Abstract—The chemistry of alkylidyne containing clusters $HM_3(\mu\text{-CX})(CO)_{10}$ and $H_3M_3(\mu_3\text{-CX})(CO)_9$ is presented—(1) structures, bonding and spectroscopic characterizations, (2) syntheses involving modification of the methylidyne substituent, (3) alkyne–alkylidyne coupling, and (4) formation of H—CX bonds. Reactions of $HRu_3(COMe)(CO)_{10}$ or $H_3Ru_3(CX)(CO)_9$ (X = OMe, Ph or alkyl) with alkynes, produce $HRu_3(\mu_3\text{-}\eta^3\text{-XCCRCR})(CO)_9$ clusters containing 1,3-dimetalloallyl ligands. Hydrogenation of these products when X = OMe or SEt gives new alkylidynes $H_3Ru_3(\mu_3\text{-CCHRCH}_2R)(CO)_9$. For X = SEt, isomerization of $HRu_3(\mu_3\text{-}\eta^3\text{-EtSCCRCR})(CO)_9$ to $Ru_3(\mu\text{-SEt})(\mu_3\text{-}\eta^3\text{-CCRCHR})(CO)_9$, a presumed intermediate in the hydrogenation reaction, occurs under mild conditions. Under CO, reductive elimination of CH_3X can be induced from $H_3Ru_3(\mu_3\text{-CX})(CO)_9$ (X = OMe, Ph, Cl or CO_2Me). Pyrolysis of $H_3Ru_3(\mu_3\text{-CX})(CO)_9$, X = CO_2Me and SEt, gives stabilized intermediates $H_2Ru_3(\mu_3\text{-CHCO}_2Me)(CO)_9$ and $HRu_3(\mu_3\text{-CH}_2SEt)(CO)_9$, respectively. Protonation of $H_3Ru_3(\mu_3\text{-CR})(CO)_9$ (R = Et or $CHPhCH_2Ph$) yields $H_3Ru_3(\mu_3\text{-HCR})(CO)_9^{1+}$, in which the alkylidene hydrogen is agostic; the protonated clusters undergo more rapid reductive elimination than the neutral precursors. The kinetics and mechanism of reductive elimination have been investigated. A mechanism is presented.

The comparison between the chemical reactivity of hydrocarbyl ligands bridging two or more metals and the reactivity of these ligands when bound to a single metal centre is clearly of fundamental interest. The chemistry of bridging hydrocarbyl ligands is also of interest because of the analogy to the chemistry of hydrocarbyl groups adsorbed on metal surfaces. The alkylidyne ligand has an extensive chemistry for monometallic complexes and is implicated in acetylene metathesis.[1] Furthermore, alkylidynes have been identified in numerous studies of surface adsorbed hydrocarbons, although little is known of the reactivity of these surface bound species.[2] Alkylidynes of metal clusters have also been known for many years. The best known class of clusters containing a bridging alkylidyne group has the general formula $Co_3(\mu_3\text{-CR})(CO)_9$; the chemistry of these compounds has been mainly found to involve modification of the alkylidyne substituent or ligand substitution on the metal atoms.[3] Comparisons of the reactivity of the alkylidyne ligand on single metal centres, on metal clusters and on metal surfaces are therefore of special interest.

Our research group has been concerned with the chemical reactivity of the cluster series having the general formula $H_3M_3(CX)(CO)_9$, M = Fe, Ru or Os and X = alkyl, aryl, alkoxy or other substituent (Fig. 1). These clusters are isoelectronic with, and close structural analogues of the $Co_3(CX)(CO)_9$ clusters. These series provide the opportunity to investigate the chemical reactivity of a variety of groups—hydride, carbonyl, M—C bond or C—X bond—as a function of the metal, methylidyne substituent and Lewis base ligands.

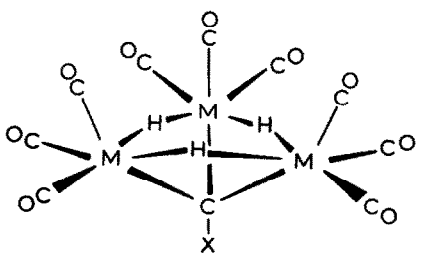

Fig. 1. Structure of $(\mu\text{-H})_3M_3(\mu_3\text{-CX})(CO)_9$ (M = Fe, Ru or Os; X = H, alkyl, aryl, halide, OMe, CO_2Me or SEt).

This review will present the chemistry of the $H_3M_3(CX)(CO)_9$ series and the related class $HM_3(CX)(CO)_{10}$: (1) structure, bonding and spectroscopic characterization, (2) syntheses involving modification of the X substituent, (3) insertion of alkynes into the M—CX bond, and (4) formation of H—CX bonds. Although this review will emphasize work done by our group on Ru clusters, results of other research groups will also be presented.

STRUCTURES, BONDING AND SPECTROSCOPY

The structures of $H_3M_3(CX)(CO)_9$ (Fig. 1: M = Fe, X = Me;[4] M = Ru, X = Cl,[5] Me,[6] C_6H_4-4-Me[7] and CH_2CMe_3;[8] M = Os, X = OBO(trimeric)[9] and CO_2H[10]) all contain a triangle of metal atoms symmetrically capped by the methylidyne ligand and with each edge of the triangle bridged by a single hydride ligand. The coordination geometry around each metal is octahedral, with facially coordinating CO ligands and mutually *cis* hydrides and methylidyne ligands. For several Ru clusters the positions of the hydride ligands have been determined directly by X-ray methods. The Ru—H—Ru angles are 97–108°, while the H—Ru—H and C—Ru—H angles are 85–87°.

Much greater structural variation is found for clusters of the general formula $HM_3(CX)(CO)_{10}$ (Fig. 2: M = Fe, X = OMe,[11] NMe_2[12] or O^{1-};[13] M = Ru, X = OMe,[14,15] NMe_2[16] or O^{1-};[17] M = Os, X = CCH_2CHMe_2,[18] Ph,[19] H,[20] $NHCMe_3$[21] or C(Ph)CC(Ph)Re$(CO)_4PMe_2Ph$[22]). Although in all of these the hydride and methylidyne bridge a common edge, the bonding of the CX ligand varies from doubly bridging to almost symmetrically triply bridging. The dihedral angle θ between the CM_2 and M_3 planes varies between 104–70°, depending upon the metal and the methylidyne substituent, with the angle decreasing as X = O^{1-} (Ru, 104°) > NMe_2 (Ru, 100°) > C(Ph)CC(Ph)Re$(CO)_4$L (Os, 99°) > OMe (Ru, 95°) > CH_2CHMe_2 (Os, 82°) > Ph (Os, 78°) > H (Os, 70°) and as M = Os > Ru > Fe; a comparison between the structures of $HRu_3(COMe)(CO)_{10}$ (θ = 94.90°) and $HRu_3(COMe)(CO)_8(C_6H_8)$ (θ = 60.70°) shows that the other ligands on the cluster also have an influence.[14] For the doubly bridging alkylidynes, there is structural and spectroscopic evidence for π-donation from the methylidyne substituent to the adjacent carbon. Thus, for $HM_3(\mu\text{-}CX)(CO)_{10}$, X = OMe or NMe_2, the $M_2(\mu\text{-}CX)$ unit is planar, the C—X bond lengths are substantially shorter than values expected for single bonds (for $HRu_3(\mu\text{-}COMe)(CO)_{10}$, 1.305 Å and for $HRu_3(\mu\text{-}CNMe_2)(CO)_{10}$, 1.280 Å), and there is restricted rotation about the C—X bond ($\Delta G^{\ddagger}$ = 56.5 kJ for $HOs_3(COMe)(CO)_{10}$[23,24] and > 80 kJ for $HOs_3(CNMeCH_2Ph)(CO)_{10}$[23]). The degree of C—X multiple bonding increases as the π-donor ability of X increases: OR < NR_2 < O^{1-}.

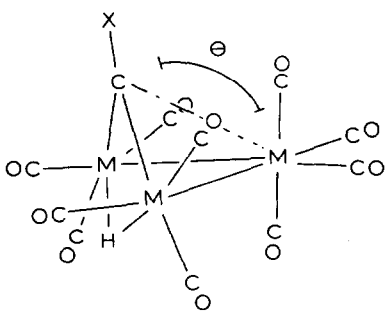

Fig. 2. Structure of $(\mu\text{-}H)M_3(\mu\text{-}CX)(CO)_{10}$ (M = Fe, Ru or Os; X = OMe, NR_2, O^-, H, or Ph).

At this time there is no explanation for the dependence of the coordination geometry, assumed by the methylidyne in the ground state, upon the identity of the metal or other ligands. The explanation for the variation of the dihedral angle θ with the nature of the methylidyne substituent may be found in the competition between X → C π-donation, which is most favourable for a doubly bridging configuration, and M → C π-donation, which is most favourable for a triply bridging one.[14]

Fenske–Hall calculations and photoelectron spectroscopy have been used to investigate the bonding in $H_3M_3(\mu_3\text{-}CX)(CO)_9$.[25] The "tilt" of the $Ru(CO)_3$ units caused by the hydride ligands gives rise to some differences between the MO's of the Ru clusters and those of the Co analogues. The Ru—H—Ru bonds are best described as three-centre, two-electron bonds with no direct Ru—Ru interaction. The methylidyne carbon atom may be described as *sp*-hybridized with delocalized bonding involving the $2p\pi$ orbitals and little delocalization of the *sp* hybrid lone pair onto the cluster. The HOMO is mainly Ru—C bonding in character, unlike the Co analogues for which the HOMO is Co—Co bonding.

The vibrational spectra of $H_3M_3(CX)(CO)_9$ (M = Ru, X = H, Me, Cl; M = Os, X = Me) have been analysed.[26,27] The metal–hydride stretching modes occur near 1350 cm^{-1}. For $H_3Ru_3(CH)(CO)_9$ the C—H stretching frequency is 2988 cm^{-1} and normal coordinate analysis found the Ru—C force constant to be 137 N m^{-1}, close to the value for the Co analogue.

^{13}C NMR spectra have been reported for both $HM_3(CX)(CO)_{10}$ and $H_3M_3(CX)(CO)_9$. The chemical shift of the methylidyne carbon varies between 370 and 118 ppm, depending upon the

Table 1. ^{13}C Chemical shift for the alkylidyne carbon

Compound	Chemical shift (ppm)	Reference
$HRu_3(COMe)(CO)_{10}$	366.5	15
$HRu_3(CNMe_2)(CO)_{10}$	312.6	28
$H_3Ru_3(CEt)(CO)_9$	232.6	29
$H_3Ru_3(CMe)(CO)_9$	219.3	27
$H_3Ru_3(CPh)(CO)_9$	213.0	30
$H_3Ru_3(CSEt)(CO)_9$	204.4	31
$H_3Ru_3(CCO_2Me)(CO)_9$	183.5 or 180.2	32
$HOs_3(COMe)(CO)_{10}$	352.2	24
$HOs_3(CCH_2CHMe_2)(CO)_{10}$	320.5 (40°C)	
	312.0 (−80°C)	18
$HOs_3(CPh)(CO)_{10}$	314.2 (17°C)	
	304.2 (−115°C)	19
$HOs_3(CH)(CO)_{10}$	219 (−100°C)	
$H_3Os_3(COMe)(CO)_9$	205.2	23
$H_3Os_3(CMe)(CO)_9$	154.7	27
$H_3Os_3(CH)(CO)_9$	118.4	20
$HFe_3(CNEt_2)(CO)_{10}$	317.3	33
$HFe_3(COMe)(CO)_{10}$	356.5	11
$H_3Fe_3(CH)(CO)_9$	232.0	34

bonding mode of the ligand, the metal and the methylidyne substituent (Table 1). In several examples the chemical shift of the methylidyne carbon has been found to be strongly temperature dependent. It has been proposed that in these instances there exists a fluxional equilibrium between isomers having different coordination modes for the methylidyne ligand.[35]

SYNTHESES OF $HM_3(CX)(CO)_{10}$ AND $H_3M_3(CX)(CO)_9$

Relatively few methylidynes of the general formula $HM_3(CX)(CO)_{10}$ have been synthesized. In 1975 Shriver *et al.* prepared $HFe_3(COMe)(CO)_{10}$ by O-methylation of $HFe_3(CO)_{11}^-$.[11,36] The Ru and Os analogues were subsequently prepared by several groups using similar routes [eq. (1)].[15,23,24] Substitution on $HM_3(CO)_{11}^-$ by CNR, followed by alkylation, gives the analogous $HM_3(CNR_2)(CO)_{10}$.[23,33] Attack by nucleophiles, $LiBHEt_3$ or LiPh on $HOs_3(COMe)(CO)_{10}$, followed by treatment with Lewis acids, has been used to generate $HOs_2(CX)(CO)_{10}$, X = H[20] or Ph;[19] $HRu_3(CX)(CO)_{10}$ has been similarly prepared.[38] Treatment of $H_2Os_3(CO)_{10}$ with 3,3-dimethylcyclopropene produces $HOs_3(CCH_2CHMe_2)(CO)_{10}$.[18]

$$M_3(CO)_{12} \xrightarrow{OH^-} HM_3(CO)_{11}^- \xrightarrow{Me^+} HM_3(COMe)(CO)_{10} \quad (1)$$
(M = Fe, Ru or Os)

$$HM_3(COMe)(CO)_{10} + (1)X^-(2)Me^+ \longrightarrow HM_3(CX)(CO)_{10}. \quad (2)$$
(M = Ru or Os; X = H^- or Ph)

The first member of the class $H_3M_3(CX)(CO)_9$, $H_3Ru_3(CMe)(CO)_9$, was prepared by the reaction of $H_4Ru_4(CO)_{12}$ ethylene;[39] subsequently the Os analogue was prepared by hydrogenation of $H_2Os_3(CCH_2)(CO)_9$, derived from ethylene and $Os_3(CO)_{12}$.[40] Fehlner and Wong more recently prepared $H_3Fe_3(CR)(CO)_9$, R = H, Me or Et, by reduction of $Fe(CO)_5$.[41] These syntheses were not adaptable to other methylidyne derivatives. In 1976 we found that hydrogenation of $HM_3(COMe)(CO)_{10}$, M = Fe, Ru or Os, gave $H_3M_3(COMe)(CO)_9$ [eq. (3)].[23] With these new methylidyne clusters in hand we sought to prepare a complete series analogous to the $Co_3(CX)(CO)_9$ series. Seyferth had earlier developed a number of syntheses involving modification of the halomethylidyne ligand. Therefore, our first goal was to convert $H_3M_3(COMe)(CO)_9$ to $H_3M_3(CX)(CO)_9$, X = halide. The approach in eq. (4) afforded the desired clusters in nearly quantitative yields.[42] Then by application of procedures developed for the Co analogues, we were able to prepare a wide variety of substituted methylidyne species [eqs (5)–(8)].[42,31]

$$HM_3(COMe)(CO)_{10} + H_2 \longrightarrow H_3M_3(COMe)(CO)_9 + CO \quad (3)$$
(M = Fe, Ru or Os)

$$H_3M_3(COMe)(CO)_9 + BX_3 \longrightarrow H_3M_3(CX)(CO)_9 \quad (4)$$
(M = Ru or Os; X = Cl or Br)

$$H_3M_3(CX)(CO)_9 + AlCl_3 + C_6H_6 \longrightarrow H_3M_3(CPh)(CO)_9 \quad (5)$$
(M = Ru or Os; X = Br or OMe)

$$H_3M_3(CX)(CO)_9 + AlCl_3 + CO \longrightarrow H_3M_3(CCO)(CO)_9^+ \quad (6a)$$
(M = Ru or Os; X = Br or OMe)

$$H_3M_3(CCO)(CO)_9^+ + ROH \longrightarrow H_3M_3(CCO_2R)(CO)_9 \quad (6b)$$

$$H_3Ru_3(CBr)(CO)_9 + NEt_3 + HSR \longrightarrow H_3Ru_3(CSR)(CO)_9 \quad (7)$$

$$H_3Ru_3(CBr)(CO)_9 + HSnBu_3 \longrightarrow H_3Ru_3(CH)(CO)_9 \quad (8)$$

$$HOs_3(CH)(CO)_{10} + X \longrightarrow HOs_3(CHX)(CO)_{10}. \quad (X = H^- \text{ or pyridine}) \quad (9)$$

Although the mechanisms of these reactions remain unknown, the reaction chemistry involving modification of the C—X unit may be considered to fall into three classes: (a) reactions which may be thought to proceed through the $H_3M_3(C)(CO)_9^{1+}$ ion, by the abstraction of halide or alkoxide from the neutral cluster [e.g. reactions (4), (5) and (6)], (b) radical reactions proceeding through $H_3M_3(C)(CO)_9$ [e.g. reactions (7) and (8)], and (c) reactions which proceed by nucleophilic attack on the alkylidyne carbon [reaction (9)]. The $Co_3(CX)(CO)_9$ clusters display reactivities analogous to that of $H_3M_3(CX)(CO)_9$.

The apparent radical chemistry of the cluster in the presence of reducing agents has been proposed to follow the $S_{RN}1$ mechanism. Electron transfer to $H_3Ru_3(CBr)(CO)_9$ followed by halide ion expulsion could form the $H_3Ru_3(C)(CO)_9$ radical, which may abstract hydrogen from donor substrates to form $H_3Ru_3(CH)(CO)_9$, or may add to substrates such as thiols.[31]

The chemistry of the $H_3M_3(C)(CO)_9^{1+}$ ion is more thoroughly understood, although the cation may never exist in a free form. In the presence of large quantities of the reactive substrate the cation may be trapped without rearrangement. For example, in benzene the aryl product is obtained. However, in an unreactive medium, the cation picks up CO from solution to form the ketenylidene $H_3M_3(CCO)(CO)_9^{1+}$. The chemistry of this species is quite interesting. Attack by nucleophiles such as HX = ROH, R_2NH or H_2O generates the corresponding acyls $H_3M_3(CCOX)(CO)_9$.[10,38,42] Deprotonation forms $H_2M_3(CCO)(CO)_9$; an X-ray crystallographic study of the Os cluster found an upright μ_3-η^1 bonding mode for the CCO ligand.[43] The neutral ketenylidene is also formed by pyrolysis of $HOs_3(CH)(CO)_{10}$.

Shapley has demonstrated nucleophilic addition and substitution on the alkylidyne carbon of $HM_3(CX)(CO)_{10}$ (M = Ru or Os; X = OMe or H).[19,20,38] In several instances the addition products can be isolated, but the reactions can be quite complex. At this time there are no definitive examples of nucleophilic attack on the alkylidyne carbon of clusters of the class $H_3M_3(CX)(CO)_9$. This suggests that the chemical reactivity of the alkylidyne ligand may depend strongly upon its coordination mode.

INSERTION OF ALKYNES INTO THE M—CX BOND

Alkyne–alkylidyne coupling is a reaction of some interest for monometallic alkylidyne complexes since it is the central step in the alkyne metathesis reaction.[44] Alkyne–alkylidyne coupling has also been noted on polymetallic systems,[37] although less is known about the mechanism of the reaction.

Stoichiometric hydrogenations of alkynes by $H_3Ru_3(CX)(CO)_9$ (X = OMe, Me, Ph or $CH_2CH_2CMe_3$) yield the corresponding *cis*-alkene; in each case a second equivalent of alkyne combines with the cluster residue to produce clusters of the general formula $HRu_3(C(X)C(R)CR)(CO)_9$ (Fig. 3), in which alkyne–alkylidyne coupling has generated a μ_3-η^3-1,3-dimetalloallyl ligand. For X = OMe these same clusters may be obtained in better yields by direct reaction of $HM_3(COMe)(CO)_{10}$, M = Ru or Os, with the alkyne.[29]

Clusters of this class have been previously synthesized through a variety of pathways. The clusters $HRu_3(\mu_3$-η^3-$RCCR'CR'')(CO)_9$ have been obtained from reactions of alkenes, dienes or alkynes with $Ru_3(CO)_{12}$.[45] Interestingly, a hydroxy derivative $HOs_3(\mu_3$-η^3-$HOCCHCH)(CO)_9$ is formed from $Os_3(CO)_{10}(NCMe)_2$ and acetylene in wet THF; in this reaction a CO ligand is the source of the "hydroxymethylidyne" fragment.[46] The stability of these clusters and the numerous pathways for their formation suggests that the μ_3-η^3-C_3R_3 fragment may also be a common intermediate during reactions of hydrocarbons adsorbed on metal surfaces.

The reactions of $H_3M_3(CX)(CO)_9$ or $HM_3(COMe)(CO)_{10}$ with alkynes provide an excellent opportunity to study alkyne–alkylidyne coupling in trimetallic cluster systems. Two regioisomers are obtained with unsymmetrical alkynes. The two regioisomers from the terminal alkynes are easily identified by virtue of their ^1H NMR spectra, in which the coupling constant between the hydride and the hydrogen on the central carbon is *ca* 3 Hz, but no coupling is observed between the hydride and the hydrogen on the terminal carbon. The ratio of the isomers $[HRu_3(C(X)C(R^1)CR^2)(CO)_9]/[HRu_3(C(X)C(R^2)CR^1)(CO)_9]$ depends upon the

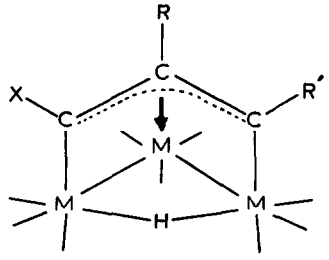

Fig. 3. Structure of $HM_3(\mu_3$-η^3-$XCCRCR')(CO)_9$ (M = Ru or Os; X = OMe, SEt, Ph or alkyl; R and R' = H or alkyl).

identities of the alkyne substituents: (R^1, R^2), ratio = (H, Ph), 3:1; (H, Bu), 2:1; (H, CMe_3), 20:1; (H, CO_2Me), 2:1; (H, OEt), 1:0; (Me, C_7H_{15}), 3:1; (CO_2Me, Ph), 2:1. The isomer distribution is kinetically determined, since the isomers do not interconvert even at temperatures far in excess of that required for coupling. Apparently both steric and electronic properties influence the orientation of coupling. Comparison of the isomer ratios from 1-hexyne and from 3,3-dimethylbutyne indicates that bulkier substituents prefer the terminal carbon. However, since the sterically similar substituents OEt and Bu give rise to very different isomer ratios, electronic effects are also important.

The steric and electronic requirements for alkyne–alkylidyne coupling are still poorly understood. Bis(trimethylsilyl)acetylene, trimethylsilylacetylene and dimethyl acetylenedicarboxylate give little or no coupled products with $HRu_3(COMe)(CO)_{10}$. Furthermore, coupled products could not be isolated from reactions of 2-butyne with $HFe_3(COMe)(CO)_{10}$ or with $HRu_3(CNMe_2)(CO)_{10}$. Obviously, the coupling is sensitive to the nature of the alkyne, the metal and the alkylidyne substituent.

The carbon–carbon bond formation in these Ru_3 clusters is reminiscent of carbon chain growth on metal surfaces in the Fischer–Tropsch reaction,[47] in which CO is reduced with hydrogen to give alkanes and water. The major products from CO hydrogenation are linear hydrocarbons, but minor products are branched hydrocarbons, primarily 2-methyl branched. Since alkylidyne species have been identified on metal surfaces and may come together to form alkynes, we considered the possibility that the cluster reaction might act as a model for carbon chain growth on metal surfaces. If an adsorbed CH fragment were to couple with an adsorbed "alkyne" HC_2R, then the products would be linear and 2-methyl branched hydrocarbon chains. Pertinent to this analogy, is the report of the formation of $HOs_3(\mu_3\text{-}\eta^3\text{-}HOCCHCH)(CO)_0$ from water, CO, acetylene and $Os_3(CO)_{10}(NCMe)_2$.[46]

To investigate this analogy we treated $HRu_3(C(OMe)C(R)CR)(CO)_9$ with hydrogen (1–4 atm, 90–110°C). In each case the major cluster products isolated were $H_4Ru_4(CO)_{12}$ and $H_3Ru_3(CCHRCH_2R)(CO)_9$ (15–90%). A minor product from the hydrogenation of $HRu_3(C(OMe)CHCH)(CO)_9$ was identified as $H_2Ru_3(MeC_2OMe)(CO)_9$ (Fig. 4);[48] this product shows that hydrogen can migrate from, as well as to, the hydrocarbon framework. The isolation of alkylidyne and alkyne products, indeed suggested the possibility of carbon chain growth by the coupling of C_1 and C_2 fragments to give dimetalloallyl species.

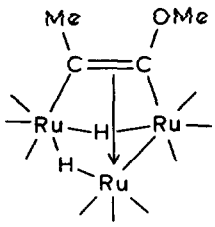

Fig. 4. Structure of $(\mu\text{-H})_2Ru_3(\mu_3\text{-}\eta^3\text{-MeCCOMe})(CO)_9$.

The mechanism of the hydrogenation reaction was investigated. Hydrogenation of $DRu_3(C(OMe)C(H)CCMe_3)(CO)_9$ produced exclusively $H_3Ru_3(CCH_2CHDCMe_3)(CO)_9$, indicating transfer of the hydride to the 3-carbon, prior to the addition of molecular hydrogen. Comparison of the rates of reaction of $HRu_3(C(OMe)C(H)CR)(CO)_9$, R = Bu and CMe_3, showed that bulkier substituents on the 3-carbon facilitate the hydrogenation, and consistent with this, hydrogenation of $HRu_3(MeOCC(H)COEt)(CO)_9$ produces primarily $H_3Ru_3(CCH_2CH_2OEt)(CO)_9$. These observations suggest that the hydride ligand is transferred to the 3-carbon early in the reaction. Low yields precluded further kinetic studies.

No alkylidyne products are obtained by hydrogenation of $HRu_3(C(X)C(R)CR)(CO)_9$ when X = H, alkyl or NMe_2. However, hydrogenation of $HRu_3(C(SEt)C(Me)CMe)(CO)_9$ does form $H_3Ru_3(CCHMeCH_2Me)(CO)_9$. Thus, a relatively weak C—X bond is required to allow rearrangement under conditions mild enough to allow isolation of the product.

More information concerning intermediates in the hydrogenation was obtained by careful analysis of the products from the coupling of alkynes RC_2R, R = Me or Ph, with $H_3Ru_3(CSEt)(CO)_9$. Although the major product of the reaction is the expected $HRu_3(C(SEt)C(R)CR)(CO)_9$, a minor product was found to be $Ru_3(CCRCHR)(SEt)(CO)_9$; the structure of this product (Fig. 5), determined by X-ray crystallography for R = Ph, is closely related to the possible intermediate in the hydrogenation process.[49] The hydride ligand has been transferred

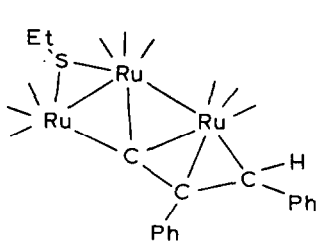

Fig. 5. Structure of $Ru_3(\mu_3\text{-}\eta^3\text{-CCPhCHPh})(\mu\text{-SEt})(CO)_9$.

to the 3-carbon and the CSEt bond has been cleaved, as is required in the hydrogenation. Although the alkylidyne carbon is triply bridging, there are only two Ru—Ru bonds. Presumably, the strong Ru—S bonds are responsible for retention of the SEt moiety in the cluster, whereas pyrolysis of $HRu_3(MeOCCRCR)(CO)_9$ does not form an analogous, stable product. Pyrolysis of $HRu_3(EtSCCRCR)(CO)_9$ at 70°C forms $Ru_3(CCRCHR)(SEt)(CO)_9$ in nearly quantitative yield; preliminary kinetic measurements have found a first order rate law with a rate constant of $7.6 \times 10^{-6}\ s^{-1}$ at 70°C. Thus, $Ru_3(CCRCHR)(SEt)(CO)_9$ seems to be a possible intermediate in the hydrogenation of $HRu_3(EtSCCRCR)(CO)_9$ to $H_3Ru_3(CCHMeCH_2Me)(CO)_9$.

From the results obtained so far we can propose the mechanism shown in Fig. 6 for alkyne–alkylidyne coupling and subsequent hydrogenation.

This work has shown that: (1) alkyne–alkylidyne coupling occurs on trimetallic clusters as well as for monometallic species, but μ_3-η^3-bridging makes the cluster-bound metallocycles much more stable, and (2) hydrogenation of 1,3-dimetalloallyls can form alkylidynes. These reactions provide a pathway for hydrocarbon chain growth on polymetallic units, which may be related to hydrocarbon chain growth on metal surfaces. Although the μ_3-η^3-C_3R_3 fragment has not yet been identified on a metal surface, the stability of these clusters and the large variety of paths which have been shown to lead to clusters of this class suggest that the fragment is likely to be an important product of hydrocarbon adsorption in heterogeneous catalysis. Further studies of the mechanism of the isomerization and hydrogenation reactions are in progress.

REDUCTIVE ELIMINATION OF H—CX BONDS

Reductive eliminations of C—H bonds from metals are the product-releasing steps in many catalytic processes. The mechanism is well understood for monometallic complexes,[50] but not for metal clusters or surfaces. Reactions of $H_3M_3(CX)(CO)_9$ with CO (1–35 atm, 60–110°C) produce CH_3X and $Ru_3(CO)_{12}/Ru(CO)_5$ when X = Ph, CO_2Me, Cl or H;[51] when X = OMe, dimethyl ether can be identified after decomposition under a CO/H_2 mixture. Elimination of CH_3X from $H_3M_3(CX)(CO)_9$ may model desorption of alkanes from metal surfaces. With this in mind, we undertook an investigation of the kinetics and mechanism of this reaction.

Calvert and Shapley have previously demonstrated the reverse process, "adsorption" of a methyl group by sequential C—H oxidative additions to give methylene and methylidyne fragments (Fig. 7).[52] Importantly, a facile equilibrium

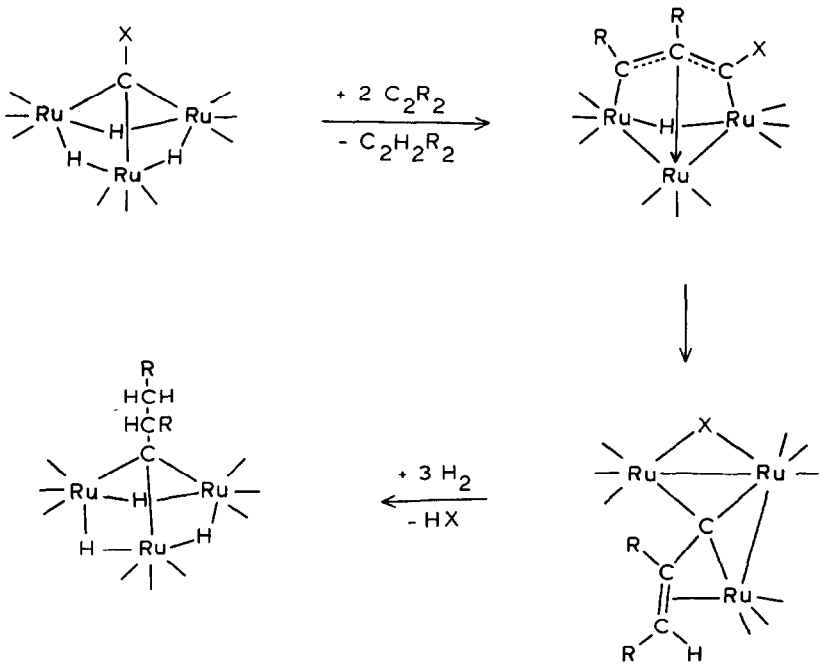

Fig. 6. Reaction pathway for alkyne–alkylidyne coupling and hydrogeneration of a 1,3-dimetalloallyl ligand. (X = OMe or SEt.)

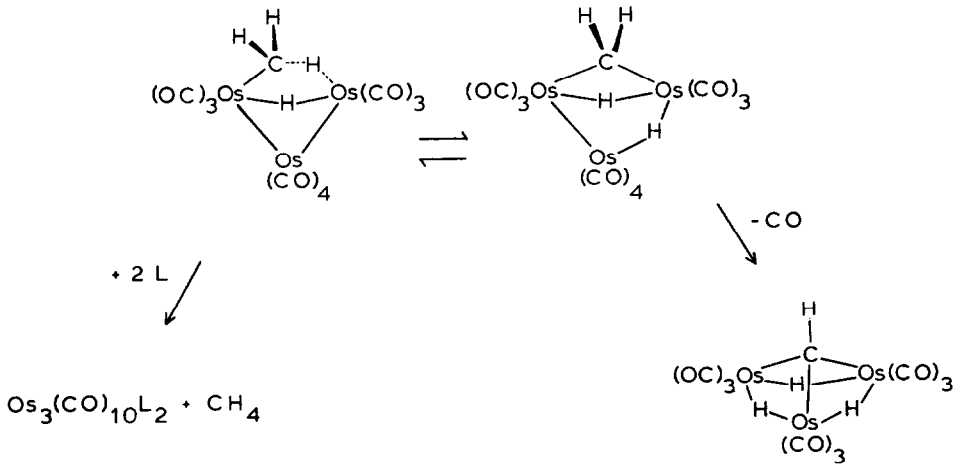

Fig. 7. Interconversion of alkyl, alkylidene and alkylidyne ligands on a Os_3 cluster.

between hydridomethylene and a methyl ligand with an agostic hydrogen was demonstrated. Furthermore, $HOs_3(CH_3)(CO)_{10}$ reacted under mild conditions with Lewis bases to form methane. These Os clusters provide valuable models for intermediates in the reductive elimination, but the difficulty and expense of obtaining substantial quantities make kinetic studies of this system impractical.

Based upon our results and those of others we can propose the mechanism shown in Fig. 8 for the reductive elimination from $H_3M_3(CX)(CO)_9$, M = Ru or Os. The basis for this proposition is given below.

That C—H elimination from $H_3Ru_3(CX)(CO)_9$ occurs in a sequential manner is suggested by the isolation of stabilized alkylidene and alkyl intermediates. Pyrolysis of $H_3Ru_3(CCO_2Me)(CO)_9$ in the absence of CO forms $H_2Ru_3(CHCO_2Me)(CO)_9$ in 56% yield (Fig. 9).[32] This product is formed by reductive elimination of a single C—H bond followed by coordination of the acyl to the unsatu-

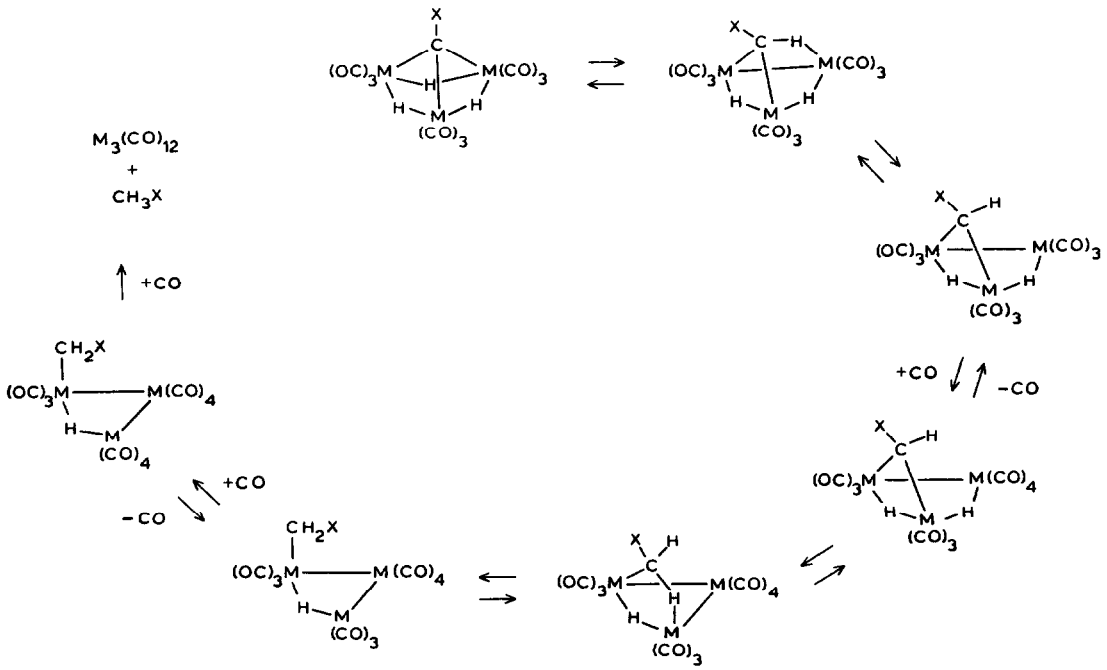

Fig. 8. Mechanism for reductive elimination of CH_3X from $H_3M_3(\mu_3\text{-}CX)(CO)_9$ (X = H, alkyl, Cl, Ph or CO_2Me; M = Ru or Os).

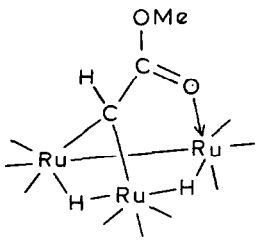

Fig. 9. Structure of $(\mu\text{-H})_2Ru_3(\mu_3\text{-}CCO_2Me)(CO)_9$.

rated metal site thus created. Pyrolysis of $H_3Ru_3(CSEt)(CO)_9$ yields $HRu_3(CH_2SEt)(CO)_9$ (Fig. 10); in this case the sulphur atom stabilizes the two vacant sites formed by reductive elimination.[31] Under CO, complete elimination of CH_3X ultimately yields $Ru_3(CO)_{12}$, which is in equilibrium with $Ru(CO)_5$ under the reaction conditions.

A number of lines of evidence indicate that the rate of C—H reductive elimination increases for successive steps. First, no intermediate alkylidene is observed during pyrolysis of $H_3Ru_3(CSEt)(CO)_9$, suggesting that formation of $H_2Ru_3(CHSEt)(CO)_9$ is slower than its conversion to $HRu_3(CH_2SEt)(CO)_9$. Second, direct comparison of the reactivity of the $H_2Os_3(CH_2)(CO)_{10}/HOs_3(CH_3)(CO)_{10}$ equilibrium mixture found that the rate of conversion of $H_2Os_3(CH_2)(CO)_{10}$ to $HOs_3(CH_3)(CO)_{10}$ is slower than the reaction of CO with the latter, forming methane and $Os_3(CO)_{12}$. Third, structural evidence suggests that the Ru—C bond strength decreases upon each successive C—H elimination; the Ru—C bond lengths decrease in the order: $H_3Ru_3(CR)(CO)_9 < H_2Ru_3(CHCO_2Me)(CO)_9 < HRu_3(CH_2SEt)(CO)_9$.[31]

A study of the mechanism of the reductive elimination process was undertaken. A crossover experiment revealed that the acetates formed from a mixture of $H_3Ru_3(CO_2Et)(CO)_9$ and $D_3Ru_3(CO_2Me)(CO)_9$ were labelled in a manner consistent with intramolecular formation of at least two of the three C—H bonds. The rate-determining step involves formation of only the first C—H bond. The rate law for toluene elimination from $H_3Ru_3(CPh)(CO)_9$ was determined to be as shown in eq. (10). The near-zero entropy of activation for the limiting rate constant, a, is consistent with an intramolecular rate-determining step. Kinetic isotope effects were unexpectedly less than or equal to one, being 0.64 for X = Ph and 1.00 for X = CO_2Me.

$$\text{rate} = \frac{ac[CO]}{b + c[CO]}[H_3Ru_3(CPh)(CO)_9]. \quad (10)$$

Although several pre-equilibria may be postulated to account for the kinetics, the most attractive, shown in Fig. 11, involves reversible migration of a hydrogen atom from a position bridging a Ru—Ru vector, to a position bridging a Ru—C vector. The agostic C—H—M bond[53] has recently been established in a number of monometallic complexes, as well as in polymetallic ones. In particular there are two excellent models for this intermediate.

First, Fehlner and coworkers have shown that deprotonation of $H_3Fe_3(CH)(CO)_9$ forms $HFe_3(HCH)(CO)_9^{1-}$, shown by ^1H and ^{13}C NMR spectroscopy to contain a Fe—H—C bridge. Further work by this group has shown that $H_3Fe_3(CH)(CO)_9$ exists in solution in equilibrium with $H_2Fe_3(HCH)(CO)_9$ and $HFe_3(H_2CH)(CO)_9$ (Fig. 12).[34]

Second, although the equilibrium constant for the tautomerization is not so favourable for the agostic Ru analogues, we have found that dissolution of $H_3M_3(CR)(CO)_9$, where M = Ru and R = Et or $CHPhCH_2Ph$, or M = Os and R = Me, in fluorosulphonic or trifluoromethanesulphonic acid forms $H_3M_3(HCR)(CO)_9^{1+}$ (Fig. 13), by protonation of the M—C bond. These cations have been characterized by NMR spectroscopy.[30] For $H_3Ru_3(HCEt)(CO)_9^{1+}$, the chemical shift of the agostic hydrogen is −9.45 ppm while a singlet resonance at −18.37 ppm is found for the three hydride ligands. The propylidene α carbon resonance occurs at 143.3 ppm (d) with a coupling constant to the agostic hydrogen of 58 Hz. These values of the spectral parameters are very similar to corresponding values for $H_2Fe_3(HCH)(CO)_9^{1-}$. Protonation of the Ru—C bond is expected since the HOMO is Ru—C bonding in character.[25] The proposed structure should give rise to two signals for the hydride ligands. To account for the obser-

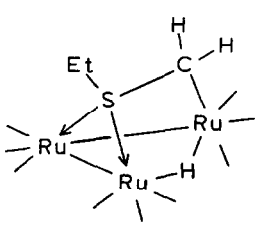

Fig. 10. Structure of $(\mu\text{-H})Ru_3(\mu_3\text{-}CH_2SEt)(CO)_9$.

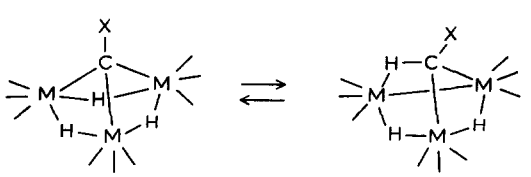

Fig. 11. Equilibrium between ground state $(\mu\text{-H})_3M_3(\mu_3\text{-}CX)(CO)_9$ and the higher energy tautomer $(\mu\text{-H})_2M_3(\mu_3\text{-}HCX)(CO)_9$ with an agostic hydrogen.

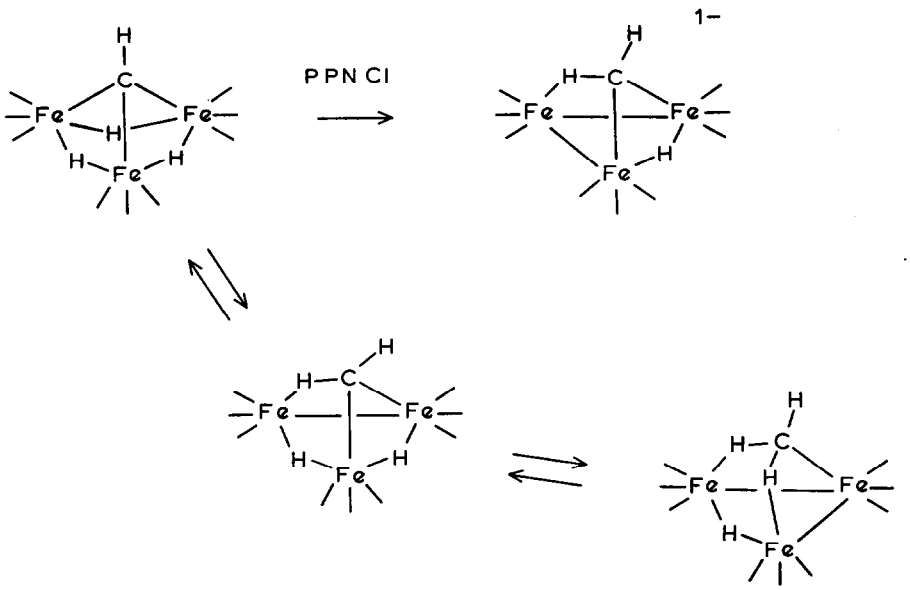

Fig. 12. Interconversions between various tautomers of $H_4Fe_3(C)(CO)_9$ and deprotonation of $(\mu\text{-}H)_3Fe_3(\mu_3\text{-}CH)(CO)_9$ to give $(\mu\text{-}H)Fe_3(\mu_3\text{-}HCH)(CO)_9^-$.

vation of only a single hydride resonance, we must postulate that the hydrides are averaged by some dynamic process; however, there is no evidence for line broadening in the NMR spectrum even at −80°C. Fluxional migration of the agostic hydrogen to each of the three M—C edges would explain the observed spectrum. The exchange process must be intramolecular, because ^{13}C-hydride coupling is retained. No exchange occurs between the agostic hydrogen and the hydride ligands on the NMR timescale. Isotopic labelling has shown that exchange between the agostic hydrogen and the metal hydrides does not take place over a period of several hours at 25°C.

The protonated clusters undergo much faster reductive elimination than the neutral precursors. Shapley has found that dissolution of $H_3Os_3(CH)(CO)_9$ in sulphuric acid gives methane and $H_2Os_3(O_3SO)(CO)_9$.[54] Dissolution of $H_3Ru_3(CR)(CO)_9$, R = H, Ph, Et, $CHPhCH_2Ph$, in trifluoromethanesulphonic acid results in the formation of the corresponding alkane RH and a variety of Ru species including $HRu_3(CO)_{12}^+$, $HRu(CO)_5^+$ and what may be $H_2Ru_3(O_3SCF_3)(CO)_9^+$. The alkane product was isolated in the cases of R = $CHPhCH_2Ph$ and Ph. Although the alkyl derivatives are moderately stable ($t_{1/2} \sim 24$ h for $CHPhCH_2Ph$), dissolution of benzylidyne or methylidyne clusters causes immediate decomposition.

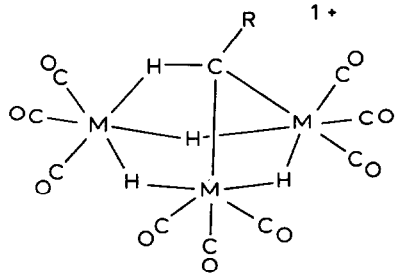

Fig. 13. Proposed structure for $(\mu\text{-}H)_3M_3(\mu_3\text{-}HCR)(CO)_9^+$ (M = Ru or Os; R = Et or $CHPhCH_2Ph$).

The pre-equilibrium between $H_3Ru_3(CX)(CO)_9$ and its agostic tautomer accounts nicely for the inverse isotope effect for the reductive elimination of CH_3X, since the vibrational modes of an agostic hydrogen should be considerably higher in energy than those of a bridging hydride (e.g. stretching frequencies of *ca* 2600 cm^{-1} for C—H—M vs 1350 cm^{-1} for M—H—M). If only the stretching modes are considered, the equilibrium isotope effect upon the equilibrium constant for the equilibrium shown in Fig. 11 can be calculated to be 0.54 (cf. 0.64 for reductive elimination from $H_3Ru_3(CPh)(CO)_9$).

The rate-determining step following the pre-equilibrium tautomerization to the agostic alkylidene intermediate, is cleavage of the C—H—Ru bond to form an unsaturated Ru centre. Addition of CO to the unsaturated cluster produces a saturated alkylidene of the formula $H_2M_3(\mu\text{-}CHX)(CO)_{10}$. Stable analogues of this alkylidene intermediate are $H_2Ru_3(CHCO_2Me)(CO)_9$ and $H_2Os_3(CH_2)(CO)_{10}$.[55] Methylidyne substituents which can act as Lewis bases, such as CO_2Me, $C(O)NR_2$ or SEt, greatly

accelerate the reductive elimination reaction. In these cases, the fact that the relative rates increase in the same order as the basicity of the substituent ($C(O)OMe < C(O)NR_2 < SEt$), and the fact that stable products can be isolated in which the substituents are coordinated to a metal centre, suggest that the acceleration is due to direct attack of the substituent upon a metal atom as the agostic bond is cleaved.

The next step in the reductive elimination of the alkane is reversible conversion of $H_2M_3(\mu\text{-}CHX)(CO)_{10}$ to $HM_3(\mu\text{-}HCHX)(CO)_{10}$, a tautomer containing an agostic bond. Indeed, Shapley has shown that in solution, $H_2Os_3(CH_2)(CO)_{10}$ is in equilibrium with $HOs_3(HCH_2)(CO)_{10}$, a slightly less stable tautomer ($K_{eq} = 0.28$).[52] These workers have established the same tautomeric equilibrium for $H_2Os_3(CHMe)(CO)_{10}/HOs_3(HCHMe)(CO)_{10}$ ($K_{eq} = 0.14$); in this system β-elimination from the ethyl group is thermodynamically favoured, but α-elimination is *ca* 100 times faster at 19°C.[56]

The next step in the proposed mechanism is cleavage of the agostic bond of $HM_3(HCHX)(CO)_{10}$, forming an unsaturated metal centre, followed by coordination of CO to give the hydridoalkyl $HM_3(CH_2X)(CO)_{10}$. Stable analogues of these intermediates are $HOs_3(CH_2CO_2R)(CO)_{10}$ (Fig. 14),[57] $HOs_3(RCHOMe)(CO)_{10}$,[58] $HOs_3(MeCHSPh)(CO)_{10}$,[59] $HOs_3(NCO)$(succinoyl)$(CO)_{10}$[60] and $HRu_3(CH_2SEt)(CO)_9$.

Finally, reductive elimination of the third C—H bond and coordination of CO would produce $M_3(CO)_{12}$ and CH_3X. If fact, both $HOs_3(HCH_2)(CO)_{10}$ and $HOs_3(CH_2CO_2Et)(CO)_{10}$ react with Lewis bases under very mild conditions (room temperature and below) in this fashion. In the latter case an intermediate of the probable formula $HOs_3(CH_2CO_2Et)(CO)_{10}(PMe_2Ph)$ was observed by NMR spectroscopy during the reaction with PMe_2Ph.[61]

An alternative path for "desorption" of the hydrocarbon from the cluster alkyl is β-elimination, producing an alkene and a metal hydride. In fact, decomposition of $H_3Ru_3(CCHPhCH_2Ph)(CO)_9$ under CO produces exclusively alkenes —CH_2=CPhCH_2Ph and *cis*- and *trans*-MeC(Ph)=CHPh,[62] while fumarate esters are the only products of the reaction between stabilized alkyls $HOs_3(C(CO_2R)CH_2CO_2R)(CO)_{10}$ and Lewis bases.[61] Thus, β-elimination, when possible, is the prefered path for decomposition of hydridoalkyl clusters.

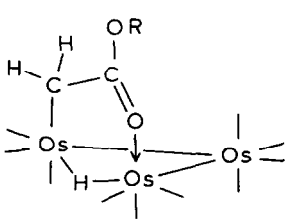

Fig. 14. Proposed structure of $HOs_3(CH_2CO_2Et)(CO)_{10}$.

At this point, isolatable analogues are available for all the probable intermediates in the "desorption" of an alkane, adsorbed as alkylidyne, from a small molecular cluster. Determinations of the energetics and mechanism are only beginning. These studies should continue to provide analogies applicable to metal surface chemistry.

CONCLUSION

Since the structures and compositions of cluster compounds vary so widely, it is not surprising that generalizations concerning chemical reactivity are difficult to come by. However, cluster chemistry is unique from the chemistry of monometallic complexes in that: (1) Bonding of hydrocarbyl ligands to several metal centres is the rule in cluster chemistry. (2) One may expect facile hydrogen migration from metal to carbon as well as from metal to metal, and the various tautomers may differ only slightly in energy. (3) The wide variety of bonding modes available for hydrocarbyls on clusters makes the number of potential reaction pathways much greater than for monometallic complexes. (4) Metal clusters have already provided useful models for the bonding of hydrocarbyl ligands to metal surfaces and will continue to provide useful models for reaction mechanisms.

REFERENCES

1. (a) M. H. Chisholm, K. Folting, D. M. Hoffman and J. C. Huffman, *J. Am. Chem. Soc.* 1984, **106**, 6794; (b) R. R. Schrock, M. L. Listemann and L. G. Sturgeoff, *J. Am. Chem. Soc.* 1982, **104**, 4291; (c) J. H. Wengrovius, J. Sancho and R. R. Schrock, *J. Am. Chem. Soc.* 1981, **103**, 3932; (d) G. J. Leigh, M. T. Rahman and D. R. M. Walton, *J. Chem. Soc., Chem. Commun.* 1982, 541.
2. (a) L. L. Kesmodel, L. H. Dubois and G. A. Somorjai, *J. Chem. Phys.* 1979, **70**, 2180; (b) T. P. Beebe, Jr, M. R. Albert and J. T. Yates, Jr, *J. Catal.* 1985, **96**, 1; (c) M. M. Hills, J. E. Parmetcr and W. H. Weinberg, *J. Am. Chem. Soc.* 1987, **109**, 4224; (d) Ts. S. Marinova and K. L. Kostov, *Surf. Sci.* 1987, **181**, 573; (e) M. M. Hills, J. E. Parmeter and W. H. Weinberg, *J. Am. Chem. Soc.* 1986, **108**, 7215; (f) K. M. Ogle and J. M. White, *Surf. Sci.* 1986, **165**, 234; (g) B. E. Koel, B. E. Bent and G. A. Somorjai,

Surf. Sci. 1984, **146**, 211; (h) J. E. Parmeter, M. M. Hills and W. H. Weinberg, *J. Am. Chem. Soc.* 1987, **109**, 72.
3. (a) G. Palyi, F. Piacenti and L. Marko, *Inorg. Chim. Acta Rev.* 1970, **4**, 109; (b) D. Seyferth, *Adv. Organomet. Chem.* 1976, **24**, 97; (c) B. R. Penfold and B. H. Robinson, *Acc. Chem. Res.* 1973, **6**, 73.
4. K. S. Wong, K. J. Haller, T. K. Dutta, D. M. Chipman and T. P. Fehlner, *Inorg. Chem.* 1982, **21**, 3197.
5. N. J. Zhu, C. Lecomte, P. C. Coppens and J. B. Keister, *Acta Cryst.* 1982, **B38**, 1286.
6. G. M. Sheldrick and J. P. Yesinowski, *J. Chem. Soc., Dalton Trans.* 1975, 873.
7. M. R. Churchill, T. P. Duggan, J. B. Keister and J. W. Ziller, *Acta Cryst.* 1987, **C43**, 203.
8. M. Castiglioni, G. Gervasio and E. Sappa, *Inorg. Chim. Acta* 1982, **49**, 217.
9. S. G. Shore, D.-Y. Jan, W.-L. Hsu, L.-Y. Hsu, S. Kennedy, J. C. Huffman, T.-C. L. Wang and A. G. Marshall, *J. Chem. Soc., Chem. Commun.* 1984, 392.
10. J. Krause, D.-Y. Jan and S. G. Shore, *J. Am. Chem. Soc.* 1987, **109**, 4416.
11. D. F. Shriver, D. Lehman and D. Strope, *J. Am. Chem. Soc.* 1975, **97**, 1594.
12. F. H. Herbstein, *Acta Cryst.* 1981, **B37**, 339.
13. E. Iiskola, T. A. Pakkanen, T. T. Pakkanen and T. Venalainen, *Acta Chem. Scand.* 1983, **A37**, 125.
14. M. R. Churchill, L. R. Beanan, H. J. Wasserman, C. Bueno, Z. Abdul Rahman and J. B. Keister, *Organometallics* 1983, **2**, 1179.
15. B. F. G. Johnson, J. Lewis, A. G. Orpen, P. R. Raithby and G. Suss, *J. Organomet. Chem.* 1979, **173**, 187.
16. M. R. Churchill, B. G. DeBoer and F. J. Rotella, *Inorg. Chem.* 1976, **15**, 1843.
17. B. F. G. Johnson, J. Lewis, P. R. Raithby and G. Suss, *J. Chem. Soc., Dalton Trans.* 1979, 1356.
18. M. Green, A. G. Orpen and C. J. Schaverein, *J. Chem. Soc., Chem. Commun.* 1984, 37.
19. W.-Y. Yeh, J. R. Shapley, Y. J. Li and M. R. Churchill, *Organometallics* 1985, **4**, 767.
20. J. R. Shapley, M. E. Cree-Uchiyama, G. M. St. George, M. R. Churchill and C. Bueno, *J. Am. Chem. Soc.* 1983, **105**, 140.
21. R. D. Adams and N. M. Golembeski, *Inorg. Chem.* 1979, **18**, 2255.
22. A. A. Kordize, O. A. Kizas, N. E. Kolobova, A. I. Yanovsky and Yu. T. Struchkov, *J. Organomet. Chem.* 1986, **302**, 413.
23. J. B. Keister, M. W. Payne and M. J. Muscatella, *Organometallics* 1983, **2**, 219.
24. P. D. Gavens and M. J. Mays, *J. Organomet. Chem.* 1978, **162**, 389.
25. D. E. Sherwood, Jr and M. B. Hall, *Organometallics* 1982, **1**, 1519.
26. I. A. Oxton, *Spectrochimica Acta* 1982, **38A**, 181.
27. J. Evans and G. S. McNulty, *J. Chem. Soc., Dalton Trans.* 1984, 79.
28. D. M. Dalton, D. J. Barnett, T. P. Duggan, J. B. Keister, P. T. Malik, S. P. Modi, M. R. Shaffer and S. A. Smesko, *Organometallics* 1985, **4**, 1854.
29. L. R. Beanan and J. B. Keister, *Organometallics* 1985, **4**, 1713.
30. D. K. Bower and J. B. Keister, *J. Organomet. Chem.* 1986, **312**, C33.
31. M. R. Churchill, J. W. Ziller, D. M. Dalton and J. B. Keister, *Organometallics* 1987, **6**, 806.
32. M. R. Churchill, T. S. Janik, T. P. Duggan and J. B. Keister, *Organometallics* 1987, **6**, 799.
33. J. A. S. Howell and P. Mathur, *J. Chem. Soc., Dalton Trans.* 1982, 43.
34. T. K. Dutta, J. C. Vites, G. B. Jacobsen and T. P. Fehlner, *Organometallics* 1987, **6**, 842.
35. (a) L. J. Farrugia, *J. Organomet. Chem.* 1986, **310**, 67; (b) A. A. Aitchison and L. J. Farrugia, *Organometallics* 1986, **5**, 1103.
36. H. A. Hodali and D. F. Shriver, *Inorg. Chem.* 1979, **18**, 1236.
37. (a) J. Ros, G. Commenges, R. Mathieu, X. Solans and M. Font-Altaba, *J. Chem. Soc., Dalton Trans.* 1985, 1087; (b) M. H. Chisholm, J. A. Heppert and J. C. Huffman, *J. Am. Chem. Soc.* 1984, **106**, 1151.
38. J. S. Holmgren and J. R. Shapley, *Organometallics* 1984, **3**, 1322.
39. A. J. Canty, B. F. G. Johnson, J. Lewis and J. R. Norton, *J. Chem. Soc., Chem. Commun.* 1972, 1331.
40. A. J. Deeming and M. Underhill, *J. Chem. Soc., Chem. Commun.* 1973, 277.
41. K. S. Wong and T. P. Fehlner, *J. Am. Chem. Soc.* 1981, **103**, 906.
42. J. B. Keister and T. L. Horling, *Inorg. Chem.* 1980, **19**, 2304.
43. J. R. Shapley, D. S. Strickland, G. M. St. George, M. R. Churchill and C. Bueno, *Organometallics* 1983, **2**, 185.
44. (a) M. R. Churchill, J. W. Ziller, J. H. Freudenberger and R. R. Schrock, *Organometallics* 1984, **3**, 1554; (b) J. H. Freudenberger, R. R. Schrock, M. R. Churchill, A. L. Rheingold and J. W. Ziller, *Organometallics* 1984, **3**, 1563.
45. (a) O. Gambino, M. Valle, S. Aime and G. A. Vaglio, *Inorg. Chim. Acta* 1974, **8**, 71; (b) M. Castiglioni, L. Milone, D. Osella, G. A. Vaglio and M. Valle, *Inorg. Chem.* 1976, **15**, 394; (c) M. I. Bruce, M. A. Cairns and M. Green, *J. Chem. Soc., Dalton Trans.* 1972, 1293; (d) S. Aime, G. Jannon, D. Osella, A. J. Arce and A. J. Deeming, *J. Chem. Soc., Dalton Trans.* 1984, 1987.
46. B. E. Hanson, B. F. G. Johnson, J. Lewis and P. R. Raithby, *J. Chem. Soc., Dalton Trans.* 1980, 1852.
47. (a) C. K. Rofer-DePoorter, *Chem. Rev.* 1981, **81**, 447; (b) E. L. Muetterties and J. Stein, *Chem. Rev.* 1979, **79**, 479.
48. M. R. Churchill, J. C. Fettinger, J. B. Keister, R. F. See and J. W. Ziller, *Organometallics* 1985, **4**, 2112.
49. D. K. Bower, J. W. Ziller, M. R. Churchill and J. B. Keister, unpublished results.
50. For leading references see: (a) R. A. Periana and R. G. Bergman, *J. Am. Chem. Soc.* 1986, **108**, 7332; (b) W. D. Jones and F. J. Feher, *J. Am. Chem. Soc.* 1986, **108**, 4814; (c) W. D. Jones and F. J. Feher, *J. Am. Chem. Soc.* 1985, **107**, 620; (d) R. H. Crabtree,

E. M. Holt, M. Lavin and S. M. Morehouse, *Inorg. Chem.* 1985, **24**, 1986; (e) A. H. Janowicz and R. G. Bergman, *J. Am. Chem. Soc.* 1983, **105**, 3929.
51. T. P. Duggan, D. J. Barnett, M. J. Muscatella and J. B. Keister, *J. Am. Chem. Soc.* 1986, **108**, 6076.
52. R. B. Calvert and J. R. Shapley, *J. Am. Chem. Soc.* 1977, **99**, 5225; 1978, **100**, 6544.
53. M. Brookhart and M. L. H. Green, *J. Organomet. Chem.* 1983, **250**, 395.
54. R. L. Keiter, D. S. Strickland, S. R. Wilson and J. R. Shapley, *J. Am. Chem. Soc.* 1986, **108**, 3846.
55. R. B. Calvert, J. R. Shapley, A. J. Schultz, J. M. Williams, S. L. Suib and G. D. Stucky, *J. Am. Chem. Soc.* 1978, **100**, 6240.
56. M. Cree-Uchiyama, J. R. Shapley and G. M. St. George, *J. Am. Chem. Soc.* 1986, **108**, 1316.
57. J. B. Keister and J. R. Shapley, *J. Am. Chem. Soc.* 1976, **98**, 1056.
58. E. Boyar, A. J. Deeming, A. J. Arce and Y. De Sanctis, *J. Organomet. Chem.* 1984, **276**, C45.
59. E. Boyar, A. J. Deeming, K. Henrick, M. McPartlin and A. Scott, *J. Chem. Soc., Dalton Trans.* 1986, 1431.
60. J. L. Zuffa and W. L. Gladfelter, *J. Am. Chem. Soc.* 1986, **108**, 4669.
61. J. B. Keister, Ph.D. thesis, University of Illinois (1978).
62. T. P. Duggan, Ph.D. thesis, University at Buffalo (1987).

Polyhedron Vol. 7, No. 10/11, pp. 859–870, 1988
Printed in Great Britain

0277–5387/88 $3.00+.00
© 1988 Pergamon Press plc

THE ADDITION OF SMALL MOLECULES TO $(\eta\text{-}C_5H_5)_2Rh_2(CO)(CF_3C_2CF_3)$—IX.* C—H BOND ACTIVATION IN THE REACTIONS WITH DIENES, POLYENES AND ARENES; THE CRYSTAL AND MOLECULAR STRUCTURE OF $[(\eta\text{-}C_5H_5)_2Rh_2\{C(CF_3)=C(CF_3)H\}]_2(C_6H_4)$

RON S. DICKSON† and SUSAN M. JENKINS

Department of Chemistry, Monash University, Clayton, Victoria, 3168, Australia

and

BRIAN W. SKELTON and ALLAN H. WHITE

Department of Physical and Inorganic Chemistry, The University of Western Australia, Nedlands, Western Australia, 6009, Australia

(*Accepted* 5 *November* 1987)

Abstract—The sunlight assisted reactions of $(\eta\text{-}C_5H_5)_2Rh_2(CO)(CF_3C_2CF_3)$ with acyclic dienes (1,3-butadiene, allene and 1-methyl-1,2-butadiene) and cyclic polyenes (1,5-cyclooctadiene, norbornadiene, 1,4- and 1,3-cyclohexadiene, cyclopentadiene, methylcyclopentadiene, cycloheptatriene and cyclooctatetraene) result in facile C—H bond activation and the formation of $(\eta\text{-}C_5H_5)_2Rh_2\{C(CF_3)C(CF_3)H\}$(polyene-H). Often, two or more structural isomers of the product are identified. In some instances, a subsequent reaction with more $(\eta\text{-}C_5H_5)_2Rh_2(CO)(CF_3C_2CF_3)$ gives $[(\eta\text{-}C_5H_5)_2Rh_2\{C(CF_3)C(CF_3)H\}]_2$(polyene-2H). With arenes (benzene, chlorobenzene, toluene and dichlorobenzenes), the activation of two C—H bonds occurs simultaneously to give $[(\eta\text{-}C_5H_5)_2Rh_2\{C(CF_3)C(CF_3)H\}]_2$(arene-2H). The structure of $[(\eta\text{-}C_5H_5)_2Rh_2\{C(CF_3)C(CF_3)H\}]_2(C_6H_4)$, which is derived from the reaction with benzene, was confirmed by single crystal X-ray diffraction studies. It is monoclinic, space group $P2_1/c$ with $a = 16.958(6)$, $b = 9.119(5)$, $c = 24.74(1)$ Å and $\beta = 118.57(4)°$. The structure was solved by direct methods and refined by least-squares to the R value of 0.037 for 3870 observed reflections. The σ-bonded rhodium atoms adopt *meta* positions and are coplanar with the ring carbons. One π-bonded rhodium is above and the other below the plane of the ring. The π-electron density in the ring is essentially localized.

In a previous paper,[2] a number of reactions of the type shown in eq. (1) were described. The reactions occur under mild conditions

$$2(\eta\text{-}C_5H_5)_2Rh_2(CO)(CF_3C_2CF_3) + \text{alkene} \xrightarrow{\text{sunlight}} (\eta\text{-}C_5H_5)_2Rh_2\{C(CF_3)C(CF_3)H\}(\text{alkene-H}) + (\eta\text{-}C_5H_5)_2Rh_2(CO)_2(CF_3C_2CF_3) \quad (1)$$

with a variety of alkenes including ethylene, terminal, internal and cyclic alkenes. We now report an extension of this study to reactions involving acyclic and cyclic dienes, cyclic polyenes and arenes. Our interest in these systems was prompted by three considerations—would these less reactive substrates be activated under similarly mild conditions; would it be possible to activate more than one C—H bond in particular substrates, and what factors would influence the stereo- and regioselectivity of these reactions? Some answers to these questions are provided.

* For Part VIII, see ref. 1.

† Author to whom correspondence should be addressed.

RESULTS AND DISCUSSION

Acyclic dienes

Butadiene reacts with $(C_5H_5)_2Rh_2(CO)(CF_3C_2CF_3)$ to yield $(C_5H_5)_2Rh_2(CO)_2(CF_3C_2CF_3)$ plus the products (**1a**) and (**1b**). These two isomers are readily identified on the basis of ^1H NMR data (see Experimental, Table 3), with the presence or absence of a low field μ-CH resonance near $\delta 9$ being diagnostic.[2] The isomers result from terminal or internal C—H bond cleavage, respectively, and the product ratio (**1a**):(**1b**) of 3:1 indicates a preference for terminal C—H bond cleavage. This ratio seems not to depend on the reaction conditions, and is unchanged for reactions carried out over several days in the absence of light and those irradiated with sunlight for 2 h. We are aware of just two other examples of C—H bond activation in acyclic dienes by binuclear metal complexes;[3,4] in each, only terminal C—H bond cleavage occurs. Related reactions between 1,3-dienes and polynuclear metal carbonyls apparently involve C—H bond activation but lead to complex product mixtures.[5,6]

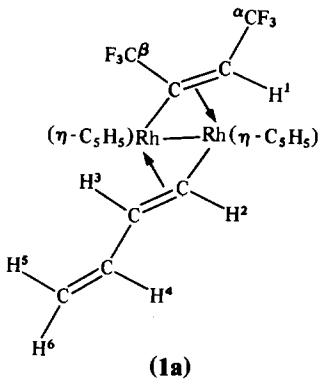

(**1a**)

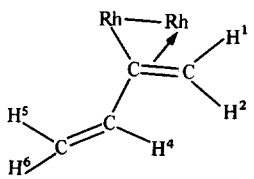

(**1b**)*

* In this and all subsequent structural diagrams,

Rh—Rh represents

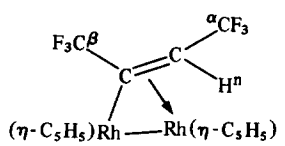

The products (**1a**) and (**1b**) undergo further reaction with $(\eta\text{-}C_5H_5)_2Rh_2(CO)(CF_3C_2CF_3)$ when the solutions are irradiated with sunlight. Each reaction involves cleavage of a second C—H bond to give the products (**2a**) and (**2b**) [obtained from (**1a**)] or (**2b**) [from (**1b**)]. Although these tetranuclear products have low solubility in most organic solvents, satisfactory ^1H and ^{19}F NMR spectra were obtained, and these spectra provided the basis for the structural assignments. The presence of only two C_5H_5 or CF_3 resonances in the spectra of (**2a**) indicate that it is a symmetrical molecule. In the spectra of (**2b**) however, a separate resonance for each individual group is observed. Only a minor amount of (**2b**) was isolated from the reaction of (**1a**), indicating that activation of the terminal C—H bond is again strongly favoured. This is further supported by the absence of isomer (**2c**), which would be formed if two internal C—H bonds were activated. We are not aware of any previous examples of the sequential activation of two C—H bonds in an acyclic diene.

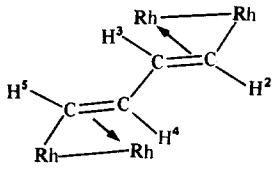

(**2a**)

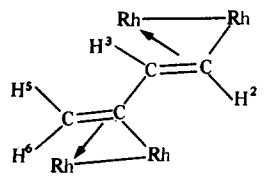

(**2b**)

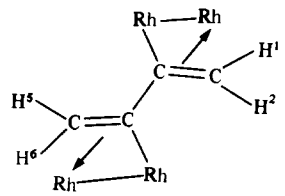

(**2c**)

Several complexes are known with intact allenes coordinated as η^2,η^2-bridging ligands to dinuclear metal centres.[7-11] In other examples, η^1,η^3-allyl complexes are obtained from dinuclear complexes and allenes.[12] No examples are known to us in which a C—H bond of an allene is cleaved to give an allenyl–metal complex. We have generated allene by decarboxylation of diketene;[11] the decarboxylation is induced under mild conditions by $(\eta\text{-}C_5H_5)_2Rh_2(CO)(CF_3C_2CF_3)$ which concomitantly cleaves a C—H bond to give $(\eta\text{-}C_5H_5)_2Rh_2\{C(CF_3)C(CF_3)H\}(CH{=}C{=}CH_2)$. NMR results are consistent with the structure (**3**, $R^3 = R^4 = H$). In the ^1H NMR spectrum, two quartets ($J = 3$ Hz) are observed near $\delta 5$ in addition to the characteristic low field signal for μ-CH^2 and the high field quartet of triplets for $CH(CF_3)$. Spin decoupling experiments establish that the quartets arise because $H^{3\text{ or }4}$ couples equally with $H^{4\text{ or }3}$, H^2 and Rh. A closely related complex (**3**, $R^3 = R^4 =$ Me) is formed from $(\eta\text{-}C_5H_5)_2Rh_2(CO)(CF_3C_2CF_3)$ and 3-methyl-1,2-butadiene. In the ^1H NMR spectrum of this complex, the methyl resonances are detected as doublets, the magnitude of the ^5J couplings of $Me^{3,4}$ to H^2 being 1.2 and 1.8 Hz.

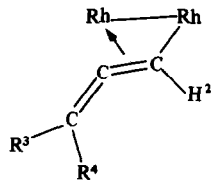

(3)

The allene complex (3, $R^3 = R^4 = H$) incorporates terminal C—H bonds on the coordinated allenyl group, and it was of interest to determine if these could be activated by reaction with a further amount of $(\eta\text{-}C_5H_5)_2Rh_2(CO)(CF_3C_2CF_3)$. A second C—H bond cleavage did indeed occur, producing one major product (4). The ^1H and ^{19}F NMR data indicate that this is a symmetrical molecule, but it is not possible to distinguish between the alternative structures (**4a**) and (**4b**). On the basis of previous work with 1-alkenes, (**4b**) would be

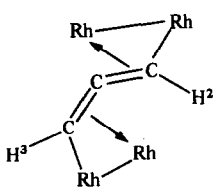

(4a)

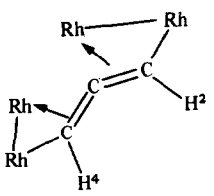

(4b)

favoured on steric grounds. A minor product was also detected and spectroscopic results indicate that it has the same formula as (**4b**) but a less symmetrical structure. During TLC, the minor product isomerizes to the major product. Terminal C—H bonds are not available in the complex (3, $R^3 = R^4 = Me$) and so a related reaction with this complex was not possible.

Cyclic polyenes

Previous experience has shown that harsh conditions are generally needed to activate C—H bonds in cyclic polyenes,* a major exception being our facile activation of cyclic monoenes with $(\eta\text{-}C_5H_5)_2Rh_2(CO)(CF_3C_2CF_3)$ in the presence of sunlight.[2] Given the interesting results with acyclic dienes described above, we decided to extend our study to include some cyclic polyenes.

The initial reactions between the dirhodium complex and the symmetrical dienes, 1,5-cyclooctadiene, norbornadiene and 1,4-cyclohexadiene proceed as expected. For example, the reaction with 1,4-cyclohexadiene gives (**5**). However, some differences in behaviour emerge when these alkenyl–dirhodium complexes are treated with more $(\eta\text{-}C_5H_5)_2Rh_2(CO)(CF_3C_2CF_3)$. With the 1,4-cyclohexadienyl derivative (**5**), further reaction gives a product which we suggest is (**6a**) rather than

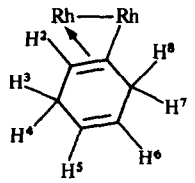

(5)

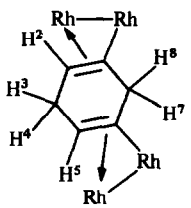

(6a)

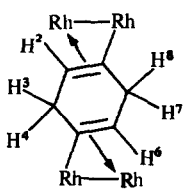

(6b)

(**6b**). The basis for this assignment is that different pairs of methylene proton resonances are detected in the NMR spectrum, whereas all methylene protons should be equivalent in (**6b**) provided the ring remains planar. A corresponding reaction occurs with the norbornadienyl–dirhodium complex. Again, two products are possible, but only one is obtained. NMR results reveal a single resonance for the two hydrogens on the bridge-head carbons and this is more consistent with structure (**7b**) rather than (**7a**). In contrast to these two systems, further

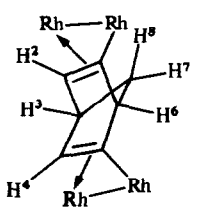

(7a)

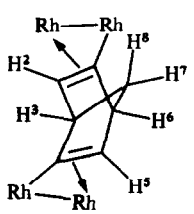

(7b)

activation of the C—H bonds could not be achieved with the cyclooctadienyl–dirhodium complex. This lack of reactivity can be rationalized if it is assumed that the cyclooctadienyl ligand has a tub configuration [see (**8**)] in the complex. The relatively

* Examples can be found in refs 13 and 14.

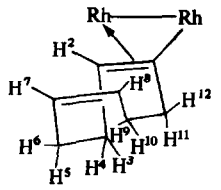

(8)

close proximity of all the alkenyl hydrogens would then inhibit the approach of a second Rh_2-unit.

The reaction between $(\eta\text{-}C_5H_5)_2Rh_2(CO)(CF_3C_2CF_3)$ and 1,3-cyclohexadiene gives two products (**9a**) and (**9b**). The individual isomers are readily identified from ^1H NMR results. The product ratio (**9a**):(**9b**) of 3:2 indicates a preference for attack at the 1-position of the cyclic diene; this preference is less pronounced but consistent with that shown with 1,3-butadiene where the ratio of (**1a**):(**1b**) was 3:1. Other analogies with the acyclic diene can be drawn as (**9a**) reacts further with $(C_5H_5)_2Rh_2(CO)(CF_3C_2CF_3)$ to form both (**10a**) and (**10b**), whereas (**9b**) produces (**10b**) exclusively.

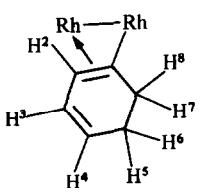

(9a)

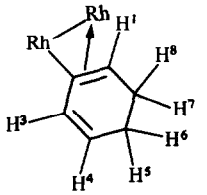

(9b)

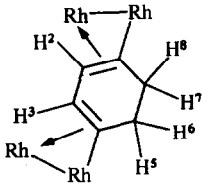

(10a)

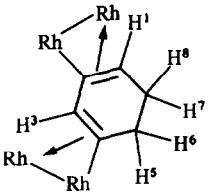

(10b)

To determine if the same behaviour applies to other asymmetric cyclic dienes, corresponding reactions were undertaken with cyclopentadiene. The reaction gave approximately equal amounts of (**11a**) and (**11b**), and each isomer reacted further with a second equivalent of $(\eta\text{-}C_5H_5)_2Rh_2(CO)$

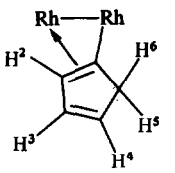

(11a)

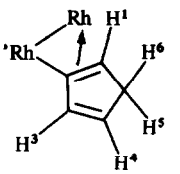

(11b)

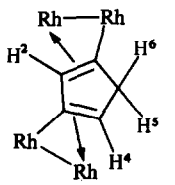

(12a)

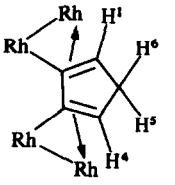

(12b)

$(CF_3C_2CF_3)$ to give tetranuclear products. The complex (**11a**) gave only (**12a**), but (**11b**) yielded both (**12a**) and (**12b**). These results contrast with those of the 1,3-cyclohexadienyl system, and hence a common pattern of behaviour is not evident.

Four products were formed in the analogous reaction with methylcyclopentadiene. NMR data identifies these as the isomers (**13a**)–(**13d**); in the crude product, the ratio of (**13a**+**13b**):(**13c**+**13d**) is approximately 4:3, but there is significant isomerization of the minor isomers to the major ones during chromatography. There was no evidence for the other possible isomers in which the methyl group is located on the saturated ring carbon. The ^1H NMR spectrum of a freshly prepared sample of methylcyclopentadiene revealed the presence of two isomers 1- and 2-methyl-1,3-cyclopentadiene (mol ratio 4:3),* thereby providing a rationale for the above results. There is no formation of tetranuclear complexes when the isomers (**13a**)–(**13d**) are treated

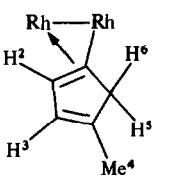

(13a)

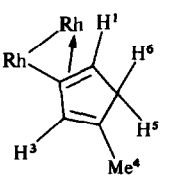

(13b)

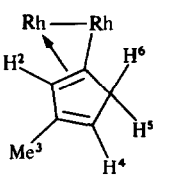

(13c)

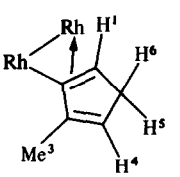

(13d)

* In contrast, W. D. Jones and J. A. Maguire report (*Organometallics* 1987, **6**, 1301) that free methylcyclopentadiene is present as a 47:47:6 mixture of the 1-, 2- and 5-methyl isomers.

with more $(\eta\text{-}C_5H_5)_2Rh_2(CO)(CF_3C_2CF_3)$. This is consistent with other results which establish that there is a steric barrier to the methyl group occupying the position shown in (**14**). It is interesting that the tetranuclear complex (**15**) has been isolated

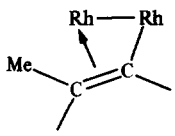

(**14**)

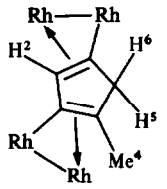

(**15**)

in a separate study.[15] Thus, the sunlight assisted reaction between $(\eta\text{-}C_5H_5)_2Rh_2(CO)(CF_3C_2CF_3)$ and $(\eta^5\text{-}MeC_5H_4)Mn(CO)_2\cdot THF$ gives several products, one of which is $[(\eta\text{-}C_5H_5)_2Rh_2\{C(CF_3)C(CF_3)H\}]_2(MeC_5H_2)$. The structure of complex (**15**) has been confirmed from single crystal X-ray diffraction data.

To establish the full scope of these reactions, C—H bond activation in two other cyclic polyenes was studied. With cyclooctatetraene, the expected product (**16**) was obtained, and in the corresponding reaction with 1,3,5-cycloheptatriene the three isomeric products (**17a**)–(**17c**) were identified. Each of these cycloheptatrienyl products reacts further with $(C_5H_5)_2Rh_2(CO)(CF_3C_2CF_3)$, but mixtures of isomers are obtained and they are difficult to separate or characterize spectroscopically. Surprisingly, the cyclooctatetraenyl complex (**16**) resists further reaction with $(\eta\text{-}C_5H_5)_2Rh_2(CO)(CF_3C_2CF_3)$, and so its behaviour resembles that of the cyclooctadiene derivative (**8**). It is difficult to rationalize this lack of further C—H bond activation in (**16**). Even if the coordinated cyclooctatetraenyl ligand adopts a tub configuration as suggested for (**8**), there are still four exposed alkenyl C—H sites. We have no explanation for the peculiar behaviour of the C_8-systems.

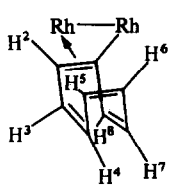

(**16**)

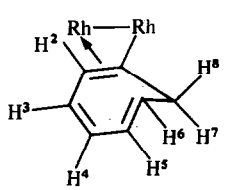

(**17a**)

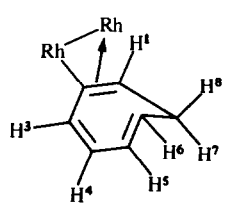

(**17b**)

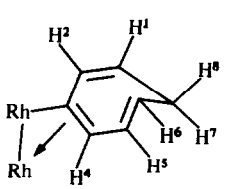

(**17c**)

Overall, this set of reactions with cyclic polyenes establishes that activation of one C—H bond can be achieved under mild conditions with all systems, regardless of ring size, and the extent and location of the polyunsaturation. In most conjugated systems, there is generally some preference for C—H bond cleavage at the 1-position of 1,3-dienes. Sequential activation of a second C—H bond occurs in many systems and often there is a preferred site of attack. However, the factors that influence this preference are difficult to discern. It is interesting to note that tetranuclear products are not formed in the initial reactions between $(C_5H_5)_2Rh_2(CO)(CF_3C_2CF_3)$ and the cyclic polyenes, where the free ligand is in excess. It appears, therefore, that the activation of a second C—H bond is more difficult to achieve than the first.

There are few relevant examples with which to compare these results. Some polynuclear complexes of the type $[Os_4(CO)_{11}(nbd\text{-}H)H_3]$, and $[Ru_3(CO)(cod\text{-}H)H]$ have been investigated,[13,16,17] and there are more recent studies[18,19] of photochemical reactions between $Re_2(CO)_{10}$ and a limited range of cyclic polyenes. In the latter, there seems to be preference for attack at the 2-position of cyclic 1,3-dienes.

Arenes

A single product is isolated from the sunlight assisted reaction between benzene and $(\eta\text{-}C_5H_5)_2Rh_2(CO)(CF_3C_2CF_3)$. Unexpectedly, this is the tetranuclear product $[(\eta\text{-}C_5H_5)_2Rh_2\{C(CF_3)C(CF_3)H\}]_2(benzene\text{-}2H)$. No evidence is obtained for the prior formation of the binuclear complex $(\eta\text{-}C_5H_5)_2Rh_2\{C(CF_3)C(CF_3)H\}(benzene\text{-}H)$, when the reaction is monitored over the early stages. The NMR spectra of the tetranuclear complex are consistent with structure (**18**) in which there is *meta*-coordination of the σ-bonded rhodium atoms. To determine if similar behaviour is observed with substituted arenes, reactions were carried out with chlorobenzene and toluene. Two tetranuclear compounds were obtained with chlorobenzene, with (**19a**, X = Cl) being the major and (**19b**, X = Cl)

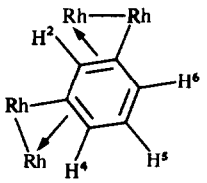

(18)

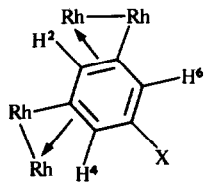

(19a)

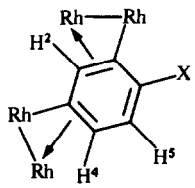

(19b)

the minor product. Toluene gave only a single product of structure (**19a**, X = Me). The formation of only one product in this latter reaction indicates that the aromatic protons adjacent to a methyl group may be protected in some way from activation. The observation that *p*-xylene failed to react at all with $(\eta\text{-}C_5H_5)_2Rh_2(CO)(CF_3C_2CF_3)$ provided some support for this idea. It seemed likely, then, that formation of a binuclear product (**20**) might be favoured in the reaction with *o*-xylene. The fact that no product was obtained from this reaction lends support to the premise that double activation is a requirement with arenes. Similar behaviour was observed with dichlorobenzenes. Thus, *m*- and *p*-dichlorobenzenes failed to react, whereas *o*-dichlorobenzene gave mainly (**21a**). In the latter reaction, (**21b**) was isolated as a minor product, and a trace amount of a third product, spectroscopically characterized as (**22**) was obtained.

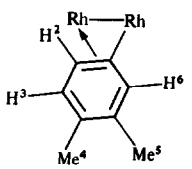

(20)

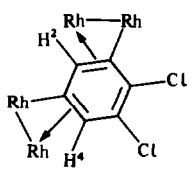

(21a)

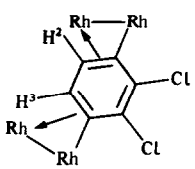

(21b)

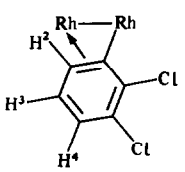

(22)

Overall, a common pattern of behaviour has emerged in the reactions of this collection of arenes. Thus, simultaneous activation of two C—H bonds occurs, and when this is prohibited by substituent effects, there is no activation at all. Triple activation was never observed, and is presumably not possible due to steric constraints. In seeking an explanation for the observed behaviour of arenes, we were interested to establish what effect the coordinated rhodium atoms had on the aromaticity of the arenes. Consequently, we decided to determine the crystal and molecular structure of one of these tetranuclear complexes; the benzene system (**18**) was chosen.

A diagram of the molecule is shown in Fig. 1 and some of the more important bond parameters are listed in Table 1. As predicted from spectroscopic results, two rhodium atoms, Rh(2) and Rh(3) are σ-bonded to the ring carbons and they occupy *meta* positions; these metal atoms are approximately coplanar with the ring carbons. The remaining rhodium atoms, Rh(1) and Rh(4), are π-attached to the ring bonds C(1)—C(2) and C(5)—C(6), respectively; they are situated above and below the ring plane in the same manner as previously observed[20] for the $\eta^2,\eta^{2'}$-bonded arene complex $[(\eta\text{-}C_5Me_5)Re(CO)_2]_2(\mu\text{-}C_6H_6)$. These placements are consistent with the π-bonding requirements of the metal atoms. The C—C distances within the arene ring indicate significant localization of the π-electron density. Thus, only C(3)—C(4) retains double bond character, with C(1)—C(6), C(2)—C(3) and C(4)—C(5) being significantly elongated. The distances for C(1)—C(2) and C(5)—C(6) are consistent with metal-coordinated alkene distances. The geometries for the two $Rh_2C(CF_3)$=$C(CF_3)H$ units are similar to those described previously[2] for the related complexes $(\eta\text{-}C_5H_5)_2Rh_2\{C(CF_3)C(CF_3)H\}(CHCF_2)$ and $(\eta\text{-}C_5H_5)_2Rh_2\{C(CF_3)C(CF_3)H\}(CHCHCN)$.

The most significant structural feature is the clear indication that the C_6-ring has lost its aromatic character. Perhaps the consequent loss of resonance energy leads, in some way, to the need for double activation of the aromatic systems.

There are some previous examples of the use of metal complexes to activate C—H bonds in arenes. These include some recent reports,[21-25] in which electron-deficient mononuclear metal complexes are used and activation of one C—H bond is achieved. In the related reaction of the lutetium complex $(\eta\text{-}C_5Me_5)_2LuH$ with benzene, sequential double activation was achieved,[26] but the two σ-bonded metal atoms were positioned in a *para* arrangement. Earlier work[14,27] with Os_3-clusters led to activation of adjacent C—H bonds and gave some μ_3-cyclohexa-3,5-diene-1,2-diylidene com-

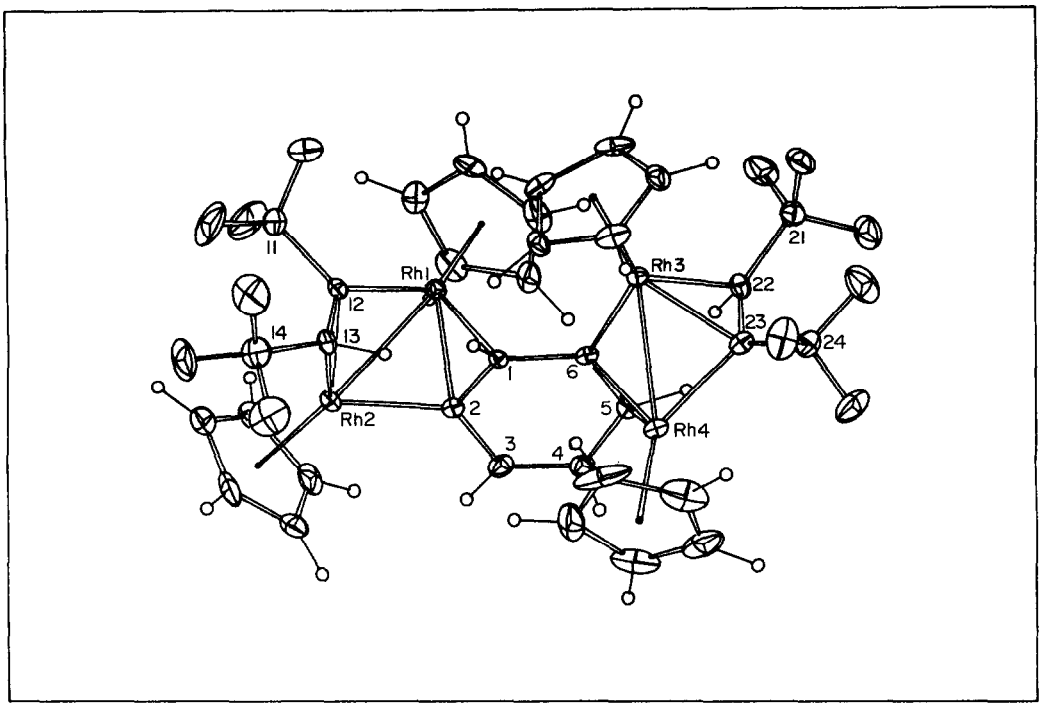

Fig. 1.

Table 1. Selected bond lengths and angles for $[(\eta\text{-}C_5H_5)_2Rh_2\{C(CF_3)C(CF_3)H\}]_2(C_6H_4)$

(a) Bond lengths (Å)		(b) Bond angles (°)	
Rh(1)—Rh(2)	2.627(1)	Rh(2)—Rh(1)—C(12)	51.3(2)
Rh(3)—Rh(4)	2.603(1)	Rh(1)—Rh(2)—C(2)	53.4(2)
Rh(1)—C(1)	2.200(7)	Rh(4)—Rh(3)—C(6)	53.2(2)
Rh(1)—C(2)	2.164(7)	Rh(3)—Rh(4)—C(23)	50.7(2)
Rh(1)—C(12)	2.028(8)		
Rh(2)—C(2)	2.059(10)	C(2)—C(1)—C(6)	124.1(6)
Rh(2)—C(12)	2.087(8)	Rh(2)—C(2)—C(1)	125.0(6)
Rh(2)—C(13)	2.127(8)	Rh(2)—C(2)—C(3)	119.6(7)
Rh(3)—C(6)	2.048(8)	C(1)—C(2)—C(3)	115.2(8)
Rh(3)—C(22)	2.106(8)	C(2)—C(3)—C(4)	121.0(8)
Rh(3)—C(23)	2.057(9)	C(3)—C(4)—C(5)	122.9(7)
Rh(4)—C(5)	2.240(7)	C(4)—C(5)—C(6)	119.9(8)
Rh(4)—C(6)	2.141(7)	C(1)—C(6)—C(5)	116.3(7)
Rh(4)—C(23)	2.056(9)	Rh(3)—C(6)—C(1)	116.6(5)
		Rh(3)—C(6)—C(5)	127.0(7)
C(1)—C(2)	1.41(1)		
C(1)—C(6)	1.47(1)	Rh(1)—C(12)—C(13)	123.2(6)
C(2)—C(3)	1.49(1)	Rh(4)—C(23)—C(22)	122.3(7)
C(3)—C(4)	1.35(1)		
C(4)—C(5)	1.43(1)		
C(5)—C(6)	1.42(1)		
C(12)—C(13)	1.415(9)		
C(22)—C(23)	1.421(9)		

Table 2. Yields and analytical data for products obtained from $(C_5H_5)_2Rh_2(CO)(CF_3C_2CF_3)$ and polyenes

Product[a] (% yield), m.p. (°C)		Analysis[b] C	H	F	MS (P^+)
1,3-Butadiene	**1a**(25), 151–152	39.4(39.2)	2.9(2.9)	20.5(20.6)	552
	1b(8), 130–131	39.5	2.9	20.5	552
	2a(27), > 250	36.9(36.8)	2.7(2.5)	21.4(21.4)	1050
	2b(9 or 34),[c] 155–157	36.6	2.5	21.7	1050
Allene	**3**($R^3 = R^4 = H$)(43), 130–131	37.9(38.0)	2.4(2.6)	21.3(21.2)	538
	4(45), > 250	36.2(35.9)	2.5(2.3)	22.2(22.0)	1036
3-Methyl-1-2-butadiene	**3**($R^3 = R^4 = Me$)(34), 143–145	40.5(40.3)	3.3(3.2)	20.1(20.1)	566
1,4-Cyclohexadiene	**5**(39), 160–161	41.9(41.6)	3.2(3.1)	19.8(19.7)	578
	6a(33), > 250	38.2(38.0)	2.6(2.6)	21.4(21.2)	1076
Norbornadiene	[d](41), 204–206	43.1(42.7)	3.2(3.1)	19.5(19.3)	590
	7b(33), > 250	38.5(38.6)	2.7(2.6)	20.9(20.9)	1088
1,5-Cyclooctadiene	**8**(37), 148–149	43.8(43.6)	3.8(3.7)	19.1(18.8)	606
1,3-Cyclohexadiene	**9a**(18), 179–180	41.8(41.6)	3.2(3.1)	19.8(19.7)	578
	9b(15), 165–166	41.9	3.2	20.0	578
	10a(14), > 250	38.2(38.0)	2.7(2.6)	21.2(21.2)	1076
	10b(20 or 36),[e] > 250	38.3	2.8	21.4	1076
Cyclopentadiene	**11a**(17), 162–163	40.6(40.5)	2.7(2.9)	20.1(20.2)	564
	11b(16), 162–164	40.8	2.8	20.3	564
	12a(36 or 26),[f] > 250	37.5(37.3)	2.4(2.4)	21.7(21.5)	1062
	12b(9), > 250	37.2	2.6	21.5	1062
Methylcyclopentadiene	**13a**(10), 200–202	41.8(41.6)	3.3(3.1)	20.0(19.7)	578
	13b(10), 150–151	41.8	3.2	19.9	578
	13c(8), 183-184	41.9	3.4	19.7	578
	13d(8), 153(dec.)	41.7	3.3	19.8	578
Cyclooctatetraene	**16**(34), 175–176	44.4(43.9)	3.1(3.0)	18.9(18.9)	602
1,3,5-Cycloheptatriene	**17a**(12), 162–163	42.9(42.7)	3.3(3.1)	19.5(19.3)	590
	17b(13), 175–177	42.8	3.3	19.3	590
	17c(12), 154–155	43.0	3.4	19.6	590
Benzene	**18**(42), 240(dec.)	38.4(38.0)	2.6(2.4)	21.4(21.2)	1074
Chlorobenzene	**19a**(X = Cl)(34), > 250	37.0(36.8) [Cl, 3.2(3.2)]	2.5(2.3)	20.8(20.6)	1108
	19b(X = Cl)(5), > 250	37.1 [Cl, 3.3]	2.5	20.7	1108
Toluene	**19a**(X = Me)(34), 248–249	38.2(38.6)	2.5(2.6)	20.8(20.9)	1088
o-Dichlorobenzene	**21a**(34), 190 (dec.)	35.9(35.7) [Cl, 6.3(6.2)]	2.3(2.1)	20.2(19.9)	1142
	21b(5), > 250	36.0 [Cl, 6.2]	2.2	20.1	1142
	22(1), 156–158	—	—	—	645

[a] In all reactions, the complexes $(C_5H_5)_2Rh_2(CO)_2(CF_3C_2CF_3)$[28] and $(C_5H_5)_3Rh_3(CO)(CF_3C_2CF_3)$[29] were formed in yields of approximately 45–50% and ⩽ 3%, respectively.

[b] Calculated values in parentheses.

[c] From **1a** and **1b**, respectively.

[d] Product analogous to **5**.

[e] From **9a** and **9b**, respectively.

[f] From **11a** and **11b**, respectively.

Table 3. NMR chemical shift (δ) and coupling constant (J) data for solutions of representative examples[a] of the products in $CDCl_3$

Product	^1H (300 MHz) δ,[b] multiplicity, rel. area, assignment[c]	J (Hz)	^{19}F (282.4 MHz) δ,[b] multiplicity,[c] assignment[c]	J (Hz) $F^\alpha F^\beta$,	HF^α,	RhF^α
(1a)	9.22, ddd, 1H, H^2 5.77, ddd, 1H, H^4 5.49, s, 5H, C_5H_5 5.20, s, 5H, C_5H_5 5.16, d, 1H, H^5 4.91, d, 1H, H^6 3.46, ddd, 1H, H^3 1.50, qt, 1H, H^1	$H^4H^5 = 17.7$ $H^4H^6 = 10.1$ $H^2H^3 = 11.1$ $H^3H^4 = 9.5$ $F^\beta H^1 = 9.6$ $RhH^2 = 3.1, 1.3$ $RhH^3 = 2.0$ $RhH^1 = 2.0, 2.0$	48.63, q, F^β 53.96, m, F^α	12.2,	9.6,	2.0
(1b)	7.02, dd, 1H, H^4 5.45, s, 5H, C_5H_5 5.28, s, 5H, C_5H_5 4.88, dd, 1H, H^5 4.51, dd, 1H, H^6 3.44, m, 1H, H^2 1.60, qt, 1H, H^3 1.29, t, 1H, H^1	$H^4H^5 = 16.8$ $H^4H^6 = 10.0$ $H^5H^6 = 1.7$ $F^\alpha H^3 = 9.7$ $RhH^3 = 2.0, 2.0$ $RhH^1 = 2.5, 2.5$	49.46, q, F^β 53.53, m, F^α	12.2,	9.7,	2.0
(2a)	9.33, dm, 2H, H^2+H^5 5.60, s, 10H, $2\times C_5H_5$ 5.26, s, 10H, $2\times C_5H_5$ 3.01, dm, 2H, H^3+H^4 1.22, qm, 2H, H^1+H^6	$H^2H^3 = H^4H^5 = 9.7$ $F^\alpha H^1 = F^{\alpha'}H^6 = 9.9$	47.42, q, $F^\beta+F^{\beta'}$ 52.51, m, $F^\alpha+F^{\alpha'}$	13.1,	9.9,	2.8
(2b)	9.27, ddd, 1H, H^2 5.47, s, 5H, C_5H_5 5.45, s, 5H, C_5H_5 5.25, s, 5H, C_5H_5 5.24, s, 5H, C_5H_5 3.98, dd, 1H, H^3 3.37, m, 1H, H^5 1.67, qm, 1H, $H^{1\text{or}4}$ 1.47, qm, 1H, $H^{1\text{or}4}$ 1.32, m, 1H, H^6	$H^2H^3 = 10.8$ $F^{\alpha'}H^4 = 9.7$ $F^\alpha H^1 = 9.7$ $RhH^3 = 1.0$ $RhH^2 = 2.1, 1.0$	47.85, q, $F^{\beta\text{or}\beta'}$ 49.55, q, $F^{\beta\text{or}\beta'}$ 53.42, m, $F^{\alpha\text{or}\alpha'}$ 54.16, m, $F^{\alpha\text{or}\alpha'}$	12.9, 12.6,	9.7, 9.7,	2.4 2.1
(3) $(R^3 = R^4 = H)$	8.86, m, 1H, H^2 5.52, s, 5H, C_5H_5 5.37, s, 5H, C_5H_5 5.30, q, 1H, $H^{3\text{or}4}$ 4.78, q, 1H, $H^{3\text{or}4}$ 1.79, qt, 1H, H^1	$F^\alpha H^1 = 10.0$ $RhH^1 = 1.9, 1.9$ $H^2H^3 \sim H^2H^4 \sim H^3H^4 \sim 3.0$	50.63, q, F^β 53.66, m, F^α	12.7,	10.0,	2.8
(5)	5.59, m, 1H, H^5 5.44, s, 5H, C_5H_5 5.42, m, 1H, H^6 5.23, s, 5H, C_5H_5 3.84, qm, 2H, H^7+H^8 2.92, dm, 1H, $H^{3\text{or}4}$ 2.70, m, 1H, H^2 2.45, dm, 1H, $H^{3\text{or}4}$	$H^3H^4 = 21.5$ $H^7H^8 = 20.7$ $F^\alpha H^1 = 9.8$ $RhH^1 = 2.1, 2.1$	48.73, q, F^β 53.16, m, F^α	13.3,	9.8,	2.7

Table 3 (*continued*)

Product	^{1}H (300 MHz) δ,[b] multiplicity, rel. area, assignment[c]	J (Hz)	^{19}F (282.4 MHz) δ,[b] multiplicity,[c] assignment[c]	J (Hz) $F^{\alpha}F^{\beta}$,	HF^{α},	RhF^{α}
(6a)[d]	5.68, d, 5H, C_5H_5 5.57, s, 5H, C_5H_5 5.41, s, 5H, C_5H_5 5.40, s, 5H, C_5H_5 5.37, m, 2H, H^7+H^8 4.28, ddm, 1H, $H^{3\text{or}4}$ 3.73, dm, 1H, $H^{4\text{or}3}$ 2.67, m, 1H, $H^{2\text{or}5}$ 2.52, m, 1H, $H^{2\text{or}5}$ 1.18, qt, 1H, $H^{1\text{or}4}$ 1.08, qt, 1H, $H^{1\text{or}4}$	$H^3H^4 = 19.3$ $RhC_5H_5 = 0.6$ $F^{\alpha}H^1 = 10.1$ $RhH^1 = 2.0, 2.0$ $F^{\alpha'}H^4 = 10.1$ $RhH^4 = 2.0, 2.0$ $H^{3\text{or}4}H^{2\text{or}5} = 5.5$	46.83, q, $F^{\beta\text{or}\beta'}$ 47.58, q, $F^{\beta\text{or}\beta'}$ 51.69, m, $F^{\alpha\text{or}\alpha'}$ 51.88, m, $F^{\alpha\text{or}\alpha'}$	13.2, 13.2,	10.1, 10.1,	2.6 2.6
(11a)	6.47, m, 1H, $H^{3\text{or}4}$ 6.28, m, 1H, $H^{3\text{or}4}$ 5.55, s, 5H, C_5H_5 5.00, s, 5H, C_5H_5 3.80, m, 1H, H^2 3.57, qm, 2H, H^5+H^6 1.39, qt, 1H, H^1	$H^5H^6 = 22.6$ $F^{\alpha}H^1 = 9.7$ $RhH^1 = 1.9, 1.9$	48.78, q, F^{β} 53.70, m, F^{α}	13.1,	9.7,	2.7
(11b)	6.99, m, 1H, H^3 6.03, m, 1H, H^4 5.57, s, 5H, C_5H_5 4.94, s, 5H, C_5H_5 3.41, br.s, 1H, H^1 2.99, dm, 1H, $H^{5\text{or}6}$ 2.47, dm, 1H, $H^{5\text{or}6}$ 1.41, qt, 1H, H^2	$H^5H^6 = 23.1$ $F^{\alpha}H^2 = 9.8$ $RhH^2 = 1.9, 1.9$	49.16, q, F^{β} 53.45, m, F^{α}	13.1,	9.8,	2.6
(16)	6.95, d, 1H, H^8 5.90, ddd, 1H, H^4 5.82, dt, 1H, H^3 5.81, dd, 1H, H^6 5.68, dm, 1H, H^5 5.36, s, 5H, C_5H_5 5.33, s, 5H, C_5H_5 5.18, dd, 1H, H^7 2.64, br.s, 1H, H^2 1.71, qt, 1H, H^1	$H^7H^8 = 11.6$ $H^6H^7 = 3.8$ $H^5H^6 = 11.3$ $H^3H^4 = 11.3$ $H^3H^5 = 1.2$ $H^2H^3 = 1.2$ $H^2H^4 = 0.9$ $H^4H^5 = 3.8$ $F^{\alpha}H^1 = 9.6$ $RhH^1 = 2.0, 2.0$	49.16, q, F^{β} 53.10, m, F^{α}	13.2,	9.6,	2.8
(18)	7.36, d, 1H, H^6 6.11, dd, 1H, H^5 5.55, s, 5H, C_5H_5 5.52, s, 5H, C_5H_5 4.93, s, 5H, C_5H_5 4.91, s, 5H, C_5H_5 4.18, br.s, 1H, H^2 3.12, d, 1H, H^4 1.09, qm, 1H, $H^{1\text{or}3}$ 0.88, qm, 1H, $H^{1\text{or}3}$	$H^5H^6 = 8.8$ $H^4H^5 = 6.0$ $F^{\alpha}H^1 = 9.6$ $F^{\alpha}H^3 = 9.6$	48.12, q, $F^{\beta\text{or}\beta'}$ 48.67, q, $F^{\beta\text{or}\beta'}$ 53.66,[e] m, $F^{\alpha}+F^{\alpha'}$	12.8, 12.6,	9.6, 9.6,	2.0 2.0

[a] Data for all other products are presented in Supplementary Table SUP-5 (Available from the Editor).

[b] ^{1}H, $\delta(Me_4Si) = 0.00$; ^{19}F, $\delta(CCl_3F) = 0.00$.

[c] ^{1}H assignments according to numbering scheme in structural diagrams; CF_3 assignments according to scheme in structure (**1a**); all CF_3 resonances of equal intensity unless indicated otherwise.

[d] Spectra measured in d_6-acetone.

[e] Relative area 6F.

plexes. To our knowledge, the activation of C—H bonds in arenes has not previously been achieved with binuclear complexes and the simultaneous activation of two *meta* C—H bonds has not been reported before.

EXPERIMENTAL

The general procedures and instrumentation used are described in previous papers.[2,30] Dienes, polyenes and arenes were commercial samples; gases were used as received, and liquids were distilled before use. Cyclopentadiene and methylcyclopentadiene were obtained by cracking the appropriate dimer in the presence of iron powder.[31] Allene was produced *in situ* from diketene.[11]

A ten-fold excess of the appropriate unsaturated organic compound was condensed into an evacuated Carius tube containing $(\eta\text{-}C_5H_5)_2Rh_2(CO)(CF_3C_2CF_3)$ in hexane. The tube was placed in sunlight, that had passed through a glass window pane, and left until the colour of the solution had changed from green to orange (generally 30–120 min). The solvent was then removed under reduced pressure and the products extracted with the minimum quantity of dichloromethane (more polar solvents were generally required for the tetranuclear products). The products were separated by TLC on 20×20 cm plates with a 1:1 silica gel G-HF_{254} mixture as adsorbent. In general, the separation of dinuclear products required eluent mixtures of petroleum spirit (b.p. 40–60°C) and Et_2O (9:1 or 4:1). Tetranuclear products required more polar mixtures. The results for individual reactions are summarized in Table 2 and NMR spectroscopic data used to characterize the complexes are in Table 3.

Crystallographic study

Crystal data. $C_{34}H_{26}F_{12}Rh_4$, $M = 1048$, monoclinic, $a = 16.958(6)$, $b = 9.119(5)$, $c = 24.74(1)$ Å, $\beta = 118.57(4)°$, $U = 3360(3)$ Å^3; space group $P2_1/c$, $Z = 4$, $D_c = 2.07$, $D_m = 2.11(1)$ g cm^{-3}, $F(000) = 2072$. Specimen: $0.08 \times 0.24 \times 0.09$ mm. $A^*_{min,max} = 1.12, 1.21$.

Data collection. Syntex $P2_1$ diffractometer, Mo-K_α radiation ($\lambda = 0.7106_9$ Å, graphite monochromated), $2\theta/\theta$ scan mode, $2\theta_{max} = 50°$, temp. = 295 K, 5773 data measured, 3870 with $I > 3\sigma(I)$, corrected for absorption.

Structure solution and refinement. Direct methods, full matrix least-squares. The structure was refined without problems to final R values of $R = 0.037$, $R' = 0.032$ [$w = 1/\sigma^2(F)$; $\sigma^2(I) = \sigma^2\text{diff}(I) + 0.00012\sigma^4(I)$]. Non-hydrogen atoms were assigned anisotropic thermal parameters; (x, y, z, U_{iso})H were included constrained at estimated values.

Final atomic coordinates and anisotropic thermal parameters, full lists of atom geometries, and lists of F_o/F_c have been deposited with the Editor as supplementary material. Computer programs and sources of scattering factor data are given in refs 32 and 33.

Acknowledgements—We thank the Australian Research Grants Scheme for financial support (R.S.D., A.H.W.), the Australian Government for a postgraduate scholarship (S.M.J.), and Johnson Matthey for the loan of rhodium trichloride.

REFERENCES

1. R. S. Dickson, G. D. Fallon, R. J. Nesbit and H. Pateras, *Organometallics* 1987, **6**, 2517.
2. R. S. Dickson, G. D. Fallon, S. M. Jenkins, B. W. Skelton and A. H. White, *J. Organomet. Chem.* 1986, **314**, 333.
3. K-H. Franzreb and C. G. Kreiter, *Z. Naturforsch.* 1982, **37b**, 1058.
4. M. D. Fryzuk, T. Jones and F. W. B. Einstein, *J. Chem. Soc., Chem. Commun.* 1984, 1556.
5. O. Gambino, M. Valle, S. Aime and G. A. Vaglio, *Inorg. Chim. Acta* 1974, **8**, 71.
6. R. P. Ferrari and G. A. Vaglio, *J. Organomet. Chem.* 1979, **182**, 245.
7. P. Racanelli, G. Pantini, A. Immerzi, G. Allegra and L. Porri, *J. Chem. Soc., Chem. Commun.* 1969, 301.
8. M. H. Chisholm, L. A. Rankel, W. I. Bailey, F. A. Cotton and C. A. Murillo, *J. Am. Chem. Soc.* 1977, **99**, 1261.
9. W. I. Bailey, M. H. Chisholm, F. A. Cotton, C. A. Murillo and L. A. Rankel, *J. Am. Chem. Soc.* 1978, **100**, 802.
10. Y. N. Al-Obaidi, P. K. Baker, M. Green, N. D. White and G. E. Taylor, *J. Chem. Soc., Dalton Trans.* 1981, 2321.
11. W. A. Herrmann, J. Weichmann, M. L. Ziegler and H. Pfisterer, *Angew. Chem. Int. Ed. Engl.* 1982, **21**, 551.
12. See, for example, R. E. Colborn, A. F. Dyke, S. A. R. Knox, K. A. Mead and P. Woodward, *J. Chem. Soc., Dalton Trans.* 1983, 2099.
13. A. J. Canty, A. J. P. Domingo, B. F. G. Johnson and J. Lewis, *J. Chem. Soc., Dalton Trans.* 1973, 2056.
14. A. J. Deeming and M. Underhill, *J. Chem. Soc., Dalton Trans.* 1974, 1415.
15. R. S. Dickson and M. J. Liddell, unpublished results.
16. E. G. Bryan, B. F. G. Johnson, J. W. Kelland and J. Lewis, *J. Chem. Soc., Chem. Commun.* 1976, 254.
17. S. Bhaduri, B. F. G. Johnson, J. W. Kelland, J. Lewis, P. R. Raithby, S. Rehani, G. M. Sheldrick

and K. Wong, *J. Chem. Soc., Dalton Trans.* 1979, 562.
18. K-H. Franzreb and C. G. Kreiter, *J. Organomet. Chem.* 1983, **246**, 189.
19. C. G. Kreiter, K-H. Franzreb, W. Michels, U. Schubert and K. Ackermann, *Z. Naturforsch.* 1985, **40b**, 1188.
20. H. van der Heijden, A. G. Orpen and P. Pasman, *J. Chem. Soc., Chem. Commun.* 1985, 1576.
21. W. D. Jones and J. A. Maguire, *Organometallics* 1986, **5**, 590.
22. M. D. Fryzuk, P. A. MacNell and N. T. McManus, *Organometallics* 1987, **6**, 882.
23. M. V. Baker and L. D. Field, *J. Am. Chem. Soc.* 1986, **108**, 7433.
24. M. Hackett, J. A. Ibers, P. Jernakoff and G. M. Whitesides, *J. Am. Chem. Soc.* 1986, **108**, 8094.
25. H. Werner, A. Höhn and M. Dziallis, *Angew. Chem. Int. Ed. Engl.* 1986, **25**, 1090.
26. P. L. Watson, *J. Chem. Soc., Chem. Commun.* 1983, 276.
27. R. J. Goudamit, B. F. G. Johnson, J. Lewis, P. R. Raithby and M. J. Rosales, *J. Chem. Soc., Dalton Trans.* 1983, 2257.
28. R. S. Dickson, A. P. Oppenheim and G. N. Pain, *J. Organomet. Chem.* 1982, **224**, 377.
29. R. S. Dickson, C. Mok and G. N. Pain, *J. Organomet. Chem.* 1979, **166**, 385.
30. R. S. Dickson, G. D. Fallon, F. I. McLure and R. J. Nesbit, *Organometallics* 1987, **6**, 215.
31. R. S. Dickson, B. Dobney and F. W. Eastwood, *J. Chem. Educ.* 1987, **64**, 898.
32. J. A. Ibers and W. C. Hamilton (Eds) *International Tables for X-ray Crystallography*, Vol. 4. Kynoch Press, Birmingham (1974).
33. S. R. Hall and J. M. Stewart, *The XTAL 2.2 User's Manual.* Universities of Western Australia and Maryland (1987).

Polyhedron Vol. 7, No. 10/11, pp. 871–879, 1988
Printed in Great Britain

0277–5387/88 $3.00+.00
Pergamon Press plc

THEORETICAL STUDIES OF (μ-CR) BRIDGING COMPLEXES

ELUVATHINGAL D. JEMMIS† and BHARATAM V. PRASAD

School of Chemistry, University of Hyderabad, Central University P.O., Hyderabad-500 134, India

(*Accepted* 5 *November* 1987)

Abstract—Scrambling of substituents on the C_3R_3 bridging ligands in $L_2W(\mu\text{-}C_3R_3)(\mu\text{-}CR)WL_2$ is studied using Extended Hückel calculations by two pathways: deinsertion and cyclopropenium ring formation. The reaction of $L_2W(\mu\text{-}CR)_2WL_2$ with allenes to give $L_2W(\mu\text{-}CHC(CR_2)_2)(\mu\text{-}CR)WL_2$ is also studied. The electronic structure of $CpMeW(\mu\text{-}CMe)_2WMeCp$ is compared to that of $L_2W(\mu\text{-}CR)_2WL_2$.

Bimetallic systems bridged by small organic molecules are of current interest.‡[1] Carbyne bridged (μ-CR) complexes are of special interest, mainly because of their catalytic implications.[2] Several reactions of bridging CH or CR groups have been reported recently.[3] Bimetallic systems bridged by two such carbynes, **1**, are especially interesting, because of the delocalization of the 4 π electrons of the M_2C_2 ring.[4–8,9(b)] Some of these react selectively with small organic molecules.[9–11] We have studied the aromatic behaviour and reactivity of these complexes using molecular orbital theory.[11] **1** reacts specifically with those molecules having π bonds in orthogonal planes. Thus, alkynes, allenes, ketenes etc. but not alkenes react with **1**.[9–11] Reaction of alkynes with **1** results in the formation of a carbon–carbon bond as shown in Scheme 1.[9(a),(b)] Allene reacts with **1** to give **4**. The reaction with alkyne first yields an adduct, **2**, which finally results in an η^3-didehydroallyl bridging complex, **3**. Formation of **2** and its MO correlation to **3** have been discussed.[11] The C_3R_3 bridge in **3** scrambles the CR units to give a product with a bulkier group on the central carbon atom. Here, we analyse two pathways for this process: One involves essentially a deinsertion step. Formation of a bridged cyclopropenyl ring and its rotation along a C3 axis and reformation of the product is another. We also discuss the formation of **4**. The electronic structure of the recently reported 1,3-dimetallacyclobutadiene, $(C_5Me_5)MeW(\mu\text{-}CMe)_2WMe(C_5Me_5)$,[8] **5**, is compared to that of **1** at the end.

The Fragment Molecular Orbital (FMO) method within the Extended Hückel approximation is used in obtaining the electronic structures.[12] All the calculations were carried out on models where the terminal ligands were CH_3 and the substituents on bridging carbon fragments were hydrogens. **5** is modelled by $CpCH_3W(\mu\text{-}CH)_2WCpCH_3$. The details of geometric and atomic parameters used in the Extended Hückel calculations are given in the appendix.

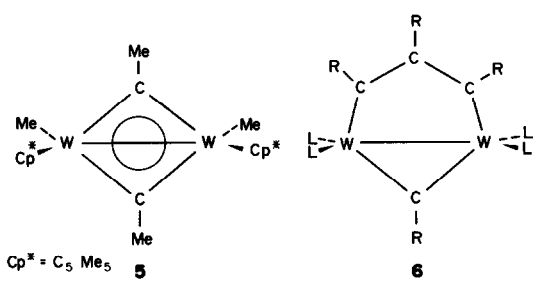

THE C—C BOND FORMATION AND THE DEINSERTION PATHWAY FOR SCRAMBLING

One possible pathway for the conversion of **2** → **3**, involves the formation of a transition state having a six membered ring, **6**, formed by the in-plane movement of the acetylene and CH. The C3 unit then rotates around an axis perpendicular to the M—M axis to give **3**. We studied the for-

† Author to whom correspondence should be addressed.

‡ Theoretical studies on single carbyne bridged bimetallic systems are in progress.

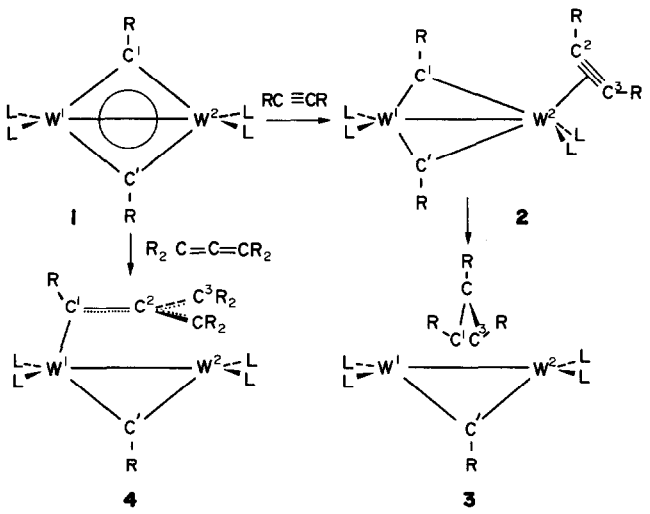

Scheme 1.

mation of **6** and its conversion to **3** separately. The formation of **6** indicates a barrier of 2.8 eV. An optimized reaction coordinate should give a smaller barrier and the Walsh diagram is given in Fig. 1. The HOMO (a') orbital initially goes up in energy due to the decrease in the bonding interaction between the acetylene π^* and the nearest metal, and then comes down mainly due to the reformation of the metal–metal bond. The M—M bond is decreased from 2.915 to 2.544 Å. HOMO−1 shows an increase in energy due to the increasing antibonding interaction between the terminal carbons of the allyl group and also an increasing δ^* interaction between the metals. The LUMO+1 (δ^*) orbital comes down due to a decrease in the antibonding interaction between the π of the alkyne and δ^* of the metal, and the increasing π combination within the allylic carbons. The MOs corresponding to the new C—C σ and π bonds formed are buried among lower lying ligand orbitals and mix well with other ligand based orbitals because of their lower symmetry. Therefore, it was not practical to point any out.

Conversion of **6** to **3** involves twisting the allylic part of **6** by 90° and correspondingly adjusting the

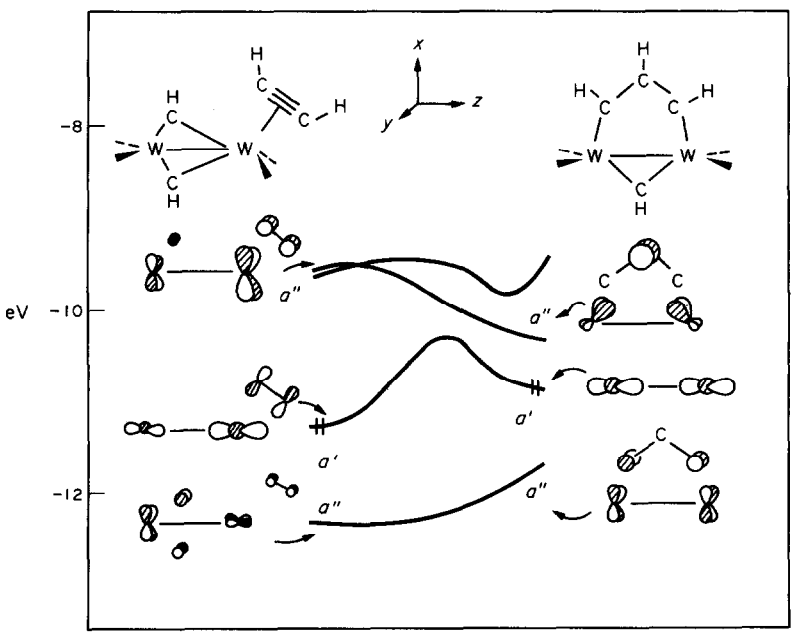

Fig. 1. Walsh diagram for the conversion of **2** → **6**. C_s symmetry is maintained.

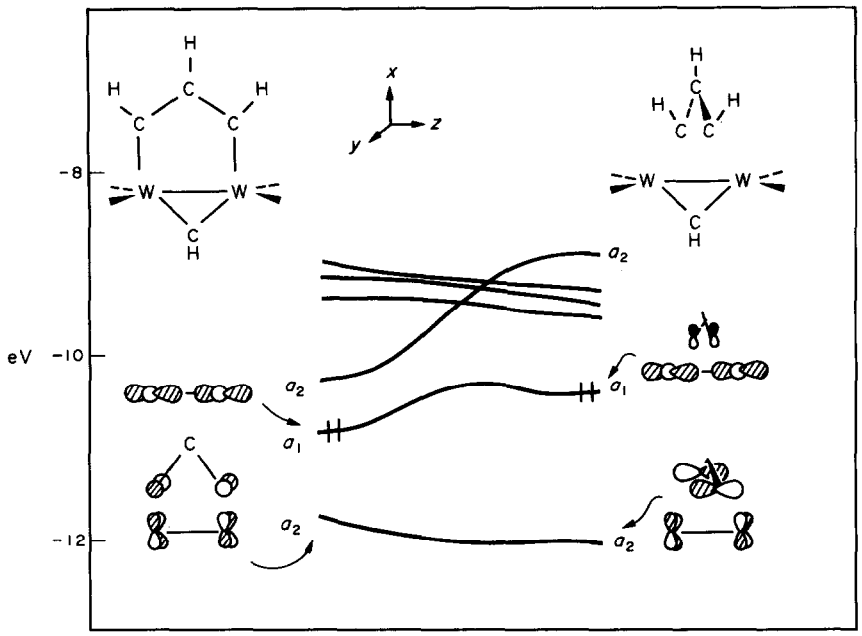

Fig. 2. Walsh diagram for the conversion of **6** → **3**. C_2 symmetry is maintained.

distance between the C_3R_3 and the bimetallic fragment. The process has only C_2 symmetry and the energy barrier for the process is around 1.68 eV. The Walsh diagram (Fig. 2) shows that the σ HOMO (a_1) gradually increases in energy due to an increase in the antibonding combination with the terminal carbons of the allyl part. The non-bonding π^* combination of the allylic group remains almost constant because it retains a δ type of interaction with the δ^* orbital of the M—M combination in the HOMO − 1 (a_2). In this process, the M—M distance is kept constant. No other change is observed in the Walsh diagram. The above discussion indicates that the conversion of **2** to **3** through transition state **6** is an allowed process.

Experimental studies on the insertion reaction have shown that the kinetically favoured product retains the substituents on the alkynes in the 1,2 positions,[9(b)] but the thermodynamic product has the bulkier carbon substituent on the central carbon of the bridging C_3 ligand. The thermodynamic preferences can be simply attributed to the steric factors, both in the ground state and the transition state. The transformation of the kinetic product to the thermodynamic one (the scrambling of the C_3R_3 group) takes place with ease. An alkyne deinsertion along the lines described for the C—C bond formation, together with alkyne rotation can account for the scrambling. If the processes from **2** to **6** and **6** to **3** are reversible, the new alkyne formed in **6** can include the original bridging because the two end carbons of the C_3 units are equivalent. To make way for the formation of the thermodynamically more favoured product from any possible set of starting materials, both a rotation of the acetylene in **2** and a dissociation–association step have to be involved. We find that rotation of the alkyne in **2** along an axis perpendicular to the C—C bond and passing through the metal, is a possible pathway, involving a barrier of only 1.5 eV. This is lower than that for **2** to **6** or **6** to **3**. It should be emphasized here that these values are only to be taken as a crude estimate, as the method we use cannot give reliable energy differences. This scrambling mechanism, which involves deinsertion, demands that the rotation of the allylic group as in **6** → **3** should be observed. The detailed experiments of Chisholm *et al.*[9(b)] do not indicate any such process, probably because the barrier for such a process may be higher than is possible thermally. This, in addition to the thermodynamics of the bonds involved does not allow us to support this mechanism conclusively, even though this is the simplest possible mechanism.

SCRAMBLING PROCESS INVOLVING A CYCLOPROPENIUM RING FORMATION

A general scheme which encompasses all the observed rearrangements was proposed by Chisholm *et al.*[9(b)] This involves the formation of the $L_2W(\mu\text{-}\eta^1,\eta^2\text{-cyclopropenyl})WL_2$ transition state, **7**. It is envisaged that the transition state has the cyclopropenyl ring parallel to the L_2W—WL_2

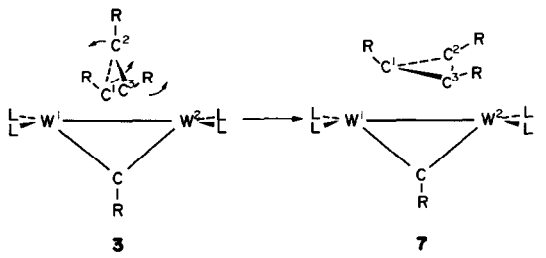

Scheme 2.

plane, as shown in Scheme 2. This involves the formation of a cyclopropenium ring by bringing the terminal carbon of C_3R_3 closer. Ring opening or closing in the normal cyclopropenium cation is not feasible thermally, but the presence of the transition metal changes the picture dramatically. Many experimental[14] and theoretical studies[13] are available on these systems. The cyclopropenium ion ring opening is complete in the case of d^8-ML_2 complexes. Experimental results suggest that the ring opening is partial in several other systems.[14]

A Walsh diagram for the conversion of **3** to **7** is plotted in Fig. 3. A least motion path is defined by pushing the terminal carbons of the allylic bridging ligand upwards and pulling the central carbon downwards. This is the only path which can have at least C_s symmetry. The total energy increases continuously and the Walsh diagram shows HOMO–LUMO crossing towards the end of the process. As is clearly shown in Fig. 3, the $3a''$ (HOMO − 1), **8** of **3** goes up in energy precipitously to become the LUMO, **9** of **7**. Correspondingly, the $3a'$ of **3** comes down slightly to become the HOMO of **7**. The $3a''$ becomes destabilized due to the decrease in the δ type of bonding interaction of the non-bonding allyl π^* orbital with the δ^* orbital of M—M in **3**. There is an avoided crossing between $2a''$ *and* $3a''$ which exchanges their character. The HOMO of **3**, the M—M σ bond, now becomes the HOMO − 1.

In **7**, the HOMO–LUMO gap is small. The forbidden symmetry of the reaction may be an artifact of the reaction coordinate assumed and the restriction (C_s symmetry) imposed on the studied reaction path. A minor change in **7** (as shown in **10**) would

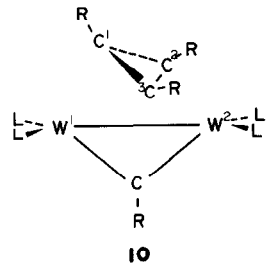

avoid the HOMO–LUMO crossing. A reaction coordinate which lacks any symmetry restrictions is also tried. The conversion should be analysed only on the basis of variation of energy levels. Slight

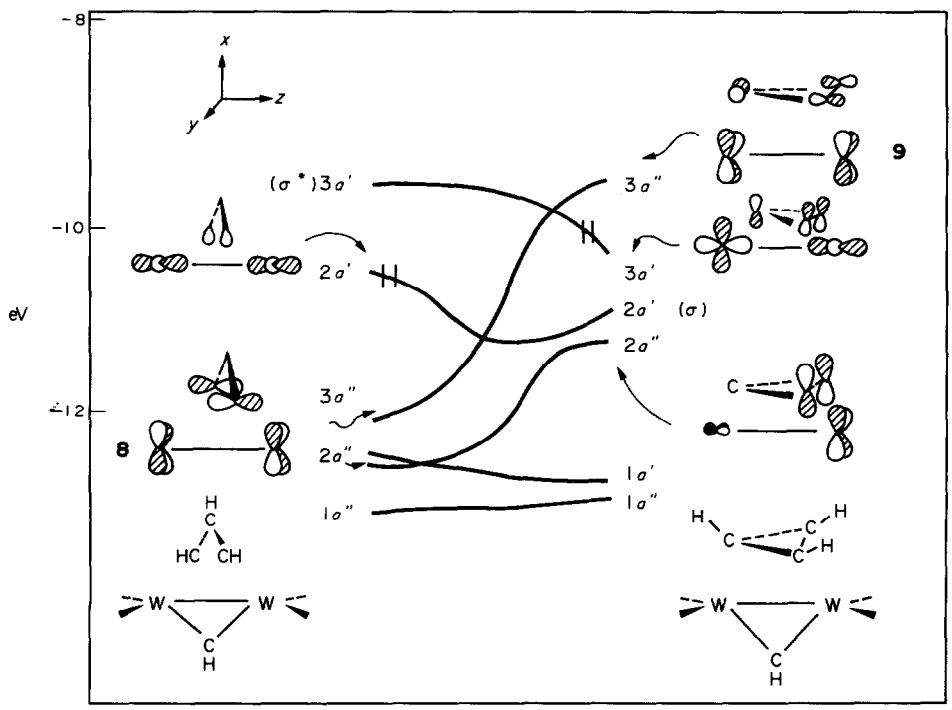

Fig. 3. Walsh diagram for the conversion of **3** → **7** (C_s symmetry). Only important orbitals are shown.

changes in the geometric parameters like increasing the M—M distance or changes in the C—C distances, make the transition state **7** more stable and the energy barrier small.

Rotation of the cyclopropenyl ring, either in **7** or **10** along a pseudo C3 axis and the return to the ring opened structure **3** by breaking a different C—C bond results in complete scrambling. Rotation of the C_3R_3 ring along an axis passing through the ring centroid and the M—M mid point in **7** produced a tiny barrier (less than 0.2 eV), slightly preferring the structure which lacks any symmetry. This indicates that rotation is a facile process. At this stage, steric factors may play a role in preferentially opening a C—C bond which is opposite to the carbon containing bulky substituents, leading to the observed thermodynamically favoured products.

REACTION OF $L_2W(\mu\text{-CR})_2WL_2$ WITH ALLENE

Allene satisfies the necessary conditions required for its reaction with **1** and is experimentally found to give **4**[10,11] (Scheme 3). A plausible mechanism, via the formation of an intermediate (allene adduct), **11** and the transition state, **12**, is proposed.[11] Here, we trace the reaction using the molecular orbital methods and analyse the electronic structure of the final complex, **4**.

Conversion of **1** and allene to **11** is a smooth process, where the HOMO becomes stabilized due to the increasing bonding interaction between the σ orbital of **1** and the in-plane π^* orbital of the allene. No other orbital shows any considerable change during the process. The electronic structure of **11** is similar to the corresponding alkyne adduct. The conversion of **11** to **12** is a symmetry allowed process but with a high energy barrier. The Walsh diagram is similar to Fig. 1. Conversion of **12** to **4** does not retain any symmetry and the barrier is small, so, formation of **4** along the lines discussed should be an allowed process.

The electronic structure of **4** is studied using the FMO method between fragments **13** and **14**. Figure 4 gives the interaction diagram. The orbital pattern of fragment **13** can be easily obtained from the well known L_2M—ML_2 and carbyne fragments, and hence is not discussed in detail. It has three occupied metal orbitals with the following electronic configuration in the frontier range: $1a'\ (\pi)^2$, $2a'\ (\sigma)^2$, $1a''\ (\delta)^0$, $2a''\ (d^*)^0$, $3a'\ (\pi^*)^0$, $4a'\ (\sigma^*)^0$ and $5a'\ (\sigma)^0$. (Symmetry labels are given assuming C_s symmetry rather than C_{2v}, as **4** has only C_s symmetry.) Fragment **14** is like trimethylmethylene except for the lack of one hydrogen. The framework of $CHC(CH_2)_2$ resembles that of trimethylenemethane and it can also be considered as having a carbyne (CH) attached to the central carbon of the allylic system. The four orbitals of the allylic part are clearly describable as in $1a'$, $2a'$, $1a''$ and $3a'$. The contribution from the CH group is through an *sp* hybrid as in $2a'$ and $3a'$. The CH group in addition has a *p* orbital lying in the plane of the C4 unit, $2a''$. The orbitals involved are shown clearly in Fig. 4. Its interaction with fragment **13** gives **4**. The HOMO in **4** is a slightly destabilized $2a'$ (σ) orbital of fragment **13**. This indicates the presence of a metal–metal (σ) single bond even though it has such a long bond length (2.855 Å). The $1a''$ orbital of fragment **14** becomes stabilized by its interaction with the LUMO (δ^*) orbital of fragment **13**, which is pushed up to high energy. The HOMO (δ) of fragment **13** stabilizes the $2a''$ of fragment **14**. The metal–metal σ^* combination remains unaffected and becomes the LUMO of **4**. In this case also, the second CH group is unreactive because of the absence of the metal–metal δ^* LUMO which is used to accept electrons from allene.

ELECTRONIC STRUCTURE OF $(C_5Me_5)MeW(\mu\text{-CMe})_2WMe(C_5Me_5)$, 5

Electronic structure studies on 1,3-dimetallacyclobutadienes reported so far are with simple alkyl ligands.[11,15] In **5**, an alkyl group on each metal

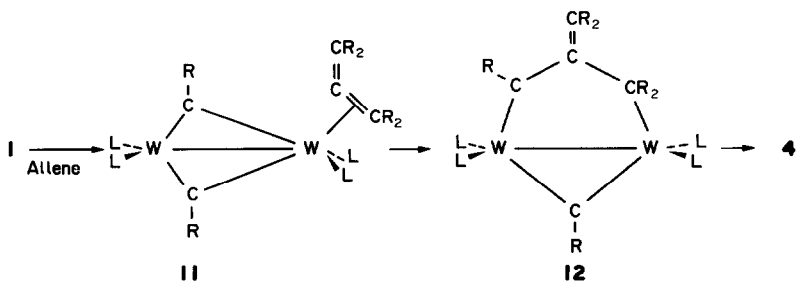

Scheme 3.

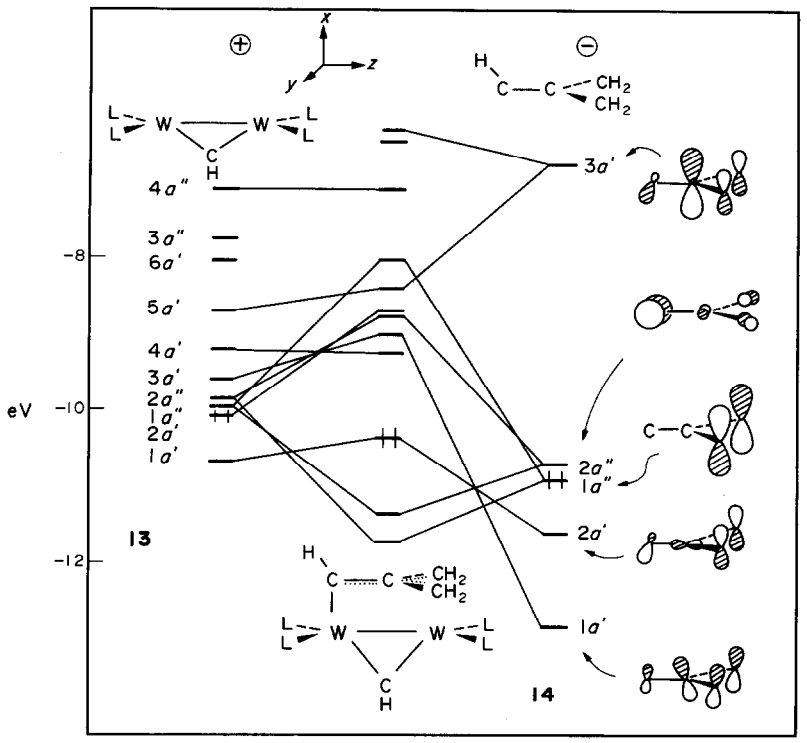

Fig. 4. Interaction diagram for the construction of the orbitals of $L_2W(\mu\text{-}CRC(CR_2)_2)(\mu\text{-}CR)WL_2$ from $L_2W(\mu\text{-}CR)WL_2$ and $RCC(CR_2)_2$. Only the orbitals of the later fragment are shown.

is replaced by a Cp*. The electronic structure of $Cp^*MeW(\mu\text{-}CMe)_2WMeCp^*$ is analysed here. Assuming that CR is a 3− ligand, the oxidation state of the metal is 5+ (d^1). There are 16 electrons around W in **5** as opposed to the 12 electron count found in **1**. The electronic structure of **1** (R = $SiMe_3$, L = CH_2SiMe_3) has a metal–metal (d_z2-d_z2) bond as the HOMO and a ($d_{xy}-d_{xy}$)δ^* as the LUMO. The HOMO−1 shows the delocalization that removes the antiaromatic character from the four-membered ring. Extended Hückel calculations on **5** show that it has the same orbital pattern as that of **1** (R = $SiMe_3$, L = CH_2SiMe_3). The HOMO corresponds to a M—M σ bond and the LUMO is a δ^* ($d_{xy}-d_{xy}$) orbital. The HOMO–LUMO gap is around 0.82 eV), which is of the same order as that in **1**. Here also, the aromatic nature of the molecule can be traced to the HOMO−1 orbital. Neither a change due to Cp* nor to out-of-plane bending in **5** over **1** seems to cause any change in the electronic structure. (The corresponding planar structure is less stable by 4 kcal mol^{-1}.) We expect this molecule to have a similar reactivity to that of **1**, with small organic molecules, which have two orthogonal π orbitals, like alkynes, allene, ketenes, etc. but not with alkenes. A word of caution is in order here—the bulky terminal ligands may cause some hindrance to the incoming reagent, also, **5** is already strained and puckered in order to release it. So, the formation of an intermediate adduct with an alkyne, which is shown to be crucial, may be difficult, because it involves the out-of-plane bending of terminal ligands. With Cp ligands instead of Cp* the steric problems should be reduced.

Scrambling of substituents on the C_3R_3 ligands in $L_2W(\mu\text{-}C_3R_3)(\mu\text{-}CR)WL_2$ is studied in detail. The deinsertion path demands a rotation of the C3 unit between **3** and **6**. The cyclopropenium ring formation path would demand the transition state to be more like **10** than **7**. Reaction of **1** with allenes is shown to be a symmetry allowed process, but with a high energy barrier. The electronic structure of **5** is very similar to that of **1**.

Acknowledgements—We thank the University Grants Commission for financial assistance and the University of Hyderabad's computer centre for computations.

REFERENCES

1. (a) W. A. Herrmann, *Angew. Chem. Int. Ed. Engl.* 1982, **21**, 117; (b) W. A. Herrmann, *J. Organomet. Chem.* 1983, **250**, 319; (c) M. H. Chisholm, D. M. Hoffman and J. C. Huffman, *Chem. Soc. Rev.* 1985,

14, 69; (d) M. H. Chisholm, B. K. Conroy, K. Folting, D. M. Hoffmann and J. C. Huffman, *Organometallics* 1986, **5**, 2457; (e) M. H. Chisholm, D. L. Clark, D. M. Hoffman and J. C. Huffman, *Organometallics* 1987, **6**, 1532; (f) P. J. Blower, M. H. Chisholm, D. L. Clark and B. W. Eichhorn, *Organometallics* 1986, **5**, 2125; (g) M. H. Chisholm, B. K. Conroy, B. W. Eichhorn, K. Folting, D. M. Hoffman, J. C. Huffman and N. S. Marchant, *Polyhedron* 1987, **6**, 783; (h) J. C. Green, M. L. H. Green, D. O. Hare, R. R. Watson and J. A. Bandy, *J. Chem. Soc., Dalton Trans.* 1987, 391; (i) F. A. Cotton and K. R. Dunbar, *J. Am. Chem. Soc.* 1987, **109**, 2199; (j) E. L. Hoel, *Organometallics* 1986, **5**, 587; (k) M. D. Curtis, L. Messerle, J. J. D'Errico, H. E. Solis, I. C. Barcelo and M. W. Butler, *J. Am. Chem. Soc.* 1987, **109**, 3603; (l) C. J. Caseuit, M. R. DuBois and J. Mason, *Inorg. Chem.* 1987, **26**, 1889; (m) B. E. Bursten and R. H. Cayton, *J. Am. Chem. Soc.* 1986, **108**, 8241; (n) B. E. Bursten and D. L. Clark, *Polyhedron* 1987, **6**, 695; (o) D. M. Hoffman, R. Hoffmann and C. R. Fisel, *J. Am. Chem. Soc.* 1982, **104**, 3858; (p) M. J. Calhorda and R. Hoffmann, *Organometallics* 1986, **5**, 2181; (q) E. D. Jemmis and P. N. V. Pavan Kumar, *J. Am. Chem. Soc.* 1988, **110**, 125.

2. (a) A. Yamamoto, *Organotransition Metal Chemistry, Fundamental Concepts and Applications*, Wiley Interscience, New York (1986); (b) L. L. Kesmodel, L. H. DuBois and G. A. Somorjai, *Chem. Phys. Lett.* 1978, **56**, 267; (c) R. J. Koestner, J. C. Frost, P. C. Stair, M. A. Vanttove and G. A. Somorjai, *Surf. Sci.* 1982, **116**, 85; (d) R. R. Schorock, *Am. Chem. Soc. Symp. Ser.* 1983, **211**, 369; (e) J. A. Beck, S. A. R. Knox, R. E. D. Stansfield, F. G. A. Stone, M. J. Winter and P. Woodward, *J. Chem. Soc., Dalton Trans.* 1982, 195.
3. (a) J. C. Jeffery, K. A. Mead, H. Razay, F. G. A. Stone, M. J. Went and P. Woodward, *J. Chem. Soc., Chem. Commun.* 1981, 867; (b) J. C. Jeffery, I. Moore, H. Razay and F. G. A. Stone, *J. Chem. Soc., Chem. Commun.* 1981, 1255; (c) M. Green, J. A. K. Howard, S. J. Porter, F. G. A. Stone and D. C. Tyler, *J. Chem. Soc., Dalton Trans.* 1984, 2553; (d) J. C. Jeffery, K. A. Mead, H. Razay, F. G. A. Stone, M. J. Went and P. Woodward, *J. Chem. Soc., Dalton Trans.* 1984, 1383; (e) J. C. Jeffery, I. Moore, H. Razay and F. G. A. Stone, *J. Chem. Soc., Dalton Trans.* 1984, 1581; (f) N. M. Boag, R. J. Goodfellow, M. Green, B. Hessner, J. A. K. Howard and F. G. A. Stone, *J. Chem. Soc., Dalton Trans.* 1983, 2585; (g) E. Delgado, J. Hein, J. C. Jeffery, R. L. Raterman, F. G. A. Stone and L. J. Farrugia, *J. Chem. Soc., Dalton Trans.* 1987, 1191; (h) D. L. Davies, M. J. Parrott, P. Sherwood and F. G. A. Stone, *J. Chem. Soc., Dalton Trans.* 1987, 1201; (i) M. E. Garcia, J. C. Jeffery, P. Sherwood and F. G. A. Stone, *J. Chem. Soc., Dalton Trans.* 1987, 1209; (j) P. G. Byrne, M. E. Garcia, J. C. Jeffery, P. Sherwood and F. G. A. Stone, *J. Chem. Soc., Dalton Trans.* 1987, 1215; (k) J. A. K. Howard, A. P. James, A. N. d. M. Jelfs, C. M. Nunn and F. G. A. Stone, *J. Chem. Soc., Dalton Trans.* 1987, 1221; (l) P. G. Byrne, M. E. Garcia, N. H. Tran-Hvy, J. C. Jeffery and F. G. A. Stone, *J. Chem. Soc., Dalton Trans.* 1987, 1243; (m) G. P. Elliott, J. A. K. Howard, K. Mise, I. Moore, C. M. Nunn and F. G. A. Stone, *J. Chem. Soc., Dalton Trans.* 1986, 2091; (n) E. Delgado, J. C. Jeffery and F. G. A. Stone, *J. Chem. Soc., Dalton Trans.* 1986, 2105; (o) M. Green, J. A. K. Howard, A. P. James, A. N. d. M. Jelfs, C. M. Nunn and F. G. A. Stone, *J. Chem. Soc., Dalton Trans.* 1986, 1967; (p) S. V. Hoskins, A. P. James, J. C. Jeffery and F. G. A. Stone, *J. Chem. Soc., Dalton Trans.* 1986, 1709; (q) D. G. Evans, J. A. K. Howard, J. C. Jeffery, D. B. Lewis, G. E. Lewis, M. J. Gross-Ophoff, M. J. Parrott and F. G. A. Stone, *J. Chem. Soc., Dalton Trans.* 1986, 1723; (r) C. P. Casey, P. J. Fagan and W. H. Miles, *J. Am. Chem. Soc.* 1982, **104**, 1134; (s) C. P. Casey and P. J. Fagan, *J. Am. Chem. Soc.* 1982, **104**, 4950; (t) C. P. Casey and P. J. Fagan, *J. Mol. Catal.* 1983, **21**, 762; (u) C. P. Casey and P. J. Fagan, *J. Am. Chem. Soc.* 1982, **104**, 7360; (v) C. P. Casey, S. R. Marder and P. J. Fagan, *J. Am. Chem. Soc.* 1983, **105**, 7197; (w) C. P. Casey, M. W. Meszaros, S. R. Marder and P. J. Fagan, *J. Am. Chem. Soc.* 1984, **106**, 3680; (x) C. P. Casey, S. R. Marder and B. R. Adams, *J. Am. Chem. Soc.* 1985, **107**, 7700; (y) C. P. Casey, S. R. Marder and A. L. Rheingold, *Organometallics* 1985, **4**, 763; (z) C. P. Casey, M. A. Gohdes and M. W. Meszaros, *Organometallics* 1986, **5**, 196; (A) C. P. Casey, S. R. Marder, R. E. Colborn and P. A. Goodson, *Organometallics* 1986, **5**, 199; (B) C. P. Casey and E. A. Austin, *Organometallics* 1986, **5**, 584; (C) C. P. Casey and D. M. Roddick, *Organometallics* 1986, **5**, 436; (D) C. P. Casey, M. W. Meszaros, P. J. Fagan, R. K. Bly, S. R. Marder and E. A. Austin, *J. Am. Chem. Soc.* 1986, **108**, 4043; (E) C. P. Casey, M. W. Meszaros, P. J. Fagan, R. K. Bly and R. E. Colborn, *J. Am. Chem. Soc.* 1986, **108**, 4053; (F) C. P. Casey, M. W. Meszaros, S. R. Marder, R. K. Bly and P. J. Fagan, *Organometallics* 1986, **5**, 1873; (G) C. P. Casey, M. W. Meszaros, R. E. Colborn, D. M. Roddick, W. H. Miles and M. A. Gohdes, *Organometallics* 1986, **5**, 1879.
4. (a) F. Huq, W. Mowat, A. C. Skapski and G. Wilkinson, *J. Chem. Soc., Chem. Commun.* 1971, 1477; (b) W. Mowat and G. Wilkinson, *J. Chem. Soc., Dalton Trans.* 1973, 1120; (c) R. A. Anderson, A. L. Gayler and G. Wilkinson, *Angew. Chem. Int. Ed. Engl.* 1976, **15**, 609; (d) M. Boachmann, G. Wilkinson, A. M. R. Galas, M. B. Hursthouse and K. M. A. Malik, *J. Chem. Soc., Dalton Trans.* 1980, 1797.
5. (a) M. H. Chisholm, F. A. Cotton, M. W. Extine and B. R. Stults, *Inorg. Chem.* 1976, **15**, 2252; (b) M. H. Chisholm, F. A. Cotton, M. W. Extine and C. A. Murrilo, *Inorg. Chem.* 1978, **17**, 696.
6. F. A. Cotton, W. Schwotzer and E. S. Shamshoum, *Organometallics* 1983, **2**, 1167.
7. P. E. Fanwick, A. E. Ogilvy and I. P. Rothwell, *Organometallics* 1987, **6**, 73.
8. A. J. Liu, R. C. Murray, J. C. Dewan, B. D. San-

tarsiero and R. R. Schrock, *J. Am. Chem. Soc.* 1987, **109**, 4282.

9. (a) M. H. Chisholm, J. A. Heppert and J. C. Huffman, *J. Am. Chem. Soc.* 1984, **106**, 1151; (b) M. H. Chisholm, J. C. Huffman and J. A. Heppert, *J. Am. Chem. Soc.* 1985, **107**, 5116; (c) M. H. Chisholm and J. A. Heppert, *Adv. Organomet. Chem.* 1986, **27**, 97; (d) M. H. Chisholm, J. A. Heppert, J. C. Huffman and W. E. Streib, *J. Chem. Soc., Chem. Commun.* 1985, 1771; (e) M. C. Azar, K. J. Chetcuti, C. Eigenbrot and K. A. Green, *J. Am. Chem. Soc.* 1985, **107**, 7209; (f) S. R. Finnimore, S. A. R. Knox and G. E. Taylor, *J. Chem. Soc., Chem. Commun.* 1980, 411; (g) R. S. Dickson, G. S. Evans and G. D. Fallon, *J. Organomet. Chem.* 1982, **236**, C49; (h) L. R. Heanan, Z. A. Rahman and J. B. Keister, *Organometallics* 1983, **2**, 1062.
10. M. H. Chisholm, K. Folting, J. A. Heppert and W. E. Streib, *J. Chem. Soc., Chem. Commun.* 1985, 1755.
11. E. D. Jemmis and B. V. Prasad, *J. Am. Chem. Soc.* 1987, **109**, 2560.
12. (a) R. Hoffmann and W. N. Lipscomb, *J. Chem. Phys.* 1962, **36**, 2179; (b) R. Hoffmann, *J. Chem. Phys.* 1963, **39**, 1397; (c) H. Fujimoto and R. Hoffmann, *J. Phys. Chem.* 1974, **78**, 1167.
13. E. D. Jemmis and R. Hoffmann, *J. Am. Chem. Soc.* 1980, **102**, 2570.
14. (a) R. M. Tuggle and D. L. Weaver, *J. Am. Chem. Soc.* 1970, **92**, 5523; (b) P. D. Frisch and G. P. Khare, *Inorg. Chem.* 1979, **18**, 781; (c) R. M. Tuggle and D. L. Weaver, *Inorg. Chem.* 1972, **11**, 2237; (d) P. D. Frisch, R. G. Posey and G. P. Khare, *Inorg. Chem.* 1978, **17**, 402; (e) R. G. Posey, G. P. Khare and P. D. Frisch, *J. Am. Chem. Soc.* 1977, **99**, 4863; (f) W. E. Caroll, M. Green, J. A. K. Howard, M. Pfeffer and F. G. A. Stone, *Angew. Chem.* 1977, **89**, 838; *J. Chem. Soc., Dalton Trans.* 1978, 1472; (g) J. P. Visser and J. E. Ramakers-Blom, *J. Organomet. Chem.* 1972, **44**, C63; (h) W. Wong, S. J. Singer, W. D. Pitts, S. F. Watkins and W. H. Baddley, *J. Chem. Soc., Chem. Commun.* 1972, 672; (i) A. Kesey, P. M. Bailey and P. M. Maitlis, *J. Chem. Soc., Chem. Commun.* 1977, 178; (j) H. Hoberg, R. Krause-Going, C. Kruger and J. C. Sekutowski, *Angew. Chem.* 1977, **89**, 179; (k) M. Evans, M. Hursthouse, E. W. Randall, E. Rosenberg, L. Minole and M. Valle, *J. Chem. Soc., Chem. Commun.* 1972, 545; (l) W. A. Herrmann, E. Herdweek and C. Weber, *Angew. Chem. Int. Ed. Engl.* 1986, **25**, 563; (m) J. W. Egan Jr, R. P. Hughes and A. L. Rheingold, *Organometallics* 1987, **6**, 1578.
15. M. H. Chisholm, J. A. Heppert, E. M. Kober and D. L. Lichtenberger, *Organometallics* 1987, **6**, 1065.

APPENDIX

The geometric parameters (internal coordinates) for structures are given in Table 1. In structures **7** and **10**, *d* is taken as the mid point of the two metals and *d'* is the centroid of the cyclopropenium ring.

Process **2** → **6** is described by the in-plane movement of the alkyne in **2** towards C^1. W—W and C^1—C^2 distances decreased and the C^2—C^3 distance increased. The terminal ligands on W^2 are brought back to the $L_2W^1W^2$ plane. The process maintains C_s symmetry. Process **6** → **3** is designed to maintain C_2 symmetry. Rotation of the allyl ligand along the M—M mid point and C^2 axis is performed in six equal intervals. C_s symmetry is maintained in process **3** → **7**. C^2 is brought down and C^1 and C^3 are pushed upwards as shown in Scheme 2. This process is also studied in six steps.

Table 1.

Parameter	Structure 1	2	3	4	5	6	7	10
W^1—W^2	2.550	2.915	2.550	2.858	2.606	2.550	2.550	2.550
W^1—C′	1.910	1.730	1.910	1.972	1.960	1.910	1.910	1.910
W^2—C′	1.910	2.158	1.910	1.972	1.960	1.910	1.910	1.910
W^1—C^1	1.910	1.730	2.220	1.928	1.960	1.926	1.922	2.136
W^2—C^2		2.000	2.450				2.111	1.948
W^2—C^3		2.000	2.220			1.926	2.111	1.948
W—C(L)	2.100	2.100	2.100	2.100	2.199	2.100	2.100	2.100
C^1—C^2			1.410	1.470		1.410	1.410	1.410
C^2—C^3		1.300	1.410	1.440	1.410	1.410	1.410	
d—*d'*							1.790	1.790
d'—C^2							0.866	0.866
C^1—C^2—C^3			106.0	120.0		106.0	60.0	60.0
W^1—C′—W^2	79.9	86.7	79.0	86.2	83.3	79.9	79.9	79.9
W^1—C^1—W^2	79.9	86.9	69.9		83.3			
W^1—W^2—C(L)	125.0	125.0	125.0	125.0	115.6	125.0	125.0	125.0
W^2—W^1—C(L)	125.0	115.0	125.0	125.0	115.6	125.0	125.0	125.0
C(L)—W—C(L)	110.0	103.0	110.0	110.0		110.0	110.0	110.0
W^1—W^2—C(μ-C^2)	48.1	45.2	60.3		48.4			
d—*d'*—C^2							90.0	118.0

Distances are in angstrom units and angles in degrees.

Polyhedron Vol. 7, No. 10/11, pp. 881–902, 1988
Printed in Great Britain

0277–5387/88 $3.00+.00
© 1988 Pergamon Press plc

SYNTHESIS OF CATIONIC DIIRON μ-VINYLCARBYNE COMPLEXES

CHARLES P. CASEY,* MARK S. KONINGS and SETH R. MARDER

Department of Chemistry, University of Wisconsin, Madison, WI 53706, U.S.A.

(*Accepted* 5 *November* 1987)

Abstract—Reaction of the diiron μ-ethylidyne complex $[C_5H_5(CO)Fe]_2(\mu\text{-}CO)(\mu\text{-}C\text{—}CH_3)^+BF_4^-$ (**1**) with *p*-tolualdehyde gave a 92% yield of the μ-vinylcarbyne complex $[C_5H_5(CO)Fe]_2(\mu\text{-}CO)(\mu\text{-}C\text{-}E\text{-}CH{=}CHC_6H_4\text{-}p\text{-}CH_3)^+BF_4^-$ (**4**) which was characterized by spectroscopy and single crystal X-ray diffraction. **1** reacted with *para*-substituted benzaldehydes, cinnamaldehyde, pivalaldehyde, acetone, cyclohexanone, and isophorone to give similar vinylcarbyne complexes in 18–95% isolated yields. Propylidyne complex $[C_5H_5(CO)Fe]_2(\mu\text{-}CO)(\mu\text{-}C\text{—}CH_2CH_3)^+PF_6^-$ (**12**) reacted with *p*-tolualdehyde to give vinylcarbyne complex $[C_5H_5(CO)Fe]_2(\mu\text{-}CO)[\mu\text{-}C\text{-}E\text{-}C(CH_3){=}CHC_6H_4\text{-}p\text{-}CH_3]^+PF_6^-$ (**13**) in 83% yield. These new condensations are suggested to proceed by nucleophilic attack of a neutral μ-alkenylidene complex on a protonated aldehyde or ketone followed by dehydration. **1** reacted with isobutyraldehyde to give vinylcarbyne complex $[C_5H_5(CO)Fe]_2(\mu\text{-}CO)[\mu\text{-}C\text{-}E\text{-}CH{=}CHCH(CH_3)_2]^+BF_4^-$ (**20B**) which rearranged under the reaction conditions to give μ-alkenyl complex $[C_5H_5(CO)Fe]_2(\mu\text{-}CO)[\mu\text{-}\eta^1,\eta^2\text{-}E\text{-}CH{=}CHCH{=}C(CH_3)_2]^+BF_4^-$ (**21B**) in 88% yield. Reaction of diiron pentenylidene complex $[C_5H_5(CO)Fe]_2(\mu\text{-}CO)(\mu\text{-}C{=}CHCH_2CH_2CH_3)$ (**9**) with the hydride abstracting reagent $(C_6H_5)_3C^+PF_6^-$ gave vinylcarbyne complex $[C_5H_5(CO)Fe]_2(\mu\text{-}CO)(\mu\text{-}C\text{-}E\text{-}CH{=}CHCH_2CH_3)^+PF_6^-$ (**18P**) in 80% yield. Alkenylidene complex $[C_5H_5(CO)Fe]_2(\mu\text{-}CO)[\mu\text{-}C{=}C(CH_3)CH_2CH_3]$ (**35**), reacted with $(C_6H_5)_3C^+PF_6^-$ via preferential abstraction of a secondary allylic hydrogen to give a 3.8 : 1 ratio of vinylcarbyne complexes. $[C_5H_5(CO)Fe]_2(\mu\text{-}CO)[\mu\text{-}C{=}C(CH_3)CH_2C_6H_4\text{-}p\text{-}CH_3]$ (**38**), reacted with $(C_6H_5)_3C^+PF_6^-$ via preferential abstraction of a primary allylic hydrogen to give an 8.4 : 1 ratio of vinylcarbyne complexes.

Cationic diiron μ-vinylcarbyne complexes were first prepared by Rosenblum by reaction of $\eta\text{-}C_5H_5(CO)_2FeLi$ with cyclopentene oxide and with norbornene oxide followed by strong acid work-up, eq. (1).[1] However, vinylcarbyne complexes were not obtained with epoxides of other cyclic or acyclic alkenes.

We recently communicated two new methods for the synthesis of vinylcarbyne complexes.[2,3] One method involves allylic hydride abstraction from neutral diiron μ-alkenylidene complexes.[2] The other method utilizes a condensation reaction between cationic diiron μ-alkylidyne complexes and aldehydes, ortho esters, or ketones, eq. (2).[3] These complementary procedures provide access to a wide variety of vinylcarbyne complexes. In this paper, we report full details on the synthesis of cationic diiron μ-vinylcarbyne complexes.

Vinylcarbyne complexes are useful starting materials for the synthesis of functionalized μ-alkenylidene complexes. Nucleophiles such as $NaCH(CO_2CH_2CH_3)_2$ (C. P. Casey and M. S. Konings, unpublished observations) and PMe_3^2 add regioselectively to the remote vinyl carbon atom of vinylcarbyne complexes to generate alkenylidene complexes as shown in eq. (3).

Vinylcarbyne complexes have interesting electronic properties. We have found that vinylcarbyne complexes have unusually low barriers to rotation of the entire vinylcarbyne ligand.[4] Fenske–Hall calculations[5] reveal that a low barrier to vinylcarbyne rotation exists because the bridging carbyne carbon has orthogonal *p*-orbitals which can accept electron

* Author to whom correspondence should be addressed.

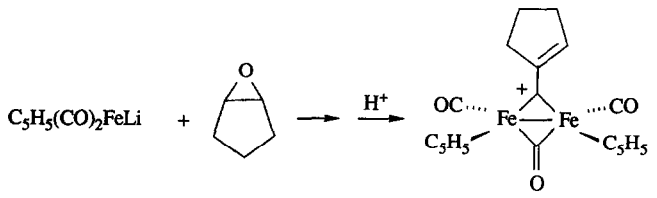

(1)

Eq. (1)

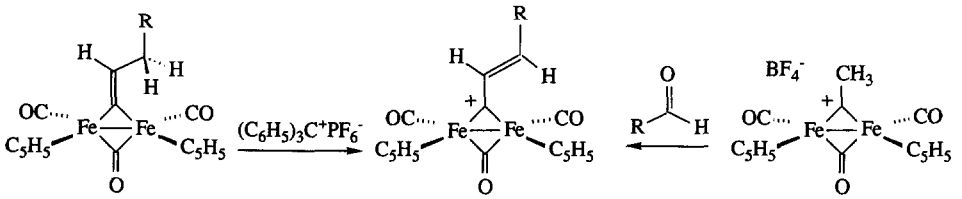

(2)

Eq. (2)

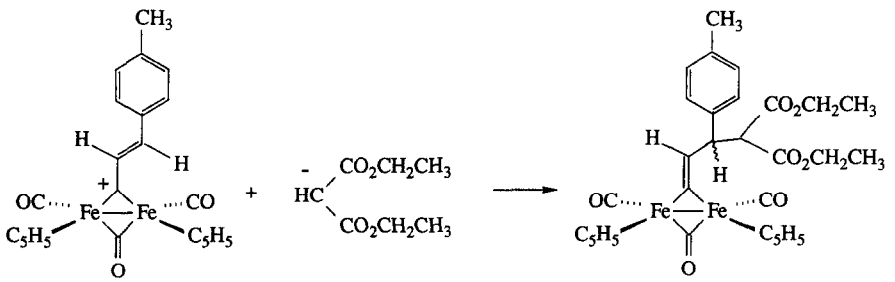

(3)

Eq. (3)

density from the vinyl group throughout rotation (Fig. 1).

RESULTS AND DISCUSSION

Synthesis of vinylcarbyne complexes by condensation

The condensation of *para*-substituted benzaldehydes with μ-ethylidyne diiron complex $[C_5H_5(CO)Fe]_2(\mu\text{-}CO)(\mu\text{-}C\text{—}CH_3)^+BF_4^-$ (**1**)[1] occurred smoothly and in high yield in either THF or CH_2Cl_2. For example, when *p*-tolualdehyde was added to a suspension of the red ethylidyne complex **1** in THF at 40°C the *p*-tolyl substituted vinylcarbyne complex $[C_5H_5(CO)Fe]_2(\mu\text{-}CO)(\mu\text{-}C\text{-}E\text{-}CH{=}CHC_6H_4\text{-}p\text{-}CH_3)^+BF_4^-$ (**4**) gradually precipitated from solution over 24 h and was isolated in 92% yield as analytically pure brilliant purple microcrystals. In CD_2Cl_2 at 38°C, the half-life for the condensation of *p*-tolualdehyde (0.05 M) with **1** (0.02 M) was about 2 h. Similarly, the condensation of **1** with *p*-nitrobenzaldehyde, benzaldehyde, *p*-anisaldehyde, *p*-hydroxybenzaldehyde, and *p*-dimethylaminobenzaldehyde led to the formation of high yields of the vinyl carbyne complexes $[C_5H_5(CO)Fe]_2(\mu\text{-}CO)(\mu\text{-}C\text{-}E\text{-}CH{=}CHC_6H_4\text{-}p\text{-}X)^+BF_4^-$ [**2**, X = NO_2; **3**, X = H; **5**, X = OCH_3; **6**, X = OH; **7**, X = $N(CH_3)_2$]. Multigram quantities of aryl substituted vinylcarbyne complexes were easily prepared by this condensation reaction, eq. (4).

The formation of vinylcarbyne complexes can be explained by the mechanism shown in Fig. 2. In the first step of this mechanism, a cationic alkylidyne complex and an aldehyde are proposed to be in equilibrium with a neutral alkenylidene complex and a protonated aldehyde. Pettit[6] and others[7,8] have shown that alkylidyne complexes can be reversibly deprotonated to yield alkenylidene complexes. We have found that the pentylidyne complex $[C_5H_5(CO)Fe]_2(\mu\text{-}CO)(\mu\text{-}C\text{—}CH_2CH_2CH_2CH_3)^+PF_6^-$ (**8P**)[1,8] is approximately as acidic as trifluoroacetic acid by studying the equilibrium between **8** and pentenylidene complex $[C_5H_5(CO)Fe]_2(\mu\text{-}CO)(\mu\text{-}C{=}CHCH_2CH_2CH_3)$ (**9**)[8] in the presence of trifluoroacetic acid in CD_2Cl_2 (C. P. Casey and E. A. Austin, unpublished observations).

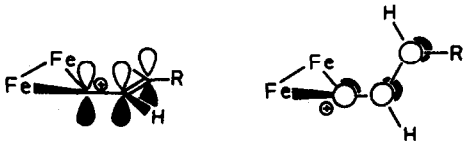

Fig. 1.

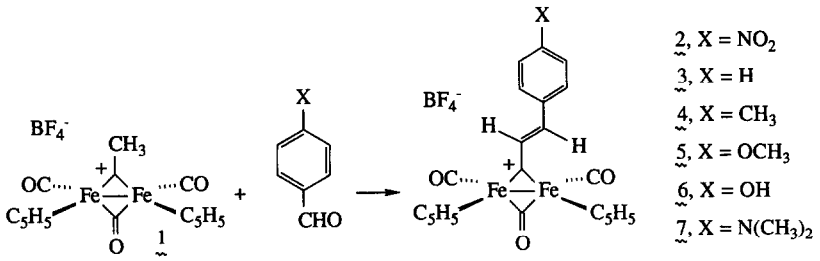

(4)

Eq. (4)

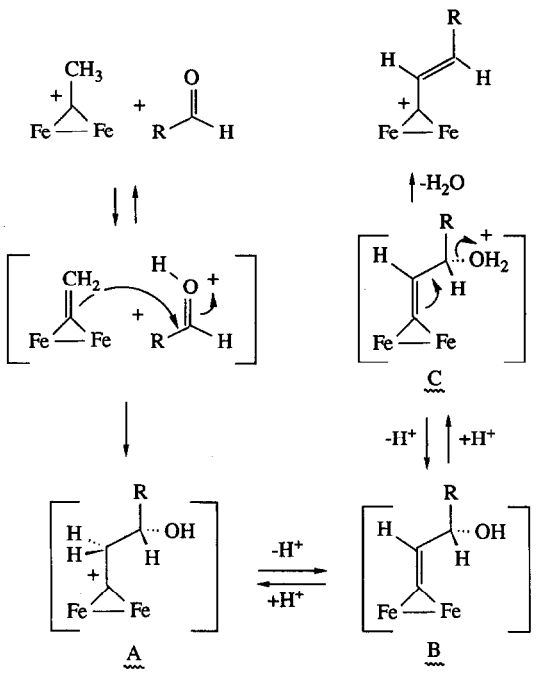

Fig. 2.

In the key carbon–carbon bond forming step in this mechanism, the alkenylidene complex functions as a carbon nucleophile and attacks the carbonyl carbon of the protonated aldehyde to produce alkylidyne intermediate **A**. The driving force for this reaction is the formation of a carbon–carbon bond and of a cationic carbon center stabilized by two strongly electron donating iron centers. Deprotonation of **A** produces the neutral hydroxy substituted alkenylidene intermediate **B**. Protonation of the hydroxy group of **B** followed by loss of water from the protonated intermediate **C** then produces the vinylcarbyne complex.

The formation of vinylcarbyne complexes in this new condensation reaction is not reversible. A CD_2Cl_2 solution containing the *p*-tolyl substituted vinylcarbyne complex **4** (0.007 M), *p*-dimethylaminobenzaldehyde (0.02 M), and water (0.08 M) was monitored by ^1H NMR. After 11 days at 38°C, no (< 5%) formation of *p*-tolualdehyde or the *p*-dimethylaminophenyl substituted vinylcarbyne complex **7** was observed; however, about 68% of **4** had decomposed. Similarly, when a solution of *p*-tolualdehyde, **7**, and H_2O was monitored over 11 days, no formation of *p*-dimethylaminobenzaldehyde or **4** was observed and 50% decomposition of **7** was seen, eq. (5).

Vinylcarbyne complexes were characterized by ^1H and ^{13}C NMR and IR spectroscopy. For brevity only the spectra of *p*-tolyl substituted complex **4** will be discussed in detail. The key features of the ^1H NMR spectrum of **4** are the low field doublets due to *trans* vinyl hydrogens at δ 10.26 (d, $J = 14.9$ Hz, μ-C—CH) and δ 8.09 (d, $J = 14.9$ Hz, μ-C—CH=C*H*). The two cyclopentadienyl groups gave rise to a single resonance at δ 5.67. Since the solid state structure of **4** has inequivalent Cp ligands,[3] the observation of a single Cp resonance in the ^1H NMR spectrum implies that a rapid fluxional process, such as rotation of the vinylcarbyne ligand, occurs in solution.[4]

In the ^{13}C NMR spectrum of **4**, the bridging carbyne carbon appears far downfield at δ 439.9. The resonances for the bridging and terminal carbonyls appeared at δ 254.3 and 208.9, respectively. Vinyl carbon atoms in **4** were observed at δ 153.4 and 152.4. The bridging carbyne carbon resonance of **4** is ~ 60 ppm less downfield than that of starting ethylidyne complex **1** (δ 497.9). The downfield

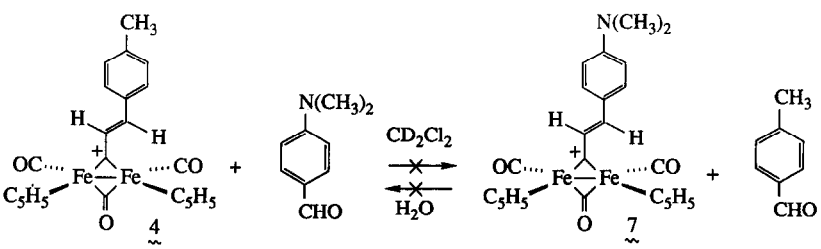

(5)

Eq. (5)

Table 1. Spectral properties and σ_p^+ values

Compound	X	σ_p^{+a}	^{1}H NMR C_5H_5	^{13}C NMR μ-C	^{13}C NMR C_5H_5	IR Symmetric	IR Bridging
2	NO_2	0.740	5.73	451.2	93.5	2040	1853
3	H	0.0	5.68	44.30	93.0	2038	1847
4	CH_3	−0.256	5.67	439.9	93.1	2033	1848
5	OCH_3	−0.648	5.64	431.6	92.8	2028	1842
6	OH	−0.853	5.63	428.1	92.5	2024	1838
7	$N(CH_3)_2$	−1.7[b]	5.49	395.2	91.8	1019	1837
Correlation coefficient, ρ			0.96	0.95	0.97	0.97	0.94

[a] Values are those given by C. G. Swain and E. C. Lupton, Jr., *J. Am. Chem. Soc.* 1968, **90**, 4328.
[b] Value given by P. R. Wells, *Chem. Rev.* 1963, **63**, 771.

chemical shifts of carbene and bridging carbyne carbons have been associated with a low lying LUMO localized in the carbene or carbyne carbon.[9] The LUMO of bridging carbyne complexes has a major contribution from the bridging carbyne carbon *p*-orbital perpendicular to the Fe_2-μ-C plane.[10] Conjugation of this *p*-orbital on **4** with the vinyl group results in a more diffuse LUMO than in the case of **1** and a smaller downfield chemical shift is observed. A similar effect was seen for $Cp(CO)_2Fe{=}CMe_2^+$ (δ 419.0) and $Cp(CO)_2Fe{=}CH{-}CH{=}CMe_2^+$ (δ 316.7).[11]

IR spectroscopy indicates that these vinylcarbyne complexes have *cis* terminal carbonyl ligands.[8] For **4**, a high energy symmetric stretch and a lower energy asymmetric stretch were observed at 2033 (vs) cm^{-1} and 2000 (m) cm^{-1} in addition to the bridging carbonyl stretch at 1848 (s) cm^{-1} in CH_2Cl_2 solution. Electron donor groups in the *para* position of the vinylcarbyne complexes **2**–**7** bring about a decrease in the IR stretching frequencies of the bridging and terminal carbonyl groups. Electron donation from the aryl substituent is fed into the iron centers and results in increased iron to carbonyl back-bonding. Similarly, electron donor *para* substituents bring about upfield shifts in the ^{1}H and ^{13}C NMR resonances of the Cp groups, again indicating an increase in electron density at the Fe_2-μ-C core. In all these cases, good correlations (ρ = 0.94–0.97) were obtained when the spectral properties were plotted vs the σ_p^+ values of the *para* substituent (Table 1) and are consistent with our observation that the magnitude of the barrier to vinylcarbyne rotation increases as better electron donor groups are placed on the remote vinyl carbon.[4]

Condensation of **1** with other non-enolizable aldehydes also occurs cleanly. Reaction of **1** with pivalaldehyde in CH_2Cl_2 led to the isolation of the t-butyl substituted vinylcarbyne complex $[C_5H_5(CO)Fe]_2(\mu\text{-}CO)[\mu\text{-}C\text{-}E\text{-}CH{=}CHC(CH_3)_3]^+ BF_4^-$ (**10**) in 83% yield. Condensation of **1** with cinnamaldehyde yielded the more highly conjugated vinylcarbyne complex $[C_5H_5(CO)Fe]_2(\mu\text{-}CO)(\mu\text{-}C\text{-}E,E\text{-}CH{=}CHCH{=}CHC_6H_5)^+BF_4^-$ (**11**) in 92% yield, eq. (6).

Longer chain alkylidyne complexes also react with aldehydes to produce vinylcarbyne complexes. When a suspension of propylidyne complex $[C_5H_5(CO)Fe]_2(\mu\text{-}CO)(\mu\text{-}C{-}CH_2CH_3)^+PF_6^-$ (**12**)[8] was stirred in neat *p*-tolualdehyde at ambient temperature for 20 h, **12** slowly dissolved and the vinylcarbyne complex $[C_5H_5(CO)Fe]_2(\mu\text{-}CO)[\mu\text{-}C\text{-}E\text{-}C(CH_3){=}CHC_6H_4\text{-}p\text{-}CH_3]^+PF_6^-$ (**13**) was isolated in 83% crude yield. Similarly, pentylidyne complex $[C_5H_5(CO)Fe]_2(\mu\text{-}CO)(\mu\text{-}C{-}CH_2CH_2CH_2CH_3)^+ BF_4^-$ (**8B**) reacted with neat *p*-tolualdehyde at ambient temperature over 42 h to produce vinylcarbyne complex $[C_5H_5(CO)Fe]_2(\mu\text{-}CO)[\mu\text{-}C\text{-}E\text{-}C(CH_2CH_2CH_3){=}CHC_6H_4\text{-}p\text{-}CH_3]^+BF_4^-$ (**14**) in

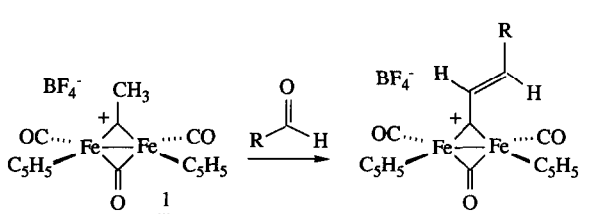

(6)

Eq. (6)

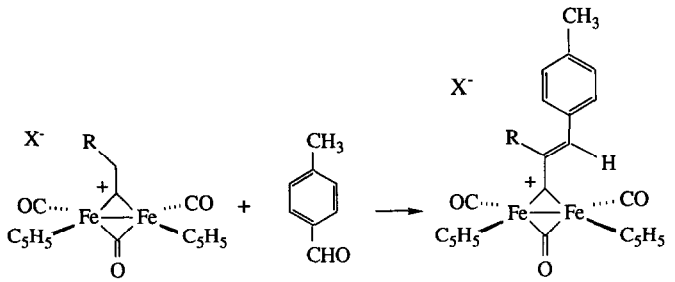

12, R = CH_3; X = PF_6
8, R = n-Pr; X = BF_4

13, R = CH_3; X = PF_6
14, R = n-Pr; X = BF_4

(7)

Eq. (7)

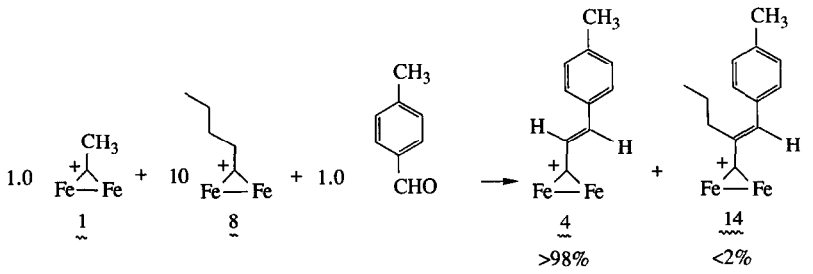

(8)

Eq. (8)

77% isolated yield as a 4.4:1 ratio of *cis* and *trans* isomers **14c** and **14t**, eq. (7).

The condensation reactions of these longer chain alkylidyne complexes are significantly slower than those of ethylidyne complex **1**. In a competition experiment, ethylidyne complex **1** (0.057 mmol) and pentylidyne complex **8B** (0.57 mmol) were allowed to compete for a deficiency of *p*-tolualdehyde (0.057 mmol), eq. (8). NMR analysis of the red–brown powder obtained upon precipitation of the CH_2Cl_2 solution with diethyl ether revealed the presence of ethylidyne condensation product **4**. No pentylidyne condensation product **14** was detected (2% detection limit). From this data, we calculate that ethylidyne complex **1** is at least 500 times more reactive than pentylidyne complex **8B**. We had previously found that substituted alkylidyne complexes **8P** and **12** rearrange to μ-alkenyl complexes upon heating.[12] Due to the thermal sensitivity and low reactivity of **8** and **12**, high yields of condensation products are best obtained by running the reactions in neat aldehyde.

Ethylidyne complex **1** is much less reactive towards ketones than aldehydes. Under conditions where the reaction of **1** with aldehydes is complete in 24 h (4 equivalents of aldehyde in CD_2Cl_2 at 23°C) the condensation of **1** with acetone or cyclohexanone is very slow ($t_{1/2} \sim 30$ days). However, condensations of **1** with neat ketones occur on a convenient time scale.

1 condensed cleanly with neat cyclohexanone over 18 h at 16°C to yield vinylcarbyne complex $[C_5H_5(CO)Fe]_2(\mu\text{-}CO)(\mu\text{-}C{-}CH{=}CCH_2CH_2CH_2CH_2CH_2)^+BF_4^-$ (**15**) in 76% crude yield. Pure **15** was obtained in 44% yield by recrystallization from THF. Condensation of **1** with neat

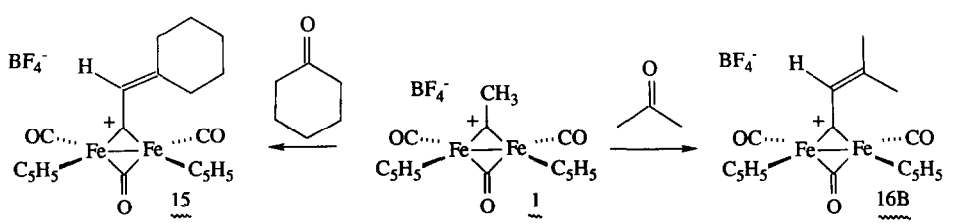

(9)

Eq. (9)

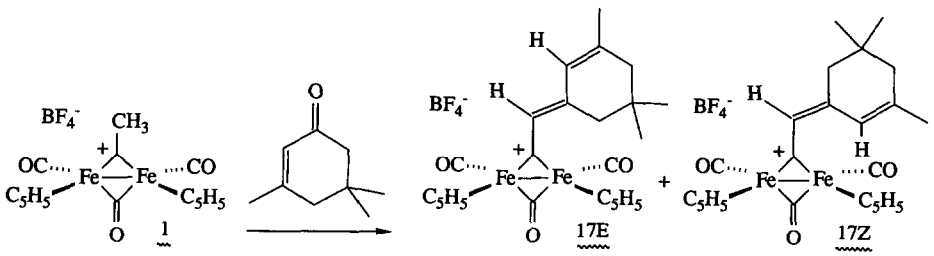

(10)

Eq. (10)

acetone proceeded smoothly to generate vinylcarbyne complex $[C_5H_5(CO)Fe]_2(\mu\text{-CO})[\mu\text{-C—CH=C}(CH_3)_2]^+BF_4^-$ (**16B**) in 83% yield, eq. (9).

Neat isophorone condensed slowly with ethylidyne complex **1** (4–5 days) to give two isomeric vinylcarbyne complexes $[C_5H_5(CO)Fe]_2(\mu\text{-CO})[\mu\text{-C-}E\text{-CH=CCH=C}(CH_3)CH_2C(CH_3)_2CH_2]^+BF_4^-$ (**17E**) and $[C_5H_5(CO)Fe]_2(\mu\text{-CO})[\mu\text{-C-}Z\text{-CH=CCH=C}(CH_3)CH_2C(CH_3)_2CH_2]^+BF_4^-$ (**17Z**) in a 2.8:1 ratio in 50% crude yield, eq. (10). Pure **17** enriched in **17E** (**17E**:**17Z** ~ 8:1) was obtained in 18% yield after careful recrystallization from CH_2Cl_2–ether. The structure of the major isomer was shown to be **17E** by NOE experiments. Irradiation of the quartet at δ 6.59 (q, J = 1.5 Hz, μ-C—CH=C—C*H*) due to a vinyl proton on the major isomer led to a 42% increase in the signal of the other vinyl proton of the major isomer at δ 9.58 (s, μ-C—CH). Similarly, irradiation of the δ 9.58 resonance led to a 10% increase in the δ 6.59 resonance. These large NOEs unambiguously establish the structure of the major isomer as **17E**.

The reactions of ethylidyne complex **1** with enolizable aldehydes proved to be complex. Reaction of propanal with a THF suspension of **1** led to a mixture of many products which did not contain any of the desired vinylcarbyne complex $[C_5H_5(CO)Fe]_2(\mu\text{-CO})(\mu\text{-C-}E\text{-CH=CHCH}_2CH_3)^+BF_4^-$ (**18B**). An authentic sample of the corresponding PF_6^- salt **18P** was prepared by reaction of $(C_6H_5)_3C^+PF_6^-$ with alkenylidene complex $[C_5H_5(CO)Fe]_2(\mu\text{-CO})(\mu\text{-C=CHCH}_2CH_2CH_3)$ (**9**) and was shown to be unstable ($t_{1/2}$ = 1.5 h, 25°C) in THF solution. Attempted condensation of **1** with propanal in CH_2Cl_2 led to a complex mixture of products containing some **18B** (< 20%). Similarly, reaction of **1** with 3-phenylpropanal in CH_2Cl_2 led to the observation of the desired vinylcarbyne complex $[C_5H_5(CO)Fe]_2(\mu\text{-CO})(\mu\text{-C-}E\text{-CH=CHCH}_2CH_2C_6H_5)^+BF_4^-$ (**19**) as a major component of the crude reaction mixture, but repeated attempts to obtain pure **19** failed, eq. (11).

In contrast to the reaction of ethylidyne complex **1** with propanal and 3-phenylpropanal, reaction of **1** with isobutyraldehyde in CH_2Cl_2 for 15 h at 37°C led to the isolation of a single, pure product. However, instead of the expected vinylcarbyne complex $[C_5H_5(CO)Fe]_2(\mu\text{-CO})[\mu\text{-C-}E\text{-CH=CHCH}(CH_3)_2]^+BF_4^-$ (**20B**), its rearrangement product the μ-alkenyl complex $[C_5H_5(CO)Fe]_2(\mu\text{-CO})[\mu\text{-}\eta^1,\eta^2\text{-}E\text{-CH=CHCH=C}(CH_3)_2]^+BF_4^-$ (**21B**) was obtained in 88% yield, eq. (12). The observation of a low field ^1H NMR resonance at δ 12.03 (d, J = 11.8 Hz) for the μ-CH proton and of a ^{13}C NMR resonance at δ 173.2 for the μ-C carbon were crucial in establishing the structure of **21B**.

When the reaction of **1** with isobutyraldehyde in CD_2Cl_2 at 38°C was monitored by ^1H NMR using hexamethylbenzene as an internal standard, the initial formation of vinylcarbyne complex **20B** was noted (19% after 1 h). At longer reaction times, the resonances for **20B** increased and the formation of μ-alkenyl rearrangement product **21B** was observed

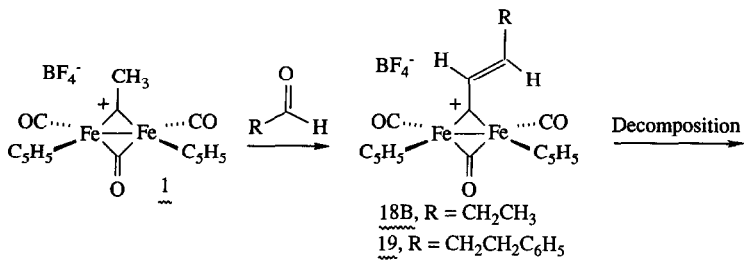

18B, R = CH_2CH_3
19, R = $CH_2CH_2C_6H_5$

(11)

Eq. (11)

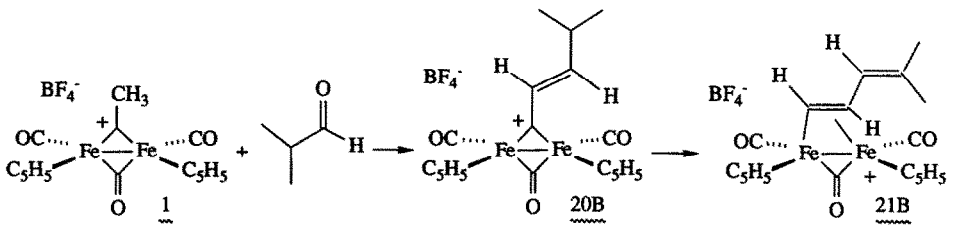

(12)

Eq. (12)

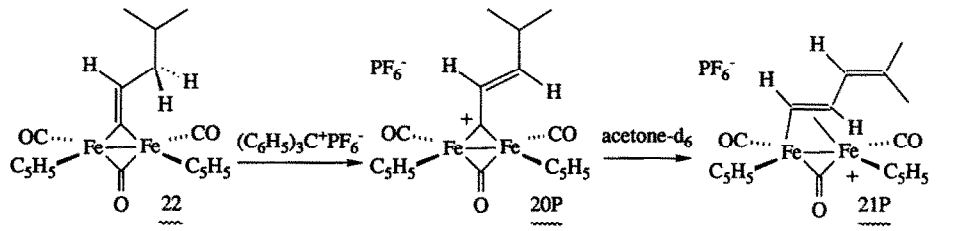

(13)

Eq. (13)

(31% of **20B** and 29% of **21B** after 3 h). At still longer reaction times, the resonances for **20B** decreased as those of **21B** continued to increase (11% of **20B** and 61% of **21B** after 5 h). After 6 h only resonances for **21B** (76%) were seen and no **20B** was observed (5% detection limit).

An authentic sample of vinylcarbyne complex **20** as the corresponding PF_6^- salt **20P** was prepared in 88% yield by reaction of $(C_6H_5)_3C^+PF_6^-$ with μ-alkenylidene complex $[C_5H_5(CO)Fe]_2(\mu\text{-}CO)[\mu\text{-}C{=}CHCH_2CH(CH_3)_2]$ (**22**). The isomerization of vinylcarbyne complex **20P** (0.03 M) in acetone-d_6 at 23°C to μ-alkenyl complex **21P** was monitored by ^1H NMR and found to occur with $t_{1/2}$ of 3 h, eq. (13).

The rearrangement of vinylcarbyne complex **20** to μ-alkenyl complex **21** can be explained by the sequence of reactions shown in Scheme 1. Reversible deprotonation of vinylcarbyne complex **20** generates dienylidene intermediate **D**. A similar deprotonation of a vinylcarbyne complex was observed previously.[2] Protonation of **D** can also occur at the β-carbon to produce the cationic allylcarbyne intermediate **E**. Reversible protonation of μ-alkenylidene complexes is a well-known facile process (Refs 6–8; C. P. Casey and E. A. Austin, unpublished observations). The key step in this mechanism is the 1,2-hydride migration that converts alkylidyne intermediate **E** into μ-alkenyl product **21**. Electron donating alkyl groups on the β-carbon

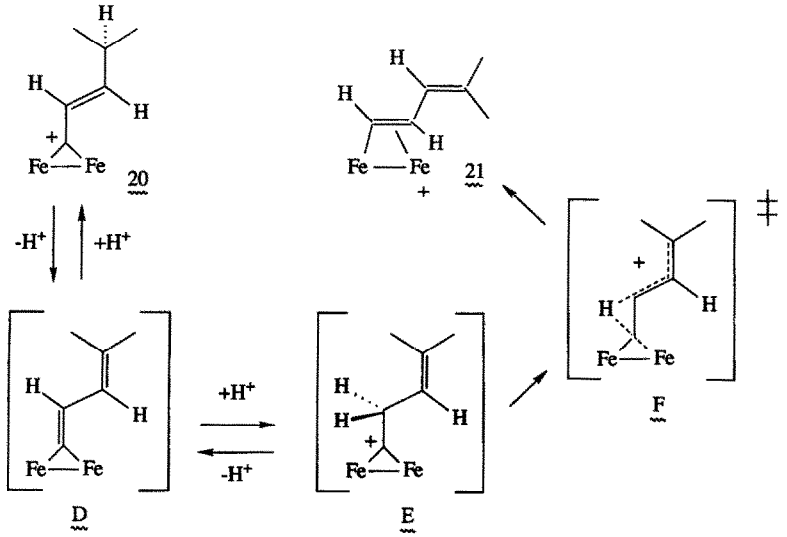

Scheme 1.

of μ-alkylidyne complexes dramatically accelerate the rearrangement to μ-alkenyl complexes.[12] Alkylidyne complexes with a single β-alkyl substituent normally require heating to 90°C for rearrangement to μ-alkenyl complexes. The more rapid isomerization of **E** to **21** is attributed to the enhanced electron donor ability of the β-dimethylvinyl substituent that stabilizes transition state **F**.

The failure to observe similar rearrangements for vinylcarbyne complexes **18** and **19** is somewhat surprising. Evidently the rearrangements of these vinylcarbyne complexes which possess only a single electron donor alkyl substituent on the β-vinyl carbon in transition state **F** are sufficiently slow that they do not effectively compete with alternate decomposition pathways.

A similar rearrangement was seen in the reaction of **1** with cyclohexanecarboxyaldehyde which led to the isolation of μ-alkenyl complex $[C_5H_5(CO)Fe]_2(\mu\text{-}CO)(\mu\text{-}\eta^1,\eta^2\text{-}E\text{-}CH{=}CHCH{=}CCH_2CH_2CH_2CH_2CH_2)^+BF_4^-$ (**23**) in 65% yield, eq. (14). When this reaction was followed by ^1H NMR, the initial build-up of vinylcarbyne complex $[C_5H_5(CO)Fe]_2(\mu\text{-}CO)(\mu\text{-}C\text{-}E\text{-}CH{=}CHCHCH_2CH_2CH_2CH_2CH_2)^+BF_4^-$ (**24**) and its subsequent conversion to **23** were observed. As in the case of the formation of μ-alkenyl complex **21** from isobutyraldehyde, the presence of an electron donor β-disubstituted vinyl group in the key allylcarbyne intermediate similar to **E** leads to the rearrangement reaction.

To further probe the electronic requirements for these rearrangements, we studied the reaction of **1** with phenylacetaldehyde and found that condensation followed by rearrangement occurred to produce the μ-alkenyl complex $[C_5H_5(CO)Fe]_2(\mu\text{-}CO)(\mu\text{-}\eta^1,\eta^2\text{-}E,E\text{-}CH{=}CHCH{=}CHC_6H_5)^+BF_4^-$ (**25**). In this case, a single phenyl substituent on the vinyl group of the key allylcarbyne intermediate is sufficiently electron donating to allow rearrangement. **25** was found to be in equilibrium with a further rearrangement product $[C_5H_5(CO)_2Fe][C_5H_5(CO)Fe](\mu\text{-}\eta^1,\eta^4\text{-}E,E\text{-}CH{=}CHCH{=}CHC_6H_5]^+BF_4^-$ (**26**), eq. (15). This further rearrangement will be the subject of a subsequent paper.

The reactivity of ethylidyne complex **1** with other carbonyl compounds was briefly explored. The reactions of **1** with methyl formate, acetic anhydride, benzoyl chloride, or acetyl chloride led

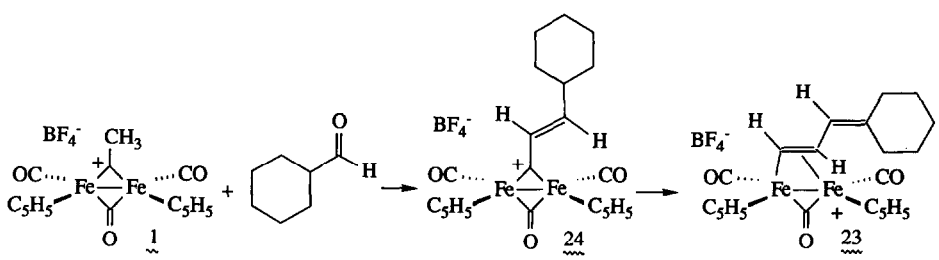

(14)

Eq. (14)

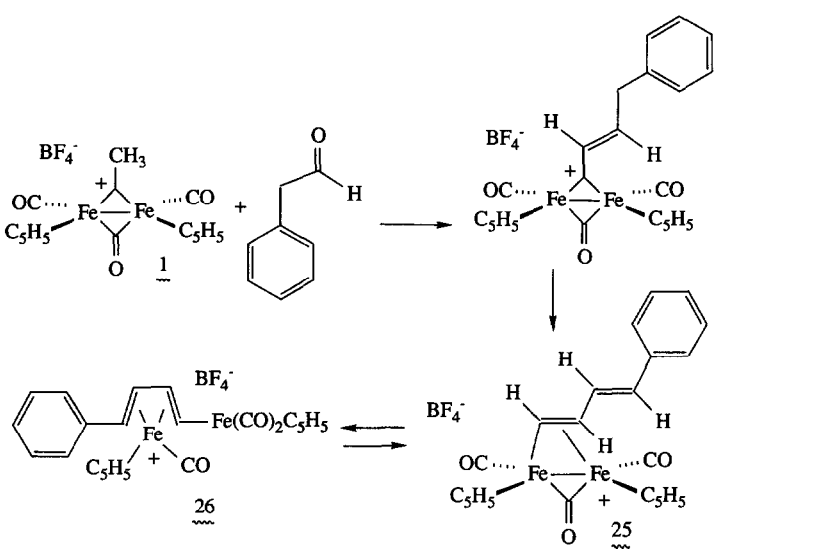

(15)

Eq. (15)

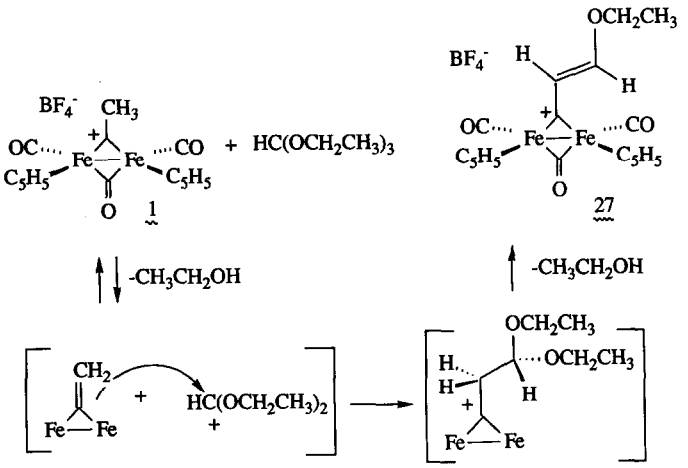

(16)

Eq. (16)

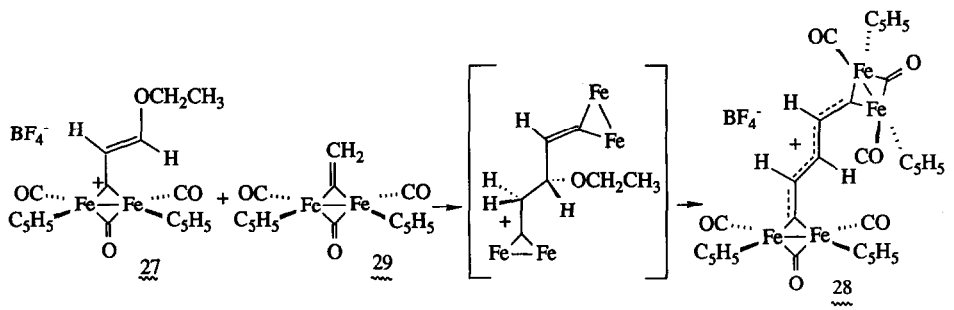

(17)

Eq. (17)

either to reisolation of starting material **1** or to the observation of a mixture of **1** and unidentified decomposition products.

However, **1** condensed cleanly with triethyl *ortho*formate to yield the ethoxy substituted vinylcarbyne complex $[C_5H_5(CO)Fe]_2(\mu\text{-}CO)(\mu\text{-}C\text{-}E\text{-}CH{=}CHOCH_2CH_3)^+BF_4^-$ (**27**) in 77% yield, eq. (16). Careful crystallization of **27** was necessary to remove 5–10% of a contaminating tetrairon vinylcarbyne complex $\{[C_5H_5(CO)Fe]_2(\mu\text{-}CO)\}_2(\mu\text{-}C_5H_3)^+BF_4^-$ (**28**).[13]

Pure tetrairon complex **28** was obtained in 85% yield as pink–brown microcrystals from the reaction of ethenylidene complex $[C_5H_5(CO)Fe]_2(\mu\text{-}CO)(\mu\text{-}C{=}CH_2)$ (**29**)[7] with ethoxy substituted vinylcarbyne complex **27** as shown in eq. (17). This reaction is proposed to occur by nucleophilic attack of the remote ethenylidene carbon of **29** on the remote vinyl carbon of **27** followed by elimination of ethanol.

Nucleophilic replacement of the ethoxy group of **27** in a reaction with dimethylamine was also observed. When dimethylamine was added to a THF solution of **27** at −78°C, a color change from red–orange to orange occurred instantly. Orange, microcrystalline $[C_5H_5(CO)Fe]_2(\mu\text{-}CO)[\mu\text{-}C\text{-}E\text{-}CH{=}CHN(CH_3)_2]^+BF_4^-$ (**30**) gradually precipitated from solution and was isolated in 84% yield. **30** is the only vinylcarbyne complex with a sufficiently high rotation barrier about the carbyne

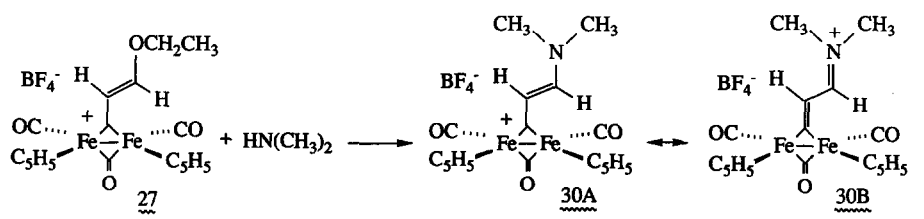

(18)

Eq. (18)

carbon to vinyl carbon bond to exhibit two Cp resonances in the ^1H and ^{13}C NMR at room temperature.[4] This indicates the importance of resonance structures **30A** and **30B**, eq. (18).

Synthesis of vinylcarbyne complexes by hydride abstraction

A second method for the preparation of diiron vinylcarbyne complexes involves allylic hydride abstraction from alkenylidene complexes with $(C_6H_5)_3C^+PF_6^-$. A wide variety of μ-alkenylidene complexes are readily available via deprotonation of cationic μ-alkylidyne complexes. The alkylidyne complexes in turn can be synthesized either by the addition of the C—H bond of methylidyne complex $[C_5H_5(CO)Fe]_2(\mu\text{-CO})(\mu\text{-CH})^+PF_6^-$ (**31**) across the carbon–carbon double bond of alkenes in a hydrocarbation reaction,[8] or by the reaction of lithium reagents with $[C_5H_5(CO)_2Fe]_2(\mu\text{-CO})_2$ followed by treatment with strong acid.[1]

When a CH_2Cl_2 solution of μ-pent-1-enylidene complex **9** and $(C_6H_5)_3C^+PF_6^-$ was stirred at 0°C for 1 h μ-pent-2-enylidyne complex **18P** was isolated as a red precipitate in 80% yield, eq. (19). As indicated earlier, efforts to prepare **18** via condensation of ethylidyne complex **1** with propanal were unsuccessful.

Reaction of μ-(3-methyl)but-1-enylidene complex $[C_5H_5(CO)Fe]_2(\mu\text{-CO})[\mu\text{-C}{=}CHCH(CH_3)_2]$ (**32**)[8] with $(C_6H_5)_3C^+PF_6^-$ led to abstraction of the tertiary allylic hydride and μ-(3-methyl)but-2-enylidyne complex **16P** was isolated in 77% yield. The related BF_4^- salt **16B** was prepared in 83% yield by condensation of **1** with acetone as described earlier, eq. (20).

Reaction of $[C_5H_5(CO)Fe]_2(\mu\text{-CO})(\mu\text{-C}{=}CCH_2CH_2CH_2CH_2)$ (**33**)[12] with $(C_6H_5)_3C^+PF_6^-$ led to hydride abstraction and formation of vinylcarbyne complex $[C_5H_5(CO)Fe]_2(\mu\text{-CO})(\mu\text{-C—C}{=}CHCH_2CH_2CH_2)^+PF_6^-$ (**34P**) in 71% yield. Earlier, Rosenblum had prepared the BF_4^- salt **34B** from the reaction of $C_5H_5(CO)_2FeLi$ with cyclopentene oxide followed by treatment with strong acid,[1] eq. (21).

To determine the selectivity for the abstraction of primary versus secondary allylic hydrides, the reaction of $[C_5H_5(CO)Fe]_2(\mu\text{-CO})[\mu\text{-C}{=}C(CH_3)CH_2CH_3]$ (**35**)[8] with $(C_6H_5)_3C^+PF_6^-$ was studied. The product of secondary allylic hydride abstraction was selectively formed and a 3.8 : 1 mixture of vinylcarbyne complexes $[C_5H_5(CO)Fe]_2(\mu\text{-CO})[\mu\text{-C-}E\text{-C}(CH_3){=}CHCH_3]^+PF_6^-$ (**36**) and $[C_5H_5(CO)Fe]_2(\mu\text{-CO})[\mu\text{-C—C}(CH_2CH_3){=}CH_2]^+PF_6^-$ (**37**) was isolated, eq. (22). However, the reaction of

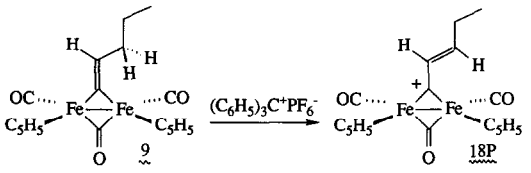

(19)

Eq. (19)

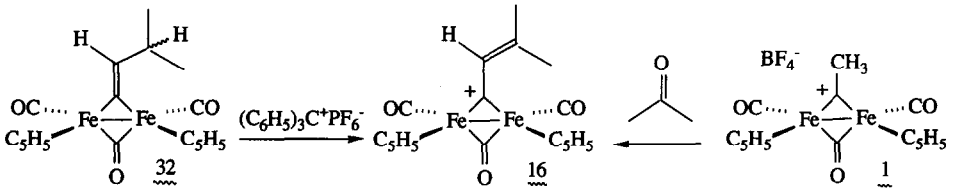

(20)

Eq. (20)

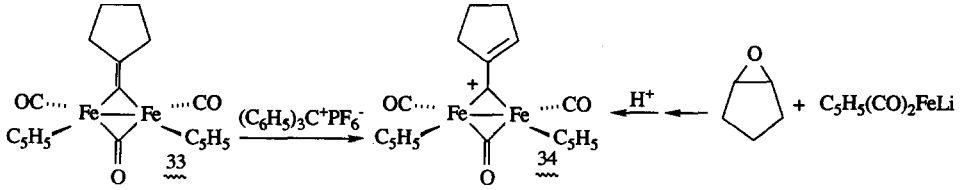

(21)

Eq. (21)

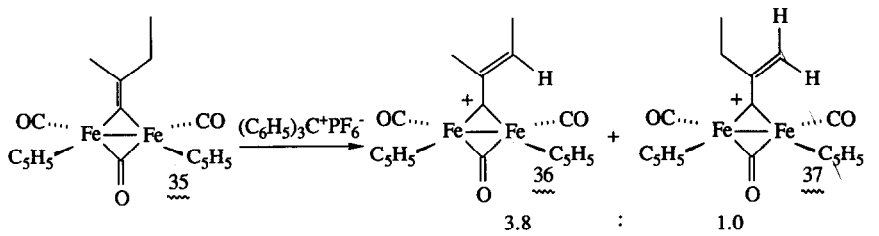

(22)

Eq. (22)

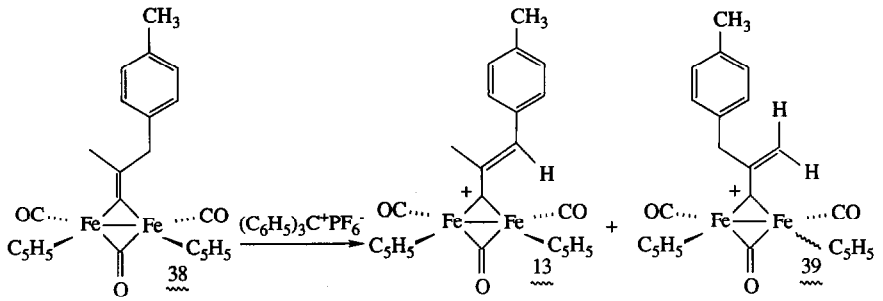

(23)

Eq. (23)

alkenylidene complex $[C_5H_5(CO)Fe]_2(\mu\text{-}CO)[\mu\text{-}C{=}C(CH_3)CH_2C_6H_4\text{-}p\text{-}CH_3]$ (**38**) with $(C_6H_5)_3C^+PF_6^-$ led to selective abstraction of a primary hydride in preference to abstraction of a benzylic hydride and an 8.4 : 1 mixture of $[C_5H_5(CO)Fe]_2(\mu\text{-}CO)[\mu\text{-}C{-}C(CH_2C_6H_4\text{-}p\text{-}CH_3){=}CH_2]^+PF_6^-$ (**39**) (as a 2.8 : 1 mixture of *cis* and *trans* isomers, **39c** and **39t**) and $[C_5H_5(CO)Fe]_2(\mu\text{-}CO)(\mu\text{-}C\text{-}E\text{-}CH{=}CHC_6H_4\text{-}p\text{-}CH_3)^+PF_6^-$ (**13**) were formed, eq. (23). Alkenylidene complex $[C_5H_5(CO)Fe]_2(\mu\text{-}CO)[\mu\text{-}C{=}C(CH_3)CH(CH_3)_2]$ (**40**) (C. P. Casey, M. W. Meszaros and S. R. Marder, unpublished observations), containing primary and tertiary allylic hydrogens, underwent only primary hydride abstraction upon treatment with $(C_6H_5)_3C^+PF_6^-$ to yield vinylcarbyne complex $[C_5H_5(CO)Fe]_2(\mu\text{-}CO)\{\mu\text{-}C{-}C[CH(CH_3)_2]{=}CH_2\}^+PF_6^-$ (**41**) in 63% yield as a 2.4 : 1 mixture of *cis* and *trans* isomers **41c** and **41t**. These results clearly demonstrate that the product selectivity is not controlled by the ability of electron donor substituents to stabilize the electron deficient vinylcarbyne group. Subtle conformational effects must be influencing the kinetic selectivities observed.

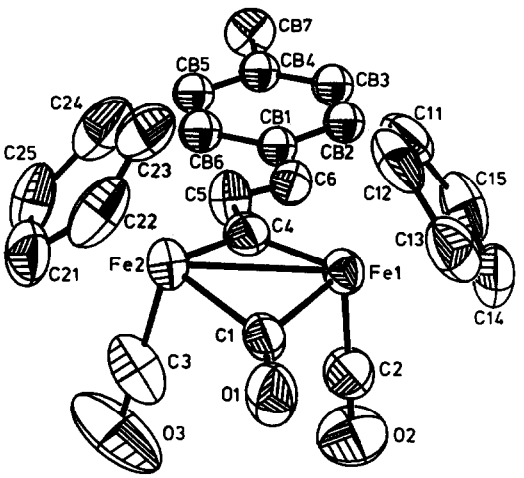

Fig. 3. Structure of **4**, BF_4^- and hydrogens omitted for clarity.

Crystal structures of vinylcarbyne complexes

In order to more completely define the bonding within vinylcarbyne complexes, the X-ray crystal structures of the *p*-tolyl substituted vinylcarbyne complex **4**, tetrairon vinylcarbyne complex **28**,* and dimethylamino substituted vinylcarbyne complex **30** were determined. Overall geometries and atom labelling schemes for **4**, **28** and **30** are presented in Figs 3, 4 and 5 respectively. A summary of important bond lengths and angles for **4**, **28** and **30** is presented in Tables 2, 3 and 4.†

* The results presented here contain further refinement of the structure of **28** beyond that presented in Ref. 13.

† A complete list of bond lengths and angles, as well as atomic coordinates and thermal parameters for **28** and **30**, are available as supplementary material. A complete list of bond lengths and angles, and atomic coordinates and thermal parameters for **4** are available as supplementary material from Ref. 3.

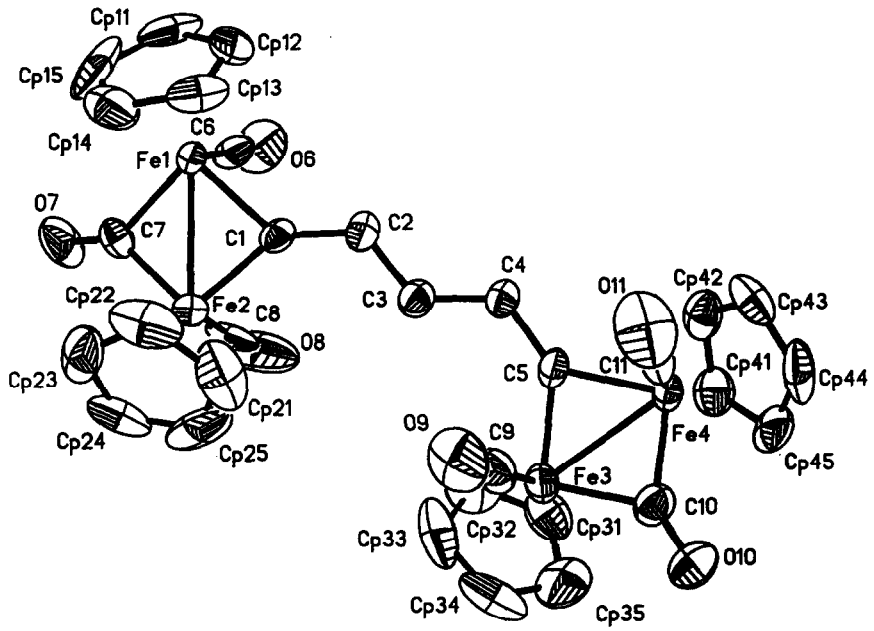

Fig. 4. Structure of **28**, BF_4^- and hydrogens omitted for clarity.

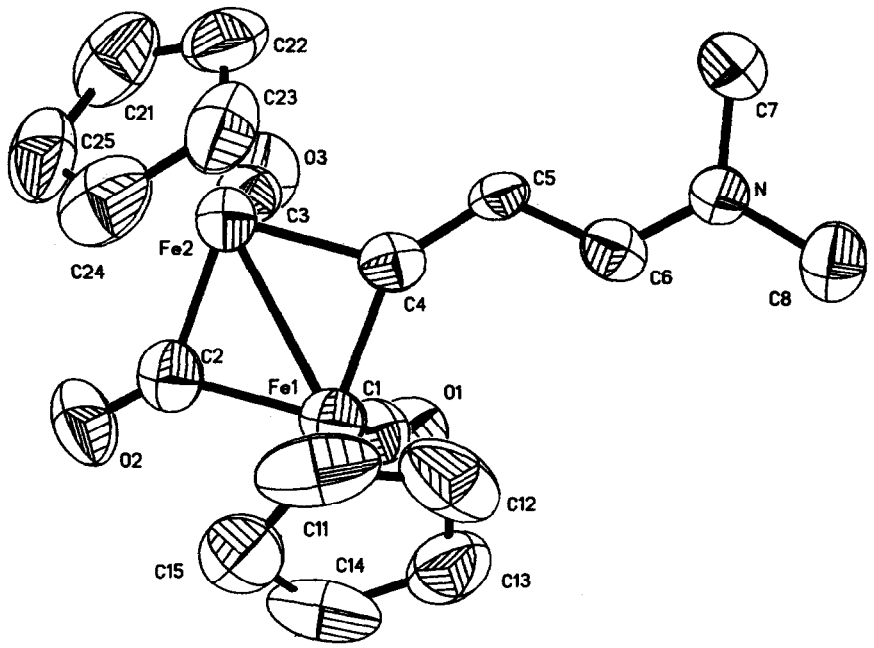

Fig. 5. Structure of **30**, BF_4^- and hydrogens omitted for clarity.

Table 2. Selected bond lengths and angles for **4**

Bond lengths (Å)		Bond angles (deg)	
Fe(1)—Fe(2)	2.507(1)	Fe(1)—C(4)—C(5)	141.6(5)
Fe(1)—C(4)	1.833(6)	Fe(2)—C(4)—C(5)	132.5(5)
Fe(2)—C(4)	1.848(6)	C(4)—C(5)—C(6)	123.9(6)
C(4)—C(5)	1.422(8)	C(5)—C(6)—Cb(1)	126.3(5)
C(5)—C(6)	1.335(8)		
C(6)—Cb(1)	1.472(7)		

Table 3. Selected bond lengths and angles for **28**

Bond lengths (Å)		Bond angles (deg)	
Fe(1)—Fe(2)	2.498(1)	Fe(1)—C(1)—C(2)	134.4(5)
Fe(3)—Fe(4)	2.506(2)	Fe(2)—C(1)—C(2)	141.7(5)
Fe(1)—C(1)	1.894(7)	Fe(3)—C(5)—C(4)	138.2(6)
Fe(2)—C(1)	1.860(7)	Fe(4)—C(5)—C(4)	136.8(6)
Fe(3)—C(5)	1.884(7)	C(1)—C(2)—C(3)	124.9(7)
Fe(4)—C(5)	1.854(7)	C(2)—C(3)—C(4)	127.5(7)
C(1)—C(2)	1.352(10)	C(3)—C(4)—C(5)	125.1(7)
C(2)—C(3)	1.382(10)		
C(3)—C(4)	1.370(11)		
C(4)—C(5)	1.377(10)		

Table 4. Selected bond lengths and angles for **30**

Bond lengths (Å)		Bond angles (deg)	
Fe(1)—Fe(2)	2.508(2)	Fe(1)—C(4)—C(5)	142.7(6)
Fe(1)—C(4)	1.853(8)	Fe(2)—C(4)—C(5)	132.8(7)
Fe(2)—C(4)	1.881(7)	C(4)—C(5)—C(6)	122.5(8)
C(4)—C(5)	1.377(10)	C(5)—C(6)—N	126.7(8)
C(5)—C(6)	1.391(11)	C(6)—N—C(7)	123.1(7)
C(6)—N	1.295(9)	C(6)—N—C(8)	121.6(7)
N—C(7)	1.439(11)		
N—C(8)	1.454(11)		

The nearly planar geometry of the two iron atoms and the entire vinylcarbyne ligand is the most striking structural feature of these complexes. For **4**, the maximum deviation from planarity is the 0.18 Å displacement of Fe(2); for **28** the maximum deviation from planarity is the 0.22 Å displacement of Fe(4); and for **30**, the maximum deviation from planarity is the 0.11 Å displacement of an *N*-methyl carbon (C7). The observed planar conformation maximizes conjugation of the vinylcarbyne ligand with an electron deficient μ-alkylidyne carbon *p*-orbital perpendicular to the planar system.

For *p*-tolyl substituted vinylcarbyne complex **4**, the vinylcarbyne ligand is best described as having a localized double bond within the vinyl unit [C(5)—C(6), 1.335(8) Å] and a single bond between the μ-alkylidyne carbon and the vinyl group [C(4)—C(5), 1.422(8) Å]. The C(4)—C(5) bond is slightly but significantly shortened relative to a normal sp^2–sp^2 carbon–carbon single bond and indicates some delocalization of positive charge out onto the vinylcarbyne ligand as depicted in resonance structure **4B**.

For the amino substituted vinylcarbyne complex **30**, there is more extensive delocalization of positive charge out onto the vinylcarbyne ligand as depicted in resonance structures **30A** and **30B**. Evidence for this delocalization comes from the observation of similar carbon–carbon bond lengths in the vinylcarbyne group [C(4)—C(5), 1.376(10) Å; C(5)—C(6), 1.392(12) Å] and of a short bond from

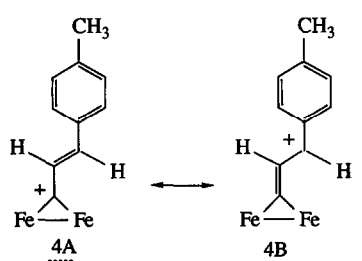

Structures 4A and 4B

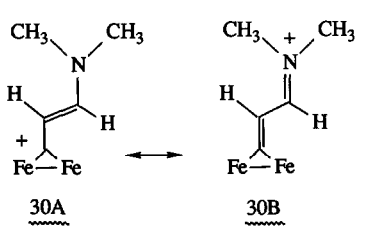

Structures 30A and 30B

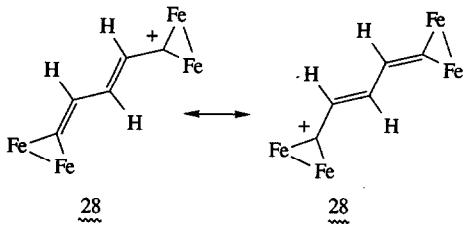

28 28

Structure 28

the amino nitrogen to the vinyl carbon [N—C(6), 1.297(10) Å].

For the tetrairon vinylcarbyne complex **28**, the near equivalence of all the carbon–carbon bond lengths [1.37(1) Å] of the μ-C_5H_3 ligand is readily understood in terms of the two equivalent resonance forms for this planar delocalized π-system.

Conclusion

We have developed two complementary procedures for the synthesis of a wide variety of μ-vinylcarbyne diiron complexes in good yield. One involves hydride abstraction from μ-alkenylidene complexes; its major limitation is the low selectivity for abstraction of different types of allylic hydrogens. The second procedure involves the condensation of μ-alkylidyne complexes with carbonyl compounds. This procedure works extremely well for non-enolizable aldehydes. Multigram quantities of analytically pure microcrystalline products are easily obtained, especially from aromatic aldehydes. The reaction of ethylidyne complex **1** with enolizable aldehydes is very sensitive to the nature of the aldehyde and in no case have pure vinylcarbyne complexes been isolated. For enolizable aldehydes with two β-alkyl substituents, μ-alkenyl complexes were obtained as rearrangement products derived from an initially formed unstable vinylcarbyne complex. The condensation of **1** with ketones is slow and requires the use of neat ketone to obtain reasonable reaction rates. The reactions of longer chain alkylidyne complexes with aldehydes are also slow but reasonable yields can be obtained by using neat aldehyde.

We are currently investigating the reactions of these new vinylcarbyne complexes with nucleophiles (Ref. 2; C. P. Casey, M. S. Konings and S. R. Marder, in preparation), and are actively pursuing methods to release the hydrocarbyl fragment from the metal center in a synthetically useful manner.

EXPERIMENTAL

^{1}H NMR spectra were obtained on a Bruker WP200, WP270, or AM500 spectrometer. ^{13}C NMR spectra were obtained on a JEOL FX200 spectrometer operating at 50.1 MHz or an AM500 spectrometer operating at 126 MHz; samples contain 0.07 M $Cr(acac)_3$ as a shiftless relaxation agent. CD_2Cl_2 was dried over P_2O_5. Acetone-d_6 was dried over 4 Å molecular sieves or B_2O_3. CD_3NO_2 was dried over CaH_2. CD_3CN was dried over 4 Å molecular sieves and stored over CaH_2. NMR samples were prepared on a vacuum line and sealed under a positive flow of N_2. IR spectra were recorded on a Beckman 4230 or 4250 spectrometer and calibrated with polystyrene film or on a Mattson Polaris FT-IR spectrometer. Mass spectra were obtained on a KRATOS MS-80 mass spectrometer. Elemental analyses were performed by Schwarzkopf Microanalytical Laboratories or Galbraith Laboratories. Air sensitive compounds were handled using standard high vacuum line of Schlenk procedures and glovebox manipulations. Diethyl ether, THF, and hexane were distilled from degassed, purple solutions of sodium and benzophenone immediately prior to use. Acetone was dried over B_2O_3. CH_2Cl_2 was distilled from CaH_2. *p*-Tolualdehyde, isophorone, cyclohexanone, triethyl *ortho*formate, and phenylacetaldehyde were distilled on a short path column from $MgSO_4$. Other aldehydes were used as purchased.

$[C_5H_5(CO)Fe]_2(\mu\text{-}CO)(\mu\text{-}C\text{-}E\text{-}CH{=}CHC_6H_4\text{-}p\text{-}CH_3)^+BF_4^-$ (**4**)

A suspension of **1** (2.10 g, 4.77 mmol) and *p*-tolualdehyde (1.64 g, 14.3 mmol) in THF (150 cm^3) were stirred at 40°C for 22 h under N_2. The volume of solvent was reduced to 10 cm^3 by evaporation under high vacuum and a purple microcrystalline solid was isolated by filtration on a reversible Schlenk filter frit, washed four times with 2 cm^3 portions of solvent distilled from the filtrate, and dried under vacuum to give **4** (2.37 g, 92%). ^{1}H NMR (acetone-d_6, 270 MHz): δ 10.26 (d, J = 14.9 Hz, μ-C—CH), 8.20 (d, J = 8.2 Hz, *o*-C_6H_4), 8.09 (d, J = 14.9 Hz, μ-C—CH=C*H*), 7.45 (d, J = 8.1 Hz, *m*-C_6H_4), 5.67 (s, 10H, C_5H_5), 2.45 (s, CH_3). $^{13}C\{^1H\}$ NMR (acetone-d_6, 50.1 MHz): δ 439.9 (μ-C); 254.3 (μ-CO); 208.9 (CO); 153.4, 152.4 (μ-C—*C*H=*C*H); 146.8 (*p*-C_6H_4); 133.5, 131.6 (*o*,*m*-C_6H_4); 132.8 (*ipso*-C_6H_4); 93.1 (C_5H_5); 22.2 (CH_3). IR (CH_2Cl_2): 2033 (vs), 2000 (m), 1848 (s) cm^{-1}. Anal. Found: C, 51.06; H, 3.76. Calc. for $C_{23}H_{19}BF_4Fe_2O_3$: C, 50.98; H, 3.53%.

$[C_5H_5(CO)Fe]_2(\mu\text{-}CO)(\mu\text{-}C\text{-}E\text{-}CH{=}CHC_6H_4\text{-}p\text{-}NO_2)^+BF_4^-$ (**2**)

1 (1.65 g, 3.75 mmol) and *p*-nitrobenzaldehyde (1.14 g, 7.50 mmol) were stirred in THF (175 cm^3)

at 35°C for 26 h. The volume of solvent was reduced to 30 cm^3 and diethyl ether (50 cm^3) was added. The resulting dark purple microcrystalline solid was isolated by filtration, washed three times with 5 cm^3 portions of solvent, and dried under vacuum to give **2** (1.88 g, 87%). ^1H NMR (acetone-d_6, 270 MHz): δ 10.35 (d, J = 15.6 Hz, μ-C—CH), 8.52 (d, J = 9.0 Hz, o-C_6H_4), 8.39 (d, J = 8.9 Hz, m-C_6H_4), 8.05 (d, J = 15.2 Hz, μ-C—CH=C*H*), 5.73 (s, 10H, C_5H_5). $^{13}C\{^1H\}$ NMR (acetone-d_6, 126 MHz): δ 451.2 (μ-C); 252.5 (μ-CO); 208.2 (CO); 157.4, 144.5 (μ-C—*C*H=*C*H); 150.3 (p-C_6H_4), 141.5 (*ipso*-C_6H_4); 133.1 (o-C_6H_4); 125.0 (m-C_6H_4); 93.5 (C_5H_5). IR (CH_2Cl_2): 2040 (vs), 2015 (sh), 1853 (s) cm^{-1}. Anal. Found: C, 45.96; H, 2.94; N, 2.34. Calc. for $C_{22}H_{16}BF_4Fe_2NO_5$: C, 46.13; H, 2.82; N, 2.45%.

$[C_5H_5(CO)Fe]_2(\mu\text{-}CO)(\mu\text{-}C\text{-}E\text{-}CH{=}CHC_6H_5)^+BF_4^-$ (3)

1 (200 mg, 0.455 mmol) and benzaldehyde (89 mg, 0.91 mmol) were stirred in THF (20 cm^3) at 36°C for 25 h. The volume of solvent was reduced to 5 cm^3 and a purple microcrystalline solid was isolated by filtration, washed once with 2 cm^3 of solvent, and dried under vacuum to give **3** (181 mg, 75%). ^1H NMR (acetone-d_6, 270 MHz): δ 10.27 (d, J = 15.0 Hz, μ-C—CH), 8.30 (d, J = 7.5 Hz, o-C_6H_4), 8.07 (d, J = 15.0 Hz, μ-C—CH=C*H*), 7.73 (t, J = 7.4 Hz, p-C_6H_4), 7.62 (t, J = 7.7 Hz, m-C_6H_4), 5.68 (s, 10H, C_5H_5). $^{13}C\{^1H\}$ NMR (acetone-d_6, 126 MHz): δ 443.0 (μ-C); 253.9 (μ-CO); 208.4 (CO); 152.6, 151.9 (μ-C—*C*H=*C*H); 135.1 (*ipso*-C_6H_5); 134.6 (p-C_6H_5); 132.9, 130.5 (o,m-C_6H_5); 93.0 (C_5H_5). IR (CH_2Cl_2): 2038 (vs), 2005 (m), 1847 (s) cm^{-1}. Anal. Found: C, 50.12; H, 3.23. Calc. for $C_{22}H_{17}BF_4Fe_2O_3$: C, 50.06; H, 3.25%.

$[C_5H_5(CO)Fe]_2(\mu\text{-}CO)(\mu\text{-}C\text{-}E\text{-}CH{=}CHC_6H_4\text{-}p\text{-}OCH_3)^+BF_4^-$ (5)

1 (250 mg, 0.568 mmol) and p-anisaldehyde (92 mg, 0.85 mmol) were stirred in THF (30 cm^3) at 40°C for 25 h. The volume of solvent was reduced to 20 cm^3 and diethyl ether (15 cm^3) was added. A purple microcrystalline solid was isolated by filtration, washed twice with 2 cm^3 portions of solvent, and dried under vacuum to give **5** (250 mg, 79%). ^1H NMR (acetone-d_6, 270 MHz): δ 10.20 (d, J = 14.6 Hz, μ-C—CH), 8.31 (d, J = 8.9 Hz, o-C_6H_4), 8.13 (d, J = 14.8 Hz, μ-C—CH=C*H*), 7.23 (d, J = 8.9 Hz, m-C_6H_4), 5.64 (s, 10H, C_5H_5), 4.00 (s, CH_3). $^{13}C\{^1H\}$ NMR (acetone-d_6, 50.1 MHz): δ 431.6 (μ-C); 255.1 (μ-CO); 209.1 (CO); 166.7 (p-C_6H_4); 155.1, 151.5 (μ-C—*C*H=*C*H); 136.5 (o-C_6H_4), 127.8 (*ipso*-C_6H_4); 116.8 (m-C_6H_4); 92.8 (C_5H_5); 56.9 (CH_3). IR (CH_2Cl_2): 2028 (vs), 2001 (m), 1842 (s) cm^{-1}. Anal. Found: C, 49.69; H, 3.51. Calc. for $C_{23}H_{19}BF_4Fe_2O_4$: C, 49.52; H, 3.43%.

$[C_5H_5(CO)Fe]_2(\mu\text{-}CO)(\mu\text{-}C\text{-}E\text{-}CH{=}CHC_6H_4\text{-}p\text{-}OH)^+BF_4^-$ (6)

1 (500 mg, 1.14 mmol) and p-hydroxybenzaldehyde (208 mg, 1.70 mmol) were stirred in CH_2Cl_2 (40 cm^3) at 40°C for 30 h. The volume of solvent was reduced to 5 cm^3 and diethyl ether (10 cm^3) was added. A purple–brown microcrystalline solid was isolated by filtration, washed twice with 5 cm^3 portions of solvent, and dried under vacuum to give **6** (587 mg, 95%). ^1H NMR (acetone-d_6, 270 MHz): δ 10.17 (d, J = 14.7 Hz, μ-C—CH), 10.00 (s, OH), 8.25 (d, J = 8.7 Hz, o-C_6H_4), 8.12 (d, J = 14.6 Hz, μ-C—CH=C*H*), 7.12 (d, J = 8.7 Hz, m-C_6H_4), 5.63 (s, 10H, C_5H_5). $^{13}C\{^1H\}$ NMR (acetone-d_6, 50.1 MHz): δ 428.1 (μ-C); 255.3 (μ-CO); 208.9 (CO); 165.3 (p-C_6H_4); 155.8, 150.9 (μ-C—*C*H=*C*H); 136.9 (o-C_6H_4); 126.7 (*ipso*-C_6H_4); 118.2 (m-C_6H_4); 92.5 (C_5H_5). IR (THF): 2024 (vs), 1996 (m), 1838 (s) cm^{-1}. Anal. Found: C, 48.32; H, 3.29. Calc. for $C_{22}H_{17}BF_4Fe_2O_4$: C, 48.59; H, 3.15%.

$[C_5H_5(CO)Fe]_2(\mu\text{-}CO)[\mu\text{-}C\text{-}E\text{-}CH{=}CHC_6H_4\text{-}p\text{-}N(CH_3)_2]^+BF_4^-$ (7)

1 (250 mg, 0.568 mmol) and p-dimethylaminobenzaldehyde (128 mg, 0.852 mmol) were stirred in THF (30 cm^3) at 40°C for 25 h. The volume of solvent was reduced to 5 cm^3. A green–grey microcrystalline solid was isolated by filtration, washed once with THF (2 cm^3), twice with diethyl ether (2 cm^3 portions), and dried under vacuum to give **7** (291 mg, 90%). ^1H NMR (acetone-d_6, 270 MHz): δ 9.94 (d, J = 13.8 Hz, μ-C—CH), 8.17 (br s, o-C_6H_4), 8.07 (d, J = 13.8 Hz, μ-C—CH=C*H*), 7.07 (d, J = 9.2 Hz, m-C_6H_4), 5.49 (s, 10H, C_5H_5), 3.35 (s, 6H, CH_3). $^{13}C\{^1H\}$ NMR: (acetone-d_6, 50.1 MHz): δ 395.2 (μ-C); 258.7 (μ-CO); 210.0 (CO); 158.5, 148.4 (μ-C—*C*H=*C*H); 157.7 (p-C_6H_4), 138.4 (o-C_6H_4), 122.6 (*ipso*-C_6H_4); 114.6 (m-C_6H_4); 91.8 (C_5H_5); 41.0 (CH_3). IR (CH_2Cl_2): 2019 (vs), 1995 (m), 1827 (s) cm^{-1}. Anal. Found: C, 50.33; H, 3.77; N, 2.23. Calc. for $C_{24}H_{22}BF_4Fe_2NO_3$: C, 50.49; H, 3.88; N, 2.45%.

$[C_5H_5(CO)Fe]_2(\mu\text{-}CO)[\mu\text{-}C\text{-}E\text{-}CH{=}CHC(CH_3)_3]^+BF_4^-$, (10)

1 (250 mg, 0.568 mmol) and pivalaldehyde (1.9 g, 14 mmol) were stirred in CH_2Cl_2 (10 cm^3) at 40°C

for 16 h. Solvent and excess aldehyde were removed under reduced pressure. CH_2Cl_2 (2 cm^3) was added and the solution was filtered. Diethyl ether (30 cm^3) was added over 30 min to produce a red precipitate which was isolated by filtration and dried under vacuum to give **10** (241 mg, 83%). ^1H NMR (acetone-d_6, 270 MHz): δ 9.44 (d, J = 15.0 Hz, μ-C—CH), 7.41 (d, J = 15.0 Hz, μ-C—CH=C*H*), 5.62 (s, 10H, C_5H_5), 1.37 (s, 9H, CH_3). $^{13}C\{^1H\}$ NMR: δ 451.7 (μ-C), 251.6 (μ-CO), 206.8 (CO), 167.9 (μ-C—CH=*C*H), 152.2 (μ-C—*C*H), 91.6 (C_5H_5), 35.3 (Cq), 26.7 (CH_3). IR (CH_2Cl_2): 2036 (vs), 2003 (m), 1853 (s) cm^{-1}. Anal. Found: C, 46.92; H, 3.87. Calc. for $C_{20}H_{21}BF_4Fe_2O_3$: C, 47.30; H, 4.17%.

$[C_5H_5(CO)Fe]_2(\mu$ - CO)(μ - C - *E,E* - CH=CHCH=$CHC_6H_5)^+BF_4^-$ (**11**)

1 (200 mg, 0.455 mmol) and *trans*-cinnamaldehyde (11 mg, 0.909 mmol) were stirred in CH_2Cl_2 (20 cm^3) at 35°C for 6 h. Solvent was removed under reduced pressure. CH_2Cl_2 (2 cm^3) was added and the solution was filtered. Diethyl ether (25 cm^3) was added and a black powder was isolated by filtration, washed four times with 5 cm^3 portions of solvent, and dried under vacuum to give **11** (234 mg, 93%). ^1H NMR (acetone-d_6, 270 MHz): δ 9.64 (d, J = 14.1 Hz, μ-C—CH), 8.08 (d, J = 15.5 Hz, μ-C—CH=CHCH=C*H*), (dd, J = 14.1, 10.3 Hz, μ-C—CH=C*H*), 7.83 (m, 2H, C_6H_5), 7.57 (dd, J = 15.3, 10.9 Hz, μ-C—CH=CHC*H*), 7.53 (m, 3H, C_6H_5), 5.63 (2, 10H, C_5H_5). $^{13}C\{^1H\}$ NMR (acetone-d_6, 50.1 MHz): δ 434.3 (μ-C); 254.3 (μ-CO); 206.8 (CO); 156.1, 154.8, 154.0, 137.1, 132.3, 130.2, 129.6, 129.1 (vinyl and aryl); 92.7 (C_5H_5). IR (CH_2Cl_2): 2038 (vs), 2006 (m), 1846 (s) cm^{-1}. Anal. Found: C, 51.72; H, 3.83. Calc. for $C_{24}H_{19}BF_4Fe_2O_3$: C, 52.04; H, 3.46%.

$[C_5H_5(CO)Fe]_2(\mu$ - CO)(μ - C - *E* - C(CH_3)=CHC_6H_4-*p*-$CH_3)^+PF_6^-$ (**13**)

12[8] (350 mg, 0.684 mmol) was stirred in *p*-tolualdehyde (5 g) at 25°C for 20 h. Diethyl ether (50 cm^3) was added and a brown powder was isolated by filtration, washed five times with 5 cm^3 portions of solvent, and dried under vacuum to give **13** (345 mg, 83%). ^1H NMR analysis revealed 5% of $C_5H_5Fe(CO)_3^+$ as an impurity. Analytically pure **13** was obtained by washing a CH_2Cl_2 solution (50 cm^3) of **13** (340 mg, 0.559 mmol) with saturated aqueous $NaHCO_3$ (50 cm^3). The CH_2Cl_2 layer was separated, dried ($MgSO_4$) and filtered. The volume of solvent was reduced to 5 cm^3 to yield a purple microcrystalline solid which was isolated by filtration, washed with 2 cm^3 of solvent, and dried under vacuum to give **13** (200 mg, 48%). ^1H NMR (acetone-d_6, 270 MHz): δ 8.31 (s, μ-C—C=CH), 8.00 (d, J = 8.2 Hz, *o*-C_6H_4), 7.50 (d, J = 8.1 Hz, *m*-C_6H_4), 5.72 (s, 10H, C_5H_5), 3.27 [s, C(CH_3)], 2.46 (s, *p*-CH_3). $^{13}C\{^1H\}$ NMR (acetone-d_6, 50.1 MHz): δ 451.0 (μ-C); 253.8 (μ-CO); 208.7 (CO); 161.6, 158.5 (μ-C—*C*H=*C*H); 145.2 (*p*-C_6H_4); 132.9 (*ipso*-C_6H_4); 133.9, 131.1 (*o,m*-C_6H_4); 93.2 (C_5H_5); 25.0, 22.9 (CH_3). IR (CH_2Cl_2): 2028 (vs), 2003 (m), 1845 (s) cm^{-1}. Anal. Found: C, 46.63; H, 3.61. Calc. for $C_{24}H_{21}F_6Fe_2O_3P$: C, 46.94; H, 3.45%.

cis- *and* trans-$[C_5H_5(CO)Fe]_2(\mu$-CO)[μ-C-*E*-C($CH_2CH_2CH_3$)=CHC_6H_4-*p*-$CH_3]^+BF_4^-$ (**14**)

8[1,8] (250 mg, 0.519 mmol) was stirred in *p*-tolualdehyde (3 g) at 25°C for 42 h. Solvent was removed under reduced pressure and THF (5 cm^3) was added and the solution was filtered. The solvent was removed under reduced pressure and CH_2Cl_2 (2 cm^3) and then diethyl ether (25 cm^3) were added to give a red–black powder which was isolated by filtration and dried under vacuum to give **14** (235 mg, 77%, 4.4:1 *cis*:*trans*). ^1H NMR (acetone-d_6, 270 MHz) for **14c**: δ 8.21 (s, μ-C—C=CH), 7.98 (d, J = 8.4 Hz, *o*-C_6H_4), 7.51 (d, J = 8.3 Hz, *m*-C_6H_4), 5.72 (s, 10H, C_5H_5), 3.65 (m, $CH_2CH_2CH_3$), 2.46 (s, *p*-CH_3), 1.90 (m, CH_2CH_3), 1.19 (t, J = 7.1 Hz, CH_3); for **14t**: δ 8.02 (s, μ-C—C=CH), 7.88 (d, J = 8.2 Hz, *o*-C_6H_4), 7.47 (d, J = 8.2 Hz, *m*-C_6H_4), 5.49 (s, 10H, C_5H_5), 3.80 (m, $CH_2CH_2CH_3$), 2.44 (s, *p*-CH_3), 1.81 (m, CH_2CH_3), 1.09 (t, J = 7.0 Hz, CH_3). $^{13}C\{^1H\}$ NMR (acetone-d_6, 126 MHz) for **14c**: δ 452.6 (μ-C); 253.9 (μ-CO); 209.1 (CO); 167.0, 157.4 (μ-C—*C*—CH); 145.3 (*p*-C_6H_4); 133.0 (*ipso*-C_6H_4); 133.8, 131.3 (*o,m*-C_6H_4); 93.4 (C_5H_5); 39.6 [C(CH_2)]; 23.0, 21.9 ($CH_2CH_2CH_3$, *p*-CH_3); 14.2 (CH_3); for **14t**: δ 457.7 (μ-C); 252.0 (μ-CO); 207.8 (CO); 172.4, 144.5 (μ-C—*C*=CH); 143.5 (*p*-C_6H_4); 132.4, 131.0 (*o,m*-C_6H_4); 94.8 (C_5H_5); 39.8 [C(CH_2)]; 23.7, 21.8 ($CH_2CH_2CH_3$, *p*-CH_3), 14.5 (CH_3), (*ipso*-C_6H_4, not observed). IR (CH_2Cl_2): 2033 (vs), 2009 (s), 1850 (s) cm^{-1}. Anal. Found: C, 53.55; H, 4.36. Calc. for $C_{26}H_{25}BF_4Fe_2O_3$: C, 53.48; H, 4.32%.

$[C_5H_5(CO)Fe]_2(\mu$ - CO)(μ - C—CH=C$CH_2CH_2CH_2CH_2CH_2)^+BF_4^-$ (**15**)

1 (250 mg, 0.568 mmol) was stirred in cyclohexanone (11 g) at 0°C for 12 h and 28°C for 11 h under vacuum. Solvent was removed under reduced pressure and THF (10 cm^3) and diethyl ether (20

cm^3) were added. A red powder was isolated by filtration, washed three times with 5 cm^3 portions of solvent, and dried under vacuum to give **15** (241 mg, 82%). ^1H NMR analysis revealed several impurities. Suspension of the solid in THF (25 cm^3) gave red microcrystals which were isolated by filtration and dried under reduced pressure to give pure **15** (130 mg, 44%). ^1H NMR (acetone-d_6, 270 MHz): δ 9.62 (μ-C—CH), 5.59 (s, 10H, C_5H_5), 3.08 [t, J = 5.5 Hz, C=CC(CH_2)(CH_2)], 2.66 [t, J = 6.1 Hz, C=C(CH_2)(CH_2)], 1.96 (pentet, J = 5.5 Hz, CH_2), 1.78 (m, CH_2CH_2). $^{13}C\{^1H\}$ NMR (acetone-d_6, 126 MHz): δ 438.1 (μ-C); 252.3 (μ-CO); 207.2 (CO); 167.8 (μ-C—CH=*C*); 154.2 (μ-C—*C*H). IR: 2035 (vs), 2000 (m), 1851 (s) cm^{-1}. Anal. Found: C, 48.42; H, 4.23. Calc. for $C_{21}H_{21}BF_4Fe_2O_3$: C, 48.52; H, 4.07%.

$[C_5H_5(CO)Fe]_2(\mu$ - CO)[μ - C—CH=C$(CH_3)_2]^+BF_4^-$ (**16B**)

1 (200 mg, 0.455 mmol) was stirred in acetone (32 g) at 23°C for 25 h. The volume of solvent was reduced to 5 cm^3 and the solution was filtered. The solvent was removed under reduced pressure and CH_2Cl_2 (2 cm^3) and diethyl ether (20 cm^3) were added to give a red precipitate of **16B** (193 mg, 88%), which was isolated by filtration. This material was shown by ^1H NMR to be contaminated with a small amount (< 5%) of $C_5H_5Fe(CO)_3^+BF_4^-$. ^1H NMR (acetone-d_6, 270 MHz): δ 9.69 (s, μ-C—CH), 5.60 (s, 10H, C_5H_5), 2.48 (s, CH_3), 2.37 (s, CH_3).

$[C_5H_5(CO)Fe]_2(\mu$-CO)[μ-C—CH=CCH=C(CH_3) $CH_2C(CH_3)_2CH_2]^+BF_4^-$ (**17**)

1 (125 mg, 0.284 mmol) was stirred in isophorone (11 g) at room temperature for 125 h. Solvent was removed under reduced pressure, THF (5 cm^3) was added, and the solution was filtered. Solvent was removed under reduced pressure and CH_2Cl_2 (2 cm^3) and diethyl ether (25 cm^3) were added to give a dark brown powder which was isolated by filtration and dried under reduced pressure to give **17** (99 mg, 62%). ^1H NMR analysis revealed a 2.8:1 ratio of **17E**:**17Z** approximately 80% pure. Repeated crystallizations failed to give pure **17**. Pure **17** was obtained in low yield enriched in **17E** (**17E**:**17Z**, 8:1) by vapour diffusion of diethyl ether into a concentrated CH_2Cl_2 solution of **17** (29 mg, 18%). ^1H NMR (acetone-d_6, 270 MHz) for **17E**: δ 9.60 (s, μ-C—CH), 6.59 (q, J = 1.5 Hz, μ-C—CH=CC*H*), 5.55 (s, 10H, C_5H_5), 3.01 (d, J = 1.5 Hz, CH_2), 2.37 (m, CH_2), 2.01 (d, J = 1.9 Hz, C=CCH_3), 1.04 [s, C$(CH_3)_2$]. $^{13}C\{^1H\}$ NMR (acetone-d_6, 126 MHz) for **17E**: 421.3 (μ-C); 209.4 (CO); 166.4, 155.7, 155.3, 128.5 (μ-C—*C*H=*CC*H=*C*); 93.3 (C_5H_5); 47.0, 41.6 (CH_2); 27.9 [C(*C*$H_3)_2$], 28.2, 26.3 [*C*$(CH_3)_2$, C=*CC*H_3] (μ-CO not observed). IR (CH_2Cl_2): 2038 (vs), 1999 (m), 1844 (s) cm^{-1}. While the crystalline material contained no NMR detectable impurities, repeated attempts to obtain fully satisfactory elemental analyses failed. Anal. Found: C, 50.85; H, 4.35. Calc. for $C_{24}H_{25}BF_4Fe_2O_3$: C, 51.48; H, 4.50%.

$[C_5H_5(CO)Fe]_2(\mu$ - CO)(μ - C - *E* - CH=CHCH_2 $CH_3)^+PF_6^-$ (**18P**)

9[8] (2.33 g, 5.91 mmol) and $(C_6H_5)_3C^+PF_6^-$ (2.25 g, 5.74 mmol) were stirred in CH_2Cl_2 (25 cm^3) at 0°C for 1.5 h. The volume of solvent was reduced to 15 cm^3 and a red microcrystalline solid was isolated by filtration. The solid was washed with CH_2Cl_2 until the washings were only slightly colored and then the solid was dried under vacuum to give **18P** (2.54 g, 82%). ^1H NMR (acetone-d_6, 270 MHz): δ 9.53 (dt, J = 14.6, 1.3 Hz, μ-C—CH), 7.55 (dt, J = 14.6, 6.6 Hz, μ-C—CH=C*H*), 5.62 (s, 10H, C_5H_5), 2.66 (m, CH_2), 1.33 (t, J = 7.5 Hz, CH_3). $^{13}C\{^1H\}$ NMR (CD_3NO_2, 50.1 MHz): δ 451.1 (μ-C); 253.8 (μ-CO); 208.2 (CO); 164.8, 157.6 (μ-C—*C*H=*C*H); 93.2 (C_5H_5); 30.0 (CH_2), 11.9 (CH_3). IR (CH_2Cl_2): 2037 (vs), 2005 (m), 1850 (s) cm^{-1}. Anal. Found: C, 40.39; H, 3.39. Calc. for $C_{18}H_{17}F_6Fe_2O_3P$: C, 40.19; H, 3.19%.

$[C_5H_5(CO)Fe]_2(\mu$-CO)(μ-C-*E*-CH=CHCH_2CH_2 $C_6H_5)^+BF_4^-$ (**19**)

1 (250 mg, 0.568 mmol) and 3-phenylpropanal (147 mg, 1.14 mmol) were stirred in CH_2Cl_2 (75 cm^3) at 35°C for 13 h. The volume of solvent was reduced to 10 cm^3 and the solution was filtered. The volume of solvent was reduced to 2 cm^3 and diethyl ether (50 cm^3) was added. A red precipitate was isolated by filtration, washed with 5 cm^3 of solvent and dried under vacuum (274 mg). ^1H NMR analysis revealed the presence of **19** (~ 60% pure). Repeated crystallizations failed to give pure **19**. ^1H NMR (acetone-d_6, 270 MHz): δ 9.47 (dt, J = 14.8, 1.1 Hz, μ-C—CH), 7.46 (dt, J = 14.8, 6.9 Hz, μ-C—CH=C*H*), 7.20 (m, C_6H_5), 5.56 (s, 10H, C_5H_5), 3.14 (m, CH_2), 2.56 (m, CH_2).

$[C_5H_5(CO)Fe]_2(\mu$-CO)[μ-η^1,η^2-*E*-CH=CHCH= $C(CH_3)_2]^+BF_4^-$ (**21B**)

1 (200 mg, 0.568 mmol) and isobutyraldehyde (157 mg, 1.36 mmol) were stirred in CH_2Cl_2 (75 cm^3) at 37°C for 15 h. Solvent was removed under

reduced pressure and acetone (15 cm^3) was added. The solution was stirred at 37°C for 2 h to insure the complete isomerization described in the text and filtered. Solvent was removed under reduced pressure and CH_2Cl_2 (2 cm^3) and diethyl ether (40 cm^3) were added. A red precipitate was isolated by filtration, washed twice with 5 cm^3 portions of solvent, and dried under vacuum to give **21B** (197 mg, 88%). ^1H NMR (acetone-d_6, 270 MHz): δ 12.03 (d, $J = 11.8$ Hz, μ-CH), 6.13 (d, $J = 10.5$ Hz, μ-CH=CHC*H*), 5.60 (s, 10H, C_5H_5), 4.73 (t, $J = 10.9$ Hz, μ-CH=C*H*), 1.86 (s, CH_3), 1.85 (s, CH_3). ^{13}C NMR (acetone-d_6, 126 MHz): δ 243.9 (μ-CO), 211.7 (CO), 173.2 (d, $J = 157$ Hz, μ-CH), 146.4 [s, *C*$(CH_3)_2$], 128.1 (d, $J = 160$ Hz, μ-CH=C*H*CH), 95.9 (d, $J = 157$ Hz, μ-CH=*C*H), 91.4 (d, $J = 183$ Hz, C_5H_5), 26.4 (CH_3), 19.1 (CH_3). IR (CH_2Cl_2): 2024 (s), 1998 (m), 1853 (m) cm^{-1}. Anal. Found: C, 45.92; H, 4.01. Calc. for $C_{19}H_{19}BF_4Fe_2O_3$: C, 46.21; H, 3.88%.

$[C_5H_5(CO)Fe]_2(\mu$-CO)[μ-C-*E*-CH=CHCH$(CH_3)_2]^+PF_6^-$ (**20P**)

22 (162 mg, 0.397 mmol) and $(C_6H_5)_3C^+PF_6^-$ (146 mg, 0.377 mmol) were stirred in CH_2Cl_2 (10 cm^3) at 0°C for 45 min then at 25°C for 30 min. The volume of solvent was reduced to 5 cm^3 and diethyl ether (20 cm^3) was added. A red precipitate was isolated by filtration, washed twice with 5 cm^3 portions of solvent and dried under vacuum to give **20P** (184 mg, 88%). ^1H NMR (acetone-d_6, 270 MHz): δ 9.48 (dd, $J = 14.8$, 1.1 Hz, μ-C—CH), 7.42 (dd, $J = 14.9$, 6.9 Hz, μ-C—CH=C*H*), 5.60 (s, 10H, C_5H_5), 2.89 (octet d, $J = 6.7$, 1.1 Hz, CH=CHC*H*), 1.33 (d, 6H, CH_3). $^{13}C\{^1H\}$ NMR (acetone-d_6, 126 MHz): δ 451.5 (μ-C); 253.2 (μ-CO); 208.2 (CO); 166.9, 155.0 (μ-C—*C*H=*C*H); 92.8 (C_5H_5); 33.8 (CH); 20.4 (CH_3). IR (CH_2Cl_2): 2019 (vs), 2007 (m), 1852 (s) cm^{-1}. Anal. Found: C, 40.93; H, 3.74. Calc. for $C_{19}H_{19}F_6Fe_2O_3P$: C, 41.27; H, 3.46%.

$[C_5H_5(CO)Fe]_2(\mu$-CO)[μ-C=CHCH_2CH$(CH_3)_2$] (**22**)

31[8,14] (350 mg, 0.723 mmol) was suspended in CH_2Cl_2 (50 cm^3). 3-Methyl-1-butene (0.50 atm, 350 cm^3, 25°C, 7.2 mmol) was added and the solution stirred at 0°C for 2 h. Trimethylamine (0.50 atm, 350 cm^3, 25°C, 7.2 mmol) was added. Solvent was removed under reduced pressure and the residue was purified by chromatography (alumina, 2 × 15 cm, 1:1 diethyl ether–hexanes eluant) to give **22** (241 mg, 82%) as a red powder. ^1H NMR (acetone-d_6, 270 MHz): δ 7.11 (dd, $J = 8.1$, 5.9 Hz, μ-C=CH), 4.95 (s, C_5H_5), 4.90 (s, C_5H_5), 2.82 (dt, $J = 13.7$, 5.9 Hz, C*H*H), 2.54 (dt, $J = 13.7$, 8.1 Hz, CH*H*), 1.82 [nonet, $J = 6.7$ Hz, C*H*$(CH_3)_2$], 1.05 (d, $J = 6.7$ Hz, CH_3), 1.01 (d, $J = 6.6$ Hz, CH_3). ^{13}C NMR (acetone-d_6, 126 MHz): δ 271.5 (μ-C), 266.4 (μ-CO), 213.0 (CO), 212.9 (CO), 139.7 (d, $J = 153$ Hz, μ-C=*C*H), 88.7 (d, $J = 178$ Hz, C_5H_5), 88.0 (d, $J = 178$ Hz, C_5H_5), 46.9 (t, $J = 126$ Hz, CH_2), 23.1 (q, $J = 124$ Hz, CH_3), 22.6 (q, $J = 124$ Hz, CH_3). IR (CH_2Cl_2): 1997 (vs), 1906 (m), 1785 (s) cm^{-1} HRMS. Found: 408.0113. Calc. for $C_{19}H_{20}Fe_2O_3$: 408.0111.

$[C_5H_5(CO)Fe]_2(\mu$-CO)(μ-η^1,η^2-*E*-CH=CHCH=CCH$_2$CH$_2$CH$_2$CH$_2$CH$_2$)$^+BF_4^-$ (**23**)

1 (250 mg, 0.568 mmol) and cyclohexanecarboxyaldehyde (221 mg, 1.70 mmol) were stirred in CH_2Cl_2 (20 cm^3) at 35°C for 18 h. Solvent was removed under reduced pressure and THF (5 cm^3) was added. The solution was filtered to remove small amounts of $C_5H_5Fe(CO)_3^+$ and solvent was removed under reduced pressure. CH_2Cl_2 (2 cm^3) and diethyl ether (20 cm^3) were added to produce a red–brown powder which was washed twice with 5 cm^3 portions of solvent and dried under vacuum to give **23** (197 mg, 65%). ^1H NMR (acetone-d_6, 270 MHz): δ 12.05 (d, $J = 11.6$ Hz, μ-CH), 6.07 (d, $J = 10.4$ Hz, μ-CH=CHC*H*), 5.63 (s, 10H, C_5H_5), 4.80 (t, $J = 11.2$ Hz, μ-CH=C*H*), 2.39 [m, C=C(*C*H_2)(CH_2)], 2.33 [m, C=C(CH_2)(*C*H_2)], 1.62 (m, 6H, $CH_2CH_2CH_2CH_2CH_2$). ^{13}C NMR (acetone-d_6, 126 MHz): δ 243.9 (μ-CO); 211.8 (CO); 173.6 (d, $J = 159$ Hz, μ-CH); 154.0 (s, μ-CH=CHCH=*C*); 125.1 (d, $J = 154$ Hz, μ-CH=CH*C*H); 95.3 (d, $J = 147$ Hz, μ-CH=*C*H); 91.1 (d, $J = 183$ Hz, C_5H_5); 37.9, 30.5, 28.3, 26.9 (CH_2, one obscured by solvent). IR (CH_2Cl_2): 2024 (s), 1997 (m), 1852 (m) cm^{-1}. Anal. Found: C, 49.29; H, 4.36. Calc. for $C_{22}H_{23}BF_4Fe_2O_3$: C, 49.49; H, 4.34%.

$[C_5H_5(CO)Fe]_2(\mu$-CO)(μ-η^1,η^2-*E,E*-CH=CHCH=CHC$_6$H$_5$]$^+BF_4^-$ (**25**)

1 (120 mg, 0.273 mmol) and phenylacetaldehyde (92 mg, 0.82 mmol) were stirred in CH_2Cl_2 (75 cm^3) at 37°C for 18 h. Solvent was removed under reduced pressure and THF (10 cm^3) was added. The solution was filtered and solvent was removed under reduced pressure. CH_2Cl_2 (5 cm^3) and diethyl ether (25 cm^3) were added to give an orange–brown powder which was isolated by filtration and dried under vacuum to give a mixture (see text) of **25** and **26** (120 mg, 81%). For **25**: ^1H NMR (acetone-d_6, 500 MHz): δ 12.27 (d, $J = 12.4$ Hz, μ-CH), 7.62 (m, 2H, C_6H_5), 7.37 (m, 3H, C_6H_5), 7.20 (d, $J = 15.0$ Hz, μ-CH=CHCH=C*H*), 7.11 (dd,

J = 15.6, 9.8 Hz, μ-CH=CHC*H*), 5.67 (s, 10H, C_5H_5), 4.69 (t, J = 11.2 Hz, μ-CH=C*H*). For **26**: δ 7.55 (m, 2H, C_6H_5), 7.33 (m, 3H, C_6H_5), 7.33 (dd, J = 11.6, 5.8 Hz, 1H, μ-CH=CHC*H*, obscured by C_6H_5, established through decoupling experiments), 6.78 (ddd, J = 13.5, 5.8, 0.7 Hz, μ-CH=C*H*), 5.38 (s, C_5H_5), 5.21 (s, C_5H_5), 4.65 (d, J = 13.4 Hz, μ-CH), 2.57 (d, J = 11.6 Hz, μ-CH=CHCH=C*H*).

$[C_5H_5(CO)Fe]_2(\mu\text{-}CO)(\mu\text{-}C\text{-}E\text{-}CH{=}CHOCH_2CH_3)^+BF_4^-$ (27)

1 (2.00 g, 4.55 mmol) and $HC(OCH_2CH_3)_3$ (20 g, 140 mmol) were stirred in CH_2Cl_2 (20 cm³) at 35°C for 2 h. Solvent and excess $HC(OEt)_3$ were removed under reduced pressure. Acetone (20 cm³) was added and the solution was filtered at −78°C. Solvent was removed under reduced pressure and THF (10 cm³) and diethyl ether (2 cm³) were added to give an oil which crystallized upon sonication (5 min) and was isolated by filtration. The solid was washed twice with 10 cm³ portions of solvent and dried under vacuum to give **27** (1.83 g, 77%). ^{1}H NMR (acetone-d_6, 270 MHz): δ 9.23 (d, J = 11.0 Hz, μ-C—CH), 8.66 (dq, J = 11.0, 0.5 Hz, μ-C—CH=C*H*), 5.52 (s, 10H, C_5H_5), 4.80 (qd, J = 7.1, 0.5 Hz, CH_2), 1.53 (t, J = 7.1 Hz, CH_3). $^{13}C\{^1H\}$ NMR (acetone-d_6, 50.1 MHz): δ 410.3 (μ-C), 256.0 (μ-CO), 208.9 (CO), 177.1 (μ-C—CH=*C*H), 142.1 (μ-C—*C*H), 92.0 (C_5H_5), 74.5 (CH_2), 14.8 (CH_3). IR (CH_2Cl_2): 2019 (vs), 2007 (m), 1852 (s) cm^{-1}. This material showed no impurities by ^{1}H NMR but failed to give a satisfactory analysis. Anal. Found: C, 42.83; H, 3.27. Calc. for $C_{18}H_{17}BF_4Fe_2O_4$: C, 43.60; H, 3.46%. Crystallization from acetone gave an analytically pure acetone solvate of **27**. Anal. Found: C, 44.49; H, 3.82. Calc. for $C_{18}H_{17}BF_4Fe_2O_4 \cdot 0.5C_3H_6O$: C, 44.62; H, 3.84%.

$\{[C_5H_5(CO)Fe]_2(\mu\text{-}CO)\}_2(\mu\text{-}C_5H_3)^+BF_4^-$ (28)

A mixture of **27** (100 mg, 0.202 mmol) and **29**[7] (77 mg, 0.22 mmol) was stirred in CH_2Cl_2 (5 cm³) for 5 min at ambient temperature. A rapid color change from red to deep purple was observed and microcrystals precipitated from solution. The volume of solvent was reduced to 2 cm³ and diethyl ether (20 cm³) was added. Pink–brown microcrystals were isolated by filtration, washed twice with 2 cm³ portions of solvent, and dried under vacuum to give **28** (138 mg, 85%). ^{1}H NMR (acetone-d_6, 270 MHz): δ 9.10 (d, J = 12.6 Hz, 2H, μ-C—CH), 7.73 (t, J = 12.6 Hz, μ-C—CH=C*H*), 5.44 (s, 20H, C_5H_5). IR (CH_2Cl_2): 2010 (vs), 1990 (sh), 1830 (s), 1822 (s) cm^{-1}. Anal. Found: C, 46.30; H, 2.79. Calc. for $C_{31}H_{23}BF_4Fe_4O_6$: C, 46.44; H, 2.89%.

$[C_5H_5(CO)Fe]_2(\mu\text{-}CO)[\mu\text{-}C\text{-}E\text{-}CH{=}CHN(CH_3)_2]^+BF_4^-$ (30)

27 (100 mg, 0.202 mmol) was dissolved in THF (15 cm³) at −78°C. $HN(CH_3)_2$ (350 cm³, 0.13 atm, 23°C, 1.9 mmol) was condensed in at −78°C. An instant color change from red–orange to orange was observed. After 2 min orange microcrystals precipitated from solution. The crystals were isolated by filtration, washed three times with 2 cm³ portions of solvent and dried under vacuum to give **30** (84 mg, 84%). ^{1}H NMR (acetone-d_6, 270 MHz): δ 8.85 (d, J = 11.1 Hz, μ-C—CH), 8.41 (d septets, J = 11.1, 0.7 Hz, μ-C—CH=C*H*), 5.35 (s, C_5H_5), 5.31 (s, C_5H_5), 3.71 (d, J = 0.7 Hz, CH_3), 3.56 (d, J = 0.8 Hz, CH_3). $^{13}C\{^1H\}$ NMR (acetone-d_6, 50.1 MHz): δ 355.7 (μ-C), 261.1 (μ-CO), 210.9 (CO), 164.6 (μ-C—CH=*C*H), 137.0 (μ-C—*C*H), 91.1 (C_5H_5), 90.5 (C_5H_5), 47.4 (CH_3), 40.4 (CH_3). IR (Nujol): 2001 (vs), 1964 (m), 1828 (s) cm^{-1}. Anal. Found: C, 43.46; H, 3.81; N, 2.68. Calc. for $C_{18}H_{18}BF_4Fe_2O_3N$: C, 43.69; H, 3.67; N, 2.83%.

$[C_5H_5(CO)Fe]_2(\mu\text{-}CO)[\mu\text{-}C{-}CH{=}C(CH_3)_2]^+PF_6^-$ (16P)

32[8] (148 mg, 0.38 mmol) and $(C_6H_5)_3C^+PF_6^-$ (139 mg, 0.36 mmol) were stirred in CH_2Cl_2 (10 cm³) at 0°C for 1.5 h. The volume of solvent was reduced to 6 cm³ and a red precipitate was isolated by filtration, washed with CH_2Cl_2 until the washings were only slightly colored, and dried under vacuum to give **16P** (147 mg, 77%). ^{1}H NMR (acetone-d_6, 270 MHz): δ 9.68 (μ-C—CH), 5.60 (s, C_5H_5), 2.48 (d, J = 0.7 Hz, CH_3), 2.34 (s, CH_3). $^{13}C\{^1H\}$ NMR (CD_3NO_2, 50.1 MHz): δ 440.2 (μ-C), 254.3 (μ-CO), 208.7 (CO), 163.2 (μ-C—CH=*C*), 158.1 (μ-C—*C*H), 93.7 (C_5H_5), 29.4 (CH_3), 23.4 (CH_3). IR (CH_2Cl_2): 2030 (vs), 2000 (m), 1850 (s) cm^{-1}. Anal. Found: C, 40.34; H, 3.33. Calc. for $C_{18}H_{17}F_6Fe_2O_3P$: C, 40.19; H, 3.19%.

$[C_5H_5(CO)Fe]_2(\mu\text{-}CO)(\mu\text{-}C{-}\overline{C{=}CHCH_2CH_2}\overline{)}^+PF_6^-$ (34P)

32[12] (170 mg, 0.42 mmol) and $(C_6H_5)_3C^+PF_6^-$ (154 mg, 0.40 mmol) were stirred in CH_2Cl_2 at 0°C for 30 min and then at ambient temperature for 1 h. The volume of solvent was reduced to 5 cm³ and hexane (3 cm³) was added. A precipitate was isolated by filtration, washed with solvent and dried under vacuum to give **34P** (155 mg, 71%). ^{1}H NMR

(acetone-d_6, 200 MHz): δ 7.55 (m, μ-C—C═CH), 5.64 (s, 10H, C_5H_5), 3.66 (m, CH_2C═CH), 2.85 (m, C═CHCH_2), 2.32 (m, $CH_2CH_2CH_2$). $^{13}C\{^1H\}$ NMR (CD_3NO_2, 50.1 MHz): δ 444.6 (μ-C), 252.1 (μ-CO), 207.3 (CO), 172.0 (μ-C—*C*), 163.2 (μ-C—C═*C*H), 93.1 (C_5H_5), 40.2 (*C*H_2C═CH), 38.0 (C═CH*C*H_2), 25.7 (CH_2*C*H_2CH_2). IR (CH_2Cl_2): 2030 (vs), 2000 (m), 1853 (s) cm^{-1}. Anal. Found: C, 41.19; H, 3.58. Calc. for $C_{19}H_{17}F_6Fe_2O_3P$: C, 41.46; H, 3.12%.

Reaction of [C_5H_5(CO)Fe]$_2$(μ - CO)[μ - C═C(CH_3)CH_2CH_3] (**35**) *with* $(C_6H_5)_3C^+PF_6^-$

35[8] (194 mg, 0.49 mmol) and $(C_6H_5)_3C^+PF_6^-$ (184 mg, 0.47 mmol) were stirred in CH_2Cl_2 (10 cm^3) at 0°C for 1 h. The volume of solvent was reduced to 5 cm^3 and hexane (4 cm^3) was added. A brown powder was isolated by filtration, washed three times with 9 cm^3 portions of solvent, and dried under vacuum to give a 3.8 : 1 mixture of **36** : **37** (237 mg, 90%). The ^1H NMR (acetone-d_6, 270 MHz) of a mixture of **36** : **37** was assigned. For **36**: δ 7.67 (q, J = 7.2 Hz, μ-C—C═CH), 5.65 (s, 10H, C_5H_5), 2.89 (s, μ-C—CCH_3), 2.25 (d, J = 7.2 Hz, CHCH_3); for **37**: δ 6.38 (br s, μ-C—C═C*H*H), 6.25 (br s, μ-C—C═CH*H*), 5.69 (s, 10H, C_5H_5), 3.23 (q, J = 7.0 Hz, C$H_2$$CH_3$), 1.39 (t, J = 7.0 Hz, CH_3).

[C_5H_5(CO)Fe]$_2$(μ - CO)[μ - C═C(CH_3)$CH_2C_6H_4$ - *p*-CH_3] (**38**)

13 (250 mg, 0.407 mmol) and $N(CH_2CH_3)_4^+$ $HFe(CO)_4^-$ (185 mg, 0.611 mmol) were stirred in THF (30 cm^3) at 25°C for 30 min. Solvent was removed under reduced pressure. The residue was chromatographed (alumina, diethyl ether) to give pure **38** (84 mg, 44%). ^1H NMR (acetone-d_6, 270 MHz): δ 7.36 (d, J = 7.9 Hz, 2H, C_6H_4), 7.13 (d, J = 7.9 Hz, 2H, C_6H_4), 5.03 (s, C_5H_5), 4.96 (s, C_5H_5), 4.25 (d, J = 15.2 Hz, C*H*H), 4.06 (d, J = 14.9 Hz, CH*H*), 2.32 (s, CH_3), 2.30 (s, CH_3). $^{13}C\{^1H\}$ NMR (acetone-d_6, 126 MHz): δ 271.2, 261.7 (μ-C); 213.4, 213.2 (CO); 140.6, 139.7, 135.3 (*para*, *ipso* and μ-C═*C*); 129.5, 128.9 (*ortho*, *meta*); 85.2, 85.1 (C_5H_5); 48.7 (CH_2); 25.3, 20.9 (CH_3). IR (CH_2Cl_2): 1997 (s), 1956 (m), 1785 (m) cm^{-1}. HRMS Found: 470.0265. Calc. for $C_{24}H_{22}Fe_2O_3$: 470.0261.

Reaction of [C_5H_5(CO)Fe]$_2$(μ - CO)[μ - C═C(CH_3)$CH_2C_6H_4$ - *p* - CH_3] (**38**) *with* $(C_6H_5)_3C^+PF_6^-$

38 (65 mg, 0.14 mmol) and $(C_6H_5)_3C^+PF_6^-$ (51 mg, 0.13 mmol) were stirred in CH_2Cl_2 (1 cm^3) at 0°C for 1 h and then at ambient temperature for 15 min. Diethyl ether (1 cm^3) was added and a red–brown precipitate was isolated by filtration, washed with 1 cm^3 portions of solvent until the washings were colorless, and dried under vacuum (39 mg, 49%). The ^1H NMR (acetone-d_6, 200 MHz) of the 1 : 6.2 : 2.2 mixture of **13** : **39c** and **39t** was assigned. For **39c**: δ 7.32 (d, J = 7.9 Hz, 2H, C_6H_4), 7.23 (d, J = 7.9 Hz, 2H, C_6H_4), 6.34 (br s, μ-C—C═C*H*H), 6.01 (br s, μ-C—C═CH*H*), 5.69 (s, 10H, C_5H_5), 4.54 (br s, C$H_2C_6H_4$-*p*-CH_3), 2.33 (s, CH_3); for **39t**: δ 7.44 (d, J = 7.9 Hz, 2H, C_6H_4), (remaining C_6H_4 obscured by **39c** C_6H_4), 6.13 (br s, μ-C—C═C*H*H), 5.95 (br s, μ-C—C═CH*H*), 5.43 (s, 10H, C_5H_5), 4.59 (br s, C*H*HC_6H_4-*p*-CH_3), 4.57 (br s, CH*H*C_6H_4-*p*-CH_3), 2.31 (s, CH_3).

Cis- *and* trans-[C_5H_5(CO)Fe]$_2$(μ-CO){μ-C—C[CH(CH_3)$_2$]═CH_2}$^+PF_6^-$ (**41**)

40 (C. P. Casey, M. W. Meszaros and S. R. Marder, unpublished observations) (160 mg, 0.39 mmol) and $(C_6H_5)_3C^+PF_6^-$ (145 mg, 0.37 mmol) were stirred in CH_2Cl_2 (3 cm^3) at 0°C for 1 h. Hexane (2 cm^3) was added and a red precipitate was isolated by filtration, washed with solvent and dried under vacuum. Concentration of the mother liquor gave additional **41** (129 mg, 63% 2.4 : 1 *cis* : *trans*). ^1H NMR (acetone-d_6, 270 MHz) for **41C**: δ 6.36 (br s, μ-C—C═C*H*H), 6.23 (br s, μ-C═CH*H*), 5.63 (s, C_5H_5), 3.44 (septet, J = 7.0 Hz, CH), 1.41 (d, J = 7.0 Hz, 6H, CH_3); for **41t**: δ 6.27 (br s, μ-C—C═C*H*H), 6.21 (br s, μ-C—C═CH*H*), 5.43 (s, 10H, C_5H_5), 3.84 (septet, J = 7.0 Hz, CH), 1.57 (d, J = 7.0 Hz, CH_3), 1.32 (d, J = 7.0 Hz, CH_3). $^{13}C\{^1H\}$ NMR (CD_3NO_2, 50.1 MHz) for **41c**: 472.7 (μ-C), 252.1 (μ-CO), 207.3 (CO), 185.0 (μ-C—*C*), 120.4 (C═*C*H_2), 94.2 (C_5H_5), 37.0 (CH), 24.0 (CH_3), 22.0 (CH_3); for **41t**: 250.6 (μ-CO), 209.1 (CO), 183.2 (μ-C—*C*), 122.9 (C═*C*H_2), 95.3 (C_5H_5), 37.9 (CH), 24.7 (CH_3), 24.0 (CH_3), (μ-C not observed). IR (CH_2Cl_2): 2039 (vs), 2011 (s), 1860 (m) cm^{-1}. Anal. Found: C, 41.56; H, 3.60. Calc. for $C_{19}H_{19}F_6Fe_2O_3P$: C, 41.34; H, 3.47%.

Crystallography

A summary of crystal data and intensity collection is presented in Table 5. Data reduction, solution, and refinement of the structures were performed with the SHELXTL structure determination package (Nicolet XRD Corp., Madison, WI) similar to that described previously.[15] For **28** and **30** second orientations of the BF_4 counterion were located on a difference map and refined to 13 and 17% occupancy respectively. For both **28**

Table 5. Summary of crystal data and intensity collection

	4	28	30
Empirical formula	$C_{23}H_{19}BF_4Fe_2O_3$	$C_{31}H_{23}BF_4Fe_4O_6$	$C_{18}H_{18}BF_4Fe_2O_3N$
Formula weight	541.898	801.713	494.845
Crystal dimension, mm	$0.45 \times 0.39 \times 0.30$	$0.80 \times 0.30 \times 0.05$	$0.40 \times 0.05 \times 0.05$
Temperature, K	297	297	297
Cell parameters			
a, Å	10.444(2)	8.715(2)	16.403(3)
b, Å	12.994(3)	27.586(9)	9.237(1)
c, Å	16.827(3)	12.974(3)	14.416(2)
β, deg	90.76(2)	98.20(2)	113.72(1)
Space group	$P2_1/n$	$P2_1/c$	$P2_1/c$
Z	4	4	4
Calculated density g cm^{-3}	1.58	1.72	1.64
Absorption coefficient, μ, cm^{-1}	13.24	18.10	15.04
Nicolet diffractometer[a]	P3/F	P3/F	P3/F
Scan type	Wycoff	θ–2θ	θ–2θ
Scan range,			
deg below 2θ-K_α	1.0[b]	1.0	0.7
deg below 2θ-K_α	1.0	1.0	0.7
Scan speed	4.0–29.3	3.5–29.3	1.5–14.65
Background/scan ratio	1.00	1.00	0.05
2θ limits, deg	3.00–45.00	3.00–50.67	4.00–42.93
Max $\sin\theta/\lambda$, Å^{-1}	0.539	0.602	0.515
Absorption correction	Psi-scan method	Psi-scan method	None
Unique data, theoretical	3341	7092	2286
$F_0 > 3\sigma(F_0)$	2286[c]	3716	1615
P; weight $= [\sigma^2(F)+p^2F^2]^{-1}$	0.001	0.00021	0.0016
Discrepancy indices			
R, %	5.85	6.74	6.62
Rw, %	6.10	5.53	5.93
Observation/variable ratio	9.5	9.0	6.1
Final difference ρ_{max}, e/Å^3	0.46	0.83	0.57

[a] Diffractometer equipped with a graphite monochromated Mo-K_α radiation source.
[b] Scan range and background offset.
[c] $F_0 > 2.5\sigma(F_0)$.

and **30** the major and minor orientations of the BF_4 counterion were constrained to be approximately tetrahedral with similar isotropic thermal factors for the minor orientation. Some disorder of the BF_4 counterion for **4** was evident from the large thermal parameters of the fluorine atoms but a suitable disorder model was not found. The phenyl and Cp groups of **4** were refined as rigid bodies. Atomic coordinates have been deposited with the Cambridge Crystallographic Data Centre.

Acknowledgements—Funding from the National Science Foundation is gratefully acknowledged. We thank Dr Kenneth J. Haller and Dr Robert E. Palermo for help with the crystal structures, and Dr Robert E. Colborn for helpful discussions. MSK thanks SOHIO for a fellowship. SRM thanks W. R. Grace Company for a fellowship.

REFERENCES

1. M. Nitay, W. Priester and M. Rosenblum, *J. Am. Chem. Soc.* 1978, **100**, 3620.
2. C. P. Casey and S. R. Marder, *Organometallics* 1985, **4**, 411.
3. C. P. Casey, M. S. Konings, R. E. Palermo and R. E. Colborn, *J. Am. Chem. Soc.* 1985, **107**, 5296.
4. C. P. Casey, M. S. Konings, S. R. Marder and Y. Takezawa, *J. Am. Chem. Soc.* (submitted).
5. M. B. Hall and R. F. Fenske, *Inorg. Chem.* 1972, **11**, 768.
6. S. C. Kao, P. P. Y. Lu and R. Pettit, *Organometallics* 1982, **1**, 911.
7. G. M. Dawkins, M. Green, J. C. Jeffery and F. G. A. Stone, *J. Chem. Soc., Chem. Commun.* 1980, 1120.
8. C. P. Casey, M. W. Meszaros, P. J. Fagan, R. K. Bly, S. R. Marder and E. A. Austin, *J. Am. Chem. Soc.* 1986, **108**, 4043.

9. R. F. Fenske, In *Organometallic Compounds: Synthesis Structure and Theory* (Edited by B. L. Shapiro). Texas A&M University Press, College Station, Texas (1983).
10. B. E. Bursten and R. H. Cayton, *J. Am. Chem. Soc.* 1986, **108**, 8241.
11. C. P. Casey, W. H. Miles and H. Tukada, *J. Am. Chem. Soc.* 1985, **107**, 2924.
12. C. P. Casey, S. R. Marder and B. R. Adams, *J. Am. Chem. Soc.* 1985, **107**, 7700.
13. C. P. Casey, M. S. Konings and K. J. Haller, *J. Organomet. Chem.* 1986, **301**, C55.
14. C. P. Casey, P. J. Fagan and W. H. Miles, *J. Am. Chem. Soc.* 1982, **104**, 1134.
15. K. J. Haller and J. H. Enemark, *Inorg. Chem.* 1978, **17**, 3552.

Polyhedron Vol. 7, No. 10/11, pp. 903–918, 1988
Printed in Great Britain

0277–5387/88 $3.00+.00
© 1988 Pergamon Press plc

METAL ALKOXIDES: MODELS FOR METAL OXIDES—XIII.† NMR SPECTROSCOPIC AND THEORETICAL INVESTIGATIONS INTO THE REDUCTION OF ALKYNES BONDED TO HEXAALKOXIDES OF DIMOLYBDENUM AND DITUNGSTEN

MALCOLM H. CHISHOLM,‡ BRIAN K. CONROY, DAVID L. CLARK and JOHN C. HUFFMAN

Department of Chemistry and Molecular Structure Center, Indiana University, Bloomington, IN 47405, U.S.A.

(*Accepted* 5 *November* 1987)

Abstract—In reactions between $M_2(OR)_6(py)_x$ compounds, where M = Mo and W, R = Np (Np = neopentyl), *i*-Pr and *t*-Bu, $x = 0$ or 2, and alkynes (1 : 1 stoichiometry) in hydrocarbon/pyridine solvents at or below room temperature, $M_2(OR)_6(py)_x(\mu\text{-}C_2R_2)$ complexes are formed and have previously been shown to adopt one of three different structural types. Based on the local coordination geometry about each metal atom, these structural types can be described as octahedral–octahedral, **I**, octahedral–trigonal-bipyramidal, **II**, and trigonal-bipyramidal–trigonal-bipyramidal, **III**. All $Mo_2(\mu\text{-}C_2R_2)$ containing complexes adopt structure **I** while the $W_2(\mu\text{-}C_2R_2)$ complexes adopt one of **I**, **II**, or **III**, depending on the alkyne and the alkoxide. A comparison of structures and C—C bond distances in the $\mu\text{-}C_2R_2$ ligand reveals that the C—C bond distance is dependent on the structural type and increases in the order **I** < **II** < **III** and Mo < W. The magnitudes of $^1J_{^{13}C-^{13}C}$ for the $M_2(\mu\text{-}C_2H_2)$ moieties show an inverse correlation with d(C—C). Fenske–Hall molecular orbital calculations performed on the model compounds $M_2(OH)_6(NH_3)_x(\mu\text{-}C_2H_2)$, where M = Mo and W and $x = 1$ or 2, reveal that the major factor contributing to the reduction of the alkyne in **I**, **II**, and **III**, is the local coordination geometry about each metal atom. Trigonal-bipyramidal coordinated metals and monoalkoxy-bridged $M_2(\mu\text{-}C_2R_2)$ complexes reduce the alkyne more than octahedral coordinated metal atoms and di-alkoxy-bridged structures, respectively. The reduction of the alkynes for M = W > Mo can be traced to the relative orbital energetics and radial extension of the metal atomic orbitals. The influence of the supplemental Lewis base ligand NH_3 is found to be small. The effect of alkoxide π-donation is seen in calculations employing a frozen π orbital approach. It is demonstrated that alkoxide π-donation to the metal atom enhances metal π back-donation into the alkyne π^* orbitals.

During our investigations of the organometallic chemistry associated with molybdenum and tungsten supported by alkoxide ligands, we have proposed that alkoxide clusters of these metals may act as homogeneous models for heterogeneous metal oxide catalysts.[2] In both systems the metals are in middle to high oxidation states supported by strong π-donating oxygen ligands. The use of alkoxide ligands has two pronounced effects: (1) it solubilizes the cluster units and (2) the nuclearity of the cluster can be controlled by steric effects associated with the OR ligands. The chemistry of discrete dinuclear, trinuclear and tetranuclear clusters can then be studied.

$M_2(OR)_6L_x$ compounds (M = Mo, W; R = Np, *i*-Pr, *t*-Bu; $x = 0$, 2) react with small unsaturated molecules, e.g. RC≡CR,[3–17] C≡O,[18–24] $R_2C{=}O$,[25] RC≡N,[13,26–28] RN≡C,[29] N≡O,[30–33] and

† For Part XII, see ref. 1.

‡Author to whom correspondence should be addressed.

$R_2NC{\equiv}N$,[34,35] to produce either a large reduction in the coordinated C—E multiple bond or a cleavage of the C—E function.

In the reactions of $M_2(OR)_6L_x$ with alkynes ($R'C{\equiv}CR'$), a wide variety of compounds are formed depending on (1) the metal, (2) the steric bulk of the alkoxide or the alkyne substituents, (3) the stoichiometry of the reaction and (4) the reaction temperature. Isolated products include $M_2(OR)_6L_x(\mu\text{-}C_2R'_2)$,[3-6,10,15] $[L_x(RO)_3M{\equiv}CR']_y$,[6,9,11-16] $M_3(OR)_9(\mu_3\text{-}CR')$,[7-11] $M_2(OR)_6L_x(\mu\text{-}C_4R'_4)$,[3,4,7,11] and $W_2(OR)_6(\mu\text{-}C_4R'_4)(\eta^2\text{-}C_2R'_2)$.[3-5,7,9,11]

The $M_2(OR)_6L_x(\mu\text{-}C_2R'_2)$ complexes of molybdenum appear to adopt structure **I**[3,4] while the tungsten complexes adopt structures **I**, **II** and **III**,[5,6,10] shown below. The $W_2(\mu\text{-}C_2R'_2)$ complexes favour structure **III** over structure **I** and **II** when sterically bulky combinations of alkoxide and alkyne are used.

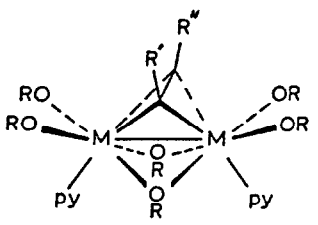

I

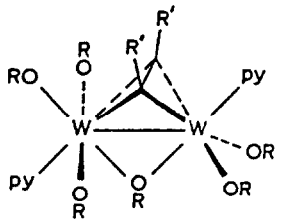

II

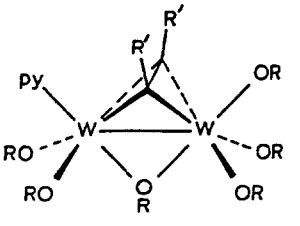

III

Upon further investigation, it was found that $W_2(O\text{-}t\text{-}Bu)_6(py)(\mu\text{-}C_2H_2)$ was in equilibrium with $(t\text{-}BuO)_3W{\equiv}CH$ in toluene-d_8 solution [eq. (1)] in a 5 : 1 ratio, respectively.[6]

$$W_2(O\text{-}t\text{-}Bu)_6(py)(\mu\text{-}C_2H_2) \rightleftharpoons 2(t\text{-}BuO)_3W{\equiv}CH + py. \quad (1)$$

Changing the alkoxide to the slightly larger *t*-amyloxide ($OCMe_2Et$) changed the equilibrium ratio to *ca* 1 : 5, favouring the alkylidyne.[11] Schrock *et al.* found that increasing the steric bulk of the reactant molecules favoured carbon–carbon bond cleavage [eq. (2)].[12-14]

$$W_2(O\text{-}t\text{-}Bu)_6 + RC{\equiv}CR \rightarrow 2(t\text{-}BuO)_3W{\equiv}CR. \quad (2)$$

$$R = Me, Et, Pr$$

In this report we will use metal–metal and carbon–carbon bond distances, carbon–carbon coupling constants in the $M_2(\mu\text{-}C_2H_2)$ moieties, and Fenske–Hall molecular orbital calculations to investigate the reduction of alkynes by $M_2(OR)_6L_x$ compounds.

EXPERIMENTAL

Computational procedures

We have employed the model systems $M_2(OH)_6(NH_3)_x(C_2H_2)$, where M = Mo and $x = 2$, and M = W and $x = 1$ or 2, to investigate the nature of $M_2(\mu\text{-}C_2H_2)$ bonding. The coordinates for these model compounds were idealized to either C_{2v} or C_s point symmetry, but otherwise bond lengths, bond angles and dihedral angles were taken from the crystal structures of $Mo_2(O\text{-}i\text{-}Pr)_6(py)_2(\mu\text{-}C_2H_2)$,[4] $W_2(O\text{-}i\text{-}Pr)_6(py)_2(\mu\text{-}C_2H_2)$,[6] $W_2(ONp)_6(py)_2(\mu\text{-}C_2H_2)$[10] and $W_2(O\text{-}t\text{-}Bu)_6(py)(\mu\text{-}C_2H_2)$.[6] A summary of the structural parameters employed in this study is listed in Table 1.

Molecular orbital calculations were performed using the Fenske–Hall method, which has been discussed in detail elsewhere[36] and its applications reviewed.[37] The Fenske–Hall method is an approximate Hartree–Fock–Roothaan SCF–LCAO procedure, and the final results depend only upon the chosen atomic basis set and internuclear distances. SCF calculations were performed in the atomic basis on the C_2H_2, $(NH_3)_x$ ($x = 1$ or 2) and $M_2(OH)_6$ fragments, and on the $M_2(OH)_6(NH_3)_x(\mu\text{-}C_2H_2)$ compounds. To aid in the interpretation of orbital interactions, the converged wave functions were transformed into a basis consisting of the canonical orbitals of the isolated C_2H_2 and $M_2(OH)_6(NH_3)_x$ fragments. All of the calculations described in this paper were performed at the Indiana University Computational Chemistry Center using a VAX 11/780 computer system.

All atomic wave functions were generated by a best fit to Herman–Skillman atomic calculations using the method of Bursten *et al.*[38] Contracted double-ζ representations were used for Mo 4*d* and W 5*d* AO's as well as C, O, and N 2*p* AO's. Basis functions for the metal atoms were derived for a +1 oxidation state with the valence *s* and *p* exponents fixed at 1.55 for Mo 5*s* and 5*p*, and 1.80

Table 1. Structural parameters for $M_2(OH)_6(NH_3)_x(\mu\text{-}C_2H_2)$ model compounds of Mo and W

Distance[a]	I[b]	I[c]	II[d]	III[e]	Fixed[f]
M—M	2.554	2.567	2.609	2.665	2.614
M—C	2.088	2.097	2.164	2.107	2.104
			2.084	2.092	
C—C	1.368	1.394	1.390	1.441	1.408
M—μO	2.146	2.143	2.070	2.083	2.075
			2.012	1.999	
M—O_t	1.942	1.941	1.961	1.938	1.940
			1.927	1.919	
M—N	2.312	2.312	2.314	2.267	2.291
			2.274	—	
O—H	0.960	0.960	0.960	0.960	0.960
N—H	1.010	1.010	1.010	1.010	1.010
C—H	0.960	0.960	0.960	0.960	0.960
Angle[g]					
C—C—H	137.0	140.5	136.8	135.5	137.6
M—O_t—H	135.5	134.6	133.8	149.0	135.0
			136.2	152.4	
M—μO—H	125.3	124.9	133.9	139.6	135.0
			132.7	138.9	
H—N—H	112.0	112.0	112.0	112.0	112.0

[a] Distances are in Angstroms.
[b] For M = molybdenum.
[c] For M = tungsten.
[d] When two numbers are given, the first number refers to the distances or angles from the octahedral metal and the second number refers to the trigonal-bipyramidal metal.
[e] When two numbers are given, the first number refers to the distances or angles from the pyridine coordinated metal and the second number refers to the non-pyridine coordinated metal.
[f] These parameters were assumed for calculations described in the text and for the results given in Table 5.
[g] Angles are in degrees.

for W 6*s* and 6*p* orbitals.† Examination of a variety of Xα optimized atomic orbital bases for the metal atoms with various valence *s* and *p* exponents showed no effect on the *general* conclusions presented herein. An exponent of 1.16 was used for the H 1*s* atomic orbital since it minimizes the energy of methane.[39]

Synthetic methods and spectroscopic studies

Standard experimental techniques for the manipulation of air- and water-sensitive materials were used. The known compounds were prepared as previously described.[4,6,10,40,41]

^{13}C NMR spectra were recorded on a Nicolet NT-360 spectrometer at 90 MHz or on a Varian XL-300 at 75 MHz in benzene-d_6 or toluene-d_8 solvent. The ^{13}C NMR spectra for $M_2(OR)_6(py)_x(\mu\text{-}C_2H_2)$ were obtained using labelled ethyne (ethyne-1,2-$^{13}C_2$ 92 mol% ^{13}C). The ^{13}C labelled ethyne was purchased from MSD Isotopes and used without purification. ^{13}C NMR chemical shifts are in ppm relative to the C_6D_6 triplet of benzene-d_6 set at δ 128.0 or the methyl-carbon of toluene-d_8 set at δ 20.4. The ^{13}C—^{13}C coupling constants reported for the ethyne adducts were obtained by use of gated ^1H decoupling techniques.

RESULTS AND DISCUSSION

Bonding considerations

The presence of three structural types for the alkoxide-supported $M_2(\mu\text{-}C_2H_2)$ compounds raises

† Valence *s* and *p* orbital exponents were those that kept the populations of the Mo atomic 5*s* and 5*p* orbitals and W atomic 6*s* and 6*p* orbitals less than 0.1

several questions concerning the role of structural geometry on the reduction and cleavage of the alkyne ligand in this system. The reduction of the C≡C bond is an important first step in alkyne metathesis reactions and a detailed understanding of alkyne reduction in these systems is clearly desirable. In particular, what is the effect of (1) the metal, (2) the local geometry, (3) the M—M distance, (4) the presence of π-donating alkoxide ligands and (5) the presence of Lewis bases on the dimetal centre with regard to the reduction of the alkyne? We have used Fenske–Hall molecular orbital calculations in an attempt to answer these questions and to gain insight into the nature of the bonding in these complexes.

Linear vs bent C_2H_2

Although the result is known,[42] it is useful to review briefly the changes that occur in the molecular orbitals when linear C_2H_2 bends upon coordination to a metal. The orbitals of C_2H_2 that are important for M—C bonding are the C—C π and π* orbitals. In linear C_2H_2, the π and π* orbital pairs are each doubly degenerate. Bending the C_2H_2 molecule in the plane of the page lifts the degeneracy of the π and π* orbital pairs as shown in Fig. 1. For simplicity, the π orbitals of bent C_2H_2 are referred to as $\pi_\parallel$ and $\pi_\perp$ being parallel or perpendicular to the metal–metal bond in the $M_2(\mu\text{-}C_2H_2)$ complexes, respectively. The $\pi_\parallel$ and $\pi_\parallel^*$ orbitals are not contained in the plane of the bend (as shown in IV) and are relatively unperturbed by the bending process as demonstrated by the C—C overlap populations in Table 2 and the relative orbital energetics in Fig. 1. The small decrease in the C—C overlap populations of the $\pi_\parallel$ and $\pi_\parallel^*$ orbitals (Table 2) can be attributed primarily to an elongation of the C—C distance and not to a change in the C—C—H angle.

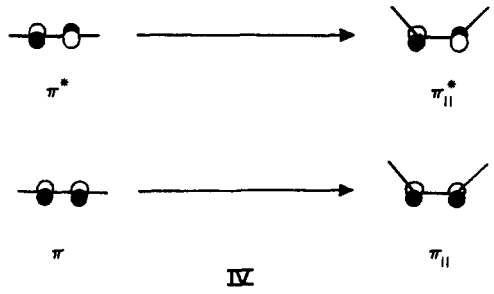

IV

The $\pi_\perp$ and $\pi_\perp^*$ orbitals of C_2H_2 are contained within the plane of the bend, and the bending process promotes a rehybridization of *s* and *p* atomic orbital character as shown in V. This rehybridization results in a dramatic decrease in the antibonding character of the $\pi_\perp^*$ orbital, as revealed in the overlap populations listed in Table 2, and a concomitant lowering in orbital energy (Fig. 1). The consequent stabilization of the π* orbitals that results from both a bending of the C_2H_2 molecule

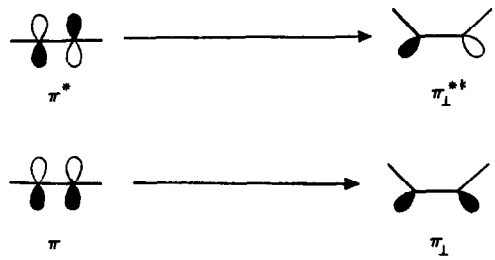

V

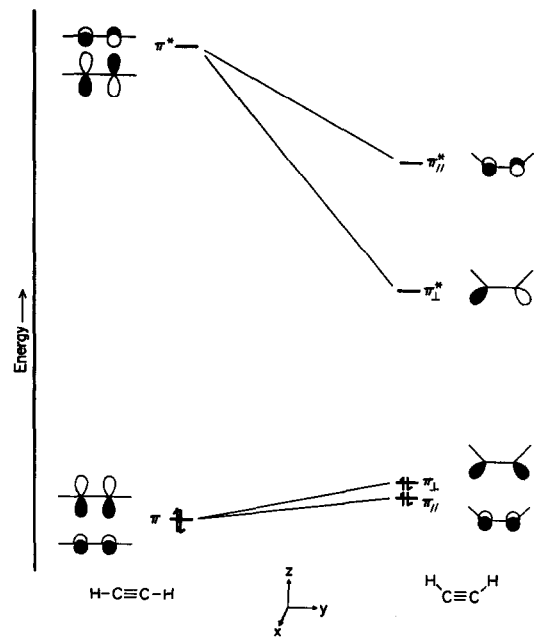

Fig. 1. Molecular orbital diagram comparing the valence π and π* orbitals of C_2H_2 in linear and bent geometries.

Table 2. C—C overlap populations[a] for an uncoordinated C_2H_2 ligand at the internuclear distances relevant for free C_2H_2 and the bent C_2H_2 moiety in $W_2(O\text{-}i\text{-}Pr)_6(py)_2(\mu\text{-}C_2H_2)$

Compound	Overlap populations			
	$\pi_\parallel$	$\pi_\perp$	$\pi_\perp^*$	$\pi_\parallel^*$
Linear C_2H_2	0.296	0.296	−0.727	−0.727
Bent C_2H_2	0.256	0.154	−0.260	−0.525

[a] Overlap populations for a single electron occupying the molecular orbital.

and the lengthening of the C—C distance will have important consequences towards the interaction of C_2H_2 with the M_2 centre.

The C_{2v}-$W_2(OH)_6(NH_3)_2$ fragment, I′

In order to investigate the bonding interactions between C_2H_2 and the $M_2(OR)_6(py)_x$ moieties, we have used the model compounds $M_2(OH)_6(NH_3)_x$ (μ-C_2H_2). The use of OH in place of OR reduces the number of molecular orbitals in the calculations but allows us to maintain oxygen lone pair interactions with the metal. NH_3 was chosen to represent the pyridine ligands despite the fact that pyridine has a π system because the long M—N distances (*ca* 2.3 Å) preclude any significant π-interaction with the metal atoms.

A simple way to discuss the bonding interactions between the C_2H_2 ligand and the W_2 unit in the $W_2(\mu$-$C_2H_2)$ compounds is to examine the interactions in terms of fragment MO's. The tungsten model compound for structure **I**, C_{2v}-$W_2(OH)_6(NH_3)_2(\mu$-$C_2H_2)$, can be decomposed into C_{2v}-$W_2(OH)_6(NH_3)_2$, **I′**, and C_2H_2 fragments. The important metal-based fragments of **I′** are shown schematically in VI along with a local coordinate system for each metal atom.

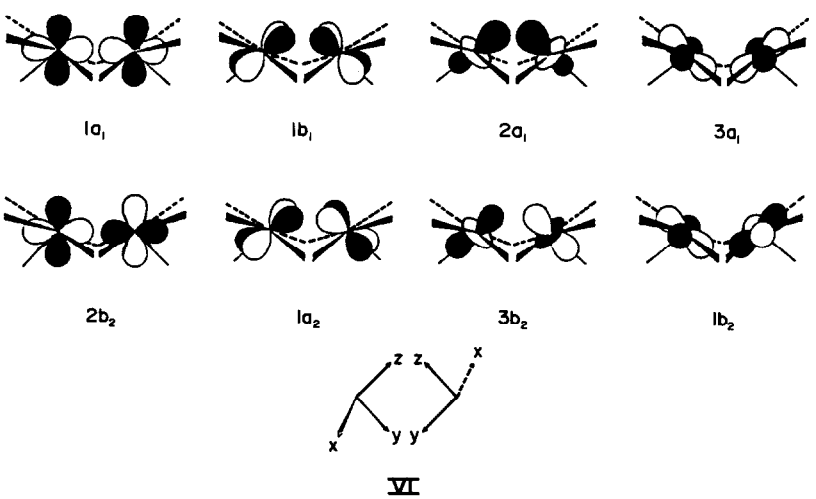

VI

Using this local coordinate system, the important metal-localized MO's of **I′** can be visualized in terms of combining two square-based-pyramidal metal fragments "hinged" along a common edge. In- and out-of-phase combinations of two metal d_z^2 atomic orbitals yield the $2a_1$ and $3b_2$ M—M σ-bonding and -antibonding fragment MO's, respectively. The $2a_1$ fragment MO is hybridized away from the terminal NH_3's to minimize M—N antibonding. In a similar fashion, the in- and out-of-phase combinations of two d_{xz} atomic orbitals would give rise to the $1b_1$ and $1a_2$ π-bonding and -antibonding orbitals, respectively,while the d_{yz} atomic orbitals give rise to the $1a_1$ and $2b_2$ σ-bonding and -antibonding orbitals, respectively. The last two fragment MO's of importance to our discussion are the in-and out-of-phase combinations of two d_{x2-y2} atomic orbitals producing the $3a_1$ and $1b_2$ fragment MO's of **I′**. The six metal *d*-electrons occupy the $1a_1$, $1b_1$ and $2a_1$ M—M bonding orbitals as seen on the left of Fig. 2. The M—M σ-bonding and -antibonding $3a_1$ and $1b_2$ fragment orbitals lie high in energy as a result of strong π-donor interactions with the OH ligands. This has been discussed in detail elsewhere.[19]

M—M *and* M—C *bonding in complexes of structure* **I** *for* W *and* Mo

The π and π^* orbital pairs of the alkyne ligand are involved in metal–carbon bonding interactions. The alkyne ligand bonds to the dinuclear centre via a synergistic mechanism of electron donation from filled alkyne π orbitals to empty metal *d*-orbitals, and backbonding results from electron donation from filled metal *d*-orbitals to unoccupied alkyne π^* orbitals. The relative magnitude and nature of the metal–alkyne bonding interactions are similar in nature, but different in magnitude for the tungsten and molybdenum analogues. We first describe the interaction of C_2H_2 with **I′** (**I′** = C_{2v}-$M_2(OH)_6(NH_3)_2$) of tungsten in detail.

As shown in Fig. 2, the C_2H_2 $\pi_\parallel$ orbital has b_2 symmetry in the C_{2v} point group and can interact with W_2 fragment orbitals of the same symmetry. From simple perturbation theory, the magnitude of the interaction will depend on the relative orbital

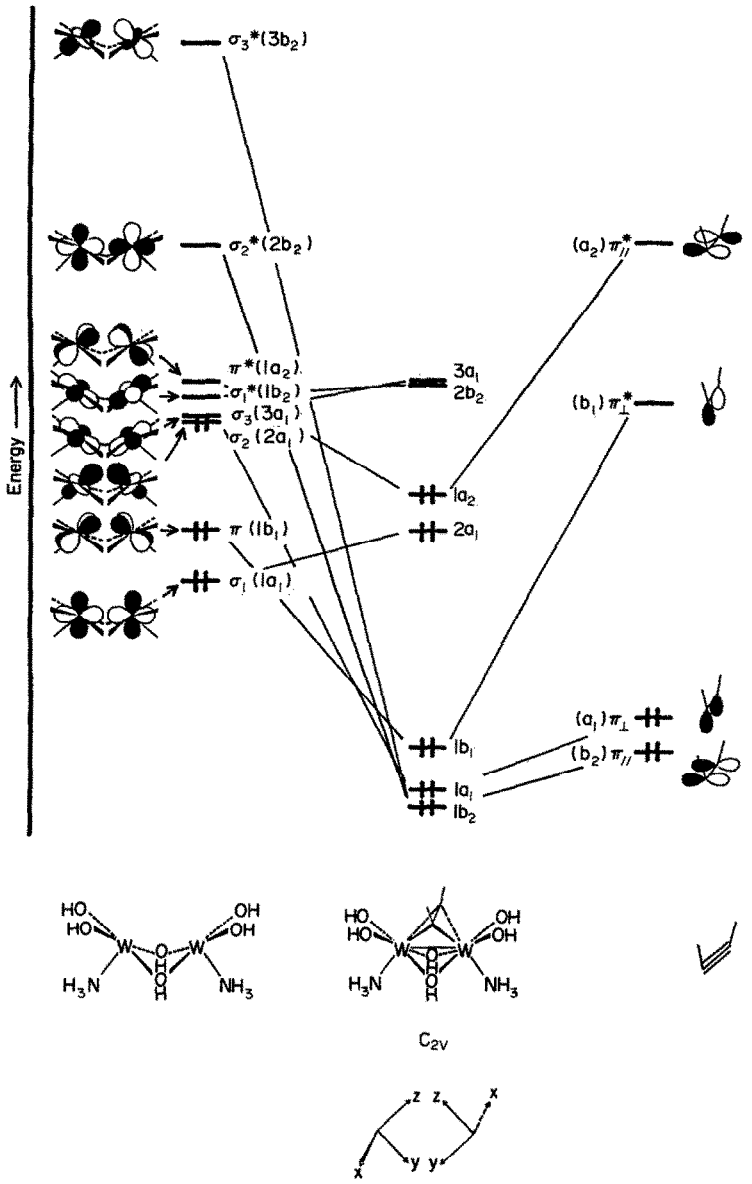

Fig. 2. Fragment molecular orbital diagram showing the perturbation of C_{2v}-$W_2(OH)_6(NH_3)_2$ [I′] fragment orbitals by interaction with a bent C_2H_2 moiety. Orbital occupation by electrons is denoted by bars. Only the important metal- and acetylene-based fragments are shown.

energetics and degree of overlap between the M_2 and C_2 fragments.[44] In the I′ fragment of tungsten, no single b_2 fragment orbital is spatially oriented to produce good overlap with the b_2 $\pi_\parallel$ orbital of C_2H_2. As a result, the b_2 interaction forces a rehybridization of the $2b_2$ and $3b_2$ fragment orbitals of I′ in order to maximize the M—C b_2 bonding interaction. The forced rehybridization of the $2b_2$ and $3b_2$ orbitals of I′ is shown qualitatively in VII and the resulting $1b_2$ W—C bonding orbital of the

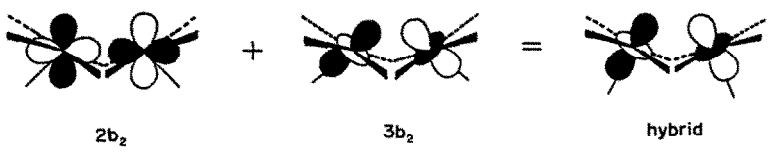

VII

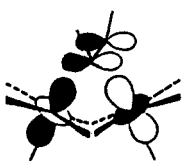

$1b_2$

VIII

$W_2(\mu\text{-}C_2H_2)$ moiety is shown in VIII. The $1b_2$ fragment orbital of I′ also has the correct symmetry to interact with the b_2 C_2H_2 $\pi_\parallel$ orbital but there is negligible overlap. Therefore the $1b_2$ orbital of fragment I′ is relatively unperturbed by interaction with the C_2H_2 moiety and becomes the $2b_2$ orbital (LUMO) of the $W_2(\mu\text{-}C_2H_2)$ compound.

The C_2H_2 $\pi_\perp$ orbital has a_1 symmetry and interacts primarily with the $2a_1$ W—W σ-bonding orbital of I′ resulting in the $1a_1$ W—C bonding MO of I, shown in IX.

$1a_1$

IX

Both the $1a_1$ and $3a_1$ fragment orbitals of I′ have the correct symmetry to interact with the C_2H_2 $\pi_\perp$ fragment orbital but have negligible overlap. The $3a_1$ fragment orbital of I′ transfers essentially unperturbed into the $3a_1$ MO of I. The $1a_1$ fragment orbital of I′ mixes somewhat with the $2a_1$ fragment orbital of I′ to give the $2a_1$ MO of I which is destabilized relative to its parent orbital, the $1a_1$ of I′. The resulting $2a_1$ MO represents the primary component of the W—W σ-bond in I.

We can gain a relative measure of the magnitude of the alkyne π-interaction with the W_2 centre through the aid of fragment overlap populations. The total overlap population between the W_2 and C_2H_2 fragments is 0.327 for the b_2 interaction, while the overlap population for the a_1 interaction is only 0.225. The b_2 interaction has a better overlap than the a_1 interaction, even though the b_2 fragment orbitals are energetically further away than the a_1 fragment orbitals. The balance between orbital energetics and the magnitude of the overlap, results in a situation where both a_1 and b_2 alkyne π orbitals are stabilized by approximately the same amount.

The $2b_2$ and $3a_1$ orbitals of I′, the LUMO and SLUMO (second lowest unoccupied molecular orbital), have just been described as transferring essentially unperturbed from the I′ fragment. However, there is a reordering which takes place between these two orbitals as they are transferred from their parent $1b_2$ and $3a_1$ orbitals of I′ to the $2b_2$ and $3a_1$ orbitals of I. While the overlap populations between the $1b_2$ and $3a_1$ orbitals of I′ and the $\pi_\parallel$ and $\pi_\perp$ orbitals of C_2H_2, respectively, are small, the overlap population for the a_1 interaction is larger than the b_2 interaction. This switches the order of the $3a_1$ and $1b_2$ orbitals of I′ such that the $3a_1$ orbitals of I (M—M σ-bonding) is higher in energy than the $2b_2$ orbital of I (M—M σ-antibonding).

The C_2H_2 π^* fragment orbitals are involved in strong, covalent interactions with I′. The C_2H_2 $\pi_\perp^*$ fragment orbital interacts with the $1b_1$ fragment orbital of I′ resulting in the formation of the $1b_1$ W—C bonding MO of I. In a similar fashion, the C_2H_2 $\pi_\parallel^*$ fragment orbital of I′ interacts with the $1a_2$ orbital of I′ to give the $1a_2$ W—C bonding orbital of I as shown in Fig. 2. The resulting $1a_2$ and $1b_1$ M—C bonding orbitals are illustrated in X.

$1a_2$ $1b_1$

X

The bonding picture shown in Fig. 2 has the components of four M—C bonds. The $1a_1$ and $1b_2$ orbitals are predominantly alkyne π in character and represent alkyne π-donation to the M_2 centre. The $1b_1$ and $1a_2$ orbitals have more balanced contributions from both M_2 and alkyne fragments and represent strong, covalent π-backbonding interactions.

We can now discuss the qualitative similarities and differences between the Mo and W analogues of the formula $M_2(OH)_6(NH_3)_2(\mu\text{-}C_2H_2)$ having C_{2v} point symmetry, structure I. The overall bonding picture is found to be very similar with the primary difference being their fragment orbital energies, degree of overlap with the C_2H_2 ligand and the degree of rehybridization of M_2 fragment orbitals.

In general, the fragment MO's constructed from W 5*d* atomic orbitals are higher in energy than the corresponding fragments constructed from Mo 4*d* atomic orbitals. Thus for π-backbonding into vacant alkyne π^* orbitals, the W-based fragments are

Table 3. Mulliken populations of the canonical orbitals of bent C_2H_2 and the C_2H_2 moiety in $M_2(OH)_6(NH_3)_x(\mu\text{-}C_2H_2)$

Compound	Structure	Mulliken populations				π-density	
		$\pi_\parallel$	$\pi_\perp$	$\pi^*_\perp$	$\pi^*_\parallel$	π_ρ	π^*_ρ
Bent C_2H_2		2.000	2.000	0.000	0.000	4.000	0.000
C_{2v}-$Mo_2(OH)_6(NH_3)_2(\mu\text{-}C_2H_2)$	I	1.631	1.672	0.742	0.537	3.303	1.279
C_{2v}-$W_2(OH)_6(NH_3)_2(\mu\text{-}C_2H_2)$	I	1.666	1.705	0.788	0.633	3.371	1.421
C_s-$W_2(OH)_6(NH_3)_2(\mu\text{-}C_2H_2)$	II	1.625	1.737	0.886	0.652	3.362	1.538
C_s-$W_2(OH)_6(NH_3)(\mu\text{-}C_2H_2)$	III	1.570	1.754	1.002	0.818	3.324	1.820

energetically closer and have better overlap with alkyne π* orbitals than their Mo counterparts. In a similar fashion, for π-donation from filled alkyne π orbitals into vacant metal orbitals, the Mo-based fragments are energetically closer than their W counterparts.

The lower energy Mo_2 fragment orbitals result in a greater degree of rehybridization of a_1 orbitals, and now the $1a_1$ M—M σ-bonding orbital has a primary interaction with the alkyne $\pi_\perp$ orbital. This is the same result found by Hoffmann *et al.* in their studies of alkyne complexes employing the Extended Hückel Method.[42]

The important message from the orbital picture presented here, is that the alkyne ligand is both a better π-acceptor and weaker π-donor to the W compounds than to the Mo compounds. These observations are supported by an examination of the Mulliken populations (or orbital occupancies) of the canonical orbitals of the C_2H_2 moiety in the $M_2(\mu\text{-}C_2H_2)$ compounds listed in Table 3. Since the π* orbitals of free C_2H_2 are empty, populations greater than 0.000 represent a measure of the degree of π-backbonding from the M_2 centre, and populations less than 2.000 for a π orbital represents π-donation to the M_2 centre. From Table 3 the synergistic nature of $M_2(\mu\text{-}C_2H_2)$ bonding in these systems is demonstrated via the loss of alkyne π density and the gain in alkyne π* density for all three geometric types. The greater decrease in $\pi_\parallel$ and $\pi_\perp$ populations of structure **I** for Mo *relative* to W reveals the slightly greater π-donation to Mo *relative* to W. In a similar fashion, the larger increase in $\pi^*_\parallel$ and $\pi^*_\perp$ populations for the W analogue reveals the stronger π-backbonding for W *relative* to Mo.

Again, these results can be attributed to the *relative* energetics and magnitude of overlap between W 5*d* and Mo 4*d* fragment orbitals with C_2H_2. Both interactions represent C—C bond weakening and M—C bond strengthening for W compounds *relative* to Mo compounds and are consistent with the longer C—C bond in the W complex. In general, π-backbonding is the dominant M—C bonding mechanism. These results parallel those found in earlier studies on $M_2(\mu\text{-}CX)$ compounds (X = O,[19] NR^{29}) of Mo and W which emphasized the greater reducing strength of the W≡W bond relative to the Mo≡Mo bond towards unsaturated substrate molecules.

A comparison of the I′, II′ *and* III′ *ditungsten fragments*

During the course of our studies on the $M_2(\mu\text{-}C_2H_2)$ compounds, we realized that the C—C distance (Table 1), and hence the degree of alkyne reduction, is different in the three structural types found for $W_2(\mu\text{-}C_2H_2)$ containing compounds. For all three structural types, the C_2H_2 moiety uses both π and π* orbital pairs in $W_2(\mu\text{-}C_2H_2)$ bonding.

The *primary* difference in the magnitude of alkyne reduction can be traced to the geometry of the W_2 fragments **I′**, **II′** and **III′**. The W_2 fragment geometry controls the relative orbital energetics and spatial orientation of the fragment orbitals. This, in turn, determines the magnitude of orbital interactions between the W_2 and C_2H_2 fragments in structural types **I**, **II** and **III**.

To understand this, compare the W_2 fragment orbitals of the W_2 fragments **I′**, **II′** and **III′** illustrated in XI below. These W_2 fragments originate

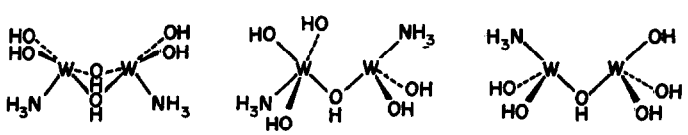

I′ II′ III′

XI

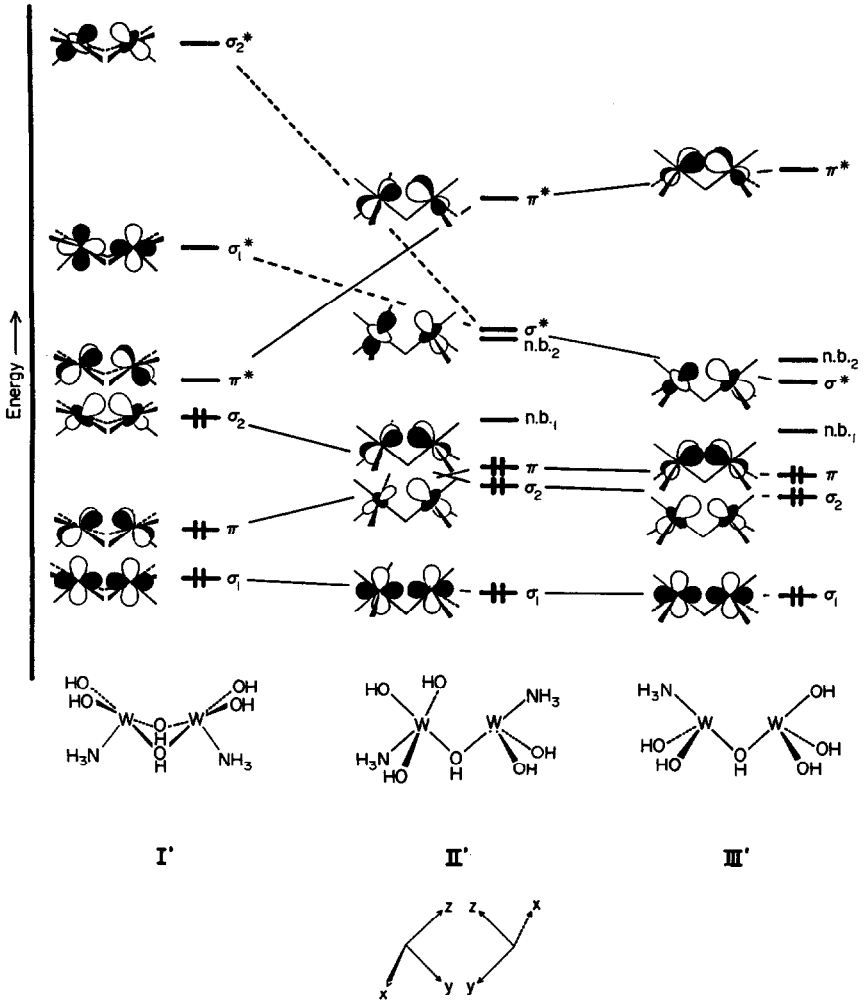

Fig. 3. Molecular orbital diagram comparing the valence fragment orbitals of $W_2(OH)_6(NH_3)_x$ fragments with local oct–oct (left), oct–tbp (centre) and tbp–tbp (right) geometries. Orbital occupation by electrons is denoted by bars. Only the important metal-based fragment orbitals are shown.

from the fused octahedral–octahedral units in **I**, octahedral–trigonal-bipyramid units in **II** and trigonal-bipyramid–trigonal-bipyramid units in **III** counting the C_2H_2 ligand as a common vertex for each metal atom. We shall refer to these fragments as **I′**, **II′** and **III′**, respectively.

The relative orbital energetics of W_2 fragments **I′**, **II′** and **III′** are compared in Fig. 3. Since the W_2 fragments are not all of the same symmetry, we use the simplistic orbital designations σ, σ^*, π and π^* for easy comparison between the three fragments.

Differences between the fragment orbital energetics in **I′**, **II′** and **III′** can be understood in terms of the combination of ML_5 (square-based pyramid) and ML_4 (trigonal-bipyramid minus one equatorial vertex) units. The W_2 fragments will be constructed from the remnants of an octahedral "t_{2g}" set and from hybrid orbitals pointing to the missing vertices of an octahedron. The "t_{2g}" remnants will be low-lying and the hybrid counterparts will be high-lying. For example, compare the octahedral origin of the π^* orbitals in Fig. 3 for geometry **I′** and **III′** shown in XII.

XII

In geometry **I′**, the π^* orbital is constructed from "t_{2g}" orbitals and therefore is relatively low-lying in Fig. 3. In contrast, the π^* counterpart in geometry **III′** is constructed from hybrid orbitals pointing to the missing vertices of an octahedron. As a result, this π^* orbital is destabilized relative to

its counterpart in **I′**. Since geometry **II′** is composed of both "t_{2g}" orbitals and hybrid orbitals, the π^* orbital for geometry **II′** is intermediate in relative energy between its π^* counterpart in **I′** and **III′**.

The W_2 fragment orbital which becomes the M—M σ-bond in the $W_2(\mu\text{-}C_2H_2)$ complexes is labelled σ_1 in Fig. 3. This orbital is unaffected by changing the geometry from **I′** to **II′** to **III′**.

The σ_2 and σ^* orbitals in Fig. 3 undergo somewhat more complicated changes as a function of the changing structure. Besides the factors mentioned affecting the π and π^* orbitals, i.e. "t_{2g}" remnants being low-lying and hybrid orbitals being high-lying, the effect of the asymmetry between the two metals in **II′** and **III′** is realized. In **II′** and **III′**, there is an uneven contribution from each metal in the σ_2 and σ^* orbitals.

It was demonstrated for structure type **I** that the $W_2(\mu\text{-}C_2H_2)$ bonding is dominated by strong, covalent π-backbonding interactions between W_2 fragment orbitals of π symmetry (Fig. 3) and alkyne π^* orbitals. Since this π-backbonding is the dominant interaction, we can anticipate the relative magnitude of π-backbonding to be **III** > **II** > **I** based on the relative orbital energetics and spatial orientation of the W_2 π and π^* fragment orbitals shown in Fig. 3.

Since the W_2 fragment π and π^* orbitals of **III′** are composed of hybrid orbitals, they are energetically closer to the alkyne π^* orbitals than their W_2 fragment π and π^* counterparts in **II′** and **I′**. Moreover, the nature of the hybridization in the W_2 fragment π and π^* orbitals in **III′** is such that the hybrids are strongly polarized towards the incoming C_2H_2 orbitals. As a result, we anticipate **III′** to have the strongest π-backbonding interaction with the alkyne ligand of the three structures.

We can use the Mulliken populations of the canonical orbitals of the C_2H_2 moiety in each structural type to gauge the *relative* degree of alkyne reduction. We begin our discussion by noting that electron occupation of π^* orbitals will contribute more to the weakening of the C—C bond than a loss of electron density from the bonding π orbitals. This is a well-known consequence of orbital interactions[43] and is illustrated by the C—C overlap populations (a measure of bond strength) of Table 2 where a linear C_2H_2 π orbital contributes 0.296 and a π^* orbital −0.717 to the C—C overlap population. With this background we can compare the total electron occupation of π and π^* orbitals of the alkyne moiety in $M_2(\mu\text{-}C_2H_2)$ compounds shown in Table 3. In Table 3 the total occupation of π and π^* orbitals are denoted as π_ρ and π_ρ^*, respectively.‡ Note that all the $M_2(\mu\text{-}C_2H_2)$ containing compounds display a π orbital occupation (π_ρ in Table 3) which is relatively constant between *ca* 3.2–3.4. By contrast, the total occupation of π^* orbitals (π_ρ^* in Table 3) steadily increases from *ca* 1.3 to 1.8 in the order Mo < W and **I** < **II** < **III**. From this data, we reiterate that π-backbonding into alkyne π^* orbitals is the dominant C—C bond weakening process and further illustrates the effect of structural change on π-backbonding in the order **III** > **II** > **I** and W > Mo for the series of compounds under study. This ordering of C—C bond weakening is further amplified by the C—C overlap population which gives a measure of relative C—C bond strength. One can see that C—C bond strength is inversely proportional to the degree of π-backbonding.

The changes in the relative energy and order of the fragment orbitals in Fig. 3 seem to explain the changes in the reduction of the C_2H_2 moiety in the three $M_2(\mu\text{-}C_2H_2)$ containing structures, as reflected by the Mulliken populations. The picture is a little more complicated than this, however, because there are two other important orbitals in fragments **II′** and **III′**, those structures containing only one bridging alkoxide, that have not been considered.

In fragment **I′**, the molecular orbitals composed of two d_{xy} atomic orbitals are M—O σ-antibonding and lie high in energy, out of the bonding picture. In fragments **II′** and **III′**, these orbitals are M—O π-antibonding and find themselves amongst the M—M bonding and antibonding fragment orbitals shown in Fig. 3. These are M—M nonbonding orbitals and are labelled n.b.$_1$ and n.b.$_2$ in Fig. 3.

When the alkyne moiety interacts with W_2 fragments **II′** and **III′**, the W_2 n.b.$_1$ and n.b.$_2$ and π^* orbitals mix to form a new hybrid orbital shown in XIII for fragment **III′**. This new hybrid is now

‡ Total occupation of π orbitals calculated as arithmetic sum of $\pi_\parallel$ and $\pi_\perp$ Mulliken population. Total π^* occupation calculated as arithmetic sum of $\pi_\parallel^*$ and $\pi_\perp^*$ Mulliken population.

XIII

Table 4. Selected overlap populations between II′ and III′ and C_2H_2 fragments

	n.b.$_1/\pi_\parallel^*$	n.b.$_2/\pi_\parallel^*$	$\pi^*/\pi_\parallel^*$
II′	0.220	0.070	0.061
III′	0.195	0.101	0.169

spatially oriented so as to afford better M—C overlap in the resulting M—C bonding orbital shown in XIV. A similar rehybridization takes place for the

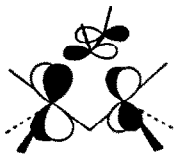

XIV

interaction between C_2H_2 and fragment II′. The fragment overlap populations for this interaction, given in Table 4, show that all three fragment orbitals contribute substantially to M—C bonding.

Population changes: real or artifactual?

Thus far we have argued that changes in the calculated Mulliken populations of the alkyne moiety occur as a direct result of metal–alkyne bonding and provide a *relative* measure of alkyne reduction in each structural type. However, the C—C, M—M and M—C bond distances differ in each structural type, and this could have an effect on the Mulliken populations. In order to test that the *relative* trends observed in the populations are not biased by the structural parameters employed, we undertook a series of calculations in which all three structural types used identical W—W, C—C, W—C and W—O distances and W—O—H angles (Table 1). The Mulliken populations of the C_2H_2 moiety for the three tungsten structures from this study are given in Table 5. The general trend of π-back-bonding and alkyne reduction based on these populations and the resultant π^* orbital occupation (π_ρ^*) given in Table 5 is still in the order **III** > **II** > **I**.

Effect of oxygen to metal π-donation

Alkoxides, which are strong π-donor ligands, will have a destabilizing influence on the metal *d*-block electrons relative to σ-donor ligands, while π-accepting ligands such as carbon monoxide will stabilize the electrons in the metal *d*-block. Since the relative energy of the fragment orbitals in I′, II′ and III′ have been described as having a direct correlation with the reduction of the C_2H_2 ligand in these complexes, we sought to investigate the role of alkoxide π-donations towards reduction of the ancillary alkyne ligand in these molecules. We can separate the alkoxide σ and π interactions through what we will refer to as a "frozen π orbital" method.[44] To accomplish this we first reconverge a calculation on each model compound with linear W—O—H angles and note that variation in this angle has a negligible effect on the Mulliken populations of the C_2H_2 moiety. With linear M—O—H angles, the O—H π orbitals are pure atomic *p* in character and in the canonical basis they are partitioned in the Fock and overlap matrices, in a fashion similar to the partitioning of the matrices of a diatomic molecule into core and valence regions, as illustrated by Roothaan.[45] The π orbitals are then deleted from variational treatment as described by Lichtenberger and Fenske[46] and we will refer to them as "frozen π orbitals". With this method we can effectively "switch off" the alkoxide π interaction to examine the σ-only interaction in the absence of the π. The results of "freezing" the hydroxide π lone-pair orbitals in the canonical basis are quite revealing. Table 6 lists the Mulliken populations of the C_2H_2 ligand in compounds **I**, **II** and **III** with frozen OH π lone-pairs and may be com-

Table 5. Selected Mulliken populations of the canonical orbitals of bent C_2H_2 and the C_2H_2 moiety in the molecules $W_2(OH)_6(NH_3)_x(\mu\text{-}C_2H_2)$ using fixed structural parameters[a]

Compound	Structure	Mulliken populations				π-density	
		$\pi_\parallel$	$\pi_\perp$	$\pi_\perp^*$	$\pi_\parallel^*$	π_ρ	π_ρ^*
Bent C_2H_2		2.000	2.000	0.000	0.000	4.000	0.000
C_{2v}-$W_2(OH)_6(NH_3)_2(\mu\text{-}C_2H_2)$	**I**	1.662	1.708	0.817	0.649	3.370	1.466
C_s-$W_2(OH)_6(NH_3)_2(\mu\text{-}C_2H_2)$	**II**	1.610	1.745	0.916	0.685	3.355	1.601
C_s-$W_2(OH)_6(NH_3)_2(\mu\text{-}C_2H_2)$	**III**	1.591	1.742	0.971	0.747	3.333	1.718

[a] Only the angles necessary to define a new geometry were varied. Parameters are listed in Table 1.

Table 6. Selected Mulliken populations of the canonical orbitals of the C_2H_2 moiety in the molecules $W_2(OH)_6(NH_3)_x(\mu\text{-}C_2H_2)$ with frozen hydroxide π orbitals

Compound	Structure	Mulliken populations				π-density	
		$\pi_\parallel$	$\pi_\perp$	$\pi^*_\perp$	$\pi^*_\parallel$	π_ρ	π^*_ρ
C_{2v}-$W_2(OH)_6(NH_3)_2(\mu\text{-}C_2H_2)$	I	1.630	1.680	0.770	0.560	3.310	1.330
C_s-$W_2(OH)_6(NH_3)_2(\mu\text{-}C_2H_2)$	II	1.633	1.760	0.815	0.537	3.393	1.352
C_s-$W_2(OH)_6(NH_3)(\mu\text{-}C_2H_2)$	III	1.558	1.781	0.996	0.687	3.339	1.683

pared with those in Table 3 where OH π-donation is allowed. Most notable is the dramatic decrease in the population of the π^* orbitals of C_2H_2 in each structural type as a result of "switching off" the OH π-donation. This π-donation from the alkoxide ligands, enhances π-backbonding to the alkyne ligand as evidenced in a decrease by the C_2H_2 π^* population, relative to those where OH π lone-pairs are allowed to interact. Thus we conclude that π-donor interactions with alkoxide ligands enhance π-backbonding to the π^* orbitals of the ancillary C_2H_2 ligand in all three structural types.

Effect of Lewis base

In a previous paper,[19] we discussed the effect of Lewis base addition on the reduction of CO when bound to an $M_2(OR)_6$ unit. It was found that coordination of a Lewis base *trans* to the CO ligand enhanced the extent of CO reduction. In this study we find that Lewis base association does *not* substantially affect the reduction of C_2H_2 because (1) the Lewis base either does not coordinate *trans* to the C_2H_2 ligand or (2) if it does, the orbitals affected are not involved in metal to C_2H_2 π-backbonding which is the major contributor to C_2H_2 reduction.

C—C *distances and* ^{13}C—^{13}C *coupling constants in perpendicular alkyne adducts*

The term dimetallatetrahedrane is often used to describe a perpendicular bridged alkyne complex. However, the C—C bond distances in most $M_2(\mu\text{-}C_2R_2)$ containing compounds are close to 1.34 Å,[42] the C—C distance found for C—C double bonds. The C—C distances in the $W_2(\mu\text{-}C_2R_2)$ complexes supported by alkoxides are amongst the longest reported. Indeed, the C—C distance for μ-C_2H_2 in $W_2(O\text{-}t\text{-}Bu)_6(py)(\mu\text{-}C_2H_2)$, 1.44(1) Å,[6] is the longest reported and approaches that for the central C_4 unit in $C_4(t\text{-}Bu)_4$, 1.48(1) Å.[47] It is not unreasonable to expect that the C—C bond distance and the C—C bond order reduction should show a correlation. Regrettably, the typical esd in a C—C distance close to a heavy metal is one or two hundredths of an Angstrom which leads to uncertainties in comparing distances within these compounds.

We were attracted to the notion that the value of $^1J_{^{13}C-^{13}C}$ for the μ-C_2H_2 ligand might correlate with C—C bond order reduction. There is, in fact, a rough inverse correlation between $^1J_{^{13}C-^{13}C}$ and C—C bond distance. Note the values of d(C—C) and $^1J_{^{13}C-^{13}C}$ listed in Table 7 and see Fig. 4.†

However, within the specific group of compounds that we have carried out Fenske–Hall molecular orbital calculations on, there is no direct correlation between C_2H_2 π^* occupation and $^1J_{^{13}C-^{13}C}$ (see Table 8). This is perhaps not surprising because the range of $^1J_{^{13}C-^{13}C}$ is very small and the magnitude of this coupling constant is also very small, cf. $^1J_{^{13}C-^{13}C}$ = 171 Hz in HC≡CH and 67 Hz in $CH_2{=}CH_2$.[50]

Coupling constants have been described as arising from three types of interactions; orbital–dipole, magnetic spin–dipole and Fermi contact interactions.[51] Of these, the Fermi contact interaction is usually considered to contribute the largest amount to the magnitude of the coupling constant.[51] As a result, several empirical equations have been developed to predict one-bond coupling constants.[52] Each of these formulae use the percent-s-character of the interacting nuclei to predict the magnitude of the coupling. The assumption in these equations is that the coupling constant is of a reasonably large value such that the Fermi contact term dominates. If, however, the coupling constant is in the low range, the Fermi contact term becomes no more important than the magnetic spin–dipole and orbital–dipole terms.[51] Thus the percent-s-model for coupling constants may breakdown. Table 8 shows the carbon 2s–carbon 2s overlap populations for the three tungsten model compounds. A direct comparison of the overlap populations with $^1J_{^{13}C-^{13}C}$ shows the lack of a correlation.

Some of the predictive equations for one-bond

† $^1J_{^{13}C-^{13}C}$ for the edge of the tetrahedron is $C_4(t\text{-}Bu)_4$ is 9.4 Hz.[49]

Table 7. Selected bond distances and ^{13}C NMR data for $M_2(OR)_6(py)_x(\mu\text{-}C_2R'_2)$ compounds and related carbonyl derivatives

Compound	Structure type	M—M[a]	C—C[a]	$\delta(^{13}C)$[b]	$^1J_{^{13}C-^{13}C}$	Ref.
$Mo_2(OPr^i)_6(py)_2(\mu\text{-}C_2H_2)$	I	2.554(1)	1.368(6)	163.4[d]	28.2	this work
$Mo_2(ONp)_6(py)_2(\mu\text{-}C_2H_2)$	I	—	—	166.7[e]	26.9	this work
$Mo_2(OBu^t)_6(\mu\text{-}C_2H_2)$	[f]	—	—	127.1[g]	23.2	this work
$W_2(OPr^i)_6(py)_2(\mu\text{-}C_2H_2)$	I	2.567(1)	1.39(2)	166.3[h]	11.4	this work
$W_2(ONp)_6(py)_2(\mu\text{-}C_2H_2)$	II	2.610(1)	1.39(2)	133.2	19.0	this work
$W_2(OBu^t)_6(py)(\mu\text{-}C_2H_2)$	III	2.665(1)	1.44(1)	121.9[i]	10.3	this work
$Co_2(CO)_6(\mu\text{-}C_2H_2)$[j]	μ_2	2.464(1)	1.327(6)	71.1[k]	56.0	48[l]
$Cp_2Mo_2(CO)_4(\mu\text{-}C_2H_2)$	μ_2	2.980(1)	1.337(5)	61.9	43.4	this work

[a] Distances are in Angstroms.
[b] Chemical shifts are in ppm relative to Me_4Si.
[c] Coupling constants are in Hz.
[d] −40°C, C_7D_8.
[e] −65°C, C_7D_8.
[f] Structure unknown.
[g] −20°C, C_7D_8.
[h] 25°C, C_7D_8.
[i] 25°C, C_5D_5N/C_6D_6.
[j] The distances shown are for the closely related $Co(CO)_4(PMe_3)_2(\mu\text{-}C_2H_2)$ complex. The M—M and C—C distances of $Co_2(CO)_6(\mu\text{-}C_2H_2)$ are not known.
[k] 25°C, C_6D_6.
[l] Original values were obtained using a 60 MHz NMR spectrometer. The compound was synthesized and analysed in our laboratories using a 360 MHz spectrometer. The values were found to correlate well with the originally reported values, however, for the sake of consistency, our values are entered here.

coupling constants include an energy term, ΔE.[53] If we assume that ΔE is proportional to the HOMO–LUMO gap, a correlation does appear, as shown in Table 8. The model compound with the largest calculated HOMO–LUMO gap, **II**, also has the largest $^1J_{^{13}C-^{13}C}$ for the actual compound, $W_2(ONp)_6(py)_2(\mu\text{-}C_2H_2)$. Model compound **I** for tungsten has an intermediate HOMO–LUMO gap and $^1J_{^{13}C-^{13}C}$ for $W_2(O\text{-}i\text{-}Pr)_6(py)_2(\mu\text{-}C_2H_2)$, and **III** has the smallest HOMO–LUMO gap and $^1J_{^{13}C-^{13}C}$ for $W_2(O\text{-}t\text{-}Bu)_6(py)(\mu\text{-}C_2H_2)$. Therefore the trend in C—C coupling constants seems to depend more

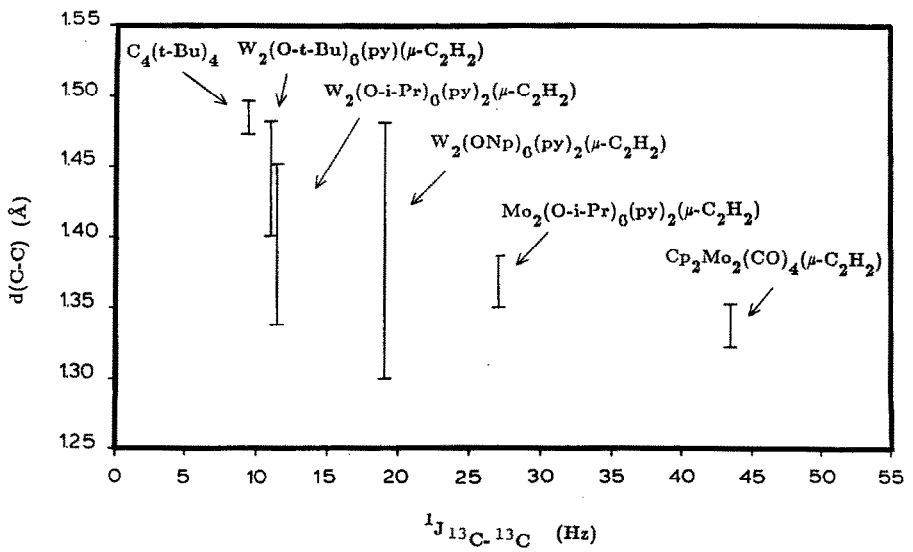

Fig. 4. Comparison of C—C distance with $^1J_{^{13}C-^{13}C}$ in selected $M_2(\mu\text{-}C_2H_2)$ compounds and $C_4(t\text{-}Bu)_4$. The vertical bars indicate the esd in the C—C distances.

Table 8. Selected properties of the $W_2(OH)_6(NH_3)_x(\mu\text{-}C_2H_2)$ model compounds and the $W_2(OR)_6(py)_x(\mu\text{-}C_2H_2)$ compounds

Property	Structural type I	II	III
π^* occupation	1.421	1.538	1.820
C_{2s}-C_{2s} overlap population	0.233	0.216	0.185
$^1J_{^{13}C-^{13}C}$ (Hz)	11.4	19.0	10.3
HOMO–LUMO gap (eV)	2.88	3.22	2.80
$\delta(^{13}C)$	166.6	133.2	121.9
Mulliken atomic charge	−0.529	−0.591	−0.657

on ΔE than on C2*s*–C2*s* bonding in this low range of the magnitude of $^1J_{^{13}C-^{13}C}$.

As a final note, the carbon-13 chemical shifts of the C_2H_2 moiety in the $W_2(\mu\text{-}C_2H_2)$ complexes were found to vary with structure. A comparison of the carbon-13 chemical shifts with the Mulliken atomic charge on the alkyne carbon atoms shows a direct correlation (see Table 8). This may be due to a change in the shielding of the carbons as the π-electron density about the C_2H_2 ligands changes.[54] It seems reasonable that π- backbonding in the order **III** > **II** > **I** places increased electron density on carbon and this is reflected in the decrease in negative charge on carbon in the same order, **III** > **II** > **I**.

CONCLUSIONS

There are many examples of alkynes bridging a dimetal centre. For those that have been crystallographically characterized, very few have alkyne carbon–carbon bond lengths approaching the carbon–carbon bond lengths found in the $M_2(OR)_6(py)_x(\mu\text{-}C_2R_2')$ complexes. There are a number of reasons for this. Most of the alkyne bridging dimers involve middle to late transition metals in low oxidation states with partial or total CO ligand environments. In contrast, we show that π-donation from alkoxide ligands enhances π-backbonding and hence C—C reduction.

In general, as a metal progresses from left to right across the transition series, the added electrons are inefficiently shielded from the effective nuclear charge and the resultant energy of the *d*-block falls in energy. For high oxidation state metals, the Z_{eff} is even higher and the *d*-block drops more.[55] CO, a π-withdrawing ligand, effectively increases the electronegativity of a metal by lowering the metal-*d*-block while π-donating ligands decrease the electronegativity of a metal by raising the metal-*d*-block.[55] Also, the metal-*d*-block of early third row transition metals are generally higher than those of the second and first row transition metals, for middle to high oxidation states, because of the increased shielding of the core electrons.[55] The net sum of the various effects is that the metal-*d*-block of the alkoxide supported $M_2(\mu\text{-}C_2R_2)$ complexes is much higher than those of most other $M_2(\mu\text{-}C_2R_2)$ complexes.

With the metal-*d*-block higher in energy, a better energy match is made between the filled metal orbitals and the empty π^* orbitals of C_2H_2. Therefore, while the π-donation of electrons from C_2R_2 to M_2 in alkoxy supported $M_2(\mu\text{-}C_2R_2)$ complexes appears to be very similar to those of the Cp and CO supported $M_2(\mu\text{-}C_2R_2)$ complexes,[42] the π-acceptance of electrons to C_2R_2 from M_2 is superior. This reduces the alkyne to a much greater extent, even to the point of cleaving the carbon–carbon bond.

The changes in M—M, M—C and C—C bond distances and M—O—H bond angles in **I**, **II** and **III** have little affect on the reduction of the C_2H_2 ligand. When comparing the molybdenum and tungsten complexes of **I**, the tungsten complex is found to have a larger reducing potential than molybdenum,as would be expected by the Z_{eff} differences listed above. Turning off the π-donation from the alkoxide ligands decreases the ability of the M_2 centre to reduce the alkyne ligand. Also, the presence of Lewis bases on the $M_2(\mu\text{-}C_2R_2)$ complexes are shown to have little effect on the reduction of the alkyne ligand. This leads us to conclude that the steric interactions between the OR, py and C_2R_2 ligands on the dimetal framework combine to determine the geometry adopted (**I**, **II** or **III**), and the geometry determines the extent of reduction of the alkyne ligand.

It is interesting to speculate about non-alkoxide-bridged $M_2(OR)_6(\mu\text{-}C_2R_2')$ structures and the reaction pathway leading to C—C and M—M cleavage.

Calculations employing hypothetical geometries could well shed light on the various possibilities. However, this is a matter for future consideration.

Acknowledgements—We thank the Department of Energy, Office of Basic Research, Chemical Sciences Division, for support. D.L.C. was the Indiana University General Electric Fellow, 1985/86. We also thank Dr Suzanne Harris of Exxon Research and Engineering, and Adjunct Professor at Indiana University, for helpful discussions.

REFERENCES

1. M. H., Chisholm, D. L. Clark, J. C. Huffman and C. A. Smith, *Organometallics* 1987, **6**, 1280.
2. (a) M. H. Chisholm, *ACS Symp. Ser.* 1983, **211**, 243; (b) M. H. Chisholm, *J. Solid State Chem.* 1985, **57**, 120.
3. M. H. Chisholm, J. C. Huffman and I. P. Rothwell, *J. Am. Chem. Soc.* 1981, **103**, 4245.
4. M. H. Chisholm, K. Folting, J. C. Huffman and I. P. Rothwell, *J. Am. Chem. Soc.* 1982, **104**, 4389.
5. M. H. Chisholm, K. Folting, D. M. Hoffman, J. C. Huffman and J. Leonelli, *J. Chem. Soc., Chem. Commun.* 1983, 589.
6. M. H. Chisholm, K. Folting, D. M. Hoffman and J. C. Huffman, *J. Am. Chem. Soc.* 1984, **106**, 6794.
7. M. H. Chisholm, D. M. Hoffman and J. C. Huffman, *J. Am. Chem. Soc.* 1984, **106**, 6806.
8. M. H. Chisholm, K. Folting, J. A. Heppert, D. M. Hoffman and J. C. Huffman, *J. Am. Chem. Soc.* 1985, **107**, 1234.
9. M. H. Chisholm, B. K. Conroy and J. C. Huffman, *Organometallics* 1986, **5**, 2384.
10. M. H. Chisholm, B. K. Conroy, K. Folting, D. M. Hoffman and J. C. Huffman, *Organometallics* 1986, **5**, 2457.
11. M. H. Chisholm and B. K. Conroy, unpublished results.
12. M. L. Listemann and R. R. Schrock, *Organometallics* 1985, **4**, 74.
13. R. R. Schrock, M. L. Listemann and L. G. Sturgeoff, *J. Am. Chem. Soc.* 1982, **104**, 4291.
14. J. H. Freudenberger, S. F. Pedersen and R. R. Schrock, *Bull. Soc. Chim. de France* 1985, 349.
15. H. Strutz and R. R. Schrock, *Organometallics* 1984, **3**, 1600.
16. F. A. Cotton, W. Schwotzer and E. S. Shamshoum, *Organometallics* 1983, **2**, 1167.
17. F. A. Cotton, W. Schwotzer and E. S. Shamshoum, *Organometallics* 1983, **2**, 1340.
18. M. H. Chisholm, D. M. Hoffman and J. C. Huffman, *Organometallics* 1985, **4**, 986.
19. P. J. Blower, M. H. Chisholm, D. L. Clark and B. W. Eichhorn, *Organometallics* 1986, **5**, 2125.
20. M. H. Chisholm, F. A. Cotton, M. W. Extine and R. L. Kelly, *J. Am. Chem. Soc.* 1979, **101**, 7645.
21. M. H. Chisholm, J. C. Huffman, J. Leonelli and I. P. Rothwell, *J. Am. Chem. Soc.* 1982, **104**, 7030.
22. M. H. Chisholm, J. C. Huffman and R. L. Kelly, *J. Am. Chem. Soc.* 1979, **101**, 7615.
23. F. A. Cotton and W. Schwotzer, *J. Am. Chem. Soc.* 1983, **105**, 5639.
24. F. A. Cotton and W. Schwotzer, *J. Am. Chem. Soc.* 1983, **105**, 4955.
25. T. P. Blatchford, M. H. Chisholm, K. Folting and J. C. Huffman, *J. Chem. Soc., Chem. Commun.* 1984, 1295.
26. M. H. Chisholm, J. C. Huffman and N. S. Marchant, *J. Am. Chem. Soc.* 1983, **105**, 6162.
27. M. H. Chisholm, K. Folting, J. C. Huffman and J. P. Rothwell, *J. Am. Chem. Soc.* 1982, **104**, 4389.
28. M. H. Chisholm, D. M. Hoffman and J. C. Huffman, *Inorg. Chem.* 1983, **22**, 2903.
29. M. H. Chisholm, D. L. Clark, D. Ho and J. C. Huffman, *Organometallics* 1987, **6**, 1532.
30. M. H. Chisholm, J. C. Huffman and R. L. Kelly, *Inorg. Chem.* 1980, **19**, 2762.
31. M. H. Chisholm, F. A. Cotton, M. W. Extine and R. L. Kelly, *J. Am. Chem. Soc.* 1978, **100**, 3354.
32. M. H. Chisholm, F. A. Cotton, M. W. Extine and R. L. Kelly, *Inorg. Chem.* 1979, **18**, 116.
33. M. H. Chisholm, F. A. Cotton, M. W. Extine and W. W. Reichert, *Inorg. Chem.* 1978, **17**, 2944.
34. M. H. Chisholm, J. C. Huffman and N. S. Marchant, *J. Am. Chem. Soc.* 1983, **105**, 6162.
35. M. H. Chisholm, K. Folting, J. C. Huffman and N. S. Marchant, *Polyhedron* 1984, **3**, 1033.
36. M. B. Hall and R. F. Fenske, *Inorg. Chem.* 1972, **11**, 768.
37. (a) R. F. Fenske, *Prog. Inorg. Chem.* 1976, **21**, 179; (b) R. F. Fenske, *Pure Appl. Chem.* 1971, **27**, 61.
38. B. E. Bursten, J. R. Jensen and R. F. Fenske, *J. Chem. Phys.* 1978, **68**, 3320.
39. W. J. Hehre, R. F. Steward and J. A. Pople, *J. Chem. Phys.* 1969, **51**, 2657.
40. R. S. Dickson and P. J. Fraser, *Adv. Organomet. Chem.* 1974, **12**, 323.
41. W. I. Bailey, Jr, M. H. Chisholm, F. A. Cotton and L. A. Rankel, *J. Am. Chem. Soc.* 1978, **100**, 5764.
42. For example: D. M. Hoffman, R. Hoffmann and C. R. Fisel, *J. Am. Chem. Soc.* 1982, **104**, 3858.
43. T. A. Albright, J. K. Burdett and M.-H. Whangbo, *Orbital Interactions in Chemistry*. John Wiley, New York (1985).
44. M. H. Chisholm and D. L. Clark, *Comments Inorg. Chem.* 1987, **6**, 23.
45. C. C. J. Roothaan, *Rev. Mod. Phys.* 1951, **23**, 69.
46. D. L. Lichtenberger and R. F. Fenske, *J. Chem. Phys.* 1976, **64**, 4247.
47. H. Irngartinger, A. Goldman, R. Jahn, M. Nixdorf, H. Rodewald, G. Maier, K. D. Malsch and R. Emrich, *Angew. Chem. Int. Ed. Engl.* 1984, **23**, 993.
48. S. Aime, D. Osella, E. Giamello and G. Granozzi, *J. Organomet. Chem.* 1984, **262**, C1.
49. W. Luttke, T. Loerzer, R. Machinek, L. H. Franz, K. D. Malsch and G. Maier, *Angew. Chem. Int. Ed. Engl.* 1983, **22**, 878.
50. J. B. Stothers, *Carbon-13 NMR Spectroscopy*, Chap. 10. Academic Press, New York (1972).

51. J. A. Pople and O. P. Santry, *Mol. Phys.* 1964, **8**, 1.
52. For example: M. D. Newton, J. M. Schulman and M. M. Manus, *J. Am. Chem. Soc.* 1974, **96**, 17.
53. For example: P. S. Pregosin and R. W. Kunz, ^{31}P *and* ^{13}C *NMR of Transition Metal Phosphine Complexes.* Springer, New York (1979).
54. A. Carrington and A. D. McLachlan, *Introduction to Magnetic Resonance*, p. 63. Chapman and Hall, London (1979).
55. J. E. Huheey, *Inorganic Chemistry, Principles of Structure and Reactivity*, 2nd Edn. Harper & Row, New York (1978).

Polyhedron Vol. 7, No. 10/11, pp. 919–930, 1988
Printed in Great Britain

0277–5387/88 $3.00+.00
© 1988 Pergamon Press plc

A STUDY OF THE REACTION BETWEEN $Mo_2(OCH_2CMe_3)_6(\mu\text{-}\eta^1,\eta^2\text{-}NCNR_2)$ COMPOUNDS (R = Me AND Et) AND 2-BUTYNE

M. H. CHISHOLM,* J. C. HUFFMAN and NANCY S. MARCHANT

Department of Chemistry and Molecular Structure Center, Indiana University, Bloomington, IN 47405, U.S.A.

(*Received* 5 *November* 1987)

Abstract—The compound $Mo_2(ONp)_6(\mu\text{-}\eta^1,\eta^2\text{-}NCNEt_2)$ reacts with MeC≡CMe (2 equiv.) in hydrocarbon solvents at *ca* 0°C to give $Mo_2(ONp)_6(\mu\text{-}C_4Me_4)(NCNEt_2)$, **I**, which is shown to be structurally related to the previously characterized compound $Mo_2(ONp)_6(\mu\text{-}C_4H_4)py$ obtained in the reaction between $Mo_2(ONp)_6$ and HC≡CH (2 equiv.) in the presence of pyridine (py = pyridine and Np = neopentyl). Compound **I** is unstable in hydrocarbon solutions at room temperature. It rapidly and reversibly loses $NCNEt_2$ and addition of py or PMe_3 leads to the compounds $Mo_2(ONp)_6(\mu\text{-}C_4Me_4)L$, where L = py or PMe_3. Compound **I** also reacts by C—C and N—H bond formation to give $Mo_2(ONp)_6(\mu\text{-}C_4Me_3CH_2C(NEt_2)NH)$, **II**. A mechanism for the conversion of **I** to **II** is proposed to involve (i) initial dissociation of $NCNEt_2$, (ii) C—H bond cleavage of a β-CMe group and (iii) insertion of the C≡N moiety into the Mo—H bond with C—C bond formation. Rate studies show that the conversion of **I** to **II** is suppressed by the addition of excess py or PMe_3 supporting the view that initial dissociation of $NCNEt_2$ is required in a rapid pre-equilibrium step. The new compounds **I** and **II** have been characterized by elemental analyses, IR spectroscopy, ^1H and ^{13}C NMR spectroscopy and single crystal X-ray studies.

It was recently shown that $W_2(OR)_6(py)_n(\mu\text{-}C_2R'_2)$ compounds which contain a perpendicular bridging alkyne ligand react with nitriles. The reactions proceed under mild conditions to give coupling of the $\mu\text{-}C_2R_2$ and R″CN groups, inserting either one or two R″CN units to form five or seven membered heterocyclic rings, e.g. as in $W_2(O\text{-}t\text{-}Bu)_6(\mu\text{-}CHCHCPhN)$ and $W_2(ONp)_6(\mu\text{-}N(CMe)_4N)(py)$ where Np = neopentyl.[1]

In light of these reactions we examined the reactivity of $Mo_2(ONp)_6(\mu\text{-}R_2NCN)$[2] compounds toward alkynes in order to compare the reactivity of bridging alkyne ligands and bridging nitrile ligands. It was anticipated that similar C—C bond forming reactions might result. A preliminary aspect of this work has appeared.[3]

RESULTS AND DISCUSSION

Synthesis

The reaction of $Mo_2(ONp)_6(\mu\text{-}R_2NCN)$ compounds with excess ethyne proceeds rapidly at low temperature (*ca* −78°C) to give scarlet solutions which upon warming to room temperature change to deep brown solutions. Removing the solvent *in vacuo* from the scarlet solution resulted in isolation of $Mo_2(ONp)_6(\mu\text{-}Et_2NCN)$. Low temperature NMR spectroscopic studies on the reaction of $Mo_2(ONp)_6(\mu\text{-}Me_2NCN)$ and C_2H_2 showed two singlets of equal intensity, δ 9.94 and 9.40 ppm, which may be attributable to a bound C_2H_2 unit. Signals were also present in the region 2.8–3.4 ppm which may be attributed to a bound Me_2NCN ligand. The alkyne signals broadened and collapsed into the baseline upon warming the sample. Collectively, this information is consistent with initial alkyne adduct formation which is readily reversible, and the adduct reacts further upon warming. A reaction product was not purifiable and only polyacetylene and unreacted $Mo_2(ONp)_6(\mu\text{-}NCNMe_2)$ are obtained.

$Mo_2(ONp)_6(\mu\text{-}Et_2NCN)$ and C_2Me_2 follow a similar reaction scheme. However, a brown crystalline compound may be isolated from hexane solutions which have been warmed to room temperature for 10 min and then cooled to −15°C.

* Author to whom correspondence should be addressed.

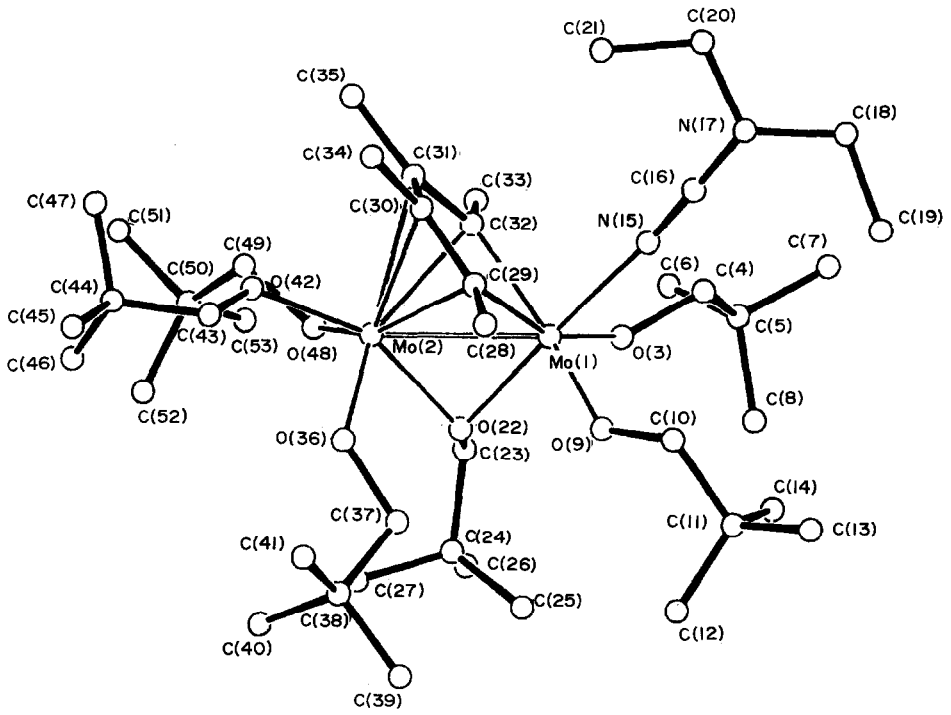

Fig. 1. A ball-and-stick drawing of $Mo_2(ONp)_6(\mu\text{-}C_4Me_4)(NCNEt_2)$ using the numbering scheme found in Tables 1 and 2.

Solid state and molecular structure of $Mo_2(ONp)_6(\mu\text{-}C_4Me_4)(NCNEt_2)$

Figure 1 shows a ball-and-stick drawing of the molecular structure of $Mo_2(ONp)_6(\mu\text{-}C_4Me_4)(NCNEt_2)$, **I**, found in the solid state. The bridging $NCNEt_2$ ligand in $Mo_2(ONp)_6(R_2NCN)$ becomes terminally bound, and two equivalents of alkyne have coupled to form a metallocyclopentadiene moiety which is π-bonded to the neighbouring molybdenum atom. Pertinent bond distances and angles are given in Tables 1 and 2, respectively. Compound **I** is closely related to a previously characterized complex, $Mo_2(ONp)_6(\mu\text{-}C_4H_4)(py)$, which is formed in the reaction between $Mo_2(ONp)_6(py)_2$ and excess acetylene.[4] Table 3 shows a comparison of the pertinent bond distances and angles for these two compounds.

Each molybdenum is in a distorted octahedral environment if the $\mu\text{-}C_4Me_4$ ligand is considered to

Table 1. Selected bond distances (Å) for the $Mo_2(ONp)_6(\mu\text{-}C_4Me_4)(NCNEt_2)$ molecule

A	B	Distance	A	B	Distance
Mo(1)	Mo(2)	2.6393(15)	Mo(2)	C(32)	2.369(6)
Mo(1)	O(3)	1.959(4)	O(3)	C(4)	1.408(8)
Mo(1)	O(9)	1.918(5)	O(9)	C(10)	1.406(8)
Mo(1)	O(22)	2.073(4)	O(22)	C(23)	1.440(7)
Mo(1)	N(15)	2.168(6)	O(36)	C(37)	1.439(8)
Mo(1)	C(29)	2.158(7)	O(42)	C(43)	1.400(8)
Mo(1)	C(32)	2.131(6)	O(48)	C(49)	1.418(8)
Mo(2)	O(22)	2.150(4)	N(15)	C(16)	1.146(8)
Mo(2)	O(36)	1.922(5)	N(17)	C(16)	1.317(8)
Mo(2)	O(42)	2.015(4)	N(17)	C(18)	1.471(10)
Mo(2)	O(48)	1.941(4)	N(17)	C(20)	1.477(9)
Mo(2)	C(29)	2.295(7)	C(29)	C(30)	1.383(10)
Mo(2)	C(30)	2.432(6)	C(30)	C(31)	1.450(10)
Mo(2)	C(31)	2.407(7)	C(31)	C(32)	1.395(9)

Table 2. Selected bond angles (°) for the $Mo_2(ONp)_6(\mu\text{-}C_4Me_4)(NCNEt_2)$ molecule

A	B	C	Angle	A	B	C	Angle
Mo(2)	Mo(1)	O(3)	126.11(13)	O(48)	Mo(2)	C(30)	126.58(22)
Mo(2)	Mo(1)	O(9)	112.22(14)	O(48)	Mo(2)	C(31)	93.34(21)
Mo(2)	Mo(1)	O(22)	52.63(12)	O(48)	Mo(2)	C(32)	84.71(21)
Mo(2)	Mo(1)	N(15)	130.16(15)	C(29)	Mo(2)	C(30)	33.86(24)
Mo(2)	Mo(1)	C(29)	56.09(18)	C(29)	Mo(2)	C(31)	60.99(24)
Mo(2)	Mo(1)	C(32)	58.39(17)	C(29)	Mo(2)	C(32)	66.62(23)
O(3)	Mo(1)	O(9)	105.79(20)	C(30)	Mo(2)	C(31)	34.87(23)
O(3)	Mo(1)	O(22)	89.22(18)	C(30)	Mo(2)	C(32)	58.85(23)
O(3)	Mo(1)	N(15)	87.46(20)	C(31)	Mo(2)	C(32)	33.96(22)
O(3)	Mo(1)	C(29)	159.73(22)	Mo(1)	O(3)	C(4)	131.0(4)
O(3)	Mo(1)	C(32)	90.94(23)	Mo(1)	O(9)	C(10)	140.4(4)
O(9)	Mo(1)	O(22)	93.50(18)	Mo(1)	O(22)	Mo(2)	77.33(14)
O(9)	Mo(1)	N(15)	86.93(21)	Mo(1)	O(22)	C(23)	121.5(4)
O(9)	Mo(1)	C(29)	89.39(23)	Mo(2)	O(22)	C(23)	128.1(4)
O(9)	Mo(1)	C(32)	162.75(23)	Mo(2)	O(36)	C(37)	130.4(4)
O(22)	Mo(1)	N(15)	176.64(18)	Mo(2)	O(42)	C(43)	128.3(4)
O(22)	Mo(1)	C(29)	103.45(21)	Mo(2)	O(48)	C(49)	126.3(4)
O(22)	Mo(1)	C(32)	90.87(20)	Mo(1)	N(15)	C(16)	173.3(5)
N(15)	Mo(1)	C(29)	79.88(23)	C(16)	N(17)	C(18)	120.5(6)
N(15)	Mo(1)	C(32)	89.67(23)	C(16)	N(17)	C(20)	118.0(6)
C(29)	Mo(1)	C(32)	73.36(26)	C(18)	N(17)	C(20)	117.5(6)
Mo(1)	Mo(2)	O(22)	50.04(11)	N(15)	C(16)	N(17)	177.7(8)
Mo(1)	Mo(2)	O(36)	103.78(14)	N(17)	C(18)	C(19)	111.7(7)
Mo(1)	Mo(2)	O(42)	152.27(13)	N(17)	C(20)	C(21)	112.3(6)
Mo(1)	Mo(2)	O(48)	112.54(13)	Mo(1)	C(29)	Mo(2)	72.63(20)
Mo(1)	Mo(2)	C(29)	51.28(17)	Mo(1)	C(29)	C(28)	122.1(5)
Mo(1)	Mo(2)	C(30)	74.35(16)	Mo(1)	C(29)	C(30)	118.5(5)
Mo(1)	Mo(2)	C(31)	75.23(16)	Mo(2)	C(29)	C(28)	124.5(5)
Mo(1)	Mo(2)	C(32)	50.01(16)	Mo(2)	C(29)	C(30)	78.5(4)
O(22)	Mo(2)	O(36)	84.74(18)	C(28)	C(29)	C(30)	119.1(6)
O(22)	Mo(2)	O(42)	157.00(17)	Mo(2)	C(30)	C(29)	67.6(4)
O(22)	Mo(2)	O(48)	82.65(17)	Mo(2)	C(30)	C(31)	71.6(4)
O(22)	Mo(2)	C(29)	96.67(21)	Mo(2)	C(30)	C(34)	129.7(5)
O(22)	Mo(2)	C(30)	124.36(19)	C(29)	C(30)	C(31)	114.9(6)
O(22)	Mo(2)	C(31)	116.58(20)	C(29)	C(30)	C(34)	125.8(7)
O(22)	Mo(2)	C(32)	82.90(20)	C(31)	C(30)	C(34)	119.3(7)
O(36)	Mo(2)	O(42)	82.35(19)	Mo(2)	C(31)	C(30)	73.5(4)
O(36)	Mo(2)	O(48)	118.17(19)	Mo(2)	C(31)	C(32)	71.5(4)
O(36)	Mo(2)	C(29)	90.40(22)	Mo(2)	C(31)	C(35)	125.5(5)
O(36)	Mo(2)	C(30)	110.18(22)	C(30)	C(31)	C(32)	112.0(6)
O(36)	Mo(2)	C(31)	144.78(22)	C(30)	C(31)	C(35)	120.3(6)
O(36)	Mo(2)	C(32)	152.27(21)	C(32)	C(31)	C(35)	127.6(6)
O(42)	Mo(2)	O(48)	86.78(18)	Mo(1)	C(32)	Mo(2)	71.60(19)
O(42)	Mo(2)	C(29)	102.36(22)	Mo(1)	C(32)	C(31)	120.7(5)
O(42)	Mo(2)	C(30)	78.15(20)	Mo(1)	C(32)	C(33)	118.6(5)
O(42)	Mo(2)	C(31)	84.29(21)	Mo(2)	C(32)	C(31)	74.5(4)
O(42)	Mo(2)	C(32)	116.47(21)	Mo(2)	C(32)	C(33)	122.0(4)
O(48)	Mo(2)	C(29)	151.10(21)	C(31)	C(32)	C(33)	120.6(6)

occupy a pair of *cis* sites for each Mo atom, with two Mo—C σ bonds for Mo(1) and two π bonds for Mo(2). The terminal alkoxide ligands show some π donation to the dimetal centre having Mo—O bond lengths of 1.94 Å.[5] The bridging alkoxide ligand may be considered a 1-ligand to Mo(1) and a dative ligand to Mo(2) based on the bond lengths. Mo(1) may be considered to be formally in oxidation state 5+ while Mo(2) is in oxidation state 3+. The Mo—Mo distance, 2.6393(15) Å, indicates that there is a single bond between the metal centres.

The Mo—N dative bond lengths are comparable

Table 3. Internuclear distances (Å) associated with the central $M_2(\mu\text{-}C_4)$ moiety in $Mo_2(ONp)_6(\mu\text{-}C_4Me_4)(Et_2NCN)$ (A) and $Mo_2(ONp)_6(\mu\text{-}C_4H_4)(py)$ (B)

Bond	A	B
M(1)—M(2)	2.6393(15)	2.69(1)
M(1)—C(1)	2.131(6)	2.12(2)
M(1)—C(4)	2.158(7)	2.12(2)
M(2)—C(1)	2.369(6)	2.39(2)
M(2)—C(4)	2.295(7)	2.39(2)
M(2)—C(2)	2.407(1)	2.34(2)
M(2)—C(3)	2.432(6)	2.34(2)
C(1)—C(2)	1.395(9)	1.47(3)
C(3)—C(4)	1.383(10)	1.47(3)
C(2)—C(3)	1.450(10)	1.43(6)
M(1)—N	2.168(6)	2.15(3)

in **I** and $Mo_2(ONp)_6(C_4H_4)(py)$ being 2.168(6) and 2.15(3) Å, respectively. There appears to be involvement of the amide lone pair in the cyanamide, as the Et_2N—C bond length is 1.317(8) Å, the C≡N distance is 1.146(8) Å, and the amide N is planar. This type of interaction was predicted for terminal N bound cyanamides on the basis of Extended-Hückel calculations.[6]

Solution behaviour

In toluene-d_8 solution, compound **I** is fluxional and a low temperature limiting spectrum is not frozen-out on the ^{1}H NMR time-scale at 360 MHz and −80°C. The solution behaviour is further complicated by the presence of an equilibrium involving **I**, $Mo_2(ONp)_6(\mu\text{-}C_4Me_4)$ and Et_2NCN. The position of this equilibrium will be influenced by both temperature and concentration with both of these factors complicating the interpretation of dynamic solution behaviour. At a temperature of 60°C compound **I** reacts rapidly (t_∞ *ca* 1 h) in NMR tubes to give **II**. Conversion of **I** to **II** takes *ca* 2 h at 20°C.

The lability of the Et_2NCN ligand in **I** is seen in a number of NMR tube reactions. (1) Addition of either of the donor ligands pyridine and PMe_3 gave $Mo_2(ONp)_6(\mu\text{-}C_4Me_4)(L)$ compounds where L = py or PMe_3. These compounds, $Mo_2(ONp)_6(\mu\text{-}C_4Me_4)(L)$ have been characterized by ^{1}H NMR studies and appear to be related to the fully characterized analogue $Mo_2(ONp)_6(\mu\text{-}C_4Me_4)(py)$.[4] The PMe_3 adduct gives NMR spectra consistent with a static structure at room temperature, while the pyridine adduct is fluxional. (2) The addition of excess Et_2NCN to **I** in tolune-d_8 leads to one sharp set of signals for the Et_2NCN species present in solution at 22°C, 360 MHz. (3) The ^{13}C NMR spectrum of **I*** in toluene-d_8, where **I*** represents the ^{13}C-labelled compound incorporating $Et_2N^{13}CN$, shows a broad signal at δ 129 ppm at 22°C, 90.8 MHz which sharpens on cooling to give a signal at 132 ppm assignable to the cyanide carbon atom. The signal for the free ligand $Et_2N^{13}CN$ occurs at δ 118 ppm.

Of particular note in the ^{1}H NMR spectrum of **II** was the presence of seven AB quartets of equal intensity and only three Me signals derived from the C_4Me_4 ligand of **I**. Reactions employing $N^{13}CNCEt_2$ revealed that the high field AB quartet is coupled to ^{13}C ($^2J_{C-H}$ = 6.1 Hz), as shown in Fig. 2. This was suggestive of C—C bond formation involving the $N^{13}CNEt_2$ carbon. A broad singlet at 5.07 ppm, a band at 3358 cm^{-1} in the IR spectrum, along with a shift in the C≡N stretching frequency from 2205 to 1590 cm^{-1} were indicative of the formation of a $CH_2C(NEt_2)NH$ unit. Coordination of the NH function to a Mo atom was anticipated but to which Mo atom was uncertain. Furthermore, which methyl of the μ-C_4Me_4 ligand (α or β) had reacted could not be ascertained.

Solid state and molecular structure of $Mo_2(\mu\text{-}C_4Me_3CH_2C(NEt_2)NH)$, **II**

A single crystal suitable for X-ray crystallography was obtained from a concentrated toluene solution of **II** and the resulting structure is shown in Fig. 3. It should be pointed out that the space group for the compound was chiral and only one of the two possible enantiomers eventually crystallized. Pertinent bond distances and angles of the crystallized compound are given in Tables 4 and 5 respectively.

The bicyclic system may be viewed as having a dative bond from the NH unit to Mo(1), 2.167(7) Å. A partial double bond system exists in the N—C—N portion since the amide N is planar and the N≡C distance has lengthened to 1.319(10) Å and the C—N amide distance is 1.353(10) Å. At room temperature rotation about the Et_2N—C is just approaching the NMR time-scale as shown in Fig. 2. The C—C distances within the flyover ring are nearly equivalent and average 1.42 Å, supporting the view that the ring system may be viewed as a metallacyclopentadiene ligand.

The Mo atoms are still in a pseudo-octahedral environment, and the overall oxidation state of the dimetal centre has not changed from compound **I**. The Mo—Mo distance is 2.7108(18) Å and is slightly longer than in compound **I**, 2.6393(15) Å, but still with the distances assignable to a Mo—Mo single bond.[5]

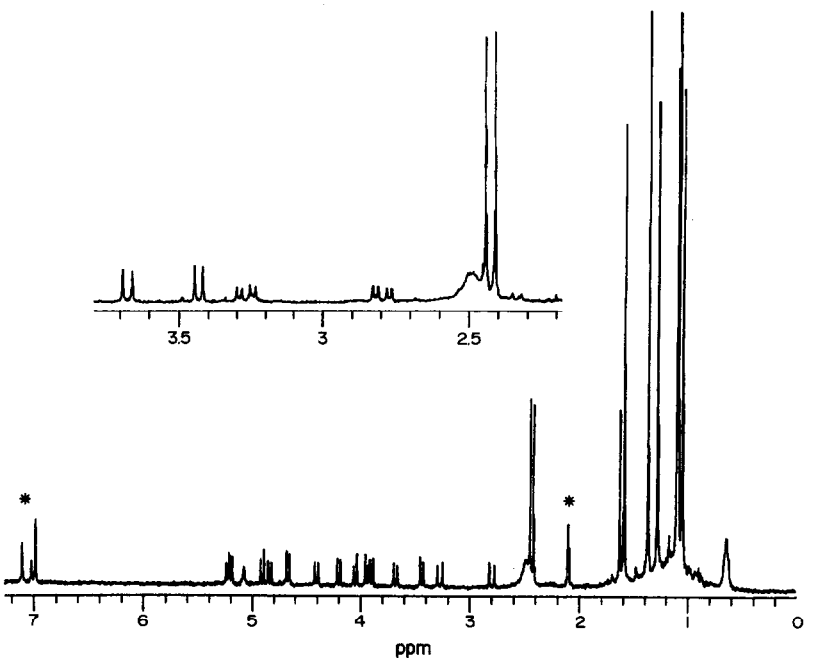

Fig. 2. A ^{1}H NMR spectrum of $Mo_2(ONp)_6(\mu\text{-}C_4Me_3CH_2C(NEt_2)NH)$ taken at room temperature in toluene-d_8(*), and an insert showing the carbon-13 coupling to the high field AB quartet in $Mo_2(ONp)_6(\mu\text{-}C_4Me_4CH_2^{13}C(NEt_2)NH)$.

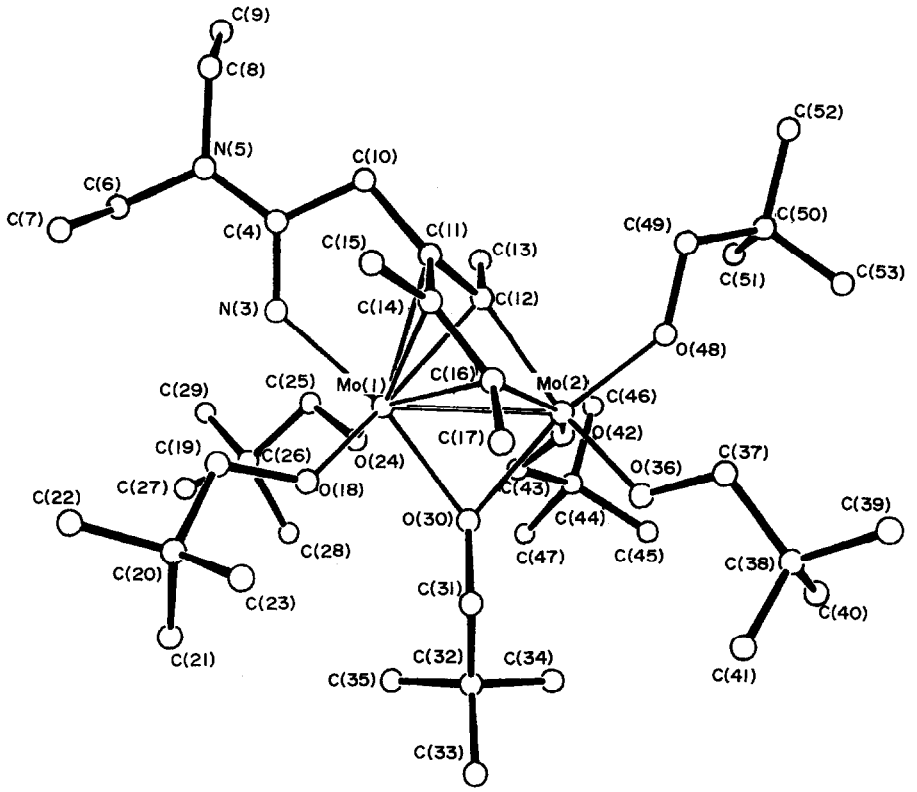

Fig. 3. A ball-and-stick drawing of $Mo_4(ONp)_6(\mu\text{-}C_4Me_3CH_2C(NEt_2)NH)$ using the numbering scheme found in Tables 4 and 5.

Table 4. Selected bond distances (Å) for the $Mo_2(ONp)_6(\mu\text{-}C_4Me_3CH_2C(NEt_2)NH)$ molecule

A	B	Distance	A	B	Distance
Mo(1)	Mo(2)	2.7108(18)	O(18)	C(19)	1.397(10)
Mo(1)	O(18)	1.938(5)	O(24)	C(25)	1.422(10)
Mo(1)	O(24)	1.944(5)	O(30)	C(31)	1.424(9)
Mo(1)	O(30)	2.135(5)	O(36)	C(37)	1.432(1)
Mo(1)	N(3)	2.167(7)	O(42)	C(43)	1.407(10)
Mo(1)	C(11)	2.335(8)	O(48)	C(49)	1.391(11)
Mo(1)	C(12)	2.319(8)	N(3)	C(4)	1.319(10)
Mo(1)	C(14)	2.264(8)	N(5)	C(4)	1.353(10)
Mo(1)	C(16)	2.299(8)	N(5)	C(6)	1.465(10)
Mo(2)	O(30)	2.127(5)	N(5)	C(8)	1.472(11)
Mo(2)	O(36)	1.950(5)	C(4)	C(10)	1.500(11)
Mo(2)	O(42)	1.890(6)	C(10)	C(11)	1.510(11)
Mo(2)	O(48)	1.920(6)	C(11)	C(12)	1.414(12)
Mo(2)	C(12)	2.118(8)	C(14)	C(16)	1.411(11)
Mo(2)	C(16)	2.164(8)			

Reaction pathway

A possible reaction pathway leading to the formation of **II** may be based on the C—H activation chemistry established for $(C_5Me_5)_2MR_2$ compounds where M = Ti, Zr, Hf, Th, and W.[7–11] C—H activation is also known for $Mo_2R_2(OR)_4$ compounds where β-H elimination from alkyl ligands was found to be facile and reversible under conditions where the bulk of the alkoxide ligand and the alkyl group permitted an open coordination site.[12] In the present case, loss of cyanamide from **I** leads to an unsaturated intermediate, which upon a fluxional process involving the alkoxide ligands would open a coordination site next to the MoC_4Me_4 ring. This intermediate could undergo β-H abstraction from the metallapentadiene ring to form metal hydride and metallafulvelene ligands. The cyanamide would then insert into either the M—H bond or the "tucked in" position on the ring as shown in Scheme 1. Cyanamide ligands have been shown to insert into (a) M—H bonds, e.g. in reactions with $Os_3(H)_2(CO)_{10}$,[13] and (b) M=CR_2 bonds as in reactions with $(CO)_5M{=}CPh(R')$ compounds where M = W or Cr.

It was decided to study the conversion of **I** to **II** in more detail in order to gain a better understanding of the reaction and possible mechanism. Accordingly, a series of rate studies were undertaken. All of the experiments were followed via ^1H NMR spectroscopy. The increasing concentration of the final product was determined in relationship to the protio impurities of the solvent (toluene-d_8).

Initial experiments showed that Et_2NCN was in rapid equilibrium between the bound and free states. Indeed, the equilibrium is faster than the NMR time scale even at −75°C. In crossover experiments with excess Me_2NCN, **II** was virtually quantitatively converted to $Mo_2(ONp)_6(\mu\text{-}C_4Me_4)(NCNMe_2)$, **II′**. Compounds in which the cyanamide donor ligand has been replaced by pyridine or PMe_3 also react, at slower rates, with free cyanamide to produce **II**. The relative rate of reaction found for various L is Et_2NCN > py > PMe_3 which is the inverse of the donor ability of the ligand L. These data indicate that the pre-equilibrium process is governed by the relative donor ability of the ligand L. Table 6 shows the specific rate data for each study.

While following the conversion of **I** to **II**, no intermediates are visible via NMR spectroscopy. Therefore, if an intermediate metal hydride compound is formed, it must react quickly to form the final product and may be assumed to be in a steady state of formation and reaction. Accordingly, the following reaction expression and rate law were determined as a possible mechanism for the conversion of **I** to **II** in the case of L being Et_2NCN. $[M_2]$ represents the total concentration of the dinuclear metal compounds contained in the equilibrium K_1.

$$\underset{\text{A}}{Mo_2(ONp)_6(C_4Me_4)(Et_2NCN)} \overset{K_1}{\rightleftharpoons} \underset{\text{B}}{Mo_2(ONp)_6(C_4Me_4)} + \underset{\text{L}}{Et_2NCN}$$

Fast equilibrium

Table 5. Selected bond angles (°) for the $Mo_2(ONp)_6(C_4Me_3CH_2C(NEt_2)NH)$ molecule

A	B	C	Angle	A	B	C	Angle
Mo(2)	Mo(1)	O(18)	126.65(15)	O(36)	Mo(2)	C(16)	84.63(27)
Mo(2)	Mo(1)	O(24)	99.77(18)	O(42)	Mo(2)	O(48)	94.85(25)
Mo(2)	Mo(1)	O(30)	50.38(14)	O(42)	Mo(2)	C(12)	88.6(3)
Mo(2)	Mo(1)	N(3)	141.12(18)	O(42)	Mo(2)	C(16)	153.43(25)
Mo(2)	Mo(1)	C(11)	74.50(20)	O(48)	Mo(2)	C(12)	88.49(28)
Mo(2)	Mo(1)	C(12)	49.05(20)	O(48)	Mo(2)	C(16)	104.94(27)
Mo(2)	Mo(1)	C(14)	75.82(20)	C(12)	Mo(2)	C(16)	74.6(3)
Mo(2)	Mo(1)	C(16)	50.37(19)	Mo(1)	O(18)	C(19)	132.2(5)
O(18)	Mo(1)	O(24)	106.36(23)	Mo(1)	O(24)	C(25)	134.6(5)
O(18)	Mo(1)	O(30)	88.83(21)	Mo(1)	O(30)	Mo(2)	78.98(18)
O(18)	Mo(1)	N(3)	86.97(24)	Mo(1)	O(30)	C(31)	125.2(5)
O(18)	Mo(1)	C(11)	126.81(27)	Mo(2)	O(30)	C(31)	125.9(5)
O(18)	Mo(1)	C(12)	158.64(26)	Mo(2)	O(36)	C(37)	128.8(5)
O(18)	Mo(1)	C(14)	96.19(26)	Mo(2)	O(42)	C(43)	143.9(5)
O(18)	Mo(1)	C(16)	93.10(24)	Mo(2)	O(48)	C(49)	139.8(6)
O(24)	Mo(1)	O(30)	80.88(22)	Mo(1)	N(3)	C(4)	129.1(6)
O(24)	Mo(1)	N(3)	86.26(25)	C(4)	N(5)	C(6)	120.8(6)
O(24)	Mo(1)	C(11)	117.85(27)	C(4)	N(5)	C(8)	121.6(7)
O(24)	Mo(1)	C(12)	94.89(27)	C(6)	N(5)	C(8)	117.6(7)
O(24)	Mo(1)	C(14)	154.06(26)	N(3)	C(4)	N(5)	125.4(7)
O(24)	Mo(1)	C(16)	150.03(26)	N(3)	C(4)	C(10)	114.4(7)
O(30)	Mo(1)	N(3)	164.75(23)	N(5)	C(4)	C(10)	120.2(7)
O(30)	Mo(1)	C(11)	124.62(24)	N(5)	C(6)	C(7)	112.4(7)
O(30)	Mo(1)	C(12)	96.85(23)	N(5)	C(8)	C(9)	113.8(8)
O(30)	Mo(1)	C(14)	112.80(25)	C(4)	C(10)	C(11)	109.1(7)
O(30)	Mo(1)	C(16)	76.89(24)	Mo(1)	C(11)	C(10)	117.9(5)
N(3)	Mo(1)	C(11)	68.91(26)	Mo(1)	C(11)	C(12)	71.7(4)
N(3)	Mo(1)	C(12)	92.34(28)	Mo(1)	C(11)	C(14)	69.2(4)
N(3)	Mo(1)	C(14)	82.25(27)	C(10)	C(11)	C(12)	125.8(8)
N(3)	Mo(1)	C(16)	117.97(26)	C(10)	C(11)	C(14)	119.4(8)
C(11)	Mo(1)	C(12)	35.4(3)	C(12)	C(11)	C(14)	113.7(7)
C(11)	Mo(1)	C(14)	36.2(3)	Mo(1)	C(12)	Mo(2)	75.16(24)
C(11)	Mo(1)	C(16)	62.25(28)	Mo(1)	C(12)	C(11)	72.9(5)
C(12)	Mo(1)	C(14)	62.6(3)	Mo(1)	C(12)	C(13)	124.2(6)
C(12)	Mo(1)	C(16)	68.4(3)	Mo(2)	C(12)	C(11)	119.3(6)
C(14)	Mo(1)	C(16)	36.02(27)	Mo(2)	C(12)	C(13)	122.8(6)
Mo(1)	Mo(2)	O(30)	50.64(14)	C(11)	C(12)	C(13)	117.9(7)
Mo(1)	Mo(2)	O(36)	121.28(16)	Mo(1)	C(14)	C(11)	74.6(5)
Mo(1)	Mo(2)	O(42)	98.65(16)	Mo(1)	C(14)	C(15)	124.6(5)
Mo(1)	Mo(2)	O(48)	141.11(17)	Mo(1)	C(14)	C(16)	73.3(4)
Mo(1)	Mo(2)	C(12)	55.79(21)	C(11)	C(14)	C(15)	121.7(7)
Mo(1)	Mo(2)	C(16)	54.90(20)	C(11)	C(14)	C(16)	114.9(7)
O(30)	Mo(2)	O(36)	85.43(21)	C(15)	C(14)	C(16)	123.3(7)
O(30)	Mo(2)	O(42)	84.19(22)	Mo(1)	C(16)	Mo(2)	74.73(24)
O(30)	Mo(2)	O(48)	167.91(21)	Mo(1)	C(16)	C(14)	70.7(4)
O(30)	Mo(2)	C(12)	103.52(24)	Mo(1)	C(16)	C(17)	122.3(5)
O(30)	Mo(2)	C(16)	80.04(24)	Mo(2)	C(16)	C(14)	117.2(6)
O(36)	Mo(2)	O(42)	115.38(24)	Mo(2)	C(16)	C(17)	123.6(5)
O(36)	Mo(2)	O(48)	84.11(23)	C(14)	C(16)	C(17)	119.2(7)
O(36)	Mo(2)	C(12)	155.4(3)				

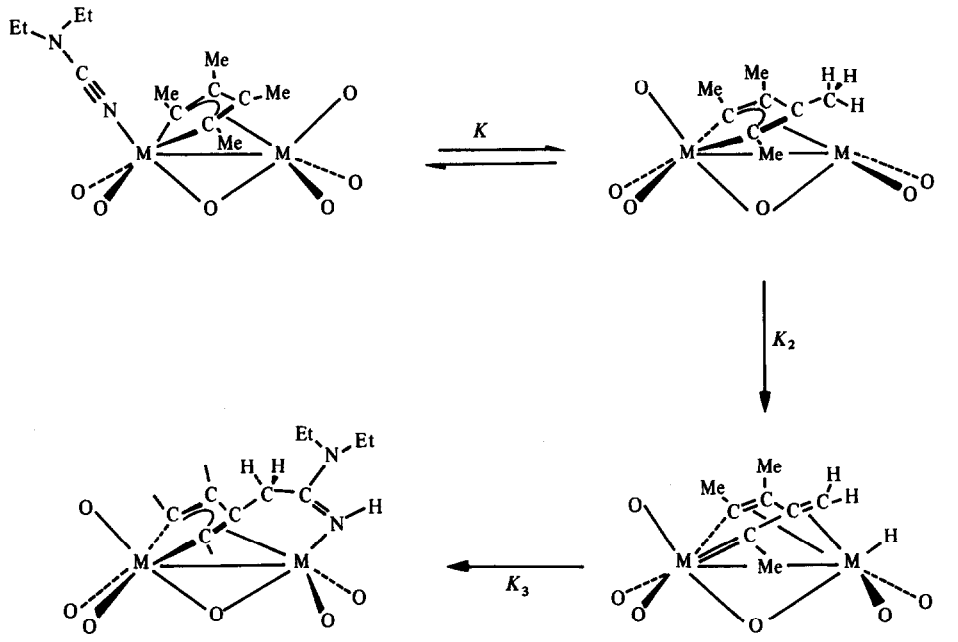

Fig. 4. A possible reaction pathway for the conversion of compound **I** to compound **II**.

$$\underset{\text{B}}{Mo_2(ONp)_6(C_4Me_4)} \xrightarrow{k_2} \underset{\text{C}}{Mo_2(ONp)_6(C_4Me_3CH_2)(H)}$$

Rate determining step

$$\underset{\text{C}}{Mo_2(ONp)_6(C_4Me_3CH_2)(H)} + \underset{\text{L}}{Et_2NCN} \xrightarrow{k_3} \underset{\text{D}}{Mo_2(ONp)_6(C_4Me_3CH_2C(NEt_2)NH)}$$

Very very fast

$$\frac{d[D]}{dt} = \frac{k_2K_1[M_2]}{K_1+[L]}.$$

Table 6. The rate data for the conversion of compound **I** to compound **II**

T	$[M_2]$ M	k_{obs} (s) $\times 10^3$	Cor. Coeff.
42.9	0.0325	0.195	0.988
47.6	0.0325	0.315	0.994
52.3	0.0325	0.856	0.986
56.8	0.0325	1.220	0.974
49.0	0.0217	0.405	0.991
49.0	0.0217 + 10 Et_2NCN	0.395	0.953
52.3	0.0325 + 7 Et_2NCN	0.900	0.87
52.3	0.0325 L = PMe_3	0.371	0.993
52.3	0.0325 L = py	0.662	0.977

If the reaction in Scheme 1 is correct, the rate determining step is the β-H abstraction from the MoC_4Me_4 ring. Activation parameters taken at 43.0, 47.6, 52.3 and 57.0°C yielded $\Delta H^{\dagger}_{obs} = 28.4 \pm 3.6$ kcal mol^{-1} and $\Delta S^{\dagger}_{obs} = +14.25 \pm 11.22$ eu. The value for $\Delta H^{\dagger}$ is consistent with a relatively high enthalpic process being the dominant factor. Although the error margin in the $\Delta S^{\dagger}_{obs}$ value is extremely large, $\Delta S^{\dagger}$ is at least zero to very positive indicating that incorporation of Et_2NCN must be occurring after the rate determining step. A large positive entropy value would be consistent with the loss of Et_2NCN in the pre-equilibrium process before the rate determining step.[14]

The rate expression also shows dependence on [L], and by varying [L] the value of k_2 may be determined. It was found that adding up to 10 equivalents of Et_2NCN had no effect on the rate. Therefore, it was assumed when [L] was equal to one equivalent that K_1 was much greater than [L] and the rate law could be altered to that shown below. In this case the observed rate constant would reflect only the rate determining step.

$$\frac{d[D]}{dt} = k_2[M_2].$$

In the development of this reaction scheme other possible mechanisms have been ignored. These mechanisms include attack of free cyanamide on the C—H bond of the MoC_4Me_4 ring, and a direct coupling between a π-bound cyanamide with the

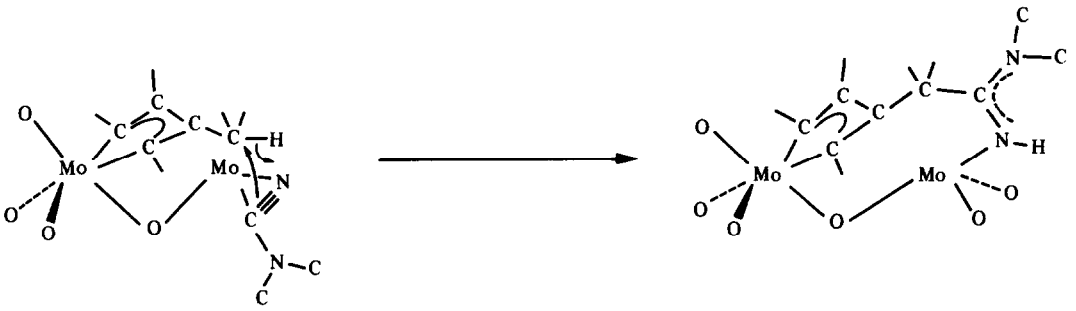

Scheme 1.

methyl of the flyover ring involving a 1,3-hydrogen shift as shown in Scheme 1. Both of these schemes would be dependent on the concentration of cyanamide and would be expected to give second order or even more complicated kinetics rather than the simple first order kinetics observed. Attack of free cyanamide would also be expected to have negative entropy of activation.

The kinetic data are consistent with C—H activation and H abstraction on the MoC_4Me_4 ring. Hydrogen abstraction is becoming recognized as a viable and relatively widespread reaction in permethylated cyclopentadienyl metal complexes.[9] This type of reaction has not been seen before for μ-C_4R_4 ligands involving bimetallic complexes. Nevertheless, the occurrence of this type of reaction in dinuclear compounds having a metallacyclopentadiene ring is not unexpected, and emphasizes the comparison between metallacyclopentadiene ligands and cyclopentadiene ligands. This reaction also shows that dinuclear metal alkoxide compounds may undergo the same type of reactions previously seen for monomeric metal complexes.

It may be expected, based on this work, that C—H activation in $W_2(OR)_4(\mu\text{-}C_4R'_4)L$ compounds may prove to be yet an additional mode of activity.[16]

EXPERIMENTAL

Reagents and general techniques

General procedures and the preparation of $Mo_2(ONp)_6(R_2NCN)$ have been described.[3] Dry and oxygen-free solvents were used in all preparations and all manipulations were carried out under inert atmospheres (N_2) using dry box and Schlenk techniques. Elemental analyses were performed by Alfred Bernhart Microanalytisches Laboratorium, West Germany.

^{1}H NMR spectra were recorded on a Nicolet NT-360 360-MHz spectrometer in dry and oxygen-free toluene-d_8 or benzene-d_6. ^{13}C NMR spectra were recorded on a Nicolet NT-360 or a Varian XL-300. The ^{13}C NMR spectra were obtained for the μ-Et_2NCN using ^{13}C-labelled Et_2N^*CN.[15] All ^{1}H NMR chemical shifts are in ppm relative to protio impurities in the solvent. ^{13}C NMR chemical shifts are in ppm relative to the *ipso* carbon of toluene-d_8 at δ 137.5.

IR spectra were obtained on a Perkin–Elmer 283 spectrophotometer as Nujol mulls between CsI plates.

$Mo_2(ONp)_6(\mu\text{-}C_4Me_4)(NCNEt_2)$

$Mo_2(ONp)_6(\mu\text{-}NCNEt_2)$ (0.240 g, 0.29 mmol) was dissolved in hexane (5 cm^3) and was frozen at liquid N_2 temperature. C_2Me_2 (0.738 mmol) was condensed into the flask using a calibrated gas line. The solution was rapidly warmed to room temperature and stirred vigorously for 15 min. During this time the solution turned scarlet and then brown. Just as the brown colour became dominant the flask was cooled to -15°C. After 24 h brown diamond shaped crystals were filtered from the blue solution. Reduction of the solvent volume led to second and third crops of crystals. Total crystalline yield was *ca* 60% based on Mo.

Analysis. Found: C, 55.87; H, 9.48; N, 3.03. Calc.: C, 56.08; H, 9.63; N, 3.04%. IR: 2207(m), 1345(sh), 1255(w), 1239(w), 1211(w), 1070(vs,br), 1038(sh), 1020(s), 930(w), 905(w), 800(w,br), 752(w), 720(w), 650(s), 625(m), 460(m,br) cm^{-1}. ^{1}H NMR (toluene-d_8, room temperature): δ 2.11, 0.653 (q, t, Et_2N); 2.4, 1.8 (vbr, C_4Me_4); 1.15 (br, OCH_2-*t-Bu*). ^{13}C NMR (room temperature): 129.1 ppm (vbr, Et_2NCN); (-60°C, toluene-d_8): 132 ppm (Et_2NCN).

$Mo_2(ONp)_6(\mu\text{-}C_4Me_3CH_2C(NEt_2)NH)$

$Mo_2(ONp)_6(\mu\text{-}C_4Me_4)(NCNEt_2)$ (0.250 g) was dissolved in toluene (10 cm^3) and heated to 60°C for 2 h while stirring rapidly. The solution was

concentrated to approximately 1 cm^3 *in vacuo* and cooled to −15°C. The compound precipitated as a powder. After repeated attempts, a single crystal was crystallized from concentrated toluene.

Analysis. Found: C, 55.79; H, 9.43; N, 3.01. Calc.: C, 56.08; H, 9.63; N, 3.04%. IR: 3358(vw), 1590(s), 1340(sh), 1275(w), 1255(m), 1210(w), 1190(w), 1091(s), 1071(s), 1058(s), 1020(s), 800(br,m), 645(s), 450(br,w). ^1H NMR (toluene-d_8, room temperature): δ 5.08 (brs, NH); 5.23, 5.20, 4.90, 4.84, 4.68, 4.40, 4.05, 3.95, 3.90, 3.68, 3.44 (d of AB quartets, OCH_2-t-Bu, J_{HH} = 9–11 Hz); 3.29, 2.80 (d of AB quartet, J_{HH} = 16 Hz, $CCH_2C(NEt_2)MH$); 2.45, 2.42, 1.63 (s, C_4Me_3); 1.59, 1.37, 1.28, 1.11, 1.09, 1.05 (s, OCH_2-*t-Bu*); 2.49, 0.656 (br qt, t, NEt_2). ^{13}C NMR (toluene-d_8, room temperature): 170 ppm (J_{CH} = 6.1 Hz, $CH_2C(NEt_2)NH$).

$Mo_2(ONp)_6(C_4Me_3CH_2(NMe_2)NH)$

$Mo_2(ONp)_6(\mu\text{-}C_4Me_4)(NCNEt_2)$ (0.010 g, 0.01 mmol) was dissolved in benzene-d_6 (0.5 cm^3) and excess Me_2NCN (5 μl) was added via syringe. The solution was frozen and sealed under vacuum in an NMR tube. The reaction was heated to 65°C for 2 h. The resultant solution was spectroscopically identified via ^1H NMR spectroscopy.

^1H NMR (benzene-d_6, room temperature): δ 5.31, 5.25, 5.00, 4.83, 4.78, 4.34, 4.26, 4.11, 3.90, 3.75, 3.40 (d of AB quartets, J_{HH} = 9–11 Hz, OCH_2-t-Bu); 4.91 (s, br, NH); 3.17, 2.72 (d of AB quartet, J_{HH} = 15 Hz, $C_4Me_3CH_2$); 2.49, 2.48, 1.76 (s, C_4Me_3); 1.634, 1.392, 1.309, 1.147, 1.108, 1.055 (s, OCH_2-*t-Bu*); 2.21, 0.757 (q,t, free Et_2NCN); 1.93, 1.922 (s, $CH_2C(NMe_2)NH$); 1.842 (s, free Me_2NCN).

$Mo_2(ONp)_6(\mu\text{-}C_4Me_4)(PMe_3)$

$Mo_2(ONp)_6(\mu\text{-}C_4Me_4)(NCNEt_2)$ (30 mg, 0.0325 mmol) was dissolved in toluene-d_8 (1 cm^3). The solution (0.5 cm^3) was transferred to a NMR tube with a gas tight Teflon plug. PMe_3 (3.5 equiv.) was condensed into the tube using a calibrated gas line. The tube was warmed to room temperature and characterized via ^1H NMR spectroscopy.

^1H NMR (toluene-d_8, room temperature): δ 3.51, 4.23, 4.00, 4.15 (s,s,d,vbr, OCH_2-t-Bu); 2.13, 1.90, 1.89 (s, C_4Me_4); 1.37, 1.30, 1.09, 1.07 (s, 1:1:2:2, OCH_2-*t-Bu*); 0.89 (d, J_{PH} = 7.95 Hz, bound PMe_3); 0.79 (d, J_{PH} = 2.2 Hz, free PMe_3); 2.26, 0.79 (q, t, Et_2NCN).

$Mo_2(ONp)_6(C_4Me_4)(py)$

(a) $Mo_2(ONp)_6$ (0.28 g, 0.392 mmol) was dissolved in hexane (5 cm^3) and py (1 cm^3). The solution was frozen at liquid N_2 temperature and C_2Me_2 (2.5 equiv.) was condensed into the evacuated flask using a calibrated gas line. The solution was rapidly warmed to room temperature and stirred at room temperature for 4 h. The solvent was evaporated *in vacuo* and the residue was checked by ^1H NMR spectroscopy which showed a mixture of $Mo_2(ONp)_6(\mu\text{-}C_2Me_2)(py)$ and $Mo_2(ONp)_6(\mu\text{-}C_4Me_4)(py)$. The remaining sample was redissolved in hexane (7 cm^3) and C_2Me_2 (2.5 equiv.) was reintroduced into the flask using the previously described method and allowed to stir for 12 h. The solvent was concentrated to 1 cm^3 and cooled to −15°C and microcrystalline $Mo_2(ONp)_6(\mu\text{-}C_4Me_4)(py)$ was collected and characterized via ^1H NMR spectroscopy.

^1H NMR (benzene-d_6, room temperature, all signals are very broad): δ 8.68, 6.74, 6.48 (*o*, *p*, *m* protons of py), 5.38, 4.47, 4.39, 4.22, 3.70 (br, OCH_2-t-Bu); 2.18 (s, C_4Me_4); 1.46, 1.36, 1.12 (s, OCH_2-*t-Bu*).

(b) $Mo_2(ONp)_6(C_4Me_4)(NCNEt_2)$ (10 mg) was dissolved in benzene-d_6 and placed in a NMR tube. The sample was checked for authenticity via ^1H NMR spectroscopy and excess py (5 cm^3) was injected into the sample via syringe through a rubber septum. The sample was than identified via ^1H NMR and compared to authentic samples of $Mo_2(ONp)_6(\mu\text{-}C_4Me_4)(py)$.

Kinetic studies

$Mo_2(ONp)_6(\mu\text{-}C_4Me_4)(NCNEt_2)$ was weighed and dissolved in toluene-d_8 (1 cm^3) in a volumetric flask. The solution (0.5 cm^3) was measured into a NMR tube and sealed. The sample was stored in an ice bath until studied. The sample was then inserted into the NMR probe which was heated to a specific reaction temperature. Two signals (1.61 and 1.52 ppm) were integrated and the average A_t/A_0 value from both peaks was used in the determination of the rate given in Table 6. The reactions were followed for three half-lives.

Crystallographic studies

General operating procedures and listings of programs have been previously described.[17] A summary of crystal data is given in Table 7.

$Mo_2(ONp)_6(\mu\text{-}C_4Me_4)(NCNEt_2)$. Transfer and

Table 7. Summary of crystal data

	I	II
Empirical formula	$Mo_2C_{43}H_{78}N_2O_6$	$Mo_2C_{43}H_{88}N_2O_6$
Colour of crystal	red/brown	black
Crystal dimensions (mm)	0.18 × 0.18 × 0.22	0.20 × 0.30 × 0.40
Space group	$P2_1/a$	$P2_12_12_1$
Cell dimensions		
Temperature (°C)	−159	−153
a (Å)	11.892(5)	11.101(4)
b (Å)	32.487(18)	17.177(9)
c (Å)	13.919(6)	25.766(14)
β (°)	111.38(2)	
Z (molecules/cell)	4	4
Volume (Å^3)	5007.48	4913.34
Calculated density (g cm^{-3})	1.208	1.245
Wavelength (Å)	0.71069	0.71069
Molecular weight	910.98	921.06
Linear absorption coefficient (cm^{-1})	5.274	5.274
Detector to sample distance (cm)	22.5	22.5
Sample to source distance (cm)	23.5	23.5
Average omega scan width at half height	0.25	0.25
Scan speed (deg min^{-1})	4.0	6.0
Scan width (deg + dispersion)	2.0	1.5
Individual background (s)	5	6
Aperture size (mm)	3.0 × 4.0	3.0 × 4.0
Two-theta range (°)	6–45	6–45
Total number of reflections collected	7199	3716
Number of unique intensities	6560	3631
Number of $F > 0.0$		3475
Number of $F > 3.0\sigma(F)$	4486	3200
$R(F)$	0.0487	0.0419
$Rw(F)$	0.0486	0.0435
Goodness of fit for the last cycle	0.854	0.758
Maximum delta/sigma for last cycle	0.05	0.05

I = $Mo_2(ONp)_6(\mu\text{-}C_4Me_4)(NCNEt_2)$; II = $Mo_2(ONp)_6(\mu\text{-}C_4Me_3CH_2C(NEt_2)NH)$.

characterization were by the usual methods with the space group being uniquely determined to be $P2_1/a$ (a non-standard setting of $P2_1/c$).

The structure was solved by direct methods and Fourier techniques and refined by full-matrix least squares. Hydrogen atoms were located in a difference Fourier phased on the non-hydrogen parameters. Attempts to refine the hydrogen met with limited success, with *ca* 10% failing to converge to reasonable positions. For this reason the located positions were used to place all hydrogens in fixed idealized positions for the remainder of the refinement.

A final difference map was featureless, the largest peak being 0.59 e Å^{-3}. No absorption correction was made.

$Mo_2(ONp)_6(\mu\text{-}C_4Me_3CH_2C(NEt_2)NH)$. A small crystal was selected, transferred to the goniostat and cooled to −153°C for characterization and data collection. A systematic search of a limited hemisphere of reciprocal space yielded a set of reflections which exhibits orthorhombic symmetry. The systematic extinction of $h00$ for $h = 2n+1$, $0k0$ for $k = 2n+1$, and 001 for $1 = 2n+1$ identified the space group as $P2_12_12_1$.

The structure was solved by using a combination of direct methods and heavy atom techniques. The structure was refined by full-matrix least-squares, using 3200 reflections having $F > 3.0\sigma(F)$. Hydrogen atoms were included in fixed calculated positions. All non-hydrogen atoms were refined using anisotropic thermal parameters. The final R was 0.042. The final difference map was essentially featureless, the final peak being 0.4 e Å^{-3}. The enantiomer was checked, and the proper one is displayed in this report.

Supplementary materials

Atomic positional parameters are available from the Cambridge Crystallographic Data Centre and a complete listing of bond lengths and angles together with F_o and F_c values have been deposited with the Editor at Queen Mary College.

Acknowledgements—We thank the Department of Energy, Basic Science Division, Chemistry Program and the Wrubel Computing Center for support.

REFERENCES

1. M. H. Chisholm, D. M. Hoffman and J. C. Huffman, *J. Am. Chem. Soc.* 1984, **106**, 6815.
2. M. H. Chisholm, J. C. Huffman and N. S. Marchant, *Organometallics* 1987, **6**, 1073.
3. M. H. Chisholm, J. C. Huffman and N. S. Marchant, *Organometallics* 1986, **5**, 602.
4. M. H. Chisholm, K. Folting, J. C. Huffman and I. P. Rothwell, *J. Am. Chem. Soc.* 1982, **104**, 4389.
5. M. H. Chisholm, *Polyhedron* 1983, **2**, 681.
6. H. F. Haneike and R. S. Drago, *J. Am. Chem. Soc.* 1968, **90**, 5112.
7. C. McDade, J. C. Green and J. E. Brecaw, *Organometallics* 1982, **1**, 1629.
8. J. E. Bercaw, *Adv. Chem. Ser.* 1978, **167**, 135.
9. J. E. Bercaw and A. R. Bulls, A.C.S. Lecture 131 190, A.C.S. National Meeting (Chicago).
10. J. W. Bruno, G. M. Smith, T. J. Mark, C. K. Fair, A. J. Schultz and J. M. Williams, *J. Am. Chem. Soc.* 1986, **108**, 40.
11. F. G. N. Cloke, J. C. Green, M. L. H. Green and C. P. Morley, *J. Chem. Soc., Chem. Commun.* 1985, 945.
12. M. H. Chisholm and R. Tatz, *Organometallics* 1986, **5**, 1590.
13. J. Banford, M. J. Mays and P. R. Raithby, *J. Chem. Soc., Dalton Trans.* 1985, 1355.
14. J. H. Espenson, *Chemical Kinetics and Reaction Mechanisms*. McGraw-Hill, New York (1981).
15. H. Fischer and U. Schubert, *Angew. Chem. Int. Ed. Engl.* 1981, **20**, 461.
16. M. H. Chisholm, B. K. Conroy, B. W. Eichhorn, K. Folting, D. M. Hoffman, J. C. Huffman and N. S. Marchant, *Polyhedron* 1987, **6**, 783.
17. M. C. Chisholm, K. Folting, J. C. Huffman and C. C. Kirkpatrick, *Inorg. Chem.* 1984, **24**, 1021.

Polyhedron Vol. 7, No. 10/11, pp. 931–941, 1988
Printed in Great Britain

0277–5387/88 $3.00+.00
© 1988 Pergamon Press plc

SYNTHESIS AND REACTIVITY OF 1,2-DIOSMACYCLES

JOSEF TAKATS

Department of Chemistry, University of Alberta, Edmonton, Alberta, Canada, T6G 2G2

(*Accepted* 5 *November* 1987)

Abstract—Photolysis of $Os_3(CO)_{12}$ in the presence of alkenes with filtered radiation ($\lambda >$ 370 nm) leads to fragmentation of the cluster and gives mononuclear $Os(CO)_4(\eta^2$-alkene) derivatives and dinuclear 1,2-diosmacyclobutanes, $Os_2(CO)_8(\mu$-η^1,η^1-CHRCHR′). Attempts to extend the photochemical method to the preparation of other types of diosmacycles met with little success. As an alternative synthetic approach the exchange of ethylene in $Os_2(CO)_8(\mu$-η^1,η^1-$C_2H_4)$, **3a**, for other unsaturated organic substrates was explored. Reaction of **3a** with alkynes gave diosmacyclobutenes, whereas with dienes regiospecific 1,2-addition was observed. The scope and limitations of the exchange reactions are reviewed. The properties of the diosmacycles and of the product obtained via hydride abstraction from **3a** are outlined.

Interest in the chemistry of dimetallacycles can be traced to the now often verified postulate that such species are involved as key intermediates in a variety of chemical reactions and that they may serve as useful models for the bonding and transformation of unsaturated organic substrates on metal surfaces.[1] Although the importance of these compounds is well recognized, the number of examples, with the exception of dimetallacyclopropanes[2] (i.e. alkylidene bridged dimetallic complexes) and those resulting from alkyne addition to dimetallic complexes,[3] is still rather small.

It is the purpose of this article to give a brief overview of our discovery, albeit serendipitous, of a convenient photochemical synthesis of 1,2-diosmacyclobutanes[4] and the utilization of these compounds for the preparation of other diosmacycles. Emphasis will be on the work from the author's laboratory, although relevant work from other groups will be also mentioned.

PHOTOCHEMICAL SYNTHESIS OF 1,2-DIOSMACYCLOBUTANES, $Os_2(CO)_8(\mu$-η^1,η^1-CHRCHR′)

The successful preparation of a range of $Ru(CO)_4(\eta^2$-alkene) compounds via photolysis of $Ru_3(CO)_{12}$ (**1–Ru**) in the presence of alkenes[5] [eq. (1)] prompted us to investigate the similar photoreaction with $Os_3(CO)_{12}$(**1–Os**).

$$Ru_3(CO)_{12} + \text{alkene} \xrightarrow[\text{hydrocarbon, RT}]{h\nu,\ \lambda > 370\text{ nm}} 3Ru(CO)_4(\eta^2\text{-alkene}). \quad (1)$$

The goal being to complete the series of iron triad $M(CO)_4(\eta^2$-alkene) (M = Fe, Ru, Os) compounds and compare their properties.

However a potential problem presented itself. It was well documented at the time, that whereas near-UV irradiation of $Ru_3(CO)_{12}$ in the presence of CO, C_2H_4 and PPh_3 led to photofragmentation,[6] the reaction between $Os_3(CO)_{12}$ and PPh_3 resulted in photosubstitution.[7] Indeed the success of the reaction shown in eq. (1) resides in the use of selective excitation into the first allowed electronic band of $Ru_3(CO)_{12}$ at 380 nm, which is known to have $\sigma \rightarrow \sigma^*$ (Ru—Ru) character and therefore leads to facile and synthetically efficient photofragmentation.† The different reactivity of $Os_3(CO)_{12}$ was attributed to a reversal in the relative order of the two lowest energy absorptions. In the case of osmium, the predominantly $\sigma \rightarrow \sigma^*$ (Os—Os) transition being associated with the second band at 330 nm. Accordingly, the first synthetic reactions with $Os_3(CO)_{12}$ utilized Pyrex filtered radiation ($\lambda > 280$ nm) to ensure excitation into the $\sigma \rightarrow \sigma^*$ transition. A π-acidic alkene, methyl acrylate, was chosen as the organic substrate in order to favour the formation

† Reaction (1) proceeds in 100% yield by IR spectroscopy. Isolated yields are somewhat lower and depend on the nature of the ligand, the most stable compounds are obtained with strongly π-acidic alkenes.

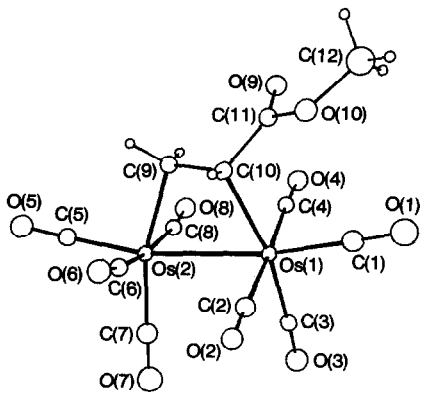

Fig. 1. Molecular structure of $Os_2(CO)_8(\mu\text{-}\eta^1,\eta^1\text{-}CH_2CHCO_2CH_3)$,[9] **3b**. Relevant bond distances (Å): Os(1)—Os(2) = 2.8850(1), Os(1)—C(10) = 2.223(9), Os(2)—C(9) = 2.203(9), C(9)—C(10) = 1.52(1). Torsional angle Os—Os and C—C 23.0°.

of a stable product. Although $Os_3(CO)_{12}$ was consumed, mixtures of carbonyl–alkene complexes were obtained which defied separation and characterization. Undaunted, if a bit sceptical, the same reaction was tried with near-UV radiation. Serendipity smiled and formation of carbonyl–alkene complexes of osmium was again observed.† After some initial difficulties, it was ascertained[9] that the crude reaction product was in fact a mixture of two compounds [eq. (2)], the anticipated monomeric **2b** and the unexpected diosmacyclobutane derivative **3b**, Fig. 1.

$$Os_3(CO)_{12} + CH_2CHCO_2CH_3 \xrightarrow[\text{benzene, 15°C}]{h\nu,\ \lambda > 370\ nm} Os(CO)_4(\eta^2\text{-}CH_2CHCO_2CH_3) \quad \mathbf{2b}$$
$$+ Os_2(CO)_8(\mu\text{-}\eta^1,\eta^1\text{-}CH_2CHCO_2CH_3). \quad \mathbf{3b} \qquad (2)$$

While this work was in progress we have learned that Norton and co-workers[10] have synthesized the unsubstituted 1,2-diosmacyclobutane, **3a**, via a very different reaction sequence [eq. (3)]. Prompted by the successful preparation of **3a** without the stabilizing electron withdrawing substituents on carbon, the photoreaction under a continuous ethylene purge was carried out and, gratifyingly, gave a mixture of $Os(CO)_4(\eta^2\text{-}C_2H_4)$, **2a** and **3a**.

$$Os_3(CO)_{12} \rightarrow Na_2[Os_2(CO)_8]$$
$$Na_2[Os_2(CO)_8] + TsOCH_2CH_2OTs \rightarrow Os_2(CO)_8(\mu\text{-}\eta^1,\eta^1\text{-}C_2H_4). \quad \mathbf{3a} \qquad (3)$$

Since **2a** is volatile and consequently removed during the evaporation of the solvent, the isolation of **3a** is very simple‡ and makes the photochemical route the preparative method of choice[11] for this interesting and synthetically very useful material. Extension of this method to other olefins has met with moderate success. In our hands,[12] substituted diosmacyclobutanes were observed with propylene, methylvinyl ketone, dimethylfumerate (DMF) and dimethyl maleate (DMM). Other workers reported similar results with 1-octene,[13] 5,6-dimethylidene-7-oxabicyclo[2.2.1]-hept-2-ene[14] and propylene, 1-butene, styrene, tert-butylethylene.[15]

The molecules exhibit relatively rich IR spectra in the terminal carbonyl region with a characteristic absorption above 2100 cm^{-1}. Another typical feature is the high field position of the carbon atoms of the Os_2C_2 ring in the ^{13}C NMR spectrum (cf. **3a**, $\delta_C = -25.2$ ppm). The stability of the diosmacyclobutanes is a function of both steric and electronic factors. Thus the propylene bridged compound is much less stable than **3a** which in turn is less stable than **3b** and other diosmacyclobutanes having electron withdrawing substituents at the bridgehead carbon atoms. Although the reaction with π-acidic alkenes is not always without complication, nor does it guarantee the universal formation of dimetallacyclic compounds. For instance, the photoreaction with DMM proceeded with isomerization of the alkene and formation of all possible mono- and dinuclear compounds [eq. (4)]. Contrary to this, the reaction with **1–Ru** gave only $Ru(CO)_4(\eta^2\text{-DMM})$.[5]

$$Os_3(CO)_{12} + DMM \xrightarrow[\text{benzene, 15°C}]{h\nu,\ \lambda > 370\ nm} Os(CO)_4(\eta^2\text{-DMM}) + Os(CO)_4(\eta^2\text{-DMF}) + Os_2(CO)_8(\mu\text{-DMM}) + Os_2(CO)_8(\mu\text{-DMF}). \quad \mathbf{3c} \quad \mathbf{3d} \qquad (4)$$

The structures of **3c** and **3d**, shown in Figure 2, also emphasize another characteristic of the com-

† From a recent study by Bensten and Wrighton,[8] it is clear that severe overlap of the absorption bands at room temperature is the cause of the early difficulties and for the success of the filtered radiation approach. In other words irradiation with $\lambda > 370$ nm gives suitable excitation into the tail-end of the $\sigma \rightarrow \sigma^*$ band without affecting the higher energy band which, under Pyrex filtered radiation is also excited and causes further reaction of the primary photoproducts.

‡ Yields of up to 86% based on the presumed stoichiometry of eq. (2) (57% based on osmium carbonyl) have been achieved. The average yield of several synthetic runs (0.5 g of $Os_3(CO)_{12}$) is approximately 45% based on osmium.

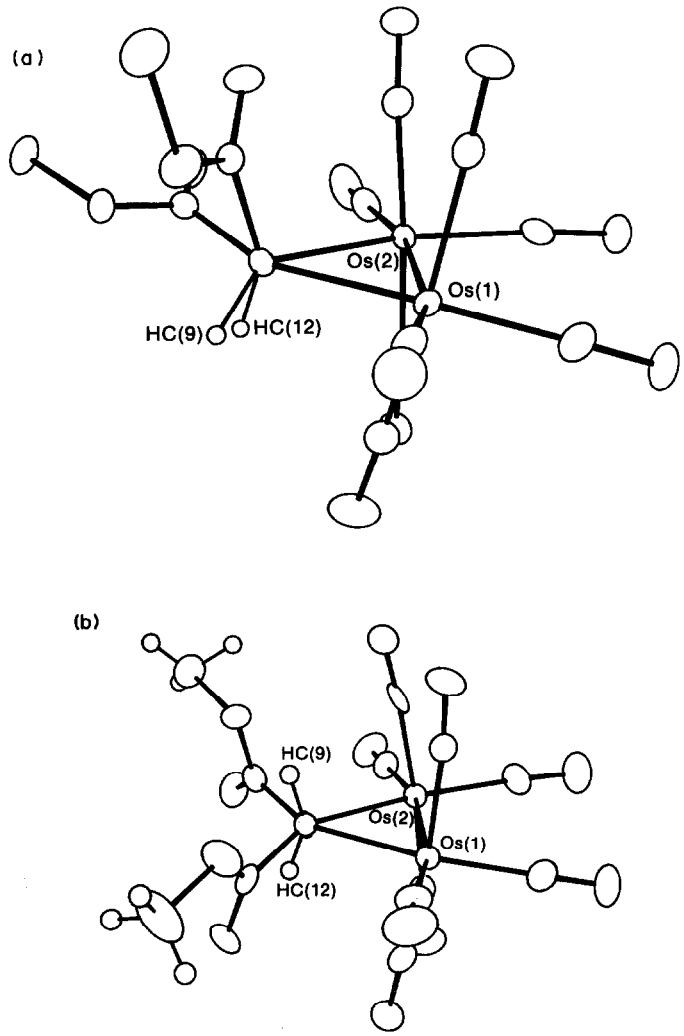

Fig. 2. Views of (a) $Os_2(CO)_8(\mu$-DMM), **3c**, and (b) $Os_2(CO)_8(\mu$-DMF), **3d**, looking down the C(9)—C(12) vector.[12] Relevant bond distances (Å) **3c**: Os(1)—Os(2) = 2.8788(4), Os(1)—C(9) = 2.220(7), Os(2)—C(12) = 2.202(6), C(9)—C(12) = 1.54(1); **3d**: Os(1)—Os(2) = 2.8719(4), Os(1)—C(9) = 2.205(6), Os(2)—C(12) = 2.221(7), C(9)—C(12) = 1.501(9). Torsional angle Os—Os and C—C: **3c** 18.5°; **3d** 23.2°.

pounds, the puckered nature of the four-membered ring. However, the conformational mobility of the ring is high.

No reaction between **1–Os** and tetrafluoroethylene, perfluoro-2-butene and maleic anhydride was observed, although a diosmacyclobutane based on the latter π-acidic olefin is available via an alternate route (see below).

Thus it appears, at least to this author, that even after several thoughtful reports, all the details of the photofragmentation of **1–Os**[8,13] and **1–Ru**[16] are still not completely understood. What seems irrefutable is that at some stage $M_3(CO)_{12}$ (M = Fe, Ru, Os) breaks down to mononuclear, $M(CO)_4$ and dinuclear, $M_2(CO)_8$ fragments probably stabilized by some supportive ligands. Based on this consideration it was of interest to establish whether the interception of the dinuclear osmium fragment by other unsaturated organic substrates may lead to a potentially general synthetic strategy for a variety of diosmacyclic compounds.

PHOTOREACTION OF $Os_3(CO)_{12}$ WITH ALKYNES

Although the thermal reaction of **1–Os** with alkynes has resulted in a rich derivative chemistry,[17] the corresponding photoreaction remained, surprisingly, untouched. With the precedent established by the saturated 1,2-diosmacyclobutanes, the

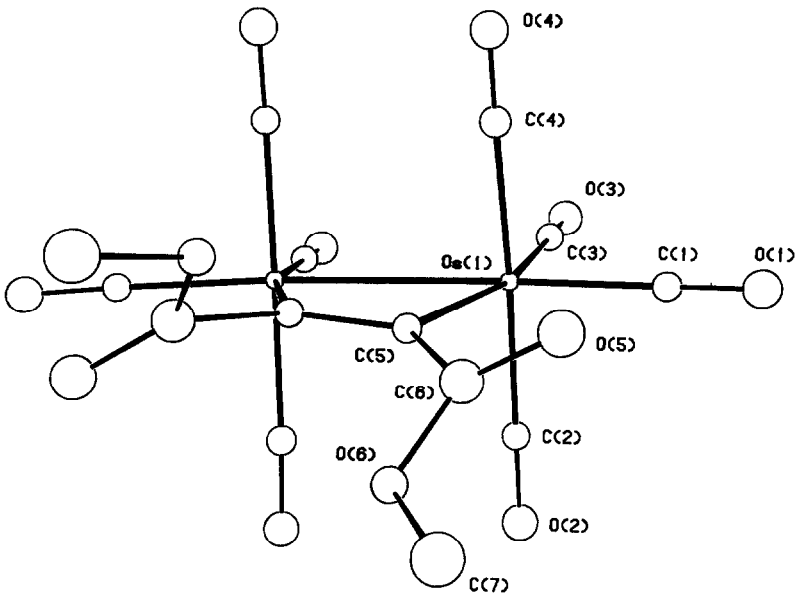

Fig. 3. Molecular structure of $Os_2(CO)_8(\mu\text{-}\eta^1,\eta^1\text{-DMAD})$,[19] **4–Os**. Relevant bond distances (Å): Os(1)—Os(1) = 2.8975(1), Os(1)—C(5) = 2.138(5); C(5)—C(5)′ = 1.33(1). Torsional angle Os—Os and C—C 8.4°.

less common "parallel" bonding mode of the alkyne[18] (i.e. formation of 1,2-diosmacyclobutene) was anticipated from the photoreaction.

Since activated alkenes afforded the most stable diosmacyclobutanes, the choice of dimethylacetylenedicarboxylate (DMAD, $C_2(CO_2CH_3)_2$) was obvious. Unfortunately the reaction resulted in the formation of a mixture of products [eq. (5)].

$$Os_3(CO)_{12} + DMAD \xrightarrow[\text{benzene, RT}]{h\nu > 370\,nm}$$

$$Os_2(CO)_8(\mu\text{-}\eta^1,\eta^1\text{-DMAD}) \quad \textbf{4–Os}$$

$$+ Os_2(CO)_6(DMAD)_4 + C_6(CO_2CH_3)_6 \quad \textbf{5–Os}$$

$$+ \text{unidentified compound(s).} \qquad (5)$$

Because of separation difficulties only two osmium containing products could be isolated, in low yields.[19] Compound **4–Os** is the desired 1,2-diosmacyclobutene, Fig. 3. As expected from the more rigid parallel alkyne bridge, the four membered ring in **4–Os** is less puckered than in the saturated relatives, the Os—C and C—C distances are also in accord with the unsaturated nature of **4–Os**. Not surprisingly, the compound is also more stable than the diosmacyclobutanes and undergoes thermal CO substitution by PPh_3, as opposed to alkene loss from and fragmentation of the saturated four membered Os_2C_2 rings.[12] Interestingly, and perhaps as a result of the enhanced stability of the unsaturated dimetallacyclobutenes, the analogous diruthenacyclobutene, **4–Ru**, is also accessible from the photoreaction between $Ru_3(CO)_{12}$ and DMAD [eq. (6)].[20] The compounds **4–Os** and **4–Ru** are isomorphous and isostructural.

$$Ru_3(CO)_{12} + DMAD \xrightarrow[\text{pentane, RT}]{h\nu > 370\,nm}$$

$$Ru_2(CO)_8(\mu\text{-}\eta^1,\eta^1\text{-DMAD}) \quad \textbf{4–Ru}$$

$$+ Ru_2(CO)_6(DMAD)_4 + C_6(CO_2CH_3)_6. \quad \textbf{5a–Ru, 5b–Ru} \qquad (6)$$

As with osmium, this reaction is accompanied by the formation of another product, **5–Ru**. Indeed, in this case the material is present under two isomeric forms, **5a–Ru** and **5b–Ru**. Spectroscopic work showed that the osmium compound corresponds to isomer **5a**.

The structures of the osmium compound, **5a–Os**, and the isomeric **5b–Ru** are shown in Fig. 4. The compounds are seen to arise from what can be considered "head-to-tail", **5a** and "head-to-head", **5b**, dimerization of the 16 electron metallacyclopentadiene, $M(CO)_3[C_4(CO_2CH_3)_4]$, [eq. (7)].

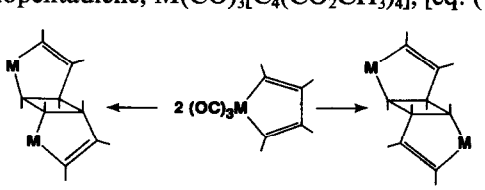

(7)

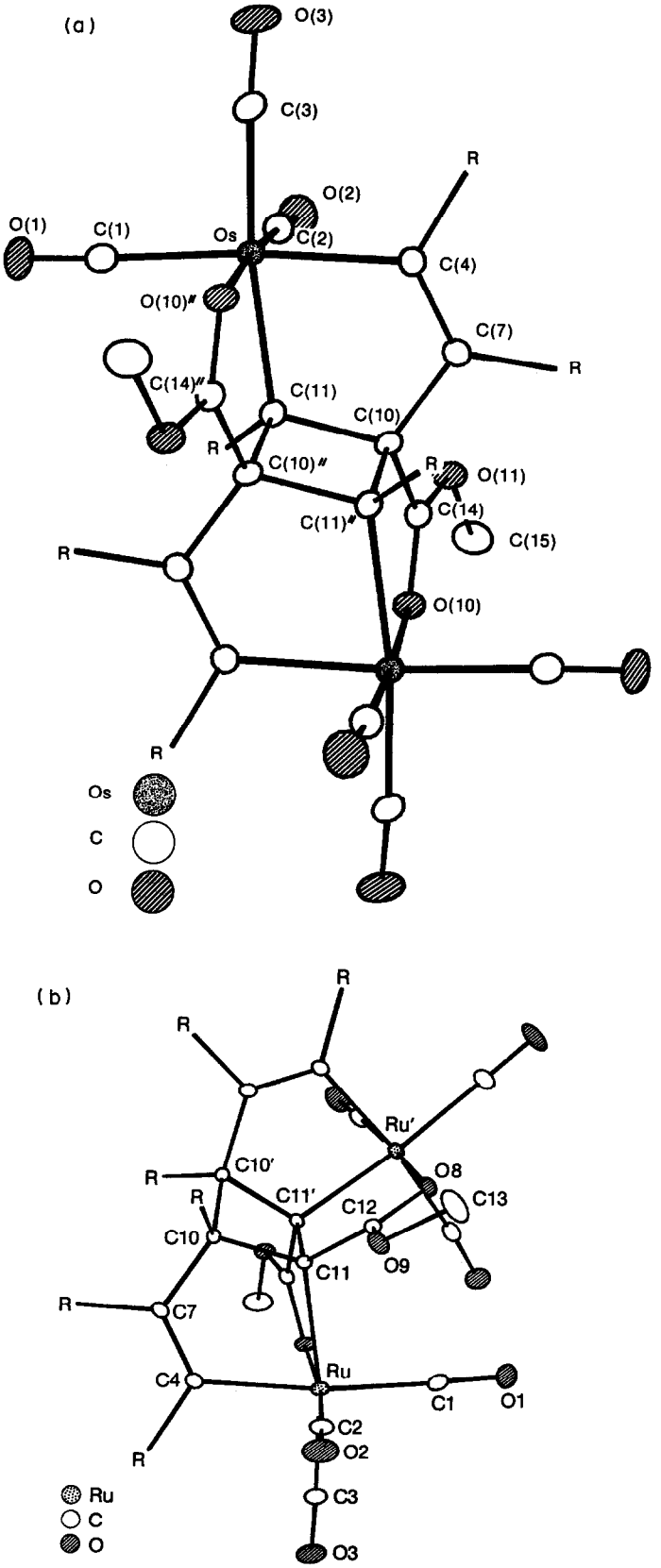

Fig. 4. Perspective views of (a) $Os_2(CO)_6(DMAD)_4$,[19] **5a–Os** and (b) $Ru_2(CO)_6(DMAD)_4$,[20] **5b–Ru**. Primed atoms are related by the centre of symmetry and the C_2 axis of symmetry, respectively. R represents the CO_2CH_3 group.

End-on coordination of a carboxylate oxygen donor completes the electronic demand of each metal. This is clearly evidenced by the lengthening of the C=O distance (~ 1.25 vs 1.19 Å for the unbound moieties) and the appearance of a low frequency C=O stretching frequency absorption around 1600 cm^{-1}. The coupling of the alkyne units is thus different from the usual sequential addition of one to four alkyne units to dimetallic centres.[3(a),(c)] It is noteworthy that from a thermal reaction Bruce *et al.*[21] identified two ruthenium containing compounds, $Ru_3(CO)_7(DMAD)_4$ and $Ru_2(CO)_6(DMAD)_2$, both different from the photoproducts described here.

The photoreaction of **1–Os** was also carried out with bis(trimethylsilyl)acetylene (BTMSA), hexafluorobut-2-yne (HFB), diphenylacetylene (DPA) and acetylene. Although the reaction with BTMSA led to the isolation of the first simple tetracarbonyl alkyne osmium compound,[22] $Os(CO)_4(\eta^2$-BTMSA) and paved the way for the preparation of the analogous ruthenium compound,[22] the other alkynes gave disappointing results. The reactions led to complicated and difficult to separate mixtures of products, many accessible from thermal reactions. Diosmacyclobutenes were seen with HFB and DPA, but isolated yields were exceedingly small.

ALKENE EXCHANGE IN $Os_2(CO)_8(\mu$-η^1,η^1-$CH_2CHR)$ (R = CO_2CH_3, H)

The problems encountered already in the photoreaction of $Os_3(CO)_{12}$ with certain alkenes and even more extensively with alkynes, clearly indicated the necessity of an alternate synthetic route if we hoped to extend the number of known diosmacycles. Since, naively, we envisaged the formation of $Os_2(CO)_8(\mu$-$C_2H_4)$, **3a**, as arising from the interception of nascent $Os_2(CO)_8$ by ethylene, it seemed plausible that reversal of this process, [eq. (8)], could yield the reactive diosmium fragment which could then be scavenged by other unsaturated organic substrates giving other diosmacycles.

(8)

The attractive feature of such an approach was the ready availability of **3a** in moderate yields (see above).

Although from the isolobal relation between **3a** and cyclobutane,[23] fragmentation of **3a**, as shown in eq. (8), is a symmetry forbidden process,† Trinquier and Hoffman[24] have shown that the activation barrier to such a dinuclear reductive elimination process is significantly lowered when the leaving groups are tied together, as in **3a**. Indeed, anticipating some of the results, elimination of ethylene from **3a** is facile and in solution occurs already at around 30°C, albeit slowly. More surprisingly, some recent very elegant experiments by Norton[25] have established that the elimination is stereospecific and as such, contrary to the symmetry rules, most probably proceeds via a concerted process.

Exchange reactions with alkynes

The initial experiment between $Os_2(CO)_8(\mu$-η^1,η^1-$CH_2CHCO_2CH_3)$ **3b**, and DMAD was encouraging. Although a temperature of 80°C was required to give convenient conversion rates, a yield of 47% of the diosmacyclobutene, **4–Os**, was obtained.[19]‡ However, the high temperature necessary for exchange was deleterious with other alkynes and consequently contemporary exchange reactions involve **3a** [eq. (9)].[27]

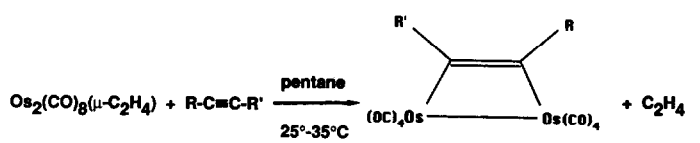

(9)

R	R′	Yield (%)
CO_2Me	CO_2Me	50 (68§)
Ph	Ph	20 (32§)
H	COMe	70
H	CO_2Me	70
CF_3	CF_3	5–20

It should be noted that the thermal exchange reaction can also be used to prepare saturated diosmacyclobutanes which are more robust than **3a** and/or **3b**. Heating **3b** with excess maleic anhydride

† The forward reaction, or further reaction of $Os_2(CO)_8$ with double or triple bonds is also a symmetry forbidden thermal process. It is the organometallic analogue of the organic $[2\pi_s+2\pi_s]$ cycloaddition reaction.

‡ For the use of DMAD as a trapping agent in a related dimetalla-Diels–Alder reaction ($[4\pi_s+2\pi_s]$ cycloaddition) involving the six-membered benzodicobaltacyclohexane ring, $Cp_2Co_2(\mu$-$CO)_2(\mu$-*o*-xylylene), see Hersch and Bergman.[26]

§ The yields in parentheses refer to photochemical exchange reaction.

gave $Os_2(CO)_8(\mu\text{-}\eta^1,\eta^1\text{-}CHCHC(O)OC(O)$ in 54% isolated yield. This material, as indicated before, is not accessible via photolysis.

The improved yield of **4–Os** and the isolation of the DPA and HFB bridged compounds in quantities sufficient for full characterization, clearly indicate the superiority of the thermal exchange method over the photolysis of $Os_3(CO)_{12}$ and alkynes. Unfortunately the procedure is not universal in its application. Already the reaction with DPA is accompanied by the formation of other products including $Os_3(CO)_{12}$, a ubiquitous by-product in many reactions. Similar problems have been encountered with acetylene and HFB. Indeed the parent diosmacyclobutene, $Os_2(CO)_8(\mu\text{-}\eta^1,\eta^1\text{-}HCCH)$, has so far defied isolation. Also puzzling is the reaction with HFB which also gave mixtures of products. That the problem is not associated with some peculiar property of the product diosmacyclobutene, $Os_2(CO)_8(\mu\text{-}\eta^1,\eta^1\text{-}HFB)$, is evidenced by an interesting and unusual alternate synthesis which can be extended to the RuRu and mixed RuOs compounds as well. In a very interesting development we have discovered that the 18 electron $M(CO)_4(\eta^2\text{-}HFB)$ (M = Ru, Os) complexes react further with the respective pentacarbonyls to produce dimetallacyclobutenes in good yields [eq. (10)].[28] No solid state structural work is yet available, but the proper formulation of the compounds was ascertained by spectroscopic techniques, the ^{13}C NMR spectra being especially valuable.

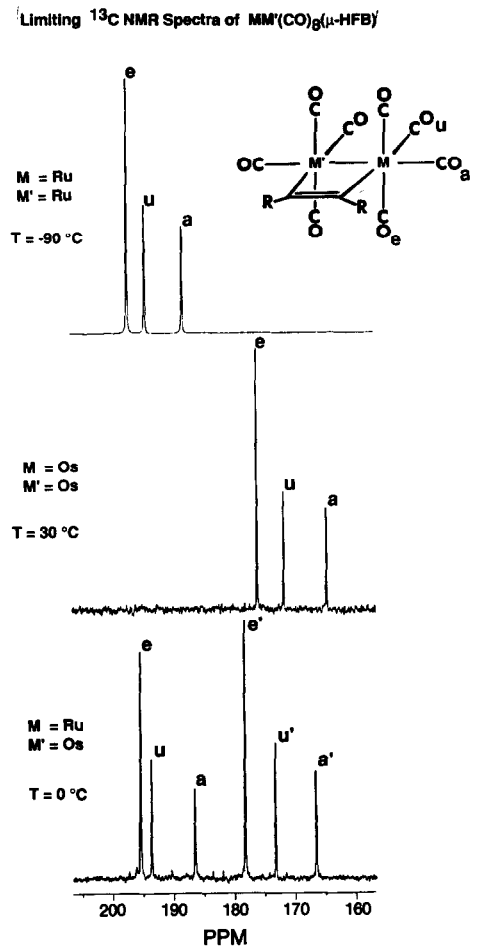

Fig. 5. Limiting ^{13}C NMR spectra of $MM'(CO)_8(\mu\text{-}\eta^1,\eta^1\text{-}HFB)$ molecules.[28]

$$M(CO)_4(\eta^2\text{-}HFB) + M'(CO)_5 \xrightarrow[\text{alkane}]{\Delta} MM'(CO)_8(\mu\text{-}\eta^1,\eta^1\text{-}HFB) \quad (10)$$

			△	Yield
M = Ru	M′ = Ru	MM′ = RuRu	25°C	73%
Os	Os	OsOs	60°C	66%
Ru	Os	RuOs	25°C	77%

The limiting spectra are shown in Fig. 5. The number and intensity distribution of the peaks are clearly consistent with the proposed structures. The spectra provide a nice illustration of the predictable upfield shifts of the carbonyl signals as the metal triad is descended.[29] With the exception of the OsOs compound, which is rigid at room temperature, the molecules are fluxional. The intermetallic carbonyl exchange proceeds most plausibly via the "merry-go-round" process[30] which exchanges the environments of carbonyl groups lying in a plane, leaving one, the unique CO *trans* to the parallel alkyne bridge, invariant. The activation energy for interchange follows RuRu (11.0 kcal mol^{-1}) < RuOs (14.4 kcal mol^{-1}) < OsOs (static at room temperature).

Exchange reactions with dienes

The thermal reaction between **3a** and 1,3-dienes was initiated with the hope of producing diosmacycles with different ring sizes. Indeed as shown in eq. (11), the reaction in principle can proceed via 1,2- and/or 1,4-addition, yielding four-and six-membered diosmacycles, respectively. Although the 1,2-type addition with **3a** is now firmly established, in view of the precedented dimetalla-Diels–Alder type reaction,[26] the 1,4-addition can not be dismissed lightly.

The reaction between **3a** and diethylmuconate (MUCO) gave $Os_2(CO)_8(MUCO)$ in good yield.[31] The complex ^{13}C NMR spectrum, Fig. 6, clearly implies the formation of a 1,2-adduct. Trace amounts of an isomeric product were also isolated from this reaction which may be the symmetric 1,4-

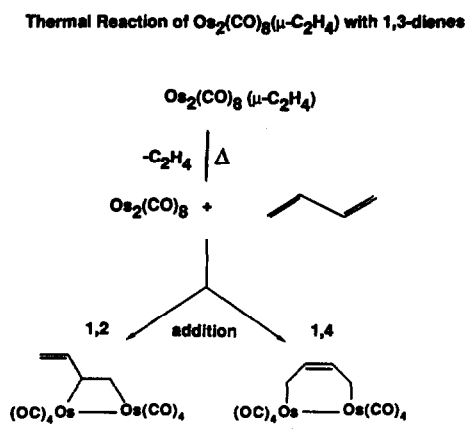

(11)

adduct. Efforts are underway to identify appropriate reaction conditions to favour the Diels–Alder path. Similar 1,2-addition occurred with two heterodienes,[31] Table 1. The reaction with the diazadiene ligand gave the aza-diosmacyclobutane $Os_2(CO)_8(\mu\text{-}\eta^1,\eta^1\text{-Gpi})$, in 35% isolated yield (^{13}C NMR spectrum, Fig. 7) and represents a new type of bonding of this ligand system on dimetallic centres.[32] The reaction with *trans*-benzalacetone gave only a single, *trans* adduct and as such represents an interesting example of regio- and stereospecific 1,2-addition. Thus, although our initial goal of preparing diosmacycles with a larger ring size has been temporarily aborted, the prospect of obtaining diosmacycles with different heteroatoms and functional groups for further derivatization is nevertheless encouraging.

It would be less than candid to close this section by giving the impression that the thermal exchange reactions are not without difficulties. Problems were encountered especially with "unactivated" dienes. In an effort to promote the 1,4-addition, the reactions with cyclopentadiene (CpH), 2,3-dimethyl-1,3-butadiene (DMBU) and 2-trimethylsiloxy-1,3-butadiene (TSBU) were carried out. No reaction was observed with CpH. The reaction with DMBU gave mostly $Os_3(CO)_{12}$ and a small amount of $Os(CO)_3(\eta^4\text{-DMBU})$, whereas with TSBU a very slow 1,2-addition to the unsubstituted double bond occurred.[31] Believing that at least part of the difficulties are associated with the thermal fragility of the newly formed diosmacycles, current efforts are centred on the photochemically induced ethylene exchange from **3a**.

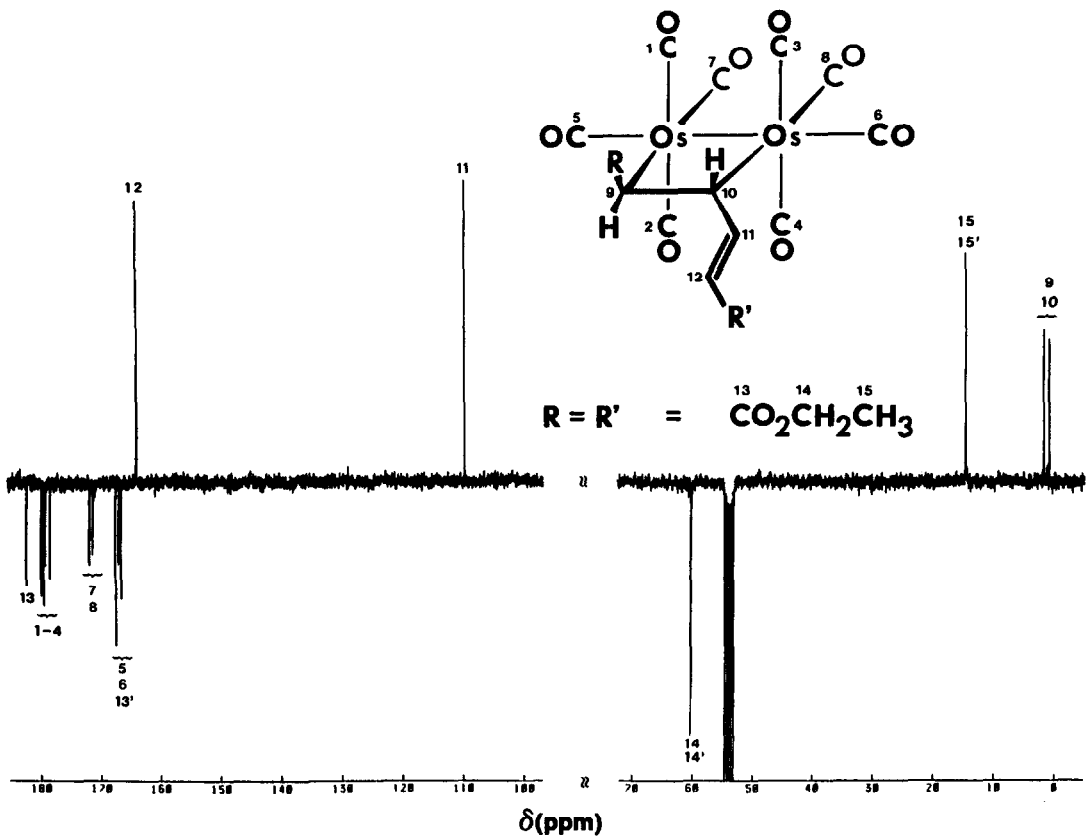

Fig. 6. APT ^{13}C NMR spectrum of $Os_2(CO)_8(\mu\text{-}\eta^1,\eta^1\text{-diethylmuconate})$.[31]

Table 1. Thermal reaction of $Os_2(CO)_8(\mu\text{-}C_2H_4)$ with "dienes"

Diene		Product(s)	Addition
(1)	(MUCO)	$Os_2(CO)_8(\mu\text{-MUCO})$	1,2 (C,C)
(2)	(GpI)	$Os_2(CO)_8(\mu\text{-GpI})$	1,2 (C,N)
(3)	(BEAC)	$Os_2(CO)_8(\mu\text{-BEAC})$	1,2 (C,C)

REACTIVITY OF THE DIOSMACYCLOBUTANES: HYDRIDE ABSTRACTION FROM $Os_2(CO)_8(\mu\text{-}C_2H_4)$

An important aspect of the chemistry of dimetallacyclic compounds is the thesis that such molecules may serve as useful models for the surface transformations of unsaturated organic substrates. As a first test of hydrogen mobility, hydride abstraction from $Os_2(CO)_8(\mu\text{-}C_2H_4)$, **3a**, was investigated. The reaction of **3a** with Ph_3CBF_4 proceeded readily and gave the $\mu\text{-}\eta^1,\eta^2$-vinyl complex **6** in excellent yield [eq. (12)].[33]

$$\mathbf{3a} + Ph_3CBF_4 \xrightarrow[4RT]{CH_2Cl_2} [Os_2(CO)_8(\mu\text{-}\eta^1,\eta^2\text{-}C_2H_3)]BF_4 \quad (12)$$

6 (92%)

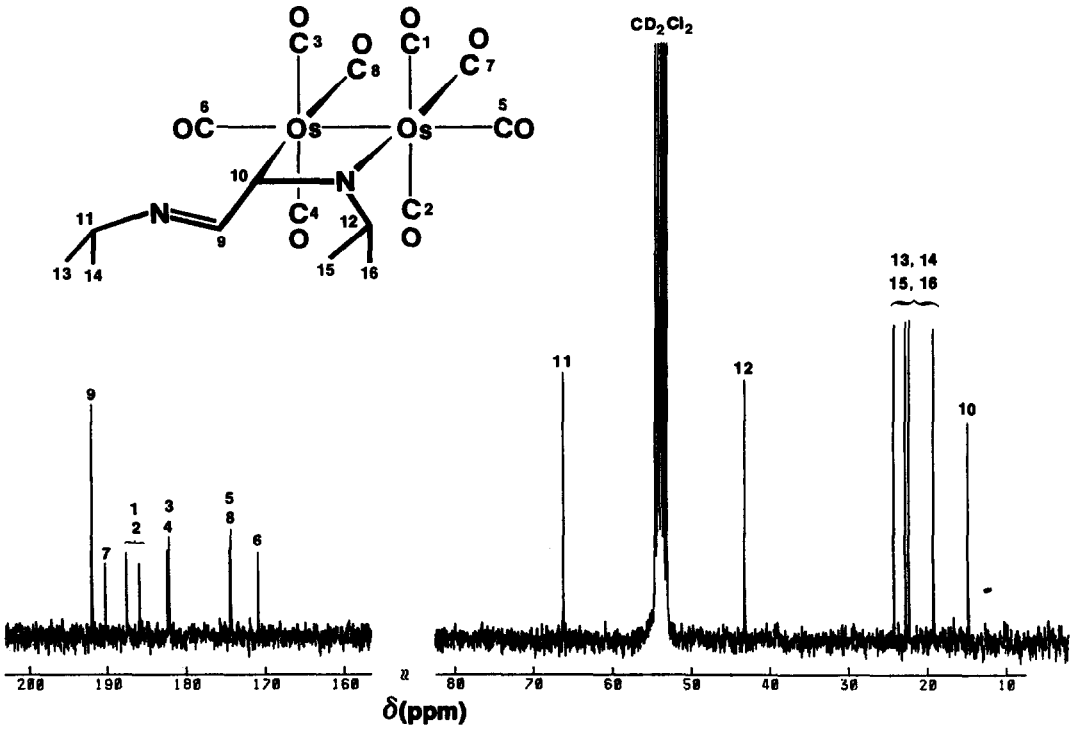

Fig. 7. ^{13}C NMR spectrum of $Os_2(CO)_8(\mu\text{-}\eta^1,\eta^1\text{-C-glyoxalbis(isopropylimine)})$.[31]

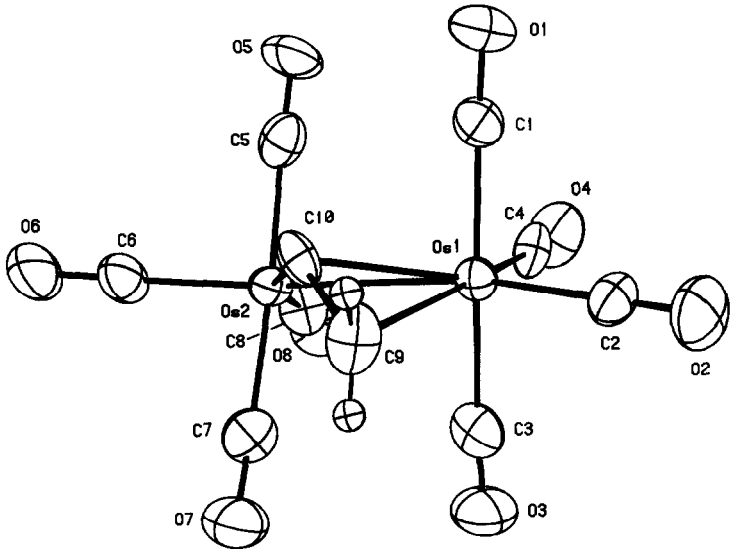

Fig. 8. Molecular structure of $Os_2(CO)_8(\mu\text{-}\eta^1,\eta^2\text{-}CHCH_2)^+$, **6**.[33] Relevant bond distances (Å): Os(1)—Os(2) = 2.8569(5), Os(2)—C(10) = 2.061(9), Os(1)—C(10) = 2.30(1), Os(1)—C(9) = 2.34(1), C(9)—C(10) = 1.41(2).

The structure of **6** is shown in Fig. 8. A characteristic feature of the μ-CH moiety in related vinyl bridged cationic species is the μ-carbenoid nature of this group, which is reflected in the low field NMR position of the μ-CH carbon and hydrogen atoms[34] and the nearly symmetrical metal–carbon distances.[35] This type of behaviour is manifested in the present complex as well, although perhaps to a more limited extent. Indeed the μ-CH (δ = 8.56 ppm) and μ-CH (δ = 134.9 ppm) resonance positions are at higher, whereas the CH_2 signal (δ = 64.8 ppm) is at lower field than expected. Also, the Os(2)—C(10) interaction, 2.06(1) Å is significantly shorter than the Os(1)—C(10), 2.30(1) Å distance, indicative of a greater contribution from σ,π-vinyl type bonding in this compound.† Interestingly the bonding changes appear to have a noticeable effect on both physical and chemical properties of **6**. Thus, contrary to other μ-η^1,η^2-vinyl complexes which are fluxional in solution,[34,37] **6** remains rigid up to 90°C Also, as opposed to the normal behaviour of the related compounds which undergo hydride addition to the β-carbon of the μ-vinyl group and generate μ-carbene complexes,[34] hydride attack on **6** initially occurs at the α-carbon and regenerates the original 1,2-diosmacyclobutane, **3a**.

Attempts to deprotonate **6** proved unsuccessful. Even hindered bases like KO^{t}Bu and DBU acted as nucleophiles and $NaN(SiMe_3)_2$ led to decomposition. The reaction with PMe_3 gave a single product. The ^{13}C NMR features at −21.2 ppm (d, J_{P-C} = 25.9 Hz, $CHPMe_3$) and −28.6 ppm (d, J_{P-C} = 8.3 Hz, CH_2), clearly show the formation of a substituted 1,2-diosmacyclobutane [eq. (13)].

$$\mathbf{6} + PMe_3 \xrightarrow[RT]{\text{acetone}} [Os_2(CO)_8(\mu\text{-}\eta^1,\eta^1\text{-}CH_2CHPMe_3]BF_4. \quad (13)$$

CONCLUSION

A serendipitous discovery led to the synthesis of a modest number of saturated 1,2-diosmacyclobutanes. The hope that the simple photochemical route could be extended and would allow the preparation of a wide range of diosmacyclic compounds proved short lived. This resulted in a search for a more rational synthesis of such compounds. Although not without problems, the thermally and/or photochemically induced ethylene exchange reaction from $Os_2(CO)_8(\mu\text{-}\eta^1,\eta^1\text{-}C_2H_4)$ has already proved useful in this regard. The scope of this reaction and the chemistry of the derived diosmacycles is of continuing interest to us.‡

† A more pronounced distortion of the bridging vinyl group in $W_2Cl_3(NMe_2)_2(CHCH_2)(PMe_2Ph)_2$, led Chisholm[36] to postulate a tendency towards "terminal" metal–carbene type interaction of the CH moiety in this compound.

‡ The utility of $Os_2(CO)_9$ as a source of $Os_2(CO)_8$ for reactions with unsaturated substrates is being explored by J. R. Norton and his co-workers, personal communication.

Acknowledgements—I would like to thank NSERC (Canada) and the University of Alberta for generous financial support. The work described here would not have been possible without the dedication and hard work of my able co-workers whose names are listed in the references. I would especially like to acknowledge the fruitful collaboration and stimulating exchange of ideas with Dr F. W. Grevels of M.P.I. für Strahlenchemie, Mülheim, FRG.

REFERENCES

1. Two recent reviews deal with the chemistry of hydrocarbon-bridged dinuclear transition metal complexes. (a) C. P. Casey and J. D. Audett, *Chem. Rev.* 1986, **86**, 339; (b) J. R. Moss and L. G. Scott, *Coord. Chem. Rev.* 1984, **60**, 171.
2. W. A. Hermann, *J. Organomet. Chem.* 1983, **250**, 319; W. A. Herman *Adv. Organomet. Chem.* 1982, **20**, 159.
3. (a) M. D. Curtis, *Polyhedron* 1987, **6**, 759; (b) M. Chisholm, B. K. Conroy, B. W. Eichhorn, K. Falting, D. M. Hoffman, J. C. Huffman and N. S. Marchant, *Polyhedron* 1987, **6**, 783; (c) S. A. R. Knox, *Pure Appl. Chem.* 1984, **56**, 81; (d) R. S. Dickson, G. D. Fallon, S. M. Jenkins and R. J. Nesbit, *Organometallics* 1987, **6**, 1240.
4. For a delightful account of the origin of the word "serendipity" and its place in science see P. Laszlo, *Nou. J. Chimie* 1983, **7**, 675.
5. F.-W. Grevels, J. G. A. Reuvers and J. Takats, *J. Am. Chem. Soc.* 1981, **103**, 4069.
6. B. F. G. Johnson, J. Lewis and M. V. Twigg, *J. Chem. Soc., Dalton Trans* 1975, 1876.
7. D. R. Taylor, M. Altobelli and H. B. Gray, *J. Am. Chem. Soc.* 1980, **102**, 3022.
8. J. G. Bensten and M. S. Wrighton, *J. Am. Chem. Soc.* 1987, **109**, 4518.
9. M. R. Burke, J. Takats, F.-W. Grevels and J. G. A. Reuvers, *J. Am. Chem. Soc.* 1983, **105**, 4092.
10. K. M. Motyl, J. R. Norton, C. K. Schauer and O. P. Anderson, *J. Am. Chem. Soc.* 1982, **104**, 7325.
11. F.-W. Grevels, J. R. Norton, J. Takats *et al.*, *Inorg. Synth.*, to be submitted.
12. M. R. Burke, Ph.D. thesis, University of Alberta, Edmonton (1987).
13. A. J. Poë amd C. V. Sekhar, *J. Am. Chem. Soc.* 1986, **108**, 3673.
14. Ph. Vioget, M. Bonivento, R. Roulet and P. Vogel, *Helv. Chim. Acta* 1984, **67**, 1630.
15. J. R. Norton, personal communication of unpublished results.
16. (a) J. Malito, S. Markiewicz and A. J. Poë, *Inorg. Chem.* 1982, **21**, 4335; (b) M. F. Desrosiers, D. A. Wink, R. Trautman, A. E. Friedman and P. C. Ford, *J. Am. Chem. Soc.* 1986, **108**, 1917; (c) J. G. Bensten and M. S. Wrighton, *J. Am. Chem. Soc.* 1987, **109**, 4530.
17. P. R. Raithby and M. J. Rosales, *Adv. Inorg. Chem. Radiochem.* 1985, **29**, 169.
18. D. M. Hoffman, R. Hoffmann and C. A. Friesel, *J. Am. Chem. Soc.* 1982, **104**, 3858.
19. M. R. Burke and J. Takats, *J. Organomet. Chem.* 1986, **302**, C25.
20. R. G. Ball, M. R. Gagné and J. Takats, to be submitted.
21. M. I. Bruce, J. G. Matisons, B. W. Skelton and A. H. White, *J. Organomet. Chem.* 1983, **251**, 249.
22. R. G. Ball, M. R. Burke and J. Takats, *Organometallics* 1987, **6**, 1918.
23. (a) R. Hoffmann, *Angew. Chem. Int. Ed. Engl.* 1982, **21**, 711; (b) T. A. Albright, J. K. Burdett and M.-H. Whangbo, *Orbital Interactions in Chemistry*. Wiley-Interscience, New York (1985).
24. G. Trinquier and R. Hoffmann, *Organometallics* 1984, **3**, 370.
25. R. T. Hembre, C. P. Scott and J. R. Norton, *J. Am. Chem. Soc.* 1987, **109**, 3468.
26. W. H. Hersch and R. G. Bergman, *J. Am. Chem. Soc.* 1983, **105**, 5846.
27. M. R. Burke, F. Seils and J. Takats, to be submitted.
28. M. R. Gagné and J. Takats, *Organometallics*, in press.
29. B. E. Mann and B. F. Taylor, ^{13}C *NMR Data for Organometallic Compounds*. Academic Press, New York (1981).
30. E. Bond and E. Muetterties, *Chem. Rev.* 1978, **28**, 639.
31. F. Seils and J. Takats, unpublished results.
32. G. van Koten and K. Vrieze, *Adv. Organomet. Chem.* 1982, **21**, 151.
33. F.-W. Grevels, W. A. Kiel and J. Takats, unpublished results.
34. (a) A. F. Dyke, S. A. R. Knox, M. J. Morris and P. J. Naish, *J. Chem. Soc., Dalton Trans.* 1983, 1417; (b) C. P. Casey, S. R. Marder and B. R. Adams, *J. Am. Chem. Soc.* 1985, **107**, 7700.
35. A. G. Orpen, *J. Chem. Soc., Dalton Trans.* 1983, 1427 and refs therein.
36. K. J. Ahmed, M. H. Chisholm, K. Folting and J. C. H. Hoffmann, *J. Am. Chem. Soc.* 1986, **108**, 989.
37. J. R. Shapley, S. I. Richter, M. Tachikawa and J. B. Keister, *J. Organomet. Chem.* 1975, **95**, C43.

Note added in proof. The parent diosmacyclobutene, $Os_2(CO)_8(\mu\text{-}\eta^1,\eta^1\text{-}C_2H_2)$, has since been isolated and characterized. Seen in the exchange reactions between **3a** and acetylene, the cleanest preparation so far discovered involves self condensation of $Os(CO)_4(\eta^2\text{-}C_2H_2)$; G.-Y. Kiel, F. Seils and J. Takats, unpublished results.

Polyhedron Vol. 7, No. 10/11, pp. 943–954, 1988
Printed in Great Britain

0277–5387/88 $3.00+.00
© 1988 Pergamon Press plc

ELECTRONIC STRUCTURE OF PIANO-STOOL DIMERS—VII. INTERRELATIONSHIPS AMONG THE ELECTRONIC STRUCTURE, REACTIVITY AND CONFORMATIONAL PREFERENCES OF HYDROCARBYL-BRIDGED PIANO-STOOL DIMERS†

BRUCE E. BURSTEN‡ and ROGER H. CAYTON

Department of Chemistry, The Ohio State University, Columbus, OH 43210, U.S.A.

(*Accepted* 5 *November* 1987)

Abstract—The electronic structure of a number of hydrocarbyl-bridged piano-stool dimers has been calculated by using the non-empirical Fenske–Hall molecular orbital method. It is shown that there is a close connection between a number of electronic structural factors (e.g. the number of available metal-based orbitals, the number and energies of available orbitals on the hydrocarbyl bridge, and the electronic competition between the hydrocarbyl bridge and the ancillary ligands) and the reactivities and conformational preferences of the dimers. Examples are chosen from both low-valent dimers with π-acid ancillary ligands and high-valent dimers with predominantly σ-donor ligands.

Piano-stool dimer frameworks [species adhering to the general formula $[CpM]_2L_n$, $(Cp = \eta^5\text{-}C_5H_5)$] provide, in many cases, a convenient template for the coordination and experimental manipulation of a number of hydrocarbyl moieties. The synthetic versatility afforded by these species has fueled the recent development of a rich and diverse chemistry within this area. The electronic structure and bonding of complexes comprising this class are equally diverse and are quite dependent upon the number and type of ligands L, nature of the transition metal M, as well as the various geometries assumed. We have previously demonstrated a close relationship between the electronic structure of piano-stool dimers and their reaction chemistry and geometric preferences.[1,2] In this contribution, we will examine several of the electronically-driven properties of hydrocarbyl-bridged piano-stool dimers. We will also make an effort to delineate those characteristics imparted to the dimers by the hydrocarbyl bridges, and to draw comparisons between low-valent and high-valent systems.

Before detailing our molecular orbital approach into the electronic structure of specific hydrocarbyl-bridged systems, it will be beneficial to illustrate the derivation of the orbitals of a piano-stool dimer for a general case. Because of the multitude of geometries observed for this class we have neither the time nor space for an in-depth analysis of each here. Therefore, in light of this restriction, we will focus on a specific geometry keeping in mind that similar derivations are possible for the other structure types.

The piano-stool dimer framework, $[CpML]_2(\mu\text{-}L)_2$, is a very common structure type in this class and is assumed by nearly all of the $Cp_2M_2L_4$ systems. The structure of the *cis* isomer is shown below. The geometry about each metal centre resembles that of a three-legged piano-stool (hence the term piano-stool dimer) (see Structure 1). There

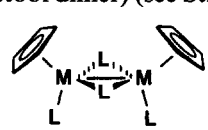

Structure 1.

have been a number of theoretical treatments applied to compounds adhering to this basic structure;[2,3] we have, however, developed a method which we have found to be particularly useful in elucidating the separate σ and π effects of various

† For part VI see ref. 1.

‡ Author to whom correspondence should be addressed. Camille and Henry Dreyfus Foundation Teacher–Scholar (1984–1989) and Fellow of the Alfred P. Sloan Foundation (1985–1987).

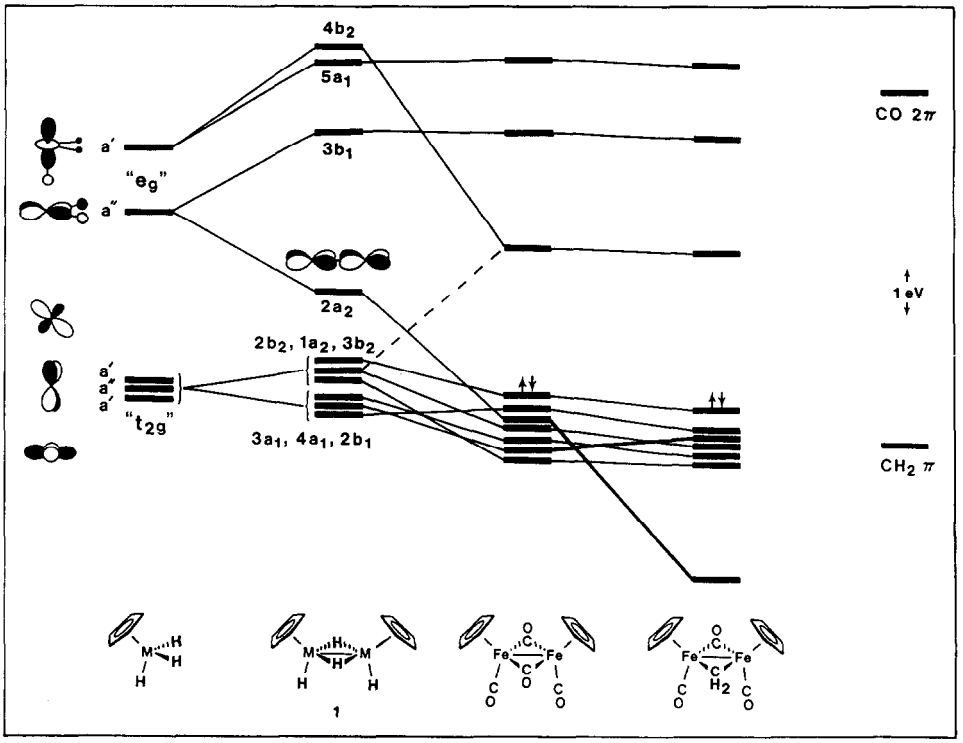

Fig. 1. MO diagram illustrating the derivation of the orbitals of the piano-stool dimers $[CpFe(CO)]_2(\mu\text{-}CO)_2$ and $[CpFe(CO)]_2(\mu\text{-}CO)(\mu\text{-}CH_2)$ from those of $[CpMH]_2(\mu\text{-}H)_2$.

ligands, L. First the appropriate "σ-only" framework is constructed using L = H, followed by "turning on" the π-effects by substituting H with the ligand under investigation.† Figure 1 depicts the frontier orbitals of the σ-only framework $[CpMH]_2(\mu\text{-}H)_2$, **1**, as calculated by the Fenske–Hall method (calculational details are provided in the Appendix). Since the metal centres of **1** are in a three-legged piano-stool environment, the orbitals of **1** are correlated to the orbitals of the appropriate monomeric piano-stool hydride. The metal-based orbitals of three-legged piano-stool complexes are well-known,[4] and are illustrated on the left of Fig. 1. As is the case for other $CpML_3$ complexes, the $CpMH_3$ species can be treated as a pseudo-octahedral system by virtue of its *fac*-MH_3 "legs". As a result, its metal-based orbitals are split into two groups resembling the O_h t_{2g} and e_g sets. The "t_{2g}" set is composed of three metal-based non-bonding orbitals, whereas the "e_g" set contains two orbitals that are antibonding between M and both the H 1*s* and the Cp π_2 orbitals. The similarity of these orbitals to the t_{2g} and e_g sets of an O_h ML_6 compound illustrates how $CpML_3$ species "remember" their O_h parentage.

Inasmuch as the structure of **1** keeps the metal centres in a pseudo-octahedral environment, its metal-based orbitals can be viewed as resulting from dimerization of the orbitals of $CpML_3$. The MO's of **1** that are derived from the "t_{2g}" orbitals are split slightly (< 1.0 eV for M = Fe), a splitting that is due entirely to a very weak M—M interaction. Those derived from the "e_g" orbitals are uniformly destabilized with the exception of the $2a_2$ orbital, which is substantially stabilized. The $2a_2$ is a M—M π^* orbital that, due to the generation of a nodal plane bisecting the M—M vector upon dimerization, cannot by symmetry contain any μ-H character. It is thus converted from a M—H antibonding orbital into a non-bonded one, and therefore ends up close in energy to the "t_{2g}"-based orbitals.

The simple picture derived for the σ-only framework, **1**, can be used as a basis for the subsequent consideration of the electronic structure of more complicated piano-stool dimer systems of this same basic geometry. The H ligands can be replaced by π-acid or π-donor ligands of varying strength and the metal-based frontier orbitals may be followed as they are stabilized or destabilized accordingly.

† A more detailed derivation by this method is outlined for $Cp_2M_2L_4$ complexes in ref. 2e and for $Cp_2M_2L_6$ complexes in ref. 1.

In this way a qualitative picture of a seemingly complicated bimetallic system can be constructed with relative ease. We have included the case for the well-known dimer, $[CpFe(CO)]_2(\mu\text{-}CO)_2$,† to the right of **1** in Fig. 1. The π-acid CO ligands serve to stabilize the metal-based orbitals with which they are allowed to interact. We could just have easily replaced the H ligands of **1** with O ligands to form the known compound, $[CpMoO]_2(\mu\text{-}O)_2$,[6] and followed the subsequent destabilization of the metal-based orbitals due to the π-donor ability of O. We need not concern ourselves with the CO or O σ interactions as they have been qualitatively accounted for by the σ-only H ligands in framework **1**. The σ-donor strengths of various ligands will, of course, differ from that of H, but the orbitals resulting from such interactions generally do not lie in the important frontier orbital region. Thus, for most qualitative applications (such as those to be presented here) it is not essential to modify the M—L σ interactions. With mixed ligand sets (as is the case for most hydrocarbyl-bridged piano-stool dimers) the competitive π-effects (and, to a lesser extent, σ-effects) become more complicated; nevertheless, they may be conveniently accounted for using this approach. The methylene-bridged system, $[CpFe(CO)]_2(\mu\text{-}CO)(\mu\text{-}CH_2)$, **3**, is provided to the right of $[CpFe(CO)]_2(\mu\text{-}CO)_2$ in Fig. 1 as an example. The π-effects associated with the substitution of a CO bridge with a CH_2 bridge are minor and can easily be traced. As shown in Fig. 1, the CH_2 ligand possesses just one π orbital (in contrast to the degenerate 2π set in CO) that is closer in energy, and hence interacts more strongly with a metal-based orbital (the $2a_2$ orbital in framework **1**). The lack of a second π orbital for CH_2 causes a slight destabilization of one metal-based orbital (the orbital that had previously been stabilized by CO interaction). The remainder of the MO picture changes little. While it is true that some subtle electronic effects can only be discerned via MO calculations, the approach outlined above can often go a long way in developing a qualitative understanding of the electronic structure of many piano-stool dimers. Such a treatment can be viewed in the same spirit as Hoffmann's isolobal analogy, which provides simple qualitative descriptions of mononuclear fragments.[7]

With regard to correlation of the calculational results to the experimental observations, we have found that the Fenske–Hall MO method provides reliable results when applied to hydrocarbyl-bridged transition metal dimers.[2] We will begin our discussion with an examination of electronic structural effects on the reactions of simple electrophiles and nucleophiles with hydrocarbyl-bridged dimers. Several guidelines must be kept in mind when using MO theory to explain chemical reactivity: (1) The electronic structure of a *reactant* provides information concerning possible sites of reactivity, or the *kinetic* product of a reaction. (2) In order to obtain information pertaining to the *thermodynamic* product, one must consider the electronic structures of the possible *products* of the reaction in question. (3) We will be considering only reactions which proceed via *orbital* control or *charge* control. (4) For reactions which are orbitally-controlled, the HOMO will direct an *electrophilic* attack, and the LUMO will direct a *nucleophilic* attack.

PROTONATION OF μ-CH_2 COMPLEXES

The simplest electrophile is the proton. It has been shown that the treatment of a series of closely related methylene-bridged piano-stool dimers with strong acids yields a variety of results [eqs. (1)–(3)]. For example, Herrmann found that protonation of the complex $[CpMn(CO)_2]_2(\mu\text{-}CH_2)$, **2**, resulted in no apparent reactivity [eq. (1)].[8] However, Casey *et al.* showed that treatment of $[CpFe(CO)]_2(\mu\text{-}CO)(\mu\text{-}CH_2)$, **3**, with strong, non-coordinating acids resulted in the formation of an agostic, methyl-bridged cation [eq. (2)].[9] Herrmann *et al.* noted yet a different type of reactivity by moving farther across the periodic table to $[CpRh(CO)]_2(\mu\text{-}CH_2)$, **4**, and upon protonation of this dimer observed the formation of a hydride-bridged cation [eq. (3)].[10] The potential driving forces behind such diverse reactivity can be uncovered via the electronic structures of the parent methylene-bridged dimers.

Figure 2 illustrates the frontier MO diagrams of the methylene-bridged compounds **2**, **3** and **4′** (**4′** is the Co analogue of the Rh complex **4**).‡ A comparison of the three electronic structures allows us to highlight several features. First, the highest occupied

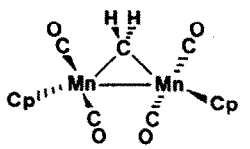

2

$\xrightarrow{H^+}$ N.R. (1)

† The crystal structure of *cis*-$[CpFe(CO)]_2(\mu\text{-}CO)_2$ has been reported.[5] The electronic structure has been investigated by a number of methods.[2(c)–(e),3(a)–(d)]

‡ The Co analogue was used to model the Rh complex (**4**) in order to provide a more direct comparison to the other two methylene-bridged compounds containing first row transition metals, Mn and Fe. Calculations on the Rh complex yield similar results.

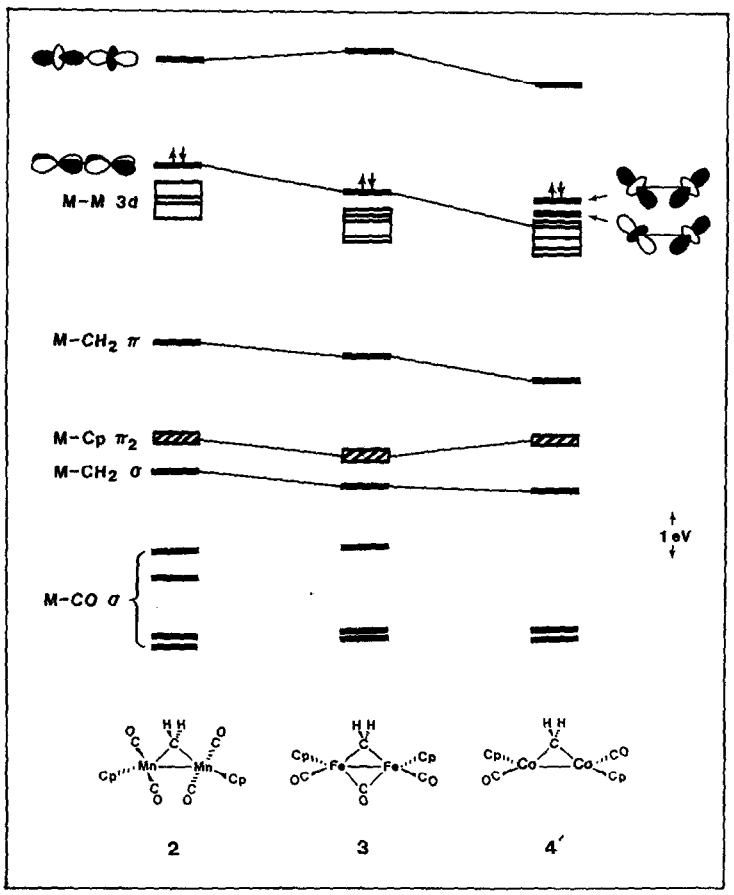

Fig. 2. Comparative MO diagrams of the methylene-bridged compounds **2**, **3**, and **4'**. The arrows indicate the highest occupied MO.

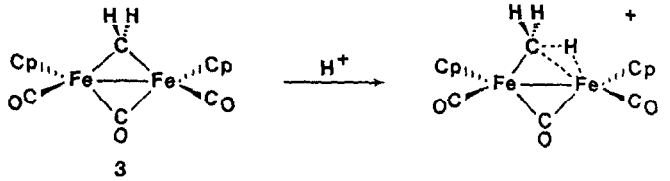

(2)

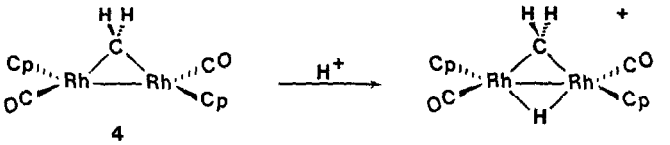

(3)

molecular orbitals are primarily metal-based 3*d* orbitals that are, for the most part, metal–ligand non-bonding. For **2**, this group is comprised of five such orbitals, including the HOMO which is Mn–Mn π^* in character.[11] The HOMO of **3** is similar to that found for **2** (Fe—Fe π^*). However, since **3** contains only three CO ligands, an additional metal-based orbital is present in its group of now six occupied metal orbitals; it has one less metal-based orbital "removed" by M—L σ-interactions. In **4'**, which has one less CO ligand than **3**, there are now seven metal-based 3*d* orbitals in the -8 to -10 eV region. In addition, the removal of a μ-CO on proceeding from **3** to **4'** markedly changes the nature of the HOMO and second-highest occupied MO (SHOMO) of **4'** relative to those of **2** or **3**. The two highest occupied MO's are the symmetric and antisymmetric (with respect to the C_2 axis) linear

combinations of hybrid orbitals directed toward the vacant bridge position.† In **3**, which is geometrically very similar to **4'**, the orbitals that are the analogues of the HOMO and SHOMO of **4'** are strongly destabilized and (less strongly) stabilized, respectively, via interaction with the 5σ and one of the 2π orbitals of the μ-CO ligand.

The LUMO of each dimer is essentially a M—M σ^* interaction that is isolated by, in each case, > 2.5 eV from the next lowest virtual orbitals. The HOMO–LUMO separation calculated from each compound is similar: **2** = 2.20, **3** = 2.95, **4'** = 2.42 eV. The occupied orbitals below the metal-based sets are arranged in a similar pattern for all three dimers. Highest in energy is the M—CH_2 π-type interaction, with the M—Cp π_2 orbitals at slightly lower energy. Below the Cp orbitals are found the M—CH_2 and M—CO σ interactions.

As was mentioned earlier, the electronic structure of a reactant provides information on the site of attack, or kinetic product of a reaction. Thus for compounds **2**, **3** and **4'**, we will primarily be interested in the nature of the HOMO for an electrophilic, orbital-controlled reaction and the Mulliken atomic charges for the case of a charge-controlled reaction. Considering first the two reactions which yield products [eqs (2) and (3)], we can identify the electronic effects which lead to their formation. The HOMO of **3** is an Fe—Fe π^* orbital which is oriented perpendicular to the bridge plane, causing it to lie in the plane of the Cp ligands and the terminal CO ligands. Therefore the HOMO is sterically inaccessible to incoming electrophiles, which would appear to retard an orbital-controlled reaction pathway. If the reaction were to be charge-controlled, the electrophile would seek out the most negative site on the complex. In the case of **3**, the most negative site is the methylene carbon ($q_c = -0.52$ e, see Table 1). Hence it would appear that the charge-controlled pathway is more favourable in the protonation of **3**, thereby inducing protonation at the methylene carbon.‡ The observed product is indeed a methyl-bridged cation which displays some interesting electronic interactions and fluxional behaviour in its own right.[2b]

The formation of the hydride-bridged cation from the protonation of **4** can also be rationalized with the aid of its electronic structure. As with **3**, the most negative site calculated for **4'** is the methylene carbon atom. In fact, the μ-CH_2 carbon of **4'** is even more negative ($q_c = -0.63$ e) than that of **3**, indicating even greater charge transfer from the metal atoms to the methylene bridge. This would seem to indicate that a charge-controlled protonation of the μ-CH_2 bridge of **4** would constitute a viable reaction pathway. Although we cannot rule out the charge-controlled route, in this case an orbital-controlled mechanism appears just as likely. In the MO diagram of **4'** (Fig. 2) the HOMO was calculated to be a symmetric M—M bonding interaction oriented towards the "open" bridging position, thereby providing a sterically accessible, filled orbital for electrophilic attack. The protonation product exhibits a hydride-bridged metal–metal bond wherein the proton interacts with the HOMO of **4'**. Although it is impossible to say which kinetic pathway (charge-controlled or orbital-controlled) is utilized initially in the protonation of **4**, it is clear that the character and availability of the HOMO facilitates the formation of the observed thermodynamic product.

Table 1. Mulliken atomic charges in $[CpMn(CO)_2]_2$ (μ-CH_2) (**2**), $[CpFe(CO)]_2(\mu$-CO)(μ-CH_2) (**3**) and $[CpCo(CO)]_2(\mu$-CH_2) (**4'**)

	2	**3**	**4'**
M	+0.49	+0.39	+0.59
C(μ-CH_2)	−0.53	−0.52	−0.63
C(μ-CO)	—	−0.02	—
O(μ-CO)	—	−0.20	—
C(t-CO)	+0.05[a]	+0.11	+0.01
O(μ-CO)	−0.08[a]	−0.06	0.00

[a] Average charge of atoms for the two t-COs.

The lack of reactivity found for the Mn dimer **2** is not as clear. Based on the electronic properties operating in the reactions of the Fe and Rh dimers, we would predict that **2** would react in a manner similar to **3**. From Fig. 2 we find that the HOMO of **2** is a Mn—Mn π^* orbital and is rendered sterically inaccessible by the Cp and CO ligands. Like dimers **3** and **4'**, the methylene carbon of **2** is calculated to be the most negative site ($q_c = -0.53$ e). Therefore we would expect **2** to follow a protonation pathway similar to the Fe dimer **3** to yield a methyl-bridged cation. Calculations performed on a methyl-bridged manganese dimer indicate that, like $[CpFe(CO)]_2(\mu$-CO)(μ-$CH_3)^+$, an asymmetric methyl bridge would be favoured over a symmetric bridging structure.[13] However, the calculations also show that the stabilization gained from an asymmetric methyl bridge in the iron system is greater

† Similar frontier orbitals were found by P. Hofmann using the EHMO approach.[12]

‡ It is possible that a sterically-accessible, filled orbital below the HOMO could direct an orbitally-controlled mechanism, and such a possibility has been previously addressed in ref. 3d.

than that of the manganese species, and although a charge-controlled protonation of **2** at the μ-CH_2 carbon is predicted kinetically, it may be that the relative thermodynamic instability of the product impedes its formation and isolation.

NUCLEOPHILIC ATTACK OF μ-CH COMPLEXES

It has been established that a number of nucleophilic addition reactions on transition metal complexes are directed by their LUMO.[14] We have found such to be the case for two isovalent methylidyne-bridged piano-stool dimers, namely $[CpFe(CO)]_2(\mu\text{-}CO)(\mu\text{-}CH)^+$, **5**[9] and $[CpFe(\mu\text{-}NO)]_2(\mu\text{-}CH)^+$, **6**.[15] Both complexes contain the bridging methylidyne unit; **5** contains three CO groups whereas **6** contains two NO ligands. As is evident in eqs (4) and (5), these two compounds demonstrate markedly different reactivity with nucleophiles.

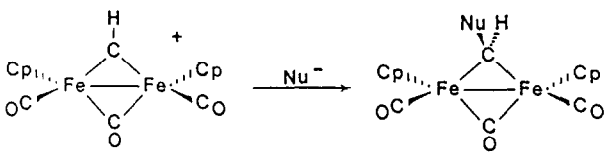

5 (4)

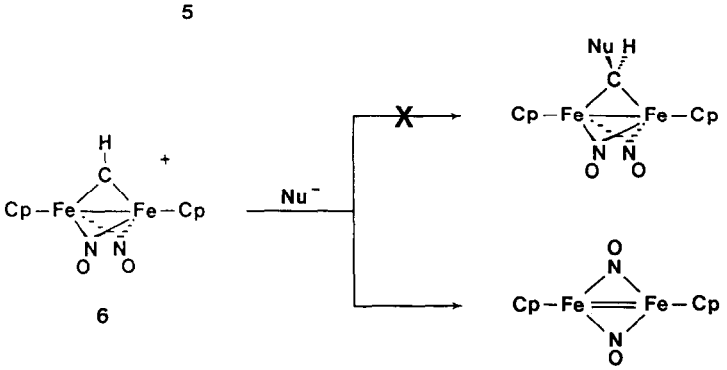

6 (5)

Compound **5** readily forms adducts with a wide variety of nucleophiles, attack occurring in all cases at the methylidyne carbon.[16] Even very weak nucleophiles such as CO and alkenes have been shown to react. In contrast, the treatment of **6** with nucleophiles produces no adducts comparable to those of **5**, and the complex apparently decomposes to yield $[CpFe(\mu\text{-}NO)]_2$ as the only tractable organometallic product.[15] The site specificity of nucleophilic attack on **5**, as well as the lack of nucleophilic addition observed for **6**, can be explained on the basis of their electronic structures.

The MO diagrams of **5** and **6** are shown in Fig. 3. The occupied MO's of these two methylidyne-bridged piano-stool dimers are similar to one another. Once again, the highest occupied MO's in each complex are a set of primarily metal-based 3*d* orbitals. As before, the presence of one fewer NO ligand in **6** than there are CO ligands in **5** results in the generation of one more metal-based orbital in **6** than in **5**. Below these are the Fe—CH π-bonding interactions in which the denotations $\perp$ and $\parallel$ refer to the orientation of the CH π orbitals as either perpendicular or parallel to the Fe—Fe vector. Just below these orbitals are found the Cp π_2 bonding levels, with the Fe—CH σ interaction at still lower energy. The major difference that exists between the electronic structures of **5** and **6** is due to the virtual orbitals. The LUMO of **5** is the Fe—CH $\pi_\perp$ antibonding level, 50% of which is due to contribution from the μ-CH carbon 2*p* orbital. Just above this orbital in energy lies the Fe—Fe σ^* interaction. The virtual orbitals of **6** are exactly reversed. The LUMO is the Fe—Fe σ^* interaction and above this orbital lies the Fe—CH $\pi_\perp$ antibonding level. Therefore, as long as nucleophilic addition reactions are orbitally-controlled in this system, the LUMO of **5** offers a sterically accessible orbital containing a high degree of μ-CH character. Hence the electronic structure would support nucleophilic attack at the μ-CH carbon atom of **5**. On the other hand, the LUMO of **6** is quite sterically inaccessible as it lies along the Fe—Fe vector and between the Cp ligands. In this case nucleophilic additions are retarded from occurring at the LUMO, and compound **6** does not form analogous products.

We would not expect a charge-controlled mechanism to operate in the nucleophilic addition reactions of these systems since the most positive sites on both **5** and **6** are the metal centres, and there is no evidence for attack at these sterically congested sites.

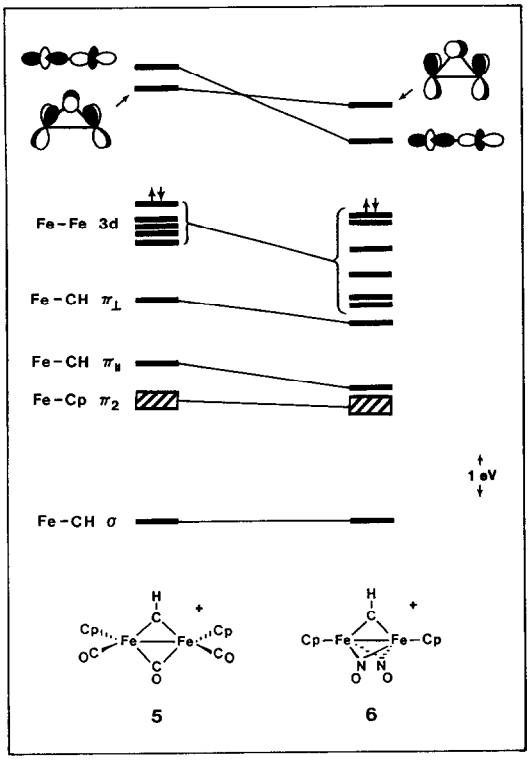

Fig. 3. Comparative MO diagrams of the methylidyne-bridged compounds **5** and **6**. The arrows indicate the highest occupied MO.

CONFORMATIONAL PREFERENCES IN μ-CH COMPLEXES

Thus far we have utilized MO theory to analyse certain reactivity patterns exhibited by a few hydrocarbyl-bridged systems. In doing so we have concentrated on the electronic structure of the reactants involved in order to elucidate the possible sites of reactivity. In this section we utilize the MO calculations to determine geometric preferences in similar hydrocarbyl-bridged systems.

We will focus our attention on two alkylidyne-bridged molecules, $[CpFe(\mu\text{-}NO)]_2(\mu\text{-}CH)^+$, **6** and $[Cp^*W(CH_3)]_2(\mu\text{-}CCH_3)$, **7** ($Cp^* = \eta^5\text{-}C_5Me_5$).[17] In the previous section we have already briefly addressed the reactivity of **6** with nucleophiles. Complex **6** was prepared from the reaction of its methylene-bridged parent compound, $[CpFe(NO)]_2(\mu\text{-}CH_2)$, **8**, with the trityl cation [eq. (6)].[15] IR spectroscopic monitoring of eq. (6) indicated that the NO ligands changed from terminal coordination in **8** to a bridging mode in **6**. The reason for the bridging NO preference in **6** can be explained through a fragment analysis of the possible limiting geometries for this complex.

Figure 4 displays the MO diagrams for the bridging NO isomer, **6** and the terminal NO isomer, $[CpFe(NO)]_2(\mu\text{-}CH)^+$, **9**. Fragment analysis is used to view each isomer as a CH^+ moiety interacting with its respective $Cp_2Fe_2(NO)_2$ framework. Through such an analysis we can isolate the electronic driving force responsible for the geometric preference of isomer **6** over isomer **9**. The CH^+ 2σ orbital (the carbon-based "lone pair") interacts to about the same extent with either $Cp_2Fe_2(NO)_2$ framework. The CH^+ $1\pi_\parallel$ interactions are also similar with both frameworks, in either case involving the C_2 ($Cp_2Fe_2(NO)_2$) or mirror-plane ($Cp_2Fe_2(NO)_2$) antisymmetric metal-based orbitals (17*b* and 18*b* in **9**; $8b_1$ and $9b_1$ in **6**). At first glance, the interactions of the CH^+ $1\pi_\perp$ orbital with the two frameworks look very similar; however, it is the nature of the framework orbital with which the $1\pi_\perp$ can interact that determines the fate of the NO ligation mode. In the terminal NO geometry (left side), the 16*b* framework orbital interacts with the CH $1\pi_\perp$ orbital. The 16*b* orbital is 56% Fe and 42% NO 2π in character, and thus the CH $1\pi_\perp$ orbital is involved in competition with a substantial amount of NO 2π character for the same metal orbital. In the bridging NO geometry (right side) the $8b_2$ framework orbital interacts with the CH $1\pi_\perp$ orbital. The $8b_2$ orbital is 81% Fe and only 16% NO 2π in character. Hence, the CH $1\pi_\perp$ orbital is competing with much less NO 2π character for the same metal orbital than in the terminal NO geometry. Accordingly, the CH^+ fragment displays a stronger interaction with the metal centres when the NO ligands are in a bridging geometry, thus achieving a better separation of Fe—CH and Fe—NO π interactions. For ligands that lack a $\pi_\perp$ orbital (such as CH_2) the electronic preference for bridging NO ligands would be removed. That this is the case is seen, of course, in the observed geometry of **8**.[14]

All of the systems we have thus far looked at are low-valent systems with π-acid ancillary ligands. Many of the same types of arguments can be used

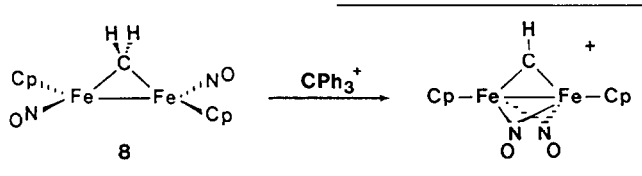

(6)

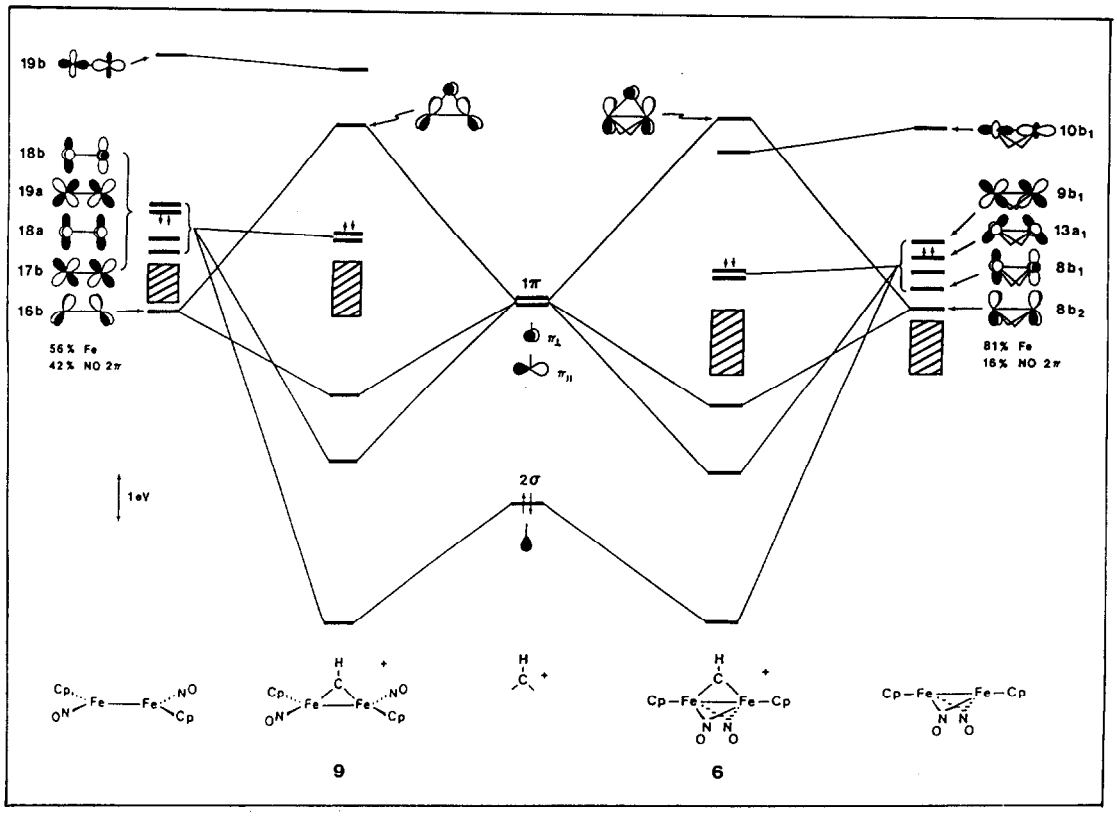

Fig. 4. The orbital interaction diagram for $Cp_2Fe_2(NO)_2(\mu\text{-}CH)^+$ in conformations **6** and **9**. The arrows indicate the highest occupied MO.

for high-valent hydrocarbyl-bridged dimers as well. Recently Schrock and co-workers synthesized and structurally characterized an interesting bis-alkylidyne-bridged piano-stool dimer of the formulation $[Cp^*W(CH_3)]_2(\mu\text{-}CCH_3)_2$, **7**.[17] This complex can formally be considered as a 1,3-dimetallacyclobutadiene and is structurally and electronically (*vide infra*) analogous to a variety of such compounds of the formulation $[WX_2]_2(\mu\text{-}CSiMe_3)_2$ (X = OR, R), recently investigated by Chisholm and Heppert.[18] The Schrock dimetallacycle, **7**, can be considered a derivative of the Chisholm alkyl system wherein one terminal alkyl ligand on each tungsten atom has been replaced by a Cp* ligand. The structure of **7** differs from those of Chisholm in one significant regard, however. Unlike the Chisholm systems, the $W_2(\mu\text{-}CR)_2$ dimetallacyclic core of **7** is decidely non-planar (as shown below) with the μ-CR ligands bent up towards the Cp* ligands (dihedral angle = 155°) (see Structure 2). Such a structural perturbation would seem sterically unfavourable in that the μ-CMe ligands are closer to the bulky C_5Me_5 ligands than they would be in a planar structure. A bent core would also seem to be unfavourable electronically, in a qualitative sense, due to the apparent weakening of the conjugated π system.†

Structure 2.

Since it is clear that the structural deformation in **7** must be electronic in origin, we have investigated its source via MO calculations on the model piano-stool dimer $[CpW(CH_3)]_2(\mu\text{-}CH)_2$ (**7′**). We will derive the MO scheme for **7′** in the same manner as was outlined earlier for the case of a general piano-stool dimer of the structure type $[CpML]_2(\mu\text{-}L)_2$. In this way we can separate the σ and π effects of the ligands in order to explain the geometric preference for a bent W_2C_2 core. The left side of Fig. 5 shows the MO diagram of the σ-only framework for the fictitious $[CpW(CH_3)]_2(\mu\text{-}H)_2$. The orbital energetics of this framework are similar to those shown earlier for the general $[CpMH]_2(\mu\text{-}H)_2$ system. This is not surprising considering the structural simi-

† A full paper describing the electronic structure of **7** in detail, and its relationship to other 1,3-dimetallacyclobutadiene systems is in preparation.

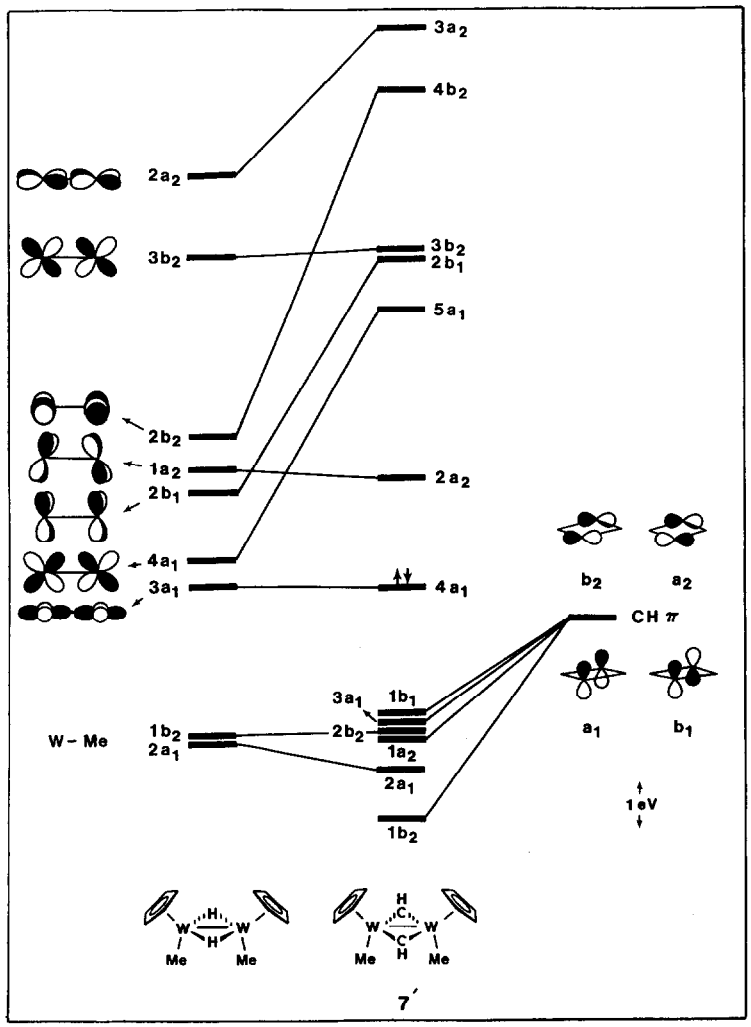

Fig. 5. Frontier orbital diagram of 7′ and its correlation to the σ-only framework $[CpWMe]_2(\mu\text{-}H)_2$. The arrows indicate the highest occupied MO.

larities and that CH_3 is predominantly a σ donor like H. The metal-based orbitals begin with the $3a_1$ orbital. The three highest lying "e_g" orbitals are not shown here since they are not subsequently affected by CH π interaction. It should be noted that the splitting within the "t_{2g}" set is somewhat greater than with the $[CpMH]_2(\mu\text{-}H)_2$ framework (M = Fe), indicating a stronger W—W interaction. The shape of the $2b_2$ orbital warrants some comment. Simple dimerization of the orbitals of the "t_{2g}" set from $CpMH_3$ (Fig. 1) would result in the generation of an orbital similar in shape to the $3a_1$ orbital, but M—M antibonding in character. However, an allowed mixing of this antibonding orbital with a higher energy b_2 combination takes place to produce the $2b_2$ orbital (see Scheme 1) shown in Fig. 5. This serves to decrease the W—W anti-bonding character among the filled MOs, thus facilitating stronger overall W—W bonding.

When the μ-H ligands are replaced by μ-CH ligands, the π interactions are "turned on". The resulting frontier MO diagram is shown in the centre of Fig. 5, in which a planar W_2C_2 core has been assumed, along with its correlation to the orbitals of the σ-only framework. The π orbitals of the two CH ligands transform as $a_1+a_2+b_1+b_2$ representations under C_{2v} symmetry, and they find symmetry matches with four appropriate W-based orbitals. This results in the generation of four W—CH π bonding MOs that are predominantly of CH character with corresponding antibonding orbitals that are mostly metal-based. Above the manifold of π bonding orbitals is the HOMO of the complex, the metal-based bonding $4a_1$ orbital that,

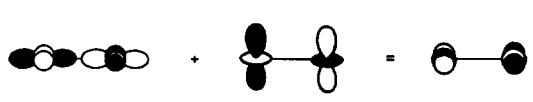

Scheme 1.

by symmetry, cannot interact with CH π orbitals. The LUMO is a W—W orbital of approximate δ^* symmetry (see discussion below) that similarly is unable to interact with CH π orbitals of the bridging ligands. This MO description is in complete accord with that recently advanced by Chisholm *et al.* for the $M_2R_4(\mu\text{-}CR')_2$ (M = Ta, W, Re) systems.[19]

Why does **7** contain a bent rather than a planar W_2C_2 core? The introduction of two *cis* Cp* ligands destroys the W_2C_2 mirror plane symmetry found in the Chisholm systems and allows for the generation of slightly asymmetric frontier orbitals. The driving force behind the bending of the W_2C_2 core lies in the W—CH π interactions. The CH π combinations corresponding to a_1, b_1 and b_2 symmetry each find W-based orbitals of the correct symmetry located rather low in energy, close to that of the CH π orbitals. However, the CH a_2 combination must interact with a W-based a_2 orbital ($2a_2$ in the σ-only framework) which is quite high in energy. Another W-based a_2 orbital matches-up much better energetically (the $1a_2$ in the σ-only framework), but in a planar geometry this orbital has zero overlap and cannot interact with the CH a_2 combination. As is evident in Fig. 5, the $1a_2$ orbital of $[CpW(CH_3)]_2(\mu\text{-}H)_2$ is mostly W—W δ^*, but there is a small mixing of W—W π^* interaction as well. This leads to a "tipping" of the orbitals such that they point towards the "Cp* side" of the W_2H_2 core. Bending the μ-CH ligands up towards the Cp ligands allows the CH a_2 set to overlap with this low-energy W-based a_2 orbital and provides an overall greater interaction. Also, such an interaction destabilizes the $2a_2$ orbital of **7'**, thus causing an increase in the HOMO–LUMO separation, which may also contribute to its stability.† Although bending the W_2C_2 core does increase the a_2 interaction, it is done at the expense of the W—CH a_1 and b_1 interactions. Hence, at some point in the distortion from planarity, the stabilization gained from a more favourable a_2 interaction will be offset by weakening the other π interactions. This is most easily seen in the Walsh diagram in Fig. 6. Figure 6(a) depicts the fate of the frontier orbitals of **7'** upon decreasing the dihedral angle ϕ from 180 (planar) to 100°. The orbitals most affected are the W—CH a_2 π-bonding orbital ($1a_2$), which is stabilized as ϕ decreases, and its antibonding counterpart ($2a_2$, LUMO), which is destabilized accordingly. When ϕ becomes < 130°, the W—CH b_1 interaction ($2b_1$) begins to rise very

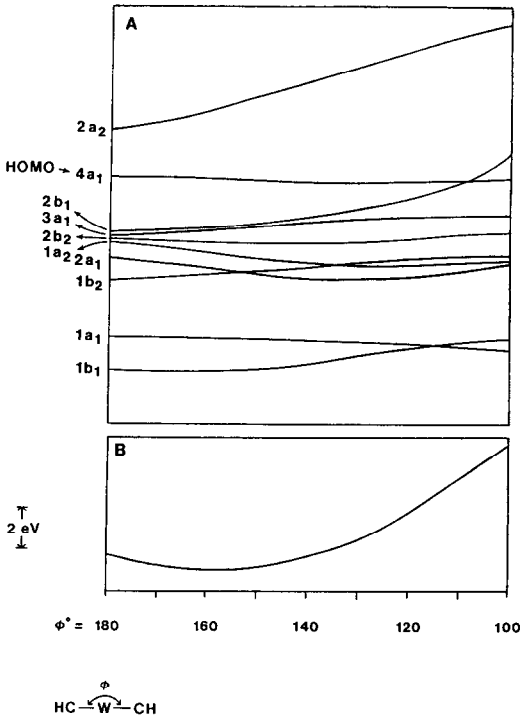

Fig. 6. (A) Walsh diagram for the variation of the dihedral angle ϕ for **7'**. (B) Energy profile for the variation of ϕ in **7'**.

quickly in energy. This is due to a C—C antibonding interaction that begins to dominate this orbital when the distance between the CH ligands is lessened. Figure 6(b) shows the summation of the orbital energies for the filled orbitals included in the Walsh diagram of Fig. 6(a). This includes the μ-CH σ and π interactions, the CH_3 σ interactions and the W—W σ interaction. The Cp orbitals are not affected by this structural perturbation and therefore are not shown. The energy decreases down to $\phi \approx 155°$ due to the more favourable a_2 interaction, then rises rapidly as the $2b_1$ orbital begins to dominate the picture. If the sum of orbital energies is used as an approximate total energy, then the calculations indicate that a bent core with $\phi = 155°$ is 15.5 Kcal mol^{-1} lower in energy than the planar geometry.

It is interesting that **7** prefers a *cis* Cp* arrangement rather than the sterically less hindered *trans* conformation. Similar calculations performed on the *trans*-**7'** isomer indicate it to be 11.8 Kcal mol^{-1} *more* stable than the planar *cis*-**7'** geometry, but still 3.7 Kcal mol^{-1} *less* stable than *cis*-**7'** with a bent W_2C_2 core. In contrast to the *cis* isomer, bending the W_2C_2 core in *trans*-**7'** does not lead to a lower energy geometry. This is due primarily to the lack of stabilization in its a_2-type interaction upon bending. The $2a_u$ orbital is the low-energy, W-based orbital

† Chisholm *et al.* found that substituting X = OR for X = R in $[WX_2]_2(\mu\text{-}CSiMe_3)_2$ caused a similar increase in the HOMO–LUMO separation as well as resulting in more stable complexes.[19]

of *trans*-**7′** that is comparable to the $2a_2$ orbital of *cis*-**7′**. As in *cis*-**7′**, the Cp rings in *trans*-**7′** induce a tipping of the metal-based orbitals such that the $2a_u$ is no longer pure W—W δ^*. As shown in Structure 3, however, the *trans* arrangement of the Cp ligands dictates that the orbitals rotate in a "conrotary" fashion. As a result, the $2a_u$ orbital of *trans*-**7′** is less effective at interacting with "bent" CR ligands than was the $2a_2$ orbital of *cis*-**7′**.

$2a_2$ $2a_u$

cis - 7′ trans - 7′

Structure 3.

We can use the Walsh diagram of Fig. 6 to offer predictions concerning the core geometries of the unknown d^0–d^0 and d^2–d^2 dimetallacycles, *cis*-$[CpM(R)]_2(\mu\text{-}CR')_2$ (M = Ta, Re). The Ta system would have two less electrons than **7′** and these would be removed from the $4a_1$ HOMO. This orbital is energetically invariant to the bending of the core and thus the Ta complex should display a geometry similar to that of **7′**, i.e. it should contain a puckered Ta_2C_2 cycle. The Re system, on the other hand, contains two more electrons than **7′** and these would occupy the $2a_2$ LUMO of **7′**. This would remove the motivation for a bent M_2C_2 core inasmuch as the $2a_2$ orbital rises rapidly as the system is made non-planar. Thus we would expect *cis*-$[CpRe(R)]_2(\mu\text{-}CR')_2$ to have a planar (or nearly so) Re_2C_2 core. We look forward to the experimental testing of these predictions.

REFERENCES

1. B. E. Bursten and R. H. Cayton, *Organometallics*, in press.
2. (a) J. P. Blaha, B. E. Bursten, J. C. Dewan, R. B. Frankel, C. L. Randolph, B. A. Wilson and M. S. Wrighton, *J. Am. Chem. Soc.* 1985, **107**, 4561; (b) B. E. Bursten and R. H. Cayton, *Organometallics* 1986, **5**, 1051; (c) B. E. Bursten and R. H. Cayton, *J. Am. Chem. Soc.* 1986, **108**, 8241; (d) B. E. Bursten and R. H. Cayton, *J. Am. Chem. Soc.* 1987, **109**, 6053; (e) B. E. Bursten, R. H. Cayton and M. G. Gatter, *Organometallics*, in press.
3. (a) E. D. Jemmis, A. R. Pinhas and R. Hoffmann, *J. Am. Chem. Soc.* 1980, **102**, 2576; (b) M. Benard, *Inorg. Chem.* 1979, **18**, 2782; (c) M. Benard, *J. Am. Chem. Soc.* 1978, **100**, 7740; (d) G. Granozzi, E. Tondello, M. Benard and I. Fragala, *J. Organomet. Chem.* 1980, **194**, 83.
4. (a) B. E. R. Schilling, R. Hoffmann and D. L. Lichtenberger, *J. Am. Chem. Soc.* 1979, **101**, 585; (b) D. L. Lichtenberger and R. F. Fenske, *J. Organomet. Chem.* 1976, **117**, 253; (c) D. L. Lichtenberger and R. F. Fenske, *J. Am. Chem. Soc.* 1976, **98**, 50; (d) T. A. Albright, P. Hofmann and R. Hoffmann, *J. Am. Chem. Soc.* 1977, **99**, 7546 and refs therein.
5. R. F. Bryan, P. T. Greene, M. J. Newlands and D. S. Field, *J. Chem. Soc.* (*A*) 1970, 3068.
6. Preparation: M. Cousins and M. L. H. Green, *J. Chem. Soc.* 1964, 1567; M. Cousins and M. L. H. Green, *J. Chem. Soc.* (*A*) 1969, 16; M. J. Bunker and M. L. H. Green, *J. Chem. Soc., Dalton Trans.* 1981, 847; M. J. Bunker, A. DeCian and M. L. H. Green *J. Chem. Soc., Chem. Commun.* 1977, 59. Crystal structure: C. Couldwell and K. Prout, *Acta. Cryst.* 1978, **B34**, 933; Crystal structure for the C_5Me_5 derivative: H. Arzoumanian, A. Baldy, M. Picrrot and J.-F. Petrignani, *J. Organomet. Chem.* 1985, **294**, 327.
7. R. Hoffmann, *Science* 1981, **211**, 995.
8. W. A. Herrmann, *Adv. Organomet. Chem.* 1982, **20**, 159.
9. C. P. Casey, P. J. Fagan and W. H. Miles, *J. Am. Chem. Soc.* 1982, **104**, 1134.
10. W. A. Herrmann, J. Plank, D. Riedel, M. L. Ziegler, K. Weidenhammer, E. Guggolz and B. Bulbach, *J. Am. Chem. Soc.* 1981, **103**, 63.
11. Lichtenberger *et al.* obtained similar results also via the Fenske–Hall method: D. C. Calabro, D. L. Lichtenberger and W. A. Herrmann, *J. Am. Chem. Soc.* 1981, **103**, 6852.
12. P. Hofmann, *Angew. Chem. Int. Ed. Engl.* 1979, **18**, 544.
13. B. E. Bursten and R. H. Cayton, unpublished results.
14. See, for example, T. F. Block, R. F. Fenske and C. P. Casey, *J. Am. Chem. Soc.* 1976, **98**, 441.
15. C. P. Casey and D. M. Roddick, *Organometallics* 1986, **5**, 436.
16. (a) C. P. Casey and P. J. Fagan, *J. Am. Chem. Soc.* 1982, **104**, 4950; (b) C. P. Casey, P. J. Fagan and V. W. Day, *J. Am. Chem. Soc.* 1982, **104**, 7360; (c) C. P. Casey, M. W. Meszaros, P. J. Fagan, R. K. Bly, S. R. Marder and E. A. Austin, *J. Am. Chem. Soc.* 1986, **108**, 4043.
17. A. H. Liu, R. C. Murray, J. C. Dewan, B. D. Santarsiero and R. R. Schrock, *J. Am. Chem. Soc.* 1987, **109**, 4282.
18. M. H. Chisholm and J. A. Heppert, *Adv. Organomet. Chem.* 1986, **26**, 97 and refs therein.
19. M. H. Chisholm, J. A. Heppert, E. M. Kober and D. L. Lichtenberger, *Organometallics* 1987, **6**, 1065.
20. M. B. Hall and R. F. Fenske, *Inorg. Chem.* 1972, **11**, 768.
21. B. E. Bursten, J. R. Jensen and R. F. Fenske, *J. Chem. Phys.* 1978, **68**, 3320.
22. W. J. Hehre, R. F. Stewart and J. A. Pople, *J. Chem. Phys.* 1969, **51**, 2657.
23. D. L. Lichtenberger and R. F. Fenske, *J. Chem. Phys.* 1976, **64**, 4247.

APPENDIX

Molecular orbital calculations were performed on an IBM 3081-D computer system using the Fenske–Hall non-empirical approximate MO method.[20] All atomic basis functions were generated by using the method of Bursten *et al.*[21] Contracted double-ζ representations were used for the Mn, Fe and Co 3*d* AOs, W 5*d* AOs and C, N and O 2*p* AOs. An exponent of 1.16 was used for the H 1*s* AOs.[22] The basis functions for Mn, Fe and Co were derived for the +1 oxidation state with the 4*s* exponents fixed at 2.0, 2.0 and 2.2, respectively, and the 4*p* exponents fixed at 1.8, 1.8 and 2.0, respectively. The basis functions for W were derived for the +3 oxidation state with the 6*s* and 6*p* exponents fixed at 1.8 and 1.6, respectively. The CO and NO 3σ orbitals as well as the first three occupied Cp orbitals were filled with 2.0 electrons and deleted from the basis transformation sets. The CO and NO 6σ orbitals as well as all virtual orbitals above the e_2'' level of Cp were filled with 0.0 electrons and deleted from the basis transformation sets.[23]

In all calculations the Cp rings were idealized to local D_{5h} symmetry. All C—H bond lengths were set at 1.08 Å. The atomic coordinates used in the calculation of model complex **1** were taken from the crystal structure of *cis*-$[CpFe(CO)]_2(\mu\text{-}CO)_2$[5] and were idealized to C_{2v} symmetry. The following Fe—H bond lengths were assumed: Fe—*t*H = 1.55 Å, Fe—μH = 1.65 Å. The atomic coordinates for $CpMH_3$ were obtained from a direct fragmentation of **1**. The atomic coordinates for $[CpFe(CO)]_2(\mu\text{-}CO)_2$ were reported in earlier work.[2(c)] Details of the structures used in the calculations of **2**, **3**, **4′**, **5** and **6** were also reported earlier.[2(c),(d)] For the model complex **7′**, the atomic parameters were taken from the crystal structure of **7**[17] and idealized to C_{2v} symmetry. The model complex, $[CpW(CH_3)]_2(\mu\text{-}H)_2$, was constructed with a planar W_2H_2 core and a W—H distance of 1.90 Å. Calculations on **7′** with bent W_2C_2 cores were performed keeping the W—μC distance and W—μC—W angle the same, and varying only the dihedral angle between W—μC—W planes. The atomic coordinates for *trans*-**7′** were obtained by rotating one $CpW(CH_3)$ group of *cis*-**7′** 180°, idealizing the complex to C_{2h} symmetry.

As specified in the text, many of the calculations were performed using a fragment analysis. The CO and CH_2 ligands were converged as neutral fragments. The Cp and CH_3 ligands were converged as mono-anions, and the CH ligands of **5** and **6** were converged as mono-cations. In the case of the NO ligand, it was converged as NO^+ for *t*-NO and NO^- for μ-NO geometries. The CH ligands of **7′** were treated as neutral fragments. All calculations were converged using a self consistent field iterative method until the largest deviation in orbital populations was less than 0.0010 in successive cycles.

Polyhedron Vol. 7, No. 10/11, pp. 955–960, 1988
Printed in Great Britain

0277–5387/88 $3.00+.00
© 1988 Pergamon Press plc

C—C AND C—H BOND FORMATION IN THE CHEMISTRY OF TRIRUTHENIUM CLUSTERS

M. J. SAILOR and D. F. SHRIVER*

Department of Chemistry, Northwestern University, Evanston, IL 60208, U.S.A.

(*Accepted* 5 *November* 1987)

Abstract—The μ_3-acetyl cluster $[Ru_3(CO)_9(\mu_3\text{-}CO)(\mu_3\text{-}CC(O)CH_3)]^-$ (**1**), readily adds CO to produce the acylketene clusters $[Ru_3(CO)_7(\mu\text{-}CO)_3(\mu_2\text{-}\eta^2\text{-}CH_3C(O)CCO)]^-$ and under moderate CO pressures a mobile equilibrium is established between these two species. The phosphine-substituted acetyl cluster $[Ru_3(CO)_8(\mu\text{-}CO)(PPh_3)(\mu_3\text{-}CC(O)CH_3)]^-$ does not add CO under conditions in which the parent cluster **1** does. The acetyl cluster **1** also reacts with H^- or OH^-, to produce the complex $[Ru_3(CO)_6(\mu\text{-}CO)_3(\mu_3\text{-}\eta^2\text{-}CHC(O)CH_3)]^{2-}$, which has been characterized spectroscopically. Mobile C—C and C—H formation is characteristic of these three-metal cluster systems and it is attributed to the variety of multi-site ligand–metal interactions that are possible with a three-metal ensemble.

Recently an extensive chemistry has been observed for the ketenylidene ligand, CCO, in a variety of three-metal clusters, and in particular for anionic ketenylidenes such as $[Ru_3(CO)_6(\mu\text{-}CO)_3(\mu_3\text{-}CCO)]^{2-}$.[1–5] Several routes to cationic, neutral and anionic ketenylidenes have been devised.[1–11] The generation of the CCO group in these clusters can be described formally as the coupling of a cluster-bound carbide atom with a CO molecule. Furthermore, in the anionic ketenylidene clusters the CO group is readily displaced. Thus reaction with alkylating agents,[2–5] nucleophiles,[12] or electrophilic metal complexes[13,14] can result in scission of the C—C bond of CCO, eqs (1)–(3).

$$[Fe_3(CO)_9(\mu_3\text{-}CCO)]^{2-} + CH_3I \rightarrow [Fe_3(CO)_{10}(\mu_3\text{-}CCH_3)]^- \quad (1)$$

$$[CoFe_2(CO)_9(\mu_3\text{-}CCO)]^- + PMe_3 \rightarrow [CoFe_2(CO)_9(\mu_3\text{-}CPMe_3)]^- + CO \quad (2)$$

$$[Fe_3(CO)_9(\mu_3\text{-}CCO)]^{2-} + Cr(CO)_3(NCCH_3)_3 \rightarrow [CrFe_3C(CO)_{13}]^{2-}. \quad (3)$$

The above reactions demonstrate that the CO of CCO can be quite labile in these clusters.

An unusual example of the lability of the CO moiety of CCO is provided by the acylketene cluster $[Ru_3(CO)_7(\mu\text{-}CO)_3(\mu_2\text{-}\eta^2\text{-}CH_3C(O)CCO)]^-$ (**2**). This compound exists in equilibrium with $[Ru_3(CO)_9(\mu_3\text{-}CO)(\mu_3\text{-}CC(O)CH_3)]^-$ (**1**) under a CO atmosphere, eq. (4).[15] The acylketene complex **2** reverts to **1** on removal of the CO atmosphere, and it was previously characterized *in situ* by two-dimensional ^{13}C NMR spectroscopy on a highly ^{13}C-enriched sample.[15] In this report we describe some of the factors involved in this C—C bond forming reaction, as well as a related reaction involving C—H bond formation on complex **1**.

RESULTS AND DISCUSSION

Although the formation of the acylketene moiety of **2** is observed on the addition of CO to **1**, an isotopic tracer experiment has shown that the ketenyl CO is derived from an originally cluster-bound CO ligand rather than the external carbon monoxide.[15] Similar CO-insertion reactions have been observed in several osmium carbonyl clusters containing the μ-CH_2 group.[16] In an attempt to elucidate the factors responsible for the formation of the unusual acylketene cluster **2** of eq. (4), we investigated the reaction of **1** with other ligands. Treatment of the acetyl cluster **1** with PPh_3 does not lead to the phosphine-substituted analogue of **2**. Rather, simple substitution of phosphine for CO occurs. Thus, reaction of PPh_3 with ^{13}C-enriched

*Author to whom correspondence should be addressed.

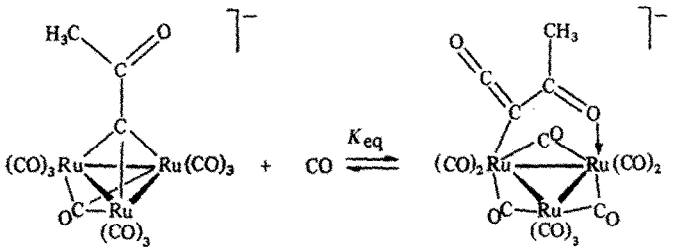

1 2

(4)

Eq. 4

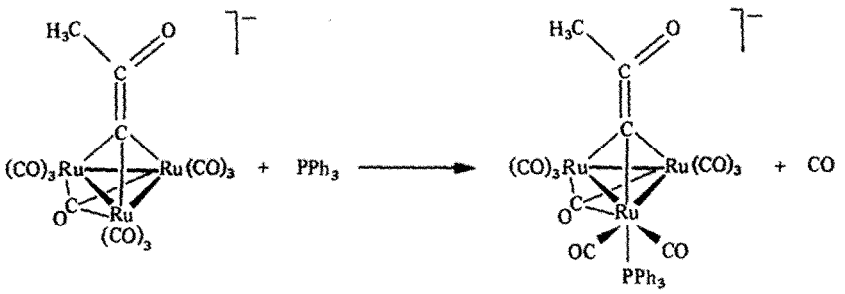

1 3

(5)

Eq. 5

$[Ru_3(CO)_9(\mu_3\text{-}CO)(\mu_3\text{-}CC(O)CH_3)]^-$ in CD_2Cl_2 in a sealed NMR tube results in a ^{13}C NMR signal for free CO at 183.4 ppm and resonances that have been assigned to the phosphine-substituted acetylmethylidyne cluster **3**, eq. (5). Additionally, when a solution of $[Ru_3(CO)_8(\mu\text{-}CO)(PPh_3)(\mu_3\text{-}CC(O)CH_3)]^-$ (**3**) is placed under an atmosphere of CO, we see no spectroscopic evidence for reaction. These results suggest that the forward reaction represented by eq. (4) is less favoured for the phosphine-substituted cluster **3** than for the carbonyl complex **1**. Similar results are obtained with $P(OMe)_3$.

We have previously reported that H_2 will also react with $[Ru_3(CO)_9(\mu_3\text{-}CO)(\mu_3\text{-}CC(O)CH_3)]^-$.[15] Addition of H_2 to **1** results in loss of one CO ligand and formation of a carbon–hydrogen bond, eq. (6). Equation (6) is similar to eq. (4) because in the course of the reaction the oxygen atom of the acetyl ligand enters into an interaction with the metals, at the expense of a metal–carbon interaction. The O → Ru bonding arrangement apparently is important in the C—C and C—H bond forming reactions of eqs (4) and (6), because treatment of either of the products with $CH_3OSO_2CF_3$ results in alkylation of the acetyl oxygen atom and disruption of the C—C or C—H bond. In both cases a vinylidene cluster is produced (Scheme 1).[15]

A μ_3-η^2-$CHC(O)CH_3$ ligand can also be generated by reaction of $[Ru_3(CO)_9(\mu_3\text{-}CO)(\mu_3\text{-}CC(O)CH_3)]^-$ with hydride or hydroxide, eq. (7). The dinegative complex **7** has been characterized spectroscopically. The configuration of the capping ligand was established by ^{13}C and ^1H NMR spectra of a sample of **7** that was enriched with ^{13}C. The NMR data are summarized and compared to two related, previously characterized clusters containing the μ_3-η^2-$CHC(O)CH_3$ ligand in Table 1. Although the ^1H

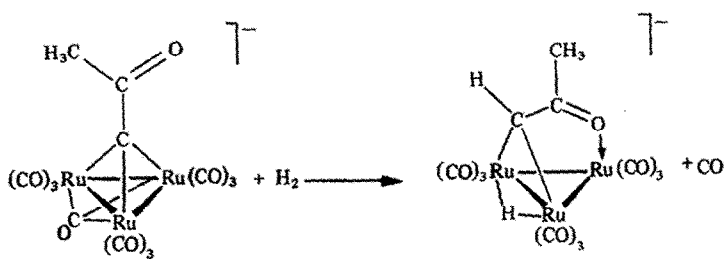

(6)

Eq. 6

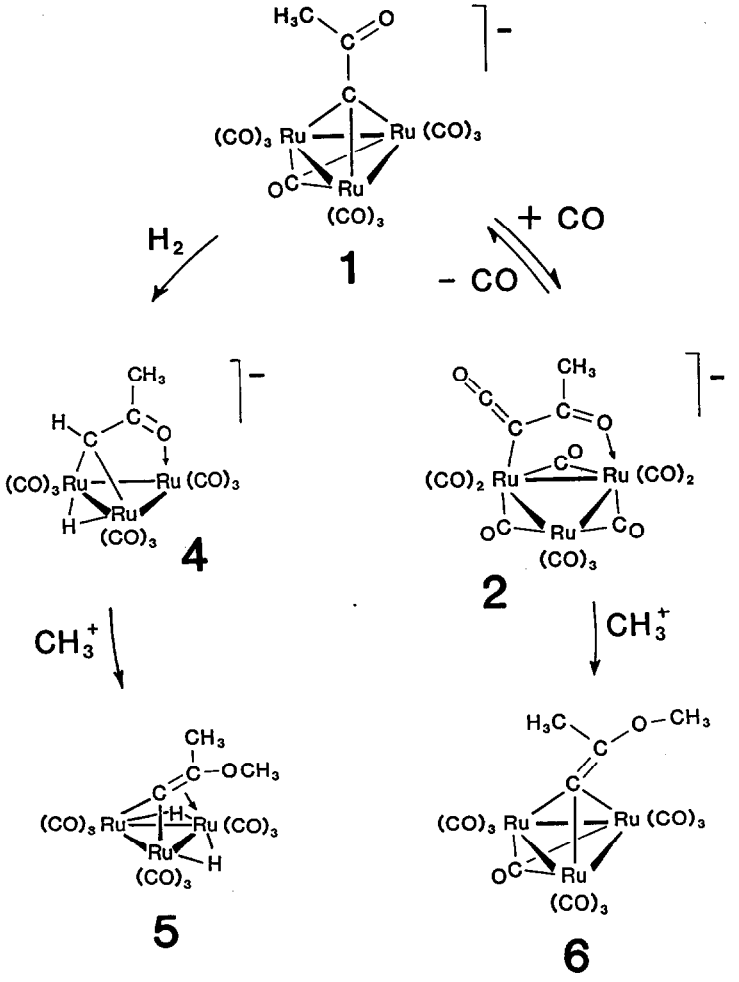

Scheme 1.

NMR signal of the unique proton in the $CHC(O)CH_3$ ligand of **7** is more than 2 ppm upfield of the corresponding resonances of the complexes $[HRu_3(CO)_9(\mu_3\text{-}\eta^2\text{-}CHC(O)CH_3)]^-$ (**8**) and $H_2Ru_3(CO)_9(\mu_3\text{-}\eta^2\text{-}CHC(O)CH_3)$ (**9**), the associated $^1J_{CH}$ coupling constant is comparable. The high-field ^1H NMR shift for the unique proton in **7** may be a reflection of the CO ligand disposition, which is different in **7** than in either of the other two clusters **8** or **9**. Although the anionic and neutral complexes $[HRu_3(CO)_9(\mu_3\text{-}\eta^2\text{-}CHC(O)CH_3)]^-$ and $H_2Ru_3(CO)_9(\mu_3\text{-}\eta^2\text{-}CHC(O)CH_3)$ contain only terminal CO ligands, the IR and ^{13}C NMR data indicate that dinegative $[Ru_3(CO)_6(\mu\text{-}CO)_3(\mu_3\text{-}\eta^2\text{-}CHC(O)CH_3)]^{2-}$ contains three bridging carbonyl ligands. Presumably the carbonyl ligands of **7** more effectively

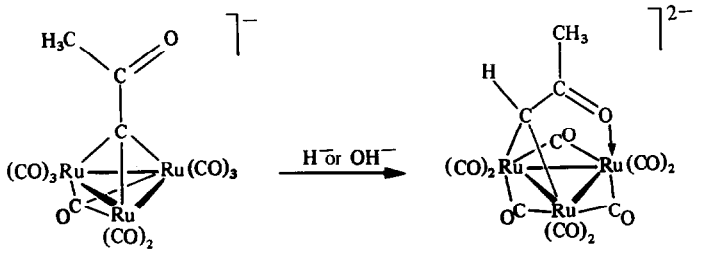

(7)

Eq. 7

Table 1. ^{13}C and ^{1}H NMR shifts and coupling constants for the μ_3-η^2-CHC(O)CH_3 ligand[a]

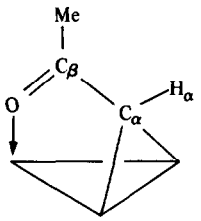

Compound	^{13}C NMR (ppm) C_α	C_β	^{1}H NMR (ppm) H_α	Me	^{1}J (HZ) C_α-C_β	C_α-H_α
$[Ru_3(CO)_9(L)]^{2-}$	56.9	216.1	1.46	1.45	49	140
$[HRu_3(CO)_9(L)]^{-}$[b]	77.5	230.7	4.03	1.79	46	141
$H_2Ru_3(CO)_9(L)$[b]	74.3	239.5	4.16	1.99	43	143

[a] L is defined as the μ_3-η^2-$C_\alpha H_\alpha C_\beta$(O)Me group. All measurements made in CD_2Cl_2 solution on ^{13}C-enriched complexes.
[b] Ref. 15.

shield the unique proton, resulting in the higher-field ^{1}H NMR resonance.

With respect to the carbonyl ligand disposition, the isoelectronic series of μ_3-η^2-CHC(O)CH_3 clusters **7**, **8** and **9** is similar to the series of ketenylidene clusters $H_2Ru_3(CO)_9(\mu_3\text{-CCO})$, $[HRu_3(CO)_9(\mu_3\text{-CCO})]^-$ and $[Ru_3(CO)_6(\mu\text{-CO})_3(\mu_3\text{-CCO})]^{2-}$.[2] Presumably the presence of the bridging carbonyl groups in the dinegative compounds partially alleviates the high negative charge in these complexes. A set of variable-temperature ^{13}C NMR spectra in the CO-region of **7** is presented in Fig. 1. The low-temperature spectrum indicates that the molecule possesses a mirror plane that contains the μ_3-η^2-CHC(O)CH_3 ligand (excluding the methyl hydrogens from consideration), a bridging CO, two ter-

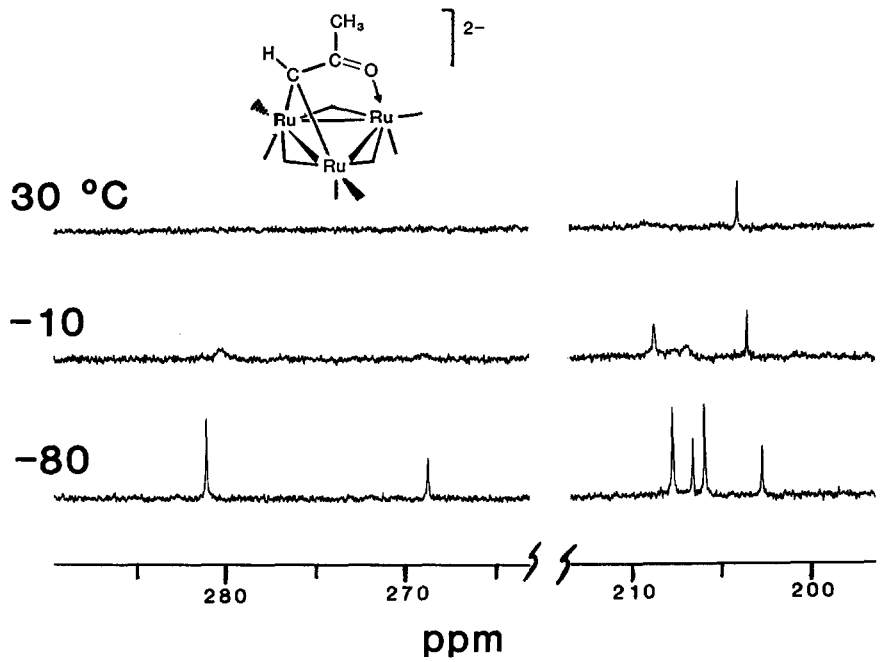

Fig. 1. Variable-temperature ^{13}C NMR spectrum (100.58 MHz) of $[Ru_3(CO)_6(\mu\text{-CO})_3(\mu_3\text{-}\eta^2\text{-CHC(O)}CH_3)]^{2-}$, **7**, showing the carbonyl ligand fluxionality.

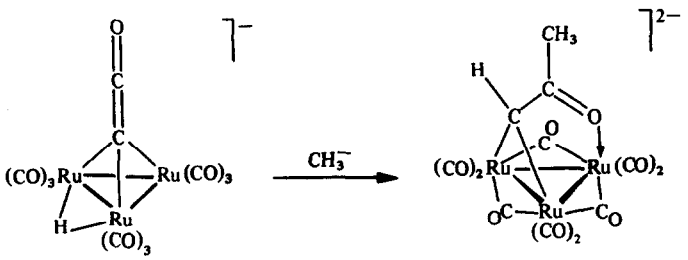

(8)

Eq. 8

minal carbonyl ligands and a ruthenium vertex. On raising the temperature, exchange between all but one of the carbonyl ligands becomes fast on the NMR timescale, as evidenced by the broadening of all but one of the ^{13}C NMR signals for the CO ligands. The unique CO ligand is presumed to be *trans* to the O → Ru interaction, in line with the previous interpretation of the VT-^{13}C NMR spectra of **8**.[15]

As might be expected, the compounds $[HRu_3(CO)_9(\mu_3\text{-}\eta^2\text{-}CHC(O)CH_3)]^-$ (**8**) and $H_2Ru_3(CO)_9(\mu_3\text{-}\eta^2\text{-}CHC(O)CH_3)$ (**9**) can be synthesized from $[Ru_3(CO)_6(\mu\text{-}CO)_3(\mu_3\text{-}\eta^2\text{-}CHC(O)CH_3)]^{2-}$ (**7**) by successive protonation. It is interesting that addition of hydride or hydroxide to **1** results in C—H bond formation to generate **7**, but that subsequent addition of H^+ to **7** occurs at the metal framework rather than the carbon atom. Thus the $\mu_3\text{-}\eta^2\text{-}CHC(O)CH_3$ moiety is apparently a relatively stable ligand. Another indication of the stability of the $\mu_3\text{-}\eta^2\text{-}CHC(O)CH_3$ group is that the cluster $[Ru_3(CO)_6(\mu\text{-}CO)_3(\mu_3\text{-}\eta^2\text{-}CHC(O)CH_3)]^{2-}$ can also be synthesized by reaction of the ketenylidene cluster $[HRu_3(CO)_9(\mu_3\text{-}CCO)]^-$ with $LiCH_3$, eq. (8). In reaction (8) the CH_3^- group is presumed to attack the carbonyl carbon of the CCO ligand to form a μ_3-acetyl ligand. In the course of the transformation, the metal-bound hydride migrates to the apical carbon atom of the former μ_3-CCO ligand. Apparently, in these anionic clusters the $\mu_3\text{-}\eta^2\text{-}CHC(O)CH_3$ ligand is favoured over a $\mu_3\text{-}CC(O)CH_3$ moiety.

CONCLUDING REMARKS

In this work we have discussed two related processes involving the activation of a cluster-bound carbon atom and these can be systematized by the following formal description. In the μ_3-acetyl cluster $[Ru_3(CO)_9(\mu_3\text{-}CO)(\mu_3\text{-}CC(O)CH_3)]^-$, the replacement of a carbon-to-ruthenium bond with an O → Ru interaction can be considered to generate an "unsaturation" at the capping carbon atom. The carbon can either couple with H to form a $\mu_3\text{-}\eta^2\text{-}CHC(O)CH_3$ ligand, or with CO to form a $\mu_2\text{-}\eta^2\text{-}CH_3C(O)CCO$ moiety. In these anionic clusters, the barrier to C—C and C—H bond formation and cleavage is apparently very low.

EXPERIMENTAL

General

All manipulations were carried out under a dry dinitrogen atmosphere using standard Schlenk and syringe techniques[17] or in a Vacuum Atmospheres drybox. Solvents were distilled from the appropriate drying agents before use: CH_2Cl_2 and CD_2Cl_2 from P_2O_5; THF and Et_2O from sodium and benzophenone. The compounds $[PPN][Ru_3(CO)_9(\mu_3\text{-}CO)(\mu_3\text{-}CC(O)CH_3)]$, $[PPN][HRu_3(CO)_9(\mu_3\text{-}CCO)]$ and ^{13}C-enriched $[PPN][Ru_3(*CO)_9(\mu_3\text{-}*CO)(\mu_3\text{-}*C*C(O)CH_3)]$ were prepared as described previously.[2] Potassium tri-secbutylborohydride ("K-selectride", 1.0 M solution in THF, Aldrich) and methyllithium (low-halide 1.4 M solution in Et_2O, Aldrich) were used as received. Elemental analyses were performed by Elbach Analytical Laboratories.

Infrared spectra were obtained on Nicolet 7199 Fourier transform or Perkin–Elmer 283 infrared spectrometers. Multinuclear NMR spectra on ^1H, ^{31}P and ^{13}C were obtained on either JEOL FX-270 or Varian XL-400 NMR spectrometers, and were referenced to residual solvent protons, external 20% H_3PO_4 in D_2O, or the ^{13}C NMR signal of the solvent carbon atoms, respectively. Unless otherwise noted, the ^{13}C NMR data reported are on ^{13}C-enriched materials. The data for J_{CC} reported were measured from the ^{13}C–^{13}C satellite peaks from samples *ca* 30% enriched with ^{13}C. Note that the ^{13}C-enriched starting material $[Ru_3(*CO)_9(\mu_3\text{-}*CO)(\mu_3\text{-}*C*C(O)CH_3)]^-$ was not enriched at the methyl carbon.

Synthesis and characterization of $[PPN][Ru_3(CO)_9(PPh_3)(\mu_3\text{-}CC(O)CH_3)]$, **3**

A 30 mg sample of $[PPN][Ru_3(*CO)_9(\mu_3\text{-}*CO)(\mu_3\text{-}*C*C(O)CH_3)]$ (* denotes ^{13}C enrichment of *ca* 20%) and a 6 mg sample of triphenylphosphine, were loaded into a 5 mm NMR tube

fitted with a concentric Teflon valve. Approximately 0.5 cm^3 of CD_2Cl_2 was vacuum transferred into the tube at liquid nitrogen temperature. ^1H NMR (taken 15 min after sealing and warming the NMR tube): phenyl protons (PPh_3 and $[PPN]^+$); 2.41 (s, CH_3 of **3**); 2.36 (s, CH_3 of **1**); 1.87 (s, CH_3 of **2**) ppm. After 8 h the signals for **1** and **2** had almost disappeared and the only detectable product was species **3**. ^{31}P NMR: 35.95 (PPh_3 of **3**); 21.54 ($[PPN]^+$); −5.12 (free PPh_3) ppm. ^{13}C NMR (−90°C): 274.6 ($J_{CP} = 7$ Hz, μ-CO); 212.7 ($^1J_{CC} = 44$ Hz, $C\underline{C}(O)CH_3$); 204.1 ($J_{CP} = 10$ Hz, 2 CO's); 199.6 (br, 6CO's); 193.5 ($J_{CP} = 29$ Hz, $^1J_{CC} = 42$ Hz, $\underline{C}C(O)CH_3$); 183.4 (dissolved CO); 31.4 ($CC(O)\underline{C}H_3$) ppm. The methyl carbon was unenriched in these experiments; thus the signal was too weak to discern any associated ^{13}C–^{13}C coupling satellites. IR(ν_{CO}, THF): 2065(vw), 2035(m), 1982(vs), 1947(sh), 1916(w), 1655(w). There was also a small resonance at 203.3 ppm that was assumed to be an impurity. Reaction of **1** with a five-fold excess of PPh_3 for two days led to an approximately 1 : 1 mixture of **3** and a species with an ^1H NMR resonance at 2.45 ppm, tentatively assigned to a bis-phosphine adduct.

Synthesis and characterization of $[PPN]_2[Ru_3(CO)_6(\mu\text{-}CO)_3(\mu_3\text{-}\eta^2\text{-}CHC(O)CH_3)]$, **7**

A 150 mg sample of $[PPN][Ru_3(CO)_9(\mu_3\text{-}CO)(\mu_3\text{-}CC(O)CH_3)]$ was dissolved in 2 cm^3 of THF. Eight drops of 4 M KOH in methanol solution was added with stirring, at which point the colour of the solution had changed from yellow to red–orange. A solution of 0.2 g of [PPN]Cl in 2 cm^3 of methanol was added to the solution, followed by 10 cm^3 of Et_2O. A red oil was produced, which was separated from the supernatant and extracted into THF. Filtration and addition of diethylether produced 140 mg (69%) of **7** as a yellow powder. Anal. Calc. (found) for $C_{84}H_{64}O_{10}P_4N_2Ru_3$: C, 59.70 (59.12); H, 3.82 (3.97); P, 7.34 (5.57); Ru, 17.96 (17.75). IR (ν_{CO}, Nujol): 1988(w), 1932(vs), 1886(m), 1869(m), 1800(vw), 1741(s). ^1H NMR (CD_2Cl_2, 25°C): 1.46 (1H, $C\underline{H}C(O)CH_3$); 1.45 (3H, $CHC(O)C\underline{H}_3$) ppm. ^{13}C NMR (CD_2Cl_2, −80°C): 281.2, 268.9 (2 : 1, μ-CO's); 216.1 ($^1J_{CC} = 49$ Hz, $CH\underline{C}(O)CH_3$); 207.7, 206.6, 205.9, 202.7 (2 : 1 : 2 : 1, CO's); 56.1 ($^1J_{CC} = 49$ Hz, $\underline{C}HC(O)CH_3$) ppm. In the proton coupled spectrum the 56.1 ppm peak is split into a doublet, $^1J_{CH} = 140$ Hz. In the ^1H NMR spectrum of ^{13}C-enriched $[HRu_3(*CO)_6(\mu\text{-}*CO)_3(\mu_3\text{-}\eta^2\text{-}*CH*C(O)CH_3)]^{2-}$, ^{13}C satellites of 140 Hz are observed on the 1.46 ppm resonance. Addition of successive aliquots of $HBF_4 \cdot Et_2O$ to a sample of **7** in a CD_2Cl_2 solution in an NMR tube generates $[HRu_3(CO)_9(\mu_3\text{-}\eta^2\text{-}CHC(O)CH_3)]^-$ and $H_2Ru_3(CO)_9(\mu_3\text{-}\eta^2\text{-}CHC(O)CH_3)$ sequentially, as determined by ^1H NMR. Complex **7** was also produced by addition of K-selectride to a solution of **1** in THF (identified by IR), or alternatively by addition of a LiMe solution to $[HRu_3(CO)_9(\mu_3\text{-}CCO)]^-$ in Et_2O at −78°C. In the latter case the product **7** was identified by IR and ^1H NMR spectroscopy.

Acknowledgement—This research was supported by the NSF Synthetic Inorganic and Organometallic Chemistry program.

REFERENCES

1. M. J. Sailor and D. F. Shriver, *Organometallics* 1985, **4**, 1476.
2. M. J. Sailor, C. P. Brock and D. F. Shriver, *J. Am. Chem. Soc.* 1987, **109**, 6015.
3. M. J. Went, M. J. Sailor, P. L. Bogdan, C. P. Brock and D. F. Shriver, *J. Am. Chem. Soc.*, in press.
4. J. W. Kolis, E. M. Holt, M. A. Drezdzon, K. H. Whitmire and D. F. Shriver, *J. Am. Chem. Soc.* 1982, **104**, 6134.
5. J. W. Kolis, E. M. Holt and D. F. Shriver, *J. Am. Chem. Soc.* 1983, **105**, 7307.
6. D. Seyferth, G. H. Williams and C. L. Nivert, *Inorg. Chem.* 1977, **4**, 758.
7. J. B. Keister and T. L. Horling, *Inorg. Chem.* 1980, **19**, 2304.
8. J. S. Holmgren and J. R. Shapley, *Organometallics* 1984, **3**, 1322.
9. A. C. Sievert, D. S. Strickland, J. R. Shapley G. R. Steinmetz and G. L. Geoffroy, *Organometallics* 1982, **1**, 214.
10. (a) A. M. Crespi and D. F. Shriver, *Organometallics* 1986, **5**, 1750; (b) A. M. Crespi, M. J. Went, S. S. Sunshine and D. F. Shriver, *Organometallics* 1988, **7**, 214.
11. P. L. Bogdan. Ph.D. Thesis, Northwestern University (1987).
12. S. Ching, M. Sabat and D. F. Shriver, *J. Am. Chem. Soc.* 1987, **109**, 4722.
13. J. W. Kolis, E. M. Holt, J. A. Hriljac and D. F. Shriver, *Organometallics* 1984, **3**, 496.
14. (a) J. A. Hriljac, P. N. Swepston and D. F. Shriver, *Organometallics* 1985, **4**, 158; (b) J. A. Hriljac, E. M. Holt and D. F. Shriver, *Inorg. Chem.* 1987, **26**, 2943.
15. M. J. Sailor, M. Sabat and D. F. Shriver, *Organometallics*, in press.
16. (a) E. D. Morrison, G. R. Steinmetz, G. L. Geoffroy, W. C. Fultz and A. L. Rheingold, *J. Am. Chem. Soc.* 1984, **106**, 4783; (b) E. D. Morrison and G. L. Geoffroy *J. Am. Chem. Soc.* 1985, **107**, 3541.
17. D. F. Shriver and M. A. Drezdzon, *Manipulation of Air-Sensitive Compounds*, 2nd edn. John Wiley, New York (1986).

Polyhedron Vol. 7, No. 10/11, pp. 961–965, 1988
Printed in Great Britain

0277–5387/88 $3.00+.00
© 1988 Pergamon Press plc

INTERCONVERSION OF BENZYLIDYNE AND METHYLBENZYNE TRIOSMIUM COMPLEXES

WEN-YANN YEH, HEINZ-JOSEF KNEUPER and JOHN R. SHAPLEY*

Department of Chemistry, University of Illinois, Urbana, IL 61801, U.S.A.

(*Accepted* 5 *November* 1987)

Abstract—Pyrolysis of $H_3Os_3(CO)_9(\mu_3\text{-}CC_6H_5)$ (**1**) in a sealed glass tube at 220°C gives the known methylbenzyne complex $H_2Os_3(CO)_9(\mu_3,\eta^2\text{-}C_6H_3CH_3)$ (**2**), previously prepared from $Os_3(CO)_{10}(NCCH_3)_2$ and toluene. Similar pyrolysis (220°C) of **2** either as a solid or in tridecane solution shows significant conversion to **1**, demonstrating reversibility. Pyrolysis of $H_3Os_3(CO)_9(\mu_3\text{-}CC_6D_5)$ (**1**-d_5) provides **2**, which shows scrambling of the deuterium atoms into all sites by ^1H NMR. However, pyrolysis of a mixture of **1** and $D_2Os_3(CO)_9(\mu_3,\eta^2\text{-}C_6D_3CD_3)$ (**2**-d_8) gives **2** which is also just partially deuterated in all proton sites. Thus, intermolecular hydrogen/deuterium exchange accompanies the benzylidyne/methylbenzene interconversion.

Organotriosmium cluster compounds undergo a variety of transformations in which the organic moiety is changed by proton transfers to and/or from the metal framework.[1] As part of out interest in alkylidyne triosmium clusters, we have investigated the properties of $H_3Os_3(CO)_9(\mu_3\text{-}CC_6H_5)$ (**1**).[2,3] To our surprise, heating this compound leads to the methyl-substituted benzyne complex $H_2Os_3(CO)_9(\mu_3,\eta^2\text{-}C_6H_3CH_3)$ (**2**);[4,5] furthermore, this transformation is reversible [see eq. (1)]. In this

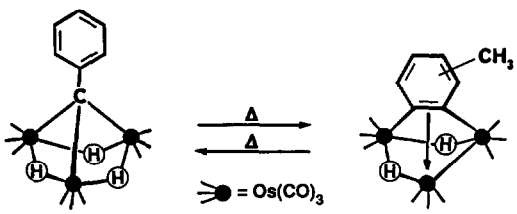

1 2 (1)

paper we describe our information concerning this dramatic interconversion.

EXPERIMENTAL

$H_3Os_3(CO)_9(\mu_3\text{-}CBr)$ was prepared by Keister's method.[6] $H_3Os_3(CO)_9(\mu_3\text{-}CC_6H_5)$ was prepared as described by Strickland.[2] $H_2Os_3(CO)_9(\mu_3,\eta^2\text{-}C_6H_3CH_3)$ was prepared from $Os_3(CO)_{10}(NCCH_3)_2$[7] and toluene.[5] Aluminum trichloride (Mallinckrodt, AR), benzene-d_6 (Aldrich) and toluene-d_8 (Aldrich) were used directly as received. Tridecane and benzene were distilled from sodium before use. Preparative thin-layer chromatographic (TLC) plates were prepared from Silica Gel GF (Type 60, E. Merck). ^1H NMR spectra were obtained on a Nicolet NT-360 spectrometer at 360 MHz or on a GE GN-500 spectrometer at 500 MHz. IR spectra were recorded either on a Perkin–Elmer 281 B spectrometer or on a Perkin–Elmer 1750 FT spectrometer. Microanalyses and mass spectra were determined by the personnel of the respective service facilities in the School of Chemical Sciences at the University of Illinois.

Preparation of $H_3Os_3(CO)_9(\mu_3\text{-}CC_6D_5)$ (**1**-d_5)

Aluminum trichloride (50 mg, 0.38 mmol) was placed in an oven-dried 50 cm^3 Schlenk flask equipped with a magnetic stir bar and an oven-dried 35 cm^3 pressure-equalizing addition funnel, topped with a rubber serum stopper. The system was evacuated for 30 min and then nitrogen gas was admitted. A solution of $H_3Os_3(CO)_9(\mu_3\text{-}CBr)$ (49 mg, 0.053 mmol) in benzene-d_6 (5 cm^3) was transferred into the addition funnel via a cannula through the serum stopper. It then was added dropwise to the flask over a period of 30 min, forming

* Author to whom correspondence should be addressed.

an orange slurry. A mixture of aqueous sodium bicarbonate (10%, 20 cm^3) and benzene (10 cm^3) was then poured into the flask. The organic layer was transferred to a separatory funnel, washed with distilled water (3×5 cm^3), dried over magnesium sulphate, filtered and the solvent was removed on a rotary evaporator. The residue was subjected to TLC, eluting with *n*-pentane. Isolation of the material forming the single yellow band gave $H_3Os_3(CO)_9(\mu_3\text{-}CC_6D_5)$ (44 mg, 0.048 mmol, 90%), which showed an IR spectrum in the carbonyl region identical to that of **1**. The level of deuteration for $H_3Os_3(CO)_9(\mu_3\text{-}CC_6D_5)$ was *ca* 90%, based on ^1H NMR data (acetone-d_6, 17°C): δ 7.76 (s, 0.2H), 7.23 (s, 0.1H), 7.02 (s, 0.2H), −18.49 (s, 3H).

Pyrolysis of **1** *in vacuo*

A sample of **1** (17 mg, 0.018 mmol) was sealed in glass tubing *in vacuo* (0.1 mmHg), and the tube placed in a silicone oil bath at 220°C. After 40 min, the tube was removed from the bath, cooled to room temperature and opened in air. The brown residue was extracted with dichloromethane and subjected to TLC, eluting with *n*-pentane/dichloromethane (9:1 *v/v*). The starting material was recovered from the second, yellow band (3 mg, 18%). Isolation of the material forming the first yellow band gave the methylbenzyne complex $H_2Os_3(CO)_9(\mu_3,\eta^2\text{-}C_6H_3CH_3)$ (**2**)[4,5] (8 mg, 47%). IR (C_6H_{12}): ν_{CO}, 2109(m), 2080(vs), 2070(w), 2055(vs), 2034(vs), 2023(s), 2007(vs), 2002(s), 1988(sh), 1984(s) cm^{-1}. ^1H NMR ($CDCl_3$, 16°C, mixture of two isomers, **A** and **B**, **A**:**B** = 4:1) **A**: δ 7.76 (d, 1H, J = 8 Hz), 7.63 (s, 1H), 6.65 (d, 1H, J = 8 Hz), 2.27 (s, 3H), −19.00 (s, s−); **B**: δ 7.66 (d, 1H, J = 8 Hz), 7.01 (d, 1H, J = 7 Hz), 6.66 (m, 1H), 2.40 (s, 3H), −18.62 (s, 1H).

Pyrolysis of **1**-d_5 *in vacuo*

This reaction was carried out and worked up in a fashion identical with that above. The ^1H NMR spectrum ($CDCl_3$, 17°C) of the methylbenzyne complex indicated that the deuterium atoms scrambled in all sites of both isomers **A** and **B** (see Fig. 1).

Pyrolysis of **1** *in presence of toluene*-d_8

This reaction was conducted as above, except that two drops of toluene-d_8 were added to the tube before sealing. After work-up, the ^1H NMR and mass spectra of both products showed no evidence for deuterium incorporation.

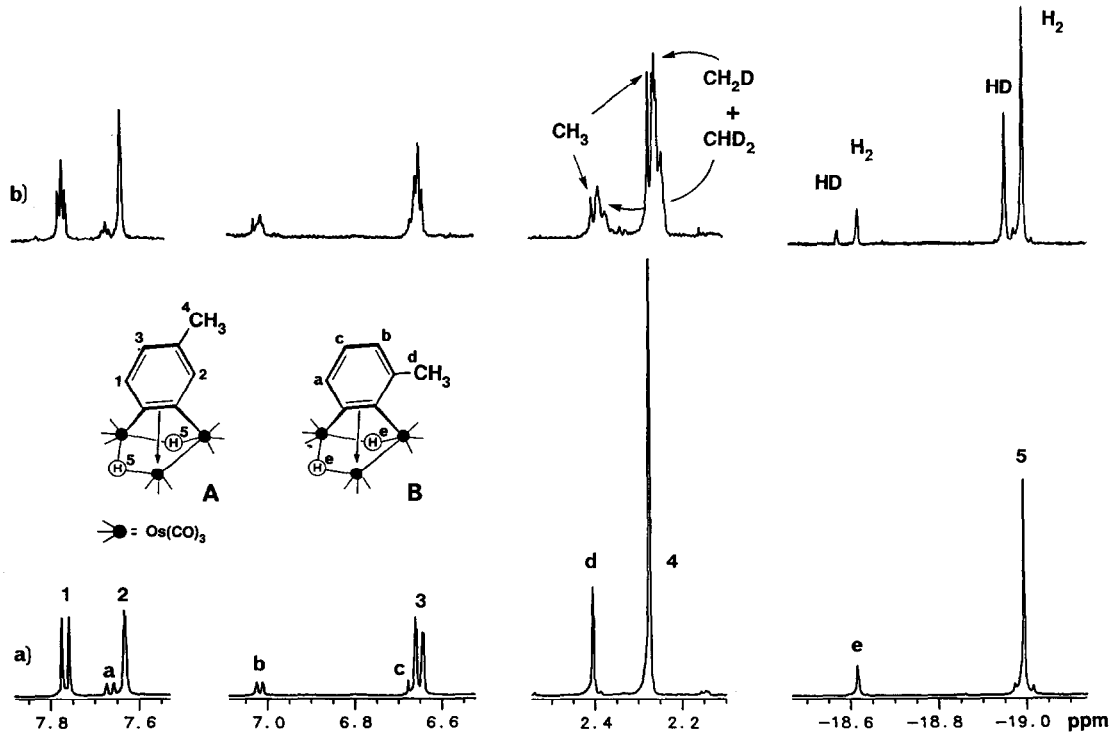

Fig. 1. ^1H NMR spectra (500 MHz, $CDCl_3$, 17°C) of (a) **2** and (b) **2**-d_5.

Pyrolysis of **2** *in solution*

A solution of **2** (9 mg, 0.001 mmol) in tridecane (1 cm^3) was evacuated and sealed in glass tubing. The tube was heated at 220°C in a silicone oil bath for 60 min, then cooled to room temperature and opened in air. The resulting brownish-yellow mixture was subjected to TLC, eluting with *n*-pentane/dichloromethane (9:1 *v/v*). The starting material was recovered from the first yellow band (6 mg, 67%). Compound **1** was isolated from the second yellow band (1 mg, 10%).

Pyrolysis of **2** *in vacuo*

A sample of **2** (11 mg, 0.012 mmol) was sealed in an oven-dried glass tube under vacuum, and the tube placed in a silicone oil bath at 220°C. After 40 min, the tube was removed from the bath, cooled to room temperature and opened in air. The residue was dissolved in dichloromethane and subjected to TLC, eluting with *n*-pentane/dichloromethane (9:1 *v/v*). Compounds **2** (6 mg, 55%) and **1** (1 mg, 9%) were isolated and identified.

Pyrolysis of **2** *in presence of* CO *or* H_2

Two samples of **2** were treated as above except that they were sealed under 0.1 atm of CO or H_2, respectively. Only **2** was recovered from the former tube and **2** with just a trace of **1** was obtained from the latter tube.

Preparation of $(\mu\text{-D})_2Os_3(CO)_9(\mu_3,\eta^2\text{-}C_6D_3CD_3)$ (**1**-d_8)

$Os_3(CO)_{10}(CH_3CN)_2$ (31 mg, 0.033 mmol) and toluene-d_8 (1 cm^3) were placed in an oven-dried glass tube. The solution was frozen with a liquid nitrogen bath and the tube sealed under vacuum. The tube was then placed in an oil bath at 100°C for 60 min, cooled to room temperature and opened in air. The volatile materials were removed under vacuum and the residue subjected to TLC, eluting with *n*-pentane. $(\mu\text{-D})_2Os_3(CO)_9(\mu_3,\eta^2\text{-}C_6D_3CD_3)$ (11 mg, 0.012 mmol, 36%) was obtained from the first, yellow band. The level of deuteration was > 95%, and no loss of label after TLC was observed.

Vacuum pyrolysis of $(\mu\text{-D})_2Os_3(CO)_9(\mu_3,\eta^2\text{-}C_6D_3(CD_3))$ *mixed with* $H_2Os_3(CO)_9(\mu_3,\eta^2\text{-}C_6H_3(CH_3))$

A mixture of **1** (2.3 mg) and **2**-d_8 (2.1 mg) was pyrolysed and worked up according to the procedure described above. The ^1H NMR spectrum of the recovered methylbenzyne mixture showed complete scrambling of the deuterium label ($CDCl_3$, 17°C, **A**:**B** = 4:1); **A**: δ 7.76 (s, d, 0.4H), 7.63 (s, d, 0.4H), 6.65 (s, d, 0.4H), 2.27 (s, 0.9H, CH_3), 2.25 (br, 0.9H, CH_2D and CHD_2), −18.96 (s, 0.2H, μ-(HD)), −19.00 (s, 0.7H, μ-(HH)); **B**: δ 7.66 (s, d), 7.01(br), 6.66(m), 2.40 (s, CH_3), 2.38 (br, CH_2D and CHD_2), −18.57 (s, μ-(HD)), −18.62 (s, μ-(HH)).

RESULTS AND DISCUSSION

Interconversion of **1** *and* **2**

Pyrolysis of solid **1** at 220°C for 40 min affords $H_2Os_3(CO)_9(\mu_3,\eta^2\text{-}C_6H_3(CH_3))$ (**2**) (47%) and recovered **1** (18%) together with some decomposed materials. The methylbenzyne complex **2** has been characterized by IR, ^1H NMR and mass spectroscopy and the results are in close agreement with those reported by Deeming[4] and by Lewis.[5] The IR (ν_{CO}) absorption pattern resembles that recorded for the parent species $H_2Os_3(CO)_9(\mu_3,\eta^2\text{-}C_6H_4)$;[8] the benzyne structure of this complex has been established by X-ray crystallography.[5] The ^1H NMR spectrum of **2** [Fig. 1(a)] shows the existence of two isomers, **A** and **B** in *ca* 4:1 ratio, which cannot be separated by TLC. Assignment of the major isomer **A** as the 1,2,4-substituted complex has been based on the ring proton coupling constants.[4,5]

Pyrolysis of solid **2** *in vacuo* at 220°C for 40 min produces **1** (9%), recovered **2** (55%), and some decomposed materials. Similar results are obtained by heating a tridecane solution of **2** in a sealed tube at 220°C for 60 min. Although these conversions do not achieve equilibrium, they do establish that a mixture of **1** and **2** can be approached from either direction.

Deuterium labelling experiment

The selectively labelled complex $H_3Os_3(CO)_9(\mu_3\text{-}CC_6D_5)$ (**1**-d_5) is prepared cleanly from $H_3Os_3(CO)_9(\mu_3\text{-}CBr)$, $AlCl_3$ and benzene-d_6. Pyrolysis of **1**-d_5 gives **2**-d_5. However, the ^1H NMR spectrum of this product, as illustrated in Fig. 1(b), shows complete scrambling of the deuterium atoms (and hence the protons), so that the intensities of the ring proton, methyl and hydride resonances are approximately in a 4:5:3 ratio. Moreover, an isotope effect is observed for the methyl resonances (0.02 ppm upfield shift) as well as the hydride resonances (0.04 ppm downfield shift) upon replacing a hydrogen atom with a deuterium atom.

Cross-over experiment

The ^{1}H NMR spectrum of the recovered complex **2**, generated by pyrolysis of $H_2Os_3(CO)_9(\mu_3,\eta^2\text{-}C_6H_3CH_3)$ mixed with $(\mu\text{-}D)_2Os_3(CO)_9(\mu_3,\eta^2\text{-}C_6D_3CD_3)$ (1.1 : 1), is essentially the same as that shown in Fig. 1(b). The isotope effects make it obvious that intermolecular scrambling of the deuterium atoms (and the protons) has occurred.

Possible mechanism

Our observations on the interconversion of **1** and **2** certainly show an intermolecular component to the reaction system. However, whether this component is required for the fundamental interconversion of the organic moieties, or is incidental to it, is not so clear. The inhibition by CO and by H_2 imply reversible dissociation of these species, and the intermolecular H/D scrambling established by the crossover experiment is likely to be caused by exchange of $H_2/HD/D_2$ between cluster intermediates. On the other hand there is no exchange with free toluene, so that the C_7 moiety remains bound to one or more metal centres throughout the interconversion. Although it is certainly possible to envision reversible fragmentation to a lower nuclearity, there is ample precedent for the rearrangement to occur on a triosmium framework.[1]

Key stages in the interconversion of **1** and **2** relate to the distribution of hydrogen atoms on the C_7 moiety. Compound **1** has no hydrogen atoms attached to the benzylidyne carbon atom, whereas compound **2** has this carbon centre converted to a methyl group, with three attached hydrogen atoms. Obvious important intermediates, then, are complexes with *one* or *two* hydrogen atoms attached to this carbon, respectively. On the other hand, compound **2** has *two* ring carbons attached to the metal framework, whereas **1** has none. Thus, likely intermediate structures should be similar to **I** and **II**.

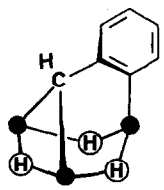

I

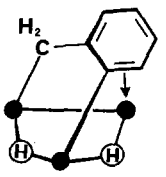

II

Proceeding from **1**, we expect that one phenyl C—H bond undergoes oxidative addition concomitant with migration of a hydride ligand to the alkylidyne carbon (see **I**). Close precedents for this behaviour are the rearrangements of the benzylidyne compound **3** [eq. (2)][9] and the ester-substituted alkylidyne compounds **5** [eq. (3), M = Ru;[10] Os[11]].

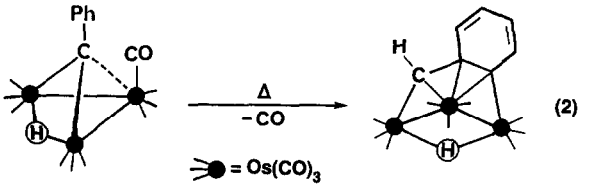

3 4

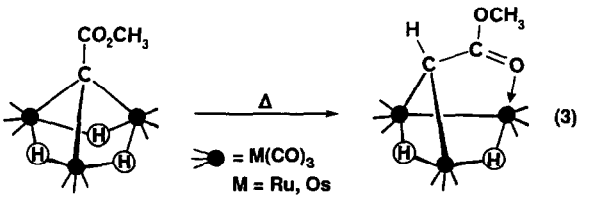

5 6

Migration of a second hydride ligand to the benzylic carbon centre could be accompanied by a change in the ring coordination (see **II**). Precedents for this step include the rearrangement shown in eq. (4)[12] as well as the structure of complex **9** derived from phenol [eq. (5)],[13] which contains an isoelectronic

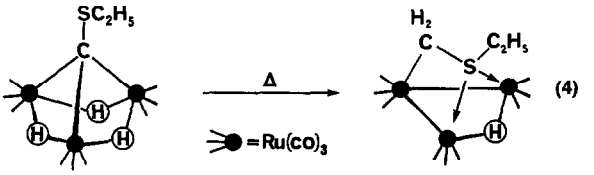

7 8

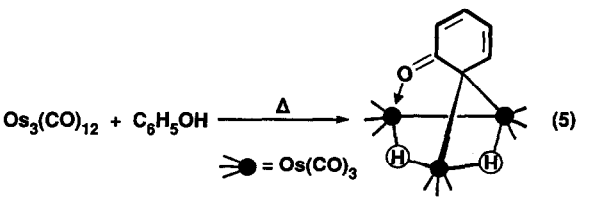

9

organic moiety. Formation of **2** is completed by transfer of the third hydride ligand and cleavage of the second ring C—H bond. In other work we have shown that exchange between the ring protons and the metal protons in **2** is fast at 90°C;[14] this dynamic process also interconverts the two positional isomers of **2** [eq. (6)].

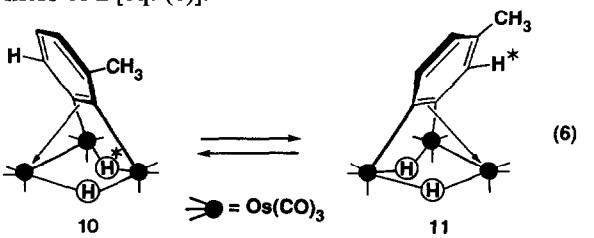

10 11

Finally, it is likely that species similar to **1** and **2** are involved in the chemisorption of toluene on metal surfaces.[15] Friend and Muetterties[16] found that the methyl protons of toluene undergo exchange with deuterium over nickel surfaces under mild conditions, followed by exchange of the ring protons at higher temperatures. The interconversion of **1** and **2** together with the extensive H atom scrambling involved, provides a compelling molecular model for the surface reactions.[17]

Acknowledgements—This work was supported by the National Science Foundation grant CHE 84-07233 (to J.R.S.). H.-J. Kneuper thanks the Deutsche Forschungsgemeinschaft (Bonn) for a fellowship. The GE GN-500 NMR spectrometer was purchased in part by funds from NSF Grant CHE 85-14500 to the School of Chemical Sciences.

REFERENCES

1. A. J. Deeming, *Adv. Organometal. Chem.* 1986, **26**, 1.
2. D. S. Strickland, Ph.D. Thesis, University of Illinois (1983).
3. S. G. Shore, D.-Y. Jan, W.-L. Hsu, S. Kennedy, J. C. Huffman, T.-C. L. Wang and A. G. Marshall, *J. Chem. Soc., Chem. Commun.* 1984, 392.
4. K. A. Azam, C. C. Yin and A. J. Deeming, *J. Chem. Soc., Dalton Trans.* 1978, 1201.
5. R. J. Goudsmit, B. F. G. Johnson, J. Lewis, P. R. Raithby and M. J. Rosales, *J. Chem. Soc., Dalton Trans.* 1983, 2257.
6. J. B. Keister and T. L. Horling, *Inorg. Chem.* 1980, **19**, 2304.
7. M. Tachikawa and J. R. Shapley, *J. Organometal. Chem.* 1977, **124**, C19.
8. A. J. Deeming, R. E. Kimber and M. Underhill, *J. Chem. Soc., Dalton Trans.* 1973, 2589.
9. W.-Y. Yeh, J. R. Shapley, Y.-J. Li and M. R. Churchill, *Organometallics* 1985, **4**, 767.
10. M. R. Churchill, T. S. Janik, T. P. Duggan and J. B. Keister, *Organometallics* 1987, **6**, 799.
11. D. S. Strickland and J. R. Shapley, *Organometallics*, submitted for publication, see also ref. (2).
12. M. R. Churchill, J. W. Ziller, D. M. Dalton and J. B. Keister, *Organometallics* 1987, **6**, 806.
13. K. A. Azam, A. J. Deeming, I. P. Rothwell, M. B. Hursthouse and L. New, *J. Chem. Soc., Chem. Commun.* 1978, 1086.
14. H.-J. Kneuper and J. R. Shapley, *Organometallics* 1987, **6**, 2455.
15. M.-C. Tsai and E. L. Meutterties, *J. Am. Chem. Soc.* 1982, **104**, 2534.
16. C. M. Friend and E. L. Meutterties, *J. Am. Chem. Soc.* 1981, **103**, 773.
17. (a) E. L. Muetterties, *Chem. Soc. Rev.* 1982, **11**, 283; (b) A. L. Johnson, E. L. Muetterties and J. Stöhr, *J. Am. Chem. Soc.* 1983, **105**, 7183.

Polyhedron Vol. 7, No. 10/11, pp. 967–978, 1988
Printed in Great Britain

0277–5387/88 $3.00+.00
© 1988 Pergamon Press plc

THE STRUCTURE, BONDING AND TRANSFORMATION BEHAVIOUR OF IMINIUM, AMINOCARBENE AND AMINOCARBYNE LIGANDS IN TRIOSMIUM CLUSTER COMPLEXES

RICHARD D. ADAMS,* JAMES E. BABIN and HOON-SIK KIM

Department of Chemistry, University of South Carolina, Columbia, SC 29208, U.S.A.

(*Accepted* 5 *November* 1987)

Abstract—A summary of recent developments in the study of the reactions of tertiary amines with triosmium cluster complexes is presented. The relationships between iminium ion ligands, dimethylaminocarbene ligands and dimethylaminocarbyne ligands in several series of triosmium carbonyl cluster complexes are described. The transformations are dominated by binuclear C—H activation processes. Novel ligand coordination modes were characterized by crystallographic methods.

Fischer carbenes are one of the most thoroughly studied of all the ligand systems known to organometallic chemistry.[1] Discoveries involving the chemistry of carbene complexes have contributed to our understanding of catalytic reactions such as the Ziegler–Natta polymerization of olefins,[2] the olefin metathesis reaction[3] and the Fischer–Tropsch reaction.[4] Transition metal carbene complexes have also found applications in organic synthesis.[5]

Until recently, however, the chemistry of carbene ligands in transition metal clusters has received very little attention.[6–11] The lack of significant work in this area may be attributable largely to difficulties encountered in the synthesis of cluster complexes containing carbene ligands. The most common method of carbene ligand synthesis in mononuclear metal complexes, namely, the nucleophilic/electrophilic treatments of carbonyl ligands,[12] does not work well when applied to cluster compounds. Kaesz showed that the acetyl ligand in the complex, $[Os_3(CO)_{11}(COMe)]^-$, generated by the treatment of $Os_3(CO)_{12}$ with MeLi, could not be alkylated to yield a methoxycarbene cluster [eq. (1)].[8]

In addition, complexes containing Fischer carbene ligands have been shown to undergo facile transformations that involve the cleavage of C—H bonds on the α-positioned carbon atom [eq. (2)].[9] In other cases they have been found to combine with seemingly "innocent" ligands [eq. (3)].[11]

An alternative route to the synthesis of carbene ligands is the addition of carbene precursors to the metal complex. Imidoyl chlorides[13] and iminium salts[14] have been employed previously in the synthesis of mononuclear carbene complexes. We have recently found that trimethylamine can serve as a precursor to dimethylaminocarbene ligands by activation of the C—H bonds on one of the methyl groups. The reaction of $Os_3(CO)_9(\mu_3\text{-}CO)(\mu_3\text{-}S)$, **1** with NMe_3 at 125°C yields the trinuclear cluster $Os_3(CO)_8[C(H)NMe_2](\mu_3\text{-}S)(\mu\text{-}H)_2$, **2**, which contains a dimethylaminocarbene ligand, $C(H)NMe_2$.[15] Thermolysis of the cluster $Os_3(CO)_8(NMe_3)(\mu_3\text{-}SC_6H_4)(\mu\text{-}H)_2$, **3**, at 98°C results in the formation of three isomeric hexanuclear carbene clusters $Os_6(CO)_{16}[C(H)NMe_2](\mu_4\text{-}S)(\mu_3\text{-}S)(\mu\text{-}H)_2$, **4**, that contain a dimethylaminocarbene ligand.[16]

While searching for other reagents that may serve

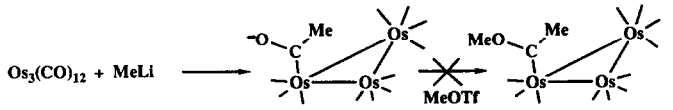

(1)

*Author to whom correspondence should be addressed.

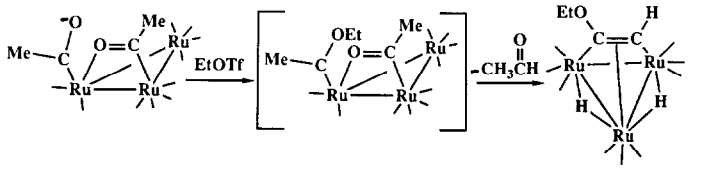

(2)

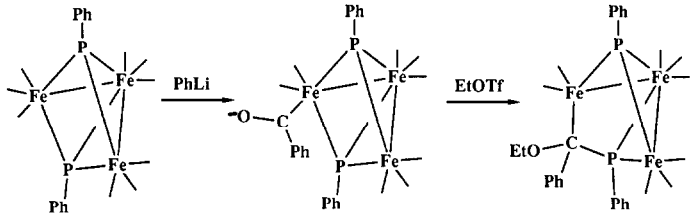

(3)

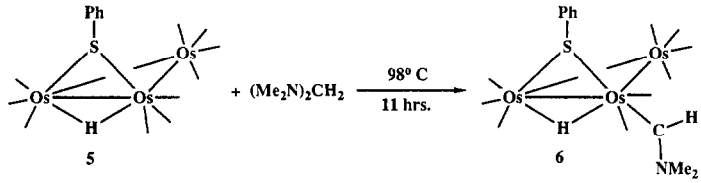

(4)

as useful precursors for carbene ligands, we discovered that tetraalkyldiaminomethanes can also react with transition metal cluster complexes to yield carbene-containing products.[17,18] For example, the reaction of $Os_3(CO)_{10}(\mu\text{-SPh})(\mu\text{-H})$, **5** with $CH_2(NMe_2)_2$ results in the formation of the aminocarbene containing cluster $Os_3(CO)_9[C(H)NMe_2](\mu\text{-SPh})(\mu\text{-H})$; **6** [(eq. (4)].

While the pathway for the transformation of the diamine reagent into carbene ligands has not been established, we have amassed significant evidence to suggest that iminium ion ligands are key intermediates. In this report we will summarize our recent studies involving the synthesis and reactivity of cluster compounds that contain dimethylaminocarbene ligands and will discuss the relationships that we have observed between iminium ion, aminocarbene and aminocarbyne ligands.

SYNTHESIS OF CARBENE CONTAINING CLUSTERS

The aminocarbene cluster $Os_3(CO)_8[C(H)NMe_2](\mu_3\text{-S})(\mu\text{-H})_2$, **2**, was obtained from the reaction of $Os_3(CO)_9(\mu_3\text{-CO})(\mu_3\text{-S})$, **1**, with trimethylamine at 125°C [eq. (5)].[15] Compound **2** was characterized structurally, see Fig. 1 and the dimensions of the carbene ligand were found to be very similar to those in mononuclear metal complexes, (e.g. a planar nitrogen atom, a carbene C—N distance of 1.28 (2) Å and methyl C—N distances of 1.48 (2) Å). The ^1H NMR spectrum of **2** showed a resonance at $\delta = +11.18$ ppm indicative of the hydrogen atom of a terminal secondary carbene ligand.[14(a)]

In contrast to reaction **5** the reaction of $Os_3(CO)_{12}$, **7**, with trimethylamine [eq. (6)], yielded three products in low yield, $Os_3(CO)_{10}(\mu\text{-HC}{=}\text{NMe})(\mu\text{-H})$, **8**, $Os_3(CO)_9(\mu_3\text{-HC}{=}\text{NMe})(\mu\text{-H})$, **9** and $Os_3(CO)_{10}(\mu\text{-CNMe}_2)(\mu\text{-H})$, **10**.[20] Compounds **8** and **9** were formed by C—H activation processes and by the elimination of methane. Compound **10** contains a dimethylaminocarbyne ligand which was derived by C—H activation and elimination of H_2 from the NMe_3 molecule. No carbene

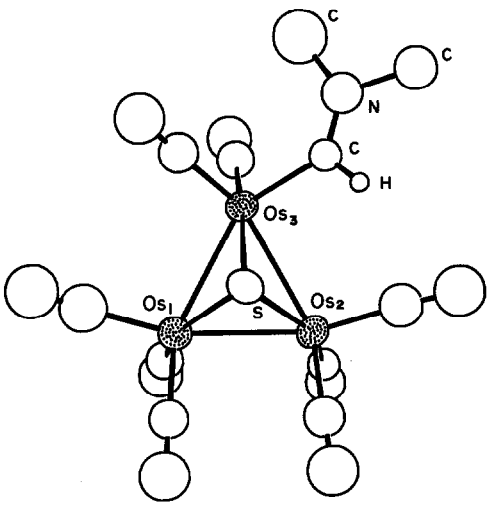

Fig. 1.

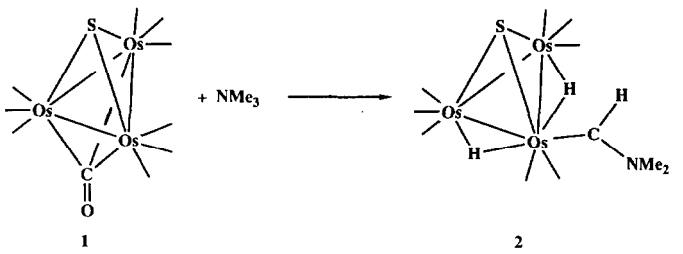

(5)

1 2

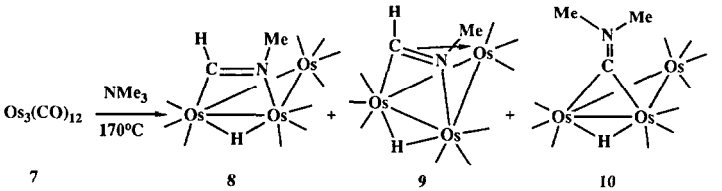

(6)

7 8 9 10

containing products were isolated from this reaction.

Compound **2** exhibits remarkable stability even at temperatures in excess of 150°C, but has been found to serve as an effective catalyst for the metathesis of alkyl groups between tertiary amines [eq. (7)].[21]

$$Et_3N + Pr_3N \xrightarrow[MeOH,\ 145°C]{2} Et_2NPr + EtNPr_2. \quad (7)$$

An extensive study aimed at determining the mechanism of this reaction has been performed and the available evidence indicates that the carbene ligand plays an intimate role in the catalytic process.[22]

Unfortunately, due to the great stability of compound **2** we have not yet succeeded in isolating new products derived from transformations of this carbene ligand. To study the chemistry of the carbene ligand in clusters more thoroughly, it thus, seemed desirable to synthesize other clusters with carbene ligands which might display greater reactivity. Our efforts were rewarded by the preparation of compound **6** from the reaction of **5** with $CH_2(NMe)_2$ at 98°C [eq. (4)]. Compound **6** is structurally very similar to the parent compound, **5**, but has a dimethylaminocarbene ligand coordinated to one of the osmium atoms that contains the bridging thiolato ligand, Fig. 2. The carbene hydrogen signal appears in the ^1H NMR spectrum at a characteristically low field position of +11.71 ppm. Possible intermediates for the formation of this carbene complex will be discussed later in this report. First, we will discuss the reactivity of compound **6** and its derivatives.

PHOTOLYSIS OF $Os_3(CO)_9[C(H)NMe_2](\mu\text{-}SPh)(\mu\text{-}H)$, 6

Photolysis of compound **5** under a carbon monoxide atmosphere yields $Os_3(CO)_9(\mu_3\text{-}CO)(\mu_3\text{-}S)$, **1**, through cleavage of the sulphur–carbon bond and the elimination of benzene. [eq. (8)].[23]

Photolysis of compound **6** however, proceeds in a completely different fashion to yield two products, both of which involve an initial CO dissociation from the $Os(CO)_4$ group. [eq. (9)].

One product, $Os_3(CO)_8[C(H)NMe_2](\mu_3\text{-}SC_6H_4)(\mu\text{-}H)_6$, **11** contains a triply bridging SC_6H_4 ligand

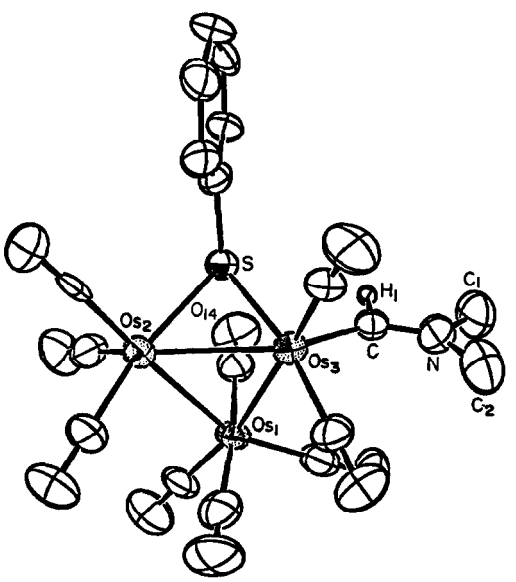

Fig. 2.

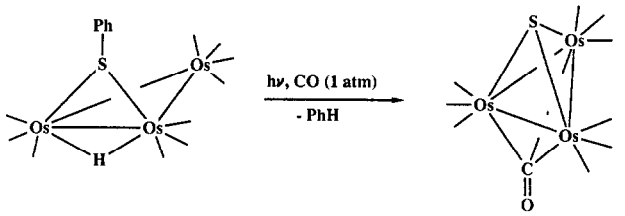

5 1 (8)

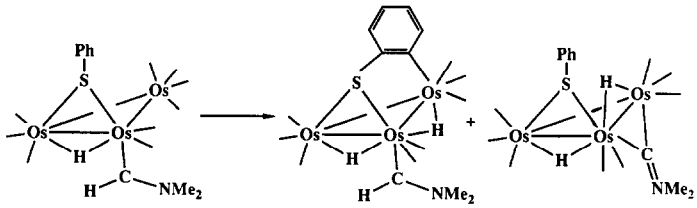

6 11 12 (9)

formed by an *ortho*-metallation of the phenyl group at the third metal. The dimethylaminocarbene ligand was unchanged in the transformation of **10** to **11**.[18]

The second product is $Os_3(CO)_8(\mu\text{-}CNMe_2)(\mu\text{-}SPh)(\mu\text{-}H)_2$, **12**. This complex contains a dimethylaminocarbyne ligand which bridges an edge of the cluster. The carbyne ligand was derived from the carbene ligand in **6** by an oxidative addition of the carbene C—H bond at the adjacent metal atom. The first mononuclear carbyne complexes that were discovered by Fischer were also derived from carbene ligands. These transformations, however, involved Lewis acid promoted activation of C—X bonds where X = Cl, Br, I, $SnPh_3$, SeC_6H_4R, $PbPh_3$ and TePh.[24] The transformation of **6** to **12** is the first example of a *binuclear* activation of a carbene C—H bond.

Compound **12** was also characterized structurally, Fig. 3. The metrical parameters of the carbyne ligand, Os—C = 2.11(2) and 2.00(2) Å and C—N = 1.30(2) Å, are very similar to those found in the carbyne clusters $M_3(CO)_{10}(\mu\text{-}CNMe_2)(\mu\text{-}H)$ M = Os, **8**[25] and Ru, **13**.[26] The short C—N distance indicates a significant degree of multiple bonding between these atoms.[18]

Compound **11** was converted to **12** in a refluxing hexane solution, suggesting that **11** could be an intermediate in the formation of **12**. To test this possibility, the methanethiolato analogue of **10**, $Os_3(CO)_9[C(H)NMe_2](\mu\text{-}SMe)(\mu\text{-}H)$, **14** was prepared. Photolysis of **14** also resulted in a carbene–carbyne transformation to yield $Os_3(CO)_9(\mu\text{-}CNMe_2)(\mu\text{-}SMe)(\mu\text{-}H)$, **15**. In a similar experiment a perflourinated analogue of **6**, $Os_3(CO)_9[C(H)NMe_2](\mu\text{-}SC_6F_5)(\mu\text{-}H)$, **16**, was converted to the aminocarbyne cluster $Os_3(CO)_8(\mu\text{-}CNMe_2)(\mu\text{-}SC_6F_5)(\mu\text{-}H)_2$, **17**. These experiments indicate that **11** is not a necessary intermediate in the formation of **12**. The formation of **11** is merely an alternative way for the intermediate to relieve the unsaturation caused by the loss of CO from **6**.

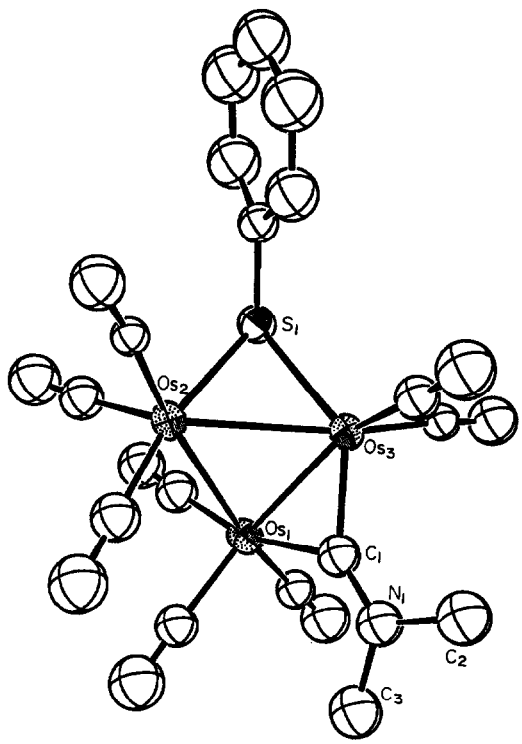

Fig. 3.

HIGH TEMPERATURE PYROLYSIS OF $Os_3(CO)_9[C(H)NMe_2](\mu$-SPh)($\mu$-H), 6

When **5** is pyrolyzed in the absence of solvent in a sealed glass tube at 200°C, benzene elimination occurs and is followed by condensation reactions to yield a wide variety of sulphido–osmium clusters [eq. (10)].[15]

$$\underset{\mathbf{5}}{Os_3(CO)_{10}(\mu\text{-SPh})(\mu\text{-H})} \xrightarrow{200°C} \underset{\mathbf{18}}{Os_3(CO)_9S_2} + \underset{\mathbf{19}}{Os_4(CO)_{12}S} + \underset{\mathbf{20}}{Os_4(CO)_{12}S_2} + \underset{\mathbf{21}}{Os_5(CO)_{15}S} + \underset{\mathbf{22}}{Os_6(CO)_{16}S_2} + \underset{\mathbf{23}}{Os_7(CO)_{20}S_2}. \quad (10)$$

It seemed possible that pyrolysis of **6**, might also yield higher nuclearity clusters, containing carbene ligands.

Pyrolysis of **6** at 200°C resulted in the formation of five products: $Os_3(CO)_9(\mu_3\text{-S})(\mu\text{-H})_2$, **24**, $Os_3(CO)_{10}(\mu\text{-CNMe}_2)(\mu\text{-H})$, **8**, $Os_3(CO)_{10}(\mu\text{-CNMe}_2)(\mu\text{-SPh})$, **25**, $Os_6(CO)_{15}(\mu_3\text{-S})(\mu\text{-CNMe}_2)(\mu\text{-SPh})$, **26** and a red compound which was not completely characterized, **27**.[27] Compounds **24**[28] and **8**[20] have been observed previously.

The remaining products are new. Compound **25** consists of an open triangular cluster of three osmium atoms with the non-bonding osmium–osmium distance bridged by a benzenethiolate ligand and a dimethylaminocarbyne ligand. It is structurally very similar to the cluster $Os_3(CO)_{10}(\mu\text{-OMe})_2$.[29] The carbyne ligand is similar to those observed in **12**[18] and **8**.[20]

The structure of **26** consists of a square pyramidal cluster of five osmium atoms capped on the base by a quadruply bridging sulphido ligand. Two adjacent edges of the square base are bridged by an $Os(CO)_3$ group and a dimethylaminocarbyne ligand. The bond between the basal and edge bridging osmium atoms are also bridged by a benzenethiolato ligand.

THERMOLYSIS OF $Os_3(CO)_8(\mu\text{-CNMe}_2)(\mu\text{-SPh})(\mu\text{-H})_2$, 12

While benzene elimination from **6** was evidently side-tracked by the greater reactivity of the carbene ligand, the product **12** still contained the groups necessary for benzene formation and it seemed plausible that a pyrolysis of **12** might induce the elimination of benzene.

Thermolysis of **12** in refluxing octane did induce cleavage of the sulphur–carbon bond, but the elimination of benzene did not occur. Instead, the phenyl group was transferred from the sulphur atom to the carbyne carbon atom and the new complex $Os_3(CO)_8[C(Ph)NMe_2](\mu_3\text{-S})(\mu\text{-H})_2$, **28** was formed [eq. (11)].[18]

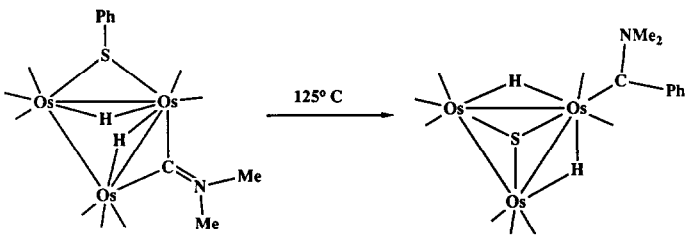

12 28 (11)

Curiously, this product is simply the phenyl–carbene analogue of **2**, Fig. 4. It also exhibits activity towards the *trans*-alkylation reaction. A crossover experiment consisting of the thermolysis of a mixture of **12** and $Os_3(CO)_8(\mu\text{-CNEt}_2)(\mu\text{-S-tol})(\mu\text{-H})_2$, **29**, was performed to determine if the shift of the phenyl group occurred by an intra- or intermolecular pathway. The results given in eq. (12) are consistent only with an intramolecular pathway.

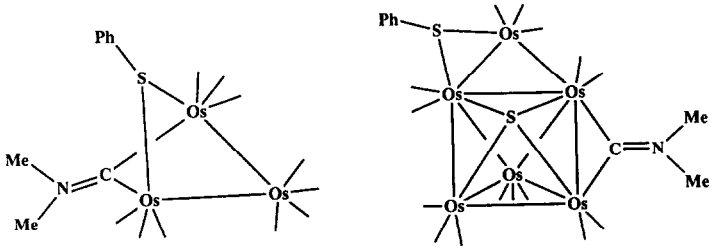

25 26

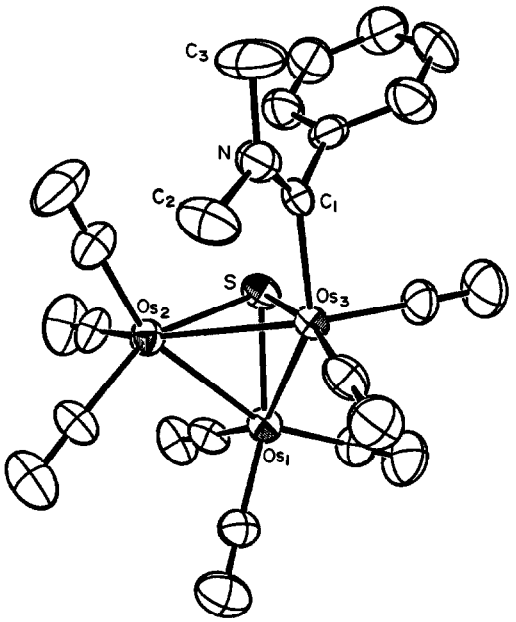

Fig. 4.

It seemed plausible that the mechanism might involve *ortho*-metallated-phenyl intermediates, but the transformation of $Os_3(CO)_8(\mu\text{-}CNMe_2)(\mu\text{-}SC_6F_5)(\mu\text{-}H)_2$, **15** to $Os_3(CO)_8[C(C_6F_5)NMe_2](\mu_3\text{-}S)(\mu\text{-}S)_2$, **33**, strongly indicates that *ortho*-metallated intermediates are not necessary.

A sigmatropic shift process such as those shown in Scheme 1 through which the C—S bond is activated by the third metal of the cluster was proposed.[18] These processes seem reasonable in view of the apparent P—C bond activation induced by the third metal atom of the cluster in the compound $Ru_3(CO)_9(\mu\text{-}PPh_2)(\mu\text{-}H)$, **34**.[30]

The thermolysis of **15**, was also studied.[31] This reaction does not proceed by cleavage of the sulphur–carbon bond, but instead involves a cluster condensation that yields the hexanuclear product $Os_6(CO)_{12}(\mu\text{-}CNMe_2)_2(\mu_3\text{-}SCH_3)_2(\mu\text{-}H)_2$, **35** [eq. (13)]. Compound **35** was found to consist of a novel

$$\begin{array}{l} Os_3(CO)_8(CNMe_2)(SPh)H_2,\ \mathbf{12} \\ \quad + \\ Os_3(CO)_8(CNEt_2)(S\text{-tol})H_2,\ \mathbf{29} \end{array} \xrightarrow{125^\circ C} \begin{array}{c} Os_3(CO)_8[C(Ph)NMe_2](S)H_2,\ \mathbf{28}\ (52\%) \\ + \\ Os_3(CO)_8[C(tol)NMe_2](S)H_2,\ \mathbf{30}\ (0\%) \\ + \\ Os_3(CO)_8[C(Ph)NEt_2](S)H_2,\ \mathbf{31}\ (0\%) \\ + \\ Os_3(CO)_8[C(tol)NEt_2](S)H_2,\ \mathbf{32}\ (43\%) \end{array} \quad (12)$$

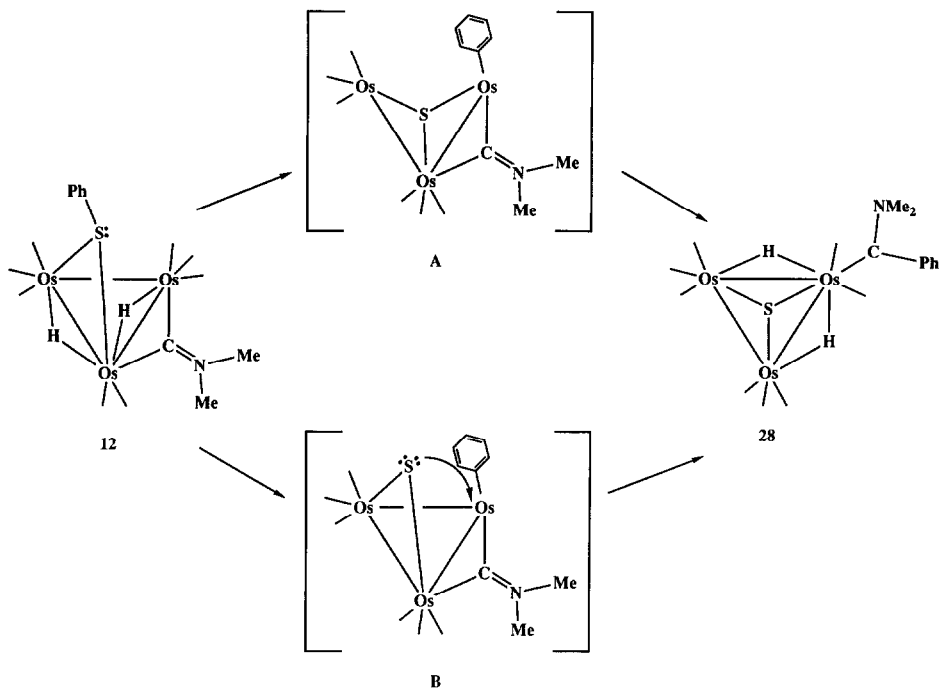

Scheme 1.

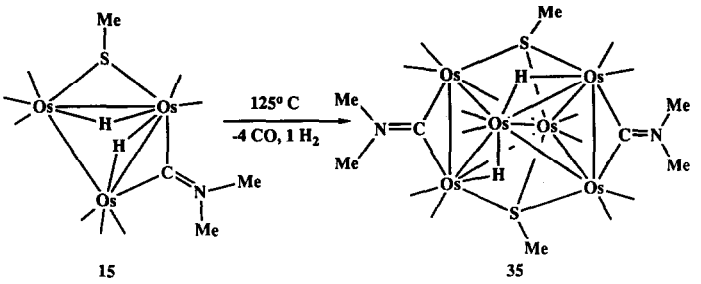

15 35 (13)

edge-fused bitetrahedron of six metal atoms. Bridging carbyne ligands span opposite edges of the cluster. There are also two triply bridging methanethiolato ligands.

SYNTHESIS AND REACTIVITY OF CLUSTERS CONTAINING IMINIUM ION LIGANDS

A point of great interest is the mechanism for the formation of the carbene ligands from the tetraalkyldiaminomethanes. The first insight into the mechanism of carbene formation was obtained from the reaction of the carbyne containing cluster **12** with tetramethyldiaminomethane. Two products were formed that were found to be isomers with the formula $Os_3(CO)_7(\mu\text{-}CNMe_2)(H_2CNMe_2)(\mu\text{-}SPh)(\mu\text{-}H)$, **36** and **37**[32] [eq. (14)].

Compound **36** contains a π-complexed *N,N*-dimethyliminium ligand in addition to bridging benzenethiolato and dimethylaminocarbyne ligands, Fig. 5. This type of bonding has been observed for iminium ligands in mononuclear metal complexes.[33] The short C—N distance of 1.42(2) Å indicates the existence of a significant amount of C—N multiple bonding.

Compound **37** also contains an *N,N*-dimethyliminium ligand, but in this case the iminium ligand bridges an edge of the cluster, Fig. 6. The C—N distance of 1.50(2) Å, is slightly longer than that of a normal C—N single bond.[34] This ligand may be described more accurately as a bridging dimethylaminomethyl ligand.

When heated to reflux in a heptane solution under a CO atmosphere, **36** was converted into **37**. This

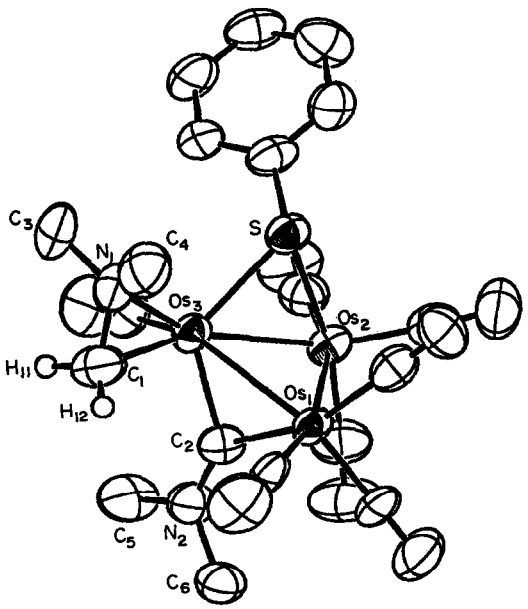

Fig. 5.

transformation involves a shift of the carbyne ligand, from one pair of metal atoms to another. Intermediates containing terminal and triply bridging carbyne ligands have been proposed, Scheme 2. The initial step may involve a CO induced cleavage of the Os—N bond in **36** to yield a terminal dimethylaminomethyl ligand. The nitrogen atom may then attack the second osmium atom to form the bridging iminium ligand.

The formation of **36** most likely proceeds by formation of a CO-substituted intermediate such as

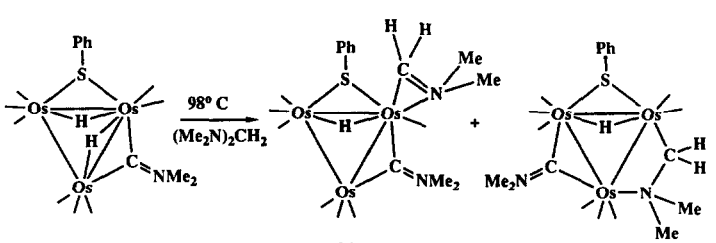

12 36 37 (14)

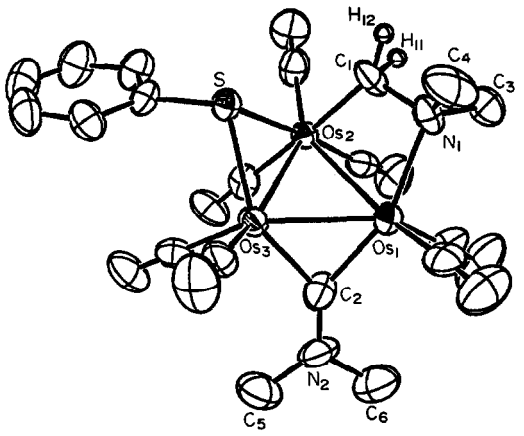

Fig. 6.

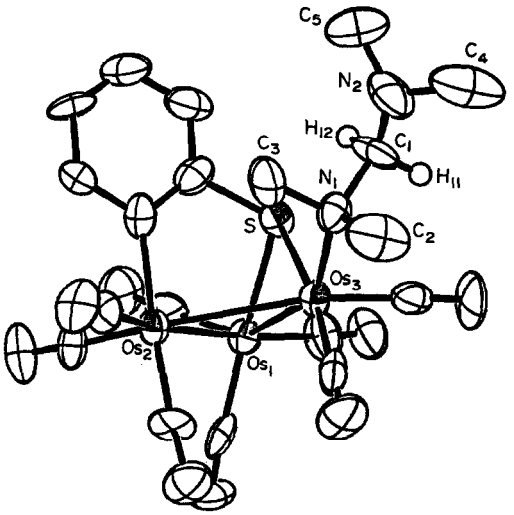

Fig. 7.

$Os_3(CO)_7(\mu\text{-}CNMe_2)(Me_2NCH_2NMe_2)(\mu\text{-}SPh)(\mu\text{-}H)_2$, **38**. A coordinated diamine ligand was found in the cluster $Os_3(CO)_8(Me_2NCH_2NMe_2)(\mu\text{-}SC_6H_4)(\mu\text{-}H)_2$, **39**, obtained from the reaction of **3** with $CH_2(NMe_2)_2$, Fig. 7.[33] A diamine ligand of this type could undergo cleavage of a carbon–nitrogen bond and eliminate a dimethylamido grouping. A proton is also eliminated in this process. This would combine with the dimethylamido group to yield dimethylamine.

Thermolysis of compound **37** results in an activation of both C—H bonds of the methylene group of the iminium ligand to yield the cluster $Os_3(CO)_7(\mu\text{-}CNMe_2)_2(\mu\text{-}SPh)(\mu\text{-}H)$, **40**,[35] which contains two dimethylaminocarbyne ligands. Details of this transformation have not yet been established.

An iminium containing cluster, $Os_3(CO)_8(\eta^2\text{-}HC(Ph)NMe_2)(\mu_3\text{-}S)(\mu\text{-}H)$, **41**, was obtained by heating the *ortho*-metallated cluster **11** in refluxing $CHCl_3$ [eq. (15)], Fig. 8.[36] The formation of **41** occurs by a transfer of the metallated-phenyl group

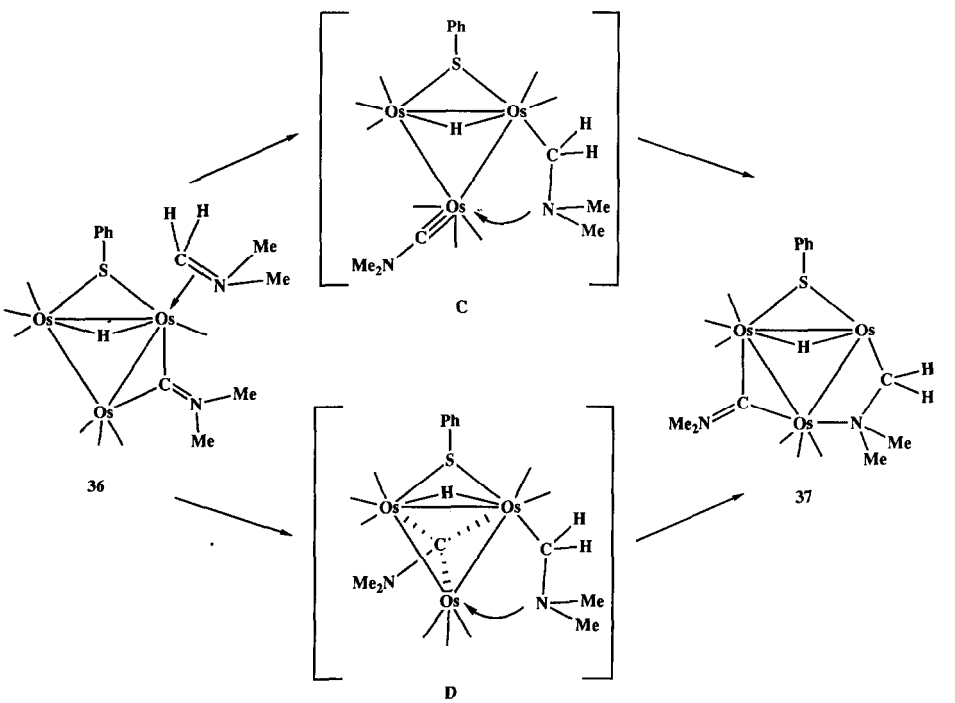

Scheme 2.

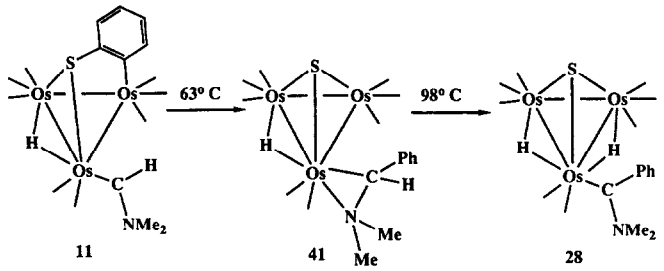

(15)

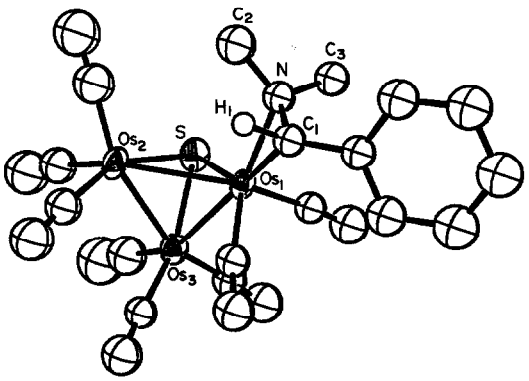

Fig. 8.

from the sulphur and metal atoms to the carbene carbon atom. In this case the iminium C—N distance of 1.48(3) Å is similar to that of a C—N single bond.[37]

Treatment of **41** in refluxing heptane resulted in a nearly quantitative transformation to the phenylcarbene cluster **28**.[36] This conversion must proceed by activation of the iminium C—H bond. Compound **41** may be an analogue of the intermediate traversed in the formation of **2**, from the reaction of **1** with NMe_3.[15]

An interesting series of products was obtained from the reaction of $Os_3(CO)_{10}(\mu\text{-}H)_2$, **42** with $CH_2(NMe_2)_2$. The first product is $Os_3(CO)_{10}(\mu\text{-}\eta^2\text{-}H_2CNMe_2)(\mu\text{-}H)$, **43**, which contains a bridging *N,N*-dimethyliminium ligand.[25] (Fig. 9.)

When compound **43** was heated to 98°C, two products were obtained. One of these is $Os_3(CO)_{10}(\mu\text{-}CNMe_2)(\mu\text{-}H)$, **10**. The other is the new compound $Os_3(CO)_9(\mu_3\text{-}\eta^2\text{-}C(H)NMe_2)(\mu\text{-}H)_2$, **44**, which contains a dihapto triply bridging dimethylaminocarbene ligand.[38] This product was characterized structurally, see Fig. 10. The carbene C—N distance of 1.46(5) Å, is similar to that of a C—N single bond and is significantly longer than those in terminal carbene ligands (e.g. C—N = 1.28 Å).

The conversion of **43** to **44** is believed to occur by a binuclear C—H activation process that is initiated by the loss of CO from the $Os(CO)_4$ group, eq. (16). The vacant coordination site on the intermediate **E** reacts by an oxidative addition of the methylene C—H bond.

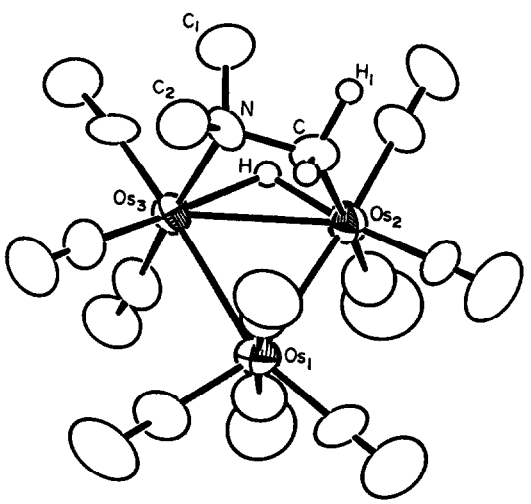

Fig. 9.

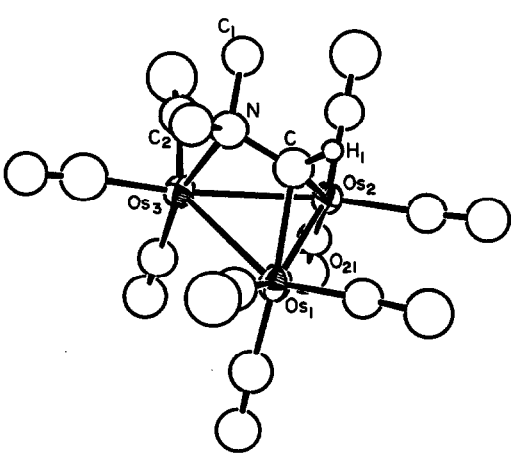

Fig. 10.

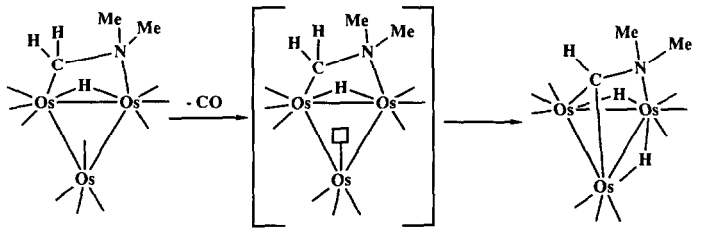

43 E 44

(16)

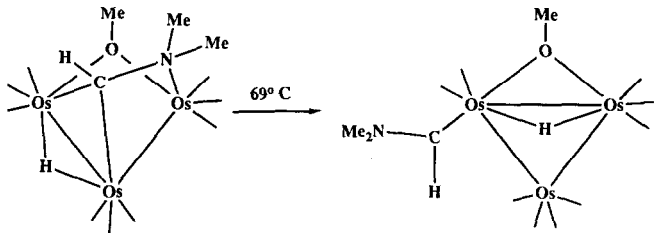

46 47

(17)

Compound **44** can be converted to **10** at 125°C under a CO atmosphere; but there appears to be a second route for the conversion of **43** to **10**, since **44** is not converted to **10** under the conditions of the original reaction.

Another complex containing a triply bridging carbene ligand was formed from the reaction of $Os_3(CO)_{10}(\mu\text{-OMe})(\mu\text{-H})$, **45**, with tetramethyldiaminomethane. This compound $Os_3(CO)_9(\mu_3\text{-}\eta^2\text{-}C(H)NMe_2)(\mu\text{-OMe})(\mu\text{-H})$, **46**, was isolated along with an analogue of the thiolato carbene cluster, **5**, $Os_3(CO)_9[C(H)NMe_2](\mu\text{-OMe})(\mu\text{-H})$, **47**.[38]

Compound **46** contains only two metal–metal bonds. When heated to 69°C, the Os—N bond is cleaved, the cluster closes to a triangle and the carbene ligand is shifted into a terminal bonding mode, eq. (17).

CONCLUSION

In the course of studying several systems, we have observed all the elements of the transformation series involving iminium, aminocarbene and aminocarbyne ligands (e.g. Scheme 3). Reaction of the diaminomethane reagents with hydride containing clusters results initially in substitution prod-

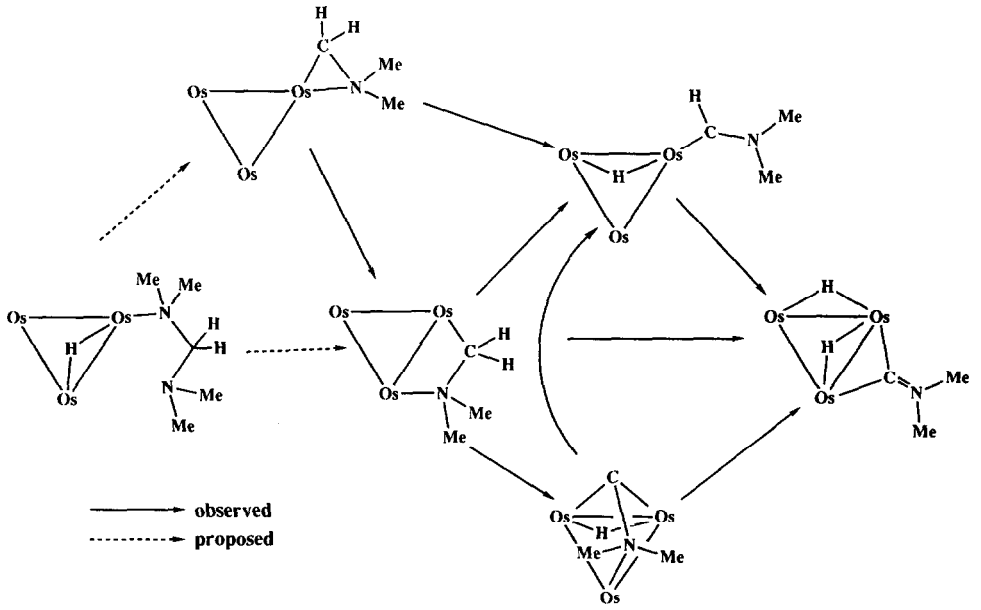

Scheme 3.

ucts. A carbon–nitrogen bond in this coordinated diamine may then be cleaved, apparently by a hydride abstraction/nucleophilic displacement process, to yield either π-complexed or bridging *N,N*-dimethyliminium ligands. The π-complexed iminium ligands can be converted to bridging iminium ligands, or be transformed to carbene ligands by C—H activation processes. By a second C—H activation process, the carbene ligands may be converted to carbyne ligands.

These transformations illustrate the importance of polynuclear ligand coordinations in the chemistry of transition metal cluster compounds.[39] The isolation of bridging iminium, aminocarbene and aminocarbyne ligands in these systems suggests that intermediates with bridged ligands must play key roles in these cluster-based ligand transformations.

It is hoped that other carbene containing clusters will be synthesized by using the methodology reported herein. The study of clusters containing carbene ligands is still in its infancy, but its future now appears to be as promising and as exciting as the study of mononuclear metal carbene complexes was 20 years ago.

REFERENCES

1. For Reviews on Carbene Chemistry See: (a) D. J. Cardin, B. Cetinkaya and M. F. Lappert, *Chem. Rev.* 1972, **72**, 545; (b) F. A. Cotton and C. M. Lukehart, *Prog. Inorg. Chem.* 1972, **16**, 487; (c) F. J. Brown, *Prog. Inorg. Chem.* 1980, **27**, 1; (d) E. O. Fischer, *Pure Appl. Chem.* 1970, **24**, 407; (e) E. O. Fischer, *Pure Appl. Chem.* 1972, **30**, 353; (f) E. O. Fischer, U. Schubert and H. Fischer, *Pure Appl. Chem.* 1978, **50**, 857; (g) E. O. Fischer, *Adv. Organomet. Chem.* 1976, **14**, 1; (h) M. F. Lappert, *J. Organomet. Chem.* 1975, **100**, 139; (i) R. R. Schrock, *Acc. Chem. Res.* 1979, **12**, 98; (j) K. H. Dötz, H. Fischer, P. Hofmann, F. R. Kreissl, U. Schubert and K. Weiss, *Transition Metal Carbene Complexes.* Verlag Chemie, Weinheim (1983).
2. (a) H. Sinn and W. Kaminsky, *Adv. Organomet. Chem.* 1980, **18**, 99; (b) P. Pino and R. Mülhaupt, *Angew. Chem. Int. Ed. Engl.* 1980, 857.
3. (a) E. O. Fischer, G. Kreis, C. G. Kreiter, J. Müller, G. Huttner and H. Lorenz, *Angew. Chem. Int. Ed. Engl.* 1973, **12**, 564; (b) E. O. Fischer and U. Schubert, *J. Organomet. Chem.* 1975, **100**, 59; (c) S. M. Rocklage and R. R. Schrock, *J. Am. Chem. Soc.* 1982, **104**, 3077; (d) N. Calderon, J. P. Lawrence and E. A. Ofstead, *Adv. Organomet. Chem.* 1979, **17**, 449; (e) R. H. Grubbs, *Coord. Chem. Rev.* 1978, **24**, 1.
4. (a) R. R. Schrock, *Acc. Chem. Res.* 1979, **12**, 98; (b) H. Henrici-Olivé and S. Olivé, *Catalyzed Hydrogenation of Carbon Monoxide*, Chap. 9. Springer, New York (1984).
5. J. P. Collman, L. S. Hegedus, J. R. Norton and R. G. Finke, *Principles and Applications of Organotransition Metal Chemistry*, 2nd Edn, Chap. 16 and refs therein. University Science, Mill Valley (1987).
6. (a) T. V. Ashworth, M. Berry, J. A. K. Howard, M. Laguna and F. G. A. Stone, *J. Chem. Soc., Dalton Trans.* 1980, 1615; (b) M. F. Lappert and P. L. Dye, *J. Chem. Soc., Dalton Trans.* 1977, 2172.
7. C. M. Jensen, T. J. Lynch, C. B. Knobler and H. D. Kaesz, *J. Am. Chem. Soc.* 1982, **104**, 4679.
8. C. M. Jensen, C. B. Knobler and H. D. Kaesz, *J. Am. Chem. Soc.* 1984, **106**, 5926.
9. C. M. Jensen and H. D. Kaesz, *J. Am. Chem. Soc.* 1983, **105**, 6969.
10. J. R. Shapley, W. Y. Yeh, M. R. Churchill and Y. Li, *Organometallics* 1985, **4**, 1898.
11. G. D. Williams, G. L. Geoffroy, R. R. Whittle and A. L. Rheingold, *J. Am. Chem. Soc.* 1985, **107**, 729.
12. (a) E. O. Fischer, H. J. Beck, C. G. Kreiter, J. Lynch, J. Muller and E. Winkler, *Chem. Ber.* 1972, **105**, 162; (c) E. O. Fischer and H. Fischer, *Chem. Ber.* 1974, **107**, 657; (d) M. Y. Darensbourg and D. J. Darensbourg, *Inorg. Chem.* 1970, **9**, 32; (e) J. A. Connor and E. M. Jones, *J. Chem. Soc., Dalton Trans.* 1973, 2119.
13. (a) M. F. Lappert and A. J. Oliver, *J. Chem. Soc., Dalton Trans.* 1974, 65; (b) P. B. Hitchcock, M. F. Lappert, G. M. McLaughlin and A. J. Oliver, *J. Chem. Soc., Dalton Trans.* 197, **4**, 68; (c) H. Brunner and J. Wachter, *J. Organomet. Chem.* 1978, **155**, C29; (d) H. Brunner, H. G. Kerkien and J. Wachter, *J. Organomet. Chem.* 1982, **224**, 301.
14. (a) A. J. Hartshorn, M. F. Lappert and K. Turner, *J. Chem. Soc., Dalton Trans.* 1978, 348; (b) C. W. Fong and G. Wilkinson, *J. Chem. Soc., Dalton Trans.* 1975, 1100.
15. R. D. Adams, H. S. Kim and S. Wang, *Inorg. Chem.* 1985, **107**, 6107.
16. R. D. Adams, J. E. Babin and H. S. Kim, *Inorg. Chem.* 1986, **25**, 4319.
17. R. D. Adams, J. E. Babin and H. S. Kim, *Organometallics* 1986, **5**, 1924.
18. R. D. Adams, J. E. Babin and H. S. Kim, *J. Am. Chem. Soc.* 1987, **109**, 1414.
19. (a) J. A. Connor and O. S. Mills, *J. Chem. Soc.* (*a*) 1969, 334; (b) E. K. Barefield, A. M. Carrier, D. J. Sepelak and D. G. Van Derveer, *Organometallics* 1982, **1**, 103; (c) B. Cetinkaya, M. T. Lappert, G. M. McLaughlin and K. Turner, *J. Chem. Soc., Dalton Trans.* 1974, 1591.
20. C. C. Yin and A. J. Deeming, *J. Organomet. Chem.* 1977, **133**, 123.
21. (a) S. I. Marahashi, T. Hirano and T. J. Yano, *J. Am. Chem. Soc.* 1978, **100**, 348; (b) R. M. Laine and R. B. Wilson Jr, *J. Am. Chem. Soc.* 1985, **107**, 361; (c) Y. Shvo and R. M. Laine, *J. Chem. Soc., Chem. Commun.* 1980, 753; (d) S. I. Murahashi, N. Yoshimura, T. Tsumiyama and R. Kojima, *J. Am. Chem. Soc.* 1983, **105**, 5002. (e) R. M. Laine, D. W. Thomas and L. W. Cary, *J. Am. Chem. Soc.* 1982, **104**, 1763.
22. R. D. Adams, J. E. Babin, H. S. Kim and S. Wang, report in preparation.

23. R. D. Adams., I. T. Horvath and H. S. Kim, *Organometallics* 1984, **3**, 548.
24. (a) H. Fischer, A. Motsch and W. Kleine, *Angew. Chem. Int. Ed. Engl.* 1978, **17**, 842; (b) E. O. Fischer. W. Kleine, F. R. Kreissl, H. Fischer, P. Friedrich and G. Huttner, *J. Organomet. Chem.* 1977, **128**, C49; (c) E. O. Fischer, H. Fischer, V. Schubert and R. B. A. Pardy, *Angew. Chem. Int. Ed. Engl.* 1979, **18**, 871; (d) E. O. Fischer, D. Himmelrich, R. Cai, H. Fischer, U. Schuber and B. Zimmer-Gasser, *Chem. Ber.* 1981, **114**, 3209; (e) H. Fischer, E. O. Fischer and R. Cai, *Chem. Ber.* 1982, **115**, 2707; (f) H. Fischer, E. O. Fischer, R. Cai and P. Himmelreich, *Chem. Ber.* 1983, **116**, 1009.
25. R. D. Adams and J. E. Babin, *Organometallics*, in press.
26. M. R. Churchill, B. G. DeBoer and F. J. Rotella, *Inorg. Chem.* 1976, **15**, 1843.
27. R. D. Adams and J. E. Babin, *Organometallics* 1987, **6**, 2236.
28. A. J. Deeming and M. Underhill, *J. Organomet. Chem.* 1972, **42**, C60.
29. V. I. Allen, R. Mason and P. B. Hitchcock, *J. Organomet. Chem.* 1977, **140**, 297.
30. S. A. MacLaughlin, A. J. Carty and N. J. Taylor, *Can. J. Chem.* 1982, **60**, 87.
31. R. D. Adams and J. E. Babin, *Inorg. Chem.* 1987, **26**, 980.
32. R. D. Adams, J. E. Babin and H. S. Kim, *Organometallics* 1987, **6**, 749.
33. R. D. Adams and J. E. Babin, unpublished results.
34. (a) E. W. Abel, R. S. Rowley, R. Mason and K. M. Thomas, *J. Chem. Soc., Chem. Commun.* 1974, 72; (b) D. J. Sepelak, C. G. Pierpont, E. K. Barefield, J. T. Budz and C. A. Poffenberger, *J. Am. Chem. Soc.* 1976, **98**, 6178; (c) S. S. Crawford, C. B. Knobler and H. D. Kaesz, *Inorg. Chem.* 1977, **16**, 3201.
35. R. D. Adams and J. E. Babin, report in preparation.
36. R. D. Adams and J. E. Babin, *J. Am. Chem. Soc.* 1987, **109**, 6872.
37. *International Tables for X-Ray Crystallography*, Vol. III, p. 276, Table 4.2.4. Kynoch Press, Birmingham, U.K. (1975).
38. R. D. Adams and J. E. Babin, *Organometallics* 1987, **6**, 1364.
39. (a) R. D. Adams and I. T. Horvath, *Prog. Inorg. Chem.* 1985, **33**, 127; (b) E. L. Muetterties, *Bull. Soc. Chim. Belg.* 1976, **85**, 451.

Polyhedron Vol. 7, No. 10/11, pp. 979–985, 1988
Printed in Great Britain

0277–5387/88 $3.00+.00
© 1988 Pergamon Press plc

REACTIONS OF ACETYLENIC ALDEHYDES, ETHERS AND CARBOXYLIC ACIDS WITH TRIOSMIUM AND TRIRUTHENIUM CLUSTERS

ALEJANDRO J. ARCE and YSAURA DE SANCTIS

Instituto Venezolano de Investigaciones Cientificas, Chemistry Center, Apartado 21827, Caracas 1020-A, Venezuela

and

ANTONY J. DEEMING*

Department of Chemistry, University College London, 20 Gordon Street, London WC1H 0AJ, U.K.

(*Accepted* 5 *November* 1987)

Abstract—The hydrido cluster $[Os_3H_2(CO)_{10}]$ reacts with $CH{\equiv}CCHO$ to give $[Os_3H(CO)_{10}(CH_2{=}CCHO)]$ in which the ligand is bridging as a three-electron donor through the oxygen and the unsaturated α-carbon atom. On thermolysis in refluxing cyclohexane, two compounds are formed. One is the isomer $[Os_3H(CO)_{10}(cis\text{-}CH{=}CHCHO)]$ which has an open structure with two Os—Os bonds, since the organic ligand is now a five-electron donating bridge. The other product is the dinuclear derivative $[Os_2H(CO)_6(cis\text{-}CH{=}CHCHO)]$. The clusters $[Os_3H_2(CO)_{10}]$, $[Os_3(CO)_{10}(MeCN)_2]$ and $[Ru_3(CO)_{10}(MeCN)_2]$ react with $CH{\equiv}CCH_2OMe$ to give $[M_3(CO)_{10}(CH{=}CCH_2OMe)]$ (M = Ru or Os), $[Os_3(CO)_9(RCCHCOCH{=}CR)]$ and $[Os_3(CO)_9\{(RC_2H)_2CO\}]$ (R = CH_2OMe), where the last two correspond to alkyne-coupled products. $[Os_3H_2(CO)_{10}]$ and $[Os_3(CO)_{10}(MeCN)_2]$ react smoothly with $CH{\equiv}CCO_2H$ to give, as expected, the carboxylato derivative $[Os_3H(CO)_{10}(CH{\equiv}CCO_2)]$ which contains an uncoordinated alkyne group. With the aim of producing linked clusters we reacted this compound with $[M_3(CO)_{10}(MeCN)_2]$ (M = Ru or Os) to give the two linked clusters in high yields: $[Os_6H(CO)_{20}(\mu^5\text{-}CH{\equiv}CCO_2)]$ and $[Os_3Ru_3H(CO)_{20}(\mu^5\text{-}CH{\equiv}CCO_2)]$.

We have been interested in the coordination and rearrangements of small organic ligands containing oxygen atoms in trinuclear clusters, in view of the importance of oxy-ligands of various sorts in the chemical modification of CO in clusters. Previously, we have reported studies on oxy-ligands derived from aldehydes (saturated[1] or unsaturated[2]), unsaturated ethers,[3] ketones (saturated[1] or unsaturated)[4] and formyl derivatives of heterocycles,[5] among others.

Organic oxy-ligands readily coordinate through an oxygen atom by chelation, or bridging in triosmium clusters when this is geometrically allowed.[2,3] For example, αβ-unsaturated aldehydes RCH=CHCHO, react with triosmium clusters by competitive oxidative additions with cleavage of a vinylic C—H bond to give compounds of the type $[Os_3H(CO)_{10}(RC{=}CHCHO)]$, or with cleavage of the aldehydic C—H bond to give μ-acyl clusters of the type $[Os_3H(CO)_{10}(RCH{=}CHCO)]$ (Scheme 1).[3]

In both cluster products the oxygen atom of the organic carbonyl ligand is coordinated, even though one could easily envisage alternative structures in which there is η^2-coordination through the available C=C bond. Indeed, if the organic carbonyl group is not set up for bridging or chelation, as is the case

*Author to whom correspondence should be addressed.

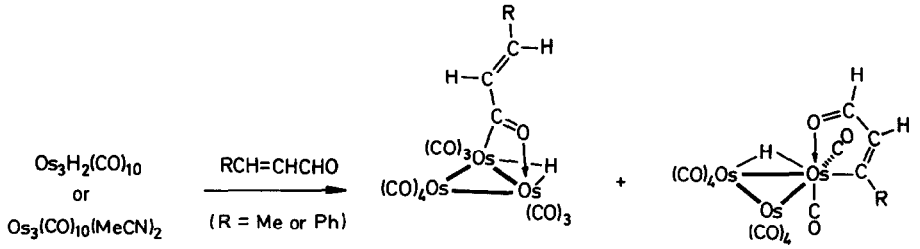

Scheme 1.

with $[Os_3H(CO)_{10}(trans\text{-}CH{=}CHCH_2CH_2COMe)]$, then η^2-alkene coordination is found and the ketone remains uncoordinated. This particular compound contains a normal μ,η^2-vinyl bridge. Chemistry related to that in Scheme 1 is found for $\alpha\beta$-unsaturated ketones except, of course that, μ-acyl complexes are not accessible. We have found that the mode of coordination of the cyclometallated product depends upon the substituents at carbon. Thus $CH_2{=}CHCOMe$ and $RCH{=}CHCOMe$ (R = Me or Ph) give related compounds but of different structure (see Scheme 2).[4] Both types of product have the stoichiometry $[Os_3H(CO)_{10}(RC{=}CHCOMe)]$ (R = H, Me, or Ph) and both are formed by cyclometallation with oxidative addition involving β-C—H bond cleavage. However, if R is bigger than a hydrogen atom η^2-coordination of the alkene is apparently prevented (most likely for steric reasons). The organic ligand is a three-electron donor and a closed triangular metal cluster is formed. When R = H the ligand can donate five electrons and the cluster opens out since only two Os—Os bonds are then required. Oxygen coordination occurs whatever.

In this paper we describe the syntheses of several triosmium and triruthenium clusters derived from the reactive clusters $[Os_3H_2(CO)_{10}]$, $[Os_3(CO)_{10}(MeCN)_2]$ and $[Ru_3(CO)_{10}(MeCN)_2]$ with prop-2-ynal ($CH{\equiv}CCHO$), prop-2-ynoic acid ($CH{\equiv}CCO_2H$) and methyl prop-2-ynyl ether ($CH{\equiv}CCH_2OMe$). We believed that the alkyne function would strongly bond to the cluster and donate four electrons and that this might work against oxygen atom coordination. In the case of $CH{\equiv}CCH_2OMe$ no coordination through the oxygen atom was observed, as expected for a weakly coordinating ether group in the presence of the strongly coordinating alkyne function. This contrasts with methyl vinyl ether which gives an insertion product $[Os_3H(CO)_{10}(\mu\text{-}MeCHOMe)]$ with ether coordination.[3] Only alkyne and coupled alkyne products were obtained from $CH{\equiv}CCH_2OMe$, i.e. the only reactions to occur are through the alkyne function. With triosmium clusters, $CH{\equiv}CCHO$ reacts by coordination and insertion, while $CH{\equiv}CCO_2H$ reacts initially through coordination of the carboxylate group rather than through the alkyne. However, we could subsequently synthesize compounds with the $CH{\equiv}CCO_2$ ligand bridging two M_3 clusters by bonding to two metal atoms at one cluster and to three at the other, so that $CH{\equiv}CCO_2$ behaves as a μ_5-seven-electron donor.

RESULTS AND DISCUSSION

The alkyne $CH{\equiv}CCH_2OMe$ reacts with $[Os_3H_2(CO)_{10}]$, $[Os_3(CO)_{10}(MeCN)_2)]$ and $[Ru_3(CO)_{10}(MeCN)_2]$ to give compounds **(1)**–**(4)** (Scheme 3). The structures are based on ν(CO) IR and ^{1}H NMR spectra which are quite characteristic for these known types of compound.[6]

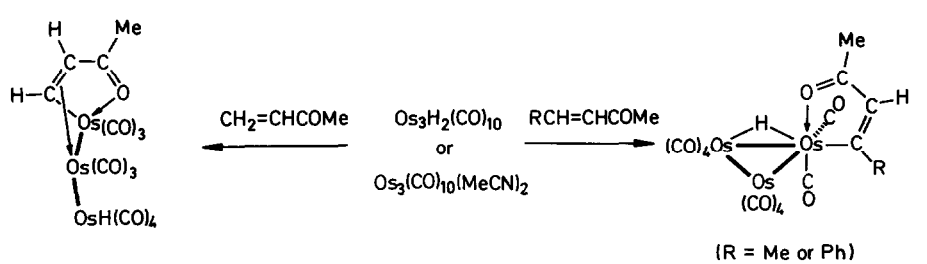

Scheme 2.

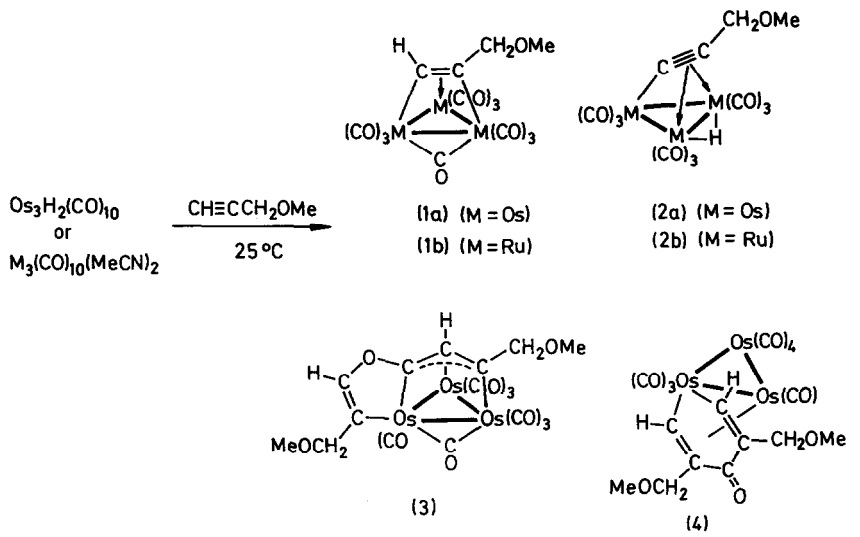

Scheme 3.

Compounds (**1a**) and (**1b**) adopt the usual bridging CO structure [ν(CO) 1850 and 1880 cm^{-1}, respectively] and ready decarbonylation of these compounds above 85°C affords compounds (**2a**) and (**2b**) almost quantitatively. Compound (**2b**) is unstable in solution and in air. The ^1H NMR spectra of compounds (**1a**) and (**1b**) require that there is mobility of the alkyne ligand with respect to the metal triangles, leading to exchange of the diastereotopic CH_2 protons. The osmium compound (**1a**) shows separate signals for these protons (an AB-quartet) at room temperature, but this is well above the coalescence temperature for the ruthenium compound (**1b**) and an AB-quartet is only observed for the CH_2 group at −73°C. The process giving this exchange is an enantiomerization. Rotation of the alkyne (in conjunction with CO migration) occurs by the plane of the ligand passing through an angle orthogonal to the metal plane and back into a tilted orientation. The formulations of compounds (**3**) and (**4**) shown in Scheme 3 are based on IR and ^1H NMR spectroscopic data (Table 1) which were compared with those of analogous compounds obtained from the reactions of $[Os_3(CO)_{12}]$ with PhC≡CH[7] and $[Os_3H_2(CO)_{10}]$ with RC≡CH.[8]

The cluster $[Os_3H_2(CO)_{10}]$ reacts with prop-2-ynal (CH≡CCHO) under mild conditions to afford, in moderate yields, the compound $[Os_3H(CO)_{10}(CH_2CCHO)]$ (**5**). By comparison of the IR and ^1H NMR data with those of $[Os_3H(CO)_{10}(PhCH{=}CCHO)]$,[2] we were able to assign the structure shown in Scheme 4. The organic carbonyl is coordinated [ν(CO) 1515 cm^{-1}] and the ^1H NMR spectrum of (**5**) shows two doublets at δ 7.40 and 7.30 (J = 2.3 Hz) corresponding to *gem* coupling and a low field singlet at δ 9.5 for the CHO proton. Thus compound (**5**) is closely related in structure to the oxidative addition (cyclometallation) product of cyclohex-2-enone, $[Os_3H(CO)_{10}C_6H_7O)]$, which we have already reported.[9] On thermolysis of compound (**5**) an interesting isomerization to $[Os_3H(CO)_{10}(cis\text{-}CH{=}CHCHO)]$ (**6**) occurs. Compound (**6**) was isolated together with the closely related dimer (**7**) formed by loss of an $Os(CO)_4$ group (Scheme 4). The aldehydic and

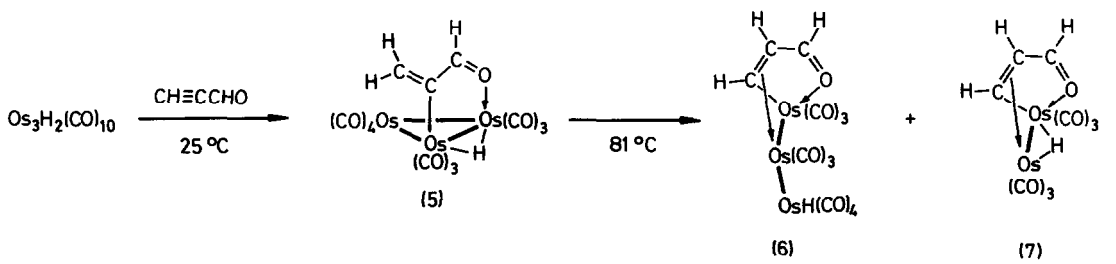

Scheme 4.

Table 1. Some spectroscopic data for the compounds (**1**)–(**9**)

Compound	ν(CO)[a] (cm^{-1})	^1H NMR[b]
$[Os_3(CO)_{10}(CH^x{=}CCH_2^{yz}OMe^w)]$ (**1a**)	2100m, 2061vs, 2055vs, 2020s, 2004m, 1848 (μ-CO)	9.3(s,x) 4.1(d,y) $J_{xy} = 14$ 3.5(d,z) 3.3(s,w)
$[Ru_3(CO)_{10}(CH^x{=}CCH_2^{yz}OMe^w)]$ (**1b**)	2096w, 2058vs, 2052vs, 2026s, 2006m, 1880(μ-CO)	8.3(s,x) 3.8(s,yz) 3.3(s,w) 3.4(d,y) $J_{yz} = 1.7$[c] 4.0(d,z)
$[Os_3H(CO)_9(C{\equiv}CCH_2^xOMe^y)]$ (**2a**)	2100m, 2075s, 2054s, 2020vs, 2013vs, 1982m	5.0(s,x) 3.6(s,y) −23.6(s,OsH)
$[Ru_3H(CO)_9(C{\equiv}CCH_2^xOMe^y)]$ (**2b**)	2102m, 2082s, 2066s, 2036vs, 2006m, 1975w	4.6(s,x) 3.5(s,y) −21.0(s,RuH)
$[Os_3(CO)_9(Me^xOCH_2^{yz}C{=}CH^pOCCH^qCCH_2^{yz}OMe^x)]$ (**3**)	2096m, 2060vs, 2032vs, 2026sh, 2011m, 1990m, 1846(μ-CO)	8.9(s,q) 7.2(s,p) 4.8, 4.2(d,yz) $J_{yz} = 12$ 4.6, 4.4(d,yz) $J_{yz} = 4$ 3.5, 3.4(s,x)
$[Os_3(CO)_9\{(CH^x{=}CCH_2^{yz}OMe^w)_2CO\}]$ (**4**)	2094m, 2060vs, 2050vs, 2021s, 2012m, 2000m, 1978w, 1635(C=O)	6.1(s,x) 4.6, 3.9(d,yz) $J_{yz} = 15$ 3.5(s,w)
$[Os_3H(CO)_{10}(CH_2^{xy} = CCH^zO)]$ (**5**)	2100m, 2062vs, 2050s, 2022vs, 2008m, 2002s, 1996br, 1985m, 1968m, 1515(CHO)	9.5(s,z) 7.4, 7.3(d,xy) $J_{xy} = 2.3$ −12.8(s,OsH)
$[Os_3H(CO)_{10}(CH^x{=}CH^yCH^zO)]$ (**6**)	2112m, 2078vs, 2050s, 2024vs, 2018vs, 2010s, 1994m	9.0(m,z) 8.4(m,z) 4.9(m,y) −9.1(s,OsH)
$[Os_2H^w(CO)_6(CH^x{=}CH^yCH^zO)]$ (**7**)	2098m, 2062vs, 2020s, 2008s, 1990m, 1980m	9.2(m,z) 7.5(m,x) 4.4(m,y) −11.5(d,OsH) $J_{wx} = 1.6$
$[Os_3H(CO)_{10}(CH^x{\equiv}CCO_2)]$ (**8**)	2110m, 2072vs, 2061s, 2024vs, 2014vs, 1980m	2.8(s,x) −10.5(s,OsH)
$[Os_6H(CO)_{20}(CH^x{\equiv}CCO_2)]$ (**9a**)	2112vw, 2102w, 2074vs, 2062s, 2056sh, 2032sh, 2025s, 2010vs, 1982m, 1860(μ-CO)	10.1(s,x) −10.5(OsH)
$[Os_3Ru_3H(CO)_{20}(CH^x{\equiv}CCO_2)]$ (**9b**)	2112vw, 2102w, 2076vs, 2064s, 2054sh, 2036sh, 2026s, 2010vs, 1982m, 1896(μ-CO)	9.0(s,x) −10.6(s,OsH)

[a] Cyclohexane solutions.

[b] 100 MHz spectra at room temperature (J in Hz) in $CDCl_3$ except for (**1b**) which is in CD_2Cl_2: chemical shifts (δ) given with multiplicities and assignments in parentheses.

[c] Recorded at −73°C.

[d] Couplings between H^x, H^y and H^z were not analysed.

C=C groups are both coordinated in compound (**6**) and the cluster has opened up in the isomerization from (**5**) to (**6**) since only two Os—Os bonds are required on the basis of electron-counting (data in Table 1). The *cis* geometry at the double bond allows the ligand to chelate; the ^{1}H NMR shift for the hydride is rather low for a triosmium hydride (δ −9.1) and almost certainly this is terminally bonded. The structure shown in Scheme 4 for compound (**6**) is based on the similarity of the ν(CO) absorptions to those of the cluster [$Os_3H(CO)_{10}$(*cis*-CH=CHC$_5$H$_4$N)] formed by cyclometallation of 2-vinylpyridine.[10] The X-ray structure of this compound is just like that shown for (**6**) but with the formyl (CHO) group replaced by the 2-pyridyl (C$_5$H$_4$N) group. The hydride ligand in the 2-vinylpyridine derivative is terminal and the ^{1}H NMR hydride shift is likewise rather low. Similarly very strong evidence allowed the structure of the related ketone in Scheme 2 to be established.

The dimeric compound [$Os_2H(CO)_6$(*cis*-CH=CHCHO)] (**7**) compares spectroscopically, very closely with [$Os_2H(CO)_6$(*cis*-MeCH$_2$C=CHCOMe)] obtained from the reaction of [$Os_3H_2(CO)_{10}$] and hex-5-en-2-one.[11]

The CH=CHCHO ligand donated five-electrons so the structure shown for compound (**7**) in Scheme 4 is most likely. The ^{1}H NMR spectrum (Table 1) confirms the overall composition of the *cis*-CH=CHCHO ligand. In support of our proposed structure, the analogous dinuclear compound [$Ru_2H(CO)_6$(PhC=CHCOMe)] of known X-ray structure[12] corresponds directly with our representation of (**7**). In compounds (**5**), (**6**) and (**7**) the aldehydic group remains coordinated [e.g. ν(CO) 1515 cm^{-1} for (**5**)]. Just like the ketones shown in Scheme 2, the aldehydes [$Os_3H(CO)_{10}$(RC=CHCHO)] (R = Me or Ph) and [$Os_3H(CO)_{10}$(CH=CHCHO)] (**6**) adopt different structures.

The clusters [$Os_3(CO)_{10}(MeCN)_2$] and [$Os_3H_2(CO)_{10}$] both react with CH≡CCO$_2$H under mild conditions to afford good yields (58% from the bis-acetonitrile compound) of the carboxylate derivative [$Os_3H(CO)_{10}$(CH≡CCO$_2$)] (**8**) shown in Scheme 5. The ν(CO) absorption spectrum is essentially identical to that of the reported carboxylate [$Os_3H(CO)_{10}$(HCO$_2$)][13] and the ^{1}H NMR spectrum shows two singlets at δ −10.5 and 2.8, indicating that the acetylenic group is uncoordinated (CH proton for the free ligand at δ 3.0). Based on the well-known reactivity of alkynes towards trinuclear clusters, we decided to react compound (**8**) with labile trinuclear clusters in order to get linked triangular clusters. [$Os_3(CO)_{10}(MeCN)_2$] and [$Ru_3(CO)_{10}(MeCN)_2$] react with compound (**8**) in a 1 : 1 mol ratio at room or below room temperature, to give very good yields of two new clusters: [$Os_6H(CO)_{20}$(CH≡CCO$_2$)] (**9a**) and [$Os_3Ru_3H(CO)_{20}$(CH≡CCO$_2$)] (**9b**), respectively (Scheme 5). The ν(CO) absorption spectra of (**9a**) and (**9b**) can be reproduced almost exactly by a combination of the spectra of compound (**8**) and either (**1a**) or (**1b**). The ν(CO) absorptions at 1860 and 1896 cm^{-1} for compounds (**9a**) and (**9b**) are associated with the metal-bridging CO ligand and are very characteristic of clusters of the type [$M_3(CO)_{10}$(alkyne)]. The ^{1}H NMR spectra [singlets at δ −10.5 and 10.1 for (**9a**) and at δ −10.5 and 9.0 for (**9b**)] show the characteristic signals around δ 9–10 for μ_3-terminal alkynes. The structures depicted for (**9a**) and (**9b**) in Scheme 5 are most likely. We are now trying to grow good crystals for an X-ray structure determination in order to confirm our assessment that these compounds contain seven-electron donating μ_5-ligands. Although we have

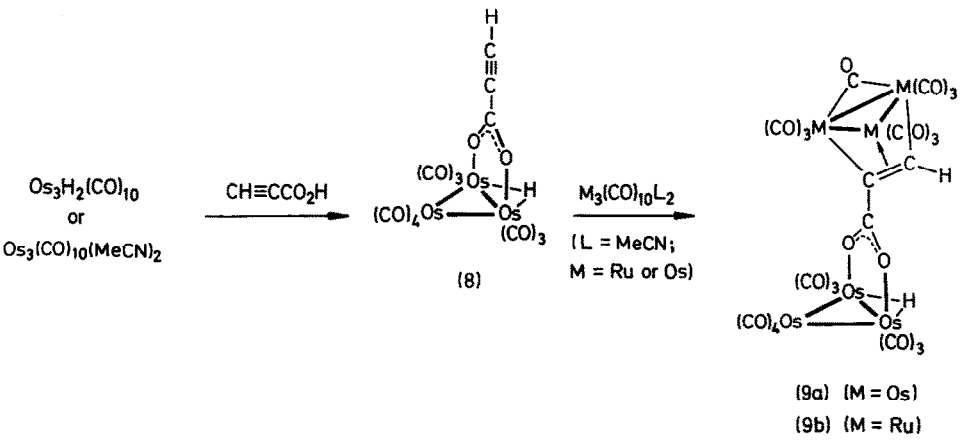

Scheme 5.

not done it yet, it should be quite simple to thermally decarbonylate compounds (**9a**) and (**9b**) to give the clusters $[Os_6H_2(CO)_{19}(C{\equiv}CCO_2)]$ and $[Os_3Ru_3H_2(CO)_{19}(C{\equiv}CCO_2)]$ which would contain eight-electron donating C_3O_2 ligands. This is a remarkable number of electrons to be donated by a ligand with so few atoms.

EXPERIMENTAL

The starting clusters $[Os_3H_2(CO)_{10}]$,[14] $[Os_3(CO)_{10}(MeCN)_2]$[15] and $[Ru_3(CO)_{10}(MeCN)_2]$[16] were prepared as described previously. Methyl prop-2-ynyl ether and prop-2-ynoic acid were purchased from Aldrich and purified prior to use. Prop-2-ynal was synthesized according to the literature.[17] All solvents were purified by conventional methods and all reactions were carried out under nitrogen. Products were isolated by preparative TLC using Merck SiO_2 (H. Type 60).

Methyl prop-2-ynyl ether

(i) A solution of $[Os_3(CO)_{10}(MeCN)_2]$ (0.210 g) and $CH{\equiv}CCH_2OMe$ (0.02 cm^3) in dichloromethane (50 cm^3) was stirred at room temperature for 5 h. After removal of solvent *in vacuo*, the red–orange residue was separated by TLC [eluant: petroleum ether (b.p. 40–60°C)/diethylether, 10/1 by volume] to give four bands. The main yellow band gave $[Os_3(CO)_{10}(CH{=}CCH_2OMe)]$ (**1a**) (0.060 g, 30%) and the second yellow–orange band gave $[Os_3(CO)_9(MeOCH_2C{=}CHOCCHCCH_2OMe)]$ (**3**) (0.063 g, 20%). The other two bands gave very small quantities of compounds which were not characterized.

(ii) The purified ether (0.5 cm^3) was added to a yellow solution of $[Ru_3(CO)_{10}(MeCN)_2]$ (0.175 g) in dichloromethane (30 cm^3) at −20°C which became red in 5 min. Separation as above gave only two bands. The main one gave $[Ru_3(CO)_{10}(CH{=}CCH_2OMe)]$ (**1b**) (0.084 g, 46%) as an orange solid and $[Ru_3(CO)_{12}]$ (0.043 g, 25%).

(iii) A solution of $[Os_3H_2(CO)_{10}]$ (0.025 g) and the ether (0.5 cm^3) in dichloromethane (50 cm^3) was stirred at room temperature for 4 h. Removal of the solvent under vacuum and separation of the residue by TLC [eluant: petroleum ether (b.p. 40–60°C)/diethylether, 10/1 by volume] gave several species of which two were characterized as $[Os_3(CO)_9\{(HC_2CH_2OMe)_2CO\}]$ (**4**) (0.180 g, 65%) as purple crystals and $[Os_3(CO)_{10}(CH{=}CCH_2OMe)]$ (**1a**) (0.068 g, 25%) as yellow crystals. Other products which increased in number on extended reaction time were not characterized.

Prop-2-ynal

A solution of $[Os_3H_2(CO)_{10}]$ (0.200 g) and $CH{\equiv}CCHO$ (0.09 cm^3) in dichloromethane (40 cm^3) was stirred at room temperature for 5 h and set aside at −20°C overnight. After removal of the solvent *in vacuo*, the orange residue was separated by chromatography (eluant: pentane/diethylether, 20/1 by volume) to give one yellow band yielding $[Os_3H(CO)_{10}(CH_2{=}CCHO)]$ (**5**) (0.085 g, 40%) as orange crystals.

Prop-2-ynoic acid

A solution of $[Os_3(CO)_{10}(MeCN)_2]$ (0.200 g) and $CH{\equiv}CCO_2H$ (0.5 cm^3) in THF (30 cm^3) was heated under reflux for 45 min. Removal of the solvent and TLC (eluant: pentane) produced one main yellow band giving $[Os_3H(CO)_{10}(CH{\equiv}CCO_2)]$ (**8**) (0.116 g, 58%) as yellow crystals.

Thermolysis of $[Os_3(CO)_{10}(CH{=}CCH_2OMe)]$ (**1a**) *in refluxing* n-*octane*

A solution of compound (**1a**) (0.050 g) in octane (20 cm^3) was refluxed for 5 min. TLC work-up as above gave one yellow crystalline compound, $[Os_3H(CO)_9(C{\equiv}CCH_2OMe)]$ (**2a**) (0.030 g, 75%).

Thermolysis of $[Ru_3(CO)_{10}(CH{=}CCH_2OMe)]$ (**1b**) *in refluxing cyclohexane*

A solution of compound (**1b**) (0.070 g) in cyclohexane (30 cm^3) was heated under reflux for 30 min. TLC separation gave $[Ru_3H(CO)_9(C{\equiv}CCH_2OMe)]$ (**2b**) (0.038 g, 55%) as a pale yellow solid.

Thermolysis of $[Os_3H(CO)_{10}(CH_2{=}CCHO)]$ (**5**) *in refluxing cyclohexane*

A solution of compound (**5**) (0.080 g) in cyclohexane (50 cm^3) was refluxed for 6 h, after which time the IR spectrum showed no more change. TLC work-up [eluant: petroleum ether (b.p. 40–60°C)] gave two yellow bands which yielded $[Os_3H(CO)_{10}(CH{=}CHCHO)]$ (**6**) (0.030 g, 40%) and $[Os_2H(CO)_6(CH{=}CHCHO)]$ (**7**) (0.017 g, 30%).

Reaction of $[Os_3H(CO)_{10}(CH{\equiv}CCO_2)]$ (**8**) *with* $[Os_3(CO)_{10}(MeCN)_2]$

A solution of the bis-acetonitrile compound (0.110 g) in dichloromethane (20 cm^3) was added to a yellow–orange solution of compound (**8**) (0.094 g) in dichloromethane (15 cm^3). The mixed solution

became red in 1 min and was stirred at room temperature for 13 h. Removal of the solvent and TLC separation [eluant: petroleum ether (b.p. 40–60°C)] gave one main yellow band resulting in $[Os_6H(CO)_{20}(CH{\equiv}CCO_2)]$ (**9a**) (0.126 g, 70%) as yellow–orange crystals.

Reaction of $[Os_3H(CO)_{10}(CH{\equiv}CCO_2)]$ (**8**) *with* $[Ru_3(CO)_{10}(MeCN)_2]$

The bis-acetonitrile compound (0.085 g) was added to a yellow–orange solution of compound (**8**) (0.116 g) in dichloromethane (20 cm^3) at −20°C which after warming to room temperature became orange–red in 20 min. After removal of the solvent, TLC work-up [eluant: petroleum ether (b.p. 40–60°C)/diethylether, 10/1 by volume] gave $[Os_3Ru_3H(CO)_{20}(CH{\equiv}CCO_2)]$ (**9b**) (0.144 g, 75%) as an orange solid and some $[Ru_3(CO)_{12}]$ (0.020 g, 14%).

Acknowledgement—We thank Johnson Matthey Ltd for a loan of ruthenium trichloride.

REFERENCES

1. K. A. Azam, A. J. Deeming and I. P. Rothwell, *J. Chem. Soc., Dalton Trans.* 1981, 91.
2. A. J. Arce, Y. De Sanctis and A. J. Deeming, *J. Organomet. Chem.* 1985, **295**, 365.
3. E. Boyar, A. J. Deeming, A. J. Arce and Y. De Sanctis, *J. Organomet. Chem.* 1984, **276**, C45.
4. A. J. Deeming, P. J. Manning, I. P. Rothwell, M. B. Hursthouse and N. P. C. Walker, *J. Chem. Soc., Dalton Trans.* 1984, 2039.
5. A. J. Arce, Y. De Sanctis and A. J. Deeming, *J. Organomet. Chem.* 1986, **311**, 371.
6. S. Aime, A. Tiripicchio, M. Tiripicchio Camellini and A. J. Deeming, *Inorg. Chem.* 1981, **20**, 2027.
7. O. Gambino, R. P. Ferrari, M. Chinone and C. A. Vaglio, *Inorg. Chim. Acta* 1975, **12**, 155.
8. J. F. Blount, L. F. Dahl, C. Hoogzand and W. Hübel, *J. Am. Chem. Soc.* 1966, **88**, 292.
9. K. A. Azam, A. J. Deeming and I. P. Rothwell, *J. Organomet. Chem.* 1979, **178**, C20; K. A. Azam, A. J. Deeming and I. P. Rothwell, *J. Chem. Soc., Dalton Trans.* 1981, 91.
10. K. Burgess, H. D. Holden, B. F. G. Johnson, J. Lewis, M. B. Hursthouse, N. P. C. Walker, A. J. Deeming, P. J. Manning and R. Peters, *J. Chem. Soc., Dalton Trans.* 1985, 85.
11. A. J. Arce, E. Boyar and A. J. Deeming, *J. Organomet. Chem.* 1987, **320**, 385.
12. A. J. P. Domingos, B. F. G. Johnson, J. Lewis and G. M. Sheldrick, *J. Chem. Soc., Chem. Commun.* 1973, 912.
13. J. R. Shipley, G. M. St. George, M. R. Churchill and F. J. Hollander, *Inorg. Chem.* 1982, **21**, 3295.
14. S. A. R. Knox, J. W. Koepke, M. A. Andrews and H. D. Kaesz, *J. Am. Chem. Soc.* 1975, **97**, 3942.
15. B. F. G. Johnson, J. Lewis and D. A. Pippard, *J. Chem. Soc., Dalton Trans.* 1981, 407.
16. G. A. Foulds, B. F. G. Johnson and J. Lewis, *J. Organomet. Chem.* 1985, **296**, 147.
17. J. C. Sauer, *Org. Synth.* 1963, **IV**, 813.

Polyhedron Vol. 7, No. 10/11, pp. 987–999, 1988
Printed in Great Britain

0277–5387/88 $3.00+.00
© 1988 Pergamon Press plc

ALLYL AND μ-ALLYL COMPLEXES FROM REACTIONS OF A HYDRIDO-BRIDGED MOLYBDENUM–MANGANESE COMPLEX WITH DIENES: CRYSTAL STRUCTURES OF $(\eta\text{-}C_5H_5)(CO)_2Mo(\mu\text{-}PPh_2)Mn(\eta^3\text{-}C_3H_5)(CO)_3$ AND $(\eta\text{-}C_5H_5)(CO)Mo(\mu\text{-}\sigma:\eta^4\text{-}C_5H_9)(\mu\text{-}PPh_2)Mn(CO)_3$

CAROLINE M. HAY, ANDREW D. HORTON, MARTIN J. MAYS* and PAUL R. RAITHBY

University Chemical Laboratory, Lensfield Road, Cambridge, CB2 1EW, U.K.

(*Accepted* 5 *November* 1987)

Abstract—The complex $(\eta\text{-}C_5H_5)(CO)_2Mo(\mu\text{-}H)(\mu\text{-}PPh_2)Mn(CO)_4$ reacts under photolysis with the dienes allene, 1,1-dimethylallene, 1,3-butadiene and 2-methyl-1,3-butadiene to give heterodimetallic allyl complexes in which the allyl ligand is bonded to either the Mn atom, the Mo atom or, alternatively, to both metal atoms. The crystal structure of two of these complexes, $(\eta\text{-}C_5H_5)(CO)_2Mo(\mu\text{-}PPh_2)Mn(\eta^3\text{-}C_3H_5)(CO)_3$ and $(\eta\text{-}C_5H_5)(CO)Mo(\mu\text{-}\sigma:\eta^4\text{-}C_5H_9)(\mu\text{-}PPh_2)Mn(CO)_3$, have been determined by X-ray diffraction. In the former the allyl ligand is η^3-bonded to the manganese atom, which is also coordinated by three CO groups, the bridging PPh_2 group and the Mo atom [Mo—Mn = 3.038(1) Å]. In the latter complex the *syn*-$CH_3CHC(CH_3)CH_2$ allyl ligand is η^3-bonded to the Mo atom and also via coordination of one C—H bond of the CH_2 group to the Mn atom. The Mo atom is additionally coordinated by an $\eta\text{-}C_5H_5$ ligand, a CO group, the PPh_2 group and the Mn atom [Mo—Mn = 2.800(1) Å]. In the presence of CO, the μ-allyl complexes are in equilibrium in solution with complexes of proposed formula $(\eta\text{-}C_5H_5)(CO)(\eta^3\text{-allyl})Mo(\mu\text{-}PPh_2)Mn(CO)_4$, containing the allyl ligand bonded exclusively to the Mo atom, but these latter complexes lose CO and revert to the μ-allyl complexes readily on attempted isolation. The μ-allyl complex $(\eta\text{-}C_5H_5)(CO)Mo(\mu\text{-}\sigma:\eta^4\text{-}C_4H_7)Mn(CO)_3$ gives a 1:1 adduct with $P(OMe)_3$ in which the coordination of the allyl C—H bond to the Mn atom is replaced by bonding of the $P(OMe)_3$ group. The μ-allyl complexes can be deprotonated with $LiBu^n$ giving anionic species which are postulated to contain μ-allylidene ligands. One such species, $[(\eta\text{-}C_5H_5)(CO)Mo(\mu\text{-}\sigma:\eta^3\text{-}CH_3CHCHCH)(\mu\text{-}PPh_2)Mn(CO)_3]^-$, has been reacted with CD_3COOD to regenerate the corresponding allyl complex; the added deuterium atom is located exclusively at the site involved in the interaction with the Mn atom.

The reaction of unsaturated organic molecules with dimetallic or polymetallic complexes containing μ-H ligands has proved to be a useful route to complexes containing bridging hydrocarbyl ligands.[1–5] Certain complexes with μ-H ligands such as $Os_3(\mu\text{-}H)_2(CO)_{10}$ react with a wide variety of unsaturated organic substrates under mild conditions[2,6] but other homometallic complexes such as $Mn_2(\mu\text{-}H)(\mu\text{-}PPh_2)(CO)_8$[3] and $(\eta\text{-}C_5H_5)_2Co_2(\mu\text{-}H)(\mu\text{-}PMe_2)_2$[7] generally require thermal or photochemical activation or the use of activated organic substrates.

Although many heterometallic complexes containing μ-H ligands are now known there have been few studies on the reactions of these species with unsaturated organic molecules,[8–10] even though it might be expected that the polarity of the the heterometallic bonds would lead to greater reactivity as compared to related homometallic species. We have recently reported the synthesis of the heterodimetallic complex $(\eta\text{-}C_5H_5)(CO)_2MoMn(\mu\text{-}H)(\mu\text{-}PPh_2)(CO)_4$ (**1**)[11,12] and we now describe the reactions of this complex with dienes, which lead to allyl complexes of three different types, in which the allyl ligand is η^3-bonded to the Mo or Mn atom or, alternatively, η^4-bonded as a bridge between the

* Author to whom correspondence should be addressed.

metal atoms. The deprotonation of the (η^4-allyl)-bridged complexes has also been studied. Preliminary accounts of part of this work have been published.[11,13]

RESULTS AND DISCUSSION

(a) *Reactions of* (1) *with dienes*

The reactions of complex **1** with the four dienes, allene, 1,1-dimethylallene, butadiene and 2-methyl-1,3-butadiene give the new complexes (η-C_5H_5)$(CO)_2$Mo(μ-PPh_2)Mn(η^3-allyl)$(CO)_3$ (allyl = C_3H_5, **2a**; C_4H_7, **2b**; C_5H_9, **2c**), (η-C_5H_5)(CO)Mo(μ-σ:η^4-allyl)(μ-PPh_2)$Mn(CO)_3$ (allyl = C_3H_5, **3a**; C_4H_7, **3b**; C_5H_9, **3c**) and (η-C_5H_5)(CO)(η^3-C_4H_7)Mo(μ-PPh_2)$Mn(CO)_4$(**4b**), the proposed structures of which are shown in Fig. 1. Reaction takes place on UV irradiation in hexane–benzene (3 : 1) solution at room temperature and the mixtures of products obtained were separated by TLC. Complexes of type **2**, in which the η^3-allyl ligand is bonded exclusively to the Mn atom, were obtained from all four dienes and complexes of type **3**, containing an η^4-allyl ligand bridging the two metal atoms, from each diene apart from 1,1-dimethylallene. A product of type **4** in which the η^3-allyl ligand is bonded exclusively to the Mo atom was only isolated (**4b**) in the reaction of **1** with 1,3-butadiene, although spectroscopic evidence was obtained for the existence of **4a** and **4c** in solution in equilibrium with, respectively, **3a** and **3c** under favourable conditions (see below).

The ^{1}H NMR spectra of **2a–2c** indicate the presence in solution of two isomers for each of these complexes. Thus, the spectrum of **2a** at room temperature shows, in addition to resonances assigned to phenyl and two cyclopentadienyl groups, resonances due to ten η^3-allyl hydrogens. The ratio of the intensities of the cyclopentadienyl and η^3-allyl resonances of the two isomers, indicates that the relative concentrations are *ca* 4 : 1. The resonances due to the η^3-allyl hydrogens in the two isomers have been assigned on the basis of their distinctive chemical shifts and ^{1}H–^{1}H coupling constants. In particular, in each isomer, the central allyl hydrogen couples to the *syn* and *anti* hydrogens with coupling constants of *ca* 6 and *ca* 11–13 Hz, respectively. Selective irradiation of each of the η^3-allyl resonances in the ^{1}H NMR spectrum of **2a** results in the collapse of a resonance due to a corresponding hydrogen in the other isomer. Thus, for example, irradiation of an *anti* allyl hydrogen in the major isomer results in the collapse of one of the *anti* allyl hydrogens in the minor isomer and vice versa. These results are consistent with the operation of a fluxional process, which interconverts the two isomers of **2a** at a rate too slow to result in broadening of the resonances, but sufficiently rapid to result in spin saturation transfer between them.[14] A similar fluxional process, occurring at a slightly greater rate, is presumably responsible for the broadening of the allyl and cyclopentadienyl resonances in the ^{1}H NMR spectrum of complex **2b** at 293 K compared to the well resolved spectrum at 278 K. The two isomers of the η^3-*syn*-1-methylallyl complex,

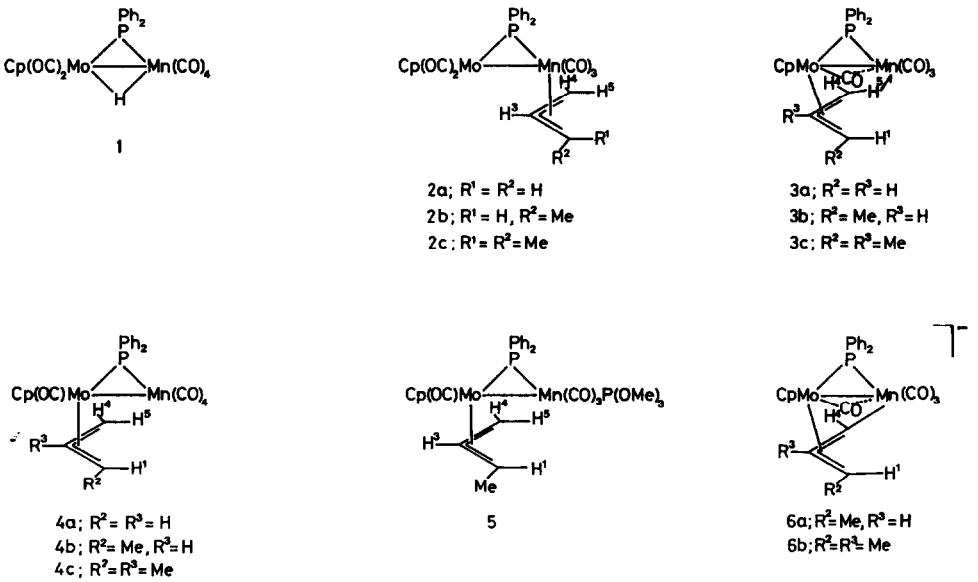

Fig. 1. Proposed structures for the new complexes.

2b, are present in a ratio of *ca* 3 : 1. The two isomers of the η^3-1,1-dimethylallyl complex, **2c**, formed on reaction of **1** with either 1,1-dimethylallene or 2-methyl-1,3-butadiene, are present in the same ratio, 18 : 7, in each case (as shown by the well resolved ^{1}H NMR spectrum at 293 K); this is further evidence that the two isomers of each of the η^3-allyl complexes are readily interconverted by a process which is nevertheless slow on the NMR time scale.

The ^{13}CO NMR spectra of complexes **2a** and **2b** each show the expected five resonances attributable to the carbonyl ligands of the major isomer but the signal intensities were such that only two of the minor isomer carbonyl resonances were observed. Two of the major carbonyl resonances of **2b**, a doublet at δ 244.0 ($^2J_{PC}$ = 23.1 Hz) and a sharp singlet at δ 235.7 ppm, are very similar to the resonances due to the two carbonyl ligands on Mo in **1** [a doublet at δ 242.2 ($^2J_{PC}$ = 25.9 Hz) and a singlet at δ 234.8 ppm]. These two resonances may therefore be assigned to two carbonyl ligands on Mo in **2b**, whilst the other three major resonances may be assigned to three carbonyl ligands on Mn.

In order to confirm that the allyl ligand in the complexes **2** is bonded to the Mn atom and in the hope of obtaining further information about the isomerism of **2** in solution, an X-ray diffraction study of **2a** was undertaken. Suitable crystals of **2a** were grown by slow cooling of a solution in hexane–CH_2Cl_2 (1 : 1). The molecular structure of **2a** is shown in Fig. 2; Table 1 lists the final bond lengths and interbond angles.

The central carbon of the η^3-allyl group is disordered over two sites, with occupancy factors of 57% C(2A) and 43% C(2B). The structure shown in Fig. 2 is derived by inclusion of only the major central carbon site, C(2A). The angle between the two allyl planes, C(1A)—C(2A)—C(3A) and C(1A)—C(2B)—C(3A), is 131.8° and the two structures are related by a *ca* 180° rotation of the allyl fragment about the Mn–allyl axis. The disorder in the allyl fragment of **2a** prevents an accurate assessment of the bonding in this ligand. The average Mn—C(terminal, allyl) bond distance [2.204(5) Å] is slightly longer than the average Mn—C(central, allyl) distance for the disordered atom [2.156(9)

Table 1. Selected bond lengths and angles for $(\eta^5\text{-}C_5H_5)(CO)_2Mo(\mu\text{-}PPh_2)Mn(\eta^3\text{-}C_3H_5)(CO)_3$ (**2a**)

Bond lengths (Å)			
Mn(1)—Mo(1)	3.038(1)	P(1)—Mn(1)	2.282(1)
P(1)—Mo(1)	2.376(1)	C(1A)—Mn(1)	2.221(5)
C(11)—Mo(1)	1.964(4)	C(2A)—Mn(1)	2.118(7)
C(12)—Mo(1)	1.934(4)	C(2B)—Mn(1)	2.194(9)
C(1P)—Mo(1)	2.390(4)	C(3A)—Mn(1)	2.187(5)
C(2P)—Mo(1)	2.352(5)	C(21)—Mn(1)	1.846(4)
C(3P)—Mo(1)	2.301(4)	C(22)—Mn(1)	1.813(4)
C(4P)—Mo(1)	2.330(4)	C(23)—Mn(1)	1.824(4)
C(5P)—Mo(1)	2.366(4)	C(2A)—C(1A)	1.303(9)
C(101)—P(1)	1.835(3)	C(2B)—C(1A)	1.418(12)
C(201)—P(1)	1.834(3)	C(3A)—C(2A)	1.383(10)
		C(3A)—C(2B)	1.215(12)
Bond angles (°)			
P(1)—Mo(1)—Mn(1)	48.0(1)	P(1)—Mn(1)—Mo(1)	50.7(1)
C(11)—Mo(1)—Mn(1)	86.1(1)	C(1A)—Mn(1)—Mo(1)	137.4(1)
C(11)—Mo(1)—P(1)	108.1(1)	C(1A)—Mn(1)—P(1)	86.7(1)
C(12)—Mo(1)—Mn(1)	121.0(1)	C(2A)—Mn(1)—Mo(1)	160.3(2)
C(12)—Mo(1)—P(1)	82.9(1)	C(2A)—Mn(1)—P(1)	117.3(2)
C(12)—Mo(1)—C(11)	80.2(2)	C(2A)—Mn(1)—C(1A)	34.9(2)
C(21)—Mn(1)—Mo(1)	90.6(1)	C(2B)—Mn(1)—Mo(1)	166.0(3)
C(21)—Mn(1)—P(1)	89.2(1)	C(2B)—Mn(1)—P(1)	121.3(3)
C(22)—Mn(1)—Mo(1)	69.6(1)	C(2B)—Mn(1)—C(1A)	37.5(3)
C(22)—Mn(1)—P(1)	120.2(1)	C(3A)—Mn(1)—Mo(1)	157.0(2)
C(22)—Mn(1)—C(21)	88.3(2)	C(3A)—Mn(1)—P(1)	152.4(2)
C(23)—Mn(1)—Mo(1)	85.7(1)	C(3A)—Mn(1)—C(1A)	65.7(2)
C(23)—Mn(1)—P(1)	91.1(1)	C(3A)—Mn(1)—C(2A)	37.4(3)
C(23)—Mn(1)—C(21)	174.9(2)	C(3A)—Mn(1)—C(2B)	32.2(3)
C(23)—Mn(1)—C(22)	87.2(2)	Mn(1)—P(1)—Mo(1)	81.4(1)
C(3A)—C(2A)—C(1A)	125.6(7)	C(3A)—C(2B)—C(1A)	130.2(9)

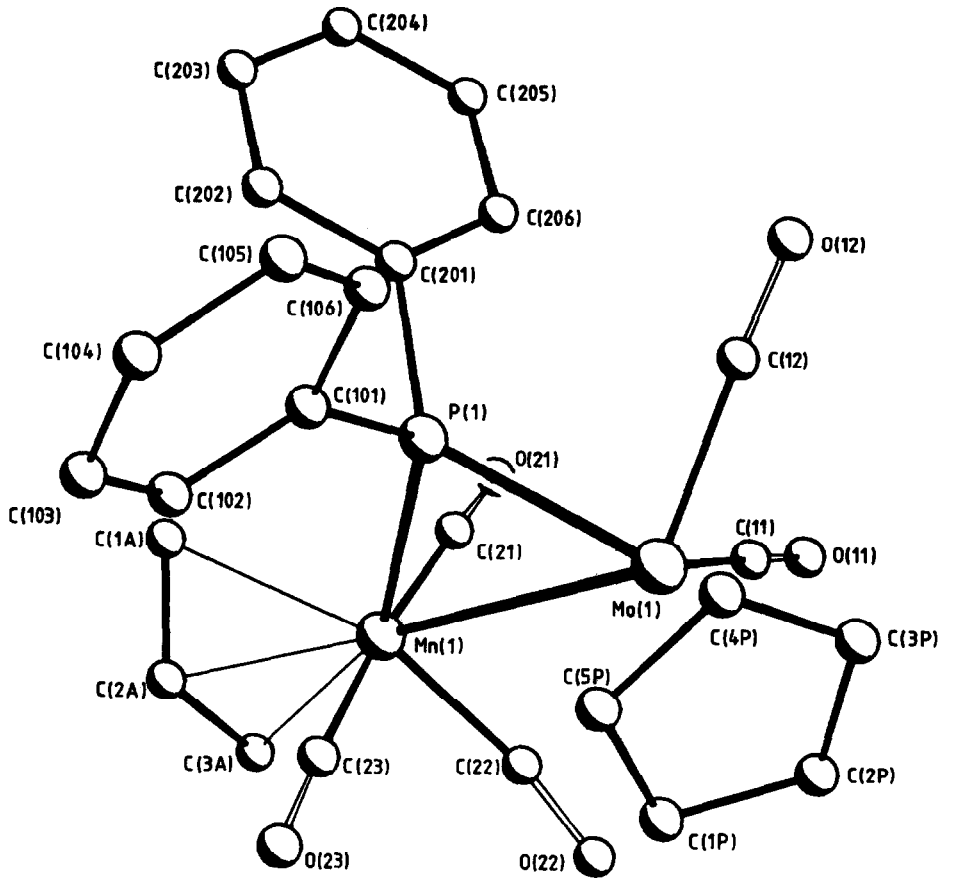

Fig. 2. Molecular structure of $(\eta\text{-}C_5H_5)(CO)_2Mo(\mu\text{-}PPh_2)Mn(\eta^3\text{-}C_3H_5)(CO)_3$ (**2a**) showing the crystallographic numbering.

Å]. Although the two axial carbonyl ligands at Mn are perpendicular to the Mo—Mn vector, as in complex **1**, the equatorial carbonyl ligand in the complex occupies the space taken up by the hydride ligand in **1** [Mo—Mn—CO(*trans* to PPh_2) angle, 69.6(1)° in **2a**, compared to 116.2(2)° in **1**]. For comparison, the average Mo—Mn—CO(*trans* to PPh_2) angle in $[Mn_2(\mu\text{-}PPh_2)(CO)_8]^-$, in which *two* carbonyls have moved towards the space previously occupied by the bridging hydride ligand in $[Mn_2(\mu\text{-}H)(\mu\text{-}PPh_2)(CO)_8]$, is 88.5(3)°.[15] Although CO(22) is non-linear [Mn—CO interbond angle of 170.5(3)°], the large separation of C(22) and Mo(1) [2.946 Å] and the lack of a semi-bridging carbonyl absorption band in the IR [ν(CO)] spectrum of **2a** confirms the absence of any semi-bridging character for CO(22). The reduced π-acid character of the η^3-allyl ligand, compared to a carbonyl ligand, leading to increased electron density on Mn, may explain the slightly reduced average Mn—CO bond distance in **2a** [1.828(4) Å] compared to that in **1** [1.838(6) Å].

The geometry of the ligands at Mo is, apart from the loss of the hydride ligand, little altered from that in **1**. Although the complex obeys the 18-electron rule overall, the Mo centre is electron poor and the Mn centre electron rich. This is counteracted to some extent by increased electron donation from phosphorus to Mo as reflected in the short Mo—P bond [2.376(1) Å] in **2a** compared to that in **1** [2.435(1) Å]. In contrast, the Mn—P distance [2.282(1) Å] is only slightly shorter than in **1** [2.294(2) Å]. The reduction in the Mn bond distance may perhaps be ascribed to the poor π-acid character of the η^3-allyl ligand, which increases the electron density available for π-back bonding from Mn to phosphorus. The loss of the [μ-H] ligand in **1** is accompanied by a reduction in the Mo—Mn bond distance [3.088(1) Å in **1** as compared to 3.038(1) Å in **2a**]. The reduction in the Mo—P and Mo—Mn bond distances in **2a** from those found in **1** accounts for the similar bite angles at phosphorus in the two complexes [81.4(1)° in **2a** and 81.5(1)° in **1**].

The structures of **2a**–**2c** in solution are almost certainly closely related to that found for **2a** in the solid state and we propose that the two isomers for

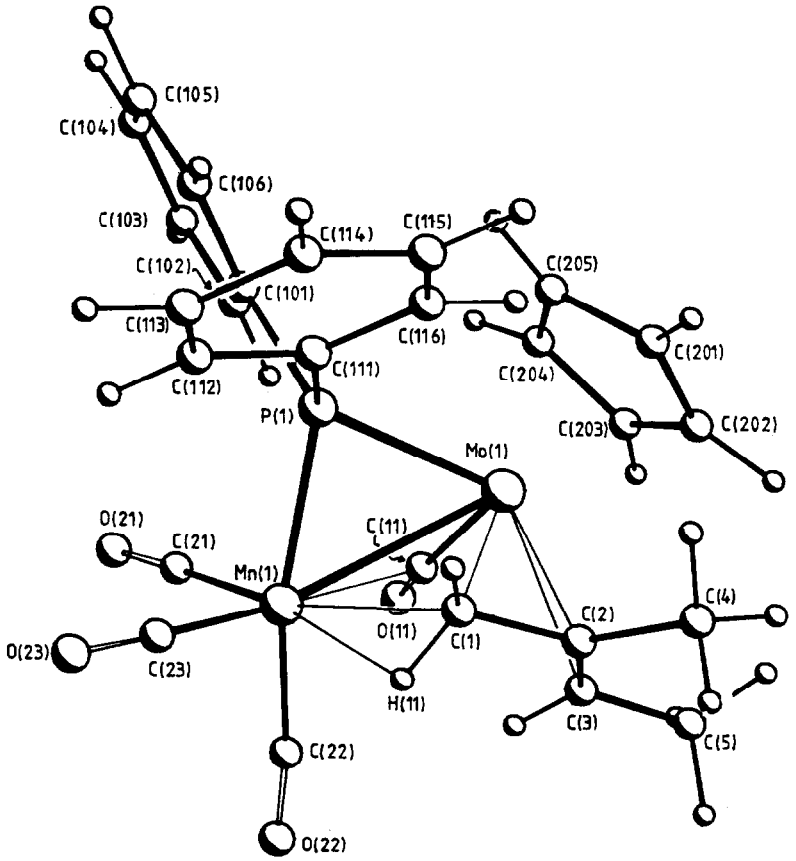

Fig. 3. Molecular structure of $(\eta\text{-}C_5H_5)(CO)Mo(\mu\text{-}\sigma:\eta^4\text{-}C_5H_9)(\mu\text{-}PPh_2)Mn(CO)_3$ (**3c**) showing the crystallographic numbering scheme.

each complex differ only in the orientation of the η^3-allyl ligand relative to the rest of the molecule. The mechanism of interconversion of the isomers may involve a *ca* 180° rotation about the Mn–allyl axis; similar isomerization has been observed in other η^3-allyl complexes[16,17] and it is possible that the two isomers of **2a** may be structurally related to the disorder of the η^3-allyl ligand over the two sites in the crystal structure of the complex.

The molecular structure of **3c** in the solid state has also been determined by X-ray diffraction. Suitable crystals of **3c** were grown by slow evaporation of a solution in hexane–CH_2Cl_2 (1 : 1). The structure of **3c** is shown in Fig. 3; Table 2 list the final bond lengths and interbond angles.

The C_5H_9 ligand is coordinated via the η^3-allyl group to Mo and via a three-centre "agostic" interaction[18] of an *anti* C—H bond to Mn. The η^3-allyl group adopts the *exo* conformation relative to the cyclopentadienyl ligand on Mo; the bonding may perhaps best be described as of the σ–π type, since the Mo—C (allyl, terminal) bond distances are significantly different [Mo—C(1), 2.276(4) Å and Mo—C(3), 2.397(4) Å] and C(2)—C(3) [1.392(6) Å] is slightly shorter than C(1)—C(2) [1.431(5) Å]. In addition the deviation of 0.71 Å of the agostic hydrogen atom, H(11), from the C(1)—C(2)—C(3) plane compared to 0.01 Å for H(12), 0.06 Å for C(4), 0.32 Å for H(31) and 0.01 Å for C(5) provides some evidence for a departure from sp^2 hybridization at C(1). On the other hand, the relatively short Mo—C(2) (allyl, central) separation [2.239(4) Å] suggests that the σ–π component of the bonding is less than for the highly asymmetric allyl ligand in $(\eta\text{-}C_5H_5)MoI(\eta^3\text{-}C_5H_5)(NO)$.[19]

A number of polynuclear complexes containing a C...H...M interaction have been reported[18] but few of these have been heteronuclear complexes.[20] A similar agostic interaction to that in **3c**, involving a formal sp^2 C—H bond of an η^3-allyl group, has been observed previously in the crystal structure of $[(\eta\text{-}C_5H_5)_2Mo_2(\mu\text{-}C_8Me_8H)]^+$.[21] The increased Mn...C(1) [2.346(4) Å] and Mn...H(11) [2.02(4) Å] separations in **3c** compared to the corresponding values [2.196(5) and 1.88(8) Å] in the Mo_2 complex indicate that the "agostic" bonding interaction in

Table 2. Selected bond lengths and angles for $(\eta^5\text{-}C_5H_5)(CO)Mo(\mu\text{-}\sigma:\eta^4\text{-}C_5H_9)(\mu\text{-}PPh_2)Mn(CO)_3$ (**3c**)

Bond lengths (Å)			
Mn(1)—Mo(1)	2.800(1)	P(1)—Mn(1)	2.267(1)
P(1)—Mo(1)	2.428(1)	C(11)—Mn(1)	2.507(4)
C(201)—Mo(1)	2.382(4)	C(21)—Mn(1)	1.776(4)
C(202)—Mo(1)	2.352(4)	C(22)—Mn(1)	1.838(4)
C(203)—Mo(1)	2.312(4)	C(23)—Mn(1)	1.790(4)
C(204)—Mo(1)	2.309(4)	C(1)—Mn(1)	2.346(4)
C(205)—Mo(1)	2.341(4)	H(11)—Mn(1)	2.023(36)
C(11)—Mo(1)	1.944(4)	C(101)—P(1)	1.841(3)
C(1)—Mo(1)	2.276(4)	C(111)—P(1)	1.829(2)
C(2)—Mo(1)	2.239(4)	C(2)—C(1)	1.431(5)
C(3)—Mo(1)	2.397(4)	H(11)—C(1)	0.955(38)
C(5)—C(3)	1.497(6)	C(3)—C(2)	1.392(6)
		C(4)—C(2)	1.517(5)
Bond angles (°)			
P(1)—Mo(1)—Mn(1)	50.8(1)	P(1)—Mn(1)—Mo(1)	56.1(1)
C(11)—Mo(1)—Mn(1)	60.7(1)	C(11)—Mn(1)—Mo(1)	42.5(1)
C(11)—Mo(1)—P(1)	94.4(1)	C(11)—Mn(1)—P(1)	84.8(1)
C(1)—Mo(1)—Mn(1)	53.9(1)	C(21)—Mn(1)—Mo(1)	113.6(1)
C(1)—Mo(1)—P(1)	72.9(1)	C(21)—Mn(1)—P(1)	93.7(1)
C(1)—Mo(1)—C(11)	103.5(2)	C(21)—Mn(1)—C(11)	82.7(2)
C(2)—Mo(1)—Mn(1)	82.8(1)	C(22)—Mn(1)—Mo(1)	110.5(1)
C(2)—Mo(1)—P(1)	109.4(1)	C(22)—Mn(1)—P(1)	165.7(1)
C(2)—Mo(1)—C(11)	105.8(1)	C(22)—Mn(1)—C(11)	81.2(2)
C(2)—Mo(1)—C(1)	36.9(1)	C(22)—Mn(1)—C(21)	87.7(2)
C(3)—Mo(1)—Mn(1)	83.6(1)	C(23)—Mn(1)—Mo(1)	144.2(1)
C(3)—Mo(1)—P(1)	129.8(1)	C(23)—Mn(1)—P(1)	98.0(1)
C(3)—Mo(1)—C(11)	76.1(2)	C(23)—Mn(1)—C(11)	172.4(2)
C(3)—Mo(1)—C(1)	62.3(1)	C(23)—Mn(1)—C(21)	90.1(2)
C(3)—Mo(1)—C(2)	34.7(1)	C(23)—Mn(1)—C(22)	96.2(2)
H(11)—Mn(1)—Mo(1)	72.9(11)	C(1)—Mn(1)—Mo(1)	51.6(1)
H(11)—Mn(1)—P(1)	95.7(11)	C(1)—Mn(1)—P(1)	74.7(1)
H(11)—Mn(1)—C(11)	99.1(10)	C(1)—Mn(1)—C(11)	86.3(1)
H(11)—Mn(1)—C(21)	170.6(11)	C(1)—Mn(1)—C(21)	164.6(2)
H(11)—Mn(1)—C(22)	83.5(11)	C(1)—Mn(1)—C(22)	101.2(2)
H(11)—Mn(1)—C(23)	87.6(11)	C(1)—Mn(1)—C(23)	101.2(2)
H(11)—Mn(1)—C(1)	23.8(11)	Mn(1)—P(1)—Mo(1)	73.1(1)
C(1)—H(11)—Mn(1)	97.5(25)	C(5)—C(3)—C(2)	125.3(4)
C(3)—C(2)—C(1)	117.9(3)		
C(4)—C(2)—C(1)	118.2(4)		
C(4)—C(2)—C(3)	123.9(4)		

3c is the weaker. It is also weaker in **3c** than in the mononuclear manganese complex $Mn(\eta^3\text{-}C_6H_8Me)(CO)_3$[22] as indicated by the reduced Mn...H distance and the shift to higher field of the "agostic" hydrogen in the ^1H NMR spectrum of the latter complex. Thus a reduction in the Mn...H distance from 2.02(4) Å in **3c** to 1.84(1) Å in $Mn(\eta^3\text{-}C_6H_8Me)(CO)_3$ is accompanied by an upfield ^1H NMR shift from δ −7.64 to −13.7 (5-*endo*-methyl isomer).

The "agostic" C—H group in **3c** occupies the coordination site of the fourth carbonyl ligand in **1**: the other most significant changes in the coordination at the manganese atom compared to that in **1** are the replacement of the bridging hydride in **1** by a semi-bridging carbonyl interaction, and the resultant movement back of CO(21) from the Mo–Mn vector; the Mo—Mn—CO(21) interbond angle increases from the corresponding value of 89.8(2)° in **1** to 113.6(1)° in **3c**. The semi-bridging nature of CO(11) is indicated by the Mo—CO(11) and Mn—CO(11) distances [1.944(4) and 2.507(4) Å

respectively] and by the Mo—C(11)—O(11) interbond angle [161.9(3)°]. The Mn centre in **3c** is electron poor, even if the agostic group is considered as donating two electrons so that the complex obeys the 18-electron rule overall, and this electron deficiency is compensated for by the semi-bridging carbonyl ligand, the reduced Mn—P distance of 2.267(1) Å [compared to 2.294(2) Å in **1**] and the short Mo—Mn bond distance of 2.800(1) Å [compared to 3.088(1) Å in **1**] which may indicate an Mo—Mn bond order of greater than one. The reduction in the Mo—Mn bond length is accompanied by a reduction in the bite angle at phosphorus [73.1(0)° in **3c** compared to 81.5(0)° in **1**].

The ^{1}H NMR spectra of the complexes **3a**–**3c** show in each case a high field resonance which may be assigned to an agostic hydrogen atom, indicating that the structure found for **3c** in the solid state is maintained in solution. Thus for **3b** this signal is at δ −7.51 and the geometrical and electronic distortion introduced into the allyl ligand as a result of the C...H...Mn interaction is reflected in the large geminal coupling constant between H^5 and the *syn* hydrogen, H^4, of 7.3 Hz, and in the unusually low coupling constant (for an *anti* hydrogen) of 6.3 Hz between H^5 and the central allyl hydrogen, H^3. In contrast, the other *anti* hydrogen, H^1, is coupled to H^3 with a coupling constant of 10.2 Hz. The chemical shifts of H^3, δ 4.49, H^1, δ 2.58, and the methyl substituent, Me^2, δ 1.65, are within the range normally observed for η^3-allyl complexes. The *syn* hydrogen atom in **3b**, H^4, gives rise to a resonance at the unusually high field value of δ −0.74 ppm. There is no indication from the crystal structure determination that H^4 interacts directly with the Mn atom, and the high field shift is presumably associated with the agostic interaction in which the other hydrogen atom, H^5, attached to the same carbon atom as H^4, is involved. This may also account for the large ^{31}P–^{1}H coupling constant for H^4 of 168 Hz.

The ^{13}C NMR spectrum of **3b** shows four ^{13}CO resonances which may be assigned on the basis of their relative chemical shifts to a carbonyl ligand on Mo and three carbonyl ligands on Mn. Two ^{13}C–^{1}H coupling constants for the carbon in the "agostic" C—H group of 162.7 and 123.5 Hz are observed, which may be compared with the corresponding couplings of 167.7 and 163.3 Hz for the other terminal and central allyl carbons. The reduced coupling constant for the agostic C—H bond of 123.5 Hz may be attributed to the reduction in electron density along the C–H vector as a result of interaction with the Mn centre. A similar reduction from *ca* 120–130 Hz to *ca* 75–100 Hz has been observed for agostic C—H bonds involving an sp^3 hybridized carbon.[18]

Complex **4b**, a red crystalline material obtained in 10% yield in the direct reaction of **1** with 1,3-butadiene, was more conveniently prepared in 83% yield by treatment of a solution of **3b** with CO followed by slow crystallization under CO. Loss of CO from **4b** takes place readily even in the solid state at room temperature and **4b** is converted essentially quantitatively to **3b** when N_2 is passed through a hexane solution of the complex. Satisfactory microanalytical data for **4b** could not be obtained and the complex was characterized by its spectroscopic properties. Thus the allyl resonances in the ^{1}H NMR spectrum of **4b** are closely similar to those assigned to the *exo* isomer of the dimolybdenum allyl complex $(\eta\text{-}C_5H_5)_2Mo_2(\eta^3\text{-}C_4H_7)(\mu\text{-}PPh_2)(CO)_3$.[23] Whereas in the dimolybdenum complex ^{1}H NMR signals due to an *endo* isomer are also observed, the spectrum of **4b** indicates that only one isomer is present in solution.

The yield of **4b** relative to that of **3b** is increased if the reaction of **1** with 1,3-butadiene is carried out at a lower temperature (see Experimental section). This suggests that the initial products of the reaction are **2b** and **4b** with subsequent formation of **3b** by CO loss from **4b**. Complexes **4a** and **4c** lose CO so readily that they are not present in detectable concentrations in the product mixtures formed on reaction of **1** with the appropriate dienes at room temperature, although low concentrations of **4a** were detected by IR spectroscopy during the reaction of **1** with allene at 253 K. Saturation of a benzene solution of **3a** at room temperature with CO gave an equilibrium mixture of **4a** and **3a**, with a ratio **4a** : **3a** of *ca* 3 : 2. Complexes **4a** and **4c** were only characterized by their IR spectra which are closely similar to that of **4b**; all attempts at isolation led only to their complete conversion to **3a** and **3c** respectively.

The product ratio of Mn–allyl to Mo–allyl complexes formed in the reactions of **1** with dienes depends critically on the diene used, as shown in Table 3. The increased steric crowding at the Mo centre compared to the Mn centre, as a result of the bulky cyclopentadienyl ligand at Mo, could result in preferred attack of bulky dienes at Mn rather than Mo. This may explain the higher proportion of the Mn–allyl product formed on reaction of **1** with 1,1-dimethylallene (100%) as compared to the reaction with allene (85%). Steric effects are perhaps also important in the reaction of **1** with 2-methyl-1,3-butadiene, which results in two different allyl ligands depending on the metal centre to which the ligand is coordinated. Thus the 1,1-dimethylallyl ligand on Mn in **2c** is derived from attack of the

Table 3. Proportions of allyl products formed on reaction of **1** with dienes at room temperature

Diene	Mn–allyl complex **2**	Mo–allyl complexes **3**+**4**
1,1-Dimethylallene	100%	0%
Allene	85%	15%
1,3-Butadiene	21%	79%
2-Methyl-1,3-butadiene	20%	80%

hydride ligand on the more sterically hindered end of the diene, whilst the *syn*-1,2-dimethylallyl ligand on Mo in **3c** is derived from attack on the less hindered end. On the other hand electronic as well as steric factors are known to be important in determining the mode of metal hydride addition to substituted butadienes in mononuclear complexes.[24] Thus, for example, whereas $HCo(CO)_4$ adds to the more basic double bond in 2-methyl-1,3-butadiene to give a 1,1-dimethylallyl complex, the less acidic $IrH(CO)_2(PPh_3)_2$ adds to the less basic double bond.[24] Clearly a much more comprehensive study would be needed to determine the relative importance of steric and electronic factors in the addition of dienes to dinuclear complexes such as **1**.

(b) *Addition reaction of* $(\eta\text{-}C_5H_5)(CO)Mo(\mu\text{-}\sigma:\eta^4\text{-}C_4H_7)(\mu\text{-}PPh_2)Mn(CO)_3$ (**3b**)

Agostically bonded C—H ligands are usually readily displaced by two-electron donor ligands such as CO, PR_3 and RNC.[25–27] In the case of **3b**, however, as described above, reaction with CO at room temperature and atmospheric pressure leads to an equilibrium in solution which favours the agostically bonded complex. Reaction of **3b** with $P(OMe)_3$ is more favourable to adduct formation but also fails to proceed to completion. Thus, addition of 1.3 equivalents of $P(OMe)_3$ to a $CDCl_3$ solution of **3b** in an NMR tube results in the near instantaneous formation of a red complex in solution, formulated on the basis of its ^1H NMR spectrum as $(\eta\text{-}C_5H_5)(CO)(\eta^3\text{-}C_4H_7)Mo(\mu\text{-}PPh_2)Mn(CO)_3[P(OMe)_3]$ (**5**). The presence of two sets of five ^1H NMR signals in an intensity ratio of 1 : 1 : 3 : 1 : 1 due to the allyl protons in **5** indicates that **5** exists in solution as a mixture of two isomers. The chemical shifts and coupling constants of the allyl protons for both isomers of **5** are very similar to those of **4b** and to those of the *exo* isomer of $(\eta\text{-}C_5H_5)_2Mo_2(\eta^3\text{-}C_4H_7)(\mu\text{-}PPh_2)(CO)_3$.[23] The *exo* and *endo* isomers of the dimolybdenum complex show resonances with widely differing chemical shifts, suggesting that the isomerism of **5** is not of this type. A more likely explanation is that the two isomers result from the $P(OMe)_3$ ligand in **5** occupying alternative coordination sites on the Mn atom. All four CO sites on the Mn atom in **4b** are non-equivalent and there are thus four possibilities for the location of the $P(OMe)_3$ ligand in **5** which cannot be distinguished on the basis of the available data.

The reaction of **3b** with a slight excess of $P(OMe)_3$ as above proceeds only *ca* 72% towards completion, as judged by the ^1H NMR spectrum of the mixture. Addition of a total of *ca* 16 equivalents of $P(OMe)_3$ results in the reaction going *ca* 95% towards completion. The reaction is, however, reversible as indicated by the slow reformation of **3b** on attempted TLC purification of **5**. There was no evidence for loss of CO rather than $P(OMe)_3$ to give $P(OMe)_3$ substituted complexes analogous to **3b**. The ligand PPh_3 did not react with **3b** over a period of 24 h but further studies are needed to determine whether this is due to steric or electronic factors.

(c) *Deprotonation of the μ-allyl complexes* **3b** *and* **3c**

Reaction of **3b** or **3c** with an excess of $LiBu^n$ in THF leads to an air unstable orange–olive solution in each case, the IR [ν(CO)] spectrum of which shows absorption bands shifted to lower frequency compared to **3b** or **3c**. Addition of excess CD_3CO_2D to the solution formed from **3b** and $LiBu^n$ gives monodeuterated **3b** for which the ^1H NMR spectrum reveals that the deuterium atom is located exclusively at the agostic site. On the basis of the IR spectra and the deuteration experiments it is proposed that the orange–olive solutions obtained on deprotonation of **3b** and **3c** contain respectively the anions $[(\eta\text{-}C_5H_5)(CO)Mo(\mu\text{-}\sigma:\eta^3\text{-}C_4H_6)(\mu\text{-}PPh_2)Mn(CO)_3]^-$ (**6a**) and $[(\eta\text{-}C_5H_5)(CO)Mo(\mu\text{-}\sigma:\eta^3\text{-}C_5H_8)(\mu\text{-}PPh_2)Mn(CO)_3]^-$ (**6b**) with the structures shown in Fig. 1. The bridging organic group in **6a** and **6b** may be described as a μ-allylidene ligand, with an η^3-allyl linkage to the Mo atom and a π-bond to the Mn atom, although there are a number of other possible representations.[28] Similar bridging ligands have been identified in a number of other dinuclear complexes.[21,29,30]

The protonation of the anion **6a** to give the uncharged complex **3b** is closely related to the protonation of $(\eta\text{-}C_5H_5)_2Mo_2(\mu\text{-}C_8Me_8)$ to give $[(\eta\text{-}C_5H_5)_2Mo_2(\mu\text{-}C_8Me_8H)]^+$.[21] Unlike the Mo_2 com-

plex, however, there is no evidence that the agostic deuterium in [$^2H_1$]-**3b** can migrate over the organic ligand. Thus the deuterium remains located at the same position on the ligand in [$^2H_1$]-**3b** over long periods in an NMR tube in $CDCl_3$ solution at room temperature. Furthermore in [$^2H_1$]-**4b**, formed on treatment of [$^2H_1$]-**3b** with CO as previously described, the deuterium resides exclusively at the H^5 position and no exchange is observed with H^4.

EXPERIMENTAL

All reactions were carried out under an N_2 atmosphere in N_2-saturated solvents distilled from an appropriate drying agent and stored over 4 Å molecular sieves. Work-up procedures were generally performed in air. The instrumentation used to obtain spectroscopic data has been previously described.[15] The ^{13}C spectra are ^1H gated decoupled unless otherwise stated. ^1H and ^{13}C chemical shifts are given in ppm relative to $SiMe_4$ = 0.0 ppm. ^{31}P NMR chemical shifts are given relative to $P(OMe)_3$ with upfield shifts negative. All NMR spectra were recorded at 293 K unless otherwise stated. Preparative thin layer chromatography (TLC) was carried out on commercial Merck plates coated with a 0.25 mm layer of silica. The complex (η-C_5H_5)$(CO)_2$Mo(η-H)(μ-PPh_2)Mn$(CO)_4$ (**1**) was prepared as previously described.[12] All other reagents were obtained from the usual commercial suppliers and used without further purification.

Reaction of **1** *with dienes*

(a) *With allene at room temperature.* Complex **1** (0.114 g, 0.2 mmol) was dissolved in 30 cm^3 hexane, 10 cm^3 benzene and the solution saturated with allene. Irradiation with UV light (Hanovia, medium pressure lamp) for 4 h at room temperature gave a dark red solution. After removal of the solvent on a rotary evaporator, the residue was dissolved in CH_2Cl_2 and applied to the base of TLC plates. Elution with hexane–CH_2Cl_2 (3:1) gave, after removal of solvent on a rotary evaporator (highest R_f value complexes first), **1** (0.010 g, 9%), dark red crystalline (η-C_5H_5)$(CO)_2$Mo(μ-PPh_2)Mn(η^3-C_3H_5)$(CO)_3$ (**2a**) (0.072 g, 62%) and orange crystalline (η-C_5H_5)(CO)Mo(μ-σ:η^4-C_3H_5)(μ-PPh_2)Mn$(CO)_3$ (**3a**) (0.012 g, 11%) together with several other compounds in very low yields.

Found: C, 51.3; H, 3.5. Calc. for (η-C_5H_5)$(CO)_2$Mo(μ-PPh_2)Mn(η^3-C_3H_5)$(CO)_3$ (**2a**) ($C_{25}H_{20}MnMoO_5P$): C, 51.6; H, 3.5%. Mass spectrum: *m/e* 554 $[M-CO]^+$. IR(*n*-hexane) ν_{max} (CO): 2034m, 1952sh, 1947m and 1877m cm^{-1}. NMR (*J* values in Hz): $^1H(CD_2Cl_2)$; major isomer (80%), δ 7.6–7.0 (m, 10H, Ph), 5.05 (s, 5H, C_5H_5), 4.95 (obscured, H^3), 3.60 (m, 1H, H^4), 3.41 (m, J_{23} = 6.3, 1H, H^2), 2.27 (d, J_{13} = 11.2, 1H, H^1), 1.06 (d, J_{35} = 12.7, 1H, H^5) ppm; minor isomer (20%), δ 5.14 (s, 5H, C_5H_5), 4.60 (m, J_{13} = 11.9, J_{35} = 11.9, 1H, H^3), 3.60 (m, 1H, H^4), 2.90 (m, 1H, H^2), 2.56 (d, 1H, H^5) 2.51 (d, 1H, H^1) ppm. ^{13}C ($CDCl_3$, 243 K); major isomer, δ 243.9 (d, $^2J_{PC}$ = 23.5, 1MoCO), 236.6 (s, 1CO), 235.5 (s, 1CO), 216.5 (d, $^2J_{PC}$ = 13.0, 1MnCO), 212.3 (d, $^2J_{PC}$ = 13.3, 1MnCO), 143.1–127.5 (m, Ph), 93.3 (s, C_5H_5), 89.3 (s, CH_2CHCH_2), 48.5 (s, CH_2CHCH_2), 47.2 (s, CH_2CHCH_2) ppm; minor isomer, δ 236.0 (s, 1CO), 215.9 (d, $^2J_{PC}$ = 10, 1MnCO), 143.1–127.5 (m, Ph), 93.5 (s, C_5H_5), 89.8 (s, CH_2CHCH_2), 49.5 (s, CH_2CHCH_2), 48.3 (s, CH_2CHCH_2) ppm. ^{31}P ($CDCl_3$, 243 K); major isomer, δ 57.2 (s, μ-PPh_2); minor isomer, δ 54.8 (s, μ-PPh_2) ppm.

Found: C, 51.5; H, 3.6. Calc. for (η-C_5H_5)(CO)Mo(μ-σ:η^4-C_3H_5)(μ-PPh_2)Mn$(CO)_3$ (**3a**) ($C_{24}H_{20}MnMoO_4P$): C, 52.0; H, 3.6%. Mass spectrum: *m/e* 554 $[M]^+$; $[M-nCO]^+$ (*n* = 2–4). IR (*n*-hexane) ν_{max}(CO): 2014s, 1938m, 1924m and 1840w cm^{-1}. NMR (*J* values in Hz): $^1H(CDCl_3)$, δ 7.7–7.2 (m, 10H, Ph), 5.14 (s, 5H, C_5H_5), 4.59 (dddd, J_{13} = 10.6, J_{23} = 6.7, J_{34} = 6.6, J_{35} = 6.0, 1H, H^3), 2.53 (d, 1H, H^1), 1.64 (d, 1H, H^2), −0.57 (ddd, $^3J_{PH}$ = 17.1, J_{45} = 6.4, 1H, H^4), −7.51 (dd, 1H, H^5) ppm.

(b) *With allene at* 253 *K.* An identical procedure to that followed for the room temperature reaction was used. IR monitoring of the reaction solution indicated the formation of an additional product, (η-C_5H_5)(CO)(η^3-C_3H_5)Mo(μ-PPh_2)Mn$(CO)_4$ (**4a**) the amount of which, in comparison to **3a**, decreased as the reaction proceeded. However, on work-up of the mixture the product distribution was the same as in the room temperature reaction and no **4a** could be isolated.

(c) *With* 1,1-*dimethylallene.* Complex **1** (0.114 g, 0.2 mmol) and 1,1-dimethylallene (excess) were used at room temperature as in (a) above to give **1** (0.036 g, 32%) and dark red (η-C_5H_5)$(CO)_2$Mo(μ-PPh_2)Mn(η^3-C_5H_9)$(CO)_3$ (**2c**). Found: C, 51.3; H, 3.9. Calc. for **2c** ($C_{27}H_{24}MnMoO_5P$): C, 53.1; H, 3.9%. IR(*n*-hexane) ν_{max}(CO): 2026m, 1948s, 1942s, 1918m and 1875m cm^{-1}. Mass spectrum: *m/e* 596. NMR (*J* values in Hz): $^1H(CDCl_3)$; major isomer (72%), δ 7.8–7.0 (m, 10H, Ph), 5.01 (s, 5H, C_5H_5), 4.65 (dd, J_{35} = 12.2, J_{34} = 6.7, 1H, H^3), 3.68 (ddd, $^3J_{PH}$ = 4.6, J_{45} = 2.9, 1H, H^4), 2.08 (s, 3H, Me^2), 1.36 (s, 3H, Me^1), 1.26 (dd, 1H, H^5) ppm; minor isomer (28%), δ 5.12 (s, 5H, C_5H_5), 4.21 (dd,

$J_{35} = 11.5$, $J_{34} = 6.9$, 1H, H^3), 3.04 (m, $^3J_{PH} = 4$, 1H, H^4), 2.63 (d, 1H, H^5), 2.06 (s, 3H, Me^2), 1.52 (s, 3H, Me^1) ppm.

(d) *With* 1,3-*butadiene at room temperature.* Complex **1** (0.114 g, 0.2 mmol) and 1,3-butadiene (large excess bubbled into solution) were used at room temperature as in (a) above to give **1** (0.01 g, 9%), dark red (η-C_5H_5)$(CO)_2$Mo(μ-PPh_2)Mn(η^3-C_4H_7)$(CO)_3$ (**2b**) (0.021 g, 18%), dark red (η-C_5H_5)(CO)(η^3-C_4H_7)Mo(μ-PPh_2)$Mn(CO)_4$ (**4b**) (0.012 g, 10%) and orange crystalline (η-C_5H_5)(CO)Mo(μ-σ:η^4-C_4H_7)(μ-PPh_2)$Mn(CO)_3$ (**3b**) (0.065 g, 57%).

Found: C, 52.1; H, 3.5. Calc. for (η-C_5H_5)$(CO)_2$Mo(μ-PPh_2)Mn($\eta^3C_4H_7$)$(CO)_3$ (**2b**) ($C_{26}H_{22}MnMoO_5P$): C, 52.4; H, 3.7%. IR(*n*-hexane) ν_{max}(CO): 2029m, 1951sh, 1946s, 1923m and 1876m cm^{-1}. NMR (*J* values in Hz): $^1H(CD_2Cl_2$ at 278 K); major isomer (74%), δ 7.8–7.0 (m, 10H, Ph, 5.00 (s, 5H, C_5H_5), 4.79 (ddd, $J_{35} = 11.8$, $J_{13} = 10.7$, $J_{34} = 7.1$, 1H, H^3), 3.46 (ddd, $^3J_{PH} = 3$, $J_{45} = 1$, 1H, H^4), 3.05 (dq, $J_{12} = 6.2$, 1H, H^1), 1.96 (d, 3H, Me^2), 0.77 (dd, 1H, H^4) ppm; minor isomer (26%), δ 5.13 (s, 5H, C_5H_5), 4.40 (ddd, $J_{35} = 11.1$, $J_{13} = 10.0$, $J_{34} = 5.9$, 1H, H^3), 3.27 (dq, $J_{12} = 6.2$, 1H, H^1), 2.68 (m, $^4J_{PH} = 3$, 1H, H^4), 2.23 (d, 1H, H^5), 1.97 (d, 3H, Me^2) ppm. $^{13}C(CDCl_3$, 243 K); major isomer, δ 244.0 (d, $^2J_{PC} = 23.1$, 1MoCO), 236.5 (s, 1MnCO), 235.7 (s, 1MoCO), 216.8 (d, $^2J_{PC} = 15.0$, 1MnCO), 212.3 (s, 1MnCO), 143.3–127.4 (m, Ph), 93.2 (s, C_5H_5), 91.3 (s, $CH_2CHCHCH_3$), 65.2 (s, $CH_2CHCHCH_3$), 43.1 (s, $CH_2CHCHCH_3$), 19.4 (s, $CH_2CHCHCH_3$) ppm; minor isomer, δ 236.1 (s, 1CO); 216.1 (d, $^2J_{PC} = 10.1$, 1MnCO), 143.3–127.4 (m, Ph), 93.4 (s, C_5H_5), 91.2 (s, $CH_2CHCHCH_3$), 67.8 (s, $CH_2CHCHCH_3$), 43.0 (s, $CH_2CHCHCH_3$), 19.0 (s, $CH_2CHCHCH_3$) ppm.

Spectroscopic data for (η-C_5H_5)(CO)(η^3-C_4H_7)Mo(μ-PPh_2)$Mn(CO)_4$ (**4b**). Mass spectrum: *m/e* 568 $[M-CO]^+$, $[M-nCO]^+$ ($n = 1$, 3–5). IR(*n*-hexane) ν_{max}(CO): 2049s, 1984m, 1963sh, 1958s and 1948m cm^{-1}. NMR (*J* values in Hz): $^1H(CDCl_3)$: δ 7.7–7.1 (m, 10H, Ph), 5.02 (s, 5H, C_5H_5), 3.95 (ddd, $J_{35} = 11.8$, $J_{13} = 11.0$, $J_{34} = 7.8$, 1H, H^3), 2.12 (dq, $J_{12} = 6.3$, 1H, H^1), 1.74 (d, 3H, Me^2), 1.46 (ddd, $J_{45} = 4.9$, $^3J_{PH} = 2.3$, 1H, H^4), −0.44 (ddd, $^3J_{PH} = 9.7$, 1H, H^5).

Found: C, 52.8; H, 3.9; P, 5.2. Calc. for (η-C_5H_5)(CO)Mo(μ-σ:η^4-C_4H_7)(μ-PPh_2)$Mn(CO)_3$ (**3b**) ($C_{25}H_{22}MnMoO_4P$): C, 52.8; H, 3.9; P. 5.5%. Mass spectrum: *m/e* 568 $[M]^+$, $[M-nCO]^+$ ($n =$ 2–4). IR (*n*-hexane) ν_{max}(CO): 2011s, 1935m, 1921m and 1831w cm^{-1}. NMR (*J* values in Hz): $^1H(CDCl_3)$, δ 7.6–7.2 (m, 10H, Ph), 5.10 (s, 5H, C_5H_5), 4.49 (ddd, $J_{13} = 10.2$, $J_{34} = 6.3$, $J_{35} = 6.3$, 1H, H^3), 2.58 (dq, $J_{12} = 6.2$, 1H, H^1), 1.65 (d, 3H, Me^2), −0.74 (ddd, $^3J_{PH} = 16.8$, $J_{45} = 7.3$, 1H, H^4), −7.51 (dd, 1H, H^5) ppm. ^{13}C (243 K): δ 238.6 (d, $^2J_{PC} = 7.1$, 1MoCO), 224.0 (d, $^2J_{PC} = 19.1$, 1MnCO), 223.0 (d, $^2J_{PC} = 15.7$, 1MnCO), 221.3 (d, $^2J_{PC} = 15.9$, 1MnCO), 143.8–126.7 (m, Ph), 92.8 (d, $J_{CH} = 178.1$, C_5H_5), 83.6 (d, $J_{CH} = 163.3$, CH_2 $CHCHCH_3$), 72.2 (d, $J_{CH} = 161.7$, $CH_2CHCHCH_3$), 19.3 (q, $J_{CH} = 126.0$, $CH_2CHCHCH_3$), 6.1 (ddd, $J_{CH} = 162.7$, 123.5, $^2J_{PC} = 20.1$, $CH_2CHCHCH_3$) ppm. $^{31}P(CDCl_3$, 243 K): δ −31.1 (s, μ-PPh_2).

(e) *With* 1,3-*butadiene at* 258 *K.* Experiment (d) above was repeated at 258 K; IR monitoring after 6 h indicated an approximate relative product distribution of **2b**:**4b**:**3b** of *ca* 1:3:1 with *ca* 70% of **1** remaining unreacted.

(f) *With* 2-*methyl*-1,3-*butadiene.* Complex **1** (0.114 g, 0.2 mmol) and 2-methyl-1,3-butadiene (0.5 cm^3, large excess) were used at room temperature as in (a) above, to give **1** (0.045 g, 39%), **2c** (0.01 g, 8%) and orange crystalline (η-C_5H_5)(CO)Mo(μ-σ:η^4-C_5H_9)(μ-PPh_2)$Mn(CO)_3$ (**3c**).

Found: C, 52.6; H, 4.1. Calc. for **3c** ($C_{26}H_{24}$ $MnMoO_4P$): C, 53.6; H, 4.2%. Mass spectrum: *m/e* 582 $[M]^+$, $[M-nCO]^+$ ($n = 2$–4). IR(*n*-hexane) ν_{max}(CO): 2012s, 1933m, 1924s and 1828w cm^{-1}. NMR (*J* values in Hz): $^1H(CDCl_3)$, δ 7.6–7.2 (m, 10H, Ph), 5.01 (s, 5H, C_5H_5), 2.29 (q, $J_{12} = 6.3$, 1H, H^1), 1.94 (s, 3H, Me^3), 1.68 (d, 3H, Me^2), −0.66 (dd, $^3J_{PH} = 18.2$, $J_{45} = 7.2$, 1H, H^4), −7.68 (d, 1H, H^5) ppm. $^{13}C(CDCl_3$ at 243 K), δ 239.9 (d, $^2J_{PC} = 8.8$, 1MoCO), 224.1 (d, $^2J_{PC} = 19.1$, 1MnCO), 222.6 (d, $^2J_{PC} = 15.6$, 1MnCO), 220.7 (d, $^2J_{PC} = 14.6$, 1MnCO), 144.3–127.7 (m, Ph), 99.2 [s, $CH_2C(CH_3)CH(CH_3)$], 93.7 (s, C_5H_5), 70.0 [s, $CH_2C(CH_3)CH(CH_3)$], 23.6 [s, $CH_2C(CH_3)CH(CH_3)$], 16.0 [s, $CH_2C(CH_3)CH$ (CH_3)], 9.9 [m, $CH_2C(CH_3)CH(CH_3)$] ppm.

Interconversion of allyl and μ-allyl complexes

(a) *Reaction of* **3a** *with* CO. Complex **3a** (0.015 g, 0.026 mmol) was dissolved in 30 cm^3 benzene and stirred under 1 atm CO for 3 h. The colour of the solution changed from orange to red and IR monitoring indicated that **4a** and **3a** were present in a ratio of *ca* 7:3 [IR for **4a** (*n*-hexane) ν_{max}CO: 2050s, 1985s, 1960s and 1943s cm^{-1}]. Prolonged exposure (3 days) of the solution to CO did not alter this ratio but led to the slow formation of unidentified new products. Attempted TLC separation of the mixture of **4a** and **3a** was unsuccessful due to the slow conversion of **4a** to **3a** on the plates.

(b) *Reaction of* **3b** *with* CO. Complex **3b** (0.015 g, 0.026 mmol) was treated with CO as in (a) above, to give, after 3 h, a mixture of **4b** and **3b** in a ratio,

as judged by IR monitoring, of *ca* 9 : 1. Prolonged exposure of the solution to CO did not lead to any change in the IR spectrum. Red crystalline **4b** (0.013 g, 84%) was obtained on slow crystallization of the above solution under CO.

(c) *Reaction of* **3c** *with* CO. Complex **3c** (0.015 g, 0.026 mmol) treated with CO as in (a) above, to give, after 18 h, a mixture of **4c** and **3c** in a ratio, as judged by IR monitoring, of *ca* 3 : 2 [IR for **4c** (*n*-hexane) ν_{max}(CO): 2049s, 1984m, 1963sh, 1958s and 1947m cm^{-1}]. As in (a), prolonged exposure to CO did not alter this ratio and led only to the slow formation of new products; attempted TLC separation of **4c** and **3c** was unsuccessful due to the slow conversion of **4c** to **3c**.

(d) *Conversion of* **4b** *to* **3b**. Complex **4b** (0.012 g, 0.02 mmol) was dissolved in 15 cm^3 hexane, 5 cm^3 benzene and the solution stirred at 291 K under N_2 for 18 h to give **3b** (0.01 g, 88%) as the only product on TLC separation.

(e) *Reaction of* **3b** *with* $P(OMe)_3$. Complex **3b** (0.006 g, 0.01 mmol) was dissolved in $CDCl_3$ (0.5 cm^3) in an NMR tube and $P(OMe)_3$ (0.0015 cm^3, 0.013 mmol) added. ^1H NMR monitoring of the reaction showed the rapid but incomplete formation of two isomers of $(\eta\text{-}C_5H_5)(CO)(\eta^3\text{-}C_3H_5)Mo(\mu\text{-}PPh_2)Mn(CO)_3P(OMe)_3$ (**5**) with a ratio **3b** : **5** of *ca* 1 : 3. Addition of a large excess of $P(OMe)_3$ (0.018 cm^3, 0.15 mmol) gave an equilibrium ratio of **3b** : **5** of *ca* 1 : 20. Attempted TLC separation of the complexes failed due to the slow conversion of **5** to **3b** on the plates.

Spectroscopic data for $(\eta\text{-}C_5H_5)(CO)(\eta^3\text{-}C_4H_7)Mo(\mu\text{-}PPh_2)Mn(CO)_3[P(OMe)_3]$ (**5**). NMR (*J* values in Hz): $^1H(CDCl_3)$; isomer 1 (50%), δ 7.8–7.0 (m, 10H, Ph), 4.93 (s, 5H, C_5H_5), 3.92 (ddd, $J_{35} = 10.8$, $J_{13} = 10.1$, $J_{34} = 7.0$, 1H, H^3), 3.78 (d, $^3J_{PH} = 10.6$, 9H, OMe), 1.99 (dq, $J_{12} = 6.1$, 1H, H^1), 1.66 (d, 3H, Me^2), 1.37 (ddd, $J_{45} = 4.5$, $^3J_{PH} = 2$, 1H, H^4), −0.42 (ddd, $^3J_{PH} = 10.8$, 1H,

Table 4. Summary of crystal data for **2a** and **3c**

Empirical formula	$C_{25}H_{20}MnMoO_5P$	$C_{26}H_{24}MnMoO_4P$
Molecular weight	582.26	582.30
Crystal habit	orange	red
Crystal colour	block	rectangular block
Crystal dimensions (mm)	0.28 × 0.30 × 0.41	0.17 × 0.20 × 0.53
Cell dimensions (at 293 K)		
a (Å)	11.422(1)	10.337(1)
b (Å)	11.747(1)	15.743(1)
c (Å)	18.220(1)	15.281(1)
β (°)	100.83(1)	102.49(1)
Volume (Å^3)	2401	2428
Crystal system	monoclinic	monoclinic
Space group	$P2_1/c$	$P2_1/c$
Z	4	4
Calculated density (g cm^{-3})	1.61	1.59
F(000)	1168	1176
Absorption coefficient (cm^{-1})	10.81	11.49
Scan step width (°)	0.04	0.04
No. steps in scan	24	24
Scan time per step (s)	0.5–2.0	0.5–2.0
Two-theta range (°)	5–50	5–50
Index limits	$\pm h, +k, \pm l$	$\pm h, -k, \pm l$
Total No. reflections collected	9390	9413
No. unique reflex	4234	4281
R(int)	0.027	0.041
No. with $F > 4\sigma(F)$	3799	3772
Transmission factors		
max.	0.751	0.835
min.	0.654	0.620
Weighting scheme	2.806/ $[\sigma^2(F)+0.0005F^2]$	3.935/ $[\sigma^2(F)+0.0005F^2]$
R(*F*)	0.036	0.037
$R_w(F)$	0.040	0.042
Max. Δ/σ for last cycle	0.70	0.04

H^5); isomer 2 (50%), δ 4.90 (s, 5H, C_5H_5), 3.77 (obscured, H^3), 2.26 (dq, $J_{13} = 10.1$, $J_{12} = 6.2$, 1H, H^1), 1.74 (d, 3H, Me^2), 1.09 (ddd, $J_{34} = 7.0$, $J_{45} = 4.5$, $^3J_{PH} = 2$, 1H, H^4), −0.27 (ddd, $^3J_{PH} = 10.4$, $J_{35} = 10.4$, 1H, H^5) ppm. $^{31}P(CDCl_3)$, δ 54.9 [m, $P(OMe)_3$], 37.3 [m, $P(OMe)_3$], 29.0 (m, μ-PPh_2), 23.5 (m, μ-PPh_2) ppm.

(f) *Attempted reaction of* **3b** *with* PPh_3. Complex **3b** (0.006 g, 0.01 mmol) and PPh_3 (0.021 g, 0.08 mmol) were dissolved in benzene (10 cm^3). IR and TLC monitoring over 24 h showed that no reaction had occurred.

Deprotonation of μ-allyl complexes

(a) *Deprotonation of* **3b** *with* $LiBu^n$. Complex **3b** (0.007 g, 0.012 mmol) was dissolved in 10 cm^3 THF and a large excess of $LiBu^n$ (0.06 cm^3 of 15% wt solution in hexane) was added to give (10 s) an olive–orange solution. This solution was treated with CD_3CO_2D (1 drop, excess) to give [$^2H_1$]-**3b** (0.005 g, 70%; mass spectrum, *m/e* 569, $[M]^+$). The olive–orange solution was shown by IR monitoring not to contain any **3b** [IR(THF) ν_{max}(CO): 1954s, 1946m, 1851s cm^{-1}] and the species giving rise to the observed IR spectrum is formulated as Li[(η-C_5H_5)(CO)Mo{μ-σ:η^3-C_4H_6}(μ-PPh_2)Mn(CO)$_3$] (**6a**).

(b) *Deprotonation of* **3c** *with* $LiBu^n$. This experiment was carried out in an identical manner to that in (a) to give an olive–orange solution [IR(THF) ν_{max}(CO): 1944s, 1852s, 1820m cm^{-1}] the species present being formulated as Li[(η-C_5H_5)(CO)Mo{μ-σ : η^3-C_5H_8}(μ-PPh_2)Mn(CO)$_3$] (**6b**).

X-ray crystallography

The crystals in both structure determinations were mounted on glass fibres with epoxy resin. All X-ray measurements were made using a Stoe–Siemens four-circle diffractometer operating with graphite monochromated Mo-K_α radiation (λ = 0.71069 Å) in the ω/θ scan mode. The data sets were corrected for absorption using face indexing techniques. The structures were solved using a combination of Patterson (Mo and Mn) and Fourier difference techniques, and refined by blocked least-squares techniques with all non-hydrogen atoms, except the allyl group in **2a**, assigned anisotropic thermal parameters. Phenyl, methyl and cyclopentadienyl hydrogens were fixed in idealized positions and refined with common isotropic temperature factors. Other hydrogen atoms were directly located and refined freely with isotropic temperature factors. Details of crystal data and data collection and refinement parameters are given in Table 4.*

Acknowledgements—We thank Dr A. G. Kent for valuable discussion and the S.E.R.C. and BP Chemicals Limited for financial support.

REFERENCES

1. A. J. Deeming and S. Hasso, *J. Organomet. Chem.* 1976, **114**, 313; J. R. Shapley, J. B. Keister, M. R. Churchill and B. G. DeBoer, *J. Am. Chem. Soc.* 1975, **97**, 4145.
2. K. Burgess, *Polyhedron* 1984, **3**, 1175.
3. J. A. Iggo, M. J. Mays, P. R. Raithby and K. Henrick, *J. Chem. Soc., Dalton Trans.* 1983, 205.
4. K. Henrick, J. A. Iggo, M. J. Mays and P. R. Raithby, *J. Chem. Soc., Chem. Commun.* 1984, 209; K. Henrick, J. A. Iggo, A. C. Kemball, M. J. Mays, M. McPartlin and P. R. Raithby, *J. Chem. Soc., Dalton Trans.* 1987, 2669.
5. T. Adatia, K. Henrick, A. D. Horton, M. J. Mays and M. McPartlin, *J. Chem. Soc., Chem. Commun.* 1986, 1206.
6. A. J. Deeming, *Transition Metal Clusters* (Edited by B. F. G. Johnson), Chap. 6, p. 391. John Wiley, Chichester (1980).
7. R. Zolk and H. Werner, *Angew. Chem. Int. Ed. Engl.* 1985, **24**, 577; H. Werner and W. Hofmann, *Angew. Chem. Int. Ed. Engl.* 1979, **18**, 158.
8. G. L. Geoffroy, *Acc. Chem. Res.* 1980, **13**, 469.
9. P. A. Tooley, L. W. Arndt and M. Y. Darensbourg, *J. Am. Chem. Soc.* 1985, **107**, 2422.
10. R. P. Rosen, J. B. Hoke, R. R. Whittle, G. L. Geoffroy, J. P. Hutchinson and J. A. Zubieta, *Organometallics* 1984, **3**, 846.
11. A. D. Horton, M. J. Mays and P. R. Raithby, *J. Chem. Soc., Chem. Commun.* 1985, 247.
12. A. D. Horton, M. J. Mays and M. McPartlin, *J. Chem. Soc., Dalton Trans.* 1987, 1557.
13. A. D. Horton, M. J. Mays and M. McPartlin, *J. Chem. Soc., Chem. Commun.* 1987, 424.
14. S. Forsen and R. A. Hoffman, *J. Chem. Phys.* 1963, **39**, 2892.
15. J. A. Iggo, M. J. Mays, P. R. Raithby and K. Henrick, *J. Chem. Soc., Dalton Trans.* 1984, 633.
16. A. Davison and W. C. Rode, *Inorg. Chem.* 1967, **6**, 2124.
17. J. W. Faller, C.-C. Chen, M. J. Mattina and A. Jakubowski, *J. Organomet. Chem.* 1973, **52**, 361.
18. M. Brookhart and M. L. H. Green, *J. Organomet. Chem.* 1983, **250**, 395.
19. J. W. Faller, D. F. Chodosh and D. Karahira, *J. Organomet. Chem.* 1980, **187**, 227.

* Final atomic, positional and thermal parameters, bond lengths and angles, and tables of F_o vs F_c have been deposited as supplementary material with the Editor from whom copies are available on request. Atomic coordinates have also been submitted to the Cambridge Crystallographic Data Centre.

20. J. C. Jeffery, A. G. Orpen, W. T. Robinson, F. G. A. Stone and M. J. Went, *J. Chem. Soc., Chem. Commun.* 1984, 396.
21. M. Green, N. C. Norman, A. G. Orpen and C. J. Schaverein, *J. Chem. Soc., Dalton Trans.* 1984, 2455.
22. A. J. Shultz, R. G. Teller, M. A. Beno, J. M. Williams, M. Brookhart, W. Lamanna and M. B. Humphrey, *Science* 1983, **220**, 197; M. Brookhart, W. Lamanna and A. R. Pinhas, *Organometallics* 1983, **2**, 638.
23. A. D. Horton, Ph.D. Thesis, University of Cambridge, 1986.
24. C. K. Brown, W. Mowat, G. Yagupsky and G. Wilkinson, *J. Chem. Soc.* (*A*) 1971, 850 and references therein.
25. G. F. Schmidt and M. Brookhart, *J. Am. Chem. Soc.* 1985, **107**, 1443.
26. M. Brookhart, W. Lamanna and A. R. Pinhas, *Organometallics* 1983, **2**, 638.
27. S. D. Ittel, F. D. Van-Cutledge and J. P. Jesson, *J. Am. Chem. Soc.* 1979, **101**, 6905.
28. A. F. Dyke, J. E. Guerchais, S. A. R. Knox, J. Roue, R. L. Short, G. E. Taylor and P. Woodward, *J. Chem. Soc., Chem. Commun.* 1981, 537.
29. J. C. Jeffery, I. Moore, H. Razay and F. G. A. Stone, *J. Chem. Soc., Chem. Commun.* 1981, 1255.
30. W. E. Carroll, M. Green, A. G. Orpen, C. J. Schaverien, I. A. Williams and A. J. Welch, *J. Chem. Soc., Dalton Trans.* 1986, 1021.

Polyhedron Vol. 7, No. 10/11, pp. 1001–1014, 1988
Printed in Great Britain

0277–5387/88 $3.00+.00
© 1988 Pergamon Press plc

REACTION OF OLEFINS AND DIENES WITH BINUCLEAR RHODIUM HYDRIDE COMPLEXES TO GENERATE BRIDGING ALKENYL, DIENYL AND DIENE UNITS

MICHAEL D. FRYZUK† and WARREN E. PIERS

Department of Chemistry, University of British Columbia, 2036 Main Mall, Vancouver, British Columbia, Canada V6T 1Y6

(*Accepted* 5 *November* 1987)

Abstract—Some members of the family of coordinatively unsaturated rhodium hydride dimers of the formula $[\{R_2P(CH_2)_nPR_2\}Rh]_2(\mu\text{-}H)_2$ (**1a**: $n = 2$, R = Pr^i; **1b**: $n = 3$, R = Pr^i) were found to react stoichiometrically with olefins and dienes. The reactivity towards olefins is influenced by the steric properties of the ancillary bisphosphine ligand. Compound **1a** reacts with a variety of simple olefins to yield binuclear bridging alkenyl–hydride complexes of the formula $[(dippe)Rh]_2(\mu\text{-}\eta^2\text{-}\sigma\text{-}RC{=}CH(R)(\mu\text{-}H)$, whereas **1b**, which incorporates the more sterically bulky dippp ligand, reacts only with ethylene. The μ-alkenyl ligand in these complexes exhibits the well known "windshield wiper" fluxionality, with a $\Delta G^{\ddagger}$ of 12.2(2) kcal mol^{-1} found for $[(dippe)Rh]_2(\mu\text{-}\eta^2\text{-}\sigma\text{-}HC{=}CH_2)(\mu\text{-}H)$, **2a**. The proposed mechanism for these reactions involves a dehydrogenation of the dihydride by one equivalent of olefin, followed by reaction of a second equivalent of alkene with the transient $[(P_2)Rh]_2$ d^9–d^9 Rh(0) dimer. Dihydrides **1a** and **1b** also react with 1,3-dienes (butadiene, isoprene and piperylene) to afford binuclear products. Two distinct bonding modes for the diene ligand are found: a $\mu\text{-}\eta^4\text{-}\sigma$ mode, and a $\mu\text{-}\eta^3\text{-}\eta^3$ mode in which the diene ligand is partially sandwiched between the two metal centres. The distribution of products is governed by the steric requirements of both the chelating phosphine ligand and the diene. In some cases, mononuclear methyl substituted allyl complexes are produced either as side products, or as the major products. The binuclear compounds may alternatively be synthesized via reaction between the chlorobridged dimers $[\{R_2P(CH_2)_nPR_2\}Rh]_2(\mu\text{-}Cl)_2$ ($n = 2,3$; R = Pr^i) and magnesium diene reagents; indeed this route provides an avenue to compounds not accessible via the dihydride/diene reaction.

Small unsaturated hydrocarbon molecules such as olefins and dienes react with mononuclear transition metal hydrides with fairly predictable results. With olefins, metal alkyls are the kinetic products while with dienes, allyl derivatives can be obtained. The conversion of a mononuclear metal hydride to a metal alkyl or an allyl by reaction with respectively, an olefin or a diene, constitutes one of the fundamental processes involved in organometallic chemistry,[1] namely olefin insertion. Other fundamental processes that are known for mononuclear systems are β-elimination, oxidative addition/reductive elimination and migratory CO insertion/deinsertion. A knowledge of these basic stoichiometric transformations is crucial to the optimization of the corresponding catalytic cycles involved in the homogeneous hydrogenation of these hydrocarbon molecules.[2]

With polynuclear metal hydrides, the reaction of these simple hydrocarbons is not so predictable. In fact, there is no corresponding library of fundamental processes with which to model transformations at complexes with more than one metal centre. It may well be that the same fundamental processes detailed for mononuclear systems above, hold for polynuclear metal derivatives either acting in parallel at each metal centre or in series at separate metal centres. A more exciting possibility is that new primary processes,[3] pertaining only

† Author to whom correspondence should be addressed.

to polynuclear metal systems, are required to adequately explain observed transformations. For example, a hydrocarbyl ligand bridging two or more metal centres may undergo a rearrangement that is not possible for a mononuclear metal complex and more importantly, that is not describable using the aforementioned primary processes.

Our approach to examining the primary processes associated with polynuclear metal complexes was to take a simple, well defined system involving two metal centres and examine the reactions with unsaturated hydrocarbons. Our rationale was straightforward: since a derivative with two metals is the simplest type of polynuclear metal complex possible, complexity associated with higher clusters can be avoided. In addition, we had access[4] to binuclear complexes with hydride ligands and thus allowed comparison to mononuclear metal hydrides. The family of coordinatively unsaturated rhodium hydride dimers of the formula $[\{R_2P(CH_2)_nPR_2\}Rh]_2(\mu\text{-}H)_2$ (**1a**: $n = 2$, $R = Pr^i$; **1b**: $n = 3$, $R = Pr^i$; **1c**: $n = 2$, $R = OPr^i$) provide a versatile set of starting materials. In this symposium-in-print, we detail the reactivity of these binuclear rhodium hydrides with olefins and dienes.

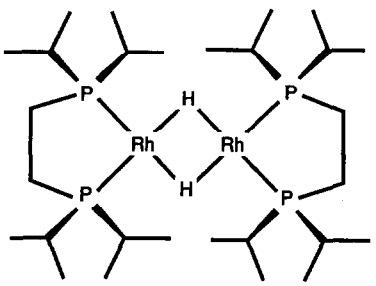

1a

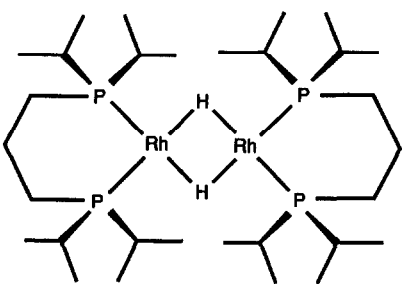

1b

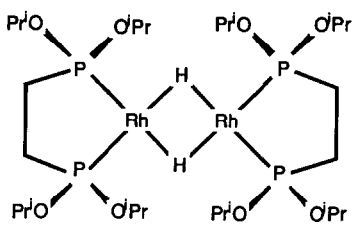

1c

RESULTS AND DICUSSION

Olefins

As was reported earlier,[5] reaction of these binuclear rhodium hydride complexes with simple olefins leads to the formation of bridging alkenyl–hydrides as shown in eq. (1). The scope of this reaction appears to correlate with the steric and electronic properties of the ancillary chelating phosphine ligand. For example, complex **1a**, $[(dippe)Rh]_2(\mu\text{-}H)_2$ (dippe = 1,2-bis(diisopropylphosphino)ethane) having the five-membered chelate rings, reacts with simple terminal olefins and internal olefins, but does not react with bulkier olefins such as *t*-butylethylene and cyclic olefins such as cyclooctene. Presumably, approach by these olefins to the reactive $Rh_2(\mu\text{-}H)_2$ core is impeded by the isopropyl substituents of the dippe ligands. The complex **1b**, $[(dippp)Rh]_2(\mu\text{-}H)_2$ (dippp = 1,3-bis(diisopropylphosphino)propane[6]), which has the six-membered chelate rings, only reacts with ethylene to generate the corresponding vinyl–hydride complex **2b**. This reaction is quite slow requiring 1–2 h to proceed to completion; by contrast, the reaction of **1a** with ethylene proceeds within minutes even at −20°C. The larger bite angle of the dippp[7] ligand as compared to the dippe[5] could conceivably force the isopropyl substituents to be in closer proximity to the $Rh_2(\mu\text{-}H)_2$ core, thereby retarding olefin approach. Alternatively, the difference in reactivity of these two binuclear complexes might be electronic in nature since it has been shown[8] earlier that the P_2 bite angle can dramatically affect the energy of the HOMO in certain d^9 complexes. Evidence that electronic effects are important comes from the attempted reaction of olefins with **1c**, $[(dipope)Rh]_2(\mu\text{-}H)_2$ (dipope =

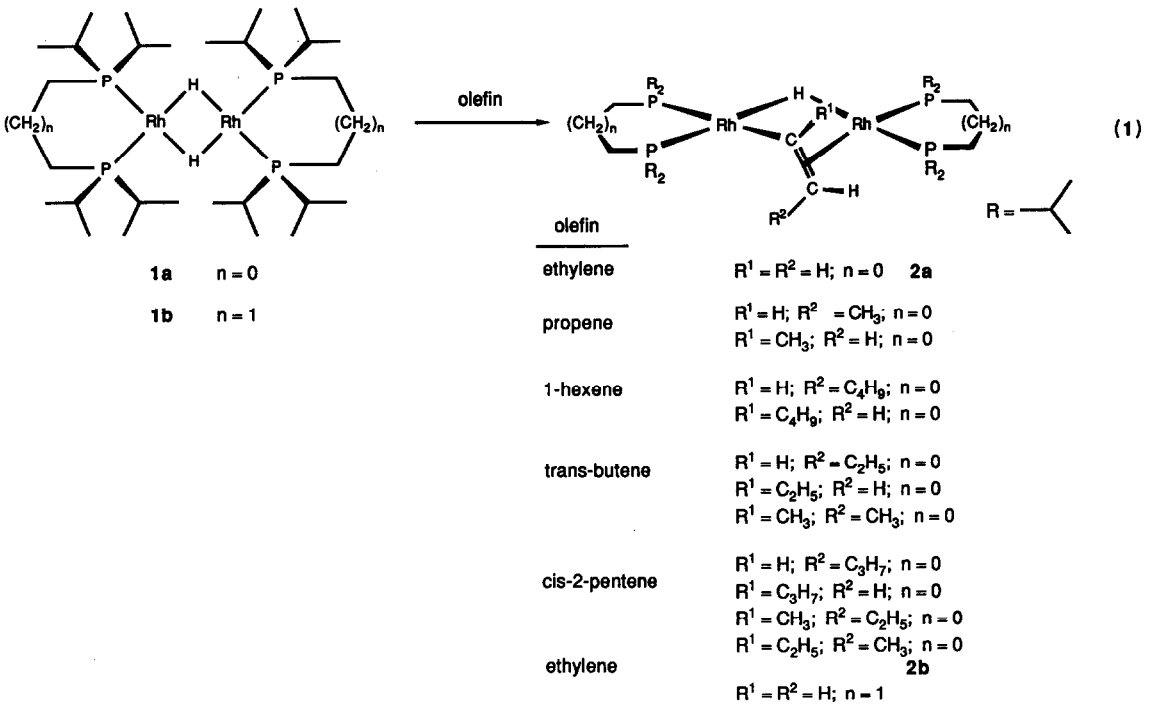

Eq. (1)

1,2-bis(diisopropoxyphosphino)ethane), the corresponding complex with electron-withdrawing substituents on the phosphorus donors; with this derivative, there is no measurable reaction with ethylene or any other mono-olefin. A similar result was reported[10] for the related binuclear complex $[\{Pr^iO)_3P\}_2Rh]_2(\mu\text{-}H)_2$ having the monodentate, electron-withdrawing phosphite ligands.

The reaction of $[(dippe)Rh]_2(\mu\text{-}H)_2$, **1a**, with substituted olefins, generates isomeric products in approximately 1 : 1 ratios.[5] As shown in eq. (1), the two isomers produced in the reaction with propene differ in the positioning of the methyl group of the μ-propenyl ligand either being *cis* or geminal with respect to the σ-bound rhodium atom. The *E*-isomer having the methyl substituent *trans* to the rhodium was not detected, again presumably because the bulky isopropyl groups on the dippe ligand either destabilize this particular product or impede an intermediate in its formation. The use of internal olefins such as *trans*-butene or *cis*-2-pentene generates a mixture of products with the major components being those expected of the corresponding terminal olefins, 1-butene and 1-pentene, respectively; although the internal alkenyl–hydride derivatives are detectable, clearly they react at a rate which is competitive with olefin isomerization to the more reactive terminal olefins. Once again the steric requirements of this reaction are quite pronounced as judged by the decreasing rates of conversion as the olefin becomes more bulky.

Alkenyl–hydride fluxionality

The solution behaviour of a bridging alkenyl ligand is well documented.[5,9] In the binuclear rhodium complexes described above, this so-called "windshield wiper" process (Fig. 1) equilibrates the

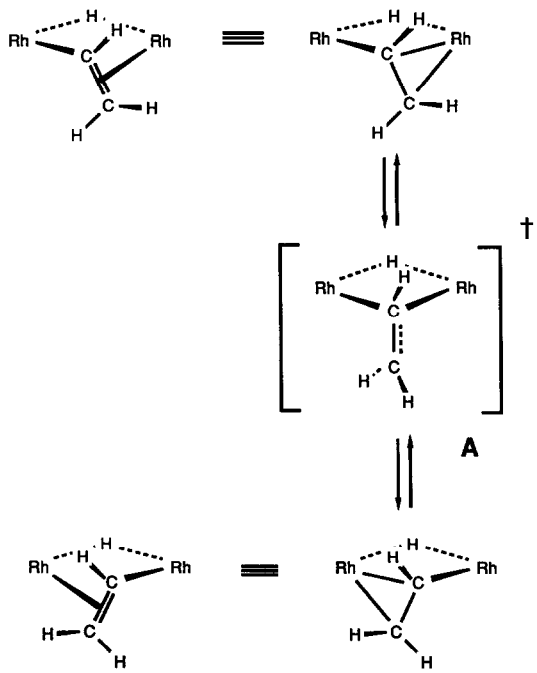

Fig. 1. "Windshield wiper" process to explain the fluxional behaviour of the vinyl–hydride complexes **2a** and **2b**. The symmetrical transition state **A** is also shown.

two metal centres and exchanges the pairs of phosphorus nuclei A and B, and C and D, rapidly at room temperature. A highly symmetrical transition state such as **A** in Fig. 1 is consistent with the high temperature limit for these derivatives. Further evidence for **A** is found in the one-bond carbon–hydrogen ($^1J_{C,H}$) and carbon–carbon ($^1J_{C,C}$) coupling constants of the bridging vinyl ligand of the ^{13}C-labelled complexes **2a** and **2b**. In the fast exchange regime, the smaller $^1J_{C,H}$ of 127 and 132 Hz for the α-C as compared to $^1J_{C,H}$ of 148–151 Hz for the β-carbon are suggestive of considerable sp^3 character about C_α. The observed $^1J_{C,C}$s in **2a** and **2b** are about 6–8 Hz lower than those normally found in η^4-bound diene complexes, but are of the same order of magnitude as the C_1–C_2 coupling constants found in early transition metal derivatives wherein the diene binds in the η^4-σ^2-π fashion.[11] Therefore, it is reasonable to invoke that some single bond character is inherent in the C_α—C_β bond in the vinyl–hydrides **2a** and **2b**.

At low temperatures, the slow exchange spectrum can be obtained. The $^{31}P\{^1H\}$ NMR spectrum of the dippe dineyl–hydride **2a** shows four inequivalent phosphine environments (Fig. 2), completely in agreement with the μ-η^2-σ vinyl–hydride structure found in the solid-state. Simulation of this spectrum as an ABCDXY spin system (Fig. 2: A, B, C, D = ^{31}P; X, Y = ^{103}Rh) shows that substantial coupling through three and four bonds exists via the hydride bridge between P_1 and P_2 ($^4J_{AB}$), P_1 and Rh_2 ($^3J_{AY}$) and P_2 and Rh_1 ($^3J_{BX}$). Such strong couplings through the bridge have been observed[4(c),12] previously in systems of the type $[P_2Rh]_2(\mu\text{-}H)(\mu\text{-}X)$ where $X = NR_2$, OR″. Presumably these arise because the geometry around the metal is distorted through steric interactions between the X ligand and the proximate phosphorus donors, such that the phosphorus nuclei *cis* to X are nearly *trans* disposed across the Rh—Rh vector thus enhancing magnetic communication between each side of the metal complex.

As the temperature is raised, P_1/P_2 and P_3/P_4 coalesce and decoalesce as complex multiplets of doublets (Fig. 2). A $\Delta G‡$ of 12.2 ± 0.2 kcal mol^{-1} has been determined for this process in **2a** and is

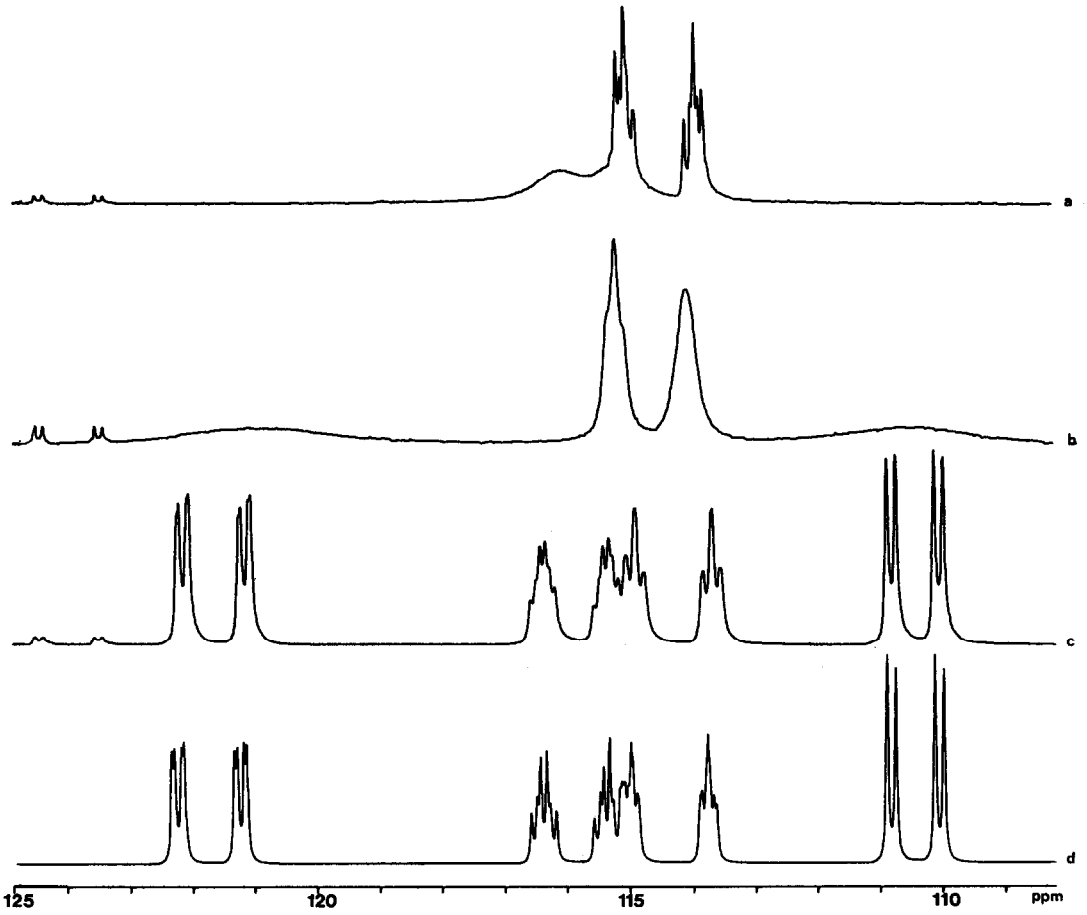

Fig. 2. Variable temperature $^{31}P\{^1H\}$ NMR (162.2 MHz, C_7D_8) spectra of $[(doppe)Rh]_2(\mu\text{-}\eta^2\text{-}\sigma\text{-}CH{=}CH_2)(\mu\text{-}H)$, **2a**; spectrum **a**: $T = 333$ K; spectrum **b**: $T = 283$ K; spectrum **c**: $T = 203$ K; spectrum **d**: simulation of the low temperature limit (see Experimental for parameters).

slightly larger than the value of 10.3 kcal mol^{-1} that was found[10(a)] for $(CO)_{10}Os_3(\mu\text{-H})(\mu\text{-CH=CH}_2)$, but identical with the value reported for the complex $(CO)_7(PPh_3)Re_2(\mu\text{-H})(\mu\text{-CH=CH}_2)$.[13]

Mechanism of formation

The formation of the observed alkenyl–hydride products **2** from the starting dihydride precursors **1** requires that two equivalents of olefin be consumed: one equivalent to *dehydrogenate* the dihydride dimers and the remaining equivalent to become the alkenyl–hydride unit. The use of the deuterium labelled complex, $[(dippe)Rh]_2(\mu\text{-D})_2$, d_2-**1a**, and ethylene shows no incorporation of deuterium into the vinyl–hydride product **2a**, clearly consistent with this *dehydrogenation* step.

In Scheme 1 possible mechanisms for the formation of the observed products are represented. The coordinatively unsaturated dihydride dimers must first react with the olefin to generate an olefin complex **B** which undergoes insertion, followed by binuclear reductive elimination to generate the binuclear rhodium(0) dimer **C** and one equivalent of alkane. The subsequent reaction with the second equivalent of alkene can follow path **a** or path **b**. In path **a**, the olefin coordinates to one metal centre of the dimer **C**, and the second metal centre activates the vinylic C—H bond by an oxidative addition. This is the most commonly assumed pathway[13] for the formation of alkenyl–hydride complexes. An intriguing alternative pathway is presented in **b** wherein the olefin inserts into the metal–metal bond of the binuclear rhodium(0) dimer **C** to produce a bridging alkanediyl linkage in **D** which subsequently undergoes a binuclear β-elimination to generate the observed products. Both pathways **a**

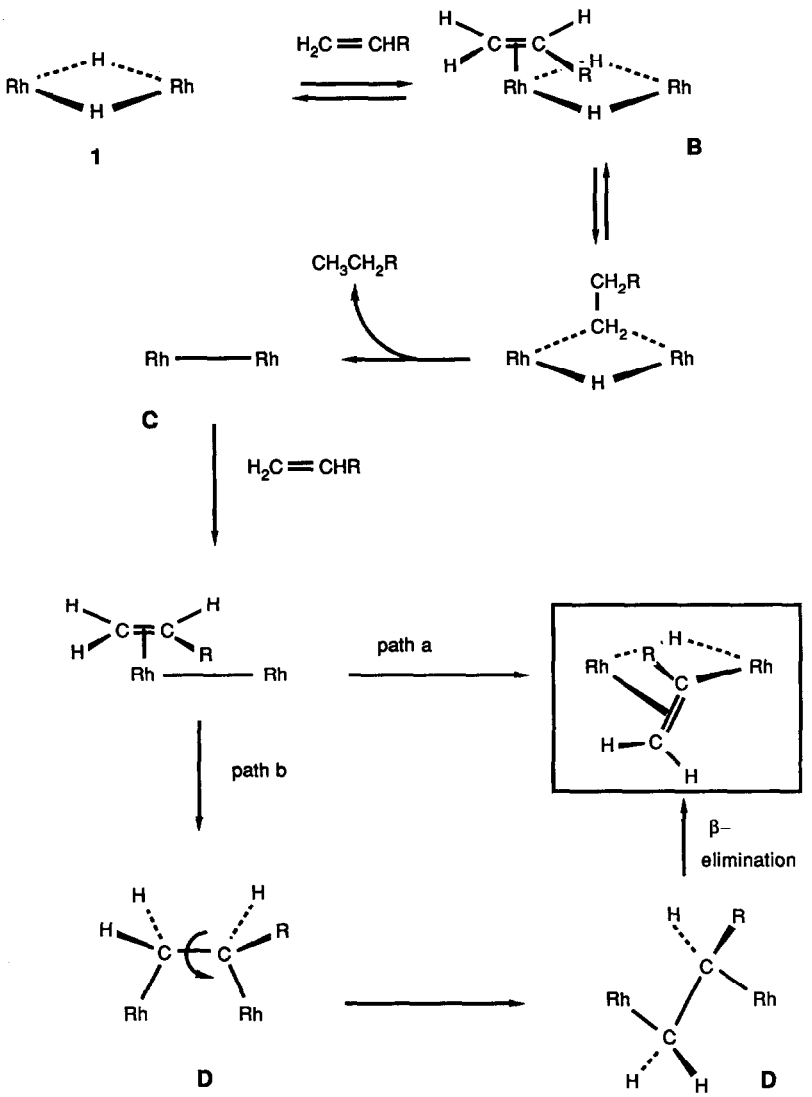

Scheme 1.

and **b** are consistent with all of the labelling studies. Recent stereochemical studies[14] on the reaction of, formally, $H_2C{=}CH_2$ and "$(CO)_4Os{=}Os(CO)_4$" show that this process corresponds to a 2+2 concerted cycloaddition to generate a diosmacyclobutane derivative. In the mechanism shown in Scheme 1, path **b** also corresponds to a 2+2 cycloaddition between the double bond of the olefin and the *single* bond of **D**, the binuclear rhodium(0) complex. Our attempts to determine the stereochemical course of the reaction of olefins with purported **C** using *cis*-1,2-d_2-ethylene and *cis*-1,2-d_2-propylene were thwarted by the scrambling and isomerization side-reactions. The use of tetrafluoroethylene as a possible trap for a species like **D** with a β-elimination stabilized 1,2-alkanediyl bridge was unsuccessful since the only product isolated from the reaction with $[(dippe)Rh]_2(\mu\text{-}H)_2$ **1a** was the fluorobridged dimer $[(dippe)Rh]_2(\mu\text{-}F)_2$.

While we have no evidence to distinguish between path **a** and path **b**, we have been able to follow the progress of the reaction in the early stages by running the reaction at low temperature. Thus the interaction of 1-butene with the dippe dimer **1a** at $-78°C$ generates an intensely magenta-coloured solution which by $^{31}P\{^1H\}$ NMR spectroscopy shows the presence of another species besides signals for **1a** and the diastereomeric butenyl hydride products. The four extra peaks are attributable to the intermediate **B** (Scheme 1) in which the olefin is η^2-bound to one of the rhodium centres. Raising the temperature in the presence of excess olefin, resulted in the disappearance of the signals due to this intermediate and the completion of the reaction. A similar intermediate has been detected[7] in the reaction of **1a** with 1,3-butadiene. The reaction of terminal olefins and even ethylene with the dippp dimer **1b** is so slow that this type of intermediate has never been observed. It is conceivable that an increase of the steric crowding about the inner $Rh_2(\mu\text{-}H)_2$ core in **1b**, as discussed above, may hinder olefin coordination even at low temperatures.

Dienes

The reaction of the dimers **1a**, **1b** and **1c** with 1,3-butadiene has been reported[15,16] but will be briefly recounted here. The dippe dimer **1a** reacts quite cleanly with 1,3-butadiene to generate two isomeric, binuclear complexes of the formula $[(dippe)Rh]_2 \cdot C_4H_6$ as shown in eq. (2). The solution behaviour of this isomeric mixture is complex;[7] not only are the two derivatives $[(dippe)Rh]_2(\mu\text{-}H)(\mu\text{-}\eta^4\text{-}\sigma\text{-}C_4H_5)$, **3a** and $[(dippe)Rh]_2(\mu\text{-}\eta^3\text{-}\eta^3\text{-}C_4H_6)$, **4a**, in equilibrium above $-20°C$ (by ^1H NMR spectroscopy), but the butadienyl–hydride core of **3a** is itself undergoing intramolecular rearrangements on the NMR time scale.

The analogous reaction of the dippp dimer, **1b**, generates only one binuclear product, the non-fluxional complex $[(dippp)Rh]_2(\mu\text{-}\eta^3\text{-}\eta^3\text{-}C_4H_6)$, **4b**, in approximately 60% yield along with 30% of mononuclear 1-methylallyl complexes as shown in eq. (3). Both of the binuclear types of products are unusual and represent new binding and activation modes for 1,3-butadiene on two metal centres. In particular, the derivatives **4a** and **4b**, having the $\mu\text{-}\eta^3\text{-}\eta^3\text{-}C_4H_6$ are termed[16] "partial butadiene sandwich" complexes since the butadiene ligand is sandwiched between the two metal centres. $^{31}P\{^1H\}$ NMR spectroscopy is particularly diagnostic[7] for each binding mode, given the symmetry of the individual complexes and the fact that the $\mu\text{-}\eta^4\text{-}\sigma\text{-}C_4H_5$ core is

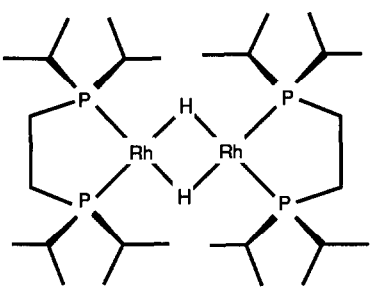

1a

excess

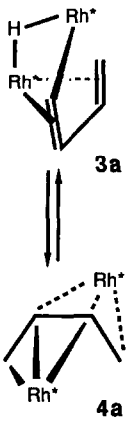

3a **4a**

(2)

Rh* = Rh(dippe)

Eq. (2)

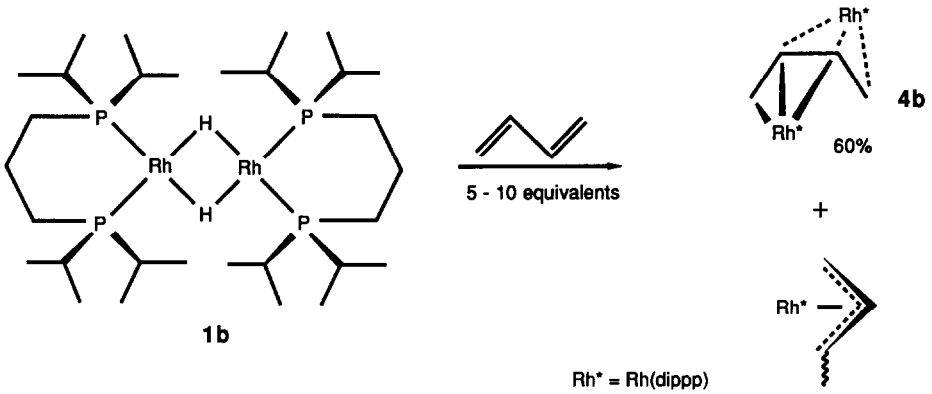

(3)

Eq. (3)

fluxional while the μ-η^3-η^3-C_4H_6 unit is rigid on the NMR time scale. The reaction of the dipope dimer **1c** with 1,3-butadiene is totally different. Alkenyl–hydride complexes are formed in a similar way to those found by reaction of olefins with **1a** and **1b**. These alkenyl–hydride derivatives are thermally sensitive particularly in the presence of excess butadiene.[15]

The X-ray crystal structures of the butadienyl–hydride complex **3a**, having the five-membered chelate ring dippe ligands, and the sandwich derivative with the six-membered chelate ring dippp ligands **4b**, have been reported.[7,15,16] Although in the dippe system the butadienyl–hydride form (μ-η^4-σ-C_4H_5), **3a**, is more thermodynamically preferred in solution than the sandwich isomer (μ-η^3-η^3-C_4H_6), **4a**, none of the former can be detected in the dippp system. The reason for this may be related again to the steric demands of the two chelating bidentate ligands. The solid-state structure of **3a** indicates that the isopropyl groups of the dippe ligand on the σ-bound rhodium centre are close to the dienyl–hydride core, and this in turn suggests that the dippp ligand having the larger chelate bite angle would place the isopropyl substituents even closer to the core ligands in the butadienyl–hydride isomer. Such is not the case from examination of the solid-state structure of the sandwich derivative **4b** since in the bridging sandwich mode, the μ-η^3-η^3-C_4H_6 moiety is placed between two skewed (dippp)Rh units. This destabilization of the dienyl–hydride form by steric crowding was sufficiently intriguing to us that we examined the reaction of methyl substituted butadienes, namely isoprene (2-methyl-1,3-butadiene) and piperylene (*cis*/*trans*-1-methyl-1,3-butadiene), with the electron-rich, binuclear dihydride complexes **1a** and **1b**. In addition, we also briefly examined the effect of bulkier substituents on the phosphorus donors using a new synthetic procedure with "magnesium butadiene".

Reaction of [(dippe)Rh]$_2$(μ-H)$_2$ *with isoprene and piperylene*

The dihydride **1a** reacts readily with isoprene and piperylene, but the reaction times are significantly longer as compared to the analogous reaction with 1,3-butadiene, which is rapid even at −20°C. Although shorter reaction times can be obtained by the use of excess diene, this also decreases the proportion of binuclear products. Optimal production of binuclear products with reasonable reaction times are possible with 5–10 equivalents of the diene.

The reaction with isoprene is summarized in eq. (4). A *syn*/*anti* mixture of the mononuclear 2,3-dimethylallylrhodium complexes is obtained as the major product with the binuclear isoprenyl–hydride derivatives **5a**/**5a′** as the minor component; the best ratio of mononuclear to binuclear products is approx. 4:1. Unfortunately, the binuclear complexes could not be separated from the mononuclear dimethylallyl products by fractional crystallization or chromatography and this complicated NMR analysis. Although we could not detect any of the binuclear isomeric isoprenyl sandwich derivative [(dippe)Rh]$_2$(μ-η^3-η^3-C_5H_8), at best we can say that there is less than 10% since this is probably the limit of detectability given the complex pattern of overlapping signals. The complexity of the spectra also precluded meaningful data from ^{13}C and ^{31}P spectra; however, from the variable temperature $^1H\{^{31}P\}$ NMR spectra, we were able to observe that the isoprenyl–hydride species, **5a**/**5a′**, are fluxional and apparently interconvert between the two possible diastereomeric forms as shown in eq. (4). Support for this comes from the hydride resonance at −8.34 ppm that appears as a broad triplet (with broad-band ^{31}P decoupling) at ambient temperatures; as the temperature is lowered the pattern becomes more complex, consistent with two

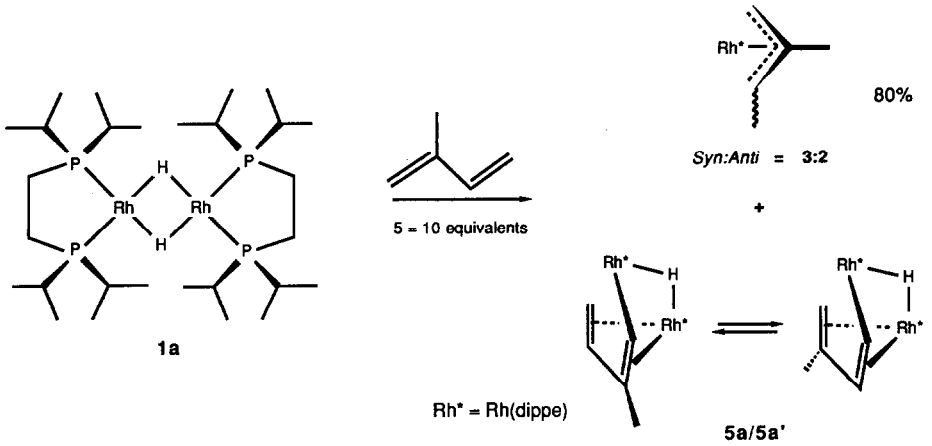

(4)

Eq. (4)

species both having inequivalent ^{103}Rh nuclei coupled to the bridging hydride ligand. Other resonances downfield were observed, in particular, a doublet at 1.5 ppm is attributed to the methyl group on the isoprenyl ligand; as the temperature is lowered, this doublet broadens and sharpens into two doublets of equal intensity again consistent with the slow exchange limit for the diastereomeric isoprenyl–hydride complexes **5a/5a'**. Other resonances were observed to broaden and coalesce, but we have been unable to assign these peaks with certainty. Nonetheless, to explain the rearrangements in the high temperature limit, one must invoke a process to exchange both rhodium centres and both ends of the isoprenyl ligand, all of which require substantial bond-breaking and bond-making. One possible process is shown in Scheme 2 and is a modification of a process already proposed by us to explain the fluxionality of the butadienyl–hydride **3a** and its conversion to the butadiene sandwich complex **4a**. Dissociation of one end of the isoprenyl ligand followed by a "windshield wiper" process (see Fig. 1) interconverts the two rhodium centres on any one particular diastereomeric isoprenyl–hydride complex **5a**. To interconvert the diastereomers, we suggest a binuclear

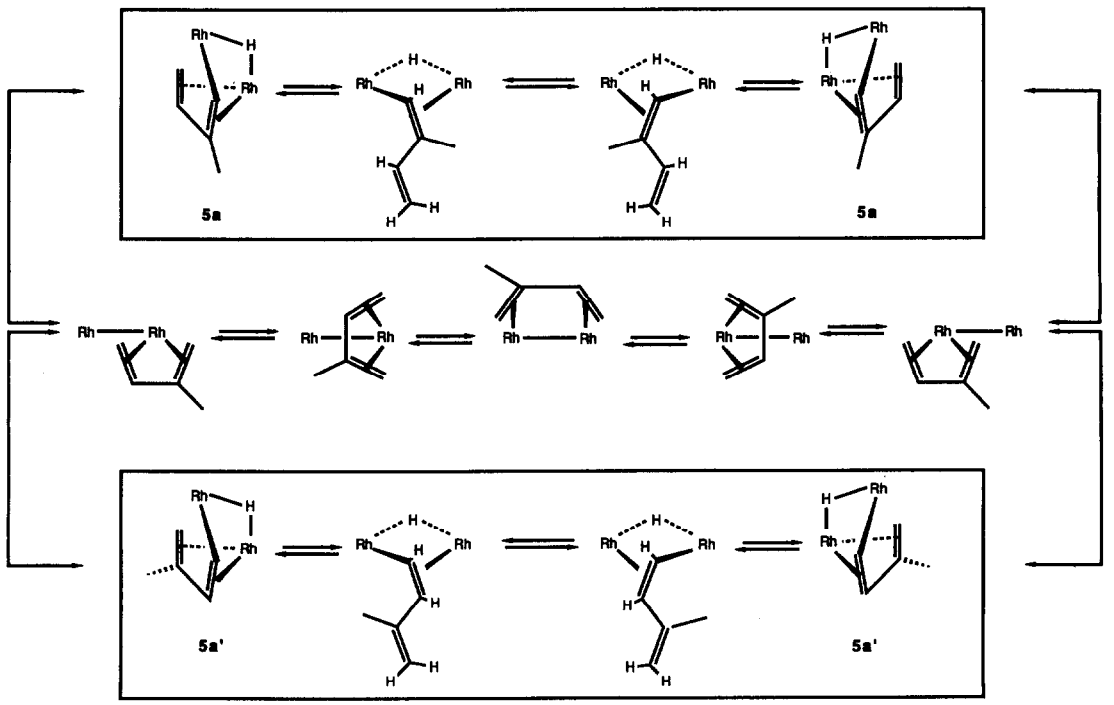

Scheme 2.

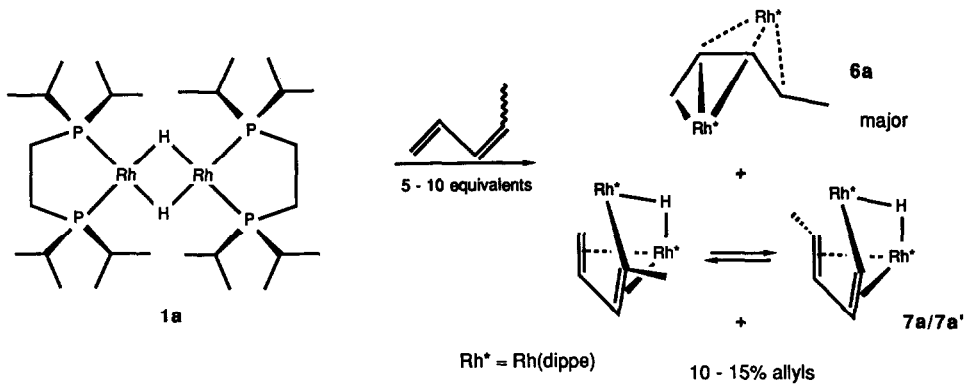

(5)

Eq. (5)

reductive elimination of the hydride and the isoprenyl ligands to generate an η^4-isoprene ligand bound to a formally Rh(0) dimer. By analogy to Scheme 1, the C—H bond can be cleaved either by oxidative addition or by insertion of one of the double bonds of the isoprene unit into the Rh—Rh single bond, followed by a binuclear β-elimination.

The reaction of $[(dippe)Rh]_2(\mu\text{-}H)_2$, **1a**, with piperylene was more straightforward and is summarized in eq. (5). The binuclear products are now the major components with the mononuclear substituted-allyl complexes spectroscopically observed in only 10–15% yield. The binuclear products are a 4:1 mixture of the *syn*-piperylene sandwich **6a** and piperylenyl–hydride diastereomers **7a/7a'** and can be isolated, as a mixture, in approximately 50% yield with only a slight contamination of the tenacious allyl side products. The behaviour of this mixture in solution is similar to that already discussed for the prototype butadiene reaction; the piperylene sandwich **6a** is in equilibrium with the piperylenyl–hydride diastereomers **7a/7a'**, but in this case the equilibrium favours the sandwich derivative. This observation is consistent with our analysis of the steric requirements of this reaction, since the presence of the methyl group at the 1-position of butadiene has reversed the thermodynamic preference found for the (unsubstituted) butadiene reaction products with $[(dippe)Rh]_2(\mu\text{-}H)_2$, **1a**. Unfortunately, we were unable to obtain an accurate ratio of the diastereomers **7a** and **7a'** due to the complexity of the spectra.

Reaction of $[(dippp)Rh]_2(\mu\text{-}H)_2$ *with isoprene and piperylene*

The sluggish reactivity of $[(dippp)Rh]_2(\mu\text{-}H)_2$, **1b**, with unsaturated hydrocarbons has already been discussed in its reaction with ethylene. The corresponding reaction with isoprene is also very slow proceeding over a period of 6–7 days to produce a mixture of exclusively mononuclear dimethylallyl complexes. As no binuclear products were observed, this reaction is not appropriate for discussion here.

The reaction of the dippp dimer **1b** with *cis/trans*-piperylene also generates mononuclear substituted allyl derivatives, but not exclusively; also formed is the binuclear piperylene sandwich complex **6b** in approximately 20% spectroscopic yield as shown in eq. (6). Separation of **6b** from the complex mixture of allyl complexes (at least five derivatives could be detected although not unambiguously assigned) was not possible but spectroscopic characterization of **6b** was and there is no doubt of its formulation as the *syn*-piperylene sandwich complex. The corresponding piperylene–hydride isomers were not detected, in line with the destabilization of the dienyl–hydride isomer by substitution on the diene.

Alternate preparation: the "magnesium butadiene" route

It is quite clear that the reaction of 1,3-dienes with the electron-rich binuclear hydride complexes **1a** and **1b** can be complicated by the formation of mononuclear allyl side-products either as minor constituents or as the major components. Because of our interest in the binuclear products of these reactions, we examined other possible synthetic routes to these materials. One rational sequence which proved to be successful was the reaction of "magnesium butadiene"[17] $([Mg \cdot C_4H_6 \cdot 2THF]_n)$ with chlorobridged dimers of rhodium(I) as shown in eq. (7). Using this procedure, we have been able to prepare[7] binuclear compounds in very high yields with only a trace formation of the mononuclear allyl side-products. Of particular importance is the fact that we can now access compounds for which the corresponding hydride dimer is not available; for example, because $[(dtbpp)Rh]_2(\mu\text{-}H)_2$, where

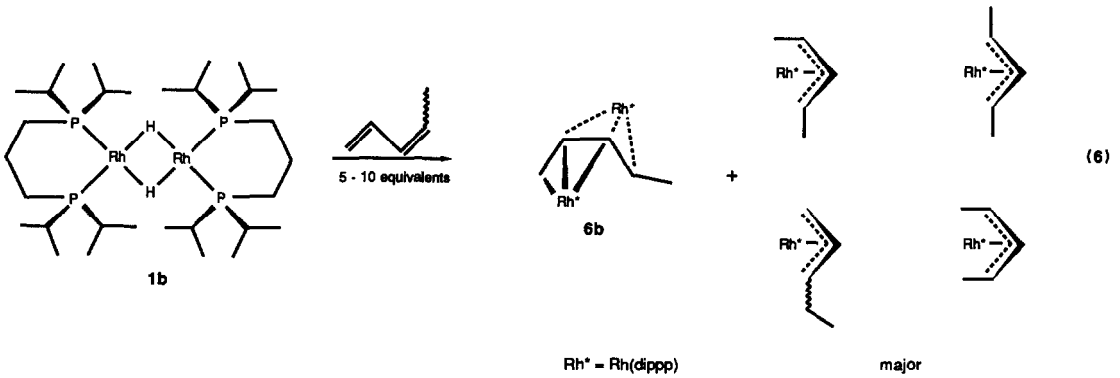

(6)

Eq. (6)

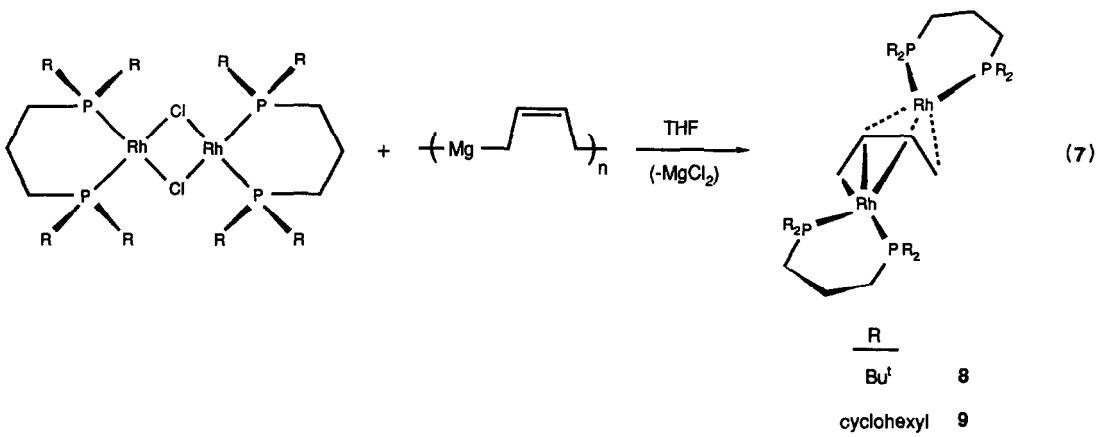

(7)

Eq. (7)

dtbpp = 1,3 - bis(ditertiarybutylphosphino)propane, is thermally unstable,[18] reactions with dienes are not feasible. However, the "magnesium butadiene" route generates the corresponding butadiene sandwich complex $[(dtbpp)Rh]_2(\mu\text{-}\eta^3\text{-}\eta^3\text{-}C_4H_6)$, **8**, in excellent yield. The corresponding chelating phosphine with cyclohexyl substituents, dcypp = 1,3-bis(dicyclohexylphosphine)propane, has also been utilized on rhodium(I) using this alternative route to produce the butadiene sandwich complex $[(dcypp)Rh]_2(\mu\text{-}\eta^3\text{-}\eta^3\text{-}C_4H_6)$, **9**; the relative insolubility of this latter derivative has precluded $^{13}C\{^1H\}$ NMR data collection, although the $^{31}P\{^1H\}$ and ^1H NMR spectra are diagnostic for the sandwich formulation. The availability† of other "magnesium diene" reagents makes this an attractive procedure for more complex systems.

† In fact, recently we have obtained the compound $[(dippp)Rh]_2(\mu\text{-}\eta^3\text{-}\eta^3\text{-}C_5H_8)$ from $[(dippp)Rh]_2(\mu\text{-Cl})_2$ and "magnesium isoprene".[20] This compound was unavailable via the **1b** plus isoprene route, illustrating the utility of the magnesium diene synthesis.

CONCLUSIONS

The reaction of simple olefins with these binuclear rhodium hydride complexes appears to be under steric control in the formation of alkenyl–hydride derivatives. In fact, it is quite remarkable that chelate ring size has such an effect on the relative rates of these reactions. In an attempt to formulate a mechanism for this process, we have suggested that an important step is insertion of an olefin into a Rh—Rh bond. Although speculative, such a transformation would constitute a new primary process for polynuclear metal systems.

In this work we have also outlined two new activation modes for 1,3-dienes on a bimetallic fragment: (i) the bridging dienyl–hydride core represented by $\mu\text{-}\eta^4\text{-}\sigma$-dienyl, which is remarkably mobile between metal centres, and (ii) the partial diene sandwich form represented by $\mu\text{-}\eta^3\text{-}\eta^3$-diene. These products are the result of the interaction of a 1,3-diene with a binuclear rhodium hydride derivative; however, mononuclear allyl derivatives are also sometimes formed as the predominant species. The use of the "magnesium butadiene" route

circumvents this and generates the binuclear complexes in excellent yields. We have already suggested a mechanism to account for the binuclear and mononuclear products of the reaction of 1,3-butadiene with **1a** and **1b**. What emerges from this study is the extent of rearrangement of the core in the dienyl–hydride isomers. Not only is there a process which exchanges both ends of the binuclear metal fragment (via the modified "windshield wiper" rearrangement), but a more complex process is also operative to exchange the ends of the dienyl unit. We suggest that this unique rearrangement involves both metal centres and requires that the 1,3-diene shunts from η^4 to *cis*-μ-η^2-η^2 back to η^4, but now on the adjacent metal (see Scheme 2). Such massive structural rearrangements are undoubtedly a result of the coordinatively unsaturated, electron-rich nature of the dirhodium core and bode well for the activation of other small organic molecules.

EXPERIMENTAL

General procedures

The general procedures used in this work have been described in detail elsewhere.[5,7] The dienes isoprene and piperylene were purchased from Aldrich Chemical Co. (the piperylene came as a 90% mixture of *cis*/*trans* isomers, with 10% cyclopentene) and were dried over 3 Å molecular sieves. They were then vacuum transferred into storage vessels, thoroughly degassed via the freeze–pump–thaw routine and stored in the dark. The ligands $R_2P(CH_2)_3PR_2$, (R = Pr^i,[6] and cyclohexyl[20]) were prepared using literature procedures and for R = Bu^t, Otsuka's procedure was employed.

Reaction of [(dippp)Rh]$_2$(μ-H)$_2$ *with ethylene*

A solution of **1b** (0.075 g, 0.10 mmol) in toluene (5 cm^3) was loaded into a thick-walled reactor bomb equipped with a 5 mm Kontes needle valve. The vessel was attached to a vacuum line and degassed; ethylene was then admitted to a pressure of 1 atm. A slow deep green to red colour change was observed over a period of 2–3 h. The toluene was removed under reduced pressure and the residue recrystallized from minimum hexanes, from which 0.067 g (86%) of the deep red crystals of **2b** were isolated. ^{1}H NMR (C_6D_6, ppm): RhC*H*=CH$_t$H$_c$, 9.79 (m, J_{H_t} = 17.5 Hz, J_{H_c} = 9.5 Hz, $J_{H-^{13}C}$ = 132.4 Hz, additional couplings to three phosphorus nucleus, J_P = 3.3, 3.3, 3.8 Hz); RhCH=C*H$_t$H$_c$*, 5.40 (m, J_{H_t} = 3.6 Hz, $J_{H-^{13}C}$ = 148.3 Hz, $J_P \approx 4$ Hz); RhCH=C*H$_t$*H$_c$, 4.53 (dd, $J_{H-^{13}C}$ = 151.9); C*H*(CH$_3$)$_2$, 1.8–2.2 (3 br overlapping d of sp); CH(C*H*$_3$)$_2$ and PC*H*$_2$C*H*$_2$C*H*$_2$P, 1.0–1.6; Rh—*H*—Rh, −9.76 (m). ^{13}C{^{1}H} NMR (C_6D_6, ppm): Rh^{13}C*H*=^{13}CH$_2$, 201.7 (m); Rh^{13}CH=^{13}C*H*$_2$, 69.6 (d, J_{C-C} = 35.4 Hz); ligand resonances, 18–32. Anal. Calc. for $C_{32}H_{72}P_4Rh_2$: C, 48.85; H, 9.24. Found: C, 48.89; H, 9.15%.

Spectral simulation of the low temperature limit spectrum of **2a**

The simulation of the ^{31}P{^{1}H} NMR spectrum for **2a** at −70°C was carried out using the program UBCPANIC.† Using measured coupling constants, a close fit was obtained by manual iteration. A line width of 7 Hz was used to obtain the calculated trace found in Fig. 2(d). Chemical shift and coupling constant assignments are based on the following spin system:

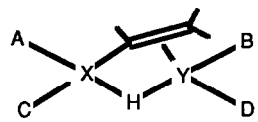

Chemical shifts: δ_A = 114.5; δ_B = 115.9; δ_C = 110.5; δ_D = 121.8 ppm.
Coupling constants: J_{AB} = 15.8; J_{AC} = 22.2; J_{AD} = 0.0; J_{AX} = 196.1; J_{AY} = 6.0; J_{BC} = 0.0; J_{BD} = 25.0; J_{BX} = 25.0; J_{BY} = 162.8; J_{CD} = 0.0; J_{CX} = 123.9; J_{CY} = 0.0; J_{DX} = 7.5; J_{DY} = 160.9; J_{XY} = 4.0 Hz.

Reactions of [(dippe)Rh]$_2$(μ-H)$_2$ *and* [(dippp)Rh]$_2$ (μ-H)$_2$ *with tetrafluoroethylene*

An identical procedure was employed for both of these reactions. The hydrides (**1a** or **1b**) were dissolved in toluene and loaded into a small, thick-walled reactor bomb equipped with a 5 mm Kontes needle valve. The vessel was attached to a vacuum line, and about 5 equivalents of tetrafluoroethylene were vacuum transferred into the bomb. The reaction was immediate for **1a**, while **1b** took about 0.5 h to react completely. The solids isolated had very similar ^{1}H NMR spectra to the chlorobridged dimers [(dippe)Rh]$_2$(μ-Cl)$_2$ and [(dippp)Rh]$_2$(μ-Cl)$_2$,[7] and the ^{31}P{^{1}H} spectra consisted of a complex multiplet indicative of the AA′A″A‴MM′XX′ spin system expected for the fluorobridged dimers

† PANIC: Parameter Adjustment in NMR by Iteration Calculation. PANIC is a minicomputer version of larger LAOCOON type programs used with the Bruker Aspect 2000 software package.

[(dippe)Rh]$_2$(μ-F)$_2$ and [(dippp)Rh]$_2$(μ-F)$_2$. Data for [(dippe)Rh]$_2$(μ-F)$_2$: ^{1}H NMR (C_6D_6, ppm): C*H*(CH$_3$)$_2$, 1.90 (br m); CH(C*H*$_3$)$_2$, 1.49, 1.18 (dd, ^3J_H = 7.6, 6.4 Hz, ^3J_P = 14.4, 13.6 Hz); PC*H*$_2$C*H*$_2$P, 0.92 (m, ^2J_P = 9.2 Hz). ^{31}P{^{1}H} NMR (C_6D_6, ppm referenced to P(OCH$_3$)$_3$ at 141.0): 109.1 (m). Data for [(dippp)Rh]$_2$(μ-F)$_2$: ^{1}H NMR (C_6D_6, ppm): C*H*(CH$_3$)$_2$, 1.90 (br m); CH(C*H*$_3$)$_2$, 1.52, 1.25 (dd, ^3J_H = 7.2, 7.2 Hz, ^3J_P = 13.2, 12.0 Hz); PC*H*$_2$ CH$_2$C*H*$_2$P, ~ 1.4 (partially obscured); PCH$_2$ C*H*$_2$CH$_2$P, 0.75 (br m). ^{31}P{^{1}H} NMR (C_6D_6, ppm referenced to P(OCH$_3$)$_3$ at 141.0): 59.3 (m). Anal. Calc. for $C_{30}H_{68}P_4F_2Rh_2$: C, 45.24; H, 8.60. Found: C, 45.60; H, 9.00%.

Reaction of [(dippe)Rh]$_2$(μ-H)$_2$ *with isoprene*

A solution of **1a** (0.10 g, 0.14 mmol) in toluene (10 cm^3) was loaded into a reactor bomb and degassed on a vacuum line. Approximately 10 equivalents of isoprene were then introduced into the system, and the reaction was stirred at room temperature until the green to orange colour change was complete (4–6 h). The solvent was removed *in vacuo* to leave 0.110 g (≈ 95% by mass balance) of an orange oil consisting of a *syn*:*anti* mixture of 1,2-dimethylallylrhodium(I)dippe compounds (80% by NMR), and about 20% of the equilibrating binuclear isomers **5a** and **5a′**. ^{1}H NMR (C_7D_8, ppm), *syn*-1,2-dimethylallylrhodium(I)dippe: C*H*$_s$(H$_a$), 3.40 (s); C*H*$_a$(CH$_3$), 3.07 (m, J_{CH_3} = 6.4 Hz, J_P = 4.0 Hz); C*H*$_a$(H$_s$), 2.37 (s); CC*H*$_3$(H$_a$), 2.09 (dt, J_P = 4.8 Hz); C—C*H*$_3$, 1.65 (d, J_{Rh} = 1.5 Hz). ^{1}H NMR (C_7D_8, ppm), *anti*-1,2-dimethylallylrhodium(I)dippe: C*H*$_s$(CH$_3$), 4.38 (m, J_{CH_3} = 6.8 Hz); C*H*$_s$(H$_a$), 3.41 (s); C*H*$_a$(H$_s$), 2.32 (d, J_P = 7.4 Hz); C—C*H*$_3$, 1.63 (d, J_{Rh} = 1.6 Hz); CC*H*$_3$(H$_s$), 1.32 (m). ^{1}H NMR (C_7D_8, ppm): broad signals for dienyl protons appear at 5.90 and 2.63 ppm at ambient temperature; C—C*H*$_3$, 1.5 (d, room temp.); 1.6, 1.4 (d, J = 6–8 Hz, −70°C); Rh—*H*—Rh, −8.36 (br m). Analytically pure samples were unobtainable.

Reaction of [(dippe)Rh]$_2$(μ-H)$_2$ *with piperylene*

A procedure analogous to that described above for the reaction of **1a** and isoprene was employed. This reaction took 4–5 h for completion, and produced 0.045 g (42%) of a solid consisting of a mixture of the binuclear products **7a** and **6a**, as traces of contaminating mononuclear allyl products. ^{1}H and ^{13}C{^{1}H} NMR data for **6a** are included in Tables 1 and 2. ^{31}P{^{1}H} NMR (C_6D_6, ppm referenced to P(OCH$_3$)$_3$ at 141.0), **6a**: 102.9 (dm, J_{Rh} = 239.3 Hz); 96.2 (dm, J_{Rh} = 240.1 Hz); 88.5 (2 overlapping dm, J_{Rh} ≈ 187–193 Hz, 2P). ^{1}H NMR (C_6D_6, ppm), **8a**: dienyl proton resonances at 3.98 and 5.77 (br m, ambient temp.); Rh—*H*—Rh, −7.83 (m, J_{Rh} = 25.1 Hz). ^{31}P{^{1}H} NMR (C_6D_6, ppm referenced to P(OCH$_3$)$_3$ at 141.0): 94.8 (d, $J_{Rh(av)}$ = 167.8 Hz).

Reaction of [(dippp)Rh]$_2$(μ-H)$_2$ *with piperylene*

An analogous procedure to that described above for the reactions of **1a** with isoprene and piperylene was employed. An oily, extremely soluble (hexane) orange solid was obtained (91% by mass balance), consisting of a complex mixture of 1,3-dimethylallylrhodium(I)dippp, and 1-ethylallylrhodium(I) dippp isomers, as well as the binuclear product **6b** (20% by NMR). ^{1}H and ^{13}C{^{1}H} NMR data for **6b** are included in Tables 1 and 2. ^{31}P{^{1}H} NMR (C_6D_6, ppm referenced to P(OCH$_3$)$_3$ at

Table 1. ^{1}H and ^{13}C{^{1}H} NMR data[a] for the partial sandwich compounds **4a/b**, **6a/b**, **8** and **9**

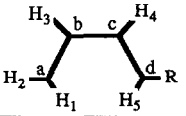

Compound	R	H_1	H_2	H_3	H_4	H_5	CH_3	C_a	C_b	C_c	C_d
4a	H	0.75	2.66	4.85				40.0	63.2		
4b	H	0.87	2.65	4.78				37.9	60.2		
6a	CH_3	0.95	2.59	4.71	4.93	1.61	2.00	37.6	56.5	67.4	50.5
6b	CH_3	0.65	2.32	4.57	4.71	----[b]	2.03	36.8	57.2	66.5	48.6
8	H	0.86	2.98	4.90				39.5	60.1		
9	H	0.73	2.56	4.79				----[b]	59.8		

[a]PPM, C_6D_6. [b]Signal obscured by ligand resonances and/or impurities.

Table 2. Coupling constants[a] in partial diene sandwich complexes

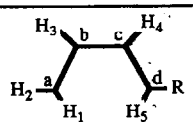

Compound	R	$J_{1,2}$	$J_{1,3}$	$J_{2,3}$	$J_{3,3'}$	$J_{3,4}$	$J_{4,5}$	$J_{5,Me}$	$J_{a,P}$	$J_{a,Rh}$	$J_{b,P}$	$J_{c,P}$	$J_{d,P}$	$J_{d,Rh}$
4a	H	4.0	10.3	----[b]	----[b]				36.5	10.5	19.8			
4b	H	3.9	10.8	6.6	4.5				35.0	10.0	18.0			
6a	CH_3	4.5	12.4	6.4		5.2	11.2	5.6	37.2	9.1	21.6	19.3	44.1	10.6
6b	CH_3	3.2	12.0	6.2		4.4	11.1	5.6	35.2	10.1	----[c]	19.4	36.5	10.4
8	H	3.8	10.4	6.3	4.0				35.9	10.0	16.0			
9	H	3.9	10.0	6.3	4.2				----[c]	----[c]	18.2			

[a]Hertz. [b]Unobtainable due to poor resolution. [c]Signal obscured by ligand resonances and/or impurities.

141.0): 54.7 (dm, J_{Rh} = 235.0 Hz); 48.6 (dm, J_{Rh} = 234.8 Hz); 35.3 (2 overlapping dm, $J_{Rh} \approx$ 152–158 Hz).

Synthesis of [(dcypp)Rh]$_2$(μ-Cl)$_2$

To a vigorously stirred suspension of [(COD)Rh]$_2$(μ-Cl)$_2$ (0.250 g, 0.51 mmol) in THF (30 cm^3) was added in one portion, a solution of 1,3-bis(dicyclohexylphosphino)propane, dcypp (0.442 g, 1.02 mmol) in THF (10 cm^3). The disappearance of all solid [(COD)Rh]$_2$(μ-Cl)$_2$ along with a deepening of the orange colouring of the solution was followed by precipitation of the bright orange product. The product suspension was reduced in volume to 40 cm^3 and cooled to −30°C to complete product precipitation. The product was collected on a fine porosity frit, and washed with three 15 cm^3 portions of cold hexanes (0.522 g, 0.45 mmol, 89.7%). ^{1}H NMR (C_6D_6, ppm): ligand resonances, 0.9–2.1 (br m). ^{31}P{^{1}H} (C_6D_6, ppm referenced to P(OCH$_3$)$_3$ at 141.0): 35.37 (d, J_{Rh} = 187.6 Hz). Anal. Calc. for $C_{54}H_{100}P_4Cl_2Rh_2$: C, 56.40; H, 8.76. Found: C, 56.09; H, 8.70%.

Synthesis of [(dtbpp)Rh]$_2$(μ-Cl)$_2$

To a stirred suspension of [$(C_2H_4)_2$Rh]$_2$(μ-Cl)$_2$ (0.250 g, 0.64 mmol) in THF (50 cm^3), was added dropwise a solution of 1,3-bis(ditertiarybutylphosphino)propane, dtbpp (0.429 g, 1.28 mmol) in THF (5 cm^3) over a period of 5 min. A deep red solution resulted, which was allowed to stir for 15 min before removal of the THF *in vacuo*. The remaining red powder was washed with two 10 cm^3 portions of cold hexanes and isolated by filtration (0.526 g, 87%). ^{1}H NMR (C_6D_6, ppm): C(CH_3)$_3$, 1.53 (d, J_P = 12.0 Hz); $CH_2CH_2CH_2$, 1.31 (br m^3 J_H = 7.6 Hz), $CH_2CH_2CH_2$, 1.09 (br m). ^{31}P{^{1}H} NMR (C_6D_6, ppm referenced to P(OCH$_3$)$_3$ at 141.0): 52.99 (d, J_{Rh} = 197.7 Hz).

Synthesis of [(dtbpp)Rh]$_2$(μ-η^3-η^3-C_4H_6)

A solution of [(dtbpp)Rh]$_2$(μ-Cl)$_2$ (0.040 g, 0.043 mmol) in THF (15 cm^3), was cooled to −30°C. A similarly cooled suspension of magnesium butadiene (0.011 g, 0.049 mmol) in THF (2 cm^3) was added dropwise to the deep red rhodium solution. Upon warming, this red colouring gave way to an orange–yellow solution, which was pumped down, extracted with 3 × 15 cm^3 portions of hexanes, and filtered through a celite pad. The hexane solution was concentrated to about 5 cm^3 and cooled. The product was collected as bright yellow crystals (0.034 g, 87.2%). ^{31}P{^{1}H} NMR (C_6D_6, ppm referenced to P(OCH$_3$)$_3$ at 141.0): P_A, 67.43 (d of m, J_{Rh} = 236.2 Hz); P_B, 47.88 (dd, J_{AB} = 24.0 Hz, J_{Rh} = 183.1 Hz).

Synthesis of [(dcypp)Rh]$_2$(μ-η^3-η^3-C_4H_6)

A THF suspension of [(dcypp)Rh]$_2$(μ-Cl)$_2$ (0.185 g, 0.16 mmol) and magnesium butadiene (0.045 g, 0.20 mmol), were loaded into a reactor bomb and stirred at 70°C until the suspension went clear (0.5–1 h). The resulting orange solution was pumped down and extracted with 3 × 50 cm^3 portions of hexanes. Concentration of this solution resulted in the precipitation of a yellow powder which was collected on a fine porosity frit (0.162 g, 90%). Approximately 5% of this powder was 1-methylallyl derivatives which was inseparable from the main product.

Acknowledgements—Financial support for this work was provided by NSERC of Canada in the form of an operating grant to M.D.F. and a postgraduate scholarship to W.E.P. We would also like to thank Johnson Matthey for a generous loan of $RhCl_3$.

REFERENCES

1. J. P. Collman, L. S. Hegedus, J. R. Norton and R. G. Finke, *Principles and Applications of Organotransition Metal Chemistry*, pp. 383–394. University Science Books, Mill Valley California (1987).
2. G. W. Parshall, *Homogeneous Catalysis*, pp. 12–19. John Wiley, New York (1980).
3. N. E. Schore, C. S. Ilenda, M. A. White, H. E. Bryndza, M. G. Matturo and R. G. Bergman, *J. Am. Chem. Soc.* 1984, **106**, 7451.
4. (a) M. D. Fryzuk, *Organometallics* 1982, **1**, 408; (b) M. D. Fryzuk, *Can. J. Chem.* 1983, **61**, 1347; (c) M. D. Fryzuk, M.-L. Jang, T. Jones and F. W. B. Einstein, *Can. J. Chem.* 1986, **64**, 174.
5. M. D. Fryzuk, T. Jones and F. W. B. Einstein, *Organometallics* 1984, **3**, 185.
6. K. Tani, E. Tanigawa, Y. Tatsubo and S. Otsuka, *J. Organomet. Chem.* 1985, **279**, 87.
7. M. D. Fryzuk, W. E. Piers, T. A. Albright, S. J. Rettig, F. W. B. Einstein and T. Jones, *J. Am. Chem. Soc.*, to be submitted.
8. S. Otsuka, *J. Organomet. Chem.* 1980, **200**, 191.
9. (a) J. R. Shapley, S. I. Richter, M. Tachikawa and J. R. Keister, *J. Organomet. Chem.* 1975, **94**, C43; (b) R. F. Gerlach, D. N. Duffy and M. D. Curtis, *Organometallics* 1983, **2**, 1172; (c) J. A. Iggo, M. J. Mays, P. R. Raithby and K. Hendrick, *J. Chem. Soc., Dalton Trans.* 1983, 205; (d) R. B. King, P. M Treichel and F. G. A. Stone, *J. Am. Chem. Soc.* 1961, **83**, 3600; (e) Y. N. Al-Obaidi, P. K. Baker, M. Green, N. D. White and G. E. Taylor, *J. Chem. Soc., Dalton Trans.* 1981, 2321; (f) P. Caddy, M. Green, L. E. Smart and N. White, *J. Chem. Soc., Chem. Commun.* 1978, 839; (i) J. R. Keister and J. R. Shapley, *J. Organomet. Chem.* 1975, **85**, C29; (j) A. J. Deeming, S. Hasso and M. Underhill, *J. Organomet. Chem.* 1974, **80**, C53; (k) J. J. Guy, B. E. Reichert and G. M. Sheldrick, *Acta. Cryst.* 1976, **B32**, 3319, (l) A. D. Clauss, M. Tachikawa. J. R. Shapley and C. G. Pierpont, *Inorg. Chem.* 1981, **20**, 1528.
10. A. J. Sivak and E. L. Muetterties, *J. Am. Chem. Soc.* 1979, **101**, 4878.
11. R. Benn and A. Rufinska, *J. Organomet. Chem.* 1987, **323**, 305.
12. S. T. McKenna, R. A. Andersen and E. L. Muetterties, *Organometallics* 1986, **5**, 2233.
13. P. O. Nubel and T. L. Brown, *J. Am. Chem. Soc.* 1984, **106**, 3474.
14. R. T. Hembre, C. P. Scott and J. R. Norton, *J. Am. Chem. Soc.* 1987, **109**, 3468.
15. M. D. Fryzuk, T. Jones and F. W. B. Einstein, *J. Chem. Soc., Chem. Commun.* 1984, 1556.
16. M. D. Fryzuk, W. E. Piers and S. J. Rettig, *J. Am. Chem. Soc.* 1985, **107**, 8259.
17. S. S. Wreford and J. F. Whitney, *Inorg. Chem.* 1981, **20**, 3918.
18. W. E. Piers and M. D. Fryzuk, unpublished observations.
19. (a) H. Yasuda, Y. Nakano, K. Natsukawa and H. Tani, *Macromolecules* 1978, **11**, 586; (b) H. Yasuda, Y. Kajihara, K. Mashima, K. Nagasuna, K. Lee and A. Nakamura, *Organometallics* 1982, **1**, 388.
20. K. Issleib and D.-W. Muller, *Chem. Ber.* 1959, **92**, 3175.

Polyhedron Vol. 7, No. 10/11, pp. 1015–1021, 1988
Printed in Great Britain

0277–5387/88 $3.00+.00
© 1988 Pergamon Press plc

1,3-DITUNGSTACYCLOBUTADIENES—III. A COMPARISON OF THE INFLUENCE OF THE SUPPORTING LIGANDS, Pr^iO VERSUS Me_3SiCH_2, ON THE REACTIVITY OF THE $M_2(\mu\text{-}CR)_2$ CORE TOWARD ALKYNES

MALCOLM H. CHISHOLM† and CYNTHIA D. ONTIVEROS

Department of Chemistry, Indiana University, Bloomington, IN 47405, U.S.A.

(*Accepted* 5 *November* 1987)

Abstract—The compounds $X_4W_2(\mu\text{-}CSiMe_3)_2$ react with alkynes to give $X_4W_2(\mu\text{-}C(R)C(R')C(SiMe_3))(\mu\text{-}CSiMe_3)$, **II**, where X = Me_3SiCH_2 and OPr^i, but the reaction profile differs with X. For X = Me_3SiCH_2, the reaction proceeds in a step-wise manner to give first a 1:1 π-adduct, $X_4W_2(\mu\text{-}CSiMe_3)_2(\eta^2\text{-}C_2RR')$, **I**, and then by carbon–carbon bond formation **II**. For reactions involving X = OPr^i and ethyne, there is NMR evidence at −78°C for the formation of a transient species, **I**, but in general the reactions between $(Pr^iO)_4W_2(\mu\text{-}CSiMe_3)_2$ and alkynes obey second-order kinetics. The activation parameters for reactions involving $Me_3SiC{\equiv}CH$ with $X_4W_2(\mu\text{-}CSiMe_3)_2$ reveal that for X = OPr^i, $\Delta S^\ddagger$ is very large and negative, −43 eu, typical of organic cycloaddition reactions involving sterically encumbered reagents while the $\Delta H^\ddagger$ values are very small. For X = Me_3SiCH_2, $\Delta S^\ddagger$ values are only medium in magnitude and negative, consistent with a unimolecular reaction involving an ordered transition state but $\Delta H^\ddagger$ values are notably larger than for those observed for X = OPr^i. The compounds **II** show rearrangements within the μ-C(R)C(R′)C($SiMe_3$) ligands that are dependent on X such that the $\Delta S^\ddagger$ parameters, −16 and +9 eu, lie in the order of magnitude X = Pr^iO > Me_3SiCH_2 while the $\Delta H^\ddagger$ values are in the reverse order. A comparison of these activation parameters for C—C bond formation and rearrangements as a function of X may be understood in terms of the role of π-donation from the RO ligands to W.

Previously we have examined the reactivity of alkylidyne-bridged complexes of formula $X_4M_2(\mu\text{-}CSiMe_3)_2$, where M = Ta and W and X = CH_2SiMe_3.[1,2] For M = W, the d^1–d^1 dinuclear centre provides a template for reactions with π-acids such as alkynes and allenes, whereas no reactivity is observed for the d^0–d^0 compound (M = Ta). In the reactions involving alkynes, initial 1 : 1 π complexes were isolated or detected by NMR spectroscopy. The available data, including an X-ray structure[2] of $(Me_3SiCH_2)_4W_2(\mu\text{-}CSiMe_3)_2(\eta^2\text{-}PhC_2Me)$, are consistent with a Valence Bond description shown in **I** for the 1 : 1 alkyne adducts.

A further reaction occurs involving alkyne–alkylidyne C—C bond formation to give a μ-C(R)C(R′)C($SiMe_3$) ligand which may be called a dimetallaallyl ligand. See the article by Jeffery and Went in this issue. These dimetallaallyl compounds are shown in **II**. Subsequently, rearrangements of the substituents with the μ-C(R)C(R′)C($SiMe_3$) ligand may occur such that the CR/CR′/$CSiMe_3$ groups are scrambled.

During these initial studies, reactions involving $(Pr^iO)_4W_2(\mu\text{-}CSiMe_3)_2$ were also examined with the alkynes C_2H_2 and $Me_3SiC{\equiv}CH$ and, though the

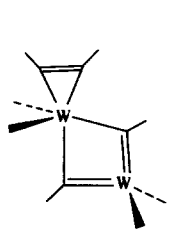

I

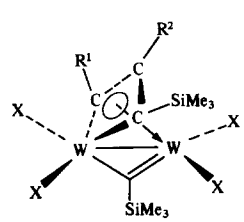

II

†Author to whom correspondence should be addressed.

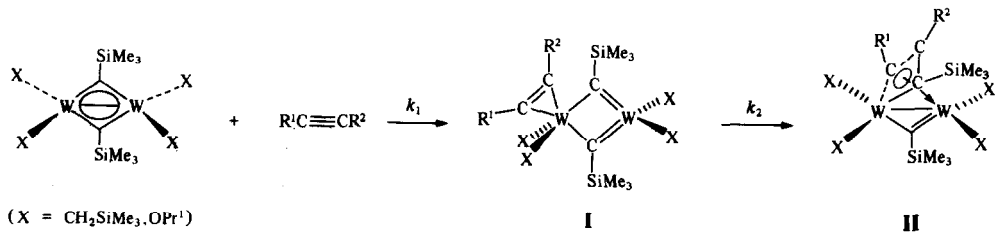

Scheme 1.

reactions proceeded qualitatively in the same manner, certain differences were noted. In particular, (i) alkyne adducts of type **I** were not isolable, though $(Pr^iO)_4W_2(\mu\text{-}CSiMe_3)_2(\eta^2\text{-}*C_2H_2)$ was detectable by low temperature ^{13}C NMR spectroscopy (*C represents 92.5 atom % ^{13}C) and (ii) the rearrangement within the C(R)C(R′)C($SiMe_3$) ligand was notably slower for X = OPr^i than for X = CH_2SiMe_3.

In this paper we describe quantitative studies of the reaction involving $(Pr^iO)_4W_2(\mu\text{-}CSiMe_3)_2$ and $Me_3SiC{\equiv}CH$ and compare these to related findings[2] for $(Me_3SiCH_2)_4W_2(\mu\text{-}CSiMe_3)_2$. We furthermore present a comparative study of the μ-C(R)C(R′)C($SiMe_3$) scrambling as a function of the supporting ligands, X, OPr^i vs CH_2SiMe_3.

RESULTS

1. *Alkyne–alkylidyne* (C—C) *coupling*

We can now present a general scheme for the alkyne insertion reaction, the C—C bond forming reaction, based on that shown in Scheme 1. In the case of X = CH_2SiMe_3, reactions give 1 : 1 alkyne adducts, **I**, more rapidly than **I** goes to **II**, i.e. $k_1 > k_2$. We have no evidence for reversible steps k_{-1} and k_{-2}. By contrast, when X = OPr^i, the alkyne adduct **I** has only been detected at −78°C for reactions involving $*C_2H_2$, where *C represents 92.5 atom % ^{13}C. Thus, kinetic studies of C—C bond formation for X = OPr^i reveal that $k_2 > k_1$ and studies were carried out under pseudo first-order reaction conditions. Specifically, samples of $(Pr^iO)_4W_2(\mu\text{-}CSiMe_3)_2$ in toluene-d_8 were allowed to react with excess $Me_3SiC{\equiv}CH$ in the temperature range −50 to +22°C and progress of the reaction was monitored by ^1H NMR spectroscopy. A listing of specific conditions and of k_{obs} and second-order rate constants determined in these studies is given in Table 1. The activation parameters were evaluated from Eyring plots and these together with a comparison of similar data for X = CH_2SiMe_3 are summarized in Table 2.

Rather interestingly, the $\Delta G^{\ddagger}_{298}$ values are essentially identical for X = CH_2SiMe_3 and OPr^i, although this is only at 298 K. The two reactions differ most markedly in their $\Delta S^{\ddagger}$ values, with that for X = OPr^i being large in magnitude and negative, −43 eu, consistent with a sterically encumbered bimolecular process. The $\Delta S^{\ddagger}$ value for X = CH_2SiMe_3 is negative but modest by comparison, −15 eu, implying a sterically ordered transition state. This is, of course, a unimolecular process whereas, for X = OPr^i, $\Delta S^{\ddagger}$ reflects the entropic barrier associated with k_1.

The $\Delta H^{\ddagger}$ values for X = CH_2SiMe_3 (15 ± 1 kcal mol^{-1}) and OPr^i (7.3 ± 0.2 kcal mol^{-1}) reveal that enthalpically the alkoxy groups favour C—C bond formation.

Table 1. First-order rate constants (k_{obs}) and derived second-order rate constants for the reaction of $(Pr^iO)_4W_2(\mu\text{-}CSiMe_3)_2$ with excess Me_3SiCCH in toluene-d_8 solution

T(K)	Equiv of Me_3SiCCH	k_{obs} (s^{-1})	$k_r = \frac{K_{obs}}{[Me_3SiCCH]_{av}}$ $M^{-1}s^{-1}$
223	10	5.55×10^{-5}	1.12×10^{-4}
233	10	1.17×10^{-4}	2.37×10^{-4}
251	10	3.86×10^{-4}	7.82×10^{-4}
243	10	2.51×10^{-4}	5.08×10^{-4}
243	20	4.98×10^{-4}	5.04×10^{-4}
243	5	1.28×10^{-4}	5.22×10^{-4}

Table 2. Activation parameters for the formation of $X_4W_2(\mu\text{-CSiMe}_3)(\mu\text{-C(SiMe}_3)\text{C(H)C(SiMe}_3))$ in toluene-d_8 solution

$X = CH_2SiMe_3$[a]	$\Delta H^{\ddagger} = 15.2 \pm 1.2$ kcal mol^{-1}
	$\Delta S^{\ddagger} = -15 \pm 5$ eu
	$\Delta G^{\ddagger}_{298} = 19.7 \pm 2.7$ kcal mol^{-1}
$X = Pr^iO$[b]	$\Delta H^{\ddagger}_{obs} = 7.3 \pm 0.2$ kcal mol^{-1}
	$\Delta S^{\ddagger}_{obs} = -43.1 \pm 1.0$ eu
	$\Delta G^{\ddagger}_{obs} = 20.1 \pm 0.5$ kcal mol^{-1}

[a] Activation parameters are those associated with the reaction $X_4W_2(\mu\text{-CSiMe}_3)_2(\eta^2\text{-C(SiMe}_3)\text{C(H)}) \rightarrow X_4W_2(\mu\text{-CSiMe}_3)(\mu\text{-C(SiMe}_3)\text{C(H)C(SiMe}_3))$.

[b] Activation parameters are those associated with the reaction $X_4W_2(\mu\text{-CSiMe}_3)_2 + Me_3SiCCH \rightarrow X_4W_2(\mu\text{-CSiMe}_3)(\mu\text{-C(SiMe}_3)\text{C(H)C(SiMe}_3))$.

2. C(R)/C(R′)/C(SiMe$_3$) *scrambling in* II

For the rearrangement reaction we selected ethyne insertion products, since these undergo clean (quantitative) conversion to the β-CSiMe$_3$ derivative, i.e. **III** → **IV**. It should be emphasized that this

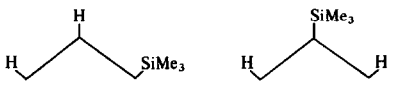

III **IV**

is truly a CR/CR′/CSiMe$_3$ scrambling and does not involve R, R′, SiMe$_3$ migrations, since reactions employing $*C_2H_2$ show that carbon–hydrogen bonds are retained. This is apparent from ^{13}C—H couplings.†

For X = CH$_2$SiMe$_3$, the rearrangement is relatively rapid at room temperature and kinetic studies were carried out in toluene-d_8 in the temperature range 0 to +18°C. For X = OPr^i, the rearrangement is sluggish at room temperature and rate measurements were carried out in toluene-d_8 at +80–110°C. In both cases we observed first-order kinetics and reactions were followed for approximately three half-lives. A summary of rate data is given in Table 3 and activation parameters are given in Table 4.

† ^{13}C proton-coupled spectral data (90.8 MHz) for: **IIIa**, $(Me_3SiCH_2)_4W_2(\mu\text{-}C\text{(H)}C\text{(H)C(SiMe}_3))(\mu\text{-CSiMe}_3)$, $^1J_{^{13}C-^1H} = 160$, 135.8 Hz; **IVa**, $(Me_3SiCH_2)_4W_2(\mu\text{-}C\text{(H)C(SiMe}_3)C\text{(H)})(\mu\text{-CSiMe}_3)$, $^1J_{^{13}C-^1H} = 161$, 156 Hz; **IIIb**, $(PrO^i)_4W_2(\mu\text{-}C\text{(H)}C\text{(H)C(SiMe}_3))(\mu\text{-CSiMe}_3)$, $^1J_{^{13}C-^1H} = 163$, 160 Hz; **IVb**, $(PrO^i)_4W_2(\mu\text{-}C\text{(H)C(SiMe}_3)C\text{(H)})(\mu\text{-CSiMe}_3)$, $^1J_{^{13}C-^1H} = 151$ Hz.

Table 3. Rate constants for the rearrangement process $X_4W_2(\mu\text{-C(H)}C\text{(H)C(SiMe}_3))(\mu\text{-CSiMe}_3) \xrightarrow{k} X_4W_2(\mu\text{-C(H)C(SiMe}_3)C\text{(H)})(\mu\text{-CSiMe}_3)$

X = CH$_2$SiMe$_3$		X = Pr^{i}O	
T (K)	$k(\times 10^{-4}\ s^{-1})$	T (K)	$k(\times 10^{-4}\ s^{-1})$
274.0	0.45±0.02	354.5	1.88±0.09
279.0	1.10±0.06	366.5	4.80±0.17
284.5	2.13±0.09	373.0	8.15±0.77
291.0	6.65±0.15	383.0	19.1±0.7

While the $\Delta H^{\ddagger}$ values do not differ significantly (24 kcal mol^{-1} for X = CH$_2$SiMe$_3$ vs 21 kcal mol^{-1} for X = OPr^i), there is a pronounced difference in the $\Delta S^{\ddagger}$ values (−16 eu for X = OPr^i vs +9 eu for X = CH$_2$SiMe$_3$). Thus while the enthalpic contribution is greater for X = CH$_2$SiMe$_3$, the entropic term becomes rate-limiting in the temperature region of interest.

DISCUSSION

Having summarized the facts we may proceed to the speculation of the differing roles of Me$_3$SiCH$_2$ vs OPr^i. We shall assume that the differences are essentially electronic in origin, i.e. that steric factors for OPr^i are comparable to those for CH$_2$SiMe$_3$, or at least not limiting with respect to 1 : 1 π-complex formation. This seems reasonable from considerations of space filling drawings of the starting compounds $X_4W_2(\mu\text{-CSiMe}_3)_2$ for X = OPr^i vs CH$_2$SiMe$_3$ and also because the compound $W_2(CH_2SiMe_3)_2(OPr^i)_4$ can coordinate *two* molecules of MeC≡CMe.[3]

1. *Alkyne–alkylidyne coupling*: C—C *bond formation*

We suggest that the different reaction profile for X = CH$_2$SiMe$_3$ vs OPr^i arises from the π-donating

Table 4. Activation parameters for the rearrangement reaction $X_4W_2(\mu\text{-C(H)}C\text{(H)C(SiMe}_3))(\mu\text{-CSiMe}_3) \xrightarrow{k} X_4W_2(\mu\text{-C(H)C(SiMe}_3)C\text{(H)})(\mu\text{-CSiMe}_3)$

$X = CH_2SiMe_3$	$\Delta H^{\ddagger} = 24.0 \pm 1.3$ kcal mol^{-1}
	$\Delta S^{\ddagger} = +9.3 \pm 4.2$ eu
	$\Delta G^{\ddagger}_{298} = 21.2 \pm 2.5$ kcal mol^{-1}
$X = Pr^iO$	$\Delta H^{\ddagger} = 21.2 \pm 0.7$ kcal mol^{-1}
	$\Delta S^{\ddagger} = -16.3 \pm 2.0$ eu
	$\Delta G^{\ddagger}_{298} = 26.1 \pm 1.3$ kcal mol^{-1}

ability of the alkoxide ligands. The latter act as π-buffers and decrease the strength of alkyne-to-tungsten bonding[4] in the 1 : 1 alkyne adduct, **I**. This is seen in an examination of the NMR parameters previously obtained for 1 : 1 adducts involving $*C_2H_2$, which are listed in Table 5. (a) The chemical shift values reflect the π^x donor properties of the C_2H_2 ligand.[5] The δ value of 217 ppm is typical of a π^4 donor while δ 187 ppm is indicative of a π^3 donor, i.e. the alkyne and the alkoxide ligands compete for vacant metal d_π orbitals to a comparable extent. (b) The relative magnitude of $^1J_{W-C}$ and $^1J_{C-C}$ are inversely related for the two compounds in a manner consistent with stronger W—C_2 bonding when X = CH_2SiMe_3 relative to X = OPr^i.

These are, however, ground state effects. The alkoxy π-donor ligands will have a destabilizing effect on the approach of the alkyne ligand since in the starting compound, $(Pr^iO)_4W_2(\mu\text{-}CSiMe_3)_2$, the alkyne–tungsten bonding orbitals are otherwise engaged in M—OR π-bonding. Thus formation of the alkyne adduct will be less favoured for X = OPr^i than for X = CH_2SiMe_3 on both thermodynamic and kinetic grounds.

The fact that $\Delta H^\ddagger$ is less for C—C bond formation when X = OPr^i relative to X = CH_2SiMe_3 could be attributed to (i) formation of a less stable alkoxide supported 1 : 1 π-complex and/or (ii) electronic factors that may actually promote C—C bond formation, i.e. their π-donor capability may allow them to mix O p atomic orbitals with μ-C alkylidyne C p orbitals and alkyne π/π^* orbitals, to lower the electronic barrier to C—C bond formation.

For X = OPr^i, the $\Delta S^\ddagger$ value was found to be large in magnitude and negative, −43 eu, indicative of an associative bimolecular process in which extensive restriction of degrees of freedom has occurred on formation of the transition state. It should be noted that activation entropies have been evaluated in a number of Diels–Alder [4+2] cycloaddition reactions and $\Delta S^\ddagger$ values typically lie in the range −35 to −45 eu.[6]

Table 5. Selected ^{13}C NMR data for $X_4W_2(\mu\text{-}CSiMe_3)_2(\eta^2\text{-}*C_2H_2)$[a]

δ	216.8 ppm	187.3 ppm
$^1J_{^{183}W-^{13}C}$	33.0 Hz	23.7 Hz
$^1J_{^{13}C-^{13}C}$	42.0 Hz	49.0 Hz

[a] ^{13}C NMR spectral data pertain to the acetylenic carbon resonances in the labelled compounds $X_4W_2(\mu\text{-}CSiMe_3)_2(\eta^2\text{-}*C_2H_2)$ where *C represents 92.5 atom % ^{13}C; recorded in toluene-d_8 at −70°C, 90.8 MHz.

2. C(R)/C(R′)/C($SiMe_3$) *scrambling*

The kinetic data obtained in this study indicate that for the C(R)/C(R′)/C($SiMe_3$) rearrangement process, when X = OPr^i, the entropic term becomes rate-limiting. Our ability to previously isolate and structurally characterize[1] $(Pr^iO)_4W_2(\mu\text{-}C(H)C(H)C(SiMe_3))(\mu\text{-}CSiMe_3)$ was largely due to the significant entropy of activation for its rearrangement to $(Pr^iO)_4W_2(\mu\text{-}C(H)C(SiMe_3)C(H))(\mu\text{-}CSiMe_3)$, **III** → **IV**. Had the $\Delta S^\ddagger$ value been comparable to that for X = CH_2SiMe_3, the rate of rearrangement would have been comparable to the rate of formation of the μ-C(H)C(H)C($SiMe_3$) ring. This was, in fact, the case for reactions employing PhC≡CH where X = CH_2SiMe_3 which gave rise to isomers wherein all three substituents within the metallaallyl ligand had been scrambled. The fact that these isomers had formed at similar rates indicated that kinetic control in the C—C bond forming step was not apparent in this instance.

A possible mechanism for the rearrangement process within the μ-C(R)C(R′)C($SiMe_3$) ring, which invokes the formation of a $W_2(\mu\text{-}\eta^1,\eta^2\text{-}$cyclopropene) intermediate, is shown in Scheme 2. It should be emphasized that we have no evidence for the reversibility of the reactions depicted in Scheme 1 and we can rule out any mechanism involving alkyne deinsertion in a number of instances on kinetic grounds.

The rearrangement of the substituents in the μ-C(R)C(R′)C($SiMe_3$) ligand, which shows a significantly greater ordering in the transition state when X = OPr^i relative to X = CH_2SiMe_3, could again be explained qualitatively on electronic grounds. If the alkoxides have specific metal d_π orbital bonding preferences in the ground state, then rotations about M—O—C bonds will have electronic barriers. It may be that the electronic barrier to rearrangement within the μ-C_3 ligand, the formation of the μ-cyclopropene intermediate, is coupled to such rotations about M—O—C bonds. An orbital analysis of the effects of RO-π-donation on $W_2(\mu\text{-}C_3)$ rearrangements could be useful in evaluating these points.

CONCLUDING REMARKS

The reactions between $X_4W_2(\mu\text{-}CSiMe_3)_2$ (M—M) compounds, where X = CH_2SiMe_3 or OPr^i, and alkynes follow different reaction profiles. (See Scheme 3.) For X = CH_2SiMe_3 there is a two-step reaction sequence in the formation of the 1,3-dimetallaallyl products, **II**, in which the alkyne–alkylidyne coupling step, **I** → **II**, is notably slower

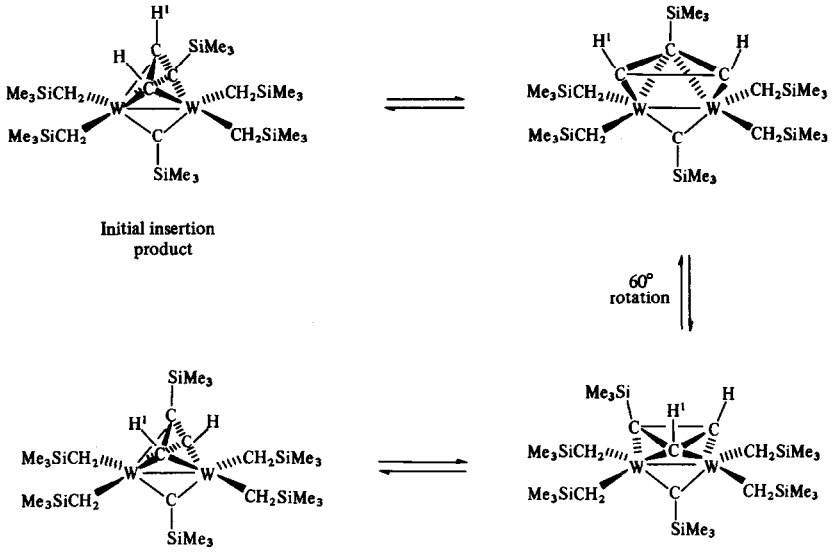

Scheme 2. Proposed rearrangement mechanism.

than the initial formation of the 1 : 1 alkyne adduct, I. For X = OPr^i, C—C bond formation follows biomolecular kinetics and there is evidence for only the fleeting existence of 1 : 1 alkyne adducts, I. The rate of rearrangement within the metallaallyl ligand, subsequent to C—C bond formation, is also significantly influenced by the nature of X.

It seems reasonable to attribute the relative rate in the formation of the 1 : 1 alkyne adducts, I, to the influence of the π-donating alkoxide ligands. The latter act as π-buffers weakening both the alkyne–tungsten bonding in I and suppressing the rate of formation of I. The role of the alkoxide ligands in the subsequent C—C bond forming step is less clear. The lower values of $\Delta H^{\ddagger}$ could arise from either a destabilization of I or a direct assistance in C—C bond formation—a π-orbital involvement in the transition state for C—C bond formation. Similarly, the marked difference in the $\Delta S^{\ddagger}$ values for the rearrangement within the μ-C_3 ring may have an electronic origin. A rotation about M—O—C bonds, which would alter O to W π-bonding, may be coupled with the formation of the cyclopropene ring intermediate.

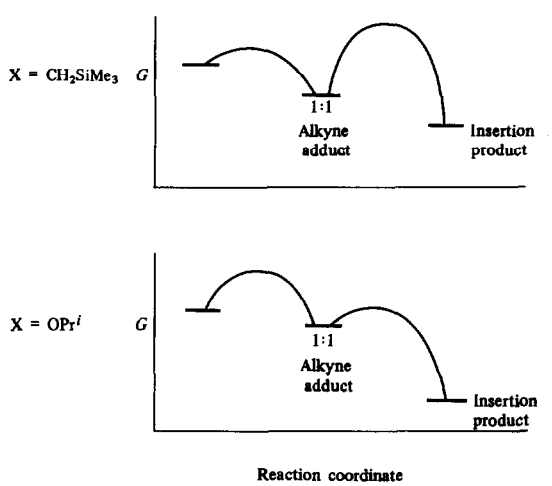

Scheme 3. Qualitative reaction profile of allyne insertion reactions.

The role played by the π-donating OPr^i ligands may perhaps be clarified by devising experiments wherein the degree of π-donation has been effectively reduced. For example, experiments may involve either the use of weaker π-donating alkoxides (e.g. OAr) or the addition of excess alcohol to the reaction. In the latter instance, hydrogen bonding involving oxygen lone pairs would effectively decrease the extent of π-donation of the OR ligand. This has been seen before to have pronounced effects on M—M and M—O distances in compounds of the formula $Mo_2(OR)_4L_4$ (M≡M), where L = ROH or py.[7] In addition, molecular orbital analyses of the type previously reported by Jemmis and Prasad[8] could be extended to include an evaluation of the influence of π-donor alkoxides as supporting ligands. Experimental studies on mixed alkyl/alkoxide ditungsten systems such as the *gem*-disubstituted compound $(RO)_2W(\mu\text{-}CSiMe_3)_2W(CH_2SiMe_3)_2$ and the *syn* or *anti* compounds $(RO)(Me_3SiCH_2)W(\mu\text{-}CSiMe_3)_2W(CH_2SiMe_3)(OR)$ could further probe the role of alkoxide ligands in π-complexation, alkyne-alkylidyne coupling and isomerization processes. Further studies are in progress.

EXPERIMENTAL

General procedures

All procedures were carried out under a dry nitrogen atmosphere using standard Schlenk and glovebox techniques. $(Me_3SiCH_2)_4W_2(\mu\text{-}CSiMe_3)_2$ and $(Pr^iO)_4W_2(\mu\text{-}CSiMe_3)_2$ were prepared by previously published procedures.[1,9] Acetylene (Matheson) was used without further purification and transferred using a calibrated vacuum line. Me_3SiCCH (Petrarch) was deoxygenated and stored over 3 Å sieves and transferred via a microlitre syringe. Toluene-d_8 was degassed using a dry nitrogen purge and dried over 3 Å sieves. All solid reagents were weighed and transferred in a nitrogen-filled vacuum atmospheres drybox.

Reaction rates were monitored by ^1H NMR spectroscopy using a Nicolet NT-360 spectrometer equipped with an automated kinetics software program (KINET) and with a variable temperature unit. Probe temperatures ($T < 0°C$) were calibrated against an external MeOH standard.

Kinetics

(a) *Insertion of* Me_3SiCCH *into* $X_4W_2(\mu\text{-}CSiMe_3)_2$ (X = OPr^i, CH_2SiMe_3). All NMR samples were prepared by charging 5 mm tubes with 20 mg of $(Pr^iO)_4W_2(\mu\text{-}CSiMe_3)_2$ and adding 0.5 cm^3 of toluene-d_8 via a microlitre syringe. The tubes were sealed with septum caps, cooled to $-78°C$ and predetermined excess quantities of Me_3SiCCH were injected into the tubes. The samples were warmed briefly (< 10 s) in order to ensure mixing of the tube contents and were then placed into the precooled NMR probe. After allowing for thermal equilibration (several min), NMR spectra were acquired periodically using preset delays and acquisition times loaded into the KINET sub-program. The rate of formation of **II**, the alkyne insertion product, $(Pr^iO)_4W_2(\mu\text{-}C(SiMe_3)C(H)C(SiMe_3))(\mu\text{-}CSiMe_3)$, was determined from the absolute integral intensities of the $-OCH(Me)_2$ resonances. In each instance, data were acquired for ≥ 2.5 half-lives. Rate data conformed to simple pseudo first-order kinetics giving linear plots of ln [**II**] vs time and relative rate constants were obtained from linear regression analyses. Relative rate constants were determined at four temperatures using a ten-fold excess of alkyne. Second-order rate constants were then obtained from linear plots of k_{obs} vs $[alkyne]_{av}$. Activation parameters were obtained from a plot of $\ln k_r$ (time^{-1}) vs T^{-1} and linear regression analyses.

(b) *Rearrangement of* $X_4W_2(\mu\text{-}C(H)C(H)C(SiMe_3))(\mu\text{-}CSiMe_3)$, **III**, *to* $X_4W_2(\mu\text{-}C(H)C(SiMe_3)C(H))(\mu\text{-}CSiMe_3)$, **IV**. All NMR samples used to study the kinetics of rearrangement were prepared in the following manner. In a drybox, samples of either $(Me_3SiCH_2)_4W_2(\mu\text{-}CSiMe_3)_2$, (40 mg, 0.045 mmol) or $(Pr^iO)_4W_2(\mu\text{-}CSiMe_3)_2$ (40 mg, 0.052 mmol) were placed in 5 mm NMR tubes equipped with glass extensions. Toluene-d_8 (0.5 cm^3) was added via a syringe and the solutions were then cooled to $-196°C$. Acetylene (1 equiv) was condensed above the frozen solution and the tubes were flame sealed under vacuum. All samples were kept at $-196°$ prior to use. For reactions involving $(Me_3SiCH_2)_4W_2(\mu\text{-}CSiMe_3)_2$, the NMR sample tubes were warmed from $-196°C$ to a predetermined temperature using a suitable slush bath for a fixed period of time, then cooled to $-78°C$ to quench the reaction, and placed into an NMR probe precooled to $-50°C$ for data acquisition.† The rate of formation of the rearrangement product, $(Me_3SiCH_2)_4W_2(\mu\text{-}C(H)C(SiMe_3)C(H))(\mu\text{-}CSiMe_3)$, was monitored by integration of the (μ-C*H*CSi Me_3C*H*) resonances. Rate data were treated as for irreversible consecutive first-order reactions,[12] $A \xrightarrow{k_1} B \xrightarrow{k_2} C$ with the assumption that $k_1 > k_2$. Thus, the concentration of C, the rearranged dimetallaallyl product, which may be expressed as

$$[C] = [A]_0 \times \left[1 - \frac{k_2}{k_2 - k_1}\exp(-k_1 t) + \frac{k_1}{k_2 - k_1}\exp(-k_2 t)\right]$$

reduces to $[C]/[A]_0 = -k_2 t$. Plots of ln ($[C]/[A]_0$) vs time (where A represents the alkyne mono-adduct) gave linear plots over 2.5 half-lives. Relative rate constants were determined at four temperatures and activation parameters were derived from a plot of $\ln k_r$ (time^{-1}) vs T^{-1} and linear regression analyses. Reported errors are those obtained from least-squares standard deviations.

Sample tubes containing $(Pr^iO)_4W_2(\mu\text{-}CSiMe_3)_2$ were warmed in oil baths at predetermined temperatures for timed intervals. The reaction was then quenched by submerging the tubes into an ice/salt bath and the tubes were then placed into the NMR probe (22°C) for data acquisition. The rate of formation of the rearranged product **IVb**, $(Pr^iO)_4W_2(\mu\text{-}C(H)C(SiMe_3)C(H))(\mu\text{-}CSiMe_3)$, was monitored by integration of the (μ-C(H)C(Si*Me*$_3$)C(H)) resonances. Rate data were again treated as for irreversible consecutive first-order reactions,[10]

† In order to obtain accurate integrations it was necessary to acquire data at $-50°C$ at which temperature the fluxional behaviour associated with the μ-C_3R_3 scrambling process was frozen out.

$A \xrightarrow{k_1} B \xrightarrow{k_2} C$, but in this case A represents the starting compound, $(Pr^iO)_4W_2(\mu\text{-}CSiMe_3)_2$, and k_1 represents k_{obs}. Since $k_{obs} > k_2$, the concentration of C, the rearranged dimetallaallyl product, can be expressed as $[C] = -[A]_0k_2t$. Plots of $\ln([C]/[A]_0)$ vs time gave linear plots over three half-lives from which relative rate constants were derived. Rate constants were determined at four temperatures and activation parameters were derived from Eyring plots of $\ln k_r(\text{time}^{-1})$ vs T^{-1} and linear regression analyses. Reported errors are those obtained from least squares standard derivations.

Acknowledgements—We thank the donors of the Petroleum Research Fund administered by the American Chemical Society and the National Science Foundation for support.

REFERENCES

1. M. H. Chisholm, J. C. Huffman and J. A. Heppert, *J. Am. Chem. Soc.* 1985, **107**, 5116.
2. M. H. Chisholm and J. A. Heppert, *Adv. Organomet. Chem.* 1986, **26**, 97.
3. M. H. Chisholm and B. W. Eichhorn, results to be published.
4. M. H. Chisholm, J. A. Heppert, E. M. Kober and D. L. Lichtenberger, *Organometallics* 1987, **6**, 1065.
5. J. L. Templeton and B. C. Ward, *J. Am. Chem. Soc.* 1980, **102**, 3288.
6. J. Sauer and R. Sustmann, *Angew. Chem. Intl. Ed. Engl.* 1980, **19**, 779.
7. M. H. Chisholm, K. Folting, J. C. Huffman and R. J. Tatz, *J. Am. Chem. Soc.* 1984, **106**, 1153.
8. E. D. Jemmis and B. V. Prasad, *J. Am. Chem. Soc.* 1987, **109**, 2560.
9. M. H. Chisholm, F. A. Cotton, M. W. Extine and C. A. Murillo, *Inorg. Chem.* 1978, **17**, 696.
10. (a) J. H. Espenson, *Chemical Kinetics and Reaction Mechanisms*, p. 66. McGraw-Hill, New York (1981); (b) R. G. Wilkins, *The Study of Kinetics and Mechanism of Reactions of Transition Metal Complexes*, p. 22. Allyn and Bacon, Boston (1974).

Polyhedron Vol. 7, No. 10/11, pp. 1023–1034, 1988
Printed in Great Britain

0277–5387/88 $3.00+.00
© 1988 Pergamon Press plc

INTRAMOLECULAR CARBYNE–CARBYNE COUPLING ON EXPOSURE OF $[\mu_3\text{-}\eta^1\text{-}CR^1][\mu_3\text{-}\eta^1\text{-}CR^2][CpCo]_3$ CLUSTERS TO SULPHUR AND SELENIUM: A NOVEL SYNTHESIS OF 1-COBALTA-2,5-DIHETEROCYCLOPENT-3-ENES

K. P. C. VOLLHARDT* and E. C. WALBORSKY

Department of Chemistry, University of California, and the Materials and Chemical Sciences Division, Lawrence Berkeley Laboratory, Berkeley, CA 94720, U.S.A.

(*Accepted* 5 *November* 1987)

Abstract—The trinuclear cobalt biscarbyne clusters $[\mu_3\text{-}\eta^1\text{-}CR^1][\mu_3\text{-}\eta^1\text{-}CR^2][CpCo]_3$ (**1**) react with sulphur (or selenium) to give the CpCo dithiolenes (or selenolenes) **2**. This degradation is thought to proceed via electrophilic attack of the chalcogen, a step modelled by the addition of CH_3S^+ to **1a** to furnish **6**, characterized by X-ray crystallography. Labelling experiments aimed at elucidating the mechanistic features of the formation of **2** were inconclusive because of the occurrence of CpCo-scrambling.

Sulphur is a well-known poison to catalysts of industrial significance.[1] Here we present a report on the reaction of trinuclear cobalt $\mu_3\text{-}\eta^1$-biscarbyne clusters with sulphur and selenium which causes the disassembly of the metal framework and the intramolecular coupling of the carbyne fragments to yield cobaltadithiolenes and -selenolenes, respectively, a process that is of possible relevance to surface-mediated transformations.[2] There is a considerable body of literature dealing with the events that occur when transition metal clusters are exposed to sulphur.[2(c),3] Some of these lead to metalladithiolenes,[4] molecules of structural and electronic interest, often by mechanisms which are obscure. The results summarized in this manuscript are unique and add to the diversity of the reactivity patterns that are possible in such processes.

This investigation was inspired by the observation that the clusters $[\mu_3\text{-}\eta^1\text{-}CR^1][\mu_3\text{-}\eta^1\text{-}CR^2][CpCo]_3$ (**1**), readily available by the reaction of $CpCo(CO)_2$[5] or $CpCo(CH_2{=}CH_2)_2$[6] with alkynes, are remarkably resilient to oxidation with O_2.[7] However, exposure to an excess of elemental sulphur for two days in boiling chloroform provided the mononuclear η^5-cyclopentadienylcobalt dithiolenes **2** [eq. (1)] in unusually high yield (Table 1). While the generation of the known[8] bis-μ_3-sulphido species **3** (10% yield) was only ascertained in the case of the reaction of **1b**, it is assumed to be a by-product in all the other degradations. The structural assignments of **2** were based on the characteristic[4] spectral and the analytical data.

*Author to whom correspondence should be addressed.

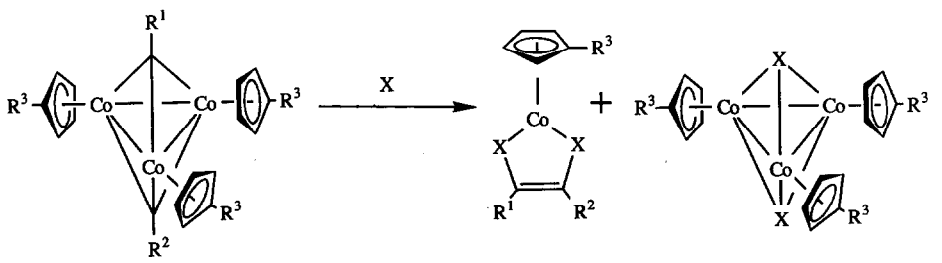

(1)

1

2 (X = S)
5 (X = Se)

3 (R^3 = H, X = S)

Table 1. Results of the reaction of **1** with sulphur

Cluster	R^1	R^2	R^3	X	1-Colbata-2,5-dihetero-cyclopent-3-ene % Yield
1a[5]	$CH_3CH_2CH_2CH_2$	$CH_3CH_2CH_2CH_2$	H	S	**2a**, 99
1b[5]	C_6H_5	C_6H_5	H	S	**2b**, 99
1c[5]	$C_2Si(CH_3)_3$	$C_2Si(CH_3)_3$	H	S	**2c**, 33
1d	C_6H_5	C_2H_5	H	S	**2d**, 98
1e	C_6H_5	C_6D_5	H	S	**2e**, 95
1f[5]	CO_2CH_3	CO_2CH_3	H	S	**2f**, 90
1g	C_6H_5	C_6H_5	CH_3	S	**2g**, 97
1a[5]	$CH_3CH_2CH_2CH_2$	$CH_3CH_2CH_2CH_2$	H	Se	**5**, 97

Phenyl, alkoxycarbonyl and remarkably, appended ethynyl groups, appear to be tolerated by the reaction conditions, the latter albeit not completely. It is probably of mechanistic significance that the sulphurization of **1c** gives **2c** and none of **2h**, a feasible product should any of the reacting metal species undergo migration along the triple bonds.[9] That the ethynyl substituents are not entirely inert is evidenced by the isolation of a small amount (5%) of the unusual bisdithiolene **4**. Its structure follows from spectral and analytical data. Thus, the ^1H NMR spectrum exhibited the expected four singlet signals and a parent ion at *m/z* 594 in conjunction with a fragmentation pattern consistent with that of other dithiolene complexes was seen in the mass spectrum. The formation of **4** can be envisioned to involve the intermediacy of **2c**, in which one of the triple bonds functions as an internal trap for the excess cyclopentadienylcobalt fragments generated from the starting cluster.

As a demonstration of the potential generality of the chalcogen degradation reaction, selenium transformed **1a** to **5** in virtually quantitative yield, although relatively higher temperatures were needed compared with the analogous sulphur reaction.

The mechanistic details of the conversion of **1** to **2** were of obvious interest. ^1H NMR monitoring of the progress of the degradation in the presence of either sulphur or selenium did not allow the detection of any intermediates. A clue to the intramolecular nature of the coupling of the two carbyne fragments as observed in **2** was provided by the reaction of **1d** which did not furnish any crossover products. A more rigorous experiment involved deuterium-labelled **1e** which resulted in **2e** cleanly, the absence of deuterium scrambling being readily ascertained by mass spectral analysis. At the time of its discovery,[2(d)] such a bond-forming reaction between cluster-bound carbyne units had only one precedence in related double-decker clusters.[9(b)] Since then, several of these unusual couplings have been observed, not only featuring trinuclear CpCo-systems[10] but also others.[11]

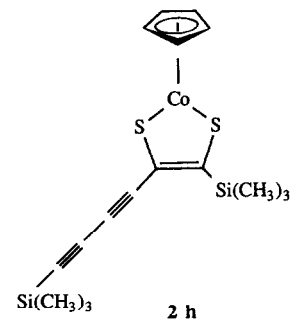

2 h

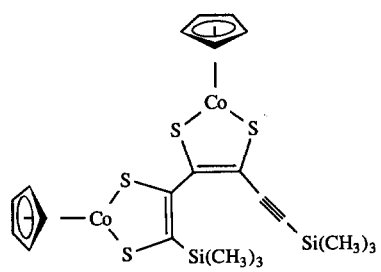

4

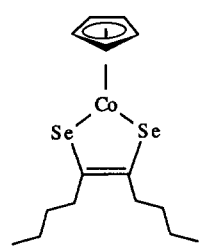

5

Considering that alkynes convert to compounds of type **2** in the presence of CpCo and sulphur (or selenium),[4(a)] the possibility of the intermediacy of the free alkyne $R^1C{\equiv}CR^2$ derived from **1** had to be considered as a mechanistic pathway in the present work. However, admixture of external 5-decyne to **1b** followed by addition of sulphur resulted in the formation of only **2b**, ruling out any mechanisms

in which carbyne–carbyne coupling followed by alkyne dissociation was responsible for the observed products.

The established[7,10] nucleophilicity of clusters of the type **1** made it appear reasonable to assume that whatever form of sulphur[12] attacked them, it was of an electrophilic nature. To establish the feasibility of this notion, which has precedence in the literature,[13] dimethyl(methylthio)sulphonium tetrafluoroborate,[14] a source of CH_3S^+, was allowed to react with **1a** in nitromethane for 1 h [eq. (2)]. This treatment afforded a black crystalline salt, **6**, whose

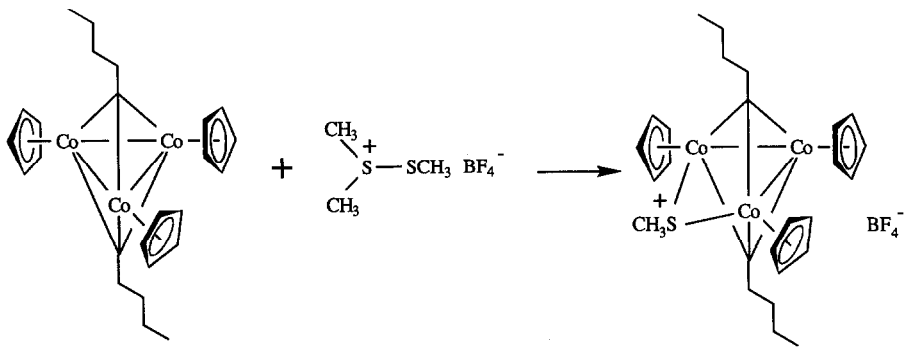

(2)

1a **6**

structure was initially assigned based only on spectral and analytical data. In particular, the chemical ionization mass spectrum showed a parent ion at *m/z* 584 for the cationic portion of the salt. More diagnostic was the ^{1}H NMR spectrum which exhibited two singlets in the chemical shift range typical for cyclopentadienyl ligands (δ = 5.08, 4.81 ppm) in a ratio of 1 : 2. Of further note was the apparent non-equivalence of the two butyl groups, best indicated by the two distinct triplets assigned to the two sets of terminal methyl protons. Assuming the geometry about the sulphur atom to be tetrahedral, these data would be consistent with the structure of an edge-on bound methylsulphonium salt as depicted by **6**. To corroborate this assignment and to rule out other feasible structural alternatives, an X-ray structural analysis was carried out, the results of which confirmed the initial formulation (Fig. 1, Table 2).

On inspection of the structural parameters, it is interesting to note that the sulphur has indeed adopted a tetrahedral geometry and the molecule has attained C_{2v}-symmetry. The Co2—Co3 distance has lengthened to 2.738 Å, an increase of almost 0.4 Å from that observed in $[\mu_3\text{-}\eta^1\text{-}CH]_2[CpCo]_3$.[15] The Co2,3—Co1 distances are 2.38 Å, relatively unchanged from those seen in the parent system. A slight compression of the Co1–carbyne of approximately 0.015 Å and elongation of the Co2,3–carbyne carbon bonds of nearly 0.1 Å is evident.

Although perhaps of dubious relevance with respect to the mechanism of the conversion of **1** to **2**, **6** did convert to **2a** (78%) on exposure to sulphur under the conditions used to degrade **1a** to the same product.

While it was clear that intramolecular carbyne–carbyne coupling was occurring in the reactions of **1** with sulphur (and presumably also selenium), the molecularity of this process with respect to the CpCo unit remained to be established. To this end,

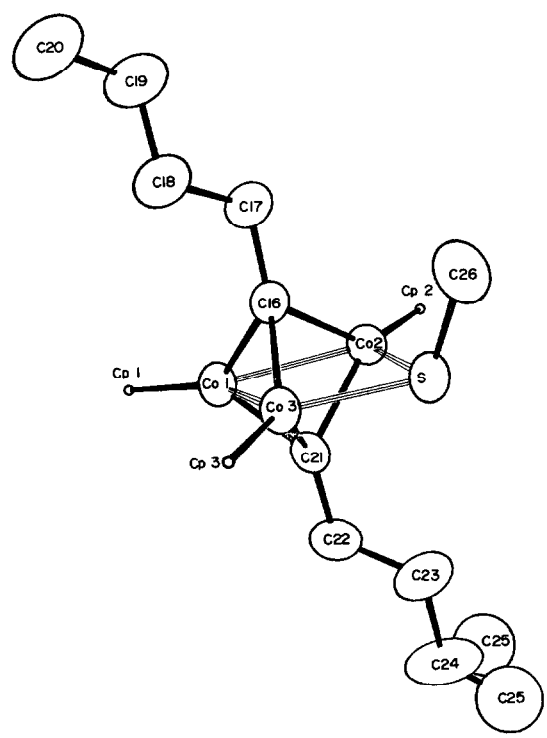

Fig. 1. ORTEP drawing of **6**. Ellipsoids are scaled to represent the 50% probability surface. There is some disorder at the terminus of one of the butyl substituents.

Table 2. Bond lengths (Å) and angles (°) for **6**

Intramolecular angles				Intramolecular distances		
Atom 1	Atom 2	Atom 3	Angle	Atom 1	Atom 2	Distance
Co2	Co1	Co3	70.10(1)	Co1	Co2	2.387(1)
C16	Co1	C21	86.12(11)	Co1	Co3	2.380(1)
Co2	Co1	Cp1[a]	145.0	Co2	Co3	2.738(1)
Co3	Co1	Cp1	144.9	S	Co2	2.219(1)
C16	Co1	Cp1	136.8	S	Co3	2.218(1)
C21	Co1	Cp1	137.1	S	C16	2.729(2)
Co1	Co2	Co3	54.84(1)	S	C21	2.614(3)
Co1	Co2	S	106.64(2)	C16	Co1	1.829(2)
C16	Co2	C21	79.59(10)	C16	Co2	1.944(2)
Co1	Co2	Cp2[a]	127.7	C16	Co3	1.959(2)
Co3	Co2	Cp2	177.1	C21	Co1	1.817(2)
S	Co2	Cp2	125.4	C21	Co2	1.946(2)
C16	Co2	Cp2	136.6	C21	Co3	1.956(3)
C21	Co2	Cp2	134.3	Co1	C1	2.076(3)
Co1	Co3	Co2	55.06(1)	Co1	C2	2.093(3)
Co1	Co3	S	106.86(2)	Co1	C3	2.076(3)
C16	Co3	C21	78.97(10)	Co1	C4	2.056(3)
Co1	Co3	Cp3[a]	129.0	Co1	C5	2.064(3)
Co2	Co3	Cp3	174.9	Co1	Cp1[a]	1.715
S	Co3	Cp3	123.7	Co2	C6	2.035(3)
C16	Co3	Cp3	139.3	Co2	C7	2.053(3)
C21	Co3	Cp3	133.6	Co2	C8	2.105(3)
Co1	C16	Co2	78.43(9)	Co2	C9	2.080(3)
Co1	C16	Co3	77.80(9)	Co2	C10	2.064(3)
Co2	C16	Co3	89.10(10)	Co2	Cp2[a]	1.721
Co1	C16	C17	133.21(19)	Co3	C11	2.098(3)
Co2	C16	C17	125.71(18)	Co3	C12	2.082(3)
Co3	C16	C17	133.47(19)	Co3	C13	2.078(3)
Co1	C21	Co2	78.65(10)	Co3	C14	2.072(3)
Co1	C21	Co3	78.12(10)	Co3	C15	2.054(3)
Co2	C21	Co3	89.11(11)	Co3	Cp3[a]	1.725
Co1	C21	C22	133.45(20)	S	C26	1.812(3)
Co2	C21	C22	128.52(19)	C16	C17	1.505(3)
Co3	C21	C22	130.28(19)	C17	C18	1.503(4)
Co2	S	Co3	76.19(2)	C18	C19	1.503(4)
Co2	S	C26	111.17(11)	C19	C20	1.476(5)
Co3	S	C26	110.21(11)	C21	C22	1.502(4)
C16	C17	C18	117.5(2)	C22	C23	1.519(5)
C17	C18	C19	113.9(3)	C23	C24	1.550(5)
C18	C19	C20	116.6(3)	C24	C25	1.368(8)
C21	C22	C23	115.2(3)	C24	C25′	1.173(12)
C22	C23	C24	110.7(4)	B	F1	1.365(4)
C23	C24	C25	110.7(4)	B	F2	1.340(4)
C23	C24	C25′	129.7(8)	B	F3	1.358(5)
C5	C1	C2	108.7(4)	B	F4	1.346(5)
C1	C2	C3	108.3(4)	C1	C2	1.367(6)
C2	C3	C4	109.3(4)	C2	C3	1.329(6)
C3	C4	C5	106.8(4)	C3	C4	1.390(6)
C4	C5	C1	106.9(4)	C4	C5	1.384(6)
C10	C6	C7	109.3(4)	C5	C1	1.375(6)
C6	C7	C8	110.8(4)	C6	C7	1.326(6)
C7	C8	C9	109.4(4)	C7	C8	1.279(6)
C8	C9	C10	106.2(4)	C8	C9	1.345(7)
C9	C10	C6	104.3(4)	C9	C10	1.438(7)

Table 2. (*continued*)

Intramolecular angles				Intramolecular distances		
Atom 1	Atom 2	Atom 3	Angle	Atom 1	Atom 2	Distance
C15	C11	C12	108.3(4)	C10	C6	1.344(7)
C11	C12	C13	110.2(4)	C11	C12	1.326(6)
C12	C13	C14	105.2(4)	C12	C13	1.380(6)
C13	C14	C15	106.4(4)	C13	C14	1.398(7)
C14	C15	C11	109.9(4)	C14	C15	1.372(7)
F1	B	F2	110.2(3)	C15	C11	1.325(6)
F1	B	F3	109.6(3)			
F1	B	F4	109.5(4)			
F2	B	F3	108.9(4)			
F2	B	F4	108.8(3)			
F3	B	F4	109.8(3)			

[a] Cp1, Cp2 and Cp3 are the centroids of the cyclopentadienide ligands.

another crossover experiment was devised involving methyl labelled **1g**. To also address the possibility of a potentially regioselective (albeit mechanistically rather obscure) metal attachment pathway, this compound was reacted with sulphur in the presence of **1e**. The outcome of this experiment revealed the occurrence of scrambling of the labelled CpCo unit to give **2b**, **2e**, **2g** and **7** [see eq. (3)].

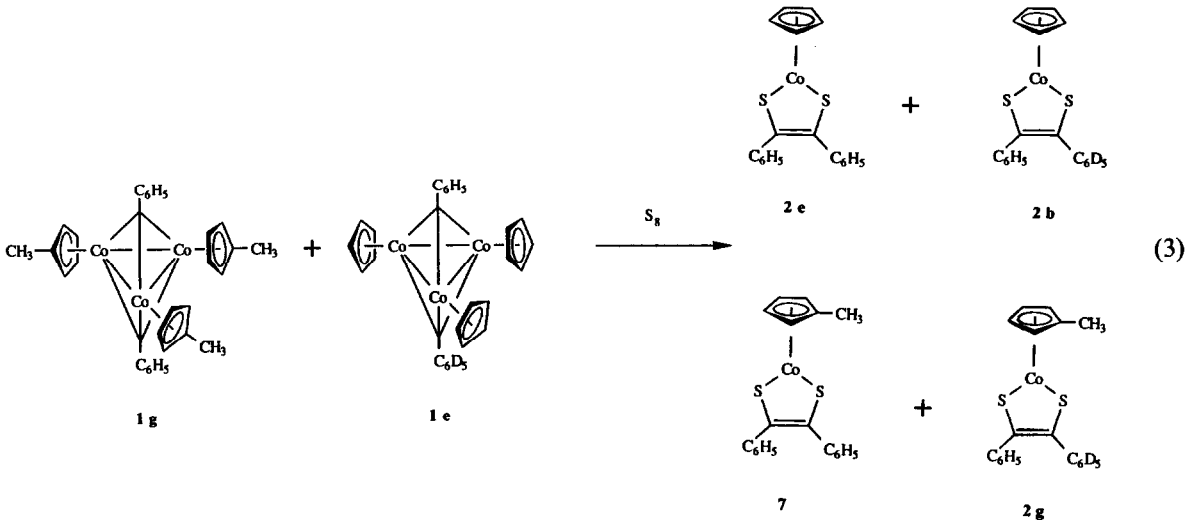

(3)

Although one could have construed this result as being indicative of an intermolecular mechanism by which the metal units progressed to **2**, a control experiment in which **2e** and **2g** were heated in chloroform to give an equilibrium mixture with **2b** and **7** negated the validity of that conclusion. Transpositions of this type had been known in metalladithiolenes,[4,16] but had never been rigorously scrutinized mechanistically. The observation of scrambling in the transformation of **2e** in the presence of **2g** provided an opportunity to do so. Three processes can be envisaged as a rationale for this molecular reorganization: exchange of Cp, CpCo or $CpCoS_2$ (or $R^1R^2C_2$). The feasibility of the first option was made likely by literature precedence for Cp exchange[17] and the fact that exposure of **2g** to nine equivalents of sodium cyclopentadienide in boiling THF afforded **2b** and starting material in a roughly equimolar ratio. This experiment suggested the possibility that trace quantities of anionic Cp could function as reactive intermediates in the observed scrambling. The second option had been implied in previous reports[4,16] but was never proven. The possibility of alkyne exchange also had to be considered seriously, based on some literature analogies[18] and the finding that **2b**, when treated with dimethyl butynedioate in boiling CH_2Cl_2 gave **2f**

(18%), diphenylacetylene (45%) and dimethyl 4,5-diphenylthiophene-2,3-dicarboxylate (10%).

To differentiate between these three modes, a series of crossover experiments was designed aimed at revealing the conservation (or lack thereof) of the presence of the various bonds which are involved. These utilized selenium as a label for sulphur and rhodium as a label for cobalt. To probe the possibility of alkyne exchange, a solution of **2g** and **5** was heated to 90°C for 12 h, after which the reaction was stopped and the mixture separated by HPLC to give the respective pairs of dithiolenes **2b**, **2g** and diselenolenes **5**, **8** [see eq. (4)]. These were then

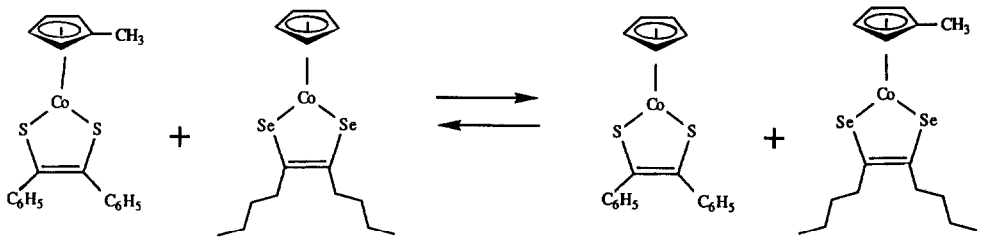

(4)

2g **5** **2b** **8**

analysed by both ^{1}H NMR and mass spectroscopy to reveal only exchange products in which the chalcogen had remained attached to the alkyne fragment. This finding ruled out the possibility that alkyne units were being transferred in these processes and suggested that the reaction of **2b** with dimethyl butynedioate followed an independent (and as yet unexplored) pathway.

To distinguish between Cp and Cpmetal exchange it was necessary to label the metal centre. This goal was reached by the preparation of rhodium dithiolene **9** via an adaptation of the Bönnemann–Schrauzer procedure.[4(a)] Exposure of **9** to **10** (obtained in an analogous way from (η^5-$CH_3C_5H_4$)$Co(CO)_2$, 5-decyne, and S_8) in xylene at 130°C showed products **11** and **2g**, determined by mass spectral analysis to be derived only from cyclopentadienylrhodium or methylcyclopentadienylcobalt exchange [see eq. (5)]. This experiment eliminates the consideration of cyclopentadienyl ligand transfer in the degradation of **1**, leaving only Cpmetal exchange as a viable mechanism. It therefore appears that the reaction of **2g** with cyclopentadienylanion is mechanistically unrelated to the transformations which constitute the main body of this report.

Although the details by which cyclopentadienylmetal exchange occurs in these processes are not known, several possibilities present themselves. The first to be considered is a dissociative pathway in which **2** would split into cyclopentadienylcobalt and the corresponding dithioketone. While such a mechanism is attractive because of its topological simplicity, it seems unlikely, as the organometallic fragment produced contains a highly coordinatively unsaturated 14e configuration. Indeed, attempts to trap such a complex were unsuccessful. Thus, addition of disodium 1,2-dicyanoethene-1,2-dithiolate to a heated solution of **2a** gave only recovered starting material.

A more likely scenario draws again from literature precedence which shows that metalladithiolenes are capable of forming diverse dimeric structures incorporating bridging enedithiolate ligands,[18] all of which could be intermediates in the exchange reactions uncovered in this work.

Finally, although more of the details by which

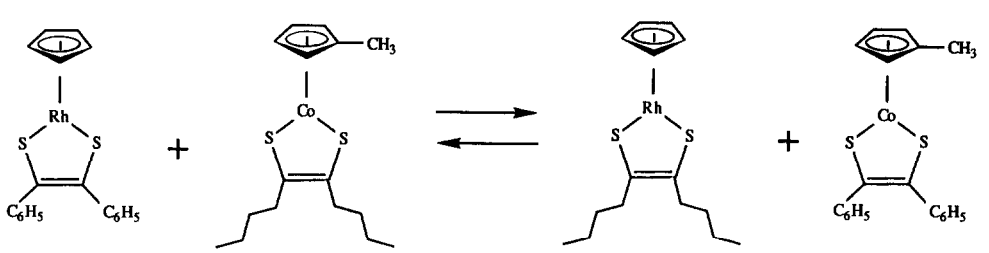

(5)

9 **10** **11** **2g**

clusters **1** transform in the presence of chalcogens remain to be established, it is likely that after sulphur has attacked one of the cobalt–cobalt bonds, migration into a carbyne–metal bond takes place, as observed for NO^+ and HCO^+,[10] to, in the present case, furnish a cluster bound thioacyl group, a species that has been the result of a number of related reactions of metal clusters with sulphur or sulphur-containing reagents.[19]

EXPERIMENTAL

General procedures

Unless otherwise noted, materials were obtained from commercial suppliers and used without further purification. THF was purified by distillation from sodium–benzophenone ketyl under N_2 and hydrocarbon solvents by stirring over H_2SO_4 for several hours. This treatment was repeated until the H_2SO_4 remained colourless. The organic layer was washed five times with 5% aqueous bicarbonate, five times with H_2O, twice with aqueous $KMnO_4$, again H_2O, then dried over $MgSO_4$, and distilled from CaH_2. Solvents and solutions were deoxygenated either by bubbling a vigorous stream of nitrogen through the liquid for several hours or by subjecting the latter to several freeze–evacuation–thaw cycles. All reactions involving cobalt were executed in deoxygenated solvents and under an inert atmosphere. Melting points (open Pyrex capillary) are uncorrected. ^1H NMR spectra were recorded at 250 or 200 MHz on instruments equipped with Cryomagnets Inc. magnets and Nicolet model 1180 data collection systems. ^1H NMR data are tabulated in the order: multiplicity (s, singlet; d, doublet; t, triplet; q, quartet; quin, quintet; sex, sextet; m, multiplet), coupling constant(s) in Hz and number of hydrogens (H). Chemical shifts are reported in ppm downfield from TMS, referenced to the residual proton peak of deuterated solvent as follows: δ $CHCl_3$, 7.24; C_6D_5H, 7.15; $CD_3C(O)CD_2H$, 2.04; CD_2HCN, 1.09 ppm. ^{13}C NMR chemical shifts are reported in ppm downfield from TMS, referenced to the respective central peaks of the perdeuteriobenzene ($\delta = 127.0$ ppm) or deuteriochloroform triplet ($\delta = 77.0$ ppm). Infrared absorptions were measured on a Perkin–Elmer infrared spectrophotometer model number 681. Mass spectral data are tabulated as m/z (relative intensity) and were obtained with Atlas MS-12 (low resolution) or Consolidated 12-110B (high resolution) mass spectrometers. Elemental analyses were provided by the Microanalytical Laboratory in the College of Chemistry, University of California, Berkeley, California. All chromatography was carried out with Alfa alumina (neutral) which had been deactivated by adding 5% H_2O *w/w*. High pressure liquid chromatography was performed with an Altex model 110A pump and an Altex model 153 UV detector using, linked in series, two Ultrasphere ODS 10 mm × 25 cm, 5μ particle columns (reverse phase). All crystallizations took place in hexane at −78°C.

General procedure for the preparation of bis(μ_3-η^1-alkylidyne)tris(η^5-cyclopentadienylcobalt) complexes[5]

Decalin (300 cm^3) was placed in a 500 cm^3 round bottom flask equipped with a magnetic stirbar and a reflux condenser stoppered with a rubber septum pierced by two 20 gauge syringe needles, one of which reaches a position just above level, the other functioning as a pressure release. The solvent was heated to reflux and exposed to a nitrogen purge for 2 h. A decalin solution (20 cm^3) containing the alkyne (1 equiv) and $CpCo(CO)_2$ (3 equiv) was then added via syringe pump to the boiling solvent with continued nitrogen purge over 6 h. After boiling the resulting mixture for an additional 4 h, it was filtered through glass wool and the solvent removed via vacuum transfer. The residue was dissolved in CH_2Cl_2 and preadsorbed onto alumina, then chromatographed on alumina with hexane and hexane–ether mixtures to afford the desired biscarbyne clusters.

(μ_3-η^1-Benzylidyne)(μ_3-η^1-propylidyne)tris(η^5-cyclopentadienylcobalt) (**1d**)

Following the general protocol for the preparation of biscarbyne clusters, the following reagents were used: 1-phenyl-1-butyne (1 g, 7.69 mmol) and $CpCo(CO)_2$ (4.15 g, 23 mmol). This reaction afforded **1d** (1.56 g, 41%): maroon crystals, m.p. 155–157°C; IR (NaCl) 2960m, 2935m, 1415w, 1160w, 1005m, 800s cm^{-1}; ^1H NMR (250 MHz, $CDCl_3$) δ 2.16 (t, $J = 7$ Hz, 3 H), 4.94 (s, 15 H), 5.19 (q, $J = 7$ Hz, 2 H), 7.41 (m, 3 H), 8.18 (br d, $J = 7$ Hz, 2 H); mass spectrum m/z 502 (M^+, 89), 370 (60), 247 (32), 189 (100), 124 (17). Exact mass. Found: 501.9949. Calc. for $C_{25}H_{25}Co_3$: 501.9952. Analysis. Found: C, 60.00; H, 5.02. Calc. for $C_{25}H_{25}Co_3$: C, 59.76; H, 5.02%.

(μ_3-η^1-Benzylidyne)(μ_3-η^1-pentadeuteriobenzylidyne)tris(η^5-cyclopentadienylcobalt) (**1e**)

Diphenylacetylene-d_5[20] (1.0 g, 5.46 mmol) and $CpCo(CO)_2$ (3.0 g, 16.7 mmol) were converted to **1e** (1.29 g, 42.5%): maroon crystals; mass spectrum m/z 555 (M^+, 100), 370 (26), 189 (90), 124 (49).

Bis(μ_3-η^1-benzylidyne)tris(η^5-methylcyclopentadienylcobalt) (**1g**)

Diphenylacetylene (500 mg, 2.8 mmol) and (η^5-$CH_3C_5H_4$)$Co(CO)_2$ (1.6 g, 8.2 mmol) transformed to **1g** (1.2 g, 74%): maroon crystals, m.p. 131–132°C; IR (NaCl) 2920w, 1570m, 1432m, 800s, 700s cm^{-1}; ^1H NMR (200 MHz, C_6D_6) δ1.28 (s, 9 H), 4.21 (br s, 6 H), 4.38 (br s, 6 H), 7.45 (m, 6 H), 8.38 (br d, J = 8 Hz, 4 H); mass spectrum m/z 592 (M^+, 46), 372 (100), 316 (30), 267 (33), 217 (49), 178 (24). Exact mass. Found: 592.0414. Calc. for $C_{32}H_{31}Co_3$: 592.0422. Analysis. Found: C. 65.20; H, 5.38. Calc. for $C_{32}H_{31}Co_3$: C, 64.94; H, 5.29%.

General procedure for sulphur degradations

In a 50 cm^3 round bottom flask equipped with a stirbar was placed $CHCl_3$ (35 cm^3) and an excess of sulphur (~ 0.6 mmol) while N_2 was bubbled through the solution for several hours. The cluster (~ 0.2 mmol) was added, the mixture boiled for 2 days, alumina (5 g) added and the solvent removed on a rotary evaporator. The reaction mixture, thus preadsorbed, was placed on top of an alumina column and chromatographed using hexane and hexane–ether mixtures.

Degradation of bis(μ_3-η^1-pentylidyne)tris(η^5-cyclopentadienylcobalt) (**1a**)

According to the above general procedure, **1a** (100 mg, 0.196 mmol) and sulphur (20 mg, 0.63 mmol) were transformed into **2a** (63 mg, 99%): purple crystals, m.p. 62–64°C; IR (NaCl) 2960m, 2940m, 1470w, 1410w, 1000m cm^{-1}; ^1H NMR (200 MHz, C_6D_6) δ 0.84 (t, J = 7.3 Hz, 6 H), 1.33 (quin, J = 7.5 Hz, 4 H), 1.78 (sex, J = 8 Hz, 4 H), 2.78 (t, J = 7.4 Hz, 4 H), 4.69 (s, 5 H); mass spectrum m/z 326 (M^+, 77), 241 (39), 188 (83), 44 (100). Exact mass. Found: 326.0581. Calc. for $C_{15}H_{23}CoS_2$: 326.0556.

Degradation of bis(μ_3-η^1-benzylidyne)tris(η^5-cyclopentadienylcobalt) (**1b**)

Complex **1b** (100 mg, 0.18 mmol) and sulphur (20 mg, 0.63 mmol) were allowed to react as above to furnish **2b** (66 mg, 99%): blue crystals, m.p. 113–114°C; IR (KBr) 3050w, 1598m, 1490m, 1440m, 755s, 680s cm^{-1}; ^1H NMR (250 MHz, C_6D_6) δ 4.71 (s, 5 H), 6.95 (m, 6 H), 7.45 (m, 4 H); ^{13}C NMR (50 MHz, $CDCl_3$) δ 79.61, 127.14, 127.85, 129.02, 142.24, 168.82; mass spectrum m/z 366 (M^+, 74), 188 (100), 178 (91), 124 (61). Analysis. Found: C, 62.72; H, 4.18; S, 17.2. Calc. for $C_{19}H_{15}CoS_2$: C, 62.28; H, 4.13; S, 17.5%.

A second more polar compound was then isolated and characterized as **3** (8 mg, 10%): black plates, m.p. > 250°C (ref. 8 > 250°C; ^1H NMR (250 MHz, $CDCl_3$) δ 4.65 (s); mass spectrum m/z 436 (M^+, 11), 189 (79), 124 (100).

Degradation of bis[μ_3-η^1-(3-trimethylsilyl)-2-propynylidyne]tris(cyclopentadienylcobalt) (**1c**)

Following the general procedure, **1c** (100 mg, 0.17 mmol) and sulphur (20 mg, 0.63 mmol) were converted to **2c** (23 mg, 33%): aquamarine crystals, m.p. 115–116°C; IR (KBr) 2960w, 2060w, 1010w, 800w cm^{-1}; ^1H NMR (250 MHz, C_6D_6) δ 0.23 (s, 9 H), 4.35 (s, 5 H); mass spectrum m/z 406 (M^+, 20), 279 (35), 188 (41), 183 (33), 149 (94), 57 (100). Exact mass. Found: 406.0111. Calc. for $C_{17}H_{23}CoS_2Si_2$: 406.0111. A second more polar compound turned out to be **4** (5 mg, 5%): forest green crystals, m.p. 187–189°C; IR (NaCl) 2060w, 1460m, 730m cm^{-1}; ^1H NMR (250 MHz, $CDCl_3$) δ 0.24 (s, 9 H), 0.28 (s, 9 H), 4.35 (s, 5 H), 4.42 (s, 5 H); mass spectrum m/z 594 (M^+, 8.5), 522 (36), 366 (19), 189 (8.1), 44 (100). Exact mass. Found: 593.9274. Calc. for $C_{22}H_{28}Co_2S_4Si_2$: 593.9276.

Degradation of (μ_3-η^1-benzylidyne)(μ_3-η^1-propylidyne)tris(cyclopentadienylcobalt) (**1d**)

Reaction of **1d** (100 mg, 0.20 mmol) with sulphur (20 mg, 0.63 mmol) afforded **2d** (62 mg, 98%): blue crystals, m.p. 110–111°C; IR (KBr) 3100w, 2950w, 1455m, 1430m, 1405m, 835m, 742m, 740m cm^{-1}; ^1H NMR (250 MHz, $CDCl_3$) δ 1.31 (t, J = 7 Hz, 3 H), 2.83 (q, J = 7 Hz, 2 H), 4.67 (s, 5 H), 7.11 (m, 3 H), 7.43 (m, 2 H); ^{13}C NMR (50 MHz, $CDCl_3$) 16.43, 31.09, 79.28, 127.31, 127.97, 128.45, 142.70, 167.69, 174.12; mass spectrum m/z 318 (M^+, 36), 188 (100), 149 (13), 124 (35). Analysis. Found: C, 56.28; H, 4.71; S, 19.76. Calc. for $C_{15}H_{15}CoS_2$: C, 56.59; H, 4.76; S, 20.14%.

Degradation of **1e**

Complex **1e** (100 mg, 0.18 mmol) and sulphur (20 mg, 0.63 mmol) transformed to **2e** (66 mg, 99%): blue crystals, m.p. 113–114°C; mass spectrum m/z 371 (M^+, 45), 188 (100), 183 (33).

Degradation of **1f**

Complex **1f** (100 mg, 0.195 mmol) and sulphur (20 mg, 0.63 mmol) converted to **2f** (58 mg, 90%): red violet crystals, m.p. 112–114°C; IR (KBr)

2950m, 2910m, 1710s, 1365m cm^{-1}; ^1H NMR (250 MHz, C_6D_6) δ 3.52 (s, 6 H), 4.40 (s, 5 H); mass spectrum m/z 330 (M^+, 75), 188 (100), 168 (39), 124 (82). Exact mass. Found: 329.9429. Calc. for $C_{11}H_{11}CoO_4S_2$: 329.9449.

Degradation of **1g**

Complex **1g** (100 mg, 0.17 mmol) and sulphur (20 mg, 0.63 mmol) provided **2g** (62 mg, 97%): blue crystals, m.p. 165–166°C; IR (KBr) 3050w, 1595m, 1475m, 1460m, 1420m, 1020m, 745m, 690m cm^{-1}; ^1H NMR (250 MHz, C_6D_6) δ 1.80 (s, 3 H), 4.52 (br, s, 2 H), 4.66 (br, s, 2 H), 6.95 (m, 6 H), 7.48 (m, 4 H); mass spectrum m/z 380 (M^+, 82), 202 (100), 178 (45). Exact mass. Found: 380.0106. Calc. for $C_{20}H_{17}CoS_2$: 380.0076.

Degradation of **1a** *with selenium*

Complex **1a** (100 mg, 0.196 mmol) was dissolved in toluene (25 cm^3) in a 50 cm^3 round bottom flask containing a stirbar. The solution was purged with nitrogen for 2 h and selenium (1.0 g, 13 mmol) added. The reaction mixture was heated for 2 days, the solvent removed and the residue purified by chromatography on alumina eluting with hexane and hexane–ether mixtures to furnish **5** (78 mg, 94%): dark violet crystals, m.p. 72–73°C; IR (KBr) 2975w, 2915w, 1450w, 1410w, 1009m, 995m cm^{-1}; ^1H NMR (250 MHz, C_6D_6) δ 0.847 (t, $J = 7$ Hz, 6 H), 1.27 (m, 4 H), 1.83 (m, 4 H), 3.01 (t, $J = 7$ Hz, 4 H) 4.59 (s, 5 H); mass spectrum m/z 422 (M^+, 9.0), 420 (8.2), 286 (23), 284 (770), 124 (62), 44 (100). Exact mass. Found: 421.9474. Calc. for $C_{15}H_{23}CoSe_2$: 421.9461. Analysis. Found: C, 42.93; H, 5.61. Calc. for $C_{15}H_{23}CoSe_2$: C, 42.87; H, 5.53%.

Preparation of the sulphonium salt **6**

In a 100 cm^3 round bottom flask equipped with a stirbar, **1a** (275 mg, 0.539 mmol) dissolved in nitromethane (50 cm^3) was added to dimethyl-(thiomethyl)sulphonium tetrafluoroborate (105 mg, 0.54 mmol) and the mixture stirred at ambient temperature for 2 h. The solvent was removed via vacuum transfer and the residue triturated with benzene to remove any residual starting material. The remainder was dissolved in acetone and the product crystallized by vapour diffusion using hexane over 2 days leading to **6** (320 mg, 92%): black prisms, m.p. > 300°C; ^1H NMR (250 MHz, CD_3CN) δ 1.21 (s, 3 H), 1.28 (t, $J = 8$ Hz, 3 H), 1.36 (t, $J = 7$ Hz, 3 H), 2.05 (m, 4 H), 2.53 (m, 2 H), 2.99 (m, 2 H), 4.81 (s, 10 H), 5.08 (s, 5 H), 5.27 (m, 4 H); CI mass spectrum m/z 557 (M^+ of cation, 1.7), 473 (1.7), 431 (5.7), 189 (100). Analysis. Found: C, 47.32; H, 5.36; S, 4.53. Calc. for $C_{26}H_{36}BCo_3F_4S$: C, 48.46; H, 5.64; S, 4.53%.

Crystal structure determination of **6**

Shiny black crystals were grown from an acetone–hexane bilayer. One of these was cleaved and a fragment of dimensions $\sim 0.21 \times 0.23 \times 0.32$ mm mounted on a glass fibre in air using polychromate cement. Crystal parameters at 25°C: $a = 8.8230(6)$, $b = 20.331(25)$, $c = 15.3307(14)$ Å, $\beta = 101.088(7)°$, $V = 2699$ Å^3, space group $P2_1/c$; weight = 644.24 amu, $Z = 4$, $d_{calc} = 1.585$ g cm^{-3}, $\mu_{calc} = 109.36$ cm^{-1}. Data measurement parameters: diffractometer, Enraf–Nonius CAD-4; monochromatic radiation, Mo-K_α ($\lambda = 0.71073$ Å); highly-orientated graphite ($2\theta_m = 12.2$) perpendicular mode, assumed 50% perfect; detector, crystal scintillation counter with PHA; aperture → crystal = 173 mm, vertical aperture = 3.0 mm, horizontal aperture = 2+1 tan(θ) mm (variable); reflections measured: $+H+K\pm L$; 2θ range 3–45°; scan type θ–2θ; scan speed, 0.66–6.7 (θ, ° min^{-1}; scan width, $\Delta\theta = 0.55+0.347$ tan θ; background, measured over an additional 0.25 ($\Delta\theta$) added to each end of the scan; number of reflections collected, 3916; number of unique reflections, 3525; intensity standards, 553, 239, 0 12 1; measured every 2 h of X-ray exposure time; no decay in intensity was observed; orientation, three reflections were checked after every 250 measurements; no reorientation was necessary during data collection; unit cell parameters and their esds were derived from a least-squares fit to the setting angles of the unresolved Mo-K_α components of 24 reflections with 2θ near 28°; the esds of all parameters are given in parentheses, right-justified to the least significant digits.

Structure solution and refinement: the 3916 raw intensity data were converted to values of the structure factor amplitudes and their esds by correction for scan speed, background, and Lorentz and polarization effects. Inspection of the azimuthal scan data revealed a $\pm 5\%$ variation in intensity. At the end of refinement an absorption correction was performed based on the measured shape and size of the crystal and a $10 \times 10 \times 8$ Gaussian grid of internal points. The maximum transmission factors were 0.84 and 0.70, respectively. Rejection of systematically absent and redundant data yielded 3525 unique data.

The three cobalt atoms were located by analysis of a three-dimensional Patterson map. Location of the other non-hydrogen atoms proceeded via standard Fourier and least-squares techniques. Analysis

of the disorder for C25—C25′ was performed by applying different occupancies until the isotropic thermal parameters were approximately equal. Over a broad range of occupancy distributions there was no significant change in the residuals. Prior to the last cycles of least squares refinement the idealized positions of all hydrogen atoms (except those on C24 and C25) were calculated and their contribution included in structure factor calculations. The final residuals for 315 variables refined against 2953 data for which $F^2 > 3\sigma(F^2)$, $R = 3.32\%$, $R_w = 4.93\%$, and GOF = 2.401. The R value for all 3525 data was 4.40%.

The quantity minimized by the least-squares program was $\Sigma w(|F_o| - |F_c|)^2$, where w is the weight of a given observation. The p-factor used to reduce the weight of intense reflections was set to 0.03 throughout the refinement. The analytical forms of the scattering factor tables for the neutral atoms were used and all non-hydrogen values corrected for both the real and imaginary components of anomalous dispersion. Inspection of the residuals ordered in ranges of $|F_o|$ and parity, and value of the individual indices showed no unusual features or trends. There was no evidence of secondary extinction in the low-angle, high intensity data. Reflections with low sin θ/λ were systematically poor in fit, probably due to the observed disorder. The largest peak in the final difference Fourier map had an electron density of 0.55 $e^- Å^{-3}$. The atomic positional and thermal parameters as well as structure factor tables have been deposited with the editor as supplementary material.

Notes on the structure of **6**. Molecules of the cationic part are well separated from each other and from their counterion. There are no particularly close contacts between molecules. Each cation core has approximate 2 mm (C_{2v}) symmetry. One plane is defined by the three cobalt atoms, the sulphur and the cyclopentadiene centroids, Cp1, Cp2 and Cp3. An orthogonal plane includes Cp1, Co1, S, C16, C21 and the methyl carbon C26. The three Cp ligands are all planar. The torsional angles of the rings about the Co-centroid vector differ quite significantly from the mirror ideal values. The internal distances in the Cp ligands show clear systematic and random errors due to the very large amplitudes of vibrational motion about the Co-centroid axis. Thermal motion effects and those of disorder are also evident at the distal ends of the carbyne ligands, e.g. C19—C20, C24—C25 and C24—C25′. The sulphur is bridging Cp2 and Cp3 in the plane of Co1, Co2 and Co3 and displays a pyramidal environment. A Co2—Co3 distance of 2.738(1) Å is consistent with the absence of any significant metal–metal bond. Comparison of the three Co—C(carbyne) bonds indicates a strengthening of the linkage to the unique metal centre Co1, at the expense of the other two. There is also a slight and probably *not* significant, difference in the Co—Cp distances between the two types of chemically non-equivalent cobalt atoms. The C_5H_9 ligands adopt basically an extended *trans* configuration, their planes oriented in different directions (probably due to packing forces); C16—C20 aligns roughly parallel to the plane defined by Co2, C16 and C21, and C21—C25 is approximately parallel to that incorporating Co1, C16 and C21.

Conversion of **6** to **2a**

The salt **6** (25 mg, 0.039 mmol) and sulphur (10 mg, 0.39 mmol) in acetonitrile were heated to reflux for 48 h. The solvent was removed on a rotary evaporator and the residue chromatographed on alumina to afford **2a** (10 mg, 78%).

Mixed degradation of **1e** *and* **1g**

Complexes **1e** (50 mg, 0.084 mmol) and **1g** (50 mg, 0.091 mmol) were allowed to react with sulphur (20 mg, 0.63 mmol) under standard conditions. The so-generated mixture was analysed by mass spectroscopy to reveal the presence of equimolar amounts of **2b**, **e**, **g** and **7**.

Reaction of **2e** *with* **2g**

In a 25 cm^3 round bottom flask, a $CHCl_3$ solution (10 cm^3) containing **2e** (10 mg, 0.027 mmol) and **2g** (10 mg, 0.026 mmol) was heated to reflux for 24 h. The reaction mixture was filtered through alumina and the products analysed by mass spectroscopy to reveal the parent ions of the four dithiolenes **2b**, **e**, **g** and **7** present in roughly equal intensity.

Reaction of **2g** *with* NaCp · DME *complex*

Methylcyclopentadienylcobalt(diphenyldithiolene) **2g** (50 mg, 0.13 mmol) was dissolved in THF (15 cm^3), NaCp · DME (200 mg, 1.12 mmol) added and the reaction mixture boiled for 24 h. The solvent was then removed on a rotary evaporator and the residue chromatographed on alumina to afford **2b** and **2g** as a roughly equimolar mixture, analysed by mass spectroscopy.

Reaction of dimethyl butynedioate with cyclopentadienylcobalt(diphenyldithiolene) (**2b**)

The dithiolene **2b** (50 mg, 0.136 mmol) was dissolved in CH_2Cl_2 (15 cm^3) and the solution heated

to reflux. A first portion of dimethyl butynedioate (200 mg, 0.141 mmol) was added, followed after 12 h by a second (200 mg, 0.070 mmol), and after 36 h a third (200 mg, 0.070 mmol). After 48 h, the solvent was removed and the reaction mixture purified by chromatography on silica gel eluting with hexane and hexane–ether mixtures. The first compound to be isolated was diphenylacetylene (11 mg, 45%), the second the fluorescent dimethyl 4,5-diphenylthiophene-2,3-dicarboxylate (5 mg, 10%): m.p. 90–92°C (ref. 21 92°C); mass spectrum m/z 352 (M^+), and the third the red violet **2f** (8 mg, 18%).

Crossover between **2g** *and* **5**

A mixture of **2g** (5 mg, 0.013 mmol) and **5** (5 mg, 0.012 mmol) was dissolved in benzene (1 cm^3) and heated in a sealed tube for 24 h at 110°C. The crude product was filtered through alumina and purified by reverse phase HPLC, eluting with acetonitrile to give mixtures of **2b** and **g** and **5** and **8**, respectively, analysed by mass spectroscopy.

η^5 - Cyclopentadienylrhodium(3,4 - diphenyldithio - lene) (**9**)

A cyclooctane solution (10 cm^3) containing $CpRh(CO)_2$[22] (1.0 g, 4.4 mmol) and diphenylacetylene (794 mg, 4.4 mmol) was added via syringe pump over 0.66 h to a boiling solution of sulphur (600 mg, 18.75 mmol) in cyclooctane (100 cm^3). After heating to reflux for an additional 1.5 h, the solution was cooled to room temperature, the solvent removed and the residue chromatographed on alumina eluting with hexane and hexane–ether mixtures to provide **9** (458 mg, 25%): red–violet crystals, m.p. > 250°C; IR (KBr) 1600m, 1495m, 1442s, 1070m, 919m, 758s, 690s cm^{-1}; ^1H NMR (250 MHz, acetone-d_6) δ 7.20 (br s, 10 H), 5.78 (s, 5 H); mass spectrum m/z 410 (M^+, 55), 232 (2), 178 (100), 176 (23), 149 (25). Exact mass. Found: 409.9668. Calc. for $C_{19}H_{15}RhS_2$: 409.9659.

η^5-Methylcyclopentadienylcobalt(3,4-dibutyldithio-lene) (**10**)

A cyclooctane solution (10 cm^3) containing (η^5-$CH_3C_5H_4$)$Co(CO)_2$ (1.0 g, 5.15 mmol) was added over 0.66 h via a syringe pump to boiling cyclooctane (75 cm^3) containing sulphur (330 mg, 10.3 mmol) and 5-decyne (700 mg, 5.15 mmol). The mixture was heated for an additional hour, the solvent removed and the residue purified by chromatography to afford **10** (472 mg, 27%): purple crystals, m.p. 116–118°C; IR(NaCl) 2960m, 2910m, 1460m, 1020w cm^{-1}; ^1H NMR (250 MHz, C_6D_6) δ 0.85 (t, J = 7 Hz, 6 H), 1.32 (m, 4 H), 1.72 (s, 3 H), 1.84 (m, 4 H), 3.03 (t, J = 7 Hz, 4 H), 4.56 (br s, 2 H), 4.57 (br s, 2 H); mass spectrum m/z 340 (M^+, 61), 225 (40), 202 (65), 44 (100). Exact mass. Found: 340.0747. Calc. for $C_{16}H_{25}CoS_2$: 340.0730.

Crossover between **9** *and* **10**

A solution of **9** (5 mg, 0.015 mmol) and **10** (5 mg 0.012 mmol) in *m*-xylene (5 cm^3) was heated to reflux for 48 h. An aliquot was filtered through alumina and the solvent removed under reduced pressure. The residue was then analysed by mass spectroscopy, revealing the presence of approximately equimolar amounts of **9**, **10**, **11** and **2g**.

Acknowledgement—This work was supported by the Director, Office of Energy Research, Office of Basic Energy Sciences, Chemical Sciences, Chemical Sciences Division of the U.S. Department of Energy under Contract No. DE-AC-03-76 SFO 0098 and the NSF (CHE-8504987). The crystal structure analysis was carried out by Dr F. J. Hollander, U.C. Berkeley X-ray Crystallographic Facility. Atomic positional parameters have been deposited with the Cambridge Crystallographic Data Centre. We thank Johnson Matthey for a gift of rhodium chloride hydrate.

REFERENCES

1. L. L. Hegedus and R. W. McCabe, *Catalyst Poisoning*. Marcel Dekker, New York (1984); R. A. Meyers, *Coal Desulfurization*. Marcel Dekker, New York (1977).
2. (a) E. L. Muetterties and M. J. Krause, *Angew. Chem. Int. Ed. Engl.* 1983, **22**, 135; (b) A. B. Anderson, *J. Catal.* 1981, **67**, 129; (c) R. D. Adams, J. E. Babin and M. Tasi, *Organometallics* 1987, **6**, 1717, and refs therein; (d) For a preliminary report, see: K. P. C. Vollhardt and E. C. Walborsky, *J. Am. Chem. Soc.* 1983, **105**, 5507.
3. See for example, (a) H. Vahrenkamp, *Angew. Chem. Int. Ed. Engl.* 1975, **14**, 322; (b) H. Vahrenkamp, *Adv. Organomet. Chem.* 1983, **22**, 169; (c) E. Sappa, A. Tiripicchio and P. Braunstein, *Coord. Chem. Rev.* 1985, **65**, 219; (d) L. Marko and B. Marko-Monostory, Complexes with sulphur-containing ligands, in *The Organic Chemistry of Iron* (Edited by E. A. Koerner von Gustorf, F.-W. Grevels and I. Fischler). Academic Press, New York (1981).
4. (a) M. Kajitani, R. Ochiai, N. Kobayashi, T. Akiyama and A. Sugimori, *Chem. Lett.* 1987, 245; (b) N. J. Harris and A. Underhill, *J. Chem. Soc., Dalton Trans.* 1987, 1683; (c) M. S. Ansari, J. Chandrasekaran and S. Sarkar, *Inorg. Chim. Acta* 1987, **130**, 155; (d) H. A. Harris, A. D. Rae and L. F. Dahl, *J. Am. Chem. Soc.* 1987, **109**, 4739; (e) S. Boyde, C.

D. Garner, J. A. Joule and D. F. Rowe, *J. Chem. Soc., Chem. Commun.* 1987, 800; (f) A. C. Filippou and E. O. Fischer, *J. Organomet. Chem.* 1987, **330**, C1 and the refs therein.
5. J. R. Fritch and K. P. C. Vollhardt, *Angew. Chem. Int. Ed. Engl.* 1980, **19**, 559.
6. B. Eaton, J. M. O'Connor and K. P. C. Vollhardt, *Organometallics* 1986, **5**, 394.
7. D. E. Van Horn and K. P. C. Vollhardt, *J. Chem. Soc., Chem. Commun.* 1982, 203.
8. A. Otsuka, A. Nakamura and T. Yoshida, *Liebigs Ann. Chem.* 1968, **719**, 54.
9. (a) J. R. Fritch and K. P. C. Vollhardt, *Angew. Chem. Int. Ed. Engl.* 1979, **18**, 409; (b) N. T. Allison, J. R. Fritch, K. P. C. Vollhardt and E. C. Walborsky, *J. Am. Chem. Soc.* 1983, **105**, 1384.
10. A. Goldhaber, K. P. C. Vollhardt, E. C. Walborsky and M. Wolfgruber, *J. Am. Chem. Soc.* 1986, **108**, 516; K. P. C. Vollhardt and M. Wolfgruber, *Angew. Chem. Int. Ed. Engl.* 1986, **25**, 929.
11. See (a) G. A. McDermott and A. Mayr, *J. Am. Chem. Soc.* 1987, **109**, 580; (b) R. R. Schrock, *Acc. Chem. Res.* 1986, **19**, 342; (c) M. H. Chisholm, B. K. Conroy, J. C. Hoffman and N. S. Marchant, *Angew. Chem. Int. Ed. Engl.* 1986, **25**, 446; (d) Y. Chi, J. R. Shapley, M. R. Churchill and Y. Li, *Inorg. Chem.* 1986, **25**, 4165; (e) W.-Y. Yeh and J. R. Shapley, *J. Organomet. Chem.* 1986, **315**, C29; (f) Y. Chi and J. R. Shapley, *Organometallics* 1985, **4**, 1900 and refs therein.
12. F. N. Tebbe, E. Wasserman, W. G. Peet, A. Vatvars and A. Hayman, *J. Am. Chem. Soc.* 1982, **104**, 4971.
13. See H. Werner, G. Luxenburger, W. Hofmann and M. Nadvornik, *J. Organomet. Chem.* 1987, **323**, 161; K. Burgess, *Polyhedron* 1984, **11**, 1175; W. A. Herrmann, C. Bauer and J. Weichmann, *J. Organomet. Chem.* 1983, **243**, C21; W. Hofmann and H. Werner, *Angew. Chem. Int. Ed. Engl.* 1981, **20**, 1014; M. P. Brown, J. R. Fisher, R. J. Puddephatt and K. R. Seddon, *Inorg. Chem.* 1979, **18**, 2808; A. L. Balch, L. S. Benner and M. M. Olmstead, *Inorg. Chem.* 1979, **18**, 2996; M. P. Brown, J. R. Fisher, S. J. Franklin, R. J. Puddephatt and K. R. Seddon, *J. Chem. Soc., Chem. Commun.* 1978, 749 and refs therein.
14. H. Meerwein, K.-F. Zenner and R. Gipp, *Liebigs Ann. Chem.* 1965, **688**, 67.
15. V. W. Day, J. R. Fritch and K. P. C. Vollhardt, unpublished results (consult V. W. D. for details).
16. J. A. McCleverty, *Prog. Inorg. Chem.* 1968, **10**, 49.
17. H. E. Bryndza and R. G. Bergman, *Inorg. Chem.* 1981, **20**, 2988; H. Werner and H.-J. Kraus, *J. Chem. Soc., Chem. Commun.* 1978, 814; H. Werner, H.-J. Kraus, U. Schubert and K. Ackermann, *Chem. Ber.* 1982, **115**, 2905; R. J. Cross and A. J. McLennan, *J. Chem. Soc., Dalton Trans.* 1983, 359: P. E. Garrou, *Adv. Organomet. Chem.* 1984, **23**, 95 and refs therein.
18. K. Roesselet, K. E. Doan, S. D. Johnson, P. Nicholls, G. L. Miessler, R. Kroeker and S. H. Wheeler, *Organometallics* 1987, **6**, 480; M. J. H. Russell, C. White, A. Yates and P. M. Maitlis, *J. Chem. Soc., Dalton Trans.* 1978, 849; A. L. Balch, *Inorg. Chem.* 1971, **10**, 388; A. L. Balch, *J. Am. Chem. Soc.* 1969, **91**, 6962; A. L. Balch, I. G. Dance and R. H. Holm, *J. Am. Chem. Soc.* 1968, **90**, 1139; R. B. King and M. B. Bisnette, *Inorg. Chem.* 1967, **6**, 469; J. Locke and J. A. McCleverty, *Inorg. Chem.* 1966, **5**, 1157; R. B. King, *J. Am. Chem. Soc.* 1963, **85**, 1587 and refs therein.
19. E. Delgado, J. Hein, J. C. Jeffery, A. L. Ratermann, F. G. A. Stone and L. J. Farrugia, *J. Chem. Soc., Dalton Trans.* 1987, 1191; M. R. Churchill, J. W. Ziller, D. M. Dalton and J. B. Keister, *Organometallics* 1987, **6**, 806; R. D. Adams and S. Wang, *Organometallics* 1985, **4**, 1902; E. Delgado, A. T. Emo, J. C. Jeffery, N. D. Simmons and F. G. A. Stone, *J. Chem. Soc., Dalton Trans.* 1985, 1323.
20. S. Safe, *J. Labeled Comp.* 1970, **6**, 197.
21. G. N. Schrauzer and V. Mayweg, *Z. Naturforsch. B.* 1964, **19**, 192.
22. R. S. Dickson and G. R. Tailby, *Aust. J. Chem.* 1970, **23**, 1531.

Polyhedron Vol. 7, No. 10/11, pp. 1035–1043, 1988
Printed in Great Britain

0277–5387/88 $3.00+.00
© 1988 Pergamon Press plc

CONTRASTS IN THE CHEMISTRY OF TRINUCLEAR CLUSTER COMPLEXES OF OSMIUM AND RUTHENIUM. FORMATION OF A FISCHER CARBENE OR A FUNCTIONALIZED μ_3,η^2-VINYLIDENE GROUP

HERBERT D. KAESZ† and CRAIG M. JENSEN

Department of Chemistry and Biochemistry, University of California, Los Angeles, CA 90024-1569, U.S.A.

(*Accepted* 5 *November* 1987)

Abstract—The complex $Os_3(CO)_{12}$ (**1**) is alkylated with organolithium reagents to give $[Li][Os_3\{\eta^1\text{-}C(O)R\}(CO)_{11}]$ ([Li][**2**]). Attempts at electrophilic alkylation of such salts has been unsuccessful. Acidification of a tetrahydrofuran (THF) solution of [Li][**2**] leads to $Os_3(CO)_{11}(THF)$ (**3**).

Metathesis of [Li][**2**] with [PPN]Cl ($[PPN]^+ = (Ph_3P)_2N]^+$) accompanied by exchange of THF by $CHCl_3$, leads to a solution of $[PPN][Os_3\{1,2\text{-}\mu\text{-}O{=}C(Me)\}(CO)_{10}]$ ([PPN][**4**]). Acidification of the latter gives $Os_3\{1,2\text{-}\mu\text{-}H;\ 1,2\text{-}\mu\text{-}O{=}C(Me)\}(CO)_{10}$ (**5**). Alkylation of [PPN][**4**] with $ROSO_2CF_3$ gives the bis-acyl derivative $Os_3\{\eta^x\text{-}C(O)R\}\{\mu\text{-}O{=}C(Me)\}(CO)_9$ (**6**). This reacts with water to give a small amount of $Os_3\{1,2\text{-}\mu\text{-}X;\ 1,2\text{-}\mu\text{-}O{=}C(Me)\}(CO)_{10}$ (**7**, X = Cl, or I) along with the two principal products, the Fischer carbene complex $Os_3\{1,2\text{-}\mu\text{-}H;\ 1,2\text{-}\mu\text{-}O{=}C(Me)\}\{1\text{-}C(OR)Me\}(CO)_9$ (**8**, R = CH_3, CD_3, C_6H_5), and $Os_3\{1,2\text{-}\mu\text{-}(OH);\ 1,2\text{-}\mu\text{-}O{=}C(Me)\}(CO)_{10}$ (**9**).

Complex **5** is deprotonated by alkyl lithium reagents at 25°C; at −30°C, however, it is alkylated to give $[Li][Os_3\{C(O)R\}\{\mu\text{-}H,\mu\text{-}O{=}C(Me)\}(CO)_9]$ ([Li](**10**)). Electrophilic alkylation of this salt with $R'OSO_2CF_3$ at 25°C leads to cluster complexes containing a Fischer carbene group, $Os_3\{1\text{-}\eta^1\text{-}C(OR')R\}\{1,2\text{-}\mu\text{-}H;\ 1,2\text{-}\mu\text{-}O{=}C(Me)\}(CO)_9$ (**8**, R = R′ = Me; R = Me, R′ = Et; R = Ph, R′ = Et) in high yield.

Treatment of $Ru_3\{1,2\text{-}\mu\text{-}H;\ 1,2\text{-}\mu\text{-}O{=}C(Me)\}(CO)_{10}$ (**11**) with LiR at −30°C leads to $[Li][Ru_3\{C(O)R\}\{\mu\text{-}H,\mu\text{-}O{=}C(Me)\}(CO)_9]$ ([Li][**12**]). Electrophilic alkylation of these salts, however, leads to the elimination of acetaldehyde along with the formation of double C—H oxidative addition products, $Ru_3\{\mu\text{-}H\}_2\{\eta^2,\mu_3\text{-}C(OEt){=}C(H)\}(CO)_9$ (**13**). Starting with Me_2NH instead of alkyllithium in this sequence gives $Ru_3\{\mu\text{-}H\}_2\{\eta^2,\mu_3\text{-}C(OEt)N(Me)C(H)\}(CO)_9$ (**14**).

A few years ago[1] we noted that despite the passing of 18 years since the isolation of the first heterocarbene complex by Fischer and Maasböl,[2] there had been no report of the synthesis of such a functional group on a cluster complex of nuclearity three or higher. Formation of one (or two) Fischer carbene groups on dinuclear carbonyls had been reported[3] and the migration or transfer of a preformed Fischer carbene group had been achieved in the reaction of $M\{C(OMe)Ph\}(CO)_5$ (M = Cr or W) with zero-valent platinum complexes (giving di- and trinuclear complexes containing a $\{\mu$-C(OMe)Ph$\}$ group).[4] A tri-iron complex containing the η^1-$CS_2(CH)_2$ group had been obtained in the reaction of 1,3-dithiole-2-thione with $Fe_2(CO)_9$.[5]

ATTEMPTS TO FORM A FISCHER CARBENE GROUP ON $Os_3(CO)_{12}$

Our investigations with $Os_3(CO)_{12}$ (**1**) are summarized in Scheme 1. The lithium salt of the acyl anion $[Os_3\{\eta^1\text{-}C(O)CH_3\}(CO)_{11}]^-$ ([**2**]$^-$) is formed instantaneously by treatment of **1** with methyl lithium at 0°C.[6] Care must be taken in the stoi-

† Author to whom correspondence should be addressed.

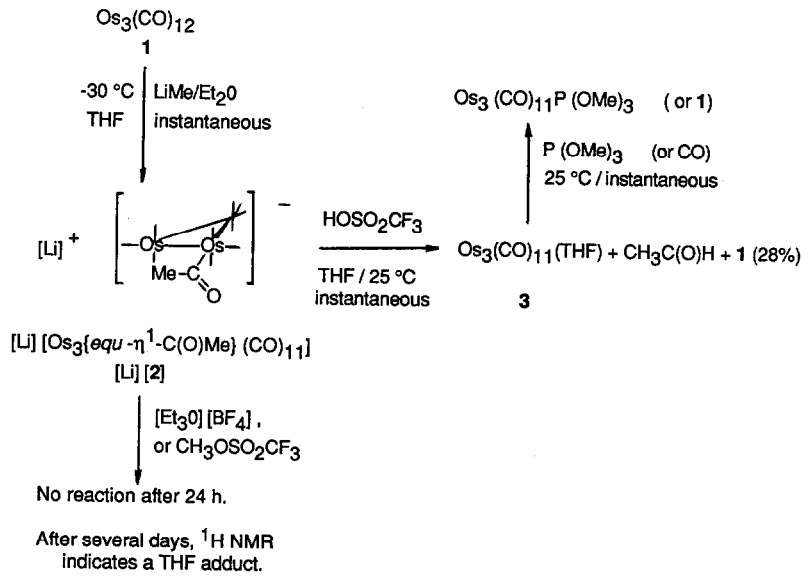

Scheme 1.

chiometry since $Os_3(CO)_{12}$ can absorb two mols of alkyl lithium reagent.[7]

The anionic complex $[2]^-$ is shown in Scheme 1 with the acyl group in the *equatorial* position, as deduced from the $\{^1H\}^{13}C$ NMR at $-85°C$.[1(b)] This spectrum contains seven resonances in the carbonyl region (δ 196.3–173.5) with an intensity pattern 2:4:1:1:1:1:1; the resonance for the acyl carbon of the $\{\eta^1$-C(O)R$\}$ group is observed at δ 238.8 ppm. The carbonyl group resonances coalesce to an averaged signal at room temperature, indicating fluxionality for this anion. Information about the first-formed (kinetic) product is thus lost; this might well have been the anion with an axial-acyl group, deriving from initial attack of the nucleophile at the carbon of an axial CO group, where this is expected to be favoured.

Alkylation of [Li][2] at 25°C proved to be slow and fraught with the usual complications,[8] see Scheme 1. After about 8 h the principal solution constituents are $Os_3(CO)_{11}$(THF) (**3**) and a corresponding amount of acetaldehyde. Some $Os_3(CO)_{12}$ is also obtained as by-product. Complex **3** is not isolated but its presence is confirmed by ^1H NMR and by its instantaneous reaction with $P(OMe)_3$, as shown in Scheme 1. We ascribe the formation of acetaldehyde to protonation of $[2]^-$ by trifluoromethylsulphonic acid[9] produced in the hydrolysis of the alkylating agent by traces of water in the system; protonation of metal acylates is known to give aldehydes.† In support of this conclusion, addition of a stoichiometric amount of trifluoromethylsulphonic acid to a THF solution of [Li][2] results in the instantaneous formation of **3** along with a stoichiometric amount of acetaldehyde.

Under rigorously anhydrous conditions, no alkylation is seen. After 16 h, polymerization of the THF solution[11] is observed.

CONVERSION OF $[Li][Os_3\{\eta^1$-C(O)CH$_3\}$(CO)$_{11}]$ ([Li][2]) INTO $[PPN][Os_3\{\mu$-O=C(CH$_3)\}$(CO)$_{10}]$ ([PPN][4])

We next sought to perform the electrophilic alkylation of $[2]^-$ in chloroform as its $[PPN]^+$ salt, see Scheme 2. This salt is formed by metathesis of [Li][4] with [PPN]Cl. The substitution of solvents, however, is accompanied by appreciable conversion of $[2]^-$ into $[Os_3\{\mu$-O=C(CH$_3)\}$(CO)$_{10}]^-$ ($[4]^-$).[6] A part of this transformation occurs during the removal of the THF under reduced pressure and is completed in chloroform.

ALKYLATION OF [PPN][4]

Methyl triflate is added to the solution of [PPN][4] and, after 2 h, the anion is completely converted to a neutral derivative, (**6**). The reactivity of $[4]^-$ towards alkylating agents was compared to that of $[2]^-$; we observed no alkylation of $[2]^-$ before polymerization of the THF sets in, while $[4]^-$

† The formation of aldehyde may result from either protonation at the metal followed by reductive elimination of the aldehyde,[10(a)] or from protonation at oxygen to give a hydroxycarbene followed by rearrangement to the aldehyde.[10(b)]

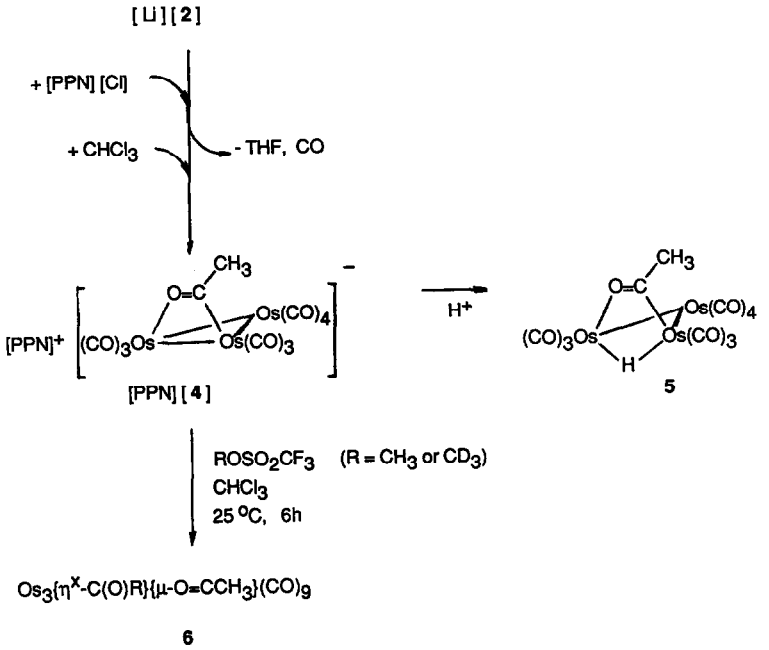

Scheme 2.

shows partial alkylation to **6** in about the same time (in THF).

The $\{^1H\}$ ^{13}C NMR of **6** is shown in Fig. 1. Nine resonances of equal intensity are seen in the region δ 186–173 ppm, denoting a cluster with nine CO groups, each in a different environment; the CO groups do not exchange at room temperature. The remaining signals attributable to **6** consist of two pairs of resonances at δ 283.8, 269.1, 50.2 and 49.4 ppm. One (low field)–(high field) pair must represent the original $\{\mu$-O=C(Me)$\}$ group, while the other pair represents the functional group formed during the electrophilic alkylation.

There are two possibilities for the site of alkylation in $[\mathbf{4}]^-$. One is the formation of a new acyl group arising from alkylation at a metal centre in $[\mathbf{4}]^-$ followed by migration to coordinated CO. This would parallel the formation of $[Fe\{\eta^1$-C(O)Me$\}(CO)_2\{\mu$-$P(C_6H_5)_2\}Fe(CO)_3]^-$ (in the reaction of $[Fe(CO)_3\{\mu$-$P(C_6H_5)_2\}Fe(CO)_3]^{2-}$ with CH_3I).[12] Such a reaction would give a bis-acyl derivative $Os_3\{\eta^x$-C(O)R$\}\{\mu$-O=C(Me)$\}(CO)_9$ (**6**-bis-acyl; $R = CH_3$ or CD_3); in such a derivative, the {-C(O)R} group would probably be dihapto to attain a 48 e^- count on the cluster.

A second possibility is O-alkylation of $[\mathbf{4}]^-$ to form an alkoxy–carbyne derivative,[13,14,15] namely $Os_3\{\eta^x$-C(OR)$\}\{\mu$-O=C(Me)$\}(CO)_9$ (**6**-alkoxy–carbyne). It has not as yet been possible to obtain a definitive characterization of **6** owing to its extreme reactivity (see below). We have proposed a bis-acyl formulation for **6** based on the chemical shifts of the resonances mentioned above; while the resonance of the carbyne carbon in the triply-bridged alkoxycarbyne group in $Os_3\{\mu$-H$\}_3\{\mu_3$-C(OMe)$\}(CO)_9$ is observed at δ 205.5 ppm,[14] this resonance in other alkoxy–carbyne complexes occurs below 300 ppm.[13,15] Still, the structure of **6** must be regarded as an open question, and to reflect this in the present account, we write the formula as $Os_3\{\eta^x$-CO(R)$\}\{\mu$-O=C(Me)$\}(CO)_9$.

FORMATION OF A FISCHER CARBENE COMPLEX IN THE REACTION OF 6 WITH H_2O

Attempts to purify **6** by silica gel column chromatography results in its conversion to the three products shown in Scheme 3 (R=CH_3). The Fischer carbene containing cluster complex $Os_3\{1$-η^1-C(OMe)Me$\}\{1,2$-μ-H;1,2-μ-O=C(Me)$\}(CO)_9$ (**8**) is obtained in 38% yield; its structure was determined by X-ray diffraction.[1] The {μ-hydroxy,μ-acyl} complex $Os_3\{1,2$-μ-(OH);1,2-μ-O=C(Me)$\}(CO)_{10}$ (**9**) is obtained in about the same yield. A halogen bridged complex $Os_3\{1,2$-μ-Cl;1,2-μ-O=C(Me)$\}(CO)_{10}$ (**7**, X = Cl) is a minor by-product in this reaction. This arises from the presence of a chloride ion in the mixture owing to incomplete precipitation of LiCl in the metathesis of [PPN]Cl with [Li][**2**].

In order to trace the origin of the methyl group in the above conversion, we alkylated [PPN][**4**] with $CD_3OSO_2CF_3$, Scheme 2 ($R = CD_3$). The complex

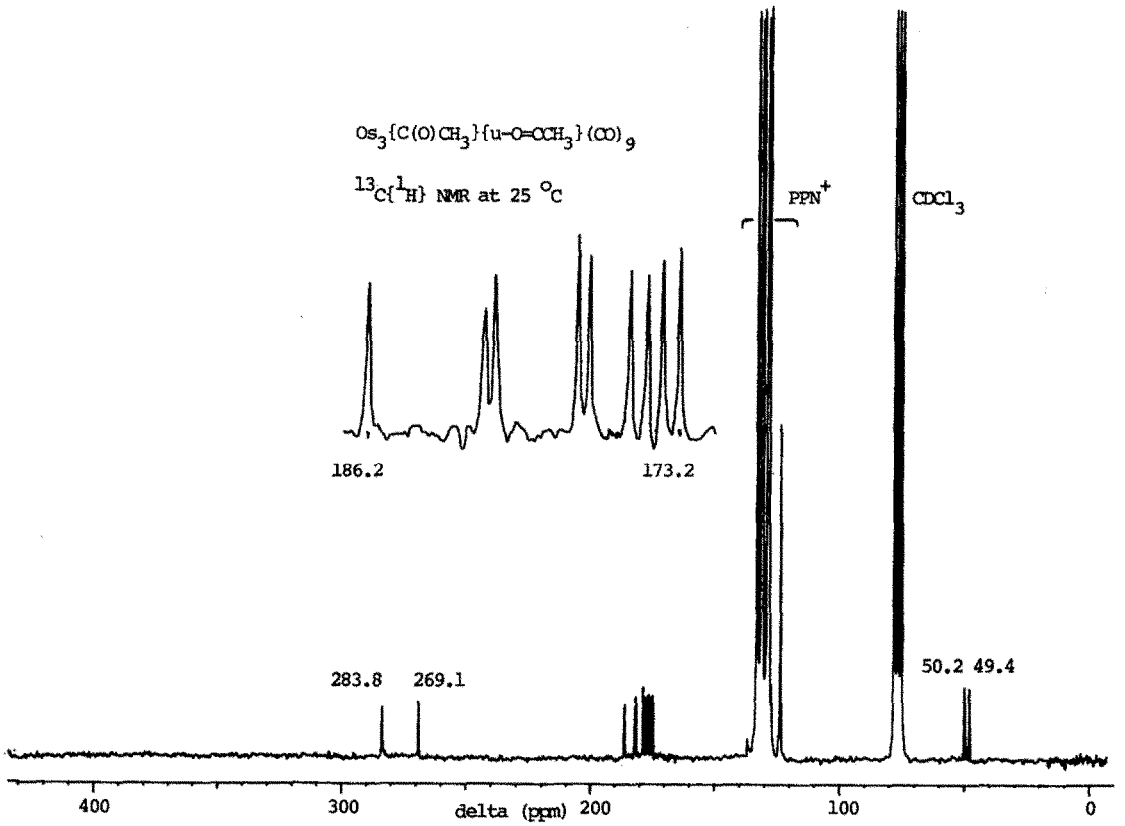

Fig. 1. $^{13}\{^{1}H\}$ NMR of $Os_3\{\eta^x\text{-}C(O)CH_3\}\{\mu\text{-}O{=}CCH_3\}(CO)_9$ (**6**), at 25°C, $CDCl_3$ solution; carbonyl group resonances are at δ 186.2, 185.6, 180.1, 179.7, 178.8, 178.1, 177.3, 175.5, 173.2. (*cf.* Dissertation, C. M. Jensen, UCLA, 1984).

6-d$_3$ was examined by ^2H NMR and found to contain the deuterium label only in the $\{\eta^x\text{-}CO(R)\}$ group, i.e. $Os_3\{\eta^x\text{-}CO(CD_3)\}\{\mu\text{-}O{=}C(Me)\}(CO)_9$. No scrambling of the deuterium label is observed in this complex over 1 week at room temperature (under exclusion of air and moisture).

Addition of water to a solution of **6-d$_3$** (Scheme 3, R = CD_3) followed by removal of the chloroform solvent and extraction with petroleum ether, results in the disappearance of the resonance corresponding to the $\{\eta^x\text{-}CO(CD_3)\}$ group in the ^2H NMR and its replacement by resonances cor-

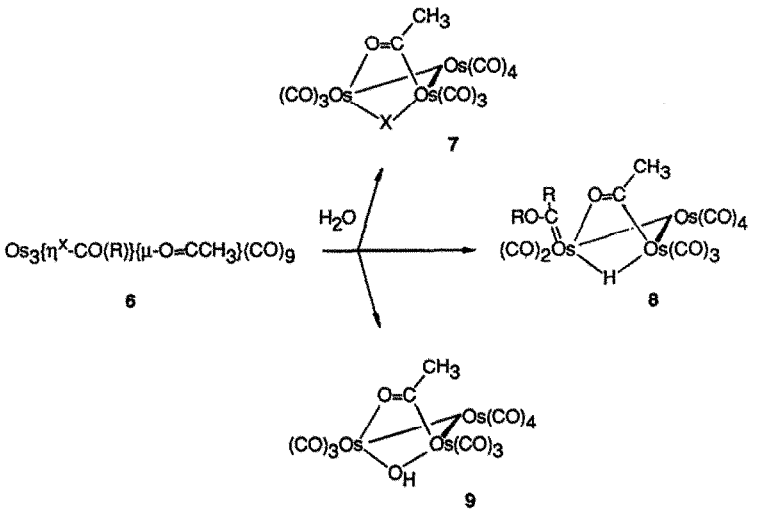

Scheme 3.

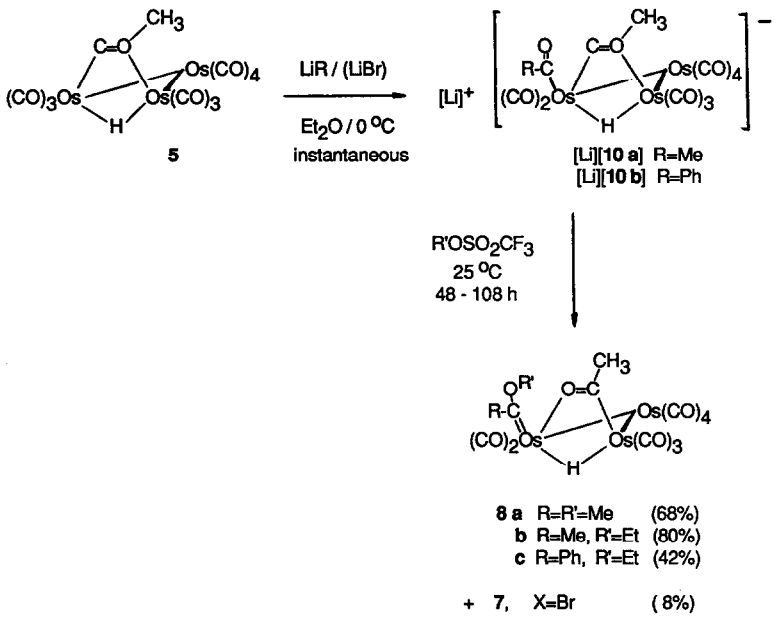

Scheme 4.

responding to the CD_3 and OCD_3 groups of the carbene moiety of **8-d$_6$**. Chromatography of the petroleum ether extracts on silica gel produces **8-d$_3$**: $Os_3\{\eta^1\text{-}C(OCD_3)CH_3\}\{1,2\text{-}\mu\text{-}H;1,2\text{-}\mu\text{-}O{=}C(Me)\}(CO)_{10}$; loss of the label on the carbene methyl group results from H/D exchange on silica gel, owing to the acidic nature of these protons.[16] No label is detected in complex **9** which is also produced in this reaction. In transformations of the CD_3-labelled materials, the minor by-product is $Os_3\{1,2\text{-}\mu\text{-}I;1,2\text{-}\mu\text{-}O{=}C(Me)\}(CO)_{10}$ (**7**, X = I). This arises from reaction of residual $[I]^-$ which is introduced in the preparation of the methyltriflate-d_3 by the reaction of silver triflate with CD_3I.

The conversion of **6-d$_3$** into **8-d$_6$** and **9** by water does not involve the μ-acyl group. To achieve the regiospecific transfer of a $-CD_3$ group while also explaining the observed product distribution, we have proposed attack of a water molecule on **6** followed by proton transfer to a second molecule of **6** leading to the ionic species [**A**$^-$] and [**B**$^+$] as shown in eq. (1).

$$2Os_3\{\eta^x\text{-}CO(R)\}\{\mu\text{-}O{=}C(Me)\}(CO)_9 + H_2O$$
$$= [Os_3\{\eta^x\text{-}CO(R)\}\{\mu\text{-}O{=}C(Me)\}\{(OH)\}(CO)_9]^-([\mathbf{A}]^-) + [Os_3\{\eta^x\text{-}CO(R)\}\{\mu\text{-}O{=}C(Me)\}\{H\}(CO)_9]^+([\mathbf{B}]^+). \quad (1)$$

Our proposal for the transfer of a $-CD_3$ group and a pair of electrons from [**A**]$^-$ to [**B**]$^+$ (assuming a bis-acyl structure in **6**) is shown in Scheme 4 of ref. 1. The structure of **6** and the details of the regiospecific "disproportionation" of -R groups are still open questions at this time.

THE FISCHER REACTION SEQUENCE ON $Os_3\{1,2\text{-}\mu\text{-}H;1,2\text{-}\mu\text{-}O{=}C(Me)\}(CO)_{10}$ (5)

Having obtained **8** unexpectedly in the aforementioned reactions, we were led to attempt its direct synthesis from **5**. This proved successful as summarized in Scheme 4. Titration of **5** in diethylether at −30°C with LiMe (also in diethylether, low bromide content) produces $[Li][Os_3\{\eta^1\text{-}C(O)Me\}\{1,2\text{-}\mu\text{-}H;1,2\text{-}\mu\text{-}O{=}C(Me)\}(CO)_9]$ ([Li][**10a**]). This is remarkable in view of the Brönsted acidity of cluster hydrides,†[17] where acidity, however, is not kinetically favoured at slightly lowered temperature. At room temperature, deprotonation rather than nucleophilic alkylation is observed (see discussion for triruthenium complexes, below).

Warming the solution of [Li][**10a**] to 25°C and treating it with a slight excess of $CH_3OSO_2CF_3$ leads, after 36 h stirring, to **8a** (R = CH_3) in 68% yield. Longer reaction time does not increase the amount of **8a** produced. Instead, increasing amounts of the *ethoxy* carbene derivative $Os_3\{1\text{-}\eta^1\text{-}C(OEt)Me\}\{1,2\text{-}\mu\text{-}H;1,2\text{-}\mu\text{-}O{=}C(Me)\}(CO)_9$ (**8b**) are obtained in yields approaching 10% in 70 h. Formation of this product results from the *trans*-alkylation reaction between $CH_3OSO_2CF_3$ and the

† The cluster hydrogen is removed as a proton in the reaction of hydrido-cluster complexes with H^-.[17(d)]

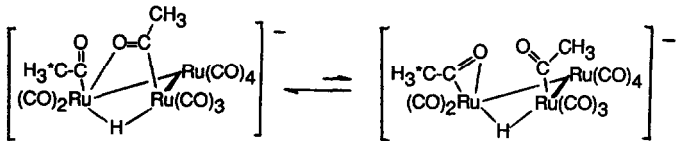

η^1,μ-[12]$^-$ η^2,η^1-[12]$^-$

Scheme 5.

diethylether.[9] When [Li][**10**] is alkylated directly with ethyl triflate, **8b** is obtained in 80% yield (48 h reaction time). In these reaction sequences, the minor by-product is the bromide complex $Os_3\{1,2\text{-}\mu\text{-Br};1,2\text{-}\mu\text{-O=C(Me)}\}(CO)_{10}$ (**7**, X = Br), arising from reaction of LiBr originating in the LiMe solution.

Titration of **5** with LiC_6H_5 in diethylether at −30°C produces a solution of [Li][**10b**], see Scheme 4. Alkylation at 25°C with a slight excess of $EtOSO_2CF_3$ requires 108 h to form $Os_3\{1\text{-}\eta^1\text{-C(OEt)}C_6H_5\}\{1,2\text{-}\mu\text{-H};1,2\text{-}\mu\text{-O=C(Me)}\}(CO)_9$ (**8c**) in 42% yield. Again, a minor amount of **7** (8%) is obtained.

O-alkylation of the salts Li[**10**] in diethylether contrasts the chemistry of iron acylates,† which undergo alkylation at the metal centre with this combination of solvent and counter ion. A long reaction time and/or excess of reagent is usually required for the alkylation of cluster anions.[8(b),13] This is presumably due to delocalization of charge on the cluster framework.

THE FISCHER REACTION SEQUENCE ON $Ru_3\{\mu\text{-H},\mu\text{-O=C(CH}_3)\}(CO)_{10}$ (11)

Titration of **11** with $LiCH_3$ in diethylether at −30°C leads to its instantaneous conversion to $[Li][Ru_3\{\eta^1\text{-C(O)CH}_3\}\{\mu\text{-H},\mu\text{-O=C(CH}_3)\}(CO)_9]$ ([Li][**12**]). Complete spectroscopic data for this anion have recently been published;[19] two distinct methyl resonances are seen in [**12**]$^-$, indicating that the two different types of acyl group do not exchange on the NMR time scale; experiments with ^{13}C and deuterium labelled complexes (mentioned below) indicate that there is no exchange at longer periods as well. Such exchange would require conversion of the μ-acyl group in the η^1,μ-isomer to an η^1-acyl group, as shown in Scheme 5. However, the coordinative unsaturation thus created must draw the original η^1-acyl group into η^2-bonding, cf. $Ru(PPh_3)_2(I)\{\eta^2\text{-C(O)Me}\}$.[20] The η^2,η^1-tautomer of the bis-acyl anion would explain the non-interconversion of the two acyl groups, and could also account for variability in O-alkylation observed in the anions [**12**]$^-$ R = Ph, or CMe_3, as discussed below.

It should be noted that despite the thermodynamic acidity of cluster-bonded hydrogen atoms,[17] these prove to be kinetically slow to remove, as also observed for the hydrido triosmium complex **5**. By contrast, *only deprotonation is observed* in the treatment of **11** with $LiCH_3$ at 25°C, to give the salt $[Li][Ru_3\{\mu\text{-O=C(CH}_3)\}(CO)_{10}]$.[19]

Alkylation of [Li][**12**] with $C_2H_5OSO_2CF_3$ at 25°C leads, after 48 h, to $Ru_3\{\mu\text{-H}\}_2\{\eta^2,\mu_3\text{-C(OEt)=C(H)}\}(CO)_9$ (**13**) in 80% yield; acetaldehyde is obtained as a by-product; this is illustrated in Scheme 6 for isotopically labelled material, discussed below.

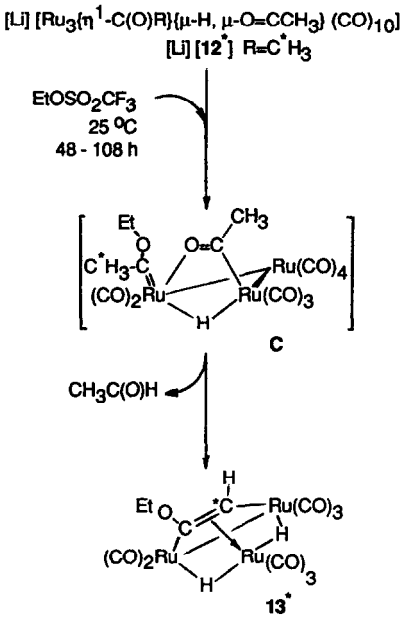

Scheme 6.

† O-alkylation has been found to occur in special systems where the acylate complexes are phosphine substituted,[18(a)] or where the acylate contains a C_6Cl_5, C_6F_5 or $N(Me)_2$ group,[18(b)] or where HmPA is utilized as a cosolvent.[18(c)]

Compound **13** was characterized by spectroscopic means, as a heteroatom substituted homologue of ethyne complexes earlier observed in the reaction of olefines,[21]† or acetylenes[23] with $Ru_3(CO)_{12}$. The structure of a close analogue, $Ru_3\{\mu\text{-}H\}_2\{\eta^2,\mu_3\text{-}C(OMe)\text{=}C(OMe)\}(CO)_9$ (isolated as one of the products in the hydrogenation of $Ru_3\{\mu\text{-}H,\eta^3,\mu_3\text{-}C(H)C(H)C(OMe)\}(CO)_9$) has been reported.[24]

Using $Li^{13}CH_3$ in the reaction with **11** gives rise to the regiospecifically ^{13}C-labelled product, $Ru_3\{\mu\text{-}H\}_2\{\eta^2\mu_3\text{-}C(OEt)\text{=}^{13}C(H)\}(CO)_9$ (***13**), see Scheme 6. The regiospecificity of ^{13}C in this product establishes that the non-exchange of acyl groups observed in the NMR of $[\mathbf{12}]^-$,[19] persists over a longer time frame, and is also consistent with the regiospecific alkylation shown in intermediate **C** in Scheme 6. The regiospecificity indicated in Scheme 6 has been confirmed in two other experiments.[19] In the first of these, regiospecifically labelled starting material (**11**-^{13}**C**) [see eq. (2)] is synthesized from $Ru_3(CO)_{12}$ and $Li^{13}CH_3$. When this is treated with unlabelled $LiCH_3$, followed by alkylation, the trinuclear product $Ru_3\{\mu\text{-}H\}_2\{\eta^2\mu_3\text{-}C(OEt)\text{=}C(H)\}(CO)_9$ (**13**) is obtained containing no ^{13}C incorporation.

$$Ru_3\{\mu\text{-}H,\mu\text{-}O\text{=}C(^{13}CH_3)\}(CO)_{10} \quad \mathbf{11}\text{-}^{13}\mathbf{C}$$

$$\xrightarrow[\text{(ii) } EtOSO_2CF_3]{\text{(i) } LiCH_3} \mathbf{13} + {}^{13}CH_3C(O)H \quad (2)$$

$$Ru_3\{\mu\text{-}H,\mu\text{-}O\text{=}C(CD_3)\}(CO)_{10} \quad \mathbf{11}\text{-}\mathbf{CD_3}$$

$$\xrightarrow[\text{(ii) } EtOSO_2CF_3]{\text{(i) } LiCH_3} \mathbf{13} + CD_3C(O)H. \quad (3)$$

Similarly, starting with **11**-$\mathbf{CD_3}$ [see eq. (3)] there is no deuterium incorporation into the triruthenium product.[19]

EFFECT OF CO

Under an atmosphere of CO, acetaldehyde is still eliminated from the initial alkylation product but oxidative addition is temporarily *prevented*; IR indicates the presence of a new complex, presumably $Ru_3\{C(OEt)CH_3\}(CO)_{11}$. This has eluded characterization owing to its rapid conversion to **13** under conditions attempted for its isolation or purification;[19] removal of the CO above a solution of the new complex results in its rapid conversion to **13**. Addition of excess triphenylphosphine to a solution of the new complex results in the instantaneous formation of $Ru_3(CO)_9\{P(C_6H_5)_3\}_3$.[25]

USE OF LiPh OR $LiCMe_3$ TO INITIATE THE FISCHER REACTION SEQUENCE

Reaction of **11** with other organo-lithium reagents, followed by alkylation with $C_2H_5OSO_2CF_3$, is shown in Scheme 7. These routes also give **13** along with the corresponding aldehyde RC(O)H. This suggests intermediate **D** in Scheme 7, in contrast to intermediate **C** in Scheme 6, arising perhaps through alkylation of the tautomer η^2,η^1-$[\mathbf{12}]^-$ (Scheme 5). The phenacyl or *t*-butyl-acyl groups ($RC(O)^-$, R = Ph or CMe_3) of η^1,μ-$[\mathbf{12}]^-$ (Scheme 5) must somehow be deactivated towards O-alkylation. In the case of the *t*-butyl derivative, it would be steric hindrance, while in the phenacyl anion it would be due to deactivation of the oxygen atom by the phenyl group. For related reports where similar considerations of an η^1-form for a coordinated acyl group may be of importance, see the O-alkylation of $[Fe_3\{\mu_3\text{-}O\text{=}CMe\}(CO)_9^-]$,[8(b)] or the protonation of a μ-acyl group in $Cp_2Zr(\eta^2\text{-}O\text{=}CMe)Mo(CO)_3Cp$.[26]

ABSENCE OF H/D EXCHANGE IN DOUBLE C—H OXIDATIVE ADDITION PRODUCTS

The deuterium labelling experiment described in eq. (3) above indicates that there is no scrambling between cluster-bonded hydrogen atoms formed in the double oxidative addition and the eliminated aldehyde. The aldehyde must be formed and elim-

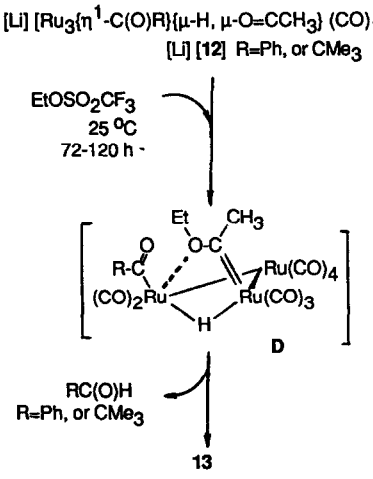

Scheme 7.

† For a review of other cluster complexes of these and related fragments see ref. 22.

inated in a step *preceding* the double oxidative addition.

ISOLATION AND CHARACTERIZATION OF $Ru_3\{\mu\text{-}H\}_2\{\eta^2,\mu_3\text{-}C(OEt)NMeC(H)\}(CO)_9$ (14)

Substitution of $HNMe_2$ for RLi in the Fischer sequence on **11** gives deep orange crystals of **14** in 45% yield, see Scheme 8. The structure shown for **14** is consistent with a variety of spectroscopic data.[19] An intermediate like **C** in Scheme 6 containing the $\{\eta^1\text{-}C(NMe_2)(OEt)\}$ carbene group must be traversed.

COMPETITION BETWEEN THE DOUBLE C—H OXIDATIVE ADDITION PROCESS AND EXTERNAL REAGENTS

Aromatic hydrocarbons

The alkylation of [Li][**12**] was carried out in the presence of C_6H_5F or $C_6H_5CF_3$ to see whether C—H activation of these could compete with the *intramolecular* double oxidative addition, to compare with studies on mono-nuclear complexes,[27] in which it is observed that certain intramolecular C—H oxidative additions are *slower* than C—H addition of an external hydrocarbon. In the competition experiments, the aromatic hydrocarbons are added just before alkylation of $[\mathbf{12}]^-$; IR spectra taken at various intervals show the absorptions of the anion being replaced by those of **13**, with no bands of any other compounds evident. The same results are obtained in the presence of trifluorotoluene.[19]

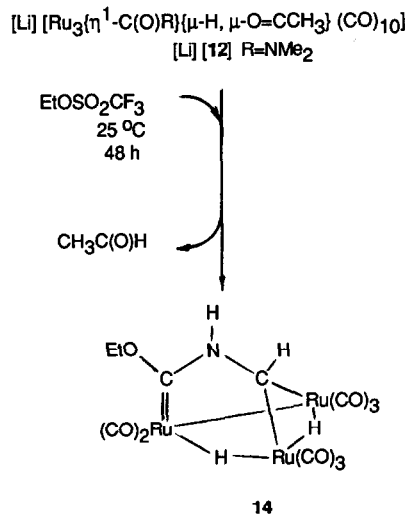

Scheme 8.

CONCLUSION

A Fischer carbene group can be constructed on edge double-bridged $\{\mu\text{-}H,\mu\text{-}O{=}C(Me)\}$ triosmium complexes. The same reaction sequence on triruthenium complexes undoubtedly leads to analogous but unstable complexes.

Products isolated in the triruthenium system must derive from further transformations on the complexes first formed in the Fischer reaction sequence. These transformations involve reductive elimination of an aldehyde (an overall four-electron donor in its separate precursor parts), followed by the double oxidative addition of a C-methyl of a Fischer carbene group. *Both of these processes occur at the unprecedented mild temperature of* 25°C. There are many examples of double oxidative addition products, but all have been formed at significantly higher temperatures. For example, trinuclear reaction intermediates containing double oxidatively added groups are postulated in the H/D exchange in amines catalysed by $Ru_3(CO)_{12}$ and $Rh_6(CO)_{16}$ at 150°C.[28] Another example of double oxidative addition is the complex $Os_3\{\mu\text{-}H\}_3\{\mu_3\text{-}C(H)\}(CO)_9$, obtained in the thermolysis of $Os_3\{\mu\text{-}H,\mu\text{-}O{=}C(CH_3)\}(CO)_9$ or $Os_3\{\mu\text{-}H,\mu\text{-}O(CH{=}CH_2)\}(CO)_9$ at 150°C,[29(a)] or in the thermolysis of $Os_3\{\mu\text{-}H,\mu\text{-}CH_3\}(CO)_{10}$ at 100°C.[29(b)] In this same vein, the complex $Os_3\{\mu\text{-}H\}_2\{\eta^2\mu_3\text{-}C(R)P(R')_2\}(CO)_9$ is obtained in the thermolysis of $Os_3(CO)_{11}P(R')_3$ at 150°C.[29(c)]

The higher temperatures required to achieve coordinative unsaturation on the metal cluster complexes in these other examples, masked the temperature at which double oxidative additions may occur, which in this work are shown to take place at ambient temperature. These results provide clues to two other observations in the literature. Firstly, to the extensive transformation reported in isolation of the complex $Ru_3\{\mu\text{-}H,\mu,\eta^3\text{-}C(Ph){-}C_6H_4\}(CO)_9$,[30] from the reaction of $Ru_3(CO)_{12}$ with LiPh, and secondly, to the dehydrogenation of triethyl amine by $Os_3(CO)_{10}(NCCH_3)_2$ leading to $HOs_3\{\mu\text{-}^-CHCH{=}^+NEt_2\}(CO)_{10}$ in refluxing benzene.[31]

It is also significant that oxidative addition in the triruthenium system is *prevented* under an atmosphere of CO. The coordinatively unsaturated intermediate(s) formed by the loss of the aldehyde can obviously be intercepted by this nucleophile, although *not* by the two aromatic hydrocarbons tested (C_6H_5X, X = F or CF_3). The rate of the internal oxidative additions observed must thus fall somewhere between the rate of attack by these two types of external reagents.

Acknowledgement—This work was supported by a grant from the National Science Foundation (CHE 84-05517).

REFERENCES

1. (a) C. M. Jensen, T. J. Lynch, C. B. Knobler and H. D. Kaesz, *J. Am. Chem. Soc.* 1982, **104**, 4679; (b) C. M. Jensen, C. B. Knobler and H. D. Kaesz, *J. Am. Chem. Soc.* 1984, **106**, 5926.
2. E. O. Fischer and A. Maasböl, *Angew. Chem. Int. Ed. Eng.* 1964, **3**, 580.
3. (a) E. O. Fischer, E. Offhaus and D. Nöthe, *Chem. Ber.* 1972, **105**, 3027; (b) C. P. Casey, C. R. Cyr, R. L. Anderson and D. F. Marten, *J. Am. Chem. Soc.* 1975, **97**, 3053; (c) E. W. Post and K. L. Waters, *Inorg. Chim. Acta.* 1978, **26**, 29; (d) E. O. Fischer, T. L. Lindner, H. Fischer, G. Huttner and P. Friedrich, *Z. Naturforsch. Teil B* 1977, **32**, 648.
4. T. V. Ashworth, M. Berry, J. A. K. Howard, M. Laguna and F. G. A. Stone, *J. Chem. Soc., Dalton Trans.* 1980, 1615.
5. A. Benoit, J.-Y. Le Marouille, C. Mahe, H. Patin, *J. Organomet. Chem.* 1982, **233**, C51.
6. A. Mayr, Y. C. Lin, N. M. Boag and H. D. Kaesz, *Inorg. Chem.* 1982, **21**, 1704.
7. C. M. Jensen, Y.-J. Chen and H. D. Kaesz, *J. Am. Chem. Soc.* 1984, **106**, 4046.
8. (a) A. W. Parkins, E. O. Fischer, G. Huttner and D. Regler, *Angew. Chem.* 1970, **82**, 635; (b) W. Wong, K. W. Chiu, G. Wilkinson, A. M. R. Galas, M. Thornton-Pett and M. B. Hursthouse, *J. Chem. Soc., Dalton Trans.* 1983, 1557.
9. T. Gramstad and R. N. Haszeldine, *J. Chem. Soc.* 1956, 173.
10. (a) M. P. Cooke, *J. Am. Chem. Soc.* 1970, **92**, 6080; (b) E. O. Fischer and A. Maasböl, *Chem. Ber.* 1967, **100**, 2444.
11. H. Meerwein, D. Delfs and H. Morschel, *Angew. Chem.* 1960, **74**, 927.
12. (a) J. P. Collman, R. K. Rothrok, R. G. Finke and F. Rose-Munch, *J. Am. Chem. Soc.* 1977, **99**, 7381.
13. P. D. Gavens and M. J. Mays, *J. Organomet. Chem.* 1978, **162**, 389.
14. J. B. Keister, *J. Chem. Soc., Chem. Commun.* 1979, 214.
15. W.-Y. Yeh, J. R. Shapley, J. W. Ziller and M. R. Churchill, *Organometallics* 1986, **5**, 1757.
16. C. G. Kreiter, *Angew. Chem.* 1968, **80**, 402.
17. (a) B. Fontal, Ph.D. Thesis, University of California at Los Angeles (1969); (b) H. D. Kaesz and R. B. Saillant, *Chem. Rev.* 1972, **72**, 231; (c) R. G. Pearson and P. C. Ford, *Comments Inorg. Chem.* 1982, **1**, 279; (d) J. C. Bricker, C. C. Nagel and S. G. Shore, *J. Am. Chem. Soc.* 1982, **104**, 1444.
18. (a) H. L. Conder and M. Y. Darensbourg, *Inorg. Chem.* 1974, **13**, 506; (b) E. O. Fischer, H. J. Beck, C. G. Kreiter, J. Lynch, J. Müller and H. Winkler, *Chem. Ber.* 1972, **105**, 162; (c) M. F. Semmelhack and R. Tamura, *J. Am. Chem. Soc.* 1983, **105**, 4099.
19. C. M. Jensen and H. D. Kaesz, *J. Organomet. Chem.* 1987, **330**, 133.
20. W. R. Roper, G. E. Taylor, J. M. Waters and L. J. Wright, *J. Organomet. Chem.* 1979, **182**, C46.
21. A. J. Deeming and M. Underhill, *J. Chem. Soc., Dalton Trans* 1974, 1419.
22. E. Sappa, A. Tiripicchio and P. Braunstein, *Chem. Rev.* 1983, **83**, 203.
23. G. Cetini, O. Gambino, E. Sappa and M. Valle, *J. Organomet. Chem.* 1969, **17**, 437.
24. M. R. Churchill, J. C. Fettinger, J. B. Keister, R. F. See and J. W. Ziller, *Organometallics* 1985, **4**, 2112.
25. M. I. Bruce, J. G. Matisons and B. K. Nicholson, *J. Organomet. Chem.* 1983, **247**, 321.
26. B. Longato, J. R. Norton, J. C. Huffman, J. A. Marsella and K. G. Caulton, *J. Am. Chem. Soc.* 1981, **103**, 209.
27. W. D. Jones and F. J. Feher, *J. Am. Chem. Soc.* 1982, **104**, 4240.
28. (a) R. M. Laine, D. W. Thomas, L. W. Cary and S. E. Buttrill, *J. Am. Chem. Soc.* 1978, **100**, 6527; (b) Y. Shvo, D. W. Thomas and R. M. Laine, *J. Am. Chem. Soc.* 1981, **103**, 2461.
29. (a) A. J. Deeming and K. A. Azam, *J. Mol. Catal.* 1977, **3**, 207; (b) R. B. Calvert and J. R. Shapley, *J. Am. Chem. Soc.* 1977, **99**, 5225; (c) A. J. Deeming and M. Underhill, *J. Chem. Soc., Dalton Trans.* 1973, 2727.
30. A. W. Parkins, E. O. Fischer, G. Huttner and D. Regler, *Angew. Chem.* 1970, **82**, 635.
31. J. R. Shapley, M. Tachikawa, M. R. Churchill and R. A. Lashewycz, *J. Organomet. Chem.* 1978, **162**, C39.

Polyhedron Vol. 7, No. 10/11, pp. 1045–1052, 1988
Printed in Great Britain

0277–5387/88 $3.00+.00
© 1988 Pergamon Press plc

CARBON-13 NMR SHIFTS OF BRIDGING ACETYLIDES IN POLYNUCLEAR COMPLEXES

ARTHUR J. CARTY,* ANDREW A. CHERKAS and LESLIE H. RANDALL

Guelph-Waterloo Centre for Graduate Work in Chemistry, Waterloo Campus, University of Waterloo, Waterloo, Ontario, Canada N2L 3G1

(*Accepted* 5 *November* 1987)

Abstract—Carbon-13 NMR data for a range of iron group polynuclear acetylide complexes with μ_2-η^2, μ_3-η^2 and μ_4-η^2 alkynyl groups are presented. For doubly bridging μ_2-η^2-acetylides of Fe, Ru and Os, the C_α resonance lies in the range 65–110 ppm downfield of TMS, while C_β shifts cover the range 90–110 ppm. In μ_3-η^2-complexes C_α lies in the region 115–220 ppm and is always downfield of C_β (43–153 ppm). For μ_4-η^2-acetylides, C_α is also downfield of C_β with values lying in the ranges 185–230 and 91–165 ppm, respectively. Comments on the most appropriate experimental parameters for the observation of ^{13}C spectra of acetylides and techniques for assigning resonances are included.

Among C_2 hydrocarbyl groups the acetylide or alkynyl ligand -C≡CR occupies a unique position. It has the highest degree of unsaturation and the greatest versatility as a bridging ligand, being capable of functioning as a one, three or five electron donor when considered as a radical. For reviews on acetylide chemistry see ref. 1(a–c). Examples of coordination modes illustrating these donor characteristics are shown in Scheme 1. The organometallic chemistry of the alkynyl group is thus characterized by its structural variety, by the diversity of its reaction chemistry and utility as a source of other C_2 hydrocarbyls including alkenyls, vinylidenes, alkylidenes, alkylidynes and alkyls (Scheme 2).†

Although a large number of mono- and polynuclear alkynyl complexes have been characterized,† ^{13}C NMR data for bridging alkynyl carbon atoms are sparse, particularly in comparison with ^{13}C shifts for other hydrocarbyl ligands. There is an obvious reason for this lack of data. Alkynyl *sp*-hybridized carbon atoms are generally assumed to have long relaxation times and Nuclear Overhauser Enhancement effects are small or negligible. Thus ^{13}C resonances of alkynyl carbon atoms are often difficult to detect without long accumulation times. One solution to this problem is ^{13}C isotopic substitution but this is expensive and may be time consuming. Another difficulty even when good quality ^{13}C NMR spectra are available, is the assignment of ^{13}C resonances to the α- and β-carbons of the -C_α≡C_βR group. A lack of systematic information on ^{13}C shifts and their cor-

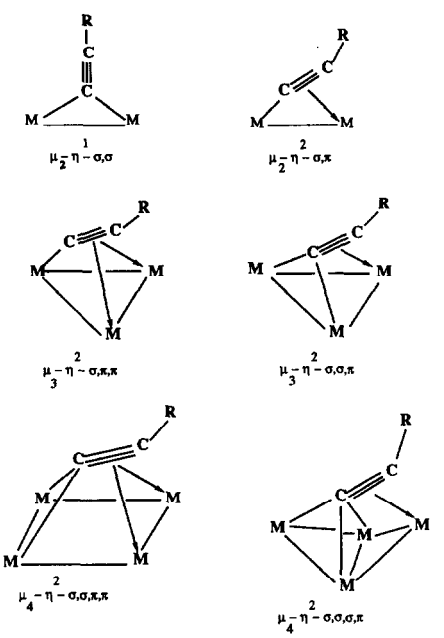

Scheme 1. Bonding modes of acetylides.

*Author to whom correspondence should be addressed.

† For some recent work on acetylide chemistry without acetylide ^{13}C NMR data see ref. 1(d–o). Work with acetylides which does include ^{13}C NMR data is included in refs 2–14.

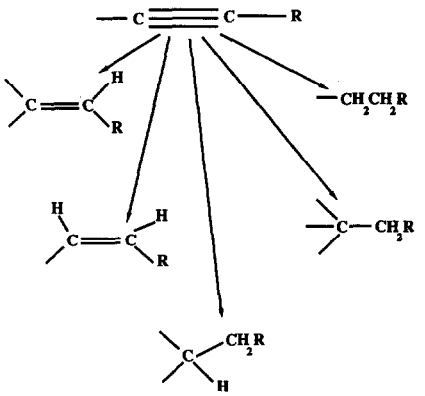

Scheme 2.

relation with the structural parameters and bonding mode is a serious shortcoming in this regard.

In this study we set out to: (i) expand the data available for ^{13}C shifts in polynuclear acetylides; (ii) describe some experimental techniques useful in assigning ^{13}C resonances; (iii) correlate the chemical shifts for alkynyl carbon atoms, with the type of bonding mode; (iv) assess the influence of the metal atom on ^{13}C shifts down a triad.

EXPERIMENTAL

The compounds for which ^{13}C NMR parameters are reported herein were synthesized and characterized as described elsewhere. References are included in the appropriate tables.

NMR techniques

The ^{13}C NMR spectra were obtained on Bruker WH-400, AM-250 or AC-200 spectrometers and were referenced internally to the solvent ($CDCl_3$ = 77.0 relative to TMS). Typically, 100–200 mg of each complex was used to obtain the ^{13}C NMR spectra. The best results were obtained from the AC-200 spectrometer which is equipped with an Aspect 3000 computer. A digitization of 64K data points was generally used to obtain satisfactory line shapes (Hz/pt = 0.43). The optimum conditions for data accumulation were a relaxation delay of 7 s with a pulse angle of 40° (3.5 μs). A more complete discussion of the optimization of pulsed Fourier transform experiments can be found in ref. 15. Spectra were recorded at 300 K under temperature controlled conditions and samples were contained in 5 mm tubes. Total acquisition times were typically in the range of 4–8 h, with the most difficult sample [$Ru_5(CO)_{13}(\mu_4$-η^2-C≡C-*i*-Pr)(μ-PPh_2)] requiring a

RESULTS AND DISCUSSION

Assignment of ^{13}C resonances for acetylides

Acetylide resonances, like ^{13}CO metal carbonyl signals are generally of low intensity since quaternary carbon atoms typically exhibit longer relaxation times than protonated carbons and exhibit little Nuclear Overhauser Enhancement. However, it should be stressed that to our knowledge no relaxation studies of transition metal coordinated acetylenic carbon atoms have yet been published. In order to obtain useful ^{13}C acetylide spectra, acquisition parameters must be optimized or alternatively enriched samples used. The former entails the use of a suitable relaxation delay and a pulse angle of less than 90°. We have found that a relaxation delay of 7 s and a pulse angle of approximately 40° gave optimal results in our hands.

The presence of heteronuclear coupling reduces the intensities of ^{13}C signals; however this coupling has proved to be advantageous for peak assignments. In phosphido-bridged complexes such as $M_2(CO)_6(\mu_2$-η^2-C≡CR)(μ-PPh_2),[2] the resonance with the larger phosphorus–carbon coupling has been empirically assigned to the alpha carbon atom (Fig. 1).[2] To unequivocally assign the C_α and C_β resonances we undertook a series of proton coupled experiments. The results for $Ru_2(CO)_6(\mu_2$-η^2-C≡C-*i*-Pr)(μ-PPh_2) are shown in Fig. 2. The fully coupled spectrum shows a complex pattern consisting of a doublet of doublets of septets for C_β and a doublet of doublets for C_α. In general, we have observed that remote coupling to proton nuclei four bonds removed does not occur. Thus for R = $C(CH_3)_3$, the beta carbon is a doublet of decets while the alpha carbon resonance remains as a doublet uncoupled to any protons (Fig. 3). We have found that the *t*-butyl group in particular serves as a very useful probe for the assignment of ^{13}C resonances in alkynyl complexes since in the proton coupled spectra it is immediately evident from a comparison of intensities, which is the uncoupled C_α resonance.

μ_2-η^2-acetylides

The range of ^{13}C shifts for these edge bridging alkynyl groups is ~ 45 ppm. Comparison with the

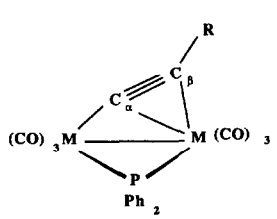

Fig. 1. Central core of $M_2(CO)_6(\mu_2$-η^2-C≡CR)(μ-PPh_2),

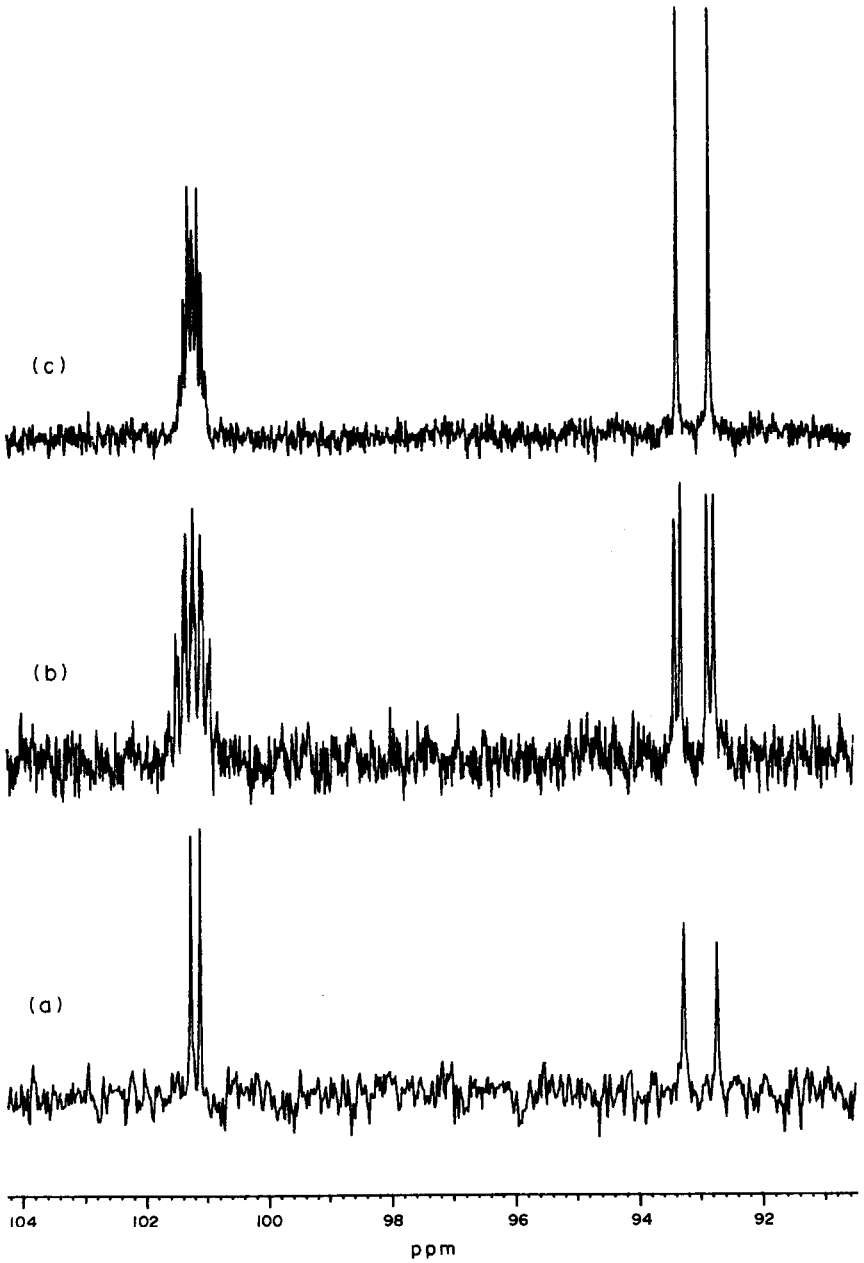

Fig. 2. $^{13}C\{^1H\}$ NMR spectra of the acetylide region of $Ru_2(CO)_6(\mu_2\text{-}\eta^2\text{-}C{\equiv}C\text{-}i\text{-}Pr)(\mu\text{-}PPh_2)$ under conditions of (a) broad band decoupling; (b) gated decoupling (fully proton coupled with NOE), and (c) selective proton decoupling (irradiation at the frequency of the methine proton, $CHMe_2$).

^{13}C shift scales for $\mu_3\text{-}\eta^2$- and $\mu_4\text{-}\eta^2$-groups (Scheme 3) shows that although there is some overlap particularly for C_β, the C_α resonance generally moves to lower field in the sequence $\mu_2\text{-}\eta^2 < \mu_3\text{-}\eta^2 < \mu_4\text{-}\eta^2$ as the number of metals interacting with the hydrocarbyl increases. Deshielding of C_α can probably be attributed to the development of a positive charge density on this atom due to coordination to electrophilic $M(CO)_n$ fragments.

The series $M_2(CO)_6(\mu_2\text{-}\eta^2\text{-}C{\equiv}CR)(\mu\text{-}PPh_2)$ (M = Fe, Ru, Os; R = Ph, *t*-Bu, *i*-Pr) **1** illustrates two effects (Table 1). (a) A metal effect on $\delta(^{13}C)$: generally C_α which is bound to two metals moves downfield in the order Fe > Ru > Os, while the position of the C_β resonance (C_β is coordinated to only one metal) remains relatively unchanged. (b) An effect of the R group: for the $\mu_2\text{-}\eta^2$-acetylides listed in Table 1, C_α is at higher field than C_β except in the cases of M = Fe, Ru; R = Ph, where the order is reversed. This suggests that the electronic properties of the R group have an influence on the ^{13}C NMR shifts (see also ref. 3). The coupling

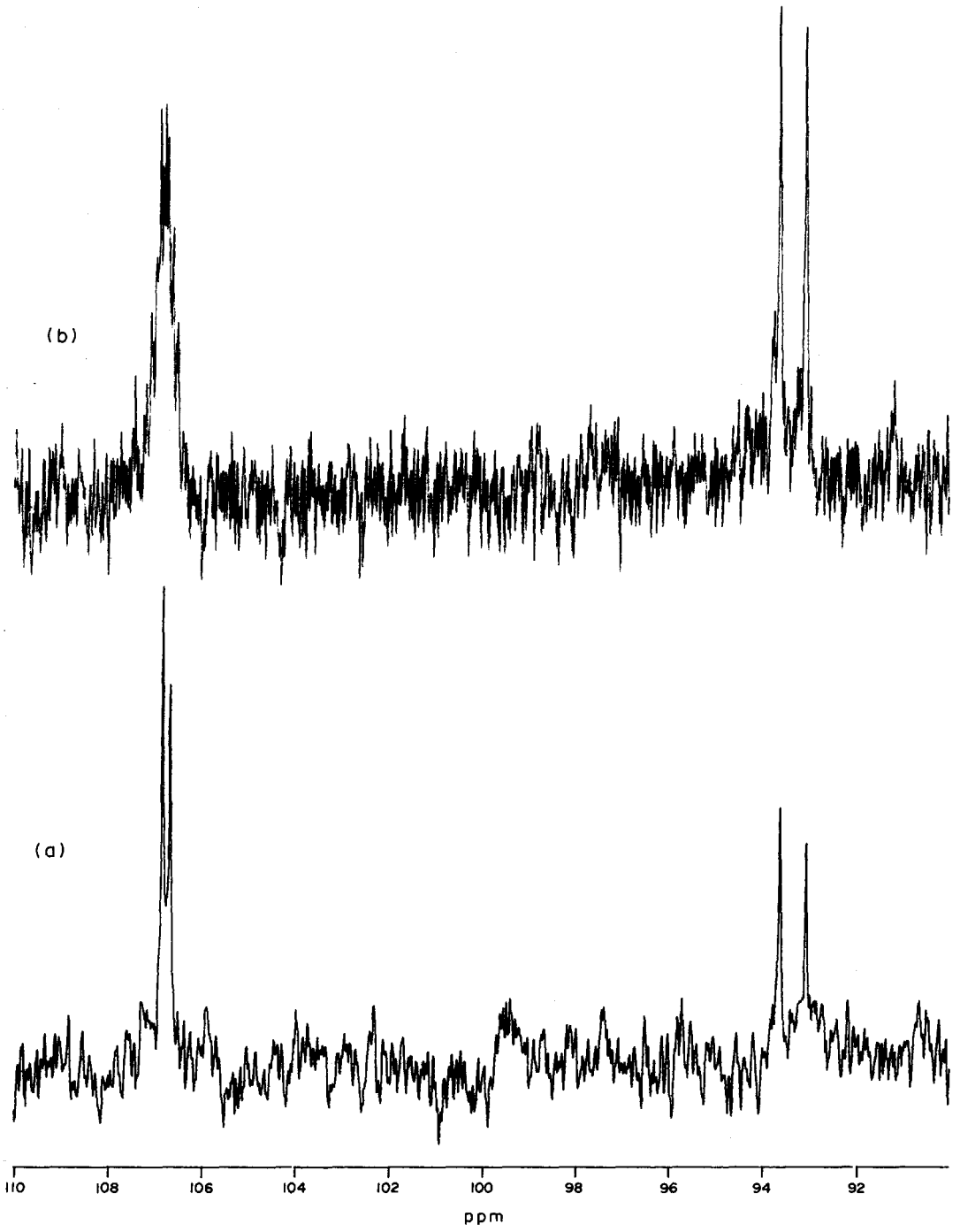

Fig. 3. $^{13}C\ \{^1H\}$ NMR spectra of the acetylide region of $Ru_2(CO)_6(\mu_2\text{-}\eta^2\text{-}C{\equiv}C\text{-}t\text{-}Bu)(\mu\text{-}PPh_2)$: (a) broad band decoupling; (b) gated decoupling.

constants $J_{^{31}P-^{13}C}$ are greater for C_α than for C_β in each case, with the values of J_{P-C_α} decreasing in the sequence Fe > Ru > Os. The $J_{^{31}P-^{13}C_\beta}$ parameters change relatively little down the triad.

Three trinuclear complexes $M_3(CO)_7(\mu_2\text{-}\eta^2\text{-}C{\equiv}CR)_2(\mu\text{-}PPh_2)_2$ (M = Ru, R = *i*-Pr; M = Os, R = Ph, *i*-Pr) of type **2** with edge bridging alkynyl ligands, have been characterized. Assignments

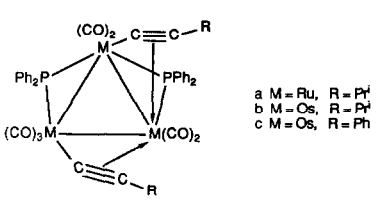

2

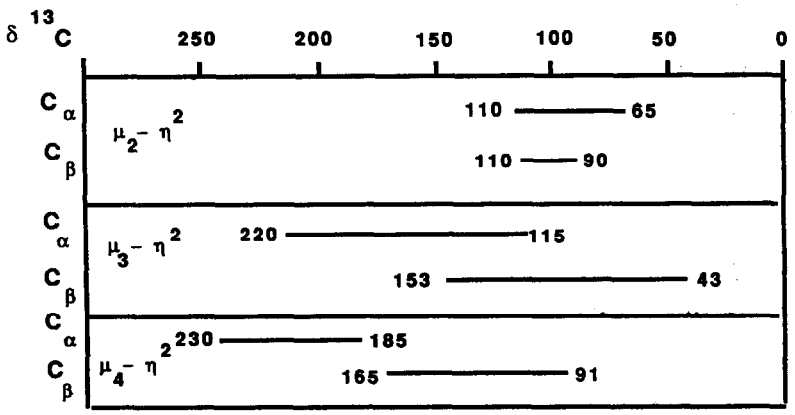

Scheme 3. Range of ^{13}C resonances for bridging acetylides.

(Table 2) are based on $^{31}P—^{13}C$ coupling constants. A similar pattern of chemical shifts to those in type **1** complexes is seen with C_α at higher field than C_β. However the $J_{^{31}P—^{13}C}$ values are significantly smaller in the trinuclear compounds.

Two other complexes which provide valuable new data are the phosphinoalkyne substituted binuclear compound $Ru_2(CO)_5(\mu_2\text{-}\eta^2\text{-}C{\equiv}C\text{-}t\text{-}Bu)(\mu\text{-}PPh_2)(Ph_2PC{\equiv}C\text{-}t\text{-}Bu)$ **3** and the triosmium

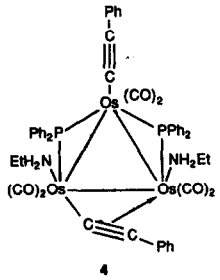

4

Table 1. Acetylide ^{13}C $\{^1H\}$ NMR resonances for $M_2(CO)_6(\mu_2\text{-}\eta^2\text{-}C{\equiv}CR)(\mu\text{-}PPh_2)$, (M = Fe, Ru, Os, R = Ph, *t*-Bu, *i*-Pr), (**1**). (Refs. 1(c), 2) in $CDCl_3$ at 50.3 MHz ($J_{^{31}P—^{13}C}$ in Hz)

M	R	C_α	$^2J_{^{31}P—^{13}C}$	C_β	$^2J_{^{31}P—^{13}C}$
Fe	Ph	110.0(d)	52.9	91.7(d)	7.7
Fe	*t*-Bu	97.7(d)	53.4	106.3(d)	8.0
Fe	*i*-Pr	98.2(d)	52.7	101.0(d)	7.7
Ru	Ph	105.4(d)	27.5	92.7(d)	7.7
Ru	*t*-Bu	93.4(d)	27.8	106.7(d)	7.8
Ru	*i*-Pr	93.0(d)	27.4	101.2(d)	8.0
Os	Ph	86.0(d)	19.8	90.4(d)	9.3
Os	*t*-Bu	73.1(d)	19.5	103.7(d)	9.5
Os	*i*-Pr	72.5(d)	18.9	97.2(d)	9.5

Table 2. Acetylide ^{13}C $\{^1H\}$ NMR resonances for $M_3(CO)_7(\mu_2\text{-}\eta^2\text{-}C{\equiv}CR)_2(\mu_2\text{-}PPh_2)_2$, (M = Ru, R = *i*-Pr (**2a**), M = Os, R = *i*-Pr (**2b**), M = Os, R = Ph (**2c**), in $CDCl_3$, 50.3 MHz ($^2J_{^{31}P—^{13}C}$ in Hz) (ref. 3)

Compound	C_α	$^2J_{^{31}P—^{13}C}$	$^2J_{^{31}P—^{13}C}$	C_β	$^2J_{^{31}P—^{13}C}$	$^2J_{^{31}P—^{13}C}$
2a	85.6(dd)	16.0	14.0	101.0(d)	6.4	—
	100.2(dd)	7.4	2.4	109.8(d)	< 5	—
2b	66.1(dd)	15.9	13.3	80.5(d)	4.5	—
	97.7(dd)	7.4	3.6	107.7(dd)	4.7	2.1
2c	74.9(dd)	16.2	12.9	96.5(d)	5.4	—
	93.7(dd)	8.4	3.0	105.7(d)	< 5	—

Table 3. Acetylide ^{13}C $\{^1H\}$ resonances for $Ru_2(CO)_5(Ph_2PC{\equiv}CBu^t)(\mu_2\text{-}\eta^2\text{-}C{\equiv}CBu^t)(\mu\text{-}PPh_2)$ (**3**) (ref. 4) and $Os_3(CO)_6(\mu_2\text{-}\eta^2\text{-}C{\equiv}CPh)(\eta^1\text{-}C{\equiv}CPh)(\mu\text{-}PPh_2)_2(NEtH_2)_2$ (**4**) (ref. 3) in $CDCl_3$, 50.3 MHz ($J_{^{31}P-^{13}C}$ in Hz)

Compound	Acetylide	C_α	$J_{^{31}P-^{13}C}$	$J'_{^{31}P-^{13}C}$	C_β	$J_{^{31}P-^{13}C}$	$J'_{^{31}P-^{13}C}$
3a	—PC≡CBu^t(trans)	75.1(d)	86.2	—	120.7(dd)	10.8	1.0
b	—PC≡CBu^t(cis)	75.1(d)	86.2	—	117.6(d)	11.9	—
a	μ_2-η^2-(trans)	104.9(dd)	26.4	17.7	107.6(dd)	8.5	2.9
b	μ_2-η^2-(cis)	98.3(dd)	29.0	6.0	106.3(dd)	8.0	< 2
4	μ_2-η^2	98.9(t)	22.4	22.4	105.7(t)	12.3	12.3
	η^1	101.1(t)	12.0	12.0	109.1(s)	—	—

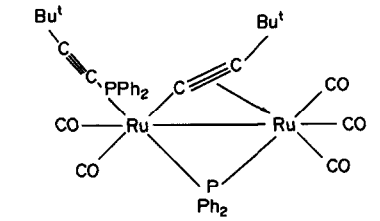

3a

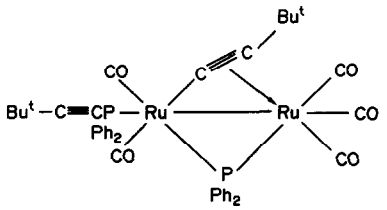

3b

Fig. 4. The two isomers of $Ru_2(CO)_5(Ph_2PC{\equiv}C\text{-}t\text{-}Bu)(\mu_2\text{-}\eta^2\text{-}C{\equiv}C\text{-}t\text{-}Bu)(\mu\text{-}PPh_2)$ **3a** ("trans"), **3b** ("cis").

species $Os_3(CO)_6(\mu_2\text{-}\eta^2\text{-}C{\equiv}CPh)(\eta^1\text{-}C{\equiv}CPh)(\mu\text{-}PPh_2)_2(NEtH_2)_2$ **4** (Table 3). In both of these complexes the acetylide ^{13}C resonances lie in the same region of the spectrum and pose a problem for assignments. For **3** an additional complication is the existence of *trans* and *cis* isomers **3a** and **3b** in which the phosphinoalkyne is respectively *trans* to the μ-PPh_2 and *cis* to the fluxional acetylide **3a** or *cis* to the μ-PPh_2 group and *cis* to the acetylide **3b** (Fig. 4). A doublet resonance due to C_α of the $Ph_2PC{\equiv}C\text{-}t\text{-}Bu$ ligand is readily recognized by virtue of a large $^1J_{^{31}P-^{13}C}$ of 86.2 Hz and the presence of isomers, with the *trans* species predominant is readily apparent from the number of ^{13}C peaks. Comparison with the ^{13}C spectrum of $Ru_2(CO)_6(\mu_2\text{-}\eta^2\text{-}C{\equiv}C\text{-}t\text{-}Bu)(\mu\text{-}PPh_2)$ shows that two sets of double doublets centred at 107.6 and 106.3 ppm lie close to the C_β peak position in the unsubstituted complex. These are attributed to C_β of the μ_2-η^2-acetylide in the *trans* and *cis* isomers **3a** and **3b**. The C_α resonances in **3a** and **3b** are assigned to double doublets at 104.9 and 98.3 ppm, respectively, with the former exhibiting the greater change compared to the parent. The *trans* isomer **3a** also has the largest (17.7 Hz) coupling to the phosphorus atom of the phosphinoalkyne.

Complex **4** provides a novel example, for a cluster compound, of a terminal η^1-bound alkynyl group. Here the phosphido bridges are respectively *cis* to the η^1-ligand and *trans* to the μ_2-η^2-acetylide. We attribute a singlet at 109.1 ppm to C_β, the uncoordinated atom of the η^1-acetylide and a resonance at 98.9 ppm with a $^2J_{^{31}P-^{13}C}$ value of 22.4 Hz, comparable to that in $Os_2(CO)_6(\mu_2\text{-}\eta^2\text{-}C{\equiv}CPh)(\mu\text{-}PPh_2)$ (19.8 Hz), to C_α of the μ_2-η^2-ligand. The remaining triplets were assigned on the basis of proton coupled spectra. It is worth noting here that η^1- and μ_2-η^2-alkynyl groups appear in the same spectral region.

μ_3-η^2-acetylides

Structurally these face bridging acetylides can be considered as "alkylidyne–carbides" in which a μ_3-CR unit and a bare carbide-like carbon atom occupy adjacent vertices in a skeletal framework. For example, the M_3C_2 framework of the 50-electron species $M_3(CO)_9(\mu_3\text{-}\eta^2\text{-}C{\equiv}C\text{-}i\text{-}Pr)(\mu\text{-}PPh_2)$ (M = Ru, Os) closely approximates an open-hinged butterfly arrangement of three metal atoms and an alkylidyne carbon, with a carbide-like carbon atom coordinated between the wings of the butterfly.[5] The "bare" acetylide carbon atom is thus four connected in these structures. Not surprisingly in view of the structural features, the C_α resonances in $Os_3(CO)_9(\mu_3\text{-}\eta^2\text{-}C{\equiv}CR)(\mu\text{-}PPh_2)$ (R = Ph, *t*-Bu, *i*-Pr) **5** [Table 4(a)] lie substantially downfield of the C_α shifts in the binuclear series $Os_2(CO)_6(\mu_2\text{-}\eta^2\text{-}C{\equiv}CR)(\mu\text{-}PPh_2)$. In each case C_α resonates at lower field than C_β. Moreover the C_β shifts are less positive (i.e. more upfield) than for the μ_2-η^2-complexes of the same acetylide. The net effect is a much greater

Table 4(a). Acetylide ^{13}C $\{^1H\}$ NMR resonances for $Os_3(CO)_9(\mu_3\text{-}\eta^2\text{-}C{\equiv}CR)(\mu\text{-}PPh_2)$, R = Ph (**5a**), *t*-Bu (**5b**), *i*-Pr (**5c**), (ref. 5), in $CDCl_3$ at 100 MHz ($^2J_{^{31}P-^{13}C}$ in Hz)

Compound	C_α	$^2J_{^{31}P-^{13}C}$	C_β	$^2J_{^{31}P-^{13}C}$
5a	125.1(d)	12.2	43.3(d)	9.1
5b	117.1(d)	11.7	59.5(d)	5.0
5c	116.8(d)	12.1	52.6(d)	7.0

Table 4(b). Acetylide ^{13}C $\{^1H\}$ NMR resonances for $M_3(CO)_9(\mu_3\text{-}\eta^2\text{-}C{\equiv}C\text{-}t\text{-}Bu)_2\{\mu\text{-}P(C{\equiv}C\text{-}t\text{-}Bu)_2\}$, M = Fe(**6a**), Ru(**6b**), Os(**6c**), (ref. 6), in $CDCl_3$ at 62.9 MHz ($J_{^{31}P-^{13}C}$ in Hz)

Compound	Acetylide	C_α	$J_{^{31}P-^{13}C}$	C_β	$J_{^{31}P-^{13}C}$
6a	$\mu_3\text{-}\eta^2$	147.6(d)	10.2	74.7(s)	—
	PC≡C-*t*-Bu	78.1(d)	obscured	114.9(d)	5.4
	PC≡C-*t*-Bu′	74.4(d)	79.0	110.2(d)	3.3
6b	$\mu_3\text{-}\eta^2$	134.5(d)	9.6	76.2(d)	7.5
	PC≡C-*t*-Bu	79.6(d)	68.2	112.5(d)	10.8
	PC≡C-*t*-Bu′	75.2(d)	75.8	107.6(d)	7.9
6c	$\mu_3\text{-}\eta^2$	116.6(d)	14.4	65.1(d)	7.3
	PC≡C-*t*-Bu	77.2(d)	131.5	111.3(d)	13.0
	PC≡C-*t*-Bu′	73.5(d)	103.2	107.0(d)	10.9

Table 5. $\mu_3\text{-}\eta^2$ ^{13}C $\{^1H\}$ NMR resonances for some other compounds

Compound	C_α	C_β	Ref.
$Ru_3(CO)_9(\mu_3\text{-}\eta^2\text{-}C{\equiv}C\text{-}i\text{-}Pr)(\mu\text{-}PPh_2)$	134.4(d) $^2J_{^{31}P-^{13}C}$ = 33.4 Hz	103.8(s)	1(c), 5
$(\mu\text{-}H)Ru_3(CO)_8[P(OEt)Ph_2](\mu_3\text{-}\eta^2\text{-}C{\equiv}C\text{-}t\text{-}Bu)$	165.7(s)	112.2(s)	1(c), 4
$(\mu\text{-}H)Ru_3(CO)_9(\mu_3\text{-}\eta^2\text{-}C{\equiv}C\text{-}t\text{-}Bu)$	164.2(s)	110.6(s)	7
$[Fe_3(CO)_9\{\mu_3\text{-}\eta^2\text{-}C{\equiv}COC(O)CH_3\}]^-$	172.9(s)	132.2(s)	8(a)
$[Fe_3(CO)_9(\mu_3\text{-}\eta^2\text{-}C{\equiv}CCH_3)]^-$	184.7(s)	99.5(s)	9
$Fe_2W(\mu_3\text{-}\eta^2\text{-}C{\equiv}CC_6H_4Me\text{-}4)(CO)_8(\eta^5\text{-}C_5H_5)$	172.9(s)	112.7(s)	10
$Fe_2W(\mu_3\text{-}\eta^2\text{-}C{\equiv}CMe)(CO)_8(\eta^5\text{-}C_5H_5)$	165.7(s)	108.3(s)	10
$Fe_2Mo(\mu_3\text{-}\eta^2\text{-}C{\equiv}CMe)(CO)_8(\eta^5\text{-}C_5H_5)$	181.8(s)	95.9(s)	10
$\{Fe_3(CO)_9(\mu_3\text{-}\eta^2\text{-}C{\equiv}COEt)\}^-$	160.9(s)	148.5(s)	8(b)
$\{Fe_3(CO)_9(\mu_3\text{-}\eta^2\text{-}C{\equiv}COMe)\}^-$	160.4(s)	147.6(s)	8(b)
$CpNiFe_2(CO)_6(\mu_3\text{-}\eta^2\text{-}C{\equiv}C\text{-}t\text{-}Bu)$	192.0(s)	141.0(s)	11
$CpNiFe_2(CO)_5(PPh_3)(\mu_3\text{-}\eta^2\text{-}C{\equiv}C\text{-}t\text{-}Bu)$	219.4(d)	136.2(d) $J_{^{31}P-^{13}C}$ = 43 Hz	11
$Cp_2W_2Fe(CO)_6(\mu_3\text{-}\eta^2\text{-}C{\equiv}CC_6H_4Me\text{-}4)$	168.5(s)	153.8(s)	12

chemical shift separation between the α- and β-carbon atoms than in the edge bridging cases.

A complete triad of alkynyl clusters $M_3(CO)_9(\mu_3\text{-}\eta^2\text{-}C{\equiv}C\text{-}t\text{-}Bu)\{\mu\text{-}P(C{\equiv}C\text{-}t\text{-}Bu)_2\}$ **6**, has recently been characterized. Similar trends in $\delta(^{13}C)$ are evident [Table 4(b)] with C_α downfield of C_β in all cases. A "metal-effect" on the C_α shifts is observed with an upfield shift in the sequence Fe < Ru < Os. Coupling constants $J_{^{31}P-^{13}C}$ between the phosphido bridge ^{31}P nucleus and C_α lie in the fairly narrow range 9.6–14.4 Hz for these compounds. Much larger $^1J_{^{31}P-^{13}C}$ couplings are observed for the alkynyl groups on the phosphido bridge.

Table 5 lists a number of other ^{13}C shifts for homo- and heteronuclear $\mu_3\text{-}\eta^2$-acetylides. Assignment of C_α and C_β resonances in many of these cases appears to have been largely empirical although for $PPN[Fe_3(CO)_9(CCOC(O)CH_3)]$ ^{13}C isotopic labelling confirmed that the $CCOC(O)CH_3$ resonance was downfield of the substituted carbon atom.[8] In

Table 6. $^{13}C\{^1H\}$ NMR acetylide shifts for μ_4-η^2-acetylides ($J_{^{31}P-^{13}C}$ in Hz)

Compound	C_α	$J_{^{31}P-^{13}C}$	C_β	$J_{^{31}P-^{13}C}$	Ref.
$Ru_5(CO)_{13}(\mu_4\text{-}\eta^2\text{-}C{\equiv}C\text{-}i\text{-}Pr)(\mu\text{-}PPh_2)$	218.8(d)	2.7	164.0(d)	3.0	13
$(\mu\text{-}H)Ru_4(CO)_{10}(\mu_3\text{-}OH)(\mu_4\text{-}\eta^2\text{-}C{\equiv}C\text{-}t\text{-}Bu)(\mu\text{-}PPh_2)$	226.9(d)	12.3	118.6(s)	—	4
$(\eta^5\text{-}C_5H_5)_2Ni_2Fe_2(CO)_5(\mu_4\text{-}\eta^2\text{-}C{\equiv}CPh)(\mu\text{-}PPh_2)$	187.7(s)	—	91.6(s)	—	14

all cases reported C_α and C_β are well separated with $\Delta\delta$ values ranging between 15–86 ppm, and C_α downfield of C_β.

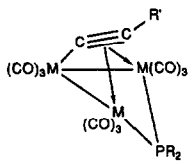

5

M = Os, R = Ph

a R' = Ph
b R' = Bu^t
c R' = Ph

6

R = Bu^t, R = C_2Bu^t

a M = Fe
b M = Ru
c M = Os

μ_4-η^2-acetylides

Few examples of this type of bonding mode have been documented and ^{13}C data is very limited for obvious reasons. Clusters with a single μ_4-acetylide on a metal framework consisting of at least four atoms have high molecular weights and a low weight percentage of alkynyl carbon, making detection of ^{13}C signals a tedious task. Table 6 lists data for three such complexes. The C_α shifts are downfield of C_β in all cases and δ values for C_α and C_β are well downfield of their counterparts in μ_2-η^2- and μ_3-η^2- complexes. It would seem from the C_α ^{13}C shifts in these clusters that the μ_4- carbon atom is quite electron deficient. Indeed these shifts approach the values for coordinated carbonyls and alkylidenes.

REFERENCES

1. (a) R. Nast, *Coord. Chem. Rev.* 1982, **47**, 89; (b) E. Sappa, A. Tiripicchio and P. Braunstein, *Chem. Rev.* 1983, **83**, 202; (c) A. J. Carty, *Pure Appl. Chem.* 1982, **54**, 113; (d) A. J. Deeming, M. S. B. Felix, P. A. Bates and M. B. Hursthouse, *J. Chem. Soc., Chem. Commun.* 1987, 461; (e) M. Cowie and S. J. Loeb, *Organometallics* 1985, **4**, 852; (f) N. W. Alcock, T. J. Kemp, P. G. Pringle, P. Bergamini and O. Traverso, *J. Chem. Soc., Dalton Trans.* 1987, 1659; (g) D. P. Markham, B. L. Shaw and M. Thornton-Pett, *J. Chem. Soc., Chem. Commun.* 1987, **5**, 1005; (h) D. Nucciarone, N. J. Taylor and A. J. Carty, *Organometallics* 1986, **5**, 2565; (i) A. J. Deeming, S. Donovan-Mtunzi and K. Hardcastle, *J. Chem. Soc., Dalton Trans.* 1986, 543; (j) D. M. McEwan, D. P. Markham, P. G. Pringle and B. L. Shaw, *J. Chem. Soc., Dalton Trans.* 1986, 1809; (k) E. Boyar, A. J. Deeming and E. K. Shariff, *J. Chem. Soc., Chem. Commun.* 1986, 577; (l) K. W. Lee, W. T. Pennington, A. W. Cordes and T. L. Brown, *J. Am. Chem. Soc.* 1985, **107**, 631; (m) P. O. Nubel and T. L. Brown, *Organometallics* 1984, **3**, 29; (n) S. P. Deraniyagala and K. R. Grundy, *Organometallics* 1985, 424; (o) A. J. Carty, S. A. MacLaughlin, J. Van Wagner and N. J. Taylor, *Organometallics* 1982, **1**, 1013.
2. (a) G. N. Mott and A. J. Carty, *Inorg. Chem.* 1983, **22**, 2726; (b) A. A. Cherkas, L. H. Randall, S. A. McLaughlin, G. N. Mott, N. J. Taylor and A. J. Carty, *Organometallics*, in press.
3. A. A. Cherkas, N. J. Taylor and A. J. Carty, unpublished results.
4. S. A. MacLaughlin, Ph.D. Thesis, University of Waterloo (1983).
5. (a) A. J. Carty, S. A. MacLaughlin and N. J. Taylor, *J. Organomet. Chem.* 1981, **204**, C27; (b) D. Nucciarone, S. A. MacLaughlin, N. J. Taylor and A. J. Carty, *Organometallics* 1987, **7**, 106.
6. B. Bobbie, A. J. Carty and N. J. Taylor, unpublished results.
7. S. Aime, O. Gambino, L. Milone, E. Sappa and E. Rosenberg, *Inorg. Chim. Acta*, 1975, **15**, 53.
8. (a) J. A. Hriljac and D. F. Shriver, *Organometallics*, 1985, **4**, 2225; (b) J. A. Hriljac and D. F. Shriver, *J. Am. Chem. Soc.* 1987, **109**, 6010.
9. D. DeMontauzon and R. Mathieu, *J. Organomet. Chem.* 1983, **252**, C83.
10. M. Green, K, Marsden, I. D. Salter, F. G. A. Stone and P. Woodward, *J. Chem. Soc., Chem. Commun.* 1983, 446.
11. E. Sappa, *J. Organomet. Chem.* 1987, **323**, 83.
12. L. Busetto, J. C. Jeffery, R. M. Mills, F. G. A. Stone, M. J. Went and P. Woodward, *J. Chem. Soc., Dalton Trans.* 1983, 101.
13. (a) A. J. Carty, S. A. MacLaughlin and N. J. Taylor, *J. Am. Chem. Soc.* 1981, **103**, 2456; (b) S. A. MacLaughlin, N. J. Taylor and A. J. Carty, *Organometallics* 1983, **2**, 1194.
14. C. Weatherell, N. J. Taylor, A. J. Carty, E. Sappa and A. Tiripicchio, *J. Organomet. Chem.* 1985, **291**, C9.
15. D. Shaw, *Fourier Transform NMR Spectroscopy*, 2nd Edn. Elsevier, New York (1984).

Polyhedron Vol. 7, No. 12, pp. 1053–1061, 1988
Printed in Great Britain

0277–5387/88 $3.00+.00
© 1988 Pergamon Press plc

DIRECT SYNTHESIS, SPECTRAL AND MAGNETIC PROPERTIES OF *TRANS*-ANIONO(1,4,10,13-TETRAOXA-7,16-DIAZACYCLOOCTADECANE-7-ACETATO)COPPER(II) COMPLEXES

STANISŁAW P. KASPRZYK* and RYSZARD A. KOLIŃSKI

Institute of Organic Chemistry, Polish Academy of Sciences, 01-224 Warsaw, Poland

and

JERZY MROZIŃSKI*

Institute of Chemistry, University of Wrocław, 50-383 Wrocław, Poland

(*Received* 9 *November* 1987; *accepted* 4 *January* 1988)

Abstract—7-Carboxymethyl-7,16-diaza-18-crown-6 acid hydrates ($LH \cdot H_2O$) and their copper(II) complexes [CuLX], (X = Cl, Br, NO_3, ClO_4 and CH_3CO_2) were obtained. The earlier X-ray investigation of the [CuLCl] complex, as well as the IR and UV-vis spectral evidence for the complexes revealed the inner chelate structure with the six-coordinated copper(II) ion embedded inside the macrocyclic ligand (deformed octahedral, 4+2, N,N, CO_2^-,X^-,O,O-coordination sphere) and the *trans* arrangement of the CO_2 and X ligands. The spectral data, the conductivity measurements and the chemical properties show the existence of the macrocyclic inclusion cation $[CuL]^+$ and the formulation of the complexes as the $[(CuL)^+X^-]$ inner salts. The magnetic moments of the complexes amount to 1.76–1.83 BM at room temperature and 1.3–0.92 BM at 4.2 K. These results revealed the monomeric form of the complexes with the occurrence of the intermolecular (through space) magnetic super-exchange interactions of copper(II) paramagnetic centres.

Macrobicyclic aminoethers (cryptands) have excellent complexing properties for metal ions. A characteristic feature of these ligands is their selectivity, which is adjustable toward various metal ions by the design of a suitable topology for the molecule, the choice of suitable binding atoms and the choice of ligand layer properties.[1] All these structural features are built into the ligand molecule during its often tedious and difficult synthesis.

We aimed to imitate the complexing properties of cryptands by using simpler molecules, namely, macromonocyclic compounds with pendant arms containing charged binding sites, i.e. carboxylate or other anionic groups. We expected that the ligands of such a flexible structure would be able to adopt the topology related to cryptands in complexes and thus, these ligands would have the selectivity of cryptands. We further expected that the occurrence of metal ion–carboxylate bonds would increase the desired stability of complexes, whereas coordination with numerous ligating heteroatoms of the macrocycle would positively contribute to the selectivity of the ligand towards specific metal ions. We also hoped that the synthesis of pendant ligands should be much easier than that of corresponding macrobicyclic ones.

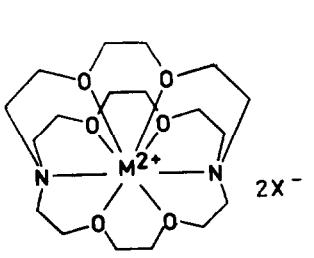

Cryptand [2.2.2]

Cryptate $[M^{2+} \subset 2.2.2]$

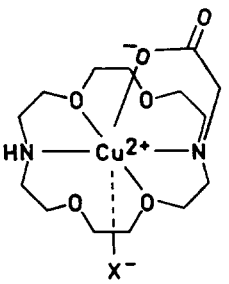

Ligand L^-

Complex [CuLX]

* Authors to whom correspondence should be addressed.

We report here the synthesis of 1,4,10,13-tetraoxa-7,16-diazacyclooctadecane-7-acetic acid and its stable copper(II) complexes.

RESULTS AND DISCUSSION

1,4,10,13-Tetraoxa-7,16-diazacyclooctadecane-7-acetic acid (LH) was first obtained as an intermediate in the synthesis of 16-dodecanoyl-1,4,10,13-tetraoxa-7,16-diazacyclooctadecane-7-acetic acid[2] by a mono-N-alkylation of 1,4,10,13-tetraoxa-7,16-diazacyclooctadecane with sodium chloroacetate. However, the acid LH has neither been isolated in a pure state nor characterized.

We obtained the acid by the method quoted above[2] and we have improved its isolation by the application of a cation exchange resin and by crystallization from methanol. Thus, we have obtained the acid LH as a crystalline monohydrate, m.p. 130–132°C.

The relevant IR spectral properties of the solid acid monohydrate $LH \cdot H_2O$ are the occurrence of a very strong carboxylate band at 1580 cm^{-1} (an antisymmetric νCO_2^- vibration), the lack of the symmetric νCO_2^- band and the occurrence of broad bands at 2710s, 2600sh, 2340m cm^{-1} assigned to the νN^+—H vibration. The low frequency of the νCO_2^- band suggests the presence of the $NCH_2CO_2^-$ group[3] with an uncharged nitrogen atom, and the occurrence of the ammonium bands weakly separated from the νCH_2 bands[4] suggests the protonation of the secondary amino group. The H_2O absorption bands were observed at 3535s and 3490s (νO—H) and 1635s cm^{-1} (δH_2O). All these bands disappeared on vacuum drying of the acid at 110°C. Very strong νC—O (ether) bands were observed at 1130, 1115 and 1100 cm^{-1}. The quoted IR spectral evidence allowed us to propose the zwitterionic structure for the acid monohydrate $LH \cdot H_2O$.

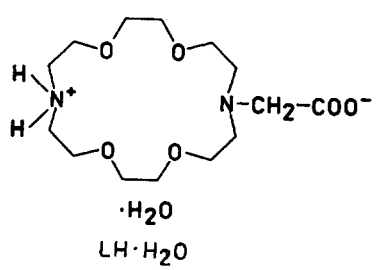

$LH \cdot H_2O$

The synthesis of copper(II) complexes from the acid LH is quite straightforward; equimolar quantities of the acid and the CuX_2 salt are dissolved in a suitable solvent, generally methanol, triethylamine is added in order to deprotonate the ammonium group of the ligand and to bind the HX acid formed during the reaction, and the reaction mixture is refluxed. Concentration of the solution leads to the crystallization of the appropriate complexes [CuLX], which are recrystallized in order to obtain analytical samples.

$$LH + CuX_2 + NEt_3 \rightarrow [CuLX] + HN^+Et_3X^-$$

$$X^- = Cl^-, Br^-, NO_3^-, ClO_4^-, CH_3CO_2^-. \quad (1)$$

Elemental analysis of compounds [CuLX] revealed that the 1 : 1 : 1 copper : macrocyclic ligand : ligand X^- complexes were obtained. In the case of copper(II) diperchlorate tetrahydrate, a hydrated $[CuLClO_4] \cdot H_2O$ complex was obtained.

The good solubility of the complexes in organic solvents i.e. [CuLCl] in chloroform, $[CuLCH_3CO_2]$ in acetone, etc. is indicative of the inner-chelate structure of these complexes. Upon dissolution in water or in other polar solvents, a partial or total dissociation of the complexes occurs to yield the solvated cation $[CuL \cdot Solv]^+$ and the anion X^-. This was confirmed by the immediate precipitation of AgCl or AgBr by adding aqueous silver nitrate to aqueous solutions of the complexes.

$$[CuLX] + Solvent \rightarrow [CuL \cdot Solv]^+ + X^-. \quad (2)$$

The conductivity measurements of the 0.001 M aqueous solutions of [CuLCl] and $[CuLClO_4] \cdot H_2O$ at 25°C gave molar conductivities of 111 and 207 Ω^{-1} cm^2 mol^{-1}, respectively. The conductivity $\Lambda_{[CuL]^+}$ of the macrocation $[CuL]^+$ was calculated to be 32 ± 3 Ω^{-1} cm^2 mol^{-1} from the known values of the conductivity of Cl^- and ClO_4^- anions. The relatively low value for the $[CuL]^+$ cation conductivity results undoubtedly from its small mobility, owing to the bulkiness of the cation.

The steric structure of the [CuLX] complex was established by the X-ray investigation[5] revealing that this is an inclusion complex with the copper(II) cation located within the cavity of the macrocycle. The molecule belongs to the orthorhombic system, space group *Pbca*, with cell dimensions $a = 1273.4$, $b = 1196.5$, $c = 2325.2$ pm, and $Z = 8$. The closest coordination sphere of the copper ion is formed by two nitrogen atoms, one oxygen atom of the carboxylate group and the chlorine; the bond lengths are: Cu—N_7 206.5, Cu—N_{16} 202.0, Cu—O^- 192.9 and Cu—Cl^- 226.1 pm. The next two atoms closest to the copper ion are the oxygen atoms O_4 and O_{13} of the macrocycle at distances 276.7 and 275.3 pm, respectively. Thus, the [CuLCl] and the other [CuLX] complexes are of the (4+2) coordination type, i.e. they have deformed octahedral

coordination spheres. The 18-membered ring of the ligand is too large for binding the copper ion with all of its heteroatoms; oxygen atoms O_1 and O_{10} are too far away to be bonded.

The Cu—Cl and Cu—O^- (carboxyl) distances, are only slightly shorter than the sum of corresponding ionic radii ($Cu—Cl_{calc.} = 69+181 = 250$ pm, $\Delta(Cu—Cl_{calc.} - Cu—Cl_{obs}) = 250-226 = 24$ pm; $Cu—O^-_{calc.} = 69+145 = 214$ pm, $\Delta(Cu—O^-_{calc.} - Cu—O^-_{obs}) = 214-193 = 21$ pm). This proves that the bonds have only little covalent character and explains their easy dissociation.

The relative configuration of the carboxylate group and the Cl^- anion in the coordination sphere of the [CuLCl] complex is *trans*, and that of the carboxylate group and the hydrogen of the N—H group is *cis*, without any hydrogen bonding between them. The same configuration and structure are proposed for the remaining [CuLX] complexes. The properties and structures of the [CuLX] complexes suggest that the latter exist as neutral salts of a monovalent, positively charged inclusion copper(II) cation, "a macrocation" $[CuL]^+$, with X^- anions, i.e. a $[(CuL)^+X^-]$ structure. In the macrocation, one charge of the dipositive copper(II) cation is neutralized by the carboxylate group of the macrocyclic ligand:

$$Cu^{2+} + L^- \rightarrow [CuL]^+ \qquad (3)$$

and the whole macrocation is stabilized by the coordination bonds of the copper ion with the macrocycle ligating atoms. This concept was further confirmed by some X^- metathesis reactions of the [CuLX] complexes[6] and by the IR spectral evidence (see below).

IR spectra

Generally, the IR spectra of the [CuLX] complexes in the 4000–600 cm^{-1} region are very similar to each other (Table 1). They clearly consist of the spectrum of the macrocyclic ligand, more precisely speaking that of the coordinated ligand in the inclusion cation $[CuL]^+$, and the spectra of ligands X and water (if present) superimposed onto the $[CuL]^+$ spectrum. This strongly confirms our hypothesis of the occurrence of the inclusion cation $[CuL]^+$ in these compounds.

The most distinct absorption bands of the cation $[CuL]^+$ are:

(i) A sharp νN—H band in the range 3270–3245 cm^{-1}. According to the X-ray structure[5] of [CuLCl], this band is assigned to the free, non-hydrogen bonded N—H group. The νN—H band of $[CuLCH_3CO_2]$ at 3162 cm^{-1} is indicative of an intermolecular hydrogen bonding of the N—H group, probably to a carboxylate group, as it is shifted to 3270 cm^{-1} in solution (Table 1). In the case of the perchlorate hydrate complex $[CuLClO_4]\cdot H_2O$ a broad νO—H band centred at 3450 cm^{-1} is superimposed onto the sharp νN—H band (3250 cm^{-1}) and a δH_2O band is discernible as a shoulder (1670 cm^{-1}) on the νC=O band (1650 cm^{-1}).

(ii) A very strong νC=O absorption band in the range 1660–1640 cm^{-1} proves a unidentate coordination of the ligand carboxylate group

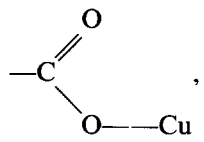

Table 1. Characteristic IR absorption bands of [CuLX] complexes [ν_{max} (cm^{-1})]

Complex	[CuLX][a]	Ligand L			Ligand X[b]
		νN—H	νC=O (CO_2^-)	νC—O (CO_2^-)	
[CuLCl]	Solid	3250m	1650vs	1370s	
	$CHCl_3$ soln	3272m	1647vs	1380s	
[CuLBr]	Solid	3250m	1651vs	1370s	
$[CuLNO_3]$	Solid	3245m	1660vs	1356s	1482s, 1291s, 1006s, 792w, 733m, 725sh
$[CuLCH_3CO_2]$	Solid	3162m	1662vs	1386s	1610vs, 1332s,
	$CHCl_3$ soln	3270m	1642vs	1383s	1613vs, 1346s
$[CuLClO_4]\cdot H_2O$	Solid	3250m[c]	1650vs	1368s	(1100vs)[d], 637s, 626s

[a] Solid samples as paraffin oil mulls and KBr pellets.

[b] See description in the text.

[c] H_2O bands at 3450s br cm^{-1} (νO—H) and 1670sh cm^{-1} (δH_2O) were observed.

[d] Four bands at 1145, 1125, 1110 and 1090 cm^{-1}, all very strong, were observed, but in this region overlapping with strong νC—O ether bands occurred.

this vibration having a distinct carbonyl character, rather than its assignment to the antisymmetric mode of the carboxylate group vibration.

(iii) A strong νC—O$^-$ (carboxyl) absorption band in the range 1386–1356 cm^{-1} corroborates the assignment of (ii).

(iv) All spectra contain sets of strong νC—O (either) bands in the 1150–1045 cm^{-1} region (five–seven bands).

The spectra of the solid complexes and those of their chloroform solutions show only minor differences in band positions (except for the hydrogen bonded N—H group), and indicate the same structure of complexes in both phases.

A very important piece of structural information results from the IR spectra of the coordinated ligands X (Table 1). For [CuLCl] and [CuLBr] complexes we observed the νCu—Cl and νCu—Br bands at 238 and 187 cm^{-1}, respectively (tentative assignments). For [CuLNO$_3$], the observed NO_3 bands reveal the unidentate coordination, Cu—O—NO$_2$, of the nitrate anion.[7] For the [CuL ClO_4]·H$_2$O complex, we observed the ClO_4^- vibration modes as a set of very strong bands around 1100 cm^{-1}, which were superimposed on the νC—O (ether) bands, and two strong, sharp bands at 636 and 626 cm^{-1} characteristic of a unicoordinated, Cu—O—ClO$_3$, perchlorate anion.[7] The acetato complex, [CuLCH$_3$CO$_2$], has two carboxylate groups: one, in the macrocyclic ligand and another in the acetate anion. Both of the carboxylate groups were found unicoordinated to the copper ion. Their IR frequencies were assigned by analogy to the other [CuLX] complexes.

Electronic spectra

The spectra of solid and dissolved [CuLX] complexes are as should be expected for the six-coordinated d^9 copper cation complexes, having low symmetry of the coordination sphere (asymmetric or close to C_{2v}). Two very broad asymmetric or weakly split absorption bands were observed (see Table 2). The first occurred at 48100–34100 cm^{-1} in the spectra of solid complexes and at 38000–33900 cm^{-1} in the spectra of methanolic solutions of the complexes; it was assigned to the charge-transfer transition.[8] A blue shift (*ca* 6000–2000 cm^{-1}) of this band was observed in aqueous solutions. The *d–d* transition bands (the second band) occurred at 14800–14400 cm^{-1} in the spectra of both the solid and dissolved complexes.[8] Two weak inflections on this band were detected at 18000–16000 and at 13600–13400 cm^{-1}.

The UV spectra of all [CuLX] complexes are also quite similar to each other. This can be explained by the similarity of the spectrochemical properties of the coordination sphere of the complexes, in which only one ligand X is changed when going from one complex to another. Moreover, all the ligands, X are soft acids, which induce only small changes in the ligand fields. Another factor could be a similar position of the dissociation equilibrium [eq. (2)] for all complexes. If the equilibrium is strongly shifted to the right, the spectrum of each complex originates from the same species, [CuL·Solv]$^+$, and this may explain their similarity.

Magnetic investigations

The magnetic susceptibilities of the [CuLX] complexes were examined by the Faraday method in a temperature range of 290–4.2 K (Table 3). The basic difference in the magnetic properties of complexes was observed in the low temperature range. For the chloride and bromide complexes a drastic decrease in the $\chi_{Cu}T$ product value is observed, from

Table 2. Electronic spectra of [CuLX] complexes (cm^{-1})

Compound	Reflection spectra (solid state) Charge transfer		*d–d*		Absorption spectra (methanolic solution) Charge transfer		*d–d*[a]
[CuLCl]	—	35300	18200sh	14400	—	37700(6080) 33900sh(3640)	14600(48.9)
					41700sh(2790)[b]	35800(3575)[b]	14700(56.5)[b]
[CuLBr]	48100	34100	18200sh	14400	—	34400(5250)	14800(51.6)
[CuLNO$_3$]	47200	35700	18020sh	14800	—	36400(3760)	14450(59.1)
[CuLCH$_3$CO$_2$]	—	36400	18200sh	14700	—	38000(5090)	14700(45.1)
[CuLClO$_4$]·H$_2$O	—	38500	—	14700	—	36600(3870)	14400(58.7)
					41700sh(1300)[b]	36200(1660)[b]	15150(26.8)[b]

[a]A very broad band with weak shoulders at 16000–18000 cm^{-1} and 13400–13600 cm^{-1}.
[b]Aqueous solutions.

Table 3. Magnetic data of [CuLX] complexes

Complex	Magnetic susceptibility $\chi_{Cu}^{corr} \times 10^6$ ($cm^3\ mol^{-1}$)		Magnetic moment $\mu_{eff} = 2.83(\chi_{Cu}^{corr}\ T)^{1/2}$ (BM)		Constant[a]	
	Temperature		Temperature		Curie C	Weiss θ
	4.2 K	290 K	4.2 K	290 K	($cm^3\ mol^{-1}\ K$)	(K)
[CuLCl]	50400	1460	1.30	1.84	0.430	−3.3
[CuLBr]	25400	1330	0.92	1.76	0.401	−7.2
[CuLNO$_3$]	102000	1370	1.83	1.79	0.395	0.7
[CuLCH$_3$CO$_2$]	116000	1650	1.98	1.96	0.495(0.477)	−11.9(−4.1)
[CuLClO$_4$]·H$_2$O	139000	1520	2.16	1.88	0.435	2.4

[a] Curie and Weiss constants were calculated in the temperature range 4.2–290 K, and for the [CuLCH$_3$CO$_2$] compound also in the range 14–290 K (in brackets).

0.425 and 0.385 $cm^3\ mol^{-1}$ K at 290 K, to 0.212 and 0.107 $cm^3\ mol^{-1}$ K at 4.2 K, respectively. This is related to a drastic lowering of the magnetic moment value, from 1.84 and 1.76 BM at 290 K to 1.30 and 0.92 BM at 4.2 K, respectively. This is most likely connected with the presence of super-exchange magnetic interactions between the copper(II) paramagnetic centres of different molecules of the complex in the crystal lattice.

Since the complexes examined have monomeric forms and do not contain any bridge system bonding the copper ions, a magnetic super-exchange via space or hydrogen bonded systems must be involved, which can thus take place at quite long distances between the interacting magnetic centres.[9–13] An interaction of this type was observed earlier in monomeric hexahalogenorhenates(IV) via the halogenide ions, even when the rhenium–rhenium distance was close to 1000 pm and depended on the halogen involved in super-exchange.[14–19] Antiferromagnetic super-exchange interactions increase in the order F < Cl < Br < I, i.e. with the increasing covalent character of the metal–X bond.

This is consistent with the observations for [CuLCl] and [CuLBr] complexes. For the bromide complex, the magnetic super-exchange effect considerably exceeds that for the chloride complex (Fig. 1, Table 3).

In the crystal lattice of the [CuLCl] complex, the shortest copper–copper distance is 647 pm. Since the shortest Cl—Cl distance from the adjacent complex molecules is 660 pm, and the Cu—Cl bond lengths are 226.1 pm, the magnetic super-exchange path Cu—Cl... Cl—Cu involving the d_π–p_π orbitals from Cu—Cl bonds and the p_π–p_π overlapping orbitals of the Cl atoms is equal to about 1100 pm.

The suggestion about the relation between the kind of ligand X and the effect of the magnetic interaction (based upon the studies of the chloride and bromide complexes) was confirmed also for other [CuLX] complexes, i.e. acetate, nitrate and perchlorate.

The acetate complex, [CuLCH$_3$CO$_2$], in the temperature range 290–14 K (Fig. 1) shows magnetic properties which are similar to those of the chloride and bromide complexes, i.e. a drastic decrease in the $\chi_{Cu}T$ product value upon lowering the temperature from 0.480 to 0.239 $cm^3\ mol^{-1}$ K at 290 and 14 K, respectively. This is characteristic of antiferromagnetic interactions in molecular systems. As a result of the magnetic super-exchange, the magnetic moment of the complex declines from 1.96 BM at 290 to 1.35 BM at 14 K. Below 14 K, an anomalous constant increase in the $\chi_{Cu}T$ product value to 0.489 $cm^3\ mol^{-1}$ K is observed, which may suggest a transition to the long ordering magnetic phase at the lowest temperatures.

The nitrate complex at 290–4.2 K (Fig. 1) exhibits a practically constant value of the $\chi_{Cu}T$ product, 0.408 ± 0.010 $cm^3\ mol^{-1}$ K, which is related to the magnetic moment value 1.81 ± 0.02 BM. Magnetic properties of the nitrate complex can result either from complete isolation of the magnetic centres of the complex or from a possible compensation of the intermolecular antiferro- and ferromagnetic interactions in the crystal lattice.

Upon temperature lowering, the perchlorate complex [CuLClO$_4$]·H$_2$O shows an increase in the $\chi_{Cu}T$ product value (Fig. 1), from 0.440 to 0.580 $cm^3\ mol^{-1}$ K at 290 and 4.2 K, respectively, and an increase in the magnetic moment, from 1.88 to 2.16 BM. The rapid increase in the $\chi_{Cu}T$ product value at temperatures below 20 K may suggest the

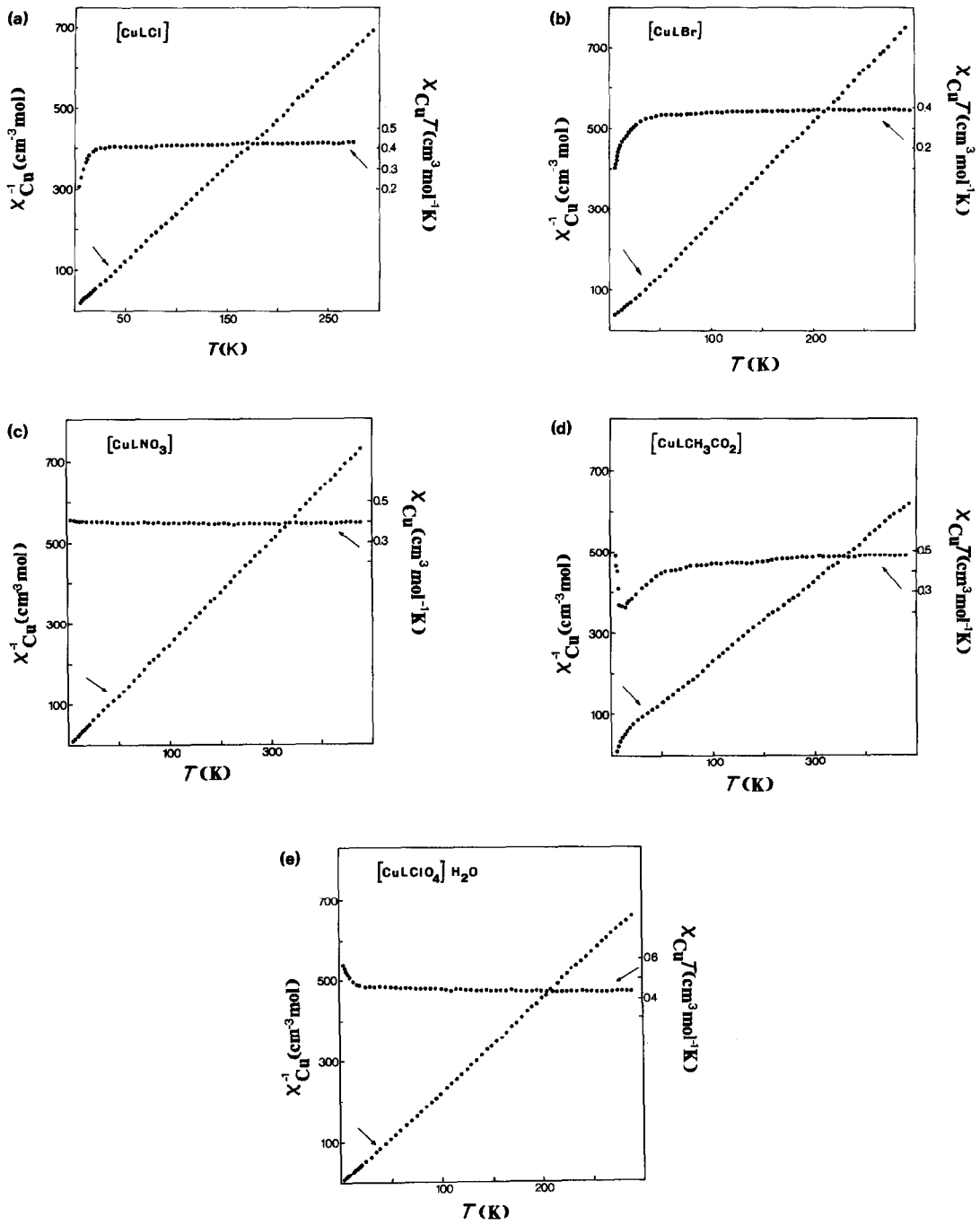

Fig. 1. Temperature dependence of the product $\chi_{Cu}T$ and that of χ_{Cu}^{-1} for the [CuLX] complexes.

presence of a phase transition to a magnetically ordered state at temperatures below the liquid helium temperature.

EPR spectra

The EPR spectra of [CuLX] complexes were measured at room and lower temperatures.

The chloride complex shows a rhombic spectrum at room temperature ($g_1 = 2.05_0$, $g_2 = 2.07_2$, $g_3 = 2.21_6$ and $\langle g \rangle = 2.11_3$) and at 170 K ($\langle g \rangle = 2.11_4$). The bromide complex exhibits identical axial spectra at room temperature ($g_\perp = 2.05_4$, $g_\parallel = 2.22_6$, $\langle g \rangle = 2.11_3$) and at 180 K ($\langle g \rangle = 2.11_1$). In both of them the area between the parallel and perpendicular part of the spectrum

contains a very complicated super-hyperfine pattern derived from the interaction of the electron spin of the copper ion with the nitrogen nuclei ($I = 1$), bromide nuclei ($I = 3/2$), as well as with the nuclei of the Cu^{63} and Cu^{65} isotopes.

The acetate complex, at room temperature, shows a single, asymmetric signal ($g = 2.07_8$), while the temperature lowering (to 180 K) is accompanied by the appearance of a weak parallel component. The continued temperature lowering (to 77 K) results in the appearance of a weak rhombic line ($g_1 = 2.05_4$, $g_2 = 2.10_7$ and $g_3 = 2.18_7$) with the average spectroscopic splitting factor $\langle g \rangle = 2.11_7$.

Thus, at low temperatures, all three complexes, i.e. the chloride, bromide and acetate have an almost identical average spectroscopic splitting factor value, $\langle g \rangle = 2.11_{1-7}$.

The nitrate complex shows an axial spectrum at room temperature ($g_\perp = 2.06_2$, $g_\parallel = 2.24_8$ and $\langle g \rangle = 2.12_6$) and at 180 K $\langle g \rangle = 2.12_8$.

The perchlorate complex is characterized by the lack of an EPR signal in the range 290–77 K.

The results of low-temperature magnetic investigations together with the EPR results revealed that the [CuLX] complexes are very interesting macrocyclic compounds in which intermolecular magnetic interactions take place. In the latter, the effects of magnetic super-exchange depend strongly upon the ligand X and the character of the Cu—X bond.

EXPERIMENTAL

Materials

1,4,10,13-Tetraoxa-7,16-diazacyclooctadecane (m.p. 115–116°C) was obtained according to Kulstad and Malmsten,[20] or Kryptofix 22 (Merck) recrystallized from acetone (m.p. 115–116°C) was used. Commercial reagents and copper(II) salts were used without further purification.

Physical measurements

Conductance of 0.001 M aqueous solutions of complexes was measured at 25°C on a laboratory conductometer model N 572. IR spectra were recorded in paraffin oil mulls and in KBr pellets on a Perkin–Elmer 180 spectrometer. Electronic spectra in solution were recorded in the range 200–1000 nm on a Cary 14 spectrometer. Reflectance spectra of the undiluted compounds were measured in the 350–1500 nm region on a Beckman UV spectrometer and those of Li_2CO_3 diluted compounds in the 200–800 nm region on a Hitachi 356 spectrometer. EPR spectra of the solid samples were measured on a Jeol JES-ME-3X spectrometer in the temperature range 290–77 K. The spectra were analysed by means of a manganese standard (Mn^{2+} in MgO). Magnetic susceptibilities were measured using the Faraday method with a Cahn RG-HV electrobalance. Magnetic measurements were carried out on a polycrystalline samples (weight *ca* 60 mg) in the temperature range 290–4.2 K and a magnetic field of *ca* 0.505 T. Magnetic susceptibilities of all of the samples were found to be field independent. The susceptibilities were corrected for the diamagnetism of all the constituent atoms using Pascal's constants[21] and the TIP of the copper(II) ion. The calibrant employed was $HgCo(SCN)_4$, for which $\chi_g = 16.44$ cm^3 g^{-1} at 293 K.[22] The temperature was determined with an accuracy of about ± 0.1 K.

1,4,10,13 - *Tetraoxa* - 7,16-*diazacyclooctadecane* - 7 - *acetic acid monohydrate*, $LH \cdot H_2O$

1.89 g of chloroacetic acid (20 mmol) in 50 cm^3 of water was adjusted to a pH value of *ca* 9.5 using 4 N NaOH and added dropwise over a period of 4 h, to a boiling solution of 7.86 g of 1,4,10,13-tetraoxa-7,16-diazacyclooctadecane (30 mmol, 50% excess) in 40 cm^3 of water. The reaction mixture was refluxed for 10 h. It was then adjusted to a pH *ca* 12 using 4 N NaOH and extracted with chloroform (3×100 cm^3) to remove any unreacted aminoether. The aqueous layer was concentrated *in vacuo* and passed through an ion exchange column (Amberlite IR-120, H^+ form). The column was washed with water until the pH was *ca* 7, followed by eluation of the desired product by 4N NH_3(aq). The latter eluate was collected and evaporated *in vacuo* to dryness. The remaining white solid acid $LH \cdot H_2O$ was recrystallized from 96% ethanol. Yield 70%. M.p. 130–132°C. IR (solid sample mull in paraffin oil) bands at 3535s, 3490s (νOH, disappeared on drying), 2710m, 2340br (νN^+H_2), 1635s (δH_2O, disappeared on drying), 1575vs (antisymmetric νCO_2^-), 1130, 1115, 1100vs (νC—O—C) cm^{-1}. ^{1}H NMR (D_2O/DSS) 3.15 (m, 8H, N—C$\underline{H}_2$—CH_2—O), 3.41 (s, 2H, N—C$\underline{H}_2$—COOH), 3.70 (s, 8H, O—C$\underline{H}_2$—C$\underline{H}_2$—O), 3.76 (m, 8H, O—C$\underline{H}_2$—CH_2—N).

trans - *Chloro*(1,4,10,13 - *tetraoxa* - 7,16 - *diazacyclooctadecane* - 7 - *acetato*) *copper*(II), [CuLCl]

170.5 mg of $CuCl_2 \cdot 2H_2O$ (1 mmol) was dissolved in 20 cm^3 of methanol and added to 338 mg of $LH \cdot H_2O$ (1 mmol) in 20 cm^3 of methanol. A few drops of triethylamine were added to the reaction mixture and the dark blue solution was refluxed for

Table 4. Elemental analysis

Compound	Calc. (%) C	H	N	Cu	Found (%) C	H	N	Cu
$LH \cdot H_2O$ $C_{14}H_{30}N_2O_7$	49.7	8.9	8.3	—	49.4	8.9	8.3	—
[CuLCl][a] $C_{14}H_{27}ClCuN_2O_6$	40.2	6.5	6.7	15.2	40.0	6.6	6.6	15.2
[CuLBr][b] $C_{14}H_{27}BrCuN_2O_6$	36.3	5.8	6.0	13.7	36.6	6.1	5.9	13.7
$[CuLNO_3]$ $C_{14}H_{27}CuN_3O_9$	37.8	6.1	9.4	14.3	37.8	6.4	9.2	14.1
$[CuLCH_3CO_2]$ $C_{16}H_{30}CuN_2O_8$	43.5	6.8	6.3	14.4	43.1	7.2	6.1	13.9
$[CuLClO_4] \cdot H_2O$ $C_{14}H_{29}ClCuN_2O_{11}$	33.6	5.8	5.6	12.7	33.7	5.6	5.3	12.4

[a] % Cl; Calc. 8.5; found 8.6.
[b] % Br; Calc. 17.3; found 17.3.

1 h. Then, the solution was concentrated *in vacuo* and was left overnight in the refrigerator yielding dark blue crystals of [CuLCl], which were filtered off, washed with ethanol and dried over P_4O_{10}.

trans - *Bromo*(1,4,10,13 - *tetraoxa* - 7,16 - *diaza-cyclooctadecane-7-acetato*) *copper*(II), [CuLBr], trans - *nitrato*(1,4,10,13 - *tetraoxa* - 7,16 - *diaza-cyclooctadecane-7-acetato*) *copper*(II), $[CuLNO_3]$ *and* trans-*perchlorato*(1,4,10,13-*tetraoxa*-7,16-*diazacyclooctadecane-7-acetato*) *copper*(II) *hydrate*, $[CuLClO_4] \cdot H_2O$

These were prepared in the same manner as the complex [CuLCl] using $CuBr_2$, $Cu(NO_3)_2 \cdot 3H_2O$ and $Cu(ClO_4)_2 \cdot 6H_2O$, respectively.

trans - *Acetato*(1,4,10,13 - *tetraoxa* - 7,16 - *diazacyclooctadecane* - 7 - *acetato*) *copper*(II), $[CuLCH_3CO_2]$

338 mg of $LH \cdot H_2O$ (1 mmol) was dissolved in 20 cm^3 of methanol and added to a slurry of 200 mg of $Cu(CH_3CO_2)_2 \cdot H_2O$ in 50 cm^3 of methanol. A few drops of triethylamine were added to the reaction mixture and the dark blue solution was refluxed for 1 h. The methanol was removed *in vacuo* followed by the addition of 10 cm^3 of acetone and a few drops of triethylamine. The solution was left overnight in the refrigerator yielding a dark blue powder of $[CuLCH_3CO_2]$ which was filtered off and dried *in vacuo* over P_4O_{10}.

Elemental analysis of all complexes is given in Table 4.

Acknowledgement—This work has been financed by the Polish Academy of Sciences within the research project CPBP 01.12.

REFERENCES

1. J. M. Lehn, *Structure Bonding* 1973, **16**, 1.
2. S. Shinkai, H. Kinda, Y. Araragi and O. Manabe, *Bull. Chem. Soc. Japan* 1983, **56**, 559.
3. K. Nakamoto, *Infrared and Raman Spectra of Inorganic and Coordination Compounds*, p. 313. Wiley, New York (1978).
4. K. Nakanishi and P. Solomon, *Infrared Absorption Spectroscopy*, p. 34. Holden-Day, San Francisco (1977).
5. P. Gluziński, J. W. Krajewski, S. P. Kasprzyk, J. Bleidelis, A. Mishnyov and A. Kemme, *J. Cryst. Spect. Res.* 1987, **17**, 495.
6. S. P. Kasprzyk, in preparation.
7. M. R. Rosenthal, *J. Chem. Ed.* 1973, **50**, 331.
8. A. B. P. Lever, *Inorganic Electronic Spectroscopy*, p. 356, 553. Elsevier, Amsterdam (1984).
9. R. E. Coffman and G. R. Buettner, *J. Chem. Phys.* 1979, **83**, 2387.
10. T. R. Felthouse, E. J. Laskowski and D. N. Hendrickson, *Inorg. Chem.* 1977, **16**, 1077.
11. M. Verdaguer, J. Gouteron, S. Jeannin and O. Kahn, *Inorg. Chem.* 1984, **23**, 4291.
12. E. G. Bakalbassis, C. A. Tsipis and J. Mroziński, *Inorg. Chem.* 1985, **24**, 3548.
13. E. G. Bakalbassis, J. Mroziński and C. A. Tsipis, *Inorg. Chem.* 1986, **25**, 3684.
14. B. N. Figgis, J. Lewis, R. S. Nyholm and R. D. Peacock, *Discuss. Faraday Soc.* 1958, **26**, 103.
15. R. H. Busey and E. Sonder, *J. Chem. Phys.* 1962, **36**, 93.

16. V. J. Minkiewicz, G. Shirane, B. C. Frazier, R. G. Wheeler and F. B. Dorain, *J. Phys. Chem. Sol.* 1968, **29**, 881.
17. H. W. Willemsen, R. L. Armstrong and P. M. Meincke, *J. Low Temp. Phys.* 1977, **26**, 299.
18. J. Mroziński, *Bull. Ac. Pol. Chim.* 1978, **26**, 789.
19. J. Mroziński, *Bull. Ac. Pol. Chim.* 1980, **28**, 559.
20. S. Kulstad and L. A. Malmsten, *Acta Chim. Scand.* 1979, **B33**, 469.
21. E. K. König, *Magnetic Properties of Coordination and Organometallic Transition Metal Complexes.* Springer, Berlin (1966).
22. B. N. Figgis and R. S. Nyholm, *J. Chem. Soc.* 1958, 4190.

Polyhedron Vol. 7, No. 12, pp. 1063–1065, 1988
Printed in Great Britain

0277–5387/88 $3.00+.00
© 1988 Pergamon Press plc

SOME NEW RUTHENIUM(III) SCHIFF BASE COMPLEXES: A PHOTOELECTRON SPECTROSCOPIC STUDY

M. M. TAQUI KHAN* and SHEKHAR SRIVASTAVA

Coordination Chemistry Division, Central Salt & Marine Chemicals Research Institute, Bhavnagar 364002, India

(*Received* 30 *September* 1987; *accepted after revision* 13 *January* 1988)

Abstract—Three complexes of ruthenium(III) with Schiff bases of the type $K[Ru(SB)Cl_2]$ (where SB = bisacetylacetoneethylenediimine, bisbenzoylacetoneethylenediimine and bisbenzoylacetone 1,2-propylenediimine) were prepared and characterized by elemental analysis, conductivity measurements, UV-vis, IR, ESR, magnetic susceptibility and XPS data. The report involves the first synthesis of simple Ru(III) Schiff base complexes without a π-acidic ligand.

Although a number of ruthenium(III) coordination complexes have been reported[1–3] complexes with Schiff base ligands are relatively less known. Various Schiff base complexes of Ru(II) with appended CO and PPh_3 groups were reported by Wilkinson *et al.*[4] Simple Ru(III) and Ru(II) Schiff base complexes without the appended π-acidic groups are not known. We report here three simple ruthenium(III) complexes with Schiff bases prepared from $K_2[RuCl_5(H_2O)]$ as a convenient starting material and characterized by physicochemical and spectroscopic data.

EXPERIMENTAL

The complex $K_2[RuCl_5(H_2O)]$[5] and the Schiff bases $acac_2en$, $benac_2en$ and $benac_2$propylenediimine[6] were prepared, purified and characterized according to literature procedures.

Preparation of the Schiff base complexes

(1) Dichlorobis(acetylacetone)ethylenediimine - ruthenium(III).

(2) Dichlorobis(benzoylacetone)ethylenediimine - ruthenium(III).

(3) Dichlorobis(benzoylacetone)propylenediimine-ruthenium(III).

To an ethanolic solution of the appropriate Schiff base (1 mmol) in 10 cm^3 of EtOH, an aqueous solution of $K_2[RuCl_5(H_2O)]$ (1 mmol) in 10 cm^3 of water was added. The mixture was allowed to reflux for 5–6 h. After completion of the reaction checked by TLC, the solvent was evaporated on a rotary evaporator and the residue was dissolved in absolute ethanol and filtered. The filtrate was allowed to run over a column of silica gel. Ethanol was removed on a rotary evaporator and the residue recrystallized with ethanol : diethyl ether (1 : 1). The yields of complexes **1–3** were ~ 80%.

The microanalyses of complexes **1–3** were carried out at the Australian Mineral Development Laboratory, Australia. Conductance measurements in methanol were made at room temperature using a Digisun Electronics conductivity bridge. The electronic spectra were recorded on a Shimadzu UV-160 spectrophotometer. IR spectra were recorded in Nujol mulls on a Perkin–Elmer spectrophotometer. Magnetic susceptibility was measured by the Faraday method using a Cahn magnetic susceptibility system at room temperature. $Hg[Co(CNS)_4]$ was used as a standard for calibration. The electron spin resonance (ESR) spectra were measured on a Brucker 300 ESR instrument with 100 KHz modulation. The spectral g values were calibrated with a DPPH standard.

The X-ray photoelectron spectra were recorded on a VG Scientific ESCA-3 MKII electron spectrometer. The $Mg_{\alpha}K$ X-ray line (1253.6 eV) was used for photoexcitation. The Cu $2p_{3/2}$ (Eb = 932.8 ± 0.2) and Au $4f_{7/2}$ (Eb = 83.8 ± 0.1) lines were used to calibrate the instrument and Ag $3d_{5/2}$ (Eb = 368.2) was used for cross checking.[7] All

*Author to whom correspondence should be addressed.

the spectra were recorded using the same spectrometer parameters of 50 eV pass energy and 4 mm slit width. The reduced full width at half maximum (FWHM) at the Au $4f_{7/2}$ (Eb = 83.8 eV) level under these conditions was 1.2 eV.

The powdered sample was mixed with higher purity silver powder to reduce the charging effect. A thin layer of such a sample was pressed on a gold metal gauze which was welded to a nickel sample holder. The Ag $3d_{5/2}$ level (Eb = 368.2 eV) obtained from this sample was sharp and did not show any observable shift. Thus the charging of the samples if present at all was negligible.[8] The spectra were recorded in triplicate in the region of interest. In most of the cases the binding energies were reproducible within ± 0.1 eV. The usual least-squares fitting procedures of determining peak position, line widths and areas were used.

RESULTS AND DISCUSSION

Complexes **1–3** are reddish-brown in colour, air stable with high melting points. They are soluble in all common organic solvents except benzene and ether. Elemental analyses were within $\pm 0.5\%$ for C, H. N and Cl. The observed molar conductances in methanol were 120, 124 and 130 Ω^{-1} cm^2 mol^{-1}, respectively for complexes **1–3**, indicating that all these complexes are 1 : 1 electrolytes with the composition K[Ru(SB)Cl_2].[9]

An intense band at ~ 324 nm in the UV spectrum of K[Ru(acac$_2$en)Cl_2] and two bands at ~ 314 and ~ 248 nm for K[Ru(benac$_2$en)Cl_2] and ~ 308 and ~ 262 nm, for K[Ru(benac$_2$propylenediamine)Cl_2] are attributed to a π–π^* transition due to pseudo-aromaticity of the acetylacetonate and benzoylacetonate complex ring.[10–12] The electronic spectrum of complex **1** K[Ru(acac$_2$en)Cl_2] shows two weak *d–d* transition bands at ~ 699 and ~ 506 nm. Complexes K[Ru(benac$_2$en)Cl_2] **2** and K[Ru(benac$_2$propylenediimine)Cl_2] **3** show only one single *d–d* transition band at ~ 404 and ~ 402 nm, respectively. These peaks have been assigned to a *d–d* transition of spin paired $(2_{2g})^5$ ruthenium(III).[13] The IR bands observed in the region 1590–1560 and 1515–1480 cm^{-1} in the spectra of complexes **1–3** are assigned to perturbed carbonyl and (C=C/C=N) stretching vibrations, respectively.[11,14] The ν M—Cl is observed as a single peak at 330 cm^{-1} indicating a *trans* configuration of the complexes.

The magnetic moment (μ_{eff}) of complexes **1–3** are 1.93, 2.18 and 2.19 BM, respectively, at room temperature corresponding to one unpaired electron spin. The ESR spectra of solid complexes **1–3** exhibited axial distortion with $g_\parallel$ *ca* 1.8–2.4 and $g_\perp$ *ca* 1.75–1.9 at room temperature. None of the ESR spectra of these complexes **1–3** revealed hyperfine splitting due to nuclear interaction with ruthenium.

The binding energies data of the N 1*s*, O 1*s*, Cl 2*p* and Ru $3p_{3/2,1/2}$ photoelectron peaks for K_2[Ru$Cl_5(H_2O)$], acac$_2$en, benac$_2$en and benac$_2$ propylenediimine Schiff base ligands with their metal complexes are listed in Table 1. It may be seen that the O 1*s* BE value in the starting complex K_2[$RuCl_5(H_2O)$] is observed at 534.2 eV for coordinated water, but in complexes **1–3** only one symmetrical O 1*s* peak was observed in the range 532.9–532.4 eV as also with the respective ligands. From

Table 1. Ru $3p_{3/2,1/2}$ N 1*s*, O 1*s* and Cl 2*p* binding energies (eV) in K_2[$RuCl_5(H_2O)$], Schiff base ligands and K[Ru(SB)Cl_2] complexes[a]

Complex	Ru^{3+} Ru $3p_{3/2}$	Ru $3p_{1/2}$	N 1*s*	O 1*s*	Cl 2*p*
K_2[$RuCl_5(H_2O)$]	466.4 (5.2)	489.8 (4.8)	—	534.2 (4.3)	199.2 (3.3)
acac$_2$en	—	—	400.8 (3.1)	532.4 (4.8)	—
K[Ru(acac$_2$en)Cl_2]	464.7 (4.0)	486.8 (4.2)	401.2 (2.4)	532.9 (2.6)	199.6 (3.2)
benac$_2$en	—	—	400.2 (3.6)	531.9 (3.8)	—
K[Ru(benac$_2$en)Cl_2]	464.6 (4.0)	486.7 (4.6)	400.9 (2.8)	532.5 (2.6)	199.4 (3.2)
benac$_2$propylenediimine	—	—	399.1 (2.6)	531.8 (2.6)	—
K[Ru(benac$_2$propylenediimine)Cl_2]	464.7 (4.1)	486.8 (3.8)	400.2 (2.6)	532.4 (2.8)	199.5 (3.2)

[a] Full width at half maximum (FWHM) of the peak is given in parentheses.

the XPS data, it may be concluded that coordinated water is absent in complexes **1–3**. It may be further noted that of all the three Schiff base ligands, O 1*s* and N 1*s* binding energies are maximums for $acac_2en$ and minimums for $benac_2$ propylenediimine. Using Siegbahn's generalization[15,16] one may conclude that the maximum effective positive charge on the oxygen and nitrogen atom is for $acac_2en$ Schiff base and the minimum is for $benac_2$propylenediimine. The decreasing order of effective positive charge on O 1*s* and N 1*s* in these Schiff base ligands is: $acac_2en > benac_2en >$ $benac_2$propylenediimine. It is clear that the phenyl group of $benac_2en$ increases the electron density on the oxygen and nitrogen atoms and this electron density was comparatively more in $benac_2$-propylenediimine oxygen and nitrogen atoms due to the presence of one methyl group in propylenediimine. The trend of O 1*s* and N 1*s* binding energies in the metal complexes **1–3** was the same as in the ligand 1 > 2 > 3 (Table 1). The values of O 1*s* and N 1*s* binding energies in the metal complexes were, however, more positive than their free ligand (Table 1). One can conclude from these observations that oxygen and nitrogen atoms of the Schiff base ligands are coordinated to the Ru(III) ion.

The Ru $3p_{3/2.1/2}$ photoelectron peaks of complexes **1–3** are about the same (Fig. 1), but less than the starting complex, $K_2[RuCl_5(H_2O)]$. This further suggests that the electronegative oxygen and nitrogen atoms of the Schiff base are coordinated to the Ru(III) ion. The electron density on the ruthenium(III) in complexes **1–3** is more than that for the chloro complex $K_2[RuCl_5(H_2O)]$. The Ru $3p_{3/2}$ and Ru $3p_{1/2}$ photoelectron peaks in complexes **1–3** are broad and asymmetric towards higher BE values having one shake up satellite.[17]

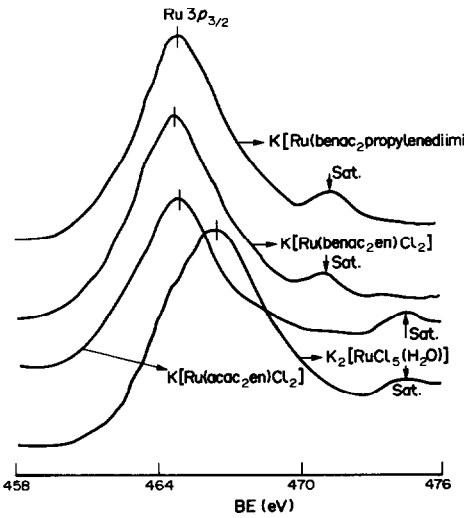

Fig. 1. Ru $3p_{3/2}$ photoelectron spectra in metal complexes.

The Cl 2*p* photoelectron spectra of complexes **1–3** have shown BE values in the range 199.6–199.5 eV, as in the starting complex, $K_2[RuCl_5(H_2O)]$ (Cl 2*p* BE = 199.2 eV), which suggests that in each of the three complexes **1–3** the chloride ion is coordinated in the inner coordination sphere of the metal ion. The binding energy of the outer sphere chloride should be less than 198.3 eV.[18,19] These data thus support the conclusion which was arrived at on the basis of conductivity and IR data, for the presence of *trans* coordinated chloride groups in the complexes.

Since there was more than one type of carbon in these complexes, the signals due to C $1s_{1/2}$ overlapped and one broad signal was obtained. The data of C $1s_{1/2}$ could not be therefore utilized for the structural analysis.

REFERENCES

1. K. S. Seddon, *Coord. Chem. Rev.* 1981, **35**, 41.
2. K. S. Seddon, *Coord. Chem. Rev.* 1982, **41**, 79.
3. K. S. Seddon, *Coord. Chem. Rev.* 1985, **67**, 171.
4. J. R. Thornback and G. Wilkinson, *J. Chem. Soc., Dalton Trans.* 1978, **2**, 110.
5. E. E. Mercer and R. R. Buckley, *Inorg. Chem.* 1965, **4**, 1692.
6. P. J. MacCarthy, R. J. Hovey, K. Veno and A. E. Martell, *J. Am. Chem. Soc.* 1955, **77**, 5820.
7. S. Evans, *Handbook of X-ray and Ultraviolet Photoelectron Spectroscopy* (Edited by D. Briggs), p. 128. Hayden, Rochelle Park, New Jersey (1975).
8. W. Jolly, *Coord. Chem. Rev.* 1974, **13**, 47.
9. W. J. Greary, *Coord. Chem. Rev.* 1971, **7**, 81.
10. R. C. Aggarwal, D. S. Surya Narayana and V. C. Sekhar, *Ind. J. Chem.* 1982. **21A**, 419.
11. S. C. Comning and R. E. Sievers, *Inorg. Chem.* 1970, **9**, 1131.
12. R. C. Aggarwal and D. S. Surya Narayana, *Ind. J. Chem.* 1984, **23A**, 1044.
13. M. M. Taqui Khan and V. Vijay Sen Reddy, *Inorg. Chem.* 1986, **25**, 208.
14. J. M. Heigh, N. P. Slabbert and D. A. Thornton, *J. Mol. Struct.* 1971, **7**, 199.
15. K. Seigbahn, C. Nordling, A. Fahlman, R. Nordberg, H. Hamrin, J. Hedman, G. Johnson, T. Bergmark, K. S. Karlsson, I. Lindgren and B. Lindberg, *ESCA, Atomic Molecular and Solid State Structure by Means of Electron Spectroscopy*. Almquist & Wiksell, Uppsala (1967).
16. K. Sieghbahn, C. Nordling, G. Johnson, J. Hedman, P. Hedan, K. Hamrin, U. Gelius, T. Bergmark, L. Werme, R. Manne and Y. Baer, *ESCA, Applied to Free Molecules*. North–Holland, Amsterdam (1969).
17. S. Srivastava, *Applied Spectrosc. Rev.* 1986, **22**, 401.
18. V. I. Nefedov, I. V. Prokofeva, A. E. Bukonova, L. K. Schubochkin, Ya. V. Salyn and V. L. Pershin, *Russ. J. Inorg. Chem.* 1974, **19**, 859.
19. V. I. Nefedov and M. A. Porai-Koshit, *Materials Res. Bull.* 1972, **7**, 1543.

Polyhedron Vol. 7, No. 12, pp. 1067–1070, 1988
Printed in Great Britain

0277–5387/88 $3.00+.00
© 1988 Pergamon Press plc

ISOLATION OF $[Rh(DIOLEFIN)X_2]^-$ SPECIES AND THEIR REACTIONS WITH P- OR N-DONOR LIGANDS, TIN(II) HALIDES AND CARBON MONOXIDE

M. A. GARCIA, M. A. GARRALDA* and L. IBARLUCEA

Catedra de Quimica Inorganica, Facultad de Quimica, Universidad del Pais Vasco, San Sebastian, Spain

(*Received* 27 *October* 1987; *accepted after revision* 13 *January* 1988)

Abstract—Anionic $[Rh(diolefin)X_2]^-$ species (X = Cl, Br) have been prepared and their reactions studied. The reactions with monodentate ligands led to neutral tetracoordinated complexes, and with N-donor bidentate ligands (Rh : LL = 2 : 1) gave Rh(X)(diolefin)(LL), $[Rh(diolefin)(LL)]^+[Rh(diolefin)X_2]^-$, or [Rh(diolefin)(LL)]X compounds, depending on the nature of LL or X. Reactions with carbon monoxide involved diolefin displacement. A trichlorostannato complex was obtained from the $[Rh(COD)Cl_2]^-$ species. Reactions of $[Rh(COD)Br]_2$ with bidentate N-donor ligands were also studied.

The reaction between $[Rh(diolefin)Cl]_2$ and some bidentate N-donor ligands (Rh : LL = 2 : 1) may give, depending on the nature of LL, ion-pair $[Rh(diolefin)(LL)]^+[Rh(diolefin)Cl_2]^-$ complexes, that contain diolefinic rhodium(I) anions.[1–4] While anionic carbonylated rhodium(I) species $[Rh(CO)_2X_2]^-$ have been extensively studied[5–12] and the crystal structure of $[Rh(CO)_2Cl_2]^-$ has been determined,[6–8] similar diolefinic $[Rh(diolefin)X_2]^-$ species have received less attention. $AsPh_4[Rh(COD)Cl_2]$ has been isolated[13] and the molecular structure of an ionic complex containing the $[Rh(COD)Cl_2]^-$ anion has been reported.[14]

In the present paper, we describe the synthesis of different $[Rh(diolefin)X_2]^-$ species and their reactivity with mono- and bidentate ligands containing N- or P-donor atoms, with carbon monoxide and with tin(II) halides.

RESULTS AND DISCUSSION

$[Rh(diolefin)X_2]^-$ species may be easily prepared by the reaction of $[Rh(diolefin)X]_2$ dimers with a stoichiometric amount of the corresponding halide as the salt of bulky cations that favour precipitation [eq. (1)]

$$[Rh(diolefin)X]_2 + 2RX \rightarrow 2R[Rh(diolefin)X_2]. \quad (1)$$

The complexes (**I–III**) thus obtained (see Table 1) are yellow and air stable, behave as 1 : 1 electrolytes in acetone solution and their IR spectra show, along with the bands due to the corresponding cations and diolefins, one or two bands in the far-IR due to ν (Rh—X). The ^{1}H-NMR spectra of the two anions containing 1,5-cyclooctadiene (X = Cl, Br) show three groups of resonances, around 4.3, 2.4 and 1.7 ppm. These values agree with those found in the literature for the anion $[Rh(COD)Cl_2]^-$ isolated as the tetraphenylarsonium salt by a more complicated method.[13] The anion $[Rh(NBD)Cl_2]^-$ shows the corresponding signals around 3.8, 3.6 and 1.1 ppm. All these signals are very similar to those corresponding to the starting dimers $[Rh(diolefin)X]_2$.[15]

The reactivity of $[Rh(COD)X_2]^-$ with aliphatic diamines (LL) depends on the degree of N-substitution in the diamine. Thus, when LL = ethylenediamine (en), pentacoordinated neutral Rh(X)(COD)(en) compounds are obtained, irrespective of the stoichiometric ratios employed (Rh : LL = 2 : 1 or 1 : 1) [eq. (2)]

$$Et_4N[Rh(COD)X_2] + en \rightarrow Rh(X)(COD)(en) + Et_4NX, \quad (2)$$

but when the more crowded LL = N,N,N′,N′-tetramethylethylenediamine (tmen) is used, no reaction occurs and the starting products are recovered unchanged.

*Author to whom correspondence should be addressed.

The anions $[Rh(COD)X_2]^-$ react with bidentate heterocyclic N-donor ligands to give products that depend on the type of halogen, X. Thus, $Et_4N[Rh(COD)Cl_2]$ reacts with 2,2′-bipyridine (bipy), 1,10-phenanthroline (phen), 5,6-dimethyl-1,10-phenanthroline (5,6-Me_2phen) or 4,7-diphenyl-1,10-phenanthroline (4,7-Ph_2phen) to yield ion-pair compounds $[Rh(COD)(LL)]^+[Rh(COD)Cl_2]^-$ when Rh : LL = 2 : 1 or ionic tetracoordinated [Rh(COD)(LL)]Cl when Rh : LL = 1 : 1. These products may also be obtained by the reaction of $[Rh(COD)Cl]_2$ with these ligands.[3,16] On the other hand, the reaction of $Et_4N[Rh(COD)Br_2]$ with these ligands gave only tetracoordinated ionic [Rh(COD)(LL)]Br complexes, irrespective of the stoichiometric ratios employed (Rh : LL = 2 : 1 or 1 : 1). The elemental analyses, molar conductivities and yields for the complexes obtained (**IV–VII**) are collected in Table 1.

$$[Rh(COD)X_2]^- \xrightarrow{(i)} 1/2[Rh(COD)(LL)]^+[Rh(COD)X_2]^- + X^- \quad (3)$$
$$\xrightarrow{(ii)} [Rh(COD)(LL)]X + X^-$$

(i) = 1/2LL (X = Cl); (ii) = LL (X = Cl, Br).

These results indicate a lower tendency to form the ion-pair compounds, when the anionic species contain bromine.

Monodentate P- or N-donor ligands, such as quinoline (quin) or triphenylphosphine, react easily with $[Rh(diolefin)X_2]^-$ species (Rh : L = 1 : 1), and displace one halide atom, yielding neutral tetracoordinated compounds [eq. (4)]

$$Et_4N[Rh(COD)X_2] + L \rightarrow Rh(X)(COD)L + Et_4NX \quad (4)$$

L = quin, Ph_3P.

Carbon monoxide displaces the coordinated diolefin, leading to the well-known dicarbonylated anions $[Rh(CO)_2Cl_2]^-$[5] identified through the IR spectra of the solutions obtained.

$Et_4N[Rh(COD)Cl_2]$ reacts with $SnCl_2$ but needs Rh : Sn = 1 : 3 molar ratios to react completely and give $(Et_4N)_2[Rh(SnCl_3)_3(COD)]$,[17] while $Et_4N[Rh(COD)Br_2]$ does not react with $SnBr_2$ under the same conditions and the starting product is recovered unchanged.

In the light of the above results, we have studied the reaction between $[Rh(COD)Br]_2$, prepared *in situ* from $[Rh(COD)Cl]_2$,[1] and bidentate N-donor ligands (Rh : LL = 2 : 1). The reaction with LL = bipy, phen, 5,6-Me_2phen, 4,7-Ph_2phen or tmen, gave ion-pair compounds [eq. (5)]

$$[Rh(COD)Br]_2 + LL \rightarrow [Rh(COD)(LL)]^+[Rh(COD)Br_2]^- \quad (5)$$

The complexes obtained are collected in Table 1 (**X–XVI**), they behave as 1 : 1 electrolytes in acetone solution and their IR spectra show bands due to ν (Rh—Br) of the anion $[Rh(COD)Br_2]^-$. In keeping with previous suggestions[18] we could attribute the behaviour of $[Rh(COD)Br]_2$, to a bridge cleavage mechanism via five-coordinate intermediates that could avoid free bromine appearing in solution.

The reaction of $[Rh(COD)Br]_2$ with ethylenediamine, 2,9-dimethyl-1,10-phenanthroline (2,9-Me_2phen) or 2,9-dimethyl-4,7-diphenyl-1,10-phenanthroline (2,9-Me_2-4,7-Ph_2phen) (Rh : LL = 1 : 1 or 2 : 1) gave only pentacoordinated neutral compounds Rh(Br)(COD)(LL) (**XV–XVII**), analogous to those obtained from $[Rh(COD)Cl]_2$[3,4] [eq. (6)]

$$[Rh(COD)Br]_2 + 2LL \rightarrow 2Rh(Br)(COD)(LL). \quad (6)$$

These compounds behave as non-electrolytes in acetone solution and their IR spectra show one band around 200 cm^{-1} that may be due to ν (Rh—Br), thus confirming the bromine being bonded to the rhodium atom. Rh(Br)(COD)(en) shows bands due to the coordinated diamine at ν (N—H) = 3190 ($\Delta\nu$ = 180), 3170 ($\Delta\nu$ = 200) and 3080 ($\Delta\nu$ = 205) cm^{-1}. The band at the higher frequency is split, probably due to crystal lattice effects. The ν (N—H) decreases upon coordination are smaller than in the analogous Rh(Cl)(COD)(en).[4]

EXPERIMENTAL

$[Rh(COD)Cl]_2$, *in situ* $[Rh(COD)Br]_2$[1] and $[Rh(NBD)Cl]_2$[19] compounds were prepared by published methods. The C, H and N microanalysis were carried out with a Perkin–Elmer 240C microanalyser. Conductivities were measured in *ca* 2.5×10^{-4} M acetone solutions with a Metrhom E518 conductimeter. Proton NMR spectra were recorded at room temperature with an XL-200 Varian spectrometer with tetramethylsilane as the internal standard and deuterochloroform as the solvent. IR spectra were recorded on a Perkin–Elmer 598 spectrophotometer in the range 4000–200 cm^{-1} using Nujol mulls between polyethylene sheets and

Table 1. Analytical, conductivity and IR data and yields for the isolated compounds

Compound	Found (calc.) %C	%H	%N	Λ_M (Ω^{-1} cm^2 mol^{-1})	ν (Rh—X) (cm^{-1})	Yield (%)
Et_4N[Rh(COD)Cl_2] (I)	45.3 (46.4)	7.4 (7.8)	3.2 (3.4)	106	270(sh) 258(s)	61
$AsPh_4$[Rh(NBD)Cl_2] (II)	56.2 (57.3)	4.3 (4.3)	—	112	275(m) 260(m)	76
Et_4N[Rh(COD)Br_2] (III)	38.4 (38.3)	7.1 (6.4)	2.8 (2.8)	136	188(s)	74
[Rh(COD)(phen)]Br (IV)	49.9 (51.0)	4.3 (4.3)	5.9 (5.9)	[a]	—	52
[Rh(COD)(bipy)]Br (V)	46.9 (48.4)	4.7 (4.5)	6.1 (6.3)	109	—	70
[Rh(COD)(5,6-Me_2phen)]Br (VI)	50.4 (52.9)	4.5 (4.8)	5.6 (5.6)	121	—	75
[Rh(COD)(4,7-Ph_2phen)]Br (VII)	60.1 (61.6)	4.8 (4.5)	4.3 (4.5)	114	—	66
Rh(Br)(COD)(quin) (VIII)	47.5 (48.6)	4.8 (4.6)	3.5 (3.3)	10	193(s)	53
Rh(Cl)(COD)(quin) (IX)	54.0 (54.3)	5.0 (4.5)	4.4 (3.7)	10	285(sh) 265(m)	31
[Rh(COD)(4,7-Ph_2phen)][Rh(COD) Br_2] (X)	51.8 (52.5)	4.4 (4.4)	3.3 (3.1)	96	178(m)	72
[Rh(COD)(phen)][Rh(COD)Br_2] (XI)	43.8 (44.1)	4.3 (4.2)	3.7 (3.7)	[a]	191(s)	69
[Rh(COD)(5,6-Me_2phen)][Rh(COD)Br_2] (XII)	45.4 (45.6)	4.6 (4.6)	3.4 (3.5)	[a]	179(s)	65
[Rh(COD)(bipy)][Rh(COD)Br_2] (XIII)	42.7 (42.3)	4.3 (4.4)	4.1 (3.8)	104	190(m)	47
[Rh(COD)(tmen)][Rh(COD)Br_2] (XIV)	36.0 (37.8)	5.8 (5.8)	4.1 (4.0)	116	195(s)	79
Rh(Br)(COD)(2,9-Me_2phen) (XV)	51.6 (52.9)	4.8 (4.8)	5.4 (5.6)	2	202(s)	48
Rh(Br)(COD)(2,9-Me_2-4,7-Ph_2phen) (XVI)	61.6 (62.6)	5.0 (4.9)	4.5 (4.3)	2	202(s)	85
Rh(Br)(COD)(en) (XVII)	33.6 (34.2)	5.7 (5.7)	7.2 (8.0)	[a]	202(s)	65

[a] Insoluble in acetone.

with a Nicolet 60SX spectrophotometer in the range 500–140 cm^{-1}, using polyethylene pellets.

Preparation of Et_4N[Rh(COD)X_2] *complexes*

To 5 cm^3 of dichloromethane solutions of [Rh(COD)X]$_2$ (0.12 mmol), the appropriate Et_4NX (0.24 mmol) was added. Upon addition of diethyl ether yellow precipitates were formed, filtered off, washed with diethyl ether and air-dried.

Preparation of Ph_4As[Rh(NBD)Cl_2]

Addition of Ph_4AsCl (0.24 mmol) to 5 cm^3 of a dichloromethane solution of [Rh(NBD)Cl]$_2$ (0.12 mmol), followed by addition of n-hexane gave a yellow solid that was filtered off, washed with n-hexane and air-dried.

Reactions of Et_4N[Rh(COD)X_2]

(i) *Reaction with ethylenediamine.* Addition of ethylenediamine (0.12 mmol) to solutions of Et_4N[Rh(COD)X_2] (0.12 mmol) in 5 cm^3 of dichloromethane yield yellow solids that were filtered off, washed with dichloromethane and air dried. The solids obtained were identified as Rh(X)(COD)(en).

(ii) *Reaction with phenanthroline type ligands.* To Et_4N[Rh(COD)X_2] (0.12 mmol) solutions in 5 cm^3 of dichloromethane, the corresponding stoi-

chiometric amounts (0.12 mmol) of 1,10-phenanthroline, 2,2′-bipyridine, 5,6-dimethyl-1,10-phenanthroline or 4,7-diphenyl-1,10-phenanthroline were added, whereupon the solution turned red or violet. The formed [Rh(COD)(LL)]Br complexes precipitated immediately as red crystals when LL = 1,10-phenanthroline or 5,6-dimethyl-1,10-phenanthroline were added and required elimination of CH_2Cl_2 and addition of acetone when LL = 2,2′-bipyridine (red crystals) or 4,7-diphenyl-1,10-phenanthroline (violet crystals) was used. The complexes obtained were filtered off, washed with acetone and air-dried.

(iii) *Reaction with triphenylphosphine.* Ph_3P (0.08 mmol) was added to yellow solutions of $Et_4N[Rh(COD)X_2]$ (0.08 mmol) in 5 cm^3 of CH_2Cl_2/MeOH (1 : 1) whereupon the solutions became orange. The elimination of dichloromethane yielded orange Rh(X)(COD)(Ph_3P) compounds that were filtered off, washed with methanol and air-dried.

(iv) *Reaction with quinoline.* Quinoline (0.12 mmol) was added to 5 cm^3 of yellow dichloromethane solutions of $Et_4N[Rh(COD)X_2]$ (0.12 mmol). Addition of methanol (3 cm^3) and elimination of dichloromethane led to yellow precipitates of Rh(X)(COD)(quin) complexes that were filtered off, washed with methanol and air-dried.

(v) *Reaction with carbon monoxide.* Carbon monoxide (P = 1 atm) was bubbled through dichloromethane solutions of $Et_4N[Rh(COD)X_2]$ (0.12 mmol) for 30 min. IR spectra of the yellow solutions obtained confirmed the formation of $Et_4N[Rh(CO)_2X_2]$ complexes.

(vi) *Reaction with tin*(II) *halides.* $SnCl_2 \cdot 2H_2O$ (0.30 mmol) in 5 cm^3 of methanol was added to 5 cm^3 of $Et_4N[Rh(COD)Cl_2]$ (0.10 mmol) in dichloromethane. The addition of Et_4NCl (0.10 mmol) followed by elimination of dichloromethane gave $(Et_4N)_2[Rh(SnCl_3)_3(COD)]$ that was filtered off, washed with methanol and air-dried.

$Et_4N[Rh(COD)Br_2]$ did not react with $SnBr_2$ under the same conditions.

Preparation of $[Rh(COD)(LL)]^+[Rh(COD)Br_2]^-$ *complexes*

Addition of the corresponding ligand (0.06 mmol) to 5 cm^3 of dichloromethane solutions of *in situ* prepared $[Rh(COD)Br]_2$ (0.06 mmol) gave red solids when LL = 1,10-phenanthroline, 2,2′ bipyridine or 5,6-dimethyl-1,10-phenanthroline. When LL = 4,7-diphenyl-1,10-phenanthroline or N,N,N′,N′-tetramethylethylenediamine, addition of diethyl ether was necessary to afford precipitation of the corresponding compounds. The complexes obtained were filtered off, washed with diethyl ether and air-dried.

Preparation of Rh(Br)(COD)(LL) *complexes*

0.12 mmol of the corresponding ligand were added to 5 cm^3 of dichloromethane solutions of *in situ* prepared $[Rh(COD)Br]_2$ (0.06 mmol). When LL = ethylenediamine, a yellow solid appeared immediately. When LL = 2,9-dimethyl-1,10-phenanthroline or 2,9-dimethyl-4,7-diphenyl-1,10-phenanthroline, addition of diethyl ether gave yellow solids. The complexes thus obtained, were filtered off, washed with diethyl ether and air-dried.

Acknowledgement—We thank the CAICYT for financial support.

REFERENCES

1. J. Chatt and L. M. Venanzi, *J. Chem. Soc.* 1957, 4735.
2. D. M. Roe and G. Massey, *J. Organomet. Chem.* 1971, **28**, 273.
3. V. García, M. A. Garralda and L. Ibarlucea, *Transition Met. Chem.* 1985, **10**, 288.
4. M. A. Garralda and L. Ibarlucea, *J. Organomet. Chem.* 1986, **311**, 225.
5. L. M. Vallarino, *Inorg. Chem.* 1965, **4**, 161.
6. E. Cetinkaya, A. W. Johnson, M. F. Lappert, G. M. McLaughlin and K. W. Mir, *J. Chem. Soc., Dalton Trans.* 1974, 1236.
7. C. K. Thomas and J. A. Stanko, *Inorg. Chem.* 1971, **10**, 566.
8. F. W. B. Einstein and C. R. S. M. Hampton, *Can. J. Chem.* 1971, **49**, 1901.
9. A. R. Sanger, *J. Chem, Soc., Dalton Trans.* 1981, 228.
10. J. V. Kingston, *Inorg. Nucl. Chem. Lett.* 1968, **4**, 65.
11. J. V. Kingston, F. T. Mahmoud and G. R. Scollary, *J. Inorg. Nucl. Chem.* 1972, **34**, 3197.
12. H. A. Hudali, J. V. Kingston and H. A. Tayim, *Inorg. Chem.* 1979, **18**, 1391.
13. B. Crociani, U. Belluco and P. Sandrini, *J. Organomet. Chem.* 1979, **177**, 385.
14. M. C. Bonnet, I. Tkatchenko, R. Faure and H. Loiseleur, *Nouv. J. Chim.* 1983, **7**, 601.
15. H. C. Volger, M. M. P. Gaasbeek, H. Hogeveen and K. Vrieze, *Inorg. Chim. Acta* 1969, **3**, 145.
16. G. Zassinovich, G. Mestroni and A. Camus, *J. Organomet. Chem.* 1975, **91**, 379.
17. M. Kretschmer, P. S. Pregosin and H. Ruegger, *J. Organomet. Chem.* 1983, **241**, 87.
18. B. Denise and G. Pannetier, *J. Organomet. Chem.* 1978, **148**, 155.
19. E. W. Abel, M. A. Bennett and G. Wilkinson, *J. Chem. Soc.* 1959, 3178.

Polyhedron Vol. 7, No. 12, pp. 1071–1077, 1988
Printed in Great Britain

0277–5387/88 $3.00 + .00
© 1988 Pergamon Press plc

CLUSTER SYNTHESIS—XX. THE SYNTHESIS, AND CRYSTAL AND MOLECULAR STRUCTURE OF $Ru_6(CO)_{17}(\mu_4\text{-}\eta^2\text{-}HC_2Ph)(\mu_4\text{-}S)$

RICHARD D. ADAMS,* JAMES E. BABIN, MIKLOS TASI and THOMAS A. WOLFE

Department of Chemistry, University of South Carolina, Columbia, SC 29208, U.S.A.

(*Received* 23 *September* 1987; *accepted after revision* 18 *January* 1988)

Abstract—The reaction of $Ru_5(CO)_{15}(\mu_4\text{-}S)$ with HC_2Ph at 68°C has resulted in the formation of the complex $Ru_5(CO)_{13}(\mu\text{-}CO)(\mu_4\text{-}\eta^2\text{-}HC_2Ph)(\mu_4\text{-}S)$, **1** in 60% yield. Compound **1** was found to react with $Ru(CO)_5$ at 80°C to yield the enlarged cluster $Ru_6(CO)_{17}(\mu_4\text{-}\eta^2\text{-}HC_2Ph)(\mu_4\text{-}S)$, **2** in 53% yield. Compound **2** was characterized structurally. Crystal data: $Ru_6SO_{17}C_{25}H_6$, $M = 1216.80$, monoclinic, $P2_1/c$ (No. 14), $a = 11.050(2)$, $b = 22.503(5)$, $c = 29.26(1)$ Å, $\beta = 90.80(3)°$, $V = 7276(4)$ Å^3, $D_c = 2.27$ g cm^{-3}, $Z = 8$, λ(Mo-K_α) = 0.71073 Å (graphite monochromator) $\mu = 24.9$ cm^{-1}. Methods: MITHRIL, difference Fourier, full-matrix least-squares. Refinement of 4647 reflections ($F^2 \geqslant 3\sigma(F^2)$), ($1° < 2\theta < 42°$), gave R and R_w values of 0.049 and 0.048, respectively. Data/parameters ratio = 9.54, highest peak in final difference Fourier = 0.79 e Å^{-3}. The molecule consists of a distorted square of four ruthenium atoms that contains a quadruply bridging sulphido ligand on one side of the cluster and a quadruply bridging alkyne ligand on the other side. $Ru(CO)_4$ groups bridge adjacent edges of the cluster. The $Ru(CO)_4$ groups can be cleaved off sequentially by treatment with CO at 80°C/1 atm.

In recent years, much of our research has focused on developing procedures for the synthesis of osmium carbonyl clusters that contain sulphido ligands.[1] In an expansion of our studies of cluster synthesis, we have recently focused on the element ruthenium. We have discovered high yield syntheses for the compounds $Ru_3(CO)_9(\mu_3\text{-}CO)(\mu_3\text{-}S)$ and $Ru_3(CO)_9(\mu_3\text{-}S)_2$, both of which have been found to be useful reagents for the preparation of new high nuclearity sulphido ruthenium carbonyl clusters.

We have now extended these studies to include sulphidoruthenium carbonyl clusters which contain alkyne ligands.[4] In the course of these studies, we have discovered a new route to the compound $Ru_5(CO)_{13}(\mu\text{-}CO)[\mu_4\text{-}\eta^2\text{-}HC_2Ph](\mu_4\text{-}S)$, **1**, and have prepared and structurally characterized the new higher nuclearity cluster $Ru_6(CO)_{17}[\mu_4\text{-}\eta^2\text{-}HC_2Ph](\mu_4\text{-}S)$, **2**. These results are described herein.

* Author to whom correspondence should be addressed.

EXPERIMENTAL

General

All reactions were performed under a nitrogen atmosphere. Reagent grade solvents were stored over 4 Å molecular sieves. $Ru_3(CO)_{12}$ was purchased from Strem Chemical Company and was used as received. Phenylacetylene was purchased from Aldrich Chemical Company and was vacuum distilled before use. CP grade carbon monoxide was purchased from Linde Company and was used without further purification. $Ru(CO)_5$ was prepared by the reported method.[5] $Ru_5(CO)_{15}(\mu_4\text{-}S)$ was prepared as previously reported.[3]

All chromatographic separations were performed in air. TLC separations were performed on plates (0.25 mm Kieselgel 60 F_{254}, E. Merck, West Germany) purchased from Bodman Chemicals, U.S.A. IR spectra were recorded on a Nicolet 5DXB FT-IR spectrophotometer. ^{1}H NMR spectra were recorded on a Bruker AM-300 spectrometer operating

at 300 MHz. Elemental analyses were performed by Desert Analytics, Tucson, Arizona.

Preparation of $Ru_5(CO)_{13}(\mu\text{-CO})[\mu_4\text{-}\eta^2\text{-}HC_2Ph](\mu_4\text{-S})$, **1**

40 mg (0.042 mmol) of $Ru_5(CO)_{15}(\mu_4\text{-S})$ and 2.3×10^{-2} cm^3 (0.209 mmol) of HC_2Ph was added to 40 cm^3 of hexane. This mixture was refluxed for 15 min. During this time, the $Ru_5(CO)_{15}(\mu_4\text{-S})$ dissolved and the solution turned dark green. The solvent was removed *in vacuo*. The residue was dissolved in a minimal amount of CH_2Cl_2 and was chromatographed by TLC on silica gel. Elution with hexane/CH_2Cl_2, 95/5 solvent mixture yielded 26 mg of $Ru_5(CO)_{13}(\mu\text{-CO})[\mu_4\text{-}\eta^2\text{-}HC_2Ph](\mu_4\text{-S})$, **1**, 60%, as a green band.

Preparation of $Ru_6(CO)_{17}[\mu_4\text{-}\eta^2\text{-}HC_2Ph](\mu_4\text{-S})$, **2**

40 mg (0.039 mmol) of compound **1** was dissolved in 30 cm^3 cyclohexane and brought to a reflux. A 100 cm^3 cyclohexane solution of $Ru(CO)_5$ (0.422 mmol) was added from a dropping funnel over a period of approximately 30 min. The reaction solution was then refluxed for an additional 15 min. The solution was concentrated and chromatographed over a Florisil column using hexane solvent. The first yellow band was $Ru_3(CO)_{12}$. A second black band was eluted with CH_2Cl_2 and was subsequently purified further by TLC. Elution with a hexane/CH_2Cl_2, 95/5, solvent mixture yielded 0.5 mg of $Ru_4(CO)_9(\mu\text{-CO})_2[\mu_4\text{-}\eta^2\text{-}HC_2Ph](\mu_4\text{-S})$, **3**, 2%, as an orange band, 6.7 mg of unreacted **1** and 20.9 mg of $Ru_6(CO)_{17}[\mu_4\text{-}\eta^2\text{-}HC_2Ph](\mu_4\text{-S})$, **2**, 53%, as a brown band. IR for **2**: [ν(CO)in hexane] 2115(vw), 2091(s), 2074(vs), 2050(m), 2043(s), 2030(vs), 2023(s), 2009(m), 1999(vw), 1987(vw), 1962(w), 1956(w). ^{1}H NMR (in CD_2Cl_2) 7.27–7.19 (m, 3H), 7.09–7.05 (m, 2H), 7.21 (s, 1H). Found: C, 25.1; H, 0.5. Calc. for $Ru_6SO_{17}C_{25}H_6$: C, 24.7; H, 0.5%. The yields of compounds **2** and **3** were calculated on the basis of the amount of **1** consumed.

Reaction of **1** *with* CO

15.9 mg (0.015 mmol) of **1** was dissolved in 25 cm^3 of cyclohexane. The solution was heated to reflux (80°C) for 5 h under a CO purge. The cyclohexane was removed *in vacuo*. The residue was dissolved in a minimal amount of CH_2Cl_2 and was chromatographed by TLC on silica gel. Elution with hexane/CH_2Cl_2, 95/5, solvent mixture yielded 7.5 mg of **3**, 60%, as an orange band, 0.7 mg of unreacted **2**, and 0.5 mg of **2**, 3%, as a brown band. The yields of compounds **2** and **3** were calculated on the basis of the amount of **1** consumed.

Reaction of **2** *with* CO

16.6 mg (0.014 mmol) of **2** was dissolved in 25 cm^3 of cyclohexane. The solution was heated to reflux (80°C) for 3 h under a CO purge. Work-up as described above yielded 4.6 mg of compound **3**, 51%, 3.0 mg of **1**, 27% and 3.6 mg of unreacted **2**. The yields of compounds **1** and **3** were calculated on the basis of the amount of **2** consumed.

CRYSTALLOGRAPHIC ANALYSES

Crystals of **2** were grown by slow evaporation of solvent from benzene solutions at 5°C. The data crystal was mounted in a thin-walled glass capillary. Diffraction measurements were made on a Rigaku AFC6 automatic diffractometer by using Mo-K_α radiation. The unit cell was determined and refined from 25 randomly selected reflections obtained by using the AFC6 automatic search, centre, index and least-squares routines. Crystal data, data collection parameters and results of the analyses are listed in Table 1.* All data processing was performed on a Digital Equipment Corp. MICROVAX II computer by using the Molecular Structure Corp. TEXSAN structure solving program library. Neutral atom scattering factors were obtained from the standard sources.[6(a)] Anomalous dispersion corrections were applied to all non-hydrogen atoms.[6(b)] Full-matrix least-squares refinements minimized the function

$$\sum_{hkl} W(|F_{obs}| - |F_{calc}|)^2$$

where

$$W = 1/\sigma(F)^2, \quad \sigma(F) = \sigma(F_{obs}^2)2/F_{obs}$$

and

$$\sigma(F_{obs}^2) = [\sigma(I_{raw})^2 + (PR_{obs})^2]^{1/2} L_p.$$

Compound **2** crystallized in the monoclinic crystal system. The space group $P2_1/c$ was determined by the systematic absences observed in the data. Compound **2** crystallizes with two independent molecules in the asymmetric unit. Metal atom positions were determined by direct methods

* Complete tables of bond lengths, angles and thermal parameters for (1)–(3) and observed and calculated structure factors for (1)–(3) have been deposited as supplementary material with the Editor, from whom copies are available on request. Atomic coordinates have been submitted to the Cambridge Crystallographic Data Centre.

Table 1. Crystallographic data for the structural analysis for compound **2**

(a)		
	Formula	$Ru_6SO_{17}C_{25}H_6$
	Temperature (±3°C)	23°C
	Space group	$P2_1/c$, No. 14
	a (Å)	11.050(2)
	b (Å)	22.503(5)
	c (Å)	29.26(1)
	β (deg)	90.80(3)
	V (Å^3)	7276(6)
	M_r	1216.8
	Z	8
	ρ_{calc} (g cm^{-3})	2.22
(b)	Measurement of intensity data	
	Radiation	Mo-K_α (0.71073 Å)
	Monochromator	Graphite
	Detector aperture (mm)	
	horizontal	2.0
	vertical	2.0
	Crystal faces:	010, 0$\bar{1}$0, 001 00$\bar{1}$, 1$\bar{1}$0, $\bar{1}$02
	Crystal size (mm):	0.06 × 0.18 × 0.19
	Crystal orientation:	
	lattice direction; deg from θ-axis	[100]; 6.06
	Reflections measured	$+h$, $+k$, $\pm l$
	Max 2θ	42°
	Scan type	Moving crystal– stationary counter
	ω-Scan width $(A + 0.347 \tan\theta)°$	$A = 1.10$
	Background: time at	$\frac{1}{4}$ addition scan at each end of scan
	ω-Scan rate (deg min^{-1})*	4.0[a]
	Data used ($F^2 \geq 3.0\sigma(F^2)$)	4647
(c)	Treatment of data	
	Absorption correction:	Not applied
	coefficient (cm^{-1}):	24.9
	P-factor	0.02
	Final residuals R_F	0.049
	R_{wF}	0.048
	Esd of unit weight observation	1.51
	Largest shift/error	
	Value of final cycle	0.03
	Largest peak in final diff. Fourier (e Å^{-3})	0.79
	No. of variables	487

[a] Rigaku software uses a multiple scan technique. If the $I/\sigma(I)$ ratio is less than 10.0, a second scan is made and the results are added to the first scan, etc. A maximum of three scans was permitted per reflection.

(MITHRIL). All other non-hydrogen atoms were located by subsequent difference Fourier syntheses. Due to the large size of the calculations, only atoms heavier than oxygen were refined with anisotropic thermal parameters. In the later stages of refinement one mole of benzene solvent that had co-crystallized per 2 moles of **2** was located. This was added to the analysis and satisfactorily refined. Hydrogen atom positions were calculated by assuming idealized geometries. Their positions were not refined but their contributions were added to the structure factor calculations.

RESULTS

When $Ru_5(CO)_{15}(\mu_4\text{-S})$ was allowed to react with HC_2Ph at 68°C, the compound $Ru_5(CO)_{13}(\mu\text{-CO})(\mu_4\text{-}\eta^2\text{-}HC_2Ph)(\mu_4\text{-S})$, **1** was formed in 60% yield. Compound **1** was obtained previously in low yield by cluster enlargement in the reaction of $Ru_4(CO)_9(\mu\text{-CO})_2(\mu_4\text{-}\eta^2\text{-}HC_2Ph)(\mu_4\text{-S})$, **3** with $Ru(CO)_5$.[4] We have now found that **1** can also be enlarged by reaction with $Ru(CO)_5$ to yield $Ru_6(CO)_{17}(\mu_4\text{-}\eta^2\text{-}HC_2Ph)(\mu_4\text{-S})$, **2** in 53% yield. Compound **2** was obtained in trace amounts from the reaction of **3** with $Ru(CO)_5$.[4]

Compound **2** has been characterized by a single-crystal X-ray diffraction analysis. It was found to contain two independent molecules in the asymmetric crystal unit. Both molecules are structurally similar. An ORTEP diagram of the molecular structure of **2** is shown in Fig. 1. Selected intramolecular bond distances and angles are listed in Tables 2 and 3, respectively. The molecule consists of an approximately square cluster of four ruthenium atoms, Ru(1), Ru(2), Ru(3) and Ru(4) that contains a quadruply bridging sulphido ligand on one side of the cluster and a quadruply bridging HC_2Ph ligand on the other side. The four metal atoms together with the sulphido ligand and two alkyne carbon atoms could be viewed as a larger cluster of seven atoms that has an idealized shape of a pentagonal bipyramid. The pentagonal plane includes the sulphido ligand, the two carbon atoms and the two metal atoms, Ru(1) and Ru(3). This portion of the molecule is very similar to those found in **1** and **3** which have also been structurally characterized.[4] Compound **2** also contains two $Ru(CO)_4$ groups that bridge adjacent apical–equatorial

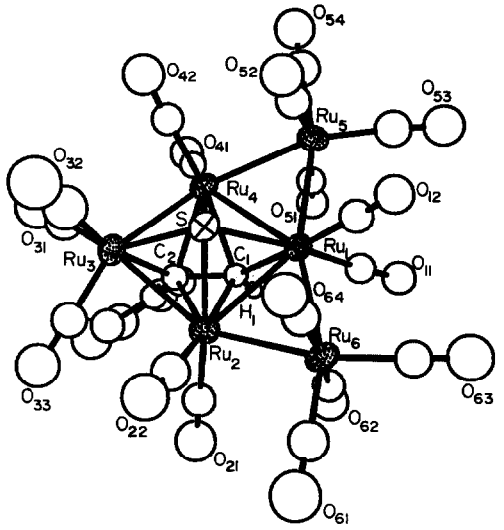

Fig. 1. An ORTEP diagram of the molecular structure of $Ru_6(CO)_{17}(\mu_4\text{-}\eta^2\text{-}HC_2Ph)(\mu_4\text{-S})$, **2** showing 50% probability thermal ellipsoids.

Table 2. Intramolecular distances for $Ru_6(CO)_{17}(\mu_4\text{-}\eta^2\text{-}HC_2Ph)(\mu_4\text{-S})$, **2**[a]

Atom	Atom	Distance	Atom	Atom	Distance
Ru(1a)	C(1a)	2.12(2)	Ru(2b)	S(1b)	2.493(5)
Ru(1a)	S(1a)	2.419(5)	Ru(2b)	Ru(6b)	2.732(3)
Ru(1a)	Ru(6a)	2.754(2)	Ru(2b)	Ru(3b)	2.794(2)
Ru(1a)	Ru(5a)	2.770(2)	Ru(3a)	C(2a)	2.18(2)
Ru(1a)	Ru(2a)	2.787(2)	Ru(3a)	S(1a)	2.434(5)
Ru(1a)	Ru(4a)	2.788(2)	Ru(3a)	Ru(4a)	2.753(2)
Ru(1b)	C(1b)	2.08(2)	Ru(3b)	C(2b)	2.13(2)
Ru(1b)	S(1b)	2.432(5)	Ru(3b)	S(1b)	2.445(6)
Ru(1b)	Ru(4b)	2.753(2)	Ru(3b)	Ru(4b)	2.744(2)
Ru(1b)	Ru(6b)	2.770(2)	Ru(4a)	C(2a)	2.31(2)
Ru(1b)	Ru(5b)	2.790(2)	Ru(4a)	S(1a)	2.491(5)
Ru(1b)	Ru(2b)	2.823(2)	Ru(4a)	Ru(5a)	2.738(2)
Ru(2a)	C(2a)	2.35(2)	Ru(4b)	C(2b)	2.34(2)
Ru(2a)	S(1a)	2.470(5)	Ru(4b)	S(1b)	2.485(5)
Ru(2a)	Ru(6a)	2.732(2)	Ru(4b)	Ru(5b)	2.739(2)
Ru(2a)	Ru(3a)	2.766(2)	C(1a)	C(2a)	1.43(2)
Ru(2b)	C(2b)	2.31(2)	C(1b)	C(2b)	1.41(2)
C(a)	$O(a)_{av.}$	1.15(2)	C(a)	$C(b)_{av.}$	1.38(2)
C(b)	$O(b)_{av.}$	1.16(2)	C(a)	$C(b)_{av.}$	1.37(2)

[a] Distances are in angstroms. Estimated standard deviations in the least significant figure are given in parentheses.

Table 3. Intramolecular bond angles for $Ru_6(CO)_{17}(\mu_4\text{-}\eta^2\text{-}HC_2Ph)(\mu_4\text{-}S)$, **2**[a]

Atom	Atom	Atom	Angle	Atom	Atom	Atom	Angle
C(1a)	Ru(1a)	S(1a)	81.8(5)	Ru(4b)	Ru(1b)	Ru(2b)	80.97(6)
C(1a)	Ru(1a)	Ru(6a)	100.7(4)	Ru(6b)	Ru(1b)	Ru(5b)	161.10(9)
C(1a)	Ru(1a)	Ru(5a)	97.3(4)	Ru(6b)	Ru(1b)	Ru(2b)	58.46(6)
C(1a)	Ru(1a)	Ru(2a)	53.5(4)	Ru(5b)	Ru(1b)	Ru(2b)	139.49(8)
C(1a)	Ru(1a)	Ru(4a)	53.0(4)	C(2a)	Ru(2a)	S(1a)	79.7(4)
S(1a)	Ru(1a)	Ru(6a)	92.8(1)	C(2a)	Ru(2a)	Ru(6a)	133.3(4)
S(1a)	Ru(1a)	Ru(5a)	96.7(1)	C(2a)	Ru(2a)	Ru(3a)	49.6(4)
S(1a)	Ru(1a)	Ru(2a)	56.1(1)	C(2a)	Ru(2a)	Ru(1a)	79.1(4)
S(1a)	Ru(1a)	Ru(4a)	56.6(1)	S(1a)	Ru(2a)	Ru(6a)	92.2(1)
Ru(6a)	Ru(1a)	Ru(5a)	160.67(8)	S(1a)	Ru(2a)	Ru(3a)	55.1(1)
Ru(6a)	Ru(1a)	Ru(2a)	59.09(6)	S(1a)	Ru(2a)	Ru(1a)	54.4(1)
Ru(6a)	Ru(1a)	Ru(4a)	139.23(8)	Ru(6a)	Ru(2a)	Ru(3a)	147.23(8)
Ru(5a)	Ru(1a)	Ru(2a)	139.57(8)	Ru(6a)	Ru(2a)	Ru(1a)	59.87(6)
Ru(5a)	Ru(1a)	Ru(4a)	59.02(6)	Ru(3a)	Ru(2a)	Ru(1a)	96.06(7)
Ru(2a)	Ru(1a)	Ru(4a)	80.56(7)	C(2b)	Ru(2b)	S(1b)	79.0(4)
C(1b)	Ru(1b)	S(1b)	79.5(5)	C(2b)	Ru(2b)	Ru(6b)	128.5(4)
C(1b)	Ru(1b)	Ru(4b)	52.4(5)	C(2b)	Ru(2b)	Ru(3b)	48.2(4)
C(1b)	Ru(1b)	Ru(6b)	95.5(5)	C(2b)	Ru(2b)	Ru(1b)	78.5(4)
C(1b)	Ru(1b)	Ru(5b)	102.0(5)	S(1b)	Ru(2b)	Ru(6b)	97.0(1)
C(1b)	Ru(1b)	Ru(2b)	51.8(5)	S(1b)	Ru(2b)	Ru(3b)	54.7(1)
S(1b)	Ru(1b)	Ru(4b)	56.9(1)	S(1b)	Ru(2b)	Ru(1b)	54.0(1)
S(1b)	Ru(1b)	Ru(6b)	97.5(1)	Ru(6b)	Ru(2b)	Ru(3b)	151.21(8)
S(1b)	Ru(1b)	Ru(5b)	92.7(1)	Ru(6b)	Ru(2b)	Ru(1b)	59.81(6)
S(1b)	Ru(1b)	Ru(2b)	56.1(1)	Ru(3b)	Ru(2b)	Ru(1b)	94.74(7)
Ru(4b)	Ru(1b)	Ru(6b)	139.35(8)	C(2a)	Ru(3a)	S(1a)	84.0(5)
Ru(4b)	Ru(1b)	Ru(5b)	59.24(6)	C(2a)	Ru(3a)	Ru(4a)	54.5(5)
C(2a)	Ru(3a)	Ru(2a)	55.3(5)	S(1b)	Ru(4b)	Ru(1b)	55.0(1)
S(1a)	Ru(3a)	Ru(4a)	57.0(1)	Ru(5b)	Ru(4b)	Ru(3b)	148.01(8)
S(1a)	Ru(3a)	Ru(2a)	56.3(1)	Ru(5b)	Ru(4b)	Ru(1b)	61.05(6)
Ru(4a)	Ru(3a)	Ru(2a)	81.54(7)	Ru(3b)	Ru(4b)	Ru(1b)	97.51(7)
C(2b)	Ru(3b)	S(1b)	83.5(5)	Ru(4a)	Ru(5a)	Ru(1a)	60.82(6)
C(2b)	Ru(3b)	Ru(4b)	55.6(5)	Ru(4b)	Ru(5b)	Ru(1b)	59.71(6)
C(2b)	Ru(3b)	Ru(2b)	53.8(5)	Ru(2a)	Ru(6a)	Ru(1a)	61.04(6)
S(1b)	Ru(3b)	Ru(4b)	56.9(1)	Ru(2b)	Ru(6b)	Ru(1b)	61.74(6)
S(1b)	Ru(3b)	Ru(2b)	56.4(1)	Ru(1a)	S(1a)	Ru(3a)	116.5(2)
Ru(4b)	Ru(3b)	Ru(2b)	81.63(7)	Ru(1a)	S(1a)	Ru(2a)	69.5(1)
C(2a)	Ru(4a)	S(1a)	80.0(5)	Ru(1a)	S(1a)	Ru(4a)	69.2(1)
C(2a)	Ru(4a)	Ru(5a)	131.0(4)	Ru(3a)	S(1a)	Ru(2a)	68.6(1)
C(2a)	Ru(4a)	Ru(3a)	50.0(4)	Ru(3a)	S(1a)	Ru(4a)	67.9(1)
C(2a)	Ru(4a)	Ru(1a)	79.7(4)	Ru(2a)	S(1a)	Ru(4a)	93.2(2)
S(1a)	Ru(4a)	Ru(5a)	95.9(1)	Ru(1b)	S(1b)	Ru(3b)	115.9(2)
S(1a)	Ru(4a)	Ru(3a)	55.0(1)	Ru(1b)	S(1b)	Ru(4b)	68.1(1)
S(1a)	Ru(4a)	Ru(1a)	54.2(1)	Ru(1b)	S(1b)	Ru(2b)	69.9(1)
Ru(5a)	Ru(4a)	Ru(3a)	150.89(8)	Ru(3b)	S(1b)	Ru(4b)	67.6(1)
Ru(5a)	Ru(4a)	Ru(1a)	60.17(6)	Ru(3b)	S(1b)	Ru(2b)	68.9(1)
Ru(3a)	Ru(4a)	Ru(1a)	96.32(7)	Ru(4b)	S(1b)	Ru(2b)	93.3(2)
C(2b)	Ru(4b)	S(1b)	78.7(4)	C(2a)	C(1a)	Ru(1a)	134(1)
C(2b)	Ru(4b)	Ru(5b)	135.9(4)	C(2b)	C(1b)	Ru(1b)	138(1)
C(2b)	Ru(4b)	Ru(3b)	48.8(4)	C(1a)	C(2a)	Ru(3a)	124(1)
C(2b)	Ru(4b)	Ru(1b)	79.5(4)	C(1a)	C(2a)	Ru(4a)	70(1)
S(1b)	Ru(4b)	Ru(5b)	92.7(1)	C(1a)	C(2a)	Ru(2a)	70(1)
S(1b)	Ru(4b)	Ru(3b)	55.5(1)	Ru(3a)	C(2a)	Ru(4a)	75.6(6)
Ru(3a)	C(2a)	Ru(2a)	75.2(5)				
Ru(4a)	C(2a)	Ru(2a)	101.2(7)				
C(1b)	C(2b)	C7(1b)	117(2)				
C(1b)	C(2b)	Ru(3b)	123(1)				
C(1b)	C(2b)	Ru(2b)	70(1)				
C(1b)	C(2b)	Ru(4b)	67(1)				
Ru(3b)	C(2b)	Ru(2b)	77.9(6)				
Ru(3b)	C(2b)	Ru(4b)	75.6(5)				
Ru(2b)	C(2b)	Ru(4b)	102.5(7)				

[a] Angles are in degrees. Estimated standard deviations in the least significant figure are given in parentheses.

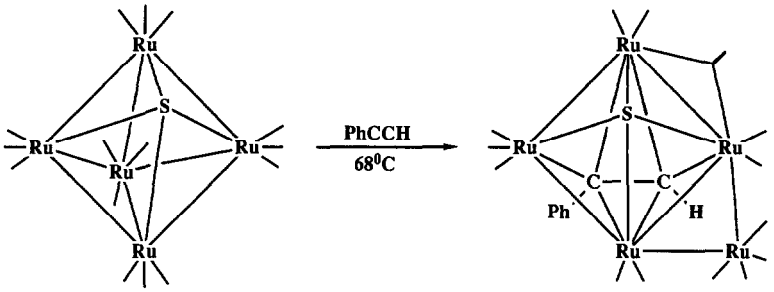

1

Scheme 1.

edges, Ru(1)—Ru(4) and Ru(1)—Ru(6), of the cluster. Compounds **1** and **3** have one and two bridging carbonyl ligands on these sites, respectively. Structurally, the substitution of a bridging group with a bridging $Ru(CO)_4$ group produces a significant lengthening of the bridged metal–metal bond (e.g. Ru(1)—Ru(2) = 2.787(2) Å [2.823(2) Å] and Ru(1)—Ru(4) = 2.788(2) Å [2.753(2) Å] in **2** vs the Ru(1)—Ru(2) = 2.6954(6) Å in **1**; and Ru(1)—Ru(2) = 2.7188(8) Å and Ru(1)—Ru(4) = 2.7293(9) Å in **3**). The value in brackets is for the second independent molecule. The Ru—Ru distances to the bridging $Ru(CO)_4$ groups, 2.732(2)–2.790(2) Å are not unusual.[7] There are no other significant differences in the metal–ligand bonding between **2**, and **1** and **3**.

Electron counting procedures reveal that the cluster violates the Effective Atomic Number Rule by being deficient by the amount of two electrons. Inspection of the molecular geometry shows no evidence of a localized form of electronic unsaturation. Thus, it is believed that this unsaturation is distributed throughout the cluster as a unit. In accord with this, it is found that **2** obeys the electronic requirements of the Skeletal Electron Pair Theory.[8]

DISCUSSION

$Ru_5(CO)_{15}(\mu_4\text{-S})$ contains a square pyramidal cluster of five metal atoms with a quadruply bridging sulphido ligand spanning the square base. It reacts with HC_2Ph by the loss of one carbonyl ligand to form **1** in which the square pyramid is converted to a $Ru(CO)_4$ bridged square of four metal atoms, Scheme 1. It was not established if the CO loss is a prerequisite to the HC_2Ph addition. In fact, in our studies of sulphido–osmium carbonyl clusters, we observed that the reaction of $Os_4(CO)_{12}(\mu_3\text{-S})$ with HC_2Ph proceeds by an addition of the alkyne to the sulphur atom, and after a sequence of polyhedral rearrangements, a decarbonylation step yields $Os_4(CO)_{11}(\mu_4\text{-}HC_2Ph)(\mu_4\text{-S})$ which is an analogue of **3**.[9] It is possible that the reaction of $Ru_5(CO)_5(\mu_4\text{-S})$ with alkynes is also initiated by alkyne–sulphur interactions.

Compound **1** was made previously by us from the reaction of **3** with $Ru(CO)_5$.[4] Small amounts of **2** were also obtained in this reaction and were believed to be formed by the addition of a mononuclear ruthenium carbonyl unit to **1**. This is supported by our current study which shows that **2** can

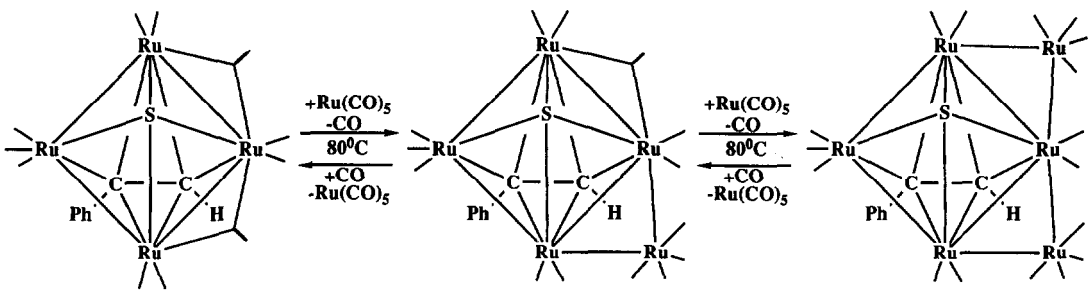

3 1 2

Scheme 2.

be made in good yield from **1** by the reaction with $Ru(CO)_5$. Under a CO atmosphere, **2** is degraded to **1** and **3** by the sequential removal of the bridging $Ru(CO)_4$ groups, Scheme 2. A similar cluster growth/degradation sequence was observed to occur for the cluster series $Ru_5(CO)_{15}(\mu_4\text{-S})$, $Ru_6(CO)_{18}(\mu_4\text{-S})$, $Ru_7(CO)_{21}(\mu_4\text{-S})$.[3] While the facile addition and elimination of mononuclear metal carbonyl fragments might be viewed as an advantage in the scheme of cluster synthesis in general, the equilibria that are generated under these conditions also make the isolation of a selected species in good yield more difficult.

Acknowledgements—The research was supported by the National Science Foundation under Grant No. CHE-8612862. The AM-300 NMR spectrometer was purchased with funds from the National Science Foundation, Grant No. CHE-8411172.

REFERENCES

1. R. D. Adams, *Polyhedron* 1985, **4**, 2003.
2. R. D. Adams, J. E. Babin and M. Tasi, *Inorg. Chem.* 1986, **25**, 4514.
3. R. D. Adams, J. E. Babin and M. Tasi, *Organometallics* 1988, **7**, 503.
4. R. D. Adams, J. E. Babin, M. Tasi and T. A. Wolfe, *Organometallics* 1987, **6**, 2228.
5. R. Hug, A. J. Poë and S. Charola, *Inorg. Chim. Acta.* 1980, **38**, 121.
6. *International Tables for X-ray Crystallography*, Vol. IV, (a) Table 2.2B, pp. 99–101, (b) Table 2.3.1, pp. 140–149. Kynoch Press, Birmingham, U.K.
7. M. I. Bruce, in *Comprehensive Organometallic Chemistry* (Edited by G. Wilkinson, F. G. A. Stone and E. W. Abel), Chap. 32.6. Pergamon Press, Oxford, U.K. (1982).
8. D. M. P. Mingos, *Accts Chem. Res.* 1984, **17**, 311.
9. R. D. Adams and S. W. Wang, *J. Am. Chem. Soc.* 1987, **109**, 924.

Polyhedron Vol. 7, No. 12, pp. 1079–1088, 1988
Printed in Great Britain

0277-5387/88 $3.00+.00
Pergamon Press plc

ALKYLIMIDO AND OXO ARYLS OF RHENIUM. X-RAY STRUCTURES OF $(Bu^tN)_2ReCl_2(o\text{-}MeC_6H_4)$ AND $MO_2(2,6\text{-}Me_2C_6H_3)_2$, M = Re AND Os

CINDY J. LONGLEY, PAUL D. SAVAGE and GEOFFREY WILKINSON*

Chemistry Department, Imperial College of Science and Technology, London SW7 2AY, U.K.

and

BILQUIS HUSSAIN and MICHAEL B. HURSTHOUSE*

Chemistry Department, Queen Mary College, London E1 4NS, U.K.

(*Received* 17 *December* 1987; *accepted* 19 *January* 1988)

Abstract—The compounds $(Bu^tN)_3Re(aryl)$, (aryl = *o*-tol, xylyl and mes†), have been prepared from $(Bu^tN)_3Re(OSiMe_3)$ and the appropriate Grignard reagents. The aryls have been converted to the corresponding dichloride compounds, $(Bu^tN)_2ReCl_2(aryl)$ by treatment with HCl. The X-ray crystal structure of $(Bu^tN)_2ReCl_2(o\text{-tol})$ has been determined. The compound has square pyramidal geometry with one linear (basal site) and one bent (axial site) imido group, which formally suggests a 16e configuration.

The interaction of xylyl magnesium bromide with $[Me_3NH][ReO_4]$ or Re_2O_7 gives the diamagnetic rhenium(V) complex $[(xylyl)_2ReO_2]_2Mg(THF)_2$, which can be oxidized to the paramagnetic rhenium compound, $ReO_2(xylyl)_2$. Interaction of $ReO_3(OSiMe_3)$ with either xylyl or mesityl Grignard yields $ReO_2(aryl)_2$ directly in higher yield. The molecule is tetrahedral.

The interaction of OsO_4 with xylyl magnesium bromide yields $OsO_2(xylyl)_2$. The geometries of the O_2MC_2 units in $MO_2(xylyl)_2$, M = Re and Os, are analogous to those found in the corresponding mesityl derivatives, with the O—Os—O angle much larger than the O—Re—O angle (139° vs 121°).

Following studies on d^0-imidoaryl compounds of Cr, Mo and W[1] [various ^{t}BuN compounds of Mo(VI) such as $(Bu^tN)MoCl(CH_2Bu)_3$ have also been reported, see ref. 1(c)] of the type, $(Bu^tN)_2M(aryl)_2$, we now report the preparation of similar rhenium derivatives. Rhenium(VII)bis (imido)neopentylidene complexes have been studied by Schrock *et al.*[2(a)–(c)] with a view to finding an alkene metathesis catalyst, but the d^0-imido aryl compounds have not been reported. The trialkyl complexes, $(Bu^tN)_3ReR_3$ (R = Me, CH_2Ph, CH_2SiMe_3), are obtained in good yield from $(Bu^tN)_2ReCl_3$[2(a),(b)] and the mixed alkyl/halide species, $(Bu^tN)_2ReClR_2$ (R = Me, CH_2SiMe_3) are also known.[2(b)]

We have made the tris(imido)aryl compounds, $(Bu^tN)_3Re(aryl)$ (aryl = *o*-tol, xylyl, mes) and converted these to the corresponding $(Bu^tN)_2ReCl_2$ (aryl) by treatment with HCl. An analogous alkyl complex $(RN)_2ReCl_2(CH_2Bu^t)$ (R = 2,6-diisopropylphenyl) has been obtained from the reaction of 0.65 equiv of $Zn(CH_2Bu^t)_2$ with $(RN)_2Re(py)Cl_3$,[2(c)] but no crystal structure is reported.

Further work on oxo aryl compounds of rhenium has led to the isolation of $[(xylyl)_2ReO_2]_2Mg(THF)_2$ and its oxidation to the paramagnetic $ReO_2(xylyl)_2$. An alternative higher yield synthesis of $ReO_2(xylyl)_2$ and of $ReO_2(mes)_2$ from $ReO_3(OSiMe_3)$ is also reported. The similar dioxo compound, $OsO_2(xylyl)_2$, has been obtained by interaction of OsO_4 and the Grignard reagent.

*Authors to whom correspondence should be addressed.

† *o*-tol = 2-methylphenyl, xylyl = 2,6-dimethylphenyl, mes (mesityl) = 2,4,6-trimethylphenyl.

Table 1. Physical properties and analytical data

Compound	Colour	M.p.(°C)	Analysis (%)[a] C	H	N	O
$(Bu^tN)_3Re(o\text{-tol})$	Yellow	47–48	46.3 (46.7)	6.3 (6.6)	8.4 (8.6)	
$(Bu^tN)_3Re(xylyl)$	Yellow	65	47.5 (47.6)	7.3 (7.1)	8.2 (8.3)	
$(Bu^tN)_3Re(mes)$	Yellow	69	48.8 (48.6)	7.3 (7.3)	7.9 (8.1)	
$(Bu^tN)_2ReCl_2(o\text{-tol})$	Yellow	135	36.9 (36.7)	5.2 (5.1)	5.8 (5.7)	14.5 (Cl) (14.5)
$(Bu^tN)_2ReCl_2(xylyl)$	Yellow–green	122	37.2 (38.1)	5.7 (5.4)	5.4 (5.6)	
$(Bu^tN)_2ReCl_2(mes)$	Yellow	125–127	39.3 (39.4)	5.7 (5.6)	5.4 (5.4)	
$[ReO_2(xylyl)_2]_2Mg(THF)_2$	Purple	132	47.0 (46.9)	5.2 (5.1)		9.8 (9.4)
$ReO_2(xylyl)_2$	Red	138–140	44.8 (44.8)	4.4 (4.2)		7.4 (7.5)
$OsO_2(xylyl)_2$	Green	144	44.8 (44.4)	[b]		7.2 (7.4)

[a] Found (required).
[b] No hydrogen analysis possible in presence of Os.

Physical and analytical data for new compounds are given in Table 1 and NMR spectroscopic data in Table 2.

RESULTS AND DISCUSSIONS

(1) *Imido aryl compounds of rhenium*

The imido aryl complexes were prepared from $(Bu^tN)_3Re(OSiMe_3)$[3] by the reaction

$$(Bu^tN)_3Re(OSiMe_3) + (aryl)MgBr \xrightarrow[RT]{hexane} (Bu^tN)_3Re(aryl) + Mg(OSiMe_3)Br$$

which is analogous to that used in the preparation of d^0-imidoaryl derivatives of Cr, Mo and W.[1]

The products are bright yellow, low-melting solids that are air-stable, although on prolonged exposure they appear to be hygroscopic; they can be recrystallized from acetonitrile or diethyl ether and are stable in hydrocarbons; $(Bu^tN)_3Re(o\text{-tol})$ decomposes in halogenated solvents. As well as unreactivity towards oxygen, the compounds do not react with carbon monoxide even at 50 atm, in contrast to the behaviour of $(Bu^tN)_2Cr(mes)_2$.[1] This stability is presumably due to the steric protection afforded by the *o*-methyl group on the arene ring and the bulky *t*-butyl groups on nitrogen inhibiting insertion reactions.

The room temperature ^1H NMR spectra of the compounds show only singlets for the *t*-butylimido functions and the spectra are unchanged on cooling to −50°C. The *ortho*-hydrogen in $(Bu^tN)_3Re(o\text{-tol})$ is shifted to low-field as expected. The room temperature ^{13}C NMR spectrum also shows that the three *t*-butylimido groups are equivalent with peaks at 32.3 (CH_3) and 69.2 (Me_3C) for $(Bu^tN)_3Re(xylyl)$.

The mass spectra all show parent ions with the characteristic rhenium isotope pattern and the subsequent loss of imido and alkyl groups. The IR spectra show weak aromatic stretches at 1550–1600 cm^{-1}.

Attempts to prepare the analogous phenyl and *p*-(*t*-butyl)phenyl derivatives gave oils that could not be crystallized.

The treatment of the tris(imido)aryl compounds with excess HCl in ether [cf. ref. 2(b), (c)] produces one equivalent of Bu^tNH_3Cl and the corresponding dichlorocomplex $(Bu^tN)_2ReCl_2(aryl)$. These compounds may also be prepared by treating $(Bu^tN)_2ReCl_3$[2(a)] with one equivalent of the appropriate aryl Grignard reagent. Golden crystals are obtained on concentrating ether solutions of $(Bu^tN)_2ReCl_2(o\text{-tol})$ and $(Bu^tN)_2ReCl_2(mes)$; the xylyl complex was isolated as a yellow–green powder. The compounds are higher melting than their precursors and decompose slowly on exposure to air both in the solid state and in solution. They are sparingly soluble in hexane, but quite soluble in

Table 2. ^{1}H nuclear magnetic resonance data

Compound	δ (ppm)	Assignment
$(Bu^tN)_3Re(o\text{-tol})^a$	8.05(dd)	1H *o-H*—C_6H_3
	7.10(m)	3H *m,p-H*$_3$—C_6H_2
	2.44(s)	3H *o*-C*H*$_3$
	1.41(s)	27H CC*H*$_3$
$(Bu^tN)_3Re(xylyl)^b$	7.25(d)	2H *m-H*$_2$—C_6H_1
	7.07(t)	1H *p-H*—C_6H_2
	2.68(s)	6H *o*-C*H*$_3$
	1.36(s)	27H CC*H*$_3$
$(Bu^tN)_3Re(mes)^a$	7.06(br.s)	2H *m-H*$_2$—C_6
	2.65(s)	6H *o*-C*H*$_3$
	2.21(s)	3H *p*-C*H*$_3$
	1.41(s)	27H CC*H*$_3$
$(Bu^tN)_2ReCl_2(o\text{-tol})^b$	7.92(m)	1H *o-H*—C_6H_3
	7.07(m)	3H *m,p-H*$_3$—C_6H_2
	2.47(s)	3H *o*-C*H*$_3$
	1.10(s)	18H CC*H*$_3$
$(Bu^tN)_2ReCl_2(xylyl)^b$	7.10(m)	3H *m,p-H*$_3$—C_6
	2.37(s)	6H *o*-C*H*$_3$
	1.10(s)	18H CC*H*$_3$
$(Bu^tN)_2ReCl_2(mes)^b$	6.94(m)	2H *m-H*$_2$—C_6
	2.38(s)	6H *o*-C*H*$_3$
	2.10(s)	3H *p*-C*H*$_3$
	1.12(s)	18H CC*H*$_3$
$[ReO_2(xylyl)_2]_2Mg(THF)_2^b$	6.91(d)	8H *m-H*$_2$—C_6H_1
	6.65(t)	4H *p-H*—C_6H_2
	3.57(m)	8H α-C*H*$_2$(THF)
	3.2–2.6, 2.14 (br.m)	24H *o*-C*H*$_3$
	1.25(m)	8H *p*-C*H*$_2$(THF)
$OsO_2(xylyl)_2^b$	7.15(d)	4H *m-H*$_2$—C_6H_1
	6.92(t)	2H *p-H*—C_6H_2
	2.37(s)	12H *o*-CH_3

[a] In $CDCl_3$.
[b] In C_6D_6.

benzene and ether, and very soluble in dichloromethane.

Again, all three compounds show a parent ion in the mass spectrum, the peaks being complicated by the presence of both rhenium and chlorine isotopes.

The structure of the *o*-tolyl compound has been determined by X-ray crystallography. A diagram of the molecule is given in Fig. 1, bond lengths and angles are given in Table 3. The molecular geometry is logically described as square pyramidal with the *t*-butylimido group containing N(2) occupying the axial site. The *trans* angles in the basal plane are then 146.4(2) [C(4)—Re—Cl(1)] and 151.4(3)° [N(1)—Re—Cl(2)] and the axial/equatorial angles are 100–109°.

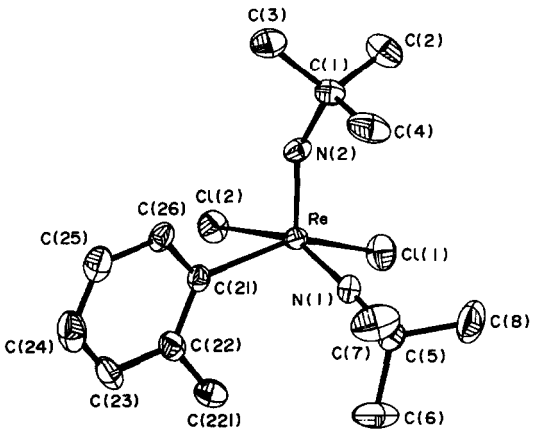

Fig. 1. The structure of $ReCl_2(NBu^t)_2(2\text{-}MeC_6H_4)$.

Table 3. Selected bond lengths and angles for $ReCl_2(NBu^t)_2$(*o*-tolyl)

(a) Bond lengths (Å)			
Cl(1)—Re(1)	2.372(5)	Cl(2)—Re(1)	2.410(4)
N(1)—Re(1)	1.715(9)	N(2)—Re(1)	1.708(10)
C(21)—Re(1)	2.148(8)	C(5)—N(1)	1.445(12)
C(2)—C(1)	1.552(18)	C(3)—C(1)	1.508(18)
C(4)—C(1)	1.536(18)	N(2)—C(1)	1.470(13)
C(6)—C(5)	1.538(18)	C(7)—C(5)	1.503(20)
C(8)—C(5)	1.521(20)	C(23)—C(22)	1.395
C(21)—C(22)	1.395	C(221)—C(22)	1.536(17)
C(24)—C(23)	1.395	C(25)—C(24)	1.395
C(26)—C(25)	1.395	C(21)—C(26)	1.395
(b) Bond angles (°)			
Cl(2)—Re(1)—C((1)	81.3(2)	N(1)—Re(1)—Cl(1)	92.1(3)
N(1)—Re(1)—Cl(2)	151.4(3)	N(2)—Re(1)—Cl(1)	109.4(4)
N(2)—Re(1)—Cl(2)	100.3(4)	N(2)—Re(1)—N(1)	108.1(5)
C(21)—Re(1)—Cl(1)	146.4(2)	C(21)—Re(1)—Cl(2)	81.0(3)
C(21)—Re(1)—N(1)	89.9(1)	C(21)—Re(1)—N(2)	101.8(4)
C(5)—N(1)—Re(1)	176.4(7)	C(3)—C(1)—C(2)	110.8(11)
C(4)—C(1)—C(2)	109.6(12)	C(4)—C(1)—C(3)	110.0(13)
N(2)—C(1)—C(2)	107.6(9)	N(2)—C(1)—C(3)	108.5(11)
N(2)—C(1)—C(4)	110.3(9)	C(1)—N(2)—Re(1)	150.5(7)
C(6)—C(5)—N(1)	109.1(10)	C(7)—C(5)—N(1)	110.0(11)
C(7)—C(5)—C(6)	109.7(15)	C(8)—C(5)—N(1)	106.1(10)
C(8)—C(5)—C(6)	108.9(15)	C(8)—C(5)—C(7)	112.8(16)
C(21)—C(22)—C(23)	120.0	C(221)—C(22)—C(23)	117.3(7)
C(221)—C(22)—C(21)	122.7(7)	C(24)—C(23)—C(22)	120.0
C(25)—C(24)—C(23)	120.0	C(26)—C(25)—C(24)	120.0
C(21)—C(26)—C(25)	120.0	C(22)—C(21)—Re(1)	119.2(2)
C(26)—C(21)—Re(1)	120.8(2)	C(26)—C(21)—C(22)	120.0

The geometries of the imido groups, and the resulting implications for the electronic configuration of the metal are interesting. Were both imido groups to act as normal 4e donors with a linear MNR unit, the metal atom would have a formal 18e configuration. The imido group in the basal site containing N(1) is linear and typical of a 4e interaction (Re=N—R), but the imido group occupying the axial site is bent (Re—N—C = 150°), suggesting that this group is tending to act as two electron donor $\left(\begin{array}{c} Re{=}\ddot{N} \\ \diagdown \\ R \end{array}\right)$. Unusually, however, the formal M—N double bond is slightly shorter than the formal M—N triple bond, and we can only presume that this is a reflection of the stronger π-bond overlap capability at the axial site.

If this is a true picture of the bonding, then, in the absence of any other interactions, the metal would seem to be adopting a 16e configuration. Several compounds containing both linear and bent imido groups exist, but in all cases bar one the complexes would have a maximum count of 20 or more if both NR groups were 4e donors.[4] Examples are $Os(NBu^t)_2O_2$,[5] $Mo(NPh)_2(S_2CNCEt_2)_2$[6] and $Re_3(NBu^t)_4O_5(OSiMe_3)_3$.[3(a)] In the latter, one of the bent (154.9°) imido groups has a Re—N bond distance 0.01 Å *shorter* than that of the linear (157.8°) group. For this complex and for $Os(NBu^t)_2O_2$ the bent and linear *t*-butylimido groups are reported to be indistinguishable by NMR. Similarly, the ^1H NMR spectra for $Re(NBu^t)_2Cl_2$(aryl) show only a singlet for the *t*-butyl groups, even on cooling to −50°C. The only example in which a bent imido ligand is bound to a metal with a formal electron count less than 18 is the complex[7] $[Mo_4S_4(S_2CNBu^t_2)(N\text{-}p\text{-tol})_4]$ in which one of the four terminal imido ligands is bent to an angle of 157° (the others are 164, 170 and 173°). This geometry is explained in terms of a steric interaction involving a neighbouring molecule.

In our structure there are no short contacts either *intra-* or *inter*molecular involving atoms of the bent *t*-butylimido ligand. We have examined in detail other geometrical features of the molecule, especially at the methyl group C(221) on the *o*-tolyl ligand, which is positioned below the basal plane of

the square pyramid and *trans* to the axial imido group. Although one of the methyl hydrogens is close to the metal (H(223)···Re = 2.82 Å), there does not seem to be any deformation of the CH_3 group and the *o*-tolyl ligand is bonding symmetrically (i.e. with approximately equal Re—C—C angles). It is possible, however, that this apparently "normal" geometry is masking the true picture. A non-interacting methyl group may well be repelled by steric interactions and lead to unsymmetrical *o*-tolyl bonding. The geometry as found, may thus indeed arise from an agostic C—H···Re interaction and this may be the source of the "missing" 2e contribution to the metal electron count.

Finally, it may be noted that the structure of $Re(NBu^t)_2Cl_3$ was held to be trigonal bipyramidal with equatorial imido ligands, because the *t*-butyl groups give a singlet in the NMR spectrum.[2(a)] Similarly, NMR spectra for $Re(NBu^t)_2R_3$ (R = Me, CH_2Ph, CH_2SiMe_3) are said to indicate a trigonal bipyramidal structure with one type of imido and two types of alkyl groups.[2(b)] A trigonal bipyramid containing equatorial imido and an axial neopentyl group has also been suggested for $Re(NAr)_2(CH_2Bu^t)Cl_2$ (Ar = 2,6-diisopropylphenyl) on the basis of ^1H NMR data.[2(c)] Since, for the aryl discussed here, NMR indicates equivalence, either the molecule is non-rigid or has a structure in solution different than that in the solid state. X-ray data on one or more of Schrock's $(Bu^tN)_2ReR_3$ compounds is desirable and is now being undertaken.

These bis(imido) derivatives may adopt different geometries depending on the nature of the other three ligands, but in most cases the solution NMR data may not be regarded as conclusive evidence for a particular solid state structure.

(2) *Oxo aryl compounds of rhenium*(V) *and* (VII)

The synthesis of oxorhenium(V,VI) aryls and the X-ray crystal structures of $ReO_2(mes)_2$ and $ReO(mes)_4$ have been described[8] while comparable alkyls have also been studied.[9] For both alkyls and aryls, anionic species such as $[(mes)_2ReO_2]_2Mg(THF)_2$ were usually formed initially in the alkylation of $(Me_3NH)(ReO_4)$ or Re_2O_7, and these species could be oxidized to the neutral compounds, e.g. $ReO_2(mes)_2$. It may be noted that salts of the related anion $[ReO_2(CH_2CMe_3)_2]^-$ have recently been described;[10(a)] the first oxorhenium alkylate anion, $[ReO(CH_2SiMe_3)_4]^-$, was obtained some time ago by chemical (Na/Hg) or electrochemical (1e) reduction of $ReO(CH_2SiMe_3)_4$.[10(b)]

(a) *Synthesis of* $[(xylyl)_2ReO_2]_2Mg(THF)_2$. The interaction of $Me_3NH[ReO_4]$ or Re_2O_7 with seven equivalents of xylylmagnesium bromide per rhenium atom in THF gives diamagnetic air-sensitive red–purple crystals of $[(xylyl)_2ReO_2]Mg(THF)_2$ from diethyl ether. The compound is soluble in aromatic hydrocarbons and ethers but decomposes rapidly in halogenated solvents like the analogous mesityl compound.[8]

The IR spectrum contains peaks at 1025, 1005, 920, 900 and 860 cm^{-1} that can be assigned to the skeletal vibrations of THF;[11] these partially mask the Re=O stretches although shoulders at 992 and 943 cm^{-1} are probably ν(Re=O) bands. In view of structural determinations on similar compounds[8,9] we assume that these tetrahedral $[(xylyl)_2ReO_2]^-$ units are coordinated to solvated Mg^{2+} via only one oxygen. A bridging stretch would therefore be expected at lower frequency, compared to the 975 and 930 cm^{-1} stretches of the neutral $ReO_2(xylyl)_2$ compound (see below), and this stretch is probably obscured by the broad THF vibrations.

Unlike the situation for the analogous mesityl complex,[8] the ^{13}C NMR spectrum proved to be more useful than the ^1H NMR spectrum. At ambient temperatures the latter shows the usual doublet and triplet pattern for the aromatic protons at δ 6.65 and 6.91 ppm while the broad THF peaks appear at δ 1.25 and 3.57. However, the *ortho*-methyl on the arene ring groups show complicated patterns—two sharp peaks (δ 2.14 and 2.79) and a broad hump between δ 2.6–3.2, possibly caused by restricted rotation about the Re—C_α bond and the non-equivalence of the *ortho*-methyls of the xylyl ligands. The ^{13}C-{^1H} spectrum shows six unique aromatic carbons at δ 124.3, 125.3, 126.4, 130.2, 137.7 and 150.0, coordinated THF at δ 25.3 and 68.8 and a broad peak at δ 29.6, presumably due to the non-equivalent *ortho*-methyls.

(b) *Synthesis of* $ReO_2(xylyl)_2$. In THF the above rhenium(V) complex is rapidly oxidized by dry oxygen or by addition of aqueous H_2O_2 to give bright red solutions of the paramagnetic $ReO_2(xylyl)_2$. However, better yields can be obtained from the interaction of xylyl Grignard and $ReO_3(OSiMe_3)$, where the product is formed directly, oxidation being avoided. The mesityl analogue[8] can similarly be prepared in higher yields in this way. The expected initial product of this reaction, i.e. $ReO_3(xylyl)$, however, proved difficult to isolate (as did the mesityl, ReO_3mes), although there is evidence for it in the mass spectrum of the crude product before recrystallization.

The IR spectrum of $ReO_2(xylyl)_2$ shows two strong peaks at 975 and 930 cm^{-1} for the ν(Re=O) stretches of the "ReO_2" unit and like $ReO_2(mes)_2$, the compound shows high air and thermal stability in the solid state. However, on exposure to air,

solutions of the complex slowly turn from bright red to pale yellow.

The mass spectrum shows the parent ion doublet, *m/e* 429 and 427 and subsequent losses of both xylyl groups. The electron spin resonance spectrum (293 K, X-band) of $ReO_2(xylyl)_2$ prepared under anaerobic conditions showed a band with a six-line hyperfine structure ($g_{iso} = 1.967$, $A_{iso} = 0.0194$ cm^{-1}). When the temperature of the solution was lowered, the spectrum gradually resolved into a complicated pattern showing, at 98 K, more than two sets of six rhenium hyperfine lines with unequal spacing. The *Q*-band spectrum showed that this pattern corresponds to a molecule with rhombic symmetry with the *z*- and *x*-axes well apart, whereas the *y*-axis lies in between ($g_z > g_y > g_x$ and $A_z > A_x > A_y$). The parameters for the *z*-axis ($g_z = 2.094$, $A_z = 0.0337$) and the *x*-axis ($g_x = 1.865$, $A_x = 0.0244$) were derived directly from the *y*-axis ($g_y = 1.943$, $A_y = -4 \times 10^{-4}$) and were calculated from the isotropic and anisotropic values by using the equations

$$g_y = 3g_{iso} - g_z - g_x \quad \text{and} \quad A_y = 3A_{iso} - A_z - A_x.$$

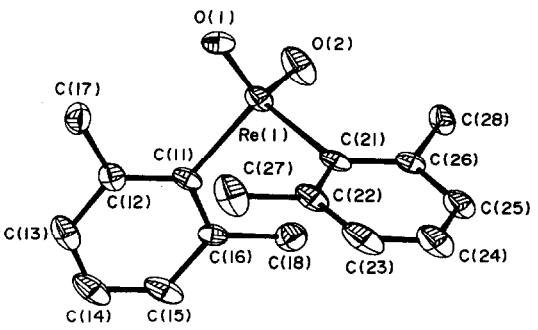

Fig. 2. The structure of $ReO_2(2,6\text{-}Me_2C_6H_3)_2$.

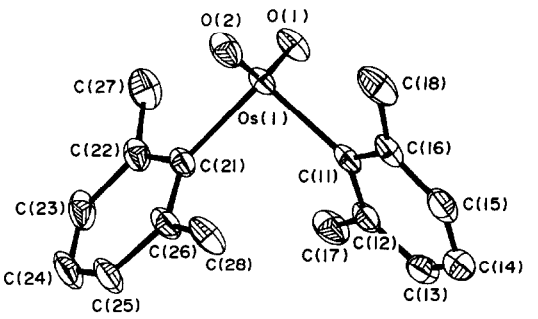

Fig. 3. The structure of $OsO_2(2,6\text{-}Me_2C_6H_3)$.

(3) *Synthesis of* $OsO_2(xylyl)_2$

The reaction of OsO_4 with aryl Grignards and aluminium aryls has yielded both aryls and oxo aryls,[8,12] namely $Os(C_6H_5)_4$, $Os(o\text{-}MeC_6H_4)_2$ and $OsO_2(mes)_2$. Interaction of OsO_4 with seven equivalents of xylylmagnesium bromide in THF with subsequent oxidation of the deep red solution (which presumably contains an unisolated anionic species), leads to moderate yields of the diamagnetic, air stable $OsO_2(xylyl)_2$ as green crystals.

As well as the xylyl peaks, the IR spectrum shows two strong peaks at 960 and 915 cm^{-1} (both with shoulders at 970 and 926 cm^{-1}, respectively, probably due to lattice effects) that can be assigned as ν(Os=O) stretches of the OsO_2 unit; these compare favourably with values for the analogous mesityl compound.

The ^{1}H NMR spectrum shows a sharp peak at δ 2.37 readily assigned to the *ortho*-methyls of the arene ring, a triplet at δ 6.92 (1,*p*-H) and a doublet at δ 7.15 (2,*m*-H). The ^{13}C-{^{1}H} spectrum shows the *ortho*-methyls at δ 28.9 and of the four unique aromatic carbons only three appear at δ 126.7, 131.0 and 146.5 ppm. This phenomenon occurs in other high oxidation state aryl compounds, e.g. $OsPh_4$ and $OsO_2(mes)_2$. The mass spectrum of the compound shows the parent ion $OsO_2R_2^+$ and the ions OsO_2R^+, OsR_2^+, $OsOR^+$ and OsR^+ with patterns as expected for the isotopes ^{192}Os, ^{190}Os, ^{189}Os and ^{188}Os.

(4) *Structures of* $MO_2(xylyl)_2$, M = Re *and* Os

The structures of both xylyl compounds have been determined by X-ray crystallography and are analogous to those of the corresponding mesityl derivatives.[9] Thus, the considerable difference in the deformation of the O_2MC_2 "tetrahedral" geometry involving the O—M—O angles found in the mesityl structures is again found here, where the O—Os—O angle is 139.2(3)° and the O—Re—O angle is 121.3(4)° (cf. 136.1(3)° and 121.5(4)° for the respective mesityls). Furthermore, there is no indication of xylyl methyl-to-metal interactions and the xylyl rings bond quite symmetrically, with M—C—C angles of 119–121°. Diagrams of the two structures are given in Figs 2 and 3; bond lengths and angles are given in Table 4.

EXPERIMENTAL

Microanalyses were by Pascher, Remagen. Spectrometers: IR, Perkin–Elmer 683 (spectra in Nujol mulls, values in cm^{-1}); NMR, Bruker WM-250 and JEOL FX 900 (data in ppm relative to $SiMe_4$); mass, Kratos MS902, at 70 eV; ESR, Varian E-9 (*X*-band) and Bruker ER 20000-SRC (*Q*-band). The following were prepared as before: Re_2O_7,[12] $ReO_3(OSiMe_3)$,[11] $(Me_3NH)ReO_4$[9] and $(Bu^tN)_3Re(OSiMe_3)$.[3] Solvents were refluxed over sodium or

Table 4. Bond lengths and angles for $ReO_2(xylyl)_2$ and $OsO_2(xylyl)_2$

$ReO_2(xylyl)_2$		$OsO_2(xylyl)_2$	
(a) Bond lengths (Å)			
O(1)—Re(1)	1.686(7)	O(1)—Os(1)	1.699(5)
O(2)—Re(1)	1.672(6)	O(2)—Os(1)	1.688(5)
C(11)—Re(1)	2.065(7)	C(11)—Os(1)	2.058(6)
C(21)—Re(1)	2.069(7)	C(21)—Os(1)	2.060(6)
C(12)—C(11)	1.430(9)	C(12)—C(11)	1.427(7)
C(16)—C(11)	1.413(8)	C(16)—C(11)	1.403(7)
C(13)—C(12)	1.376(10)	C(13)—C(12)	1.395(9)
C(17)—C(12)	1.505(10)	C(17)—C(12)	1.512(10)
C(14)—C(13)	1.384(12)	C(14)—C(13)	1.384(13)
C(15)—C(14)	1.376(12)	C(15)—C(14)	1.360(12)
C(16)—C(15)	1.380(11)	C(16)—C(15)	1.400(8)
C(18)—C(16)	1.514(12)	C(18)—C(16)	1.515(10)
C(22)—C(21)	1.431(8)	C(22)—C(21)	1.413(8)
C(26)—C(21)	1.421(8)	C(26)—C(21)	1.420(8)
C(23)—C(22)	1.396(10)	C(23)—C(22)	1.392(9)
C(27)—C(22)	1.489(11)	C(27)—C(22)	1.516(11)
C(24)—C(23)	1.363(12)	C(24)—C(23)	1.399(12)
C(25)—C(24)	1.377(12)	C(25)—C(24)	1.348(12)
C(26)—C(25)	1.390(10)	C(26)—C(25)	1.370(8)
C(28)—C(26)	1.497(10)	C(28)—C(26)	1.525(10)
(b) Bond angles (°)			
O(2)—Re(1)—O(1)	121.3(4)	O(2)—Os(1)—O(1)	139.1(2)
C(11)—Re(1)—O(1)	106.5(3)	C(11)—Os(1)—O(1)	101.5(3)
C(11)—Re(1)—O(2)	109.5(3)	C(11)—Os(1)—O(2)	108.4(3)
C(21)—Re(1)—O(1)	110.3(3)	C(21)—Os(1)—O(1)	107.1(3)
C(21)—Re(1)—O(2)	106.8(3)	C(21)—Os(1)—O(2)	98.2(3)
C(21)—Re(1)—C(11)	100.4(3)	C(21)—Os(1)—C(11)	93.9(3)
C(12)—C(11)—Re(1)	122.1(5)	C(12)—C(11)—Os(1)	120.6(4)
C(16)—C(11)—Re(1)	119.2(5)	C(16)—C(11)—Os(1)	118.6(4)
C(16)—C(11)—C(12)	118.6(6)	C(16)—C(11)—C(12)	120.7(5)
C(13)—C(12)—C(11)	119.4(6)	C(13)—C(12)—C(11)	117.3(6)
C(17)—C(12)—C(11)	123.0(6)	C(17)—C(12)—C(11)	124.5(6)
C(17)—C(12)—C(13)	117.7(6)	C(17)—C(12)—C(13)	118.1(6)
C(14)—C(13)—C(12)	121.5(7)	C(14)—C(13)—C(12)	121.8(7)
C(15)—C(14)—C(13)	119.3(7)	C(15)—C(14)—C(13)	119.9(7)
C(16)—C(15)—C(14)	121.8(7)	C(16)—C(15)—C(14)	121.7(7)
C(15)—C(16)—C(11)	119.5(7)	C(15)—C(16)—C(11)	118.2(6)
C(18)—C(16)—C(11)	122.2(7)	C(18)—C(16)—C(11)	123.6(5)
C(18)—C(16)—C(15)	118.3(7)	C(18)—C(16)—C(15)	118.1(6)
C(22)—C(21)—Re(1)	121.3(5)	C(22)—C(21)—Os(1)	118.2(5)
C(26)—C(21)—Re(1)	119.2(5)	C(26)—C(21)—Os(1)	122.3(4)
C(26)—C(21)—C(22)	119.5(6)	C(26)—C(21)—C(22)	119.2(5)
C(23)—C(22)—C(21)	118.2(7)	C(23)—C(22)—C(21)	119.1(6)
C(27)—C(22)—C(21)	124.9(7)	C(27)—C(22)—C(21)	123.8(6)
C(27)—C(22)—C(23)	116.9(6)	C(27)—C(22)—C(23)	117.1(6)
C(24)—C(23)—C(22)	121.5(7)	C(24)—C(23)—C(22)	120.4(7)
C(25)—C(24)—C(23)	120.8(7)	C(25)—C(24)—C(23)	119.3(6)
C(26)—C(25)—C(24)	120.9(7)	C(26)—C(25)—C(24)	123.2(7)
C(25)—C(26)—C(21)	119.0(6)	C(25)—C(26)—C(21)	118.6(6)
C(28)—C(26)—C(21)	122.3(7)	C(28)—C(26)—C(21)	123.5(6)
C(28)—C(26)—C(25)	118.7(7)	C(28)—C(26)—C(25)	118.0(6)

sodium–benzophenone under nitrogen and distilled before use; all manipulations were carried out *in vacuo* or under purified argon or dinitrogen.

Tris(t-*butylimido*)(2-*methylphenyl*)*rhenium*(VII)

To a stirred solution of $(Bu^tN)_3Re(OSiMe_3)$[3] (1g, 2.05 mmol) in hexane (50 cm^3) was added *o*-tolylmagnesium bromide (1.1 cm^3 of a 1.9 mol dm^{-3} solution in Et_2O, 2.1 mmol) at −78°C. The solution was allowed to warm to room temperature and stirred for 2 h. The solvent was removed *in vacuo* and the residue extracted with hexane (20 cm^3), the solution was filtered and the clear yellow solution evaporated. The residue was recrystallized from concentrated Et_2O or hexamethyldisiloxane solutions at −21°C, to give a yellow crystalline solid. Yield, *ca* 45%. Mass spectrum: *m/e* 491 (32%), $^{187}Re(NBu^t)_3(C_7H_7)^+$; 489 (18%), $^{185}Re(NBu^t)_3(C_7H_7)^+$; 420 (9%), $^{187}Re(NBu^t)_2(C_7H_7)^+$; 418 (4%), $^{185}Re(NBu^t)_2(C_7H_7)^+$. IR: 1580w, 1366s, 1270(sh), 1260m, 1230s, 1210s, 1131m, 1090(br), 1050w, 1025(br), 935w, 915w, 824m, 805s, 738vs, 605m, 565w, 535w, 492m.

Tris(t-*butylimido*)(2,6-*dimethylphenyl*)*rhenium*(VII)

As for $(Bu^tN)_3Re$(*o*-tol) from $(Bu^tN)_3Re(OSiMe_3)$ (1g, 2.05 mmol) and xylylmagnesium bromide (1.8 cm^3 of a 1.2 mol dm^{-3} solution in Et_2O, 2.15 mmol). The orange–yellow residue obtained from the hexane extract was recrystallized from acetonitrile at −21°C to give yellow needles. Yield, *ca* 50%. Mass spectrum: *m/e* 505 (100%), $^{187}Re(NBu^t)_3(C_8H_9)^+$; 503 (60%), $^{185}Re(NBu^t)_3(C_8H_9)^+$; 490 (100%), $^{187}P—Me^+$; 488 (54%), $^{185}P—Me^+$; 448 (55%), $^{187}P—Bu^t$; 446 (14%), $^{185}P—Bu^{t+}$; 434 (51%), $^{187}P—NBu^{t+}$; 432 (39%), $^{185}P—NBu^{t+}$. IR: 1400w, 1355s, 1265s, 1225s, 1209s, 1130m, 1021(br), 904s, 803s, 762s, 708m, 611w, 600m, 532w, 499m, 484m, 455w. NMR. $^{13}C-\{^1H\}$ (C_6D_6): 32.3 [s, CMe_3], 33.7 (s, *o*-Me), 69.2 [s, *C*, Me_3], 126.6, 127.9, 146.3 (C_6H_4).

Tris(t - *butylimido*)(2,4,6 - *trimethylphenyl*)*rhenium* (VII)

As for $(Bu^tN)_3Re$(xylyl) from $(Bu^tN)_3Re(OSiMe_3)$ (1 g, 2.05 mmol) and mesitylmagnesium bromide (2.1 cm^3 of a 0.98 mol dm^{-3} solution in THF, 2.06 mmol). Bright yellow crystals were obtained from concentrated MeCN or Et_2O solutions at −21°C. Yield, *ca* 50%. Mass spectrum: *m/e* 519 (69%), $^{187}Re(NBu^t)_3(C_9H_{11})^+$; 17 (82%), $^{185}Re(NBu^t)_3(C_9H_{11})^+$; 504 (44%), $^{187}P—Me^+$; 502 (24%), $^{185}P—Me^+$. IR: 1595w, 1353s, 1258s, 1223s, 1205s, 1127m, 1085(br), 1025(br), 905m, 842s, 801s, 750w, 705w, 600(br), 493(br), 450w.

Di(t - *butylimido*)*dichloro*(2 - *methylphenyl*)*rhenium* (VII)

To a stirred solution of $(Bu^tN)_3Re$(*o*-tolyl) (0.5 g, 1.0 mmol) in Et_2O (30 cm^3) was added a solution of HCl in Et_2O (7 cm^3 of a 0.5 mol dm^{-3} solution) at −78°C. The solution was allowed to warm to room temperature and stirred for *ca* 3 h, then filtered from Bu^tNH_3Cl, and the filtrate evaporated. The yellow–green residue was recrystallized from Et_2O to give golden crystals. Yield, 60%. Mass spectrum: *m/e* 494 (4%), 492 (15%), 490 (21%), 488 (12%), $Re(NBu^t)_2Cl_2(C_7H_7)^+$ ($^{187,185}Re$ and $^{37,35}Cl$ isotopes); 457 (11%), 455 (35%), 453 (20%), $Re(NBu^t)_2Cl(C_7H_7)^+$; 421 (26%), 419 (15%), $Re(NBu^t)Cl_2(C_7H_7)^+$; 401 (8%), 399 (24%), 397, $Re(NBu^t)_2Cl_2^+$; 366 (34%), 365 (50%), 364 (100%), 363 (31%), 362 (55%), $Re(NBu^t)_2Cl^+$; 91 (31%) $C_7H_7^+$, 57 (35%), $C_4H_9^+$. IR: 1576w, 1565w, 1450s, 1361s, 1257s, 1245s, 1215m, 1192s, 1238w, 1118w, 1090(br), 1055m, 1025(br), 950(br), 928w, 841m, 800s, 747vs, 646w, 605(br), 508w, 470w, 447w.

Di(t - *butylimido*)*dichloro*(2,6 - *dimethylphenyl*)*rhenium*(VII)

As for $(Bu^tN)_2ReCl_2$(*o*-tol) from $(Bu^tN)_3Re$(xylyl) (0.5 g, 0.99 mmol) and HCl in Et_2O (7 cm^3 of a 0.5 mol dm^{-3} solution, 3.5 mmol). The solution, which became blue–green, was filtered from Bu^tNH_3Cl and concentrated to give a yellow–green precipitate which was recrystallized from Et_2O. Yield, 45%. Mass spectrum: *m/e* 506 (24%), 505 (12%), 504 (61%), 502 (20%), $Re(NBu^t)_2Cl_2(C_8H_9)^+$ ($^{187,185}Re$ and $^{37,35}Cl$ isotopes); 457 (11%), 455 (35%), 453 (20%), $Re(NBu^t)_2Cl(C_8H_9)^+$; 105 (53%) $C_8H_9^+$. 57 (100%) $C_4H_9^+$. IR: 1571w, 1360s, 1250m, 1220w, 1210w, 1175(br), 1160w, 1130w, 1020(br), 905s, 800m, 771vs, 720w, 710w, 625w, 604w, 562w, 475w.

Di(t-*butylimido*)*dichloro*(2,4,6-*trimethylphenyl*)*rhenium*(VII)

As for $(Bu^tN)_2ReCl_2$(*o*-tol) from $(Bu^tN)_3Re$(mes) (0.3 g, 0.58 mmol) and HCl in Et_2O (4 cm^3 of a 0.5 mol dm^{-3} solution, 2 mmol). The blue–green solution was filtered and concentrated to give a yellow powder which was recrystallized from Et_2O. Yield, 58%. Mass spectrum. *m/e* 520 (32%), 518 (79%), 516 (30%), $Re(NBu^t)_2Cl_2(C_9H_{11})^+$ ($^{157,158}Re$ and $^{37,38}Cl$ isotopes); 485 (10%), 483 (55%), 481 (30%), $Re(NBu^t)_2Cl(C_9H_{11})^+$; 119 (30%), $C_9H_{11}^+$;

57 (98%), $C_4H_9^+$. IR: 1595w, 1360s, 1288m, 1240m, 1215m, 1173(br), 1119m, 1025(br), 995w, 855s, 799(br), 709m, 630w, 607w, 550w, 473w.

Bis(tetrahydrofuran)magnesium bis[dioxodi(2,6-dimethylphenyl)rhenate(V)]

To a cooled (−78°C) suspension of Re_2O_7 (1.30 g, 2.68 mmol) in THF (45 cm^3) was added xylylmagnesium bromide (31.3 cm^3 of a 1.20 mol dm^{-3} solution in Et_2O, 37.6 mmol). The mixture was allowed to warm slowly and was held at room temperature for *ca* 1 h. The resulting red–purple solution was evaporated and the residue extracted with Et_2O (3 × 20 cm^3), filtered and concentrated to *ca* 40 cm^3 to afford, on cooling to −20°C, red–purple crystals. Yield, 18%, IR: 1572m, 1555w, 1348w, 1299w, 1250w, 1215m, 1180w, 1160w, 1120w, 1075s, 1025(vbrs), 1005(sh), 992(sh), 943(sh), 920s, 900(sh), 860s, 822(sh), 760s, 709m, 678m, 551m, 520w, 471m, 440w. NMR: $^{13}C\text{-}\{^1H\}$: δ 25.3 (s, β-CH_2, THF), 29.6 (br, *o*-CH_3), 68.8 (s, α-CH_2, THF), 124.3, 125.3, 126.4, 130.2, 137.7 and 150.0 (s, C_6H_3).

Dioxodi(2,6-dimethylphenyl)rhenium(VI)

To a stirred solution of $O_3Re(OSiMe_3)$ (0.85 g, 2.64 mmol) in THF (30 cm^3) was added xylylmagnesium bromide (4.4 cm^3 of a 1.20 mol dm^{-3} solution in Et_2O, 5.28 mmol) and the solution was warmed to room temperature and stirred for 2 h. The resulting red solution was evaporated and the residues were extracted into Et_2O (3 × 25 cm^3), which was filtered, concentrated to *ca* 45 cm^3 and cooled at −20°C overnight to yield dark red crystals. Yield, 63%. Mass spectrum: *m/e* 429 (51%), $^{187}ReO_2R_2^+$; 427 (35%), $^{185}ReO_2R_2^+$; 324 (7%), $^{187}ReO_2R^+$; 332 (16%), $^{185}ReO_2R^+$; 308 (12%), $^{187}ReOR^+$; 306 (4%), $^{185}ReOR^+$; 105 (100%), R^+; 91 (73%), $C_7H_7^+$. IR: 3000m, 1566m, 1230m, 1165m, 1115w, 1026s, 975s, 930s, 855w, 770s, 705w. ESR: $g_{iso} = 1.967$, $A_{iso} = 0.0194$, $g_z = 2.0937$, $A_z = 0.0377$, $g_y = 1.943$, $A_y = -4.0 \times 10^{-4}$, $g_x = 1.865$, $A_x = 0.0244$, energies in cm^{-1}.

Dioxodi(2,6-dimethylphenyl)osmium(VI)

To a stirred solution of OsO_4 (0.5 g, 1.98 mmol) in THF (35 cm^3) at −78°C was added xylylmagnesium

Table 5. Crystal data, details of intensity measurement and refinement

Formula	$C_{15}H_{25}Cl_2N_2Re$	$C_{16}H_{18}O_2Re$	$C_{16}H_{18}O_2Os$
M	478.460	428.504	432.504
Crystal system	Monoclinic	Triclinic	Triclinic
Space group	*Cc*	$P\bar{1}$	$P\bar{1}$
a (Å)	9.725(2)	8.192(1)	9.113(1)
b (Å)	13.671(1)	8.575(1)	12.354(1)
c (Å)	14.039(2)	12.522(2)	7.064(1)
a (°)	90.0	77.87(1)	85.89(6)
b (°)	92.73(2)	71.21(1)	91.50(8)
c (°)	90.0	62.30(1)	68.49(8)
U (Å^3)	1864.29	735.39	736.78
Z	4	2	2
D (g cm^{-3})	1.704	1.935	1.949
F(000)	904	410	412
μ (cm)	68.46	83.42	82.95
θ-range	1.5, 25.0	1.5, 30.0	1.5, 30.0
h, k, l range	−11–> 11	−9–> 9	−10–> 10
	0–> 16	0–> 10	−14–> 14
	0–> 16	−14–> 14	0–> 8
Total no. of reflections	1838	2590	2856
No. of unique reflections	1701	2582	2594
Significance test	$F_o > 3\sigma(F_o)$	$F_o > 3\sigma(F_o)$	$F_o > 4\sigma(F_o)$
No. of observed reflections	1595	2368	2399
No. of refined parameters	167	244	244
Weighting scheme parameter *g* in $w = 1/[\sigma^2(F_o)+gF_o^2]$	0.0003	0.00052	0.0012
Final *R*	0.0182	0.0273	0.0209
Final R_w	0.0188	0.0289	0.0225

bromide (40.5 cm^3 of a 0.3 mol dm^{-3} solution in Et_2O, 13.8 mmol). The mixture was allowed to warm slowly to room temperature and was held there for 1 h. The solvent was removed and oxygen-saturated hexane (60 cm^3) was added to the residue and the mixture stirred overnight. The green filtered extract was concentrated to *ca* 15 cm^3 and cooled to −20°C to give green crystals. Yield, 0.38 g, 44%. Mass spectrum: *m/e* 434 (58%), $^{192}OsO_2R_2^+$: 432 (42%), $^{190}OsO_2R_2^+$; 431 (28%), $^{189}OsO_2R_2^+$; 432 (23%), $^{188}OsO_2R_2^+$; 416 (7%), $^{190}OsOR_2^+$; 400 (7%), $^{190}OsR_2^+$; 327 (18%), $^{190}OsO_2R^+$; 313 (49%), $^{192}OsOR^+$; 311 (35%), $^{190}OsOR^+$; 298 (21%), $^{192}OsO(R—Me)^+$; 296 (17%), $^{190}OsO(R—Me)^+$; 295 (11%), $^{190}OsR^+$; 210 (42%), R_2^+; 195 (12%), $R_2—Me^+$; 180 (14%) $R_2—2Me^+$; 105 (95%), R^+; 91 (100%), $C_7H_7^+$; 77 (68%), $C_6H_5^+$. IR: 1556m, 1261w, 1238s, 1196w, 1165(sh), 1160s, 1117w, 1025(sh), 1010s, 1000m, 960s, 926(sh) 915(vsbr), 890(sh), 770vs, 750m, 706s, 556m. NMR: $^{13}C-\{^1H\}$: 28.9 (s, *o*-Me) and 126.7, 131.0 and 146.5 (s, ring carbons).

X-ray crystallography

All crystallographic measurements were made at room temperature (293 K) on crystals sealed in thin-walled glass capillaries, using a CAD4 diffractometer operating in the ω-2θ scan mode with graphite monochromated Mo-K_α radiation ($\lambda = 0.71069$ Å) as previously described.[13] The structures were solved via standard heavy atom procedures and refined using full-matrix least squares, with scattering factors calculated using data from ref. 14. All non-hydrogen atoms were refined anisotropically, hydrogens were included in experimentally determined positions with isotropic displacement factor coefficients, but with the C—H bond lengths constrained to a value of 0.96 Å. Details of crystal data, intensity measurements and refinements are given in Table 5.*

* Atomic coordinates, thermal parameters, full lists of bond lengths and angles of lists of F_o/F_c values have been deposited as supplementary data with the Editor, from whom copies are available on request. Atomic coordinates have also been deposited with the Cambridge Crystallographic Data Centre.

Acknowledgements—We thank the SERC for a studentship (C.J.L.) and for provision of X-ray facilities and Johnson Matthey PLC for the loan of osmium.

REFERENCES

1. (a) A. C. Sullivan, G. Wilkinson, M. Motevalli and M. B. Hursthouse, *J. Chem. Soc., Chem. Commun.* 1986, 1398; (b) A. C. Sullivan, G. Wilkinson, M. Motevalli and M. B. Hursthouse, *J. Chem. Soc., Dalton Trans.* 1988, 53; (c) D. E. Ehrenfeld, J. Kress, B. D. Moore, J. A. Osborn and G. Schoettel, *J. Chem. Soc., Chem. Commun.* 1987, 129.
2. (a) D. S. Edwards and R. R. Schrock, *J. Am. Chem. Soc.* 1982, **104**, 68; (b) D. S. Edwards, L. V. Biondi. J. W. Zeller, M. R. Churchill and R. R. Schrock, *Organometallics* 1983, **2**, 1505; (c) A. D. Horton, R. R. Schrock and J. H. Freidenberger, *Organometallics* 1987, **6**, 893.
3. (a) W. A. Nugent and R. L. Harlow, *J. Chem. Soc., Chem. Commun.* 1979, 1105; (b) W. A. Nugent, *Inorg. Chem.* 1983, **22**, 965.
4. W. A. Nugent and B. L. Haymore, *Coord. Chem. Rev.* 1980, **31**, 123.
5. W. A. Nugent, R. L. Harlow and R. J. McKinney, *J. Am. Chem. Soc.* 1979, **101**, 7265.
6. B. L. Haymore, G. A. Maatta and R. A. D. Wentworth, *J. Am. Chem. Soc.* 1979, **101**, 2063.
7. K. L. Wall, K. Folting, J. C. Huffman and R. A. D. Wentworth, *Inorg. Chem.* 1983, **22**, 2366.
8. P. Stavropoulos, P. G. Edwards, T. Behling, G. Wilkinson, M. Motevalli and M. B. Hursthouse, *J. Chem. Soc., Dalton Trans.* 1987, 169.
9. P. Stavropoulos, P. G. Edwards, G. Wilkinson, M. Motevalli, K. M. Abdul Malik and M. B. Hursthouse, *J. Chem. Soc., Dalton Trans.* 1985, 2167.
10. (a) S. Cai, D. M. Hoffman, J. C. Huffman, D. A. Wierda and H. G. Woo, *Inorg. Chem.* 1987, **26**, 3693; (b) K. Mertis, D. H. Williamson and G. Wilkinson, *J. Chem. Soc., Dalton Trans.* 1975, 607.
11. A. Palm and E. R. Bissell, *Spectrochim. Acta* 1960, **16**, 459; (b) J. M. Eyster and E. W. Prohotsky, *Spectrochim. Acta* 1974, **30A**, 2041.
12. P. Stavropoulos, P. D. Savage, R. P. Tooze, G. Wilkinson, B. Hussain, M. Motevalli and M. B. Hursthouse, *J. Chem. Soc., Dalton Trans.* 1987, 557.
13. M. B. Hursthouse, R. A. Jones, K. M. A. Malik and G. Wilkinson, *J. Am. Chem. Soc.* 1979, **101**, 4128.
14. *International Tables for X-Ray Crystallography*, Vol. 4. Kynoch Press, Birmingham (1974).

Polyhedron Vol. 7, No. 12, pp. 1089–1093, 1988
Printed in Great Britain

0277–5387/88 $3.00+.00
© 1988 Pergamon Press plc

COBALT(II) AND ZINC(II) COMPLEXES OF CYSTEINE CONTAINING DIPEPTIDES

I. SÓVÁGÓ,* T. KISS and K. VÁRNAGY

Department of Inorganic and Analytical Chemistry, L. Kossuth University, 4010 Debrecen, Hungary

and

B. DECOCK-LE RÉVÉREND

Laboratoire de Chimie Macromoléculaire, Université des Sciences et Techniques de Lille, France

(*Received* 28 *September* 1987; *accepted after revision* 19 *January* 1988)

Abstract—Formation of the proton, zinc(II) and cobalt(II) complexes of GlyCys and CysGly was studied by pH-metric, spectrophotometric and ^{1}H-NMR methods. CysGly forms stable bis-complexes with both metal ions, with cysteine-like (S,N)-coordination. (S,O)-coordination is favoured, however, in the zinc(II) and cobalt(II) complexes of GlyCys. The binding mode is supported by the deprotonation micro-constants of the ligands and protonated complexes, and by the results of spectrophotometric and NMR studies. Amide deprotonation and coordination can not be observed below pH 10 in any of the systems studied.

In a previous paper,[1] equilibrium and spectroscopic results on the nickel(II) complexes of simple cysteinyl dipeptides were reported. In accordance with expectations, it was found that the presence of the thiol group significantly changes the binding mode of the peptide molecules as compared to aliphatic dipeptides.[2] The interactions of glutathione and mercaptopropionylglycine with nickel(II) and copper(II) also reveal the considerable effect of thiol groups.[3–5] Solution equilibria of peptide complexes of other transition metal ions have scarcely been studied, because stable complexes are not present around the physiological pH range. Histidyl peptides (i.e. glycylhistidine and derivatives) are so far the only exception. Here, there is a significant influence on the complex formation with zinc(II) and cobalt(II) ions: amide deprotonation and coordination to zinc(II) and cobalt(II) ions around pH 7 was proved by equilibrium[6] and NMR studies.[7] In aliphatic dipeptides, cobalt(II) induces amide deprotonation[8] only above pH 10. On the other hand, O_2 uptake of the cobalt(II) peptide complexes and the corresponding cobalt(III) complexes were extensively studied.[9,10]

Little data on the complexes of thiol containing peptides with zinc(II) and cobalt(II) are available. Studies on mercaptopropionylglycine suggest that amide deprotonation does not occur,[4,11] but this process has been proposed in the zinc(II)–glutathione system,[12] at pH above 10.5.

In the present study, equilibrium and spectroscopic data are reported for glycyl–L-cysteine (GlyCys) and L-cysteinyl–glycine (CysGly) with zinc(II) and cobalt(II), and the effect of the thiol group on peptide coordination is discussed.

EXPERIMENTAL

L-Cysteine containing peptides (CysGly and GlyCys) were prepared by procedures described earlier.[1] N-acetyl-D-penicillamine was a commercial product of Fluka. Metal ion stock solutions were prepared in the form of chloride salts and their

*Author to whom correspondence should be addressed.

concentrations were checked gravimetrically via the oxinates.

In the pH-metric studies, the ligand concentration varied between $1–4 \times 10^{-3}$ mol dm^{-3}, while the metal ion to ligand ratios ranged from 1 : 1 to 1 : 3. Argon was bubbled through the samples (5 cm^3) to ensure the absence of oxygen and carbon dioxide, and to mix the solutions during titration with carbonate-free potassium hydroxide. The removal of oxygen contamination was crucial for cobalt(II) complexes, which are readily oxidized in slightly basic solution. Measurements were made with a Radiometer pHM 84 pH-meter with a GK 2421 C combined electrode and an ABU 80 automatic burette. The purities of the peptides and their concentrations in solution were checked by potentiometric titration. The calculation of [H$^+$] ion concentration from the measured pH and the other details of the pH-metric procedure, have been described previously.[13] All pH-metric studies were carried out at 298 K, at a constant ionic strength of 0.2 mol dm^{-3} KCl. Stability constants were calculated with PSEQUED, a general computational program.[14]

The dissociation micro-constants of the ligands were determined by pH-spectrophotometric titration, the dissociation of the SH group being monitored separately on the UV-band of the thiolate. The measurements were carried out as described earlier,[15,16] using a Beckman Acta MIV double-beam recording spectrophotometer. The same instrument was used to obtain the visible spectra of cobalt(II) complexes in an oxygen-free atmosphere.

^{1}H-NMR spectra of the zinc(II)–GlyCys system were recorded on a WP 200SY impulse FT NMR spectrophotometer in D_2O. The zinc(II) and ligand concentrations were 2.3×10^{-3} and 5×10^{-3} mol dm^{-3}, respectively.

RESULTS AND DISCUSSION

The pH-metrically and spectrophotometrically determined dissociation constants, are listed in Table 1. The fully protonated forms of the peptide molecules have three dissociation constants, the first relates to the dissociation of the carboxyl group. Similarly to cysteine itself[15] the pK_2 and pK_3, however, cannot be ascribed unambiguously to the dissociation of the ammonium group and the thiol group because these processes overlap. Thus, the real acidity of the individual groups must be characterized by micro-constants. These values, together with those for cysteine, are also given in Table 1.

It can be seen from Table 1 that for both peptides the NH_3^+ group is more acidic than the SH group ($k_2/k_3 < 1$), whereas the acidity sequence is just the opposite for cysteine ($k_2/k_3 = 1.62$). This can mainly be attributed to the greater distance of the strong electron-releasing carboxylate group from the NH_3^+ group in the peptides, so, that the acidity of the terminal NH_3^+ group is higher in the Cys-peptides than in cysteine. The overlap between the two dissociation processes is relatively small; the second proton dissociates mainly from the NH_3^+ group, the proportion of this being 91% in GlyCys and 83% in CysGly.

To check the validity of these micro-constants, they can be compared with the pK values of various model compounds. Thus, in the case of CysGly, for instance, the presence of the SH group increases the acidity of the NH_3^+ group by 8.19–7.01 = 1.18 log units, as compared with $pK_{NH_3^+} = 8.19$ for GlyAla.[13] There is a similar increase in the acidity of the NH_3^+ group due to the SH group in the case of cysteine. This can be seen when pk_3 for cysteine is compared to $pK_{NH_3^+}$ for alanine[17] (9.68–8.52 = 1.16 log units).

Stability constants of cobalt(II) and zinc(II) complexes with CysGly, GlyCys and N-acetyl-D-penicillamine (NAP) are collected in Table 2.

Table 1. Dissociation macro-constants (pK) and micro-constants (pk)[a] of the ligands at 25°C and $I = 0.2$ mol dm^{-3}

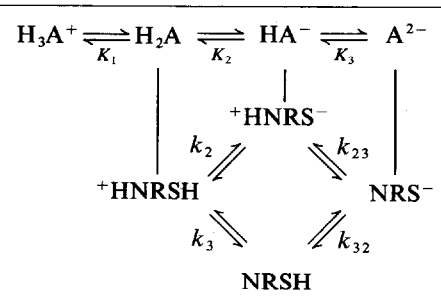

	GlyCys	CysGly	Cys
pK_1	2.73±0.02	3.13±0.01	1.86
pK_2	8.04±0.02	6.94±0.02	8.10
pK_3	9.48±0.02	9.37±0.02	10.16
pk_2 (SH)	9.14±0.03	7.78±0.05	8.31±0.06
pk_3 (NH_3^+)	8.08±0.02	7.01±0.02	8.52±0.07
pk_{23}	8.38±0.03	8.53±0.05	9.95±0.06
pk_{32}	9.44±0.03	9.30±0.03	9.74±0.07
k_2/k_3	0.09	0.17	1.62

[a] Although k generally stands for rate constants, it is widely used for the notation of equilibrium constants of processes at the molecular level (microscopic processes).

Table 2. Stability constants (log β_{pqr})[a] of cobalt(II) and zinc(II) complexes with CysGly, GlyCys and N-acetyl-D-penicillamine at 25°C and $I = 0.2$ mol dm^{-3}

	CysGly		GlyCys		NAP	
	Co(II)	Zn(II)	Co(II)	Zn(II)	Co(II)	Zn(II)
MA	6.65±0.05	8.15±0.04	—	—	4.63±0.08	6.85±0.05
MA_2	13.29±0.03	15.96±0.03	10.03±0.04	11.60±0.03	10.10±0.04	14.03±0.03
MA_2H	—	—	18.47±0.05	20.28±0.04	—	—
MA_2H_2	—	—	25.78±0.04	27.86±0.04	—	—
MA_2H_{-1}	—	—	—	1.87±0.06	—	—
log (K_1/K_2)	0.01	0.34	—	—	−0.84	−0.33
$pK^{MA_2H_2}_{MA_2H}$	—	—	7.31	7.60	—	—
$pK^{MA_2H}_{MA_2}$	—	—	8.44	8.68	—	—

[a] $\beta_{pqr} = \dfrac{[M_pA_qH_r]}{[M]^p[A]^q[H]^r}$.

It is clear from Table 2 that CysGly forms only mono- and bis-complexes with both metal ions; this result is analogous to that obtained for the complexation with nickel(II).[1] From the small log (K_1/K_2) values, it is also obvious that the formation of bis-complexes is especially favoured. The equilibrium results for L-cysteine and D-penicillamine[11,18] show the same trend, but an overall comparison of the stability constants of CysGly and L-cysteine (or D-penicillamine) is not possible for several reasons. The presence of the carboxylate group in L-cysteine makes two types of coordination possible with this compound [(S,O)- and (S,N)-coordination]. Steric factors preclude (S,O)-coordination of the peptide molecule via the carboxylate and thiol groups, and therefore the formation of various protonated complexes is ruled out. On the other hand, polynuclear complexes were formed with L-cysteine with all the metal ions studied, but such species were negligible in the nickel(II)–CysGly system.[1]

Equilibrium calculations on the cobalt(II) and zinc(II) complexes also ruled out polynuclear complex formation which can be interpreted in terms of steric requirements of the CysGly molecule.

The equilibrium relations of dipeptides containing N-terminal cysteinyl residues are therefore very simple. The formation of bis-complexes is almost exclusive, and the strong cysteine-like coordination, via the amino and thiol groups, precludes the possibility of amide deprotonation and coordination. The absorption spectra of the cobalt(II)–CysGly system (in a 1 : 3 molar ratio) lend support to these findings. An absorption maximum appears at $\lambda = 520$ nm which corresponds to that for the cobalt(II)–L-cysteine system.[11] The same process was observed with N-terminal histidyl peptides, where the stable histidine-like coordination favours bis-complex formation and precludes peptide amide ionization.[6]

In the case of GlyCys where the cysteine is in the C-terminal position, steric requirements exclude (S,N)-coordination (8-membered chelate ring), but (S,O)-coordination is possible (6-membered chelate ring), and the complexes of N-acetyl-D-penicillamine (NAP) were therefore also studied. (Polynuclear complex formation is characteristic of N-acetyl-L-cysteine,[3,11] and thus N-acetyl-D-penicillamine is a better model for comparison.) Corresponding stability constants are collected in Table 2. As an illustration, the concentration distribution curves of species formed in the zinc(II)–GlyCys system as a function of pH are depicted in Fig. 1.

It can be seen from Table 2 that only mono- and bis-complexes are formed with NAP, in which coordination can occur via the thiol-sulphur and carboxylate-oxygen donors. The formation of bis-complexes is especially favoured as indicated by the negative log (K_1/K_2) values. If similar complex formation processes are assumed for GlyCys, and it is borne in mind that it has three dissociable protons (thiol, ammonium and carboxyl), the formation of protonated species is also to be expected. The existence of bis-complexes is again favoured and reliable stability constants can therefore not be obtained for complexes of type [MA] and $[MAH]^+$. (Their concentrations do not reach 5% of the total metal ion concentration.)

The structures of the species $[MA_2H_2]$, $[MA_2H]^-$ and $[MA_2]^{2-}$ can therefore be explained by (S,O)-coordination and the stepwise deprotonation processes can be ascribed to the dissociation of the non-coordinated terminal NH_3^+ groups of the glycine residues. This assumption is supported by the fact

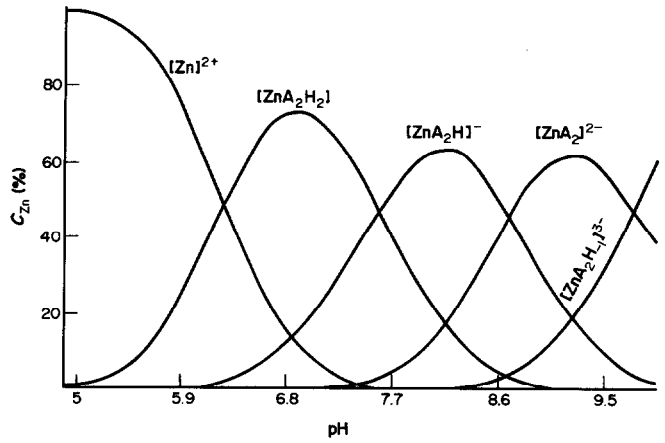

Fig. 1. Concentration distribution of complexes formed in the zinc(II)–GlyCys system, as a function of pH. $c_{Zn^{2+}} = 1.033 \times 10^{-3}$, $c_A = 3.256 \times 10^{-3}$ mol dm^{-3}.

that $pK^{MA_2H_2}_{MA_2H^2}$ and $pK^{MA_2H}_{MA_2^2}$ (see Table 2) correspond fairly well to the pk_3, characteristic of the dissociation of the terminal NH_3^+ group of the ligand ($pk_3 = 8.08$) and are much lower than the pk_2 characteristic of the dissociation of the SH group. However, the difference between $pK^{MA_2H_2}_{MA_2H^2}$ and $pK^{MA_2H}_{MA_2^2}$ differs from 0.6 log units (the statistical case for the ratio of the stepwise deprotonation constants of a molecule containing two acidic groups of the same acidity), suggesting that ammonium group deprotonation and hydroxo complex formation take place simultaneously. In the zinc(II)–GlyCys system a further proton dissociation with $pK^{MA_2}_{MA_2H_{-1}} = 9.73$ takes place (followed by hydrolysis and precipitation), which seems to confirm the above assumption. The spectrophotometric results of the cobalt(II)–GlyCys system support the (S,O)-binding mode of the ligand.

The absorption maximum of the CoA_2H_2 complex of GlyCys appears around $\lambda = 700$ nm, and is characteristic of a tetrahedral cobalt(II) complex.[11] Similar geometry is present in other (S,O)-coordinated cobalt(II) complexes, while octahedral coordination is characteristic of (N,S)-coordination.[11] Increase in the pH of this solution does not lead to any spectral changes, supporting the assumption that only deprotonation of the ammonium group takes place, which results in the formation of the species $[CoA_2H]^-$ and $[CoA_2]^{2-}$. In the case of the zinc(II)–GlyCys system, ^{1}H-NMR studies were carried out to prove the occurrence of (S,O)-coordination. In solutions containing zinc(II) and GlyCys in 1:2 molar ratio the chemical shift of the glycyl-CH_2 protons was observed only in the pH range of 7–9. The low-frequency chemical shift supports the deprotonation of the free ammonium group, while the "inactivity" of the cysteinyl-CH and CH_2-protons suggests that the coordination probably occurs via the thiol and carboxylate donor groups.[1]

To summarize the results on the GlyCys complexes, it can be stated that (S,O)-coordination is characteristic of both of the metal ions studied. This result, however, is different from that obtained for nickel(II)–GlyCys, where deprotonation and coordination of the amide group occurred, resulting in the formation of an $[NiAH_{-1}]^-$ species, coordinated via amino, amide and sulphur donor atoms.

The coordinating ability of GlyCys therefore differs from that of GlyHis, where amide coordination was characteristic for all metal ions studied. However, this result is not surprising if it is remembered that nickel(II) generally induces amide deprotonation in dipeptides. On the other hand, nickel(II) does not prefer (S,O)-coordination, which is favoured for cobalt(II) and zinc(II); this precludes the possibility of amide deprotonation in the corresponding GlyCys complexes.

REFERENCES

1. H. Kozlowski, B. Decock-Le Révérend, D. Ficheux, C. Loucheux and I. Sóvágó, *J. Inorg. Biochem.* 1987, **29**, 187.
2. H. Sigel and R. B. Martin, *Chem. Rev.* 1982, **82**, 385.
3. I. Sóvágó and R. B. Martin, *J. Inorg. Nucl. Chem.* 1981, **43**, 425.
4. Y. Sugiura, Y. Hirayama, H. Tanaka and H. Sakurai, *J. Inorg. Nucl. Chem.* 1975, **37**, 2367.
5. Y. Sugiura, Y. Hirayama, H. Tanaka and K. Ishizu, *J. Am. Chem. Soc.* 1975, **97**, 5577.
6. E. Farkas, I. Sóvágó and A. Gergely, *J. Chem. Soc., Dalton Trans.* 1983, 1545.
7. D. L. Rabenstein, S. A. Daignault, A. A. Isab, A. P.

Arnold and M. M. Shoukry, *J. Am. Chem. Soc.* 1985, **107**, 6437.
8. M. S. Michailidis and R. B. Martin, *J. Am. Chem. Soc.* 1969, **91**, 4683.
9. M. T. Barnet, H. C. Freeman, D. A. Buckingham, I. Hsu and D. J. van der Hehn, *J. Chem. Soc., Chem. Commun.* 1970, 367.
10. W. R. Harris and A. E. Martell, *J. Am. Chem. Soc.* 1977, **99**, 6746.
11. B. Harman and I. Sóvágó, *Inorg. Chim. Acta* 1983, **80**, 75.
12. B. J. Fuhr and D. L. Rabenstein, *J. Am. Chem. Soc.* 1973, **95**, 6944.
13. A. Gergely and I. Nagypál, *J. Chem. Soc., Dalton Trans.* 1977, 1104.
14. L. Zékány and I. Nagypál, in *Computational Methods for the Determination of Stability Constants* (Edited by D. Leggett). Plenum Press, New York (1985).
15. J. T. Edsall, R. B. Martin and B. R. Hollingworth, *Proc. Nat. Acad. Sci. U.S.* 1958, **44**, 505.
16. T. Kiss and B. Tóth, *Talanta* 1982, **29**, 539.
17. A. Gergely and I. Sóvágó, *J. Inorg. Nucl. Chem.* 1973, **35**, 4355.
18. I. Sóvágó, A. Gergely, B. Harman and T. Kiss, *J. Inorg. Nucl. Chem.* 1979, **41**, 1629.

Polyhedron Vol. 7, No. 12, pp. 1095–1100, 1988
Printed in Great Britain

0277–5387/88 $3.00+.00
© 1988 Pergamon Press plc

SYNTHESIS AND THERMAL STABILITY OF LANTHANIDE ORGANOMETALLICS INVOLVING CYCLOPENTADIENYL AND ACETYLACETONATO CHELATE LIGANDS

ZHONGWEN YE,* YONGFEI YU and HUAIZHU MA

Institute of Organic Chemistry, Anhui Normal University, Wuhu, Anhui, China

(*Received* 16 *December* 1987; *accepted* 19 *January* 1988)

Abstract—Two series of lanthanide organometallics of the general formulae, $Cp_2Ln(acac)$ and $CpLn(acac)_2$ (Cp = cyclopentadienyl; Ln = Nd, Sm, Gd, Dy, Er; Hacac = acetylacetone), have been synthesized and characterized. These compounds are not very stable to heat and tend to disproportionate into Cp_3Ln and $Ln(acac)_3$ at moderate temperatures. The sequence of thermal stability of the compounds of these two series has been determined and discussed in connection with the lanthanide contraction effect.

It is well-known that almost all organolanthanide compounds are very sensitive to moisture and air, but they have excellent thermal stability and many of them can be purified by sublimation. We have reported that either dicyclopentadienyl samarium acetate or halides,[1] or ytterbium organometallics involving both cyclopentadienyl and β-diketonato chelate ligands tend to disproportionate[2] at a moderately high temperature. Up to now, only a few ytterbium organometallics involving both cyclopentadienyl and β-diketonato chelate ligands have been synthesized.[2,3] The analogous lanthanide organometallics, except ytterbium, have not been reported. The purpose of this paper is to expand the scope of investigation to the lanthanides other than ytterbium. We have synthesized two series of lanthanide organometallics involving both cyclopentadienyl and acetylacetonato chelate ligands and compared their thermal stability.

RESULTS AND DISCUSSION

By reaction of the tricyclopentadienyl lanthanides with one or two equivalents of acetylacetone at room temperature in THF, ten new compounds have been synthesized. They are:

1:1 Ratio of reactants		1:2 Ratio of reactants	
$Cp_2Nd(acac)$	**(1)**	$CpNd(acac)_2$	**(2)**
$Cp_2Sm(acac)$	**(3)**	$CpSm(acac)_2$	**(4)**
$Cp_2Gd(acac)$	**(5)**	$CpGd(acac)_2$	**(6)**
$Cp_2Dy(acac)$	**(7)**	$CpDy(acac)_2$	**(8)**
$Cp_2Er(acac)$	**(9)**	$CpEr(acac)_2$	**(10)**

*Author to whom correspondence should be addressed.

All compounds were identified by elemental analysis, IR (Table 1) and MS (Table 2).

All ten compounds exhibit four characteristic Cp absorption peaks at approx. 3100, 1400, 1010, 780 cm^{-1} and an absorption peak at about 250 cm^{-1} for the Ln—C of the π-bonded Cp group.[4] All of them exhibit the characteristic C···O and C···C multiple absorption bands of O-chelate complexes.[5]

Due to the large radii and coordination unsaturation of lighter lanthanides, their organometallics involving both Cp and Cl ligands, such as, Cp_2LnCl and $CpLnCl_2$ (Ln = La, Ce, Pr, Nd), have not been synthesized. Recently, Chen *et al.*[6] reported the successful preparation of $CpNdCl_2 \cdot 3THF$ and $Cp_2NdCl \cdot THF$ by improving the traditional preparative conditions, although the two compounds are both solvated and unstable at room temperature. Here, the facile preparation of the unsolvated and room-temperature stable $Cp_2Nd(acac)$ and $CpNd(acac)_2$ is obviously due to stabilization of the species by the chelation effect.

The mass spectra of all the compounds were recorded at different temperatures and revealed that all compounds display their molecule ion peak M^+ and fragments thereof at comparatively low temperatures, but neither the ion peak for M_2 nor that for THF could be found. It is obvious that all of these compounds are unsolvated monomers. Secondly, the MS data reveal that these compounds tend to disproportionate at moderately high temperatures. We adopt the lowest temperature of vaporization at which the disproportionation reaction begins to be observed as a standard in order to compare the relative thermal stability of all the compounds. In the course of gradually raising the

Table 1. Analytical and part of IR[a] data for the compounds **1–10**

Compounds $(C_5H_5)_nLn(CH_3COCHCOCH_3)_{3-n}$	Yield (%)	M.p. (°C)[b] (d = decomp.)	Colour	Analysis[c] % Found (calc.) Ln	C	H	IR (cm^{-1}) 1500–1600 cm^{-1}		
$n = 2$, Ln = Nd (**1**)	60	450(d)	Purple	38.5 (38.6)	47.6 (48.2)	5.2 (4.5)	1517	1524	1590
$n = 1$, Ln = Nd (**2**)	53	390(d)	Purple	34.8 (35.4)	44.0 (44.2)	4.9 (4.7)	1517	1525	1584
$n = 2$, Ln = Sm (**3**)	51	164	Yellow	39.7 (39.6)	47.6 (47.4)	5.2 (4.5)	1515	1522	1583
$n = 1$, Ln = Sm (**4**)	59	113	Pale Yellow	36.8 (36.3)	43.4 (43.5)	5.0 (4.6)	1515	1522	1584
$n = 2$, Ln = Gd (**5**)	57	150	Pale Yellow	41.1 (40.7)	46.9 (46.6)	4.8 (4.4)	1516	1526	1580
$n = 1$, Ln = Gd (**6**)	59	150	Pale Yellow	37.8 (37.4)	43.0 (42.8)	4.8 (4.5)	1514	1534	1584
$n = 2$, Ln = Dy (**7**)	52	480(d)	Yellow	40.9 (41.5)	46.3 (46.0)	4.6 (4.4)	1516	1522	1580
$n = 1$, Ln = Dy (**8**)	54	85	Yellow	38.0 (38.2)	41.5 (42.3)	5.1 (4.5)	1518	1523	1597
$n = 2$, Ln = Er (**9**)	61	60	Pink	42.1 (42.2)	45.0 (45.4)	4.5 (4.3)	1517	1522	1588
$n = 1$, Ln = Er (**10**)	64	114	Pink	39.2 (38.8)	41.7 (41.8)	4.7 (4.4)	1519	1522	1592

[a] IR were recorded on a Perkin–Elmer 983(G) (CsI crystal plate, Nujol and Fluorolube mulls) instrument.

[b] Melting points were determined in sealed argon-filled capillaries and were uncorrected.

[c] Elemental analysis results for Ln were obtained by a published method.[4] The elemental analysis data for C and H were obtained on Yanaco MT-2 analyser.

temperature, $CpLn(acac)_2$, initially disproportionates into $Cp_2Ln(acac)$ and $Ln(acac)_3$ and then further into Cp_3Ln and $Ln(acac)_3$. The disproportionate reaction of $CpLn(acac)_2$ presumably involves the following equilibria:

$$2CpLn(acac)_2 \rightleftharpoons Cp_2Ln(acac) + Ln(acac)_3$$

$$3Cp_2Ln(acac) \rightleftharpoons 2Cp_3Ln + Ln(acac)_3.$$

The reversibilities of the above disproportionation reactions have been verified by their reverse reactions. The purified products of the reverse reactions, $CpLn(acac)_2$ and $Cp_2Ln(acac)$, are all characterized by elemental analyses and MS. So, we conclude that, for the same lanthanide metal, the compound of the type $CpLn(acac)_2$ is much less thermally stable than that of $Cp_2Ln(acac)$. Evans[7] pointed out that ligand rearrangement and reversible modification of the coordination geometry may be relatively facile in the absence of orbital factors, as long as electrostatic demands are met. We suggest that the lability of the η^5-Cp ligand[8] is the cause of the disproportionation reactions. It is also possible that the disproportionation takes place via an intermediate bimolecular complex in which the Cp groups are bonded in an η^5-fashion to one molecule and in an η^1-fashion to a second molecule of the complex. The transfer of one Cp group from one molecule to another may initiate the disproportionation reaction. Since the transfer of one Cp group is more facile than the transfer of two Cp groups at the same time, therefore, $CpLn(acac)_2$ is thermally less stable than $Cp_2Ln(acac)$.

From the MS data, we also conclude that the sequence of thermal stability of the compounds of either the $CpLn(acac)_2$ or $Cp_2Ln(acac)$ series is: Er > Dy > Gd > Sm > Nd.

Evidently, the dependence of thermal stability on ionic radii of the rare earths implies that attraction forces among Ln^{3+} and anionic ligands are important in determining the relative stability. These forces should become greater as the radius of the metal ion decreases. For this reason, the thermal stability of lanthanide organometallics involving both Cp and acac ligands is firmly connected to the lanthanide contraction effect.

Comparing with the MS data in the previous paper,[2] we ought to point out that $Cp_2Yb(acac)$ is much more thermally stable than $Cp_2Ln(acac)$ (Ln = Nd, Sm, Gd, Dy, Er), as $Cp_2Yb(acac)$ begins to disproportionate at 200°C. But, $CpYb(acac)_2$ begins to disproportionate at 50°C and is apparently less thermally stable than the other rare earth analogues.

EXPERIMENTAL

All manipulations on these lanthanide organometallics were carried out in an atmosphere of purified argon using Schlenk techniques or a glovebox. All solvents were refluxed and distilled over either finely divided $LiAlH_4$ or the sodium ketyl of benzophenone under argon immediately before use. The acetylacetone was dried over anhydrous Na_2SO_4 and distilled under argon.

Cp_3Ln (Ln = Nd, Sm, Gd, Dy, Er) was prepared by a published procedure.[9]

General method of synthesis of $Cp_2Ln(acac)$ *or* $CpLn(acac)_2$

To a suspension of Cp_3Ln (1 equiv.) in *n*-hexane was added acetylacetone (1 or 2 equiv.). After stirring for 1 day, the *n*-hexane was removed *in vacuo* and the resulting solid was recrystallized from THF/*n*-hexane (twice) to afford $Cp_2Ln(acac)$ or $CpLn(acac)_2$.

Yields, analyses and physical properties of all ten compounds are listed in Table 1.

Preparation of anhydrous $Ln(acac)_3$

Acetylacetone (3.50 g, 0.035 mol) was added to a suspension of anhydrous Cp_3Ln (0.01 mol) in *n*-hexane. The reaction mixture was stirred for 10 h and then, the *n*-hexane was removed *in vacuo*. The resulting solid was dried for 3 h to afford $Ln(acac)_3$. The products were characterized by elemental analyses and IR.

Reactions of $Ln(acac)_3$ *with* $Cp_2Ln(acac)$

A suspension of 4 mmol $Ln(acac)_3$ and 4 mmol $Cp_2Ln(acac)$ in *n*-hexane was allowed to react under stirring at room temperature for 1 day. The *n*-hexane was removed *in vacuo* and the resulting solid was recrystallized from THF/*n*-hexane (thrice). Each product, $CpLn(acac)_2$ (Ln = Nd, Sm, Gd, Dy or Er), was characterized by elemental analyses and MS.

Reactions of $Ln(acac)_3$ *with* Cp_3Ln

A suspension of 4 mmol $Ln(acac)_3$ and 8 mmol Cp_3Ln in *n*-hexane was allowed to react at room temperature. After stirring for 1 day, the *n*-hexane was removed *in vacuo* and the resulting solid was recrystallized from THF/*n*-hexane (thrice). Each product, $Cp_2Ln(acac)$ (Ln = Nd, Sm, Gd, Dy or Er), was characterized by elemental analyses and MS.

Table 2. MS data[a] for compounds **1–10** at different temperatures of vaporization

Compounds $Cp_nLn(acac)_{3-n}$ ($Cp = C_5H_5$, acac = $CH_3COCHCOCH_3$) and mol. species	Temperature of vaporization (°C)	Main peaks, m/e[b]
(1) $n = 2$, Ln = Nd, M = $Cp_2Nd(acac)$, M′ = $Nd(acac)_3$, M″ = Cp_3Nd	40, 65, 90	371(M), 306(M—Cp), 272(M—acac), 249(M—2Cp), 207(M—Cp—acac),
	120, 130, 150	439(M′), 371(M), 337(M″), 306(M—Cp), 272(M—acac), 241(M—2Cp), 207(M—Cp—acac)
(2) $n = 1$, Ln = Nd, M = $CpNd(acac)_2$, M′ = $Nd(acac)_3$, M″ = Cp_3Nd, M‴ = $Cp_2Nd(acac)$	50, 65, 80	405(M), 340(M—Cp), 306(M—acac), 241(M—Cp—acac), 207(M—2acac),
	90, 100, 110	439(M′), 405(M), 371(M‴), 340(M—Cp), 306(M—acac), 241(M—Cp—acac), 207(M—2acac)
	120, 150, 200	439(M′), 405(M), 371(M‴), 340(M—Cp), 337(M″), 306(M—acac), 241(M—Cp—acac), 207(M—2acac)
(3) $n = 2$, Ln = Sm, M = $Cp_2Sm(acac)$, M′ = $Sm(acac)_3$, M″ = Cp_3Sm	50, 100, 130	381(M), 361(M—Cp), 282(M—acac), 251(M—2Cp), 217(M—Cp—acac),
	150, 200, 250	449(M′), 381(M), 347(M″), 316(M—Cp), 282(M—acac), 251(M—2Cp), 217(M—Cp—acac)
(4) $n = 1$, Ln = Sm, M = $CpSm(acac)_2$, M′ = $Sm(acac)_3$, M″ = Cp_3Sm, M‴ = $Cp_2Sm(acac)$	50, 70, 90	415(M), 350(M—Cp), 316(M—acac), 251(M—Cp—acac), 217(M—2acac),
	110, 120, 135	449(M′), 415(M), 381(M‴), 350(M—Cp), 316(M—acac), 251(M—Cp—acac), 217(M—2acac)
	150, 200, 240	449(M′), 415(M), 381(M‴), 350(M—Cp), 347(M″), 316(M—acac), 251(M—Cp—acac), 217(M—2acac)
(5) $n = 2$, Ln = Gd, M = $Cp_2Gd(acac)$, M′ = $Gd(acac)_3$, M″ = Cp_3Gd	60, 100, 150	387(M), 322(M—Cp), 288(M—acac), 257(M—2Cp), 223(M—Cp—acac),
	165, 200, 230	455(M′), 387(M), 353(M″), 322(M—Cp), 288(M—acac), 257(M—2Cp), 223(M—Cp—acac)

(6)	$n = 1$, Ln = Gd, M = $CpGd(acac)_2$, M′ = $Gd(acac)_3$, M″ = Cp_3Gd, M‴ = $Cp_2Gd(acac)$	60, 85, 120	421(M), 356(M—Cp), 322(M—acac), 257(M—Cp—acac), 223(M—2acac),
		130, 140, 150	455(M′), 421(M), 387(M‴), 356(M—Cp), 322(M—acac), 257(M—Cp—acac), 223(M—2acac)
		165, 200, 240	455(M′), 421(M), 387(M‴), 356(M—Cp), 353(M″), 322(M—acac), 257(M—Cp—acac), 223(M—2acac)
(7)	$n = 2$, Ln = Dy, M = $Cp_2Dy(acac)$, M′ = $Dy(acac)_3$, M″ = Cp_3Dy	70, 100, 160	393(M), 328(M—Cp), 294(M—acac), 263(M—2Cp), 229(M—Cp—acac),
		185, 200, 250	461(M′), 393(M), 359(M″), 328(M—Cp), 294(M—acac), 263(M—2Cp), 229(M—Cp—acac)
(8)	$n = 1$, Ln = Dy, M = $CpDy(acac)_2$, M′ = $Dy(acac)_3$, M″ = Cp_3Dy, M‴ = $Cp_2Dy(acac)$	70, 90, 130	427(M), 362(M—Cp), 328(M—acac), 263(M—Cp—acac), 229(M—2acac),
		150, 165, 170	461(M′), 427(M), 393(M‴), 362(M—Cp), 328(M—acac), 263(M—Cp—acac), 229(M—2acac)
		180, 200, 250	461(M′), 427(M), 393(M‴), 362(M—Cp), 359(M″), 328(M—acac), 263(M—Cp—acac), 229(M—2acac)
(9)	$n = 2$, Ln = Er, M = $Cp_2Er(acac)$, M′ = $Er(acac)_3$, M″ = Cp_3Er	100, 150, 180	395(M), 330(M—Cp), 296(M—acac), 265(M—2Cp), 231(M—Cp—acac),
		195, 200, 250	463(M′), 395(M), 361(M″), 330(M—Cp), 296(M—acac), 265(M—2Cp), 231(M—Cp—acac)
(10)	$n = 1$, Ln = Er, M = $CpEr(acac)_2$, M′ = $Er(acac)_3$, M″ = Cp_3Er, M‴ = $Cp_2Er(acac)$	80, 115, 145	429(M), 364(M—Cp), 330(M—acac), 265(M—Cp—acac), 231(M—2acac)
		165, 170, 180	463(M′), 429(M), 395(M‴), 364(M—Cp), 330(M—acac), 265(M—Cp—acac), 231(M—2acac)
		190, 210, 240	463(M′), 429(M), 395(M‴), 364(M—Cp), 361(M″), 330(M—acac), 265(M—Cp—acac), 231(M—2acac)

[a] MS spectra were recorded on a VG ZAB–HS organic mass spectrometer.

[b] MS data are given for isotopes ^{142}Nd, ^{152}Sm, ^{158}Gd, ^{164}Dy and ^{166}Er. The peak patterns correspond to theoretical values based on the natural abundance of isotopes.

Acknowledgements—Projects are supported by the Science Fund of the Chinese Academy of Science. Mr Pin Li is thanked for recording the MS.

REFERENCES

1. Zhongwen Ye, Huaizhu Ma and Yongfei Yu, *J. Less-Common Metals*, 1986, **126**, 405.
2. Huaizhu Ma and Zhongwen Ye, *J. Organomet. Chem.* 1987, **326**, 369.
3. G. Bielang and R. D. Fischer, *Inorg. Chem. Acta* 1979, **36**, L389.
4. C. Qian, C. Ye, H. Lu, Y. Li, J. Zhou and Y. Ge, *J. Organomet. Chem.* 1983, **247**, 161.
5. K. Nakamoto, *Infrared and Raman Spectra of Inorganic and Coordination Compounds*, 3rd Edn, p. 249. Wiley-Interscience, New York (1977).
6. G. Yang, Y. Fan, Z. Jin, Y. Xing and W. Chen, *J. Organomet. Chem.* 1987, **322**, 57.
7. W. J. Evans, *Adv. Organomet. Chem.* 1985, **24**, 131.
8. K. W. Bagnall, in T. J. Marks and R. D. Fischer (Eds), *Organometallics of the f-Elements*, p. 221. Reidel, Dordrecht (1979).
9. J. M. Birmingham and G. Wilkinson, *J. Am. Chem. Soc.* 1954, **76**, 6210.

Polyhedron Vol. 7, No. 12, pp. 1101–1105, 1988
Printed in Great Britain

0277–5387/88 $3.00+.00
© 1988 Pergamon Press plc

CHELATES OF ACETYLFERROCENE BENZOYLHYDRAZONE WITH LANTHANIDES

MA YONGXIANG* and ZHAO GANG

Department of Chemistry, Lanzhou University, China

(*Received* 15 *December* 1987; *accepted* 19 *January* 1988)

Abstract—The chelates, $Ln(HL)_2Cl_3 \cdot nH_2O$ of acetylferrocene benzoylhydrazone with 15 lanthanide(III) metals have been prepared and characterized by elemental analysis, IR, UV, molar conductance, TG and DTA. It was found that the ligand coordinates to the central ions in the keto form, and some chloride ions and water molecules participate in coordination to the metal ion. The chelates are 1 : 1 electrolytes in methanol and DMF, and are more thermostable than their ligand due to the formation of chelate rings.

Due to their biological activity, especially as potent inhibitors for many enzymes, the coordination chemistry of aroylhydrazines and related compounds is a subject of extensive studies.[1] Edwards *et al.*[2] have shown that the replacement of aromatic groups by the ferrocenyl moiety in the penicillins and cephalosphorins improves their antibiotic activity. Some transition metal chelates with α-N-aroyl-β-ferrocenylidenehydrazides have been synthesized by Patil *et al.*[3] However, the chelates of this ligand with lanthanide metals have not been reported so far. In this paper, we report the synthesis of the chelates of acetylferrocene benzoylhydrazone with lanthanide(III) chloride, and discuss their IR, UV, molar conductance, thermagravimetry (TG) and differential thermal analysis (DTA).

EXPERIMENTAL

Methods and materials

Acetylferrocene was prepared according to the literature method.[4] Benzoylhydrazine was chemical reagent grade. The ligand, acetylferrocene benzoylhydrazone (HL) was obtained and purified by the literature method.[3] Lanthanide(III) chlorides were prepared from their oxides and hydrochloric acid.

Syntheses of lanthanide chelates

The chelates were prepared by mixing lanthanide(III) chloride (0.0005 mol) in ethanol–triethyl *ortho*-formate and acetylferrocene benzoylhydrazone (0.001 mol) in warm ethanol and refluxing the solution for 9 h. The mixture was then concentrated to the appropriate volume. The solid which formed when the mixture was cooled was filtered, washed several times with ethanol–ether and dried *in vacuo*. Yield above 82%. Elemental analysis and some physical properties of products obtained are listed in Table 1.

Measurements

The IR spectra were made on KBr pellets using a NIC-5DX spectrophotometer. UV spectra were recorded in the 200–500 nm region in methanol with a DJ-240 spectrophotometer. Electrolytic conductivities were carried out using a DDS-IIA molar conductometer using methanol and dimethylformamide (DMF) as solvents at 25°C. TG and DTA measurements were made in a nitrogen atmosphere between room temperature and 800°C using a Thermoflex TG-DTA meter (Japan).

RESULTS AND DISCUSSION

These chelates of acetylferrocene benzoylhydrazone with lanthanide metals are insoluble in non-polar solvents such as pentane and benzene,

* Author to whom correspondence should be addressed.

Table 1. Physical properties and elemental analyses of chelates $Ln(HL)_2Cl_3 \cdot nH_2O$[a]

Chelate	Formula	M.p. (°C)	Colour	Elemental analysis (%)[b] C	H	N	Cl
I	$Y(HL)_2Cl_3 \cdot 2H_2O$	178[c]	Brown	49.4 (49.3)	4.3 (4.3)	6.2 (6.0)	11.6 (11.4)
II	$La(HL)_2Cl_3 \cdot H_2O$	180	Brown	47.7 (47.7)	4.2 (4.0)	6.2 (5.9)	11.3 (11.2)
III	$Ce(HL)_2Cl_3 \cdot 3H_2O$	173	Brown	45.9 (46.0)	4.0 (4.3)	6.4 (5.6)	11.0 (11.7)
IV	$Pr(HL)_2Cl_3 \cdot 3H_2O$	175	Brown	47.2 (47.6)	4.3 (4.3)	6.3 (5.8)	11.1 (10.8)
V	$Nd(HL)_2Cl_3 \cdot H_2O$	181	Brown	47.5 (47.4)	4.1 (4.0)	6.3 (5.8)	11.2 (11.0)
VI	$Sm(HL)_2Cl_3 \cdot 2H_2O$	185	Red–brown	46.3 (46.3)	4.0 (4.1)	6.4 (5.7)	10.1 (10.8)
VII	$Eu(HL)_2Cl_3 \cdot 2H_2O$	187	Red–brown	45.9 (46.2)	4.1 (4.1)	6.2 (5.7)	10.5 (10.8)
VIII	$Gd(HL)_2Cl_3 \cdot 2H_2O$	182	Red–brown	45.8 (46.0)	4.0 (4.0)	6.4 (5.6)	10.4 (10.7)
IX	$Tb(HL)_2Cl_3 \cdot 3H_2O$	185	Brown	44.1 (45.1)	4.1 (4.2)	6.1 (5.5)	10.5 (10.5)
X	$Dy(HL)_2Cl_3 \cdot 3H_2O$	181	Red–brown	44.3 (44.5)	3.9 (4.1)	6.1 (5.5)	10.6 (10.4)
XI	$Ho(HL)_2Cl_3 \cdot 3H_2O$	184	Brown	44.9 (44.8)	4.0 (4.1)	6.3 (5.5)	10.7 (10.4)
XII	$Er(HL)_2Cl_3 \cdot 3H_2O$	183	Red–brown	44.6 (44.7)	4.0 (4.1)	6.0 (5.5)	10.5 (10.4)
XIII	$Tm(HL)_2Cl_3 \cdot H_2O$	174	Brown	46.6 (46.2)	3.9 (3.8)	6.1 (5.7)	10.2 (10.8)
XIV	$Yb(HL)_2Cl_3 \cdot 5H_2O$	180	Red–brown	42.9 (42.9)	4.0 (4.3)	5.6 (5.3)	10.3 (10.0)
XV	$Lu(HL)_2Cl_3 \cdot 3H_2O$	186	Red–brown	44.6 (44.4)	4.0 (4.1)	5.8 (5.4)	10.6 (10.4)

[a] $HL = C_5H_5FeC_5H_4CMe{=}NNHCOC_6H_5$.
[b] Calculated values are given in parentheses.
[c] M.p. of all chelates are their decomposition points.

but soluble in DMF, methanol, ethanol and acetonitrile. These chelates are hygroscopic. Their elemental analyses show that $LnCl_3 \cdot nH_2O$ (Ln = lanthanide) forms chelates without loss of chloride ions and they conform to the formula $Ln(HL)_2Cl_3 \cdot (1\text{–}5)H_2O$. Their molar conductance, IR and UV spectra, TG and DTA measurements suggest the structure shown in Fig. 1.

IR spectra

The IR frequencies along with their relative assignments are given in Table 2. The IR spectra of these chelates are similar to those of the ligand. They appear as characteristic bands of amide I, ν (C=O), azomethine ν (C=N) and amide II.[5] Usually the ν (C=O) and ν (C=N) bands are shifted by *ca* 30–50 and 15–25 cm^{-1}, respectively to lower frequencies compared with the parent ligand. The hydrazone residue acts as a neutral bidentate

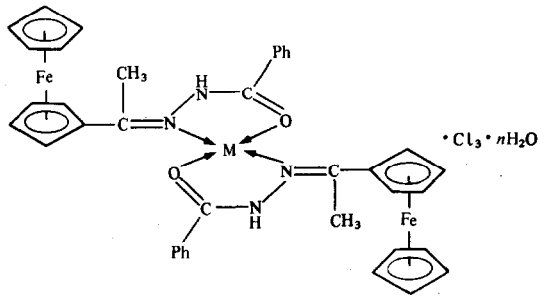

Fig. 1. Proposed structure for the chelates, Fc = $C_5H_5FeC_5H_4$ $n = 1$, M = La, Nd, Tm; $n = 2$, M = Y, Sm, Eu, Cd; $n = 3$, M = Ce, Pr, Dy, Ho, Er, Lu; $n = 4$, M = Tb; $n = 5$, M = Yb.

Table 2. Important IR frequencies (cm^{-1}) of the ligand and its chelates

Chelate	Amide I ν (C=O)	ν (C=N)	ν (N—N)	ν (M—N)	ν (M—O)
HL	1645vs[a]	1526s	910m		
I	1611br,s	1520s	910m	546w	376w
II	1612br,s	1520s	910m	543w	374w
III	1608br,s	1521s	910m	537w	380w
IV	1600br,s	1523s	911m	548w	378w
V	1593br,s	1520br,s	910m	546m	375w
VI	1595br,s	1521s	910m	546m	375w
VII	1600br,s	1520s	910m	545m	378w
VIII	1597br,s	1523br,s	910m	550w	380w
IX	1601br,s	1520br,s	911m	546w	376m
X	1596br,s	1520br,s	913m	548m	381m
XI	1598br,s	1520br,s	911m	550w	385w
XII	1592br,s	1515br,s	910m	543w	376m
XIII	1595br,s	1516br,s	910m	548m	375m
XIV	1601br,s	1520br,s	910m	546w	373w
XV	1615br,s	1520br,s	915m	546w	375w

[a] vs = very strong, s = strong, m = medium, w = weak and br = broad.

ligand in these chelates and is coordinated to the central Ln(III) ion via the carbonyl oxygen atom and the azomethine nitrogen atom. The ν (N—N) band appears at 910 cm^{-1}.[6] The bands observed at *ca* 1435, 1100, 820, 491 and 395 cm^{-1} are attributed to the ferrocenyl group as the ν (C—C), δ (C—H), π-CH, and g(Fe–ring), respectively.[7] The stretching vibration frequency ν (O—H) of water appears in the range 3300–3500 cm^{-1}.[8] The ν (N—H) and ferrocenyl group ν (C—H) stretching are covered by the ν (O—H). In the far-IR region, two new bands which are observed at *ca* 548 and 380 cm^{-1} may be attributed to ν (Ln ← N) and ν (Ln ← O), respectively.

UV spectra

UV-vis absorption spectra of the ligand and its chelates in methanol are shown in Table 3. UV spectra of these chelates show that the *K* band of the ligand at 296 nm is shifted to lower wavelength 290–294 nm; there is a shoulder peak similar to that of the ligand at *ca* 220–230 nm, which can be attributed to the $\pi \rightarrow \pi^*$ transition on azomethine. The very weak but single peak at 260 nm in the spectra of these chelates, which is not clear in that of the ligand, may be due to the *B* band of the cyclopentadienyl ring.[9] The band at 202 nm can be attributed to the E_2 band of benzene. The band around 450 nm may be due to charge-transfer from the 3*d* orbitals on iron to either the non-bonding or antibonding orbitals on the cyclopentadienyl ring ($d \rightarrow \pi^*$ transition).[10] Thus, these small changes in the wavelength of these chelates as compared to that of the parent ligand suggest that the lanthanide(III) ions are bonded to the acetylferrocene benzoylhydrazone entity.

Electrolytic conductance

Dissolving the lanthanide chelates in methanol and DMF afforded a dark brown solution. The

Table 3. UV spectra of the ligand and its chelates

Chelate	Absorption peaks (nm, λ max) (1)	(2)	(3)	(4)	(5)
HL	202	220–230sh[a]		296	450
I	202	220–230sh	270	294	451
II	202	220–230sh	270	294	450
III	201	220–230sh	263	294	450
IV	202	220–230sh	262	292	450
V	202	220–230sh	255	292	451
VI	202	220–230sh	257	291	450
VII	202	220–230sh	261	293	450
VIII	202	220–230sh	258	291	451
IX	202	220–230sh	259	291	450
X	202	220–230sh	256	291	451
XI	202	220–230sh	254	290	450
XII	202	220–230sh	256	293	451
XIII	202	220–230sh	255	294	450
XIV	202	220–230sh	258	293	450
XV	202	220–230sh	256	292	450

[a] sh = shoulder.

Table 4. Molar conductances of the chelates at 25°C

Chelate	In methanol conc. (10^{-3} mol)	λ_m (Ω^{-1} cm^2 mol^{-1})	In DMF conc. (10^{-3} mol)	λ_m (Ω^{-1} cm^2 mol^{-1})
I	1.03	101.0	1.28	65.0
II	1.04	104.2	1.08	68.1
III	0.96	93.5	1.11	65.4
IV	1.12	92.9	1.07	67.5
V	1.07	98.5	1.09	68.7
VI	1.04	89.5	1.05	66.7
VII	1.11	85.7	1.19	61.2
VIII	0.98	90.1	1.06	66.6
IX	1.12	105.2	1.06	69.2
X	1.07	96.3	1.14	62.1
XI	1.03	123.1	1.01	69.5
XII	1.01	99.7	1.01	67.8
XIII	1.11	91.7	1.06	53.3
XIV	1.08	94.3	0.99	56.1
XV	1.07	97.1	1.05	58.9

Conc. = concentration.

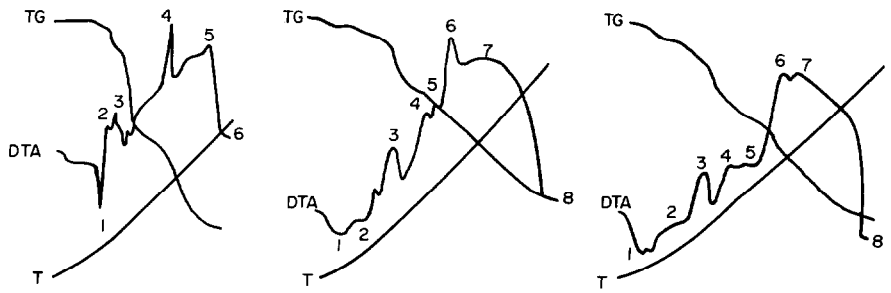

Fig. 2. TG–DTA diagram of (a) HL 1—168, 2—200, 3—224, 4—420, 5—570, 6—648°C. (b) $Pr(HL)_2Cl_3 \cdot 3H_2O$ 1—70, 2—180, 3—240, 4—380, 5—417, 6—470, 7—560, 8—756°C. (c) $Tb(HL)_2Cl_3 \cdot 4H_2O$ 1—90, 2—167, 3—250, 4—331, 5—410, 6—527, 7—587, 8—786°C.

molar conductances (Table 4) of these solutions approach those reported for 1 : 1 electrolytes.[11] It is fairly evident that there are two chloride ions which participate in coordination.

TG and DTA

In order to investigate their thermal properties we measured weight-loss and decomposition temperature of the ligand and its two chelates by the TG and DTA methods (Fig. 2). The TG–DTA diagram of the ligand [Fig. 2(a)] shows that the ligand melts at 168°C and begins to decompose at 200°C accompanied by the release of heat. It loses weight intensely at about 224 and 570°C, but only slightly between 268–420°C. The TG–DTA diagram of the chelate $Pr(HL)_2Cl_3 \cdot 3H_2O$ [Fig. 2(b)] indicates that this chelate loses about 2.5% of its weight at 70°C, which corresponds to the loss of one molecule of water (calculated value 2.0%). It then loses *ca* 5% of its weight at 180°C, perhaps indicating that the other two molecules of water break away from the chelates (calculated value 5.4%). It appears that the former is crystal water and the latter is coordinated water. The chelate decomposes exothermically and continuously at 240, 380, 417, 470 and 560°C. The TG–DTA diagram of the chelate $Tb(HL)_2Cl_3 \cdot 4H_2O$(c) indicates that the chelate loses 5.3% of its weight at 90°C. This should be due to the release of its three molecules of water (calculated value equals 5.8%). The other molecule of water is lost endothermally at 167°C (found 2.5, calc. 2.5%). The chelate continues to decompose exothermally at 250, 331, 410, 527 and 587°C and is complete at 786°C.

It can be seen from the aforementioned data that

in these chelates, the coordination numbers of the central ions are different, i.e. those of Pr(III) and Tb(III) equal eight and seven, respectively.

REFERENCES

1. M. F. Iskander, L. El. Sayed and M. A. Lasheen, *Inorg. Chim. Acta* 1976, **16**, 147.
2. E. I. Edwards, R. Epton and G. Marr, *J. Organomet. Chem.* 1975, **85**, C23.
3. S. R. Patil, U. N. Kantak and D. N. Sen, *Inorg. Chim. Acta* 1982, **63**, 261; S. R. Patil, U. N. Kantak and D. N. Sen, *Inorg. Chim. Acta* 1983, **68**, 1.
4. P. J. Graham, R. V. Lindsey, G. W. Parshall, M. L. Peterson and G. M. Whitman, *J. Am. Chem. Soc.* 1957, **79**, 3416.
5. M. Mashima, *Bull. Chem. Soc. Japan* 1962, **35**, 1882; M. Mashima, *Bull. Chem. Soc. Japan* 1963, **36**, 210.
6. R. C. Aggarwal and K. K. Narang, *Indian J. Chem.* 1971, **9**, 1413.
7. K. Nakamoto, *Infrared Spectra of Inorganic and Coordination Compounds*, 2nd Edn. Wiley-Interscience, New York (1970).
8. G. V. Yukhnevich, *Russian Chem. Rev.* 1963, **32**, 1397.
9. S. I. Goldberg, D. W. Wayo and J. A. Afalford, *J. Org. Chem.* 1963, **28**, 1708.
10. M. Rosenblum, J. O. Santer and W. G. Jowells, *J. Am. Chem. Soc.* 1963, **85**, 1450.
11. W. J. Geary, *Coord. Chem. Rev.* 1971, **7**, 81.

Polyhedron Vol. 7, No. 12, pp. 1107–1120, 1988
Printed in Great Britain

0277–5387/88 $3.00+.00
© 1988 Pergamon Press plc

POLYHEDRAL REARRANGEMENTS IN CLUSTERS

ALISON RODGER and BRIAN F. G. JOHNSON

University Chemical Laboratory, Lensfield Road, Cambridge, CB2 1EW, U.K.

(*Received* 18 *December* 1987; *accepted* 21 *January* 1988)

Abstract—Alternative reaction mechanisms for the rearrangements of cluster compounds containing from five to twelve atoms (or units of atoms) are deduced using purely geometrical arguments and the fact that cluster structures are determined by strong attractive forces between component units. This forms the first stage of a two-stage procedure. The results of the first stage apply to all clusters of a given geometry and the second stage involves quantitative consideration of the electronic states of a given system to determine the relative energetics of the geometrically determined mechanisms.

The rearrangement mechanisms for transition metal cluster compounds might be expected to proceed differently from those for either transition metal complexes or main group cluster compounds such as boranes and carboranes.[1] Transition metal clusters have two or more metal atoms which are bonded to one another, so not all metal electron density is available for metal–ligand bonding. In addition, ligands may attach terminally to one metal atom or else be bridged between two or more metal atoms. The main differences between transition metal clusters and boron etc. clusters are in the involvement of *d*-electrons in the bonding between cluster atoms, and the difference in mass between metal atoms and ligand atoms.

Despite these differences, reactions of all systems have a common feature, namely that each step of the reaction proceeds along a normal mode of vibration of the system.[2] A number of symmetry selection rules (SSR) can then be derived, which restrict the symmetry (and hence geometry) changes that are possible in each step of a reaction. Such an approach is general and classical in nature, in that no account is taken of the details of electronic structure in a particular system. It can be seen as the first stage in a two stage approach to investigate cluster rearrangements. The first stage, from geometrical and symmetry arguments, elicits all potentially feasible reaction mechanisms for systems of a given geometry. The second stage, the quantum refinement, involves quantitative calculations on specific systems to determine which of these geometrically feasible reactions is the most probable pathway. In some instances there may not be a feasible process, thus indicating for example a non-fluxional system. The dependence of cluster energy on the details of electronic structure means it is not possible to make any but the most qualitative general conclusions about the relative merits of proposed mechanisms. Separate calculations must be performed for each system of interest. However, it is precisely this lack of general quantitative conclusion that makes the two stage approach of this work so valuable as it separates off that part of the problem which is dependent only on geometry, thus enabling valuable general conclusions to be made which provide a background for quantitative calculations if required.

If all the normal modes of a system are determined, then the initial stages of potential reaction pathways are apparent. For transition metal clusters determining normal modes is seldom easy, and usually impossible with currently available techniques, due to the large number of component atoms of each cluster. However, some of the special features of transition metal clusters mean that an approximate determination of normal modes, and hence mechanisms, can often be made. These are helpful in the interpretation of experimental mechanistic data. Of particular value to us are (i) the difference in mass between the metal atoms in the metal polyhedron, M_m, and the atoms in the ligand system L_l, and (ii) the comparatively short range

nature of metal–metal interactions. (i) results in most of the normal modes of the system being able to be classified as largely M_m or largely L_l. (Notable exceptions to this are those vibrations which account for the rearrangement of M_m with L_l.[3]) As a result, the normal modes which are relevant for rearrangements within M_m can be approximated by the normal modes of M_m in isolation from the ligands. Once symmetry allowed mechanisms for an isolated M_m polyhedron have been determined it is necessary to consider the effect of the ligand motion to which the reacting motion is coupled. In general, the effect of the ligands will alter the relative energetics of any postulated motion from that suggested by consideration of M_m alone. No additional SSR can be introduced by the ligand system since if anything it reduces the symmetry of M_m. Thus, consideration of the ligand system can be postponed to the second stage in the study of reaction mechanisms. (ii) provides us with an approximate criterion for selecting those mechanisms which are most likely to be energetically unfeasible. Thus, strictly speaking it is part of the second stage but we shall introduce it at the beginning to reduce the dimensions of the problem. If the M—M interaction is short range, then it is energetically expensive to break or significantly stretch many M—M links. Keppert's empirical parametrization of the atom–atom interactions in the core of a cluster in terms of an attractive and a repulsive inverse distance dependence illustrates how short range the transition metal interactions are, compared with closo borane systems.[4] His optimized exponents for boranes are two and one, whereas for transition metals he finds the exponents should be somewhere from one to ten depending on the system. Woolley[5] has rigorously determined, using metallic bonding arguments, the metal–metal interaction energy for systems with high connectivity, the cohesive energy, to be $\Sigma A\sqrt{z}/R^5$ where A is a constant, z is the connectivity (i.e. the number of nearest neighbours), R is the nearest neighbour distance and the sum is over metal atoms.

The above discussion leads us to three hypotheses which will provide the *modus operandi* for the analysis of M_m rearrangements which is contained in the next Section.

Hypothesis 1. In order to determine possible mechanisms metal polyhedron rearrangements can be considered in isolation from ligand motion, the effect of ligand motion being on the relative energetics of postulated mechanisms.

Hypothesis 2. Rearrangement reactions of M_m proceed by successive breaking and formation of single M—M links.

Hypothesis 3. The point symmetry of a reacting system is the highest symmetry consistent with (a) the atom–atom linkages present in the system, and (b) reactant and product geometry.

The justification of Hypothesis 3 follows from consideration of the potential energy surface of the system being studied. The Taylor series expansion of potential energy in terms of a normal coordinate indicates that high symmetry points are either stable or completely unstable (i.e. not semi stable) with respect to motion along that coordinate.[2,6] Since we generally know the symmetry of the (stable) reactant in a rearrangement, we can deduce whether a given high symmetry structure is stable or unstable. It should be noted that throughout this work point symmetry operations are defined in a labelled atom sense; i.e. in order to claim a common symmetry element two structures must have a given type of symmetry operation (say a C_2 rotation) which relates the same atoms in the two structures.

Hypothesis 2 implies that for a system with triangular faces, if the diamond–square-diamond rearrangement[7] illustrated in Fig. 1 is possible for the chosen link breakage, then it will take place. If it is not possible because *a* and *d* of Fig. 1 are already linked, then either *b* or *c* rotate or *b*–*c* reforms. The single diamond–square–diamond rearrangement has fallen into a certain amount of disfavour as a result of the extended Hückel calculations of Gimarc and Ott[8,9] on main group systems, which indicate that it defies orbital symmetry if an equatorial link of a trigonal bipyramid

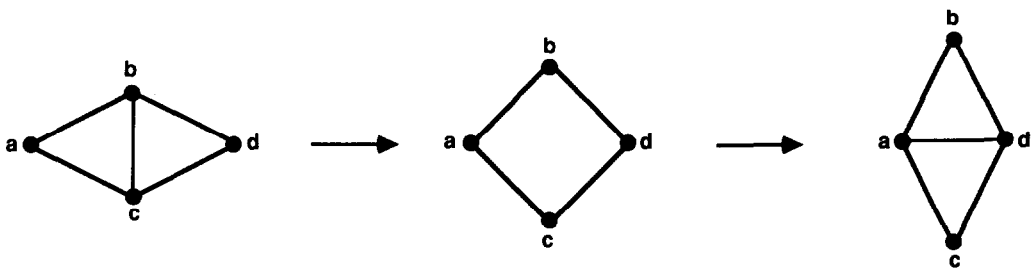

Fig. 1. The diamond–square–diamond rearrangement.

or a link between two atoms of order five connectivity in a tricapped trigonal prism is broken. Conclusions from such a study (if they apply to transition metal systems which is by no means obvious at this stage of our knowledge) form the second stage of a mechanistic study—the energetic stage. As an aside it should be noted that orbital symmetry arguments strictly determine how probable a reaction mechanism is, although the vocabulary used is often to say "allowed" or "forbidden" by orbital symmetry.

Hypothesis 2 is less appropriate for systems with low degrees of connectivity than for those systems with high degrees of connectivity since next-nearest neighbour distances can be small in systems of low formal connectivity and so next-nearest neighbour interactions can make a significant contribution to the stability of the system. For example, the vertices of a dodecahedron have three nearest neighbours and six next nearest neighbours at $\sin 108/\sin 36 = 1.6$ times the nearest neighbour distances. So next nearest neighbour interactions account for 20% of the nearest neighbour interaction energy in a dodecahedron. Hypothesis 2 also contains the implicit assumption that the energy required to break links cannot be provided by a resulting net contraction of the cluster, i.e. the assumption that breaking links does not enable the r^{-5} contribution to the stability to increase without the repulsive contribution to the energy coming significantly in to play. Once again this assumption is less likely to be valid for the low connectivity systems since in high connectivity systems more links are required to be broken to enable much contraction to occur. It is for these reasons that we shall limit our consideration to $m = 5$–12 systems.

The nature of Hypothesis 2 tends to suggest that M_m rearrangement reactions are generally, though not always, multi-step. Thus, the symmetry selection rule procedure (SSRP) of refs 2 and 10 cannot be used directly to generate reaction mechanisms as was the case for the corresponding metal complexes. However, it is still a useful tool since it can often (i) indicate whether a given break/link process is concerted or non-concerted, (ii) restrict the links which can be broken in a high symmetry (C_{nv} or higher) reactant or intermediate (since Hypothesis 2 requires only one breakage and the symmetry selection rules define the possible symmetries of the next stable species), and (iii) indicate whether the next step of a reaction is a distortion of the system rather than a link breakage. A more direct application of point symmetry is that it is a convenient way of cataloguing which links are equivalent in a system.

In this work we shall be focusing on the rearrangement of the metal polyhedron of a transition metal cluster. At the present time little, except for what has been deduced by analogy with main group clusters (a potentially hazardous way of proceeding), is known about these. Our aim in this study is to investigate M_m rearrangements systematically based on the hypotheses given above. The applicability and limitations of the work are then immediately apparent. We shall be able to derive symmetry allowed rearrangement mechanisms for M_m which if not comprehensive at least provide a starting point and a systematic study against which later work can be compared. Additional rearrangement mechanisms can be derived in the same manner by, for example, relaxing Hypothesis 2. We shall focus on the most common metal polyhedra found for $m = 5$–12. Exactly the same principles can be applied to other geometries.

Before proceeding to investigate particular rearrangement processes, we must develop the notation with which to express our analysis. Pictorially the clusters are represented by solid shapes for atoms (or units of atoms) with lines joining nearest neighbours. The number of links that each atom possesses (denoted its order) is indicated by the shape which represents it. Thus, an atom with three links is represented by a triangle, an atom with four links by a square and so on. Each atom is numbered and retains that number throughout a reaction sequence. The links which are in front of the clusters are drawn as solid lines and those behind as broken lines. If the link *a*–*b* is broken and *c*–*d* formed in a step this is indicated "*a*/*b*,*c*–*d*". Although not explicitly included in this work, a table indicating the orders of the atoms at each stage of a reaction pathway is helpful. Finally, since we are considering rearrangement reactions between identical structures, the net effect of a reaction pathway can be indicated using permutation notation. For example, if, as in Fig. 2(a), atom 2 is replaced by atom 4, atom 4 by atom 5, atom 5 by atom 2 and atoms 1 and 3 remain unchanged, we may write, $P = (1,2,5)(3)(4)R = (1,2,5)R$ where R = reactant and P = product. Although a convenient form of notation, this is not unique since we could also have written $P = (2,5)(3,4)R$. We shall therefore adopt the convention that the permutation notation used must rearrange the fewest number of atoms. (Even this is not necessarily unique.)

We are now in a position to consider rearrangements of particular clusters beginning with those of five atoms. The smaller clusters are treated fully and in some detail. To do so for the larger clusters is impracticable and unnecessary since many of the symmetry allowed mechanisms are energetically

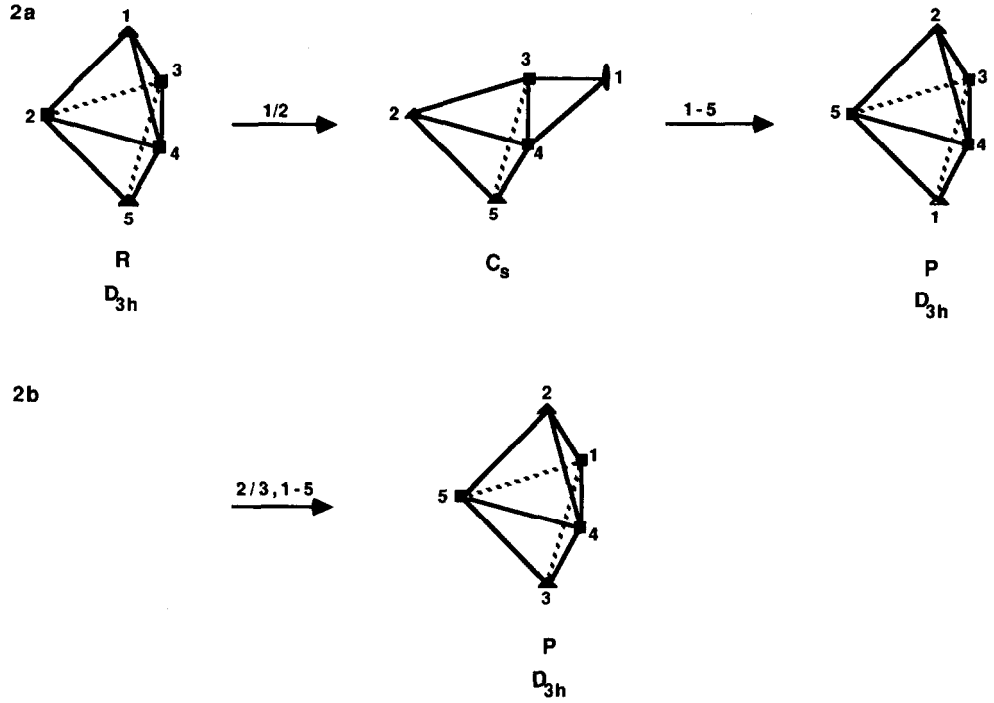

Fig. 2. Reaction mechanisms for five atom cluster rearrangements.

unfeasible and can be ignored on that basis. The next eight sections are very formalistic in content. The results are clearly summarized in Figs 2–9 using the notation discussed above.

FIVE ATOM CLUSTERS

The most stable five atom M_m structure is the D_{3h} trigonal bipyramid shown in Fig. 2. It has two distinct types of links, viz. 1–2 and 2–3. In accord with Hypothesis 2 we shall consider the effect of breaking one of these links as the first step in any rearrangement process.

Breaking edge 1–2 is followed by the relaxation and linking illustrated in Fig. 2(a) since the two atoms opposite 1–2, namely 3–4, are already joined. The net effect of this mechanism is a migration of an atom from one face of a (distorted) tetrahedron to another. By the SSRP this is potentially a symmetry allowed concerted reaction along an E'' vibration of R which results in $P_1 = (1,2,5)R$.

Breaking 2–3 results in the linking of 2 and 5 (by Hypothesis 2) giving the product illustrated in Fig. 2(b). Once again this is potentially a symmetry allowed concerted reaction, this time along an E' vibration, with $P_2 = (1,2,5,3)R$.

These two mechanisms are the only possibilities for M_5 polyhedra. Repeated application of either can result in any trigonal bipyramidal structure. There is no obvious classical reason to suggest which of these mechanisms is more likely to be the dominant. Consideration of the details of the electronic structure of the main group cluster $C_2B_3H_5$ by extended Hückel calculations[9] has shown that the mechanism of Fig. 2(b) does not conserve orbital symmetry for that system. Thus, for $C_2B_3H_5$, state selection rules enable us to conclude that the mechanism of Fig. 2(a) is the dominant one. The same conclusion cannot be immediately applied to transition metal clusters since their bonding involves *d*-electrons. This case must be treated on its own merits so we can only conclude that one or both (or perhaps neither, in which case the cluster is non-fluxional) of the mechanisms is significant. In fact, even for other *s–p* bonded systems, the ordering of the molecular orbitals may be different and so the state selection rules different.

SIX ATOM CLUSTERS

The most common stable six atom M_m structure is the octahedron. In the course of analysing it we shall also examine the bicapped tetrahedron. Other structures such as the capped square pyramid and the trigonal prism can be treated in an analogous manner. There are six distinct types of octahedral products possible from the octahedral reactant

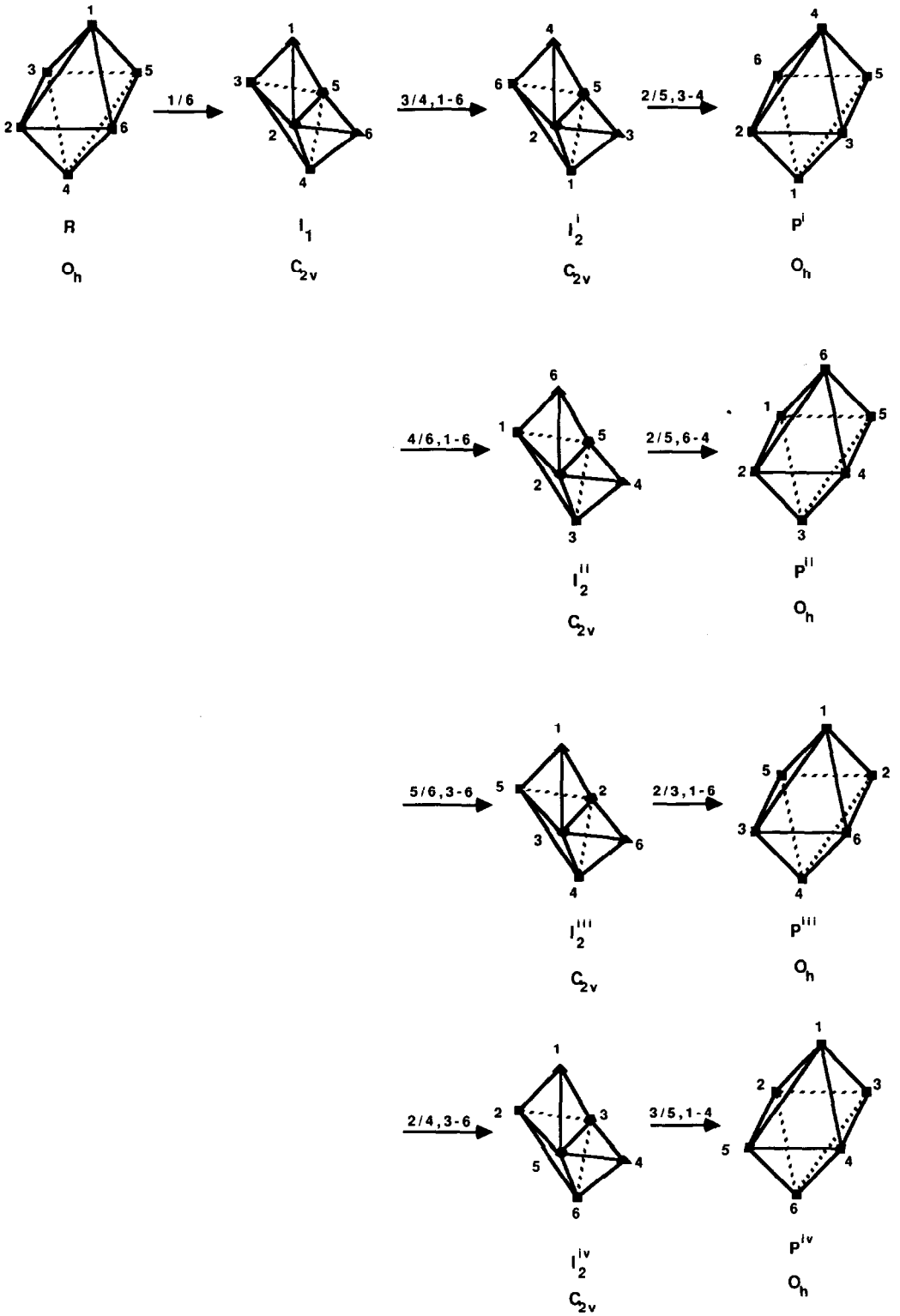

Fig. 3. Energetically feasible reaction mechanisms for six atom cluster rearrangements.

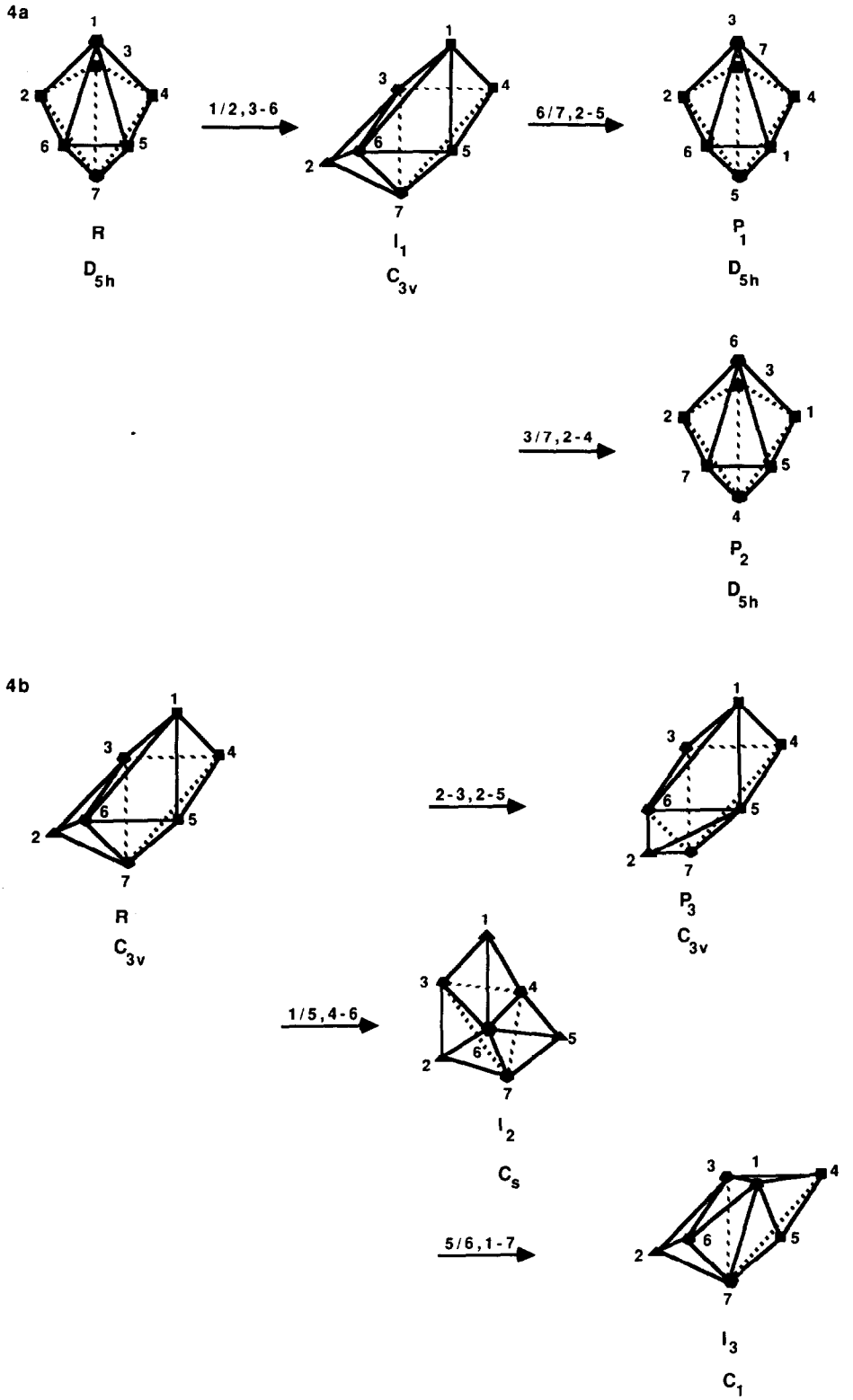

Fig. 4. Energetically feasible reaction mechanisms for seven atom pentagonal bipyramid and capped octahedron cluster rearrangements.

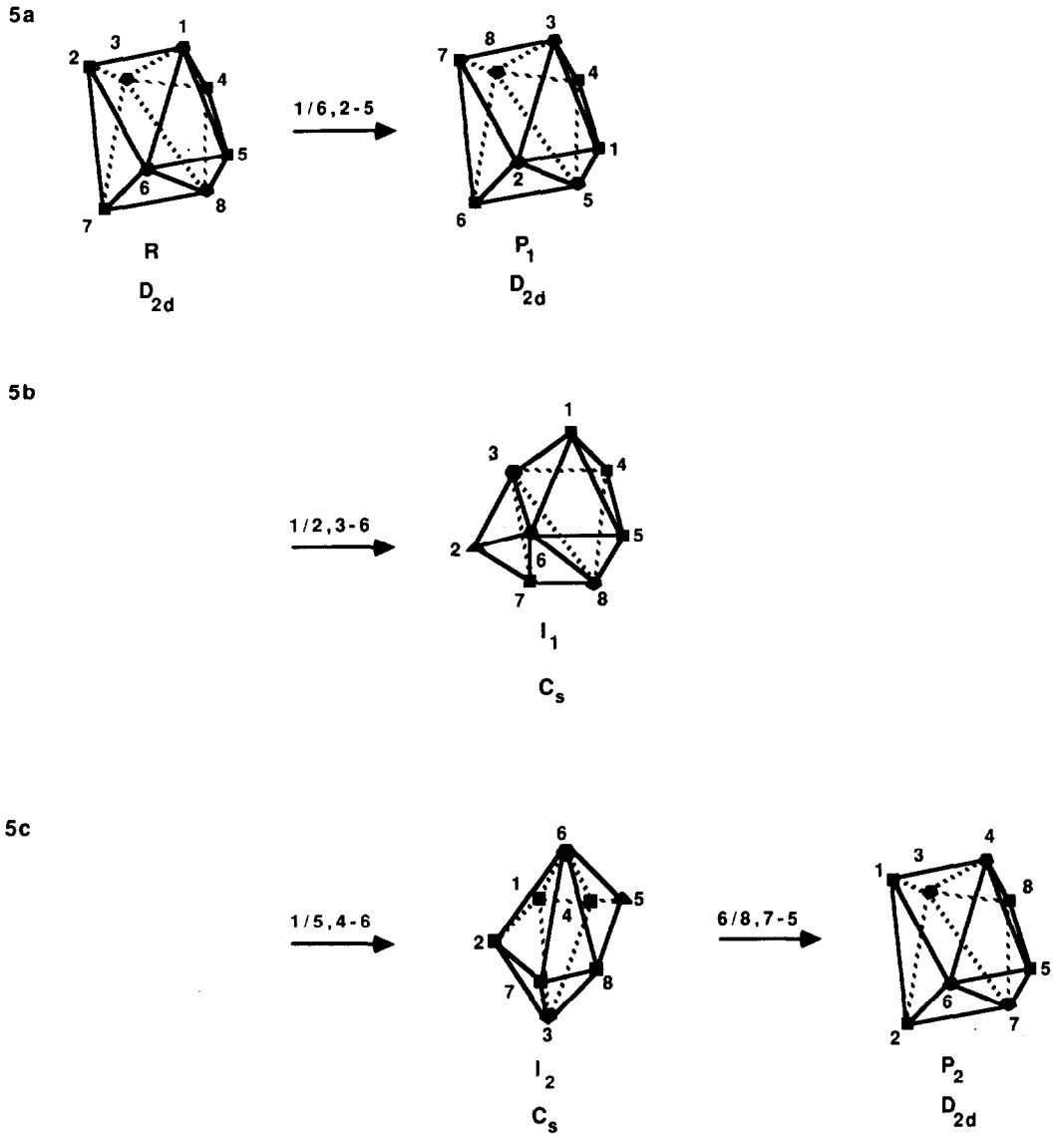

Fig. 5. Energetically feasible reaction mechanisms for eight atom cluster rearrangements.

of Fig. 3. Typical examples of each are P_1 = (1,4)$R[O_h]$, P_2 = (2,3)$R[C_{2v}]$, P_3 = (4,5,6)$R[D_3]$, P_4 = (4,6,5)$R[D_3]$, P_5 = (2,3)(4,6)$R[D_3]$, P_6 = (3,5)(4,6)$R[D_3]$ (the point groups in square brackets are the intersection of the R and P point groups). All routes from R to P_i must be at least two step since any SSRP-allowed concerted step requires two or more M—M links to be simultaneously broken.

We shall now proceed to derive feasible cluster rearrangement mechanisms using Hypotheses 1–3, and noting any additional information given by the SSRP about each step. All links of R are equivalent so we choose one to be broken as the first step, say 1–6. The system then relaxes according to Fig. 1 resulting in the C_{2v} bicapped tetrahedron intermediate, I_1, of Fig. 3(a). (This is a symmetry allowed step via a T_{1u} vibration.) I_1 has three distinct links. We shall consider the effect of breaking each in turn.

(1) If 2–5 is broken the system returns to R.
(2) If 3–4 is broken, 1–6 will be linked and the system will relax to an equivalent structure I'_2 = (1,4)(3,6)I_1. The transition state for this step can be envisaged from Fig. 3 with both 3–4 and 1–6 half-formed and stretched. This step may be concerted.
(3) If 6–4 is broken, 1–6 will be linked and the

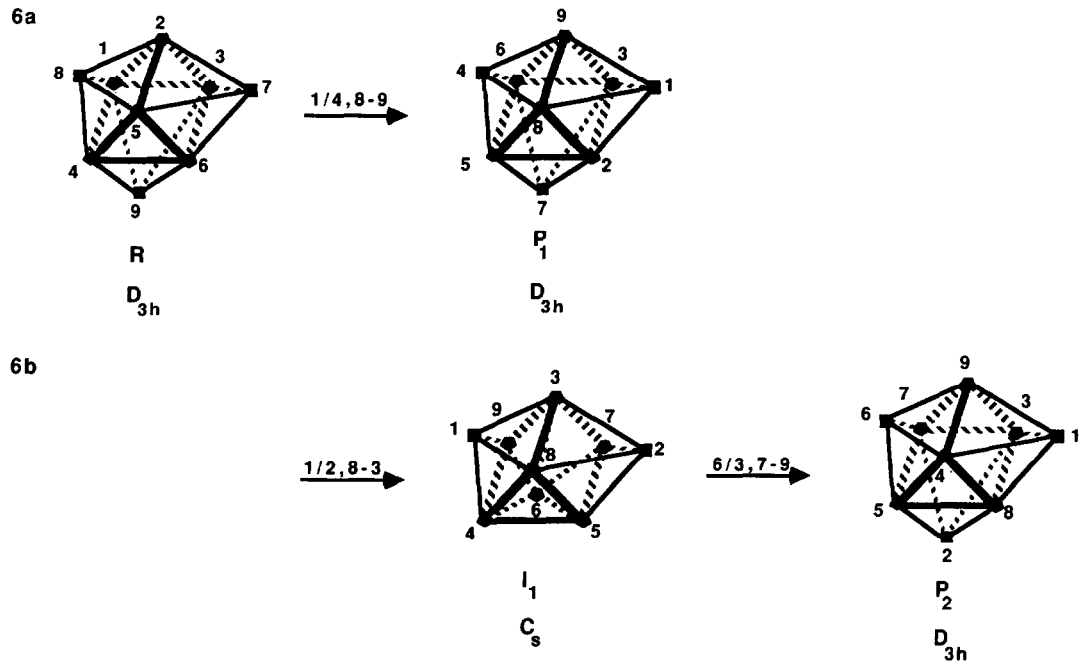

Fig. 6. Energetically feasible reaction mechanisms for nine atom cluster rearrangements.

system will relax to an equivalent structure $I_2^{ii} = (1,6,4,3)I_1$. This step may be concerted.

(4) The fourth type of link is represented by 5–6. If it is broken, 6 will continue to migrate around the cluster until it links with 3. This results in yet another bicapped triangular pyramid $I_2^{iii} = (2,3,5)I_1$. This process, by the SSRP, is non-concerted and since 5–6 does not lie on any symmetry planes of I_1, the first step is a distortion of the system to a lower symmetry.

(5) Finally, if 2–4 is broken, 6 will migrate until it links with 3, resulting in $I_2^{iv} = (2,5,3)(4,6)I_1$. By the SSRP this process is also non-concerted and once again the first step is a geometry distortion.

Any one of the I_2 intermediates can then react concertedly to give an octahedron simply by breaking the link between the fifth order atoms and joining the third order atoms. Figure 3 illustrates these possibilities viz. $P^{i} = R$, $P^{ii} = R$, $P^{iii} = (2,6)R$ and $P^{iv} = (4,6,5)R$. Alternatively, another bicapped tetrahedron to bicapped tetrahedron step can be inserted. Examination of the break link processes for R to $P^{i} = P^{ii} = R$ indicate why there is no net reaction: all new links are broken and all breaks reformed during the reaction. It is interesting to note that R to P^{iv} effects the same rearrangement as a Bailar twist but via a different route. It is by no means obvious which of R to P^{iii} or R to P^{iv} is more energetically feasible but repeated application of either can result in any one of the possible products.

SEVEN ATOM CLUSTERS

The two most common M_7 geometries are the pentagonal bipyramid and the capped octahedron.

Pentagonal bipyramid

A pentagonal pyramid has only two distinct types of links, 1–2 and 2–3 in Fig. 4. If 2–3 of Fig. 4(a) is broken, then the only link that can possibly be formed is 1–7. Such a strained structure is unlikely, especially when compared with the mechanism of Fig. 4(a), so will not be considered further. If the link 1–2 of R is broken, by Hypothesis 2, 6 and 3 become linked thus forming a capped octahedron. Breakage of either 6–7 or 3–7 will result in the new pentagonal bipyramids: $P_1 = (1,3,5,7)R$ and $P_2 = (1,6,7,4)R$. Figure 4(a) thus summarizes the most direct rearrangement for pentagonal bipyramids. Each step is symmetry allowed by the SSRP, so potentially concerted. Alternative pathways follow from inserting any of the pathways determined below for rearrangements of capped octahedra.

Capped octahedron

R in Fig. 4(b) has four distinct types of links. The effect of breaking 6–7 is illustrated in Fig. 4(a). We now consider the others. If 2–3 of R is broken, atom 2 is free to migrate from the 6–7–3 face to the 6–7–5 face and form a link with atom 5 resulting in $P_3 = (3,6,5,4)R$. This mechanism enables atoms of

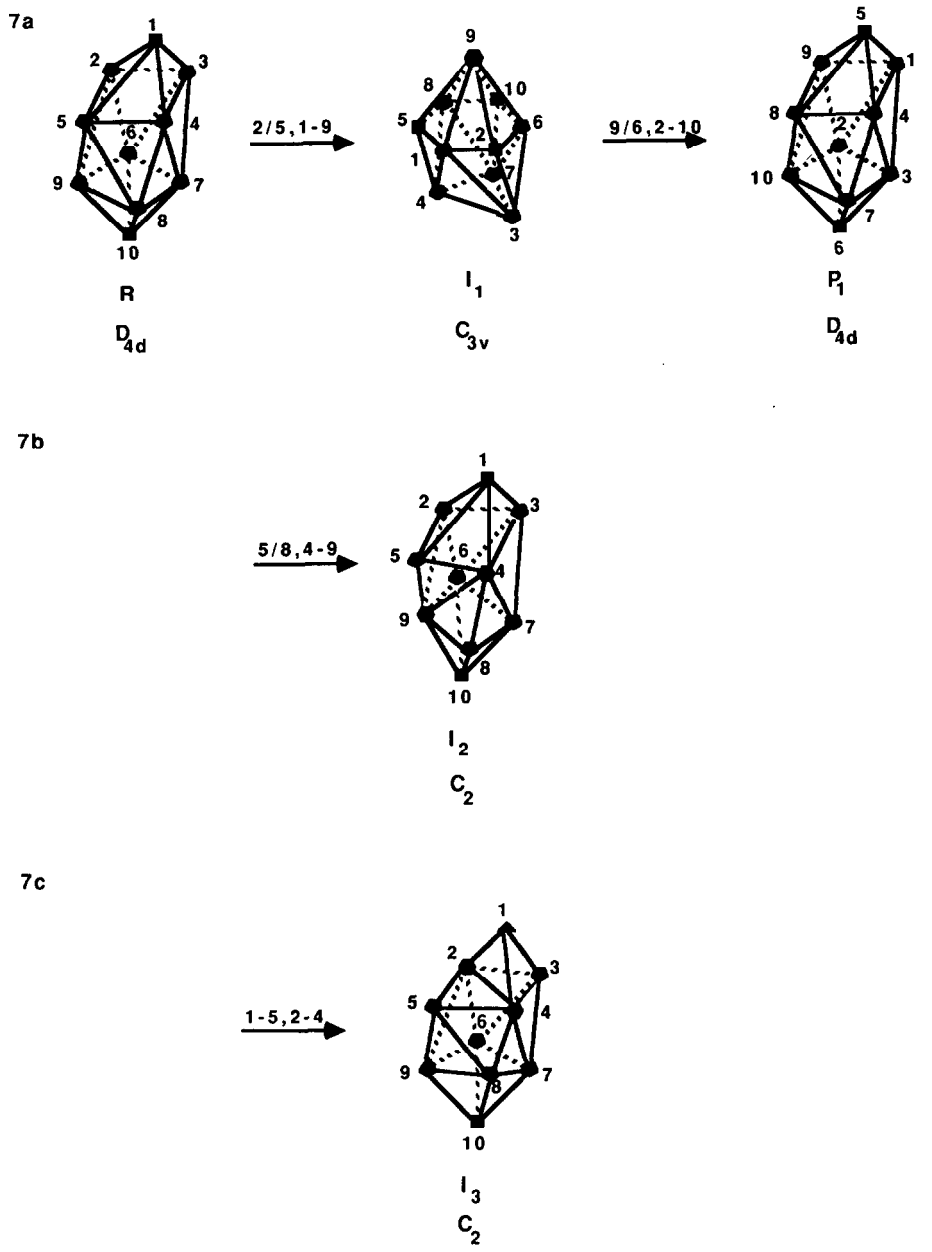

Fig. 7. Energetically feasible reaction mechanisms for ten atom cluster rearrangements.

order four and five to interchange, but atom 2 always remains of order three. Thus complete rearrangement is not possible by this mechanism. Breaking 1–5 or 5–6 of *R* results in the formation, respectively, of 4–6 or 1–7 and the structures I_3 and I_4 of Fig. 4(b). I_3 and I_4 and the possible structures in the succeeding steps are significantly less stable for M_7 than the structures of Fig. 4(a). These mechanisms are therefore unlikely to be significant causes of rearrangement in seven atom systems and will not be explicitly enumerated here.

In conclusion then there are two energetically feasible rearrangement mechanisms for seven atom clusters. That of Fig. 4(a) is a two step mechanism applicable either to pentagonal bipyramids or capped octahedra. That of Fig. 4(b) provides a means for the cap on the capped octahedron to migrate from face to face. It could easily be an intermediate step in a Fig. 4(a) rearrangement.

EIGHT ATOM CLUSTERS

The most common, though not necessarily the most stable, M_8 structure is the D_{2d} triangulated

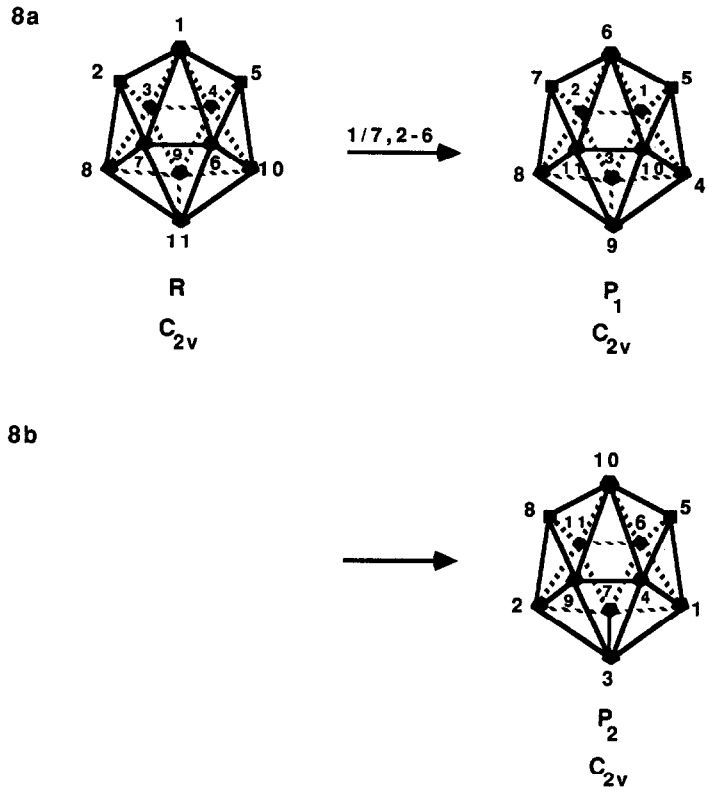

Fig. 8. Energetically feasible reaction mechanisms for 11 atom cluster rearrangements.

dodecahedron of Fig. 5. We shall explore the effect of breaking its three distinct types of links. The simplest reaction pathway results from breaking 1–6 and joining 2–5 giving $P_1 = (1,3,8,5)(2,7,6)R$ as illustrated in Fig. 5(a). Successive application of this symmetry allowed concerted mechanism (via an E vibration) will enable any atom rearrangement to be produced. If 1–2 of R is broken than 3 and 6 will be linked making I_1, a C_s capped capped octahedron. There are then a number of possibilities depending upon which of the nine types of links are broken. One of these possibilities (breaking 7–8) leads to an equivalent structure which will probably relax back to the reactant. Breaking 6–8 is a more circuitous higher energy route to a P_1-like product. The remainder go via significantly energetically unfavourable structures compared with the Fig. 5(a) mechanism.

The final possible first step to be considered is the breaking of 1–5 and formation of 4–6 resulting in I_2 of Fig. 5(c). By the SSRP this cannot be a concerted process since all normal modes of a D_{2d} system retain at least one symmetry operation and 1–5 does not lie on any symmetry elements. The first step of the reaction must therefore be a distortion of the geometry to a lower symmetry. As I_2 has eleven types of links it is not immediately apparent what the next step should be. Breaking 5–6 or 5–8 leads to an equivalent structure which permutate the atoms in any product, but does not provide a route to that product. They are therefore potential intermediate steps. Breaking 6–8 and forming 5–7 leads to $P_2 = (1,4,8,7,2)R$ as indicated in Fig. 5(c). This process is the reverse of that used to get from R to I_2 so cannot be concerted. The remaining possibilities go via unstable structures so do not provide competitive mechanisms.

In conclusion then, there are two energetically feasible rearrangement mechanisms for eight atom clusters. That of Fig. 5(a) being a one step mechanism and that of Fig. 5(c) being four step (two break-link processes). Repetition of either could lead to any arrangement of atoms in the product. Alternatively, additional intermediate steps between I_2 and equivalent structures may be inserted.

NINE ATOM CLUSTERS

The most common M_9 structure is the D_{3h} tricapped triangular prism structure of Fig. 6. It has three distinct types of links. Breaking 1–4 and linking 8–9 results in $P_1 = (1,6,2,9,7)(4,5,8)R$, which is a one step rearrangement reaction via an E' vibration as illustrated in Fig. 6(a). If 1–2 of R

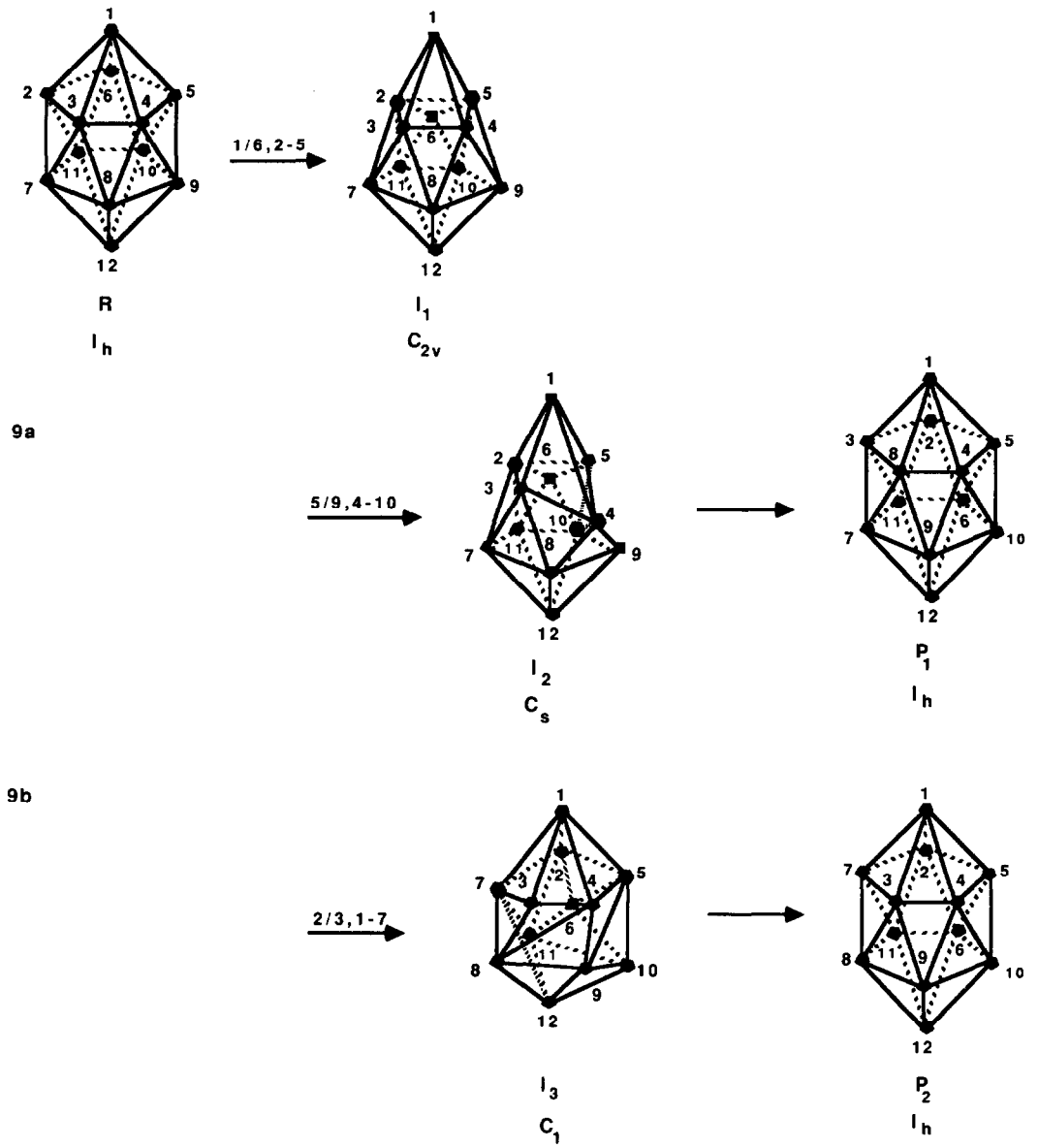

Fig. 9. Energetically feasible reaction mechanisms for 12 atom cluster rearrangements.

is broken, then 8–3 will be linked giving I_1 of Fig. 6(b) which gives $P_2 = (1,7)(2,9)(4,5)(6,8)R$ if 6–3 is broken and 9–7 is formed (the converse of the first step). Alternative second steps are more circuitous and proceed via less stable structures. Upon breaking 1–8, 2–4 might perhaps link up. However this is such a strained structure that it is more probable that it will relax back to *R*.

Two rearrangement mechanisms similar to those deduced in this work are also reported by Guggenberger and Muetterties[11] based on a "points on a sphere" repulsion calculation. The difference lies in the fact that the Fig. 6(b) mechanism of this work, in accord with Hypothesis 2, consists of two successive link breaks and formations whereas their second mechanism is seen as a simultaneous breaking of both links. In light of Hypothesis 2, we cannot therefore catagorically adopt their conclusion that the Fig. 6(a) mechanism is the more energetically feasible, though it is likely that this is so. At this stage it is appropriate to mention the extended Hückel calculation of Gimarc and Ott on the main group cluster $B_9H_9^{2-}$.[10] They showed that the mechanism of Fig. 6(a) is energetically unfeasible on the basis of orbital symmetry not being conserved between reactant and product. As they note, this is consistent with the experimentally observed stability of $B_9H_9^{2-}$. Once again we note that care

must be taken in extrapolating this conclusion to other types of tricapped triangular prisms.

TEN ATOM CLUSTERS

The most stable M_{10} structure is the D_{4d} structure illustrated in Fig. 7 which has three different types of linkages. If 2–5 is broken and 1–9 formed we get the C_{3v} structure I_1 of Fig. 7(a) by a one step process (E_1 or E_3 vibration). There are seven distinct links in I_1. Breaking any one of them could set the system on a path to the required product structure. However, most of them are circuitous, proceeding via comparatively unstable intermediates. The most direct route to a product comes from breaking 9–6 (or 9–8) and the formation of 2–10 (5–10) which is the reverse of a step like the first step. This results in $P_1 = (1,5,8,7,3)(2,9,10,6)R$. If 5–8 of R is broken and 4–9 joined the C_2 intermediate I_2 of Fig. 7(b) results by a concerted process. This structure is rather strained as is any further intermediate en route to a product. It is therefore most likely that it relaxes back to R. If 1–5 of R is broken and 2–4 joined, the C_2 intermediate I_3 of Fig. 7(c) results. I_3 is also strained compared with I_1 so any mechanism proceeding via I_3 will be much less probable than that of Fig. 7(a). We can therefore conclude that the Fig. 7(a) mechanism is the only feasible one for rearrangements of ten atom clusters.

ELEVEN ATOM CLUSTERS

The most common M_{11} structure is the C_{2v} one illustrated in Fig. 8. Since R has C_{2v} symmetry, by the SSRP the first reaction step must retain all symmetry operations, or the C_2 axis, or one of the reflection planes. Thus there are four types of links which can be broken in the first step. Representatives of these types being 9–11, 1–2, 2–8, 7–6. Alternatively, the first step may simply be a geometry distortion that removes two symmetry elements, in which case the second step could involve the breaking of 1–7, or 2–7, or 8–11, or 8–7, or 7–11 type bonds.

The simplest rearrangement reaction follows from distorting the geometry then breaking 1–7, followed by the formation of 2–6. As illustrated in Fig. 8(a) this results in $P_1 = (1,6,10,4)(2,7,11,9,3)R$. For transition metal clusters, where the cohesive energy goes as the square root of the connectivity,[5] the link between highest order atoms requires the least energy to break it. Thus not only is this mechanism the simplest, but it is also energetically favourable as 1–7 connects the highest order atoms in the cluster and so is the weakest link. Repeated application can lead to any arrangement of atoms. Breaking 7–2 or 7–6 results in the formation of, respectively, 1–8 or 1–11. Atom 1 in such structures is of order seven and the structure as a whole is strained, so we shall not pursue these further.

Alternative mechanisms to that of Fig. 8(a) can be determined. For example if 9–11 is broken and 8–10 joined the "nearest" product obtained by breaking 1–2 and forming 3–7, then breaking 8–7 and forming 2–11, and finally breaking 8–3 and forming 2–9 is $P_2 = (1,10)(2,8)(3,11)(4,6)(7,9)R$ of Fig. 8(b). Other possibilities can be contrived, however other first steps do not suggest the route to the product and they proceed by structures less stable than the simple mechanism of Fig. 7(a).

TWELVE ATOM CLUSTERS

The icosahedron is the most common M_{12} structure. Any rearrangement of such a cluster must proceed by breaking one of the 20 identical links, say 1–6 in Fig. 9, which gives the C_{2v} intermediate I_1 after the formation of 2–5. There are then ten distinct types of links to be considered. Of these, 2–5 can be ignored as it leads back to R. Breaking 1–3 or 6–2 results in the comparatively unstable intermediate with atoms of order seven and three. Breaking 3–7 requires an atom of order seven in a rather strained structure, so this can also be ignored.

The symmetry allowed second steps of breaking 5–9, or 3–4, or 12–8 effectively result in the same mechanism by a different ordering of the same steps. We shall consider the path where the weakest link (determined on connectivity grounds) is broken at each stage. If 5–9 is broken and 4–10 formed then I_2 of Fig. 9(a) results. The lowest energy sequence is therefore 5/9, 4–10 [giving I_2 of Fig. 9(a)]; 3/4, 1–8; 2/7, 3–11; 10/11, 6–12 and finally 8/12, 7–9, which gives the product $P_1 = (2,3,8,9,10,6)R$.

Finally we consider the effect of breaking 2–3, or 12–7, or 4–8 in I_1. Each of these effectively results in the same mechanisms and each by symmetry requires a geometry distortion as the first step. Once again we shall follow the reaction along its most probable course by breaking the weakest links. Thus 2/3, 1–7 [I_3 of Fig. 9(b)]; 7/12, 8–11; 4/8, 3–9; 5/9, 4–10 and finally 10/11, 6–12 resulting in the product $P_2 = (2,7,8,9,10,6)R$.

Of course other possibilities can easily be envisaged by forcing a different third step into each of the above two sequences. However, these are the ones which result from following through from a reactant icosahedron to a product icosahedron via a path with intermediates strained as little as possible. Qualitatively there does not seem to be much to choose between the two mechanisms of Fig. 9.

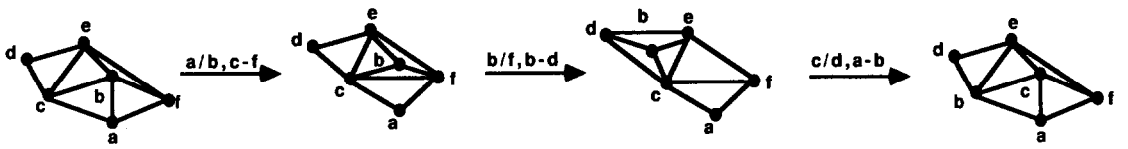

Fig. 10. General polyhedral rearrangement mechanism previously proposed.[1]

CONCLUSION

Using the hypotheses proposed in the introduction and the SSRP it has been possible to perform the first stage of a two stage approach to study the rearrangement reactions of the metal polyhedron of a transition metal cluster, viz. the classical geometrical derivation of rearrangement mechanisms for M_m units of five to 12 atoms. For the smaller systems it was possible to investigate all possible reaction pathways, however, with increasing complexity it became necessary to rely on qualitative energy arguments to limit our consideration to those mechanisms which might be significant. (Thus, qualitatively introducing the energetic stage into the first stage.) As one might expect for systems where the structures are determined by different criteria, the rearrangement mechanisms for transition metal clusters (where the structure is determined by strong attractive forces), often proved to be different from those for corresponding normally bonded compounds and also may be expected to differ from those of main group clusters.

The second stage of investigating reaction mechanisms, namely the determination of the relative feasibility of the proposed mechanisms, was only briefly touched upon. Some account was given to strain arguments to eliminate mechanisms, and reference was made to boron hydride calculations of Gimarc and Ott, though at this stage it is not possible to know how they relate to transition metal systems. A general conclusion to be made is that for each geometry type at least one relatively simple feasible mechanism has emerged. This is in accord with observed fluxional behaviour of metal polyhedra, although more detailed consideration of the energetics of each symmetry allowed mechanism is required before definite conclusions can be drawn. The ligand motion which is coupled to metal motion can no longer be ignored when one is asking questions about energetics, so the second stage is by no means a simple one. From this work it is possible to provide a framework for a study of the energetics and to limit the mechanisms which it may otherwise have seemed necessary to study.

The question arises as to whether these reaction mechanisms, for systems which differ quite dramatically in structure, have features in common. Can a general polyhedral rearrangement pathway be proposed which is applicable to all systems? A general mechanism has been proposed[1] which can be schematically expressed as in Fig. 10(a) and can be summarized as:

(i) a cap is extruded onto the surface of the polyhedron,
(ii) the cap migrates to another face,
(iii) the cap sinks back into the polyhedron.

Analysis of this mechanism shows that it effects the exchange of two neighbouring atoms of order four. This is precisely the route from R to P^{iii} in Fig. 3. It cannot be used to explain the equivalence of all links in the structures with atoms of orders other than four. Slight variants of the mechanism do however occur in a number of the mechanisms determined in this paper. For example, in Figs 4(a) and 5(a), a cap is formed and instead of migrating it "sinks back" into a different position in the polyhedron. It also appears partially in some instances, for example the mechanisms of Figs 2(a) and 4(b) involve only step (ii) above. Thus, on the basis of this study we must conclude that there is not a general energetically feasible mechanism for clusters of five to twelve atoms but there are similarities between the mechanisms. Most importantly, we can conclude that we can approach the determination of reaction mechanisms in the same systematic manner for all triangulated systems. The variety of actual mechanisms which have resulted is due to a range of vertex orders in the clusters. For systems of 13 atoms and higher, the approach used in this work requires some modification to account for the significant contribution to the metal polyhedron stability from the next nearest neighbour metal atoms.

REFERENCES

1. B. F. G. Johnson, *J. Chem. Soc., Chem. Commun.* 1986, 27.
2. A. Rodger and P. E. Schipper, *Chem. Phys.* 1986, **107**, 329; *J. Phys. Chem.* 1987, **91**, 189.
3. B. F. G. Johnson, D. Braga and E. A. Marseglia, submitted for publication.
4. D. J. Fuller and D. L. Keppert, *Inorg. Chem.* 1984, **23**, 3273.
5. R. G. Woolley, *Transition Metal Clusters* (Edited by B. F. G. Johnson). John Wiley, London (1980).

6. R. G. Pearson, *Symmetry Rules for Chemical Reactions*. John Wiley (1976).
7. W. N. Lipscomb, *Science* (Washington D.C.) 1966, **153**, 373.
8. B. M. Gimarc and J. J. Ott, *Inorg. Chem.* 1986, **25**, 83.
9. B. M. Gimarc and J. J. Ott, *Inorg. Chem.* 1986, **25**, 2708.
10. A. Rodger and P. E. Schipper, *Inorganic Chemistry*, 1988, **27**, 458.
11. L. J. Guggenberger and E. L. Muetterties, *J. Am. Chem. Soc.* 1976, **98**, 7221.

Polyhedron Vol. 7, No. 12, pp. 1121–1128, 1988
Printed in Great Britain

0277–5387/88 $3.00+.00
© 1988 Pergamon Press plc

THE SYNTHESIS, PROPERTIES AND CRYSTAL STRUCTURE OF THE COPPER(I)–THIOLATO–THIOXANTHATO COMPLEX $Cu_8(SC_5H_{11})_4(S_2CSC_5H_{11})_4$

RAJ K. CHADHA,* RAJESH KUMAR and DENNIS G. TUCK†

Department of Chemistry and Biochemistry, University of Windsor, Windsor, Ontario, Canada N9B 3P4

(*Received* 19 *August* 1987; *accepted after revision* 21 *January* 1988)

Abstract—The copper(I) thiolate $CuSC_5H_{11}$ (CuSR; R = —$C(CH_3)_2CH_2CH_3$) dissolves in carbon disulphide to yield $Cu_8(SR)_4(S_2CSR)_4$. The crystal structure of this substance is monoclinic, with $a = 31.532(26)$, $b = 20.700(6)$, $c = 23.725(10)$ Å, $\beta = 114.16(3)°$, $V = 14129(13)$ Å^3, $Z = 8$ and space group $C2/c$. The molecule is a complex cage of copper atoms ligated by RS and $RSCS_2$ ligands. The structure breaks down on thermal loss of CS_2 or on electrochemical oxidation. Reaction with PPh_3 or $PPhCy_2$ (Cy = cyclohexyl) gives the 1 : 2 adducts of CuS_2CSR, which are also unstable to loss of CS_2.

The range of structures identified amongst the complexes formed by copper(I) and alkyl or aryl thiolate ligands, with or without neutral donors, is indeed surprising. As we note in the Discussion below, these complexes vary in terms of the stereochemistry at copper, of the degree of molecularity, and in consequence of the Cu—S bond distances and angles. The present paper reports the preparation of a carbon disulphide insertion product of copper(I) thiolate $CuSC_5H_{11}$ (C_5H_{11} = 2-methyl-2-butyl), shown by X-ray crystallography to have the unusual cage structure $Cu_8(SC_5H_{11})_4(S_2CSC_5H_{11})_4$. The latter reacts further with tertiary phosphines to give species which are formally 1 : 2 adducts of $CuS_2CSC_5H_{11}$ and PR_3. A preliminary report of part of this work has already appeared.[1]

EXPERIMENTAL

General

Solvents were distilled from either calcium hydride, phosphorus pentoxide or molecular sieves as appropriate and stored over the same reagent. Copper metal for electrolysis was as a foil, which was washed with nitric acid and then water, and dried before use. All other materials were used as supplied.

Copper was determined by atomic absorption spectrophotometry and microanalysis was carried out by Guelph Chemical Laboratories. IR spectra were recorded on a Nicolet 5DX spectrometer and mass spectra on a MAT CH-5 instrument operating in the EI mode. ^{1}H NMR spectra were obtained with a Perkin–Elmer 20 instrument and ^{31}P spectra on a Bruker 90 spectrometer.

Reaction of $CuSC_5H_{11}$ *with* CS_2

(i) Copper metal was oxidized electrochemically in an acetonitrile solution of $C_5H_{11}SH$ to give $CuSC_5H_{11}$; details of this and related syntheses have been given elsewhere.[2]

(ii) When carbon disulphide (50 cm^3) was added to $CuSC_5H_{11}$ (0.5 g, 3.0 mmol) with stirring, the solid immediately dissolved to give a clear red solution. Stirring was continued at room temperature for up to 12 h, although we subsequently found that the duration of this stirring had no effect on the nature of the final product. Excess CS_2 was then removed *in vacuo* and the red–brown residue was recrystallized from tetrahydrofuran–methanol. Yield 92%. Found: C 32.3; H 5.6; Cu 30.4. Calc. for $Cu_8(SC_5H_{11})_4(S_2CSC_5H_{11})_4$: C 32.3; H 5.4; Cu 31.0%. M.p. 140°C.

The ^{1}H NMR spectrum of this substance is discussed below. The mass spectrum in the *m/e* range

* Present address: Department of Chemistry, University of Manitoba, Winnipeg, Manitoba, Canada R3T 2N2.

†Author to whom correspondence should be addressed.

0–800 available to us did not show any fragments above $m/e = 666$; as for the other ions reported, this represents the most intense peak in a complex manifold whose relative intensities were successfully fitted to a computer generated pattern based on the known isotopic abundances of C, H, S and Cu for the ion $[CuSC_5H_{11}]_4^+$. Other ions in the high mass region of the spectrum are at $m/e = 595$, $[(CuSC_5H_{11})_3CuS]^+$: 524, $[CuSC_5H_{11}CuS]_2^+$: 453, $[CuSC_5H_{11}Cu_3S_3]^+$: 382, $Cu_4S_4^+$: 350, $Cu_4S_3^+$ and 168, $CuSC_5H_{11}^+$. A number of relatively intense ions in this region at 202, 235, 263, 285, 313, 335 and 501 do not apparently contain copper on the evidence of the isotopic abundance patterns. The integrated ion current in this region ($m/e > 200$) was approximately 3% of the total spectrum. Significant ions in the low m/e region were identified at 76, CS_2^+: 71, $C_5H_{11}^+$ and 61, $C_2H_5S^+$.

Reactions of $Cu_8(SC_5H_{11})_4(S_2CSC_5H_{11})_4$, **1**, *with* PR_3

A. (i) Solid PPh_3 (0.97 g, 3.70 mmol) was gradually added to a solution of **1** (0.38 g, 0.23 mmol, or 1.85 mmol of $CuSR \cdot \frac{1}{2}CS_2$) in a mixture of *n*-pentane (20 cm^3) and CS_2 (2 cm^3). A thick yellow precipitate was immediately thrown down. The reaction mixture was stirred at room temperature for 3–4 h, after which the precipitate was collected, washed with *n*-pentane and dried *in vacuo* at room temperature. Recrystallization was effected from toluene-*n*-pentane mixtures (1 : 10 *v/v*). Yield 90%.

(ii) The above procedure was repeated with 0.30 g of **1** (0.18 mmol, or 1.47 mmol of $CuSR \cdot \frac{1}{2}CS_2$) in 20 cm^3 of *n*-pentane. A heavy yellow precipitate appeared on the addition of PPh_3 (0.77 g, 2.9 mmol) and this was collected as before. No products could be isolated from the filtrate.

(iii) The precipitate thrown down from an experiment as in (i) above was stirred for 3–4 h with a large excess of PPh_3. No change in appearance was observed and subsequent analysis showed that the composition of the product was unchanged by this procedure.

The products from procedures (i)–(iii) were identical, being $CuS_2CSC_5H_{11} \cdot 2Ph_3P$. Found: C 65.8, H 5.6, Cu 9.0. Calc. for $C_{42}H_{41}P_2S_3Cu$: C 65.7, H 5.4, Cu 8.3%. ^1H NMR spectrum (CS_2): 7.13 (br, 30 H), 1.80 (t, 2H), 1.36 (s, 6H), 0.90 (q, 3H) ppm relative to Me_4Si. $^{31}P\{^1H\}$ resonance in CS_2 at -0.605 ppm relative to 85% H_3PO_4; PPh_3 in same solvent $+5.691$ ppm. The EI mass spectrum of this compound in the region $m/e > 200$ was essentially identical with that of **1** except for the presence of a peak at $m/e = 262$, Ph_3P^+.

B. When a three-fold excess of dicyclohexylphenylphosphine was used in place of Ph_3P with **1** (0.32 g, 0.20 mmol; 1.56 mmol calculated as $CuSC_5H_{11} \cdot \frac{1}{2}CS_2$) in 20 cm^3 *n*-pentane, a deep yellow solution resulted. Slow removal of the solvent *in vacuo* with cooling produced a yellow–orange precipitate which was washed with cold *n*-pentane and dried *in vacuo*. Yield 60%. Found Cu 8.7. Calc. for $CuS_2CSC_5H_{11} \cdot 2(C_6H_{11})_2PC_6H_5$: Cu 8.1%. $^{31}P\{^1H\}$ in CS_2: 6.18 ppm (-1.534 for $(C_6H_{11})_2PPh$ in CS_2). ^1H NMR: 7.23 (m, 10H), 1.44 (m, 55H). The EI mass spectrum of this substance was almost identical with that of **1**, except for $m/e = 274$, $(C_6H_{11})_2PC_6H_5^+$.

Thermal stability of **1**

(i) A solution of **1** (0.05 g, 0.24 mmol calculated as $CuSC_5H_{11} \cdot \frac{1}{2}CS_2$) in benzene (15 cm^3) was refluxed. A rapid (~15 min) change of colour from red–brown to pale yellow was observed. After a further 1 h of refluxing, the mixture was taken to dryness *in vacuo* to give a gummy solid, which was triturated with *n*-pentane. The resultant yellow solid was identified as $CuSC_5H_{11}$ (Found: Cu 37.8; Calc. Cu 38.2%).

(ii) A suspension of **1** (0.15 g, 0.73 mmol calculated as $CuSC_5H_{11} \cdot \frac{1}{2}CS_2$) in 10 cm^3 methanol was refluxed for 2 h. No colour change was observed and subsequent analysis showed that the recovered solid was the unchanged starting material.

(iii) A sample of **1** was heated to 100°C under reduced pressure (72.5 cm Hg) for 10 min. No colour change was observed and the m.p. of the substance was unchanged. In contrast, a sample which had been heated to 150°C (5 min) and then cooled to room temperature, showed signs of decomposition at 120°C, and turned black during a subsequent m.p. determination.

Cyclic voltammetry

Solutions of **1** (0.001 M) in acetonitrile–tetrahydrofuran mixtures (2 : 1 *v/v*) containing tetraethylammonium perchlorate (0.1 M) as the supporting electrolyte were studied with a Mandel Scientific electrochemistry unit, using a conventional three-electrode arrangement at a scan rate of 400 mv s^{-1}. The cyclic voltammagram showed a sharp oxidation peak at -0.14 V (relative to SCE). This reaction is irreversible and the scan showed no other features of interest. No colour change was observed, but a yellow–brown precipitate, not identified, was observed in the vessel at the end of the experiment.

Table 1. Summary of crystal data, intensity collection and structural refinement for $Cu_8(SC_5H_{11})_4(S_2CSC_5H_{11})_4$

Cell constants	$a = 31.532(26)$, $b = 20.700(6)$, $c = 23.725(10)$ Å, $\beta = 114.16(3)$
Cell volume (Å^3)	14129(13)
Crystal system	Monoclinic
Space group	$C2/c$
Mol. wt	1636.4
Z	8
ρ_c (g cm^{-3})	1.54
ρ_o (g cm^{-3})	1.50
Abs. coeff. μ (cm^{-1})	27.58
Min. abs. corr.	1.436
Max. abs. corr.	1.714
Radiation	Mo-K_α $\lambda = 0.71069$ Å
Monochromator	Highly oriented graphite
Temp (°C)	21
2θ angle (°)	4–45
Scan type	Coupled θ (crystal)/2θ (counter)
Scan width	$K_{\alpha_2} - 1°$ to $K_{\alpha_2} + 1°$
Scan speed (° min^{-1})	Variable, 2.02–4.88
Background time/scan time	0.5
Total reflections measured	10297 $(+h, +k, \pm l)$
Unique data used	4307 $[I > 2\sigma(I)]$
Number of parameters (NP)	412 (199,213)
$R = (\Sigma \|\|F_o\| - \|F_c\|\|/\Sigma\|F_o\|)$	0.0745
$R_w = [\Sigma w(\|F_o\| - \|F_c\|)^2/\Sigma w\|F_o\|^2]^{\frac{1}{2}}$	0.0741
$\Delta\rho$max (eÅ^{-3})	0.7
Shift error (max)	0.5

Crystallographic analysis of **1**

A red–brown transparent crystal, 0.13 × 0.19 × 0.34 mm, was mounted along its longest dimension on a Syntex $P2_1$ diffractometer and data collected at room temperature (~25°C) by the procedures described previously.[3] Intensities of three check reflections were monitored after every 60 reflections; no significant decay was observed during the time required for data collection. The cell parameters were measured and refined from data from 15 strong high angle ($15 < 2\theta < 30°$) reflections. Data used in structure determination were corrected for Lorentz and polarization effects, and analytically for absorption. The unit cell dimensions and other pertinent data are given in Table 1. The density was measured by the flotation method in ethanol–hexachlorobutadiene mixtures containing a drop of diethylamine to render these solvents miscible. This approach was necessary because of the high solubility of **1** in most organic solvents.

The systematic absences (hkl, $h+k = 2n+1$; $h0l, l = 2n+1$) are consistent with either $C2/c$ or Cc space groups; the former was used and later assumed to be correct because of the successful refinement of the structure. The structure was solved by direct methods using the program SHELX. The copper atoms were all found from the E-map, and the sulphur and carbon atoms from the difference Fourier syntheses. The structure was refined in blocks during the least squares analysis, with Cu(1) and Cu(2) in every cycle, Cu(3)—Cu(8) and S(1)—S(14) (199 variables) in alternate cycles with S(15), S(16) and C(1)—C(44) (213 variables). The refinement gave unreasonable C—C distances, in the range 1.10–1.72 Å, and these distances were subsequently constrained within the limits 1.40–1.54 Å. Hydrogen atoms were not included in the calculation and the final refinement was carried out with anisotropic temperature factors for copper and sulphur atoms only. Unit weights were used in the initial stages, while in the final cycles the weighting scheme used was of the form $w^{-1} = \sigma^2(F) + 0.0001F^2$. The refinement minimizing the function $(|F_o| - |F_c|)^2$ converged at $R = 0.0745$ and $R_w = 0.0741$; these relatively high R values are due to the high thermal motion of the carbon atoms and there may also be some positional disorder in certain carbon atoms.

The computer programs and the source of scattering factors were those used in earlier work.[3] Important bond lengths and angles for the copper,

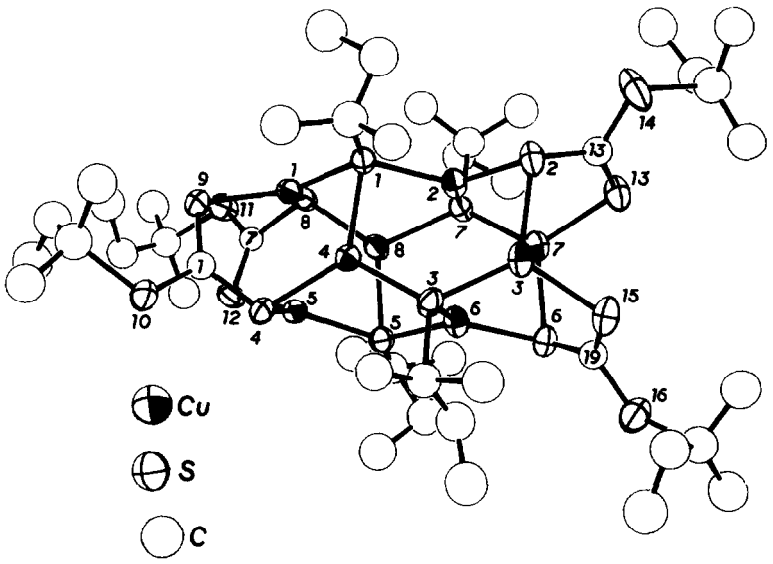

Fig. 1. Structure of $Cu_8(SC_5H_{11})_4(S_2CSC_5H_{11})_4$, showing the atom labelling scheme. Copper and sulphur atoms are drawn as 30% probability ellipsoids, while the amyl carbon atoms shown are represented by circles of arbitrary radius.

the sulphur, and the carbon next to the sulphur, are given in Table 2. Tables of anisotropic thermal parameters for copper and sulphur atoms, bond lengths and angles other than those in Table 2, a unit cell packing diagram, observed and calculated structure factors, and atomic coordinates have been deposited with the Editor,* from whom copies may be obtained.

RESULTS AND DISCUSSION

Preparative

As we have reported earlier, the synthesis of CuSR compounds by direct oxidation of a sacrificial anode is a simple and efficient method.[2] The resultant thiolato complexes are insoluble in the common organic solvents, but $CuSC_5H_{11}$ dissolves readily in carbon disulphide to give the octacopper complex **1**, whose structure is discussed below. This is another example of the *in situ* insertion of CS_2 into the M—S bond of an existing thiolato complex, as opposed to those syntheses which depend on the prior reaction of CS_2 with a thiolate anion to give $RSCS_2^-$ which then reacts to form the appropriate thioxanthate derivative.[4] In the present case, as with the reaction of $Cd(SPh)_2$ with CS_2 to give $Cd(SPh)(S_2CSPh)$,[5] the product corresponds stoichiometrically to the insertion of CS_2 into only half of the Cu—S bonds of $CuSC_5H_{11}$.

The octacopper cage **1** reacts readily with Ph_3P or Cy_2PhP to give products of formal stoichiometry $CuS_2CSC_5H_{11} \cdot 2PR_3$, independent of the reaction conditions, so that the adducts are of the copper(I) thioxanthate and not of the mixed ligand starting material. This clearly implies a drastic rearrangement of the CuS cage, since the tridentate thiolato ligands in **1** are in fact bonded to copper atoms in the core of the structure (see below). In view of the wide variety of structures reported for copper(I)–thiolato complexes, there is little point in speculating about the actual structure of these thioxanthate adducts in the absence of X-ray crystallographic results.

The structure of $Cu_8(SC_5H_{11})_4(S_2CSC_5H_{11})_4$ (1)

The molecular structure of **1** is based on a Cu_8S_{12} cage, shown in Fig. 1 and in a simpler form in Fig. 2, and the complexity of the structure is the

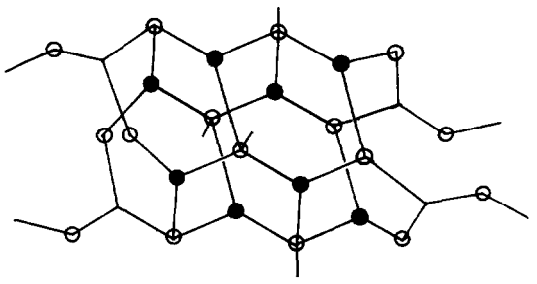

Fig. 2. Simplified diagram of $Cu_8(SC_5H_{11})_4(S_2CSC_5H_{11})_4$ showing the two layers of $Cu_4(SC_5H_{11})_2$ held together by four amylthiocarbonate groups.

* Atomic coordinates have also been deposited with the Cambridge Crystallographic Data Centre.

Table 2. Interatomic distances (Å) and angles (°) for copper, sulphur and carbon atoms shown in Fig. 1

Cu(1)—S(1)	2.240(6)	S(1)—Cu(1)—S(8)	118.2(2)
Cu(1)—S(8)	2.271(7)	S(1)—Cu(1)—S(9)	122.6(2)
Cu(1)—S(9)	2.263(5)	S(8)—Cu(1)—S(9)	118.7(2)
Cu(2)—S(1)	2.254(4)	S(1)—Cu(2)—S(2)	115.9(2)
Cu(2)—S(2)	2.286(6)	S(1)—Cu(2)—S(7)	115.2(2)
Cu(2)—S(7)	2.295(7)	S(2)—Cu(2)—S(7)	127.2(2)
Cu(3)—S(2)	2.270(6)	S(2)—Cu(3)—S(3)	121.8(2)
Cu(3)—S(3)	2.237(5)	S(2)—Cu(3)—S(15)	117.8(2)
Cu(3)—S(15)	2.277(5)	S(3)—Cu(3)—S(15)	119.7(2)
Cu(4)—S(1)	2.301(5)	S(1)—Cu(4)—S(3)	111.7(2)
Cu(4)—S(3)	2.245(5)	S(1)—Cu(4)—S(4)	130.0(2)
Cu(4)—S(4)	2.292(5)	S(3)—Cu(4)—S(4)	116.9(2)
Cu(5)—S(4)	2.270(6)	S(4)—Cu(5)—S(5)	120.3(2)
Cu(5)—S(5)	2.250(5)	S(4)—Cu(5)—S(12)	115.7(2)
Cu(5)—S(12)	2.276(6)	S(5)—Cu(5)—S(12)	123.3(3)
Cu(6)—S(3)	2.292(6)	S(3)—Cu(6)—S(5)	112.5(2)
Cu(6)—S(5)	2.259(6)	S(3)—Cu(6)—S(6)	125.5(2)
Cu(6)—S(6)	2.284(5)	S(5)—Cu(6)—S(6)	120.6(2)
Cu(7)—S(6)	2.281(6)	S(6)—Cu(7)—S(7)	121.7(2)
Cu(7)—S(7)	2.251(5)	S(6)—Cu(7)—S(13)	116.1(2)
Cu(7)—S(13)	2.276(6)	S(7)—Cu(7)—S(13)	121.4(2)
Cu(8)—S(5)	2.287(5)	S(5)—Cu(8)—S(7)	112.1(2)
Cu(8)—S(7)	2.267(5)	S(5)—Cu(8)—S(8)	128.6(2)
Cu(8)—S(8)	2.282(5)	S(7)—Cu(8)—S(8)	117.7(2)
		Cu(1)—S(1)—Cu(2)	120.1(3)
		Cu(1)—S(1)—Cu(4)	71.5(2)
		Cu(2)—S(1)—Cu(4)	87.4(2)
		Cu(1)—S(1)—C(25)	120.9(7)
		Cu(2)—S(1)—C(25)	118.6(7)
		Cu(4)—S(1)—C(25)	105.3(8)
S(2)—C(13)	1.743(17)	Cu(2)—S(2)—Cu(3)	74.5(2)
		Cu(2)—S(2)—C(13)	111.5(8)
		Cu(3)—S(2)—C(13)	102.9(7)
		Cu(3)—S(3)—Cu(4)	120.4(2)
		Cu(3)—S(3)—Cu(6)	75.1(2)
		Cu(4)—S(3)—Cu(6)	89.7(2)
		Cu(3)—S(3)—C(30)	120.1(7)
		Cu(4)—S(3)—C(30)	119.4(6)
		Cu(6)—S(3)—C(30)	106.7(9)
S(4)—C(1)	1.739(16)	Cu(4)—S(4)—Cu(5)	75.7(2)
		Cu(4)—S(4)—C(1)	110.4(7)
		Cu(5)—S(4)—C(1)	105.1(7)
		Cu(5)—S(5)—Cu(6)	119.6(3)
		Cu(5)—S(5)—Cu(8)	72.0(2)
		Cu(6)—S(5)—Cu(8)	86.9(2)
		Cu(5)—S(5)—C(40)	119.0(8)
		Cu(6)—S(5)—C(40)	120.9(8)
		Cu(8)—S(5)—C(40)	104.6(8)
S(6)—C(19)	1.718(22)	Cu(6)—S(6)—Cu(7)	74.3(2)
		Cu(6)—S(6)—C(19)	109.3(6)
		Cu(7)—S(6)—C(19)	104.9(7)
		Cu(2)—S(7)—Cu(7)	73.5(2)
		Cu(2)—S(7)—Cu(8)	86.7(2)
		Cu(7)—S(7)—Cu(8)	119.9(2)
S(8)—C(7)	1.753(18)	Cu(1)—S(8)—Cu(8)	77.8(2)
		Cu(1)—S(8)—C(7)	102.6(6)
		Cu(8)—S(8)—C(7)	113.7(6)

Table 2—*continued*

S(9)—C(1)	1.656(18)		
		S(4)—C(1)—S(9)	126.6(10)
S(10)—C(1)	1.746(17)		
		S(4)—C(1)—S(10)	107.8(10)
S(11)—C(7)	1.720(18)	S(9)—C(1)—S(10)	125.5(10)
S(12)—C(7)	1.660(17)	Cu(5)—S(12)—C(7)	102.2(7)
S(13)—C(13)	1.664(23)	Cu(7)—S(13)—C(13)	101.8(7)
S(14)—C(13)	1.733(22)		
S(15)—C(19)	1.634(24)	Cu(3)—S(15)—C(19)	100.9(6)
S(16)—C(19)	1.769(19)		
		S(8)—C(7)—C(11)	108.0(9)
		S(8)—C(7)—S(12)	125.4(11)
		S(11)—C(7)—S(12)	126.5(11)

combination of several interesting detailed features.

The arrangements of the copper atoms is a convenient starting point, since these form an array of distorted tetrahedra. There are a number of reports of polymeric inorganic[6] and organometallic[7] copper compounds, but in general these possess higher symmetry in terms of the copper atom array than in the present case. The Cu_8 cage is linked together by a series of sulphur atoms of either RS^- or $RSCS_2^-$ ligands, with mono-, bi- and tridentate coordination. The thiolato sulphur atoms, S(1), S(3), S(5) and S(7) each bridge three copper atoms in an approximately tetrahedral $CSCu_3$ arrangement [e.g. C—S(1)—Cu(1), Cu(2), Cu(4)]. It has been suggested elsewhere[2] that the polymeric structure of CuSR compounds is due to cross-linking through sulphur atoms, which at its simplest can be written as in Structure 1. The nature of the thiolate bonding

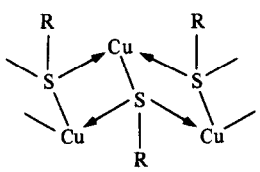

Structure 1.

in **1** appears to support this suggestion, since the same $CSCu_3$ site is involved in both cases. The thioxanthate ligands provide sulphur atoms which are of two types, namely non-bridging [S(9), S(12), S(13) and S(15)], or doubly bridging [S(4), S(8), S(2) and S(6)]; each of the latter bridges two copper atoms, as in S(4), Cu(4), Cu(5), with pyramidal geometry at each bidentate sulphur.

Each copper atom in the structure is coordinated by three sulphur atoms; atoms 1, 3, 5 and 7 are attached to a non-bridging, a doubly-bridging and a triply-bridging sulphur atom, while atoms 2, 4, 6 and 8 are ligated by one non-bridging and two triply-bridging sulphurs. The average sum of the bond angles on all the copper atoms is 358.8°, so that each is in a slightly distorted CuS_3 plane. There is some difference in the average value for copper atoms 1, 3, 5 and 7 (359.3°) and 2, 4, 6 and 8 (358.4°), but the major difference between the two groups is that for 2, 4, 6 and 8 the average is the result of two small and one large value, while for 1, 3, 5 and 7 the angles are clustered more closely about the mean (see Table 2). This deviation from trigonal symmetry is presumably related to the effect of the bridging sulphur atoms in the coordination kernel of this group of copper atoms.

The overall cage structure includes eight six-membered rings in the boat form, as in Cu(1)—S(1)—Cu(4)—S(4)—C(1)—S(9), and these can be regarded collectively as a core which is capped by two eight-membered rings [e.g. Cu(3) — S(2) — C(13) — S(13) — Cu(7) — S(6) — C(19)—S(15)—Cu(3)]. An approximately two-fold axis passes through the centre of the cage. In terms of the insertion process by which **1** is formed, the reaction presumably takes place at the boundaries of a $(CuSR)_n$ oligomer (see above) and the final structure retains some of the features of that unit. The Cu···Cu distances are in the range 2.652(3)–3.250(4) Å, with an average value of 2.92(1) Å, implying a non-bonding interaction (cf. ref. 2 for a discussion of this point).

As a consequence of the variety of copper(I) thiolate structures which have been studied, there is a large number of Cu—S bond distances against which the present results can be compared. The values for Cu—S (thiolate) lie in the range 2.237(5)–2.301(5) Å, while for Cu—S (thioxanthate) the range is 2.263(5)–2.295(5) Å. The reported Cu—S distances in complexes with doubly-bridging sul-

phur atoms attached to alkyl groups are in the range 2.402(2)–2.451(2) Å in $(Ph_3P)_2CuS_2COEt$[8] and 2.411(5)–2.479(5) Å in $(Ph_3P)_2Cu(S_2CSCH_2SCS_2)$ $Cu(PPh_3)_2$,[8] and these clearly represent longer bonds than those found for **1**, as do the distances of 2.308–2.406 Å in Cu_4 $(dppm)_4(CS_3)_2$ (dppm = diphenylphosphinomethane)[9] whose structure involves six-membered CuSCuPCP and CuSCSCuS rings. The present values are close to those in the $Cu(SPh)_3^-$ anion[10,11] where the ranges are 2.274(4)–2.335(4) Å or 2.239(2)–2.258(2) Å, depending on the cation, but a detailed comparison with oligomeric structures involving phenylthiolate ligands does not seem justified.

Stability of $Cu_8(SC_5H_{11})_4(S_2CSC_5H_{11})_4$ *and adducts*

It is clear that the reaction of $CuSC_5H_{11}$ with CS_2 to give **1** is reversed in refluxing benzene and such reversibility is found with other thioxanthates.[4,5] The breakdown of the cage structure of **1** under these conditions is complete and rapid, and there is no evidence for intermediate structures of lower molecularity than in **1**. A comparison of the results for a solution in benzene (b.p. 80°C) and a suspension in methanol (b.p. 65°C) points to the importance of homogeneous decomposition. The thermal stability of the solid at 100°C again underlines this, and we conclude that the cage structure is remarkably stable to thermal decomposition by heterogeneous elimination of CS_2. It seems probable that in benzene solution there are fluxional changes like those reported for various adamantane-like $[M_4(SR)_{10}]^{2-}$ anions[12] and that these provide an accessible path for decomposition, but are obviously not available in the solid state.

The EI mass spectrum of **1** is then explicable in terms of the high energy decomposition.

$$Cu_8(SR)_4(S_2CSR)_4 \xrightarrow{-CS_2} (CuSR)_n \xrightarrow{EI} \text{ions}$$

so that the EI spectrum is not that of **1** itself, but of its decomposition product CuSR. The insolubility of $CuSC_5H_{11}$ in all solvents except CS_2 prevents a direct test of this conclusion. The mass spectra of the 1:2 adducts of PR_3 with $CuS_2CSC_5H_{11}$ are almost identical with that of **1**, and again we suggest that the sequence is

$$CuS_2CSR \cdot 2PR_3 \xrightarrow[-PR_3]{-CS_2} (CuSR)_n \xrightarrow{EI} \text{ions}.$$

The decomposition of **1** observed in the cyclic voltammetry also illustrates the finely balanced stability of the structure. The removal of an electron is not accommodated by a structural rearrangement, as is the case in many transition metal clusters, but rather by an irreversible collapse of the cage. The decomposition of $Cu_8(SR)_4(S_2CSR)_4$ to $(CuSR)_n$ on either an oxidative or thermal reaction emphasises that cages are both more labile and more fragile entities than clusters, which depend on both M—M and M–ligand bonding for their stability.

Spectroscopic results

The IR spectra of **1** and its PR_3 adducts convey little structural information, other than confirming the presence of the neutral ligands. Strong bands at 885 and 822 cm^{-1} in **1** are assigned to ν(C—S) of the $C_5H_{11}SCS_2$ ligand, following earlier reports,[13,14] and similar modes are observed in the adducts with PPh_3 (990, 885 cm^{-1}) and $PPhCy_2$ (984, 889 cm^{-1}).

The ^1H NMR spectrum of **1** in CS_2 solution can be assigned in the light of the structural determination. There are two C_5H_{11} environments, depending on whether the ligand is —SR or —S_2CSR and the spectrum is the superimposition of two sets of signals. The terminal CH_3 of —$C(CH_3)_2$ CH_2CH_3 gives a pair of triplets, centred at 0.70 and 0.72 ppm from Me_4Si; since the thioxanthate group is more electron-withdrawing than the sulphur of thiolate, the upfield resonance is assigned to $CH_3CH_2C(CH_3)_2S$. Similarly, the CH_2 groups of RS and $RSCS_2$ generate a pair of quartets at 1.74 + 1.76 ppm (mid-points). The resonances of the α-CH_3 groups appear as a pair of doublets at 1.23 + 1.25 and 1.46 + 1.48 ppm. Two effects are at issue here. The two CH_3 environments, close to S^- or SCS_2^-, should produce resonances more widely separated than for the terminal CH_3, and in addition each ligand has a pair of diastereotopic CH_3 groups. Whether the latter effect is dominant over the former in terms of the separation of the signals is not clear at this point.

Acknowledgement—This work was supported in part by Operating Grants (to D.G.T.) from the Natural Sciences and Engineering Research Council of Canada.

REFERENCES

1. R. K. Chadha, R. Kumar and D. G. Tuck, *J. Chem. Soc., Chem. Commun.* 1986, 188.
2. R. K. Chadha, R. Kumar and D. G. Tuck, *Can. J. Chem.* 1987, **65**, 1336.
3. M. A. Khan, R. C. Steevensz, D. G. Tuck, J. G. Noltes and P. W. R. Corfield, *Inorg. Chem.* 1980, **19**, 3407.
4. D. Coucouvanis, *Prog. Inorg. Chem.* 1979, **26**, 301.
5. S. J. Black, F. W. B. Einstein, P. C. Hayes, R. Kumar and D. G. Tuck, *Inorg. Chem.* 1986, **25**, 4181.

6. I. G. Dance, M. L. Scudder and L. J. Fitzpatrick, *Inorg. Chem.* 1985, **24**, 2547 and refs therein.
7. J. G. Noltes and G. van Koten, *Comprehensive Organometallic Chemistry* (Edited by G. Wilkinson, F. G. A. Stone and E. W. Abel), Vol. 2, p. 14. Pergamon Press, Oxford (1982).
8. C. Bianchini, C. A. Ghilardi, A. Meli, S. Midollini and A. Orlandini, *Inorg. Chem.* 1985, **24**, 932.
9. A. M. M. Lanfredi, A. Tiripicchio, A. Camus and N. Marsich, *J. Chem. Soc., Chem. Commun.* 1983, 1126.
10. D. Coucouvanis, C. N. Murphy and S. K. Kanodia, *Inorg. Chem.* 1980, **19**, 2993.
11. C. D. Garner, J. R. Nicholson and W. Clegg, *Inorg. Chem.* 1984, **23**, 2148.
12. K. S. Hagen, D. W. Stephan and R. H. Holm, *Inorg. Chem.* 1982, **21**, 3928.
13. D. Coucouvanis, S. J. Lippard and J. A. Zubieta, *J. Am. Chem. Soc.* 1970, **92**, 3342.
14. D. G. Lewis, S. J. Lippard and J. A. Zubieta, *J. Am. Chem. Soc.*, 1972, **94**, 1563.

Polyhedron Vol. 7, No. 12, pp. 1129–1130, 1988
Printed in Great Britain

0277–5387/88 $3.00+.00
© 1988 Pergamon Press plc

COMMUNICATION

SYNTHESIS AND STRUCTURAL CHARACTERIZATION OF A BINUCLEAR OXOMOLYBDENUM(VI) TROPOLONATE COMPLEX, $(n\text{-}Bu_4N)_2[Mo_2O_6(trop)_2]$, DISPLAYING THE NOVEL $[MoO_2(\mu\text{-}O)_2MoO_2]^0$ CORE

SHUNCHENG LIU and JON ZUBIETA*

Department of Chemistry, State University of New York at Albany, Albany, NY 12222, U.S.A.

(*Received* 25 *November* 1987; *accepted* 19 *January* 1988)

Abstract—Reaction of $(n\text{-}Bu_4N)_2[Mo_2O_7]$ with tropolone ($C_7H_6O_2$) in acetonitrile yields $(n\text{-}Bu_4N)_2[Mo_2O_6(trop)_2]$. The title complex is a unique example of a binuclear oxomolybdenum(VI) species exhibiting the $[MoO_2(\mu\text{-}O)_2MoO_2]^0$ core. Crystal data: monoclinic space group $P2_1/c$, $a = 10.092(2)$, $b = 14.867(3)$, $c = 17.002(4)$ Å, $\beta = 93.05(1)°$, $V = 2547.4(11)$ Å^3, $Z = 2$, $D_{calc.} = 1.37$ g cm^{-3}; 3764 reflections to give $R = 0.035$.

Catecholato complexes of transition metals are of fundamental chemical interest as models for metal sites in metalloproteins,[1] in the investigation of ligand-centred redox processes[2] and in the preparation of metal–semiquinone species.[3] The chemistry of molybdenum–catecholato species has been explored extensively by Pierpont[4] and others[5,6] and shown to present a variety of novel structural types. The tropolonato ligand, the seven-numbered ring analogue of the catecholato group, has also been demonstrated to react with molybdate in aqueous solution to yield a dioxomolybdate(VI) complex, $[MoO_2(trop)_2]$.[7] By exploiting the synthetic potential of polyoxomolybdate species soluble in non-aqueous solvents,[8] we have prepared and structurally characterized the binuclear Mo(VI) complex, $(n\text{-}Bu_4N)_2[Mo_2O_6(trop)_2]$, which presents the first example of the $[MoO_2(\mu\text{-}O)_2MoO_2]^0$ core. The oxo group is ubiquitous to the chemistry of Mo(VI) and Mo(V), and a variety of oxomolybdenum cores have been structurally characterized: $[MoO_2]^{2+}$, $[MoO_3]^0$ and $[Mo_2O_5]^{2+}$ for Mo(VI) and $[Mo_2O_3]^{4+}$, $[Mo_2O_4]^{2+}$ and $[MoO]^{3+}$ for Mo(V).[9,10] To our knowledge, the $[Mo_2O_6]^0$ core of $[Mo_2O_6(trop)_2]^{2-}$ is unique.

$(n\text{-}Bu_4N)_2[Mo_2O_6(trop)_2]$ was prepared from the reaction of $(n\text{-}Bu_4N)_2[Mo_2O_7]$ with an equimolar amount of tropolone in acetonitrile. Addition of ether, followed by cooling at 4°C for 3 days, gave bright yellow–orange crystals in 65% yield.† The IR spectrum is characterized by strong bands at 920 and 894 cm^{-1} assigned to ν_s(Mo=O) and ν_{as}(Mo=O), respectively, and a band at 1600 cm^{-1} associated with ν(C=C). The electronic spectrum shows bands at 388 and 325 nm with extinction coefficients of 3×10^3 and 9×10^3 M^{-1} cm^{-1}, respectively. The complex crystallizes in the monoclinic space group $P2_1/c$ with $a = 10.092(2)$, $b = 14.867(3)$, $c = 17.002(4)$ Å, $\beta = 93.05(1)°$, $V = 2547.4(11)$ Å^3, $Z = 2$ (based upon binuclear formulation), $D_{calc.} = 1.32$ g cm^{-3}. Structure solution and refinement based upon 3764 reflections with $F_o \geqslant 6\sigma(F_o)$(Mo-$K_\alpha$, $\lambda = 0.71073$ Å) converged at $R = 0.035$.‡

* Author to whom correspondence should be addressed.

† Elemental Analysis: Found: C, 54.2; H, 8.3; N, 2.7. Calc. for $C_{46}H_{82}N_2O_{10}Mo_2$: C, 54.4; H, 8.1; N, 2.8%.

‡ Final atomic positional and thermal parameters, bond lengths and angles, and F_o/F_c values have been deposited as supplementary material with the Editor, from whom copies are available on request. Atomic coordinates have also been submitted to the Cambridge Crystallographic Data Centre.

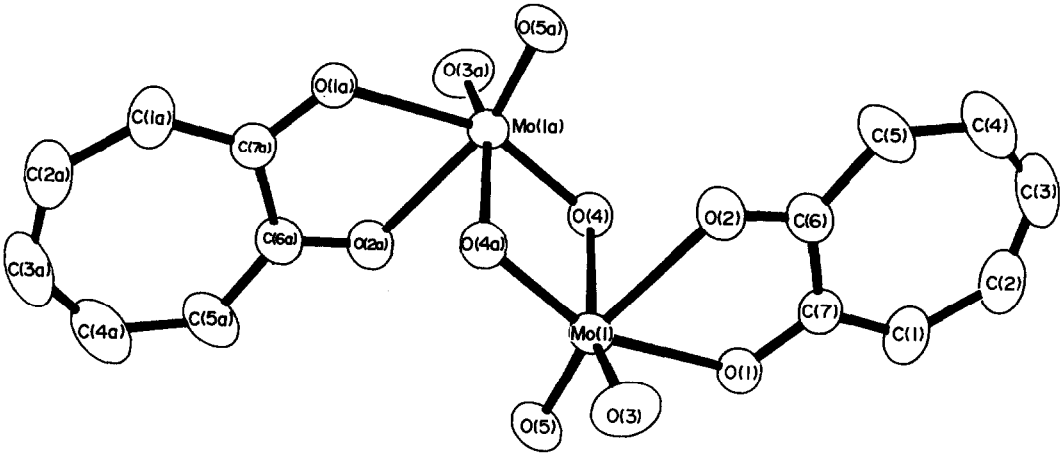

Fig. 1. ORTEP view of the structure of $[Mo_2O_6(trop)_2]^{2-}$, showing the atom-labelling scheme. Selected bond lengths (Å) and angles (°): Mo(1)—O(1), 2.190(2); Mo(1)—O(2), 2.252(2); Mo(1)—O(3), 1.729(2); Mo(1)—O(4), 2.215(2); Mo(1)—O(4a), 1.807(2); Mo(1)—O(5), 1.715(2); C(7)—O(1), 1.285(4); C(6)—O(2), 1.262(4); Mo(1)—Mo(1a), 3.153(1); O(1)—Mo(1)—O(2), 70.2(1); O(1)—Mo(1)—O(3), 93.2(1); O(1)—Mo(1)—O(4), 80.9(1); O(1)—Mo(1)—O(5), 86.7(1); O(2)—Mo(1)—O(3), 86.3(1); O(2)—Mo(1)—O(4), 75.2(1); O(2)—Mo(1)—O(5), 155.7(1); O(3)—Mo(1)—O(4), 161.5(1); O(3)—Mo(1)—O(5), 103(1); O(4)—Mo(1)—O(5), 94.1(1).

The structure of $[Mo_2O_6(trop)_2]^{2-}$ is shown in Fig. 1, and selected bond lengths and angles are presented in the caption. The crystallographically unique halves of the binuclear dianion are related by a centre of symmetry at the midpoint of the Mo(1)—Mo(1a) vector. The most unusual feature of the structure is the presence of the unique structural core $[Mo_2O_6]^0$. The metrical parameters associated with the core are not unanticipated. Thus, the Mo(1)—O(2) distance is significantly longer than Mo(1)—O(1) as a consequence of the *trans* influence of the terminal oxo-group O(5), relative to that of the bridging oxo-group O(4a). In a similar fashion, the molybdenum-bridging oxo distances are non-equivalent, 2.215(2) and 1.807(2) Å for Mo(1)—O(4) and Mo(1)—O(4a), respectively, due to the significant *trans* influence of the terminal oxo group O(3) and the negligible *trans* influence of O(1). The Mo(1)—Mo(1a) distance of 3.153(1) Å is consistent with the absence of a Mo—Mo interaction, as expected for a binuclear Mo(VI)-d^0 complex, and contrasting with the distance of *ca* 2.70 Å observed for $[(\mu\text{-O})_2Mo_2(V)]$ centres where a metal–metal bond is invoked.

Although the complex is electrochemically active, the well-behaved process appears to be associated with the ligand. In common with Type II oxomolybdate(VI) species,[11] the metal based reductions occur at potentials below −1.9 V and appear as ill-behaved multi-electron processes.

Acknowledgement—This work was supported by NSF Grant CHE8514634 to J. Zubieta.

REFERENCES

1. K. N. Raymond and C. Carrano, *Acc. Chem. Res.* 1979, **12**, 183; L. Que Jr, *Struct. Bonding (Berlin)* 1980, **40**, 39.
2. S. D. Pell, R. B. Salmonson, A. Abelleira and M. J. Clark, *Inorg. Chem.* 1984, **23**, 385; J. R. Bradbury and F. A. Schultz, *Inorg. Chem.* 1986, **25**, 4414 and refs therein.
3. K. Broadley, N. G. Connelly and W. E. Geiger, *J. Chem. Soc., Dalton Trans.* 1983, 121; P. Mathur and G. C. Dismukes, *J. Am. Chem. Soc.* 1983, **105**, 7093.
4. M. W. Lynch, D. N. Hendrickson, B. J. Fitzgerald and C. G. Pierpont, *J. Am. Chem. Soc.* 1984, **106**, 2041; C. G. Pierpont and R. M. Buchanan, *J. Am. Chem. Soc.* 1975, **97**, 6450; R. J. Buchanan and C. G. Pierpont, *Inorg. Chem.* 1979, **18**, 1616; C. G. Pierpont and H. M. Downs, *J. Am. Chem. Soc.* 1975, **97**, 2123; M. E. Cass and C. G. Pierpont, *Inorg. Chem.* 1986, **25**, 122; C. G. Pierpont and H. M. Downs, *Inorg. Chem.* 1975, **14**, 343.
5. W. P. Griffith, C. A. Pumphrey and C.-A. Rainey, *J. Chem. Soc., Dalton Trans.* 1986, 1125; S. Bristow, J. H. Enemark, C. D. Garner, M. Minelli, G. A. Morris and R. B. Ortega, *Inorg. Chem.* 1985, **24**, 4070.
6. S. Liu, S. N. Shaikh and J. Zubieta, *Inorg. Chem.* 1987, **26**, 4304; S. N. Shaikh and J. Zubieta, unpublished results.
7. W. P. Griffith, C. A. Pumphrey and A. C. Skapski, *Polyhedron* 1987, **6**, 891.
8. V. W. Day and W. G. Klemperer, *Science* 1985, **228**, 533.
9. E. I. Stiefel, *Prog. Inorg. Chem.* 1977, **22**, 1.
10. B. Spivack and Z. Dori, *Coord. Chem. Rev.* 1975, **17**, 99.
11. M. T. Pope, *Inorg. Chem.* 1972, **11**, 1973.

Polyhedron Vol. 7, No. 12, pp. 1131–1134, 1988
Printed in Great Britain

0277-5387/88 $3.00 + .00
© 1988 Pergamon Press plc

COMMUNICATION

EQUILIBRIA OF THE H^+–MoO_4^{2-}–SeO_3^{2-} SYSTEM IN AQUEOUS 1 M Na(Cl) MEDIUM

T. OZEKI, A. YAGASAKI, H. ICHIDA and Y. SASAKI*

Department of Chemistry, Faculty of Science, The University of Tokyo, 7-3-1 Hongo, Bunkyo-ku, Tokyo 113, Japan

(*Received* 22 *December* 1987; *accepted* 1 *February* 1988)

Abstract—The equilibria $pH^+ + qMoO_4^{2-} + rSeO_3^{2-} \rightleftharpoons (H^+)_p(MoO_4^{2-})_q(SeO_3^{2-})_r$ have been investigated by potentiometry at 25°C in 1 M Na(Cl). The data have been explained by the formation of the following ternary species denoted by (p,q,r) according to the equation above: (10,5,2), (11,5,2), (14,8,2) and (15,8,2). ^{77}Se NMR spectra have also been recorded at various hydrogen ion concentrations.

A large number of heteropolyanions have been isolated and their crystal structures have been determined in the last two decades. These works have made a great contribution to the heteropolyanion chemistry. However, preparative works do not give us any information on the stability or lability of polyanions in solution. There is always a possibility that a certain species was isolated only because it was less soluble than the species predominant in solution.

As part of our project to study the solution chemistry of heteropolyanions, we have carried out a potentiometric investigation of the H^+–MoO_4^{2-}–SeO_3^{2-} system. We have also measured the ^{77}Se NMR of this system. ^{77}Se is a good NMR nucleus with $I = 1/2$, moderate sensitivity and large chemical shifts.[1] We anticipated that ^{77}Se NMR would be a good probe for the investigation of the title system.

EXPERIMENTAL

Chemicals

NaCl (Matsunaga, JIS Primary Standard) was heated at 140°C for *ca* 8 h before use. The molybdate stock solution was prepared as described elsewhere.[2] SeO_2 (Wako, I) was purified by double sublimation.[3]

Emf measurement

The same apparatus as in our previous report was employed.[2] The temperature was kept constant at 25.0 ± 0.1°C throughout the experiment. Nine titrations were performed and 254 data points were collected. The data covered the ranges $5.8 > -\log h > 2.0$, $58.9 > B/\text{mM} > 33.2$, $48.8 > C/\text{mM} > 4.3$, and $0.8 \leqslant B/C \leqslant 10.0$, where h is the concentration of the free hydrogen ion. B stands for the total concentration of molybdate and C that of selenite. In most cases stable emf values were attained within 5 min. However, we found somewhat slower equilibria in the range $B/C \geqslant 3$ when $-\log h$ was around 4.5.

NMR measurement

^{77}Se NMR spectra were recorded on a JEOL FX-90Q spectrometer at 17.03 MHz. Chemical shift values were externally referenced to pure $(CH_3)_2Se$ by the sample replacement method. However, most spectra were recorded by using an aqueous saturated SeO_2 solution as a secondary reference. The spin-lattice relaxation times (T_1) were evaluated by the inversion-recovery method. The T_1/s (and $\Delta\nu$/Hz) values of peak 2 in Fig. 1 were 5.2(5.36) and 1.2(16.07) at pH of 6.16 and 2.25, respectively. The pH of the sample solution was measured by an ordinary pH-meter. The difference between the pH and $-\log h$ values was found to be less than 0.1.

*Author to whom correspondence should be addressed.

Analysis of the data

The equilibria in solution can generally be written as

$$pH^+ + qMoO_4^{2-} + rSeO_3^{2-} \rightleftharpoons (H^+)_p(MoO_4^{2-})_q(SeO_3^{2-})_r.$$

The complex on the right hand side will simply be referred to as (p,q,r) and its formation constant β_{pqr}. The search for the best set of (p,q,r) and β_{pqr} was performed with the least-squares program LETAGROPVRID, version ETITR.[4] The function $U = \Sigma(H_{calc.} - H)^2$ has been minimized, where $H_{calc.}$ and H stand for calculated and actual total hydrogen concentrations over the zero level (H_2O, MoO_4^{2-} and SeO_3^{2-}).

Binary systems

Since there was no former report on the binary H^+–SeO_3^{2-} equilibria in 1.0 M Na(Cl), three separate titrations were performed to determine the formation constants of this system. A total of 125 emf data points were collected. The data covered the ranges $6.9 > -\log h \geqslant 2.0$ and $10.6 < C/\text{mM} < 34.5$. The titration curves did not show any sign of concentration dependence. This means that only monomeric species existed in the range investigated. The system was well explained by (0,0,1), (1,0,1) and (2,0,1) with the formation constants $\log\beta_{1,0,1} = 8.28 \pm 0.04$ and $\log\beta_{2,0,1} = 10.64 \pm 0.04$. These values were in accord with the change of the chemical shift of peak 1 observed in the ^{77}Se NMR (see Fig. 1). The final $\sigma(H)$* was 0.32 mM.

For the H^+–MoO_4^{2-} equilibria the constants we reported elsewhere[5,6] were used.

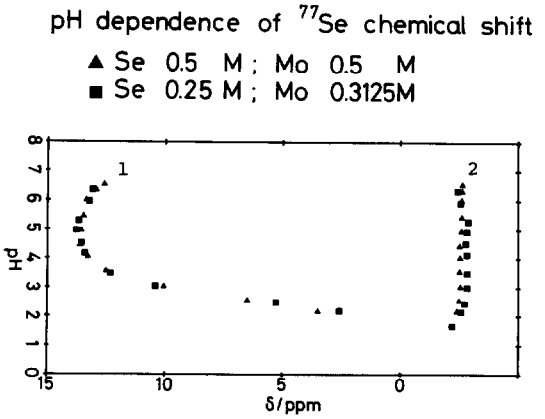

Fig. 1. Plot of ^{77}Se chemical shifts vs pH. (1) $(p,0,1)$ (2) $(p,5,2)$. ▲: $B = 0.5$ M, $C = 0.5$ M; ■: $B = 0.3125$ M, $C = 0.25$ M.

However, the residuals in the least-squares analysis of the emf data showed some systematic trends: they were unsatisfactorily large in the ranges (1) $-\log h < 3$ and (2) $B/C > 4$. We made a further analysis as follows.

Low ratio data

Several calculations were carried out to determine the formation constant of (10,5,2) by using the experimental points of low B/C ratios ($B/C \leqslant 2.5$, 145 points). The least-squares calculation gave $\sigma(H) = 0.62$ mM with $\log\beta_{10,5,2} = 71.41 \pm 0.04$ when (10,5,2) was introduced to the system as the only ternary species. Here again the residuals showed a systematic deviation as h increased. This systematic deviation disappeared after the introduction of (11,5,2). The ^{77}Se NMR

RESULTS AND DISCUSSION

A preliminary pqr-analysis[7] strongly favoured (10,5,2).[8] In fact, the introduction of a single ternary species of (10,5,2) to the system resulted in a $\sigma(H)$ value as low as 0.91 mM. The ^{77}Se NMR spectra of the solution of $B/C = 1$ showed that about 40% of Se in solution is bound in a single ternary species, in a wide $-\log h$ range, which is consistent with the formation of a strong heteropoly species whose q/r ratio is 2.5 (see Fig. 2).

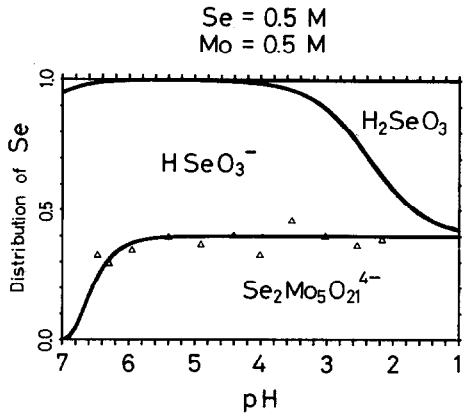

Fig. 2. Distribution of Se as a function of pH. Experimental points are indicated by triangles. $B = 0.5$ M, $C = 0.5$ M.

* $\sigma(H)$ is defined $[U/(m-n)]^{1/2}$, where m is the number of data points and n is the number of complexes. See ref. 4 for details.

spectra also indicated the protonation of (10,5,2). The shift of peak 2, which was assigned to the Mo_5Se_2 species, showed a slight change in the very acidic region (see Fig. 1). The least-squares calculation with both (10,5,2) and (11,5,2) converged with $\sigma(H) = 0.35$ mM and gave $\log\beta_{10,5,2} = 71.39 \pm 0.02$ and $\log\beta_{11,5,2} = 72.63 \pm 0.01$.

High ratio data

While the low B/C ratio data were explained satisfactorily, there was still a discrepancy between the calculated and observed titration curves in the high B/C ratio even after the introduction of (11,5,2). A *pqr*-analysis on the whole range of data, where the constants for (10,5,2) and (11,5,2) were fixed to the values described in the preceding paragraph, revealed that there were one or more ternary species whose (average) $z_{q+r}[= p/(q+r)]$ was *ca* 1.4.†

In Table 1 tentative models and the formation constant of each species are given. We have selected these two models out of numerous possible ones because of their simplicity. The composition of (14,8,2) coincides with that of $Se_2Mo_8O_{31}^{6-}$ reported in the literature.[9] The species (10,5,2) has the same composition as $Se_2Mo_5O_{21}^{4-}$ which was isolated as an ammonium salt previously.[10] We have isolated a sodium salt of the anion and the X-ray diffraction study has revealed it has the structure shown in Fig. 3.[11] We presume this structure is maintained in solution. Possible protonation sites are indicated by asterisks in the figure.‡

Table 1. Proposed models and $\log\beta_{pqr}$ of each species

	Model (a)	Model (b)
(10,5,2)	71.32±0.02	71.40±0.02
(11,5,2)	72.73±0.04	72.74±0.03
(14,8,2)	97.97±0.02	—
(15,8,2)	101.04±0.03	—
(11,7,1)	—	74.37±0.03
(12,7,1)	—	77.71±0.03
U/mM^2	21.3	24.5
$\sigma(H)$/mM	0.30	0.32

Figure 4 illustrates the distribution of molybdate in each species based on model (a) in Table 1. Formation of the ternary species starts at around $-\log h = 6$, which is a common feature of heteropolymolybdate systems which have tetrahedral

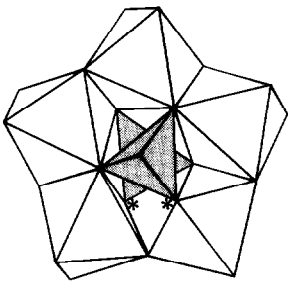

Fig. 3. Structure of $[Se_2Mo_5O_{21}]^{4-}$.

† It has been pointed out that the ordinary *pqr*-analysis only gives information on the proton consumption of the species in the search when applied to a complicated system like the current one, although it works more effectively for simpler systems. See ref. 14.

‡ The bond order[12] calculation showed that the oxygen atoms doubly shared by one Mo atom and one Se atom are slightly more basic than the others.

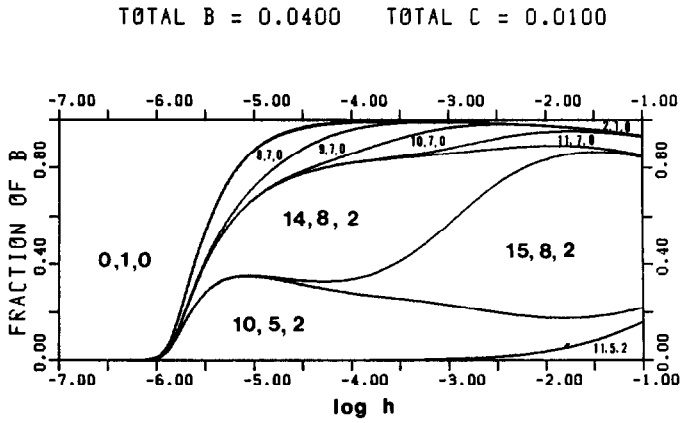

Fig. 4. Distribution of Mo among different species at $B/C = 4$. $B = 0.04$ M, $C = 0.01$ M.

heteroatoms.[8,13–15] The diagram also tells us that (p,8,2) are weak. Notable amounts of isopolymolybdates exist even at such a low B/C ratio as 4. This type of weak heteropolyanions have also been found in the molybdophosphonate[14] and molybdoarsonate[15] systems.

Although we started ^{77}Se NMR measurements in order to fully characterize the H^+–MoO_4^{2-}–SeO_3^{2-} system, this was not possible with our spectrometer because of its limited sensitivity. Precipitation prevented us from preparing a solution of high B/C ratios with high Se content. We are planning a further investigation of this system using a spectrometer with a higher frequency.

REFERENCES

1. See for example: H. Kolshorn and H. Meier, *J. Chem. Res. (S)* 1977, 338 and refs cited therein.
2. H. Takahama and T. Sasaki, *Bull. Chem. Soc. Jpn.* 1983, **56**, 895.
3. G. Brauer, *Handbook of Preparative Inorganic Chemistry*, 2nd edn, p. 428. Academic Press, New York (1963).
4. P. Brauner, L. G. Sillén and R. Whiteker, *Arkiv Kemi* 1969, **31**, 365.
5. A. Yagasaki and Y. Sasaki, *Bull. Chem. Soc. Jpn.* 1987, **60**, 763.
6. A. Yagasaki, Ph.D. Thesis, The University of Tokyo (1987).
7. L. Pettersson, *Acta Chem. Scand. A* 1975, **29**, 677.
8. T. Ozeki, M.Sc. Dissertation, The University of Tokyo (1985).
9 (a) A. Rosenheim and L. Drause, *Z. Anorg. Chem.* 1921, **118**, 184; (b) W. Prandtl, *Z. Anorg. Chem.* 1913, **93**, 45.
10. H. Ichida, H. Fukushima and Y. Sasaki, *Nippon Kagaku Kaishi* 1986, 1521.
11. H. Ichida, T. Ozeki, A. Yagasaki and Y. Sasaki, manuscript in preparation.
12. I. D. Brown and K. K. Wu, *Acta Cryst. B* 1976, **32**, 1957.
13. L. Pettersson, I. Andersson and L.-Ö. Ohman, *Inorg. Chem.* 1986, **25**, 4726.
14. A. Yagasaki, I. Andersson and L. Pettersson, *Inorg. Chem.* 1987, **26**, 3926.
15. A. Yagasaki and Y. Sasaki, *Bull. Chem. Soc. Jpn* 1987, **60**, 3925.

Polyhedron Vol. 7, No. 12, pp. 1135–1136, 1988
Printed in Great Britain

0277-5387/88 $3.00+.00
Pergamon Press plc

COMMUNICATION

A RAPID AND DIRECT ELECTROCHEMICAL SYNTHESIS OF $K_2[MoOF_5]$

MUKUL C. CHAKRAVORTI* and DEBASIS BANDYOPADHYAY

Department of Chemistry, Indian Institute of Technology, Kharagpur-721302, India

(*Received* 25 *January* 1988; *accepted* 9 *February* 1988)

Abstract—A single-step synthesis of $K_2[MoOF_5]$ has been made by the oxidation of a sacrificial molybdenum anode in a solution containing 20% HF followed by the addition of KF. This electrosynthesis represents a significant improvement over the existing methods.

The preparation of oxo and μ-oxofluoro complexes of quinquevalent molybdenum (e.g. $K_2[MoOF_5]$, $Cs_2[Mo_2O_4F_4]$, $Cs_4[Mo_2O_4F_6]$ etc.) by chemical means starting from $MoO(OH)_3$ has been developed earlier in our laboratory.[1–3] We have now achieved a rapid single-step preparation of $K_2[MoOF_5]$ by electrochemical anodic dissolution of molybdenum metal in aqueous hydrofluoric acid. Although the electrochemical synthesis of chloro complexes by oxidation of a sacrificial metal anode is already known,[4,5] the electrosynthesis of analogous fluoro complexes does not appear to have been previously reported.

EXPERIMENTAL

Molybdenum metal was used as supplied by Johnson Matthey & Co. Ltd, U.K. in the form of a rod (diameter ~ 5 mm). All other chemicals used were of A.R. or G.R. quality of reputed manufacturers. The analysis of molybdenum, fluorine and potassium, the determination of the oxidation state of molybdenum, recording of spectra and measurement of magnetic susceptibility were made by the methods described earlier.[6,7]

Electrochemical procedure

The electric power was supplied by a dc power supply (Aplab, India). The experiment was performed in a 100 cm^3 polythene beaker fitted with a rubber stopper through which three polythene tubes were inserted. A molybdenum rod (weighed previously) and a platinum foil each connected with platinum wire electrical leads were inserted through two of the tubes. The tube containing the rod was filled up with mercury for easy contact with the lead. The third tube served to permit the escape of hydrogen gas generated at the cathode. 10 cm^3 of 20% aqueous hydrofluoric acid was placed in a beaker and the electrodes were dipped in the solution. The molybdenum rod and platinum foil were connected to the positive and negative terminals of the power supply, respectively. Completion of the circuit gave a current of 1.0 A for an applied voltage of 6 V. As the electrochemical reactions proceeded, hydrogen gas was evolved at the cathode and the solution gradually became greenish in colour and warm. The electrolysis was continued for 2.5 h. During the electrolysis, part of the anode disintegrated into small particles which deposited at the bottom of the vessel. The current remained almost steady. After switching off the circuit the solution was filtered and 2.0 g of potassium fluoride dissolved in a minimum volume of 20% HF was

* Author to whom correspondence should be addressed.

added to it. A green microcrystalline precipitate appeared within 2 min of stirring. This was filtered and dried by pressing between folds of filter paper followed by keeping it in a desiccator over sulphuric acid and sodium hydroxide pellets.

The molybdenum rod was washed with water followed by ether, dried in a desiccator and weighed.

RESULTS AND DISCUSSION

The characterization of the complex was made by the usual methods. Analysis gave, found: Mo, 32.8; F, 32.5; K, 27.5. Calc. for $K_2[MoOF_5]$: Mo, 33.6; F, 33.3; K, 27.3%.

The oxidation number of molybdenum in the complex has been found to be 4.98. The complex is paramagnetic with a μ_{eff} value of 1.62 BM at 26°C. The IR spectrum shows bands at 980(s), 943sh(w) and 910(m) cm^{-1} which is in agreement with the spectrum reported earlier.[1,2]

In a typical experiment 1.5 g of the metal was dissolved and 2.5 g of the product was isolated. The yield based on the weight of metal dissolved was about 56%. The electrochemical efficiency (the number of moles of metal dissolved per Faraday of electricity passed) was 0.16 mol F^{-1}. The deviation of this value from the theoretical value is attributed to the disintegration of the anode and the slight variation of current during the electrolysis.

Acknowledgements—One of the authors (D.B.) gratefully acknowledges the financial support given to him by the Council of Scientific and Industrial Research, India.

REFERENCES

1. M. C. Chakravorti and S. C. Pandit, *Inorg. Synth.* 1982, **21**, 170.
2. M. C. Chakravorti and S. C. Pandit, *J. Coord. Chem.* 1976, **5**, 85.
3. M. C. Chakravorti and A. K. Bera, *Transition Met. Chem.* 1983, **8**, 83.
4. M. J. Taylor and D. G. Tuck, *Inorg. Synth.* 1983, **22**, 135.
5. C. Oldham and D. G. Tuck, *J. Chem. Educ.* 1982, **59**, 420.
6. M. C. Chakravorti and S. C. Pandit, *Indian J. Chem.* 1971, **9**, 1306.
7. M. C. Chakravorti and S. C. Pandit, *J. Inorg. Nucl. Chem.* 1973, **35**, 3644; 1974, **36**, 2265.

Polyhedron Vol. 7, No. 12, p. 1137, 1988.
Pergamon Press plc. Printed in Great Britain.

CORRIGENDUM

Aqueous redox chemistry of dinuclear clusters. A mechanistic study of proton oxidative addition to the $Mo_2Cl_8^{4-}$ ion and the homogeneous reduction of $Mo_2(\mu-X)(\mu-Cl)_2Cl_6^{3-}$, X = H, Cl, by aqueous chromium(II). C. Mertis, M. Kravaritou, A. Shehadeh and D. Katakis (*Polyhedron,* Vol. 6, No. 11, pp. 1975–1980, 1987).

(i) The units (min^{-1}) for k_{obs} in Fig. 5 should be inserted.

(ii) The scale for the three lines in Fig. 4 is not the same. The corrections are: the value -1.0 corresponds to -6.5; values for the 6M line should be multiplied by 10^{-1}.

Polyhedron Vol. 7, No. 13, pp. 1139–1145, 1988
Printed in Great Britain

0277–5387/88 $3.00+.00
Pergamon Press plc

SPECTRAL IDENTIFICATION OF $Al_3Cl_{10}^-$ IN 1-METHYL-3-ETHYLIMIDAZOLIUM CHLOROALUMINATE MOLTEN SALT

C. J. DYMEK, JR. and J. S. WILKES

Frank J. Seiler Research Laboratory, U.S. Air Force Academy, Colorado Springs, CO 80840-6528, U.S.A.

and

M.-A. EINARSRUD and H. A. ØYE*

Institute of Inorganic Chemistry, The Norwegian Institute of Technology, 7034 Trondheim, Norway

(*Received* 24 *August* 1987; *accepted* 5 *January* 1988)

Abstract—The IR specular reflection of molten 1-methyl-3-ethylimidazolium (MEI) $Al_3Cl_{10}^-$ is reported. After elimination of vibrational bands due to MEI^+, $Al_2Cl_7^-$ and Al_2Cl_6, the following bands were assigned to $Al_3Cl_{10}^-$: 583, 540, 488, 424, 361, 293 and 174 cm^{-1}. MNDO–MOPAC calculations were carried out and the predicted frequencies and intensities agreed remarkably well with the experimental spectrum.

In molten mixtures of $AlCl_3$ with MCl (M^+ being an alkali ion or an organic cation), the anionic species Cl^-, $AlCl_4^-$ and $Al_2Cl_7^-$ are well recognized and the latter two have been characterized spectroscopically.[1–5] Evidence for the existence of minor amounts of higher polymers, $Al_nCl_{3n+1}^-$ with $n \geqslant 3$ has been found in melts with more than 66 mol % $AlCl_3$.[2,3,5,6,7,8] While $AlCl_4^-$, $Al_2Cl_7^-$ and Al_2Cl_6 are well characterized, only a few weak spectral bands or shoulders have been attributed to higher polymers. The stoichiometry of the higher polymers has also been uncertain. Generally the formation of higher polymers is more likely with larger M^+ cations.[3]

The two components 1-methyl-3-ethylimidazolium chloride (MEICl) and $AlCl_3$ are completely miscible. A recent thermodynamic study[9] of acidic mixtures ($X_{AlCl_3} > 0.5$) of MEICl and aluminum chloride showed a much stronger dependence of the $AlCl_3$ activity on melt composition than for alkali chloride–aluminum chloride mixtures. Vapour pressure measurements gave $AlCl_3$ activity as high as 0.53 at 76.7 mol % $AlCl_3$. However, with the addition of MEICl, the $AlCl_3$ activity drops off sharply to 0.30 and 0.14 for 73.8 and 70.5 mol % $AlCl_3$, respectively. A straightforward explanation of this behaviour is the presence of substantial amounts of $Al_3Cl_{10}^-$ and no other high polymers. Based on a thermodynamic model,[9] the following relative amounts were predicted at 250°C and 75 mol % $AlCl_3$: $Al_3Cl_{10}^- = 50\%$, $Al_2Cl_7^- = 33\%$ and $Al_2Cl_6 = 17\%$. The relative amount of $Al_3Cl_{10}^-$ in the MEICl–$AlCl_3$ melts is substantially higher than in alkali chloride–$AlCl_3$ melts. This melt should then provide an excellent opportunity to characterize the $Al_3Cl_{10}^-$ ion spectroscopically and at the same time serve as a check on the thermodynamic model.

EXPERIMENTAL

A melt with 25 mol % MEICl–75 mol % $AlCl_3$ and a pure MEICl melt were prepared.[10] The melts were added to a cell described in detail earlier[5] and their IR specular reflection spectra were obtained with a Bruker IFS 113v Fourier transform instrument. The spectra of these films (< 10 μm) were recorded after letting a piston press the melt against a diamond window (Type II A, D. Drukker and Zn). Thick samples (2–3 mm) were used as a ref-

*Author to whom correspondence should be addressed.

erence to avoid false band splitting.[11,12] The averaged spectra consisted of 400 single scans obtained with a DTGS detector at a resolution of 8 cm^{-1}. A 3.5 μm Mylar beam splitter was used in the frequency range 150–700 cm^{-1}.

RESULTS

Figure 1, curves (a) and (b) show the spectra of the melt having the stoichiometric composition $MEIAl_3Cl_{10}$ at 200°C. The melt film was slightly thicker for the lower spectrum. Figure 1, curve (c) gives the spectrum of MEICl at the same temperature. The goal of the present work was to characterize the Al-species, $Al_3Cl_7^-$, $Al_2Cl_{10}^-$ and Al_2Cl_6. Although the spectrum of MEICl was recorded over the range 4000–150 cm^{-1}, it is only shown here in the range 700–150 cm^{-1}, with the purpose of eliminating bands in the spectrum of $MEIAl_3Cl_{10}$ not belonging to Al-species. By comparing curves (b) and (c), the following bands in curve (b) can be eliminated as due to MEI^+: 643, possibly 616, 247, 228, 204 and 154 cm^{-1}. The remaining band frequencies are given in the figure. The following uncertainties in the band positions are estimated for the reflection spectra:

—2 cm^{-1} for narrow bands with medium or less intensity.
—5 cm^{-1} for broad bands, well defined shoulders and narrow bands with high intensity.
—10 cm^{-1} for very strong and broad bands and less defined shoulders.

The band positions are to some extent dependent upon the melt thickness.

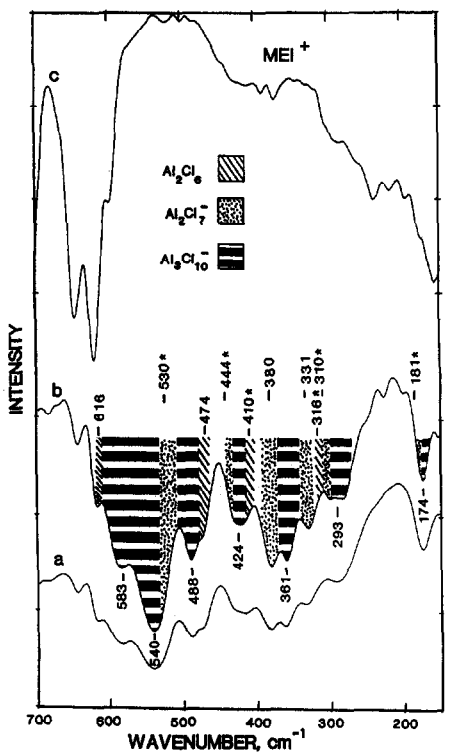

Fig. 1. IR reflectance spectra of a molten mixture of 25 mol % 1-methyl-3-ethylimidazolium chloride (MEICl) and 75 mol % aluminum chloride (a) and (b), and of MEICl (c) at 200°C. The (a) spectrum has been recorded on a melt with a slightly higher thickness than the melt in the (b) spectrum.

The assignment of peaks (or parts of broad bands) to Al_2Cl_6 and $Al_2Cl_7^-$ are based on previous analyses of inorganic melts.[3,13] The bands assigned to $Al_2Cl_7^-$ and Al_2Cl_6 which do not show up as a peak or a pronounced shoulder, but which are given based on previous evidence,[3,13] are marked with an asterisk.

In a previous IR study,[5] the $Al_3Cl_{10}^-$ ion was looked for in a NaCl–$AlCl_3$ melt having the composition $NaAl_3Cl_{10}$. Due to the lower stability of $Al_3Cl_{10}^-$ in this melt, the strong peak at 540 cm^{-1} only appeared as a shoulder, giving a frequency shift of the maximum to 533 cm^{-1}. A shoulder at 361 cm^{-1} was, however observed in agreement with one of the presently observed peaks.

Several Raman studies[2,3,6] have been performed on melts which are high in $AlCl_3$ content, and bands due to high polymers, i.e. $Al_3Cl_{10}^-$, have been reported. All the papers reported a peak in the region 390–395 cm^{-1} which we do not observe, although it may be hidden as a shoulder on the 380 cm^{-1} peak. In addition, peaks at 493 and 177 cm^{-1} [3] and 297 cm^{-1} [6] were reported. These frequencies correspond closely to frequencies found in the present IR study.

SPECTRAL CALCULATIONS

Semi-empirical molecular orbital calculations were carried out on the $Al_3Cl_{10}^-$ species to provide guidance in the analysis of the spectrum. The MNDO (Modified Neglect of Diatomic Overlap) model[14] as incorporated in the MOPAC program[15] was used. The MOPAC program has been successfully used in studying chloroaluminate species.[16] It readily calculates optimum geometries, heats of formation, force constants of normal modes and other molecular parameters from the input initial geometries. In this work, we also used MOPAC to calculate vibrational modes along with their frequencies and transition dipoles.

The initial geometry input for $Al_3Cl_{10}^-$ was constructed by simply adding an $AlCl_3$ group to one of the terminal Cls in the geometry of $Al_2Cl_7^-$.[16] The

most stable configuration was calculated to have a heat of formation of -589.8 kcal mol^{-1} and the structure shown in Fig. 2(a). The characteristic feature of the "stretched" structure is that atoms 1–5–6–7–10 are in a plane, and chlorines 2 and 11 are staggered relative to the central chlorines, 8 and 9. Thus the symmetry is C_{2v}.

It should be noted that the calculation is for an isolated gas phase molecule, while our interest is in $Al_3Cl_{10}^-$ in the liquid phase surrounded by an ionic environment. In previous work,[16] this environment was simulated by arranging ions in a cluster around the ion or ions of interest, significantly lengthening the time required for the computations. Calculations on reaction energetics were improved (by comparison with experimental data) by including surrounding ions. However, the calculated vibrational frequencies and normal modes were virtually unchanged. Therefore, in the present calculations on $Al_3Cl_{10}^-$, we did not attempt to simulate the ionic environment.

In the melt, $Al_3Cl_{10}^-$ is not expected to stay rigidly in the most stable configuration. The activation energies for rotation around the single bridge bond are small (about 1 kcal mol^{-1}) and so the $Al_3Cl_{10}^-$ will twist and be in several different conformations. In order to account for this twisting structure, in predicting the IR spectrum, calculations were performed for two other structures, "winged" and "cart" [Fig. 2(b), (c)]. The "winged" structure was obtained by positioning atoms 6–9–5–1 and 6–9–7–10 each in a plane. In the optimized geometry, the bonds 10–7 and 5–1 are twisted out of plane by 24 and 17°, respectively. The "cart" structure was optimized from an initial geometry in which atoms 1–5–6–7–10 formed a plane. The plane was retained (0.3° deviation), but the central and terminal chlorines were optimized in a staggered structure. The "winged" and the "cart" structures were 0.6 and 1.2 kcal, respectively, less stable than the stretched structure.

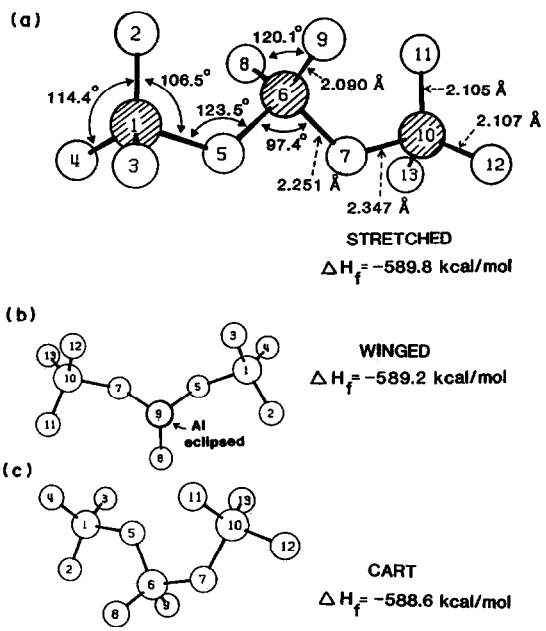

Fig. 2. The three optimized $Al_3Cl_{10}^-$ conformations for which calculations are carried out.

Table 1 gives calculated and experimental frequencies. The calculation is carried out for all three structures. The frequencies are given as bold face numbers in cm^{-1}. The numbers in parentheses refer to intensity. The experimental frequencies are listed as s—strong; m—medium; w—weak and sh—shoulder, while the calculated intensities are given as the square of the transition dipole multiplied by the frequency. Calculated stretching modes which contribute more than 10% to the total vibrational energy are listed. All 12 stretching frequencies are listed, but of the 21 bending modes, only those with intensities greater than one are given. The bonded atoms listed as m_1+m_2 signify stretching, and m_1-m_2 signify compression following the pictorial representations of the normal mode's output by MOPAC. The atom numbers refer to the structures given in Fig. 2.

In Table 1, column 4, the average values for the band locations and intensities are calculated. The values for the different models and the average do not give an exact description of the vibrations, but important features are illustrated. The band locations are found to be quite insensitive to the different conformations, while this is not the case for the intensities. Only for the vibrations that are calculated to be close together, i.e. the terminal antisymmetric and the outer symmetric bridge modes, do cross-overs in band location occur. Experimentally, both bands are found to be broad as expected from the calculations. Another noteworthy feature is the calculated strong increase in intensity for the terminal symmetric stretching modes when the structure is no longer "stretched".

In Fig. 3 calculated and experimental frequencies are compared. The strongest single mode, the 595 cm^{-1} "cart" mode, is set equal to 100 and the other intensities are given relative to this. A close correspondence is found between calculated and experimental values with respect to both band location and intensity. The calculated frequencies tend, however, to be a little higher than the experimental values.

The following comments apply to the bands given in cm^{-1} assigned to $Al_3Cl_{10}^-$:

Table 1. Calculated and experimental vibrations for $Al_3Cl_{10}^-$ as well as experimental vibrations for $Al_2Cl_7^-$ and Al_2Cl_6

I. "Stretched"		II. "Winged"		III. "Cart"		Ave. I, II, III	Experimental frequency	Main vibrational stretch modes
							616 (w)	Al_2Cl_6, terminal antisym.
605 (17.5)	6+9, 6−8	**601** (34.7)	6+9, 6−8	**595** (39.6)	6−9, 6+8	**600** (30.4)	**583** (m)	Central antisym.
581 (24.7)	10−11, 1−2 10+12, 10+13 1+3	**574** (14.9)	10+13, 10−11 10−12	**580** (18.3)	10+13, 1−2 10−11, 1+3			
578 (0.8)	1+2, 10−11 1−3, 1−4 10+13, 10+12	**577** (11.2)	1+2, 1−3 10+12	**579** (17.6)	1−2, 10+11 10−13, 1+3 1+4	**576** (55.4)	**540** (s)	Terminal antisym.
573 (10.0)	10+12, 10−13	**580** (26.8)	10+12, 10−11	**573** (16.9)	10+12, 10−11 10−13, 10+7			
570 (6.7)	1+4, 1−3	**571** (11.6)	1−4, 1+3 1+2	**574** (6.8)	1+4, 1−3 1−2, 1+5			
505 (5.0)	6+8, 6+9 6−7, 6−5	**510** (10.3)	6−8, 6−9 6+7, 6+5	**503** (11.3)	6−8, 6−9 6+5, 6+7	**506** (8.9)	**488** (m)	Central sym.
							474 (sh)	Al_2Cl_6, terminal sym.
425 (0.0002)	6−7, 6+6	**429** (0.6)	6−7, 6+5	**440** (5.1)	6−7, 6+5	**431** (1.9)		Inner, antisym. bridge w/outer Al-atoms counteracting

408 (0.1)	10+11, 10+12 10+13, 1+2 1+4, 1+3	**407** (4.5)	10+11, 10+13 10+12, 1+2 1+4, 1+3	**407** (8.0)	1−2, 1−3 1−4, 10−12	**407** (4.2)	**424** (m)	Terminal sym.
							380 (m)	$Al_2Cl_7^-$, terminal sym.
373 (27.0)	6+5, 6−7	**376** (32.4)	6+5, 6−7	**381** (24.8)	6+7, 6−5 10+13, 10+11	**377** (28.1)	**361** (m)	Inner, antisym. bridge w/reinforcement from outer Al-atoms
352 (0.4)	6+7, 6+5 10−7, 1−5	**353** (2.1)	6+5, 6+7 1−5, 10−7	**352** (4.8)	6+7, 10−7 6+5, 1−5	**352** (2.4)		Mainly inner sym. bridge
							331 (m)	$Al_2Cl_7^-$, antisym. bridge
311 (0.2)	1−5, 10−7	**306** (2.4)	1−5	**294** (3.6)	1+5	**299** (14.2)	**301** (m) **293** (m)	Mainly outer sym. bridge
293 (13.5)	10+7, 1−5	**290** (14.3)	10−7, 1+5	**302** (10.2)	10−7, 1+5 6−5		**287** (m)	Outer antisym. bridge
				176 (3.1)				
160 (0.4)		**163** (1.6)		**159** (1.2)		**161** (4.3)	**174** (w)	Bending mode mainly involving bridge
154 (1.8)		**160** (3.7)		**153** (1.2)				

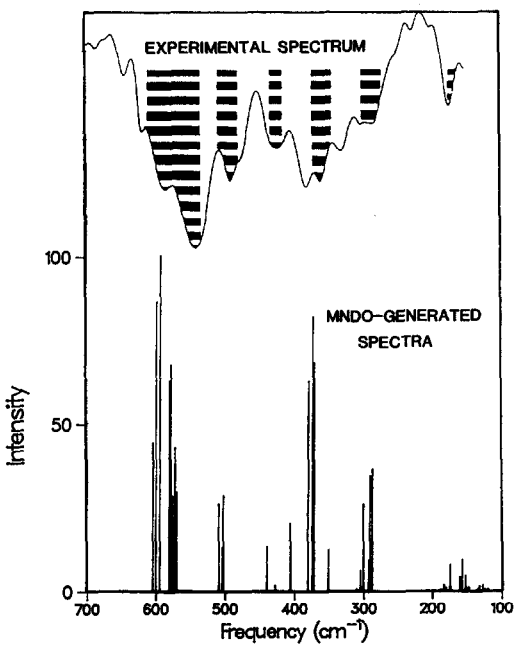

Fig. 3. Comparison of the experimental reflection spectrum with combined MNDO-generated spectra for the three structures given in Fig. 2.

583: the central antisymmetric stretching mode is found at the highest frequency as expected.

540: the four terminal antisymmetric stretching modes are calculated to be strong and close together with partial cross-overs. The experimental band is found to be broad and strong as expected.

488: the central symmetric stretching mode is also strong in accordance with calculations.

424: the terminal symmetric band is the only stretching mode for which the calculations predict a lower frequency. This mode is, however, expected to give the strongest interaction with the surroundings, with all six terminal chlorines vibrating. This interaction may well result in an increase of the experimental frequency relative to the calculated values. An alternative explanation is to assign the 424 cm^{-1} band to a combination of $Al_2Cl_7^-$, Al_2Cl_6 and the weak $Al_3Cl_{10}^-$ mode predicted at 431 cm^{-1}. The symmetric stretching mode is unobserved in the region, 390–395 cm^{-1}, where a Raman band has been reported.[2,3,6]

361: three inner bridge modes are predicted at 431, 377 and 352 cm^{-1}. Of these, the 431 and 352 modes are predicted to be weak. In accordance with this, only the inner antisymmetric bridge with intensity reinforcements from the outer Al atoms are clearly observed, while the two weak bands may be hidden by the 424 and 331 cm^{-1} bands, respectively.

293: this may be only one band, the splitting being
(304) caused by electronic noise. The band is due to
(287) outer symmetric and antisymmetric stretching, the cross-overs giving a broad band.

174: this band is due to bridge bending frequencies. The calculated frequencies are a little lower than the experimental.

CONCLUSION

The MNDO–MOPAC calculations predict the observed frequencies and intensities remarkably well, in spite of the fact that the model considers an isolated $Al_3Cl_{10}^-$ ion and has no adjustable parameters. The vibrational modes were assigned based on the empirical rules and comparison with $AlCl_4^-$, $Al_2Cl_7^-$ and Al_2Cl_6 before the MNDO model was applied. The MNDO vibrational analysis confirmed the results. This generally good agreement indicates that discrepancies between the theoretical and experimental spectra may be due to shifts in the experimental frequencies caused by interactions with surrounding ions, rather than to imperfections in the MNDO method.

The $Al_3Cl_{10}^-$ ion having low symmetry and shifting conformations is particularly rewarding to study by IR spectroscopy because all the modes become allowed. We were indeed able to assign 10 of the 12 calculated stretching modes and can probably also see the modes predicted at 432 and 352 cm^{-1} as part of the 424 and 331 cm^{-1} bands.

The present method of calculating intensity as the mean of three arbitrary but carefully chosen models can be improved. A future development of the MNDO–MOPAC calculation may be to generate conformations statistically and give the conformations weight according to their Boltzmann energy.

Finally, the spectra give a qualitative check on the conclusion of the thermodynamic study where the ratio of the species $Al_2Cl_7^-/Al_3Cl_{10}^-/Al_2Cl_6$ were predicted to be 2/2/1.[9] By comparing the present spectrum with the spectra for 67 and 100 mol % $AlCl_7$ in Fig. 6 in ref. 5 the predicted ratios are confirmed within the limits of uncertainty.

Acknowledgements—H. A. Øye gratefully acknowledge a National Research Council fellowship. Thanks are expressed to Jeff Boon for preparing the sample. Helpful discussions with Dr J. J. P. Stewart are much appreciated. We also thank Missy Landess for her prompt and expert word-processing of the manuscript.

REFERENCES

1. S. J. Cyvin, P. Klaeboe, E. Rytter and H. A. Øye, *J. Chem. Phys.* 1970, **52**, 2776.
2. G. Torsi, G. Mamantov and G. M. Begun, *Inorg. Nucl. Chem. Letters* 1970, **6**, 553.
3. E. Rytter, H. A. Øye, S. J. Cyvin, B. N. Cyvin and P. Klaeboe, *Inorg. Nucl. Chem.* 1973, **35**, 1185.
4. R. J. Gale and R. A. Osteryoung, *Inorg. Chem.* 1980, **19**, 2240.
5. J. Hvistendahl, P. Klaeboe, E. Rytter and H. A. Øye, *Inorg. Chem.* 1984, **23**, 706.
6. F. W. Poulsen, *J. Raman Spectros.* 1981, **11**, 302.
7. T. Matsumoto and K. Ichikawa, *J. Am. Chem. Soc.* 1984, **106**, 4316.
8. L. Heerman and W. D'Olieslager, *Inorg. Chem.* 1985, **24**, 4704.
9. C. J. Dymek Jr, C. L. Hussey, J. S. Wilkes and H. A. Øye, *Proc. Joint Int. Symp. Molten Salts*, The Electrochemical Society, Honolulu, 1987, **87-7**, 93.
10. J. S. Wilkes, J. A. Levisky, R. A. Wilson and C. L. Hussey, *Inorg. Chem.* 1982, **21**, 1263.
11. J. Hvistendahl, E. Rytter and H. A. Øye, *Appl. Spectroscos.* 1983, **37**, 182.
12. E. Rytter, *Spectrochim. Acta* 1987, **43A**, 523.
13. M.-A. Einarsrud, *Thesis Nr 52*, Institute of Inorganic Chemistry, The Norwegian Institute of Technology, p. 118 (1987).
14. M. J. S. Dewar and W. Thiel, *J. Am. Chem. Soc.* 1977, **99**, 4899.
15. J. J. P. Stewart, *Quantum Chem. Prog. Exchange Bull.* 1986, **6**, 91; QCPE Program 455, Version 3.1.
16. L. P. Davis, C. J. Dymek Jr, J. J. P. Stewart, H. P. Clark and W. J. Lauderdale, *J. Am. Chem. Soc.* 1985, **107**, 5041.

Polyhedron Vol. 7, No. 13, pp. 1147–1152, 1988
Printed in Great Britain

0277–5387/88 $3.00+.00
© 1988 Pergamon Press plc

COORDINATION COMPOUNDS OF ETHYLHYDRAZINE AND 2,2,2-TRIFLUOROETHYLHYDRAZINE; CRYSTAL AND MOLECULAR STRUCTURE OF DICHLOROTETRAKIS(2,2,2-TRIFLUOROETHYLHYDRAZINE) NICKEL(II)

AZILAH ABD. RAHMAN,* M. P. BROWN, MARJORIE M. HARDING, C. ELIZABETH KEGGAN and D. NICHOLLS†

Donnan Laboratories, The University, Liverpool L69 3BX, U.K.

(*Received* 21 *October* 1987; *accepted* 21 *January* 1988)

Abstract—Ethylhydrazine (EH) forms the complexes $MX_2(EH)_2$ (M = Co, Ni; X = Cl; M = Co, X = Br), $NiBr_2(EH)_2(H_2O)$ and $MX_2(EH)$ (M = Zn, Cd; X = Cl; M = Zn, X = Br). Spectroscopic evidence suggests that these all contain bridging hydrazine ligands, the cobalt and nickel complexes containing six coordinated metal atoms while the zinc and cadmium complexes are tetrahedral. 2,2,2-Trifluoroethylhydrazine (TFEH) in contrast, forms six coordinate complexes of the type $MX_2(TFEH)_4$ (M = Co, Zn, X = Br; M = Co, Ni, X = NCS; M = Ni, X = Cl) for which spectroscopic evidence points to unidentate coordination by the hydrazine. An X-ray crystal structure determination on $NiCl_2(TFEH)_4$ confirms that the hydrazine bonds to nickel through the NH_2 nitrogen only, in a tetragonal structure with axial chlorine atoms. One bis(TFEH) complex $ZnBr_2(TFEH)_2$ and one hexakis (TFEH) complex, $NiBr_2(TFEH)_6$, have also been isolated.

Hydrazine complexes of metal(II) ions are of two principal types. By far the more common are compounds of the type $MX_2(N_2H_4)_2$ in which the hydrazine is acting as a bidentate bridging ligand in a six coordinate structure around the metal.[1] Complexes containing unidentate hydrazine are less common; they can sometimes be prepared by crystallization from anhydrous hydrazine e.g. $[Co(N_2H_4)_6]Cl_2$.[2] The complexes $M(N_2H_4)_2(N_2H_3CO_2)_2$ (M = Zn, Mn, Co, Ni) also contain unidentate hydrazines along with bidentate hydrazine carboxylate ligands.[3,4] With mono-substituted hydrazine ligands, e.g. methylhydrazines[5] and phenylethylhydrazine,[6] the bridging mode of bonding again predominates, but one remarkable complex of phenylhydrazine,[7] $[(\eta^5\text{-}C_5H_5)Mo(NO)I(NH_2NHPh)]_2[BF_4]_2$ represents the only established example of a hydrazine acting as a chelating ligand. With disubstituted hydrazines such as N,N-dimethylhydrazine, $Me_2N^1N^2H_2$, steric and electronic effects become important; the ligand is known to act as unidentate through N^1 in $CoCl_2(Me_2NNH_2)_2$,[2] unidentate through N^2 in $[RuH(cod)(NH_2NMe_2)]_3[PF_6]$[8] and bridging in $[RuCl(H)(cod)]_2(NH_2NMe_2)$[9] (cod = cyclo-octa-1,5-diene).

In this paper we report on attempts to prepare complexes of the monosubstituted hydrazines, ethylhydrazine (EH) and 2,2,2-trifluoroethylhydrazine (TFEH). These monosubstituted hydrazines $RNHNH_2$ differ in the relative electron withdrawing effect of the two R groups CH_3CH_2 and CF_3CH_2; this is likely to affect their relative basicities and tendencies to bond in a bridging fashion. In order to confirm the spectroscopic evidence for the mode of bonding of TFEH, a crystal structure determination has been carried out on $[Ni(TFEH)_4Cl_2]$.

EXPERIMENTAL

Experimental techniques were as described previously[10] except that reflectance spectra were re-

* Present address: Pusat Asasi Sains, University of Malaya, Kuala Lumpur, Malaysia.

† Author to whom correspondence should be addressed.

Table 1. Complexes of ethylhydrazine (EH) and 2,2,2-trifluoroethylhydrazine (TFEH): colours and analytical data

Complex	Colour	Elemental analysis[a] (%) C	H	N	M
$CoCl_2(EH)_2$	Pink	19.1 (19.2)	6.3 (6.4)	21.3 (22.4)	23.5 (23.6)
$CoBr_2(EH)_2$	Pink	14.5 (14.2)	4.7 (4.7)	16.5 (16.5)	17.1 (17.4)
$NiCl_2(EH)_2$	Blue	19.2 (19.2)	6.4 (6.4)	22.2 (22.4)	23.2 (23.5)
$NiBr_2(EH)_2(H_2O)$	Blue–green	13.2 (13.5)	4.6 (5.0)	15.9 (15.7)	16.6 (16.5)
$ZnCl_2(EH)$	White	12.1 (12.2)	3.9 (4.1)	13.5 (14.3)	33.9 (33.3)
$ZnBr_2(EH)$	White	8.6 (8.4)	2.8 (2.8)	9.5 (9.8)	23.3 (22.9)
$CdCl_2(EH)$	White	9.7 (9.9)	3.3 (3.3)	11.0 (11.5)	46.6 (46.2)
$CoBr_2(TFEH)_4$	Orange	18.2[b] (14.2)	2.8 (3.0)	16.6 (16.6)	8.7 (8.7)
$Co(NCS)_2(TFEH)_4$	Pink	18.3 (19.0)	3.2 (3.2)	22.2 (22.2)	—
$NiCl_2(TFEH)_4$	Blue	16.5 (16.4)	3.3 (3.4)	18.8 (19.1)	9.9 (10.0)
$Ni(NCS)_2(TFEH)_4$	Violet	19.0 (19.0)	3.3 (3.2)	21.7 (22.2)	9.3 (9.3)
$NiBr_2(TFEH)_6$	Blue	16.6 (16.0)	3.1 (3.3)	17.6 (18.6)	—
$ZnBr_2(TFEH)_2$	White	10.3 (10.6)	2.2 (2.2)	11.9 (12.4)	—
$ZnBr_2(TFEH)_4$	White	14.3 (14.1)	3.1 (2.9)	15.5 (16.4)	—

[a] Theoretical percentages in parentheses.
[b] Because of the poor C figure, F was estimated; found, 33.7 (33.8).

corded on a Perkin–Elmer 330 spectrophotometer over the range 40,000–6,600 cm^{-1}.

Anhydrous cobalt(II) halides were prepared by dehydration of the hydrated salts at 100°C *in vacuo*. Ethylhydrazine was prepared via Fischer's synthesis as modified by Condon and Thakker,[11] it was dried by distillation from barium oxide. 2,2,2-Trifluoroethylhydrazine was obtained as a 70% aqueous solution (ex Aldrich) and was used as such.

The complexes (Table 1) were prepared from the metal salts and appropriate ligand in a variety of solvents. No single solvent was found satisfactory for the preparation of all the complexes so that their isolation proved more difficult than that of complexes of hydrazine and methylhydrazine.[5]

Ethanol was the most commonly used preparative solvent for complexes of EH but ether or water usually proved better for the precipitation of pure complexes of TFEH. Thus the EH complexes of cobalt and nickel halides were prepared by heating, under reflux, ethanolic solutions of the metal halide (anhydrous cobalt halides were necessary but hydrated nickel halides gave satisfactory results) with an excess of the ligand under an atmosphere of nitrogen [to prevent oxidation of cobalt(II)]. The complexes either precipitated immediately or upon cooling the mixtures to 0°C. They were filtered off, washed with ethanol and ether and dried *in vacuo*. An ethanol–ether mixture (1 : 1) was found to be the best medium from which to precipitate the zinc complexes of EH. The preparation of $[Ni(TFEH)_4Cl_2]$ is fully described below because of its importance in this paper. The other TFEH complexes were prepared, however, using concentrated solutions of the metal salts in ether, ($CoBr_2(TFEH)_4$ and $ZnBr_2(TFEH)_2$), or water, ($Co(NCS)_2(TFEH)_4$, $Ni(NCS)_2(FTEH)_4$, $NiBr_2(TFEH)_6$) as the crystallization medium. The zinc complex $ZnBr_2(TFEH)_4$ was obtained by precipitation from an ethereal solution using ethanol. In all cases an excess of the ligand was used (i.e. > 6 : 1 ligand : metal); when the metal salts were in excess, only impure compounds or mixtures were isolated.

Preparation of $[Ni(TFEH)_4Cl_2]$

Nickel(II) chloride hexahydrate (0.48 g) was dissolved in hot ethanol (15 cm^3) and TFEH (2 cm^3) was slowly added until a dark blue solution was obtained. This was heated to boiling and then allowed to cool in a refrigerator for several days. The bright blue crystals which had grown were filtered off washed with ethanol and ether and dried *in vacuo*.

Crystal and molecular structure of $[Ni(TFEH)_4Cl_2]$

The material as prepared above contained suitable crystals for X-ray structure determination. Preliminary oscillation and Weissenberg photographs indicated a triclinic crystal; the intensities of 1540 unique reflections, to $\theta_{max} = 60°$, were recorded on a Stoe Siemens AED2 diffractometer at Edinburgh University, for a crystal of dimensions $0.4 \times 0.4 \times 0.2$ mm^3.

Table 2. Magnetic moments, molar conductivities and electronic spectra of ethylhydrazine (EH) and 2,2,2-trifluoroethylhydrazine (TFEH) complexes

Complex	Magnetic moments μ_{eff}(BM) at 20°C	Molar conductivities λ (Ω^{-1} mol^{-1} cm^3)	Electronic spectra ($cm^{-1} \times 10^3$) solid state (reflectance)	Solution spectra [ε ($lmol^{-1}$ cm^{-1}) in parentheses]
$CoCl_2(EH)_2$	4.97	[a]	35.7, 27.8sh, 20.2, 19.4sh, 17.0sh, 8.4	[a]
$CoBr_2(EH)_2$	5.03	[a]	35.3, 20.9, 19.6, 18.7sh, 16.3sh, 8.7	[a]
$NiCl_2(EH)_2$	3.12	[a]	34.5, 26.0, 15.5, 9.0	[a]
$NiBr_2(H_2O)(EH)_2$	3.41	[a]	34.1, 25.3, 17.1sh, 15.5, 8.4	[a]
$ZnCl_2(EH)$	Diamagnetic	[b] 7.9	36.6	
$CdCl_2(EH)$	Diamagnetic	[b] 12.8	38.6	
$COBr_2(TFEH)_4$	3.81		31.0, 22.2, 19.8sh, 11.6, 7.9	
$Co(NCS)_2(TFEH)_4$	5.39	[a]	34.1, 21.6sh, 20.6, 9.8	
$NiCl_2(TFEH)_4$	3.30	[c] 17.8 [d] 1.2	27.4, 17.4, 12.9sh, 10.6, 8.7	[c] 26.7(13), 16.4(7.5) 8.8(4.7)
$Ni(NCS)_2(TFEH)_4$	3.09	[d] 10.8	27.8sh, 18.0, 10.8	[d] 17.5(16), 10.6(13)
$NiBr_2(TFEH)_6$	3.49	[d] 6.3	obsc., 17.4, 10.5	
$ZnBr_2(TFEH)_2$	Diamagnetic	[a]	35.1	
$ZnBr_2(TFEH)_4$	Diamagnetic	[a]	36.1	

[a] Insoluble in suitable solvents.
[b] $\sim 10^{-3}$ M in DMSO.
[c] $\sim 10^{-3}$ M in acetonitrile.
[d] $\sim 10^{-3}$ M in nitromethane.
sh = shoulder.
obs = obscured under charge transfer band.

The structure was solved from a nickel phased electron density map and then refined using SHELX76;[12] the assumption of space group $P\bar{1}$ proved satisfactory. Hydrogen atoms were placed at stereochemically expected positions and their coordinates refined with N—H and C—H distances restrained. All non-hydrogen atoms were treated as anisotropic. Unit weights were used. Refinement converged to $R = 0.063$, for 1505 reflections with $|I| > 3\sigma(I)$. The largest peaks in the final electron density difference map are *ca* 0.4 e A^{-3}, but appear to have no chemical significance.

*Crystal data**

Crystals of $C_8H_{20}Cl_2F_{12}N_8Ni$, MW 585.75 are triclinic, with $a = 5.864(1)$, $b = 8.923(1)$, $c = 11.016(2)$ Å, $\alpha = 101.23(1)$, $\beta = 94.38(1)$, $\gamma = 100.68(1)°$, $U = 551.78$ Å^3, $D_m = 1.78$ g cm^{-3}, $Z = 1$, $D_x = 1.763$ g cm^{-3}. Space group $P\bar{1}$, Cu-K_α radiation, $\lambda = 1.5418$ Å, $\mu = 46.52$ cm^{-1}.

* Atomic coordinates, tables of thermal parameters, and observed and calculated structure factors have been deposited with the Editor as supplementary data; atomic coordinates have also been deposited with the Cambridge Crystallographic Data Centre.

RESULTS AND DISCUSSION

Ethylhydrazine complexes of cobalt(II), nickel (II), zinc(II) and cadmium(II) (Table 1) have been isolated. When iron(III) chloride or bromide in ethanolic solution were treated with the ligand, only black oils were obtained and copper(II) chloride, when similarly treated, gave only a white precipitate of copper(I) chloride. The pink cobalt(II) complexes $CoX_2(EH)_2$ have magnetic moments and electronic spectra (Table 2) typical of pseudo-octahedral complexes; the bands around 8,500 cm^{-1} being assigned to the $^4T_{1g} \rightarrow {}^4T_{2g}$ transition, the bands at 17,000 (chloride) and 16,300 cm^{-1} (bromide) to the $^4T_{1g} \rightarrow {}^4A_{2g}$ transition and those at 20,200 (chloride) and 19,600 cm^{-1} (bromide) to the $^4T_{1g} \rightarrow {}^4T_{1g}$(P) transition. These complexes were not indefinitely stable in dry air; they slowly changed colour first to violet and then to blue. The reflectance spectra recorded during these changes showed the slow disappearance of the bands in the 19–20,000 cm^{-1} region and the growth of a band

at 15,200 (chloride) or 14,400 cm^{-1} (bromide) (assignable to the $^4A_2 \rightarrow {}^4T_1(P)$ transition in a tetrahedral complex) and the formulae of the complexes approached $CoX_2(EH)$. A similar effect was observed when $CoBr(EH)_2$ was heated *in vacuo* to 100°C for 24 h; the blue residue had an empirical formula close to $CoBr_2(EH)$ and gave the same spectrum as the blue material obtained at room temperature. Thus the bis(ethylhydrazine) complexes appear to evolve 1 mol of ligand and the cobalt to change from an octahedral to a tetrahedral environment. A similar transformation was noted for cobalt(II) complexes of phenelzine.[6] Curiously it was not possible to isolate pure mono (ethylhydrazine) complexes from solutions containing an excess of cobalt(II). The spectral and magnetic data on the bis(ethylhydrazine)nickel(II) complexes again clearly show pseudo-octahedral coordination around the nickel, the three peaks being assigned to the transitions $^3A_{2g} \rightarrow {}^3T_{2g}$ (~ 9000 cm^{-1}), $^3A_{2g} \rightarrow {}^3T_{1g}(F)$ ($\sim 15{,}500$ cm^{-1}) and $^3A_{2g} \rightarrow {}^3T_{1g}(P)$ ($\sim 26{,}000$ cm^{-1}). There is evidence of splitting of the $^3T_{1g}(F)$ band in the bromide complex arising from tetragonality ($^3B_{1g} \rightarrow {}^3E_g$ and $^3B_{1g} \rightarrow {}^3A_{2g}$ transitions). The positions of these transitions are as expected for a NiN_4X_2 chromophore, i.e. very close to those found in $Ni(py)_4Cl_2$,[13] so that our complexes must contain bridging ethylhydrazine. The IR spectrum of $NiBr_2(EH)_2(H_2O)$ confirms that the water molecule is present as lattice water.

The IR spectra of the bis(ethylhydrazine) complexes of cobalt(II) and nickel(II) are similar. The shift in the N—N stretching band (Table 3) from 1110 cm^{-1}, observed for the free ligand, to around 1170 cm^{-1} in the complexes indicates a bridging mode for the hydrazine. A similar shift in ν(N—N) is observed when hydrazine becomes a bridging ligand.[14] The M—Cl stretches in these complexes are in the region usually found[15] for terminal metal–chlorine bonds in six coordinate complexes. The non-appearance of ν(M—Br) above 200 cm^{-1} is also expected in such a structure. It is almost certain, therefore, that these complexes possess a polymeric structure with bridging ethylhydrazines and terminal halides as found in $Co(N_2H_4)_2Cl_2$[1] and $Co(MeNHNH_2)_2Cl_2$.[2]

A less likely, but possible structure for these bis (ethylhydrazine) complexes is one containing bidentate ethylhydrazine(2−) ligands. Such a bonding mode has been found recently[16] in $[VCl_2(H_2NNMePh)_2(NNMePh)]Cl$ and the scarcity of bis(trifluoroethylhydrazine) complexes (see later) may be attributable to the lesser tendency to form hydrazide(2−) complexes arising from the presence of the electron withdrawing CF_3 groups on the ligand. In nickel and cobalt chemistry however, the occurrence of η^{2-}-NNHEt ligands in six coordinate complexes containing terminal metal–halogens would require unusually high oxidation states for the metals. The general insolubility of the complexes also supports the preferred polymeric structure.

Mono(ethylhydrazine) complexes are formed by zinc chloride. These complexes show, (Table 3), ν(M—X) in the regions expected for terminal halogens in tetrahedral structures[15] while the ν(N—N) bands are in similar positions to those of the cobalt

Table 3. Some important IR bands in complexes of ethylhydrazine (EH) and 2,2,2-trifluoroethylhydrazine (TFEH)

Compound	ν(CN)	ν(NN)	ν(CS)	δ(NCS)	ν(MN)	ν(MX)
EH		1110				
$CoCl_2(EH)_2$		1175			295, 279	251, 249
$CoBr_2(EH)_2$		1175			288, 280	
$NiCl_2(EH)_2$		1179			302, 280	250
$NiBr_2(EH)_2(H_2O)$		1172				
$ZnCl_2(EH)$		1169			338	325, 278
$ZnBr_2(EH)$		1164			382	260, 255
$CdCl_2(EH)$		1162			375	340, 310
TFEH		1148				
$CoBr_2(TFEH)_4$		1145			261, 230	
$Co(NCS)_2(TFEH)_4$	2070	1150	790	470, 450	230	
$NiCl_2(TFEH)_4$		1153			275	238
$Ni(NCS)_2(TFEH)_4$	2090	1160	795, 781	471	258	
$NiBr_2(TFEH)_6$		1158			290, 275	
$ZnBr_2(TFEH)_2$		1152			360	230
$ZnBr_2(TFEH)_4$		1162			370	

and nickel complexes. These complexes thus probably contain tetrahedrally coordinated zinc and cadmium atoms in polymeric structures with bridging ethylhydrazine. The polymeric structure may be broken down in dimethylsulphoxide in which the compounds behave as non-electrolytes.

Trifluoroethylhydrazine formed complexes less readily then hydrazine,[2] methylhydrazines,[5] ethylhydrazine and phenylethylhydrazine,[6] the reactions generally requiring concentrated solutions of the metal salt and heat. Even then precipitation and crystal growth were slow. This is most likely to be due to the lower basicity of the hydrazine which results from the electron withdrawing effect of the trifluoromethyl group. As with ethylhydrazine, an excess of the ligand was necessary in order to isolate pure complexes. In contrast to the reactions of hydrazine however, trifluoroethylhydrazine yielded bis(ligand) complexes only rarely (Table 3); several tetrakis(TFEH) complexes have been isolated and one hexakis(TFEH) complex. Further, some of these complexes are soluble in nitromethane in which they behave as weak or non-electrolytes. It seems likely therefore that the TFEH complexes are not polymeric and that only unidentate TFEH is present. The electronic spectra of the cobalt(II) tetrakis(TFEH) complexes are clearly indicative of six coordination around the cobalt; the 9,800 cm^{-1} peak in $Co(NCS)_2(TFEH)_4$ assigned to the $^4T_{1g} \rightarrow {}^4T_{2g}$ transition is in fact split in $CoBr_2(TFEH)_4$ into the two components at 11,560 (^4E_g) and 7,900 cm^{-1} ($^4B_{2g}$) expected in a tetragonal field. The magnetic moment of this complex is surprisingly low at room temperature; it may arise from an equilibrium between spin states as has been observed in similar tetragonal complexes such as $CoBr_2$(diacetyldihydrazone).[17] The similarity of the ligand field strengths of —NCS and TFEH again result in no tetragonal splitting being observed in $Ni(NCS)_2(TFEH)_4$. With the chloro complex $NiCl_2(TFEH)_4$ however the transitions to the ^3E_g (8,700 cm^{-1}), $^3B_{2g}$ (10,600 cm^{-1}), $^3A_{2g}$ (12,900 cm^{-1}) and ^3E_g (17,400 cm^{-1}) are all visible resulting from a tetragonal D_{4h} structure. The hexakis(TFEH) complex of nickel(II) bromide shows no splitting in its spectral bands which are in very similar positions to those in $[Ni(MeCN)_6]^{2+}$;[18] it may therefore contain the $[Ni(TFEH)_6]^{2+}$ cation. Because of its surprisingly low conductivity in nitromethane we carried out conductivity studies over the concentration range 10^{-3}–10^{-6} M and found that the Onsager plot of Λ_M against C (C = concentration in gram moles per litre) has the characteristic curve shape found for weak electrolytes. The complex is thus heavily ion-paired at the higher concentration.

Some important IR bands in complexes of TFEH are given in Table 3. In the free ligand we assign the band at 1148 cm^{-1} to ν(N—N) (bands at 1305 and 1268 cm^{-1} being assigned to C—F stretching bands). The complexes show only a slight shift to higher frequencies for this band indicating that the TFEH is bonded from one nitrogen atom only. The complexes $Co(NCS)_2(TFEH)_4$ and $Ni(NCS)_2(TFEH)_4$ exhibit bands assignable to ν(CN), ν(CS) and δ(NCS) in the regions characteristically found[19] with N-bonded thiocyanates. Zinc bromide curiously forms a bis- and a tetrakis (TFEH) complex; the IR spectra imply (through the presence and absence of ν(Zn—Br) that these complexes may be tetrahedral and octahedral, respectively.

In order to provide unambiguous proof of structure, an X-ray diffraction study has been carried out on $NiCl_2(TFEH)_4$. The compound is confirmed to be $NiCl_2(H_2N \cdot NH \cdot CH_2 \cdot CF_3)_4$ with molecular

Table 4. Selected interatomic distances (Å) and angles (°) in $NiCl_2(H_2N \cdot NH \cdot CH_2 \cdot CF_3)_4$

Ni(1)—Cl(1)	2.444(2)
Ni(1)—N(1)	2.091(6)
Ni(1)—N(11)	2.120(5)
N(2)—N(1)	1.427(8)
N(2)—C(3)	1.43(1)
C(3)—C(4)	1.46(1)
C(4)—F(5)	1.36(1)
C(4)—F(6)	1.30(1)
C(4)—F(7)	1.32(1)
N(11)—N(12)	1.44(1)
N(12)—C(13)	1.45(1)
C(13)—C(14)	1.47(1)
C(14)—F(15)	1.33(1)
C(14)—F(16)	1.34(1)
C(14)—F(17)	1.35(1)
Cl(1)—Ni(1)—N(1)	89.0(2)
Cl(1)—Ni(1)—N(11)	89.1(1)
N(1)—Ni(1)—N(11)	91.8(2)
N(1)—N(2)—C(3)	115.0(6)
Ni(1)—N(1)—N(2)	115.3(4)
N(2)—C(3)—C(4)	112.6(7)
Ni(1)—N(11)—N(12)	114.4(4)
N(11)—N(12)—C(13)	114.9(5)
N(12)—C(13)—C(14)	115.4(6)
Cl(1)—Ni(1)—N(1)—N(2)	−52.9(4)
N(11)—Ni(1)—N(1)—N(2)	36.2(4)
Cl(1)—Ni(1)—N(11)—N(12)	−142.8(4)
C(3)—N(2)—N(1)—Ni(1)	168.4(5)
N(1)—N(2)—C(3)—C(4)	84.8(8)
N(2)—C(3)—C(4)—F(5)	−60.6(10)
Ni(1)—N(11)—N(12)—C(13)	−161.8(4)
N(12)—C(13)—C(14)—F(15)	−61.4(9)

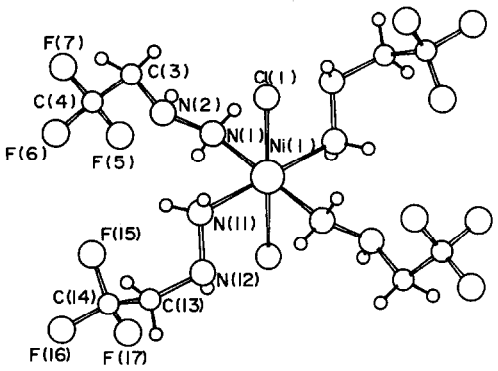

Fig. 1. A view of the $NiCl_2(TFEH)_4$ molecule (hydrogen atoms are shown unlabelled).

symmetry $\bar{1}(i)$ and octahedrally coordinated nickel; the molecule is illustrated in Fig. 1. The hydrazine is seen to be unidentate through the more basic NH_2 nitrogen atom. Selected bond lengths and angles are given in Table 4 and it is seen that the two chemically equivalent but crystallographically inequivalent ligands are not significantly different from each other or from expected values.

Acknowledgement—We are grateful to Dr R. O. Gould, Edinburgh University for recording the intensity data.

REFERENCES

1. A. Ferrari, A. Braibanti, G. Bigliardi and F. Dallavalle, *Acta Cryst.* 1965, **19**, 548.
2. D. Nicholls, M. Rowley and R. Swindells, *J. Chem. Soc.* (*A*) 1966, 950.
3. A. Ferrari, A. Braibanti, G. Bigliardi and A. M. Lanfredi, *Z. Krist* 1965, **122**, 259.
4. E. N. Maslen, C. L. Ralston, B. W. Skelton and A. H. White, *Australian J. Chem.* 1975, **41**, 739.
5. A. Anagnostopoulos and D. Nicholls, *J. Inorg. Nuclear Chem.* 1976, **38**, 1615.
6. Azilah Ab. Rahman, David Nicholls and John M. Tsangaris, *J. Coord. Chem.* 1986, **14**, 327.
7. N. A. Bailey, P. D. Frisch, J. A. McCleverty, N. W. J. Walker and J. Williams, *J. Chem. Soc., Chem. Commun.* 1975, 350.
8. T. V. Ashworth, M. J. Nolte and E. Singleton, *J. Chem. Soc., Dalton Trans.* 1978, 1040.
9. T. V. Ashworth, M. J. Nolte, R. H. Reimann and E. Singleton, *J. Chem. Soc., Dalton Trans.* 1978, 1043.
10. C. N. Elgy and D. Nicholls, *J. Inorg. Nucl. Chem.* 1981, **43**, 2025.
11. F. E. Condon and D. C. Thakkar, *Org. Prep. Proced. Int.* 1973, **5(S)**, 219.
12. G. M. Sheldrick, SHELX program for crystal structure determination, University Chemical Laboratory, Cambridge (1976).
13. J. S. Merriam and J. R. Perumareddi, *J. Phys. Chem.* 1975, **79**, 142.
14. D. N. Sathyanarayana and D. Nicholls, *Spectrochim. Acta.* 1974, **34A**, 1445.
15. J. R. Ferraro, *Low Frequency Vibrations of Inorganic and Coordination Compounds.* Plenum Press, New York (1971).
16. J. Bultitude, L. F. Larkworthy, D. C. Povey, G. W. Smith, J. R. Dilworth and G. J. Leigh, *J. Chem. Soc., Chem. Commun.* 1986, 1748.
17. M. R. Harrison and D. Nicholls, *Transition Met. Chem.* 1984, **9**, 144.
18. B. J. Hathaway and D. G. Holah, *J. Chem. Soc.* 1964, 2400.
19. K. Nakamoto, *Infrared and Raman Spectra of Inorganic and Coordination Compounds*, 3rd Edn. John Wiley (1978).

Polyhedron Vol. 7, No. 13, pp. 1153–1158, 1988
Printed in Great Britain

0277–5387/88 $3.00+.00
© 1988 Pergamon Press plc

INVESTIGATION OF THE EFFECT OF THE AMINOCARBOXYLATO CHELATE CONFORMATION ON THE OPTICAL ACTIVITY OF THE *CIS*(NO_2),*TRANS*(NH_2)-BIS(AMINOCARBOXYLATO)DINITROCOBALT/ATE(III) ISOMERS

N. JURANIĆ, M. J. MALINAR, P. N. RADIVOJŠA, SNEŽANA ZARIĆ, D. VUČELIĆ, MILANKA VUČIĆ and M. B. ČELAP*

Institute of Chemistry, Faculty of Sciences, University of Beograd and Institute of General and Physical Chemistry, Beograd, Yugoslavia

(*Received* 22 *December* 1987; *accepted* 21 *January* 1988)

Abstract—In the *cis*(NO_2),*trans*(NH_2)-bis(aminocarboxylato)dinitrocobalt/ate(III) isomers, containing glycinato, S-alaninato, S-*n*-valinato, S-valinato, S-*n*-leucinato, S-leucinato, S-*i*-leucinato and S-arginine ligands, respectively, it was found that in the Λ-isomers circular dichroic spectra are determined by the configurational contribution to the optical activity. This is connected in the case of optically active ligands with the chair conformation of the chelate rings and the equatorial position of the ring side group. In the Δ-isomers, λ-conformation of the aminocarboxylato chelate rings and the axial position of the ring side groups induce a considerable contribution to the optical activity, which varies from complex to complex. NMR spectroscopy showed that these variations are related to small changes in the chelate ring conformation in such a way that a more axial position of a ring side group induces a larger contribution. The λ-conformation of a S-aminocarboxylato chelate ring induces a large negative contribution to the circular dichroism of the investigated complexes.

In aminocarboxylatocobalt(III) complexes, the optical activity may arise[1] from the configurational dissymetry of the chelate rings (assymmetry of donor atoms[2]) arrangement, the conformational assymmetry of a chelate ring and from the vicinal effect of an assymmetric centre in an optically active aminocarboxylato ligand. The vicinal contribution to the optical activity in aminocarboxylatocobalt(III) complexes has been considered as an important contribution, while the conformational contribution of an α-aminocarboxylato ring was considered to be of small importance, due to the almost planar arrangement of ring atoms.[3–10] However, in order to extract the vicinal contribution from the total optical activity of a complex, i.e. to separate it from the configurational contribution, an additive and equal vicinal contribution to the optical activity of a diastereomeric pair of a complex has been assumed.[3,4,8] Such an approach has not allowed the investigation of the effect of unequal steric constraints, imposed on the aminocarboxylato ligand in a diastereomeric pair of a complex, on its contribution to the optical activity. It seems that this effect was usually small, which inhibited investigations in this direction. But in the *cis*(NO_2),*trans*(NH_2)-bis(aminocarboxylato)dinitrocobaltate(III) complexes, which contain sterically demanding nitro groups as ligands, a large difference in the effect of aminocarboxylato ligand conformation on the optical activity of their diastereomers has been suggested.[9] Because of that, this series of complexes seems to allow investigation of the effect of the aminocarboxylato chelate ring conformation on the optical activity. However, in earlier work,[9] the optical isomers of *cis*-(NO_2),*trans*(NH_2) - bis(aminocarboxylato)dinitrocobaltate(III) complexes have been separated by fractional crystallization,† which preclude the isolation of optically pure substances and

* Author to whom correspondence should be addressed.

† Their absolute configuration was assumed from circular dichroic spectra[9] and later confirmed by crystal structure analysis.[11,12]

the corresponding CD data, which are essential for the above mentioned investigation. We have decided to devise a new procedure for the preparation of some of the optically pure isomers and to use them for such an investigation.

RESULTS AND DISCUSSION

Circular dichroic spectra of the investigated isomers are presented in Figs 1 and 2, and in Table 1 the wavelength and dichroism of their dichroic maximum in the region of the first *d–d* electronic transition are tabulated. The results differ considerably from those previously reported,[9] mainly due to the higher optical purity of the optical isomers produced in the present work.

As is seen, the diastereomers having a positive sign Cotton effect in the region of the first *d–d* transition and having the Λ-absolute configuration, exhibit approximately the same CD spectra, irrespective of the type of optically active aminocarboxylato ligand used. There is also only a small difference between the corresponding spectrum of the analogous glycinato complex, which does not possess the vicinal contribution, and the spectra of the complexes with S-aminocarboxylato ligands. The situation is quite different with those diastereomers having a dominant negative Cotton effect and Δ-absolute configuration. In these cases maximal dichroism is more than doubled in the transition from the glycinato to S-valinato or S-isoleucinato complexes.

To understand the observed data it is necessary to consider the structures of the investigated diastereomers,[11-12] general features of which are presented in Fig. 3. In the Λ-isomers the chelate ring side group is strongly repulsed by the bulk nitro group and occupies the equatorial position; because of this the chelate ring adopts the strained chair conformation. In the isomers of Δ-absolute configuration the chelate ring side group is not in the vicinity of a nitro group but it is orientated towards a relatively small coordinated oxygen atom, and therefore the chelate ring adopts a slightly puckered λ-conformation, with the side group in an axial position. This arrangement is not strained, since the same ring conformation is found in a structurally closely related glycinato complex.[13]

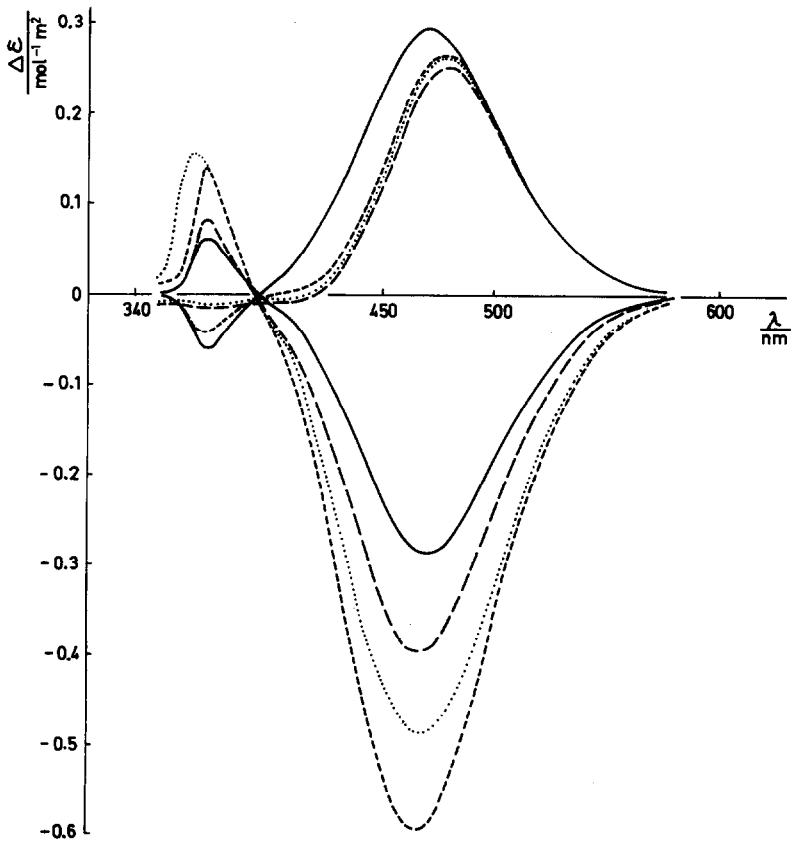

Fig. 1. Circular dichroic spectra of the *cis*(NO_2),*trans*(NH_2) - bis(aminocarboxylato)dinitrocobalt/ate(III) complexes containing glycinato ——, S-alaninato — — —, S-*n*-valinato ····, or S-valinato – – – – ligands. The positive dominant Cotton effect corresponds to Λ-diastereomers.

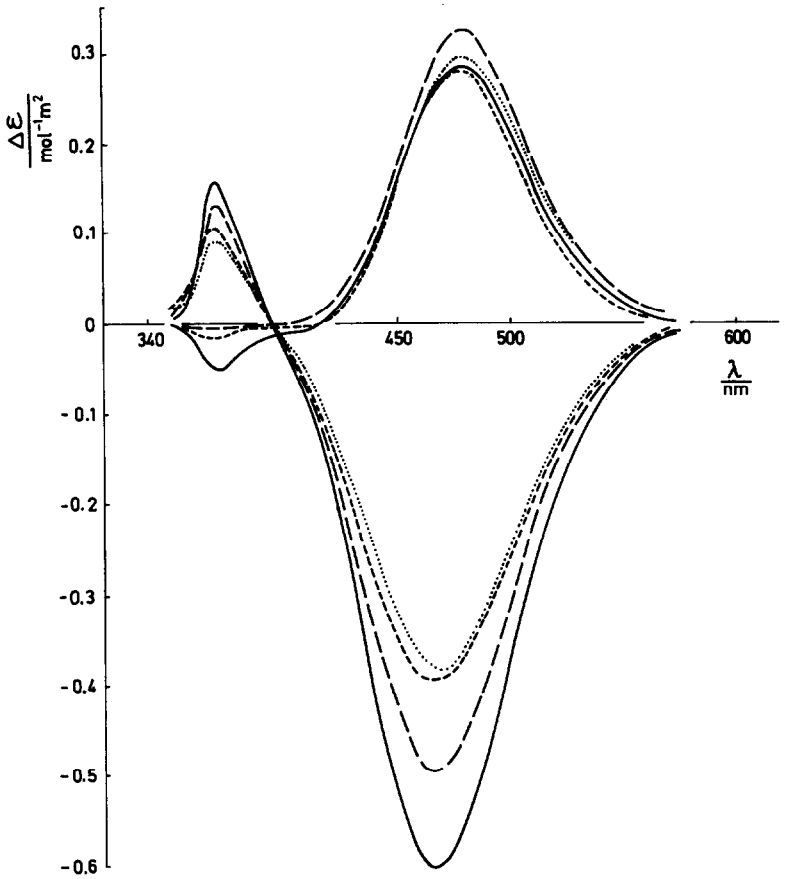

Fig. 2. Circular dichroic spectra of the *cis*(NO_2),*trans*(NH_2) - bis(aminocarboxylato)dinitrocobalt/ate(III) complexes containing S-leucinato ····, S-*n*-leucinato ----, S-arginine ———, or S-*i*-leucinato —— ligands. The positive dominant Cotton effect corresponds to Λ-diastereomers.

By applying the concept of the Quadrant rule for conformational and vicinal contributions to the optical activity of octahedral complexes, suggested by Bosnich and Harrowfield,[14] the effect of the ligand conformation on the activity of the considered isomers could be explained as shown in Fig. 4. In the Λ-isomer the chelate ring chair conformation and equatorial position of the side group would produce small or no net optical activity. Contrary to this, in the Δ-isomer a strong negative cir-

Table 1. Wavelength (λ, nm) of the circular dichroic maximum in the region of the first electronic *d–d* transition and the corresponding dichroism (Δε, $mol^{-1}m^2$), and the proton chemical shift of the aminocarboxylato ligand α-hydrogen (δ, ppm) for the Λ- and Δ-isomers of the investigated bis (aminocarboxylato)dinitrocobalt/at(III) complexes

Complex[a]	Λ-isomer λ	Λ-isomer Δε	Λ-isomer δ	Δ-isomer λ	Δ-isomer Δε	Δ-isomer δ
cis(NO_2),*trans*(NH_2)						
-Ag[Co(NO_2)$_2$(gly)$_2$]	475	+0.298	3.66(equat.)	475	−0.298	3.77(axial)
-Ag[Co(NO_2)$_2$(S-ala)$_2$]	475	+0.25	3.76	467	−0.38	3.93
-K[Co(NO_2)$_2$(S-nva)$_2$]	480	+0.261	3.66	468	−0.478	3.87
-K[Co(NO_2)$_2$(S-val)$_2$]	477	+0.263	3.65	467	−0.596	3.90
-K[Co(NO_2)$_2$(S-nle)$_2$]	478	+0.290	3.67	467	−0.393	3.84
-Na[Co(NO_2)$_2$(S-leu)$_2$]	477	+0.294	3.67	468	−0.383	3.85
-Na[Co(NO_2)$_2$(S-ile)$_2$]	477	+0.292	3.66	466	−0.603	3.90
-[Co(NO_2)$_2$(S-argH)$_2$]Cl	478	+0.326	3.70	467	−0.496	3.89

[a] The content of crystallization water in some of the diastereomers is given in Table 2.

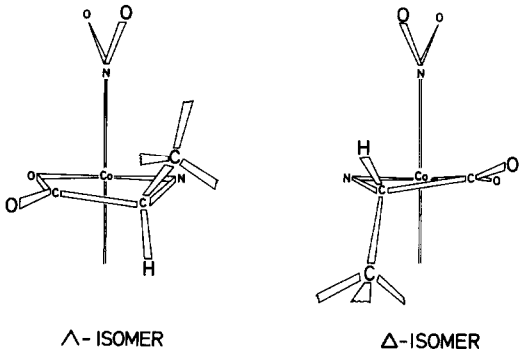

Fig. 3. Main structural feature of the investigated bis(S-aminocarboxylato)dinitrocobalt/ate(III) diastereomers.

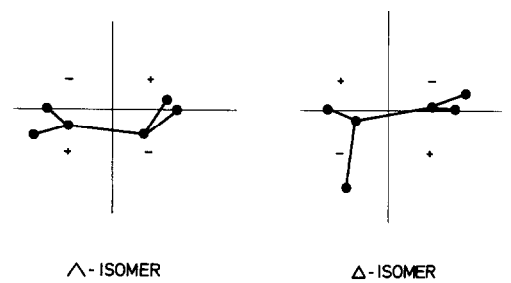

Fig. 4. Aminocarboxylato ligands skeletal atom projection according to the Quadrant rule for their conformational and vicinal contribution to the optical activity of the investigated isomers.

cular dichroism would be predicted on the assumption that the aminocarboxylato chelate ring having the λ-conformation generates negative circular dichroism in the region of the first *d–d* electronic transition. It may be further concluded that Λ-isomers, containing S-aminocarboxylato ligands, possess almost solely a configurational contribution to the optical activity and therefore exhibit circular dichroism similar to that of the corresponding complex with the glycinato ligand. In this isomer the circular dichroism does not depend significantly on the kind of the aminocarboxylato ligand, because the chelate ring side group protrudes into the equatorial region where no constraints for larger group accomodation exists. In the Δ-isomer, the aminocarboxylato ligand is flexible. The dominant steric constraint on a chelate ring side group in this case would be the intraligand interaction with the carboxylato oxygen atom,[15] which may cause a certain change in the orientation of a bulk side group. According to the same rule one can conclude that a more axially oriented side group would enhance the negative contribution to the circular dichroism in the region of the first absorption band. Therefore, we suggest that the large variation in the circular dichroism of the Δ-isomers, containing S-aminocarboxylato ligands, is due to the conformational and vicinal contribution to the optical activity, which would be the largest for the most axially oriented aminocarboxylato chelate ring side group.

To substantiate the proposed correlation between the chelate ring side group's spatial position and its contribution to the optical activity of the investigated diastereomers we examined their proton NMR spectra. In particular, the chemical shift of the hydrogen atom on the α-carbon atom of the aminocarboxylato ligand was considered, because the spatial positioning of this hydrogen atom is directly related to the positioning of the side group, i.e. when a side group is in an equatorial position the hydrogen atom is in an axial position and *vice versa*. The chemical shifts of the considered hydrogen atom are influenced by the neighbouring magnetic anisotropy of cobalt(III)[16] and carboxylato group.[17] Both influences predict that the chemical shift of this hydrogen atom becomes progressively smaller when the hydrogen atom is moving from an equatorial to an axial position. In accordance with this prediction, the experimental data (Table 1) show that in the diastereomers of Λ-absolute configuration the chemical shift is always smaller than in the diastereomers of Δ-absolute configuration. Besides, the small variations in the chemical shifts among the diastereomers of Λ–absolute configuration could be well explained as a consequence of the different substituents on the α-carbon atom. This effect becomes unimportant when the difference in the hydrogen chemical shift between the members of a diastereomeric pair is considered. This difference varies notably with the kind of aminocarboxylato ligand and it is related to the difference in circular dichroism between diastereomers, as is shown in Fig. 5. Since in the Λ-isomers the circular dichroism has almost the same value for all the investigated aminocarboxylato ligands (the side group orientation cannot vary appreciably), the correlation presented in the figure is proof that in the Δ-isomer the more axially oriented side group induces a larger conformational contribution to the circular dichroism. From the figure it can also be concluded that the bulkiest chelate ring side groups on the first side carbon atom (encountered in the valinato and isoleucinato ligands) are positioned the furthest away in the axial direction (in accordance with the predicted repulsion from the carboxylato oxygen atom).

In conclusion, we point out that our results suggest that the strong negative circular dichroism is associated with the λ-conformation of the aminocarboxylato chelate ring of the S-amino acids. These results may be valuable in the analyses of the

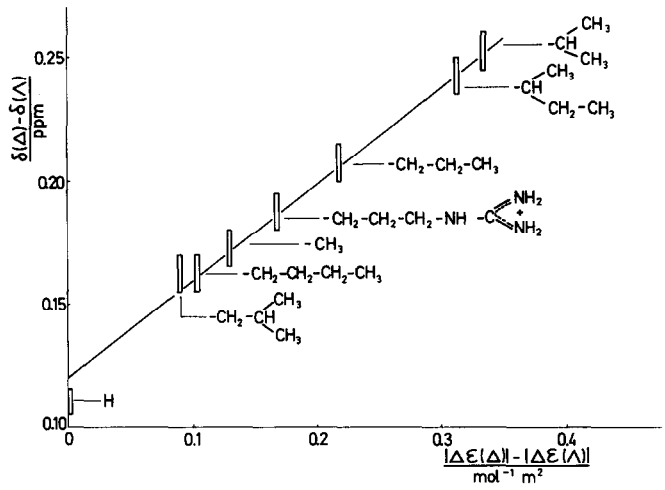

Fig. 5. Correlation between the dichroism and the α-proton chemical shift differences in a diastereomeric pair of the investigated complexes. The formulas represent the α-carbon side groups.

CD spectra of octahedral aminocarboxylato complexes.

EXPERIMENTAL

Preparations

Enantiomers of silver cis(NO_2), trans(NH_2)-*diglycinatodinitrocobaltate*(III). These were obtained by a previously described procedure.[18,19]

Diastereomers of the cis(NO_2),trans(NH_2)-*bis*(*aminocarboxylato*)*dinitrocobaltate*(III) *complex.* These were synthesized according to the procedure described by Ćelap *et al.*[9] The procedure was modified by prolonging the heating of the reaction mixture to 2 h and the mixture of diastereomer obtained was resolved by column chromatography. After the reaction was over, the hot solution was filtered off and the filtrate evaporated to dryness on a rotatory evaporator; the dry residue was extracted with 95% ethanol and evaporated to dryness. The mixture obtained was dissolved in a small amount of water and poured on a Dowex 1-X4 (200–400 mesh, 24 cm length and 4 cm o.d.) column in the chloride form. The column was first washed with water and then elution was carried out with a 0.2 M potassium chloride solution until the first zone was completely eluted, and then with a 0.5 M solution. In the cases of the leucine and isoleucine complexes, instead of potassium chloride, sodium chloride was used. From the eluate of the first zone, the Δ-diastereomer was obtained, whereas the eluate of the third zone yielded the corresponding Λ-diastereomer (the second and the fourth zones were found to contain the corresponding *cis,cis,cis*-diastereomers). When the eluates of the individual zones started to elute from the column, they were collected in portions of about 50–100 cm^3 and each portion was immediately evaporated on a rotatory evaporator (30°C). Each dry residue was extracted with absolute ethanol and the filtered extracts kept in a refrigerator. The united extracts of one zone were then evaporated to dryness on a rotatory evaporator, and the dry residue was extracted again with absolute ethanol. The filtered extract was concentrated to a small volume on a rotatory evaporator until the crystals began to separate, and then left to stand overnight in a refrigerator. The separated crystals were filtered off and washed with ethanol and ether. The filtrate was again concentrated and cooled in a refrigerator yielding an additional amount of the corresponding substance. The substances thus obtained were almost optically pure and their yields are given in Table 2. The diastereomers obtained, except those of the S-alanine complex, were purified as follows. The Δ-diastereomers were purified by pouring their solutions again onto a Dowex 1-X4 column (200–400 mesh, 4 cm length and 2.5 cm o.d.). The elution (with a 0.2 M solution) and the isolation of substances was carried out as already described. The Λ-diastereomers were purified by extracting them with absolute ethanol and evaporating the extracts obtained on a rotatory evaporator until the crystals started to separate. The optically pure diastereomers of the S-alanine complex were obtained by dissolving about 0.5 g of the corresponding potassium salt, obtained as described above, in 10 cm^3 of water and by adding a 1 M silver nitrate solution (20% more than the equivalent amount). The solution was then filtered off to remove the white precipitate of silver chloride formed as impurity and the filtrate was kept overnight in a refrigerator.

Table 2. The yields and specific optical rotations $[\alpha]_D^{20^\circ}$ of the *cis*(NO_2),*trans*(NH_2)-bis(aminocarboxylato)cobaltate(III) diastereomers separated by ion exchange chromatography

No.	Diastereomer	Yield (%)	$[\alpha]_D^{20^\circ}$
1	Δ-Ag[Co(NO_2)$_2$(S-ala)$_2$]	9	−573
2	Λ-Ag[Co(NO_2)$_2$(S-ala)$_2$]	23	+343
3	Δ-K[Co(NO_2)$_2$(S-nva)$_2$]·H_2O	9	−790
4	Λ-K[Co(NO_2)$_2$(S-nva)$_2$]·H_2O	30	+232
5	Δ-K[Co(NO_2)$_2$(S-val)$_2$]·$2H_2O$	4	−795
6	Λ-K[Co(NO_2)$_2$(S-val)$_2$]	32	+165
7	Δ-K[Co(NO_2)$_2$(S-nle)$_2$]·$2H_2O$	15	−666
8	Λ-K[Co(NO_2)$_2$(S-nle)$_2$]	22	+267
9	Δ-Na[Co(NO_2)$_2$(S-leu)$_2$]·H_2O	11	−607
10	Λ-Na[Co(NO_2)$_2$(S-leu)$_2$]·H_2O	29	+294
11	Δ-Na[Co(NO_2)$_2$(S-ile)$_2$]	8	−690
12	Λ-Na[Co(NO_2)$_2$(S-ile)$_2$]	40	+189

The Δ-diastereomer crystallized out in dark brown, cube-like crystals, whereas the Λ-diastereomer separated out in the form of needle-like crystals. The optical rotations of the isomers obtained are given in Table 2.

Diastereomers of cis(NO_2),trans(NH_2)-*bis*(S-*arginine*)*dinitrocobalt*(III) *chloride*. These were prepared by an earlier described procedure.[20]

Measurements

Optical rotation. This was measured with a Perkin–Elmer 141 MC polarimeter, using 2×10^{-3} M aqueous solutions.

CD spectra. These were recorded on a JASCO Dichrograph model 500A, using the same solutions.

NMR spectra. These were recorded on a Varian FT-80A spectrometer, using D_2O solutions and DTS as an internal standard.

Acknowledgment—The authors are grateful to the Serbian Republic Research Fund for financial support.

REFERENCES

1. Y. Saito, Inorganic molecular dissimmetry, in *Inorganic Chemistry Concepts*, Vol. 4, p. 137. Springer, Berlin (1979).
2. S. Fijinami, M. Miyamae, T. Miura and K. Fushimi, *Bull. Chem. Soc. Japan* 1986, **59**, 43.
3. C. T. Lin and B. E. Douglas, *Inorg. Chem.* 1964, **3**, 1356.
4. B. E. Douglas and S. Yoneda, *Inorg. Chem.* 1965, **4**, 1561.
5. R. G. Denning and T. S. Piper, *Inorg. Chem.* 1960, **5**, 1056.
6. S. Larsen, K. J. Watson, A. M. Sargeson and K. R. Turnbull, *J. Chem. Soc., Chem. Commun.* 1986, 847.
7. S. K. Hall and B. E. Douglas, *Inorg. Chem.* 1969, **8**, 372.
8. N. Matsuoka, J. Hidaka and Y. Shimura, *Bull. Chem. Soc. Japan* 1970, **9**, 719; N. Matsuoka, J. Hidaka and Y. Shimura, *Bull. Chem. Soc Japan* 1975, **48**, 458.
9. M. B. Ćelap, R. G. Denning, D. J. Radanović and T. J. Janjić, *Inorg. Chim. Acta* 1971, **5**, 9.
10. F. S. Richardson, *Inorg. Chem.* 1972, **11**, 2366.
11. W. H. Watson, D. R. Johnson, M. B. Ćelap and B. Kamberi, *Inorg. Chim. Acta* 1972, **8**, 591.
12. R. Herak, B. Prelesnik, Lj. Manojlović-Muir and K. W. Muir, *Acta Cryst.* 1974, **B30**, 229.
13. P. Vasić, R. Herak and S. Djurić, *Acta Cryst.* 1976, **B32**, 91.
14. B. Bosnich and J. McB. Harrowfield, *J. Am. Chem. Soc.* 1972, **94**, 3425.
15. K. Sakaguchi, K. Morito and H. Yoneda, *Inorg. Chim. Acta* 1979, **37**, 209.
16. N. Juranić, M. B. Ćelap, D. Vučelić, M. J. Malinar and P. N. Radivojša, *Inorg. Chem.* 1980, **19**, 802.
17. R. G. Denning, M. B. Ćelap and D. J. Radanović *Inorg. Chim. Acta* 1968, **2**, 58.
18. T. J. Janjić, M. B. Ćelap and P. Spevak, *Glasnik Hem. Društva Beograd* 1962, **27**, 111.
19. M. B. Ćelap, D. J. Radanović and T. J. Janjić, *Inorg. Chem.* 1965, **4**, 1494.
20. M. B. Ćelap, M. J. Malinar, P. N. Radivojša and Lj. Solujić, *Inorg. Synth.* 1985, **23**, 91.

Polyhedron Vol. 7, No. 13, pp. 1159–1167, 1988
Printed in Great Britain

0277–5387/88 $3.00+.00
© 1988 Pergamon Press plc

THE KINETICS OF THE REACTION BETWEEN *TRANS*-DICHLOROBIS(1,2-DIAMINOETHANE)COBALT(III) PERCHLORATE AND MONOAMINES IN DIMETHYLFORMAMIDE—I. SPECTROPHOTOMETRIC AND SPECTROPOLARIMETRIC MEASUREMENTS

A. M. THOMPSON and D. A. HOUSE*

Department of Chemistry, University of Canterbury, Christchurch, New Zealand

(*Received* 21 *December* 1987; *accepted* 27 *January* 1988)

Abstract—The title reaction is first-order in both complex and amine concentrations and second order rate constants were obtained spectrophotometrically ($k_2^{spectro}$) under pseudo-first-order conditions (excess amine). For amines of the type RCH_2NH_2, the rate is proportional to pK_a, but steric factors are important. Thus, $k_2^{spectro}$ values for *n*-, *sec*- and *iso*-butylamine (with approximately constant pK_a) are in the ratio 1 : 0.41 : 0.37, respectively, and likewise 1 : 0.46 : 0.33 for benzylamine, α-Me- and N-Me-, respectively. The spectrophotometric method essentially monitors the rate of loss of the *trans*-dichloro- by all paths and the rate of coordination of the monoamine was more securely measured by monitoring the rate of increase in optical activity (k_2^{CD}) using chiral amines. Where comparable data are available, k_2^{CD} is usually less than $k_2^{spectro}$, and $k_2^{spectro}$ data are probably composite quantities.

Chloropentaaminecobalt(III) complexes of the type $[CoCl(en)_2(monoamine)]^{2+}$ are almost always prepared by the reaction between the *trans*-dichlorobis(ethylenediamine)cobalt(III) cation and the monoamine in a suitable solvent (usually water).†[2–6] Although this reaction is of considerable synthetic utility, very few studies of the rate have been reported. Yields certainly vary with the nature of the amine and the time for completion on a synthetic scale varies from minutes[7,8] to weeks.[9] Data from the synthetic studies are summarized by the statement "the yields of $[CoCl(en)_2(A)]^{2+}$ run parallel to the basicity of the amine. At the same time, the marked influence of basicity on complex formation may sometimes be overshadowed by the effect of other factors which cannot be strictly defined at present."[5]

The stereochemistry of the product has also been the subject of much speculation.[1] For many complexes, the *cis* configuration has been established by resolution[6] or by X-ray structure[10,11] but for at least one amine (theophylline), both *cis*- and *trans*-$CoCl(en)_2\{theoplylline(-1)\}^+$ have been characterized.[12,13]

A kinetic study of the reaction between *trans*-$CoCl_2(en)_2^+$ and amines in methanol[14,15] (followed conductometrically), shows that the methoxide ion makes an important contribution to the reaction rate. In DMF alone, the rate is $\sim 10^3$ times slower.

In this investigation, we report a more detailed spectrophotometric study of the reaction between *trans*-$[CoCl_2(en)_2]ClO_4$ and some 23 monoamines (Fig. 1) in DMF.

EXPERIMENTAL

trans-$[CoCl_2(en)_2]ClO_4$ was prepared by literature procedures[16(a)] and the amines and DMF (Reagent Grade) were used as supplied without further purification. Amine solutions in DMF (0.1–0.3 M) were prepared by weight and standardized by titration in aqueous solution using 0.100 M HCl and

*Author to whom correspondence should be addressed.

† Between 1904–1923 there were 11 unpublished dissertations produced by students of A. Werner, University of Zurich, on various aspects of this reaction.[1]

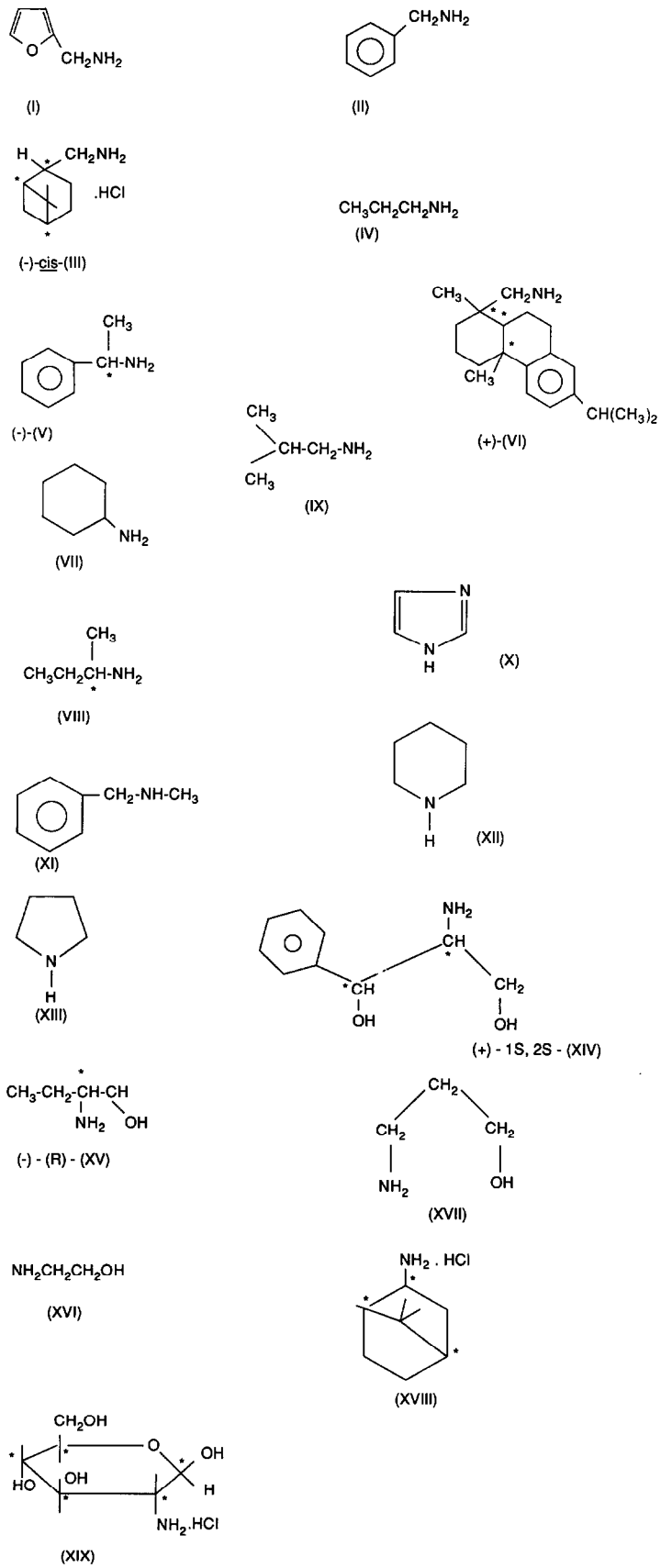

Fig. 1. Representative amines used in this investigation. Chiral centres are marked* with the sign of rotation at the Na_D lines in parentheses.

Table 1. Activation parameters associated with $k_2^{spectro}$ or k_2^{CD} (25°C)

Amine	$10^3\ k_2^{spectro}$ ($M^{-1}\ s^{-1}$)	$10^3\ k_2^{CD}$ ($M^{-1}\ s^{-1}$)	E_a (kJ mol^{-1})	$\Delta S^{\#}_{298}$ ($JK^{-1}\ mol^{-1}$)
Imidazole (X)	0.0457		147.5±2.8	+139±6
(+)-Dihydroabietylamine (VI)	1.74		83.5±2.9	−26±6
3-Methoxypropylamine	4.00		61.2±0.3	−94±1
(±)-α-Me-Benzylamine (V)	1.09		54.3±0.6	−128±2
(−)-α-Me-Benzylamine (V)	0.823		53.3±2.2	−133±5
(−)-α-Me-Benzylamine (V)		0.893	90.6±4.9	−8±10
(−)-2-Aminobutane-1-ol (XV)		1.11	60.5±1.9	−107±4
(+)-2-Amino-1-phenyl-1,3-propanediol (XIV)		0.356	68.4±0.9	−90±2

screened methyl-red indicator.* A Varian Superscan recording spectrophotometer was used for all absorption spectral measurements and a JASCO ORD/CD/UV-5 recording spectropolarimeter for all CD measurements.

The reaction rate was investigated using a sequence of experiments of increasing sophistication.

(1) The amine solution (5 cm^3, $\geqslant 0.1$ M) was added to 20 mg of *trans*-$[CoCl_2(en)_2]ClO_4$ in a screw-capped vial at room temperature and subjected to visual examination from time to time. The initial green solution changed through purple to grey to red and allowed a rough estimate (essentially fast or slow) of the rate.[17] In many cases, red crystals of some chloropentaamine salt deposited after 2–3 weeks.

(2) Small amounts of *trans*-$[CoCl_2(en)_2]ClO_4$ (~ 7 mg) were added to DMF solutions of the amine in a 1.00 cm spectrophotometer cell maintained at 25.0°C using circulating water from a temperature controlled water bath. Repeat scan techniques (5 min cycles) gave the position of isobestic points and provided an approximate measure of half-life.

(3) The above procedures were repeated using fixed-wavelength techniques (500 nm) to obtain a plot of absorbance vs time. Mean pseudo-first-order rate constants ($k_{obs}^{spectro}$ ± the standard deviation) were the average of 10–15 point-by-point calculations over 2–3 half-lives using the expression $t \times k_{obs}^{spectro} = \ln[(A_\infty - A_o)(A_\infty - A_t)^{-1}]$.

These data were converted to $k_2^{spectro}$ using the expression:

$$k_2^{spectro} = k_{obs}^{spectro}\,[\text{amine}]^{-1}.$$

Overall reproducibility from completely independent experiments, was about 5%.

*The mixed indicator is prepared from one part 0.2% methyl-red in alcohol and three parts of 0.1% bromocresol-green in alcohol.[16(b)]

(4) For some of the more interesting systems, activation parameters (Table 1) were obtained from the variation of $k_2^{spectro}$ with temperature using standard calculations[18] and $k_2^{spectro}$ (25°C) values were obtained by extrapolation. The variation of $k_{obs}^{spectro}$, $k_2^{spectro}$ and $k_2^{spectro}$ (calc.) (calculated from the activation parameters) with temperature, is shown in Tables 2 and 3.

(5) Where chiral amines were available, similar methods were used to monitor the increase in CD with time in the 650–300 nm region (Table 4). Concentrations were slightly modified to accommodate the use of a jacketed 5.00 cm reaction cell. Once a suitable wavelength had been established from the repeat scan CD measurements, kinetic data were accumulated using fixed wavelength techniques.

RESULTS

The rate of solvolysis of *trans*-$CoCl_2(en)_2^+$ in DMF is $8.5 \times 10^{-7}\ s^{-1}$ ($t_{1/2} \sim 3.8$ days) at 25°C ($E_a = 88.6$ kJ mol^{-1}, $\Delta S^{\#}_{298} = -63\ J\ K^{-1}\ mol^{-1}$).[19] Addition of > 10 times of an excess of the monoamine (pseudo-first-order conditions) causes a much more rapid colour change from green to red which can be monitored spectrophotometrically at 25°C ($t_{1/2} \sim$ 10–50 min). Repeat scan techniques were initially used to establish the presence and position of isosbestic points (Table 5) and kinetic data were obtained by monitoring the rate of increase in absorbance at 500 mm. Near this wavelength, the *trans*-dichloro parent has a minimum (525 nm, $\varepsilon = 6.5\ M^{-1}\ cm^{-1}$) and the chloropentaamine product a maximum (e.g. *cis*-$CoCl(en)_2(NH_2(CH_2)_3OCH_3)^{2+}$ 523.5 nm, $\varepsilon = 77.2\ M^{-1}\ cm^{-1}$). In general, satisfactory isosbestic points and constant "infinity" values were obtained, but there were occasional systems where "drifting" was noticeable.

For one amine system (3-methoxypropylamine), $k_{obs}^{spectro}$ were determined over a five-fold variation in

Table 2. $k_2^{spectro}$ (M^{-1} s^{-1}) data for the reaction between *trans*-[$CoCl_2(en)_2$] ClO_4 and amines in DMF at various temperatures

Amine	Conc. (M)	T (°C)	10^4 $k_{obs}^{spectro}$ (s^{-1})	10^3 $k_2^{spectro}$ [a] (M^{-1} s^{-1})	10^3 $k_2^{spectro}$ (calc.)[b] (M^{-1} s^{-1})
Imidazole (X)	0.205	48.0	0.66±0.01	0.322±0.007	0.324
		50.0	0.93±0.03	0.45±0.01	0.456
		52.0	1.33±0.06	0.65±0.03	0.639
		54.0	1.90±0.06	0.93±0.03	0.892
		56.0	2.51±0.08	1.22±0.04	1.24
		58.0	3.48±0.08	1.69±0.04	1.71
3-Methoxypropylamine	0.0524	25.0	2.33±0.24	4.45±0.45	
	0.105		4.23±0.26	4.04±0.25	
	0.157		6.00±0.33	3.82±0.21	
	0.182		7.82±0.47	4.29±0.26	
	0.220		8.61±0.24	3.91±0.12	
			8.22±0.20	3.74±0.09	
	0.262		11.0±0.62	4.21±0.24	
		25.0		mean 4.06±0.26	4.00
	0.220	29.9	13.1±0.2	5.96±0.11	5.96
	0.235	35.0	20.8±1.8	8.83±0.76	8.91
	0.235	39.9	30.5±2.6	13.0±1.1	12.9
	0.235	47.2	52.2±3.5	22.2±1.5	22.1
α-Methyl-benzylamine (V)	(−)0.220	24.0	1.71±0.08	0.777±0.036	0.765
	(±)0.195	25.0	2.13±0.09	1.09±0.04	1.09
	(−)	25.0			0.822
	(−)0.220	27.2	2.15±0.08	0.978±0.034	0.963
	(±)0.203	29.5	3.00±0.20	1.50±0.10	1.51
	(−)0.210	31.1	2.72±0.13	1.30±0.06	1.27
	(±)0.203	31.5	3.50±0.20	1.73±0.08	1.74
	(±)0.203	34.0	4.20±0.30	2.10±0.10	2.07
	(−)0.210	34.6	3.06±0.15	1.46±0.07	1.61
	(±)0.203	36.8	4.90±0.20	2.50±0.10	2.50
	(−)0.210	39.9	4.90±0.20	2.33±0.09	2.29
	(±)0.203	40.0	6.30±0.20	3.10±0.10	3.11
	(−)0.210	47.2	7.86±0.12	3.74±0.06	3.65
(+)-Dehydroabietylamine (VI)	0.170	34.0	7.88±0.4	4.64±0.2	4.67
	0.170	36.6	10.9±0.6	6.40±0.4	6.14
	0.170	40.0	14.2±0.9	8.36±0.5	8.73
	0.170	43.1	21.1±1.0	12.4±0.7	12.0
	0.208	44.5	27.4±1.0	13.2±0.5	13.7
	0.170	48.0	33.5±1.0	19.7±0.8	19.4

[a] $k_2^{spectro}$ calculated from the expression $k_2^{spectro} = k_{obs}^{spectro}$ [amine]$^{-1}$.
[b] $k_2^{spectro}$ calculated from the activation parameters cited in Table 1.

amine concentration. These data (Table 6) showed that $k_2^{spectro}$, calculated from the expression, $k_2^{spectro} = k_{obs}^{spectro}$ [amine]$^{-1}$, were essentially constant and the rate of reaction can be represented as:

$$\frac{-d[trans\text{-}CoCl_2(en)_2^+]}{dt} = \frac{d[product]}{dt} = k_2[Co(III)][amine].$$

The plot of $k_{obs}^{spectro}$ vs [3-methoxypropylamine] was linear, with the intercept at the origin, indicating negligible background solvation during the course of the reaction.

This situation was assumed to prevail for all amines investigated and when occasionally checked, constant $k_2^{spectro}$ values were obtained with variation in amine concentration. Table 5 lists $k_2^{spectro}$ data at 25°C for a variety of monoamines and aminoalcohols.

During the course of this data accumulation it

Table 3. k_2^{CD} (M^{-1} s^{-1}) data for the reaction between *trans*-$[CoCl_2(en)_2]$ ClO_4 and amines in DMF at various temperatures

Amine	T (°C)	10^3 k_2^{CD} (M^{-1} s^{-1})	10^3 k_2^{CD} (calc.)[a] (M^{-1} s^{-1})
(−)-α-Methylbenzylamine	25.0		0.893
	36.9	3.90±0.05	3.63
	39.6	4.68±0.22	4.92
	43.2	6.88±0.30	7.32
	46.3	10.3±0.14	10.2
	50.9	17.1±0.10	16.6
(−)-(R)-2-Aminobutan-1-ol (XV)	25.0		1.11
	29.9	1.69±0.02	1.65
	32.2	1.97±0.02	1.97
	40.1	3.61±0.08	3.60
	43.9	4.43±0.10	4.76
	47.6	6.18±0.20	6.19
	51.5	8.54±0.10	8.13
(+)-2-Amino-1-phenyl-1,3-propanediol (XIV)	25.0		0.356
	43.0	1.69±0.05	1.71
	44.4	1.95±0.06	1.92
	50.1	3.03±0.07	3.04
	56.8	5.16±0.17	5.09
	59.9	6.35±0.42	6.42

[a]Calculated from the activation parameters cited in Table 1.

became apparent that in some systems, *cis*-$CoCl_2(amine)_2^+$ was not the sole product. The kinetic conditions (10-fold excess amine in DMF) are different from the usual synthetic conditions (1.2-fold excess amine in water) and base catalysed solvolysis or substitution of the second coordinated chloro ligand is possible. Thus we suspect that $k_2^{spectro}$ is a composite quantity, reflecting the loss of *trans*-$CoCl_2(en)_2^+$ by all paths.

A more reliable measure of the rate of coor-

Table 4. Wavelengths of CD max. or min. induced by the coordination of chiral amines to *trans*-$[CoCl_2(en)_2]$ ClO_4 in DMF

Amine	λ (nm)
(−)-(R)-2-Aminobutan-1-ol (XV)	550(−), 480(+), 400(−)
Isorotatory points	524, 436, 340
(−)-2-Amino-1-phenyl-1,3-propanediol (XIV)	575(+), 485(−), 390(+)
Isorotatory points	554, 426, 352
(−)-α-Methylbenzylamine (V)	555(−). 480(+), 400(−)
Isorotatory points	490, 460
(+)-Bornylamine. HCl[a,b] (XVIII)	555(−), 470(+)
Isorotatory points	515, 400
(−)-3-Aminomethylpinane. HCl[a] (III)	550(−), 465(+)
Isorotatory points	510, 390
(+)-D-glucosamine. HCl[a] (XIX)	480(−)
Isorotatory points	410

[a] Measured in the presence of excess triethylamine.

[b] Synthesized by the method of J. B. Cohen, *Practical Organic Chemistry*, 3rd Edn, p. 297. MacMillan, London (1924).

Table 5. $k_2^{spectro}$ data ($M^{-1}\ s^{-1}$) for various monoamines at 25°C in DMF

Amine[a]	pK_a[b]	$10^3\ k_2^{spectro}$	Isosbestic points
Class A: RCH_2NH_2			
Furfurylamine (I)	8.89	1.58±0.05	410 430 590
Benzylamine (II)	9.33	2.34±0.03	595
2-Methoxyethylamine	9.4	1.86±0.05	348 401 432 586
3-Methoxypropylamine[c]	10.1	4.00±0.07	347 398 430 582
(−)-Myrtanylamine (III)	10.6	6.51±0.20	348 411 432 584
n-Octylamine	10.65	4.49±0.12	402 429 584
n-Butylamine (IV)	10.77	7.50±0.40	348 407 434 582
iso-Butylamine (IX)	10.83	2.75±0.09	347 403 432 585
Class B: $RC(R_1)(R_2)NH_2$			
(±)-α-Methylbenzylamine (V)[c]	9.35	1.09±0.07	403 440 586
(−)-α-Methylbenzylamine[c]	9.35	0.823±0.039	405 441 586
		0.893±0.042[c,d] CD	
(+)-Dehydroabietylamine (VI)	10.3	1.74±0.06[c]	405 437 588
Cyclohexylamine (VII)	10.66	3.41±0.1	595
sec-Butylamine (VIII)	10.72	3.05±0.04	350 412 439 590
Class C: R_1NHR_2			
Imidazole (X)[c]	6.99	0.0457±0.0009	582
N-Me-Benzylamine (XI)[c]	9.58	0.785±0.03	592
Diethylamine	10.49	2.09±0.18	595
N-Me-*n*-Butylamine	10.9	2.28±0.11	596
Piperidine (XII)	11.2	3.40±0.19	598
Pyrrolidine (XIII)	11.27	4.74±0.12	593
Class D: aminoalcohols			
(+)-2-Amino-1-phenyl-1,3-propandiol (XIV)	8.0	1.49±0.09	599
		0.356±0.024[c,d] CD	
(−)-2-Aminobutane-1-ol (XV)	9.5	3.51±0.11	587
		1.11±0.04[c,d] CD	
Ethanolamine (XVI)[d]	9.5	4.96±0.10	593
3-Aminopropane-1-ol (XVII)[d]	10.11	7.89±0.21	593

[a] For amine structure see Fig. 1.
[b] See ref. 23.
[c] For activation parameters see Table 1.
[d] k_2^{CD} data (see text).

Table 6. Variation of $k_{obs}^{spectro}$ vs amine concentration in DMF at 25.0°C[a]

[Amine][b] (mM)	$10^4\ k_{obs}^{spectro}$[c] (s^{-1})	$10^3\ k_2^{spectro}$[d] ($M^{-1}\ s^{-1}$)
52.4	2.33±0.24	4.45±0.45
105	4.23±0.26	4.04±0.25
157	6.00±0.33	3.82±0.21
182	7.82±0.47	4.29±0.26
220	8.61±0.24	3.91±0.12
262	11.0±0.62	4.21±0.24

[a] *t*-$[CoCl_2(en)_2]^+$ concentration ~ 10 mM.
[b] Amine = 3-methoxypropylamine.
[c] Observed pseudo-first-order rate constant.
[d] $k_2^{spectro} = k_{obs}^{spectro}\ [amine]^{-1}$.

dination of the monoamine to the Co(III) centre was obtained by measuring the rate of increase in the circular dichroism induced by a chiral monoamine (Fig. 2). *trans*-$CoCl_2(en)_2^+$ is achiral, but a coordinated chiral monoamine will produce induced circular dichroism at the $CoCl(N_5)^{2+}$ chromophore.[20] The intensity of this induced CD is related to the nature of the amine and decreases rapidly as the site of the asymmetric centre in the ligand is progressively remote from the metal centre. We investigated the chiral amines (III), (V), (VI), (XVIII) and (XIX) and chiral aminoalcohols (XIV) and (XV) (Table 4) but only (V), (XIV) and (XV) gave induced CD of sufficient intensity to evaluate kinetic parameters (Table 5).

Preliminary data were also obtained for $k_2^{spectro}$ in

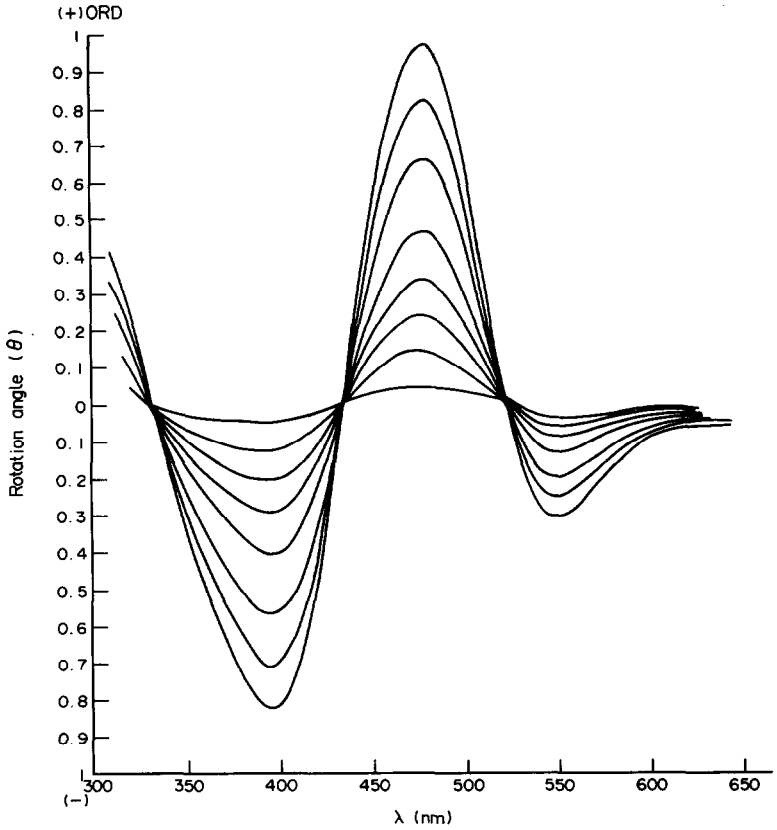

Fig. 2. CD spectral scans for the reaction of *t*-$CoCl_2(en)_2^+$ with (−)-(R)-2-aminobutan-1-ol in DMF in 25°C. Times reading upwards at 480 nm are 0, 9, 17, 27, 42, 74, 112 and 184 min.

other dipolar aprotic solvents (DMSO and DMA). In general $k_2^{spectro}$ values were within experimental error for DMF and DMA, but distinctly smaller (0.8–0.3 times) in DMSO. Controlled addition of 2% H_2O to DMF resulted in a two-fold increase in $k_2^{spectro}$ and reproducible data could not be obtained on addition of 4% H_2O.

DISCUSSION

Despite the probability that $k_2^{spectro}$ data are composite quantities, we believe that *cis*-$CoCl(en)_2(amine)^{2+}$ represents a considerable proportion (> 25%) of the product, from the reaction under investigation, as red crystals frequently deposit from aged reactant solutions used in preliminary investigations. Support for this comes from a comparison of $k_2^{spectro}$ with k_2^{CD} for chiral aminoalcohols where k_2^{CD} represents $\frac{1}{4}$ to $\frac{1}{3}$ of the $k_2^{spectro}$ values. The fact that the plot of $k_2^{spectro}$ vs [amine] is linear and passes through the origin merely indicates that all "by-product" reactions are proportional to [amine] as well.

With due respect for the uncertainties in the nature of the reaction, it is apparent that the amines can be placed into about four categories.

Class A—primary amines unsubstituted in the α-position, Class B—primary amines substituted in the α-position, Class C—secondary amines and Class D—aminoalcohols. Within each class, plots of $-\log k_2^{spectro}$ vs pK_a (amine) are linear, but displaced successively upwards (i.e. slower) in the order D < A < B < C (Fig. 3), to give a set of four, almost parallel, lines.

A linear plot is to be expected if the SN_1CB mechanism is operating, as the first step involves the base-assisted removal of a proton from the complex, forming its conjugate base. The position of the equilibrium will depend on the strength of the base, as measured by the pK_a of its conjugate acid.

$$t\text{-}CoCl_2(en)_2^+ + :B \overset{k_1}{\Leftrightarrows} BH^+ + CoCl_2(en)(en{-}H)$$

$$CoCl_2(en)(en{-}H) \xrightarrow{k_2} CoCl(en)(en{-}H)^+ + Cl^-$$
rate determining

$$CoCl(en)(en{-}H)^+ + BH^+ \xrightarrow{k_3} CoCl(en)_2(B)^{2+}.$$

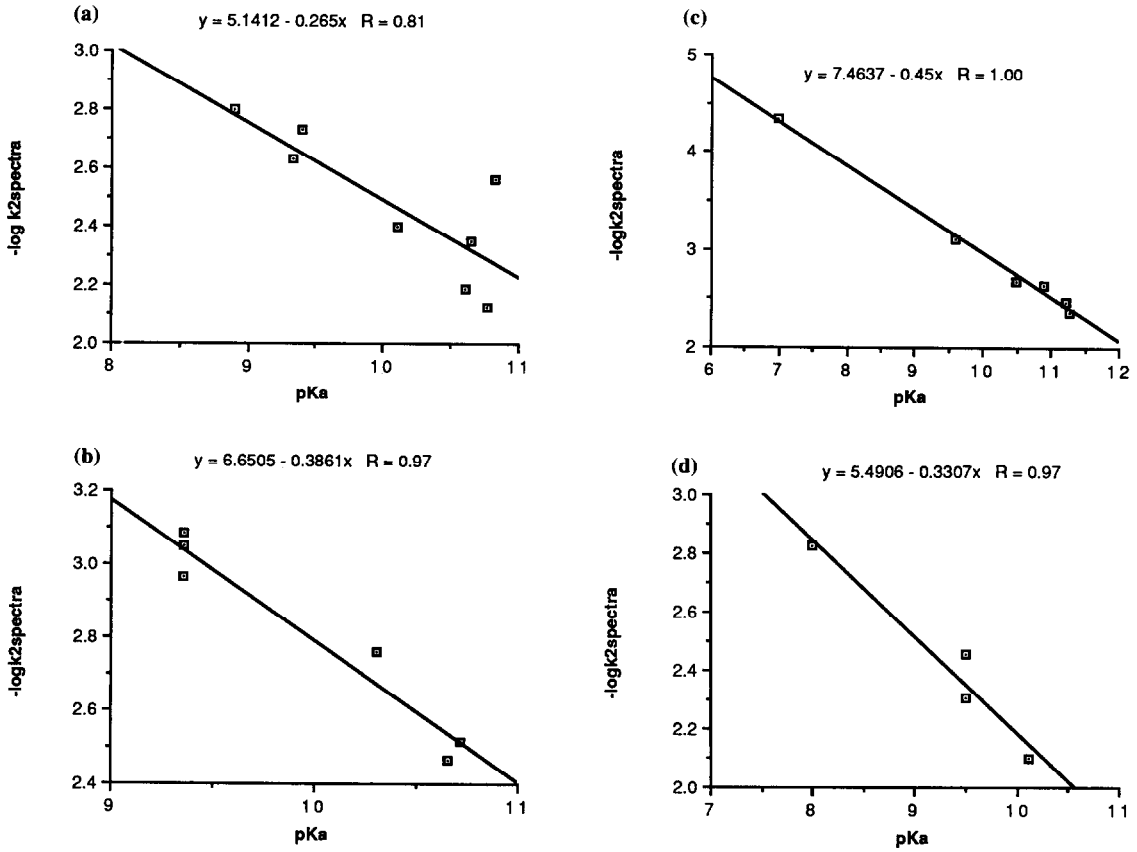

Fig. 3. Plots of $-\log k_2^{spectro}$ vs pK_a (amine) at 25°C (Table 5). (a) Primary amines unsubstituted in the α-position. (b) Primary amines substituted in the α-position. (c) Secondary amines. (d) Aminoalcohols.

Therefore, the general dependence of reactivity is on the base strength. Most interesting, is the fact that under the conditions employed, the reaction with pyridine (pk_a = 5.25) is extremely slow and yet quite satisfactory yields are rapidly obtained using conventional synthetic procedures.[1,4,21] Obviously, in pure DMF, py is too weak to act as a facile proton acceptor, while in water,[21] there are sufficient OH^- ions generated to allow the efficient production of the conjugate base.

Activation parameters for both $k_2^{spectro}$ and k_2^{CD} (Table 1) indicate an overall general trend of large negative values for $\Delta S^{\#}$. This is different from the trend observed in aqueous base hydrolysis reactions where large positive $\Delta S^{\#}$ values are the norm.[6] We attribute this effect to the fact that the species removing the protons in the present reaction are neutral rather than negative, and the charge neutralization that accounts for the large position $\Delta S^{\#}$, in conventional base hydrolysis,[22] is absent.

Aminoalcohols are the most reactive of the bases studied here, when compared with aliphatic amines of similar pK_a values. Autoionization is possible for those systems (similar to the generation of MeO^- in MeOH plus amine[14,15]) and the resulting alkoxide ion is expected to be several orders of magnitude more effective in conjugate base formation. When O-alkylated, the amino alcohols "revert" to the "normal" aliphatic amine values.

$$ROH + :B \Leftrightarrow RO^- + BH^+.$$

Acknowledgement—We thank the New Zealand Universities Grants Committee for funds to purchase instruments used in this work.

REFERENCES

1. R. Feenstra (1904), R. Vogel (1905), W. E. Boes (1910), M. Rosner (1910), R. Samanek (1912), J. C. A. Vink (1912), F. Klaus (1913), R. Plischke (1913), E. Luscher (1917), A. Fischer (1919) and W. A. Redeker (1923).
2. J. Meisenheimer and E. Kiderlen, *Justus Liebigs Annln Chem.* 1924, **438**, 238.

3. A. Ablov, *Bull. Soc. Chim. Fr.* 1936, **3**, 2270; A. Ablov, *Bull. Soc. Chim. Fr.* 1937, **4**, 1783.
4. J. C. Bailar Jr and L. B. Clapp, *J. Am. Chem. Soc.* 1945, **67**, 171.
5. M. J. Davies, P. Mamalis, V. Petrow, B. Sturgeon, G. H. Beaven, E. R. Holiday and A. E. Johnson, *J. Pharm. Pharmac.* 1952, **4**, 448.
6. D. A. House, *Coord. Chem. Rev.* 1977, **23**, 223 and refs cited therein.
7. D. A. House, G. Hall, A. J. Matheson, W. T. Robinson, Foo Chuk Ha and C. B. Knobler, *Inorg. Chim. Acta* 1980, **39**, 257.
8. D. A. House, *J. Chem. Ed.* 1976, **53**, 124.
9. I. J. Kindred and D. A. House, *Inorg. Chim. Acta* 1975, **14**, 185.
10. O. Bortin, *Acta Chem. Scand.* 1976, **30A**, 475.
11. J. McB. Harrowfield, B. W. Skelton, A. H. White and F. R. Wilner, *Aust. J. Chem.* 1986, **39**, 339 and refs cited therein.
12. T. J. Kistenmacher, *Acta Cryst.* 1975, **31B**, 85.
13. T. J. Kistenmacher and D. J. Szalda, *Acta Cryst.* 1975, **31B**, 90.
14. A. S. Janardan, V. Kesavan and D. S. Mahadevappa, *Curr. Sci.* 1980, **49**, 738.
15. A. S. Janardan, V. Kesavan and D. S. Mahadevappa, *Aust. J. Chem.* 1980, **33**, 1485.
16. (a) D. A. House, *Helv. Chim. Acta* 1985, **68**, 1872; (b) A. I. Vogel, *Quantitative Chemical Analysis*, 3rd Edn, p. 255. Longmans (1961).
17. R. G. Pearson, C. R. Boston and F. Basolo, *J. Am. Chem. Soc.* 1953, **75**, 3089.
18. A. J. Cunningham, D. A. House and H. K. J. Powell, *J. Inorg. Nucl. Chem.* 1971, **33**, 572.
19. I. R. Lantzke and D. W. Watts, *Aust. J. Chem.* 1967, **20**, 2623.
20. C. J. Hawkins, *Absolute Configuration of Metal Complexes*. Wiley Interscience, New York (1971).
21. G. Coulter and M. Krishnamurthy, *J. Inorg. Nucl. Chem.* 1977, **39**, 1969.
22. J. O. Edwards, F. Monacelli and G. Ortaggi, *Inorg. Chim. Acta* 1974, **11**, 47 (esp. Section 8).
23. D. Perrin, *Dissociation Constants of Organic Bases in Aqueous Solution*. Butterworth, London (1972).

Polyhedron Vol. 7, No. 13, pp. 1169–1173, 1988
Printed in Great Britain

0277–5387/88 $3.00+.00
© 1988 Pergamon Press plc

INTERACTION OF THE DIPHENYLDICHALCOGENS, $C_6H_5EEC_6H_5$ (E = S, Se AND Te), WITH THE TETRAMERIC HALOGENOTRIMETHYLPLATINUMS. THE FORMATION AND CHARACTERIZATION OF $[\{PtX(CH_3)_3\}_2C_6H_5TeTeC_6H_5]$ (X = Br AND I) AND A DYNAMIC NUCLEAR MAGNETIC RESONANCE STUDY OF $[\{PtI(CH_3)_3\}_2C_6H_5TeTeC_6H_5]$

EDWARD W. ABEL,* MICHAEL A. BECKETT, KEITH G. ORRELL, VLADIMIR ŠIK and DAVID STEPHENSON

Department of Chemistry, University of Exeter, Exeter EX4 4QD, U.K.

and

HARKESH B. SINGH and NARASIMHAN SUDHA

Department of Chemistry, Indian Institute of Technology, Powai, Bombay 400076, India

(*Received* 12 *January* 1988; *accepted* 27 *January* 1988)

Abstract—$Te_2(C_6H_5)_2$ undergoes reaction with $[\{PtX(CH_3)_3\}_4]$ (X = Br, I) in chloroform solution to yield the bimetallic products $[\{PtX(CH_3)_3\}_2\{Te_2(C_6H_5)_2\}]$. These complexes have been characterized by elemental analysis and low temperature multi-element (^1H, ^{13}C, ^{125}Te, ^{195}Pt) NMR studies. $[\{PtCl(CH_3)_3\}_4]$ was unreactive towards $Te_2(C_6H_5)_2$, and similarly $Se_2(C_6H_5)_2$ and $S_2(C_6H_5)_2$ failed to bring about the fission of the tetranuclear $[\{PtX(CH_3)_3\}_4]$ (X = Cl, Br, I) molecule. $[\{PtI(CH_3)_3\}_2\{Te_2(C_6H_5)_2\}]$ was found to be fluxional over the temperature range −20 to +65°C, and a dynamic NMR study of the complex revealed two different modes of fluxionality. The lower energy process has been ascribed to the concerted/correlated double inversion of the coordinated tellurium atoms ($\Delta G^{\ddagger} = 59.7 \pm 0.1$ kJ mol^{-1}), and the higher energy fluxion ($\Delta G^{\ddagger} = 64.5 \pm 0.03$ kJ mol^{-1}) is attributed to an intermetallic ligand commutation of the two tellurium atoms between the two platinum atoms, leading to exchange of the three platinum methyl environments.

There have been extensive investigations of the interaction of organic sulphides and selenides with trimethylplatinum halides;[1] and in particular we have found that the dialkyldichalcogens produced[2–5] the binuclear complexes $[\{PtX(CH_3)_3\}_2$ REER], R = alkyl, E = S and Se. Similar isoelectronic and isostructural complexes of the rhenium carbonyl halides have been reported $[\{ReX(CO)_3\}_2$ REER], E = S, Se and Te, R = alkyl and aryl.[6] The absence of any reported diaryldichalcogen complex of Pt(IV) has prompted us to look at these reactions.

*Author to whom correspondence should be addressed.

EXPERIMENTAL

All reactions were performed under dry nitrogen in Schlenk glassware. $C_6H_5SSC_6H_5$ and C_6H_5Se SeC_6H_5 were used as purchased and $[\{PtX(CH_3)_3\}_4]$ (X = Cl, Br and I) and $C_6H_5TeTeC_6H_5$ were prepared by standard methods.

^1H, ^{13}C-$\{^1H\}$, ^{125}Te-$\{^1H\}$ and ^{195}Pt-$\{^1H\}$ NMR spectra were recorded in $CDCl_3$ solution on a Bruker AM250 F.T. spectrometer operating at 250.1, 62.9, 78.9 and 53.5 MHz, respectively. For ^1H and ^{13}C-$\{^1H\}$ experiments $Si(CH_3)_4$ was used as an internal standard. ^{125}Te-$\{^1H\}$ spectra were referenced to $Te(CH_3)_2$ and ^{195}Pt-$\{^1H\}$ spectra to the standard frequency (Ξ) of 21.4 MHz. All chemi-

cal shifts are quoted as positive to high frequency (low field) of 0 ppm. For the dynamic NMR study, computations of total NMR bandshapes were carried out as previously described,[7] and matching of computer simulated and experimental spectra was performed visually. Activation energies were based upon standard least-squares fitting of Arrhenius and Eyring plots. Errors quoted are those obtained according to the definition of Binsch and Kessler.[8]

Preparation of [{PtI(CH_3)$_3$}$_2${$Te_2(C_6H_5)_2$}]

[{PtI(CH_3)$_3$}$_4$] (0.400 g, 0.25 mmol) was dissolved in chloroform (5 cm^3) with gentle warming. To this solution was added crystalline $Te_2(C_6H_5)_2$ (0.23 g, 0.56 mmol). The ditelluride rapidly dissolved and the solution became dark red. After 1 h at room temperature hexane (25 cm^3) was added to the reaction mixture and the vessel cooled to −20°C overnight. Dark red crystals of the product were obtained and further recrystallized from chloroform/hexane (0.371 g, 60% yield). M.p. 160–162°C; C, 19.0 (18.9); H, 2.4 (2.4)%. The analogous bromide [{PtBr(CH_3)$_3$}$_2${$Te_2(C_6H_5)_2$}] was similarly prepared in 48% yield as orange crystals, m.p. 155–160°C (dec.); C, 20.7 (20.6); H. 2.7 (2.7)%.

Static NMR data for [{PtI(CH_3)$_3$}$_2${$Te_2(C_6H_5)_2$}]

(In $CDCl_3$ at −20°C), ^{1}H: δ 2.18, 6H, ^2J(Pt—H) 72.0 Hz, $PtCH_3$ *trans* Te; δ 1.41, 6H, ^2J(Pt—H) 74.7 Hz, $PtCH_3$ *trans* I; δ 1.15, 6H, ^2J(Pt—H) 75.4 Hz, $PtCH_3$ *trans* I; δ 7.3–7.5 m, 6H, δ 8.0–8.1 m, 4H, {$Te_2(C_6H_5)_2$}. ^{13}C-{^{1}H}: δ 10.51, ^1J(Pt—C) 620.0 Hz, $PtCH_3$ *trans* Te; δ 7.18 ^1J(Pt—C) 667.4 Hz, $PtCH_3$ *trans* I; δ 8.75, ^1J(Pt—C) 657.1 Hz, $PtCH_3$ *trans* I; δ 138.6, 130.8. 130.1, 110.2, {$Te_2(C_6H_5)_2$} ^{195}Pt{^{1}H}: δ 1058.5, ^1J(Pt—^{125}Te) 950 Hz, ^1J(Pt—^{125}Te) 790 Hz. ^{125}Te-{^{1}H}: δ 840.1, ^1J(Pt—Te) 949 Hz.

Static NMR data for [{PtBr(CH_3)$_3$}$_2${$Te_2(C_6H_5)_2$}]

(In $CDCl_3$ at −50°C). ^{1}H: δ 1.91, 6H, ^2J(Pt—H) 70.1 Hz, $PtCH_3$ *trans* Te; δ 1.28, 6H, ^2J(Pt—H) 76.9 Hz, $PtCH_3$ *trans* I; δ 1.04, 6H, ^2J(Pt—H) 77.7 Hz, $PtCH_3$ *trans* I, δ 7.2–7.5 m, 6H, δ 8.0 m, 4H, {$Te_2(C_6H_5)_2$} ^{13}C-{^{1}H}: at −20°C, δ 13.04 ^1J(Pt—C) 631.8 Hz, $PtCH_3$ *trans* I; δ 3.16, ^1J(Pt—C) 689.8 Hz, $PtCH_3$ *trans* I; δ 1.25, ^1J(Pt—C) 691.4 Hz, $PtCH_3$ *trans* I; δ 139.1, 130.8, 130.1, 108.8, {$Te_2(C_6H_5)_2$}. ^{195}Pt-{^{1}H}: δ 1578.3, ^1J(Pt^{125}—Te) 881 Hz; ^{125}Te-{^{1}H}: δ 783.1, ^1J(Pt—Te) 881 Hz.

NMR data of $Te_2(C_6H_5)_2$

(In $CDCl_3$ at −20°C). ^{13}C-{^{1}H}: δ 137.4, 129.4, 128.1, 107.9. ^{125}Te-{^{1}H}: δ +422.

Dynamic NMR data for [{PtI(CH_3)$_3$}$_2${$Te_2(C_6H_5)_2$}]

Parameters for the computer simulation of ^{1}H spectra were extracted from the ^{1}H static low temperature data above and T_2^* was calculated, from the experimental half-height band width $\Delta\nu_{1/2}$, as 0.193 s. First-order rate constants obtained for synchronous/correlated double tellurium atomic inversion over a range of temperatures were obtained (Table 1). Energy data obtained from these values are $\Delta G^\ddagger = 59.7 \pm 0.1$ kJ mol^{-1}, $\Delta H^\ddagger = 60 \pm 2$ kJ mol^{-1}, $\Delta S^\ddagger = 1.6 \pm 7$ J K^{-1} mol^{-1}, $E_a = 63 \pm 2$ kJ mol^{-1}, $\log_{10}(A/s^{-1}) = 13.3 \pm 0.4$.

First order rate constants for the double tellurium inversion in the temperature range 303–338 K were extrapolated from the above data; and the first-order rate constants for methyl scrambling could be obtained from the computer simulated and experimental spectra (Table 1). The Arrhenius and Eyring activation energy parameters for the methyl scrambling process calculated from these first-order rate constants are $\Delta G^\ddagger = 64.5 \pm 0.03$ kJ mol^{-1}, $\Delta H^\ddagger = 76 \pm 0.7$ kJ mol^{-1}, $\Delta S^\ddagger = 37 \pm 2$ J K^{-1} mol^{-1}, $E_a = 78 \pm 0.7$, $\log_{10}(A/s^{-1}) = 15.2 \pm 0.1$.

RESULTS AND DISCUSSION

Diphenyldisulphide and diphenyldiselenide have both been reported[6] to form the binuclear com-

Table 1. First order rate constants for the synchronous/correlated double tellurium atom inversion, Eq–Eq and of the intermetallic ligand commutation process, Ax–Eq

	$PtCH_3$ exchange rate constants (s^{-1})	
Temp. (K)	Eq–Eq	Ax–Eq
263	3	
268	10	
273	22	
278	35	
283	50	
288	85	
293	140	
298	220	
303	340	50
308	520	85
313	784	140
318	1167	230
323	1716	370
328	2495	550
333	3584	800
338	5095	1200

plexes $[Re_2(CO)_6X_2\{E_2(C_6H_5)_2\}]$, (X = Cl, Br, I; E = S, Se). Despite prolonged reaction times and a range of conditions we have failed to obtain the corresponding isoelectronic and isostructural complexes of Pt(IV) from the reactions between the $[\{PtX(CH_3)_3\}_4]$ tetramer and diphenyldisulphide and diphenyldiselenide. Similarly, there appears to be no reaction between $[\{PtCl(CH_3)_3\}_4]$ and diphenylditelluride. In contrast, however, the reactions between $Te_2(C_6H_5)_2$ and the corresponding bromide and iodide tetramers $[\{PtX(CH_3)_3\}_4]$ (X = Br and I) proceed rapidly in chloroform at room temperature to produce the binuclear species (Fig. 1).

$$[\{PtX(CH_3)_3\}_4] + 2Te_2(C_6H_5)_2 \rightarrow 2[\{PtX(CH_3)_3\}_2\{Te_2(C_6H_5)_2\}] \quad (X = Br, I).$$

These orange–red crystalline products are formed in good yield and appear to be air stable in both solid and solution.

Low temperature NMR studies

These binuclear complexes were found to be fluxional in solution like the corresponding binuclear Pt(IV) complexes of dialkyldisulphides and dialkyldiselenides. At low temperatures fluxionality is halted and NMR parameters for the "static" molecules may be obtained. Multinuclear NMR data (^1H, ^{13}C, ^{125}Te, ^{195}Pt) for these two new complexes are recorded in the experimental section.

The low temperature ^1H and $^{13}C\text{-}\{^1H\}$ spectra of the complexes are consistent with the structure shown in Fig. 1. This *trans* (DL) configuration for the complexes is also that adopted in the solid state for the analogous binuclear rhenium(I) complexes and the corresponding platinum(IV) complexes of the dialkyl–disulphides and –diselenides.

At low temperature the ^1H NMR spectra of these complexes show the expected aromatic ^1H signals (relative intensity 10) at δ 7.2–8.1 and also three low frequency signals (each one of relative intensity six). These are the ^{195}Pt-coupled hydrogens of the platinum methyl groups. Of these three separate $PtCH_3$ signals, the one at highest frequency is assigned to the axial $PtCH_3$ groups *trans* to the Te atoms, and the other two are the equatorial $PtCH_3$ groups *trans* to the halide atoms. These equatorial $PtCH_3$ resonances have $^2J(^{195}Pt—^1H)$ and $^1J(^{195}Pt—^{13}C)$ coupling constants in the ranges expected[9] for $PtCH_3$ groups *trans* to bridging halides, whilst the $^2J(^{195}Pt—^1H)$ values for the $PtCH_3$ groups *trans* to Te are at the high end of the ranges already observed[3] in the related $S_2(CH_3)_2$ and $Se_2(CH_3)_2$ complexes.

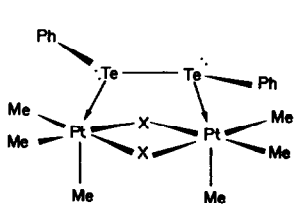

Fig. 1. Proposed *trans* structure of $[\{PtX(CH_3)_3\}_2\{Te_2(C_6H_5)_2\}]$.

The ^{125}Te spectra of these materials show coupling to ^{195}Pt with $^1J(^{125}Te—^{195}Pt)$ of *ca* 900 Hz. The ^{125}Te resonances of the complexes are 361 ppm (X = Br) and 417 ppm (X = I) to the high frequency side of the free ligand value of δ 422 ppm. The magnitudes of the $^1J(^{125}Te—^{195}Pt)$ coupling constants are confirmed by ^{195}Pt spectra where satellites from ^{125}Te nuclei (natural abundance 7%) and ^{123}Te nuclei (natural abundance 0.89%) can be seen. Moreover, $^1J(^{125}Te—^{195}Pt)$ and $^1J(^{123}Te—^{195}Pt)$ are, as expected, in proportion to the magnetogyric ratios of the ^{123}Te and ^{125}Te nuclei.

^{13}C and ^{125}Te data were obtained for the free ligand $Te_2(C_6H_5)_2$ at −20°C and are noted in the experimental section. Both ^{13}C and ^{125}Te spectra of $Te_2(C_6H_5)_2$ showed exchange broadening at raised temperatures. This has previously been seen in the spectra of diarylditellurides and has been attributed to an exchange reaction.[10] The ^{125}Te signal in $Te_2(C_6H_5)_2$ was sensitive to temperature and shifts of *ca* 0.3 ppm K^{-1} were observed over the range −20 to +20°C.

Dynamic NMR studies of the complex $[\{PtI(CH_3)_3\}_2\{Te_2(C_6H_5)_2\}]$

There are reversible changes both in the number and shape of the $PtCH_3$ signals in the ^1H spectrum of this complex on warming from −20 to +65°C. Between −20 and +20°C the two individual equatorial $PtCH_3$ signals broaden and coalesce. A further increase in temperature causes broadening of the axial PtMe signal and its eventual coalescence with the single averaged equatorial $PtCH_3$ signal at *ca* +50°C. Above this temperature the single $PtCH_3$ signal sharpens and its ^{195}Pt satellites are visible at +65°C. These fully reversible changes indicate that the complex is undergoing a series of fluxional rearrangements, or alternatively that ligand dissociation/recombination may be occurring. However, ^{13}C NMR spectra of the complex in the presence of free $Te_2(C_6H_5)_2$ show that at +50°C no ligand exchange is taking place, and thus the spectral changes observed in the $PtCH_3$ region of the ^1H spectrum are intramolecular in origin.

These changes, involving two stage collapse of the $PtCH_3$ region of the ^1H NMR spectra are remi-

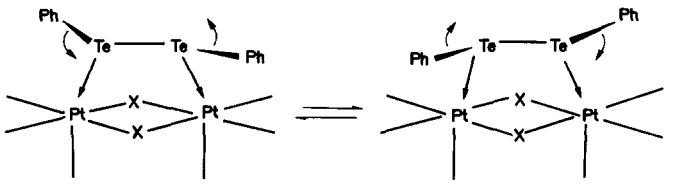

Fig. 2. Synchronous or correlated tellurium atomic inversions in $[\{PtX(CH_3)_3\}_2\{Te_2(C_6H_5)_2\}]$.

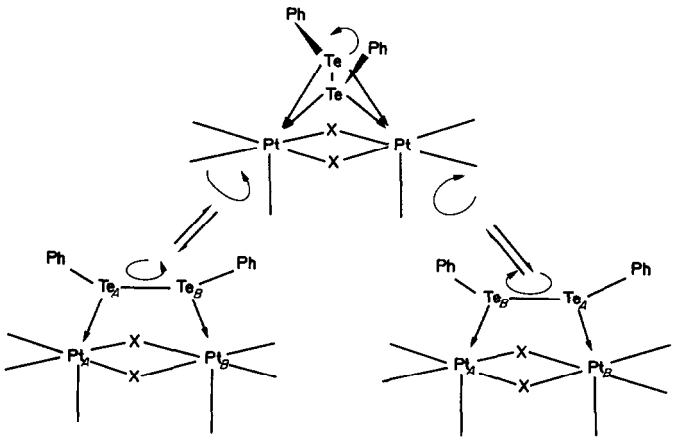

Fig. 3. Intermetallic ligand commutation in $[\{PtX(CH_3)_3\}_2\{Te_2(C_6H_5)_2\}]$, showing the proposed facile fluxionality of the methyl groups in the effectively seven coordinate platinum atoms.

niscent of those observed[4] for the binuclear complexes of disulphides and diselendides. The lower energy process for which only the equatorial $PtCH_3$ signals are averaged can be attributed to the double chalcogen inversion which can involve the tellurium ligand atoms in either synchronous or correlated inversions (Fig. 2). The higher energy process, in which all three $PtCH_3$ signals are averaged, is ascribable to a ligand commutation process, Fig. 3, the transition state of which involves seven coordinate Pt(IV). In this transition state the rotational scrambling of all $PtCH_3$ groups would be a facile process.

The equatorial $PtCH_3$ region of the ^1H NMR spectrum of $[\{PtI(CH_3)_3\}_2\{Te_2(C_6H_5)_2\}]$ was simulated over the temperature range 0–25°C in intervals of 5°C in order to evaluate the process of double tellurium inversion, Fig. 2. $\Delta G^{\ddagger}$ for this transformation was found to be 59.7 ± 0.1 kJ mol^{-1}, and values for $\Delta S^{\ddagger}$ and $\log_{10}(A/s^{-1})$ (see Experimental) indicated the process to be strictly intramolecular. Unfortunately the sulphur and selenium analogues could not be prepared to obtain comparative values of $\Delta G^{\ddagger}$. However, double sulphur and selenium inversions in comparable dialkyldichalcogen complexes have values for $\Delta G^{\ddagger}$ of 40.7 kJ mol^{-1} $[\{PtBr(CH_3)_3\}_2\{S_2(CH_3)_2\}]$ and 53.4 kJ mol^{-1} $[\{PtBr(CH_3)_3\}_2\{Se_2(CH_3)_2\}]$, respectively.[4] Thus the values for the activation energies of such double inversions are clearly seen as S < Se < Te and are in accord with the order indicated previously in a series of mononuclear complexes of Pt(II).[11]

The higher temperature fluxionality, which then averages the axial and equatorial $PtCH_3$ groups, has a value for $\Delta G^{\ddagger}$ of 64.5 kJ mol^{-1} for this intermetallic ligand commutation/methyl scrambling process, Fig. 3. Comparing this with the corresponding values[4] for sulphur commutation (in $[\{PtX(CH_3)_3\}_2\{S_2(CH_3)_2\}]$) of 61.3–62.4 kJ mol^{-1} and selenium commutation (in $[\{PtX(CH_3)_3\}_2\{Se_2(CH_3)_2\}]$) of 65.1–65.2 kJ mol^{-1}, we see that the activation energy for this particular fluxional process is virtually insensitive to the nature of the commuting chalcogen atom, in contrast to the great sensitivity for the inversion process. Whilst values of $\Delta S^{\ddagger}$ and $\log_{10}(A/s^{-1})$ are high (see Experimental), they are not unreasonably so for a unimolecular process of this complexity.

REFERENCES

1. E. W. Abel, S. K. Bhargava and K. G. Orrell, *Prog. Inorg. Chem.* 1984, **32**, 1.
2. E. W. Abel, A. R. Khan, K. Kite, K. G. Orrell, V. Šik, T. S. Cameron and R. Cordes, *J. Chem. Soc., Chem. Commun.* 1979, 713.

3. E. W. Abel, A. R. Khan, K. Kite, K. G. Orrell and V. Šik, *J. Chem. Soc., Dalton Trans.* 1980, 1169.
4. E. W. Abel, A. R. Khan, K. Kite, K. G. Orrell and V. Šik, *J. Chem. Soc., Dalton Trans.* 1980, 2220.
5. E. W. Abel, A. R. Khan, K. Kite, K. M. A. Malik and M. A. Mazid, *J. Organometal. Chem.* 1982, **235**, 121.
6. F. Calderazzo, D. Vitali, R. Poli, J. L. Atwood, R. D. Rogers, J. M. Cummings and I. Bernal, *J. Chem. Soc., Dalton Trans.* 1981, 1004; J. Korp, I. Bernal, J. L. Atwood, F. Calderazzo and D. Vitali, *J. Chem. Soc., Dalton Trans.* 1979, 1492 and refs therein.
7. E. W. Abel, K. Kite, K. G. Orrell, V. Šik and B. L. Williams, *J. Chem. Soc., Dalton Trans.* 1981, 2439.
8. G. Binsch and H. Kessler, *Angew. Chem., Int. Edn. Engl.* 1980, **19**, 411.
9. E. W. Abel, A. R. Khan, K. Kite, K. G. Orrell and V. Šik, *J. Chem. Soc., Dalton Trans.* 1980, 1175.
10. P. Granger, S. Chapelle, W. R. McWhinnie and Ali Al-Rubaie, *J. Organometal. Chem.* 1981, **220**, 149.
11. R. J. Cross, T. H. Green and R. Keat, *J. Chem. Soc., Chem. Commun.* 1974, 207; R. J. Cross, T. H. Green and R. Keat, *J. Chem. Soc., Dalton Trans.* 1976, 1150.

Polyhedron Vol. 7, No. 13, pp. 1175–1186, 1988
Printed in Great Britain

0277–5387/88 $3.00+.00
Pergamon Press plc

EQUILIBRIA IN COMPLEXES OF N-HETEROCYCLES—XLVI.* POLYMORPHISM AND SOLVATOCHROMISM IN SOME SALTS OF THE TRIS-(1,10-PHENANTHROLINE) NICKEL(II) ION†

R. D. GILLARD‡ and S. H. MITCHELL

Department of Chemistry, University College, P.O. Box 78, Cardiff CF1 1XL, Wales, U.K.

(*Received* 6 *November* 1987; *accepted* 1 *February* 1988)

Abstract—The extensive polymorphism among hydrated racemic and resolved salts of tris-1,10-phenanthrolinenickel(II), notably the iodides, $[Ni(phen)_3]I_2 \cdot nH_2O$, is described.

Phenanthroline is a popular ligand. Many compounds have been prepared[1–6] and much work on tris-complexes has included the kinetics and mechanisms of the racemization of the octahedral tris-complexes in solid[7–9] and solution[10,11] phases.

The tris-(1,10-phenanthroline)nickel (II) cation is easy to make and resolve.[12–14] It has been used to resolve other complex anions by the unusual method of clay column chromatography, where $D\text{-}(-)_{589}\text{-}[Niphen_3]^{2+}$ is adsorbed on sodium–montmorillonite and the complex to be resolved is passed through this material.[15] Another method of resolving (partially) $[Ni(phen)_3]^{2+}$ is based on the Pfeiffer effect.[16] $[M(phen)_3]^{2+}$ complexes have classically shown this effect[17,18] and a number have been investigated; M = Zn,[17] Ru indirectly on solubility grounds;[19] and Zn, Ni, Co, Mn, Cd, Hg.[20,21] Enantiomerization of $[Ni(phen)_3]^{2+}$ has been studied in (−)-2,3-butanediol[22] for which the equilibrium constant 1.062 $[K_{25°}(-)/(+)]$ is found and in aqueous solution containing[16] (−)-malic acid.

Recent work[7,8] on rates of racemization of solid salts of $[Ni(phen)_3]^{2+}$ indicates that different phases may exist. No crystallographic information was presented with the kinetic data, nor is it available at all. It may be that the various reports concern different phases. (Certainly, polymorphism and/or the existence of several solvates is known for a number of phenanthroline-containing compounds, for example *cis*-$[M(phen)_2Cl_2]Cl \cdot nH_2O$, with[1] M = Ir, $n = 2$ or 3; M = Co, Rh or Cr with[5] up to five phases identified; M = Co and Cr.[3])

It is surprising that there have been no studies using powder diffraction or crystal structures for these simple salts of $[Ni(phen)_3]^{2+}$, although one report says that $[Ni(phen)_3]I_2$ is amorphous.[9,36] The literature certainly reveals (Table 1) that the state of hydration of some salts is variable or at least hard to determine.

We have now established the crystal and molecular structure of one of the stable forms of $[Ni(phen)_3]I_2 \cdot 3H_2O$ (reported elsewhere) and established the polymorphism in both racemic and optically active systems, which we describe here.

The present distinction between phases is based almost exclusively on X-ray powder diffractograms and photographs. As powders, many of the compounds are very similar in colour (pink or salmon-pink). In many cases, the powder pattern and degree of hydration were particularly difficult to determine because of changes that began when the compounds were removed from solution. For this reason, good crystals only (when available) were used to determine the hydration number and precautions were taken when recording powder patterns.

EXPERIMENTAL

$[Ni(phen)_3]X_2 \cdot nH_2O$. Typically: 1,10-phenanthroline monohydrate (1.0 g, 5.05×10^{-3} moles) was stirred in water (40 cm^3) and an aqueous solution of a nickel salt (e.g. $NiSO_4 \cdot 7H_2O$, 0.45 g, 1.6×10^{-3} moles) was added dropwise, giving (over

* Part XLV—D. W. Clack and R. D. Gillard, *Inorg. Chim. Acta* 1988, **141**, 37.

† Presented, in part, at the NZIC Conference, University of Otago, Dunedin, (August 1986).

‡ Author to whom correspondence should be addressed.

Table 1. Reported states of hydration and solvation for salts of racemic (±) or resolved (+, −) $[Ni(phen)_3]X_2 \cdot nS$

X	S	n (±)	n (+) or (−)	Ref.
Cl	H_2O	4		23
		6		24–26
		7		27
		8		4
		10		28, 29
			8	14
Br	H_2O	5		4
		6		24
		7		18
			5	14
I	H_2O	2		4, 24
		3		1
		7		25
			4	30
NO_3	H_2O	9		18
SO_4[a]	H_2O	9		18
		14		29
ClO_4	H_2O	0.5		25
		1		4
		2		12
			2	30, 32, 33
			3	12, 31
IO_3	H_2O		6.5	34
Cl	CH_2Cl_2	2		35
	CH_3OH	2		35
	CH_3OH+H_2O	1+1		22
	CH_3OH+H_2O		2+2	22

[a] Here, $SO_4 = 2X$.

a few minutes) a clear burgundy solution. The complex cation was precipitated by the addition of an excess of the appropriate anion. For the chloride, it is necessary to dilute the solution with acetone to effect precipitation. The solids were recrystallized by dissolution in water (with or without heating) and reprecipitation.

Chloride and bromide salts were prepared from $NiCl_2$ and $NiBr_2$, while the iodide salt was prepared from $NiCl_2$ or $NiSO_4$.

(+)- and (−)-$[Ni(phen)_3]I_2 \cdot nH_2O$. $[Ni(phen)_3]^{2+}$ was resolved by the method of Dwyer and Gyarfas.[12] The chloride was the starting material, and the enantiomers were precipitated as iodide rather than perchlorate salts. Both enantiomers were recrystallized by washing them through a filter paper with cold water into an aqueous potassium iodide solution so that they precipitated immediately. The purity of the enantiomers was established by polarimetry. (Sucrose was the calibrant.) Solutions were prepared and their optical rotation measured immediately. Electronic spectra were then recorded and the concentration in solution calculated as $[Ni(phen)_3]I_2 \cdot 3H_2O$. The specific rotations, $[\alpha]_D$, of (+)- and (−)-$[Ni(phen)_3](ClO_4)_2 \cdot 3H_2O$ have already been determined: (+)- and (−)-$[Ni(phen)_3](ClO_4)_2 \cdot 3H_2O$ $[\alpha]_D^{15°}$, $H_2O = 1463$;[12] (+)-$[Ni(phen)_3](ClO_4)_2 \cdot 3H_2O$ $[\alpha]_D^{25°}$, H_2O/acetone (50% v/v) = +1476;[13] (−)-$[Ni(phen)_3](ClO_4)_2 \cdot 3H_2O$ $[\alpha]_D^{25°}$, H_2O/acetone (50% v/v) = −1482.[13]

If a molar rotation [M] is defined by $[M] = r/(lM)$ (r = rotation, degrees; l = cell path, decimeters; M = molarity) then $[\alpha] = 1000$ [M]/mol. wt. The molar rotation calculated for $[Ni(phen)_3]^{2+}$ from the perchlorate salt is ~ 1260 ($[\alpha] = 1479$). This number was used to calculate the purity (enantiomeric excess) of the iodide salt assuming that the anion does not affect the rotation. In all determinations, the concentration of the complex is less than 10^{-3} molar.

The purity of the freshly prepared resolved salts (phase B) is 98% for the (+)-isomer, and 92% for its (−)-enantiomer. After 16 months (now phase B′), the purity was still > 80%.

X-ray powder diffraction

Tables 2–5 give the recorded patterns. Three recording methods were used; chiefly Guinier photographs, but also diffractograms and Debye–Scherrer photographs. Guinier photographs took 3–4 h to record and are difficult to measure, because the complex is a weak reflector and the lines are broad. A diffractometer was used to record a few patterns; these were recorded rapidly at 2°2θ/min to ensure minimal changes.

More detail is present in diffractograms because band profiles and intensities may be readily examined. When available, these were used as sources for the results in the tables. Identification of the phases initially precipitated was made difficult by the ready loss of water, accompanied by colour changes observed before and after a scan. Guinier X-ray powder photographs required relatively long exposures, and there must necessarily then be uncertainty as to whether the observed colour changes were accompanied by structural changes. The changes may have been extremely rapid, depending on the prevailing environmental conditions and only the pattern of the more stable final phase was obtained.

The original crystal morphology and/or colour were good indicators of the parent phase and with

Table 2. X-ray powder patterns for phases of $[Ni(phen)_3]I_2 \cdot nH_2O$

Phase	B	D	$(I/I_0)^a$	B′	C′
	10.281w	10.402	8	9.826w	9.612s
	9.165s	9.212	3	8.385vw	7.468vw
	8.153s	8.153	4	7.437vw	6.889vw
	7.468vw	7.595	2	6.810m	6.371s
	6.997vw	7.053	4	6.394s	5.887s
	6.681vw	6.150	9	5.717s	5.626vw
	6.416w	5.735	100	5.471w	5.324w
	6.303m	5.421	7	5.356vw	4.758m
	5.965w	4.996	5	5.096w	4.364w
	5.644s	4.821	4	4.969w	4.095vs
	5.556s	4.569	4	4.439m	3.892m
	4.506m	4.428	4	4.332w	3.802s
	4.385w	4.185	17	4.142m	3.466w
	4.076s	4.049	38	3.810vs	3.232w
	3.986m	4.017	13	3.693w	2.801w
	3.858m	3.875	27	3.493vw	2.640vw
	3.801s	3.809	18	3.421w	
	3.670vw	3.711	43	3.153w	
	3.597w	3.433	6	3.079vw	
	3.568w	3.287	6		
	3.254vw	3.107	18		
	3.084vw	3.032	12		
		3.010	10		
		2.866	12		
		2.801	8		
		2.767	8		
		2.684	12		

[a] For phase D.

suitable precautions [(a) using crushed rather than ground crystals; (b) leaving the material damp, with water or aq. KI; (c) mulling in Nujol; (d) encapsulating damp material between sellotape layers] a diffraction pattern of the parent phase was obtained.

Crystal phases of $[Ni(phen)_3]I_2 \cdot nH_2O$

When the tris-(1,10-phen)nickel(II) cation, prepared from either $NiCl_2$ or $NiSO_4$, is precipitated with aqueous potassium iodide, a number of different coloured compounds are produced.

(i) *Racemic phases.* If a concentrated aqueous solution of potassium iodide is rapidly added to a solution of a salt of the complex, a lilac–pink precipitate is produced (phase A). At low iodide concentration only, this rapidly (minutes) changes to a new salmon-pink phase (B). This change does not happen with a higher concentration of iodide. Alternatively, *slow* addition of aqueous potassium iodide to precipitate the complex gives phase (B) directly. If the iodide concentration is not too high, phases A or B recrystallize over several days giving rose-red rhombs of a third phase (C). A fourth phase (D), also salmon-pink, was prepared by rapidly treating a solution of the iodide salt with a concentrated aqueous solution containing an excess of KI.

Phase A: the identification of this as a distinct phase is based on its colour, lilac–pink. All attempts to record a powder pattern (Guinier) resulted in phase B, B′, or C type patterns being recorded. Similarly, attempts to prepare a dry powder for thermogravimetric analysis resulted in a colour change to salmon-pink indicating a phase change. Refrigeration of the damp material immediately after preparation retains the colour.

Phase B and B′: good crystals (pale rose-pink) of phase B may be prepared by recrystallization from hot water. But unless the crystallizing solution and mother liquor is cooled these readily recrystallize to give phase C. Crystals freshly removed from solution and dried on a filter paper, show a great variability in water content (Table 6). Water con-

Table 3. X-ray powder pattern of $[Ni(phen)_3]I_2 \cdot 3H_2O$ (phase C)

hkl	d_c	I_c	d_0	*hkl*	d_c	I_c	d_0
110	12.683	24	12.538vw	112	4.555	65	4.564vs
200	9.954	26	9.936vw	31$\bar{2}$	4.508	28	4.484vw
			9.261vw	202	4.194	15	4.171vw
011	8.774	31	8.672vw	33$\bar{1}$	4.150	13	4.124vw
11$\bar{1}$	8.732	10		32$\bar{2}$	4.073	12	4.058w
210	8.517	33	8.465vw	212	4.064	44	
			8.230vw	41$\bar{2}$	4.014	22	4.004vw
111	7.472	23					3.875vw
21$\bar{1}$	7.395	85	7.345m	041	3.824	14	
220	6.341	100	6.326m	14$\bar{1}$	3.820	70	3.810s
211	5.989	55	5.965w	240	3.802	28	
31$\bar{1}$	5.923	39		222	3.736	39	3.371m
121	5.873	22	5.484w	43$\bar{1}$	3.693	19	
22$\bar{1}$	5.835	8		24$\bar{1}$	3.684	10	
			5.662vw	421	3.675	39	3.670m
			5.539vw	302	3.669	10	
10$\bar{2}$	5.352	15	5.324vw	50$\bar{2}$	3.620	75	3.612s
130	5.288	22	5.262vw	34$\bar{1}$	3.452	13	3.453w
002	5.186	23	5.140vw	322	3.351	58	3.345w
11$\bar{2}$	5.090	84	5.068s	600	3.318	12	
221	5.066	38		52$\bar{2}$	3.314	26	3.308w
32$\bar{1}$	5.026	32	4.997vw	53$\bar{1}$	3.268	15	
400	4.977	7	4.942vw	12$\bar{3}$	3.266	31	
012	4.946	7		610	3.252	39	3.249m
031	4.849	53	4.835m	113	3.210	11	
13$\bar{1}$	4.841	35		44$\bar{1}$	3.175	27	3.198vw
311	4.829	21		32$\bar{3}$	3.169	18	3.164w
410	4.764	87	4.758m	61$\bar{2}$	3.154	7	3.116vw
102	4.740	14					3.074vw
131	4.590	49		123	3.041	14	3.043vw
23$\bar{1}$	4.572	46		42$\bar{3}$	3.015	8	3.008vw

tents between 14.1 and 11.2% (7.8–6.0 H_2O) were found by thermogravimetry.

Air-drying begins a process of transformation, shown by a change from pale rose-pink to orange. Water is lost to varying degrees, probably depending on the environmental conditions (Table 6). Samples presumably in equilibrium with the atmosphere gave water contents of 10.0–4.5%. (5.3–2.2 H_2O). Below 6.6% (3.0 H_2O), a new salmon-pink–orange phase (B′) is found.

Oven dehydrated samples of phase B give a phase B′ pattern and when rehydrated (95% RH, Na_2SO_4) gave back—in one instance—phase B′ and—in another—phase C, with water contents of 4.8 and 5.2%, respectively.

Phases C and C′: phase C grows rapidly by the recrystallization of phases A and B, which even when merely damp, will transform into good crystals. Rose-red rhombs grow by the accretion of the complex from its immediate surroundings with a gradually expanding cleared zone around each crystal. Phase C is a trihydrate. We report its crystal structure elsewhere. It is reasonably stable: air-drying does not cause loss of water. Dehydration by heating gives a cream-coloured powder, phase C′, which rehydrates readily to reform the present trihydrate. Analysis for $[Ni(phen)_3]I_2 \cdot 3H_2O$: Found: C, 47.5; H, 3.6; H, 9.4; H_2O, 5.9. Calc. for $C_{36}H_{30}I_2N_6NiO_6$: C, 47.7; H, 3.3; N, 9.3; H_2O, 6.0%.

Phase D: this was obtained only once, when an aqueous solution of the iodide was precipitated with a concentrated aqueous solution of potassium iodide. The salmon-pink precipitate was filtered off, washed with water and the X-ray powder diffractogram recorded on the damp material. Dehydration by heating (110°C) gave phase B′ (mustard colour).

(ii) *Chiral phases.* The phase system of (+)- or (−)-$[Ni(phen)_3]I_2 \cdot nH_2O$ is similar to that of the

Table 4. X-ray powder patterns of (+)- and (−)-$[Ni(phen)_3]I_2 \cdot nH_2O$ and the racemization product

(+)-B d_0	(−)-B′ d_0	I/I_0	B_{rac} d_0	I/I_0	(−)-C d_0	(−)-C′ d_0
10.494m	9.825	20	11.120	19	15.781w	16.289
10.105m	7.917	14	9.212	18	14.488w	9.664vs
9.612vw	7.778	13	8.445	23	12.109m	8.116w
9.358vw	6.915	25	7.628	19	10.982w	7.390m
8.889w	6.745	23	7.405	20	9.638s	6.942vw
8.505w	5.876	39	6.451	28	8.801s	6.758m
8.267vw	5.698	38	6.015	11	8.210w	6.005m
7.864w	5.300	40	5.886	11	7.830w	5.886s
7.595w	5.147	33	5.698	58	7.612w	5.716vw
7.225m	4.914	18	5.573	68	7.254vs	5.617s
6.997w	4.634	45	5.200	10	6.915s	5.471vw
6.732vw	4.353	29	5.133	17	6.558vw	5.308s
6.558w	4.156	31	5.096	17	6.129vw	4.133vw
6.325m	4.076	40	4.975	17	5.985vw	4.821m
6.150w	4.017	22	4.682	17	5.847w	4.646vw
5.975w	3.900	100	4.500	41	5.608vw	4.563vw
5.809m	3.833	60	4.363	18	5.170vw	4.506vw
5.626m	3.746	21	4.195	52	5.111w	4.444vw
5.488w	3.625	68	4.081	100	4.982w	4.301m
5.364vw	3.516	12	3.917	89	4.834m	4.220w
5.238m	3.479	16	3.891	84	4.646vw	4.104w
5.111m	3.388	9	3.817	32	4.439vw	4.022w
4.854m	3.314	12	3.707	14	4.395vw	3.917w
4.783w	3.290	14	3.554	24	4.327m	3.842m
4.483w	3.249	15	3.496	48	4.230w	3.769w
4.406m	3.203	16	3.237	23	4.104w	3.685w
4.321w	3.110	35	3.153	23	4.040m	3.600w
4.086s	2.980	27	3.058	23	3.942w	3.533w
4.035vs	2.862	15	3.045	23	3.801w	3.472w
3.908w	2.824	22	2.990	20	3.746w	3.401w
3.825s	2.752	11	2.884	10	3.640w	3.344w
3.769m	2.676	21	2.813	19	3.593w	3.314vw
3.662w	2.614	14	2.726	13	3.506vw	3.249w
3.640w			2.638	6	3.462w	3.203vw
3.459w			2.546	8	3.388vw	3.105vw
3.360w			2.479	23	3.341vw	3.053vw
3.249w					3.278w	2.988vw
3.164w					3.243vw	2.956vw
3.131vw					3.192w	
3.078w						
2.978vw						
2.940vw						
2.893w						
2.848vw						
2.820vw						
2.792vw						

racemate. Observations and comments concerning colour and stability are similar for both systems.

The chiral phase B is readily prepared by adding aqueous potassium iodide to a solution of the enantiomer. In contrast to the racemic case, phase C is difficult to prepare because it is necessary to recrystallize phase B at low temperature (2°C), to keep the solution concentration as low as possible, while at the same time maintaining some transfer to the new phase. With the bulk of the complex in the solid state, racemization is much slower.

Other salts: other salts of $[Ni(phen)_3]^{2+}$, namely

Table 5. X-ray powder patterns of $[Ni(phen)_3]X_2 \cdot nH_2O$

X = Cl	Br	ClO_4
10.749vs	11.120vw	9.717s
7.694vw	10.652s	9.117w
5.372w	7.899w	8.714vw
4.406w	7.563m	7.761vw
4.240w	6.370w	6.915s
3.817s	6.108w	6.440s
3.597m	5.906w	6.303vw
3.332w	5.488w	5.790m
3.249vw	5.356m	5.388m
2.581vw	5.185vw	5.111w
2.535vw	4.982vw	5.024w
	4.808vw	4.783brw
	4.395vw	4.658w
	4.132vw	4.552vw
	4.040s	4.483vw
	3.833vs	4.385m
	3.561w	4.095w
	3.493w	3.934vw
	3.433w	3.858vs
	3.260vw	3.738w
	3.110brw	3.692vw
	3.027brw	3.604vw
	2.862brw	3.540vw
	2.788brw	3.472vw
		3.426w
		3.363vw
		3.308vw
		3.169w
		3.027brvw
		2.813vw
		2.784w

Br, Cl, NO_3, ClO_4 gave compounds, precipitated as hydrates, that were stable and did not change colour on air-drying, although some water of crystallization was lost. The bromide salt was the most variable. Good plum-red crystals were produced and care was taken to remove surface water before analysis. Thus, the variability of water content found between successive runs can be attributed only to occluded water. No X-ray powder photograph showed sufficient similarity with any other (including iodide phases) to indicate isomorphous phases, nor was any salt found to be polymorphic.

Thermal reactions: Thermogravimetric analysis (Table 6) was used chiefly to determine water content. Crystals were removed from solution immediately before use and dried on a filter paper; because of the high volume to surface ratio, there are unlikely to be serious errors due to adhering surface water. The thermogravimetric analysis shows results similar to those found by others;[9,26,36] water is lost readily at low temperature; by 120°C, water loss is complete, although heating is not necessary. Then follows the loss of 1.0 phen in a discrete step beginning at about 180 (Cl^-), 240 (Br^-), and 320°C (I^-, all phases) giving pale-green $Ni(phen)_2X_2$. Beyond this stage, loss of phen is indistinct and merges with sublimation of NiX_2.

$[Ni(phen)_3]I_2 \cdot 3H_2O$ (phase C) was heated in a differential scanning calorimeter so that colour changes could be correlated with thermal/heat changes and temperature. Runs were from room temperature to at least the onset of decomposition of the complex (loss of phenanthroline). The compound began as a salmon-pink powder which changed to orange–salmon-pink at the beginning of an endotherm due to water loss (66°C). By 88°C the compound was yellow–mustard-yellow and at 100°C, the end of the endotherm, mustard-yellow. Thereafter there were no changes till ~ 280°C when a green tint was apparent. Thermograms show that it is at about this temperature that phenanthroline begins to be lost.

Diffraction patterns were recorded from a sample

Table 6. Hydration states of some salts $[Ni(phen)_3]X_2 \cdot nH_2O$

X	$\%H_2O$[a]	n	
Cl	15.9	7.1	
Br	16.0[b]	8.0	
NO_3	14.0	6.5	rose crystals
NO_3	20.0	10.0	rose crystals
	(+)- or (−)-I		
	7.6	3.9	salmon-pink, phase B
	(±)-I Phase C		
	5.9	3.0	air dry red–rose crystals
	(±)-I Phase B and B′		
	Crystals freshly removed from solution:		
	14.1[c]	7.8	
	12.4	6.7	
	12.2	6.6	
	11.4	6.1	
	11.2	6.0	
	Air dried crystal and powders:		
	10.0	5.3	salmon-pink
	9.9	5.2	orange crystals
	6.6	3.3	phase B′
	4.5	2.2	orange–pink/orange flakes

[a] By thermogravimetry.
[b] Other samples gave 14.2, 15.0, 15.2, 18.6%.
[c] Calculated; $6H_2O$, 11.2; $7H_2O$, 12.9; $8H_2O$, 14.4%.

of racemic phase C that had been heated to 110°C and cooled to room temperature, and on the reheated sample as it cooled. A pair of lines at 3.802 and 3.892 Å in the hot sample coalesce as the sample cools, to a peak at 3.810 Å. Finally at room temperature they are separate again, at 3.778 and 3.867 Å. Another line at 4.095 Å in the hot sample becomes two lines at 4.049 and 4.124 Å at room temperature. These differences point to a further subtle phase change as phase C is heated; this is substantiated by the change from cream at room temperature to mustard-yellow when hot.

Colour changes are not only associated with loss of water and heating. A sample of racemic phase B was heated to drive off water and then sealed in a glass tube. At room temperature it was cream but in liquid nitrogen changed back to a weak pink.

To investigate possible connections between the phase systems of the racemic and chiral phases, a sample of the chiral phase B, (−)-$[Ni(phen)_3]I_2 \cdot nH_2O$, was heated so as to racemize it.[9] A sample was heated for 7 days at 190°C, which is much longer than required to complete racemization.

The product gave the normal electronic spectrum of $[Ni(phen)_3]^{2+}$ and had no C.D. spectrum. Its X-ray powder pattern (Table 4) does not correspond to any previously recorded for a racemic salt. This new phase is designated B_{rac}.

RESULTS

Infrared spectra

There have been several studies of the IR spectra of tris-phenanthroline metal complexes.[25,37–39] The spectra for divalent and trivalent metal complexes are quite similar. Phenanthroline ligand modes are little shifted and are similar to those in 1,10-phen · H_2O. There was no evidence for a correlation between any of the ligand bands and the nature of the metal centre.[25,38]

The identities of the modes of phenanthroline (free or complexed) have been little studied. Knowledge of metal–ligand (Ni and Fe) modes is much more complete. The metal isotope effect has been used[25] to identify metal–ligand bands between 500 and 150 cm^{-1}.

Despite these complexes being hydrates, the water modes have attracted no mention whatsoever. In view of the extensive phase system of $[Ni(phen)_3]I_2 \cdot nH_2O$, we looked at IR spectra to find distinctions that might relate to structural differences. Spectra are recorded in Table 7.

Table 7. Some corresponding IR bands of $[Ni(phen)_3]I_2 \cdot nH_2O$ and 1,10-phen · H_2O[b]

	phen · H_2O	Phase B	Phase C
H_2O			3550w
H_2O			3455s
H_2O	3380s	3405s	3420s
H_2O	1646m		
	1618m	1626m	1627m
	1588m	1607w	1608m
	1562m	1582m	1588m
			1581m
	1505s	1516s	1517s
	1493m	[a]	1496m
	1423s	1425s	1421s
	1347m	1341w	1340w
			1337w
	1296w	1306w	1305w
			1253w
	1219w	1224w	1221m
		1208w	1206w
		1196w	1194w
		1169w	
	1143w	1142m	1143m
	1138w		1137w
	1092m	1104m	1103m
	1079w		1092w
	1037w		1002w
			982w
	988w	~ 970brm	971w
			948w
	883w	870m	869m
	854s	849s	848s
		845s	843s
	778w		777w
	766w	770w	763w
	738s	724s	722s
	723w		
	623m	643w	643m
Evans window(+)[c]			563w
H_2O			530m
			513m
Evans window(+)	509w		
H_2O		~ 505brm	
	499w		
H_2O			493s
H_2O			480s
H_2O			442w
phen	411m	425w	425m
H_2O			394s
ν(Ni—N)		300m	300m
ν(Ni—N)		252w	253m
ν(Ni—N)		244w	

[a] Obscured by Nujol.
[b] Unlabelled bands are due to 1,10-phenanthroline.
[c] Positive component of an Evans window.

Ligand modes

Very little difference was found between the various phases of the iodide or other salts; the anhydrous materials could be distinguished from hydrates by the slight difference in the splitting pattern for a few modes. Some modes previously undetected appeared on dehydration because they were no longer obscured by a broad water mode(s) ($\sim$ 500 cm^{-1}), and in the hydrate spectra, Evans windows associated with this band caused slight obscuring of some bands.

(a) M–L modes: there was only one band readily accessible found at the same position (300(2) cm^{-1}) in all the iodide phases. (b) Water bands: water bands were observed only in two regions: 3600–3200 cm^{-1} and 600–300 cm^{-1}. No bands were found in the region 1700–1600 cm^{-1} (HOH bend), this being for the most part obscured by phen bands.

The water bands between about 600 and 300 cm^{-1} are libration modes. The structure of phase C is known to contain three unique water molecules in general positions in the cell, each of which hydrogen bonds to iodide. This structure is probably as simple as that of any other hydrate or polymorph. Consequently many distinct libration (and other) modes might be expected for all the hydrated phases.

$[Ni(phen)_3]I_2 \cdot 3H_2O$ (phase C)

There are two groups of absorptions in the spectrum of $[Ni(phen)_3]I_2 \cdot 3H_2O$ (Table 8) some at least of which arise from libration modes. The group at the higher wavenumber 570–470 cm^{-1} has a good deal of structure, arising probably from a combination of water and phen bands, and Evans windows. Window minima occurring at 557 and 506 cm^{-1} would be responsible in part for the apparent peaks at 563 and 513 cm^{-1}. However, the weak bands of phen observed at 508 and 481 cm^{-1} in the anhydrous salt and at 509 and 499 cm^{-1} in phen $\cdot H_2O$ might contribute to the bands at 513 and 493 or 480 cm^{-1}.

To confirm the position of the libration modes of water, $[Ni(phen)_3]I_2(H_2O,D_2O)$ was prepared by recrystallization from aqueous solutions with different D_2O contents. As the D_2O content increased, a pair of bands at 493 and 480 cm^{-1} and the bands at 530 and 394 cm^{-1} weaken, while a band grows at 360 cm^{-1}. It appears that an Evans window at 486 cm^{-1} is in fact dividing a water band to give the pair of bands seen at 492 and 481 cm^{-1}.

Libration modes are expected[39] to show marked isotopic shifts (1.35–1.41 for H_2O/D_2O). Although two sets of bands were found to move on deuteration, only the one new band appears (360 cm^{-1}). If this band is due to movement of the libration mode at about 486.5 cm^{-1}, then its isotopic shift is 1.35 (486.5/360), confirming it or the group of bands in this region as a libration mode. A similar isotopic shift for the other band at 394 cm^{-1} would place it at 292 cm^{-1} in the deuterate but no absorption occurs with that frequency. Instead, if the 394 cm^{-1} band has moved into the region 360–320 cm^{-1} then the isotopic ratio is 1.16 (394/340). This might indicate that the mode is more influenced by hydrogen bonding to iodide.

The presence of an O—H band at 3455 cm^{-1} in the sample prepared from pure D_2O indicates that there must still be protons present. It seems unlikely that this absorption at 3455 cm^{-1} could stem from

Table 8. Water and other bands of $[Ni(phen)_3]I_2 \cdot 3H_2O$ (phase C), in the regions 4000–2000 and 600–250 cm^{-1}

	[a]	$3H_2O$	50% D_2O[b]	100% D_2O[b]
ν(O—H)		3550w		
ν(O—H)	3475	3455s	3490	3455
ν(O—H)		3420s		
ν(O—D)			$\sim$ 2520	$\sim$ 2505
ν(O—D)			$\sim$ 2470	
ν(O—D)			$\sim$ 2330	$\sim$ 2370
phen windows[c](+)		563	561	562
phen?			543	544
H_2O		530		
phen + windows[c]	508	513	512	512
window minimum		506		
phen?			502	506
H_2O		493	492	496
window minimum		486	486	488
H_2O + phen		480s	481	483
phen	481			
		442	444	444
phen	424	425	425	425
H_2O		394s	394	
				390
				383
D_2O or HOD			361	360
Rot $\cdot H_2O$			350	350
Rot $\cdot H_2O$			333	332
Rot $\cdot H_2O$			324	325
Ni—N	298	300	300	300
Ni—N	250	253		

[a] Sample dried by heating.

[b] This is the composition of the water used for recrystallizing the sample.

[c] See text.

an overtone or a combination band. This incomplete exchange probably accounts for the continued presence of the bands at 483 and 496 cm^{-1} (H_2O or HOD bands).

Phase B

$[Ni(phen)_3]I_2 \cdot nH_2O$ (phase B) has broad featureless water bands at 3380 and 505 cm^{-1}. The 505 cm^{-1} band obscures weak phen bands. Oven-drying causes conversion to phase B′, the loss of water bands and the appearance of weak phen bands at 550, 512, 485 and 427 cm^{-1}. Phase B′ is also produced when phase B is treated with dry ether; the colour changes from salmon-pink to cream with a pink flush, and weak water bands appear at 3520, 3420 and 400 cm^{-1}.

Reaction with organic solvent

As already mentioned, treatment of $[Ni(phen)_3]I_2 \cdot nH_2O$ (phase B) with dry diethyl ether causes an immediate change from salmon-pink to cream with a pink flush, indicative of the loss of water. A thermogram on the product shows a rapid loss of 3.8% up to 94°C (heating rate 2°C/min), and a gradual loss of phenanthroline from 140°C. This is a temperature much lower than for an untreated sample under the same conditions. If this "dry" phase B (now phase B′) is rapidly air-dried, a new very asymmetric band is observed at 400 cm^{-1}. This band does not occur on the oven-dried sample or with phase C similarly treated. Its near coincidence with the librational mode of phase C and presence of unusual O—H stretching bands suggests water in an unusual environment, and/or since it is near a moderately strong mode of free phen and phen is more readily lost than usual, possibly a Ni—N bond has been disrupted.

Phase C in diethyl ether loses its water only slowly (days) changing to a creamy-pink. Its IR spectrum is like the trihydrate but with weaker water bands.

Oven dehydrated samples of $[Ni(phen)_3]I_2 \cdot nH_2O$, phases B or C when placed in dichloromethane, 1,2-dichloroethane or chloroform ($CaCl_2$ or P_4O_{10} dry) immediately recover their salmon-pink colour. In addition some dissolves slowly to give yellow solutions. After some time in dichloromethane, red–rose crystals grow; these are probably a dichloromethane solvate but their composition was not determined.

The solvate $[Ni(phen)_3]Cl_2 \cdot 2CH_2Cl_2$ has been described[35] but the crystals were yellow. The difference in the anion might account for this difference. Certainly water is not required to produce a pink-coloured chloride salt, witness[35] the ethanol solvate $[Ni(phen)_3]Cl_2 \cdot 2EtOH$ which is pink.

Soxhlet extraction of anhydrous $[Ni(phen)_3]I_2$ by 1,2-dichloroethane resulted in a dark yellow solution from which dark red tablets (brown–mustard when powdered) grew when the solvent was slowly evaporated. The absence of water is shown by the IR spectrum. A thermogram gave a loss of 18.0% from about 50°C, equivalent to 1.9 (1,2-dichloroethane) molecules; thus the formula is $[Ni(phen)_3]I_2 \cdot 2CH_2ClCH_2Cl$.

When the iodide salt was crystallized from 30% (*v/v*) aqueous acetone, plum-coloured crystals were produced, which show a large loss of 21.4% from room temperature and a minor loss of 2.8% from 180°C. If all the loss is associated with acetone, then 4.7 moles are indicated. However it seems more likely that water and acetone combine in giving the total loss; mixed water–methanol solvates, $[Ni(phen)_3]Cl_2 \cdot CH_3OH \cdot H_2O$ and (+)- or (−)-$[Ni(phen)_3]Cl_2 \cdot 2CH_3OH \cdot H_2O$ have been described.[22]

CONCLUSIONS AND DISCUSSION

The relationships found between the racemic phases of the iodide salts of $[Ni(phen)_3]^{2+}$, prepared from aqueous solution and by drying are shown below:

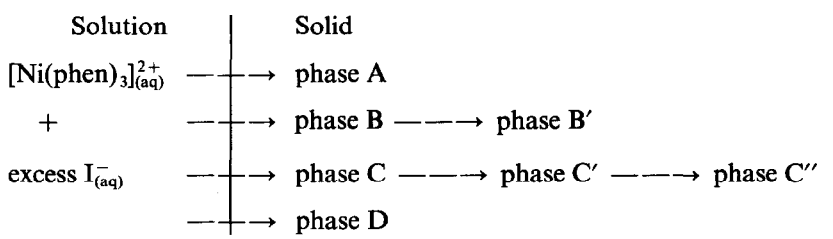

Phases A, B, C, and D crystallize directly from solution. All are hydrates; phase C is a trihydrate and phase B probably a 6- or 7-hydrate. The hydration states of phase A and D are not known.

Drying the hydrate phases brings about conversion to phases B′ and C′; these may have a small amount of water present in the lattice or be anhydrous. Heating phase C′ brings about a further change to phase C″. In general, the phases that crystallize as hydrates are pink. Partial drying

causes a change to salmon-pink–orange and finally cream with a pinkish tint for the anhydrous material. Heating the anhydrous salt produces a mustard-yellow compound. Clearly, water is involved in determining the colour.

A similar relationship was found between the phases of resolved $[Ni(phen)_3]I_2 \cdot nH_2O$. However, fewer phases were discovered. Completely analogous colour changes were observed.

Solution		Solid
(+)- or (−)-$[Ni(phen)_3]^{2+}_{(aq)}$	→	phase B ——→ phase B′
+ excess $I^-_{(aq)}$	→	phase C ——→ phase C′

Chiral phase B′ racemizes to give a new phase (B_{rac}).

The situation here with $[Ni(phen)_3]I_2 \cdot nH_2O$ is similar to that[40] for (+)-$[Co(en)_3]X_3 \cdot nH_2O$ ($X = Br^-$ or I^-), wherein the presence of water affects the rate of racemization and its loss causes a phase change. During racemization, however, the X-ray powder diffraction pattern of the chiral salt does not change even though there is a 50–70% loss of optical activity. No new lines were found but the authors conclude[40] that a new racemic phase does form.

Colours and phases

Colour differences are also found in different solutions of the nickel complex and this raises the question of the nature of the species involved. In water, $[Ni(phen)_3]^{2+}$ is burgundy–pink and with iodide can be extracted or dissolved in organic solvents to give yellow solutions. The related property has been used in the determination of iron; $[Fe(phen)_3]I_2$ (blood-red in water) is extracted into chloroform (colour yellow) and its concentration determined[41] colorimetrically.

$[FeL_3]X_2$ (L = phen or bipy; $X = I^-$, ClO_4^- and others) association complexes have been identified in solution by Johansson.[42–44] Solubility measurements in water show that iodide and perchlorate form strong outersphere complexes, $\{[Fe(phen)_3]X\}^{(2-n)+}$ ($X = I^-$, $n \leqslant 4$; ClO_4^-, $n \leqslant 3$), with the anions said to occupy pockets between the phenanthroline ligands.[42] The varying degree of association in $[M(phen)_3]^{2+}$ (M = Fe and Ru) in a variety of solvents has been attributed[45] to the varying dielectric constant of the solvent. The solvating ability of the solvent accounts for the solubility properties of $[M(phen)_3]$ salts in a number of ways. Because organic solvents are poor at solvating ions, they ought to favour neutral species such as $\{[M(phen)_3]I_2\}^0_{(solv)}$. Their formation would explain[42] why $[M(phen)_3]^{2+}$ can be extracted into chloroform, nitrobenzene, or dichloromethane, whereas only a small proportion of it remains in aqueous solution. (Certainly, the circular dichroism of (+)-$[Ni(phen)_3]^{2+}$ in aqueous and dichloroethane solutions are quite different[11] indicating that the chromophores present differ.)

In contrast, water is very good at solvating ions but a poor solvator of neutral organic molecules. Despite this, aqueous solutions of $[Ni(phen)_3]^{2+}$ have been shown[46] to salt-in toluene and nitrobenzene; a nitrobenzene solvate, $[Fe(phen)_3]I_2 \cdot 2H_2O \cdot PhNO_2$ has been prepared in which $PhNO_2$ indeed occupies pockets.[47] The presence of 2,2′-bipyridine in solution likewise increases[44] the solubility of $[Fe(bipy)_3](ClO_4)_2$. An explanation is that organic molecules occupy (displacing the anion if present or necessary) the outer coordination sphere because the anions are more readily solvated. A similar relationship with L-malic acid[16] or (−)-2,3-butanediol[22] has been held responsible for the enantiomerization (Pfeiffer effect)[21] of $[Ni(phen)_3]^{2+}$.

The observation[48] that NaOH suppresses the solubility of $[Ni(phen)_3]X_2$ ($X = I^-$ or ClO_4^-) in aqueous solution is more difficult to explain. If the species $[Ni(phen)_3](OH)_n^{(2-n)+}$ form, then effectively an extra free anion is available; this is like adding iodide (or perchlorate) to the system. Now the solubility of $[Ni(phen)_3]X_2$ is the amount of all the nickel species present in solution. So whether more or less dissolves in the presence of hydroxide will depend on the relative stabilities of the $[Ni(phen)_3](OH)_n^{(2-n)+}$ and/or mixed species.

The colour differences found[49] for salts of $[Rh(bipy)_3]X_3$ and $[Rh(terpy)_2]X_3$ (X = halide, SCN^-, ClO_4^-) in solid and solution are of a nature similar to those for $[Ni(phen)_3]I_2 \cdot nH_2O$, traced to the shift of a charge-transfer band to lower energy as the anion-complex gegen ion distance decreases. Solvent properties also determine the position of the charge-transfer bands of N-alkylpyridinium iodides[50] and of the Schilt–Barbieri compound $[Fe(phen)_2(CN)_2]^0$.[51,52]

The charge-transfer band could of course change the colour of the compounds not by moving to different energy but simply by changing shape.[53] In the case of $[Ni(phen)_3]I_2 \cdot nH_2O$, the pink colour arises from a *d–d* band (513 nm, $\varepsilon = 220$ mol^{-1} dm^{-2}, $^3T_{1g} \leftarrow {}^3A_{2g}$ of O_h parentage) and the yellow colour from a charge-transfer band which

encroaches on the visible spectrum. Being a much stronger transition, it dominates the observed colour when it moves into the visible region.

The reason for the development of the yellow colour is probably that water in the solid or solution phases solvates (at least partially) the anion. Removing the water causes the anion and the complex cation to associate more closely and the charge transfer band shifts into the visible region. To what extent the presence of species $\{[Ni(phen)_3]I_n\}^{(2-n)+}$ affects the colour is not easily determined because the iodide salts are not very soluble. The ready formation[42] of the neutral species $\{[Ni(phen)_3]I_2\}^0$, poorly solvated by water, probably accounts for this. In $[Ni(phen)_3]I_2 \cdot 3H_2O$, phase C, which is rose-red, the complex molecules and iodide are held apart because the iodide is embedded in a hydrogen bonded network with water. However, no water molecules actually intrude between it and the complex, so removing water would probably result directly in reducing the distance and a shift to lower energy of the charge-transfer band.

The thermochromism (pink at −196°C and mustard-yellow at 100°C) found for $[Ni(phen)_3]I_2$ (phase B′) is also probably linked to a change of the charge-transfer band in one of the two ways above. Lattice changes might bring about a separation of the iodide and complex cations, or the vibrationally excited states could be depopulated by cooling, giving the usual loss[53] of "hot" bands.

Our work on the phases of $[Ni(phen)_3]I_2 \cdot nH_2O$ bears on the subject of solid state racemization in that previously the variety of phases involved and their relation to water have not been recognized. Such detail is an important factor in understanding the mechanism and kinetics involved.[7] Phase changes during dehydration or resulting from it have been implicated as being responsible for the rapid initial loss of optical activity of solid salts of tris-phen or tris-bipy complexes of iron,[9] nickel[9] and cobalt.[8] A mechanism proposed for this is that escaping water expands the lattice leading to the easier formation of the transition state.[54] With all the water gone, a new condensed phase forms as shown by the mustard-yellow colour arising from the now closer association of iodide and the $[Ni(phen)_3]^{2+}$ units. Undoubtedly this new phase contains a large number of defects which participate in the subsequent racemization.

Fujiwara and Yamamoto report[9] that they used anhydrous complexes. They state that "dehydration was accompanied by slight colour changes"; however we find considerable changes to accompany dehydration. Thus their compounds were not actually anhydrous, nor are they amorphous as stated.[9,36] An initial loss of water would accompany the observed initial rapid loss of optical activity. Water has been shown to depress the racemization of $[Fe(phen)_3]Br_2$ at room temperature[9] and the pressure induced racemization[32] of $[Ni(phen)_3](ClO_4)_2$.

Gomes has pointed out[55] that it is difficult to relate activation energies or rate constants to mechanism in solid state reactions. The present work would add the further caveat that just as in any mechanistic study, a material balance is a prerequisite, so, in work on solid coordination compounds as complicated as those of these N-heterocyclic ligands, it is vital to identify the particular phase or solvate in hand.

REFERENCES

1. L. H. Berka, R. R. Gagne, G. E. Philippon and C. E. Wheeler, *Inorg. Chem.* 1970, **9**, 2705.
2. J. L. Kahl, K. Hanck and K. DeArmond, *J. Inorg. Nucl. Chem.* 1979, **41**, 495.
3. M. P. Hancock, J. Josephsen and C. E. Schaffer, *Acta Chem. Scand.* 1976, **A30**, 79.
4. C. M. Harris and E. D. McKenzie, *J. Inorg. Nucl. Chem.* 1967, **29**, 1047.
5. E. D. McKenzie and R. A. Plowman, *J. Inorg. Nucl. Chem.* 1970, **32**, 199.
6. C. M. Harris and E. D. McKenzie, *J. Inorg. Nucl. Chem.* 1961, **19**, 372.
7. P. O'Brien, *Polyhedron* 1983, **2**, 233.
8. T. Fujiwara, *Bull. Chem. Soc. Jpn.* 1983, **56**, 122.
9. T. Fujiwara and Y. Yamamoto, *Inorg. Chem.* 1980, **19**, 1903.
10. M. Yamamoto, T. Fujiwara and Y. Yamamoto, *Inorg. Nucl. Chem. Lett.* 1979, **15**, 37.
11. R. D. Gillard and P. A. Williams, *Trans. Met. Chem.* 1977, **2**, 14.
12. F. P. Dwyer and E. C. Gyarfas, *Proc. R. Soc. New South Wales*, 1949, **83**, 232.
13. G. B. Kauffman and L. T. Takahashi, *Inorg. Synth.* 1966, **8**, 227.
14. T. Fujiwara and Y. Yamamoto, *Inorg. Nucl. Chem. Lett.* 1979, **15**, 397.
15. A. Yamagishi, *Inorg. Chem.* 1982, **21**, 3393; A. Yamagishi, *J. Chem. Soc., Chem. Commun.* 1981, 1128; A. Yamagishi, *J. Chem. Soc., Chem. Commun.* 1981, 1168.
16. S. Kirschner and N. Ahmad, *J. Am. Chem. Soc.* 1968, **90**, 1910.
17. P. Pfeiffer and K. Quehl, *Ber.* 1931, **64**, 2667.
18. P. Pfeiffer and Y. Nakatsuka, *Ber.* 1933, **66**, 415.
19. F. P. Dwyer, E. C. Gyarfas and M. F. O'Dwyer, *Nature* 1951, **167**, 1036.
20. S. Kirschner, K. Magnell and K. H. Pearson, *Rev. Chim.* 1966, **17**, 588.
21. S. Kirschner, N. Ahmad and K. Magnell, *Coord. Chem. Rev.* 1968, **3**, 201.
22. B. Bosnich and D. W. Watts, *Inorg. Chem.* 1975, **14**, 47.

23. J. Sullivan and J. C. Fanning, *J. Inorg. Nucl. Chem.* 1969, **31**, 49.
24. K. Akabori and H. Matsuo, *J. Inorg. Nucl. Chem.* 1973, **35**, 267.
25. B. Hutchinson, J. Takemoto and K. Nakamoto, *J. Am. Chem. Soc.* 1970, **92**, 3335.
26. G. N. Natu, S. B. Kulkarni and P. S. Dhar, *J. Thermal Anal.* 1982, **23**, 101.
27. K. Yoshitani, M. Yamamoto and Y. Yamamoto, *Bull. Chem. Soc. Jpn.* 1983, **56**, 1978.
28. L. J. Matienzo, L. I. Yin, S. O. Grim and W. E. Swartz, *Inorg. Chem.* 1973, **12**, 2762.
29. P. Pfeiffer and F. Tappermann, *Z. Anorg. Allg. Chem.* 1933, **215**, 273.
30. T. Fujiwara and Y. Yamamoto, *Inorg. Nucl. Chem. Lett.* 1975, **11**, 635.
31. J. Bolard and F. Plique, *C.R. Acad. Sci. Paris, Ser. C*, 1969, **268**, 598.
32. G. E. Humiston and J. E. Brady, *Inorg. Chem.* 1969, **8**, 1773.
33. A. Tatehata, T. Kumamaru and Y. Yamamoto, *J. Inorg. Nucl. Chem.* 1971, **33**, 3427.
34. N. I. Lobanov, *Russ. J. Inorg. Chem.* 1967, **12**, 1363.
35. D. G. Holah and C. N. Murphy, *Can. J. Chem.* 1971, **49**, 2726.
36. K. Akabori, H. Matsuo and Y. Yamamoto, *J. Inorg. Nucl. Chem.* 1973, **35**, 2679.
37. A. A. Schilt and R. C. Taylor, *J. Inorg. Nucl. Chem.* 1959, **9**, 211.
38. R. G. Inskeep, *J. Inorg. Nucl. Chem.* 1962, **24**, 763.
39. G. H. Thomas, M. Falk and O. Knop, *Can. J. Chem.* 1974, **52**, 1029.
40. C. Kutal and J. C. Bailar, *J. Phys. Chem.* 1972, **76**, 119.
41. F. Vydra and R. Pribil, *Talanta* 1959, **3**, 72.
42. L. Johansson, *Chemica Scripta* 1976, **9**, 30.
43. L. Johansson, *Chemica Scripta* 1976, **10**, 72.
44. L. Johansson, *Chemica Scripta* 1976, **10**, 149.
45. T. Takamatsu, *Bull. Chem. Soc. Jpn.* 1974, **47**, 118.
46. E. Iwamoto, M. Yamamoto and Y. Yamamoto, *Inorg. Nucl. Chem. Lett.* 1974, **10**, 1069.
47. T. Fujiwara, E. Iwamoto and Y. Yamamoto, *Inorg. Chem.* 1984, **23**, 115.
48. L. P. Morgenthaler and D. W. Margerum, *J. Am. Chem. Soc.* 1962, **84**, 710.
49. C. M. Harris and E. D. McKenzie, *J. Inorg. Nucl. Chem.* 1963, **25**, 171.
50. E. M. Kosower, *J. Am. Chem. Soc.* 1958, **80**, 3253.
51. J. Burgess, *Spectrochim. Acta* 1970, **A26**, 1369.
52. J. Burgess, *Spectrochim. Acta* 1970, **A26**, 1957.
53. R. D. Gillard and G. Wilkinson, *J. Chem. Soc.* 1963, 5885 and refs therein.
54. J. E. House, *Thermochim. Acta* 1980, **38**, 59.
55. W. Gomes, *Nature* 1961, **192**, 865.

Polyhedron Vol. 7, No. 13, pp. 1187–1195, 1988
Printed in Great Britain

0277–5387/88 $3.00+.00
© 1988 Pergamon Press plc

COMPLEX SPECIES IN AQUEOUS SOLUTION OF 4-CHLORO-1,2-PHENYLENEDIAMINE-N,N,N′,N′-TETRAACETIC ACID WITH Co(II), Ni(II) AND Cu(II), AND OF 3,4-TOLUENEDIAMINE-N,N,N′,N′-TETRAACETIC AND *ORTHO*-PHENYLENEDIAMINE-N,N,N′,N′-TETRAACETIC ACIDS WITH Cu(II)

F. BRITO

Laboratorio de Equilibrios en Solución, Escuela de Química, Facultad de Ciencias, Universidad Central de Venezuela, Caracas, Venezuela

and

A. MEDEROS,* J. V. HERRERA, S. DOMINGUEZ and M. HERNANDEZ-PADILLA

Departamento de Química Inorgánica, Universidad de La Laguna, Tenerife, Canary Islands, Spain

(*Received* 8 *January* 1988; *accepted* 1 *February* 1988)

Abstract—The complex species formed in aqueous solution between 4-chloro-1,2-phenylenediamine-N,N,N′,N′-tetraacetic acid (4-Cl-o-PDTA) and Co(II), Ni(II) and Cu(II), and between 3,4-toluenediamine-N,N,N′,N′-tetraacetic (3,4-TDTA) and *ortho*-phenylenediamine-N,N,N′,N′-tetraacetic (*o*-PDTA) acids and Cu(II), were studied at 25°C and ionic strength 0.1 M in KCl. Potentiometric investigations were carried out at metal:ligand ratios 2:1, 1:1 and 1:2. The concentration of metal was 2 mM (ratios 2:1, 1:1 and 1:2), 1.5 mM (ratio 1:1) and 1 mM (ratio 1:1). The applications of the least-squares computer program LETAGROP to the experimental potentiometric data, in the pH ranges studied, indicate that the following complex species are formed (ligands H_4C): 4-Cl-*o*-PDTA acid: $[CoHC]^-$, $[CoC]^{2-}$, $[NiHC]^-$, $[NiC]^{2-}$, CuH_2C, $[CuHC]^-$ and $[CuC]^{2-}$; 3,4-TDTA acid: CuH_2C, $[CuHC]^-$ and $[CuC]^{2-}$; *o*-PDTA acid: CuH_2C, $[CuHC]^-$, $[CuC]^{2-}$ and $[Cu(OH)C]^{3-}$. These ligands, 4-Cl-*o*-PDTA, 3,4-TDTA and *o*-PDTA, are potentially hexadentate ligands with a coordination sphere, as occurs in the case of EDTA.

The greater proximity of the nitrogen atoms in methylcarboxylic tetraacids derived from aromatic diamines in *ortho* positions (Fig. 1), permits the simultaneous coordination of both to the same metallic cation. Moreover, the proximity of the four methylcarboxylate groups enhances the formation of a large number of chelate rings. Both effects considerably increase the stability constants of the complexes formed in aqueous solution, such that despite the lesser basicity of the aromatic amines with respect to the aliphatic ones, the coordinating capacity of these ligands is close to that of EDTA. The hexadentate coordinating capacity has been proven by way of an X-ray diffraction ana-

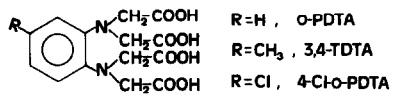

Fig. 1. Structural formulae of *o*-PDTA, 3,4-TDTA and 4-Cl-*o*-PDTA.

*Author to whom correspondence should be addressed.

lysis of the crystal structure for the complexes Co(II)–*o*-PDTA[1] (*o*-PDTA = *ortho*-phenylenediamine-N,N,N′,N′-tetraacetic acid), Mn(II)–*o*-PDTA, Cu(II)–*o*-PDTA and Zn(II)–*o*-PDTA.[2] In accordance with this behaviour as potentially hexacoordinated ligands, studies have been carried out on the complexing capacity, in aqueous solution, of *o*-PDTA acid with the divalent transition-metal cations, Mn, Co, Ni, Cu and Zn;[3] on *o*-PDTA and 3,4-TDTA acids (3,4-TDTA = 3,4-toluenediamine-N,N,N′,N′-tetraacetic acid) with alkaline and alkaline earth cations;[4] and on *o*-PDTA, 3,4-TDTA and 4-Cl-*o*-PDTA acids (4-Cl-*o*-PDTA = 4-chloro-1,2-phenylenediamine-N,N,N′,N′-tetraacetic acid) with Be(II).[5] Contrary to this is the behaviour of diaminetetracarboxylic ligands derived from aromatic *meta*- or *para*-diamines, which can only coordinate an N atom of the ligand to the same metallic cation and are potentially tridentate ligands, as confirmed by our studies in aqueous solution, of the coordinating capacity of the *m*-PDTA (*m*-PDTA = *meta*-phenylenediamine-N,N,N′,N′-tetraacetic) and *p*-PDTA (*p*-PDTA = *para*-phenylenediamine-N,N,N′,N′-tetraacetic) acids with Be(II),[6] Cu(II)[7] and Co(II).[8]

The present work is a continuation of our studies on the coordinating capacity in aqueous solution of tetramethylcarboxylic acids derived from *ortho*-diamines, of 4-Cl-*o*-PDTA acid with Co(II), Ni(II) and Cu(II), and of 3,4-TDTA and *o*-PDTA acids with Cu(II).

EXPERIMENTAL

Reagents

o-PDTA acid was obtained following a modification of the method developed by McCandlish *et al.*[1] with a significant increase in the yield of this synthesis.[9] Adopting a similar technique, the monopotassic salt of 3,4-TDTA acid[9] and the monosodic salt of 4-Cl-*o*-PDTA acid[10] were prepared for the first time and used as a base product in the titrations, since the acids did not precipitate from their respective aqueous solutions when the pH decreased.

The metal solutions (in the form of the chloride) were evaluated: Co(II) and Cu(II), electrolytically[11,12] and complexometrically;[13] Ni(II), gravimetrically with dimethylglyoximate.[11] A carbonate-free sodium hydroxide solution was prepared according to the School of Sillén[14] and standardized against potassium hydrogen phthalate. KCl was prepared by recrystallization of KCl (KCl, $CoCl_2$, $NiCl_2$, $CuCl_2$, HCl and NaOH, Merck, analytical grade).

Apparatus and titration procedures

The potentiometric titrations in aqueous solution were carried out in an inert argon atmosphere at 25 ± 0.05°C, $I = 0.1$ M in KCl, using a Radiometer Type PHM-64 potentiometer, a Radiometer G 202 B glass electrode and a K 401 calomel electrode. The cell constants were determined according to the method of Biedermann and Sillén,[15] the liquid junction potentials being found to be negligible within the margins of $[H^+]$ studied.

Measurements were taken of the ligands alone at the following concentrations: *o*-PDTA (1.17 mM), 3,4-TDTA (2 mM) and 4-Cl-*o*-PDTA (2 mM); and the ligands in the presence of metallic cation at the following concentrations and ligand : metal ratios: $C_M = 2$ mM (ratios 2 : 1, 1 : 1 and 1 : 2), $C_M = 1.5$ mM (ratio 1 : 1) and $C_M = 1$ mM (ratio 1 : 1).

Data treatment

The experimental potentiometric data were analysed by means of the NERNST/LETA/GRAFICA version[16] of the LETAGROP program,[17] based on a generalized form of the least-squares method that establishes the best model and best values of the β_{pqr} constants, minimizing the function $U = \Sigma (Z_{exp} - Z_{calc})^2$, Z being the average number of dissociated protons for the concentration of ligand (Z_C) or for the total concentration of metal (Z_B). The LETAGROP calculations also give standard deviations $\sigma(Z)$ and $\sigma(\log \beta_{pqr})$.[18] The computations were performed on a Burroughs 6700 computer (Facultad de Ciencias, Universidad Central de Venezuela, Caracas).

From the LETAGROP calculations corresponding to the potentiometic titrations of the ligands it is found that $pK_w = 13.694 \pm 0.018$.

The presence of the $[Cu_2(OH)_2]^{2+}$ species, which is the major hydrolytic species of Cu(II),[19] has been taken into account in the calculations for the ligand–Cu(II) systems.

The calculations are begun by fitting the 4-Cl-*o*-PDTA–Co(II) system, since Co(II) is the least complexing cation. The final values are the result of the simultaneous fit of the five potentiometric titrations. The values found for $-\log \beta_{pqr}$ are taken as reference for the subsequent fit of the remaining systems, in the order 4-Cl-*o*-PDTA–Ni(II), 4-Cl-*o*-PDTA–Cu(II), *o*-PDTA–Cu(II) and 3,4-TDTA–Cu(II), respectively. The calculations show that the MH_2C species for Co(II) and Ni(II) is not present in significant amounts, since $-\log \beta_{pqr} \simeq 0$. The $[Cu(OH)C]^{3-}$ species was discarded for 4-Cl-*o*-PDTA and 3,4-TDTA acids at the pH intervals studied.

RESULTS AND DISCUSSION

Ionization constants of the acids

From the values obtained for the constants β_{pr} corresponding to equilibrium (1):

$$pH^+ + rH_4C \rightleftharpoons [H_p(H_4C)_r]^{p+} \quad (1)$$

the ionization constants of the acids (K_i) given in Table 1 could readily be determined.

The values found for the pK_i are in excellent agreement with those previously found for the three ligands at the same ionic strength and temperature,[9,10] and with those found also for the three ligands[5] at 25°C and $I = 0.5$ M in $NaClO_4$, and at 25°C and $I = 1$ M for *o*-PDTA acid.[3] The values of pK_4 indicate that the basic strength of the C^{4-} anions follow the order 3,4-TDTA > *o*-PDTA > 4-Cl-*o*-PDTA, as expected from the electron donor inductive effect of the methyl radical in 3,4-TDTA acid and from the effect of the withdrawal of electronic density exerted by the Cl atom on the aromatic ring and on the N atoms in the 4-Cl-*o*-PDTA acid. The diagrams of the distribution of species as a function of $-\log[H^+]$ (Fig. 2 for the *o*-PDTA and 3,4-TDTA acids; for 4-Cl-*o*-PDTA[10]) calculated in accordance with the values of $-\log\beta_{pr}$ given in Table 1, show that the monoprotonated species HC^{3-}, with a fundamentally betainic structure,[9,20] is most basic for 3,4-TDTA acid.

Stability constants of the complexes formed

The analysis of the experimental data of the metal–ligand systems studied by the NERNST/LETA/GRAFICA version[16] of the LETAGROP program[17] allowed us to calculate the β_{pqr} constants for the complex species formed for each ligand, defined by means of equilibrium (2):

$$pH^+ + qM^{2+} + rH_4C \rightleftharpoons [H_pM_q(H_4C)_r]^{(p+2q)+}. \quad (2)$$

The model that best fits the experimental results for each system is that which corresponds to the complex species indicated in Table 2.

The validity of similarity is proven in Figs 3(a), 4(a) and 5(a), where an excellent fit can be observed between the experimental Z vs $-\log[H^+]$ curves (Z_C, Figs 3(a) and 4(a); Z_B, Fig. 5(a)) and those calculated from the values of β_{pqr} given in Table 2. Analogous curves are obtained for the 4-Cl-*o*-PDTA–Co(II) and 3,4-TDTA–Cu(II) systems. Although models were tested that included the possible presence of complex species with an excess of ligand and with an excess of metal, the results indicate that they are not present in significant amounts.

The values of log K corresponding to the stability constants of the complex species found, according to the equilibria

$$M^{2+} + H_2C^{2-} \rightleftharpoons MH_2C \quad (3)$$

$$M^{2+} + HC^{3-} \rightleftharpoons [MHC]^- \quad (4)$$

Table 1. Ionization constants of 4-Cl-*o*-PDTA, 3,4-TDTA and *o*-PDTA (25°C, $I = 0.1$ M in KCl)

	$-\log\beta_{pr}$			
pr[a]	4-Cl-*o*-PDTA	3,4-TDTA	pr	*o*-PDTA
			11	0.574±0.132
11	3.396±0.012	2.898±0.004	−11	−2.877±0.067
−11	−3.621±0.015	−3.531±0.006	−21	−6.477±0.043
−21	−8.463±0.024	−8.245±0.008	−31	−11.234±0.018
−31	−14.359±0.027	−15.247±0.013	−41	−17.876±0.021
No. of titrations/No. of experimental points	2/72	2/68		2/86
Standard deviation [$\sigma(Z)$]	0.017	0.006		0.009
$-\log[H^+]$ range	2.75–8.05	2.67–8.71		1.60–9.50
Equilibrium	pK_i			
H_5C^+–H_4C				0.6
H_4C–H_3C^-	3.40	2.90		2.88
H_3C^-–H_2C^{2-}	3.62	3.53		3.60
H_2C^{2-}–HC^{3-}	4.84	4.72		4.76
HC^{3-}–C^{4-}	5.90	7.00		6.64

[a] The use of the monosodium salt of 4-Cl-*o*-PDTA acid and the monopotassium salt of 3,4-TDTA acid led to the calculated real values of pr of 11, −11, −21 and −31, respectively.

$$M^{2+} + C^{4-} \rightleftharpoons [MC]^{2-} \quad (5)$$

$$M^{2+} + C^{4-} + OH^- \rightleftharpoons [M(OH)C]^{3-} \quad (6)$$

are also given in Table 2, being readily obtained from the values of the β_{pqr} in Table 2, and taking into account the values of β_{pr} constants of the acids presented in Table 1.

The values of $pK_i = -\log K_i$ corresponding to the ionization of the complex species, according to the equilibria

$$MH_2C \rightleftharpoons [MHC]^- + H^+ \quad (7)$$

$$[MHC]^- \rightleftharpoons [MC]^{2-} + H^+ \quad (8)$$

$$[MC]^{2-} \rightleftharpoons [M(OH)C]^{3-} + H^+ \quad (9)$$

are also given in Table 2, and are readily obtained from the values of the β_{pqr} constants in Table 2, by means of the equation

$$pK_i = \log \beta_{-n11} - \log \beta_{-(n+1)11}.$$

For comparison purposes, data reported in the literature on the values of $\log K$ of metallic complexes of EDTA,[21] *o*-PDTA[3] ($I = 1$ M in $NaClO_4$) are given in Table 3, as well as those of tetramethylcarboxylic acids derived from *meta*- and *para*-phenylenediamines: *m*-PDTA,[8] *p*-PDTA,[8] 2,4-TDTA[22] (2,4-TDTA = 2,4-toluene-

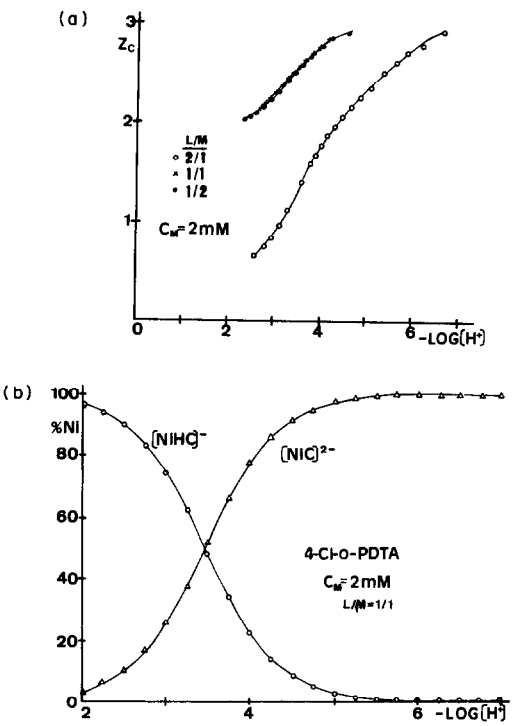

Fig. 3. For the 4-Cl-*o*-PDTA–Ni(II) system: (a) Z_C vs $-\log[H^+]$ curves; full curves have been calculated using the β_{pqr} constants in Table 2. (b) Species distribution as a function of $-\log[H^+]$.

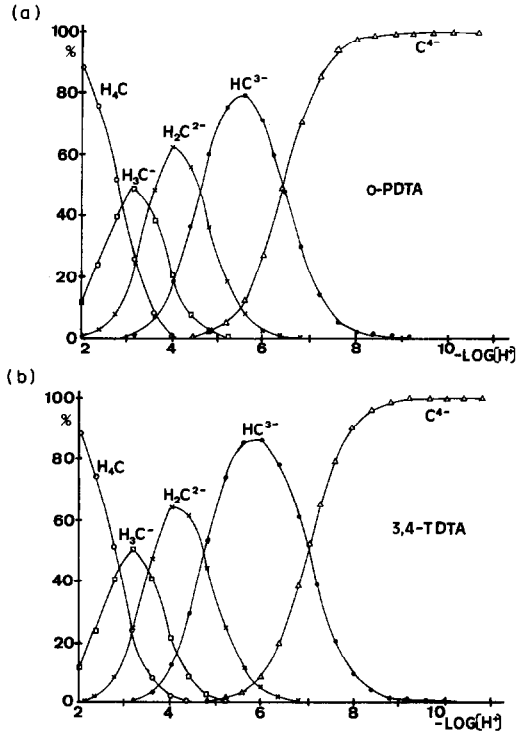

Fig. 2. Species distribution as a function of $-\log[H^+]$: (a) *o*-PDTA and (b) 3,4-TDTA.

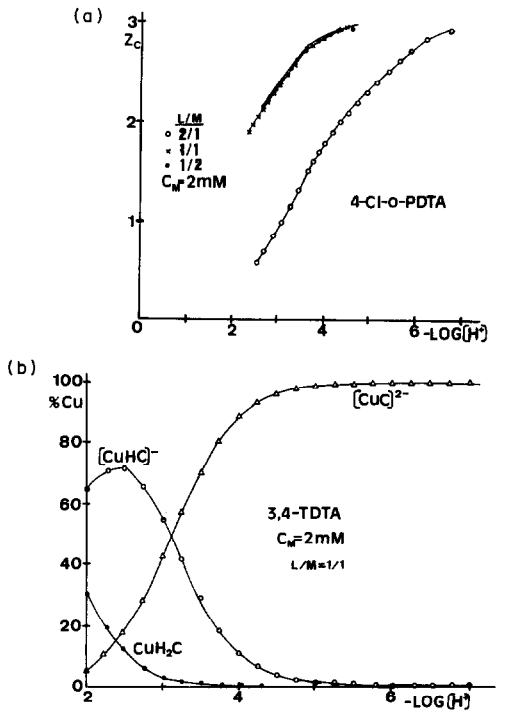

Fig. 4. (a) Z_C vs $-\log[H^+]$ curves for the 4-Cl-*o*-PDTA–Cu(II) system; full curves have been calculated using the β_{pqr} constants in Table 2. (b) Species distribution as a function of $-\log[H^+]$ for the 3,4-TDTA–Cu(II) system.

Table 2. Stability constants of the complexes of 4-Cl-*o*-PDTA with Co(II), Ni(II) and Cu(II); 3,4-TDTA with Cu(II); and *o*-PDTA with Cu(II) (25°C, $I = 0.1$ M in HCl)

	$-\text{Log}\,\beta_{pqr}$					
	4-Cl-*o*-PDTA			3,4-TDTA		*o*-PDTA
pqr[a]	Co(II)	Ni(II)	Cu(II)	Cu(II)	*pqr*	Cu(II)
−111			5.753±0.016	5.544±0.058	−211	2.175±0.070
−211	1.109±0.010	4.042±0.008	3.933±0.001	3.865±0.005	−311	0.296±0.062
−311	−1.611±0.002	0.576±0.008	0.786±0.004	0.753±0.004	−411	−2.768±0.041
					−511	−13.786±0.000
No. of titrations/No. of experimental points	5/146	5/130	5/143	5/150		5/114
Standard deviation [$\sigma(Z)$]	0.018	0.012	0.025	0.007		0.061
$-\text{Log}[H^+]$ range	2.37−7.01	2.38−6.71	2.42−6.80	2.40–7.80		2.25−11.02
Equilibrium			Log *K*			
(3)			9.37	9.08		8.65
(4)	9.57	12.50	12.40	12.11		11.53
(5)	12.75	14.93	15.15	16.00		15.11–15.21[b]
(6)						17.80
Equilibrium			pK_i			
(7)			1.82	1.68	1.88	1.8[b]
(8)	2.72	3.47	3.15	3.11	3.06	3.04[b]
(9)					11.02	11.4[b]

[a] The use of the monosodium salt of 4-Cl-*o*-PDTA and the monopotassium salt of 3,4-TDTA led to real values of *pqr* of −111, −211 and −311, respectively.
[b] 25°C, $I = 1$ M in $NaClO_4$.[3]

Table 3. Stability constants of metal complexes of EDTA, *o*-PDTA, *m*-PDTA, *p*-PDTA, 2,4-TDTA, 2,6-TDTA and 2,6-PDTA

	Log K											
	EDTA[a]			*o*-PDTA[b]			*m*-PDTA		*p*-PDTA	2,4-TDTA	2,6-TDTA	2,6-PDTA
Equilibrium	Co(II)	Ni(II)	Cu(II)	Co(II)	Ni(II)	Cu(II)	Co(II)[c]	Cu(II)[d]	Cu(II)[d]	Cu(II)[e]	Cu(II)[e]	Cu(II)[e]
(3)				5.88[f]	6.68[f]	9.03[f]	2.06	4.47	4.69		3.39	
(4)	9.09[f]	11.55[f]	11.53[f]	9.29[f]	10.39[f]	11.84[f]	3.33	6.65	6.95	5.21	4.68	5.10
(5)	16.26	18.52	18.70	13.18	13.48	15.21	5.02	8.22	8.16	7.48	6.11	6.68
(6)			21.2[g]			17.56[h]						
Equilibrium						pK_i						
(7)				1.2	0.9	1.8	3.73	2.82	2.61		3.23	
(8)	3.0	3.2	3.0	2.52	3.32	3.04	4.06	4.18	4.90	4.32	4.71	4.65
(9)			11.2[g]	12	11.5	11.4						

[a] 25°C, $I = 0.1$ M.[21]
[b] 25°C, $I = 1$ M in $NaClO_4$.[3]
[c] 25°C, $I = 0.1$ M in KCl.[8]
[d] 25°C, $I = 0.1$ M in KCl.[7]
[e] 25°C, $I = 0.1$ M in KCl.[22]
[f] Converted from the original data.
[g] Converted from the original data, assuming that p$K_w = 13.70$.
[h] Converted from the original data, assuming that p$K_w = 13.75$.

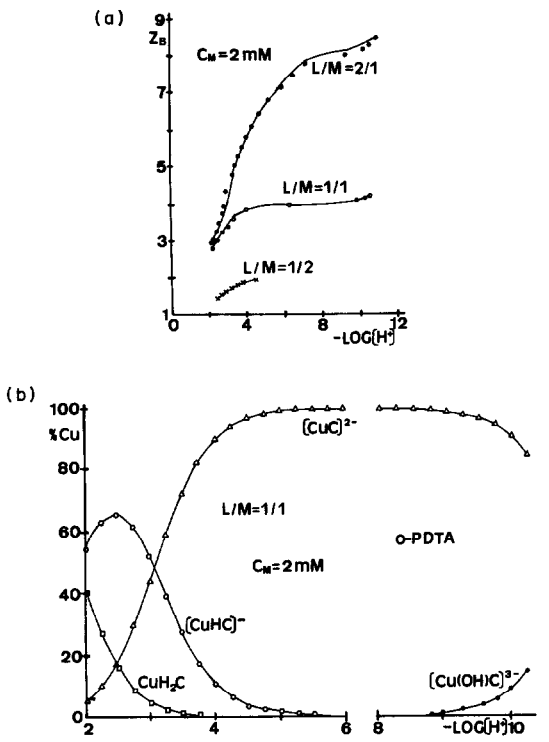

Fig. 5. For the *o*-PDTA–Cu(II) system: (a) Z_B vs $-\log[H^+]$ curves; full curves have been calculated using the β_{pqr} constants in Table 2. (b) Species distribution as a function of $-\log[H^+]$.

diamine-N,N,N′,N′-tetraacetic acid), 2,6-TDTA[22] (2,6-TDTA = 2,6-toluenediamine-N,N,N′,N′-tetraacetic acid) and 2,6-PDTA[22] (2,6-PDTA = 2,6-pyridinediamine-N,N,N′,N′-tetraacetic acid).

The special conformation of the tetramethylcarboxylic ligands derived from *meta*- and *para*-phenylenediamines implies that a metallic cation can only be bonded to a single, potentially tricoordinating, iminodiacetic group of one and the same ligand.[7,22] In the case of *m*-PDTA, in aqueous solution as with Co(II),[8] or forming crystalline solids as with Cu(II),[23] a metallic cation can be bonded to iminodiacetic groups of different ligands, forming M_2(*m*-PDTA)$_2$ dimeric species. The data presented in Tables 2 and 3 for the CuC^{2-} species indicate that the values of log *K* for the ligands derived from *meta*- and *para*-phenylenediamines are practically half of those corresponding to the ligands derived from *ortho*-phenylenediamines. That is, the tetramethylcarboxylic ligands derived from *ortho*-phenylenediamines are potentially hexadentate, and use both iminodiacetic groups in order to bond them to the same metallic cation, as has been proven with the crystalline solids studied.[1,2] *o*-PDTA, 3,4-TDTA and 4-Cl-*o*-PDTA are, therefore, strong complexing agents, although somewhat less than EDTA because of the lower basicity of the aromatic amines with respect to the aliphatic amines and because of the distortions of the octahedral symmetry imposed by the planar N—C—C—N structure which includes both N atoms.[1-3]

However, compared to EDTA, these distortions facilitate the formation of stable protonated complexes; the values of log *K* for the MHC^- complexes are practically identical, or somewhat higher for the complexes of *o*-PDTA, 3,4-TDTA and 4-Cl-*o*-PDTA with respect to EDTA. If the values of log *K* for the $CuHC^-$ species [equilibrium (4)] of *o*-PDTA, 3,4-TDTA and 4-Cl-*o*-PDTA are compared to the log *K* values of the CuC^{2-} species [equilibrium (5)] of *m*-PDTA and *p*-PDTA, which only bond an iminodiacetic group to the Cu(II), it is observed that in the $CuHC^-$ complexes of the acids derived from *ortho*-phenylenediamines, the ligand utilizes both iminodiacetic groups to bond itself to the Cu(II) as a tetra- or pentadentate ligand. In the $CuHC^-$ complexes of the ligands derived from *meta*- or *para*-phenylenediamines, one iminodiacetic group is bonded to the metal and the other to the proton[7,22] [equilibrium (8), Table 3]. The values of pK_i [equilibrium (8), Tables 2 and 3], indicate that in *o*-PDTA, 3,4-TDTA and 4-Cl-*o*-PDTA the proton of the $[MHC]^-$ complex is not firmly bonded to the N atom, but is a carboxylic proton, possibly due to the repulsion of the very close metallic cation which is preferentially bonded to both N atoms.

The formation of the MH_2C complex species, proven by us for Cu(II) with the *o*-PDTA, 3,4-TDTA and 4-Cl-*o*-PDTA, takes place more readily with these ligands than with EDTA, very probably due to the distortion of the octahedral symmetry mentioned earlier.[3] Log *K* for the CuH_2C complexes [equilibrium (3), Tables 2 and 3] of *o*-PDTA, 3,4-TDTA and 4-Cl-*o*-PDTA is somewhat greater than log *K* for the $[CuC]^{2-}$ complexes [equilibrium (5), Table 3] of *m*-PDTA and *p*-PDTA, which seems to indicate that in the CuH_2C complexes the ligand is tetradentate. This totally carboxylic second proton is much more readily lost, as is to be expected, in the complexes of the acids derived from *ortho*-phenylenediamines, than in those derived from *meta*- and *para*-phenylenediamines [equilibrium (7), Tables 2 and 3], because in the former the proton is subjected to a greater repulsion due to the close proximity of the metallic cation and another proton.

The $[MC]^{2-}$ complexes of *o*-PDTA, 3,4-TDTA and 4-Cl-*o*-PDTA are, therefore, strong complexes, the ligand acting as a hexadentate one. For this

reason, the M_2C bimetallic species is not formed, nor are complexes with an excess of the ligand, in contrast to *m*-PDTA and *p*-PDTA.[7] The diagrams for the distribution of the species of M(II) as a function of $-\log[H^+]$ were calculated from the values of β_{pr} given in Table 1, those of β_{pqr} in Table 2 and for Cu(II), those of β_{pq}.[19] They are plotted in Fig. 3(b) for the 4-Cl-*o*-PDTA–Ni(II) system (analogous to the 4-Cl-*o*-PDTA–Co(II) system), in Fig. 4(b) for the 3,4-TDTA–Cu(II) system (analogous to the 4-Cl-*o*-PDTA–Cu(II) system), and in Fig. 5(b) for the *o*-PDTA–Cu(II) system. The diagrams show that at pH 2 the metal is already practically 100% complexed. For comparison purposes, it should be noted that in the *m*-PDTA–Co(II) system,[8] the metal is only practically complexed at pH 6 with $C_M = 10$ mM. For the $[MC]^{2-}$ complexes of Co(II), Ni(II) and Cu(II), corresponding to 4-Cl-*o*-PDTA, the Irving and Williams sequence is fulfilled, but the stability of the Ni(II) complexes is close to that of the Cu(II) complexes, as occurs with EDTA (Tables 2 and 3).

Figures 3(a) and 4(a) (analogous to the other systems studied) display graphically the non-formation of M_2C and MC_2 species. The 1 : 1 and 1 : 2 ligand : metal curves coincide, since the M_2C species is not formed and the metal is almost totally complexed in the MC species. The 2 : 1 ligand : metal curve is shifted to the right in accord with titration of the excess of the non-complexed ligand. $Z_C \to 3$, as is to be expected, upon utilizing the starting ligand H_3C^-.

Figure 3(b) shows that for Ni(II), the 1 : 1 complex is practically $[NiHC]^-$ at pH 2 (to 97%), $[NiHC]^-$ and $[NiC]^{2-}$ up to 50% at pH 3.5 and $[NiC]^{2-}$ up to 100% at pH > 6. The almost non-formation of either the NiH_2C or the CoH_2C species for 4-Cl-*o*-PDTA, in contrast to the formation of the CuH_2C species, may be due to the greater symmetry of the coordinating polyhedron for the complex $[NiHC]^-$ with respect to $[CuHC]^-$, due to the requirements of the metallic cation. Figure 4(b) for the 3,4-TDTA–Cu(II) system (analogous to the 4-Cl-*o*-PDTA–Cu(II) system) shows that at pH < 3.3 the protonated species predominate, with a maximum for the $[CuHC]^-$ species at pH 2.6, the proportion of the CuH_2C species increasing at lower pHs. Figure 5(b) displays similar behaviour for the *o*-PDTA–Cu(II) system, the protonated species predominating at pH < 3.3, the $[CuC]^{2-}$ species being the sole species at 100% complexation between pH 5.5–8.5.

The hydrolysis of the $[CuC]^{2-}$ species begins at pH > 8.5, to form the $[Cu(OH)C]^{3-}$ species. This hydrolysis is also observed in Fig. 5(a), where Z_B vs $-\log[H^+]$ curves are plotted. With the ligand : metal ratio 1 : 1, $Z_B > 4$ at pH > 8.5 (starting ligand H_4C), and with the ratio of 2 : 1, $Z_B > 8$ at pH > 8.5, indicating the titration of an acidity supplementary to that of the ligand, due to the formation of the complex $[Cu(OH)C]^{3-}$. Figure 5(b) indicates that the complex $[Cu(OH)C]^{3-}$ is formed starting from $[CuC]^{2-}$. The chelate ion $[CuC]^{2-}$ in the solid state is not aquated,[2] the formation reaction thus being

$$[CuC]^{2-} + OH^- \rightleftharpoons [Cu(OH)C]^{3-}$$

and the hexadentate ligand becomes pentadentate. The alternative would be that at a pH below 8.5, in aqueous solution, the complex $[CuC]^{2-}$ is aquated, in accord with the aquation reaction

$$[CuC]^{2-} + H_2O \rightleftharpoons [Cu(H_2O)C]^{2-}$$

the hexadentate ligand becomes pentadentate, and the subsequent hydrolysis reaction occurs

$$[Cu(H_2O)C]^{2-} \rightleftharpoons [Cu(OH)C]^{3-} + H^+,$$

but no evidence is available to enable a choice to be made between the two alternatives.

The values of $\log K$ for the complex $[CuC]^{2-}$ (Table 2) indicate that 3,4-TDTA is the strongest chelating agent, very probably due to the electron donor effect of the methyl radical which increases the electronic density on the N atoms. In contrast, no appreciable difference has been observed in this work in the coordinating capacity of 4-Cl-*o*-PDTA and *o*-PDTA with Cu(II).

Acknowledgements—This work has been carried out under the Agreement of Scientific and Academic Cooperation signed in 1984 between the Faculty of Chemistry of the University of La Laguna (ULL) and the Faculty of Science of the Central University of Venezuela (UCV). We wish to thank the Computer Center of the Faculty of Science (UVC) for computer time at Burroughs 6700; CONICIT (Caracas, Grant No. 51.78.31.S1–1228), CDCH (UCV, Grant No. C–03.12/83) and the Education Council of the Canary Islands Government (Grant No. 86/22.04.85) for financial support.

REFERENCES

1. E. F. K. McCandlish, T. K. Michael, J. A. Neal, E. C. Lingafelter and N. J. Rose, *Inorg. Chem.* 1978, **17**, 1383.
2. N. Nakasuka, S. Azuma, C. Katayama, M. Honda, J. Tanaka and M. Tanaka, *Acta Crystallogr., Sect. C: Cryst. Struct. Commun.* 1985, **C41**, 1176; S. Azuma, N. Nakasuka and M. Tanaka, *Acta Crystallogr., Sect. C: Cryst. Struct. Commun.* 1986, **C42**, 673; N. Nakasuka, S. Azuma and M. Tanaka, *Acta Crystallogr., Sect. C: Cryst. Struct. Commun.* 1986, **C42**, 1482.
3. N. Nakasuka, M. Kunimatsu, K. Matsumura and M. Tanaka, *Inorg. Chem.* 1985, **24**, 10; K. Matsu-

mura, N. Nakasuka and M. Tanaka, *Inorg. Chem.* 1987, **26**, 1419.
4. A. Mederos, J. V. Herrera and J. M. Felipe, *An. Quím.* 1985, **81**, 152; A. Mederos, J. V. Herrera and J. M. Felipe, *An. Quím.* 1987, **83**, 22.
5. A. Mederos, J. M. Felipe, M. Hernández-Padilla, F. Brito, E. Chinea and K. Bazdikian, *J. Coord. Chem.* 1986, **14**, 277.
6. A. Mederos, S. Domínguez, M. Hernández-Padilla, F. Brito and E. Chinea, *Bol. Soc. Quím. Perú* 1984, **50**, 277.
7. A. Mederos, J. M. Felipe, F. Brito and K. Bazdikian, *J. Coord. Chem.* 1986, **14**, 285.
8. F. Brito, A. Mederos, P. Gili, S. Domínguez and P. Martín Zarza, *J. Coord. Chem.* in press.
9. A. Mederos, J. V. Herrera, J. M. Felipe and M. L. Quesada, *An. Quím.* 1984, **80B**, 281.
10. A. Mederos, J. V. Herrera, J. M. Felipe and M. Hernández-Padilla, *An. Quím.* 1986, **82B**, 150.
11. I. M. Kolthoff, E. B. Sandell, E. J. Mechan and S. Bruckenstein, *Quantitative Chemical Analysis*, 4th Edn. Macmillan, London (1969).
12. F. Bermejo Martínez, *Tratado de Química Analítica*, 6th Edn. Dossat, Madrid (1981).
13. G. Schwarzenbach, *Las complexonas en el Análisis Químico*. Atlas, Madrid (1959).
14. F. Brito and N, Ingri, *An. Quím.* 1960, **56B**, 165.
15. G. Biedermann and L. G. Sillén, *Ark. Kemi* 1953, **5**, 425.
16. F. Brito and J. M. Gonçalves, Project No. 51.78.31-S1-1228. CONICIT, Caracas, Venezuela (1981).
17. R. Arnek, L. G. Sillén and O. Wahlberg, *Ark. Kemi* 1969, **31**, 353.
18. L. G. Sillén, *Acta Chem. Scand.* 1962, **16**, 159; L. G. Sillén and B. Warnqvist. *Ark. Kemi* 1969, **31**, 341.
19. R. N. Sylva and M. R. Davidson, *J. Chem. Soc., Dalton Trans.* 1979, 232.
20. A. Mederos, F. G. Manrique, J. V. Herrera, M. Alvarez-Romero and J. M. Felipe, *An. Quím.* 1986, **82B**, 133.
21. A. E. Martell and R. M. Smith, *Critical Stability Constants*, Volume 1. Amino Acids, pp. 206–207. Plenum Press, New York (1974).
22. A. Mederos. A. Benitez, A. Rancel, R. Guerra, F. Brito, K. Bazdikian and J. Bruzal, *J. Coord. Chem.* 1986, **15**, 85.
23. M. L. Rodriguez, P. Gili, A. Mederos, P. Martín-Zarza, S. Domínguez and A. Perez-Monje, Reunión Científica del Grupo Especializado de Química Inorgánica de la Real Soc. Esp. de Química, Salamanca, Spain, Com. P-53 (1987).

Polyhedron Vol. 7, No. 13, pp. 1197–1202, 1988
Printed in Great Britain

0277–5387/88 $3.00+.00
© 1988 Pergamon Press plc

THE PENTACYANONITROSYLFERRATE ION—V*. THE COURSE OF THE REACTIONS OF NITROPRUSSIDE WITH A RANGE OF THIOLS

ANTHONY R. BUTLER, ADRIANNE M. CALSY-HARRISON and CHRISTOPHER GLIDEWELL†

Chemistry Department, University of St. Andrews, KY16 9ST, U.K.

and

POUL E. SØRENSEN

Chemistry Department A, The Technical University of Denmark, DK-2800, Lyngby, Denmark

(*Received* 14 *January* 1988; *accepted* 1 *February* 1988)

Abstract—Thiols RSH (RSH = MeSH, cysteine, N-acetylcysteine, 2-methylcysteine, N-acetyl-2-methylcysteine, penicillamine, N-acetylpenicillamine and glutathione) react with nitroprusside ($[Fe(CN)_5NO]^{2-}$, pentacyanonitrosylferrate(2−)) to give, via the intermediates $[Fe(CN)_5N(O)SR]^{3-}$ and $[Fe(CN)_5NO]^{3-}$, the pentacoordinate iron(I) complex $[Fe(CN)_4NO]^{2-}$. The fate of this complex depends crucially upon the reaction conditions; in the presence of oxygen, $[Fe(CN)_4NO]^{2-}$ can reform $[Fe(CN)_5NO]^{2-}$ to give an effective stoichiometry of RS^- to $[Fe(CN)_5NO]^{2-}$ substantially greater than 1 : 1; in the absence of oxygen and with a stoichiometric ratio of 1 : 1, the $[Fe(CN)_4NO]^{2-}$ follows a well established pathway to yield $[Fe(CN)_6]^{4-}$, Fe^{2+} and NO; in the absence of oxygen and with an excess of the RS^- ligand, substitution occurs at $[Fe(CN)_4NO]^{2-}$ to give firstly $[Fe(NO)_2(SR)_2]^-$ and subsequently $[Fe_2(SMe)_2(NO)_4]$ (where R = Me) or $[Fe_4S_3(NO)_7]^-$ (when R = H). For every R except R = H, decomposition of the initial adduct $[Fe(CN)_5N(O)SR]^{3-}$ yields the disulphide RSSR; when R = H, elemental sulphur is formed.

The kinetics of the reactions of thiols RSH and thiolate anions RS^- with the nitroprusside ion, pentacyanonitrosylferrate(2−) $[Fe(CN)_5NO]^{2-}$, have been rather extensively studied.[2–5] The initial step in the reaction is attack by the thiolate anion RS^- on the nitrogen atom of the nitrosyl ligand:[5] this is comparable to the initial step in the reactions of other oxygen-, nitrogen- and carbon-centred[6–15] nucleophiles with nitroprusside, eq. (1):

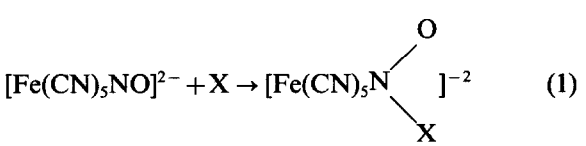

$$[Fe(CN)_5NO]^{2-} + X \rightarrow [Fe(CN)_5N(O)X]^{-2} \quad (1)$$

where X = ^-OH (ref. 6), ^-SH (ref. 2), NH_2R (refs 7, 8), ^-NHR (ref. 9), NHR_2 (ref. 10), $^-CHR_2$ (refs 1, 11–14), ^-SR (refs 3–5, 16, 17).

In some cases,[3] the primary intermediate $[Fe(CN)_5N(O)SR]^{3-}$ has been observed to decay to a paramagnetic species, characterized by $g = 2.024$, $A(^{14}N) = 15$ G (1N), which can also be obtained by reduction of nitroprusside electrochemically,[3] or by use of borohydride, ascorbic acid, quinol or dithionite,[3] or superoxide.[18] This paramagnetic species, commonly described in the literature as $[Fe(CN)_5NO]^{3-}$ (although formulations such as $[Fe(CN)_5NOH]^{2-}$ and $[Fe(CN)_5NO_2]^{5-}$ have also been suggested), is[19] in fact $[Fe(CN)_4NO]^{2-}$, presumably formed in every case by very fast[20] dissociation of $[Fe(CN)_5NO]^{3-}$. Apart from these observations[3] of $[Fe(CN)_4NO]^{2-}$, together with the identification[3] of the disulphide RSSR cor-

*For Part IV, see ref. 1.

†Author to whom correspondence should be addressed.

responding to the initial thiol RSH when RSH was PhSH,[3] $PhCh_2SH$[3] or cysteine,[4] essentially nothing is known of the subsequent course of the reaction between nitroprusside and thiols.

In this paper we report the determination of the reaction stoichiometry and the final products, and the identification of a number of the intermediates, for a wide range of thiols.

RESULTS

Final products

For all the thiols RSH examined in this study, except H_2S, the final products of similar reactions were the corresponding disulphide, identified in most examples by ^1H and ^{13}C NMR spectroscopy, and hexacyanoferrate(II) $[Fe(CN)_6]^{4-}$ again identified[21] by ^{13}C NMR spectroscopy. When H_2S was the thiol, $[Fe(CN)_6]^{4-}$ was again formed along with elemental sulphur. Nitrogen(II) oxide was identified as a product of the reactions of several thiols with nitroprusside.

The products and intermediates which were unambiguously identified are summarized, for each of the thiols studied, in Table 1.

Reaction stoichiometry

When the primary adduct $[Fe(CN)_5N(O)SR]^{3-}$ formed from nitroprusside and thiolate anions decomposes, the characteristic[3,4,5] purple colour fades: however if the thiolate is in excess, then aeration of the faded solution regenerates the purple adduct. The sequence of aeration, followed by fading of the newly purple solution, followed by further aeration can be repeated many times; in this way, nitroprusside has been made[4] to oxidize up to ten molar equivalents of cysteine to cystine.

We have confirmed these observations[4] and find from NMR titrations that, in air, typical stoichiometric ratios of thiolate: nitroprusside lie in the range 2:1 to 4:1. However, when oxygen is rigorously excluded, the reaction stoichiometry is precisely 1:1. The simplest rationalization of the effect of oxygen is in terms of eq. (2):

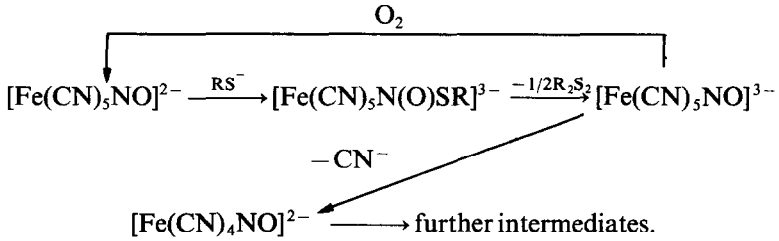

(2)

Table 1. Formation[a] of intermediates and products in the reactions of RS^- with $[Fe(CN)_5NO]^{2-}$

RSH	$[Fe(CN)_5N(O)SR]^{3-}$ λ_{max} (nm)	Intermediates $[Fe(CN)_4NO]^{2-}$	Intermediates $[Fe(NO)_2(SR)_2]^-$	Final products $[Fe(CN)_6]^{4-}$	Final products RSSR
H_2S	570	+	+[b]	+	[c]
MeSH	522	+	+[b]	+	[d]
Cysteine	522	+	−	+	[d]
N-acetylcysteine	522	+	+[e]	+	+
2-Methylcysteine	521	n.s.	−	+	+
N-acetyl-2-methylcysteine	520	+	+[e]	n.s.	n.s.
Penicillamine[f]	526	n.s.	−	+	+
N-acetylpenicillamine	525	+	+[e]	+	+
Glutathione[g]	520	+	−	+	+

[a] Product observed, +; product not observed, −; not studied, n.s.; $[Fe(CN)_4NO]^{2-}$ and $[Fe(NO)_2(SR)_2]^-$ identified by EPR spectroscopy; $[Fe(CN)_6]^{4-}$ and RSSR identified by ^{13}C NMR spectroscopy, except as noted.

[b] Observed only with excess of RS^-.

[c] Elemental sulphur (but not HSSH) isolated and identified by mass spectrometry.

[d] Water-insoluble RSSR isolated prior to identification.

[e] Observed as a minor product in reactions at 1:1 stoichiometry.

[f] 2,2-Dimethylcysteine.

[g] Ref. 30.

The reduced anion $[Fe(CN)_5NO]^{3-}$ is known[20] from pulse radiolysis work to be the primary product of electron attachment to nitroprusside, which furthermore undergoes[20] very rapid dissociation to yield $[Fe(CN)_4NO]^{2-}$. This latter cyanoferrate is that observed by EPR spectroscopy in the reactions of thiolates with nitroprusside (ref. 2 and Table 1), and probably arises by the same route; the $[Fe(CN)_5NO]^{3-}$ having been formed by the loss of $RS^{\bullet}$ or $\frac{1}{2}R_2S_2$ from the purple adduct $[Fe(CN)_5N(O)SR]^{3-}$.

The intermediate $[Fe(CN)_5NO]^{3-}$ is formed by a reaction between RS^- and $[Fe(CN)_5NO]^{2-}$ of 1 : 1 stoichiometry: in the absence of air it all decays to $[Fe(CN)_4NO]^{2-}$. However, in the presence of oxygen at least part of the $[Fe(CN)_5NO]^{3-}$ is oxidized, reforming $[Fe(CN)_5NO]^{2-}$ which can react with further RS^-, so giving an overall stoichiometry, in air, with the ratio RS^- : $[Fe(CN)_5NO]^{2-}$ greater than 1 : 1.

While the recycling back to $[Fe(CN)_5NO]^{2-}$ was observed with most of the thiols in Table 1 (and with homocysteine), no such recycling was observed with the sterically hindered thiols $HSCMe_2CH(NH_2)COOH$ (penicillamine) and $HSCEt_3$.

Identified intermediates

The initial adduct is[4] of type $[Fe(CN)_5N(O)SR]^{3-}$: for a wide range of thiols RSH, except for H_2S, the adduct has λ_{max} in the range 520–526 nm (Table 1). Thioglycolic acid and 2-mercaptoethanol gave[3] similar adducts having λ_{max} of 522 nm.

The hydrogen sulphide anion HS^- is a unique thiolate, because of the possibility of further proton loss from its initial adduct with nitroprusside. The kinetics of the reaction of HS^- with nitroprusside were interpreted[2] in terms of an initial species A, which was then converted to a second species B. The formation of A was first-order in each of nitroprusside and HS^-, while the conversion of A to B was first-order in A only, and was independent of both pH and HS^- concentration.[2] A and B were identified[2] as $[Fe(CN)_5N(O)SH]^{3-}$ and $[Fe(CN)_5NOS]^{4-}$, respectively, although λ_{max} for A, 570 nm, is markedly different from that of other $[Fe(CN)_5N(O)SR]^{3-}$ species (Table 1). Nor has the constitution of B been fully established.[22]

Loss of either $RS^{\bullet}$ or $\frac{1}{2}R_2S_2$ from the primary adduct $[Fe(CN)_5N(O)SR]^{3-}$ yields the known[20] $[Fe(CN)_5NO]^{3-}$, which in the absence of oxygen decays[20] to the paramagnetic $[Fe(CN)_4NO]^{2-}$.[23] When RSH is cysteine, the decay of the primary adduct $[Fe(CN)_5N(O)SR]^{3-}$ has been shown[4] to follow first-order kinetics: this suggests that the initial decay products are $[Fe(CN)_5NO]^{3-}$ and the thiyl radical $RS^{\bullet}$, eq. (3), but it has not yet proven possible to detect or trap such thiyl radicals in these reactions:

$$[Fe(CN)_5N(O)SR]^{3-} \rightarrow [Fe(CN)_5NO]^{3-} + RS^{\bullet}. \quad (3)$$

The square-pyramidal[23] five-coordinate complex $[Fe(CN)_4NO]^{2-}$ is substitution labile[24] and in the presence of a 10–20-fold molar excess of RS^- (for R = H or Me) the characteristic[19] EPR spectrum of $[Fe(CN)_4NO]^{2-}$ is rapidly replaced by those of the known[25] dinitrosyl complexes $[Fe(NO)_2(SH)_2]^-$ and $[Fe(NO)_2(SMe)_2]^-$; (R = H: $g = 2.027$, $A(^{14}N) = 2.7$ G, $A(^1H) = 0.5$ G; R = Me: $g = 2.027$, $A(^{14}N) = 2.1$ G, $A(^1H) = 2.1$ G). The resulting conversion of an $\{Fe(NO)\}^7$ complex to an $\{Fe(NO)_2\}^9$ complex is yet another example of the very easy interconversion of $[Fe(NO)]^{2+}$ and $[Fe(NO)_2]^+$ fragments.

The mononuclear dinitrosyls $[Fe(NO)_2(SH)_2]^-$ and $[Fe(NO)_2(SMe)_2]^-$ are known[25,26] precursors of tetranuclear $[Fe_4S_3(NO)_7]^-$ and dinuclear $Fe_2(SMe)_2(NO)_4$, respectively: on a preparative scale, similar oxygen-free reactions of $[Fe(CN)_5NO]^{2-}$ with an excess of HS^- or MeS^- gave isolated purified yields of $Na[Fe_4S_3(NO)_7]$ (when $RS^- = HS^-$, yield 26%) or $Fe_2(SMe)_2(NO)_4$ (when $RS^- = MeS^-$, yield 7.2%).

Similar paramagnetic species having g values slightly higher than the primary paramagnetic complex $[Fe(CN)_4NO]^{2-}$ have previously been observed[3] in reactions between $[Fe(CN)_5NO]^{2-}$ and $HOCH_2CH_2SH$, $HSCH_2COOH$ or PhSH: these species were not identified,[3] but the formulation $[Fe(CN)_5NHSR]^{3-}$ (containing the neutral radical ligand $RSNH^{\bullet}$) was suggested. We can now, with some confidence, reassign these in every case as $[Fe(NO)_2(SR)_2]^-$, having R = CH_2CH_2OH, CH_2COOH and Ph, respectively.

The observation noted above, that with an excess of HS^- nitroprusside yields $[Fe(CN)_4NO]^{2-}$ which in turn reacts with HS^- to give $[Fe(NO)_2(SH)_2]^-$, must call into question the published[2] interpretation of the kinetics of the reaction of $[Fe(CN)_5NO]^{2-}$ with HS^-: typical molar ratios of HS^- to $[Fe(CN)_5NO]^{2-}$ were[2] 80 : 1. Hence the interpretation[2] of species A and B as $[Fe(CN)_5N(O)SH]^{3-}$ and $[Fe(CN)_5NOS]^{4-}$, respectively, seems unlikely to be complete. Under the conditions used in the kinetic study,[2] we have identified, in succession $[Fe(CN)_4NO]^{2-}$, $[Fe(NO)_2(SH)_2]^-$ and $[Fe_4S_3(NO)_7]^-$, but we have no unambiguous evidence for the existence of $[Fe(CN)_5NOS]^{4-}$. The identified intermediates are summarized in Table 1.

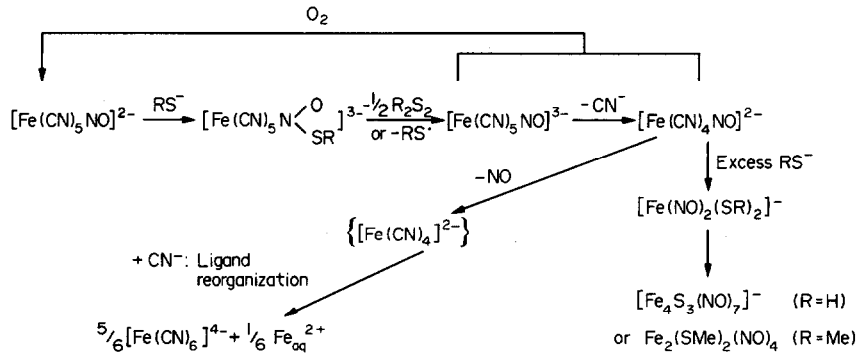

Scheme 1.

Reaction mechanism

The overall mechanistic scheme for the reaction between nitroprusside and thiols is given in Scheme 1. In terms of this scheme, three distinct reaction pathways can be defined dependent upon the initial ratio of RS^- to $[Fe(CN)_5NO]^{2-}$ and upon the presence or absence of atmospheric oxygen.

(i) *Oxygen present.* Part or all of the $[Fe(CN)_5NO]^{3-}$ (or possibly $[Fe(CN)_4NO]^{2-}$ and CN^-) is oxidized back to $[Fe(CN)_5NO]^{2-}$. If a molar excess of RS^- over initial $[Fe(CN)_5NO]^{2-}$ is present, the reformed $[Fe(CN)_5NO]^{2-}$ will react with further RS^- to give an effective stoichiometric ratio of RS^- to $[Fe(CN)_5NO]^{2-}$ greater than 1 : 1.

(ii) *Oxygen absent and no initial excess of* RS^-. All of the $[Fe(CN)_4NO]^{2-}$ loses NO and after re-addition of the cyanide ion lost earlier and ligand reorganization, yields $[Fe(CN)_6]^{4-}$, together with Fe^{2+}_{aq}.

(iii) *Oxygen absent and* RS^- *present in excess.* Ligand substitution occurs in $[Fe(CN)_4NO]^{2-}$ to yield, after nitrosyl ligand migration[25] and redox disproportionation,[25] $[Fe(NO)_2(SR)_2]^-$.

With the single exception of the postulated intermediate, $[Fe(CN)_4]^{2-}$ arising from loss of NO from $[Fe(CN)_4NO]^{2-}$, all of the intermediates and products in Scheme 1 have been identified and characterized, mainly by us, but $[Fe(CN)_5NO]^{3-}$ and Fe^{2+}_{aq} by others.[20,27]

In Table 1, we summarize the identified intermediates and products for each of the thiols studied in the present work. In addition to the results of Table 1, we note that $[Fe(CN)_4NO]^{2-}$ was formed, although not identified as such,[3] when RSH was $HSCH_2CH_2OH$, $HSCH_2COO^-$, HSPh and $HSCH_2Ph$.

Kinetics

The kinetics of the initial adduct-forming step, eq. (4), have been studied by Wilkins[5] for a range of thiols, using temperature-jump methods and the values of k_f and k_d established.

$$[Fe(CN)_5NO]^{2-} + RS^- \underset{k_d}{\overset{k_f}{\rightleftharpoons}} [Fe(CN)_5N(O)SR]^{3-}. \quad (4)$$

We have extended the range of thiols studied to include penicillamine $HSCMe_2CH(NH_2)COOH$, N-acetylpenicillamine and homocysteine $HSCH_2CH_2CH(NH_2)COOH$. The relaxations were effectively first-order and with nitroprusside in excess over the thiol the relaxation time τ is given by eq. (5):

$$\tau^{-1} = k_f[Fe(CN)_5NO]^{2-} + k_d. \quad (5)$$

The resulting values of k_f and k_d are given in Table 2 and confirm further that the variation of k_f and k_d with structural variation adjacent to the thiol centre is very slight. For all the thiols studied, here and elsewhere,[5] the overall range of k_f and k_d is small. In all cases k_f is of the order of 10^4 s^{-1} dm^3 mol^{-1}.

Table 2. Rate constants for adduct-forming equilibria

Thiol	pH	k_f (s^{-1} dm^3 mol^{-1})	k_d (s^{-1})
Penicillamine	11.2	1.50×10^4	3.90×10^3
N-acetylpenicillamine	11.2	1.75×10^4	2.55×10^3
Homocysteine	10.5	1.33×10^4	2.47×10^3

DISCUSSION

The course of the reaction between RS^- and $[Fe(CN)_5NO]^{2-}$ established above (Scheme 1) is clearly entirely different from those which have been described for other nucleophiles such as OH^-,[6] primary and secondary amines,[7-10] and simple carbanions.[11-14] In such cases the initial adduct $[Fe(CN)_5N(O)X]^{2-}$ arising from the addition of the nucleophile X to nitroprusside [eq. (1)] decomposes in a dissociation reaction giving $[Fe(CN)_5H_2O]^{3-}$ and XNO which undergoes further reaction. The eventual products from XNO are NO_2^- (when $X = OH^-$), ROH (when $X = RNH_2$),[7,8] R_2NNO (when $X = R_2NH$),[10] or $R_2C=NOH$ (when $X = {}^-CHR_2$).[11-14] For each of these nucleophile types, the nitrosyl ligand is incorporated into the final products: when $X = RNH_2$, the final products are ROH and N_2 where one atom of the each dinitrogen molecule arises from the nitrosyl ligand of $[Fe(CN)_5NO]^{2-}$, and the other atom from RNH_2.

In contrast, the reaction of $[Fe(CN)_5NO]^{2-}$ with RS^- does not generate any product which incorporates the nitrosyl ligand. A strict parallel with the reactions of amines and carbanions would suggest that the S-nitrosothiol, RSNO, is the primary product XNO. However, we have never observed such products, even from reactions using thiols like N-acetylpenicillamine which are known[28] to form highly stable S-nitroso derivatives. Rather, the reactions proceed as indicated in Scheme 1 and the nitrosyl ligand is liberated as neutral NO. For reactions *in vitro* in the absence of oxygen, the NO is lost from the reaction and is readily identified by IR spectroscopy. In reactions *in vivo*, the NO may be trapped, for example, by haem groups, as a nitrosylhaem.[29,30]

Now that the course of the reactions of thiols with nitroprusside have been delineated, it seems probable that several of the kinetic studies of these reactions[3-5] will require re-evaluation.

EXPERIMENTAL

Except where stated otherwise, thiols were purchased from Sigma and were used as received. NaSH and NaSMe were prepared by the reaction of metallic sodium with H_2S or Me_2S_2, in ethanol or liquid ammonia, respectively. A sample of Et_3CSH was kindly donated by Prof. Sir Derek Barton, FRS.

Preparation of 2-methylcysteine

A mixture of acetaldehyde (158 cm^3), hippuric acid (56.5 g) and sodium acetate (26.0 g) was refluxed in acetic anhydride (158 cm^3) for 3 h. The mixture was cooled and ice-cold water was added to precipitate 4-ethylidene-2-phenyl-5-oxazolone (44.1 g, 75%): δ (^1H) ($CDCl_3$ solution); 2.2 (d, 3H), 6.8 (q, 1H), 7.6–8.1 (m, 5H). A solution of oxazolone (39.7 g) in toluene (210 cm^3) was added slowly, at 5–10°C, to a solution formed from sodium metal (10.6 g) and benzyl mercaptan (25 cm^3) in dry methanol (200 cm^3). The mixture was stirred overnight and then acidified with aqueous HCl (Congo Red). The solvent was removed and the resulting syrup was dissolved in glacial acetic acid (500 cm^3) and refluxed for 1 h. The mixture was cooled to 4°C overnight and the resulting precipitate filtered off and washed successively with acetic acid and water to provide 1-(N-benzoylamino)-2-benzylthiobutyric acid (21.0 g, 30%). This was suspended in a mixture of 85% formic acid (325 cm^3), concentrated hydrochloric acid (325 cm^3), and water (325 cm^3), and the whole refluxed for 4 h. The solvent mixture was removed and the residue extracted with hot petroleum (b.p. 60–80°C) (2 × 250 cm^3) and then with hot water (2 × 250 cm^3). The aqueous extract was filtered, neutralized with ammonia and concentrated to 65 cm^3. Cooling this solution precipitated 1-amino-2-benzylthiobutyric acid (11.0 g, 77%): δ (^1H) ($CDCl_3$ solution); 1.3 (d, 3H), 2.1 (s, 2H), 3.4 (m, 1H), 3.7 (s, 2H), 5.0 (d, 1H), 7.3 (m, 5H).

The foregoing amino acid (2.0 g) was dissolved in a solution of sodium (0.83 g) in liquid ammonia (55 cm^3). Ammonium chloride (1.86 g) was added and the solvent removed. Concentrated hydrochloric acid (0.70 cm^3) was added and the solid residue extracted with ether (3 × 30 cm^3). The residue was then extracted with warm ethanol (3 × 15 cm^3). The ethanol was removed and replaced by 120 cm^3 of ether/ethanol (10:1 *v/v*), and the resulting solution was cooled overnight to yield 2-methylcysteine (0.31 g, 26%).

Instruments

NMR spectra were recorded on a Bruker AM-300 spectrometer, EPR spectra on a Bruker ER200D spectrometer with d-*t*-butyl nitroxide as the standard for the measurement of line positions, and electronic spectra on a Pye-Unicam SP8-100 spectrophotometer. Fast kinetics were measured using a Messenlager *T*-jump apparatus.

REFERENCES

1. A. R. Butler, A. M. Calsy and C. Glidewell, *J. Organomet. Chem.*, in press.
2. P. A. Rock and J. H. Swinehart, *Inorg. Chem.* 1966, **5**, 1058.

3. D. Mulvey and W. A. Waters, *J. Chem. Soc., Dalton Trans.* 1975, 951.
4. P. J. Morando, E. B. Borghi, L. M. de Schteingart and M. A. Blesa, *J. Chem. Soc., Dalton Trans.* 1981, 435.
5. M. D. Johnson and R. G. Wilkins, *Inorg. Chem.* 1984, **23**, 231.
6. J. H. Swinehart and P. A. Rock, *Inorg. Chem.* 1966, **5**, 573.
7. A. R. Butler, C. Glidewell, J. Reglinski and A. Waddon, *J. Chem. Res.* 1984, (S), 279, (M) 2768.
8. L. Dózsa, V. Kormos and M. T. Beck, *Inorg. Chim. Acta* 1984, **84**, 69.
9. R. Nast and J. Schmidt, *Z. Naturforsch. B* 1977, **23B**, 469.
10. J. Casado, M. Mosquera, M. F. Rodriguez Prieto and J. Vazquez Tato, *Ber. Bunsenges. Phys. Chem.* 1985, **89**, 735.
11. J. H. Swinehart and W. G. Schmidt, *Inorg. Chem.* 1967, **6**, 232.
12. S. K. Wolfe and J. H. Swinehart, *Inorg. Chem.* 1968, **7**, 1855.
13. N. Y. M. Iha and H. E. Toma, *Inorg. Chim. Acta* 1984, **81**, 181.
14. A. R. Butler, C. Glidewell, V. Chaipanich and J. McGinnis, *J. Chem. Soc., Perkin Trans 2* 1986, 7.
15. For a review: A. R. Butler and C. Glidewell, *Chem. Soc. Rev.*, in press.
16. K. Antal, I. Banyai and M. T. Beck, *J. Chem. Soc., Dalton Trans.* 1985, 1191.
17. M. Jakševac-Mikša, V. Hankonyi and V. Karas-Gašparec, *Z. Phys. Chem. (Leipzig)* 1980, **261**, 1041.
18. H. P. Misra, *J. Biol. Chem.* 1984, **259**, 12678.
19. C. Glidewell and I. L. Johnson, *Inorg. Chim. Acta* 1984, **132**, 145.
20. R. P. Cheney, M. G. Sijmic, M. Z. Hoffman, I. A. Taub and K.-D. Asmus, *Inorg. Chem.* 1977, **16**, 2187.
21. A. R. Butler, C. Glidewell, A. S. McIntosh, D. Reed and I. H. Sadler, *Inorg. Chem.* 1986, **25**, 970.
22. E. J. Baran and A. Müller, *Angew Chem. Int. Ed. Engl.* 1969, **8**, 890.
23. J. Schmidt, H. Kühr, W. L. Dorn and J. Kopf, *Inorg. Nucl. Chem. Letts* 1974, **10**, 55.
24. J. Fiedler and J. Mašek, *Inorg. Chim. Acta* 1984, **81**, 117.
25. A. R. Butler, C. Glidewell, A. R. Hyde and J. C. Walton, *Polyhedron* 1985, **4**, 797.
26. A. R. Butler and C. Glidewell, *Adv. Inorg. Chem.* 1988, **32**, 335.
27. N. G. Giniyatullin and Yu. M. Kargin, *Izv. Vysch. Uchebn. Zaved. Khim. Khim. Tekhnol.* 1976, **19**, 1668; *Chem. Abs.* 1977, **86**, 64862 r.
28. L. Field, R. V. Dilts, R. Ravichandran, P. G. Lenhert and G. E. Carnahan, *J. Chem. Soc., Chem. Commun.* 1978, 249.
29. A. R. Butler, C. Glidewell, I. L. Johnson and A. S. McIntosh. *Inorg. Chim. Acta* 1987, **138**, 159.
30. A. R. Butler, A. M. Calsy-Harrison, C. Glidewell, I. L. Johnson, J. Reglinski and W. E. Smith, *Inorg. Chim. Acta* 1988, **151**, 281.

Polyhedron Vol. 7, No. 13, pp. 1203–1206, 1988
Printed in Great Britain

0277–5387/88 $3.00+.00
© 1988 Pergamon Press plc

THE MECHANICAL NATURE OF THE *TRANS*-EFFECT IN LIGAND SUBSTITUTION REACTIONS OF SQUARE-PLANAR COMPLEXES

A. V. BABKOV

Sechenov First Moscow Medical Institute, 2 B. Pirogovskaya St, Moscow, U.S.S.R.

(*Received* 21 *October* 1986; *accepted* 5 *February* 1988)

Abstract—The kinetic *trans*-effect in associative ligand substitution reactions of square-planar complexes is explained theoretically on the basis of the angular deformability of the bond in the *trans*-activating ligands. The ability of these ligands, under the condition of low energy input, to leave the plane of the complex determines the ease with which the transition of the complex into the pentacoordinate state takes place in the substitution process. The most general property of ligands exhibiting a strong *trans*-effect is the large angular unfolding of the donor orbital in the direction of the central atom. This facilitates coordination between the bond-cleaving process and the formation of chemical bonds in the intermediate compound.

The idea of the *trans*-effect[1–3] emerged in the course of the development of the theoretical concepts about the nature of the Chernyaev *trans*-influence.[3] Despite the considerable progress made in the research on the *trans*-effect during the last three decades on the basis of the chemical bond theory and quantum-chemical calculations,[4,5] there is still no complete and consistent explanation of this phenomenon. There was insufficient knowledge as to what factors determine the *trans*-effect and the interrelationship between the *trans*-effect and the mutual influence of the ligands. There was also no clear understanding about the nature of the so-called σ-*trans*-effect. These difficulties were largely due to a failure up to now to explain the mechanism of the *trans*-effect. The theory of the π-*trans*-effect explains to a certain extent the reduced energy of the transition state in the presence of a π-acceptor ligand in the *trans*-position with respect to the leaving group. However, this theory does not consider how the *trans*-activating ability of the ligand is realized in the formation of the pentacoordinate intermediate. Thus, it seems that the *trans*-effect, which is clearly evident in experiments, becomes nebulous when it is analysed theoretically.

The purpose of the present work is to formulate a mechanical approach to explaining the *trans*-effect and to substantiate this approach with the help of electronic concepts.

We shall regard the location line of the central atom and the two ligands (one of which represents the leaving group) as the active coordinate of the complex, and the ligands on this coordinate in the *trans*-position with respect to the leaving group as the *trans*-activating ligand (conditionally). Here we shall consider mainly square-planar complexes of platinum(II) since the *trans*-effect appears most clearly in the reactions of these complexes.

It has been reliably established[6,7] that associative ligand substitution reactions pass through a pentacoordinate trigonal–bipyramidal intermediate. The leaving group (L), entering group (E) and *trans*-activating group (A) in the intermediate are on a trigonal plane. When the angle L—Pt—A is 180° in the starting complex, it is close to 120° in the intermediate compound (Fig. 1). Therefore, in the course of the substitution reaction a bending of the active coordinate takes place. If the complex contains at least one ligand which relatively easily (at a low energy input) deviates from the complex plane, it will determine the flexibility of the coordinate. And it is this coordinate which will become active in the substitution reaction.

It is usually thought that in the substitution process the leaving group becomes displaced from the plane of the complex. However, this view was not subjected to direct verification and it may well have prevented a correct understanding of the mechanism of the *trans*-effect. Let us try to explain this phenomenon from the "other end" of the active

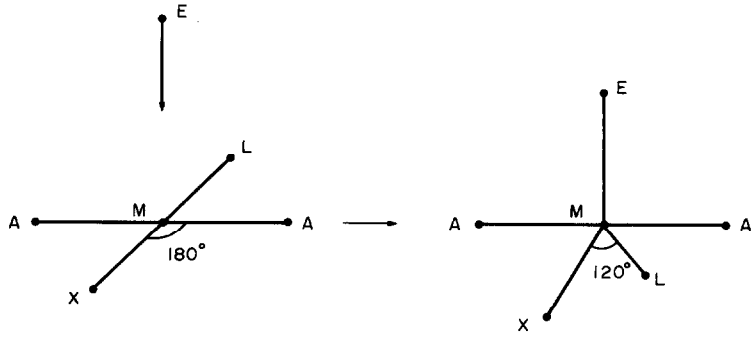

Fig. 1. Deflection of the active coordinate of the complex during transition into the pentacoordinate state.

coordinate. Let us assume that the *trans*-effect is a manifestation of the angular mobility of the *trans*-activating ligand, in other words, of the ability of its bond with the central atom to undergo angular deformation, with this bond remaining sufficiently strong, stronger than the bond of the leaving group. What is meant here by angular deformability is the fact that the bending of the bond in the direction in which the ligand leaves the complex plane requires only a small amount of energy. Of the two ligands, the one which can be removed from the plane of the complex with less energy is characterized by a larger angular deformation of the bond. Further, the stability of the metal–ligand bond and the angular deformation of this same bond will be considered as two different and relatively independent characteristics; thus, for example, the stable M—A bond can be simultaneously characterized by a large angular deformation.

As a result of the deformation of the complex, along the active (flexible) coordinate a site becomes free in the coordination sphere of the central atom for the attachment of a fifth ligand. Regardless of whether the given mobile (in the sense defined above) ligand has a *trans*-influence on the second ligand, which is aligned on the same coordinate, this second ligand, owing to the ease with which it deviates from the plane of the complex, facilitates the formation of a pentacoordinated intermediate compound upon a small increase in potential energy. The second ligand on the active coordinate appears in the trigonal plane as if accidentally, irrespective of its own properties and of the mutual influence of the ligands. This shows that the concept of the "*trans*-activating" ligand is of a conditional nature. Actually, the *trans*-effect amounts to labilization of the complex; and this labilization is the more pronounced, the greater the angular mobility of at least one of the ligands that makes up its composition. This phenomenon is of the nature of the *trans*-effect owing to the specific geometry of the pentacoordinated intermediate. Therefore, we can consider that the very presence of the *trans*-effect confirms the trigonal–bipyramidal structure of the intermediate compound in associative substitution reactions in square-planar complexes.

The pentacoordinate intermediate $M(X)_2ALE$ goes over to the plane of the tetracoordinate complex, detaching in the process one of the ligands located in the trigonal plane. Depending on the strength of the bonds between the A, L and E ligands and the central atom, the following cases are possible.

(1) The least stable is the bond of ligand L which does not deform easily. This ligand splits off from the inner sphere of the complex; and the apparent cause of its quick substitution is the *trans*-effect of ligand A with its readily deformable bond.

(2) The readily deformable M—A bond is at the same time the least stable. In this case the *trans*-effect is absent. Ligand A itself becomes a leaving group characterized by a sufficiently high rate of substitution. Complexes $[PtdienX]^+$ can serve as an example (here, $X = Cl^-, I^-$). Trident ligand N-(2-aminoethyl)-1,2-diaminoethane (dien) should be characterized by sufficient rigidity of the bonds and the substitution of X proceeds through the angular deformation of Pt—X bonds. With $X = I^-$ the rate constant of the conversion into thiourea is greater than in the case where $X = Cl^-$.[8] This corresponds to the position of ligands in a series of decreasing *trans*-labilizing ability, which, according to what has been said above, should coincide with a series of decreasing angular mobility of the same ligands.

(3) The least stable is the bond of the fifth attached ligand E, which should play the role of the entering group. However, in the majority of elemental transformations the intermediate compound decomposes, followed by the detachment of this ligand. Therefore, the substitution proceeds at a slow rate. For example, in the $[PtdienX]^+$ com-

plexes under consideration, the exchange of Cl^- takes place at a higher rate constant than the substitution of I^- by Cl^-.[9] Further, one can assume that a stable complex, in which the ligands are characterized by a high angular mobility, in reacting with solvent molecules becomes transformed into the trigonal–bipyramidal state. A considerable portion of its molecules can remain in this state in solution.

It should be emphasized that the proposed approach in explaining the *trans*-effect holds true also in the presence of three identical ligands in the trigonal plane of the complex; for example, in the case of the substitution reactions of the type:

$$PtX_4^{2-} + X^{*-} \rightarrow PtX_3X^{*2-} + X^-.$$

The deformation of the active coordinate for such reactions is determined by the angular mobility of both the ligands in the molecule.

The mechanical concept of the *trans*-effect makes it possible to have an effective approach to analysing the properties of the electronic structure which determine this phenomenon. The most important factor on which the angular deformation of bonds depends is apparently the ease with which free p_z-orbitals of metal can be drawn into sp^3d-hybridization when a pentacoordinate complex is formed. This should be facilitated by the presence, in the donor atoms of the ligands, of electron pairs on orbitals characterized by a large angular unfolding in the direction of the central atom. To such orbitals belong spherical as well as sufficiently diffuse (expanded) nodular orbitals. The angular deformation is accompanied by a weakening of the bond due to a decrease in the density of overlapping of the ligand orbital with the dsp^2-orbital of the metal. However, in the case where the orbital of the ligand is strongly spread in the direction of the central atom and has a large transverse diameter, the decrease in the overlapping density with the dsp^2-orbital is considerably compensated for by the transfer of electron density onto the p_z-orbital of the metal. It is this concurrent weakening of the interaction between the donor atom in the ligand and one orbital of the metal, on the one hand, and an intensification of the interaction between the donor atom in the ligand and another orbital, on the other, that facilitates the formation of a pentacoordinate complex with a relatively small increase in potential energy.

This principle of the concurrence of the weakening and stabilization of bonds makes it possible to explain the strong *trans*-effect of the hydride ion, which has electrons on a spherical *s*-orbital. In hydride complexes of Pt(II) this orbital, even at a small angular deformation, becomes effectively

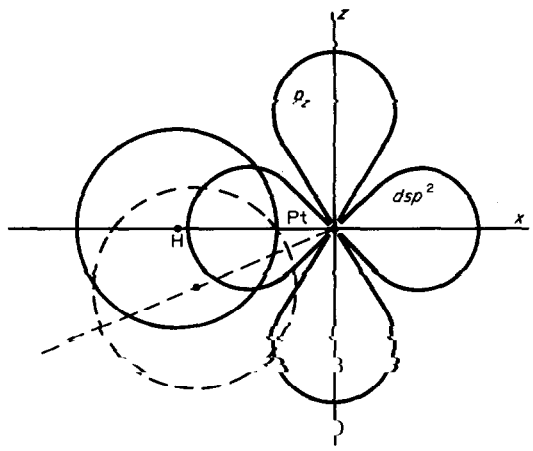

Fig. 2. Overlapping of the spherical orbital of the hydride ion with the $6p_z$-orbital of platinum during angular deformation of the bond.

overlapped with the $6p_z$-orbital of Pt (Fig. 2). Phosphines, which are characterized by a strong *trans*-effect, also form σ-bonds with platinum owing to the presence of an electron pair which is predominantly *s*-type. Olefins, which exhibit a very pronounced *trans*-effect, are one more example of ligands having expanded, strongly unfolded orbitals towards the central atom. The mechanism of the overlapping of orbitals in the Pt complex formed with ethylene, as proposed by Chatt and Duncanson,[10] clearly shows a large unfolding of the $2p\pi$-orbitals of ethylene in the direction of the Pt atom. Ligands with donor atoms that have narrow pointed hybrid orbitals such as, for instance, ammonia and saturated amines, exhibit a weak *trans*-effect. This is due to the fact that the effective transfer of electron density onto the $6p_z$-orbital of Pt can begin only when the angular deformation of the bond is sufficiently large, which requires a corresponding increase in the activation energy. Ammonia forms a strong bond with Pt but it does not fall into the group of σ-donor ligands having a strong *trans*-effect because of the high density of its donor orbital.

If one and the same donor atom forms part of the composition of ligands in different hybrid states, the *trans*-effect will apparently increase in the order $sp^3 < sp^2 < sp$, i.e. with an increase in the *s*-character of the electron cloud. For example, the *trans*-effect of the saturated amine is smaller than that of pyridine, and that of pyridine is smaller than that of nitrile. However, in the case of pyridines and nitriles the situation becomes complicated owing to the possibility of formation of π-bonds.

In a series of ligands of the same type, such as

halide ions, the *trans*-effect increases with an increase in the ion radius, i.e. in the same direction as the changes in the size of the donor electron cloud. Simultaneously, the donor properties of the halogen ligand are enhanced. Thus, the stability of the bond and the *trans*-effect change in the same direction.

It is true, in the case of π-acceptor ligands that the formation of π-bonds does not decrease the angular mobility of the ligands, but on the contrary increases it. Partly, this can be explained by $\sigma\pi$-synergism, i.e. by an increase in the stability of the σ-bond and a corresponding decrease in the internuclear distance as a result of π-bond formation. Also, the angular deformation capacity apparently arises from the symmetry of the π-bonds, since a decrease in the overlapping of π-orbitals in one region is accompanied by an increase in the overlapping of π-orbitals in another region.

Thus, our explanation of the *trans*-effect encounters no basic difficulties from the point of view of the electron structure of the complex compounds and makes it possible from a uniform position to understand the causes of a strong *trans*-effect in ligands of a different nature, such as a hydride ion and olefins. A common property of all *trans*-activating ligands is the presence of donor orbitals with large orbital unfolding in the direction of the central atom, in other words, with a large transverse diameter. The factor which facilitates angular deformation of the bonds is the presence of π-bonds between the *trans*-activating ligand and the central atom.

Of great interest and apparently very complex is the question concerning the interdependence between the *trans*-effect and the mutual influence of ligands. However, within the framework of the proposed approach to an understanding of the *trans*-effect, the question about the mutual influence of ligands in the kinetics of substitution reactions can be formulated more definitely: the mutual influence of ligands can change the flexibility of the active coordinate of the complex and correspondingly affect the reaction rate. Thus, a clear differentiation of the *trans*-effect and the mutual influence of ligands makes it possible to forecast that the latter in different forms (*cis* and *trans*) can result in either an increase or a decrease in the rate constant of substitution reactions. A more detailed analysis of this question is outside the scope of this study.

CONCLUSIONS

(1) The *trans*-effect is explained as being due to the angular mobility of *trans*-activating ligands.

(2) The nature of the *trans*-effect basically differs from the *trans*-influence. The mutual influence of ligands can either increase or decrease the *trans*-effect.

(3) The *trans*-activating ability of ligands and the ability of ligands to be substituted are realized through the same mechanism of angular deformation of the complex along the active coordinate. Of the two ligands on this coordinate, the one with a stronger linkage becomes the *trans*-activating group and the one with a weaker linkage—the leaving group.

(4) The most general property of ligands that determines their *trans*-activating ability is the presence of a donor electron pair in an orbital, which is characterized by a large angular spreading in the direction of the central atom.

Acknowledgement—The author wishes to thank Dr N. N. Zheligovskaya for helpful discussions of this paper.

REFERENCES

1. T. G. Appleton, H. C. Clark and L. E. Manzer, *Coord. Chem. Rev.* 1973, **10**, 335.
2. F. R. Hartley, *Chem. Soc. Rev.* 1973, **2**, 163.
3. I. I. Chernyaev, *Ann. Inst. Platine* (*USSR*) 1926, **4**, 243.
4. D. R. Armstrong, R. Fortune and P. G. Perkins, *Inorg. Chim. Acta* 1974, **9**, 9.
5. D. R. Armstrong, R. Fortune, P. G. Perkins and R. J. Dickinson, *Inorg. Chim. Acta* 1976, **17**, 73.
6. C. H. Langford and H. B. Gray, *Ligand Substitution Processes*, Chap. 2. Benjamin Franklin Press, New York (1965).
7. F. Basolo and R. G. Pearson, *Mechanism of Inorganic Reactions*, Chap. 5. John Wiley, New York (1968).
8. U. Belluco, R. Ettore, F. Basolo, R. G. Pearson and A. Turco, *Inorg. Chem.* 1966, **5**, 591.
9. H. B. Gray, *J. Am. Chem. Soc.* 1962, **84**, 1548.
10. J. Chatt and L. A. Duncanson, *J. Chem. Soc.* 1953, 939.

Polyhedron Vol. 7, No. 13, pp. 1207–1209, 1988
Printed in Great Britain

0277–5387/88 $3.00+.00
© 1988 Pergamon Press plc

COMMUNICATION

ISOLATION AND STRUCTURE OF $[Re_2Cl_7(dto)]^-$. A QUADRUPLY BONDED INTERMEDIATE IN AN INTRAMOLECULAR DISPROPORTIONATION REACTION

BRUCE J. HEYEN and GREGORY L. POWELL†

Department of Chemistry, Abilene Christian University, Abilene, Texas 79699, U.S.A.

(*Received* 29 *December* 1987; *accepted* 1 *February* 1988)

Abstract—The preparation and structural characterization of $(n\text{-}Bu_4N)[Re_2Cl_7(dto)]$ (dto = 3,6-dithiaoctane) is described. Crystallographic parameters at 20°C are $a = 11.299$ (3), $b = 11.552$ (4), $c = 14.645$ (4) Å, $\alpha = 108.19$ (2)°, $\beta = 104.07$ (2)°, $\gamma = 88.65$ (3)°, $Z = 2$, and space group $P\bar{1}$. This compound is the first example of a quadruply bonded complex of the type $[Re_2X_7(LL)]^-$. The anion has a slightly staggered structure in which the dto ligand coordinates in an equatorial–axial arrangement on one Re atom. The Re–Re bond distance is 2.248 (1) Å. This complex is an air-stable intermediate in the formation of triply bonded $Re_2Cl_5(dto)_2$ from quadruply bonded $(n\text{-}Bu_4N)_2[Re_2Cl_8]$.

The rich chemistry of quadruply bonded dirhenium(III) complexes includes two examples of intramolecular disproportionation reations. Compounds of the type $Re_2(O_2CR)_2X_4L_2$ react with PPh_3 in refluxing alcohols (ROH) to yield the complexes $(RO)_2Cl_2Re—ReCl_2(PPh_3)_2$ with retention of the quadruple bond,[1,2] while $[Re_2Cl_8]^{2-}$ reacts with excess 2,5-dithiahexane (dth) to give the triply bonded complex $Cl_4Re—Re(dth)_2Cl$.[3,4] In our investigations of the reactions of $[Re_2Cl_8]^{2-}$ with other dithioether ligands, we have isolated a new quadruply bonded dirhenium(III) complex of the type $[Re_2Cl_7(LL)]^-$ that is an air-stable intermediate in the formation of another triply bonded $Re_2Cl_5(LL)_2$ compound.

The reaction between $(n\text{-}Bu_4N)_2[Re_2Cl_8]$[5] and 3,6-dithiaoctane (dto)‡ was carried out in ethanol at 55°C. After 6 h, $(n\text{-}Bu_4N)[Re_2Cl_7(dto)]$ was produced as a green powder in 82% yield. Found: C, 25.9; H, 4.8. Calc. for $C_{22}H_{50}NS_2Cl_7Re_2$: C, 26.1; H, 4.9%. The results were the same regardless of whether a large excess or a stoichiometric amount of dto was used. However, at reflux temperatures (80°C and higher) a second product, brown $Re_2Cl_5(dto)_2$, was also formed. Found: C, 16.8; H, 3.4. Calc. for $C_{12}H_{28}S_4Cl_5Re_2$: C, 16.9; H, 3.3%. Both products are air-stable and soluble in CH_2Cl_2. The UV-vis. spectrum of $(n\text{-}Bu_4N)[Re_2Cl_7(dto)]$ exhibits a relatively strong absorption band centred at 732 nm ($\varepsilon = 1346$) that is typical of the $\delta \rightarrow \delta^*$ transition in quadruply bonded Re_2 species.[6] Such an absorption is absent in the UV-vis. spectrum of $Re_2Cl_5(dto)_2$, with bands at 589, 508, 444 and 382 nm.

The structure of $(n\text{-}Bu_4N)[Re_2Cl_7(dto)]$ has been determined by X-ray crystallography§ and a view

†Author to whom correspondence should be addressed.

‡3,6-Dithiaoctane was purchased from Pfaltz & Bauer, Inc. and used as received. All reactions were carried out under a nitrogen atmosphere using standard vacuum line techniques.

§Crystal data for $(n\text{-}Bu_4N)[Re_2Cl_7(dto)]$ at 20°C; $a = 11.299(3)$, $b = 11.552(4)$, $c = 14.645(4)$ Å, $\alpha = 108.19(2)°$, $\beta = 104.07(2)°$, $\gamma = 88.65(3)°$, $Z = 2$, $d_{calc.} = 1.913$ g cm^3, and space group $P\bar{1}$. Crystals were grown by slow diffusion of hexane into a CH_2Cl_2 solution of the complex. Data collection, data reduction and an empirical absorption correction based on psi scans for five reflections were performed by Crystalytics Company, Lincoln, Nebraska. Solution and refinement of the structure were carried out on a VAX-11/785 computer at Abilene Christian University with use of the SDP-VAX software package. A Patterson map was used to find the positions of the two Re atoms. Full-matrix least squares refinement of 307 parameters using 3324 reflections with $F_o^2 > 3\sigma(F_o^2)$ gave residuals of $R = 0.048$ and $R_w = 0.058$. Atomic coordinates have been deposited with the Cambridge Crystallographic Data Centre.

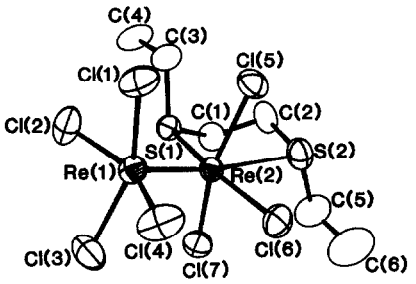

Fig. 1. ORTEP view of the anion in $(n\text{-}Bu_4N)[Re_2Cl_7(dto)]$. Thermal ellipsoids are at the 50% probability level. Selected bond distances (Å) and angles (deg) are Re(1)—Re(2) = 2.248(1), Re(2)—S(1) = 2.455(3), Re(2)—S(2) = 2.906(5), avg. Re—Cl = 2.322[6], Re(1)—Re(2)—S(1) = 95.3(1), Re(1)—Re(2)—S(2) = 172.3(1), avg. Re—Re—Cl = 102 [2].

of the anion appears in Fig. 1. The dto ligand is unsymmetrically chelated to the rhenium atom Re(2). The seven chloride ligands along with the sulphur atom S(1) occupy equatorial sites, while S(2) binds in an axial position to give a distorted square-pyramidal coordination geometry for Re(1) and a distorted octahedral geometry for Re(2). The rotational conformation is nearly eclipsed with an average L—Re—Re—L torsion angle of 2.25°. The structure is perhaps best thought of as a modification of the $[Re_2Cl_8]^{2-}$ structure by replacement of one chloride ligand with one sulphur atom of the dto ligand and subsequent binding of the second sulphur atom along the Re—Re axis (see Scheme 1). This is the first example of a quadruply bonded Re_2 compound with no bridging ligands and only one axial ligand. The axial Re—S bond is much weaker than the equatorial, reflecting the strength of the metal–metal bond. The Re—Re distance in $[Re_2Cl_7(dto)]^-$ is slightly longer than that in $(n\text{-}Bu_4N)_2[Re_2Cl_8]$,[7] 2.248 (1) vs 2.222 (2) Å, respectively.

To our knowledge, $[Re_2Cl_7(dto)]^-$ is the first example of a quadruply bonded anion of the type $[Re_2X_7(LL)]^-$. Recently, Bakir and Walton reported the isolation of the first examples of quadruply bonded complexes containing monoanionic $[Re_2Cl_7L]^-$ units, namely $(n\text{-}Bu_4N)_2[(Re_2Cl_7)_2(\mu\text{-}L—L)]$, where L—L is either $Ph_2PC{\equiv}CPPh_2$ or *trans*-$Ph_2PCH{=}CHPPh_2$.[8] Although no crystal structure was determined, the suggested arrangement involves replacement of one of the chloride ligands on each of the two $[Re_2Cl_8]^{2-}$ units with one phosphorus atom of the L—L ligand (see **1**). The

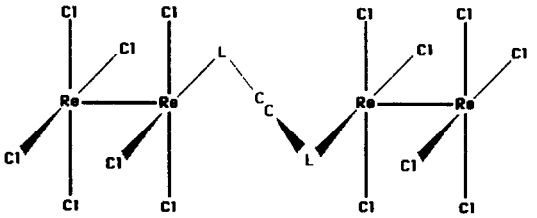

1

rigid C—C backbone of the diphosphine ligands prevents them from chelating one Re atom as the dithioether ligand does in $[Re_2Cl_7(dto)]^-$. However, no examples of dimers with only one chelating bidentate ligand have ever been observed in the many previous studies of reactions between $[Re_2X_8]^{2-}$ and the more flexible diphosphines and dithioethers.[6,9] One such reaction of particular relevance is the aforementioned reaction of $[Re_2Cl_8]^{2-}$ with excess 2,5-dithiahexane (dth) to yield $Re_2Cl_5(dth)_2$, a compound with a staggered structure in which both dth ligands chelate one Re atom (see **2**). This product of intramolecular disproportionation was the first example of a compound containing a metal–metal triple bond,[3] and its molecular geometry and one-electron paramagnetism (μ_{eff} = 1.72 BM) led to its assignment as the zwitterion $[Cl_4Re]^-[Re(dth)_2Cl]^+$.[4]

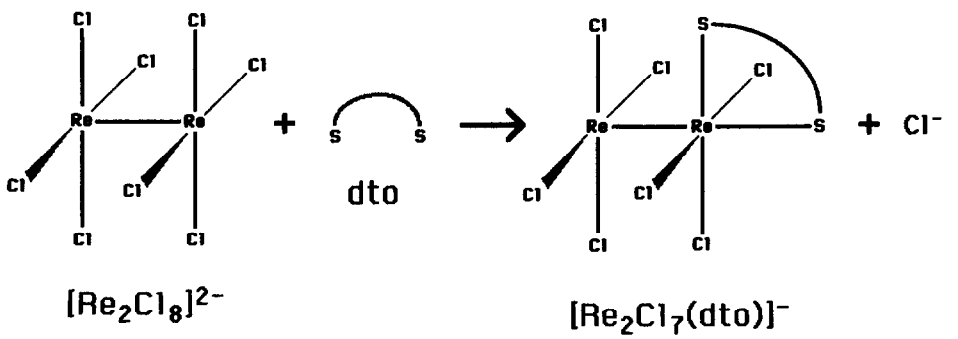

Scheme 1.

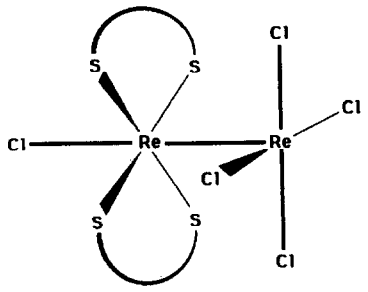

2

Further reaction of $(n\text{-}Bu_4N)[Re_2Cl_7(dto)]$ with dto in refluxing ethanol results in the formation of $Re_2Cl_5(dto)_2$ in up to 62% yield. This involves reduction of the Re(III)—Re(III) core to an Re(II)—Re(III) core with concomitant reduction in the metal–metal bond order. The new compound $Re_2Cl_5(dto)_2$ is paramagnetic ($\mu_{eff} = 1.85$ BM) at room temperature. A crystal structure determination (still in progress) has confirmed a structure analogous to that of $Re_2Cl_5(dth)_2$ with an Re—Re distance of 2.278 (1) Å. This is only the second example of a complex with the stoichiometry $Re_2Cl_5L_4$ and the structure **2**. With the isolation and characterization of the title compound, it is logical to assume that triply bonded $Re_2Cl_5(LL)_2$ species are formed through an intermediate of formula $[Re_2Cl_7(LL)]^-$, with coordination of a second diothioether ligand on the Re atom to which the first dithioether is already bonded.

The reactivity of dithioethers towards multiply bonded dimers is not well understood. An important question arising from the present work is whether or not the dto ligand initially coordinates to a vacant axial site of $[Re_2Cl_8]^{2-}$. We are currently studying the interactions of other $RS(CH_2)_nSR$ ligands with complexes containing triple and quadruple M—M bonds. A report of our results, along with a more detailed account of the work presented in this paper, will be submitted later.[10] We are also investigating the reactivity of $[Re_2Cl_7(dto)]^-$ toward a variety of reagents. It could prove to be a useful precursor in the synthesis of new types of multiply bonded dirhenium compounds.

Acknowledgement—We are grateful to The Robert A. Welch Foundation for financial support.

REFERENCES

1. A. R. Chakravarty, F. A. Cotton, A. R. Cutler, S. M. Tetrick and R. A. Walton, *J. Am. Chem. Soc.* 1985, **107**, 4795.
2. A. R. Chakravarty, F. A. Cotton, A. R. Cutler and R. A. Walton, *Inorg. Chem.* 1986, **25**, 3619.
3. M. J. Bennett, F. A. Cotton and R. A. Walton, *J. Am. Chem. Soc.* 1966, **88**, 3866.
4. M. J. Bennett, F. A. Cotton and R. A. Walton, *Proc. R. Soc. London, A* 1968, **303**, 175.
5. T. J. Barder and R. A. Walton, *Inorg. Chem.* 1982, **21**, 2510.
6. F. A. Cotton and R. A. Walton, *Multiple Bonds Between Metal Atoms*. Wiley, New York (1982).
7. F. A. Cotton, B. A. Frenz, B. R. Stults and T. R. Webb, *J. Am. Chem. Soc.* 1976, **98**, 2768.
8. M. Bakir and R. A. Walton, *Polyhedron* 1987, **6**, 1925.
9. A. C. Price and R. A. Walton, *Polyhedron* 1987, **6**, 729 and refs therein.
10. B. J. Heyen and G. L. Powell, to be submitted to *Inorg. Chem.*

Polyhedron Vol. 7, No. 13, pp. 1211–1216, 1988
Printed in Great Britain

0277–5387/88 $3.00+.00
© 1988 Pergamon Press plc

COMMUNICATION

^{3}C- AND ^{1}H-NMR STUDY OF SOME Pt(II) COMPLEXES WITH DITHIOCARBAZIC LIGANDS

A. M. GIULIANI* and E. TROTTA

ITSE–CNR, Area della Ricerca di Roma, C.P. 10-00016 Monterotondo Stazione, Italy

(*Received* 9 *November* 1987; *accepted after revision* 18 *February* 1988)

Abstract—Pt(II) complexes with singly- and doubly-deprotonated dithiocarbazic ligands have been examined by ^{1}H- and ^{13}C-NMR. Complexation induces a deshielding of all the ligand resonances, except that of the thiono carbon. The shielding of C(1) is greater in complexes with singly-deprotonated rather than with twice-deprotonated ligands. The upfield shift may be connected with a decrease of the C=S bond order. The ensemble of the experimental NMR results indicates that considerable differences in bond order, electron density distribution and stereochemistry exist between the complexes with singly- and doubly-deprotonated ligands.

Dithiocarbazic acid derivatives, R′NHNHCSSR† (= L), constitute a class of very versatile ligands. They can be coordinated in the neutral (L), singly-deprotonated (L—H) and doubly-deprotonated (L—2H) anionic forms, giving rise to three different series of complexes; they can moreover act as monodentate S-ligands or bidentate (SN)-chelating agents.[1,2]

Reported and discussed here are the ^{1}H- and ^{13}C-NMR spectral data of Pt(II) complexes with the following dithiocarbazic ligands, in the singly- or doubly-deprotonated forms:

I. R = CH_3; R′ = H
IV. R = $PhCH_2$; R′ = H
VII. R = CH_3; R′ = $PhCH_2$
IX. R = $PhCH_2$; R′ = $PhCH_2$
XI. R = CH_3; R′ = Ph
XIII. R = CH_3; R′ = Pr^{i}
XVI. R = CH_3; R′ = Bu^{t}
XIX. R = CH_3; R′ = Hex^{n}
XXII. R = $PhCH_2$; R′ = Hex^{n}

* Author to whom correspondence should be addressed.

† Numbering of the atoms follows the IUPAC convention

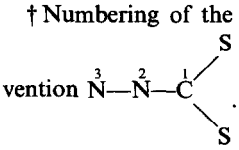

EXPERIMENTAL

All the products were donated by Drs F. Tarli and L. Suber of ITSE-CNR. The ^{1}H- and ^{13}C-NMR spectra were recorded with a Bruker WP-200 spectrometer operating at 4.7 T (NMR service of the Area della Ricerca di Roma, CNR). The deuterated solvent (Merck UVASOL) was used for reference and field-frequency lock. All chemical shift data are given relative to TMS; the experiments were run at 27 ± 1°C. The choice of solvent, chloroform or dimethylsulphoxide, has been mainly dictated by solubility reasons.

RESULTS AND DISCUSSION

The ^{1}H-NMR spectra for the Pt(II) complexes with singly-deprotonated ligands are collected in Table 1, together with those of ligands **I**, **IV** and **XVI**. The parameters for the other ligands and for the complexes with doubly-deprotonated ligands have been reported previously.[3]

A downfield shift is observed for the S—CH_3 and the R′ resonances upon ligation, while the S—CH_2 spectral position is essentially unaffected. Satellites of ^{195}Pt are observed for the N(3)H resonances indicating coordination through the terminal nitrogen atoms; the satellites are broader than the cen-

Table 1. ^{1}H-NMR data for the Pt(II) complexes with singly-deprotonated dithiocarbazic ligands. Chemical shifts are in ppm from TMS; coupling constants to ^{195}Pt, in Hz, are reported in parentheses. ($B_0 = 4.7$ T)

Compound	No.	Solvent	δ (ppm) N(3)H	N(3)R α	N(3)R β	Others	N(2)H	SR′ α	SR′ β
$H_2NNHCSSCH_3$ (= L_1)	**I**	DMSO-d_6	5.2; 7.8				10.74	2.39; 2.32	
c-Pt(L_1—H)$_2$	**IIa**	DMSO-d_6	8.61 (43.9)					2.50	
t-Pt(L_1—H)$_2$	**IIb**	DMSO-d_6	8.82 (45.9)					2.47	
$H_2NNHCSSCH_2Ph$ (= L_2)	**IV**	DMSO-d_6	5.23				8.58	4.49; 4.51	7.44[m]
c-Pt(L_2—H)$_2$	**Va**	DMSO-d_6	8.82 (42.0)					4.45	7.44[m]
t-Pt(L_2—H)$_2$	**Vb**	DMSO-d_6	9.04 (42.6)					4.41	7.44[m]
c-Pt(PhL_1—H)$_2$	**XIIa**	DMSO-d_6	10.31 (51); 10.94 (53)	7.1				2.51; 2.52	
t-Pt(PhL_1—H)$_2$	**XIIb**	DMSO-d_6	11.59 (60); 11.63 (64)	7.1				2.50; 2.49	
Pt(Pr^iL_1—H)$_2$	**XIV**	DMSO-d_6	9.20 (50.8)[a]; 9.52 (60.0); 9.55 (58.0)	3.83[a] 3.44	1.18; 1.49[a] 1.20; 1.23; 1.34			2.66[a] 2.60[b]	
Bu^tL_1	**XVI**	$CHCl_3$-d_1	3.64		1.16; 1.25		8.54	2.54; 2.64	
Pt(Bu^tL_1—H)$_2$	**XVII**	DMSO-d_6	9.20 (5.40)		1.35			2.60[b]	
Pt(Hex^nL_1—H)$_2$	**XX**	$CHCl_3$-d_1	7.97; 7.98 (60–68)[c]	3.09; 3.56	1.55; 1.87	1.27; 0.87		2.54	
Pt(Hex^nL_2—H)$_2$	**XXIII**	DMSO-d_6	9.54 (44.8); 9.82 (55.2)	3.4	1.86[c]	1.29; 0.96		4.4[c]	7.44[m]

[m] Multiplet.
[a] Tentatively assigned to the *cis* isomer.
[b] Overlapping solvent.
[c] Broad.

Table 2. ^{13}C-NMR data for dithiocarbazic ligands and their Pt(II) complexes. Chemical shifts are in ppm from TMS; couplings to ^{195}Pt, in Hz, are reported in parentheses. ($B_0 = 4.7$ T)

Compound	No.	Solvent	δ (ppm) N(3)R′ α	N(3)R′ β	N(3)R′ Others	SR α	SR β	SR Others	C=S
L_1	I	$CHCl_3$-d_1				17.50			199.87
$Pt(L_1—H)_2$	II	DMSO-d_6				19.19; 19.43; 19.53			176.69; 178.75
$Pt(L_1—2H)_2$	III	DMSO-d_6				19.62			187.69
L_2	IV	$CHCl_3$-d_1				39.39	136.20	127.13(*p*); 128.74(*o*); 129.14(*m*)	198.15
$Pt(L_2—H)_2$	V	DMSO-d_6				*ca* 40[a]	138.70; 138.81	128.19(*p*); 129.47(*o*); 129.95(*m*)	178.01; 176.00
$Pt(L_2—2H)_2$	VI	DMSO-d_6				*ca* 40[a]	138.73	128.00(*p*); 129.87(*m*); 128.06(*o*)	175.82
$PhCH_2L_1$	VII	$CHCl_3$-d_1	54.62; 55.38	136.48; 138.86	[b]	17.33			205.98
$Pt(PhCH_2L_1—2H)_2$	VIII	$CHCl_3$-d_1	*ca* 77[a]	138.89	127.79(*p*); 129.04(*m*); 128.52(*o*)	19.13			183.74
$PhCH_2L_2$	IX	$CHCl_3$-d_1	55.44; 54.61	136.41	[c]	39.07; 39.23	135.77	[c]	204.36; 194.86
$Pt(PhCH_2L_2—2H)_2$	X	CH_2Cl_2-d_2	*ca* 53[a]	138.72	[d]	*ca* 41[e]	138.72	[d]	[e]
Pr^iL_1	XIII	$CHCl_3$-d_1	50.88; 51.77	20.42; 20.52		17.33			206.58; 196.44
$Pt(Pr^iL_1—H)_2$	XIV	$CHCl_3$-d_1	64.61; 65.09	21.74; 21.98		19.20; 19.37			176.56
$Pt(Pr^iL_1—2H)_2$	XV	$CHCl_3$-d_1	74.05 (71.2)	25.36		19.02 (21.4)			182.23
Bu^tL_1	XVI	DMSO-d_6	55.17; 58.52	28.21		17.35			207.65; 195.50
$Pt(Bu^tL_1—H)_2$	XVII	DMSO-d_6	66.30	28.80		19.19			178.52
$Pt(Bu^tL_1—2H)_2$	XVIII	$CHCl_3$-d_1	75.84 (77.0)	37.07		19.07 (19.5)			176.81
Hex^nL_1	XIX	$CHCl_3$-d_1	51.33	27.44	26.52; 31.45; 22.40; 13.86	17.09			205.38
			50.80						195.15

[continued overleaf

Table 2. (*continued*)

Compound	No.	Solvent	δ (ppm) N(3)R′ α	β	Others	SR α	β	Others	C=S
$Pt(Hex^nL_1—H)_2$	**XX**	$CHCl_3$-d_1	62.69; 63.13	27.60; 27.73	26.15; 31.51; 22.51; 13.98	19.11 (17.9)			178.43; 176.24
$Pt(Hex^nL_1—2H)_2$	**XXI**	$CHCl_3$-d_1	73.76 (71.5)	36.88	26.51; 31.45; 22.45; 13.97	18.98 (20.1)			182.62
Hex^nL_2	**XXII**	$CHCl_3$-d_1	51.53	27.44	26.55; 31.52; 22.46; 13.93	38.95	136.43	127.38(*p*); 128.59(*o*); 129.39(*m*)	204.18
			50.87	27.44		38.95	136.36	127.65(*p*); 128.70(*o*); 129.09(*m*)	193.63
$Pt(Hex^nL_2—2H)_2$	**XXIII**	$CHCl_3$-d_1	73.87 (70.9)	36.97	26.56; 31.48; 22.46; 13.99	40.71 (15.8)	136.26	127.69(*p*); 128.67(*o*); 129.18(*m*)	180.76

[a] Under solvent.
[b] Many signals between 128 and 129 ppm.
[c] Many signals between 127.5 and 129.5 ppm.
[d] Many signals between 127.4 and 128.8 ppm.
[e] Undetected, too low solubility.

tral peak as already observed by other authors.[4] The $^2J_{PtNH}$ couplings range between 42 and 67 Hz.

Two sets of resonances are observed for several complexes and have been attributed to the simultaneous presence of the *cis* and *trans* isomers of the $[S_2N_2]$ chromophore; assignment to one isomer or the other was based on variable temperature spectra for **II** and **V**,[2] and was made by analogy with them for the others.

Complex **XIV** exhibits three sets of resonances, accountable for by the possibility of the *trans*, but not the *cis*, isomer to exist with the isopropyl groups on the same or on opposite sides of the chromophore plane.

The two-bond coupling constants $^2J_{PtNH}$ are much smaller in the complexes with the doubly-deprotonated ligands[3] than in those with singly-deprotonated ones (42–67 vs *ca* 90 Hz). Several geminal PtH couplings have been reported in the literature,[5–7] relative to the PtCH fragment, while $^2J_{PtNH}$ is known to be negative,[8] but no general theory has been proposed for these couplings.

The $^2J_{PtCH}$ couplings are very sensitive to steric factors[7] and the large difference found between the complexes of **I** and **IV** in the singly- or in the doubly-deprotonated form might be connected to a different geometrical relationship of the Pt and the H nuclei.

The ^{13}C-NMR data for the ligands and the Pt(II) complexes with the ligands in the (L—H) or (L—2H) form are collected in Table 2. Two sets of resonances are observed for the complexes with (L—H) ligands, in agreement with the existence of *cis* and *trans* isomers, as already found by ^{1}H-NMR. The greater complexity of the ^{1}H- relative to the ^{13}C-spectrum of **XIV** is probably connected with the solvent difference.

All resonances show a marked downfield shift upon complexation, except the thiono carbon. The shift is larger for the α carbon of the R′ substituent and it increases going from the singly- to the doubly-deprotonated ligand. This downfield shift reflects the expected reduction of electron density resulting from ligation. On the other hand, the upfield shift of the thiono carbon resonance indicates a build up of electronic density on the atom. The shielding is consistent with a lowering of the C=S bond order, as already observed for Pt(II) and Pt(IV) thioamido complexes[9] and for the S-methyl dithiocarbazato ligand.[10]

The X-ray data are in agreement with this hypothesis; for instance, the C=S bond length is 1.667 Å for the ligand PhL_1 and 1.705 Å for its complex $Pt(PhL_1—2H)_2$.[11] The effect is greater with the singly-deprotonated than with the doubly-deprotonated ligands, suggesting that the σ donor ability of the sulphur atom towards the metal is greater in the former case.

The $^2J_{PtSC}$ couplings are of the order of 5–10 Hz, considerably smaller than the literature values for monothio-β-diketonate Pt(II) complexes.[12] This finding may be connected with the different value of the PtSC angle, suggesting a strong dependence of the coupling on stereochemistry.

The two-bond couplings $^2J_{PtNC}$ (of the order of 70–77 Hz) observed for the complexes with doubly-deprotonated, but not with singly-deprotonated ligands are considerably larger than those reported for other classes of Pt complexes.[8,13,14]

The $^nJ_{PtNC}$ values depend significantly on the π-bond order[15] and on the bond angles; our experimental results suggest the existence of marked differences in the bond angles and/or π-bond order between the two classes of dithiocarbazato complexes. IR spectral data[3] support this hypothesis.

The $^3J_{PtNCC}$ couplings, which obey a Karplus-type relationship,[13] have been found to be zero, giving a value close to 90° for the dihedral angle ϕ. The X-ray data for **VIII**[3] give a ϕ value of 99.2°, while for **XV** the two values of ϕ are 120.6 and 115.6°,[16] indicating that the solution average conformation is different from the crystal structure.

The $^4J_{PtSCSC}$ couplings (16–21 Hz) of ^{195}Pt to the SCH_3 are unusually large, the reported values for *cis*-$[Pt(NH_3)_2X_2]^{2+}$ complexes being of the order of 11 Hz.[15] Some π bonding involving the sp^3 hybrid orbitals of sulphur (the CSC angle is 103.1° in **VIII**[3] and 104° in **XV**[16]) and the metal may be envisaged as in agreement with the observed deshielding of SCH_3 upon complexation.

Acknowledgements—The authors wish to thank Drs F. Tarli and L. Suber for the gift of the products and Dr M. Bonamico and co-workers for the communication of the unpublished X-ray data.

REFERENCES

1. A. Monaci and F. Tarli, *J. Chem. Soc., Dalton Trans.* 1980, 499.
2. C. Battistoni, A. M. Giuliani, E. Paparazzo and F. Tarli, *J. Chem. Soc., Dalton Trans.* 1984, 1293.
3. V. Fares, A. M. Giuliani, P. Imperatori, L. Suber and F. Tarli, *J. Chem. Soc., Dalton Trans.* 1987, 1035.
4. R. H. Crabtree, B. E. Segmuller and R. J. Uriarte, *Inorg. Chem.* 1985, **24**, 1949.
5. T. G. Appleton, J. R. Hall and T. G. Jones, *Inorg. Chim. Acta* 1979, **32**, 127.
6. N. H. Agnew, T. G. Appleton and J. R. Hall, *Inorg. Chim. Acta* 1980, **41**, 85.
7. B. Crociani, T. Boschi and P. Uguagliati, *Inorg. Chim. Acta* 1981, **48**, 9.

8. L. E. Erickson, J. E. Sarneski and C. N. Reilley, *Inorg. Chem.* 1978, **17**, 1701.
9. J.-M. Bret, P. Costan, G. Commenges and J.-P. Laurent, *Polyhedron* 1983, **2**, 901.
10. S. Manogaran and D. N. Sathyanarayana, *J. Mol. Struct.* 1983, **99**, 267.
11. G. Dessy and V. Fares, *Acta Cryst.* 1980, **B36**, 2266.
12. M. Das and D. T. Haworth, *J. Inorg. Nucl. Chem.* 1981, **43**, 515.
13. L. E. Erikson, J. E. Sarneski and C. N. Reilley, *Inorg. Chem.* 1975, **14**, 3007.
14. L. E. Erikson, J. E. Sarneski and C. N. Reilley, *Inorg. Chem.* 1978, **17**, 1711.
15. G. V. Fazakerley and K. R. Koch, *Inorg. Chim. Acta* 1979, **36**, 13.
16. M. Bonamico, V. Fares and P. Imperatori, private communication.

Polyhedron Vol. 7, No. 13, pp. 1217–1219, 1988
Printed in Great Britain

0277-5387/88 $3.00+.00
Pergamon Press plc

COMMUNICATION

KrF_2/MnF_4 ADDUCTS FROM KrF_2/MnF_2 INTERACTION IN HF AS A ROUTE TO HIGH PURITY MnF_4

KAREL LUTAR, ADOLF JESIH and BORIS ŽEMVA*

"Jožef Stefan" Institute, "Edvard Kardelj" University of Ljubljana,
61000 Ljubljana, Yugoslavia

(*Received* 12 *November* 1987; *accepted* 18 *February* 1988)

Abstract—In the system KrF_2–MnF_2–HF two new adducts, $2KrF_2 \cdot MnF_4$ and $KrF_2 \cdot MnF_4$ have been synthesized. The 2 : 1 adduct decomposes in a dynamic vacuum at −45°C yielding KrF_2 and the 1 : 1 adduct, which is stable in a dynamic vacuum up to −25°C. $KrF_2 \cdot MnF_4$ decomposes further at room temperature to krypton, fluorine, krypton difluoride and manganese tetrafluoride. This reaction is a useful synthetic route for the preparation of pure manganese tetrafluoride.

The xenon fluoride chemistry of manganese has been investigated in the past.[1,2,3] Mn^{2+} or Mn^{3+} is oxidized by xenon difluoride or xenon hexafluoride to Mn^{4+} and at the same time both xenon fluorides act as good fluoride ion donors and form corresponding xenon(II) and xenon(VI) fluoromanganates(IV).[1,2] The reaction between NH_4MnF_3 and XeF_6 yields ammonium xenon(VI) hexafluoromanganate(IV), which is the first known ammonium xenon(VI) fluorometalate.[3] Recently these studies were extended to reactions with KrF_2 as a strong fluorinating agent, in combination with XeF_6 as a moderately good fluoride-ion donor, in anhydrous hydrogen fluoride. This synthetic route yielded xenon(VI) fluoroargentate(III)[4] and was used in the case of manganese with the intention of synthesizing xenon(VI) fluoromanganates with manganese in a higher oxidation state than 4+. Because only known xenon(VI) fluoromanganates(IV) were synthesized, the system MnF_2–KrF_2 in HF as a solvent without XeF_6 was further investigated. This paper describes the preparation and some of the properties of KrF_2 adducts with manganese(IV) fluoride and the synthetic route to high purity manganese(IV) fluoride.

* Author to whom correspondence should be addressed.

RESULTS AND DISCUSSION

The reaction between manganese difluoride and an excess of krypton difluoride in HF as solvent yields oily, dark red krypton difluoride–manganese tetrafluoride adducts. After removal of the solvent, the curve of weight-loss versus time of pumping was recorded at −45°C (Fig. 1). From the change in the slope of the curve it could be concluded that the adduct $2KrF_2 \cdot MnF_4$ exists. It is unstable at this temperature and loses KrF_2 yielding $KrF_2 \cdot MnF_4$. The 1 : 1 adduct is stable at −25°C and is without measurable vapour pressure. Its colour is a little darker than the 2 : 1 adduct. The 1 : 1 compound decomposes to KrF_2, Kr and fluorine, and MnF_4 at higher temperatures. At −10°C the decomposition rate is *ca* 2 mol % h^{-1} and at 0°C about 8 mol % h^{-1}. At room temperature $KrF_2 \cdot MnF_4$ decomposes to krypton, fluorine and managanese tetrafluoride, as shown by analysing the evolved gases. The analysis of decomposition gases at room temperature showed 48.2 vol % of fluorine and the rest was pure krypton as was shown by mass spectrometry. When MnF_4 was reacted again with KrF_2 in HF as the solvent, again an oily, dark red substance was obtained. Neither adducts give Raman spectra, either at −196°C directly in the reaction vessel together with excess KrF_2 and HF,

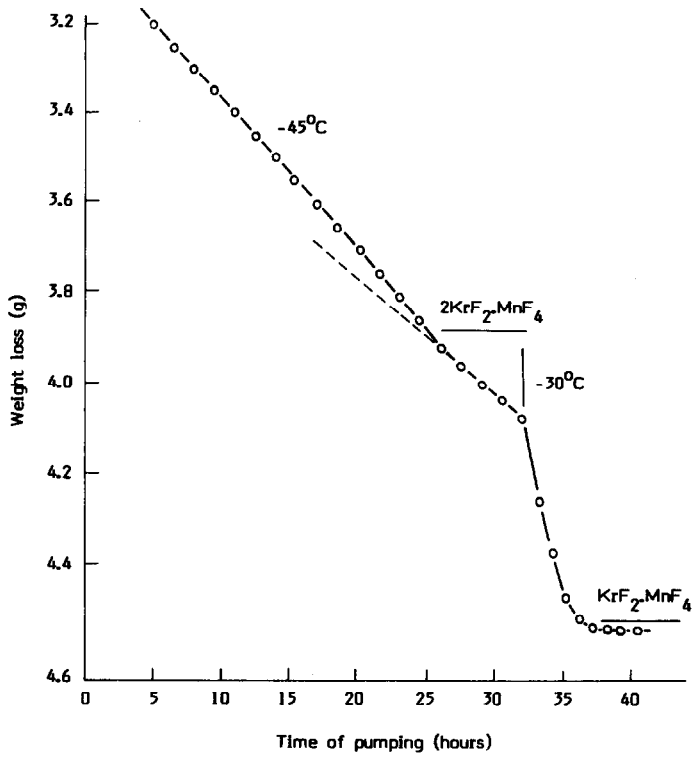

Fig. 1. Weight loss vs time of pumping curve for the reaction between 5.29 mmol of MnF_4 with 47 mmol of KrF_2 at $-45°C$.

or at high temperatures when they were already separated from excess KrF_2 and the solvent.

The reaction between manganese difluoride and excess krypton difluoride in HF (solvent) at room temperature, after pumping off krypton, fluorine, excess KrF_2 and HF, yields pure deep blue manganese tetrafluoride: chemical analysis: Found: Mn, 41.9; F, 57.4. Calc. for MnF_4: Mn, 42.0; F, 58.0%.

$$MnF_2 + nKrF_2 \xrightarrow[20°C]{HF} MnF_4 + (z+1)Kr + zF_2 + (n-z-1)KrF_2 \qquad n \geqslant 10.$$

This reaction represents the simplest route so far for the preparation of pure MnF_4 in high yield. MnF_4 was prepared up until now in small yield (20 mg h^{-1}) from manganese(II) or manganese(III) compounds in a stream of fluorine at 550°C,[5,6] by fluorinating manganese powder in a fluidized bed at 600–700°C,[7,8] or by fluorination under high pressure (2–3 kbars) and high temperature (300–500°C).[9]

Magnetic susceptibility measurements confirm that the manganese tetrafluoride obtained is pure. The compound follows the Curie–Weiss law with a magnetic moment of 3.85 BM and a Weiss constant $\Theta = 10$ K. Since the Weiss constant is small, the super exchange coupling Mn(IV)–F–Mn(IV) must be weak. These magnetic susceptibility measurements are in agreement with literature data.[5,6] MnF_4 synthesized by this method is amorphous and no X-ray powder patterns were obtained.

EXPERIMENTAL

General apparatus and techniques

The synthetic procedure for working with the metal fluoride or oxide–KrF_2–XeF_6–HF systems is described elsewhere.[4]

In a typical experiment MnF_2 (5 mmol) was weighed into a FEP reaction vessel. Then a few cm^3 of anhydrous HF were distilled and condensed onto the MnF_2. Krypton difluoride was added by sublimation at $-196°C$. The FEP reaction vessel was connected to an expansion vessel for the removal of the krypton and fluorine generated by the reaction and/or krypton difluoride decomposition. The reaction vessel was then slowly warmed up to room temperature. After the reaction was completed, the volatiles were pumped off at $-45°C$ (isolation of $2KrF_2 \cdot MnF_4$), $-30°C$ (isolation of $KrF_2 \cdot MnF_4$) or at room temperature (isolation of MnF_4). The

stoichiometry of the reaction was followed using mass balance throughout the experiment with an accuracy of ± 5 mg.

Routine characterization of materials

Routine characterization (Raman spectroscopy, X-ray powder photography, magnetic susceptibility measurements) of materials was carried out as described elsewhere.[4]

Chemical analysis

The amount of total fluorine was determined by an ion-selective electrode in the presence of appropriate buffer solutions and masking reagents. The amount of manganese was determined by direct complexometric titration in alkaline media in the presence of a visual indicator.[10]

Reagents

Manganese difluoride was used as supplied by Riedel de Haën (analysis of MnF_2. Found: Mn, 58.2; F, 39.7. Calc.: Mn, 59.1; F, 40.9%). Krypton difluoride was prepared by irradiation of a liquified mixture of fluorine and krypton with near-UV light at -196°C.[11] Fluorine was prepared and purified in this laboratory.[12] Additional purification was performed by a photochemical method.[13] Commercial anhydrous hydrogen fluoride was purified by a modified method as described elsewhere,[14] and before use it was treated with krypton difluoride.

Acknowledgements—This material is based on work supported by the U.S.–Yugoslav Joint Fund for Scientific and Technological Cooperation, in cooperation with the National Science Foundation under Grant No. 552. The financial support of the Research Community of Slovenia is also acknowledged. The authors are grateful to Miss B. Sedej for chemical analysis.

REFERENCES

1. B. Žemva, J. Zupan and J. Slivnik, *J. Inorg. Nucl. Chem.* 1971, **33**, 3953.
2. M. Bohinc, J. Grannec, J. Slivnik and B. Žemva, *J. Inorg. Nucl. Chem.* 1976, **38**, 75.
3. B. Žemva and J. Slivnik, *J. Fluorine Chem.* 1981, **17**, 375.
4. K. Lutar, A. Jesih and B. Žemva, *Rev. Chem. Min.* 1986, **23**, 565.
5. R. Hoppe, W. Dähne and W. Klemm, *Naturwiss.* 1961, **48**, 429.
6. R. Hoppe, W. Dähne and W. Klemm, *Liebigs Ann.* 1962, **658**, 1.
7. H. W. Roesky and O. Glemser, *Angew. Chem.* 1963, **75**, 920; *Angew. Chem. (Int. Edn)* 1964, **3**, 47.
8. H. W. Roesky, O. Glemser and K. H. Hellberg, *Chem. Ber.* 1965, **98**, 2046.
9. R. Hoppe, *Israel J. Chem.* 1978, **17**, 48.
10. A. K. Covington, *Ion-Selective Electrode Methodology*, CRC Press, Boca Roton (1984); R. Pribil, *Applied Complexometry*, Pergamon Press, Oxford (1982).
11. J. Slivnik, A. Šmalc, K. Lutar, B. Žemva and B. Frlec, *J. Fluorine Chem.* 1975, **5**, 273.
12. J. Slivnik, A. Šmalc and A. Zemljič, *Vestn. Slov. Kem. Društ.* 1965, **12**, 17.
13. A. Šmalc, K. Lutar and J. Slivnik, *J. Fluorine Chem.* 1975, **6**, 287.
14. H. Simmons Booth (ed.), *Inorganic Syntheses*, Vol. I, p. 134. McGraw Hill, New York (1939).

Polyhedron Vol. 7, No. 13, pp. 1221–1223, 1988
Printed in Great Britain

0277–5387/88 $3.00+.00
Pergamon Press plc

COMMUNICATION

SYNTHESIS AND CHARACTERIZATION OF BIS(CYCLOPENTADIENYL)BIS(HEXAFLUOROANTIMONATO) TITANIUM(IV)*

TH. KLAPÖTKE

Institut für Anorganische und Analytische Chemie, Technische Universität Berlin, D-1000 Berlin 12, F.R.G.

(*Received* 14 *March* 1988; *accepted* 23 *March* 1988)

Abstract—Reaction of titanocene dichloride with two equivalents of silver hexafluoroantimonate in sulphur dioxide quantitatively yields $Cp_2Ti(SbF_6)_2$ ($Cp = \eta^5$-C_5H_5) and AgCl. The titanocene bishexafluoroantimonate was recrystallized from SO_2 and characterized by chemical analysis, ^1H NMR, IR and mass spectroscopy.

Transition metal halides have been reported to possess Lewis base qualities and it has been assumed that the metal–halide bond is not broken in the complexes formed.[1] Adduct formation between Cp_2TiF_2 and Lewis acids (e.g. BF_3 and PF_5) has been investigated. However, by these reactions and by treatment of Cp_2TiCl_2 with two equivalents of $AgBF_4$ (or $AgPF_6$) only oils could be obtained.[2] The isolation of Cp_2TiF_2 has been reported from reactions involving fluorine-containing reagents such as the silver salts of CF_3S^-,[3] BF_4^-, PF_6^-, SbF_6^- and AsF_6^-;[4] but in these cases no complex of the type $Cp_2Ti(MF_6)_2$† was either isolated or identified. Titanocene derivatives containing MF_6^- groups, directly coordinated to the Cp_2Ti centre, have not previously been described, so this was the reason to study this particular problem in organometallic chemistry. The synthesis of a compound like $Cp_2Ti(MF_6)_2$ seemed to be of interest in terms of the Cp_2Ti—MF_6 bond situation (ionic or Ti—F bond interaction with reduced MF_6 symmetry: $O_h \rightarrow C_{4v}$), its stability (decomposition routes and mechanism), and last but not least the possibility that $(Cp_2Ti(NR_3)_2^{2+}(SbF_6^-)_2)$ (known as a stable complex[5]) may be the only preparation of $(Cp_2Ti(SO_2)_2^{2+}(SbF_6^-)_2)$. The first results on this project are reported in this paper.

Reaction of Cp_2TiCl_2 with two equivalents of $AgSbF_6$ (Alfa) in SO_2 at −20°C quantitatively yielded the precipitation of AgCl and led to the formation of $Cp_2Ti(SbF_6)_2$ (**1**) according to eq. (1).

$$Cp_2TiCl_2 + 2AgSbF_6 \xrightarrow[-20°C]{SO_2(l)} Cp_2Ti(SbF_6)_2 + 2AgCl\downarrow. \quad (1)$$

(1)

1, which is highly soluble in SO_2 (deep red solution), was separated from AgCl by filtration (D4) and recrystallized from the same solvent at room temperature (yield, 94%). The chemical analysis ($C_{10}H_{10}F_{12}Sb_2Ti$, M = 649,55 g mol^{-1}. Found: C, 18.3; H, 1.35. Calc. for $C_{10}H_{10}F_{12}Sb_2Ti$: C, 18.5; H, 1.55%) of the deep red microcrystalline air- and moisture-sensitive solid is in very good agreement with the composition $Cp_2Ti(SbF_6)_2$ and there is no evidence for coordinated SO_2.

While the ^1H NMR spectrum of Cp_2TiF_2 consists of a triplet in the Cp region,[3,6] in the ^1H NMR spectrum of **1** (SO_2 solution, relative to TMS) only one very sharp singlet appears in the Cp range at δ = 7.25 ppm (δ, Cp_2TiCl_2 = 6.65 ppm). This value and the low-field shift, compared with Cp_2TiCl_2, indicate a partial dissociation of **1** in solution

* Organo-transition metal chemistry of highly fluorinated ligand systems (Organo-Übergangsmetall-Chemie hochfluorierter Ligand-Systeme): first communication.

† (M = pnictogen).

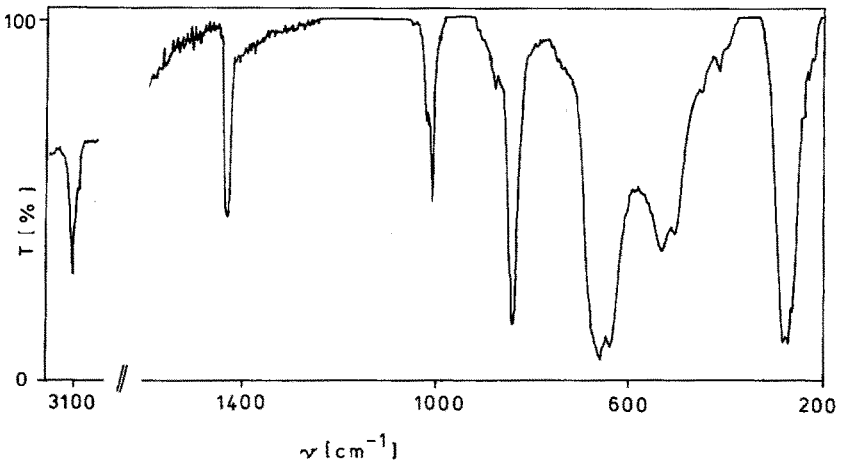

Fig. 1. IR spectrum of solid $Cp_2Ti(SbF_6)_2$ in the regions 1600–200 cm^{-1} and 3200–3000 cm^{-1} (Perkin–Elmer 457).

according to eq. (2) (cf. ref. 4).

$$\mathbf{1} \xrightarrow{SO_2(l)} (Cp_2Ti(SO_2)_2^{2+}(SbF_6^-)_2). \qquad (2)$$

The mass spectrum of **1** (electron-impact, 70 eV, 60°C) does not show a peak due to the molecular ion but to one corresponding to $CpTiF_3$. This fact and also the appearance of SbF_3^+ indicate that a fluorine transfer from the SbF_6 group to the transition metal occurs as a decomposition reaction at low temperature. The base peak is given by Cp^+.

Figure 1 shows the IR spectrum of **1**, obtained with the pure powdered compound. IR values and assignments are given in Table 1.

All bands due to the Cp_2Ti fragment are quite strong and nearly unchanged compared with those of Cp_2TiF_2. In the spectrum of Cp_2TiF_2, bands at 564 and 539 cm^{-1} have been assigned to the Ti—F symmetric and asymmetric stretching modes, respectively.[7] However, in **1** these bands are shifted to 535 and 505 cm^{-1}. This indicates weaker Ti—F bonds in **1** compared with Cp_2TiF_2. This is in agreement with a fluorine bridged structure where a "divalent" fluorine is coordinated to both the Cp_2Ti group and a "SbF_5" unit. The lower symmetry (C_{4v}) of the SbF_6 system (O_h in SbF_6^-) with five short (strong) and one long (weak) Sb—F bonds leads as expected to a splitting of the ν_3 and ν_4 bands at 650 and 285 cm^{-1}, respectively.[8–10]

Table 1. IR frequencies of $Cp_2Ti(SbF_6)_2$

Frequency (cm^{-1})	Assignment
3110 s	ν-CH
1435 s	ω-CC
1025 m,sh	δ-CH
1015 s	δ-CH
845 vs	γ-CH
665 vs	ν_{eq}-SbF_4 } ν^{12}
640 vs	ν_{ax}-SbF } ν^{12}
535 s	ν_s-TiF
505 s	ν_{as}-TiF
287 vs	δ-SbF_4 } ν^{12}
275 vs	δ-SbF_4 } ν^{12}

While $Cp_2Ti(PF_6)_2$ seems to be unstable in the solid state, the antimony analogue is described as the first stable and well characterized titanocene MF_6 (M = pnictogen) compound in the present paper. Our interest will now be extended to the AsF_6 compounds, as the fluorine affinity of AsF_5 is significantly higher than that of PF_5[11] and therefore the preparation of $Cp_2Ti(AsF_6)_2$ seems to be very likely.

Acknowledgements—Thanks are given to P. Gowik (TU Berlin) for cooperation in the experimental work and to A. Stöckel (TU Berlin) for carrying out the mass spectroscopy. I also thank M. Schriver for the ^1H NMR spectra and helpful discussions.

REFERENCES

1. M. Pankowski, B. Demerseman, G. Bouquet and M. Bigorgne, *J. Organomet. Chem.* 1972, **35**, 155; T. J. Marks, J. Kristoff, A. Alich and D. F. Shriver, *J. Organomet. Chem.* 1971, **33**, C35.
2. H. C. Clark and A. Shaver, *J. Coord. Chem.* 1975, **4**, 243.
3. R. B. King and N. Welcman, *Inorg. Chem.* 1969, **8**, 2540.

4. G. Doyle and R. S. Tobias, *Inorg. Chem.* 1967, **6**, 1111.
5. K. Berhalter and U. Thewalt, *J. Organomet. Chem.* 1987, **332**, 123.
6. A. N. Nesmeyanov, O. V. Nogina, E. I. Fedin, V. A. Dubovitskii, B. A. Kvasov and P. V. Petrovskii, *Dokl. Adad. Nauk. S.S.S.R.* 1972, **205**, 857.
7. P. M. Drucė, B. M. Kingston, M. F. Lappert, R. C. Srivastava, M. J. Frazer and W. E. Newton, *J. Chem. Soc. A* 1969, 2814.
8. S. Buffagni, L. M. Vallarino and J. V. Quagliano, *Inorg. Chem.* 1964, **3**, 671.
9. H. C. Clark and R. J. O'Brien, *Inorg. Chem.* 1963, **2**, 1020.
10. K. Seppelt, *Z. Anorg. Allg. Chem.* 1978, **899**, 87.
11. T. E. Mallouk, G. L. Rosenthal, G. Müller, R. Brusasco and N. Bartlett, *Inorg. Chem.* 1984, **23**, 3167.
12. T. Birchall, P. A. W. Dean and R. J. Gillespie, *J. Chem. Soc. A* 1971, 1777.

Polyhedron Vol. 7, No. 13, p. 1225, 1988
Pergamon Press plc. Printed in Great Britain

BOOK REVIEWS

Gmelin Handbook of Inorganic Chemistry, Sn–organotin Compounds, part 14. Dimethyltin–, diethyltin– and dipropyltin–oxygen compounds. Sn–Tin/System No. 46. Published by Gmelin Institute for Inorganic Chemistry of the Max Planck Society for the Advancement of Science, 8th Edn. Springer, Berlin, 1987. ISBN 3-540-93551-7, xiv+248 pp, 13 figs. DM1119.

This 14th Gmelin volume on organotin compounds, like all the previous ones, has been compiled by Herbert and Ingeborg Schumann. It deals with dimethyltin–, diethyltin– and dipropyltin–oxygen compounds, that is the hydroxides, alkoxides, peroxides, carboxylates and derivatives of inorganic oxyacids such as the nitrates, sulphates and phosphates. The text is wholly in English and the literature is covered up to the end of 1985.

General preparative methods for a particular group of compounds are given, then the members of the group are tabulated with data such as mp, bp and IR and NMR spectra. Important members are then listed individually and their preparations and properties, particularly their IR and NMR spectra, are discussed in detail. When the structures have been determined by X-ray diffraction, they are illustrated and labelled with their important dimensions.

The book begins with a bibliography of the relevant literature which has been published since the end of 1982, continuing that which appeared in Vol. 11, and it concludes with 34 pages of empirical formula and ligand formula indexes.

The printing and presentation are above reproach. Like its predecessors, this volume will be invaluable to organotin chemists.

Department of Chemistry **PROF. A. G. DAVIES**
University College London
20 Gordon Street
London WC1H 0AJ, U.K.

Gmelin Handbook of Inorganic Chemistry, Cu–organocopper Compounds, part 4. Cu–Copper/ System No. 60. Published by Gmelin Institute for Inorganic Chemistry of the Max Planck Society for the Advancement of Science, 8th Edn. Springer, Berlin, 1987. ISBN 3-540-93555-X, xii+272 pp., 86 figs. DM1249.

This volume covers mononuclear compounds carrying two or more ligands bonded through carbon, as well as all dinuclear to octanuclear and polymeric compounds. Related mononuclear compounds carrying one carbon-bonded ligand have already been discussed in Vols 1, 2 and 3. The literature is covered up to the end of 1986, and the text is wholly in English.

The presentation follows the familiar pattern. A general description of a group of compounds is given, the properties and the reactions of compounds within the group are tabulated, and important members are then discussed in detail. There are 86 figures illustrating the structures of compounds which have been studied by X-ray diffraction.

The organocopper compounds are finding increasing applications in organic synthesis and these Gmelin volumes provide an invaluable guide to the relevant literature. A complete formula and ligand index of the four volumes on organocopper compounds is to appear shortly as Vol. 5.

Department of Chemistry **PROF. A. G. DAVIES**
University College London
20 Gordon Street
London WC1H 0AJ, U.K.

Polyhedron Vol. 7, No. 14, pp. 1227–1230, 1988
Printed in Great Britain

0277–5387/88 $3.00+.00
© 1988 Pergamon Press plc

SPECTROPHOTOMETRIC STUDY OF THE COMPLEXATION REACTIONS BETWEEN ALKALINE EARTH CATIONS AND MUREXIDE IN SOME NON-AQUEOUS SOLUTIONS

SOHEILA KASHANIAN, MOHAMMAD BAGHER GHOLIVAND, SIAVASH MADAENI, ALIREZA NIKRAHI and MOJTABA SHAMSIPUR*

Department of Chemistry, Razi University, Bakhtaran, Iran

(*Received* 7 *July* 1987; *accepted* 13 *October* 1987)

Abstract—The complexation reactions between alkaline earth cations and murexide in methanol, dimethylformamide and dimethylsulphoxide solutions have been studied spectrophotometrically at 25°C. The formation constants of the resulting 1 : 1 complexes were determined. In all solvents used, the stabilities of the murexide complexes vary in the order $Ca^{2+} > Sr^{2+} > Ba^{2+} > Mg^{2+}$. There is an inverse relationship between the stabilities of the complexes and the Gutmann donicity of the solvents.

Murexide, the ammonium salt of purpuric acid (I),

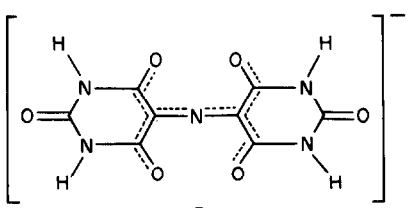

I

has been known for a long time as a good indicator for the calcium ion[1–4] and some other alkaline earth cations[5] in aqueous solutions. At neutral pH, murexide is present as a monovalent anion in which the negative charge is distributed among the N-bridge atom and four neighbouring oxygens. Chelation of the metal cations by this ligand involves then the contribution from the bridge nitrogen as well as from the neighbouring oxygen atoms. Since the Ca^{2+}–murexide equilibrium is very rapidly established in aqueous[6] and methanol[7] solutions, the ligand has been used in the kinetic studies of calcium cryptates using the stopped-flow method.[8] The use of murexide as a metal indicator in the study of the dynamics of Mg^{2+}–bicarbonate interactions by means of stopped-flow and temperature-jump methods has also been reported.[9]

Despite the important role of murexide as a metal indicator in the determination of alkaline earth cations as well as in the thermodynamic and kinetic studies of their complexes, the alkaline earth–murexide interactions have only been studied in aqueous solutions,[6,10–12] and information about their interactions in non-aqueous solutions is quite sparse.

It was of interest to us, to study the effect of solvent properties on the stoichiometry and stability of the murexide complexes with alkaline earth cations. In this paper we report a spectrophotometric study of the murexide complexes with Mg^{2+}, Ca^{2+}, Sr^{2+} and Ba^{2+} ions in methanol, dimethylformamide and dimethylsulphoxide solutions at 25°C.

EXPERIMENTAL

Reagent grade magnesium chloride, calcium chloride, strontium nitrate (all from Merck Co.), barium chloride (Fluka) and murexide (Merck) were dried over P_4O_{10} *in vacuo* for 72 h. Methanol (Baker, MeOH), dimethylformamide (Fisher, DMF) and dimethylsulphoxide (Fisher, DMSO) were purified and dried by the previously reported methods.[13] All spectra were obtained with a Model 34 Beckman UV–vis. spectrometer at 25°C.

The formation constants of 1 : 1 complexes between murexide and alkaline earth cations were determined by the absorbance measurements at several wavelengths of the spectra of solutions in which varying concentrations of the metal ions

* Author to whom correspondence should be addressed.

(1.0×10^{-5}–1.0×10^{-4} M) were added to a fixed concentration of murexide (2.0×10^{-5} M) in different solvents. Attainment of equilibrium was checked by the observation of no further change in the spectra after several hours. Errors associated with the formation constants were reported as ± standard deviations.

RESULTS AND DISCUSSION

The spectra of murexide and its alkaline earth complexes were obtained. All of the complexes are distinguished by a strong spectral shift in comparison to the free murexide in all three solvents used. The resulting spectra in DMSO solution are shown in Fig. 1. The spectral behaviour of murexide complexes is quite unique in all three solvents studied, consisting of strong and ion specific absorption shifts towards shorter wavelengths. Generally, the electrostatic interactions of a bound metal ion would not be able to produce such a pronounced effect on the electrostatic structure of a dye molecule, and hence on its spectrum. It is reasonable to assume that the twisting of the two rings of the murexide molecule relative to each other (around the N-bridge axis), brought about by metal ion complexation, is responsible for such spectral behavior.

The stoichiometry of the alkaline earth–murexide complexes in MeOH, DMF and DMSO solutions were examined by the method of continuous variations, introduced by Ostromisslensky[14] and Job.[15] Two samples of the resulting plots are shown in Fig. 2. It was found that the metal ion to ligand mole ratio in the alkaline earth–murexide complexes is 1 : 1. Moreover, the existence of a well defined isosbestic point in the spectra of murexide upon titration with alkaline earth cations (Fig. 3) is also a good indication for a simple 1 : 1 complexation equilibrium.

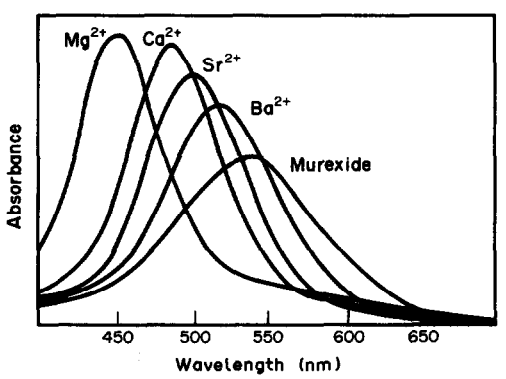

Fig. 1. Visible spectra for murexide and its alkaline earth complexes in DMSO.

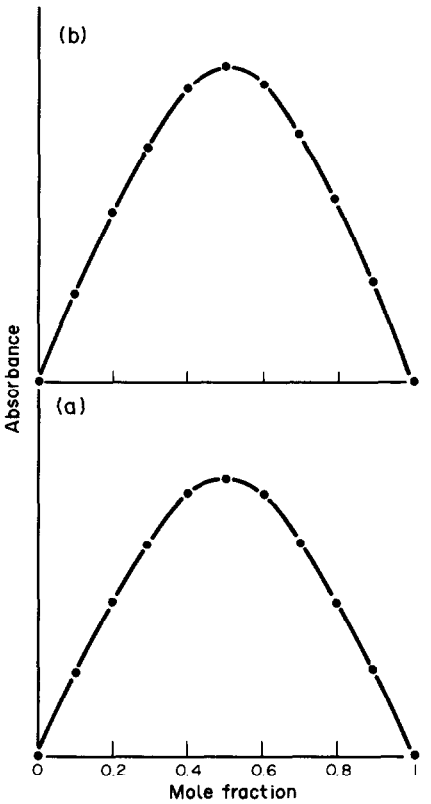

Fig. 2. Continuous variation plots for Ca^{2+}–murexide in DMSO (a) and Sr^{2+}–murexide in DMF (b).

In order to determine the stability of metal ion–murexide complexes, the spectra of a series of solutions of fixed murexide concentration and varying amounts of the alkaline earth cations were recorded. In all cases, maximum absorption of the free and complexed murexide molecules were separated by about 20–90 nm. All spectra presented satisfactory isosbestic points. The deviations of spectra from isosbestic points were at the most ±5%. The spectra of mixtures of strontium ion and murexide in DMSO solutions are shown in Fig. 3. All calculated formation constants of the resulting 1 : 1 complexes in MeOH, DMF and DMSO solutions are presented in Table 1. The corresponding reported values in aqueous solution[10] are also included for comparison. The relationship between the stabilities of the complexes and crystal radii of the cations[18] are shown in Fig. 4.

All of the solvents used have relatively high dielectric constants (Table 1) and at the very low salt concentrations we used (10^{-4}–10^{-5} M), the amount of ion pairing with free alkaline earth cations, and especially with large complex ions is

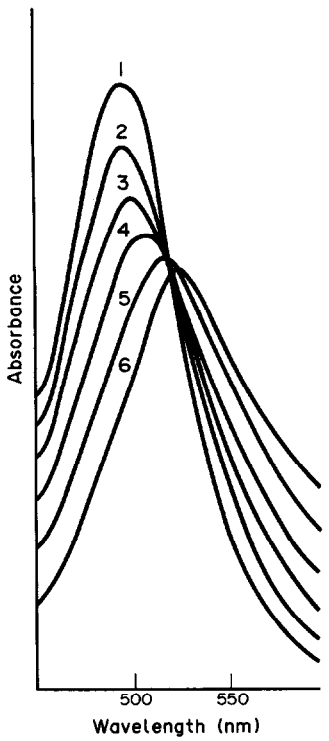

Fig. 3. Visible spectra for titration of murexide (2.0×10^{-5} M) with the Sr^{2+} ion in DMSO at 25°C. Respective concentrations of the Sr^{2+} ion in different solutions are: 1, 8.0×10^{-5} M; 2, 6.0×10^{-5} M; 3, 4.0×10^{-5} M; 4, 2.0×10^{-5} M; 5, 1.0×10^{-5} M; 6, murexide alone.

negligible. Therefore, the nature of the anion should not influence the complexation reaction.

Figure 1 shows that the absolute binding strength of the alkaline earth complexes with murexide decreases monotonically with increasing ionic size from Mg^{2+} to Ba^{2+} (both $\Delta\lambda_{max}$ and $\Delta\varepsilon$ are largest for the smallest cation). In contrast, the results given in Table 1 show a decrease in the stability of the resulting murexide complexes in the order $Ca^{2+} > Sr^{2+} > Ba^{2+} > Mg^{2+}$ in MeOH, DMF and DMSO solutions as well as in aqueous solution. However, it should be noticed that the thermodynamic stability constants are not just a measure of the absolute strength of the complexes, but a measure of the relative strength as compared to the ionic solvation. Remember that the species involved in the complexation reaction (i.e. cation, murexide and their complex) are all carrying either positive or negative charges. Thus the maximum K_f for the Ca^{2+} ion complex results from a balance between the binding and solvation energies. Figure 4 shows that the selectivity of murexide for alkaline earth cations follows the same trend in various solvents.

Table 1. Log K_f of different alkaline earth–murexide complexes in various solvents at 25°C

Solvent	D^a	DN^b	Cation	Log K_f
MeOH	32.7	25.7[c]	Mg^{2+}	3.85±0.10
			Ca^{2+}	6.09±0.09
			Sr^{2+}	5.68±0.10
			Ba^{2+}	5.40±0.11
DMF	36.7	26.6	Mg^{2+}	3.57±0.07
			Ca^{2+}	4.98±0.09
			Sr^{2+}	4.52±0.09
			Ba^{2+}	4.43±0.07
DMSO	46.7	29.8	Mg^{2+}	3.22±0.07
			Ca^{2+}	4.64±0.06
			Sr^{2+}	4.35±0.09
			Ba^{2+}	4.05±0.07
H_2O[d]	78.5	33.0[c]	Mg^{2+}	0.0
			Ca^{2+}	2.70
			Sr^{2+}	2.45
			Ba^{2+}	2.14

[a] D = dielectric constant, ref. 16.
[b] DN = donor number, ref. 16.
[c] Ref. 17.
[d] Data from ref. 10.

From Table 1, it is obvious that the solvent plays a very fundamental role in the complexation reaction. There is an inverse relationship between the donating ability of the solvents, as expressed by the Gutmann donor number,[16] and the stability of the complexes. This result is not surprising, since the solvent molecules acting as electron donating ligands can compete with murexide for the alkaline earth cations in solution. Among the solvents used

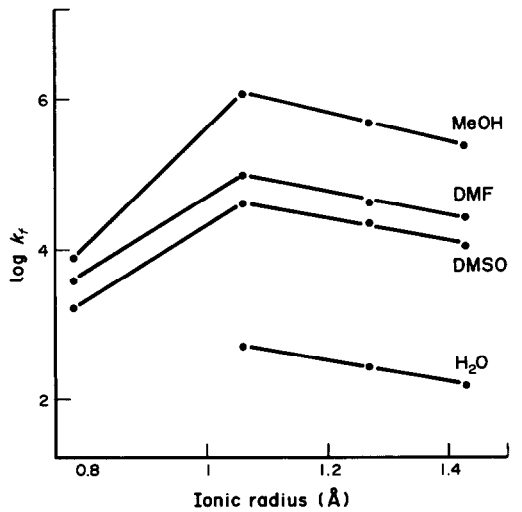

Fig. 4. Stability constants of the alkaline earth–murexide complexes vs ionic radii of the cations in various solvents.

in this study, DMSO is the one with the highest donicity and, therefore, competes the most with murexide molecules for the cations, which in turn results in the least stable murexide complexes in the series. The results in water, which is a better donating solvent,[17] nicely follow the lines of the argument. The same solvent effect has already been reported for different alkali and alkaline earth complexes in various solvents.[19-22]

REFERENCES

1. G. Schwartzenbach and H. Gysling, *Helv. Chim. Acta* 1949, **32**, 1314.
2. H. Ostertag and M. E. Rinck, *Chim. Anal.* 1952, **34**, 108.
3. W. T. G. M. Smeets and L. Seekles, *Nature* 1952, **169**, 802.
4. A. Scarpa, *Methods Enzymol.* 1972, **24B**, 343.
5. D. S. Russel, J. B. Campbell and S. S. Berman, *Anal. Chim. Acta* 1961, **25**, 81.
6. G. Geier, *Helv. Chim. Acta* 1968, **51**, 94.
7. H. Diebler, M. Eigen, G. Ilgenfritz, G. Maass and R. Winkler, *Pure Appl. Chem.* 1969, **20**, 93.
8. V. M. Loyola, R. Pizer and R. G. Wilkins, *J. Am. Chem. Soc.* 1977, **99**, 7185.
9. R. C. Palet, F. Garland and G. Atkinson, *J. Sol. Chem.* 1975, **4**, 161.
10. H. Ostertag, *Comp. Rend.* 1960, **250**, 1061.
11. G. Geier, *Helv. Chim. Acta* 1967, **50**, 1879.
12. D. Guo and E. Wang, *Fenxi Huaxue* 1982, **10**, 277.
13. M. S. Greenberg and A. I. Popov, *Spectrochim. Acta* 1975, **31A**, 697.
14. I. Ostromisslensky, *Ber. Deut. Chem. Ges.* 1911, **44**, 268.
15. P. Job, *Ann. Chim. (Paris)* 1928, **9**, 113.
16. V. M. Gutmann and E. Wychera, *Inorg. Nucl. Chem. Lett.* 1966, **2**, 257.
17. M. S. Greenberg, R. L. Bonder and A. I. Popov, *J. Phys. Chem.* 1973, **77**, 2449.
18. J. M. Lehn, *Struct. Bonding* 1973, **16**, 1.
19. M. B. Gholivand and M. Shamsipur, *Inorg. Chim. Acta* 1986, **121**, 53.
20. M. B. Gholivand, S. Kashanian and M. Shamsipur, *Polyhedron* 1987, **6**, 535.
21. M. Shamsipur and A. I. Popov, *Inorg. Chim. Acta* 1980, **43**, 243.
22. E. Schmidt, A. Hourdakis and A. I. Popov, *Inorg. Chim. Acta* 1981, **52**, 91.

Polyhedron Vol. 7, No. 14, pp. 1231–1237, 1988
Printed in Great Britain

0277–5387/88 $3.00+.00
© 1988 Pergamon Press plc

PREPARATION, PROPERTIES AND REACTIVITY OF GOLD COMPLEXES WITH SOME HETEROCYCLIC DITHIOCARBAMATES AS LIGANDS

FABRIZIA FORGHIERI, CARLO PRETI,* LORENZO TASSI and GIUSEPPE TOSI

Department of Chemistry, University of Modena, Via G.Campi, 183, 41100 Modena, Italy

(*Received* 8 *October* 1987; *accepted* 16 *December* 1987)

Abstract—The syntheses, properties and reactivity of the gold complexes AuRdtc, $Au(Rdtc)_3$, $Au(Rdtc)_2X$ and $Au(Rdtc)X_2$ (X = Cl, Br; Rdtc = piperidine-, morpholine-, thiomorpholine-, piperazine-, N-methylpiperazine-, N-phenylpiperazine- and 4-phenylpiperidinedithiocarbamate) are reported. Elemental analysis, electrical conductance measurements, spectral (electronic and IR), magnetic susceptibility and thermogravimetric studies were used for characterization. The dithiocarbamato ligands exhibit both bidentate behaviour acting as S,S′-donors and monodentate behaviour acting as S-donors, depending on the type of the complex. The diamagnetic behaviour confirms the low-spin d^8 configuration for Au(III) complexes and some metal–ligand and metal–halide stretches have been assigned.

As a part of our studies on the coordinating behaviour of the heterocyclic dithiocarbamate ligands towards transition metals, we report in this paper the synthesis, properties and reactivity of new complexes of gold(I) and gold(III) with the ligands indicated in Structure 1.

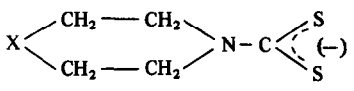

Structure 1.

We have previously described the complexes with *d*- and *p*-block metals, their reactivity towards nitrogen donor ligands, their mass spectral investigations and their structural characterization by XPS techniques.[1–7] It is of interest to monitor the influence of the different heterocyclic groups bearing different substituents in the ring, on the C⋯N and C⋯S bonds and, consequently, on the electron structure of the complexes. The nature of the heterocycle influences the behaviour of the dithiocarbamates through variation in the electron-releasing ability of the different amines.

* Author to whom correspondence should be addressed.

RESULTS AND DISCUSSION

The analytical data for the ligands and the complexes are reported in Tables 1 and 2, respectively. The complexes obtained were characterized by conductivity measurements, magnetic moment studies, electronic, IR and far-IR spectra and thermal analyses (TG and DTG techniques). In Table 3 the most important IR bands with their assignments are listed. The electronic spectra data for the dithiocarbamato derivatives are collected in Table 4.

$X = CH_2$	Pipdtc
= O	Morphdtc
= S	Timdtc
= NH	Pzdtc
$= N-CH_3$	N−MePzdtc
$= N-C_6H_5$	N−PhPzdtc
$= HC-C_6H_5$	4−PhPipdtc

The compounds are stable at room temperature, insensitive to atmospheric oxygen and moisture, and are soluble in N,N′-dimethylformamide, pyridine, benzene, nitrobenzene and nitromethane. Conductance measurements in nitrobenzene and N,N′-dimethylformamide solution are indicative of 1 : 1 electrolytes for compounds of the $Au(Rdtc)_2X$-

Table 1. Analytical data for the dithiocarbamate sodium salts and for the thiuramdisulphides

Compounds	Found (required) % C	H	N	S
$C_6H_{10}NS_2Na \cdot 2H_2O$ (PipdtcNa · $2H_2O$)	33.0 (32.9)	6.5 (6.4)	6.4 (6.4)	29.1 (29.2)
$C_5H_8NOS_2Na \cdot 2H_2O$ (MorphdtcNa · $2H_2O$)	27.0 (27.1)	5.4 (5.5)	6.4 (6.3)	28.9 (29.0)
$C_5H_8NS_3Na \cdot 2H_2O$ (TimdtcNa · $2H_2O$)	25.1 (25.3)	5.1 (5.1)	5.9 (5.9)	40.6 (40.5)
$C_5H_9N_2S_2Na \cdot 3H_2O$ (PzdtcNa · $3H_2O$)	25.2 (25.2)	6.2 (6.3)	11.9 (11.8)	27.0 (26.9)
$C_6H_{11}N_2S_2Na \cdot 2H_2O$ (N-MePzdtcNa · $2H_2O$)	30.6 (30.7)	6.6 (6.5)	11.8 (11.9)	27.3 (27.4)
$C_{11}H_{13}N_2S_2Na \cdot 2H_2O$ (N-PhPzdtcNa · $2H_2O$)	44.7 (44.6)	5.6 (5.8)	9.5 (9.5)	21.5 (21.6)
$C_{12}H_{14}NS_2Na \cdot 2H_2O$ (4-PhPipdtcNa · $2H_2O$)	48.7 (48.8)	6.1 (6.1)	4.8 (4.7)	21.8 (21.7)
$C_{12}H_{20}N_2S_4$ (Pip_2tds)	44.9 (45.0)	6.3 (6.3)	8.7 (8.7)	40.2 (40.0)
$C_{10}H_{16}N_2O_2S_4$ ($Morph_2tds$)	37.0 (37.0)	5.0 (5.0)	8.7 (8.6)	39.7 (39.5)
$C_{10}H_{16}N_2S_6$ (Tim_2tds)	33.7 (33.7)	4.5 (4.5)	7.8 (7.8)	54.0 (53.9)
$C_{10}H_{18}N_4S_4$ (Pz_2tds)	37.3 (37.2)	5.4 (5.6)	17.5 (17.4)	39.8 (39.8)
$C_{12}H_{22}N_4S_4$ (N-$MePz_2tds$)	41.1 (41.1)	6.4 (6.3)	16.0 (16.0)	36.5 (36.6)
$C_{22}H_{26}N_4S_4$ (N-$PhPz_2tds$)	55.7 (55.7)	5.5 (5.5)	11.8 (11.8)	26.9 (27.0)
$C_{24}H_{28}N_2S_4$ (4-$PhPip_2tds$)	61.0 (61.0)	6.0 (6.0)	5.9 (5.9)	26.9 (27.1)

type; all the remaining compounds were non-conducting in the above solvents, hence the absence of ionic species is indicative of the covalent nature of these complexes.[8]

IR spectra

The IR spectra of the ligands and their gold complexes are given in Table 3. The thioureide band in the range 1440–1470 cm^{-1} of the free ligands indicates considerable double-bond character of the carbon–nitrogen bond, this band being between the stretching frequencies of ν(C=N) and ν(C—N), which lie at 1690–1640 and 1350–1250 cm^{-1}, respectively. This fact could be explained by taking into account that the electron-releasing ability of the heterocyclic group which, by forcing high electron density on the sulphur atom via the π system, produces greater double-bond character of the carbon–nitrogen bond whose stretching vibration, as a consequence, increases.

All complexes reported here show bands assigned to ν(C···N) in the 1560–1480 cm^{-1} range; in addition the 1 : 3 gold(III) derivatives show a second band between 1470–1445 cm^{-1}; this fact clearly indicates that the dithiocarbamate groups are linked to the central metal ion in different ways.

On passing from the dithiocarbamato sodium salts to the complexes, the ν(C···N) mode is shifted to higher energies and in particular undergoes blue shifts in the order Au(I) < Au(III). As regards the halo-derivatives, the ν(C···N) band is shifted to higher frequency following the order $Au(Rdtc)X_2 > Au(Rdtc)_2X$. This sequence is due to the increase in electronegativity deriving from the increase of halide atoms in the complexes, and this fact promotes a higher positive charge on the nitrogen atom.

Taking into account the structure of the dithioanions which can be represented by the formalism shown in Scheme 1(a)–(d), we can conclude that the contribution from structure (d) is greater in the bishalo-derivatives and decreases on passing to the monohalo-derivatives and from gold(III) to gold(I).

The band in the region 1020–970 cm^{-1} can be attributed to the prevailing contribution of ν(C···S); this value enables a decision to be made as to whether the dithio-ligand moiety is mono- or bidentate. The presence in the spectra of all the complexes (except the 1 : 3 gold derivatives), of only one strong band at about 1000 cm^{-1} strongly supports bidentate coordination of the dithio-ligand, a doublet being expected in the 1000 ± 70 cm^{-1} range

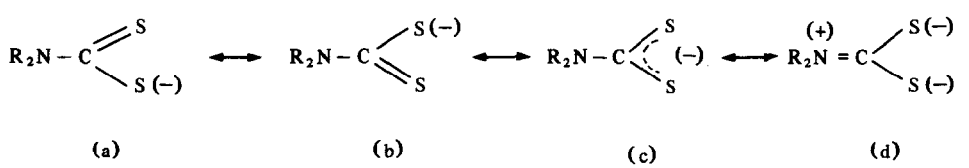

(a) (b) (c) (d)

Scheme 1.

Table 2. Analytical data for the gold complexes

Compounds	Colour	Found (required) % N	C	H	S
$Au(Pzdtc)_3$	Pale brown	12.3 (12.3)	26.2 (26.5)	3.6 (4.0)	28.2 (28.3)
$Au(Pzdtc)_2Cl$	Brown	9.9 (10.1)	21.9 (21.6)	3.1 (3.3)	23.0 (23.1)
$Au(Pzdtc)Cl_2$	Brown	6.5 (6.5)	13.9 (14.0)	2.1 (2.1)	14.8 (14.9)
$Au(Pzdtc)Br_2$	Brown	5.0 (5.4)	11.6 (11.6)	1.6 (1.8)	12.5 (12.4)
$Au(N\text{-}MePzdtc)_3$	Brown	11.6 (11.6)	30.0 (29.9)	4.6 (4.6)	26.6 (26.6)
$Au(N\text{-}MePzdtc)Cl_2$	Red–brown	6.6 (6.3)	16.5 (16.3)	2.5 (2.5)	14.9 (14.5)
$Au(N\text{-}MePzdtc)Br_2$	Ochre	5.3 (5.3)	13.7 (13.5)	2.1 (2.1)	12.3 (12.0)
$Au(N\text{-}PhPzdtc)_3$	Hazel–brown	9.2 (9.2)	43.8 (43.6)	4.2 (4.3)	21.2 (21.2)
$Au(N\text{-}PhPzdtc)_2Cl$	Pale brown	8.0 (7.9)	37.6 (37.4)	3.7 (3.7)	18.0 (18.1)
$Au(N\text{-}PhPzdtc)Cl_2$	Pale brown	5.7 (5.5)	26.7 (26.2)	2.7 (2.6)	13.0 (12.7)
$Au(N\text{-}PhPzdtc)_2Br$	Hazel–brown	7.2 (7.5)	35.0 (35.2)	3.5 (3.5)	17.0 (17.1)
$Au(N\text{-}PhPzdtc)Br_2$	Hazel–brown	4.9 (4.7)	22.6 (22.2)	2.2 (2.2)	11.3 (10.8)
$Au(Pipdtc)_3$	Dark violet	6.3 (6.2)	31.9 (31.9)	4.5 (4.5)	28.4 (28.4)
$Au(Pipdtc)_2Cl$	Brown	5.1 (5.1)	26.1 (26.1)	3.6 (3.6)	22.8 (23.2)
$Au(Pipdtc)Cl_2$	Light green	3.2 (3.3)	16.3 (16.8)	2.3 (2.3)	14.9 (15.0)
$Au(Pipdtc)_2Br$	Brown	4.7 (4.7)	24.2 (24.1)	3.2 (3.4)	21.8 (21.5)
$Au(Pipdtc)Br_2$	Yellow–ochre	2.7 (2.7)	13.6 (13.9)	1.7 (1.9)	12.4 (12.4)
$Au(4\text{-}PhPipdtc)_3$	Pale green	4.8 (4.6)	47.6 (47.7)	4.6 (4.7)	21.3 (21.2)
$Au(4\text{-}PhPipdtc)_2Cl$	Green	4.0 (4.0)	40.4 (40.9)	4.0 (4.0)	18.2 (18.2)
$Au(4\text{-}PhPipdtc)Cl_2$	Pale yellow	2.8 (2.8)	28.5 (28.6)	2.8 (2.8)	12.8 (12.7)
$Au(4\text{-}PhPipdtc)_2Br$	Yellow–green	3.8 (3.7)	37.7 (38.5)	3.6 (3.8)	17.0 (17.1)
$Au(4\text{-}PhPipdtc)Br_2$	Orange	2.5 (2.4)	24.4 (24.3)	2.3 (2.4)	10.8 (10.8)
$Au(Morphdtc)_3$	Brown	6.2 (6.1)	26.0 (26.3)	3.5 (3.5)	28.0 (28.1)
$Au(Morphdtc)_2Cl$	Pale Brown	5.1 (5.0)	21.7 (21.6)	2.9 (2.9)	22.9 (23.0)
$Au(Morphdtc)Cl_2$	Light green	3.3 (3.2)	14.1 (14.0)	1.9 (1.9)	15.7 (14.9)
$Au(Morphdtc)_2Br$	Pale brown	4.7 (4.7)	20.4 (20.0)	2.7 (2.7)	21.4 (21.3)
$Au(Morphdtc)Br_2$	Yellow–green	2.8 (2.7)	12.1 (11.6)	1.6 (1.6)	12.6 (12.4)
$Au(Timdtc)_3$	Brown	5.7 (5.7)	24.3 (24.6)	3.3 (3.3)	39.4 (39.4)
$Au(Timdtc)_2Cl$	Pale brown	5.0 (4.8)	20.6 (20.4)	2.9 (2.7)	32.6 (32.7)
$Au(Timdtc)Cl_2$	Light brown	3.0 (3.1)	13.2 (13.4)	1.8 (1.8)	21.5 (21.6)
$Au(Timdtc)_2Br$	Pale brown	4.6 (4.4)	19.3 (19.0)	2.6 (2.5)	30.3 (30.4)
$Au(Timdtc)Br_2$	Yellow	2.9 (2.6)	11.4 (11.2)	1.8 (1.5)	18.3 (18.0)
Au(Pzdtc)	Brown	7.5 (7.8)	16.8 (16.8)	2.5 (2.5)	17.8 (17.9)
Au(N-MePzdtc)	Grey–green	7.5 (7.5)	19.4 (19.4)	3.0 (3.0)	17.1 (17.2)
Au(N-PhPzdtc)	Grey–green	6.5 (6.4)	30.4 (30.4)	3.1 (3.0)	14.9 (14.8)
Au(Pipdtc)	Dark brown	3.9 (3.9)	20.1 (20.2)	2.9 (2.8)	18.0 (17.9)
Au(4-PhPipdtc)	Light green	3.3 (3.2)	33.2 (33.3)	3.2 (3.2)	14.8 (14.8)
Au(Morphdtc)	Pale yellow	4.0 (3.9)	17.0 (16.7)	2.2 (2.2)	17.7 (17.8)
Au(Timdtc)	Pale green	3.7 (3.7)	15.6 (16.0)	2.0 (2.1)	25.4 (25.6)

for monodentate behaviour.[9–11] On the contrary, a split band in the 1020–970 cm^{-1} range for gold(III) tris-derivatives suggests that monodentate dithiocarbamato groups are present in the complexes. Further confirmation comes from an analysis of the position of the $\nu(C{\cdots}N)$ mode; in fact this band undergoes upward shifts for bidentate behaviour and it would undergo downward shifts or, at least, it would remain unchanged having the same value as for the free sodium dithiocarbamate in the case of monodentate coordination.[12]

Turning now to the 1:3 gold derivatives, from the behaviour of the $\nu(C{\cdots}N)$ and $\nu(C{\cdots}S)$ stretching modes, we propose the simultaneous presence of bidentate and monodentate dithiocarbamato groups. In all the other complexes, the presence of only one $\nu(C{\cdots}S)$ band and the shift of the $\nu(C{\cdots}N)$ mode towards higher energies point to a bidentate behaviour of the ligands. The vibrational modes in the 580–470 cm^{-1} range can be ascribed to the contribution of $\nu(CS)+\delta(SCS)$, but it is interesting to point out that the band in this range must involve some 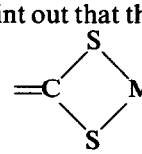 ring deformation, as dem-

Table 3. Most important IR bands (cm^{-1}) for the ligands and for the gold complexes

Compounds	ν(C⋯N)	ν(C⋯S)	ν(CS)+δ(SCS)	ν(M—S)	ν(M—X)
PzdtcNa	1460vs	1000vs	560m	—	—
N-MePzdtcNa	1450vs	995s	540m	—	—
N-PhPzdtcNa	1465vs	975m	524m	—	—
PipdtcNa	1465vs	965vs	525m	—	—
4-PhPipdtcNa	1469vs	958ms	530m	—	—
MorphdtcNa	1440vs	990s	535m	—	—
TimdtcNa	1458vs	995s	490ms	—	—
$Au(Pzdtc)_3$	1545vs, 1460ms	1020s, 990s	575m	425m, 400m	—
$Au(Pzdtc)_2Cl$	1530vs	1010m	570m	428m, 398m	—
$Au(Pzdtc)Cl_2$	1535vs	1005m	572m	420m, 395m	345m, 325m
$Au(Pzdtc)Br_2$	1535vs	1000m	580m	422m, 385m	245m, 222m
$Au(N\text{-}MePzdtc)_3$	1535vs, 1455ms	1000s, 970ms	535m	435m, 382m	—
$Au(N\text{-}MePzdtc)Cl_2$	1540vs	1000s	550m	410m, 372sh	348m, 325m
$Au(N\text{-}MePzdtc)Br_2$	1555vs	995s	545m	402m, 370sh	249m, 224m
$Au(N\text{-}PhPzdtc)_3$	1550vs, 1450ms	1010s, 995ms	530m	420m, 390m	—
$Au(N\text{-}PhPzdtc)_2Cl$	1545vs	1010s	525m	415m, 385sh	—
$Au(N\text{-}PhPzdtc)Cl_2$	1550vs	1015s	525m	440m, 395m	355m, 330m
$Au(N\text{-}PhPzdtc)_2Br$	1545vs	1000s	515m	419m, 387sh	—
$Au(N\text{-}PhPzdtc)Br_2$	1550vs	1020s	520m	418m, 390m	246m, 238m
$Au(Pipdtc)_3$	1550vs, 1460ms	1010s, 990s	515m	428m, 382m	—
$Au(Pipdtc)_2Cl$	1530vs	1015s	520m	415m, 395sh	—
$Au(Pipdtc)Cl_2$	1550vs	995s	530m	410m, 390sh	356ms, 335m
$Au(Pipdtc)_2Br$	1540vs	1005m	520m	420m, 393m	—
$Au(Pipdtc)Br_2$	1555vs	1010m	530m	417m, 392m	247m, 236m
$Au(4\text{-}PhPipdtc)_3$	1540vs, 1470ms	1020m, 1000s	525m	415m, 385m	—
$Au(4\text{-}PhPipdtc)_2Cl$	1540vs	995m	525m	410m, 390m	—
$Au(4\text{-}PhPipdtc)Cl_2$	1550vs	995m	520m	415m, 385m	345m, 330m
$Au(4\text{-}PhPipdtc)_2Br$	1545vs	990m	520m	418m, 390m	—
$Au(4\text{-}PhPipdtc)Br_2$	1550vs	995m	525m	416m, 386m	248m, 225m
$Au(Morphdtc)_3$	1540vs, 1445ms	1020vs, 1000s	540m	430m, 398m	—
$Au(Morphdtc)_2Cl$	1530vs	1010s	540m	412m, 398sh	—
$Au(Morphdtc)Cl_2$	1540vs	1010s	535m	410m, 380sh	354m, 324m
$Au(Morphdtc)_2Br$	1530vs	1000s	540m	409m, 388m	—
$Au(Morphdtc)Br_2$	1560vs	1000s	540m	408m, 388m	245m, 224m
$Au(Timdtc)_3$	1535vs, 1455ms	990s, 975s	480m	409m, 393m	—
$Au(Timdtc)_2Cl$	1540vs	1000s	475m	410m, 392m	—
$Au(Timdtc)Cl_2$	1530vs	1010m	470m	408m, 394m	340m, 324m
$Au(Timdtc)_2Br$	1535vs	1000s	470m	410m, 395m	—
$Au(Timdtc)Br_2$	1545vs	1000s	475m	410m, 392m	248m, 218m
Au(Pzdtc)	1530s	1010m	565m	419m, 395m	—
Au(N-MePzdtc)	1480ms	990m	535m	430m, 378m	—
Au(N-PhPzdtc)	1540vs	1015m	520m	410m, 387m	—
Au(Pipdtc)	1545vs	1000m	515m	408m, 380m	—
Au(4-PhPipdtc)	1545vs	995m	530m	400m, 380m	—
Au(Morphdtc)	1525vs	990ms	540m	425m, 390m	—
Au(Timdtc)	1540vs	1000ms	490m	405m, 390m	—

onstrated by a detailed IR isotopic study on $^{58}Ni(II)$, $^{62}Ni(II)$, $^{63}Cu(II)$ and $^{65}Cu(II)$ dithio-complexes.[2]

The vibrational modes involving the heteroatom of the ring are unchanged relative to the free ligands, so any coordination to the metal via these oxygen, sulphur and nitrogen atoms is excluded.

In the far-IR region, the bands of the ligands appear unchanged in the spectra of the complexes. New bands, absent in the spectra of the starting materials, are observed in the 440–370 cm^{-1} range and they can be assigned to the metal–sulphur stretching mode according to the normal coordinate analysis of the dithiocarbamato complexes and pre-

Table 4. Main absorption bands in the solid state electronic spectra of the complexes

Compounds	max (cm^{-1})
$Au(Pzdtc)_3$	36760, 32780, 31250, 23800, 17860
$Au(Pzdtc)_2Cl$	36360, 29325, 24390, 19610, 17390
$Au(Pzdtc)Cl_2$	36290, 29200, 22180, 17750
$Au(Pzdtc)Br_2$	36360, 31240, 27770, 20000, 16660
$Au(N\text{-}MePzdtc)_3$	36360, 31250, 24390, 18180
$Au(N\text{-}MePzdtc)Cl_2$	35100, 29850, 22220, 17860
$Au(N\text{-}MePzdtc)Br_2$	35080, 30770, 22730, 17390
$Au(N\text{-}PhPzdtc)_3$	36800, 31150, 23810, 18200
$Au(N\text{-}PhPzdtc)_2Cl$	37170, 32150, 22220, 17820
$Au(N\text{-}PhPzdtc)Cl_2$	36750, 30670, 24090, 18350
$Au(N\text{-}PhPzdtc)_2Br$	36360, 32260, 22990, 17820
$Au(N\text{-}PhPzdtc)Br_2$	36200, 30670, 24950, 17700
$Au(Pipdtc)_3$	36360, 32150, 30770, 23530, 20000, 17090
$Au(Pipdtc)_2Cl$	36100, 32050, 24390, 20410, 16000
$Au(Pipdtc)Cl_2$	35710, 30770, 24100, 19230, 18000
$Au(Pipdtc)_2Br$	36350, 32150, 24390, 21730, 17400
$Au(Pipdtc)Br_2$	36230, 31050, 26660, 20000, 18000
$Au(4\text{-}PhPipdtc)_3$	36350, 33900, 21740, 20000, 17900
$Au(4\text{-}PhPipdtc)_2Cl$	35970, 32150, 22170, 18600
$Au(4\text{-}PhPipdtc)Cl_2$	35850, 30770, 24390, 17390
$Au(4\text{-}PhPipdtc)_2Br$	36360, 32000, 22220, 18180
$Au(4\text{-}PhPipdtc)Br_2$	36000, 31270, 24240, 18000
$Au(Morphdtc)_3$	37030, 30400, 23530, 17090
$Au(Morphdtc)_2Cl$	37730, 31350, 29410, 23530, 19050, 16950
$Au(Morphdtc)Cl_2$	36360, 34960, 29410, 24350, 18520
$Au(Morphdtc)_2Br$	37300, 30770, 24450, 19700, 17100
$Au(Morphdtc)Br_2$	37040, 31060, 24390, 19700, 16960
$Au(Timdtc)_3$	36760, 31350, 29850, 24450, 22220, 16660
$Au(Timdtc)_2Cl$	36900, 30770, 24400, 20000, 17390
$Au(Timdtc)Cl_2$	36490, 30300, 21500, 17390
$Au(Timdtc)_2Br$	36360, 30860, 23810, 19050, 16390
$Au(Timdtc)Br_2$	36350, 29850, 20400, 17240

vious work on gold derivatives.[13,14] It is noteworthy that ν(Au—S) increases in frequency as the oxidation number of the gold ion increases.

The bands present at 356–324 and at 249–218 cm^{-1} in the chloro- and bromo-bishalo-derivatives, respectively, are attributed to the ν(Au—Cl) and ν(Au—Br) stretching frequencies for terminal halides.[14,15] The above mentioned metal–halide modes have not been found in the spectra of the $Au(Rdtc)_2X$-type complexes, in agreement with the conductivity measurement results indicative of the 1 : 1 electrolyte character of these compounds.

Electronic spectra

The solid state electronic spectra of the complexes are reported in Table 4; these derivatives show absorptions in the 37730–26660 cm^{-1} range, which can be attributed to intramolecular charge-transfer due to the chromophore group NCS_2.[16] The band at higher energy is a $\pi^* \leftarrow \pi$ transition located mainly in the N···C···S group.[17,18] The position of this band is sensitive to the number of the dithiocarbamato groups linked to the central atom showing the sequence

$$Au(Rdtc)_3 > Au(Rdtc)_2X > Au(Rdtc)X_2.$$

The nature of the halogen has little influence on the position of this band and in general the sequence Cl > Br is observed. The second band at about 32000–29000 cm^{-1} is attributed to a second $\pi^* \leftarrow \pi$ transition of the S···C···S group.[19]

All the gold(III) complexes give a characteristic spectrum on the low energy side of the main charge-transfer edge. These transitions can be attributed to *d–d* bands, whose position is clearly indicative of a square-planar environment for the metal in these complexes. The most intense band between 24500–

22000 cm^{-1} can be assigned to the $^1A_{1g} \rightarrow {}^1E_g$ band corresponding to the $d_{xy} \rightarrow d_{xz},d_{yz}$ transition, while the second weaker band, accompanied in some cases by a shoulder at lower energy, can be attributed to the first spin-allowed transition $^1A_{1g} \rightarrow {}^1A_{2g}$.[20] All the complexes are diamagnetic according to the low-spin configuration of the metal ion.

Thermogravimetric studies

Thermal analyses, performed using TG and DTG techniques, indicate that all the complexes undergo decomposition, transforming the dithiocarbamates into polysulphides and giving metallic gold as the end-product. The data give metal analyses in accord with the formulae given in Table 1.

Reactivity

The gold(I) derivatives of the AuRdtc-type give, by reaction with the corresponding thiuramdisulphide, the gold(III) trisdithiocarbamates as final products; in this reaction Au(I) is oxidized to Au(III) according to the scheme:

$$AuRdtc + R_2tds \rightarrow Au(Rdtc)_3.$$

Analogous to the above reported reaction, the dihaloaurate(I) ion is oxidized with thiuramdisulphide to obtain the complex $Au(Rdtc)_2X$:

$$AuX_2^- + R_2tds \rightarrow Au(Rdtc)_2X.$$

The oxidative reaction of AuRdtc with halogens in methylene chloride produces the $Au(Rdtc)X_2$ complexes:

$$AuRdtc + X_2 \rightarrow Au(Rdtc)X_2.$$

The compounds of the $Au(Rdtc)_2X$-type react with $MAuX_4$ (M = Na, K) in methylene chloride to give ionic complexes $[AuX_4]^-[Au(Rdtc)_2]^+$ which easily rearrange, by boiling in methylene chloride, to the non-ionic isomers $Au(Rdtc)X_2$. These last compounds, by reaction in methylene chloride with the dithiocarbamate sodium salts produce complexes of the type $Au(Rdtc)_2X$:

$$Au(Rdtc)X_2 + RdtcNa \rightarrow Au(Rdtc)_2X + NaX.$$

EXPERIMENTAL

Preparation of the ligands

The sodium salts of the ligands were obtained by treating piperazine and 4-phenylpiperidine in dry diethylether and isopropyl alcohol; piperidine, morpholine, thiomorpholine, N-methylpiperazine and N-phenylpiperazine in dry diethylether with CS_2 and adding NaOH with vigorous stirring over 4 h using molar ratios of amine : CS_2 : NaOH = 1 : 1 : 1. The crude products were recrystallized from isopropyl alcohol.

The thiuramdisulphides have been prepared by treating an aqueous solution of the corresponding sodium dithiocarbamates with a slight excess of potassium esacyanoferrate(III), $K_3[Fe(CN)_6]$, at 0–5°C. The precipitates so formed were filtered, washed several times with cold water and dried over P_4O_{10}. The analytical data are summarized in Table 1.

Preparation of the complexes

Commercial $NaAuCl_4$ and $KAuBr_4$ of high purity grade were used. The preparation of the 1 : 3 gold derivatives was performed in water, starting with $NaAuCl_4$ having a metal to ligand stoichiometrical ratio of 1 : 3 or by the reaction of the gold(I) dithiocarbamates with the corresponding thiuramdisulphides in a 1 : 1 stoichiometrical ratio.

The gold(I) complexes were prepared by starting with $MAuX_4$ (X = Cl, Br) in aqueous solution cooled to 0°C, carefully reducing these with a water solution of Na_2SO_3 (0.1 M) until the solution became colourless and then treating with an aqueous solution of the ligands in a 1 : 1 molar ratio.

The gold(III) chloro- and bromo-derivatives were obtained by metathetical reactions starting with a water solution of $MAuX_4$ and the dithiocarbamate sodium salts in 1 : 1 or 1 : 2 metal to ligand molar ratios in the same solvent.

The $Au(Rdtc)_2X$-type complexes can be obtained by treating a gold(I) solution, prepared according to the method described above, with thiuramdisulphides dissolved in methanol, in a 1 : 1 molar ratio. A second way consists of reaction of the compounds $Au(Rdtc)X_2$ in methylene chloride with the dithiocarbamato sodium salts dissolved in methanol.

Compounds of the $Au(Rdtc)X_2$-type can be obtained starting with $Au(Rdtc)_2X$ and $MAuX_4$, (M = Na, K; X = Cl, Br) and refluxing in methylene chloride under stirring, or by oxidative reaction of the AuRdtc derivatives with halogens in methylene chloride at room temperature.

All the precipitates were filtered, washed with ethanol, diethylether and dried over P_4O_{10}.

Electronic spectra

The electronic spectra were recorded with a Shimadzu MPS-50L spectrophotometer in the solid state in the 5000–45000 cm^{-1} region. Samples were prepared by grinding the complexes on a filter paper as a support.

IR spectra

The IR spectra have been recorded in the 4000–50 cm^{-1} range with a Perkin–Elmer 180 spectrophotometer at the "Centro Interdipartimentale Grandi Strumenti" of Modena University. The spectra in the 4000–400 cm^{-1} range were measured for KBr discs or Nujol mulls. Far-IR spectra were measured on Nujol mulls suported between polyethylene sheets. Atmospheric water was removed from the spectrophotometer housing by flushing with dry nitrogen.

Magnetic susceptibility measurements

These measurements were carried out by Gouy's method at room temperature. The molecular susceptibilities were corrected for the diamagnetism of the component atoms by the use of Pascal's constants. All the complexes were diamagnetic.

Conductivity measurements

These measurements were carried out with a WTW LBR type conductivity bridge for freshly prepared 10^{-3} M solutions in DMF at 25 ± 0.1°C.

Thermal analyses

Thermogravimetric analyses (TG and DTG) were performed in air on a Mettler TG50 thermobalance equipped with a Mettler TC10TA processor. A scan rate of 10°C min^{-1} was used.

Analyses

Carbon, nitrogen, hydrogen and sulphur were determined with a Carlo Erba 1106 elemental analyser.

Acknowledgements—We thank Dr Celsino Govoni for his experimental work, Mr G. Goldoni for elemental analyses, the "Centro Interdipartimentale Grandi Strumenti" of Modena University for recording the IR spectra and the "Ministero della Pubblica Istruzione" (MPI) of Italy for the financial support.

REFERENCES

1. A. C. Fabretti, C. Preti, L. Tassi, G. Tosi and P. Zannini, *Aust. J. Chem.* 1986, **39**, 605 and refs therein.
2. H. O. Desseyn, A. C. Fabretti, F. Forghieri and C. Preti, *Spectrochim. Acta* 1985, **41A**, 1105.
3. A. Benedetti, C. Preti and G. Tosi, *J. Mol. Struct.* 1983, **98**, 155.
4. A. Benedetti, C. Preti, L. Tassi, G. Tosi and P. Zannini, *J. Mol. Struct.* 1985, **129**, 107.
5. C. Furlani, G. Polzonetti, C. Preti and G. Tosi, *Inorg. Chim. Acta* 1983, **73**, 105.
6. C. Furlani, G. Polzonetti, C. Preti and G. Tosi, *Gazz. Chim. Ital.* 1983, **113**, 609.
7. G. Polzonetti, C. Preti and G. Tosi, *Polyhedron* 1986, **5**, 1969.
8. W. J. Geary, *Coord. Chem. Rev.* 1971, **7**, 81.
9. F. Bonati and R. Ugo, *J. Organomet. Chem.* 1967, **10**, 257.
10. T. N. Srivastava and V. Kumar, *J. Organomet. Chem.* 1976, **107**, 55.
11. G. St. Nikolov, N. Jordanov and K. Daskalova, *Inorg. Nucl. Chem. Lett.* 1970, **6**, 723.
12. C. O'Connor, J. D. Gilbert and G. Wilkinson, *J. Chem. Soc. (A)* 1969, 84.
13. K. Nakamoto, J. Fujita, R. A. Condrate and Y. Morimoto, *J. Chem. Phys.* 1963, **39**, 423.
14. P. T. Beurskens, H. J. A. Blaauw, J. A. Cras and J. J. Steggerda, *Inorg. Chem.* 1968, **7**, 805.
15. J. R. Ferraro, *Low-frequency Vibrations of Inorganic and Coordination Compounds*. Plenum Press, New York (1971).
16. C. K. Jorgensen, *Inorganic Complexes*. Academic Press, London (1963).
17. C. K. Jorgensen, *J. Inorg. Nucl. Chem.* 1962, **24**, 1571.
18. F. Takami, S. Wakahara and T. Maeda, *Tetrahedron Lett.* 1971, **28**, 2645.
19. M. J. Janssen, *Rec. Trav. Chim. Pays-Bas* 1960, **79**, 1066.
20. A. B. P. Lever, *Inorganic Electronic Spectroscopy*. Elsevier, Amsterdam (1984).

Polyhedron Vol. 7, No. 14, pp. 1239–1242, 1988
Printed in Great Britain

0277–5387/88 $3.00+.00
© 1988 Pergamon Press plc

HYDROGENATION OF ALKENES BY DIRUTHENIUM(II) TETRAACETATE

ALAN J. LINDSAY, GREGORY McDERMOTT and GEOFFREY WILKINSON*

Chemistry Department, Imperial College of Science and Technology, London SWY 2AY, U.K.

(*Received* 22 *January* 1988; *accepted* 9 *February* 1988)

Abstract—The metal–metal bonded carboxylates, $Ru_2(\mu\text{-}O_2CR)_4$, R = CH_3 and CF_3 have been studied as catalysts for the homogeneous hydrogenation of alk-1-enes. Evidence for interaction of H_2 with $Ru_2(O_2CMe)_4$ and of complex formation between alk-1-enes and the carboxylates has been obtained.

Both the ruthenium acetate compounds $Ru_2(O_2CCH_3)_4Cl$ and $[Ru_3O(O_2CCH_3)_6(H_2O)_3](O_2CCH_3)$ have been used as catalysts for the homogeneous hydrogenation of alkenes.[1,2] The former and its triphenylphosphine reaction product,[1] exhibit catalytic activity in the presence of strong, non-complexing acids and excess triphenylphosphine; in these cases the active system appears to involve cationic alkene–bis(triphenylphosphine)-ruthenium(II) species,[3] $[Ru(PPh_3)_2(alkene)]^{2+}$. The oxo-triruthenium cluster acts as a hydrogenation catalyst at elevated temperatures (> 80°C) in dimethylformamide, and mechanistic studies indicate that only one ruthenium centre of the ion $[Ru_3O(O_2CCH_3)_4(DMF)]^+$ is active in coordinating both the hydrogen and alkene molecules and in mediating the subsequent hydride transfer to the alkene.[2] Other catalytically active ruthenium complexes have been prepared[3] from the oxo-centred species but none retain the triruthenium centre.

All these ruthenium systems catalyse the reduction of terminal alkenes but have varying selectivities for the reduction of internal and cyclic alkenes. For example, protonated $Ru_2(O_2CCH_3)_4Cl$ solutions will not reduce cyclooctene whereas the oxo-centred cluster readily reduced cyclohexene. The extent of substrate isomerization during these reductions is usually less than 5%, which is in marked contrast to that observed for the system using rhodium acetate $Rh_2(O_2CCH_3)_4$.[4]

We now report the use of $Ru_2(O_2CCH_3)_4$[5] as a catalyst precursor for the homogeneous hydrogenation of alkenes and alkynes to alkanes. The complex is effective in methanol under ambient conditions and the reduction proceeds with no isomerization of the unsaturated substrate. Unlike the ruthenium acetate system noted earlier, $Ru_2(O_2CCH_3)_4$ does not require elevated temperatures or additional acid or phosphine ligands to induce catalytic activity.

RESULTS AND DISCUSSION

Methanolic solutions of $Ru_2(O_2CCH_3)_4$ hydrogenate terminal and cyclic monoenes, and terminal alkynes homogeneously at room temperature under 1 atm of hydrogen. Comparative rates given in Table 1 indicate the reactivity order, cyclic alkene > terminal alkene > terminal alkyne: hydrogenation occurs at similar rates in ethanol and in dimethylformamide but is markedly slower in CH_3CN and CH_2Cl_2 and does not occur in THF and benzene. No hydrogenation of internal monoenes, dienes or of other compounds such as ketones and imines was observed.

In the absence of alkene, diruthenium(II) tetraacetate takes up one molecule of hydrogen per dimeric unit. In the absence of hydrogen, there is evidently the formation of an alkene adduct with $Ru_2(O_2CCH_3)_4$. Thus the initial electronic absorption spectrum of $Ru_2(O_2CCH_3)_4$ in methanol (λ 445 nm, $\varepsilon = 880$ dm^3 mol^{-1} cm^{-1}) changes upon the addition of hydrogen or alkene to the solution as shown in Figs 1 and 2, respectively. NMR spectra of the reacting solutions of $Ru_2(O_2CCH_3)_4$ showed considerable line broadening indicating that the paramagnetism of the catalyst species was retained throughout. Upon completion of a hydrogenation

* Author to whom correspondence should be addressed.

Table 1. Representative hydrogenations using $[Ru_2(O_2CCH_3)_4]$[a]

Substrate	Time (min)[b]
Hex-1-ene	70
Oct-1-ene	85 (96)[c]
Cyclohexene	63
Cyclooctene	79 (300)[c]
Styrene	125
Hex-1-yne	570
Oct-1-ene	94[d]
Oct-1-ene	90[e]
Oct-1-ene	340[f]

[a] Reaction conditions: 50 cm^3 of 2 mM methanolic solution of complex, 25°C, 1 atm H_2, catalyst : substrate 1 : 15.

[b] Time for complete hydrogenation.

[c] Time for "complete" hydrogenation using $[Rh_2(O_2CCH_3)_4]$ under identical conditions.

[d,e,f] Solvent = ethanol, DMF, acetonitrile, respectively.

reaction the $Ru_2(O_2CCH_3)_4$ was easily recovered and could be reused without appreciable loss of activity.

No detailed mechanistic studies have been undertaken but the kinetics for the hydrogenation appear to be first-order in alkene at low alkene concentration for the solvents and substrates used; in all cases hydrogen consumption levelled off at an amount close to that required for complete hydrogenation of the unsaturated substrate. Analysis of the final solution by gas–liquid chromatography confirmed the complete conversion of the alkene or alkyne to alkane and the absence of any isomerization products. The absence of isomerization suggests that $Ru_2(O_2CCH_3)_4$ may be of more practical use than the rhodium analogue $Rh_2(O_2CCH_3)_4$, which leads to isomerization of

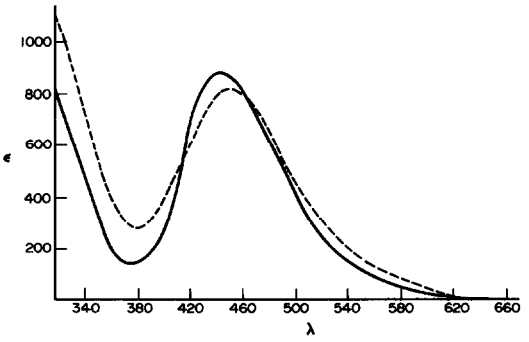

Fig. 1. Change in the electronic spectrum of $Ru_2(O_2CCH_3)_4$ in CH_3OH after stirring under hydrogen (1 h). Initial spectrum ——, hydrogenated spectrum – – –.

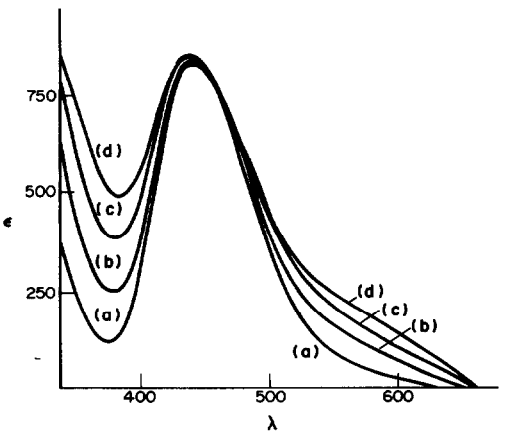

Fig. 2. Changes in the electronic spectrum on sequential addition of octene to $Ru_2(O_2CCH_3)_4$, 3 cm^3, 0.9 mM methanol solution at 25°C; (a) no octene; (b) 1.14 mM; (c) 2.4 mM; (d) 3.7 mM.

alk-1-enes.[4] The absorption of dihydrogen noted above suggests the formation of a hydride complex but the paramagnetism of the solutions and low solubilities prevented any characterization by IR and NMR spectra. Concentration of the hydride-containing solution under hydrogen results only in precipitation of the $Ru_2(O_2CCH_3)_4$. For the trioxoruthenium cluster[2] and rhodium(II) acetate[4] systems the initial activation step has been proposed to occur by hydrogenolysis for example:

$$Rh_2(O_2CCH_3)_4 + H_2 \rightleftharpoons HRh_2(O_2CCH_3)_3 + H^+ + {}^-O_2CCH_3. \quad (1)$$

Hydrogen uptake has also been observed for the oxo-centred triruthenium species and an inverse dependence of hydrogen uptake rate on free acetate concentration is observed;[2] a similar dependence has been observed for $Ru_2(O_2CCH_3)_4$ and the reaction with hydrogen is doubtless as in eq. (1). The requirement of a polar solvent (MeOH, DMF) for hydride formation suggests that solvation of the proton is necessary in addition to solvating the complex. In the hydrogenation cycle, we hence have the reactions (solvated methanol omitted):

$$Ru_2(O_2CMe)_4 + H_2 \rightleftharpoons HRu_2(O_2CMe)_3 + H^+ + MeCO_2^-$$

$$Ru_2(O_2CMe)_4 + \text{alkene} \rightleftharpoons Ru_2(O_2CMe)_4(\text{alkene})$$

$$HRu_2(O_2CMe)_3 + \text{alkene} \rightleftharpoons Ru_2(O_2CMe)_3(\text{alkyl})$$

$$Ru_2(O_2CMe)_3(\text{alkyl}) + H^+ + MeCO_2^- \rightarrow Ru_2(O_2CMe)_4 + \text{alkane}.$$

There is no change in oxidation state of the ruthenium in any reaction and H-transfer to coor-

dinated alkene doubtless occurs at the same ruthenium atom.

In the second step it is assumed as usual that π-complex formation occurs between the alkene and the hydride species followed by an insertion of the coordinated alkene into the ruthenium–hydride bond to form an alkyl complex.[6] The most facile route for hydrogen transfer would be obtained when the alkene is π-bonded to the ruthenium–hydride centre as shown in **1**.

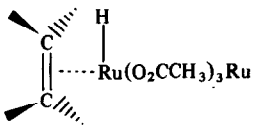

(1)

The absence of alk-1-ene isomerization indicates that the alkyl formation is irreversible unlike the analogous dirhodium(II) system where reversible alkyl formation results in significant isomerization.[4]

Although it might be expected on the basis of the above mechanism that the addition of a strong base, such as triethylamine, would favour hydrogenolysis and metal–hydride formation, the rate of hydrogenation is strongly inhibited by addition of triethylamine. Electronic spectra suggest that this results from the blocking of sites by axial coordination of the amine (L) through formation of an adduct of type $LRu_2(O_2CCH_3)_4L$, examples of which have been reported.[7]

Acidification of a methanolic solution of $Ru_2(O_2CCH_3)_4$ with an excess of a strong non-complexing acid such as HBF_4 produces a red colouration. The low catalytic activity of this red solution is however enhanced by the addition of triphenylphosphine and the yellow–brown solution so formed readily catalyses the hydrogenation of terminal and cyclic monoenes under hydrogen (cf. ref. 3); however, on standing, yellow $Ru(O_2CCH_3)_2(PPh_3)_2$ is deposited.

The complexing of the alkene noted above is not observed with $Rh_2(O_2CCH_3)_4$, but alkene complexing has been reported for the trifluoroacetate, $Rh_2(O_2CCF_3)_4$.[8] This adduct formation may be attributed to the electron deficient nature of the rhodium atoms in the trifluoroacetate complex compared to the acetate species. It is reasonable to assume that similar 1 : 1 adduct formation occurs in the ruthenium(II) system given the similarity in spectral shifts and the relatively electron deficient ruthenium centres in the tetraacetate. The absence of 2 : 1 complexes is probably due to the decreased acceptor capabilities of the 1 : 1 ruthenium adducts as observed for the rhodium(II) species.[9]

$Rh_2(O_2CCH_3)_4$ has been used as a catalyst for a variety of organic transformations including the autooxidation of alkenes[10] and the dehydrogenation of alcohols.[11] However, the air-sensitive nature of $Ru_2(O_2CCH_3)_4$ prevents its use as an autooxidation catalyst because of decomposition, while cleavage of the dimeric unit occurs with CO[7] thus preventing its use as a hydroformylation catalyst.

Hydrogenations using $Ru_2(O_2CCF_3)_4$

Qualitatively, we observe that the complex $Ru_2(O_2CCF_3)_4$ takes up hydrogen in the presence of terminal and cyclic monoenes on a significantly slower timescale than $Ru_2(O_2CCH_3)_4$. The times required for hydrogenation of alkenes, using the same conditions as for the $Ru_2(O_2CCH_3)_4$ experiments were about 18–24 h, regardless of whether a terminal or cyclic monoene was the substrate. The slowness of hydrogen uptake for the $Ru_2(O_2CCF_3)_4$ system is understandable in that the more electron-poor trifluoroacetato complex should be slower to add hydrogen than the corresponding acetato complex.

The electronic spectra of solutions following the addition of aliquots of alkene to a CH_2Cl_2 solution of $Ru_2(O_2CCF_3)_4$ show that the complex coordinates alkene, as judged by the change in the extinction coefficient (initially > 455 nm, ε 590 dm^3 mol^{-1} cm^{-1}) and slight shift in the λ_{max} for the absorption in the visible region similar to Fig. 2. A plot of $1/\Delta A$ vs 1/[alkene] provided evidence for a 1 : 2 complex between $Ru_2(O_2CCF_3)_4$ and alkene (L) presumably forming adducts of the type $LRu_2(O_2CCF_3)_4L$.

EXPERIMENTAL

Hydrated ruthenium "trichloride" was from Johnson Matthey plc. The carboxylates, $Ru_2(O_2CCH_3)_4$[5] and $Ru_2(O_2CCF_3)_4$[7] were prepared as before.[5] Solvents and substrates were rigorously purified and thoroughly degassed prior to use. Hydrogen was passed through an Englehard "Deoxo" catalyst before admission to the vacuum system.

Electronic spectra were recorded on a Perkin–Elmer 551 spectrophotometer. Successive injections of alkene into a 10^{-3} M solution of $Ru_2(O_2CCF_3)_4$ were made until the limiting λ_{max} of the complex could be determined. GLC analysis was carried out using a Perkin–Elmer Sigma 1B gas chromatographic system: for alkane and isomerized alkene detection a 4 m column of 15% Carbowax 20 M on Chromosorb (W.80–100 mesh) was used.

Hydrogen uptakes were measured using a mercury-filled gas burette and the thermostatted reaction flask was fitted with a Teflon stirrer rotating at the gas–liquid interface.

Acknowledgements—We thank Johnson Matthey plc for the loan of ruthenium and the SERC for support.

REFERENCES

1. P. Legzdins, R. W. Mitchell, G. L. Rempel, J. D. Ruddick and G. Wilkinson, *J. Chem. Soc.* (*A*) 1970, 3322.
2. S. A. Fouda and G. L. Rempel, *Inorg. Chem.* 1979, **18**, 1.
3. R. W. Mitchell, A. Spencer and G. Wilkinson, *J. Chem. Soc., Dalton Trans.* 1973, 846.
4. B. C. Y. Hui, W. K. Teo and G. L. Rempel, *Inorg. Chem.* 1973, **12**, 758.
5. A. J. Lindsay, G. Wilkinson, M. Motevalli and M. B. Hursthouse, *J. Chem. Soc., Dalton Trans.* 1985, 2321.
6. P. S. Hallman, B. R. McGarvey and G. Wilkinson, *J. Chem. Soc.* (*A*) 1968, 3143.
7. A. J. Lindsay, M. Motevalli, M. B. Hursthouse and G. Wilkinson, *J. Chem. Soc., Dalton Trans.* 1987, 2723.
8. M. P. Doyle, S. N. Mahapatro, A. C. Carghey, M. S. Chinn, M. R. Colsman, N. K. Harn and A. N. Redwine, *Inorg. Chem.* 1987, **26**, 3070.
9. R. S. Drago, J. R. Long and R. Cosmano, *Inorg. Chem.* 1982, **21**, 2196.
10. A. F. Noels, A. J. Hubert and P. Teyssie, *J. Organomet. Chem.* 1979, **166**, 79.
11. S. Shimoda, T. Kojima and Y. Saito, *J. Mol. Catal.* 1983, **18**, 99.

Polyhedron Vol. 7, No. 14, pp. 1243–1244, 1988
Printed in Great Britain

0277–5387/88 $3.00+.00
© 1988 Pergamon Press plc

OPTICALLY ACTIVE COORDINATION COMPOUNDS—XLVII.* ISOMERISM IN TRIS(S-CYSTEINATO)COBALT(III)

PETER S. CARTWRIGHT and R. D. GILLARD†

Department of Chemistry, University College, P.O. Box 78, Cardiff CF1 1XL, U.K.

(*Received* 2 *December* 1987; *accepted* 9 *February* 1988)

Abstract—The red O,S-bonded linkage isomer of tris(S-cysteinato)cobaltate(III) has the facial geometry and forms stereospecifically.

α-Amino-acids such as glutamic acid, histidine or cysteine with functional side-chains have three possible binding sites for metal ions. In the case of cysteine, shown as its di-anion, I, these are N, O

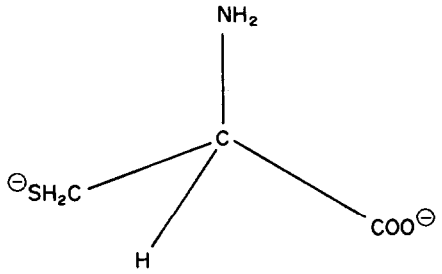

(I)

and S. When cysteine acts as a bidentate ligand in forming a chelate ring, three linkage isomers are possible: N,O; N,S and O,S.

Schubert[2] studied the reaction between cobalt (III) and L-cysteine in basic aqueous solution, and the oxidation of the resulting unstable green potassium tris(cysteinato)cobaltate(III) with hydrogen peroxide to give a yellow sulphinate. Neville[3] deduced that the green compound was the N,S-bonded linkage isomer by comparison of its electronic spectrum with that of tris(2-aminoethanethiolato)cobalt(III). He also prepared the red tris(cysteinato-O,S)cobaltate(III) isomer and proved the O,S mode of coordination by comparison with tris(N-formylcysteinato)cobaltate (III). Gorin[4] rectified some errors in his student's (Neville's) earlier paper, but confirmed the mode of coordination of both the red and green linkage isomers.

We report here the stereoselectivity of the formation of the *red* isomer, and some of its properties, to accompany our earlier work[1] on the green isomer and its derivatives.

EXPERIMENTAL

tris(L-*cysteinato*-O,S)*cobalt*(III) *tetrahydrate*

The method of preparation is essentially that used by Gorin.[4] 3.15 g (0.002 mole) of L-cysteine hydrochloride was dissolved in 6.0 cm^3 of 1.0 M $Co(NO_3)_2 \cdot 6H_2O$ and 8.203 g (0.10 mole) of anhydrous sodium acetate was added (the resulting pH was 5.1). The reaction flask under an inverted litre beaker, with a dish containing water to minimize evaporation, was stirred continuously for 16 h. The thick reddish-brown paste formed was treated with 20 cm^3 of 5.8 M HCl and the mixture was filtered: the filter-cake was washed with 25 cm^3 of water and dried at 100°C for 2.5 h. The crushed product was added to 500 cm^3 of 0.05 M KOH solution. After stirring for 1 h and filtering, the burgundy solution was acidified to pH 2 with concentrated HCl and the stringy, red precipitate allowed to stand for 10 min. Most of the clear solution was decanted before filtration, which is slow. To facilitate subsequent drying, the red product was pressed gently while washing away the brown bis-cysteinato complex with 100 cm^3 of H_2O. Preparations which are not thoroughly washed give analyses low in C and N. The tris(L-cysteinato-O,S)cobalt(III) tetrahydrate was dried for 48 h over conc. H_2CO_4 *in vacuo*. (wt = 1.65 g, 61% yield). Found: C 21.9; H 3.9; N 8.3, H_2O (by TGA), 15.0. Calc. for "H_3[Co(L-cysteinato(2−)O,S)$_3$]$4H_2O$", $C_9H_{26}CoN_3O_{10}S_3$: C 22.0; H 5.3; N 8.6; H_2O 14.7%. The residue from TGA was a

*For Part XLVI, see ref. 1.

†Author to whom correspondence should be addressed.

grey ash. The low value for the hydrogen content in combustion analysis is a common experience for hydrated compounds.

The compound has a green metallic sheen when dry, forming cherry-red solutions in dilute base. In more concentrated base (> 1 M), decomposition occurs to give a brown–yellow solution, presumably containing a bis-cysteinato complex. The tris complex is insoluble in water, ethanol, dilute acids, THF, ether, acetone, benzene, DMF, DMSO or hexane. However, it dissolves in concentrated sulphuric acid to give a red solution and is reprecipitated on dilution (like the water-insoluble β-facial-isomer of [Co(L-ala-O)$_3$]).

RESULTS AND DISCUSSION

The proton magnetic resonance of the compound at 35°C in D_2O (NaOD) shows only three doublets of doublets, at 3.56 (assigned to the asymmetric carbon proton) and at 3.10 and 2.88, both assigned to methylene protons. This typical [ABX] splitting pattern is consistent with all three cysteinate ligands being equivalent, i.e. with the facial structure.

The circular dichroism and electronic spectra are shown in Table 1. The high extinction coefficient (*ca* 24,000) of the lowest energy transition at 508 nm confirms the presence of S^-—Co(III) bonds. The circular dichroism in this band is made up of two overlapping components of opposite sign, leading to rather small asymmetry factors. The circular dichroism reveals a clear transition at 327 nm ($\Delta\varepsilon = +4.6$) whereas the isotropic absorption spectrum shows only a shoulder in this region.

Attempts to modify crystal morphology were unsuccessful; a solution of the complex was made up in dilute base and (a) water was allowed to evaporate slowly or (b) ethanol was diffused slowly into solution or (c) hydrochloric acid was slowly added until the equivalence point. They all resulted in the same red gelatinous precipitate.

A solution of this red O,S-bonded linkage isomer gives no reaction with hydrogen peroxide, merely forming the voluminous red precipitate of the solid acid as the solution becomes acidic; oxidation of the thiolate group to the sulphinate of the well-known resolving agent [Co(L-cysu)$_3$]$^{3-}$ does of course occur,[1,5] when a basic solution of the *green* N,S-bonded isomer is treated with hydrogen peroxide, and is also observed[6] for other N,S-bonded cysteinates, such as [Co(en)$_2$(cys-O)]$^+$, where the sulphinate forms via the sulphenate.

Table 1. Electronic spectra of facial [Co(L-cysteinato (2-)O,S]$^{3-}$ in dilute base

Isotropic absorption		Circular dichroism		
λ	ε	λ	$\Delta\varepsilon$	Ref.
510	24,700	—	—	4
508	24,230	567	+12.7	[a]
		511	−17.3	[a]
417	8400	—	—	4
414	7680	420[b]	+5[b]	[a]
362[c]	3900[c]	373[c]	+1.3[c]	[a]
330[d]	5000[d]	327	+4.6	[a]
270	9800	—	—	4
273	7810	280	−6.0	[a]

[a] This work: these spectra are reproduced on p. 74 of the Ph.D. thesis of P.S.C., University of Wales (1987).
[b] A plateau, *ca* 450–410 nm.
[c] A local minimum.
[d] Shoulder.

Both the known isomers of [Co(S-cys-O)$_3$]$^{3-}$ form stereoselectively (in the sense of geometric, linkage and optical isomerism). The syntheses differ (green N,S-isomer with five-membered rings from [Co(NH$_3$)$_6$]Cl$_3$ in strongly basic solution; red O,S-isomer with six-membered rings from Co(II) and air oxidation) but in each case the less probable* facial isomer results.

Of the three possible homoleptic linkage isomers, the only one not yet made is the tris(N,O)-bonded structure, which is of course commonplace[7] among bidentate amino acidates like glycine and alanine.

* The probability of a bidentate chelating ligand forming, on an octahedral metal ion, the meridianal as against the facial isomer is 3:1. The statistical proportions for the case of meridianal (*cis–trans*, 1,2,4) as against facial (*cis–cis*, 1,2,3) among unidentate ligands differ from the chelated case.

REFERENCES

1. P. S. Cartwright, R. D. Gillard and E. R. J. Sillanpaa, *Polyhedron* 1987, **6**, 105.
2. M. P. Schubert, *J. Am. Chem. Soc.* 1933, **55**, 3336.
3. R. G. Neville and G. Gorin, *J. Am. Chem. Soc.* 1956, **78**, 4893.
4. G. Gorin, J. F. Spessard, G. A. Webber and J. P. Oliver, *J. Am. Chem. Soc.* 1959, **87**, 3191.
5. M. Kita, K. Yamanari and Y. Shimura, *Bull. Chem. Soc. Japan*, 1982, **55**, 2873.
6. C. P. Sloan and J. H. Kruger, *Inorg. Chem.* 1979, **14**, 1481.
7. R. D. Gillard, S. H. Laurie, D. C. Price, D. A. Phillips and C. F. Weick, *J. Chem. Soc., Dalton Trans.* 1974, 1385.

Polyhedron Vol. 7, No. 14, pp. 1245–1262, 1988
Printed in Great Britain

0277–5387/88 $3.00+.00
© 1988 Pergamon Press plc

OXOVANADIUM(IV) AND AMINO ACIDS—I. THE SYSTEM L-ALANINE+VO^{2+}; A POTENTIOMETRIC AND SPECTROSCOPIC STUDY

J. COSTA PESSOA and L. F. VILAS BOAS

Centro de Quimica Estrutural, Complexo Interdisciplinar, Instituto Superior Tecnico, 1096 Lisbon, Portugal

and

R. D. GILLARD* and R. J. LANCASHIRE†

Department of Chemistry, University College, P.O. Box 78, Cardiff CF1 1XL, Wales, U.K.

(*Received* 25 *January* 1988; *accepted* 9 *February* 1988)

Abstract—The equilibria in aqueous solution in the system L-alanine+VO^{2+} have been studied by a combination of pH-potentiometric and spectroscopic methods (EPR, visible absorption and circular dichroism) in the pH range 1.5–13. For pH > 4, high ligand to metal ratios were used. The results of the various methods are made self-consistent, then rationalized assuming an equilibrium model including the species MAH, MA, MAH_{-2}, MA_2H_2, MA_2H, MA_2, MA_2H_{-1}, $M_2A_2H_{-2}$, $M_2A_2H_{-3}$ (where HA denotes L-alanine) and several hydrolysis products; their formation constants and individual electronic spectra (isotropic and circular dichroism) are given. The isomerism arising from the combination of the lop-sided oxovanadium ion with the asymmetric carbon ligand is analysed.

The biochemistry of vanadium has attracted increasing interest,[1–6] particularly in studies related to its accumulation in certain tunicates[7–10] and in the mushroom *Amanita muscaria*.‡[10–17]

The VO^{2+} ion is a useful paramagnetic probe of protein structure; it would be useful to know the nature of its amino acid complexes in solution and the preference exhibited by VO^{2+} for various potential chelating combinations with those α-amino acids like serine having additional coordinating groups.

Although knowledge of such complex equilibria of VO^{2+} in the presence of amino acids is relevant in understanding its possible interaction with likely biological ligands, few reliable data exist. The equilibria in aqueous solutions containing VO^{2+} and amino acids have been reviewed recently.[18] Several experimental methods have been used and the isolation of solids has also been claimed.§[19]

This first part introduces our study and gives detailed results for L-alanine+VO^{2+} in the pH range 2–12. The development of the series will then be: (2) L-serine and L-threonine: (3) L-cysteine and D-penicillamine; (4) L-aspartic and L-glutamic acids. Some work has been presented in a preliminary form.[20–24]

In pH-potentiometric investigations of solutions containing VO^{2+} + N-donor ligands, relatively high

* Author to whom correspondence should be addressed.

† Now at University of the West Indies, Kingston 7, Jamaica.

‡ The occurrence of vanadium in mushrooms (50 species) was surveyed by H, Meisch, J. A. Schmitt and W. Rienle, *Z. Naturforsch.* 1978, **33c**, 1, who found background levels in all but *A. muscaria*. The hazardous nature of vanadium, chiefly vanadate, for marine life in general is also documented (see NERC report 1977/8, HMSO, London (1978).

§ When solids of known structure can be isolated from solutions at labile equilibrium between a metal ion and an optically active ligand, a comparison of their CD spectra (as discs or mulls) with those of their solutions can be informative, as found with vanadyl(+)tartrato species or with copper(II) amino acid complexes (R. D. Gillard and S. H. Laurie, *J. Chem. Soc., Chem. Commun.* 1969, 489; *J. Chem. Soc.* 1970, 59). We have not yet isolated pure crystalline compounds from any aqueous oxovanadium(IV)–amino acid system.

pH is necessary to achieve an appropriate free ligand concentration for complex formation. At pH > 4, however, hydrolysis of the VO^{2+} ion takes place and oxidation to V(V) may also be significant unless careful deoxygenation is carried out. Another difficulty is that the nature (and formation constants) of the hydrolysis products of VO^{2+} in the pH range 5–12 is not well understood.

Tomiyasu and Gordon[25] studied the system glycine + VO^{2+} in the pH range 2–7 mainly by spectrophotometric measurements. They used large ratios of glycine to VO^{2+} to suppress metal precipitation and explained their results assuming that the system is characterized by model I in Table 1. At pH $\gtrsim$ 7, Tomiyasu and Gordon[25] report that, even with a glycine : vanadium ratio of 100, the absorbance of the solution decreases and the system is markedly less stable with respect to hydrolysis.

Fábián and Nagypál[26] studied the same system using a very high excess of glycine and characterized it assuming model II in Table 1. This is certainly a better approximation to the "real" situation existing in VO^{2+} + glycine solutions than model I. However, in both cases, the only species included not containing coordinated glycine are VO^{2+}, $[VO(OH)]^+$ and $[(VO)_2(OH)_2]^{2+}$.

The hydrolysis of oxovanadium(IV) has recently been reviewed.[27] The nature of species present in neutral or basic solutions is still controversial but it is clear that for pH > 5 other hydrolysis products predominate which should be included in any equilibrium model, especially for systems like L-Ala + VO^{2+} where—even using high ligand-to-metal ratios—for pH > 7–8, solutions have a brown colour, in contrast to Ser, Thr, Cys or Asp + VO^{2+}.

Two OH^- : VO^{2+} stoichiometries seem reasonable in the pH range 5–11; (i) 5 : 2 (e.g. $[(VO)_2(OH)_5^-]_n$ and (ii) 6 : 2 (e.g. $[(VO)_2(OH)_6^{2-}]_n$). Probably a 5 : 2 stoichiometry predominates in this pH range,[27–29] although the value of n is not known (evidently it depends on the total vanadium concentration). Assuming that $[(VO)_2(OH)_5]^-$ predominates in the pH range 9–12, Komura *et al.* determined its formation constant* in 0.1 M $LiClO_4$ and $T = 25°C$, $\beta_{20-5} = 1.4 \times 10^{-22}$.

We have now studied solutions containing oxovanadium(IV) and amino acid by combining the results of potentiometric and spectroscopic techniques. Fábián and Nagypál[26,30] have discussed the possibility and accuracy of pH-metric equilibrium studies at high ligand-to-metal ratios; an important conclusion was that if complex formation takes place in a pH region where the protonation of the ligand has no significant buffer effect, the potentiometric method can be used.

To estimate formation constants, we developed programs to simulate titration curves as well as methods based on spectrophotometric results. The constants were subsequently refined using MINIQUAD[31,32] and SUPERQUAD;[33,34] the results obtained with these two programs were compared.

Visible isotropic spectra (VIS spectra), circular dichroism spectra (CD spectra) and EPR spectra were recorded within a wide range of amino acid and metal concentrations and amino acid : metal ratios. Spectrophotometric results are analysed by the SQUAD[35–37] program.

The formation constants calculated correspond to the general reaction:

$$xVO^{2+} + yAlaO^- + zH^+ \rightleftharpoons (VO)_x(AlaO)_y(H)_z. \quad (1)$$

In common with biochemical studies, we call the singly charged alaninate ion L-AlaÕ. We abbreviate L-alanine as HA and the alaninate ion is then A^-.

For the formulation $(VO)_x(AlaO)_y(H)_z$ we normally use the abbreviation $M_xA_yH_z$. For each species $M_xA_yH_z$ proposed in our final equilibrium model, possible structures are discussed.

MATERIALS AND METHODS

Reagents

All solutions were prepared in an inert atmosphere (high purity dinitrogen passed through soda-lime and glass wool). All measurements were performed at 25.0°C with solutions containing 2.25 M $NaNO_3$.

Stock solutions of the $VO(H_2O)_5^{2+}$ ion in perchlorate media were prepared by the stoichiometric addition of barium perchlorate to vanadyl sulphate (Merck) at 80°C. The solutions were kept acidic by the addition of small amounts of $HClO_4$; normally the final $HClO_4$ concentration was around 0.1 M, this was determined by Gran's procedure.[38] The oxovanadium(IV) stock solutions were analysed by titration with standard $KMnO_4$. Stock $NaNO_3$ solutions, prepared from anhydrous $NaNO_3$ (Merck pa) oven-dried at 110°C for 48 h, usually contain a small amount of base and this was taken into account; similar problems were reported by Johansen and Jøns[39] for KNO_3 (Merck pa).

L-Alanine (BDH) for stock solutions was dried for 5 days (in a desiccator with silica gel *in vacuo*). Their concentration was checked by titration with strong base. N,N-dimethyl-D-alanine (chromato-

* In the final calculation[29] of β_{20-5}, $K_w = 1.0 \times 10^{-14}$ replaced 1.66×10^{-14} used in the rest of that work. We recalculated β_{20-5} taking the latter value for K_w.

Table 1. Compositions and formation of the species in the L-Ala + VO^{2+} system, assuming various equilibrium models, with comparable data.[25,26] Values for $\log \beta_{xyz}$ of eq. (1) are given

Species	Gly + VO^{2+} [a] Model I[25]	Gly + VO^{2+} [a] Model II[26]	L-Ala + VO^{2+} [b] Model IX[c]	L-Ala + VO^{2+} [b] Final (High L/M)[d]
MLH	10.06(0.02)	10.81(0.02)	11.16(0.01)	11.16(0.01)
ML	6.23(0.05)[e]	6.51(0.03)	6.87(0.02)	6.87(0.02)
ML_2H_2	—	—	21.4(0.1)	21.4(0.2)
ML_2H	—	16.63(0.04)	17.6(0.1)	17.6(0.1)
ML_2	10.96(0.06)	11.82(0.05)	12.4(0.1)	12.4(0.1)
$M_2L_2H_{-2}$	—	5.1(0.4)	5.8(0.2)	5.8(0.2)
ML_2H_{-1}	—	4.1(0.06)	4.4(0.2)	4.4(0.2)
$M_2L_2H_{-3}$	—	−1.7(?)[f]	−0.8(>)	−1.3(0.2)
MLH_{-1}	—	1.3(0.3)	—	—
MLH_{-2}	—	−6.3(0.3)	—	−6.7(0.2)
ML_3H_{-2}	—	8(?)[f]	—	—
M_2LH_{-2}	—	−0.7(?)[f]	—	—
H_2L	11.94	12.11	12.49	12.49
HL	9.60	9.64	9.96	9.96
MH_{-1}	−6.00	−6.07	−5.98	−5.98
M_2H_{-2}	−6.88	−6.59	−6.95	−6.95
M_2H_{-5}	—	—	−22.22[g]	−22.22
MH_{-3}	—	—	[h]	—

[a] 1 M $NaClO_4$; 25°C.

[b] 2.25 M $NaNO_3$; 25°C; $2 \lesssim pH \lesssim 8$.

[c] From the SUPERQUAD calculation (including standard deviations) on potentiometric titrations: $CHI^2 = 21.22$. c.f. $CHI^2 = 29.93$ for the model where MA_2H_2 is omitted, which gives values of 17.83, 12.41, 6.87, 4.77, −0.19, for the species ML_2H to $M_2L_2H_{-3}$ with remaining values (MLH, H_2L, MH_{-1}) unchanged, as explained in the text. Other models for explaining potentiometric results are analysed in the doctoral thesis of J. Costa Pessoa ("Estudos de Complexos de Oxovanadio(IV) com Alguns Aminoacidos", Instituto Superior Técnico, Lisbon, 1986): they all have in common the ligand species, the hydrolysed ions and the complex species MLH, ML, ML_2H_2, ML_2H, ML_2, $M_2L_2H_{-2}$ and vary only among minor species.

[d] These are our final values for the species formed in the systems with high L/M, self-consistent between potentiometry—model IX of this table, VIS—Table 3 and CD—Tables 3 and 4.

[e] Tomiyasu and Gordon[25] included the complex resulting from dissociation of H^+ from MGH (NH_2 uncoordinated).

[f] Fábián and Nagypál[26] included these species, of uncertain existence.

[g] Approximated from the value of β_{20-5} obtained[29] for a 0.1 M $LiClO_4$ medium, with correction for the ionic strength difference. When β_{20-5} is included in our potentiometric models as a constant to be refined, the final set of species is the same and the value refines to 10^{-23}–10^{-22} with low standard deviations.

[h] Not included in SUPERQUAD calculations: this species is certainly important for pH > 11: probably $10^{-18} > \beta_{10-3} > 10^{-19}$.

graphically pure, kindly supplied by Dr S. Weinstein, Weizmann Institute of Science, Israel) and L-alanine ethyl ester hydrochloride (Aldrich) were dried for 5 days (desiccator with silica gel) before preparing their stock solutions. The NaOH solutions were prepared from Titrisol® solutions and their concentration was determined by several titrations with standard HCl. The solutions were kept in an inert atmosphere in polyethylene bottles.

Instrumentation

For potentiometric titrations we used a special glass vessel with a double wall, with entries for the

glass electrode (Corning 003 11 101J), calomel reference electrode (Corning 476 109 00K), thermometer, nitrogen and base from the burette (Radiometer Autoburet ABU12). The emf measurements were made with a Corning EEL Digital 112-Research pH meter. Visible spectra were recorded with a Cary 17 spectrophotometer and circular dichroism spectra with a Roussel–Jouan Dicrographe MK III using anaerobic cells. Cell compartments were kept at 25.0°C with circulating water from a thermostatted bath. Unless otherwise stated, by VIS spectra we always mean a representation of ε_m values vs λ (ε_m = absorption/$b \times C_{VO}$; b = optical path) and by CD spectra a representation of $\Delta\varepsilon_m$ values vs λ ($\Delta\varepsilon_M$ = (differential absorption)/$b \times C_{VO}$)). The X-band EPR spectra were recorded at 77 K (on glasses made by freezing solutions in liquid N_2) mainly with a Bruker-ESR-ER 200tt connected to a Bruker-B-MN C5 EPR and to a Bruker EPR Data System (linked to a Nicolet 1180 computer). A few of the spectra were recorded on a Varian E109 spectrometer. MINIQUAD[31,32] and the program used to simulate EPR spectra[40] were run in an Eclipse S/140 data general computer (and a Calcomp 565 plotter); SQUAD[35–37] and SUPERQUAD[33,34] were run in a VAX 11/780 digital computer.

Calibration procedure

For calibration, we assumed that the measured potential depends on $[H^+]$ according to eq. (2).

The pH measuring system was calibrated by titrating dilute HCl (2–10 mmol l^{-1}) by standard NaOH (0.2 M), three or four times daily. For the acidic region of each titration, the Gran method was used to calculate V_e. Then we calculated

(i) the average $E_A^{0'}$ (and standard deviation) assuming a slope $S = 59.157$ mV;

(ii) the $E_A^{0'}$ and S values (and standard deviations) by a linear least squares method ($E_A^{0'} = E^{0'}$ for the acidic region).

The value of S obtained in (ii) was used to check whether the "measuring system" has a Nernstian slope. The MINIPOT program[41] was then used to refine a value of $E^{0'}$ for the acidic region (keeping $S = 59.157$); the value obtained was considered correct for $[H^+]$ calculations. Several tests were also made for the S, J_H and $E^{0'}$ values. In the calibration procedure used for the titration curves in the L-Ala+VO^{2+} system, the acid pH range was 2.3–3.3 (therefore $J_H = 0$). The calibration was considered satisfactory only if $J_H = 0$ and S and $E^{0'}$ approximately coincide with the initial values.

$$E = E^{0'} + S \times \log[H^+] + J_H[H^+] + J_{OH} \times [OH^-]. \quad (2)$$

For the basic region of each titration curve and using the value of $E^{0'}$ obtained in the acidic region ($E_A^{0'}$), the Gran method was used to calculate V_e and

(iii) K_w^* assuming $S = 59.157$;

(iv) K_w^* and S by a linear least-squares method.

The value of S obtained in (iv) was used to check that the "measuring system" has a Nernstian slope in the basic region. A constant value of $-\log K_w^* = 13.82 \pm 0.02$ was found; K_w^* is a conditional constant dependent on the apparatus and electrode used. It does not correspond exactly to the ionic product of water, K_w, for solutions containing 2.25 M $NaNO_3$. The MINIPOT program[41] was also used to refine values for $E^{0'}$, J_{OH}, S and/or $\log K_w^*$. The calibration was considered satisfactory only if $J_{OH} = 0$ and if S and K_w^* approximately coincided with the initial values. The value obtained for K_w^* was used in all protonation and formation constant calculations.

Calibrations from data at pH 2.3–3.3 and 10.5–11.0 may introduce errors into results collected outside these regions. However, the use of buffers would probably introduce greater errors (since the change in liquid-junction potential due to differences in composition between buffers and test solutions may amount to several millivolts[42]) and in practice, even greater errors are probably generated by the transfer of reference electrodes between solutions of different electrolytes.[43]

The acidity constants of L-Ala in 2.25 M $NaNO_3$ are such (pK_{a1} 2.5 and pK_{a2} 10) that the calibration used is adequate for their determination (especially for pK_{a1}). For the L-Ala+VO^{2+} system, with ligand to metal ratios 1–10, the calculations are based on pH values in the range 2.4–4.0 and the calibration is also adequate. However, for titration curves with high ligand-to-metal ratios (40–110) and other pH measurements in the range 3.5–9.5, our method of electrode calibration may introduce some errors. Similar approximated procedures are of course used in many other laboratories.

General experimental conditions

Five titration curves ($C_{Ala} = 3–8 \times 10^{-2}$ M) were obtained to determine the protonation constants of L-Ala in 2.25 M $NaNO_3$; NaOH (2 M) was used. For L-Ala+VO^{2+}, 14 titration curves were measured with initial oxovanadium(IV) concentrations in the range $1–20 \times 10^{-3}$ and L-Ala 5×10^{-4}–0.45 M. Titrations involving pH measurements in the

range 2–4 and 4.5–8 were performed using ligand-to-metal ratios of 0.5–12 and 48–108, respectively.

A total of 60 VIS spectra and 82 CD spectra (visible region) were used for the refinement of constants and calculation of spectra of individual species, with total oxovanadium(IV) and L-Ala concentrations in the range $2–40 \times 10^{-3}$ and $2–60 \times 10^{-2}$ M, respectively. Ligand-to-metal ratios were in the range 0.5–97.

RESULTS

EPR studies

The EPR spectra recorded with "solutions" containing VO^{2+} and L-Ala at 77 K are typical VO^{2+} axial spectra. The region that corresponds to $A_{\parallel}$ and $M_I = 5/2$ and 7/2 gives more information about the type and number of species present. In Fig. 1, we include the high-field region of the EPR spectra of "solutions" with metal-to-ligand ratios of 53.9 at several values of pH. Clearly, as the pH is increased, the peaks corresponding to $A_{\parallel}$ and $M_I = 5/2$ and 7/2 shift to lower field values (in an approximately continuous manner) until pH = 5.0. This means that in this pH range more than one species exists with rather similar $A_{\parallel}$ values (see Fig. 1).

Between pH 5.0 and 6.2, one can see two distinct peaks. As the pH is increased, their relative intensities invert and for pH > 6.2 only the peaks corresponding to the species with lower $A_{\parallel}$ are detected. The g and A ($\perp$ and $\parallel$) parameters obtained by simulation of the spectra at pH 6.2 are consistent with a formulation $VO(AlaO)_2$ with N_2O_2 coordination in the equatorial plane. This spectrum coincides with those of VO^{2+} + L-Ser (or L-Thr) solutions at pH 6.0 with comparable ligand-to-metal ratios.[20,21]

For pH > 6.2, the spectra apparently correspond to that of only one species and (except for intensity) are very similar (at least till pH 11.3) to the one recorded at pH 6.2, only a slight shift of the $M_I = 5/2$ and 7/2 peaks being detected. Several g and A ($\perp$ and $\parallel$) values calculated by spectra simulation[40] are included in Table 2.

Starting with VO^{2+} + L-Ala solutions at (a) pH 4.4 or (b) pH 4.8 with ligand-to-metal ratios of 97 and $C_{VO} = 2 \times 10^{-3}$ M, and progressively adding stock VO^{2+} solution, the position and relative intensities of the several peaks hardly change down to ligand-to-metal ratios of 9.4 ($C_{VO} - 1.4 \times 10^{-2}$ M) and 15.8 ($C_{VO} - 9.3 \times 10^{-3}$ M) for (a) and (b) respectively. Similar experiments at pH 5.9 and 9.2 started with VO^{2+} : L-Ala of 1 : 54, till respective ratios of 15 ($C_{VO} = 0.044$ M) and 11.4 ($C_{VO} = 0.05$ M) were reached. The several peaks are unchanged. Except at pH 9.2, further addition of VO^{2+} stock solution precipitated $VO(OH)_2$. No EPR signal was detected for any solution in the region corresponding to $g \simeq 4$.

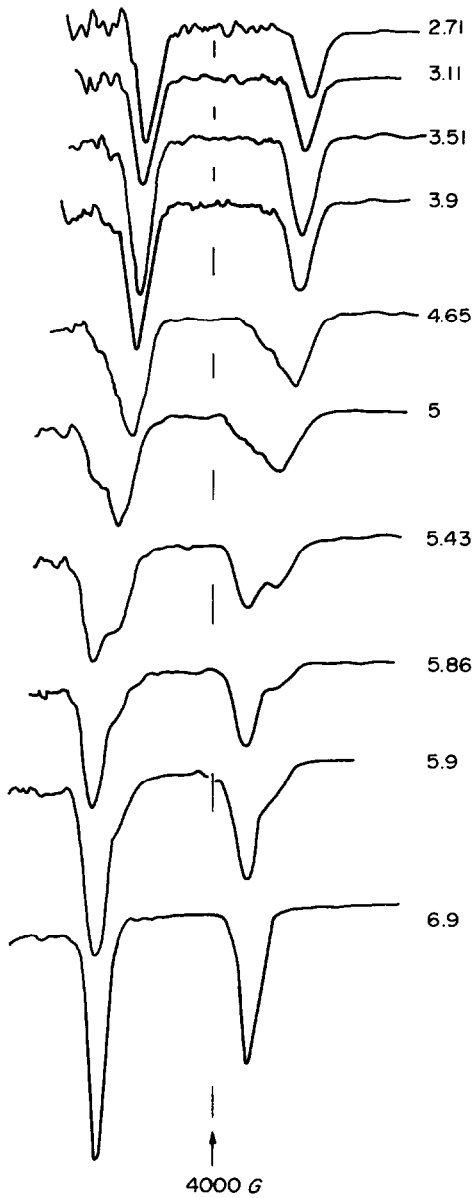

Fig. 1. High-field range of the first derivative EPR spectra at 77 K of frozen "solutions" containing L-Ala and VO^{2+} with a L/M ratio of 53.9. The total vanadium concentration is in the range $7.1–8.7 \times 10^{-3}$ M. Gain $= 2 \times 10^5$ and the modulation is in the range 1.6–2.5 depending on the spectra. pH values are indicated.

Circular dichroism and visible absorption spectra

Figure 2 includes visible spectra of solutions with a ligand-to-metal ratio of 53.9. For pH < 3, except

Table 2. Vanadium hyperfine coupling constants and g values calculated by simulation of EPR spectra recorded at 77 K[43] of "solutions" containing VO^{2+} + L-Ala with high ligand-to-metal ratios

L/M ratio	C_{VO} ($\times 10^3$)	pH	$g_\perp$	$g_\parallel$	$A_\perp$ ($cm^{-1} \times 10^4$)	$A_\parallel$
53.9	7.88	3.43	1.973	1.934	64	177
53.9	7.50	8.80	1.972	1.945	54	165
40.0	15	1.1	1.971	1.931	70	181
40.0	15	2.3	1.975	1.933	63	173
40.0	15	4.0	1.976	1.935	62	170
40.0	15	6.2	1.976	1.944	55	164
40.0	15	6.6	1.976	1.944	55	164
40.0	15	10.4	1.973	1.947	52	160
40.0	15	13.4	1.974	1.948	50	161
$VOSO_4$[a]		1.1	1.970	1.925	68	180
		13.4	1.974	1.948	50	162

[a] The solution contains glycerol, but no amino acid.

for the ε_m values, the spectra are similar to the spectra of aqueous oxovanadium(IV) solutions. For pH > 3, the spectra reveal an increase of the ligand field around VO^{2+}. For pH > 6, the general increase in ε_m (especially for $450 < \lambda < 600$ nm) suggests hydrolysis and/or oxidation of VO^{2+}.

The CD spectra of the same solutions show enormous modifications in the pH range 1.8–12 (Figs 3, 4 and 5). Up to pH 6, the $|\Delta\varepsilon_m|$ values gradually increase (Fig. 6) and the λ_{max} of band II shifts to longer wavelengths, consistent with increased complex formation and a change in the ligand from predominantly monodentate at pH < 2.5 to predominantly bidentate for pH > 3–4.

For pH > 6, the $|\Delta\varepsilon_m|$ values generally decrease except in the pH range 8–9.8 where different types of behaviour may be observed (Fig. 6). This is consistent with the gradual hydrolysis of the complexes that predominate at pH 6. For pH > 12.1, no CD spectrum is detected; this shows that no L-Ala is then coordinated to vanadium(IV).

If solutions with high alanine-to-metal ratios that have been kept at pH 9–10 are acidified, equilibration is fast and the CD spectra coincide with those of freshly prepared solutions with the same pH (if dilution is not extensive), so no extensive VO^{2+} oxidation or L-Ala racemization has occurred. However if solutions that have been kept at pH > 11–12 are acidified, depending on the final

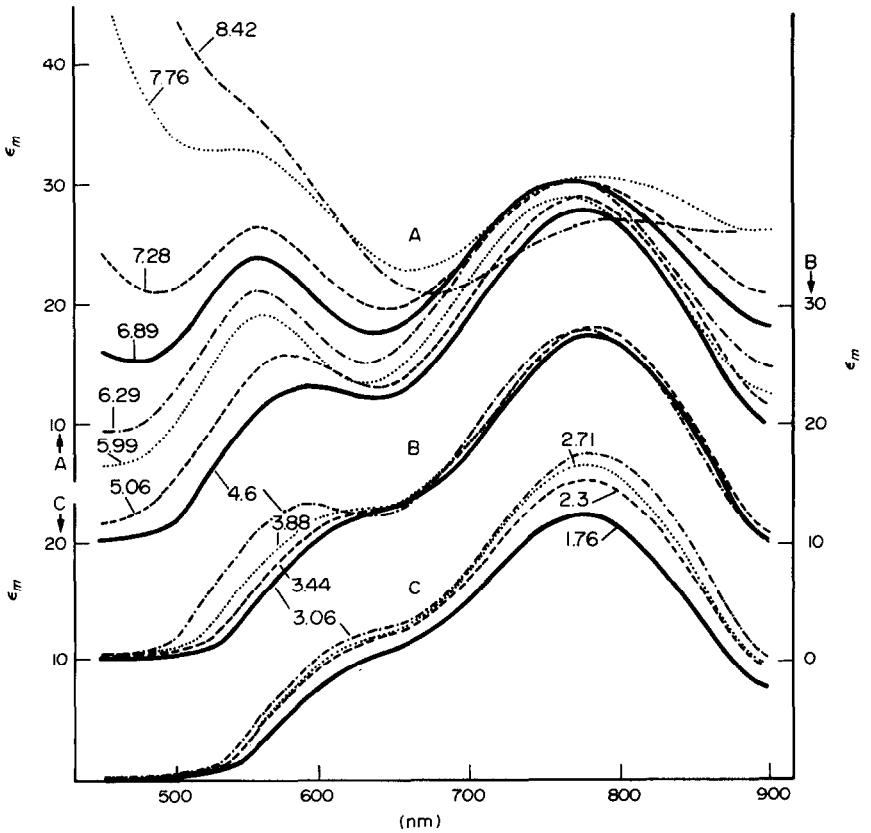

Fig. 2. Visible spectra of solutions containing L-Ala + VO^{2+} with ligand-to-metal ratios of 53.9 and $C_{VO} = 8–10 \times 10^{-3}$ M. The pH corresponding to each spectrum is indicated. Note the different scales on the ε_m axes for A, B and C. The CD spectra for the same solutions are in Figs 3 and 4.

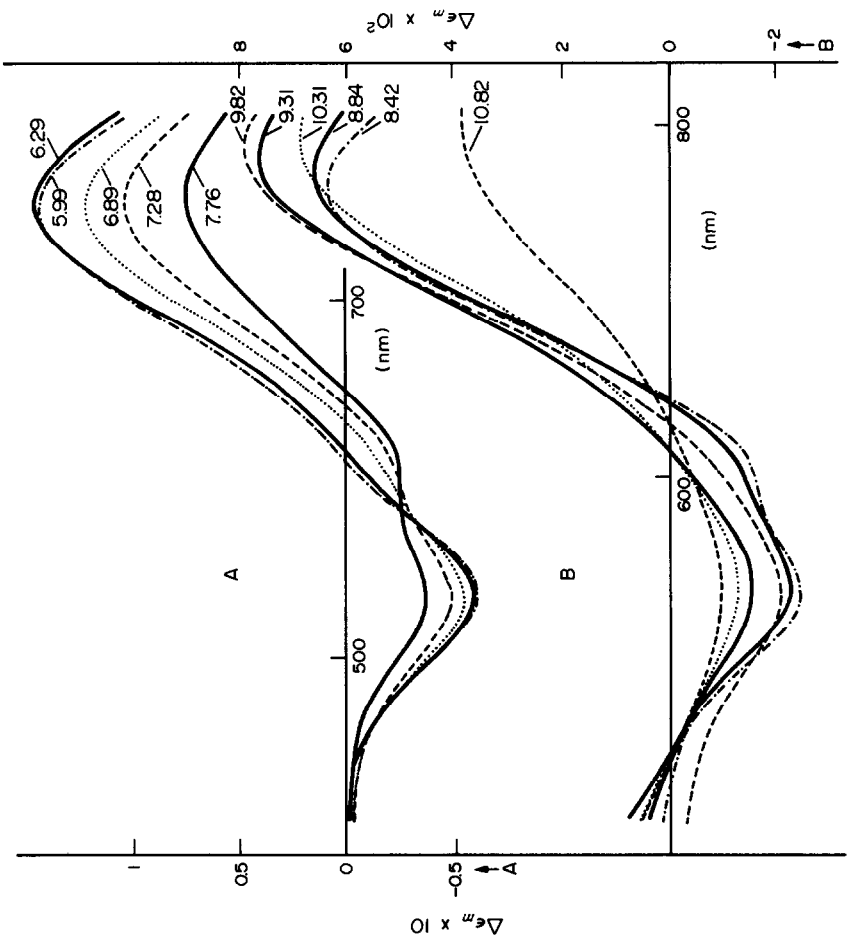

Fig. 4. CD spectra of solutions containing L-Ala + VO^{2+} with the ligand-to-metal ratio of 53.9 and $C_{VO} = 9 - 10 \times 10^{-3}$ M. The pH corresponding to each spectrum is indicated. Note the different scales for A (left) and B (right). The isotropic absorption spectra for these solutions are in Fig. 2.

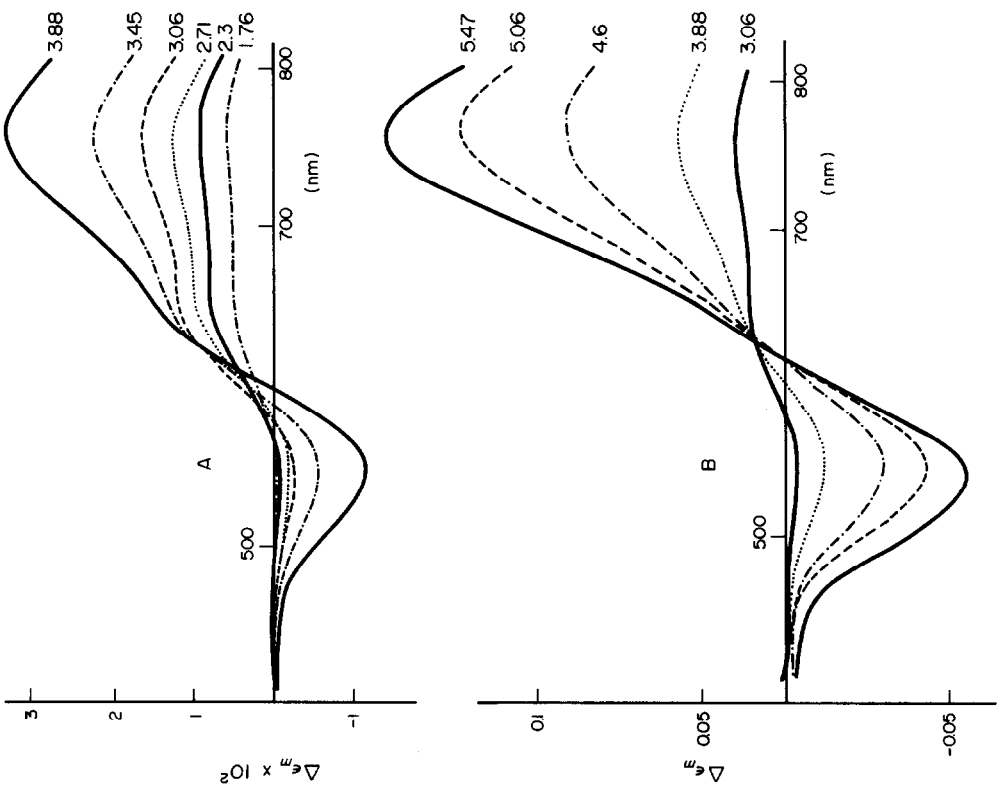

Fig. 3. CD spectra of solutions containing L-Ala + VO^{2+} with the ligand-to-metal ratio of 53.9 and $C_{VO} = 8 - 10 \times 10^{-3}$ M. The pH corresponding to each spectrum is indicated. Note the different scales for A and B. The isotropic absorption spectra for these solutions are in Fig. 2.

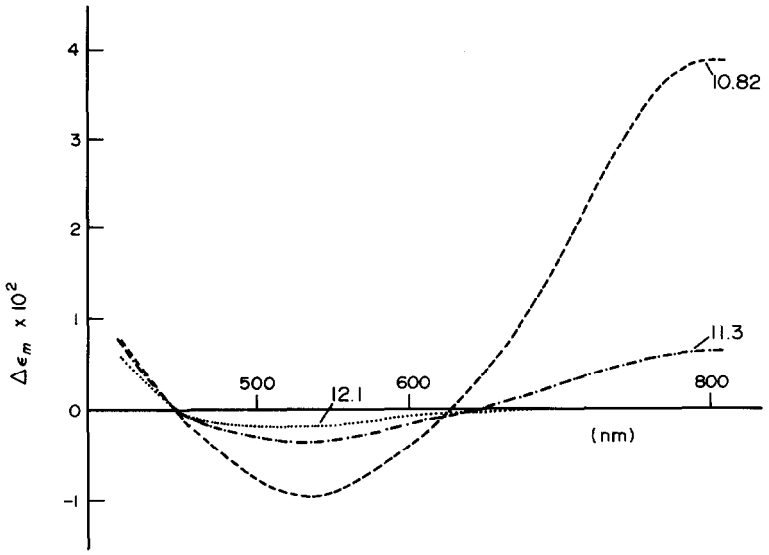

Fig. 5. CD spectra of solutions containing L-Ala + VO^{2+} with the ligand-to-metal ratio of 53.9 and $C_{VO} = 9\text{–}10 \times 10^{-3}$ M. The pH corresponding to each spectrum is indicated.

pH, the rate of equilibration varies, consistent with extensive polymerization of vanadium(IV) for pH > 12.[44] For low vanadium(IV) concentrations, $VO(OH)_3^-$ would predominate.[45]

Figure 7 gives several examples of spectra at fixed pH (= 2.26, 2.62, 3.50 and 4.00), varying the alanine-to-vanadium ratio (0.5 to 5.0). The CD spectra change quite drastically as the total alanine concentration is increased (for low alanine-to-vanadium ratios). The changes in the VIS spectra are much less pronounced.

Spectra have also been recorded at fixed pH (4.4, 4.8, 5.9 and 9.2) at varying but high alanine: vanadium. The total concentration of the L-Ala in solution is constant and the concentration of VO^{2+} is varied. At pH 4.4, the VIS and CD spectra show minor changes between alanine: vanadium ratios of 97 ($C_{VO} = 1.8 \times 10^{-3}$ M) and 12.1 ($C_{VO} = 1.4 \times 10^{-2}$ M). For lower L/M ratios, changes in CD spectra are rather pronounced, probably due to hydrolysis of the complexes. At pH 4.8, the VIS and CD spectra gradually change (the

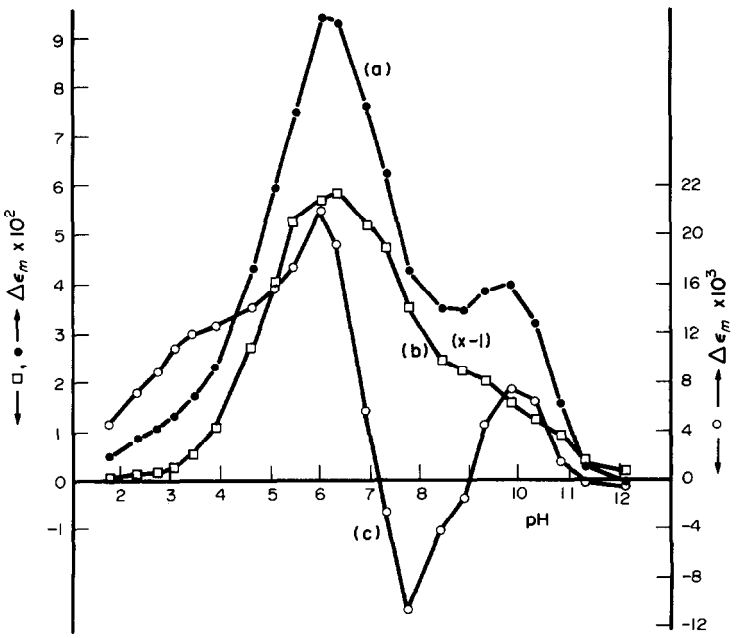

Fig. 6. Change with pH of the $\Delta\varepsilon_m$ values of L-Ala + VO^{2+} solutions with a ligand-to-metal ratio of 53.9 (Figs 3–5) at three different wavelengths. (a) 697, (b) 532 [$\Delta\varepsilon_m \times (-1)$] and (c) 637 nm.

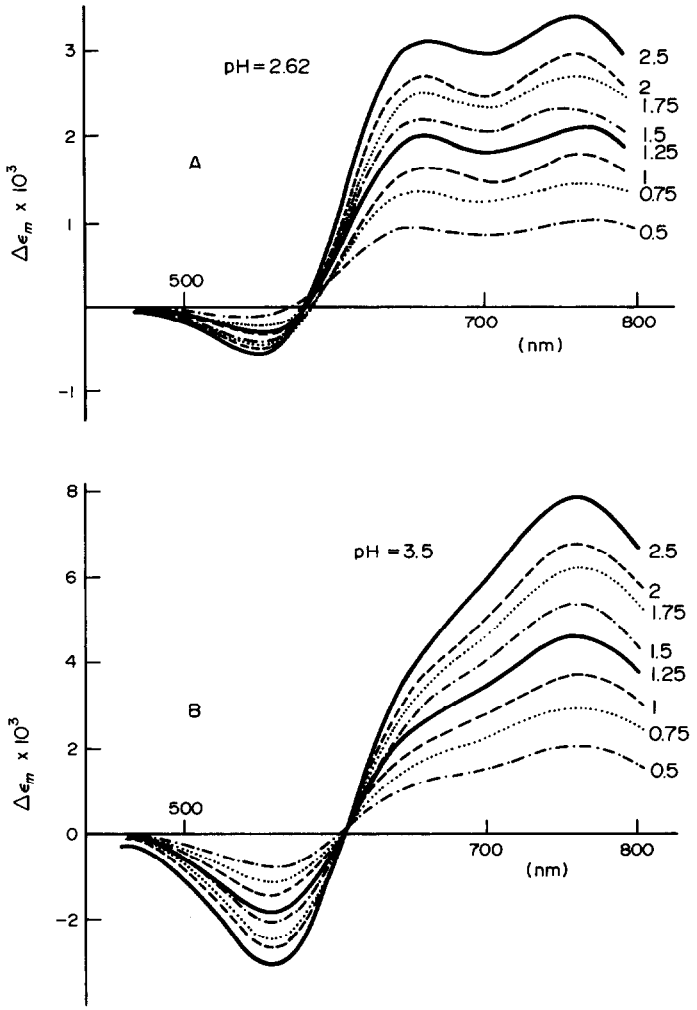

Fig. 7. CD spectra of solutions containing L-Ala and VO^{2+} with $C_{VO} = 3.3\text{–}4.0 \times 10^{-2}$ M. The solutions were prepared by adding the same volume of VO^{2+} stock solution, varying the volume of the L-Ala stock solution and adjusting the pH. The L/M ratios are indicated.

$|\Delta\varepsilon_m|$ values decrease and ε_m increase) between L/M = 97 and 21, but the changes are small. For L/M < 20, the ε_m values in the VIS spectra increase drastically; the $|\Delta\varepsilon_m|$ decrease significantly. At pH 5.9 and 9.2, the CD spectra change quite drastically as the L/M ratio varies between 55 and 20 (Fig. 8).

The results in Fig. 8 can be explained only by an equilibrium, at pH 5 and 9.2, between at least two vanadium-containing species with different degrees of polymerization.

Between pH 4 and 8, vanadium(IV) must be mainly coordinated to alanine, otherwise $VO(OH)_2$ would precipitate, but the importance of a soluble oxovanadium(IV) hydrolysis product may gradually increase. Thus species with different degrees of polymerization must involve complexes of VO^{2+} containing alanine (at, say, pH 6) but not necessarily at pH 9.2. Therefore the main features of the spectra of Fig. 8A could be explained assuming equilibria of the type:

$$VO(AlaO)_2 \text{ (and other monomeric complexes)} \underset{\text{L/M increasing}}{\overset{\text{L/M decreasing}}{\rightleftharpoons}} (VO)_2(AlaO)_2(OH)_2 \text{ (and other polymeric species).} \quad (3)$$

With L/M = 54 and $C_{VO} = 6\text{–}10 \times 10^{-3}$ M, while EPR spectra hardly vary in the pH range 6–11, the CD and VIS spectra change drastically (Figs 2–5). A possible hydrolysis product of $VO(AlaO)_2$, $VO(AlaO)_2(OH)^-$, (corresponding to $VO(GlyO)_2(OH)^-$ considered by Fábián and Nagypál[26] as a hydrolysis product in the range $6 \lesssim$ pH $\lesssim 8$) probably has an EPR spectrum similar to that of its parent $VO(AlaO)_2$. In fact, if the OH^- group is assumed to be equatorial, the values estimated for $g_\parallel$ and $A_\parallel$[46] are 1.950 and 164.2×10^{-4} cm^{-1} for $VO(AlaO)_2(OH)^-$, and 1.948 and 165.6×10^{-4} cm^{-1} for $VO(AlaO)_2$ (see below). In

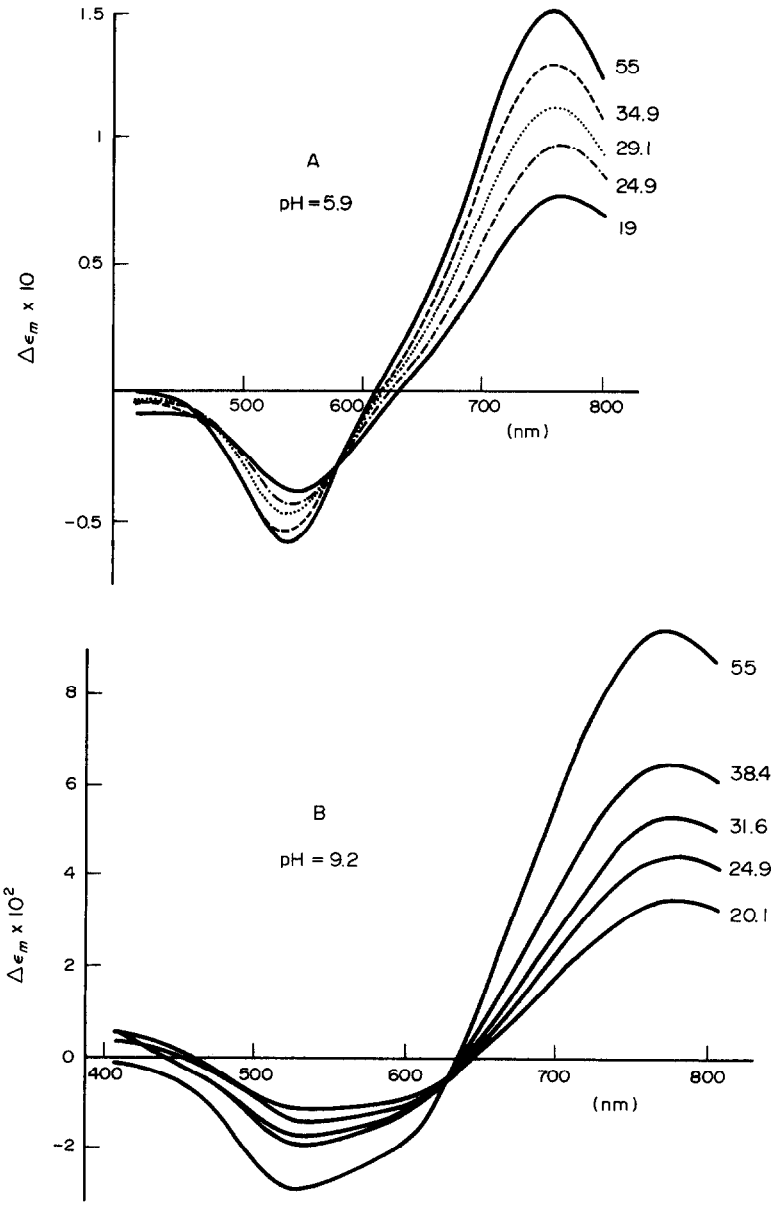

Fig. 8. CD spectra of solutions containing L-Ala and VO^{2+} with $C_{VO} = 1\text{–}2.7 \times 10^{-2}$ M (L/M ratios are indicated). The solutions were prepared by varying the volume of the VO^{2+} stock solution; the total alanine concentration is approximately the same in all cases.

contrast, one would expect very different contributions to the CD spectra from $VO(AlaO)_2$ and $VO(AlaO)_2(OH)^-$, especially if the OH^- is equatorial.

In solutions containing VO^{2+} and N,N-dimethyl-D-alanine with L/M = 1, as the pH is increased from 1.4 to 3.3, the $|\Delta\varepsilon_m|$ values gradually increase, as in similar L-Ala + VO^{2+} solutions. For pH > 3.0, the $|\Delta\varepsilon_m|$ values are substantially lower than for L-Ala + VO^{2+} solutions with the same pH, metal and ligand concentrations. With solutions containing VO^{2+} and L-alanine–ethyl–ester with L/M = 2, $\Delta\varepsilon_m \simeq 0$ in the range $400 < \lambda < 800$ nm between pH 1.7 and 2.3. For $2.3 \lesssim$ pH $\lesssim 4$ the $|\Delta\varepsilon_m|$ values are approximately ten times lower than with "similar" L-Ala + VO^{2+} solutions.

These experiments show that for low pH values ($\lesssim 2.5$) the NH_2 group is not coordinated to VO^{2+}.

Potentiometry

The protonation constants calculated by the MINIQUAD and SUPERQUAD programs prac-

tically coincide. From MINIQUAD, for L-alanine in solutions containing 2.25 M $NaNO_3$ (at 25°C): $pK_{a1} = 2.53$ and $pK_{a2} = 9.96$. These values will be used in all our calculations.

Formation curves calculated from our titration curves show the same trends as found by Fábián and Nagypál[26] for $Gly + VO^{2+}$, so we do not comment further.

The system is quite complicated. Calculations involving the refinement of β_{xyz} values of all possible species that may form (i.e. $M_xA_yH_z$ with x, y, and z quite general) always gave results with no physical meaning. We therefore chose the following strategy for the calculations.

(i) From curves of solutions with low L/M, "titration points" were selected to correspond to "solutions" where only MAH and MA (and VO^{2+}) co-exist (several iterations were needed to select these "titration points"). Taking only these "titration points", the MINIQUAD and SUPERQUAD programs were used to calculate the corresponding β_{111} and β_{110} values (the results practically coincide). These results satisfy the criteria proposed by Braibanti and colleagues.[47] They also agree with those we calculated from VIS and CD spectra of solutions with L/M ratios of 1–4 and $2 < pH < 3$ using the MINISPEF program[48] and other simple programs.[22] The β_{111} obtained correlates well with the formation constants obtained by others[49] for several monocarboxylates and for the corresponding complex with glycine.[26]

(ii) Taking β_{111} and β_{110} as known constants, the MINIQUAD and SUPERQUAD programs were used to calculate the β_{xyz} of other species now including the full set of the "complete" titration curves.

Our best model (model IX) obtained following this procedure is in Table 1.

Besides the usual criteria used to select equilibrium models of speciation using these sorts of programs (CHI^2 and R values, standard deviations etc.), we have used a comparison with the spectroscopic results. It is this self-consistency between thermodynamic and spectroscopic results which constitutes the novelty of our method of speciation. Several other models, differing from that in Table 1 in minor respects, were acceptable if the species MA_2H_2 is not included. However, by including MA_2H_2, almost all formation constants have lower CHI^2 and standard deviations. Moreover, calculations involving CD spectra in the pH range 2.6–3.5 also suggest that (besides MAH and MA), MA_2H_2 must be included to get satisfactory CD spectra for the individual species and to simulate the experimental spectra of the solutions.[22]

For each species in Table 1, the actual values obtained in the whole set of calculations performed with MINIQUAD and SUPERQUAD lie between the maximum and minimum values presented.

In model IX, we include a plausible range for each of the $\log \beta_{xyz}$ values, established by critical examination of all calculations performed with these programs. Species important for $pH > 6$ show a wider range of values probably due to the uncertainty in the value assumed for β_{20-5}. We emphasize that if β_{20-5} is included as a constant to be refined, a value of $\beta_{20-5} \gtrsim 6 \times 10^{-23}$ is always obtained with a low standard deviation.

The CHI^2 values corresponding to the models which contributed to Table 1 are relatively high (20–70). However, these values are reasonable because: the system is quite complicated; β_{20-5} is not accurately known; and many different titration curves (with two different NaOH concentrations, 0.2 and 2 M) in two different pH ranges are included (2.1–4.0 and 4.5–8.0).

Spectrometry

In solutions containing VO^{2+} and L-amino acids, in the visible spectra, only vanadium complexes contribute to the ε_m or $\Delta\varepsilon_m$ values observed. This fact removes the limitation of potentiometry to regions of pH where the ligand has no significant buffer effect. Therefore, when calculating formation constants based on CD or VIS spectra, one is in a more favourable situation for species that are important for $pH > 5$–6 because a wider range of L-Ala and VO^{2+} concentrations can be used as well as solutions with $pH > 8$.

Table 3 summarizes results with the program SQUAD for solutions in the pH range 1.8–6.2. In all cases, the ε (or $\Delta\varepsilon$) values for species MAH, MA, MA_2H_2, MA_2H and MA_2 are considered as parameters to be refined. Except for β_{120} in CDlO, the values obtained for the constants are within the range obtained in the calculations with MINIQUAD and SUPERQUAD. Therefore one may accept as correct the values for β_{122}, β_{121}, β_{120} and β_{22-2} in the last column of Table 1.

Taking β_{111}, β_{112}, β_{122}, β_{121}, β_{120} and β_{22-2} as known constants, the VIS and CD spectra of species MAH, MA, MA_2H_2, MA_2H and MA_2 were calculated using SQUAD[35–37] based on experimental spectra in the pH range 1.8–5.1. We used a step by step procedure, following the order: VIS spectra: (i) MAH and MA_2H_2, (ii) MA_2H, (iii) MA and (iv) MA_2. CD spectra: (i) MAH, (ii) MA_2H, (iii) MA, (iv) MA_2H_2 and (v) MA_2. For example, in the calculation of the CD spectra of MA [step (iii)], after having included the CD spectra of MAH and MA_2H in the input file [they were calculated in steps

Table 3. Calculations using the program SQUAD[35,37] based on experimental VIS and CD spectra in the pH range 1.8–6.2[a,b]

Calculation number	Number of iteration cycles	$\log\beta_{122}$ (SD)	$\log\beta_{121}$ (SD)	$\log\beta_{120}$ (SD)	pH range of experimental spectra used in the calculations (and number of spectra included)
VIS1	3	21.417 (0.084)	—	—	1.8–4.8 (23)
VIS2[c]	3	21.447 (0.080)	—	—	1.8–4.8 (23)
VIS3	4	21.303 (0.095)	—	—	1.8–5.1 (25)
VIS4	6	—	17.632 (0.074)	—	1.8–4.8 (23)
VIS5	5	21.459 (0.082)	17.649 (0.075)		1.8–5.1 (25)
CD1	3	21.284 (0.042)	—	—	1.8–5.1 (38)
CD2[c]	3	21.547 (0.038)	—	—	1.8–5.1 (38)
CD3[c]	4	21.331 (0.053)	—	—	1.8–4.8 (36)
CD4[d]	4	21.199 (0.066)	—	—	1.8–4.8 (36)
CD5	3	—	17.292 (0.034)	—	1.5–5.1 (38)
CD6	3	—	17.572 (0.018)	—	1.8–5.1 (38)
CD7[c]	4	21.261 (0.072)	17.593 (0.044)	—	1.8–4.6 (21)
CD8[c]	3	21.537 (0.039)	17.569 (0.019)	—	1.8–4.8 (36)
CD9	17	21.280 (0.063)	—	12.572 (0.021)	1.8–6.2 (43)
CD10	6		17.965 (0.014)[e]	12.966 (0.018)[e]	1.8–6.2 (43)

[a] Unless otherwise specified the values for the formation constants were: $\log\beta_{111} = 11.16$, $\log\beta_{122} = 21.39$, $\log\beta_{110} = 6.87$, $\log\beta_{121} = 17.52$, $\log\beta_{120} = 12.42$ and $\log\beta_{22-2} = 5.80$; the ε_{xyz} (VIS spectra) or $\Delta\varepsilon_{xyz}$ (CD spectra) values are calculated for the corresponding complex species.

[b] The spectral region covered is 480–820 nm for VIS spectra and 447–777 nm for CD spectra (at 5.0 nm intervals). All CD data used (Δabs. and Δε values) were multiplied by 10^4.

[c] $\Delta\varepsilon_{22-2}$ not refined in the calculation.

[d] Taking $\log\beta_{121} = 17.60$ as fixed constant.

[e] These β values are too high. Probably other species are important in the pH range 5.1–6.2 that have not been included, e.g. MA_2H_{-1} and $M_2A_2H_{-3}$.

(i) and (ii)], a set of experimental spectra was first chosen; then, the CD spectra of MA, MA_2H_2 and MA_2 were calculated using SQUAD. The values obtained for $\Delta\varepsilon_{110}$ were then included in the input file of SQUAD as known parameters. Step (iv) (calculation of the CD spectra of MA_2H_2) was then executed. The spectra so obtained were similar to those from a single calculation of all five spectra using the whole set of experimental results. The VIS spectra are in Fig. 9, the CD spectra in Fig. 10A.

For pH > 6, the VIS spectra reflect the increase in importance of the hydrolysis of VO^{2+}. For pH > 8, bands I and II cannot be located. Oxidation of a small fraction of the total V(IV) may also have a substantial effect on the spectra. We therefore made no calculations with SQUAD using VIS spectra of solutions with pH > 5.1.

Table 4 summarizes some results obtained with SQUAD for the CD spectra (high L/M ratios) in the "high" pH range. The CD spectra of $M_2A_2H_{-2}$, MA_2H_{-1}, $M_2A_2H_{-3}$ and MAH_{-2} obtained in calculation CD14 are in Fig. 10B.

DISCUSSION

The proposed equilibrium model—the set of species that should be included to explain all the experimental potentiometric and spectroscopic results (with plausible values for their formation constants)—is in Table 1. For low L/M ratios, MAH^{-1} [$\beta = 50$–$150(?)$] and other complex species might possibly be important.

For pH > 11, $VO(OH)_3^-$ [$\beta = 10^{-18}/10^{-19}(?)$, probably $\beta \sim 10^{-18}$] and oligomeric species may form. Johnson and Schlemper[44] identified a deep-brown species with the stoichiometry $V_{18}O_{42}^{12-}$, which may be prepared from concentrated $VOSO_4$ solutions at pH near 14, but remarked that it is not stable in dilute solutions. The equilibrium relationship between the monomer and oligomer is not known in detail. The formation of oligomeric species at high pH (> 11–12) may account for the slow re-establishment of the equilibrium that may be observed when acidifying these solutions.

The concentration distribution of the complexes

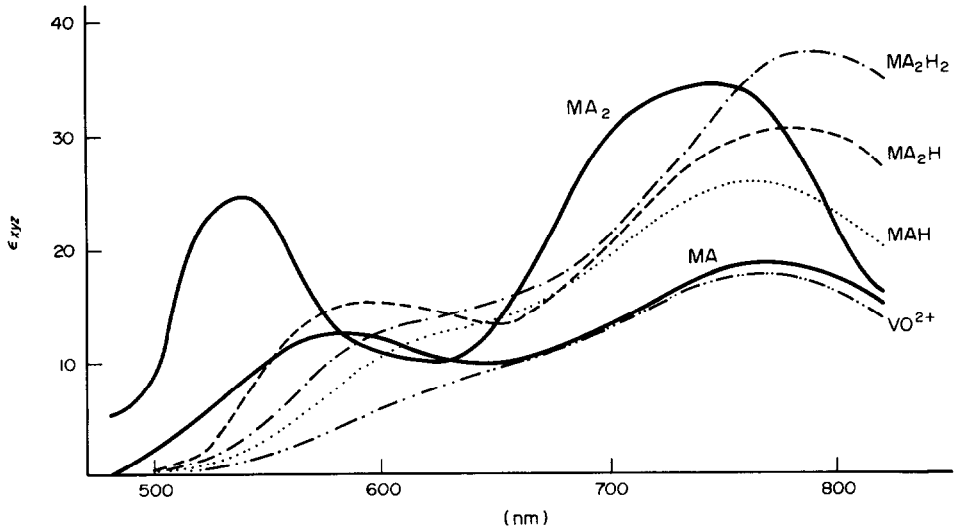

Fig. 9. Visible spectra (calculated using the SQUAD program) for complex species that may form in solutions containing L-Ala and VO^{2+} (high L/M ratios) in the range $1.6 \lesssim pH \lesssim 5.1$ ($\log \beta_{xyz}$ in Table 1).

formed in the L-Ala+VO^{2+} system calculated for L/M = 53.9 and a total vanadyl concentration close to those corresponding to the EPR, VIS and CD spectra of Figs 1–5, is represented in Fig. 11.

On a semi-quantitative basis, the concentration distribution shown explains the evolution of VIS and CD spectra of Figs 3–6, namely:

(i) maximum $|\Delta\varepsilon_m|$ values are obtained when MA_2 has a maximum concentration;

(ii) the odd behaviour of the CD spectra in the range $7.5 \lesssim pH \lesssim 9.5$ may be explained by the effect of MA_2 and $M_2A_2H_{-2}$ decreasing in concentration and M_2H_{-5} first increasing and then decreasing in concentration;

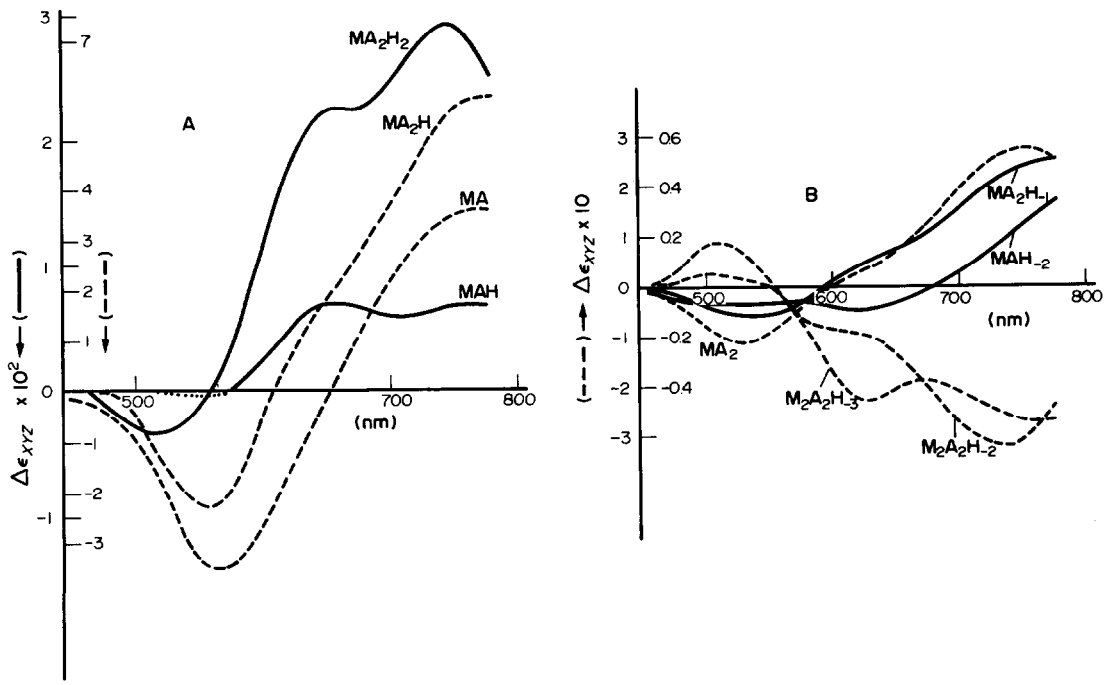

Fig. 10. CD spectra (calculated using the SQUAD program) for the species $M_xA_yH_z$ that may form in solutions containing L-Ala and VO^{2+} (high L/M ratios) in the pH range 1.6–12 ($\log \beta_{xyz}$ in Table 1). A Species that predominate at pH < 6, B Species that predominate at pH > 6. Note the different scales for A and B.

Table 4. Calculations of CD spectra and/or formation constants of species $M_2A_2H_{-2}$, MA_2H_{-1}, $M_2A_2H_{-3}$ and MAH_{-2} using SQUAD, based on experimental CD spectra of L-Ala+VO^{2+} solutions (high L/M ratios) in the pH range 4.4–10

Calculation number	CD11	CD12	CD13	CD14	CD15[a]
$\log\beta_{22-2}$	5.773	—	5.575	—	—
(SD)	(0.011)	Δε refined	(0.042)	Δε refined	Δε refined
$\log\beta_{12-1}$	—	—	—	4.503	5.409[b]
(SD)		Δε refined	Δε refined	(0.031)	(0.072)
$\log\beta_{22-3}$	—	−0.922[c]	—	−1.349[d]	—
(SD)		(0.019)		(0.054)	
$\log\beta_{11-2}$	—	—	−4.569[e]	−6.718[d]	—
(SD)			(0.020)	(0.144)	
Number of iteration cycles	3	4	7	6	5
pH range[f] (and number of experimental spectra included	4.4–6.2 (12)	4.6–10.8 (20)	4.6–10.8 (20)	4.6–10.8 (20)	4.6–10.8 (20)

[a] The fit of the calculated and experimental spectra is not good. This probably results from not having included other species important in this pH range.

[b] The value obtained is too high and the CD spectrum obtained for MA_2H_{-1} is not acceptable.

[c] The β_{22-3} obtained seems to be high and the calculated CD spectrum is not what one would expect from the observation of the experimental spectra.

[d] The values obtained may be considered reasonable taking into account the experimental CD spectra and the calculations with MINIQUAD and SUPERQUAD (MAH_{-2} is not an important species for pH < 8.0 and the β_{22-3} value is not well defined).

[e] The value obtained is too high. If correct one would refine satisfactory β_{11-2} values in the calculations with the MINIQUAD and SUPERQUAD. This probably results from not having included in the calculation other species important in this pH range.

[f] Although Δε values ($\neq 0$) are obtained in the range $10.8 \lesssim$ pH $\lesssim 12$, experimental CD spectra in this pH range were not included owing to (i) possible formation of other hydrolysis products of V(IV), (ii) higher risk of V(IV) oxidation, (iii) increasing inaccuracy in pH measurements and (iv) sluggish equilibria.

(iii) at extreme pH values, $\simeq 1.6$ and $\simeq 12$, the $\Delta\varepsilon_m$ values observed should be approximately proportional to $\Delta\varepsilon_{111}$ and $\Delta\varepsilon_{11-2}$, respectively.

On a quantitative basis, the VIS and CD spectra calculated using SQUAD, taking the formation constants of Table 1 and the VIS and CD spectra of Figs 9 and 10, almost coincide with the corresponding experimental spectra.

Estimation of formation constants in similar systems

Figure 12 shows a representation of the $\log\beta^A$ obtained in this work for the L-Ala+VO^{2+} system and the $\log\beta^G$ values obtained by Fábián and Nagypál[26] for the related system Gly+VO^{2+} at the same temperature but in a 1 M $NaClO_4$ medium. The linear plot can be used to estimate $\log\beta$ values for MAH_{-1} and MG_2H_2, assuming that the values for MGH_{-1} and MA_2H_2 are correct.

This type of plot (Fig. 12) can also be used to estimate formation constants of corresponding species, for example in VO^{2+} + L-leucine, L-valine, L-phenylalanine or L-methionine systems, if the corresponding pK_{a1} and pK_{a2} are known in the appropriate medium. For other amino acids (like L-serine) containing other groups that may coordinate to VO^{2+}, this type of plot may also be used for species with the same stoichiometry and type of coordination.[50]

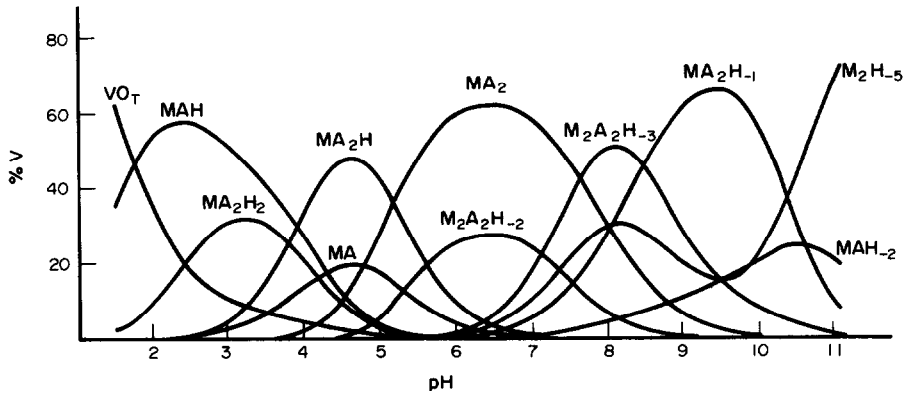

Fig. 11. Concentration distributions of the complexes formed in the VO^{2+} + L-Ala system in solutions with $C_{VO} = 8.0 \times 10^{-3}$ M and L/M = 53.9, calculated using the β_{xyz} values of Table 1.

Possible structure of the complexes

Because the vanadyl ion is lop-sided, chelates of oxovanadium(IV) may form more isomers than apparently analogous mono-atomic metal centres. For example, for 1 : 1 complexes of a N,O-coordinating chelate like glycine, two enantiomers (I) and (II) may form in equal concentrations:

In the case of L-Ala, similar 1 : 1 complexes (III) and (IV), respectively, are not enantiomers; in (III) [akin to (I)] the $-CH_3$ is "parallel" to the V=O group and in (IV) it will be "antiparallel". The equilibrium between (III) and (IV) is not pH dependent and unless one uses an experimental technique that does permit distinction between (III) and (IV), the determined formation constant β_{110} will correspond to the sum β_{110}(III) + β_{110}(IV).

For complexes of say L-alaninate with a MA_2 stoichiometry, three isomers (V), (VI) and (VII) may form in different concentrations, again, the formation constant β^A_{120} corresponds to the sum β^A_{120}(V) + β^A_{120}(VI) + β^A_{120}(VII).

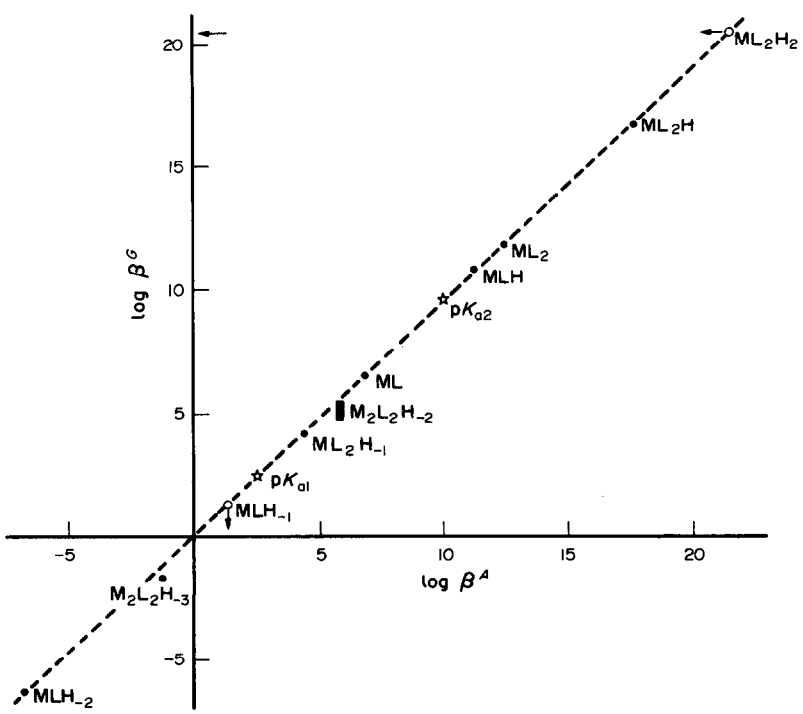

Fig. 12. Representation of $\log \beta^G_{xyz}$ obtained by Fábián and Nagypál[26] for the Gly + VO^{2+} system in 1 M $NaClO_4$ medium and $\log \beta^A_{xyz}$ obtained in this work for the L-Ala + VO^{2+} system. The pK_{a1} and pK_{a2} are also represented.

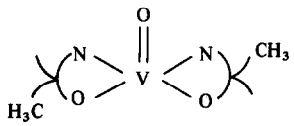

(V) *(cis)*

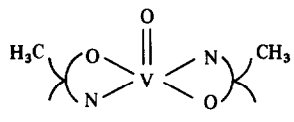

(VI) *(trans)*

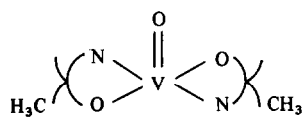

(VII) *(trans)*

EPR, VIS and CD spectra of the isomeric species (III) and (IV) or (V)–(VII) should differ. However, as the concentration ratios of (III)/(IV) and (V)/(VI)/(VII) are not dependent on pH, C_{Ala} or C_{VO}, at least in a first approximation, it was not possible to distinguish the several isomers corresponding to MA and MA_2 stoichiometries (nor, indeed, for other stoichiometries where different types of isomers may also be envisaged). Furthermore, in the pH range where MA_2 predominates, the EPR spectra seem to involve the contribution of one species only. This could be due either to the existence of only one isomer [for example (V)] or to isomers (V)–(VII) having very similar g and A parameters.

The MAH stoichiometry probably corresponds to a complex with the R—COO^- group coordinated in an equatorial position. For the MA_2H_2 stoichiometry, at least two isomers may be considered, as two carboxylate groups coordinated in equatorial positions may either be *cis* or *trans*.

The MA stoichiometry may correspond to structures (III) and (IV). For MA_2H, as the vanadyl ion is lop-sided, four structures may be envisaged considering one L-AlaO^- as bidentate and the other coordinated by the R—COO^- group (coordination involving the NH_2 group is not likely). For either MA or MA_2H stoichiometries, other structures may be envisaged if one considers the possibility of coordinating one of the R—COO^- groups in an axial position.

Using the R—COO^- and R—NH_2 contributions to $g_\parallel$ and $A_\parallel$ ($\times 10^{-4}$ cm^{-1}) proposed by Chasteen[46] for additivity calculations assuming equatorial coordination, leads to 1.935, 179.7 for MAH, 1.937, 176.8 for MA_2H_2, 1.940, 174.1 for MA and 1.942, 171.2 for MA_2H. Therefore, as MAH, MA_2H_2, MA, MA_2H (and VO^{2+}) gradually interconvert in the range $1.6 < pH < 4.0$, it is not surprising that the EPR spectra in this pH region show no clear contribution from the different species.

In the equilibrium model proposed, for $pH > 6.2$ the species that may be important are: MA_2, MA_2H_{-1}, $M_2H_2H_{-2}$, $M_2A_2H_{-3}$, MAH_{-2} and the hydrolysis products of VO^{2+} ($[(VO)_2(OH)_5^-]_n$, $VO(OH)_3^-$ and oligomeric species). However, as mentioned above, for $pH > 6.2$ the EPR spectra apparently correspond to the spectra of only one (or two) vanadyl complex moieties and they are all very similar to the one recorded at pH 6.2 (Fig. 1 and Table 2). We will now examine briefly how this might be explained.

For MA_2 stoichiometry, the most plausible structures are (V)–(VII). Using Chasteen's[46] parameters to predict $g_\parallel$ and $A_\parallel$ for these structures, gives $g_\parallel = 1.948$ and $A_\parallel = 165.6 \times 10^{-4}$ cm^{-1} (no correction exists differentiating *cis* and *trans* coordination). For the MA_2H_{-1} stoichiometry, if coordination involves two R—COO^- groups, one R—NH_2 and one OH^- coordinated in the equatorial plane and H_2O in the axial position, the prediction is similar: $g_\parallel = 1.950$ and $A_\parallel = 164.2 \times 10^{-4}$ cm^{-1} (if the axial position is not occupied by an H_2O molecule, estimates of $g_\parallel$ and $A_\parallel$ are no longer "safe").

Therefore for such structural types, the estimated parameters approximately coincide with $g_\parallel$ and $A_\parallel$ obtained by simulating the EPR spectra in the pH range 6.2–10 (Table 2).

In the case of the stoichiometries $M_2A_2H_{-2}$ and $M_2A_2H_{-3}$, where many different structures may be envisaged, there are two possible situations: (i) the actual structures are such that their EPR spectra are similar to those of MA_2 and MA_2H_{-1} and (ii) these species are EPR silent. Possibly the latter explanation is correct. In fact, $(VO)_2(OH)_2^{2+}$ and the soluble hydrolysis species (except VO$(OH)_3^-$) that may be important for $pH > 6$ are EPR silent; [45,51] it has also been suggested that $(Cu)_2(AlaO)_2(OH)_2$ is EPR silent.[52]

At pH 13.4, EPR spectra of VO^{2+} and L-Ala+VO^{2+} solutions with high L/M ratios practically coincide (Table 2) and no CD spectra are observed. Therefore, at this pH, L-AlaO^- is not coordinated to VO^{2+}.

In the range $10 < pH < 12$ the important stoichiometries are MA_2H_{-1}, MAH_{-2} and V(IV) hydrolysis products, and no important changes of the EPR spectra may apparently be predicted; in fact, assuming for MAH_{-2} that the equatorial positions are occupied by a bidentate L-AlaO^- ligand and two OH^-, the estimates are $g_\parallel = 1.955$ and $A_\parallel = 160.2 \times 10^{-4}$ cm^{-1}, values similar to those observed for $VO(OH)_3^-$.

As a final point, the values of molar circular dichroism for the visible transitions of the bis-

chelated $[VO(L\text{-}AlaO)_2]$ (MA_2) ($\Delta\varepsilon = +0.26$ for the red-near IR band and -0.11 for the yellow-green absorption) are considerably larger than for other species like $[VO(L\text{-}AlaO)]^+$ (MA) ($+0.035$ and -0.035) or "$VO(L\text{-}AlaO)_2H_2$" (MA_2H_2) ($+0.028$ and -0.068). The rough correspondence between the numbers of chelate rings and molar circular dichroism for d–d transitions in simple compounds of transition metal ions (originally noticed[53] by Mathieu) is again found.

Acknowledgements—J.C.P. and L.F.V.B. thank the Instituto Nacional de Investigação Cientifica e Tecnologica (INIC), Fundaçao Calouste Gulbenkian and the British Council for financial support.

REFERENCES

1. K. Schwarz and D. B. Milne, *Science* 1971, **174**, 426.
2. N. D. Chasteen, *Struct. Bonding* (*Berlin*) 1983, **53**, 105.
3. K. Kustin, G. C. McLeod, T. R. Gilbert and Le Baron R. Briggs, *Struct. Bonding* (*Berlin*) 1983, **53**, 139.
4. D. W. Boyd and K. Kustin, *Adv. Inorg. Biochem.* 1984, **6**, 311.
5. R. L. Robson, R. R. Eady, T. H. Richardson, R. W. Miller, M. Hawkins and J. R. Postgate, *Nature* 1986, **322**, 388; J. M. Arber, B. D. Dobson, R. R. Eady, P. Stevens, S. S. Hasnain, C. D. Garner and B. E. Smith, *Nature* 1987, **325**, 372.
6. E. de Boer, Y. V. Kooyk, M. G. M. Tromp, H. Plat and R. Wever, *Biochem. Biophys. Acta* 1986, **869**, 48; E. de Boer, M. G. M. Tromp, H. Plat, B. E. Krenn and R. Wever, *Biochem. Biophys. Acta* 1986, **872**, 104; H. Vilter and D. Rehder, *Inorg. Chim. Acta* 1987, **136**, L7.
7. R. C. Bruening, E. M. Oltz, J. Furukawa, K. Nakanishi and K. Kustin, *J. Am. Chem. Soc.* 1985, **107**, 5298.
8. R. J. Seltzer, *Chem. Engng News* 1985, **63**, 67.
9. P. Frank, R. M. K. Carlson and K. O. Hodgson, *Inorg. Chem.* 1986, **25**, 470.
10. S. G. Brand, C. J. Hawkins and D. L. Parry, *Inorg. Chem.* 1987, **26**, 627 and refs therein.
11. R. D. Gillard and R. J. Lancashire, *Phytochemistry* 1984, **23**, 179.
12. J. Felcman, M. C. T. A. Vaz and J. J. R. Fraústo da Silva, *Inorg. Chim. Acta* 1984, **93**, 101.
13. M. A. Nawi and T. L. Riechel, *Inorg. Chim. Acta* 1984, **93**, 131.
14. G. Bemski, J. Felcman, J. J. R. Fraústo da Silva, I. Moura, J. J. G. Moura, M. C. T. A. Vaz and L. F. Vilas-Boas, in *Frontiers in Bioinorganic Chemistry* (Edited by A. V. Xavier), p.97. VCH Verlagsgesellschaft, Weinheim (1986).
15. H. Kneifel and E. Bayer, *J. Am. Chem. Soc.* 1986, **108**, 3075.
16. G. Anderegg, E. Koch and E. Bayer, *Inorg. Chim. Acta* 1987, **127**, 183.
17. M. A. Nawi and T. L. Riechel, *Inorg. Chim. Acta* 1987, **136**, 33.
18. L. F. Vilas-Boas and J. Costa Pessoa, in *Comprehensive Coordination Chemistry* (Edited by G. Wilkinson, R. D. Gillard and J. A. McCleverty) Sect. 33.5.9.2. Pergamon Press, Oxford (1987).
19. W. U. Malik, R. B. Bemóri and V. Asnaf, *Ind. J. Chem.* 1976, **14A**, 542; Y. Xu, X. Li, L. Yu, C. Liu, J. Lu and W. C. Liu, *Jiegou Huaxue*, 1982, **1**, 55 (*Chem. Abs.* 1983, **98**, 136 555r); O. F. Khodzhaev, U. M. Shodiev, Z. M. Musaev, Ya. S. Usmankhodzhaeva and N. A. Parpiev, *Uzb. Khim. Zh.* 1984, 15, (*Chem. Abs.* 1984, **102**, 105 090g); U. M. Shodiev, O. F. Khodzhaev and N. A. Parpiev, *Dokl. Akad. Nauk USSR*, 1984, 35 (*Chem. Abs.* 1984, **103**, 47 216k); L. Xi and Y. Xu, *Kexue Tongbao* (Foreign Lang. Edn), 1985, **30**, 340; U. M. Shodiev, Z. M. Musaev, O. F. Kodzhaev, Ya. S. Usmankhodzhaeva and N. A. Parpiev, *Uzb. Khim. Zh.* 1985, 59, (*Chem. Abs.* 1985, **104**, 156 745a).
20. R. D. Gillard, R. J. Lancashire, J. Costa Pessoa and L. Vilar-Boas, *Comunicação 3A11, 2° Encontro Nacional de Quimiçã*, Porto (1979).
21. J. Costa Pessoa and L. Vilas-Boas, *1980 Autumn Meet. Chem. Soc.* University College, Cardiff (1980).
22. R. D. Gillard, J. Costa Pessoa and L. Vilas-Boas, *Comunicação C31.9, 5° Encontro Nacional de Química*, Porto (1982).
23. R. D. Gillard, R. J. Lancashire, J. Costa Pessoa and L. Vilas-Boas, *Comunicação PA54, 6° Encontro Nacional de Química*, Aveiro (1983).
24. R. D. Gillard, R. Marques, J. Costa Pessoa and L. Vilas-Boas, *Comunicação 5CP12, 9° Encontro Nacional de Química*, Coimbra (1986).
25. H. Tomiyasu and G. Gordon, *J. Coord. Chem.* 1973, **3**, 47.
26. I. Fábián and I. Nagypál, *Inorg. Chim. Acta* 1982, **62**, 193.
27. Ref. 18, section 33.5.5.1.2.
28. L. P. Ducret, *Ann. Chim.* (*Paris*) 1951, **S12**, **V6**, 705.
29. A. Komura, M. Hayashi and H. Imanaga, *Bull. Chem. Soc. Japan* 1977, **50**, 2927.
30. I. Fábián and I. Nagypál, *Talanta* 1982, **29**, 71.
31. A. Sabatini, A. Vacca and P. Gans, *Talanta* 1974, **21**, 53.
32. P. Gans, A. Sabatini and A. Vacca, *Inorg. Chim. Acta* 1976, **18**, 237.
33. P. Gans, A. Sabatini and A. Vacca, *Inorg. Chim. Acta* 1983, **79**, 219.
34. P. Gans, A. Sabatini and A. Vacca, *J. Chem. Soc., Dalton Trans.* 1985, 1195.
35. D. J. Leggett and W. A. E. McBryde, *Anal. Chem.* 1975, **47**, 1065.
36. D. J. Leggett, *Anal. Chem.* 1977, **49**, 276.
37. D. J. Leggett, S. L. Kelly, L. R. Shine, Y. T. Wu, D. Chang and K. M. Kadish, *Talanta* 1983, **30**, 579.
38. G. Gran, *Acta Chem. Scand.* 1950, **4**, 559; G. Gran, *Analyst* 1952, **77**, 661; F. J. C. Rossotti and H. S. Rossotti, *J. Chem. Ed.* 1965, **42**, 375.

39. E. S. Johansen and O. Jøns, *Talanta* 1984, **31**, 743.
40. T. D. Smith, J. F. Boas and J. R. Pilbrow, *Aust. J. Chem.* 1974, **27**, 2535.
41. F. Gaizer and A. Puskás, *Talanta* 1981, **28**, 565.
42. R. G. Bates, *CRC Crit. Rev. Anal. Chem.* 1981, **10**, 247.
43. D. P. Brezinski, *Analyst* 1983, **108**, 425.
44. G. K. Johnson and E. O. Schlemper, *J. Am. Chem. Soc.* 1978, **100**, 3645.
45. M. M. Iannuzzi and P. H. Rieger, *Inorg. Chem.* 1975, **14**, 2895.
46. N. D. Chasteen, *Biological Magnetic Resonance*, Vol. 3, p. 53. Plenum Press, New York (1981).
47. A. Braibanti, F. Dallavalle, G. Mori and M. Pasquali, *Gazz. Chim. Ital.* 1983, **1113**, 407.
48. F. Gaizer and A. Puskás, *Talanta* 1981, **28**, 925.
49. A. Lorenzotti, D. Leonesi, A. Cingolani and P. Bernardo, *J. Inorg. Nucl. Chem.* 1981, **43**, 737; A. Lorenzotti, D. Leonesi, A. Cingolani and A. Turolla, *Gazz. Chim. Ital.* 1983, **113**, 229; A. Lorenzotti, D. Leonesi and A. Cingolani, *Inorg. Chim. Acta* 1981, **52**, 149.
50. R. D. Gillard, J. Costa Pessoa and L. Vilas-Boas, to be published.
51. J. Francavilla and N. D. Chasteen, *Inorg. Chem.* 1975, **14**, 2860.
52. R. D. Gillard, R. J. Lancashire and P. O'Brien, *Trans. Met. Chem.* 1980, **5**, 340.
53. J.-P. Mathieu, *Volume Commem.* Victor Henri, p. 111. Desoer, Liege (1946); for a later extension, see R. D. Gillard, *J. Inorg. Nucl. Chem.* 1964, **26**, 657.

Polyhedron Vol. 7, No. 14, pp. 1263–1266, 1988
Printed in Great Britain

0277–5387/88 $3.00+.00
© 1988 Pergamon Press plc

METAL-DIRECTED SYNTHESIS OF THE NEW POTENTIALLY PENTADENTATE AMINOALCOHOL LIGAND 5-AMINO-5-METHYL-3,7-DIAZANONAN-1,9-DIOL BASED ON ETHANOLAMINE

GEOFFREY A. LAWRANCE,* THERESE M. MANNING and MARGARET A. O'LEARY

Department of Chemistry, The University of Newcastle, New South Wales 2308, Australia

(*Received* 24 *November* 1987; *accepted* 9 *February* 1988)

Abstract—Reaction of the copper(II) complex of ethanolamine in basic methanol with formaldehyde and nitroethane produces the cation (5-methyl-5-nitro-3,7-diaza-1-oxynonan-9-ol)copper(II). Reduction with zinc in aqueous hydrochloric acid yields the hydrochloride salt of the new aminoalcohol 5-amino-5-methyl-3,7-diazanonan-1,9-diol. This molecule has the capacity to act as a pentadentate N_3O_2 ligand to metal ions, illustrated by the synthesis and characterization of a chlorocobalt(III) complex of the ligand.

The facile syntheses of new multidentate polyamine ligands have been described recently, in which reaction relies on the condensation of two coordinated and *cis*-disposed primary amines with formaldehyde and nitroethane.[1–4] A new six-membered chelate ring is built during this reaction [eq. (1)]. Further, reduction of the nitro-substituted macrocyclic copper(II) complexes with zinc in aqueous acid [eq. (2)] forms a new class of macrocycles with a pendant primary amine on the ring.[2,5] A reaction based on $[Cu(en)_2]^{2+}$ (en = ethane-1,2-diamine) produces both a dicapped macrocycle and a half-capped molecule which yields the pentaamine L_1.[2,6]

Apart from reactions involving polyamines, only the aminothioether $(H_2NCH_2CH_2SCH_2)_2CH_2$ has been reacted by the method outlined in eq. (1).[7] Since the groups binding the metal ion in addition to the reacted *cis* primary amines apparently do not affect ring formation as presented in eq. (1), we believed that a dialcohol analogue of L_1 could be accessible by the reaction of the known ethanolamine complex of copper(II).[8] We have pursued the synthesis of firstly L_2 and then the desired L_3

* Author to whom correspondence should be addressed.

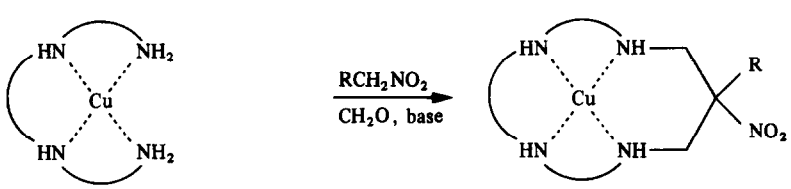

(1)

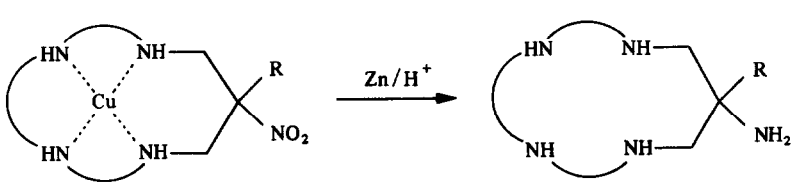

(2)

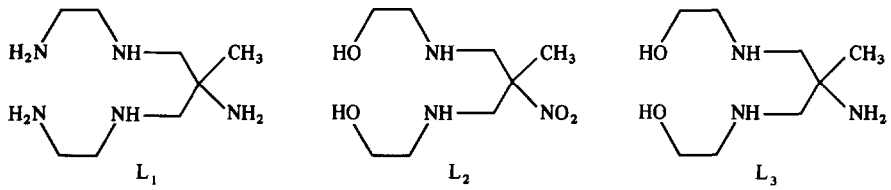

Structure 1.

molecule (see Structure 1) and the details are reported here.

EXPERIMENTAL

Syntheses

$[Cu(NH_2CH_2CH_2OH_{1/2})_2](NO_3)$. This known compound was prepared essentially as described.[8] To a warm solution of $Cu(NO_3)_2 \cdot 2H_2O$ (6 g) in methanol was added with stirring a solution of ethanolamine (10 cm^3) in methanol (20 cm^3). The bright blue suspension was warmed and stirred for 2 h, then the blue crystals were collected (3.4 g, 53%). The product can be recrystallized as the perchlorate salt from water on addition of $NaClO_4$.

$[Cu(L_2—H)](ClO_4)$. Triethylamine (0.5 cm^3) was added to a suspension of the above complex (3 g, 12.2 mmol) in methanol (100 cm^3). The mixture was warmed and nitroethane (1.0 cm^3, 14 mmol) and formaldehyde (4 cm^3, 37% aq, 52 mmol) were added. The deep green mixture was warmed at ~ 50°C and stirred for 2 h, during which solids dissolved to give an emerald green solution. On standing overnight, the blue crystals which deposited, were collected, washed with a little cold water to remove some green material, then washed with propanol and ether and dried. Further standing of the filtrate yielded a second crop (0.8 g, 20%). The product was recrystallized from water by addition of $NaClO_4$. An alternative method of separation involves dilution of the reaction mixture with water, sorption on a column of SP-Sephadex C-25 resin, and elution with 0.2 dm^3 mol^{-1} $NaClO_4$. The desired product can be recovered as the only blue band and crystallized by concentration and standing. Found: C, 24.8; N, 10.5. Calc. for $C_8H_{18}ClCuN_3O_8$; C, 25.1; H, 4.7; N, 10.9%. IR (KBr disc); $\nu_{as}(NO_2)$ 1553 cm^{-1}, $\nu_s(NO_2)$ 1345 cm^{-1}. Electronic spectrum (water): λ_{max} 610 nm ($\varepsilon = 65$ dm^3 mol^{-1} cm^{-1}), 260 nm ($\varepsilon = 3170$). Voltammetry ($E_{1/2}$, V, vs Ag—AgCl in 0.1 mol dm^{-3} aq. $NaClO_4$): −0.56 [Cu(II)—(I)]; −0.92 (—NO_2 → —NHOH).

$L_3 \cdot 3HCl \cdot \frac{1}{2}H_2O$. Zinc dust (1 g) was added to a solution of $[Cu(L_2—H)](ClO_4)$ (0.58 g) in water (50 cm^3) containing concentrated HCl (8 cm^3). The mixture was stirred at room temperature for 1 h, filtered through cellulose to remove Cu and Zn, then sorbed onto a column (7.5 × 3 cm) of Dowex 50W × 2 cation exchange resin. The column was washed with 0.5 mol dm^{-3} HCl to remove Zn^{2+}, then eluted with 2 mol dm^{-3} HCl to recover the ligand. The solution was rotary evaporated to dryness, triturated with ethanol, then diethyl ether, then dried *in vacuo* at 60°C for 4 h (0.28 g, 65%). The product was recrystallized from water–ethanol and dried as before. Found: C, 31.4; H, 8.1; N, 13.5. Calc. for $C_8H_{25}Cl_3N_3O_{2.5}$: C, 31.0; H, 8.1; N, 13.6%. ^1H NMR (D_2O): δ 1.66 (3H, s), 3.59 (4H, s), 3.4 (4H, m), 3.9 (4H, m). ^{13}C NMR (D_2O): δ 20.15, 51.8, 52.9, 53.9, 57.1.

$[Co(L_3)Cl]Cl \cdot H_2O$. Excess $CoCl_2 \cdot 6H_2O$ (~ 0.4 g) was added to a solution of $L_3 \cdot 3HCl$ (~ 0.2 g) in water (50 cm^3) and the pH was raised to eight with NaOH. The solution was warmed and H_2O_2 (30%, 2 cm^3) added. Following filtration, concentrated HCl (5 cm^3) was added and the solution left to stand overnight. The cherry-red solution was diluted and sorbed onto a column of Dowex 50W × 2 cation exchange resin, and eluted with 2 mol dm^{-3} HCl. A major purple band was collected, rotary evaporated to dryness, triturated with propanol and dried *in vacuo* at 50°C for 6 h. A second minor red band turned purple on standing in HCl and appeared to be simply the aqua rather than the chloro complex isolated. The isolated complex was very soluble in water or water–alcohol mixtures and could not readily be recrystallized. As isolated, it proved to be relatively pure. Found: C, 28.8; H, 6.9; N, 12.45. Calc. for $C_8H_{22}Cl_2CuN_3O_3$: C, 28.4; H, 6.8; N, 12.4%. Electronic spectrum (water, pH 1): λ_{max} 548 (ε 174 dm^3 mol^{-1} cm^{-1}), 382 (ε 132). ^1H NMR (D_2O/DCl): δ 1.57 (CH_3, s), 3.0–4.0 (—CH_2—, m), 5.4, 7.3 (NH, br), 8.2 (OH); (D_2O/NaOD): δ 1.27 (CH_3, s), 2.4–3.0 (—CH_2—N, m), 3.1–3.5 (—CH_2—O, m). ^{13}C NMR (D_2O): δ 18.7, 53.6, 56.3, 57.9, 65.5.

Physical methods

Electronic spectra were recorded using a Hitachi 220A spectrophotometer. IR spectra were recorded on compounds dispersed in KBr discs using a Nicolet MX-1 Fourier-transform spectrometer. Electrochemical measurements were performed

with a Bioanalytical Systems Inc. CV-27 controller and a conventional three-electrode system with an Ag—AgCl reference electrode and argon purge gas. The ^1H and ^{13}C NMR spectra were recorded using a JEOL FX-90Q spectrometer; chemical shifts are cited vs $SiMe_4$.

RESULTS AND DISCUSSION

Reaction of the copper(II) complex of ethanolamine with formaldehyde and nitroethane does not proceed as cleanly as similar reactions with ethane-1,2-diamine or related polyamines.[1-4] Nevertheless, a ~ 20% yield of the blue $[Cu(L_2)]^{2+}$ complex was obtained from a reaction mixture which also contains very soluble and uncharacterized green species. The relative instability of the aminoalcohol complex under the basic reaction conditions probably affects the yield; with the analogous propanolamine complex, we have not been able to obtain any of the desired product. Although chromatography on SP-Sephadex offers the simplest way of separating the desired product from other species, we were also able to separate the complex by direct crystallization from the reaction mixture. The new six-membered ring formed between the two ethanolamine chelates generates a new tetradentate ligand with nitro and methyl substituents on the central carbon of the six-membered ring. The nitro group is readily characterized by strong IR vibrations near 1550 and 1350 cm^{-1} (ν_{as} and ν_s, respectively), and by an irreversible multielectron reduction in voltammetry experiments (near −0.9 vs Ag–AgCl). The product, with a CuN_2O_2 chromophore, has an electronic maximum in the visible region at lower energy (610 nm) than the known analogue with a CuN_4 chromophore (529 nm), where NH_2 groups replace the OH groups,[2] consistent with the locations of these donors in the spectrochemical series.

The cation formed between Cu(II) and L_2 carries an overall charge of 1+, due to deprotonation of one alcohol group. This is also observed for the bis(ethanolamine)copper(II) cation, where structural investigations defined this as, in effect, a dimer with strong hydrogen-bonding interactions between the OH group on one cation and an O^- group on the adjacent cation.[8] It is presumed that the analogous arrangement also exists here, see Structure 2. The alternate arrangement is for a monomer

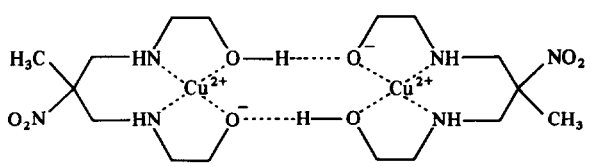

Structure 2.

Table 1. Comparison of the ^1H and ^{13}C NMR spectra of the ligands $L_1 \cdot 5HCl$ and $L_3 \cdot 3HCl$ in D_2O[a]

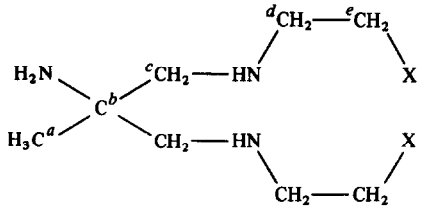

Group	X = OH		X = NH_2	
	$\delta(^{13}C)$	$\delta(^1H)$	$\delta(^{13}C)$	$\delta(^1H)$
a	20.15	1.66 (s)	20.75	1.46 (s)
b	53.9	—	55.0	—
c	52.9	3.59 (s)	53.3	3.56 (s)
d	51.8	3.4 (m)	47.0	3.35 (m)
e	57.1	3.9 (m)	37.0	3.45 (m)

[a] Shifts cited vs $SiMe_4$; ^1H-decoupled ^{13}C spectra; all amines deuterated.

with the hydrogen bond operating in an intramolecular fashion to form a pseudo-macrocycle.

The $[Cu(L_2)]^+$ cation readily dissociates in aqueous acid and the ligand is reduced cleanly in the presence of zinc dust to the amine analogue L_3. This stable polyaminoalcohol carries two alcohol groups, two secondary amines and one primary amine, all potentially capable of coordinating to a metal ion. Therefore it represents a new potentially pentadentate saturated ligand with mixed nitrogen and oxygen donors. The similarity to the pentaamine L_1, which has been characterized structurally and shown to coordinate to cobalt(III) as drawn below (X = NH_2),[6] is apparent. The NMR spectra of the ligands L_1 and L_3 are compared in Table 1, with assignments. The very soluble cobalt(III) complex of L_3 was isolated as a 1+ cation, presumably with a CoN_3O_2Cl chromophore and one deprotonated hydroxyl group. The single symmetric low-energy electronic transition at 548 nm is consistent with a *fac*-CoN_3X_3 geometry like that in Structure 3 (X = OH), as is the

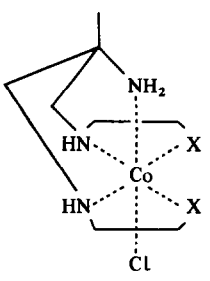

Structure 3.

observation of five resonances in the ^{13}C decoupled NMR. The L_1 analogue, of known stereochemistry, likewise shows five resonances in the ^{13}C NMR spectrum. Evidently, L_3 can act as a pentadentate ligand at least for cobalt(III). It represents a new and relatively simply prepared mixed N,O-donor ligand.

Acknowledgement—Support of this research by the Australian Research Grants Scheme is gratefully acknowledged.

REFERENCES

1. P. Comba, T. W. Hambley and G. A. Lawrance, *Helv. Chim. Acta* 1985, **68**, 2332.
2. P. Comba, N. F. Curtis, G. A. Lawrance, A. M. Sargeson, B. W. Skelton and A. H. White, *Inorg. Chem.* 1986, **25**, 4260.
3. G. A. Lawrance and M. A. O'Leary, *Polyhedron* 1987, **6**, 1291.
4. P. Comba, N. F. Curtis, G. A. Lawrance, M. A. O'Leary, B. W. Skelton and A. H. White, *J. Chem. Soc., Dalton Trans.* 1988, 497.
5. N. F. Curtis, G. J. Gainsford, T. W. Hambley, G. A. Lawrance, K. R. Morgan and A. Siriwardena, *J. Chem. Soc., Chem. Commun.* 1987, 295.
6. P. V. Bernhardt, T. W. Hambley and G. A. Lawrance, to be published.
7. G. A. Lawrance, M. Rossignoli, B. W. Skelton and A. H. White, *Aust. J. Chem.* 1988, **41**, in press.
8. J. A. Bertrand, E. Fujita and D. G. Van Derveer, *Inorg. Chem.* 1980, **19**, 2022.

Polyhedron Vol. 7, No. 14, pp. 1267–1271, 1988
Printed in Great Britain

0277-5387/88 $3.00+.00
© 1988 Pergamon Press plc

SYNTHESIS OF UNUSUAL MIXED LIGAND TELLURIUM(IV) DITHIOCARBAMATES WITH PERCHLORATE. CRYSTAL AND MOLECULAR STRUCTURE OF PERCHLORATOTRIS(DIETHYLDITHIOCARBAMATO)TELLURIUM(IV)

SP. CHIDAMBARAM and G. ARAVAMUDAN*

Department of Chemistry, Indian Institute of Technology, Madras-600 036, India

M. SESHASAYEE

Department of Physics, Indian Institute of Technology, Madras-600 036, India

and

T. A. SHIBANOVA and V. I. SIMONOV

Institute of Crystallography, Academy of Sciences of the USSR, Leninsky Pr., 59, Moscow, 117333, U.S.S.R.

(*Received* 11 *August* 1987; *accepted after revision* 9 *February* 1988)

Abstract—Synthetic and structural aspects of perchlorato complexes of tellurium(IV) with different dithiocarbamates (dtc) [($R_1R_2NCS_2$) where $R_1 = R_2$ = methyl, ethyl, *n*-propyl, *i*-propyl; $R_1R_2 = (CH_2)_5$(piperidine), $C_2H_4OC_2H_4$ (morpholine)] are reported. The crystal structure of TeL_3ClO_4 (where L = diethyl dtc) has been determined. The crystals of the complex are monoclinic, space group $P2_1/n$, $a = 11.379(3)$, $b = 17.745(7)$, $c = 14.016(8)$ Å, $\gamma = 103.30(2)°$, $V = 2754.2$ Å^3, $F(000) = 1352$, $D_x = 1.61$ mg M^{-3}. The final R and R_w values are 0.047 and 0.058, respectively for 5224 unique reflections. Tellurium displays a distorted dodecahedral stereochemistry formed by two interposing trapezoids, one resulting from the four sulphurs of two L groups and the other from the two sulphurs of the third L and the two oxygens of the perchlorate ion. The average Te—S distance 2.648(2) Å is close to that reported in other tris(dithiocarbamato)tellurium(IV) complexes. The perchlorate is weakly coordinated to tellurium(IV), with the average Te—O distance being 2.994(8) Å. The unusual coordination of perchlorate (as a bidentate ligand) to tellurium(IV) dithiocarbamate is reported for the first time.

In acid media tellurium(IV) mostly gives tetrakis complexes on the addition of excess dithiocarbamates ($R_1R_2NCS_2$).[1-4] Recently, mixed ligand complexes of the type TeL'_3X[5-7] (L′ = N(2-hydroxyethyl)-N-methyldithiocarbamate, X = Cl, SCN), TeL''_3X[8] (L″ = bis(2-hydroxyethyl)dithiocarbamate, X = Cl), TeL'''_3X[9] (L‴ = 2,2′-iminodiethanoldithiocarbamate, X = SCN), TeL_3Ph[10] L = diethyldithiocarbamate) and TeL'_2I_2, featuring six and seven-coordinated tellurium, have been prepared and their crystal structures reported.[11] Most of the dtc mixed ligand complexes were readily prepared by weakening the coordinating ability of the ligand by attaching electron withdrawing or solvent interacting moieties to the R_1 and R_2 groups. In the case when $R_1 = R_2$ = ethyl, where only electron donating groups are attached, mixed ligand complexes[12,13] were formed under non-aqueous conditions.

Most unexpectedly we observed that in perchloric acid medium, L readily interacts with Te(IV) to give two complexes, one red in colour and the other yellow. Analysis indicated that these were not the

* Author to whom correspondence should be addressed.

tetrakis dtc complexes of tellurium(IV), which are formed quantitatively in hydrochloric or sulphuric acid media. The molecular formulae of the red and yellow complexes are found to be $Te_3L_9ClO_4(OH)_2$ and TeL_3ClO_4, respectively. Synthetic aspects of the complexes and the crystal structure of TeL_3ClO_4 are reported here. The unusual coordination of perchlorate to tellurium(IV) is discussed based on a structural investigation. In addition to L, the study was extended to dimethyl, di-*n*-propyl, di-*i*-propyl, morpholyl and piperidenyl dtc complexes.

EXPERIMENTAL

Tellurium dioxide, sodium dimethyl dtc, morpholine, piperidine, di-*n*-propylamine, di-*i*-propylamine (all from Aldrich) and sodium diethyl dtc (s.d. chem., India) were used. Dithiocarbamates of the corresponding amines were prepared by conventional methods.[14] IR spectra were recorded on Perkin–Elmer 781 and 983 IR spectrometers, using Nujol mulls and potassium bromide discs.

Preparation of the complexes

Method (i): $Te_3L_9ClO_4(OH)_2$. 0.16 g of TeO_2 (1 mmol) dissolved in 5 cm^3 of 1 M sodium hydroxide was acidified with 20 cm^3 of 4 N perchloric acid (solution A). A solution of 6 mmol of the sodium salt of L dissolved in 25 cm^3 of water was added to solution A with continuous stirring. A red precipitate was obtained. It was extracted with 15 cm^3 of dichloromethane and the solution was evaporated to a small volume by suction. Addition of 10 cm^3 of ethyl acetate gave red needle shaped crystals. Found: Te, 20.5; C, 29.2; H, 4.9; N, 6.7; S, 31.2; Cl, 2.0. Calc. for $Te_3L_9(ClO_4)(OH)_2$: Te, 20.6; C, 29.2; H, 5.0; N, 6.8; S, 31.2; Cl, 1.9%.

The percentage yield of the complex is 87%. The crystal data were collected but the structure could not be solved due to the poor quality of the crystal (high mosaic properties, poorly diffracting) and hence data was poor. The compound is prone to hydrolytic decomposition.

Method (ii): *Perchloratotris(diethyldithiocarbamato)tellurium*(IV): $[TeL_3ClO_4]$. Methanol (25 cm^3) was added to solution A and 25 cm^3 of a methanolic solution of 6 mmol of the sodium salt of L was added. A yellow crystalline solid separated. This was filtered and washed with ether. Found: Te, 18.9; C, 26.8; H, 4.4; N, 6.2; S, 28.5; Cl, 5.5. Calc. for $TeL_3(ClO_4)$: Te, 19.0; C, 26.8; H, 4.5; N, 6.2; S, 28.6; Cl, 5.3.

The percentage yield of the complex is 83%. Single crystals of the above complex were prepared by dissolving 50 mg of the complex in 2 cm^3 of dichloromethane and evaporating the solution at room temperature after the addition of 5 cm^3 of ethyl acetate and 0.1 cm^3 of 6 N perchloric acid. The compound was stable indefinitely under dry conditions but was best preserved under liquid paraffin.

General method of preparation for other dtc *tellurium*(IV) *perchlorate complexes*

Method (i) was used as a general method of preparation for other dithiocarbamates. N,N-dimethyl dtc formed only the $Te_3L_9(ClO_4)(OH)_2$ [type I] complex. Attempts to prepare the TeL_3ClO_4 [type II] complex with it were unsuccessful. Morpholino and piperidino dtcs formed only type II complexes while the preparation of the type I complex was unsuccessful. When $R_1 = R_2 = i$-propyl or *n*-propyl, both type I and type II complexes were formed. However, the type II complex of *n*-propyl dtc was prepared with difficulty, using a higher concentration of perchloric acid. The type I complex of N,N-di-*n*-propyl dtc was comparatively more stable than its diethyl dtc complex. The structure determination of the above reported complexes is being taken up.

Crystal data of $Te_3(dedtc)_9ClO_4(OH)_2$

$C_{45}H_{90}N_9S_{18}Te_3ClO_4(OH)_2$: $f_w = 1847$, $a = 13.827(2)$, $b = 22.853(3)$, $c = 24.631(3)$ Å, $\lambda = 0.71069$, $V = 7783.37$ $Å^3$. Space group *Pcan*, μ(Mo-K_α) = 15.51 mm^{-1}, $Z = 4$, $F(000) = 3727$. Crystal data were collected with an Enraf–Nonius CAD 4 diffractometer. Graphite monochromated Mo-K_α radiation was used. Complete structure elucidation was not possible due to the poor quality of the crystal. Only the central tellurium atom and the surrounding sulphur atoms were located.

Crystal data of $Te(dedtc)_3ClO_4$ (*at* 23°C)

$C_{15}H_{30}N_3S_6TeClO_4$: $f_w = 670.5$, $a = 11.379(3)$, $b = 17.745(7)$, $c = 14.016(8)$ Å, $\gamma = 103.30(2)°$, $V = 2754.2$ $Å^3$. Space group $P2_1/n$, $Z = 4$, $F(000) = 1352$, $D_x = 1.61$ mg M^{-3}, μ(Mo-K_α) = 15.3 mm^{-1}. A crystal of size $0.2 \times 0.37 \times 1.0$ mm^3 was mounted on an Enraf–Nonius CAD-4F automatic diffractometer. Graphite monochromated Mo-K_α (0.71069 Å) radiation was used. The intensity data were collected by the ω scan technique, maximum $\sin\theta/\lambda = 0.7$ $Å^{-1}$. 5395 independent reflections with $I > 3\sigma(I)$ were collected. After merging 171 reflections, $R_{int} = 0.154$. The tellurium atom was located using the Patterson map and all the peaks corresponding to other non-

hydrogen atoms were located using difference Fourier maps. Least-squares refinement of positional and thermal parameters was carried out using the *SHELX-76*[15] program. Twenty-five out of 30 hydrogens appeared in the subsequent Fourier and difference Fourier maps and were refined isotropically. Convergence was reached at $R = 0.047$ and $R_w = 0.058$ [where w is the weighting scheme used) $= 1/(\sigma^2(F_0)+0.0599|F_0|^2]$. The maximum peak in the final difference Fourier map was 2.3 e $Å^{-3}$, but was chemically meaningless.

Neutral atomic scattering factors of the non-hydrogens,[16] the hydrogens[17] and the anomalous scattering factors[18] were used in the structure elucidation. The final positional coordinates of non-hydrogens are deposited* and Table 1 contains the bond lengths and bond angles. Figures 1 and 2 depict the molecule and the packing of the molecule, respectively, and were drawn using the ORTEP[19] program.

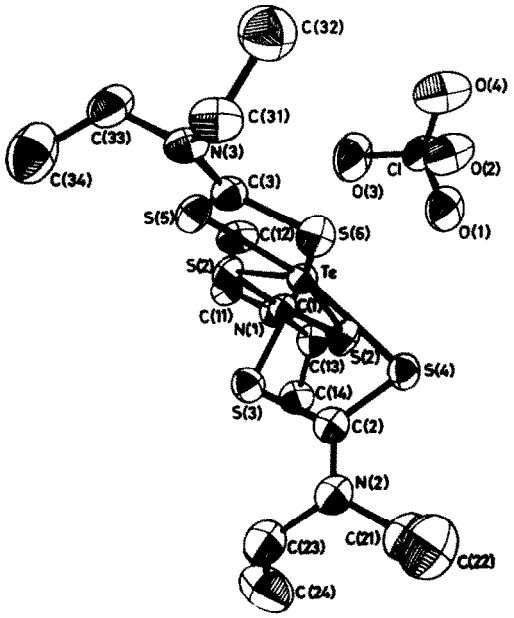

Fig. 1. Perspective of the molecule.

RESULTS AND DISCUSSION

Tellurium(IV) gave two types of perchlorato dtc complexes, one of composition $Te_3(dtc)_9ClO_4(OH)_2$ was red in colour, and the other of composition $Te(dtc)_3ClO_4$ was yellow in colour. Both types of complex were highly soluble in dichloromethane and moderately in chloroform, but unlike the $Te(dtc)_4$ complexes, they were insoluble in benzene and carbon tetrachloride. The complexes were stable under anhydrous conditions, but on the addition of an excess of the sodium salt of dtc in a methanolic medium, they were converted to the corresponding $Te(dtc)_4$ complexes.

The composition of the complexes prepared, along with the ν_{C-N} and ν_{C-S} frequencies observed in them are given in Table 2. The assignment of these frequencies were made based on the data available[14] for dtc complexes of other metals. The ν_{C-N} frequency for the perchlorate complexes was slightly higher than for the corresponding $Te(dtc)_4$ complexes. In all the perchlorate complexes a broad band was observed at around 1100 cm^{-1} which was ascribed to the perchlorate group. However, it was difficult to conclude from IR spectral consideration whether ClO_4^- was strongly bonded to Te(IV). Also, it was difficult to pick out the Te—S and Te—O frequencies from the large number of bands observed in the far-IR region.

Crystal structure of TeL_3ClO_4 (*refer to Table* 1 *and Figs* 1 *and* 2)

In tetrakisdithiocarbamate complexes of Te(IV), the central tellurium atom exhibits distorted dodecahedral coordination with eight sulphurs.[1] In the perchlorato complex, the perchlorate replaces one of the dithiocarbamates and acts as a very weak bidentate ligand through two of its oxygen atoms. As is usual, the dodecahedron is considered to comprise two interposing trapezoids. The first trapezoid contains Te, S_3, S_4, S_5, S_6 atoms and the other is

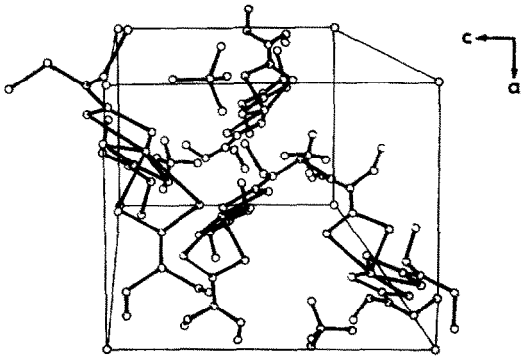

Fig. 2. Molecular packing in the unit cell of the molecule down the *b*-axis.

* Lists of atomic coordinates of non-hydrogens, hydrogen bond lengths, bond angles of the hydrogen atoms, mean plane calculations, anisotropic thermal parameters and the structure factor tables are deposited with The Institüt für Anorganische Chemie (IAC).

Table 1. Some important bond lengths (Å) and bond angles (°) with their standard deviation in parentheses

	Bond lengths (Å)		
Te—S(1)	2.426(2)	Te—S(2)	2.790(3)
Te—S(3)	2.590(2)	Te—S(4)	2.732(2)
Te—S(5)	2.598(3)	Te—S(6)	2.753(2)
Te—O(1)	3.124(7)	Te—O(3)	2.876(9)
S(1)—C(1)	1.780(9)	S(2)—C(1)	1.692(9)
C(1)—N(1)	1.303(11)	N(1)—C(11)	1.482(12)
C(11)—C(12)	1.508(14)	N(1)—C(13)	1.476(12)
C(13)—C(14)	1.500(13)	S(3)—C(2)	1.740(8)
S(4)—C(2)	1.717(9)	C(2)—N(2)	1.320(8)
N(2)—C(21)	1.494(9)	C(21)—C(22)	1.527(12)
N(2)—C(23)	1.453(10)	C(23)—C(24)	1.482(18)
S(5)—C(3)	1.744(7)	S(6)—C(3)	1.704(8)
C(3)—N(3)	1.329(8)	N(3)—C(31)	1.494(9)
C(31)—C(32)	1.508(13)	N(3)—C(33)	1.483(10)
C(33)—C(34)	1.513(14)	Cl—O(1)	1.437(8)
Cl—O(2)	1.403(7)	Cl—O(3)	1.408(8)
Cl—O(4)	1.436(8)		
	Bond angles (°)		
S(1)—Te—S(2)	68.8(2)	S(3)—Te—S(4)	67.2(2)
S(5)—Te—S(6)	66.8(2)	Te—S(1)—C(1)	92.0(4)
Te—S(2)—C(1)	82.1(4)	S(1)—C(1)—N(1)	118.2(6)
S(2)—C(1)—N(1)	124.7(6)	C(1)—N(1)—C(11)	122.8(6)
C(1)—N(1)—C(13)	121.3(6)	N(1)—C(11)—C(12)	111.2(7)
N(1)—C(13)—C(14)	112.9(7)	C(11)—N(1)—C(13)	115.9(6)
S(1)—C(1)—S(2)	117.1(5)	S(3)—C(2)—S(4)	117.0(5)
S(3)—C(2)—N(2)	119.5(6)	S(4)—C(2)—N(2)	123.5(6)
C(2)—N(2)—C(21)	120.9(6)	C(2)—N(2)—C(23)	122.4(6)
N(2)—C(21)—C(22)	110.3(6)	N(2)—C(23)—C(24)	114.4(7)
C(21)—N(2)—C(23)	116.7(6)	Te—S(3)—C(2)	89.7(4)
Te—S(4)—C(2)	85.6(4)	Te—S(5)—C(3)	89.7(4)
Te—S(6)—C(3)	85.5(4)	S(5)—C(3)—S(6)	117.6(5)
S(5)—C(3)—N(3)	118.6(5)	S(6)—C(3)—N(3)	123.8(5)
C(3)—N(3)—C(31)	120.5(5)	C(3)—N(3)—C(33)	121.7(5)
N(3)—C(31)—C(32)	111.8(6)	N(3)—C(33)—C(34)	112.7(6)
C(31)—N(3)—C(33)	117.7(5)		

made up of Te, S_1, S_2, O_1, O_3 atoms. The interplanar angle between them is found to be 88.4(2)° which is comparable to 86.5° in Te(bis(2-hydroxyethyl)dtc)$_4$,[1] 88.5° in Te(morphdtc)$_4$,[2] 89.8° in Te((hydroxyethyl)methyl dtc)$_4$[3] and 90.0° in Te(diethyl dtc)$_4$.[4] The geometry of the sulphur around the tellurium is very similar to that observed in other tris(dithiocarbamato)tellurium(IV) complexes featuring chloride,[7,8,12] thiocyanate[6,9] and iodide,[20] as additional ligands. Five of the sulphurs are weakly bonded (Te—S distance varies from 2.590(2) to 2.790(3) Å) and these form a puckered pentagonal girdle around the tellurium. The sixth sulphur atom is closely bonded to tellurium at a distance of 2.426(2) Å, which is only slightly longer than the sum of the single covalent radii for tellurium and sulphur, namely 2.36 Å.

The average Te—O bond distance is found to be 2.994(8) Å which is very much longer than the sum of the covalent radii, 1.98 Å, but is however, shorter than the sum of the van der Waals radii of 3.50 Å.[21] This clearly shows that the coordination of the two oxygens of the perchlorate to tellurium(IV) is very weak indeed and in support of this, no perturbation is observed in the γ_3 region of the perchlorate in the IR spectrum and therefore it appears as if it is ionic.

The average intraligand S—Te—S angle is 67.6(3)°, which is more than the angle in the eight-coordinated TeL_4 (65.0°). In nickel dtcs where four-coordination was found, the average S—Ni—S

Table 2. Perchlorate dtc Te(IV) complexes

Complex	ν_{C-N} (cm^{-1})	ν_{C-S} (cm^{-1})
NaDEDTC	1476	986
$Te(DEDTC)_4$	1483	984
$Te(DEDTC)_9ClO_4(OH)_2$	1491	983(w)
$Te(DEDTC)_3ClO_4$	1500	982
NaDMeDTC	1490	960
$Te(DMeDTC)_4$	1520	960
$Te_3(DMeDTC)_9ClO_4(OH)_2$	1525	940(w)
Na(D-*n*-propDtc)	1470	975
$Te(D\text{-}n\text{-}propDtc)_4$	1485	970
$Te_3(D\text{-}n\text{-}propDtc)_9ClO_4(OH)_2$	1510	960
Morpholino(morpholineDtc)	1455	995
$Te(morphDtc)_4$	1480	980
$Te(morphDtc)_3ClO_4$	1480	
Na(pipDtc)	1470	965
$Te(pipDtc)_4$	1480	955
$Te(pipDtc)_3ClO_4$	1500	
Na(D-*i*-propdtc)	1460	950
$Te(D\text{-}i\text{-}propdtc)_4$	1475	935
$Te(D\text{-}i\text{-}propdtc)_3ClO_4$	1490	

angle reported was 79.3(1).[22] It was also found that on heating TeL_4[23] or on keeping the TeL_4[1] solution, TeL_2 and L—L form, relieving the steric strain over tellurium. So the feasible substitution of dtc by perchlorate may be due to the smaller size of the perchlorate ion, which lowers the steric strain over tellurium and retains the dodecahedral configuration around it, thus satisfying the stereochemical requirement. We also observed that the feasibility of the substitution of perchlorate increases with increase in size of the substituent in the dtc ($R_1 = R_2 = Me < Et < n\text{-}Pr < i\text{-}Pr$).

The C—S bond lengths vary between 1.692(9) and 1.780(9) Å with an average of 1.730(9) Å. The C—N bond lengths are between 1.303(9) and 1.327(8) Å having an average of 1.317(9) Å. This indicates that the C—S and C—N bonds exhibit partial double bond character due to the usual mesomeric shift of electrons from the nitrogens to the sulphur found in the dithiocarbamate complexes. N—C and C—C bond lengths and bond angles around them are normal and no abnormal short-contacts were observed.

Acknowledgement—We thank B. V. Merinov for his assistance in making the X-ray measurements.

REFERENCES

1. G. C. Rout, M. Seshasayee, G. Aravamudan and K. Radha, *Acta Cryst.* 1984, **C40**, 1142.
2. S. Esparas and S. Husebye, *Acta Chem. Scand.* 1975, **A29**, 185.
3. S. Husebye, *Acta Chem. Scand.* 1979, **A33**, 485.
4. S. Husebye and S. E. Svaeran, *Acta Chem. Scand.* 1973, **27**, 763.
5. G. Aravamudan, Chhaya Janakiram and B. G. Sejekan, *Phosphorus and Sulphur* 1978, **5**, 185.
6. S. Husebye and A. G. Thowson, *Acta Chem. Scand.* 1981, **A35**, 386.
7. S. Husebye and A. G. Thowson, *Acta Chem. Scand.* 1981, **A35**, 443.
8. G. V. N. Apparao, M. Seshasayee, G. Aravamudan and K. Radha, *Inorg. Chem.* 1983, **22**, 2590.
9. G. C. Rout, M. Seshasayee, G. Aravamudan and K. Radha, *J. Cryst. Spect. Res.* 1984, **14**, 193.
10. S. Esparas, S. Husebye and S. E. Svaeran, *Acta Chem. Scand.* 1971, **25**, 3539.
11. G. V. N. Apparao, M. Seshasayee, G. Aravamudan and K. Radha, *Acta Cryst.* 1983, **C39**, 1018.
12. K. V. Deuton, W. Schnabel and G. Klar, *Phosphorus and Sulphur* 1980, **9**, 93.
13. W. Schnabel, K. V. Deuton and G. Klar, *Phosphorus and Sulphur* 1982, **13**, 345.
14. D. Coucouvanis, *Prog. Inorg. Chem.* 1970, **11**, 233.
15. G. M. Sheldrick, *SHELX-76, Program for Crystal Structure Determination.* University of Cambridge, Cambridge, U.K. (1976).
16. D. T. Cromer and J. B. Mann, *Acta Cryst.* 1968, **A24**, 321.
17. R. F. Stewart, E. R. Davidson and W. T. Simpson, *J. Chem. Phys.* 1965, **42**, 3175.
18. D. T. Cromer and D. J. Libermann, *J. Chem. Phys.* 1970, **53**, 1891.
19. C. K. Johnson, 'ORTEP' report ORNL-3794. Oakridge National Laboratory, Oak Ridge, TN (1965).
20. SP. Chidambaram, G. Aravamudan, M. Seshasayee, M. R. Snow and E. R. T. Tiekink, to be published.
21. A. Bondi, *J. Phys. Chem.* 1964, **68**, 441.
22. K. Ramalingam, K. Radha, G. Aravamudan, C. Mahadevan, Ch. Subramanian and M. Seshasayee, *Acta Cryst.* 1984, **C40**, 1839.
23. O. Foss, *Acta Chem. Scand.* 1953, **7**, 226.

Polyhedron Vol. 7, No. 14, pp. 1273–1278, 1988
Printed in Great Britain

0277–5387/88 $3.00+.00
© 1988 Pergamon Press plc

MONOMERIC Pt(II) AND Pd(II) COMPLEXES WITH CREATININE. CRYSTAL STRUCTURE OF TETRAKIS-(CREATININE) PLATINUM(II) DIPERCHLORATE

M. MITEWA, G. GENCHEVA, P. R. BONTCHEV* and O. ANGELOVA

Department of Chemistry, Sofia University, A. Ivanov Avenue 1, 1126 Sofia, Bulgaria

and

J. MACICEK

Institute of Applied Mineralogy, Bulgarian Academy of Sciences, Rakovski Str. 92, 1000 Sofia, Bulgaria

(*Received* 1 *October* 1987; *accepted after revision* 9 *February* 1988)

Abstract—Pt(II) and Pd(II) complexes with creatinine, $C_3H_2N_2(O)(CH_3)NH_2$, were synthesized. Potentiometric and IR spectroscopic analyses were carried out. A model for the coordination of the ligands to the central atoms was confirmed by X-ray structural investigation of $Pt(creat)_4(ClO_4)_2$. The compound $[Pt(C_4H_7N_3O)(ClO_4)_2]$ crystallizes in the monoclinic crystal system, space group $C2/c$, $a = 15.748(5)$, $b = 15.763(7)$, $c = 24.843(8)$ Å, $\beta = 106.84(4)°$, $V = 5902$ Å^3, $Z = 8$. The refinement of the structure by the least-squares method gave $R = 0.051$ and $R_w = 0.054$ for 1527 observed reflections with $I > 2\sigma(I)$. The structure consists of $Pt(creat)_4^{2+}$ complex cations, possessing approximate $D2$ symmetry and rotationally disordered perchlorate anions. The Pt atom is square-planarly coordinated by the endocyclic N atoms of four creatinine ligands. The Pt—N bond lengths range from 2.00(2) to 2.03(1) Å and the N—Pt—N angles from 88.4(9) to 91.8(8)°. The ligands are almost planar and tilted towards the PtN_4-plane by 82.1(8)–93.5(9)°.

Creatinine is a final product of the creatinine metabolism.[1,2] Considering the possibility of it existing in imino- or/and amino-tautomeric forms (**I, II**) and the presence of several donor groups we presume that creatinine may coordinate to metal ions in different ways according to the metal ions' nature and the reaction conditions.

Recently we have started a systematic investigation on the creatinine coordination to different metal ions.[3–5] The complexation of this important bioligand is scarcely studied—only data concerning its complexes with Hg(II), Cd(II), Co(II), Zn(II), Cu(II), Ag(I), Pd(II) and Pt(II) have been reported.[1–9] In the latest studies on the complex formation with Pt(II) and Pd(II) it was demonstrated[5,9] that variation of the reaction conditions leads to different types of M(II) complexes as well as to the formation of a paramagnetic Pt(III) complex, most probably, an analogue of pyridonate– and pyrrolidonate–platinum blues.[10,11]

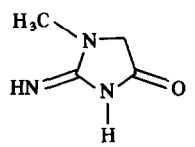

I

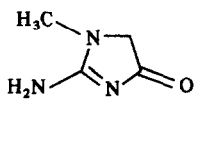

II

In the present paper we report the results of the IR spectroscopic study of M(II) complexes, formed as a product of the $M(II)Cl_4^{2-}$ (M = Pt, Pd) reaction with creatinine at a ligand (L) excess L : M > 4, as well as the X-ray crystal study of $Pt(creat)_4(ClO_4)_2$, particularly since we obtained crystals suitable for structural analysis.

*Author to whom correspondence should be addressed.

EXPERIMENTAL

Synthetic and analytical procedures

Complexes with a general formula $M(II)(creat)_4A_2$ (M = Pt, Pd; A = tetraphenylborate (TPB), perchlorate) were prepared by mixing the aqueous solutions of the corresponding MCl_4^{2-} (5×10^{-2} M) and creatinine (5×10^{-2} M) at a ligand excess L:M > 4. The reaction mixture was stirred for 1 h at room temperature and the complexes formed were precipitated with perchlorate or TPB, filtered off and washed with water. $(NH_4)_2MCl_4$ of Fluka (puriss) and other reagents of AR grade were used. The composition of the complexes formed was determined by an elemental analysis. Pt and Pd were estimated gravimetrically after treating the complexes with conc. H_2SO_4 and heating to a constant weight.

IR and potentiometric studies

The IR spectra were recorded on a Perkin–Elmer 580 spectrophotometer (KBr discs). The potentiometric studies were performed with a precise digital pH-meter Radelkis OP-208 equipped with Cl^- selective (Crytur, ČSSR) and standard calomel electrodes. A two-vessel cell with a graphite bridge at constant temperature (25±0.1°C) and constant ionic strength (μ = 0.1 M KNO_3) was used.

Crystal data and structure solution

The essential crystallographic information is summarized in Table 1. A white prismatically shaped crystal with the approximate dimensions 0.15 × 0.20 × 0.12 mm was mounted on a glass capillary and analysed on the computer controlled Enraf-Nonius CAD4 diffractometric system CAD4SDP44M at the Institute of Applied Mineralogy. For the monoclinic crystal system the space group $C2/c$ was chosen according to the systematic absences and confirmed by the subsequent successful structure solution. Accurate cell constants were obtained from a least-squares refinement of the setting angles of 22 reflections in the range $15 < \theta < 16°$. Graphite monochromatized Mo-K_α radiation was employed. The diffraction data were collected at a temperature of 292 K, using the $\omega/2\theta$ scan technique. The intensities of three standard reflections were monitored in order to check the instrument and crystal stability. The intensity variation was < 0.1% and no decay correction was applied. The structure was solved by the heavy-atom method. In the final full-matrix least-squares refinement, anisotropic temperature factors for Pt

Table 1. Crystal data and experimental details

Molecular weight	846.47
Crystal system	Monoclinic
Space group	$C2/c$
a (Å)	15.748(5)
b (Å)	15.763(7)
c (Å)	24.843(8)
β(°)	106.84(4)
V (Å^3)	5902(1)
Z	8
D_x (g cm^{-3})	1.905
μ (cm^{-1})	50.59
F(000)	3328
Max $\sin(\theta)/\lambda$	0.481
hkl limits	−15/15, −14/14, −23/0
Reflections measured	6054
Transmission factor range	79.222–99.955
Reflections unique	1620
R_{int} ($\|F\|$)	0.050
Reflections unobserved	1966, $I < 2\sigma(I)$
Minimization function	$M = \sum W(\|F_o\| - \|F_c\|)$
Weighting scheme	$W = 4F_o^2/[\sigma(F_o)^2]^2$
R	0.051
R_w	0.054
S	1.056
Max. (Δ/σ)	2.045
Max. ($\Delta\rho$)	1.026 e Å^{-3}

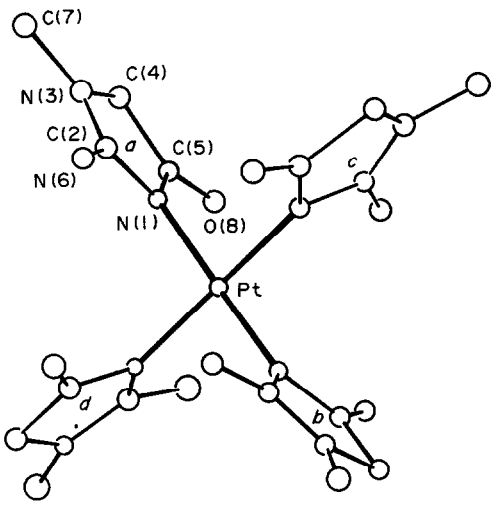

Fig. 1. ORTEP drawing of the complex cation. The atom and ring labelling schemes are given. The hydrogen atoms are not depicted.

and isotropic for all the other atoms, were applied with H-atoms being ignored. The extinction effect was neglected. Atomic scattering factors and anomalous dispersion coefficients for neutral atoms were used as coded in the SDP/PDP V3.0 crystallographic package. Selected interatomic distances and angles are given in Table 2. Listings of the observed and calculated structure factors, positional and thermal parameters and least-square planes have been deposited as supplementary data with the Editor, from whom copies may be obtained on request. Atomic coordinates have also been deposited with the Cambridge Crystallographic Data Centre. Figure 1 depicts the geometry and atom-labelling scheme of the complex cation. The packing of the molecules within the unit cell is represented in Fig. 2.

RESULTS AND DISCUSSION

On the basis of the analytical data obtained (Table 3) it was assumed that the complexation at a ligand excess (L : M ranging from 4 : 1 to 10 : 1) resulted in the formation of $[M(II)(creat)_4]^{2+}$ complexes. Additional evidence for the composition of the complexes was obtained by potentiometric determination of the liberated chloride in the course of the $(PtCl_4)^{2-}$ and creatinine reaction. It was found that at the end of the reaction the total amount of Cl^- liberated in the solution is equal to the calculated one in the case when all Cl^- ions are substituted by creatinine molecules in the inner coordination sphere of Pt(II).

IR results

The cationic complexes formed were precipitated with TPB or perchlorate and their characteristic IR spectra are represented in Table 3.

The IR spectra of the $M(II)(creat)_4(ClO_4)_2$ and $M(II)(creat)_4(TPB)_2$ complex salts are similar, suggesting an analogous structure of the complex cation. The $\nu_{C=O}$ bands were observed in the region

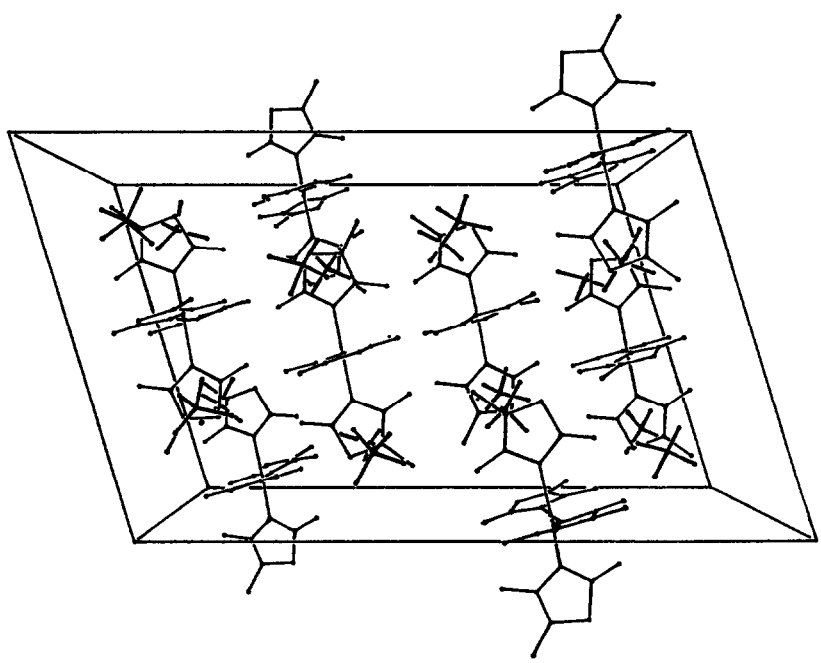

Fig. 2. The unit cell content viewed along the *b* axis.

Table 2. Interatomic distances (Å) and angles (°) within the cation and the perchlorate anion with e.s.ds in parentheses

Pt—N(1a)	2.03(1)	N(6a)—C(2a)	1.30(2)
Pt—N(1b)	2.00(1)	N(6b)—C(2b)	1.32(3)
Pt—N(1c)	2.01(2)	N(6c)—C(2c)	1.35(3)
Pt—N(1d)	2.02(2)	N(6d)—C(2d)	1.29(3)
O(8a)—C(5a)	1.25(3)	C(4a)—C(5a)	1.49(3)
O(8b)—C(5b)	1.27(2)	C(4b)—C(5b)	1.52(3)
O(8c)—C(5c)	1.18(3)	C(4c)—C(5c)	1.57(4)
O(8d)—C(5d)	1.25(3)	C(4d)—C(5d)	1.52(4)
N(1a)—C(2a)	1.40(3)	C(11)—O(11)	1.48(3)
N(1a)—C(5a)	1.36(2)	C(11)—O(12)	1.36(2)
N(1b)—C(2b)	1.35(3)	C(11)—O(13)	1.40(3)
N(1b)—C(5b)	1.36(3)	C(11)—O(14)	1.46(2)
N(1c)—C(2c)	1.38(3)	C(11)—O(11′)	1.53(4)
N(1c)—C(5c)	1.37(3)	C(11)—O(12′)	1.47(4)
N(1d)—C(2d)	1.44(3)	C(11)—O(13′)	1.50(4)
N(1d)—C(5d)	1.34(3)	C(11)—O(14′)	1.39(4)
N(3a)—C(2a)	1.34(3)	C(12)—O(21)	1.48(3)
N(3a)—C(4a)	1.46(3)	C(12)—O(22)	1.38(2)
N(3a)—C(7a)	1.51(3)	C(12)—O(23)	1.39(3)
N(3b)—C(2b)	1.35(3)	C(12)—O(24)	1.50(3)
N(3b)—C(4b)	1.49(3)	C(12)—O(21′)	1.47(4)
N(3b)—C(7b)	1.50(2)	C(12)—O(22′)	1.49(4)
N(3c)—C(2c)	1.33(3)	C(12)—O(23′)	1.50(5)
N(3c)—C(4c)	1.38(3)	C(12)—O(24′)	1.37(4)
N(3c)—C(7c)	1.52(3)		
N(3d)—C(2d)	1.33(4)		
N(3d)—C(4d)	1.40(3)		
N(3d)—C(7d)	1.51(3)		
N(1a)—Pt—N(1b)	177.3(8)	N(1b)—C(2b)—N(3b)	112(2)
N(1a)—Pt—N(1c)	88.4(8)	N(1b)—C(2b)—N(6b)	126(2)
N(1a)—Pt—N(1d)	90.4(9)	N(3b)—C(2b)—N(6b)	122(2)
N(1b)—Pt—N(1c)	89.5(8)	N(1c)—C(2c)—N(3c)	112(2)
N(1b)—Pt—N(1d)	91.8(9)	N(1c)—C(2c)—N(6c)	123(3)
N(1c)—Pt—N(1d)	178.6(7)	N(3c)—C(2c)—N(6c)	126(2)
C(2a)—N(1a)—C(5a)	107(2)	N(1d)—C(2d)—N(3d)	108(2)
C(2b)—N(1b)—C(5b)	106(2)	N(1d)—C(2d)—N(6d)	118(2)
C(2c)—N(1c)—C(5c)	107(2)	N(3d)—C(2d)—N(6d)	133(2)
C(2d)—N(1d)—C(5d)	107(2)	N(3a)—C(4a)—C(5a)	99(1)
C(2a)—N(3a)—C(4a)	113(2)	N(3b)—C(4b)—C(5b)	95(2)
C(2a)—N(3a)—C(7a)	124(2)	N(3c)—C(4c)—C(5c)	101(2)
C(4a)—N(3a)—C(7a)	123(2)	N(3d)—C(4d)—C(5d)	101(2)
C(2b)—N(3b)—C(4b)	112(1)	O(8a)—C(5a)—N(1a)	123(2)
C(2b)—N(3b)—C(7b)	129(2)	O(8a)—C(5a)—C(4a)	125(2)
C(4b)—N(3b)—C(7b)	119(2)	N(1a)—C(5a)—C(4a)	112(2)
C(2c)—N(3c)—C(4c)	113(2)	O(8b)—C(5b)—N(1b)	122(2)
C(2c)—N(3c)—C(7c)	124(2)	O(8b)—C(5b)—C(4b)	123(2)
C(4c)—N(3c)—C(7c)	123(2)	N(1b)—C(5b)—C(4b)	115(2)
C(2d)—N(3d)—C(4d)	113(2)	O(8c)—C(5c)—C(4c)	127(2)
C(2d)—N(3d)—C(7d)	122(2)	O(8c)—C(5c)—C(4c)	127(2)
C(4d)—N(3d)—C(7d)	124(2)	N(1c)—C(5c)—C(4c)	107(2)
N(1a)—C(2a)—N(3a)	109(2)	O(8d)—C(5d)—N(1d)	125(2)
N(1a)—C(2a)—N(6a)	124(2)	O(8d)—C(5d)—C(4d)	126(2)
N(3a)—C(2a)—N(6a)	127(2)	N(1d)—C(5d)—C(4d)	110(2)
O(11)—Cl(1)—O(12)	111(2)	O(21)—Cl(2)—O(22)	106(2)
O(11)—Cl(1)—O(13)	114(2)	O(21)—Cl(2)—O(23)	109(2)
O(11)—Cl(1)—O(14)	111(2)	O(21)—Cl(2)—O(24)	103(1)
O(12)—Cl(1)—O(13)	116(2)	O(22)—Cl(2)—O(23)	115(2)
O(12)—Cl(1)—O(14)	108(2)	O(22)—Cl(2)—O(24)	113(2)
O(13)—Cl(1)—O(14)	95(1)	O(23)—Cl(2)—O(24)	112(2)
O(11′)—Cl(1)—O(12′)	117(3)	O(21′)—Cl(2)—O(22′)	106(3)
O(11′)—Cl(1)—O(13′)	104(2)	O(21′)—Cl(2)—O(23′)	109(2)
O(11′)—Cl(1)—O(14′)	111(2)	O(21′)—Cl(2)—O(24′)	107(2)
O(12′)—Cl(1)—O(13′)	88(2)	O(22′)—Cl(2)—O(23′)	116(2)
O(12′)—Cl(1)—O(14′)	115(2)	O(22′)—Cl(2)—O(24′)	107(2)
O(13′)—Cl(1)—O(14′)	121(2)	O(23′)—Cl(2)—O(24′)	112(3)

Table 3. Elemental analysis and selected IR data

Compound	Calc. (%)	Found (%)	$\nu_{C=O}$ (cm^{-1})	ν_{NH_2} (cm^{-1})	δ_{NH_2} (cm^{-1})
$Pt(creat)_4(TPB)_2$	15.2	14.9	1705	3390	1665
				3330	
$Pd(creat)_4(TPB)_2$	8.9	9.1	1710	3345	1665
				3320	
$Pt(creat)_4(ClO_4)_2$	23.1	22.5	1725	3410	1675
				3315	1655
				3290	
				3215	
$Pd(creat)_4(ClO_4)_2$	14.1	13.8	1720	3405	1650
				3315	1670
				3295	
				3215	

1725–1705 cm^{-1}, showing unequivocally that $>C=O$ groups are not involved in the coordination. A number of bands were observed in the region 3400–3200 cm^{-1}, where ν_{NH_2} symmetric and asymmetric vibrations appear. These data show that the ligand is present in the complex as its amino-tautomer form (II). At the same time the existence of two pairs of bands for ν_{NH_2} (two bands due to δ_{NH_2}, respectively) in the case of M(II) $(creat)_4(ClO_4)_2$ shows the formation of two different types of H-bonds, in contrast to M(II) $(creat)_4(TPB)_2$.

In the IR spectra of $M(II)(creat)_4(TPB)_2$ the $\nu_{C=O}$ bands are observed at lower frequencies (Table 3) indicating stronger H-bond formation between C=O and NH_2 groups.

These spectroscopic data, however, were not sufficient to determine the details of the coordination mode and the stereochemistry of the complexes.

Description of the structure of $Pt(creat)_4(ClO_4)_2$

The crystal structure consists of $Pt(creat)_4^{2+}$ cations and perchlorate anions disposed in general positions. The complex cation possesses approximate D_2 symmetry. The platinum atom has its usual nearly perfect square-planar coordination with Pt—N(1) bond lengths ranging from 2.00(2) to 2.03(1) Å and N(1)—Pt—N(1) angles from 88.4(9) to 91.8(8)°.

The four creatinine ligands are planar within 0.02 Å. The Pt atom is displaced from the ligand planes (a–d) by 0.185(1), 0.197(1), 0.076(1) and 0.194(1) Å, respectively. The tilt angles between adjacent ligand planes are a–c 99.8(9), a–d 90.4(9), b–c 86.8(1.1) and b–d 77.4(1.1)°. The tilting between the PtN_4-plane and ligand planes ranges from 82.1(8) to 93.5(9)°. This originates from intramolecular steric factors and is supported by the intermolecular hydrogen bonding between the amino-hydrogen atoms and the H-bond acceptors—carbonyl groups of the ligands and the perchlorate anions.* The shortest N(6)···O(8) distances are: 2.87(2) (a-d), 2.90(3) (d–b), 2.90(3) (c–b) and 2.92(3) (b–d) and N(6)—O(No.): 2.86(4) (a–24′), 2.95(3) (b–12), 2.84(4) (c–14′), 2.97(3) Å (d–22).

The ClO_4^- ions in the structure are surrounded by four creatinine ligands, which are parallel in pairs, and are rotationally disordered. The disordering scheme chosen presumes full occupancy of the Cl positions and approximately 60 and 40% occupancy of the bifurcated O-sites. The Cl—O distances range from 1.36(2) to 1.53(4) Å (av. 1.45(3) Å) and the O—Cl—O angles from 87(2) to 120(2)°.

* The H-bonding scheme was deduced from the calculated positions of the amino-hydrogen atoms presuming their coplanarity with the ligands.

REFERENCES

1. S. Muralidharan, K. S. Nagaraja and M. R. Udupa, *Polyhedron* 1984, **3**, 619.
2. S. Muralidharan, K. S. Nagaraja and M. R. Udupa, *Trans. Met. Chem.* 1984, **9**, 218.
3. M. Mitewa, P. R. Bontchev and K. Kabassanov, *Polyhedron* 1985, **4**, 1159.
4. P. R. Bontchev, M. Mitewa, V. I. Nefedov and Ya. E. Salyn, *Proc. XXIV ICCC* p. 720. Athens, Greece (1986).

5. P. R. Bontchev, M. Mitewa, G. Gencheva, J. Macicek, O. Angelova and V. I. Nefedov, *Proc. 11th Conf. Coord. Chem.* p. 37. Smolenice, CSSR (1987).
6. A. J. Canty, M. Fife and B. M. Gatehouse, *Inorg. Chem.* 1978, **7**, 1467.
7. M. D. Udupa and B. Krebs, *Inorg. Chim. Acta* 1979, **33**, 241.
8. M. D. Udupa and B. Krebs, *Inorg. Chim. Acta* 1981, **55**, 153.
9. F. J. Martin-Gil and J. Martin-Gil, *Inorg. Chim. Acta* 1987, **137**, 131.
10. J. D. Woollins and P. F. Kelly, *Coord. Chem. Rev.* 1985, **65**, 115.
11. Th. V. O'Halloran and S. Lippard, *Israel J. Chem.* 1985, **25**, 130.

Polyhedron Vol. 7, No. 14, pp. 1279–1284, 1988
Printed in Great Britain

0277–5387/88 $3.00+.00
© 1988 Pergamon Press plc

COMPLEXES OF THE TYPE $Mo_2(O_2CR)_2X_2(L—L)$ IN WHICH THE BIDENTATE PHOSPHINE LIGANDS L—L STRADDLE THE Mo≡Mo BOND

MOHAMMED BAKIR and RICHARD A. WALTON*

Department of Chemistry, Purdue University, West Lafayette, IN 47907, U.S.A.

(*Received* 11 *December* 1987; *accepted* 12 *February* 1988)

Abstract—The reactions of $Mo_2(O_2CCH_3)_2Cl_2(PPh_3)_2$ with the bidentate phosphine ligands $Ph_2PCH_2CH_2PPh_2$(dppe), $Ph_2PCH{=}CHPPh_2$(dppee) and *o*-$C_6H_4(PPh_2)_2$(dppbe) yield purple complexes of the stoichiometry $Mo_2(O_2CCH_3)_2X_2(L—L)$ in which the acetate ligands are believed to be *cis* and the L—L ligands bridge the dimolybdenum core so that their P atoms are *anti* to one another. The relationship of these complexes to the previously reported complex $Mo_2(O_2CCH_3)_2Cl_2$(dppm), where dppm = $Ph_2PCH_2PPh_2$, is discussed. These complexes have been characterized on the basis of their electrochemical redox properties, and electronic absorption and NMR (^1H and $^{31}P\{^1H\}$) spectral measurements.

Our recent isolation and characterization of geometric isomers of the series of triply bonded dirhenium(II) complexes *cis*- and *trans*-$Re_2(O_2CR)_2X_2(dppm)_2$ (R = CH_3 or C_2H_5; X = Cl or Br; dppm = $Ph_2PCH_2PPh_2$),[1] in which the halide ligands X are axially bound, has led us to examine whether complexes of this or a similar type could be isolated in the case of the quadruply bonded dimolybdenum(II) core, in spite of the proclivity of the latter to form (at best) weak axial interactions with various ligands.[2] In this report we describe such a study in which the phosphine ligands $Ph_2PCH_2PPh_2$(dppm), $Ph_2PCH_2CH_2PPh_2$(dppe), $Ph_2PCH{=}CHPPh_2$(dppee) and *o*-$C_6H_4(PPh_2)_2$(dppbe) have been used.

EXPERIMENTAL

Starting materials

The compounds $Mo_2(O_2CCH_3)_4$,[3] $Mo_2(O_2CCH_3)_2Cl_2(PR_3)_2$, where R = Ph or *n*-Bu,[4] were prepared by standard literature procedures, while $Mo_2(O_2CCH_3)_2Cl_2$(dppm) was prepared by a modified version of the procedure [see Section (b)] described by Green *et al.*[4] The ligands PPh_3, dppbe and dppe were purchased from Strem Chemicals and dppee was purchased from Pressure Chemical Company. Solvents used in the preparation of the complexes were of commercial grade and were deoxygenated prior to use.

Reaction procedures

All reactions were performed in a nitrogen atmosphere with the use of standard vacuum line techniques.

(a) *Preparation of* $Mo_2(O_2CCH_3)_2Br_2(PPh_3)_2$

A mixture of $Mo_2(O_2CCH_3)_4$ (0.20 g, 0.47 mmol), PPh_3 (0.31 g, 1.18 mmol), THF (10 cm^3) and Me_3SiBr (0.30 cm^3) was stirred at room temperature for 20 min. A red–pink solid was filtered off, washed with THF, hexanes and diethyl ether and then dried in vacuum; yield 0.24 g (52%). Found: 47.6; H, 3.6. Calc. for $C_{40}H_{36}Br_2Mo_2O_4P_2$: C, 48.3; H, 3.6%.

(b) *Preparation of* $Mo_2(O_2CCH_3)_2Cl_2$(dppm)

A mixture of $Mo_2(O_2CCH_3)_2Cl_2(PPh_3)_2$ (0.20 g, 0.22 mmol), dppm (0.11 g, 0.30 mmol) and THF (5 cm^3) was stirred at room temperature for 20 min. A red–purple solid was filtered off, washed with THF (~ 2 cm^3), hexanes and diethyl ether, and then dried; yield 0.12 g (72%). Found: C, 45.9; H, 3.9. Calc. for $C_{29}H_{28}Cl_2Mo_2O_4P_2$: C, 46.4; H, 3.8%. This product was unstable even at 0°C and after a few hours its colour had changed to brown.

*Author to whom correspondence should be addressed.

When a freshly prepared sample of $Mo_2(O_2CCH_3)_2Cl_2$(dppm) (0.10 g, 0.13 mmol) was refluxed in THF (10 cm^3) for 6 h, the colour of the reaction mixture changed from red–purple to dark green. The reaction mixture was cooled to room temperature and an excess of diethyl ether was added. A dark brown solid was filtered off and the green filtrate was evaporated to dryness. The resulting green residue was recrystallized from CH_2Cl_2/diethyl ether to afford dark green crystals of $Mo_2Cl_4(dppm)_2$ which were filtered off, washed with hexanes and diethyl ether, and dried; yield 0.03 g (22%). The identity of this product was confirmed by its electrochemical and spectroscopic properties.[5]

(c) *Preparation of* $Mo_2(O_2CCH_3)_2Cl_2$(L—L), *where* L—L = dppee, dppbe *or* dppe

(i) $Mo_2(O_2CCH_3)_2Cl_2$(dppee). A mixture of $Mo_2(O_2CCH_3)_2Cl_2(PPh_3)_2$ (0.40 g, 0.44 mmol), dppee (0.22 g, 0.56 mmol) and THF (10 cm^3) was stirred at room temperature for 1 h. A purple solid was filtered off, washed with THF, hexanes and diethyl ether, and dried *in vacuo*; yield 0.30 g (87%). Found: C, 46.8; H, 3.3; Cl, 8.6. Calc. for $C_{30}H_{28}Cl_2Mo_2O_4P_2$: C, 46.4; H, 3.6; Cl, 9.1%.

(ii) $Mo_2(O_2CCH_3)_2Cl_2$(dppbe)·THF. This product was obtained as a purple solid by the use of a procedure very similar to that described in (i); yield 55%. Found: C, 50.5; H, 4.0. Calc. for $C_{38}H_{38}Cl_2Mo_2O_5P_2$: C, 50.7; H, 4.3%.

(iii) $Mo_2(O_2CCH_3)_2Cl_2$(dppe). A procedure similar to (i) gave the title product as a purple insoluble solid; yield 93%. Found: C, 46.2; H, 4.3; Cl, 10.0. Calc. for $C_{30}H_{30}Cl_2Mo_2O_4P_2$: C, 46.2; H, 3.9; Cl, 9.1%.

(d) *Preparation of* $Mo_2(O_2CCH_3)_2Br_2$(L—L), *where* L—L = dppee *or* dppbe

(i) $Mo_2(O_2CCH_3)_2Br_2$(dppee). A mixture of $Mo_2(O_2CCH_3)_2Br_2(PPh_3)_2$ (0.20 g, 0.20 mmol), dppee (0.10 g, 0.25 mmol) and THF (10 cm^3) was stirred at room temperature for 20 min. A purple solid was filtered off, washed with THF, hexanes and diethyl ether, and dried *in vacuo*; yield 0.15 g (86%). Found: C, 42.1; H, 3.3. Calc. for $C_{30}H_{28}Br_2Mo_2O_4P_2$: C, 41.6; H, 3.3%.

(ii) $Mo_2(O_2CCH_3)_2Br_2$(dppbe). A reaction similar to (i) but with a reaction time of 1 h gave this product in the usual way; yield 87%. Found: C, 44.5; H, 3.5. Calc. for $C_{34}H_{30}Br_2Mo_2O_4P_2$: C, 44.6; H, 3.3%.

(e) *Reactions of* $Mo_2(O_2CCH_3)_2Cl_2$(L—L), *where* L—L = dppee *or* dppbe, *with bidentate phosphines in the presence of* Me_3SiCl

(i) *Reaction of* $Mo_2(O_2CCH_3)_2Cl_2$(dppee) *with* dppee *in* THF. A mixture of $Mo_2(O_2CCH_3)_2Cl_2$ (dppee) (0.10 g, 0.13 mmol), dppee (0.07 g, 0.17 mmol), THF (10 cm^3) and Me_3SiCl (0.2 cm^3) was stirred at room temperature for 24 h. The green–brown solid that resulted was filtered off, washed with THF, hexanes and diethyl ether, and dried. This product was extracted with CH_2Cl_2 to leave a small quantity of an insoluble green solid (*ca* 0.2 mg) which was identified as α-$Mo_2Cl_4(dppee)_2$ on the basis of its electrochemical properties.[6] The brown CH_2Cl_2 washings were evaporated to dryness and the resulting brown residue was recrystallized from CH_2Cl_2/diethyl ether, the crystals washed with diethyl ether and then dried; yield 0.07 g (48%). This product was identified as β-$Mo_2Cl_4(dppee)_2$ from its electrochemical properties.[6]

When this reaction was carried out for 40 min under reflux conditions, only the brown isomer β-$Mo_2Cl_4(dppee)_2$ was isolated; yield 55%.

(ii) *Reaction of* $Mo_2(O_2CCH_3)_2Cl_2$(dppee) *with* dppm. A mixture of $Mo_2(O_2CCH_3)_2Cl_2$(dppee) (0.10 g, 0.13 mmol), dppm (0.07 g, 0.19 mmol), THF (10 cm^3) and Me_3SiCl (0.2 cm^3) was stirred at room temperature for 20 h. A green solid was filtered off, washed with THF, hexanes and diethyl ether, and dried; yield 0.08 g (58%). Found: C, 56.2; H, 5.3. Calc. for $C_{50}H_{44}Cl_4Mo_2P_4$: C, 55.9; H, 4.1%. The properties of this product are in accord with its formulation as $Mo_2Cl_4(dppm)_2$.[5]

(iii) *Reaction of* $Mo_2(O_2CCH_3)_2Cl_2$(dppbe) *with* dppbe. A mixture of $Mo_2(O_2CCH_3)_2Cl_2$(dppbe)·THF (0.11 g, 0.12 mmol), dppbe (0.07 g, 0.16 mmol), THF (10 cm^3) and Me_3SiCl (0.10 cm^3) was stirred at room temperature for 14 h. A green solid was filtered off, washed with THF, CH_2Cl_2, hexanes and diethyl ether, and then dried; yield 0.06 g (37%). This product was identified as α-$Mo_2Cl_4(dppbe)_2$ from its electrochemical and spectroscopic properties.[7]

Physical measurements

IR spectra were recorded as Nujol mulls with the use of a Perkin–Elmer 1800 FTR spectrophotometer. Electronic absorption spectra were recorded as CH_2Cl_2 solutions or Nujol mulls on a HP 8451A spectrophotometer. Electrochemical measurements were made on CH_2Cl_2 solutions of the complexes which contained tetra-*n*-butylammonium hexafluorophosphate (TBAH) as the

supporting electrolyte. The $E_{p,a}$ and $E_{1/2}$ ($= E_{p,a} + E_{p,c}/2$) values were referenced to the silver–silver chloride (Ag–AgCl) electrode at room temperature and are uncorrected for junction potentials. Voltammetric experiments were performed using a Bioanalytical Systems Inc. model CV-1A instrument in conjunction with a Hewlett-Packard model 7035 *x–y* recorder. ^1H and $^{31}P\{^1H\}$NMR spectra were obtained on a Varian XL-200 spectrometer. For the ^1H NMR spectra, the resonances were referenced internally to the residual protons in the incompletely deuterated solvent, whereas for the $^{31}P\{^1H\}$NMR spectra an internal deuterium lock and an external reference, 85% H_3PO_4, were used.

Elemental microanalyses were performed by Dr H. D. Lee of the Purdue University Microanalytical Laboratory.

RESULTS AND DISCUSSION

Complexes of the type $Mo_2(O_2CCH_3)_2X_2(L—L)$, where X = Cl or Br and L—L = dppm, dppe, dppee or dppbe, have been prepared from the reaction of $Mo_2(O_2CCH_3)_2X_2(PPh_3)_2$[4] with L—L in THF at room temperature. We found no evidence for the formation of stable compounds of stoichiometry $Mo_2(O_2CCH_3)_2X_2(L—L)_2$. These compounds are the first examples of dimolybdenum(II) complexes that contain one bridging bidentate phosphine ligand and two bridging acetato groups. In the course of this study we have also isolated the pink complex $Mo_2(O_2CCH_3)_2Br_2(PPh_3)_2$ from the reaction of $Mo_2(O_2CCH_3)_4$ with PPh_3 and Me_3SiBr in THF at room temperature. Of the compounds we isolated that contain bidentate phosphine ligands, only $Mo_2(O_2CCH_3)_2Cl_2(dppm)$ was reported previously (as it's THF solvate).[4] On the basis of a partial characterization of this complex, a structure that contains both a unidentate and a bidentate acetato-group was proposed.[4] However, as we shall discuss later, the instability of this complex complicates its spectroscopic characterization and it may in fact be structurally related to other compounds of the type $Mo_2(O_2CCH_3)_2X_2(L—L)$.

The electrochemical properties and electronic absorption spectra of these complexes are listed in Table 1 along with related data for $Mo_2(O_2CCH_3)_2Cl_2(PR_3)_2$ (R = Ph or *n*-Bu), whose preparations were described previously,[4] and $Mo_2(O_2CCH_3)_2Br_2(PPh_3)_2$, which is reported here for the first time. Cyclic voltammetric data for freshly prepared solutions of these complexes in 0.1 M TBAH—CH_2Cl_2 show a single irrevers-

Table 1. Cyclic voltammetric and electronic absorption spectral data for $Mo_2(O_2CCH_3)_2X_2(L—L)$ and $Mo_2(O_2CCH_3)_2X_2(PR_3)_2$

Compound	Voltammetric potentials ($E_{p,c}$)[a]	Electronic absorption spectra (nm)[b]
$Mo_2(O_2CCH_3)_2Cl_2(dppm)$	~ +0.90	~ 528 530[c]
$Mo_2(O_2CCH_3)_2Cl_2(dppe)$[d]	—	528,[c] ~ 380 sh[c]
$Mo_2(O_2CCH_3)_2Cl_2(dppee)$	+0.95	554(1190), ~ 400 sh 556,[c] 400 sh[c]
$Mo_2(O_2CCH_3)_2Br_2(dppee)$	~ +1.0	550(1210), 400 sh 550[c]
$Mo_2(O_2CCH_3)_2Cl_2(dppbe)\cdot THF$	+0.90	546(1060), ~ 380 sh ~ 540,[c] ~ 400 sh[c]
$Mo_2(O_2CCH_3)_2Br_2(dppbe)$	+0.96	550(1370), ~ 400 sh ~ 550[c]
$Mo_2(O_2CCH_3)_2Cl_2(PPh_3)_2$	+0.98	526(1740), ~ 390 sh 526, ~ 380 sh
$Mo_2(O_2CCH_3)_2Br_2(PPh_3)_2$	~ +1.15	535, 400 sh ~ 525, ~ 400 sh
$Mo_2(O_2CCH_3)_2Cl_2(P—n\text{-}Bu_3)_2$	+0.90	512(1630), 372(450)

[a] In V vs Ag—AgCl. Recorded on solutions in 0.1 M TBAH—CH_2Cl_2 using a Pt-bead electrode. Data obtained at $v = 200$ mV s^{-1}.

[b] Recorded on CH_2Cl_2 solutions (unless otherwise stated): ε_{max} values are given in parentheses.

[c] Solid state spectrum measured as a Nujol mull.

[d] Insoluble in CH_2Cl_2.

ible oxidation at $E_{p,a} \simeq +1.0$ V vs Ag—AgCl. This oxidation corresponds to the configuration change $\sigma^2\pi^4\delta^2 \rightarrow \sigma^2\pi^4\delta^1$ (i.e. oxidation of Mo_2^{4+} to Mo_2^{5+}) and is characteristic of complexes that contain the quadruply bonded Mo_2^{4+} core.[8]

In the electronic absorption spectra of all the complexes listed in Table 1, the $\delta \rightarrow \delta^*$ transition[2] is seen as an intense band in the region 510–560 nm. A second weaker feature is observed close to 400 nm. The similarity in the electronic absorption spectra and electrochemical properties of the purple coloured complexes $Mo_2(O_2CCH_3)_2X_2$(L—L) imply a basic similarity in structure. These spectra are in turn similar to those reported previously for the monodentate phosphine derivatives $Mo_2(O_2CPh)_2X_2(P—n\text{-}Bu_3)_2$, where X = Cl or Br, in benzene solution,[9] and for $Mo_2(O_2CCH_3)_2Cl_2(P—n\text{-}Bu_3)_2$ and $Mo_2(O_2CCH_3)_2X_2(PPh_3)_2$, where X = Cl or Br, in CH_2Cl_2 as reported herein (Table 1). In the case of the latter species, λ_{max} for the lowest energy transition ($\delta \rightarrow \delta^*$) is between 510 and 540 nm.

X-ray crystallographic data for several complexes of this type that contain monodentate phosphine ligands show that there is either a *cis*- or *trans*-arrangement of carboxylate groups (structures **1** and **2**). In the case of $Mo_2(O_2CCH_3)_2Cl_2$

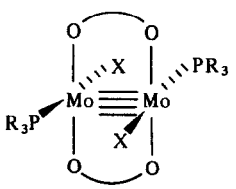

1

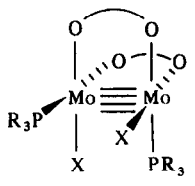

2

$(P—n\text{-}Bu_3)_2$,[4] $Mo_2(O_2CPh)_2X_2(P—n\text{-}Bu_3)_2$[10] and $Mo_2(O_2CCH_3)_2(OSiMe_3)_2(PMe_3)_2$,[11] the structures determined have proven to be those of molecules of type **1**, whereas the orange and red isomeric forms of $Mo_2(O_2CCMe_3)_2Cl_2(PEt_3)_2$ that were prepared correspond to structures **1** and **2**, respectively.[12] In this same context, the red and orange coloured isomers designated as α- and β-$Mo_2(O_2CCH_3)_2X_2(PEt_3)_2$ by Green *et al.*,[4] probably correspond to **2** and **1**, respectively.

Because of the conformational constraints inherent in the six-membered rings that are formed when the dppe, dppee and dppbe ligands form intramolecular ligand bridges between pairs of multiply bonded metal atoms, the complexes $Mo_2(O_2CCH_3)_2X_2$(L—L) most likely possess structure **3**, which is a close relative of **2**. This is especially true when the overall rotational geometry is expected to remain eclipsed, as is invariably the case with quadruply bonded Mo_2^{4+} species.[2] Alternative structures in which there are either *cis* or *trans* pairs of μ-acetato ligands but the phosphine atoms of the bridging L—L ligands are *syn* to one another (rather than *anti* as in **3**) are not favoured.

The ^1H NMR and $^{31}P\{^1H\}$ NMR spectral properties of $Mo_2(O_2CCH_3)_2X_2$(L—L), where X = Cl or Br and L—L = dppee or dppbe, and $Mo_2(O_2CCH_3)_2Cl_2(PPh_3)_2$ are listed in Table 2. ^1H NMR spectra were recorded in CD_2Cl_2 and, in all instances, showed the correct relative intensities for the phenyl protons and acetate methyl protons. The data for $Mo_2(O_2CCH_3)_2Cl_2(PPh_3)_2$ show only one singlet for the methyl resonance rather than the several singlets between δ +2.5 and +2.8 that were reported previously.[4] In the case of $Mo_2(O_2CCH_3)_2Cl_2$(dppbe), additional resonances at δ +1.82 and +3.68 are due to the one mole of lattice THF that is present in the crystalline samples. The $^{31}P\{^1H\}$ NMR spectra of these same complexes (recorded in CH_2Cl_2) each display a singlet. For $Mo_2(O_2CCH_3)_2Cl_2(PPh_3)_2$, the chemical shift of a freshly prepared sample was δ +36.7. Singlets at δ +32.0, +26.0 and +23.0 (relative intensity 1.0 : 0.1 : 0.05) have been reported[4] for a CD_2Cl_2 solution of this complex.

In the case of the purple complex $Mo_2(O_2CCH_3)_2Cl_2$(dppm), the presence of a monodentate acetato ligand had been inferred from a band at 1710 cm^{-1} in the IR spectrum.[4] However, we found that for several different preparative samples of this complex only a very weak feature was present at $\simeq$ 1700 cm^{-1} and, accordingly, we conclude that the IR spectral evidence is not convincing in this regard. Note that the ease with which this complex decomposes in solution and in the solid state makes its characterization quite difficult. The ^1H NMR spectra of freshly prepared CD_2Cl_2 solutions of this compound exhibit a complex pattern between δ +7.0 and +7.6 (phenyl protons), a multiplet at $\delta \simeq +4.6$ (—CH_2— of dppm) and singlets at δ +3.0, +2.9 (actually a closely spaced "doublet"), +2.6 and $\simeq$ +2.0. After 2 h, the spectrum of this same solution showed the growth of a pentet at $\delta \simeq +4.3$ (—CH_2— of $Mo_2Cl_4(dppm)_2$)[5] and an increase in the intensity of the singlet at $\delta \simeq +2.0$. The original singlets at δ +3.0, +2.9 and +2.6 had decreased in intensity and the phenyl region of the spectrum had changed significantly. The resonance at $\delta \simeq +2.0$ is probably due to acetic acid. Note that when the solid samples decompose they clearly give off acetic acid (odour!).

The $^{31}P\{^1H\}$NMR spectrum of a solution of the dppm complex in CH_2Cl_2 (recorded within 15 min of its preparation) showed a singlet

Table 2. NMR spectral data for $Mo_2(O_2CCH_3)_2X_2(L—L)$ and $Mo_2(O_2CCH_3)_2X_2(PPh_3)_2$

Compound[a]	^1H NMR (δ)[b]			$^{31}P\{^1H\}$[c]
	Phenyl	—CH=CH—	$—CH_3$	
$Mo_2(O_2CCH_3)_2Cl_2(dppee)$	7.0–7.5	7.85[d]	2.94	+29.7
$Mo_2(O_2CCH_3)_2Br_2(dppee)$	7.1–7.5	7.83[d]	2.95	+29.3
$Mo_2(O_2CCH_3)_2Cl_2(dppbe)\cdot THF$[e]	7.1–7.8		2.78	+34.3
$Mo_2(O_2CCH_3)_2Br_2(dppbe)$	7.1–7.8		2.78	+33.8
$Mo_2(O_2CCH_3)_2Cl_2(PPh_3)_2$	7.2–7.6		2.57	+36.7

[a] $Mo_2(O_2CCH_3)_2Cl_2(dppe)$ was too insoluble in CD_2Cl_2 for satisfactory NMR spectral data to be obtained.

[b] All resonances downfield of TMS. Spectra recorded in CD_2Cl_2.

[c] Spectra recorded in CH_2Cl_2.

[d] AA'XX' pattern.

[e] Additional proton resonances at δ +3.68(m) and +1.82(m) arise from the methylene resonances of the lattice THF.

at δ +28.9 assignable to the authentic complex $Mo_2(O_2CCH_3)_2Cl_2(dppm)$. This signal decayed very rapidly as new singlets appeared at δ +28.5 and +23.2 (due to two distinct chemical species). These in turn disappeared as features at δ +16.4 and +4.6 developed. The resonance at δ +16.4 is due to $Mo_2Cl_4(dppm)_2$.[5]

The available spectroscopic evidence indicates that $Mo_2Cl_4(dppm)_2$ is one of the final products of the decomposition of $Mo_2(O_2CCH_3)_2Cl_2(dppm)$, thereby supporting the earlier observation[4] that green crystals of $Mo_2Cl_4(dppm)_2$ eventually separate from solutions of this complex. This decomposition is enhanced by heating $Mo_2(O_2CCH_3)_2Cl_2(dppm)$ in THF. After a reaction period of 6 h, $Mo_2Cl_4(dppm)_2$ is present in *ca* 22% yield. The nature of the remaining molybdenum containing species has not yet been ascertained.

The ease with which $Mo_2(O_2CCH_3)_2Cl_2(L—L)$ can be converted into $Mo_2Cl_4(L—L)_2$ (L—L = dppee or dppbe) by reaction with Me_3SiCl and additional ligand L—L in THF led us to attempt the synthesis of mixed ligand complexes of this type, viz., $Mo_2Cl_4(L—L)(L—L')$. However, since the reaction between a mixture of $Mo_2(O_2CCH_3)_2Cl_2(dppee)$, dppm and Me_3SiCl gave $Mo_2Cl_4(dppm)_2$ rather than $Mo_2Cl_4(dppee)(dppm)$, further reactions have not been carried out at this time.

CONCLUSION

The reactions of $Mo_2(O_2CCH_3)_2X_2(PPh_3)_2$ with bidentate phosphines, L—L provide a convenient route to $Mo_2(O_2CCH_3)_2X_2(L—L)$, but we find no evidence for the formation of $Mo_2(O_2CCH_3)_2X_2(L—L)_2$ which would be structural analogues of the recently prepared $Re_2(O_2CCH_3)_2X_2(L—L)_2$.[1] Although the complexes with L—L = dppe, dppee and dppbe almost certainly are of structure type **3**, some doubt remains as to the structure of $Mo_2(O_2CCH_3)_2Cl_2(dppm)$. While it may well possess structure **3**, we suspect that isomerization occurs upon its dissolution in CH_2Cl_2 (this is also the case in CH_3CN),[4] followed by decomposition to give $Mo_2Cl_4(dppm)_2$, acetic acid and other unidentified species. The isomerization of $Mo_2(O_2CCH_3)_2Cl_2(dppm)$ from **3** to a structure in which dppm bridges the Mo_2 unit such that the P atoms are *syn* to one another (see structures A and C in ref. 4), may be favoured by the formation of a stable five-membered ring in which the Mo_2P_2 unit is planar.

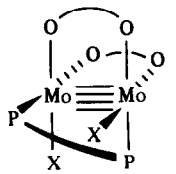

3

Acknowledgement—We thank the National Science Foundation (Grant No. CHE85-06702) for research support.

REFERENCES

1. A. R. Cutler, D. R. Derringer, P. E. Fanwick and R. A. Walton, *J. Am. Chem. Soc.*, accepted for publication.
2. F. A. Cotton and R. A. Walton, *Multiple Bonds*

Between Metal Atoms. John Wiley, New York (1982).
3. A. B. Brignole and F. A. Cotton, *Inorg. Synth.* 1972, **13**, 87.
4. M. L. Green, G. Parkin, J. Bashkin, J. Fail and K. Prout, *J. Chem. Soc., Dalton Trans.* 1982, 2519.
5. W. S. Harwood, J.-S. Qi and R. A. Walton, *Polyhedron* 1986, **5**, 15.
6. M. Bakir, F. A. Cotton, L. R. Falvello, C. Simpson and R. A. Walton, *Inorg. Chem.*, submitted for publication.
7. M. Bakir and R. A. Walton, unpublished results.
8. T. C. Zietlow, D. D. Klendworth, T. Nimry, D. J. Salmon and R. A. Walton, *Inorg. Chem.* 1981, **20**, 947.
9. J. San Filippo, Jr. and H. J. Sniadoch, *Inorg. Chem.* 1976, **15**, 2209.
10. J. A. Potenza, R. J. Johnson and J. San Filippo, Jr., *Inorg. Chem.* 1976, **15**, 2215.
11. G. S. Girolami, V. V. Mainz and R. A. Anderson, *J. Am. Chem. Soc.* 1982, **104**, 2041.
12. J. D. Arenivar, V. V. Mainz, H. Ruben, R. A. Anderson and A. Zalkin, *Inorg. Chem.* 1982, **21**, 2649.

Polyhedron Vol. 7, No. 14, pp. 1285–1287, 1988
Printed in Great Britain

0277–5387/88 $3.00+.00
© 1988 Pergamon Press plc

METHYL TRANSFER IN THE REACTION OF $IrMe_3(PMe_2Ph)_3$ WITH $Cu(NCMe)_4^+$

DAN ALVAREZ JR and KENNETH G. CAULTON*

Department of Chemistry, Indiana University, Bloomington, IN 47405, U.S.A.

(*Received* 26 *January* 1988; *accepted* 12 *February* 1988)

Abstract—$Cu(NCMe)_4BF_4$ reacts with *fac*-$IrMe_3(PMe_2Ph)_3$ in THF to yield *cis,mer*-$[IrMe_2(NCMe)(PMe_2Ph)_3]BF_4$, together with an unstable copper product which could not be trapped (added PPh_3) and was not further characterized. The geometry of the iridium-containing product was established by detailed multi-nuclear NMR studies, including heteronuclear decoupling. The same product results from a 1:1 reaction of *fac*-$IrMe_3(PMe_2Ph)_3$ with $HBF_4 \cdot OEt_2$ in CH_3CN.

We reported earlier numerous examples of using $Cu(NCMe)_4^+$ as a source of the naked[1,2] (or nearly naked[3]) electrophile Cu^+ which functions as a building block for heterometallic polyhydride clusters. In every instance, a terminal hydride ligand serves to link Cu^+ to the second transition metal through hydride bridges. We have now explored a generalization of this concept by studying whether another "one-electron donor" ligand, —CH_2R, can form heterometallic bridges to yield mixed-metal alkyl clusters.[4,5] Heterometallic clusters containing unactivated ("typical") saturated alkyl ligands are virtually unknown.

EXPERIMENTAL

All manipulations were carried out under an inert N_2 atmosphere using standard Schlenk line and glovebox techniques. THF and benzene were dried by refluxing over Na/benzophenone and CH_3CN was dried by refluxing over P_4O_{10}. ^1H and ^{31}P NMR spectra were obtained on a Nicolet 360 MHz spectrometer. $Ir(CH_3)_3(PMe_2Ph)_3$ was made by a literature procedure.[6] $CDCl_3$ was stirred over P_4O_{10} and vacuum distilled. IR spectra were obtained as Nujol mulls between KBr plates using a Perkin–Elmer 283 spectrophotometer. Mass spectra were obtained using a DS-55 Mass Spectrometry Data system on a Kratos MS80 mass spectrometer. Microanalysis was performed by Malissa and Reuter Analytische Laboratorien, F.R.G.

* Author to whom correspondence should be addressed.

$Cu(CH_3CN)_2O_3SCF_3$

A solution of CF_3SO_3H (10.0 g, 66.63 mmol; CAUTION: Corrosive!) in 40 cm^3 CH_3CN was added (Teflon cannula) to a suspension of Cu_2O (4.77 g, 33.32 mmol) in 85 cm^3 of cold (0°C) CH_3CN. The reaction mixture was allowed to warm to room temperature and stirred for 2 h. The solution was then filtered, concentrated and held at −20°C for 24 h. This yielded large transparent crystals which became opaque when filtered and placed under vacuum. After 36 h *in vacuo* at room temperature, no further changes were observed. $Cu(CH_3CN)_2O_3SCF_3$ was isolated as a grey–white powder (12.01 g, 61%). IR: 2290 cm^{-1} sharp/medium, 2215 cm^{-1} sharp/weak: CH_3CN. FAB/MS confirmed the presence of Cu^+ and $^-O_3SCF_3$ but no parent ion was found. Found: C, 20.2; H, 2.1. Calc. for $CuC_5H_6F_3N_2O_3S$: C, 20.4; H, 2.0%.

$[Ir(CH_3)_2(NCCH_3)(PMe_2Ph)_3]BF_4$ *from* $Ir(CH_3)_3(PMe_2Ph)_3$ *and* $Cu(NCCH_3)_4BF_4$

fac-$Ir(CH_3)_3(PMe_2Ph)_3$ (0.15 g, 0.23 mmol) and $Cu(CH_3CN)_4BF_4$ (0.072 g, 0.23 mmol) were each weighed into separate Schlenk flasks. To each flask, 40 cm^3 THF was added and the resulting solutions were each cooled to −78°C and allowed to stir at this temperature for 10 min. The $IrMe_3(PMe_2Ph)_3$ solution was then added to the $Cu(MeCN)_4BF_4$ via a cannula and the resultant solution was allowed to stir at −78°C for 25 min. The clear solution was then allowed to warm to room temperature. After stirring at 25°C for 1 h, the solution had turned

yellow with the deposition of a small amount of green solid. The solution was then filtered to yield a clear yellow solution. THF was then removed *in vacuo* from the filtrate and the resultant yellow solid was washed with 40 cm^3 benzene to leave a white benzene-insoluble powder of $[Ir(CH_3)_2(NCMe)(PMe_2Ph)_3]BF_4$. The benzene washings turned blue in air, indicating the presence of an organocopper compound. ^1H NMR (360 MHz, $CDCl_3$): 7.37 (m, Ph); 7.20 (m, Ph); 2.14 (s, CH_3CN, 3H); 1.64 (t, $J = 3.5$, PMe, 6H); 1.48 (t, $J = 3.3$, PMe, 6H); 1.35 (d, $J = 7.9$, PMe, 6H); 0.18 (m, 6H). $^{31}P\{^1H\}$ NMR (146 MHz, $CDCl_3$): −35.2 (d, $J = 16.3$, 2P); −49.1 (t, $J = 16.3$, 1P).

$[Ir(CH_3)_2(NCCH_3)(PMe_2Ph)_3]BF_4$ *from* $Ir(CH_3)_3(PMe_2Ph)_3$ *and* $HBF_4 \cdot Et_2O$

A 40 cm^3 CH_3CN solution of $Ir(CH_3)_3(PMe_2Ph)_3$ (0.050 g, 0.077 mmol) was cooled to 0°C. To this solution was added 7.1×10^{-3} cm^3 of $HBF_4 \cdot Et_2O$ (0.012 g, 0.077 mmol). The resulting mixture was allowed to warm to room temperature. The solvent was then removed *in vacuo* to yield a white powder. ^1H NMR confirmed the formation of $[Ir(CH_3)_2(NCCH_3)(PMe_2Ph)_3]BF_4$.

RESULTS AND DISCUSSION

Our initial studies involved an attempt to produce and isolate a μ-alkyl compound from the reaction of Cp_2ZrMe_2 with $[Cu(NCMe)_4]BF_4$ in THF. These resulted in polymerization of THF. Simultaneously, Jordan *et al.*[7] reported similar results in the reaction of $AgPF_6$ with Cp_2ZrMe_2 and reasoned that fluoride abstraction from PF_6^- by a Zr(IV) electrophile was followed by PF_5-catalysed ring-opening polymerization. We therefore sought a copper electrophile with an anion more inert than BF_4^-, obtaining it according to eq. (1).

$$Cu_2O + 2HO_3SCF_3 \xrightarrow{MeCN} \underset{\mathbf{1}}{2Cu(NCMe)_2O_3SCF_3} + H_2O. \quad (1)$$

Reagent **1** reacts with Cp_2ZrMe_2 in THF to give a dark green, insoluble precipitate whose physical properties discouraged further study. We next sought to incorporate a more stable alkyl group into the system and, to this end, investigated $Cp_2Zr(CH_2Ph)_2$. This bisbenzyl complex reacts with **1** to produce Cu^0 and $PhCH_2CH_2Ph$, the latter identified by ^1H NMR; replacement of **1** by $[Cu(NCMe)_4]BF_4$ in this reaction again gives Cu^0 and bisbenzyl.

We next decided to examine a more robust polyalkyl compound and one which was a close analogue to the *fac*-$H_3Ir(PMe_2Ph)_3$ case we had studied previously. Reaction of $[Cu(NCMe)_4]BF_4$ with *fac*-$IrMe_3(PMe_2Ph)_3$ in THF occurs below 25°C to give a yellow solution from which increasing amounts of a green precipitate form with the passage of time. Optimally, filtration of the yellow solution from the green precipitate after short (< 1 h) reaction times, rapid solvent removal *in vacuo* and washing of the solid residue with benzene, leaves behind a white solid whose ^{31}P NMR shows an AX_2 pattern ($J_{AX} = 16$ Hz) consistent with all three of the structures **I–III**. The ^1H NMR chemical shift and integration proves the presence of one MeCN. The presence of three P*Me* ^1H NMR chemical shifts rules out structure **I**. The triplet multiplicity of two of the three P*Me* resonances indicates a *mer* configuration of the phosphines, with the three chemical shifts due to diastereotopic methyl groups on the *trans* pair of phosphines. This excludes structure **III** and is consistent with structure **II**. While structure **II** has two inequivalent IrMe groups, the pattern observed in the 360 MHz ^1H NMR of the product cannot be better defined than as being a "multiplet".

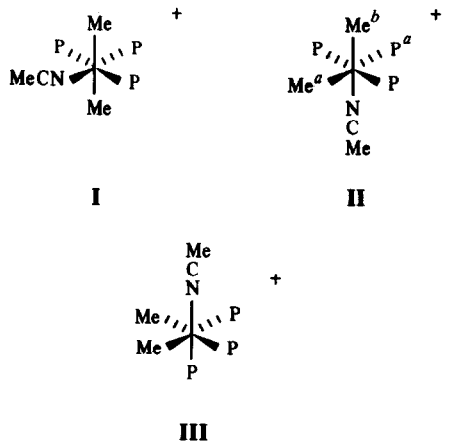

In order to resolve this apparent discrepancy, selective $^1H\{^{31}P\}$ NMR experiments were carried out. First, complete decoupling of both ^{31}P types collapses all methyl signals (IrMe and PMe) to singlets. In the IrMe region, two barely resolved (0.02 ppm) signals are observed near 0.18 ppm. If the two mutually *trans* phosphorus nuclei are selectively decoupled, the upfield IrMe signal is a singlet and the downfield signal is a doublet. The downfield IrMe peak is thus assigned as the one *trans* to the unique phosphorus (Me^a in **II**). If the unique phosphorus is decoupled, both IrMe peaks are resolved into (nearly overlapping) triplets; the *trans* phosphines couple to *both* methyls and thus show larger *cis* coupling than P^a does in **II**.

As final confirmation of this stoichiometry and structure, an independent synthesis of this iridium complex was accomplished by acidolysis (equimolar $HBF_4 \cdot OEt_2$) of *fac*-$IrMe_3(PMe_2Ph)_3$ in CH_3CN at or below 25°C.

In summary, $IrMe_3(PMe_2Ph)_3$ reacts with $[Cu(NCMe)_4]BF_4$ in THF under mild conditions [eq. (2)] to quantitatively* transfer a methyl group (net transfer of CH_3^-), with the resulting electrophile $IrMe_2(PMe_2Ph)_3^+$ being efficiently quenched by back-transfer of a molecule of acetonitrile.

$$[Cu(NCMe)_4]BF_4 + fac\text{-}IrMe_3(PMe_2Ph)_3 \rightarrow [IrMe_2(NCMe)(PMe_2Ph)_3]BF_4 + CuMe. \quad (2)$$

Our attempts to trap the CuMe product by running the reaction in the presence of PPh_3 were without success.† Decomposition of CuMe in the reaction medium leads to an insoluble green (presumably divalent copper) product and later to the deposition of copper metal. The cationic iridium product contains a rearranged IrP_3 skeleton (i.e. *fac* → *mer*) and avoids competitive (i.e. *trans*) positioning on Ir of the two strong *trans* influence methyl groups.

We have employed an oxidation-resistant [Ir(III)] alkyl and an electrophile which is (at worst) a weak oxidant in our quest for an $Ir(\mu\text{-}CH_3)_nCu^+$ species. While we are successful in avoiding a net oxidation of the iridium alkyl, any bridging species, while an obvious candidate as a reaction intermediate in eq. (2) is not observed. Instead, net ligand transfer takes place, and Cu^+ behaves towards CH_3^- in a manner formally similar to its more common role in halide[8] or phosphine[9] abstraction.

We feel the weight of evidence supports the methyl transfer as evolving from a 1 : 1 intermediate or transition state. For example, while a 2 : 1 reaction of $H_3Ir(PMe_2Ph)_3$ with $Cu(NCMe)_4^+$ forms a 2 : 1 complex,[2] two *fac*-$IrMe_3(PMe_2Ph)_3$ reacts with one $Cu(NCMe)_4^+$ to leave one mole of $IrMe_3(PMe_2Ph)_3$ unreacted. At the other extreme, Jordan *et al.* have considered[10] a mechanism where two alkyl groups are removed, and then conproportionation with unaltered reagent dialkyl complex (i.e. back-transfer of one alkyl) gives the observed monoalkyl products. In our system, the reaction of *fac*-$IrMe_3(PMe_2Ph)_3$ with 2 $Cu(NCMe)_4^+$ proceeds exactly according to eq. (2), with no evidence of any $IrMe(NCMe)_2(PMe_2Ph)_3^{2+}$ product.

The possibility that one-electron transfer (rather than net methyl transfer) is the actual event which follows the 1 : 1 encounter of $Cu(NCMe)_4^+$ and $IrMe_3(PMe_2Ph)_3$ has been discussed for the $Cp_2Fe^+/Cp_2Zr(CH_2Ph)_2$ case by Jordan *et al.*[11]

Acknowledgements—We thank the National Science Foundation for partial financial support and Johnson Matthey Co. for material support. Wyatt Mills is thanked for valuable discussions.

REFERENCES

1. L. F. Rhodes, J. C. Huffman and K. G. Caulton, *J. Am. Chem. Soc.* 1983, **105**, 5137.
2. L. F. Rhodes, J. C. Huffman and K. G. Caulton, *J. Am. Chem. Soc.* 1984, **106**, 6874.
3. L. F. Rhodes, J. C. Huffman and K. G. Caulton, *J. Am. Chem. Soc.* 1985, **107**, 1759.
4. For a review of μ-hydrocarbyls, see J. Holton, M. F. Lappert, R. Pearce and P. I. W. Yarrow, *Chem. Rev.* 1983, **83**, 135.
5. For an example of CH_3 bridging two zirconium centres, see R. M. Waymouth, B. O. Santarsiero, R. J. Coots, M. J. Bronowski and R. H. Grubbs, *J. Am. Chem. Soc.* 1986, **108**, 1427.
6. J. Chatt and B. L. Shaw, *J. Chem. Soc.* (*A*) 1966, 1836.
7. R. F. Jordan, W. E. Dasher and S. F. Echols, *J. Am. Chem. Soc.* 1986, **108**, 1718.
8. P. Braunstein, M. A. Luke, A. Tiripicchio and M. Tiripicchio-Camellini, *Angew. Chem. Int. Ed. Engl.* 1987, **26**, 768.
9. S. A. Levitre, C. C. Tso and A. R. Cutler, *J. Organometal. Chem.* 1986, **308**, 253.
10. R. F. Jordan, W. E. Dasher and S. F. Echols, *J. Am. Chem. Soc.* 1986, **108**, 1718.
11. R. F. Jordan, R. E. LaPointe, C. S. Bajgur, S. F. Echols and R. Willett, *J. Am. Chem. Soc.* 1987, **109**, 4111.

* The reaction was also monitored by ^1H NMR in $CDCl_3$ solvent. While a green precipitate was observed immediately, compound **II** is the only iridium phosphine product observed.

† We will report separately on the full characterization of $(Ph_3P)_3CuMe$ by an independent route: P. Coan (unpublished).

Polyhedron Vol. 7, No. 14, pp. 1289–1298, 1988
Printed in Great Britain

0277–5387/88 $3.00+.00
© 1988 Pergamon Press plc

THE REVERSIBLE ADDUCT FORMATION OF GROUP III TRIALKYLS WITH RELATIVELY INVOLATILE PHOSPHINES; X-RAY CRYSTAL STRUCTURES OF $(Me_3M)_2 \cdot (Ph_2PCH_2)_2$ (M = Al, Ga, In) AND $(Me_3Al)_3 \cdot (Ph_2PCH_2CH_2)_2PPh$

DONALD C. BRADLEY,* HALINA CHUDZYNSKA, MARC M. FAKTOR,† DARIO M. FRIGO, MICHAEL B. HURSTHOUSE,* BILQUIS HUSSAIN and LESLEY M. SMITH

Department of Chemistry, Queen Mary College, University of London, Mile End Road, London E1 4NS, U.K.

(*Received* 26 *January* 1988; *accepted* 18 *February* 1988)

Abstract—The following adducts of Group III trialkyls with phosphines have been prepared, either by direct reaction in hydrocarbon solution or by displacement of ether from the metal trialkyl etherate: $Me_3M \cdot PPh_3$ (M = Ga, In); $Me_3In \cdot P(2\text{-}MeC_6H_4)_3$; $(R_3M)_2 \cdot (Ph_2PCH_2)_2$ (R = Me, M = Al, Ga, In; R = Et, M = Ga, In; R = Bu^i, M = Al); $(Me_3M)_3 \cdot (Ph_2PCH_2CH_2)_2PPh$ (M = Al, Ga, In) and $(Me_3M)_4 \cdot (Ph_2PCH_2CH_2PPhCH_2)_2$ (M = Al, Ga, In). The compounds were analysed by ^1H and ^{31}P NMR. The ^{31}P NMR spectra of $(Me_3M)_2 \cdot (Ph_2PCH_2)_2$ (M = Ga, In) showed little change between 193 K and room temperature. Thermal dissociation of the adducts *in vacuo* gave the free metal trialkyl with no detectable contamination by the respective phosphine. Crystals of $(Me_3M)_2 \cdot (Ph_2PCH_2)_2$ (M = Al, Ga, In) are iso-structural and the molecules contain two distorted tetrahedral metals bridged by the $(Ph_2PCH_2)_2$; the M—P distances are 2.544(4), 2.546(4) and 2.755(4) Å, respectively. The X-ray crystal structure of $(Me_3Al)_3 \cdot (Ph_2PCH_2CH_2)_2PPh$ shows the molecule to contain distorted tetrahedral aluminium atoms bonded to each of the three phosphorus atoms, with Al—P distances of 2.536(9) and 2.510(9) Å for the terminal and central moieties, respectively; the unit cell contains two such molecules plus one benzene molecule (the crystallizing solvent).

The trialkyls of Group III and their adducts with amines and phosphines have been successfully used for the Metal–Organic Chemical Vapour Deposition (MOCVD) of III–V semiconductors.[1,2] The adducts reported hitherto[3–6] have mainly been volatile compounds whose principal advantages over the parent trialkyls in MOCVD have been reduced fire and toxicity hazards with consequently greater ease of purification and handling.[2] An alternative approach, reported herein, is the formation of adducts with relatively involatile bases which have weak adduct bonds. Thus, safety and ease of purification are maximized and the purified adduct can then be thermolytically dissociated to release the volatile metal trialkyl R_3M either prior to loading into the MOCVD reactor, or *in situ*.

The process can be generally illustrated thus:

$$xR_3M(g) + B(s) \rightleftharpoons (R_3M)_x \cdot B(s). \quad (1)$$

The equilibrium constant K which defines the equilibrium partial pressure of the trialkyl over the adduct P_{R_3M} is given by the following:

$$K = \frac{(P_{R_3M})^x a_B}{a_{(R_3M)_xB}} \quad (2)$$

$$\ln K = \frac{-\Delta H}{RT} + \frac{\Delta S}{R} \quad (3)$$

where a_B and $a_{(R_3M)_xB}$ are the activities of the base and adduct, respectively, and ΔH and ΔS are the enthalpy and entropy change associated with the above reaction. The value of ΔS will be largely dominated by the entropy of vaporization of R_3M and so to a first approximation may be independent of the nature of B. Under these circumstances the

* Authors to whom correspondence should be addressed.
† Deceased.

value of K will be largely determined by the value of ΔH, a term containing the enthalpy of vaporization of R_3M (once again independent of the nature of B) and the enthalpy of complex formation in the condensed phase ΔH_c.

An ideal candidate for B must possess a very much lower vapour pressure than R_3M at normal temperatures, but must also have a specific value of ΔH_c upon reaction with R_3M: if it is too large then the dissociation reaction will only proceed appreciably at very high temperatures which may be both inconvenient and lead to further thermolysis of R_3M itself; if ΔH_c is too low there will be a substantial partial pressure of the pyrophoric R_3M over the adduct even at room temperature, therefore losing all the advantages of the adduct process.

An additional criterion for a base if the adduct is to be used for *in situ* generation of R_3M in the MOCVD reactor is that both base and adduct must have fairly high melting points, neither must the latter form a very low melting eutectic when depleted of the metal trialkyl. From eq. (2), if the base and adduct are solid then their activities are unity and the value of P_{R_3M} is independent of the extent of depletion from the system, i.e. the source is time-independent. If the sample melts however, the activities of the base and adduct will rise and fall respectively as the sample is depleted; the value of P_{R_3M} will gradually decrease with time.

The vapour pressures of PPh_3, $P(2\text{-}MeC_6H_4)_3$ and $(Ph_2PCH_2)_2$ (diphos) were known to be low,[7] and furthermore it was thought from a simplistic viewpoint that the presence of electron-withdrawing aryl groups on the phosphorus would reduce the ability of the lone pairs to coordinate, therefore giving the desired relatively weak aducts with R_3M. Although the vapour pressures of $(Ph_2PCH_2CH_2)_2PPh$ (triphos) and $(Ph_2PCH_2CH_2PPhCH_2)_2$ (tetraphos) were not known, they are clearly even less volatile than those listed above.

Therefore, the five phosphines mentioned above were thought to be possible candidates for reversible adduct formation with R_3M.

RESULTS AND DISCUSSION

Displacement of diethyl ether from $Me_3M \cdot OEt_2$ by the respective phosphine in the appropriate molar ratio gave $Me_3M \cdot PPh_3$ (M = Ga, In), $(Me_3M)_2 \cdot$diphos (M = Ga, In; diphos = $(Ph_2PCH_2)_2$), $(Me_3Ga)_3 \cdot$triphos (triphos = $(Ph_2PCH_2CH_2)_2PPh$) and $(Me_3Ga)_4 \cdot$tetraphos (tetraphos = $(Ph_2PCH_2CH_2PPhCH_2)_2$). Direct reaction of R_3M with the respective phosphine in hydrocarbon solution and in the appropriate molar ratio gave $Me_3Al \cdot PPh_3$, $Me_3In \cdot P(2\text{-}MeC_6H_4)_3$, $(Me_3Al)_2 \cdot$diphos, $(Et_3M)_2 \cdot$diphos (M = Ga, In), $(Bu^i_3Al)_2 \cdot$diphos, $(Me_3M)_3 \cdot$triphos (M = Al, In) and $(Me_3M)_4 \cdot$tetraphos (M = Al, In). The compound $Me_3Al \cdot PPh_3$ has already been reported[8] but was prepared here to test its thermal dissociation properties.

All the compounds were white, crystalline solids except $(Me_3In)_3 \cdot$triphos which was isolated as an oil which could not be crystallized. They reacted much more slowly upon exposure to the atmosphere than the parent trialkyls: in the solid, $t_{1/2}$ values of up to 1 h were observed for some. Only $(Et_3In)_2 \cdot$diphos appeared to be sensitive to daylight, decomposing to a grey metallic solid (indium) after several days.

All the compounds were analysed by ^1H NMR and most by ^{31}P NMR; selected data are presented in Table 1. As has been observed previously, the ^1H NMR chemical shifts of the alkyl groups on the metal are invariably shifted downfield relative to the uncomplexed moiety, but the extent of this shift does not appear to be simply related to adduct bond strength.[6] It has been reported however, that the chemical shifts of the protons on the Lewis base, particularly those on the carbons α to the pnicogen, are normally more shielded in the complex;[6] the reverse is found in all the phosphine adducts reported here. No such generalizations can be made for the ^{31}P NMR chemical shifts: only the Me_3Ga moiety was shown invariably to produce a downfield shift upon adduct formation; the other R_3M gave either upfield or downfield shifts depending upon R and the phosphine, and in fact Me_3In produced downfield shifts in the central P atoms of triphos and tetraphos, but upfield shifts in the terminal ones. The P—P coupling constants for triphos, tetraphos and their adducts were obtained by computer simulation; the values found in the adducts were invariably greater than those in the free phosphines.

The differences between the values for δ_P in the adducts and respective uncoordinated phosphines were surprisingly small in many cases, e.g. < 2.5 ppm for the diphos adducts. It was thought that this may be due to the complexes dissociating at least partially in solution; therefore variable temperature ^{31}P NMR was performed on solutions of diphos, $(Me_3Ga)_2 \cdot$diphos, $(Me_3In)_2 \cdot$diphos, $(Me_3Ga)_2 \cdot$diphos + diphos and $(Me_3In)_2 \cdot$diphos + diphos (the mixtures being present in a 1 : 1 molar ratio). The results are presented in Table 2. The δ_P for each solution moves upfield as the temperature is lowered. For diphos, this must be a solvent anisotropy effect but for the other solutions may include a changing degree of dissociation. The δ_P of $(Me_3In)_2 \cdot$diphos is upfield of diphos and

Table 1. Selected NMR signals for the compounds in C_6D_6

Compound	δ_H (ppm) R_3M	Phosphine Alkyl	Phosphine Aryl[c]	δ_P (ppm) P_A[a]	P_B[a]	J_{PP} (Hz)
PPh_3	—	—	7.01, 7.44	−6.26	—	—
$P(2\text{-}MeC_6H_4)_3$	—	2.42	7.01	−30.76	—	—
Diphos	—	2.20	7.02, 7.35	−13.81	—	—
Triphos	—	1.93[c]	7.04, 7.39	−18.01	−14.08	AB 28.3
Tetraphos	—	1.80[c]	7.05, 7.39	−18.11	−14.02	AB 28.0[b] AA′ 24.0[b]
Me_3Al	−0.35	—	—	—	—	—
Bu^i_3Al	0.29d, 1.04d, 1.95 hept	—	—	—	—	—
Me_3Ga	−0.10	—	—	—	—	—
Et_3Ga	0.50q, 1.22t	—	—	—	—	—
Me_3In	−0.18	—	—	—	—	—
Et_3In	0.53q, 1.42t	—	—	—	—	—
$Me_3Al \cdot PPh_3$	−0.07	—	7.06, 7.50	−9.37	—	—
$Me_3Ga \cdot PPh_3$	0.17	—	7.00, 7.45	−5.49	—	—
$Me_3In \cdot PPh_3$	0.15	—	7.00, 7.45	−8.96	—	—
$Me_3In \cdot P(2\text{-}MeC_6H_4)_3$	−0.15	2.45	7.01	−29.19	—	—
$(Me_3Al)_2 \cdot$ diphos	−0.17	2.62	7.00, 7.47	−14.01	—	—
$(Bu^i_3Al)_2 \cdot$ diphos	0.51d, 1.10d, 2.10 hept	2.47	7.01, 7.45	−12.88	—	—
$(Me_3Ga)_2 \cdot$ diphos	0.15	2.52	6.99, 7.41	−11.38	—	—
$(Et_3Ga)_2 \cdot$ diphos	0.80q, 1.48t	2.51	7.00, 7.44	Not obtained	—	—
$(Me_3In)_2 \cdot$ diphos	0.07	2.51	6.99, 7.40	−15.02	—	—
$(Et_3In)_2 \cdot$ diphos	0.96q, 1.61t	2.51	7.05, 7.47	Not obtained	—	—
$(Me_3Al)_3 \cdot$ triphos	−0.22	2.39[c]	6.99, 7.50	−17.44	−13.95	AB 33.5
$(Me_3Ga)_3 \cdot$ triphos	0.10	2.30[c]	7.00, 7.46	−14.17	−10.90	AB 32.8
$(Me_3In)_3 \cdot$ triphos	0.12	2.25[c]	7.04, 7.47	−17.91	−15.29	AB 33.6
$(Me_3Al)_4 \cdot$ tetraphos	−0.25	2.24[c]	6.97, 7.50	−17.57	−14.02	AB 34.5[b] AA′ 28.9[b]
$(Me_3Ga)_4 \cdot$ tetraphos	0.06	2.21[c]	7.00, 7.50	−14.64	−11.23	AB 32.2[b] AA′ 27.4[b]
$(Me_3In)_4 \cdot$ tetraphos	0.02	2.09[c]	6.97, 7.45	−18.05	−15.12	AB 32.2[b] AA′ 28.2[b]

[a] For triphos and tetraphos moieties, P_A (and $P_{A'}$) refer to the more central P atom(s).
[b] Calculated assuming $J_{P_BP_{B'}} = 0$ Hz.
[c] Complex multiplets, median reported.

changes only slightly with temperature (much less so than diphos itself); that of $(Me_3Ga)_2 \cdot$ diphos is downfield of diphos, so its small but significant upfield shift as the temperature is lowered cannot be due to greater association. As expected, the δ_P for each of the mixtures of $(Me_3M)_2 \cdot$ diphos + diphos was intermediate between the values for the adduct and free diphos. For indium, only one signal was detected down to 193 K implying either that the adduct was totally dissociated, or a 1 : 1 adduct

Table 2. Variable temperature ^{31}P NMR chemical shifts (ppm in $C_6D_5CD_3$) of selected species

Temperature (K)	Diphos	$(Me_3Ga)_2 \cdot$ diphos	$(Me_3Ga)_2 \cdot$ diphos + diphos	$(Me_3In)_2 \cdot$ diphos	$(Me_3In)_2 \cdot$ diphos + diphos
Room (295–305)	−12.20	−11.33	−11.34	−15.34	−14.25
263	—	—	—	−15.58	−14.78
223	—	—	—	−15.70	−15.26
193	−14.31	−11.55	−12.64[a]	−15.66	−15.54

[a] Signal flanked by spinning side-bands at ±16 Hz, relative intensity 1/8.

is formed (a fluxional four-coordinate or non-fluxional chelate complex), or that exchange between adduct components was rapid even at this temperature. The first is unlikely since the chemical shifts are different from the free phosphines; attempts to isolate a 1:1 adduct have failed and evidence from measuring the partial pressure of Me_3M over the diphos adducts suggests that the 1:1 adduct at temperatures of 40–150°C is unstable with respect to the 2:1 adduct + diphos; the facile exchange of adduct components at low temperature has been observed previously[6] and seems the most likely explanation. For gallium, one signal was found at ambient temperature but at 193 K the signal at δ −12.64 was flanked by two smaller signals of equal intensity (1:8 relative to the central peak) at 16 Hz either side of the main signal. These are believed to be spinning side-bands but this has not been verified; we can find no plausible explanation for these satellites which are based upon "freezing out" of fluxionality. Furthermore, both the ^{31}P and ^1H NMR spectra of $Et_3Ga \cdot (Ph_2P)_2CH_2$ were largely unchanged between ambient and 193 K.[9]

The variable temperature NMR evidence implies that for $(Me_3M)_2 \cdot$diphos (M = Ga, In) there is no substantial association as the temperature is lowered, as would be expected for a partially dissociated complex. On the other hand, a totally dissociated moiety would give δ_H and δ_P values virtually identical with the free moieties, which is not observed; therefore it must be concluded that these adducts are associated in solution at these temperatures and concentrations (*ca* 5%), even though the changes in δ_P upon adduct formation are often small. Variable temperature NMR was not performed on the other adducts.

Each adduct was heated *in vacuo* and the resulting volatiles, which were analysed by ^1H NMR, showed the respective metal trialkyl with no signals corresponding to the phosphine. The sample temperature at which condensed volatiles first became visible to the naked eye varied between 40°C for $Me_3In \cdot P(2\text{-}MeC_6H_4)_3$ and 115°C for $(Me_3Al)_2 \cdot$diphos, both at 10^{-2} mmHg; these temperatures are thought to correspond broadly with the adduct bond strengths. For the adducts with PPh_3 and diphos, these bond strengths, based upon the ease of thermal dissociation, followed the series:

$$Al > Ga \sim In.$$

This order is similar to that found for adducts between Me_3M and diphos by dissociation pressure measurements,[10] *viz.*

$$Al \gg In > Ga.$$

Furthermore, for a given Lewis acid the bond strengths appeared to be in the order:

$$PPh_3 \sim \text{diphos} > \text{triphos} \sim \text{tetraphos} > P(2\text{-}MeC_6H_4)_3.$$

Interestingly, when uncomplexed diphos or any of the adducts containing triphos and tetraphos were crystallized from benzene then this solvent was clathrated into the crystals. Prolonged drying at just above room temperature and 10^{-2} mmHg gave crystals which still showed the presence of benzene in the ^1H NMR; in fact the benzene can be seen in the X-ray crystal structure of $(Me_3Al)_3 \cdot$triphos (*vide infra*). Furthermore, the benzene was observed in the ^1H NMR of the metal alkyls obtained by thermal dissociation of these adducts. This phenomenon was not observed for the diphos adducts provided there was no excess diphos present.

X-ray crystal structure determination showed that the three complexes $(Me_3M)_2 \cdot$diphos (M = Al, Ga, In) are isostructural with two distorted tetrahedral metal centres linked across a centre of symmetry by the bridging diphos. The structure of the indium complex as a representative of the group, is shown in Fig. 1; selected bond lengths and angles are given in Table 3. The bond lengths show that the covalent radii of Al and Ga are very similar, and are *ca* 0.2 Å smaller than that for In. Detailed comparison of M—P and M—C distances,

Table 3. Selected bond lengths (Å) and angles (deg) for $(Me_3M)_2 \cdot$diphos

	Al	Ga	In
M—P	2.544(4)	2.546(4)	2.755(4)
M—C(1)	1.967(5)	1.973(5)	2.175(6)
M—C(2)	1.967(5)	1.977(5)	2.161(6)
M—C(3)	1.957(5)	1.980(5)	2.177(7)
P—C(11)	1.819(4)	1.820(4)	1.822(4)
P—C(21)	1.817(4)	1.820(4)	1.819(4)
P—C(4)	1.835(4)	1.841(4)	1.841(4)
C(1)—M—P(1)	98.7(2)	98.5(2)	96.1(2)
C(2)—M—P(1)	103.2(2)	102.7(2)	101.7(3)
C(3)—M—P(1)	104.1(2)	103.3(2)	100.8(3)
C(1)—M—C(2)	116.5(3)	116.7(3)	118.8(4)
C(1)—M—C(3)	116.4(3)	116.9(3)	116.5(4)
C(2)—M—C(3)	114.5(3)	114.7(2)	116.7(4)
C(4)—P—M	116.1(2)	116.3(2)	116.6(2)
C(11)—P—M	111.4(2)	111.7(2)	113.5(2)
C(21)—P—M	114.3(2)	114.5(2)	112.3(2)
C(11)—P—C(4)	101.8(2)	101.6(2)	104.5(2)
C(21)—P—C(4)	104.8(2)	104.6(2)	101.9(2)
C(11)—P—C(21)	107.4(2)	106.8(2)	106.9(2)

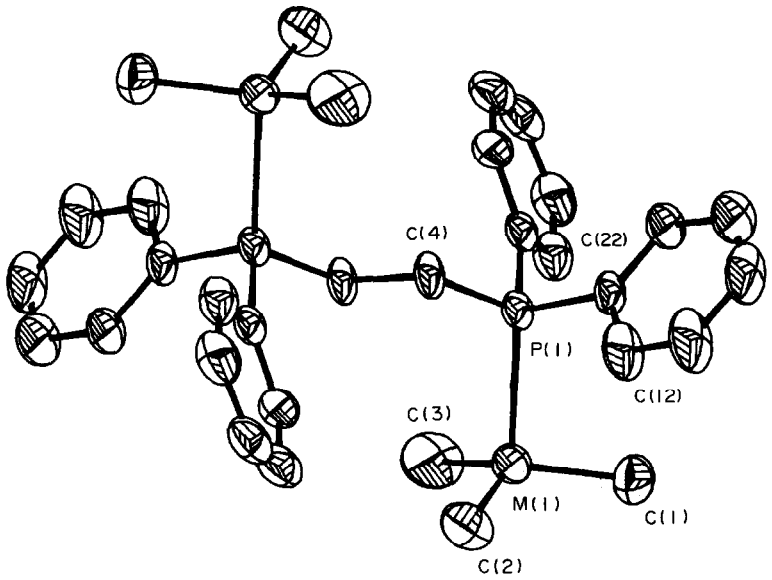

Fig. 1. X-ray crystal structure of $(Me_3In)_2 \cdot$ diphos to show the numbering scheme.

using M—C distances as the basis for covalent radii changes, indicate a slight shortening (0.015 Å) of the Ga—P distance compared with the difference between the Al—C and Ga—C distances, and a slightly larger increase (0.03 Å) in the In—P distance. This is perhaps surprising in view of the relative bond strengths as reflected by thermal dissociation (see above and ref. 10). The In—P distance, 2.755(4) Å, is substantially longer than that found for $Me_3In \cdot PMe_3$ *viz.* 2.683(4) Å,[11] and this is consistent with it being a weaker interaction[10] than in the PMe_3 adduct.[5] There is a dearth of data on Al—P and Ga—P distances from X-ray crystal data, but values of 2.53(4) and 2.52(2) Å have been determined by gas phase electron diffraction for $Me_3Al \cdot PMe_3$[12] and $Me_3Ga \cdot PMe_3$,[13] respectively. Again the analogous distances in the diphos adducts are greater, but the errors in the gas phase measurements are too large for meaningful comparisons.

The X-ray crystal structure of $(Me_3Al)_3 \cdot$ triphos is shown in Fig. 2 with selected parameters in Table 4. The triphos bridges the three distorted tetrahedral aluminium centres; the central Al—P distance of 2.510(9) Å is shorter than the terminal ones at 2.536(9) Å, either because one phenyl and two ethylene groups are less sterically crowding than *vice versa*, or because of the electron-withdrawing effect of the phenyl groups on the phosphorus lone pair. It is noted that the central Al—P distance is shorter than that obtained by electron diffraction of $Me_3Al \cdot PMe_3$ (*vide supra*), although as has already been mentioned, the error in this technique is too great for meaningful comparison. Both of the Al—P distances are slightly smaller than in the diphos adduct described above. The crystal packing diagram, Fig. 3, shows the unit cell contains one benzene molecule of crystallization per two adduct molecules.

EXPERIMENTAL

All operations were performed under an atmosphere of purified nitrogen using Schlenk-style apparatus and a glove box. Solvents were distilled from sodium benzophenone under nitrogen. Anhydrous $GaCl_3$, $InCl_3$, Me_3In, Et_3Ga, Et_3In, all phosphines and solutions of Me_3Al (in hexane), Bu^i_3Al (in toluene) and MeLi (in diethyl ether), were obtained from commercial sources. ^1H and ^{31}P NMR spectra were obtained using Bruker WP80 FT, WM250 FT, WH400 FT spectrometers and micro-analyses on some of the more important compounds were carried out by the Microanalytical Laboratory of University College, London.

(1) $Me_3Al \cdot PPh_3$

This was prepared as described previously[8] and was recrystallized from benzene (76% yield); m.p. 127–131°C. A sample of this compound (1.3 g, 3.9 mmol) was heated slowly under 10^{-2} mmHg in a trap-to-trap distillation apparatus, the receiver flask at −196°C. A distillate became visible at 105°C and the dissociation became vigorous at 120°C when the adduct melted and bubbled. Final yield of $(Me_3Al)_2$: 0.22 g, 78%.

(2) $Me_3Ga \cdot PPh_3$

To a solution of $GaCl_3$ (11.0 g, 62 mmol) in diethyl ether (40 cm^3) at 0°C was added MeLi (112

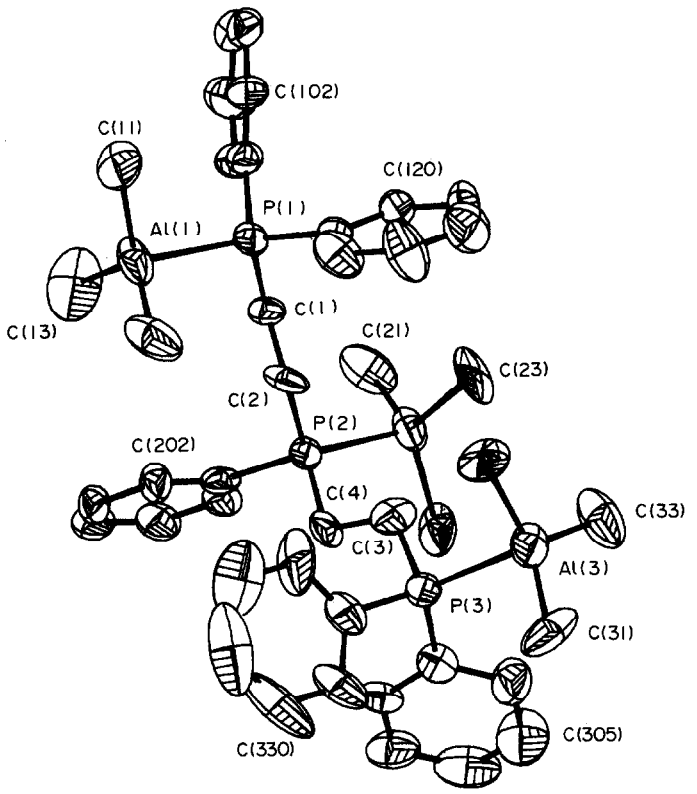

Fig. 2. X-ray crystal structure of $(Me_3Al)_3 \cdot$ triphos $\cdot 0.5C_6H_6$ to show the numbering scheme.

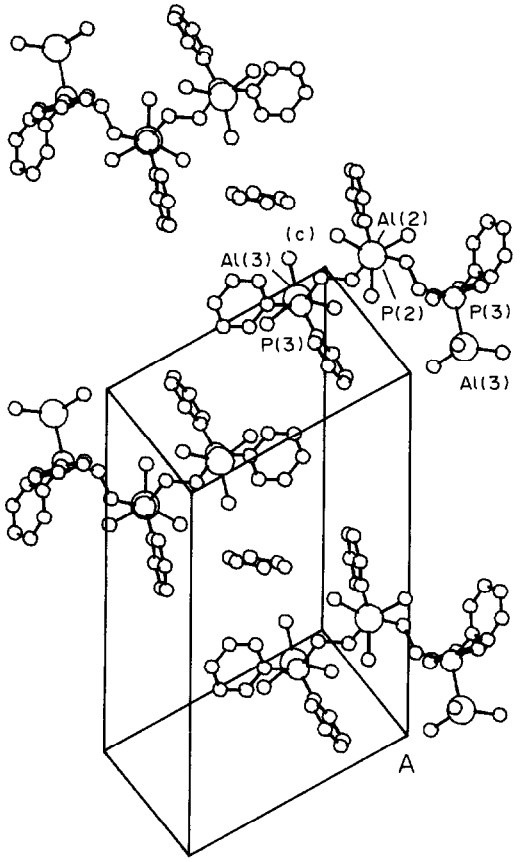

Fig. 3. Crystal packing diagram of $(Me_3Al)_3 \cdot$ triphos $\cdot 0.5C_6H_6$.

Table 4. Selected bond lengths (Å) and angles (deg) for $(Me_3Al)_3 \cdot (Ph_2PCH_2CH_2)_2PPh$

Al(1)—C(11)	1.960(14)	Al(1)—C(12)	1.979(11)
Al(1)—C(13)	1.961(14)	Al(1)—P(1)	2.535(7)
P(1)—C(101)	1.802(10)	P(1)—C(110)	1.808(10)
P(1)—C(1)	1.832(12)		
Al(2)—C(21)	1.968(11)	Al(2)—C(22)	1.973(15)
Al(2)—C(23)	1.983(15)	Al(2)—P(2)	2.504(6)
P(2)—C(2)	1.816(11)	P(2)—C(3)	1.812(10)
P(2)—C(201)	1.813(10)		
Al(3)—C(31)	1.936(12)	Al(3)—C(32)	1.965(14)
Al(3)—C(33)	1.972(13)	Al(3)—P(3)	2.531(7)
P(3)—C(301)	1.804(10)	P(3)—C(310)	1.790(10)
P(3)—C(4)	1.816(9)		
C(1)—C(2)	1.549(13)	C(3)—C(4)	1.536(15)
C(12)—Al(1)—C(11)	116.1(6)	C(13)—Al(1)—C(11)	117.2(6)
C(13)—Al(1)—C(12)	115.2(7)	P(1)—Al(1)—C(11)	101.5(4)
P(1)—Al(1)—C(12)	107.3(5)	P(1)—Al(1)—C(13)	95.5(4)
C(101)—P(1)—Al(1)	111.0(3)	C(110)—P(1)—Al(1)	121.2(3)
C(110)—P(1)—C(101)	104.7(4)	C(1)—P(1)—Al(1)	111.4(4)
C(1)—P(1)—C(101)	104.4(4)	C(1)—P(1)—C(110)	102.7(4)
C(2)—C(1)—P(1)	109.6(7)	P(2)—C(2)—C(1)	112.2(7)
Al(2)—P(2)—C(2)	114.5(4)	C(201)—P(2)—C(2)	106.2(5)
C(201)—P(2)—Al(2)	118.2(3)	C(3)—P(2)—C(2)	103.1(5)
C(3)—P(2)—Al(2)	110.9(4)	C(3)—P(2)—C(201)	102.2(5)
C(21)—Al(2)—P(2)	105.6(4)	C(22)—Al(2)—P(2)	99.8(4)
C(22)—Al(2)—C(21)	116.9(6)	C(23)—Al(2)—P(2)	99.7(4)
C(23)—Al(2)—C(21)	114.0(6)	C(23)—Al(2)—C(22)	117.1(6)
C(4)—C(3)—P(2)	114.0(7)	P(3)—C(4)—C(3)	118.8(7)
Al(3)—P(3)—C(4)	108.5(4)	C(301)—P(3)—C(4)	104.1(5)
C(301)—P(3)—Al(3)	117.7(3)	C(310)—P(3)—C(4)	105.8(5)
C(310)—P(3)—Al(3)	114.2(4)	C(310)—P(3)—C(301)	105.5(5)
C(31)—Al(3)—P(3)	101.0(5)	C(32)—Al(3)—P(3)	99.2(5)
C(32)—Al(3)—C(31)	118.3(6)	C(33)—Al(3)—P(3)	103.2(5)
C(33)—Al(3)—C(31)	116.5(6)	C(33)—Al(3)—C(32)	114.3(6)

cm^3 of 1.67 M solution, 187 mmol) dropwise over about 1 h. The ether was fractionated off at atmospheric pressure using a 16 cm Vigreux column and the $Me_3Ga \cdot OEt_2$ was distilled without the column at 98°C; yield 10.3 g, 88% based on $GaCl_3$. To $Me_3Ga \cdot OEt_2$ (3.0 g, 16 mmol) in benzene (10 cm^3) was added PPh_3 (4.2. g, 16 mmol) in benzene (40 cm^3). The ether was fractionated off as above and the remaining benzene solution was concentrated *in vacuo* to obtain crystalline $Me_3Ga \cdot PPh_3$ which was recrystallized from pentane; yield 4.2 g, 70%; m.p. 132–135°C. Found: C, 66.6; H, 6.47. $GaPC_{21}H_{24}$ requires: C, 66.9; H, 6.41%. A sample of $Me_3Ga \cdot PPh_3$ (6.0 g, 16 mmol) began to liberate Me_3Ga at 80°C/10^{-2} mmHg but the rate was more satisfactory at 90°C. Final yield of Me_3Ga: 1.3 g, 71%.

(3) $Me_3In \cdot PPh_3$

This was prepared in a similar manner to $Me_3Ga \cdot PPh_3$ using $InCl_3$ (7.2 g, 33 mmol), MeLi (76 cm^3 of 1.30 M solution, 99 mmol) and PPh_3 (10.2 g, 39 mmol). From the crude product (15.5 g) which contained excess phosphine, a sample was recrystallized twice from benzene; m.p. 130–133°C. Found: C, 59.0; H, 5.64. $InPC_{21}H_{24}$ requires: C, 59.7; H, 5.73%. Another crude sample containing $Me_3In \cdot PPh_3$ (2.9 g, 6.9 mmol) plus excess PPh_3 (0.3 g) began to liberate Me_3In at 85°C/10^{-2} mmHg but the rate was more satisfactory at 105–135°C. Final yield of $[Me_3In]_4$: 0.5 g, 45%.

(4) $Me_3In \cdot P(2\text{-}MeC_6H_4)_3$

$P(2\text{-}MeC_6H_4)_3$ (3.7 g, 12 mmol) was dissolved in benzene (80 cm^3) and cooled to −196°C. Then Me_3In (1.9 g, 12 mmol) (obtained commercially) was condensed onto the frozen solution *in vacuo*, the mixture allowed to warm to room temperature, filtered and the filtrate concentrated *in vacuo* whence crystals of $Me_3In \cdot P(2\text{-}MeC_6H_4)_3$ were obtained; yield 2.8 g, 50%; m.p. 110–125°C. A

sample of the adduct (1.6 g, 3.4 mmol) began to liberate Me_3In at 40°C/10^{-2} mmHg but the temperature was gradually raised to 80°C to obtain a satisfactory evolution rate. Final yield of $[Me_3In]_4$: 0.43 g, 79%.

(5) $(Me_3Al)_2$·diphos

A solution of Me_3Al (21 cm^3 of 2.3 M solution, 48 mmol) was added to a solution of diphos (10.2 g, 25.6 mmol) in benzene (250 cm^3). The hexane was removed using a fractionating column at atmospheric pressure and the solution cooled to room temperature, filtered and the filtrate concentrated *in vacuo* whence large crystals of $(Me_3Al)_2$·diphos were obtained; yield 9.2 g, 71% based upon Me_3Al; m.p. 163–170°C. Found: C, 67.0; H, 6.73. $Al_2P_2C_{32}H_{42}$ requires: C, 70.8; H, 7.80%. A sample of $(Me_3Al)_2$·diphos (3.0 g, 5.5 mmol) began to liberate Me_3Al at 115°C/10^{-2} mmHg but the rate was more satisfactory at 130–140°C. Final yield of $(Me_3Al)_2$: 0.71 g, 90%.

(6) $(Bu^i_3Al)_2$·diphos

A solution of Bu^i_3Al (14.4 g of 25% solution, 18.2 mmol) was added to diphos (3.6 g, 9 mmol) in benzene. Solvents were removed *in vacuo* to give the crude adduct (6.8 g). A sample of this material was recrystallized from pentane; m.p. 75–90°C. The remainder (2.05 g, 2.58 mmol) was found to start liberating Bu^i_3Al at 80°C/10^{-2} mmHg and does so at a useful rate at 120–130°C. Final yield of Bu^i_3Al: 0.9 g, 88%.

(7) $(Me_3Ga)_2$·diphos

This was prepared in a similar manner to $Me_3Ga \cdot PPh_3$ using $GaCl_3$ (6.3 g, 36 mmol), MeLi (65 cm^3 of 1.67 M solution, 109 mmol) and diphos (8.2 g, 21 mmol). The crude product (12.5 g) was recrystallized from benzene giving large, colourless crystals of $(Me_3Ga)_2$·diphos; m.p. 163–167°C. Found: C, 61.4; H, 6.73. $Ga_2P_2C_{32}H_{42}$ requires: C, 61.2; H, 6.74%. A sample of the adduct (3.32 g, 5.29 mmol) began to liberate Me_3Ga at 85°C/10^{-2} mmHg but this proceeded more rapidly at 110–130°C. Final yield of Me_3Ga: 1.11 g, 91%.

(8) $(Et_3Ga)_2$·diphos

Et_3Ga (2.7 g, 17 mmol) was condensed *in vacuo* onto a solution of diphos (3.55 g, 8.92 mmol) in benzene (40 cm^3) at −196°C. The mixture was allowed to warm to room temperature and was stirred for 30 min. The solution was concentrated *in vacuo* whence crystals were obtained; yield 5.45 g, 87%; m.p. 120–128°C. A sample of this (3.45 g, 4.85 mmol) began to liberate Et_3Ga at 80°C/10^{-2} mmHg and this continued at 120–125°C. Final yield of Et_3Ga: 1.0 g, 66%.

(9) $(Me_3In)_2$·diphos

MeLi (63 cm^3 of 1.30 M solution, 82 mmol) was added dropwise to a suspension of $InCl_3$ (6.0 g, 27 mmol) in diethyl ether (50 cm^3) at 0°C. The contents were heated to reflux for 2 h and a solution of diphos (6.0 g, 15 mmol) in benzene (200 cm^3) was added. The ether was fractionated off at atmospheric pressure and the remaining solution was filtered. Solvents were removed *in vacuo* and the crude adduct (9.78 g) was recrystallized from benzene to give large, colourless crystals of $(Me_3In)_2$·diphos; m.p. 163–166°C. Found: C, 53.8; H, 5.90. $In_2P_2C_{32}H_{42}$ requires: C, 53.5; H, 5.89%. A sample of the adduct (3.07 g, 4.28 mmol) began to liberate Me_3In at 80°C/10^{-2} mmHg but was conveniently performed at 120–130°C. Final yield of $[Me_3In]_4$: 1.01 g, 74%.

(10) $(Et_3In)_2$·diphos

This was prepared in a similar manner to $(Et_3Ga)_2$·diphos using Et_3In (67 g, 330 mmol) and diphos (82 g, 206 mmol) and the product crystallized from benzene; yield 98 g, 74%; m.p. 95–108°C. A small sample exposed to daylight had decomposed to a grey metallic material after a few days. The remainder (98 g, 122 mmol) began to liberate Et_3In at 90°C/10^{-2} mmHg which became rapid at 100–115°C. Final yield of Et_3In: 34 g, 69%.

(11) $(Me_3Al)_3$·triphos

This was prepared in a similar manner to $(Me_3Al)_2$·diphos using Me_3Al (6.0 cm^3 of 2.3 M solution, 14 mmol) and triphos (2.46 g, 4.61 mmol). Upon the removal of benzene 3.6 g was obtained ≡ 104%! From X-ray studies, the compound reformulated as $(Me_3Al)_3$·triphos·$0.5C_6H_6$. Recalculated yield: 99%. A sample of this (1.14 g, 1.44 mmol) began to liberate Me_3Al at 55°C/10^{-2} mmHg and proceeded rapidly at 70–80°C. Final yield of $(Me_3Al)_2$: 0.25 g, *ca* 80% as the distillate contained a trace of benzene.

(12) $(Me_3Ga)_3$·triphos

This was prepared in a similar manner to $Me_3Ga \cdot PPh_3$ using $GaCl_3$ (2.29 g, 13 mmol), MeLi (10 cm^3 of 1.30 M solution, 13 mmol) and triphos

(2.45 g, 4.6 mmol), and gave the crystalline adduct; yield 2.6 g, *ca* 68% ignoring the benzene of crystallization. A sample of the adduct (1.27 g, *ca* 1.4 mmol) began to liberate Me_3Ga at 50°C/10^{-2} mmHg and the temperature was gradually raised to 120°C. Final yield of Me_3Ga: 0.49 g, essentially quantitative although the distillate contained a trace of benzene.

(13) $(Me_3In)_3$ · triphos

A sample of $(Me_3In)_2$ · diphos (5.4 g, 7.5 mmol) was heated to 130°C/10^{-2} mmHg and the resulting Me_3In was condensed onto a solution of triphos (2.70 g, 5.06 mmol) in benzene (50 cm^3) at −196°C. The solution was allowed to warm to room temperature and solvents were removed *in vacuo* to leave a sticky oil (5.56 g, equivalent to 109%, so clearly some benzene had been incorporated; equivalent to 1.2 moles per mole of adduct from gravimetric estimation). Attempted recrystallization to separate from pentane, benzene and toluene was unsuccessful. Found: C, 52.5; H, 5.86. $In_3P_3C_{43}H_{60}$ requires: C, 50.9; H, 5.96%. A sample of the adduct (2.8 g, *ca* 2.8 mmol) began to liberate Me_3In at 60°C/10^{-2} mmHg but the temperature was gradually raised to 140°C. Final yield of $[Me_3In]_4$: 1.0 g, *ca* 75% but the sublimate contained a trace of benzene.

(14) $(Me_3Al)_4$ · tetraphos

This was prepared in a similar manner to $(Me_3Al)_2$ · diphos using Me_3Al (6.6 cm^3 of 2.3 M solution, 15 mmol) and tetraphos (2.55 g, 3.81 mmol). Solvents were removed *in vacuo* to leave a white powder (3.92 g, 108%, so benzene has been incorporated; equivalent to 0.93 moles of benzene per mole of adduct from gravimetric estimation). A sample of the adduct (1.58 g, *ca* 1.6 mmol) began to liberate Me_3Al at 60°C/10^{-2} mmHg but proceeded rapidly at 75–80°C. Final yield of $(Me_3Al)_2$: 0.48 g, essentially quantitative but the distillate was contaminated with a trace of benzene.

(15) $(Me_3Ga)_4$ · tetraphos

This was prepared in a similar manner to $(Me_3Ga)_2$ · diphos using $GaCl_3$ (2.35 g, 13.3 mmol), MeLi (10.3 cm^3 of 1.30 M solution, 13.4 mmol) and tetraphos (2.45 g, 3.66 mmol). The product was crystallized from benzene; yield 2.0 g, 53% based

Table 5. Crystal data, details of intensity measurements and structure

Molecular formula	$Al_2P_2C_{32}H_{42}$	$Ga_2P_2C_{32}H_{42}$	$In_2P_2C_{32}H_{42}$	$Al_3P_3C_{43}H_{60}\cdot 0.5C_6H_6$
Molecular weight	542.556	628.036	695.922	789.814
Crystal system	Triclinic	Triclinic	Triclinic	Triclinic
a (Å)	8.922(6)	8.903(3)	9.003(1)	19.968(4)
b (Å)	9.485(2)	9.485(4)	9.576(1)	12.521(3)
c (Å)	11.324(2)	11.308(3)	11.332(1)	10.346(9)
α (deg)	68.870(2)	68.922(2)	69.585(9)	96.175(6)
β (deg)	84.001(3)	83.865(2)	84.786(9)	93.917(6)
γ (deg)	66.808(3)	66.906(3)	67.302(9)	72.928(2)
Volume (Å^3)	820.86	818.97	843.59	2456.54
Space group	$P\bar{1}$	$P\bar{1}$	$P\bar{1}$	$P\bar{1}$
Z	1	1	1	2
D_c (g cm^{-3})	1.097	1.273	1.413	0.941
μ	1.65	17.52	13.55	1.60
$F(000)$	290	326	362	778
hkl, range	$0 \rightarrow 10$	$-10 \rightarrow 10$	$0 \rightarrow 10$	$-20 \rightarrow 20$
	$-11 \rightarrow 11$	$0 \rightarrow 11$	$-11 \rightarrow 11$	$-12 \rightarrow 12$
	$-13 \rightarrow 13$	$-13 \rightarrow 13$	$-13 \rightarrow 13$	$0 \rightarrow 10$
Total no. of reflections	3089	2880	2966	5287
No. of unique reflections	2884	2880	2966	5287
No. of reflections, used; ($F > 3\sigma(F)$)	2463	2574	2628	2237
No. of parameters	247	247	247	446
Weighting scheme parameter g in $w = 1/[\sigma^2(F)+gF_0^2]$	0.0002	0.0002	0.0002	0.0005
Final R	0.0345	0.0282	0.0241	0.0753
Final R_w	0.0380	0.0309	0.0247	0.0689

upon benzene-free crystals. The whole sample began to liberate Me_3Ga at 65°C/10^{-2} mmHg and was rapid at 120–130°C. Final yield of Me_3Ga: 0.76 g, *ca* 93% but this contained traces of benzene.

(16) $(Me_3In)_4$ · tetraphos

This was prepared in a similar manner to $(Me_3In)_3$ · triphos by decomposing $(Me_3In)_2$ · diphos (6.2 g, 8.6 mmol) and condensing the Me_3In onto tetraphos (3.00 g, 44.48 mmol) in benzene (60 cm^3). The compound was crystallized from benzene; yield 4.66 g, 83% based upon benzene-free crystals. Found: C, 47.9; H, 5.67. $In_4P_4C_{54}H_{78}$ requires: C, 49.5; H, 6.00%. A sample of the adduct (1.75 g, *ca* 1.34 mmol) began to liberate Me_3In at 70°C/10^{-2} mmHg but proceeded rapidly at 130–140°C. Final yield of $[Me_3In]_4$: 0.64 g; *ca* 75% but was contaminated with a trace of benzene.

X-ray crystallography

Crystals of the four compounds were sealed under nitrogen in thin-walled glass capillaries. All X-ray measurements were made on an Enraf–Nonius CAD4 using the $\omega/2\theta$ scan technique with graphite monochromated Mo-K_α radiation ($\lambda = 0.71069$ Å) following previously detailed procedures[14] and standard CAD4 software. The structures were solved via the heavy atom method and refined by full-matrix least-squares. Non-hydrogen atoms were assigned anisotropic displacement factor coefficients; hydrogens in all three diphos structures were experimentally located and freely refined with isotropic displacement factor coefficients, but were included in idealized positions in the triphos structure and refined as components of rigid groups, with group U_{iso} values. Crystal data and details of intensity measurements and refinement are given in Table 5.

Acknowledgements—We thank the Director of Research, British Telecom Research Laboratories, Martlesham Heath, Ipswich (DMF); the Procurement Executive, Ministry of Defence, D.C.V.D., sponsored by the Radar and Signals Research Establishment, Malvern (LMS) and the S.E.R.C. in part via the Joint Opto-Electronic Research Scheme (HC), for financial support and permission to publish. We also thank Mrs J. Hawkes of the U.L.I.R.S. NMR Service at Kings College for the ^{31}P spectra.

REFERENCES

1. H. M. Manasevit and W. I. Simpson, *J. Electrochem. Soc.* 1969, **116**, 1725; *J. Electrochem. Soc.* 1973, **120**, 135.
2. R. H. Moss, *J. Cryst. Growth* 1984, **68**, 78.
3. G. E. Coates, *J. Chem. Soc.* 1951, 2003.
4. G. E. Coates and R. G. Hayter, *J. Chem. Soc.* 1953, 2519.
5. G. E. Coates and R. A. Whitcombe, *J. Chem. Soc.* 1956, 3351.
6. D. C. Bradley, H. Dawes, D. M. Frigo, M. B. Hursthouse and B. Hussain, *J. Organomet. Chem.* 1987, **325**, 55.
7. D. C. Bradley, M. M. Faktor and D. M. Frigo, *Chemtronics* 1987, **2**, 22.
8. T. R. Durkin and E. P. Schram, *Inorg. Chem.* 1972, **11**, 1054.
9. H. Schmidbaur, S. Lauteschliger and G. Muller, *J. Organomet. Chem.* 1985, **281**, 25.
10. D. C. Bradley, M. M. Faktor, D. M. Frigo and D. H. Zheng, *Chemtronics* 1988, **3**, 53.
11. K. A. Aitchison, J. D. J. Backer-Dirks, D. C. Bradley and M. B. Hursthouse, unpublished results.
12. A. Almenningen, L. Fernholt and A. Haaland, *J. Organomet. Chem.* 1978, **145**, 109.
13. L. M. Golubinskaya, A. V. Golubinskii, V. S. Mastryukov, L. I. Vilkov and V. I. Bregadze, *J. Organomet. Chem.* 1976, **117**, C4.
14. R. A. Jones, M. B. Hursthouse, K. M. A. Malik and G. Wilkinson, *J. Am. Chem. Soc.* 1979, **101**, 4128.

Polyhedron Vol. 7, No. 14, pp. 1299–1303, 1988
Printed in Great Britain

0277–5387/88 $3.00+.00
© 1988 Pergamon Press plc

CRYSTAL STRUCTURE OF $[HgAg(C_4H_6NO)_2(NO_3)]_2$: A DIMERIC HETEROMETALLIC COMPLEX CONTAINING BOTH BI- AND TRINUCLEATING 2-PYRROLIDINONE ANION LIGANDS AND A FOLDED Ag—O—Ag—O RING

D. M. L. GOODGAME,† D. J. WILLIAMS and R. E. P. WINPENNY

Chemistry Department, Imperial College of Science and Technology, London SW7 2AY, U.K.

(*Received* 18 *December* 1987; *accepted* 18 *February* 1988)

Abstract—Reaction of mercuric acetate, 2-pyrrolidinone and silver nitrate leads to the formation of a dimeric mixed-metal complex, $[HgAg(C_4H_6NO)_2(NO_3)]_2$ (where C_4H_6NO is the anion of 2-pyrrolidinone). The complex has been characterized by X-ray diffraction; the crystals are orthorhombic, *Pbcn*, $a = 15.532(3)$, $b = 16.244(2)$, $c = 19.755(2)$ Å, $Z = 8$. The structure was refined on 2549 reflections to $R = 0.054$. The dimeric complex has at its centre a folded Ag_2O_2 ring with the bridging oxygen atoms being provided by the 2-pyrrolidinone anions, the first example of this compound functioning as a trinucleating ligand. There are also significant inter-dimer interactions, giving rise to unusually distorted silver coordination geometries. Further, weak electrostatic, anion-mediated interactions serve to bridge adjacent dimers so as to form loosely linked polymeric sheets.

We are exploring the ability of the anion of 2-pyrrolidinone to function as a binucleating ligand. In particular, we have found that in the presence of mercuric acetate the ring nitrogen is deprotonated leading to the formation of $Hg(C_4H_6NO)_2$ (**1**) (where C_4H_6NO is the anion of 2-pyrrolidinone). This can then react with further metal salts to produce unusual mixed-metal polymers, several of which have been characterized by X-ray analysis.[1,2] When 2-pyrrolidinone, mercuric acetate and copper(II) nitrate were reacted together, a novel layer polymer comprised of contiguous 32-membered macrocycles resulted.[1] On substituting cobalt nitrate for copper nitrate a totally different structural type was formed—a chain polymer made up of interlocking 16-membered heterobimetallic macrobicyclic links.[2] As the coordination geometry adopted by the transition metal appears to have an important influence on the overall structure of the polymer, it was felt to be important to extend our studies of the range of metals which would react with (**1**). To this end a reaction utilizing Ag^+, a monopositive cation with a proclivity for distorted coordination geometries, has been performed. A new dimeric complex $[HgAg(C_4H_6NO)_2(NO_3)]_2$ (**2**) has resulted which, whilst not having the same covalent polymeric character of the mixed metal pyrrolidinone compounds previously described,[1,2] does form polymer-like structures via weak electrostatic inter-dimer interactions.

EXPERIMENTAL

2-Pyrrolidinone (4 mmol) and mercuric acetate (2 mmol) in methanol (5 cm^3) were added to a suspension of silver nitrate (1 mmol) in 9:1 methanol–water (20 cm^3). A white microcrystalline precipitate began to form immediately. The mixture was stirred for *ca* 2 h, then filtered. The white powder was washed with methanol (2 × 5 cm^3) and dried in air. Yield: 0.3 mmol (60%). Slow evaporation of the filtrate gave, after three days, colourless crystals suitable for X-ray analysis. Found: C, 18.0; H, 2.1; N, 7.7. Calc. for $HgAg(C_4H_6NO)_2(NO_3)$: C, 17.8; H, 2.2; N, 7.8%.

X-ray studies

Crystal data. $C_{16}H_{24}O_{10}N_6Ag_2Hg_2$, orthorhombic, $a = 15.532(3)$, $b = 16.244(2)$, $c = 19.755(2)$ Å,

† Author to whom correspondence should be addressed.

$U = 4984$ Å^3, space group *Pbcn*, $Z = 8$, $M = 1077$, $D_c = 2.87$ g cm^{-3}, μCu-$K_\alpha = 365$ cm^{-1}.

Measurements. Refined unit cell parameters were obtained by centring 20 reflections on a Nicolet R3m diffractometer. Using the omega scan measuring routine, 3367 independent reflections ($\theta \leqslant 58°$) were measured with Cu-K_α radiation (graphite monochromator). Of these, 2549 had $|F_0| > 3\sigma(|F_0|)$ and were considered to be observed. Lorentz and polarization corrections were applied. A numerical absorption correction (face indexed crystal) was applied.

Structure analysis. The structure was solved by the heavy atom method, which gave the position of one of the mercury atoms. All other non-hydrogen atoms were located from subsequent ΔF maps and were refined anisotropically. The hydrogen atom positions were idealized (C—H = 0.96 Å) and assigned constrained isotropic thermal parameters $U(\mathrm{H}) = 1.2U(\mathrm{C})$.

Refinement was by block-cascade full-matrix least-squares to $R = 0.054$, $R_w = 0.058$ [$w^{-1} = \sigma^2(F) + 0.0017F^2$]. Computations were carried out on an Eclipse S140 computer using the *SHELXTL* program system.[3] Scattering factors were taken from the *International Tables for X-ray Crystallography*.[4]

Final atomic coordinates, thermal parameters and structure factors have been deposited with the Editor as supplementary data. Atomic coordinates have also been deposited with the Cambridge Crystallographic Data Centre.

RESULTS AND DISCUSSION

The X-ray structure analysis shows that the complex has the stoichiometry $HgAg(C_4H_6NO)_2(NO_3)$ and is dimeric (Fig. 1). Selected bond lengths and angles are listed in Tables 1 and 2.

The 2-pyrrolidinone ligand adopts two quite different binding modes within the dimer. The first is a binucleating interaction in which the ring nitrogen atom bonds to mercury and the exocyclic oxygen to silver. Bonding of this type has been found previously when (**1**) forms heterometallic polymers with transition metal ions.[1,2] Similar coordination also occurs in tetranuclear platinum complexes of 2-pyrrolidinone.[5] The second and novel, ligand coordination mode is trinucleating involving the exocyclic oxygen bridging two silver atoms. This leads to the formation of a folded four-membered Ag—O—Ag—O ring. Although similar Ag_2O_2 rings have been reported previously (with the oxygen atom bridging from $OTeF_5^-$,[6] tetraphenylcyclopentadienone[7] and ClO_4^-[8]) in those cases the ring is planar. In (**2**) the dihedral angle between the O(1)O(3)Ag(1) and O(1)O(3)Ag(2) planes is 165°, and the deviation of the four constituent atoms from the mean plane of the ring is *ca* 0.12 Å. This distortion can be accounted for by considering inter-dimer interactions.

A view down the *c*-axis of the unit cell (Fig. 2) shows that the dimers form parallel extended planes. The structure may be visualized in terms of two principal inter-layer interactions, back-to-back and anion mediated face-to-face. In the former, these interactions chiefly involve the Ag_2O_2 units which are oriented such that inter-dimer bonds can be formed linking the Ag atoms in one ring with bridging oxygens in the next (Fig. 3). These Ag—O bonds [Ag(1)—O(1)* = 2.72, Ag(2)—O(3)* = 2.67 Å and *vice versa*] are almost certainly responsible for the non-planar nature of the four-membered metallocycle. The oxygen atoms are displaced

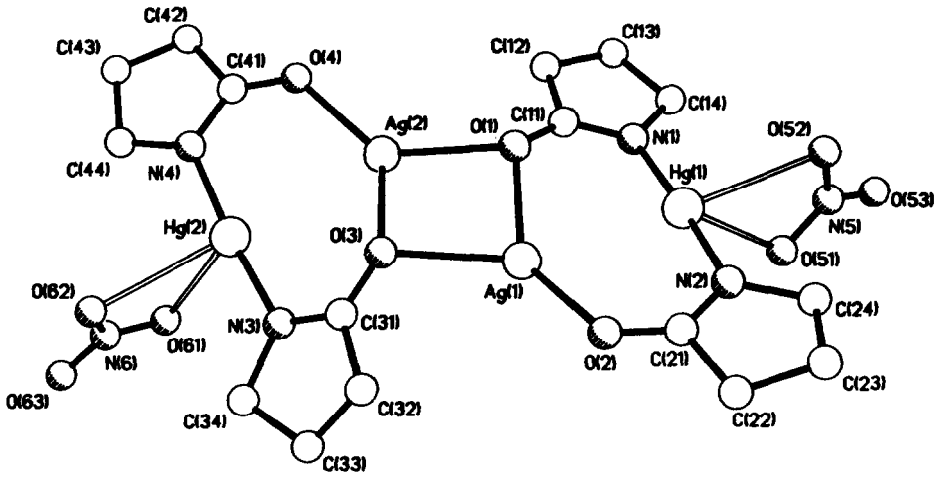

Fig. 1. Molecular structure of $Hg_2Ag_2(C_4H_6NO)_4(NO_3)_2$, giving the atom numbering scheme.

Table 1. Selected bond lengths (Å) for (**2**)

Hg(1)—N(1)	2.043(10)	Hg(1)—N(2)	2.047(12)
Hg(1)—O(51)	2.647(11)	Hg(1)—O(52)	2.769(11)
Hg(2)—N(3)	2.002(11)	Hg(2)—N(4)	2.011(10)
Hg(2)—O(61)	2.641(11)	Hg(2)—O(62)	2.797(11)
Ag(1)—O(1)	2.369(9)	Ag(1)—O(2)	2.267(10)
Ag(1)—O(3)	2.407(10)	Ag(1)—O(1)*	2.719(10)
Ag(1)—O(61)″	2.745(10)	Ag(1)—O(63)″	2.725(10)
Ag(2)—O(1)	2.435(9)	Ag(2)—O(3)	2.402(9)
Ag(2)—O(4)	2.285(10)	Ag(2)—O(3)*	2.671(10)
Ag(2)—O(51)′	2.720(10)	Ag(2)—O(53)′	2.663(10)

Table 2. Selected bond angles (deg) for (**2**)

N(1)—Hg(1)—N(2)	174.6(5)	N(1)—Hg(1)—O(51)	92.0(4)
N(1)—Hg(1)—O(52)	89.2(4)	N(2)—Hg(1)—O(51)	93.2(4)
N(2)—Hg(1)—O(52)	95.3(4)	O(51)—Hg(1)—O(52)	47.0(4)
N(3)—Hg(2)—N(4)	174.0(5)	N(3)—Hg(2)—O(61)	94.1(4)
N(3)—Hg(2)—O(62)	90.9(4)	N(4)—Hg(2)—O(61)	91.8(4)
N(4)—Hg(2)—O(62)	93.8(4)	O(61)—Hg(2)—O(62)	46.5(4)
O(1)—Ag(1)—O(2)	142.0(3)	O(1)—Ag(1)—O(3)	82.8(3)
O(1)—Ag(1)—O(1)*	87.1(3)	O(1)—Ag(1)—O(61)″	93.1(4)
O(1)—Ag(1)—O(63)″	113.4(4)	O(2)—Ag(1)—O(3)	131.2(3)
O(2)—Ag(1)—O(1)*	85.7(4)	O(2)—Ag(1)—O(61)″	83.5(4)
O(2)—Ag(1)—O(63)″	91.4(5)	O(3)—Ag(1)—O(1)*	76.7(4)
O(3)—Ag(1)—O(61)″	120.4(5)	O(3)—Ag(1)—O(63)″	81.1(4)
O(1)*—Ag(1)—O(61)″	162.8(5)	O(1)*—Ag(1)—O(63)″	147.5(4)
O(61)″—Ag(1)—O(63)″	46.5(4)	O(1)—Ag(2)—O(3)	81.5(3)
O(1)—Ag(2)—O(4)	136.7(3)	O(1)—Ag(2)—O(3)*	77.1(4)
O(1)—Ag(2)—O(51)′	118.1(4)	O(1)—Ag(2)—O(53)′	82.2(4)
O(3)—Ag(2)—O(4)	135.3(4)	O(3)—Ag(2)—O(3)*	81.3(3)
O(3)—Ag(2)—O(51)′	91.9(4)	O(3)—Ag(2)—O(53)′	117.1(4)
O(4)—Ag(2)—O(3)*	86.1(4)	O(4)—Ag(2)—O(51)′	87.5(5)
O(4)—Ag(2)—O(53)′	94.4(4)	O(3)*—Ag(2)—O(51)′	162.4(4)
O(3)*—Ag(2)—O(53)′	150.0(4)	O(51)′—Ag(2)—O(53)′	47.0(4)
Ag(1)—O(1)—Ag(2)	96.8(3)	Ag(1)—O(3)—Ag(2)	96.7(3)

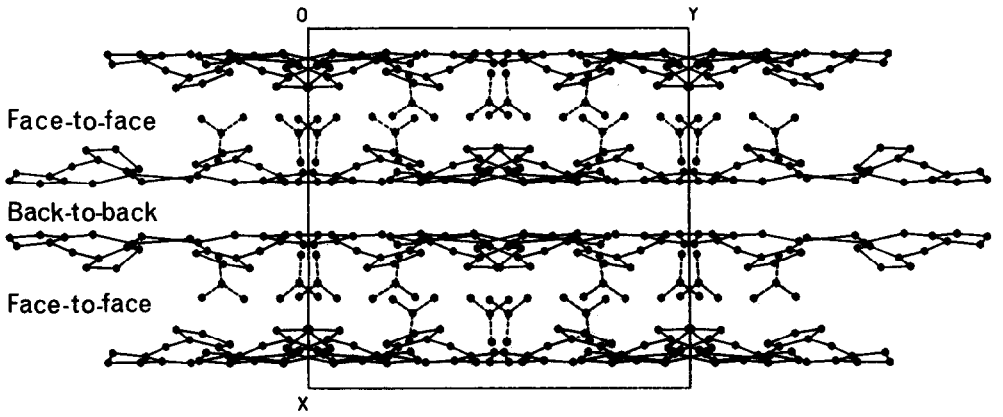

Fig. 2. The stacking of the dimers in (**2**) viewed down the crystallographic *c*-axis, showing the face-to-face and back-to-back arrangements.

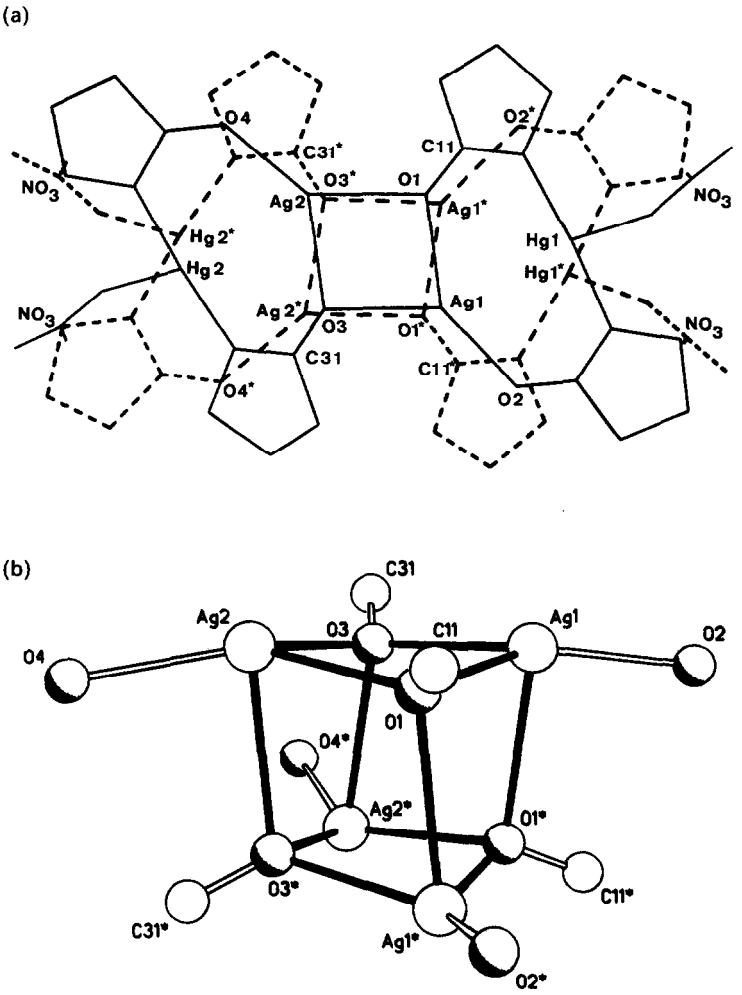

Fig. 3. The back-to-back inter-dimer stacking: (a) viewed normal to the Ag_2O_2 plane, (b) approximately edge on showing the dimer–dimer interactions.

below the plane of the Ag_2O_2 unit towards the silver atoms in the dimer beneath. The silver atoms, however, are not displaced towards the oxygen atoms in the lower dimer because of the competing interactions of the interposed nitrate anions (see below).

The region between the face-to-face layers of dimers (Fig. 2) is occupied by the nitrate anions. These provide additional structure stabilizing interlayer bridging interactions. Each nitrate can be regarded as being bidentate towards a silver atom [Ag(1)—O(61)″ = 2.75, Ag(1)—O(63)″ = 2.73 Å; Ag(2)—O(51)′ = 2.72, Ag(2)—O(53)′ = 2.66 Å] and monodentate to a mercury atom [Hg(1)—O(61)″ = 2.88; Hg(2)—O(51)′ = 2.87 Å] in one dimer, whilst simultaneously being bidentate to

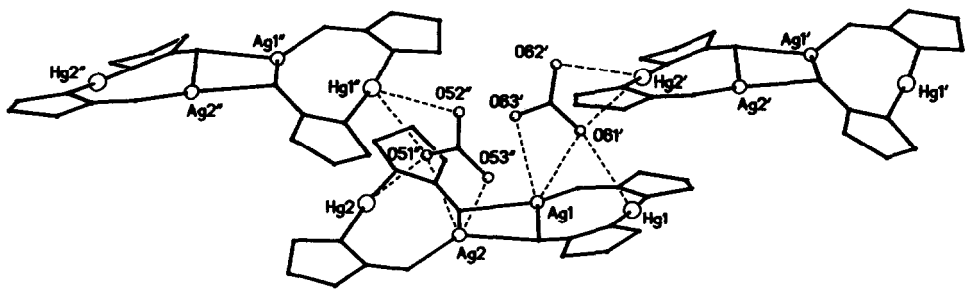

Fig. 4. The anion mediated face-to-face dimer interactions.

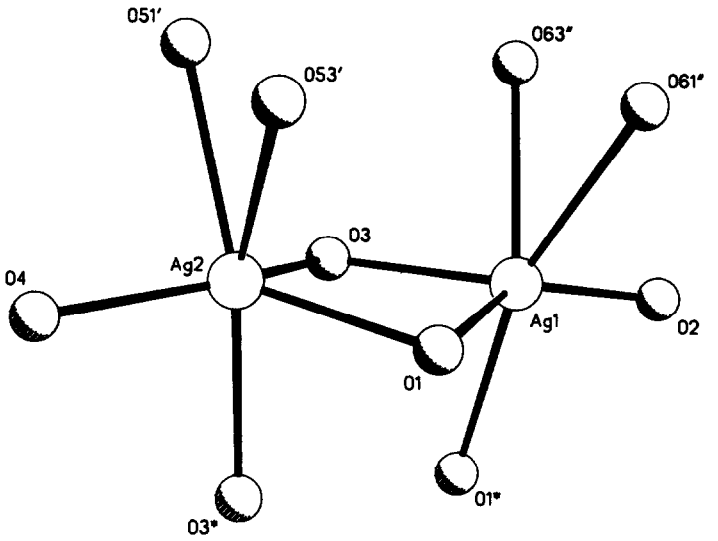

Fig. 5. A perspective view of the coordination geometries of the two silver atoms within the dimer.

a mercury atom in another [Hg(1)′—O(51)′ = 2.65, Hg(1)′—O(52)′ = 2.77 Å; Hg(2)″—O(61)″ = 2.65, Hg(2)″—O(62)″ = 2.80 Å]. (See Fig. 4.)

As a result of these intra- and inter-dimer silver–oxygen interactions, each silver atom is bound to six oxygen atoms but with a very irregular geometry (Fig. 5). In each case, three of these oxygen atoms [O(1), O(2) and O(3); O(1), O(3) and O(4)] are 2-pyrrolidinone oxygens within the dimeric unit. The non-bridging oxygens form the shortest bonds [Ag(1)—O(2) = 2.27(1), Ag(2)—O(4) = 2.29(1) Å], whilst the bridging oxygens have slightly longer bonds (ranging between 2.37(1)–2.44(1) Å]. The three remaining oxygen atoms are those involved in the inter-dimer binding and have Ag—O distances that are significantly longer (*ca* 2.7 Å, see above). The coordination geometry is perhaps best considered as a bicapped square pyramid. The two mercury atoms in the dimeric unit are, as expected, both essentially linearly coordinated to two 2-pyrrolidinone ring nitrogens (see Table 1).

In previous compounds obtained by the reaction of (**1**) with transition metal nitrates we have found that large heterometallic rings are formed, in one case as large as 32-membered[1] and in another 16-membered.[2] In (**2**), bimetallic macrocycles are also formed, though on this occasion the ring is only eight-membered, comprising one Hg, one Ag, two C, two O and two N atoms. There are two such rings in the dimer, both of which can be considered to be essentially planar, but with the silver atoms providing the major deviation from planarity [Ag(1) and Ag(2) lying ~ 0.4 and 0.6 Å, respectively from the mean planes of the ring atoms other than Ag].

The Hg···Ag contacts [Ag(1)—Hg(1) = 3.02, Ag(2)—Hg(2) = 3.07 Å] within the dimer, though less than Van der Waals, are too long for any significant degree of metal–metal bonding. The *trans*-annular Ag(1)—Ag(2) distance is 3.59 Å.

There are also inter-dimer mercury–mercury contacts but again these are too long to be of great significance, [Hg(1)—Hg(1)′ = 3.67, Hg(2)—Hg(2)′ = 3.77 Å].

Acknowledgement—We thank the SERC for the diffractometer and for a Research Studentship (to R.E.P.W.).

REFERENCES

1. D. M. L. Goodgame, D. J. Williams and R. E. P. Winpenny, *Angew. Chem. Int. Ed. Engl.* 1987, **26**, 1044.
2. D. M. L. Goodgame, D. J. Williams and R. E. P. Winpenny, *Angew. Chem. Int. Ed. Engl.* 1988, **27**, 261.
3. G. M. Sheldrick, *SHELXTL, An Integrated System for Solving, Refining and Displaying Crystal Structures from Diffraction Data*, Revision 4.1. University of Gottingen, F.R.G. (1983).
4. *International Tables for X-ray Crystallography*, Vol. IV, pp. 99–143. Kynoch Press, Birmingham, U.K. (1974).
5. K. Matsumoto, H. Takahashi and K. Fuwa, *Inorg. Chem.* 1983, **22**, 4086.
6. S. H. Strauss, M. D. Noirot and O. P. Anderson, *Inorg. Chem.* 1985, **24**, 4307.
7. P. K. Baker, K. Broadley, N. G. Connelly, B. A. Kell, M. D. Kitchen and P. Woodward, *J. Chem. Soc., Dalton Trans.* 1980, 1710.
8. I. F. Taylor and E. L. Amma, *J. Chem. Soc., Chem. Commun.* 1970, 1442.

Polyhedron Vol. 7, No. 14, pp. 1305–1310, 1988
Printed in Great Britain

0277-5387/88 $3.00+.00
© 1988 Pergamon Press plc

ALKALI METAL AND AMMONIUM PEROXODIPHOSPHATES: PREPARATION, VIBRATIONAL AND ^{31}P NMR SPECTRA, AND THE X-RAY CRYSTAL STRUCTURE OF AMMONIUM PEROXODIPHOSPHATE DIHYDRATE $(NH_4)_4[P_2O_8]\cdot 2H_2O$

WILLIAM P. GRIFFITH,* RICHARD D. POWELL and ANDRZEJ C. SKAPSKI*

Inorganic Chemistry and Chemical Crystallography Laboratories, Imperial College, London SW7 2AY, U.K.

(*Received* 4 *January* 1988; *accepted* 18 *February* 1988)

Abstract—Improved preparations are reported of $M_4[P_2O_8]\cdot nH_2O$ (M = K, $n = 0$; M = Na, $n = 18$; M = Li, $n = 4$; M = NH_4, $n = 2$), as well as their ^{31}P NMR spectra; the vibrational spectra for $Li_4[P_2O_8]\cdot 4H_2O$ are described. The X-ray crystal structure of $(NH_4)_4[P_2O_8]\cdot 2H_2O$ has been determined, its unit cell is monoclinic with $a = 15.336(2)$, $b = 9.893(2)$, $c = 8.789(1)$ Å, $\beta = 91.28(2)°$ (at 20°C), space group $C2/c$, and $Z = 4$. The structure has been refined to $R = 0.034$. The peroxodiphosphate anion consists of two phosphate tetrahedra linked by a peroxide bond.

The peroxodiphosphate ion, $[P_2O_8]^{4-}$, is a powerful oxidant ($E_0 = 2.07$ V[1]). It is used in organic oxidations,[2–4] and as an initiator in polymerizations.[5,6] Several salts have been reported and characterized by elemental analysis,[7,8] and vibrational spectra are reported for two salts.[8,9] However, no crystal structures have been determined.

In this study, lithium, sodium, potassium and ammonium peroxodiphosphate have been prepared in a pure state and the crystal structure of ammonium peroxodiphosphate dihydrate, $(NH_4)_4[P_2O_8]\cdot 2H_2O$, has been determined by single-crystal X-ray diffraction. The vibrational spectra of $Li_4[P_2O_8]\cdot 4H_2O$ are reported for the first time, and the ^{31}P NMR of the four salts measured in the solid state and in aqueous solution. The reaction of $[P_2O_8]^{4-}$ with ruthenium and its suitability as a co-oxidant for organic oxidations has been briefly investigated.

RESULTS AND DISCUSSION

X-ray crystal structure of ammonium peroxodiphosphate dihydrate, $(NH_4)_4[P_2O_8]\cdot 2H_2O$

The $[P_2O_8]^{4-}$ ion consists of two phosphate tetrahedra linked through a peroxide bond, as shown in Fig. 1; it lies on a crystallographic two-fold axis. The peroxide bond length is 1.501(3) Å, similar to those found for $(NH_4)_2[S_2O_8]$ (1.497(8) Å)[10] and $K_2[S_2O_8]$ (1.482(6) Å),[11] but appreciably longer than the value of 1.453(7) Å observed in solid hydrogen peroxide,[12] probably because of the strongly electron-withdrawing effect of the $-PO_3$ groups. The terminal P—O distances are identical within experimental error, mean 1.508(2) Å, with a P—$O_{peroxide}$ distance of 1.658(2) Å. The angles between the terminal oxygen atoms are slightly greater than tetrahedral, while those between the terminal and peroxo oxygen atoms are 99.4° for that *anti* to the peroxo group and 106.5° for the other two. The angles at the peroxo oxygen atoms are 105.7° and the *anti* O—P—O—O—P—O moiety is

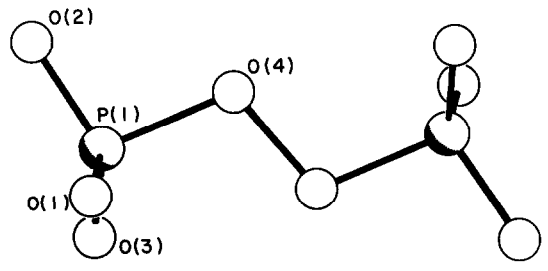

Fig. 1. The peroxodiphosphate anion, $[P_2O_8]^{4-}$, in ammonium peroxodiphosphate dihydrate.

* Authors to whom correspondence should be addressed.

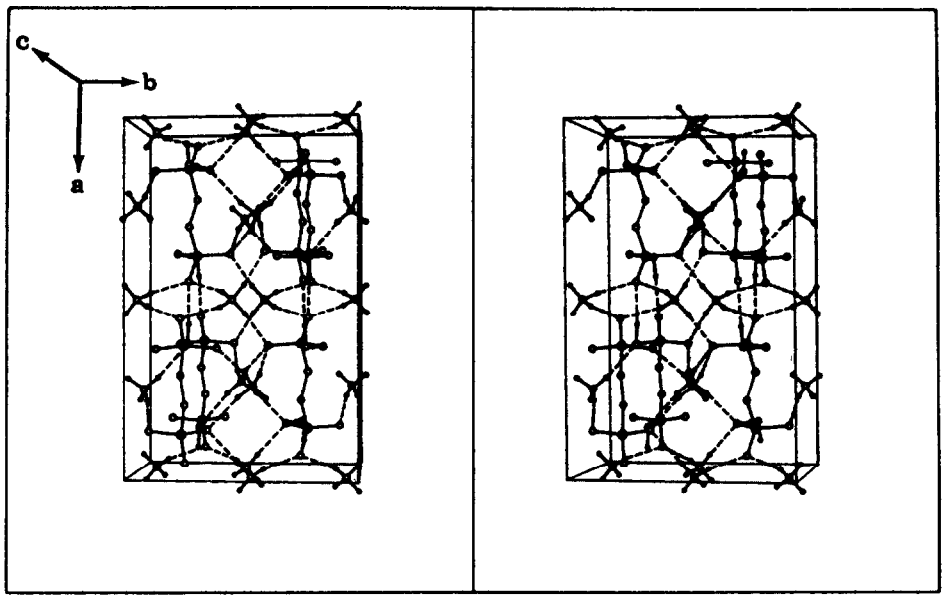

Fig. 2. Stereo view of packing in the unit cell of $(NH_4)_4[P_2O_8]\cdot 2H_2O$, showing hydrogen bonds as dotted lines.

planar. Overall, the structure is similar to that of the peroxodisulphate anion in $(NH_4)_2[S_2O_8]$[10] and $K_2[S_2O_8]$.[11] All the hydrogen atoms of the ammonium groups and the water molecules are involved in a complex network of hydrogen bonds, as shown in Fig. 2. Bond lengths, bond angles and hydrogen bond data are given in Table 1 and the unit-cell packing is shown in Fig. 2.

Vibrational spectra

The Raman[8] and IR[9] spectra of a number of salts containing the $[P_2O_8]^{4-}$ ion have been reported. We have measured such spectra for $K_4[P_2O_8]$, $Li_4[P_2O_8]\cdot 4H_2O$, $Na_4[P_2O_8]\cdot 18H_2O$ and $(NH_4)_4[P_2O_8]\cdot 2H_2O$ in the solid state and in aqueous solution; for the lithium salt these are recorded

Table 1. Selected bond lengths (Å) and bond angles (°) with estimated standard deviations in parentheses

P1—O1	1.509(2)	P1—O2	1.507(2)
P1—O3	1.508(2)	P1—O4	1.658(2)
O1—P1—O2	114.4(1)	O1—P1—O3	113.9(1)
O2—P1—O3	114.4(1)	O1—P1—O4	106.5(1)
O2—P1—O4	99.4(1)	O3—P1—O4	106.5(1)
P1—O4—O4A	105.7(2)		

Hydrogen bonds

Bond lengths				Angle at H (°)
N1—H11	0.87	N1···O2	2.82	159
N1—H12	0.92	N1···O1	2.80	174
N2—H21	0.88	N2···O2	2.82	165
N2—H22	0.85	N2···O3	2.81	170
N3—H31	0.94	N3···O1	3.04	164
N3—H32	0.88	N3···O3	2.84	169
N3—H33	0.82	N3···O5	2.87	169
N3—H34	0.88	N3···O1	2.84	171
O5—H51	0.82	O5···O3	2.74	174
O5—H52	0.90	O5···O2	2.85	175

Table 2. Vibrational spectra of $Li_4[P_2O_8]\cdot 4H_2O$

Raman (solid)	Raman (IM solution)	IR (KBr disc)	Assignments
300(1)	311(1)	361w	
390(1)	389(1)	392w	$\omega(PO_3)$
503(1)	512(2)	472w,b	
562(1)	575(1)	553m	$\delta(PO_3)$
		629w,b	
	635(1)		
		774m	τ(P—O—O—P)
790(6)	779(4)		ν_s(P—O—O—P)
894(8)	893(7)		ν_s(O—O)
		996m	ν_{as}(P—O—O—P)
1019(10)	1008(10)		$\nu_s(PO_3)$
		1092m	
1120(2)	1105(1)	1112s	$\nu_{as}(PO_3)$
1137(1)	1125(1)	1132vs	
1182(1)	1155(1)	1161s	

Relative Raman intensities in parentheses.

for the first time and are given in Table 2. Only partial assignments for $[P_2O_8]^{4-}$ were given by Simon and Richter,[8] with no polarization data.

The totally symmetric terminal PO_3 stretch $\nu_s(PO_3)$ is observed at 1008 cm^{-1} in aqueous solutions of the salts with a depolarization ratio (ρ) of 0.02. The band at 779 cm^{-1} ($\rho = 0.07$) is probably the symmetric P—O stretch [ν_s(P—O—O—P)] of the peroxo bridge, observed at 842 cm^{-1} in $[S_2O_8]^{2-}$.[11] The O—O stretch [ν_s(O—O)] we assign to the partially polarized band at 893 cm^{-1} ($\rho = 0.41$); a similar ratio, 0.34, was observed for the corresponding mode in $[S_2O_8]^{2-}$.[11] The position of this band in the solid salts $M_4[P_2O_8]\cdot nH_2O$ seems to be strongly cation-dependent: 894 cm^{-1} (M = Li), 860 cm^{-1} (Na), 843 cm^{-1} (K) and 884 cm^{-1} (NH_4). The wavenumbers for the Raman spectra of $K_4[P_2O_8]$ and $Na_4[P_2O_8]\cdot 18H_2O$ agree fairly well with those reported by Simon and Richter,[8] with the exception of the O—O stretch [ν_s(O—O)] which we find lies at 843 and 860 cm^{-1}, respectively. Also by analogy with the $[S_2O_8]^{2-}$ ion we assign the strong IR band at 774 cm^{-1} to the P—O—O—P torsion τ(P—O—O—P); the IR band at 996 cm^{-1} could arise from ν_{as}(P—O—O—P). The IR and Raman bands in the 1100–1200 cm^{-1} region will be due to asymmetric PO_3 stretches [$\nu_{as}(PO_3)$], with the corresponding deformations at 400–600 cm^{-1} and wagging modes at 300–400 cm^{-1}. Similar assignments have been proposed for $[S_2O_8]^{2-}$.[11]

^{31}P *NMR Spectra*

The ^{31}P NMR spectrum of a 0.5 M aqueous solution of $K_4[P_2O_8]$ shows a singlet with a chemical shift of δ 7.0 ppm (relative to 85% $H_3[PO_4]$) at pH 10.3. Acidification causes a shift to lower δ values, presumably due to protonation of the $[P_2O_8]^{4-}$ anion. A plot of the ^{31}P shift against pH (from pH 12 to 2) (Fig. 3) shows only one inflection, at pH

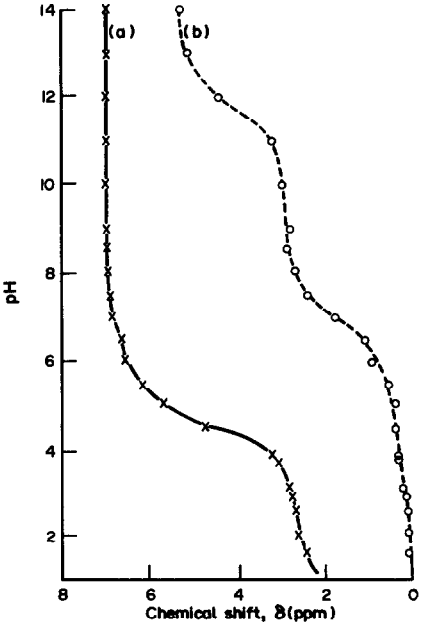

Fig. 3. Plot of pH vs ^{31}P chemical shift for aqueous 0.5 M solutions of (a) $K_4[P_2O_8]$ and (b) $K_3[PO_4]$.

4.8, although the pK_3 and pK_4 values for $H_4[P_2O_8]$ have been found from potentiometric titration data to be 5.18 and 7.68, respectively.[13] It is not clear why this discrepancy arises, since plots of the ^{31}P shift versus pH for the $H_nPO_4^{3-n}$ system give good agreement with the published values; we find the pK_a for HPO_4^{2-} is 12.3 and the pK_a for $H_2PO_4^-$ is 7.1, the same as those given in the literature.[13]

We have also recorded the ^{31}P chemical shifts for the solid salts, using ^{31}P cross-polarization magic-angle spinning. The shifts (again relative to 85% H_3PO_4) are δ 9.2 ppm (K), 8.0 ppm (Li), 5.7 ppm (NH_4) and a doublet at 10.0 and 11.0 ppm for the sodium salt. The apparent cation dependence of these shifts could arise from effects of the cations in the solid state, when they are packed next to the anions rather than independently solvated; the splitting in the sodium salt could arise from partial dehydration of the sample.

$[P_2O_8]^{4-}$ *as an oxidant*

The peroxodisulphate anion, $[S_2O_8]^{2-}$, acts as a co-oxidant for $[RuO_4]^{2-}$ in alkaline aqueous solution and the $[RuO_4]^{2-}$–$[S_2O_8]^{2-}$ system is an efficient catalytic cycle.[14] Since the $[P_2O_8]^{2-}$ anion has a similar structure and E_0 value, it was thought that it might function similarly. We find this to be so; a solution of $RuCl_3 \cdot nH_2O$ (2×10^{-5} M) in aqueous NaOH (2 M) and a large excess of $Na_4[P_2O_8] \cdot 18H_2O$ (0.06 M) does generate the red $[RuO_4]^{2-}$ ion, identified by its electronic spectrum.[15] Such solutions at 50°C slowly oxidize benzylic alcohols to the corresponding carboxylic acids (e.g. benzyl alcohol to benzoic acid and 4-methoxybenzyl alcohol to 4-methoxybenzoic acid) with turnovers of up to 100. These reactions are however much slower than those with $[S_2O_8]^{2-}$, due probably to the higher negative charge on $[P_2O_8]^{4-}$. Nevertheless such a system could well be of interest where mild organic oxidations are required.

EXPERIMENTAL

Most of the preparations of salts of $[P_2O_8]^{2-}$ appear in the patent literature and often lack specific detail; in many cases it is not clear whether the products are pure. We have devised modifications to existing preparations for these salts to give pure products.

Potassium peroxodiphosphate, $K_4[P_2O_8]$

The procedure used here is a modification of that described in recent patent literature.[16] Potassium dihydrogen *ortho*-phosphate (41.1 g, 0.3 mol), potassium hydroxide (21.9 g, 0.39 mol) and potassium nitrate (8.1 g, 0.08 mol) were dissolved in distilled water to give 80 cm^3 of solution. The mixture was then electrolysed for 6 h on three successive days, using a voltage of 6 V and a current of 0.4 A. A platinum gauze (approximately 2 cm^2) was used as the anode, giving a current density of approximately 0.2 A cm^{-2}, and a platinum wire as the cathode. Stirring was continued throughout and the preparation was carried out under a gentle flow of N_2 to prevent the formation of carbonate from atmospheric carbon dioxide. The temperature was maintained at 10°C during electrolyses. The product was then precipitated with methanol. After several recrystallizations from water/methanol the pure product was obtained by slow evaporation of an aqueous solution *in vacuo* over concentrated sulphuric acid. Found: O_2^{2-}, 9.0; K, 44.4; P, 17.7. $K_4P_2O_8$ requires: O_2^{2-}, 9.2; K, 45.2; P, 17.9%.

Lithium peroxodiphosphate tetrahydrate, $Li_4[P_2O_8] \cdot 4H_2O$

The procedure used here is a modification of that described by Creaser and Edwards.[17] Crude potassium peroxodiphosphate was prepared as follows: potassium dihydrogen *ortho*-phosphate (45.3 g, 0.33 mol), potassium hydroxide (29.7 g, 0.53 mol) and potassium fluoride (18.0 g, 0.31 mol) were dissolved in distilled water to give 80 cm^3 of solution and electrolysis was conducted as described above. The product separated as a solid and following electrolysis was filtered off and redissolved in distilled water (100 cm^3). To this was added a solution of lithium perchlorate $LiClO_4 \cdot nH_2O$ (54 g) in distilled water (150 cm^3), and the resulting thick white precipitate stirred for 15 min; it was then filtered off. The filtrate was tested for completion of reaction by adding a few drops of lithium perchlorate solution. The filtrate was then warmed to 45°C and methanol (150 cm^3) was added rapidly dropwise to the stirred solution. Repeated recrystallization from water/methanol gave the pure salt as a white powder. Found: O_2^{2-}, 11.0; Li, 9.9. $Li_4H_8P_2O_8$ requires: O_2^{2-}, 11.0; Li, 9.6%.

Sodium peroxodiphosphate octadecahydrate, $Na_4[P_2O_8] \cdot 18H_2O$

Crude potassium peroxodiphosphate was prepared as described for the lithium salt and dissolved in distilled water (100 cm^3). To this was added a solution of sodium perchlorate (61 g) in water (150 cm^3); the resulting thick white precipitate was filtered off and the filtrate warmed to 50°C. Methanol (200 cm^3) was then added quickly, with stirring and

after overnight storage at 5°C the impure product was filtered off as a white solid. This was then dissolved in the minimum quantity of water (30 cm^3), with stirring. Chilling to 0°C gave a white precipitate; this was filtered off at 0°C and recrystallized by slow evaporation of an aqueous solution *in vacuo* over concentrated sulphuric acid. Found: O_2^{2-}, 5.0; Na, 14.3. $Na_4H_{36}P_2O_{26}$ requires: O_2^{2-}, 5.3; Na, 15.2%.

Ammonium peroxodiphosphate dihydrate, $(NH_4)_4[P_2O_8]\cdot 2H_2O$

Crude potassium peroxodiphosphate was prepared as for the lithium salt and dissolved in distilled water (100 cm^3). To this was added a solution of ammonium perchlorate (55 g, 0.46 mol) in water (250 cm^3); the resulting thick white precipitate was then filtered off. The filtrate was warmed to 35°C and methanol (200 cm^3) added quickly with stirring. After overnight storage at 5°C the impure product was filtered off. Repeated recrystallization from water/methanol gave the anhydrous salt as a white powder; slow evaporation of an aqueous solution *in vacuo* over concentrated sulphuric acid gave the dihydrate as large single crystals. Found: O_2^{2-}, 10.6; N, 18.6; H, 6.6; P, 20.2. $N_4H_{20}P_2O_{10}$ requires: O_2^{2-}, 10.7; N, 18.8; H, 6.8; P, 20.8%.

X-ray crystal structure of $(NH_4)_4[P_2O_8]\cdot 2H_2O$

Single crystals of the compound were prepared as described in the Experimental. The one selected for study was a rectangular section (of approximate dimensions $0.19\times0.15\times0.07$ mm) cut from a large plate. Crystals of the dihydrate decomposed over about a week, with the loss of water of crystallization. They were, however, sufficiently stable without needing varnish coating or mounting in a Lindemann capillary to permit X-ray data collection, provided that this was commenced immediately upon mounting the crystal and completed overnight. Measurements were taken on a Nicolet R3*m*/Eclipse S140 diffractometer system with graphite-monochromated Cu-K_α radiation. Unit-cell dimensions were determined by least-squares refinement of the angular settings of 16 automatically centred reflections.

Crystal data. $N_4H_{20}P_2O_{10}$, $M = 298.13$, monoclinic, space group $C2/c$, $a = 15.336(2)$, $b = 9.893(2)$, $c = 8.789(1)$ Å, $\beta = 91.28(2)°$, $U = 1336.7$ $Å^3$ at 20°C, $Z = 4$, $D_c = 2.97$ g cm^{-3}, $F(000) = 631.9$, λ(Cu-K_α) = 1.5418 Å, μ(Cu-K_α) = 34.67 cm^{-1}.

Integrated intensities in one quadrant were measured using the ω scan technique. The 020 and 202 reflections were monitored every 50 measurements and these increased by *ca* 10% over the period of data collection (12 h); it is possible that this was due to a decrease in observed extinction. A total of 995 independent reflections were measured, to $\theta = 57°$, of which 67 were judged to be "unobserved" [$I < 3\sigma(I)$]. The data were scaled using the reference reflections and were corrected for Lorentz and polarization effects. Later an absorption correction was applied[18] based on face-indexing. All calculations and drawings were made using the program system *SHELXTL*;[18] atomic scattering factors and anomalous dispersion corrections were taken from ref. 19.

The coordinates of the independent phosphorus atom were found by direct methods and after a few cycles of least-squares refinement all the non-hydrogen atoms were located. When these were allowed to refine anisotropically the hydrogen atoms were found. All the atoms were then allowed to refine, with isotropic temperature factors for the hydrogen atoms and a weighting scheme was applied such that $w = 1/[\sigma(F_o)^2 + 0.0007F_o^2]$ for the last cycle; R reduced to 0.034, and $R' = [\Sigma w\Delta F^2/\Sigma w\Delta F_o^2]^{1/2}$ was 0.037. The final difference Fourier synthesis was featureless, with the largest remaining peak < 0.3 e A^{-2}.

Final atomic parameters, full lists of bond lengths and angles, anisotropic temperature factors of the non-hydrogen atoms, and F_o/F_c values have been deposited as supplementary material with the Editor, from whom copies are available on request.

Physical measurements

IR spectra were recorded as potassium bromide discs and liquid paraffin mulls, using a Perkin–Elmer 683 IR spectrophotometer; Raman spectra were recorded using a Spex Ramalog V Raman spectrometer and a Spex Datamate data acquisition unit. For solid state Raman spectra the samples were sealed in capillaries to prevent cation exchange. ^{31}P NMR measurements were taken on a Jeol FX-90Q NMR spectrometer for solution spectra and a Bruker MSL-300 instrument with a ^{31}P cross-polarization magic-angle spinning attachment for solid state spectra. The peroxide content was determined by treatment with ammonium ferrous sulphate followed by back titration with potassium permanganate solution; hydrogen, nitrogen and phosphorus contents were determined by the Imperial College Microanalytical Laboratory. Potassium was determined gravimetrically as the tetraphenylborate, and the lithium and sodium contents were determined by inductively coupled plasma atomic emission spectrometry.

Acknowledgements—We thank the SERC and Interox Chemicals Ltd for a grant to one of us (R.D.P.) and the SERC for the diffractometer system. We are also grateful to Mr John Davies for the determination of sodium and lithium, and Dr Chris Groombridge and Mr David Butler of Royal Holloway and Bedford New College for recording the solid state ^{31}P NMR spectra. We thank Drs P. Baxter and I. S. McKirdie, and Prof. D. F. Evans, for helpful discussions.

REFERENCES

1. P. Maruthamuthu, K. V. Seshadri and M. Santappa, *Indian J. Chem.* 1972, **10**, 762.
2. K. Tomizawa and Y. Ogata, *Toyoda Kenkyu Hokuku* 1981, **34**, 21.
3. P. Maruthamuthu and M. Santappa, *Indian J. Chem.* 1978, **16**, 43.
4. P. Maruthamuthu and M. Santappa, *Indian J. Chem.* 1974, **12**, 424.
5. S. Lenka, P. L. Nayak, A. P. Das and S. N. Mishra, *J. Polymer Sci., Polymer Chem. Ed.* 1985, **23**, 1615.
6. S. Lenka and P. L. Nayak, *J. Polymer Sci., Polymer Chem. Ed.* 1983, **21**, 1871.
7. F. Fichter and E. Gutzwiller, *Helv. Chim. Acta.* 1928, **11**, 323; S. Husain and J. R. Partington, *Trans. Faraday Soc.* 1928, **24**, 239.
8. A. Simon and H. Richter, *Naturwissenschaften* 1957, **44**, 178; A. Simon and H. Richter, *Z. Anorg. Allg. Chem.* 1960, **302**, 165.
9. D. E. C. Corbridge and E. J. Lowe, *J. Chem. Soc.* 1954, 4555; B. Malinak, J. Touzin, J. Hakelhova, N. Kocanova and J. Dusek, *Collect. Czech. Chem. Commun.* 1974, **39**, 2549.
10. B. K. Sivertsen and H. Sorum, *Z. Krist.* 1969, **130**, 449.
11. H. H. Eysel and G. Rosinger, *J. Raman Spectros.* 1987, **18**, 123.
12. W. R. Busing and H. A. Levy, *J. Chem. Phys.* 1965, **42**, 3054.
13. M. M. Crutchfield and J. O. Edwards, *J. Am. Chem. Soc.* 1960, **82**, 3533.
14. M. Schröder and W. P. Griffith, *J. Chem. Soc., Chem. Commun.* 1978, 58; G. Green, D. M. Hollingshead, S. V. Ley and M. Schröder, *J. Chem. Soc., Perkin. Trans. I*, 1984, 681.
15. R. E. Connick and C. R. Hurley, *J. Am. Chem. Soc.* 1952, **74**, 5012.
16. U.S. Patent No. 4 626 326, (2 December 1986).
17. I. I. Creaser and J. O. Edwards, *Topics Phosphorus Chem.* 1972, **7**, 379 and refs therein.
18. G. M. Sheldrick, *SHELXTL—an Integrated System for Solving, Refining and Displaying Crystal Structures from Diffraction Data*, revision 4. Nicolet Instruments Ltd, Warwick, U.K. (1983).
19. *International Tables for X-Ray Crystallography*, Vol. 4. Kynoch Press, Birmingham (1974).

Polyhedron Vol. 7, No. 14, pp. 1311–1316, 1988
Printed in Great Britain

0277–5387/88 $3.00+.00
Pergamon Press plc

SYNTHESIS OF RUTHENIUM(II) COMPOUNDS WITH *ORTHO*-OXYPYRIDINATE LIGANDS (hp). CRYSTAL STRUCTURE CHARACTERIZATION OF [Ru(η^6-*p*-$CH_3C_6H_4CH(CH_3)_2$)Cl(hp)]

P. LAHUERTA,† J. LATORRE and M. SANAÚ

Departamento de Química Inorgánica, Facultad de Químicas, Universidad de Valencia, Burjasot, 46100 Valencia, Spain

and

F. A. COTTON† and W. SCHWOTZER

Department of Chemistry and Laboratory for Molecular Structure and Bonding, Texas A&M University, College Station, TX 77843, U.S.A.

(*Received* 18 *January* 1988; *accepted* 18 *February* 1988)

Abstract—The reaction of [Ru(η^6-*p*-cymene)Cl_2]$_2$ (*p*-cymene = *p*-$CH_3C_6H_4CH(CH_3)_2$) with Nahp in THF yields [Ru(η^6-*p*-cymene)Cl(hp)] (**1**). The crystal structure of (**1**) has been determined by X-ray methods. (**1**) crystallizes in the space group *Pbca*, with $a = 16.629(2)$, $b = 10.201(3)$, $c = 17.752(2)$ Å. The compound contains one coordinated arene group, one chlorine and one hp group in a chelating coordination mode. The reaction of (**1**) with Aghp yields [Ru(η^6-*p*-cymene)(hp)$_2$] (**2**). The ^{13}C NMR spectrum at $-70°C$ is consistent with a structure Ru(η^6-*p*-cymene)(η^2-hp)(η^1-hp). At room temperature a rapid interconvertion between the two hp ligands occurs according to the observed ^1H and ^{13}C NMR spectra.

Dinuclear compounds of ruthenium in the oxidation states (II,II), (II,III) or (III,III) are well known.[1] In these dimers the metals are linked by multiple bonds of orders 2, 2.5 and 3 for the Ru_2^{4+}, Ru_2^{5+} and Ru_2^{6+} ions, respectively. Electrochemical studies have revealed that electron transfer processes interconverting these oxidation states and thus altering the bond order are relatively easy.[2] In contrast, very little is known about dinuclear complexes with the Ru_2^{2+} core for which the assumption of a single M—M bond is compatible with the MO description *viz.* a $\sigma^2\pi^4\delta^2\delta^{*2}\pi^{*4}$ configuration. We have recently observed[3] that [Ru(η^6-*p*-cymene)Cl_2]$_2$ can be electrochemically reduced to a product which, because of the lack of an ESR response, we postulate to be the dinuclear Ru(I)—Ru(I) compound. This compound has only limited stability in solution at room temperature. On the other hand, electrochemical data suggest that this dinuclear compound should be thermodynamically stable with respect to disproportionation processes by virtue of a separation of the reduction waves by 1.1 V,[3] and we assume that the decomposition is initiated by a dissociation of the dinuclear unit. We therefore attempted to synthesize Ru_2^{4+} starting materials in which the dinuclear unit is stabilized by bridging ligands such as α-oxypyridinates. We report here the results of an attempt to synthesize such dimers by reacting [Ru(η^6-*p*-cymene)Cl_2]$_2$ with Na and Ag salts of hydroxypyridine. The products thereby obtained are mononuclear complexes of Ru(II) which were characterized by chemical and spectroscopic analyses and by X-ray crystallography.

EXPERIMENTAL

Preparation of the compounds

[Ru(η^6-*p*-cymene)Cl_2]$_2$ was prepared by literature procedures.[4] Hhp was obtained from Aldrich Chemical Co. and $RuCl_3$ was obtained from Johnson Matthey. Nahp was obtained by reaction of sodium

† Authors to whom correspondence should be addressed.

methoxide in methanol with Hhp and Aghp was prepared by reacting Nahp with $AgNO_3$. ^1H NMR and ^{13}C spectra were recorded in $CDCl_3$ or CD_2Cl_2 on a Bruker AC200 spectrometer.

Ru(η^6-*p*-cymene)Cl(hp) (**1**). A mixture of 50 mg (0.081 mmol) of [Ru(η^6-*p*-cymene)Cl_2]$_2$ and 19 mg (0.162 mmol) of Nahp in 20 cm^3 of THF was stirred for 1 h. The resulting solution was concentrated under vacuum to one third of the initial volume. Slow addition of 10 cm^3 of ethyl ether gave red–orange crystals of Ru(η^6-*p*-cymene)Cl(hp). The crystallization was completed by cooling the sample overnight at −20°C. Yield 61%.

Ru(η^6-*p*-cymene)(hp)$_2$ (**2**). A mixture of 122 mg (0.334 mmol) of Ru(η^6-*p*-cymene)Cl(hp) and 64.5 mg (0.334 mmol) of Aghp in 30 cm^3 of THF was stirred for 4 h and a white precipitate was separated from the yellow solution. The solution was filtered and concentrated under vacuum to half of its initial volume; a yellow solid separated during this process. Precipitation was completed by addition of 10 cm^3 of *n*-hexane. The crystals were filtered off, washed with hexane and dried under vacuum. Yield 67%. Found: C, 54.7; H, 5.2; N, 6.1. Calc. for $C_{18}H_{22}N_2O_2Ru$: C, 56.7; H, 5.2; N, 6.6%.

X-ray procedures

The crystallographic work followed the general procedures which have been described previously.[5] The crystal parameters and procedural information corresponding to data collection and structure refinement for compound (**1**) are given in Table 1. Lorentz and polarization corrections were applied. The position of the ruthenium atom was located

Table 1.

Formula	$RuClONC_{15}H_{18}$
Formula weight	364.84
Space group	Pbca
Systematic absences	($0kl$ $k = 2n$) ($h0l$ $l = 2n$) ($hk0$ $h = 2n$)
a (Å)	16.629(2)
b (Å)	10.201(3)
c (Å)	17.752(2)
α (degrees)	90.0
β (degrees)	90.0
γ (degrees)	90.0
V (Å^3)	3011(3)
Z	8
d_{calc} (g cm^{-3})	1.610
Crystal size (mm)	0.15 × 0.2 × 0.2
μ(Mo-K_α)(cm^{-1})	5.959
Data collection instrument	Syntex $P1$
Radiation (monochromated in incident beam)	Mo-K_α (λ_α = 0.71073 Å)
Orientation reflections, number, range (2θ)	25
Temperature (°C)	22±2
Scan method	$\omega-2\theta$
Data collection range (2θ, degrees)	4–45
No. unique data, total with $F_o^2 > 3\sigma(F_o^2)$	2240 1559
Number of parameters refined	172
Trans. factors, max., min.	
R^a	0.03410
R_w^b	0.06846
Quality-of-fit indicator[c]	1.445
Largest shift/esd, final cycle	0.61
Largest peak, e Å^{-3}	0.586

[a] $R = \Sigma||F_o|-|F_c||/\Sigma|F_o|$.
[b] $R_w = [\Sigma w(|F_o|-|F_c|)^2/\Sigma w|F_o|^2]^{1/2}$; $w = 1/\sigma^2(|F_o|)$.
[c] Quality-of fit = $[\Sigma w(|F_o|-|F_c|)^2/(N_{obs}-N_{parameters})]^{1/2}$.

with the use of the direct methods program MULTAN. The remaining non-hydrogen atoms were located by using successive least-squares refinement and difference Fourier maps. The refinement converged at residuals of $R = 0.043$, $R_w = 0.068$.

Electrochemistry

Cyclic voltammograms were carried out in a three-electrode cell using a programmed function generator (305 H.Q. Instruments) connected to a 552 Amel potentiostat and were recorded with a Riken-Denshi F35 *x-z* recorder. The working and auxiliary electrode were platinum, the reference electrode was a saturated calomel electrode electrically connected to the non-aqueous solution by a "salt bridge". The solvent was THF which had been freshly distilled over Na–benzophenone. The supporting electrolyte, Bu_4NPF_6, was recrystallized from ethanol and dried at 80°C *in vacuo* for 48 h. All the electrochemical experiments were carried out under an argon atmosphere. Controlled potential electrolyses were carried out in a three-compartment cell separated by fritted glass using an Amel 552 potentiostat. Working and auxiliary electrodes were of platinum mesh. The charge transferred was calculated by recording intensity versus time during the electrolyses and carrying out an integration. The system was calibrated against cobaltocene.

RESULTS AND DISCUSSION

The reaction of $[Ru(\eta^6\text{-}p\text{-cymene})Cl_2]_2$ and Nahp (1 : 1 molar ratio) in THF gives (**1**) in good yield. This in turn reacts with Aghp in dichloromethane giving (**2**). These two compounds are solution in halogenated solvents, slightly soluble in ethyl ether and insoluble in hexane. They are fairly air stable in the solid state and in solution for short periods of time.

Structural results

The compound $[Ru(\eta^6\text{-}p\text{-cymene})Cl(hp)]$ (**1**), is a mononuclear complex of Ru(II) with a η^6-coordinated aromatic ligand. A perspective view of the molecular unit is shown in Fig. 1. Bond distances and angles are given in Tables 2 and 3.

The η^6-coordination of the aromatic ring and the small bite of the chelating ligand lead to a rather irregular coordination geometry which can be described as distorted octahedral. There is some indication of an alternation of bond lengths within the aromatic ring indicative of a contribution from the cyclohexatriene resonance structure to the overall resonance hybrid.

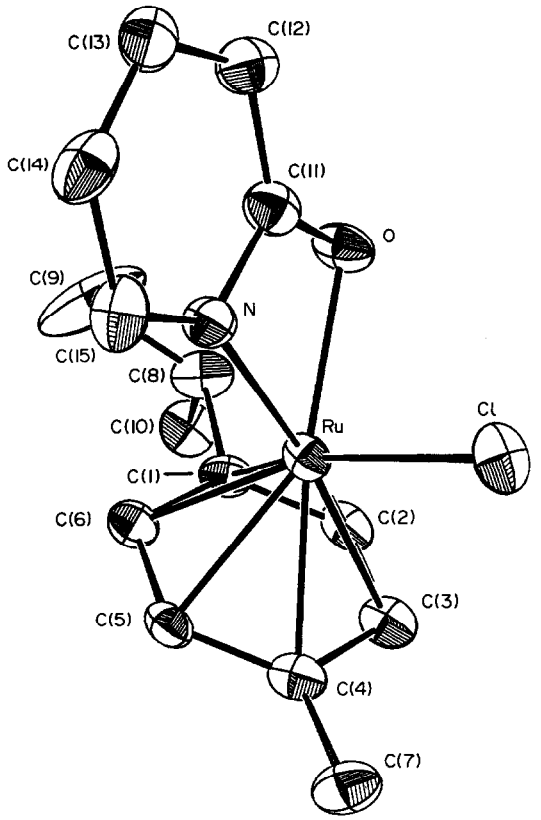

Fig. 1. Ortep view of (**1**).

The bidentate ligand, which was introduced because of its tendency to adopt the bridging mode

Table 2. Selected bond distances (Å) for compound (**1**)

Compound	1
Ru—Cl	2.396(3)
Ru—O(1)	2.153(6)
Ru—N	2.084(7)
Ru—C(1)	2.191(9)
Ru—C(2)	2.183(9)
Ru—C(3)	2.207(10)
Ru—C(4)	2.188(10)
Ru—C(5)	2.170(8)
Ru—C(6)	2.209(9)
C(1)—C(2)	1.44(1)
C(2)—C(3)	1.41(1)
C(3)—C(4)	1.48(1)
C(4)—C(5)	1.41(1)
C(5)—C(6)	1.45(1)
C(6)—C(1)	1.44(1)
C(11)—O(1)	1.30(1)

Table 3. Selected bond angles (deg) for compound (1)

Compound	1
Cl—Ru—O(1)	86.3(2)
Cl—Ru—N	85.6(2)
O—Ru—N	62.4(3)
C(6)—C(1)—C(2)	118.6(8)
C(1)—C(2)—C(3)	122.5(8)
C(2)—C(3)—C(4)	118.7(9)
C(4)—C(5)—C(6)	122.2(8)
C(5)—C(6)—C(1)	119.1(8)
N—C(11)—O	110.9(8)
C(11)—O(1)—Ru	96.6(5)
C(11)—N—Ru	63.9(6)

of ligation, assumes the less common chelating function. The bite angle L—M—L′ is 62.4(3)°. The ^{13}C and ^{1}H NMR spectroscopic results (Table 4) suggest that (**1**) in solution retains the solid state structure. There are two partially overlapping multiplets at 1.31 and 1.34 ppm in the proton spectrum which can plausibly be assigned to the inequivalent methyl groups of the isopropyl substituents. The aromatic protons appear in two blocks centred around 5.3 and 5.6 ppm, while the signals of the oxypyridinate appear as four well separated resonances with the expected doublet and triplet fine structure. Even more clearly demonstrating the lack of symmetry is the ^{13}C NMR spectrum where all the aromatic resonances appear separated.

Table 4. ^{1}H and ^{13}C NMR data for compounds (**1**) and (**2**)

Compound	T (°K)	^{1}H δ(ppm), [J Hz]	^{13}C δ(ppm)
(**1**)	303	Arene ligand	100.7; 96.1
		5.63 m (2H); 5.38 m (2H)	81.2; 80.8; 80.4; 78.8
		2.93 spt (1H)	31.3
		2.36 s (3H)	18.8
		1.34 d (3H) [6.4]; 1.31 d (3H) [5.8]	22.6; 22.2
		hp ligand	177.4
		8.00 d (1H) [5.1]; 7.45 t (1H) [8.4]	
		6.54 t (1H) [6.2]; 6.13 d (1H) [8.6]	145.1; 136.5; 111.4; 111.2
(**2**)	303	Arene ligand	101.9;[a] 95.8[a]
		5.63–5.51 (4H, AB) [6.0]	80.5; 79.8
		2.87 spt (1H)	17.6[a]
		2.27 s (3H)	30.7[a]
		1.34 d (6H) [6.9]	21.5
		hp ligand	173.0
		7.73 d (2H) [4.72]; 7.11 t (2H) [7.0]	
		6.13 t (2H) [6.2]; 6.02 d (2H) [8.5]	146.7; 136.9; 111.9; 107.5
(**2**)	204	Arene ligand	101.5;[a] 95.8[a]
			80.9; 80.4; 79.9; 77.9
			17.7[a]
			30.6[a]
			22.0; 20.8
		hp ligand	175.5; 169.5
			147.5; 146.2; 137.7; 136.6
			114.8; 109.9; 108.3; 106.2

s: singlet; d: doublet; t: triplet; m: unresolved multiplet.
[a] Signal unmodified by the temperature change.

* Solutions of compound (**2**) in halogenated solvents slowly generate small amounts of compound (**1**). This must be due to the cleavage of the Rh—O bond in the η^1-hp ligand by traces of HCl present in the solvent. It is consistent with this observation that compound (**2**) is always isolated as a yellow solid with low analytical results for C and N. The ^{1}H and ^{13}C NMR spectra are in good agreement with the proposed stoichiometry.

In compound (**2**), which according to chemical analysis* and ^{1}H NMR integration has the composition [Ru(η^6-*p*-cymene)(hp)$_2$], there is at room temperature only one set of resonances for the hp ligand in the ^{1}H as well as in the ^{13}C spectrum. Additionally, the dynamically averaged spectra suggest a plane of symmetry with only four aromatic carbon resonances and the characteristic AA′BB′

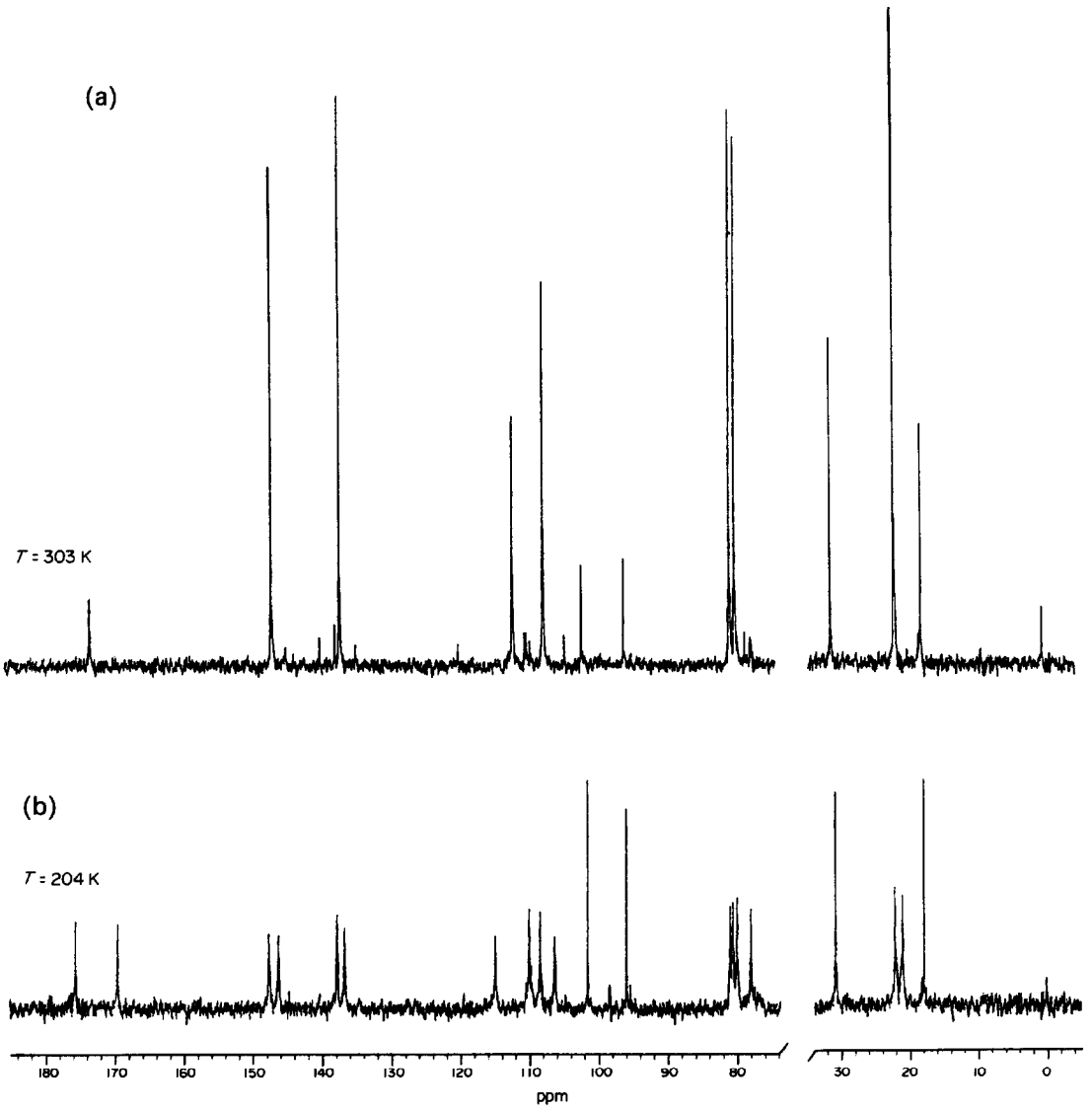

Fig. 2. ^{13}C NMR spectra of (**2**) in Cl_2CD. (a) 303 K and (b) 204 K.

pattern in the proton spectrum. Assuming an instantaneous structure with one dangling and one chelating oxypyridinate ligand, we must invoke a dynamic process that involves rapid interconversion between the dangling and chelating mode for each hp.

Ru(η^6-*p*-cymene)(η^2-hp*)(η^1-hp)

$\rightleftharpoons\!=\!=\!=\!=\!=\!\rightleftharpoons$ Ru(η^6-*p*-cymene)(η^1-hp*)(η^2-hp).

All the ^{13}C resonances corresponding to the average hp ligands in the room temperature spectrum collapse at low temperature and give two sets of signals at $-70°C$, (Fig. 2). All the arene resonances appear separated, in agreement with the lack of symmetry expected for the rigid molecule Ru(η^6-*p*-cymene)(η^2-hp)(η^1-hp).

Electrochemical results

Compounds (**1**) and (**2**) in THF irreversibly reduce at potential values of -1.38 and -1.56, respectively (vs SCE) (peak A_1). One oxidation peak at about 0.0 V is detected in all cases in the reverse sweep. No other clear oxidation peaks are observed in the potential range used -2.0, $+1.4$ V. A cyclic voltammogram typical for the two compounds is shown in Fig. 3.

Controlled potential electrolysis of compound (**1**) at room temperature on the plateau of peak A_1 results in the consumption of 1.9–2.0 Faraday mol^{-1} of Ru. Similar results are also obtained in the electrolysis of compound (**2**). The resulting dark red solutions obtained after the electrolysis oxidize at 0.0 V. One additional oxidation peak at $+1.1$ V,

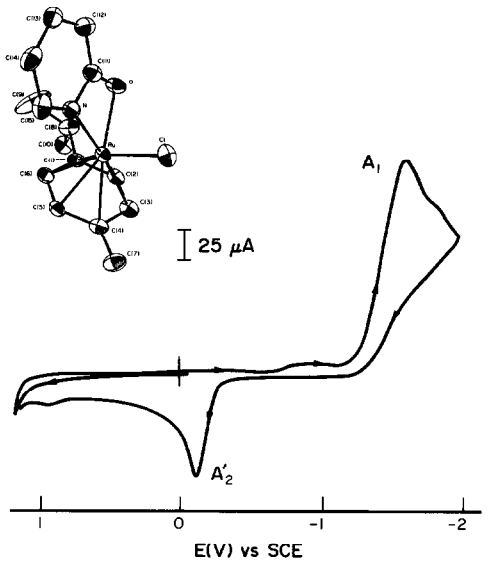

Fig. 3. Cyclic voltammogram of compound (**1**) in THF.

is also detected in the reduced solution of (**1**) and is assigned to the oxidation of chloride ions generated during the electrolysis.

These results indicate that direct reduction from Ru(II) to Ru(0) occurs without any evidence of the stabilization of Ru(I) intermediates. This is generally observed for mononuclear Ru(II) compounds as opposed to the dinuclear $[Ru(\eta^6\text{-}p\text{-cymene})Cl_2]_2$[3] which shows selective reduction from Ru(II)—Ru(II) to Ru(I)—Ru(I).

Acknowledgements—We thank the National Science Foundation and the CAICYT (Spain) for financial support under grant No. 3275/83.

REFERENCES

1. R. W. Callahan, G. M. Brown and T. J. Meyer, *Inorg. Chem.* 1975, **14**, 1443; (b) V. T. Coombe, G. A. Heath, T. A. Stephenson and D. K. Vattis, *J. Chem. Soc., Dalton Trans.* 1983, 2307.
2. J. C. Curtis, J. S. Bernstein and T. J. Meyer, *Inorg. Chem.* 1984, **24**, 385.
3. J. Latorre, Dissertation. Universidad de Valencia (1985).
4. D. A. Tocher, R. O. Gould, T. A. Stephenson, M. A. Bennett, J. P. Ennet, T. W. Matheson, L. Sawyer and V. K. Shah, *J. Chem. Soc., Dalton Trans.* 1983, 1571; (b) M. A. Bennett, N. Huang, T. W. Matteson and K. Smith, *Inorg. Synth.* 1982, **21**, 75.
5. (a) Calculations were carried out on the VAX-11/780 computer at the Department of Chemistry, Texas A&M University, College Station, TX, with a VAX-SPD software package; (b) A. Bino, F. A. Cotton and P. E. Fanwick, *Inorg. Chem.* 1979, **18**, 3558; (c) F. A. Cotton, B. A. Frenz, G. Deganello and A. Shaver, *J. Organomet. Chem.* 1973, **50**, 227; (d) A. C. T. North, D. C. Phillips and F. S. Mathews, *Acta Cryst.* 1968, **A24**, 351.

Polyhedron Vol. 7, No. 14, pp. 1317–1319, 1988
Printed in Great Britain

0277–5387/88 $3.00+.00
© 1988 Pergamon Press plc

COMMUNICATION

PHOSPHIDO AND ARSENIDO CHEMISTRY OF TIN(II). SYNTHESIS AND STRUCTURE OF $[Sn(\mu\text{-}E\text{-}t\text{-}Bu_2)Cl]_2$ (E = P, As)

ALAN H. COWLEY,* DEAN M. GIOLANDO, RICHARD A. JONES,* CHRISTINE M. NUNN and JOHN M. POWER

Department of Chemistry, The University of Texas at Austin, Austin, TX 78712-1167, U.S.A.

and

WOLF-WALTHER du MONT*

Fachbereich Chemie, Universität Oldenburg, D-2900, Oldenburg, F.R.G.

(*Received* 30 *November* 1987; *accepted* 18 *Feburary* 1988)

Abstract—The reaction of $SnCl_2$ with $E(t\text{-}Bu_2)SiMe_3$ (E = P, As) affords compounds of empirical composition $[Sn(E\text{-}t\text{-}Bu_2)Cl]_X$. An X-ray diffraction study of the arsenic compounds reveals a dimeric structure, $ClSn(\mu\text{-}As\text{-}t\text{-}Bu_2)_2SnCl$. A similar structure is assigned to the phosphorus analogue on the basis of NMR data.

The phosphido and arsenido chemistry of the main-group elements has been investigated much less extensively than that of the corresponding amides.[1] In the context of low valent group 14 compounds, duMont *et al.* reported that the reaction of $K[P\text{-}t\text{-}Bu_2]$ with $Et_3P \rightarrow SnCl_2$ (2:1 stoichiometry) afforded the dimer $[Sn(\mu\text{-}P\text{-}t\text{-}Bu_2)_2]_2$ (**1**) [eq. (1)].[2] It was later found that reaction of $Et_3P \rightarrow SnCl_2$ with $P(t\text{-}Bu)_2SiMe_3$ (1:1 stoichiometry) afforded a material of empirical composition $[Sn(P\text{-}t\text{-}Bu_2)Cl]_X$ (**2a**) [eq. (2)].[3] An arsenic analogue, $[Sn(As\text{-}t\text{-}Bu_2)Cl]_X$ (**2b**) was reported subsequently.[4] The structure assignment for **1** was consistent with ^{31}P and ^{119}Sn NMR data. Although a dimeric structure for **2a,b** was not excluded, a polymeric formulation was suggested for these compounds on the basis of their low solubilities. As part of a general study of the reactions of $E(t\text{-}Bu)_2SiMe_3$ (E = P, As) with main-group halides, we have reinvestigated the $SnCl_2$ reaction.

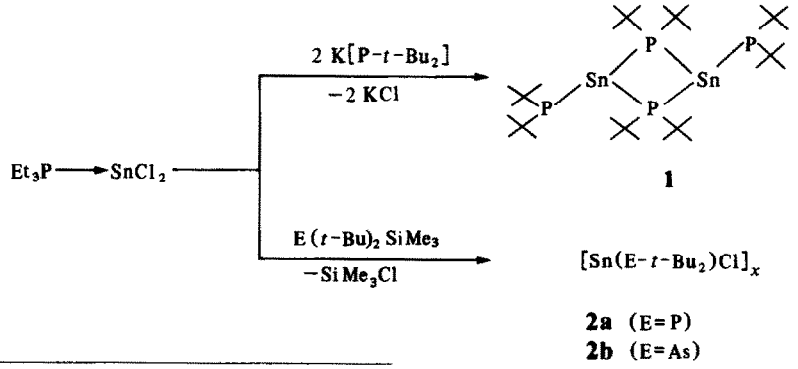

(1)

1

(2)

2a (E=P)
2b (E=As)

* Authors to whom correspondence should be addressed.

Addition of a hexane solution of $E(t\text{-Bu})_2SiMe_3$ (E = P, As) to $SnCl_2$ (in Et_2O) produced yellow slurries which upon filtration afforded microcrystalline **2a** and **2b** in 95 and 83% yields, respectively. Compounds **2a** and **2b** are poorly soluble in most common hydrocarbon and ether solvents; however, both compounds can be extracted slowly into toluene. The same products were produced when an excess of $E(t\text{-Bu})_2SiMe_3$ was employed. In fact, it is convenient to use an approximately 25% molar excess of the silyl reagent to ensure the complete reaction of $SnCl_2$. Compound **2a** can also be produced in good yields via the reaction of equimolar quantities of $Li[P\text{-}t\text{-}Bu_2]$ and $SnCl_2$. However, this methodology was not successful for the preparation of **2b** because of reduction to metallic tin.

The solid state structure of **2b** comprises discrete centrosymmetric dimers and there are no unusually short intermolecular contacts (Fig. 1).* The chloro and arsenido ligands adopt terminal and bridging positions, respectively, and the rhombohedral Sn_2As_2 core is planar. The As geometry is approximately tetrahedral, that of the Sn atom is best described as pyramidal, and there is an *anti* arrangement of the Cl ligands. Overall, the structure of

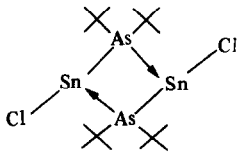

2b

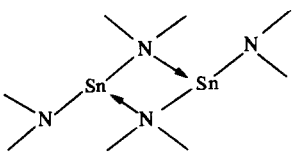

3

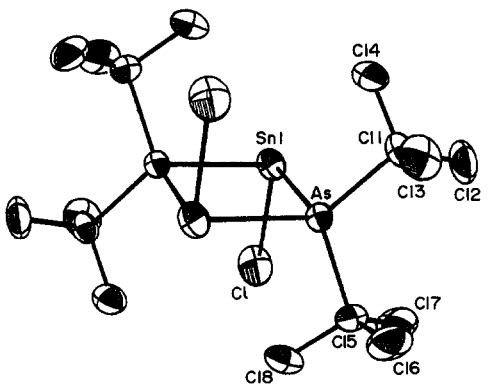

Fig. 1. ORTEP view of (**2b**); key bond lengths (Å) and angles (°): Sn(1)—As 2.773(1), Sn(1′)—As 2.776(1), Sn(1)—Cl 2.453(1), As—C(11) 2.031(2), As—C(15) 2.032(3), $[C\text{—}C]_{av}$ 1.539(4) [over the range 1.529(4) to 1.549(4)], As—Sn(1)—As 77.78(1), As—Sn(1)—Cl 98.58(2), As—Sn(1)—Cl 97.82(2), Sn(1)—As—Sn(1′) 102.22(1), C(11)—As—C(15) 111.0(1), $[Sn(1)\text{—}As\text{—}C]_{av}$ 110.9(8) [over the range 105.78(7) to 116.17(8)].

2b resembles that of $[Sn(\mu\text{-}NMe_2)NMe_2]_2$ (**3**).[5] The most important structural feature for **2b** is the As—Sn bond distance (av. 2.775(1) Å) which, to the best of our knowledge, is the first such measurement for a molecular compound. The sum of the covalent radii for Sn and As (2.63 Å) is approximately 5.6% shorter than the observed As—Sn distance.[6] Analogously for **3**, a 5.1% difference between the sum of the covalent radii for Sn and N and the (bridging) Sn—N distance is observed. For the $R_2E\text{—}SnX$ dimers (X = Cl, NMe_2) the four-membered ring core consists of alternating single and dative bonds. Since the crystallographic experiment gives the E—Sn (E = N, As) distances as an average of the two types of bonding, it is expected that the observed E—Sn distances will be somewhat longer than the corresponding sums of covalent radii.

Unfortunately, it has not been possible to obtain single crystals of **2a** suitable for X-ray diffraction study. However, on the basis of NMR data it can be concluded that **2a** is isostructural with **2b**. Significantly, the ^{119}Sn NMR spectrum of **2a** consists of a triplet (507 ppm, [t, $J(^{119}Sn\text{—}P) = 1432$ Hz]) thus demonstrating that the $t\text{-}PBu_2$ groups reside in the bridging positions. The ^{31}P NMR spectrum of **2a** consists of a singlet (−61.2 ppm)† that is considerably upfield of the chemical shifts for **1** ($P_{terminal}$ +65 ppm; P_{bridge} +20 ppm). Such an upfield shift can be attributed to the presence of chloride substituent on Sn. In fact, the ^{31}P NMR resonances for the compounds $(Me_{3-X}Cl_X)SnP\text{-}t\text{-}Bu_2$ are shifted progressively further upfield as the number of chlorides on tin is increased: −20.7 ppm, $X = 0$; −40.5 ppm, $X = 1$ and −72.3 ppm, $X = 2$.[7]

*Crystal data for **2b**: $C_{16}H_{36}As_2Cl_2Sn_2$; $M = 686.6$. Crystal data: triclinic, $P\bar{1}$ (No. 2), $a = 8.027(1)$, $b = 9.027(2)$, $c = 9.385(1)$ Å, $\alpha = 77.69(1)$, $\beta = 81.09(1)$, $\gamma = 67.40(1)°$, $V = 611$ Å^3, $Z = 1$, $D_c = 1.87$ g cm^{-3}, $\mu(Mo\text{-}K_\alpha) = 49.5$ cm^{-1}.

Crystal growth: Yellow–orange cubic single crystals of **2b** were grown by cooling a saturated toluene solution to −20°C for one week.

Intensity data: Enraf–Nonius CAD4 diffractometer at 23±2°C, $\omega - 2\theta$ scan mode within the range $3 \leqslant 2\theta \leqslant 56°$. The structure was solved by Patterson and Fourier methods by which all non-hydrogen atoms were located and refined anisotropically. Full-matrix least-squares refinement of 2463 reflections [$I > 3\sigma(I)$] from a total of 3142 unique measured reflections gave final R and R_w values of 0.034 and 0.044, respectively.

Atomic coordinates, bond lengths and angles and thermal parameters have been deposited at the Cambridge Crystallographic Data Centre. See notice to Authors, issue No. 1.

†The tin satellites appear as a doublet-of-doublets: $^1J(^{119}Sn\text{—}P) = 1426$ Hz; $^1J(^{117}Sn\text{—}P) = 1370$ Hz.

As summarized in eq. (3), **1** and **2a** can be interconverted.

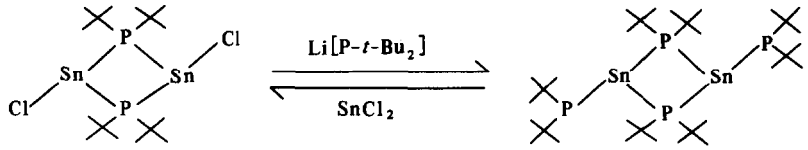

(3)

2a **1**

Thus, treatment of **2a** with one equiv. of Li[P-*t*-Bu_2] causes a rapid conversion to **1**. The reaction of **1** with $SnCl_2$ to form **2a** is, however, much slower. It seems likely that **2a** is the intermediate species in the formation of **1** from $SnCl_2$.

Acknowledgements—We are grateful to the National Science Foundation, the Robert A. Welch Foundation and the Texas Advanced Technology Research Program for financial support.

REFERENCES

1. M. F. Lappert, P. P. Power, A. R. Sanger and R. C. Srivastava, *Metal and Metalloid Amides: Syntheses, Structures and Physical and Chemical Properties*. Horwood-Wiley, Chichester, U.K. (1980).
2. W.-W. du Mont and H.-J. Kroth, *Angew. Chem., Int. Ed. Engl.* 1977, **16**, 792.
3. W.-W. du Mont and M. Grenz, *Chem. Ber.* 1985, **118**, 1045.
4. W.-W. du Mont and G. Rudolph, *Z. Naturforsch.* 1981, **36b**, 1215.
5. M. M. Olmstead and P. P. Power, *Inorg. Chem.* 1984, **23**, 413.
6. L. Pauling, *The Nature of the Chemical Bond*, p. 210. Cornell University Press, Cornell (1967).
7. H. Schumann, J. Held, W.-W. du Mont, G. Rodewald and B. Wöbke, *Adv. Chem. Ser.* 1976, **157**, 57.

Polyhedron Vol. 7, No. 15, pp. 1321–1327, 1988
Printed in Great Britain

0277–5387/88 $3.00+.00
Pergamon Press plc

NUCLEAR MAGNETIC RESONANCE INVESTIGATIONS OF THE FLUXIONALITY OF *TRANS*-PALLADIUM(II) AND -PLATINUM(II) DICHLORIDE COMPLEXES OF 1,3-DITHIOLANES—I. 1,3-DITHIOLANE AND 2,2-DIMETHYL-1,3-DITHIOLANE COMPLEXES

EDWARD W. ABEL, KEITH G. ORRELL,* KHURSHID B. QURESHI and VLADIMIR ŠIK

Department of Chemistry, University of Exeter, Exeter EX4 4QD, U.K.

(*Received* 7 *February* 1988; *accepted* 18 *February* 1988)

Abstract—The complexes *trans*-$[MCl_2(\overline{SC_2H_4SCR_2})_2]$ (M = Pd(II) and Pt(II), R = H and Me) have been synthesized and characterized. The energies of pyramidal inversion of the metal-coordinated sulphur atoms, measured by NMR bandshape analyses, are in the range 49–64 kJ mol^{-1} for the dichloro complexes. NMR observations suggest that for the 1,3-dithiolane complexes (R = H) this pyramidal inversion process is correlated with intramolecular 1,3-metallotropic shifts.

Palladium(II) and platinum(II) *trans*-dihalide complexes of cyclic sulphides have been known for a considerable time,[1–4] and certain of them have been extensively studied by variable temperature NMR in order to characterize the pyramidal inversion of the coordinated sulphur atoms.[5–6] One of these studies concerned the five-membered tetrahydrothiophen ring complexes $[MX_2\{\overline{S(CH_2)_4}\}_2]$ (M = Pd(II) and Pt(II), X = Cl, Br and I). Synthesis of the related complexes of 1,3-dithiolanes, namely $[MCl_2(\overline{SC_2H_4SCR_2})_2]$ (M = Pd(II) and Pt(II), R = H and Me), has been prompted for two reasons. We wished, firstly, to examine the influence of a second heterocyclic sulphur atom on the inversion rates of the metal-coordinated sulphur atom, and secondly to establish whether the metal underwent a 1,3-shift between the two sulphur sites analogous to the shifts in metal complexes of the open chain ligands, $MeS(CH_2S)_nMe$, *viz.* 2,4-dithiapentane ($n = 1$),[7,8] 2,4,6-trithiaheptane ($n = 2$),[9,10] 2,4,6,8-tetrathianonane ($n = 3$)[9] and the cyclic ligands 1,3-dithian, $\overline{SCH_2SCH_2CH_2CH_2}$[11–13] 1,3,5-trithian, $\overline{SCH_2SCH_2SCH_2}$,[11–13] and 1,3,5,7-tetrathian, $\overline{SCH_2SCH_2SCH_2SCH_2}$.[14,15]

We report herein the syntheses and solution ^1H NMR properties of the unsubstituted and 2,2-dimethyl substituted 1,3-dithiolane complexes $[MCl_2(\overline{SC_2H_4SCR_2})_2]$ (M = Pd(II) and Pt(II), R = H and Me), and in the following paper[16] on the 2-monosubstituted ligand complexes $[MCl_2(\overline{SC_2H_4SCHR})_2]$ (R = Me, ^{t}Bu, and Ph).

EXPERIMENTAL

Materials and preparations

Ligands. 1,3-Dithiolane was prepared by condensation of ethylenedimercaptan with formaldehyde.[17] The mercaptan (8.86 g, 0.119 mol, 9.43 cm^3) was slowly added to a formalin (2.83 g, 0.119 mol, 2.60 cm^3) solution containing a trace of HCl (1 cm^3) cooled to below 10°C. When the clear solution was gently warmed it suddenly became turbid with the separation of 1,3-dithiolane and its polymeride. The former was steam distilled and the distillate purified further by extraction with ether (2×50 cm^3). The combined ether layers were dried over $MgSO_4$. Removal of ether under reduced pressure gave the required product (2.96 g, 0.028 mol; yield 23.3%). B.p. 61°C/11 mmHg.[17]

2,2-Dimethyl-1,3-dithiolane was prepared by reacting a solution of Analar acetone (7.9 g, 0.13 mol, 10 cm^3) in benzene (100 cm^3) with ethanedithiol (12.8 g, 0.13 mol, 11.5 cm^3) in the presence of *para*-toluenesulphonic acid (0.2 g). The mixture was heated under reflux for 9 h at 65°C, during

* Author to whom correspondence should be addressed.

which time water (2.1 cm^3, 0.116 mol) was collected using a Dean and Stark apparatus. After removing the benzene by distillation at 80°C, the required product (12 g, 0.090 mol) was obtained by distillation of the residue under reduced pressure. B.p. 50°C/10 mmHg.[18]

The palladium(II) and platinum(II) complexes. These were prepared by a modified version of the procedure of Kauffman and Cowan.[19] For the *trans*-dichloro complexes this involved stirring an aqueous solution of the palladium or platinum salt K_2MCl_4 with an aqueous solution of the excess ligand for 1 h at room temperature.

Dichlorobis(1,3-dithiolane)platinum(II), $[PtCl_2(\overline{SC_2H_4SCH_2})_2]$. (A representative preparation.) K_2PtCl_4 (0.27 g, 0.67 mmol) was dissolved in water (20 cm^3) and added to an aqueous solution (20 cm^3) of 1,3-dithiolane (0.142 g, 1.34 mmol). After complete addition the reaction mixture was stirred for 1 h, the yellow product filtered and then dried over anhydrous calcium chloride. Recrystallization from chloroform gave the desired product. Analytical data are in Table 1.

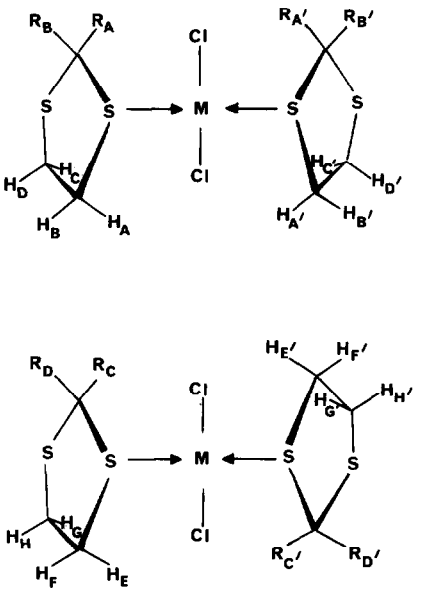

Fig. 1. General structure of *meso*- and DL-$[MCl_2(\overline{SC_2H_4SCR_2})_2]$ (M = Pd(II) or Pt(II), R = H or Me) showing the proton labelling.

NMR spectra

All spectra were recorded on a Brüker AM250 FT spectrometer operating at 250.1 MHz (^1H) and 62.9 MHz (^{13}C). All complexes were examined as solutions in $CDCl_3$ using Me_4Si as the internal reference. Sample temperature variation was achieved by a standard variable temperature unit, temperatures being considered accurate to ±1°C. Bandshape analyses of the ^1H spectra were based on at least six spectra and were performed using the authors' modified version of the DNMR program of Kleier and Binsch.[20]

RESULTS

Static NMR data

The *trans*-$[MCl_2(\overline{SC_2H_4SCR_2})_2]$ complexes all possess the same basic geometry. The tetrahedral sulphur atoms in these complexes constitute chiral centres which render the ring methylene hydrogen pairs diastereotopic and hence anisochronous in the absence of any exchange process. Because of the lower symmetry of the 1,3-dithiolane complexes compared to the tetrahydrothiophen complexes,[5] two diastereomers are possible which differ in the relationship of their isolated —CR_2— groups. (Fig. 1). A *meso* isomer arises when the groups are mutually *cis* and a DL isomer pair results when the groups are mutually *trans*. These diastereomers cannot be interconverted by any bond rotation process (e.g. rotation about the M—S bonds) but can be exchanged by atomic inversion of the pyramidal S atoms. Low temperature ^1H and ^{13}C NMR studies clearly show that no isomer exchange is occurring, and both *meso* and DL forms of the complex exist in approximately equal amounts. Rapid rotation

Table 1. Analytical data for the complexes $[MCl_2(\overline{SC_2H_4SCR_2})_2]$

				Elemental analysis (%)			
				C		H	
	Yield	M.p. (°C)	Colour	Calc.	Found	Calc.	Found
$[PdCl_2(\overline{SC_2H_4SCH_2})_2]$	70.5	110	Orange	18.5	18.5	3.1	3.0
$[PtCl_2(\overline{SC_2H_4SCH_2})_2]$	80.7	100	Yellow	15.1	14.8	2.5	2.5
$[PdCl_2(\overline{SC_2H_4SCMe_2})_2]$	54.0	210	Orange	27.0	24.3[a]	4.5	3.8[a]
$[PtCl_2(\overline{SC_2H_4SCMe_2})_2]$	78.0	210–20	Yellow	22.5	19.3[a]	3.7	3.0[a]

[a] Recrystallization tends to lead to the loss of the ligand. The quoted values are the best obtained from a number of attempts.

Table 2. Hydrogen-1 NMR shifts[a] for the complexes $[MCl_2(\overbrace{SC_2H_4SCR_2}^{})_2]$

Complex	Temp. (°C)	$R_{AA'}/R_{CC'}$	$R_{BB'}/R_{DD'}$	$H_{AA'}/H_{EE'}$	$H_{BB'}/H_{FF'}$	$H_{CC'}/H_{GG'}$	$H_{DD'}/H_{HH'}$
$[PdCl_2(\overbrace{SC_2H_4SCH_2}^{})_2]$	−40	4.74	3.90	4.21	3.47	3.53	2.98
		4.70	3.85	4.17	3.39	3.50	2.93
	20	3.91	3.91	3.17	3.17	3.17	3.17
$[PtCl_2(\overbrace{SC_2H_4SCH_2}^{})_2]$	−20	4.73	3.96	4.22	3.39	3.50	3.08
		4.68	3.92	4.17	3.36	3.45	3.06
	60	4.32	4.32	3.44	3.44	3.44	3.44
$[PdCl_2(\overbrace{SC_2H_4SCMe_2}^{})_2]$	−50	2.33	1.96	4.23	3.08	3.41	3.41
				4.17	3.01		
	30	2.09	2.09	3.75	3.75	3.49	3.49
$[PtCl_2(\overbrace{SC_2H_4SCMe_2}^{})_2]$	−30	2.15	1.98	4.33	3.15	3.49	3.49
			1.97	4.27	3.10		
	60	2.11	2.11	3.77	3.77	3.47	3.47

[a] In ppm relative to Me_4Si.

about the M ← S bonds is assumed to be occurring at all temperatures and the structures in Fig. 1 depict one arbitrarily chosen conformation.

The ^1H NMR spectral data for these complexes recorded at low temperatures are given in Table 2. The proton labelling relates to the structures in Fig. 1 and the assignments are based on experience with the tetrahydrothiophen complexes.[5] The MCl_2 moiety exerts a deshielding effect on the ring protons, particularly those attached to the carbons adjacent to the coordinated S atom and directed towards the halogen (*viz.* $R_{AA'}$, $R_{CC'}$, $H_{AA'}$, $H_{EE'}$, Fig. 1).

On warming the complexes, major spectral changes occur (see later) resulting for most cases in single signals for the R substituent protons and for the other ring methylene protons. Data for the high temperature limiting spectra are also given in Table 2. The static forms of these complexes were also characterized by their ^{13}C chemical shift data measured at low temperatures (Table 3).

Dynamic NMR studies

At low temperatures (*ca* −40°C) the ^1H spectra of the complexes $[MCl_2(\overbrace{SC_2H_4SCH_2}^{})_2]$ [M = Pd(II) and Pt(II)] consisted of a pair of almost first-order AB quartets due to the methyl protons of the isolated C(2) carbon. (Fig. 2). The two AB signals are attributed to the *meso* and DL forms but it was not possible to assign each AB system individually. On warming the complex, sulphur pyramidal inversion becomes established and the AB signals show exchange broadening. Initially this broadening is slight, leading simply to a loss of distinction between the *meso* and DL isomers. On heating to 60°C (Fig. 3) further broadening occurs leading to coalescence at approximately 30°C in the case of the platinum(II) complex (Fig. 3). By 60°C the single band has sharpened somewhat but the fast exchange limit was not reached with the chosen solvent, $CDCl_3$.

Table 3. Carbon-13 NMR shift data[a] for the complexes $[MCl_2(\overbrace{SC_2H_4SCR_2}^{})_2]$

Complex	Temp (°C)	S—*C*—S	C—*C*—S—M	*C*—C—S—M	Me
$[PdCl_2(\overbrace{SC_2H_4SCH_2}^{})_2]$	−40	42.36	39.80	36.99	—
		42.21	39.65	36.99	
$[PtCl_2(\overbrace{SC_2H_4SCH_2}^{})_2]$	−40	42.37	38.83	36.91	—
		42.24	38.67	36.91	
$[PtCl_2(\overbrace{SC_2H_4SCMe_2}^{})_2]$[b]	−30	41.82	37.11	36.33	29.50
		41.83	37.05	36.33	29.40

[a] In ppm relative to Me_4Si.

[b] Quarternary carbon shift not detected.

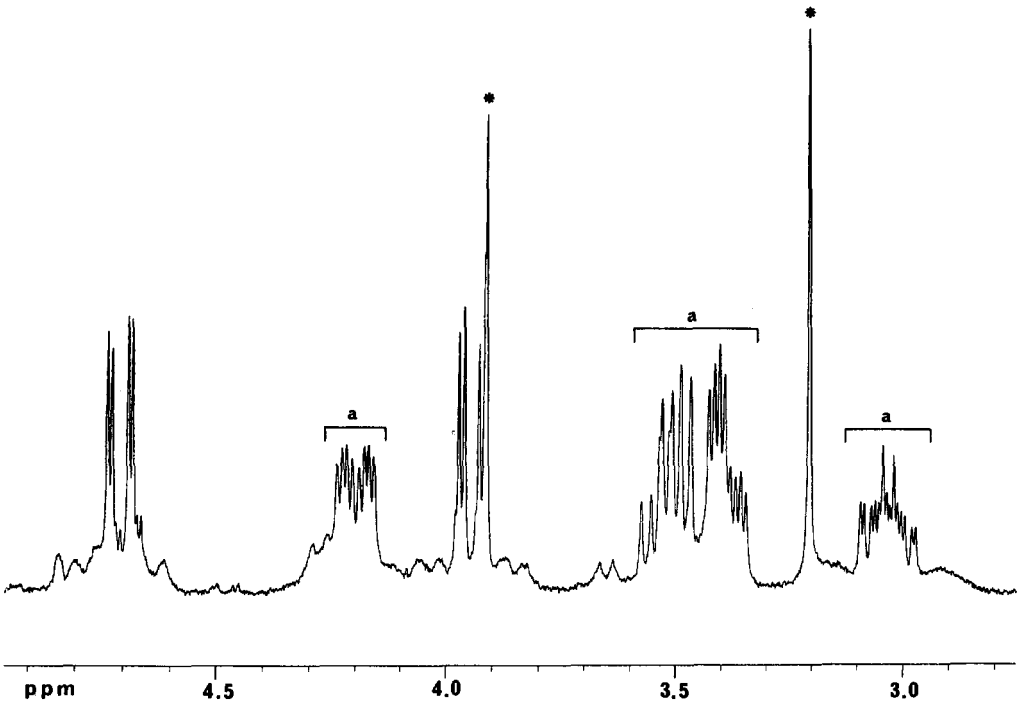

Fig. 2. 250 MHz ^{1}H spectrum of $[PtCl_2(\overline{SC_2H_4SCH_2})_2]$ at −20°C showing the *meso*–DL invertomer distinction in the —SCH_2S— signals. Additional signals due to ^{195}Pt satellites, free ligand (*) and —SC_2H_4S— (a) protons.

These changes can be rationalized in terms of independent atomic inversions of the coordinated S atoms. Such inversions exchange the *meso* isomer with the DL pair according to Fig. 4. The effect of this process on the methylene protons attached to carbon-2 (R = H, Fig. 4) is to produce a dynamic spin system of the type

$$\begin{array}{ccc} ABA'B' & \rightleftharpoons & CDD'C' \\ \downarrow\uparrow & & \downarrow\uparrow \\ D'C'CD & \rightleftharpoons & B'A'BA \end{array}$$

where the labelling refers to the local magnetic environments of the protons numbered in the order (1) to (4) in Fig. 4. Since there are no measurable scalar couplings between protons in different rings, the spin system may be simplified to

$$\begin{array}{ccc} meso\ AB & \rightleftharpoons & CD\ DL \\ \downarrow\uparrow & & \downarrow\uparrow \\ DL\ DC & \rightleftharpoons & BA\ meso. \end{array}$$

Since there are only two NMR-distinguishable species of approximately equal abundance, the spin problem is a function of a single magnitude of rate constant $k(meso \rightarrow DL)$ $[= k(DL \rightarrow meso)]$. Bandshape fittings were performed on this basis using the static parameters given in Table 4 and the results for the platinum(II) complex shown in Fig. 3. The fittings of the lower frequency portions of the spectra were hampered somewhat by overlappings with the —SCH_2CH_2S— proton signals which also exhibited exchange broadenings. However, reasonably reliable "best-fit" rate constants were deduced and from these values inversion energy data based on Arrhenius and Eyring plots were calculated (Table 5).

The 2,2-dimethyl-1,3,-dithiolane complexes $[MCl_2(\overline{SC_2H_4SCMe_2})_2]$ [M = Pd(II), Pt(II)] exhibited similar variable temperature NMR features. In these cases, the *meso*–DL interconversion arising from the sulphur pyramidal inversions was monitored by the —CMe_2— proton signals. The ^{1}H spectra of the platinum(II) complex measured in the temperature range −30 to 25°C are shown in Fig. 5. At low temperatures the *meso*–DL isomer distinction is only just apparent, the higher frequency methyl signals overlapping to give an unresolved broadened singlet. Populations of the *meso* and DL isomers are in the approximate ratio 3 : 2.

On warming the complex, the expected broadening occurred with coalescence being achieved around 10°C (Fig. 5). Bandshape fittings, using the static parameters in Table 4, were carried out using the same type of spin system as for the 1,3-dithiolane complexes, except that no scalar couplings were included. The resulting inversion energy data are given in Table 5.

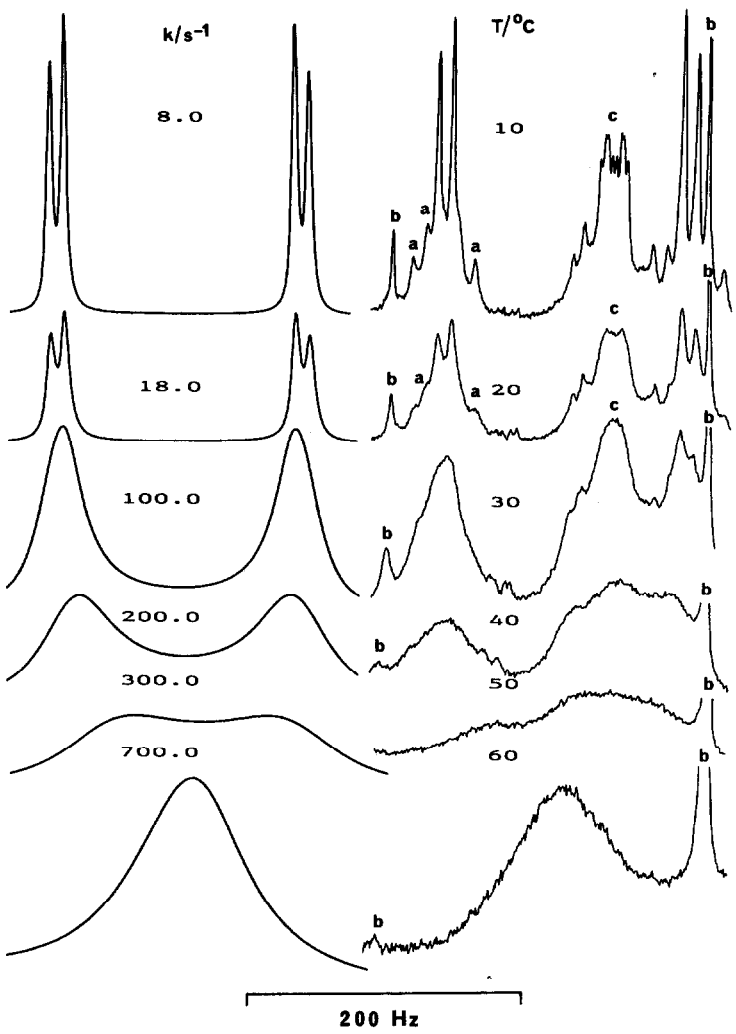

Fig. 3. Experimental and computer synthesized 250 MHz ^{1}H spectra of the —SCH_2S— region of $[PtCl_2(SC_2H_4SCH_2)_2]$ in the temperature range 10–60°C. Additional signals are due to ^{195}Pt satellites (a), free ligand (b), and —SC_2H_4S— methylene absorption (c).

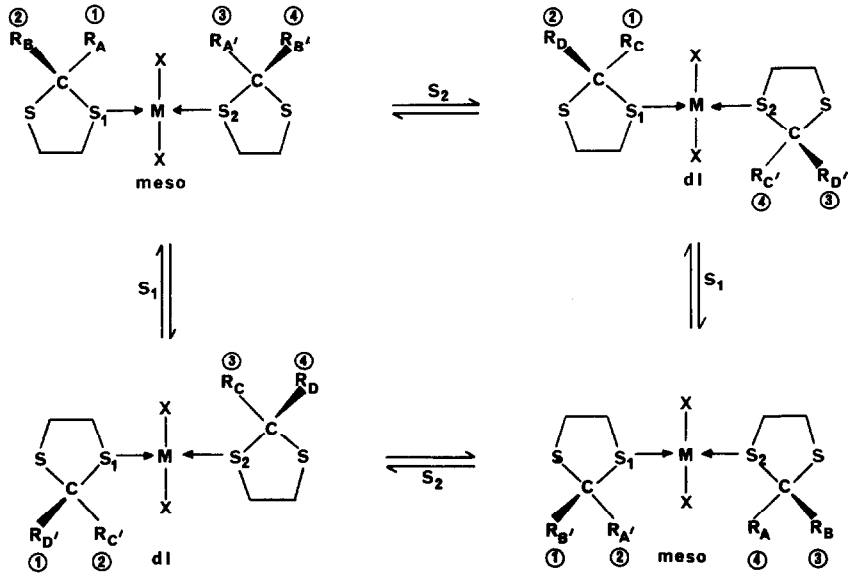

Fig. 4. The interconversion of *meso* and DL isomers due to independent pyramidal inversion of the coordinated sulphur atoms S_1 and S_2. N.B. To retain the same mutual relationship of the two rings in all cases the inversion process must be followed by a 180° rotation about the M—S bond.

Table 4. ^{1}H NMR data for $[MCl_2(\overbrace{SC_2H_4SCR_2}^{})_2]$

Complex[a]	Temp. (°C)	ν_A (Hz)[b]	ν_B (Hz)	ν_C (Hz)	ν_D (Hz)	$^2J_{AB}$ (Hz)	$^2J_{CD}$ (Hz)	T_2^* (s)[c]
$[PdCl_2(\overbrace{SC_2H_4SCH_2}^{})_2]$	−30	1180.4	967.0	1178.6	971.2	11.2	11.2	0.177
$[PtCl_2(\overbrace{SC_2H_4SCH_2}^{})_2]$	0	1178.3	987.7	1176.0	990.8	10.9	10.9	0.177
$[PdCl_2(\overbrace{SC_2H_4SCMe_2}^{})_2]$	−50	588.3	488.3	586.3	488.3	0.0	0.0	0.15
$[PtCl_2(\overbrace{SC_2H_4SCMe_2}^{})_2]$	−20	537.8	493.9	537.8	496.3	0.0	0.0	0.15

[a] $CDCl_3$ solvent.
[b] Frequency shifts measured at 250 MHz, relative to Me_4Si.
[c] Natural line width at half height = $(\pi T_2^*)^{-1}$.

Table 5. Arrhenius and Eyring energy data for fluxionality in $[MCl_2(\overbrace{SC_2H_4SCR_2}^{})_2]$ complexes

Complex[a]	E_A (kJ mol^{-1})	$\log_{10}$ (A s^{-1})	$\Delta H^\ddagger$ (kJ mol^{-1})	$\Delta S^\ddagger$ (J K^{-1} mol^{-1})	$\Delta G^\ddagger$ (kJ mol^{-1})[b]
$[PdCl_2(\overbrace{SC_2H_4SCH_2}^{})_2]$	69.7±1.0	15.1±0.2	67.4±1.0	36.3±3.8	56.6±0.1
$[PtCl_2(\overbrace{SC_2H_4SCH_2}^{})_2]$	71.0±6.1	14.0±1.0	68.4±6.0	15.2±1.2	63.9±0.2
$[PdCl_2(\overbrace{SC_2H_4SCMe_2}^{})_2]$	67.2±1.2	15.9±0.2	65.1±1.1	52.7±4.6	49.4±0.2
$[PtCl_2(\overbrace{SC_2H_4SCMe_2}^{})_2]$	79.4±1.7	16.9±0.2	77.2±1.2	71.0±4.4	56.0±0.1

[a] $CDCl_3$ solvent.
[b] At 298.15 K.

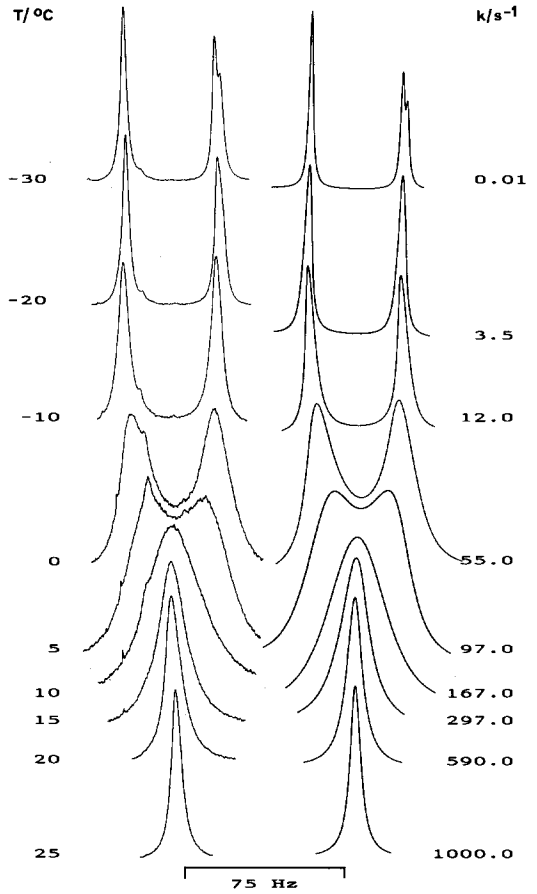

Fig. 5. Experimental and computer synthesized 250 MHz ^{1}H spectra of the methyl region of $[PtCl_2(\overbrace{SC_2H_4SCMe_2}^{})_2]$ in the temperature range −30 to 25°C.

DISCUSSION

The energy data in Table 5 display a number of noteworthy trends. Gibbs function values ($\Delta G^\ddagger$) range from 49 to 64 kJ mol^{-1}, indicating that sulphur inversion is a fairly facile process when the atom is coordinated to transition metals.[21] Attachment to platinum(II) rather than palladium(II) raises the barrier by *ca* 7 kJ mol^{-1} in accordance with previous trends.[5,22,23] The value for $[PdCl_2(\overbrace{SC_2H_4SCH_2}^{})_2]$ of 56.6 kJ mol^{-1} compares very closely with that of 56.1 for $[PdCl_2\{\overbrace{S(CH_2)_4}^{}\}_2]$ obtained previously, indicating a negligible effect on the S inversion barrier of replacing a ring methylene group by a heterocyclic S atom. Methylation of the ring at the 2-position causes an appreciable lowering (7.2–7.9 kJ mol^{-1}) of the free energy of activation for the S inversion process. This is attributed to an increase in the ground state energy of the 2,2-dimethyl ring complexes compared to the unsubstituted 1,3-dithiolane complexes, arising from the unfavourable positioning of one of the C-methyls with respect to the chloro ligand.

It is notable that in the case of the $[MCl_2(\overbrace{SC_2H_4SCH_2}^{})_2]$ [M = Pd(II), Pt(II)] complexes the —SC_2H_4S— proton signals collapse to a singlet simultaneously with the —SCH_2S— signals. This can only be attributed to a 1,3-metal shift correlated with the S inversion process. Such a process is well established in chromium and tungsten pentacarbonyl complexes of the type $[M(CO)_5L]$,[7–9,12–14] and in platinum(IV) complexes of the type

$[(PtXMe_3)_2L]$,[11,15] but this is the first report of 1,3-metal fluxions involving palladium(II) and platinum(II) atoms. In previous studies, 1,3-metal shifts have occurred subsequent to the onset of rapid sulphur inversion and the two processes have *not* been correlated. The present observations for the $[MCl_2(\overline{SC_2H_4SCH_2})_2]$ [M = Pd(II), Pt(II)] complexes are notably different in that respect. In the complexes $[MCl_2(\overline{SC_2H_4SCMe_2})_2]$, a 1,3-metal shift process was not apparent in the spectra of the Pt(II) complex up to 60°C or in the spectra of the Pd(II) complex up to 30°C, since distinct signals were always present for the $H_{AA'}/H_{BB'}$ and $H_{CC'}/H_{DD'}$ ring protons, (Table 2). Thus, the bulky $-CMe_2-$ group between the two S atoms appears to prevent easy access to the transition state associated with a 1,3-metal sulphur commutation.

The precise mechanism of the S inversion/1,3-shift fluxion is not known. However, a dissociation/recombination process can be discounted since, although scalar $^{195}Pt-^{1}H$ couplings could not be detected *after* the onset of S inversion because of residual line broadenings, separate free and coordinated ligand signals were clearly observed (*viz.* ^{1}H spectrum at 60°C, Fig. 3). The spectral changes were in all cases temperature reversible and a purely intramolecular process is thought most likely. Certainly, in the case of $[PtCl_2(\overline{SC_2H_4SCMe_2})_2]$ where no 1,3-shift occurs, the S inversion process can be assumed to be purely intramolecular by analogy with the complex $[PtCl_2\{\overline{S(CH_2)_4}\}_2]$.[5]

REFERENCES

1. R. J. H. Clark, G. Natile, V. Belluco, L. Cattalini and C. Filippino, *J. Chem. Soc.* (*A*), 1970, 659.
2. E. A. Allen, N. P. Johnson, D. T. Rosevear and W. Wilkinson, *J. Chem. Soc.* (*A*), 1970, 2137.
3. E. A. Allen and W. Wilkinson, *Spectrochim. Acta* 1972, **A28**, 725.
4. E. A. Andronov, S. I. Bakhireva, L. V. Konovalov, Y. N. Kukushkin and R. A. Vlasova, *Russ. J. Inorg. Chem.* 1973, **18**, 1732.
5. E. W. Abel, M. Booth and K. G. Orrell, *J. Chem. Soc., Dalton Trans.* 1979, 1994.
6. E. W. Abel, M. Booth and K. G. Orrell, *J. Chem. Soc., Dalton Trans.* 1980, 1582.
7. E. W. Abel, S. K. Bhargava, T. E. MacKenzie, P. K. Mittal, K. G. Orrell and V. Šik, *J. Chem. Soc., Chem. Commun.* 1982, 983.
8. E. W. Abel, T. E. MacKenzie, K. G. Orrell and V. Šik, *Polyhedron* 1987, **6**, 1785.
9. E. W. Abel, M. Z. A. Chowdhury, K. G. Orrell and V. Šik, *J. Organomet. Chem.* 1984, **262**, 293.
10. E. W. Abel, M. Z. A. Chowdhury, K. G. Orrell and V. Šik, *Polyhedron* 1984, **3**, 331.
11. E. W. Abel, M. Booth, G. D. King, K. G. Orrell, G. M. Pring and V. Šik, *J. Chem. Soc., Dalton Trans.* 1981, 1846.
12. E. W. Abel, M. Booth, K. G. Orrell and G. M. Pring, *J. Chem. Soc., Dalton Trans.* 1981, 1944.
13. E. W. Abel, G. D. King, K. G. Orrell, G. M. Pring, V. Šik and T. S. Cameron, *Polyhedron* 1983, **2**, 1117.
14. E. W. Abel, G. D. King, K. G. Orrell and V. Šik, *Polyhedron* 1983, **2**, 1363.
15. E. W. Abel, G. D. King, K. G. Orrell, V. Šik, T. S. Cameron and K. Jochem, *J. Chem. Soc., Dalton Trans.* 1984, 2047.
16. E. W. Abel, K. G. Orrell, K. B. Qureshi and V. Šik, *Polyhedron* 1988, **7**, 1329.
17. D. T. Gibson, *J. Chem. Soc.* 1930, 13.
18. R. J. Morris, Ph.D. thesis. University of Exeter (1981).
19. G. B. Kauffman and D. O. Cowan, *Inorg. Synth.* 1960, **6**, 211.
20. D. A. Kleier and G. Binsch, *DNMR3 Program 165.* Quantum Chemistry Program Exchange, Indiana University (1970).
21. E. W. Abel, K. G. Orrell and S. K. Bhargava, *Prog. Inorg. Chem.* 1984, **32**, 1.
22. E. W. Abel, S. K. Bhargava, K. Kite, K. G. Orrell, V. Šik and B. L.Williams, *Polyhedron* 1982, **1**, 289.
23. K. G. Orrell, V. Šik, C. H. Brubaker, Jr and B. McCulloch, *J. Organomet. Chem.* 1984, **276**, 267.

Polyhedron Vol. 7, No. 15, pp. 1329–1333, 1988
Printed in Great Britain

0277–5387/88 $3.00+.00
Pergamon Press plc

NUCLEAR MAGNETIC RESONANCE INVESTIGATIONS OF THE FLUXIONALITY OF *TRANS*-PALLADIUM(II) AND -PLATINUM(II) DICHLORIDE COMPLEXES OF 1,3-DITHIOLANES—II. 2-SUBSTITUTED 1,3-DITHIOLANE COMPLEXES

EDWARD W. ABEL, KEITH G. ORRELL,* KHURSHID B. QURESHI and VLADIMIR ŠIK

Department of Chemistry, University of Exeter, Exeter EX4 4QD, U.K.

(*Received* 7 *February* 1988; *accepted* 18 *February* 1988)

Abstract—The complexes *trans*-$[MCl_2(\overline{SC_2H_4SCHR})_2]$ (M = Pd(II) and Pt(II), R = Me, ^{t}Bu and Ph) have been synthesized. In $CDCl_3$ solution these complexes exist as two out of six possible NMR-distinct isomeric forms. These isomers are *not* interconverted by pyramidal S inversions since the resulting invertomers, having R groups in sterically crowded environments, are energetically unfavoured. The palladium(II) complexes show evidence of 1,3-metal shifts coupled with ligand dissociation/recombination, whereas the platinum(II) complexes are stereochemically rigid at all temperatures up to 60°C.

The preceding paper[1] examined the variable temperature solution properties of 1,3-dithiolane and 2,2-dimethyl-1,3-dithiolane complexes of palladium(II) and platinum(II) dichlorides, and showed how DL and *meso* forms of the complexes co-exist in comparable quantities in $CDCl_3$ solutions at low temperatures. In accordance with previous studies of S-coordinated Pd(II) and Pt(II) complexes,[2–6] pyramidal S inversion occurs on increasing the solution temperature and this interconverts the two isomeric forms. In the case of the 1,3-dithiolane complexes this dynamic process is accompanied by a 1,3-metal shift commutation. However, a *gem*-dimethyl group between the two S sites, as in $[MCl_2(\overline{SC_2H_4SCMe_2})_2]$, precludes this metal fluxion but slightly accelerates the S inversion process. In order to probe more thoroughly the relative ground state and transition state energies of these 1,3-dithiolane complexes, we have now synthesized the 2-substituted ligand complexes $[MCl_2(\overline{SC_2H_4SCHR})_2]$ (M = Pd(II) and Pt(II), R = Me, ^{t}Bu, and Ph), and report herein on their solution NMR properties.

* Author to whom correspondence should be addressed.

EXPERIMENTAL

Materials and preparations

Ligands. All the 2-alkyl-1,3-dithiolanes were prepared by the general method of Gibson.[7]

2-*Methyl*-1,3-*dithiolane.* This was prepared in an exactly analogous way to 1,3-dithiolane,[1] using acetaldehyde and ethanedithiol at 5°C. Yield 51.1%; b.p. of required product, 58°C/12 mmHg (58°C/12 mmHg).[8]

2-*Tertiarybutyl*-1,3-*dithiolane.* This was synthesized from ethanedithiol (5.80 g, 0.061 mol, 6.17 cm^3) and trimethylacetaldehyde (5.31 g, 0.061 mol, 6.68 cm^3) in the presence of HCl (1 cm^3) at 5°C. The reaction mixture was stirred for 1 h, heated under reflux for 2 h and then steam distilled. The crude product was purified by ether extraction (2×50 cm^3) and the ether extract dried over $MgSO_4$. On removing the solvent under reduced pressure the required product (7.2 g, 0.044 mol) was obtained. Yield 72.0%.

2-*Phenyl*-1,3-*dithiolane.* This was obtained by reacting ethanedithiol (5.28 g, 0.056 mol, 5.62 cm^3) with benzaldehyde (5.95 g, 0.056 mol, 5.68 cm^3) in

Table 1. Analytical data for the complexes $[MCl_2(\overbrace{SC_2H_4SCHR}^{})_2]$

Complex	Yield	M.p. (°C)	Colour	Elemental analysis C Calc.	C Found	H Calc.	H Found
$[PdCl_2(\overbrace{SC_2H_4SCHMe}^{})_2]$	57.6	75	Yellow	23.1	22.5	3.8	3.8
$[PtCl_2(\overbrace{SC_2H_4SCHMe}^{})_2]$	51.0	65	Yellow	19.0	17.7	3.2	3.0
$[PdCl_2(\overbrace{SC_2H_4SCHBu^t}^{})_2]$	65.0	125	Orange	33.6	32.7	5.6	5.5
$[PtCl_2(\overbrace{SC_2H_4SCHBu^t}^{})_2]$	65.0	102	Yellow–orange	28.5	27.0	4.7	4.5
$[PdCl_2(\overbrace{SC_2H_4SCHPh}^{})_2]$	57.0	112	Orange	40.0	40.0	3.7	3.7
$[PtCl_2(\overbrace{SC_2H_4SCHPh}^{})_2]$	60.0	115	Orange	34.3	34.6	3.2	3.3

the presence of HCl (1 cm^3) at 3°C. The mixture was heated under reflux for 2 h and unreacted materials removed by steam distillation. The residue was extracted with ether and dried over $MgSO_4$. Removal of ether under reduced pressure yielded a light yellow solid (5.51 g, 0.030 mol). M.p. 30°C. Yield 55.1%.

Palladium(II) *and platinum*(II) *dichloride complexes.* The Pd(II) and Pt(II) dichloride complexes of the above ligands were prepared by a literature method which involved stirring an aqueous solution of the metal salt K_2MCl_4 with an excess aqueous solution of the ligand for 1 h at room temperature.[9] Fuller details of this general method are given in the preceding paper.[1] Analytical data are presented in Table 1.

NMR spectra

All spectra were recorded on a Brüker AM250 FT spectrometer under the same conditions as described previously.[1]

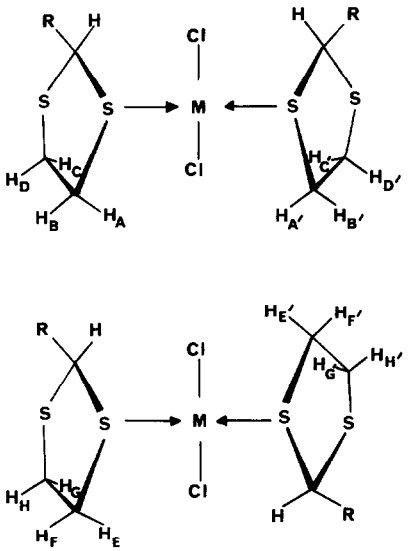

Fig. 1. The most probable solution invertomers of $[MCl_2(\overbrace{SC_2H_4SCHR}^{})_2]$ (M = Pd(II) or Pt(II), R = Me, Ph, Bu^t) showing the methylene proton labelling.

RESULTS AND DISCUSSION

The complexes $[MCl_2(\overbrace{SC_2H_4SCHR}^{})_2]$ possess tetrahedral sulphur atoms which are chiral centres, and numerous diastereomers can arise depending both on the relationship of the —CHR groups to each other and the relative dispositions of the substituents within the two groups. Two such isomers are shown in Fig. 1. None of these diastereomers can be interconverted by any bond rotation process such as M—S bond rotation, but certain exchanges can be effected by coordinated-sulphur inversions. These are depicted in Figs 2 and 3, where the species are named according to the relative positioning of the five-membered rings (viz. *meso* and DL) and the position of attachment of the R groups, namely either directed away from the halogen, (i.e. *trans* to the metal centre) or directed towards the halogen (i.e. *cis* to the metal). In each set two invertomer species are indistinguishable by normal solution NMR spectroscopy. For example in Fig. 2, *meso* (R, *trans*/*cis*) and *meso* (R, *cis*/*trans*) are identical species and in Fig. 3 DL (R, *trans*/*cis*) and DL (R, *cis*/*trans*) constitute a mirror pair.

A further consequence of the chirality of the sulphur atoms is the diastereotopic nature of the ring methylene hydrogens. In the absence of any exchange process these are anisochronous and thus the ring methylenes of each species produce ABCD type ^1H spectra.

Low temperature ^1H spectra of all the complexes, with the exception of the 2-methyl-1,3-dithiolane complexes, consisted of *pairs* of almost first-order ABCD systems for the ring methylene protons, indicating the presence of *two* out of the six NMR-

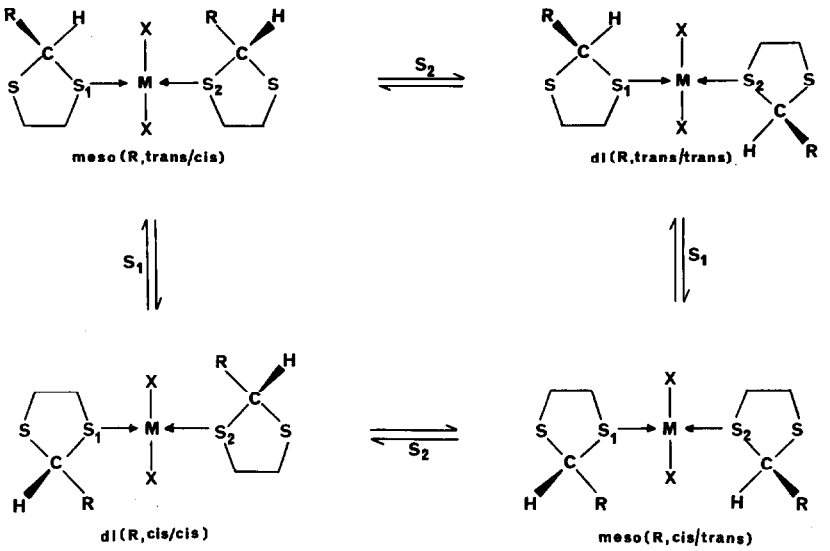

Fig. 2. The interconversion of one set of *meso* and DL invertomers due to independent pyramidal inversion of the coordinated sulphur atoms S_1 and S_2. N.B. The same mutual relationship of the two rings is maintained by performing a 180° rotation about the M—S bond after the S atom has inverted.

distinguishable invertomers. The ^1H spectrum of $[PdCl_2(SC_2H_4SCHBu^t)_2]$ at −20°C (Fig. 4) is representative of the other complexes. The proton labelling is according to Fig. 1. Assignments are based on the assumed deshielding effect of the MCl_2 moiety on the ring protons, particularly on those attached to carbons adjacent to the coordinated sulphur atoms and directed towards the halogen (*viz.* AA′, EE′, Fig. 1). However, distinction between corresponding protons in the two species is not known with any certainty. This is reflected in the chemical shift values in Table 2, which do not unambiguously distinguish between proton pairs such as AA′/EE′ etc. Due to the smaller steric effect of the methyl group compared to phenyl or *t*-butyl groups, no chemical shift distinction was obtained between the two forms of the 2-methyl-1,3-dithiolane complexes. In the cases of the phenyl and *t*-butyl substituted ligand complexes, the two species present in solution were also clearly apparent from their ^{13}C spectra (Table 3).

The palladium(II) and platinum(II) complexes exhibited somewhat different variable temperature NMR characteristics. On changing from −20 to

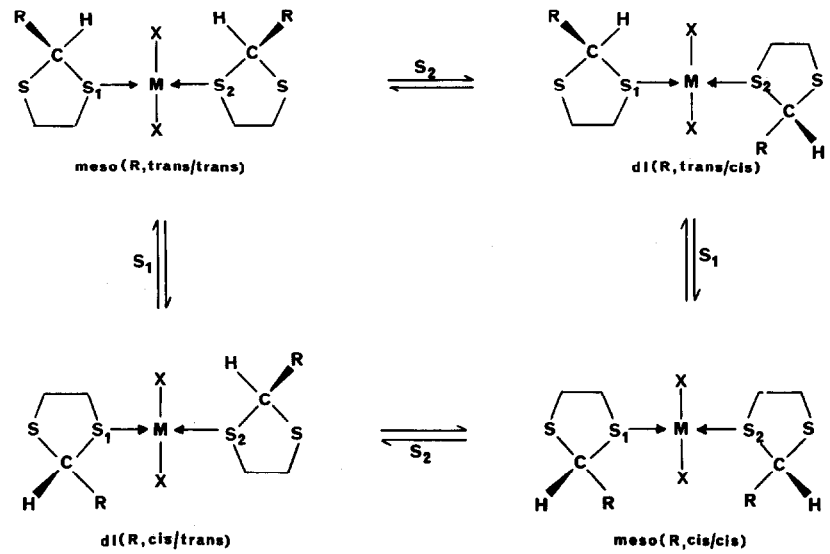

Fig. 3. The interconversion of the second set of *meso* and DL invertomers. Other caption details as for Fig. 2.

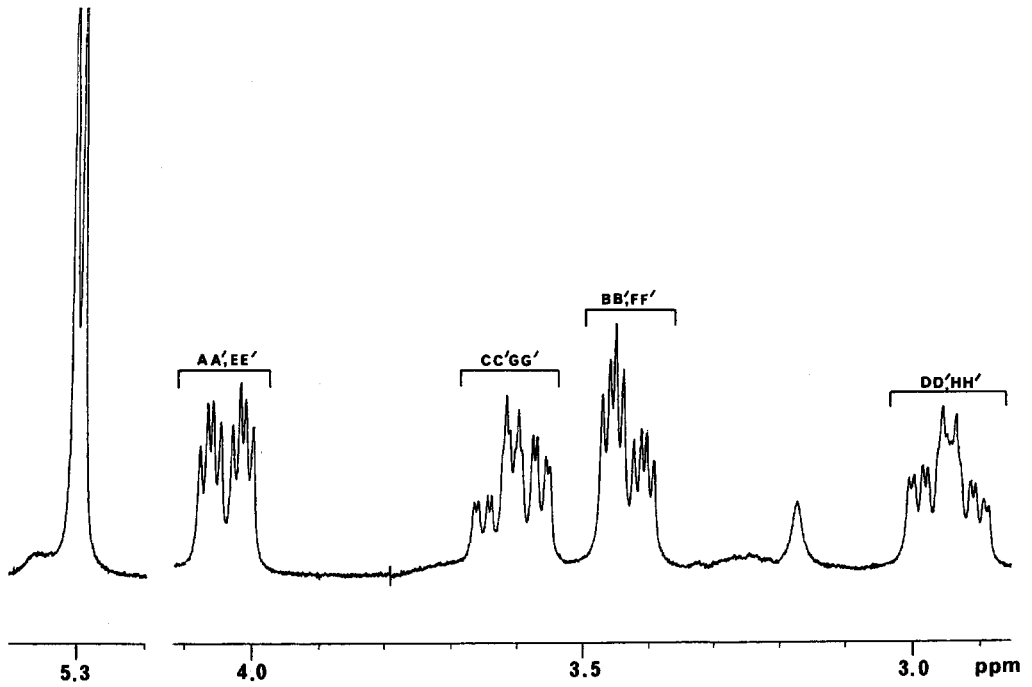

Fig. 4. The 250 MHz ^{1}H NMR spectrum of $[PdCl_2(\overline{SC_2H_4SCHBu^t})_2]$ in $CDCl_3$ at −20°C. The methylene signals are labelled according to Fig. 1.

60°C, the spectra of the Pt(II) complexes were essentially unchanged, whereas the bands in the spectra of the Pd(II) complexes showed considerable exchange broadening.

The absence of exchange processes in the Pt(II) complexes is clear evidence for the two detected invertomer species belonging to the different invertomer sets depicted in Figs 2 and 3. Steric considerations strongly favour the R substituents being directed away from the halogen (i.e. *trans* to the metal) and the favoured structures are therefore the structures shown in Fig. 1, namely DL (R, *trans/trans*) (Fig. 2) and *meso* (R, *trans/trans*) (Fig. 3). Pyramidal sulphur inversion in either species necessarily brings an R group into an unfavourable *cis* relationship to halogen, causing the resulting species to be thermodynamically unfavoured and undetected in the ^{1}H NMR spectra. Thus, no evidence of sulphur inversion is obtained from the spectra of $[PtCl_2(\overline{SC_2H_4SCHR})_2]$ complexes, which are temperature invariant up to 60°C.

The exchange broadening observed in the spectra

Table 2. Hydrogen-1 NMR shifts for the complexes $[MCl_2(\overline{SC_2H_4SCHR})_2]$

Complex	Temp. (°C)	R	CH	$H_{AA'}/H_{EE'}$	$H_{BB'}/H_{FF'}$	$H_{CC'}/H_{GG'}$	$H_{DD'}/H_{HH'}$
$[PdCl_2(\overline{SC_2H_4SCHMe})_2]$	−30	1.74	5.26	4.05	3.47	3.50	3.10
	60	1.80	5.3	~3.8	~3.8	~3.3	~3.3
$[PtCl_2(\overline{SC_2H_4SCHMe})_2]$	21	1.80	5.3	4.2	3.6	3.5	3.2
$[PdCl_2(\overline{SC_2H_4SCHBu^t})_2]$	−20	1.11	5.30	4.06	3.46	3.64	2.98
				4.01	3.41	3.58	2.92
	70	1.2	5.4	3.85	3.85	3.20	3.20
$[PtCl_2(\overline{SC_2H_4SCHBu^t})_2]$	22	1.17	5.38	4.11	3.37	3.67	3.15
				4.07	3.32	3.63	3.12
$[PdCl_2(\overline{SC_2H_4SCHPh})_2]$	−60	7.4–7.7	6.46	4.21	~3.7	~3.7	3.27
				4.16	~3.7	~3.7	3.23
	60	7.4–7.7	6.6	~3.9	~3.9	~3.45	~3.45
$[PtCl_2(\overline{SC_2H_4SCHPh})_2]$	20	7.4–7.7	6.44	4.20	3.65	3.75	~3.35

Table 3. Carbon-13 NMR shift data for the complexes $[MCl_2(\overline{SC_2H_4SCHR})_2]$

Complex	Temp. (°C)	S—C—S	C—C—S—M	C—C—S—M	>C<	Me
$[PdCl_2(\overline{SC_2H_4SCHBu^t})_2]$	−20	70.04 69.89	44.65 44.55	39.29 39.29	36.58 36.58	28.26 28.26
$[PtCl_2(\overline{SC_2H_4SCHBu^t})_2]$	−30	69.74[a] 69.57[a]	44.68[b] 44.57[b]	38.35[c] 38.35[c]	35.97[d] 35.97[d]	28.35 28.33
$[PtCl_2(\overline{SC_2H_4SCHPh})_2]$	−30	62.05 60.74	44.03 43.09	38.90 38.14	[e]	[e]

[a] ^2J(C—Pt) = 9 Hz.
[b] ^2J(C—Pt) = 8.5 Hz.
[c] ^3J(C—Pt) = 16.2 Hz.
[d] ^3J(C—Pt) = 18 Hz.
[e] Phenyl carbon shifts δ 129–135.

of the Pd(II) complexes affects both the ring methylene and methine proton signals. The former signals consist of two four-spin ABCD-type systems at low temperature (Fig. 4). On raising the temperature to *ca* 30°C two exchange-broadened signals are observed. At 60°C, the lower frequency band sharpened to a multiplet whilst the other band was still somewhat broad. These changes are consistent with an approach to an AA′BB′ spin system. The methine signal broadens on warming the complex and remains broad at 60°C. The ring methylene changes are indicative of the onset of 1,3-palladium(II)–sulphur shifts, while the broadened methine signal suggests that this commutation is accompanied by the dissociative loss of the ligand. Sulphur inversion cannot account for these changes since the methylene signals would become the ABCD-type, not AA′BB′, in the fast inversion limit. In any case the steric factors mentioned earlier preclude this as a likely possibility. The proposed 1,3-shift fluxion will interconvert the species shown in Figs 2 and 3. In particular, *meso* (R, *trans/trans*) will exchange with DL (R, *trans/trans*) and band broadening of the methylene region will result.

The dissociative nature of the 1,3-shift as evidenced by the methine signal broadening is clearly due to the R substituent on the ligand preventing easy access to the transition state for the 1,3-shift, thereby leading to dissociation. In the unsubstituted 1,3-dithiolane complexes[1] the process proceeds very much more rapidly by an intramolecular non-dissociative route which is a consequence of rapid pyramidal inversion of the coordinated sulphur atoms. The absence of pyramidal inversion in the 2-R-1,3-dithiolane complexes militates against the 1,3-shift process, which, when it does occur at elevated temperatures, involves a dissociative intermediate as a result of the steric interaction of the ring substituent. This conclusion is also compatible with the finding in the previous paper[1] that the 2,2-dimethyl-1,3-dithiolane complexes do not undergo intramolecular 1,3-metal shifts.

The absence of any fluxionality or dissociation of the platinum(II) complexes is clearly due to the greater strength of Pt—S bonds compared to Pd—S bonds. This difference is reflected in the magnitude of the sulphur inversion barriers in $[MCl_2(\overline{SC_2H_4SCR_2})_2]$, studied in the preceding paper,[1] increasing by *ca* 7 kJ mol^{-1} on changing from M = Pd(II) to M = Pt(II).

REFERENCES

1. E. W. Abel, K. G. Orrell, K. B. Qureshi and V. Šik, *Polyhedron* 1988, **7**, 1321.
2. P. Haake and P. C. Turley, *J. Am. Chem. Soc.* 1967, **89**, 4611.
3. P. Haake and P. C. Turley, *J. Am. Chem. Soc.* 1967, **89**, 4617.
4. E. W. Abel, G. W. Farrow, K. G. Orrell and V. Šik, *J. Chem. Soc., Dalton Trans.* 1977, 42.
5. E. W. Abel, A. K. S. Ahmed, G. W. Farrow, K. G. Orrell and V. Šik, *J. Chem. Soc., Dalton Trans.* 1977, 47.
6. E. W. Abel, M. Booth and K. G. Orrell, *J. Chem. Soc., Dalton Trans.* 1979, 1994.
7. D. T. Gibson, *J. Chem. Soc.* 1930, 13.
8. F. Challenger, E. A. Mason, E. C. Holdsworth and R. Emmott, *J. Chem. Soc.* 1953, 292.
9. G. B. Kauffman and D. O. Cowan, *Inorg. Synth.* 1960, **6**, 211.

Polyhedron Vol. 7, No. 15, pp. 1335–1340, 1988
Printed in Great Britain

0277–5387/88 $3.00+.00
© 1988 Pergamon Press plc

MIXED LIGAND COMPLEX FORMATION OF COPPER(II) AND ZINC(II) IONS WITH 3-HYDROXYNAPHTHOATE AND PICOLINATE IONS AS LIGANDS IN DIOXANE–WATER MIXTURES

E. CASASSAS,* R. TAULER and G. FONRODONA

Department of Analytical Chemistry, Facultat de Química, Universitat de Barcelona, Diagonal 647, Barcelona 08028, Spain

(*Received* 28 *January* 1988; *accepted* 18 *February* 1988)

Abstract—Cu(II)–hydroxynaphthoate–picolinate and Zn(II)–hydroxynaphthoate–picolinate ternary systems were studied in dioxane–water (1 : 1, *v/v*) solutions at a 0.2 mol dm^{-3} ionic strength and 25°C. From EMF data the mixed ligand complexes M(hna)(pic) for M = Cu(II) and Zn(II) and $M(hna)(pic)_2$ for M = Zn(II) were detected and their formation constants evaluated ($\log K_f = 18.94 \pm 0.03$, 18.09 ± 0.08 and 23.4 ± 0.07, respectively). Factors contributing to the stabilization of these complexes are discussed and optimum experimental conditions for their predominance established.

The binary complex formation between the picolinate ion and different metal ions has been studied in aqueous solution by Anderegg[1] and more recently by Casassas and Tauler,[2] and in dioxane–water mixtures (1 : 1, *v/v*) by Casassas and Fonrodona.[3] The binary complexation between Cu(II) and the picolinate ion takes place in very acidic medium, under conditions where the use of a glass electrode is not convenient[2] and a Cu(II) ion selective electrode must be used. Since picolinato–Zn(II) complexes do not form until higher pH values, in the case of Zn(II) systems the glass electrode can be used to obtain reliable EMF readings.

In previous work the mixed ligand complex formation between Cu(II), salicylate and picolinate ions, was studied as part of a more general study on mixed complex formation between salicylato–copper(II) ion complexes and several nitrogen bases.[4–6] In the present work a comparison is made between the complex-forming abilities of salicylate (sal) and 3-hydroxynaphthoate (hna) ions, not only as far as binary metal complexes are concerned[7] but also including ternary complex formation. In the ternary complexes with picolinate (pic) and 3-hydroxy-2-naphthoate ions as ligands, three kinds of donor groups are involved: the pyridine nitrogen atom, two carboxylate groups (one for each ligand) and the phenoxyde group of the hna ligand. In the present work the ternary systems formed by copper(II) and zinc(II) ions as the central ions and the bidentate ligands pic and hna are studied in dioxane–water solvent mixtures, at 0.2 M ionic strength and 25°C.

EXPERIMENTAL

Reagents

Picolinic acid, Hpic, (Fluka, puriss., 98%), was further purified by sublimation. Stock solutions of this ligand were prepared and standardized potentiometrically. 3-Hydroxy-2-naphtoic acid, H_2hna, (Merck, p.a.) was further doubly recrystallized from ethanol–water mixtures after treatment with activated charcoal. Fresh solutions of CO_2-free KOH (Merck, p.a.) were prepared[8] and standardized with potassium biphthalate. HNO_3 solutions were prepared by dilution of concentrated acid (Merck, p.a.) and standardized with HgO (Merck, p.a.). Stock solutions of Cu(II) and Zn(II) nitrates (Merck, 99%) were prepared and standardized by iodometric and complexometric titrations, respectively.

Dioxane (Probus, R.A.) was purified by Eigenberger's method.[9] Water used throughout was purified by a Culligan Water Purification System (resistivity 18.3 MΩ cm). All solutions were prepared

* Author to whom correspondence should be addressed.

at a ionic strength of 0.2 mol dm^{-3} with KNO_3 (Probus, R.A.) in a dioxane–water solvent (1 : 1 *v/v*).

Apparatus

EMF readings were obtained using an Orion 701A potentiometer (precision ± 0.1 mV), an Orion 9101 indicator glass electrode and an Orion 9005 Ag/AgCl (with a saturated aqueous KCl filling) reference electrode. Test solutions were stirred magnetically under a continuous stream of purified N_2 (washed with $Ba(OH)_2$ and vanadous perchlorate solution). The titrant (KOH) was added from a Metrhom E415 Multidosimat autoburette equipped with an anti-diffusion tip. All the potentiometric assembly was automatically controlled with a HP9816 microcomputer interfaced to the autoburette and the potentiometer via an HP3421A Data Acquisition/Control Unit. The stabilization criteria for the EMF readings was 0.1 mV within 90 s; if the stabilization is not achieved after 15 min, a message is printed and a new addition of titrant is performed. The titrant volume additions were preset depending on the concentrations of the reactants.

Titration procedure

All determinations were made by the well known potentiometric methods described elsewhere.[2–6] Test solutions in a dioxane–water (1 : 1 *v/v*) mixed solvent containing 0.2 mol dm^{-3} KNO_3 were used throughout in the potentiometric cell. "*In situ*" calibration of this cell using Gran's method,[10] was employed to determine the standard potential of the cell, its liquid junction potential and the initial free mineral acid concentration in each experiment. EMF readings were found to be stable within the covered pH range. Study of the formation equilibria for the mixed ligand complexes were carried out from titrations of solutions which contained the three constituents, the metal ion and the two ligands, acidified with a known amount of mineral acid using a potassium hydroxyde solution as titrant. The EMF readings obtained with the glass electrode gave enough information to fully describe the studied systems even in the case of copper(II) complexes, which are formed in a quite acidic range. In Table 1 the initial conditions for the potentiometric titrations are summarized for both the Cu(II) and Zn(II) systems.

Calculations

For the evaluation of the stability constants of the complexes, SUPERQUAD[11] and MINIQUAD[12] computer programs were used. All the calculations were carried out with an IBM 370 main-frame computer and with a HP9816 microcomputer.

Table 1. Experimental details of potentiometric determinations for the study of ternary complex formation in the Cu(II)–hydroxynaphthoate–picolinate and Zn(II)–hydroxynaphthoate–picolinate systems in dioxane–water (1 : 1, *v/v*), at 0.2 mol dm^{-3} KNO_3 and 25°C

Curve No.	Cu : hna : pic ratio	Cu (mmol)	hna (mmol)	pic (mmol)	acid (mmol)	E^0 (mV)
		Cu(II)–hydroxynaphthoate–picolinate system				
1	1 : 0.99 : 0.97	0.1025	0.1025	0.0995	0.2925	393.9
2	1 : 0.99 : 1.94	0.1025	0.1025	0.1990	0.2925	394.0
3	1 : 1.99 : 0.97	0.1025	0.2045	0.0995	0.2925	392.1
4	1 : 1.99 : 1.94	0.1025	0.2045	0.1990	0.2530	395.8
5	1 : 1 : 0.97	0.0408	0.0408	0.0396	0.2928	393.2
6	1 : 1 : 1.94	0.0408	0.0408	0.0792	0.2928	394.1
7	1 : 2 : 0.97	0.0408	0.0816	0.0396	0.2928	394.2
		Zn(II)–hydroxynaphthoate–picolinate system				
1	1 : 0.97 : 0.96	0.1031	0.1000	0.0996	0.1189	399.2
2	1 : 0.97 : 1.92	0.1030	0.1003	0.1978	0.1191	400.6
3	1 : 0.96 : 2.88	0.1035	0.0999	0.2988	0.1193	400.8
4	1 : 1.94 : 0.96	0.1035	0.2000	0.0994	0.1191	399.9
5	1 : 1.92 : 1.92	0.1035	0.1989	0.1989	0.1193	399.9
6	1 : 1.94 : 2.89	0.1030	0.1999	0.2985	0.1193	399.5

Table 2. Overall summary of the equilibrium constants obtained from the study of Cu(II)–hydroxynaphthoate–picolinate and Zn(II)–hydroxynaphthoate–picolinate systems in dioxane–water (1 : 1, *v/v*), at 0.2 mol dm^{-3} KNO_3 and 25°C

Reaction	log *K*	Reference
$H + hna \rightleftharpoons H(hna)$	13.52±0.01	13
$2H + hna \rightleftharpoons H_2(hna)$	17.17±0.01	
$Cu + hna \rightleftharpoons Cu(hna)$	10.44±0.007	7
$Cu + 2hna \rightleftharpoons Cu(hna)_2$	18.20±0.008	
$Zn + hna \rightleftharpoons Zn(hna)$	7.8±0.04	7
$H + pic \rightleftharpoons Hpic$	5.36±0.007	3
$2H + pic \rightleftharpoons H_2pic$	6.80±0.04	
$Cu + pic \rightleftharpoons Cu(pic)$	8.76±0.001	3
$Cu + 2pic \rightleftharpoons Cu(pic)_2$	16.92±0.007	
$Zn + pic \rightleftharpoons Zn(pic)$	6.10±0.05	3
$Zn + 2pic \rightleftharpoons Zn(pic)_2$	11.47±0.03	
$Zn + 3pic \rightleftharpoons Zn(pic)_3$	15.77±0.08	
$Cu + hna + pic \rightleftharpoons Cu(hna)(pic)$	18.94±0.03	—
$Zn + hna + pic \rightleftharpoons Zn(hna)(pic)$	18.09±0.08	—
$Zn + hna + 2pic \rightleftharpoons Zn(hna)(pic)_2$	23.4±0.07	

RESULTS

In Table 2 the values found for the formation constants of the mixed ligand complexes in the Cu(II)–hna–pic and Zn(II)–hna–pic systems are given, together with the protonation constants of the ligands and the formation constants of the binary complexes of these ligands with Cu(II) and Zn(II). All the values were obtained under the same experimental conditions of temperature, ionic strength and in 1 : 1 *v/v* dioxane–water mixtures. In the Cu(II)–hna–pic system only one mixed species was detected, Cu(hna)(pic) (log of formation constant 18.94±0.03), whereas in the Zn(II)–hna–pic system two mixed ligand complexes were found, Zn(hna)(pic) and $Zn(hna)(pic)_2$ (log of formation constants 18.09±0.08 and 23.4±0.07, respectively). The species $Zn(hna)_2(pic)$ was not detected under the experimental conditions used, in agreement with the non-existence of $Zn(hnca)_2$ in the related binary system. In Figs 1 and 2 the distribution plots of the two mixed ligand systems are given at conditions similar to the experimental ones. From these figures, the experimental ranges in which the formation of these species is favoured can be seen.

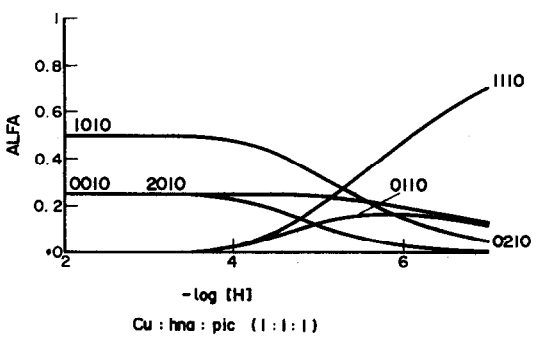

Fig. 1. Distribution plot of the species which contain the copper ion in the ternary Cu(II)–hydroxynaphthoate–picolinate system. In the figure ALFA is the ratio of each species concentration to the total copper concentration. 0, 0, 1, 0; 1, 0, 1, 0; 2, 0, 1, 0; 0, 1, 1, 0; 0, 2, 1, 0 and 1, 1, 1, 0 refer respectively, to Cu^{2+}, $Cupic^+$, $Cupic_2$, Cuhna, $Cu(hna)_2^{2-}$ and Cu(hna)(pic). The ratio of the total concentrations Cu : hna : pic is 1 : 1 : 1.

DISCUSSION

The relative stabilization of the mixed species with respect to the related binary complexes with the same number of ligands can be measured using the equilibrium constants for the so-called reproportionation reactions, given in Table 3. For all the mixed ligand complexes considered in this study, the log of the reproportionation constant, $\log K_M$ is positive, showing that the equilibrium is shifted to the formation of the mixed complex, which is favoured with respect to the formation of the related binary complexes with the same number (two or three) of ligands. One reason for this stabilization is of a statistical nature, but when this statistical contribution is allowed for, the value of the log of the new reproportionation constant ($\log K_{MB}$ in

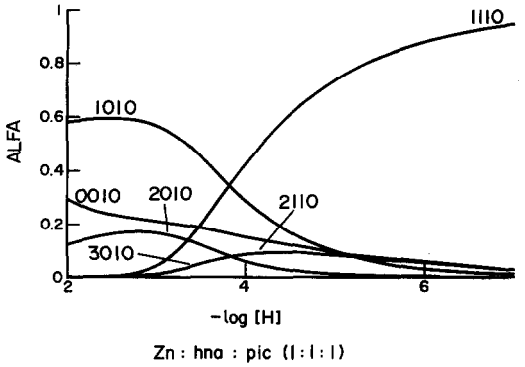

Fig. 2. Distribution plot of the species which contain the zinc ion in the ternary Zn(II)–hydroxynaphthoate–picolinate system. In the figure ALFA is the ratio of each species concentration to the total zinc concentration. 0, 0, 1, 0; 1, 0, 1, 0; 2, 0, 1, 0; 3, 0, 1, 0; 0, 1, 1, 0; 1, 1, 1, 0 and 2, 1, 1, 0 refer respectively, to Zn^{2+}, $Znpic^{+}$, $Znpic_2$, $Znpic_3$, Znhna, Zn(hna)(pic) and $Zn(hna)(pic)_2$. The ratio of the total concentrations Zn : hna : pic is 1 : 1 : 1.

Table 3) is still positive, showing that other reasons are needed to explain the observed stabilization.

The stabilization of the mixed ligand complexes relative to the binary complexes containing only one of the ligands can be measured using the constant $\Delta \log K$ (see Table 3). This constant gives a measure of how favourable the addition of a second or a third molecule of ligand on to the binary complex already formed with the other ligand is. A positive value of this constant means that the mixed complex is more favoured than the simple binary complex (with only one molecule of either ligand).

The value of the formation constant for the Cu(hna)(pic) species is very similar to that for Cu(sal)(pic),[2] showing that formation of mixed complexes is almost equally favoured in both systems irrespective of whether the molecule of one of the ligands contains a benzene or a naphthalene ring. The high values found for the stabilization constants of the mixed Zn(II) complexes are remarkable; they can be explained by a strong back-donation effect of the pic ligand, aromatic in character, through the donor N heteroatom.[14]

In Figs 3, 4, 5 and 6 the distribution plots are drawn for different total concentrations of the constituents and for different ligand to metal concentration ratios. An increase in the hna concentration causes an increase in the concentration of the 1 : 1 : 1 mixed ligand complexes [in both Cu(II) and Zn(II) systems] at low pH values, whereas an increase of pic concentration depresses

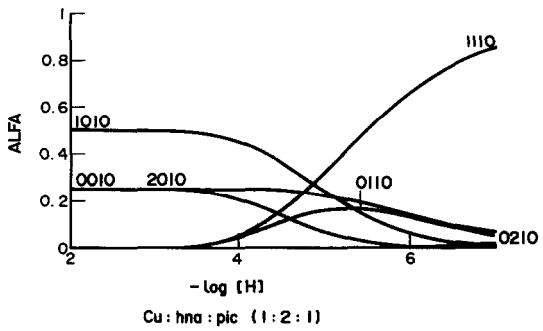

Fig. 3. Distribution plot of the species which contain the copper ion in the ternary Cu(II)–hydroxynaphthoate–picolinate system. In the figure ALFA is the ratio of each species concentration to the total copper concentration. 0, 0, 1, 0; 1, 0, 1, 0; 2, 0, 1, 0; 0, 1, 1, 0; 0, 2, 1, 0 and 1, 1, 1, 0 refer respectively, to Cu^{2+}, $Cupic^{+}$, $Cupic_2$, Cuhna, $Cu(hna)_2^{2-}$ and Cu(hna)(pic). The ratio of the total concentrations Cu : hna : pic is 1 : 2 : 1.

Table 3. Stabilization constants for the ternary systems

Reaction	Value of the log stabilization constant
$1/2Cu(pic)_2 + 1/2Cu(hna)_2 \rightleftharpoons Cu(hna)(pic)$	1.38 ($\log K_m$)[a]
$Cupic + Cu(hna) \rightleftharpoons Cu(hna)(pic)$	−0.26 ($\Delta \log K$)[b]
$Cupic + hna \rightleftharpoons Cu(hna)(pic)$	10.18
$Cu(hna) + pic \rightleftharpoons Cu(hna)(pic)$	8.50
$Zn(pic) + Zn(hna) \rightleftharpoons Zn(hna)(pic)$	4.06 ($\Delta \log K$)[b]
$Znpic_2 + Zn(hna) \rightleftharpoons Zn(hna)(pic)_2$	4.05 ($\Delta \log K$)[b]
$Znpic + hna \rightleftharpoons Zn(hna)(pic)$	11.86
$Znpic_2 + hna \rightleftharpoons Zn(hna)(pic)_2$	11.85
$Zn(hna) + pic \rightleftharpoons Zn(hna)(pic)$	10.28
$Zn(hna) + 2pic \rightleftharpoons Zn(hna)(pic)_2$	15.85

[a] $\text{Log } K_m = [MA_qB_r]/[MA_N]^{q/N}[MB_N]^{r/N}$ (where $q + r = N$).

[b] $\Delta \log K = \log K_{MA,MAB} - \log K_{M,MB}$, where $K_{MA,MAB}$ refers to the equilibrium $MAB \rightleftharpoons MA + B$, and $K_{M,MB}$ refers to $MB \rightleftharpoons M + B$.

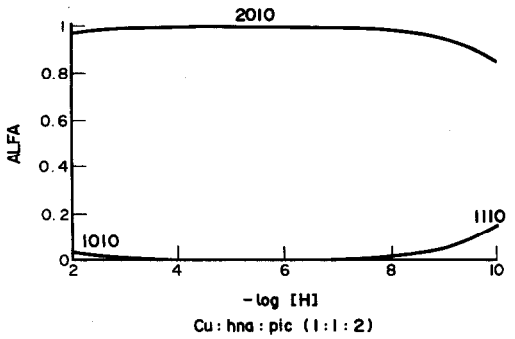

Fig. 4. Distribution plot of the species which contain the copper ion in the ternary Cu(II)–hydroxynaphthoate–picolinate system. In the figure ALFA is the ratio of each species concentration to the total copper concentration. 0, 0, 1, 0; 1, 0, 1, 0; 2, 0, 1, 0; 0, 1, 1, 0; 0, 2, 1, 0 and 1, 1, 1, 0 refer respectively, to Cu^{2+}, $Cupic^{+}$, $Cupic_2$, Cuhna, $Cu(hna)_2^{2-}$ and Cu(hna)(pic). The ratio of the total concentrations Cu : hna : pic is 1 : 1 : 2.

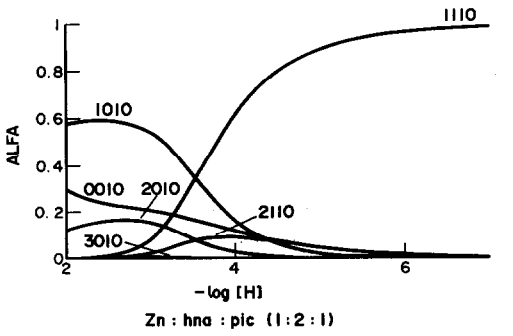

Fig. 5. Distribution plot of the species which contain the zinc ion in the ternary Zn(II)–hydroxynaphthoate–picolinate system. In the figure ALFA is the ratio of each species concentration to the total zinc concentration. 0, 0, 1, 0; 1, 0, 1, 0; 2, 0, 1, 0; 3, 0, 1, 0; 0, 1, 1, 0; 1, 1, 1, 0 and 2, 1, 1, 0 refer respectively, to Zn^{2+}, $Znpic^{+}$, $Znpic_2$, $Znpic_3$, Znhna, Zn(hna)(pic) and $Zn(hna)(pic)_2$. The ratio of the total concentrations Zn : hna : pic is 1 : 2 : 1.

Table 4. Study of optimal conditions for the maximum formation of mixed ligand complexes and for the minimum concentration of mono-protonated ortohydroxycarboxylate ligand species. pH ranges studied: 3–9 for the Cu(II)(hna)(pic) system and 2–7 for the Zn(II)(hna)(pic) system

		Optimal conditions				
System	Species	pH	R_1[a]	R_2[b]	Max[c] (%)	Min[d] (%)
Cu(II)–hna–pic	Cu(hna)(pic)	9.0	2.0	1.0	92.1	—
	H(hna)	8.5	1.0	1.0	—	6.8
Zn(II)–hna–pic	Zn(hna)(pic)	7.0	2.0	1.0	98.5	—
	$Zn(hna)(pic)_2$	6.9	1.0	2.1	98.3	—
	H(hna)	9.0	1.0	1.3	—	2.6
Cu(II)–sal–pic	Cu(sal)(pic)	9.0	2.0	1.0	87.9	—
	H(sal)	12.0	1.0	1.0	—	0.05

[a] Ratio of the ortohydroxycarboxylate ligand to the metal concentration of the solution.

[b] Ratio of the picolinate ligand to the metal concentration of the solution.

[c] Maximum concentration of the mixed ligand species.

[d] Minimum concentration of the mono-protonated ortohydroxycarboxylate ligand species.

their formation, until higher pH values are reached (pH > 8.0). On the contrary, an increase of pic concentration causes an increase in the concentration of the $Zn(hna)(pic)_2$ species.

In Table 4 the optimal conditions (pH and total concentrations) for the maximum formation of each of the mixed species are given. These conditions were evaluated from the set of protonation and stability constants found for these systems, using the optimization CSMC procedure,[15] which gives the best experimental conditions for obtaining solutions in which one specific species predominates.

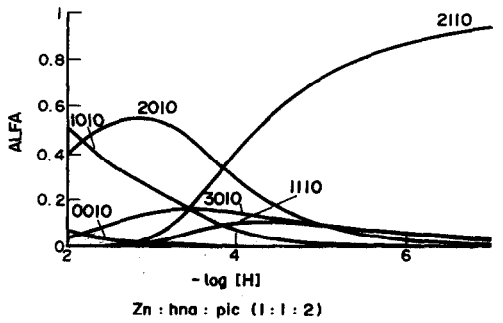

Fig. 6. Distribution plot of the species which contain the zinc ion in the ternary Zn(II)–hydroxynaphthoate–picolinate system. In the figure ALFA is the ratio of each species concentration to the total zinc concentration. 0, 0, 1, 0; 1, 0, 1, 0; 2, 0, 1, 0; 3, 0, 1, 0; 0, 1, 1, 0; 1, 1, 1, 0 and 2, 1, 1, 0 refer respectively, to Zn^{2+}, $Znpic^{+}$, $Znpic_2$, $Znpic_3$, Znhna, Zn(hna)(pic) and $Zn(hna)(pic)_2$. The ratio of the total concentrations Zn : hna : pic is 1 : 1 : 2.

REFERENCES

1. G. Anderegg, *Helv. Chim. Acta* 1960, **43**, 414.
2. E. Casassas and R. Tauler, *J. Chim. Phys.* 1984, **81**, 557.
3. E. Casassas and G. Fonrodona, *Polyhedron* 1988, **7**, 689.
4. E. Casassas and R. Tauler, *J. Chim. Phys.* 1984, **81**, 233.
5. E. Casassas and R. Tauler, *J. Chim. Phys.* 1985, **82**, 1067.
6. E. Casassas and R. Tauler, *J. Chim. Phys.* 1986, **86**, 409.
7. E. Casassas, G. Fonrodona and R. Tauler, *Polyhedron* 1987, **6**, 1517.
8. J. E. Powell and M. A. Hiller, *J. Chem. Ed.* 1957, **34**, 330.
9. A. I. Vogel, *A Textbook of Practical Organic Chemistry*, p. 177. Longmans Green, London (1961).
10. G. Gran, *The Analyst* 1952, **77**, 661; *Acta Chem. Scand.* 1950, **4**, 559.
11. P. Gans, A. Sabatini and A. Vacca, *J. Chem. Soc.*, in press.
12. A. Sabatini, A. Vacca and P. Gans, *Talanta* 1974, **21**, 53; *Inorg. Chem. Acta* 1976, **18**, 237.
13. E. Casassas and G. Fonrodona, *J. Chim. Phys.*, in press.
14. H. Sigel, *Chimie* 1967, **21**, 489; *Inorg. Chem.* 1980, **19**, 1411.
15. E. Casassas and R. Tauler, *Anal. Chim. Acta*, in press.

Polyhedron Vol. 7, No. 15, pp. 1341–1347, 1988
Printed in Great Britain

0277–5387/88 $3.00+.00
© 1988 Pergamon Press plc

LITHIUM-7 NMR STUDIES OF MACROBICYCLIC COMPLEXES IN AMBIENT TEMPERATURE MOLTEN SALTS

RICK R. RHINEBARGER and ALEXANDER I. POPOV*

Department of Chemistry, Michigan State University, East Lansing, MI 48824, U.S.A.

(*Received* 23 *November* 1987; *accepted* 22 *February* 1988)

Abstract—Complexation of the Li^+ ion by macrobicyclicdiazapolyoxa ligands (cryptands) was studied in a 45:45 mol% aluminum(III) chloride–N-(*n*-butyl)pyridinium chloride mixture at 40°C. Lithium-7 NMR measurements at this temperature and a field strength of 42.28 kG, showed that the exchange of the Li^+ ion between the "free" and complexed sites is slow, and separate resonance signals were observed for the free and complexed Li^+ ion. Conditional formation constants were obtained from the integrated areas of the resonance lines; the complex stabilities were found to decrease in the order C221·Li^+ > C222·Li^+ > C222B·Li^+. In the case of the C222·Li^+ complex, a decomplexation rate constant of $\sim 5 \times 10^2\ s^{-1}$ was obtained at the coalescence temperature of 40°C.

Solid state ^7Li NMR spectra were obtained for the C211·$LiAlCl_4$ and C222B·$LiAlCl_4$ complexes, in the static and magic angle spinning modes. These measurements indicate that the electric field gradient at the ^7Li nucleus in these complexes is small, yielding narrow resonance lines in the MAS mode.

Molten salt systems, which are liquid at room temperature, are interesting non-aqueous solvents with some unusual properties. Some ten years ago Osteryoung *et al.*[1] reported that the aluminum(III) chloride–N-(*n*-butyl)pyridinium chloride mixtures, containing 44–66 mol% of $AlCl_3$, are liquid at, or near, room temperature. Since that time numerous studies of this and similar systems have been described in the literature.

We reported previously ^7Li NMR studies of lithium chloride solutions in these melts[2] and, in particular, formation of lithium ion complexes with several crown ethers.[3] These studies indicated[2] that in the basic mixtures (< 50 mol% $AlCl_3$) lithium chloride exists as the dichloride anion, $LiCl_2^-$ and that the stabilities of the crown ether complexes with the Li^+ ion follow approximately the same trend as the one observed in many non-aqueous solvents. Unfortunately, crown ethers decompose rapidly in acidic mixtures (> 50 mol% $AlCl_3$) which, obviously, precludes complexation studies in these media.

It seems likely that with two-dimensional crown ethers the complexed lithium ion may still be bonded to a chloride ion or ions. On the other hand, macrobicyclic diazapolyoxa ligands (cryptands), originally synthesized by Lehn *et al.*[4] form very stable three-dimensional complexes (cryptates) with a variety of metal ions, and with alkali cations in particular.[5] When the size of the cation is equal to, or somewhat smaller than the cryptand cavity, the cation inside the cavity is completely insulated from the environment ("inclusive complex"[6]). It was of interest to us to investigate the complexation reactions of the lithium ion with several cryptands with different cavity sizes, and particularly to determine whether the cryptated lithium ion is still bonded to one or more chloride ions.

EXPERIMENTAL

N-(*n*-butyl)pyridinium chloride (BPCl) and aluminum(III) chloride were prepared as described previously.[2] Melt batches were prepared by mixing weighed amounts of $AlCl_3$ and of BPCl in Pyrex weighing bottles using Teflon-coated magnetic stirring bars. References to "basic melt" within the

* Author to whom correspondence should be addressed.

text refer specifically to the melt with 45.00 mol% $AlCl_3$–55.00 mol% BPCl composition. All operations were carried out in a dry box under an inert atmosphere (est. $H_2O/O_2 < 10$ ppm) at room temperature. Lithium chloride (Fisher) was dried at 100°C for three days. Lithium tetrachloroaluminate was prepared by fusing equimolar amounts of LiCl and $AlCl_3$ at 150°C in a vacuum-sealed Pyrex ampule. The melting point of $LiAlCl_4$, in a sealed capillary, was 144±2°C (ref. 7, 143.0°C). Cryptands C211, C221, C222 and C222B (monobenzo C222) were obtained from MCB Manufacturing Chem. Inc. and were used as received.

Stock solutions of lithium chloride in the basic melt (1.00 mol% LiCl in 45.00 mol% $AlCl_3$ melt) were obtained by adding appropriate amounts of LiCl to pure basic melt and stirring the solution until it became homogeneous (*ca* 24 h). Samples with different ligand/Li^+ mole ratios for NMR measurements were prepared by adding weighed amounts of the cryptands to the stock solution, stirring for 30 min and removing 0.5 g samples at the desired cryptand/lithium ion mole ratios. These samples were sealed under vacuum.

All ^7Li NMR measurements were obtained at 40 (±1)°C on a Bruker WH-180 NMR spectrometer at a resonance frequency of 69.951 MHz (field strength of 42.28 kG). Sample tubes were mounted co-axially within 10 mm o.d. NMR tubes containing the external reference solution (0.015 M LiCl in D_2O for ^2H lock). In cases where sample and reference ^7Li signals overlapped, a secondary external reference solution (0.015 M LiCl in pyridine) was used, and spectra were obtained without lock.

Chemical shifts are reported vs the external aqueous reference, and are corrected for the magnetic susceptibility of basic melt.[8] Paramagnetic shifts from the reference are indicated to be positive.

Deconvolution of the ^7Li NMR spectra to obtain integrated areas was performed by using the NTCCAP subroutine provided in the Nicolet 1180 software package.

Lithium-7 solid state NMR spectra were obtained at 22°C in the static and magic angle spinning (MAS) modes by using a Doty Scientific multinuclear solid state probe. Samples were contained in Delrin plastic rotors with end caps. Chemical shifts are referenced to the primary external reference solution (static) by sample substitution.

Elemental analyses for the C211·$LiAlCl_4$ and C222B·$LiAlCl_4$ complexes were performed by Galbraith Laboratories. These results are given in Table 1.

Table 1. Elemental analysis for C211·$LiAlCl_4$ and C222B·$LiAlCl_4$ complexes

Element	C211·$LiAlCl_4$ % theor.	C211·$LiAlCl_4$ % found	C222B·$LiAlCl_4$ % theor.	C222B·$LiAlCl_4$ % found
C	40.6	41.8	36.4	36.2
H	6.3	5.7	6.0	6.1
N	4.6	4.4	5.3	6.0
O	18.5	20.2	18.8	13.8
Li	0.9	1.1	0.8	1.5
Al	3.7	4.3	4.9	5.8
Cl	21.8	22.4	28.1	30.5

RESULTS AND DISCUSSION

Lithium-7 NMR measurements in the melt

Lithium-7 NMR spectra were obtained for samples with cryptand/lithium ion mole ratios varying from zero to 4.37:1 (C222), 3.44:1 (C221) and 1.18:1 (C222B). For C222, only mole ratios from 0.757:1 to 2.80:1 could be studied. Typical spectra for the C211, C221 and C222B·Li^+ systems are shown in Fig. 1. In each case, upfield signals are assigned to the cryptated Li^+ ion. The chemical shifts for complexed Li^+ were unaffected (within ±0.02 ppm) by changes in the cryptand/lithium ion

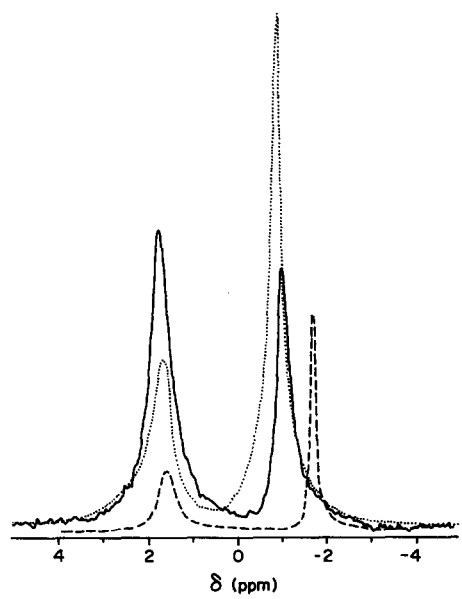

Fig. 1. Lithium-7 NMR spectra at 40°C in basic melt. —— 0.949 mol % C222B+1.00 mol % LiCl; ---- 0.988 mol % C221+0.992 mol % LiCl; ···· 0.888 mol % C211+0.985 mol % LiCl. In each case the diamagnetic signal is that of the complexed Li^+ ion.

Table 2. Lithium-7 chemical shifts for the lithium cryptates in basic $AlCl_3$–(BP)Cl melt at 40°C

Cryptand	(ppm)[a]
C211	−0.79
C221	−1.49
C222	−1.01[b]
C222B	−1.08

[a] Versus 0.015 M LiCl in D_2O external reference; corrected for the difference in magnetic susceptibility between basic melt and water; uncertainty = ±0.02 ppm.

[b] At a 1:1 C222:Li^+ mole ratio.

mole ratios. A summary of chemical shift values for these systems is given in Table 2.

As shown in Fig. 2, the high frequency signals attributable to the lithium chloro complexes, were observed to shift paramagnetically with the increasing cryptand/lithium ion mole ratio. We reported previously[2] that in the basic melt lithium chloride exists as the dichlorolithium ion $LiCl_2^-$. Concentration dependence of the ^7Li chemical shift as a function of LiCl concentration has been interpreted as being due to a dimerization equilibrium.[8]

$$2LiCl_2^- \overset{K_d}{\rightleftharpoons} Li_2Cl_4^{2-}$$

where $\log K_d = 2.82 \pm 0.39$. At an analytical LiCl concentration of 1.00 mol%, approximately 90% of the salt exists as the dilithium tetrachloro complex.

The above results indicate that observed paramagnetic shift of the "free" Li^+ ion results from the dissociation of the lithium chloro complexes when the cryptate is formed. The constancy of the chemical shifts for the cryptated lithium ion sites, as the total amount of the macrobicyclic ligand is varied, indicates that the lithium ion resides within the cryptand cavities, i.e. inclusive complexes are formed. Similar behaviour has been observed by Cahen *et al.*[9] in a ^7Li NMR study of the C211–lithium ion system in various non-aqueous solutions. It is apparent that in the basic melt, 40°C is well below the coalescence temperature for the C211, C221 and C222B·Li^+ systems. Slow exchange is observed and the signals for the "free" and complexed lithium ion sites are well resolved.

Lithium-7 NMR spectra obtained for the C222·Li^+ system in basic melt were found to be quite different from those of the other three cryptates (Fig. 3). In this case, the "free" and cryptated lithium ion signals overlapped, yielding broad (*ca* 100 Hz) lines. In addition, the upfield signal assigned to the C222·Li^+ cryptate exhibited a significant (−0.5 ppm) diamagnetic shift with increasing C222/Li^+ mole ratio. It should be noted that the linewidths of the other three systems ranged from *ca* 8 (C221) to 20 Hz (C222B). The linewidths of the C222·Li^+ complex signals decreased with increasing mole ratio, tending to values which are

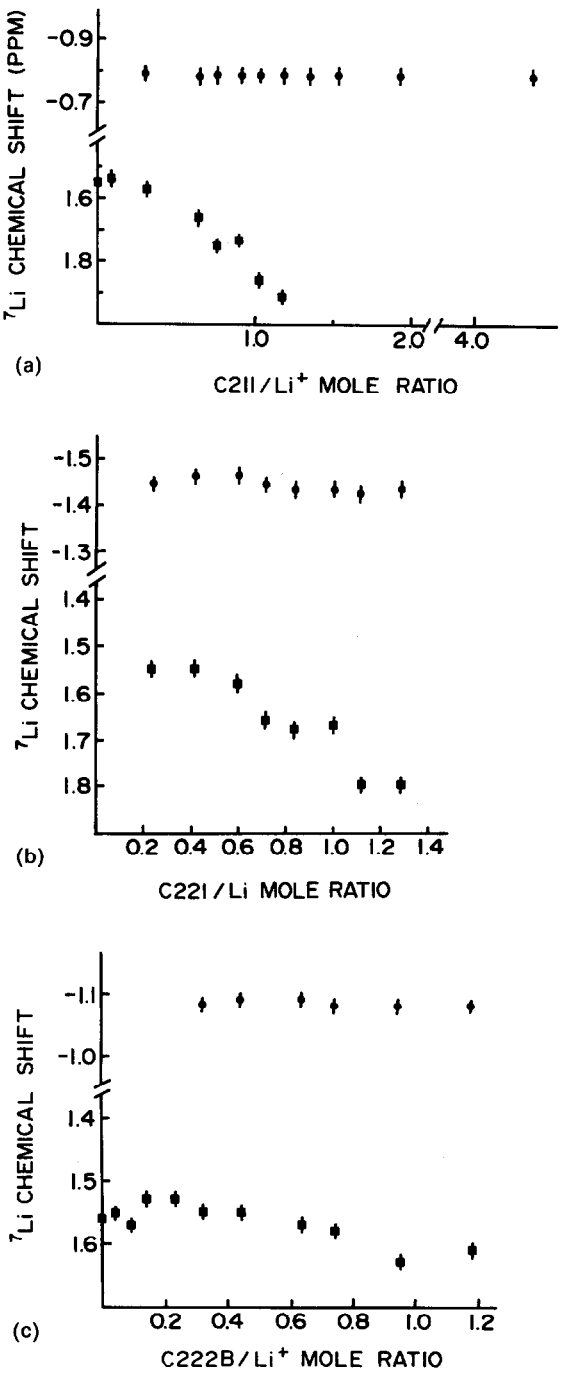

Fig. 2. Chemical shifts of the "free" (■) and cryptated (●) lithium ion signals as a function of the cryptand/lithium ion mole ratio at 40°C in basic melt; (a) C211, (b) C221 and (c) C222B.

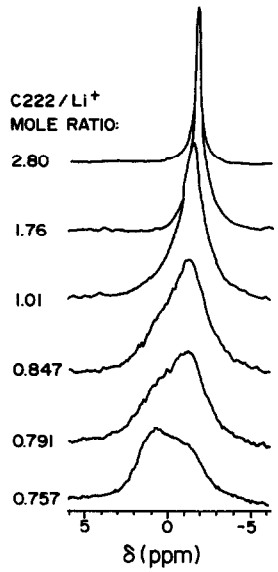

Fig. 3. Lithium-7 NMR spectra for the C222 · Li^+ system at 40°C in basic melt as a function of C222/Li^+ ratio.

similar to those observed in the other systems ($W_{1/2}$ = 13 Hz at a mole ratio of 2.80 : 1).

Thus, it appears that for the C222 · Li^+ system, 40°C is near, but slightly below the coalescence temperature. The exchange is slow and the signals for the two lithium ion sites are broadened by the exchange to the point where they overlap.

At the coalescence temperature, the rate of a first-order decomplexation process (k_{-1}) is given by eq. (1)[10]

$$k_{-1} = \pi\Delta\nu/\sqrt{2} \tag{1}$$

where $\Delta\nu = \nu_A - \nu_B$, and A and B refer to the "free" and complex sites in the absence of exchange. We assume that eq. (1) applies to the C222/Li^+ system at 40°C and that the chemical shift observed for the complex at a C222/Li^+ mole ratio of 2.80 : 1 ($\delta = \delta_B = -1.49$ ppm) is a fair approximation of the limiting chemical shift of the complex site. The chemical shift of the "free" lithium ion (site A, no C222 present) is $\delta_A = +1.55$ ppm. Thus, $\Delta\delta = 3.04$ ppm or 213 Hz at the stated resonance frequency. Substituting this value into eq. (1) yields $k_{-1} \sim 5 \times 10^2\ s^{-1}$. Cox *et al.*[11] have estimated a k_{-1} value of $> 3 \times 10^2\ s^{-1}$ for the C222/Li^+ system in methanol at 25°C. It should be noted that in our case eq. (1) does not yield the true value of the first-order decomplexation rate constant. The transfer of the lithium ion from C222 · Li^+ to $Li_2Cl_4^{2-}$ involves more then one step, therefore, the value we obtained is a "conditional" rate constant.

The NTCCAP subroutine in the Nicolet software package was used to calculate integrated areas for the signals due to "free" (δ_f) and cryptated (δ_c) lithium ion populations in the C221, C222 and C222B · Li^+ systems at 40(±1)°C in the basic melt. Assuming that the dimer must dissociate in order for formation of the cryptate complex to occur,

$$LiCl_2^- + L \overset{K_s}{\rightleftharpoons} LiL^+ + 2Cl^-$$

where L is the cryptand. We have previously noted[2] that small changes in composition in basic melt solutions of LiCl have no effect on ^{7}Li chemical shifts. Since the concentration of free chloride ions in basic melt is in a ten-fold excess of either the lithium ion or cryptand concentrations, small changes in [Cl^-] have little effect on the equilibrium reaction. Therefore, in the derivation of the equilibrium expression, we can neglect the chloride ion concentration and write,

$$K_s = \frac{[LiL^+]}{[LiCl_2^-][L]}. \tag{2}$$

We define: $D \equiv [Li_2Cl_4^{2-}]$; $M \equiv [LiCl_2^-]$; $C \equiv [LiL^+]$; [L] ≡ concentration of the free ligand; $N \equiv$ total concentration of the ligand; $P \equiv$ total concentration of the Li^+ ion and $f \equiv$ fraction of the total area due to the cryptated Li^+ ion. Equilibrium relationships and mass balance yield,

$$K_d = \frac{D}{M^2} \tag{3}$$

$$K_s = \frac{C}{M \times L} \tag{4}$$

$$N = L + C \tag{5}$$

$$P = M + 2D + C \tag{6}$$

$$C = fP. \tag{7}$$

From the above equation we easily obtain an expression for K_s in terms of known or measurable quantities, K_d, P, N and f.

$$K_s = \frac{4K_d f P}{-1 + [1 + 8K_d P(1-f)]^{1/2}[N - Pf]}. \tag{8}$$

A similar procedure was not feasible for the C211–Li^+ system due to the formation of a precipitate at mole ratios between zero and one. Samples with mole ratios of 1 : 1, or slightly above this value, remained homogeneous, but the signal for the "free" lithium ion site was too low in intensity to be detected.

The results of these calculations are given in Table 3 along with values previously reported for lithium cryptates in aqueous and some non-aqueous media.[9,12,13] In general, the stability constants for the cryptates in basic melt are smaller than those

Table 3. Comparison of lithium cryptate stability constants ($\log K_f$) in the basic melt, water and some non-aqueous solvents[a]

Solvent	Cryptand C211	C221	C222	C222B
Water	5.5	2.5_0	0.99	—
Methanol	8.0_4	5.3_8	2.6	2.19[b]
Ethanol	8.4_7	5.3_8	2.3	—
Acetonitrile	10	10.3	7.0	—
Propylene carbonate	12.4_4	9.6_0	6.9_4	—
n-Methylpropionamide	6.4_3	3.4_8	2.9_7	—
Dimethylformamide	6.8_5	3.5_8	—	—
Dimethylsulphoxide	5.8_4	2.7_7	1.0	—
Pyridine	—	—	2.94[c]	—
Basic melt	—	2.51 (±0.15)	2.06 (±0.12)	1.60 (±0.25)

[a] Ref. 11 except as noted.
[b] Ref. 12.
[c] Ref. 8.

obtained in non-aqueous solutions. It is interesting to note that in basic melt, the change in complex stabilities in going from C222 to C221 is either equal to, or less (by 2–3 $\log K_s$ units) than that found in other solvents. This apparently reduced complexation selectivity with respect to cryptand cavity size, and overall reduced stabilities, as compared to other media, is a reflection of the stability of the dilithium chloro complex in the basic melt.

As mentioned below, in the solid C222B·Li^+ complex, the cation is bonded only to the donor atoms of the ligand, i.e. lithium chloro complexes must dissociate before the above lithium cryptate can be formed. It seems quite likely that the structure of the C222B·Li^+ cryptate in the melt is very similar to that in the solid state (especially in view of the slow ambient temperature exchange of the Li^+ ion).

On the other hand, it also seems likely that in the Li^+ complexes with the two-dimensional crown ethers, the cation remains bonded to the chloride ion or ions. In such cases, the "conditional" formation constant of the crown complexes would be roughly of the same magnitude as that for the formation of the cryptate. Unfortunately, thus far, attempts to isolate a crystalline Li^+ complex with a crown ether have been unsuccessful.

In comparing the C222B·Li^+ and C222·Li^+ cryptates, it is apparent that the presence of the benzene ring in the former case reduces the decomplexation rate. The steric influence of the benzene ring may also be responsible for the slightly smaller stability constant for the C222B·Li^+ cryptate versus C222·Li^+.

Cryptate precipitates and ^{7}Li *MAS NMR*

Precipitates were observed to form in C211·Li^+ samples in the basic melt with mole ratios between zero and 1:1. This material was isolated by vacuum-filtration of the melt solution containing a *ca* 1:1 C211:Li^+ mole ratio, washing obtained crystals with benzene, and drying them under vacuum for several days. Elemental analysis of the product (Table 1) showed it to be the C211·$LiAlCl_4$ complex. A solid, analysed as C222B·$LiAlCl_4$, was obtained with the same procedure as C222B:Li^+ at mole ratios greater than 1:1. The crystal and molecular structure of this latter complex has been recently published.[14] In the basic melt the C221·Li^+ system exhibits no tendency towards precipitate formation; at 40°C samples remained homogeneous at all mole ratios studied.

Lithium-7 solid state NMR spectra (static and MAS modes) were obtained for polycrystalline samples of LiCl, $LiAlCl_4$, C211·$LiAlCl_4$ and C222B·$LiAlCl_4$. The spectra obtained from $LiAlCl_4$ and the C222B·$LiAlCl_4$ complex are shown in Figs 4 and 5. All NMR data are summarized in Table 4.

The classic Pake doublet ($m = 1/2 \rightarrow m = -1/2$ transition) was observed for LiCl in the static mode. According to Fyfe,[15] for a nucleus with a spin of 3/2 in a glass or polycrystalline powder, experiencing large quadrupolar interactions, the observed spacing of the doublet equals $(25/9)A_2$, with A_2 defined by,

$$A_2 = (3/64) + \chi^2/\nu_0 \qquad (9)$$

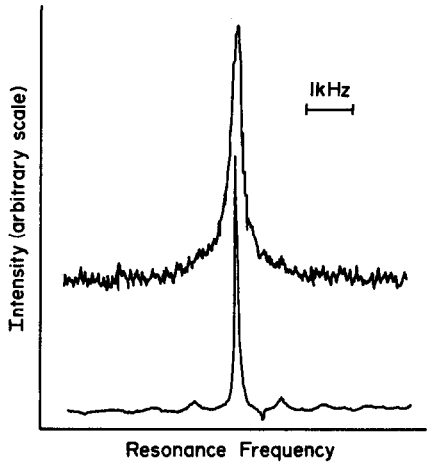

Fig. 4. Solid state ^{7}Li NMR spectra of $LiAlCl_4$. Upper spectrum—static mode; lower spectrum obtained with "magic angle" spinning.

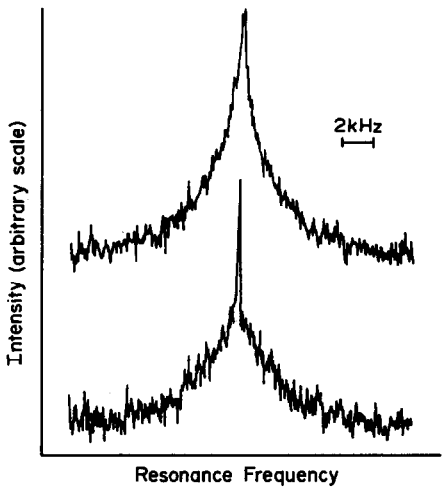

Fig. 5. Solid state ^{7}Li NMR spectra of the complex, C222B·$LiAlCl_4$. Upper spectrum—static mode; lower spectrum obtained with "magic angle" spinning.

where χ is the nuclear quadrupole coupling constant (e^2qQ/h). The observed splitting (5.5 kHz) yields $A_2 = 2000$ Hz and $\chi = 1.7$ MHz. This result is within an order of magnitude of the value for ^{7}Li in lithium silicate glasses (910 kHz) obtained by Tokuhiro *et al.*[16]

No splitting was observed in the static spectrum of $LiAlCl_4$ (Fig. 4), which indicates a smaller quadrupolar interaction for the Li nucleus in this compound. In this case,[15]

$$\Delta\nu_{1/2} = A_1 = \chi/4. \tag{10}$$

With $\Delta\nu_{1/2} = 420$ Hz, a χ value of 1.7 kHz is obtained. This very small value for χ is reasonable in view of the known crystal structure of $LiAlCl_4$ (space group $p2_1/c$), which is made up of $LiCl_6$ octahedral layers linked together by $AlCl_4$ tetrahedra.[17]

The narrowing effect of magic angle sample spinning is seen in the spectra for C222B·$LiAlCl_4$ (Fig. 5). In the spinning mode, the central transition is partially resolved from the broad background. This broadening, due to dipolar interactions, is not completely removed at the spinning rate of 2.1 kHz. By using eq. (10) and since $\Delta\nu_{1/2} = 1600$ Hz (static), a coupling constant of 6.4 kHz is obtained for this complex.

For the C211·$LiAlCl_4$ sample, stable spinning rates of > 1 kHz could not be obtained. Thus, very little reduction in the dipolar broadening was observed. In the MAS mode, the central transition was barely discernable at this spinning rate. A coupling constant of *ca* 8 kHz is estimated from $\Delta\nu_{1/2}$ of approximately 2000 Hz in the static mode.

The coupling constants for the ^{7}Li nucleus in the two cryptate complexes are quite small, indicating highly symmetric environments for the lithium ion. Evaluation of the differences in chemical shifts among the four compounds (Table 4) is difficult due to the lack of literature values for these or other lithium compounds in the solid state. Solid state ^{7}Li NMR measurements by Dye and Ellaboudy[18] show

Table 4. Lithium-7 solid state NMR results for various lithium compounds

Sample	(ppm)	Linewidth (Hz) MAS mode	Static mode	χ (kHz)
0.015 M $LiCl/D_2O$	0.0	—	19	—
LiCl	−3.2	450 @ 2.7 kHz	Splitting: 5.5 kHz	1700
$LiAlCl_4$	−0.8	58 @ 1.8 kHz	420	1.7
C222B·$LiAlCl_4$	+1.0	200 @ 2.1 kHz	1600	6.4
C211·$LiAlCl_4$	+1.0	*ca* 2000 @ 1 kHz	*ca* 2000	8

chemical shifts of −2.8 ppm for LiCl, −1.1 ppm for LiI, −0.8 ppm for C211·LiI, and −3.5 ppm for $Li^+ \cdot C211 \cdot Na^-$. Data given in Table 4 show that the cryptands effectively remove the shielding influence of the chlorine atoms in the $AlCl_4^-$ ion on the ^7Li nucleus; the shifts for LiCl and $LiAlCl_4$ are more negative (by about 2–3 ppm) than those of the cryptates. This lack of Li—Cl interactions is understandable since the lithium ion is expected to reside within the ligand cavities, a fact which has been confirmed for the C222B·$LiAlCl_4$ complex.[14]

Acknowledgement—We gratefully acknowledge the support of this study by a National Science Foundation research grant (CHE-8515474).

REFERENCES

1. R. J. Gale, B. Gilbert and R. A. Osteryoung, *Inorg. Chem.* 1978, **17**, 2728; R. J. Gale and R. A. Osteryoung, *Inorg. Chem.* 1979, **18**, 1603.
2. F. Taulelle and A. I. Popov, *Polyhedron* 1983, **2**, 889.
3. R. R. Rhinebarger, J. W. Rovang and A. I. Popov, *Inorg. Chem.* 1984, **23**, 2557.
4. B. Dietrich, J.-M. Lehn and J.-P. Sauvage, *Tetrahedron Lett.* 1969, 2882, 2889.
5. A. I. Popov and J.-M. Lehn, in *Coordination Chemistry of Macrocyclic Compounds* (Edited by G. A. Melson), Chap. 8. Plenum Press, New York (1979).
6. E. Mei, A. I. Popov and J. L. Dye, *J. Am. Chem. Soc.* 1977, **99**, 6532.
7. J. Kendall, E. D. Crittenden and H. K. Miller, *J. Am. Chem. Soc.* 1923, **45**, 976.
8. R. R. Rhinebarger, J. W. Rovang and A. I. Popov, *Inorg. Chem.* 1986, **25**, 4430.
9. Y. M. Cahen, J. L. Dye and A. I. Popov, *J. Phys. Chem.* 1975, **79**, 1289.
10. J. Sandstrom, *Dynamic NMR Spectroscopy*. Academic Press, New York (1982).
11. B. G. Cox, H. Schneider and J. Stroka, *J. Am. Chem. Soc.* 1978, **100**, 4746.
12. M. K. Chantooni and I. M. Kolthoff, *J. Solution Chem.* 1985, **14**, 1.
13. B. G. Cox, D. Knop and H. Schneider, *J. Phys. Chem.* 1980, **84**, 320.
14. D. L. Ward, R. R. Rhinebarger and A. I. Popov, *Inorg. Chem.* 1986, **25**, 2325.
15. C. A. Fyfe, *Solid State NMR for Chemists*. C.F.C. Press, Guelph, Canada (1983).
16. T. Tokuhiro, L. E. Iton and E. M. Peterson, *J. Chem. Phys.* 1983, **78**, 7473.
17. G. Mairesse, P. Barbier and J.-P. Wignacourt, *Acta Cryst.* 1979, **B35**, 1573.
18. J. L. Dye and A. S. Ellaboudy, unpublished results.

Polyhedron Vol. 7, No. 15, pp. 1349–1353, 1988
Printed in Great Britain

0277–5387/88 $3.00+.00
© 1988 Pergamon Press plc

REVERSIBLE ETHYLENE COORDINATION IN $(\eta^2\text{-}C_2H_4)Pt(PCy_3)_2$

HOWARD C. CLARK,† GEORGE FERGUSON, MARK J. HAMPDEN-SMITH,‡ BRANKO KAITNER and HEINZ RUEGGER§

Guelph-Waterloo Centre for Graduate Work in Chemistry, Guelph Campus, University of Guelph, Guelph, Ontario N1G 2W1, Canada

(*Received* 28 *January* 1988; *accepted* 22 *February* 1988)

Abstract—The complex $(\eta^2\text{-}C_2H_4)Pt(PCy_3)_2$ (**I**) exists in the equilibrium $(\eta^2\text{-}C_2H_4)Pt(PCy_3)_2 \rightleftarrows Pt^0(PCy_3)_2 + C_2H_4$ in solution, involving the reversible coordination of ethylene to the platinum(0) centre. Two dimensional ^{31}P NMR spectroscopy provides evidence for exchange between the two platinum(0) species. The X-ray crystallographic analysis of $(\mathbf{I}) \cdot 1/2C_6H_{14}$ provides evidence for weak coordination of the ethylene moiety in the solid state. I lies on a two-fold crystallographic axis which passes through Pt and the mid-point of the olefin C=C bond; principal dimensions include Pt—P 2.284(1), Pt—C(olefin) 2.137(7), C=C 1.440(7) Å, P—Pt—P 116.33(7)°, C—Pt—C 39.4(2)°. These results are interpreted in terms of possible bonding modes.

It is possible to identify a number of key steps[1] in catalytic hydrogenation cycles: (I) reversible oxidative addition–reductive elimination of hydrogen to the metal centre; (II) reversible coordination of the organic substrate; (III) insertion of the organic substrate into the M—H bond; (IV) reductive elimination of the C—H bond regenerating the original metal species. We have recently described our results related to this cycle concerning oxidative addition–reductive elimination equilibria [steps (I) and (IV)],[2] coordination of hydrogen to a platinum centre[3] [step (I)] and the insertion of acetylene into Pt—H bonds[4] [step (III)]. The present investigation is aimed at better understanding the nature of step (II). Many types of olefin complexes of platinum have been known for many years,[5] in particular $(R_3P)_2Pt(\eta^2\text{-}C_2H_4)$ complexes are excellent synthetic sources of coordinatively unsaturated $(R_3P)_2Pt^0$ species (although for bulky R groups they may be obtained by other methods[6]). It has been theoretically predicted that the olefin fragment in $(R_3P)_2Pt(\eta^2\text{-ol})$ (where ol = olefin) complexes is highly activated[7] and that the barrier to internal rotation of the olefin about the M–olefin axis is high. Hoffmann[8] has also predicted that the barrier to internal rotation will be reduced as the P—Pt—P angle is increased. For $(R_3P)Pt^0(ol)_2$ and Pt(II) (olefin) complexes, however, the barrier to olefin rotation[9] has been measured and falls in the range 10.2–13.0 kcal mol^{-1}. In this paper we provide the first evidence for reversible coordination of an ethylene ligand in $(R_3P)_2Pt(\eta^2\text{-}C_2H_4)$ complexes, together with the X-ray crystallographic analysis of $(Cy_3P)_2Pt(\eta^2\text{-}C_2H_4)$. In contrast, the complex $(Cy_2P(CH_2)_3PCy_2)Pt(\eta^2\text{-}C_2H_4)$ (**III**) does not dissociate ethylene even at 100°C in toluene.

In benzene solution, the ^1H NMR spectrum of $(\eta^2\text{-}C_2H_4)Pt(PCy_3)_2$[10] exhibits a signal which corresponds to a significant amount of free ethylene. This might arise from either a small amount of decomposition of the complex, the irreversible dissociation of coordinated ethylene or possibly the existence of an equilibrium which involves reversible coordination of the ethylene moiety to the platinum(0) centre according to eq. (1).

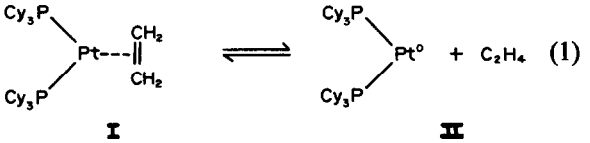

I **II** (1)

† Present address: Department of Chemistry, Dalhousie University, Halifax, Nova Scotia, Canada B3H 4J3.

‡ Author to whom correspondence should be addressed. Present address: Department of Chemistry, Indiana University, Bloomington, Indiana 47405, U.S.A.

§ Spectropin AG, Industrestrasse 26, 8117 Fallender, Zurich, Switzerland.

The ^{31}P NMR spectrum of a benzene solution of **I** does indeed show the presence of a small signal (with a good signal to noise ratio) corresponding to **II** ($\delta = 62.5$ ppm, $J_{P-Pt} = 4159$ Hz). As the temperature of this solution (in a sealed NMR tube under 1 atm of N_2) is raised, the amount of platinum(0) species, **II**, increases, consistent with previous results[2] obtained for the oxidative addition–reductive elimination equilibrium in *cis*-$H[R_3Si]Pt(PCy_3)_2$ (R = variously substituted phenyl and benzyl). On cooling the solution to room temperature, the ^{31}P NMR spectrum obtained was similar to that obtained before the temperature was raised, and therefore is consistent with the presence of an equilibrium process. In order to establish unequivocally the presence of equilibrium 1, we carried out a 2D ^{31}P chemical exchange experiment.† In the resulting contour plot, Fig. 1, off diagonal contours represent chemically exchanging ^{31}P nuclei. It can be seen that exchange occurs between the ^{31}P nuclei of $(\eta^2\text{-}C_2H_4)Pt(PCy_3)_2$ and $Pt^0(PCy_3)_2$ as shown by a crosspeak, A. There is also a crosspeak, B, between the ^{196}Pt satellites of the ^{31}P resonances of $(\eta^2\text{-}C_2H_4)^{195}Pt(PCy_3)_2$ and $^{195}Pt(PCy_3)_2$. However, most importantly, there are *no crosspeaks* between the ^{31}P nuclei bonded to non-spin-active Pt and ^{31}P nuclei bonded to ^{195}Pt. This observation rules out the possibility that the off diagonal contours result from dissociative phoshine exchange.‡ It is interesting to note that the exchange between free and coordinated ethylene does not lead to exchange broadening of the respective ^1H NMR resonances on the NMR timescale (at 400 MHz).

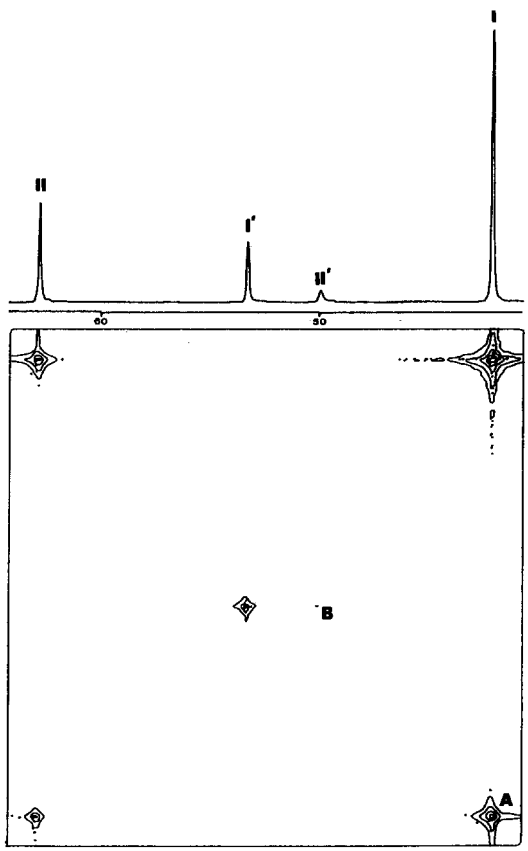

Fig. 1. The 2D ^{31}P NMR chemical exchange contour plot of a benzene solution of $(\eta^2\text{-}C_2H_4)Pt(PCy_3)_2$ at 304 K† [2D matrix: 512 W FID (32 scans) × 128], spectral frequency 161.9 MHZ. Shifts are quoted down-field from external H_3PO_4. **I'** and **II'** are the ^{195} Pt satellites of **I** and **II**, respectively.

In contrast, we observe that benzene solutions of $(\eta^2\text{-}C_2H_4)Pt(Cy_2P(CH_2)_nPCy_2)$, $n = 2$, 3 or 4,[3,12] *do not* exhibit a ^1H NMR signal corresponding to free ethylene and no evidence for dissociation analogous to that of eq. (1) was observed by ^{31}P NMR spectroscopy on heating $(\eta^2\text{-}C_2H_4)Pt(Cy_2P(CH_2)_3PCy_2)$, **III**, to 100°C in toluene-d_8.

In the hope of establishing a firm basis for the apparent difference in the strength of ethylene coordination by the platinum(0) centres, we have carried out X-ray diffraction studies on complexes **I** and **III**. The X-ray structural analysis of **III** has previously been reported[12] and unfortunately is disordered about an inversion centre; the Pt, $\eta^2\text{-}C_2H_4$ and $(CH_2)_3$ moieties are distributed over two sites. Accurate data concerning the coordination of the ethylene ligand is therefore not available. The structure of $(\eta^2\text{-}C_2H_4)Pt(PCy_3)_2 \cdot 1/3C_6H_{14}$ is shown in Fig. 2 together with some of the relevant dimensions in Tables 1 and 2.§ The molecule lies on a crys-

† The benzene solution of $(\eta^2\text{-}C_2H_4)Pt(PCy_3)_2$ was heated and some ethylene gas was removed via a one-way bleed in order to displace the equilibrium of eq. (1) to the right, prior to the two-dimensional experiment.

‡ We have previously observed exchange between the phosphine ligands of $Pt^0(PCy_3)_2$ and free PCy_3 by 2D ^{31}P NMR spectroscopy.[11]

§ $(\eta^2\text{-}C_2H_4)Pt(PCy_3)_2 \cdot 1/3C_6H_{14}$, crystal data (23°C): hexagonal $R\bar{3}c$ (No. 167), $a = 29.839(3)$, $c = 23.383(6)$ Å, $V = 18031(8)$ Å^3, $Z = 18$, d(calc.) = 1.35 g cm^{-3}, crystal size $0.12 \times 0.12 \times 0.48$ mm, Mo–K_α radiation. A total of 4576 reflections were collected, of which 4200 were unique and not systematically absent. Data were corrected for Lorentz, polarization and absorption effects. The structure was solved using the Patterson heavy atom method and remaining atoms were located in difference Fourier syntheses. Hydrogen atoms were included in the refinement, but restrained to ride on the atom to which they were bonded. The 2169 reflections for which $F^2 > 3\sigma(F^2)$ were used in refinements. The final cycles of refinement included 197 variables and converged with $R = 0.032$, $R_w = 0.039$. Atomic positional parameters have been deposited with the Cambridge Crystallographic Data Centre.

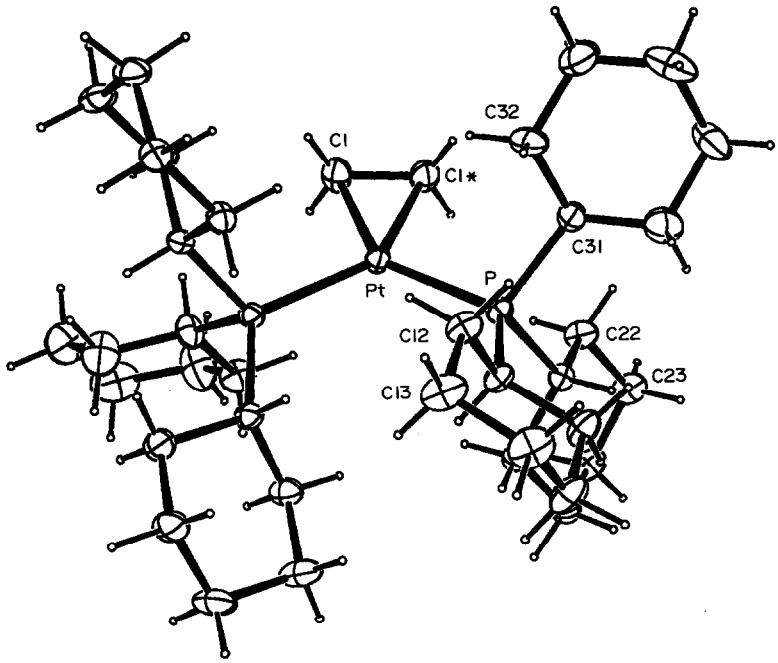

Fig. 2. The molecular structure of $(\eta^2\text{-}C_2H_4)Pt(PCy_3)_2 \cdot 1/3C_6H_{14}$. Cl* is related to Cl by a crystallographic two-fold axis. Relevant bond lengths (Å): Pt—P 2.284(1), Pt—C(1) 2.137(1), C(1)—C(1)* 1.440(7), P—C(11) 1.881(7), P—C(21) 1.861(6), P—C(31) 1.868(8); Bond angles (°): P—Pt—P* 116.33(7), P—Pt—C(1) 141.5(2), P—Pt—C(1)* 102.2(2), C(1)—Pt—C(1)* 39.4(2), Pt—C(1)—C(1)* 70.3(4).

tallographic two-fold axis which passes through Pt and the mid-point of the olefin C=C bond. The solvent molecule (C_6H_{14}) lies about a three-fold crystallographic axis. The ethylene moiety essentially lies in the PtP_2 coordination plane† and the C(1)—C(1)* bond distance of 1.440 Å is much longer than that of free ethylene (1.335 Å), but similar to that of $(\eta^2\text{-}C_2H_4)Pt(PPh_3)_2$ (1.434(13) Å).[13] The Pt—C(ethylene)bond distances of 2.137(7) Å are, however, somewhat longer than those of $(\eta^2\text{-}C_2H_4)Pt(PPh_3)_2$ (2.106(8), 2.116(9) Å).

Since there are no short intramolecular nonbonded distances between the cyclohexyl rings and the coordinated ethylene of $\eta^2\text{-}(C_2H_4)Pt(PCy_3)_2$ in the solid state, it seems unlikely that the dissociative equilibrium, 1, is entirely steric in origin. It might be expected that the basicity of the PCy_3 ligands would result in *stronger* bonding between the olefin and the platinum(0) centre if electron donation from platinum to the ethylene π^*-antibonding orbitals is predominant. However, such interaction is expected to cause a significant lengthening of the C=C distance over an analogous species with a less basic phosphine ligand (e.g. PPh_3). Since such lengthening is not observed, the weak coordination of the ethylene ligand in I may therefore result, in part, from the high *trans*-influence of the PCy_3 ligands[14] and the large P—Pt—P angle. The apparently stronger coordination of the ethylene ligand of $(\eta^2\text{-}C_2H_4)Pt(Cy_2P(CH_2)_3PCy_2)$ may then be due to the reduced *trans*-influence of the PCy_2R ligands (compared to PCy_3) as a result of the poorer overlap between the σ-bonding orbitals of Pt and P and the smaller P—Pt—P angle (113.0(4)° in III).

† Dihedral angle between the P_2Pt and PtC_2 planes = 2.6°.

Table 1. Bond distances in Å[a]

Atom 1	Atom 2	Distance	Atom 1	Atom 2	Distance
Pt	P	2.284(1)	C(21)	C(22)	1.514(10)
Pt	C(1)	2.137(7)	C(21)	C(26)	1.530(9)
C(1)	C(1)[b]	1.440(7)	C(22)	C(23)	1.527(9)
P	C(11)	1.881(7)	C(23)	C(24)	1.499(11)
P	C(21)	1.861(6)	C(24)	C(25)	1.501(12)
P	C(31)	1.868(8)	C(25)	C(26)	1.526(9)
C(11)	C(12)	1.515(9)	C(31)	C(32)	1.514(9)
C(11)	C(16)	1.530(6)	C(31)	C(36)	1.464(9)
C(12)	C(13)	1.534(12)	C(32)	C(33)	1.513(14)
C(13)	C(14)	1.504(8)	C(33)	C(34)	1.428(11)
C(14)	C(15)	1.520(12)	C(34)	C(35)	1.477(11)
C(15)	C(16)	1.511(11)	C(35)	C(36)	1.540(15)

[a] Numbers in parentheses are estimated standard deviations in the least significant digits.

[b] The coordinates of this atom are obtained by applying the transformation: $x-y, -y, 0.5-z$.

Table 2. Bond angles in degrees[a]

Atom 1	Atom 2	Atom 3	Angle	Atom 1	Atom 2	Atom 3	Angle
P	Pt	P[b]	116.33(7)	C(21)	C(22)	C(23)	110.7(5)
P	Pt	C(1)	141.5(2)	C(22)	C(23)	C(25)	112.9(6)
P	Pt	C(1)[b]	102.2(2)	C(23)	C(24)	C(25)	110.9(6)
C(1)	Pt	C(1)[b]	39.4(2)	C(24)	C(25)	C(26)	111.7(6)
Pt	C(1)	C(1)[b]	70.3(4)	C(21)	C(26)	C(25)	111.4(6)
C(11)	P	C(21)	101.1(3)	P	C(31)	C(32)	113.0(5)
C(11)	P	C(31)	108.8(3)	P	C(31)	C(36)	121.9(6)
C(21)	P	C(31)	103.4(3)	C(32)	C(31)	C(36)	112.8(6)
P	C(11)	C(12)	112.7(4)	C(31)	C(32)	C(33)	111.0(7)
P	C(11)	C(16)	118.3(5)	C(32)	C(33)	C(34)	114.4(7)
C(12)	C(11)	C(16)	109.1(5)	C(33)	C(34)	C(35)	115.2(7)
C(11)	C(12)	C(13)	111.6(6)	C(34)	C(35)	C(36)	112.6(8)
C(12)	C(13)	C(14)	110.3(7)	C(31)	C(36)	C(35)	111.2(7)
C(13)	C(14)	C(15)	111.6(6)				
C(14)	C(15)	C(16)	111.6(6)				
C(11)	C(16)	C(15)	110.8(6)				
P	C(21)	C(22)	112.7(4)				
P	C(21)	C(26)	111.7(4)				
C(22)	C(21)	C(26)	108.7(5)				

[a] Numbers in parentheses are estimated standard deviations in the least significant digits.

[b] The coordinates of these atoms are obtained by applying the transformation: $x-y, -y, 0.5-z$.

It is conceivable that for **I**, the opening of the P—Pt—P angle results in weaker coordination of the ethylene as demonstrated by Hoffman *et al.*[8] and that the energy barrier to free rotation and dissociation are now similar. It is also envisaged that if ethylene were to dissociate from **III**, [$(Cy_2P(CH_2)_3PCy_2)Pt^0$] would be extremely labile. At present we are examining the possibility of concurrent free rotation of the olefin ligands in these complexes, by preparing platinum(0) complexes containing unsymmetrical olefin ligands. Preliminary results (variable temperature ^{31}P NMR spectroscopy) show that the coordinated olefin ligand of $(\eta^2\text{-}CH_2{=}CH(C_6H_4Br\text{-}4))Pt(PCy_3)_2$ undergoes free rotation in solution at elevated temperatures.

EXPERIMENTAL

Our general experimental techniques have previously been described.[15] All solvents were dried prior to use and all reactions carried out under an atmosphere of dry N_2. ^1H and ^{31}P NMR spectra were obtained on a Bruker WH400 or AM250 instrument and temperatures were calibrated using ethylene glycol or methanol standards. ^1H NMR spectra were referenced to the proton-impurities of C_6D_6 or C_7D_8, or to TMS. ^{31}P NMR spectra were referenced to external trimethylphosphite and shifts are quoted relative to H_3PO_4 using the high frequency positive sign convention.

The 2D ^{31}P NMR experiments were carried out at 161.98 MHz and 304 K. 2D Matrix: 512 W FID (32 scans) × 128.

The preparation of the chelating diphosphine ligands and their corresponding platinum(II) dichloride complexes will be reported elsewhere.[16]

Preparation of platinum(0) (η^2-C_2H_4) complexes

For the modified procedure of Yoshida *et al.*[7] for preparing $(Cy_3P)_2Pt(\eta^2\text{-}C_2H_4)$, see ref. 3. The preparation of $(\eta^2\text{-}C_2H_4)$Pt(1,3-DCPP) (where 1,3-DCPP = 1,3-dicyclohexylphosphinopropane) is described below.

0.60 g (0.86 mmol) of (1,3-DCCP)$PtCl_2$ was placed in a 100 cm^3 Schlenk flask and 2.5 cm^3 of THF were added. The suspension was cooled in an ice bath to 0°C and stirred rapidly as sodium naphthalide solution was added dropwise. The addition was continued until the golden brown solution just remained green (indicating a slight excess of sodium naphthalide) (~ 15 min). The solution was vigorously stirred for 3 h as it warmed up to

room temperature. The solvent was removed in a vacuum and the residue pumped to ensure removal of the last traces of THF and to remove some naphthalene. The platinum(0) product was then extracted into a 50 cm^3 Schlenk flask with 3×10 cm^3 portions of warm ($\sim 40°C$) *n*-hexane, to give a pale yellow solution. The presence of a platinum(0) species was confirmed by removing a small sample (0.1 cm^3) and exposing it to air. An immediate white precipitate was observed together with loss of colour of the solution. The small flask was then placed inside a thick-walled, steel, high pressure apparatus which had previously been flushed with nitrogen. The tap of the Schlenk flask was opened and the lid of the high pressure apparatus quickly replaced and tightened down under N_2. The solution was then subjected to 1000 psi of ethylene gas for 4 h, and then filtered under nitrogen to give 0.355 g (0.54 mmol) of colourless crystals of $(\eta^2\text{-}C_2H_4)Pt(1,3\text{-DCPP})$, 62.8% yield. In an analogous experiment, after preparation of the Pt^0 species, all procedures were carried out under an ethylene atmosphere (i.e. filtration, etc.) but the yield was not increased. We have previously noted[2] that a yield of 60–64% is usual for reduction of the complexes $Cl_2Pt(Cy_2P(CH_2)_nPCy_2)$ to the corresponding Pt^0 species and it is envisaged that formation of the ethylene adduct is essentially quantitative.

Elemental analyses: $(1,3\text{-DCPP})Pt(\eta^2\text{-}C_2H_4)$: Found: C, 52.6; H, 8.9. Calc.: C, 52.8; H, 8.2%. $(PCy_3)_2Pt(\eta^2\text{-}C_2H_4)$: Found: C, 58.6; H, 8.9. Calc.: C, 58.2; H, 9.0%. M.p. **I**, 123–125°C; **III**, $\sim$ 120°C. NMR: **III**: ^{31}P, 26.7 ppm, $J_{P-Pt} = 3269$ Hz; ^1H, 2.34 ppm (C_2H_4), $J_{H-P(cis)} = 1.5$ Hz, $J_{H-P(trans)} = 3.0$ Hz, $J_{H-Pt} = 82$ Hz. **I**: ^{31}P, 42.0 ppm, $J_{P-Pt} = 3614$ Hz.

REFERENCES

1. J. P. Collman and L. S. Hegedus, *Principles and Application of Organotransition Metal Chemistry*. University Science Books, CA (1987).
2. H. C. Clark, M. J. Hampden-Smith and H. Ruegger, *Organometallics*, submitted for publication.
3. H. C. Clark and M. J. Hampden-Smith, *J. Am. Chem. Soc.* 1986, **108**, 3829.
4. H. C. Clark, G. Ferguson, A. B. Goel, E. G. Janzen, H. Ruegger, P. Y. Siew and C. S. Wong, *J. Am. Chem. Soc.* 1986, **108**, 6961.
5. For a recent review see F. R. Hartly in *Comprehensive Organometallic Chemistry*, Vol. 6, Chap. 39. Pergamon Press, Oxford (1982).
6. T. Yoshida and S. Otsuka, *Inorg. Synth.* 1979, **19**, 101.
7. T. Ziegler, *Inorg. Chem.* 1985, **24**, 1547.
8. A. Albright, R. Hoffmann, J. C. Thiebeault and D. L. Thorn, *J. Am. Chem. Soc.* 1979, **101**, 3801.
9. N. C. Hanson, M. Murray, J. L. Spencer and F. G. A. Stone, *J. Chem. Soc., Dalton Trans.* 1978, 1337.
10. Our procedure for preparing this complex has been described in detail in H. C. Clark, M. J. Hampden-Smith and H. Ruegger, *Organometallics*, submitted for publication.
11. A. Immirzi, A. Musco and B. E. Mann, *Inorg. Chim. Acta* 1977, **21**, L37.
12. G. Ferguson, M. J. Hampden-Smith and R. L. Ruhl, *Acta Cryst.* 1987, **C43**, 788.
13. (a) P.-T. Cheng, C. D. Cook, S. C. Nyburg and K. Y. Won, *Inorg. Chem.* 1971, **10**, 2210; (b) P.-T. Cheng and S. C. Nyburg, *Can. J. Chem.* 1972, **50**, 912.
14. T. G. Appleton, H. C. Clark and L. E. Manzer, *Coord. Chem. Rev.* 1973, **10**, 335.
15. H. C. Clark, M. J. Hampden-Smith and H. Ruegger, *Organometallics*, in press.
16. H. C. Clark, M. J. Hampden-Smith and H. Ruegger, manuscript in preparation.

Polyhedron Vol. 7, No. 15, pp. 1355–1361, 1988
Printed in Great Britain

0277–5387/88 $3.00+.00
© 1988 Pergamon Press plc

THE HYDROLYSIS OF THE CERIUM(III) ION, Ce^{3+}, IN AQUEOUS PERCHLORATE SOLUTIONS AT 50°C

LIBERATO CIAVATTA,† RAFFAELLA PORTO and ERMANNO VASCA

Dipartimento di Chimica dell'Università, Via Mezzocannone 4, 80134 Napoli, Italy

(*Received* 13 *November* 1987; *accepted* 26 *February* 1988)

Abstract—The hydrolysis equilibria of the Ce^{3+} ion have been studied at 50°C by measuring, with a glass electrode, the hydrogen ion concentration of $Ce(ClO_4)_3$ solutions. The Ce(III) concentration ranged from 0.1 to 1 m, while the ClO_4^- level was kept constant at 3 m by adding $LiClO_4$. Solutions containing hydrolysed species, in which at the most 0.4% of the Ce^{3+} can be transformed into reaction products without the formation of a precipitate, were prepared by constant-current coulometry. The potentiometric data have been explained in terms of $Ce(OH)^{2+}$, $Ce_2(OH)^{5+}$ and $Ce_3(OH)_5^{4+}$ complexes. Their formation constants in the inert 3 m $LiClO_4$ medium are reported.

The most careful investigation of the reaction between the Ce^{3+} ion and water is the one carried out in 1964 by Biedermann and Newman[1] who measured, at 25°C in 3 M (Li)ClO_4 media, the hydrogen ion concentration in a series of $Ce(ClO_4)_3$ solutions. The predominating reaction product was found to be $Ce_3(OH)_5^{4+}$ whereas the expected species such as $Ce(OH)^{2+}$ and $Ce_2(OH)_2^{4+}$ did not reach a sufficient concentration for detection under the chosen experimental conditions.

Concerning the formation of the intermediate species, a reinvestigation at 50°C seemed of some interest. As a matter of fact, a rise in temperature, as pointed out in previous work[2] on the hydrolysis of the La^{3+} ion at 60°C, should increase the ratios $[Ce(OH)^{2+}]/[Ce_3(OH)_5^{4+}]$ and $[Ce_2(OH)_2^{4+}]/[Ce_3(OH)_5^{4+}]$ and consequently, should make the detection of complexes bearing less than five OH^- groups more favourable.

A temperature of 50°C was considered most suitable, as indicated by the results of exploratory experiments performed at 50°C and at 60°C, since the accessible concentration range diminishes rapidly with increase in temperature. It was found that at the most 0.1% of the Ce^{3+} ions was transformed at 60°C into reaction products before the formation of a precipitate. On the other hand, Z values as high as 0.004 could be reached at 50°C.

NOTATION

A concentration of chloride ion
a_w water activity
B concentration of Ce(III)
b concentration of Ce^{3+}
$*\beta_{pq}$ equilibrium formation constant of $Ce_q(OH)_p^{3q-p}$, considering H_2O and not OH^- as reagent
$\gamma_H, \gamma_B, \gamma_{pq}$ activity coefficients of H^+, Ce^{3+}, $Ce_q(OH)_q^{3q-p}$, respectively
H Proton concentration excess, $=[ClO_4^-]+A-[Li^+]+3B$
h equilibrium concentration of H^+
K_p formation constant of all species containing p OH^- groups
χ moles of silver deposited per second on the cathode of cell(II)
Z average number of hydrogen ions set free per cerium atom.

Concentrations and equilibrium constants, if not otherwise stated, are expressed on the molal scale, m, mole kg^{-1} H_2O.

METHOD

The hydrolysis equilibria were studied by employing a glass electrode to measure, as a function of H and B, the hydrogen ion concentration, h, in a series of $Ce(ClO_4)_3$ solutions. The concentration of ClO_4^- in all test solutions was made up to 3 m by adding $LiClO_4$. Since the hydrolysis of the Ce^{3+} ion becomes measurable at $\log h < -5.0$ and, furthermore, not more than 0.4% of the Ce(III) can be transformed into hydrolysis products before precipitation ensues, a sufficient buffer capacity could be accomplished only with concentrated Ce(III) solutions. The B values ranged from 0.1 to 1 m. Over this interval Z values could be determined with an uncertainty not exceeding 1–3%, depending on B.

† Author to whom correspondence should be addressed.

In conducting measurements in a system of this type the main problem inevitably encountered is that of keeping protolytic contamination at a minimum. Taking advantage of the experience gained in similar studies,[2-4] the difficulties could be prevented by making the test solutions more alkaline by the coulometric reduction of water. Stable and reproducible potentiometric data were measured even in solutions where the concentration of OH^- ions bound to hydrolysis species was as low as 2×10^{-5} m.

The test solutions, abbreviated as TS, had the general composition

$$B\,\text{m Ce(III)}, H\,\text{m H}^+, A\,\text{m Cl}^-,$$
$$(3-3B-H+A)\,\text{m Li}^+, 3\,\text{m ClO}_4^- = \text{TS}.$$

The presence of chloride ions, between 5×10^{-3} and 0.05 m, served the purpose of avoiding salt bridges in the galvanic cell (I), for measuring h, as well as in the electrolysis cell (II), employed to decrease the acidity of TS. Measurements at constant B but different A yielded practically coincidental results, within the limits of experimental error, thus indicating the negligible effect of chloride ions on the hydrolysis reaction.

The hydrogen ion concentration in TS was determined using cell (I)

$$-\text{Ag/AgCl/TS/GE}+ \qquad \text{(I)}$$

in which GE stands for the glass electrode. The EMF of cell (I) at 50°C can be expressed, in mV, by

$$E = E'_0 + 64.115 \log (hA) + 64.115 \log \gamma_{HCl}^2 \qquad (1)$$

where E'_0 is a constant in each experiment and γ_{HCl} denotes the activity coefficient of hydrochloric acid. The standard states are defined so that the activity of a solute species tends to the value of concentration as the composition of TS approaches 3 m $LiClO_4$. At constant B, due to the low Z reached, the variations of γ_{HCl} are negligible and h can be calculated using eq. (2).

$$E = E_0 + 64.115 \log (hA). \qquad (2)$$

E_0, which is constant for a given B, was determined for each experiment, carried out as a potentiometric titration at constant B, by measuring E in solutions where the hydrolysis is suppressed, thus $h = H$. The values of E_0 and H_0, the hydrogen ion excess in the starting solution, were ascertained simultaneously on the basis of Gran diagrams.[5] In each case E_0 could be evaluated to within ± 0.1 mV, whilst H_0 was calculated with an uncertainty of 0.1%.

The electrolysis circuit consisted of

$$-\text{Pt/TS/AgCl/Ag}+ \qquad \text{(II)}$$

which was connected to a constant-current supply. When OH^- ions are generated, small but detectable amounts of silver ions are reduced on the Pt cathode. As found earlier,[2] the moles of metal deposited are proportional to the electrolysis time, and under the actual experimental conditions $\chi = (9.0 \pm 1.0) \times 10^{-11}$ mol s^{-1}. The uncertainty of χ represents deviations from the average of 15 determinations of Ag deposited in different titrations, performed at various values of A and current intensities. In correcting H using the χ value found in the same titration, the error of χ must certainly be less than 1×10^{-11} mol s^{-1}.

On the basis of these results, a 99.9% current efficiency can be maintained only with current intensities greater than 1 mA. High intensities, on the other hand, make problematic the avoidance of a local excess of base which might promote premature formation of cerium(III) hydroxide. Good results were attained with intensities in the interval from 0.03 to 0.3 mA. This implies that the use of the lowest intensity introduces in H an error of the order of 1–2%.

After each passage of current the potential of the anode of (II) was measured, but within less than a minute it deviated by less than 0.1 mV from that of the Ag/AgCl electrode of cell (I). Thus side reactions, i.e. oxidation of Ce(III) to Ce(IV), must occur to a negligible extent and the current yield of AgCl generation must be very near to the theoretical level.

In the construction of the $Z(\log h)_B$ function, which is the basis of the following calculations, we had to take into consideration another source of error, connected with protolytic impurities introduced by the inert medium salt. By a potentiometric procedure, developed recently in our laboratory,[6] the salt preparation used was found to contain in 3 m $LiClO_4$, $(5 \pm 1) \times 10^{-6}$ m of a protolytic impurity with a $pK_a = 5.55 \pm 0.15$. From these figures we estimate that at the lowest B, the Z values are affected by uncertainties of a few per cent, while in the remaining part of the reaction range the error is far below 1%.

On the attainment of equilibrium

A series of experiments was performed in order to establish conditions favourable for reaching the hydrolysis equilibria in a reasonable time. It was found that the rate of increase in alkalinity could be varied between 6×10^{-8} and 6×10^{-9} mol OH^-/(kg $H_2O \times s$) without affecting the shape and position of the $Z(\log h)_B$ curves. During each generation step the EMF of cell (I) took 10–20 min to assume a steady value which remained constant, within 0.1 mV, for several hours. Biedermann and Newman[1]

had to wait, at 25°C, for a couple of hours for constant potentials. This demonstrates the beneficial effect of a higher temperature to hasten the attainment of equilibrium.

Data for a given B falling on the same curve within the limits of the present accuracy, independently of the rate of OH^- generation, were considered to represent the equilibrium position of $Z(\log h)_B$. If the addition of strong base exceeded the level of 10^{-7} mol $OH^-/(kg\ H_2O \times s)$, the points were displaced towards higher acidities and readjustment to equilibrium proved to take a long time. Evidently, a local excess of base caused the premature precipitation of cerium(III) hydroxide which only redissolves slowly.

A titration, due to the extremely slow addition of OH^- ions, lasted for more than 15 h inevitably with a loss of accuracy, because the E_0 of cell (I) may have changed. When acidic or hydrolysed solutions were left standing overnight the E_0 drift was never found to exceed ± 0.5 mV.

EXPERIMENTAL

Materials and analysis

Cerium(III) *perchlorate.* These solutions were made from CeO_2, Aldrich of 99.999% purity, by employing the reaction:

$$CeO_2(s) + 4H^+ + I^- \rightarrow Ce^{3+} + 0.5I_2 + 2H_2O.$$

To a slurry of the oxide with 4 M $HClO_4$ having the stoichiometric requirement, azeotropic HI, a Baker p.a. product, was added dropwise and iodine was expelled on heating. When the major part of the oxide had dissolved, a dilute HI solution, 0.1 M, was used to complete the reaction paying attention so that the iodide ions did not greatly exceed the 10^{-3} m level.

The iodide ions were removed by precipitation with Ag^+ ions generated coulometrically, while a Ag/AgI indicator electrode served to localize the end-point. The final I^- concentration was estimated to be much less than 10^{-5} m.

In order to suppress heavy metal impurities, introduced by the reagents, the solution was made alkaline by generating OH^- on a Pt cathode until a permanent precipitate of cerium(III) hydroxide appeared. The solution, after standing for a week, was filtered and acidified to about 10^{-3} m.

The cerium concentration was determined gravimetrically as CeO_2. The analyses agreed to within 0.1%. The hydrogen ion excess was deduced from coulometric acid–base titrations employing a glass electrode as an indicator. The perchlorate concentration was calculated from the sum; $3B + H$.

Lithium perchlorate. This was prepared as previously described[4] but with the modification that four crystallizations, instead of three, were carried out. The salt, analysed for protolytic impurities using a potentiometric procedure soon to be published,[6] was found to contain, in 3 m $LiClO_4$ at 50°C, $(5 \pm 1) \times 10^{-6}$ m of a monoprotic acid with $pK_a = 5.55 \pm 0.15$. The effectiveness of crystallization is evident when we compare the present results with those found for an impurity of 34×10^{-6} m, in 3 m $LiClO_4$ after three crystallizations.[2]

Perchloric acid and lithium chloride. These were obtained as described previously.[2]

We also refer the reader to the same paper[2] for experimental details of EMF measurements.

THE COMPOSITION OF THE HYDROLYSIS PRODUCTS

Table 1 gives the primary $Z(\log h)_B$ data which are graphically represented in Fig. 1. The data were treated as follows. First, each set pertaining to a constant B was used to deduce the most important p values in $Ce_q(OH)_p^{3q-p}$ and the homo-ligand formation constants $K_p = K_p(B)$. Then, the most important q and preliminary $^*\beta_{pq}$ values were found from the variation of K_p with B. The data were finally treated with a numerical approach based on the principle of least-squares.

The prevailing values of p

When we consider a set of data at constant B and take into account that in our solutions the maximum Z never exceeds 0.004, then, without introducing any appreciable error, we may simplify

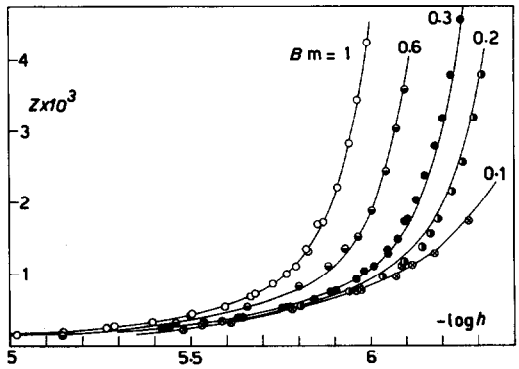

Fig. 1. Z, the average number of OH^- ions bound per Ce(III) ions, as a function of $\log h$. The curves were calculated using the constants of Table 3 and eqs (13)–(15) for medium changes.

Table 1. $Z(\log h)_B$ data

$B = 0.100$ m		
$Z \times 10^3(-\log h)$:	(a)	0.197(5.479); 0.314(5.610); 0.493(5.779); 0.801(5.968); 1.114(6.087)
	(b)	0.329(5.531); 0.531(5.783); 0.742(5.960); 0.957(6.073); 1.284(6.181); 1.723(6.274)
	(c)	0.348(5.579); 0.730(5.952); 1.130(6.117)
$B = 0.200$ m		
$Z \times 10^3(-\log h)$:		0.336(5.536); 0.533(5.805); 0.735(5.943); 0.940(6.037); 1.145(6.098); 1.351(6.147); 1.549(6.171); 1.747(6.190); 2.142(6.229); 2.556(6.261); 3.176(6.292); 3.796(6.315)
$B = 0.300$ m		
$Z \times 10^3(-\log h)$:	(a)	0.233(5.423); 0.364(5.631); 0.496(5.756); 0.630(5.844); 0.764(5.906); 0.926(5.962); 1.098(6.011); 1.291(6.051); 1.493(6.078); 1.764(6.104); 2.035(6.127); 2.374(6.148); 2.780(6.181); 3.187(6.202); 3.797(6.225); 4.577(6.254).
	(b)	0.224(5.439); 0.369(5.642); 0.517(5.769); 0.740(5.887); 1.040(5.986); 1.378(6.048); 1.754(6.089).
$B = 0.600$ m		
$Z \times 10^3(-\log h)$:		0.156(5.145); 0.324(5.458); 0.547(5.657); 0.831(5.798); 1.116(5.883); 1.353(5.929); 1.507(5.970); 1.858(6.009); 2.422(6.047); 3.002(6.076); 3.588(6.100).
$B = 0.9986$ m		
$Z \times 10^3(-\log h)$:	(a)	0.011(3.968); 0.143(5.020); 0.262(5.290); 0.442(5.506); 0.714(5.680); 0.986(5.767); 1.326(5.829); 1.734(5.873); 2.210(5.913); 2.822(5.943); 3.435(5.971); 4.251(5.993).
	(b)	0.187(5.121); 0.240(5.267); 0.323(5.393); 0.422(5.501); 0.537(5.594); 0.683(5.666); 0.859(5.731); 1.096(5.793); 1.349(5.824); 1.689(5.854).

the calculations by making

$$[Ce^{3+}] = b \simeq B = \text{constant.} \quad (3)$$

For the formation of a series of hydrolysis products, $Ce_q(OH)_p^{3q-p}$, the concentration of hydrogen ions set free per hydrolysis, BZ, is expressed by eq. (4)

$$BZ = \sum\sum p[Ce_q(OH)_p^{3q-p}]$$

$$= \sum\sum p^* \beta_{pq} b^q h^{-p} \gamma_B^q \gamma_H^{-p} \gamma_{pq}^{-1} a_w^{4p}. \quad (4)$$

It was postulated, on writing eq. (4), that each H^+ is solvated by four H_2O, as suggested by experimental[7,8] and theoretical[9] evidence, and that Ce^{3+} remains unchanged in its coordination in the reaction products. As far as when B is constant, the variation of the activity coefficients and the water activity may be neglected so that eq. (4) can be written as

$$BZ = \sum pK_p h^{-p} \quad (5)$$

where

$$K_p = \sum {}^*\beta_{pq} B^q \gamma_B^q \gamma_H^{-p} \gamma_{pq}^{-1} a_w^{4p}. \quad (6)$$

No satisfactory agreement in the entire BZ range could be found from comparison of the $BZ(\log h)$ data with normalized functions[10] representing a single p. However, points for the lowest Z fit well to the model curve calculated with $p = 1$. To explain the data we had to assume, that in addition to $Ce_q(OH)^{3q-1}$, other species also containing p' OH^- groups were present. To test the validity of this hypothesis, which may be expressed by the equation

$$BZ = K_1 h^{-1} + p' K_{p'} h^{-p'} \quad (7)$$

the data, recalculated to the form $\log(BZh)$ versus $\log h$, were superimposed onto the family of $Y_{p'}(\log u)$ curves using eqs (8) and (9) calculated with $p' = 2, 3, 4, 5, 6$ and 7:

$$Y_{p'} = \log(BZh) - \log K_1 = \log(1 + p'u^{p'-1}) \quad (8)$$

$$\log u = (1/(p'-1))\log(K_{p'}/K_1) - \log h. \quad (9)$$

The model function $Y_5(\log u)$ satisfactorily fitted the data, whereas systematic deviations were noticed in some parts of the $\log h$ range studied with any other member of the $Y_{p'}$ group. This result indicates the formation of mono- and penta-ligand complexes.

The probable values of K_1 and K_5, given in Table 2, were computed from the differences $Y_5 - \log(BZh)$ and $\log u - (-\log h)$ read off from the point of best fit.

Additional evidence for the conclusions reached using curve fitting can be obtained from a numerical approach which enables one to examine systematically how the experimental error and the underlying assumptions affect the estimation of p'. It is easily demonstrated how the sum of the concentrations of all the complexes, S, can be deduced using eq. (10)

$$S = \sum[Ce_q(OH)_p^{3q-p}] = \sum K_p h^{-p} = \int_{\ln h}^{\infty} BZ \, d\ln h. \quad (10)$$

By combining eq. (7) with (10) one has

$$\log(BZ - S) = \log(p'-1) + \log K_{p'} - p' \log h, \quad (11)$$

thus, provided only species with $p = 1$ and $p = p'$ are present, $\log(BZ - S)$ should be a linear function of $-\log h$ having a slope p'.

The integration was performed by using the trapezoid rule which avoids smoothed curves and makes direct use of the experimental points. The magnitudes of the residual integral $\int_{\ln h_0}^{\infty} BZ \, d\ln h$, where h_0 denotes the highest h at which a reliable Z could still be obtained, were estimated graphically by the extrapolation method described earlier,[3] assuming that the three lowest experimental points at each B were measured in solutions where only mono-ligand species prevail.

For a given set of data the most probable p' was computed by the method of least-squares. In order to gain an idea on the influence of random errors, the number of points considered was varied. The results are given in Table 2, the limits indicating maximum deviations from the mean of p' calculated by varying the number of points. The reasonable constancy of p' appears to justify the conclusions of the graphical approach.

Having ascertained that the main hydrolysis products are mono- and penta-ligands we next concentrated our attention upon refining the values of K_1 and K_5. The function

$$\log(5S - BZ) = \log 4 + \log K_1 - \log h \quad (12)$$

was chosen to evaluate K_1 because the contribution from the mono-ligandic term is greater in eq. (12) than in functions based on BZ. Equation (11), on the other hand, with $p' = 5$ was employed to find K_5. The results are collected in Table 2. The errors are the largest deviations from the mean values. Since the constants from eqs (11) and (12) are affected by smaller errors, they are selected as the basis for the following treatment.

Estimation of the most probable q *values*

To ascertain the number of metal ions in the predominating complexes we have to compare data of different B values. Such a comparison involves the evaluation of changes in the activity coefficients and in the water activity caused by the replacement of Li^+ with Ce^{3+}. Medium effects were corrected using the specific interaction theory, SIT.[11] According to theory, since all participants in the equilibrium are positively charged and the anionic composition of the medium remains practically unchanged, the activity coefficient of a species, i, of charge z_i, defined so that $\gamma_i \to 1$ as $[i] \to 0$ in 3 m

Table 2. Survey of the homo-ligandic equilibrium constants

B, m	$-\log K_1$ eqs (8)	$-\log K_5$ and (9)	p'	$-\log K_1$ eq. (12)	$-\log K_5$ eq. (11)
0.9986	8.87±0.03	33.24±0.05	5.2±0.2	8.86±0.02	33.24±0.04
0.600	9.17±0.03	34.04±0.05	5.2±0.5	9.16±0.02	34.05±0.05
0.300	9.59±0.03	34.99±0.10	4.8±0.6	9.58±0.02	34.96±0.06
0.200	9.79±0.02	35.66±0.10	5.3±0.3	9.79±0.01	35.66±0.04
0.100	10.10±0.05	36.5±0.2	—	10.09±0.02	—

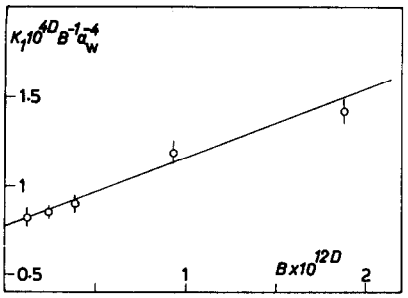

Fig. 2. $K_1 B^{-1} a_w^{-4} 10^{4D}$, eq. (16), as a function of $B \times 10^{12D}$. The line represents: $7.8 \times 10^{-10} + 3.8 \times 10^{-10} B 10^{12D}$.

$LiClO_4$ at 50°C, may be expressed as a function of the ionic strength, I

$$\log \gamma_i = -z_i^2 D \qquad (13)$$

where

$$D = 0.5339 I^{0.5}/(1+1.5I^{0.5}) - 0.2570. \qquad (14)$$

On the medium scale, $a_w \to 1$ as the composition of TS tends to 3 m $LiClO_4$. The variations of a_w with B were calculated from eq. (15)

$$\log a_w = 0.0205 B. \qquad (15)$$

Relationship (15) was deduced from osmotic coefficients published by Pitzer,[12] by assuming a linear variation between the values prevailing in 3 m $LiClO_4$ and 1 m $Ce(ClO_4)_3$.

Equation (6) for $p = 1$ can then be written as

$$K_1 10^{4D} a_w^{-4} B^{-1} = {}^*\beta_{11} + {}^*\beta_{12} B 10^{12D} + \cdots. \qquad (16)$$

The plot of the left-hand side term of eq. (16) against $B10^{12D}$ is shown in Fig. 2. It can be seen that the points, within the limits of experimental error, fall on a straight line. This means that $Ce(OH)^{2+}$ and $Ce_2(OH)^{5+}$ ions are present. Their formation constants are given in Table 3.

For $p = 5$, eq. (6) yields, neglecting species such as $Ce(OH)_5^{2-}$,

$$K_5 = {}^*\beta_{52} B^2 a_w^{20} 10^{-12D} + {}^*\beta_{53} B^3 a_w^{20} 10^{-6D} + \cdots. \qquad (17)$$

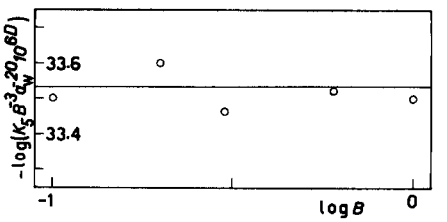

Fig. 3. $\log(K_5 B^{-3} a_w^{-20} 10^{6D})$, eq. (17), as a function of $\log B$.

As Fig. 3 shows, $\log(K_5 B^{-3} a_w^{-20} 10^{6D})$ remains constant within ± 0.05 units over the entire B range, thus demonstrating the formation of $Ce_3(OH)_5^{4+}$. The formation constant, an average of the values calculated for each point, is given in Table 3.

Refinement of the equilibrium constants

To check the results determined in the previous sections, the data were treated with methods based on the principle of least-squares. The calculations consisted of minimization of the sum

$$U = \sum((Z_i - Z_c)/Z_i)^2 \qquad (18)$$

in which Z_i is an experimental datum, while Z_c denotes a value calculated with a given set of ${}^*\beta_{pq}$. Medium changes were accounted for by eqs (13)–(15).

The minimum was afforded by the constants of Table 3. The uncertainties are three times the standard deviation, defined by the D-boundary[13] and are lower than the maximum errors estimated by graphical procedures.

The numerical treatment of the data, through the distribution of the relative error $1 - Z_c/Z_i$, yields a quantitative measure of the agreement between experimental data and the proposed model. Of a total of 82 data points, 41 are found to have a positive deviation whereas 41 have a negative deviation. The average of the positive ones amounts to 5.9%, the average of the negative ones to 5.0%. The magnitude and sign of the deviations do not exhibit an appreciable trend with B and Z.

Table 3. Calculated values of the equilibrium constants

Method	$-\log {}^*\beta_{11}$	$-\log {}^*\beta_{12}$	$-\log {}^*\beta_{53}$
Dependence of K_p on B	9.11 ± 0.05	9.46 ± 0.2	35.53 ± 0.07
Least-squares	9.13 ± 0.03	9.45 ± 0.09	35.60 ± 0.03

DISCUSSION

The main result of this work is that at 50°C the "intermediate" species $Ce(OH)^{2+}$ and $Ce_2(OH)^{5+}$, which did not reach a sufficient concentration for detection at 25°C, are readily detected according to expectation. The absence of these ions at 25°C is understandable in terms of the following arguments.

First, the constants

$$\log {}^*\beta_{11} = -9.78 \pm 0.15 \quad (19)$$

$$\log {}^*\beta_{12} = -10.4 \pm 0.2 \quad (20)$$

valid in 3 M $LiClO_4$ at 25°C, i.e. the experimental conditions used by Biedermann and Newman,[1] were evaluated. The constants in eqs (19) and (20) were obtained from the values of Table 3 and from the heats associated with the formation of $Ce(OH)^{2+}$ and $Ce_2(OH)^{5+}$. These were assumed to be identical with the ones estimated for $La^{3+} + H_2O \leftrightarrows La(OH)^{2+} + H^+$, $\Delta^*H_{11} = 33 \pm 7$ kJ mol^{-1}, and for $2La^{3+} + H_2O \leftrightarrows La_2(OH)^{5+} + H^+$, $\Delta^*H_{12} = 71 \pm 10$ kJ mol^{-1}. The enthalpy values given here were calculated by combining constants determined in 3 m $LiClO_4$ at 60°C with the quotients, valid in 3 m $LiClO_4$ at 25°C,

$$\log([La(OH)^{2+}]h/[La^{3+}]) = -9.89 \pm 0.10$$

$$\log([La_2(OH)^{5+}]h/[La^{3+}]^2) = -10.2 \pm 0.1$$

which were deduced by treating previous measurements[3] with the procedure described under "estimation of the most probable q values". The heats now proposed are slightly different from those given previously,[2] which however, were derived from constants not processed for medium changes.

The $Ce_2(OH)^{5+}$ complex with the constant given by eq. (20) would attain concentrations influencing BZ by less than 1%. On the other hand, a constant of −9.78 for $\log {}^*\beta_{11}$ would affect BZ by more than 10% at the lowest B, 0.05 M, studied by Biedermann and Newman.[1] Therefore $Ce(OH)^{2+}$ should be detectable at 25°C. We invoke kinetic factors to explain its absence. Biedermann and Newman point out that at low OH^- and Ce^{3+} concentrations "...the rate of the hydrolysis reaction can become so slow that after the addition of OH^-, h is increasing for a couple of hours". Probably $Ce(OH)^{2+}$ does not attain detectable amounts within the period of a titration.

Finally, we would like to understand how La^{3+} and Ce^{3+}, i.e. cations of the same charge and with almost identical ionic radii and electronegativities, form different polynuclear complexes, $La_2(OH)_3^{3+}$ and $Ce_3(OH)_5^{4+}$. Irregularities must be sought for in the partial filling of the 4*f* and the empty 5*d*, 6*s* and 6*p* orbitals which characterize the lanthanide series. The exploration of such irregularities may motivate a systematic, more comprehensive reinvestigation of the hydrolysis of the lanthanide cations.

Acknowledgement—This work has been financially supported by the Ministero della Pubblica Istruzione, Rome.

REFERENCES

1. G. Biedermann and L. Newman, *Arkiv Kemi* 1964, **22**, 303.
2. L. Ciavatta, M. Iuliano and R. Porto, *Polyhedron* 1987, **6**, 1283.
3. G. Biedermann and L. Ciavatta, *Acta Chem. Scand.* 1961, **15**, 1347.
4. G. Biedermann and L. Ciavatta, *Arkiv Kemi* 1964, **22**, 253.
5. G. Gran, *Analyst* 1952, **77**, 661.
6. L. Ciavatta and R. Porto, to be published.
7. D. G. Tuck and R. M. Diamond, *J. Phys. Chem.* 1961, **65**, 193.
8. D. S. Terekhova, *Zh. Strukt. Khim.* 1970, **11**, 530.
9. R. Grahn, *Arkiv Fysik* 1962, **21**, 13.
10. L. G. Sillén, *Acta Chem. Scand.* 1956, **10**, 186.
11. L. Ciavatta, *Ann. Chim. (Rome)* 1980, **70**, 551.
12. K. S. Pitzer, in *Activity Coefficients in Electrolyte Solutions* (Edited by R. M. Pytkowicz), Vol. 1. CRC Press, Boca Raton, FL (1979).
13. L. G. Sillén, *Acta Chem. Scand.* 1962, **16**, 159.

Polyhedron Vol. 7, No. 15, pp. 1363–1370, 1988
Printed in Great Britain

0277–5387/88 $3.00+.00
Pergamon Press plc

TRIANGULOTRIRHENIUM(III) ALKOXIDES. X-RAY CRYSTAL STRUCTURES OF $Re_3(\mu\text{-}Cl)_3(OBu^t)_6$ AND $Re_3(\mu\text{-}Cl)Cl(\mu\text{-}MENTHOXO)_2(MENTHOXO)_5$ AND OF $Re_2(\mu\text{-}Cl)_2(CO)_6(THF)_2$

ANTHONY C. C. WONG and GEOFFREY WILKINSON*

Chemistry Department, Imperial College of Science and Technology, London SW7 2AY, U.K.

and

BILQUIS HUSSAIN, MAJID MOTEVALLI and MICHAEL B. HURSTHOUSE*

Chemistry Department, Queen Mary College, Mile End Road, London E1 4NS, U.K.

(*Received* 11 *February* 1988; *accepted* 1 *March* 1988)

Abstract—The syntheses of triangulotrirhenium cluster alkoxides from *t*-butanol, (−)-menthol and *i*-propanol are reported and the structures of $Re_3(\mu\text{-}Cl)_3(OBu^t)_6$ and $Re_3(\mu\text{-}Cl)Cl(\mu\text{-menthoxo})_2(\text{menthoxo})_5$ determined by X-ray crystallography. Interactions with carbon monoxide and the X-ray structure of $Re_2(\mu\text{-}Cl)_2(CO)_6(THF)_2$ are reported.

We have previously reported the syntheses of various triangulotrirhenium(III) cluster alkyl species such as $Re_3(\mu\text{-}Cl)_3R_6$ (R = Me, CH_2Ph, C_6H_5, CH_2SiMe_3, $C_6H_4Me\text{-}p$)[1–4] and $Re_3(\mu\text{-}Me)_3R_6$ (R = Me, CH_2SiMe_3, CH_2Ph).[1,3,4] We have now extended the series to alkoxo clusters of rhenium(III).

Rhenium(III) alkoxides are not common, being mainly of the type $Re_2(OR)_2X_4(PPh_3)_2$[5] (R = Me, Et, Pr^n, Pr^i and X = Cl, Br). Some trinuclear cluster compounds of rhenium(III) involving Re—O bonds have however been synthesized, for example $Re_3(\mu\text{-}Cl)_3(O_2CPh)_6$[6] and $Re_3(\mu\text{-}Br)_3(\eta^3\text{-}O_3AsO)_2(Me_2SO)_3$.[7]

RESULTS AND DISCUSSION

(1) *The* t-*butoxide*

The *t*-butoxo cluster compound, $Re_3(\mu\text{-}Cl)_3(OBu^t)_6$ (1), was prepared by the interaction of $Re_3Cl_9(THF)_3$ with $NaOBu^t$, in approximately stoichiometric amounts, in tetrahydrofuran (THF). The product, obtained in good yield as deep green needles, gives intense green solutions in organic solvents and is extremely air- and moisture-sensitive. The IR spectrum shows a band at 340 cm^{-1}, assigned to the Re—Cl—Re stretching frequency by comparison to other trirhenium cluster compounds with chloride bridges.[1–3] There is also a band at 722 cm^{-1}, tentatively assigned to ν(Re—O).[8]

The ^1H NMR spectrum exhibits a singlet peak at δ 1.46 ppm due to the butyl protons, whilst the $^{13}C\{^1H\}$ spectrum has two resonances (δ 87.72 and 34.71 ppm) which were assigned, via the gated ^{13}C NMR spectrum, to the butyl quaternary (singlet) and butyl methyl [quartet, J(C—H) = 126.3 Hz] carbons, respectively. The structure of $Re_3(\mu\text{-}Cl)_3(OBu^t)_6$ has been determined by X-ray crystallography. A diagram of the molecular structure is given in Fig. 1, selected bond lengths and angles are given in Table 1. The molecule lies in a general position in the unit cell and thus has no crystallographically imposed symmetry. However, the $Re_3Cl_3O_6$ core has a structure which approximates very closely to C_{3v} (but not D_{3h}) symmetry. Thus the Re—Re distances are equal within experimental error, as are the Re—Cl distances, and the Re_3Cl_3 unit is accurately planar. The Re—O distances, however, fall into two well defined groups—three "short" (Re—O = 1.82 ± 0.02 Å) and three "long" (Re—O = 1.99 ± 0.02 Å), one of each per Re atom,

* Authors to whom correspondence should be addressed.

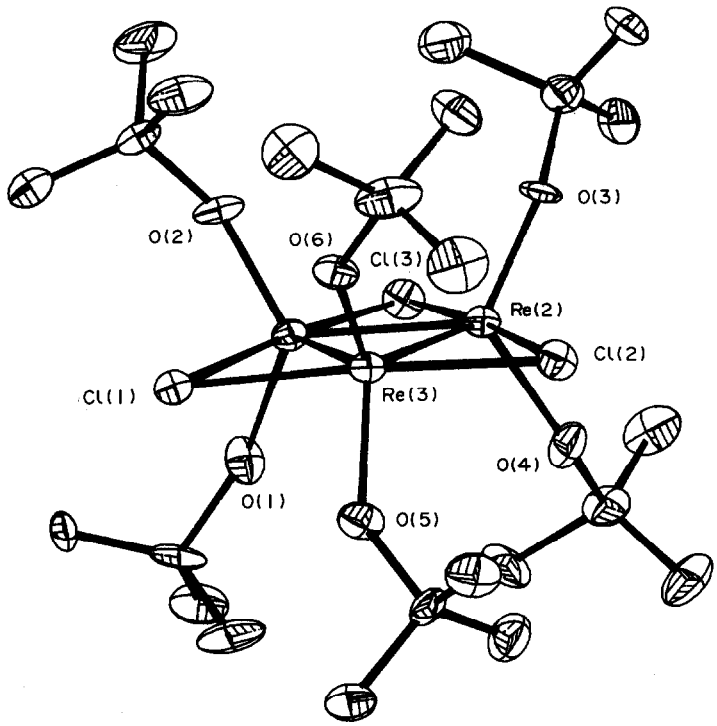

Fig. 1. The structure of $Re_3(\mu\text{-}Cl)_3(OBu^t)_6$.

with the three bonds of one type on the *same side* of the Re_3 triangle (hence the C_3 and not D_3 symmetry). The presence of short Re—O (alkoxide) bonds may well be an indication of O → Re π-bonding arising out of the electron deficiency of the Re(III) centres in Re_3 clusters where the metal has only two terminal ligands (and is thus a 16e system, assuming Re=Re double bonding along each Re—Re edge). Surprisingly however, the Re—O—C angles in all six ligands are approximately the same at 142–145°, and the angles formed by the Re—O bonds and the Re_3 plane are all very similar.

The occurrence of strong O → Re π-bonding is also reflected in increases in the Re—Cl distances (Cl can also be considered a weak π-donor) and the Re—Re distances of 0.02 and 0.05 Å, respectively, compared with those in the analogous alkyl $Re_3Cl_3(CH_2SiMe_3)_6$,[9] in which the alkyl is a pure σ-bonding ligand (in the absence, of course of Re···C—H agostic interactions).

(2) *The menthoxide*

The menthoxo cluster, $Re_3(\mu\text{-}Cl)Cl(\mu\text{-menthoxo})_2(menthoxo)_5$, was prepared by the reaction of $Re_3Cl_9(THF)_3$ with the sodium salt of natural menthol, in approximately stoichiometric quantities in tetrahydrofuran. The green–brown compound gives deep brown solutions in organic solvents. Bands of interest in the IR spectrum are at 320 and 338 cm^{-1} assigned to the metal–chloride vibrations for the bridging and terminal chlorides, respectively. The ^1H NMR spectrum is very complicated, consisting of a complex of peaks, typical of menthoxo groups between 0.5–1.8 ppm. It was not possible to differentiate between the terminal and bridging menthoxo groups.

The crystal structure of the compound has been determined by X-ray crystallography. A digram of the molecule is shown in Fig. 2, selected bond lengths and angles in Table 2. As for the butoxide, the molecule has no crystallographic symmetry, but the $Re_3(O_2Cl)(O_5Cl)$ core has an approximate plane of symmetry perpendicular to the ring and containing Cl(1), Re(1), O(1) and Cl(2).

The Re_3 triangle is isosceles with the Re—Re edge bridged by the chloride being slightly longer than the two edges bridged by oxygen (2.422 vs 2.372 Å). The bridging Re—Cl distances are very similar to those in the butoxide and the bridging Re—O distances are all very similar at 2.10 Å. In contrast to the butoxide, all terminal Re—O distances are all essentially equal and close to the average of the two types of distance found in that compound. The Re—O—C angles in these terminal alkoxides are slightly smaller than those in the butoxide, at 133–142°.

Table 1. Selected bond lengths and angles for $Re_3(\mu\text{-}Cl)_3(OBu^t)_6$

	Bond lengths (Å)		
Re(2)—Re(1)	2.438(3)	Re(3)—Re(1)	2.439(3)
Cl(1)—Re(1)	2.451(7)	Cl(3)—Re(1)	2.406(7)
O(1)—Re(1)	2.009(16)	O(2)—Re(1)	1.844(15)
Re(3)—Re(2)	2.436(3)	Cl(2)—Re(2)	2.425(7)
Cl(3)—Re(2)	2.421(7)	O(3)—Re(2)	1.794(14)
O(4)—Re(2)	1.982(16)	Cl(1)—Re(3)	2.472(7)
Cl(2)—Re(3)	2.394(7)	O(5)—Re(3)	2.001(16)
O(6)—Re(3)	1.824(14)		
	Bond angles (deg.)		
Re(3)—Re(1)—Re(2)	59.94(2)	Cl(1)—Re(1)—Re(2)	120.6(2)
Cl(1)—Re(1)—Re(3)	60.7(2)	Cl(3)—Re(1)—Re(2)	60.0(2)
Cl(3)—Re(1)—Re(3)	119.8(2)	Cl(3)—Re(1)—Cl(1)	175.1(2)
O(1)—Re(1)—Re(2)	113.8(5)	O(1)—Re(1)—Re(3)	118.1(5)
O(1)—Re(1)—Cl(1)	91.8(5)	O(1)—Re(1)—Cl(3)	83.7(5)
O(2)—Re(1)—Re(2)	116.5(6)	O(2)—Re(1)—Re(3)	120.8(5)
O(2)—Re(1)—Cl(1)	95.1(6)	O(2)—Re(1)—Cl(3)	88.7(5)
O(2)—Re(1)—O(1)	115.5(7)	Re(3)—Re(2)—Re(1)	60.15(2)
Cl(2)—Re(2)—Re(1)	119.0(2)	Cl(2)—Re(2)—Re(3)	59.0(2)
Cl(3)—Re(2)—Re(1)	59.4(2)	Cl(3)—Re(2)—Re(3)	119.3(2)
Cl(3)—Re(2)—Cl(2)	175.2(2)	O(3)—Re(2)—Re(1)	118.5(5)
O(3)—Re(2)—Re(3)	113.6(6)	O(3)—Re(2)—Cl(2)	87.5(6)
O(3)—Re(2)—Cl(3)	97.2(6)	O(4)—Re(2)—Re(1)	116.2(5)
O(4)—Re(2)—Re(3)	111.4(5)	O(4)—Re(2)—Cl(2)	84.6(5)
O(4)—Re(2)—Cl(3)	92.2(5)	O(4)—Re(2)—O(3)	120.9(8)
Re(2)—Re(3)—Re(1)	60.04(2)	Cl(1)—Re(3)—Re(1)	59.9(2)
Cl(1)—Re(3)—Re(2)	119.9(2)	Cl(2)—Re(3)—Re(1)	120.3(2)
Cl(2)—Re(3)—Re(2)	60.3(2)	Cl(2)—Re(3)—Cl(1)	176.4(2)
O(5)—Re(3)—Re(1)	112.5(5)	O(5)—Re(3)—Re(2)	117.1(5)
O(5)—Re(3)—Cl(1)	84.1(5)	O(5)—Re(3)—Cl(2)	92.7(5)
O(6)—Re(3)—Re(1)	116.7(5)	O(6)—Re(3)—Re(2)	121.9(5)
O(6)—Re(3)—Cl(1)	87.2(6)	O(6)—Re(3)—Cl(2)	95.7(6)
O(6)—Re(3)—O(5)	115.9(7)	Re(3)—Cl(1)—Re(1)	59.4(2)
Re(3)—Cl(2)—Re(2)	60.7(2)	Re(2)—Cl(3)—Re(1)	60.7(2)
C(1)—O(1)—Re(1)	144.2(12)	C(2)—O(2)—Re(1)	144.4(13)
C(3)—O(3)—Re(2)	142.5(12)	C(4)—O(4)—Re(2)	145.4(13)
C(5)—O(5)—Re(3)	141.7(13)	C(6)—O(6)—Re(3)	141.1(14)

It seemed reasonable that all the chloride groups of Re_3Cl_9 could be replaced by menthoxo groups, but the reaction of $Re_3Cl_9(THF)_3$ with an excess of sodium menthoxide in refluxing THF yielded only a brown viscous oil which we were unable to purify characterize.

(3) *The* i-*propoxide*

The reaction of $Re_3Cl_9(THF)_3$ with $NaOPr^i$ in approximately stoichiometric amounts in THF gave a deep green solution which yielded deep green crystals which were soluble in most polar organic solvents. However, we were unable to characterize the compound conclusively by analytical or spectroscopic techniques and despite numerous attempts, we were unable to obtain crystals suitable for X-ray crystallography—all samples were partially crystalline. The IR spectrum was consistent with a trirhenium isopropoxo cluster compound with Re—Cl stretches at 320 and 348 cm^{-1} and the presence of both terminal and bridging chlorides, as in the case of the menthoxide cluster. The ^1H NMR spectrum showed seven sharp doublets between 0.8–2.0 ppm, corresponding to six methyl protons each for seven isopropyl groups. There are also three multiplets at 4.29, 4.93 and 5.18 ppm, corresponding to two, three and two protons, respectively. This suggests that the product may have the molecular formula, $Re_3(\mu\text{-}Cl)(\mu\text{-}O\text{—}Pr^i)_2Cl(O\text{—}Pr^i)_5$, which seems to correlate fairly well with the analytical data.

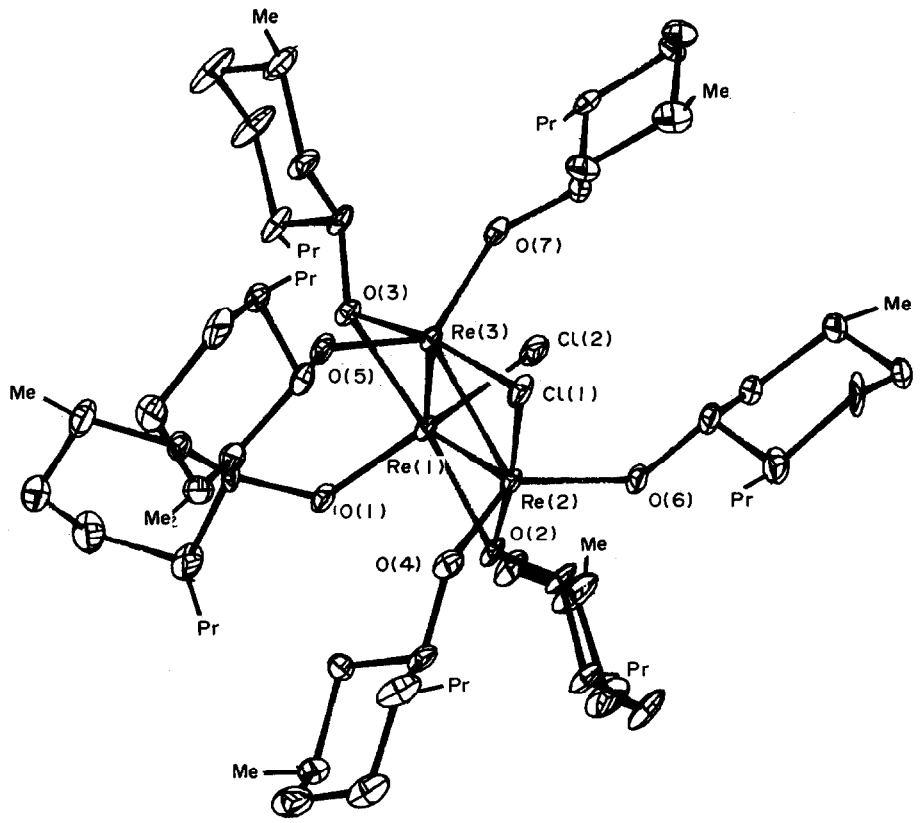

Fig. 2. The structure of $Re_3(\mu\text{-Cl})Cl(\mu\text{-menthoxo})_2(\text{menthoxo})_5$. The substituents on the menthoxo ligands are represented schematically, to reduce overlapping.

(4) *Interaction of alkoxides with* CO

The butoxide did not react with either hydrogen or carbon disulphide and the unreacted compound was recovered in both cases. However, on reaction with CO (1.8 atm) in THF at room temperature, the compound is reduced to a mixture of rhenium(I) carbonyl chlorides, $ReCl(CO)_5$, $Re_2Cl_2(CO)_8$, $[ReCl(CO)_3]_4$ and $Re_2Cl_2(CO)_6(THF)_2$. The main product is $ReCl(CO)_5$, followed by $Re_2Cl_2(CO)_6(THF)_2$; $Re_2Cl_2(CO)_8$ and $[ReCl(CO)_3]_4$ were present in small amounts in the $ReCl(CO)_5$ fraction. The carbonyl halides were identified by mass spectrometry, which showed the appropriate molecular ion peaks and fragmentation patterns, as well as good correlation with isotope cluster abundance calculations for each of the products. The solution IR spectrum of $ReCl(CO)_5$ showed two very strong bands at 1985 and 2040 cm^{-1}, as well as a medium band at 2155 cm^{-1} for the carbonyl stretching modes, which agree well with literature values.[10] $Re_2Cl_2(CO)_6(THF)_2$ was identified by analytical and spectroscopic data. The IR spectrum of $Re_2Cl_2(CO)_6(THF)_2$ shows three bands in the carbonyl stretching region at 1960, 1948 and 1928 cm^{-1} consistent with a C_{2h} symmetry and a *trans* arrangement of the THF ligands, giving rise to three IR active bands (A_2+2Bu). This structure is confirmed by X-ray crystallography study (see below).

On increasing the pressure of CO (20 atm) and the temperature (100°C) of the reaction, $Re_2Cl_2(CO)_6(THF)_2$ was no longer produced and the abundance of $Re_2Cl_2(CO)_8$ and $[ReCl(CO)_3]_4$ in $ReCl(CO)_5$ decreases. Using *t*-BuOH as solvent for the reaction (20 atm CO, 100°C), $ReCl(CO)_5$, with the same minor components as above, is formed. The reaction of $Re_3Cl_9(THF)_3$ with six equivalents of NaOMe and CO (20 atm 100°C) in methanol gives a good yield of $ReCl(CO)_5$, again with small amounts of $Re_2Cl_2(CO)_8$ and $[ReCl(CO)_3]_4$ impurities. We were unable to isolate any product containing or resulting from the alkoxo group, either as a solid or a liquid.

A diagram of the centrosymmetric, chloro-bridged dimer structure for $Re_2Cl_2(CO)_6(THF)_2$ is given in Fig. 3, and bond lengths and angles in Table 3. The chlorine bridging is symmetrical within experimental error and there is only a marginal difference between Re—C distances for carbonyls

Table 2. Selected bond lengths and angles for $Re_3(\mu\text{-Cl})Cl(\mu\text{-menthoxo})_2(menthoxo)_5$

Bond lengths (Å)			
Re(2)—Re(1)	2.368(3)	Re(3)—Re(1)	2.376(3)
Cl(2)—Re(1)	2.316(6)	O(1)—Re(1)	1.883(10)
O(2)—Re(1)	2.103(14)	O(3)—Re(1)	2.096(15)
Re(3)—Re(2)	2.422(3)	Cl(1)—Re(2)	2.439(8)
O(2)—Re(2)	2.053(16)	O(4)—Re(2)	1.877(11)
O(6)—Re(2)	1.878(13)	Cl(1)—Re(3)	2.438(6)
O(3)—Re(3)	2.084(12)	O(5)—Re(3)	1.889(15)
O(7)—Re(3)	1.882(10)	C(11)—O(1)	1.444(18)
C(21)—O(2)	1.496(28)	C(31)—O(3)	1.467(17)
C(41)—O(4)	1.438(16)	C(51)—O(5)	1.449(20)
C(61)—O(6)	1.458(17)	C(71)—O(7)	1.427(15)
Bond angles (deg.)			
Re(3)—Re(1)—Re(2)	61.4(1)	Re(3)—Re(2)—Re(1)	59.4(1)
Re(2)—Re(3)—Re(1)	59.1(1)	Cl(2)—Re(1)—Re(2)	101.4(2)
Cl(2)—Re(1)—Re(3)	97.8(2)	O(1)—Re(1)—Re(2)	113.5(4)
O(1)—Re(1)—Re(3)	119.9(5)	O(1)—Re(1)—Cl(2)	137.2(4)
O(2)—Re(1)—Re(2)	54.3(4)	O(2)—Re(1)—Re(3)	115.6(4)
O(2)—Re(1)—Cl(2)	97.5(4)	O(2)—Re(1)—O(1)	84.5(5)
O(3)—Re(1)—Re(2)	116.1(4)	O(3)—Re(1)—Re(3)	55.1(4)
O(3)—Re(1)—Cl(2)	93.7(4)	O(3)—Re(1)—O(1)	92.4(5)
O(3)—Re(1)—O(2)	166.6(5)	Cl(1)—Re(2)—Re(1)	119.6(2)
Cl(1)—Re(2)—Re(3)	60.2(2)	O(2)—Re(2)—Re(1)	56.3(4)
O(2)—Re(2)—Re(3)	115.6(4)	O(2)—Re(2)—Cl(1)	175.3(4)
O(4)—Re(2)—Re(1)	113.0(4)	O(4)—Re(2)—Re(3)	107.7(5)
O(4)—Re(2)—Cl(1)	85.9(5)	O(4)—Re(2)—O(2)	93.7(6)
O(6)—Re(2)—Re(1)	114.8(4)	O(6)—Re(2)—Re(3)	118.5(4)
O(6)—Re(2)—Cl(1)	92.6(5)	O(6)—Re(2)—O(2)	91.4(6)
O(6)—Re(2)—O(4)	125.2(5)	Cl(1)—Re(3)—Re(1)	119.4(3)
Cl(1)—Re(3)—Re(2)	60.2(2)	O(3)—Re(3)—Re(1)	55.6(5)
O(3)—Re(3)—Re(2)	114.3(5)	O(3)—Re(3)—Cl(1)	172.3(3)
O(5)—Re(3)—Re(1)	110.9(5)	O(5)—Re(3)—Re(2)	112.4(4)
O(5)—Re(3)—Cl(1)	92.3(4)	O(5)—Re(3)—O(3)	84.9(6)
O(7)—Re(3)—Re(1)	111.5(5)	O(7)—Re(3)—Re(2)	119.3(5)
O(7)—Re(3)—Cl(1)	95.6(4)	O(7)—Re(3)—O(3)	91.9(5)
O(7)—Re(3)—O(5)	125.4(7)	Re(3)—Cl(1)—Re(2)	59.6(2)
C(11)—O(1)—Re(1)	132.8(9)	Re(2)—O(2)—Re(1)	69.4(5)
C(21)—O(2)—Re(1)	121.0(8)	C(21)—O(2)—Re(2)	129.1(9)
Re(3)—O(3)—Re(1)	69.3(4)	C(31)—O(3)—Re(1)	137.4(12)

trans to chlorine (1.88(1) Å) and *trans* to THF (1.87(1) Å). The THF is weakly bonded and the carbon atoms show the usual high displacement perpendicular to the ring.

The structure of the bromine analogue, $Re_2Br_2(CO)_6(THF)_2$ has previously been determined[11] and the present structure is very similar.

EXPERIMENTAL

Microanalyses were carried out by Pascher, Remagen and Imperial College Laboratories. The following spectrometers were used: IR, Perkin–Elmer 683 (spectra in Nujol mulls or as dichloromethane solutions for $ReCl(CO)_5$, in cm^{-1}) calibrated with polystyrene; NMR, Bruker WM-250 and JEOL FX-90Q (data in ppm relative to $SiMe_4$); mass spectra, VG Micromass 7070 and Kratos MS 25. $Re_3Cl_9(THF)_3$[3] was prepared as before. All solvents were dried by standard methods and distilled and degassed before use. All syntheses and manipulations were carried out under oxygen-free nitrogen or argon. Sodium menthoxide, $NaOBu^t$ and $NaOPr^i$ were prepared by the interaction of NaH with natural menthol, *t*-butanol and *i*-propanol, respectively in THF.

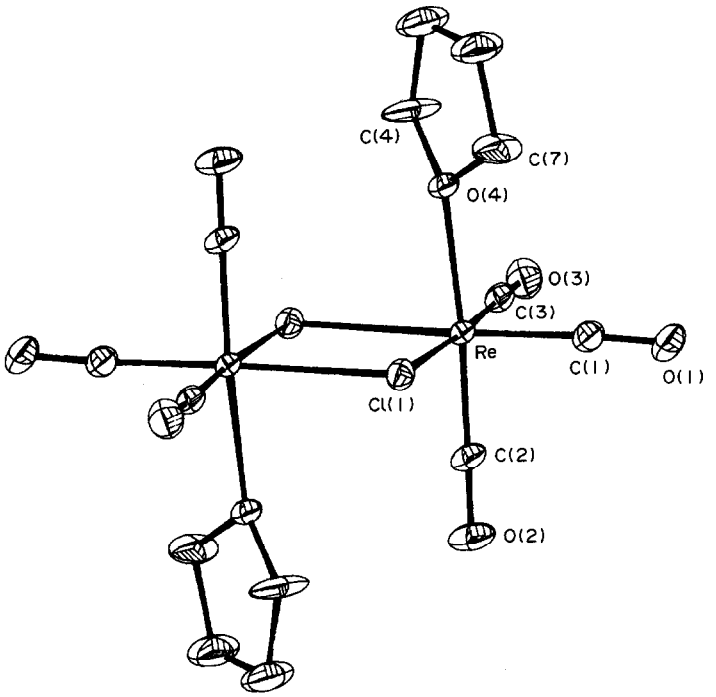

Fig. 3. The structure of $Re_2(\mu\text{-}Cl)_2(CO)_6(THF)_2$.

Hexakis(t - *butoxo*)*tris*(μ - *chloro*)*triangulotrirhenium*(III) (1)

To a stirred suspension of $Re_3Cl_9(THF)_3$ (1 g, 0.9 mmol) in THF (50 cm^3) was added $NaOBu^t$ (9.4 cm^3 of a 0.6 M solution in THF, 5.64 mmol). The red suspension darkens and eventually turns deep green. The mixture was stirred for 48 h, evaporated and the residue extracted into CH_2Cl_2 (2 × 30 cm^3). The combined extracts were filtered, concentrated

Table 3. Selected bond lengths and angles for $Re_2Cl_2(CO)_6(THF)_2$

	Bond lengths (Å)		
Cl(1)—Re(1)	2.505(6)	C(1)—Re(1)	1.882(16)
C(2)—Re(1)	1.867(16)	C(3)—Re(1)	1.877(15)
O(4)—Re(1)	2.213(10)	Re(1)—Cl(1a)	2.508(6)
O(1)—C(1)	1.166(15)	O(2)—C(2)	1.168(16)
O(3)—C(3)	1.165(16)	C(4)—O(4)	1.424(16)
C(7)—O(4)	1.404(18)	C(5)—C(4)	1.467(23)
C(6)—C(5)	1.475(25)	C(7)—C(6)	1.432(22)
	Bond angles (deg.)		
C(1)—Re(1)—Cl(1)	175.5(4)	C(2)—Re(1)—Cl(1)	92.7(6)
C(2)—Re(1)—C(1)	89.7(7)	C(3)—Re(1)—Cl(1)	95.0(5)
C(3)—Re(1)—C(1)	88.9(7)	C(3)—Re(1)—C(2)	89.2(7)
O(4)—Re(1)—Cl(1)	83.8(3)	O(4)—Re(1)—C(1)	93.6(6)
O(4)—Re(1)—C(2)	175.1(5)	O(4)—Re(1)—C(3)	94.5(5)
Re(1)—Cl(1)—Re(1a)	98.7(3)	Cl(1)—Re(1)—Cl(1a)	81.3(2)
O(1)—C(1)—Re(1)	177.6(13)	O(2)—C(2)—Re(1)	178.8(13)
O(3)—C(3)—Re(1)	177.7(12)	C(4)—O(4)—Re(1)	124.2(9)
C(7)—O(4)—Re(1)	123.3(9)	C(7)—O(4)—C(4)	107.2(12)
C(5)—C(4)—O(4)	107.3(15)	C(6)—C(5)—C(4)	106.9(14)
C(7)—C(6)—C(5)	105.2(17)	C(6)—C(7)—O(4)	110.5(15)

Key to symmetry operations relating designated atoms to reference atoms at (x, y, z).
a $-x$, $-y$, $-z$.

until saturated and then cooled at −20°C. The dark green needles were collected, washed with cold hexane (2 × 5 cm^3, −78°C) and dried *in vacuo*. The supernatant liquor provided a second crop of crystals. Yield: 0.78 g, 78% based on $Re_3Cl_9(THF)_3$. [Found: C, 25.6; H, 4.7; O, 8.7. $C_{24}H_{54}Cl_3O_6Re_3$ requires C, 26.1; H, 4.9; O, 8.7%.] IR: 1360s, 1310w, 1264w, 1241sh, 1230m, 1160s, 1025m, 930s, 906s, 785s, 722s, 561s, 489w, 372m, 340m cm^{-1}. NMR (in C_6D_6). ^1H; 1.46, s (*t*-Bu). ^{13}C-{^1H} (in CD_2Cl_2); 87.72, s (CMe_3), 34.71, s (CMe_3).

Pentakis(menthoxo)bis(μ-menthoxo)chloro(μ-chloro)triangulotrirhenium(III) (**2**)

To a stirred suspension of $Re_3Cl_9(THF)_3$ (2.67 g, 2.44×10^{-3} mol) in THF (50 cm^3) was added sodium methoxide (48 cm^3 of a 0.32 M solution in THF, 15.4 mmol) and the mixture was refluxed overnight. The deep brown solution was filtered, evaporated and the residue extracted into CH_2Cl_2 (40 cm^3). The extract was filtered, concentrated until saturated and then cooled at −20°C. The dark brown crystals were collected, washed with cold hexane (5 cm^3, −78°C) and dried *in vacuo*. The supernantant liquor provided further crops of crystals. The compound has a tendency to co-crystallize with unreacted sodium menthoxide and needs several recrystallizations from CH_2Cl_2 to purify. Alternatively, unreacted sodium menthoxide may be removed by sublimation. Yield: 1.7 g, 40% based on $Re_3Cl_9(THF)_3$. [Found: C, 46.9; H, 7.73; Cl, 4.21. $C_{70}H_{133}Cl_2O_7Re_3$ requires C, 49.0; H, 7.75; Cl, 4.12%.] IR: 1355w, 1347m, 1320s, 1280w, 1269m, 1238m, 1180m, 1160sh, 1150m, 1107m, 1094m, 1079m, 1061w, 1040m, 1009s, 991s, 969w, 950s, 920s, 910s, 880m, 851s, 808m, 774w, 727m, 700s, 687s, 652m, 602w, 502m, 461w, 338w, 320m cm^{-1}. NMR (in $CDCl_3$). ^1H; 0.5–1.8, m (menthoxo group).

Triangulotrirhenium isopropoxo compound

To a stirred suspension of $Re_3Cl_9(THF)_3$ (0.9 g, 8.23×10^{-4} mol) in THF (60 cm^3) was added $NaOPr^i$ (6 cm^3 of a 0.86 M solution in THF, 5.15×10^{-3} mol). The suspension darkened quickly and the solution, which eventually became deep green after stirring for 48 h, was evaporated and the residue extracted with CH_2Cl_2 (40 cm^3). The extract was filtered, concentrated and cooled at −20°C to give dark green crystals, which were collected, washed with cold hexane (5 cm^3, −78°C) and dried *in vacuo*. Yields: 0.3 g, 35% based on $Re_3Cl_9(THF)_3$. [Found: C, 24.1; H, 4.7; Cl, 9.0; O, 10.3. $C_{21}H_{49}Cl_2O_7Re_3$ requires C, 24.2; H, 4.7; Cl, 6.8; O, 10.7%.] IR: 1363m, 1335sh, 1320s, 1260m, 1167m, 1141w, 1122sh, 1105sh, 1098s, 1015w, 975sh, 960s, 910w, 848s, 830s, 720m, 635s, 625s, 615s, 600s, 540m, 450w, 347m, 318w, 294m cm^{-1}. NMR: (in $CDCl_3$, multiplicities and relative intensities in parenthesis). ^1H: 0.86 (d, 6), 1.02 (d, 6), 1.16 (d, 6), 1.27 (d, 6), 1.61 (d, 6), 1.82 (d, 6), 1.97 (d, 6) ($OCHMe_2$). 4.30 (m, 2), 4.93 (m, 3), 5.19 (m, 2) ($OCHMe_2$).

Reactions of alkoxides with CO

$Re_3Cl_3(OBu^t)_6$ (0.98 g, 8.88×10^{-4} mol) in THF (30 cm^3), in a pressure bottle was stirred for 4 h at room temperature under CO (2 atm). The red–brown solution was filtered, concentrated and cooled at −20°C to give colourless crystals of $ReCl(CO)_5$, which were collected, dried *in vacuo* and purified by sublimation (*ca* 80°C, under reduced pressure). Yield: 0.31 g, 32% based on $Re_3Cl_3(OBu^t)_6$. IR: ν(CO), in CH_2Cl_2 solution: 1985s, 2040s, 2155m cm^{-1}. Mass spectral data: *m/e* 327 $[Re(CO)_5]^+$, *m/e* 299 $[Re(CO)_4]^+$, *m/e* 271 $[Re(CO)_3]^+$, *m/e* 243 $[Re(CO)_2]^+$, *m/e* 215 $[Re(CO)]^+$, *m/e* 1224 $[Re_4Cl_4(CO)_{12}]^+$, *m/e* 1168 $[Re_4Cl_4(CO)_{10}]^+$, *m/e* 1140 $[Re_4Cl_4(CO)_9]^+$, *m/e* 1112 $[Re_4Cl_4(CO)_8]^+$, *m/e* 668 $[Re_2Cl_2(CO)_8]^+$, *m/e* 640 $[Re_2Cl_2(CO)_7]^+$, *m/e* 612 $[Re_2Cl_2(CO)_6]^+$, *m/e* 584 $[Re_2Cl_2(CO)_5]$. The intensities of the $Re_4Cl_4(CO)_{12}$ and $Re_2Cl_2(CO)_8$ peaks were about 10–20 times less than those for $ReCl(CO)_5$.

The supernatant was concentrated further to *ca* 2 cm^3 and then extracted into hexane (20 cm^3). The yellow–brown extract was filtered, concentrated until saturated and cooled at −20°C. The brown needles of $Re_2(\mu\text{-}Cl)_2(CO)_6(THF)_2$ were collected, washed with cold hexane (5 cm^3, −78°C) and dried *in vacuo*. The crystals were recrystallized from hexane. Yield: 0.2 g, 10% based on $Re_3Cl_3(OBu^t)_6$. [Found: C, 22.3; H, 3.8; Cl, 9.5. $C_{14}H_{16}Cl_2O_8Re_2$ requires C, 22.2; H, 2.1; Cl, 9.4%.] IR: ν(CO): 1960s, 1948s, 1928sh cm^{-1}.

Interaction of $Re_3Cl_9(OBu^t)_6$ in THF or *t*-BuOH at *ca* 20 atm and 100°C gave yields of *ca* 72% $ReCl(CO)_5$ on work up; similar conditions using $Re_3Cl_9(THF)_3$ and a slight excess of NaOMe in MeOH gave a yield of *ca* 40% $ReCl(CO)_5$.

X-ray crystallography

All crystallographic measurements were made at room temperature (293 K) on crystals sealed in thin walled glass capillaries, using a CAD4 diffractometer operating in the $\omega/2\theta$ scan mode with graphite monochromated Mo-K_α radiation ($\lambda = 0.71069$ Å) as previously described.[12] The

Table 4. Crystal data, details of intensity measurements and structure refinement

Molecular formula	$Re_3C_{24}H_{54}Cl_3O_6$	$Re_3C_{70}H_{133}O_7Cl_2$	$Re_2C_{14}H_{16}O_8Cl$
Molecular weight	1103.65	1716.264	720.118
Crystal system	Orthorhombic	Triclinic	Monoclinic
a (Å)	32.955(4)	13.787(6)	8.604(2)
b (Å)	38.406(6)	13.878(8)	10.938(3)
c (Å)	11.251(4)	13.735(8)	11.634(3)
Alpha (deg.)	90	66.89(5)	90
Beta (deg.)	90	111.51(4)	111.89(2)
Gamma (deg.)	90	115.76(5)	90
Volume (Å^3)	14240.95	2102.03	1015.96
Space group	*Fdd*2	*P*1	$P2_1/n$
Z	16	1	2
Dc (g cm^{-3})	2.06	1.347	2.353
Mu	105.74	44.46	123.12
F(000)	8352	868	610
h, *k*, *l*, range	$0 \rightarrow 13$	$-16 \rightarrow 16$	$-10 \rightarrow 10$
	$0 \rightarrow 39$	$-16 \rightarrow 16$	$0 \rightarrow 13$
	$0 \rightarrow 45$	$0 \rightarrow 16$	$0 \rightarrow 13$
Total no. of reflections	3582	7747	1980
No. of unique reflections	3298	7743	1775
Significance test	$F > 3\sigma(F)$	$F > 3\sigma(F)$	$F > 3\sigma(F)$
No. of reflections used	2656	6228	1065
No. of parameters	324	737	118
Weighting scheme paramater			
g in $w = 1/[\sigma^2(F)+gF^2]$	0.000001	0.001	0.000345
Final *R*	0.0371	0.0367	0.0286
Final *RG*	0.0382	0.0478	0.0331

structures were solved via standard heavy atom procedures and refined using full-matrix least-squares with scattering factors calculated using data from ref. 13. All non-hydrogen atoms were refined anisotropically. Hydrogens were included in idealized positions only in the THF molecule in the dimer and assigned a fixed U_{iso} value of 0.1 Å.^{2} Details of the crystal data, intensity measurements and refinement are given in Table 4.

Tables of atomic positional parameters, displacement factor coefficients, full lists of bond lengths and angles, and F_o/F_c values have been deposited as supplementary data with the Editor, from whom copies are available on request. Atomic coordinates have also been deposited with the Cambridge Crystallographic Data Centre.

Acknowledgement—We thank the S.E.R.C. for provision of X-ray facilities.

REFERENCES

1. A. F. Masters, K. Mertis, J. F. Gibson and G. Wilkinson, *Nouv. J. Chim.* 1977, **1**, 389.
2. P. G. Edwards, K. Mertis, G. Wilkinson, M. B. Hursthouse and K. M. Malik, *J. Chem. Soc., Dalton Trans.* 1980, 334.
3. K. Mertis, P. G. Edwards, G. Wilkinson, K. M. A. Malik and M. B. Hursthouse, *J. Chem. Soc., Dalton Trans.* 1981, 705.
4. A. C. C. Wong, P. G. Edwards, G. Wilkinson, M. Motevalli and M. B. Hursthouse, *J. Chem. Soc., Dalton Trans.* 1988, 219.
5. A. R. Chatravarty, F. A. Cotton, A. R. Cutter and R. A. Walton, *Inorg. Chem.* 1986, **25**, 3619.
6. P. G. Edwards, F. Felix, K. Mertis and G. Wilkinson, *J. Chem. Soc., Dalton Trans.* 1979, 361.
7. F. A. Cotton and S. J. Lippard, *J. Am. Chem. Soc.* 1966, **88**, 1882.
8. P. G. Edwards, G. Wilkinson, M. B. Hursthouse and K. M. A. Malik, *J. Chem. Soc., Dalton Trans.* 1980, 2467.
9. M. B. Hursthouse and K. M. A. Malik, *J. Chem. Soc., Dalton Trans.* 1978, 1334.
10. S. P. Schmidt, W. C. Trogler and F. Basolo, *Inorg. Synth.* 1985, **23**, 41.
11. F. Calderazzo, I. P. Mavani, D. Vitali, J. Bernal, J. D. Korp and J. L. Atwood, *J. Organomet. Chem.* 1978, **160**, 207.
12. R. A. Jones, M. B. Hursthouse, K. M. A. Malik and G. Wilkinson, *J. Am. Chem. Soc.* 1979, **101**, 4128.
13. *International Tables for X-ray Crystallography*, Vol. 4. Kynoch Press, Birmingham (1974).

Polyhedron Vol. 7, No. 15, pp. 1371–1375, 1988
Printed in Great Britain

0277–5387/88 $3.00+.00
© 1988 Pergamon Press plc

ELECTRON PARAMAGNETIC RESONANCE STUDY OF THE REACTIONS OF ROUSSIN ESTERS $Fe_2(SR)_2(NO)_4$ WITH A RANGE OF NUCLEOPHILIC ANIONS

CHRISTOPHER GLIDEWELL* and IAN L. JOHNSON

Chemistry Department, University of St Andrews, St Andrews, Fife KY16 9ST, U.K.

(*Received* 5 *November* 1987; *accepted after revision* 1 *March* 1988)

Abstract—The Roussin methyl ester $Fe_2(SMe_2)(NO)_4$ reacted with bromide or iodide to yield the known paramagnetic mononuclear complexes $[Fe(NO)_2X_2]^-$ (X = Br or I). With thiocyanate the reactions of $Fe_2(SR)_2(NO)_4$ (R = Me or Bu^t) proceeded via the S-bonded intermediates $[Fe(NO)_2(SR)(SCN)]^-$ to the N-bonded product $[Fe(NO)_2(NCS)_2]^-$: azide and cyanate gave a similar product $[Fe(NO)_2(NXY)_2]^-$, with no detectable intermediates. Nitrite yielded the known $[Fe(NO)_2(NO_2)_2]^-$ with a range of $Fe_2(SR)_2(NO)_4$ (R = Me, Et, Pr^i or Ph) in a range of solvents (CH_2Cl_2, acetone or DMF): $Fe_4S_4(NO)_4$ with nitrite in CH_2Cl_2 gave a mixture of $[Fe(NO)_2(NO_2)_2]^-$ and $[Fe(NO)_2(SH)_2]^-$. With $Fe_2(SMe)_2(NO)_4$, sulphate and chromate yielded complexes of the type, $[Fe(NO)_2(SMe)(OR)]^{2-}$ (R = CrO_3 or SO_3). The bis-chelating ligand piperazinobis(dithiocarbamate) with $Fe_2(SMe)_2(NO)_4$ gave both a five-coordinate square pyramidal mononitrosyl and a tetrahedral dinitrosyl complex, based on $Fe(NO)S_4$ and $Fe(NO)_2S_2$ chromophores, respectively. The two complexes $[Fe(NO)_2(S_2MoS_2)]^-$ and $[Fe(NO)(S_2MoS_2)_2]^{2-}$ which are formed by reaction of tetrathiomolybdate with a range of esters $Fe_2(SR)_2(NO)_4$ have been synthesized also by redox reactions from the known complexes $[Fe(NO)_2(S_2MoS_2)]^{2-}$ and $[Fe(S_2MoS_2)_2]^{3-}$, respectively.

The Roussin esters $Fe_2(SR)_2(NO)_4$ react with thiolate anions RS^- to yield[1] mononuclear paramagnetic complexes $[Fe(NO)_2(SR)_2]^-$ and with tetrathiomolybdate $[MoS_4]^{2-}$ to yield,[2] as well as $[Fe(NO)_2(SR)_2]^-$, both the heterometallic mononitrosyl $[Fe(NO)(S_2MoS_2)_2]^{2-}$ and the heterometallic dinitrosyl $[Fe(NO)_2(S_2MoS_2)]^-$. We now describe the reactions of $Fe_2(SR)_2(NO)_4$, principally $Fe_2(SMe)_2(NO)_4$, with a range of further nucleophiles to give, as previously, paramagnetic complexes readily detected by EPR spectroscopy. The side-chains of proteins and peptides contain a number of potentially nucleophilic groups, based upon oxygen, nitrogen and sulphur; as models for the formation of paramagnetic mononuclear dinitrosyliron complexes from the neutral diamagnetic esters $Fe_2(SR)_2(NO)_4$ by interaction with nucleophilic peptide side chains, we have studied the reactions of the ester $Fe_2(SMe)_2(NO)_4$ with a number of nucleophilic anions based upon these three elements, together with halide ions.

* Author to whom correspondence should be addressed.

RESULTS AND DISCUSSION

Reactions with halides

The methyl ester $Fe_2(SMe)_2(NO)_4$ reacted readily with an excess of iodide ion in DMF solution to yield the known[3] $[Fe(NO)_2I_2]^-$, characterized by $g = 2.079$, $A(^{127}I) = 20.6$ G: the bromide ion similarly yielded $[Fe(NO)_2Br_2]^-$, having $g = 2.049$, $A(^{79}Br) = 18.4$ G, $A(^{81}Br) = 20.0$ G and $A(^{14}N) = 2.5$ G. However, the chloride ion gave no complexes containing chloro ligands, but rather the two solvo complexes[1] $[Fe(NO)_2(SMe)(DMF)]$ and $[Fe(NO)_2(DMF)_2]^+$. When the solvent was changed to THF, iodide again gave $[Fe(NO)_2I_2]^-$, but bromide gave solutions which were EPR-silent, while in acetone as the solvent even iodide gave EPR-silent solutions. The ease of ring-opening in $Fe_2X_2(NO)_4$ to yield mononuclear products is greatest in a given solvent for X = I, because $Fe_2I_2(NO)_4$ has the longest and weakest Fe—Fe bond:[4] the variation with solvent, for given X, follows the order of the Gutmann donor numbers.[5]

Reactions with pseudohalides

When $Fe_2(SMe)_2(NO)_4$ reacted with (PPN)SCN [$(PPN)^+ \equiv (Ph_3PNPPh_3)^+$] in CH_2Cl_2 solution, a paramagnetic complex was formed immediately upon mixing having a 12 line EPR spectrum centred at $g = 2.029$, with the intensity ratio 1:3:5:7:9:11:11:9:7:5:3:1. The spectrum was consistent with the formulation $[Fe(NO)_2(SMe)(SCN)]^-$, having $A(^{14}N) = 4.8$ G and $A(^1H) = 2.4$ G: confirmation was obtained from the corresponding reaction between (PPN)SCN and $Fe_2(SBu^t)_2(NO)_4$ where the product $[Fe(NO)_2(SBu^t)(SCN)]^-$ exhibited no hyperfine coupling to hydrogen, only to the two nitrogens of the nitrosyl ligands. In these reactions, the softer sulphur site of the ambidentate thiocyanate has attacked iron in a simple addition reaction, eq. (1): no hyperfine coupling was detected to the remote nitrogen of the thiocyanate.

$$Fe_2(SMe)_2(NO)_4 + 2SCN^- \rightarrow 2[Fe(NO)_2(SMe)(SCN)]^- \quad (1)$$

Within 30 min of mixing, the spectrum was more complex consisting of $[Fe(NO)_2(SMe)(SCN)]^-$ and a second species of a higher g value. After 6 h, this second species was the sole paramagnetic species detectable, having a nine line spectrum centred at $g = 2.034$, with spacing 2.4 G and intensity ratio 1:4:10:16:19:16:10:4:1.

The identical spectrum was obtained by reaction of $Fe_2I_2(NO)_4$ with excess thiocyanate in DMF solution, and we attribute it to $[Fe(NO)_2(NCS)_2]^-$ in which both hyperfine couplings to nitrogen are 2.4 G. The same g value, 2.034, was obtained[6] from the complex formed from the interaction of NO gas with an aqueous mixture of Fe^{2+} and thiocyanate. Hence, although the initial product from thiocyanate and $Fe_2(SMe)_2(NO)_4$ contained thiocyanate bound through sulphur, the final product contained thiocyanate bound to iron through nitrogen: this last product is the thermodynamic one but the kinetic product depended upon attack by the soft site at the soft Fe(−I), an electron-rich d^9 centre.[1,3] While formation of the kinetic product, eq. (1) is fast, formation of the final thermodynamic product, eq. (2) takes several hours.

$$[Fe(NO)_2(SMe)(SCN)]^- + SCN^- \rightarrow MeS^- + [Fe(NO)_2(NCS)_2]^- \quad (2)$$

In contrast to the behaviour of thiocyanate, both cyanate, NCO^- and azide, N_3^-, react with $Fe_2(SMe)_2(NO)_4$ to yield a single product of the type $[Fe(NO)_2(NXY)_2]^-$ (where XY is CO or N_2, respectively) in which the iron is coordinated by four nitrogen atoms. For the cyanate complex, $g = 2.030$, and the two $A(^{14}N)$ values are 4.8 and 2.4 G in acetone solution; for the azido complex, where the line width was substantially higher, possibly because of a small hyperfine coupling to the central ^{14}N of the azide ligands, the spectral parameters were virtually identical. However, selonocyanate, $SeCN^-$ gave with $Fe_2(SMe)_2(NO)_4$, a complex and rather poorly resolved spectrum indicative of the presence of at least three paramagnetic nitrosyl complexes. In a comparative experiment, selenocyanate reacted with $Fe_2I_2(NO)_4$ to give, again, a very complex spectrum which could not be interpreted.

Reactions with oxo-anions

During the course of a study of the isotopic exchange reactions between a range of iron–sulphur nitrosyl complexes and labelled nitrite $[^{15}NO_2]^-$, we observed[7] that the esters $Fe_2(SR)_2(NO)_4$ (R = Et or Ph) with $(PPn)^+[^{15}NO_2]^-$ in CD_2Cl_2 solution gave only broad unresolved absorptions in their ^{15}N NMR spectra, indicative of paramagnetic species. We subsequently showed that $Fe_2(SR)_2(NO)_4$ (R = Me, Et or Ph) all gave $[Fe(NO)_2(NO_2)_2]^-$ with nitrite. We have now extended this series to include R = Pr^i. In the same study we observed[7] that $Fe_4S_4(NO)_4$ also reacted rapidly with $(PPN)^+[^{15}NO_2]^-$ in CD_2Cl_2 to yield the rearranged product $[Fe_4S_3(^{15}NO)_7]^-$. It has since been reported[8] that nitrite reacts, as the $(PPN)^+$ salt, with CH_2Cl_2 solvent to yield $ClCH_2ONO$, which acts as a potential source of nitrosyl chloride and the nitrosonium cation. Consequently, we have reinvestigated the reactions of $Fe_2(SR)_2(NO)_4$, and of $Fe_4S_4(NO)_4$, with $(PPN)^+[NO_2]^-$ in solvents other than CH_2Cl_2.

We have observed the same complex[7] $[Fe(NO)_2(NO_2)_2]^-$, formed from a range of esters $Fe_2(SR)_2(NO)_4$ in CH_2Cl_2, acetone and DMF. Although in aqueous solution,[6] no such complex appears to be formed from Fe^{2+}, nitrite and nitric oxide gas, in acetone at least this is an extremely stable and persistent complex. Solutions of $Fe_2(SMe)_2(NO)_4$ which have been kept in either acetone or acetone-d_6 over a period of several months at room temperature show well-developed spectra of $[Fe(NO)_2(NO_2)_2]^-$.

Although the ^{15}N NMR spectra of solutions of $Fe_4S_4(NO)_4$ and $(PPN)^+[^{15}NO_2]^-$ in CH_2Cl_2 showed no evidence for the presence of paramagnetic complexes, nevertheless EPR study of such solutions showed the presence of two mononuclear species $[Fe(NO)_2(SH)_2]^-$ and $[Fe(NO)_2(NO_2)_2]^-$. As commonly occurs,[1] a polynuclear precursor containing only mononitrosyl–

iron groups gives only dinitrosyl–iron fragments in the mononuclear products; the presence of such products renders intelligible the identity of the final product in this solvent, $[Fe_4S_3(NO)_7]^-$. In acetone solution however the ^{15}N NMR spectrum of a fresh mixture of $Fe_4S_4(NO)_4$ and $(PPN)^+[^{15}NO_2]$ showed only a broad featureless absorption indicative of the presence of paramagnetic species: EPR examination showed a single paramagnetic complex, having a five line spectrum centred at $g = 2.028$ but otherwise unidentified, which disappeared over a period of two weeks, after which time the ^{15}N NMR spectrum showed the presence of both $[Fe_4S_3(NO)_7]^-$ and $[Fe_2S_2(NO)_4]^{2-}$. Hence, we conclude that while the course of the reaction of the esters $Fe_2(SR)_2(NO)_4$ with nitrite is independent of the solvent, that of $Fe_4S_4(NO)_4$ differs markedly when CH_2Cl_2 and acetone are solvents.

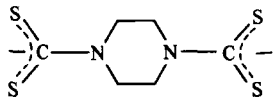

L_1

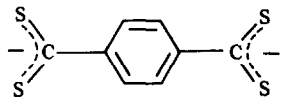

L_2

Each of $(PPN)_2[CrO_4]$ and $(PPN)_2[SO_4]$ reacted with $Fe_2(SMe)_2(NO)_4$ in acetone solution to yield paramagnetic products whose spectra characteristics were essentially identical with those of the first product, $[Fe(NO)_2(SMe)(SCN)]^-$, from the reaction of $Fe_2(SMe)_2(NO)_4$ with thiocyanate: consequently we assign to these products the formulations $[Fe(NO)_2(SMe)(OR)]^{2-}$ (where R = CrO_3 and SO_3, respectively). By contrast, the reaction of $Fe_2(SMe)_2(NO)_4$ with $(PPN)_2[S_2O_3]$ yielded, as the sole parmagnetic product, the known[1] $[Fe(NO)_2(SMe)_2]^-$. This may be compared with the formation[2] of $[Fe(NO)_2(SPh)_2]^-$ as the the sole paramagnetic product of the reaction between $Fe_2(SPh)_2(NO)_4$ and $[MoS_4]^{2-}$. No paramagnetic products were formed by either $(PPN)[MnO_4]$ or $(PPN)[ClO_4]$, possibly because of the very low nucleophilicity of these anions.

Reactions with piperazinobis(dithiocarbamate) and tetrathioterephthalate

The esters $Fe_2(SR)_2(NO)_4$ (R = alkyl) react with tetrathiomolybdate $[MoS_4]^{2-}$ to yield two paramagnetic complexes,[2] $[Fe(NO)(S_2MoS_2)_2]^{2-}$ and $[Fe(NO)_2(S_2MoS_2)]^-$. Of these, $[Fe(NO)_2(S_2MoS_2)]^-$ is analogous to the complexes[1] $[Fe(NO)_2(SR)]^-$ and contains tetrahedral[9] iron(−I), while $[Fe(NO)(S_2MoS_2)_2]^{2-}$ contains square pyramidal iron(I) and is thus analogous to the dithiocarbamate complex $Fe(NO)(S_2CNMe_2)_2$.[10] We have now studied the reactions of $Fe_2(SMe)_2(NO)_4$ with two bis-dithio ligands, piperazinobis(dithiocarbamate), L_1 and tetrathioterephthalate, L_2:

If these ligands were to be coordinated to square pyramidal iron(I) at both ends of the ligand then polymeric iron nitrosyls would ensue: the ligands L_1 and L_2 have been designed to provide, in the event of such polymer formation, respectively an insulating and a conducting fragment between successive iron centres.

Reaction of the disodium salt of the piperazino ligand L_1 with $Fe_2(SMe)_2(NO)_4$ in DMF solution such that the molar ratio of L_1 to the ester was 5 : 1 gave an EPR spectrum showing the presence of two paramagnetic species (**A**) and (**B**). Complex (**A**) was a mononitrosyl characterized by $g = 2.039$, $A(^{14}N) = 13.6$ G: such a large value of A characterizes[2] the complex as containing a square pyramidal iron(I) with a linear Fe—N—O fragment and points to the partial structure (**I**), analogous to those in $Fe(NO)(S_2CNMe_2)_2$ and $[Fe(NO)(S_2MoS_2)_2]^{2-}$. Complex (**B**) was a dinitrosyl, characterized by $g = 2.014$, $A(^{14}N) = 3.8$ G, and hence contains tetrahedral iron(−I) with again linear Fe—N—O fragments and the partial structure (**II**). It is not possible to determine from these data whether complexes (**A**) and (**B**) are monomeric or oligameric: however there is no doubt that the reactions of the ligand L_1 with $Fe_2(SMe)_2(NO)_4$ in DMF closely resemble the corresponding reactions of $[MoS_4]^{2-}$.

However, when the solvent was changed from DMF to the much less polar acetone, the course of the reaction between L_1 and $Fe(SMe)_2(NO)_4$ was

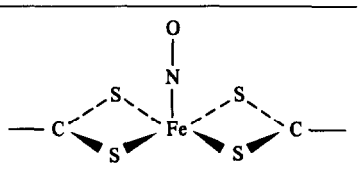

(**I**)

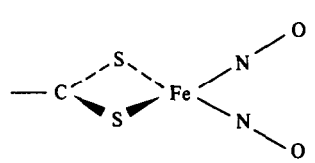

(**II**)

radically altered. The initial product had an EPR spectrum identical in type to those of the initial products formed by thiocyanate, sulphate and chromate (see above) and characterized by $g = 2.030$ with a spacing of 2.5 G: we therefore attribute this to a complex of type $[Fe(NO)_2(SMe)(S—R)]_n^{x-}$. This assignment was confirmed as in the thiocyanate reaction by comparison of the behaviour of $Fe_2(SMe)_2(NO)_4$ with that of $Fe_2(SBu^t)_2(NO)_4$. On standing for 24 h at room temperature this initial spectrum was replaced completely by that of $[Fe(NO)_2(NO_2)_2]^-$; at no stage were complexes (**A**) and (**B**) detected from either $Fe_2(SMe)_2(NO)_4$ or $Fe_2(SBu^t)_2(NO)_4$ when acetone was employed as the solvent.

In reactions of the disodium salt of ligand L_2 with both $Fe_2(SMe)_2(NO)_4$ and $Fe_2(SBu^t)_2(NO)_4$, whether in DMF or in acetone, we have not detected any square pyramidal mononitrosyl complex analogous to (**A**). In all cases, the detected products were $[Fe(NO)_2(SH)_2]^-$ and $[Fe(NO)_2(SR)_2]^-$ (R = Me or Bu^t) only.

Further study of reactions with tetrathiomolybdate

When R is an alkyl group, reaction of $Fe_2(SR)_2(NO)_4$ with $[MoS_4]^{2-}$ in DMF solution, such that the overall molar ratio Mo:Fe was 1:1, yielded[2] a mixture of $[Fe(NO)_2(SR)_2]^-$, $[Fe(NO)_2(S_2MoS_2]^-$ and $[Fe(NO)(S_2MoS_2)_2]^{2-}$, except that for R = Bu^t, the proportion of $[Fe(NO)_2(S_2MoS_2)]^-$ was negligible. Photolysis of such reaction mixtures, with an unfiltered medium pressure mercury-vapour lamp, followed a common pattern, as judged by their EPR spectra. Firstly, the trinuclear $[Fe(NO)(S_2MoS_2)_2]^{2-}$ disappeared, leaving the two dinitrosyl complexes: further irradiation caused the disappearance of $[Fe(NO)_2(S_2MoS_2)]^-$, to leave only $[Fe(NO)_2(SR)_2]^-$. Control experiments showed that similar irradiation of solutions of $Fe_2(SR)_2(NO)_4$ alone in DMF had no influence on the EPR spectra of the solvo complexes[1] $[Fe(NO)_2(DMF)_2]^+$ and $[Fe(NO)_2(DMF)(SR)]$. The complexes $[Fe(NO)_2(SR)_2]^-$ remaining after the heterometallic nitrosyls had been converted into EPR silent species appeared to be unaffected by further irradiation. When R = phenyl, the sole paramagnetic complex detectable after reaction with $[MoS_4]^{2-}$ was[2] $[Fe(NO)_2(SPh)_2]^-$: this likewise was unaffected by irradiation.

The binuclear paramagnetic dinitrosyl[1] $[Fe(NO)_2(S_2MoS_2)]^-$ is similar in stoichiometry to, but differs in redox level from, the diamagnetic di-anion[11] $[Fe(NO)_2(S_2MoS_2)]^{2-}$: this paramagnetic ion should therefore by accessible from $[Fe(NO)_2(S_2MoS_2)]^{2-}$ by mild oxidation. Reaction of a DMF solution of $(Et_4N)_2[Fe(NO)_2(S_2MoS_2)]$ with a five-fold molar excess of either $NO(BF_4)$ or $NO_2(BF_4)$ yielded an intense quintet EPR spectrum, characterized by $g = 2.027$, $A(^{14}N, 2N) = 2.0$ G, identical with that observed previously[2] in the formation of $[Fe(NO)_2(S_2MoS_2)]^-$ by reaction of $Fe_2(SR)_2(NO)_4$ with $[MoS_4]^{2-}$: thus NO^+ and NO_2^+ had effected a one-electron oxidation of the diamagnetic $[Fe(NO)_2(S_2MoS_2)]^{2-}$ to give $[Fe(NO)_2(S_2MoS_2)]^-$, eq. (3):

$$[Fe(NO)_2(S_2MoS_2)]^{2-} + NO_x^+ \rightarrow NO_x + [Fe(NO)_2(S_2MoS_2)]^-. \quad (3)$$

The trinuclear mononitrosyl[2] $[Fe(NO)(S_2MoS_2)_2]^{2-}$ is clearly related to the tri-anion[12,13] $[Fe(S_2MoS_2)_2]^{3-}$, shown by X-ray analysis[13] to contain tetrahedral iron and by magnetic susceptibility[13] and EPR[12] measurements to contain three unpaired electrons per anion. Reaction of a DMF solution of $(Et_4N)_3[Fe(S_2MoS_2)_2]$ with a five-fold molar excess of $NO(BF_4)$ yielded a very intense triplet EPR spectrum, characterized by $g = 2.024$, $A(^{14}N, 1N) = 15.0$ G, identical with that observed previously[1] in the reactions of $Fe_2(SR)_2(NO)_4$ with $[MoS_4]^{2-}$. Thus NO^+ had added to $[Fe(S_2MoS_2)_2]^{3-}$, eq. (4), so converting a tetrahedral iron complex[13] having $S = \frac{3}{2}$ into a square pyramidal iron complex[2] having $S = \frac{1}{2}$:

$$[Fe(S_2MoS_2)_2]^{3-} + NO^+ \rightarrow [Fe(NO)(S_2MoS_2)_2]^{2-}. \quad (4)$$

In $[Fe(NO)(S_2MoS_2)_2]^{2-}$, the linear Fe—N—O group (as deduced[2] from the $A(^{14}N)$ value) and the $S = \frac{1}{2}$ ground state point to a formulation containing d^7 Fe(I) coordinated by two $[MoS_4]^{2-}$ ligands: by comparison, both the X-ray data[13] and the Mössbauer spectrum[13] for $[Fe(S_2MoS_2)_2]^{3-}$ suggest a fairly high oxidation state for iron, although the electronic structure for this ion has not yet been adequately defined.

These alternative syntheses of $[Fe(NO)_2(S_2MoS_2)]^-$ and $[Fe(NO)(S_2MoS_2)_2]^{2-}$ are taken as confirmation of the constitutions derived earlier[2] from EPR data.

EXPERIMENTAL

Literature methods were used for the preparation of $Fe_2(SR)_2(NO)_4$,[2,14] $Fe_2I_2(NO)_4$,[15] $(NH_4)_2[MoS_4]$[16] and $(PPN)^+$ salts[17] [$(PPN)^+ \equiv (Ph_3PNPPh_3)^+$]; $(Et_4N)_3[Fe(S_2MoS_2)_2]$[12,13] was converted into $(Et_4N)_2[Fe(NO)_2(S_2MoS_2)]$[11] by the action of NO gas in dry DMF solution. The disodium salts of the ligands L_1 and L_2 were

prepared by standard methods[18] starting from piperazine and α,α′-dichloro-*p*-xylene, respectively. $NO(BF_4)$ and $NO_2(BF_4)$ were purchased from Aldrich and were used as received. DMF of AnalaR quality was dried over barium oxide, distilled under reduced pressure and stored under dry nitrogen. All manipulations were carried out under an atmosphere of dry nitrogen.

EPR spectra were measured in 1 mm quartz capillaries using a Bruker ER200D spectrometer with di-*t*-butyl nitroxide as the standard for the measurement of line positions. Spectral assignments were confirmed where necessary by the use of ^{15}N labelling. Photolyses were undertaken using an unfiltered medium pressure mercury-vapour lamp: experiments were generally carried out at 240 K, except where specified otherwise. ^{15}N NMR spectra were recorded using a Bruker AM-300 spectrometer, using recording conditions as previously described.[19]

REFERENCES

1. A. R. Butler, C. Glidewell, A. R. Hyde and J. C. Walton, *Polyhedron* 1985, **4**, 797.
2. A. R. Butler, C. Glidewell, I. L. Johnson and J. C. Walton, *Polyhedron* 1987, **6**, 2085.
3. A. R. Butler, C. Glidewell, A. R. Hyde and J. C. Walton, *Polyhedron* 1985, **4**, 303.
4. L. F. Dahl, E. R. de Gil and R. D. Feltham, *J. Am. Chem. Soc.* 1969, **91**, 1653.
5. V. Gutmann, *Coordination Chemistry in Non-Aqueous Solutions*. Springer, Vienna (1968).
6. L. Burlamacchi, G. Martini and E. Tiezzi, *Inorg. Chem.* 1969, **8**, 2021.
7. A. R. Butler, C. Glidewell and I. L. Johnson, *Polyhedron* 1987, **6**, 2091.
8. J. C. Fanning and L. K. Keefer, *J. Chem. Soc., Chem. Commun.* 1987, 955.
9. H. Strasdiet, B. Krebs and G. Henkel, *Z. Naturforsch.* 1986, **41b**, 1357.
10. G. R. Davies, J. A. J. Jarvis, B. T. Kilbourn, R. H. B. Mais and P. G. Owston, *J. Chem. Soc.* (*A*) 1970, 1275.
11. D. Coucouvanis, E. D. Simhon, P. Stremple and N. C. Baenziger, *Inorg. Chim. Acta* 1981, **53**, L135.
12. J. W. McDonald, G. D. Friesen and W. E. Newton, *Inorg. Chim. Acta* 1980, **46**, L79.
13. D. Coucouvanis, E. D. Simhon and N. C. Baenziger, *J. Am. Chem. Soc.* 1980, **102**, 6646.
14. A. R. Butler, C. Glidewell, A. R. Hyde, J. McGinnis and J. E. Seymour, *Polyhedron* 1983, **2**, 1045.
15. B. Haymore and R. D. Feltham, *Inorg. Synth.* 1973, **14**, 81.
16. S. H. Lawrie, D. E. Pratt and J. H. L. Young, *Inorg. Chim. Acta* 1984, **93**, L57.
17. A. Martinson and J. Songstad, *Acta Chem. Scand.* 1977, **A31**, 645.
18. Houben-Weyl, *Methoden der Organischen Chemie*, Vol. IX, p. 826, Georg Thieme, Stuttgart (1955); *Ibid*, Vol. E5, p. 914, Georg Thieme, Stuttgart (1985).
19. A. R. Butler, C. Glidewell, A. R. Hyde and J. McGinnis, *Inorg. Chem.* 1985, **24**, 2931.

Polyhedron Vol. 7, No. 15, pp. 1377–1382, 1988
Printed in Great Britain

0277–5387/88 $3.00+.00
© 1988 Pergamon Press plc

CORRELATION OF ^{31}P CHEMICAL SHIFTS AND CARBONYL STRETCHING FORCE CONSTANTS WITH SUBSTITUENT CONSTANTS FOR A SERIES OF RING-SUBSTITUTED ARENE CHROMIUM DICARBONYL TRIPHENYLPHOSPHINE COMPLEXES

THOMAS E. BITTERWOLF

Department of Chemistry, U.S. Naval Academy, Annapolis, MD 21402, U.S.A.

(*Received* 15 *October* 1987; *accepted* 1 *March* 1988)

Abstract—Fourteen mono-substituted arene chromium tricarbonyl and arene chromium dicarbonyl triphenylphosphine complexes have been prepared and characterized by IR and NMR spectroscopy. Carbonyl stretching force constants for all compounds have been calculated. Correlations of stretching forces constants of arene chromium tricarbonyl complexes with a series of substituent constants agree well with those reported in earlier studies. Similarly, both the stretching force constants and ^{31}P chemical shifts of arene chromium dicarbonyl triphenylphosphine complexes have been compared with the same series of substituent constants and were found to exhibit trends similar to those previously observed.

In our previous communications[1,2] we have demonstrated that the Taft substituent constants, σ_I and σ_R^0, and the carbonyl force constants of arene $Cr(CO)_2L$ and $CpMn(CO)_2L$ complexes vary in a regular way depending on the π acidity of the ligand L, where L is a phosphine or phosphite.

Several workers have investigated the mechanism of transmission of electron density from arene rings to a complexed metal atom or its ligands. A variety of physical parameters have been used to probe the changes in metal electron density which result from the introduction of substituents onto an arene ring. For example, carbonyl stretching frequencies and force constants, and ^{13}C NMR chemical shifts of the metal carbonyls have been measured for broad series of compounds. Senoff has exhaustively reviewed the literature on this subject up to 1979.[3] Neuse has presented a particularly thorough study of the changes in the carbonyl stretching frequencies and force constants for 28 arene chromium tricarbonyl compounds which were correlated with a set of selected substituent parameters.[4]

We have been concerned with the synthesis of a variety of arene chromium dicarbonyl phosphine compounds and have noted that the ^{31}P NMR chemical shifts appeared to be sensitive to substituents on the arene rings. A similar qualitative observation has been made by Setkina *et al.*[5] In order to determine the nature of this relationship, we have prepared a series of arene chromium dicarbonyl triphenylphosphine complexes and measured the ^1H and ^{31}P NMR chemical shifts as well as the carbonyl stretching frequencies for all compounds. The correlations between ^{31}P NMR chemical shift, carbonyl force constants and the same set of substituent constants examined by Neuse has been determined and is discussed in this communication.

RESULTS AND DISCUSSION

Fourteen mono-substituted arene chromium tricarbonyl (I) and arene chromium dicarbonyl triphenylphosphine (II) derivatives were prepared and their NMR and IR spectra recorded. In most cases it was possible to prepare good yields of the arene chromium tricarbonyl derivative by refluxing the arene with chromium hexacarbonyl in a mixture of

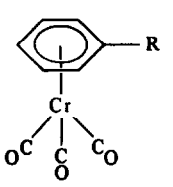

I

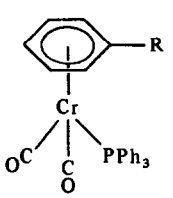

II

butyl ether and tetrahydrofuran as described by Top and Jaouen.[6] However, in the case of benzaldehyde and acetophenone, only low yields of the desired chromium complexes could be obtained. It was found that conversion of benzaldehyde and acetophenone to their dioxolane derivatives followed by metallation in the usual way gave excellent yields of the corresponding dioxolane chromium tricarbonyl derivatives which could be easily hydrolysed to the corresponding aldehyde and ketone complexes. Drefahl *et al.* adopted a similar strategy by using the diethylacetal of benzaldehyde as an intermediate in the preparation of benzaldehyde chromium tricarbonyl.[7]

Triphenylphosphine derivatives of arene chromium tricarbonyl compounds are readily prepared by photolysis in benzene.[8] Photolysis of the dioxolane chromium tricarbonyl derivatives with triphenylphosphine gave the corresponding triphenylphosphine complexes in good yield. Hydrolysis of the dioxolanes cleanly gave the aldehyde and ketone derivatives.

IR spectra were recorded for all compounds using dichloromethane as a solvent. Carbonyl stretching frequencies and stretching force constants for all compounds are recorded in Table 1. Stretching force constants for the carbonyl groups of both the arene chromium tricarbonyl and arene chromium dicarbonyl triphenylphosphine complexes were computed by using the approximations developed by Cotton and Kraihanzel.[9] IR stretching force constants for the arene chromium tricarbonyl derivatives agree very well with those reported by Neuse for the same solvent and are slightly lower than those reported by van Meurs *et al.* for isooctane solutions.[10]

Substitution of a triphenylphosphine for a carbonyl group resulted in a shift of the carbonyl stretching frequencies to lower energy, consistent with the reduced π acidity of the triphenylphosphine relative to carbonyl. The reduction in force constant upon introduction of the phosphine is highly uniform, averaging 0.879 mdyne A^{-1} with a standard deviation of about 4.3%. Carbonyl stretching frequencies and force constants are presented in Table 1.

^{1}H, ^{19}F and ^{31}P NMR spectra, as appropriate, were recorded for these compounds and were consistent with reported values. ^{31}P NMR chemical shifts are reported in Table 1. Other spectral parameters for new compounds are presented in the Experimental. Arene ring proton chemical shifts are affected only slightly when phosphine is substituted for carbonyl, while the chemical shifts of substituent methyl groups (Me, *t*-Bu, OMe, NMe_2, $SiMe_3$) are shifted downfield. ^{19}F NMR chemical shifts of the trifluoromethyl group also move to lower field [99.94 ppm for $CF_3C_6H_5Cr(CO)_3$ to 100.90 for $CF_3C_6H_5Cr(CO)_2P(C_6H_5)_3$] upon introduction of the phosphine.

Fletcher and McGlinchey have reported the ^{19}F chemical shifts of a series of *m*- and *p*-substituted fluorobenzene chromium tricarbonyl derivatives.[11] The effect of these substituents upon the chemical shifts of the fluorine was correlated using Swain–Lupton field and resonance parameters with elec-

Table 1. IR[a] and ^{31}P[b] spectral data and force constants[c]

X	$XC_6H_5Cr(CO)_3$				$XC_6H_5Cr(CO)_2P(C_6H_5)_3$				^{31}P
	A	E	k	k_i	A_1	B_1	k	k_i	
H	1973	1892	14.88	0.4218	1892	1833	14.19	0.4394	90.93
CH_3	1971	1892	14.87	0.4208	1887	1828	13.94	0.4448	91.68
$C(CH_3)_3$	1966	1887	14.79	0.4092	1883	1824	13.88	0.4466	91.90
OCH_3	1972	1892	14.87	0.4158	1886	1827	13.92	0.4385	91.90
$N(CH_3)_2$	1955	1867	14.53	0.4510	1869	1806	13.64	0.4671	93.47
$Si(CH_3)_3$	1968	1891	14.84	0.3985	1888	1833	13.98	0.4094	91.30
F	1982	1907	15.08	0.3897	1903	1847	14.19	0.4411	88.93
Cl	1981	1907	15.07	0.3847	1904	1845	14.22	0.4162	88.54
Br	1972	1897	14.92	0.3944	1892	1835	14.03	0.4320	88.31
$COCH_3$	1983	1913	15.15	0.3675	1908	1854	14.29	0.4108	86.36
CHO	1988	1919	15.23	0.3605	1917	1861	14.41	0.4269	84.85
CO_2CH_3	1983	1913	15.15	0.3675	1908	1854	14.29	0.4108	86.65
C_6H_5	1970	1893	14.87	0.4021	1889	1834	14.00	0.4157	90.58
CF_3	1988	1914	15.18	0.3908	1914	1860	14.38	0.4117	85.88

[a] Solvent CH_2Cl_2, carbonyl stretching frequencies in cm^{-1}.
[b] 85% H_3PO_4 reference, $CDCl_3$ solvent.
[c] Force constants in mdyn $Å^{-1}$.

tron donating groups being found to cause an upfield shift of the ^{19}F resonance. In this work, the upfield shift of the ^{19}F resonances resulting from substitution of a phosphine for a carbonyl [29.50 ppm for $FC_6H_5Cr(CO)_3$ and 22.55 ppm for $FC_6H_5Cr(CO)_2P(C_6H_5)_3$] is found to be roughly equivalent to the effect of placing a strongly resonance donating group, such as a methoxy or an amine, in a *para* position relative to the fluorine.

^{31}P chemical shifts were recorded and were found to be dependent upon the ring substituents as was suggested by our qualitative observations. Electron donating ring substituents cause a downfield shift of the phosphine resonance while electron withdrawing groups shift the resonance upfield. ^{31}P chemical shifts show a good correlation ($r = 0.946$) with the carbonyl stretching force constants indicating that ring substituents are exerting a proportional effect on both groups.

Following Neuse, we have examined the correlations of k(CO) arene chromium tricarbonyl, k(CO) arene chromium dicarbonyl triphenylphosphine and ^{31}P chemical shifts with several sets of substituent constants, Table 2, to determine the nature of the interaction between the metal ligands and the ring substituents. The six sets of substituent constants which were examined include σ^n, σ_p^0, σ_m, σ_p, σ_I and σ_R^0. The σ^n and σ_p^0 series are closely related and measure the effects of arene substituents on reaction centres which are isolated from the arene ring by a methylene group.[12,13] By isolating the arene ring, direct conjugation of the substituent with the reaction centre is precluded so that the observed constants reflect the total electron density changes in the ring resulting from the substituent. The σ_m and σ_p constants are traditional Hammett constants as measured by Brown and are based on the ionization of substituted benzoic acids.[14] Direct conjugation of *para* substituents such as amine and methoxy with the reaction centre will result in "exalted" substituent constants for these groups. σ_I and σ_R^0 constants have been developed by Taft and others to separate the inductive and resonance contributions of substituents.[15–17] As in the case of the σ^n and σ_p^0 constants described above, these values should be free of direct conjugation effects.

The two sets of stretching force constants and the set of ^{31}P chemical shifts were examined for correlations with all six sets of substituent constants. The resulting correlations, Table 3, substantially parallel those reported by Neuse and show that these three sets of data are best correlated by those constants which measure both the inductive and resonance contributions, i.e. σ^n and σ_p^0, of the substituents. The poor correlations for σ_I and σ_R^0 constants confirm that the substituent effect is not a simple inductive or resonance phenomenon. k(CO) arene chromium tricarbonyl and k(CO) arene chromium dicarbonyl triphenylphosphine were found to have almost identical slopes when compared to the σ_n and σ_p^0 constants. The aldehyde derivatives were found to yield data which were very far out of line with the remaining values. It is not clear whether the failure of aldehyde to conform is due to solvent effects or to intermolecular interactions between the aldehyde and the chromium atom.

The correlations presented in this work and in our previous paper illustrate the remarkably uniform interrelationships between the physical constants of these arene chromium tricarbonyl and

Table 2. Substituent constants

X	σ^n	σ_p^0	σ_m	σ_p	σ_I	σ_R^0
H	0.00	0.00	0.00	0.00	0.00	0.00
CH_3	−0.10	−0.124	−0.069	−0.170	−0.08	−0.146
$C(CH_3)_3$	−0.14	−0.174	−0.10	−0.197	—	−0.13
OCH_3	−0.09	−0.100	0.115	−0.268	0.25	−0.43
$N(CH_3)_2$	−0.24	−0.48	—	−0.83	0.10	−0.54
$Si(CH_3)_3$	—	—	−0.04	−0.07	—	0.00
F	0.18	0.212	0.337	0.062	0.52	−0.32
Cl	0.29	0.281	0.371	0.227	0.47	−0.18
Br	0.30	0.296	0.391	0.232	0.44	−0.16
$COCH_3$	0.502	0.502	0.376	0.502	0.28	0.19
CHO	0.43	0.53	—	—	0.25	—
CO_2CH_3	0.46	0.46	0.37[a]	0.45[a]	0.31[a]	0.15
C_6H_5	0.06	0.039	0.06	−0.01	0.08	−0.093
CF_3	0.53	0.505	0.43	0.54	0.41	0.13

[a] Literature values are for $CO_2C_2H_5$.

Table 3. Summary of linear regression analyses[a]

(a) Comparison of $XC_6H_5Cr(CO)_3$ carbonyl force constants with various substituent constants and $XC_6H_5Cr(CO)_2(C_6H_5)_3P$ carbonyl force constants

Sub. Const. Set	Slope (m)	Intercept (b)	Correlation
σ^n	1.24	−18.39	0.908
σ_p^0	0.596	14.88	0.959
σ_m	1.31	−19.42	0.883
σ_p	1.93	−28.75	0.943
σ_I	0.539	−7.82	0.553
σ_R^0	0.801	−12.08	0.668
k(CO)	0.924	0.236	0.901
k(CO)[b]	1.112	−2.55	0.988

(b) Comparison of $XC_6H_5Cr(CO)_2(C_6H_5)_3P$ carbonyl force constants with various substituent constants

Sub. Const. Set	Slope (m)	Intercept (b)	Correlation
σ^n	1.17	−16.33	0.890
σ^{nb}	1.18	−16.40	0.934
σ_p^0	0.576	13.78	0.895
σ_p^{0b}	0.664	−13.99	0.963
σ_m	1.06	−14.71	0.853
σ_p	1.73	−24.31	0.953
σ_I	0.564	−7.69	0.599
σ_R^0	0.762	−10.84	0.713

(c) Comparison of ^{31}P chemical shifts with various substituent constants and carbonyl force constants

Sub. Const. Set	Slope (m)	Intercept (b)	Correlation
σ^n	−0.105	9.56	0.934
σ_n^b	−0.107	9.73	0.996
σ_p^0	−0.144	10.3	0.979
σ_p^{0b}	−1.22	11.02	0.985
σ_m	−0.084	7.69	0.908
σ_p	−0.145	13.0	0.947
σ_I	−0.0521	4.91	0.646
σ_R^0	−0.0652	5.72	0.730
k(CO)	−7.96	21.20	0.946
k(CO)[b]	−7.97	21.21	0.947

[a] Data sets calculated without aldehyde derivative included.

[b] Data are presented for the relationship: $y = mx + b$. Linear regression calculations were performed using standard statistical methods. The correlation coefficient R is reflective of "goodness-of-fit" where $R = 1.0$ for a perfect straight line.

arene chromium dicarbonyl triphenylphosphine compounds. Using the carbonyl force constants as a reference, it would appear that the contributions of the phosphine and ring substituents can be treated as separate, additive quantities so that

$$\delta k(\text{CO}) = \delta k(\text{substituent}) + \delta k(\text{ligand}).$$

If this simple relationship holds for other sets of organometallic compounds, then it might be possible to determine the δ contributions for a series of ligands and substituents on different metal complexes and use these δ values as a measure of the sensitivity of a metal complex to electron donation or withdrawal.

EXPERIMENTAL

IR spectra were recorded on a Perkin–Elmer Model 1750 FT/IR spectrophotometer. NMR spectra were recorded on a Varian Associates FT80A NMR spectrometer. HPLC analysis of all compounds and reaction mixtures was conducted on a GOW-MAC Model 080-20 HPLC using a silica gel column and 3/7 THF/petroleum ether as the elutant.

Chromium hexacarbonyl was purchased from Strem. Dioxobenzaldehyde and dioxoacetophenone were prepared by literature procedures.[18] Substituted arene chromium tricarbonyl and arene chromium dicarbonyl triphenylphosphine complexes were generally prepared by literature procedures, $XC_6H_5Cr(CO)_3$: X = H,[19] CH_3,[19] CH_3O,[19] CH_3CO,[19] CH_3O_2C,[19] $(CH_3)_2N$,[19] $(CH_3)_3C$,[19] C_6H_5,[20] FC_6H_4,[21,22] ClC_6H_4,[19,22] BrC_6H_4,[23] CHO,[7] $(CH_3)_3Si$,[24] CF_3.[24] $XC_6H_5Cr(CO)_2P(C_6H_5)_3$: X = H,[5], CH_3,[25] CH_3O,[5] CH_3CO,[26] CH_3O_2C,[27] $(CH_3)_2N$,[5] $(CH_3)_3C$,[25] C_6H_5.[5] Spectral and physical properties of these compounds were compared with those reported in the literature and were consistent in all cases.

Exceptions to these procedures are described below. Photolysis reactions were conducted in an Ace doubly-jacketed photolysis vessel with a quartz inner vessel using a Hanovia medium-pressure mercury lamp. Microanalysis was conducted by Galbraith Laboratories of Knoxville, TN. All reactions were conducted under nitrogen.

Synthesis of dioxolane benzeldehyde chromium tricarbonyl

A 500 cm^3 round bottom flask outfitted with a spin bar was charged with $Cr(CO)_6$, 8.80 g (40.0 mmol) and dioxobenzeldehyde, 7.0 g (46.7 mmol). The flask was flushed with nitrogen and dibutylether (260 cm^3) and THF (30 cm^3) were added under nitrogen. The flask was outfitted with a reflux condenser and the reaction mixture refluxed for two days. The reaction mixture was filtered, reduced in volume to about 50 cm^3 and 50 cm^3 of petroleum ether was added to precipitate 9.0 g of dioxobenzaldehyde chromium tricarbonyl as a yellow powder, m.p. 70–73°C. IR: (CH_2Cl_2) 1973, 1896. ^1H NMR: ($CDCl_3$) 5.56–5.22 (m, aromatic protons), 4.17–3.98 (m, ethylene protons). Yield: 79%. Found: C, 50.2; H, 3.8. Calc. for $C_{12}H_{10}O_5Cr$: C, 49.7; H, 3.4%.

The known benzaldehyde chromium tricarbonyl can be formed from dioxobenzaldehyde chromium tricarbonyl in quantitative yield by brief reaction of the former with *p*-toluenesulphonic acid in acetone. The reaction mixture was stripped of solvent and the resulting oily residue was chromatographed on alumina using methylene chloride as an eluant. Benzaldehyde chromium tricarbonyl is recovered as a red oil.

Synthesis of dioxoacetophenone chromium tricarbonyl

In a reaction analogous to that described above for dioxobenzaldehyde, $Cr(CO)_6$, 4.40 g (20 mmol) and dioxoacetobenzene, 4.0 g (24.3 mmol), were reacted in butyl ether/THF. After removal of the reaction solvent the blue–yellow residue was taken up in hot benzene and filtered through Celite. The benzene solution was concentrated to about 5 cm^3 and petroleum ether added to precipitate 1.6 g of dioxoacetobenzene chromium tricarbonyl as a yellow crystalline solid, m.p. 87–89°C. Yield: 27%. ^1H NMR: ($CDCl_3$) 5.72–5.41 (m, 5H), 4.08 (s, 4H), 1.60 (s, 3H). Found: C, 51.9; H, 4.4. Calc. for $C_{13}H_{12}O_5Cr$: C, 51.3; H, 3.9%.

Synthesis of arene chromium dicarbonyl triphenylphoshine derivatives

In a typical reaction, 0.5 g of arene chromium tricarbonyl was photolysed overnight with a 10% molar excess of triphenylphosphine in benzene (200 cm^3) at 12°C. Photolyses were conducted in an Ace Hanovia reaction vessel equipped with a water-jacketed quartz cold finger and a water-jacketed reaction vessel. Nitrogen was bubbled through the reaction mixture throughout the photolysis. After photolysis the reaction mixture was reduced in volume to about 10 cm^3 and filtered through Celite. Addition of petroleum ether gave the desired products in 40–50% yield. Products could be further purified by recrystallization from benzene.

Data for new compounds

Fluorobenzene. Orange crystalline solid, m.p. 188–190°C. Yield: 83%. ^1H NMR: ($CDCl_3$) 7.59–6.98 (m, 15H), 4.26–3.77 (m, 5H). ^{19}F NMR: ($CDCl_3$) 22.56 (m). Found: C, 67.2; H, 4.7; P, 7.1. Calc. for $C_{26}H_{20}FCrO_2P$: C, 66.9; H, 4.3; P, 6.6%.

Chlorobenzene. Yellow–orange crystals, m.p. 186–190°C. Yield: 72%. ^1H NMR: ($CDCl_3$) 7.58–6.99 (m, 15H), 4.44–4.13 (m, 5H). Found: C, 64.7; H, 4.6; P, 6.8. Calc. for $C_{26}H_{20}ClCrO_2P$: C, 64.7; H, 4.1; P. 6.4%.

Bromobenzene. Orange plates, m.p. 168–170°C. ^1H NMR: ($CDCl_3$) 7.57–6.99 (m, 15H), 4.45 (m, 2H), 4.05 (m, 3H). Found: C, 59.0; H, 3.7; P, 5.7. Calc. for $C_{26}H_{20}BrCrO_2P$: C, 59.2; H, 3.8; P, 5.9%.

Trifluoromethylbenzene. Orange crystals, m.p. 195–198°C. Yield: 38%. ^{1}H NMR: ($CDCl_3$) 7.50–7.00 (m, 15H), 4.71 (m, 2H), 4.06 (m, 3H). ^{19}F NMR: ($CDCl_3$) 100.90 (m). Found: C, 62.8; H, 4.2; P, 6.2. Calc. for $C_{27}H_{20}F_3CrO_2P$: C, 62.8; H, 3.9; P, 6.0%.

Dioxolanebenzaldehyde. Orange crystals, m.p. 135–137°C. IR: ($CHCl_3$) 1901, 1835. ^{1}H NMR: ($CDCl_3$) 7.63–7.00 (m, 15H), 5.65 (s, 1H), 4.89 (d, 2H), 4.25 (m, 3H), 3.50 (m, 4H). ^{31}P NMR: ($CDCl_3$) 90.07 ppm. Found: C, 66.5; H, 5.0; P, 5.2. Calc. for $C_{29}H_{25}CrO_4P$: C, 66.9; H, 4.8; P, 5.9%.

Benzaldehyde. Orange crystals, m.p. 134–137°C. IR: (CH_2Cl_2) 1917, 1861, 1437 (CHO). ^{1}H NMR: ($CDCl_3$) 9.04 (s, 1H), 7.49–7.03 (m, 15H), 5.09 (d, 2H), 4.30 (t, 1H), 4.09 (t, 2H). Found: C, 68.1; H, 4.6. Calc. for $C_{27}H_{21}CrO_3P$: C, 68.1; H, 4.4%.

Dioxolaneacetophenone. Orange crystals, m.p. 128–131°C. IR: ($CHCl_3$) 1893, 1833. ^{1}H NMR: (C_6D_6) 7.65–7.02 (m, 15H), 5.26 (m, 5H), 4.18–3.99 (m, 4H), 1.64 (s, 3H). ^{31}P NMR: ($CDCl_3$) 90.75 ppm. Found: C, 67.4; H, 5.3; P, 5.1. Calc. for $C_{30}H_{27}CrO_4P$: C, 66.9; H, 5.0; P, 5.8%.

Trimethylsilylbenzene. Orange crystals, m.p. 178–182°C, ^{1}H NMR: ($CDCl_3$) 7.64–7.06 (m, 15H), 4.83 (d, 2H), 4.23 (m, 3H), 0.29 (s, 9H). Yield: 59%. Found: C, 66.3; H, 6.0; P, 6.1. Calc. for $C_{29}H_{29}SiCrO_2P$: C, 66.9; H, 5.6; P, 6.0%.

Acknowledgements—We wish to thank the Research Corporation and the Naval Academy Research Council for their continued support of this research.

REFERENCES

1. T. E. Bitterwolf, *Polyhedron* 1983, **2**, 675.
2. T. E. Bitterwolf, *Polyhedron* 1988, **7**, 409.
3. C. V. Senoff, *Coord. Chem. Rev.* 1980, **32**, 111.
4. E. W. Neuse, *J. Organometal. Chem.* 1975, **99**, 287.
5. L. A. Fedorov, P. V. Petrovskii, E. I. Fedin, G. A. Panosyan, A. A. Tsoi, N. K. Baranetskaya and V. N. Setkina, *J. Organometal. Chem.* 1979, **182**, 499.
6. S. Top and G. Jaouen, *J. Organometal. Chem.* 1979, **182**, 381.
7. G. Drefahl, H.-H. Horhold and K. Kuhne, *Chem. Ber.* 1965, **98**, 1826.
8. W. Strohmeier and H. Hellmann, *Chem. Ber.* 1963, **96**, 2859.
9. F. A. Cotton and C. S. Kraihanzel, *J. Am. Chem. Soc.* 1962, **84**, 4432.
10. F. van Meurs, J. M. A. Baas and H. van Bekkum, *J. Organometal. Chem.* 1976, **113**, 353.
11. J. L. Fletcher and M. J. McGlinchey, *Can. J. Chem.* 1975, **53**, 1525.
12. Y. Yukawa, Y. Tsuno and M. Sawada, *Bull. Chem. Soc. Japan* 1972, **45**, 1198.
13. A. J. Hoefnagel and B. M. Wepster, *J. Am. Chem. Soc.* 1973, **95**, 5357.
14. D. H. McDaniel and H. C. Brown, *J. Org. Chem.* 1958, **23**, 420.
15. R. W. Taft, Jr., N. C. Deno and P. S. Skell, *Ann. Rev. Phys. Chem.* 1958, **9**, 287.
16. R. W. Taft, E. Price, I. R. Fox, I. C. Lewis, K. K. Andersen and G. T. Davis, *J. Am. Chem. Soc.* 1963, **85**, 709.
17. R. W. Taft, E. Price, I. R. Fox, I. C. Lewis, K. K. Andersen and G. T. Davis, *J. Am. Chem. Soc.* 1963, **85**, 3146.
18. T. W. Greene, *Protective Groups in Organic Synthesis*, p. 124. Wiley, New York (1981).
19. B. Nicholls and M. C. Whiting, *Proc. Chem. Soc.* 1958, 152; B. Nicholls and M. C. Whiting, *J. Chem. Soc.* 1959, 551.
20. E. O. Fischer, N. Kriebitzsch and R. D. Fischer, *Chem. Ber.* 1959, **92**, 3214.
21. R. D. Fischer, *Chem. Ber.* 1960, **93**, 165.
22. A. C. Knipe, S. J. McGuinness and W. E. Watts, *J. Chem. Soc., Perkin II* 1981, 193.
23. K. Ofele, *Chem. Ber.* 1966, **99**, 1732.
24. F. van Meurs, J. M. van der Toorn and H. van Beekum, *J. Organometal. Chem.* 1976, **113**, 341.
25. W. R. Jackson, C. F. Pincombe, I. D. Rae, D. Rash and B. Wilkinson, *Aust. J. Chem.* 1976, **29**, 2431.
26. B. Boyer, G. Lamaty, B. Caro and G. Jaouen, *J. Organometal. Chem.* 1981, **216**, C51.
27. G. Jaouen and R. Dabard, *J. Organometal. Chem.* 1973, **61**, C36; G. Jaouen and R. Dabard, *J. Organometal. Chem.* 1974, **72**, 377.

Polyhedron Vol. 7, No. 15, pp. 1383–1388, 1988
Printed in Great Britain

0277–5387/88 $3.00+.00
Pergamon Press plc

CRYSTAL STRUCTURE AND PROPERTIES OF THE $[Cu(C_{11}H_{10}N_4)Br_2]$ COMPOUND. STEREOCHEMISTRY OF [Cu(PLANAR TRIDENTATE LIGAND)(UNIDENTATE LIGAND)$_2$] COMPLEXES

JOSE L. MESA, MARIA I. ARRIORTUA, LUIS LEZAMA, JOSE L. PIZARRO, TEOFILO ROJO* and DANIEL BELTRAN†

Departamentos de Química(Inorgánica) y Cristalografía-Mineralogía, Facultad de Ciencias, Universidad del País Vasco, Apartado 644, 48080 Bilbao, Spain

(*Received* 6 *January* 1988; *accepted* 1 *March* 1988)

Abstract—The crystal structure of the dibromo(pyridine-2-aldehyde 2′-pyridylhydrazone) copper(II) is reported. The compound crystallizes in space group $P2_1/n$, with a = 12.86(2), b = 11.944(5), c = 8.770(7) Å, β = 97.17(6)°, U = 1336(3) Å^3, Z = 4, D_m = 2.06(1), D_x = 2.10 g cm^{-3}, μ(Mo-K_α) = 78.92 mm^{-1}, $F(000)$ = 812, T = 293 K. Final R is 0.047 (R_w = 0.049) for 854 observed reflections. The structure consists of discrete molecules in which the copper(II) ion is pentacoordinate with a distorted square pyramidal geometry. The spectroscopic data are in good agreement with the structural results. The stereochemistry of several pentacoordinate complexes of type [Cu(planar tridentate ligand)(unidentate ligand)$_2$] is examined and the distortions of the coordination polyhedra are calculated.

Polydentate ligands, particularly with terdentate arrangements, can be prepared by condensing primary amines or hydrazines derived from pyridine or benzopyridine with aldehydes derived from similar starting materials. One of these ligands is the pyridine-2-aldehyde 2′-pyridylhydrazone ($C_{11}H_{10}N_4$, hereinafter paphy), whose tridentate nature was confirmed by Gerloch[1] when determining the crystal structure of [Co(paphy)Cl$_2$]. As far as we are aware, it is the only known structure of this ligand with a transition metal.

The ligand paphy forms two types of complexes when it reacts with one bivalent transition metal in a ratio of 1 : 1, [M(paphy)X$_2$] and [M(paphy)X]Y (X = halide; Y = PF_6, BPh_4). The former leads to discrete monomeric molecules, while the latter produces polynuclear species in which the X atom acts as a bridging ligand, causing magnetic interactions.[2,3]

In order to facilitate the interpretation of the physical properties of these compounds and to corroborate the predictions made by the various theories on the pentacoordinated transition metal complexes, we decided to study [Cu(paphy)Br$_2$]. This compound has been utilized as a precursor in the synthesis of a polynuclear complex (ladder-like chain).[3]

RESULTS AND DISCUSSION

The structure consists of monomeric molecules. The copper(II) ions are pentacoordinated by three nitrogens [N(1), N(2), N(3)] of the tridentate paphy molecule and the two bromine ions. The results of the single crystal X-ray diffraction study are summarized in Table 1.

Figures 1 and 2 show the [Cu(paphy)Br$_2$] molecules with the numbering system and the packing in the unit cell, respectively.

The geometry of the coordination polyhedron is better described as square pyramidal, although the influence of the rigid tridentate paphy ligand leads to deviations. Angles N(2)—Cu—N(1), N(3) [average value 78.6(9)°] deviate from 90° by about 12°, and the Cu—N(2) bond length is smaller than Cu—N(1), N(3). On the other hand, the apical bond

* Author to whom correspondence should be addressed.
† Present address: Departamento de Química Inorgánica, Facultad de Ciencias Químicas, Universidad de Valencia, 46100 Burjassot, Valencia, Spain.

Table 1. Some selected bond distances (Å), angles (°) and esds (in parentheses) of the [Cu(paphy)Br_2] complex

Cu—Br(1)	2.37(5)	Cu—Br(2)	2.62(6)
Cu—N(1)	2.03(4)	Cu—N(2)	1.98(2)
Cu—N(3)	2.01(5)	N(1)—C(1)	1.36(5)
N(1)—C(5)	1.38(3)	N(2)—C(6)	1.30(2)
N(2)—N(4)	1.35(5)	N(4)—C(7)	1.39(3)
N(3)—C(7)	1.34(2)	N(3)—C(11)	1.39(3)

Br(2)—Cu—N(1)	93.9(3)
Br(2)—Cu—N(2)	93.8(3)
Br(2)—Cu—N(3)	96.7(3)
Br(2)—Cu—Br(1)	103.2(9)
N(1)—Cu—N(3)	155.4(4)
N(2)—Cu—Br(1)	163.0(3)
N(1)—Cu—Br(1)	98.7(3)
N(1)—Cu—N(2)	79.2(5)
N(2)—Cu—N(3)	78.0(5)
N(3)—Cu—Br(1)	100.4(3)
C(1)—N(1)—C(5)	119(1)
N(1)—C(1)—C(2)	122(1)
N(1)—C(5)—C(4)	120(1)
C(7)—N(3)—C(11)	118(1)
N(3)—C(7)—C(8)	126(1)
N(3)—C(11)—C(10)	120(1)
N(1)—C(5)—C(6)	116(1)
C(5)—C(6)—N(2)	111(1)
Cu—N(2)—C(6)	103.4(4)
Cu—N(1)—C(5)	113.3(9)
Cu—N(1)—C(1)	127.4(9)
N(3)—C(7)—N(4)	117(1)
C(7)—N(4)—N(2)	112(1)
N(4)—N(2)—Cu	107.7(4)
Cu—N(3)—C(7)	114.3(7)
N(4)—C(7)—C(8)	117(1)
Cu—N(3)—C(11)	127.0(9)
N(4)—N(2)—C(6)	122(1)

length Cu—Br(2) [2.62(6) Å] is appreciably longer than the equatorial bond length Cu—Br(1) [2.37(5) Å]. Values obtained for both bond distances and angles in the paphy ligand are in good agreement with those given in the literature.[1,4]

The powder EPR spectrum of the complex shows a clear resolution of the g tensor in parallel and perpendicular components at room temperature ($g_\parallel = 2.23_3$, $g_\perp = 2.05_7$, $\bar{g} = 2.11_6$). This result is not modified at 125 K ($g_\parallel = 2.23_0$, $g_\perp = 2.05_8$, $\bar{g} = 2.11_5$). The trend of g values ($g_\parallel > g_\perp > g_0$) is indicative of a $d_{x^2-y^2}$ ground state for the [CuN_3Br_2] chromophore.[5]

In the visible region, the complex exhibits an unsymmetrical broad band centred at 14000 cm^{-1}. We tentatively assign this band to the non-resolved transitions $B_1 \rightarrow B_2$, E ($\Delta_\parallel, \Delta_\perp$) in C_{4v} symmetry. Based on this assumption, it is possible to estimate the covalence factor from the orbital contributions using the expressions: $g_\parallel = g_z = g_0 + 8u_\parallel$ and $g_\perp = g_x = g_y = g_0 + 2u_\perp$ (were $u_i = K_i^2\lambda_0/\Delta_i$ and $i = \parallel, \perp$; $\lambda_0 = 829$ cm^{-1}).[5] The value obtained, $K = 0.70$ is in good agreement with the analogous chloro-complexes of 2,2′ : 6′, 2″-terpyridine.[5]

The coordination polyhedron around the copper atom in this type of compound has been described as "distorted square pyramidal" or "distorted trigonal bipyramidal". However, these geometries are better described as regular square pyramidal (SP_r) and "tetrahedral or trigonal distorted square pyramidal" (SP_{th} and SP_{tr}, respectively) as Hathaway has pointed out.[6]

We have quantified the distortion of the coordination polyhedron of these complexes of the type [Cu(planar tridentate ligand)(unidentate ligand)$_2$] using the Muetterties and Guggenberger description[7] and by considering the regular square pyramid (SP_r) and the ideal trigonal bipyramid (TBP) as the limiting geometries. The dihedral angles and the deviation (Δ) from TBP for the ideal geometries and the title compound ($\Delta = 0.73$) are given in Table 2. The value obtained for this compound shows a topology close to the regular square pyramid (SP_r). The deviations (Δ) for the other pentacoordinate complexes are given in Table 3.

The stereochemistry of these compounds has also been examined using Kepert's model,[8-10] based on an interligand repulsion approach. The variation of angular coordinates Φ_X vs Φ_X, for the title compound, the other pentacoordinate complexes (Table 3) and the ideal geometries is displayed in Fig. 3. [Φ_X is defined as the angle between the Cu—X(unidentate ligand) and the axis perpendicular to the plane of the tridentate ligand.]

Similar results are obtained with both models. As expected, the title compound and most of the other complexes possess a topology very near to regular square pyramid (SP_r). Notwithstanding, the compound numbers 9, 10 and 11 show an unusual geometry ("reverse geometry" $\overline{SP_r}$) that may alternatively be looked at as the intermediate between two elongated square pyramids, in which the apical positions are alternatively occupied by one of the two unidentate ligands.[11]

EXPERIMENTAL

Synthesis

The [Cu(paphy)Br_2] compound has been synthesized by reaction of paphy (0.20 g, 1.01 mmol) with copper(II) bromide (0.23 g, 1.01 mmol) in ethanolic solution. Green single crystals were obtained by evaporation at room temperature of an aqueous solution containing the resulting

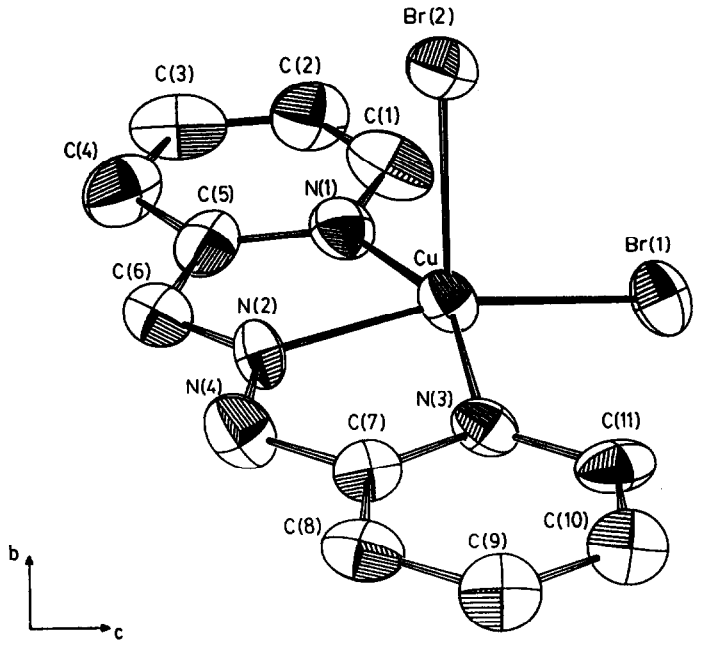

Fig. 1. Molecular structure of the $[Cu(paphy)Br_2]$ complex showing the atom numbering.

compound. Found: C, 31.6; H, 2.1; N, 13.5. $[Cu(C_{11}H_{10}N_4)Br_2]$ requires: C, 31.3; H, 2.4; N, 13.3%.

Crystal structure determination

Crystal ($0.08 \times 0.15 \times 0.22$ mm). Weissenberg photographs, monoclinic, Laue class $2/m$. Phillips PW-1100 four-circle diffractometer; Mo-K_α radiation, graphite monochromator, $\lambda = 0.71069$ Å, ω–2θ scan. The cell parameters were obtained by least squares refinement of 25 reflections ($3° < \theta < 15°$).

Crystal data. $[Cu(C_{11}H_{10}N_4)Br_2]$, $M = 421.6$, $P2_1/n$, $a = 12.86(2)$, $b = 11.944(5)$, $c = 8.770(7)$ Å, $\beta = 97.17(6)°$, $U = 1336(3)$ Å^3, $Z = 4$, $D_m = 2.06(1)$, $D_x = 2.10$ g cm^{-3}, μ(Mo-K_α) = 78.92 mm^{-1}, $F(000) = 812$. The density was measured by flotation in a bromoform/acetone mixture.

2158 unique reflections measured, 854 observed reflections [$I > 2.0\sigma(I)$], $h -10 \rightarrow 10$, $k0 \rightarrow 9$, $l0 \rightarrow 5$, $\theta_{max} = 25°$. Three standard reflections measured after every hour of X-ray exposure showed no significant intensity fluctuation. Intensities were corrected for Lorentz polarization, but not for absorption. The atomic coordinates of $[Co(paphy)Cl_2]$ published by Gerloch[1] were used as starting values for the crystal structure refinement. Final least-squares refinement of all non-H atoms were

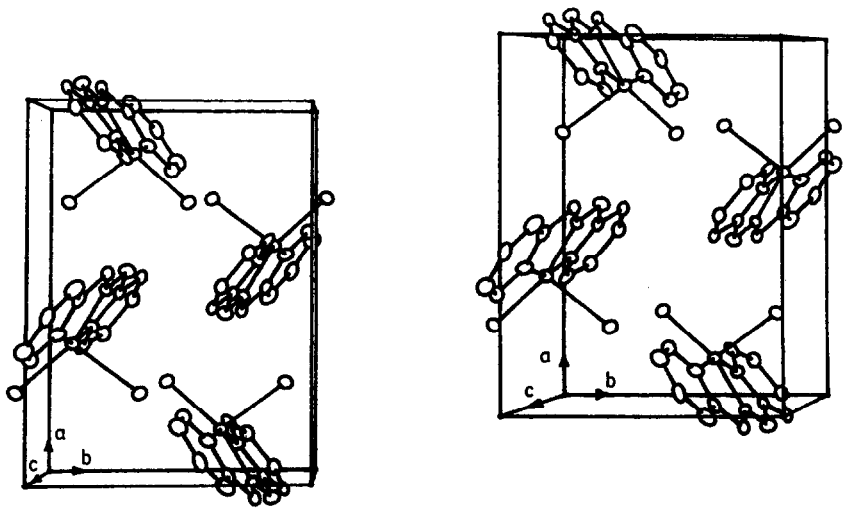

Fig. 2. Packing of the $[Cu(paphy)Br_2]$ molecules in the unit cell.

Table 2. Dihedral angles (°) and distortion of the coordination polyhedron for the [Cu(paphy)Br_2] compound and for the ideal geometries[a]

Designation	TBP	SP_{th}	SP_{tr}	[Cu(paphy)Br_2]	SP_r
δa_1	101.5	106.4	109.9	112.2	121.8
δa_3	101.5	106.4	109.9	115.2	121.8
δa_4	101.5	106.4	109.9	113.7	121.8
δa_6	101.5	106.4	109.9	116.4	121.8
δa_2	101.5	93.0	88.0	89.9	73.9
δa_5	101.5	93.0	88.0	78.4	73.9
δe_1	53.1	55.5	64.1	77.4	73.9
δe_2	53.1	55.5	64.1	67.8	73.9
δe_3	53.1	46.6	28.7	5.6	0
Δ	0	0.22	0.46	0.73	1

$$\Delta = \left|\frac{(\delta a_1+\delta a_3+\delta a_4+\delta a_6)-406.0}{182.7}\right| + \left|\frac{(\delta a_2+\delta a_5)-203.0}{248.4}\right| + \left|\frac{(\delta e_1+\delta e_2)-106.2}{187.2}\right| + \left|\frac{(53.1-\delta e_3)}{477.9}\right|.$$

[a] TBP = trigonal bipyramid; SP_{th} = tetrahedral distorted square pyramid; SP_{tr} = trigonal distorted square pyramid; SP_r = regular square pyramid.

treated anisotropically with SHELX 76[18] yielded $R = 0.047$ ($R_w = 0.049$) (function minimized: $\Sigma w[|F_o|-|F_c|]^2/\Sigma[|F_o|]^{1/2}$ with $w = 3.1285[\sigma^2|F_o|+0.000480|F_o|^2]^{-1}$). The atomic scattering factors were taken from ref. 19. The atomic coordinates of this work are available on request from the Editor and have also been deposited with the Cambridge Crystallographic Data Centre.

Physical measurements

A Brucker ER 200tt spectrometer equipped with a standard low-temperature device, operating at X-

Table 3. Angular coordinates and deviation (Δ) from TBP for several five-coordinate complexes of the type [Cu(planar tridentate ligand)(unidentate ligand)$_2$][a]

No.	Compound	Chromophore	Φ_X (°)	XCuX′ (°)	$\Phi_{X'}$ (°)	Δ	Stereochemistry	Ref.
1	[Cu(terpy)Cl](PF_6)	CuN_3Cl,Cl	102.1	90.1	12.0	0.81	SP_r	12
2	[Cu(terpy)Br](PF_6)	CuN_3Br,Br	106.3	91.4	14.9	0.75	SP_r	13
3	[Cu(terpy)(CN)](NO_3)·H_2O	CuN_3C,N	113.3	98.8	14.5	0.75	SP_r	14
4	[Cu(terpy)(ONO)(H_2O)](NO_2)·H_2O	CuN_3OO	91.4	83.9	7.5	0.74	SP_r	15
5	[Cu(terpy)Cl_2]·H_2O	CuN_3Cl_2	107.6	100.9	6.7	0.74	SP_r	16
6	[Cu(paphy)Br_2]	CuN_3Br_2	112.0	103.2	8.8	0.73	SP_r	This work
7	[Cu(paphy)Cl](PF_6)·H_2O	CuN_3Cl,Cl	110.5	103.2	7.3	0.70	SP_r	3
8	[Cu(terpy)Cl_2]	CuN_3Cl_2	115.2	104.5	10.7	0.68	SP_r	5
9	[Cu(terpy)(tda)]	CuN_3O_2	135.9	91.9	44.0	0.34	$\overline{SP}_r$	17
10	[Cu(terpy)$(NCS)_2$]	CuN_3N_2	139.1	98.1	41.0	0.30	$\overline{SP}_r$	11
11	[Cu(terpy)Br_2]	CuN_3Br_2	144.5	109.0	35.5	0.21	$\overline{SP}_r$	11

[a] Abbreviations: terpy = 2,2′:6′,2″-terpyridine; paphy = pyridin-2-aldehyde 2′-pyridilhydrazone; tda = thiodiacetate. Φ_X is the angular coordinate defined as the angle between the Cu—X(unidentate ligand) bond and the axis perpendicular to the tridentate ligand plane. XCuX′ is the angle between the unidentate ligands and the copper(II) ion. SP_r = regular square pyramid; $\overline{SP}_r$ = "reverse geometry".

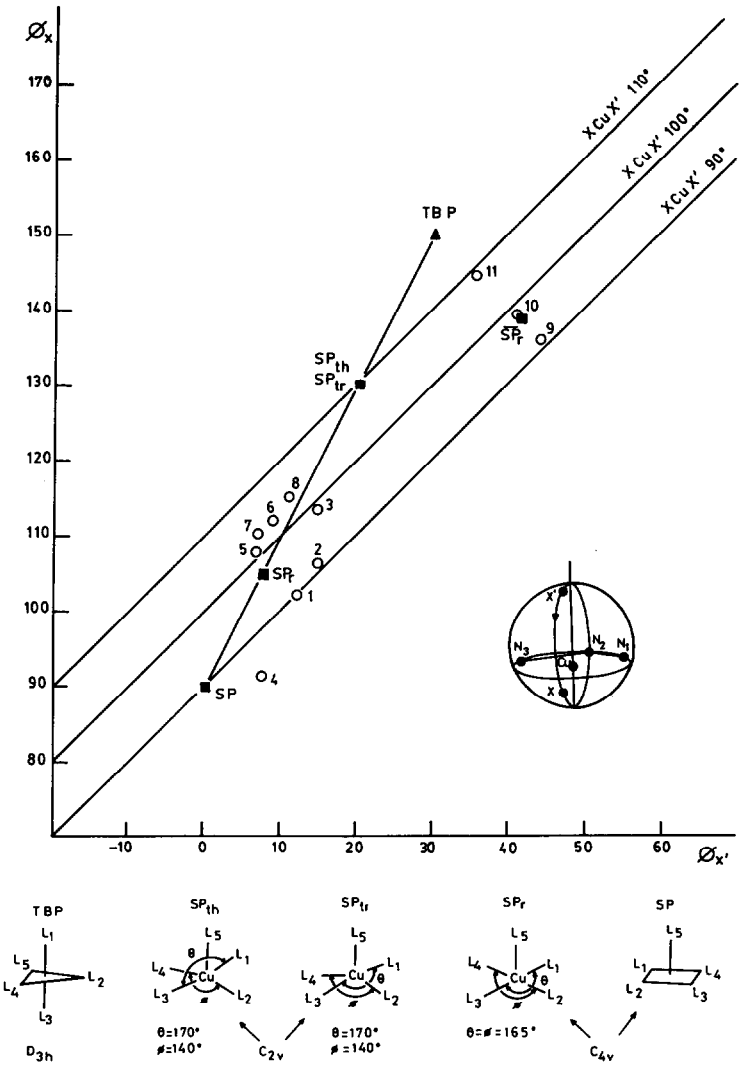

Fig. 3. Angular coordinates for molecules of the type [Cu(planar tridentate ligand)(unidentate ligand)$_2$] and for the ideal geometries.

band, calibrated by NMR probe for the magnetic field and a HP 5342A frequency counter for the microwave frequency, was used to record the EPR powder spectra of the complex at different temperatures. Visible reflectance spectra on solid powdered samples were recorded using a Cary 17 spectrometer.

Acknowledgements—This work was supported in part by grant 2930/83 from the CAICYT, which we gratefully acknowledge. J.L.M. thanks the M.E.C. for a FPI fellowship.

REFERENCES

1. M. Gerloch, *J. Chem. Soc. A* 1966, 1317.
2. J. L. Mesa, PhD thesis, University of Basque Country (1987).
3. J. L. Mesa, T. Rojo, M. I. Arriortua, J. M. Savariault, J. Galy, G. Villeneuve and D. Beltran, *Inorg. Chem.*, submitted.
4. E. Barianak, R. St. L. Bruce, H. C. Freeman, N. J. Hair and J. James, *Inorg. Chem.* 1976, **15**, 2226.
5. W. Henke, S. Kramer and D. Reinen, *Inorg. Chem.* 1983, **22**, 2858.
6. B. J. Hathaway, *Coord. Chem. Rev.* 1982, **41**, 423.
7. E. L. Muetterties and L. J. Guggenberger, *J. Am. Chem. Soc.* 1974, 1748.
8. M. C. Favas and D. L. Kepert, *Prog. Inorg. Chem.* 1980, **27**, 325.
9. D. L. Kepert, E. S. Kucharski and A. H. White, *J. Chem. Soc., Dalton Trans.* 1980, 1932.
10. D. L. Kepert, *Inorg. Chem. Concept* 1982, **6**, 1.
11. M. I. Arriortua, J. L. Mesa, T. Rojo, T. Debaerdemaeker, H. Stratemeier, D. Reinen and D. Beltran, *Inorg. Chem.*, in press.

12. T. Rojo, M. I. Arriortua, J. Darriet, G. Villeneuve, D. Beltran and J. Ruiz, *J. Chem. Soc., Dalton Trans.* 1987, 285.
13. T. Rojo, M. I. Arriortua, J. L. Mesa, R. Cortes, G. Villeneuve and D. Beltran, *Inorg. Chim. Acta* 1987, **134**, 59.
14. O. P. Anderson, A. B. Packard and M. Wicholas, *Inorg. Chem.* 1976, **15**, 1613.
15. R. Allmann, S. Kremer and D. Kucharzcyk, *Inorg. Chim. Acta* 1984, **85**, L19.
16. T. Rojo, M. Vlasse and D. Beltran, *Acta Cryst.* 1983, **C39**, 194.
17. R. P. Bonomo, E. Rizzarelli, N. Bresciani-Pahor and G. Nardin, *J. Chem. Soc., Dalton Trans.* 1982, 681.
18. G. M. Sheldrick, SHELX 76. Program for crystal structure determination. University of Cambridge, U.K. (1976).
19. *International Tables for X-ray Crystallography*, Vol. 4. Kynoch Press, Birmingham (1974).

Polyhedron Vol. 7, No. 15, pp. 1389–1391, 1988
Printed in Great Britain

0277–5387/88 $3.00+.00
© 1988 Pergamon Press plc

SYNTHESIS OF NEW BIMETALLIC [Al(III), Mg(II)]-μ-OXOISOPROPOXIDE AND ITS β-DIKETONE DERIVATIVES

HARISH K. SHARMA and PRAMESH N. KAPOOR*

Department of Chemistry, University of Delhi, Delhi-110007, India

(*Received* 18 *December* 1987; *accepted after revision* 1 *March* 1988)

Abstract—A new bimetallic-μ-oxoisopropoxide [$MgO_2Al_2(OPr^i)_4$] has been synthesized by thermal condensation of magnesium acetate (1 mol) and aluminium isopropoxide (2 mol) in refluxing decalin. The isopropoxy substitution reaction of this bimetallic [Al(III), Mg(II)]-μ-oxoisopropoxide with various β-diketones in molar ratios 1:1, 1:2 and 1:3 yielded compounds of the type [$MgO_2Al_2(OPr^i)_3(L)$], [$MgO_2Al_2(OPr^i)_2(L)_2$] and [$MgO_2Al_2(OPr^i)(L)_3$], respectively; where HL = HAcAc (acetyl acetone), HBzAc (benzoyl acetone) and HThTFA(2-thenoyl trifluoroacetone). The μ-oxo compound and its derivatives were characterized on the basis of elemental analysis, IR, ^{1}H NMR, ^{27}Al NMR and molecular weight measurements.

Metal alkoxides often provide molecular models for metal oxides.[1,2] Recently molybdenum and tungsten alkoxides in their middle oxidation states have been used as a model for the reductive cleavage of carbon monoxide to carbides and oxides via the Fischer–Tropsch reaction.[3] It has also been shown that the several atoms linked together by μ-oxo bridges possess polynuclear catalytic sites and are highly active in polymerization reactions.[4,5] A number of bimetallic-μ-oxoalkoxides possessing properties of metal alkoxides and having μ-oxo bridges of the type $(RO)_2$—Al—O—M(II)—O—Al—$(OR)_2$ where M = Cr, Co, Fe, Mn, Mo and Zn and R an alkyl group (most often propyl or butyl) have been reported.[6,7] Teyssie *et al.*[8–14] have made systematic studies on the catalytical application of these bimetallic-μ-oxoalkoxide and have shown that these compounds rank among the best catalysts in the ring opening polymerization of heterocyclic compounds like thiiranes, oxiranes and lactones. These compounds have also proved to be good catalysts in the insertion polymerization at epoxides.[6]

Since these bimetallic-μ-oxoalkoxides are highly soluble in most organic solvents and are excellent catalysts it was considered of interest to synthesize new bimetallic-μ-oxoisopropoxide using an alkaline earth metal namely magnesium in place of the transition metal. Keeping in mind their interesting properties, it was thought worthwhile to determine the structural aspects, arrangement of metal atoms and the effect of changing the isopropoxy groups on the solubility and molecularity. Therefore their isopropoxy substitution reactions with chelating β-diketones were carried out in different molar ratios.

EXPERIMENTAL

The experimental techniques and physical measurements were carried out as previously described. Isopropanol was estimated oxidimetrically using a 1N $K_2Cr_2O_7$ solution in 12.5% sulphuric acid.[15,16] Aluminium was determined gravimetrically as aluminium oxinate[17] and magnesium was estimated volumetrically using EDTA.[17]

Molecular weight measurements of bimetallic [Al(III), Mg(II)]-μ-oxoisopropoxide and its derivatives were determined in dry benzene by the cryoscopic method (depression in freezing point). The IR spectra were recorded on a Perkin–Elmer 1710(FT) spectrometer as direct film. The PMR spectra were recorded on a Jeol JNM FX 200(FT) spectrometer in $CDCl_3$ and ^{27}Al NMR was recorded on Varian FT-80 spectrometer using $AlCl_3 \cdot 6H_2O$ as a reference.

Preparation of bimetallic[Al(III), Mg(II)]-μ-*oxoisopropoxide*

The bimetallic [Al(III), Mg(II)]-μ-oxoisopropoxide was prepared by refluxing two moles of

* Author to whom correspondence should be addressed.

aluminium isopropoxide (6.77 g, 33.14 mmol) and one mole of magnesium acetate (2.36 g, 16.57 mmol) in decalin for 8 h on a fractionating column. The isopropyl acetate formed in the reaction was fractionated continuously from 80°C until the temperature rose to the boiling point of decalin (190°C). The reaction was then continued at this temperature for 1 h to ensure its completion. The excess of decalin was distilled at 40–50°C/1 mm, leaving behind a yellow solid which was dissolved in benzene. Slow evaporation of benzene gave a pale yellow glassy solid (dec. > 300°C). Yield 95%. Found: OPr^i, 67.9; Mg, 6.9; Al, 15.2. Calc: OPr^i, 68.2; Mg, 7.0; Al, 15.6%.

Reaction of bimetallic [Al(III), Mg(II)]-*μ-oxoisopropoxide with acetyl acetone* (H · AcAc) *in a molar ratio of* 1 : 1

$[MgO_2Al_2(OPr^i)_4]$ (0.45 g, 1.29 mmol) and H · AcAc (0.13 g, 1.30 mmol) were refluxed in (~ 60 cm^3) benzene for $3\frac{1}{2}$ h on an oil bath (temperature of ~ 100°C) with a fractionating column. The liberated isopropanol was fractionated at 72–78°C as the binary azeotrope of isopropanol–benzene. The azeotrope was collected and checked for completion of the reaction. The excess of solvent was removed at 40°C/1 mm and a light yellow solid product was obtained. The preparations of other β-diketones derivatives were carried out by a similar procedure and their metal analysis have been summarized in Table 1.

RESULT AND DISCUSSION

The bimetallic [Al(III), Mg(II)]-μ-oxoisopropoxide was prepared by the following reaction.

$$Mg(OAc)_2 + 2Al(OPr^i)_3 \xrightarrow[\text{decalin}]{\text{Refluxing}} [MgO_2Al_2(OPr^i)_4] + 2CH_3COOC_3H_7\uparrow.$$

The compound is soluble in most organic solvents and is highly susceptible to hydrolysis. In the IR spectra of the compound, the ν_{C-O} frequency appearing at 1630 cm^{-1} in $Mg(OAc)_2$ is absent indicating the removal of the acetyl group. The band appearing at 1340 cm^{-1} in the compound is characteristic of the *gem*-dimethyl of the isopropoxy group.[18] The bands at 1156 and 1120 cm^{-1} are the isobranching vibrations[18] of the isopropoxy moiety and the one appearing at 950 cm^{-1} is assignable to the ν_{C-O} isopropoxy bridging group.[19] The bands appearing in the region 420–450 cm^{-1} may be assigned to ν_{Al-O}[20] and those appearing in the region 650–700 cm^{-1} to the combination bands like ($\nu_{C-CH_3} + \nu_{Al-O}$) and (ring deformation + ν_{Al-O}), respectively.[20]

The ^1H NMR of the compound carried out at room temperature shows a broad overlapping doublet centred at δ 1.2 ppm probably due to the methyl protons of the overlapping bridging and non-bridging isopropoxy groups, and a multiplet centred at δ 4.2 ppm due to the methine protons of the isopropoxy groups. The ^{27}Al NMR shows a

Table 1. Analytical data

Sl. No.	Compound	Analysis Found (Calc.) Mg (%)	Al (%)
1.	$[MgO_2Al_2(OPr^i)_3(AcAc)]$	6.2 (6.3)	13.7 (14.0)
2.	$[MgO_2Al_2(OPr^i)_2(AcAc)_2]$	5.7 (5.7)	12.6 (12.7)
3.	$[MgO_2Al_2(OPr^i)(AcAc)_3]$	5.3 (5.2)	11.1 (11.6)
4.	$[MgO_2Al_2(OPr^i)_3(BzAc)]$	5.1 (5.4)	12.0 (12.0)
5.	$[MgO_2Al_2(OPr^i)_2(BzAc)_2]$	4.4 (4.4)	9.6 (9.8)
6.	$[MgO_2Al_2(OPr^i)(BzAc)_3]$	3.7 (3.7)	8.1 (8.3)
7.	$[MgO_2Al_2(OPr^i)_3(ThTFA)]$	4.8 (4.8)	10.4 (10.2)
8.	$[MgO_2Al_2(OPr^i)_2(ThTFA)_2]$	3.5 (3.6)	8.0 (8.1)
9.	$[MgO_2Al_2(OPr^i)(ThTFA)_3]$	2.7 (2.9)	6.2 (6.5)

singlet at δ 65 ppm assignable to tetrahedral geometry about the aluminium atom.[21] The dimeric nature of the compound was confirmed by molecular weight measurements carried out in dry benzene using the cryoscopic method. The β-diketone derivatives of the bimetallic [Al(III), Mg(II)]-μ-oxoisopropoxide were prepared by the following equation

$$[MgO_2Al_2(OPr^i)_4] + nLH \xrightarrow[\text{benzene}]{\text{Refluxing}} [MgO_2Al_2(OPr^i)_{4-n}(L)_n] + nPr^iOH$$

where (n = 1–3) and LH = H·AcAc, H·BzAc and H·ThTFA. All the derivatives obtained were pale yellow solids, soluble in common organic solvents and are highly susceptible to hydrolysis. It has been observed that, of the four isopropoxy groups per molecule only three could be replaced even after carrying out the 1 : 4 (molar ratio) reaction for over 30 h. The molecular weight measurements of the derivatives indicate that the 1 : 1 and 1 : 2 products are dimeric and the 1 : 3 is monomeric. The non-replacement of the fourth isopropoxy group and the monomeric behaviour of the 1 : 3 product can be explained by the fact that bimetallic μ-oxo-alkoxides are reported to have inter- and intramolecular isopropoxy bridging.[7] In the case of $[MgO_2Al_2(OPr^i)_4]$ the intermolecular bridging appears to be less stable compared to the intramolecular isopropoxy bridging which forms a stable six-membered ring structure; hence 1 : 1 and 1 : 2 products are dimeric whereas the 1 : 3 reaction proceeds by cleavage of the intermolecular isopropoxy bridge, resulting in a monomeric product.

The IR spectra of β-diketones display a strong band in the region 1600–1500 cm^{-1} due to the stretching of C=O and C=C ring groups and a broad band in the region 3200–2900 cm^{-1} due to the enolic O—H. The non-shifting of the carbonyl frequency and the disappearance of the broad O—H band in the β-diketonate derivative of the compound suggest that bonding is taking place through both terminal oxygens of the carbonyl groups. The IR spectra of these derivatives thus show that β-diketones behave as monobasic bidentate ligands as expected.

In the ^1H NMR spectra of the compounds the enolic peak at δ 13 ppm is absent and a broad overlapping doublet centred at δ 1.2 ppm in the β-diketone derivative at room temperature is due to overlapping of the methyl protons of the bridging and non-bridging isopropoxy groups. In the case of the 1 : 2 and 1 : 3 derivatives, a fairly sharp doublet centred at δ 1.3 ppm (J = 6.6 Hz) and a multiplet centred at δ 4.3 ppm are due to the bridging isopropoxy groups and singlets at δ 2.1 and 5.8 ppm are assignable to the acetyl acetonate groups. A multiplet in the region δ 7.2–7.8 ppm has been assigned to the phenyl protons of the benzoyl acetonate derivatives and signals appearing in the region δ 7.0–7.8 ppm in the 2-thenoyl trifluoroacetone derivatives are due to the thenoyl ring protons.

Acknowledgements—We are thankful to the U.G.C. for providing financial assistance and to Dr S. K. Mehrotra of the University of Texas at Austin for ^{27}Al NMR spectral studies.

REFERENCES

1. D. C. Bradley, *Coord. Chem. Rev.* 1967, **2**, 299.
2. M. H. Chisholm, *Am. Chem. Soc. Symp. Ser.* 1983, **211**, 243; M. H. Chisholm, *J. Solid State Chem.* 1985, **57**, 120.
3. M. H. Chisholm, *J. Organomet. Chem.* 1987, **334**, 77.
4. E. J. Vadenberg, *J. Polymer Sci.* 1960, **47**, 149.
5. H. Tani, O. N. Oguni, T. Araki and N. Uejama, *J. Am. Chem. Soc.* 1967, **89**, 173.
6. M. Osgan and Ph. Teyssie, *J. Polymer Sci.* (*B*) 1967, **5**, 789.
7. T. Ouhadi, J. P. Bioul, Ch. Stevens, R. Warin, L. Hocks and Ph. Teyssie, *Inorg. Chim. Acta* 1976, **19**, 203.
8. A. Hamitou, R. Jerome, A. J. Hubert and Ph. Teyssie, *Macromolecules* 1973, **6**, 651.
9. T. Ouhadi, A. Hamitou, R. Jerome and Ph. Teyssie, *Macromolecules* 1976, **9**, 927.
10. A. Hamitou, T. Ouhadi, R. Jerome and Ph. Teyssie, *J. Polymer Sci., Polymer Chem. Ed.* 1977, **15**, 865.
11. L. Hocks, J. P. Bioul, P. Durbut, A. Hamitou, J. L. Marbehant, T. Ouhadi, Ch. Stevens and Ph. Teyssie, *J. Mol. Catal.* 1977, **3**, 135.
12. A. Hamitou, R. Jerome and Ph. Teyssie, *J. Polymer Sci., Polymer Chem. Ed.* 1977, **15**, 1035.
13. Ph. Teyssie, J. P. Bioul, P. Conde, J. Druet, J. Heuschen and R. Jerome, *Am. Chem. Soc. Symp. Ser.* 1985, **286**, 97.
14. J. Heuschen, R. Jerome and Ph. Teyssie, *Macromolecules* 1981, **14**, 242.
15. D. C. Bradley, F. M. A. Halim and W. Wardlaw, *J. Chem. Soc.* 1950, 3450.
16. R. C. Mehrotra, *J. Ind. Chem. Soc.* 1954, **31**, 185.
17. A. I. Vogel, *Quantitative Inorganic Chemistry*, 4th Edn. Longmans Green, London (1978).
18. C. T. Lynch, K. S. Masdiyanni, J. S. Smith and W. J. Grawford, *Anal. Chem.* 1964, **36**, 2332.
19. V. A. Kuzunov, N. I. Kuzlova, N. Ya. Tarnova and Yu. S. Nekrasov, *Zh. Neorg. Khim.* 1979, **24**, 1526.
20. K. Nakamoto, P. J. McCarthy, A. Ruby and A. E. Martell, *J. Am. Chem. Soc.* 1961, **83**, 1066.
21. D. Mueller, D. Hoebbel and W. Gessner, *Chem. Phys. Lett.* 1981, **84**, 25.

Polyhedron Vol. 7, No. 15, pp. 1393–1396, 1988
Printed in Great Britain

0277–5387/88 $3.00+.00
© 1988 Pergamon Press plc

KINETICS OF REPLACEMENT OF BRIDGING LIGANDS IN A DIRUTHENIUM(II,III) CATION

MARIA EVERHART and JOSEPH E. EARLEY*

Department of Chemistry, Georgetown University, Washington, DC 20057, U.S.A.

(*Received* 23 *November* 1987; *accepted* 10 *March* 1988)

Abstract—Tetrakis-μ-propionatodiruthenium(II,III) cation reacts with oxalate, in acidic aqueous solution (0.10 M $LiCF_3SO_3$, $[H^+] = 0.01$ M at 29.4°C) in a two-phase process. An initial rapid change results in a small decrease in absorbance. This is ascribed to replacement of one propionate ligand by oxalate. A subsequent slower reaction, of which the rate is proportional to added oxalate concentration ($k_{bi} = 1.3\ M^{-1}\ s^{-1}$), corresponds to a relatively large increase of absorbance at 475 nm, the absorbance maximum of the product. The data indicate formation of a bis(μ-oxalato)bis(μ-propionato)diruthenium(II,III) anion with a formation constant $K_f > 2 \times 10^4\ M^{-1}$ and an extinction coefficient of $1.3 \times 10^3\ M^{-1}\ cm^{-1}$ at 475 nm. A third, much slower, change results in decomposition of that product. The occurrence of replacement of bridging ligands under mild conditions indicates that tris-μ-carboxylatodiruthenium(II,III) species (otherwise unknown) function as kinetic intermediates.

There have been many recent studies[1] dealing with structure and bonding in species such as $Ru_2(CH_3COO)_4(H_2O)_2^+$. Much of the interest in this and related compounds has centred on the detailed nature of the metal–metal bond. Enthalpies of reactions in which a number of Lewis bases (acetone, tetrahydrothiophene, acetonitrile, pyridine, etc.) formed adducts with tetrakis-μ-*n*-butyratodiruthenium(II,III) chloride have been measured and interpreted in terms of models of the metal–metal bond. That bond strongly influences the electronic orbitals involved in bonding with bases added in axial positions on the dimer.[2] We previously reported[3] that an oxalate ion replaces bridging acetate in $Ru_2(CH_3COO)_4(H_2O)_2^+$ to form $Ru_2(CH_3COO)_2(C_2O_4)_2(H_2O)_2^-$. Preparation of dimeric $Ru^{II,II}$ species containing a variety of ligands have recently been reported[4] as have additional $Ru^{II,III}$ species.[5,6] Also, a $Rh^{II,III}$ dimer containing two carboxylate bridges and two bridging triphenylphosphine ligands (coordinating through the phosphorus atom and a phenyl ring) has been reported.[7]

We now report the first kinetic study of replacement of bridging carboxylate ligands in a $Ru^{II,III}$ dimer. Replacement of the equatorial bridging ligands (studied here) is a quite different process than the previously-investigated[2] adduct-formation involving axial coordination. The axial ligands are relatively weakly bonded to the dimer and their replacement is of only minor significance to the integrity of the dimeric unit. In contrast, presence of the equatorial ligands is necessary for the preservation of the dimeric unit. We are not aware of any previously-existing evidence to indicate that dimeric mixed-valence compounds lacking one of the four bridging ligands are stable. Our observation that substitution reactions involving the equatorial ligands occur under mild conditions without disruption of the dimer unit was unexpected.

EXPERIMENTAL

The method of Mitchell, Spencer and Wilkinson for preparation of tetra-μ-acetatodiruthenium(II,III) chloride[8] was modified by using propionic acid (and propionic anhydride) rather than acetic acid (and acetic anhydride). A dark red–brown product was obtained in good yield. This salt was recrystallized from hot, concentrated propionic

* Author to whom correspondence should be addressed.

acid and then from a 50/50 ethanol–ether mixture and dried over $CaCl_2$. The UV–vis spectrum of this compound in acidic aqueous solution is quite similar to that of the corresponding tetrakis-μ-acetatodiruthenium(II,III) salt, showing an absorbance maximum at 425 nm ($\varepsilon = 6.4 \times 10^2$ M^{-1} cm^{-1}). Characterization of this product as tetrakis-μ-propionatodiruthenium(II,III) chloride is based on the method of preparation, the spectrum and on elemental analysis. Found[9]: Ru, 37.24; C, 26.77; O, 24.91; Cl, 6.49; H, 3.95. Calc. for $Ru_2(C_2H_5COO)_4Cl$: Ru, 38.14; C, 27.20; O, 24.16; Cl, 6.69; H, 3.80%.

Tetrakis-μ-propionatodiruthenium(II,III) chloride was dissolved in dilute acidic solution (0.13 g in 250 cm^3 of 8×10^{-2} mM CF_3SO_3H) to produce a yellow-orange solution which was frozen until used.

In preliminary experiments, oxalic acid solutions were added to aliquots of thawed solution of the tetrakis-μ-propionatodiruthenium(II,III) cation in perchlorate medium (0.01 M $HClO_4$, 0.10 M $LiClO_4$, 30.9°C). A change in colour of the solution from yellow–orange to red occurred over a period of several days. UV–vis spectra showed a new peak developing at 475 nm. This peak became more intense than the 425 nm peak. Eventually, the intensity of the peak at 475 nm began to decrease.

Solutions of tetrakis-μ-propionatodiruthenium (II,III) cation and various total added oxalate-ion concentrations (2–12 mM) were prepared in trifluoromethane sulphonate medium and placed in a water bath at 29.4°C. Spectra were monitored over a period of several days. The solutions were prepared, using HCF_3SO_3 and $LiCF_3SO_3$, so as to yield a final $[H^+]$ of 0.010 M and ionic strength of 0.10 M. Account was taken of oxalate acid–base equilibria, using[10] 0.09 and 4×10^{-4} M for K_1 and K_2.

The change of absorbance with time for these solutions was followed at 475 nm. An initial period of little absorbance-change was followed by a relatively fast, large increase in absorbance, giving sigmoidal absorbance vs time plots. Eventually an additional, much slower, absorbance-increase occurred.

RESULTS

Fitting the data required two exponential terms and a linear term;

$$A = (A_0 - A_1)e^{-k't} + (A_1 - A_2)e^{-k_2 t} + k''t + A_2, \quad (1)$$

where A_0, A_1 and A_2 are absorbance parameters, k' and k are rate constants, and k'' is the slope of the final (linear) absorbance-increase. Initial estimates of the parameters were obtained by appropriate linear least-squares treatments of sections of the data. Data were then displayed on a CRT and compared with the simulation that resulted from substitution of the initial parameters into eq. (1). Parameters were adjusted until agreement between data and simulation was within experimental scatter. Table 1 contains final parameters thus obtained.

Table 1. Kinetic data for reaction[a] of oxalate ion with $Ru_2(CH_3CH_2COO)_4^+$ in $CF_3SO_3^-$ media of ionic strength 0.10 M and $[H^+]$ 0.010 M at 29.4°C

$[C_2O_4^{2-}]$, mM Total	Free	A_0	A_1	A_2	$k' \times 10^3$ s^{-1}	$k \times 10^3$ s^{-1}	$k'' \times 10^2$ s^{-1}	k_{bi} M^{-1} s^{-1}
4.30	0.052	0.08	0.02	0.28	67	7.7	1.7	1.48
5.00	0.062	0.07	0.03	0.36	133	7.0	7.7	1.13
5.23	0.064	0.07	0.03	0.28	67	9.7	1.4	1.52
6.00	0.075	0.06	0.02	0.34	67	8.3	8.0	1.11
7.00	0.087	0.07	0.01	0.33	83	10.5	8.0	1.21
7.25	0.091	0.08	0.02	0.28	110	13.7	1.3	1.15
8.00	0.100	0.08	0.02	0.33	100	10.8	7.6	1.08
8.24	0.103	0.05	0.02	0.27	200	13.3	0.7	1.29
9.00	0.112	0.07	0.02	0.31	67	17.3	9.5	1.54
9.25	0.115	0.08	0.04	0.28	200	14.7	5.0	1.28
10.00	0.125	0.07	0.03	0.33	200	19.0	9.0	1.52
10.25	0.127	0.07	0.03	0.29	167	17.3	4.0	1.36
11.00	0.137	0.06	0.03	0.31	167	21.0	8.0	1.53
11.09	0.141	0.07	0.02	0.28	200	16.7	3.6	1.18
							Ave:	1.34 ± 0.15

[a] $[Ru_2(CH_3CH_2COO)_4^+] = 0.24$ mM.

Absorbance at 475 nm decreases slightly in the first portion of the reaction. In the second portion, absorbance at 475 nm increases to a value approximately 15 times greater than that reached in the first part. Absorbance parameters (A_0, A_1, A_2) needed for best fits of data did not change in a systematic way over the range of oxalate concentrations used.

Rate constants of the two faster processes varied with total oxalate concentration. Both rate constants increase with increasing oxalate concentration. The rate for the second process is linearly dependent on oxalate concentration (either total or free) with a slope of 1.3 M^{-1} s^{-1} (with respect to free oxalate concentration). Rates of the final slow increase in absorbance show no trend with variation of oxalate concentration.

DISCUSSION

Since previous attempts to prepare crystals of $Ru_2(CH_3COO)_2(C_2O_4)_2^-$ salts were unsuccessful, we chose to work with corresponding tetrapropionato-complexes as starting materials. Our attempts to prepare crystals of $Ru_2(C_2H_5COO)_2(C_2O_4)_2^-$ salts were also not successful, but our kinetic data are consistent with, and support, previous non-kinetic assignments of composition.

The straightforward interpretation of our data is that there is a two-stage reaction of the starting material with oxalate ion, followed by a slow decomposition. In perchlorate media the final process corresponds to slight decrease of absorbance; in trifluoromethylsulphonate media, a corresponding change involves a small absorbance-increase.

The spectrum of tetrakis-μ-propionatodiruthenium(II,III) does not change in the absence of oxalate ion. The first step in the observed reaction is taken to involve addition of oxalate. This leads to a product which has an extinction coefficient (at 475 nm) that is about two-thirds of that of the starting material. The initial change in absorbance is relatively small, so that the rate constant can be estimated only with a low degree of precision. During the second step, the spectrum changes more drastically. The rate constant of the second step is measurable rather precisely and turns out to be linearly dependent on free oxalate concentration. This dependence indicates that an additional oxalate ligand is being added to the product formed in the first step. Experiments were carried out at constant acid concentration; we have no evidence as to the relative activity of $H_2C_2O_4$, $HC_2O_4^-$ or $C_2O_4^{2-}$. At $[H^+] = 0.01$ M, about one per cent of the added oxalate is present as $C_2O_4^{2-}$. Previous studies[11,12] of substitution of oxalate on to transition metal ions have shown that such reactions generally involve $C_2O_4^{2-}$ rather than protonated forms of oxalate. It is likely that most, if not all, of the reaction involves $C_2O_4^{2-}$ as the nucleophile.

A stoichiometry that is consistent with our data is:

$$H^+ + Ru_2(CH_3CH_2COO)_4^+ + C_2O_4^{2-} \underset{k_2}{\overset{k_1}{\rightleftharpoons}} Ru_2(CH_3CH_2COO)_3(C_2O_4) + CH_3CH_2COOH \quad (2)$$

$$H^+ + Ru_2(CH_3CH_2COO)_3(C_2O_4) + C_2O_4^{2-} \underset{k_4}{\overset{k_3}{\rightleftharpoons}} [Ru_2(CH_3CH_2COO)_2(C_2O_4)_2]^- + CH_3CH_2COOH \quad (3)$$

$$[Ru_2(CH_3CH_2COO)_2(C_2O_4)_2]^2 \xrightarrow{k_5} Ru(C_2O_4)_3^{3-} + \text{other products.} \quad (4)$$

Our data are consistent with characterization[3] (based on IR spectra) of the solid obtained from the reaction of oxalate with tetrakis-μ-acetatodiruthenium(II,III) as a salt of bis(μ-oxalato) bis(μ-acetato)diruthenium(II,III) anion.

Since the absorbance parameters corresponding to each of the three absorbing species show no tendency to increase with increasing oxalate concentration, the reaction between oxalate and the tetrakis-μ-propionatodiruthenium(II,III) cation must be at least 90% complete at the lowest concentration of oxalate used in this study. On this basis, the extinction coefficient (at 475 nm) for the product of the second step, is calculated to be 1.3×10^3 M^{-1} cm^{-1}. This is greater than the corresponding value for the 425 nm peak characteristic of the starting material ($\varepsilon = 6.4 \times 10^2$ M^{-1} cm^{-1}). The lowest concentration of total oxalate is 4.23 mM, which corresponds to a free oxalate concentration of 0.052 mM. The equilibrium constant for the second step of this reaction [eq. (3)] must be greater than 1.9×10^4 M^{-1} s^{-1}. The second order rate constant for the second process ($k_{bi} = 1.3$ M^{-1} s^{-1}) may be identified with k_3 in eq. (3).

The high value of the equilibrium constant and the substantial increase in the extinction coefficient of the 475 nm peak that accompanies addition of the second oxalate ligand (a small decrease corresponding to the addition of the first oxalate) indicated that the substitution of one acetate group by an oxalate ion has a relatively minor affect on the chromophore, but that replacement of the second oxalate makes a substantial change in the chro-

mophore. One way that this could come about would be by substantial delocalization of electrons, involving interaction between *two* oxalates and the diruthenium(II,III) bonding-manifold, in the product of reaction (3), which would be facilitated if the oxalate ligands were *trans* in that product.[13]

There are no reports known to us of stable tris-μ-carboxylatodiruthenium(II,III) complexes in which one bridging carboxylate group has been replaced by non-bridging ligands. Nevertheless, the fact that the reactions reported here occur at measurable rates in room temperature aqueous media indicates that such species function effectively as kinetic intermediates. Substitution reactions of monomeric Ru^{III} species appear to involve largely dissociative mechanisms.[12] In order to preserve the integrity of the dimer, it seems that oxalate must be attached to the dimer unit before the initially bridging acetate is completely lost. Such a mechanism might involve either associative activation of the opening of the bridge or relatively-rapid dissociatively activated bridge-opening that normally is reversed, but sometimes is interrupted by insertion of entering oxalate. In any case, high thermodynamic stability of the quadruply bridged mixed-valence dimer evidently does not preclude reaction through kinetic intermediates having a lower number of carboxylate bridges.

REFERENCES

1. A. R. Chakravarty, *Proc. Indian Natl. Sci. Acad., Part A* 1986, **52**, 749.
2. R. S. Drago, R. Cosmano and J. Telser, *Inorg. Chem.* 1984, **23**, 4514.
3. R. N. Bose, P. A. Wagner and J. E. Earley, *Inorg. Chem.* 1984, **23**, 774.
4. A. J. Lindsay, G. Wilkinson, M. Montevalli and M. B. Harsthouse, *J. Chem. Soc., Dalton Trans* 1985, 2321.
5. A. N. Chakravarty, F. A. Cotton and W. Schwotzer, *Polyhedron* 1986, **5**, 1821.
6. F. N. Feldman, *Diss, Abstr. Int. B.* 1986, **46**, 1554.
7. A. R. Chakravarty, F. A. Cotton, D. A. Tocher and J. H. Tocher, *Organometallics* 1985, **4**, 8.
8. R. W. Mitchell, A. Spencer and G. Wilkinson, *J. Chem. Soc., Dalton Trans.* 1973, 846.
9. Elemental Analysis by Galbraith Laboratories, Knoxville, TN. Oxygen was determined at 950°C by the Perkin–Elmer 240 Elemental Analyser and may not include all the inorganic oxygen.
10. E. G. Moorehead and N. Sutin, *Inorg. Chem.* 1981, **20**, 3569.
11. P. Chaudhuri and H. Diebler, *J. Chem. Soc., Dalton Trans.* 1977, 596.
12. J. F. Ojo, O. Olubuyide and O. Oyetunjii, *J. Chem. Soc., Dalton Trans.* 1987, 957.
13. P. J. Hay, J. C. Thibeault and R. Hoffmann, *J. Am. Chem. Soc.* 1975, **97**, 4884.

Polyhedron Vol. 7, No. 15, pp. 1397–1399, 1988
Printed in Great Britain

0277–5387/88 $3.00+.00
© 1988 Pergamon Press plc

COMMUNICATION

SYNTHESIS AND STRUCTURAL CHARACTERIZATION OF *CYCLO*-PENTAKIS [BIS(μ-TRIMETHYLSILYLTHIOMETHANE)NICKEL(II)], $[Ni(SCH_2SiMe_3)_2]_5$, A PENTAMETALLIC TIARA STRUCTURE

BON-KWEON KOO,* ERIC BLOCK,† HYUNKYU KANG, SHUNCHENG LIU and JON ZUBIETA†

Department of Chemistry, State University at Albany, Albany, NY 12222, U.S.A.

(*Received* 5 *February* 1988; *accepted* 14 *April* 1988)

Abstract—Reaction of $(NEt_4)_2NiCl_4$ with $HSCH_2SiMe_3$ in acetonitrile yields lustrous dark brown crystals of $[Ni(SR)_2]_5$ (**1**). The structure of **1** consists of a nearly regular pentagon of Ni atoms, bridged by pairs of thiolate ligands and represents an unusual example of a pentametallic "tiara" structure. Crystal data: space group $P2_1/c$; $a = 16.483(3)$, $b = 22.219(4)$, $c = 23.439(4)$ Å, $\beta = 108.07(1)°$, $V = 8160.5(13)$ Å^3; current $R = 0.0611$, based on 6246 reflections.

Compounds of the general class $[M(SR)_2]_n$ of Ni, Pd and Pt have been shown to possess molecular cyclic structures with $n = 4$, 6, or 8.[1–6] The sizes of toroidal molecules $[Ni(SR)_2]_n$ appear to be determined by steric repulsions between ligand substituents or the Van der Waals volume of a guest molecule.[5] We have recently reported the synthesis and coordination properties of a second generation of sterically constrained thiolate ligands of the general class, $HSCH_{3-n}(SiR_3)_n$.[7] The structures of Sn, Cu and Ag complexes of these ligands confirm that the degree of aggregation of the metal thiolate is sensitive to the steric demands of the ligands.[7–9] As part of our studies of the general coordination properties of these ligands, we have prepared and structurally characterized a cyclic pentanuclear nickel(II) mercaptide, $[Ni(SCH_2SiMe_3)_2]_5$ (**1**). While this work was in progress, the structure of the analogous pentanuclear complex $[Ni(SC_2H_5)_2]_5$ was reported.[10]

Reaction of $(NEt_4)_2NiCl_4$ with excess $HSCH_2SiMe_3$ in acetonitrile results in a dark brown solution from which lustrous dark brown crystals of (**1**) are isolated in 25% yield upon standing at room temperature for one week. Crystal data: space group $P2_1/c$ with $a = 16.483(3)$, $b = 22.219(4)$, $c = 23.439(4)$ Å, $\beta = 108.07(1)°$, $V = 8160.5(13)$ Å^3, $Z = 4$, $D_{calc} = 1.21$ g cm^{-3}. Structure solution and refinement based on 6246 reflections with $F_o \geq 6\sigma(F_o)$ converged at a conventional discrepancy value of 0.0611.

The structure of **1** is shown in Fig. 1, and Table 1 lists selected bond lengths and angles.‡ The structure consists of an approximate pentagon of nickel atoms with two doubly bridging thiolate ligands between each adjacent pair to produce approximately square planar geometry about each metal. The cyclic molecule may also be described as five square planes linked by opposite edges to form a pentagonal prism.

In comparing the structure of **1** to the previously reported examples $[Ni(SR)_2]_n$ ($n = 4$, R = —C_5H_9NMe; $n = 6$, R = C_2H_5, —CH_2CH_2OH, —$CH_2CH(Me)OH$; $n = 8$, R = —CH_2COOEt), the obvious structural difference is in the relative conformation of the ligand substituents. There are two possible orientations of the S—C bond, either axial or equatorial to the toroid. For structures with n being even, the bond

* Permanent address: Hyosung Women's University, Department of Educational Chemistry, Daegu City, Korea.

† Authors to whom correspondence should be addressed.

‡ Tables of fractional coordinates have been deposited with the Director, Cambridge Crystallographic Data Centre.

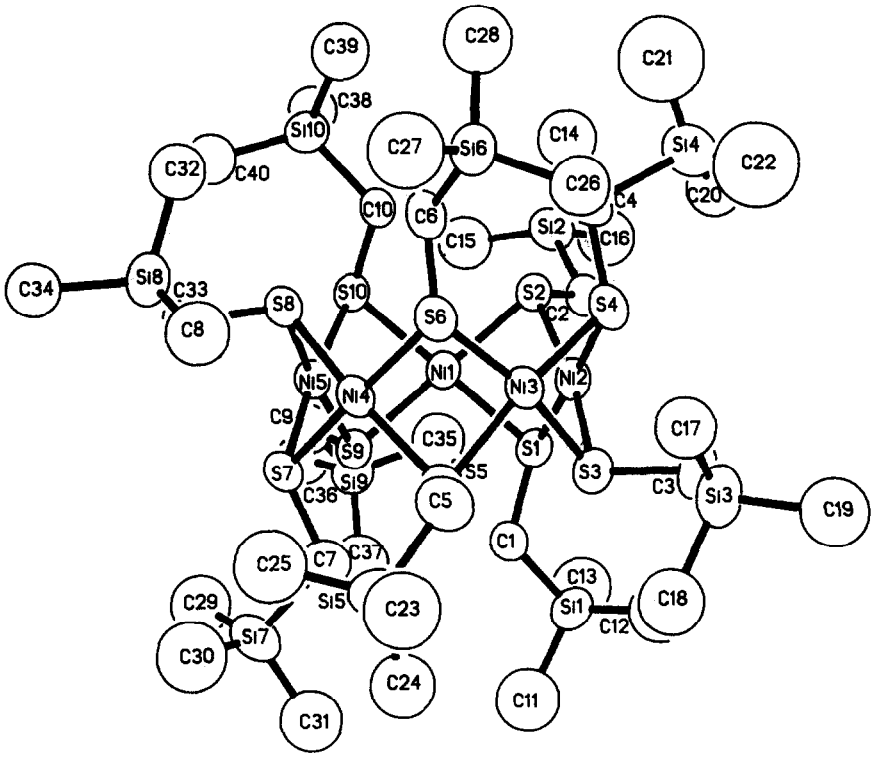

Fig. 1. ORTEP view of $[Ni(SCH_2SiMe_3)_2]_5$, showing the atom labelling scheme.

configurations alternate to minimize steric interactions. In the case of **1**, n is odd and a compromise geometry must be adopted, as illustrated in Fig. 1. The concomitant steric crowding at adjacent ligand sites associated with the S(3) and S(5) axial ligand types and the S(4) and S(6) equatorial ligand set is reflected in the θ_2 angles at Ni(3) of 89.1(1)° for S(3)—Ni—S(5) and 109.3(1)° for S(4)—Ni(3)—S(6), compared to an average value of 98.2(8)° for all θ_2 angles.

The average angle between the S_4 planes is 108.0°, the idealized value for a regular pentagonal array of nickel atoms. The average Ni—Ni distance of 2.835(8) Å confirms the correlation of increasing Ni—Ni distance with increased ring size: 2.67(1), 2.92(1) and 3.05(4) Å for $n = 4$, 6 and 8, respec-

Table 1. Selected bond lengths (Å) and angles (°)[a] for $[Ni(SCH_2SiMe_3)_2]_5$

Ni(1)—Si	2.222(3)	Ni(3)—S(5)	2.236(3)
Ni(1)—S(2)	2.220(3)	Ni(3)—S(6)	2.203(3)
Ni(1)—S(9)	2.220(3)	Ni(4)—S(5)	2.217(3)
Ni(1)—S(10)	2.223(3)	Ni(4)—S(6)	2.210(3)
Ni(2)—S(1)	2.197(3)	Ni(4)—S(7)	2.210(3)
Ni(2)—S(2)	2.216(3)	Ni(4)—S(8)	2.207(3)
Ni(2)—S(3)	2.207(3)	Ni(5)—S(7)	2.218(3)
Ni(2)—S(4)	2.209(3)	Ni(5)—S(8)	2.218(3)
Ni(3)—S(3)	2.219(3)	Ni(5)—S(9)	2.221(3)
Ni(3)—S(4)	2.228(3)	Ni(10)—S(10)	2.206(3)

Ni—S—Ni (ave)	79.6(3)
S—Ni—S (interior), θ_1	81.5(8)
S—Ni—S (exterior), θ_2	98.2(8)
S—Ni—S (*trans*), θ_3	173.1(8)

[a] Interior angles refer to endocyclic Ni_2S_2 angles; exterior angles refer to those exocyclic to the Ni_2S_2 rings.

tively. This feature is also reflected in the Ni—S—Ni angle of 79.6(3)°, compared to values of 74.3(1), 82.9(5) and 88(2)° for $n = 4$, 6 and 8, respectively.

Although the structure **1** demonstrates that suitably modified thiolate ligands can control aggregation of metal–thiolate species, the recent characterization of $[Ni(SC_2H_5)_2]_5$[10] suggests that steric effects are not the exclusive factors determining the degree of aggregation of these complexes. Suitable modifications of the ligands, such as the variations in steric bulk represented by ligand types HSC_6H_4—*o*-SiR_3, R = —C_2H_5 or —C_6H_5, and HSC_6H_3—2,6-$(SiR_3)_2$, recently synthesized by us,[11] may help to elucidate the relative importance of steric effects in determining aggregate geometry. We are currently extending these investigations to the coordination chemistries of Fe(II), Co(II) and Ni(II) with the class of ligands $HSCH_{3-n}(SiMe_3)_n$ and related ligand types.

Acknowledgement—This work was supported by a grant to Eric Block and Jon Zubieta from the National Institute of Health (Grant GM2256608).

REFERENCES

1. P. Woodward, L. F. Dahl, E. W. Abel and B. C. Crosse, *J. Am. Chem. Soc.* 1965, **87**, 5251.
2. R. O. Gould and M. M. Harding, *J. Chem. Soc. A.* 1970, 875.
3. N. R. Kunchur, *Acta Cryst. Sect. B.* 1968, **B24**, 1623.
4. W. Gaete, J. Ros, X. Solans, M. Font-Altaba and J. L. Brianso, *Inorg. Chem.* 1984, **23**, 39.
5. I. G. Dance, M. L. Scudder and R. Secomb, *Inorg. Chem.* 1985, **24**, 1201.
6. I. G. Dance, *Polyhedron* 1986, **5**, 1037 and refs therein.
7. K. Tang, M. Aslam, E. Block, T. Nicholson and J. Zubieta, *Inorg. Chem.* 1987, **26**, 1488. The development of the first generation class of sterically-hindered thiolate ligands may be traced in the publications of Koch and Millar and of Dilworth and Zubieta. See for example, S. A. Koch, R. Fikar, M. Millar and T. O'Sullivan, *Inorg. Chem.* 1984, **23**, 122, and P. T. Bishop, P. J. Blower, J. R. Dilworth and J. A. Zubieta, *Polyhedron* 1986, **5**, 363.
8. P. B. Hitchcock, H. A. Hasim, R. E. Kelly and M. Lappert, *J. Chem. Soc., Chem. Commun.* 1985, 1776.
9. Q. Yang, K. Tang, H. Liao, Y. Han, Z. Chen and Y. Tang, *J. Chem. Soc., Chem. Commun.* 1987, 1076.
10. M. Kriege and G. Henkel, *Z. Naturforsch.* 1987, **42b**, 1121.
11. E. Block, V. Eswarakrishnan, M. Gernon, G. Ofori-Okai, C. Saha, K. Tang and J. Zubieta, *J. Am. Chem. Soc.*, in press.

Polyhedron Vol. 7, No. 15, pp. 1401–1403, 1988
Printed in Great Britain

0277–5387/88 $3.00+.00
Pergamon Press plc

COMMUNICATION

A NEW TYPE OF PYRIDINE-2-THIONATO BRIDGE: X-RAY CRYSTAL STRUCTURE OF THE COMPLEX $[Re_2(MepyS)_2(CO)_6]$ WHERE MepyS IS THE 6-METHYLPYRIDINE-2-THIONATO LIGAND

ANTONY J. DEEMING* and MANZURUL KARIM

Department of Chemistry, University College London, 20 Gordon Street, London WC1H 0AJ, U.K.

and

PAUL A. BATES and MICHAEL B. HURSTHOUSE

Department of Chemistry, Queen Mary College, Mile End Road, London E1 4NS, U.K.

(*Received* 18 *February* 1988; *accepted* 3 *May* 1988)

Abstract—$[Re_2(CO)_{10}]$ reacts with pyridine-2-thione (pySH) in refluxing xylene to give the dinuclear cluster $[Re_2(pyS)_2(CO)_6]$ which contains three fused four-membered rings. The novel five-electron donating pyS bridges are easily cleaved by ligand addition and in redistribution reactions with $[Re_2(MepyS)_2(CO)_6]$, the 6-methyl-substituted derivative for which the X-ray structure is reported.

The pyridine-2-thionato (pyS) ligand is commonly monodentate through S or bidentate through S and N, but can also bridge two transition metal atoms through both heteroatoms (**A**) or just through S atoms (**B**). In both (**A**) and (**B**) the pyS ligand (counted as a radical) is a three-electron donor but it can behave as a five-electron donor in the μ_3 mode (**C**).[1–3] This communication deals with a new doubly-bridging five-electron donating mode of coordination (**D**) for which it is possible to maintain octahedral coordination at the metal atoms, unlike (**A**) which has only been found with lower coordination numbers unless there is a metal–metal bond as in the rhodium(II) dimer $[Rh_2Cl_2(\mu\text{-}pyS)_2(pySH)_2(CO)_2]$.[4]

* Author to whom correspondence should be addressed.

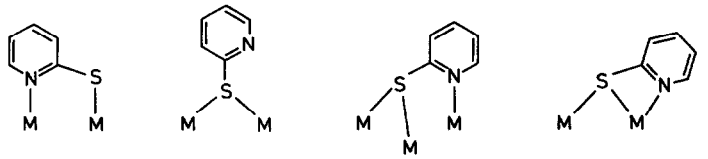

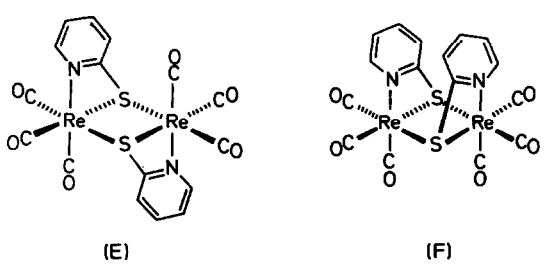

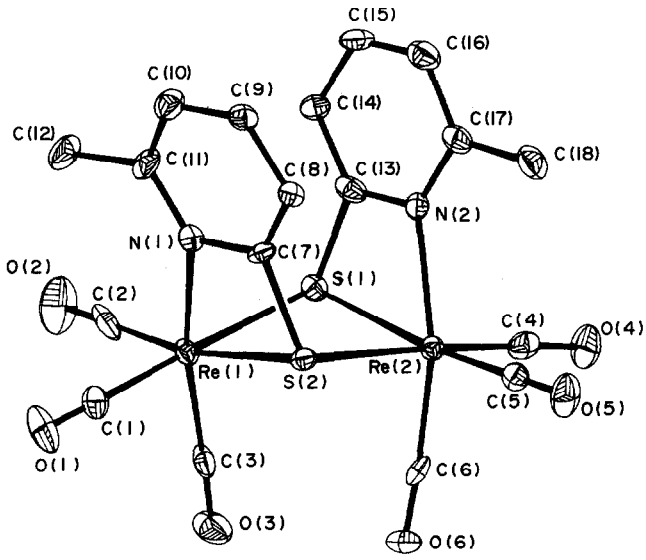

Fig. 1. The molecular structure of $[Re_2(MepyS)_2(CO)_6]$ (**2**) with hydrogen atoms omitted. Selected bond lengths (Å) and angles (°): Re(1)—S(1) 2.556(6), Re(1)—S(2) 2.529(6), Re(2)—S(1) 2.536(6), Re(2)—S(2) 2.530(6), Re(1)—N(1) 2.181(10), Re(2)—N(2) 2.194(10), Re(1)—C(1) 1.936(15), Re(1)—C(2) 1.890(17), Re(1)—C(3) 1.934(13), Re(2)—C(4) 1.873(15), Re(2)—C(5) 1.912(13), Re(2)—C(6) 1.919(13), S(1)—C(13) 1.805(12), S(2)—C(7) 1.770(11), Re(1)—S(1)—Re(2) 95.3(2), Re(1)—S(2)—Re(2) 96.2(2), S(1)—Re(1)—S(2) 80.7(2), S(1)—Re(2)—S(2) 81.1(2).

The reaction of $[Re_2(CO)_{10}]$ with pyridine-2-thione (2 mol/mol Re_2) in refluxing xylene for 48 h gave $[Re_2(pyS)_2(CO)_6]$ (**1**) (93% after chromatography on SiO_2) as pale yellow crystals. The 6-methylpyridine-2-thione and quinoline-2-thione analogues reacted similarly to give the related compounds (**2**) and (**3**) but in somewhat lower yields. The mass spectrum of (**1**) showed the parent molecular ion and ruled out a cubane-type structure like $[Re(SMe)(CO)_3]_4$[5] with non-coordinated N-atoms. Initially we considered two structures (**E**) and (**F**); the pyS ligands are equivalent in both as observed (^{1}H NMR). However, there are five IR ν(CO) absorptions for (**1**) [2039(s), 2023(vs), 1947(m), 1933(s), 1917(vs) cm^{-1} (cyclo-C_6H_{12})] supporting a non-centrosymmetric structure. Compounds (**1**), (**2**) and (**3**) have extremely similar ν(CO) spectra. A single crystal X-ray structure of the 6-methyl substituted compound (**2**) is shown in Fig. 1.* The chiral structure (**F**) with C_2 symmetry is adopted. The Re—S distances are equal and the Re_2S_2 ring is non-planar with a dihedral angle of 150.5(1)° between the Re(1)Re(2)S(1) and Re(1)Re(2)S(2) planes. What distortions there are from octahedral geometry appear to be associated with the small interligand angles of 65.8(3) and 65.6(3)° (SReN angles in chelate rings) and 80.7(2) and 81.1(2)° (SReS angles). The geometries of the chelating ligands do not seem to be substantially distorted by the sulphur atoms bridging and it is not obvious from this structure why the centrosymmetric structure (**E**) is not adopted instead.[9]

Although the dinuclear compound (**1**) is apparently strongly held by sulphur bridges and is thermally very stable, these bridges are easily cleaved. Thus the ^{1}H NMR spectrum of a $CDCl_3$ solution containing equimolar amounts of (**1**) and (**2**) showed separate signals for the two compounds but over several days at room temperature an

*Crystal data for (**2**): $C_{18}H_{12}N_2O_6Re_2S_2$, M = 788.82, monoclinic, space group $P2_1/c$, a = 10.769(2), b = 14.906(3), c = 13.274(6) Å, β = 95.33(2)°, U = 2122(1) Å^3, Z = 4, D_c = 2.470 g cm^{-3}, $F(000)$ = 1456, λ = 0.710 69 Å, μ(Mo-K_α) = 117.8 cm^{-1}, crystal size 0.63 × 0.38 × 0.25 mm. Unit cell parameters and intensity data were obtained as described previously[6] using a CAD4 diffractometer in the ω–2θ scan mode with graphite monochromated Mo-K_α radiation. 3729 unique reflections were collected ($3 \leqslant 2\theta \leqslant 50°$), scanning the segment of reciprocal space (h) −12 to 12, (k) 0 to 17, (l) 0 to 15, and reflection intensities corrected for absorption using the azimuthal-scan method. The structure was solved by routine heavy-atom methods[7] using 3273 data with $F_o > 6\sigma(F_o)$ and refined by full-matrix least-squares[8] to R = 0.032 and R_w = 0.033 (277 parameters), all non-hydrogen atoms anisotropic, H atoms in calculated positions (C—H 0.96 Å; U = 0.10 Å^2), minimizing the function $\Sigma_w(|F_o|-|F_c|)^2$ with weight $w = 1/[\sigma^2(F_o)+0.00001F_o^2]$. Atomic coordinates, bond lengths and angles, and thermal parameters have been deposited at the Cambridge Crystallographic Data Centre. See Notice to Authors, Issue No. 1.

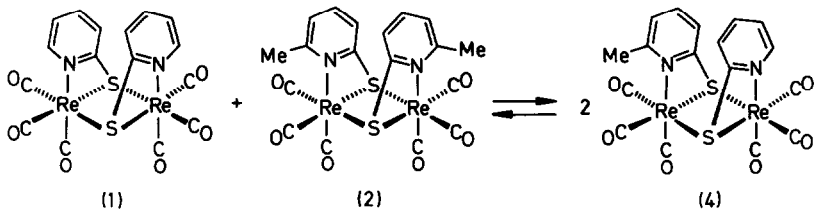

(1) (2) (4)

Scheme 1.

equilibrium was reached involving (**1**), (**2**), and the mixed form $[Re_2(pyS)(MepyS)(CO)_6]$ (**4**) in the mol ratio 1 : 1 : 2, a statistical distribution (see Scheme 1). These species are separable by TLC on silica and a solution of the mixed form (**4**) regenerates the statistical mixture over several days in $CDCl_3$. The ^1H NMR spectrum of (**4**) is sufficiently different from that of a 1 : 1 mixture of (**1**) and (**2**), that the mixture of all three can be easily analysed. This redistribution reaction could occur by cleavage of the Re—N bonds and dimerization to give a cubane structure. Reformation of dimers by cleavage could give the redistribution compounds. However, an alternative mechanism could involve dimer cleavage to give the unsaturated species $[Re(pyS)(CO)_3]$ and $[Re(MepyS)(CO)_3]$ and, consistent with this, the dimers readily react with donor molecules L (PMe_2Ph, pySH, py, MeCN etc) to give $[Re(pyS)(CO)_3L]$. For example, a solution of (**1**) in MeCN does not react immediately but overnight it forms $[Re(pyS)(CO)_3(MeCN)]$ in solution, but removal of the solvent regenerates (**1**).

Direct thermal reaction of (**1**) with PMe_2Ph in refluxing xylene results in a mixture of (**1**) (15%), the chelating pyS compound *fac*-$[Re(pyS)(CO)_3(PMe_2Ph)]$ (**5**) (9%), the monodentate pyS compound *fac*-$[Re(pyS)(CO)_3(PMe_2Ph)_2]$ (**6**) (21%), $[Re_2(pyS)_2(CO)_5(PMe_2Ph)]$ (**7**) (11%), and a trace of $[Re_2(pyS)_2(CO)_4(PMe_2Ph)_2]$ (**8**). A solution of compound (**7**) in CD_2Cl_2 at room temperature in the dark for one month underwent redistribution to give a mixture of (**1**), (**7**) and (**8**). This is unlikely to involve PMe_2Ph transfer between rhenium atoms but more likely a process like that in Scheme 1.

Acknowledgements—We thank the S.E.R.C. for support of the crystallographic work and the Association of Commonwealth Universities for a research studentship (for M.K.).

REFERENCES

1. A. J. Deeming, M. N. Meah, P. A. Bates and M. B. Hursthouse, *J. Chem. Soc., Dalton Trans.* 1988, 235.
2. A. J. Deeming, M. N. Meah, P. A. Bates and M. B. Hursthouse, *J. Chem. Soc., Dalton Trans.*, in press.
3. L. A. Oro, M. A. Ciriano, F. Viguri, A. Tiripicchio, M. Tiripicchio-Camellini and F. J. Lahoz, *Nouv. J. Chem.* 1986, **10**, 75.
4. A. J. Deeming, M. N. Meah, H. Dawes and M. B. Hursthouse, *J. Organomet. Chem.* 1986, **299**, C25.
5. W. Harrison, W. C. Marsh and J. Trotter, *J. Chem. Soc., Dalton Trans.* 1972, 1009.
6. M. B. Hursthouse, R. A. Jones, K. M. A. Malik and G. Wilkinson, *J. Am. Chem. Soc.* 1979, **101**, 4128.
7. G. M. Sheldrick, *SHELX-86 program for crystal structure solution*. University of Göttingen (1986).
8. G. M. Sheldrick, *SHELX-76 program for crystal structure determination and refinement*. University of Cambridge (1976).
9. The related dimercaptobenzothiazolato rhenium compound also has C_2 symmetry: S. Jeannin, Y. Jeannin and G. Lavigne, *Transition Met. Chem.* 1976, **1**, 195.

Polyhedron Vol. 7, No. 16/17, p. 1405, 1988
Pergamon Press plc. Printed in Great Britain

INTRODUCTION

Without a quantitative accounting of the strengths of bonds being made and broken, it is impossible to understand the course of any chemical transformation in depth. Although such considerations form an integral part of modern physical organic chemistry and the chemistry of relatively simple inorganic systems, applications to problems in organotransition metal chemistry have traditionally been retarded by a paucity of data. This picture is, however, now rapidly changing, and there is a growing awareness of the need for metal–ligand bond enthalpy information. Such information is of fundamental importance in understanding/predicting organometallic reaction pathways, the energetics of the segments of catalytic cycles, the energetics of certain metal ion-mediated enzymatic transformations, and the nature of metal–ligand bonding.

The purpose of this *Polyhedron* Symposia-in-Print is to survey the current state of knowledge in the emerging area of organotransition element metal–ligand bonding energetics. A broadly interdisciplinary view has been taken, and contributions have been assembled from recognized authorities in the areas of solution phase, gas phase, and theoretical chemistry. The authors have been given great freedom in the preparation of their contributions so that vital personal viewpoints and the most current results could be disseminated. Within each area, contributions are presented in alphabetical order of the senior authors. It is hoped that this volume will alert the scientific community to the progress, problems, and stimulating opportunities in this burgeoning field.

TOBIN J. MARKS

Polyhedron Vol. 7, No. 16/17, pp. 1409–1428, 1988
Printed in Great Britain

0277–5387/88 $3.00+.00
Pergamon Press plc

RELATIVE BOND DISSOCIATION ENERGIES FOR EARLY TRANSITION METAL ALKYL, ARYL, ALKYNYL AND HYDRIDE COMPOUNDS. EQUILIBRATION OF METALLATED CYCLOPENTADIENYL DERIVATIVES OF PERALKYLATED HAFNOCENE AND SCANDOCENE WITH HYDROCARBONS AND DIHYDROGEN

A. RAY BULLS and JOHN E. BERCAW†

Division of Chemistry and Chemical Engineering, California Institute of Technology, Pasadena, CA 91125, U.S.A.

JUAN M. MANRIQUEZ

Universidad Tecnica Federico Santa Maria, Casilla 110-V, Valparaiso, Chile

and

MARK E. THOMPSON

Present address: Department of Chemistry, Princeton University, Princeton, NJ 08544, U.S.A.

Abstract—Relative bond dissociation energies (BDEs) have been obtained by equilibrating early transition metal alkyls and hydrides with H_2 or the C—H bonds of hydrocarbons. Thus, in benzene solution $Cp^*_2HfH_2$ ($Cp^* = (\eta^5\text{-}C_5Me_5)$) equilibrates with $Cp^*_2Hf(C_6H_5)H$ and dihydrogen. From the enthalpy of the reaction, $\Delta H^0 = +6.0(3)$, the Hf—H (BDE) is calculated to be 0.8(3) kcal mol^{-1} stronger than the Hf—C_6H_5 BDE. Relative Sc—C_6H_5 and Sc—alkyl BDEs have been estimated from the equilibration of the metallated complex $Cp^*(\eta^5,\eta^1\text{-}C_5Me_4CH_2CH_2CH_2)Sc$, C_6H_6 and $Cp^*(\eta^5\text{-}C_5Me_4CH_2CH_2CH_3)ScC_6H_5$, the Sc—$C_6H_5$ BDE being 16.6(3) kcal mol^{-1} stronger than the Sc—$CH_2CH_2CH_2C_5Me_4$ BDE. From a similar reversible intramolecular metallation of $Cp^*(\eta^5\text{-}C_5Me_4CH_2CH_2CH_3)HfH_2$ to give $Cp^*(\eta^5,\eta^1\text{-}C_5Me_4CH_2CH_2CH_2)HfH$ and dihydrogen, the Hf—H BDE is estimated to be 23.0(3) kcal mol^{-1} stronger than the Hf—$CH_2CH_2CH_2C_5Me_4$ BDE. The equilibration of $Cp^*(\eta^5\text{-}C_5Me_4CH_2C_6H_5)Sc\text{—}C{\equiv}CCMe_3$ with metallated scandocene derivative $Cp^*(\eta^5,\eta^1\text{-}C_5Me_4CH_2\text{-}o\text{-}C_6H_4)Sc$ and *tert*-butylacetylene lies very far towards $Cp^*(\eta^5\text{-}C_5Me_4CH_2C_6H_5)Sc\text{—}C{\equiv}CCMe_3$, so that only a lower limit for the relative Sc—alkynyl and Sc—aryl BDEs may be determined: BDE(Sc—alkynyl) − BDE(Sc—aryl) ≥ 29(5) kcal mol^{-1}. These early transition metal–hydrocarbyl (M—R) BDEs correlate with the corresponding H—R BDEs (i.e. M—alkynyl > M—aryl > M—alkyl); however, the M—R BDEs increase more rapidly with s character for R than do the H—R BDEs. The origin of this effect is not known, but it is undoubtedly also responsible for the characteristically high M—H BDEs for transition metal hydride compounds. In order to probe the polarity of Sc—aryl bonds a series of scandocene derivatives capable of reversibly metallating at either of two differently substituted benzyl groups was prepared. The equilibrium constants for these metallated derivatives: $(\eta^5,\eta^1\text{-}C_5Me_4CH_2\text{-}o\text{-}C_6H_3\text{-}p\text{-}X)(\eta^5\text{-}C_5Me_4CH_2C_6H_4\text{-}m\text{-}CH_3)Sc \rightleftarrows (\eta^5\text{-}C_5Me_4CH_2C_6H_4\text{-}m\text{-}X)(\eta^5,\eta^1\text{-}C_5Me_4CH_2\text{-}o\text{-}C_6H_3\text{-}p\text{-}CH_3)Sc$ (X = H, CF_3, NMe_2) were determined. The small dependence of K_{eq} on the nature of X suggests that the Sc—aryl bond is essentially covalent with only a small ionic contribution.

Contribution No. 7637 from the Division of Chemistry and Chemical Engineering, California Institute of Technology, Pasadena, CA 91125, U.S.A.

† Author to whom correspondence should be addressed.

Early transition metals form many stable compounds with electronegative ligands such as halogens due to the high degree of ionic character, and concurrent strength of the M—X bond. Strong

bonds between early transition metals and oxygen- or nitrogen-containing ligands (e.g. OR, NR_2) have this same feature. Moreover, multiple M=X or M≡X bonding may also obtain by donation of one or two electron pairs from X to empty orbitals on the metal. The later, less electropositive transition metals also form strong bonds to these heteroatoms;[1] however, early metal–heteroatom bonds are generally more robust. The strength of early transition metal–carbon and early transition metal–hydrogen bonds relative to those of the middle and late transition metals is somewhat less straightforward to predict. *A priori*, we might expect that they would also be systematically greater since the bond homolysis ($L_mM^n-R \rightarrow L_mM^{n-1}+{}^{\bullet}R$) formally involves reducing the metal by one unit. Electropositive metals have higher reduction potentials (for a given oxidation state) as compared with the more electronegative transition metals to the right. Furthermore, a comparison of the electronegativities of carbon, hydrogen, and the various transition metals reveals that some ionic character ($M^{\delta+}-R^{\delta-}$; R = H, C) may be expected when M is an early transition metal. Indeed, the reactions of early metal hydrides and alkyls with protic reagents such as mineral acids and water, which rapidly evolve H_2 and RH, suggest just such polarization.† Little direct experimental evidence is available which is indicative of the amount of ionic character for early transition metal–carbon or –hydrogen bonds, however. Moreover, Mulliken populations obtained from quantum mechanical calculations are generally unreliable indicators of the ionic character of M—R bonds.[2] Likewise, little experiment evidence is available which reflects the dependence of the M—R BDE on the hybridization at the α carbon, i.e. the quantitative differences in the series: metal–alkyl vs metal–alkenyl vs metal–aryl vs metal–alkynyl.

In this manuscript we describe some experiments designed to address these issues. Although we have thus far been unable to obtain reliable absolute bond dissociation energies (BDEs), we have been able to derive accurate relative BDEs by equilibrating early transition metal alkyls and hydrides with the C—H bonds of hydrocarbons via the rapid, reversible 'sigma bond metathesis' reactions[3] characteristic of early transition metals, lanthanides and actinides [eq. (1)].

$$L_nM-R+R'-H \rightleftarrows L_nM-R'+R-H \quad (1)$$

(R, R′ = H, alkyl, alkenyl, aryl, alkynyl).

Reported for peralkylated-scandocene and -hafnocene derivatives are (i) relative M—H and M—C BDEs (M = Sc, Hf), (ii) relative bond strengths of scandium– and hafnium–carbon bonds as the hybridization at carbon is varied, and (iii) relative Sc—aryl BDEs as the aryl substituent is systematically varied.

RESULTS

Determination of relative M—H *and* M—Ph *bond dissociation energies via intermolecular equilibration*

As we have reported earlier,[3] the clean, reversible nature of the reaction of *bis*(pentamethylcyclopentadienyl)scandium hydride, Cp^*_2Sc-H ($Cp^* = (\eta^5-C_5Me_5)$) with benzene [eq. (2)] permits a determination of the relative Sc—H and Sc—C_6H_5 BDEs: the Sc—H BDE is 1.5 kcal mol^{-1} greater than the Sc—C_6H_5 BDE.

$$Cp^*_2Sc-C_6H_5+H_2 \rightleftarrows Cp^*_2Sc-H+H-C_6H_5. \quad (2)$$

In a similar manner $Cp^*_2HfH_2$ in benzene solution at ⩾ 100°C cleanly establishes an equilibrium with $Cp^*_2Hf(H)(C_6H_5)$ and dihydrogen [eq. (3)].

$$Cp^*_2HfH_2+H-C_6H_5 \rightleftarrows Cp^*_2Hf(H)(C_6H_5)+H_2. \quad (3)$$

$Cp^*_2Hf(C_6H_5)_2$ is not observed under these conditions. The enthalpy and entropy of equilibrium 3, $\Delta H^0 = +6.0(3)$ kcal mol^{-1} and $\Delta S^0 = +3.5(5)$ e.u., are obtained from the temperature dependence of the equilibrium.

Attempts to extend this approach to include equilibration of alkanes with permethylhafnocene or permethylscanodcene hydrides or alkyls were unsuccessful, possibly due to interfering reactions of the C—H bonds of the pentamethylcyclopentadienyl ligands.[3] For example, thermolysing $Cp^*_2Sc-C_6H_5$ with mesitylene, tetramethylsilane, or *n*-butane, either neat or with varying concentrations of benzene, results in the slow decomposition to a mixture of uncharacterized scandium containing products. The expected reaction products, Cp^*_2Sc-R (R = $CH_2C_6H_3$-3,5-$(CH_3)_2$, CH_2SiMe_3, $CH_2CH_2CH_2CH_3$), have been independently synthesized, and each reacts with

† Caution should be exercised in concluding too much from this type of reactivity, however, since these reactions could, in large part, be due to their very strong thermodynamic driving force. Moreover, coordination of the Brønsted acid to the metal center prior to deprotonation is likely in many cases.

benzene to generate $Cp^*_2Sc—C_6H_5$ and H—R [eq. (4)].

$$Cp^*_2Sc—R + C_6H_6 \rightleftarrows Cp^*_2Sc—C_6H_5 + H—R \quad (4)$$

$$R = CH_2C_6H_3\text{-}3,5\text{-}(CH_3)_2$$
$$= CH_2SiMe_3$$
$$= CH_2CH_2CH_2CH_3.$$

Thus, the reactions of $Cp^*_2Sc—C_6H_5$ with these hydrocarbons appear to be so thermodynamically unfavorable as to prevent build-up of detectable concentration of permethylscandocene derivatives other than $Cp^*_2Sc—C_6H_5$.

Determination of relative M—H *and* M—C *bond dissociation energies via intramolecular equilibration*

We have previously shown that bis(tetramethylneopentylcyclopentadienyl)zirconium dihydride is in facile equilibrium with the metallated mono-hydride complex and dihydrogen[4] [eq. (5)].

$$(\eta^5\text{-}C_5Me_4CH_2CMe_3)_2ZrH_2 \rightleftarrows (\eta^5\text{-}C_5Me_4CH_2CMe_3)\text{-}(\eta^5,\eta^1\text{-}C_5Me_4CH_2CMe_2CH_2)ZrH + H_2. \quad (5)$$

With the hope that these types of equilibria are quite general, we have undertaken the syntheses of compounds which would allow intramolecular equilibration via sigma bond metathesis reactions of Sc—R with the C—H bonds of appended alkyl, aryl, etc. groups. Thus, the mixed-Cp scandocene chloride **1** has been prepared as shown in eq. (6). Heating $[Cp^*ScCl_2]_n$ with one equivalent of $Li^+(C_5Me_4CH_2CH_2CH_3)^-$ yields complex **1** as an amber oil (> 90% ^1H NMR).

$$(Cp^*ScCl_2)_n + Li^+(C_5Me_4CH_2CH_2CH_3)^- \xrightarrow{110°C} Cp^*(\eta^5\text{-}C_5Me_4CH_2CH_2CH_3)ScCl + LiCl. \quad (6)$$

1

Treatment of **1** with CH_3Li yields $Cp^*(\eta^5\text{-}C_5Me_4CH_2CH_2CH_3)ScCH_3$, which rapidly eliminates methane (< 5 min at 25°C) to afford $Cp^*(\eta^5,\eta^1\text{-}C_5Me_4CH_2CH_2CH_2)Sc$ (**2**) [eq. (7)].

$Cp^*(\eta^5\text{-}C_5Me_4CH_2CH_2CH_3)$-

$$ScCl \xrightarrow{+CH_3Li,\ -LiCl} [Cp^*(\eta^5\text{-}C_5Me_4CH_2CH_2CH_3)ScCH_3] \downarrow -CH_4$$
$$Cp^*(\eta^5,\eta^1\text{-}C_5Me_4CH_2CH_2CH_2)Sc. \quad (7)$$
2

In contrast to other permethylscandocene alkyls, cyclohexane-d_{12} solutions of **2** are quite stable at 140°C. If however, solutions of **2** in cyclohexane-d_{12} are heated with 5–10 equivalents of benzene, an equilibrium consisting of **2**, C_6H_6, and a new species identified as $Cp^*(\eta^5\text{-}C_5Me_4CH_2CH_2CH_3)ScC_6H_5$ (**3**) is established [eq. (8); $\Delta H^0 = +3.5(3)$ kcal mol^{-1} and $\Delta S^0 = 10.5(5)$ e.u.].

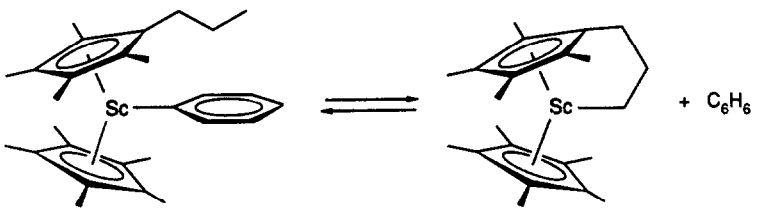

3 **2** (8)

Relative Hf—H and Hf—alkyl BDEs can be similarly obtained. The mixed-Cp hafnocene complex $Cp^*(\eta^5\text{-}C_5Me_4CH_2CH_2CH_3)HfCl_2$ (**4**) is prepared in high yield from Cp^*HfCl_3 and $Li^+(C_5Me_4CH_2CH_2CH_3)^-$ [eq. (9)].

$$Cp^*HfCl_3 + Li^+(C_5Me_4CH_2CH_2CH_3)^- \xrightarrow[\text{xylenes}]{\text{refluxing}} Cp^*(\eta^5\text{-}C_5Me_4CH_2CH_2CH_3)HfCl_2$$
4
$$+ LiCl. \quad (9)$$

Treating **4** with *n*-butyllithium under a dihydrogen atmosphere affords the dihydrido species **5** [eq. (10)].

$Cp^*(\eta^5\text{-}C_5Me_4CH_2CH_2CH_3)HfCl_2$

4

$$\xrightarrow[\substack{2.2\,n\text{-butyllithium}\\ -2\,\text{butane}}]{H_2}$$

$Cp^*(\eta^5\text{-}C_5Me_4CH_2CH_2CH_3)HfH_2 + 2LiCl.$

5 (10)

Table 1. Equilibrium data for eqs (3), (8), (11) and (14)

Equilibrium	Temperature (°C)	K_{eq}
3	100.5	5.27×10^{-5}
	109	5.91×10^{-5}
	129	8.57×10^{-5}
	144	12.1×10^{-5}
	171	18.6×10^{-5}
$\Delta H^0 = +6.0(3)$		
$\Delta S^0 = -3(1)$		
8	50	0.65
	60	0.78
	75	0.96
	89.5	1.23
	100.5	1.38
$\Delta H^0 = +3.7(3)$		
$\Delta S^0 = +11(1)$		
11	70	3.28×10^{-3}
	80	3.78×10^{-3}
	90	9.58×10^{-3}
	100.5	15.0×10^{-3}
	114	39.6×10^{-3}
$\Delta H^0 = +15.5(3)$		
$\Delta S^0 = +33(1)$		
14	59	3.56×10^{-2}
	73	5.90×10^{-2}
	86.5	9.60×10^{-2}
	98.5	17.2×10^{-2}
	113	19.0×10^{-2}
$\Delta H^0 = +8.5(3)$		
$\Delta S^0 = +19(1)$		

Dihydride **5** has not been isolated cleanly; rather a mixture of **5** and the metallated propyl hydride **6** is obtained from petroleum ether. The equilibrium shown in eq. (11) can be driven to the right by the periodic removal of H_2 from the reaction vessel, thus allowing the isolation of clean samples of **6**. Introducing dihydrogen into an NMR tube charged with **6** and benzene-d_6 re-establishes the equilibrium shown in eq. (11) with detectable concentrations of the **5** and **6**. The temperature dependence of the equilibrium (Table 1) indicates $\Delta H^0 = +15.5(3)$ kcal mol^{-1} and $\Delta S^0 = 33.5(5)$ e.u. for eq. (11).

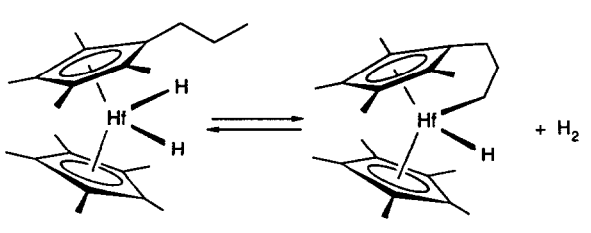

5 **6** (11)

Relative Hf—aryl and Hf—H BDEs were also determined for comparison to values obtained via the intermolecular equilibrations described above. Thus, the metallated benzyltetramethylcyclopentadienyl hafnium hydride complex Cp*(η^5,η^1-$C_5Me_4CH_2$-*o*-C_6H_4)HfH has been prepared as shown in eqs (12)–(14).

$$Cp^*HfCl_3 + Li(C_5Me_4CH_2C_6H_5) \xrightarrow[\text{xylenes}]{\text{refluxing}} Cp^*(\eta^5\text{-}C_5Me_4CH_2C_6H_5)HfCl_2 + LiCl \quad (12)$$

7

$$Cp^*(\eta^5\text{-}C_5Me_4CH_2C_6H_5)HfCl_2 \xrightarrow[(2)\,H_2,80°C,\,-2C_6H_5CH_3]{(1)\,2C_6H_5CH_2K} Cp^*(\eta^5\text{-}C_5Me_4CH_2C_6H_5)HfH_2 + 2KCl \quad (13)$$

7 **8**

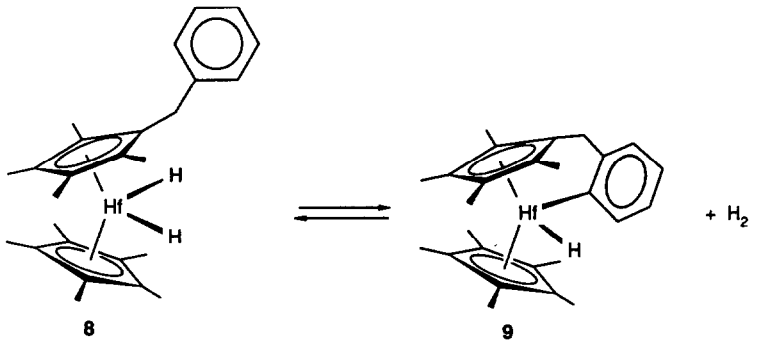

(14)

The equilibrium shown in eq. (14) is driven to the right by the periodic removal of dihydrogen from the reaction vessel. From the temperature dependence of this equilibrium a $\Delta H^0 = +8.5(3)$ kcal mol^{-1} and a $\Delta S^0 = 19(5)$ e.u. are obtained. The similarity of the enthalpy for eq. (14) to that for eq. (3) ($\Delta H^0 = +6.0(3)$ kcal mol^{-1}) suggests only a small ring strain energy for the metallated benzyl group of the (η^5,η^1-$C_5Me_4CH_2$-*o*-C_6H_4) ligand.†

Attempts to equilibrate Sc—aryl and Sc—alkynyl complexes were unsuccessful, presumably due to the exceptionally strong Sc—carbon bonds of the latter. For example, Cp*(η^5,η^1-$C_5Me_4CH_2$-*o*-C_6H_4)Sc (**10**), prepared as shown in eqs (15) and (16), reacts completely with *tert*-butylacetylene; no detectable amount of Cp*(η^5,η^1-$C_5Me_4CH_2$-*o*-C_6H_4)Sc remains.

$$[Cp^*ScCl_2]_n + Li^+(C_5Me_4CH_2C_6H_5)^- \rightarrow Cp^*(\eta^5\text{-}C_5Me_4CH_2C_6H_5)ScCl + LiCl \quad (15)$$

$$Cp^*(\eta^5\text{-}C_5Me_4CH_2C_6H_5)ScCl \xrightarrow{CH_3Li} Cp^*(\eta^5\text{-}C_5Me_4CH_2C_6H_5)Sc\text{—}CH_3 + LiCl$$
$$\downarrow -CH_4$$
$$Cp^*(\eta^5,\eta^1\text{-}C_5Me_4CH_2\text{-}o\text{-}C_6H_4)Sc. \quad \mathbf{10} \quad (16)$$

When only 0.5 equivalents of $Me_3CC{\equiv}C\text{—}H$ is used, no free acetylene remains. Thus the equilibrium constant for eq. (17) must be greater than 10^2 M^{-1}.

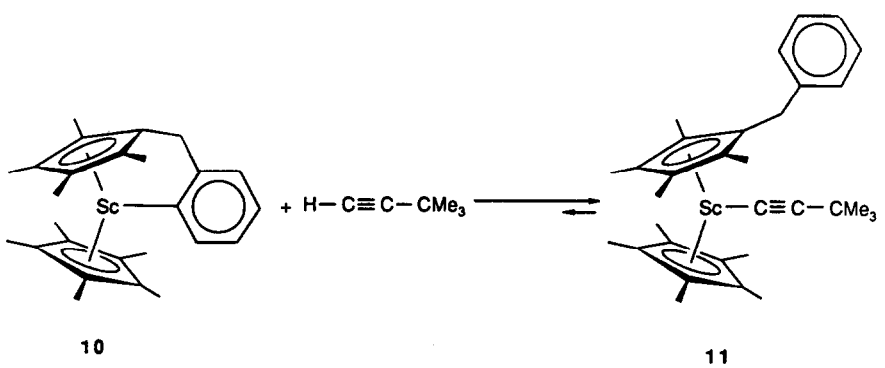

(17)

Determination of aryl substituent effects on the relative Sc—*aryl bond dissociation energies*

In order to determine the polarity of the Sc—aryl bond, a series of compounds which can metallate at either of two differently substituted benzyl groups has been prepared [eq. (18)]. Any ionic contribution to the Sc—aryl BDE, and hence, the equilibrium constant, should respond to the electron releasing or electron withdrawing power of the substituents X and Y.

Each of the substituted benzyltetramethylcyclopentadienyl anions has been prepared from the appropriate benzyl Grignard reagent and tetramethylcyclopentenone, followed by dehydration of the resulting alcohol. Treatment of the isomeric mixture of tetramethylbenzylcyclopentadienes

† The validity of this statement depends on (i) the H—C_6H_5 and (η^5-$C_5Me_4CH_2C_6H_4$-*o*-H) BDEs being equal and (ii) the Hf—aryl BDE not depending on the orientation of the phenyl ring relative to the hafnocene equatorial plane. The possibility also exists that these two effects may cancel, at least in part.

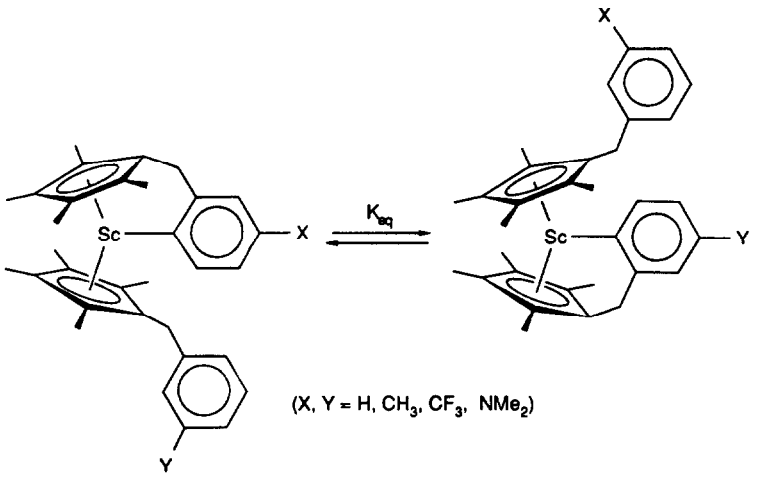

(18)

with *n*-butyllithium affords the lithium salt of the anion in moderate yield (Scheme 1).

The mixed-Cp scandocene chloride compounds: $(\eta^5\text{-}C_5Me_4CH_2C_6H_4\text{-}m\text{-}CH_3)(\eta^5\text{-}C_5Me_4CH_2C_6H_5)ScCl$ (**12**), $(\eta^5\text{-}C_5Me_4CH_2C_6H_4\text{-}m\text{-}CH_3)(\eta^5\text{-}C_5Me_4CH_2C_6H_4\text{-}m\text{-}CF_3)ScCl$ (**13**) and $(\eta^5\text{-}C_5Me_4CH_2C_6H_4\text{-}m\text{-}CH_3)(\eta^5\text{-}C_5Me_4CH_2C_6H_4\text{-}m\text{-}NMe_2)ScCl$ (**14**) are prepared by refluxing $\{(\eta^5\text{-}C_5Me_4CH_2C_6H_4\text{-}m\text{-}CH_3)ScCl_2\}_n$ with the appropriate tetramethylbenzylcyclopentadienyl anion in toluene [eq. (19)].

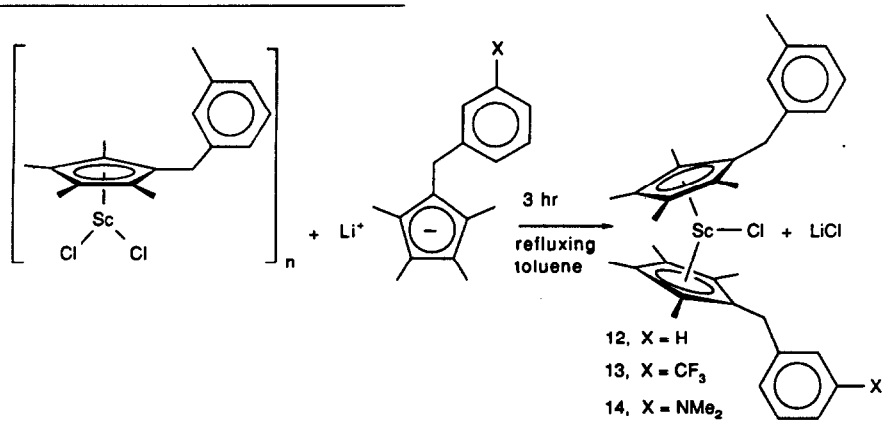

(19)

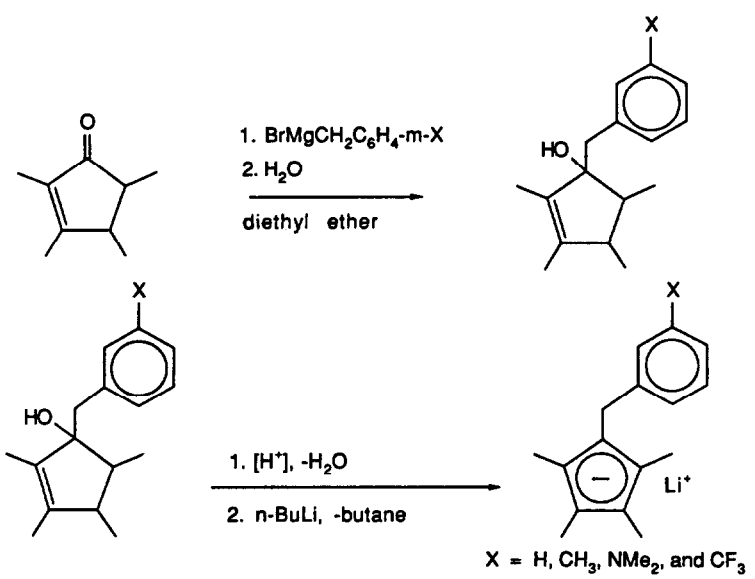

Scheme 1.

Since ^{1}H NMR analysis of the equilibrium mixture proved rather complex (even at 500 MHz), we have chosen (η^5-$C_5Me_4CH_2C_6H_4$-*m*-CH_3) as the reference substituted benzyl ligand. When metallated, e.g. for Cp*(η^5,η^1-$C_5Me_4CH_2$-*o*-C_6H_3-*p*-CH_3)Sc, the (η^5-$C_5Me_4CH_2$-*o*-C_6H_3-*p*-CH_3) resonance appears characteristically at δ 2.37. For the compounds described below, this signal consistently shifts from δ 2.05–2.11 to 2.37–2.38 on *ortho*-metallation (Table 2), thus serving as a reliable indicator.

Treating the scandium chloride (η^5-$C_5Me_4CH_2C_6H_4$-*m*-CH_3)(η^5-$C_5Me_4CH_2C_6H_5$)ScCl with one equivalent of methyllithium generates over the course of one hour one equivalent of methane and the isomeric mixture (η^5,η^1-$C_5Me_4CH_2$-*o*-C_6H_3-*p*-CH_3)(η^5-$C_5Me_4CH_2C_6H_5$)Sc (**15**) and (η^5-$C_5Me_4CH_2C_6H_4$-*m*-CH_3)(η^5,η^1-$C_5Me_4CH_2$-*o*-C_6H_4)Sc (**16**) in a 1 : 2 ratio (Scheme 2). Heating this 1 : 2 mixture overnight at 110°C in benzene-d_6 does not alter this ratio significantly. In order to establish that this 1 : 2 ratio of **15** and **16** is the equilibrium mixture, a small amount of dihydrogen was introduced to catalyse interconversion of **15** and **16**, via σ bond metathesis reactions with (η^5-$C_5Me_4CH_2C_6H_4$-*m*-CH_3)(η^5-$C_5Me_4CH_2C_6H_5$)Sc—H. Again, no change from the statistical 1 : 2 ratio is noted.

That dihydrogen does indeed interconvert **15** and **16** is supported by the following observations: (i) treating Cp*(η^5,η^1-$C_5Me_4CH_2$-*o*-C_6H_4)Sc with dihydrogen (4 atm) rapidly yields Cp*(η^5-$C_5Me_4CH_2C_6H_5$)Sc—H, (ii) heating benzene-d_6 solutions of Cp*(η^5-$C_5Me_4CH_2C_6H_5$)Sc—H under 4 atm H_2 results in H/D exchange, specifically into the *ortho* benzylic sites. Based on previous results for H/D exchange between benzene-d_6 and hydrocarbons catalysed by Cp^*_2Sc—H,[3] the likely mechanism for benzylic H/D exchange involves Cp*(η^5-$C_5Me_4CH_2C_6H_5$)Sc—H, Cp*(η^5,η^1-$C_5Me_4CH_2$-*o*-C_6H_4)Sc, and Cp*(η^5-$C_5Me_4CH_2C_6H_5$)Sc—C_6D_5 (along with H_2, HD, D_2, and $C_6H_nD_{6-n}$.†

Treating (η^5-$C_5Me_4CH_2C_6H_4$-*m*-CH_3)(η^5-C_5

† It would, of course, be preferable to demonstrate H/D exchange for the benzylic positions of **15** and **16**. The complexity of the ^{1}H NMR spectra have thwarted attempts at direct observation of deuterium incorporation, however.

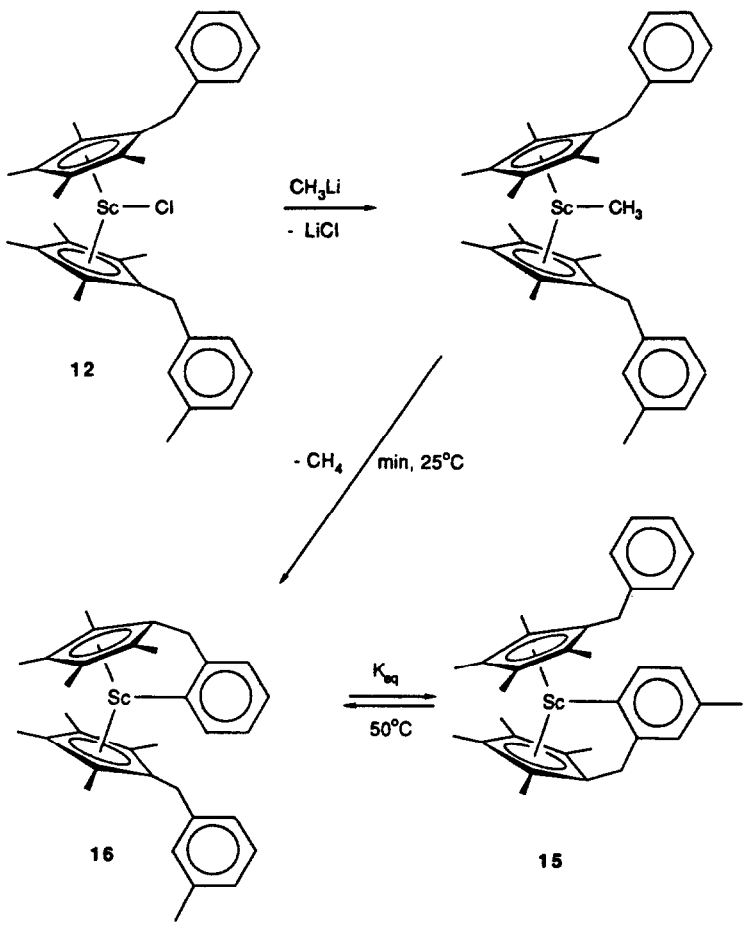

Scheme 2.

Table 2. ^{1}H and ^{13}C NMR data[a]

Compound	Assignment	δ (ppm)	Coupling[b]
$Li^{+}(C_5Me_4CH_2C_6H_4\text{-}m\text{-}CH_3)^{-}$[c]			
	$\eta^5\text{-}C_5(CH_3)_4CH_2C_6H_4\text{-}m\text{-}CH_3$	1.87 *s*	
	$\eta^5\text{-}C_5(CH_3)_4CH_2C_6H_4\text{-}m\text{-}CH_3$	3.63 *br*	
	$\eta^5\text{-}C_5(CH_3)_4CH_2C_6H_4\text{-}m\text{-}CH_3$	2.20 *s*	
	$\eta^5\text{-}C_5(CH_3)_4CH_2C_6H_4\text{-}m\text{-}CH_3$	6.6–7.0 *m*	
$Li^{+}(C_5Me_4CH_2C_6H_4\text{-}m\text{-}CF_3)^{-}$[c]			
	$\eta^5\text{-}C_5(CH_3)_4CH_2C_6H_4\text{-}m\text{-}CF_3$	1.83 *s*	
		1.87 *s*	
	$\eta^5\text{-}C_5(CH_3)_4CH_2C_6H_4\text{-}m\text{-}CF_3$	3.80 *br*	
	$\eta^5\text{-}C_5(CH_3)_4CH_2C_6H_4\text{-}m\text{-}CF_3$	7.1–7.4 *m*	
$Li^{+}(C_5Me_4CH_2C_6H_4\text{-}m\text{-}N(CH_3)_2)^{-}$[c]			
	$\eta^5\text{-}C_5(CH_3)_4CH_2C_6H_4\text{-}m\text{-}N(CH_3)_2$	1.93 *s*	
		1.90 *s*	
	$\eta^5\text{-}C_5(CH_3)_4CH_2C_6H_4\text{-}m\text{-}N(CH_3)_2$	3.60 *br*	
	$\eta^5\text{-}C_5(CH_3)_4CH_2C_6H_4\text{-}m\text{-}N(CH_3)_2$	2.80 *s*	
	$\eta^5\text{-}C_5(CH_3)_4CH_2C_6H_4\text{-}m\text{-}N(CH_3)_2$	6.3–7.0 *m*	
Cp*(η^5-$C_5Me_4CH_2CH_2CH_3$)ScCl (1)			
	$\eta^5\text{-}C_5(CH_3)_5$	1.90 *s*	
	$\eta^5\text{-}C_5(CH_3)_4CH_2CH_2CH_3$	1.85 *s*	
		2.01 *s*	
	$\eta^5\text{-}C_5Me_4CH_2CH_2CH_3$	0.79 *t*	$^{3}J_{HH} = 7$
	$\eta^5\text{-}C_5Me_4CH_2CH_2CH_3$	1.24 *m*	$^{3}J_{HH} = 7$
	$\eta^5\text{-}C_5Me_4CH_2CH_2CH_3$	2.35 *t*	$^{3}J_{HH} = 7$
Cp*(η^5,η^1-$C_5Me_4CH_2CH_2CH_2$)Sc (2)			
	$\eta^5\text{-}C_5(CH_3)_5$	1.83 *s*	
	$\eta^5,\eta^1\text{-}C_5(CH_3)_4CH_2CH_2CH_2$	1.57 *s*	
		1.97 *s*	
	$\eta^5,\eta^1\text{-}C_5Me_4CH_2CH_2CH_2$	0.77 *t*	$^{3}J_{HH} = 6.6$
	$\eta^5,\eta^1\text{-}C_5Me_4CH_2CH_2CH_2$	2.73 *tt*	$^{3}J_{HH} = 6.6$
	$\eta^5,\eta^1\text{-}C_5Me_4CH_2CH_2CH_2$	2.91 *t*	$^{3}J_{HH} = 6.6$
	$\eta^5\text{-}C_5(CH_3)_5$	11.40 *q*	$^{1}J_{CH} = 126$
	$\eta^5\text{-}C_5(CH_3)_5$	119.4 *s*	
	$\eta^5,\eta^1\text{-}C_5Me_4CH_2CH_2CH_2$	not observed	
	$\eta^5,\eta^1\text{-}C_5Me_4CH_2CH_2CH_2$	38.76 *t*	$^{1}J_{CH} = 120$
	$\eta^5,\eta^1\text{-}C_5Me_4CH_2CH_2CH_2$	28.9 *t*	$^{1}J_{CH} = 123$
	$\eta^5,\eta^1\text{-}C_5(CH_3)_4CH_2CH_2CH_2$	117.0 *s*	
		119.6 *s*	
		138.2 *s*	
Cp*(η^5-$C_5Me_4CH_2CH_2CH_3$)Sc(C_6H_5) (3)[f]			
	$\eta^5\text{-}C_5(CH_3)_5$	1.68 *s*	
	$\eta^5\text{-}C_5(CH_3)_4CH_2CH_2CH_3$	1.70 *s*	
		1.72 *s*	
	$\eta^5\text{-}C_5Me_4CH_2CH_2CH_3$	0.82 *t*	$^{3}J_{HH} = 7$
	$\eta^5\text{-}C_5Me_4CH_2CH_2CH_3$	1.22 *m*	$^{3}J_{HH} = 7$
	$\eta^5\text{-}C_5Me_4CH_2CH_2CH_3$	2.18 *t*	$^{3}J_{HH} = 7$
	$Sc(C_6H_5)$	6.81 *d*	$^{3}J_{HH} = 7$
		6.95 *t*	$^{3}J_{HH} = 7$
		7.09 *t*	$^{3}J_{HH} = 7$
Cp*(η^5-$C_5Me_4CH_2CH_2CH_3$)$HfCl_2$ (4)			
	$\eta^5\text{-}C_5(CH_3)_5$	1.93 *s*	
	$\eta^5\text{-}C_5(CH_3)_4CH_2CH_2CH_3$	1.91 *s*	
		1.99 *s*	

(*Contd.*)

Table 2. (*Contd.*)

Compound	Assignment	δ (ppm)	Coupling[b]
	η^5-$C_5Me_4CH_2CH_2CH_3$	0.82 *t*	$^3J_{HH} = 7.3$
	η^5-$C_5Me_4CH_2CH_2CH_3$	1.28 *m*	$^3J_{HH} \sim 8$
	η^5-$C_5Me_4CH_2CH_2CH_3$	2.50 *t*	$^3J_{HH} = 8.0$
Cp*(η^5-$C_5Me_4CH_2CH_2CH_3$)HfH_2 (**5**)			
	η^5-$C_5(CH_3)_5$	2.07 *s*	
	η^5-$C_5(CH_3)_4CH_2CH_2CH_3$	2.10 *s*	
		1.92 *s*	
	η^5-$C_5Me_4CH_2CH_2CH_3$	0.88 *t*	$^3J_{HH} = 8$
	η^5-$C_5Me_4CH_2CH_2CH_3$	1.41 *m*	$^3J_{HH} = 8$
	η^5-$C_5Me_4CH_2CH_2CH_3$	2.50 *t*	$^3J_{HH} = 8$
	HfH_2	15.6 *s*	
Cp*(η^5,η^1-$C_5Me_4CH_2CH_2CH_2$)HfH (**6**)			
	η^5-$C_5(CH_3)_5$	1.91 *s*	
	η^5,η^1-$C_5(CH_3)_4CH_2CH_2CH_2$	1.68 *s*	
		1.70 *s*	
		1.72 *s*	
		2.64 *s*	
	η^5,η^1-$C_5Me_4CH_2CH_2CH_2$	−0.60 *m*	
		0.31 *m*	
		1.90 *m*	
		2.02 *m*	
		2.58 *m*	
		2.78 *m*	
	HfH	13.2 *s*	
	η^5,η^1-$C_5(CH_3)_4(CH_2CH_2CH_2)$	74.09 *t*	
	η^5,η^1-$C_5(CH_3)_4(CH_2CH_2CH_2)$	37.58 *t*	$^1J_{CH} = 125$
	η^5,η^1-$C_5(CH_3)_4(CH_2CH_2CH_2)$	27.28 *t*	$^1J_{CH} = 120$
Cp*(η^5-$C_5Me_4CH_2C_6H_5$)$HfCl_2$ (**7**)[d]			
	η^5-$C_5(CH_3)_5$	2.03 *s*	
	η^5-$C_5(CH_3)_4CH_2C_6H_5$	1.97 *s*	
		2.03 *s*	
	η^5-$C_5(CH_3)_4CH_2C_6H_5$	3.80 *s*	
	η^5-$C_5(CH_3)_4CH_2C_6H_5$	6.9–7.2 *m*	
Cp*(η^5-$C_5Me_4CH_2C_6H_4$-*m*-CH_3)$Hf(CH_2C_6H_5)_2$[e]			
	η^5-$C_5(CH_3)_5$	1.75 *s*	
	η^5-$C_5(CH_3)_4CH_2C_6H_5$	1.74 *s*	
		1.76 *s*	
	η^5-$C_5(CH_3)_4CH_2C_6H_5$	3.61 *s*	
	$HfCH_2C_6H_5$	1.44 *d*	$^2J_{HH} = 13$
		1.49 *d*	$^2J_{HH} = 13$
	η^5-$C_5(CH_3)_4CH_2C_5H_5$	6.9–7.2 *m*	
	$HfCH_2C_6H_5$	6.9–7.2 *m*	
Cp*(η^5-$C_5Me_4CH_2C_6H_5$)HfH_2 (**8**)			
	$\eta^5C_5(CH_3)_5$	2.07 *s*	
	η^5-$C_5(CH_3)_4CH_2C_6H_5$	1.97 *s*	
		2.07 *s*	
	η^5-$C_5(CH_3)_4CH_2C_6H_5$	4.08 *s*	
	η^5-$C_5(CH_3)_4CH_2C_6H_5$	7.0–7.2 *m*	
	Hf-*H*	15.70	
Cp*(η^5,η^1-$C_5Me_4CH_2$-*o*-C_6H_4)HfH (**9**)			
	η^5-$C_5(CH_3)_5$	19.5 *s*	

(*Contd.*)

Table 2. (*Contd.*)

Compound	Assignment	δ (ppm)	Coupling[b]
	η^5,η^1-$C_5(CH_3)_4CH_2$-*o*-C_6H_4	1.74 *s*	
		1.87 *s*	
		1.97 *s*	
		2.02 *s*	
	η^5,η^1-$C_5Me_4CH_2$-*o*-C_6H_4	3.76 *d*	$^2J_{HH} = 17$
		3.92 *d*	$^2J_{HH} = 17$
	η^5,η^1-$C_5Me_4CH_2$-*o*-C_6H_4	7.2–7.5 *m*	
	Hf-*H*	14.15 *s*	
Cp*(η^5,η^1-$C_5Me_4CH_2$-*o*-C_6H_3-*p*-CH_3)Sc[g]			
	η^5-$C_5(CH_3)_5$	1.96 *s*	
	η^5,η^1-$C_5(CH_3)_4CH_2$-*o*-C_6H_3-*p*-CH_3	2.03 *s*	
		1.48 *s*	
	η^5,η^1-$C_5(CH_3)_4CH_2$-*o*-C_6H_3-*p*-CH_3	2.37 *s*	
	η^5,η^1-$C_5(CH_3)_4CH_2$-*o*-C_6H_3-*p*-CH_3	4.06 *s*	
	η^5,η^1-$C_5(CH_3)_4CH_2$-*o*-C_6H_3-*p*-CH_3	8.45 *d*	$^3J_{HH} = 7.4$
		7.13 *d*	$^3J_{HH} = 7.4$
		7.26 *s*	
Cp*(η^5-$C_5Me_4CH_2C_6H_5$)ScCl[e]			
	η^5-$C_5(CH_3)_5$	1.88 *s* (7 methyls)	
	η^5-$C_5(CH_3)_4CH_2C_6H_4$	1.97 *s* (2 methyls)	
	η^5-$C_5(CH_3)_4CH_2C_6H_4$	3.75 *s*	
	η^5-$C_5(CH_3)_4CH_2C_6H_4$	7.0–7.2 *m*	
Cp*(η^5,η^1-$C_5Me_4CH_2$-*o*-C_6H_4)Sc (**10**)[g]			
	η^5-$C_5(CH_3)_5$	1.95 *s*	
	η^5,η^1-$C_5(CH_3)_4CH_2$-*o*-C_6H_4	2.01 *s*	
		1.45 *s*	
	η^5,η^1-$C_5(CH_3)_4CH_2$-*o*-C_6H_4	4.08 *s*	
	η^5,η^1-$C_5(CH_3)_4CH_2$-*o*-C_6H_4	7.3–8.55 *m*	
Cp*(η^5-$C_5Me_4CH_2C_6H_5$)Sc—C≡$CCMe_3$ (**11**)			
	η^5-$C_5(CH_3)_5$	1.88 *s*	
	η^5-$C_5(CH_3)_4CH_2C_6H_4$	1.97 *s*	
		2.07 *s*	
	$C(CH_3)_3$	1.30 *s*	
	η^5-$C_5(CH_3)_4CH_2C_6H_4$	3.73 *s*	
	η^5-$C_5(CH_3)_4CH_2C_6H_4$	7.0–7.3 *m*	
(η^5-$C_5Me_4CH_2C_6H_5$)Sc(acac)$_2$[d]			
	η^5-$C_5(CH_3)_4CH_2C_6H_5$	1.87 *s*	
		1.90 *s*	
	η^2-$OC(CH_3)CH(CH_3)CO$	2.03 *s*	
	η^5-$C_5(CH_3)_4CH_2C_6H_5$	3.73 *s*	
	η^2-$OC(CH_3)CH(CH_3)CO$	5.57 *s*	
	η^5-$C_5(CH_3)_4CH_2C_6H_5$	7.0–7.3 *m*	
(η^5-$C_5Me_4CH_2C_6H_5$)$ScCl_2$[c]			
	η^5-$C_5(CH_3)_4CH_2C_6H_5$	2.03 *s*	
		2.09 *s*	
	η^5-$C_5(CH_3)_4CH_2C_6H_5$	4.0 *s*	
	η^5-$C_5(CH_3)_4CH_2C_6H_5$	6.9–7.2 *m*	
(η^5-$C_5Me_4CH_2C_6H_4$-*m*-CH_3)(η^5-$C_5Me_4CH_2C_6H_5$)ScCl (**12**)			
	η^5-$C_5(CH_3)_4CH_2C_6H_4$-*m*-CH_3	1.85 *s* (2 methyls)	
	and		
	η^5-$C_5(CH_3)_4CH_2C_6H_5$	1.95 *s* (1 methyl)	
		2.03 *s* (1 methyl)	

(*Contd.*)

Table 2. (*Contd.*)

Compound	Assignment	δ (ppm)	Coupling[b]
	η^5-$C_5(CH_3)_4CH_2C_6H_4$-*m*-CH_3	2.11 *s*	
	η^5-$C_5(CH_3)_4CH_2C_6H_4$-*m*-CH_3	3.70 *s*	
	η^5-$C_5(CH_3)_4CH_2C_6H_5$	3.70 *s*	
	η^5-$C_5(CH_3)_4CH_2C_6H_4$-*m*-CH_3	6.8–7.2 *m*	
	η^5-$C_5(CH_3)_4CH_2C_6H_5$		
(η^5-$C_5Me_4CH_2C_6H_4$-*m*-CH_3)(η^5-$C_5Me_4CH_2C_6H_5$)ScH			
	η^5-$C_5(CH_3)_4CH_2C_6H_4$-*m*-CH_3	1.89 *s*	
	and		
	η^5-$C_5(CH_3)_4CH_2C_6H_5$	1.90 *s*	
		2.02 *s*	
		2.06 *s*	
	η^5-$C_5(CH_3)_4CH_2C_6H_4$-*m*-CH_3	2.09 *s*	
	η^5-$C_5(CH_3)_4CH_2C_6H_4$-*m*-CH_3	3.79 *s*	
	η^5-$C_5(CH_3)_4CH_2C_6H_5$	3.79 *s*	
	η^5-$C_5(CH_3)_4CH_2C_6H_4$-*m*-CH_3		
	and	6.8–7.2 *m*	
	η^5-$C_5(CH_3)_4CH_2C_6H_5$		
(η^5-$C_5Me_4CH_2C_6H_4$-*m*-CH_3)Sc(acac)$_2$[d]			
	η^5-$C_5(CH_3)_4CH_2C_6H_4$-*m*-CH_3	1.87 *s*	
		1.90 *s*	
	η^5-$C_5(CH_3)_4CH_2C_6H_4$-*m*-CH_3	2.27 *s*	
	η^5-$C_5(CH_3)_4CH_2C_6H_4$-*m*-CH_3	3.70 *s*	
	η^2-$OC(CH_3)CH(CH_3)CO$	2.05 *s*	
	η^2-$OC(CH_3)CH(CH_3)CO$	5.55 *s*	
	η^5-$C_5(CH_3)_4CH_2C_6H_4$-*m*-CH_3	6.8–7.3 *m*	
(η^5-$C_5Me_4CH_2C_6H_4$-*m*-CH_3)$ScCl_2$[e]			
	η^5-$C_5(CH_3)_4CH_2C_6H_4$-*m*-CH_3	2.20 *s*	
		2.28 *s*	
	η^5-$C_5(CH_3)_4CH_2C_6H_4$-*m*-CH_3	2.07 *s*	
	η^5-$C_5(CH_3)_4CH_2C_6H_4$-*m*-CH_3	4.33 *s*	
	η^5-$C_5(CH_3)_4CH_2C_6H_4$-*m*-CH_3	6.8–7.1 *m*	
(η^5-$C_5Me_4CH_2C_6H_4$-*m*-CH_3)(η^5-$C_5Me_4CH_2C_6H_4$-*m*-CF_3)ScCl (**13**)			
	η^5-$C_5(CH_3)_4CH_2C_6H_4$-*m*-CF_3	1.80 *s*	
	and		
	η^5-$C_5(CH_3)_4CH_2C_6H_4$-*m*-CH_3	1.82 *s*	
		1.85 *s*	
		2.03 *s*	
	η^5-$C_5(CH_3)_4CH_2C_6H_4$-*m*-CH_3	2.08 *s*	
	η^5-$C_5(CH_3)_4CH_2C_6H_4$-*m*-CH_3	3.72 *s*	
	η^5-$C_5(CH_3)_4CH_2C_6H_4$-*m*-CF_3	3.72 *s*	
	η^5-$C_5(CH_3)_4CH_2C_6H_4$-*m*-CH_3		
	and	6.8–7.4 *m*	
	η^5-$C_5(CH_3)_4CH_2C_6H_4$-*m*-CF_3		
(η^5-$C_5Me_4CH_2C_6H_4$-*m*-CH_3)(η^5-$C_5Me_4CH_2C_6H_4$-*m*-CF_3)ScC_6H_5			
	η^5-$C_5(CH_3)_4CH_2C_6H_4$-*m*-CH_3	1.63 *s*	
	and		
	η^5-$C_5(CH_3)_4CH_2C_6H_4$-*m*-CF_3	1.750 *s*	
		1.758 *s*	
		1.761 *s*	
	η^5-$C_5(CH_3)_4CH_2C_6H_4$-*m*-CH_3	2.07 *s*	
	η^5-$C_5(CH_3)_4CH_2C_6H_4$-*m*-CH_3	3.45 *s*	
	η^5-$C_5(CH_3)_4CH_2C_6H_4$-*m*-CF_3	3.58 *s*	
	η^5-$C_5(CH_3)_4CH_2C_6H_4$-*m*-CH_3		(*Contd.*)

Table 2. (*Contd.*)

Compound	Assignment	δ (ppm)	Coupling[b]
	η^5-$C_5(CH_3)_4CH_2C_6H_4$-*m*-CF_3	6.7–7.5 *m*	
	Sc—C_6H_5		
(η^5-$C_5Me_4CH_2C_6H_4$-*m*-CH_3)(η^5-$C_5Me_4CH_2C_6H_4$-*m*-NMe_2)ScCl (**14**)[g]			
	η^5-$C_5(CH_3)_4CH_2C_6H_4$-*m*-NMe_2	1.86 *s*	
	and		
	η^5-$C_5(CH_3)_4CH_2C_6H_4$-*m*-CH_3	1.89 *s*	
		1.97 *s*	
		2.21 *s*	
	η^5-$C_5(CH_3)_4CH_2C_6H_4$-*m*-CH_3	2.09 *s*	
	η^5-$C_5(CH_3)_4CH_2C_6H_4$-*m*-$N(CH_3)_2$	2.59 *s*	
	η^5-$C_5(CH_3)_4CH_2C_6H_4$-*m*-$N(CH_3)_2$	3.63 *s*	
	η^5-$C_5(CH_3)_4CH_2C_6H_4$-*m*-CH_3	3.70 *s*	
	η^5-$C_5(CH_3)_4CH_2C_6H_4$-*m*-CH_3		
	and	6.4–7.2 *m*	
	η^5-$C_5(CH_3)_4CH_2C_6H_4$-*m*-$N(CH_3)_2$		
(η^5-$C_5Me_4CH_2C_6H_4$-*m*-CH_3)(η^5-$C_5Me_4CH_2C_6H_4$-*m*-NMe_2)ScC_6H_5[g]			
	η^5-$C_5(CH_3)_4CH_2C_6H_4$-*m*-CH_3	1.787 *s*	
	and		
	η^5-$C_5(CH_3)_4CH_2C_6H_4$-*m*-NMe_2	1.792 *s*	
		1.796 *s*	
		1.86 *s*	
	η^5-$C_5(CH_3)_4CH_2C_6H_4$-*m*-CH_3	2.06 *s*	
	η^5-$C_5(CH_3)_4CH_2C_6H_4$-*m*-*p*$N(CH_3)_2$	2.51 *s*	
	η^5-$C_5(CH_3)_4CH_2C_6H_4$-*m*-CH_3	3.62 *s*	
	η^5-$C_5(CH_3)_4CH_2C_6H_4$-*m*-NMe_2	3.70	
	η^5-$C_5(CH_3)_4CH_2C_6H_4$-*m*-CH_3		
	η^5-$C_5(CH_3)_4CH_2C_6H_4$-*m*-NMe_2	6.5–7.5 *m*	
	Sc—C_6H_5		
(η^5-$C_5Me_4CH_2C_6H_5$)(η^5,η^1-$C_5Me_4CH_2$-*o*-C_6H_3-*p*-CH_3)Sc (**15**)[g]			
	η^5,η^1-$C_5(CH_3)_4CH_2$-*o*-C_6H_3-*p*-CH_3	1.53 *s*	
	and		
	η^5-$C_5(CH_3)_4CH_2C_6H_5$	1.96 *s*	
		1.993 *s*	
		1.998 *s*	
	η^5,η^1-$C_5(CH_3)_4CH_2$-*o*-C_6H_3-*p*-CH_3	2.38 *s*	
	η^5-$C_5(CH_3)_4CH_2C_6H_5$	3.90 *s*	
	η^5,η^1-$C_5(CH_3)_4CH_2$-*o*-C_6H_3-*p*-CH_3	4.09 *s*	
	η^5,η^1-$C_5(CH_3)_4CH_2$-*o*-C_6H_3-*p*-CH_3		
	and	6.7–8.5 *m*	
	η^5-$C_5(CH_3)_4CH_2C_6H_5$		
(η^5-$C_5Me_4CH_2C_6H_4$-*m*-CH_3)(η^5,η^1-$C_5Me_4CH_2$-*o*-C_6H_4)Sc (**16**)[g]			
	η^5-$C_5(CH_3)_4CH_2C_6H_4$-*m*-CH_3	1.50 *s*	
	and		
	$\eta^5\eta^1$-$C_5(CH_3)_4CH_2$-*o*-C_6H_4	1.93 *s*	
		1.99 *s*	
		2.04 *s*	
	η^5-$C_5(CH_3)_4CH_2C_6H_4$-*m*-CH_3	2.06 *s*	
	η^5-$C_5(CH_3)_4CH_2C_6H_4$-*m*-CH_3	4.09 *s*	
	η^5,η^1-$C_5(CH_3)_4CH_2$-*o*-C_6H_4	3.87 *s*	
	η^5-$C_5(CH_3)_4CH_2C_6H_4$-*m*-CH_3		
	and	6.7–8.5 *m*	
	η^5,η^1-$C_5(CH_3)_4CH_2$-*o*-C_6H_4		
(η^5-$C_5Me_4CH_2C_6H_4$-*m*-CH_3)(η^5,η^1-$C_5Me_4CH_2$-*o*-C_6H_3-*p*-CF_3)Sc (**17**)[g]			
	η^5-$C_5(CH_3)_4CH_2C_6H_4$-*m*-CH_3	1.39 *s*	

(*Contd.*)

Table 2. (*Contd.*)

Compound	Assignment	δ (ppm)	Coupling[b]
	and		
	η^5,η^1-$C_5(CH_3)_4CH_2$-*o*-C_6H_3-*p*-CF_3	1.85 *s*	
		1.94 *s*	
		1.97 *s*	
	η^5-$C_5(CH_3)_4CH_2C_6H_4$-*m*-CH_3	2.06 *s*	
	η^5,η^1-$C_5(CH_3)_4CH_2$-*o*-C_6H_3-*p*-CF_3	3.78 *s*	
	η^5-$C_5(CH_3)_4CH_2C_6H_4$-*m*-CH_3	3.86 *s*	
	η^5-$C_5(CH_3)_4CH_2C_6H_4$-*m*-CH_3		
	and	6.64–8.41 *m*	
	η^5,η^1-$C_5(CH_3)_4CH_2$-*o*-C_6H_3-*p*-CF_3		
(η^5-$C_5Me_4CH_2C_6H_4$-*m*-CF_3)(η^5,η^1-$C_5Me_4CH_2$-*o*-C_6H_3-*p*-CH_3)Sc (**18**)[g]			
	η^5,η^1-$C_5(CH_3)_4CH_2$-*o*-C_6H_3-*p*-CH_3	1.51 *s*	
	and		
	η^5-$C_5(CH_3)_4CH_2C_6H_4$-*m*-CF_3	1.87 *s*	
		1.93 *s*	
		1.99 *s*	
	η^5,η^1-$C_5(CH_3)_4CH_2$-*o*-C_6H_3-*p*-CH_3	2.38 *s*	
	η^5,η^1-$C_5(CH_3)_4CH_2$-*o*-C_6H_3-*p*-CH_3	3.83 *s*	
	η^5-$C_5(CH_3)_4CH_2C_6H_4$-*m*-CF_3	4.09 *s*	
	η^5,η^1-$C_5(CH_3)_4CH_2$-*o*-C_6H_3-*p*-CH_3		
	and	6.6–8.4 *m*	
	η^5-$C_5(CH_3)_4CH_2C_6H_4$-*m*-CF_3		
(η^5-$C_5Me_4CH_2C_6H_4$-*m*-NMe_2)(η^5,η^1-$C_5Me_4CH_2$-*o*-C_6H_3-*p*-CH_3)Sc (**19**)			
and			
(η^5-$C_5Me_4CH_2C_6H_4$-*m*-CH_3)(η^5,η^1-$C_5Me_4CH_2$-*o*-C_6H_3-*p*-NMe_2)Sc (**20**)[g]			
		1.58 *s*	
		1.61 *s*	
	η^5,η^1-$C_5(CH_3)_4CH_2$-*o*-C_6H_3-*p*-CH_3	1.94 *s*	
	η^5,η^1-$C_5(CH_3)_4CH_2$-*o*-C_6H_3-*p*-NMe_2	1.95 *s*	
	η^5-$C_5(CH_3)_4CH_2C_6H_4$-*m*-CH_3	2.01 *s*	
	η^5-$C_5(CH_3)_4CH_2C_6H_4$-*m*-NMe_2	2.05 *s*	
		2.09 *s*	
		2.16 *s*	
	η^5,η^1-$C_5(CH_3)_4CH_2$-*o*-C_6H_3-*p*-$N(CH_3)_2$	2.75 *s*	
	η^5-$C_5(CH_3)_4CH_2C_6H_4$-*m*-$N(CH_3)_2$	2.47 *s*	
	η^5-$C_5(CH_3)_4CH_2C_6H_4$-*m*-CH_3	2.38 *s*	
	η^5,η^1-$C_5(CH_3)_4CH_2$-*o*-C_6H_3-*p*-CH_3	2.06 *s*	
	η^5-$C_5(CH_3)_4CH_2C_6H_4$-*m*-CH_3	3.84 *s*	
	η^5,η^1-$C_5(CH_3)_4CH_2$-*o*-C_6H_3-*p*-$N(CH_3)_2$	3.95 *s*	
	η^5,η^1-$C_5(CH_3)_4CH_2$-*o*-C_6H_3-*p*-CH_3	4.07 *s*	
	η^5-$C_5(CH_3)_4CH_2C_6H_4$-*m*-NMe_2	4.16 *s*	
	η^5,η^1-$C_5(CH_3)_4CH_2$-*o*-C_6H_3-*p*-$N(CH_3)_2$		
	η^5,η^1-$C_5(CH_3)_4CH_2$-*o*-C_6H_3-*p*-CH_3	6.3–8.5 *m*	
	η^5-$C_5(CH_3)_4CH_2C_6H_4$-*m*-NMe_2		
	η^5-$C_5(CH_3)_4CH_2C_6H_4$-*m*-CH_3		

[a] All ^{1}H NMR spectra were recorded in benzene-d_6 at 400 MHz unless otherwise noted. All signals are reference to internal tetramethylsilane unless otherwise noted.

[b] Coupling constants are reported in Hz.

[c] ^{1}H NMR spectrum recorded in THF-d_8 at 90 MHz.

[d] ^{1}H NMR spectrum recorded in $CDCl_3$ at 90 MHz.

[e] ^{1}H NMR spectrum recorded in benzene-d_6 at 90 MHz.

[f] ^{1}H NMR spectrum recorded in cyclohexane-d_{12} and referenced to the residual protio impurity.

[g] ^{1}H NMR spectrum recorded in benzene-d_6 at 500 MHz.

Note: The following abbreviations are used to denote the multiplicity of the NMR signals: *s*, singlet; *d*, doublet; *t*, triplet; *q*, quartet; *m*, multiplet; *br*, broad.

$Me_4CH_2C_6H_4$-*m*-CF_3)ScCl with one equivalent of trimethylsilylmethyllithium rapidly generates tetramethylsilane and a *ca* 1:1 mixture of (η^5-$C_5Me_4CH_2C_6H_4$-*m*-CH_3)(η^5,η^1-$C_5Me_4CH_2$-*o*-C_6H_3-*p*-CF_3)Sc (**17**) and (η^5,η^1-$C_5Me_4CH_2$-*o*-C_6H_3-*p*-CH_3)(η^5-$C_5Me_4CH_2C_6H_4$-*m*-CF_3)Sc (**18**), presumably via (η^5-$C_5Me_4CH_2C_6H_4$-*m*-CH_3)(η^5-$C_5Me_4CH_2C_6H_4$-*m*-CF_3)Sc—CH_2SiMe_3. When warmed to 50°C for a few minutes, the ratio of **17** to **18** changes to 16:1. Continued heating at 50°C results in decomposition over a period of 1–2 h; however, the ratio of **17** to **18** remains *ca* 16:1. A much more thermally robust mixture of **17** and **18** is obtained using an alternative preparation. Treating (η^5-$C_5Me_4CH_2C_6H_4$-*m*-CH_3)(η^5-$C_5Me_4CH_2C_6H_4$-*m*-CF_3)ScCl with one equivalent of phenyllithium generates the phenyl derivative (η^5-$C_5Me_4CH_2C_6H_4$-*m*-CH_3)(η^5-$C_5Me_4CH_2C_6H_4$-*m*-CF_3)Sc—C_6H_5, which is stable to loss of benzene at ambient temperature. Heating an isolated sample of (η^5-$C_5Me_4CH_2C_6H_4$-*m*-CH_3)(η^5-$C_5Me_4CH_2C_6H_4$-*m*-CF_3)Sc—C_6H_5 in benzene-d_6 to 80°C results in benzene loss and the 16:1 isomeric mixture† of (η^5-$C_5Me_4CH_2C_6H_4$-*m*-CH_3)(η^5,η^1-$C_5Me_4CH_2$-*o*-C_6H_3-*p*-CF_3)Sc (**17**) and (η^5,η^1-$C_5Me_4CH_2$-*o*-C_6H_3-*p*-CH_3)(η^5-$C_5Me_4CH_2C_6H_4$-*m*-CF_3)Sc (**18**). Thermal decomposition of this mixture is much slower, requiring several days at 80°C. The variable thermal stabilities of these compounds from batch to batch suggests decomposition is catalysed by trace impurities, but the value of K_{eq} is not in doubt [**17** ⇄ **18**, K_{eq} = 0.063(6)].

Treating (η^5-$C_5Me_4CH_2C_6H_4$-*m*-CH_3)(η^5-$C_5Me_4CH_2C_6H_4$-*m*-NMe_2)ScCl with one equivalent of LiC_6H_5 cleanly generates (η^5-$C_5Me_4CH_2C_6H_4$-*m*-CH_3)(η^5-$C_5Me_4CH_2C_6H_4$-*m*-NMe_2)ScC_6H_5. This complex has not been isolated, rather it is generated *in situ* and characterized by ^{1}H NMR. Heating benzene-d_6 solutions of (η^5-$C_5Me_4CH_2C_6H_4$-*m*-CH_3)(η^5-$C_5Me_4CH_2C_6H_4$-*m*-NMe_2)ScC_6H_5 overnight at 50°C generates C_6H_6 and a 1:1 mixture of (η^5,η^1-$C_5Me_4CH_2$-*o*-C_6H_3-*p*-CH_3)(η^5-$C_5Me_4CH_2C_6H_4$-*m*-NMe_2)Sc (**19**) and (η^5-$C_5Me_4CH_2C_6H_4$-*m*-CH_3)(η^5,η^1-$C_5Me_4CH_2$-*o*-C_6H_3-*p*-NMe_2)Sc (**20**). As with X = H and CH_3, heating solutions of the initially formed mixture at 80°C for several hours does not alter the isomeric ratio (nor does it effect decomposition). In order to assure that a true thermodynamic equilibrium had been reached, once again a small amount of dihydrogen was introduced into a benzene-d_6 solution of the phenyl derivative (η^5-$C_5Me_4CH_2C_6H_4$-*m*-CH_3)(η^5-$C_5Me_4CH_2C_6H_4$-*m*-NMe_2)Sc—C_6H_5 to catalyse rapid interconversion of **19** and **20** via (η^5-$C_5Me_4CH_2C_6H_4$-*m*-CH_3)(η^5-$C_5Me_4CH_2C_6H_4$-*m*-NMe_2)Sc—H. After heating for 20 h at 50°C no deviation from the original 1:1 ratio of (η^5,η^1-$C_5Me_4CH_2$-*o*-C_6H_3-*p*-CH_3)(η^5-$C_5Me_4CH_2C_6H_4$-*m*-NMe_2)Sc (**19**) and (η^5-$C_5Me_4CH_2C_6H_4$-*m*-CH_3)(η^5,η^1-$C_5Me_4CH_2$-*o*-C_6H_4-*p*-NMe_2)Sc (**20**) was noted. Thus, as for **15** and **16** no detectable substituent effect of the equilibrium constant for the two isomeric metallated benzyl complexes **19** and **20** was obtained.

DISCUSSION

Sigma bond metathesis has proven to be a convenient method to obtain information on the relative bond dissociation energies for these types of transition metal hydrides and hydrocarbyls. Due to interfering reactions, most likely involving the C—H bonds of the (η^5-C_5Me_5) ligands, *intermolecular* equilibrations appear to be limited to the very stable hydride and phenyl derivatives. Although our data indicate that the alkynyl complexes are even more stable, side reactions such as catalytic dimerization of terminal acetylenes to *gem*-enynes[3] preclude equilibration.

By incorporating reactive groups into the cyclopentadienyl ligands and introducing systematic variations we have capitalized on the tendency for the ligand C—H bonds to participate in the σ bond metathesis reactions. Morever, the favorable entropy associated with these intramolecular metallation reactions (ΔS^0 = 11–34 e.u.) provides an additional driving force ($T\Delta S^0$ = 3–10 kcal mol^{-1} at ambient temperature) to shift otherwise prohibitively endothermic equilibria to allow the concentrations of all participants to be accurately determined. These equilibrium constants [e.g. eqs (8), (11) and (14)] are no longer unitless, so that the issue of standard states‡ and transferability of K_{eq}'s or ΔG^0's is potentially problematic. However, by comparing ΔH^0 values obtained from the temperature dependence of the equilibrium constants, we can draw some meaningful comparisons. Another point of possible concern is the introduction of ring strain on metallation. Models suggest, and experiments appear to bear out [e.g. compare ΔH^0 values for eqs (3) and (14)] that there is little strain for a three-carbon link connecting the cyclopentadienyl ring carbon atom and the metal center. In the final series of experiments, those involving competitive metallation by scandium at either of two benzyl-substituted cyclopentadienyl ligands, the symmetry of the ligand system and the fact that the equilibrium constants are unitless completely remove these concerns.

† ^{1}H NMR integration was carried out at 50°C.

‡ We have chosen units of mole fraction in calculating the equilibrium constants for these cases.

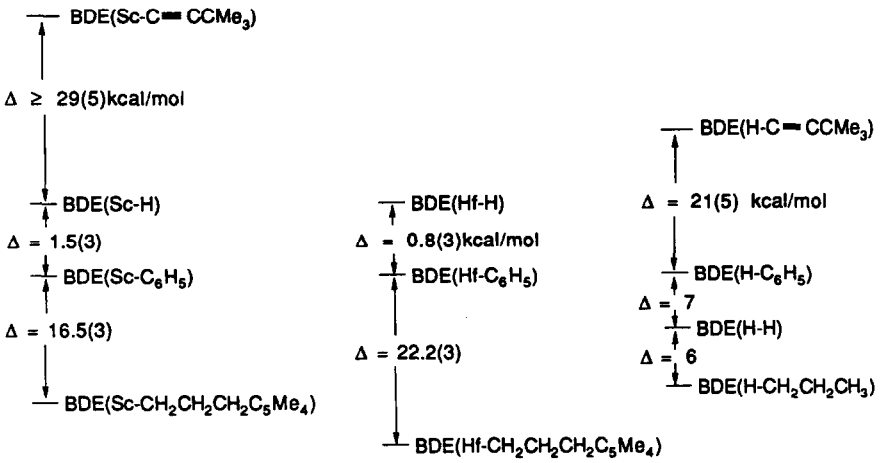

Scheme 3.

The enthalpies of the equilibrium, established by these sigma bond metathesis reactions [eq. (1)], allow the relative M—R and M—R′ bond strengths to be determined if one assumes the Benson approximation[5] and cancellation of the solvation energies.[6,7] In eq. (3), for example, since the H—C_6H_5 BDE = 110.9 kcal mol^{-1},[8] H—H BDE = 104.2 kcal mol^{-1}[9] and the heat of solvation of H_2 in benzene = −1.5 kcal mol^{-1},[10] then the +6.0(3) kcal mol^{-1} enthalpy of reaction indicates the BDE(Hf—H) is greater than BDE(Hf—C_6H_5) by (104.2–110.9+1.5+6.0) = 0.8(3) kcal mol^{-1}. In eq. (8), if the C—H BDE for Cp*(η^5-$C_5Me_4CH_2CH_2CH_2$—H)Sc—C_6H_5 is assumed to be 98 kcal mol^{-1} (the BDE for the 1° C—H bonds of propane), then the BDE(Sc—C_6H_5) is greater than BDE(Sc—$CH_2CH_2CH_2C_5Me_4$) by 16.6(3) kcal mol^{-1}, since BDE(H—C_6H_5) = 110.9 kcal mol^{-1} and ΔH^0 = +3.7(3) kcal mol^{-1}. The following ordering for Hf—R and Sc—R BDEs are calculated in an analogous manner (Scheme 3).†

Whereas the differences in metal–hydride and metal–phenyl bond strengths are essentially the same for Sc and Hf, the same cannot be said for the metal–phenyl vs metal–$CH_2CH_2CH_2C_5Me_4$ bond strengths. Some of the *ca* 6 kcal mol^{-1} discrepancy may be due to different ring strain energies for the pseudotrigonal scandium vs pseudotetrahedral hafnium. On the other hand, the total strain energy for the hafnium derivative amounts to only *ca* 2.5(3) kcal mol^{-1}, since according to equilibrium 14, the BDE(Hf—H) is greater than BDE(Hf—$C_6H_4CH_2C_5Me_4$) by 3.3(3) kcal mol^{-1}. Whatever the sources of these small effects, some general conclusions can be derived from the differences in bond strengths as the hybridization at the α carbon is varied. The order of decreasing BDEs is M—C(sp) > M—C(aryl) > M—C(sp^3), the same order as for H—C BDEs for hydrocarbons (Scheme 3). On the other hand, the relative differences for hydrogen–carbon bond strengths is small {BDE[H—C(sp)] = 132(5); BDE[H—C(aryl)] = 111; BDE[H—C(1°,sp^3)] = 98 kcal mol^{-1}} than those for the hafnium and scandium hydrocarbyls. Indeed, if the relative differences were the same, these equilibria would be essentially thermoneutral (i.e. $\Delta H^0 \approx 0$). The origin of the effect which is responsible for the M—R BDEs increasing more rapidly with s character than do the H—R BDEs is not clear; however, it undoubtedly again results in stronger M—H BDEs than would be anticipated on the basis of the correlation suggested by Bryndza, Bercaw and co-workers.[6]‡ For these early transition metal hydride compounds the BDE(M—H) is *ca* 8 kcal mol^{-1} stronger than this correlation predicts.

The sensitivity of the transition metal–carbon bond energy to s character could be a reflection of considerable ionic ($M^{\delta+}$—$C^{\delta-}$) bonding, since s character at carbon increases its electronegativity. The experiments designed to probe this aspect of the Sc—aryl bonding, equilibria 18, reveal very little substituent effect on the Sc—aryl BDE.§ Only for

† The relative positions of the (Sc—R) BDE, (Hf—R), and (H—R) BDE columns in Scheme 3 have been arbitrarily set equal at R = C_6H_5. No absolute correlation between the columns is implied.

‡ A roughly linear correlation is found for BDE(H—R) vs BDE(Sc—R) (R = alkynyl, aryl, alkyl), with a slope of 0.8, not the unity value of the Bryndza/Bercaw correlation. Similar, less-than-unity slopes have been noted by others for transition metal—hydrocarbyl bonds; see reference 7(d) and the contribution by Bergman and coworkers in this special issue of *Polyhedron*.

§ So far as we are aware, no substituent effects on the M—aryl (M = alkali or alkaline earth metal) BDEs have been examined. Thus, these results suffer from the lack of a point of reference.

para-CF_3 is a measureable difference obtained. *para*-NMe_2 exerts its effect primarily through resonant π donation. Interestingly, the phenyl ring is held perpendicular to the equatorial plane of the scandocene moiety by the link to the cyclopentadienyl ligand, i.e. in resonance with the empty π symmetry (b_2) scandium orbital. Thus, resonant donation is possible, but apparently is cancelled by the small inductive withdrawing character of the electronegative N atom. The generally small effect observed, even with the strongly withdrawing CF_3 substituent, is quite significant, and indicates little polarity for the Sc—C bond in these compounds. These experimental results are generally in accord with the picture presented by Goddard and Steigerwald[11] for the scandium–hydride bonding of Cl_2Sc—H, for which the electronegative Cl ligands (and by extension the Cp* ligands) bond primarily via the Sc 4s orbitals, with the Sc—H bonding being 3d–1s in character ($E_{3d} < E_{4s}$; hence Sc appears more electronegative[12]) and essentially covalent. It appears this same 3d character also dominates the Sc orbital used in the Sc—aryl bonding of compounds **15–20**.

EXPERIMENTAL

General considerations

All manipulations were performed using glovebox, high-vacuum[13] or Schlenk techniques. Solvents were purified by distillation from an appropriate drying agent under a N_2 atmosphere and either used immediately or vacuum-transferred from 'titanocene' or sodium–benzophenone. Benzene-d_6 and cyclohexane-d_{12} were purified by vacuum transfer from activated molecular sieves (4 Å, Linde) and then from 'titanocene'. ^1H and ^{13}C NMR spectra were recorded on Varian EM-390 (90 MHz, ^1H), JEOL GX400Q (400 MHz, ^1H; 100 MHz, ^{13}C) and Bruker WM500 (500 MHz, ^1H) spectrometers. Elemental analyses were performed by Mr Larry Henling of the CIT Analytical Laboratory.

Synthetic procedures

Preparation of $Li^+(C_5Me_4CH_2C_6H_4$-*m*-X)$^-$ [X = H,[14] CH_3, CF_3 *and* $N(CH_3)_2$].† Each ligand was prepared by the reaction of tetramethylcyclopentenone with the corresponding substituted benzyl Grignard reagent (Scheme 1), followed by dehydration with *para*-toluene sulphonic acid when needed. In each case an excess of the substituted Grignard reagent (*ca* 1.5 mol/mol of ketone) was allowed to react with tetramethylcyclopentenone. Due to the high boiling points of the ligands, purification and the final characterization was made by preparing the corresponding lithium salts.

(a) X = H. To 54 mmol of $BrMgCH_2C_6H_5$ in *ca* 100 cm^3 of diethyl ether was added 36 mmol of tetramethylcyclopentenone. The reaction mixture was refluxed overnight, then quenched with *ca* 30 cm^3 of H_2O. The organic products were extracted into diethyl ether (2×50 cm^3). The ethereal extracts were concentrated to *ca* 60 cm^3 and 0.5 g *para*-toluene sulphonic acid was added. The reaction mixture was stirred for 10 min at which time *ca* 50 cm^3 of H_2O and 1 g of $NaHCO_3$ were added. The organic product was extracted with diethyl ether (2×50 cm^3), dried over Na_2CO_4 and concentrated under high vacuum to yield 7.1 g of yellow oil. To this 7.1 g of oil in *ca* 100 cm^3 of diethyl ether (at $-80°C$) was syringed 21 cm^3 of a 1.6 M *n*-butyllithium/hexane solution. After stirring for 3 h at ambient temperatures a yellow precipitate had formed. This solid was collected by filtration, washed twice with diethyl ether and dried *in vacuo* to yield 4.2 g of $Li^+(C_5Me_4CH_2C_6H_5)^-$ (53% yield based on tetramethylcyclopentenone).

(b) X = CH_3. Following the procedure described above (for X = H), tetramethylcyclopentenone (5.0 g) and excess $BrMgCH_2C_6H_4$-*m*-CH_3 ultimately affords 4.4 g of $Li^+(C_5Me_4CH_2C_6H_4$-*m*-$CH_3)^-$ (52% based on tetramethylcyclopentenone). It should be noted that treatment of the initially isolated organic product with *para*-toluene sulphonic acid is not necessary due to spontaneous dehydration of the alcohol during work-up.

(c) X = CF_3. Again following the procedure described above (for X = H), tetramethylcyclopentanone (5.0 g) and excess $ClMgCH_2C_6H_4$-*m*-CF_3 ultimately affords 3.8 g of $Li^+(C_5Me_4CH_2C_6H_4$-*m*-$CF_3)^-$ (37% yield based on tetramethylcyclopentenone). The reaction time for the deprotonation of $HC_5Me_4CH_2C_6H_4$-*m*-CF_3 by *n*-butyllithium should be kept to a minimum (*ca* 1 h). Longer reaction times result in a darkening of the reaction mixture and a reduced yield of the lithium salt.

(d) X = NMe_2. *meta*-*N*,*N*-Dimethylaminobenzyl potassium was prepared in *N*,*N*-dimethyl-*meta*-toluidine following previously described procedures.[15] *meta*-*N*,*N*-Dimethylaminobenzylmagnesium bromide was prepared by stirring the potassium salt with anhydrous $MgBr_2$ etherate in diethyl ether, followed by filtration to

† We have found that the *meta*-methoxide derivative $Li^+(\eta^5$-$C_5Me_4CH_2C_6H_4$-*m*-OMe)$^-$ can also be prepared by methods analogous to those described here.

remove the KBr. To the filtrate was carefully added 5 g of tetramethylcyclopentenone and the resulting mixture was refluxed for 2 h. The reaction was quenched with *ca* 30 cm^3 of an aqueous solution containing 1 g of NaOH. The organic layer was separated and the aqueous layer was washed twice with 50 cm^3 portions of diethyl ether. The ether washings were combined and the volatiles were removed *in vacuo*. Residual *N,N*-dimethyl-*meta*-toluidine was removed by gently heating (30–40°C) for 2–3 h under hard vacuum. To the resulting alcohol was added 40 cm^3 of diethyl ether and 2.0 g of *para*-toluene sulphonic acid. After stirring for approximately 15 min a water layer became evident. To this mixture an aqueous solution containing 2.0 g of NaOH was added, the organic phase was separated, and the aqueous solution was washed twice with 50 cm^3 portions of diethyl ether. The solvent was removed *in vacuo* to afford 5.1 g of viscous yellow oil. To the 5.1 of crude ligand in *ca* 50 cm^3 of petroleum ether was added 12.5 cm^3 of *n*-butyllithium in hexane (1.6 M). The reaction was stirred for 2 h, then filtered to collect the precipitate. The product was washed with petroleum ether and dried to afford 2.0 g (21% based on tetramethylcyclopentenone) of pale yellow product.

$Cp^*(\eta^5\text{-}C_5Me_4CH_2CH_2CH_3)ScCl$ (**1**). $(\eta^5\text{-}C_5Me_5)ScCl_2$ (4.0 g, 15.9 mmol) and $Li(\eta^5\text{-}C_5Me_4CH_2CH_2CH_3)$[16] (3.0 g, 17.6 mmol) were heated in benzene at 110°C for three days. The solvent was removed *in vacuo* and the non-volatiles were washed into a flask with petroleum ether (40 cm^3) which was then attached to a frit assembly. The resultant suspension was filtered to remove the LiCl. Removal of the solvent *in vacuo* affords **1** as an amber oil in near quantitative yield (90–95% pure by ^1H NMR).

$Cp^*(\eta^5,\eta^1\text{-}C_5Me_4CH_2CH_2CH_2)Sc$ (**2**). $Cp^*(\eta^5\text{-}C_5Me_4CH_2CH_2CH_3)ScCl$ (2.5 g, 6.6 mmol) and $LiCH_3$ (0.145 g, 6.6 mmol) were stirred for 1 h in *ca* 20 cm^3 of benzene. The suspension was filtered and the benzene was replaced with petroleum ether. Cooling to −78°C resulted in the precipitation of product which was collected as a pale yellow solid by filtration (0.9 g, 40%). Elemental analysis: found(calculated) %C 75.22 (74.13), %H 9.33 (9.33).

$Cp^*(\eta^5\text{-}C_5Me_4CH_2CH_2CH_3)HfCl_2$ (**4**). $(\eta^5\text{-}C_5Me_5)HfCl_3$ (10.2 g, 24.3 mmol) and $Li(\eta^5\text{-}C_5Me_4CH_2CH_2CH_3)$ (4.2 g, 24.7 mmol) were refluxed in xylenes for three days under an argon atmosphere. Removal of the xylene solvent (under reduced pressure) followed by an aqueous/methylene chloride work-up[17] gave 12.6 g (95%) of **4** as off-white crystals.

$Cp^*(\eta^5,\eta^1\text{-}C_5Me_4CH_2CH_2CH_2)HfH$ (**6**). A flask was charged with **4** (4.28 g, 7.8 mmol) and *ca* 50 cm^3 of toluene. 10.7 cm^3 of a 1.6 M solution of *n*-butyllithium in hexane (2.2 equivalents of *n*-butyllithium) was added to the toluene suspension (at −78°C) under an argon flush. The argon was then replaced with one atmosphere of dihydrogen and the solution was allowed to warm with stirring. When the uptake of dihydrogen had ceased, the toluene was replaced with petroleum ether and the suspension was filtered. Removal of the petroleum ether *in vacuo* afforded an amber oil which consisted of an approximately equimolar ratio of $Cp^*(\eta^5\text{-}C_5Me_4CH_2CH_2CH_3)HfH_2$ (**5**) and $Cp^*(\eta^5,\eta^1\text{-}C_5Me_4CH_2CH_2CH_2)HfH$ (**6**). A benzene solution of this mixture was transferred to a small glass bomb which was heated to 80°C for several hours, then evacuated to remove the generated dihydrogen. After three cycles the contents of the bomb were transferred to a frit assembly and the benzene was replaced with petroleum ether. Cooling to −78°C and filtering afforded 1.8 g (50%) of **6** as a colourless powder. Elemental analysis: found (calculated) %C 55.34 (55.43), %H 7.07 (7.13).

$Cp^*(\eta^5\text{-}C_5Me_4CH_2C_6H_5)HfCl_2$ (**7**). $(\eta^5\text{-}C_5Me_5)HfCl_3$ (5.1 g, 12.1 mmol) and $Li^+(\eta^5\text{-}C_5Me_4CH_2C_6H_5)^-$ (2.7 g, 12.4 mmol) were refluxed in xylenes for three days under an argon atmosphere. Removal of the xylene solvent (under reduced pressure) followed by an aqueous/methylene chloride work-up gave 6.5 g (90%) of **7** as an off-white solid. Elemental analysis: found(calculated) %C 52.24(52.40), %H 5.53(5.75).

$Cp^*(\eta^5\text{-}C_5Me_4CH_2C_6H_5)Hf(CH_2C_6H_5)_2$. Approximately 20 cm^2 of benzene was condensed onto a mixture of **7** (1.94 g, 3.26 mmol) and excess benzylpotassium (1.39 g, 11.1 mmol). After stirring for 1 h the suspension was filtered and the benzene was replaced with petroleum ether. Cooling to −78°C and filtering afforded 1.69 g (73%) of pale yellow $Cp^*(\eta^5\text{-}C_5Me_4CH_2C_6H_5)Hf(CH_2C_6H_5)_2$.

$Cp^*(\eta^5,\eta^1\text{-}C_5Me_4CH_2\text{-}o\text{-}C_6H_4)HfH$ (**9**). A large glass bomb was charged with 1.49 g (2.10 mmol) of $Cp^*(\eta^5\text{-}C_5Me_4CH_2C_6H_5)Hf(CH_2C_6H_5)_2$ and 25 cm^3 of toluene. The bomb was cooled to −196°C, evacuated, then refilled with one atmosphere of dihydrogen (*ca* 4 atmospheres at 25°C). The solution was then stirred at 140°C for one day, recharged with dihydrogen, and stirred for a second day at 140°C. The ^1H NMR spectra of the crude reaction mixture showed the presence of $Cp^*(\eta^5\text{-}C_5Me_4CH_2C_6H_5)HfH_2$ (**8**) and $Cp^*(\eta^5,\eta^1\text{-}C_5Me_4CH_2\text{-}o\text{-}C_6H_4)HfH$ (**9**). Three cycles of heating the mixture to 80°C followed by removal of the generated dihydrogen *in vacuo* produces colourless **9**, which was isolated in 79% yield (0.88 g) from −78°C petroleum ether. Elemental analysis:

found(calculated) %C 59.39 (59.48), %H 6.51 (6.53).

Cp*(η^5-$C_5Me_4CH_2C_6H_5$)ScCl. Cp^*ScCl_2 (1.4 g, 5.5 mmol) and Li(η^5-$C_5Me_4CH_2C_6H_5$) (1.2 g, 5.5 mmol) were refluxed for 1 day in *ca* 25 cm^3 toluene. Filtering the reaction mixture and removing the solvent *in vacuo* afforded Cp*(η^5-$C_5Me_4CH_2C_6H_5$)ScCl as an amber oil which was essentially pure by ^1H NMR.

Cp*(η^5,η^1-$C_5Me_4CH_2$-*o*-C_6H_4)Sc (**10**). Cp*(η^5-$C_5Me_4CH_2C_6H_5$)ScCl (19.7 g, 4.62 mmol) and methyllithium (100 mg, 4.55 mmol) were stirred for 3 h in *ca* 20 cm^3 of benzene. The benzene solvent was replaced with petroleum ether and the LiCl was removed by filtration. Cooling the solution to −78°C and filtering afforded 0.54 g (30% yield) of colourless **10**. Elemental analysis: found (calculated) %C 79.39 (79.97), %H 8.31 (8.52).

Generation of Cp*(η^5,η^1-$C_5Me_4CH_2$-*o*-C_6H_3-*p*-CH_3)Sc. Cp^*ScCl_2 (90 mg, 0.36 mmol) and Li(η^5-$C_5Me_4CH_2C_6H_4$-*m*-CH_3) (83 mg, 0.36 mmol) were placed into a small glass bomb with 5 cm^3 of toluene and heated to 110°C for 1 day. To this reaction mixture was added $LiCH_2SiMe_3$ (34 mg, 0.36 mmol). After stirring overnight the toluene was removed *in vacuo* and the scandium product was extracted with benzene-d_6. This product, which was not isolated, exhibited a ^1H NMR spectrum consistent with Cp*(η^5,η^1-$C_5Me_4CH_2$-*o*-C_6H_3-*p*-CH_3)Sc.

(η^5-$C_5Me_4CH_2C_6H_4$-*meta*-X)Sc(acac)$_2$. (a) X = CH_3. $Sc(acac)_3$ (15.0 g, 43.9 mmol) and Li(η^5-$C_5Me_4CH_2C_6H_4$-*meta*-CH_3) (11.2 g, 48.2 mmol) were refluxed in *ca* 75 cm^3 of toluene for 12 h. The toluene was removed *in vacuo* and the air-stable product was washed three times (3 × 50 cm^3) with anhydrous methyl alcohol to remove the $Li^+(acac)^-$. The product was dried *in vacuo* to yield 11.6 g (56%) of pale yellow (η^5-$C_5ME_4CH_2C_6H_4$-*meta*-CH_3)Sc(acac)$_2$. (b) X = H. This air-stable compound was prepared in an analogous manner from 4.4 g of $Sc(acac)_3$ and 2.8 g of Li(η^5-$C_5Me_4CH_2C_6H_5$) to yield 4.1 g (71%) of product. Elemental analysis: found(calculated) %C 67.75 (68.71), %H 7.18 (7.32).

(η^5-$C_5Me_4CH_2C_6H_4$-*meta*-X)$ScCl_2$. (a) X = CH_3. (η^5-$C_5Mc_4CH_2C_6H_4$-*meta*-CH_3)Sc(acac)$_2$ (11.6 g, 24.8 mmol) and $AlCl_3$ (6.61 g, 49.6 mmol) were stirred overnight in *ca* 100 cm^3 of toluene. The resulting toluene suspension was heated to 100°C to dissolve the sparingly soluble products. Allowing the hot toluene solution to slowly cool to room temperature resulted in the precipitation of (η^5-$C_5Me_4CH_2C_6H_4$-*meta*-CH_3)$ScCl_2$, which was collected by filtration (5.2 g, 61%). (b) X = H. This compound was prepared in an analogous manner from 4.14 g of (η^5-$C_5Me_4CH_2C_6H_5$)Sc(acac)$_2$ and 2.44 g of $AlCl_3$ to yield 2.2 g (74%) of (η^5-$C_5Me_4CH_2C_6H_5$)$ScCl_2$. Elemental analysis: found (calculated) %C 59.18 (58.74), %H 6.00 (5.85).

(η^5-$C_5Me_4CH_2C_6H_4$-*m*-CH_3)(η^5-$C_5Me_4CH_2C_6H_5$)ScCl (**12**). (η^5-$C_5Me_4CH_2C_6H_5$)$ScCl_2$ (0.95 g, 2.9 mmol) and Li(η^5-$C_5Me_4CH_2C_6H_4$-*m*-CH_3) (0.67 g, 2.9 mmol) were refluxed overnight in *ca* 15 cm^3 of toluene. Filtration, followed by removal of the solvent *in vacuo* yielded **12** as an amber oil which was essentially pure by ^1H NMR.

(η^5-$C_5Me_4CH_2C_6H_4$-*m*-CH_3)(η^5-$C_5Me_4CH_2C_6H_4$-*m*-X)ScCl (**13**, X = CF_3; **14**, X = NMe_2). (**13**; X = CF_3) (η^5-$C_5Me_4CH_2C_6H_4$-*m*-CH_3)$ScCl_2$ (0.95 g, 2.79 mmol) and Li(η^5-$C_5Me_4CH_2C_6H_4$-*m*-CF_3) (0.80 g, 2.80 mmol) were refluxed for 3 h in *ca* 20 cm^3 of toluene. The toluene was replaced with petroleum ether and the solution was filtered. Cooling the petroleum ether solution to −78°C and filtering afforded 0.77 g (47%) of **13** as an off-white powder. (**14**; X = NMe_2) This compound was prepared in an analogous manner from 0.96 g (2.8 mmol) of (η^5-$C_5Me_4CH_2C_6H_4$-*m*-CH_3)$ScCl_2$ and 0.76 g (2.9 mmol) of Li(η^5-$C_5Me_4CH_2C_6H_4$-*m*-NMe_2) to yield 0.78 g (50%) of **14** as an off-white powder. Elemental analysis: found(calculated) %C 73.60 (75.05), %H 7.59 (8.10), %N 2.34 (2.50).

Synthesis of (η^5-$C_5Me_4CH_2C_6H_4$-*m*-CH_3)(η^5,η^1-$C_5Me_4CH_2$-*o*-C_6H_4)*Sc* (**16**) *and* (η^5,η^1-$C_5Me_4CH_2$-*o*-C_6H_3-*p*-CH_3)(η^5-$C_5Me_4CH_2C_6H_5$)Sc (**15**) *in a* 2 : 1 *ratio*. Methyllithium powder (60 mg, 2.7 mmol) was added to a benzene solution of **12** (1.3 g, 2.5 mmol) and the reaction mixture was stirred for 2 h. The benzene was replaced with petroleum ether and the solution was filtered. Cooling to −78°C and filtering afforded **16** and **15** in a 2 : 1 mixture (0.65 g, 54%). Elemental analysis: found(calculated) %C 81.83 (82.47), %H 8.13 (8.18).

Synthesis of (η^5-$C_5Me_4CH_2C_6H_4$-*m*-CH_3)(η^5,η^1-$C_5Me_4CH_2$-*o*-C_6H_3-*p*-CF_3)Sc (**17**) *and* (η^5,η^1-$C_5Me_4CH_2$-*o*-C_6H_3-*p*-CH_3)(η^5-$C_5Me_4CH_2C_6H_4$-*m*-CF_3)Sc (**18**) *in a* 1 : 1 (*kinetic*) *ratio*. Approximately 10 cm^3 of benzene was condensed onto a mixture of **13** (0.71 g, 1.21 mmol) and $LiCH_2SiMe_3$ (115 mg, 1.22 mmol). After stirring for 1 h the benzene was replaced with petroleum ether and the solution was filtered. Cooling the petroleum ether solution to −78°C and filtering afforded 390 mg (59%) of the two isomers in approximately a 1 : 1 ratio (^1H NMR).

(η^5-$C_5Me_4CH_2C_6H_4$-*m*-CH_3)(η^5-$C_5Me_4CH_2C_6H_4$-*m*-CF_3)ScC_6H_5. Approximately 20 cm^3 of benzene was condensed onto a mixture of **13** (0.92 g, 1.57 mmol) and phenyllithium (0.15 g, 1.79 mmol). This mixture was stirred for 1 h at room temperature and filtered. The benzene was replaced with

petroleum ether and cooled to −78°C. Filtering afforded 0.53 g (54%) of the product as an off-white powder. Elemental analysis: found(calculated) %C 73.86 (76.66), %H (6.80 (7.08).

Generation of **17** *and* **18** *in a* 16:1 *(thermodynamic) ratio.* Method (a). Heating a sample of the 1:1 mixture of (η^5-$C_5Me_4CH_2C_6H_4$-*m*-CH_3)(η^5,η^1-$C_5Me_4CH_2$-*o*-C_6H_3-*p*-CF_3)Sc and (η^5,η^1-$C_5Me_4CH_2$-*o*-C_6H_3-*p*-CH_3)(η^5-$C_5Me_4CH_2C_6H_4$-*m*-CF_3)Sc (isolated as described above) to 50°C in benzene-d_6 shifts the ratio to 16:1 within 1/2 h. This ratio was measured by integrating the benzyl methyl resonance of each isomer. Once established this ratio does not change, although decomposition is observed to slowly occur over the course of several hours. Method (b). Heating benzene-d_6 solutions of (η^5-$C_5Me_4CH_2C_6H_4$-*m*-CH_3)(η^5-$C_5Me_4CH_2C_6H_4$-*m*-CF_3)ScC_6H_5 overnight at 50°C cleanly generates benzene and a mixture of **17** and **18** in a 16:1 ratio. Samples generated in this manner do not undergo detectable decomposition until heated for several hours at 80°C.

Generation of (η^5,η^1-$C_5Me_4CH_2$-*o*-C_6H_3-*p*-CH_3)(η^5-$C_5Me_4CH_2C_6H_4$-*m*-NMe_2)Sc (**19**) *and* (η^5-$C_5Me_4CH_2C_6H_4$-*m*-CH_3)(η^5,η^1-$C_5Me_4CH_2$-*o*-C_6H_3-*p*-NMe_2)Sc (**20**) *in a* 1:1 *ratio.* Method (a). Compound **14**, 22 mg, and C_6H_5Li, 4 mg, were sealed in an NMR tube with benzene-d_6. After *ca* 15 min the ^{1}H NMR spectrum showed a single species identified as (η^5-$C_5Me_4CH_2C_6H_4$-*m*-CH_3)(η^5-$C_5Me_4CH_2C_6H_4$-*m*-NMe_2)ScC_6H_5. Heating (η^5-$C_5Me_4CH_2C_6H_4$-*m*-CH_3)(η^5-$C_5Me_4CH_2C_6H_4$-*m*-NMe_2)ScC_6H_5 overnight at 50°C resulted in the generation of C_6H_6 and a 1:1 mixture of **19** and **20**. Heating this sample to 80°C did not alter this ratio. Method (b). (η^5-$C_5Me_4CH_2C_6H_4$-*m*-CH_3)(η^5-$C_5Me_4CH_2C_6H_4$-*m*-NMe_2)ScC_6H_5 was generated as described above in a NMR tube attached to a Kontes needle valve. A catalytic amount of dihydrogen (*ca* 20 torr) was admitted to the tube which was then sealed with a torch. Heating the tube overnight at 50°C resulted in the generation of C_6H_6 and a 1:1 mixture of **19** and **20**.

Measurement of equilibrium constants

The equilibration of Cp*(η^5,η^1-$C_5Me_4CH_2CH_2CH_2$)HfH (**6**) and dihydrogen with Cp*(η^5-$C_5Me_4CH_2CH_2CH_3$)HfH_2 (**5**) [eq. (11)] was studied in the following manner. Compound **6** (16.8 mg, 0.034 mmol) was placed in a sealable NMR tube along with 0.481 g of benzene-d_6 and the tube was attached to a Kontes Teflon stoppered valve. The solvent was cooled to −78°C and the tube was evacuated. The benzene-d_6 was kept frozen at −78°C, but the remainder of the tube was allowed to warm to room temperature. Dihydrogen (282 torr) was admitted to the tube which was then sealed with a torch. The volume of space above the frozen benzene-d_6 was measured, allowing for the initial amount of dihydrogen in the NMR tube to be calculated. Subsequent equilibrations were carried out in a constant temperature ethylene glycol bath which was judged to be constant to ±0.2°C. The equation describing the equilibrium constant is given below.

$$K_{eq} = \frac{[H_2][\mathbf{6}]}{[\mathbf{5}]}.$$

The concentrations of **6** and **5** were determined from the relative heights of the resonances at δ 1.92 and 2.05, respectively. The total amount of dihydrogen in the NMR tube is given by eq. (20).

$$\text{total mmol } H_2 = (\text{mmol } H_2)_{\text{initial}} - \text{mmol } \mathbf{8} \quad (20)$$

A knowledge of the total amount of dihydrogen in the NMR tube allowed the concentration of dihydrogen in solution to be calculated as described elsewhere.[3] In order to obtain a unitless equilibrium constant the concentration of each species was expressed as a mole fraction. The equilibrium constants for eqs (3) and (14) were determined in an analogous manner.

The equilibration of **3** with benzene and **2** [eq. (8)] was studied by sealing 29 mg (0.085 mmol) of Cp*(η^5,η^1-$C_5Me_4CH_2CH_2CH_2$)Sc (**2**) in a NMR tube along with 56 mg of C_6H_6 (0.72 mmol) and 0.487 g of cyclohexane-d_{12}. The equation describing the equilibrium constant is given by:

$$K_{eq} = \frac{[C_6H_6][\mathbf{2}]}{[\mathbf{3}]}.$$

The concentrations of **2** and **3** were determined from the relative heights of their respective Cp* resonances. The total amount of C_6H_6 in the NMR tube is expressed by eq. (21).

$$\text{total mmol } C_6H_6 = (\text{mmol } C_6H_6)_{\text{initial}} - \text{mmol } \mathbf{3}. \quad (21)$$

The amount of dissolved C_6H_6 was calculated at each temperature using Henry's law. Concentrations were expressed as mole fractions in order to obtain unitless equilibrium constants.

A lower limit for the (Sc—alkynyl) BDE relative to the (Sc—aryl) BDE was established in the following manner. *tert*-Butylacetylene (0.016 mmol) was condensed into an NMR tube which contained 0.033 mmol of Cp*(η^5,η^1-$C_5Me_4CH_2$-*o*-C_6H_4)Sc (**10**) and 0.65 g of benzene-d_6 and the tube was sealed. The ^{1}H NMR spectrum revealed a 1:1 mixture of **10** and a species identified as Cp*(η^5-C_5Me_4

$CH_2C_6H_5$)Sc—C≡CCMe$_3$ (**11**); there was no evidence for unreacted *tert*-butylacetylene. Assuming as much as 2% *tert*-butylacetylene could be present yet undetected by ^{1}H NMR, lower values for K_{eq} and ΔG^0 in eq. (17) are $1.4 \times 10^2 M^{-1}$ and -3 kcal mol^{-1}, respectively. If a value for ΔS^0 of -15 e.u. is assumed, $\Delta H^0 \leqslant +7.5$ kcal mol^{-1}, and since H—C≡CCMe$_3$ BDE = 132(5) kcal mol^{-1}[8] and H—C_6H_5 BDE = 111 kcal mol^{-1},[8] the (Sc—alkynyl) BDE must be $\geqslant 29(5)$ kcal mol^{-1} stronger than the (Sc—aryl) BDE.

Acknowledgements—This work was supported by the National Science Foundation (Grant CHE-8303735) and by the Shell Companies Foundation, which are gratefully acknowledged. Use of the Southern California Regional NMR Facility, supported by the National Science Foundation Grant CHE-84-40137, is also acknowledged. The authors wish to thank Dr Jay Labinger for helpful discussions.

REFERENCES

1. H. E. Bryndza, J. C. Calabrese, M. Marsi, D. C. Roe, W. Tam and J. E. Bercaw, *J. Am. Chem. Soc.* 1986, **108**, 4805.
2. R. S. Mulliken, *Chem. Phys.* 1955, **23**, 1833.
3. M. E. Thompson, S. M. Baxter, A. R. Bulls, B. J. Burger, M. C. Nolan, B. D. Santarsiero, W. P. Schaefer and J. E. Bercaw, *J. Am. Chem. Soc.* 1987, **109**, 203, and refs therein.
4. D. R. McAlister, D. K. Erwin and J. E. Bercaw, *J. Am. Chem. Soc.* 1978, **100**, 5966.
5. S. W. Benson, *Thermochemical Kinetics*, 2nd Edn. Wiley, New York (1976).
6. H. E. Bryndza, L. K. Fong, R. A. Paciello, W. Tam and J. E. Bercaw, *J. Am. Chem. Soc.* 1987, **109**, 1444.
7. (a) A. H. Janowicz, R. A. Periana, J. M. Buchanan, C. A. Kovac, J. M. Struker, M. J. Wax and R. G. Bergman, *Pure Appl. Chem.* 1984, **56**, 13; (b) W. D. Jones and F. J. Feher, *J. Am. Chem. Soc.* 1985, **107**, 620; (c) R. G. Bergman, *Science* 1984, **223**, 902; (d) W. D. Jones and F. J. Feher, *J. Am. Chem. Soc.* 1984, **106**, 1650; (e) J. Bruno, T. J. Marks and L. R. Morss, *J. Am. Chem. Soc.* 1983, **105**, 6824; (f) M. J. Wax, J. M. Stryker, J. M. Buchanan, C. A. Kovac and R. G. Bergman, *J. Am. Chem. Soc.* 1984, **106**, 1121; (g) H. E. Bryndza, W. C. Fultz and W. Tam, *Organometallics* 1985, **4**, 939.
8. D. F. McMillen and D. M. Golden, *Ann. Rev. Phys. Chem.* 1982, **33**, 493.
9. K. A. Gingerich, *J. Chem. Phys.* 1971, **54**, 3720.
10. M. W. Cook, D. N. Hanson and B. J. Adler, *J. Phys. Chem.* 1957, **26**, 748.
11. M. L. Steigerwald and W. A. Goddard, *J. Am. Chem. Soc.* 1984, **106**, 308.
12. J. A. Labinger and J. E. Bercaw, *Organometallics* (in press).
13. B. J. Burger and J. E. Bercaw, in *New Developments in the Synthesis, Manipulation and Characterization of Organometallic Compounds* (Edited by A. Wayda and M. Darensbourg), ACS Symposium Series, 1987, **357**, 79.
14. An alternative synthesis of $C_5Me_4(CH_2C_6H_5)H$ has been published: J. P. Blaha and M. S. Wrighton, *J. Am. Chem. Soc.* 1985, **107**, 2694.
15. M. Schlosser and J. Hartmann, *Angew. Chem., Int. Ed. Engl.* 1973, **12**, 508.
16. R. S. Threlkel and J. E. Bercaw, *J. Organomet. Chem.* 1977, **136**, 1.
17. P. T. Wolczanski and J. E. Bercaw, *Organometallics* 1982, **1**, 793.

Polyhedron Vol. 7, No. 16/17, pp. 1429–1440, 1988
Printed in Great Britain

0277–5387/88 $3.00+.00
© 1988 Pergamon Press plc

THE THERMODYNAMIC DRIVING FORCE FOR C—H ACTIVATION AT IRIDIUM

PAGE O. STOUTLAND and ROBERT G. BERGMAN†

Lawrence Berkeley Laboratory and Department of Chemistry, University of California, Berkeley, CA 94720, U.S.A.

and

STEVEN P. NOLAN and CARL D. HOFF†

Department of Chemistry, University of Miami, Coral Gables, FL 33124, U.S.A.

Abstract—This paper discusses the relationship between the intermolecular oxidative addition reaction of carbon–hydrogen bonds in organic molecules to transition metal centres, and the dissociation energies of the C—H, M—H and M—R bonds that undergo changes during this process. Earlier studies of transition metal M—H and M—R bond energies are reviewed, followed by a summary of relative and absolute bond energies measured more recently for the $(\eta^5\text{-}C_5Me_5)(PMe_3)Ir(X)(Y)$ system. The M—H and M—R energies are unusually large in this system compared with most others that are presently known; an important exception are those in the thorium series, where intermolecular C—H activation is also observed. The Ir—C and Ir—H bond energy values are utilized in discussing the propensity of iridium for intermolecular C—H insertion, and in predicting thermochemistries for its R—H insertion and M(H)(R) reductive elimination reactions. Finally, the physical basis for the strong metal–carbon and –hydrogen bonds in the iridium system is discussed.

Catalytic selective functionalization of hydrocarbons has been one of the enduring goals of chemistry. While it may still be years before this goal is realized, recent exploration in this field has blossomed.[1] The goal of hydrocarbon functionalization consists of two fundamental problems, that of activation or bonding to the hydrocarbon, and functionalization once it has been activated. Central to both problems is the necessity for selectivity.

Certain alkane functionalization methods have been known for some time. Not all these processes require the use of a transition metal, and many have been shown to have free radical mechanisms (e.g. photochlorination, autoxidation).[2] In addition to requiring harsh conditions, they typically suffer from a lack of selectivity. The first attempts at using metals to functionalize alkanes were successful but left much to be desired in the areas of selectivity and efficiency.[3] These difficulties led chemists to concentrate on stoichiometric reactions between hydrocarbons and transitions metals; it is this approach which has proven most active in recent years.

At the outset, however, it was not clear that this approach was the proper one. While the overall thermodynamics for many possible alkane functionalization processes are favorable, it was believed that a possible intermediate in any functionalization scheme, a *cis*-transition metal alkyl hydride, would not be isolable due to some intrinsic weakness of the metal–carbon and metal–hydrogen bonds. This belief was not unfounded, for at the time the few known *cis*-alkyl hydrides reductively eliminated alkane at low temperatures.[4]

In the last 20 years, however (and particularly the last five), tremendous advances have been made in the area of C—H bond activation. Today, there are several examples of transition metal fragments that will insert intermolecularly in the C—H bonds of hydrocarbons forming stable *cis*-alkyl hydrides. This has raised the hopes for function-

† Authors to whom correspondence should be addressed.

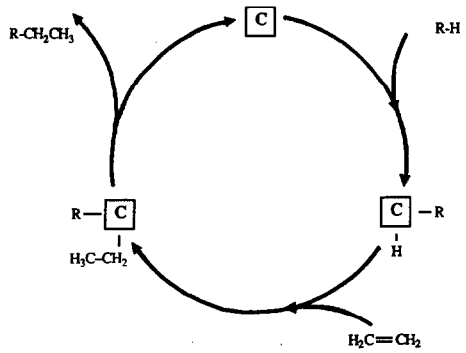

Scheme 1.

alization of alkanes in at least a stoichiometric manner from the alkyl hydrides, perhaps by using insertion reactions followed by reductive elimination.

Fundamental to this question of C—H activation and functionalization is the knowledge of the strength of the metal–carbon and the metal–hydrogen bonds, the driving force for C—H bond activation. Very little is known about such bond strengths,[5] but clearly systems capable of C—H activation are special in this regard. It is this uniqueness which has spurred our interest in these systems.

Thermodynamics of C—H *activation/ functionalization*

The isolation of stable alkyl hydrides resulting from C—H oxidative addition reactions is significant because such processes constitute the first step in simple potential functionalization cycles (e.g. Scheme 1). The latter steps, unsaturated molecule insertion and reductive elimination, are well precedented in organometallic chemistry.[6] Limited homogeneous catalytic functionalization of hydrocarbons has been achieved using organometallic complexes, and may or may not require the intermediacy of alkyl hydrides. For example, several polyhydrides have been shown to convert alkanes into alkenes in the presence of a hydrogen atom acceptor (Scheme 2).[7,8] Aromatic hydrocarbons appear to be easier to functionalize (presumably because they are easier to activate). In this area several reports of functionalization have appeared

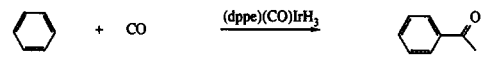

Scheme 3.

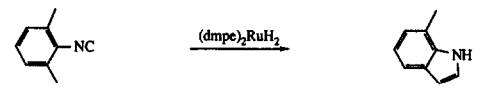

Scheme 4.

(Schemes 3, 4).[9] Unfortunately, these appear to be special cases and may not be suitable for hydrocarbons such as methane.[10]

Consider the general C—H activation and functionalization sequence in Scheme 1, which would be suitable for a wide variety of hydrocarbon substrates. An optimum process might be one in which each step has a free energy change close to, or less than zero. For the first step, this means that the sum of the M—C and M—H bond dissociation energies should not be substantially smaller than the strength of the carbon–hydrogen bond being broken. Furthermore, for reactions such as those shown the entropy of the first step at room temperature can be estimated to be close to -30 e.u. This leads to a $T\Delta S$ contribution to $\Delta G_{\text{reaction}}$ of approximately 9 kcal mol^{-1} at 25°C.[11] Thus with typical C—H bond *enthalpies* of the order of 95–110 kcal mol^{-1}, the sum of the M—C and the M—H bond dissociation enthalpies must be greater than 104–119 kcal mol^{-1} for insertion to be thermodynamically favored.

For the second step, it is desirable that the unsaturated reagent to be inserted into either the metal–carbon or the metal–hydrogen bond be one that would be amenable to large scale processes. Such a reagent should be inexpensive, abundant, and easy to handle; fitting these categories are simple olefins, acetylene, and carbon monoxide. The enthalpies of these insertion reactions can be approximated by starting with the known enthalpies of similar reactions.

For example, consider the insertion of ethylene into the M—H bond of an alkyl hydride. In order to estimate the enthalpy of the ethylene insertion

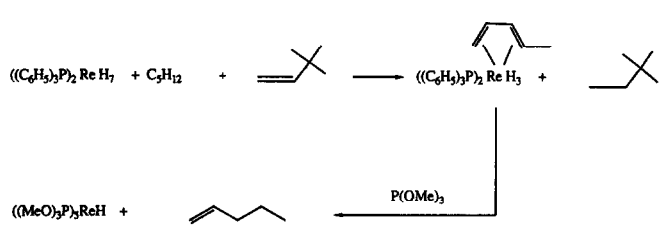

Scheme 2.

$$M(R)(H) \rightarrow {}^{\cdot}MR + H^{\cdot} \qquad \Delta H = D_{(M-H)}$$
$$^{\cdot}H + H_2C{=}CH_2 \rightarrow CH_3{-}CH_2^{\cdot} \qquad \Delta H = -38.3$$
$$CH_3CH_2^{\cdot} + RM^{\cdot} \rightarrow R{-}MEt \qquad \Delta H = -D_{(M-C)}$$
$$M(R)(H) + H_2C{=}CH_2 \rightarrow R{-}M{-}CH_2CH_3 \qquad \Delta H_{insertion} = D(M{-}H) - D(M{-}C) - 38.3$$

Scheme 5.

Table 1. Enthalpies for selected reactions (kcal mol^{-1})

Reagent	ΔH (insertion into M—H bond)	ΔH (insertion into M—R bond)
CO	$D_{(M-H)} - D_{(M-C=O)} - 15$	$D_{(M-C)} - D_{(M-C=O)} - 10$
$H_2C{=}CH_2$	$D_{(M-H)} - D_{(M-C)} - 38$	-25
HCCH	$D_{(M-H)} - D_{(M-C=C)} - 44$	$D_{(M-C)} - D_{(M-C=C)} - 40$

reaction (cf. Scheme 5), one can start [eq. (1)] with the M—H bond dissociation enthalpy (BDE), leading to H· and the M—R radical. The next quantity required in the enthalpy of addition of H· to ethylene, leading to ethyl radical. This value can be calculated accurately as −38.3 kcal mol^{-1} from the known heats of formation of these three species. Finally, one needs ΔH for combination of ·MH with the ethyl radical, which is equivalent to -BDE for the M—C bond in the final product. Using this analysis, $\Delta H_{insertion} = D_{(M-H)} - D_{(M-C)} - 38.3$ kcal mol^{-1}. Estimates for the heats of this and two other insertion reactions are given in Table 1. From Table 1 it is apparent that all the insertion reactions are thermodynamically possible unless the M—H bond energy is much larger than the M—C bond energy.

The thermodynamics of reductive elimination, the last step in such a functionalization scheme, can also be estimated if metal–carbon and metal–hydrogen bond strengths are known. However, it is clear that such reactions will not be facile, as complexes which form stable alkyl hydrides will also form very stable dialkyls, alkyl acyls, and vinyl alkyls. There is thus the need to couple this step with one that is sufficiently exothermic so that the overall free energy of the reaction is close to zero. Again, knowledge of the metal–carbon and metal–hydrogen bond strengths may help in the evaluation of the favorability of this process. It is important to remember, however, that success of these reactions will also depend on the *kinetic* barriers involved.

Metal–carbon and metal–hydrogen bond strengths

Despite recent interest in determining M—C and M—H bond strengths, there is still a paucity of information, especially for metals of the second and third rows of the transition series. Somewhat more information is available on the strengths of bonds formed with first row transition metals. Halpern, for example, has extensively studied cobalt alkyl compounds similar in structure to Coenzyme B_{12}. For these complexes it was found that the metal–carbon bond strengths typically lie in the range of 18–25 kcal mol^{-1}. The steric requirements of the alkyl group are one of the most important factors controlling the bond dissociation energy.[12] Connor has determined metal–carbon bond dissociation enthalpies for X—$Mn(CO)_5$.[13] The similarity of these BDE's is evident (Table 2). The available data on other first row organometallic compounds indicate that their metal–carbon bond dissociation enthalpies are also often less than 30 kcal mol^{-1}.[14]

Extensive information is now available from experiments done in ICR spectrometers on the strength of metal–carbon and metal–hydrogen bonds in simple cationic metal hydrides and alkyls.[15] Although the transferability of these values to organometallic compounds in solution is at best tenuous, the relative metal–carbon bond strengths

Table 2. Selected first row metal–carbon bond dissociation enthalpies

ML_n	R	D_{Co-R} (kcal mol^{-1})
[R—Co(Saloph)L]	$CH_2C(CH_3)_3$	18
	$CH(CH_3)_2$	20
	$CH_2C_6H_5$	22
	$CH_2CH_2CH_3$	25
R—$Mn(CO)_5$	$CH_2C_6H_5$	29
	$(CO)CH_3$	39
	CH_3	44
	C_6H_5	49

Table 3. Selected metal–carbon and metal–hydrogen bond dissociation enthalpies for third row transition metals and actinides

X	$(PMe_3)_2Cl(CO)Ir(I)(X)$	Cp_2WX_2	$Cp^*_2ThX_2$
H	60	72.9	97.5
CH_3	35.4	50.2	82.4
C_6H_5	—	—	90.6
C_2H_5	—	—	74.9

between a given metal and a variety of alkyl groups are certainly valuable. The strengths of metal–hydrogen bonds appear to be similar to those found in solution, ranging from 35 to 60 kcal mol^{-1}. Metal–methyl bond strengths, however, are strengthened relative to the metal–hydrogen bond in the gas phase when the metal is positively charged. Even for first row metals, metal–methyl bond dissociation enthalpies are typically 60–70 kcal mol^{-1}.

Of more relevance to this study are bond strengths for complexes in solution. A reasonable number of *average* bond energies are known for complexes such as homoleptic metal alkyls [e.g. $Hf(CH_3)_4$; $W(CH_3)_6$].[16] However, because average energies are often significantly different in magnitude from first bond dissociation energies, these numbers are of limited value in predicting reactivity. However, there appears to be a scarcity of BDE's (in either solution or the gas phase) for coordinatively saturated, third row late transition metal complexes. The limited data available suggest that we may expect significantly stronger metal–carbon bonds than are found in complexes of the first row metals. Summarized in Table 3 are metal–hydride and metal–carbon bond dissociation enthalpies for two third row transition metal systems, as well as for the actinide element thorium.[17] Both the tungsten and the thorium compounds are capable of C—H bond activation.

Information concerning the strength of the metal–hydrogen bond is more readily available, but is similarly sparse for the third row transition metals. Most of the information is for first row metals and indicates that metal–hydrogen bond strengths hover around 60 kcal mol^{-1}.[18] Studies of a wide variety of diatomic metal hydrides carried out in the gas phase show no convincing trends; few are over 60 kcal mol^{-1}, the notable exceptions being Au—H and Pt—H at 74 and 80 kcal mol^{-1}, respectively.[19] The few determinations of third row metal–hydrogen bond strengths support the belief that stronger bonds are formed to third row metals. For example, the Os—H bond strength in $H_2Os(CO)_4$ has been estimated to be 78 kcal mol^{-1}.[20] The metal–hydrogen BDE's of some other heavier transition metals are listed in Table 3, and are also significantly stronger than the 60 kcal mol^{-1} found for many first row metal hydrides.

Ir—X *BDE's for* $Cp^*(PMe_3)IrX_2$

For large organometallic molecules, the determination of relative BDE's is much easier than the determination of absolute BDE's. Several techniques allow one to determine relative bond strengths accurately. For example, measuring the temperature dependence of the equilibrium constant for a reaction of the type shown in eq. (1) allows determination of ΔH for the reaction. $\Delta H_{reaction}$ is equal to the difference in the BDE's of M—X and M—Y.

$$L_n—M—X + Y \rightleftharpoons L_n—M—Y + X. \quad (1)$$

The equilibrium method suffers from several weaknesses. First, well behaved equilibria for many compounds do not exist. Even when complexes are amenable to such studies, they are only useful for reactions with limited K_{eq} values, meaning that only nearly thermoneutral reactions can be studied for reactions with small ΔS values. The only way one can obtain relative BDE's for ligands with significantly different BDE's is by using the 'ladder' technique, where one measures a series of equilibrium constants. Errors may accumulate as the ladder is extended.

Another way to determine relative bond strengths is by using calorimetry, a technique in which one measures relative ΔH values directly. This approach to determining relative BDE's typically consists of determining ΔH for reactions which differ by only a single ligand. The results of Yoneda and Blake[21] summarized in Table 4 are an example of this. By measuring the enthalpy of the reaction shown in eq. (2), the relative Ir—X BDE's could be found knowing only the enthalpy of the reaction and the appropriate X—I BDE's.

$$(PMe_3)_2(CO)Ir(Cl) + XI \rightarrow (PMe_3)_2(CO)Ir(Cl)(X)(I). \quad (2)$$

Table 4. Relative Ir—X bond dissociation enthalpies for $(PMe_3)_2(CO)Ir(Cl)(I)(X)$

X	$D_{Ir-X}-D_{Ir-I}$
H	14
CH_3	0
$CH(CH_3)_2$	−7
$CH_2(C_6H_5)$	−17
$CO(CH_3)$	0

Table 5. Relative iridium–carbon BDE's in $(\eta^5\text{-}Me_5C_5)(PMe_3)Ir(R)(H)$

Compound	ΔD_{Ir-C} (kcal mol^{-1})
[Ir](neopentyl)	−4
[Ir](cyclohexyl)	0
[Ir](cyclopentyl)	0
[Ir](2,3-dimethylbutyl)	4
[Ir](pentyl)	6

Our work has focused on M—C and M—R bond dissociation energies in the C—H activating system $(\eta^5\text{-}C_5Me_5)(PMe_3)Ir(R)(H)$. Our first attempt at understanding the factors controlling the strengths of the metal–carbon bonds in this system involved an equilibrium study.[22] In these experiments an alkyl hydride was heated in mixtures of alkanes of varying proportions. Observation of the final amounts of the two C—H insertion products allowed determination of equilibrium constants for reactions such as that shown in eq. (3).

$$Cp^*(PMe_3)Ir(C_6H_{11})(H)+n\text{-}C_5H_{12} \rightleftharpoons Cp^*(PMe_3)Ir(C_5H_{11})(H)+C_6H_{12}. \quad (3)$$

This in turn allowed calculation of ΔG° for the reaction. Since the magnitudes of the C—H bond dissociation enthalpies in the hydrocarbons are known, the origin of $\Delta G_{reaction}$ lies entirely in the difference of the free energy contributions from the metal–carbon bonds.† Derivation of relative iridium–carbon bond dissociation enthalpies from the equilibrium constants (and thus $\Delta G^0_{reaction}$) requires separation of the enthalpic and entropic components of $\Delta G^0_{reaction}$. Normally this is done by measuring the temperature dependence of the equilibrium constant. In this case, however, the range of temperatures under which the reactions could be carried out would have led to large errors in ΔH^0 values. We instead made the assumption that the $T\Delta S$ contribution to $\Delta G^0_{r\times n}$ was close to zero.‡ The resulting relative irridium–carbon bond dissociation enthalpies are given in Table 5.

† This assumes that the strengths of the other bonds in $(\eta^5\text{-}Me_5C_5)(PMe_3)Ir(R)(H)$ do not change upon substitution of the R group. We feel that such changes would be slight, considering the similarities of the R groups used.

‡ Because of the similarity of the forward and reverse reactions, the translational component of ΔS^0 is almost certainly close to zero. Estimation of the rotational and vibrational components is more complicated, but the contributions of $T\Delta S^0_{rot}$ and $T\Delta S^0_{vib}$ to ΔG^0 are likely to be less than our uncertainty in ΔG^0.

These equilibrium studies suffered from several limitations. For example, highly volatile hydrocarbons such as methane and ethane could not be used for practical reasons. Hydrocarbons with several different types of C—H bonds could not be used due to the difficulty in interpreting the resulting mixtures of alkyl hydrides. Finally, the method we choose for analysis, ^{31}P NMR spectrometry, is subject to uncertainties on the order of 5–10% and is not particularly sensitive, being useful only for reactions with K_{eq} values between 0.005 and 200. Despite these disadvantages, the qualitative trends are clear. Perhaps most striking is that the strongest iridium–carbon bonds were formed by breaking the strongest C—H bonds; also evident is the dependence on the steric requirements of the alkyl group.

Absolute bond dissociation enthalpies are typically much more difficult to determine. One technique for determining an *upper* limit for absolute bond dissociation enthalpies kinetically involves measuring $\Delta H^\ddagger$ for a process such as that shown in eq. (4).

$$L_n—M—R \rightarrow L_n—M^\cdot + R^\cdot \quad (4)$$

If the barrier for the back reaction is sufficiently low (or if the radicals can be scavenged effectively), this provides a reasonable estimate for the BDE. Thermolysis of $(\eta^5\text{-}Me_5C_5)(PMe_3)Ir(R)(H)$ does not result in simple Ir—R or Ir—H bond homolysis; instead, reductive elimination of R—H occurs. Since the appropriate R—H bond strengths are known, we can use $\Delta H^\ddagger$ to determine an upper limit for the *sum* of the Ir—R and the Ir—H bond dissociation enthalpues [eqs. (5)–(7)].

$$(\eta^5\text{-}Me_5C_5)(PMe_3)Ir(R)(H) \rightarrow (\eta^5\text{-}Me_5C_5)(PMe_3)Ir+R—H \quad (5)$$

$$R—H \rightarrow R^\cdot + {}^\cdot H \quad (6)$$

$$\overline{(\eta^5\text{-}Me_5C_5)(PMe_3)Ir(R)(H)} \rightarrow \overline{(\eta^5\text{-}Me_5C_5)(PMe_3)Ir+R^\cdot+{}^\cdot H}. \quad (7)$$

This is shown schematically in the energy dia-

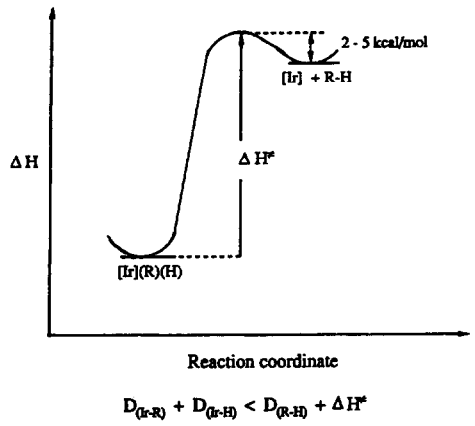

Fig. 1. Reaction coordinate diagram for the reductive elimination of RH from (η^5-Me_5C_5)(PMe_3)Ir(R)(H).

gram in Fig. 1. By measuring the temperature dependence of the rate constants for the reaction shown in eq. (5), we determine that $\Delta H^{\ddagger} = 35.6$ kcal mol^{-1} for the reductive elimination of cyclohexane. This is thus an upper limit for ΔH_5. The low kinetic selectivity of the unsaturated intermediate suggests the barrier for the reverse reaction (oxidative addition) is small, perhaps between 2 and 5 kcal mol^{-1}. Using a value of 95.5 kcal mol^{-1} (ΔH_6) for the C—H bond strength in cyclohexane leads to a value of 127–130 kcal mol^{-1} [$\Delta H_7 = \Delta H_5 + \Delta H_6 -$ (2 to 5 kcal mol^{-1})] for the sum of the iridium–carbon and iridium–hydrogen bond strengths.

Although this gave an estimate of the sum of the iridium–carbon and iridium–hydrogen bond dissociation enthalpies, as well as for some relative iridium–carbon bond BDE's, it did not provide the relative strengths of the iridium–carbon and iridium–hydrogen bonds, nor any absolute BDE's. We thus undertook calorimetric studies to determine the difference in the iridium–carbon and iridium–hydrogen bond dissociation enthalpies, which when combined with the kinetic studies allowed us to estimate *absolute* iridium–carbon and iridium–hydrogen bond strengths.[23]

Reaction of either (η^5-Me_5C_5)(PMe_3)Ir(C_6H_{11})(H) or (η^5-Me_5C_5)(PMe_3)Ir(H)$_2$ with anhydrous HCl in toluene at 25°C resulted in quantitative production of (η^5-Me_5C_5)(PMe_3)Ir(Cl)$_2$ as shown in eq. (8) and eq. (9). Subtraction of the ΔH values for these two equations leads directly to the heat of hydrogenation of the iridium–cyclohexyl bond as shown in eq. (10). Using the well-established bond strengths for H—H (104 kcal mol^{-1}) and Cy—H (96 kcal mol^{-1}) we calculated that the difference in the iridium–cyclohexyl and the iridium–hydrogen bond strengths is 23.5 kcal mol^{-1}.† Using the lower value for the sum of the iridium–cyclohexyl and the iridium–hydrogen bond strengths allowed us to estimate that the absolute bond strengths are at least 75 and 52 kcal mol^{-1}, respectively.‡

$$Cp^*(PMe_3)Ir(C_6H_{11})(H) + 2HCl \rightarrow Cp^*(PMe_3)Ir(Cl)_2 + C_6H_{12} + H_2 \quad \Delta H = -45.5 \pm 0.5 \quad (8)$$

$$Cp^*(PMe_3)Ir(H)_2 + 2HCl \rightarrow Cp^*(PMe_3)Ir(Cl)_2 + 2H_2 \quad \Delta H = -30.0 \pm 1.3 \quad (9)$$

$$Cp^*(PMe_3)Ir(C_6H_{11})(H) + H_2 \rightarrow Cp^*(PMe_3)Ir(H)_2 + C_6H_{12} \quad \Delta H = -15.5 \pm 1.8. \quad (10)$$

In a similar manner we were able to determine other iridium–carbon bond strengths. Reaction of the phenyl hydride with two mol of anhydrous HCl resulted in production of the dichloride and a mole of benzene and hydrogen [eq. (11)]. Subtraction of eq. (9) shows that hydrogenation of the phenyl hydride is virtually thermoneutral [eq. (12)]. Transferring the Ir—H bond strength from above leads to an iridium–phenyl bond dissociation enthalpy[23c] of 82 kcal mol^{-1}.

$$Cp^*(PMe_3)Ir(C_6H_5)(H) + 2HCl \rightarrow Cp^*(PMe_3)Ir(Cl)_2 + C_6H_6 + H_2 \quad \Delta H = -30.6 \pm 2.7 \quad (11)$$

$$Cp^*(PMe_3)Ir(C_6H_5)(H) + H_2 \rightarrow Cp^*(PMe_3)Ir(H)_2 + C_6H_6 \quad \Delta H = -0.6 \pm 4.0. \quad (12)$$

Calorimetric studies also allow estimation of metal–carbon bond dissociation enthalpies derived from hydrocarbons which were not suitable for equilibration studies. Reaction of (η^5-Me_5C_5)(PMe_3)Ir(CH_3)$_2$ with two mol of HCl results in production of (η^5-Me_5C_5)(PMe_3)Ir(Cl)$_2$ and two mol of methane [eq. (13)]. This allows determination of the strength of the metal methyl

† It is possible that the cyclohexyl ligand is bulky enough to destabilize other metal-ligand bonds in the molecule. This would make the iridium–cyclohexyl bond dissociation enthalpy proportionally larger.

‡ The strength of the iridium hydride bond has been confirmed by photoacoustic measurements (ref. 25a). This provides independent support for the assumption of a negligible kinetic barrier for the oxidative addition of (η^5-C_5Me_5)(PMe_3)Ir to C—H bonds.

bond (here an average) to be 56 kcal mol^{-1}. Similarly, reaction of (η^5-Me_5C_5)(PMe_3)Ir($HC{=}CH_2$)(Br) with HCl results in production of ethylene and (η^5-Me_5C_5)(PMe_3)Ir(Cl)(Br), and leads to a metal–vinyl bond strength of 71 kcal mol^{-1} [eq. (14)].

$$Cp^*(PMe_3)Ir(CH_3)_2 + 2HCl \rightarrow Cp^*(PMe_3)Ir(Cl)_2 + 2CH_4 \quad \Delta H = -68.0 \pm 1.3 \quad (13)$$

$$Cp^*(PMe_3)Ir(C_2H_3)(Br) + HCl \rightarrow Cp^*(PMe_3)Ir(Cl)(Br) + C_2H_4 \quad \Delta H = -19.3 \pm 1.2. \quad (14)$$

In order to test the transferability of the iridium–hydride bond strength to molecules with different alkyl groups, the following reactions were carried out [eqs (15)–(18)]. Within experimental error, the enthalpies of reaction are the same in all cases, indicating that changing the ancillary ligand has a negligible effect on the difference between the metal–hydrogen and metal–chlorine bond energies.

$$Cp^*(PMe_3)Ir(H)_2 + 2CCl_4 \rightarrow Cp^*(PMe_3)Ir(Cl)_2 + 2CHCl_3 \quad \Delta H = -83.0 \pm 0.6 \quad (15)$$

$$Cp^*(PMe_3)Ir(H)(Cl) + CCl_4 \rightarrow Cp^*(PMe_3)Ir(Cl)_2 + CHCl_3 \quad \Delta H = -41.8 \pm 0.7 \quad (16)$$

$$Cp^*(PMe_3)Ir(C_6H_5)(H) + CCl_4 \rightarrow Cp^*(PMe_3)Ir(C_6H_5)(Cl) + CHCl_3 \quad \Delta H = -40.9 \pm 1.4 \quad (17)$$

$$Cp^*(PMe_3)Ir(C_6H_{11})(H) + CCl_4 \rightarrow Cp^*(PMe_3)Ir(C_6H_{11})(Cl) + CHCl_3 \quad \Delta H = -43.1 \pm 1.5. \quad (18)$$

A word or two about the level of uncertainty in these values is appropriate here. In Table 6 are combined relative bond strength values determined from equilibrium studies (Table 1) with the calorimetric work described above. Prior to discussion of these data it is important to recall assumptions made in assigning the bond strengths collected in Table 2. In calculating relative BDE's from the equilibrium study discussed above, it was assumed that the entropy of reaction (4) was zero. This is probably reliable to about ± 6 e.u., yielding an uncertainty in the bond strengths of ± 2.5 kcal mol^{-1} at the temperature studied. In many cases, carbon–hydrogen bond strengths for organic molecules are only known to ± 2 kcal mol^{-1}. The calorimetric data are subject to experimental errors of similar magnitude. While direct comparison of experimental data on related complexes can often be made with good accuracy, general trends in bond strength data should probably include error bars of at least ± 5 kcal mol^{-1} at each point when dealing with complexes in solution.

Table 6. Ir—X bond dissociation enthalpies for (η^5-Me_5C_5)(PMe_3)Ir(X)$_2$

X	D_{Ir-X} (kcal mol^{-1})
$CH_2C(CH_3)_3$	48
C_6H_{11}	52
C_5H_9	52
CH_3	56
$CH_2CH(CH_3)CH(CH_3)_2$	56
C_5H_{11}	58
$CH{=}CH_2$	71
C_6H_5	82
H	74
Cl	90
Br	76
I	64

It should also be noted that the Ir—CH_3 and Ir—vinyl bond strength estimates were made in complexes of a different nature than the other Ir—C bonds (which were all alkyl hydride complexes). This was due to the difficulty of obtaining pure samples of the methyl hydride and vinyl hydride complexes in sufficient quantity to do the calorimetry. We hope the Ir—X bonds strengths are transferable between these similar systems, but it is possible that either steric or electronic factors may cause the values to be lower in the dimethyl and vinyl bromide complex than in analogous alkyl hydrides.

It is interesting to compare the relative metal–carbon/hydrogen bond dissociation enthalpies found here with those recently considered by Bryndza, Bercaw, and coworkers.[24] In their study of the relative metal–carbon, metal–oxygen and metal–nitrogen bonds in (DPPE)(Me)Pt—X and (η^5-Me_5C_5)(PMe_3)$_2$Ru—X, a 1 : 1 correlation to the analogous H—X bond dissociation enthalpies was found. A similar correlation was noted for (η^5-Me_5C_5)$_2$($OCMe_3$)Th—X. The ruthenium and platinum systems were also surprisingly insensitive to steric effects. An attempt to apply this correlation to the iridium system is shown in Fig. 2. We have not included the metal–halogen bonds in the plot because it is not expected that the correlation should

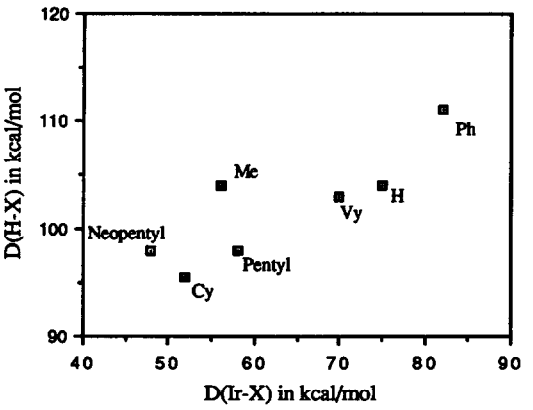

Fig. 2. Plot of Ir—X bond dissociation enthalpies in (η^5-Me_5C_5)(PMe_3)Ir(X)(H) vs the respective hydrogen–carbon BDE's.

extend beyond first row atoms. Even so, it is apparent that not all relative metal–carbon bond strengths in (η^5-C_5Me_5)(PMe_3)Ir(R)(X) correlate well with H—X bond strengths. The metal–neopentyl bond is too weak, most likely due to steric hindrance. The metal–methyl bond also deviates substantially, being weaker than the H—X bond strength would predict. Correlation of M—X and H—X bond energies would predict that the values for the metal–methyl amd metal–hydrogen bonds should be about equal; the iridium–methyl bond, however, is approximately 20 kcal mol^{-1} weaker than the iridium–hydrogen bond, consistent with early studies of first row metal complexes. The remainder of the bond strengths do lie in a straight line when plotted against the H—X bond strengths. However, the slope of the line (0.5) is significantly smaller than that observed in the earlier work.

Predictions of reactivity

We are now in a position to make some predictions concerning the reactivity of (η^5-Me_5C_5)(PMe_3)Ir(R)(H) as well as reactions of the transient intermediate (η^5-Me_5C_5)(PMe_3)Ir with other substrates. Specifically, we can make reasonable thermochemical estimates for some insertion reactions involving (η^5-Me_5C_5)(PMe_3)Ir(R)(H). Having good estimates for the Ir—R and Ir—H BDE's, we can now refer back to Table 1. Assuming the strength of a metal–acyl bond to be 0–5 kcal mol^{-1} weaker than that of a metal–pentyl bond (see Table 4),[25] we find that insertion of CO into a metal–pentyl bond has an enthalpy of reaction of -5 to -10 kcal mol^{-1}, while insertion into the metal–hydrogen bond has an enthalpy of reaction of $+10$ kcal mol^{-1}. Assuming the reactions would have to be carried out at ambient temperature or above, the $T\Delta S$ contribution to ΔG is at least 10 kcal mol^{-1}. Insertion reactions involving CO, not driven by addition of a ligand, are not thermodynamically favored.

Insertion of ethylene into the metal–hydrogen bond can be seen to have an enthalpy of reaction of -21 kcal mol^{-1}. Insertion of ethylene into the metal–carbon bond has an enthalpy of reaction of -25 kcal mol^{-1}, regardless of the nature of the complex. Despite the unfavorable entropy of reaction, both insertions will be favored at common reaction temperatures. Insertion of acetylene into either the metal–carbon or metal–hydrogen bond is favorable with enthalpies of reaction of -52 and -39 kcal mol^{-1}, respectively. The negative entropies of reaction will have little effect on such exothermic reactions, and indeed insertion into the metal–hydrogen bond has been observed with acetylene.[26]

Knowing that insertion reactions are thermodynamically feasible leads us to consider the last step in a stoichiometric functionalization scheme, reductive elimination. Since reductive elimination of R_2 or RH would result in production of the highly energetic fragment (η^5-Me_5C_5)(PMe_3)Ir, we must couple this reaction with one that will result in favorable energetics as well as being compatible with our proposed catalytic cycle. Reaction of (η^5-Me_5C_5)(PMe_3)Ir with RH is such a reaction. The enthalpies of reaction are calculated below (Table 7). In view of the feasible thermodynamics of this cycle, it must be kinetic difficulties that have prevented it from being realized.

Particularly interesting is the fact that the product of reductive elimination can again react with ethylene, completing a catalytic cycle. Unfortunately, reductive elimination reactions with the acetylene or carbon monoxide insertion products are not promising due to their endothermicity. Also, a significant kinetic barrier exists for insertion of ethylene into the M—H bond; we see no insertion products up to temperatures where reductive elimination of the alkane takes place.[27] Such problems will most likely be commonplace in these coordinatively saturated complexes. If insertion could be managed, there are significant problems to overcome before reductive elimination will be observed, not the least of which is competing lower energy pathways such as metal–carbon bond homolysis.

We can now also evaluate reactions involving (η^5-Me_5C_5)(PMe_3)Ir other than C—H insertion reactions. The enthalpies of some of the most interesting, along with some C—H insertion enthalpies, are shown in Table 8. Significant kinetic barriers may exist for the C—C insertions in this group.

Table 7. Enthalpies for selected reductive elimination/oxidative addition reactions

Reactions	ΔH (kcal mol^{-1})
[Ir](CH$_2$CH$_3$)(R)+RH → [Ir](R)(H)+CH$_3$CH$_2$—R	−4
[Ir](CH$_2$CH$_2$R)(H)+RH → [Ir](R)(H)+RCH$_2$CH$_3$	0
[Ir](CH=CH$_2$)(R)+RH → [Ir](R)(H)+H$_2$C=CHR	4
[Ir](CH—CHR)(H)+RH → [Ir](R)(H)+H$_2$C=CHR	21
[Ir](COR)(H)+RH → [Ir](R)(H)+HCOR	10

[Ir] = (η^5-Me$_5$C$_5$)(PMe$_3$)Ir

Factors influencing metal–carbon and metal–hydrogen bond strengths

The previous section highlighted the importance of having good estimates for bond dissociation energies. The myriad of combinations of different metals and ligands makes it extremely difficult to have experimental values for all possible bond dissociation enthalpies. Organic chemists have for years had a large amount of thermodynamic information available, and from this have been able to generate 'group additivity tables' which allow accurate calculation of ΔH_f for many organic molecules.[28] This in turn allows accurate estimation of enthalpies of reaction. This approach is particularly successful in organic chemistry as only a limited number of elements is involved, and there are only three stable geometries (*sp*, sp^2 and sp^3 hybridized) about carbon. The many geometries possible for transition metal complexes, and the many different ligands used, preclude this from being a practical approach for organotransition metal chemistry. There is thus the need to identify and quantify the key factors responsible for the strengths of metal–ligand bonds so that some reasonable estimates can be made for unknown metal–ligand bond strengths. These factors are discussed below.

Table 8. Calculated enthalpies of oxidative addition for selected species to '(η^5-Me$_5$C$_5$)(PMe$_3$)Ir'

A—B	$-\Delta H$ (kcal mol^{-1})
C_6H_{11}—C_6H_{11}	12
C_6H_{11}—H	29
H—H	44
C_6H_5—H	45
C_6H_5—C_6H_5	61
C—Cl	63
H_3C—CH_3	22

The effect of changing the steric requirements of an alkyl group has been studied for several systems. For example, Halpern[4] examined the effect that the steric demand of an alkyl group had on the Co—R bond strength (Table 2). In this system the metal–carbon BDE could be predicted by considering the steric requirements of the alkyl group. While not studied as extensively, the metal–alkyl bond dissociation enthalpies in (PMe$_3$)$_2$(CO)Ir(Cl)(I)(alkyl) also decrease as the steric demand of the alkyl group increases. In our investigations as well, the relative strengths of the metal–*alkyl* bonds seem to be controlled to a large extent by the steric demand of the ligand. In each of these cases, the difference between the strongest and the weakest metal–alkyl bonds was approximately 7 kcal mol^{-1}. The metal–hydrogen bonds are usually stronger; hydrogen's smaller steric demand may be one of the reasons for this.

The effect of changing the metal in a particular transition metal complex is less well understood than the effect which arises from changing a ligand. The existing evidence, however, indicates that metal–ligand bond dissociation enthalpies increase as one descends a column in the transition series of the periodic table. This behavior contrasts with non-transition metal systems, where bond energies typically decrease as one descends a column in the periodic table. Most first row metal–carbon bond dissociation enthalpies lie between 20 and 30 kcal mol^{-1}, while several recent studies of complexes containing third row metals indicate that metal–carbon bonds formed with these metals may be significantly stronger. This trend does not extend, however, to simple cationic metal alkyls in the gas phase. For example, the metal–carbon bond dissociation energy of M$^+$—CH$_3$ is 68±4 kcal mol^{-1} for M = Fe while that for M = Ru is 54±5 kcal mol^{-1}. Similarly, the M$^+$—CH$_3$ bond dissociation energies for M = Co and M = Rh are 61±4 and 47±5 kcal mol^{-1}, respectively.

In an attempt to understand more fully periodic trends in bond strengths *vis-à-vis* metal–methyl and metal–hydrogen bond strengths, Ziegler *et al.*[29] have recently performed calculations using a modified Hartree–Fock–Slater method (also known as the $X\alpha$ method) on molecules as large as X—M(CO)$_n$. Their calculations are able to accurately reproduce known bond dissociation enthalpies, and successfully model the increase in metal–carbon bond strengths that occurs as one descends a column in the periodic table. For example, the calculated M—C bond dissociation enthalpy in $(CO)_5Mn—CH_3$ is 37 kcal mol^{-1} (exp. value: 37 kcal mol^{-1}), rising to 48 kcal mol^{-1} for M = Re. Similarly, the value calculated for the M—C bond dissociation enthalpy is 38 kcal mol^{-1} in $(CO)_4Co—CH_3$ and 51 kcal mol^{-1} for the corresponding iridium complex. Two key factors were identified as responsible for this behavior. Firstly, the overlap of the ligand orbitals with the (*p*,*d*)-hybrid on the metal increases as one descends the periodic table. The second factor responsible for the particularly strong bonds formed with the third row metals is a relativistic effect which may contribute up to 10 kcal mol^{-1}. Systematic studies are clearly required if we hope to be able to quantitatively predict how changing the metal in a complex will affect the BDE's.

The effect arising from changing the alkyl/aryl group on the metal–carbon bond dissociation enthalpy is more predictable than the effect from changing the metal. As first noted by Bercaw and Bryndza[24] many metal–carbon BDE's parallel the analogous carbon–hydrogen BDE's. They noted that if the C—H BDE's are plotted against M—H BDE's, a slope of 1.0 results. This trend was observed for several different systems. One can do the same thing for the relative BDE data presented earlier, and find that this observation is generally valid. Deviations from the line occur when the alkyl/aryl group is particularly bulky, and when the alkyl group is methyl. Many of the slopes of the lines are less than 1.0, indicating that hydrocarbons which have strong C—H bonds (such as ethylene and benzene), form particularly strong M—C bonds, perhaps enhanced by π-effects involving empty metal *p* or *d* orbitals of the appropriate symmetry. Studies involving $(PMe_3)_2(CO)Ir(Cl)(I)(X)$, $(\eta^5\text{-}Me_5C_5)(PMe_3)Ir(R)(H)$, and $(CO)_5Mn—R$ suggest that the difference between the strongest and the weakest metal–carbon bonds (between a metal–phenyl and a metal–benzyl or a metal–alkyl bond for example) can be relatively large.

The effects of changing ancillary ligands on the metal, and of changing the coordination geometry about the metal on the *rates* of reactions are well documented in many cases,[30] but the effect of such changes on the BDE's are understood in only a qualitative sense. This is particularly relevant to the field of intermolecular C—H bond activation, as we would like to be able to make systematic modifications to systems known to insert into the C—H bonds of hydrocarbons, so as to improve the selectivity of the activation process, and to modify the stability of the resulting alkyl hydrides. Changing the size of the ancillary ligands seems to have the effect predicted from steric arguments, but the electronic nature of the ligand is not as well understood.

Changing the coordination geometry about the metal by using rigid ligands, or by using very bulky ligands, also affects the bond strengths in the molecule. Unfortunately, this effect is presently difficult to quantify. Theoretical papers have addressed this question,[31] and reasonably suggest that molecules which will lead to highly unstable fragments upon reductive elimination, for example, will not tend to reductively eliminate (i.e. the sum of the metal–carbon and metal–hydrogen bonds will be stronger). Experimental evidence is difficult to interpret as there have been no studies specifically directed towards trying to understand the magnitude of this effect. As an illustration, consider an octahedral iridium(III) complex such as $[Ir(H)(Cl)(p\text{-}C_6H_4Me)(CO)(PPh_3)_2]$, and one of the molecules studied by us, $(\eta^5\text{-}Me_5C_5)(PMe_3)Ir(C_6H_{11})(H)$. Upon reductive elimination of RH from either complex, the resulting metal fragment is one containing iridium(I) which is known to prefer a square planar geometry.[32] The intermediate formed by reductive elimination from the octahedral complex can easily isomerize to one of square planar geometry. In contrast, '$(\eta^5\text{-}Me_5C_5)(PMe_3)Ir$', formed by reductive elimination of cyclohexane from $(\eta^5\text{-}Me_5C_5)(PMe_3)Ir(C_6H_{11})(H)$, cannot exist in a square planar form. This results in a very unstable, reactive iridium(I) intermediate. This reactive intermediate also has a low kinetic barrier for the back reaction, insertion into a C—H bond, perhaps because it does not have to undergo a prior isomerization in order to assume in the proper geometry for insertion. Of more relevance here, however, is that the bonds formed are also much stronger for a molecule which does not have to undergo this reorganization prior to bond formation. While it is difficult to assign differences in kinetic stability solely to differences in geometry, the relative stabilities of these compounds are consistent with this idea. The octahedral complex, $[Ir(H)(Cl)(p\text{-}C_6H_4Me)(CO)(PPh_3)_2]$, will reductively eliminate at *ca* 100°C, while $(\eta^5\text{-}Me_5C_5)(PMe_3)Ir(C_6H_5)(H)$ is stable to above 200°C.[33]

CONCLUSION

Efficient and general methods for the catalytic activation and functionalization of alkanes are not yet available. We also do not yet fully understand the C—H activation process. Thermodynamic studies are a small but important step toward understanding what is necessary for C—H activation and functionalization. These studies have contributed to the small but growing body of information concerning metal–hydrogen and metal–carbon bond strengths.

Accurate absolute bond strengths in complicated organometallic systems are rare due to the errors incurred in converting the species of interest to those for which the heat of formation is known. The use of a combination of techniques (kinetic, equilibration studies, calorimetric experiments), however, is now leading to reasonable estimates for some of these values. The relative strengths of the metal–carbon bonds found here are as expected with $C_6H_5 > CHCH_2 > CH_3 > n$-alkyl $> c$-alkyl. The absolute values, however, are much larger than those found for first row metals, and the difference between the strengths of the iridium–phenyl and the iridium–methyl bonds is also much greater than found earlier for rhodium.[34] We continue to investigate these and related compounds in the hope of more fully understanding the factors which affect metal–carbon and metal–hydrogen bond dissociation enthalpies.

Acknowledgements—Support for this work by National Science Foundation Grants CHE-8618753 (C.D.H.) and by the Director, Office of Energy Research, Office of Basis Energy Sciences, Chemical Sciences Division, of the U.S. Department of Energy under Contract DE-AC03-76SF00098 (R.G.B.) is gratefully acknowledged. We also appreciate helpful discussions with Drs W. A. G. Graham, J. E. Bercaw, J. A. Labinger, and H. E. Bryndza and their willingness to disclose results prior to publication.

REFERENCES

1. For recent reviews of C—H activation see: (a) J. Halpern, *Inorg. Chim. Acta.* 1985, **100**, 41; (b) N. Aktogu, D. Baudry, D. Cox, M. Ephritikhine, H. Felkin, R. Holmes-Smith and J. Azakrzewski, *Bull. Soc. Chim. France* 1985, 381; (c) M. L. H. Green and D. O'Hare, *Pure Appl. Chem.* 1985, **57**, 1897; (d) R. H. Crabtree, *Chem. Rev.* 1985, **85**, 245.
2. (a) C. Walling, *Free Radicals in Solution.* Wiley, New York (1957); (b) E. S. Huyser, *Free Radical Chain Reactions.* Wiley, New York (1970); (c) W. A. Pryor, *Free Radicals.* McGraw-Hill, New York (1966); see also: (d) A. L. J. Beckwith and T. Duong, *J. Chem. Soc., Chem. Comm.* 1978, 413; (e) Z. Cohen, E. Keinan, Y. Mazur and T. Haim Varkony, *J. Org. Chem.* 1975, **40**, 2141 and refs therein; (f) M. D. Meyer, S. G. Stroud and E. S. Tomezsko, *Tetrahedron* 1977, **33**, 2503; (g) S. Rozen, C. Gal and Y. Faust, *J. Am. Chem. Soc.* 1980, **102**, 6861 and refs therein; (h) H. A. Olah, D. G. Parker and N. Yoneda, *Angew. Chem., Int Ed. Engl.* 1978, **17**, 909.
3. (a) J. Hanotier, P. Camerman, M. Hanotier-Bridoux and P. De Radzitzky, *J. Chem. Soc., Perkin II* 1972, 2247; (b) D. H. R. Barton, R. S. Hay-Motherwell and W. B. Motherwell, *Tetrahedron Lett.* 1983, **24**, 1979; (c) D. H. R. Barton, M. J. Gustiger and W. B. Motherwell, *J. Chem. Soc., Chem. Comm.* 1983, **41**; (c) J. A. Smegal and C. L. Hill, *J. Am. Chem. Soc.* 1983, **105**, 3515; (d) C. J. Hill, J. A. Smegal and T. J. Henley, *J. Org. Chem.* 1983, **48**, 3277; (e) J. T. Groves and T. E. Nemo, *J. Am. Chem. Soc.* 1983, **105**, 6243; (f) I. Tabushi and A. Yazaki, *J. Am. Chem. Soc.* 1981, **103**, 7371; (g) D. Mansuy, M. Fontecave and J. F. Bartoli, *J. Chem. Soc., Chem. Comm.* 1983, 253.
4. (a) L. Abis, A. Sen and J. Halpern, *J. Am. Chem. Soc.* 1978, **100**, 2915; (b) R. A. Michelin, S. Faglia and P. Uguagliati, *Inorg. Chem.* 1983, **22**, 1831 and refs therein; (c) L. Abis, R. Santi and J. Halpern, *J. Organomet. Chem.* 1981, **215**, 263 and refs therein.
5. See for example: (a) J. A. Connor, *Top. Curr. Chem.* 1977, **71**, 71; (b) J. Halpern, *Acc. Chem. Res.* 1982, **15**, 238; (c) J. Halpern, *Inorg. Chem. Acta.* 1985, **100**, 41.
6. J. P. Collman, L. S. Hegedus, J. R. Norton and R. G. Finke, *Principles and Applications of Organotransition Metal Chemistry.* University Science Books, Mill Valley, CA (1987).
7. (a) R. H. Crabtree, J. M. Mihelcic and J. M. Quirk, *J. Am. Chem. Soc.* 1979, **101**, 7738; (b) R. H. Crabtree, M. F. Mellea, J. M. Mihelcic and J. M. Quirk, *J. Am. Chem. Soc.* 1982, **104**, 107; (c) R. H. Crabtree and C. P. Parnell, *Organometallics* 1984, **3**, 1727; (d) R. H. Crabtree, P. C. Demou, D. Eden, J. M. Mihelcic, C. P. Parnell, J. M. Quirk and G. E. Morris, *J. Am. Chem. Soc.* 1982, **104**, 6994; (e) D. Baudry, M. Ephritikine and H. Felkin, *J. Chem. Soc., Chem. Comm.* 1980, 1243; (f) D. Baudry, M. Ephritikine, H. Felkin and R. Holmes-Smith, *J. Chem. Soc., Chem. Comm.* 1983, 788; (g) D. Baudry, M. Ephritikine, H. Felkin and J. Zakrzewski, *J. Chem. Soc., Chem. Comm.* 1982, 1235; (h) D. Baudry, M. Ephritikine, H. Felkin and J. Zakrzewski, *Tetrahedron Lett.* 1984, 1283; (i) N. F. Gol'dshleger, M. B. Tyabin, A. E. Shilov and A. A. Shteinman, *Zh. Fiz. Khim.* 1969, **43**, 2174; (j) L. A. Khrushch, V. V. Lavrushko, Y. S. Masharin, A. P. Moravsky and A. E. Shilov, *Nouv. J. Chim.* 1983, **7**, 729; (k) G. B. Shulpin, G. V. Nizova and A. E. Shilov, *J. Chem. Soc., Chem. Comm.* 1983, 761.
8. (a) T. Burchard and H. Felkin, *Nouv. J. Chim.* 1986, **10**, 673; (b) M. Aktogu, D. Baudryt, D. Cox, M. Ephritikhine, H. Felkin, R. Holmes-Smith and J. Zakrzewski, *Bull. Soc. Chim. Fr.* 1985, 381; (c) H. Felkin, T. Fillebeen-Khan, R. Holmes-Smith and

Y. Lin, *Tett. Lett.* 1986, 1999; (d) D. Baudry, M. Ephritikhin, H. Felkin and J. Zakezewski, *Tett. Lett.* 1984, 1283; (e) H. Felkin, T. Fillebeen-Khan, Y. Gault, R. Holmes-Smith and J. Zakrzewski, *Tett. Lett.* 1984, 1279.

9. For two recent examples, see: (a) B. J. Fisher and R. Eisenberg, *Organometallics* 1983, **2**, 764; (b) W. D. Jones and W. P. Kosar, *J. Am. Chem. Soc.* 1986, **108**, 5640.
10. (a) H. A. Witcoff and B. G. Reuben, *Industrial Organic Chemicals in Perspective.* Part 1, pp. 108–119. Wiley, New York (1980); (b) I. Dybkjear, *CEER Chem. Econ. Eng. Rev.* 1981, **13**, 17; (c) K. Weissermel and H.-J. Arpe, *Industrial Organic Chemistry.* Verlag Chemie, Weinheim (1978); (d) J. Haggin, *Chem. Eng. News* 1987, June 1, pp. 22–28. There have also been recent reports describing other routes leading to higher hydrocarbons: (e) J. A. Labinger and K. C. Ott, *J. Phys. Chem.* 1987, **91**, 2682 and refs therein: (f) H. D. Gesser, N. R. Hunter and C. B. Prakash, *Chem. Rev.* 1985, **85**, 235.
11. M. I. Page, *Angew. Chem., Int. Ed. Engl.* 1977, **16**, 449.
12. (a) J. Halpern, F. T. T. Ng and G. L. Rempel, *J. Am. Chem. Soc.* 1979, **101**, 7124; (b) F. T. T. Ng, G. L. Rempel and J. Halpern, *J. Am. Chem. Soc.* 1982, **104**, 621; (c) T. T. Tsou, M. Loots and J. Halpern, *J. Am. Chem. Soc.* 1982, **104**, 623; (d) F. T. T. Ng, G. L. Rempel and J. Halpern, *Inorg. Chim. Acta*, 1983, **77**, L165.
13. J. A. Connor, M. T. Zafarani-Moattar, J. Bickerton, N. I. El Saied, S. Suradi, R. Carson, G. Al Takhin and H. A. Skinner, *Organometallics* 1982, **1**, 1166; BDE's were adjusted upwards from those listed in this paper, due to a more accurate determination of the BDE of the Mn—Mn bond in $Mn_2(CO)_{10}$: J. L. Goodman, K. S. Peters and V. Vaida, *Organometallics* 1986, **5**, 815.
14. (a) D. L. S. Brown, J. A. Connor and H. A. Skinner, *J. Organomet. Chem.* 1974, **81**, 403; (b) M. J. Nappa, R. Santi, S. P. Diefenbach and J. Halpern, *J. Am. Chem. Soc.* 1982, **104**, 619.
15. See, for example: (a) L. F. Halle, P. B. Armentrout and J. L. Beauchamp, *Organometallics* 1982, **1**, 963; (b) P. B. Armentrout, L. F. Halle and J. L. Beauchamp, *J. Am. Chem. Soc.* 1981, **103**, 6501; (c) P. B. Armentrout and J. L. Beauchamp, *J. Am. Chem. Soc.* 1981, **103**, 784.
16. J. A. Connor, *Top. Curr. Chem.* 1977, **71**, 71 and refs therein.
17. (a) J. W. Bruno, T. J. Marks and L. R. Morss, *J. Am. Chem. Soc.* 1983, **105**, 6824; (b) J. C. G. Calado, A. R. Dias, M. S. Salem and J. A. Martinho Simões, *J. Chem. Soc., Dalton Trans.* 1981, 1174 and refs therein; (c) G. Yoneda and D. M. Blake, *Inorg. Chem.* 1981, **20**, 67.
18. R. G. Pearson, *Chem. Rev.* 1985, **85**, 41 and refs therein.
19. J. Halpern, *Inorg. Chim. Acta.* 1985, **100**, 41 and refs therein.
20. R. Calderazzo, *Ann. N.Y. Acad. Sci.* 1983, **415**, 37.
21. G. Yoneda and D. M. Blake, *Inorg. Chem.* 1981, **20**, 67.
22. J. M. Buchanan, J. M. Stryker and R. G. Bergman, *J. Am. Chem. Soc.* 1986, **108**, 1537.
23. This work has been reported in preliminary form: (a) S. P. Nolan, C. D. Hoff, P. O. Stoutland, L. J. Newman, J. M. Buchanan, R. G. Bergman, G. K. Yang and K. S. Peters, *J. Am. Chem. Soc.* 1987, **109**, 3143. Calorimetric measurements were made by using procedures described in detail elsewhere: (b) C. D. Hoff, *J. Organomet. Chem.* 1985, **282**, 201; (c) Measurements of transition metal–phenyl bond enegies are very rare. For a recent study reporting a M—Ph bond energy in porphyrins, see M. Ke, S. J. Rettig, B. R. James and D. Dolphin, *Chem. Commun.* 1987, 1110.
24. (a) H. E. Bryndza, L. K. Fong, R. A. Paciello, W. Tam and J. E. Bercaw, *J. Am. Chem. Soc.* 1987, **109**, 1444; (b) The question of including M—H bonds in this correlation has recently been discussed further: J. A. Labinger and J. E. Bercaw (submitted for publication).
25. Experimental support for this is provided in (a) S. P. Nolan, R. L. de la Vega, S. L. Mukerjee and C. D. Hoff, *Inorg. Chem.* 1986, **25**, 1160; see also (b) J. A. Connor, M. T. Zafarani-Moattar, J. Bickerton, N. I. El Saied, S. Suradi, R. Carson, H. Al Takhin and H. A. Skinner, *Organometallics* 1982, **1**, 1166.
26. P. O. Stoutland and R. G. Bergman, unpublished results.
27. P. O. Stoutland and R. G. Bergman, *J. Am. Chem. Soc.* 1985, **107**, 4581.
28. S. W. Benson, *Thermochemical Kinetics.* Wiley, New York (1968).
29. T. Ziegler, V. Tschinke and A. Becke, *J. Am. Chem. Soc.* 1987, **109**, 1351.
30. C. H. Langford and H. B. Gray, *Ligand Substitution Processes.* W. A. Benjamin, Reading, Mass. (1974).
31. J-Y. Saillard and R. Hoffmann, *J. Am. Chem. Soc.* 1984, **106**, 2006.
32. (a) F. A. Cotton and G. Wilkinson, *Advanced Inorganic Chemistry.* Wiley, New York (1980); *Comprehensive Organometallic Chemistry*, Vol. 5, (Edited by G. Wilkinson, F. G. A. Stone and E. W. Abel), Pergamon Press, New York (1982).
33. (a) L. Dahlenburg and R. Nast, *J. Organomet. Chem.* 1976, **110**, 395; (b) U. Behrens and L. Dahlenburg, *J. Organomet. Chem.* 1976, **116**, 103.
34. F. J. Feher and W. D. Jones, *J. Am. Chem. Soc.* 1984, **106**, 1650.

Polyhedron Vol. 7, No. 16/17, pp. 1441–1452, 1988
Printed in Great Britain

0277–5387/88 $3.00+.00
© 1988 Pergamon Press plc

COMPARISON OF METAL–HYDROGEN, –OXYGEN, –NITROGEN AND –CARBON BOND STRENGTHS AND EVALUATION OF FUNCTIONAL GROUP ADDITIVITY PRINCIPLES FOR ORGANORUTHENIUM AND ORGANOPLATINUM COMPOUNDS†

HENRY E. BRYNDZA,‡ PETER J. DOMAILLE and WILSON TAM

E. I. du Pont de Nemours & Company, Inc., Central Research and Development Department, Experimental Station, Wilmington, DE 19898, U.S.A.

and

LAWRENCE K. FONG, ROCCO A. PACIELLO and JOHN E. BERCAW‡

California Institute of Technology, Pasadena, CA 91125, U.S.A.

Abstract—The equilibria:

$$L_nM—X + H—Y \Leftrightarrow L_nM—Y + H—X$$

(L_nM = (DPPE)MePt or $Cp^*(PMe_3)_2Ru$; X, Y = hydride, alkoxide, hydroxide, amide, alkyl, alkynyl, hydrosulphide, cyanide) have been examined. The equilibrium constants allow for the determination of relative M—X, M—Y bond dissociation energies (BDEs) for each series of compounds. A linear correlation of L_nM—X to H—X BDEs is found for the two dissimilar metal centres. Activation barriers for phosphine dissociation from $Cp^*(PMe_3)_2RuX$ complexes have been measured and suggest the principle of functional group additivity has limited applicability in organometallic thermochemistry. The generality and predictive value of this correlation and the observations on functional group additivity are discussed.

Despite the widespread use of organometallic complexes as catalysts, synthetic reagents, interesting materials, and precursors to advanced materials, little is known about the thermochemistry of these compounds. Recent advances have led to values for some metal–hydrogen and metal–carbon bond strengths,[1] but the factors governing the reactivity of transition metal–heteroatom bonds (M—X, X = OH, OR, NR_2, PR_2, SiR_3 and SH) have been left relatively unexplored.

Early transition metal–oxygen and –nitrogen bonds are quite robust, presumably due to ligand-to-metal pi-donation of an oxygen or nitrogen lone electron pair to an empty orbital of the electrophilic metal centre.[2] In contrast, there has been a common perception that late transition metal–nitrogen and –oxygen linkages are intrinsically weak due to the mismatch or hard ligand base with soft metal acid,[3] thus explaining the relative scarcity of such complexes in the literature. Only recently has the reaction chemistry of late transition metal alkoxides and amides been examined.[4]

Recent examples of the types of reaction chemistry available to late metal–oxygen and –nitrogen bonds include CO[5] and olefin[6] insertions, β-hydride elimination[7] and 'sigma bond metathesis' reactions;[8] the last provide a means of determining relative metal–X sigma bond strengths for a series of complexes. The assumption inherent in the evaluation of this data, as well as virtually every other solution phase thermochemical investigation into organotransition metal chemistry,[9] has been the principle of functional group thermochemical addi-

† Joint contribution from the Central Research and Development Department of the E. I. du Pont de Nemours & Co., Inc. Experimental Station, Wilmington, DE 19898, U.S.A. and the California Institute of Technology, Pasadena, CA 91125, U.S.A.

‡ Authors to whom correspondence should be addressed.

tivity,[10] which has proven so appropriate in organic systems.

There have been numerous studies of the effects of *trans* labilizing, sigma-bonded ligands on M—L bond strengths for 'classical' coordination complexes.[11] However, there have been no studies where ligand loss from an organometallic complex has been investigated in a systematic way as the size of the ancillary ligand X is varied.

In this manuscript we report L_nM—X bond strengths obtained from measurements of the equilibrium constants for a series of reactions involving $Cp^*(PMe_3)_2RuX$ ($Cp^* = \eta^5$-C_5Me_5) and (DPPE)MePtX (DPPE = $Ph_2PCH_2CH_2PPh_2$) complexes.[12] We also discuss the validity of the functional group additivity assumption for a series of $Cp^*(PMe_3)_2Ru$—X species in which the *dative* bond dissociation enthalpies have been measured.[13]

METHODOLOGY AND INITIAL OBSERVATIONS

Exchange equilibria

As reported previously, addition of *N*-methyl aniline to (DPPE)MePtOMe (**1**) in THF-d_8 results in the partial conversion of starting materials to methanol and (DPPE)MePtNMePH (**2**) [eq. (1)].[14] Measurements of the concentrations of each of the components in the equilibrium by ^1H and ^{31}P NMR spectroscopy yields the equilibrium constant ($K_{eq} = 0.8 \pm 0.2$); invariant to changes in starting conditions, moderate changes in temperature, and solvent (THF-d_8 or toluene-d_8).† These observations show that entropy contributions to the equilibrium free energy are negligible‡ and that solvation effects are small.

$$\underset{\mathbf{1}}{\text{(DPPE)MePtOMe}} + \text{HNMePh} \overset{K_{eq}}{\Longleftrightarrow} \underset{\mathbf{2}}{\text{(DPPE)MePtNMePh}} + \text{HOMe.} \quad (1)$$

The thermoneutral character of this equilibrium is quite significant. If we assume the only changes represented in the equilibrium correspond to making Pt—N and H—O bonds at the expense of Pt—O and H—N bonds, the near-unity value of K_{eq} requires the Pt—O bond in (DPPE)MePtOMe to be stronger than the Pt—N bond in (DPPE)MePtNMePh by the same amount as the H—O bond in methanol is stronger than the H—N bond in N-methyl aniline. Moreover, since the equilibrium constant is not solvent dependent, gas phase bond dissociation energies of 104.5 and 87.5 kcal mol^{-1},[15] respectively, for the H—O and H—N bonds in methanol and N-methyl aniline, may be used to estimate that the Pt—O bond in (DPPE)MePtOMe is *ca* 17 kcal mol^{-1} stronger than the Pt—N bond in (DPPE)MePtNMePh. This functional group approach to solution phase bond dissociation energies has been exploited very effectively in organic§ systems and has been used in organometallic[9] thermochemistry, as well.

Another ramification of the thermoneutral character of this equilibrium concerns *heterolytic* bond dissociation constants. As illustrated in Scheme 1, the equilibrium constant for eq. (1) (K_{eq}) may be expressed as the product of the ratio of acid dissociation constants (K_a's) and the ratio of Pt—NMePh to Pt—OMe heterolytic dissociation constants (K_2 and K_1, respectively):

$$K_{eq} = \frac{K_1}{K_2} \cdot \frac{K_a(\text{HNMePh})}{K_a(\text{HOMe})}.$$

Since K_{eq} is approximately one, it follows that the relative extent of (DPPE)MePt—OMe and (DPPE)MePt—NMePh bond heterolysis (K_1/K_2) is equal to the relative acid dissociation constants for H—OMe and H—NMePh [K_a(HOMe)/K_a(HNMePh)]. Using aqueous solution values of

† The equilibrium constant is also independent of the reaction vessel wall material; e.g. Pyrex, silylated Pyrex, sapphire or quartz.

‡ Since $\Delta G_{eq} \approx 0$ and since no measurable temperature dependence of ΔG_{eq} was noted, this shows $\Delta H_{eq} \approx \Delta S_{eq} \approx 0$.

§ Throughout this manuscript we use interchangeably 'L_nM—X bond strengths', 'bond dissociation energies (BDEs)' and 'homolytic bond strengths' to mean relative *solution phase* D(M—X) values. By using gas phase D(H—X) values, we necessarily assume equivalent solvation of the functional groups on both sides of the equilibria and that the bonding of ancillary ligands (Cp*, phosphines, etc) to the metal does not appreciably change. Other studies have noted that the sublimation, dissolution and vaporization energies needed to convert such solution data to gas phase values make very small corrections to the relative bond strengths obtained when non-gaseous reagents are involved. Moreover, the values and assumptions needed to correct solution phase BDEs to gas phase numbers commonly introduce errors as large as the corrections to be made. Thus, we prefer to use the solution values obtained; we suggest the gas phase values will be similar. The applicability of this approach is evident from the utility of the thermodynamic functional group additivity tables for organic systems in solution as well as the gas phase. See: (a) S. W. Benson, *Thermochemical Kinetics*, Second Edition. Wiley, New York (1976); (b) S. W. Benson, *The Foundation of Chemical Kinetics*. Robert E. Krieger, Malabar, Florida (1982).

Heterolytic ligand dissociation

		k_{eq}
(1)	$(DPPE)MePt—OCH_3 \rightleftharpoons (DPPE)MePt^+OCH_3^-$	K_1
(2)	$(DPPE)MePt^+NCH_3(Ph)^- \rightleftharpoons (DPPE)MePt—NCH_3(Ph)$	$1/K_2$
(3)	$(DPPE)MePt—OCH_3 + NCH_3(Ph)^- \rightleftharpoons (DPPE)MePt—NCH_3(Ph) + OCH_3^-$	K_1/K_2
(4)	$H^+OCH_3^- \rightleftharpoons H—OCH_3$	$1/K_a(CH_3OH)$
(5)	$H—NCH_3(Ph) \rightleftharpoons H^+NCH_3(Ph)^-$	$K_a(HNMePh)$
(6)	$H—NCH_3(Ph) + OCH_3^- \rightleftharpoons H—OCH_3 + NCH_3(Ph)^-$	$K_a(HNMePh)/K_a(CH_3OH)$
(7)	$(DPPE)MePt—OCH_3 + H—NCH_3(Ph) \rightleftharpoons (DPPE)MePt—NCH_3(Ph) + H—OCH_3$	$\left(\frac{K_1}{K_2}\right) \times \left(\frac{K_a(HNMePh)}{K_a(CH_3OH)}\right)$

$K_1/K_2 \cong K_a(CH_3OH)/K_a(HNMePh)$
since $K \cong 1$

Scheme 1.

Table 1. Relative $L_nM—X$ bond strengths from equilibrium measurements

X	Relative D(Ru—X) (kcal mol^{-1})
(A) $Cp^*(PMe_3)_2Ru—X$ derivatives	
OH	0.0
CCPh	14.3
$CH_2C(O)CH_3$	−20.2
NHPh	−30.1
NPh_2	−37.2
SH	> −18.5
CN	> 14.2
H	−8.9
(B) (DPPE)MePt—X derivatives	
OCH_3	−15.3
OH	0.0
NPh_2	−34.5
NMePh	−32.3
$CH_2C(O)CH_3$	−19.3
SH	> −18.5
CN	> 14.2

K_a for methanol and methyl aniline† (pK_a = 16 and 25, respectively), the extent of [$NMePh^-$] dissociation from **12** in aqueous solution would be 10^9 less than [OMe^-] dissociation from **11**. While this ratio will vary as the ratio of K_a values varies with different solvents, the conclusion remains the same: the relative extent of (DPPE)MePt—X bond heterolysis parallels the relative K_a values of the H—X analogue.

The same equilibrium techniques can be used to evaluate the relative homolytic bond strengths of Pt—X bonds in a larger series: (DPPE)MePtOMe (**1**), (DPPE)MePtNMePh (**2**), (DPPE)MePtOH (**3**), (DPPE)$MePtCH_2COCH_3$ (**4**) and (DPPE)$MePtNPh_2$ (**5**) as shown in eq. (2) and listed in Table 1. Interestingly, these reactions are also essentially thermoneutral. Other reactions of (DPPE)MePtOMe with H_2S, HCN and $Cp(CO)_3MH$ (Cp = η^5-C_5H_5; M = Cr, Mo, W) have proven effectively irreversible; no evidence for any (DPPE)MePtOMe has been observed when (DPPE)MePtSH (**6**), (DPPE)MePtCN (**7**) and (DPPE)$MePtM(CO)_3Cp$ (**8**, M = Cr; **9**, M = Mo; **10**, M = W) were dissolved in 50/50 solutions of THF-d_8/CH_3OH [eq. (3)].

$$(DPPE)MePt—OMe + H—X \Leftrightarrow (DPPE)MePt—X + H—OMe \quad (2)$$

X = OH, OMe, NMePh, NPh_2, $CH_2C(O)CH_3$

$$(DPPE)MePtOMe + H—Y \rightarrow (DPPE)MePt—Y + HOMe \quad (3)$$

Y = SH, CN, $CpM(CO)_3$ (M = Cr, Mo, W).

Attempts to extend this series to other Pt—X bonds is complicated by the high reactivity of these platinum complexes and the long times required to attain equilibrium. Fortunately, the $Cp^*(PMe_3)_2$RuX system proved both kinetically more active in exchange equilibria and chemically more robust, providing further insights into M—X (M = Pt, Ru) homolytic bond strengths.

Similar equilibrium measurements carried out on the ruthenium system show thermoneutral equi-

† While it is clear that K_a values measured in aqueous solution do not accurately reflect dissociation constants in organic solvents, such as THF, the example serves to illustrate the relative ease of ligand heterolytic dissociation in a hypothetical aqueous solvent system. The use of K_a values appropriate to different solvent systems *may* change the ratio of line 6 in Scheme 1; however, any such changes, by definition, will also alter the ratio of K_1/K_2 in exactly the same way so that $K_{1solv}/K_{2solv} = K_a(HOMe)_{solv}/K_a(HNMePh)_{solv}$.

libria are established when $Cp^*(PMe_3)_2RuOH$ is combined with a variety of HX sources [eq. (4)].

$$Cp^*(PMe_3)_2Ru\text{—}OH + H\text{—}X \underset{\mathbf{11}}{} \Leftrightarrow Cp^*(PMe_3)_2Ru\text{—}X + H\text{—}OH \quad (4)$$

X = NHPh (**12**)
NPH_2 (**13**)
$CH_2C(O)CH_3$ (**14**)
CCPh (**15**).

As in the platinum case, these equilibria are insensitive to changes in temperature, solvents, wall effects and concentrations.† As before, 'irreversible' reactions were observed when $Cp^*(PMe_3)_2RuOH$ was combined with H_2S, HCN and $CpM(CO)_3H$ (M = Cr, Mo, W) [eq. (5)].

$$Cp^*(PMe_3)_2Ru\text{—}OH + H\text{—}Y \underset{\mathbf{11}}{} \rightarrow Cp^*(PMe_3)_2Ru\text{—}Y + H\text{—}OH \quad (5)$$

Y = SH (**16**)
CN (**17**)
$CpCr(CO)_3$ (**18**)
$CpMo(CO)_3$ (**19**)
$CpW(CO)_3$ (**20**).

Reaction of $Cp^*(PMe_3)_2RuH$ (**21**) with H_2O generates an equilibrium mixture of **11** and H_2; the small equilibrium constant for this reaction ($\Delta G \approx 7$ kcal mol^{-1}) limits the precision of our measurement. However, the magnitude of the equilibrium constant does, nevertheless, establish a Ru—H bond strength‡ relative to Ru—OH to within ± 2 kcal mol^{-1}. This value, and the other relative L_nM—X bond strengths obtained are listed in Table 1.

While addition of water to $Cp^*(PMe_3)_2RuSH$ failed to generate detectable amounts of the hydroxide complex **11**, addition of $HSi(OEt)_3$ establishes the equilibrium shown in eq. (6). The equilibrium constant of 0.75 appears to signal that second row main group substituents will be in nearly thermoneutral equilibrium with each other, although such Ru—X linkages are apparently substantially stronger than analogous bonds to comparable first row substituents; an observation consistent with the general effectiveness of sulphur and silicon compounds as catalyst poisons.

$$Cp^*(PMe_3)_2RuSH + HSi(OEt)_3 \underset{\mathbf{16}}{} \Leftrightarrow Cp^*(PMe_3)_2RuSi(OEt)_3 + H_2S. \underset{\mathbf{22}}{} \quad (6)$$

Equilibrium measurements for the reversible reaction of $Cp^*(PMe_3)_2RuNPh_2$ with (DPPE)MePt(OH) show only a small energetic preference for $Cp^*(PMe_3)_2RuOH$ and $(DPPE)MePtNPh_2$ [eq. (7)].

$$Cp^*(PMe_3)_2RuNPh_2 + (DPPE)MePtOH \underset{\mathbf{13}}{} \underset{\mathbf{3}}{} \Leftrightarrow (DPPE)MePtNPh_2 + Cp^*(PMe_3)_2RuOH. \underset{\mathbf{5}}{} \underset{\mathbf{11}}{} \quad (7)$$

The equilibrium constant for the reaction in eq. (7) was found to be consistent with other equilibria measured;§ this internal consistency further demonstrates the very small equilibrium solvent dependence, since the equilibrium constants are apparently unaffected when substantial amounts of protic 'co-solvents' (such as methanol, water and diphenyl amine) are present [eqs (2) and (4)], *vis-à-vis* absent [(eq. (7)]. Furthermore, this result suggests that the *combination* of ruthenium's preference for oxygen *and* the relief of steric crowding inherent on going from $Cp^*(PMe_3)_2RuNPh_2$ to $Cp^*(PMe_3)_2RuOH$ are small (3.6 kcal mol^{-1}), even in the relatively congested $Cp^*(PMe_3)_2RuX$ system.

Ru—P *Bond dissociation enthalpies*

The assumption inherent in the above evaluation of equilibrium data, as well as in virtually every other solution phase thermochemical investigation into organotransition metal chemistry,[9] has been the principle of functional group thermochemical additivity.[10] While it seems reasonable that the Ru—P bonds in $Cp^*(PMe_3)_2Ru$—X will be about as strong as those in $Cp^*(PMe_3)_2Ru$—Y, this assumption has never been tested for organometallic systems.

In order to examine M—L dative bond strengths,

† The nearly solvent independent nature of the equilibrium is further demonstrated by the fact that the [H_2O] (between 0.02 and 0.80 M), and hence the dielectric of the THF-d_8/H_2O solution, does not systematically change the measured K_{eq} values for eq. (4). Further evidence for the insensitivity of the equilibria measured to protic solvents comes from the study of eq. (7) (*vide infra*) which gives results, in the absence of protic materials, which were predicted by equilibria involving those protic organic compounds.

‡ Or, at least, the relative stability of the hydride complex (*vide infra*).

§ This equilibrium constant can be predicted by summing the following equilibria:

$$Cp^*(PMe_3)_2RuNPh_2 + HOH \Leftrightarrow Cp^*(PMe_3)_2RuOH + HNPh_2$$

$$(DPPE)MePtOH + HNPh_2 \Leftrightarrow (DPPE)MePtNPh_2 + HOH.$$

ligand exchange reactions were studied by the addition of $P(CD_3)_3$ to unlabelled $Cp^*(PMe_3)_2RuX$ complexes.[12] A large isotopic shift was observed in the ^{31}P NMR for perdeutero- *vis-à-vis* perproteophosphine (0.9 ppm at 100°C in *o*-xylene-d_{10}), and the spectral features of the Ru—PMe_3 and Ru—$P(CD_3)_3$ functional groups were found to be similarly well resolved. By measuring NOE suppressed ligand exchange kinetics† at different temperatures, the dative bond dissociation enthalpies [$\Delta H^\ddagger$ corresponding to k_1, eq. (8)] for Ru—PMe_3 linkages were obtained.‡

$Cp^*(PMe_3)_2RuX$

$$\underset{k_{-1}}{\overset{k_1}{\rightleftharpoons}} Cp^*(PMe_3)RuX + PMe_3. \quad (8)$$

A summary of the activation parameters for dative ligand loss from some of the $Cp^*(PMe_3)_2RuX$ complexes examined can be found in Table 2.§

We must stress these measurements have not determined absolute bond strengths for Ru—P linkages. We *suggest* that since the activation barrier for combination of free phosphine with the 16-electron unsaturated intermediates is likely to be a small ($\Delta H^\ddagger \approx 0$ for k_{-1}) and a fairly constant amount of energy for a variety of complexes, the differences in activation enthalpies for two complexes should be about the same as the difference in Ru—P bond strengths (Fig. 1). Support for this premise comes from the large positive free entropies of activation noted for all of these dissociations indicating the importance of 'late' (or product-like) transition states[16] for phosphine loss. This interpretation is also consistent with the observation that $k_{-1} \gg k_1$ for all derivatives studied.

Table 2. $\Delta H^\ddagger$ for phosphine dissociation from $Cp^*(PMe_3)_2Ru$—X complexes

X	$\Delta H^\ddagger$ for PMe_3 loss (kcal mol^{-1}) (± 1 kcal mol^{-1})
H	> 47
CCPh	42
CH_3	40
CH_2Ph	38
Ph	38
CH_2SiMe_3	34

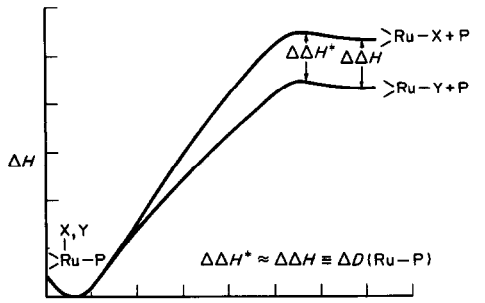

Fig. 1. Enthalpy diagram for phosphine loss from $Cp^*(PMe_3)_2RuX$ complexes assuming a small and/or constant barrier to phosphine binding to $Cp^*(PMe_3)RuX$. If this back reaction barrier is either negligible or constant then $\Delta\Delta H^\ddagger \approx \Delta\Delta H \equiv \Delta D$(Ru—P).

DISCUSSION

Ru—P *Bond strengths*

For ligands, X, which have no significant π interactions with the transition metal, these approximate Ru—P bond strengths can be ordered according to steric bulk, as shown in Table 2. Such steric trends are as expected based on previously published studies where phosphine steric requirements were varied. When $Cp^*(PMe_3)_2RuMe$ is used as a benchmark for comparison, changing the ancillary substituent to the small, rod-like phenylacetylide ligand strengthens the Ru—P interactions by about 2 kcal mol^{-1}. Conversely, when methyl is replaced by a slightly larger ligand, such as benzyl or phenyl, Ru—P bonds weaken by about the same amount. However, when methyl is substituted for something very much larger (CH_2SiMe_3) or smaller (H) *sub-*

† A numerical integration program 'GIT' was used to extract dissociation rates from the kinetic data. See ref. 14 for detailed discussion of this process. GIT was developed as an iterative integration package based on Havchem software by Dr F. J. Weigert at Du Pont CR&D.

‡ NOE suppressed kinetics were carried out with pulse delays of five T_1 periods between acquisitions. Typically four to six measurements were carried out over a 40°C temperature range. ^{31}P NMR was utilized in order to measure the concentrations of all P containing materials in solution; this also allowed quantification of the significant levels of phosphine and labelled phosphine migrating to the gas phase above the solutions. Clearly, since the $PMe_{3(soln)} \Leftrightarrow PMe_{3(gas)}$ equilibrium changes with temperature, quantification of all solution phase concentrations is critical to the accurate determination of phosphine dissociation rate constants.

§ The data collected on $Cp^*(PMe_3)_2RuX$ complexes containing nucleophilic lone electron pairs on the ancillary ligand does not directly bear on this question of functional group additivity and, so, has not been included in this manuscript. For a complete description of this work see ref. 14.

stantial deviations of more than 6 kcal mol^{-1} in the strengths of Ru—P interactions are indicated.†

These observations suggest the functional group additivity approach to organometallic thermochemistry may be quite appropriate *when substituents of similar sizes are employed. However, our data indicate caution must be exercised when thermodynamic investigations involve ligands of dissimilar sizes.*‡

This interpretation presupposes the activation barriers for adding phosphine to Cp*(PMe$_3$)RuMe and Cp*(PMe$_3$)RuCH$_2$SiMe$_3$ are the same. In fact, the barrier is likely to be *larger* for adding phosphine to the sterically more congested centre (Fig. 2) which means the differences in actual Ru—P bond strengths are *larger* than the differences in activation barriers for phosphine dissociation. *Thus our data, as applied to functional group additivity questions, represents a best-case situation. The actual differences in* Ru—P *bond strengths are likely to be larger than indicated by the data in Table 2 and the functional group additivity deviations discussed above may be conservative.*

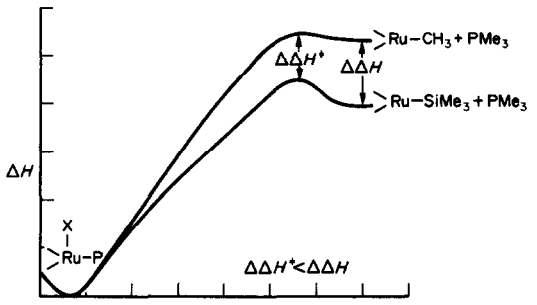

Fig. 2. Enthalpy diagram for phosphine loss from Cp*(PMe$_3$)$_2$RuCH$_3$ vs Cp*(PMe$_3$)$_2$RuCH$_2$SiMe$_3$. This figure accounts for the larger steric interactions present when PMe$_3$ approaches the bulkier complex.

Steric effects on phosphine dissociation

Another way of looking at these data, which involves no assumptions, is that the steric consequences of an ancillary ligand may have more than a 13 kcal mol^{-1} effect on the activation barrier to phosphine dissociation and this corresponds to an enormous difference in relative rates of those dissociations. In effect, this study quantifies what organometallic chemists have known intuitively for many years; steric changes to a ligated transition metal complex can dramatically affect the rates of ligand losses.

Relative σ bond strengths

The nearly thermoneutral character of the equilibria represented by eq. (9) appears to be general for a number of sigma bonded ligands. This observation naturally implies that the difference in H—X and H—Y BDEs is the same as the difference in L$_n$M—X and L$_n$M—Y BDEs, assuming that the functional group approach discussed above is equally valid for these ruthenium and platinum systems.§ Alternatively, one may take the observation that $K_{eq} \approx 1$ to indicate that heterolytic dissociation of basic ligands from these metal centres (L$_n$M—X $\Leftrightarrow$ [L$_n$M$^+$]+X$^-$) parallels the K_a values of the corresponding organic acids (H—X $\Leftrightarrow$ H$^+$ +X$^-$). The very small solvent dependence of the equilibrium constants allows quantitative estimates of relative homolytic bond strengths in these L$_n$M—X systems from the appropriate gas phase H—X bond dissociation energies.[15] This common assumption that functional groups are solvated equivalently in different complexes has proven to be valid for both organic[17] and organometallic[18] systems.

$$L_nM\text{—}X + H\text{—}Y \overset{K_{eq}}{\rightleftharpoons} L_nM\text{—}Y + H\text{—}X \quad (9)$$

[L$_n$M = (DPPE)MePt, Cp*(PMe$_3$)$_2$Ru].

An effective method of graphically illustrating the data from Table 1 is shown in Fig. 3. For this

† While differences in ground state or transition state hyperconjugative stabilizations due to the different alkyl and hydride ligands cannot be ruled out, the similarities of Ru—P bond strengths in the ruthenium benzyl, phenyl, methyl and phenylacetylide complexes suggest any such differences are insignificant compared to the magnitude of changes made by steric differences.

‡ This observation suggests, for example, the apparent thermodynamic stability of L$_n$M—H bonds, relative to L$_n$M—CH$_3$ linkages, noted in a number of studies (*vide infra*) may be due, in large part, to other bonds in those hydrides becoming stronger than in the methyl analogues. In effect the hydride complexes may be more thermodynamically stable than alkyls but this is not necessarily due to M—H being particularly strong. Another serious ramification of this information is that studies of M—X bond strengths in complexes containing other ligands (i.e. non-'naked' complexes usually present in solution) will be difficult to obtain with an uncertainty of better than ±2 kcal mol^{-1}.

§ This assumption appears justified based on the similar sizes of the X ligands employed in this study. One notable exception is the hydride. Based on the analysis (above) the significance of the Cp*(PMe$_3$)$_2$RuH data must be questioned. Clearly the small hydride ligand tends to allow stronger interactions between metal and phosphines which tends to make the complex, as a whole, more stable (*vide infra*) than it might be based on the strength of the M—H interaction alone.

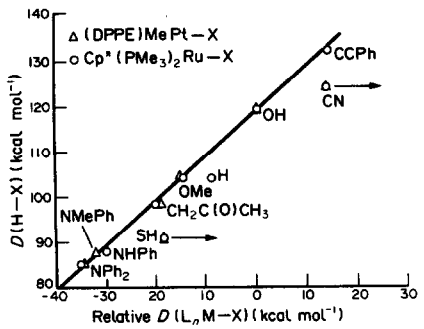

Fig. 3. H—X vs relative L_nM—X bond dissociation energies (BDEs) in kcal mol^{-1}. Data plotted from Table 1 for both (DPPE)MePt—X (△) and $Cp^*(PMe_3)_2Ru$—X (○) systems with L_nM—OH arbitrarily assigned a relative BDE of 0.0 kcal mol^{-1}. A line with an arbitrary slope of 1.0 has been drawn through the hydroxide 'point'. Data depicted for L_nM—CN and L_nM—SH are *minimum* L_nM—X bond strengths (against absolute H—X bond strengths) which, as indicated by the arrows, may be much stronger than the 9 kcal mol^{-1} deviation detectable by our experimental methods.

plot of D(H—X) vs relative $D(L_nM$—X), the L_nM—OH bond dissociation energies for (DPPE)MePtOH and $Cp^*(PMe_3)_2RuOH$ are arbitrarily assigned a relative value of zero, and a line with an arbitrary slope of one is drawn through this point. Two important conclusions can be drawn from the remarkably good correlation of relative H—X and L_nM—X bond strengths which is readily apparent: (i) the close linear fit for the bond dissociation energies of $\{Cp^*(PMe_3)_2Ru^*\}$ and $\{(DPPE)MePt^*\}$ with first row $\{X^*\}$ substituents (except for the metal cyanides and sulphides, *vide infra*) indicates that other relative L_nM—X (X = first row element) bond strengths should be predictable, even for complexes we have not yet examined, by simple extrapolation from the H—X bond strength of the organic analogue. (ii) The one-to-one correlation between L_nM—X BDEs and H—X BDEs may well be generally valid for a variety of organometallic compounds, in the absence of L_nM—X multiple bonding (*vide infra*). That the data fit so well on the line drawn for Fig. 3 is quite persuasive in this regard, since the same close correlation holds both for square planar, 16-electron, third-row (d^8) platinum complexes and for the sterically congested 'three-legged piano-stool', 18-electron, second-row (d^6) ruthenium complexes.

Extension to other systems

While examples of comparable sigma-bond strength measurements for series of organometallic complexes are rare in the literature, thermochemical data on two other organometallic systems lend support to the generality of this H—X vs relative M—X bond strength correlation. Bergman and coworkers[19] have shown that the reaction between $Cp^*(PMe_3)(H)Ir(cyclo\text{-}C_6H_{11})$ and various alkanes do not proceed to completion to generate the corresponding alkyls and cyclohexane [eq. (10)] suggesting a similar correspondence for Ir—C_6H_{11}, Ir—R [R = *cyclo*-C_5H_9, *neo*-C_5H_9, *n*-C_5H_9,$CH_2CH(CH_3)CH(CH_3)_2$] and H—*cyclo*—C_6H_{11}, H—R BDEs. Furthermore, if the (solution phase) thorium–carbon bond dissociation energies, obtained by reaction calorimetry by Bruno, Marks and Morss,[20] are evaluated in this same manner, once again, a one-to-one correlation between $Cp^*_2(OMe_3)Th$—R and H—R BDEs is evident. On the other hand, for thorium compounds with alkoxide or amide ligands, significant deviations from the one-to-one correlation are noted. For example, the $Cp^*_2(OMe_3)Th$—OR and $Cp^*_2(OCMe_3)Th$—NR_2 BDEs are greater than would be predicted† for a single sigma Th—OR or Th—NR_2 bond (i.e. by comparison to the corresponding H—OR or H—NR_2 BDE). Indeed, such deviations are entirely expected, since the coordinatively unsaturated, Lewis acidic thorium centre of these $Cp^*_2Th(IV)X_2$ complexes is a powerful π-acceptor of oxygen or nitrogen lone electron pairs, increasing the Th—OR or Th—NR_2 bond order. An estimate of the thermodynamic importance of such multiple bonds can be made from the magnitude of such deviations from the expected correlation.

$$Cp^*(PMe_3)(H)Ir(cyclo\text{-}C_6H_{11}) + HR \Leftrightarrow Cp^*(PMe_3)(H)IrR + (cyclo\text{-}C_6H_{12}) \quad (10)$$

R = *cyclo*-C_5H_9, *neo*-C_5H_9, *n*-C_5H_9, $CH_2CH(CH_3)CH(CH_3)_2$

Anomalies in the ruthenium and platinum systems

Returning to the platinum and ruthenium systems, three types of compounds studied exhibit anomalously large L_nM—X BDEs: L_nM—CN, L_nM—SH, and $Cp^*(PMe_3)_2Ru$—H (Table 1 and Fig. 3). The cyanide ligand is a moderate π-acceptor and, considering the extremely electron-rich character of

† While the data for alkoxides and amides were obtained on complexes having slightly different spectator ligand environments than the $Cp^*_2(OCMe_3)ThX$, the deviations of more than 20 kcal mol^{-1} (from the values expected based on the H—X vs Th—X plot) are large with respect to deviations seen in Th—X bonds on changing spectator ligands. For example, in the series $Cp^*_2(OCMe_3)ThEt$, $Cp^*_2(Et)ThEt$ and $Cp^*_2(Cl)ThEt$ the solution phase Th—C bond strengths range over only 4.1 kcal mol^{-1} (76.3, 73.5, 72.2 kcal mol^{-1}, respectively).

$Cp^*(PMe_3)_2Ru(II)$, considerable ruthenium-to-cyanide back donation is anticipated, which reconciles the higher than one bond order observed. The low energy of the ν (CN) (2058 cm^{-1} for **7**; cf. ν (CN) = 2240–2260 cm^{-1} for organic nitriles[21] is indeed indicative of substantial Ru≡C≡N character for $Cp^*(PMe_3)_2RuCN$ (**7**). While the platinum centre in (DPPE)MePtCN is not as electron rich as the ruthenium case, similar, though reduced, M=C multiple bonding is indicated for this complex by ν (CN) of 2128 cm^{-1}. Thus the explanation of the stability of the M—CN bonds to electron-rich late metal systems is essentially the same as found for early metal systems with π-donor ligands (i.e. multiple bond order).

Turning to the sulphides, overlap between ruthenium or platinum sigma orbitals and the $3s/3p$ orbitals of the second row main group elements may be significantly better than overlap between these metal orbitals and the $2s/2p$ orbitals of the first row elements. Such arguments, akin to those used to account for the preferences of 'hard' and 'soft' acids to bases, may be offered to explain the larger than expected L_nM—SH BDEs for **6** and **16**. In this regard, it is significant that, although $Cp^*(PMe_3)_2RuSH$ is unreactive towards a variety of first row H—X compounds, a nearly thermoneutral equilibrium is established between $Cp^*(PMe_3)_2RuSH$, $(EtO)_3SiH$, $Cp^*(PMe_3)_2RuSi(OEt)_3$, and H_2S [eq. (6)]. This observation suggests a second 'parallel' H—X vs relative L_nM—X bond strength correlation may hold for second row main group substituents. Because of the experimental limitations of our equilibrium measurements, we cannot quantify the energetic displacement between the L_nM—X and L_nM—Y (X = first row substituent; Y = second row substituent) relationships. We do, however, know the line for second row elements must lie more than 9 kcal mol^{-1} to the 'right' of the established correlation for first row substituents for these platinum and ruthenium complexes. The observation that all first row substituents show D(H—X)/D(L_nM—X) correlation with each other can be interpreted as indicating that a variety of carbon, oxygen and nitrogen sigma ligands are equally 'hard' and that only on changing rows does one find 'softer' substituents.

Although the value of the Ru—H BDE for $Cp^*(PMe_3)_2RuH$ (**21**) is rather imprecise due to the small value of the equilibrium constant found for combining **21** with H_2O,† its deviation (7 kcal mol^{-1}) from the linear correlation in Fig. 3 clearly exceeds the conservative estimate of the uncertainty in the BDE of ±2 kcal mol^{-1}. Moreover, Thompson and Bercaw[22] have found that Cp^*_2ScH reacts with benzene to establish an equilibrium mixture of Cp^*_2ScH, $Cp^*_2ScC_6H_5$, C_6H_6, and H_2, from which the thermodynamic parameters ΔH° = 6.7(3) kcal mol^{-1} and ΔS° = −1.5(1) e.u. were obtained for eq. (11). Assuming the one-to-one correlation between L_nM—X and H—X BDEs, the Sc—H BDE is 6.7 kcal mol^{-1} stronger than expected,‡ i.e. again, one finds that there is an increased stability associated with the L_nM—H bonds, amounting to approximately 7 kcal mol^{-1} for the systems considered here. Even the *average* of the two Th—H BDEs in $[Cp^*_2ThH_2]_2$ (which also includes the enthalpy of the bridging interaction between the two thorium centres, which more than compensates for the loss of translational entropy due to dimerization) obtained by reaction calorimetry deviates by only approximately 15 kcal mol^{-1}, again to the right, of the linear correlation in Fig. 4.

$$Cp^*_2ScH + C_6H_6 \Leftrightarrow Cp^*_2ScC_6H_5 + H_2. \quad (11)$$

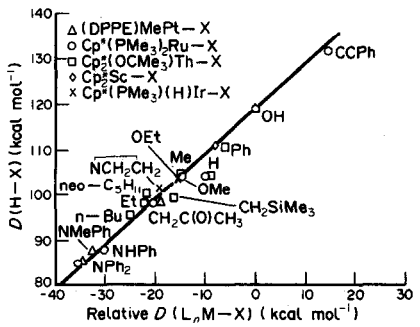

Fig. 4. Plot of H—X vs relative L_nM—X BDEs for (DPPE)MePt—X (△), $Cp^*(PMe_3)_2Ru$—X (○), Cp^*_2Sc—X (◇), $Cp^*_2(OCMe_3)Th$—X (□) and $Cp^*(PMe_3)(H)Ir$—X (x) depicted for X = singly-bonded first-row main group substituents along the arbitrary axes from Fig. 3. To put the Sc—X data on these axes the Sc—C bond in Cp^*_2Sc—Ph has been defined as −8.1 kcal mol^{-1}; the Ir—C bond in $Cp^*(PMe_3)(H)Ir$—(*cyclo*-C_6H_{11}) has been defined as −21 kcal mol^{-1} and the Th—C bond in $Cp^*_2(OCMe_3)Th$—CH_3 has been defined as −14.9 kcal mol^{-1}.

† The fact that most of the dihydrogen is in the gas phase above the solution also contributes to the error in translating the Ru—H BDE for **11** to relative gas phase values, because the enthalpy of dissolution of dihydrogen in THF, which is likely to differ substantially from the enthalpies of condensation and dissolution of the other organics used in this study, must be incorporated into the calculation. Although this quantity has not yet been measured to our knowledge, it is unlikely that it exceeds the ±2 kcal mol^{-1} uncertainty in the measurement of the equilibrium constant.

‡ Assuming a C—H BDE of 111 kcal mol^{-1} for benzene, H—H BDE of 104 kcal mol^{-1} and H_{soln} = 0.9 kcal mol^{-1} for H_2 in benzene.

While the above discussion of metal hydride bond strengths suggests these bonds are anomalously strong relative to other first row M—X bonds, it must be remembered that, as discussed above (footnote on p. 1448), the anomalously small size of the hydride ligand clearly makes the Ru—P bonds in **21** stronger than in other derivatives. Thus, analysis of equilibrium or calorimetric data will show hydride *complexes* to be anomalously stable; however, this may have little to do with the actual M—H bond strengths. Thus while the experiments described provide interesting and useful data on the stability of metal hydride complexes, it is unclear that they provide any real information on the relative strength of metal–hydrogen bonds.

The common assumption, based on the reported BDE difference between $(CO)_5Mn—H$ and $(CO)_5Mn—CH_3$, has been that 'metal–carbon' bonds in organotransition metal compounds are approximately 25 kcal mol^{-1} weaker than metal–hydrogen bonds.† Our data, and that of others cited herein, appear to indicate that (i) the difference in $L_nM—H$ and $L_nM—CH_3$ BDEs is likely to be substantially smaller, (ii) the thermodynamic stability of hydride complexes found in all of these experiments is, at least partly, due to other bonds in metal hydrides becoming stronger rather than reflecting actual increases in $D(L_nM—H)$, and (iii) one must be cautious to correct the $L_nM—R$ (R = alkyl, alkenyl, aryl, alkynyl, etc.) bond dissociation energy for the stability of $\{R^{\bullet}\}$ when discussing the relative strengths of metal–carbon and metal–hydrogen bonds. As the data of Figs 3 and 4 demonstrate, metal–carbon bond strengths may be expected to vary over a range as large as 40 kcal mol^{-1} (R = CH_2Ph to CCR′). An appropriate one-to-one comparison would be between $L_nM—H$ and $L_nM—CH_3$, since the bond dissociation energies of H—H and $H—CH_3$ are 104 and 105 kcal mol^{-1}, respectively.

Other potential anomalies

It is interesting that our ruthenium and platinum systems show no significant thermodynamic stability gain from the presence of ancillary X ligands which are π-electron donors. Clearly, π-acceptor ligands remove electron density from these metal centres and, thereby, stabilize these complexes. At this point we have no evidence for a simple π-conjugative stabilization by 'neutral' π-ligands (such as the phenyl acetylide in **15** or the phenyl substituent in Cp^*_2ThPhX), though, based on organic analogues, some stabilization might be expected. Although the stability of phenyl complexes has proven difficult to evaluate, there is some evidence[23] that these linkages may be stronger than anticipated from the $D(H—X)/D(L_nM—X)$ correlations of Figs 3 and 4. It is unclear if this type of stabilization is simply too weak to be detected in our ruthenium and platinum data, or if some other, as yet unrecognized, factors which can enhance the M—(sp^2)C bond strengths are not present in our compounds.

Interesting trends

Although the bond strength information presented here, as summarized for the $Cp^*(PMe_3)_2Ru—X$, $(DPPE)MePt—X$, $Cp^*_2(OCMe_3)Th—X$, $Cp^*_2Sc—X$ and $Cp^*(PMe_3)(H)Ir—X$ systems (X = singly-bonded first row main group substituent) in Fig. 4, is somewhat limited, we note some interesting trends. The metal–oxygen bonds examined for late metals are not, despite conventional perceptions, particularly weak. The $L_nM—OH$ bond is stronger than $L_nM—H$ and $L_nM—(sp^3)C$ bonds (as in the carbon-bound metal enolates **4** and **14**), but weaker than $L_nM—(sp)C$ bonds (as in the phenylacetylide complex **15**). Thus, the higher reactivity associated with (DPPE)MePt—OR (R = H, CH_3) bonds (*vis-à-vis* (DPPE)(OMe)Pt—Me bonds) is kinetic rather than thermodynamic in origin.[24]

Interestingly, $L_nM—O$ bond strengths are consistently stronger than the $L_nM—N$ bond strengths measured (apparently for the same reasons that H—O bonds are stronger than H—N bonds), suggesting that $L_nM—N$ bonds may be weaker than $L_nM—O$ bonds for both early and late metal systems.[25] Substituents on X that weaken H—X bonds (such as phenyl substituents) will also weaken M—X bonds for the same reasons.

The enhanced (greater than 9 kcal mol^{-1}) stability of transition metal bonds to second row main group substituents, observed in both platinum and ruthenium systems, may explain the efficiency of silicon and sulphur compounds as poisons for catalysts meant for the transformation of first row main group substrates. These second row substituents appear uniformly 'softer' than first row analogues (which also show uniform 'hardness' across the row).

Perhaps most importantly, correlation of H—X

† The $M—CH_3$ vs M—H bond strength difference of 14 kcal mol^{-1} quoted by Connor (*Organometallics* 1982, **1**, 1166) has been discussed in the more recent reviews cited in ref. 1 which take into account other experimental data, as well. We feel the cited value of 25 kcal mol^{-1} more accurately reflects the perceptions of these reviews which have been widely adopted as state-of-the-art information.

and relative M—X bond strengths is seen for widely disparate types of organometallic complexes and ligand environments. The same correlation appears general for first, second and third row transition metal complexes as well as for actinide elements. Both 16- and 18-electron complexes are included in Fig. 4 and the trend fits data for early-metal complexes as well as for late-metal derivatives. Finally, the observations concerning metal–X single bonds holds for carbon, oxygen, nitrogen and hydrogen suggesting this correlation may be general for many types of organometallic systems.

Predictions

Since the trends in M—X BDEs correlate so well with H—X BDEs, we may estimate the thermodynamics for individual steps in proposed catalytic cycles and for simple processes such as olefin or carbon monoxide insertion into L_nM—OR or L_nM—NR_2 bonds by evaluating the thermodynamics of the corresponding processes for H—OR and H—NR_2 [eq. (12)–eq. (15)].†

$$L_nM\text{—}OH + CO \Leftrightarrow L_nM\text{—}COOH \qquad \Delta H^\circ \approx -6.8 \text{ kcal mol}^{-1},$$

since

$$H\text{—}OH + CO \Leftrightarrow H\text{—}COOH \qquad \Delta H^\circ = -6.8 \text{ kcal mol}^{-1} \qquad (12)$$

$$L_nM\text{—}NH_2 + CO \Leftrightarrow L_nM\text{—}CONH_2 \qquad \Delta H^\circ \approx -7.1 \text{ kcal mol}^{-1},$$

since

$$H\text{—}NH_2 + CO \Leftrightarrow H\text{—}CONH_2 \qquad \Delta H^\circ = -7.1 \text{ kcal mol}^{-1} \qquad (13)$$

$$L_nM\text{—}OH + CH_2{=}CH_2 \Leftrightarrow L_nM\text{—}CH_2CH_2OH. \qquad \Delta H^\circ \approx -10.6 \text{ kcal mol}^{-1},$$

since

$$H\text{—}OH + CH_2{=}CH_2 \Leftrightarrow H\text{—}CH_2CH_2OH \qquad \Delta H^\circ = -10.6 \text{ kcal mol}^{-1} \qquad (14)$$

$$L_nM\text{—}NH_2 + CH_2{=}CH_2 \Leftrightarrow L_nM\text{—}CH_2CH_2NH_2 \qquad \Delta H^\circ \approx -19.2 \text{ kcal mol}^{-1},$$

since

$$H\text{—}NH_2 + CH_2{=}CH_2 \Leftrightarrow H\text{—}CH_2CH_2NH_2 \qquad \Delta H^\circ = -19.2 \text{ kcal mol}^{-1}. \qquad (15)$$

Our data also suggest that hydroxymethyl transition metal complexes, L_nMCH_2OH, should have approximately the same thermodynamic stability as the corresponding methoxy tautomer, L_nMOCH_3 (in the absence of oxygen-to-metal dative π-bonding, as, for example, with early transition metal systems), since according to Figs 3 and 4 there is a one-to-one trade-off of L_nM—C, H—O, H—C and L_nM—O BDEs [eq. (16)]. Both of these species have been proposed as key intermediates in numerous schemes for CO hydrogenation and alcohol homologation.[26] Hence, pathways which predominate via one of these two tautomers are likely to arise from a greater *kinetic* reactivity of that tautomer (assuming there is a facile interconversion of the two), since comparable concentrations of each should be present at equilibrium.

$$L_nM\text{—}CH_2OH \overset{K_{eq} \approx 1}{\Longleftrightarrow} L_nM\text{—}OCH_3. \qquad (16)$$

The relatively small difference in thermodynamic stability of M—CH_3 and M—H complexes evident in some of the species discussed in this manuscript suggests that while metal alkyl hydride complexes may never become as commonplace as metal dihydrides, alkane C—H bond activation may generally produce species which are (thermodynamically) only 5–10 kcal mol^{-1} less stable than analogous dihydrides [eq. (17)]. While most such species may not be isolable, they are, nevertheless, energetically accessible, and therefore viable, catalytic intermediates. Additionally, the same data suggests that activation of C—C bonds in ethane should be more *thermodynamically* favorable than the activation of C—H bonds in methane;‡ therefore, any complex capable of activating aliphatic C—H bonds should be thermodynamically (but not, necessarily, kinetically) able to activate C—C bonds, as well.

† Standard state used: 298.15 K, 0.1 mPa, HCO_2H(g), H_2O(g), CO(g), $HCONH_2$(g), NH_3(g), CH_3CH_2OH(g), C_2H_4(g), $CH_3CH_2NH_2$(g). S° values unavailable for $CH_3CH_2NH_2$. Values obtained from *J. Phys. Chem. Ref. Data* 1982, **11**, supplement 2.

‡ Assuming D(C—C) in ethane of 86 kcal mol^{-1}, D(H—H) $\approx$ 104 kcal mol^{-1} and D(H—C) in methane of 104 kcal mol^{-1}.

$$[L_nM] + H{-}H \Leftrightarrow L_nMH_2 \qquad \Delta H = 0\ \text{kcal mol}^{-1}$$
$$[L_nM] + H{-}CH_3 \Leftrightarrow L_nM(H)CH_3 \qquad \Delta H \approx +5\text{–}10\ \text{kcal mol}^{-1} \qquad (17)$$
$$[L_nM] + H_3C{-}CH_3 \Leftrightarrow L_nM(CH_3)_2 \qquad \Delta H \approx -2\text{–}+8\ \text{kcal mol}^{-1}$$

CONCLUSIONS

In summary, activation parameters for PMe_3 dissociation in organometallic complexes, $Cp^*(PMe_3)_2RuX$, have been obtained as a function of varying the size of X. This process, which probably involves a late transition state, provides quantitative evidence for the general perception that *sterics can play an important role in dative ligand* dynamics. In addition, the effectiveness of steric congestion in weakening Ru—P bonds suggests great care must be exercised when applying the functional group additivity assumption to thermochemical investigations in organometallic systems, and further suggests measurements of solution-phase L_nM—X bond strengths will likely have uncertainties greater than ± 2 kcal mol^{-1} because of changes in strength of other bonds in the molecules (i.e. in the L—M bonding).

We note that the observed order in L_nM—X homolytic bond strengths: L_nM—(sp)C > L_nM—O > L_nM—H > L_nM—(sp^3)C > L_nM—N might not have been predicted prior to this work. The correlation of L_nM—X bond strengths with those of the 'parent' H—X BDEs (or the stabilities of $X^{\cdot}$ radicals) allows prediction of the thermodynamics accompanying many elementary processes of interest in organotransition metal chemistry though we stress that even the several kcal mol^{-1} uncertainties inherent in our H—X/L_nM—X correlation (Figs 3 and 4) can produce marked changes in product selectivities.

The thermoneutral character of equilibria graphically represented in Figs 3 and 4 also requires a correlation of the degree of L_nM—X bond heterolysis with K_a values of the corresponding organic acids, H—X. The relative extent of anion dissociation can thus be predicted within the limitations of these data, providing information about the relative importance of this step in the reaction chemistry of L_nM—X derivatives.

Acknowledgements—The technical assistance of Martin A. Cushing, Jr, Joseph P. Foster, Jr and Elwood A. Conaway are gratefully acknowledged. We thanks Drs David M. Golden and Gregory P. Smith of the Chemical Kinetics research group at SRI International and Professor Robert G. Bergman for valuable discussions. This work was supported by the Du Pont Company and, in part, by the National Science Foundation (Grant CHE-8303735), which is gratefully acknowledged.

REFERENCES

1. For leading references see (a) J. A. Connor, *Top. Curr. Chem.* 1977, **71**, 71; (b) J. Halpern, *Acc. Chem. Res.* 1982, **15**, 238; (c) R. G. Pearson, *Chem. Rev.* 1985, **85**, 41; (d) J. Halpern, *J. Inorg. Chim. Acta* 1985, **100**, 41; (e) J. A. Martinho Simoes and J. L. Beauchamp, *Chem. Rev. 1985* (in press).
2. M. F. Lappert, D. S. Patil and J. B. Pedley, *J. Chem. Soc., Chem. Commun. 1975*, **830** and ref. 3a.
3. (a) R. G. Pearson, *J. Am. Chem. Soc.* 1963, **85**, 3533; (b) R. G. Pearson, *J. Chem. Educ.* 1968, **45**, 643.
4. (a) F. A. Cotton and G. Wilkinson, *Advanced Inorganic Chemistry*, Fourth Edition. Wiley, New York (1980); (b) R. C. Mehrotra, *Adv. Inorg. Chem. Radiochem.* 1983, **26**, 269; (c) R. A. Michelin, M. Napoli and R. J. Ros, *Organometal. Chem.* 1979, **175**, 239; (d) W. M. Rees and J. D. Atwood, *Organometallics* 1985, **4**, 402; (e) E. W. Abel, G. Farrow and I. D. H. Towle, *J. Chem. Soc., Dalton Trans.* 1979, 71; (f) S. Komiya, S. Tane-ichi, A. Yamamoto and T. Yamamoto, *Bull. Chem. Soc. Jpn.* 1980, **53**, 673; (g) D. P. Arnold and M. A. Bennett, *J. Organometallic Chem.* 1980, **199**, 119; (h) T. Yoshida, T. Okano and S. Otsuka, *J. Chem. Soc., Dalton Trans.* 1976, 993; (i) M. A. Bennett and T. Yoshida, *J. Am. Chem. Soc.* 1978, **100**, 1750; (j) H. E. Bryndza, J. C. Calabrese and S. S. Wreford, *Organometallics* 1984, **3**, 1603; (k) H. E. Bryndza, S. A. Kretchmar and T. H. Tulip, *J. Chem. Soc., Chem. Commun.* 1985, 977; (l) L. J. Newman and R. G. Bergman, *J. Am. Chem. Soc.* 1985, **107**, 5314; (m) D. R. Coulson, *J. Am. Chem. Soc.* 1976, **98**, 3111; (n) M. A. Bennett, G. B. Robertson, P. O. Whimp and T. Yoshida, *J. Am. Chem. Soc.* 1973, **95**, 3028; (o) P. K. Monaghan and R. J. Puddephatt, *Organometallics* 1984, **3**, 444; (p) D. P. Arnold and M. A. Bennett, *Inorg. Chem.* 1984, **23**, 2110; (q) B. R. Flynn and L. Vaska, *J. Am. Chem. Soc.* 1973, **95**, 5081; (r) B. N. Chaudret, D. J. Cole-Hamilton, R. S. Nohr and G. Wilkinson, *J. Chem. Soc., Dalton Trans.* 1977, 1546; (s) M. D. Fryzuk and P. A. MacNeil, *Organometallics* 1983, **2**, 355; (t) M. D. Fryzuk and P. A. MacNeil, *Organometallics* 1983, **2**, 682; (u) M. D. Fryzuk, P. A. MacNeil, S. J. Rettig, A. S. Secco and J. Trotter, *Organometallics* 1982, **1**, 918; (v) M. F. Lappert, P. P. Power, A. R. Sanger and R. C. Srivastava, *Metal and Metalloid Amides*. Ellis Horwood, Westergate, U.K. (1980); (w) W. Beck and M. Bauder, *Chem. Ber.* 1970, **103**, 58; (x) H. E. Bryndza, *Organometallics* 1985, **4**, 1686; (y) H. E. Bryndza, *Organometallics* 1985, **4**, 406; (z) H. E. Bryndza, W. C. Fultz and W. Tam, *Organometallics* 1985, **4**, 939.
5. (a) H. E. Bryndza; *Organometallics* 1985, **4**, 1686; (b) H. E. Bryndza, S. A. Kretchmar and T. H. Tulip, *J. Chem. Soc., Chem. Commun.* 1985, 977; (c) R. A.

Michelin, M. Napoli and R. Ros, *J. Organometal. Chem.* 1979, **175**, 239; (d) A. J. Deeming and B. L. Shaw, *J. Chem. Soc. A* 1969, 443; (e) M. A. Bennett and T. Yoshida, *J. Am. Chem. Soc.* 1978, **100**, 1750; (f) T. G. Appleton and M. A. Bennett, *J. Organometal. Chem.* 1973, **55**, C88.

6. (a) H. E. Bryndza, J. C. Calabrese and S. S. Wreford, *Organometallics* 1984, **3**, 1603; (b) H. E. Bryndza, *Organometallics* 1985, **4**, 406.
7. (a) H. E. Bryndza, J. C. Calabrese, M. Marsi, D. C. Roe, W. Tam and J. E. Bercaw, *J. Am. Chem. Soc.* 1986, **108**, 4805; (b) M. A. Bennett and D. P. Arnold, *J. Organometal. Chem.* 1980, **199**, C17; (c) D. P. Arnold and M. A. Bennett, *Inorg. Chem.* 1984, **23**, 2110; (d) T. Yoshida, T. Okano and S. Otsuka, *J. Chem. Soc., Dalton Trans.* 1976, 993; (e) P. K. Monaghan and R. J. Puddephatt, *Organometallics* 1984, **3**, 444; (f) R. A. Michelin, M. Napoli and R. Ros, *J. Organometal. Chem.* 1979, **175**, 239; (g) K. A. Bernard, W. M. Rees and J. D. Atwood, *Organometallics* 1986, **5**, 390.
8. (a) H. E. Bryndza, W. C. Fultz and W. Tam, *Organometallics* 1985, **4**, 939; (b) T. G. Appleton and M. A. Bennett, *Inorg. Chem.* 1978, **17**, 738.
9. J. W. Egger, *J. Organometal. Chem.* 1970, **24**, 501; (b) L. Vaska and M. F. Werneke, *Trans. N. Y. Acad. Sci., Ser. 2*, 1971, **33**, 70; (c) C. A. Tolman, *J. Am. Chem. Soc.* 1974, **96**, 2780; (d) J. Halpern, F. T. T. Ng and G. L. Rempel, *J. Am. Chem. Soc.* 1979, **101**, 7124; (e) M. J. Nappa, R. Santi, S. P. Diefenback and J. Halpern, *J. Am. Chem. Soc.* 1982, **104**, 619; (f) F. T. T. Ng, G. L. Rempel and J. Halpern, *J. Am. Chem. Soc.* 1982, **104**, 621; (g) T.-T. Tsou, M. Loots and J. Halpern, *J. Am. Chem. Soc.* 1982, **102**, 623; (h) R. S. Drage, J. G. Miller, M. A. Hoselton, R. D. Farris and M. J. Desmond, *J. Am. Chem. Soc.* 1983, **105**, 444; (i) W. D. Jones and F. J. Feher, *J. Am. Chem. Soc.* 1984, **106**, 1650; (j) A. H. Janowicz, R. A. Periana, J. M. Buchanan, C. A. Kovac, J. M. Stryker, M. J. Wax and R. G. Bergman, *Pure Appl. Chem.* 1984, **56**, 13; (k) W. D. Jones and F. J. Feher, *J. Am. Chem. Soc.* 1985, **107**, 620; (l) R. G. Bergman, *Science* 1984, **223**, 902; (m) J. W. Bruno, T. J. Marks and L. R. Morss, *J. Am. Chem. Soc.* 1983, **105**, 6824; (n) H. E. Bryndza, W. C. Fultz and W. Tam, *Organometallics* 1985, **4**, 939; (o) J. M. Buchanan, J. M. Stryker and R. G. Bergman, *J. Am. Chem. Soc.* 1986, **108**, 1537.
10. Sometimes called the 'Benson Approximation' in reference to the successful approach to organic thermochemistry outlined in S. W. Benson, *Thermochemical Kinetics*, Second Edition. Wiley-Interscience, New York (1976).
11. See, for example: C. H. Langford and H. B. Gray, *Ligand Substitution Processes*. W. A. Benjamin, Reading, Massachusetts (1966).
12. This work has been described in detail in H. E. Bryndza, L. K. Fong, R. A. Paciello, W. Tam and J. E. Bercaw, *J. Am. Chem. Soc.* 1987, **109**, 1444.
13. A full paper describing this work has been submitted for publication: H. E. Bryndza, R. A. Paciello, P. J. Domaille and J. E. Bercaw, *J. Am. Chem. Soc.* (submitted).
14. The ramifications of the thermoneutral character observed for eq. (7), in terms of homolytic and heterolytic bond strengths, has been communicated previously in H. E. Bryndza, W. C. Fultz and W. Tam, *Organometallics* 1985, **4**, 939.
15. (a) D. F. McMillen and D. M. Golden, *A. Rev. Phys. Chem.* 1982, **33**, 493; (b) D. R. Stull, E. F. Westrum and G. C. Sinke, *The Chemical Thermodynamics of Organic Compounds*. Wiley, New York (1969); (c) S. W. Benson, *Chem. Rev.* 1969, **69**, 279; (d) S. W. Benson, *Thermochemical Kinetics*, Second Edition. Wiley, New York (1976); (e) R. T. Sanderson, *Chemical Bonds and Bond Energies*, Second Edition. Academic Press, New York (1976).
16. T. H. Lowry and K. S. Richardson, *Mechanism and Theory in Organic Chemistry*, Second Edition, p. 197. Harper and Row, NewYork (1981).
17. Many examples are illustrated in S. W. Benson, *Thermochemical Kinetics*, Second Edition. Wiley, New York (1976).
18. (a) A. H. Janowicz, R. A. Periana, J. M. Buchanan, C. A. Kovac, J. M. Stryker, M. J. Wax and R. G. Bergman, *Pure Appl. Chem.* 1984, **56**, 13; (b) W. D. Jones and F. J. Feher, *J. Am. Chem. Soc.* 1985, **107**, 620; (c) R. G. Bergman, *Science* 1984, **223**, 902; (d) W. D. Jones and F. J. Feher, *J. Am. Chem. Soc.* 1984, **106**, 1650; (e) J. W. Bruno, T. J. Marks and L. R. Morss, *J. Am. Chem. Soc.* 1983, **105**, 6824; (f) M. J. Wax, J. M. Stryker, J. M. Buchanan, C. A. Kovac and R. G. Bergman, *J. Am. Chem. Soc.* 1984, **106**, 1121; (g) H. E. Bryndza, W. C. Fultz and W. Tam, *Organometallics* 1985, **4**, 939.
19. J. M. Buchanan, J. M. Stryker and R. G. Bergman, *J. Am. Chem. Soc.* 1986, **108**, 1537.
20. (a) D. C. Sonnenberger, L. R. Morss and T. J. Marks, *Organometallics* 1985, **4**, 352; (b) S. W. Bruno, H. A. Stecher, L. R. Morss, D. C. Sonnenberger and T. J. Marks, *J. Am. Chem. Soc.* 1986, **108**, 7275 and ref. 33e.
21. D. J. Pasto and C. R. Johnson, *Laboratory Text for Organic Chemistry*. Prentice-Hall, Englewood Cliffs, New Jersey (1979).
22. (a) M. E. Thompson, Thesis, California Institute of Technology (1985); (b) M. E. Thompson, S. L. Baxter, M. C. Nolan, B. D. Santarsiero, W. P. Schaefer and J. E. Bercaw, *J. Am. Chem. Soc.* (submitted).
23. J. M. Buchanan, J. M. Stryker and R. G. Bergman, *J. Am. Chem. Soc.* 1986, **108**, 1537.
24. (a) H. E. Bryndza, *Organometallics* 1985, **4**, 1686; (b) H. E. Bryndza, *Organometallics* 1985, **4**, 406; (c) H. E. Bryndza, J. C. Calabrese and S. S. Wreford, *Organometallics* 1984, **3**, 1603.
25. J. E. Bercaw, D. L. Davies and P. T. Wolczanski, *Organometallics* (in press).
26. (a) J. P. Collman and L. S. Hegedus, *Principles and Applications of Organotransition Metal Chemistry*. University Science Books, Mill Valley CA (1980); (b) G. W. Parshall, *Homogeneous Catalysis*. Wiley, New York (1980).

Polyhedron Vol. 7, No. 16/17, pp. 1453–1468, 1988
Printed in Great Britain

0277–5387/88 $3.00+.00
© 1988 Pergamon Press plc

INDUCTIVE TRANSFER AND COORDINATION OF LIGANDS IN METAL–METAL BONDED SYSTEMS

RUSSELL S. DRAGO† and CARL J. BILGRIEN

Department of Chemistry, University of Florida, Gainesville, FL 32611, U.S.A.

Abstract—Donor–acceptor complex formation between a range of neutral, dinuclear metal carboxylates and a range of Lewis bases has been monitored to obtain equilibrium constants and enthalpies for adduct formation. The acceptors studied are $Rh_2(but)_4$, $Rh_2(pfb)_4$, $Mo_2(pfb)_4$, $Ru_2(but)_4Cl$ and $Cr_2(tfa)_4(Et_2O)_2$ (but = $O_2C_4H_7^-$, pfb = $O_2C_4F_7^-$, tfa = $O_2CCF_3^-$) and the donors include oxygen, sulphur, nitrogen and phosphorous donor atom bases. Spectrophotometric and calorimetric titrations were used to measure and apportion the experimental heats. The measured enthalpies of adduct bond formation thus correspond to stepwise complexation equilibria.

Measurements with bases which varied in their covalent and electrostatic donor properties allowed definition of acid parameters to describe the dinuclear complexes by the *E* and *C* treatment. The spectral and calorimetric data point towards unusual stabilization of some of the donor–Rh dimer adduct bonds which was attributed to π-backbonding from populated Rh(II)—Rh(II) π^* orbitals to empty donor orbitals of the proper symmetry. This provides one of the first quantitative estimates of π-backbond stabilization energies in transition metal systems. The π-backbonding effects were less pronounced for adduct formation with $Ru_2(but)_4Cl$ (half-filled π^* orbitals) and not observed for $Mo_2(pfb)_4$ (unpopulated π^* orbitals).

Correlation of the first and second enthalpies of adduct formation allowed determination of inductive transfer parameters to describe the inductive effects of coordination of the first base through the metal–metal bond to influence the coordination of the second base. The lowered acidity of the second metal centre upon complex formation at the first could be quantified by this treatment and the results correlated with the nature of the metal–metal bond.

This correlation treatment was extended to IR data, ν_{CO} of $(CO)Rh_2(pfb)_4(B)$ (B = base) adducts, and EPR data, g of (TEMPO) $Rh_2(pfb)_4$ (B) adducts to demonstrate the relative *E* and *C* contributions to these spectral parameters.

Donor complexation was observed to have profound influences upon the electronic structures of the various complexes as followed by electronic spectral shifts. The $Cr_2(tfa)_4(B)_2$ adducts provided additional means for monitoring changes in electronic structure. Magnetic susceptibilities of the $Cr_2(tfa)_4(B)_2$ adducts were found to increase with B donor strength suggesting a direct exchange pathway to account for observed antiferromagnetism. Solid state measurements on three of the adducts (B = Et_2O, Et_3PO_4, HMPA) gave $-2J$ ranging from 611 to 688 cm^{-1}, values which are larger than those measured for the well-studied cupric carboxylates, $Cu_2(O_2CR)_4(B)_2$

An underlying theme in the chemistry of molecules with multiple metal centres involves metal–metal interaction to generate unique reactivity. This synergistic interplay between metal centres is implicated in a host of chemical systems. Many enzymes rely on multiple metal centres for substrate binding or for electron transport. Heterogeneous and some homogeneous catalysts utilize metal centres in close proximity. The key to understanding the reactivity of such systems is determining the ways and extents to which a second, third, etc., metal atom can influence the coordination and redox chemistry at the first metal site.

† Author to whom correspondence should be addressed.

The simplest metal clusters are those which contain two metal atoms, and we have elected to study the dinuclear metal carboxylates for our initial investigations. A considerable body of literature[1] is now available for these complexes which possess several attractive features. Beginning with a crystallographic study[2] of copper(II) acetate in 1953, a significant number of metal carboxylates have now been structurally characterized. The tetracarboxylate ligand framework is very common; examples exist for vanadium, chromium, cobalt, copper, molybdenum, technetium, ruthenium, rhodium, tungsten, rhenium and osmium. The general structure of the $M_2(O_2C)_4L_2$ molecules is shown in Fig. 1 where L represents a neutral donor molecule or coordinated anion (naked clusters with no L also abound). For M(II), neutral soluble complexes are generally available for study in non-polar non-coordinating solvents. When L is a neutral donor, adduct formation with $M_2(O_2CR)_4$ is a reversible process for which successive complexation equilibria occur. When stepwise complexation can be monitored, these equilibria provide a powerful handle on the effectiveness of the metal–metal bond in transmitting the effects of coordinating one ligand upon the coordination of the second ligand.

The axial ligand can be viewed as competing with the second metal as a ligand. A stronger metal–metal bond leads to a weaker metal–ligand interaction.[3(a)] The effect of the first metal–ligand bond upon the second is thus a secondary *trans* influence or inductive effect, transmitted through the metal–metal bond and carboxylate framework. Donor ligation exerts a perturbation upon the metal–metal interaction, which results in a weakening of the metal–metal bond.[3] Donor complexation can be monitored by changes in the electronic spectra of the dinuclear core and changes in the electronic structure can lend insight into the orbital interactions involved in ligand complexation.

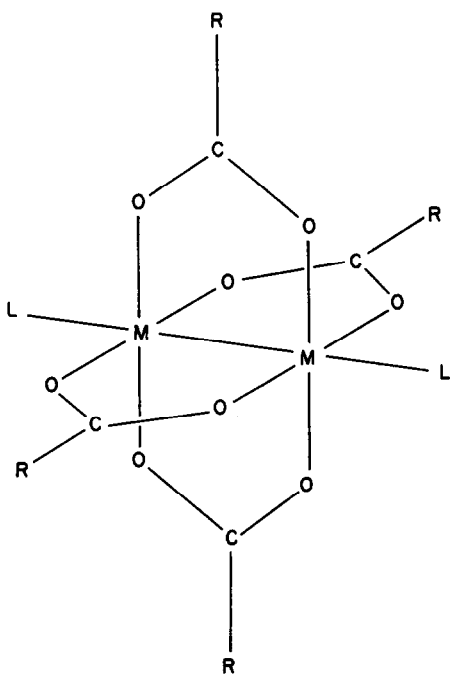

Fig. 1. General structure of $M_2(O_2CR)_4L_2$.

In any fundamental study of the coordination process two essential requirements must be met: (1) thermodynamic data must be obtained in which solvent effects are minimal or can be factored out; (2) a quantitative indication of what constitutes normal, coordinate σ-bond formation must exist. Interesting and unusual effects can then be detected instead of offered on the basis of intuition (often guided by pK_B data) about what is usual. Appropriate experimental design to minimize solvation effects has been reviewed[4(a)] and an empirical, four-parameter equation has been reported to describe bond strengths of adducts in which the interaction involves σ-bond formation. The enthalpy of interaction measured in a poorly basic, non-polar solvent can be predicted for the 'usual case' with

$$-\Delta H + W = E_A E_B + C_A C_B \qquad (1)$$

where $-\Delta H$ is the enthalpy of adduct formation, subscripts A and B represent the Lewis acid and base, and E and C roughly parallel the qualitative assignment of tendencies of acids and bases to undergo electrostatic and covalent interaction, W is a constant enthalpy contribution to the observed process. It is often zero but can be finite for a displacement reaction, cleavage of a dimeric acid, etc. One of the great advantages of this correlation is its ability to provide enthalpy values for these processes which in many cases cannot be obtained by other means. It has been shown previously that the existence of extra effects (e.g. π-backbonding or steric effects) in the coordination process can be demonstrated by first empirically determining the acid (or base) parameters on systems where the effect cannot exist. If the extra effect exists in the suspected system, the measured enthalpy will deviate from that predicted by eq. (1) in a direction consistent with the effect.[4] This approach is used in the interpretation of the enthalpy data for base coordination of the first base to estimate relative contributions of σ- and π-bonding to the measured enthalpies.

As an extension of the E and C treatment of the donor–acceptor bond, we have suggested an

inductive transfer model to describe the coordination of the second Lewis base, i.e. the Lewis acidity of the second metal centre.[5] In this model, the acid parameters of the 1:1 adducts, $E_A^{1:1}$ are reduced from that of the free acid, E_A, by an amount that is proportional, k, to the corresponding coordinated base parameter, E_B, as shown in eqs (2) and (3).

$$E_A^{1:1} = E_A - kE_B \quad (2)$$

$$C_A^{1:1} = C_A - k'C_B. \quad (3)$$

The $-\Delta H_{2:1}$ is given by

$$-\Delta H_{2:1} = E_A^{1:1}E_B + C_A^{1:1}C_B. \quad (4a)$$

Substituting eqs (2) and (3) as well as $\Delta H_{1:1} = E_AE_B + C_AC_B$ into eq. (4a) produces (4b):

$$-\Delta H_{2:1} = -\Delta H_{1:1} - kE_B^2 - k'C_B^2. \quad (4b)$$

The k and k' are proportionality constants which represent the ability of the metal–metal bond to transmit the electrostatic and covalent properties of the coordinated base. It should be emphasized that the intent of this methodology lies not only in the determination of E_A, C_A, k and k' numbers to predict unmeasured enthalpies, but also in the quantitative insight presented about the electronic nature of the metal–ligand and metal–metal bonds.

RESULTS AND DISCUSSION

1. *Synergistic influences on the Lewis acidity of some bimetallic carboxylates*

(A) $Rh_2(O_2C_4H_7)_4$. Dirhodium butyrate forms both 1:1 and 2:1 adducts with donors in the solid state.[1(a),3(a,b),6] In solution, the relative concentrations of the free acid, 1:1 adduct and 2:1 adduct are governed by the equilibria:

$$A + B \overset{K_1}{\rightleftharpoons} AB \quad (5a)$$

$$AB + B \overset{K_2}{\rightleftharpoons} AB_2. \quad (5b)$$

A representative spectrophotometric titration is shown in Fig. 2. A method for extracting the equilibrium constants from these spectral curves has been presented.[5(a)] The thermodynamic parameters that best fit the experimental data for adduct formation with a range of bases are shown in Table 1.[5(a)]

A qualitative MO scheme which illustrates the bonding interactions arising from *d* orbital overlap is shown in Fig. 3. This scheme is general for the metal carboxylate dimers, though the exact ordering and relative energy levels may differ as a function of metal atom, bridge or axial donor. The lowest energy transition, and the one seen to undergo a blue shift in Fig. 2, is $\pi^* \rightarrow \sigma^*$. $Rh_2(but)_4$ (but = $O_2C_4H_7$) functions as a Lewis acid by accepting electron density in the σ^* orbital. This interaction raises the σ^* level and a blue shift in the electronic transition is observed. Further, if the base is a π-acceptor, the Rh—Rh π^* orbital is stabilized by back donating electron density. This interaction also contributes to the magnitude of the blue shift in the $\pi^* \rightarrow \sigma^*$ transition.

Since methylene chloride undergoes a specific hydrogen-bonding interaction with Lewis bases,[7] which is interrupted when the base coordinates to the rhodium dimer, a correction needs to be applied to the $-\Delta H_{1:1}$ and $-\Delta H_{2:1}$ values of Table 1. This correction can be predicted by the E and C equation using[7] $E'_A = 1.72$ and $C'_A = -0.03$ for methylene chloride. The solvation corrected enthalpies are given in Table 2.

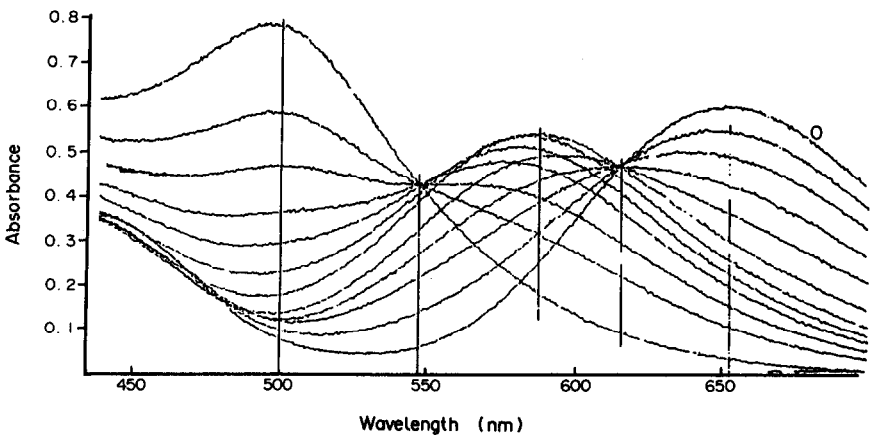

Fig. 2. Spectral titration of $Rh_2(but)_4$ with $(CH_3)_2SO$ in CH_2Cl_2.

Table 1. Thermodynamic data for the formation of 1 : 1 and 2 : 1 base adducts of various dimeric systems[a]

Acid	Base	K_1	K_2	$-\Delta H_{1:1}$ (kcal mol^{-1})	$-\Delta H_{2:1}$ (kcal mol^{-1})
$Rh_2(but)_4$[b]	Cage phosphite[c,d]	$9.1(0.7)\times10^7$	$2.6(0.1)\times10^4$	12.9(0.2)	11.3(0.2)
	Pyridine[e]	$1.115(0.001)\times10^7$	$9.88(0.05)\times10^3$	14.6(0.2)	8.5(0.2)
	1-Methylimidazole[f]	$\sim10^8$	2.1×10^3	13.7(0.4)	9.9(0.5)
	Piperidine[f]	$\sim10^8$	1.2×10^3	13.2(0.2)	8.9(0.2)
	Tetrahydrothiophene[d]	$1.7(0.1)\times10^7$	$1.9(0.3)\times10^4$	11.0(0.3)	10.3(0.4)
	4-Picoline-*N*-oxide	$8.2(0.3)\times10^4$	$1.89(0.05)\times10^2$	8.6(0.3)	5.7(0.5)
	Dimethyl sulphoxide[d]	$1.1(1)\times10^5$	$5.5(0.3)\times10^2$	6.6(0.2)	6.5(0.4)
	Acetonitrile	$1.15(0.05)\times10^3$	$1.1(0.1)\times10$	7.8(0.6)	6.8(1.5)
$Rh_2(pfb)_4$[g]	1-Methylimidazole[f,h]	$\sim10^7$	dec	19.0(0.4)	dec
	Pyridine[f]	$\sim10^7$	4.15×10^4	18.4(0.4)	15.0(0.4)
	Tetrahydrothiophene	dec			
	4-Picoline-*N*-oxide	dec			
	Dimethyl sulphoxide[h]	$6.78(0.05)\times10^5$	$6.11(0.05)\times10^3$	10.7(0.4)	8.1(0.4)
	Acetonitrile[h]	$1.43(0.23)\times10^5$	$4.53(2.0)\times10^3$	10.2(0.8)	7.4(0.5)
	Dimethyl acetamide	$2.29(0.05)\times10^5$	$1.52(0.01)\times10^3$	10.9(0.4)	9.3(0.3)
$Mo_2(pfb)_4$[f,i]	Pyridine	7.5×10^3	1.7×10^2	9.1	6.2
		9.0×10^3	3.3×10^2	8.2	4.6
		5.7×10^3	1.8×10^2	8.7	5.9
	1-Methylimidazole	dec		dec	
	Dimethyl sulphoxide	2.1×10^4	1.0×10^3	9.0	4.6
		1.7×10^4	6.76×10^2	9.5	7.3
	Dimethylacetamide	2.0×10^5	6.2×10^2	8.8	6.6
		5.0×10^4	6.6×10^2	8.8	5.3
	Bridged ether[j]	5.8×10^2	3.5×10	6.5	[1.6][k]
	Acetonitrile	7.5×10	3.9×10	5.7	[1.6][k]
	Tetrahydrothiophene	4.4×10	7.6	3.5	[1.8][k]

$Ru_2(but)_4Cl(acetone)^{f,i}$	1-Methylimidazole			8.0	
	Pyridine			7.2	
	4-Picoline-*N*-oxide			5.9	
	Dimethyl sulphoxide			2.7	
	Tetrahydrothiophene			3.2	
$Ru_2(but)_4Cl(CH_3CN)$	1-Methylimidazole			8.8	
$Cr_2(tfa)_4(Et_2O)_2^{m}$	1-Methylimidazole	dec		dec	
	Pyridine	dec		dec	
	Hexamethylphosphoramide	10^{11}	6×10^{6}	8.4(0.2)	
	Dimethyl sulphoxide	10^{9}	6×10^{4}	7.8(0.3)	6.2(0.5)
	Dimethyl acetamide	10^{9}	1×10^{5}	7.4(0.2)	5.8(0.4)
	Dimethyl formamide	10^{8}	1×10^{4}	6.5(0.3)	5.0(0.5)
	Dimethyl cyanamide	10^{8}	3×10^{3}	5.5(0.1)	4.4(0.2)
	Trimethyl phosphite	10^{8}	2×10^{3}	1.8(0.1)	1.7(0.1)
	Triethyl phosphate	10^{10}	1×10^{6}	6.4	5.0

[a] Methylene chloride solution unless otherwise noted.
[b] Ref. 5(a).
[c] Cage phosphite = 1-phospha-4-ethyl-1,5,7-trioxabicyclo[2.2.1]-octane.
[d] Measured in benzene solution.
[e] A 0.9 kcal mol^{-1} correction for the pyridine–benzene interaction is applied to each enthalpy.
[f] All values determined from calorimetric data by fixing K_1 and varying K_2 to minimize the errors in the ΔH.
[g] Ref. 5(b).
[h] Measured in toluene solution.
[i] Ref. 5(b); all measurements in toluene solution.
[j] Bridged ether = 7-oxabicyclo[2.2.1]heptane.
[k] Too small to be reliably measured.
[l] Ref. 9; all parameters correspond to base displacement of coordinated acetone or acetonitrile.
[m] Ref. 16; the enthalpies have been corrected for solvation of the base by CH_2Cl_2.

Table 2. Comparison of solvation corrected enthalpies for adduct formation between various bases and different dimeric systems[a]

Acid	Base	$-\Delta H^{1:1}_{expt}$	$-\Delta H^{1:1\,b}_{EC}$	π-stabilization	$-\Delta H^{2:1}_{expt}$	$-\Delta H^{2:1\,c}_{EC}$	π-stabilization
$Rh_2(but)_4$[d]	Cage phosphite	16.8[e]	10.3	6.5	11.3[e]	8.6	2.7
	Pyridine	16.6	12.6	4.0	10.5	9.5	1.0
	1-Methylimidazole	15.4	15.1		11.5	11.7	
	Piperidine	15.0	15.3		10.7	11.0	
	Tetrahydrothiophene	14.9[e]	11.4	3.3	10.3[e]	9.4	0.9
	4-Picoline-*N*-oxide	11.0	10.9		8.0	8.0	
	Dimethyl sulphoxide	10.5[e]	[f]		6.5[e]	[f]	
	Acetonitrile	9.3	4.8	4.5	8.3	3.8	4.5
$Rh_2(pfb)_4$[g]	1-Methylimidazole	20.3[e]	20.3		dec		
	Pyridine	18.4	17.4	1.0	15.0	13.9[h]	1.1
	Dimethyl sulphoxide	~ 12[i]	11.8		~ 8[f]	9.3[h]	
	Acetonitrile	11.5[i]	7.0	4.5	7.4[i]	5.8[k]	1.6
	Dimethyl acetamide	10.9	11.1		9.3	8.9[h]	
$Mo_2(pfb)_4$[g,i]	Pyridine	9.5(0.2)	9.4		6.5(0.2)	6.4	
	Dimethylsulphoxide	9.2(0.4)	9.0		6.1(0.3)	6.1	
	Dimethylacetamide	8.8(0.2)	8.7		6.2(0.1)	5.9	
	Bridged ether	6.5(0.2)	6.8		2	5.2	
	Acetonitrile	5.7(0.2)	5.9		small	4.6	
	Tetrahydrothiophene	5.1(0.04)	5.1		small	4.1	
$Ru_2(but)_4Cl$[j]	1-Methylimidazole	18.5	18.6				
	Pyridine	18.1	17.5	0.6			
	4-Picoline-*N*-oxide	17.1	16.8				
	Dimethyl sulphoxide	13.9	14.1				
	Tetrahydrothiophene	12.8	12.5				
	Acetonitrile	9.7	8.8	0.9			

$Cr_2(tfa)_4(Et_2O)_2$[k]	Dimethyl sulphoxide	7.8	7.5	6.2	6.2
	Dimethyl acetamide	7.4	7.3	5.7	5.5
	Dimethyl formamide	6.5	6.7	5.0	5.0
	Dimethyl cyanamide	5.5	5.4	3.4	3.3
	Trimethyl phosphite	1.8	1.8	1.9	1.9
	Triethyl phosphate	6.4	6.5	5.3	5.5
	Hexamethyl phosphoramide	8.4	8.5	—	—

[a] All enthalpies are in units of kcal mol^{-1} and were measured in methylene chloride solution unless otherwise noted. Standard deviations are in parentheses. The CH_2Cl_2 correction was applied to the base using newly refined $E = 1.71$ and $C' = -0.04$ for CH_2Cl_2. The calculated E and C values, were carried out using parameters from the new fit of the E and C master data set.[4(c)]

[b] Calculated using eq. (1).

[c] Calculated using eq. (4)

[d] Ref. 5(a).

[e] Enthalpies measured in benzene solution.

[f] ΔH_{EC} cannot be calculated since, for $Rh_2(but)_4$, Me_2SO acts as a sulphur donor and E_B and C_B have been calculated only for Me_2SO acting as an oxygen donor.

[g] Ref. 5(b).

[h] Calculated from eq. (4) using k and k' of $Rh_2(but)_4$.

[i] Enthalpies measured in toluene solution.

[j] Ref. 9.

[k] Ref. 16. Enthalpies are for the displacement reaction of diethyl ether by donor and are corrected for solvation of the base by solvent CH_2Cl_2. These are solvent corrected enthalpies for the displacement reaction. The constant W corrects for ether being displaced and being solvated by CH_2Cl_2. The 2:1 enthalpies have similarly been corrected for base solvation by CH_2Cl_2 and W includes ether displacement and solvation. The 1:1 enthalpy for triethyl phosphate was forced to fit by readjusting E_B to test the 2:1 model. These are probably better E numbers for those donors; $(EtO)_3PO$, $E = 1.20$, $C = 1.84$. The 1:1 calculated values use $E = 7.79$, $C = 0.23$ and $W = 2.4$. The 2:1 calculated values employ eq. (6) with $k = 0.998$, $k' = -0.0039$ and $W = 3.58$.

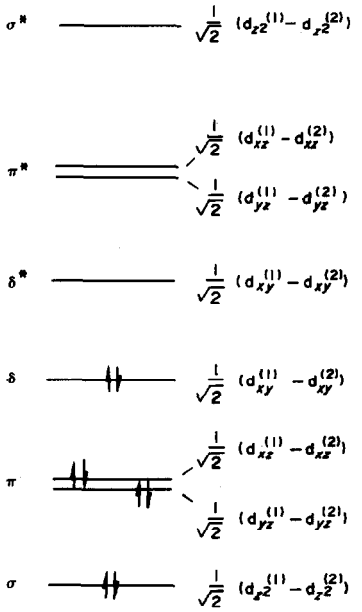

Fig. 3. Qualitative MO scheme for a dinuclear metal carboxylate in D_{4h} symmetry. (Taken with permission from ref. 1(a).)

The E and C model can illustrate the relative importance of covalent and electrostatic contributions to the σ bond and predict the magnitude of the σ-bonding interactions of Lewis acid–base adducts. Application to $Rh_2(but)_4$ is complicated by π^* metal-to-ligand backbonding ability of this acid. The solvent corrected enthalpies for only those bases (1-methylimidazole, piperidine, 4-picoline-*N*-oxide) which do not participate in π-backbonding can be utilized in an E and C fit.[5(a)] Values of 3.55 and 1.20 for E_A and C_A result[4(c)] and must necessarily be considered tentative since only three 'σ-only' enthalpies could be used.

From these parameters, 'σ-only' enthalpies can be calculated for all the acid–base pairs studied and are shown in Table 2. The measured $-\Delta H_{1:1}$ for all donors not used to determine E_A and C_A are larger than predicted for a σ-only interaction ($-\Delta H_{EC}$). The extra π-stabilization is attributed to a π-backbonding interaction and an accompanying strengthening of the σ bond. The magnitude of this π-stabilization is given in Table 2 as the difference of $-\Delta H_{1:1}$ and $-\Delta H_{EC}$.

The magnitude of the π-backbonding stabilization in these systems exceeds that found for any other acid studied thus far in the E and C work including $[Rh(CO)Cl]_2$ and $[Rh(COD)Cl]_2$. The effectiveness of the π-back donation is attributed to effective overlap between empty ligand orbitals and populated Rh dimer π^* orbitals. The dimer π^* orbitals are formed from overlap of the Rh(II) d_{xz} and d_{yz} atomic orbitals. The π^* orbitals are able to donate electron density to ligand π orbitals more effectively than a mononuclear system because of polarization of the π^* orbital as shown in Fig. 4. This polarization is a consequence of the diffuse metal d_{xz} and d_{yz} orbitals interacting when the metal–metal bond is formed. Thus, we have been able to discover an important synergistic interaction in metal clusters; π-stabilization which strengthens the coordination of π-acceptor ligands.

(B) $Rh_2(O_2C_4F_7)_4$. The bridging carboxylate ligands must certainly play a role in defining the Lewis acidity of the metal centres and may assist in the mechanism of inductive transfer. It was of interest to us, then, to explore the thermodynamics of adduct formation with $Rh_2(pfb)_4$ (pfb = perfluorobutyrate) for comparison to the unfluorinated system.[5(b)]

Electronic spectral changes upon base binding, similar to those observed for $Rh_2(but)_4$, were used to determine the equilibrium constants for 1 : 1 and 2 : 1 adduct formation. Enthalpies were determined calorimetrically with the use of these constants. Thermodynamic data determined in both toluene and methylene chloride solution are given in Table 1. As before, the methylene chloride solution data can be corrected using E'_A and C'_A for this solvent, and the solution corrected enthalpies are given in Table 2. The differences in the enthalpies of adduct formation in the toluene and the solvent corrected CH_2Cl_2 data indicates coordination of toluene to $Rh_2(pfb)_4$. The average difference of these values is attributed to a -1.3 kcal mol^{-1} bonding by toluene. The toluene solution enthalpies are corrected accordingly in Table 2 (only the $-\Delta H_{1:1}$ results are corrected as coordination of the first base probably leads to dissociation of more than one toluene).[5(a)]

An E and C fit of the solvation corrected $-\Delta H_{1:1}$ data (σ-only donors: DMSO, DMA and N-MeIm) gives the E_A and C_A values[5(b)] in Table 3 for rhodium(II) perfluorobutyrate. By comparison of these

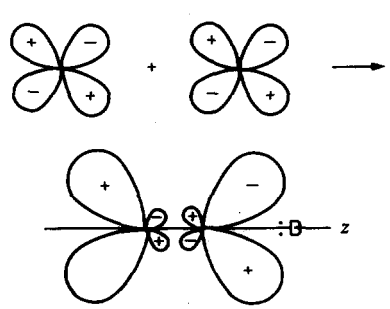

Fig. 4. Polarization of π-orbitals from metal–metal bonding.

Table 3. Comparison of the different dimer systems[a]

Acid	M_2^{n+}	d^n	BO	E_A	C_A	C_A/E_A	k	k'
$Rh_2(but)_4$	4	14	1	3.55	1.20	0.338	1.12	0.0269
$Rh_2(pfb)_4$	4	14	1	5.58	1.51	0.271		
$Mo_2(pfb)_4$	4	8	4	6.29	0.19	0.030	1.56	0.0084
$Ru_2(but)_4Cl$	5	11	2.5	8.36	0.998	0.118		
$Cr_2(tfa)_4$	4	8	4	9.17	−0.31	−0.16	0.98	−0.0045

[a] The E_A and C_A parameters as well as the k and k' values reported here differ from those previously reported for these are based on the newly refined E and C data set.[4(c)]

values to those obtained for rhodium(II) butyrate, the effect of the perfluorobutyrate ligand is seen to increase both the electrostatic and covalent acceptor properties of the rhodium dimer. The C/E ratios of the two dimers are, however, comparable. As seen in Table 2, the σ-only enthalpies predicted by the E and C equation are in good agreement with the σ-only donors used in the fit. The measured enthalpies of pyridine and acetonitrile are 1–4 kcal mol^{-1} higher than the E and C σ-only predicted values. We attribute the difference to π-stabilization (π-backbonding plus enhanced stabilization of the σ bond). As can be seen in Table 2, the relative amounts of π-stabilization are lower for $Rh_2(pfb)_4$ than $Rh_2(but)_4$, despite the stronger Lewis acidity of the former. The higher formal positive charge on the rhodium centre of the perfluorobutyrate system decreases the radial extension and lowers the energy of the π^* orbitals leading to less effective π-back-bonding.

(C) $Mo_2(O_2C_4F_7)_4$. Since one might argue that some other unusual property of metal–metal bonded systems other than π^*-backbonding is causing deviations from the E and C correlation, we turned our attention to the molybdenum metal–metal bonded dimer. Unlike the formally single metal–metal bond of the Rh(II)–Rh(II) systems, d orbital overlap gives a net quadruple bond for the Mo(II)–Mo(II) dimers. Utilizing the simple MO scheme in Fig. 3, the two d^4 Mo^{2+} ions generate a $\sigma^2\pi^4\delta^2$ configuration with no population of the π^* orbitals. Thus, the π^*-backbonding to the donor observed in the rhodium system cannot occur.

The lowest energy transition in the electronic spectrum of $Mo_2(pfb)_4$ is either a $\delta \rightarrow \delta^*$ or $\delta \rightarrow \pi^*$ transition.[10] Either of these would be rather insensitive to axial coordination and indeed, spectroscopic titrations of $Mo_2(pfb)_4$ with donors exhibit minor (if any) absorbance shifts, prohibiting the determination of K from the electronic spectra.[5(b)]

Calorimetric data must be relied on to deliver both the enthalpies and the equilibrium constants which apportion the experimental heats. This was accomplished by collecting many data points at both low and high concentrations of the base and by repetition of the titration.[5(b)] A tabulation of the best fit thermodynamic parameters is given in Table 1. Again, a noticeable inductive effect is observed in the equilibrium constants ($K_1 > 4K_2$) and enthalpies ($-\Delta H_{1:1} > -\Delta H_{2:1}$).

Calorimetric titrations with $Mo_2(pfb)_4$ were necessarily conducted in toluene solution. Previously $Rh_2(pfb)_4$ was found to undergo a 1.3 kcal mol^{-1} coordination of toluene. Should the $Mo_2(pfb)_4$ enthalpies also contain a constant contribution for toluene dissociation, the magnitude of this enthalpy would be revealed by an E, C and W analysis of the data. A fit of the enthalpy data for this acid (Table 1) to the E, C and W equation [eq. (1)] gave a negligible value of $W = 0.4$ kcal mol^{-1} (compare to the -1.3 kcal mol^{-1} for toluene coordination[5(b)] to $Rh_2(pfb)_4$ and -3.9 kcal mol^{-1} for benzene coordination[5(b)] to $Rh_2(but)_4$). The Table 1 enthalpies were not adjusted.

An E and C fit for $Mo_2(pfb)_4$ shows a good correlation between all the experimental and calculated values of $-\Delta H_{1:1}$ (Table 2), with the exception of bridged ether where steric effects may exist. The correlation is not improved upon omission of the potentially π-acceptor ligands. Thus, the lack of π-backbonding stabilization coincides with the empty π^* orbitals for this acid and provides convincing support for the existence of our proposed synergistic interaction in metal–metal bonded systems with filled π^* orbitals.

A comparison of the E_A and C_A values for $Mo_2(pfb)_4$ (Table 3) to those found for $Rh_2(pfb)_4$ shows that the two dimers differ primarily in the C_A values. Since both rhodium and molybdenum exist in the +2 oxidation state and both dimers have the same bridging ligand, the partial positive charge on each metal centre is comparable. Accordingly, the electrostatic interaction with various Lewis bases

is comparable. However, the involvement of the dimolybdenum electrons in electrode quadruple metal–metal bonding results in their not being very polarizable. A given molybdenum centre is not able to accept electron density from the ligand as effectively and distribute it over the whole molecule as effectively as can be done for the singly bonded rhodium system with polarizable electron density between the metals. A reduced C_A value for $Mo_2(pfb)_4$ results.

(D) $Ru_2(O_2C_4H_7)_4Cl$. Studies on this ruthenium acid offer the possibility to explore the effect of mixed valency in metal–metal bonded systems as a polarization mechanism for enhancing the acidity of a metal centre. The MO scheme for this dimer[11] (Fig. 5) illustrates the partial population of the π^* orbitals. Chloride ion coordination tends to make the directly bonded ruthenium have a smaller contribution to the bonding molecular orbitals of the metal–metal bond than the other ruthenium, in effect locking in a Ru(II)Ru(III)Cl type of charge distribution. If a donor of equal strength in covalent and electrostatic bonding was coordinated to Ru(II), both ruthenium atoms would have equal contributions in the essentially metal–metal molecular orbitals leading to a bond similar to that in a $Ru(II\frac{1}{2})Ru(II\frac{1}{2})$ compound. This removal of electron density from Ru(II) is similar in the molecular orbital description to the polarization mechanism in the rhodium–rhodium dimer that enhances covalent bonding. However, in this ruthenium complex it now leads to a greater increase in the positive charge on this ruthenium enhancing electrostatic bonding. This system can also provide support for π^*-backbonding synergisms. If the extent of π-back donation depends on the total amount of π^* electron density, one would expect to observe a π-stabilization effect intermediate to that observed for the rhodium and molybdenum dimers.

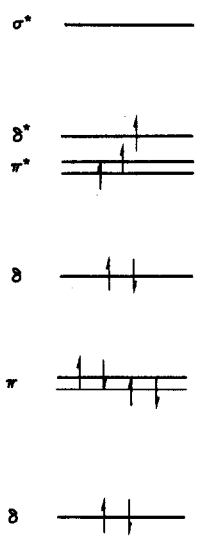

Fig. 5. Simplified MO scheme for the M—M bond in $Ru_2(but)_4Cl$.

The visible region of the electronic spectrum of $Ru_2(but)_4Cl$ in methylene chloride is typified by a band at ~ 450 nm. Little change in position or intensity is observed with concentration for various donors. Calculations,[11] resonance Raman[12] and single crystal polarized electronic spectra[13] support a (RuO) $\pi \rightarrow \pi^*$ assignment for this band; little influence would be expected from axial base coordination as observed. For determination of the thermodynamic parameters, we must then again rely on the calorimetric data alone.

The limited solubility of the free acid dictated the need to utilize a base exchange reaction. Experimental enthalpies for the exchange of donor with coordinated acetone are given[9] in Table 1 for $Ru_2(but)_4Cl$ (acetone). Following correction for specific interaction of solvent methylene chloride with free acetone and base, the experimental enthalpies were fitted to eq. (1) to deliver the E_A and C_A (Table 3) of $Ru_2(but)_4Cl$ (free acid). The calculated $W = 8.9$ (0.9) kcal mol^{-1} corresponds to the enthalpy of dissociation of the Ru–acetone adduct bond. This quantity has been added to the experimental and calculated values in Table 2 to provide data for the free acid $Ru_2(but_4)Cl$ coordinating to donors. Only the enthalpies for those donors thought to undergo only a σ interaction were included; inclusion of pyridine and acetonitrile worsens the fit. As Table 2 shows, the experimental enthalpies for adduct formation with these two donors are larger than those predicted by the E and C equation. The differences, attributed to π^*-backbonding stabilization, are discernable but lower than those observed for $Rh_2(but)_4$. The mixed valent enhancement of acidity would be expected to be reflected in large acidity for this complex. Indeed, the E value is the largest for the systems discussed thus far, the C value is considerably larger than that of molybdenum and π-backbonding is quite effective when the reduced number of electrons available is considered. This suggests a synergistic mixed valent effect that leads to a readily polarized metal–metal bond. Thus, the second metal as a ligand causes effects that a conventional ligand might not.

Quantification of inductive transfer across metal–metal bonds

Our next concern involves obtaining an appreciation of how different metal–metal bonds transmit the properties of a base coordinated at one metal

to the other metal. Accordingly, this will involve an interpretation of the 2:1 enthalpies of adduct formation.

In Table 1, the equilibrium constants and enthalpies for σ donors indicate a greatly decreased acceptor capability for coordination of the second base, relative to the first. Statistical considerations for non-interacting metal centres would lead to $K_1 = 4K_2$ if the metal centres were uncoupled. The observed ratio of K_1 to K_2 is much greater, indicating the inductive effect of base coordination at the first metal upon the second. The effect is observed after the solvation correction has been made (Table 2). Equations (2), (3) and (4b) provide the basis for the model that will be employed to quantitate inductive transfer. For metal–metal systems in which both $\Delta H_{1:1}$ and $\Delta H_{2:1}$ can be determined, all of the quantities in eq. (4b) are known except k and k'. A series of simultaneous equations each corresponding to a different σ donor base can be solved for k and k'.

For $Rh_2(but)_4$ the k and k' values are determined using the enthalpy values for 1-methylimidazole, piperidine, and 4-picoline-*N*-oxide to eliminate contributions from π effects. The values of k and k' are given in Table 3. These values are of interest for two purposes: (1) comparison to other metal carboxylates (*vide infra*) and (2) computation of σ-only values for $-\Delta H_{2:1}$. With regards to the latter point, the magnitude of π-stabilization can be estimated by calculating the σ contribution to $\Delta H_{1:1}$ and using k and k' to calculate the σ-only contribution to $\Delta H_{2:1}$. The deviation in this and the measured value is shown in Table 2 and represents π-stabilization (π bonding plus the synergistic increase in σ bonding). Of interest are the calculated π-stabilization values in the first and second adduct bonds. A weak σ donor such as acetonitrile shows comparable π-stabilization in formation of both the 1:1 and 2:1 adduct bonds. Strong σ-donors (such as pyridine) exhibit substantially decreased π-stabilization in formation of the second adduct bond. The weakened σ bond in the 2:1 adduct leads to a longer metal ligand distance and less effective π overlap. This constitutes the first quantitative estimate of the π-stabilization and allows a sorting out of the factors contributing to the effect. The σ inductive weakening of π^*-backbonding has not previously been recognized in other organometallic systems and may lead to alternative interpretation of CO stretching frequencies in metal carbonyl complexes. The often invoked idea of competitive π-backbonding decreasing the effectiveness of this interaction is not seen in the CH_3CN adducts and may be confused with the σ inductive weakening in the literature interpretations of CO frequencies.

Inductive transfer parameters (k and k') can also be calculated for $Mo_2(pfb)_4$ utilizing the four reliable $-\Delta H_{2:1}$ results are given in Table 3. It was of interest to determine k and k' for $Rh_2(pfb)_4$ to see the effect of ancillary ligands but only two enthalpies for 2:1 adducts could be determined. To broaden the application of these concepts and to determine the changes in k and k' when the metal–metal bond becomes very weak, these studies were extended to dimeric chromium carboxylates.

The dinuclear chromium carboxylates afford an opportunity to investigate the chemistry of a dimeric metal system with a weak metal–metal bond. These carboxylates are such strong Lewis acids that they are only rarely isolated without ligands coordinated to the axial acceptor sites. Coordination of the axial ligand has a pronounced effect upon the Cr—Cr distances which range from 1.99 Å for the gas phase $Cr_2(OAc)_4$ molecule[14] to 2.54 Å for[15] $Cr_2(tfa)_4(Et_2O)_2$[15] (tfa = O_2CCF_3). The rhodium and molybdenum dinuclear carboxylate adducts on the other hand display M—M bond distance ranges of only 0.12 and 0.13 Å respectively.[1(a)] The Cr_2^{4+} system provides a unique opportunity to study the role an appreciably weaker Cr—Cr bond might play in the transmission of coordination effects across the metal–metal bond.

Solution studies[16] were performed with the diethyl ether adduct, $Cr_2(tfa)_4(Et_2O)_2$. In the absence of a weak donor such as Et_2O, insolubility or complex aggregation occurs in non-coordinating solvents. Displacement of ether can be effected by donors of moderate strength, but strong donors such as pyridine decompose the complex.

The electronic spectrum of $Cr_2(tfa)_4(Et_2O)_2$ consists of visible (465 nm, 200 M^{-1} cm^{-1}) and near UV bands (333 nm, 200 M cm^{-1}). By analogy[17] to $Cr_2(OAc)_4(H_2O)_2$ the bands are assigned to a metal centred $\delta \rightarrow \pi^*$ transition (465 nm) and a $n_{p_\pi} \rightarrow \pi^*$-LMCT (333 nm). One would not expect axial donors to directly affect the orbitals involved in these transitions. Donor exchange does effect a red shift in the $\delta \rightarrow \pi^*$ transition (Table 4), though the effect is less pronounced than that observed for the rhodium dimers. The spectral changes are too slight to extract K_1 and K_2.

Following the calorimetric procedure used for $Mo_2(pfb)_4$ the equilibrium constants and enthalpies for diethyl ether exchange from $Cr_2(tfa)_4(Et_2O)_2$ were determined from calorimetric data and are shown in Table 1. In the same manner that the exchange enthalpies of $Ru_2(but)_4Cl$ (acetone) can give the parameters for $Ru_2(but)_4Cl$, so does an E, C and W fit of the $-\Delta H_{1:1}$ for base displacement of Et_2O from $Cr_2(tfa)_4(Et_2O)_2$ give the acid parameters for $Cr_2(tfa)_4(Et_2O)$. $E_A^{1:1}$ and $C_A^{1:1}$ values

Table 4. Frequency of the lowest energy electronic transition as a function of axial ligand[a]

Acid	Base	$\Delta\nu_2$ (cm^{-1})[b]	$\Delta\nu_2$ (cm^{-1})[c]	$\Delta\nu_T$ (cm^{-1})[d]
$Rh_2(but)_4$[e]	4-Picoline-*N*-oxide	860	810	1670
	Acetonitrile	1470	1210	2680
	Piperidine	2330	1360	3690
	1-Methylimidazole	2370	1440	3810
	Pyridine	2470	1700	4170
$Rh_2(pfb)_4$[f]	Dimethyl acetamide	720	420	1140
	Dimethyl sulphoxide	780	500	1380
	Acetonitrile	1490	970	2460
	Pyridine	2380	1320	3700
$Cr_2(tfa)_4(Et_2O)_2$[g]	Dimethyl cyanamide			−710
	Dimethyl formamide			−770
	Trimethyl phosphite			−1010
	Triethyl phosphate			−1160
	Dimethyl acetamide			−1160
	Tetramethyl urea			−1270
	Dimethyl sulphoxide			−1285
	Trimethyl phosphite			1720
	Hexamethyl phosphoramide			2120

[a] Methylene chloride solution.
[b] $\nu_{1:1}-\pi_0$.
[c] $\nu_{2:1}-\nu_{1:1}$.
[d] $\Delta\nu_1+\Delta\nu_2$.
[e] Ref. 5(a).
[f] Ref. 5(b).
[g] Ref. 16.

(of 7.79 and −0.23 respectively with $W = 2.4$) are obtained from the donors in Table 2. The W value of 2.4 kcal mol^{-1} is the heat required to dissociate the fraction of ether that remains coordinated and solvate it by CH_2Cl_2. These E and C values are related to the E_A and C_A of the naked carboxylate dimer, $Cr_2(tfa)_4$, by eqs (2) and (3). We need only solve for the transmission coefficients, k and k', to correct for the kE_B and $k'C_B$ ($B = Et_2O$) terms. Since the 2:1 adduct is formed by an exchange reaction, a modified form of eq. (4) is needed to determine k and k' [eq. (6)]. This procedure allows

$$-\Delta H_{2:1}+W-7.79E_B+0.23C_B = kE_B(1.08-E_B)+k'C_B(3.08-C_B) \quad (6)$$

determination of the acid parameters for $Cr_2(tfa)_4$ (Table 3), allowing direct comparison with the other metal systems. The enthalpy of the second Cr—Et_2O bond is a function of the opposite coordinated base and is thus different for each exchange reaction leading to the 2:1 adduct. The completed definition of k, k' and E and C for the naked dimer mathematically defines the coordination chemistry of this system.

The relatively large E_A and small C_A of chromium trifluoroacetate demonstrate a pronounced tendency for this Cr(II) acid centre to interact primarily in an electrostatic sense as might be expected for a first row transition metal ion. The negative C_A value does not imply that the dimer interacts covalently in an antibonding sense but simply that this is the best fit parameter to a data set in which implicit assumptions have been made in defining the magnitudes of the original parameters.[4] For all practical purposes, the C_A value merely suggests very little covalent interaction between $Cr_2(tfa)_4$ and donors. The strong Lewis acidity of the chromium dimer is consistent with the lack of experimental success in generating a dinuclear chromium carboxylate without an axial donor except in the gas phase.[14]

The low k' value for $Cr_2(tfa)_4$, which corresponds to transmission of the base covalent parameters, indicates that base binding does not serve to polarize the bonding electron density of the chromium–chromium bond, consistent with the poor orbital overlap between the chromium centres. A k value corresponding to transmission of the base electrostatic parameter is smaller than that of any of the other acids studied and is consistent with the

longer metal–metal bond distance in this compared to other metal systems. Of the three systems studied, the chromium dimer exhibits the longest metal–metal bond (2.54 Å for[15] $Cr_2(tfa)_4(Et_2O)_2$, 2.39 Å for[18] $Rh_2(OAc)_4(H_2O)_2$ and 2.09 Å for[18] $Mo_2(tfa)_4$ and should exhibit a small k based upon repulsion of the second bases' electron density with that of the coordinated base.

Trans *influence across a metal–metal bond*

Two spectral studies were undertaken to complement the calorimetry experiments and extend our systematic investigation of the inductive influence across a metal–metal bond. The EPR parameters of a coordinated spin label (TEMPO) in complexes of the type[19] $(L)Rh_2(pfb)_4(TEMPO)$ were examined along with the stretching frequency of coordinated CO in complexes of the type[20] $(L)Rh_2(pfb)_4(CO)$.

Species of the type $(B)Rh_2(pfb)_4(TEMPO)$, where B is a coordinated Lewis base and TEMPO is 2,2,6,6-tetramethyl piperidine-*N*-oxyl, were investigated by EPR to measure the influence of B on the EPR spectrum of the coordinated spin label. Methylene chloride solutions of base, $Rh_2(pfb)_4$ and TEMPO in a 9:10:1 molar ratio were examined by X-band EPR at room temperature. Most of the nitroxide existed in the unbound state, and most of that coordinated TEMPO existed as $(B)Rh_2(pfb)_4(TEMPO)$. A range of g-values was observed as B is varied in the mixed-donor 2:1 adducts whereas decreased accuracy in the measurement of the nitrogen hyperfine, A_N, shows little variation in the measured number. A tabulation of the EPR parameters is given in Table 5. The inductive effect of B upon the Rh—TEMPO bond is such that, the stronger the donor (as seen by $\Delta H_{1:1}$), the closer g is to that of free TEMPO.

The g-values were fit to a form of the E and C

Table 5. EPR parameters and CO stretching frequencies of (B) $Rh_2(pfb)_4(TEMPO)$ and (B) $Rh_2(pfb)_4(CO)$[a]

B	A_N (10^{-3} cm^{-1})	g	g_{calc}[b]	$-\Delta H_{1:1}$[c]	ν_{CO}[d] (cm^{-1})	calc ν_{CO}[e] (cm^{-1})
No base	1.57	2.0152	2.0153	0	2135.8	2135.9
Acetonitrile[f]	1.56	2.0108	(2.0131)	7.05	2129.1	(2130.0)
Methyl acetate	1.55	2.0128	2.0131	7.84		
Ethyl acetate	1.55	2.0127	2.0128	7.94	2130.8	2129.5
Acetone	1.55	2.0122	2.0123	9.23	2128.6	2128.7
p-Dioxane	1.55	2.0120	2.0122	9.64		
Triethyl phosphate				10.42	2126.2	2125.2
Dimethyl formamide	1.55	2.0114	2.0120	10.65		
Dimethyl acetamide	1.55	2.0119	2.0118	11.11	2125.4	2126.9
Bridged ether	1.55	2.0119	2.0114	11.46	2127.0	2128.0
Dimethyl sulphoxide	1.55	2.0116	2.0116	11.79	2126.2	2126.5
Tetrahydrofuran	1.55	2.0118	2.0112	12.14		
Hexamethylphosphoramide	1.55	2.0115	2.0111	13.26		
Cage phosphite[f]	1.56	2.0095	(2.0103)	13.84	2125.1	(2127.8)
Diethyl sulphide[f]	1.55	2.0093	(2.0100)	14.24	2126.1	(2128.3)
Pyridine-*N*-oxide	1.55	2.0101	2.0105	14.41		
Pyridine[g]	1.56	2.0081	(2.0093)	17.36	2122.8	(2124.5)
4-Picoline[g]	1.55	2.0083	(2.0088)	18.46	2121.5	(2124.0)
1-Methyl imidazole	1.56	2.0079	2.0080	20.29	2124.7	2123.9
Piperidine		2.0074	2.0078	20.73	2124.2	2123.2
Triethylamine		2.0069	2.0068	23.38	2121.6	2122.0
Quinuclidene				25.55	2120.8	2121.7

[a] Refs 19 and 20.

[b] Calculated from eq. (7) (see ref. 19) using refined nitroxide E_B^* and C_B^* values of 0.00133 and 0.0224 respectively with $w = 1.9740$.

[c] Enthalpy of adduct formation between $Rh_2(pfb)_4$ and B calculated from eq. (1).

[d] Measured and reported to 0.1 cm^{-1}. Accuracy is estimated to be ± 0.5 cm^{-1} as an upper limit.

[e] Calculated from eq. (7) (see ref. 20) using refined E_B^* and C_B^* values of 5.108 and 22.42 respectively with $w = 2073.6$.

[f] Systems in which metal-to-ligand π-backbonding occurs.

equation used to correlate spectral shifts [eq. (7)].[21]

$$\Delta\chi + W = E_A E_B^* + C_A C_B^*. \quad (7)$$

Here, g is substituted for $\Delta\chi$, the acid, A, is the adduct $Rh_2(pfb)_4B$ whose E_A and C_A parameters are calculated from eqs (2) and (3) using k and k' for $Rh_2(but)_4$ and E_A and C_A for $Rh(pfb)_4$. The E_B^* and C_B^* are the spectroscopic parameters for TEMPO needed to predict g and W is the value for the free nitroxide with other contributions from a non-zero intercept included. The best fit is obtained when π-acceptors are excluded as seen in Table 5. When the g-values are calculated from eq. (7) using the newly obtained W, E_B^* and C_B^* (1.9740, 0.00133 and 0.0224 respectively) the g-values for those adducts with π-acceptors are consistently higher than observed experimentally. That is, additional stabilization in the B—Rh bond, attributed to π^*-backbonding, weakens the Rh—TEMPO bond beyond what can be attributed to a σ-only interaction. This is attributed to the stronger σ bonding counterpart of the π-stabilization.

The experimental ν_{CO} values obtained when CO is bubbled through methylene chloride solutions of $Rh_2(pfb)_4$ containing excess donor are also shown in Table 5. The decrease in the carbonyl stretching frequency is dependent upon the extent of Rh to CO π^*-backbonding and the strength of the sigma bonding. The lower the value of ν_{CO}, the greater is the metal–carbon π^*-backbonding. The data indicate that stronger donors induce greater backbonding or weaker σ-bonding (or both) to CO.

As was done with the spin label g-values, the carbonyl stretching frequencies can also be correlated by eq. (7) by substituting ν_{CO} for $\Delta\chi$ and excellent agreement is obtained. Again, those donors capable of acting as π-acceptors are excluded. When the stretching frequencies for the π-acceptor base adducts are calculated from the best fit parameters (Table 5), these excluded donors all exhibit lower ν_{CO} than predicted from the σ-only parameters. Thus, the effect of the B–Rh π^*-backbond interaction is to increase the extent of π-donation to coordinated CO or weaken the σ-donation or both.

2. *Effects of axial ligation upon the MM electronic structure*

When the electronic transitions involve metal centred orbitals, the electronic spectra of the metal carboxylate dimers exhibit a pronounced dependence upon the axial ligand. For the rhodium dimers, the lowest energy transition is $\pi^* \rightarrow \sigma^*$ (Fig. 3). Adduct formation occurs with stabilization of the donor lone pair and corresponding destabilization of the MM σ^*, resulting in a blue shift for this transition. Should the donor also function as a π-acceptor, the filled π^* orbital is stabilized, shifting the $\pi^* \rightarrow \sigma^*$ transition towards high energy. The blue shifts are more pronounced for the first adduct bond formed.

For $Cr_2(tfa)_4(Et_2O)_2$, the red shift observed upon donor exchange (Table 5) arises from a weakened MM bond. The transition orbitals ($\delta \rightarrow \pi^*$) are not directly involved in bonding to axial ligands. Instead, competition for the metal d_{z^2} orbitals serves to weaken the Cr—Cr bond. The resulting decrease in d orbital overlap compresses the d orbital manifold, resulting in a red shifted $\delta \rightarrow \pi^*$ transition.

The effect of axial ligation upon orbital overlap in the $Cr_2(tfa)_4(B)_2$ adducts has a very interesting influence upon their magnetic susceptibilities.[16] An early magnetic study[22] reported magnetic moments of $\mu_{eff} = 0.74$ BM for '$Cr(F_3CCOO)_2$' and 0.85 BM for '$Cr(F_3CCOO)_2Et_2O$'. We surmised that a regular increase in magnetic moment might accompany coordination of stronger donors. Room temperature magnetic susceptibilities of various adducts, measured by the Evans method,[23] are shown in Table 6. The very satisfying trend towards larger moments with increasing donor strength confirms our expectations.

The only other first row transition metal for which a range of metal carboxylate dimers has been

Table 6. Magnetic susceptibilities and moments for $Cr_2(tfa)_4B_2$ species at 20° (Evans method) in C_6D_6[16]

	χ_M[a] $\times 10^4$	μ_{eff} (BM)[b]
$Rh_2(tfa)_4(THF)_2$	0	0
$Cr_2(tfa)_4(Et_2O)_2$	6.66	0.89
$Cr_2(tfa)_4[(MeO)_3P]_2$	6.91	0.91
[c]	6.95	0.91
$Cr_2(tfa)_4(Et_3PO_4)_2$[d]	10.94	1.15
$Cr_2(tfa)_4(DMTF)_2$[d,e]	12.40	1.22
$Cr_2(tfa)_4(Me_4Urea)_2$	14.53	1.32
$Cr_2(tfa)_4(DMF)_2$[d]	18.18	1.48
$Cr_2(tfa)_4(DMSO)_2$[d]	20.73	1.58
$Cr_2(tfa)_4(DMA)_2$[d]	20.80	1.58
$Cr_2(tfa)_4(DMCA)_2$[f]	36.90	2.11
[c]	34.52	2.04
$Cr_2(tfa)_4(HMPA)_2$[g]	47.01	2.38
$Cr_2(tfa)_4(Me_3PO)_2$	77.86	3.06

[a] Per dimer, $\pm 1 \times 10^{-4}$.
[b] Per Cr(II) atom, ± 0.35 BM.
[c] Multiple determinations.
[d] CD_2Cl_2 solution.
[e] DMTF = dimethylthioformamide.
[f] DMCA = dimethylcyanamide.
[g] HMPA = hexamethylphosphoramide.

prepared is copper. In the cupric carboxylate dimers, overlap of the half-filled $d_{x^2-y^2}$ orbitals with carboxylate orbitals allows a super exchange pathway via the carboxylate bridges. The resulting antiferromagnetic interactions range from $-2J = 217$ to 555 cm^{-1}. Axial ligation influences $-2J$, generally increasing as the terminal ligands become stronger electron pair donors.[24,25] At a given temperature, larger values of $-2J$ would give smaller experimental moments. Thus, in the cupric systems in which the super exchange pathway predominates, better donors give smaller magnetic moments. The reverse is true for the chromium series studied here and the data in Table 6 suggest a direct exchange mechanism. That is, *d* orbital overlap decreases (and the magnetic moments increase) as stronger donors compete with the *trans* metal atom for the d_{z^2} orbitals.

Three of the $Cr_2(tfa)_4B_2$ adducts were also studied in the solid state. Variable temperature (6–400 K) magnetic susceptibility data were fit to a singlet–triplet model. The calculated singlet–triplet splittings[16] were $-2J = 611$ (B = HMPA), 622 (B = Et_2O) and 688 (B = Et_3PO_4) cm^{-1}. These values lie above the range found for the copper carboxylates (217–555 cm^{-1}) indicating a more efficient exchange mechanism in the chromium carboxylates.

CONCLUSIONS

The coordination chemistry of several metal carboxylate dimers has been studied with the aim of characterizing the effects of ligation at one metal site upon the reactivity at another and upon the electronic structure of the metal–metal bond. Adduct formation of $Rh_2(but)_4$, $Rh_2(pfb)_4$, $Mo_2(pfb)_4$, $Rh_2(but)_4Cl$ and $Cr_2(tfa)_4(Et_2O)_2$ with various donors has been treated as an acid–base interaction to allow description of the metal centres in terms of the *E* and *C* model. The rhodium dimers, with filled π^* orbitals, undergo π^*-backbonding to donors capable of acting as π-acceptors. Correlation of the adduct bond enthalpies allows estimation of the relative contributions of σ- and π-stabilization to the adduct bond stabilization energy. Estimated stabilization is lower for adducts of $Rh_2(but)_4Cl$ which contain half-filled π^* orbitals, and is not found for the adducts of $Mo_2(pfb)_4$, the π^* orbitals of which are empty. The inductive transfer of base effects is a function of the metal centres. Inductive effects of base binding in adducts of $Rh_2(pfb)_4$ were further monitored by EPR (for coordinated TEMPO) and IR (for coordinated CO) and quantitatively fit to our inductive transfer model. The effects of axial ligation upon the electronic structure of adducts of the rhodium and chromium dimers was illustrated by electronic spectral shifts. Changes in the magnetic susceptibility of $Cr_2(tfa)_4B_2$ adducts with donor were interpreted in terms of a weakening of metal–metal *d* orbital overlap with progressively stronger donors, consistent with a direct exchange mechanism to describe the observed paramagnetism.

Acknowledgement—The authors acknowledge the partial support of the National Science Foundation for this research.

REFERENCES

1. For reviews, see: (a) F. A. Cotton and R. A. Walton, *Multiple Bonds Between Metal Atoms*. Wiley-Interscience, New York (1982); (b) W. C. Trogler and H. B. Gray, *Acc. Chem. Res.* 1978, **11**, 232; (c) F. A. Cotton, *Pure Appl. Chem.* 1980, **52**, 2331; (d) M. H. Chisholm and I. P. Rothwell, *Prog. Inorg. Chem.* 1982, **29**, 1; (e) T. R. Felthouse, *Prog. Inorg. Chem.* 1982, **29**, 73; (f) E. B. Boyar and S. D. Robinson, *Coord. Chem. Rev.* 1983, **50**, 109.
2. J. N. Van Niekerk and F. R. L. Schoening, *Acta Crystallogr.* 1953, **6**, 227.
3. (a) F. A. Cotton and J. G. Norman Jr, *J. Am. Chem. Soc.* 1972, **94**, 5697; (b) D. M. Collins, F. A. Cotton and C. A. Murillo, *Inorg. Chem.* 1976, **15**, 1861; (c) G. G. Cristoph and Y.-B. Koh, *J. Am. Chem. Soc.* 1979, **101**, 1422; (d) J. G. Norman Jr and H. J. Kolari, *J. Am. Chem. Soc.* 1978, **100**, 791.
4. (a) R. S. Drago, *Struct. Bond. (Berlin)* 1973, **15**, 73; (b) R. S. Drago, *Coord. Chem. Rev.* 1980, **33**, 251; (c) R. S. Drago, N. Wong, C. Bilgrien and G. C. Vogel, *Inorg. Chem.* 1987, **26**, 9. This paper lists new *E* and *C* values which were used in all the *E* and *C* calculations in this paper. The original references use the old values.
5. (a) R. S. Drago, J. R. Long and R. Cosmano, *Inorg. Chem.* 1981, **20**, 2920; (b) R. S. Drago, J. R. Long and R. Cosmano, *Inorg. Chem.* 1982, **21**, 2196; (c) R. S. Drago, *Inorg. Chem.* 1982, **21**, 1697.
6. Y.-B. Koh and G. G. Cristoph, *Inorg. Chem.* 1978, **17**, 2590.
7. R. S. Drago, J. A. Nusz and R. C. Courtright, *J. Am. Chem. Soc.* 1974, **96**, 2802.
8. R. S. Drago, S. P. Tanner, R. M. Richman and J. R. Long, *J. Am. Chem. Soc.* 1979, **101**, 2897.
9. R. S. Drago, R. Cosmano and J. Telser, *Inorg. Chem.* 1984, **23**, 4514.
10. J. G. Norman Jr, H. J. Kolari, H. B. Gray and W. C. Trogler, *Inorg. Chem.* 1977, **16**, 987.
11. J. G. Norman Jr, G. E. Renzoni and D. A. Case, *J. Am. Chem. Soc.* 1979, **101**, 5256.
12. R. J. H. Clark and L. T. H. Ferris, *Inorg. Chem.* 1981, **20**, 2759.
13. D. S. Martin, R. A. Newman and L. M. Vlasnik, *Inorg. Chem.* 1980, **19**, 3404.

14. S. N. Ketkar and M. Fink, *J. Am. Chem. Soc.* 1985, **107**, 338.
15. F. A. Cotton, M. W. Extine and G. W. Rice, *Inorg. Chem.* 1978, **17**, 176.
16. C. Bilgrien, R. S. Drago and C. J. O'Connor, *Inorg. Chem.* (submitted).
17. S. F. Rice, R. B. Wilson and E. I. Solomon, *Inorg. Chem.* 1980, **19**, 3425.
18. F. A. Cotton and J. G. Norman Jr, *J. Coord. Chem.* 1971, **1**, 161.
19. C. Bilgrien, R. S. Drago, J. R. Stahlbush and T. C. Kuechler, *Inorg. Chem.* 1985, **24**, 4268.
20. C. Bilgrien, R. S. Drago, G. C. Vogel and J. Stahlbush, *Inorg. Chem.* 1986, **25**, 2864.
21. R. S. Drago, N. O'Bryan and G. C. Vogel, *J. Am. Chem. Soc.* 1970, **92**, 3924.
22. S. Herzog and W. Kalies, *Z. Anorg. Allg. Chem.* 1967, **351**, 237.
23. D. F. Evans, *J. Chem. Soc.* 1959, 2003.
24. R. W. Jotham, S. F. A. Kettle and J. A. Marks, *J. Chem. Soc., Dalton Trans.* 1972, 428.
25. M. Melnik, *Coord. Chem. Rev.* 1982, **42**, 259.

Polyhedron Vol. 7, No. 16/17, pp. 1469–1481, 1988
Printed in Great Britain

0277–5387/88 $3.00+.00
© 1988 Pergamon Press plc

THERMOLYSIS OF THE Co—C BOND IN ADENOSYLCOBALAMIN (COENZYME B_{12})—IV. PRODUCTS, KINETICS AND Co—C BOND DISSOCIATION ENERGY STUDIES IN ETHYLENE GLYCOL

BENJAMIN P. HAY and RICHARD G. FINKE*

Department of Chemistry, University of Oregon, Eugene, OR 97403, U.S.A.

Abstract—Following an introduction outlining the key questions surrounding the adenosylcobalamin ($AdoB_{12}$) bond homolysis problem, the full details of product, kinetic and Co—C5′ bond dissociation energy studies of the thermolysis of $AdoB_{12}$ in ethylene glycol are presented. The anaerobic thermolysis of $AdoB_{12}$ in the absence of the nitroxide radical trap TEMPO proceeds with four isosbestic points to yield $100\pm2\%$ $Co(II)B_{12}$ and two nucleoside products, 8,5′-anhydroadenosine and 5′-deoxyadenosine. In the presence of $\geqslant 10^{-2}$ M TEMPO, the TEMPO-trapped Ado$^{\bullet}$ product (T-Ado) and $Co(II)B_{12}$ account quantitatively for the starting $AdoB_{12}$. From HPLC studies of the concentration of the nucleoside products vs [TEMPO], absolute rate constants at 110°C for Ado$^{\bullet}$ cyclization and its H$^{\bullet}$ abstraction from glycol solvent are obtained for the first time, $k_c(110°C) \simeq 5 \times 10^5$ s^{-1} and $k_a(110°C) \simeq 7 \times 10^3$ M^{-1} s^{-1}. Kinetic studies in the presence of added, authentic $Co(II)B_{12}$ show an inverse, linear dependence of $1/k_{obs}$ vs [$Co(II)B_{12}$], thereby providing quantitative evidence for the long sought demonstration of the $AdoB_{12} \rightleftharpoons Ado^{\bullet} + Co(II)B_{12}$ equilibrium outside of the enzyme–cofactor complex. The $Co(II)B_{12}$ dependence data also provide the previously unavailable rate constant for recombination of $Co(II)B_{12}$ and Ado$^{\bullet}$ in ethylene glycol of $k_t \simeq 3 \times 10^8$ M^{-1} s^{-1}. Next, the assumption used previously of slow homolysis by the base-off form, $k_{h,off} \ll k_{h,on}$, an assumption necessary to simplify the $AdoB_{12}$ thermolysis kinetics, is tested directly by the synthesis and thermolysis of adenosylcobinamide$^{+}OH^{-}$ and found to be valid. The base-on homolysis rate constants ($k_{h,on}$) were measured from 110 to 80°C. When combined with independently measured temperature-dependence parameters for the off$\rightleftharpoons$on axial base equilibrium, $\Delta H = -7.6\pm0.2$ kcal mol^{-1} and $\Delta S = -20.2\pm0.7$ e.u., values for the base-on homolysis activation parameters of ethylene glycol are obtained, $\Delta H^{\ddagger}_{h,on} = 34.5\pm0.8$ kcal mol^{-1}, and $\Delta S^{\ddagger} = 14\pm1$ e.u. Use of the $\Delta H^{\ddagger}_{h,on}$ data to provide an estimate of the $AdoB_{12}Co$—C5′ BDE in ethylene glycol is discussed, as are a number of additional points and conclusions that result from the present work. Key considerations that led to the nitroxide radical trapping method, and the desirable features of this method, are then discussed, with an eye towards aiding future kinetic studies and BDE determinations of Co—R and other M—R compounds.

"You will note that Vitamin B_{12} Coenzyme has a carbon–cobalt bond. This was the first known compound that was discovered that had a water stable carbon–cobalt bond. In this bond probably lies the secret of its reactivity."

So began Professor R. H. Abeles' address at a 1972 Robert A. Welch Foundation Conference.[1a] His words were prophetic; the essential function of the adenosylcobalamin (Coenzyme B_{12}) cofactor does indeed lie in the Co—C bond.

The specific proposal that reversible homolysis of the Co—C bond of adenosylcobalamin ($AdoB_{12}$) is the key to its biological function dates back even earlier than 1972.[1,2] However, this reversible homolysis, and the subsequent radical mechanism for the rearrangement steps it implied, was not immediately nor universally accepted. In fact, the homolysis/radical mechanism has been controversial,[3] even though convincing *biochemical* evidence for

*Author to whom correspondence should be addressed.

the production of radicals has existed for some time now.[2,4-6]* A key reason for the lack of acceptance of the homolysis/radical mechanism was the lack of evidence for clean, reversible *thermal* homolysis of the Co—C bond of $AdoB_{12}$ in the absence of the enzyme prior to the present studies; in fact, $AdoB_{12}$ was thought (and has been proven) to contain one of the stronger and more stable Co—C bonds.[7]

Given the lack of evidence for reversible homolysis of $AdoB_{12}$ outside the enzyme, many questions remained when we began the present studies. Does homolysis, heterolysis,[3] or some other process not involving Co—C cleavage (as others have suggested)[3d,e] preferentially occur upon heating $AdoB_{12}$ in solution in the absence of the enzyme? What $\Delta H^{\ddagger}$ and what homolytic (or heterolytic) Co—C bond dissociation energy (BDE) are involved? Is the Co—C bond in $AdoB_{12}$ one of the strongest Co—C bonds known as previous data suggested,[7] and if so why? What, both qualitatively and quantitatively, are the effects upon the Co—C cleavage and BDE of the corrin conformation, of the probability of a caged $Co^{\cdot}$ $R^{\cdot}$ pair, and what are the steric and electronic effects of both the axial 5,6-dimethylbenzimidazole and the axial adenosyl alkyl in $AdoB_{12}$? If homolysis occurs, how do the rates of homolysis in solution compare to those in the enzyme, i.e. how large is the enzymic rate acceleration of the Co—C bond homolysis? How does it compare to the rate enhancements exhibited by other enzymes and, ultimately, exactly how is this rate enhancement achieved at the molecular level? These are some of the questions we have attempted to answer throughout the present studies.[8]

The mechanistic possibilities initially confronting one when considering the homolytic cleavage of the Co—C bond of $AdoB_{12}$ are shown in Scheme 1; there are five unknown rate constants and one unknown equilibrium constant. Fortunately, several simplifications are possible. Based on the literature,[9] it seemed likely that homolysis through the base-off form should be much slower than that through the base-on form, $k_{h,off} \ll k_{h,on}$. This is, in fact, the case as will be documented herein. Scheme

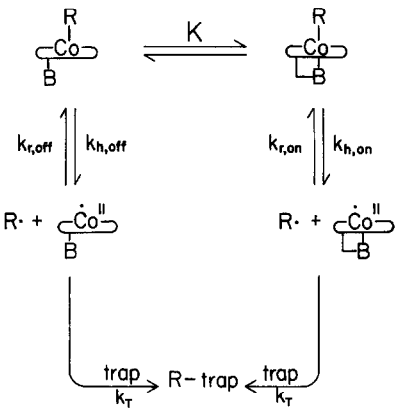

Scheme 1.

1 can be further simplified and optimized if a selective $R^{\cdot}$ trap can be found, one that reacts with $R^{\cdot}$ fast enough to prevent the diffusion-controlled recombination of free $R^{\cdot}+Co^{\cdot}$ radicals[10] (k_r, Scheme 1), yet, ideally, one that is inert to the $Co^{\cdot}$ even at temperatures of $> 100°C$! We note that important prior work employing the radical trapping technique exists, notably work using O_2 as a trap by Schrauzer and Grate[9a,b] and the pioneering work of Halpern and co-workers using B_{12}-model compounds and traps such as RSH.[11] However, it was the work of Smith, reported in 1983,[8a,12] that led to the nitroxide trapping method, the only method successful to date for use with alkylcorrins, and the method of choice in at least some other studies.[13]

In 1984 we successfully extended the nitroxide method to the B_{12} cofactor itself and communicated initial product, kinetic and Co—C BDE studies of $AdoB_{12}$ in ethylene glycol, the first such studies to be described.[14] Herein, we report the full details of those studies.

EXPERIMENTAL

(Readers requiring additional detail over and above that presented herein are directed to a Ph.D. thesis.[8c])

Adenosylcobalamin ($\geq 98\%$) was purchased from Sigma and dried to a constant weight at 80°C *in vacuo*. 5′-Deoxyadenosine and hydroxocobalamin·hydrochloride were obtained from Sigma and used as received. Hydroxocobalamin was prepared by passing an aqueous solution of hydroxocobalamin·hydrochloride down an Amberlite IRA-400 column in the basic form and recrystallizing from water–acetone. $Co(II)B_{12}$[15] and 8,5′-anhydroadenosine[16] were obtained as crystalline solids by literature methods. TEMPO

* The partial (but not 100%) stereospecificity seen in the B_{12}-dependent rearrangement reactions is another piece of evidence consistent with the radical mechanism. Note that the lack of complete stereospecificity *demands* at least some participation by a non-concerted pathway such as a radical pathway. Tightly enzyme-bound and oriented (rather than 'free') radicals that lead to partial stereospecificity are implicated. For a discussion of this point, as well as the stereochemistry of the B_{12}-dependent rearrangements, see ref. 6.

(Aldrich) was purified by sublimation (33°C, water aspirator, mp 39°C, lit. 37–39°C).[17] 5′-Deoxy-5′-[(2,2,6,6-tetramethyl-1-piperidinyl)oxy]-adenosine[18] and adenosylcobinamide$^+BF_4^-$[19] were prepared as described previously. Ethylene glycol was distilled *in vacuo* from Linde 4 Å molecular sieves. Ethylene glycol-d_4 ($\geq$ 98% $HOCD_2CD_2OH$) was obtained from Cambridge Isotopes and used as received.

Proton NMR spectra were recorded as Me_2SO-d_6 solutions on a Nicolet NT-360 spectrometer at 20 ± 1°C. HPLC analyses were carried out using a Beckman chromatograph equipped with a Gilson Holochrome variable-wavelength detector on an Alltech 300 × 4.1 mm Versapack C-18 column. Visible spectra were recorded on a Beckman DU-7 spectrophotometer thermostatted to 25.0 ± 0.2°C. The use of visible spectroscopy to monitor oxygen sensitive reactions required the construction of air-tight cuvettes. Such cuvettes, hereafter called Schlenk cuvettes, were prepared by glass blowing Teflon needle-valves onto 1-cm pathlength, Pyrex cuvettes. These Schlenk cuvettes have contained aqueous solutions at temperatures of up to 130°C without leaking (calculated internal pressure of 39 psi).

Adenosylcobalamin solutions, in ethylene glycol deoxygenated by three freeze/pump/thaw cycles, were prepared in a Vacuum Atmospheres glovebox (N_2, $\leq$ 2 ppm O_2). During the handling of $AdoB_{12}$ solutions, exposure to light was minimized by working under red lighting and keeping vessels wrapped in aluminium foil.

Anaerobic thermolysis of $AdoB_{12}$ *in ethylene glycol*

(a) *Corrin products.* To a Schlenk cuvette were added 2.5 cm^3 of an ethylene glycol solution containing 1.5×10^{-4} M $AdoB_{12}$. The sample was sealed under N_2 and its 25.0°C spectrum was recorded. The sample was then placed in a 100.0°C oil bath. Upon heating a red to yellow colour change was observed over a period of 25 h. Spectra were recorded at intervals during this reaction (see Fig. 1) by removing the cuvette from the bath, quenching the reaction by plunging the cuvette into cold water (18–20°C), allowing the cuvette to warm to 25.0°C in the thermostatted cell block of the spectrophotometer, recording the spectrum, and returning the cuvette to the bath. Superimposed visible spectra revealed isosbestic points at 337, 390, 487 and 581 nm. The final (25 h) spectrum is identical to that of authentic $Co(II)B_{12}$, exhibiting absorbance maxima at 404 and 474 nm. Since kinetic data was obtained by monitoring the reaction via visible spectroscopy, this clean $AdoB_{12}$ to $Co(II)B_{12}$ conversion has been repeated many times at $AdoB_{12}$ concentrations ranging from 5 to 30×10^{-5} M, temperatures ranging from 90 to 120°C, and in the presence of 0 to 2.0×10^{-2} M TEMPO. The same behaviour is exhibited under all these conditions, i.e. superimposed spectra show a clean, four isosbestic point conversion of $AdoB_{12}$ to $Co(II)B_{12}$.

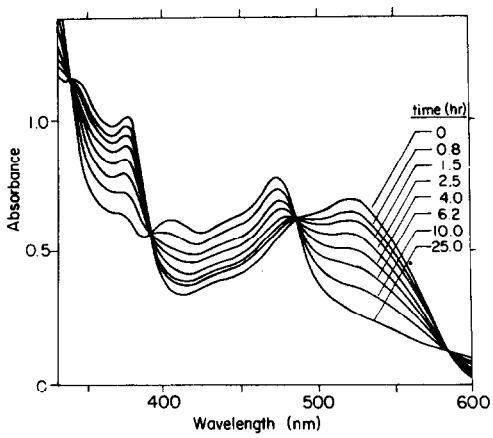

Fig. 1. Visible spectrum of the anaerobic thermolysis of $AdoB_{12}$ in ethylene glycol without added TEMPO with isosbestic points at 337, 390, 487 and 581 nm. Conditions: $[AdoB_{12}] = 9.0 \times 10^{-5}$ M; reaction temperature 100.0°C; spectra recorded at 25.0°C (see Experimental).

(b) *Isolation and identification of nucleoside products in neat ethylene glycol.* To a 100 cm^3 round-bottom flask were added 250 mg (0.16 mmol) of $AdoB_{12}$, 50 cm^3 ethylene glycol, and a stirbar. The vessel was sealed under N_2 with a greased ground glass stopper, placed in a 110.0°C oil bath, and the contents were stirred for 8 h in the absence of light. After this time the solvent was removed (10^{-3} torr, 90–95°C) and the brown residue was dissolved in a minimal amount of CH_3OH. The solution was applied to four preparative silica gel plates (20 cm × 20 cm × 1 mm, EM Reagents Silica Gel PF-254). The bands were allowed to air-dry and the plates were eluted with a 21 : 4 (v/v) *n*-butanol–H_2O solution. When the solvent had migrated to 2 cm from the top of the plates (7 h), they were removed from the tank. Upon visualization with a UV lamp, two purple bands were observed ($R_f = 0.45$–0.62 and $R_f = 0.67$–0.86). These bands were scraped from the plates and similar R_f bands combined to form an upper R_f and a lower R_f fraction. Each fraction was removed from the silica gel by repeated washings with acetone (250 cm^3 acetone/fraction). Upon removal of the acetone (water aspirator, steam bath) solid residues were obtained. The lower R_f fraction was recrystallized from water yielding

10 mg of small white needles. A 360 MHz ^{1}H NMR spectrum of this purified lower fraction was identical to that of authentic 8,5′-anhydroadenosine. ^{1}H NMR (360 MHz, Me_2SO-d_6): δ 8.08 (*s*, 1H, H-2), 7.13 (*s*, 2H, NH_2), 5.97 (*s*, 1H, H-1′), 5.53 (*d*, 1H, OH-3′), 5.24 (*d*, 1H, OH-2′), 4.60 (*d*, 1H, H-4′), 4.19 (*dd*, 1H, H-2′), 4.03 (*dd*, 1H, H-3′), 3.33 (*dd*, 1H, H-5′), 3.01 (*d*, 1H, H-5′).

The upper R_f fraction was dissolved in ethanol and yellow impurities (acetone condensation products) were removed by boiling with charcoal. After filtering and removal of the solvent (water aspirator, steam bath) 8 mg of a white amorphous solid was obtained. A 360 MHz ^{1}H NMR spectrum of this purified upper fraction was identical to that of authentic 5′-deoxyadenosine. ^{1}H NMR (360 MHz, Me_2SO-d_6): δ 8.30 (*s*, 1H, H-2 or H-8), 8.13 (*s*, 1H, H-2 or H-8), 7.27 (*s*, 2H, NH_2), 5.82 (*d*, 1H, C-1′), 5.42 (*d*, 1H, OH-2′), 5.14 (*d*, 1H, OH-3′), 4.65 (*m*, 1H, H-2′), 3.96 (*m*, 2H, H-3′ and H-4′), 1.21 (*d*, 3H, H-5′).

(c) *HPLC identification and quantitation of nucleoside products.* Samples for HPLC analysis were prepared in ethylene glycol at the same initial concentration of $AdoB_{12}$ used in the kinetic experiments, i.e. $(5–30) \times 10^{-5}$ M $AdoB_{12}$. Reactions were carried out under a variety of conditions including $(0–1.0) \times 10^{-2}$ M TEMPO and neat ethylene glycol-d_4. Such samples were prepared in the glovebox, sealed under N_2 in Schlenk cuvettes, and heated in the dark for $\geqslant 4$ half-lives (9 h) in a 110.0°C oil bath. After this time, the samples were opened to air and analysed for nucleoside content by HPLC as described in detail elsewhere.[18]

Temperature dependence of the axial-base equilibrium

An ethylene glycol solution of 1.0×10^{-4} M $AdoB_{12}$ was placed in a Schlenk cuvette and visible spectra were recorded at 5° intervals from 10.0 to 80.0°C. Values of ΔH and ΔS were calculated from 520 nm absorbance vs temperature data by the curve-fitting method described previously.[18] This method assumes that only two species, a red base-on form and a yellow base-off form, are present and that each of them exhibits a temperature-independent spectrum over the working temperature range. These assumptions are supported by the presence of isosbestic points at 389, 478 and 596 nm and a control experiment showing that adenosylcobinamide$^+BF_4^-$, a base-off form of $AdoB_{12}$, does not show any significant (< 2%) temperature dependent absorbance change at 520 nm upon heating in ethylene glycol from 10.0 to 80.0°C.

Control demonstrating the thermal stability of $Co(II)B_{12}$

To two separate Schlenk cuvettes were added 2.0 cm^3 samples of 3.0×10^{-4} M $Co(II)B_{12}$, one in ethylene glycol and the other in pH 7.0 aqueous phosphate buffer. The samples were sealed under N_2, then heated at 110°C in an oil bath. Periodically the cuvettes were removed from the oil bath, cooled to 25°C, and their visible spectra were recorded. The samples were monitored in this fashion for a total of 4 h at 110°C, revealing no detectable change (Δ abs $\leqslant$ 0.001 over this time period).

Control demonstrating the stability of $Co(II)B_{12}$ *toward oxidation by TEMPO in ethylene glycol*

Separate 2.0 cm^3 samples, each containing 2.0×10^{-4} M $Co(II)B_{12}$ and 1.0×10^{-2} M (50 eq) TEMPO in ethylene glycol, were added to two Schlenk cuvettes. One of these samples was heated in the cell block of a visible spectrometer at 40°C and spectra were recorded at 30 min intervals for a period of 3 h. The other sample was heated at 110°C in an oil bath and monitored over a period of 4 h. Periodically, the cuvettes were removed from the oil bath, cooled to 25°C, and visible spectra were recorded. In each case, no change was observed by visible spectroscopy, demonstrating that $Co(II)B_{12}$ and TEMPO do not react with one another in this solvent. Elsewhere (see pp. 158–163[8c]) we have presented electrochemical data showing why Co(II) and TEMPO are thermodynamically stable (in ethylene glycol) with respect to the formation of Co(III) and reduced TEMPO, and why this is changed somewhat in H_2O.

Kinetics of the anaerobic thermolysis of $AdoB_{12}$ *in ethylene glycol*

The rate of the thermolysis of $(5–30) \times 10^{-5}$ M $AdoB_{12}$ in ethylene glycol was monitored by visible spectroscopy at 520 nm. Thermolyses were carried out in an oil bath thermostatted to ± 0.2°C at temperatures from 90.0 to 120.0°C; spectra were recorded following cooling to 25.0°C as described above in the section entitled '*Corrin products*'. The rate of the reaction was examined under a variety of conditions including $0–2.0 \times 10^{-2}$ M TEMPO and $0–3.0 \times 10^{-4}$ M $Co(II)B_{12}$. Absorbance readings were obtained by scanning against reagent blanks containing the same [TEMPO] or [$Co(II)B_{12}$] as the $AdoB_{12}$ sample in order to subtract the absorbance of these additives. A plot of $1/k_{obs}$ vs [$Co(II)B_{12}$] was linear with a slope of $(4.6 \pm 0.3) \times 10^6$ M^{-1} s and an intercept at 8310 ± 60 s. Rate-limiting behaviour

is observed at [TEMPO] $\geqslant 5.0 \times 10^{-3}$ M and first-order plots of $\ln[(A_o - A_\infty)/(A - A_\infty)]$ vs time were linear for $\geqslant 3$ half-lives. Under these rate-limiting conditions, values of k_{obs} ($\pm 3\%$) were measured at 5° intervals from 90.0 to 120.0°C.

Kinetics of adenosylcobinamide$^+BF_4^-$ thermolysis in ethylene glycol

To a Schlenk cuvette were added 2.0 cm^3 of an ethylene glycol solution containing 1.0×10^{-4} M adenosylcobinamide$^+BF_4^-$[19] and 1.0×10^{-2} M TEMPO. The sample was sealed under N_2, thermolysed at 112.0°C, and the reaction was monitored at 380 nm by visible spectroscopy as described above. As reported for the aqueous thermolysis of adenosylcobinamide$^+OH^-$,[19] the disappearance of adenosylcobinamide$^+$ is first-order for at least a half-life and this reaction initially yields Co(II) cobinamide. Linear regression of a $\ln[(A_o - A_\infty)/(A - A_\infty)]$ vs time plot yields a value of $k_{h,off} = (5 \pm 2) \times 10^{-6}$ s^{-1}.

RESULTS

Products of the anaerobic thermolysis of AdoB$_{12}$

The anaerobic thermolysis of $(5–30) \times 10^{-5}$ M $AdoB_{12}$ in ethylene glycol was monitored by visible spectroscopy. The observed product is $100 \pm 2\%$ $Co(II)B_{12}$ (by comparison to authentic material). Superimposed visible spectra (Fig. 1) reveal that the conversion of $AdoB_{12}$ to $Co(II)B_{12}$ proceeds with four isosbestic points (337, 390, 487 and 581 nm) ruling out the build-up of other corrin products or intermediates. The same clean reaction is observed both in the absence and presence of the alkyl radical scavenger, TEMPO.

The nucleoside products of the anaerobic thermolysis of $AdoB_{12}$ were examined under a variety of reaction conditions including neat ethylene glycol, ethylene glycol-d_4, and ethylene glycol solutions containing $(0–1.0) \times 10^{-2}$ M TEMPO. While $Co(II)B_{12}$ is the only corrin product observed under all these conditions, the nucleoside product distribution was found to be condition dependent, consistent with the formation of an Ado$^\bullet$ radical intermediate.

In neat ethylene glycol, the anaerobic thermolysis of $AdoB_{12}$ yields two nucleoside products (Fig. 2). These products, 8,5′-anhydroadenosine (major) and 5′-deoxyadenosine (minor), were isolated and identified by comparison of their ^{1}H NMR spectra to those of authentic materials. HPLC provided a means of detecting and quantifying ($\pm 5\%$) these products at the visible spectroscopy concentrations $[(5–30) \times 10^{-5}$ M] employed in subsequent kinetic experiments. Over the temperature range of 90.0 to 120.0°C, the yield of 8,5′-anhydroadenosine ranges from 73 to 78% and the yield of 5′-deoxyadenosine ranges from 27 to 22%; together these two products account for $100 \pm 5\%$ of the expected nucleoside yield.

The formation of the major nucleoside product, 8,5′-anhydroadenosine, suggests the presence of a

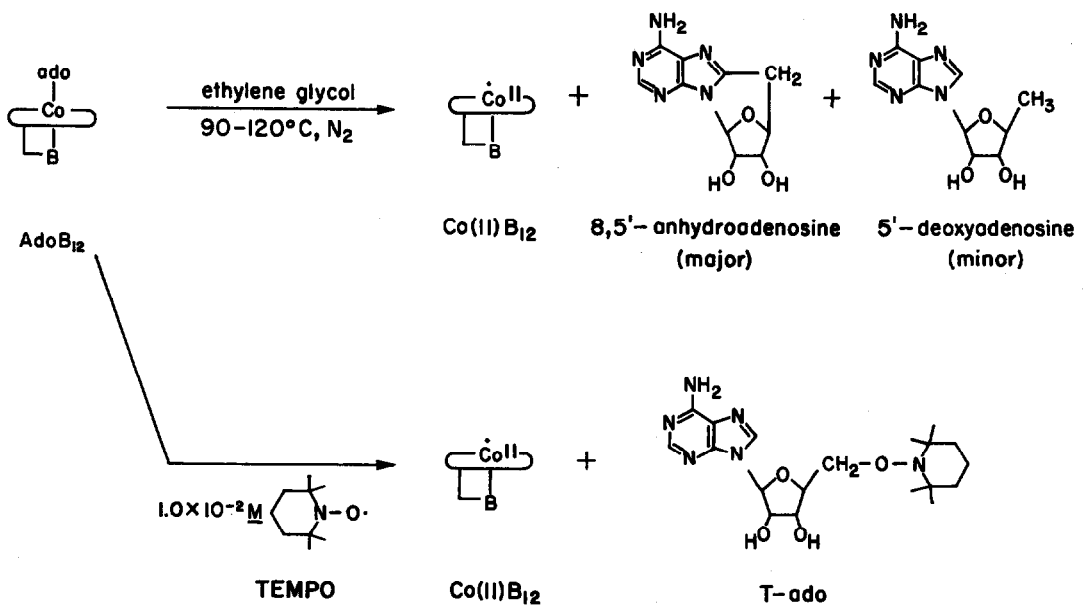

Fig. 2. Products for the thermolysis of $AdoB_{12}$ in ethylene glycol without and with added TEMPO. In each case, the mass balance is 100% within experimental error.

5′-deoxy-5′-adenosyl radical as a precursor. Such nucleoside radicals are known to undergo intramolecular cyclizations to yield products containing 8,5′-linkages.[20] In fact, 8,5′-anhydroadenosine is the only nucleoside product observed during the anaerobic photolysis of $AdoB_{12}$ in aqueous solution,[16,21] a reaction known to involve Co—C bond homolysis.[16,21,22] Furthermore, several independent syntheses of 8,5′-anhydroadenosine involve the generation of a radical centre at either the C5′ position[20e,f] or the C8 position,[20g] taking advantage of the tendency of such radicals to undergo intramolecular closure.

The minor nucleoside product, 5′-deoxyadenosine, also arises from a 5′-deoxy-5′-adenosyl radical precursor via H• abstraction of a methylene hydrogen from ethylene glycol. This pathway, which provides precedent for a proposed step in the B_{12}-dependent diol-dehydratase reaction, was demonstrated by comparing the nucleoside yields in ethylene glycol to those in ethylene glycol-d_4 (deuterated at carbons only). If H• (D•) abstraction from ethylene glycol were occurring, then running the reaction in ethylene glycol-d_4 should result in a decrease in the yield of 5′-deoxyadenosine. However, if 5′-deoxyadenosine is formed via an alternate pathway, such as H• abstraction from the corrin (or some other donor) or H^+ transfer from ethylene glycol to a 5′-deoxy-5′-adenosyl anion, then running the reaction in ethylene glycol-d_4 should not alter the product distribution. Upon comparing the 110.0°C nucleoside products in ethylene glycol to those in ethylene glycol-d_4, a substantial decrease in the yield of 5′-deoxyadenosine (and corresponding increase in the yield of 8,5′-anhydroadenosine) is observed; (22 ± 3)% in ethylene glycol vs (4 ± 1)% in ethylene glycol-d_4. This result establishes ethylene glycol as the H•(D•) source and provides the ratio $k_H/k_D \geqslant 6.7\pm1.5$ at 110.0°C. Due to the presence of a non-deuterated impurity in the ethylene glycol-d_4 ($\leqslant 2$%), this value should be regarded as a lower limit for the true k_H/k_D ratio.*

Further product studies, employing the alkyl radical scavenger TEMPO, yield results which confirm that the 5′-deoxy-5′-adenosyl radical is the precursor for both 8,5′-anhydroadenosine and 5′-deoxyadenosine. When TEMPO is present, a third nucleoside product, T-ado, is formed (see Fig. 2). As the concentration of TEMPO is increased, the yield of T-ado increases with corresponding decreases in the yields of the other two nucleoside products. The effect of $(0–1.0)\times10^{-2}$ M TEMPO on the product distribution at 110.0°C was investigated by HPLC and the results are summarized in Fig. 3.

The observed TEMPO dependence is in quantitative accord with the partial mechanism depicted in Scheme 2 involving competitive cyclization (k_c), H• abstraction (k_a), and TEMPO trapping (k_t) of (or by) the Ado• intermediate. At $\geqslant 10$ eq TEMPO, plots of [8,5′-anhydroadenosine] vs [T-ado]/[TEMPO] and [5′-deoxyadenosine] vs [T-ado]/[TEMPO] are linear and yield the important results (slopes) of $k_c/k_T = (1.12\pm0.04)\times10^{-3}$ M and k_a[ethylene glycol]$/k_T = (3.1\pm0.2)\times10^{-4}$ M, respectively (Fig. 4). With the reasonable assumption that k_T falls within the known range of $(3–5)\times10^8$ M^{-1} s^{-1} for alkyl radical scavenging by sterically hindered nitroxides,[23] the first estimates of the rate constant for cyclization of the 5′-deoxy-5′-adenosyl radical, k_c (110.0°C) $\simeq 5\times10^5$ s^{-1}, and 5′-deoxy-5′-adenosyl radical H• abstraction from ethylene glycol, k_a (110.0°C) $\simeq 7\times10^3$ M^{-1} s^{-1}, are obtained. Confidence in these rate constant estimates is fortified by the fact that they fall within the known range of rate constants for similar processes. The rate constant for H• abstraction from alcohols by methyl radicals at 25°C falls in the range of $10^2–10^4$ M^{-1} s^{-1}.[24] The intramolecular cyclization is rapid with a rate constant close to that of species such as the 5-hexenyl radical, i.e. 10^6 s^{-1} at 100°C.[25] While this is the first estimate of this rate constant, the rapidity of this 5′-deoxy-5′-adenosyl radical cyclization has previously been noted.[26]

Product studies of the anaerobic thermolysis of $AdoB_{12}$ in ethylene glycol indicate that the primary event of this reaction is Co—C bond homolysis to yield $Co(II)B_{12}$ and a 5′-deoxy-5′-adenosyl radical. Subsequent chemistry of the nucleoside radical results in the observed products. The simplest mechanism which accounts for these products is presented in Scheme 3.

Kinetics of the anaerobic thermolysis of $AdoB_{12}$ in ethylene glycol

Having postulated a mechanism, the next step is to ascertain whether observed kinetic behaviour is consistent with predicted kinetic behaviour and, of course, ideally to rule out all other plausible mechanisms. The rate law for this mechanism (see Scheme 3) was derived assuming a steady state concentration for the 5′-deoxy-5′-adenosyl radical. Given this rate law, several predictions can be made. The addition of TEMPO should result in an observed rate increase by shutting down free-radical

*Mass spectrometric confirmation that 5′-deoxyadenosine has incorporated deuterium and further studies of the k_a and k_H/k_D values at lower temperatures are in progress. R. G. Finke and Y. Wang, experiments in progress.

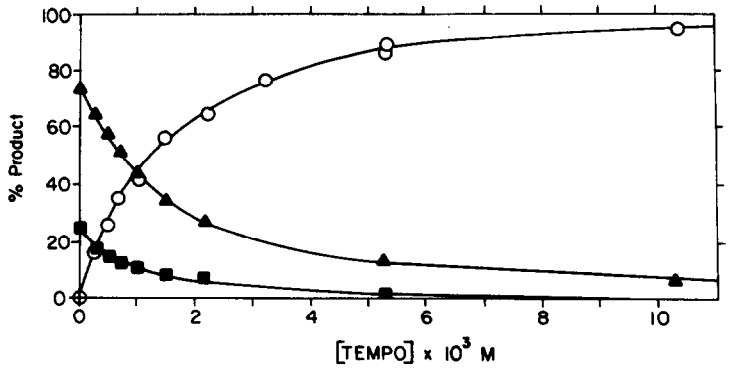

Fig. 3. Plot of the percent yields of the nucleoside products from the thermolysis of $AdoB_{12}$ (1.0×10^{-4} M) at 110°C in anaerobic ethylene glycol vs [TEMPO]; 8,5′-anhydroadenosine (▲), 5′-deoxyadenosine (■), and T-Ado (○).

recombinations. At high TEMPO concentration, where all free nucleoside radicals would be scavenged, the rate should become zero-order in [TEMPO] and first-order decay of $AdoB_{12}$ should be observed. Conversely, the addition of $Co(II)B_{12}$ should cause a rate decrease by increasing the recombination between $Co(II)B_{12}$ and 5′-deoxy-5′-adenosyl radicals.

Prior to studying the effect of added TEMPO or $Co(II)B_{12}$, the kinetic behaviour in their absence was established as a basis for comparison. In the absence of added scavenger, first-order plots for the disappearance of 1.5×10^{-4} M $AdoB_{12}$ are essentially linear for a half-life and then show a discernible downward curvature which becomes more pronounced as the reaction proceeds (see Fig. 5). This downward curvature has been shown elsewhere to be quantitatively consistent[8c,14] with recombination of $Co(II)B_{12}$ and 5′-deoxy-5′-adenosyl radicals, the amount of recombination increasing as the reaction proceeds and as $[Co(II)B_{12}]$ accumulates.

The TEMPO dependence was examined at 110.0°C using an initial $[AdoB_{12}]$ of 1.5×10^{-4} M and for [TEMPO] from 0 to 2.0×10^{-2} M. Added TEMPO decreases the downward curvature in first-order plots until [TEMPO] $\geqslant 5.0 \times 10^{-3}$ M, at which point the curvature disappears altogether and

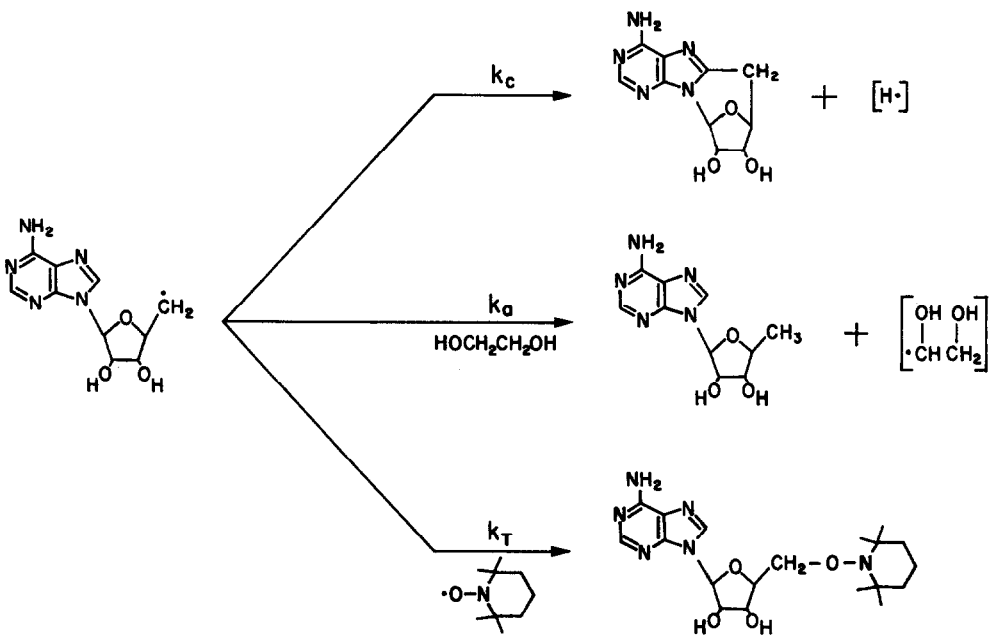

Scheme 2.

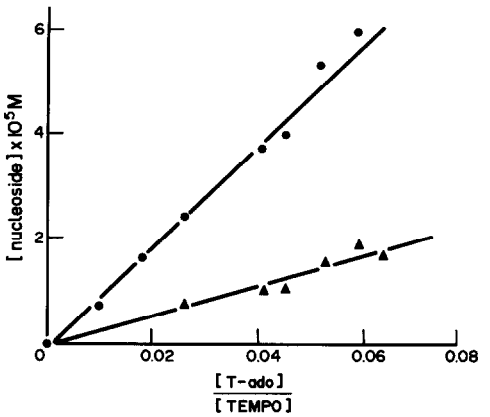

Fig. 4. Plots of nucleoside product concentrations (8,5′-anhydroadenosine (●) and 5′-deoxyadenosine (▲) vs [T-Ado]/[TEMPO]. The slopes of these plots lead to values for the rate constants k_a, k_c and k_t, as discussed in the text.

first-order plots are linear to three half-lives (Fig. 5). The presence of greater concentrations of TEMPO, up to 2.0×10^{-2} M, causes no further rate increase, thereby ruling out the presence of any direct (second-order) reaction between TEMPO and $AdoB_{12}$. A plot of k_{obs}, the slope of the best-fit line to the first two half-lives of a first-order plot, vs [TEMPO] illustrates this point (Fig. 6), and clearly shows that the rate law becomes zero-order in [TEMPO].

The $Co(II)B_{12}$ dependence was examined at 110.0°C using an initial $[AdoB_{12}]$ of 1.0×10^{-4} M and for $[Co(II)B_{12}]$ from 0 to 3.0×10^{-4} M. First-order rate constants, k_{obs}, were obtained from initial (≤ 25% reaction) rate data. In accord with the rate law, a plot of $1/k_{obs}$ vs $[Co(II)B_{12}]$ is linear (Fig. 7). The slope of this plot provides a value for k_r, the rate constant for the recombination of free

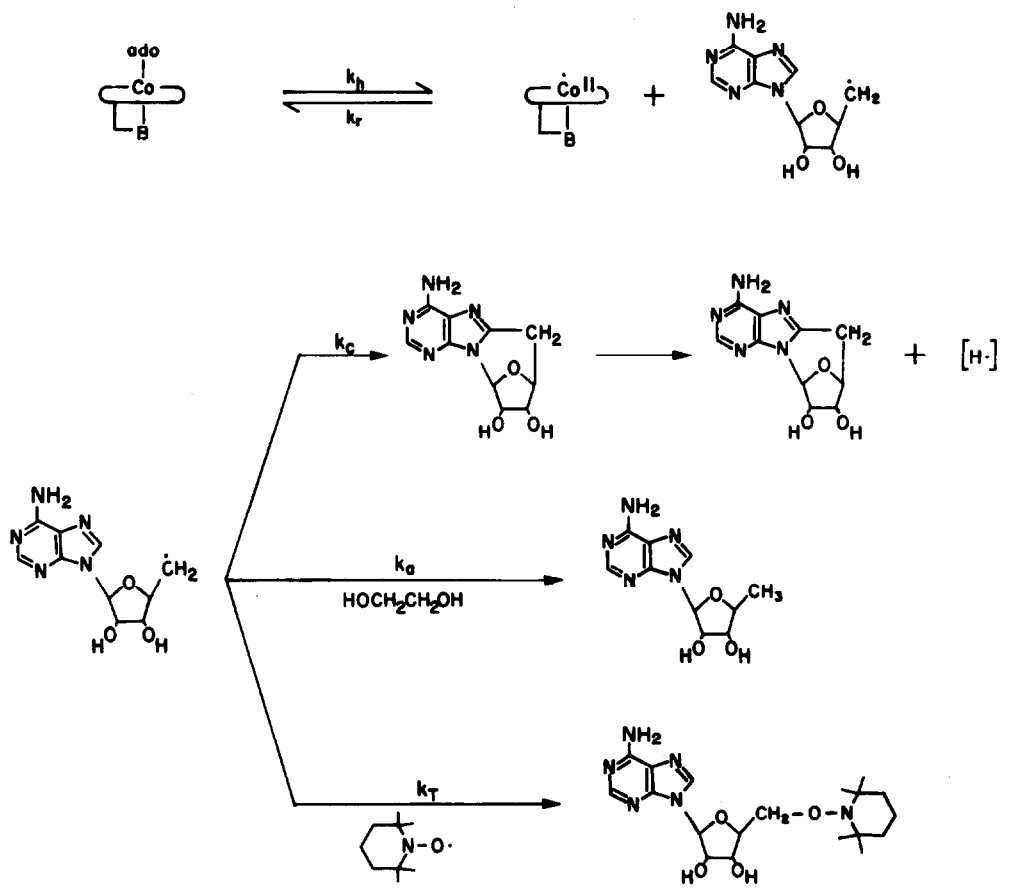

$$\frac{-d \ln AdoB_{12}}{dt} = k_h \left[\frac{k_c + k_a [HOCH_2CH_2OH] + k_T [TEMPO]}{k_c + k_a [HOCH_2CH_2OH] + k_T [TEMPO] + k_r [Co(II)B_{12}]} \right]$$

Scheme 3.

Fig. 5. First-order plots for the disappearance of $AdoB_{12}$ in the presence (△) and absence (○) of TEMPO in ethylene glycol.

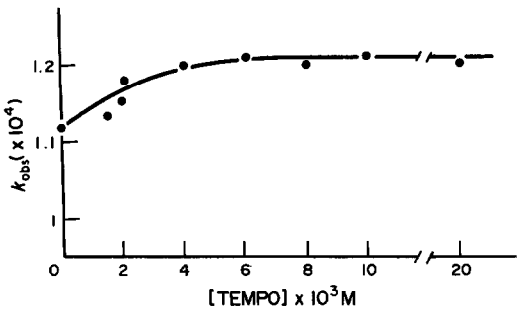

Fig. 6. Plot of k_{obs} vs [TEMPO] showing that a rate-limiting plateau (zero-order [TEMPO] dependence) has been reached. The non-zero intercept at [TEMPO] = 0 is due to the non-zero values of k_c and k_a (see text).

$Co(II)B_{12}$ and 5′-deoxy-5′-adenosyl radicals. This rate constant is related to the slope by eq. (1). Values for all the variables on the right-hand side of this relation are available: at 110.0°C the slope $= (4.6 \pm 0.3) \times 10^6$ M^{-1} s; $k_h = 1.21 \times 10^{-4}$ s^{-1}; $k_c \simeq 5 \times 10^5$ s^{-1} and k_a[ethylene glycol] $\simeq 1 \times 10^5$ s^{-1}. Inserting these values into eq. (1) yields an estimate of $k_r \simeq 3 \times 10^8$ M^{-1} s^{-1} at 110.0°C, a result which falls within the known range of $(0.5\text{–}20) \times 10^8$ M^{-1} s^{-1} for Co˙ and R˙ recombinations.[10] Significantly, along with products and other evidence consistent with homolysis, the [Co(II)] dependence provides the long sought demonstration of the *reversible, thermal* homolysis of the Co—C5′ bond of $AdoB_{12}$ in the absence of any B_{12}-binding enzyme.

$$k_r = \text{slope} \cdot k_h \cdot (k_c + k_a[\text{ethylene glycol}]). \quad (1)$$

Although unexpected initially, the relatively small magnitude of the TEMPO and $Co(II)B_{12}$ concentration dependencies (maxima of a 7% rate increase [with TEMPO] and an 8% decrease with $[Co(II)B_{12}]$ over the concentration range studied) is consistent with the rapidity of the competing radical pathways. Even though the rate of recombination, k_r, is close to the diffusion-controlled limit, when $[Co(II)B_{12}]$ is $\leqslant 5.0 \times 10^{-5}$ M (during the first half-life of the reaction) the ratio $(k_c + k_a[\text{ethylene glycol}])/k_r[Co(II)B_{12}]$ is $\geqslant 40$, so that little recombination is expected. It is only in the later stages of reaction, when $Co(II)B_{12}$ has accumulated, that recombination competes with these facile radical reactions. In the presence of $\geqslant 5.0 \times 10^{-3}$ M TEMPO, free-radical recombination is non-competitive, and the formation of free $Co(II)B_{12}$ and 5′-deoxy-5′-adenosyl radicals becomes rate-determining. All these results are consistent with, and fully supportive of, the mechanism proposed in Scheme 3.

Having established conditions where the formation of free $Co(II)B_{12}$ and 5′-deoxy-5′-adenosyl radicals is rate-determining, first-order plots yield the Co—C5′ bond homolysis rate constant, k_h (see Scheme 3). The temperature dependence of k_h was measured at 5° intervals from 90.0 to 120.0°C.* A plot of $\ln(k_h/T)$ vs $1/T$ is linear, yielding $\Delta H_h^{\ddagger} = 30.6 \pm 0.3$ kcal mol^{-1} and $\Delta S_h^{\ddagger} = 2.9 \pm 0.7$ cal mol^{-1} K^{-1}.

Axial-base temperature-dependence effects

As discussed in the introduction (see Scheme 1), the first-order rate constant for the disappearance of $AdoB_{12}$, k_h, is a composite due to the presence of the axial-base equilibrium. Over the temperature

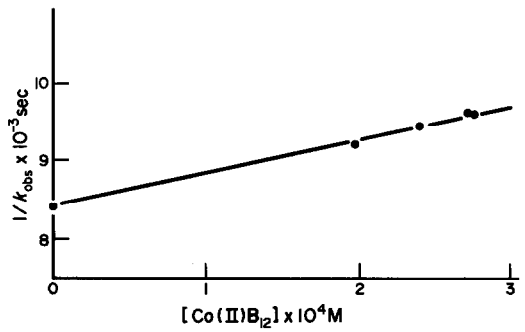

Fig. 7. Plot of $1/k_{obs}$ vs $[Co(II)B_{12}]$, providing the first direct demonstration of the $AdoB_{12} \rightleftharpoons Ado^{\cdot} + Co(II)B_{12}^{\cdot}$ equilibrium in the absence of any B_{12}-binding enzyme.

*The k_h values (s^{-1}, ±3%) and temperatures (°C, ±0.2°C) respectively, are as follows: 1.22×10^{-5}, 90.0; 2.23×10^{-5}, 95.0; 4.11×10^{-5}, 100.0; 7.13×10^{-5}, 105.0; 1.21×10^{-4}, 110.0; 2.08×10^{-4}, 115.0; 3.34×10^{-4}, 120.0.

range employed in the thermolysis study, significant amounts of both the base-on and base-off forms of $AdoB_{12}$ are present (*vide infra*); theoretically, homolysis could proceed through either form. Therefore, there are two rate constants of interest, $k_{h,on}$ and $k_{h,off}$. In accord with Scheme 1, the value k_h is related to $k_{h,on}$ and $k_{h,off}$ by eq. (2).

$$k_h = [K/(K+1)]k_{h,on} + [1/(K+1)]k_{h,off}. \quad (2)$$

Studies of Co-corrins containing other alkyl ligands have shown that alkylcobalamins (axial-base present) undergo thermal Co—C bond cleavage 10^2–10^3 times faster than alkylcobinamides (lacking the axial-base).[9] Therefore, in previous $AdoB_{12}$ studies[14,18] and on this basis, it was *assumed* that $k_{h,on} \gg k_{h,off}$, resulting in the simplification of eq. (2) to the form given below as eq. (3). This *assumption* has been verified elsewhere for $AdoB_{12}$ thermolysis in aqueous solution by comparing $k_{h,on}$ values [obtained from eq. (3)] to $k_{h,off}$ values (obtained from independent studies of adenosylcobinamide$^+OH^-$).[19] The results presented below establish that this assumption is also valid in ethylene glycol.

$$k_h = [K/(K+1)]k_{h,on}. \quad (3)$$

To test the validity of the assumed non-participation of the base-off form, adenosylcobinamide$^+BF_4^-$ was thermolysed in ethylene glycol and found to exhibit a first-order decay with a rate constant, $k_{h,off}$, of $(5 \pm 2) \times 10^{-6}$ s^{-1} at 112.0°C. Comparison of this base-off rate constant to the base-on 112.0°C value, $k_{h,on}$, of 3.4×10^{-4} s^{-1} demonstrates that the base-off form is much less reactive. When these 112.0°C rate constants are combined with the 112.0°C value for K of 0.79, eq. (2) reveals that $< 2\%$ of the observed $AdoB_{12}$ reaction proceeds through the base-off form at this temperature, a behaviour very similar to that observed in aqueous solution.[19]

The temperature dependence from 110.0 to 80.0°C of the base-off to base-on equilibrium of $AdoB_{12}$ in ethylene glycol was monitored by visible spectroscopy as described in the 'Experimental' section. The data was analysed by the curve-fitting method described previously to yield $\Delta H = -7.6 \pm 0.2$ kcal mol^{-1} and $\Delta S = -20.2 \pm 0.7$ cal mol^{-1} K^{-1} for the base-off $\rightleftharpoons$ base-on equilibrium. Extrapolating this data to the temperature range of the thermolysis study yields 59% base-on at 90.0°C but only 45% base-on at 120.0°C. Combining the k_h and K data according to eq. (3) yields values of $k_{h,on}$. These in turn provide the desired base-on Co—C bond homolysis activation parameters of $\Delta H^{\ddagger}_{h,on} = 34.5 \pm 0.8$ kcal mol^{-1} and $\Delta S^{\ddagger}_{h,on} = 14 \pm 1$ cal mol^{-1} K^{-1}.

Base-on Co—C *bond dissociation energy estimate*

In a separate article,[27] we have discussed the relationship of M—L bond dissociation energies (BDEs) to kinetic data obtained in the liquid phase. In particular, we have discussed the importance of a consideration of previously neglected radical cage effects in any attempt to relate solution Co—R homolysis enthalpies of activation, $\Delta H^{\ddagger}_h$, to *gas phase* Co—R BDEs. Since the activation enthalpy for base-on Co—C bond homolysis of $AdoB_{12}$, $\Delta H^{\ddagger}_{h,on}$, was measured using the radical scavenging method (which traps free Ado$^{\cdot}$ that have escaped the cage), it probably contains a contribution due to the enthalpy of cage escape, $\Delta H^{\ddagger}_{\eta}$. As discussed elsewhere,[27] the best current estimate is that the Co—C BDE $\simeq \Delta H^{\ddagger}_{h,on} -$ a correction, where the correction term could range from zero (no $\Delta H^{\ddagger}_{escape}$ for cage escape) to $\Delta H^{\ddagger}_{escape}$ as *estimated* by $\Delta H^{\ddagger}_{\eta}$, the enthalpy of activation for viscous flow.[28]* For ethylene glycol, $\Delta H^{\ddagger}_{\eta}$ is 4.4 kcal mol^{-1} over the 90–120°C temperature range of the thermolysis studies.[28] Therefore, in the absence of direct measurements concerning the extent and energetics of cage effects in *this* reaction, we conclude that the base-on Co—C BDE lies between 30.1 kcal mol^{-1} ($\Delta H^{\ddagger}_{escape} \simeq \Delta H^{\ddagger}_{\eta}$) to 34.5 kcal mol^{-1} ($\Delta H^{\ddagger}_{escape} \simeq 0$).† Experiments are currently in progress to measure directly the correction term for $AdoB_{12}$, a result which will allow a more accurate estimate for this M—L BDE. However, the value of 30.1 is essentially within experimental error of our earlier estimate in glycol (given in our initial communication[14]) of 31.5 ± 1.3 kcal mol^{-1} and is in good agreement with the only other reliable estimate (from studies in pH = 7.0 H_2O) of 30 ± 2 kcal mol^{-1}.[18] The subsequent $AdoB_{12}$ BDE estimate of 26 ± 2 kcal mol^{-1} has been shown to be 4 kcal mol^{-1} too low because the reaction actually studied consists of significant *heterolysis* of the Co—C5′ bond in pH = 4.3 H_2O (77% at 85°C and 45% at 110°C).[18] It is unfortunate that a recent report[13e] chose to ignore our earlier

* Calculated from $\ln(\eta)$ vs $1/T$ plot using literature viscosity data, Andrade's law, $\ln \eta = \ln A_{\eta} + E_{\eta}/RT$,[28b,c] and then $\Delta H^{\ddagger}_{\eta} = E_{\eta} - RT$.

† Our previously reported value of 31.5 ± 1.3 kcal mol^{-1} for the base-on Co—C BDE of $AdoB_{12}$[14] was obtained assuming a correction term of 3 ± 1 kcal mol^{-1}. As discussed elsewhere,[27] this correction term may be a couple of kcal mol^{-1} too low or too high, i.e. it was used initially—and still should be viewed—as a first-order approximation.

paper,[18] thereby propagating confusion on this point.*

DISCUSSION AND CONCLUSIONS

The $AdoB_{12}$ thermolysis and BDE estimate studies presented herein allow additional comparisons and conclusions to be drawn. One such conclusion is that non-radical mechanisms for the $AdoB_{12}$-dependent rearrangement reactions, such as Schrauzer's heterolysis,[3a-c] Rooney's carbene,[3e] or the Corey–Cooper–Green[3d] mechanism (involving electrocyclic cleavage of the corrin and oxidative addition of the substrate C—H bond), can now rigorously be ruled out, at least in the absence of the enzyme. These and any other non-radical mechanisms fail the test of kinetic competence, as they do not occur to any appreciable extent compared to homolysis. As for their possibility in the holoenzyme ($AdoB_{12}$ + the enzyme), others have previously noted that these mechanisms 'either dismissed or ignored' the compelling evidence obtained in studies of the B_{12}-dependent enzymes for the kinetically competent generation of $Co(II)B_{12}$ and organic radicals.[29]

Another comparison, one that yields perhaps the single most important finding of these studies, is the comparison of the rate of $AdoB_{12}$ Co—C5′ homolysis in the holoenzyme at 25°C of $\geqslant 10^2$ s^{-1}, to that obtained for base-on $AdoB_{12}$ in solution at 25°C, $k_{h,on(25°C)} = 10^{-9\pm1}$ s^{-1}.[14,18,19] The difference, an effect of $\geqslant 10^{11}$, is responsible for an enzyme Co—C5′ homolysis half-life of a few milliseconds in comparison to a solution half-life of 22 years! Discussion of this point, and the $\leqslant 10^2$ role of the axial base in B_{12} in an overall rate effect (including the axial-base) of $\geqslant 10^{13}$ is presented elsewhere.[14,18,19]

Following homolysis to $Co(II)B_{12}$ and Ado$^\bullet$, these present studies also provide chemical precedent for the second step proposed for diol dehydratase, abstraction of a $HOCH_2CH_2OH$ C—H bond by *thermally* generated[30] Ado$^\bullet$, and provide the first absolute rate constant and k_H/k_D value for this process, $k_a(110°) \simeq 7 \times 10^3$ M^{-1} s^{-1} and $k_H/k_D(110°) \geqslant 6.7 \pm 1.5$. Efforts aimed at measuring k_a and k_H/k_D in the temperature range of 25–37°C are in progress; preliminary results suggest that these measurements will allow additional insights when compared to the holoenzyme's turnover rate and k_H/k_D values (experiments in progress). This is a key reason why we chose ethylene glycol as a solvent system, it is a substrate for B_{12}-dependent diol dehydratase.

Two final areas merit brief discussion. These are: (a) some key considerations which led to the nitroxide trapping method that has been a cornerstone of our $AdoB_{12}$ thermolysis studies; and (b) recent literature citations where the nitroxide has proven to be the method of choice in other M—R thermolysis studies.[13]

As for the development of the nitroxide trapping technique, it required a Ph.D. thesis comparing the nitroxide pros and cons to those of what proved to be unsuitable traps [n-BuSH, PhSH, $HMn(CO)_5$, O_2].[8a,c,13] Key features of the nitroxide trap are: (a) that it met our criterion of *thermodynamic* stability with respect to Co(II) and trap redox side reactions (forming, for example, $Co(III)^+$ and nitroxide$^-$), at least in ethylene glycol[8c] (see pp. 159–163[8c]); (b) that it is paramagnetic to begin with, hence a diamagnetic nitroxide–R product results, one that can be *isolated* and characterized by NMR, glc or HPLC, mass spectrometry and so on; and (c) a control for possible bimolecular side reactions induced by the (paramagnetic) trap can be conducted, *ab initio*, simply by heating the cobalt alkyl and

* A valuable paper has recently appeared that measures a 4–6 kcal mol^{-1} $\Delta(\Delta H^\ddagger)$ difference (glycol vs toluene; 5 ± 1 kcal mol^{-1} from the data provided) for a series of Co—R B_{12} model compounds using the TEMPO trapping method.[13e] Unfortunately, however, this paper makes the misleading claim that 'Although an alternative explanation has been advanced[12]' (ref. 12 is our earlier communication[14]) 'we conclude that this accounts for much of the difference of *ca* 6 kcal mol^{-1} in $\Delta H^\ddagger$ previously reported for homolytic Co—C BDE reactions of 5′-adenosylcobalamin (Coenzyme B_{12}) in water and in ethylene glycol (28.6 vs 34.5 kcal mol^{-1}).' This claim is both misleading and incorrect because it ignores our earlier paper (work dated with a one year and five month earlier acceptance date[18]). Our study of $AdoB_{12}$ thermolysis in pH = 7.0 H_2O[18] had already corrected the pH = 4.3 study by showing that of the $\Delta(\Delta H^\ddagger) = 5.9$ (± 1.3) kcal mol^{-1} discrepancy in the ethylene glycol[14] vs pH = 4.3 H_2O values [$34.5(\pm 0.8) - 28.6$ (± 1) = $5.9(\pm 1.3)$], an amount equal to 4.4 (± 2.2) kcal mol^{-1} of the difference *is due to heterolysis* of the Co—C5′ bond in B_{12} in pH = 4.3 H_2O [$33(\pm 2) - 28.6(\pm 1) = 4.4(\pm 2.2)$]. The remaining 1.5 ($\pm 2.6$) kcal mol^{-1} [$5.9(\pm 1.3) - 4.4(\pm 2.2) = 1.5(\pm 2.6)$] is very likely due to the glycol vs H_2O viscosity and thus $\Delta H_\eta^\ddagger$ difference,[13c] and we previously noted that the correction factor might run as high as 4 kcal mol^{-1} (i.e. 3 ± 1 kcal mol^{-1}),[14] a value only a kcal mol^{-1} below (actually within experimental error) of the current 5 ± 1 kcal mol^{-1} *estimate*[27] (in the case of alkylcobalamins) of the proper correction factor. In summary, *both* heterolysis [$4.4(\pm 2.2)$ kcal mol^{-1}] and a solvent (viscosity) correction [$1.5(\pm 2.6)$ kcal mol^{-1}] are required to account for the previous [$5.9(\pm 1.3)$ kcal mol^{-1}] differences in the estimates of the $AdoB_{12}$ Co—C5′ BDE.

the nitroxide together (compared to a diamagnetic trap, such as a thiol, that generates a RS$^{\bullet}$ *transient*). These key features in turn allowed us, and in general allow one, to: (i) demonstrate an inverse Co(II) dependence and thus the R—Co $\rightleftharpoons$ R$^{\bullet}$ + Co(II)$^{\bullet}$ equilibrium; (ii) demonstrate whether or not the desired plateau can be attained where a rate-limiting excess of nitroxide trap is added (rate $\propto$[nitroxide]^{0}, hence the nitroxide 'reports' rather than 'causes' the chemistry), thereby avoiding bimolecular contributions that lead to incorrectly low $\Delta H^{\ddagger}$ and low (to negative) $\Delta S^{\ddagger}$; and (iii) demonstrate whether or not the final products are consistent with the proposed homolysis. (An example illustrating the importance of this latter point is available.[18]) It is also well known that reliable $\Delta H^{\ddagger}$ and $\Delta S^{\ddagger}$ values (and thus reliable, kinetically determined BDE estimates) require rate constants measured over as large a temperature range as possible.[31]

It seems likely that a consideration of the above partial list of attributes of the 'ideal' trap will prove valuable in other kinetic studies of M—R homolyses and kinetically estimated BDEs. For this reason, it has been included here even though the emphasis of the present work is the thermolysis and Co—C5′ BDE of AdoB$_{12}$ in the presence of the enzymic substrate, ethylene glycol.

Acknowledgements—Financial support was provided by NIH Grant AM-26214 and Dreyfus Teacher–Scholar and Guggenheim Fellowships to RGF while this work was in progress.

REFERENCES

1. (a) R. H. Abeles in *Proceedings Robert A. Welch Foundation, Conf. Chem. Res.*, Vol. XV, *Bio-organic Chemistry and Mechanisms* (Edited by W. O. Milligan), pp. 95–127 (1972); (b) See the acknowledgement to Professor Breslow, p. 113, and his discussion, pp. 119–120. See also footnote 3 of R. Breslow and P. L. Khanna, *J. Am. Chem. Soc.* 1976, **98**, 1297; (c) The suggestion that the AdoB$_{12}$ Co—C5′ bond is cleaved during catalysis dates back to at least 1964: R. H. Abeles and H. A. Lee, Jr, *Ann. N.Y. Acad. Sci.* 1964, **112**, 695; L. L. Ingraham, *Ann. N.Y. Acad. Sci.* 1964, **112**, 713.
2. (a) B. M. Babior, *J. Biol. Chem.* 1970, **245**, 6125. See also: P. Y. Law, D. G. Brown, E. L. Lien, B. M. Babior and J. M. Wood, *Biochem.* 1971, **10**, 3428; B. Babior and D. C. Gould, *Biochem. Biophys. Res. Commun.* 1969, **34**, 441; (b) T. H. Finlay, J. Valinsky, K. Sato and R. H. Abeles, *J. Biol. Chem.* 1972, **247**, 4197; (c) B. M. Babior, T. H. Moss and D. C. Gould, *J. Biol. Chem.* 1972, **247**, 4389; (d) S. A. Cockle, H. A. O. Hill, R. J. P. Williams, S. P. Davies and M. A. Foster, *J. Am. Chem. Soc.* 1972, **94**, 275; (e) T. H. Finlay, J. Valinsky, A. S. Mildvan and R. H. Abeles, *J. Biol. Chem.* 1973, **248**, 1285; (f) J. E. Valinsky, R. H. Abeles and J. A. Fee, *J. Am. Chem. Soc.* 1974, **96**, 4709; (g) J. E. Valinsky, R. H. Abeles and A. S. Mildvan, *J. Biol. Chem.* 1974, **249**, 2751; (h) R. G. Eagar, W. W. Bachovchin and J. H. Richards, *Biochem.* 1975, **14**, 5523; (i) J. A. Hamilton and R. L. Blakley, *Biochim. Biophys. Acta* 1969, **184**, 224.
3. (a) G. N. Schrauzer and J. W. Sibert, *J. Am. Chem. Soc.* 1970, **92**, 1022; (b) G. N. Schrauzer, W. S. Michaely and R. J. Holland, *J. Am. Chem. Soc.* 1973, **95**, 2024; (c) G. N. Schrauzer, *Angew. Chem., Int. Eng. Ed.* 1977, **16**, 233; (d) E. J. Corey, N. J. Cooper and M. L. H. Green, *Proc. Nat Acad. Sci.* 1977, **74**, 811; (e) V. Amir-Ebrahimi, R. Hamilton, M. V. Kulkarni, E. A. McIlgorm, T. R. B. Mitchell and J. J. Rooney, *J. Mol. Cat.* 1983, **22**, 21.
4. (a) K. L. Schepler, W. R. Dunham, R. H. Sands, J. A. Fee and R. H. Abeles, *Biochim. Biophys. Acta* 1975, **397**, 510; (b) J. F. Boas, P. R. Hicks, J. R. Pilbrow and T. D. Smith, *J. Chem. Soc., Faraday Trans. 2* 1978, **74**, 417; (c) J. A. Hamilton, Y. Tamao, R. L. Blakley and R. E. Coffman, *Biochemistry* 1972, **11**, 4696; (d) G. R. Buettner and R. E. Coffman, *Biochim, Biophys. Acta* 1977, **480**, 495; (e) R. E. Coffman, Y. Ishikawa, R. L. Blakley, H. Beinert and W. H. Orme-Johnson, *Biochim, Biophys. Acta* 1976, **444**, 307; (f) R. L. Blakley, W. H. Orme-Johnson and J. M. Bozdech, *Biochemistry* 1979, **18**, 2335; (g) A. Pezeshk and R. G. Coffman, *J. Chem. Soc., Dalton Trans.* 1985, 891.
5. (a) M. R. Hollaway, H. A. White, K. N. Joblin, A. W. Johnson, M. F. Lappert and O. C. Wallis, *Eur. J. Biochem.* 1978, **82**, 143; (b) A. Gaudemer, J. Zylber, N. Zylber, M. Baran-Marszac, W. E. Hull, M. Fountoulakis, A. Konig, A. Wolfle, K. Wolfle and J. Rétey, *Eur. J. Biochem.* 1981, **119**, 279; (c) O. C. Wallis, R. C. Bray, S. Gutteridge and M. R. Hollaway, *Eur. J. Biochem.* 1982, **125**, 299.
6. (a) R. G. Finke, D. A. Schiraldi and B. J. Mayer, *Coord. Chem. Rev.* 1984, **54**, 1; (b) B. T. Golding in B_{12} (Edited by D. Dolphin), Vol. 1. Wiley-Interscience, New York (1982); (c) R. M. Dixon, B. T. Golding, S. Mwesisye-Kibende and D. K. Ramakrishna Rao, *Phil. Trans. R. Soc. London* 1985, **B311**, 531; (d) J. Rétey, in *Stereochemistry* (Edited by Ch. Tamm), Chap. 6. Elsevier Biomedical Press, Amsterdam (1982); (e) D. Arigoni in *Vitamin B_{12}, Proceedings of the 3rd European Symposium. Vitamin B_{12} and Intrinsic Factor* (Edited by B. Zagalak and W. Friedrich), p. 389. W. deGruyter, Berlin (1979).
7. H. P. C. Hogenkamp, P. J. Vergamini and N. A. Matwiyoff, *J. Chem. Soc., Dalton Trans.* 1975, 2628.
8. (a) B. L. Smith, Ph.D. Dissertation, University of Oregon, 1982; (b) D. A. Schiraldi, Ph.D. Dissertation, University of Oregon, 1982; (c) B. P. Hay, Ph.D. Dissertation, University of Oregon, 1986.
9. (a) G. N. Schrauzer and J. H. Grate, *J. Am. Chem. Soc.* 1981, **103**, 541; (b) J. H. Grate and G. N. Schrauzer, *J. Am. Chem. Soc.* 1979, **101**, 4601; (c)

S. M. Chemaly and J. M. Pratt, *J. Chem. Soc., Dalton Trans.* 1980, 2274; (d) D. A. Baldwin, E. A. Betterton, S. M. Chemaly and J. M. Pratt, *J. Chem. Soc., Dalton Trans.* 1985, 1613.

10. (a) T. S. Roche and J. F. Endicott, *Inorg. Chem.* 1974, **13**, 1575; (b) J. F. Endicott and G. J. Ferraudi, *J. Am. Chem. Soc.* 1977, **99**, 243; (c) C. Y. Mok and J. F. Endicott, *J. Am. Chem. Soc.* 1977, **99**, 1276; 1978, **100**, 123; (d) A. M. Tait, M. Z. Hoffman and E. Hayon, *Int. J. Radiat. Phys. Chem.* 1976, **8**, 691; (e) W. A. Mulac and D. Meyerstein, *J. Am. Chem. Soc.* 1982, **104**, 4124; (f) H. Elroi and D. Meyerstein, *J. Am. Chem. Soc.* 1978, **100**, 5540.
11. T. T. Tsou, M. Loots and J. Halpern, *J. Am. Chem. Soc.* 1982, **104**, 623; see refs cited therein for earlier work in this series.
12. R. G. Finke, B. L. Smith, B. J. Mayer and A. A. Molinero, *Inorg. Chem.* 1983, **22**, 3677.
13. (a) A. Bakac and J. H. Espenson, *J. Am. Chem. Soc.* 1984, **106**, 5197; (b) R. Blau and J. H. Espenson, *J. Am. Chem. Soc.* 1985, **107**, 3530; (c) J. P. Collman, L. McElwee-White, P. J. Brothers and E. Rose, *J. Am. Chem. Soc.* 1986, **108**, 1332; (d) M. K. Geno and J. Halpern, *J. Am. Chem. Soc.* 1987, **109**, 1238; (e) M. K. Geno and J. Halpern, *J. Chem. Soc., Chem. Commun.* 1987, 1052.
14. R. G. Finke and B. P. Hay, *Inorg. Chem.* 1984, **23**, 3041.
15. H. U. Blaser and J. Halpern, *J. Am. Chem. Soc.* 1980, **102**, 1684.
16. K. Bernhauer and O. Müller, *Biochem. Z.* 1961, **335**, 44.
17. E. G. Rozantsev and M. B. Neiman, *Tetrahedron* 1964, **20**, 131.
18. B. P. Hay and R. G. Finke, *J. Am. Chem. Soc.* 1986, **108**, 4820.
19. B. P. Hay and R. G. Finke, *J. Am. Chem. Soc.* 1987, **109**, 8012.
20. K. Z. Keck, *Naturforsch.* 1968, **23B**, 1034; (b) K. N. V. Duong, A. Gaudemer, M. D. Johnson, R. Quillivic and J. Zylber, *Tetrahedron Lett.* 1975, **34**, 2997; (c) N. Marriagi, J. Cadet and R. Teoule, *Tetrahedron* 1976, **32**, 2385; (d) A. Matsuda, M. Tezuka and T. Ueda, *Tetrahedron* 1978, **34**, 2449; (e) A. Matsuda, K. Muneyama, T. Nishida, T. Sado and T. Ueda, *Nuc. Acid. Res.* 1976, **3** 3349; (f) J. Zylber, R. Pontikis, A. Merrien, C. Merienne, M. Baran-Marszak and A. Gaudemer, *Tetrahedron* 1980, **36**, 1579; (g) D. Gani, A. W. Johnson and M. F. Lappert, *J. Chem. Soc., Chem. Commun.* 1980, 1244.
21. (a) A. W. Johnson and N. Shaw, *J. Chem. Soc.* 1962, 4608; (b) H. P. C. Hogenkamp, *J. Biol. Chem.* 1963, **238**, 477.
22. (a) D. Dolphin, A. W. Johnson and R. Rodrigo, *Ann. N.Y. Acad. Sci.* 1964, **112**, 590; (b) H. P. C. Hogenkamp, H. A. Barker and J. S. Mason, *Arch. Biochem. Biophys.* 1963, **100**, 353; (c) D. J. Lowe, K. N. Joblin and D. J. Cardin, *Biochim. Biophys. Acta* 1978, **539**, 398; (d) V. D. Ghanekar, R. J. Lin and R. E. Coffman, *Biochem. Biophys. Res. Commun.* 1981, **101**, 215; (e) D. K. Ramakrishna Rao and M. C. R. Symons, *J. Chem. Soc., Perkin Trans. 2* 1983, 187.
23. (a) P. Schmid and K. U. Ingold, *J. Am. Chem. Soc.* 1978, **100**, 2493; (b) S. Nigam, K. D. Asmus and R. L. Willson, *J. Chem. Soc., Faraday Trans. 1* 1976, 2324; (c) A. L. J. Beckwith, V. W. Bowry, M. O'Leary, G. Moad, E. Rizzardo and D. H. Solomon, *J. Chem. Soc., Chem. Commun.* 1986, 1003.
24. J. K. Thomas, *J. Phys. Chem.* 1967, **71**, 1919.
25. D. Griller and K. U. Ingold, *Acc. Chem. Res.* 1980, **13**, 317.
26. R. T. Taylor, L. Smucker, M. L. Hanna and J. Gill, *Arch. Biochem. Biophys.* 1973, **156**, 521; (b) R. O. Brady and H. A. Barker, *Biochem. Biophys. Res. Commun.* 1961, **4**, 373.
27. T. W. Koenig, B. P. Hay and R. G. Finke, *Polyhedron* 1988, **7**, 1499.
28. (a) S. Glasstone, K. J. Laidler and H. Eyring, *Theory of Rate Processes*. McGraw-Hill, New York (1941); (b) K. Raznjevic, *Handbook of Thermodynamic Tables and Charts*. McGraw-Hill, New York (1976); (c) L. H. Thomas, R. Meatyard, H. Smith and G. H. Davis, *J. Chem. Eng. Data* 1979, **24**, 161.
29. B. T. Golding in B_{12} (Edited by D. Dolphin), Vol. 1, Chap. 15, pp. 558–560. Wiley-Interscience, New York (1982).
30. H$^{\cdot}$ abstraction from ethylene glycol by photochemically generated Ado$^{\cdot}$, but not its absolute rate constant, is known: (a) A. J. Hartshorn, A. W. Johnson, S. M. Kennedy, M. F. Lappert and J. J. MacQuitty, *J. Chem. Soc., Chem. Commun.* 1978, 643; (b) I. P. Rudakova, T. E. Ershova, A. B. Belikov and A. M. Yurkevich, *J. Chem. Soc., Chem. Commun.* 1978, 592.
31. (a) S. W. Benson in *The Foundation of Chemical Kinetics*, p. 91. McGraw-Hill, New York (1960); (b) J. O. Edwards, F. Monacelli, and G. Ortaggi, *Inorg. Chim. Acta* 1974, **11**, 47; see p. 48.

Polyhedron Vol. 7, No. 16/17, pp. 1483–1490, 1988
Printed in Great Britain

0277–5387/88 $3.00+.00
© 1988 Pergamon Press plc

DETERMINATION OF TRANSITION METAL–ALKYL BOND DISSOCIATION ENERGIES FROM KINETIC MEASUREMENTS

JACK HALPERN

Department of Chemistry, The University of Chicago, Chicago, IL 60637, U.S.A.

Abstract—Transition metal–alkyl bond dissociation energies (D_{L_nM-R}) may be deduced from kinetic measurements using the relation: $D_{L_nM-R} = \Delta H_1^{\ddagger} - \Delta H_{-1}^{\ddagger}$, where $\Delta H_1^{\ddagger}$ and $\Delta H_{-1}^{\ddagger}$ are activation enthalpies of the homolytic bond dissociation reaction and the reverse (recombination) reaction, respectively, i.e. $L_nM{-}R \rightleftharpoons L_nM^{\cdot} + R^{\cdot}$. This has come to be one of the most widely used methods for determining such bond dissociation energies in solution. The basis, scope and limitations of the method are discussed with particular reference to the following themes: (i) determination of $\Delta H_1^{\ddagger}$ and $\Delta H_{-1}^{\ddagger}$, (ii) the role and choice of free radical traps, (iii) solvent effects, (iv) magnitudes and variations of entropies of activation and (v) relation to other methods of determining transition metal–alkyl bond dissociation energies.

In 1982 we described a method for determining transition metal–alkyl bond dissociation energies (D_{M-R}, strictly bond dissociation *enthalpies*) based on measuring the kinetics of reaction (1) and using the relation of eq. (2).[1]

$$L_nM{-}R \underset{k_{-1}}{\overset{k_1}{\rightleftharpoons}} L_nM^{\cdot} + R^{\cdot} \quad (1)$$

$$D_{M-R} = \Delta H_1^{\ddagger} - \Delta H_{-1}^{\ddagger}. \quad (2)$$

Our original application of this method involved determination of the Co—C bond dissociation energies of a series of organocobalt compounds, R—Co(Saloph)py (where Saloph = N,N′-bis-salicylidene-*o*-phenylenediamine and R = propyl, neopentyl, benzyl, etc.) through a study of the reaction sequence:[1]

$$R{-}Co(Saloph)py \rightleftharpoons R^{\cdot} + Co(Saloph)py \quad (3)$$

$$R^{\cdot} + n\text{-}C_8H_{17}SH \rightarrow RH + n\text{-}C_8H_{17}S^{\cdot} \quad (4)$$

$$n\text{-}C_8H_{17}S^{\cdot} \rightarrow \tfrac{1}{2}(n\text{-}C_8H_{17}S)_2. \quad (5)$$

Overall:

$$R{-}Co(Saloph)py + n\text{-}C_8H_{17}SH \rightarrow Co(Saloph)py + RH + \tfrac{1}{2}(n\text{-}C_8H_{17}S)_2. \quad (6)$$

Since then this approach has been extensively applied by ourselves and others and has become probably the most widely used method for determining such bond dissociation energies in solution.[2–8] A principal application has been the determination of Co—C bond dissociation energies of organocobalt complexes because of the relevance of such complexes as models for coenzyme B_{12} whose biological function is triggered by homolytic Co—C bond dissociation.[9] These studies have contributed systematic information not only about the factors that influence transition metal–alkyl bond dissociation energies but also about the scope and limitation of the kinetic method of determining such energies. This paper discusses the following themes: (i) determination of $\Delta H_1^{\ddagger}$ and $\Delta H_{-1}^{\ddagger}$, (ii) the role and choice of free radical traps, (iii) solvent effects, (iv) magnitudes and variations of entropies of activation and (v) the relation of the kinetic method to other methods of determining transition metal–alkyl bond dissociation energies.

DETERMINATION OF $\Delta H_1^{\ddagger}$

The determination of $\Delta H_1^{\ddagger}$ from the temperature-dependence of k_1 is straightforward in principle. Measurement of k_1 usually requires: (1) ascertaining that thermal decomposition of L_nM—R actually proceeds through homolytic metal–carbon bond dissociation since organometallic compounds commonly decompose in other ways, e.g. by olefin elimination. If such other paths do intervene their contributions must be evaluated and subtracted from the overall rate to determine k_1,[1,10] (2) adding a suitable trap to capture the organic radical R$^{\cdot}$ (and/or, in some cases, the metal radical, $L_nM^{\cdot}$) and thereby suppress complicating side reactions, if only the recombination of $L_nM^{\cdot}$ and R$^{\cdot}$ (i.e. the k_{-1} step).

In the presence of such a radical trap (T) the reaction scheme is depicted by eqs (1), (7) and (8) [or by variants such as that desdribed by eqs (1), (7) and (10)].

$$L_nM{-}R \underset{k_{-1}}{\overset{k_1}{\rightleftharpoons}} L_nM^{\bullet} + R^{\bullet} \quad (1)$$

$$R^{\bullet} + T \xrightarrow{k_7} T{-}R. \quad (7)$$

Overall:

$$L_nM{-}R + T \rightarrow L_nM^{\bullet} + T{-}R. \quad (8)$$

In those cases where the metal radical, $L_nM^{\bullet}$, is stable and persistent (e.g. $L_5Co^{III}R \rightarrow L_5Co^{II} + R^{\bullet}$), the steady-state rate law takes the form of eq. (9). Fitting the observed dependence of the rate on the concentrations of $L_nM^{\bullet}$ and T to this equation serves to confirm the mechanistic scheme and permits evaluation of k_1 and k_{-1}/k_7

$$\frac{-d[L_nM{-}R]}{dt} = \frac{k_1k_7[L_nM{-}R][T]}{k_{-1}[L_nM^{\bullet}] + K_7[T]}. \quad (9)$$

Not uncommonly, the metal radical undergoes (reversible) dimerization according to eq. (10). In such cases, the steady-state rate law assumes the form of eq. (11). This behaviour is exemplified by the decomposition of R—Mn(CO)$_4$P in the presence of H—Mn(CO)P as the trap (R = p-CH_3O—$C_6H_4CH_2$; P = (p-CH_3O—C_6H_4)$_3$P),[11] i.e. R—Mn(CO)P $\rightleftharpoons$ R$^{\bullet}$ + $^{\bullet}$Mn(CO)$_4$P; R$^{\bullet}$ + HMn(CO)$_4$P $\rightarrow$ RH + $^{\bullet}$Mn(CO)$_4$P; 2 $^{\bullet}$Mn(CO)$_4$P $\rightleftharpoons$ Mn$_2$(CO)$_8$)P$_2$

$$2L_nM^{\bullet} \underset{k_{-10}}{\overset{k_{10}}{\rightleftharpoons}} M_2L_{2n} \quad (10)$$

$$\frac{-d[L_nM{-}R]}{dt} = \frac{k_1k_7[L_nM{-}R][T]}{k_{-1}(k_{-10}/k_{10})^{1/2}[M_2L_{2n}]^{1/2} + k_7[T]}. \quad (11)$$

Evidence that decomposition proceeds through homolytic M—C bond dissociation may also be inferred from the nature of the products, provided that the connection is unambiguous and quantitative. While the formation of the radical trapping product R—T is strongly suggestive of a free radical origin, concerns are that such a product may arise from a different route, e.g. $L_nM{-}R + T \rightarrow L_nM^{\bullet} + R{-}T$, or that the initially formed R—T product is unstable and undergoes further reactions. Furthermore, the initially formed radicals may rearrange prior to trapping or be trapped in other ways, e.g. by self-reaction or by H-abstraction from solvent. Thus, product identification alone is rarely a reliable guide to mechanism in the cases of interest. We consider establishment of the full rate law of eq. (9) or (11) to be essential to reliable application of this method and, in our own work, generally have tried to insist that this criterion be met.

Where bond dissociation energies have been deduced from studies entailing less complete rate laws, in some cases only the limiting form ($k_7[T] \gg k_{-1}[L_nM^{\bullet}]$, therefore rate = $k_1[L_nM{-}R]$), values of k_1, $\Delta H_1^{\ddagger}$ and $\Delta S_{-1}^{\ddagger}$ sometimes have agreed with those determined from more complete kinetic studies (e.g. the Co—C bond dissociation of neopentyl cobalamin).[12] In other cases there are discrepancies and the results remain controversial.[3-5,13]

DETERMINATION OF $\Delta H_{-1}^{\ddagger}$

The determination of $\Delta H_{-1}^{\ddagger}$, while again straightforward in principle, is less so in practice. Only in a few cases have the recombination rates of $L_nM^{\bullet}$ and R$^{\bullet}$ been determined directly. Two approaches to such measurements are: (1) generating $L_nM^{\bullet} + R^{\bullet}$ by flash photolytic dissociation by $L_nM{-}R$ and measuring the kinetics of recombination in real time. Such experiments have yielded $k_{-1} = ca\, 2 \times 10^9$ M^{-1} s^{-1} at 25°C for the rate constant of recombination of $CH_3^{\bullet}$ + cob(II)alamin, i.e. close to the diffusion-controlled limit.[14] Similarly, the rate constant for the combination of $PhCH_2^{\bullet}$ and Cr^{2+}(aq) has been directly determined to be $(8.5 \pm 0.6) \times 10^7$ M^{-1} s^{-1}.[15] (2) Estimating the rate of combination of $L_nM^{\bullet}$ and R$^{\bullet}$ in competition with another reaction of R$^{\bullet}$ whose rate has been determined independently (sometimes the trapping reaction itself). Thus, in our first application of this method to determining the Co—C bond dissociation energies of R—Co(Saloph)(py) compounds the trap was n-$C_8H_{17}SH$.[1] Since the rate of H atom abstraction by radicals from the latter had been independently measured ($k_7 = ca\, 10^7$ M^{-1} s^{-1} at 25°C),[16,17] measurement of k_{-1}/k_7 permitted k_{-1} to be estimated ($\gtrsim 10^8$ m^{-1} s^{-1}, i.e. also close to the diffusion-controlled limit). In yet another instance lower limits for the rate constants of combination $Co(CN)_5^{3-}$ with alkyl radicals (e.g. $Co(CN)_5^{3-} + C_2H_5^{\bullet} \xrightarrow{k_{-1}} C_2H_5{-}Co(CN)_5^{3-}$ $k_{-1} \gtrsim 10^8$ M^{-1} s^{-1}, i.e. approaching the diffusion-controlled limit) have been estimated from failure to observe competing reactions between the radicals themselves [i.e. $2C_2H_5^{\bullet} \rightarrow C_4H_{10}$ (or $C_2H_6 + C_2H_4$)].[18]

Because in virtually every case where k_{-1} has been estimated by either of these procedures it has turned out to be close to diffusion-controlled, it has generally been assumed to be so when this method of determining bond dissociations energies has been applied. There seems to be no reason to question this assumption. Indeed, the results of studies of the solvent dependence of k_1 and $\Delta H_1^{\ddagger}$, to be described

below, lend strong support to the validity of this assumption. Nevertheless, caution on this point is warranted, particularly when the method is applied to systems where, for steric or other reasons, combination may be accompanied by significant rearrangements, either of R$^\bullet$ or $L_nM^\bullet$ (or both).

ROLE AND CHOICE OF RADICAL TRAPS

The applicability of the kinetic method of determining bond dissociation energies depends upon the identification and availability of suitable radical traps. The following are some of the criteria governing the choice of the latter.

(1) *Rate and selectivity of reaction with* R$^\bullet$ *(or* $L_nM^\bullet$*)*

The trap should react selectively with R$^\bullet$ preferably (although not necessarily) to give distinctive products. Since the recombination reaction generally is close to diffusion-controlled ($k_{-1} \approx 10^8$–10^{10} M^{-1} s^{-1}) the rate constant for the trapping reaction should also be in this range, although adjustment of the concentrations may allow some latitude. In principle, selective trapping of the metal radical, $L_nM^\bullet$, also should be effective but (because R$^\bullet$ typically is much more reactive) examples of such traps are rare. One such case involves ligand substitution which, typically, is rapid for 17-electron metal radicals. An example [where Bz′ = *p*-CH_3O—$C_6H_4CH_2$ and P = (*p*-$CH_3OC_6H_4)_3P$] is:

$$Bz'\text{—}Mn(CO)_4P \xrightarrow{k_1} Bz'^\bullet + {}^\bullet Mn(CO)_4P \quad (12)$$

$${}^\bullet Mn(CO)_4P + CO \xrightarrow{\text{fast}} Mn(CO)_5 + P \quad (13)$$

$$Bz'^\bullet + {}^\bullet Mn(CO)_5 \rightarrow Bz'\text{—}Mn(CO)_5. \quad (14)$$

Overall:

$$Bz'\text{—}Mn(CO)_4P + CO \rightarrow Bz'\text{—}Mn(CO)_5 + P. \quad (15)$$

In this example k_1 (and $\Delta H^\ddagger$) can be deduced from measurements of the kinetics of the substitution reaction [eq. (15)]. Typically, in such cases the recombination of the carbon radical (R$^\bullet$) with the metal radical ($L_nM^\bullet$), in this instance Bz′$^\bullet$ with ${}^\bullet Mn(CO)_5$, is much more probable than reaction with another R$^\bullet$ ($2R^\bullet \rightarrow R_2$) since the steady-state concentration of $L_nM^\bullet$ usually greatly exceeds that of R$^\bullet$ (even when $L_nM^\bullet$ dimerizes to form $(L_nM)_2$, since $D_{M-M} \ll D_{R-R}$).[11,19]

(2) *Traps that react with both* R$^\bullet$ *and* $L_nM^\bullet$

Traps that react with both R$^\bullet$ and $L_nM^\bullet$ usually are less satisfactory than those that react with only one because of the greater difficulty of quantifying competition between the recombination and trapping steps. An example of such a trap is O_2. Its presence often decreases the steady-state concentrations of both $L_nM^\bullet$ and R$^\bullet$ so that the recombination step no longer can be detected and only k_1 can be inferred. Furthermore, since the initial trapping product ($RO_2^\bullet$) is unstable, the final oxidation products usually cannot be characterized definitively as originating from radical trapping. In one case, the homolytic Co—C bond dissociation reaction of neopentylcob(II)alamin, such use of O_2 has yielded limiting values of k_1 (and of $\Delta H^\ddagger$) that agree well with those deduced from more quantitative treatments using eq. (9),[10,12] but this procedure cannot be recommended as of general reliability.

(3) *Intrinsic radical competition reactions*

Sometimes it is unnecessary to add an external radical trap because the intrinsic further reactions of the radical products of eq. (1) and, thus, competition with the recombination step (k_{-1}), are sufficiently well defined to permit the nature of the homolytic bond dissociation step and the value of k_1 to be inferred unequivocally. Such a situation is depicted schematically by eqs (16)–(18) which give rise to the rate law, eq. (19). In such a case, k_1 and k_{-1} can be deduced from kinetic measurements if k_{17} is known independently.

$$L_nM\text{—}R \underset{k_{-1}}{\overset{k_1}{\rightleftharpoons}} L_nM^\bullet + R^\bullet \quad (16)$$

$$R^\bullet \xrightarrow{k_{17}} R'^\bullet \quad (17)$$

$$L_nM^\bullet + R'^\bullet \rightarrow L_nM\text{—}R' \quad (18)$$

$$\frac{d[L_nM\text{—}R']}{dt} = \frac{k_1 k_{17}[L_nM\text{—}R]}{k_{-1}[L_nM^\bullet] + k_{17}}. \quad (19)$$

Examples of possible reactions that could fulfill the role of eq. (17) are:

$${}^\bullet CH_2(CH_2)_3CH{=}CH_2 \rightarrow \overbrace{CH_2(CH_2)_3CH}\text{—}CH_2{}^\bullet \quad (20)$$

$$RC(=O)^\bullet \longrightarrow R^\bullet + CO. \quad (21)$$

(4) *Range of useful traps*

Several factors define and constrain the utility of potential free radical traps for the applications discussed above. Since radical traps typically are fairly reactive species, selectivity always is a matter of concern. Accordingly (as already discussed for O_2), reagents intended to trap R$^\bullet$ also may trap

$L_nM^{\cdot}$ or even react with L_nM—R. Thus, n-$C_8H_{17}SH$, which was found to be a useful trap for organic radicals ($R^{\cdot}$), formed by homolytic dissociation of the Co—C bond of R—Co(Saloph)py,[1] proved ineffective for the corresponding dissociation of R—B_{12} or R—$Co(DH)_2$ (DH_2 = dimethylglyoxime) because it reacts with these. Similarly, the attempted use of Fe^{3+} as a radical trap in a study of the decomposition of benzylcobalamin was complicated[20] by its reaction with the latter. A trap that has turned out to be widely useful for organic radicals in organic solvents (usually without interference from reaction with L_nM—R or $L_nM^{\cdot}$), is 2,2,6,6-tetramethylpiperidineoxy, TEMPO

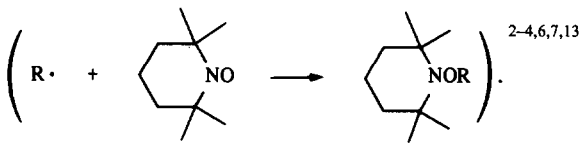

2-4,6,7,13

Satisfactory radical traps in aqueous solution still are scarce. One that has been used successfully is $Co(DH)_2$. This forms stronger bonds with alkyl radicals than most other Co(II) complexes (Table 1), hence can be used to trap radicals generated by homolytic dissociation of other Co—C bonds. This has been exploited to determine the Co—C bond dissociation of several organocobalamin compounds (R—B_{12}),[5,10] i.e.

$$R—B_{12} \rightleftharpoons R^{\cdot} + B_{12r} \quad (22)$$

$$R^{\cdot} + Co(DH)_2 \rightarrow R—Co(DH)_2. \quad (23)$$

Overall:

$$R—B_{12} + Co(DH)_2 \rightarrow R—Co(DH)_2 + B_{12r}. \quad (24)$$

Sometimes, secondary reactions following radical generation by L_nM—R bond dissociation occur in the solvent cage within which the geminate radical pair is formed. In such cases, trapping of the primary radical products by an external trap no longer is possible and cannot be invoked to establish or rule out an initial homolytic dissociation step. The following is believed to exemplify such a case.[21,22]

$$\begin{aligned} &PhCH(CH_3)—Co(DH)_2py \\ &\rightarrow \overline{PhCH(CH_3), Co(DH)_2py} \\ &\rightarrow \overline{PhCH{=}CH_2, HCo(DH)_2py} \\ &\rightarrow PhCH{=}CH_2 + HCo(DH)_2py \\ &\rightarrow [\tfrac{1}{2}H_2 + Co(DH)_2py]. \end{aligned} \quad (25)$$

SOLVENT EFFECTS

The influence of solvent may intrude upon the measurements described above in several ways, amongst them: (1) if bond dissociation is accompanied by significant changes in solvation (e.g. coordination of a solvent molecule to the vacant coordination site generated by dissociation of $R^{\cdot}$) then both the bond dissociation rate and energy are expected to be influenced by solvent. There is not much direct information about this point. Most of the applications of the kinetic method to date have involved low spin octahedral d^6 complexes (e.g. L_5Co^{III}—R or L_5Mn^{I}—R) where the product of M—R bond dissociation is a 17 electron low spin five coordinate d^7 complex. Such complexes generally show little tendency to add a sixth ligand so that solvent influences due to this are likely to be small. Support for this is provided by measurements of the bond dissociation energy of $PhCH(CH_3)$—$Co(DH)_2Py$ which yield identical values in two solvents of considerably different polarity and coordinating ability, toluene and acetone.[22] Bond dissociation processes that are accompanied by substantial changes in charge distribution (unexpected for the dissociation of neutral alkyl radicals) are, of course, expected to exhibit significant medium effects. (2) The influence of solvent on the rates of diffusional separation and encounters. Taking account of the fact that the radical products of homolytic bond dissociation are initially formed as geminate pairs which must diffuse apart before radicals can be detected and captured,

$$L_nM—R \underset{k_{recomb}}{\overset{k_{dissoc}}{\rightleftharpoons}} \overline{L_nM^{\cdot} + R^{\cdot}} \underset{k_{diff}}{\overset{k_{sep}}{\rightleftharpoons}} L_nM^{\cdot} + R^{\cdot}. \quad (26)$$

Accordingly,

$$k_1 = \frac{k_{dissoc}\,k_{sep}}{k_{recomb} + k_{sep}} \quad (27)$$

$$k_{-1} = \frac{k_{diff}\,k_{recomb}}{k_{recomb} + k_{sep}}. \quad (28)$$

For the limiting case of a diffusion controlled reaction with a small intrinsic recombination barrier ($k_{recomb} \gg k_{sep}$; $\Delta H^{\ddagger}_{recomb} \approx 0$),

$$k_1 = \frac{k_{diss}\,k_{sep}}{k_{recomb}};\ \Delta H^{\ddagger}_1 \approx \Delta H^{\ddagger}_{dissoc} + \Delta H^{\ddagger}_{sep} \quad (29)$$

$$k_{-1} = k_{diff};\ \Delta H^{\ddagger}_{-1} \approx \Delta H^{\ddagger}_{diff} (\approx \Delta H^{\ddagger}_{sep}) \quad (30)$$

where k_{diff} is the rate constant for diffusional encounters.

In most of the studies to date $\Delta H^{\ddagger}_{-1}$ has been assumed to be 2–3 kcal mol^{-1}, a value commonly identified with diffusion controlled reactions in water or organic solvents of low viscosity (e.g. toluene or acetone) and approximated by the activation enthalpy of viscous flow.[23] Because of the well recognized dependence of diffusion rates on viscosity,[23]

Table 1. Kinetic data for cobalt–alkyl bond dissociation reactions

No.	R	Chel	B	Solvent	Temp. range (°C)	$\Delta H_1^{\ddagger}$ (kcal mol^{-1})	$\Delta S_1^{\ddagger}$ (cal mol^{-1} K^{-1})	Ref.
1	$CH(CH_3)C_6H_5$	$(DH)_2$	4-CN-pyridine	Acetone	14–36	20.1	−4	22
2	$CH(CH_3)C_6H_5$	$(DH)_2$	Pyridine	Acetone	15–35	21.6	0	22
3	$CH(CH_3)C_6H_5$	$(DH)_2$	4-CH_3-pyridine	Acetone	15–35	21.8	1	22
4	$CH(CH_3)C_6H_5$	$(DH)_2$	4-NH_2-pyridine	Acetone	20–35	23.1	4	22
5	$CH(CH_3)C_6H_5$	$(DH)_2$	PPh_3	Acetone	5–25	19.3	−1	39
6	$CH(CH_3)C_6H_5$	$(DH)_2$	$PEtPh_2$	Acetone	25–46	21.3	2	39
7	$CH(CH_3)C_6H_5$	$(DH)_2$	$P(CH_2CH_2CN)_3$	Acetone	10–25	22.1	4	39
8	$CH(CH_3)C_6H_5$	$(DH)_2$	PBu_3^n	Acetone	15–35	22.8	5	39
9	$CH(CH_3)C_6H_5$	$(DH)_2$	PMe_2Ph	Acetone	10–25	25.9	10	39
10	$CH_2C(CH_3)_3$	Saloph	Pyridine	Pyridine	54–69	20.3	−6	1
11	$CH(CH_3)_2$	Saloph	Pyridine	Pyridine	43–63	21.8	−3	1
12	$CH_2C_6H_5$	Saloph	Pyridine	Pyridine	55–65	23.6	1	1
13	$CH_2CH_2CH_3$	Saloph	Pyridine	Pyridine	77–97	27.1	3	1
14	$C_6H_5CH_2$	$(DH)_2$	$P(c\text{-}C_6H_{11})_3$	Toluene	10–46	24.8	6	7
15	$C_6H_5CH_2$	$(DH)_2$	PPh_3	Toluene	47–75	27.8	6	7
16	$C_6H_5CH_2$	$(DH)_2$	$PEtPh_2$	Toluene	50–82	28.8	10	7
17	$C_6H_5CH_2$	$(DH)_2$	PBu_3^n	Toluene	62–100	30.9	13	7
18	$C_6H_5CH_2$	$(DH)_2$	PMe_2Ph	Toluene	66–100	32.4	15	7
19	$C_6H_5CH_2$	$(DH)_2$	$P(c\text{-}C_6H_{11})_3$	Ethylene glycol	35–64	29.1	17	13
20	$C_6H_5CH_2$	$(DH)_2$	PPh_3	Ethylene glycol	47–75	34.1	22	13
21	$C_6H_5CH_2$	$(DH)_2$	$PEtPh_2$	Ethylene glycol	60–88	34.8	27	13
22	$C_6H_5CH_2$	OEP	PPh_3	Toluene	50–70	25.8	2	7
23	$C_6H_5CH_2$	OEP	$PEtPh_2$	Toluene	55–90	28.1	6	7
24	$C_6H_5CH_2$	OEP	PMe_2Ph	Toluene	55–90	29.1	7	7
25	$C_6H_5CH_2$	OEP	PBu_3^n	Toluene	65–100	31.3	7	7
26	$C_6H_5CH_2$	OEP	$P(c\text{-}C_6H_{11})_3$	Toluene	73–91	31.6	2	7

questions have been raised about the appropriateness of such values of $\Delta H^{\ddagger}_{-1}$ for solvents of higher viscosity such as ethylene glycol.[3,4,13] Indeed, in a recent study that encompassed determinations of $\Delta H^{\dagger}$ for the Co–C bond dissociation of several $C_6H_5CH_2$–Co(Chel)B complexes [Chel = octaethylporphyrin (OEP) or $(DH)_2$; B = a tertiary phosphine ligand], in toluene and ethylene glycol, $\Delta H^{\dagger}$ consistently was found to be higher by *ca* 4–6 kcal in ethylene glycol.[13] This difference presumably reflects the significantly higher contributions of $\Delta H^{\ddagger}_{-1}$ in ethylene glycol to the relation of eq. (2). Thus, the correction for $\Delta H^{\ddagger}_{-1}$ in deducing D_{M-R} from measurements of $\Delta H^{\dagger}$ may be significant, particularly in solvents of high viscosity ($\gtrsim$ 6 kcal mol^{-1} in ethylene glycol).

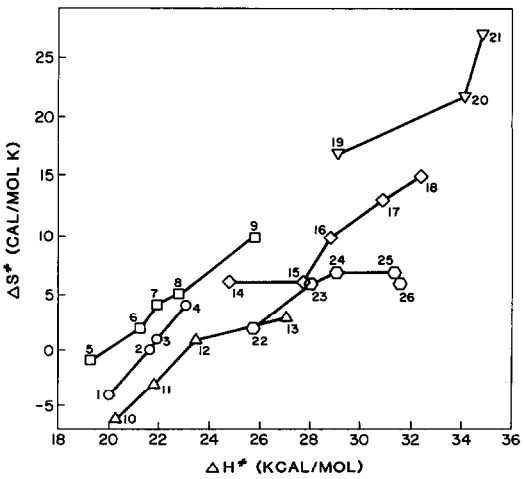

Fig. 1. Relations between entropies and enthalpies of activation for homolytic cobalt–carbon bond dissociation reactions. Numbers refer to entries in Table 1.

MAGNITUDE AND VARIATION OF $\Delta S^{\dagger}$

The bond dissociation energy (or enthalpy), D_{L_nM-R}, is related to the enthalpies of activation, $\Delta H^{\dagger}$ and $\Delta H^{\ddagger}_{-1}$, according to eq. (2). However, the magnitude of the rate constant of bond dissociation, k_1, depends also on the entropy of activation, $\Delta S^{\dagger}$.

Table 1 summarizes the results of measurements of the activation parameters of the Co—C bond dissociation reactions of an extensive array of organocobalt compounds, [R—Co(Chel)B], in which the alkyl group (R), the tetradentate equatorial ligand(s) (Chel) and the *trans*-axial ligand (B) have been systematically varied.

The variations of $\Delta H^{\dagger}$ are seen to encompass the range 19–35 kcal mol^{-1} while the corresponding values of $\Delta S^{\dagger}$ range from -6 to $+27$ cal mol^{-1} K^{-1}. Furthermore, examination of the data in Table 1 reveals that for each series of compounds with a given equatorial ligand (Chel), variation of either R or B results in a systematic partial compensation of the activation parameters such that $\Delta S^{\dagger}$ becomes increasingly positive as $\Delta H^{\dagger}$ increases. The trends are depicted in Fig. 1.

There are well recognized grounds for treating such 'compensation effects' with suspicion since they commonly have an artifactual origin reflecting the interdependence of $\Delta H^{\ddagger}$ and $\Delta S^{\ddagger}$.[24-26] However, careful examination of the trends has led us to conclude that they are indeed genuine and reflect a systematic dependence of structural features of the transition state on $\Delta H^{\dagger}$.[27] The bond dissociation process associated with $\Delta H^{\dagger}$ is substantially endothermic and the activation barrier associated with the reverse (recombination) reaction is small. Thus, the transition state for the dissociation reaction is anticipated to be 'product-like' and to become more so with increasing endothermicity, i.e. with increasing D_{Co-R} and $\Delta H^{\dagger}$ (Hammond postulate).[28] Since the entropy of the overall dissociation process is substantially positive it is expected that this should be accompanied by an increase in the entropy of activation, $\Delta H^{\dagger}$, possibly associated with increasing relaxation of the originally octahedral configuration (**1**) to the more product-like, less rigid, structure **2**. This provides a plausible explanation for the compensating dependence of $\Delta S^{\dagger}$ on $\Delta H^{\dagger}$ that we have identified as a general feature of such transition metal–alkyl bond dissociation reactions.

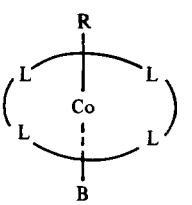

1 L_4 = Chelate

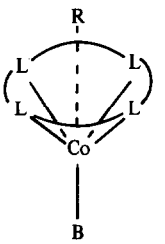

2

In this connection it is of interest that, for the series of complexes [$C_6H_5CH_2$—Co(OEP)PR_3] containing the octaethylporphyrin ligand, which we have previously concluded to be less flexible than other equatorial ligands,[7] $\Delta S^{\dagger}$ does indeed exhibit the smallest variation.

Clearly, entropic as well as enthalpic factors may contribute significantly to variation of the rates of transition metal–alkyl bond dissociation reactions. This is of some relevance in the context of attempts to elucidate and understand the mechanism of bond weakening that is responsible for the enzyme-induced Co—C bond dissociation of 5′-deoxy-

adenosylcobalamin (coenzyme B_{12}) that triggers the latter's biological action.[9]

RELATION TO OTHER METHODS OF DETERMINING TRANSITION METAL–ALKYL BOND DISSOCIATION ENERGIES

The kinetic method described here is only one of several that have been employed for determining transition metal–alkyl bond dissociation energies. Other methods will be discussed only briefly here.

Thermochemical

This is, *in principle*, the most direct approach to the determination of bond dissociation energies. The enthalpy of a process such as eq. (1) may be evaluated from the enthalpies of formation of L_nM—R, R$^\bullet$ and $L_nM^\bullet$. The frequent inaccessibility of the latter to measurement constitutes one of the limitations of this approach. Another constraint relates to the fact that the bond dissociation energy, deduced in this way, is often obtained as a relatively small difference between large numbers; therefore the precision of this method, at this stage at least, is somewhat limited. Reported applications include determinations of R—$Mn(CO)_5$ bond dissociation energies, e.g. *ca* 37 kcal mol^{-1} for CH_3—$Mn(CO)_5$.[29]

Differences in L_nM—R bond dissociation energies, for different R's, can be evaluated more readily and reliably from thermochemical measurements since such differences do not depend on a knowledge of the (often inaccessible) heat of formation of $L_nM^\bullet$. Thus, measurements of the enthalpies of oxidative addition of various X—I compounds (X = I, H, CH_3, $C_6H_5CH_2$, etc.) to *trans*-$IrCl(CO)(PMe_3)_2$ [eq. (31)] do directly yield differences between the Ir—X bond dissociation energies of the X—$IrClI(CO)(PMe_3)_2$ products.[30] In another application, determination of heats of alcoholysis [eq. (32)] has provided accurate values of the *differences* between different Th—R bond dissociation energies (R = CH_3, C_2H_5, C_6H_5, etc.)[31]

trans-$IrCl(CO(PMe_3)_2 + X—I$

$$\rightarrow X—IrClI(CO)(PMe_3)_2 \quad (31)$$

$Cp^*_2Th(R)(OR') + HOR'$

$$\rightarrow Cp^*_2Th(OR')_2 + RH \ (Cp^* = Me_5C_5). \quad (32)$$

Bond dissociation energies or differences between such bond dissociation energies sometimes can be derived from equilibrium measurements. One such application involves measurement of the temperature coefficient of the equilibrium constant (i.e. of ΔH^0) of the reversible reaction (33).[21,22] Combination of this measurement ($\Delta H_{33} = 22$ kcal mol^{-1}) with literature data for ΔH^0_{34} of reaction (34) (-2 kcal mol^{-1}) leads to a simple thermochemical cycle, for determination of $D_{Co—C}$. Thus, $D_{Co—C} = \Delta H^0_{33} + \Delta H^0_{34} = 20$ kcal mol^{-1}.[21,22] Other applications include (a) determination of differences between various Ru—X and Ru—Y bond dissociation energies from measurements of the equilibrium constants of reaction (36)[32] and (b) estimation of differences between various Ir—R bond dissociation energies from measurements of the equilibria (37)[33]

$PhCH(CH_3)—Co(DH)_2py$

$$\rightleftharpoons PhCH{=}CH_2 + Co(DH)_2py—\tfrac{1}{2}H_2 \quad (33)$$

$$PhCH{=}CH_2 + \tfrac{1}{2}H_2 \rightleftharpoons PhĊHCH_3 \quad (34)$$

Overall:

$PhCH(CH_3)—Co(DH)_2py$

$$\rightleftharpoons PhĊHCH_3 + Co(DH)_2py \quad (35)$$

$Cp^*(PMe_3)_2Ru—X + HY$

$$\rightleftharpoons Cp^*(PMe_3)_2Ru—Y + HX \quad (36)$$

$Cp^*(PMe_3)In—R + R'H$

$$\rightleftharpoons Cp^*(PMe_3)Ir—R' + RH. \quad (37)$$

Photochemical measurements

Determination of the threshold wavelength for the photolytic dissociation of a metal–alkyl bond yields an *upper limit* for the corresponding thermal bond dissociation energy. However, the suggestion that the photochemical threshold can be directly identified with the bond dissociation energy does not appear warranted.[14,34] Indeed, our determination of various cobalt–alkyl bond dissociation energies typically yield values (*ca* 20–30 kcal mol^{-1}; see Table 1) considerably lower than the photochemical thresholds for the dissociation of such bonds (*ca* 50 kcal mol^{-1}). Accordingly, this approach would appear to be of limited utility and reliability for the estimation of bond dissociation energies. However, the recently developed technique of photoacoustic calorimetry, illustrated by determination of the Mn—Mn bond dissociation energy of $Mn_2(CO)_{10}$,[35] does represent a *potentially* powerful tool for the determination of transition metal–alkyl bond dissociation energies.

Gas phase methods

The above constitute the approaches most obviously applicable to the determination of metal–

alkyl bond dissociation energies of conventional organometallic compounds, many of which are insufficiently volatile for gas phase manipulation and must be studied in solution. Other methods, notably those based on ion cyclotron resonance spectroscopy and ion beam techniques, have been developed and applied to the estimation of metal–carbon bond energies in relatively simple ionic (and, in some cases, neutral) species in the gas phase, yielding, for example, $D_{Co-CH_3} = 41$ kcal mol^{-1} and $D_{Co^+-CH_3} = 61$ kcal mol^{-1}.[36-38] The overlap of these approaches with the others cited above thus far has been small and few direct comparisons of closely related systems are available.

Each of the approaches to the determination of transition metal–alkyl bond dissociation energies discussed above has advantages and limitations. When properly applied, the kinetic method has the advantages of yielding absolute values of bond dissociation energies and of being capable of high degrees of reliability and accuracy. Application of the various different methods thus far has been largely complementary. This point is emphasized by the fact that in hardly any instances has more than one method proved applicable to determination of a given bond dissociation energy. This is unfortunate since it has limited the possibilities of calibrating the reliability and accuracy of the different methods. As the scope of the application of the various methods expands, more overlap can be expected.

Acknowledgements—Support of this research through grants from the National Institutes of Health, the National Science Foundation and the Petroleum Research Fund administered by the American Chemical Society is gratefully acknowledged.

REFERENCES

1. T. T. Tsou, M. Loots and J. Halpern, *J. Am. Chem. Soc.* 1982, **104**, 623.
2. R. G. Finke, B. L. Smith, B. J. Mayer and A. A. Molinero, *Inorg. Chem.* 1983, **22**, 3677.
3. R. G. Finke and B. P. Hay, *Inorg. Chem.* 1984, **23**, 3041.
4. R. G. Finke and B. P. Hay, *J. Am. Chem. Soc.* 1986, **108**, 4820.
5. J. Halpern, S. H. Kim and T. W. Leung, *J. Am. Chem. Soc.* 1984, **106**, 8317.
6. J. P. Collman, L. McElwee-White, P. J. Brothers and E. Rose, *J. Am. Chem. Soc.* 1986, **108**, 1332.
7. M. K. Geno and J. Halpern, *J. Am. Chem. Soc.* 1987, **109**, 1238.
8. A. Bakac and J. H. Espenson, *J. Am. Chem. Soc.* 1984, **106**, 5197.
9. J. Halpern, *Science* 1985, **227**, 869 and refs cited therein.
10. For example, S. H. Kim, H. L. Chen, N. Feilchenfeld and J. Halpern, *J. Am. Chem. Soc.* 1988, **110**, in press.
11. M. J. Nappa, R. Santi and J. Halpern, *Organometallics*, 1985, **4**, 34.
12. G. N. Schrauzer and J. H. Grate, *J. Am. Chem. Soc.* 1981, **103**, 541.
13. M. K. Geno and J. Halpern, *J. Chem. Soc., Chem. Commun.* 1987, 1052.
14. J. F. Endicott and G. J. Ferraudi, *J. Am. Chem. Soc.* 1977, **99**, 243.
15. R. J. Blau, J. H. Espenson and A. Bakac, *Inorg. Chem.* 1984, **23**, 3526.
16. M. V. Encinad, P. J. Wagner and J. C. Sciano, *J. Am. Chem. Soc.* 1980, **102**, 1357.
17. R. D. Burkhardt, *J. Phys. Chem.* 1969, **73**, 2703.
18. J. Halpern, *Pure Appl. Chem.* 1979, **51**, 2171.
19. M. J. Nappa, R. Santi, S. P. Diefenbach and J. Halpern, *J. Am. Chem. Soc.* 1982, **104**, 619.
20. R. J. Blau and J. H. Espenson, *J. Am. Chem. Soc.* 1985, **107**, 3530.
21. J. Halpern, F. T. T. Ng and G. L. Rempel, *J. Am. Chem. Soc.* 1979, **101**, 7174.
22. F. T. T. Ng, G. L. Rempel and J. Halpern, *J. Am. Chem. Soc.* 1982, **104**, 621.
23. H. H. Schuh and H. Fischer, *Helv. Chim. Acta* 1978, **61**, 2130 and refs therein.
24. J. E. Leffler, *J. Org. Chem.* 1955, **20**, 1202.
25. R. C. Peterson, *J. Org. Chem.* 1964, **29**, 3133.
26. (a) O. Exner, *Prog. Phys. Org. Chem.* 1973, **10**, 411; (b) O. Exner, *Coll. Czech Chem. Comm.* 1975, **40**, 2762.
27. J. Halpern, *Bull. Chem. Soc. Jpn* 1988, **61**, 13.
28. G. S. Hammond, *J. Am. Chem. Soc.* 1955, **77**, 334.
29. J. A. Connor, M. T. Zafarani-Maottar, J. Birkerton, N. I. El Saled, S. Suradi, R. Carson, G. A. Takhin and H. A. Skinner, *Organometallics* 1982, **1**, 1166.
30. G. Yoneda and D. M. Blake, *Inorg. Chem.* 1981, **20**, 67.
31. J. W. Bruno, T. J. Marks and L. R. Morss, *J. Am. Chem. Soc.* 1983, **105**, 6824.
32. H. E. Bryndza, L. K. Fong, R. A. Paciello, W. Tam and J. E. Bercaw, *J. Am. Chem. Soc.* 1987, **109**, 1444.
33. J. M. Buchanan, J. M. Stryker and R. G. Bergman, *J. Am. Chem. Soc.* 1986, **108**, 1537.
34. C. Y. Mok and J. F. Endicott, *J. Am. Chem. Soc.* 1978, **100**, 123.
35. J. L. Goodman, K. S. Peters and V. Vaida, *Organometallics* 1986, **5**, 815.
36. P. B. Armentrout, L. F. Halle and J. L. Beauchamp, *J. Am. Chem. Soc.* 1981, **103**, 6501.
37. P. B. Armentrout and J. L. Beauchamp, *J. Am. Chem. Soc.* 1981, **103**, 784.
38. M. L. Mandlich, L. F. Halle and J. L. Beauchamp, *J. Am. Chem. Soc.* 1984, **106**, 4403.
39. F. T. T. Ng, G. L. Rempel and J. Halpern, *Inorg. Chim. Acta* 1983, **77**, L165.

Polyhedron Vol. 7, No. 16/17, pp. 1491–1498, 1988
Printed in Great Britain

0277–5387/88 $3.00+.00
© 1988 Pergamon Press plc

THE HEAT OF REACTION OF Et—$Mo(CO)_3C_5H_5$ AND H—$Mo(CO)_3C_5H_5$ AND RELATED REACTIONS. THERMOCHEMICAL STUDY OF REDUCTIVE ELIMINATION IN ALKYL MOLYBDENUM COMPLEXES

STEVEN P. NOLAN, RAMON LOPEZ DE LA VEGA, SHAKTI L. MUKERJEE, ALBERTO A. GONZALEZ, KAI ZHANG and CARL D. HOFF*

Department of Chemistry, University of Miami, Coral Gables, FL 33124, U.S.A.

Abstract—The enthalpies of the following reactions have been measured by solution calorimetry:

$$H—Mo(CO)_3C_5H_5 + Et—Mo(CO)_3C_5H_5 \rightarrow Et—C(O)H + \tfrac{1}{2}[Mo(CO)_2C_5H_5]_2 + \tfrac{1}{2}[Mo(CO)_3C_5H_5]_2$$

$$[Mo(CO)_2C_5H_5]_2 + 2PR_3 \rightarrow [Mo(CO)_2(PR_3)C_5H_5]_2$$

$PR_3 = P(OMe)_3$ and $P(C_6H_5)_2Me$

$$R—Mo(CO)_3C_5H_5 + I_2 \rightarrow R—I + I—Mo(CO)_3C_5H_5$$

$R = C_6H_5CH_2$, $H_2C{=}CHCH_2$

$$R—Mo(CO)_3C_5H_5 + PR_3 \rightarrow R—C(O)—Mo(CO)_2(PR_3)C_5H_5$$

$R = C_6H_5CH_2$

$PR_3 = PMe_3$, PMe_2Ph, $PMePh_2$, PPh_3, $P(OMe)_3$.

The results from this work are combined with earlier data to generate estimates for Mo—X bond strengths (X = H, Cl, Br, I, CH_3, C_2H_5, C_3H_5 and $PhCH_2$). The influence of phosphine substitution on the thermochemistry of model catalytic reactions is discussed.

An overall mechanism for transition metal catalysed hydroformylation is described by eqs (1)–(4):

$$Co_2(CO)_8 + H_2 \rightarrow 2H—Co(CO)_4 \quad \text{H}_2 \text{ addition} \quad (1)$$

$$H—Co(CO)_4 + R'(H)C{=}CH_2 \rightarrow R—Co(CO)_4 \quad \text{olefin insertion} \quad (2)$$

$$R—Co(CO)_4 + CO \rightarrow R—C(O)—Co(CO)_4 \quad \text{CO insertion} \quad (3)$$

$$\begin{array}{l} R—C(O)—Co(CO)_4 \\ \quad + \\ H—Co(CO)_4 \end{array} \rightarrow \begin{array}{l} R—C(O)—H \\ \quad + \\ Co_2(CO)_8 \end{array}$$

reductive elimination. (4)

The detailed mechanism of any of these steps is complex, possibly involving coordinatively unsaturated intermediates or radical/radical pairs.[1] Such reactive species probably return to the stable platform of equations described by reactions (1)–(4). Reductive elimination can occur by reaction with either metal hydride as shown in eq. (4), or by direct reaction with H_2, shown in eq. (5):

$$R—C(O)—Co(CO)_4 + H_2 \rightarrow R—C(O)—H + H—Co(CO)_4. \quad (5)$$

Kinetic studies have shown that cleavage by H_2 is an order of magnitude slower than reductive elimination by $HCo(CO)_4$.†[2] In this paper, we consider dinuclear reductive elimination as typified by eq. (4).

Despite the complexity of the actual system, eqs (1)–(4) provide a basis for thermochemical analysis. The enthalpy of hydroformylation of typical olefins is -28 ± 2 kcal mol^{-1} [eq. (6)].[3]

$$(R')(H)C{=}CH_2 + CO + H_2 \rightarrow R—C(O)—H. \quad (6)$$

* Author to whom correspondence should be addressed.

† For a kinetic study of these reactions see ref. 2. Under actual conditions, the relative concentrations of H_2 and $HCo(CO)_4$ must be considered and may lead to more favorable cleavage by dihydrogen depending on pressure and temperature.

Therefore, the sum of the four major steps in catalysed hydroformylation obeys eq. (7), independent of the particular metal complex involved.

$$\Delta H^{\text{hydrogen}}_{\text{activation}} + \Delta H^{\text{olefin}}_{\text{insertion}} + \Delta H^{\text{carbonyl}}_{\text{insertion}} + \Delta H^{\text{reductive}}_{\text{elimination}} = -28\,\text{kcal mol}^{-1}. \quad (7)$$

A long range goal of our work is to determine the partitioning of energy for catalytic processes among the basic steps involved. This type of approach has been discussed by others[4] and a recent theoretical paper deals with the complete cycle for hydrogenations.[5] We are investigating three systems relevant to hydroformylation: R—$Mo(CO)_3C_5H_5$, R—$Mn(CO)_5$ and R—$Co(CO)_4$. We now report new data for the molybdenum system and summarize previous results to gain a view of the thermodynamic reaction profile for an active model system. Additional aspects of the themochemistry of the molbydenum system which may transfer to other systems are also discussed.

EXPERIMENTAL

Calorimetric measurements were made using either a modified Guild isoperibol or a Setaram Calvet solution calorimeter, described in detail elsewhere.[7]

RESULTS

Enthalpy of reaction of $HMo(CO)_3C_5H_5$ *and* R—$Mo(CO)_3C_5H_5$ *and of* $[Mo(CO)_2C_5H_5]_2$ *with* CO, $P(OMe)_3$ *and* PPh_2Me

In order to gain information relevant to reductive elimination, the enthalpy of reaction (8) was investigated.

$$H—Mo(CO)_3C_5H_5 + Et—Mo(CO)_3C_5H_5 \rightarrow Et—C(O)—H + \tfrac{1}{2}[Mo(CO)_3C_5H_5]_2 + \tfrac{1}{2}[Mo(CO)_2C_5H_5]_2. \quad (8)$$

At 50°C, in the presence of excess hydride, this reaction goes cleanly to completion in several hours. The kinetics and mechanism of this reaction have been investigated by Jones, Huggins and Bergman.[6] The enthalpy of reaction (8) in THF solution is -8.6 ± 0.4 kcal mol^{-1}. The aldehyde produced in reaction (8) abstracts its CO from molybdenum generating the triple bonded complex $[Mo(CO)_2C_5H_5]_2$. The enthalpy of reaction of this complex with CO [eq. (9)] is -40.3 ± 0.4 kcal mol^{-1}.[7(a)]

$$[Mo(CO)_2C_5H_5]_2 + 2CO \rightarrow [Mo(CO)_3C_5H_5]_2. \quad (9)$$

Addition of half the enthalpy of reaction (9) to reaction (8) leads to a calculated enthalpy of reaction (10) -28.7 ± 0.6 kcal mol^{-1}.

$$H—Mo(CO)_3C_5H_5 + Et—Mo(CO)_3C_5H_5 + CO \rightarrow Et—C(O)—H + [Mo(CO)_3C_5H_5]_2. \quad (10)$$

The $[Mo(CO)_2C_5H_5]_2$ dimer is an excellent precursor to a number of interesting complexes.[8] We have measured the heat of reaction of this complex with $P(OMe)_3$ and PPh_2Me as shown in eqs (11) and (12):

$$C_5H_5(CO)_2Mo{\equiv}Mo(CO)_2C_5H_5 + 2P(OMe)_3 \rightarrow C_5H_5(CO)_2Mo(P(OMe)_3)—Mo(CO)_2C_5H_5(P(OMe)_3)$$

$$\Delta H = -39.2 \pm 2.0 \text{ kcal mol}^{-1} \quad (11)$$

$$C_5H_5(CO)_2Mo{\equiv}Mo(CO)_2C_5H_5 + 2PPh_2Me \rightarrow C_5H_5(CO)_2Mo(PPh_2Me)—Mo(CO)_2C_5H_5(PPh_2Me)$$

$$\Delta H = -27.4 \pm 0.6 \text{ kcal mol}^{-1}. \quad (12)$$

These data allow calculation of the enthalpies of ligand exchange in the metal–metal bonded dimers.

Subtraction of eq. (10) from eq. (11) leads directly to reaction (13) since all other terms cancel:

$$[C_5H_5(CO)_3Mo]_2 + 2P(OMe)_3 \rightarrow [C_5H_5(CO)_2(P(OMe)_3)]_2 + 2CO. \quad (13)$$

The calculated enthalpy of reaction (13) is 1.1 ± 2.4 kcal mol^{-1}. The enthalpy for the analogous reaction with PPh_2Me is 12.9 ± 1.0 kcal mol^{-1}. The endothermic nature of these substitutions runs counter to the generally exothermic nature of reactions in which phosphines displace carbon monoxide[7] and is presumably due to steric strain in the dimer.

Enthalpy of reaction of $C_6H_5CH_2$—$Mo(CO)_3C_5H_5$ *with phosphines and phosphites*

Thermochemical data for the phosphine promoted carbonyl insertion reaction shown in eq. (14) have been reported.[7(d)]

$$R—Mo(CO)_3C_5H_5 + PR_3 \rightarrow R—C(O)—Mo(CO)_2(PR_3)C_5H_5. \quad (14)$$

Reaction (14) proceeds cleanly for R = Me and Et in THF. Reaction of the benzyl complex, shown in eq. (15), is slow in THF, but proceeds to completion in acetonitrile at 50°C:[8]

Table 1. Enthalpies of reaction (kcal mol^{-1}) of the complexes R—Mo $(CO)_3C_5H_5$ (R = H, Me, $PhCH_2$ and Et) with PR_3

PR_3	H[a]	CH_3[b]	$C_6H_5CH_2$[c]	CH_3CH_2[d]
PMe_3	−5.4(0.4)	−19.7(0.4)	−21.9(0.5)	−22.5(0.4)
$P(OMe)_3$	−4.6(0.2)	−17.2(0.2)	−17.5(0.5)	−19.8(0.4)
PMe_2Ph	−3.8(0.3)	−17.1(0.3)	−19.1(0.4)	−19.7(0.2)
$PMePh_2$	−1.6(0.2)	−14.2(0.3)	−15.8(0.5)	−18.2(0.1)
PPh_3	−1.2(0.8)	[e]	−14.1(1.2)	−15.4(0.5)

[a] In THF, product H—$Mo(CO)_2(PR_3)C_5H_5$.
[b] In THF, product $CH_3C(O)$—$Mo(CO)_2(PR_3)C_5H_5$.
[c] In CH_3CN, product $C_6H_5CH_2C(O)$—$Mo(CO)_2(PR_3)C_5H_5$.
[d] In THF, product $CH_3CH_2C(O)$—$Mo(CO)_2(PR_3)C_5H_5$.
[e] Reaction did not proceed to completion.

$$C_6H_5CH_2Mo(CO)_3C_5H_5+PR_3 \xrightarrow{H_3CCN} C_6H_5CH_2—C(O)—Mo(CO)_2(PR_3)C_5H_5. \quad (15)$$

Data for the enthalpies of reaction of R—Mo $(CO)_3C_5H_5$ complexes (R = H, CH_3, $C_6H_5CH_2$, C_2H_5) are collected in Table 1.

Enthalpy of reaction of R—$Mo(CO)_3C_5H_5$ *with* I_2 (R = $C_6H_5CH_2$ *and* H_2C=$CHCH_2$), *bond strength estimates for the complexes* X—$Mo(CO)_3C_5H_5$

Attempts to directly measure the enthalpy of iodination of H_3C—$Mo(CO)_3C_5H_5$ failed since iodination does not proceed as shown in eq. (16) but produced $H_3C(O)$—I [eq. (17)].

$$H_3C—Mo(CO)_3C_5H_5+I_2 \rightarrow I—Mo(CO)_3C_5H_5+I—CH_3 \quad (16)$$

$$H_3C—Mo(CO)_3C_5H_5+2I_2 \rightarrow I_3Mo(CO)_2C_5H_5+H_3CC(O)—I. \quad (17)$$

The enthalpy of eq. (16) was determined indirectly by subtraction of eq. (19) from eq. (18).

$$NaMo(CO)_3C_5H_5+I_2 \rightarrow I—Mo(CO)_3C_5H_5+NaI$$
$$\Delta H = -32.3\pm1.3 \text{ kcal mol}^{-1} \quad (18)$$

$$NaMo(CO)_3C_5H_5+CH_3I \rightarrow H_3C—Mo(CO)_3C_5H_5+NaI$$
$$\Delta H = -7.7\pm0.3 \text{ kcal mol}^{-1}. \quad (19)$$

This led to an enthalpy of -24.6 ± 1.6 kcal mol^{-1} for the heat of iodination of the molybdenum methyl complex as shown in eq. (16).

The lower rate of carbonyl insertion for the benzyl and allyl molybdenum derivatives suggested that iodination might proceed directly for these alkyl groups. This proved to be the case and the enthalpies of reaction in solution are reported in eqs (20) and (21):

$$C_6H_5CH_2—Mo(CO)_3C_5H_5+I_2 \rightarrow C_6H_5CH_2I+I—Mo(CO)_3C_5H_5$$
$$\Delta H = -28.8\pm1.0 \text{ kcal mol}^{-1} \quad (20)$$

$$H_2C=CHCH_2—Mo(CO)_3C_5H_5+I_2 \rightarrow H_2C=CHCH_2I+I—Mo(CO)_3C_5H_5$$
$$\Delta H = -24.1\pm0.7 \text{ kcal mol}^{-1}. \quad (21)$$

Bond strength estimates on the X—$Mo(CO)_3C_5H_5$ system have been reported.[7(e)] These data are reasonably accurate for relative values and can be placed on an absolute scale using the kinetic estimate of 32.5 kcal mol^{-1} for the Mo—Mo bond in $[Mo(CO)_3C_5H_5]_2$.[10] Using the Mo—I bond strength estimate of 51.8 kcal mol^{-1} leads to a Mo—$CH_2C_6H_5$ bond strength of 32 kcal mol^{-1} and a Mo—CH_2CH=CH_2 bond of 35 kcal mol^{-1}.*

* (a) The benzyl–Mp estimate is based on the following data:

$$PhCH_2—Mp+I_2 \rightarrow PhCH_2—I+I—Mp$$
$$\Delta H_{react.} = -28.8 \text{ kcal mol}^{-1}$$
$$\Delta H_{react.} = D(PhCH_2—Mp)+D(I—I) - D(PhCH_2—I)-D(I—Mp)-28.8$$
$$= D(PhCH_2—Mp)+36.5-45-51.8$$
$$D(PhCH_2—Mp) = 32 \text{ kcal mol}^{-1}.$$

(b) The allyl–Mp estimate is based on the following data:

$$C_3H_5—Mp+I_2 \rightarrow C_3H_5—I+I—Mp$$
$$\Delta H_{react.} = -24.1 \text{ kcal mol}^{-1}$$
$$\Delta H_{react.} = D(C_3H_5—Mp)+D(I—I) - D(C_3H_5—I)-D(I—Mp)-24.1$$
$$= D(C_3H_5—Mp)+36.5-44-51.8$$
$$D(C_3H_5—Mp) = 35 \text{ kcal mol}^{-1}.$$

(c) For bond dissociation energy values see ref. 7(e) and refs therein.

Table 2. Bond strength estimates (kcal mol^{-1}) for the complexes X—Mo $(CO)_3C_5H_5$[a]

X	BDE	X	BDE	X	BDE
H	66	CH_3	47	Mo—Mo	32.5
Cl	72.4	C_2H_5	37	Mo≡Mo	68
Br	60.5	C_3H_5	35		
I	51.8	$C_6H_5CH_2$	32		

[a] Bond strength estimates are taken from refs 7(a) and 7(e), Mo—R estimates (R = C_2H_5, C_3H_5 and $C_6H_5CH_2$) are taken from this work.

Bond strength estimates in this system are collected in Table 2.

DISCUSSION

This report deals primarily with the thermochemical reaction profile for the R—$Mo(CO)_3C_5H_5$ system. It summarizes earlier work on the heats of hydrogenation of metal–metal bonded dimers,[7(f)] carbonyl insertion,[7(d)] some aspects of ligand exchange[7(b,c)] and related reactions.[7] New data, described in the results section, are presented on reductive elimination, the enthalpy of addition of phosphines to the Mo—Mo triple bonded dimer $[Mo(CO)_2C_5H_5]_2$, the enthalpy of the phosphine promoted carbonyl insertion for $C_6H_5CH_2Mo(CO)_3C_5H_5$ and the heat of iodination of two molybdenum alkyl complexes. These data are discussed in the context of earlier studies, and an overview of our work on the R—$Mo(CO)_3C_5H_5$ system is presented.

Hydrogen addition

The enthalpies of addition of hydrogen to the metal–metal bonded dimers shown in eq. (22) were determined previously.[7(f)]

$$[C_5H_5(CO)_3M]_2 + H_2 \rightarrow 2H—M(CO)_3C_5H_5. \quad (22)$$

The reverse of reaction (22) was measured for the chromium complex by differential scanning calorimetry. Values for the other metals were determined indirectly by measuring heats of iodination and by reaction with 1,3-cyclohexadiene. The heats of hydrogenation did not show a uniform trend on descending group VI: Cr = −3.3, Mo = +6.3, W = −1.5 kcal mol^{-1}. It is generally held that metal—X bond strengths increase upon descending a group. A uniform increase in both metal–metal and metal–hydride bond strengths would lead to increasingly favorable enthalpies for reaction (22) on descending group VI (since two moles of hydride are formed from one mole of metal–metal bonded dimer). The hydrogenation of the Cr—Cr dimer is probably anomalous, since it is known to have an extremely weak metal–metal bond.[11] This is probably due to steric repulsion between adjacent ligands.

Increasing steric strain in the molybdenum dimer by ligand substitution should lead to a more favorable enthalpy of hydrogenation. This was found to be true for the $[C_5(CH_3)_5(CO)_3Mo]_2$ complex. The heat of hydrogenation was determined to be 1.8 ± 1.0 kcal mol^{-1} more favorable than for $[C_5H_5(CO)_3Mo]_2$.[7(g)] Incorporation of a phosphine ligand in the coordination sphere of the metal results in a more dramatic influence on the energetics of hydrogenation.

Several attempts were made to measure the enthalpies of hydrogenation of phosphine substituted metal–metal bonded dimers in a manner analogous to those used earlier for the complexes $[M(CO)_3C_5H_5]_2$.[7(f)] Due to side reactions none of these methods were successful.* Data on enthalpies of ligand exchange can be used to calculate the heats of hydrogenation:

$$[Mo(CO)_3C_5H_5]_2 + H_2 \rightarrow 2H—Mo(CO)_3C_5H_5 \quad (23)$$

$$2H—Mo(CO)_3C_5H_5 + 2PR_3 \rightarrow 2H—Mo(CO)_2(PR_3)C_5H_5 + 2CO \quad (24)$$

$$[Mo(CO)_3C_5H_5]_2 + 2PR_3 \rightarrow [Mo(CO)_2(PR_3)C_5H_5]_2 + 2CO \quad (25)$$

$$[Mo(CO)_2(PR_3)]_2 + H_2 \rightarrow 2H—Mo(CO)_2(PR_3)C_5H_5$$

(23) + (24) − (25).

The heat of reaction (23) is +6.3 kcal mol^{-1}. The enthalpy of phosphine substitution in H—Mo

* For example, iodination of $[Mo(CO)_2PR_3C_5H_5]_2$ does produce $I—Mo(CO)_2PR_3C_5H_5$, however $I_3Mo(CO)_2C_5H_5$ is also produced.

Table 3. Calculated enthalpies (kcal mol^{-1}) for CO insertion:

$R—Mo(CO)_2(PR_3)C_5H_5 + CO \rightarrow R—C(O)Mo(CO)_2(PR_3)C_5H_5$

Phosphine	R = CH_3	Acyl stretch[a]	R = C_2H_5	Acyl stretch[a]
PMe_3	14.8	1619	17.5	1618
$PnBu_3$	14.1	1621	16.8	1619
PMe_2Ph	13.5	1621	15.9	1620
$PMePh_2$	12.8	1624	16.5	1623
PPh_3	—	—	16.3	1624
$P(OMe)_3$	12.8	1632	15.2	1630

[a] IR data in cm^{-1}.

$(CO)_3C_5H_5$ [reaction (23)] is exothermic for both $P(OMe)_3$ (−4.6) and PPh_2Me (−1.6) as shown in Table 3. The corresponding substitution in the metal–metal bonded dimer is endothermic for both $P(OMe)_3$ (+1.1) and PPh_2Me (+12.9), as calculated in eq. (13). This leads to an enthalpy of hydrogenation of the phosphine substituted dimers of −4.5 kcal mol^{-1} for $[Mo(CO)_2(P(OMe)_3)C_5H_5]_2$ and −10.1 kcal mol^{-1} for $[Mo(CO)_2(P(C_6H_5)_2Me)C_5H_5]_2$. This shift in the heats of hydrogenation (10.8 kcal mol^{-1} for $P(OMe)_3$ and 16.4 kcal mol^{-1} for PPh_2Me) is probably due to steric strain. It should be noted that for chromium, where steric effects in the dimer are more pronounced, $Cr(CO)_2(P(OMe)_3)C_5H_5$[12] and $Cr(CO)_2(PPh_3)C_5H_5$[13] exist as free radicals which add hydrogen at room temperature and one atmosphere pressure.

Carbonyl insertion

The entrance into the thermochemical study of carbonyl insertion is reaction (26):

$$R—Mo(CO)_3C_5H_5 + PR_3 \rightarrow R—C(O)—Mo(CO)_2(PR_3)C_5H_5. \quad (26)$$

Data on the enthalpy of reaction (26) indicate a dependence on both the alkyl group and phosphine ligand (Table 1). As the alkyl group is varied the reaction becomes more exothermic in the order: $C_2H_5 > C_6H_5CH_2 > CH_3$. This does not parallel the order of kinetic reactivity where the benzyl complex is least reactive followed by methyl then the ethyl complexes.[9] It should be noted that the reactions of the benzyl complex were performed in acetonitrile while those of the other alkyl groups were done in THF. The role of solvation energies in this reaction is under investigation.[14]*

As might be expected, the enthalpy of reaction (26) depends on the phosphine ligand and spans a range of 5 kcal mol^{-1} in the order: $PMe_3 > P(OMe)_3 > PMe_2Ph > PMe_2Ph > PPh_3$ are shown in Table 1. A similar trend is observed for $H—Mo(CO)_3C_5H_5$ (see Table 1) and other ligand substitution reactions[7] of molybdenum. Thermochemically, reaction (26) can be viewed as the sum of reactions (25) and (28):

$$R—Mo(CO)_3C_5H_5 + PR_3 \rightarrow R—Mo(CO)_2(PR_3)C_5H_5 + CO \quad (27)$$

$$R—Mo(CO)_2(PR_3)C_5H_5 + CO \rightarrow R—C(O)—Mo(CO)_2(PR_3)C_5H_5. \quad (28)$$

Reaction (27) involves substitution of phosphine for carbon monoxide to produce the alkyl phosphine complex. It can not be measured directly, but it can be modelled by reaction (29) since carbonyl insertion does not occur for the metal–hydride complex.

$$H—Mo(CO)_3C_5H_5 + PR_3 \rightarrow H—Mo(CO)_2(PR_3)C_5H_5 + CO. \quad (29)$$

Thus, the enthalpy of reaction (28), insertion of carbon monoxide into the molybdenum–alkyl bond, can be approximated by subtraction of the enthalpy of reaction (29) from reaction (26). Data for this, including infrared stretching frequencies of the acyl group, are included in Table 2 for the methyl and ethyl complexes. Insertion of carbon monoxide appears to be thermodynamically more favorable for the more basic phosphines. This is reflected in the shift to lower frequencies of the acyl group stretching frequency as the basicity of the phosphine increases. Greater donation into the π^* orbitals of the acyl group may be responsible, stabilizing it relative to the alkyl. This effect, although small, is important. The entropy of carbonyl inser-

* It appears that reactions in acetonitrile are slightly more exothermic than in THF. Heats of solutions largely cancel, the principle solvent effects arise from different heats of solution of the phosphine.

tion is unfavorable, nearly balancing the enthalpy of reaction.* Minor changes in reaction enthalpies will greatly influence the relative stability of the acyl complex.

It is not possible to measure the enthalpy of carbonyl insertion into unsubstituted alkyl complexes since the acyl products are unstable.[15] Estimation of this value can be made from the data in Table 2. Since the influence of the ancillary ligand is small (2 kcal mol^{-1}) and CO is a poorer sigma donor than even $P(OMe)_3$, a reasonable estimate for insertion of CO into $Et—Mo(CO)_3C_5H_5$ is -13 ± 3 kcal mol^{-1}. It is clear that this reaction does occur, since the ethyl complex reacts smoothly with CO[7(d)] [eq. (30)].

$$Et—Mo(CO)_3C_5H_5+4CO \rightarrow Et—C(O)—C_5H_5+Mo(CO)_6. \quad (30)$$

Reductive elimination

The enthalpy of reaction (10) was determined to be -28.7 ± 0.6 kcal mol^{-1} as previously discussed. Reaction (10) can be viewed as the sum of eqs (31) and (32).

$$Et—Mo(CO)_3C_5H_5+CO \rightarrow Et—C(O)—Mo(CO)_3C_5H_5 \quad (31)$$

$$Et—C(O)—Mo(CO)_3C_5H_5+H—Mo(CO)_3C_5H_5 \rightarrow Et—C(O)—H+[Mo(CO)_3C_5H_5]_2. \quad (32)$$

Accepting a value of -13 ± 3 kcal mol^{-1} for the enthalpy of carbonyl insertion (as discussed above) leads to estimation of the enthalpy of reductive elimination, reaction (32), as -16 kcal mol^{-1}.

Olefin insertion

Several attempts were made to determine the enthalpy of olefin insertion directly. Both, the molybdenum hydride reaction with ethylene and the reverse reaction, beta-elimination, are not clean, prohibiting calorimetric measurement of olefin insertion.

$$H—Mo(CO)_3C_5H_5+C_2H_4 \rightarrow H_3C—CH_2—Mo(CO)_3C_5H_5. \quad (33)$$

In view of these observations and feeling that entropic factors could assist such a reaction, the intermolecular cyclization shown in eq. (34) was attempted but did not yield a clean product:†

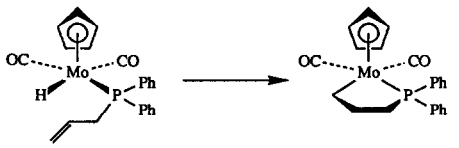

(34)

The enthalpy of hydrogen addition is known to be $+6.3$ kcal mol^{-1} and the sum of reductive elimination and carbonyl insertion is -28.7 kcal mol^{-1}. Using eq. (7), the enthalpy of olefin insertion is calculated to be -5.6 kcal mol^{-1} Combining all experimental errors and making allowance for heats of solution, this estimate is probably accurate to ±3 kcal mol^{-1}.

An independent estimate of the enthalpy of olefin insertion can be obtained using available bond strength data. Thus the heats of iodination of the molybdenum alkyl complexes described earlier led to estimates of the $Mo—CH_3$ (47), $Mo—CH_2CHC{=}CHz$ (35), and $Mo—CH_2C_6H_5$ (32) bonds shown in Table 2. Unfortunately, estimation of the Mo—Et bond strength could not be similarly obtained. Neither direct reaction with I_2, nor reaction of Et—I with $NaMo(CO)_3C_5H_5$ proceed cleanly enough to do calorimetry. Data on the tungsten complexes $R—W(CO)_3C_5H_5$ show a bond strength difference of 12 ± 2 kcal mol^{-1}[14] between the $W—CH_3$ and $W—C_2H_5$. This value is consistent with several other studies on M—X bonds.[16] Since the Mo—R bonds should be generally weaker, it seems reasonable to assume that there would be a smaller difference between the $Mo—CH_3$ and $Mo—C_2H_5$ bonds. We estimate this difference to be 10 ± 2 kcal mol^{-1}. This leads to a value for the olefin insertion reaction of -9 kcal mol^{-1}.‡ This estimate is in reasonable agreement with the value of -5.6 ± 3 obtained as described above.

CONCLUSION

The complete thermochemical profile for reactions (1)–(4) in the $R—Mo(CO)_3C_5H_5$ system is

* A reasonable estimate for this is on the order of 35 e.u. This is due primarily to the loss of translational and rotational entropy of CO(g), and should vary slightly depending on the structures of the complexes. At room temperature it can be expected to contribute on the order of 10 kcal mol^{-1} opposing carbonyl insertion.

† NMR studies in sealed tubes in C_6D_6 appeared to indicate that hydrogenation of the allyl phosphine occurred, however it appeared that several products were formed as well as insoluble precipitates.

‡ Calculated using the relative bond strength estimates in Table 2 and data from ref. 3.

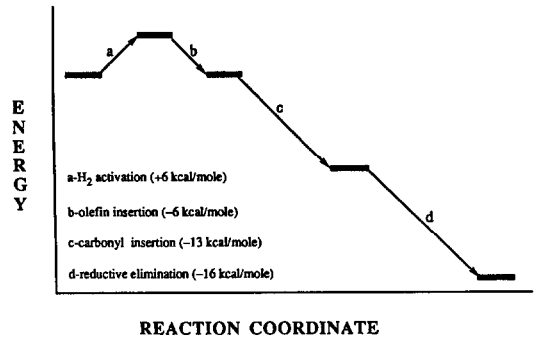

Fig. 1. Partitioning of energy for hydroformylation for X—$Mo(CO)_3C_5H_5$.

presented in Fig. 1. This includes estimated values for the enthalpies of hydrogen addition (+6 kcal mol^{-1}), olefin insertion (−6 kcal mol^{-1}), carbonyl insertion (−13 kcal mol^{-1}) and reductive elimination (−16 kcal mol^{-1}). While there are many kinetic barriers which would have to be overcome in order for the R—$Mo(CO)_3C_5H_5$ system to exhibit catalytic activity, the only thermodynamic barrier is the endothermic nature of addition of hydrogen. From the point of view of thermochemical constraints, a better system might be designed by redistributing the reaction enthalpies to increase the potential equilibrium concentration of hydride versus dimer. One way to do this is to destabilize the dimer by introduction of bulky phosphine ligands. Thermochemical cycles showed that this yielded a net favorable effect on the order of 10–15 kcal mol^{-1}. Phosphine ligands also increase (by as much as 2–4 kcal mol^{-1}) the enthalpy of carbonyl insertion. This must be done at the expense of reductive elimination and (possibly) olefin insertion. Since phosphine ligands can be degraded under active catalytic conditions and/or relaced by carbon monoxide, it seems unlikely that any practical hydroformylation catalyst could be developed for this system. Nevertheless, this study has provided important information with which work in progress on the R—$Mn(CO)_5$ and R—$Co(CO)_4$ systems can be compared.

It seems clear that thermochemical data represent only one aspect in the make-up of an active catalyst. Synthetic and kinetic work remain of prime importance. Despite this, thermochemical data of known systems not only provide fundamental information but may yield insight into designing new systems.

Acknowledgement—Support of this research by the National Science Foundation (grants CHE-8314497 and 86-18753) is gratefully acknowledged.

REFERENCES

1. J. P. Collman, L. S. Hegedus, J. R. Norton and F. G. Finke, *Principles and Applications of Organotransition Metal Chemistry*. University Science Books, Mill Valley, California (1987) and refs therein.
2. C. D. Hoff, F. Ungvary, R. B. King and L. Marko, *J. Am. Chem. Soc.* 1985, **107**, 666.
3. (a) D. R. Stull, E. F. Westrum Jr and G. C. Sinke, *The Chemical Thermodynamics of Organic Compounds*. Wiley, New York (1969); (b) J. D. Cox and G. Pilcher, *Thermochemistry of Organic and Organometallic Compounds*. Academic Press, New York (1970); (c) J. B. Pedley, R. D. Naylor and S. P. Kirby, *Thermochemical Data of Organic Compounds*. Chapman & Hall, London (1986).
4. (a) R. Shinnar and C. A. Feng, *Ind. Eng. Chem. Fundam.* 1985, **24**, 153; (b) This idea was discussed in the earlier literature as well, see for example ref. 3(a), p. 192.
5. N. Koga, C. Daniel, J. Han, X. Y. Fu and K. Morokuma, *J. Am. Chem. Soc.* 1987, **109**, 3455.
6. W. D. Jones, J. M. Huggins and R. G. Bergman, *J. Am. Chem. Soc.* 1981, **103**, 4415.
7. (a) S. P. Nolan, R. Lopez de la Vega and C. D. Hoff, *Inorg. Chem.* 1986, **25**, 4446; (b) S. P. Nolan, R. Lopez de la Vega and C. D. Hoff, *Organometallics* 1986, **5**, 2529; (c) S. P. Nolan, R. Lopez de la Vega, S. L. Mukerjee and C. D. Hoff, *Inorg. Chem.* (submitted); (d) S. P. Nolan, R. Lopez de la Vega, S. L. Mukerjee and C. D. Hoff, *Inorg. Chem.* 1986, **25**, 1160; (e) S. P. Nolan, R. Lopez de la Vega and C. D. Hoff, *J. Organomet. Chem.* 1986, **315**, 187; (f) C. D. Hoff and J. T. Landrum, *J. Organomet. Chem.* 1985, **282**, 215; (g) S. P. Nolan, C. D. Hoff and J. T. Landrum, *J. Organomet. Chem.* 1985, **282**, 365.
8. (a) R. Klinger, W. M. Butler and M. D. Curtis, *J. Am. Chem. Soc.* 1975, **97**, 3535; (b) R. B. King, *Coord. Chem. Rev.* 1976, **20**, 155; R. B. King, M. Z. Iqbal and A. D. King, *J. Organomet. Chem.* 1979, **171**, 53; (c) D. S. Ginley, C. R. Bock and M. S. Wrighton, *Inorg. Chim. Acta.* 1977, **23**, 85; (d) M. D. Curtis and R. J. Klinger, *J. Organomet. Chem.* 1978, **161**, 23; (e) M. H. Chisholm, F. A. Cotton, M. W. Extine and L. A. Rankel, *J. Am. Chem. Soc.* 1978, **100**, 807; (f) W. I. Bailey, M. H. Chisholm, F. A. Cotton, C. A. Murillo and L. A. Rankel, *J. Am. Chem. Soc.* 1978, **100**, 802.
9. P. J. Craig and M. Green, *J. Chem. Soc.* (*A*) 1969, **157**.
10. S. Amer, G. Kramer and A. Poe, *J. Organomet. Chem.* 1975, **220**, 75.
11. R. D. Adams, D. E. Collins and F. A. Cotton, *J. Am. Chem. Soc.* 1978, **96**, 749.
12. L. Y. Goh, M. J. D'Aniello Jr, S. Slater, E. L. Muetterties, I. Tavanaiepour, M. I. Chang, M. F. Fredrich and V. W. Day, *Inorg. Chem.* 1979, **18**, 192.
13. N. A. Cooley, K. A. Watson, S. Fortier and M. C. Baird, *Organometallics* 1986, **5**, 2563.

14. S. P. Nolan, R. Lopez de la Vega, S. L. Mukerjee, A. A. Gonzalez, K. Zhang, S. J. Chou and C. D. Hoff (work in progress).
15. G. Wilkinson, F. G. A. Stone and E. W. Abel, *Comprehensive Organometallic Chemistry*. Pergamon Press, Oxford (1982).
16. H. E. Bryndza, L. K. Fong, R. A. Paciello, W. Tam and J. E. Bercaw, *J. Am. Chem. Soc.* 1987, **109**, 1444.

Polyhedron Vol. 7, No. 16/17, pp. 1499–1516, 1988
Printed in Great Britain

0277–5387/88 $3.00+.00
© 1988 Pergamon Press plc

CAGE EFFECTS IN ORGANOTRANSITION METAL CHEMISTRY: THEIR IMPORTANCE IN THE KINETIC ESTIMATION OF BOND DISSOCIATION ENERGIES IN SOLUTION

THOMAS W. KOENIG,* BENJAMIN P. HAY and RICHARD G. FINKE*

Department of Chemistry, University of Oregon, Eugene, OR 97403, U.S.A.

Abstract—Following a brief review of the literature of radical cage effects in solution, the available evidence for the operation of solvent cage effects in organotransition metal chemistry is summarized. Kinetic determination of M—L bond dissociation energies (BDEs) in solution are examined within this context, emphasizing a comparison of the current gas phase reaction coordinate model vs a model more appropriate for solution work that includes solvent cage effects. The temperature dependence of the cage effect is presented in its proper mathematical form which shows that solution kinetics *cannot* be connected to BDEs without knowledge of the cage efficiency factor (F_c), except in special cases. It is pointed out that the observed activation enthalpy in solution, $\Delta H^{\ddagger}_{obs}$(soln), is a composite containing variable amounts of the difference between the activation enthalpy for the cage combination ($\Delta H^{\ddagger}_{c}$) and that for diffusive separation of the cage pair ($\Delta H^{\ddagger}_{d}$), depending on the cage efficiency factor (F_c). No *constant* correction to $\Delta H^{\ddagger}_{obs}$(soln) can be expected; a better first approximation would be to use the activation enthalpy for viscous flow of the solvent, $\Delta H^{\ddagger}_{\eta}$, although this includes the implicit assumption that $F_c = 1$. The text also attempts to analyse critically the available, relevant literature and to note areas requiring further attention. A short section in which the equations are applied to $Ni(CO)_4$ and $PhCH(CH_3)Co(DMG)_2$(Base) (and thus Ni—CO and Co—C BDEs, respectively) is included. A brief list of major points is also provided in the Summary.

The concept of a solvent caged radical pair was introduced by Franck and Rabinowitch in 1934.[1] The term "cage" refers to a hole in a liquid (solvent) that temporarily traps a pair of reactive molecules causing them to remain as neighbours for a period of time before random motion allows their separation. The probability of recombination of the radical pair is thereby increased relative to a gas phase version of the same reaction. Numerous investigations since 1934 leave little doubt about the existence of cage effects in solution radical chemistry.[2–12] These investigations include, to mention but a few, the classic contribution by Glasstone, Laidler and Eyring on the related topics of viscosity and diffusion,†[2] work on diffusion and cage effects by Noyes[3] and subsequently by Northrup and Hynes,[4] physical–organic studies of caged organic radical pairs by Szwarc,[5] Lamb and Pacifici,[6] Hammond,[7] Bartlett,[8] Singer,[9a] Pryor,§[9b] and a model of the cage contributed by one of us.[10] The phenomena of magnetic field effects on chemical reactions and CIDNP further attest to the importance of caged radical pairs‖[,11] as do recent results from organic chemistry.¶[12] A detailed review of the physical chemistry of diffusion and cage effects has also recently become available.[13]

* Authors to whom correspondence should be addressed.

† The treatments of viscosity and diffusion in ref. 2a, Chap. 9, are excellent background material for anyone interested in understanding solvent cage effects, although the latter are not discussed *per se*.

§ For one of many papers where the viscosity dependence of an organic bond homolysis rate constant is interpreted in terms of a cage effect, see ref. 9b.

‖ A computer literature search of "radical cage effects" since 1967 revealed 59 references, most of them in this area. A few lead references on magnetic field effects [11a,b] and CIDNP[11c,d,e] are noted.

¶ A 1980 review on the "Mechanism of the Thermal and Photochemical Decomposition of Azoalkanes" is available.[12c] A perusal of the data therein shows that $\Delta H^{\ddagger}_{measured}$(soln) and $\Delta S^{\ddagger}_{measured}$(soln) are often (but not always) greater than their gas phase values, for example: Table 1, compounds **3**, **9**; Table VIII, compounds **239**, **229** (p. 115).

Prototypical methods for generating a caged pair of organic radicals include the thermolysis or photolysis of azo (R—N=N—R′), peroxo (ROOR′), perester (RCO_3R') or hyponitrite (RO—N=N—OR′) precursors.[5-10] These studies from the 1960s and 1970s were largely focused on the solvent viscosity dependence of the cage effect and the mechanistic question of concerted versus non-concerted bond homolyses. The results of this period were instructive in showing that the sometimes reversible homolyses of peroxy and azo compounds involve some form of a cage effect *in all cases*. Such cage effects were neglected in some of the earlier literature.[10c] These studies also show that the viscosity dependence of the cage effect is not simple.*,†,§,[9b,10b,16-19]

A term that will become important in the attempt to determine M—L BDEs from solution thermolysis studies is the enthalpic difference for diffusive cage escape vs cage (re)combination, $\Delta(\Delta H^{\ddagger})_{d-c}$. Unfortunately, no direct measurement of $\Delta(\Delta H^{\ddagger})_{d-c}$ presently exists for a M—L homolysis and only a couple of literature studies focus upon this term. The temperature dependence of cage effects and the $\Delta(\Delta H^{\ddagger})_{d-c}$ term has been examined in the classic study of CF_3—N=N—CF_3 photolysis by Szwarc.[5b] In 14 solvents of increasing viscosity (2.3–8.9 mpoise) Szwarc found that $\Delta(\Delta H^{\ddagger})_{d-c}$ was 2.6 ± 0.1 kcal mol^{-1}, i.e. $\Delta(\Delta H^{\ddagger})_{d-c}$ *was constant* and *did not follow* the activation enthalpy for viscous flow, $\Delta H_{\eta}^{\ddagger}$, which varied from 1.4 to 5.6 kcal mol^{-1}.[5b] Similarly, Bartlett[8b] found that the cage products from the thermal decomposition of *t*-butylperoxy α-phenylisobutyrate, *t*-$BuO_2C(O)C(CH_3)_2Ph$, in 15 solvents of viscosity from 4.9 to 52.3 mpoise, gave an essentially constant $\Delta(\Delta H^{\ddagger})_{d-c}$ ($= \Delta(E_a)_{d-c}$)[8b] that varied between the close limits of $2.2(\pm 0.3)$ to $3.3(\pm 0.4)$ kcal mol^{-1}. These results were surprising at the time, and as noted by Koenig,[10b] little interpretation of them has appeared. One might infer that the $\Delta(\Delta H^{\ddagger})_{d-c}$ for the competition between diffusive cage escape and cage recombination should be essentially constant in general, even in higher viscosity solvents. However, in the Szwarc and Bartlett examples, both cage combination and diffusive separation of the cage pair require some type of cage escape, the former of N_2 or CO_2 and the latter of one partner of the reactive radical pair. In this sense, these studies are *atypical* of the types of radical pairs produced by a M—L homolysis, where a M$^{\bullet}$ $^{\bullet}$L caged pair, *without* an intervening N_2, CO_2, or other molecule, is produced.

In the *t*-butyl perbenzoate–hyponitrite (*t*-BuO—N_2—O_2CPh) case, the intervening molecule (N_2) was shown to reduce cage combination by a factor of 0.5 at 27°C in hexane relative to the peroxide (*t*-BuO—O_2CPh);[10c] unfortunately, temperature dependence and thus $\Delta(\Delta H^{\ddagger})_{d-c}$ data are not available in this case. Further evidence for "tighter" caged pairs when intervening molecules are absent comes from the recent studies of Doering.[12b] An additional point worth noting is that the phenomenological rate constant for cage combination is *not* solvent-independent and is *not* a constant[10d,e] as is often assumed.

The crucial point, then, is that the inference of a universal constant for $\Delta(\Delta H^{\ddagger})_{d-c}$ (for example, of 2–3 kcal mol^{-1} based on the Bartlett and Szwarc results) is not justified, as least at present, for systems lacking intervening molecules (such as M—L bond thermolyses). It also should be noted that the Bartlett–Szwarc observations imply significant variations in $\Delta(\Delta S^{\ddagger})_{d-c}$ (as will be discussed later).

A number of examples of cage effects in organotransition metal chemistry are now available,‖,[20,21] although in most cases to date the

---

* Noyes first showed[3a,c] that, strictly speaking, rate constants describing processes in the cage (i.e. those at short times) are not conventional ones in that a probability treatment shows these rate "constants" are functions of time. Restated, at short times under $\simeq$ 10 ps and thus at short separation distances, the solute "remembers" its last direction and velocity.[14] As a first approximation (one that improves at longer times) these effects are generally ignored and conventional (phenomenological) rate constants and expressions are often used.[3c,5-12,10b] Primary recombination (from primary radical pairs) and secondary recombination (from solvent-separated, secondary radical pairs) have been postulated.[3c] Their experimental inseparability[7] and Occam's razor lead us to follow Koenig's phenomenological treatment (using conventional rate constants, see below) of a single type of caged pair.[10b]

† In spite of the literature cited above which documents the fundamental importance and kinetic consequences of radical cage chemistry, it is of interest to note that this topic is typically absent from: undergraduate organic texts, undergraduate inorganic texts[16] and most advanced organic[17] and inorganic[18] texts. It perhaps comes as no surprise, therefore, that there is little discussion of cage chemistry in texts on organotransition metal chemistry[19] even though several important examples of cage effects are available from the literature in this area.[19a,b,20,21]

§ The comparisons of entropies from the phenomenological (Scheme 3) and spherical source[10b] models will be the subject of a separate paper.

‖ The enthalpic, as opposed to entropic, aspects of diffusion[2] and the limitations of diffusion through a continuum in properly describing diffusion out of a cage[3,4,10,13-15] (a "hole" in the continuum) are useful additions to the valuable discussion of ref. 21c.

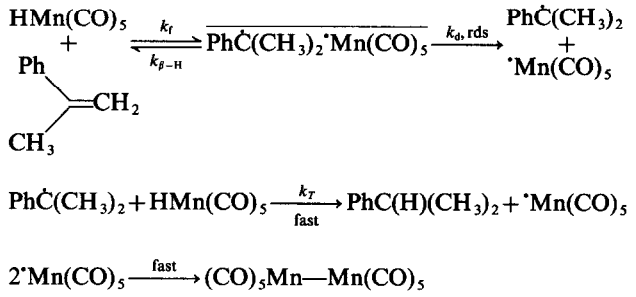

Scheme 1.

radical pair is produced by a bimolecular reaction rather than by a unimolecular M—L bond homolysis. Two exemplary cases are from the work of Halpern[20a] (Scheme 1) and Jacobsen and Bergman[21] (Scheme 2). In both of these examples, an organometallic caged pair is produced by a bimolecular reaction (with a rate constant of formation, k_f) of an olefinic material and a transition metal hydride. Cage return ($k_{\beta-H}$) in these cases is the disproportionation ($\beta-H^{\cdot}$ atom back-transfer) shown in each scheme. In the Jacobsen and Bergman example (Scheme 2) a second cage reaction occurs, radical combination to form a Mo—C bond (k_c). The reverse of k_c, shown by the dotted arrow of Scheme 2, was not studied but would be a unimolecular entry into the same caged pair, at least formally, as that given by the k_f process. Evidence was provided in both of these studies that the cage reactions (k_f, k_c) were competitive with diffusive cage escape to produce free radicals (k_d, Schemes 1 and 2).

Additional aspects of the Jacobsen and Bergman example,[21] Scheme 2, are especially illustrative. They found that cage combination to yield **A** (k_c) and diffusive cage escape (k_d) are comparable (but not identical)[21b] in low viscosity (η) solvents such as benzene or *o*-xylene (η = 0.65–0.81 cp at 20°C).[21b] However, in the viscous medium of heavy mineral oil (Nujol) (η > 200 cp at 20°C)[21b] the ratio of combination to diffusive escape became $\simeq$ 16 to 1. Furthermore, $k_{\beta-H}$ was shown to be at least 10^2 greater then k_d and k_c. The cage effect in Scheme 2 includes both the $k_{\beta-H}$ process and the k_c process, and the cage efficiency is *thus greater than 99% in this case*. If one omits $k_{\beta-H}$ and looks only at k_c vs k_d, the case of greater relevance to a M—L homolysis, the cage efficiency is still *ca* 50% in solvents such as benzene or *o*-xylene since these two rate

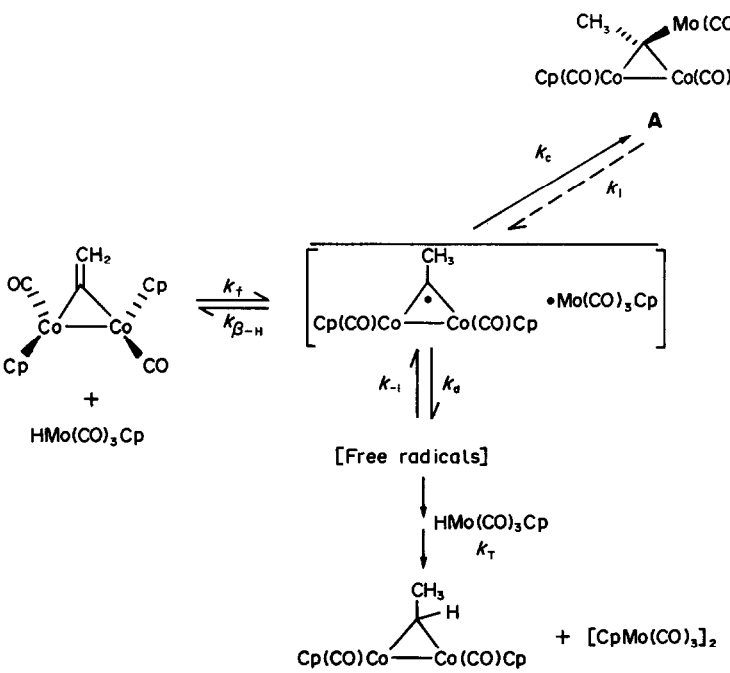

Scheme 2.

constants are roughly comparable. *Clearly, and as noted by Bergman,*[21] *sizable cage effects can exist for such organotransition metal systems, even in low viscosity solvents.* We note in passing that the origins of the high $k_{\beta-H}/k_d$ ratio are not well understood in this example[21c] nor in general.[10,14]

An important area of current organotransition metal chemistry is the estimation of M—L BDEs. This area is receiving increasing attention, as this issue of *Polyhedron* attests, with the application of calorimetry, photoacoustic calorimetry, mass spectrometry and other methods,[22,23] each of which has its own strengths and limitations. Such BDE data are crucial to the further development of organotransition metal chemistry, as they allow thermochemical predictions of the feasibility of postulated new reactions or of proposed mechanistic steps. Eventually, BDEs and other thermochemical data lead to tables of extremely valuable heats of formation, ΔH_f^0,[23d] the type of data with the broadest applicability for thermochemical predictions.

The estimation of M—L BDEs from kinetic data of M—L homolyses in the *liquid phase* has recently been applied to a number of M—L systems, especially Co—C bonds.*,†,§[24-26] Unfortunately, and as discussed in the next section, the studies to date have employed a *gas phase* reaction coordinate model.[24] The precedents above make it clear that the cage effect must be carefully considered in these reactions although, to date, cage effects have been almost completely ignored in M—L thermolyses and BDE estimates based on solution kinetic studies.[24-26]

The connection between solution phase kinetics of M—L bond cleavage and BDE involves two clearly distinct problems. The first problem is to obtain the activation parameters for the homolysis *elementary* step from the temperature dependence of the observable rate constants. We have recently provided[10a] the equations that solve this problem, equations that were previously unavailable in the cage literature (and are also provided herein as eqs (5) and (6), *vide infra*). They reveal that the observed (apparent) activation parameters are composites that include components due to the solvent cage effect. After the proper corrections to the observed activation parameters are made, one obtains the desired activation parameters for the dissociative elementary step, $\Delta H_1^{\ddagger}$(soln), be it a M—L homolysis or heterolysis. The gas phase model, mentioned above, does not recognize the cage effect, a failure that is one of the fundamental causes for considerable confusion.‖

* A reaction coordinate diagram identical to Fig. 1 herein can be found as Fig. 1 of ref. 24i.

† Following an earlier study,[25b] a study claiming to have measured the Co—C BDE on Coenzyme B_{12} in pH = 4.3 H_2O appeared.[24h] It was subsequently shown[25c] that the thermal decomposition of Coenzyme B_{12} in pH = 4.3 H_2O consists of significant amounts of heterolysis as opposed to a pure homolysis reaction (77 and 45% heterolysis at 85 and 110°C, respectively, at pH = 4.3).[25c] When the work was repeated in pH = 7 H_2O and other steps taken to eliminate the heterolysis component, a value of $\Delta H^{\ddagger}_{(\text{homolysis, base-on})}$ of 33 ± 2 kcal mol^{-1} (vs the previous heterolysis plus homolysis value of 28.6 ± 1 kcal mol^{-1})[24k] was obtained.[25c] Recently a second paper has appeared[24f] that uncovers an important 4–6 kcal mol^{-1} difference in $\Delta\Delta H^{\ddagger}_{\text{measured}}$ (glycol vs toluene) for a series of Co—R B_{12} model complexes. This paper, combined with our own work,[25c] establishes that of the $\Delta\Delta H^{\ddagger} = 5.9(\pm 1.3)$ kcal mol^{-1} discrepancy in glycol vs pH = 4.3 H_2O [$34.5(\pm 0.8) - 28.6(\pm 1) = 5.9(\pm 1.3)$], $4.4(\pm 2.2)$ kcal mol^{-1} is due to heterolysis of the Co—C bond in B_{12} [$33(\pm 2) - 28.6(\pm 1) = 4.4(\pm 2.2)$]. The remaining $1.5(\pm 2.6)$ kcal mol^{-1} [$5.9(\pm 1.3) - 4.4(\pm 2.2) = 1.5(\pm 2.6)$] is probably due to the glycol vs H_2O viscosity and the $\Delta\Delta H_{\eta}^{\ddagger}$ difference in the 85–110°C temperature range, $\Delta\Delta H_{\eta}^{\ddagger} = (4.4 - 2.1) = 2.3$ kcal mol^{-1}, as noted by Halpern and as we have discussed elsewhere.[25e]

§ A sizeable $\Delta G^{\ddagger} = 6.5$ kcal mol^{-1} for the recombination of "Co(II)(dmgBF$_2$)$_2$" [possibly the 19-electron $(H_2O)_2$Co(II)(dmgBF$_2$)$_2$] with PhCH$_2^{\cdot}$ in 25°C H_2O is cited in ref. 26d from which a $\Delta H^{\ddagger} \simeq 5(\pm 2)$ for recombination is estimated.

‖ Even though a reaction coordinate identical to Fig. 1 was published,[24a] it seems more likely, given earlier work[20a,24j] and brief but specific mention of cage effects therein,[24b,c,j] that something more along the lines of Fig. 2 was actually meant. However, an ambiguous section from a 1982 paper[24b] that appears to have caused considerable confusion is repeated below.

"Since recombination of Co(II) complexes with organic radicals has been demonstrated to be diffusion controlled[1,18] and hence expected to exhibit an activation enthalpy of *ca* 2 kcal mol^{-1}, this interpretation predicts that $\Delta H^{\ddagger}_{-1}$ should consistently be about 2 kcal mol^{-1} greater than $D_{\text{Co—R}}$."

Note that a "universal correction factor of 2 kcal mol^{-1}" was initially (and incorrectly) widely used regardless of the solvent system.[24b,c,d,h,25a,26] Further evidence for the confusion over the proper connection between $\Delta H^{\ddagger}_{\text{obs}}$ (soln) measurements and M—L BDEs is provided by two M—C BDE estimates obtained from the rates of racemization of M—C(chiral) compounds.[26b,c] The 2 kcal mol^{-1} amount is subtracted from $\Delta H^{\ddagger}_{\text{racemization}}$ measurements in spite of the fact that the racemization method potentially measures $\Delta H_1^{\ddagger}$(soln) directly, depending upon what fraction of racemization results from a cage recombination. The authors have implicitly assumed $F_c = 1$ and that no racemization occurs in the cage [i.e. that their observed racemization rates are equal to those for the disappearance of M—L in the presence of a trap (k_{obs}, Scheme 3)].

The second problem is the connection between the observed (composite) activation enthalpy (in solution) and the M—L BDE (defined in the gas phase). This problem is one that should be viewed—and kept—as distinct from the first as possible. One of the major purposes of the present paper is to carefully treat this second problem in the light of our recent[10a] solution to the first. Overall, it is hoped that the present contribution can serve as a stepping-stone for improved M—L BDE estimates based on solution kinetics and for the required additional studies of cage effects in organotransition metal chemistry.

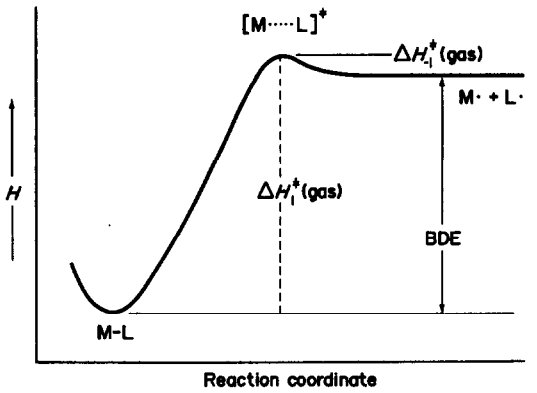

Fig. 1. Schematic gas phase reaction enthalpy vs coordinate diagram illustrating that BDE $\equiv \Delta H_1^{\ddagger}(\text{gas}) - \Delta H_{-1}^{\ddagger}(\text{gas})$. This reaction coordinate diagram is also the (oversimplified) one that has previously been used for solution phase M—L homolyses.[24]

THE KINETIC DETERMINATION OF M—L BOND DISSOCIATION ENERGIES

The gas phase model

As with any other chemical bond, a M—L BDE is defined as the enthalpy change which accompanies the dissociation of a M—L bond *in the gas phase at* 298 K. A typical enthalpy vs reaction coordinate diagram for a gas phase bond homolysis is given in Fig. 1. The BDE is related to the activation enthalpies for the forward and reverse reactions by eq. (1). In most cases, $\Delta H_{-1}^{\ddagger}(\text{gas})$ for the recombination of two reactive radicals is expected, *or assumed*, to be small.[27,28]

$$\text{BDE} \equiv \Delta H_{298}^{0} = \Delta H_1^{\ddagger}(\text{gas}) - \Delta H_{-1}^{\ddagger}(\text{gas}). \quad (1)$$

Historically, this method has worked well for many smaller organics, both because they are reasonably volatile and because either the critical assumption $\Delta H_{-1}^{\ddagger}(\text{gas}) \simeq 0$ has been justified*,[27-29] or introduces a relatively small per cent error for a *ca* 90 kcal mol^{-1} C—C bond. If it can be assumed that M$^{\cdot}$ and L$^{\cdot}$ recombinations also exhibit $\Delta H_{-1}^{\ddagger}$(gas) values of zero, then organotransition metal M—L BDEs can be obtained similarly via gas phase kinetic measurements of $\Delta H_1^{\ddagger}$(gas) alone (subject, however, to some of the problems discussed next).

Although precise gas phase values for *individual* M—L bonds in 18-*electron complexes* (the type most useful to practicing organotransition metal chemists) are presently limited,[30] efforts in this area are clearly increasing.[23a,30] Unfortunately, a large number of transition metal species are neither volatile nor otherwise rendered gaseous while still intact (e.g. even by FAB or laser desorption methods). Hence, gas phase BDE data for many organotransition metal systems are unattainable, at least presently. Furthermore, a major disadvantage of the otherwise powerful gas phase methods is that the structures and spin states of the products generally must be inferred.[31] However, in many cases the rates of unimolecular M—L dissociations can be measured in solution and, in general, the products and their spin states can be fully determined. Therefore, solution kinetic methods of estimating M—L BDEs are valuable, as is a full understanding of the problems and assumptions involved with this method.

The proper liquid phase model—one that includes the cage

Scheme 3 illustrates the M—L dissociation process in solution, including the phenomenological version of our cage effect model.[10] This scheme is central to everything that follows. It shows the particular case for M—L homolysis, but heterolytic ligand dissociations (e.g. an 18-electron M—L complex forming a 16-electron M + L) can be included

$$\text{M—L} \underset{k_c}{\overset{k_1(\text{soln})}{\rightleftharpoons}} \underset{\text{Cage pair}}{[\overline{\text{M}^{\cdot}\text{L}^{\cdot}}]} \underset{k_{-1}(\text{soln})}{\overset{k_d}{\rightleftharpoons}} \underset{\text{Free radicals}}{[\text{M}^{\cdot}]+[\text{L}^{\cdot}]} \xrightarrow[k_T]{T} \text{Trapped Product}$$

Scheme 3.

* For examples where $\Delta H_{-1}^{\ddagger}(\text{gas})$ or $\Delta H_{r,\text{obs}}^{\ddagger}(\text{soln})$ is not zero, see ref. 29.

as well.* Scheme 3 is restricted, for the purposes of this discussion,† to the case where the only possible cage reaction is recombination (k_c, fs–ns timescale); in general, other cage reactions such as disproportionation ($k_{\beta-H}$, Schemes 1, 2 and 4) are also possible. It is crucial for what follows to understand the elementary step and rate constant notation used in Scheme 3 and hereafter; a footnote§ is provided for this purpose.

The cage recombination process (k_c, Scheme 3) is conceptually distinct both from free radical recombination in solution [k_{-1}(soln), Scheme 3] and from the recombination process in the gas phase [k_{-1}(gas)]. The rate constant for diffusive cage escape, k_d, reflects‖ the effective probability per unit time that the cage pair is converted to trappable free radicals. It is also quite distinct from k_{-1}(soln) even though they both involve diffusion, since k_d denotes diffusion *out* of the cage while k_{-1}(soln) is the rate constant for diffusion *into* the cage.

The ultimate fate of the starting material (M—L), as restricted in Scheme 3,¶ is cage escape followed by reaction of *freely diffusing radicals* (ns–ms timescale) with a trapping agent (T). The trapping agent may be a hydrogen donor, such as a thiol or dihydroanthracene, or an added stable radical such as 2,2-diphenylpicrylhydrazyl (DPPH), a nitroxide or molecular oxygen.[5–9,24,25] Such trapping agents have the property of a high rate constant (k_T) for reaction with either M$^\cdot$ or L$^\cdot$. With modest ($\sim$ 0.1 M) concentrations of T, added in excess compared to M—L, all of the starting material will result in trapped product formation.**

Solution phase BDEs

It is useful to begin our discussion of solution phase BDEs by examination of the heat of reaction [ΔH^0_R(soln)] for an M—L dissociation (either homolysis or heterolysis) in the absence of a reactive trapping agent. In the gas phase, such heats of reaction are identical to the bond dissociation energy for the dissociative process, BDE $\equiv \Delta H^0_R$(gas). The

* It should be noted that bond homolysis and bond heterolysis are energetically comparable in many organotransition metal systems. Benzylmanganesepentacarbonyl furnishes an interesting example.[23a,36] The flash vacuum pyrolysis of this compound shows that bibenzyl, a product typically associated with free radical dimerization, is actually produced from an M—L heterolysis. A metastable η^5-benzylmanganesetricarbonyl intermediate[36] is the thermolytic precursor to bibenzyl; no benzyl radical dimerization is involved. The activation enthalpy (gas phase) for the heterolytic formation of the η^5 species is 24 kcal mol^{-1} whereas the BDE (gas phase) for the C—Mn bond homolysis in this compound has been estimated to be 32 $\pm$ 5 kcal mol^{-1}.[23a] As Schemes 1 and 2 show, molecule induced homolyses are common with metal hydrides. The important connection here is that a coordinatively unsaturated intermediate might react with a metal hydride, giving radical intermediates and cage chemistry. The important bond dissociation process, in such a case, would be heterolytic ligand detachment, and not homolyses, even though radicals and radical products are formed, leading to erroneous solution phase BDE estimates.

† The standard overhead bar notation is used to denote the cage pair, $\overline{M^\cdot L^\cdot}$. Following production, the chemical reactions of cage pairs can include recombination (k_c), disproportionation, isomerizations or fragmentations (β-scissions). In order to be cage (chemical) reactions, the processes must be kinetically competitive with the non-chemical reaction that is unique to the cage pair, the diffusive separation to yield free radicals (k_d). Scheme 3 is restricted to a case where the only chemical process is k_c, though this restriction is not generally necessary.

§ The notation for the elementary steps and their rate constants in Scheme 3 and thereafter requires explanation. The somewhat unusual use of k_{-1}(soln) (as other than the inverse of k_1) *is deliberate*. The rate constant k_{-1}(soln) indicates the elementary step for *free* radical recombination to form the cage pair. The use of k_1(soln) and k_{-1}(soln) as in Scheme 3 maximizes the correspondence and thereby facilitates a comparison, of Scheme 3 (and its implications) to previously proposed models[24] (Fig. 1) that ignore the cage. In particular, the equations for the composites $\Delta H^\ddagger_{obs}$(soln) and $\Delta S^\ddagger_{obs}$(soln) derived from Scheme 3 can be simplified, with certain assumptions, to what others have proposed.[24] In this way we will be able to make explicit what assumptions others have made.[24]

To summarize the notation used herein, the composite consisting of homolysis followed by cage escape will be indicated by k_{obs}, $\Delta H^\ddagger_{obs}$(soln) and $\Delta S^\ddagger_{obs}$(soln). The reverse reaction, the recombination of free radicals, will be a composite $k_{r,obs}$(soln), $\Delta H^\ddagger_{r,obs}$(soln), $\Delta S^\ddagger_{r,obs}$(soln). The elementary steps in Scheme 3 of homolysis [k_1(soln), $\Delta H^\ddagger_1$(soln), $\Delta S^\ddagger_1$(soln)], cage combination (k_c, $\Delta H^\ddagger_c$, $\Delta S^\ddagger_c$), diffusive cage escape (k_d, $\Delta H^\ddagger_d$, $\Delta S^\ddagger_d$) and cage reentry [k_{-1}(soln), $\Delta H^\ddagger_{-1}$(soln), $\Delta S^\ddagger_{-1}$(soln)], have the same meanings as they had in Schemes 1 and 2. The gas phase homolysis process [k_1(gas), $\Delta H^\ddagger_1$(gas), $\Delta S^\ddagger_1$(gas)] and the gas phase radical recombination process [k_{-1}(gas); $\Delta H^\ddagger_{-1}$(gas), $\Delta S^\ddagger_{-1}$(gas)] will be distinguished as indicated. Obviously, the k_c and k_d processes have no counterparts in the gas phase and therefore need no "(soln)" designation.

‖ See footnote * on p. 1500.

¶ See footnote † on this page.

** In practice it is important to make sure this condition holds. Ionic side reactions that occur in competition with homolysis have already contributed to the confusion in the Coenzyme B_{12} case in an unnecessary way.[24h]

gas phase usually allows one to consider the overall M—L cleavage reaction to be a single, elementary process. One of the main uncertainties in ΔH^0_R(gas) determinations is the value of $\Delta H^{\ddagger}_{-1}$(gas) but it is generally eliminated with the (sometimes incorrect) assumption that it is small, $\Delta H^{\ddagger}_{-1}$(gas) < 2 kcal mol^{-1}.

As Scheme 3 shows, the overall reaction in solution is no longer an elementary step. Figure 2 shows an enthalpy diagram that corresponds to one possible Scheme 3 reaction (without the trapping agent, T), chosen initially because it shows the slightest possible modification of the gas phase picture. Figure 2 differs from Fig. 1 only in the addition of an enthalpy barrier for the diffusive separation of the cage pair. The overall reaction is from M—L to *fully separated free radicals*. By inspection of Fig. 2, one can see that eq. (2) gives the heat of reaction in solution, ΔH^0_R(soln).

$$\Delta H^0_R(\text{soln}) = \Delta H^{\ddagger}_1(\text{soln}) + [\Delta H^{\ddagger}_d - \Delta H^{\ddagger}_{-1}(\text{soln})] - \Delta H^{\ddagger}_c. \quad (2)$$

If it is *assumed* that $\Delta H^{\ddagger}_d$ is equal to $\Delta H^{\ddagger}_{-1}$(soln) (i.e. that $\Delta H^{\ddagger}_d - \Delta H^{\ddagger}_{-1} = 0$), then eq. (2a) results.

$$\Delta H^0_R(\text{soln}) = \Delta H^{\ddagger}_1(\text{soln}) - \Delta H^{\ddagger}_c \quad (2a)$$

$$[\text{If: } \Delta H^{\ddagger}_d = \Delta H^{\ddagger}_{-1}(\text{soln})].$$

If it is *also assumed*, by analogy with gas phase work, that $\Delta H^{\ddagger}_c$ is negligible, then eq. (2b) results.

$$\Delta H^0_R(\text{soln}) = \Delta H^{\ddagger}_1(\text{soln}) \quad (2b)$$

$$[\text{If: } \Delta H^{\ddagger}_d = \Delta H^{\ddagger}_{-1}(\text{soln}),\ \Delta H^{\ddagger}_c = 0].$$

If it is *further assumed* that the difference between enthalpic effects of solvation of M—L and the transition state for M—L homolysis [defined hereafter by the useful symbol $\ddagger_1$ (Fig. 2)] is negligible, then one can equate the ΔH^0_R(soln) with the BDE.*[,32,33] Equation (2c) states this result along with its restraints, including the fact that differential solvation effects must be negligible (δ solvation = 0).

$$\text{BDE} \simeq \Delta H^{\ddagger}_1(\text{soln}) \quad (2c)$$

$$[\text{If: } \Delta H^{\ddagger}_d = \Delta H^{\ddagger}_{-1}(\text{soln}),\ \Delta H^{\ddagger}_c = 0,\ \delta \text{ solvation} = 0].$$

The above development of eq. (2c) shows how, under the right circumstances, $\Delta H^{\ddagger}_1$(soln) could give a good (even excellent) estimate of the BDE for a

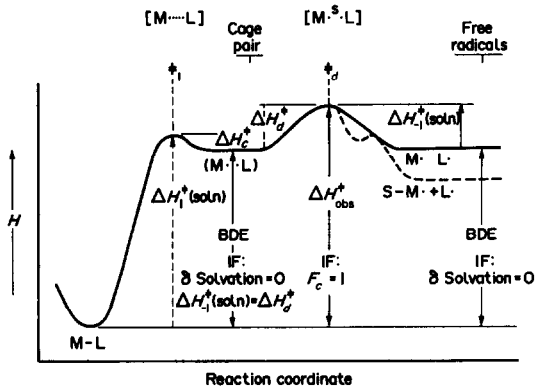

Fig. 2. *Schematic* solution phase enthalpy vs reaction coordinate diagram showing the definitions of $\Delta H^{\ddagger}_1$ (soln), $\Delta H^{\ddagger}_c$, $\Delta H^{\ddagger}_d$, $\Delta H^{\ddagger}_{obs}$(soln) (if the cage efficiency, $F_c = 1$), $\Delta H^{\ddagger}_{-1}$(soln), and $\ddagger_1$ and $\ddagger_d$. Note that the BDE, as shown in this figure, corresponds to the free radical stage (since such a large M$^{\cdot}$ and L$^{\cdot}$ separation is how a gas phase BDE (Fig. 1) is defined) and required δ solvation = 0. Note also that if $\Delta H^{\ddagger}_d = \Delta H^{\ddagger}_{-1}$ (and if δ solvation and other terms (see footnote † on p. 1507) are negligible) then the BDE will also equal the enthalpy difference from M—L to the $\overline{\text{M}^{\cdot}\text{L}^{\cdot}}$ caged pair. This figure illustrates only one set of possible enthalpies, i.e. $\Delta H^{\ddagger}_c$ is shown $\ll \Delta H^{\ddagger}_d$ but the opposite is also possible.

M—L system. The solution values *could* be at least as accurate ($\pm$2 kcal mol^{-1}) as the *best* values obtained to date via gas phase studies, even though the former are determined in solution. Extraction of an accurate $\Delta H^{\ddagger}_1$(soln) from the observable $\Delta H^{\ddagger}_{obs}$(soln) values would thus give a very useful result if it were done properly, and if the $\Delta H^{\ddagger}_{obs}$ (soln) were obtained under the appropriate conditions. However, the two crucial factors that determine the accuracy of a solution phase BDE, the enthalpic effects of differential solvation and *quantitative* correction for the cage effect, have been previously neglected in M—L BDE estimates. We examine these effects in turn in the sections that follow.

Differential solvation effects

The assumption that $\Delta H^{\ddagger}_d$ be equal to $\Delta H^{\ddagger}_{-1}$(soln) is not expected to be *exactly* correct, except fortuitously. In the case of organic radicals, both $\Delta H^{\ddagger}_d$ and $\Delta H^{\ddagger}_{-1}$(soln) are small and positive in fluid solvents like alkanes, where no specific radical–solvent complexes are formed. The $\Delta H^{\ddagger}_d - \Delta H^{\ddagger}_{-1}$(soln) difference will be nearer to zero than the individual values and the $\Delta H^{\ddagger}_d = \Delta H^{\ddagger}_{-1}$(soln) equivalence would not lead to any large error in such a case. However, for organometallic systems, specific solvation effects, on the *free radical* time scale (i.e. for radicals that have escaped the cage), could result in a large difference between $\Delta H^{\ddagger}_d - \Delta H^{\ddagger}_{-1}$(soln). Two

*The heat of solution, ΔH(solution), for organometallics in solvents such as toluene[32] or 1,2-dichloroethene[33] are often $\leqslant$ 4–5 kcal mol^{-1};[25g] it seems likely, then, that the differential heat of solution, $\Delta\Delta H$ (solution), between M—L and M$^{\cdot}$ L$^{\cdot}$ will be small, < 5 kcal mol^{-1}, at least in these solvents.

cases of specific solvation effects that may stabilize out-of-cage M$^{\cdot}$ [and thus increase $\Delta H^{\ddagger}_{-1}$(soln)] in organotransition metal systems come to mind. The first is solvent (S) addition to a 17-electron M$^{\cdot}$ to form a "19-electron"*,[34] $^{\cdot}$M—S. Since such 19-electron species are now well-known,[34a] since Tyler has recently shown their formation can be exoergic[34b] (and probably significantly exothermic), and since a 19-electron $^{\cdot}$Co(DMG)$_2$(pyridine)$_2$ complex has been isolated and crystallographically characterized[34c] (S = pyridine in this case), it seems wise to at least consider the possibility of 19-electron $^{\cdot}$M—S species (and thus that $\Delta H^{\ddagger}_{-1}$(soln) is much larger than $\Delta H^{\ddagger}_{d}$). Another way to say this is that recombination of freely diffusing M$^{\cdot}$ and L$^{\cdot}$ may actually involve $^{\cdot}$M—S in some cases. Such encounters between $^{\cdot}$M—S and L$^{\cdot}$ will initially produce a type of solvent-separated or so-called secondary radical pair, $\overline{^{\cdot}\text{M—S}\ ^{\cdot}\text{L}}$. The right side of Fig. 2 (dashed line) shows this effect in a qualitative way.

A second case of interest is in the heterolytic dissociation of an M—L bond (L = CO, PR_3 and so on) in an 18-electron complex to form L plus a 16-electron, coordinatively unsaturated fragment, M. By this example we again point out that the formalism of cage effects is not restricted to radical pairs, but rather, includes other non-ionic pairs of high reactivity. For a 16-electron M species, exothermic specific solvation to yield M—S is generally expected; for example, available estimates for $Cr(CO)_5S$ indicate that even weakly coordinating solvents like heptane or cyclohexane will have $\Delta H_{solvation} \simeq -4$ kcal mol^{-1}[35] (estimates run as high as -10 kcal mol^{-1}).[35c] An experimental point worth noting here is the need to use carefully purified solvents since, for example, the $Cr(CO)_5$—OH_2 bond energy is $\simeq 18(\pm 4)$ kcal mol^{-1}.[35c]

As we mentioned above, differential solvation effects can also enter into the value of $\Delta H^{\ddagger}_{1}$(soln). A variety of solvent effects, including those connected to size changes during reaction, could lead to an appreciable $\Delta H^{\ddagger}_{c}$. The connection of $\Delta H^{\ddagger}_{1}$(soln) to a BDE requires that solvent effects, either specific or non-specific, *must be energetically negligible at every stage of reaction from* M—L *to free radicals*. The amount of work needed to establish this condition, or correct for deviations from it, is both substantial and seldom done. The *assumption* of negligible differential solvation effects should always be stated as a restriction on the accuracy of the BDE values obtained. We use the notation δ solvation = 0 to mean that all solvent effects, besides the cage effect, are negligible.

The δ solvation = 0 statement is perhaps overly grim since solvation effects on uncharged molecules are usually not energetically large; for example, for uncharged organometallics the ΔH(solvation) (i.e. the heat for the gas phase → solution reaction) are often $\leqslant 5$ kcal mol^{-1} for lower polarity solvents.† Moreover, solvation enthalpy differences are usually smaller than individual values. Nonetheless it is important to keep distinct what is assumed from what is established in fact. The number of possibilities for failure of the δ solvation = 0 restriction in M—L dissociations is larger than the two specific cases mentioned above. The point to note here is that the δ solvation = 0 restriction applies to all of the cases, treated subsequently herein, where a BDE is derived from a $\Delta H^{\ddagger}_{obs}$(soln).

Relationships between $\Delta H^{\ddagger}_{1}$(soln) *and* $\Delta H^{\ddagger}_{obs}$(soln): *the cage effect*

The connection between $\Delta H^{\ddagger}_{1}$(soln) and $\Delta H^{\ddagger}_{obs}$(soln) is not as simple as recent literature would suggest since the cage effect has been neglected there. Scheme 3, and the equations that are derived from it, correct this oversimplification.

One of the best methods for obtaining rate constants for *free radical* formation is through the disappearance of the starting material in the presence of added trapping agent. Scheme 3 implies that, with the addition of trapping agent (T) of sufficient reactivity (k_T), the observed rate constant for the disappearance of M—L or the appearance of the trapped product (formed in 100% yield§), k_{obs}, should be related to the elementary steps of Scheme 3 via eq. (3).

$$k_{obs} = k_1\left[\frac{k_d}{k_d + k_c}\right]. \qquad (3)$$

The qualitative pictorial representation of a free energy (ΔG) reaction coordinate diagram, corresponding to the M—L homolysis and cage process in Scheme 3, is helpful here and is shown in Fig. 3.

The activation barriers for the cage processes of recombination and diffusive cage escape are shown as $\Delta G^{\ddagger}_{c}$ and $\Delta G^{\ddagger}_{d}$, respectively (Fig. 3). Note that two limiting cases of interest can be seen, one (shown with a dotted line, Fig. 3) where $\Delta G^{\ddagger}_{c}$ is $\ll \Delta G^{\ddagger}_{d}$ (so that a sizable cage effect and significant

* For 17-electron CpMo(CO)$_3^{\cdot}$ plus $X^- = I^-$, Br^- or Cl^- reacting to give 19-electron CpMo(CO)$_3X^{\cdot}$, ΔG is < -2 kcal mol^{-1} at 298 K. Since ΔS is almost surely negative, a conservative estimate is that ΔH is $\leqslant -2$ kcal mol^{-1}.

† See footnote * on p. 1505.

§ See footnote ** on p. 1504.

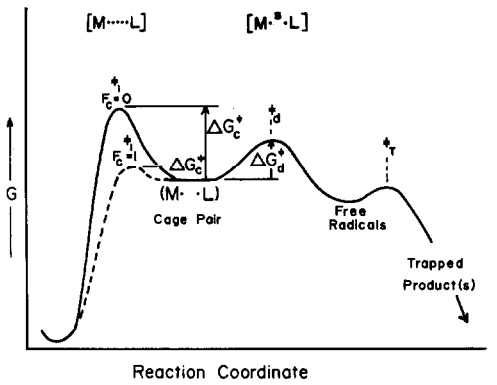

Fig. 3. *Schematic* solution phase free energy vs reaction coordinate diagram for the general cage reaction depicted in Scheme 3 showing the definitions of the transition states $\ddagger_1$, $\ddagger_d$ and $\ddagger_T$, the free energies $\Delta G_c^{\ddagger}$ and $\Delta G_d^{\ddagger}$, and the two limiting cases of the cage efficiencies, $F_c = 0$ [corresponding to $\Delta G_c^{\ddagger} \gg \Delta G_d^{\ddagger}$ (and thus to $\ddagger_1$ at higher free energy than $\ddagger_d$) and $F_c = 1$ (corresponding to $\Delta G_c^{\ddagger} \ll \Delta G_d^{\ddagger}$ and thus to $\ddagger_1$ at lower free energy than $\ddagger_d$)].

recombination exists), and one (shown with a solid line, Fig. 3) where $\Delta G_c^{\ddagger} \gg \Delta G_d^{\ddagger}$ so that no cage recombination occurs (no cage effect). The fractional cage efficiency, F_c,[10] is a very useful parameter and is defined in eq. (4).

$$F_c \equiv k_c/(k_c+k_d). \quad (4)$$

The two limiting cases can now be seen more clearly as $F_c \simeq 1$ (a large cage efficiency due to $k_c \gg k_d$), and $F_c \simeq 0$ (negligible cage efficiency since $k_d \gg k_c$ and $k_c/k_d \simeq 0$); note also that there is also a continuum of cases in between the two limits of F_c.

As we have recently[10a] shown, the activation parameters that are associated with Scheme 3 and Fig. 3 are given, in the general case (all F_c values), by eqs (5) and (6).

$$\Delta H^{\ddagger}_{obs}(soln) = \Delta H^{\ddagger}_{1}(soln) + F_c\,[\Delta H^{\ddagger}_{d} - \Delta H^{\ddagger}_{c}] \quad (5)$$

$$\Delta S^{\ddagger}_{obs}(soln) \simeq \Delta S^{\ddagger}_{1}(soln) + F_c\,[\Delta S^{\ddagger}_{d} - \Delta S^{\ddagger}_{c}]. \quad (6)$$

It should be noted that the enthalpy expression [eq. (5)] is analytic while the entropy expression [eq. (6)] is an approximation[10a] (which is good to ± 2 eu in the interval $0.9 > F_c > 0.1$, and of higher accuracy outside of that interval).

Equation (5) makes it clear that F_c, $\Delta H^{\ddagger}_{d}$ and $\Delta H^{\ddagger}_{c}$ [but *not* $\Delta H^{\ddagger}_{-1}(soln)$]* are important components of the apparent activation enthalpy [$\Delta H^{\ddagger}_{obs}(soln)$] for any reaction which occurs via Scheme 3. Equation (5) also implies curvature in the $\Delta H^{\ddagger}_{obs}(soln)$ vs $1/T$ function which is responsible for the approximate nature of eq. (6) in the $0.9 > F_c > 0.1$ interval. Equation (6) teaches that the components of $\Delta S^{\ddagger}_{obs}(soln)$ are $\Delta S^{\ddagger}_{1}(soln)$, F_c, $\Delta S^{\ddagger}_{d}$ and $\Delta S^{\ddagger}_{c}$.

These equations are quite important in showing that the cage efficiency factor (F_c) and the activation parameters of the cage reactions ($\Delta H^{\ddagger}_{d}$, $\Delta H^{\ddagger}_{c}$) must be the basis for obtaining a $\Delta H^{\ddagger}_{1}(soln)$ value for an M—L bond homolysis in solution. They are entirely different in concept to previous literature.[24-26] They also show that variations in F_c with variations in temperature must be considered before the value of $\Delta H^{\ddagger}_{1}(soln)$ and $\Delta S^{\ddagger}_{1}(soln)$ can be extracted from $\Delta H^{\ddagger}_{obs}(soln)$ and $\Delta S^{\ddagger}_{obs}(soln)$. These variations in F_c have not received any previous attention. In fact, variations in the cage effect for M—L bond dissociation reactions have been entirely ignored until our development of eqs (5) and (6).[10a]

With eqs (5) and (6) in hand, the general BDE equation [eq. (7)] is easily obtained by inserting eq. (5) into the general thermodynamic eq. (2).

$$\text{BDE} \simeq \Delta H^{\ddagger}_{obs}(soln) + (1-F_c)\cdot[\Delta H^{\ddagger}_{d} - \Delta H^{\ddagger}_{c}] - \Delta H^{\ddagger}_{-1}(soln) \quad (7)$$

[If: δ (solvation) = 0, $0 < F_c < 1$].

All restraints are relaxed in this approximation† except that differential solvation effects *again* must be absent (δ solvation = 0).

Equation (7) further illustrates that even if there was some constant value for $\Delta H^{\ddagger}_{d} - \Delta H^{\ddagger}_{c}$ [$\equiv \Delta(\Delta H^{\ddagger})_{d-c}$] that was a property of all or most solvents, the appropriate correction to $\Delta H^{\ddagger}_{obs}(soln)$ would still require values of the cage efficiency factor (F_c) and $\Delta H^{\ddagger}_{-1}(soln)$ variables. Examples of cage reactions in the organic literature and the Bergman example above (Scheme 2) show that F_c can easily vary from 0.01 to 0.99. Similarly, $\Delta H^{\ddagger}_{-1}(soln)$ will vary with solvent.

Although eq. (7) is the most general BDE equation, its use requires knowledge of F_c, $\Delta H^{\ddagger}_{d}$, $\Delta H^{\ddagger}_{c}$

* See footnote ‖ on p. 1502.

† This BDE equation is an approximation because it neglects differences in the enthalpy of the homolysis transition state ($\ddagger_1$) in solution compared to the gas phase. When the enthalpy function for the homolysis is not sharply peaked, then entropic and solvent effects will determine the *position* of the transition state, $\ddagger_1$, on the underlying potential energy (e.g. Morse) function, giving rise to different solution vs gas phase enthalpy $\Delta H^{\ddagger}$ values. If one denotes that enthalpy difference by $\delta H^{\ddagger}_{1}$, then a more exact equation is as follows, where the required $\Delta H^{\ddagger}_{-1}(gas)$ correction has also been incorporated.

$$\text{BDE} \simeq \Delta H^{\ddagger}_{1}(soln) - F_c\cdot[\Delta H^{\ddagger}_{d} - \Delta H^{\ddagger}_{c}] + \delta H^{\ddagger}_{1} - \Delta H^{\ddagger}_{-1}(gas).$$

and $\Delta H^{\ddagger}_{-1}$(soln). Since these are generally not available, BDE estimates from solution kinetic studies will generally have to proceed with simplifying conditions and assumptions. In the sections that follow, we first examine the lower limit of F_c ($F_c = 0$). In this limit, the observed activation parameters, $\Delta H^{\ddagger}_{obs}$(soln) and $\Delta S^{\ddagger}_{obs}$(soln), simplify to those of the dissociative elementary step [$\Delta H^{\ddagger}_{1}$(soln), $\Delta S^{\ddagger}_{1}$(soln)]. The $F_c = 0$ limit will also be useful in showing how the cage effect *cannot* be neglected, even when the cage efficiency factor (F_c) is negligible! The discussion then will examine the $F_c = 1$ limit. We will then return to the continuum, where F_c is a variable that can change with changing temperature, solvent and M—L structure, and will examine the simplified forms of the BDE equation that apply there.

BDE ESTIMATES IN THE LIQUID PHASE

The zero cage efficiency ($F_c = 0$) *case*

The situation in which an M—L reacts via Scheme 3 but exhibits no cage effect is depicted in the free energy profile of Fig. 3 (solid line) where $\Delta G^{\ddagger}_{c}$ is higher than $\Delta G^{\ddagger}_{d}$ ($k_d \gg k_c$, $F_c \simeq 0$). In such cases, eq. (5) simplifies so that the observed activation enthalpy [$\Delta H^{\ddagger}_{obs}$(soln)] will be equal to that for k_1 [$\Delta H^{\ddagger}_{1}$(soln)], the solution phase homolysis step of Scheme 3 [eq. (8)].

$$\left.\begin{aligned}\Delta H^{\ddagger}_{obs}(\text{soln}) &= \Delta H^{\ddagger}_{1}(\text{soln})\\ \Delta S^{\ddagger}_{obs}(\text{soln}) &= \Delta S^{\ddagger}_{1}(\text{soln})\end{aligned}\right\}(\text{If: } F_c = 0, k_c \ll k_d). \tag{8}$$

It is useful to simplify further the $\Delta G^{\ddagger}_{c} > \Delta G^{\ddagger}_{d}$ condition by eliminating entropic considerations (i.e. that $\Delta H^{\ddagger}_{c} = \Delta G^{\ddagger}_{c} > \Delta H^{\ddagger}_{d} = \Delta G^{\ddagger}_{d}$, $\Delta S^{\ddagger}_{c} = \Delta S^{\ddagger}_{d} = 0$). This simplification allows us to examine the implications of non-zero $\Delta H^{\ddagger}_{c}$ possibilities. The enthalpy profile, in this case, will be similar to the free energy profile (Fig. 3, solid curve) and $\Delta H^{\ddagger}_{c}$ will be substantial [3.2 kcal mol^{-1} more than $\Delta H^{\ddagger}_{d}$ for $F_c \leqslant 0.01$ at 350 K (77°C)].

From this point, the connection between $\Delta H^{\ddagger}_{obs}$(soln) in the liquid phase and BDE must proceed in a stepwise and careful way. Ultimately, it must be determined if the substantial $\Delta H^{\ddagger}_{c}$ is a property of the M—L molecule or a property of the solution. As already mentioned, a variety of solvation effects could lead to a significant $\Delta H^{\ddagger}_{c}$ value in solution that would not be present in the gas phase. Any connection between $\Delta H^{\ddagger}_{obs}$(soln) and BDE requires δ solvation = 0. If the system meets the δ solvation = 0 and $F_c = 0$ restrictions, and if the further assumption that $\Delta H^{\ddagger}_{d} = \Delta H^{\ddagger}_{-1}$(soln) is valid, then the observed activation enthalpy for the (reverse) free radical recombination reaction, $\Delta H^{\ddagger}_{r,obs}$(soln),* would be equal to $\Delta H^{\ddagger}_{c}$ and equal to the gas phase value $\Delta H^{\ddagger}_{-1}$(gas). Equation (7) then yields the relatively simple BDE relationship shown in eq. (9).

$$\begin{aligned}\text{BDE} &= [\Delta H^{\ddagger}_{obs}(\text{soln}) - \Delta H^{\ddagger}_{c}]\\ &= [\Delta H^{\ddagger}_{1}(\text{soln}) - \Delta H^{\ddagger}_{-1}(\text{gas})] \qquad (9)\end{aligned}$$

[If: $F_c = 0$, δ solvation = 0,
$\Delta S^{\ddagger}_{c} = 0$ so that $\Delta H^{\ddagger}_{c} = \Delta G^{\ddagger}_{c}$,
$\Delta H^{\ddagger}_{c} = \Delta H^{\ddagger}_{-1}(\text{gas}) = \Delta H^{\ddagger}_{r,obs}(\text{soln})$,
$\Delta H^{\ddagger}_{d} = \Delta H^{\ddagger}_{-1}(\text{soln})$].

The above scenario constitutes an example where the low cage efficiency ($F_c = 0$) would be a property of the M—L molecule. The $\Delta H^{\ddagger}_{c}$ in this hypothetical example is derived from the M—L bond potential function. A well-defined maximum in the enthalpy profile determines the structure of the transition state, $\ddagger_1$ (Fig. 2), in this case.

A specific example illustrating a large $\Delta H^{\ddagger}_{c}$ is useful here. The dimerization of bulky and highly delocalized triarylmethyl radicals provides a classic[37a] example where steric effects impose a *ca* 7–10 kcal mol^{-1} barrier,[29a] $\Delta H^{\ddagger}_{c}$, in the otherwise decreasing energy of a system in which a chemical bond is forming. It is quite likely that the set of conditions set forth with eq. (9) will ultimately be applicable to some M—L systems, but we don't yet know if it applies to a few or many organotransition metal systems.

There is a second important case where $F_c \simeq 0$ and where the $\Delta H^{\ddagger}_{c} = \Delta H^{\ddagger}_{-1}$(gas) equivalence can apply. It is identical in the free energy sense ($\Delta G^{\ddagger}_{c} \gg \Delta G^{\ddagger}_{d}$, Fig. 3) to the case above, but very different in the enthalpic sense. Figure 2 shows an enthalpic picture for a Scheme 3 reaction in which the activation enthalpy for the cage recombination reaction (k_c, $\Delta H^{\ddagger}_{c}$) is much smaller than the activation enthalpy for diffusive decay of the cage pair (k_d, $\Delta H^{\ddagger}_{d}$). This enthalpy picture (Fig. 2) is *not*, as it may seem, incompatible with $F_c \simeq 0$ (Fig. 3, $\Delta G^{\ddagger}_{c} > \Delta G^{\ddagger}_{d}$). One merely needs to suppose a negative $\Delta S^{\ddagger}_{c}$ that is large enough to make $k_c \ll k_d$. For example, a $\Delta S^{\ddagger}_{c} = -10$ eu (that has a likely basis from first principles[35d,38,39]) gives a $\Delta G^{\ddagger}_{c}$ of 3.5 kcal mol^{-1} at 77°C (350 K) even if $\Delta H^{\ddagger}_{c} = 0$.

Under these conditions, the rate constant for recombination of the free radicals would still be limited by surmounting $\ddagger_1$ (Fig. 2) and could be fast enough to be in the diffusion controlled range.

* See footnote § on p. 1504.

However, the value of $k_{r,obs}$(soln) would be controlled by the negative value of $\Delta S_c^{\ddagger}$ and not by $\Delta H^{\ddagger}_{-1}$(soln). The equation connecting BDE and $\Delta H^{\ddagger}_{obs}$(soln) is *not changed* in this case, i.e. eq. (9) still applies. It would be an error in this case to subtract a typical $\Delta H^{\ddagger}_{-1}$(soln) value in an attempt to obtain a BDE (although this has been suggested).[24]

A further simplification of eq. (9) is possible if $\Delta H_c^{\ddagger}$ is assumed to be negligible ($\Delta H_c^{\ddagger} \simeq 0$, the entropic barrier case); the result is eq. (9a).

$$\text{BDE} \simeq \Delta H^{\ddagger}_{obs}(\text{soln}) = \Delta H^{\ddagger}_{\dagger}(\text{soln}) \qquad (9a)$$

[If: $F_c \simeq 0, \delta$ solvation $= 0$,

$\Delta H_c^{\ddagger} \simeq \Delta H^{\ddagger}_{-1}(\text{gas}) \simeq 0, \quad \Delta S_c^{\ddagger} \ll 0,$

$\Delta H^{\ddagger}_{-1}(\text{soln}) = \Delta H_c^{\ddagger}$].

The conditions ($\Delta H_c^{\ddagger} = 0$ and $F_c = 0$) that yield eq. (9a) require an important new restriction compared to eq. (9), that $\Delta S_c^{\ddagger} \ll 0$. The sign of $\Delta S_c^{\ddagger}$ is certainly expected to be negative (in the absence of strong solvation effects), although this has not yet been clearly demonstrated. This statement ($\Delta S_c^{\ddagger} \ll 0$) is made partly on the basis that the transition state $\ddagger_1$ should be more ordered than the cage pair intermediate. The latter, by definition, allows the two cage partners the chance to move independently, ultimately leading to their separation to form free radicals. The cage pair can be considered to have entropic properties analogous to those of an M—L molecule, differing from its M—L precursor both in structure and in six vibrational frequencies that have been shifted to relatively (very) low values.[38a] These in turn should lead to a negative activation entropy for the k_c step of Scheme 3.*[,35d,38,39]

The importance of the possibility of a significantly large and negative $\Delta S_c^{\ddagger}$ is clear when one compares Fig. 2 with the $F_c = 0$, $\Delta G_c^{\ddagger} > \Delta G_d^{\ddagger}$ case in Fig. 3. Figure 2 shows a $\Delta H_c^{\ddagger}$ which is similar to Fig. 1 (gas phase) but with an added barrier ($\Delta H_d^{\ddagger}$) for the conversion of the cage pair to freely diffusing species. The enthalpy diagram (Fig. 2) would lead one to expect a large ($F_c \sim 1$) cage effect whereas the free energy profile (corresponding to the same $\Delta H_c^{\ddagger}$ but $\Delta S_c^{\ddagger} \ll 0$) shows that the cage effect is absent ($F_c = 0$)! The present situation ($\Delta S_c^{\ddagger} \ll 0$) is distinct from the one described above ($\Delta S_c^{\ddagger} = 0$, $\Delta G_c^{\ddagger} = \Delta H_c^{\ddagger}$) in that the $F_c = 0$ condition depends upon $T\Delta S_c^{\ddagger}$ and thus upon the temperature of observation. *A larger cage effect would be observed at a lower temperature.* A low temperature (photochemical) means of generating such a cage pair intermediate could give very different behaviour than that seen in thermolysis (at higher temperatures).

In closing this $F_c = 0$ section, *we note that the cage effect cannot be ignored, even when its efficiency factor,* F_c, *is negligible.* This is obvious since there are two equations relating $\Delta H^{\ddagger}_{\dagger}$(soln) to BDE [eqs (9), (9a)] for the same $F_c = 0$ limit. Schemes that do not allow for the cage pair are apt to confuse the two cases given by eqs (9) and (9a).†[,24]

The liquid phase. Efficient cage reaction ($F_c = 1$)

A different set of equations arises when F_c is not equal to zero. Before proceeding, it is useful to summarize the available evidence for cage effects *in* M—L *solution homolyses* (Fig. 3, dashed line). The evidence is several-fold, although additional studies documenting cage effects and the magnitude of F_c in M—L thermolyses are needed (some of them are in progress as part of our own work[25g]):

(1) The studies cited in the introduction[20,21] such as in Schemes 1 and 2, although not M—L homolyses, provide similar, if not identical, caged M$^{\bullet}$ and L$^{\bullet}$ pairs and thus provide good (albeit inferential) evidence for $F_c > 0$ and thus for the importance of radical cage effects in M—L homolyses.

(2) Endicott has provided *direct* evidence for cage effects by showing[40] that picosecond flash photohomolysis of the Co—C bond in adenosylcobalamin (Coenzyme B_{12}) in ambient temperature H_2O gives $k_c \simeq (1.3 \pm 1.1) \times 10^9$ s^{-1} and $k_d \simeq (0.5 \pm 0.4) \times 10^9$ s^{-1}. These values in eq. (4) give $F_c = 0.7$ with a range of 0.2–1.0, given the stated[40] error bars.

(3) Some evidence exists for a non-scavengeable fraction of products in the thermolysis or photolysis of Co—R complexes containing β-hydrogens,[24b,c] an observation generally interpreted as consistent with cage recombination[10a] and hence $F_c > 0$ (but also consistent with, and interpreted by others as evidence for, a parallel and concerted $\beta-$H elimination pathway).[41-43]

(4) In studies of Co—R homolyses using added reagents at concentrations that scavenge *free* radicals (only), an increase in ΔH_{obs}(soln) in solvents of increasing viscosity has been observed both by Halpern[24f] and ourselves.[25d,e,f] Although not interpreted previously as a cage effect,[24f] this observation is fully consistent with Scheme 3, in particular with eq. (5) and with the assumption of an increase in $\Delta H_d^{\ddagger}$ with an increase in solvent viscosity.

(5) Perhaps most importantly, such cage effects *are to be expected* in moderately viscous solvents, given the literature of radical cage effects.[1-12,14]

* See footnote § on p. 1500.

† See footnote ‖ on p. 1502.

We believe that the evidence above already establishes that F_c values for organometallic systems are not negligible; moreover, we believe it is likely that the F_c values $\geqslant 0.5$ for M—L systems will be found. If so, the F_c values will be considerably larger than those for previously studied organic radical pairs.

We therefore consider next the high cage efficiency ($F_c = 1$) limit. The BDE equation and the required restrictions are given in eq. (10).

$$\text{BDE} \simeq \Delta H^{\ddagger}_{\text{obs}}(\text{soln}) - \Delta H^{\ddagger}_{-1}(\text{soln}) \qquad (10)$$

$$[\text{If: } F_c = 1,\ \delta \text{ solvation} = 0].$$

Equation (10) is a more general version of the case suggested by Halpern[24] which has heretofore been widely accepted.[25,26] It applies to cases where the recombination of free radicals is known to be diffusion controlled, which in turn means that k_c is much greater than k_d (i.e. that $F_c = 1$). One only needs to recall eq. (9a) above to realize that a different BDE equation is appropriate if $F_c \simeq 0$. Clearly, the connection between $\Delta H^{\ddagger}_{\text{obs}}$(soln) and BDE requires a quantitative measurement of F_c, yet no quantitative values for F_c are available at the present time for any M—L system! It is also quite important to realize that, if and when eq. (10) is applicable, $\Delta H^{\ddagger}_{\text{obs}}$(soln) pertains to k_d ($\ddagger_d$) and *not* to k_1 ($\ddagger_1$) as the rate determining step. This distinction appears to have been lost in interpretations[24] of the observed activation parameters for M—L systems to date.

The liquid phase, the cage effect continuum

The actual values of F_c, for M—L systems, are expected to be somewhat removed from either limiting boundary (0 or 1). The general relationship [eq. (7)] for the continuum ($0.01 < F_c < 0.99$) can be simplified by neglecting $\Delta H^{\ddagger}_c$ ($\Delta H^{\ddagger}_c \simeq 0$) and setting $\Delta H^{\ddagger}_d$ equal to $\Delta H^{\ddagger}_{-1}$(soln). These two assumptions convert eq. (7) to (11)

$$\text{BDE} \simeq \Delta H^{\ddagger}_{\text{obs}}(\text{soln}) - F_c \cdot \Delta H^{\ddagger}_d \qquad (11)$$

$$[\text{If: } \delta \text{ solvation} = 0, \Delta H^{\ddagger}_c \simeq 0, \Delta H^{\ddagger}_d = \Delta H^{\ddagger}_{-1}(\text{soln})].$$

This equation, and its attendant restrictions, captures the essential features of the cage pair intermediate on BDE in the simplest possible way. It shows that both F_c and $\Delta H^{\ddagger}_d$ must be considered variables that will change with changing solvent. A more viscous solvent should have both a higher F_c value and a higher $\Delta H^{\ddagger}_d$ value than a less viscous solvent. The change in F_c and $\Delta H^{\ddagger}_d$ with variable solvent must be taken into account in relating $\Delta H^{\ddagger}_{\text{obs}}$(soln) to a BDE. A further approximation that is useful (at least presently) is to equate $\Delta H^{\ddagger}_d$ with the activation enthalpy for viscous flow ($\Delta H^{\ddagger}_{\eta}$) as obtained from a $\ln \eta$ vs $1/T$ plot (η = viscosity) and Andrade's law, $\ln \eta = \ln A_{\eta} + (\Delta H^{\ddagger}_{\eta} + RT)/RT$.* The result, eq. (11a), will at least explain the higher values of $\Delta H^{\ddagger}_{\text{obs}}$(soln) in solvents of high $\Delta H^{\ddagger}_{\eta}$.

$$\text{BDE} \simeq \Delta H^{\ddagger}_{\text{obs}}(\text{soln}) - F_c \Delta H^{\ddagger}_{\eta} \qquad (11a)$$

$$[\text{If: } \delta \text{ solvation} = 0, \Delta H^{\ddagger}_c = 0,$$

$$\Delta H^{\ddagger}_d = \Delta H^{\ddagger}_{-1}(\text{soln}) = \Delta H^{\ddagger}_{\eta}].$$

Determination of F_c

A key variable in each of the important eqs (5), (6), (7), (11) and (11a) is the F_c value. If F_c were known along with k_{obs} then k_1 is the result, as shown in eq. (12) [which is readily obtained from eqs (3) and (4)].

$$k_1 = \frac{k_{\text{obs}}}{(1 - F_c)}. \qquad (12)$$

Having both F_c and k_{obs} values as a function of temperature [which also gives k_1 as a function of temperature via eq. (12) and thus $\Delta H^{\ddagger}_1$(soln)] would

* At present, there are virtually no direct measurements of $\Delta H^{\ddagger}_d$ or $\Delta H^{\ddagger}_{-1}$(soln) as a function of solvent for any M—L bond thermolysis; indeed, such measurements are largely absent from all of the cage-chemistry literature.[1-15] However, Halpern has provided valuable data consistent with *the interpretation* that $\Delta H^{\ddagger}_{-1}$(soln) ranges from *ca* 2 kcal mol^{-1} in solvents such as toluene and acetone[24b,c] to *ca* 5 or more kcal mol^{-1} in more viscous solvents such as (lower temperature) ethylene glycol *if* F_c *is* 1.[24e] Our own work[25c,d,e,f] confirms the general theme (but not all aspects)[24h] of these findings. The $\Delta H^{\ddagger}_{-1}$(soln) estimates parallel estimates for the enthalpy of activation for diffusive flow obtained from the well-known $\ln \eta$ (η = viscosity) vs $1/T$ treatment.[2,13-15,44] It is crucial for the purposes of the present discussion to be aware of three points about $\Delta H^{\ddagger}_{\eta}$ values:[2,13-15,44f-l] they are only *estimates* of $\Delta H^{\ddagger}$ for diffusion through a continuum and typically underestimate it by < 1 kcal mol^{-1};[2,44f,g] they are based on viewing the solvent as a bulk, macroscopic continuum and *thus are even more uncertain estimates for the microscopic, molecular dynamics and energetics of diffusion out of the (discontinuous) cage*; they fall into two classes, $\Delta H^{\ddagger}_{\eta}$ being virtually constant for so-called "non-associated" solvents such as toluene, but $\Delta H^{\ddagger}_{\eta}$ being a function of temperature for "associated" solvents such as H-bonding H_2O or ethylene glycol[2,7,44] (in this latter case, the apparent $\Delta H^{\ddagger}_{\eta}$ decreases noticeably with increasing temperature, i.e. $\ln \eta$ vs $1/T$ plots are non-linear[2,44]). Typical values of $\Delta H^{\ddagger}_{\eta}$ are: 1.5 kcal mol^{-1} for toluene,[44a] 3.8 kcal mol^{-1} for H_2O from 8 to 25°C;[44b] 2.1 kcal mol^{-1} for H_2O from 100 to 130°C;[41c] 7.3 kcal mol^{-1} for ethylene glycol from 8 to 25°C;[44d] and 4.4 kcal mol^{-1} for ethylene glycol from 90 to 120°C.[44d,e] The η vs T data used in these $\Delta H^{\ddagger}_{\eta}$ calculations are taken from indicated sources;[44] it should also be noted that $\Delta H^{\ddagger}_{\eta} = E_{\eta} - RT$.[28b,c]

also allow a direct determination of $\Delta H_d^{\ddagger} - \Delta H_c^{\ddagger}$, as a rearranged form of eq. (5) shows, eq. (13).

$$[\Delta H_d^{\ddagger} - \Delta H_c^{\ddagger}] = \frac{\Delta H_{obs}^{\ddagger}(\text{soln}) - \Delta H_1^{\ddagger}(\text{soln})}{F_c}. \quad (13)$$

There are ways to obtain k_1 and F_c values in favourable cases. For example, racemization rate constants (k_α) can, in principle, be measured using a chiral metal complex [e.g. M—C(x)(y)(z)]. If one assumes that unrestricted rotation of the carbon group occurs in the M˙ ˙C(x)(y)(z) radical pair, then at least some racemization of M—L is expected from the homolysis and cage recombination process. If F_c is not zero and if an appropriate inversion process (an internal rotation or molecular tumbling) in the cage pair is very fast compared to k_c, then k_1 can be obtained directly. In such cases, the value of $\Delta H_1^{\ddagger}$(soln) can also be obtained directly, independent of the exact value of the cage efficiency (F_c). If the value of $\Delta H_1^{\ddagger}$(soln), so determined, is assumed to be equal to $\Delta H_1^{\ddagger}$(gas) and if $\Delta H_{-1}^{\ddagger}$(gas) is considered to be negligible, then the $\Delta H_1^{\ddagger}$(soln) value is the approximate BDE [previous eq. (2c)].

A fast intra-cage racemization process also allows a quantitative determination of F_c. This determination would be very simple in such a case. One would merely measure the disappearance of the chiral M—L in the presence of a trap (k_{obs}, Scheme 3), followed by the separate measurement of k_α. These would yield F_c, eq. (14).

$$F_c = (k_\alpha - k_{obs})/k_\alpha \qquad k_\alpha = k_1. \quad (14)$$

Under these assumptions, a relatively direct determination of $\Delta H_d^{\ddagger} - \Delta H_c^{\ddagger}$ [eq. (13)] would be possible and would valuably increase our understanding of the cage effect. The $\Delta H_d^{\ddagger} - \Delta H_c^{\ddagger}$ difference is also related to the BDE question through eq. (7), although this requires the measurement of $\Delta H_{-1}^{\ddagger}$ (soln). However, the validity of eq. (2c) could be checked if all these measurements were available.

The observed rate constants for racemization (k_α) of a chiral organometallic system are the lower limits for k_1. In other words, they may be equal to k_1 if a racemizing step, such as a rotation *at the cage pair stage*, is very fast compared to k_c. At the other extreme, the observed value of k_α could be the same as that for disappearance of the chiral M—L with an added trap (k_{obs} of Scheme 3, $k_\alpha = k_{obs}$). The latter case obtains if k_c is much greater than all racemizing processes. The interpretations of the available data[26b,c] on chiral M—L systems have implicitly assumed that $k_\alpha = k_{obs}$. Measurement of both k_{obs}, with an added trap (Scheme 3) and k_α would test the $k_\alpha = k_{obs}$ assumption (which is unlikely to be quantitatively correct).[25g]

The precedents from organic chemistry show that cage combination generally gives some retention in the cage product, even when small "spacer" molecules (N_2, CO_2) are present. The M—L cases, at least those studied to date, differ in having no such small intervening molecule and may give rise to "tight" primary radical pairs with higher k_c values. This means that the racemization rates for M—L systems will probably not count all of the cage return events.

The entropy $\Delta S_{obs}^{\ddagger}$*(soln)*

It is necessary to understand the entropy of cage systems (Scheme 3) even though entropy does not enter directly into the equations connecting $\Delta H_{obs}^{\ddagger}$ (soln) to a BDE. Furthermore, there is little discussion of $\Delta S_1^{\ddagger}$(soln), $\Delta S_c^{\ddagger}$ and $\Delta S_d^{\ddagger}$ in the existing literature. For this reason, we discuss this subject separately.

The expressions for the observed entropies* are given below.

$$\Delta S_{obs}^{\ddagger}(\text{soln}) \simeq \Delta S_1^{\ddagger}(\text{soln}) + F_c \cdot [\Delta S_d^{\ddagger} - \Delta S_c^{\ddagger}] \quad (6)$$

Limits: $\Delta S_{obs}^{\ddagger}(\text{soln}) = \Delta S_1^{\ddagger}$ (If: $F_c = 0$)

$\Delta S_{obs}^{\ddagger}(\text{soln}) = \Delta S_1^{\ddagger}(\text{soln}) + [\Delta S_d^{\ddagger} - \Delta S_c^{\ddagger}]$ (If: $F_c = 1$).

The two limiting cases are accurate but eq. (6) is an approximation that is uncertain by ± 2 eu[10a] (an inaccuracy smaller than the typical experimental error).

Previously we suggested that $\Delta S_c^{\ddagger}$ should be negative. We also suggest that $\Delta S_d^{\ddagger}$ should be positive. Indeed, the fundamental driving force for diffusive separation is disorder (i.e. the entropy of dilution or mixing). The good agreement between calculated and observed F_c values, obtainable from our spheri-

* Another definition of the activation entropy, derivable from eq. (3), is the limit of $\ln(k_{obs}/T)$ as the temperature becomes infinite [i.e. the intercept of the $\ln(k_{obs}/T)$ plot as $1/T \to 0$]. The equation for this activation entropy ($\Delta S_\infty^{\ddagger}$) is:

$$\Delta S_\infty^{\ddagger} = \Delta S_1^{\ddagger}(\text{soln}) - R\left(\ln\left[1 + e\left(\frac{\Delta S_c^{\ddagger} - \Delta S_d^{\ddagger}}{R}\right)\right]\right).$$

This equation is correct, but only in the limit $T \to \infty$. It is quite misleading because it assumes $\Delta H^{\ddagger}$ is constant over this temperature range (in general $\Delta H^{\ddagger}$ for a Scheme 3 reaction is *not* constant). Hence, this expression is of little use except if $\Delta S_c^{\ddagger} - \Delta S_d^{\ddagger} = 0$, where it teaches a small negative, $-R\ln 2$ (-1.4 eu) correction to $\Delta S_1^{\ddagger}$(soln).

cal source model[10d] of the cage, imply such randomization (a positive $\Delta S_d^{\ddagger}$). Furthermore, the Bartlett–Szwarc data consist of a *constant* $\Delta(\Delta H^{\ddagger})_{d-c}$ accompanied by variable $\Delta(\Delta S^{\ddagger})_{d-c}$ ($\equiv \Delta S_d^{\ddagger} - \Delta S_c^{\ddagger}$) values. The result is that the cage efficiency is not constant, but rather rises in viscous solvents. The $\Delta(\Delta S^{\ddagger})_{d-c}$ values in the Bartlett work range from +12 to +6 eu; their positive sign requires that $\Delta S_d^{\ddagger}$ be positive (unless $\Delta S_c^{\ddagger}$ is negative *and* $|\Delta S_c^{\ddagger}| > |\Delta S_d^{\ddagger}|$).

If $\Delta S_d^{\ddagger}$ is generally positive as expected, then a simple but extremely important point arises—*the cage is wholly enthalpic*. This is of course what Franck and Rabinowitch showed originally.[1] The cage results from repulsive potentials as molecules attempt to pass by one another or fail to do so and collide. Our suggestions of $\Delta S_d^{\ddagger} > 0$ and $\Delta S_c^{\ddagger} < 0$ mean that F_c will decrease below 0.5 as the temperature rises. This means that *higher temperature* $\Delta H_{obs}^{\ddagger}$*(soln) measurements will have smaller cage effect corrections*. Note, however, that while the cage arises by wholly enthalpic effects, *variations in* F_c *at higher temperatures are largely entropic,* $(\Delta S_d^{\ddagger} - \Delta S_c^{\ddagger})$ *effects*. Our suggestion is that F_c will almost invariably decrease with increasing temperature.

LITERATURE EXAMPLES OF SOLUTION KINETICS ESTIMATES OF M—L BDES

It is useful to conclude with the examination of some cases from the literature where the results derived here can be applied. An early, classic example of a M—L *heterolysis* is found in a study of the thermolysis of $Ni(CO)_4$. Day, Basolo and Pearson measured the rate constants for CO dissociation from $Ni(CO)_4$ in the gas phase, in hexane, and in toluene [eq. (15)].[45] The gas phase rate constants yield the relatively precise (±2%) $\Delta H_d^{\ddagger}$(gas) = 22.1 ± 0.4 kcal mol^{-1}, which can be assigned as the BDE for the $(CO)_3Ni$—CO bond if $\Delta H^{\ddagger}{}_{-1}$(gas) is neglected.

$$Ni(CO)_4 \underset{k_c}{\overset{k_1}{\rightleftharpoons}} \overline{Ni(CO)_3\,CO} \xrightarrow[k_d]{} Ni(CO)_3 + CO. \quad (15)$$

This kinetically determined BDE is in reasonable agreement with the less precise value of 25 ± 2 kcal mol^{-1} which was obtained via a Born–Haber cycle from appearance potential and electron affinity data.[46] The above example is typical in that kinetic methods usually give the most precise BDE estimates.[27,28]

When the reaction is carried out in hexane, the rate constants (k_1(25°C) = 1.0×10^{-2} s^{-1}) are about half the gas phase values (k_1(25°C) = 1.8×10^{-2} s^{-1}). This suggests a non-negligible cage effect with an F_c of approximately 0.5 and suggests that the cage escape, k_d (Scheme 3), is part of the rate-determining step. The activation enthalpy, $\Delta H_{obs}^{\ddagger}$(soln), is 24.0(±0.4) kcal mol^{-1}, 1.9(±0.6) kcal mol^{-1} larger than the gas phase value. Choosing eq. (11) for this case indicates that $F_c \cdot \Delta H_d^{\ddagger}$ is *ca* 1.9 kcal mol^{-1} so that $\Delta H_d^{\ddagger}$ is *ca* 3.8 kcal mol^{-1} assuming δ solvation = 0. Alternatively, the use of eq. (11a) and $\Delta H_{\eta}^{\ddagger}$ for hexane of 1.2 kcal mol^{-1}[144b] gives BDE ≃ 24.0 − 0.5(1.2) = 23.4 kcal mol^{-1}, a value somewhat larger (but within ±1 kcal mol^{-1}) of the gas phase kinetic estimate of 22.1 ± 0.4 kcal mol^{-1}.

Of considerable interest in this example are the precise entropy values, $\Delta S_{gas\,phase}^{\ddagger} = 8(\pm 2)$ eu and $\Delta S_{obs}^{\ddagger}$(hexane) = 13(±1) eu. The observed activation entropy has increased in hexane as expected if $\Delta S_d^{\ddagger} - \Delta S_c^{\ddagger}$ is positive. Using eq. (6), the F_c value of 0.5 and $\Delta S_1^{\ddagger}$(soln) equal to $\Delta S_1^{\ddagger}$(gas) gives the $\Delta S_d^{\ddagger} - \Delta S_c^{\ddagger}$ difference as ~ +6 eu.

The data obtained in toluene are also of interest. The measured activation parameters in toluene, $\Delta H_{obs}^{\ddagger}$(toluene) = 22.3(±0.2) kcal mol^{-1} and $\Delta S_{obs}^{\ddagger}$(toluene) = 8(±1) eu, are the same within experimental error as the gas phase values and give the same rate constant within experimental error (k_1(25°C) = 2.0×10^{-2} s^{-1}) as observed in the gas phase. The simplest explanation is that there is no cage effect in toluene so that the rate-determining step is now k_1 with no contribution from k_d. A speculative reason for this is that the better coordinating toluene forms the solvent-separated cage pair $\overline{[Ni(CO)_3(\eta^2\text{-toluene})\,CO]}$, thereby preventing recombination. An alternative possibility, that has not been ruled out, is a differential solvation effect on the heterolytic (k_1) step that fortuitously counterbalances the cage effect; however, this seems unlikely since *both* $\Delta H_{obs}^{\ddagger}$ and $\Delta S_{obs}^{\ddagger}$ are identical to the gas phase values. Additional studies of this important system in additional solvents would be very valuable, although the toxicity of $Ni(CO)_4$ is of concern. Perhaps a related but alternative system, for example $Cr(CO)_6$,[19b,35d] could be substituted.

Another example worth noting is the thermolysis of α-phenylethylCo(DMG)$_2$py, Scheme 4; it is an important and unique case where both (mechanism-independent) equilibrium (thermodynamic) measurements and kinetic estimates are available for the same series of M—L complexes in toluene solution.[24a,b] When the reaction [see Scheme 4(a)] was carried out under an atmosphere of H_2, a metastable equilibrium was obtained. Equilibrium constants were measured as a function of temperature for five different axial nitrogeneous ligands, and

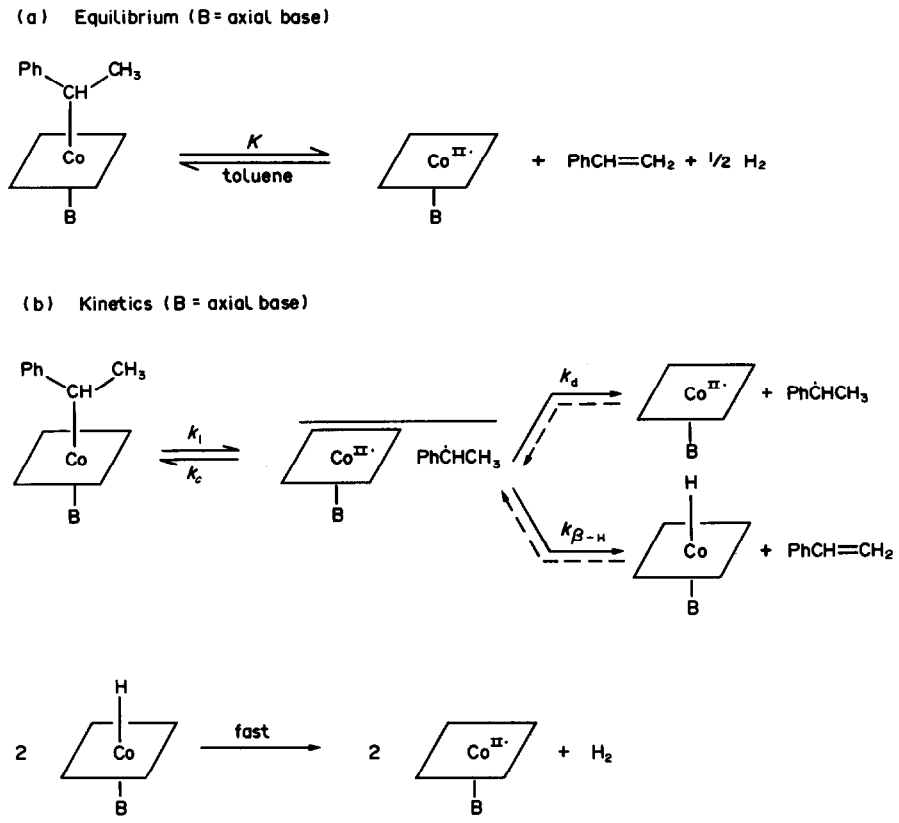

Scheme 4.

a van't Hoff plot provided ΔH for the reaction. Combining ΔH with the heats of formation of $C_6H_5CH{=}CH_2$ and the $C_6H_5C(H)(CH_3)^{\bullet}$ radical, a thermodynamic cycle yielded what was claimed[24a,b] as a Co—C BDE of 19.9 ($\pm \leqslant 0.5$) kcal mol^{-1}. However, the correct statement is that *if* one assumes δ solvation = 0, *then* the Co—C BDE is 19.9 kcal mol^{-1}.

When the reaction was carried out under N_2 in toluene, it proceeded to completion with a first-order loss of $Ph(CH_3)CH$—$Co(DMG)_2$(Base) that could be monitored spectrophotometrically [Scheme 4(b)]. Rate constants measured as a function of temperature yielded $\Delta H^{\ddagger}_{obs}$(soln) values ($\pm 0.5$ kcal mol^{-1}) that were an average of 2.0 ± 0.2 (range 1.7–2.2) higher than the thermodynamically determined BDE in toluene solution. ($\Delta H^{\ddagger}_{\eta}$ for toluene[44a] is $1.5(\pm 0.1)$ kcal mol^{-1}.)

Unfortunately, there is still uncertainty as to the nature of the rate-determining step in this example. The Bergman precedent[21] discussed back in Scheme 2 suggests that $k_{\beta-H}$ for β-hydrogen elimination might well be much faster than cage escape in this example; indeed the authors themselves speculated that[24b] "... it is probable that the β-H abstraction occurs within the solvent cage of the geminate $L(DMG)_2Co(II)^{\bullet}$, $^{\bullet}CH(CH_3)Ph$ radical pair". Moreover, a study that generates a $PhC(CH_3)_2^{\bullet}$ $^{\bullet}Co(CO)_4$ radical pair finds that β-H abstraction is competitive with cage escape[20c] and other studies confirm this finding.[20g] A reliable connection between $\Delta H^{\ddagger}_{obs}$(soln) and a Co—C BDE for this example will require a value for δ solvation and values for the components of eq. (7) [F_c, $\Delta H^{\ddagger}_d$, $\Delta H^{\ddagger}_c$ and $\Delta H^{\ddagger}_{-1}$(soln)] and perhaps also for $\Delta H^{\ddagger}_{\beta\text{-H}}$. This is another example where the superficial approach of ignoring the cage and subtracting a putative "universal correction factor of 2.0 kcal mol^{-1}" from all $\Delta H^{\ddagger}_{obs}$(soln) values is at best misleading and probably incorrect.[24b] Clearly, this example is not as well understood as one would like. Further studies, especially a value for F_c (perhaps from parallel studies where a free-radical scavenger has been added)* are needed.

* RSH free-radical scavengers, used in a separate study[24c] of $(CH_3)_2CHCo$(Saloph)py in pyridine that also involves β-H elimination, showed that most of the $(CH_3)_2CH^{\bullet}$ radicals escape the cage. However, since the solvent (py vs toluene), alkyl [$(CH_3)_2CH^{\bullet}$ vs $(Ph(CH_3)CH^{\bullet})$ and ligand ($Co(DMG)_2$ vs Co(Saloph)] are different, the relationship between these two examples, if any, is unclear.

SUMMARY

The major points discussed herein are four-fold:

(1) M—L thermolyses in solution include a cage effect in the general case, Scheme 3.

(2) The cage effect efficiency is a varaible, $0 < F_c < 1$, that is a function of temperature, solvent, pressure and variable M—L composition and structure. Furthermore, F_c values $\geqslant 0.5$ even in fluid solvents may be more common for M—L systems than for organic examples.

(3) Non-zero differential solvation effects between the gas phase and solution, δ solvation $\neq 0$, are expected. In some cases, the value of δ solvation could be a significant percentage of a $\Delta H^{\ddagger}_{obs}$(soln).

(4) Equations have been presented that provide the proper quantitative connection between $\Delta H^{\ddagger}_{obs}$ (soln) and M—L BDEs.

We note in closing that it is our intention to encourage $\Delta H^{\ddagger}_{obs}$(soln) measurements for M—L homolyses and heterolyses. Such measurements presently constitute a vital starting point for M—L BDE estimates, perhaps often good to *ca* 2–3 kcal mol^{-1} (the error bars of the best gas phase M—L BDEs currently available), once the proper equations and their indicated corrections are applied. It is hoped that the present contribution will serve as a stepping-stone for the further work necessary to obtain better M—L BDE estimates and to better understand cage effects in organo-transition metal chemistry.

Acknowledgements—Valuable comments on the manuscript were provided by Prof. David Tyler and Dr Bruce Martin. This work was supported in part by NIH Grant DK-26214.

REFERENCES

1. (a) J. Franck and E. Rabinowitch, *Trans. Faraday Soc.* 1934, **30**, 120; (b) E. Rabinowitch and W. C. Wood, *Trans. Faraday Soc.* 1936, **32**, 1381; (c) E. Rabinowitch, *Trans. Faraday Soc.* 1937, **33**, 1225.
2. (a) S. Glasstone, K. J. Laidler and H. Eyring, in *The Theory of Rate Processes*, Chap. IX. McGraw-Hill, New York (1941); (b) See also refs 13–15.
3. (a) R. M. Noyes, *J. Chem. Phys.* 1954, **22**, 1349; (b) R. M. Noyes, *Prog. Reaction Kinetics* 1961, **1**, 129; (c) R. M. Noyes, *J. Am. Chem. Soc.* 1955, **77**, 2042; (d) R. M. Noyes, *J. Am. Chem. Soc.* 1956, **78**, 5486.
4. (a) S. H. Northrup and J. T. Hynes, *J. Chem. Phys.* 1979, **71**, 871; (b) S. H. Northrup and J. T. Hynes, *J. Chem. Phys.* 1979, **71**, 884; (c) For four earlier papers in this series see: S. H. Northrup and J. T. Hynes, *J. Chem. Phys.* 1978, **69**, 5246; 5261 and refs therein.
5. (a) L. Herk, M. Feld and M. Szwarc, *J. Am. Chem. Soc.* 1961, **83**, 2998; (b) O. Dobis, J. M. Pearson and M. Szwarc, *J. Am. Chem. Soc.* 1968, **90**, 278; (c) K. Chakravorty, J. M. Pearson and M. Szwarc, *J. Am. Chem. Soc.* 1968, **90**, 283.
6. R. C. Lamb and J. G. Pacifici, *J. Am. Chem. Soc.* 1964, **86**, 914.
7. H. P. Waits and G. S. Hammond, *J. Am. Chem. Soc.* 1964, **86**, 1911 and refs therein.
8. (a) S. F. Nelsen and P. D. Bartlett, *J. Am. Chem. Soc.* 1966, **88**, 143; (b) F. E. Herkes, J. Friedman and P. D. Bartlett, *Int. J. Chem. Kinetics* 1969, **1**, 193.
9. (a) K.-W. Lee, N. Horowitz, J. Ware and L. A. Singer, *J. Am. Chem. Soc.* 1977, **99**, 2622; (b) W. A. Pryor and K. Smith, *J. Am. Chem. Soc.* 1970, **92**, 5403.
10. (a) T. Koenig and R. G. Finke, *J. Am. Chem. Soc.* 1988, **110**, 2657; (b) T. Koenig and H. Fischer, in *Free Radicals* (Edited by J. Kochi), Vol. 1, Chap. 4. John Wiley, New York (1973); (c) T. Koenig, in *Organic Free Radicals* (Edited by W. A. Pryor), Chap. 3 and refs therein, *ACS Symp. Ser.* 69, 1978; (d) T. Koenig and J. A. Hoobler, *Tetrahedron Lett.* 1972, 1803; (e) J. Owens and T. Koenig, *J. Org. Chem.* 1974, **39**, 3153; (f) R. C. Neuman Jr, *Acc. Chem. Res.* 1972, **5**, 381.
11. (a) N. J. Turro and B. Kraeutler, *Acc. Chem. Res.* 1980, **13**, 369; N. J. Turro, *Proc. Natl. Acad. Sci.* 1983, **80**, 609; (b) K. A. McLauchlan, *Sci. Prog., Oxf.* 1981, **67**, 509; (c) A. R. Lepley and G. L. Gloss (Eds), *Chemically Induced Magnetic Polarization.* Wiley, New York (1973); (d) D. Bethell and M. R. Brinkman, *Adv. Phys. Org. Chem.* 1973, **10**, 53; (e) R. Kaptein, *Adv. Free Radical Chem.* 1975, **5**, 319.
12. (a) P. S. Skell and H. N. Baxter III, *J. Am. Chem. Soc.* 1985, **107**, 2823; (b) W. von E. Doering and L. Birladeanu, *J. Am. Chem. Soc.* 1986, **108**, 7442; (c) P. S. Engel, *Chem. Rev.* 1980, **80**, 99.
13. S. A. Rice, in *Comprehensive Chemical Kinetics*, Vol. 25. Diffusion-limited reactions. Elsevier, Amsterdam (1985).
14. S. A. Rice, in *Comprehensive Chemical Kinetics*, Vol. 25. Diffusion-limited reactions. Chaps 6 and 8. Elsevier, Amsterdam (1985).
15. D. F. Evans, T. Tominaga and H. T. Davis, *J. Chem. Phys.* 1981, **74**, 1298.
16. (a) J. G. Huheey, *Inorganic Chemistry*, 3rd edn. Harper and Row, New York (1983); (b) B. Douglas, D. H. McDaniel and J. J. Alexander, *Concepts and Models of Inorganic Chemistry*, 2nd edn. John Wiley, New York (1983); (c) K. F. Purcell and J. C. Kotz, *An Introduction to Inorganic Chemistry.* Saunders College/Holt, Rinehart and Winston, Philadelphia (1980).
17. For example: (a) J. March, *Advanced Organic Chemistry: Reactions, Mechanisms and Structure*, 3rd edn, see pp. 466 and 613, which briefly discuss chemistry involving cage effects. Wiley-Interscience, New York (1985); (b) F. A. Carey and R. J. Sundberg, *Advanced*

Organic Chemistry, 2nd edn, Parts A, p. 633 and B. Plenum Press, New York (1984); (c) However, a discussion of cage effects is contained in: T. H. Lowry and K. S. Richardson, *Mechanism and Theory in Organic Chemistry*, 2nd edn. Harper and Row, New York (1981).

18. For example: (a) F. A. Cotton and G. Wilkinson, *Advanced Inorganic Chemistry*, 4th edn. Wiley-Interscience, New York (1980); (b) K. F. Purcell and J. C. Kotz, *Inorganic Chemistry*. W. B. Saunders, Philadelphia (1977).
19. (a) Cage effects are discussed, as one might expect, by Kochi in his organometallics text: J. K. Kochi, *Organometallic Mechanisms and Catalysis*, Academic Press, New York (1978) (see the index listing under cage processes); (b) Another exception is the following, where cage effects in M—L dissociations and ligand substitution reactions (p. 251) and oxidative addition (p. 308) are briefly discussed: J. P. Collman, L. S. Hegedus, J. R. Norton and R. G. Finke, *Principles and Applications of Organotransition Metal Chemistry*. University Science Books, Mill Valley, CA (1987); (c) J. D. Atwood, *Inorganic and Organometallic Mechanisms*. Brooks/Cole, Monterey, CA (1985); (d) C. M. Lukehart, *Fundamental Transition Metal Organometallic Chemistry*, Brooks/Cole, Monterey, CA (1985); (e) A. Yamamoto, *Organotransition Metal Chemistry: Fundamental Concepts and Applications*. John Wiley, New York (1986).
20. For example: (a) R. L. Sweany and J. Halpern, *J. Am. Chem. Soc.* 1977, **99**, 8335; (b) R. Sweany, S. C. Butler and J. Halpern, *J. Organomet. Chem.* 1981, **213**, 487; (c) T. E. Nalesnik and M. Orchin, *J. Organomet. Chem.* 1981, **222**, C5; (d) T. E. Nalesnik and M. Orchin, *Organometallics* 1982, **1**, 222; (e) Y. Matsui and M. Orchin, *J. Organomet. Chem.* 1983, **244**, 369; (f) J. W. Connolly, *Organometallics* 1984, **3**, 1333; (g) J. F. Garst, T. M. Bockman and R. Batlaw, *J. Am. Chem. Soc.* 1986, **108**, 1689; (h) B. Wassink, M. J. Thomas, S. C. Wright, D. J. Gillis and M. C. Baird, *J. Am. Chem. Soc.* 1987, **109**, 1995; (i) R. M. Bullock and E. G. Samsel, *J. Am. Chem. Soc.* 1987, **109**, 6542.
21. (a) E. N. Jacobsen and R. G. Bergman, *J. Am. Chem. Soc.* 1985, **107**, 2023; (b) See Table V.[21a]; (c) See the discussion, pp. 2028–2029.[21a]
22. (a) H. A. Skinner and J. A. Connor, *Pure and Applied Chem.* 1985, **57**, 79; (b) G. Pilcher and H. A. Skinner, in *The Chemistry of the Metal–Carbon Bond* (Edited by F. R. Hartlye and S. Patai), Chap. 2. John Wiley, New York (1982); (c) J. A. Connor, *Top. Cur. Chem.* 1977, **71**, 71; (d) J. U. Mondal and D. M. Blake, *Coord. Chem. Rev.* 1982, **47**, 205; (e) For a series of papers by Hoff and coworkers see: S. P. Nolan and C. D. Hoff, *J. Organomet. Chem.* 1985, **290**, 365 and refs therein.
23. (a) J. A. Simões, J. C. Schultz and J. L. Beauchamp, *Organometallics* 1985, **4**, 1238; (b) See ref. 22c, pp. 71–74 and refs 1 and 2 therein; (c) See the refs cited in: J. W. Bruno, T. J. Marks and L. R. Morss, *J. Am. Chem. Soc.* 1983, **105**, 6824; (d) S. W. Benson, *Thermochemical Kinetics*. McGraw-Hill, New York (1960).
24. (a) J. Halpern, F. T. T. Ng and G. L. Rempel, *J. Am. Chem. Soc.* 1979, **101**, 7124; (b) F. T. T. Ng, G. L. Rempel and J. Halpern, *J. Am. Chem. Soc.* 1982, **104**, 621; (c) T. T. Tsou, M. Loots and J. Halpern, *J. Am. Chem. Soc.* 1982, **104**, 623; (d) F. T. T. Ng, G. L. Rempel and J. Halpern, *Inorg. Chim. Acta.* 1983, **77**, L165; (e) M. K. Geno and J. Halpern, *J. Am. Chem. Soc.* 1987, **109**, 1238; (f) M. K. Geno and J. Halpern, *J. Chem. Soc., Chem. Commun.* 1987, 1052; (g) J. Halpern, *Bull. Chem. Soc. Jpn* 1988, **61**, 13. We thank Prof. Halpern for a preprint; (h) J. Halpern, S.-H. Kim and T. W. Leung, *J. Am. Chem. Soc.* 1984, **106**, 8317; (i) J. Halpern, *Pure Appl. Chem.* 1979, **51**, 2171; (j) J. Halpern, *Pure Appl. Chem.* 1983, **55**, 1059; (k) J. Halpern, *Pure Appl. Chem.* 1986, **58**, 575.
25. (a) R. G. Finke, B. L. Smith, B. J. Mayer and A. A. Molinero, *Inorg. Chem.* 1983, **22**, 3677; (b) R. G. Finke and B. P. Hay, *Inorg. Chem.* 1984, **23**, 3041; (c) B. P. Hay and R. G. Finke, *J. Am. Chem. Soc.* 1986, **108**, 4820; (d) B. P. Hay and R. G. Finke, *J. Am. Chem. Soc.* 1987, **109**, 8012; (e) R. G. Finke and M. Waddington, submitted; (f) B. P. Hay and R. G. Finke, *Polyhedron* 1988, **7**, 1469; (g) R. G. Finke and B. D. Martin, experiments in progress.
26. (a) J. P. Collman, L. McElwee-White, P. J. Brothers and E. Rose, *J. Am. Chem. Soc.* 1986, **108**, 1332; (b) Y. Ohgo, K. Orisaku, E. Hasegawa and S. Takeuchi, *Chem. Lett.* 1986, 27; S. Baba, Y. Ohgo and S. Takeuchi, *Bull. Chem. Soc. Jpn* 1987, **60**, 3967; (c) J. W. Suggs and C. H. Jun, *J. Am. Chem. Soc.* 1986, **108**, 4679; (d) A. Bakac and J. H. Espenson, *J. Am. Chem. Soc.* 1984, **106**, 5197.
27. D. F. McMillen and D. M. Golden, *Ann. Rev. Phys. Chem.* 1982, **33**, 493.
28. (a) J. A. Kerr, *Chem. Rev.* 1966, **66**, 465; (b) N. E. O'Neal and S. W. Benson, in *Free Radicals* (Edited by J. Kochi), Vol. 2. John Wiley, New York (1973); (c) S. W. Benson, *Thermochemical Kinetics*. McGraw-Hill, New York (1960).
29. (a) K. U. Ingold, in *Free Radicals* (Edited by J. K. Kochi), Vol. 1, Chap. 2, pp. 50–56. John Wiley, New York (1973); (c) See the discussion pp. 496–499 in ref. 27; (c) For examples cited by Koenig,[10b] see p. 179 and ref. 75 therein; (d) For an older discussion of this problem see pp. 278, 281–283 and 347–351 of ref. 28b.
30. J. P. Collman, L. S. Hegedus, J. R. Norton and R. G. Finke, *Principles and Applications of Organotransition Metal Chemistry*, Chap. 4.3, p. 239 and refs therein. University Science Books, Mill Valley, CA (1987).
31. J. L. Beauchamp, A. G. Stevens and R. R. Corderman, *Pure Appl. Chem.* 1979, **51**, 967.
32. J. W. Bruno, T. J. Marks and L. R. Morss, *J. Am. Chem. Soc.* 1983, **105**, 6824.
33. J. U. Mondal and D. M. Blake, *Coord. Chem. Rev.* 1982, **47**, 205 (see Table 7).
34. (a) A. E. Stiegman and D. R. Tyler, *Comm. Inorg.*

Chem. 1986, **5**, 215; (b) C. E. Philbin, C. A. Granatir and D. R. Tyler, *Inorg. Chem.* 1986, **25**, 4806; (c) G. D. Fallon and B. M. Gatehouse, *Cryst. Struct. Comm.* 1978, **1**, 263.

35. (a) A. J. Lees and A. W. Adamson, *Inorg. Chem.* 1981, **20**, 4381; (b) S. P. Church, F.-W. Grevels, H. Hermann and K. Schaffner, *Inorg. Chem.* 1985, **24**, 418; (c) G. K. Yang, K. S. Peters and V. Vaida, *Chem. Phys. Lett.* 1986, **125**, 566; J. D. Simon and K. S. Peters, *Chem. Phys. Lett.* 1983, **98**, 53; (d) K. E. Lewis, D. M. Golden and G. P. Smith, *J. Am. Chem. Soc.* 1984, **106**, 3905; (e) D. R. Tyler and D. P. Petrylak, *J. Organomet. Chem.* 1981, **212**, 389.
36. Hsing-Yeh Parker, C. E. Klopfenstein, R. A. Wielesek and T. Koenig, *J. Am. Chem. Soc.* 1985, **107**, 5276; Hsing-Yeh Parker, PhD dissertation, University of Oregon (1985).
37. (a) C. Walling, *Free Radicals in Solution*, pp. 530–534. John Wiley, New York (1957); (b) W. P. Neumann, W. Uzick and A. K. Zarkadis, *J. Am. Chem. Soc.* 1986, **108**, 3762.
38. (a) S. W. Benson, *Thermochemical Kinetics*, 2nd edn. John Wiley, New York (1976); S. W. Benson, *Foundations of Chemical Kinetics*. McGraw-Hill, New York (1960); (b) K. N. Houk and N. G. Rondan, *J. Am. Chem. Soc.* 1984, **106**, 4293.
39. C. Doubleday Jr, R. N. Camp, H. F. King, J. W. McIver Jr, D. Mullally and M. Page, *J. Am. Chem. Soc.* 1984, **106**, 447.
40. J. F. Endicott and T. Lo Netzel, *J. Am. Chem. Soc.* 1979, **101**, 4000.
41. (a) J. H. Grate and G. N. Schrauzer, *J. Am. Chem. Soc.* 1979, **101**, 4601; (b) G. N. Schrauzer and J. H. Grate, *J. Am. Chem. Soc.* 1981, **103**, 541.
42. K. N. V. Duong, A. Ahond, C. Merienne and A. J. Gaudemer, *J. Organomet. Chem.* 1973, **55**, 375.
43. H. B. Gjerde and J. H. Espenson, *Organometallics* 1982, **1**, 435.
44. (a) *International Critical Tables*, 1st edn, Vol. VII, p. 214. McGraw-Hill, New York (1930); (b) *Handbook of Chemistry and Physics*, 59th edn, p. F-51. CRC Press, Boca Raton, FL (1978); (c) K. K. Innes, *J. Phys. Chem.* 1956, **60**, 817; (d) L. H. Thomas, R. Meatyard, H. Smith and G. H. Davis, *J. Chem. Eng. Data* 1979, **24**, 161; (e) K. Raznjevic, *Handbook of Thermodynamic Tables and Charts*, McGraw-Hill, New York (1976); (f) H.-H. Schuh and H. Fischer, *Helv. Chim. Acta* 1978, **61**, 2130; (g) H. Schuh and H. Fischer, *Int. J. Chem. Kinetics* 1976, **8**, 341; (h) K. Tyuzyo, *Bull. Chem. Soc. Jpn* 1957, **30**, 782; (i) R. H. Ewell and H. Eyring, *J. Chem. Phys.* 1937, **5**, 726; (j) L. Herk, M. Feld and M. Szwarc, *J. Am. Chem. Soc.* 1961, **83**, 2998; (k) R. C. Lamb and J. G. Pacifici, *J. Am. Chem. Soc.* 1964, **86**, 914; (l) O. Dobis, J. M. Pearson and M. Szwarc, *J. Am. Chem. Soc.* 1986, **90**, 278.
45. J. P. Day, F. Basolo and R. G. Pearson, *J. Am. Chem. Soc.* 1968, **90**, 6927.
46. A. E. Stevens, C. S. Feigerle and W. C. Lineberger, *J. Am. Chem. Soc.* 1982, **104**, 5026.

Polyhedron Vol. 7, No. 16/17, pp. 1517–1529, 1988
Printed in Great Britain

0277–5387/88 $3.00+.00
© 1988 Pergamon Press plc

A NEW APPROACH TO MEASURING ABSOLUTE METAL–LIGAND BOND DISRUPTION ENTHALPIES IN ORGANOMETALLIC COMPOUNDS. THE $[(CH_3)_3SiC_5H_4]_3U$-SYSTEM

LAUREL E. SCHOCK, AFIF M. SEYAM, MICHAL SABAT and TOBIN J. MARKS*

Department of Chemistry, Northwestern University, Evanston, IL 60208, U.S.A.

Abstract—Absolute uranium–ligand bond disruption enthalpies in the series Cp''_3UR ($Cp'' = \eta^5$-$Me_3SiC_5H_4$) have been measured by halogenolytic isoperibol titration calorimetry of $Cp''_3U/Cp''_3UI/Cp''_3UR$ ensembles. Derived $D(Cp''_3U—R)$ values in toluene solution are (kcal mol^{-1}, R): 62.4(0.4), I; 28.9(1.7), *n*-Bu; 25.6(3.1), Bz; 39.3(2.3), CH_2SiMe_3; 44.8(1.1), Me; 48.5(2.2), vinyl; 86.7, C≡CPh. $D(Cp''_3U \leftarrow L)$ values (kcal mol^{-1}, 95% confidence limits) in toluene solution were also determined for L = CO [10.3(0.2)] and THF [9.8(0.2)]. The magnitudes of the D(U—R) values appear to reflect a combination of steric and electronic factors, and suggest that D(U—I) is less sensitive to ancillary ligation (more transferable) then D(U–alkoxide). The complex Cp''_3U(vinyl) crystallizes in the triclinic space group $P\bar{1}$ with two molecules in a unit cell of dimensions $a = 11.298(1)$, $b = 13.997(2)$, $c = 9.460(2)$ Å, and $\alpha = 97.00(1)$, $\beta = 105.98(1)$ and $\gamma = 96.94(1)°$. Least-squares refinement led to a value for the conventional R index (on F) of 0.0196 for 4373 reflections having $2\theta_{Mo\text{-}K_\alpha} < 50°$ and $I > 3\sigma(I)$. The molecule possesses a conventional pseudotetrahedral Cp_3MX geometry with U—C(ring) = 2.759(4) Å (average), U—C(α, vinyl) = 2.436(4) Å, ∢ U—C(α, vinyl)—C(β, vinyl) = 137.7(3)°, ∢ Cg—U—Cg = 116.4, 117.2, 120.0 and ∢ Cg—U—C(α, vinyl) = 95.1, 100.0, 100.1°. All hydrogen atoms were located and U—H(Cα, vinyl) = 2.93(4) Å. The metrical parameters evidence severe non-bonded repulsions between the vinyl ligand and the Cp'' ligands, as well as between different Cp'' ligands. The quantity D(M—I) − D(M—CH_3) is proposed as a gauge of metal–ligand bonding.

The current intense activity in organometallic thermochemistry[1,2] reflects the growing perception that metal–ligand bond energy data can provide unique insights into reaction pathways and metal–ligand bonding. Interest in this laboratory stems from our desire to better understand unusual transformations involving actinide, lanthanide and early transition metal complexes, as well as to predict new chemical transformations. Initial efforts[3] focused upon determining relative solution phase homolytic bond disruption enthalpies, D (as defined in eq. (1); note: all fragments are in structurally/electronically relaxed states),† by alcoholytic isoperibol titration calorimetry.[4]

$$D(L_nM—R) = \Delta H_f^\circ(L_nM) + \Delta H_f^\circ(R\cdot) - \Delta H_f^\circ(L_nM—R). \quad (1)$$

L_n = ancillary ligands.

Here R is understood to mean a hydrocarbyl, hydride, dialkylamide, etc. fragment. This approach assumes that the L_nM portion of the complex remains invariant and that the enthalpy of protonolysis can be expressed as the difference in enthalpies of bonds being made and broken [eqs (2), (3), where X = OR'].[3]

$$L_nM—R + HX \rightarrow L_nM—X + RH + \Delta H_{rx} \quad (2)$$

$$\Delta H_{rx} = D(L_nM—R) + D(H—X) - D(L_nM—X) - D(R—H). \quad (3)$$

*Author to whom correspondence should be addressed.

Observed and calculated structure-factor amplitudes are available from the Editor.

† This parameter is variously referred to as bond disruption enthalpy, bond dissociation enthalpy, bond enthalpy and bond energy. We employ the terminology of Pilcher and Skinner.[2(a)]

Furthermore, if $D(L_nM—X)$ is known accurately, the derived $D(L_nM—R)$ values can be placed on an absolute scale. It is assumed here that D values determined in non-polar solvents should reasonably approximate gas-phase data, however an actual conversion to the gas phase can be performed if necessary enthalpies of vaporization, sublimation and solution are available.[3] In initial organoactinide thermochemistry,[3] we showed that the derived *relative* $D(L_nAn—R)$ values (An = actinide) are extremely informative for understanding a large number of $L_nAn—R \rightarrow L_nAn—R''$ reaction patterns. In addition, it was of interest to place the data on an at least approximately absolute basis by estimating $D(L_nAn—OR')$. This was achieved using existing actinide[5] and group 4[5,6] absolute thermochemical data and the admittedly crude approximation of eq. (4) where M = Ti, Zr, Hf; X = halide and $\bar{D}$ denotes average bond dissociation enthalpy.

$$\frac{D(L_nAn—OR')}{\bar{D}(AnX_4)} \approx \frac{\bar{D}[M(OR)_4]}{\bar{D}(MX_4)}. \quad (4)$$

Subsequent studies have extended the approach of eqs (2) and (3) to group 4 metals, lanthanides and to halogenolytic calorimetry [eqs (5), (6)].[7,8]

$$L_nM—R + X_2 \rightarrow L_nM—X + RX + \Delta H_{rx}(5) \quad (5)$$

$$\Delta H_{rx}(5) = D(L_nM—R) + D(X—X) - D(L_nM—X) - D(R—X). \quad (6)$$

Beyond the above approximations, the more rigorous derivation of absolute metal–ligand bond enthalpies presents a challenge and all existing approaches (e.g. total combustion,[2(a,b)] pulsed laser pyrolysis,[2(f)] kinetic,[2(c,h)9] photoacoustic,[2(j),10] two-electron oxidative addition/reductive elimination [2(d),(j)]) have constraints which suggest limited applicability to many systems of current interest. We present here an approach to measuring absolute metal–hydrocarbyl (hydride, etc.) bond disruption enthalpies based upon one-electron redox processes. In essence, $L_nM/L_nMX/L_nMR$ ensembles are utilized to obtain absolute values of $D(L_nM—X)$ and $D(L_nM—R)$ as shown in eqs (7)–(11) where $\Delta H_{rx}(5)$ and $\Delta H_{rx}(8)$ are measured by titration calorimetry.

$$L_nM—R + X_2 \rightarrow L_nM—X + RX \quad \Delta H_{rx}(5) \quad (7)$$

$$L_nM—X \rightarrow L_nM + 1/2\,X_2 \quad \Delta H_{rx}(8) \quad (8)$$

$$X\cdot \rightarrow 1/2X_2 \quad 1/2\,D(X—X) \quad (9)$$

$$R—X \rightarrow R\cdot + X\cdot \quad D(R—X) \quad (10)$$

$$L_nM—R \rightarrow L_nM + R\cdot \quad D(L_nM—R). \quad (11)$$

Although we illustrate this approach with $L_nM = C\overset{''}{p}_3U$ ($C\overset{''}{p} = \eta^5$-$Me_3SiC_5H_4$), the generality of the method should be apparent. The present study provides an important calibration of the eq. (4) approximation for uranium. In view of the results and in an effort to assess the influence of U—R distance and steric crowding on $D(U—R)$, we also report a structural analysis of $C\overset{''}{p}_3UCH{=}CH_2$ by single-crystal X-ray diffusion.

EXPERIMENTAL

General methods

All procedures were performed using standard techniques for air-sensitive compounds. ^{1}H NMR spectra were recorded on a Jeol FX-90 (90 MHz), Jeol FX-270 (270 MHz) or Varian XL-400 (400 MHz) spectrometer. IR spectra were recorded on a Perkin–Elmer 283 spectrometer with Nujol mulls sandwiched between salt (KBr, NaCl) plates in an o-ring sealed, air-tight holder. Elemental analyses were performed by Dornis and Kolbe Mikroanalytisches Laboratortium, Müllheim, F.R.G.

Syntheses

The compounds $C\overset{''}{p}_3U$ (**1**) and $C\overset{''}{p}_3UCl$ (**2**) were prepared as described by Brennan *et al.*[11]

$C\overset{''}{p}_3UMe$ (**3**). To a solution of 1.00 g (1.46 mmol) of $C\overset{''}{p}_3UCl$ in 15 cm^3 of diethyl ether at −78°C was added by syringe 1.2 cm^3 (1.4 M, 1.7 mmol) of MeLi·LiBr in diethyl ether. The reaction mixture was stirred at −78°C for 15 h, then at room temperature for 0.5 h. The solvent was then removed *in vacuo* and *ca* 10 cm^3 of pentane distilled into the reaction vessel. The solution was stirred at room temperature and then filtered. After washing the precipitate on the frit twice with *ca* 5 cm^3 of pentane, the solution was reduced in volume to *ca* 5 cm^3 and then cooled to −78°C. The resulting orange needles were collected by cold filtration and dried *in vacuo* at −20°C. Upon warming to room temperature, the crystals became a red liquid (0.79 g, 81% yield).

^{1}H NMR (C_6D_6): δ 8.33 (s, 6 H); −5.67 (s, 27 H); −6.27 (s, 6 H); −199.02 (s, 3 H). IR (Nujol, cm^{-1}): 3100 (m), 1950 (w, br), 1410 (s), 1318 (m), 1250 (vs), 1180 (vs), 1110 (m), 1068 (sh), 1045 (vs), 902 (vs), 815 (vs, br), 750 (vs), 588 (s), 632 (s), 620 (s), 525 (w), 497 (w, br), 424 (m), 403 (w). Analysis. Found: C, 45.26; H, 6.25. Calc. for $C_{25}H_{42}Si_3U$: C, 45.16; H, 6.37%.

$C\overset{''}{p}_3U(n\text{-Bu})$ (**4**). To a solution of 1.10 g (1.61 mmol) of $C\overset{''}{p}_3UCl$ in 25 cm^3 of toluene at −78°C

was added by syringe 1.0 cm^3 (1.6 M, 1.6 mmol) of *n*-BuLi in hexane. The solution was stirred at −78°C for 11 h and then at room temperature for 2 h. The red solution was then filtered and evaporated to dryness. The resulting solid was next dissolved in *ca* 5 cm^3 pentane and the resulting solution cooled slowly to −78°C to give 1.03 g of dark red crystals which were collected by filtration (90% yield).

^{1}H NMR (C_6D_6): δ 1.22 (s, 6 H); −2.11 (s, 6 H); −4. 26 (s, 27 H); −11.92 (t, 3 H); −20.20 (m, 2 H); −24.46 (m, 2 H); −190.01 (d, 2 H). IR (Nujol, cm^{-1}): 1251 (s), 1180 (m), 1140 (m), 901 (m), 831 (vs), 781 (s), 776 (sh), 750 (m), 718 (w), 707 (w), 632 (w), 618 (w). Analysis. Found: C, 47.36; H, 6.73. Calc. for $C_{28}H_{48}Si_3U$: C, 47.57; H, 6.84%.

$C\overline{p}''_3U(CH_2SiMe_3)$ (**5**). Diethyl ether (20 cm^3) was distilled into a reaction apparatus containing 1.05 g (1.53 mmol) of $C\overline{p}''_3UCl$ and 0.15 g (1.59 mmol) of $LiCH_2SiMe_3$ at −78°C. The reaction was allowed to warm up to room temperature with stirring and was stirred for an additional 20 h. The solvent was then removed *in vacuo* to give a red oil. Pentane (*ca* 20 cm^3) was distilled into the vessel and the resulting solution filtered. The filtrate was reduced to *ca* 3 cm^3 and slowly cooled to −78°C. After filtration and drying *in vacuo*, 0.78 g of dark red crystals were obtained (69% yield).

^{1}H NMR (toluene-d_8): δ −0.73 (s, 6 H); −0.83 (s, 6 H); −4.40 (s, 27 H); −8.69 (s, 9 H); −207.11 (s, 2 H). IR (Nujol, cm^{-1}): 1250 (s), 1178 (m), 1067 (w), 1042 (s), 915 (sh), 900 (s), 830 (vs), 777 (s), 750 (s), 717 (sh), 685 (w), 666 (w), 631 (m), 618 (m). Analysis. Found: C, 45.49; H, 6.87. Calc. for $C_{28}H_{50}Si_4U$: C, 45.63; H, 6.84%.

$C\overline{p}''_3UBz$ (**6**). Diethyl ether (10 cm^3) was distilled into a reaction apparatus containing 1.00 g (1.46 mmol) of $C\overline{p}''_3UCl$ and 0.31 g (1.50 mmol) of LiBz·1.5 THF. The solution was stirred for 2 h at −78°C and then for an additional 10 h at room temperature. The solvent was then removed *in vacuo* and *ca* 10 cm^3 of pentane distilled into the vessel. The resulting solution was filtered and the precipitate remaining on the frit was washed twice with *ca* 5 cm^3 of pentane. The filtrate was then reduced in volume to *ca* 5 cm^3 and cooled slowly to −78°C. After recrystallization from 5 cm^3 of pentane, 0.77 g of black crystals were obtained (71% yield).

^{1}H NMR (toluene-d_8): δ 1.24 (t, 2 H); 0.46 (s, 6 H); −0.43 (s, 6 H); −3.71 (t, 1 H); −4.20 (s, 27 H); −22.90 (d, 2 H); −213.66 (s, 2 H). IR (Nujol, cm^{-1}): 1600 (m), 1250 (s), 1207 (m), 1177 (m), 1070 (w), 1042 (s), 1001 (w), 965 (m), 960 (sh), 900 (s), 830 (vs), 797 (sh), 779 (s), 749 (s), 737 (sh), 717 (sh), 694 (m), 686 (sh), 631 (m), 618 (m), 557 (w), 520 (w). Analysis. Found: C, 50.10; H, 6.30. Calc. for $C_{31}H_{47}Si_3U$: C, 50.25; H, 6.26%.

$C\overline{p}''_3U(CCPh)$ (**7**). Diethyl ether (20 cm^3) was distilled into a reaction apparatus at −78°C containing 1.00 g (1.46 mmol) of $C\overline{p}''_3UCl$ and 0.17 g (1.57 mmol) of LiCCPh.[12] The reaction mixture was stirred for 2 h at −78°C and then for a further 1 h at room temperature. The solvent was removed and the golden brown residue dried *in vacuo*. Pentane (*ca* 15 cm^3) was then distilled into the vessel and the solution stirred at room temperature. The solution was then filtered and the precipitate remaining on the frit was washed with *ca* 10 cm^3 of pentane. The filtrate was reduced in volume to *ca* 5 cm^3 and cooled slowly to −78°C to give black crystals. Recrystallization from 3 cm^3 of pentane yielded 0.90 g of black brick-like crystals (82% yield).

^{1}H NMR (C_6D_6): δ 15.15 (s, 6 H); 6.40 (t, 1 H); −1.52 (t, 2 H); −6.61 (d, 2 H); −6.93 (s, 27 H); −8.68 (s, 6 H). IR (Nujol, cm^{-1}): 2050 (m, br), 1601 (m), 1576 (sh), 1490 (s), 1410 (w), 1262 (sh), 1248 (s), 1240 (sh), 1198 (m), 1177 (s), 1070 (w), 1046 (sh), 1040 (s), 1024 (w), 900 (s), 830 (vs), 780 (vs), 750 (s), 718 (sh), 688 (s), 630 (m), 618 (m), 532 (w), 544 (w). Analysis. Found: C, 50.99; H, 5.93. Calc. for $C_{32}H_{44}Si_3U$: C, 51.18; H, 5.90%.

$C\overline{p}''_3UCHCH_2$ (**8**). Diethyl ether (20 cm^3) was distilled into a reaction apparatus containing 0.87 g (1.27 mmol) of $C\overline{p}''_3UCl$ and 0.051 g (1.50 mmol) of $LiCHCH_2$ at −78°C. The reaction mixture was stirred for 45 h at −78°C and then allowed to warm to room temperature over *ca* 1.5 h. The solvent was then removed *in vacuo* and the residue extracted with *ca* 5 cm^3 of pentane. The volume of the filtrate was then reduced to *ca* 3 cm^3 and the solution slowly cooled to −78°C to give dark red, rectangular crystals (0.80 g, 93% yield).

^{1}H NMR (C_6D_6): δ 34.30 (d, 1 H); 10.01 (s, 6 H); −5.06 (s, 6 H); −6.68 (s, 27 H); −8.30 (d, 1 H); −163.00 (t, 1 H). IR (Nujol, cm^{-1}): 1250 (s), 1195 (w), 1178 (m), 1042 (s), 964 (w), 918 (w), 900 (s), 832 (vs), 778 (s), 750 (s), 718 (w), 685 (w), 618 (m). Analysis. Found: 45.98; H, 6.20. Calc. for $C_{26}H_{42}Si_3U$: C, 46.13; H, 6.25%.

$C\overline{p}''_3UI$ (**9**). Toluene (5 cm^3) was distilled into a frit reaction apparatus containing 0.10 g (0.15 mmol) of $C\overline{p}''_3U$ and 0.02 g (0.08 mmol) of I_2. The green solution immediately became red and after several minutes of stirring, the volatiles were removed *in vacuo*. The residue was next extracted with pentane, filtered and the resulting filtrate cooled to −78°C. The resulting red needle-like crystals were then collected by filtration and dried *in vacuo* to give 0.10 g of product (86% yield).

^{1}H NMR (toluene-d_8): δ 3.43 (s, 6 H); −3.85 (s, 27 H); −6.78 (s, 6 H). IR (Nujol, cm^{-1}):

1251 (s), 1178 (m), 1042 (s), 900 (s), 835 (vs), 790 (s), 752 (m), 720 (m), 686 (w), 632 (m), 618 (w). Analysis. Found: C, 37.14; H, 5.04. Calc. for $C_{24}H_{39}Si_3IU$: C, 37.11; H, 5.06%.

NMR titrations

Prior to a calorimetric experiment, a solution containing a measured quantity of the uranium compound of interest in C_6D_6 or toluene-d_8 was placed in a Wilmad screw-capped NMR tube fitted with a septum. This solution was titrated with a standard solution of I_2 in C_6D_6 by injecting the latter in portions through the septum with a syringe, followed by vigorous shaking. The titration was monitored by ^1H NMR to determine if the reaction was quantitative and sufficiently rapid for accurate calorimetry. This was found to be the case for Cp''_3U and all Cp''_3UR complexes.

Titration calorimetry

The anaerobic calorimeter design[13] employed in these studies and the experimental procedure used[7(b)] are described elsewhere. Briefly, ampoules containing measured quantities of the organouranium complex are broken in the toluene-filled calorimeter reaction dewar and the heat of solution in toluene measured. Next, a solution of the titrant in toluene is titrated into the reaction dewar and the enthalpy of the reaction per mol of titrant is obtained by the procedure described in the above two references. For reaction of Cp''_3U with THF or CO, a solution of Cp''_3U in toluene was titrated into a toluene solution containing an excess of THF or CO.

X-ray crystallographic study of $Cp''_3UCH{=}CH_2$ (7)

Crystals of $Cp''_3UCH{=}CH_2$ were grown by slow cooling of pentane solutions. Specimens suitable for X-ray analysis were sealed in glass capillaries under an inert atmosphere. All measurements were performed on an Enraf–Nonius CAD4 diffractometer at −120°C using Mo-K_α radiation. Experimental details are given in Table 1. Intensities of four standard reflections were remeasured after every 3 h of X-ray exposure and showed no significant decay. Intensity data were subsequently corrected for Lorentz-polarization effects and empirical absorption corrections were applied from psi scans of eight Bragg reflections. The transmission factors were in the range 0.44–1.00. All calculations were performed on a VAX11/730 computer using the TEXSAN crystallographic software package.[14] The structure was solved by heavy-atom methods (Patterson and Fourier techniques). The full-matrix least-squares refinement with anisotropic thermal parameters for all non-hydrogen atoms gave a final R of 0.0196 ($R_w = 0.0254$). All H atoms were located from difference Fourier maps and were included in the refinement with isotropic thermal parameters. The largest peak in the final difference density map (1.45 e Å^{-3}) was located in the vicinity of the U atom.

Table 1. Summary of crystal structure data

Formula	$C_{26}H_{42}Si_3U$
m	676.90
Crystal size (mm)	0.43 × 0.27 × 0.18
Crystal system	Triclinic
Space group	$P\bar{1}$
a (Å)	11.298(1)
b (Å)	13.997(2)
c (Å)	9.460(2)
α (deg)	97.00(1)
β (deg)	105.98(1)
γ (deg)	86.94(1)
V (Å^3)	1427.2(7)
Z	2
d_{calc} (g cm^{-3})	1.58
μ (Mo-K_α) (cm^{-1})	55.3
Radiation	Graphite-monochromated Mo-K_α, $\lambda = 0.71069$ Å
Scan type	$\theta/2\theta$
2θ range (deg)	4–50
Scan width (deg)	$0.80+0.35\tan\theta$
Unique data	5005
Unique data with $I > 3\sigma(I)$	4373
No. of parameters	439
$R(F)$	0.0196
$R_w(F)$	0.0254
GOF	0.90

RESULTS

Synthesis and chemistry

Complexes of the type Cp''_3UR ($Cp'' = \eta^5$-$Me_3SiC_5H_4$) were prepared from Cp''_3UCl[11] and lithium reagents using procedures we have described elsewhere[15] [eq. (12)].

$$Cp''_3UCl + RLi \xrightarrow[\text{or ether}]{\text{toluene}} Cp''_3UR + LiCl$$

3, R = CH_3

4, R = *n*-Bu

5, R = CH_2SiMe_3

6, R = Bz

7, R = $CH{=}CH_2$

8, R = C≡CPh. (12)

Table 2. Enthalpies of solution in toluene, enthalpies of reaction with I_2 in toluene (per mol of I_2), and the derived bond disruption enthalpies of $C\overline{p}_3U$ and $C\overline{p}_3UR$ complexes in kcal mol^{-1}

Compound	ΔH_{soln}[a]	$-\Delta H_{rxn}$[a]	$D(U—R)_{soln}$[b]	R
$C\overline{p}_3UI$ (**9**)	3.82(0.53)			
$C\overline{p}_3U$ (**1**)	4.49(0.14)	89.3(0.4)	62.4(0.4)	I
$C\overline{p}_3U(n\text{-Bu})$ (**4**)	5.22(0.39)	46.9(0.3)	28.9(1.7)	*n*-Bu
$C\overline{p}_3UBz$ (**6**)	5.13(0.11)	40.5(0.2)	25.6(3.1)	Bz
$C\overline{p}_3UCH_2SiMe_3$ (**5**)	3.82(0.95)	41.8(0.5)	39.3(2.3)	CH_2SiMe_3
$C\overline{p}_3UMe$ (**3**)	0.44(0.30)[c]	39.4(0.4)	44.8(1.1)	Me
$C\overline{p}_3UCHCH_2$ (**8**)	5.10(0.50)	38.3(0.5)	48.5(2.2)[d]	vinyl
$C\overline{p}_3UC{\equiv}CPh$ (**7**)	5.08(0.19)	16.1(0.4)	86.7[e]	C≡CPh

[a] Quantities in parentheses are 95% confidence limits (see text).

[b] Quantities in parentheses are derived from 95% confidence limits in present calorimetric data plus reported uncertainties in literature data used to calculate D(U—R) (see text).

[c] This substance is a liquid at room temperature.

[d] A standard deviation is not reported for D(vinyl–I).[20(d)] We take it to be the average of the standard deviations of the other D(R—I) data used in Table 2.

[e] Based upon an estimated D(R—I) value (see text).

These new compounds were characterized by standard methodology (see Experimental for details). In contrast to results in the Cp_3UR series,[15] all attempts to prepare secondary alkyls (e.g. Ph) resulted in decomposition to unknown products.

On monitoring by ^1H NMR spectroscopy, solutions of the complexes $C\overline{p}_3U$ and $C\overline{p}_3UR$ are seen to undergo a quantitative and rapid reaction with I_2 as shown in eqs (13) and (14).

$$C\overline{p}_3U + 1/2I_2 \rightarrow C\overline{p}_3UI \qquad (13)$$

$$C\overline{p}_3UR + I_2 \rightarrow C\overline{p}_3UI + RI. \qquad (14)$$

The complex $C\overline{p}_3UI$ was also synthesized on a preparative scale and characterized by standard techniques. Reactions of $(RC_5H_4)_3U$ with CO (R = $SiMe_3$) and THF (R = CH_3) [eq. (15)] have been characterized by Andersen *et al.*[11,16]

$$(RC_5H_4)_3U + L \rightarrow (RC_5H_4)_3U \leftarrow L \qquad (15)$$

$$L = CO, THF.$$

Thermochemistry

Calorimetry data pertaining to eqs (13) and (14) are set out in Table 2. In all cases, titration endpoints were found at stoichiometries consistent with the expected chemistry. The derivation of D(U—R) values from solution data assumes that solvation effects in toluene are minor or at least cancel out. The organouranium ΔH_{soln} data in Table 2 confirm this and literature data or reasonable estimation procedures indicate the ΔH_{soln} values for RI products,[17] THF (estimated),[17] and CO[18] will be less than *ca* 1 kcal mol^{-1}. For I_2 in benzene, ΔH_{soln} is a somewhat larger 3.85(0.05) kcal mol^{-1}.[17] However, this contribution largely cancels in the derivation of D(U—R) [eqs (7)–(10)]. Experimental calorimetry data in Table 2 are reported with 95% confidence limits.[19] For the derivation of D(U—I) and D(U—R), requisite $D(I_2)$ and D(R—I) data are taken from the literature[20] and the reported experimental uncertainties are incorporated in our calculations. In the case of R = —C≡CPh, D(R—I) has not been reported. It was estimated from existing D(R—H) data[20(a)] using the reasonable proportionality of eq. (16).

$$\frac{D(R—I)}{D(R—H)} \approx \frac{D(Ph—I)}{D(Ph—H)}. \qquad (16)$$

Calorimetry data pertaining to eq. (15) are presented in Table 3. Measurements were made by titrating a toluene solution of **1** into a solution containing an excess of CO or THF. Values of D(U—L) assume 1 : 1 complex formation[11,16] and are reported with 95% confidence limits.

Table 3. Enthalpies of reaction of $C\overline{p}_3U$ (**1**) with Lewis bases in toluene (per mol of **1**) and derived $C\overline{p}_3U$—L bond disruption enthalpies in kcal mol^{-1}

Compound	Reagent(L)	$-\Delta H_{rxn}$[a]	D(U—L)[a]
$C\overline{p}_3U$	CO	10.3(0.2)	10.3(0.2)
$C\overline{p}_3U$	THF	9.8(0.2)	9.8(0.2)

[a] Quantities in parentheses are 95% confidence limits (see text).

Molecular structure of $(Me_3SiC_5H_4)_3UCH{=}CH_2$ (7)

The structural analysis indicates that crystals of 7 are composed of unassociated, mononuclear $Cp''_3UCH{=}CH_2$ molecules as shown in Fig. 1. Final atomic coordinates and anisotropic displacement parameters for all atoms of 7 are given in Tables 4 and 5,* respectively, according to the atom-labelling scheme of Fig. 1. Bond lengths and angles are given in Table 6. The present study is unique in that all hydrogen atoms could be located and refined. The basic structural motif of 7 is the pseudo-tetrahedral Cp_3MX configuration found in numerous organoactinides.[21] The average U—C(ring) distance is found to be 2.759 (4,25,71,15) Å,† the Cg—U—Cg (Cg = ring centre-of-gravity) angles 116.4° (ring 1—U—ring 2), 117.2° (ring 1—U—ring 3), 120.0° (ring 2—U—ring 3), and the Cg—U—C(1) angles, 95.1° (ring 1), 100.0° (ring 2), and 100.2° (ring 3). These parameters compare favourably with corresponding values of 2.733(1) Å, 117.0°(av), 100.0°(av) in $(BzC_5H_4)_3UCl$;[22] 2.74 Å, 117.2(av), 99.7°(av) in Cp_3UF;[23] 2.74 Å, 117.3°(av), 99.7°(av) in Cp_3U(2-methylallyl);[24] and 2.77(6) Å, 116.2°(av), 101.9°(av) in $[(MeC_5H_4)_3U]_2S$.[25] Parameters in other Cp_3UR complexes (R = C≡CPh,[26] *n*-butyl,[27] C≡CH[28] and *p*-methylbenzyl[27] are closely comparable.

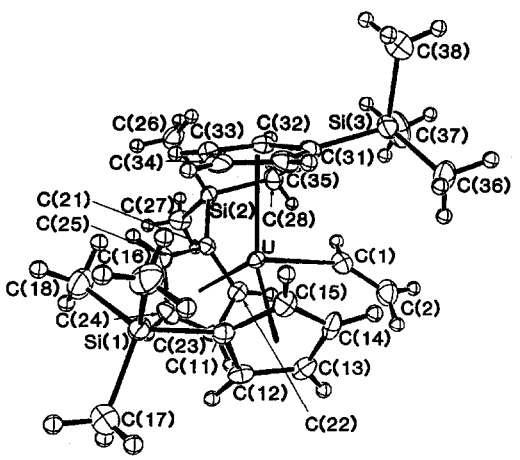

Fig. 1. Perspective drawing of the molecular structure of $(Me_3SiC_5H_4)_3UCH{=}CH_2$ (7). The shapes of the ellipsoids correspond to 30% probability contours of atomic displacement. Ring labelling code: ring 1, C(11)—C(15); ring 2, C(21)—C(25); ring 3, C(31)—C(35).

The U—C(1) distance in 7, 2.436(4) Å, can be compared to the U—C(*sp*) sigma bond distances of 2.32(2) and 2.36(3) Å in $Cp_3UC{\equiv}CPh$[26] and $Cp_3UC{\equiv}CH$,[28] respectively. Corresponding distances for U—C(sp^3) complexes are 2.43(2) Å in Cp_3U(*n*-butyl)[27], 2.54(2) Å in Cp_3U(*p*-methylbenzyl)[27] and 2.48(3) Å in Cp_3U(2-methylallyl).[23] While the precision of these data does not permit extensive metrical analysis, a comparison with the extensive data base for more electron-rich square-planar Pt(II) hydrocarbyl complexes[29] is interesting. In both series, the contraction in metal–carbon sigma bond distances for an $sp^3 \rightarrow sp^2 \rightarrow sp$ carbon is in the direction expected.[30] However, the dispersion in Pt—C distances (Pt–acetylide ≈ 1.99 Å; Pt–vinyl ≈ 2.03 Å; Pt–alkyl ≈ 2.10 Å) appears to be somewhat less than in the Cp_3U—R system, especially for C(*sp*) vs C(sp^2). Possible explanations for what may be a slight contraction in the U—C≡C— distance include actinide–acetylide π-bonding[31] (*vide infra*, analogous to that in actinide alkoxides[32]), the greater polarity of actinide–hydrocarbyl bonding, as well as lessened intramolecular non-bonded repulsions versus α-substituted alkyls (*vide infra*).

The U—C(1)—C(2) angle of 137.7(3)° in 7 is somewhat in excess of angles nearer 125° in platinum metal vinyl complexes.[29] Anomalously large metal–C(α)–C(β) angles have been noted in a number of actinide hydrocarbyls,[27,33] and have been ascribed to various combinations of non-bonded repulsions and α-C—H···metal interactions (**A**).[21(a)-(c),33,34]

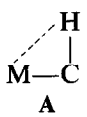

A

All hydrogen atoms were located in the present structure determination and the U—H(1) distance was found to be 2.93(4) Å. Bearing in mind a U(IV) → Th(IV) ionic radius correction[35] of +0.04 Å, this parameter can be compared to C(α)—H···Th contacts of 2.597(9) and 2.648(9) Å in $Cp'_2Th(CH_2CMe_3)_2$[33] as well as to Th—H(terminal) and Th—H(bridge) distance of 2.03(1) and 2.29(3) Å, respectively, in $[Cp'_2Th(\mu\text{-}H)H]_2$.[36] The magnitude of the interaction is clearly weaker in 7.

A number of rather severe interligand non-bonded interactions are evident in the molecular structure of 7. These include close contacts to C(1) by C(22) (3.003(5) Å), C(31) (3.247(5) Å), C(14) (3.290(5) Å), C(13) (3.312(5) Å), C(32) (3.520(6) Å)

* See footnote on p. 1517 regarding the supplementary material.

† The first number in parentheses following an averaged value of a bond length or angle is the estimated standard deviation of an individual datum. The second and third numbers are the average and maximum deviations from the averaged value, respectively. The fourth number represents the number of individual measurements that are included in the average value.

Table 4. Positional parameters for $(Me_3SiC_5H_4)_3UCH{=}CH_2$ (7)

Atom	x	y	z	Atom	x	y	z
U	−0.1128(1)	0.216002(9)	0.22019(1)	H(15)	0.137(4)	0.336(3)	0.264(4)
Si(1)	0.2054(1)	0.25140(8)	0.5581(1)	H(16)A	0.296(6)	0.395(4)	0.672(7)
Si(2)	−0.47631(9)	0.15447(8)	0.2372(1)	H(16)B	0.318(7)	0.371(5)	0.514(8)
Si(3)	−0.2643(1)	0.42890(8)	−0.0707(1)	H(16)C	0.211(5)	0.418(4)	0.548(6)
C(1)	−0.2082(4)	0.1744(3)	−0.0423(4)	H(17)A	0.387(6)	0.168(5)	0.579(8)
C(2)	−0.1746(5)	0.1409(3)	−0.1618(5)	H(17)B	0.300(5)	0.100(4)	0.613(6)
C(11)	0.1382(3)	0.2156(3)	0.3564(4)	H(17)C	0.379(5)	0.183(4)	0.737(7)
C(12)	0.1149(3)	0.1200(3)	0.2834(4)	H(18)A	0.068(8)	0.194(7)	0.69(1)
C(13)	0.0813(3)	0.1228(3)	0.1293(5)	H(18)B	0.125(4)	0.289(4)	0.769(6)
C(14)	0.0859(3)	0.2193(3)	0.1028(4)	H(18)C	0.024(6)	0.293(4)	0.631(7)
C(15)	0.1230(3)	0.2748(3)	0.2407(4)	H(22)	−0.294(3)	0.035(3)	0.073(4)
C(16)	0.2631(4)	0.3758(3)	0.5798(6)	H(23)	−0.092(4)	−0.011(3)	0.218(4)
C(17)	0.3314(4)	0.1632(4)	0.6267(5)	H(24)	−0.037(4)	0.078(3)	0.467(5)
C(18)	0.0931(5)	0.2505(4)	0.6711(5)	H(25)	−0.225(3)	0.174(3)	0.496(4)
C(21)	−0.3087(3)	0.1238(3)	0.2696(4)	H(26)A	−0.595(5)	0.262(4)	0.330(6)
C(22)	−0.2570(3)	0.0554(3)	0.1784(4)	H(26)B	−0.469(4)	0.325(4)	0.336(5)
C(23)	−0.1381(4)	0.0289(3)	0.2575(5)	H(26)C	−0.461(5)	0.253(4)	0.470(7)
C(24)	−0.1128(3)	0.0797(3)	0.4007(5)	H(27)A	−0.523(5)	0.041(4)	0.382(6)
C(25)	−0.2171(3)	0.1383(3)	0.4081(4)	H(27)B	−0.541(5)	−0.014(5)	0.219(7)
C(26)	−0.5036(4)	0.2620(3)	0.3629(5)	H(27)C	−0.630(6)	0.062(4)	0.270(6)
C(27)	−0.5498(4)	0.0495(3)	0.2803(6)	H(28)A	−0.628(5)	0.173(4)	0.024(5)
C(28)	−0.5495(4)	0.1737(4)	0.0407(5)	H(28)B	−0.520(4)	0.225(3)	−0.001(5)
C(31)	−0.2147(3)	0.3921(3)	0.1201(4)	H(28)C	−0.540(6)	0.124(5)	−0.029(7)
C(32)	−0.2892(3)	0.3595(3)	0.2032(4)	H(32)	−0.374(3)	0.337(3)	0.156(4)
C(33)	−0.2216(4)	0.3640(3)	0.3527(4)	H(33)	−0.251(4)	0.340(3)	0.422(5)
C(34)	−0.1037(4)	0.3974(3)	0.3649(5)	H(34)	−0.039(4)	0.408(3)	0.450(5)
C(35)	−0.1000(4)	0.4144(3)	0.2242(5)	H(35)	−0.039(4)	0.445(3)	0.200(5)
C(36)	−0.1407(5)	0.4043(4)	−0.1665(6)	H(36)A	−0.157(5)	0.435(5)	−0.265(7)
C(37)	−0.4090(5)	0.3699(5)	−0.1828(6)	H(36)B	−0.132(4)	0.334(4)	−0.196(5)
C(38)	−0.2922(7)	0.5622(4)	−0.0474(7)	H(36)C	−0.061(8)	0.419(6)	−0.111(9)
H(1)	−0.299(4)	0.173(3)	−0.061(5)	H(37)A	−0.417(8)	0.312(7)	−0.18(1)
H(2)A	−0.227(5)	0.127(4)	−0.260(6)	H(37)B	−0.476(6)	0.388(5)	−0.116(7)
H(2)B	−0.087(4)	0.128(3)	−0.157(4)	H(37)C	−0.444(6)	0.393(5)	−0.272(7)
H(12)	0.119(4)	0.062(3)	0.334(3)	H(38)A	−0.357(6)	0.578(5)	0.013(7)
H(13)	0.063(4)	0.067(4)	0.056(5)	H(38)B	−0.312(6)	0.591(5)	−0.136(7)
H(14)	0.071(3)	0.244(3)	0.012(5)	H(38)C	−0.227(6)	0.596(5)	0.019(8)

and C(23) (3.580(6) Å). Such contacts are considerably less than the sum of van der Waals radii for CH_3 or CH_2 groups (4.0 Å).[30(a)]* In addition, close ring–ring contacts include C(12)—C(23) = 3.128(5) Å, C(12)—C(24) = 3.169(5) Å, C(15)—C(35) = 3.085(6) Å, C(15)—C(34) = 3.403(6) Å, C(21)—C(32) = 3.462(5) Å, C(25)—C(33) = 3.260(6) Å and C(21)—C(33) = 3.489(5) Å. In comparison, the structures of $Cp'_2Th(CH_2CMe_3)_2$,[33] $Cp'_2Th(CH_2SiMe_3)_2$[37] and $Me_2Si[C_5Me_4]_2Th(CH_2SiMe_3)_2$[38] evidence few interligand C—C nonbonded contacts below 3.50 Å and none below 3.40 Å, arguing for considerably greater crowding in the $(Me_3SiC_5H_4)_3UR$ system. Hindered alkyl group rotation about the U—R bond has previously been observed in Cp_3UR complexes.[15]

* Sums of van der Waals radii for cofacial arene–arene interactions are *ca* 3.4 Å.[30(a)]

DISCUSSION

Comparison to other actinide results

The present thermochemical data provide a first glimpse of organoactinide metal–ligand bond disruption enthalpies not anchored to the D(U—OR′) approximation of eq. (4). It is found that the absolute value of $D(Cp''_3U—I)$ is 62.4(0.4) kcal mol^{-1}. This result can be compared to $D_1(UI_4) = 66(8)$ kcal mol^{-1} calculated from literature thermochemical data.[39] Thus, it appears that Cp″ and I ancillary ligands have a similar influence on D_1(U(IV)—I).

Table 5. Thermal parameters for non-hydrogen atoms of $(Me_3SiC_5H_4)_3UCH{=}CH_2$ (7)

Atom	U11	U22	U33	U12	U13	U23
U	0.01611(8)	0.01429(8)	0.01686(8)	−0.00088(5)	0.00575(5)	0.00047(5)
Si(1)	0.0227(5)	0.0278(6)	0.0197(5)	0.0014(4)	0.0067(4)	−0.0002(4)
Si(2)	0.0197(5)	0.0274(5)	0.0230(5)	0.0011(4)	0.0089(4)	0.0042(4)
Si(3)	0.0310(6)	0.0299(6)	0.0303(6)	0.0028(4)	0.0120(4)	0.0115(5)
C(1)	0.029(2)	0.021(2)	0.028(2)	−0.006(2)	0.006(2)	0.003(2)
C(2)	0.046(3)	0.035(2)	0.026(2)	−0.003(2)	0.008(2)	0.002(2)
C(11)	0.016(2)	0.026(2)	0.022(2)	−0.000(1)	0.006(1)	0.003(2)
C(12)	0.018(2)	0.024(2)	0.032(2)	−0.003(1)	0.009(2)	0.001(2)
C(13)	0.022(2)	0.034(2)	0.029(2)	0.001(2)	0.009(2)	−0.006(2)
C(14)	0.026(2)	0.042(2)	0.019(2)	−0.003(2)	0.012(2)	0.002(2)
C(15)	0.021(2)	0.026(2)	0.027(2)	−0.005(2)	0.010(1)	0.002(2)
C(16)	0.035(2)	0.031(2)	0.035(3)	−0.003(2)	0.007(2)	−0.008(2)
C(17)	0.036(2)	0.043(3)	0.031(2)	0.007(2)	0.008(2)	0.010(2)
C(18)	0.039(2)	0.051(3)	0.030(2)	0.003(2)	0.016(2)	0.002(2)
C(21)	0.021(2)	0.021(2)	0.023(2)	−0.003(1)	0.009(1)	0.006(1)
C(22)	0.027(2)	0.019(2)	0.026(2)	−0.006(1)	0.010(2)	−0.000(2)
C(23)	0.031(2)	0.014(2)	0.045(2)	0.000(2)	0.020(2)	0.003(2)
C(24)	0.022(2)	0.027(2)	0.033(2)	−0.002(2)	0.005(2)	0.014(2)
C(25)	0.029(2)	0.024(2)	0.019(2)	−0.003(2)	0.007(2)	0.004(2)
C(26)	0.032(2)	0.042(3)	0.033(2)	0.003(2)	0.018(2)	0.001(2)
C(27)	0.027(2)	0.033(2)	0.047(3)	−0.002(2)	0.016(2)	0.008(2)
C(28)	0.030(2)	0.041(3)	0.027(2)	−0.001(2)	0.003(2)	0.006(2)
C(31)	0.024(2)	0.017(2)	0.030(2)	0.002(1)	0.010(2)	0.007(2)
C(32)	0.021(2)	0.018(2)	0.033(2)	0.002(1)	0.010(2)	0.003(2)
C(33)	0.035(2)	0.022(2)	0.024(2)	0.006(2)	0.012(2)	0.004(2)
C(34)	0.036(2)	0.014(2)	0.028(2)	0.003(2)	−0.002(2)	−0.007(2)
C(35)	0.028(2)	0.017(2)	0.039(2)	−0.002(2)	0.010(2)	0.007(2)
C(36)	0.056(3)	0.041(3)	0.041(3)	−0.003(2)	0.030(2)	0.008(2)
C(37)	0.036(3)	0.077(4)	0.039(3)	−0.012(3)	−0.003(2)	0.025(3)
C(38)	0.086(4)	0.039(3)	0.054(3)	−0.015(3)	0.030(3)	0.018(3)

Table 6. Bond distances (Å) and angles (deg.) for $(Me_3SiC_5H_4)_3UCH{=}CH_2$ (7)

U	C(1)	2.436(4)	Si(2)	C(27)	1.865(4)
U	C(11)	2.748(3)	Si(2)	C(28)	1.861(4)
U	C(12)	2.762(4)	Si(3)	C(31)	1.864(4)
U	C(13)	2.753(4)	Si(3)	C(36)	1.860(5)
U	C(14)	2.744(4)	Si(3)	C(37)	1.859(5)
U	C(15)	2.752(4)	Si(3)	C(38)	1.872(6)
U	C(21)	2.818(3)	C(1)	C(2)	1.315(6)
U	C(22)	2.789(4)			
U	C(23)	2.730(4)			
U	C(24)	2.717(4)			
U	C(25)	2.755(4)	C(11)	Si(1)	C(16) 107.5(2)
U	C(31)	2.830(4)	C(11)	Si(1)	C(17) 107.6(2)
U	C(32)	2.759(4)	C(11)	Si(1)	C(18) 113.9(2)
U	C(33)	2.721(4)	C(21)	Si(2)	C(26) 111.8(2)
U	C(34)	2.729(4)	C(21)	Si(2)	C(27) 106.9(2)
U	C(35)	2.781(4)	C(21)	Si(2)	C(28) 111.5(2)
Si(1)	C(11)	1.865(4)	C(31)	Si(3)	C(36) 111.3(2)
Si(1)	C(16)	1.860(5)	C(31)	Si(3)	C(37) 111.9(2)
Si(1)	C(17)	1.863(5)	C(31)	Si(3)	C(38) 105.8(2)
Si(1)	C(18)	1.872(5)	U	C(1)	C(2) 137.7(3)
Si(2)	C(21)	1.868(4)			
Si(2)	C(26)	1.868(5)			

Reference to the absolute $D(Cp''_3U—R)$ values in Table 2 reveals several noteworthy features. First, the D(U—R) data span a wide range—*ca* 58 kcal mol^{-1} with D(U—C≡CPh) conspicuously at the high end of the range. Second, where R functionalities are similar or identical, the present $D(Cp''_3U—R)$ values are lower by *ca* 20 kcal mol^{-1} than the analogous $D(Cp'_2U(R)—R)$ parameters derived from alcoholytic calorimetry and the application of eq. (4).[3(c)] However, within both the Cp''_3UR and Cp'_2AnR_2 (An = Th, U) series, relative bond enthalpies follow qualitatively similar (but not quantitatively identical—*vide infra*) trends, with Me $\gtrsim$ CH_2SiMe_3 $\geqslant$ *n*-Bu > Bz.

The origins of the disparity between D(U—R) values derived from Cp''_3U/Cp''_3UR iodinolysis and from Cp'_2UR_2 alcoholysis/eq. (4) appear to reside in several difficultly quantifiable steric and electronic factors. The foregoing structural discussion suggests the Cp''_3AnR complexes are significantly more congested than Cp'_2AnR_2 analogues. Severe non-bonded interligand repulsions are expected to destabilize the U—R bond.[2(h)] Comparison of $D(L_nAn—Me) - D(L_nAn—R)$ pairs (An = Th, U) for relatively bulky R groups supports this picture. Thus, for Me/CH_2SiMe_3, the above difference is *ca* 5.0(3.4) kcal mol^{-1} in the Cp''_3UR series versus 2.0(6.8) kcal mol^{-1} in the Cp'_2UR_2 series[3(c)] and *ca* 1.0(3.9) kcal mol^{-1} in the Cp'_2ThR_2 series.[3(a)] For Me/*n*-Bu, the difference is *ca* 16.0(2.8) kcal mol^{-1} in the Cp''_3UR series versus *ca* 10.0(3.2) kcal mol^{-1} in the Cp'_2ThR_2 series. Furthermore, for Me/Bz, the difference in D values is 19.2(4.2) kcal mol^{-1} in the Cp''_3UR series versus 12(2.2) kcal mol^{-1} in the Cp'_2ThR_2 series and 6.0(6.2) kcal mol^{-1} in the Cp'_2UR_2 series. Such trends are in accord with greater steric repulsions in the Cp''_3UR series. The quantity $D(L_nU—I) - D(L_nU—R)$ provides another potential index of differential, L_nU-based steric or other (*vide infra*) effects on bond enthalpies. It is found that the iodinolyses[40] of Cp_3U(*n*-Bu) and Cp'_2UMe_2 proceed with $\Delta H_{rx} = -47.4(0.6)$ and $-41.0(0.3)$ (average) kcal mol^{-1}, respectively. These data are nearly identical to the corresponding Cp''_3UR values of $-46.9(0.3)$ (R = *n*-Bu) and $-39.4(0.4)$ (R = Me) kcal mol^{-1}, respectively (Table 2), arguing that for these relatively non-bulky ligands, differential Me/*n*-Bu/I L_nU-based steric/other effects are small. As noted earlier, $D_1(UI_4)$ and $D(Cp''_3U—I)$ are also identical to within experimental error. There is presently insufficient physiochemical information to judge whether there are major, electronically-based U—R or U—I bonding differences in Cp''_3UR and Cp'_2UR_2 complexes. Neither available theoretical[31,34,41] nor photoelectron spectroscopic data[42] evidence any obvious Cp_3AnR/Cp'_2AnR_2 An—R bonding differences.

Another major factor in understanding $D(Cp''_3U—R)/D(Cp'_2U(R)—R)$ relationships concerns the transferability of D(M—OR′) data, i.e. are $D(M(OR')_4) \rightarrow D(U(OR')_4) \rightarrow D(L_nU—OR')$ conversions strictly valid for M = Ti, Zr, Hf, and L_n = cyclopentadienyl ligands? Limitations on transferability are likely to be both steric and electronic in origin. In regard to eq. (4), it has previously been shown that very good transferability of D values are obtained between group 4 tetrahalides and Th, U tetrahalides.[3(a),(c)] Moreover, halide/alkoxide transferability within group 4 complexes is generally good.[3(a)(c)] In regard to $M(OR')_4 \rightarrow U(OR')_4$ and $U(OR')_4 \rightarrow Cp'_2U(OR')_2$ transferability, the latter seems most problematic both on steric and electronic grounds. This conversion requires a substantial increase in formal metal coordination number and likely in interligand non-bonded repulsion. Furthermore, the U—OR′ σ and π bonding should be sensitive to the rather large Cp′-induced changes in metal electron density.*[41,42] The strongest substantiation of this hypothesis is recent $Cp'_2ZrR_2/Cp'_2Zr(OR')_2$ calorimetry[7] which shows that the quantity $D(Cp'_2Zr(OR')—OR') - D(Cp'_2Zr(Cl)—Cl)$ is *ca* 25 kcal mol^{-1} less than in reported $\bar{D}(Zr(OR')_4) - \bar{D}(ZrCl_4)$ data[6] ($\bar{D}(ZrCl_4)$ is within 1 kcal mol^{-1} of $D_1(ZrCl_4)$[5]). These observations and the aforementioned $D_1(UI_4)/D(Cp''U—I)$ results argue that a halogen is a more reliable "anchor" ligand than alkoxide for placing $L_nM—R$ bond disruption enthalpies of varying L_n on an absolute scale. However, such D(M—X) − D(M—OR) disparities themselves are informative in regard to understanding ancillary ligand effects on metal–ligand bonding.

The present results place $Cp''_3U—R$ bond disruption enthalpies on an absolute footing and strongly suggest, but do not rigorously establish, that $Cp_3U—R$ and $Cp'_2U(R)—R$ data can be placed on the same absolute scale (using D(U(IV)—I) as an anchor). In regard to other actinides as well as lanthanides and related early transition metals, absolute bond disruption enthalpies have not been rigorously established and research is progressing in this direction.[43(a)]

In regard to understanding organouranium chemistry, the present results convey suggestions as to why Cp_3UH has never been isolated, despite

*The low energy "$5f^2$" ionization signals occur at experimentally indistinguishable energies for the two classes of uranium complexes.

numerous synthetic attempts. If D(U—H) is taken to be 10 kcal mol^{-1} greater than D(U—CH_3),[3(c)] then bimolecular H_2 elimination from such hydrides [eq. (17)] may be sufficiently close to thermoneutrality to be entropically driven (as well as driven by typical work-up procedures).

$$2C\overset{''}{p}_3UH \rightarrow 2C\overset{''}{p}_3U + H_2 \qquad (17)$$

$$\Delta H_{calc.} \approx +5 \text{ kcal mol}^{-1}.$$

In addition, what is likely to be a highly associated structure[21] of insoluble Cp_3U may provide an additional driving force. In the same vein, the apparent instability of $C\acute{p}_2U(Cl)H$[43(b)] [eq. (18)] may be rationalized by these same considerations.

$$3C\acute{p}_2U(Cl)H \rightarrow [C\acute{p}_2U(Cl)]_3 + 3/2\,H_2 \qquad (18)$$

Comparison to d-*element systems*

Presently available absolute metal–ligand bond disruption enthalpies for organotransition metal complexes span a wide range, from *ca* 20 kcal mol^{-1} for the alkyls of Co(III)N_4 complexes [2(c),(h),44] to 40–80 kcal mol^{-1} for $C\acute{p}Ir(PMe_3)(R)H$ alkyls and aryls.[2(j),45] These values are no doubt governed by a complex combination of steric and electronic factors, the latter describable in terms of metal–ligand electronegativity differences[2(g)], metal–ligand orbital overlap and repulsion,[46,47] metal redox characteristics[3(c)] and metal hybridization/promotion energy properties.[47] In the case of $C\overset{''}{p}_3UR$ complexes, the D(U—R) values do not conform to the general pattern that transition metal bond enthalpies are greatest towards the bottom and left of the Periodic Table. The most obvious reasons appear to involve the aforementioned large inter-ligand non-bonded repulsions and uranium-centred electronic factors evident in the general facility of U(IV) → U(III) oxidation state changes [cf. eq. (1)].[39,48] The latter electronic trends forecast substantially higher absolute D(Th—R) values.

As noted previously,[3(a),(c),49] relative actinide D(M—H) − D(M—alkyl) values are small compared to those in the middle and late transition metal complexes, reflecting differences in metal–ligand bond polarity[3] and metal–ligand orbital repulsions.[46] This same bond enthalpy pattern has now been demonstrated for group 4 complexes as well.[7] Another readily accessible gauge of metal–ligand bonding patterns may be D(M—I) − D(M—CH_3). The present values for actinides are rather large in comparison to most transition metal data. As can be seen in Table 7, there is a general progression of decreasing D(M—I) − D(M—CH_3) values towards the right of the transition metals. Such a trend can be viewed as arising from the greater polarizability of iodine[50] (energetic adjustment to different bond polarity situations[3(c),50]) or decreasing attraction/increasing repulsion[46] between metal orbitals and filled iodine orbitals as the metal d shell is filled.

The relative magnitudes of D(M—R) and D(H—R) parameters are another potential index of metal–ligand bonding characteristics. In several systems, a roughly linear correlation has been reported for D(M—R) and D(R—H),[2(i)] which sug-

Table 7. Values of D(M—I) − D(M—CH_3) for various organotransition metal complexes in kcal mol^{-1}

Fragment	D(M—I) − D(M—CH_3)	References
$C\overset{''}{p}_3U$—	18	This work
$C\acute{p}_2U$<	16	43
Cp_2W<	13	2(k)
$C\acute{p}_2Zr$<	13	7
Cp_2Mo<	10	2(k)
$Mn(CO)_5$—	10	2(f)
$C\acute{p}Ir(PMe_3)$<	8	2(j), 45(a)
$CpMo(CO)_3$—	7	45(b)
cis-$Pt(PPh_3)_2$<	2	2(d)
$(PMe_3)_2Ir(Cl)(CO)$<	0	2(d)

gests similar bonding characteristics. Several situations may, however, be expected to produce significant deviations from this proportionality. These include cases of prodigious steric interactions, multihapto/π bonding hydrocarbyl ligands such as d^0, f^0 benzyls,[51] possibly acetylides or vinyls, possibly systems with "agostic" C—H interactions, and of course, η^3-allyl, η^5-Cp,Cp′, etc. It has also been suggested[2(i)] that deviations in this proportionality might occur for ligands of obvious π-donor character (OR, NR_2) bound to π-acceptor centres such as Cp'_2Th. A plot of $D(Cp''U—R)$ versus $D(R—H)$ data is shown in Fig. 2. To first order, the relationship holds for the hydrocarbyl ligands with greatest deviations for *n*-BU (D(U—R) is lower than anticipated) and Bz (D(U—R) is greater than anticipated). The former deviation may reflect steric repulsion, while the latter may simply indicate differences in σ-bonding . That both R = vinyl and C≡CPh fall on the sample plot argues against major U—R π-bonding effects. The deviation of I from the proportionality is rather large and indicates that the D(M—R)/D(R—H) relationship is less general than previously implied. In other thermochemical studies,[7] we report very large deviations from this relationship for alkoxide, aryloxide, amide and halide ligands bound to early transition metals. Different classes of ligands fall onto different D(M—R)/D(R—H) plots indicating that such relationships are only valid for ligand systems having similar metal–ligand bonding.[7]

The present study also provides the first thermochemical data on an actinide carbonyl complex (Table 3). The U—CO bond disruption enthalpy, *ca* 10 kcal mol^{-1}, can be contrasted with early transition metal D(M—CO) values of 39.7(0.9) kcal mol^{-1} for $Cp'_2Zr(CO)_2$[7] and 41.3(0.9) kcal mol^{-1} for $Cp_2Ti(CO)_2$,[52] which are in the range reported for typical zero-valent homoleptic carbonyls.[2(b),(f)] Clearly the U—CO bond disruption enthalpy is low and in fact is comparable to $D(Cp''_3U—THF)$ (Table 3). In view of the reported Cp''_3UCO C—O stretching energy (1976 cm^{-1}), which suggests bonding similar to that in typical transition metal complexes, the low bond enthalpy is difficult to explain in the absence of severe interligand nonbonded repulsions.

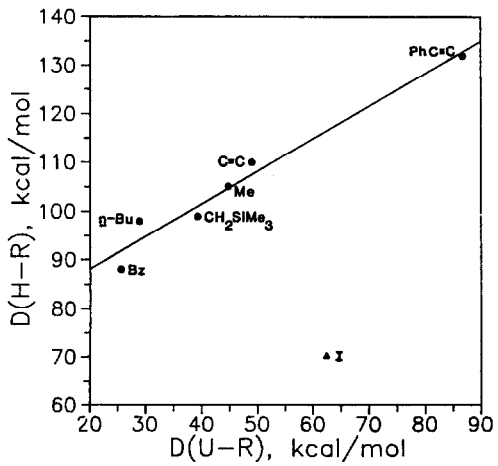

Fig. 2. Plot of $D[(Me_3SiC_5H_4)_3U—R]$ values measured in this study vs the corresponding D(R—H) values.

CONCLUSIONS

The results of this study indicate that the thermochemistry of $L_nM/L_nMX/L_nMR$ ensembles is an effective means to measure absolute metal–ligand bond disruption enthalpies. Our findings significantly complement earlier studies of relative actinide–ligand bond enthalpies[3] by providing a calibration of bond enthalpy transferability from one coordination environment to another. Assuming that literature $D(M(OR)_4)$ data are reliable, it is concluded that D(M—I) is more securely transferable than D(M–alkoxide). The magnitudes of the derived absolute $D(Cp''_3U—R)$ values appear to reflect a combination of both steric and electronic factors, with $D(M—I) - D(M—CH_3)$ differences offering a useful probe of the coordination environment and bonding.

Acknowledgements—We are grateful to NSF for support of this research under grant CHE8306255. L.E.S. thanks the Dow Chemical Company for a fellowship.

REFERENCES

1. See other articles in this Symposium-in-Print.
2. (a) G. Pilcher and H. A. Skinner, in *The Chemistry of the Metal–Carbon Bond* (Edited by F. R. Hartley and S. Patai), pp. 43–90. Wiley, New York (1982); (b) J. A. Connor, *Top. Curr. Chem.* 1977, **71**, 71; (c) J. Halpern, *Acc. Chem. Res.* 1982, **15**, 238; (d) J. U. Mondal and D. M. Blake, *Coord. Chem. Rev.* 1982, **47**, 205; (e) M. Mansson, *Pure Appl. Chem.* 1983, **55**, 417; (f) H. A. Skinner and J. A. Connor, *Pure Appl. Chem.* 1985, **57**, 79; (g) R. G. Pearson, *Chem. Rev.* 1985, **85**, 41; (h) J. Halpern, *Inorg. Chim. Acta* 1985, **100**, 41; (i) H. E. Bryndza, L. K. Fong, R. A. Paciello, W. Tam and J. E. Bercaw, *J. Am. Chem. Soc.* 1987, **109**, 1444; (j) S. P. Nolan, C. D. Hoff, P. O. Stoutland, L. J. Newman, J. M. Buchanan, R. G. Bergman, G. K. Yang and K. G. Peters, *J. Am. Chem. Soc.* 1987, **109**, 3143 and refs therein; (k) A. R. Dias, M. S. Salema and J. A. Simoes, *J. Organometal. Chem.* 1981, **222**, 69.

3. (a) J. W. Bruno, T. J. Marks and L. R. Morss, *J. Am. Chem. Soc.* 1983, **105**, 6824; (b) D. C. Sonnenberger, L. R. Morss and T. J. Marks, *Organometallics* 1985, **4**, 352; (c) J. W. Bruno, H. A. Stecher, L. R. Morss, D. C. Sonnenberger and T. J. Marks, *J. Am. Chem. Soc.* 1986, **108**, 7275.
4. (a) G. A. Vaughn, *Thermometric and Enthalpimetric Titrimetry*, Chaps 1 and 2. Van Nostrand-Reinhold, New York (1973); (b) H. J. V. Tyrrell and A. E. Beezer, *Thermometric Titrimetry*, Chaps 1–3. Chapman and Hall, London (1968); (c) J. K. Grime (Ed.), *Analytical Solution Calorimetry*. Wiley, New York (1985).
5. D. D. Wagman, W. H. Evans, V. B. Parker, R. H. Schumm and R. L. Nuttall, NBS Tech. Note (U.S.) No. 270–8 (1981).
6. M. F. Lappert, D. S. Patil and J. B. Pedley, *J. Chem. Soc., Chem. Commun.* 1975, 830. $\bar{D}(M(OR)_4)$ values were obtained from the heats of alcoholysis of the corresponding MCl_4 compounds.
7. (a) L. E. Schock and T. J. Marks, Abstracts, 193rd ACS Nat. Meet., Denver, CO, INOR 440 (5–10 April, 1987); (b) L. E. Schock and T. J. Marks, *J. Am. Chem. Soc.*, in press.
8. S. P. Nolan and T. J. Marks, research in progress.
9. M. K. Geno and J. Halpern, *J. Chem. Soc., Chem. Commun.* 1987, 1052 and refs therein.
10. L. J. Rothberg, J. D. Simon, M. Bernstein and K. S. Peters, *J. Am. Chem. Soc.* 1983, **105**, 3464.
11. J. G. Brennan, R. A. Andersen and A. Zalkin, *Inorg. Chem.* 1986, **25**, 1756.
12. R. Ilsong, R. Membo and T. Shigeru, *Tetrahedron Lett.* 1969, **52**, 5493.
13. L. E. Schock and T. J. Marks, submitted for publication.
14. P. N. Swepston, *TEXSAN, Version 2.0, TEXRAY Structure Analysis Program Package*. Molecular Structure Corporation, College station, TX (1986).
15. T. J. Marks, A. M. Seyam and J. R. Kolb, *J. Am. Chem. Soc.* 1973, **95**, 5529.
16. J. G. Brennan, R. A. Andersen and J. L. Robbins, *J. Am. Chem. Soc.* 1986, **108**, 335.
17. K.-H. Hellwege (Ed.), *Landolt-Bornstein*, Vol. 2. Springer, Berlin (1976).
18. E. Wilhelm and R. Battino, *J. Chem. Therm.* 1973, **5**, 117.
19. D. P. Shoemaker, C. W. Garland and J. I. Steinfeld, *Experiments in Physical Chemistry*, 3rd edn, pp. 27–58. McGraw–Hill, New York (1974).
20. (a) D. F. McMillan and D. M. Golden, *Ann. Rev. Phys. Chem.* 1982, **33**, 493; (b) A. M. Doncaster and R. Walsh, *J. Chem. Soc., Faraday Trans. I* 1976, **72**, 2908; (c) J. E. Huheey, *Inorganic Chemistry*, 3rd edn, pp. A28–A40. Harper and Row, New York (1983); (d) S. W. Benson, *Thermochemical Kinetics*, 2nd edn, p. 309. John Wiley, New York (1976).
21. (a) T. J. Marks and A. Streitwieser, Jr, in *The Chemistry of the Actinide Elements* (Edited by J. J. Katz, G. T. Seaborg and L. R. Morss), 2nd edn, Chap. 22. Chapman and Hall, London (1986); (b) T. J. Marks, *ibid.* Chap. 23; (c) T. J. Marks and R. D. Ernst, in *Comprehensive Organometallic Chemistry* (Edited by G. W. Wilkinson, F. G. A. Stone and E. W. Abel), Chap. 21. Pergamon Press, Oxford (1982); (d) E. C. Baker, G. W. Halstead and K. N. Raymond, *Struct. Bond.* 1976, **25**, 23 and refs therein.
22. J. Leong, K. O. Hodgson and K. N. Raymond, *Inorg. Chem.* 1973, **12**, 1329.
23. R. R. Ryan, R. A. Penneman and B. Kanellakopulos, *J. Am. Chem. Soc.* 1975, **97**, 4258.
24. G. W. Halstead, E. C. Baker and K. N. Raymond, *J. Am. Chem. Soc.* 1975, **97**, 3049.
25. J. G. Brennan, R. A. Andersen and A. Zalkin, *Inorg. Chem.* 1976, **25**, 1761.
26. J. L. Atwood, C. F. Haines, M. Tsutsui and A. E. Gebala, *J. Chem. Soc., Chem. Commun.* 1973, 452.
27. G. Perego, M. Cesari, F. Farina and G. Lugli, *Acta Cryst.* 1976, **B32**, 3034.
28. J. L. Atwood, M. Tsutsui, N. Ely and A. E. Gebala, *J. Coord. Chem.* 1976, **5**, 209.
29. F. R. Hartley, in *Comprehensive Organometallic Chemistry* (Edited by G. W. Wilkinson, F. G. A. Stone and E. W. Abel), Chap. 39 and refs therein. Pergamon Press, Oxford (1982).
30. (a) L. Pauling, *The Nature of the Chemical Bond*, 3rd edn, Chap. 7. Cornell University Press, Ithaca, NY (1960); (b) *Tables of Interatomic Distances and Configuration in Molecules and Ions*, Spec. Pub. No. 18. Chemical Society, London (1965).
31. K. Tatsumi and A. Nakamura, *J. Organometal. Chem.* 1984, **272**, 141.
32. (a) B. E. Bursten, M. Casarin, D. E. Ellis, I. Fragalà and T. J. Marks, *Inorg. Chem.* 1986, **25**, 1257; (b) M. R. Duttera, V. W. Day and T. J. Marks, *J. Am. Chem. Soc.* 1984, **106**, 2907; (c) F. A. Cotton, D. O. Marler and W. Schwotzer, *Inorg. Chim. Acta* 1984, **95**, 207; (d) F. A. Cotton, D. O. Marler and W. Schwotzer, *Inorg. Chim. Acta* 1984, **85**, L31.
33. J. W. Bruno, G. M. Smith, T. J. Marks, C. K. Fair, A. Schultz and J. M. Williams, *J. Am. Chem. Soc.* 1986, **108**, 40.
34. K. Tatsumi and A. Nakamura, *J. Am. Chem. Soc.* 1987, **109**, 3195.
35. R. D. Shannon, *Acta Cryst. Sect. A.* 1976, **32**, 751.
36. R. W. Broach, A. J. Schultz, J. M. Williams, G. M. Brown, J. M. Manriquez, P. J. Fagan and T. J. Marks, *Science* 1979, **203**, 172.
37. J. W. Bruno, T. J. Marks and V. W. Day, *J. Organometal. Chem.* 1983, **250**, 237.
38. (a) C. M. Fendrick, L. D. Schertz, V. W. Day and T. J. Marks, *Organometallics*, in press; (b) C. M. Fendrick, E. A. Mintz, L. D. Schertz, T. J. Marks and V. W. Day, *Organometallics* 1984, **3**, 819.
39. L. R. Morss, in *The Chemistry of the Actinides* (Edited by J. J. Katz, G. T. Seaborg and L. R. Morss), Chap. 17. Chapman and Hall, London (1986).
40. L. E. Schock, A. M. Seyam and T. J. Marks, unpublished results.
41. B. E. Bursten and A. Fang, *J. Am. Chem. Soc.* 1983, **105**, 6495.

42. (a) E. Ciliberto, G. Condorelli, P. J. Fagan, J. M. Manriquez, I. Fragalà and T. J. Marks, *J. Am. Chem. Soc.* 1981, **103**, 4755; (b) I. Fragalà, in *Organometallics of the* f-*elements* (Edited by T. J. Marks and R. D. Fischer), Chap. 13 and refs therein. Reidel, Dordrecht, Holland (1979).
43. (a) S. P. Nolan, L. E. Schock, A. M. Seyam and T. J. Marks, unpublished results; (b) P. J. Fagan, J. M. Manriquez, T. J. Marks, C. S. Day, S. H. Vollmer and V. W. Day, *Organometallics* 1982, **1**, 170.
44. B. P. Hay and R. J. Finke, *J. Am. Chem. Soc.* 1986, **108**, 4820.
45. (a) P. O. Stoutland, R. G. Bergman, S. P. Nolan and C. D. Hoff, *Polyhedron* 1988, **7**, 1429 (we thank these authors for permission to quote their data); (b) S. P. Nolan, R. Lopez de la Vega, S. L. Mukerjee, A. A. Gonzalez, K. Zhang and C. D. Hoff, *Polyhedron* 1988, **7**, 1491 (we thank these authors for permission to quote their data).
46. (a) T. Ziegler, V. Tschinke and A. Becke, *J. Am. Chem. Soc.* 1987, **107**, 1351; (b) T. Ziegler, V. Tschinke, L. Verslius, E. J. Baerends and W. Ravenek, *Polyhedron* 1988, **7**, 1625 (we thank these authors for permission to quote their data).
47. J. B. Schilling, W. A. Goddard III and J. L. Beauchamp, *J. Am. Chem. Soc.* 1987, **109**, 5565, 5573 and refs therein.
48. J. J. Katz, L. R. Morss and G. T. Seaborg, in *The Chemistry of the Actinide Elements* (Edited by J. J. Katz, G. T. Seaborg and L. R. Morss), Chaps 14.5 and 14.6. Chapman and Hall, London (1986).
49. J. W. Bruno, M. R. Duttera, C. M. Fendrick, G. M. Smith and T. J. Marks, *Inorg. Chim. Acta* 1984, **94**, 271.
50. R. G. Parr and R. G. Pearson, *J. Am. Chem. Soc.* 1983, **105**, 7512.
51. E. A. Mintz, K. G. Moloy. T. J. Marks and V. W. Day, *J. Am. Chem. Soc.* 1982, **104**, 4692.
52. A. R. Dias, P. B. Dias, H. P. Diego, A. M. Galvão, M. E. Minas da Piedade and J. A. M. Simoes, *Organometallics* 1987, **6**, 1427.

Polyhedron Vol. 7, No. 16/17, pp. 1531–1544, 1988
Printed in Great Britain

0277–5387/88 $3.00+.00
© 1988 Pergamon Press plc

THERMOCHEMISTRY OF $M(\eta^5\text{-}C_5H_5)_2L_n$ COMPLEXES (M = Ti, Mo, W)

ALBERTO R. DIAS and JOSÉ A. MARTINHO SIMÕES

Centro de Química Estrutural, Complexo I, Instituto Superior Técnico, 1096 Lisboa Codex, Portugal

Abstract—The available thermochemical data for the title compounds are summarized and discussed. Metal–ligand bond enthalpies are derived for a variety of ligands through a simple method that involves both the experimental standard enthalpies of formation and theoretical calculations. It is suggested that this method may be used to predict the energetics of new complexes with fair accuracy. In addition, the method provides estimates of metal–ligand stepwise bond dissociation enthalpies. Some of these estimates are compared with recent experimental results obtained for bis(pentamethylcyclopentadienyl) titanium complexes.

If the ability to estimate new data is used as a criterion to assess the development of organometallic thermochemistry, we will be compelled to conclude that our present knowledge in this area is still rather incipient, particularly for molecules containing *d* and *f* elements. This situation contrasts with the one observed for organic substances, for which several reliable prediction schemes are available,[1–3] but is not surprising, given the large number of elements and hence the different chemical bonds that can be involved in organometallic species. Moreover, even if it were assumed that these schemes could be extended to metal compounds, the size of the data bank required to derive a suitable set of "bond terms" or "group contributions" would be several orders of magnitude larger than for organic compounds. Unfortunately, the virtually infinite variety of bonds and groups in organometallic complexes, hindering the existence of traditional prediction schemes, is also the reason why the development of estimation methods becomes so important. Alternative (though eventually less reliable) procedures have thus to be found.

The simplest and most commonly used method to estimate the enthalpy change of any chemical reaction, in the absence of enthalpy of formation data, is to consider the bonds cleaved and formed. For example, the enthalpy of reaction (1) will be obtained if the difference between M—L and M—L′ bond dissociation enthalpies is available.

$$X_nML(g) + L'(g) \rightarrow X_nML'(g) + L(g). \quad (1)$$

Devising an estimation method for these quantities is apparently easier than for enthalpies of formation, since $\Delta H_f^0(X_nML,g)$ or $\Delta H_f^0(X_nML',g)$ would require energetic information on each chemical bond in the complexes, and it is also less demanding in terms of size of the experimental data bank.

The thermochemical studies on bis(cyclopentadienyl) compounds of the type $M(Cp)_2L_n$ ($Cp = \eta^5\text{-}C_5H_5$; L = H, alkyl, aryl, carbonyl, halogen, etc.) carried out in our laboratory enabled us to address some issues that may contribute to improved reliability of estimated metal–ligand bond dissociation enthalpies and standard enthalpies of formation. As the structural features of the fragment $M(Cp)_2$ are nearly constant in many complexes, indicating that its enthalpy content is not significantly changed, attention can be concentrated on the "reactive" side of the molecules, i.e. the bonds M—L. The dependence of the strengths of these bonds on the metal and its oxidation state, and on the number, types and geometrical constraints of ligands, has been examined in a wide variety of cases. It is the purpose of the present paper to summarize both the method used to derive metal–ligand bond enthalpies from experimental data and the main conclusions drawn from these studies. Pre-

liminary values of some recently determined bond enthalpies are also included in the discussion.

CALCULATION OF BOND ENTHALPIES FROM EXPERIMENTAL DATA

Enthalpies of reaction of $M(Cp)_2L_n$ complexes with several substances, typically HCl or I_2 solutions, have been determined with a reaction–solution calorimeter described in detail elsewhere.[4] These measurements, together with auxiliary enthalpies of solution and literature data, led to the standard enthalpies of formation of the crystalline complexes.

Unlike combustion calorimetry, reaction–solution calorimetry is not an "absolute" method, i.e. it normally yields a difference between the enthalpies of formation of two complexes. It is therefore necessary that one of these quantities is available so that the other can be calculated. All the $\Delta H_f^0[M(Cp)_2L_n,c]$ values listed here have been obtained using the reported standard enthalpies of formation of the related dichloride molecules, $M(Cp)_2Cl_2$, which were derived from static (Mo, Ti) and rotating (W) bomb combustion experiments.[5,6] Although the first of these methods is not considered very reliable for studying such compounds, we have accepted these values as references, in the absence of further information. Incidentally, $\Delta H_f^0[W(Cp)_2Cl_2,c] = -71.1 \pm 2.5$ kJ mol^{-1} (static-bomb) is close to the recent rotating-bomb result, -63.5 ± 7.7 kJ mol^{-1}.

The standard enthalpies of formation of *gaseous* $M(Cp)_2L_n$ complexes, necessary for evaluating metal–ligand bond enthalpies, were determined by measuring or estimating the standard enthalpies of sublimation of those molecules. Whenever possible, ΔH_s^0 values were obtained from Knudsen cell experiments (the Knudsen cell is a modified version of the one reported in ref. 7), but in most cases they had to be estimated. A thorough discussion of this subject shows that enthalpies of sublimation of analogous complexes usually fall in a narrow range, thus allowing reasonably accurate estimates.[8]

As happens with any molecule containing several types of ligands, the determination of the enthalpy associated with a given bond from the enthalpy of formation in the gas state depends strongly on the enthalpies ascribed to the remaining bonds. In the case of the bis(cyclopentadienyl) complexes, the difficulty of estimating M—Cp bond enthalpies was avoided by considering the "reference" complexes

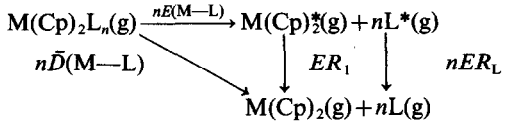

Scheme 1.

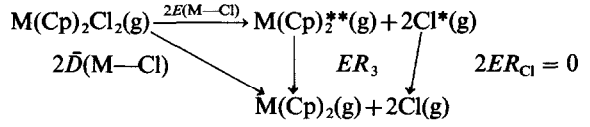

Scheme 2.

$M(Cp)_2Cl_2$ and by using two different concepts of bond enthalpies: *bond enthalpy terms*, E(M—L), and *mean bond dissociation enthalpies*, $\bar{D}$(M—L). These quantities are related through Schemes 1 and 2, from which eqs (2) and (3) were derived.

$$E(\text{M—L}) = E(\text{M—Cl}) + \frac{n}{2}\Delta H_f^0(\text{L*,g}) - \Delta H_f^0(\text{Cl,g}) - \{\Delta H_f^0[\text{M(Cp)}_2\text{L}_n\text{,g}] - \Delta H_f^0[\text{M(Cp)}_2\text{Cl}_2\text{,g}]\}/2 + (ER_3 - ER_1)/2 \quad (2)$$

$$\bar{D}(\text{M—L}) = E(\text{M—Cl}) + \frac{n}{2}\Delta H_f^0(\text{L,g}) - \Delta H_f^0(\text{Cl,g}) - \{\Delta H_f^0[\text{M(Cp)}_2\text{L}_n\text{,g}] - \Delta H_f^0[\text{M(Cp)}_2\text{Cl}_2\text{,g}]\}/2 + ER_3/2. \quad (3)$$

The asterisks indicate non-reorganized fragments, i.e. fragments retaining the geometry they had in the initial complex. ER_1, ER_3 and ER_L are the energies associated with the relaxation of the fragments to their ground states.

Bond enthalpy terms E(M—L) and E(M—Cl) do not contain the reorganization energies of the fragments. They should therefore be a better measure of the M—L "bond strengths", affording more meaningful correlations with other structural parameters (e.g. bond lengths) than $\bar{D}$(M—L). This point is relevant for the evaluation of E(M—L) and $\bar{D}$(M—L) through eqs (2) and (3). An estimate of M—Cl bond enthalpy in $M(Cp)_2Cl_2$ can be made by considering the bond enthalpy in the homoleptic molecule MCl_m. If M—Cl bond lengths are similar in both molecules, then E(M—Cl) = $\bar{D}$(M—Cl) in MCl_m can be *transferred* to the dichloride complex, i.e. is identified with E(M—Cl) in $M(Cp)_2Cl_2$.† This was indeed the procedure used to calculate E(M—L) data collected in the tables: for molybdenum and tungsten ($m = 6$) E(M—Cl) were taken as 303.8 and 347.3 kJ mol^{-1}, respectively, and for titanium ($m = 4$) E(M—Cl) = 430.5 kJ mol^{-1}.[5]

If $\bar{D}$(M—Cl) in MCl_m was identified with $\bar{D}$(M—Cl) in the complex,† then $ER_3 = 0$. As indi-

† The assumption that $\bar{D}$(M—Cl) in MCl_m is identical to $\bar{D}$(M—Cl) [and not to E(M—Cl)] in $M(Cp)_2Cl_2$ has been used in ref. 5.

cated by extended Hückel molecular orbital calculations, this conclusion does not hold for the molybdenum and tungsten dichlorides ($ER_3 \sim -82$ and -103 kJ mol^{-1}, respectively), although it is reasonable for the titanium analogue ($ER_3 \sim -11$ kJ mol^{-1}). Like ER_3, the reorganization energies ER_1 have also been estimated from curves where the total energy of the fragments $M(Cp)_2$ is plotted as a function of the angle Cp—M—Cp (θ). The most stable geometry of the isolated fragment is achieved with $\theta = 140$ and 180° for metals having two and four d electrons, respectively. As θ is usually close to 130° in $M(Cp)_2L_n$ complexes, this accounts for the large reorganization energies for molybdenum and tungsten fragments as compared with titanium.[9] The dependence of the $M(Cp)_2$ energy on the M–Cp distance is less important. Besides, for each metal, these bond lengths are rather constant.

The extended Hückel results have always been handled in a semi-quantitative way. Accordingly, the bond enthalpies collected in the tables are not affected by the "corrections" in eqs (2) and (3). It must be noted, however, that in the case of E(M—L), eq. (2), the reorganization term $(ER_3 - ER_1)/2$ is usually small since the angle θ is fairly similar for most complexes. Examples and exceptions are shown in the next section.

A pragmatic approach can be followed to obtain the enthalpies of formation of non-reorganized species, ΔH_f^0(L*,g), which are also required to calculate E(M—Cl) by eq. (2).[10] For anionic ligands, it is first considered that the geometry of L* is the same in the complex and in the molecule LH, implying that ΔH_f^0(L*,g) can be derived from Scheme 3 or eq. (4). Secondly, E(M—L) is identified with the respective Laidler term.[1]

$$\Delta H_f^0(\text{L*,g}) = E(\text{L—H}) + \Delta H_f^0(\text{LH,g}) - \Delta H_f^0(\text{H,g}) = D(\text{L—H}) - ER_L + \Delta H_f^0(\text{LH,g}) - \Delta H_f^0(\text{H,g}). \quad (4)$$

A simple calculation involving, for instance, the methyl radical, demonstrates that the introduction of Laidler terms in eq. (4) leads to physically meaningless results: ER_L, given by the difference between $D(CH_3\text{—H})$ (439.7 kJ mol^{-1})[11] and E(C—H) ($= \bar{D}$(C—H) = 415.8 kJ mol^{-1}), is *positive*, implying that the C_{3v} configuration of the free radical

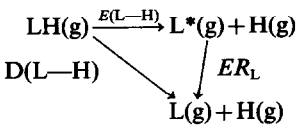

Scheme 3.

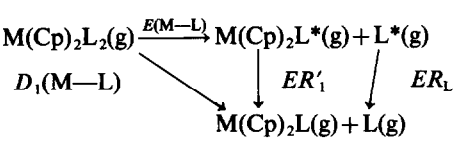

Scheme 4.

should be more stable than D_{3h}. Despite this lack of physical meaning, the procedure has the advantage of yielding E(M—L) data that are consistent with the Laidler scheme and eventually can be used to make predictions. Moreover, as shown below, estimates of stepwise bond dissociation enthalpies are independent of the value chosen for E(L—H).

If necessary, the assumption of identical geometries of L* in LH and in $M(Cp)_2L_n$ can be corrected by computing their energy difference. As illustrated in the next section, this has occasionally been made by using the Hückel, MINDO-3 or MNDO methods.

The estimation of metal–ligand partial (or stepwise) bond dissociation enthalpies follows from the above method in a straightforward manner. The first bond dissociation enthalpy, D_1(M—L), is calculated using eq. (5), derived from Scheme 4, where the symbols have the usual meaning.

$$D_1(\text{M—L}) = E(\text{M—L}) + ER'_1 + ER_L. \quad (5)$$

As E(M—L) is transferred from eq. (2) and it relies on eq. (4), D_1(M—L) becomes independent of the value ascribed to E(L—H). In other words, ER_L is cancelled when eq. (5) is used. The reorganization energy ER'_1 is also estimated through the extended Hückel approximation by optimizing the structure of the free fragment $M(Cp)_2L$.[12]

The second metal–ligand bond dissociation enthalpy, D_2(M—L), is simply the difference between $2\bar{D}$(M—L) and D_1(M—L). The Hückel calculations for several systems (L = Cl, H, CH_3, SCH_3; M = Mo, Ti) indicate that ligand to metal π-donation results in larger values of $D_2 - D_1$ than σ-donation (see Table 10).

STANDARD ENTHALPIES OF FORMATION AND BOND ENTHALPY DATA

As stated previously, the standard enthalpies of formation of all the bis(cyclopentadienyl) complexes reported here rely on combustion results for $\Delta H_f^0[M(Cp)_2Cl_2,c]$. It must be emphasized that a revision of the static-bomb values (Mo, Ti) will not affect the metal–ligand bond enthalpy data: $\Delta H_f^0[M(Cp)_2Cl_2,c]$ is cancelled in eqs (2) and (3), since the same value was used to derive

Table 1. Standard enthalpies of formation of halogen complexes (kJ mol^{-1})[a]

Complex	ΔH_f^0(c)	ΔH_s^0	ΔH_f^0(g)
$Ti(Cp)_2Cl_2$	-383.2 ± 7.5	118.8 ± 2.1	-264.4 ± 7.8
$Ti(Cp)_2I_2$	-148.4 ± 13.1	(120 ± 10)[b]	-28.4 ± 16.5
$Mo(Cp)_2Cl_2$	-95.8 ± 2.5	(100.4 ± 4.2)	4.6 ± 4.9
$Mo(Cp)_2Br_2$	9.7 ± 12.7	(100.4 ± 4.2)	110.1 ± 13.4
$Mo(Cp)_2I_2$	69.8 ± 7.8	(100.4 ± 4.2)	170.2 ± 8.9
$W(Cp)_2Cl_2$	-63.5 ± 7.7	(104.6 ± 4.2)	41.1 ± 8.8
$W(Cp)_2Br_2$	15.7 ± 13.9	(104.6 ± 4.2)	120.3 ± 14.5
$W(Cp)_2I_2$	65.4 ± 10.5	(104.6 ± 4.2)	170.0 ± 11.3

[a] Data from refs 4, 5, 6, 14 and 15.
[b] Estimated values in parentheses.

$\Delta H_f^0[M(Cp)_2L_n,c]$. A different conclusion is drawn for M—Cp bond enthalpy terms, which, by a first approximation, can be obtained from eq. (6).

$$E(M—Cp) = \Delta H_f^0(M,g)/2 + \Delta H_f^0(Cp,g) + \Delta H_f^0(Cl,g) - \Delta H_f^0[M(Cp)_2Cl_2,g]/2 - E(M—Cl). \quad (6)$$

As E(M—Cl) is constant, because it is transferred from MCl_m, an increase in the enthalpy of formation of the complex will imply a decrease of E(M—Cp).

Some enthalpies of formation shown in the tables were recalculated by using recent literature data.† This applies particularly to the tungsten complexes, whose values were adjusted to the recently reported $\Delta H_f^0[W(Cp)_2Cl_2,c]$.[6] Enthalpies of formation of ligands or radicals, necessary to derive M—L bond enthalpies, are given in the Appendix.

Halogen complexes

Table 1 collects the available standard enthalpies of formation of these bis(cyclopentadienyl) derivatives. Except for the dichlorides, all the values were obtained from reaction-solution calorimetric results.[4,14,15] The bond enthalpy data are shown in Table 2 and include metal–halogen and metal–cyclopentadienyl bond enthalpy terms, and metal–halogen mean bond dissociation enthalpies. As stated before, no corrections due to ER_1, ER_3 and ER_{Cp} were included in those values. This hardly affects E(M—X), since $(ER_3—ER_1)/2$ must be close to zero, i.e. Cp—M—Cp angles are likely to be similar in $M(Cp)_2Cl_2$ and $M(Cp)_2X_2$ (X = Br, I). The same applies to $\bar{D}$(Ti—X) (X = Cl, Br, I),

† $\Delta H_f^0[M(Cp)_2Br_2,c]$ were recalculated from new data for $\Delta H_f^0(CBr_4,c) - \Delta H_f^0(CHBr_3,1)$ in ref. 13.

Table 2. Metal–halogen and metal–cyclopentadienyl bond enthalpies (kJ mol^{-1})[a]

Complex	E(M—X)	$\bar{D}$(M—X)	E(M—Cp)
$Ti(Cp)_2Cl_2$	430.5 ± 1.3	430.5 ± 1.3	318 ± 10
$Ti(Cp)_2I_2$	298 ± 9	298 ± 9	
$Mo(Cp)_2Cl_2$	303.8 ± 7.1	303.8 ± 7.1	404 ± 12
$Mo(Cp)_2Br_2$	242 ± 10	242 ± 10	
$Mo(Cp)_2I_2$	207 ± 9	207 ± 9	
$W(Cp)_2Cl_2$	347.3 ± 0.8	347.3 ± 0.8	443 ± 10
$W(Cp)_2Br_2$	298 ± 7	298 ± 7	
$W(Cp)_2I_2$	268 ± 5	268 ± 5	

[a] Data not including reorganization energies ER_1 and ER_3.

because ER_3 is negligible, but not so for $\bar{D}$(Mo—X) and $\bar{D}$(W—X), whose corrections are predicted to be significant (see previous section). As for E(M—Cp), the values displayed are also upper limits, since ER_{Cp} was not considered.

The usual trends E(M—Cl) > E(M—Br) > E(M—I) and E(Ti—X) > E(W—X) > E(Mo—X) are observed in Table 2, but a striking feature is apparent: E(Ti—Cp) < E(Ti—Cl), while an inverse relationship is noted for molybdenum and tungsten. Although the *absolute* values in the table may be controversial (only differences E(M—X) − E(M—Cl) and $\bar{D}$(M—X) − $\bar{D}$(M—Cl), for each metal, can be trusted), it seems hard to believe that the transferability produces errors of *ca* 100 kJ mol^{-1}. Interestingly, the trend for titanium is also observed for zirconium and hafnium,[16] in agreement with the known chemistry of these complexes (e.g. the stability of $M(Cp)Cl_3$ complexes and the lability of M—Cp bonds for group 4*d* metals).

It is finally noted that E(W—Br) = 296 ± 7 kJ mol^{-1} in WBr_6 ($\Delta H_f^0(WBr_6,g)$ and $\Delta H_f^0(TiI_4,g)$

Table 3. Standard enthalpies of formation of oxygen and sulphur complexes (kJ mol^{-1})[a]

Complex	ΔH_f^0(c)	ΔH_s^0	ΔH_f^0(g)
$Ti(Cp)_2(OPh)_2$	−393.7±8.0	(97±8)[b]	−296.7±11.3
$Ti(Cp)_2(OC_6H_4Me\text{-}2)_2$	−448.9±8.2	(104±8)	−344.9±11.5
$Ti(Cp)_2(OC_6H_4Me\text{-}3)_2$	−408.1±8.1	(104±8)	−304.1±11.4
$Ti(Cp)_2(OC_6H_4Me\text{-}4)_2$	−448.7±7.9	(104±8)	−344.7±11.3
$Ti(Cp)_2(OC_6H_4Cl\text{-}2)_2$	−440±22	(90±10)	−350±24
$Ti(Cp)_2(O_2CPh)_2$	−789.7±8.1	(112±8)	−677.7±11.4
$Ti(Cp)_2(O_2CCCl_3)_2$	−1095±19	(130±8)	−965±20
$Ti(Cp)_2(O_2CCF_3)_2$	−2251.2±8.2	(108±8)	−2143.2±11.4
$Ti(Cp)_2(O_2C_{14}H_8)$	−322.6±12.7	(165±8)	−157.6±15.0
$Ti(Cp)_2(SEt)_2$	−211.3±8.2	(106±10)	−105.3±12.9
$Ti(Cp)_2(SPr\text{-}n)_2$	−267.5±9.7	(108±8)	−159.5±12.5
$Ti(Cp)_2(SPh)_2$	34.0±7.9	(113±10)	147.0±12.7
$Ti(Cp)_2(S_2C_6H_3Me)$	−30.3±9.5	(110±10)	79.7±13.8
$Mo(Cp)_2(O_2CPh)_2$	−500.7±3.4	(94±10)	−406.7±10.6
$Mo(Cp)_2(O_2CCF_3)_2$	−1984.2±4.2	(90±10)	−1894.2±10.8
$Mo(Cp)_2(O_2C_6H_4)$	−130.6±2.9	(100±8)	−30.6±8.5
$Mo(Cp)_2(O_2C_{10}H_6)$	−80.3±3.2	(135±8)	54.7±8.6
$Mo(Cp)_2(O_2C_{14}H_8)$	−53.3±10.4	(145±8)	91.7±13.1
$Mo(Cp)_2(SO_4)$	−650.4±3.4	(72±10)	−578.4±10.6
$Mo(Cp)_2(SPr\text{-}n)_2$	−10.7±5.3	(90±10)	79.3±11.3
$Mo(Cp)_2(SPr\text{-}i)_2$	−22.7±5.3	(90±10)	67.3±11.3
$Mo(Cp)_2(SBu\text{-}n)_2$	−96.0±5.5	(92±10)	−4.0±11.4
$Mo(Cp)_2(SBu\text{-}t)_2$	−68.3±4.3	(92±10)	23.7±10.9
$Mo(Cp)_2(SC_{10}H_{21}\text{-}n)_2$	−361.5±4.3	(105±10)	−256.5±10.9
$Mo(Cp)_2(SPh)_2$	282.0±4.8	(95±10)	377.0±11.1
$W(Cp)_2(O_2CPh)_2$	−455.8±8.2	(98±10)	−357.8±12.9
$W(Cp)_2(O_2CCF_3)_2$	−1925.6±8.2	(94±10)	−1831.6±12.9
$W(Cp)_2(O_2C_6H_4)$	−105.2±7.8	(104±8)	−1.2±11.2
$W(Cp)_2(SEt)_2$	70.3±9.0	(92±10)	162.3±13.5
$W(Cp)_2(SPr\text{-}n)_2$	16.6±9.2	(94±10)	110.6±13.6
$W(Cp)_2(SPh)_2$	327.5±9.1	(99±10)	426.5±13.5

[a] Data from refs 18–21.

[b] Estimated values in parentheses.

quoted from ref. 17) and E(Ti—I) = 294±2 kJ mol^{-1} in TiI_4[17] are in excellent agreement with E(W—Br) and E(Ti—I) in Table 2, which, we recall, rely on E(W—Cl) and E(Ti—Cl) from WCl_6 and $TiCl_4$. This seems to indicate that reliable predictions of the enthalpies of formation of the complexes $M(Cp)_2F_2$ can easily be made using eq. (2) together with E(M—F) values obtained from the available data for $\Delta H_f^0(MF_n,g)$:[17] $\Delta H_f^0[M(Cp)_2F_2,g]$ −656, −369 and −367 kJ mol^{-1}, respectively for M = Ti, Mo and W [E(M—F) = 585, 449 and 510 kJ mol^{-1}].

Oxygen and sulphur complexes

The standard enthalpies of formation of these molecules, obtained by reaction–solution calorimetry,[18–21] are collected in Table 3 and were used to derive metal–oxygen and metal–sulphur bond enthalpy terms and bond dissociation enthalpies (Tables 4 and 5). The available molecular structures for some complexes in these tables show that the geometry of $M(Cp)_2$ fragment is nearly constant for each metal and similar to the one in the respective dichloride.[18–20,22,23] This constancy is assumed for the remaining molecules and implies that the correction terms $(ER_3 - ER_1)/2$ are not significant. For instance, in the case of the molybdenum sulphate molecule, the angle Cp—M—Cp is 134°, corresponding to $(ER_3 - ER_1)/2 \sim -13$ kJ mol^{-1}.

In the absence of steric effects, metal–oxygen bond enthalpy terms for each metal fall in a narrow range, suggesting that the average values for Ti (452 kJ mol^{-1}), Mo (333 kJ mol^{-1}) and W (365 kJ

Table 4. Metal–oxygen bond enthalpies (kJ mol^{-1})[a]

Complex	E(M—O)	$\bar{D}$(M—O)
$Ti(Cp)_2(OPh)_2$	462±9	373±11
$Ti(Cp)_2(OC_6H_4Me\text{-}2)_2$	454±9	365±11
$Ti(Cp)_2(OC_6H_4Me\text{-}3)_2$	430±9	341±11
$Ti(Cp)_2(OC_6H_4Me\text{-}4)_2$	457±9	368±11
$Ti(Cp)_2(OC_6H_4Cl\text{-}2)_2$	440±10	351±12
$Ti(Cp)_2(O_2CPh)_2$	455±9	440±6
$Ti(Cp)_2(O_2CCCl_3)_2$	464±9	446±11
$Ti(Cp)_2(O_2CCF_3)_2$	451±9	433±11
$Ti(Cp)_2(O_2C_{14}H_8)$	417±9	
$Mo(Cp)_2(O_2CPh)_2$	327±12	312±10
$Mo(Cp)_2(O_2CCF_3)_2$	334±12	316±14
$Mo(Cp)_2(O_2C_6H_4)$	299±9	
$Mo(Cp)_2(O_2C_{10}H_6)$	300±9	
$Mo(Cp)_2(O_2C_{14}H_8)$	300±10	
$Mo(Cp)_2(SO_4)$	338±9	
$W(Cp)_2(O_2CPh)_2$	365±10	349±7
$W(Cp)_2(O_2CCF_3)_2$	365±10	347±11
$W(Cp)_2(O_2C_6H_4)$	346±5	

[a] Data not including reorganization energies ER_1 and ER_3.

mol^{-1}) can be used to estimate standard enthalpies of formation of other complexes within *ca* ±20 kJ mol^{-1}. Furthermore, the average for titanium is not far from the mean value of E(Ti—O) in $Ti(OR)_4$ molecules (R = alkyl), 466 kJ mol^{-1}.[19]

The low values for the bidentate ligands 1,2-benzenodiolate, 1,2-naphthalenodiolate and 9,10-phenanthrenodiolate were not included in the above averages since they are believed to reflect relatively high strain energies (40–80 kJ mol^{-1}).[21] An opposite conclusion is drawn for the complex $Mo(Cp)_2(SO_4)$. The "normal" E(Mo—O) value indicates a negligible strain in the sulphate moiety, this being supported by the molecular structure of the complex and by extended Hückel calculations.[19]

Table 5. Metal–sulphur bond enthalpies (kJ mol^{-1})[a]

Complex	E(M—S)	$\bar{D}$(M—S)
$Ti(Cp)_2(SEt)_2$	326±10	341±10
$Ti(Cp)_2(SPr\text{-}n)_2$	331±10	347±10
$Ti(Cp)_2(SPh)_2$	358±10	344±10
$Ti(Cp)_2(S_2C_6H_3Me)$	333±10	
$Mo(Cp)_2(SPr\text{-}n)_2$	220±12	235±13
$Mo(Cp)_2(SPr\text{-}i)_2$	217±12	233±13
$Mo(Cp)_2(SBu\text{-}n)_2$	241±12	256±12
$Mo(Cp)_2(SBu\text{-}t)_2$	206±9	221±9
$Mo(Cp)_2(SC_{10}H_{21}\text{-}n)_2$	243±12	259±12
$Mo(Cp)_2(SPh)_2$	251±12	237±12
$W(Cp)_2(SEt)_2$	261±10	277±10
$W(Cp)_2(SPr\text{-}n)_2$	266±10	281±10
$W(Cp)_2(SPh)_2$	288±10	274±10

[a] Data not including reorganization energies ER_1 and ER_3.

Recommending "constant" metal–oxygen bond enthalpy terms in $M(Cp)_2L_n$ complexes for each metal is obviously an over-simplification that can only be allowed because our present data are both scarce and not very precise (this being mainly a consequence of estimated enthalpies of sublimation). A somewhat similar situation is found for metal–sulphur bond enthalpy terms. Defining average E(M—S) values is probably the most judicious use for the data in Table 5, particularly when the uncertainty intervals are considered. However, if the individual values are accepted, several trends are apparent. First, there seems to be an increase of E(M—SR) with the length of the *n*-alkyl chain. The observation of a similar pattern in the case of the above mentioned $Ti(OR)_4$ molecules lends some support to that trend. Secondly, a large value (35 kJ mol^{-1}) is noted for the difference E(Mo—SBu-*n*) − E(Mo—SBu-*t*), reflecting expected steric effects in the *t*-butyl complex.

An interesting comparison between oxygen and sulphur bidentate ligands is provided by the complex $Ti(Cp)_2(S_2C_6H_3Me)$. The value obtained for E(Ti—S) indicates a negligible strain in the metallacycle. The larger size of the sulphur atom, compared with oxygen, causing a relaxation of the five-membered ring, has been used as a possible explanation for that different behaviour.[20] The same pattern is observed in cyclic organic molecules $(CH)_{n-1}X$ (X = CH_2, O, NH or S), discussed by Cox and Pilcher.[1] For $n = 5$ the strain energy decreases by about 15 kJ mol^{-1} when oxygen is replaced by sulphur.

The usefulness of the bond enthalpy term concept is evidenced by the oxygen and sulphur bidentate complexes: E(M—O) and E(M—S) provide the only energetic information on these bonds, since the enthalpies of formation of the free biradicals are not available, and therefore mean bond dissociation enthalpies could not be calculated.

Nitrogen and phosphorus complexes

The metal–nitrogen bond enthalpy data (Table 7) were derived from the reaction–solution calorimetric standard enthalpies of formation (Table 6)[9,14] by the common procedure, i.e. eqs (2) and (3). However, Scheme 3 or eq. (4) were not used for the neutral ligand azobenzene. Instead, ΔH_f^0(L*,g) relies on a MNDO result for the reorganization

Table 6. Standard enthalpies of formation of nitrogen and phosphorus complexes (kJ mol^{-1})[a]

Complex	ΔH_f^0(c)	ΔH_s^0	ΔH_f^0(g)
$Ti(Cp)_2(N_3)_2$	436.4±8.4	(70±10)[b]	506.4±13.1
$Ti(Cp)_2(NC_8H_6)_2$	181.9±12.1	(109±10)	290.9±15.7
$Ti(Cp)_2(N_2Ph_2)$	338.8±16.7	(90±15)	428.8±22.4
$Ti(Cp)_2(PMe_3)_2$	−261.9±17.1	(90±10)	−171.9±19.8
$Mo(Cp)_2(N_2Ph_2)$	563.7±8.6	(70±15)	633.7±17.3

[a] Data from refs 9, 14 and 25.
[b] Estimated values in parentheses.

energy of azobenzene to the *cis*-conformation (−198 kJ mol^{-1}).[14] Also, as $\bar{D}$(M—N) are meaningless parameters in this case, only values of $D(M—N_2Ph_2) = 2\bar{D}(M—N)$ are presented in Table 7.

Although $(ER_3 - ER_1)/2$ corrections are seen to be negligible for the titanium complexes with L = N_3 and N_2Ph_2, and assumed to be so for the remaining Ti and Mo molecules,[9,14] the Hückel calculations indicate that a large negative correction [$ER_3 \sim -82$ kJ mol^{-1}; see eq. (3)] should be applied to the value of $D(Mo—N_2Ph_2)$ in Table 7. As discussed before, ER_3 is not significant for the titanium analogues.

The calculation method was also slightly modified for evaluating $E(Ti—N_3)$ because N—N bond lengths are considerably different in the complex and in N_3H.[9] Extended Hückel calculations indicate that the fragment N_3 is stabilized in the complex by *ca* 48 kJ mol^{-1}. This correction, which implies a negative adjustment to the value obtained from eqs (2) and (4), is included in Table 7. The average between $E(Ti—N_3)$ and $E(Ti—NC_8H_6)$, 339 kJ mol^{-1}, can be compared with $E(Ti—NR_2) \sim 311$ kJ mol^{-1} in $Ti(NR_2)_4$ (R = Me, Et). ($E(Ti—Nr_2)$ were recalculated in 8 from data in ref. 24.) E(Ti—N) for the azobenzene complex is lower than the corresponding values for the monodentate ligands. The geometry of coordinated N_2Ph_2, a distorted *cis* form, does not seem to favour both σ- and π-bonding with the metal atom.[14]

The standard enthalpy of formation of $Ti(Cp)_2(PMe_3)_2$ was recently determined by reaction-solution calorimetry, allowing us to obtain $E(Ti—PMe_3)$ and $\bar{D}(Ti—PMe_3)$.[25] As in the case of azobenzene, eq. (4) was not used to evaluate ΔH_f^0(L*,g). MNDO calculations give a negligible reorganization energy (−5 kJ mol^{-1}) for PMe_3.[26] This correction is not included in the result shown in Table 7 and the same happens with $(ER_3 - ER_1)/2 \sim -4$ kJ mol.† The thermochemistry of other bis(cyclopentadienyl) complexes containing metal–phosphorus bonds are presently being investigated. For the moment it is of interest to stress that Ti—PMe_3 and Ti—CO bond strengths are comparable (see below).

† The structural data of $Ti(Cp)_2(PMe_3)_2$ is included in ref. 22.

Complexes containing metal–hydrogen and metal–carbon bonds

Table 8 summarizes all the available standard enthalpies of formation of these bis(cyclopentadienyl) derivatives. With the exception of $\Delta H_f^0[Ti(Cp)_2(CH_2Ph)_2,c]$, which was determined by static-bomb combustion calorimetry,[5] the data were derived from reaction–solution calorimetric measurements.[14,27] Preliminary results for Mo $(Cp)_2Et_2$, $Mo(Cp)_2(n\text{-}Bu)_2$ and $Mo(Cp)_2(C_2H_4)$ are

Table 7. Metal–nitrogen and metal–phosphorus bond enthalpies (kJ mol^{-1})[a]

Complex	E(M—L)	D or $\bar{D}$(M—L)
$Ti(Cp)_2(N_3)_2$	329±10	385±22
$Ti(Cp)_2(NC_8H_6)_2$	348±10	
$Ti(Cp)_2(N_2Ph_2)$	290±12[b]	381±24[c]
$Ti(Cp)_2(PMe_3)_2$	162±12	162±12
$Mo(Cp)_2(N_2Ph_2)$	195±12[b]	192±23[c]

[a] Data not including reorganization energies ER_1 and ER_3.
[b] Bond enthalpy term for *one* M—N bond. Values include the MNDO result for the reorganization energy of azobenzene to the *cis*-conformation (−198 kJ mol^{-1}).
[c] M—N_2Ph_2 bond dissociation enthalpy (*cis*-azobenzene as a product). See also note [a].

Table 8. Standard enthalpies of formation of complexes containing metal–hydrogen and metal–carbon bonds (kJ mol^{-1})[a]

Complex	ΔH_f^0(c)	ΔH_s^0	ΔH_f^0(g)
$Ti(Cp)_2Me_2$	−26.6±9.6	(79.5±8.4)[b]	52.9±12.7
$Ti(Cp)_2(Me)Cl$	−234.7±8.1	(110±10)	−124.7±12.9
$Ti(Cp)_2Ph_2$	262.2±8.9	(88±8)	350.2±12.0
$Ti(Cp)_2(Ph)Cl$	−79.2±7.8	(120±10)	40.8±12.7
$Ti(Cp)_2(C_6H_4Me\text{-}3)_2$	166.8±9.4	(95±8)	261.8±12.3
$Ti(Cp)_2(C_6H_4Me\text{-}4)_2$	169.6±9.6	(95±8)	264.6±12.5
$Ti(Cp)_2(C_6H_4CF_3\text{-}4)_2$	−1142.6±8.3	(110±8)	−1032.6±11.5
$Ti(Cp)_2(C_6H_4OMe\text{-}4)_2$	−91.8±8.5	(104±8)	12.2±11.7
$Ti(Cp)_2(CH_2Ph)_2$	195.8±5.0	(83.7±8.4)	279.5±9.8
$Ti(Cp)_2Fc_2$[c]	488.2±12.1	(150±15)	638.2±19.3
$Ti(Cp)_2(CO)_2$	−295.3±12.9	84.2±3.5	−211.1±13.4
$Mo(Cp)_2H_2$	210.3±5.7	81.4±1.0	291.7±5.8
$Mo(Cp)_2Me_2$	262.4±4.0	70.4±4.2	332.8±5.8
$Mo(Cp)_2Et_2$	[219.2±3.3][d]	93.7±1.8	[312.9±3.8]
$Mo(Cp)_2(n\text{-}Bu)_2$	[143.5±4.6]	(105±10)	[248.5±11.0]
$Mo(Cp)_2(C_2H_4)$	284.6±8.2	(80±10)	364.6±12.9
$W(Cp)_2H_2$	222.4±8.8	84.1±1.6	306.5±8.9
$W(Cp)_2(H)I$	176.3±11.3	(100±5)	276.3±12.4
$W(Cp)_2Me_2$	271.0±8.1	(74.6±4.2)	345.6±9.1

[a] Data from refs 5, 14, 29 and 30.
[b] Estimated values in parentheses.
[c] Fc = ferrocenyl.
[d] Preliminary values in brackets. See footnote † on this page.

also reported,† together with recent measurements of the standard enthalpies of sublimation of the $M(Cp)_2H_2$ (M = Mo, W)[29] and $Mo(Cp)_2Et_2$.[30]

The analysis of M—L bond enthalpy values (Table 9) for the complexes $M(Cp)_2(L)L'$ ($L \neq L'$) will be made below. The remaining E(M—L) and $\bar{D}$(M—L) were calculated by the methods already described. In the case of the carbonyl complex, ΔH_f^0(L*,g) relies directly on a MINDO/3 calculation which yields a negligible value (−2 kJ mol^{-1})[14] for ER_{CO}. As the structure of the ethylene complex is not available, the calculation of the reorganization energy of C_2H_4 was not attempted and thus only the Mo—C_2H_4 bond dissociation enthalpy is shown.

As happens with the bis(cyclopentadienyl) derivatives mentioned previously, the available crystal structures for the complexes in Tables 8 or 9,[22,31]‡ together with extended Hückel calculations, indicate that corrections $(ER_3 - ER_1)/2$ are relatively small,† except for $Mo(Cp)_2H_2$, where the angle Cp—Mo—Cp, 145.8°,[31] is substantially larger than the one in $Mo(Cp)_2Cl_2$, 130.5°,[33] leading to $(ER_3 - ER_1)/2 \sim -33$ kJ mol^{-1}. This implies that E(Mo—H) presented in Table 9 is a high upper limit and it is reasonable to draw a similar conclusion for the tungsten analogue, whose structure is not known.

It has been mentioned that ER_3 is small for titanium and relatively large for molybdenum and tungsten. Significant corrections (about −42 and −52 kJ mol^{-1} for Mo and W, respectively) may therefore affect $\bar{D}$(Mo—L) and $\bar{D}$(W—L) in Table 9.

A broad look at the titanium–carbon and molybdenum–carbon bond enthalpy terms suggests that, for predictive purposes, the averages 290 kJ mol^{-1} (Ti) and 135 kJ mol^{-1} (Mo) can be defined, enabling us to estimate new enthalpies of formation within *ca* ±20 kJ mol^{-1}. These estimates can, however, be improved by considering some trends evidenced in the table. For instance, E(Ti–methyl) is 15–25 kJ mol^{-1} lower than E(Ti–aryl) and E(Mo—C) decreases with the length of the *n*-alkyl chain.

† A small correction due to the dilution of the HCl–ether solution used in the experimental study is not included in the values for the ethyl and butyl complexes. Although this correction will not affect significantly the bond enthalpy data, it will be included when the results are fully reported.[28]

‡ The angle Cp—Mo—Cp in the complex $Mo(Cp)_2(n\text{-}Bu)_2$, 135.2 implies $(ER_2 - ER_1)/2 \sim -16$ kJ mol^{-1}.[32]

Table 9. Metal–hydrogen and metal–carbon bond enthalpies (kJ mol^{-1})[a]

Complex	E(M—L)	D or $\bar{D}$(M—L)
$Ti(Cp)_2Me_2$	274±5	298±6
$Ti(Cp)_2(Me)Cl$	293±11	
$Ti(Cp)_2Ph_2$	287±9	331±10
$Ti(Cp)_2(Ph)Cl$	290±13	
$Ti(Cp)_2(C_6H_4Me\text{-}3)_2$	299±10	342±10
$Ti(Cp)_2(C_6H_4Me\text{-}4)_2$	297±10	341±10
$Ti(Cp)_2(C_6H_4CF_3\text{-}4)_2$	297±10	340±10
$Ti(Cp)_2(C_6H_4OMe\text{-}4)_2$	305±9	349±10
$Ti(Cp)_2(CH_2Ph)_2$	280±12	237±9
$Ti(Cp)_2Fc_2$[b]	278±11	(331±12)[c]
$Ti(Cp)_2(CO)_2$	174±8	172±8
$Mo(Cp)_2H_2$	257±8	257±8
$Mo(Cp)_2Me_2$	142±8	166±8
$Mo(Cp)_2Et_2$	(137±11)[d]	(147±9)
$Mo(Cp)_2(n\text{-}Bu)_2$	(127±12)	(134±12)
$Mo(Cp)_2(C_2H_4)$		57±20[e]
$W(Cp)_2H_2$	311±4	311±4
$W(Cp)_2(H)I$	273±14	
$W(Cp)_2Me_2$	197±3	221±3

[a] Data not including reorganization energies ER_1 and ER_3.

[b] Fc = ferrocenyl.

[c] Estimate based on D(Fc—H) ~ $D(C_6H_5$—H).

[d] Preliminary values in parentheses. See footnote † on previous page.

[e] Mo—C_2H_4 bond dissociation enthalpy. See also note [a].

Mixed complexes and stepwise bond dissociation enthalpies

The calculation of E(Ti—Me) and E(Ti—Ph) in the complexes $Ti(Cp)_2(L)Cl$ can be made through eq. (7), derived from two schemes similar to 4, one for the complex and the other for $M(Cp)_2Cl_2$.[27] The reorganization energies associated with the fragments $M(Cp)_2Cl$ from the complex and from $M(Cp)_2Cl_2$ are represented by ER'_{13} and by ER'_3, respectively (the subscript 13 indicates a mixed complex, i.e. that the initial complex contains both the ligand of interest and a halogen; 3 means that the initial complex is the dichloride). Equation (8) was also obtained from the two schemes and includes the *first* M—L bond dissociation enthalpy, D_1(M—L).

$$E(\text{M—L}) = E(\text{M—Cl}) + \Delta H_f^0(\text{L}^*,\text{g}) - \Delta H_f^0(\text{Cl,g}) - \{\Delta H_f^0[\text{M(Cp)}_2\text{(L)Cl,g}] - \Delta H_f^0[\text{M(Cp)}_2\text{Cl}_2\text{,g}]\} + (ER'_3 - ER'_{13}) \quad (7)$$

† See ref. 12. The reorganization energy for the fragment $Ti(Cp)_2Ph$ was calculated as −41 kJ mol^{-1}.[26]

$$D_1(\text{M—L}) = E(\text{M—Cl}) + \Delta H_f^0(\text{L,g}) - \Delta H_f^0(\text{Cl,g}) - \{\Delta H_f^0[\text{M(Cp)}_2\text{(L)Cl,g}] - \Delta H_f^0[\text{M(Cp)}_2\text{Cl}_2\text{,g}]\} + ER'_3. \quad (8)$$

E(Ti—Me) and E(Ti—Ph) in Table 9 were obtained by transferring E(Ti—Cl) from $TiCl_4$ and by assuming that the geometry of the $Ti(Cp)_2Cl$ fragment is similar in the mixed complexes and in the dichloride, implying $ER'_{13} \sim ER'_3$. It is seen that for the complexes $Ti(Cp)_2Ph_2$ and $Ti(Cp)_2(Ph)Cl$, E(Ti—Ph) is remarkably constant, but the same is not observed for $Ti(Cp)_2Me_2$ and $Ti(Cp)_2(Me)Cl$: the titanium–metal bond is strengthened in the mixed complex. Although this strengthening is not unusual,[34] it must be stressed that E(Ti—Cl) was transferred from $TiCl_4$ and hence from $Ti(Cp)_2Cl_2$. If the titanium–chloride bond is also stronger in the mixed complex, then E(Ti—Me) in Table 9 will be an upper limit.

The third mixed complex in Table 9 is $W(Cp)_2(H)I$, for which E(W—H) = 273 kJ mol^{-1} was obtained. The calculation of this bond enthalpy term was made by a slight modification of the method outlined in eq. (7). The reference molecule $W(Cp)_2Cl_2$ was replaced by $W(Cp)_2I_2$ and E(W—I) was taken as 268 kJ mol^{-1} (Table 2). Also, in the absence of structural data for the iodohydride complex, it was assumed that $ER'_{13} \sim ER'_3$.

The fact that the value of E(W—H) in the mixed complex is substantially lower than E(W—H) in $M(Cp)_2H_2$ apparently indicates that this bond enthalpy cannot be transferred between the two molecules. Recall, however, that the value for the dihydride in Table 9 is not corrected by the difference $(ER_3 - ER_1)/2$, which, in the case of tungsten, is estimated to be *ca* −37 kJ mol^{-1}. If this correction is applied, the value for the dihydride will match the one for the iodohydride. Although this good agreement may be fortuitous, it illustrates the importance of reorganization energies when transferring bond enthalpy terms.

Several reorganization energies of fragments $M(Cp)_2L$ from complexes $M(Cp)_2(L)L'$ ($L = L' \neq Cl$, ER'_1; $L = L' = Cl$, ER'_3; $L \neq L' = Cl$, ER'_{13}), together with values of the stepwise bond dissociation enthalpies D_1(M—L) and D_2(M—L'), calculated with data in the previous tables and eqs (5) or (8), are collected in Table 10.† Several *qualitative* conclusions can be drawn from these values. One, fragments such as $M(Cp)_2Cl$ and $M(Cp)_2Ph$, associated with large reorganization energies, lead to considerable differences D_2(M—L) − D_1(M—L). Two, the titanium–methyl first bond dissociation energy in $Ti(Cp)_2Me_2$ is predicted to be higher than in $Ti(Cp)_2(Me)Cl$, since the

Table 10. Estimated stepwise bond dissociation enthalpies (kJ mol^{-1})

$M(Cp)_2(L)L'$	Fragment	ER'^a	D_1(M—L)	D_2(M—L')
$Ti(Cp)_2Cl_2$	$Ti(Cp)_2Cl$	−41	390	471
$Ti(Cp)_2(Me)Cl$	$Ti(Cp)_2Cl$	(−41)[b]	276	471
$Ti(Cp)_2Me_2$	$Ti(Cp)_2Me$	−11	287	309
$Ti(Cp)_2(Ph)Cl$	$Ti(Cp)_2Cl$	(−41)[b]	292	471
$Ti(Cp)_2Ph_2$	$Ti(Cp)_2Ph$	−41	290	372
$Ti(Cp)_2(CO)_2$	$Ti(Cp)_2CO$	−2	170	174
$Mo(Cp)_2Cl_2$	$Mo(Cp)_2Cl$	−65	238	369
$Mo(Cp)_2H_2$	$Mo(Cp)_2H$	−11	246	268
$Mo(Cp)_2Me_2$	$Mo(Cp)_2Me$	(−17)[c]	149	183

[a] Reorganization energy of the fragment.

[b] Identical structures of the fragment in the complex and in $Ti(Cp)_2Cl_2$ were assumed.

[c] The structure of the complex was estimated. See ref. 12.

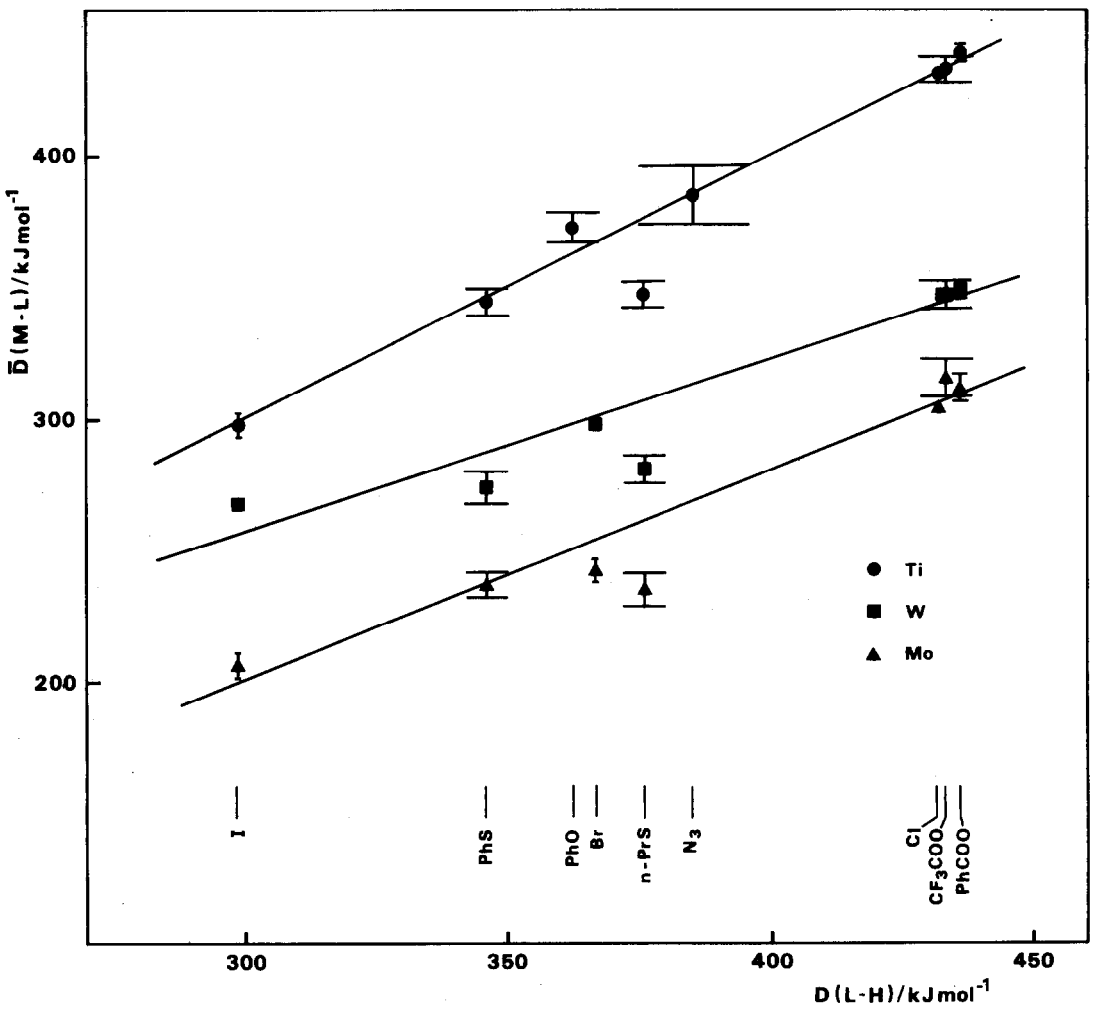

Fig. 1. Metal–ligand mean bond dissociation enthalpies vs ligand–hydrogen bond dissociation enthalpies for halogen, nitrogen, oxygen and sulphur ligands.

reorganization energy of $Ti(Cp)_2Cl$ is larger than $Ti(Cp)_2Me$. Three, $D_2(M—L) > D_1(M—L)$, as could be expected, because $D_2(M—L)$ refers to the species $M(Cp)_2L$, where the metal is in a lower oxidation state and/or is coordinated to a smaller number of ligands.

Although we strongly favour a qualitative view of the data in Table 10, recent preliminary thermochemical results involving several titanium bis(pentamethylcyclopentadienyl) complexes, viz. $Ti(Cp^*)_2Me_2$, $Ti(Cp^*)_2Me$, $Ti(Cp^*)_2Ph$, $Ti(Cp^*)_2Cl_2$ and $Ti(Cp^*)_2Cl$, showed that those estimates may also have some quantitative value.[35] The following $D_1(Ti—L)$ were directly obtained from the standard enthalpies of formation of the corresponding Ti(III) and Ti(IV) complexes (kJ mol^{-1}): $D_1(Ti—Me) = 271 \pm 21$, $D_1(Ti—Ph) = 269 \pm 28$, $D_1(Ti—Cl) = 380 \pm 20$. All are in fair agreement with the predictions in the table.

CONCLUDING REMARKS

The present paper shows that the energetics of $M(Cp)_2L_n$ complexes can be reasonably predicted by a judicious use of the "bond enthalpy term method", even when the enthalpies of formation of the radicals L are not available. In addition, the recent comparison with the experimental data for the bis(pentamethylcyclopentadienyl) titanium molecules gives some credit to the estimates of stepwise Ti—L bond dissociation enthalpies. The usefulness of the method to analyse the thermochemical data of other families of compounds has also been tested.[36]

As mentioned before, the bond enthalpy term method relies on the Laidler scheme. It is thus not surprising that some of the features observed for organic molecules are reflected in metal–ligand terms. For instance, the Laidler scheme recom-

Table 11. Auxiliary thermochemical data (kJ mol^{-1})[a]

L	Ref.	ΔH_f^0(L,g)	D(L—H)	E(L—H)[b]	$D-E$
H	39	217.997	436.0	436.0	0
Cl	39	121.302	431.6	431.6	0
Br	39	111.86	366.2	366.2	0
I	39	106.762	298.4	298.4	0
PhO[c]	11	48 ± 10	362 ± 10	451	−89
PhCOO	40	-76.3 ± 3.0	435.8 ± 3.4	451	−15
CCl_3COO	41	-213 ± 13	(433 ± 10)	451	−18
CF_3COO	42	(-815.7 ± 10)	(433 ± 10)	451	−18
$C_6H_4O_2$				451	
$C_{10}H_6O_2$				451	
$C_{14}H_8O_2$				451	
SO_4				451	
RS[d]	11, 43		375.7 ± 8.4	360	16
PhS	11, 44	240.2 ± 8.4	345.8 ± 8.4	360	−14
$MeC_6H_3S_2$				360	
N_3	45	461 ± 21	385 ± 21	377	8
C_8H_6N				377	
Me	11	146.9 ± 0.6	439.7 ± 0.8	415.8	24
Et	46	119 ± 4	421 ± 4	411	10
n-Bu		(74 ± 8)	(418 ± 8)	411	7
Ph[e]	11	328.9 ± 8.4	464.0 ± 8.4	421	43
$PhCH_2$	11	200 ± 6	368 ± 4	411	−43
Cp	47	260 ± 9	347 ± 10		
C_2H_4	48	52.2 ± 1.2			
CO	39	-110.53 ± 0.17			
cis-N_2Ph_2	48, 49	455.7 ± 2.5			
PMe_3	48	-101.1 ± 5.3			

[a] Gas-phase data. Estimated values in parentheses.

[b] Laidler terms from ref. 1 (± 8 kJ mol^{-1}) or calculated from tabulated enthalpies of formation.

[c] The same bond dissociation enthalpy was used for L = MeC_6H_4O and ClC_6H_4O.

[d] R = alkyl.

[e] The same bond dissociation enthalpy was used for L = MeC_6H_4, $CF_3C_6H_4$ and $MeOC_6H_4$.

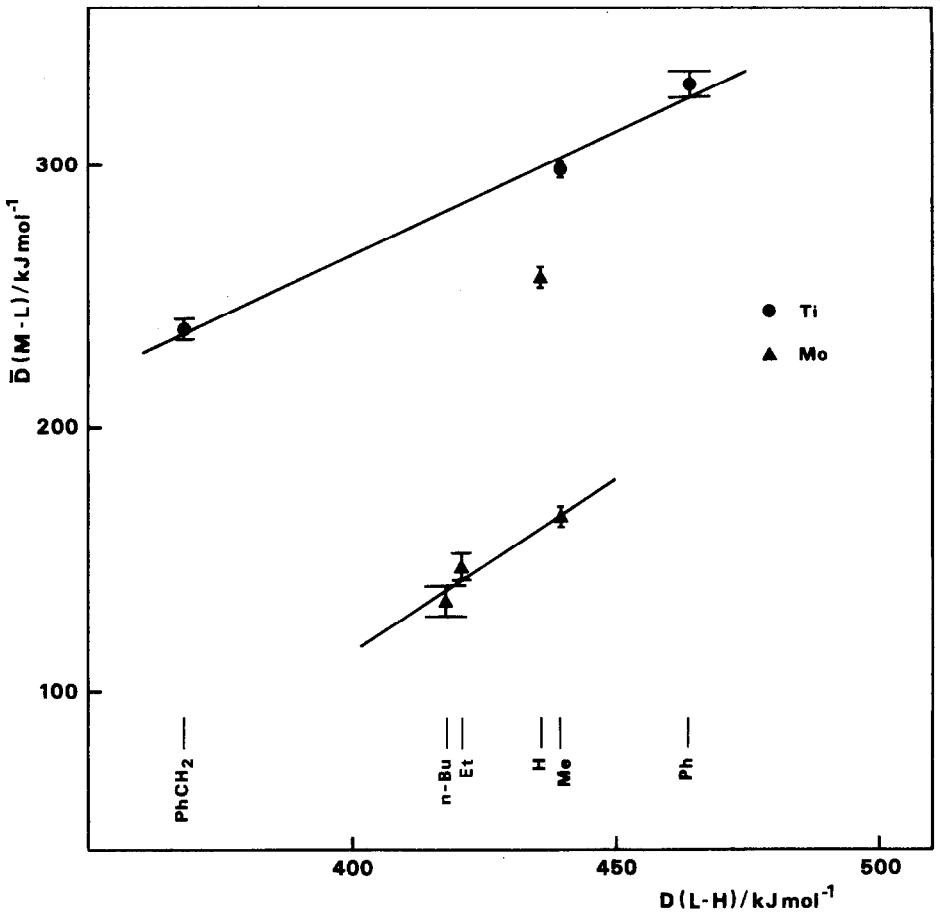

Fig. 2. Metal–carbon and metal–hydrogen mean bond dissociation enthalpies vs ligand–hydrogen bond dissociation enthalpies.

mends a single term for O—H and S—H bonds,[1] also being possible to define average M—O and M—S terms, within, *ca* ±20 kJ mol^{-1}. As metal–ligand bond strengths are more sensitive to the chemical environment than the hydrogen–ligand bonds, it is not surprising that the interval is relatively wide. Other examples showing parallel trends between Laidler terms and metal–ligand terms can be found in the tables mentioned above (compare, e.g. Ti—Ph and Ti—Me bond terms, Table 9, with E(Ph—H) and E(Me—H), Table 11).

The most common attempt to "reduce" organometallic thermochemistry to organic and inorganic thermochemistry consists of plotting metal–ligand bond dissociation enthalpies vs ligand–hydrogen bond dissociation enthalpies. It is indeed observed that such plots often lead to good linear variations, thus allowing the prediction of new values.[37] The same type of correlation for the Ti, Mo and W bis(cyclopentadienyl) complexes is shown in Figs 1 and 2. As expected for these metals, the data for σ-donor ligands (Fig. 2) does not fit the lines obtained for π-donor ligands (Fig. 1). It is also noted that $\bar{D}$(M—SPr-*n*) are significantly lower than the values predicted on the basis of the correlations in Fig. 1. It is very unlikely that the deviation is due to wrong estimates of the enthalpies of sublimation of the complexes: it would be necessary to decrease these quantities by *ca* 60 kJ mol^{-1} to obtain a good fit of the three points. Instead, the deviation may be attributed to the larger polarizability of the sulphur atom as compared with oxygen. However, an identical discrepancy is not observed in the case of PhS. $\bar{D}$(Mo—H), on the other hand, is clearly above the line defined with three Mo–alkyl bonds in Fig. 2, even if the correction $ER_3/2$ (~ -42 kJ mol^{-1}) is applied.

Although the previous correlations deal with *mean* bond dissociation enthalpies and therefore important features may be hidden, they seem less successful than recently proposed plots between the standard enthalpies of formation of crystalline complexes and the enthalpies of formation LH (for anionic ligands) or L (for neutral ligands) in their

standard reference state (rs),[38] i.e. their stable physical state at 298.15 K and 1 atm. An advantage of these latter correlations over the ones involving bond dissociation enthalpies is that they allow estimation of the enthalpies of formation of complexes even in the absence of data for D(L—H), this being particularly important in the case of bidentate (e.g. SO_4, $O_2C_6H_4$) and neutral (e.g. C_2H_4, N_2Ph_2) ligands. Interestingly, it can be shown that the plots D(M—L) vs D(L—H) and ΔH_f^0(complex, c) vs ΔH_f^0(ligand, rs) are mathematically equivalent, provided that a cancellation of sublimation and vaporization enthalpies occurs. This matter will be further explored in a future publication.

We have deliberately omitted important chemical implications of the thermochemical data surveyed in the tables above, some of which can be found in the papers where those values were originally reported. Although the main purposes of acquiring thermochemical values are understanding reactivity and providing new insights into the nature of chemical bonds, a broad view of organometallic energetics is rather desirable at the present stage. The development of new and more accurate estimation procedures will undoubtedly be fostered both by the massive amount of thermochemical data that is currently being obtained in some laboratories and by the growing efforts of theoretical chemists to produce reliable values of enthalpies of formation and bond dissociation enthalpies.

REFERENCES

1. J. D. Cox and G. Pilcher, *Thermochemistry of Organic and Organometallic Compounds*. Academic Press, London and New York (1970).
2. S. W. Benson, *Thermochemical Kinetics*. Wiley, New York (1976).
3. J. B. Pedley, R. D. Naylor and S. P. Kirby, *Thermochemical Data of Organic Compounds*. Chapman and Hall, London (1986).
4. J. C. G. Calado, A. R. Dias, J. A. Martinho Simões and M. A. V. Ribeiro da Silva, *Rev. Port. Quím.* 1979, **21**, 129.
5. V. I. Tel'noi and I. B. Rabinovich, *Usp. Khim.* 1977, **46**, 1337.
6. M. E. Minas da Piedade, L. Shaofeng and G. Pilcher, *J. Chem. Therm.* 1987, **19**, 195.
7. J. C. G. Calado, A. R. Dias, M. E. Minas da Piedade and J. A. Martinho Simões, *Rev. Port. Quím.* 1980, **22**, 53.
8. G. Pilcher and J. A. Martinho Simões, Energetics of Organomet. Species, manuscript in preparation.
9. See e.g. M. J. Calhorda, R. Gomes da Costa, A. R. Dias and J. A. Martinho Simões, *J. Chem. Soc., Dalton Trans.* 1982, 2327.
10. A. R. Dias and J. A. Martinho Simões, *Rev. Port Quim.* 1982, **24**, 191.
11. D. F. McMillen and D. M. Golden, *Ann. Rev. Phys. Chem.* 1982, **33**, 493.
12. M. J. Calhorda, A. R. Dias, A. M. Galvão and J. A. Martinho Simões, *J. Organomet. Chem.* 1986, **307**, 167.
13. J. Bickerton, M. E. Minas da Piedade and G. Pilcher, *J. Chem. Therm.* 1984, **16**, 661.
14. A. R. Dias, P. B. Dias, H. P. Diogo, A. M. Galvão, M. E. Minas da Piedade and J. A. Martinho Simões, *Organometallics* 1987, **6**, 1427.
15. J. C. G. Calado, A. R. Dias and J. A. Martinho Simões, *J. Organomet. Chem.* 1980, **195**, 203.
16. G. Pilcher and H. A. Skinner, *The Chemistry of Metal–Carbon Bond* (Edited by F. R. Hartley and S. Patai), Chap. 2. Wiley, New York (1982).
17. D. R. Stull and H. Prophet, *JANAF Thermochemical Tables* (2nd Edn). National Bureau of Standards, Washington, D. C. (1971).
18. M. J. Calhorda, A. R. Dias, J. A. Martinho Simões and C. Teixeira, *J. Chem. Soc., Dalton Trans.* 1984, 2659.
19. M. J. Calhorda, M. A. A. F. de C. T. Carrondo, A. R. Dias, A. M. T. S. Domingos, J. A. Martinho Simões and C. Teixeira, *Organometallics* 1986, **5**, 660.
20. M. J. Calhorda, M. A. A. F. de C. T. Carrondo, A. R. Dias, C. F. Frazão, M. B. Hursthouse, J. A. Martinho Simões and C. Teixeira, submitted for publication.
21. M. D. Ribeiro da Silva, Tese de Doutoramento, Faculdade de Ciências do Porto (1985).
22. D. Cozak and M. Melnik, *Coord. Chem. Rev.* 1986, **74**, 53.
23. M. A. A. F. de C. T. Carrondo, M. J. Calhorda and M. B. Hursthouse, *Acta Cryst.* 1987, **C43**, 880.
24. M. F. Lappert, D. S. Patil and J. B. Pedley, *J. Chem. Soc., Chem. Commun.* 1975, 830.
25. P. B. Dias, A. R. Dias and J. A. Martinho Simões, unpublished results.
26. M. J. Calhorda and A. M. Galvão, unpublished data.
27. See M. J. Calhorda, A. R. Dias, M. E. Minas da Piedade, M. S. Salema and J. A. Martinho Simões, *Organometallics* 1987, **6**, 734 and refs cited therein.
28. A. R. Dias, M. E. Minas da Piedade and J. A. Martinho Simões, unpublished results.
29. A. R. Dias, H. P. Diogo, M. E. Minas da Piedade, J. A. Martinho Simões, A. S. Carson and E. H. Jamea, unpublished results.
30. A. R. Dias, M. E. Minas da Piedade and J. A. Martinho Simões, unpublished results.
31. A. J. Schultz, K. L. Stearley, J. M. Williams, R. Mink and G. D. Stucky, *Inorg. Chem.* 1977, **16**, 3303.
32. M. A. A. F. de C. T. Carrondo, A. M. T. S. Domingos and A. M. Galvão, unpublished data.
33. K. Prout, T. S. Cameron and R. A. Forder, *Acta Cryst.* 1974, **B30**, 2290.
34. See e.g. J. W. Bruno, H. A. Stecher, L. R. Morss, D. C. Sonnenberger and T. J. Marks, *J. Am. Chem. Soc.* 1986, **108**, 7275.

35. A. R. Dias, M. S. Salema, J. A. Martinho Simões, J. W. Pattiasina and J. H. Teuben, *J. Organomet. Chem.*, in press.
36. J. A. Martinho Simões and J. L. Beauchamp, to be submitted to *Chem. Rev.*
37. H. E. Bryndza, L. K. Fong, R. A. Paciello, W. Tam and J. E. Bercaw, *J. Am. Chem. Soc.* 1987, **109**, 1444.
38. A. R. Dias, J. A. Martinho Simões, C. Teixeira, C. Airoldi and A. P. Chagas, *J. Organomet. Chem.* 1987, **335**, 71.
39. CODATA Recommended Key Values for Thermodynamics, *J. Chem. Therm.* 1978, **10**, 903.
40. C. E. H. Baum and S. F. Mellish, *Trans. Faraday Soc.* 1951, **47**, 1216.
41. A. R. Dias, M. S. Salema and J. A. Martinho Simões, *Rev. Port. Quím.* 1984, **26**, 227.
42. J. C. G. Calado, A. R. Dias, M. S. Salema and J. A. Martinho Simões, *J. Chem. Soc., Dalton Trans.* 1981, 1174.
43. B. K. Janousek, K. J. Reed and J. I. Brauman, *J. Am. Chem. Soc.* 1980, **102**, 3125.
44. S. W. Benson, *Chem. Rev.* 1978, **78**, 23.
45. M. J. Pellerite, R. L. Jackson and J. I. Brauman, *J. Phys. Chem.* 1981, **85**, 1624.
46. P. D. Pacey and J. H. Wimalasena, *J. Phys. Chem.* 1984, **88**, 5657.
47. D. J. DeFrees, R. T. McIver Jr and W. J. Hehre, *J. Am. Chem. Soc.* 1980, **102**, 3334.
48. J. B. Pedley and J. Rylance, *Sussex-N.P.L. Computer Analysed Thermochemical Data: Organic and Organometallic Compounds.* University of Sussex, Brighton, U.K. (1977).
49. F. W. Schulze, H. J. Petrick, H. K. Cammenga and H. Klinge, *Z. Physik. Chem. (Munich)* 1977, **107**, 1.
50. M. W. Chase Jr, J. L. Curnutt, J. R. Downey Jr, R. A. McDonald, A. N. Syverud and E. A. Valenzuela, JANAF Thermochemical Tables, 1982 Supplement, *J. Phys. Chem. Ref. Data* 1982, **11**, 695.
51. V. L. Glushko and L. V. Gurvich, *Thermochemical Constants of Individual Compounds*, Vol. 1. Nauka, Moscow (1978).
52. G. Pilcher, *CATCH Tables, Nitrogen Compounds.* University of Sussex, Brighton, U.K. (1972).
53. A. R. Dias, M. S. Salema and J. A. Martinho Simões, *J. Organomet. Chem.* 1981, **222**, 69.
54. G. Pilcher, unpublished results.

APPENDIX

The auxiliary data used to calculate metal–ligand bond enthalpies are collected in Table 11.[11,39–49] The standard enthalpies of formation of gaseous LH_n molecules ($n = 1$ or 2) were taken from the following references: L = halogen (ref. 39); L = PhO, MeC_6H_4O, PhCOO, CF_3COO, RS, PhS, C_8H_6N, Me, Et, *n*-Bu, Ph, $PhCH_2$, $CF_3C_6H_4$, $MeOC_6H_4$, Cp (ref. 48); L = SO_4 (average between the values in refs 50 and 51, -737 ± 8 kJ mol^{-1}); L = Fc (taken as 227.6 ± 4.2 kJ mol^{-1}, by using the enthalpy of formation of the crystal in ref. 5 and an average value for the enthalpy of sublimation); L = N_3 (ref. 52); L = 2-ClC_6H_4O (estimated as -145 ± 11 kJ mol^{-1} in ref. 53); L = CCl_3COO (ref. 48, together with an experimental value for the enthalpy of sublimation,[54] gives -428.3 ± 8.4 kJ mol^{-1}); L = $C_{14}H_8O_2$ (estimated as -144 ± 6 in ref. 21); L = $C_6H_4O_2$, $C_{10}H_6O_2$ (-267.8 ± 1.7 and -181.3 ± 4.7 kJ mol^{-1}, respectively; ref. 21); L = $MeC_6H_3S_2$ (estimated as 108 ± 6 kJ mol^{-1} in ref. 18).

Polyhedron Vol. 7, No. 16/17, pp. 1545–1555, 1988
Printed in Great Britain

0277–5387/88 $3.00+.00
© 1988 Pergamon Press plc

Rh—Rh, Rh—H, Rh—C AND Rh—O BOND ENERGIES IN (OEP)Rh COMPLEXES: THERMODYNAMIC CRITERIA FOR ADDITION OF M—H AND M—M BONDS TO C—O AND C—C MULTIPLE BONDS

BRADFORD B. WAYLAND

Department of Chemistry and the Laboratory for Research on the Structure of Matter, University of Pennsylvania, Philadelphia, PA 19104-6323, U.S.A.

Abstract—Thermodynamic measurements and reactivity studies are used in estimating (Rh—Rh), (Rh—H), (Rh—C) and (Rh—O) bond dissociation energies (BDE) in octaethylporphyrin rhodium, [(OEP)Rh], complexes. Temperature dependence of the proton NMR line broadening of $[(OEP)Rh]_2$ is used as a kinetic method for estimating the (Rh—Rh) BDE as 16.5 ± 0.8 kcal mol^{-1}. Thermodynamic cycles are presented that provide values for the (Rh—H) BDE in (OEP)Rh—H (62 kcal mol^{-1}) and (Rh—C) BDE in (OEP)Rh—CHO (58 kcal mol^{-1}). Transfer of bond energy values from organic compounds to the organic fragments in organometallic species is used as a means of establishing general thermodynamic criteria for addition reactions of metal hydrides and metal–metal bonded complexes, with compounds that contain C—O and C—C multiple bonds. Approximate bond energy analysis is applied to the (OEP)Rh system in anticipating reactivity, estimating (Rh—C) and (Rh—O) bond energies and in recognizing steric effects.

Metal hydride addition to C—O and C—C multiple bonds is a fundamental step in the metal catalysed hydrogenation of CO_2, CO, aldehydes, ketones, esters, amides, alkenes and alkynes. One of the general goals of organometallic catalysis research has been to discover metallo species that accomplish these reactions, and provide an opportunity to evaluate the chemical and physical properties of complexes that can potentially function as intermediates in catalytic reactions. When designing a metal complex to accomplish one of these reactions, the synthetic chemist considers both the thermodynamic and kinetic feasibility of the process. There has been relatively little reliable thermodynamic data available for organometallic compounds and thus kinetic–mechanistic thinking has dominated this area, even though thermodynamic factors ultimately limit the range of observable reactivity accessible to a particular metallo system.

The approach to designed organometallic reactivity described in this article is focused on obtaining the desired organometallic species as a thermodynamic product of an addition reaction. The mechanistic approach to directed synthesis of organometallic complexes is much more sophisticated from the synthetic chemistry point of view, but the thermodynamic approach has the challenge of identifying metal complexes that react spontaneously with the appropriate reagents (H_2, CO, CO_2, $CH_2{=}CH_2$, etc.) to yield the desired organometallic product at equilibrium.

The scope of metal hydride addition reactions that are thermodynamically favourable is largely defined by the difference between the (M—H) and (M—C) or (M—O) bond energies. Using thermodynamic data, primarily from first transition series metal complexes, Halpern concluded that transition metal–carbon bonds are weak (M—C ~ 25–30 kcal mol^{-1}) and the difference in (M—H) and (M—C) bond energies is relatively large [(M—H) − (M—C) ~ +25–30 kcal mol^{-1}].[1] This guideline set of (M—C) and (M—H) bond energies thermodynamically excludes first transition series metal complexes from reactions such as the addition of a metal hydride to CO or oxidative addition of unactivated hydrocarbons to metal centres.[1] Both of these types of reactions that are thermodynamically unfavourable for first transition series metal complexes are now well established in the chemistry of second and third transition metal species.[2–7] These observations provide qualitative evidence that a different range of (M—H) and (M—C) bond energies is manifested by these systems.

The organometallic chemistry of rhodium porphyrins has yielded important examples of unusual and in several cases unprecedented reactivity.[2,3,8-11] Systemizing the known chemistry and anticipating new reactivity benefits from a knowledge of the thermodynamic factors associated with both the metallo species [(M—H), (M—C), (M—O), (M—M) bond energies] and the organic substrates. This paper summarizes the organometallic reaction chemistry and thermodynamic studies of rhodium octaethylporphyrin, (OEP)Rh, complexes that reflect the (Rh—Rh), (Rh—H), (Rh—C) and (Rh—O) bond energies manifested by this system. Bond energies derived from thermodynamic properties of organic molecules are used in establishing approximate general thermodynamic criteria for addition reactions of metal hydrides and metal–metal bonded complexes to C—O and C—C multiple bonds. The (OEP)Rh system is used in illustrating several potential applications of this bond energy model.

RESULTS AND DISCUSSION

Octaethylporphyrin rhodium hydride, (OEP)Rh—H, was the first metallohydride reported to accomplish the addition with CO to produce observable equilibrium concentrations of an η^1-carbon bonded metallo formyl complex, (OEP)Rh—CHO.[2] Unfavourable thermodynamic factors rather than kinetics are generally responsible for the difficulty in accomplishing the general reaction, (M—H + CO ⇆ M—CHO). Observation of this reaction for the (OEP)Rh—H complex suggested the occurrence of an unusual set of M—H and M—C bond energies. As a guide to the scope of organometallic reactions accessible to this system, approximate thermochemical relationships were developed for metal hydride addition reactions with C—O and C—C multiple bonds in terms of bond energies associated with the organic fragments (CO_2H, HCO, CH_2OH, CH_2CH_3, $CH{=}CH_2$) estimated from thermodynamic data on organic molecules[12-16] (Table 1, footnote *b*). The anticipated enthalpy change (ΔH^0) for a reaction can be described in terms of the difference between the (M—H), (M—C), (M—O) and (M—M) bond dissociation energies and an enthalpy change for the organic unit (Table 1). As a representative example, the enthalpy change for the general reaction M—H + CO ⇄ M—CHO can be described as a set of bond energies [ΔH^0 = (M—H) + (C≡O) − (M—C) − (C=O) − (C—H)]. Evaluation of the organic fragments, [(C≡O) − (C=O)] = 70 kcal mol^{-1} and (C—H) = 87 kcal mol^{-1} for an aldehydic C—H group, results in the approximate relationship (ΔH^0 = (M—H) − (M—C) − 17 kcal mol^{-1}) (Table 1). The enthalpy change ΔH^0 for the addition of a metal hydride carbon monoxide to form an η^1-carbon bonded formyl complex is anticipated to be negative when (M—H) BDE exceeds the (M—C) BDE by less than 17 kcal mol^{-1}. Each of the (M—H) addition reactions in Table 1 corresponds to two reactant molecules combining to form a single molecule of product, and the entropy change for a reaction of this type is in the range of −(25–30) cal K^{-1} mol^{-1}. Estimates for ΔG^0 (298 K) in Table 1 were obtained by using $\Delta S^0 = -27$ eu ($-T\Delta S^0$ (298 K) = +8 kcal mol^{-1}). Applying this estimate to the general formyl reaction gives ΔG^0 (298 K) ~ (M—H) − (M—C) − 9 kcal mol^{-1}, which means that ΔG^0 (298 K) will be negative if the (M—H) BDE exceeds the (M—C) BDE by no more than 9 kcal. Results from this type of approximate bond energy analysis applied to addition reactions of metal hydrides to CO_2, CO, H_2CO, RCHO, R_2CO, $CH_2{=}CH_2$ and HC≡CH to form both carbon and oxygen bonded organometallic compounds are found in Table 1. Reactions of M—M bonded dimers with H_2, O_2 and a set of C—O and C—C multiply bonded compounds have also been analysed and the results also appear in Table 1. Bond energy analysis for this series of reactants establishes an order of difficulty in accomplishing these addition reactions, (CO_2 > CO > H_2CO > $CH_2{=}CH_2$ > CH≡CH) (Table 1). Approximate enthalpy relationships also establish general criteria for the formation of M—C or M—O bonded species, providing a means of estimating (M—C) and (M—O) bond energies, and assisting in identifying the presence of steric effects. Results from both thermodynamic and reactivity studies of (OEP)Rh—H and $[(OEP)Rh]_2$ will be discussed in terms of this bond energy model.

In order to establish a quantitative foundation for the thermochemistry of the (OEP)Rh system, experimental studies have been carried out that directly relate to the (Rh—Rh), (Rh—H) and (Rh—C) bond energies. The (Rh—Rh) BDE in $[(OEP)Rh]_2$ has been estimated by kinetic methods and used in conjunction with thermodynamic values from equilibrium studies that provide values for the (Rh—H) BDE in (OEP)Rh—H and the (Rh—C) BDE in (OEP)Rh—CHO.

Estimation of the (OEP)Rh—Rh(OEP) *dissociation energy from proton NMR line broadening*

(OEP)Rh(II) occurs predominantly as a diamagnetic Rh—Rh bonded dimer in hydrocarbon

Table 1. Thermochemical estimates for M—H and M—M addition reactions of M—H and M—M bonded complexes

Reaction	(I)[a,b] $\Delta H^0 = (M—H)-(M—C)+X$ $X = \Delta H^0+(M—C)-(M—H)$ X kcal mol^{-1}	(II)[c,b] [(M—H)−(M—C)] kcal mol^{-1} ΔG^0 (298 K) = 0
$CO_2+M—H \rightleftarrows M—CO_2H$	−9	1
$CO+M—H \rightleftarrows M—CHO$	−17	9
$H_2CO+M—H \rightleftarrows M—CH_2OH$	−31	23
$RCHO+M—H \rightleftarrows M—CH(R)OH$	−27	19
$R_2CO+M—H \rightleftarrows M—C(R)_2OH$	−25	17
$CH_2=CH_2+M—H \rightleftarrows M—CH_2CH_3$	−36	28
$CH_3CH_2=CH_2+M—H \rightleftarrows MCH_2CH_2CH_3$	−36	28
$CH\equiv CH+M—H \rightleftarrows M—CH=CH_2$	−45	37
	$\Delta H^0 = (M—O)-(M—H)+X$ $X = \Delta H^0+(M—O)-(M—H)$ X kcal mol^{-1}	(M—H)−(M—O) ΔG^0 (298 K) = 0
$CO_2+M—H \rightleftarrows M—OC(O)H$	+4	−12
$H_2CO+M—H \rightleftarrows M—OCH_3$	−21	13
$RCHO+M—H \rightleftarrows M—OCH_2R$	−15	7
$R_2CO+M—H \rightleftarrows M—OC(R)_2H$	−12	4
	$\Delta H^0 = (M—M)-2(M—C)+X$ $X = \Delta H^0+2(M—C)-(M—M)$ X kcal mol^{-1}	2(M—C)−(M—M) ΔG^0 (298 K) = 0
$CO+M—M \rightleftarrows M—C(O)—M$	70	78
$2CO+M—M \rightleftarrows M—C(O)—C(O)—M$	70	86
$CH_2=CH_2+M—M \rightleftarrows M—CH_2—CH_2M$	64	72
$CH\equiv CH+M—M \rightleftarrows M—CH=CH—M$	56	64
$H_2+M—M \rightleftarrows 2M—H$	$\Delta H^0 = (M—M)-2(M—H)+104$	$\Delta G^0 \cong \Delta H^0$
$O_2+M—M \rightleftarrows M—O—O—M$	$\Delta H^0 = (M—M)-2(M—O)+81$	$\Delta G^0 \cong (M—M)-2(M—O)+89$

[a] Column I lists the anticipated enthalpy change (X) for the reorganization of the organic fragment between product and reactant in terms of ΔH^0 for the reaction and differences in (M—H), (M—C), (M—O) and (M—M) bond dissociation energies. The value of X is evaluated using bond energy data for the reactant and the organic fragment in the organometallic product as described in footnote *b*.

[b] The (C—C), (C—H) and (O—H) bond energies (kcal mol^{-1}) used for the organic fragments were obtained from data for the organic molecule that most closely resembles the organic ligand. As an example, the bond energy parameters for the CH_2OH group of M—CH_2OH were obtained from the parameters for CH_3OH [(C—H) = 94, (OH) = 104]. The bond energy data for organic oxygenates are found in ref. 12, pp. 516 and 517, Table 4. RC(O)—H (87), $HOCH_2$—H (94), HOCH(R)—H (93), $HOCH(R)_2$—H (91), RO(O)C—H (93), RO—H (104), RC(O)O—H (106), HC(O)—CH_3 (82), $CH_3C(O)$—CH_3 (81), CH_3—CH_2R (85), RC(O)O—CH_3 (81). The bond energy data used for the purely hydrocarbon units are Laidler parameters from ref. 16, p. 592, Table 50. (C≡C) = 183.3, (C=C) = 133.0, (C—C) = 85.4, (=C—H_2) = 101.2, (≡C—H) = 104.2, $(C—H)_p$ = 98.2, $(C—H)_s$ = 97.4, $(C—H)_t$ = 96.5. Bond energy values for the (C=O) and (C—O) were estimated from ΔH^0 values for addition reactions of CO, CO_2, H_2CO, RCHO, and R_2CO with H_2 and CH_4.[15,16] (C≡O) = 257, (C=O) = 187, (C—O) = 100, $\overline{(C=O)}_{CO_2}$ = 192.

[c] Column II lists the differences in (M—H), (M—C), (M—O) and (M—M) bond energies that are anticipated to produce a standard free energy difference of zero at 298 K (ΔG^0 (298 K) = 0). These estimates are based on using $\Delta S^0 \sim -27$ eu for these addition reactions, ($\Delta G^0 = \Delta H^0 - T\Delta S^0$; ΔG^0 (298 K) $\cong \Delta H^0 + 8$ kcal mol^{-1}).

solvents. Approach of the two (OEP)Rh(II) fragments is restricted by the porphyrin macrocyclic ligands, which results in a relatively weak Rh—Rh bond. The ^{1}H NMR of $[(OEP)Rh]_2$ at room temperature consists of sharp resonances, but as the temperature is raised all of the ^{1}H NMR peaks of the porphyrin ligand broaden. This broadening is ascribed to the exchange of the diamagnetic dimer, $[(OEP)Rh]_2$ (S = O), with the paramagnetic monomer, (OEP)Rh$^\cdot$ (S = 1/2) (eq. 1). The contribution of the exchange reaction to the line width ($T_2^{-1} = \pi\Delta\nu_{1/2}$) is given by the expression $T_{2(EX)}^{-1} = \tau_d^{-1}[A\tau_p/2]^2[1+(A\tau_p/2)^2]^{-1}$

$$[(OEP)Rh]_2 \rightleftarrows 2(OEP)Rh^\cdot \qquad (1)$$

where τ_d and τ_p are the lifetimes of the nuclear spin states in the diamagnetic and paramagnetic species and A is the electron–nuclear coupling constant for the observed nucleus.[17,18] When $(A\tau_p/2) \gg 1$ then $T_{2(EX)}^{-1} = \tau_d^{-1}$ and the forward rate constant (k_f) is given by ($\tau_d^{-1} = k_f$) for the exchange reaction. Temperature dependence of k_f yields the activation enthalpy (ΔH_f^*) for the forward process. This type of experiment has been previously used to evaluate dissociation energies of organic peroxides.[19] In the specific case of (OEP)Rh where the values for A and τ_p are unknown, only the activation energy ΔH_f^* can be confidently determined. Temperature dependence of the exchange rate [$T_{2(EX)}^{-1} = k_f$ (constant)] derived from line broadening of the methine porphyrin hydrogens results in an activation energy (ΔH_f^*) of 18.5±0.8 kcal mol^{-1} for the homolytic dissociation of $[(OEP)Rh]_2$ (eq. 1).[20] The ΔH_f^* (18.5 kcal mol^{-1}) for $[(OEP)Rh]_2$ can be compared with the value ($\Delta H_f^* = 20.6$ kcal mol^{-1}) obtained for the homolytic dissociation of the analogous Rh—Rh bonded dimethylglyoxime complex, $[Rh(DMG)_2(Ph_3P)]_2$, by kinetic trapping of the Rh(II) species.[21] The forward activation energy (ΔH_f^*) corresponds to an upper limit for the desired Rh—Rh bond dissociation energy ($\Delta H_1^0 = \Delta H_f^* - \Delta H_r^*$). Radical recombination reactions related to the reverse of reaction (1) are usually diffusion controlled and have small activation energies ($\Delta H_r^* \sim 2$ kcal mol^{-1}).[22] Using an estimate of 2 kcal mol^{-1} for ΔH_r^* results in an estimate for ΔH_1^0 of 16.5 kcal mol^{-1}. The small (Rh—Rh) BDE in $[(OEP)Rh]_2$ contributes to the dominant mechanistic role that the metallo radical, (OEP)Rh$^\cdot$, has in the reactivity of $[(OEP)Rh]_2$ in hydrocarbon media.[2,8,11]

Estimate of the Rh—H *bond energy in* (OEP)Rh—H

$(OEP)Rh_2$ reacts with H_2 in C_6D_6 to produce an equilibrium distribution with the metallo hydride, [(OEP)Rh—H] [reaction (2)].

$$[(OEP)Rh]_2 + H_2 \rightleftarrows 2(OEP)Rh\text{—}H. \qquad (2)$$

The criteria for a M—M bonded dimer to react with H_2 to form measurable quantities of metallohydride by reaction (2) is simply that ΔH_2^0 is negative ($\Delta S_2^0 \sim 0$). ΔH_2^0 can be described as a series of bond energies [ΔH_2^0 = (Rh—Rh)+(H—H)−2(Rh—H)]. Knowledge of the Rh—Rh BDE (16.5 kcal mol^{-1}) and observation that reaction (2) occurs, establishes that the (Rh—H) BDE is greater than 60 kcal mol^{-1} [2(Rh—H) = (H—H)+(Rh—Rh)−ΔH_2^0 = (104.2+16.5−ΔH_2^0)].

Equilibrium constants for reaction (2) have been determined at a series of temperatures in benzene by integration of the ^{1}H NMR and are used in deriving thermodynamic values for (2), ($\Delta H_2^0 = -3\pm1$ kcal mol^{-1}; $\Delta S_2^0 \sim 0.8\pm1$ eu).[23] The relatively slow rate for reaction (2) requires that the system should be equilibrated outside the NMR for periods of hours to days. Rigorous exclusion of light is required in order to avoid the photoreaction that produces the reverse of (2). ΔH_2^0 is small and the relative error could be large, but the absolute error is less than 1 kcal mol^{-1}. A value for the Rh—H bond dissociation energy is obtained by using ΔH_1^0, ΔH_2^0 and ΔH_f^0(H$^\cdot$) to give Thermodynamic cycle 1.

Thermodynamic cycle 1 (Rh—H BDE)

$1/2[(OEP)Rh]_2 \rightarrow (OEP)Rh^\cdot$	$1/2\Delta H_1^0 =$ 8.2 kcal mol^{-1}
$(OEP)Rh\text{—}H \rightarrow 1/2[(OEP)Rh]_2 + 1/2H_2$	$-1/2\Delta H_2^0 =$ 1.5 kcal mol^{-1}
$1/2H_2 \rightarrow H^\cdot$	$\Delta H_f^0 =$ 52.1 kcal mol^{-1}
$(OEP)Rh\text{—}H \rightarrow (OEP)Rh^\cdot + H^\cdot$	$\Delta H^0 =$ 61.8 kcal mol^{-1}.

Evaluation of Thermodynamic cycle 1 results in a (Rh—H) BDE of approximately 62 kcal mol^{-1}. Calorimetric methods were used by Drago to obtain an average Rh—H bond energy of 57.6 kcal mol^{-1} in $Rh(Cl)(P(4\text{-tolyl})_3)_3(H)_2$[24] and the ν_{Rh-H} stretching frequencies [(OEP)Rh—H] = 2220 cm^{-1}; ($Rh(Cl)(P(4\text{-tolyl})_3)_3(H)_2$) = 2034 cm^{-1} qualitat-

ively correlate with the Rh—H bond energies. A (Rh—H) BDE of 62 kcal mol^{-1} for (OEP)Rh—H is clearly in the range expected for a second row transition metal hydride[25] and judging from the unusually high Rh—H stretching frequency for (OEP)Rh—H, the (Rh—H) BDE of 62 kcal mol^{-1} is probably at the high end of the range of Rh—H bond energies.

Quantitative comparison of the Rh—H and Co—H bond energies in (OEP)M—H complexes has not been possible because (OEP)Co(II) in the presence of H_2 fails to produce observable concentrations of (OEP)Co—H. Absence of an observable reaction places an upper limit of ~ 56 kcal mol^{-1} for the (Co—H) BDE (ΔH^0 = (H—H) − 2(Co—H); ΔG^0 (298 K) ~ (H—H) − 2(Co—H) + 8 kcal mol^{-1}). The (Rh—H) BDE must be greater than the (Co—H) BDE by at least 6 kcal mol^{-1}. The (Ir—H) BDE in (OEP)Ir—H has also eluded experimental determination because the equilibrium constant for the reaction of $[(OEP)Ir]_2$ with H_2 is too large to be conveniently measured by NMR methods, which indicates that the (Ir—H) BDE is larger than the value for (Rh—H). This qualitative conclusion is also supported by comparison of the M—H stretching frequencies (ν_{Rh-H}, [(OEP)Rh—H] = 2220 cm^{-1}, ν_{Ir-H}, [(OEP)Ir—H] = 2343 cm^{-1}). The ordering of M—H bond energies is undoubtedly Ir—H > Rh—H > Co—H, but experimental determination of the differences in these bond energies has not yet been achieved. The difference between the Co—H and Rh—H is dominated by improved bonding overlap of the 4*d* orbitals, but the difference between the Rh—H and Ir—H is apparently dominated by relativistic effects that produce orbital contractions, which become particularly important for the third transition series.[26]

Estimate of the Rh—C *bond energy in* (OEP)Rh—CHO

(OEP)Rh—H in benzene or toluene reacts reversibly with CO to produce an equilibrium distribution with the metalloformyl complexes, (OEP)Rh—CHO [reaction (3)].

$$(OEP)Rh—H + CO \rightleftarrows (OEP)Rh—CHO. \quad (3)$$

Thermodynamic values for reaction (3), ($\Delta H_3^0 = 13 \pm 1$ kcal mol^{-1}; $\Delta S_3^0 = -29 \pm 3$ eu), were obtained by measuring the temperature dependence of the equilibrium constant by NMR methods.[27] A thermodynamic cycle can be constructed to give a value for the (Rh—C) BDE from ΔH_3^0, the Rh—H BDE and thermodynamic parameters for the formyl radical[12,13] (Thermodynamic cycle 2).

Thermodynamic cycle 2 (Rh—C BDE)

(OEP)Rh—CHO → (OEP)Rh—H + CO	$-\Delta H_3^0 = +13$ kcal mol^{-1}
(OEP)Rh—H → (OEP)Rh$^{\cdot}$ + H$^{\cdot}$	$\Delta H^0 = +62$ kcal mol^{-1}
CO + H$^{\cdot}$ → $^{\cdot}$CHO	$\Delta H^0 = -17$ kcal mol^{-1}
(OEP)Rh—CHO → (OEP)Rh$^{\cdot}$ + $^{\cdot}$CHO	$\Delta H^0 = +58$ kcal mol^{-1}.

The relatively large (Rh—C) BDE (~ 58 kcal mol^{-1}) and small difference in (Rh—H) and (Rh—C) bond energies (~ 4 kcal mol^{-1}) provides an operational explanation for the range of unusual organometallic chemistry associated with rhodium porphyrins which is not observed for cobalt porphyrins.[2,8-10,11] A (Rh—C) BDE of 58 kcal mol^{-1} in (OEP)Rh—CHO is approximately twice the Co—C bond energy (Co—C ~ 28 kcal mol^{-1}) recently reported for a (OEP)Co–alkyl complex.[22(b)] Rh—C bonds are expected to be stronger than Co—C bonds due to improved bonding overlap of the 4*d* orbitals, but differences in the magnitude observed for the (OEP)M complexes must be predominantly of steric origin.[26(a)] Unfavourable interactions between the occupied metal orbitals and the ligand unit are a particularly prominent steric effect in M—C bonding. Unfavourable steric effects probably make a larger contribution to the Co—C bond because the smaller radial distribution of the 3*d* valence orbitals compared to the 4*d* requires a shorter M—C bond distance to maximize the bonding overlap. Near convergence of the Rh—H and Rh—C bond energies must also result from an unusually small effective steric interference between the (OEP)Rh and CHO fragments in (OEP)Rh—CHO. An inversion in the order of bond strengths (M—C > M—H) has been observed for gas phase metal ion species[28] and a decrease in unfavourable steric interactions through contraction of the occupied metal orbitals has been proposed as the fundamental origin of this effect.[26] The relatively high oxidation state [Rh(III)], electron delocalization from the occupied metal orbitals to the ligands and the nature of the formyl ligand may all contribute favourably to the (OEP)Rh—CHO binding.

An alternate approach to estimating the (Rh—C)

BDE in (OEP)Rh—CHO is achieved by evaluating the expression that relates ΔH_3^0 and the bond energies, $[\Delta H_3^0 = (Rh—H) - (Rh—C) + [(C\equiv O) - (C=O)] - (C—H)]$. Similarity of the Rh—CHO unit to an organic aldehyde[2,3,26] provides justification for using thermodynamic data on organic molecules to estimate $[(C\equiv O) - (C=O)]$ and (C—H) bond energies. Using $[(C\equiv O) - (C=O) = 70$ kcal mol^{-1} and (C—H) = 87 kcal mol^{-1} for an aldehydic C—H bond, $\Delta H_3^0 = -13$ kcal mol^{-1}, and a (Rh—H) BDE of 62 kcal mol^{-1} results in an estimate of 57 kcal mol^{-1} for the (Rh—C) BDE in (OEP)Rh—CHO. Excellent agreement between the (Rh—C) BDE estimated from the bond energy analysis (57 kcal mol^{-1}) and the thermodynamic cycle (58 kcal mol^{-1}) suggests that the bond energy approach can be used to establish general criteria for the difference in (M—H) and (M—C) bond energies required to obtain substantial equilibrium concentrations of M—CHO from M—H and CO. The anticipated enthalpy change for the general reaction M—H + CO ⇄ M—CHO is given by the expression $\Delta H^0 = (M—H) - (M—C) - 17$ kcal mol^{-1} and ΔG^0 (298 K) = (M—H) − (M—C) − 9 kcal mol^{-1} (Table 1). In order for ΔH^0 and ΔG^0 (298 K) to be negative the (M—H) BDE cannot exceed the (M—C) BDE by more than 17 and 9 kcal mol^{-1}, respectively. This is a relatively stringent thermodynamic requirement that very few metallo systems have fulfilled. The only metallohydrides that have been reported to accomplish the simple reaction corresponding to insertion of CO into the M—H bond to form an η^1-carbon bonded formyl (M—H + CO ⇄ M—CHO) are the rhodium porphyrins,[2] related rhodium macrocycles[3] and Cp_2^*VH.[29] The closely related (OEP)Ir—H reacts with CO to produce the six-coordinate CO adduct (OEP)Ir(H)(CO) without any evidence for a formyl complex, (OEP)Ir—CHO or (OEP)Ir(CO)(CHO).[27] Failure of the (OEP)Ir system to meet the criteria that (M—H) − (M—C) < 9 kcal mol^{-1}, must result from an increase in the (Ir—H) BDE beyond that of (Rh—H), which is not compensated by a proportionate increase in the (Ir—C) BDE.

Floriani has reported that $Cp_2^*V—H$ reacts with CO to produce $Cp_2^*V(CHO)(CO)$ which contains an η^1-carbon bonded formyl unit.[29] This process can be viewed as the reaction of an intermediate hydrido carbonyl complex $Cp_2^*V(H)(CO)$ with CO to form $Cp_2^*V(CHO)(CO)$. Depicted in this way, the (V—H) BDE in $Cp_2^*V(H)(CO)$ must be less than 9 kcal mol^{-1} stronger than the (V—CHO) BDE in $Cp_2^*V(CHO)(CO)$. It is particularly interesting that the set of (M—H), (M—C) and (M—O) bond energies required to produce an η^1-carbon bonded formyl can occur for an early transition metal complex (d^2 case). Strong (M—O) bonding generally produces η^2-C and O bonded formyl units which have been implicated in the reactions of early transition metal hydrides with CO.[30]

There is very little thermodynamic data available on reactions of metal hydrides with CO to produce metalloformyls that can be used in testing the applicability of the anticipated general relationship that $\Delta H^0 = (M—H) - (M—C) - 17$ kcal mol^{-1}. The only solution data available other than for the rhodium porphyrin hydride systems are on the reactions of $Cp_2Th(H)(OR)$ complexes with CO that produce η^2 formyl complexes[31] which are not encompassed by this bond energy scheme. Gas phase studies of the ions $[(CO)_4Fe]^-$, $[(CO)_4Fe—H]^-$ and $[(CO)_4Fe—CHO]^-$ by Squires have yielded the following mean bond energies (Fe—H) = 69.5 kcal mol^{-1}, (Fe—CHO) = 43.9 kcal mol^{-1} and a ΔH^0 of +10.3 kcal mol^{-1} for the reaction of $[(CO)_4Fe—H]^- + CO \rightarrow [(CO)_4Fe—CHO]^-$.[32] Evaluation of the general expression ($\Delta H^0 = (M—H) - (M—C) - 17$ kcal mol^{-1}) for this specific example results in an estimate of +9 kcal mol^{-1} for ΔH^0 ($\Delta H^0 = 70 - 44 - 17 = +9$ kcal mol^{-1}) which compares favourably with the experimental value of +10.3 kcal mol^{-1}. Unfortunately, the reported accuracy of the experimental results[32] is insufficient to provide a stringent test for the estimate of ΔH^0 from the M—H and M—C bond energies.

Reactions of metal hydrides with aldehydes and ketones

Addition of a metal hydride to an aldehyde can potentially produce an alkoxide or an α-hydroxyalkyl complex (M—H + RCHO ⇄ M—CH(R)OH; M—H + RCHO ⇄ M—OCH_2R). Rhodium porphyrin (Por) hydrides react with aldehydes to produce α-hydroxyalkyl complexes as the only observed products,[2(a),9] [(Por)Rh—H + RCHO ⇄ (Por)Rh—CH(R)OH, (R = H, alkyl, aryl)]. Ketones such as acetone apparently fail to react with porphyrin rhodium hydrides to form observable concentrations of α-hydroxyalkyl or alkoxide products.

(OEP)Rh—H reacts reversibly with aldehydes, RCHO (R = H, alkyl, aryl), to form α-hydroxyalkyl complexes [reaction (4)].[9]

$$(OEP)Rh—H + RCHO \rightleftarrows (OEP)Rh—CH(R)OH \quad (R = H, alkyl, aryl). \quad (4)$$

There is no evidence at present for the formation

of alkoxides in these reactions. The enthalpy change for eq. (4) when RCHO is formaldehyde is approximated by the expression ($\Delta H_4^0 \cong$ (Rh—H) − (Rh—C) − 31 kcal mol^{-1}) and (ΔG_4^0 (298 K) ~ (Rh—H) − (Rh—C) − 23 kcal mol^{-1}) (Table 1). Evaluating these expressions for the (OEP)Rh system (Rh—H) = 62 kcal mol^{-1}, (Rh—C) ~ 58 kcal mol^{-1} yields $\Delta H_4^0 \sim -27$ kcal mol^{-1} and $\Delta G_4^0 \sim -18$ kcal mol^{-1}. An estimate of the equilibrium constant ($K \sim 1.6 \times 10^{13}$) indicates that it is far too large to be determined by NMR methods which is compatable with our observations on this complex.[9] We are currently studying the series of aldehydes RCHO, (R = $(CH_2)_nCH_3$, n = 1–5) and find that conveniently observable equilibria occur for eq. (4). Thermodynamic values for the reaction of (OEP)Rh—H with pentanal to form (OEP)Rh—CH($(CH_2)_3CH_3$)OH have been obtained ($\Delta H_4^0 = -9.8 \pm 0.5$ kcal mol^{-1}, $\Delta S_4^0 = 23 \pm 2$ eu).[33] Bond energy analysis for the reaction M—H + R—CHO ⇄ M—CH(R)OH (R = alkyl) provides an expression that can be used in estimating the effective (Rh—C) BDE, (ΔH_4^0 = (Rh—H) − (Rh—C) − 27 kcal mol^{-1}) (Table 1). Using (Rh—H) = 62 kcal mol^{-1} and $\Delta H_4^0 = -9.8$ kcal mol^{-1} results in an estimate of 45 kcal mol^{-1} for the (Rh—C) bond energy in (OEP)Rh—CH($(CH_2)_3CH_3$)OH. A Rh—C bond energy of ~ 45 kcal mol^{-1} reflects a substantial steric effect associated with substituting an alkyl group for hydrogen. The unfavourable steric effects of alkyl substitution are also illustrated by the lack of an observable reaction between (OEP)Rh—H and ketones.

The thermodynamic requirements for the addition of a metal hydride to formaldehyde to produce substantial equilibrium concentrations of a hydroxymethyl complex, ($\Delta G^0 < 0$; (M—H) − (M—C) < 23 kcal mol^{-1}), is much less stringent than the criteria for producing a metalloformyl species, ($\Delta G^0 < 0$; (M—H) − (M—C) < 9 kcal mol^{-1}). It is surprising that examples of producing hydroxymethyl complexes from the addition of metal hydrides to formaldehyde are so rare.[34] First transition series metal complexes such as $HMn(CO)_5$[35] appear to fulfil the proposed thermodynamic criteria and many second and third row metallohydrides must be thermodynamically capable of accomplishing this reaction..[36] Addition of metal hydrides to RCHO (R = alkyl, aryl) are expected to remain less common because the steric effects of alkyl substitution substantially reduce the effective (M—C) BDE. At this time only rhodium porphyrin hydrides have been reported to accomplish the general reaction [M—H + RCHO ⇄ M—CH(R)OH (R = H, alkyl, aryl)].

Approximate Rh—C *bond energy in* (OEP)Rh—C(O)—Rh(OEP)

Knowledge of the (Rh—Rh) BDE in $[(OEP)Rh]_2$ permits the estimation of the (Rh—C) BDE from thermodynamic values for additional reactions. $[(OEP)Rh]_2$ reacts with CO in toluene to produce equilibria with both a 1 : 1 complex, $[(OEP)Rh]_2CO$ and a metalloketone complex, (OEP)Rh—C(O)—Rh(OEP) [reactions (5) and (6)].

$$[(OEP)Rh]_2 + CO \rightleftarrows [(OEP)Rh]_2CO \quad (5)$$

$$[(OEP)Rh]_2 + CO \rightleftarrows (OEP)Rh—C(O)—Rh(OEP). \quad (6)$$

Thermodynamic values for eq. (5) ($\Delta H_5^0 = 10 \pm 1$ kcal mol^{-1}; $\Delta S_5^0 = -26 \pm 3$ eu) and eq. (6) ($\Delta H_6^0 = -12 \pm 1$ kcal mol^{-1}; $\Delta S_6^0 = -30 \pm 3$ eu) have been obtained by NMR methods.[37] The enthalpy change in eq. (6) (ΔH_6^0) can be expressed as a series of bond dissociation energies, [ΔH_6^0 = (Rh—Rh) + (C≡O) − 2(Rh—C) − (C=O)] and evaluation of this expression, ($\Delta H_6^0 = -12$ kcal mol^{-1}; (Rh—Rh) = 16.5 kcal mol^{-1}; (C≡O) − (C=O) = 70 kcal mol^{-1}), results in an estimate of 49 kcal mol^{-1} for the average (Rh—C) BDE in (OEP)Rh—C(O)—Rh(OEP). The estimated (Rh—C) BDE of the metallo ketone, (Rh—C ~ 49 kcal mol^{-1}), is significantly smaller than the value of (OEP)Rh—CHO (Rh—C ~ 58 kcal mol^{-1}) which is presumably a manifestation of the steric effects resulting from having two bulky (OEP)Rh units bonding a single carbonyl carbon.

Considerations of the reactions of metal hydrides with aldehydes and ketones to form alkoxides: implications for the (Rh—O) *BDE*

Addition of a metal hydride to the carbonyl unit of an aldehyde or ketone can produce α-hydroxyalkyl, M—C(R)(R′)OH, or alkoxide complexes, M—OC(R′)(R)H. Approximate bond energy analysis for these two reactions is found in Table 1. Competition between producing the α-hydroxyalkyl and alkoxide can be described by the isomerization process [reaction (7)].

$$M—CR(R')OH \rightleftarrows M—OCR(R)'H \quad (R,R' = H, alkyl). \quad (7)$$

The anticipated enthalpy change in eq. (7) (ΔH_7^0) from the bond energy analysis is ΔH_7^0 = (M—C) − (M—O) + 10 kcal mol^{-1}; $\Delta S_7^0 \sim 0$; $\Delta H_7^0 \sim \Delta G_7^0$. This approximate analysis indicates that formation of an alcohol organic unit is favoured over an alkoxide unit by ~ 10 kcal mol^{-1}

which is approximately the difference between the O—H and C—H bond energies in these fragments. Application of this analysis indicates that approximately equal amounts of α-hydroxyalkyl and alkoxide will occur when the (M—O) BDE exceeds the (M—C) BDE by ~ 10 kcal mol^{-1} ($\Delta H^0_7 = 0$). If the (M—C) and (M—O) bond energies are equal then the α-hydroxyalkyl is favoured by ~ 10 kcal mol^{-1}, ($\Delta H^0_7 \sim \Delta G^0_7 \sim +10$ kcal mol^{-1}; K_5 (298 K) $\sim 4.6 \times 10^{-8}$) which would preclude observing the alkoxide in competition with the α-hydroxyalkyl.

As previously discussed, the reaction of (OEP)Rh—H with aldehydes forms α-hydroxyalkyl complexes as the only observed products. Failure to observe the alkoxide in the reaction of pentanal, where the (Rh—C) BDE in (OEP)Rh—CH(CH_2)$_3$$CH_3$)OH is ~ 45 kcal mol^{-1}, places an upper limit of ~ 55 kcal mol^{-1} for the (Rh—O) BDE in the alkoxide. We hoped that the two alkyl groups in a ketone would sterically inhibit (Rh—C) bond formation and permit the observation of the alkoxide without competition from the α-hydroxyalkyl, but the reaction of (OEP)Rh—H with acetone and other ketones does not produce any observable addition products. The absence of alkoxides formed from the reactions of aldehydes and ketones with (OEP)Rh—H places an upper limit on the (Rh—O) BDE in alkoxides at ~ 55 kcal mol^{-1}, but does not provide any information on the probable range of (Rh—O) bond energies. The observed reaction of [(OEP)Rh]$_2$ with O_2 to form (OEP)Rh—O—O—Rh(OEP) provides an estimate of 53 kcal mol^{-1} as a lower limit for the (Rh—O) BDE in bridged peroxo complexes, (M—M + O_2 ⇆ M—O—O—M; ΔH^0 = (M—M) − 2(M—O) + 81 kcal mol^{-1}; ΔG^0 (298 K) ~ (M—M) − 2(M—O) + 89 kcal mol^{-1}) (Table 1). Although no measured thermodynamic data are available that directly relate to the (Rh—O) BDE in (OEP)Rh complexes, it is clear that the (OEP)Rh—O single bond is of moderate strength (50–55 kcal mol^{-1}) and comparable to the range of (OEP)Rh—C bond energies. Analogous Co(II) complexes are known to form μ-peroxo dimers. Thermodynamic studies of Co(II) complexes reacting with O_2 to form bridging peroxo complexes (Co—O—O—Co) typically give ΔH^0 values of ~ −30 kcal mol^{-1},[37,38] which provides an estimate of ~ 55 kcal mol^{-1} for the Co—O single bond in bridged peroxo dimers, (ΔH^0 = −2(M—O) + 81 kcal mol^{-1}). The limited observations available suggest that the (OEP)Rh—O and (OEP)Co—O bond energies are comparable. The near equivalence of the (Rh—O) and Co—O bond energies compared to the wide divergence of the (Rh—C) and (Co—C) bond energies further emphasizes the special susceptibility of M—C bonds to steric effects.

Additional reactions of metal hydrides and metal–metal bonded complexes with alkenes and alkynes

Addition of metal hydrides to alkenes is thermodynamically less demanding (ΔH^0 = (M—H) − (M—C) − 36 kcal mol^{-1}) than addition to C—O multiple bonds (ΔH^0 = (M—H) − (M—C) − (9–31) kcal mol^{-1}) (Table 1). The reported reactions of (OEP)Rh—H with alkenes to produce the alkyl complexes are too highly exothermic to give measurable equilibria (ΔH^0 ~ (Rh—H) − (Rh—C) − 36 kcal mol^{-1} = −(Rh—C) + 26 kcal mol^{-1}; ΔG^0 (298 K) ~ −(Rh—C) + 34 kcal mol^{-1}), which only means that the (Rh—C) BDE is greater than 34 kcal mol^{-1}. Addition of [(OEP)Rh]$_2$ to CH_2=CH_2 produces (OEP)Rh—CH_2CH_2—Rh (OEP), which is also too highly favoured to provide measurable equilibria (ΔH^0 = (Rh—Rh) − (Rh—C) kcal mol^{-1}, ΔG^0 = ΔH^0 + 8 kcal mol^{-1}; ΔG^0 (298 K) = 2(Rh—C) + 88 kcal mol^{-1}) which implies that the (Rh—C) BDE is greater than 44 kcal mol^{-1}. Halpern has reported thermodynamic values for the addition of (OEP)Rh—H with styrene to form (OEP)RhCH_2CH(C_6H_5)Rh(OEP), (ΔH^0 = −11.2 ± 2.5 kcal mol^{-1}).[11] Substituting ΔH^0 = −11.2 kcal mol^{-1} and (Rh—Rh) = 16.5 kcal mol^{-1} in the general expression (ΔH^0 = (Rh—Rh) − 2(Rh—C) + 64 kcal mol^{-1}) (Table 1) results in an estimate of 46 kcal mol^{-1} for the average (Rh—C) bond energy, in (OEP)Rh—CH_2 CH(C_6H_5)—Rh(OEP), which again reflects the unfavourable effects of substitution on the carbon centre bonded to the (OEP)Rh unit.

Addition reactions of metal hydrides with alkynes are the least thermodynamically demanding reactions considered in this paper and virtually any transition metal hydride should be capable of accomplishing this reaction (ΔH^0 = (M—H) − (M—C) − 45 kcal mol^{-1}); ΔG^0 = (M—H) − (M—C) − 37 kcal mol^{-1}.

Comments on the addition of metal hydrides with CO_2

Addition reactions of CO_2 are more thermodynamically demanding than any of the other unsaturated molecules considered in this study (Table 1). Addition of a metal hydride to CO_2 can produce either a metallo carboxylic acid, M—CO_2H, or a formate complex, M—OC(O)H, and bond energy analyses for both of these reactions appear in Table 1, (M—H + CO_2 → M—OC(O)H; ΔH^0 = (M—H) − (M—O) + 4 kcal

mol^{-1}; ΔG^0 (298 K) $\sim \Delta H^0 + 8$ kcal mol^{-1}), (M—H + $HCO_2 \rightarrow$ M—CO_2H; ΔH^0 = (M—H) − (M—C) − 9 kcal mol^{-1}; ΔG^0 (298) $\sim \Delta H^0 + 8$ kcal mol^{-1}). The bond energy expression for the isomerization reaction M—$CO_2H \rightarrow$ M—OC(O)H is ΔH^0 = (M—C) − (M—O) + 13 kcal mol^{-1} which means that the carboxylic acid complex is favoured over the η^1-formate complex unless the (M—O) BDE exceeds the (M—C) BDE by more than 13 kcal mol^{-1}. This result is largely a consequence of the preference for forming an OH bond over that of a C—H bond. In the specific case of the (OEP)Rh system the carboxylic acid complex is favoured over the formate by $\sim$ 20 kcal mol^{-1}, although it turns out that both complexes are thermodynamically unstable relative to (OEP)Rh—H and CO_2.

Formation of substantial equilibrium concentrations of a transition metal η^1-formate complex requires the (M—O) BDE to exceed the (M—H) BDE by more than 12 kcal mol^{-1} ($\Delta G^0 \sim$ (M—H) − (M—O) + 12 kcal mol^{-1}) (Table 1). Using 60 kcal mol^{-1} as a typical (M—H) BDE suggests that (M—O) bond energies in excess of 72 kcal mol^{-1} are required for this reaction. Unoccupied metal $d\pi$ orbitals available for pi bonding with oxygen and bidentate binding of formate[39] can contribute to achieving the required effective M—O bond energies. The facile reactions of $[(CO)_5MH]^-$, (M = Cr, W, Mo), compounds with CO_2 are particularly interesting because these metals have filled $d\pi(d^6$ cases) and yield monodentate formate complexes.[40] In this unusual case the M—H bonds must be particularly weak in order for the proposed criteria (M—O) > (M—H) + 12 kcal mol^{-1} to be fulfilled. The reaction of (OEP)Rh—H with CO_2 to form (OEP)Rh—OC(O)H is clearly excluded by the relatively small (Rh—O) BDE (50–55 kcal mol^{-1}), (ΔG^0 (298 K) $\sim$ 62 − (50–55) + 12 kcal mol^{-1}; $\Delta G^0 \sim$ +19–24 kcal mol^{-1}).

The bond energy analysis for the reaction to form a metallocarboxylic acid complex, (M—H) + CO_2 $\rightarrow$ (M—CO_2H), suggests that the (M—H) BDE and (M—C) BDE must be virtually equal in order for ΔG^0 to be negative, (ΔH^0 = (M—H) − (M—C) − 9 kcal mol^{-1}; ΔG^0 (298 K) = (M—H) − (M—C) − 1 kcal mol^{-1}) (Table 1). The formation of a metallocarboxylic acid complex by this reaction must fulfil stringent thermodynamic criteria which to our knowledge have not yet been achieved by any metal hydride. There are no reported direct thermodynamic studies for the addition of a metal hydride to CO_2 to form a transition metal carboxylic acid complex that can be used as a reliable test for the anticipated general relationship (ΔH^0 = (M—H) − (M—C) − 9 kcal mol^{-1}). Thermodynamic data for $[(CO)_4$FeX$]^-$ (X = H, CO_2H) can be used in deriving the (Fe—H) BDE (69.5 kcal mol^{-1}), (Fe—C) BDE ($\sim$ 46 kcal mol^{-1}) and a ΔH^0 of $\sim$ +15 kcal mol^{-1} for the reaction $[(CO)_4Fe—H]^- + CO_2 \rightarrow [(CO)_4Fe—CO_2H]^-$.[32] Evaluating the general expression using (Fe—H) = 69.5 kcal mol^{-1} and (Fe—C) = 46 kcal mol^{-1} provides an estimate of +16 kcal mol^{-1} for ΔH^0 which compares favourably with the mean experimental value of +15 kcal mol^{-1}. Good agreement between experimental ΔH^0 and the bond energy relationship estimate, provides justification in using estimates of bond energies in anticipating thermodynamic values for the reaction M—H + $CO_2 \rightleftarrows$ M—CO_2H. Evaluating the expressions ΔH^0 = (M—H) − (M—C) − 9 kcal mol^{-1} and $\Delta G^0 = \Delta H^0 + 8$ kcal mol^{-1}, for the (OEP)Rh system, [(Rh—H) = 62 kcal mol^{-1}; (Rh—C) $\sim$ 58 kcal mol^{-1}] provides estimates of $\Delta H^0 \sim -5$ kcal mol^{-1} and $\Delta G^0 \sim +3$ kcal mol^{-1} for the reaction (OEP)Rh—H + $CO_2 \rightleftarrows$ (OEP)Rh—CO_2H. Even though the thermodynamic estimates are crude, it is clear that (OEP)Rh—H is at the thermodynamic threshold for reacting with CO_2 to produce large equilibrium concentrations of the carboxylic acid complex, (OEP)Rh—CO_2H, and it appears highly probable that a metal hydride related to (OEP)Rh—H will accomplish this important reaction.

CONCLUSION

Evaluation of (Rh—Rh), (Rh—H) and (Rh—C) bond dissociation energies in $[(OEP)Rh]_2$, (OEP)Rh—H and (OEP)Rh—CHO, respectively, provides an entry point in understanding the unusual reactivity associated with the (OEP)Rh system. A relatively weak Rh—Rh bond ($\sim$ 16.5 kcal mol^{-1}) permits facile bond homolysis for metallo radical reaction mechanisms and has a favourable thermodynamic effect on addition reactions of $[(OPE)Rh]_2$ with CO and alkenes. A normal (Rh—H) BDE ($\sim$ 62 kcal mol^{-1}) in (OEP)Rh—H coupled with an unusually large (Rh—C) BDE ($\sim$ 58 kcal mol^{-1}) in (OEP)Rh—CHO provides an example in transition metal chemistry where the M—H and M—C bond energies nearly converge.

The use of bond energies derived from thermodynamic properties of organic molecules has proven useful in providing guideline thermodynamic criteria for organometallic reactions in terms of (M—M), (M—H), (M—C) and (M—O) bond energies. The observed addition of (OEP)Rh—H to CO where the thermodynamic criteria are relatively stringent [(M—H) − (M—C) < 9 kcal mol^{-1}] (Table 1) assures that addition reactions with formaldehyde, ethene and ethyne are

thermodynamically favourable [(M—H) − (M—C) < 30–45 kcal mol^{-1}] (Table 1), unless steric effects become dominant. Alkyl substitution for hydrogen in these organic units reduces the (Rh—C) BDE by up to 10 kcal mol^{-1} per alkyl substituent, which can result in not fulfilling the relatively undemanding thermodynamic criteria for these classes of addition reactions.

Addition of a (OEP)Rh—H to aldehydes invariably produces the α-hydroxyalkyl complex (OEP)Rh—CH(R)OH in preference to the alkoxide, (OEP)Rh—OCH_2R, even when the (Rh—C) BDE (~ 45 kcal mol^{-1}) falls below the (Rh—O) bond energy (~50–55 kcal mol^{-1}). More favourable contributions of ~ 10 kcal mol^{-1} to the thermodynamics associated with forming an α-hydroxyalkyl unit compared to an alkoxy group is responsible for this result. Similarly, metallo carboxylic acid complexes, M—CO_2H, are preferred to formate complexes, M—OC(O)H, unless the (M—O) BDE exceeds the (M—C) BDE by more than 12 kcal mol^{-1}. Bond energy estimates predict that (OEP)Rh—H is close to fulfilling the criteria for the addition of CO_2 to form (OEP)Rh—CO_2H (ΔG^0 (298 K) ~ 3 kcal mol^{-1}) and these encouraging thermodynamic estimates have stimulated our current search for a metal hydride related to (OEP)Rh—H that manifests this currently unrealized type of reactivity.

Acknowledgement—We wish to acknowledge the National Science Foundation and the Department of Energy, Division of Chemical Sciences, Office of Basic Energy Sciences for support of this research.

REFERENCES

1. J. Halpern, *Acc. Chem. Res.* 1982, **15**, 238.
2. (a) B. B. Wayland, S. L. Van Voorhees and C. Wilker, *Inorg. Chem.* 1986, **25**, 4039; (b) B. B. Wayland, A. Duttaahmed and B. A. Woods, *J. Chem. Soc., Chem. Commun.* 1983, 142; (c) B. B. Wayland, B. A. Woods and R. Pierce, *J. Am. Chem. Soc.* 1982, **104**, 302; (d) B. B. Wayland and B. A. Woods, *J. Chem. Soc., Chem. Commun.* 1981, 700.
3. S. L. Van Voorhees and B. B. Wayland, *Organometallics* 1987, **6**, 204.
4. C. K. Ghosh and W. A. Graham, *J. Am. Chem. Soc.* 1987, **109**, 4726.
5. W. D. Jones and F. J. Feher, *J. Am. Chem. Soc.* 1984, **106**, 1650.
6. (a) R. G. Bergman and A. H. Janowicz, *J. Am. Chem. Soc.* 1983, **105**, 3929; (b) J. M. Buchanan, J. M. Stryker and R. G. Bergman, *J. Am. Chem. Soc.* 1986, **108**, 1537.
7. (a) R. H. Crabtree, *Chem. Rev.* 1985, **85**, 245; (b) J. Halpern, *Inorg. Chim. Acta.* 1985, **100**, 41.
8. (a) B. B. Wayland and K. J. Del Rossi, *J. Organomet. Chem.* 1984, **C27**, 276; (b) K. J. Del Rossi and B. B. Wayland, *J. Am. Chem. Soc.* 1985, **107**, 7941; (c) B. B. Wayland and K. J. Del Rossi, *J. Chem. Soc., Chem. Commun.* 1986, 1653.
9. S. L. Van Voorhees and B. B. Wayland, *Organometallics* 1985, **4**, 1887; (b) B. B. Wayland, B. A. Woods and V. M. Minda, *J. Chem. Soc., Chem. Commun.* 1982, 634.
10. B. B. Wayland, B. A. Woods and V. L. Coffin, *Organometallics* 1986, **5**, 1059.
11. R. S. Paonessa, N. C. Thomas and J. Halpern, *J. Am. Chem. Soc.* 1985, **107**, 4333.
12. D. F. McMillen and D. M. Golden, *Ann. Rev. Phys. Chem.* 1982, **33**, 493.
13. J. A. Kerr, *Chem. Rev.* 1966, **66**, 465.
14. D. D. Wagman, W. H. Evans, V. B. Parker, I. Halow, S. M. Bailey and R. H. Schumm, NBS Technical Note 270-3. Institute for Basic Standards, National Bureau of Standards (1986).
15. J. D. Cox and G. Pilcher, *Thermochemistry of Organic and Organometallic Compounds*. Academic Press, New York (1970).
16. J. B. Pedley, R. D. Naylor and S. P. Kibry, *Thermochemical Data of Organic Compounds* (2nd edn). Chapman and Hall, London (1986).
17. (a) H. M. McConnell and S. B. Berger, *J. Chem. Phys.* 1957, **27**, 230; (b) R. W. Kreilich and S. I. Weissman, *J. Am. Chem. Soc.* 1966, **88**, 264.
18. C. S. Johnson Jr, *Advances in Magnetic Resonance*, Vol. I, p. 33. Academic Press, New York (1965).
19. R. Kreilick and D. J. Williams, *J. Am. Chem. Soc.* 1968, **90**, 2775.
20. B. B. Wayland, M. D. Farnos and V. L. Coffin, *Inorg. Chem.* 1988, in press.
21. J. H. Espenson and V. Tinner, *J. Am. Chem. Soc.* 1981, **103**, 2120.
22. (a) F. T. Ng, G. L. Rempel and J. Halpern, *J. Am. Chem. Soc.* 1982, **104**, 621; (b) M. K. Geno and J. Halpern, *J. Am. Chem. Soc.* 1987, **109**, 1238.
23. M. D. Farnos, Ph.D. Thesis, University of Pennsylvania (1987). K_2 (294 K) = 116±8, K_2 (335 K) = 60±10.
24. R. S. Drago, J. G. Miller, M. A. Hoselton, R. D. Farris and M. J. Desmond, *J. Am. Chem. Soc.* 1983, **105**, 444.
25. R. G. Pearson, *Chem. Rev.* 1985, **85**, 41.
26. (a) T. Ziegler, V. Tschinke and A. Becke, *J. Am. Chem. Soc.* 1987, **109**, 1351; (b) T. Ziegler, G. T. Snijders and E. J. Baerends, *J. Chem. Phys.* 1981, **74**, 1271.
27. M. D. Farnos, B. A. Woods and B. B. Wayland, *J. Am. Chem. Soc.* 1986, **108**, 3659.
28. (a) M. L. Mandich, I. F. Halle and J. L. Beauchamps, *J. Chem. Soc.* 1984, **106**, 4403; (b) P. B. Armentrout, L. F. Halle and J. L. Beauchamp, *J. Am. Chem. Soc.* 1981, **103**, 6501.
29. C. Floriani, *Pure Appl. Chem.* 1983, **55**, 1.
30. P. T. Wolczanski and J. E. Bercaw, *Acc. Chem. Res.* 1980, **13**, 121.
31. (a) P. J. Fagan, K. G. Moloy and T. J. Marks, *J. Am. Chem. Soc.* 1981, **103**, 6959; (b) P. J. Fagan, E. A. Maatta and T. J. Marks, *ACS Symp. Ser.* 1981,

152, 52; (c) P. J. Fagan, J. M. Manriquez, T. J. Marks, S. H. Vollmer, C. S. Day and V. W. Day, *J. Am. Chem. Soc.* 1981, **103**, 2206; (d) D. C. Sonnenberger, L. R. Morss and T. J. Marks, *Organometallics* 1985, 352.

32. K. R. Lane, S. Sallans and R. R. Squires, *Organometallics* 1985, **4**, 408.
33. S. L. Van Voorhees, Ph.D Thesis, University of Pennsylvania (1987).
34. J. A. Gladysz, *Adv. Organomet. Chem.* 1982, **20**, 1.
35. J. A. Connor, M. T. Zafarani-Moattar, J. Bickerton, N. I. El Saied, S. Suradi, R. Carson, G. A. Takhin and H. A. Skinner, *Organometallics* 1982, **1**, 1166.
36. (a) G. Yoneda and D. M. Blake, *Inorg. Chem.* 1981, **20**, 67; (b) S. P. Nolan, C. D. Hoff, P. O. Stoutland, L. J. Newman, J. M. Buchanan, R. G. Bergman, G. K. Yang and K. S. Peters, *J. Am. Chem. Soc.* 1987, **109**, 3143; (c) H. E. Bryndza, L. K. Fong, R. A. Paciello, W. Tam and J. E. Bercaw, *J. Am. Chem. Soc.* 1987, **109**, 1444.
37. V. L. Coffin, W. R. Brennen and B. B. Wayland, *J. Am. Chem. Soc.* 1987, in press.
38. E. C. Niederhoffer, J. H. Timmons and A. E. Martell, *Chem. Rev.* 1984, **84**, 137.
39. D. R. Roberts, G. L. Geoffroy and M. G. Bradley, *J. Organomet. Chem.* 1980, **198**, C75.
40. (a) D. J. Darensbourg and R. A. Kudaroski, *Adv. Organomet. Chem.* 1983, **22**, 129; (b) S. G. Slater, B. F. Schumann and D. J. Darensbourg, *Organometallics* 1982, **1**, 1662; (c) D. J. Darensbourg and A. Rokicki, *J. Am. Chem. Soc.* 1982, **104**, 349.

Polyhedron Vol. 7, No. 16/17, pp. 1559–1572, 1988
Printed in Great Britain

0277–5387/88 $3.00+.00
© 1988 Pergamon Press plc

THE GAS PHASE CHEMISTRY OF BARE AND LIGATED TRANSITION METAL IONS: CORRELATIONS OF REACTIVITY WITH ELECTRONIC STRUCTURE—I. M^+ AND MCO^+

J. ALLISON,* A. MAVRIDIS† and J. F. HARRISON

Department of Chemistry, Michigan State University, East Lansing, MI 48824, U.S.A.

Abstract—In the gas phase, univalent cations such as Cr^+, $CrCO^+$, $Cr(CO)_2^+$, etc. have been generated, and their chemistry with neutral molecules characterized, using a number of mass spectrometric techniques. Presented here are results of *ab initio* calculations on two transition metal ion–monocarbonyl molecules, $ScCO^+$ and $CrCO^+$. These calculations suggest that the bonding in such systems is predominantly electrostatic in nature; this information is used to evaluate existing data on the gas phase chemistry of a variety of bare and ligated first-row transition metal ions.

Since the early 1970s, a substantial number of publications on the gas phase chemistry of transition metal and metal-containing ions with organic molecules have appeared.[1] Using a variety of mass spectrometric techniques, bare metal ions such as Fe^+, Co^+ and Ni^+ as well as ligated metal ions such as $CrCO^+$, $Co(CO)_2^+$, $Ni(PF_3)_3^+$, CoO^+, etc. can be generated, manipulated, and their chemistry studied. The chemistry of these 'exotic' gas phase species has the potential for providing insights into the fundamental aspects of organometallic chemistry and catalysis.

Currently, there are a number of experimental techniques used to generate gas phase metal and metal-containing ions such as surface ionization and laser ionization. However, early work in this area utilized electron impact ionization (EI) on volatile species (ML_n) such as $Ni(CO)_4$, $Fe(CO)_5$, $Cr(CO)_6$ and $Co(CO)_3NO$ to generate various atomic metal ions, M^+. Also formed are the various ML_n^+ ions that are seen in the mass spectra of these compounds. Thus, there is a considerable amount of information available on how M^+ and ML^+ ions react with organic molecules. We will focus our discussion here on the monoligated metal ions, to determine how and why their chemistry varies when compared to the free M^+ species.

Historically, this area of research was largely descriptive in nature.[1] Most of the work was directed towards understanding the mechanisms through which reaction products are formed. Recently, these systems have received attention from electronic structure theorists.[2] The experimental and theoretical methods each have strengths and limitations. Gas phase experiments can be used to identify both exothermic and endothermic reactions, and cross sections/rate constants can be determined for bimolecular reactions. However, only the m/z values of the reactants and products are determined in mass spectrometric experiments. No direct information is available on the states of reactants and products, their vibrational and rotational temperatures, and geometrical structures. In contrast, high level *ab initio* calculations can be used to accurately determine geometries and electron distributions in species such as CrO^+. Such calculations yield bond dissociation energies, although the substantial contribution from the electron correlation to these bond energies precludes them being calculated as reliably as other features, such as geometries. The combination of experimental and theoretical efforts is required in this area of research, to identify the structure/function relationships that cannot be realized by experimental data alone.

Discussed here are data that address the question: how does the chemistry of a bare, first row transition metal ion (M^+) change when a ligand (L) is added? The focus is mainly on the carbonyl ligand, CO. Correlations between the observed chemistry and theoretical descriptions of various M^+ and ML^+ ions will be presented.

*Author to whom correspondence should be addressed.
†On leave from The Department of Chemistry, University of Athens, Athens, Greece.

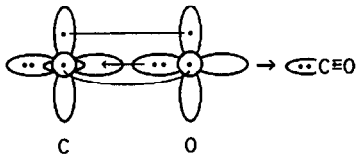

Scheme 1.

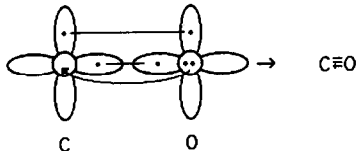

Scheme 2.

Classical description of the metal–CO bond

Consider first the CO molecule, which we may imagine as being formed in one of two ways. In the first, the C and O are asymptotically both in $^3P_{m=0}$ states, see Scheme 1. A dative bond is formed in the σ system with O contributing two electrons from its $2p_\sigma$ orbital to the empty C $2p_\sigma$ orbital. As the electrons flow into the carbon orbital the C $2s$ electrons hybridize away from the O atom and form the characteristic lone pair on the C. The second possibility has both the carbon and oxygen approach in their $^3P_{\pm 1}$ states, see Scheme 2. In this representation the dative bond is in the π system and the σ bond has much more carbon $2p_\sigma$ character to it than in the previous ($m = 0$) structure, and the C lone pair is essentially a $2s^2$ electron pair. These two localized views of the CO bonding have the same overall $^1\Sigma^+$ symmetry and of course both contribute to the CO wave function, see Scheme 3.

The more donor ability (Lewis basicity) as represented by

$$|C{\equiv}O\rangle$$

the less π acceptor ability the CO will have. The classic Dewar–Chatt[3] mechanism for the interaction of a transition metal with CO is shown in Scheme 4.

This coupling of the σ donor/π acceptor character allows a synergism which can increase the M—CO bond strength substantially. Note that if the metal is able to donate d_π electrons to CO they will contribute to the anionic character which will decrease

$$|^1\Sigma^+\rangle \equiv \cos\theta\,|C{\equiv}O\rangle + \sin\theta\,|C{\equiv}O\rangle$$
$$\equiv \cos\theta\,|\sigma\ \text{donor}\rangle + \sin\theta\,|\pi\ \text{acceptor}\rangle$$

Scheme 3.

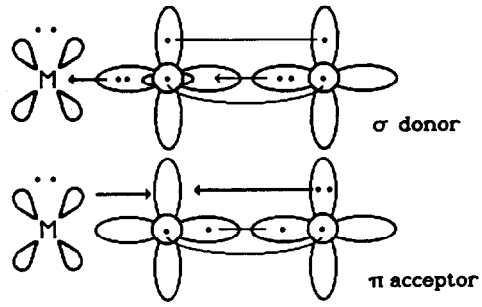

Scheme 4.

the π acceptor ability and therefore increase the σ donor ability (see Scheme 5). If the metal has no σ valence electrons to repel the CO σ electrons, a significant donation can occur, resulting in a large metal–CO bond energy. The strength of this bond will be decreased if the metal has σ valence electrons or does not have d_π electrons available for back donation. With this analysis in mind it would seem that the bonding in MCO^+ could be very similar to that in the neutral MCO if the electron which is removed on ionization is not critical to the σ–π synergism. In the subsequent discussion we will argue that this is not the case, i.e. the bonding in MCO^+ is essentially different from that in the neutral MCO.

Recently, Bauschlicher *et al.*[4,5] have explored the Dewar–Chatt mechanism for the bonding of a single CO to a transition metal atom. In a series of *ab initio* calculations on various metal–carbonyl systems they have used the Constrained Space Orbital Variation technique to analyse the energetic consequences of the σ donation–π acceptor steps in the M—CO bonding. In all cases studied, it was found that the metal-to-CO π back donation is more important than the donation of CO σ electron density to the metal when the $3d_\sigma$ and $4s$ shells are empty, and becomes increasingly weaker as the $3d_\sigma$ and $4s$ shells are filled.

Experimental data on the M^+—CO *bond*

Prior to this work, little was known of the bonding in such ionic complexes, or of the strength of the M^+—CO bond. Using appearance potential measurements,[6] heats of formation for a variety of

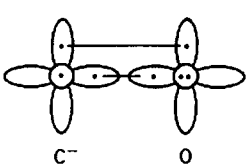

Scheme 5.

ionic species have been determined successfully; thus one might expect that data from EI or photoionization studies of compounds such as $Ni(CO)_4$ could be used to determine values such as $\Delta H_f(NiCO^+)$. From this, the bond energy $D(Ni^+—CO)$ could be calculated. Unfortunately, this is not the case. For example, the appearance potential of the $CrCO^+$ ion from EI on $Cr(CO)_6$ is 14.9 eV.[7] From this, $\Delta H_f(CrCO^+) = 235$ kcal mol^{-1} is calculated. Using $\Delta H_f(Cr^+) = 250.3$ kcal mol^{-1} and $\Delta H_f(CO) = -26.4$ kcal mol^{-1},[8] this would suggest that $D(Cr^+-CO) = -11.1$ kcal mol^{-1}, i.e. that the bond has a negative bond energy. In such experiments, the appearance potential for the bare metal ion does not give the correct $\Delta H_f(M^+)$. It has been suggested that what is being measured is the energy required to form the metal ion in some excited state, M^{+*}, that reflects the electronic configuration of the metal in the neutral compound. Thus, appearance energy data from mass spectrometric experiments did not provide useful information on the M^+—CO bond.

Some of the earliest experiments involving gas phase species such as MCO^+ were studies of ligand displacement reactions.[9,10] The results suggested that M^+—L interactions in the gas phase did not necessarily parallel M—L interactions in condensed phases—that is, a strongly bound ligand in an organometallic compound may not be strongly bound to M^+ in the gas phase. (For example, in the gas phase hexane appears to be more strongly bound to a transition metal ion than does CO.[11])

A variety of ligand displacement reactions were studied in the 1970s. Reactions such as eq. (1)

$$FeCO^+ + L \rightarrow FeL^+ + CO \qquad (1)$$

were observed[9] for a number of π and n donor bases (L). If reaction (1) occurs in the gas phase, the reaction is assumed to be exothermic or thermoneutral, implying that $D(Fe^+—CO) < D(Fe^+—L)$. Ligands such as CH_3F, CH_3Cl, H_2O, HCN, NH_3, NO and C_2H_4 were observed to displace CO from Fe^+. HCl, however, did not. It was noted that all of these 'ligands' were better Lewis acids than CO, except for HCl. Thus, there appeared to be a correlation between M^+-affinity and H^+-affinity. The exception was NO, P.A.(NO) = 127 kcal mol^{-1} < P.A.(CO) = 143 kcal mol^{-1}, which is also unique in that it was the only ligand studied that had an unpaired electron.

Results similar to those for $FeCO^+$ were also reported for $CoCO^+$. $CoCO^+$ was generated by EI on $Co(CO)_3NO$, thus a variety of $Co(CO)_n^+$ and $CoNO(CO)_n^+$ species were generated and studied.[10] In addition to ligand displacement studies, that allowed for an ordering of ligands in terms of their relative M^+-affinities, the number of COs displaced by a ligand could be used as a measure of relative $D(M^+—L)$s. For example, in the reaction

$$Co(CO)_3NO^+ + L \rightarrow Co(CO)_{3-n}NO(L)^+ + nCO \qquad (2)$$

C_2H_4 will displace one CO from $Co(CO)_3NO^+$, AsH_3 will displace two and PH_3 will displace three. The implication is that $D(Co^+—L)$ increases for the series $C_2H_4 < AsH_3 < PH_3$. Again, this correlates with the proton affinities—the ligand with the greatest gas phase basicity displacing the most COs in reaction (2).

Thus, while CO is considered to be a 'strong' ligand in organometallic chemistry, this does not seem to be the case in these gas phase ionic species. This early work suggested that M^+—L bonding may have a substantial electrostatic component, although this would contradict the more conventional descriptions of metal–ligand bonding common to organometallic chemistry.[12]

In addition to the unusual behaviour displayed by NO in deviating from the proton affinity correlation of relative $D(M^+—L)$ values, it was observed that NO could not be displaced by ligands that displaced CO from a metal centre.[10] Thus, reactions such as (3)

$$CoNO^+ + L \rightarrow CoL^+ + NO \qquad (3)$$

were not observed. Also, in reactions such as (2), while one or more CO could be displaced, the NO could not. Thus, the behaviour of NO as a ligand in these gas phase studies was very different from that observed for the variety of other ligands studied. Similar studies showed that 'Li^+ affinities'[10] paralleled proton affinities, with NO not being an exception in terms of its relative bond energy to Li^+.

Theoretical description of the M^+—CO *bond* (M = 1*st row transition metal*)

Although there have been several theoretical studies[4,5] of the interaction of a transition metal and a carbonyl there have been very few studies of the corresponding ions.[5] Accordingly we have recently embarked upon a systematic theoretical study of the positive ions of the transition metal monocarbonyls. Presented here are our results for $ScCO^+$ and $CrCO^+$. We chose to begin with Sc^+ because there are two electrons in the valence shell ($4s^13d^1$) allowing extensive *ab initio* calculations of the interaction between Sc^+ and CO with a modest computational effort. In addition, the low-lying

electronic states of Sc^+, corresponding to the configuration $3d^2$, allow us to explore the effect of the $4s$ occupancy. Cr^+ is a d^5 ion and has the advantage of being spherically symmetric (^6S ground state) and therefore, when it interacts with CO, only one low-lying molecular electronic state is formed.

THE FRAGMENTS

The transition metal ions

The electronic configuration of the Sc^+ ion is [argon core]$4s^13d^1$ or simply $4s^13d^1$. This gives rise to ^3D and ^1D states with the triplet being the ground state.[13] The lowest state of the $3d^2$ configuration is of ^3F symmetry and lies 0.596 eV above the ground ^3D state. The electronic configuration of Cr^+ is $3d^5$ and results in a ground state of ^6S symmetry and the lowest state of the first excited configuration $4s^13d^4$ is of ^6D symmetry and lies 1.5 eV above the ^6S. The relative energies of these states as well as the corresponding states in Ti^+ and V^+ are shown in Fig. 1. The metal basis set used in these calculations is described in ref. 14. There are three sets of data shown; the experimental separation, the separations calculated at an SCF level and the separations calculated using an MCSCF theory that allows a limited (radial) correlation among the valence orbitals. This shows that the splittings calculated at the MCSCF level are in reasonable agreement with experimental data.

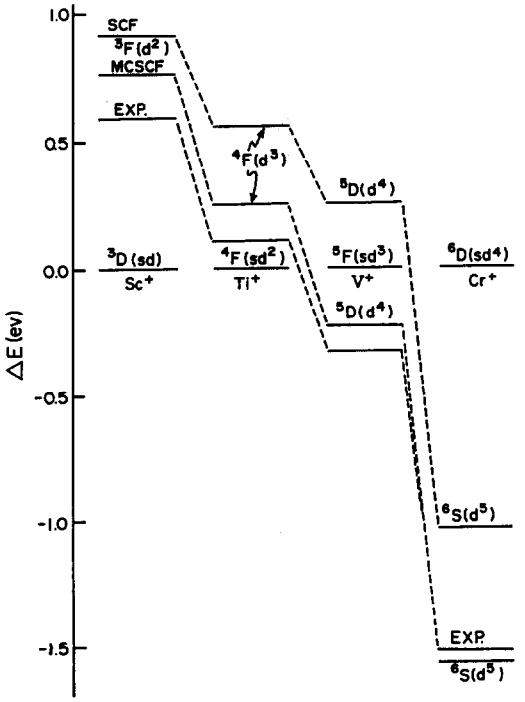

Fig. 1. The relative energies of the $4s3d^n$ and $3d^{n+1}$ configurations of the first four transition metal ions.

The CO molecule

The SCF description of CO ($^1\Sigma^+$) results in the electronic configuration

$$1\sigma^2 2\sigma^2 3\sigma^2 4\sigma^2 5\sigma^2 1\pi^4$$

with an approximate description being that 1σ is the O $1s$ orbital; 2σ, the C $1s$; 3σ, the O $2s$; 4σ, the C—O sigma bond and 5σ the lone pair on the carbon. The 1π is a mixture of C and O p_π orbitals polarized toward the O atom. The GVB description used in this study keeps the 1σ, 2σ and 3σ orbitals at the SCF level and correlates the 4σ, 5σ and $1\pi^4$, e.g.

$$(4\sigma^2 - \lambda 6\sigma^2)(5\sigma^2 - \mu 7\sigma^2)(1\pi_x^2 - \gamma 2\pi_x^2)(1\pi_y^2 - \gamma 2\pi_y^2).$$

For internal calibration purposes we also constructed an MCSCF wavefunction for CO in which all spin couplings between the 4σ, 5σ, 6σ and 7σ orbitals were included. In C_{2v} symmetry the function contains 306 configuration state functions. The basis set used for both C and O is the Duijneveldt[15] $11s$, $7p$ set, augmented with an additional s and p selected in an even tempered way, and two single-component d functions on C and O. The resulting $12s,8p,2d$ basis was contracted to $4s,4p,2d$ following Rafenetti's[16] recommendations. The potential energy curves for the SCF, GVB and MCSCF[17] functions are shown in Fig. 2. Table 1 compares the calculated spectroscopic parameters with experiment. Figure 3 shows the variation of the dipole moment with internuclear separation for the three wavefunctions. Note that the SCF solution predicts the wrong sign for the dipole but that both the GVB and the MCSCF descriptions predict a sign in agreement with experiment, i.e. $C^{\delta-}O^{\delta+}$.

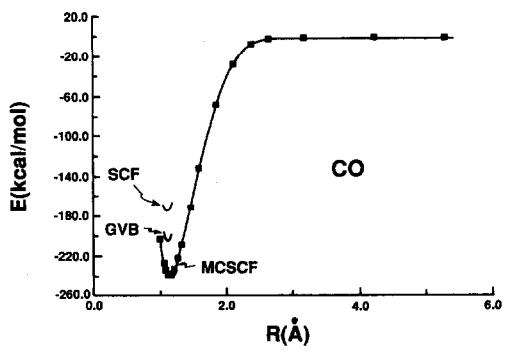

Fig. 2. Potential energy curves for CO at the SCF, GVB and MCSCF level.

Table 1. Comparison of calculated and experimentally-determined spectroscopic constants for CO

Variable	SCF	GVB	MCSCF	Experimental[a]
R_e (Å)	1.1129	1.1245	1.1414	1.1283
D_o (kcal mol^{-1})	174.7	204.8	236.0	255.8
ω_e (cm^{-1})	2409	2304	2169	2169.81
$\chi_e\omega_e$ (cm^{-1})	11.6	12.3	13.1	13.288
E_{min}(au)[b]	−112.777071	−112.843864	−112.911329	

[a] Taken from ref. 26.
[b] Electronic energy at the minimum of the calculated potential curve.

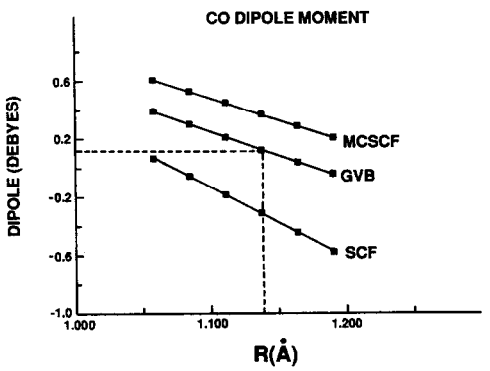

Fig. 3. Variation of the dipole moment of CO with internuclear separation. A positive dipole moment corresponds to $C^{\delta-}$—$O^{\delta+}$. The horizontal dotted line indicates the experimental dipole moment of 0.12 Debyes, which is also the value predicted by the GVB wavefunction at the C—O bond length (1.138 Å) used in the M^+CO calculations.

THE MOLECULES

$ScCO^+$

When Sc^+ in its ground ^3D state approaches the C end of CO colinearly, three molecular states are possible according to whether the 3*d* electron is in a $d_\sigma(^3\Sigma^+)$, $d_\pi(^3\Pi)$ or $d_\Delta(^3\Delta)$ orbital. The GVB wavefunction for these states has the schematic form

$$\sim 4s^1 3d^1(4\sigma^2-\lambda 6\sigma^2)(5\sigma^2-\mu 7\sigma^2)$$
$$(1\pi_x^2-\gamma 2\pi_x^2)(1\pi_y^2-\gamma 2\pi_y^2) \quad (4)$$

where the 4*s* and 3*d* electrons are triplet-coupled. The interaction energy as a function of the Sc—C separation (the CO separation is fixed at 1.138 Å) is shown in Fig. 4; also included are the curves for the singlet states arising from the ^1D state of Sc^+. The equilibrium bond lengths and bond energies for these and other calculations are collected in Table 2. Analysis of the GVB wavefunction suggests that very little electron density has been interchanged between the metal ion and the CO ligand. The relative bond energies of the triplets follow the order $\Delta > \Pi > \Sigma^+$, while the singlet states vary as $\Pi > \Delta > \Sigma^+$. Recent studies[4,5] on the neutral transition metal monocarbonyls suggest that, if the metal has an occupied 4*s* orbital, the initial M—CO interaction will be repulsive. The fact that the calculated interactions for Sc^+ and CO are attractive at long distances, even though Sc^+ has an occupied 4*s* orbital, suggests that the electrostatic interaction between Sc^+ and CO is important. If μ, Θ and Ω are the dipole, quadrupole and octapole moment tensor elements along the internuclear axis of CO, relative to the centre of mass, and α is the corresponding dipole polarizability, the interaction energy can be written as

$$\Delta E = -\mu/R^2+\Theta/R^3-\Omega/R^4-\alpha/2R^4. \quad (5)$$

The fourth order term involving the quadrupole moment of Sc^+ and the dipole moment of CO is negligible and not shown above. Using $\mu = +0.04885$, $\Theta = -1.6019$, $\Omega = +3.9577$ and $\alpha = 16.06$ [all values are in atomic units (au)], all

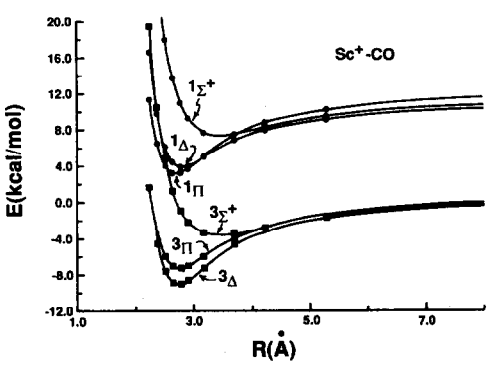

Fig. 4. Interaction energies for the low-lying triplet and singlet states of $ScCO^+$ calculated with the GVB technique. Zero energy corresponds to $Sc^+(^3D)+CO(^1\Sigma^+)$.

Table 2. Equilibrium bond lengths and bond energies for various $ScCO^+$, $CrCO^+$ and $LiCO^+$ electronic states[a]

Molecule	State	R_e(Å)	ΔE (kcal mol^{-1})
$ScCO^+$	$^3\Delta$	2.739	9.1
	$^3\Delta$ (CI)	2.697	10.2
	$^3\Pi$	2.755	7.3
	$^3\Sigma^+$	3.385	3.4
	$^1\Delta$	2.804	6.9
	$^1\Pi$	2.711	7.6
	$^1\Sigma^+$	3.504	3.2
	$^3\Sigma^-$	2.471	13.5
$ScOC^+$	$^3\Delta$	2.469	5.5
$CrCO^+$	$^6\Sigma^+$	2.479	13.5
	$^6\Sigma^+$ (CI)	2.335	14.9
	$^4\Pi$	2.250	21.5
$LiCO^+$	$^1\Sigma^+$	2.259	16.5[b]

[a] All results refer to GVB calculations, except where noted.

[b] A. Mavridis and J. F. Harrison, unpublished results.

calculated from the CO GVB wavefunction, we calculated ΔE as a function of the Sc—C distance. The results of this calculation are shown as the solid curve on Fig. 5. The *ab initio* electrostatic expression given above tracks the energy variation rather well and suggests that the dominant interaction between CO and Sc^+ is electrostatic, and that the bond energies are determined by that separation at which the electrostatic attraction gives way to the Pauli repulsion between the Sc 4*s*,3*d* electrons and the CO lone pair. This apparently happens first when the 3*d* electron is in the $3d_\sigma$ orbital, second for the $3d_\pi$ and last for the $3d_\Delta$ orbital—consistent with their spatial extension along the internuclear axis.

If CO appraoches Sc^+ (^3F) and the two *d* electrons on Sc^+ are in the $d^1_{\pi x}d^1_{\pi y}$ configuration, the resulting electronic state of $ScCO^+$ has $^3\Sigma^-$ symmetry. The interaction energy in the 4-pair GVB model is plotted in Fig. 6. Note that the interaction energy is well represented at large distances by the electrostatic multipole expansion. The absence of a d_σ or 4*s* electron on Sc^+ allows the CO to approach closer than in those states that correlate with a $4s^13d^1$ configuration. While the electrostatic representation for the energy fails at short Sc—C separations, this could be due to the importance of terms omitted from eq. (5), or simply due to the penetration of the electron densities of the two fragments. These two are, of course, not independent.

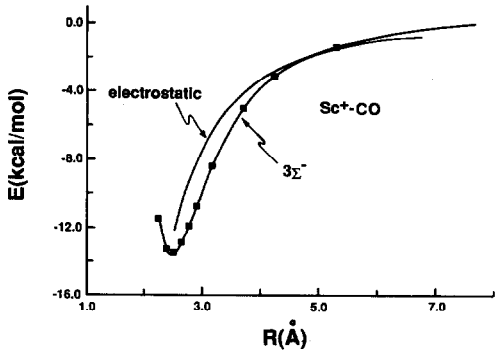

Fig. 6. Comparison of the *ab initio* interaction energy in the lowest $^3\Sigma^-$ state of $ScCO^+$ with the calculated electrostatic energy.

To assess the effect of configuration interaction (CI) on these systems we constructed the SCF + 1 + 2 function for the $^3\Delta$ state using the GVB orbitals. While the absolute energies dropped by 81 kcal mol^{-1}, the interaction energy remained essentially the same as the GVB calculation. The GVB and CI results are plotted in Fig. 7.

In Fig. 8 we show the GVB $^3\Delta$ interaction energy for the colinear approach of Sc^+ from the O end of CO. Note that while the Sc^+—O bond length (in Sc^+—OC) of 2.47 Å is significantly shorter than the

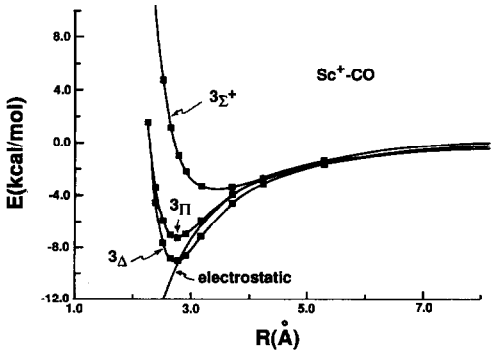

Fig. 5. Comparison of the electrostatic interaction between a point charge and CO with the *ab initio* GVB interaction energies for the $^3\Delta$, $^3\Pi$ and $^3\Sigma^+$ states.

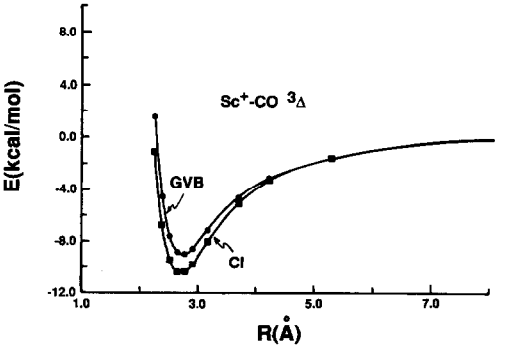

Fig. 7. Comparison of the GVB and SCF + 1 + 2 potential curves for $ScCO^+$($^3\Delta$).

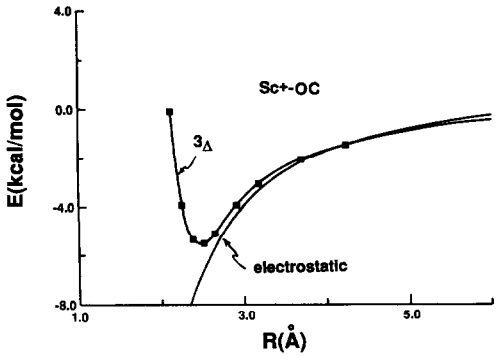

Fig. 8. Comparison of the GVB and electrostatic interactions for Sc^+—$OC(^3\Delta)$.

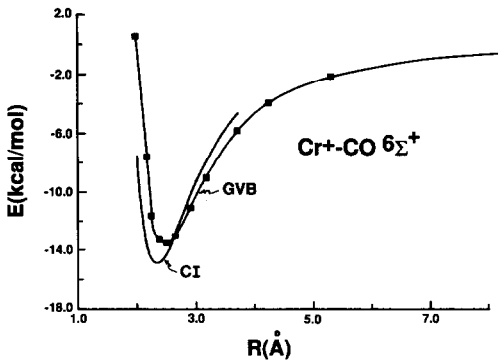

Fig. 10. Comparison of the GVB and SCF+1+2 potential curves for $CrCO^+(^6\Sigma^+)$.

Sc^+—C bond length (in Sc^+—CO) of 2.74 Å, the bond energies (5.5 and 9.1 kcal mol^{-1}, respectively) favour approach at the C end. The interaction energy for Sc^+—OC is well represented by an electrostatic calculation, using the same CO parameters as in the C-side approach (Fig. 8).

$CrCO^+$

When the ground state of Cr^+ (d^5,^6S) approaches CO, the resultant electronic state has $^6\Sigma^+$ symmetry. The interaction energy calculated with the GVB function equivalent to eq. (4) is shown in Fig. 9. Also plotted on Fig. 9 is the interaction energy curve for the $^3\Sigma^-$ state of $ScCO^+$. The resemblance is striking and suggests that the fundamental mechanism which leads to bonding in both molecules is very similar and largely electrostatic.

Interestingly, if one promotes the $3d_\sigma$ electron of Cr^+ to a $3d_\pi$ orbital, and allows the resulting configuration

$$3d_\sigma^0 3d_{\pi x}^2 3d_{\pi y}^1 3d_{\Delta+}^1 3d_{\Delta-}^1$$

to interact with CO, a much shorter and a much stronger Cr^+—C bond is formed. Our preliminary GVB results suggest that, upon this excitation of the Cr^+, the bond length in the $CrCO^+$ thus formed is reduced to 2.25 Å, and the bond strength is increased to 21.5 kcal mol^{-1}. The increase in bond energy observed on promotion of the d_σ electron appears to reflect the fact that this promotion allows the Cr^+ and CO to move closer to each other. Thus, the shortened bond results in an increased electrostatic interaction.

A comparison of the GVB result with an SCF+1+2 result for $CrCO^+$ is shown in Fig. 10. As in $ScCO^+$ the CI increases the bond energy by approximately 1 kcal mol^{-1} but, unlike the $ScCO^+$ result, the CI predicts a significantly shorter bond length than the GVB calculation.

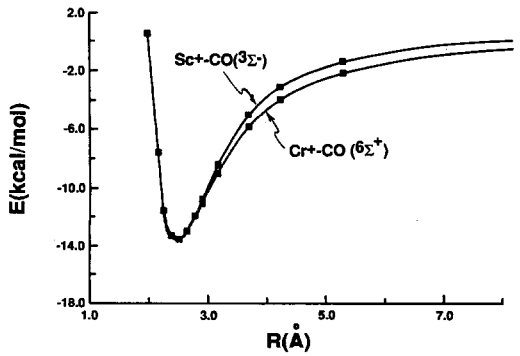

Fig. 9. Comparison of the Sc^+—CO and Cr^+—CO interaction energies at the GVB level.

Relationship to previous calculations

In a recent publication, Bauschlicher[5] reports the results of calculations on NiCO and $NiCO^+$. Both have bond energies of ~1.1 eV, but rather different bonding characteristics. The neutral NiCO has the Ni atom in the $3d^{10}$ configuration and correlates with the Ni ^1S excited state, while the positive ion has a hole in the d_σ orbital and correlates with the ^2D ground state of Ni^+. The Ni—C bond length is 1.70 Å in the neutral and 2.10 Å in the ion. Bauschlicher notes that while the neutral metal contributes a significant number of electrons via its d_π orbitals to the CO fragment the positive ion contributes virtually none. He suggests that Ni^+ binds electrostatically to the CO, as we have found for Sc^+ and Cr^+. It has also been suggested, by Orti *et al.*,[2g] that Cu^+ binds electrostatically to CO.

Implications and consequences of the calculated structure of MCO^+

Why do the first row transition metal positive ions bond differently from the neutrals to CO?

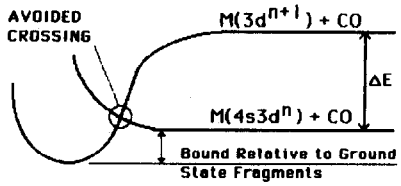

Scheme 6.

When CO approaches a neutral transition metal atom with an electronic configuration $4s^13d^n$, there is an initial repulsion[11] due to the 5σ(CO)—$4s$(M) interaction (a Pauli principle effect). If the $4s$ electron is singlet coupled to one of the $3d$ electrons, electronic states belonging to the excited configuration $4s^03d^{n+1}$ with a d_π^2 occupancy have the same spin symmetry as the $4s^13d^n$ states and can 'mix' in a Valence Bond sense, one has the situation shown in Scheme 6. Whether or not the upper state is bound, relative to the ground state fragments, depends on ΔE and the intrinsic M—CO bond strength. For a transition metal *cation*, the long range interaction with CO is electrostatic and therefore always bonding, whether the metal is in a ground or excited state (M^{+}*).

In the diagram shown in Scheme 7, the quantity E_e denotes the electrostatic interaction energy between the ground state M^+ and CO; the bond energy for the excited state is equal to $\{E_e+\delta E_e\}$. Does the ground state of the molecule MCO^+ always correlate with the ground state fragments? That is, under what circumstances could the additional binding energy (δE_e) of the metal in the excited state be greater than the excitation energy (ΔE)? There seems to be at least two extreme possibilities that could lead to positive values of δE_r: (a) when the *electrostatic* interaction is greater for M^{+}* than for M^+ and (b) when M^{+}* corresponds to an electronic configuration that favours the σ donation/π acceptor mechanism. (Of course, some combination of these two extremes could also be realized.) For example, consider Fe^+. The ground state ion has a $4s^13d^6$ configuration (^6D), and there

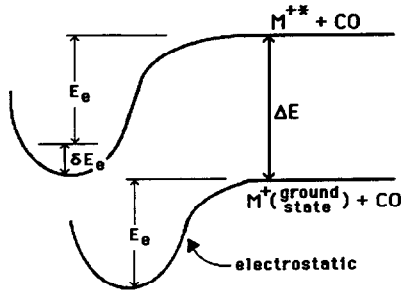

Scheme 7.

are low lying states of the $3d^7$ configuration (^4F state, $\Delta E = 5.4$ kcal mol^{-1}). A closer approach (shorter bond length), and thus a larger electrostatic interaction energy would be expected for $Fe^+(^4F)$—CO relative to $Fe^1(^6D)$—CO. The $Fe^+(^4F)$ would also have an increased opportunity for backbonding, i.e. for the d_π^2 electrons to back donate into the CO 2π* orbitals. For $Fe^+(^4F)$, the ideal state would correspond to the configuration $3d_\sigma^1 3d_{\pi x}^2 3d_{\pi y}^2 3d_{\Delta+}^1 3d_{\Delta-}^1$, i.e.

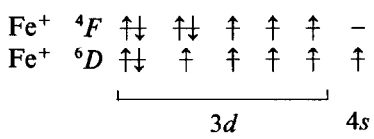

Although the opportunity exists here for increasing δE_e as a result of backbonding for this state, would it occur? In response to this question, consider the following: the $^3\Sigma^-$ state of $ScCO^+$ correlates with the ^3F state of Sc^+ ($d_{\pi x}^1 d_{\pi y}^1$) and has a calculated equilibrium Sc^+—C bond length of 2.47 Å, with a bond energy of 13.6 kcal mol^{-1}. The electrostatic energy, calculated using eq. (5) for this Sc^+—C separation, is approximately 12.8 kcal mol^{-1}. For the $^4\Pi$ state of $CrCO^+$, which correlates with the Cr^+ configuration $3d_\sigma^0 3d_{\pi x}^2 3d_{\pi y}^1 3d_{\Delta+}^1 3d_{\Delta-}^1$, the calculated bond length is 2.25 Å, the calculated bond energy is 21.5 kcal mol^{-1}, and the electrostatic energy from eq. (5) is approximately 16 kcal mol^{-1}. For $NiCO^+$, the calculated[5] Ni^+—C bond length is 2.10 Å, the calculated bond energy is 25.3 kcal mol^{-1}, and the estimate from eq. (5) is 20.1 kcal mol^{-1}. The increasing importance of terms of order $1/R^5$, of course, results in the rapidly deteriorating ability of eq. (5) to accurately represent the electrostatic interaction energy at small separations. However, the correlation of the *ab initio* results with electrostatics suggests that little dative bonding/backbonding takes place in these ionic species, and that the bond energies for both M^+—CO and M^{+}*—CO species are dominated by electrostatics. (Note that the ground state of Li^+ cannot bond to CO by a Dewar–Chatt mechanism; even so, the data in Table 2 for $LiCO^+$ correlate with the $ScCO^+$ and $CrCO^+$ results listed, further supporting the dominance of the electrostatic mechanism for these ions.) It follows, then, that the bond energies are determined by how close the M^+ and CO can approach before repulsive terms become significant. This would predict that bond lengths will decrease, and $D(M^+$—CO)s increase, as the ionic radii of the various M^+ ions decrease. In the case of Fe^+, the ^4D excited state would then form a stronger bond to CO than would its ^6D ground state, because the excited state atomic ion is smaller (the $3d$ orbitals

are more compact than the 4*s* orbital). An example of the opposite situation would be Co^+, with a $3d^8$ (^3F) ground state configuration, and a low-lying ^5F excited state ($3d^74s^1$). In this case, the excited state would be more weakly bound than the ground state, i.e. δE_e will be negative.

In response to the question of whether the global MCO^+ ground states correlate to the ground state fragments, in light of the above discussion, we have considered the ground and low-lying configurations of the various metal ions of the first transition series. $TiCO^+$ and $FeCO^+$ appear to be the only candidates for a situation where δE_e could be both positive, and greater than ΔE. Thus, these two MCO^+ species may indeed correlate with excited states of the corresponding metal ions. This question is being explored computationally in this laboratory.

The possibility that the cations of the transition metal elements could bond electrostatically to CO molecules has some intriguing consequences. First of all, in such a molecule the CO group would not modify the electronic structure of the transition metal ion. An ion with a $4s3d^n$ configuration would remain an *in situ* $4s3d^n$ in the monocarbonyl. To the extent that the chemistry of the ion is determined by its electronic configuration one would anticipate similar chemistry for M^+ and MCO^+.

Not only would the electronic configuration of M^+ and MCO^+ remain the same but so would the spin. Is the spin relevant to the chemistry of M^+, MCO^+ or any transition metal-containing ion? This question has been recently discussed by Armentrout *et al.*[18] One knows from carbene chemistry[19] that singlet carbenes insert into C—H bonds while triplet carbenes abstract. These processes conserve the electronic spin in the reaction for if a triplet carbene were to insert into a C—H bond the spin multiplicity would change. For example

$$:CH_2(\text{triplet}) + R{-}H(\text{singlet}) \rightarrow R{-}CH_3(\text{singlet})$$

would be spin forbidden, while

$$:CH_2(\text{triplet}) + R{-}H(\text{singlet}) \rightarrow CH_3^{\cdot}(\text{doublet}) + R^{\cdot}(\text{doublet})$$

is allowed, provided the products are coupled into a triplet state. While electronic spin is a much better quantum number for carbon than for the transition metal cations, an examination of the atomic spectra[13] of the bare transition metal ions suggests that spin might be a good quantum number, at least when the energy spacing between the LS coupling terms is larger than the energy spacing within the terms; this situation is often obtained for the low-lying electronic states.

Thus, in the chemistry of transition metal ions, there are at least two options: (a) the electronic spin is a good quantum number and must be conserved in the reaction; or (b) the spin can easily change and is not a factor in the reactivity. While option (b) is uninteresting in that it yields no predictive capabilities, there are some consequences of option (a). Consider, for example the reaction of Co^+ with CH_3I.[20] Two products are observed:

$$Co^+ + CH_3I \rightarrow CoI^+ + CH_3^{\cdot} \quad 73\%$$
$$\rightarrow CoCH_3^+ + I^{\cdot} \quad 27\%.$$

The ground state of Co^+ is a triplet d^8 configuration with two singly occupied orbitals and could react to form the products shown here and conserve spin. However, it has been proposed that this reaction (and others which follow) occurs by an insertion mechanism.[20] If, in the initial insertion reaction

$$Co^+ + CH_3I \rightarrow [CH_3{-}Co^+{-}I]$$

spin was conserved, the Co^+ would have to uncouple a singlet-coupled d^2 electron pair and use these electrons to bond to the CH_3 and I fragments. This it could do by *in situ* promotion of a *d* electron to an *s* orbital, and mixing a triplet state of the $4s^13d^7$ configuration into the evolving wavefunction. The product would then be a triplet which might indeed be the ground state for $CH_3{-}Co^+{-}I$. While this is possible it presumably would result in an activation barrier which could make it problematic as to whether it is energetically possible for the triplet to react. If this direct insertion channel is precluded by a large activation barrier, perhaps the insertion process takes place in "two steps", as shown here:

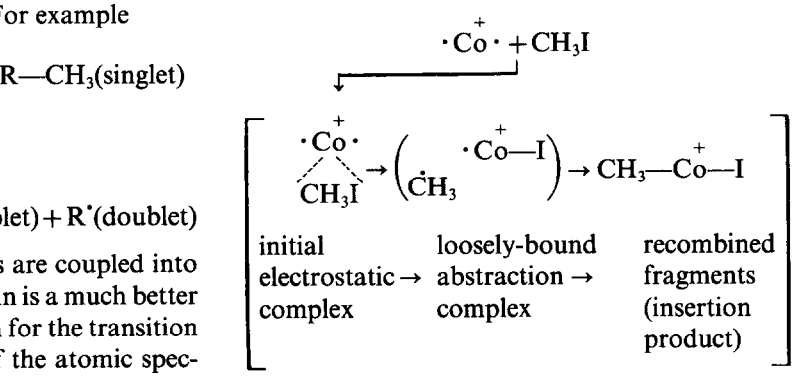

First a spin-allowed abstraction occurs, followed by the recombination of the two radicals. This mechanism allows a triplet Co^+ to form a singlet insertion product, provided the products of the abstraction are able to recombine on a lower spin

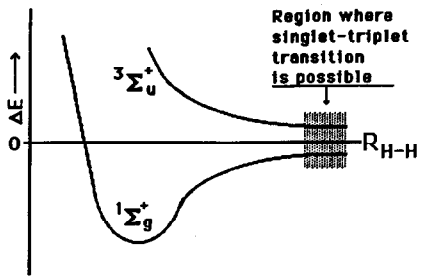

Scheme 8.

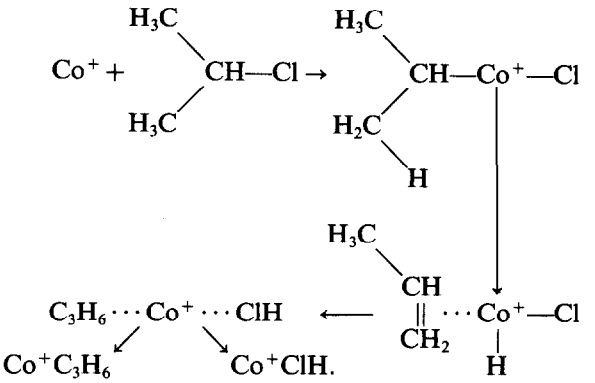

surface. For this to happen the products would have to be separated to the extent that a "small" spin–orbit interaction would allow the required surface change. This is similar to the reaction of two H atoms to form H_2. While the ground state in this case is the $^1\Sigma_g^+$, at large separations the energy difference between this singlet and the $^3\Sigma_u^+$ is very small, and a small spin–orbit interaction could take one from the triplet to the singlet surface, see Scheme 8.

This mechanism, where one substitutes an abstraction and subsequent recombination for a concerted insertion is sensible only if the fragments involved in the abstraction reaction remain sufficiently close (loosely-bound abstraction complex) so that the recombination is efficient and yet are separated sufficiently to permit a small spin–orbit interaction to induce the required surface change. One way for this to happen is if the neutral abstraction fragments are from a large, easily polarizable molecule. Thus, spin considerations may require these details as part of the overall 'insertion' mechanism.

Experimental observations: the gas phase chemistry of M^+ *vs* MCO^+

The ion/molecule reaction products shown here for Co^+ have been observed for a number of other first row transition metal ions:[20]

$$Co^+ + i\text{-}C_3H_7Cl \rightarrow C_3H_7^+ + CoCl \quad 35\% \quad (6)$$

$$\rightarrow CoC_3H_6^+ + HCl \quad 60\% \quad (7)$$

$$\rightarrow CoHCl^+ + C_3H_6 \quad 5\%. \quad (8)$$

Reaction (6) is a halide abstraction, that is frequently observed when the ionization energy of the alkyl radical involved is sufficiently low. The products in (7) and (8) are proposed to be formed as follows:

The metal ion first forms a complex with the polar neutral molecule. Following this, the metal inserts into the polar C—Cl bond. If the alkyl group is an ethyl group or larger, and possesses a H atom on a C atom that is β to the metal, this H will shift onto the metal, then onto the Cl. The result is that the metal has choreographed the degradation of propyl chloride to propene and HCl. These two ligands thus formed compete for a site on the metal[21] and, as the distribution of products shows, the retention of propene is favoured [consistent with the observation that P.A.(HCl) < P.A.(C_3H_6)].

The two possible scenarios for insertion presented above would lead to different consequences in terms of the final products. If, on insertion, the overall spin of the system changes, the products may be formed in excited states. That is, products such as $CoC_3H_6^+$ may be singlets, although the ground state of this species (if electrostatically bound) would be a triplet. When a CO is attached to Co^+, the following products are formed from iso-propyl chloride:

$$CoCO^+ + i\text{-}C_3H_7Cl \rightarrow CoCOC_3H_6^+ + HCl \quad 16\%$$

$$\rightarrow CoCOHCl^+ + C_3H_6 \quad 17\%$$

$$\rightarrow CoC_3H_6^+ + CO + HCl \quad 67\%.$$

The same reaction occurs, with retention of propene favoured over that of HCl. While $CoCO^+$ does react with propyl chloride, $CoNO^+$ does not, suggesting that NO is covalently bonded to Co^+.

As a second example,[20] the reaction products of Co^+ and $CoCO^+$ with isopropanol are given below.

$$Co^+ + i\text{-}C_3H_7OH \rightarrow C_3H_7^+ + CoOH \quad 12\%$$

$$\rightarrow CoC_3H_6^+ + H_2O \quad 48\%$$

$$\rightarrow CoH_2O^+ + C_3H_6 \quad 40\%$$

$$CoCO^+ + i\text{-}C_3H_7OH \rightarrow CoCOC_3H_6^+ + H_2O \quad 21\%$$

$$\rightarrow CoC_3H_6^+ + H_2O + CO \quad 21\%$$

$$\rightarrow CoC_3H_7OH^+ + CO \quad 58\%.$$

Again, both Co^+ and $CoCO^+$ induce the dehydration of propanol. In comparing the distribution of products from propanol and propyl chloride, retention of H_2O occurs more frequently than retention of HCl, with retention of propene favoured over both, consistent with the proton affinity ordering $PA(C_3H_6) > PA(H_2O) > PA(HCl)$. It can be difficult to compare reaction products of M^+ and MCO^+ to determine if the chemistry of the metal changes due to the presence of the ligand because the ligand appears to reside on the metal as the reaction proceeds. Thus, when $CoCO^+$ reacts with e.g. propanol, the complex that dissociates to give the observed products is $Co^+(CO)(H_2O)(C_3H_6)$. It is the relative metal–ligand binding energies that determine which of these ligands will be lost, and the distribution of products. This also suggests that the $CoC_3H_7OH^+$ products in the $CoCO^+$ reaction above exist, at least in part, as $Co^+(H_2O)(C_3H_6)$. Similar reactions are also observed in comparing the chemistry[20] of Fe^+ with $FeCO^+$, and the reactions of Ni^+ with $NiCO^+$. Thus, the Co appears to be a 'spectator' in such reactions. Its presence does not appear to alter the chemistry of the metal ion, consistent with the electrostatic bonding scheme suggested by the earlier experimental results and the *ab initio* calculations presented here.

The reactions of M^+ and MCO^+ are not *always* the same. We have noted that the order in which metal insertion occurs into the various skeletal bonds of larger molecules such as octane appears to be different when a CO is attached to the metal.[22] This may reflect a steric effect which affects the relative stabilities of the various $M^+(CO)(R_1)(R_2)$ insertion intermediates that may be formed upon insertion into various (R_1—R_2) skeletal bonds.

There are also cases reported in which the MCO^+ *group* appears to insert into a bond, although these are not commonly evident. One system in which this was reported is in the reactions of Co^+ with amines. While Co^+ has been observed to insert into a variety of polar bonds[1] such as C—Cl, C—OH, C—SH, C—NO_2, etc., it does not appear to insert into the C—NH_2 bond of primary amines. Reaction products reflecting the insertion into C—C and C—H bonds are observed,[23] e.g.

$$Co^+ + i\text{-}C_3H_7NH_2 \rightarrow C_3H_8N^+ + CoH \quad 24\%$$
$$\rightarrow CoC_3H_7N^+ + H_2 \quad 52\%$$
$$\rightarrow CoC_2H_5N^+ + CH_4 \quad 24\%.$$

When a mixture of $Co(CO)_3NO$ and a primary amine are subjected to EI, and the resulting ions allowed to react in an ICR experiment, one product that is frequently formed is $CoCH_3NH_2^+$. This ion is a reaction product of Co^+, for amines larger than ethylamine, formed via insertion into the R—CH_2NH_2 bond. However, $CoCH_3NH_2^+$ is also formed when the amine is ethylamine. If Co^+ was the precursor, this would suggest an unusual reaction in which CH_2: would be lost:

$$Co^+ + CH_3CH_2NH_2 \rightarrow CoCH_3NH_2^+ + CH_2:.$$

However, double resonance experiments[23] show that the ionic precursor is *not* Co^+, but instead $CoCO^+$, suggesting the following mechanistic sequence:

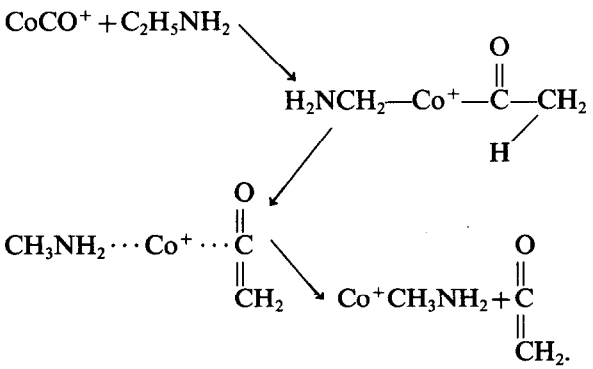

Thus, the Co^+ and the CO appear to insert into the C—C bond, with the CH_3 group being bound to the CO, forming an acetyl–metal complex. These are now Hs that are β to the metal that can shift, resulting not in the loss of CH_2, but ketene.

Such reactions may be common, but difficult to detect. For example, in the reaction

$$CoCO^+ + C_3H_7Cl \rightarrow CoC_3H_6^+ + HCl + CO$$

the neutral(s) lost may be HCOCl, formed by active participation of the CO, however this cannot be determined in these experiments.

Another example of a reaction in which the CO is actively involved is in the chemistry of $CrCO^+$ with diethyl ether.[24] Cr^+ reacts by the insertion/H-shift/competitive ligand loss mechanism, inserting into a C—O bond:

$$Cr^+ + C_2H_5\text{—}O\text{—}C_2H_5 \rightarrow C_2H_5\text{—}Cr^+\text{—}OC_2H_5$$
$$\downarrow$$
$$\downarrow$$
$$CrC_2H_4O^+ + C_2H_6 \leftarrow (C_2H_6)Cr^+(C_2H_4O)$$

This reaction is reasonable, since the poorer ligand, ethane, is lost exclusively, with the ligand retained being presumably acetaldehyde. However, when $CrCO^+$ reacts, the observed products are

$$CrCO^+ + C_2H_5OC_2H_5 \rightarrow CrC_4H_{10}O^+ + CO \quad 79\%$$
$$\rightarrow \text{“}CrCOC_2H_6^+\text{”} + C_2H_4O \quad 21\%.$$

Loss of C_2H_4O would reflect *retention* of ethane over acetaldehyde when the CO is attached, which would violate the proton affinity rule. However, the reaction product could be explained by invoking insertion of the $CrCO^+$ moiety intact:

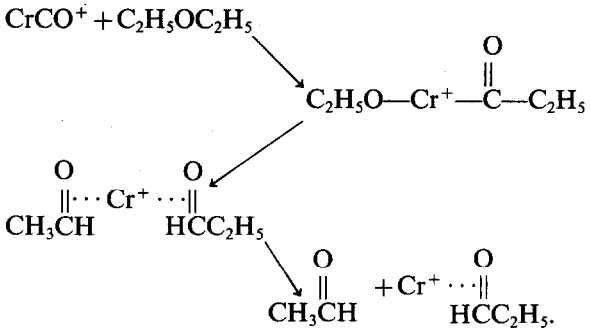

By this mechanism, acetaldehyde and propionaldehyde would be competing as ligands on Cr^+, with the ligand characterized by the lower PA being lost. Therefore the "$Cr(CO)(C_2H_6)^+$" ion should actually be a Cr^+-propionaldehyde structure.

Thus, there are cases in which the CO is involved in the chemistry of the metal ion to which it is attached. The question arises as to how the apparent "MCO^+" insertion occurs. Consider the reaction discussed above for $CoCO^+$ with ethylamine. How is the "MCO^+" insertion intermediate formed?

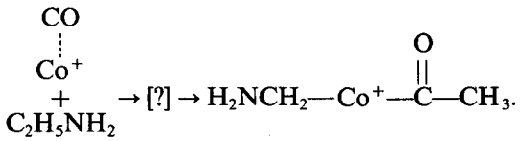

There are a number of possible mechanisms. Three are suggested by the structures shown here.

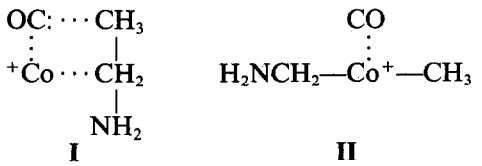

I **II**

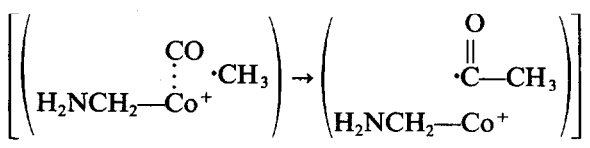

III

Intermediate **I** suggests the possibility of the direct interaction of the metal with one C and the CO with the second C of the C—C bond in a concerted manner. Intermediate **II** suggests a scenario in which the metal first inserts into the C—C bond. The CH_3 and CO groups are next converted into a CH_3CO group. (It should be noted that reactions involving the process R—M—CO → M—C(O)—R have received considerable attention in the literature recently,[25] to determine whether this rearrangement is more accurately described as an R-migration to the CO, or as a CO insertion into the R—M bond.) In **III**, the mechanism discussed previously for the insertion process is utilized. The Co^+ forms a bond to the CH_2NH_2 fragment, and a loosely-bound electrostatic complex with the CH_3 fragment. The CH_3 then has the option of approaching the metal, *or* the CO, to form a bond. If the CH_3 attacks the CO, the resulting $CH_3CO\cdot$ radical can then bond to the metal.

These various mechanisms can be evaluated by considering information such as the energy that must be supplied to break the C—C bond and the Co^+—CO bond, and the energy released when the Co^+—C bonds and the CH_3—CO bond are formed. The C—C bond energy in ethylamine is 82 kcal mol^{-1}.[8] The presence of the amino group weakens this bond slightly, when compared to a C—C bond energy of 87 kcal mol^{-1} in ethane.[8] The singlet–triplet spacing in CO ($X^1\Sigma^+ - a^3\Pi$) is large, 139 kcal mol^{-1}.[26] Based on the calculations presented here, we estimate the Co^+—CO bond energy to be approximately 10 kcal mol^{-1}. With these numbers, reaction via intermediate **I** would seem unlikely. If the CO remains a singlet, direct interaction with the methyl group could not occur, and the energy produced upon formation of the initial electrostatic complex would not be sufficient to induce conversion of the CO to a higher spin state. Intermediate **II** can be formed, i.e. Co^+ can insert into the C—C bond in an exothermic process. If the sum of the two Co^+—C bonds formed is approximately 100 kcal mol^{-1}, the insertion would be exothermic by 20 kcal mol^{-1}. It has been suggested that $(CO)Co^+CH_3$ is more stable than $CoC(O)CH_3^+$ by approximately 20 kcal mol^{-1}.[27] However, this was an estimate made using thermochemical approximations[27] such as: $D(RCo^+—CO) = 35$ kcal mol^{-1}; $D[Co^+—C(O)R] = 60$ kcal mol^{-1}; and $D(Co^+—CO) = D[(H_3C)Co^+—C(O)R] = 40$ kcal mol^{-1}. If, as suggested in this work, the Co^+—CO binding energy is considerably weaker than 40 kcal mol^{-1}, CH_3 'migration' onto the CO could occur exothermically. The mechanism suggested by **III** is attractive. The reaction

$$\cdot CH_3 + CO(^1\Sigma^+) \rightarrow CH_3CO\cdot$$

is *exothermic* by 21.4 kcal mol^{-1}.[8] Thus, CH_3 can react with the CO, and the resulting radical can

bond to the metal ion. The mechanism for insertion proposed here would allow for ligands such as CO to become actively involved in the chemistry, even though the ligand itself is not 'activated' by the metal, but only electrostatically bound.

CONCLUSIONS

Theoretical attention to these ionic organometallic systems is allowing us to go back to early data of this area of research, and begin to understand in much greater detail how observed reactions occur. Thus, we are beginning to understand some of the relationships between electronic structure and reactivity for these gas phase systems.

The possibility that M^+—CO bonding is dominated by an electrostatic, rather than the traditional Dewar–Chatt scheme may explain why attempts to model systems such as the water–gas shift reaction via gas phase ionic studies have not been successful,[28] since the CO is not 'activated' by the metal ion.

The system discussed here shows that the opportunity to form a dative bond is overshadowed by electrostatic interactions at these M^+–ligand separations for first row transition metal ions. One may expect other ligands such as water, ammonia, polar organic compounds, etc. to be bound in this way as well. The strength of the metal–ligand interaction would then be reflected in the ligand's multipole moments and polarizability.

There could be some interesting geometrical implications that result from an electrostatic bonding description. For example, suppose that olefins are only bound electrostatically to univalent transition metal ions in the gas phase. Since the C=C double bond in, e.g. ethylene, appears to be more polarizable along the bond axis, than perpendicular to the axis,[29] an electrostatic M^+–(ethylene) complex may take the geometry shown in IV. For a M^+–(1-butene) complex, consideration of interactions of the M^+ with not only the polarizable double bond, but the polarizable ethyl group, leads one to envisage the geometry as shown in V.

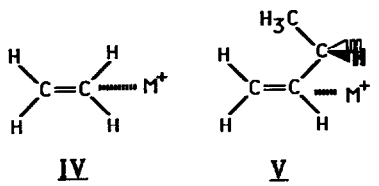

IV V

It is interesting to note that M^+–olefin reactions frequently proceed via M^+ insertion into the allyl C—H bond;[30] the description in V places the M^+ in close proximity to this bond.

The exception to this bonding scheme would be, of course, ligands such as NO that could form covalent bonds. Publications which follow from this group will focus on those ligands/fragments that have the option of bonding as CO (i.e. approaching M^+ with its lone pair), *or* bonding through a single electron (covalently), *or* through bonding schemes in which three electrons on the ligand are involved. These ligands include NO, Cl, OH and NH_2.

Acknowledgement—This work was partially supported under NSF Grant CHE8519752 (J.F.H.).

REFERENCES

1. For a recent review, see J. Allison, *Prog. Inorg. Chem.* 1986, **34**, 627.
2. See, for example: (a) A. E. Alvarado-Swaisgood, J. Allison and J. F. Harrison, *J. Phys. Chem.* 1985, **89**, 2517; (b) A. E. Alvarado-Swaisgood and J. F. Harrison, *J. Phys. Chem.* 1985, **89**, 5198; (c) E. A. Carter and W. A. Goddard, III, *J. Phys. Chem.* 1984, **88**, 1485; (d) E. A. Carter and W. A. Goddard, III, *J. Am. Chem. Soc.* 1986, **108**, 2180; (e) J. F. Harrison, *J. Phys. Chem.* 1986, **90**, 3313; (f) J. B. Schilling, W. A. Goddard, III and J. L. Beauchamp, *J. Phys. Chem.* 1987, **91**, 4470; (g) M. Merchan, I. Nebot-Gil, R. Gonzalez-Luque and E. Orti, *J. Chem. Phys.* 1987, **87**, 1690.
3. (a) M. J. S. Dewar, *Bull. Soc. Chim. France*, 1951, **18**, C79; (b) J. Chatt and L. A. Duncanson, *J. Chem. Soc.* 1953, 2939.
4. (a) C. W. Bauschlicher, Jr, P. S. Bagus, C. J. Nelin and B. O. Roos, *J. Chem. Phys.* 1986, **85**, 354; (b) C. W. Bauschlicher, Jr and P. S. Bagus, *J. Chem. Phys.* 1984, **81**, 5889.
5. C. W. Bauschlicher, Jr, *J. Chem. Phys.* 1986, **84**, 260.
6. (a) G. Distefano, *J. Res. NBS*, 1970, **74a**, 233; (b) R. E. Winters and R. W. Kiser, *Inorg. Chem.* 1964, **3**, 699; (c) S. M. Schildcrout, G. A. Pressley, Jr and F. E. Stafford, *J. Am. Chem. Soc.* 1967, **89**, 1617; (d) A. Foffani, S. Pignataro, B. Cantone and F. Grasso, *Z. Physik. Chem.* 1965, **45**, 79.
7. R. E. Winters and R. W. Kiser, *Inorg. Chem.* 1965, **4**, 157.
8. Thermochemical data taken from (a) J. L. Franklin, J. G. Dillard, H. M. Rosenstock, J. T. Herron, K. Draxl and F. H. Field, *Ionization Potentials, Appearance Potentials, and Heats of Formation of Gaseous Positive Ions*, Nat. Stand. Ref. Data Ser., Nat. Bur. Stand. 1969, **26**; (b) H. M. Rosenstock, K. Draxl, B. W. Steiner and J. T. Herron, *J. Phys. Chem. Ref. Data*, 1977, **6**.
9. M. S. Foster and J. L. Beauchamp, *J. Am. Chem. Soc.* 1971, **93**, 4924.
10. J. Allison and D. P. Ridge, *J. Am. Chem. Soc.* 1977, **99**, 35.
11. B. S. Larsen and D. P. Ridge, *J. Am. Chem. Soc.* 1984, **106**, 1912.
12. See, for example, F. A. Cotton and G. Wilkinson,

Advanced Inorganic Chemistry. Wiley Interscience, New York (1972).
13. C. E. Moore, *Atomic Energy Levels*, Natl. Stand. Ref. Data Ser. NSRDS–NBS, Circ. No. 35, Vol. 2.
14. A. Mavridis, A. E. Alvarado-Swaisgood and J. F. Harrison, *J. Phys. Chem.* 1986, **90**, 2584.
15. F. B. Duijneveldt, IBM Research Laboratory, San Jose, CA. 1971; IBM Technical Research Report No. RJ-945.
16. R. C. Raffenetti, *J. Chem. Phys.* 1973, **58**, 4452.
17. All calculations were performed on an FPS-164, jointly supported by Michigan State University's Chemistry Department and the Office of the Provost, using the Argonne National Laboratory Collection of QUEST–164 codes.
18. R. H. Schultz and P. B. Armentrout, *J. Phys. Chem.* 1987, **91**, 4433.
19. See, for example, W. Kirmse, (Ed.), *Carbene Chemistry*. Academic Press, New York (1971).
20. (a) J. Allison and D. P. Ridge, *J. Am. Chem. Soc.* 1976, **98**, 7445; (b) J. Allison and D. P. Ridge, *J. Am. Chem. Soc.* 1979, **101**, 4998.
21. A. Tsarbopoulos and J. Allison, *Organometallics* 1984, **3**, 86.
22. R. M. Stepnowski and J. Allison, presented at the *34th ASMS Conference on Mass Spectrometry and Allied Topics*, Cincinnati, OH, 8–13 June, 1986, p. 610 (Extended Abstracts Compilation).
23. B. Radecki and J. Allison, *J. Am. Chem. Soc.* 1984, **106**, 946.
24. S. K. Huang and J. Allison, *Organometallics* 1983, **2**, 883.
25. See, for example: (a) A. Cameron, V. H. Smith and M. C. Baird, *Organometallics* 1983, **2**, 465; (b) J. D. Cotton and R. D. Markwell, *Organometallics* 1985, **4**, 937; (c) S. P. Nolan, R. L. de la Vega, S. L. Mukerjee and Carl D. Hoff, *Inorg. Chem.* 1986, **25**, 1160; (d) N. Koga and K. Morokuma, *J. Am. Chem. Soc.* 1986, **108**, 6136; (e) T. Ziegler, L. Versluis and V. Tschinke, *J. Am. Chem. Soc.* 1986, **108**, 612.
26. K. P. Huber and G. Herzberg, *Constants of Diatomic Molecules*. Van Nostrand, New York (1979).
27. L. F. Halle, W. E. Crowe, P. B. Armentrout and J. L. Beauchamp, *Organometallics* 1984, **3**, 1694.
28. J. Allison, unpublished results.
29. J. O. Hirschfelder, C. F. Curtiss and R. B. Bird, *Molecular Theory of Gases and Liquids*. Wiley, New York (1954).
30. P. B. Armentrout, L. F. Halle and J. L. Beauchamp, *J. Am. Chem. Soc.* 1981, **103**, 6624.

Polyhedron Vol. 7, No. 16/17, pp. 1573–1581, 1988
Printed in Great Britain

0277–5387/88 $3.00+.00
© 1988 Pergamon Press plc

PERIODIC TRENDS IN GAS PHASE M—H AND M—C BOND ENERGIES

P. B. ARMENTROUT* and R. GEORGIADIS

Chemistry Department, University of Utah, Salt Lake City, UT 84112, U.S.A.

Abstract—Thermochemistry of simple transition metal species as determined by guided ion beam mass spectrometry is reviewed. Compounds which are discussed include metal hydrides (both ionic and neutral), metal methyls (ionic and neutral), ionic metal methylidenes and metal methylidynes, and bis-methyl metal ions. The periodic trends in this thermochemistry are discussed with an eye on developing ways of applying the data to condensed phase species.

A truly comprehensive enumeration of organometallic thermochemistry is an impossible task due to the sheer number of combinations of metals, ligands and environments. Alternatively, one can seek to identify the major trends in such thermochemistry in the hope of being able to accurately estimate values of interest in many systems. The possibility that gas phase organometallic chemistry may be able to contribute to this goal is one of its intriguing promises. This possibility seems reasonable since trends in metal thermochemistry can be analysed routinely in the gas phase without the stability restrictions imposed by the 18-electron rule. Thus, specific metal–ligand bond energies can be measured for all transition metals each having exactly the same ligand sphere.

In relating such gas phase thermochemistry to condensed phase species, it is important to realize that gas phase metal–ligand bond energies *will not equal* the metal–ligand bond energy of a saturated metal centre. For example, it is unrealistic to expect that the bond dissociation energy (BDE) of diatomic CoH or CoH^+ will be equivalent to that for H—$Co(CO)_4$. The relationship between the gas and condensed phase thermochemistry is more elusive, but of substantial value if it can be found. In this paper, we compile thermochemical results from recent studies in our laboratory and discuss useful ways of thinking about these numbers in an effort to develop ties to the "real" world of transition metal chemistry.

* Author to whom correspondence should be addressed. NSF Presidential Young Investigator, 1984–1989; Alfred P. Sloan Fellow.

EXPERIMENTAL

The methodology we have used in our laboratory to measure gas phase bond dissociation energies has been detailed before in several places.[1–4] Rather than reiterate the instrumental details, suffice it to say that we measure the absolute probability for reaction (1) or (2) while varying the kinetic energy available to the reactants.

$$M^+ + RX \rightarrow MX^+ + R \quad (1)$$

$$\rightarrow MX + R^+. \quad (2)$$

In these reactions, M represents a transition metal, X is the ligand of interest and R is a suitable donor of X. The systems are chosen such that these reactions are endothermic and therefore require the addition of kinetic energy to proceed. The results are then analysed in some detail to determine the threshold for the reaction, E_T. This is the minimum kinetic energy required for the reaction to occur.

In the limit that there is no activation barrier in excess of the endothermicity, the bond dissociation energy of the species produced in reaction (1) can be obtained from the threshold value for reaction (1) by using

$$D^0(M^+—X) = \Delta H_f(X) + \Delta H_f(R) - \Delta H_f(RX) - E_T. \quad (3)$$

In simple bond exchange processes, eq. (3) can be simplified by noting that

$$D^0(R—X) = \Delta H_f(X) + \Delta H_f(R) - \Delta H_f(RX). \quad (4)$$

Similarly, for the species produced in reaction (2), eq. (5) holds,

$$D^0(\text{M—X}) = \Delta H_f(\text{X}) + \Delta H_f(\text{R}^+) - \Delta H_f(\text{RX}) - IP(\text{M}) - E_T, \quad (5)$$

where IP(M) is the ionization potential of the metal. This may also be simplified by using the relation

$$D^0(\text{R—X}) + IP(\text{R}) = \Delta H_f(\text{X}) + \Delta H_f(\text{R}^+) - \Delta H_f(\text{RX}). \quad (6)$$

These equations demonstrate that another requirement of the species RX is that the heats of formation, ΔH_f(R), $\Delta H_f(\text{R}^+)$, ΔH_f(X) and ΔH_f(RX), should be reasonably well known.

There are several factors which influence the accuracy of BDEs derived using the beam method. The first is the assumption that there is no activation energy in excess of the reaction endothermicity. This is equivalent to there also being no barrier to reaction in the opposite (exothermic) direction. Since the long-range ion-induced dipole potential is often sufficiently strong to overcome small barriers,[5] exothermic ion–molecule reactions are often (though not always) observed to proceed without an activation energy. The converse must also be true. Endothermic ion–molecule reactions often proceed (though this is not guaranteed) once the available energy exceeds the thermodynamic threshold.

This assumption is one which we have tested directly for a number of simple endothermic reactions where the thermochemistry of all species involved is well known.[3,4,6–9] In all these cases, no activation barriers are found, although this sometimes requires very good sensitivity.[3] Unfortunately, such direct checks for transition metal-containing species are rare since there are few alternate experimental determinations having better accuracy. However, high quality theoretical results on diatomic metal hydrides are available.[10–12] These values average 2 ± 3 kcal mol^{-1} lower than the experimental values derived in our studies, a typical error for such calculations. Note that if activation barriers were present, the true bond energies would be larger making the agreement with theory even worse.

A second limitation on the beam results concerns the characterization of the internal energy of the reactants. Since this energy is presumably available to the reaction, it must be inevitably accounted for in the energy balance eqs (3) and (5). This is not a particular problem for the neutral reagents since these have well characterized internal temperatures of 300 K. (Although as the neutral reactant increases in size, the sheer number of modes makes the total energy available in internal energy appreciable.) It is a problem for the ionic reactant, however, since the production of ions is, by its very nature, an energetic process. In studies of atomic metal ions, this problem can only evidence itself in electronic excitation. Studies in our laboratories have shown that the electronic energy, E_{el}, is usually available to cause reaction,[13–19] but need not be.[15–17] A good example of the problems this effect has on the derived thermochemistry is the case of FeH^+ and $FeCH_3^+$ as measured from reactions of Fe^+ with H_2 and C_2H_6. Early studies[20,21] made the reasonable assumption that the Fe^+ reactant was in its ground state and found bond energies of 58 ± 5 and 68 ± 4 kcal mol^{-1}, respectively. More recent studies obtain raw data which are qualitatively very similar, but interpret the data to find BDEs of 50 ± 1.4[15] and 58 ± 2 kcal mol^{-1},[22] respectively. The main difference lies in the fact that the reactivity of Fe^+ in these studies is dominated by its first excited state. This state has an E_{el} of about 7 kcal mol^{-1}, a value which clearly explains most of the discrepancies between the early and recent results.

The problem with internal energy effects is one reason why gas phase ion studies have infrequently included ligated metals. The addition of vibrational and rotational degrees of freedom to the electronic ones makes the production of a characterized metal complex even more difficult. These problems are pervasive and not unique to beam studies. One means of overcoming this problem is the use of flowing afterglow or drift tube techniques where a high pressure bath gas is always present to thermalize the ions. The combination of such experimental methods with beam or ICR techniques is a powerful means of studying metal–ligand complex ions which are being developed in several laboratories.

A final consideration in the accuracy of the BDEs derived using the beam method is the determination of the threshold energy, E_T. This has been one of the sticking points in ion beam technology since the theory behind chemical threshold phenomena is not well established. The general approach is to use a reasonably versatile form for the threshold dependence of the reaction cross-section, namely

$$\sigma(E) = \sigma_0(E - E_T)^n / E^m \quad (7)$$

where σ_0 is the scaling factor, E is the relative kinetic energy, and n and m are adjustable parameters.[2,23] As discussed above, E_T may need to be corrected for internal energy effects. In early applications[20,21,23–25] of this form to metal ion chemistry, the data were not sufficiently precise that E_T could be determined unambiguously while allowing σ_0, n and m to vary independently. Several reasonable assumptions were used to limit the number of freely varying parameters in eq. (7) to over-

come this limitation. Technology has now progressed[1] to the point that the data are sufficiently precise that these constraints are no longer needed. Tests of the early assumptions show that, while attractive, they are probably not correct in many circumstances.[2,3] Generally, early results tend to obtain high BDEs, although by no systematic amount since this depends heavily on the particular system. One example is $D^0(CoCH_3^+)$ derived from reactions of Co^+ with ethane. This system does not suffer from problems with electronic states, yet early results[24] report a BDE of 61 ± 4 kcal mol^{-1} while more recent results obtain 51 ± 4 kcal mol^{-1}.[26] The data are very similar in both studies but the interpretation differs leading to assignment of a different threshold.

METAL HYDRIDE IONS

We start by considering the simplest transition metal species, the diatomic metal hydride ions. The bond dissociation energies of the first row MH^+ species, Table 1, have been discussed several times in the past.[10,12,18,20,25,27] These works point out that

Table 1. Ionic transition metal bond dissociation energies[a]

M	$D^0(M^+—H)$	$D^0(M^+—CH_3)$	$D^0(M^+—CH_2)$	$D^0(M^+—CH)$
Sc	56.2(2.3)[b]	59(3)[b]	$\geqslant$ 93(3)[b]	
Ti	54.2(2.5)[c]	58(3)[d]	93(4)[d]	121(4)[d]
V	48.2(1.4)[e]	50(2)[f]	76(1.4)[f]	114(2)[f]
Cr	32.5(2.0)[g]	30(5)[h]	54(4)[h]	75(7)[h]
Mn	48.4(3.4)[i]	51(5)[j]	94(7)[k]	
Fe	49.8(1.4)[l]	58(2)[m]	82(5)[n]	101(5)[n]
Co	46.6(1.4)[o]	51(4)[h]	84(5)[k,n]	100(5)[n]
Ni	39.5(1.8)[o]	47(5)[h,k]	86(6)[k]	
Cu	22.1(3.0)[o]	30(3)[h]		
Zn	60(5)[p], 55(3)[h]	71(3)[q]		
Y	59(3)[r]			
Zr	55(3)[r]			
Nb	54(3)[r]		109(7)[s]	145(8)[s]
Mo	42(3)[r]			
Ru	41(3)[t]	54(5)[t]		
Rh	36(3)[u]	47(5)[t]	91(5)[s]	102(7)[s]
Pd	47(3)[u]	59(5)[t]		
Ag	16(3)[r]			

[a] Values are in kcal mol^{-1} at 300 K. Uncertainties are in parentheses.

[b] L. Sunderlin, N. Aristov and P. B. Armentrout, *J. Am. Chem. Soc.* 1987, **109**, 78.

[c] Ref. 19.

[d] L. Sunderlin and P. B. Armentrout, *J. Phys. Chem.* 1988, **92**, 1209.

[e] Ref. 13.

[f] Ref. 2 and N. Aristov and P. B. Armentrout, *J. Phys. Chem.* 1987, **91**, 6178.

[g] Ref. 17.

[h] Ref. 26.

[i] Ref. 14.

[j] P. B. Armentrout, in *Laser Applications in Chemistry and Biophysics* (Edited by M. A. El-Sayed), *Proc. SPIE*, 1968, **620**, 38.

[k] Ref. 20. The value for $D^0(Mn^+—CH_2)$ is almost certainly too high since these results have not been analysed with respect to the different states of Mn^+, a very significant effect (ref. 14).

[l] Ref. 15.

[m] Ref. 22.

[n] Ref. 28(a).

[o] Ref. 16.

[p] P. L. Po, T. P. Radus and R. F. Porter, *J. Phys. Chem.* 1980, **82**, 520.

[q] Ref. 3.

[r] Ref. 27.

[s] Ref. 28(b).

[t] Ref. 25.

[u] J. L. Elkind and P. B. Armentrout, unpublished work.

Cr^+ and Cu^+ have weak BDEs because these metal ions have very stable ground state configurations, namely a half-filled shell, $3d^5$ for Cr^+ and a filled shell, $3d^{10}$ for Cu^+. To form a covalent bond to either of these ions, one of the electrons must be removed from this very stable environment. This concept can be formalized in terms of a promotion energy, E_p, defined as the energy necessary to take a metal atom (ion or neutral) in its ground state to an electron configuration where there is one electron in the $4s$ orbital. It is also important to include the loss of exchange energy involved in spin decoupling this electron from the $3d$ electrons. E_p is easily calculated as the mean energy of the electronic states which have $4s3d^{n-1}$ configurations where the $4s$ electron is high-spin and low-spin coupled to the $3d$ electrons.[25,27] A plot of the first row MH^+ BDEs versus this promotion energy, Fig. 1, shows an excellent correlation. If E_p is alternately defined as the excitation to a $4s3d^{n-1}$ configuration, but the $3d\sigma$ orbital is the bonding orbital and is spin decoupled, then a correlation almost as good as Fig. 1 is obtained.[27] This implies that the dominant binding orbital on the metal is the $4s$ orbital but that there is significant $3d\sigma$ character as well. These ideas are quite consistent with results of *ab initio* calculations.[10,12]

For the second row MH^+ BDEs, the correlation with E_p is not bad if one excludes PdH^+ although it is not as good as for the first row, Fig. 1. The strong deviation of Pd^+ can be related to the fact that its ground state electron configuration is $4d$.[9] This suggested to us that Pd^+ may utilize a $4d\sigma$ orbital to bond with hydrogen, rather than the $5s$.[27]

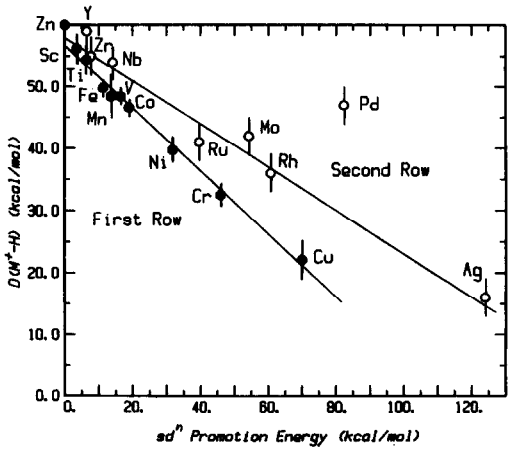

Fig. 1. First row (closed symbols) and second row (open symbols) transition metal ion hydride bond energies vs the atomic metal ion promotion energy to an sd^n spin-decoupled state (see text). The lines are linear regression fits to the first and second row data (excluding Pd).

Such a bond requires no promotion energy since the electron in the singly occupied $4d$ orbital is already decoupled from all the other electrons. *Ab initio* calculations verify this hypothesis and suggest that the amount of d character in the metal bonding orbital is much larger for the second row metals, especially Rh and Pd, than for the first row metals.[12]

When $E_p = 0$, the maximum MH^+ BDE can occur since the metal is in the most suitable state for bonding. For the first row, this occurs at ~ 57 kcal mol^{-1} and for the second row, at ~ 59 kcal mol^{-1}. We have argued previously[27] that this maximum BDE is a good estimate of intrinsic transition metal hydrogen bond energies, even if the metal is ligated. This argument contends that electronic promotion required for the atomic metal ions can be achieved by the ligands. The ligand environment can serve to place a single electron in an orbital which is directional and sterically unhindered, directly comparable to the $4s$ orbital for the first row atomic metal ions. Examples of condensed phase complexes which appear to conform to this prediction include the 18-electron species, $HCo(CO)_4$ and $[HCo(CN)_5^{3-}]_{aq}$, which both have Co—H BDEs of 58 kcal mol^{-1},[29] and $[H_2—IrCl(CO)(PPh_3)_2]$ which has a mean Ir—H BDE of 60 kcal mol^{-1}.[30]

METAL METHYL IONS

One of the early gas phase thermochemical results which contrasted with condensed phase dogma was the determination that $D^0(Co^+—CH_3)$ exceeded $D^0(Co^+—H)$ by almost 10 kcal mol^{-1}.[24] This result can be explained by noting that isolobal arguments suggest that a methyl group and a hydrogen atom should bond similarly.[31] It therefore seems reasonable that they both form strong covalent bonds with transition metals in the absence of other mediating effects (e.g. steric crowding). This has since been confirmed by detailed calculations.[32,33] For gas phase ions, the metal methyl BDEs may be stronger due to the increased polarizability of the methyl group compared to a hydrogen atom.[24] This effect could lead to a difference of 5–6 kcal mol^{-1}.[33] Nevertheless, this result was surprising to most condensed phase inorganic chemists since the limited data available for metal–carbon bond strengths indicated that they were almost half as strong as metal–hydrogen bond stengths.[34] As recently contended by Halpern,[34] the combination of the gas phase and condensed phase data suggests that steric effects are largely responsible for the weak condensed phase M—C bond strengths. Calculations show that the reduction of steric strain in cationic species can be attributed in part to electronic effects.[32]

Further investigation of the gas phase metal methyl BDEs finds a somewhat more complex picture. Table 1 lists the BDEs for first row MCH_3^+ species and Fig. 2 shows them vs E_p. For metals on the right-hand side of the periodic table (Fe, Co, Ni, Cu and Zn), the M^+—CH_3 BDEs are stronger than the M^+—H BDEs by 8 ± 2 kcal mol^{-1}. For Sc, Ti, V, Cr and Mn, however, the metal methyl bond energies are stronger by 2 ± 3 kcal mol^{-1}. Within these groups, the relative values of $D^0(M^+—CH_3)$ parallel those of $D^0(M^+—H)$ which indicates that the periodic trends and promotion energy ideas discussed above continue to be of value for the M^+—CH_3 species. The dichotomy between the metal methyl BDEs of the left side and right side metals remains to be explained.

One possible explanation is that the metals on the right side have higher *IP*s (average of 7.8 eV for Fe—Cu and 9.4 eV for Zn) compared with those on the left (average of 6.7 eV for Sc—Cr and 7.4 eV for Mn). Thus, the metal ions on the right have a higher affinity for electrons and may form a somewhat stronger bond due to the polarizability effects. Another interesting suggestion is that there are agostic[35] M···H—C interactions[36] in which a C—H bonding electron pair donates into an empty metal orbital, the $3d\pi$ in the M—C—H plane. This interaction is favoured by small M—C—H bond angles although this type of motion also reduces the overlap between the metal's 4*s* and the methyl's sp^3 radical orbital.[36,37] Since an agostic interaction should preferentially occur when there is an empty 3*d* orbital, Sc^+, Ti^+ and V^+ are the most likely candidates for this behaviour. From Mn^+ to Cu^+, a 3*d* orbital can only be empty if the metal is in a low-spin state, an energetically costly situation. Indeed, Calhorda and Simoes[36] find theoretical evidence for agostic interactions for Ti^+ and Fe^+ (in a singlet state), but not for Cr^+, Ni^+, or Fe^+ (in a triplet state). (They did not examine Fe^+ in a quintet state, the analogue of the ground state of FeH^+.) When compared with the experimental BDE data, these observations suggest that if agostic interactions are present, they *weaken* the metal–methyl bond energy. The dominant effect here may be the reduced overlap between the methyl radical orbital and the metal 4*s*.

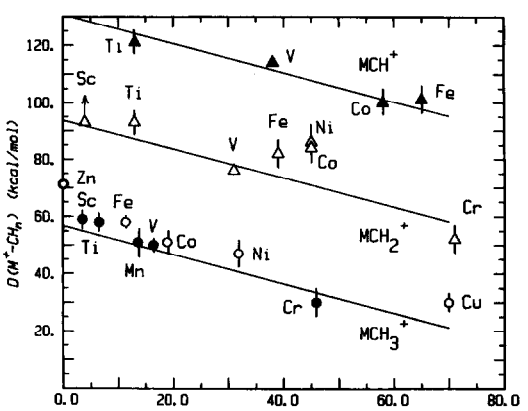

Fig. 2. Bond dissociation energies for first row transition metal ions to methyl (closed circles for left side metals, open circles for right side metals), methylidene (open triangles) and methylidyne (closed triangles) vs atomic metal ion promotion energy. The lower line is the linear regression fit representing the first row MH^+ bond energies vs the promotion energy shown in Fig. 1. The other two lines have the same slope but have been displaced upwards by 37 and by 74 kcal mol^{-1}.

METAL METHYLIDENE AND METHYLIDYNE IONS

In the first study of a series of MCH_n^+ BDEs (where $n = 1$–3), we discovered that the V^+—CH_3, V^+—CH_2 and V^+—CH bond strengths increase roughly with the organic analogues, CH_3—CH_3, CH_2=CH_2 and CH≡CH, respectively.[38] While intuitively reasonable, this simple correlation between the bond energy and the bond order for transition metal compounds had never before been documented. The data in Table 1 show that Sc^+, Ti^+ and Cr^+ also follow this type of correlation, and Hettich and Freiser have similarly documented it for Rh^+, Nb^+ and La^+ species.[39] *Ab initio* calculations by Harrison have also seen this trend for Cr^+.[11(b)]

While these simple correlations are qualitatively useful, their utility should not be overinterpreted. This is illustrated by the recent calculations of Carter and Goddard[40] who find that the ground state of $RuCH_2^+$ is a metal methylidene having a covalent M=C double bond. However, there are low-lying excited states which are metal–carbenes [i.e. they have a donor–acceptor bond between Ru^+ and $CH_2(^1A_1)$], and these states have BDEs which are comparable to the ground state BDE. The relationship between the bond energy and the bond order is muddied in such species. There is no reason to believe that $RuCH_2^+$ is unique in this regard.

It is also of interest to know whether the promotion energy ideas discussed for the singly bonded transition metal species extend to multiply bonded species. While the calculation of E_p is more complicated than for singly bound species, this procedure has been outlined elsewhere.[41] This comparison is shown in Fig. 2. The data are sufficiently incomplete that no definitive correlations are evident. The lines shown in Fig. 2 are the slope of the line in Fig. 1 displaced by 37 kcal mol^{-1} for

each additional formal bond order. The fact that these lines come close to the data for both metal methylidene BDEs and metal methylidyne BDEs is intriguing. It may suggest that the intrinsic M—C π bond is worth about 37 kcal mol^{-1}, 65% of the M—C σ bond. In this regard, it is interesting to note that Harrison and co-workers[42] have made a comparable analysis of their calculated bond energies for $TiCH^+$, VCH^+ and $CrCH^+$. Based on this, they suggest that there is an intrinsic $M^+{\equiv}CH$ bond of about 129 kcal mol^{-1}, in remarkably good agreement with the intercept of the MCH^+ line in Fig. 2.

NEUTRAL METAL HYDRIDES AND METHYLS

In seeking to apply gas phase ion thermochemistry to condensed phase chemistry, it is important to understand the influence of the charge. One means of addressing this is to compare ionic and neutral BDEs for simple species. As discussed in the Experimental, it is possible to obtain the bond energies of simple neutral transition metal species using the beam method, reaction (2). We have done this for several metal hydride diatoms and metal methyl species, Table 2. Data for the metal hydrides are also available from a variety of other sources. Comparison of the various D^0(MH) values is generally fairly good but the discrepancies that do exist demonstrate that no one method can be considered definitive at present.

Comparison of the D^0(MH) and $D^0(MCH_3)$ finds very similar values in cases where D^0(MH) appears secure, namely V, Cr, Co, Ni and Zn. For these five cases, D^0(MH) exceeds $D^0(MCH_3)$ by an average of $\sim 2 \pm 2$ kcal mol^{-1}. This is in keeping with the isolobal argument discussed above and also the idea that polarization effects cause $D^0(M^+{-}CH_3)$ to exceed $D^0(M^+{-}H)$. It is also pertinent that there is no systematic difference between the left and right side metals.

Table 2. Neutral transition metal methyl and hydrogen BDEs[a]

		D^0(M—H)				
M	$D^0(M{-}CH_3)$	Beam	TB[b]	SLSF[c]	KM[d]	Spec[e]
Sc[f]	32(7)				48(2)	
Ti	46(7)					
V	37(9)	41(4)		38(3)		
Cr	41(7)			41(3)	< 45	
Mn	< 30[g]				< 32	[58]
Fe	37(7)	46(3)[h]	43(6)	30(3)	< 43	
Co	45(5)	47(3)	54(10)	42(3)	45(3)	[74]
Ni	54(4)	59(4)	65(6)		59(2)	⩽ 71
Cu	55(4)	60(5)			60(1)	63(1)
Zn	19(3)[i]					20(1)
Mo		53(5)	46(3)			
Ru			56(5)			
Rh			59(5)			
Pd			56(6)			

[a] Values are in kcal mol^{-1} at 300 K. Unless otherwise noted, values are from R. Georgiadis, N. Aristov, R. H. Schultz and P. B. Armentrout, work in progress. Uncertainties are in parentheses.

[b] Ref. 43.

[c] Ref. 44.

[d] Ref. 45.

[e] K. P. Huber and G. Herzber, *Molecular Spectra and Molecular Structure IV, Constants of Diatomic Molecules*. Van Nostrand-Reinhold, New York (1979). Brackets indicate uncertain data.

[f] The large difference between D^0(Sc—H) and $D^0(Sc{-}CH_3)$ suggests that one or both of these values is unreliable.

[g] P. B. Armentrout, in *Laser Applications in Chemistry and Biophysics* (Edited by M. A. El-Sayed), *Proc. SPIE*, 1986, **620**, 38.

[h] Ref. 22.

[i] Ref. 3.

Figure 3 compares the neutral metal methyl BDEs with the ionic ones. A naive view holds that neutrals and ions having the same number of valence electrons might exhibit similar bond energies. This is clearly not the case in any quantitative fashion although it can be seen that both the neutral and ionic series each exhibit two minima in the periodic variation (at Mn and Zn, and at Cr^+ and Cu^+). What is surprising is that these minima are shifted in the *opposite* direction expected for isoelectronic species, i.e. Cr^+ and Cu^+ have two fewer electrons than Mn and Zn, respectively. These results can again be qualitatively understood using the promotion energy ideas. The key difference between the neutral metal atoms and the atomic metal ions is that the ground state configuration of the neutrals is generally $4s^23d^{n-2}$ while it is $3d^n$ for the ions, e.g. Ti is $4s^23d^2$ while V^+ is $3d^4$. Thus, formation of a covalent M(4*s*)—H(1*s*) bond involves promotion of a 4*s* electron out of a *stable* filled sub-shell. This means that the promotion energies for the neutral atoms will ordinarily be higher than for the ions, e.g. $E_p(\mathrm{Ti}) = 26$ kcal mol^{-1} while $E_p(V^+) = 16$ kcal mol^{-1}. As can be seen in Fig. 3, this means that the neutral BDEs are typically less than the ionic BDEs. The clear exceptions of Cr and Cu have $4s3d^5$ and $4s3d^{10}$ ground state configurations where the 4*s* electron is already in an orbital suitable for bonding, i.e. E_p is relatively low (11 and 0 kcal mol^{-1}, respectively).

A plot of the neutral metal hydride bond energies vs promotion energy, defined as above, is shown in Fig. 4. The correlation is not as good as for the ionic metal hydrides, although the same general trend appears to exist. This and a related correlation to the electron affinity of the atomic metals has been discussed previously.[43,44] One reason for the reduced correlation may be a stronger contribution of 4*p* orbital character in the bonding of MH compared with MH^+.[46] At present, another likely factor is that the accuracy of the neutral thermochemistry is substantially less than for the ion thermochemistry. It will be interesting to keep track of this correlation as the thermochemical values improve.

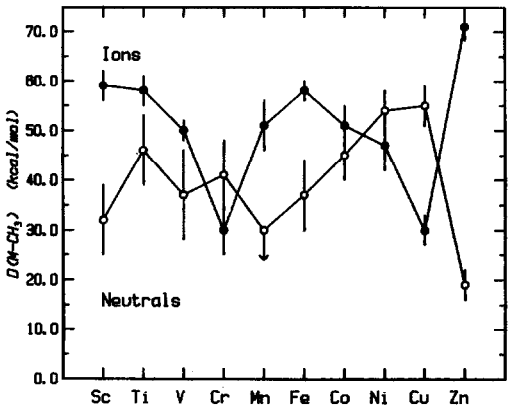

Fig. 3. Periodic variation in the bond energies for ionic (closed symbols) and neutral (open symbols) first row metal methyl species. The arrow indicates a value which is an upper limit.

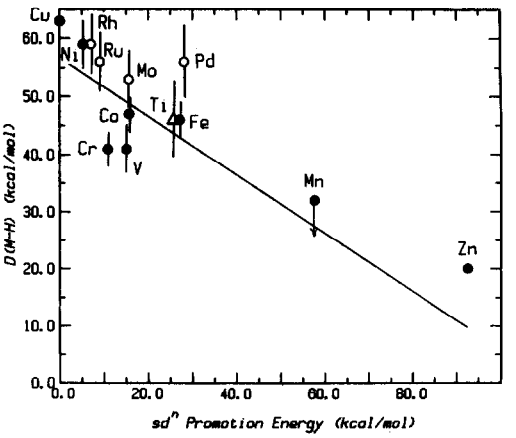

Fig. 4. First row (closed circles) and second row (open circles) neutral transition metal hydride bond energies vs the atomic metal ion promotion energy to an sd^n spin-decoupled state (see text). The triangle indicates a value for $D^0(\mathrm{Ti—CH_3})$. The line is the linear regression fit representing the first row MH^+ bond energies vs the promotion energy shown in Fig. 1. The arrow indicates a value which is an upper limit.

SECOND METAL–LIGAND BOND ENERGIES

To understand oxidative addition and reductive elimination processes, it is important to know both the first and second metal ligand BDE. For radical species like hydrogen atoms and alkyls, the experimental determination of this second bond energy is unfortunately more difficult than determining the first BDE. Nevertheless, this type of information is available for several systems, Table 3. It can be seen that the first and second BDEs are quite similar for Sc^+, V^+ and Co^+, but very different for Zn^+. They may also be similar for Fe^+ and Ni^+, although only limits to the second BDEs are presently available.

Promotion energy ideas can again qualitatively account for these results. E_p for Sc^+ is small (3.5 kcal mol^{-1})[27] and for ScR^+ is ≈ 0 since this species has only one non-bonding electron. For V^+ and Co^+, E_p is 16 and 19 kcal mol^{-1}, respectively, and for VR^+ and CoR^+, it is ~ 18 and ~ 26 kcal

Table 3. First and second bond dissociation energies for ML_2^+ species[a]

M^+—R	$D^0(M^+—R)^b$	$D^0(RM^+—R)$
Sc^+—H	56(2)	59(4)[c]
Sc^+—CH_3	59(3)	60(5)[d]
V^+—CH_3	50(2)	48(5)[e]
Fe^+—CH_3	58(2)	> 38(2)[f]
Co^+—CH_3	51(4)	59(5)[g]
Ni^+—CH_3	47(5)	> 49(5)[h]
Zn^+—CH_3	71(3)	27(3)[i]

[a] Values are in kcal mol^{-1} at 300 K. Uncertainties are in parentheses.

[b] Values are from Table 1.

[c] L. Sunderlin, L. Aristov and P. B. Armentrout, *J. Am. Chem. Soc.* 1987, **109**, 78.

[d] L. Sunderlin and P. B. Armentrout, work in progress.

[e] N. Aristov and P. B. Armentrout, work in progress.

[f] Derived from results of R. C. Burnier, G. D. Byrd and B. S. Frieser, *J. Am. Chem. Soc.* 1981, **103**, 4360.

[g] Derived from results of M. A. Hanratty, J. L. Beauchamp, A. J. Illies, P. van Koppen and M. T. Bowers, *J. Am. Chem. Soc.* 1988, **110**, 1.

[h] Derived from results of L. F. Halle, W. E. Crowe, P. B. Armentrout and J. L. Beauchamp, *Organometallics* 1984, **3**, 1694.

[i] Ref. 3.

mol^{-1},[41] respectively. Thus, the first and second bond energies should be comparable in these cases. For Zn^+, the situation changes drastically. The first bond to Zn^+ is strong since there is an unpaired electron in a 4*s* orbital ($4s3d^{10}$ configuration) and thus $E_p = 0$. Formation of a second covalent bond to Zn^+ requires disruption of the filled $3d^{10}$ shell. This leads to a very weak second bond.

SUMMARY

The measurement of gas phase BDEs of transition metal species is just emerging from its infancy. The technological and theoretical tools necessary to obtain both accurate and precise values using beam techniques have only recently been developed, as have competing methods (such as photodissociation[28] and proton affinity measurements[43,44]). In combination with values from more established techniques (such as high temperature mass spectrometry[45] and spectroscopy), this gas phase thermochemistry provides a wealth of data which can be analysed for its periodic trends. As outlined above, these analyses can provide intrinsic bond energies for ionic and neutral metal hydrides (57–60 kcal mol^{-1}), ionic and neutral metal methyls [2–8 kcal mol^{-1} higher than $D^0(MH^+)$ for cationic species, and ~ 2 kcal mol^{-1} less than $D_0(MH)$ for neutral species], ionic metal methylidenes (~ 94 kcal mol^{-1}) and ionic metal methylidynes (~ 130 kcal mol^{-1}). Further, the periodic trends can help to identify influential factors in determining the strength or weakness of a bond. These include electronic (essentially hybridization) and polarization effects. Continued studies on even more complex transition metal species should enable even closer relationships between gas and condensed phase thermochemistry to be forged.

Acknowledgements—The authors would like to thank N. Aristov, J. L. Elkind, R. H. Schultz and L. Sunderlin for their contributions to these studies. This work is funded by the National Science Foundation Grant No. 8608847 and 8796289. We would also like to thank Monsanto Corporation for their generous support.

REFERENCES

1. K. M. Ervin and P. B. Armentrout, *J. Chem. Phys.* 1985, **83**, 166.
2. N. Aristov and P. B. Armentrout, *J. Am. Chem. Soc.* 1986, **108**, 1806.
3. R. Georgiadis and P. B. Armentrout, *J. Am. Chem. Soc.* 1986, **108**, 2119.
4. K. M. Ervin and P. B. Armentrout, *J. Chem. Phys.* 1986, **84**, 6738.
5. V. L. Talrose, P. S. Vinogradov and I. K. Larin, in *Gas Phase Ion Chemistry* (Edited by M. T. Bowers), Vol. 1, pp. 305–347. Academic Press, New York (1979).
6. K. M. Ervin and P. B. Armentrout, *J. Chem. Phys.* 1987, **86**, 2659.
7. M. E. Weber, J. L. Elkind and P. B. Armentrout, *J. Chem. Phys.* 1986, **84**, 1521.
8. J. L. Elkind and P. B. Armentrout, *J. Phys. Chem.* 1984, **88**, 5454.
9. B. H. Boo and P. B. Armentrout, *J. Am. Chem. Soc.* 1987, **109**, 3549.
10. J. B. Schilling, W. A. Goddard and J. L. Beauchamp, *J. Am. Chem. Soc.* 1986, **108**, 582.
11. (a) M. A. Vincent, Y. Yoshioka and H. F. Schaefer, *J. Phys. Chem.* 1982, **86**, 3905; (b) A. E. Alvarado-Swaisgood, J. Allison and J. F. Harrison, *J. Phys. Chem.* 1985, **89**, 2517; (c) A. E. Alvarado-Swaisgood and J. F. Harrison, *J. Phys. Chem.* 1985, **89**, 5198; (d) A. K. Rappe and T. H. Upton, *J. Chem. Phys.* 1986, **85**, 4400; (e) M. Dupuis, B. L. Hammond and W. A. Lester, private communication.
12. L. G. M. Pettersson, C. W. Bauschlicher, S. R. Langhoff and H. Partridge, *J. Chem. Phys.* 1987, **87**, 481.
13. J. L. Elkind and P. B. Armentrout, *J. Phys. Chem.* 1985, **89**, 5626.
14. J. L. Elkind and P. B. Armentrout, *J. Chem. Phys.* 1986, **84**, 4862.

15. J. L. Elkind and P. B. Armentrout, *J. Am. Chem. Soc.* 1986, **108**, 2765; J. L. Elkind and P. B. Armentrout, *J. Phys. Chem.* 1986, **90**, 5736.
16. J. L. Elkind and P. B. Armentrout, *J. Phys. Chem.* 1986, **90**, 6576.
17. J. L. Elkind and P. B. Armentrout, *J. Chem. Phys.* 1987, **86**, 1868.
18. J. L. Elkind and P. B. Armentrout, *J. Phys. Chem.* 1987, **91**, 2037.
19. J. L. Elkind and P. B. Armentrout, *Int. J. Mass Spect. Ion Proc.*, in press.
20. P. B. Armentrout, L. F. Halle and J. L. Beauchamp, *J. Am. Chem. Soc.* 1981, **102**, 6501.
21. L. F. Halle, P. B. Armentrout and J. L. Beauchamp, *Organometallics* 1982, **1**, 963.
22. R. H. Schultz, J. L. Elkind and P. B. Armentrout, *J. Am. Chem. Soc.* 1988, **110**, 411.
23. P. B. Armentrout and J. L. Beauchamp, *J. Chem. Phys.* 1981, **74**, 2819.
24. P. B. Armentrout and J. L. Beauchamp, *J. Am. Chem. Soc.* 1981, **103**, 784.
25. M. L. Mandich, L. F. Halle and J. L. Beauchamp, *J. Am. Chem. Soc.* 1984, **106**, 4403.
26. R. Georgiadis and P. B. Armentrout, work in progress.
27. J. L. Elkind and P. B. Armentrout, *Inorg. Chem.* 1986, **25**, 1078.
28. (a) R. L. Hettich and B. S. Freiser, *J. Am. Chem. Soc.* 1986, **108**, 2537; (b) R. L. Hettich and B. S. Freiser, *J. Am. Chem. Soc.* 1986, **108**, 5086.
29. (a) F. Ungvary, *J. Organomet. Chem.* 1972, **36**, 363; (b) B. de Vries, *J. Catal.* 1962, **1**, 489.
30. L. Vaska, *Acct. Chem. Res.* 1968, **1**, 335.
31. J.-Y. Saillard and R. Hoffmann, *J. Am. Chem. Soc.* 1984, **106**, 2006.
32. T. Ziegler, V. Tschinke and A. Becke, *J. Am. Chem. Soc.* 1987, **109**, 1351.
33. J. B. Schilling, W. A. Goddard and J. L. Beauchamp, *J. Am. Chem. Soc.* 1987, **109**, 5573.
34. J. Halpern, *Acct. Chem. Res.* 1982, **15**, 238; J. Halpern, *Inorg. Chim. Acta* 1985, **100**, 41.
35. M. Brookhart and M. L. H. Green, *J. Organomet. Chem.* 1983, **250**, 395.
36. M. J. Calhorda and J. A. Simoes, *Organometallics* 1987, **6**, 1188.
37. O. Eisenstein and Y. Jean, *J. Am. Chem. Soc.* 1985, **107**, 1177.
38. N. Aristov and P. B. Armentrout, *J. Am. Chem. Soc.* 1984, **106**, 4065.
39. R. L. Hettich and B. S. Freiser, *J. Am. Chem. Soc.* 1986, **108**, 3543.
40. E. A. Carter and W. A. Goddard, *J. Am. Chem. Soc.* 1986, **108**, 2180.
41. M. Tolbert and J. L. Beauchamp, *J. Am. Chem. Soc.* 1986, **108**, 7509.
42. A. Mavridis, A. E. Alvarado-Swaisgood and J. F. Harrison, *J. Phys. Chem.* 1986, **90**, 2584. These authors cite an average intrinsic MCH^+ BDE of 146 kcal mol^{-1} which we have corrected for the 17 kcal mol^{-1} splitting between $CH(^2\Pi)$ and $CH(^4\Sigma)$.
43. M. A. Tolbert and J. L. Beauchamp, *J. Phys. Chem.* 1986, **90**, 5015.
44. L. Sallans, K. R. Lane, R. R. Squires and B. S. Freiser, *J. Am. Chem. Soc.* 1985, **107**, 4379; R. R. Squires, *J. Am. Chem. Soc.* 1985, **107**, 4385.
45. A. Kant and K. A. Moon, *High. Temp. Sci.* 1981, **14**, 23; 1979, **11**, 55.
46. J. Demuynck and H. F. Schaefer, *J. Chem. Phys.* 1980, **72**, 311.

Polyhedron Vol. 7, No. 16/17, pp. 1583–1603, 1988
Printed in Great Britain

0277–5387/88 $3.00+.00
© 1988 Pergamon Press plc

REACTIVITY, PHOTOCHEMISTRY AND THERMOCHEMISTRY OF SIMPLE METAL–LIGAND IONS IN THE GAS PHASE

STEVEN W. BUCKNER and BEN S. FREISER†

Herbert C. Brown Laboratory of Chemistry, Purdue University, West Lafayette, IN 47907, U.S.A.

Abstract—In this review we discuss recent results from our laboratory on the chemistry, photochemistry and thermodynamics of simple metal–ligand ionic species in the gas phase. Using laser desorption coupled to Fourier transform mass spectrometry, we have successfully generated numerous highly unsaturated metal–ligand ions including bare metal carbenes, methyls, hydrides, nitrenes and amides. The combination of photodissociation, ion–molecule reactions and other techniques has made possible the determination of a wide variety of metal–ligand ion bond dissociation energies. Reactivity studies on these species reveal gas phase catalytic cycles including olefin homologation and Fe^+ catalysed production of N—C bonds from NH_3, olefins and N_2O. General trends are observed in the reactions of MOH^+, MH^+, MCH_3^+, and MNH_2^+ with alkanes; MO^+ and MS^+ with alkanes; and MNH^+, MCH_2^+ and MO^+ with alkenes.

Research in gas-phase transition metal ion chemistry has undergone extremely rapid growth within the last ten years. Since the first observation of metal ion activation of saturated organic compounds by Allison, Freas and Ridge,[1] transition metal ions and small organometallic ions have been observed to be highly reactive and interesting species.[2,3] Catalysing the growth in the understanding of these chemical systems has been the evolution in the types of instrumental techniques which are being brought to bear on this problem, including ion-beam techniques,[4] Fourier transform mass spectrometry (FTMS)[5,6] and flowing afterglow.[7] In addition, new advances in sources, including laser desorption[8] and surface ionization,[9] and in structural techniques, including collision-induced dissociation (CID)[10] and photodissociation,[11] have begun to allow a more detailed study and understanding of the energetics and mechanisms of gas-phase transition metal ion systems.

In this review we discuss recent results from our laboratory on the chemistry, photochemistry and thermodynamics of a variety of gas-phase transition metal–ligand ions. The Experimental section will include a discussion of laser desorption for the production of bare metal ions, Fourier Transform mass spectrometry for trapping and detection, and the methodology involved in collision-induced dissociation and photodissociation. The Discussion section will cover the methods used for preparing various highly unsaturated gas-phase metal–ligand ions, for determining ion structure and metal ion–ligand bond strengths by photodissociation, collision-induced dissociation and ion-molecule reaction studies, and for monitoring the gas-phase reactivity of metal ion–ligand species. Emerging trends in the last two areas will also be discussed.

EXPERIMENTAL

The majority of the results described in this paper were obtained on a prototype Nicolet FTMS-1000 Fourier transform mass spectrometer equipped with a 5.2 cm cubic trapping cell situated between the poles of a Varian 15-in electromagnet maintained at 0.9 T. A diagram of this cell along with the laser desorption source is shown in Fig. 1. The transmitter plates have been replaced by 80% transmittance screens to allow light from an arc lamp into the cell for photodissociation experiments. The screens only decrease the detected ion current by a small amount. Photodissociation experiments on $Ni(Cp)(NO)^+$ (Cp = cyclopentadienyl) were carried out on a conventional ion cyclotron resonance (ICR) spectrometer operated in the trapping mode. Some of the reactivity studies on the transition metal–amide complexes were performed on a newly

† Author to whom correspondence should be addressed.

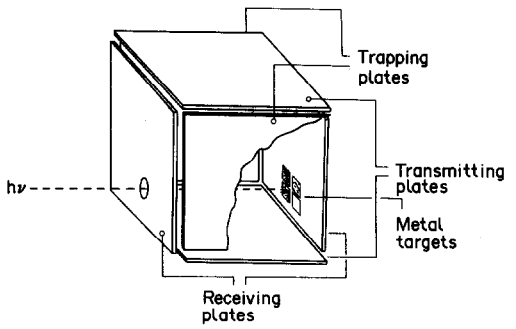

Fig. 1. Diagram of the FTMS trapping cell showing laser irradiation of metal targets for production of metal ions. Receiving plates have recently been replaced by 80% transmittance screens to permit irradiation of the cell with light from an arc lamp for photodissociation experiments.

acquired Nicolet FTMS-2000 Fourier transform mass spectrometer equipped with a differentially pumped dual cell configuration and a 3.0 T superconducting magnet.

The theory and instrumentation of ICR spectrometry and FTMS have been the subject of a number of recent reviews.[12] Briefly, an ion in a magnetic field is constrained to a circular orbit at a characteristic frequency proportional to the magnetic field and inversely proportional to the mass-to-charge ratio (m/z) of the ion. If the ion is placed between two plates and a radio frequency (rf) field having the same frequency as the cyclotron frequency of the ion is applied to the plates, the ion will absorb energy and its velocity and radius of orbit will increase. This process is used in four main ways in our laboratory, (1) ion detection, (2) ion ejection, (3) collision-induced dissociation and (4) to study endothermic reactions.

In FTMS, detection is achieved by first exciting all of the ions to a larger orbit by applying what is termed an rf "chirp", a 0–2.5 MHz sweep in ~ 0.5 ms.[5] This process also results in the ions moving in a coherent fashion, whereby each ion of the same m/z is in the same position in its orbit. The coherent motion of the ions induces an oscillating signal (image current) on the two receiving plates, see Fig. 2. This signal is amplified, digitized and sent to the computer, where it is Fourier transformed producing the frequency domain or mass spectrum.

Fig. 2. Schematic depiction of the basic principles of FTMS. Coherent motion of ions in the cell produces an image current signal which is digitized and Fourier transformed. The result is a frequency or mass spectrum.

Ion ejection is a process where a high energy rf pulse excites selected ions to orbits larger than the size of the cell causing them to be annihilated (neutralized) on the cell plates.[13] Using this technique, an ion of specific m/z can be isolated from a whole population of ions by ejecting all of the other ions from the cell. This allows the selected ion to be further investigated without complications from the other ions.

Collision-induced dissociation (CID) also involves excitation of a selected ion at its cyclotron frequency by an rf pulse.[10(b)] The kinetically excited ion is then permitted to collide with a target gas, which is usually argon maintained at a static background pressure of $\sim 1 \times 10^{-5}$ torr, after which it then undergoes fragmentation. The resulting fragment ions will often be diagnostic of the parent ion structure. However, rearrangements can occur prior to fragmentation and, thus, structures cannot always be unambiguously assigned from CID alone.

A technique similar in operation to CID can be used to synthesize ions by endothermic reactions.[14] A metal ion can be accelerated by an rf pulse at its cyclotron frequency in the presence of a reagent gas, as exemplified by reaction (1).

$$(Sc^+)\dagger + C_2H_6 \rightarrow ScH^+ + C_2H_5. \qquad (1)$$

This allows formation of many metal–ligand ion species which cannot be prepared directly from thermalized ions by exothermic reactions (e.g. ScH^+). Another advantage of this technique is that the threshold energy observed for process (1) yields a value for the bond energy of the product (e.g. $D^0(Sc^+—H)$).

We have found pulsed laser desorption/ionization to be a particularly convenient method for generating virtually any metal ion from its pure metal rod or foil for study by FTMS. The fundamental (1064 nm) or frequency doubled (532 nm) output of a pulsed Quanta Ray Nd:YAG laser is used for production of metal ions. However, the process is essentially independent of the wavelength and simply requires sufficient laser power, ~ 10^8 W cm^{-2}. Metal ions produced at high laser powers can have excess kinetic and electronic energy.[15] The photodissociation studies described here, therefore, were carried out using a high background pressure of buffer gas ($\sim 1 \times 10^{-5}$ torr Ar) to permit the ions to undergo thermalizing collisions. Similar precautions were taken for the reaction studies and, in many cases, also involved reisolation of metal–ligand precursors after trapping ~ 250–500 ms

in $\sim 1 \times 10^{-6}$ torr reagent gas. Non-composite pseudo first order decay kinetic plots indicated that these methods produce predominantly thermalized ions, although a small population of non-thermal ions cannot be completely ruled out. Another possible source of non-thermal ions is from exothermic reactions.[16] For example, when thermalized Fe^+ reacts with cyclopentene to form Fe(cyclopentadiene)$^+$, reaction (2), much of the reaction exothermicity ($\sim$ 25–30 kcal mol^{-1}) remains with the ionic product.

$$Fe^+ + c\text{-}C_5H_8 \rightarrow (Fe(c\text{-}C_5H_6)^+)^* + H_2. \quad (2)$$

The evidence for this is that the $Fe(c\text{-}C_5H_6)^+$ product ion exhibits non-linear kinetics in its subsequent reactions. Trapping the $(Fe(c\text{-}C_5H_6)^+)^*$ in excess argon prior to reaction, however, cools the ion and yields linear kinetic plots.

Reagents used for formation of metal–ligand ions are admitted into the trapping cell through a General Valve Corp. series 9 pulsed solenoid valve. This allows the reagent to be pumped away prior to isolation of the appropriate metal–ligand ion, eliminating any complicating secondary reactions with that reagent during subsequent reaction sequences. A second pulsed valve has just been installed on our FTMS-1000 to permit even more control over the preparation of various reactant ions as exemplified below. Pulsed valve introduction of the reagents in FTMS has been previously discussed in detail.[17]

Photodissociation experiments are performed by irradiating the trapped (typically 2–10 s) ions with light from a 2.5 kW Hg–Xe arc lamp, used in conjunction with a Schoeffel 0.25 m monochromator set for 10 nm resolution. Photodissociation spectra are obtained by monitoring the appearance of ionic photoproducts as a function of the wavelength of light. Photodissociation onsets (the longest wavelength at which photoproducts are observed) are confirmed using white light and cut-off filters.

DISCUSSION

Ion synthesis

In our laboratory, gas-phase metal–ligand ions are prepared by one of three techniques, (1) from exothermic reactions,[18] (2) by CID of larger organometallic ions,[19] or (3) from endothermic reactions driven by kinetic excitation.[14(b)] Though (1) is the simplest and most commonly used method for the synthesis of ions, (2) and (3) allow generation of ions inaccessible by (1). For example, no reagent gas has yet been found to generate MH^+ (M = Fe, Co, Ni) in appreciable quantities directly by exothermic reaction with M^+.

$$M^+ + CH_3ONO \xrightarrow{-NO} MOCH_3^+$$

$$\xrightarrow[Ar]{CID} MH^+ + CH_2O \quad (3)$$

(M = Fe, Co, Ni).

Collisional activation of $MOCH_3^+$, generated from methyl nitrite, however, produces MH^+ in large abundance, [reaction (3)].[19(a)] As an example of method (3), $CrCH_2^+$ can be generated by accelerating Cr^+ into cyclopropane, reaction (4).[16]

$$(Cr^+)^\dagger + c\text{-}C_3H_6 \rightarrow CrCH_2^+ + C_2H_4. \quad (4)$$

$CrCH_2^+$ has not yet been observed as a reaction product from any exothermic reaction of Cr^+.

One difficulty often encountered in ion synthesis is secondary reactions with the parent neutral. For example, $FeOH^+$, formed in reaction (5), reacts further with CH_3NO_2 as in reactions (6)–(9). These secondary reactions can obscure any reactivity studies which would subsequently be done on $FeOH^+$ and renders photodissociation experiments impossible. This problem can be circumvented, however, by adding the initial reagent through a pulsed valve so, during the formation and isolation of the ion of interest (e.g. $FeOH^+$), the reactant gas (e.g. CH_3NO_2) is pumped away. The selected ion can then be permitted to react with a second reagent in the absence of the first.

$$Fe^+ + CH_3NO_2 \rightarrow FeOH^+ + CH_2NO \quad (5)$$

$$FeOH^+ + CH_3NO_2 \begin{cases} \rightarrow Fe(OH)_2^+ + CH_2NO & (6) \\ \rightarrow Fe(OH)(H_2O)^+ + CHNO & (7) \\ \rightarrow FeCH_2NO_2^+ + H_2O & (8) \\ \rightarrow Fe(OH)(CH_3NO_2)^+. & (9) \end{cases}$$

A typical reaction sequence is shown in Fig. 3. Initially, the laser and the first pulsed valve are fired. Thus, M^+ (in this case Fe^+) is formed in the presence of a high pressure of the first reagent gas (in this case N_2O). After an appropriate reaction period ($\sim$ 400 ms), this reagent is pumped away and ML^+ (FeO^+ in this case) can be isolated by swept double resonance ejection pulses. At this point, ML^+ can undergo reaction with a second reagent gas which is either present at a lower static background pressure ($\sim 1 \times 10^{-6}$ torr), or is pulsed in by the second pulsed valve. One possibility is that the second reagent gas is required to prepare the desired reactant ion. For example, Fig. 3(d) shows formation of $FeNH^+$ from the reaction of FeO^+ with NH_3, which has been introduced via a second pulsed valve. After isolation, the ion of interest is reacted

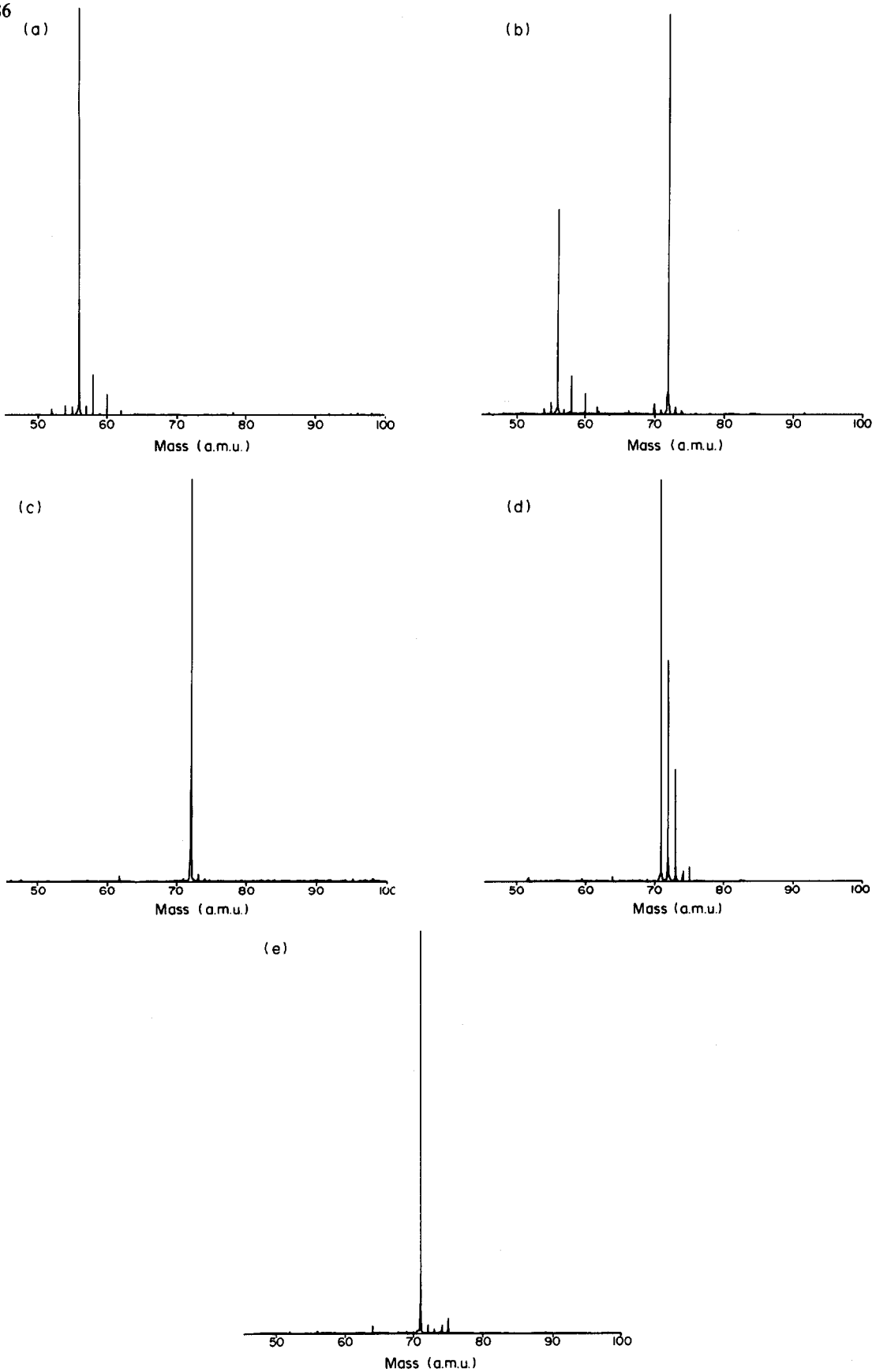

Fig. 3. Reaction sequence for gas-phase synthesis of $FeNH^+$. (a) Laser desorption of iron foil to produce Fe^+ (peaks at $m/z = 52$, 58 and 60 are due to impurities of Cr and Ni). (b) Reaction of Fe^+ with N_2O to produce FeO^+. (c) Isolation of FeO^+. (d) Reaction of FeO^+ with NH_3. (e) Isolation of $FeNH^+$.

with a background reagent gas. The final product ions may then be structurally interrogated by a variety of methods as discussed below.

Structural determination

In general a mass spectrum only reveals the mass-to-charge ratio of ions. In order to verify a proposed reaction mechanism, however, it is clearly necessary to determine both reactant and product ion structures. No one technique can definitively determine all ion structures, so a number of useful methods have been developed.

Collision-induced dissociation and photodissociation. Daughter ions produced upon fragmentation of ions will often be diagnostic for parent ion structure. Energy sufficient for dissociation can be put into an ion via energetic collisions (CID) or photons (photodissociation). These two techniques are very complementary, since they often produce significantly different dissociation products due to the nature of the excitation processes.[20] The low energy CID process is a multi-collision process and, as such, involves sequential addition of rotational and vibrational energy to the ion. This is in contrast to photodissociation where initially the ion undergoes an instantaneous electronic excitation. For example, MCH_2^+ (M = Fe, Co) undergoes CID via direct cleavage of CH_2 to produce M^+, reaction (10), whereas photodissociation of MCH_2^+ produces MCH^+, MC^+ and M^+, reactions (11)–(13).[21]

$$MCH_2^+ \xrightarrow{Ar} M^+ + CH_2$$

0–100 eV laboratory collision energy (10)

$$MCH_2^+ + h\nu \longrightarrow MCH^+ + H^\cdot \quad (11)$$

$$(M = Fe, Co) \longrightarrow MC^+ + H_2 \quad (12)$$

$$\longrightarrow M^+ + CH_2. \quad (13)$$

As a further illustration of these methods, photodissociation and collision-induced dissociation have been used to differentiate four $NiC_4H_8^+$ isomers generated by reactions (14)–(17).[20,22]

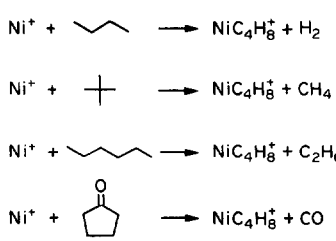

(14)

(15)

(16)

(17)

A comparison of the neutral losses upon collision-induced and photo-induced dissociation of these isomers is given in Table 1. The photodissociation spectra of these ions are shown in Fig. 4(a)–(d). Photodissociation has an additional advantage in structure differentiation in that differences in the photodissociation spectra, as well as different photoproducts, will often be observed. In addition, photodissociation spectra are characteristic of the ion structure *prior* to excitation and, therefore, are less susceptible than CID to misinterpretations due to rearrangements.

Table 1. Neutral losses from collision-induced dissociation and photodissociation of four $NiC_4H_8^+$ isomers

Structure	Neutral losses CID	PDS
	C_2H_4 C_4H_8	C_2H_4 C_4H_8
	C_4H_8	C_4H_8 CH_4
	H_2 C_4H_8	H_2 C_4H_8 C_2H_4 CH_3
	H_2 C_2H_4 C_4H_8	H_2 C_2H_4 C_4H_8

The proposed structures (I–IV) are shown for the

(I) reaction 14 (II) reaction 15 (III) reaction 16 (IV) reaction 17

products of reactions (14)–(17). As can be seen in Table 1, CID and photodissociation both can easily differentiate the four isomers. Also evident, as in the $FeCH_2^+$ example discussed above, these two techniques can produce different fragments from the same ion. For example, Ni(isobutene)$^+$ undergoes photodissociation to lose CH_4 as well as the entire ligand, whereas CID produces only direct cleavage of the isobutene. This is also interesting in light of an endothermic reaction study of Co^+ with isobutene which showed formation of $CoC_3H_4^+$ with loss of CH_4.[23]

Two isomers of $FeC_4H_6^+$ have also been investigated by photodissociation. Fe(butadiene)$^+$ can be generated by reaction (18), and undergoes CID via direct cleavage of butadiene.

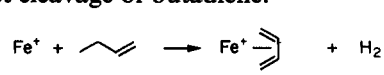

(18)

The photodissociation spectrum for this ion, which produces Fe^+ exclusively, is shown in Fig. 5(a).

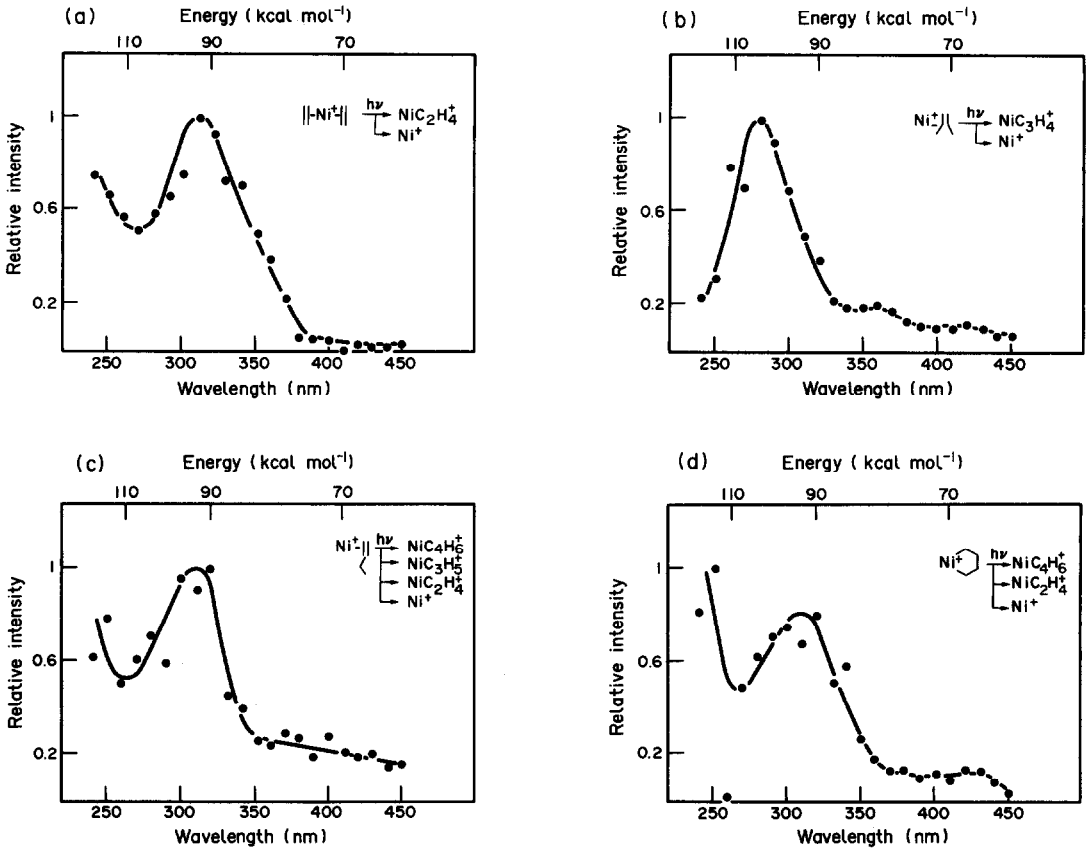

Fig. 4. Photodissociation spectra of four $NiC_4H_8^+$ isomers. (a) Ni(bis-ethylene)$^+$. (b) Ni(isobutene)$^+$. (c) Ni(1-butene)$^+$. (d) Nickel metallacyclopentane$^+$.

Electron impact ionization of trimethylene-methane(iron)tricarbonyl at 30 eV electron energy produces $FeC_4H_6^+$, reaction (19).

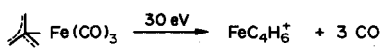

(19)

Collision-induced dissociation and photodissociation both yield loss of C_2H_2, C_2H_4 and C_4H_6. The photodissociation spectrum for this ion is shown in Fig. 5(b). These observations, along with the observation of the displacement of C_2H_4 by 1-butene, reaction (20), indicate the ion produced in reaction (19) may have rearranged upon electron impact to an iron–ethylene–acetylene complex, structure (V).

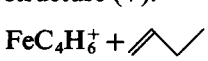

(20)

In any event CID and photodissociation provide clear evidence for the existence of at least two $FeC_4H_6^+$ isomers.

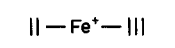

(V)

Ion-molecule reactions. In analogy to solution phase qualitative analysis, ion–molecule reaction chemistry can be used to differentiate isomers, since they will generally display different reactivities. The main two methods used in this category are H/D exchange reactions[24] and ligand displacement reactions. H/D exchange is performed by trapping a selected ion in a static background of a deuterating reagent such as D_2, C_2D_4, or C_3D_6. The number of exchangeable H atoms will be characteristic of the ionic structure. For example, $RhC_3H_6^+$ reacts with D_2 to exchange 5 H atoms, reaction (21), providing evidence for a rapid equilibrium between the hydrido–allyl structure (VI) and the propene structure (VII).[24(a)]

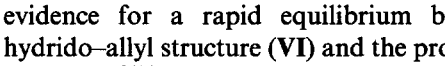

(21)

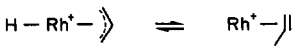

(VI) (VII)

Another interesting example involves the reactions of Fe^+, Co^+ and Ni^+ with cyclobutanone to

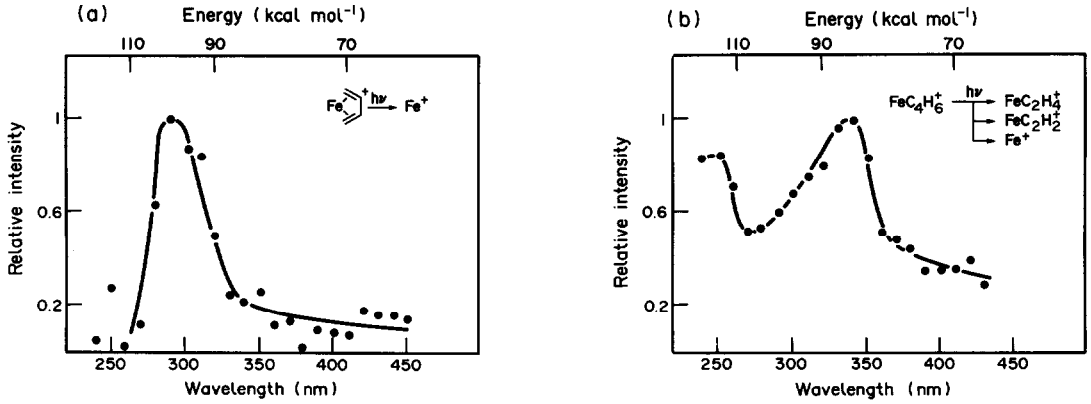

Fig. 5. Photodissociation spectra of two $FeC_4H_6^+$ isomers. (a) Fe(butadiene)$^+$. (b) $FeC_4H_6^+$ generated from electron impact on trimethylenemethane(iron)tricarbonyl.

generate $MC_3H_6^+$, reaction (22).[25]

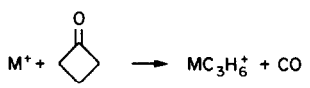

(22)

Using C_2D_4 as the deuterating reagent, it was found that $FeC_3H_6^+$ generated in this way has a stable metallocyclobutane structure (**VIII**), while $CoC_3H_6^+$ and $NiC_3H_6^+$ apparently isomerize to the propene structure (**IX**). The implications of these results are discussed by the authors, as well as the differentiation of other isomeric ions.

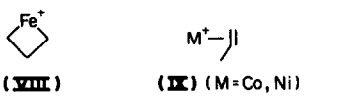

(VIII) (IX) (M=Co, Ni)

Ligand displacement, as shown in reaction (20), will produce displacement of a more weakly bound ligand by a more strongly bound ligand. For instance, benzene will displace an H atom from Co^+. $CoNH_2^+$ reacts with benzene to displace NH_2, exclusively, suggesting that $CoNH_2^+$ has an amide structure (**X**) and not a hydrido–nitrene structure, (**XI**).[26]

$$Co^+—NH_2 \qquad H—Co^+—NH$$
$$\text{(X)} \qquad\qquad \text{(XI)}$$

Another prime example by Beauchamp and coworkers was the differentiation of structures **I** and **IV** using HCN as the reagent gas.[27] In this case structure **I** was observed to undergo the sequential displacement of one and then two molecules of C_2H_4 with HCN, while structure **IV** is completely unreactive with HCN. This result provided significant evidence for the notion that bare metal ions can undergo C—C insertion in alkanes. An extension of this work was performed in our laboratory on a variety of Fe^+, Co^+ and Ni^+ olefin complexes.[3(d),22]

Techniques for the determination of metal–ligand bond strengths

The determination of absolute bond energies for metal–ligand systems is of primary importance to organometallic chemistry. Bond energies aid in understanding structure and bonding as well as in determining the feasibility of various reaction mechanisms.

Several complementary techniques have been developed for the determination of metal–ligand bond energies of ionic species in the gas phase including: (1) appearance potentials,[28] (2) thermal ion–molecule reactions,[18(b),(c)] (3) endothermic reaction thresholds,[4,14] (4) ligand equilibria,[29,30] (5) photodissociation thresholds[20,31] and (6) competitive CID.[32] Methods (2) and (5) are the main techniques used in our laboratory and are, therefore, described in the greatest detail below.

Photodissociation. Photodissociation, process (23),

$$AB^+ + h\nu \rightarrow A^+ + B \qquad (23)$$

is controlled by three factors: (a) the ion must first absorb a photon, (b) the photon energy must exceed the enthalpy for process (23) and (c) the quantum yield for photodissociation must be greater than zero. Thus, photodissociation cut-offs can be attributed to either spectroscopic or thermodynamic factors. If the first allowed electronic state lies above the energy for process (23), then the photodissociation threshold will be determined by spectroscopic factors (see Fig. 6) and yield only an upper limit for the enthalpy of process (23). If an allowed electronic state lies at the same energy as process (23), or a high density of states lies in this energy range, then the threshold will be determined by thermodynamic factors and will yield an absolute

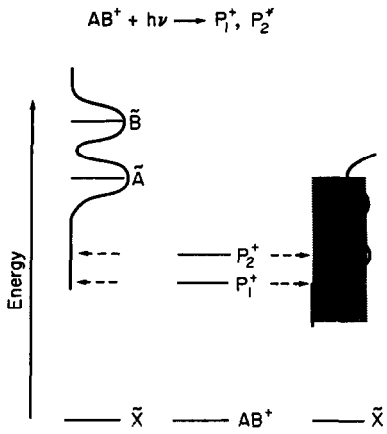

Fig. 6. Energy level diagram showing cases where photodissociation thresholds are determined by spectroscopic factors, due to a low density of low-lying electronic states (left) and thresholds determined by thermodynamic factors due to a high density of low-lying electronic states (right).

value for the bond energy. In general, photodissociation onsets of organic ions tend to be spectroscopically determined, while data from our laboratory suggest that many metal ion species yield thermodynamic thresholds. Due to the presence of the metal, a high density of low-lying electronic states results in a broad absorption in the vicinity of the bond dissociation energy. For example, the photoappearance spectrum for Fe^+, obtained by irradiating FeO^+, is shown in Fig. 7. The threshold at 420 ± 10 nm implies $D^0(Fe^+—O) = 68 \pm 5$ kcal mol^{-1}, in excellent agreement with a value of $D^0(Fe^+—O) = 68 \pm 3$ kcal mol^{-1} obtained in an ion-beam study by Beauchamp *et al.*[33] This clearly indicates that the threshold is due to the thermodynamics of the photodissociation process, involving a simple bond cleavage to produce ground state products.

Often, multiple products are observed from photodissociation. For example, $FeCH_2^+$ undergoes photodissociation in the vis–UV region to give three product ions, reactions (24)–(26).[21]

$$FeCH_2^+ + h\nu \longrightarrow FeCH^+ + H^\cdot \quad (24)$$
$$\longrightarrow FeC^+ + H_2 \quad (25)$$
$$\longrightarrow Fe^+ + CH_2. \quad (26)$$

For this type of situation, each photoproduct can be measured as a function of wavelength. If rapid internal conversion to a vibrationally excited ground state occurs with subsequent randomization of the energy, then thresholds for higher energy photoproducts can also yield absolute thermodynamic values. Photoappearance spectra for reactions (25) and (26) are shown in Fig. 8. Photodissociation thresholds for $FeCH^+$ and FeC^+ imply $D^0(Fe^+—CH) = 101 \pm 5$ kcal mol^{-1} and $D^0(Fe^+—C) = 94 \pm 5$ kcal mol^{-1}, in reasonable agreement with $D^0(Fe^+—CH) = 115 \pm 20$ kcal mol^{-1} [34] and $D^0(Fe^+—C) \sim 89$ kcal mol^{-1} [34] obtained from ion-beam experiments. These results indicate that, for $FeCH_2^+$ at least, the thresholds for higher energy products can be attributed to thermodynamic factors.

Ion–molecule reactions. In the gas phase, the attraction between an ion and the permanent and/or induced dipole of the neutral is long range and in general leads to an interaction with little or no activation barrier. Thus, if an ion–molecule reaction is observed in the gas phase, the free energy of reaction (27) can be assumed to be negative.

$$A^+ + B \rightarrow C^+ + D \quad \Delta G_{rxn} < 0. \quad (27)$$

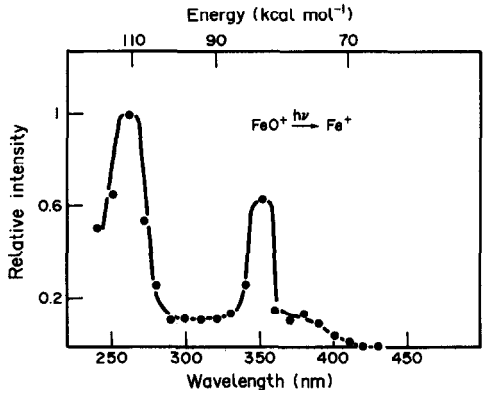

Fig. 7. Photodissociation spectrum of FeO^+ with the threshold at 420 nm indicating $D^0(Fe^+—O) = 68 \pm 5$ kcal mol^{-1}.

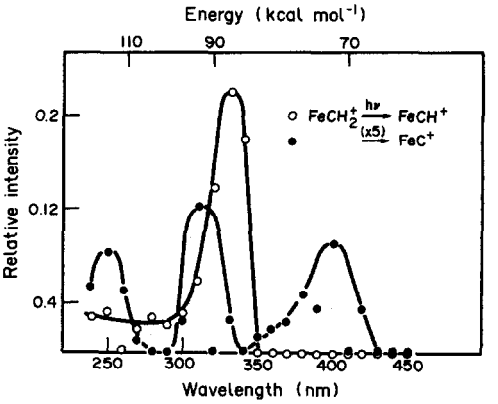

Fig. 8. Photoappearance spectra for $FeCH^+$ and FeC^+ produced upon photodissociation of $FeCH_2^+$.

Furthermore, since entropy effects are often negligible, the enthalpy of the reaction can also be assumed to be negative. Thus, limits on the heats of formation can be derived from the observation of a reaction. For example, from the observation of reaction (28)

$$(M = Fe, Co) \quad MOH^+ + NH_3 \rightarrow MNH_2^+ + H_2O \quad (28)$$

and using the known heats of formation for H_2O, NH_3 and MOH^+, $\Delta H_f(MNH_2^+)$ can be derived from eq. (29).

$$\Delta H_f(MNH_2^+) < \Delta H_f(NH_3) + \Delta H_f(MOH^+) - \Delta H_f(H_2O). \quad (29)$$

Then, from $\Delta H_f(MNH_2^+)$, lower limits for the bond energies of $D^0(Co^+—NH_2) > 56 \pm 3$ kcal mol^{-1} and $D^0(Fe^+—NH_2) > 58 \pm 3$ kcal mol^{-1} are obtained.[26] Upper limits can also be derived using a similar procedure.

$$FeNH_2^+ + \text{propene} \rightarrow Fe(\text{allyl})^+ + NH_3. \quad (30)$$

Reaction (30), for example, indicates $D^0(Fe^+—NH_2) < 72 \pm 7$ kcal mol^{-1}, using previously reported heats of formation for the other species. Finally, from the upper and lower brackets, a value of $D^0(Fe^+—NH_2) = 67 \pm 12$ kcal mol^{-1} is obtained.

Two important ion–molecule reactions frequently used to determine thermochemistry are proton transfer[31] and ligand displacement reactions.[19(b)] An example of the former is the reaction of MOH^+ (M = Fe, Co) with various bases, reaction (31):

$$MOH^+ + B \rightarrow MO + BH^+ \quad (B = \text{various bases}). \quad (31)$$

For $CoOH^+$, proton transfer is observed with pyridine or stronger bases but is not observed with 1-propylamine or weaker bases indicating PA(pyridine) > PA(CoO) > PA(1-propylamine). Using this result in eq. (32) yields $D^0(Co^+—OH) = 71 \pm 6$ kcal mol^{-1}, in good agreement with $D^0(Co^+—OH) = 71 \pm 3$ kcal mol^{-1} obtained from photodissociation.[31]

$$\Delta H_f(MOH^+) = \Delta H_f(MO) + \Delta H_f(H^+) - PA(MO). \quad (32)$$

Ligand displacement reactions can also be used to determine bond energy limits, as in reaction (33), which indicates 68 ± 5 kcal mol^{-1} = $D^0(Co^+—\text{benzene}) > D^0(Co^+—NH_2)$.[26]

$$CoNH_2^+ + \text{benzene} \rightarrow Co(\text{benzene})^+ + NH_2^{\bullet}. \quad (33)$$

Thermodynamic information derived from ion–molecule reactions must clearly be viewed with caution. Absence of a reaction may be due to kinetic and not thermodynamic factors. Competing reaction channels may prevent observation of all exothermic pathways. Also, ion–molecule reactions which are slightly (1–3 kcal mol^{-1}) endothermic can still be observed, though they will proceed very slowly ($k^{II} < 5\%$ of Langevin rate).[35,36] This is because the equilibrium is being driven by an infinite excess of one reagent. For example, in the $CoOH^+$ case, reaction (31), no CoO is present to be reprotonated by BH^+, so thermoneutral or slightly endothermic reactions can be observed. Finally, as discussed earlier, care must be taken to ensure that the reactant ions are thermalized. Thus, it is important to have other techniques to verify thermochemical values.

Other techniques. The most common method used to corroborate the thermodynamic results obtained by photodissociation and ion–molecule reactions is competitive CID. This technique was first developed by Cooks and coworkers to obtain proton affinity information,[32] but can be generalized to other cation affinities (including metal ions) and anion affinities. In particular, a metal cation centre which contains two ligands will undergo collisional activation via competitive loss of the ligands. In general, loss of the more weakly bound ligand should be favoured in the dissociation process. For example, CID of Mg(EtOH)(*n*-PrOH)$^+$ favours production of Mg(*n*-PrOH)$^+$ over Mg(EtOH)$^+$ indicating $D^0(Mg^+—n\text{-PrOH}) > D^0(Mg^+—\text{EtOH})$.[37] A second example is the observation that CID of $CoC_6H_7^+$ yields $CoC_6H_6^+$ indicating 52 ± 4 kcal mol^{-1} = $D^0(Co^+—H) < D^0(Co^+—\text{benzene})$.[18(b)] One difficulty with this approach has recently been suggested. Restrictions on the change in angular momentum during the dissociation process may affect the relative rates of dissociation and hence the product distributions, regardless of the relative bond dissociation energies.[38]

Another powerful approach, which yields accurate relative bond energies, is to determine the equilibrium constant for ligand displacement, as exemplified by reaction (34).

$$Mg(i\text{-PrOH})^+ + n\text{-BuOH} \underset{k_r}{\overset{k_f}{\rightleftharpoons}} Mg(n\text{-BuOH})^+ + i\text{-PrOH}. \quad (34)$$

This value can be obtained from the ratio of the partial pressures of the ligands in the cell and from the ratio of the steady-state ion populations at equilibrium. K_{eq} can also be obtained from the relation

$K_{eq} = k_f/k_r$, by measuring the forward and reverse rate constants for reaction (34) in two separate experiments. From $\Delta G = -RT \ln K$ and again assuming ΔS is small, an accurate value (± 0.1 kcal mol^{-1}) for the difference in binding energies for the two ligands can be obtained. Table 2 shows the ladder of relative bond strengths for various oxygen bases bound to Mg^+ obtained by ligand exchange equilibria.[37] The absolute bond energies shown in the table were derived from photodissociation experiments.

Finally, endothermic reactions can be used to determine metal–ligand bond strengths. For example, translationally excited Co^+ reacts with ethane as in reaction (35).

$$(Co^+)^\dagger + C_2H_6 \rightarrow CoCH_3^+ + CH_3^\cdot. \qquad (35)$$

The threshold energy for production of $CoCH_3^+$ of 1.82 ± 0.62 eV gives the endothermicity for the reaction.[14(b)] From the known heats of formation for the other species, $D^0(Co^+—CH_3) = 46 \pm 14$ kcal mol^{-1} was obtained, in comparison to $D^0(Co^+—CH_3) = 61 \pm 4$ kcal mol^{-1} obtained from an ion-beam experiment[39] and $D^0(Co^+—CH_3) = 57 \pm 7$ kcal mol^{-1} determined by photodissociation.[20] Results from measuring endothermic thresholds using FTMS must be viewed with caution, however, since the spread in translational energies in the instrument is not well characterized and the signal-to-noise is low near threshold. In addition, the elimination of barriers, which normally accompanies thermal reactions due to the formation of an intimate ion-induced dipole collision complex, may not occur at higher energies where scattering type collisions occur.

Summary of thermodynamic results

As discussed above for photodissociation and ion–molecule reactions, there are assumptions made for every technique and spectroscopic, kinetic and other factors may be the controlling influence as opposed to thermodynamic factors. For this reason, it is essential that each thermodynamic value be checked by as many techniques as possible. Table 3 lists the results obtained in our laboratory by photodissociation, ion–molecule reactions,

Table 2. Relative and absolute gas phase ligand binding energies to Mg^+ for various organic molecules[a]

Ligand (L)	Measured $\Delta G_{exchange}$[b]	$D^0(Mg^+—L)$ Rel.[c]	Abs.[d]
MeCOEt		7.64	68
Me_2CO	1.24	6.40	67
THF[e]	1.05, 1.20	5.41	66
Et_2O	0.23	5.16	66
n-PrCHO	0.52, 1.61	4.60	66
n-BuOH	0.86, 1.45	3.87	65
EtCHO	1.76, 0.30	3.67	65
i-PrOH	0.72, 0.93	3.59	65
n-PrOH		2.95	64
MeCHO	0.68, 1.17	2.28	63
EtOH	0.52	1.77	63
MeOH	1.77	0.00	61

[a] All data are in kcal mol^{-1}.
[b] For the equilibrium reaction (34) in text.
[c] Values (± 0.2 kcal mol^{-1}) are relative to $D^0(Mg^+—MeOH) = 0.00$ kcal mol^{-1}.
[d] Absolute values (± 5 kcal mol^{-1}) assigned from photodissociation results, see text.
[e] Tetrahydrofuran.

Table 3. Bond dissociation energies for various gaseous ions obtained by various methods (see text). All values in kcal mol^{-1}

Bond	PDS	I—M reactions	Competitive CID	Endothermic reactions	Ref.	Lit.	Ref.
Co^+—CH_2	84±5			81±7	14(b), 21	84±7	57
Co^+—CH	100±5				21		
Co^+—C	90±5				21	98	34
Fe^+—CH_2	82±5				21	96±5	58
Fe^+—CH	101±5				21	115±20	34
Fe^+—C	94±5				21	89	34
Rh^+—CH_2	89±5	94±5			49,50		
Rh^+—CH	102±7				50		
Rh^+—C	> 120	164±16			50, 59		
La^+—CH_2	106±5	> 93			50, 54		
La^+—CH	125±8				50		
La^+—C	102±8				50		
Nb^+—CH_2	109±5	112±5			50, 51		
Nb^+—CH	145±8				50		
Nb^+—C	> 88				50		
Fe^+—S	65±5	74 > x > 59			48		
Co^+—S	62±5	74 > x > 59			48		
Ni^+—S	60±5				48		
Fe^+—CH_3	65±5				20	69±5	60
Co^+—CH_3	57±7			46±14	14(b), 20	61±4	33
Co^+—CH_3CN	> 61±4				19(b)		
Fe^+—O	68±5				20	68±3	33
$NiCp^+$—NO	< 43±3				56	41.9±1	61
Fe_2^+—H				52±16	14(b)		
V^+—C_6H_6	62±5	> 49			20,47		
$VC_6H_6^+$—C_6H_6	57±7				20		
Co^+—C_6H_6	68±5	66±7	> 48		18(b), 19(b), 20		
Fe^+—C_6H_6	55±5				20		
Fe^+—H			55±5		18(b)	47±4, 60±3	62,63
Ni^+—C_3H_5	< 60	> 55			20		
Fe^+—butadiene	48±5	60 > x > 45			20		
Ni^+—$2C_2H_4$	80±5	74±2			20		
Rh^+—C_6H_6	66±7	> 49			16, 24(a)		
Nb^+—C_6H_6	66±7	> 60	< 73		16		
Co^+—OH	71±3	71±6			31		
Fe^+—OH	73±3	77±6			31		
Fe^+—(c-C_5H_6)	51±5				16		
Co^+—Cp		85±10			53		
$CoCp^+$—Cp		118±10			53		
$CoCp^+$—butadiene		> 57			53		
Co^+—butadiene		< 52			18(a)		
Co^+—C_3H_5		> 72			18(a)		
Co—CH_4		49±11			18(a)		
Co^+—toluene			> 48		44		
Fe^+—Cp		> 66			18(b)		
Fe^+—NH_2		67±12			26		
Co^+—NH_2		65±8			26		
V^+—NH		100±7			16		
VN—H^+		220±7			16		
V—N		110±10			16		
Fe^+—NH	61±5	54±14			16		
FeO—H^+		219±5			31		
CoO—H^+		219±5			31		

PDS = photodissociation.
I—M Reactions = ion–molecule reactions.

endothermic reaction thresholds and competitive CID. These values are also compared where available with other literature values, primarily from ion-beam experiments, and good agreement is observed in general.

Of particular note are the high bond strengths of MNH_2^+ (M = Fe, Co). Primary amide complexes of later transition metals have not been observed in condensed phase, which has been attributed to the unfavourable nitrogen *p*/metal *d* interaction which would presumably make the M—N bond extremely weak.[40] Furthermore, earlier gas-phase studies had also suggested the possibility of an extremely weak Co^+—NH_2 bond (< 19 kcal mol^{-1}).[41] CH_3CN displaces $CH_3^•$ from $CoCH_3^+$ but does not displace $NH_2^•$ from $CoNH_2^+$ in accordance with the bond energies in Table 3 indicating $D^0(Co^+—NH_2) > D^0(Co^+—CH_3)$. This trend is the opposite of that observed in solution studies.[42]

An interesting correlation for the determination of bond energy/bond order relationships has recently been suggested by Aristov and Armentrout.[43] Plots of M^+—L bond energies versus those of the corresponding carbon analogues are observed to be linear with distinct regions appearing which correspond to single, double and triple bonds. Using the values from Table 3, plots for Fe^+, Co^+, Rh^+, Nb^+, La^+ and V^+ are shown in Fig. 9(a)–(d). Single bond regions are defined by M^+—H bonds and double bonds are defined by M^+—CH_2 bonds, in line with recent theoretical results. One immediate feature of these plots is the propensity of early transition metal ions to form multiple bonds to oxygen and nitrogen containing ligands, in contrast to their later transition metal counterparts which form primarily single bonds. This is believed to be due to the empty *d*-orbitals in the early transition metals which are available for multiple bonding.

Interestingly, this type of correlation is also observed for the neutral V—L species (see Fig. 10). Thermochemical values for VN were derived using reactions (36)–(38) and the other data used were

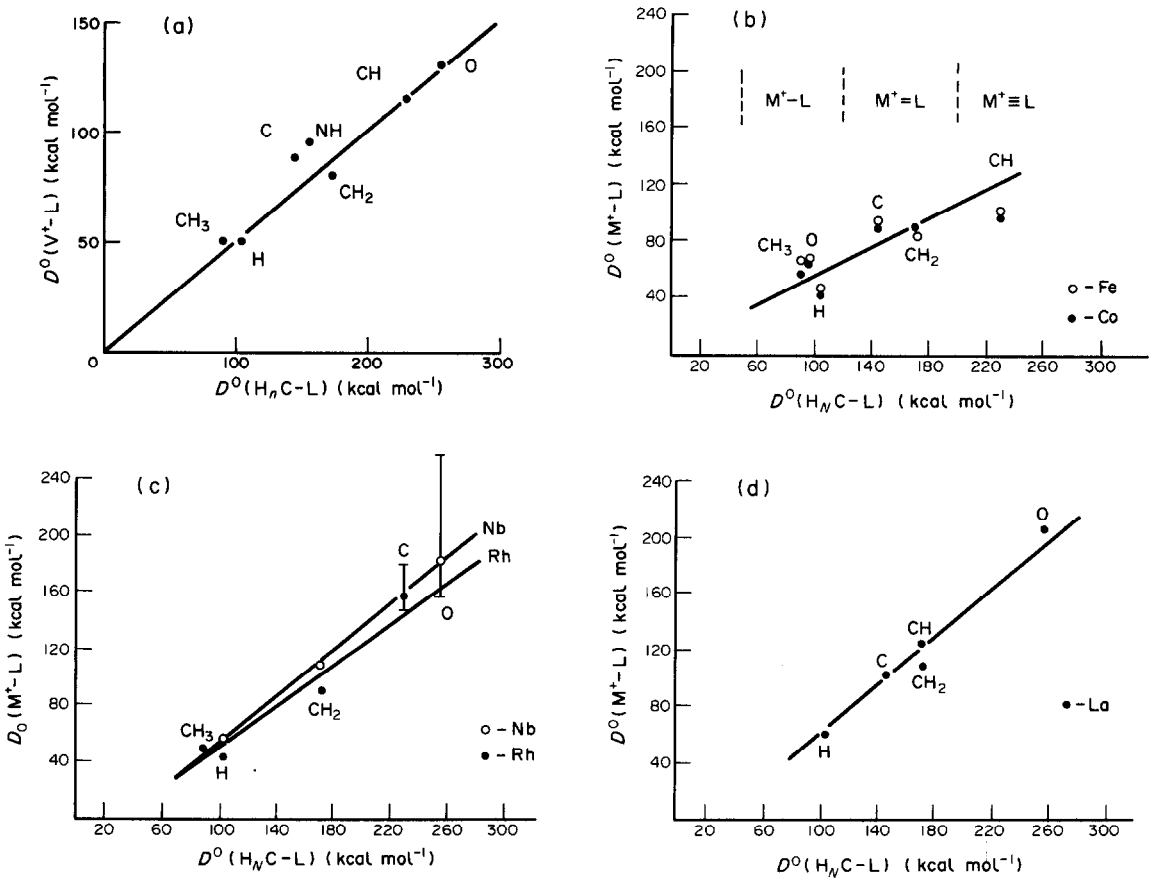

Fig. 9. Correlation of metal ion–ligand bond dissociation energies ($D^0(M^+—A)$ with the corresponding carbon analogues $D^0(H_NC—A)$. (a) V^+—L. (b) Fe^+—L, Co^+—L. (c) Nb^+—L, Rh^+—L. (d) La^+—L.

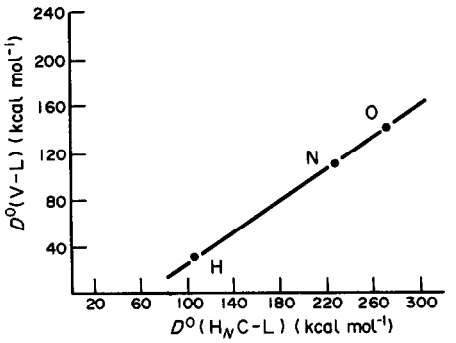

Fig. 10. Correlation of the neutral vanadium–ligand bond dissociation energies with the corresponding carbon analogues.

taken from the literature.

$$V^+ + NH_3 \rightarrow VNH^+ + H_2$$

implies $D^0(V^+—NH) > 93\,\text{kcal mol}^{-1}$ (36)

$$VNH^+ + H_2O \rightarrow VO^+ + NH_3$$

implies $D^0(V^+—NH) < 107\,\text{kcal mol}^{-1}$ (37)

$$VNH^+ + B \rightarrow VN + BH^+$$

implies $PA(VN) = 220 \pm 6\,\text{kcal mol}^{-1}$. (38)

These plots must be viewed with caution, though. The idea that M^+—L bond energies should correlate with their organic analogues is clearly an oversimplification, as multiple bonds in condensed phase inorganic species are often weaker than single bonds.

Reactivity of ML^+

In this section we will discuss the reactivity of various ligated atomic metal ions (M = Fe, Co, Ni, V, Rh, Nb, La; L = H, CH_3, NH_2, OH, O, S, NH, CH_2, π-type ligands) with various alkanes and alkenes. First a discussion of the reactivity of bare atomic metal ions will be useful for comparison.

There have been numerous studies of the reactivity of atomic metal ions with organic compounds,[2] making possible a good understanding of the driving force behind their reactivity. By far the most heavily studied metal ions have been Fe^+, Co^+ and Ni^+. These metal ions react with hydrocarbons predominantly by attacking the C—C bonds, as exemplified by the proposed mechanism in Scheme 1. This is in contrast to solution where organometallic complexes of these metals only activate C—H bonds. One explanation for the gas phase behaviour is that C—C bond insertion is more thermodynamically favourable than C—H insertion, since C—C bonds are weaker than C—H bonds and M^+–alkyl bonds are stronger than M^+—H bonds.

In contrast to the reactivity of the first row groups 8–10 metal ions, the other metal ions studied to date have been observed to predominantly activate C—H bonds in hydrocarbons. A survey of the reactivity of Fe^+, Co^+, Ti^+, Rh^+, Ta^+, Y^+ and Nb^+ with methane through propane is shown in Table 4.

The discussions of ML^+ reactivity will be broken up into groups with similar reactivity. L = H, CH_3, NH_2, OH; where predominant formation of metal–alkyl and metal–allyl occurs upon the loss of the original ligand. L = O, S; where the loss of H_2O and H_2S occurs with formation of an activated M^+–alkene complex which further decomposes. L = CH_2, NH; where formation of a four-centred intermediate leads to catalytic homologation reactions, and lastly L = various π-type ligands.

L = H, CH_3, OH, NH_2. The reactivity of these ligands is governed by the expected behaviour of a singly bonded-sigma bound species.[16,18(a)(b),19(a),44] One of the main reaction pathways with small hydrocarbons is shown in Scheme 2. Again, oxidative addition is the first step of the reaction. For FeL^+, CoL^+ and NiL^+ it is interesting to note that initial insertion occurs across C—H bonds. This is in contrast to the bare atomic metal species which almost exclusively attack C—C bonds. An increased preference for C—H bond activation relative to C—C bond activation is observed for all ligated Fe^+, Co^+ and Ni^+ species studied to date. After the initial oxidative addition, rapid reductive

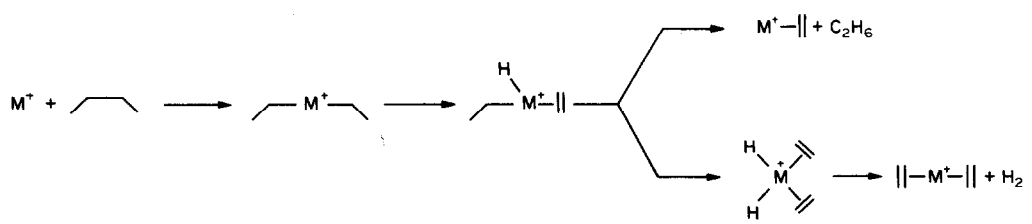

Scheme 1.

Table 4. Reactions of various metal ions with small alkanes

		Nb^+	Ta^+	Fe^+	Co^+	Rh^+	Ti^+	Y^+	V^+
CH_4	MCH_2^+	NR	100	NR	NR	NR	NR	NR	NR
C_2H_6	$MC_2H_4^+$	64	10	NR	NR	100	100	100	NR
	$MC_2H_2^+$	36	90	0	0	0	0	0	0
C_3H_8	$MC_3H_6^+$	0	0	24	69	94	100	75	100
	$MC_3H_4^+$	85	78	0	0	6	0	25	0
	$MC_3H_2^+$	15	22	0	0	0	0	0	0
	$MC_2H_4^+$	0	0	76	31	0	0	0	0

elimination of HL can occur with the formation of M^+–alkyl which, in many cases, is internally excited due to the reaction exothermicity. This excited M^+–alkyl complex can further decompose via the loss of H_2 to form an M^+–allyl ion; however, this is not the only reaction pathway available. As shown in Table 5, dehydrogenation or dealkylation with retention of the initial ligand is also observed.

For bare metal ions, the general trend in reactivity is $Fe^+ > Co^+ > Ni^+$. For the ligated species, however, a reversal is observed, with $NiD^+ > CoD^+ > FeD^+$ [19(a)] and $CoL^+ > FeL^+$ (L = CH_3, OH). Though $D^0(Co^+—allyl) > 76$ kcal mol^{-1} [18(a)] is greater than $D^0(Fe^+—allyl) = 56 \pm 7$ kcal mol^{-1},[45] $D^0(Co^+—CH_3) = 61 \pm 4$ kcal mol^{-1} is lower than $D^0(Fe^+—CH_3) = 69 \pm 5$ kcal mol^{-1}. Thus, the overall thermodynamics of metal–alkyl formation appears to favour Fe^+, while metal–allyl formation appears to favour Co^+. Since the overall thermodynamics do not seem to account for the reduced reactivity of FeL^+ relative to CoL^+, kinetic barriers for the initial insertion or elimination of H_2 or HL may be present. Since $FeOH^+$ and FeH^+ react with larger linear alkanes mainly via the loss of the initial ligand, a barrier to the elimination of H_2 or H_2O seems less likely than a barrier to initial insertion. This may also account for the trend in reactivity $CoD^+ > CoOH^+ > CoCH_3^+$ and $FeD^+ > FeOH^+ > FeCH_3^+$.

Subsequent reactions of M^+–allyl, formed in the above reactions, proceed via dehydrogenation to generate M(allyl)(alkene)$^+$ complexes.[44] Coupling of the ligands was ruled out in most cases by ligand displacement of the alkene using CH_3CN or another alkene.

L = O, S. An oxygen ligand can enhance or suppress the reactivity of a metal ion depending on the metal–oxide bond strength. For FeO^+, which has a relatively low bond strength, $D^0(Fe^+—O) = 68 \pm 5$ kcal mol^{-1},[33] there is enhanced reactivity relative to Fe^+ (see Table 6).[46] Two reaction pathways are observed with the main reaction pathway shown in Scheme 3. As for all ligated species, the C—H insertion pathway is greatly enhanced. The main reaction pathway involves the loss of H_2O to form a highly activated Fe(alkene)$^+$ complex which subsequently decomposes by further dehydrogenation, dealkylation or loss of the alkene ligand. This activated complex arises due to the exothermicity of H_2O loss ($\sim$ 56 kcal mol^{-1}) which is also responsible for the enhanced reactivity of FeO^+ relative to Fe^+. The other pathway observed

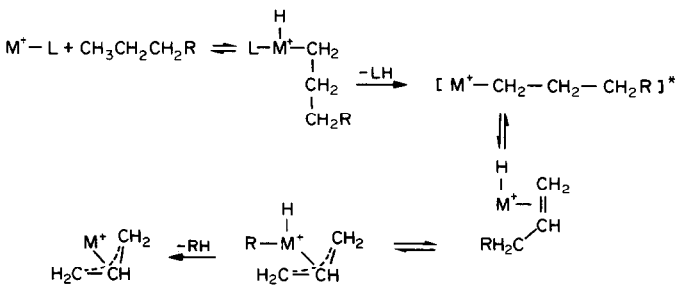

Scheme 2.

Table 5. Product distributions for the reactions of ML^+ with various alkanes (L = H, CH_3, OH, NH_2)

Reactant	Products	FeD^+	CoD^+	NiD^+	$FeCH_3^+$	$CoCH_3^+$	$FeOH^+$	$CoOH^+$	$FeNH_2^+$
CH_4	$MH^+ + CH_3D$	NR	NR	20	NR	NR	NR	NR	NR
	$MCH_3^+ + HL$			80					
C_2H_6	$MC_2H_5^+ + HL$	NR	100	100	NR	NR	NR	NR	NR
C_3H_8	$MC_3H_7^+ + HL$	100			NR	29	NR		NR
	$MC_3H_5^+ + HL + H_2$		100	100		70		100	
	$MC_3H_6L^+ + H_2$								
	$C_3H_7^+ + MCH_4$					1			
c-C_3H_6	$MC_2H_5^+ + C_2H_4$	× ×	× ×	× ×	100	87			
	$MC_3H_5^+ + HL$					4	100	100	100
	$MC_4H_7^+ + H_2$					7			
n-C_4H_{10}	$MC_4H_9^+ + HL$	40			NR		NR		NR
	$MC_4H_7^+ + HL + H_2$	60	100	23		100		48	
	$MC_3H_5^+ + HL + CH_4$			77				5	
	$MC_2H_4L^+ + C_2H_6$							18	
	$MC_4H_8L^+ + H_2$							29	
n-C_5H_{12}	$MC_5H_{12}L^+$	× ×	× ×	× ×	NR		NR		30
	$MC_5H_{10}L^+ + H_2$							9	
	$MC_5H_8L^+ + 2H_2$							5	70
	$MC_5H_9^+ + HL + H_2$					74		51	
	$MC_4H_7^+ + 2CH_4$					2			
	$MC_3H_6L^+ + C_2H_6$							20	
	$MC_3H_5^+ + HL + C_2H_6$					16		11	
	$MC_2H_4L^+ + C_3H_8$							4	
	$C_5H_{11}^+ + CoCH_4$					8			

NR indicates no reaction was observed ($k^{II} < 10^{-12}$ cm^3 mol^{-1} s^{-1}).
× × indicates the reaction was not performed.

for FeO^+ with alkanes involves C—C insertion with loss of an alkyl radical, Scheme 4.

VO^+ has a decreased reactivity relative to V^+, exhibiting a slower reaction rate and less extensive dehydrogenation.[47] The high V^+—O bond strength, $D^0(V^+—O) = 131 \pm 5$ kcal mol^{-1},[43] appears to suppress the reactivity without a significant change in reaction pathways due to coordinative saturation. Loss of H_2O is not observed as this is an endothermic reaction pathway.

A study of MS^+ (M = Fe, Co, Ni)[48] revealed similar reactivity to that observed for FeO^+, but the C—C cleavage pathway involving radical loss products is almost completely suppressed. The overall reactivity of MS^+ is somewhat lower than that for FeO^+, with less extensive dehydrogenation observed. This was accounted for as being due to the lower exothermicity of H_2S loss relative to H_2O loss.

$$Fe^+ + C_2H_6 \longrightarrow FeC_2H_4^+ + H_2$$
$$\Delta H(\text{reaction})\ \text{kcal mol}^{-1} \sim 0 \quad (39)$$

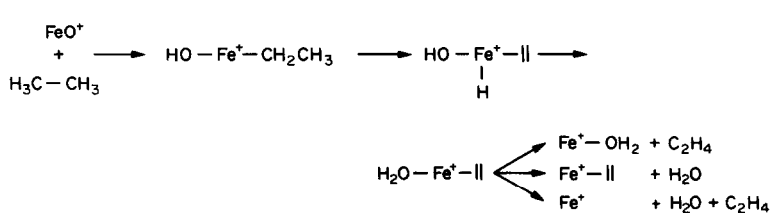

Scheme 3.

Table 6. Product distributions for the reaction of Fe^+ and FeO^+ with linear alkanes

Alkane	Fe^+ Neutral lost	Fe^+ % of total	FeO^+ Neutral lost	FeO^+ % of total
CH_4	NR		NR	
C_2H_6	NR		H_2O	70
			C_2H_4	20
			$H_2O+C_2H_4$	10
	CH_4	76	H_2O	50
	H_2	24	CH_3	20
			$H_2O+C_3H_6$	20
			C_3H_6	10
	C_2H_6	60	H_2O, H_2	60
	CH_4	29	H_2O, C_2H_4	30
	$2H_2$	3		
	H_2	8	H_2O, C_4H_8	10
	C_3H_8	43	H_2O, C_2H_4	44
	CH_4	22	H_2O, C_3H_6	27
	H_2	16	H_2O, CH_4	15
	C_2H_6	15	CH_3CH_2	9
	CH_4, H_2	4	H_2O, C_5H_{10}	5
	C_4H_{10}	31	H_2O, C_3H_6	34
	H_2	27	H_2O, C_2H_4	21
	CH_4	13	H_2O, $3H_2$	15
	C_3H_8	11	CH_3CH_2	14
	C_2H_6	11	H_2O, C_2H_4, H_2	9
	C_2H_6, H_2	7	H_2O, C_4H_8	7

$$FeS^+ + C_2H_6 \longrightarrow FeC_2H_4^+ + H_2S$$

$$\Delta H(\text{reaction})\,\text{kcal mol}^{-1} \sim -8 \quad (40)$$

$$FeO^+ + C_2H_6 \longrightarrow FeC_2H_4^+ + H_2O$$

$$\Delta H(\text{reaction})\,\text{kcal mol}^{-1} \sim -51 \quad (41)$$

$$FeO^+ + C_2H_6 \longrightarrow Fe(H_2O)^+ + C_2H_4 \quad (42)$$

$$FeO^+ + C_2H_6 \longrightarrow Fe^+ + (C_2H_6O). \quad (43)$$

Reactions (39)–(41) show the overall exothermicity of reaction of FeL^+ (L = O, S) and Fe^+ with ethane.

L = CH_2, NH. Transition metal carbenes are very important in organometallic chemistry due to their presence as intermediates in many important catalytic processes. Because of this and the fact that they can be easily generated, there have been numerous studies on their chemistry and photochemistry.

Table 7 shows product distributions for the reactions of $RhCH_2^+$, $FeCH_2^+$ and $CoCH_2^+$ with a few alkanes and alkenes. These carbenes exhibit very complex chemistry including migratory insertion, olefin metathesis, olefin homologation and other pathways.[18(c)–(e),49]

Scheme 5 shows proposed reaction pathways for $CoCH_2^+$ with ethane. Numerous steps show migratory insertion of CH_2 into an M—C bond. Analogous behaviour is seen with $RhCH_2^+$ and $FeCH_2^+$ with alkanes and also with MCH_3^+

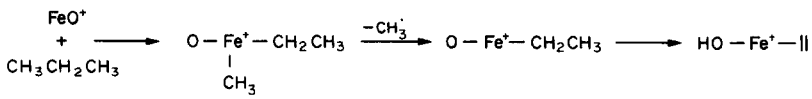

Scheme 4.

Table 7. Product distributions for reactions of MCH_2^+ with various hydrocarbons (M = Fe, Co, Rh)

Reactant	Product	$FeCH_2^+$	$CoCH_2^+$	$RhCH_2^+$
C_2H_4	$M^+ + C_3H_6$	100	100	30
	$MC_3H_4^+ + H_2$			70
C_3H_6	$M^+ + C_4H_8$	32	31	8
	$MC_2H_4^+ + C_2H_4$	62	54	27
	$MC_3H_4^+ + CH_4$			26
	$MC_4H_4^+ + 2H_2$			23
	$MC_4H_6^+ + H_2$	6	15	16
C_2H_6	$M^+ + C_3H_8$	NR	58	8
	$MC_2H_4^+ + CH_4$		28	92
	$MC_3H_6^+ + H_2$		14	
C_3H_8	$M^+ + C_4H_{10}$	16	18	× ×
	$MC_2H_4^+ + C_2H_6$	8	13	
	$MC_3H_6^+ + CH_4$	70	59	
	$MC_4H_6^+ + 2H_2$	2	1	
	$MC_4H_8^+ + H_2$	4	9	

NR indicates no reaction was observed ($k^{II} < 10^{-12}$ cm^3 mol^{-1} s^{-1}).

× × indicates the reaction was not performed.

(M = Fe, Co) with alkenes.[18(f)] It was proposed that the positive charge on the metal centre makes the unsaturated carbon electrophilic. The alkyl group then migrates with its bonding pair onto the unsaturated carbon.

$RhCH_2^+$ and $NbCH_2^+$ are observed to react with both H_2 and CH_4, reactions (44)–(46).[49,50] Reaction (44) is proposed to have a four-centred intermediate like structure (**XII**).

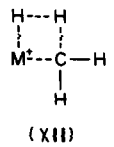

(XII)

$$(M = Nb, Rh) \quad MCH_2^+ + H_2 \rightarrow M^+ + CH_4 \quad (44)$$

$$RhCH_2^+ + CH_4 \rightarrow Rh^+ + C_2H_6 \quad (45)$$

$$NbCH_2^+ + CH_4 \rightarrow NbC_2H_4^+ + H_2. \quad (46)$$

Four-centred intermediates are also proposed for the reactions of MCH_2^+ (M = Fe, Co) and $FeNH^+$ with alkenes.[16,18] For example, $FeCD_2^+$ reacts with ethene (for products see Table 7) as in reactions (47) and (48). A mechanism which accounts for this is shown in Scheme 6, with a four-centred intermediate. Metallocyclic intermediates of this type

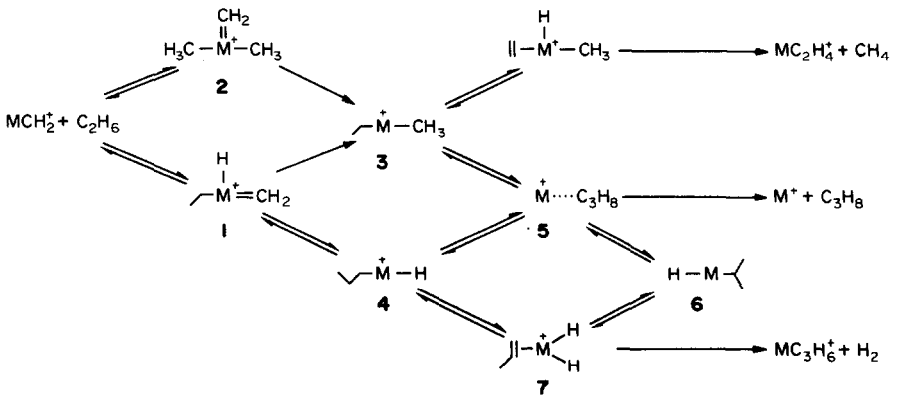

Scheme 5.

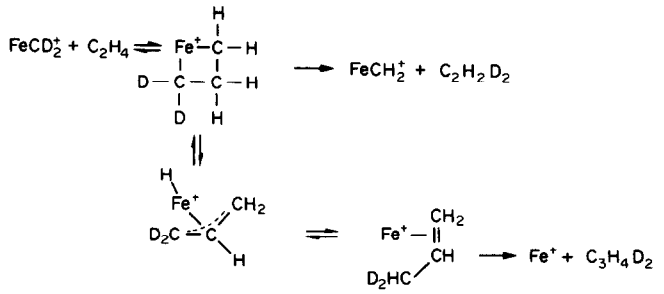

Scheme 6.

have also been observed in condensed phase.

$$FeCD_2^+ + C_2H_4 \longrightarrow Fe^+ + C_3H_4D_2 \quad (47)$$
$$\longrightarrow FeCH_2^+ + C_2H_2D_2. \quad (48)$$

$FeNH^+$ reacts with ethene via several reaction pathways including a metathesis reaction to form $FeCH_2^+$ and a homologation reaction to produce Fe^+.[16] These products indicate Fe^+ catalysed formation of an N—C bond, reaction (49), which is one of the first of its kind.

$$N_2O + NH_3 + C_2H_4 \xrightarrow{Fe^+} C_2H_5N + H_2O + N_2. \quad (49)$$

A mechanism consistent with these results is shown in Scheme 7.

The reaction of FeO^+ with C_2H_4 generates products analogous to those in the $FeNH^+/C_2H_4$ reaction. This suggests a generalized mechanism for reaction of the isoelectronic series $FeNH^+$, $FeCH_2^+$, FeO^+ with C_2H_4, Scheme 8.

Multiply charged metal ions have been observed to react almost exclusively via rapid charge exchange. Recently, however, we reported that Nb^{2+} reacts with CH_4 as in reactions (50)–(52).[51] $NbCH_2^{2+}$ formed in reaction (52) is observed to undergo rapid proton transfer to form $NbCH^+$. These studies yielded $D^0(Nb^{2+}—CH_2) = 197 \pm 10$ kcal mol^{-1} in comparison to $D^0(Nb^+—CH_2) = 109 \pm 5$ kcal mol^{-1}.

$$Nb^{2+} + CH_4 \longrightarrow Nb^+ + CH_4^+ \quad (50)$$
$$\longrightarrow NbH^+ + CH_3^+ \quad (51)$$
$$\longrightarrow NbCH_2^{2+} + H_2. \quad (52)$$

The effect of a multiple charge on the bond energies and reactivities of metal–ligand species will be the subject of further investigation.

L = *π-type ligands*. A number of novel reactions have been observed in the reactions of metal–olefin ion complexes. All of the reactions with hydrocarbons so far have involved some neutral losses (dehydrogenation, dealkylation, dehydration, loss of a ligand, etc.) to eliminate excess energy and stabilize the newly formed complex. However, $RhC_7H_6^+$, formed in reaction (53), reacts with H_2 to undergo the hydrogenation reaction (54).[52]

$$Rh^+ + \text{toluene} \rightarrow RhC_7H_6^+ + H_2 \quad (53)$$

$$RhC_7H_6^+ + H_2 \rightarrow RhC_7H_8^+. \quad (54)$$

This reaction is observed to go to completion with a rate constant of $(6 \pm 3) \times 10^{-11}$ cm^3 molecule^{-1} s^{-1}. The product ion, $RhC_7H_8^+$, was proposed to be stabilized by IR radiative stabilization.

$Co(Cp)^+$ reacts with alkanes by similar pathways to $Co(allyl)^+$.[53] As previously discussed, $Co(allyl)^+$ reacts mainly via dehydrogenation without coupling of the ligands. In a novel reaction, $Co(Cp)(alkene)^+$ complexes for C_5 and C_6 alkenes undergo collisionally activated dehydrocyclization to form $Co(Cp)_2^+$. As expected, this reaction occurs more readily for linear alkenes than for branched alkenes. $Co(Cp)^+$ also reacts with trans-1,3-pentadiene to

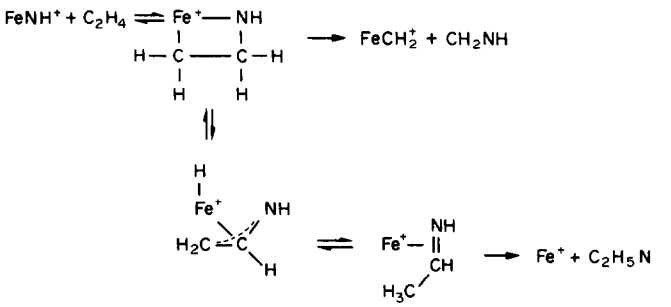

Scheme 7.

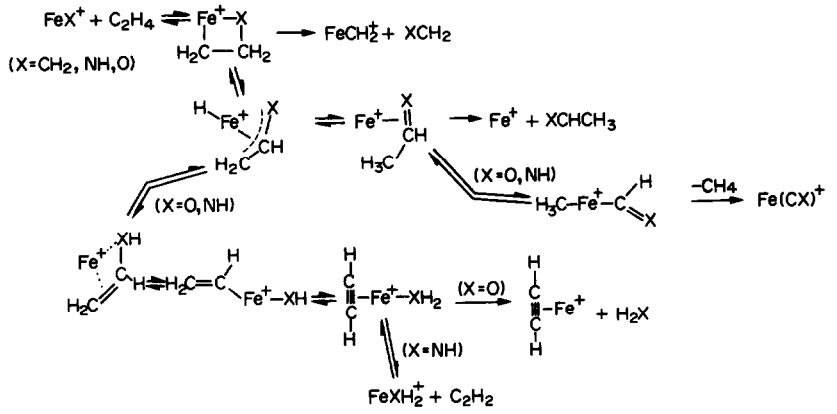

Scheme 8.

form $Co(Cp)_2^+$, reaction (55).

$$Co(Cp)^+ + \text{⌒⌒} \longrightarrow Co(Cp)_2^+ + H_2 + H^\cdot \quad (55)$$

Studies of M(alkene)$^+$ show that enhancement or reduction of available reaction routes can occur upon attachment of an alkene.[16,45,54] For Fe^+, reaction with 1-butene produces Fe(butadiene)$^+$, exclusively.[45] Fe(butadiene)$^+$ reacts with linear butenes via numerous reaction routes, reactions (56)–(59).

$$FeC_4H_6^+ + \text{linear butenes} \begin{cases} \rightarrow Fe(C_4H_6)_2^+ + H_2 & (56) \\ \rightarrow Fe(C_4H_6)C_2H_4^+ + C_2H_4 & (57) \\ \rightarrow FeC_6H_6^+ + C_2H_6 + H_2 & (58) \\ \rightarrow Fe(C_4H_6)CH_2^+ + C_3H_6. & (59) \end{cases}$$

In contrast, Sc^+, Y^+ and La^+ react more slowly and with fewer reaction pathways in their secondary reactions with alkanes relative to their primary reactions.[16,54] For example, La(alkene)$^+$ only reacts with C_3—C_5 cyclic alkenes, whereas La^+ reacts with C_2 and larger linear, cyclic and branched alkanes.

CONCLUSION

FTMS has been proven to be an excellent technique for generating and studying highly unsaturated metal–ligand ions. Many novel species including bare metal carbenes, alkyls, hydrides, amides, nitrenes, etc. can be prepared. Subsequent ion–molecule reactions and photodissociation have been used to derive thermodynamic information which is useful for proposing mechanisms and structures. The development of these tools will allow a fuller understanding of the effect of ligands on gas-phase metal ion reactivity.

Future directions for this research will be to investigate the effect of a second ligand on the bond strength of the first ligand as well as its effect on the overall reactivity. We have also recently observed marked changes in the reactivity of small transition metal cluster ions upon the addition of a ligand.[55] Clearly, the surface has just been scratched!

Acknowledgements—Metal–ligand ion research in our laboratory is supported by the Division of Chemical Sciences in the Office of Basic Energy Research in the United States Department of Energy (DE-FG02-87ER13766) and the National Science Foundation (CHE-8612234). S.W.B. also acknowledges the W. R. Grace Company for providing fellowship support.

REFERENCES

1. J. Allison, R. B. Freas and D. P. Ridge, *J. Am. Chem. Soc.* 1979, **101**, 1332.
2. For a review of gas phase metal–ion chemistry, see: J. Allison, in *Progress in Inorganic Chemistry*, Vol. 34, p. 628. (Edited by S. J. Lippard.) Wiley-Interscience, New York (1986).
3. (a) J. Allison and D. P. Ridge, *J. Am. Chem. Soc.* 1979, **101**, 4998; (b) A. Tsarbopoulos and J. Allision, *Organometallics* 1984, **3**, 86; (c) R. C. Burnier, G. D. Byrd and B. S. Freiser, *J. Am. Chem. Soc.* 1981, **103**, 4360; (d) D. B. Jacobson and B. S. Freiser, *J. Am. Chem. Soc.* 1983, **105**, 5797; (e) R. Houriet, L. F. Halle and J. L. Beauchamp, *Organometallics* 1983, **2**, 1818; (f) J. L. Elkind and P. B. Armentrout, *J. Am. Chem. Soc.* 1986, **108**, 2765; (g) D. A. Weil and C. L. Wilkins, *J. Am. Chem. Soc.* 1986, **108** 2765; (h) D. A. Peake and M. L. Gross, *J. Am. Chem. Soc.* 1987, **109**, 600; (i) C. Schulze, H. Schwarz, D. A. Peake and M. L. Gross, *J. Am. Chem. Soc.* 1987, **109**, 2368.
4. (a) J. L. Elkind and P. B. Armentrout, *J. Chem. Phys.* 4862, **84**, 1986; (b) P. B. Armentrout, J. L. Beauchamp and R. V. Hodges, *J. Chem. Phys.* 1977, **66**, 4683.
5. (a) M. B. Comisarow and A. G. Marshall, *Chem. Phys. Lett.* 1974, **25**, 282; (b) M. B. Comisarow and A. G. Marshall, *Chem. Phys. Lett.* 1974, **26**, 489; (c)

M. B. Comisarow and A. G. Marshall, *Can. J. Chem.* 1974, **52**, 1997.
6. (a) B. S. Freiser, *Talanta* 1985, **32**, 697; (b) T. J. Carlin, M. B. Wise and B. S. Freiser, *Inorg. Chem.* 1981, **20**, 2743.
7. (a) R. Tonkyn and J. C. Weisshaar, *J. Phys. Chem.* 1986, **90**, 2305; (b) D. Wang and R. R. Squires, *Organometallics* 1985, **6**, 697.
8. R. B. Cody, R. C. Burnier, W. D. Reents Jr, T. J. Carlin, D. A. McCrery, R. K. Lengal and B. S. Freiser, *Int. J. Mass Spec. Ion Phys.* 1980, **33**, 37.
9. (a) R. Georgiadis and P. B. Armentrout, *J. Am. Chem. Soc.* 1986, **108**, 2119; (b) P. B. Armentrout and J. L. Beauchamp, *Chem. Phys.* 1980, **48**, 315.
10. (a) D. A. Peake, M. L. Gross and D. P. Ridge, *J. Am. Chem. Soc.* 1984, **106**, 4307; (b) R. B. Cody and B. S. Freiser, *Int. J. Mass Spec. Ion Phys.* 1982, **41**, 199; (c) R. G. Cooks, *Collision Spectroscopy*. Plenum, New York (1978).
11. R. C. Dunbar, *Gas Phase Ion Chemistry*, Vol. 3, Chap. 20. (Edited by M. T. Bowers.) Academic Press, New York (1984).
12. (a) D. A. Laude, C. L. Johlman, R. S. Brown, D. A. Weil and C. L. Wilkins, *Mass Spec. Rev.* 1986, **5**, 107 and refs cited within; (b) A. G. Marshall, *Acc. Chem. Res.* 1985, **18**, 316.
13. M. B. Comisarow, G. Parisod and V. Grassi, *Chem. Phys. Lett.* 1978, **57**, 413.
14. (a) M. Bensimon and R. Houriet, *Int. J. Mass Spec. Ion. Proc.* 1986, **72**, 93; (b) R. A. Forbes, L. M. Lech and B. S. Freiser, *Int. J. Mass Spec. Ion. Proc.* 1987, **77**, 107.
15. H. Kang and J. L. Beauchamp, *J. Phys. Chem.* 1985, **89**, 3364.
16. L. M. Lech, S. W. Buckner, Y. Huang, T. J. MacMahon, J. R. Gord and B. S. Freiser, unpublished results.
17. T. J. Carlin and B. S. Freiser, *Anal. Chem.* 1983, **55**, 571.
18. (a) D. B. Jacobson and B. S. Freiser, *J. Am. Chem. Soc.* 1984, **106**, 3891; (b) D. B. Jacobson and B. S. Freiser, *J. Am. Chem. Soc.* 1984, **106**, 3900; (c) D. B. Jacobson and B. S. Freiser, *J. Am. Chem. Soc.* 1985, **107**, 67; (d) D. B. Jacobson and B. S. Freiser, *J. Am. Chem. Soc.* 1985, **107**, 2605; (e) D. B. Jacobson and B. S. Freiser, *J. Am. Chem. Soc.* 1985, **107**, 4373; (f) D. B. Jacobson and B. S. Freiser, *J. Am. Chem. Soc.* 1985, **107**, 5876.
19. (a) T. J. Carlin, L. Sallans, C. J. Cassady, D. B. Jacobson and B. S. Freiser, *J. Am. Chem. Soc.* 1983, **105**, 6320; (b) D. B. Jacobson and B. S. Freiser, *J. Am. Chem. Soc.* 1984, **106**, 4623; (c) D. B. Jacobson and B. S. Freiser, *J. Am. Chem. Soc.* 1984, **106**, 5351.
20. R. L. Hettich, T. C. Jackson, E. M. Stanko and B. S. Freiser, *J. Am. Chem. Soc.* 1986, **108**, 5086.
21. R. L. Hettich and B. S. Freiser, *J. Am. Chem. Soc.* 1986, **108**, 2537.
22. D. B. Jacobson and B. S. Freiser, *J. Am. Chem. Soc.* 1983, **105**, 736.
23. P. B. Armentrout, L. F. Halle and J. L. Beauchamp, *J. Am. Chem. Soc.* 1981, **103**, 6624.
24. (a) G. D. Byrd and B. S. Freiser, *J. Am. Chem. Soc.* 1982, **104**, 5944; (b) D. B. Jacobson and B. S. Freiser, *J. Am. Chem. Soc.* 1985, **107**, 72.
25. D. B. Jacobson and B. S. Freiser, *Organometallics* 1984, **3**, 513.
26. S. W. Buckner and B. S. Freiser, *J. Am. Chem. Soc.* 1987, **109**, 4715.
27. L. F. Halle, R. Houriet, M. Kappes, R. H. Staley and J. L. Beauchamp, *J. Am. Chem. Soc.* 1982, **104**, 6293.
28. E. Murad, *J. Chem. Phys.* 1980, **73**, 1381.
29. R. R. Corderman and J. L. Beauchamp, *J. Am. Chem. Soc.* 1976, **98**, 3998.
30. (a) R. W. Jones and R. H. Staley, *Int. J. Mass Spec. Ion. Phys.* 1981, **39**, 35; (b) J. S. Uppal and R. H. Staley, *J. Am. Chem. Soc.* 1982, **104**, 1235.
31. C. J. Cassady and B. S. Freiser, *J. Am. Chem. Soc.* 1984, **106**, 6176.
32. (a) R. G. Cooks and T. L. Kruger, *J. Am. Chem. Soc.* 1977, **99**, 1279; (b) S. A. McLuckey, D. Cameron and R. G. Cooks, *J. Am. Chem. Soc.* 1981, **103**, 1313; (c) S. A. McLuckey, A. E. Schoen and R. G. Cooks, *J. Am. Chem. Soc.* 1982, **104**, 848.
33. P. B. Armentrout and J. L. Beauchamp, *J. Am. Chem. Soc.* 1981, **103**, 784.
34. J. L. Beauchamp, private communication.
35. M. Mautner, *J. Am. Chem. Soc.* 1982, **104**, 5.
36. L. Sallans, K. R. Lane, R. R. Squires and B. S. Freiser, *J. Am. Chem. Soc.* 1985, **107**, 4379.
37. L. Operti, E. C. Tews and B. S. Freiser, *J. Am. Chem. Soc.*, in press.
38. P. B. Armentrout, private communication.
39. P. B. Armentrout and J. L. Beauchamp, *J. Am. Chem. Soc.* 1981, **103**, 784.
40. M. F. Lappert, P. P. Power, A. R. Sanger and R. C. Srivastava, *Metal and Metalloid Amides*. Ellis Horwood Ltd, West Sussex, U.K. (1980).
41. (a) J. Allison and B. D. Radecki, *J. Am. Chem. Soc.* 1984, **106**, 946; (b) S. J. Babinec and J. Allison, *J. Am. Chem. Soc.* 1984, **106**, 7718.
42. H. E. Bryndza, L. K. Fong, R. A. Paciello, W. Tam and J. E. Bercaw, *J. Am. Chem. Soc.* 1987, **109**, 1444.
43. N. Aristov and P. B. Armentrout, *J. Am. Chem. Soc.* 1984, **106**, 4065.
44. C. J. Cassady and B. S. Freiser, *J. Am. Chem. Soc.* 1986, **108**, 5690.
45. D. B. Jacobson and B. S. Freiser, *J. Am. Chem. Soc.* 1983, **105**, 7484.
46. T. C. Jackson, D. B. Jacobson and B. S. Freiser, *J. Am. Chem. Soc.* 1984, **106**, 1252.
47. T. C. Jackson, T. J. Carlin and B. S. Freiser, *J. Am. Chem. Soc.* 1986, **108**, 1120.
48. T. C. Jackson, T. J. Carlin and B. S. Freiser, *Int. J. Mass Spec. Ion. Proc.* 1986, **72**, 169.
49. D. B. Jacobson and B. S. Freiser, *J. Am. Chem. Soc.* 1985, **107**, 5870.
50. R. L. Hettich and B. S. Freiser, *J. Am. Chem. Soc.* 1987, **109**, 3543.
51. S. W. Buckner and B. S. Freiser, *J. Am. Chem. Soc.* 1987, **109**, 1247.

52. D. B. Jacobson and B. S. Freiser, *J. Am. Chem. Soc.* 1984, **106**, 1159.
53. D. B. Jacobson and B. S. Freiser, *J. Am. Chem. Soc.* 1985, **107**, 7399.
54. Y. Huang, M. B. Wise, D. B. Jacobson and B. S. Freiser, *Organometallics* 1987, **6**, 346.
55. S. W. Buckner, J. R. Gord and B. S. Freiser, *J. Chem. Phys.* 1988, **88**, 3678.
56. R. C. Burnier and B. S. Freiser, *Inorg. Chem.* 1979, **18**, 906.
57. P. B. Armentrout and J. L. Beauchamp, *J. Chem. Phys.* 1981, **74**, 2819.
58. P. B. Armentrout, L. F. Halle and J. L. Beauchamp, *J. Am. Chem. Soc.* 1981, **103**, 6501.
59. D. B. Jacobson, G. D. Byrd and B. S. Freiser, *Inorg. Chem.* 1984, **23**, 553.
60. L. F. Halle, P. B. Armentrout and J. L. Beauchamp, *Organometallics* 1982, **1**, 963.
61. S. Evans, M. F. Guest, I. H. Hillier and E. F. Orchard, *J. Chem. Soc., Faraday Trans. II* 1974, **70**, 417.
62. J. L. Elkind and P. B. Armentrout, *Inorg. Chem.* 1986, **25**, 1078.
63. D. B. Jacobson, private communication.

Polyhedron Vol. 7, No. 16/17, pp. 1605–1608, 1988
Printed in Great Britain

0277-5387/88 $3.00+.00
© 1988 Pergamon Press plc

GAS-PHASE FIRST BOND DISSOCIATION ENERGIES IN TRANSITION-METAL CARBONYLS

G. P. SMITH

Departmental of Chemical Kinetics, SRI International, Menlo Park, CA 94025, U.S.A.

Abstract—Bond dissociation energy values for a group of transition-metal carbonyl compounds and derivatives in the gas phase are given and discussed. Metals include Fe, Cr, Mo, W and Mn. New preliminary values of 38 and 44 kcal mol^{-1} are reported for $Mn_2(CO)_9$—CO and $MnBr(CO)_4$—CO.

The rapid, recent growth in the study of heterogeneous and homogeneous catalysis has been prompted by the importance of many such industrial processes in synthesis, fuel refining and environmental controls, as well as a basic desire to examine the large ensemble of elements involved. To understand these mechanisms and to improve or replace them requires quantitative determinations of the relationships between structure, bonding and reactivity. One key need in this area is a thermodynamic and kinetic data base for the relevant bond scissions. This information is also important to the mechanisms of organometallic chemical and photochemical deposition processes used in electronics manufacturing.

Transition-metal carbonyls and their derivatives are an important class of the above-mentioned compounds. They are known to catalyse and to be intermediates in industrially important processes, including hydroformylation, acetic acid synthesis and related processes. Although there are many hundreds of papers on the reaction chemistry of metal carbonyls, until recently the basic data on the energy required to remove the key first ligand, the bond dissociation energy (BDE), had not been well determined. Indeed, one reason for the paucity of gas-phase organometallic BDE data is the great tendency of the parent and product species to react on hot surfaces. With the arrival of new laser methods, techniques are now becoming available to build such a data base. This, in turn, will also allow comparisons to values in solution, single ligands bound to metal atoms (the last bond energy), bond strengths to bulk surfaces or clusters and the average bond strength for all ligands in the compound (a thermodynamic quantity). With enough values, predictions of BDEs for many other compounds by group-additivity-type relations should then become possible.

In this paper, we will briefly describe one such method, laser powered homogeneous pyrolysis (LPHP), which uses a pulsed-IR laser as the heating source. Cool walls prevent surface reactions. Our previously published results will be summarized without portending to be a complete review on the subject. Finally, a few new results on manganese carbonyl BDEs will be reported, and the implications to general BDE trends and to other mechanistic studies will be discussed.

EXPERIMENTAL

The LPHP technique is fully described elsewhere.[1] A flow of gases is directed into a cylindrical irradiation cell at 30–100 torr pressure, and then into a mass spectrometer for analysis. The gas mixture contains SF_6 infrared absorber, a majority of nitrogen bath gas and small quantities of the organometallic, and of a standard compound (thermometer) whose kinetic decomposition rate constant parameters (log A and E) are known. A logarithmic plot of the relative yields, $\ln(kt)$, has a slope of the relative activation energies, from which the unknown BDE can be determined. (This assumes there is no additional kinetic barrier to the decomposition.) A value can also be deduced from single-temperature measurements, provided one has a good estimate of the A-factor from transition-state theory or measurements on similar compounds. In cases where secondary or catalytic reactions may interfere, the use of trapping agents or separate sequential runs with the unknown and standard may be necessary.

The basic physics of the LPHP method, as docu-

mented by various diagnostics,[2] are as follows. A pulsed-CO_2 laser vibrationally excites the absorber, without multiphoton decomposition. Rapid intermolecular energy transfer collisions quickly heat all components of the mixture within the irradiated region to a high and true temperature on the microsecond time scale of the laser pulse. Unimolecular reactions begin. The hot gas at higher pressure then expands outwards and cools, typically from 800 to 650 K for the carbonyl experiments. At the speed of sound for our heated volume of 1.8 cm diameter, this takes 15 μs. At this point, pressures have equalized and further unimolecular reactions are quenched by the cooling. Further transport cooling and mixing proceeds and concludes before the next laser pulse.

PREVIOUS RESULTS

Table 1 summarizes most of the results from our previous studies of transition-metal carbonyl BDEs.[1] The $Cr(CO)_6$ decomposition was measured relative to the dicyclopentadiene retro-Diels–Alder reaction, and the other carbonyls relative to chromium. The additional values are derived from gas-phase thermodynamic heats of formation measured calorimetrically,[3] since the monodentate carbonyl BDE also gives the unsaturated fragment heat of formation. Thus, many BDEs can be derived from one measurement, which illustrates the need for a larger thermodynamic data base as well. The gas-phase BDE value for nickel tetracarbonyl is from a photodetachment experiment,[4] and is included for completeness.

Since these results and comparisons to other relevant work are fully discussed in ref. 1, and another paper[5] in this symposium addresses the Group 6 compounds in detail, only the main conclusions will be summarized here. For all the carbonyls of our studies except chromium, the first bond dissociation was the strongest and rate-determining one. Reasonable values of log $A \simeq 15.5$ were found. Since the ground state of $Fe(CO)_4$ is a triplet to which dissociation is spin forbidden, the iron values probably correspond to singlet production, as expected kinetically.

Table 1. Metal carbonyl bond dissociation energies (kcal mol^{-1})

$M(CO)_n$—L		D(298)	E(avg)
$Fe(CO)_5$		41.5	28.0
$Cr(CO)_6$		36.8	26.0
$Mo(CO)_6$		40.5	36.0
$W(CO)_6$		46.0	43.0
$Ni(CO)_4$	(ref. 4)	25.0	35.0
$Fe(CO)_4C_2H_4$		37.2	
$Fe(CO)_4Fe(CO)_5$		41.0	
$W(CO)_5$pyridine		39.5	
$W(CO)_5$pyrazine		35.5	
$W(CO)_5$pyrazole		33.0	
$W(CO)_5$piperidine		44.7	
$W(CO)_5NCCH_3$		42.7	

A comparison of the BDE with the average bond energy of all the CO ligands, E,[3] is also given in Table 1. The deviations are at least 10 kcal for period 4, and clearly indicate the danger of using the average and thermodynamic value for the often unknown, kinetically important first BDE. That is, the simple bond additivity principle of transferability[3] appears inapplicable. The only example in period 6, tungsten, however, shows enough good agreement to suggest the possible utility of this simpler procedure for accurately estimating BDEs for the heaviest transition metals.

One can also generalize, perhaps prematurely, certain trends in the BDE values. Going down Group 6, the bond energies increase. Compared to CO, ethylene and the aromatic nitrogen heterocycles appear to be weaker ligands, while the bonds to piperidine and acetonitrile are roughly as strong. However, when one compares[1] these implications with some of the known solution kinetics results, discrepancies exist. This suggests alternate mechanisms or solvent effects, which will also need to be separated out and characterized in order to understand the whole process. The value for the η^2 ethylene bond is interestingly, and perhaps fortuitously, 0.4 times that in the η^5 ferrocene.[6,7] The thermodynamically derived value[8] for $Fe_2(CO)_9$ must be applied with caution to kinetics, since several bonds must be broken or rearranged in this bridged compound, and the lack of additional barriers cannot be presumed.

MANGANESE CARBONYLS

We first attempted a conventional very low pressure pyrolysis (VLPP) experiment on $Mn_2(CO)_{10}$, similar to our earlier work on and evaluation[15] of main group alkyl compounds. This was prompted by the reported observation of equilibria with $Mn(CO)_5$ in a graphite flow reactor by mass spectroscopy,[10] accompanied by a BDE value of 21 kcal mol^{-1}. We observed clear signs of catalytic decomposition at the 500 K temperatures of ref. 10, an occurrence previously seen for several other organometallic compounds. It is also worth noting that compounds with low BDEs near 25 kcal mol^{-1} will not be amenable to gas-phase studies. Given a

moderate A-factor of $10^{15.5}$, lifetimes range from 6 min at room temperature to only 20 μs at 500 K. Thus studies giving such low values must be carefully examined.

Two LPHP experiments were performed on $Mn_2(CO)_{10}$, at 773 K and 782 K according to the $Mo(CO)_6$ standard used in this instance. Addition of an excess of PF_3 as a trap had no effect on the manganese carbonyl disappearance rate, no trapped products were observed, and metal particulates were formed similar to the other carbonyls. This indicated complete decomposition with the initial bond scission being the rate-determining step.[1] A marked tendency of the compound to stick to surfaces was observed by the mass spectrum time decay when the gas flow was diverted around the carbonyl pick-up reservoir. Unfortunately, this prevented the aquisition of more data points and the operation over a wide enough range of temperatures to obtain the usual relative $\ln(kt)$ plot.

An activation energy for dissociation, and hence a BDE, can still be determined from the data if one knows the decomposition path and can estimate an A-factor. Some early kinetics evidence suggested Mn—Mn bond scission was occurring.[9,10] However, more recent studies using ligand substitution,[11] isotope substitution,[12] and sonolysis[13] clearly show that CO loss is the predominant thermal decomposition mechanism. Thus we can assume an A-factor of $10^{15.5}$ similar to those measured (and expected from transition-state theory) for the other carbonyls. Then these experiments give a BDE of 38 ± 2 kcal mol^{-1} for CO loss from $Mn_2(CO)_{10}$. This value is in good agreement with the 37 kcal activation energy measured for the ligand substitution reaction in solution.[11] Our attempts to use PF_3 to trap $Mn_2(CO)_9$ or CCl_4 to trap $Mn(CO)_5$ were unsuccessful due to the subsequent complete decomposition to metal atoms. (In fact, the particles or some earlier decomposition product catalysed the conversion of CCl_4 to C_2Cl_6.)

We also performed two preliminary LPHP experiments to measure $Mn(CO)_5Br$ decomposition relative to $Fe(CO)_5$, at 787 and 809 K. Again, assuming $\log A = 15.5$, we derive a BDE for CO loss of 44 ± 2 kcal mol^{-1}. It appears that the substitution of a bromine increases the bond strength to the CO. This suggests that the bromine increases the backbonding to the CO by donating electron density through Π bonding with empty metal d orbitals, rather than by withdrawing electron density by virtue of its electronegativity. Following the pattern seen for most of the other period 4 carbonyls, these BDEs are much higher than the average value of 25 kcal mol^{-1} given for all CO ligands.[3] Finally, it should also be remembered that $Mn_2(CO)_9$ is probably a bridged structure,[14] and some of the rearrangement to this most stable form may occur after the CO dissociation kinetics measured above. Thus, the kinetic value above is an upper limit to the thermodynamic BDE value and the radical heat of formation.

Relative BDEs for a large series of monosubstituted manganese carbonyls have been measured calorimetrically,[3] and could be put on an absolute basis by knowing the Mn—Mn BDE in $Mn_2(CO)_{10}$. In addition, this bond is active in the compound's photochemistry. In view of the CO dissociation kinetics described above, previously reported low values for the Mn—Mn scission appear unreliable. Can any limits on this value be deduced from the above CO BDE number? A-factors for scission into two bulky polyatomic fragments, tetramethyl butane for example, are usually 10^{16} or greater. The solution data[12] indicate less than 5% of the bond scission at 423 K is Mn—Mn scission. This requires the Mn—Mn bond be at least 4 kcal stronger than the Mn—CO bond, which then also predicts less than 20% of our measured LPHP reaction at 775 K is Mn—Mn bond scission. Thus the data suggest the metal–metal BDE in $Mn_2(CO)_{10}$ is greater than 42 kcal mol^{-1}, and the lower limits shown in Table 2 can be derived from the relative values.[3] This result is consistent with the value of 38 ± 5 kcal mol^{-1} from a photoacoustic calorimetry study in solution[15] and the value of 41 ± 9 kcal mol^{-1} from a recent appearance potential result.[16]

The relative values and trends in these BDEs are discussed in ref. 3, but the significance of the actual

Table 2. Manganese carbonyl bond dissociation energies (kcal mol^{-1})

$Mn(CO)_n$—L	$D(298)$
$Mn_2(CO)_9$—CO	38
$MnBr(CO)_4$—CO	44
$Mn(CO)_5$—$Mn(CO)_5$	>42
$Mn(CO)_5$—Br	>77
$Mn(CO)_5$—Cl	>90
$Mn(CO)_5$—I	>66
$Mn(CO)_5$—H	>70
$Mn(CO)_5$—CH_3	>56
$Mn(CO)_5$—phenyl	>60
$Mn(CO)_5$—benzyl	>40
$Mn(CO)_5$—acetyl	>50
$Mn(CO)_5$—benzoyl	>41
$Mn(CO)_5$—CF_3	>61
$Mn(CO)_5$—$COCF_3$	>55

values can now be addressed. Bonds stronger than about 60 kcal will be difficult to break, the ligands less labile, and slow participants in kinetic processes under operating conditions. The halides are very tightly held, in the expected order as well. The Mn—Br bond in $MnBr(CO)_5$ is over 30 kcal stronger than the Mn—CO BDE observed in the LPHP experiment. This is consistent with the hypothesis in the last paragraph that halogen pΠ orbital overlap with empty metal $d\Pi$ orbitals results in electron donation to the metal, which in turn increases the strength of backbonding to the CO. The hydrocarbon radical BDEs show the same trends as in carbon and tin based systems,[17] including the resonance stabilization gained by the dissociated benzyl. The family of manganese BDEs are roughly equal to those known for mercury systems, but lower than the comparable tin values.[17]

The manganese BDEs for methyl, acetyl and CO are considerably below the high hydrogen atom BDE. Thus steps involving the former ligands can be considered more probable in catalytic mechanisms, while one would expect hydrogen ligands involved in any such steps to tend to remain firmly attached and relatively inactive. This extra 14 kcal stability shown in the H vs CH_3 BDE makes hydrogen more difficult to activate than carbon. For example, carbonylation of hydrocarbons is favoured over that of hydrogen (Fischer–Tropsch) because the insertion step to form $Mn(CO)_5CHO$ will be endothermic, given a reasonable estimate of its enthalpy.[3] Another consequence pointed out in ref. 3 is that the $Mn(CO)_5C_2H_5$ decomposition path to eliminate ethene and form the stable hydride is only 25 kcal mol^{-1} endothermic. One final result of the strong BDEs found here is that the product-forming binuclear reductive elimination step in hydroformylation appears to be endothermic in the gas phase, suggesting the importance of the solvent to the mechanism of aldehyde formation.

More precise experiments will be needed to better measure the heat of formation of $Mn(CO)_5$ and thus to determine well a whole series of relevant gas phase BDEs. This work does illustrate the advantage of when one can also do a series of calorimetric determinations on related, volatile organometallics. A full series of LPHP experiments on $Mn_2(CO)_{10}$ in the future would help refine the CO BDE value, and at least set a better limit on the metal–metal BDE than the rough value given above. In addition, we hope to use a new molecular beam sampling mass spectrometer apparatus to identify the products by directly sampling from the laser pyrolysis region. In the meantime, the manganese BDE values in Table 2 should be applicable to mechanistic studies of Group 7 homogeneous catalysis, and values for comparison from other groups remaining to be measured.

Acknowledgements—It is a great pleasure to thank my colleagues in this work, Karan Lewis, David Golden and Richard Laine.

REFERENCES

1. K. E. Lewis, D. M. Golden and G. P. Smith, *J. Am. Chem. Soc.* 1984, **106**, 3905.
2. D. M. McMillen, K. E. Lewis, G. P. Smith and D. M. Golden, *J. Phys. Chem.* 1982, **86**, 709.
3. J. A. Connor, *Curr. Top. Chem.* 1977, **71**, 71; J. A. Connor, M. T. Zafaranin-Moattar, J. Bickerton, N. I. El Saied, S. Suradi, R. Carson, G. Al Takhin and H. A. Skinner, *Organometallics* 1982, **1**, 1166.
4. A. E. Stevens, C. S. Feigerle and W. C. Lineberger, *J. Am. Chem. Soc.* 1982, **104**, 5026.
5. G. K. Yang, V. Vaida and K. S. Peters, *Polyhedron* 1988, **7**, 1619.
6. K. E. Lewis and G. P. Smith, *J. Am. Chem. Soc.* 1984, **106**, 4650.
7. The second BDE for ferrocene given in ref. 6 should be raised to 67 kcal mol^{-1} if one uses the recommended value for the cyclopentadienyl heat of formation given by D. F. McMillen and D. M. Golden in *A. Rev. Phys. Chem.* 1982, **33**, 493.
8. The value given in ref. 1 is miscalculated.
9. R. A. Jackson and A. Poe, *Inorg. Chem.* 1978, **17**, 997.
10. D. R. Bidinosti and N. S. McIntyre, *Can. J. Chem.* 1970, **48**, 593.
11. H. Wawersik and F. Basolo, *Inorg. Chem. Acta* 1969, **3**, 113; *Chem. Commun.* 1966, p. 366.
12. N. J. Coville, A. M. Stolzenberg and E. L. Muetterties, *J. Am. Chem. Soc.* 1983, **105**, 2499.
13. K. S. Suslick and P. F. Schubert, *J. Am. Chem. Soc.* 1983, **105**, 6042.
14. A. F. Hepp and M. S. Wrighton, *J. Am. Chem. Soc.* 1983, **105**, 5934.
15. J. L. Goodman, K. S. Peters and V. Vaida, *Organometallics* 1986, **5**, 815.
16. J. A. Martinho Simões, J. C. Schultz and J. L. Beauchamp, *Organometallics* 1985, **4**, 1238.
17. G. P. Smith and R. Patrick, *Int. J. Chem. Kinet.* 1983, **15**, 167.

Polyhedron Vol. 7, No. 16/17, pp. 1609–1618, 1988
Printed in Great Britain

0277–5387/88 $3.00+.00
© 1988 Pergamon Press plc

HYDRIDE TRANSFER TO TRANSITION-METAL CARBONYLS IN THE GAS PHASE. FORMATION AND RELATIVE STABILITIES OF ANIONIC FORMYL COMPLEXES

KELLEY R. LANE and ROBERT R. SQUIRES*

Department of Chemistry, Purdue University, West Lafayette, IN 47907, U.S.A.

Abstract—The hydride binding energies of $Fe(CO)_5$, $Cr(CO)_6$, $Mo(CO)_6$ and $W(CO)_6$ ($HA(M(CO)_n) = D[(CO)_{n-1}MCO—H^-]$) have been estimated from bimolecular hydride transfer reactions in the gas phase. Hydride transfer to the metal carbonyls yields the corresponding anionic formyl complexes and the hydride affinity bracketing experiments establish $HA(Fe(CO)_5) = 56 \pm 4$ kcal mol^{-1} and $HA(Cr(CO)_6) = HA(Mo(CO)_6) = HA(W(CO)_6) = 44 \pm 4$ kcal mol^{-1}. Gas-phase heats of formation and metal–carbon bond strengths for the metal formyl anions are derived from the hydride binding energies. The hydride affinity ordering for the metal carbonyls parallels their relative reactivities towards nucleophilic addition in solution and correlates with the relative magnitudes of their CO-stretching force constants (k_{CO}). The new metal formyl data are combined with known or estimated heats of formation for metal hydrides to show that CO-insertion into the metal–hydrogen bond is thermodynamically unfavourable for these systems.

A major growth area in organometallic chemistry over the last decade has involved the search for efficient, homogeneous catalysts which can affect the conversion of C_1 oxygenates and other small molecules into more complex organic compounds of practical value. Many clever strategies for CO and CO_2 reduction, carbon–carbon bond formation and functional group manipulation have emerged from the extensive experimental activity in this area.[1–10] Transition-metal formyl complexes, hydridometal carbonyls, metal oxy-carbenes (Fischer carbenes) and α-hydroxy metal alkyls are commonly invoked as reactive intermediates in both catalytic and stoichiometric CO reduction reactions.[1–5] A wide variety of transition metal formyls[11] and hydridocarbonyls[2,12–14] are known as stable species in solution. Many have been generated independently under conditions where the kinetic and mechanistic details of their role in CO reduction cycles could be assessed. The critical thermochemical data that are necessary to define a complete picture of these catalytic cycles are largely absent, however, owing to the high reactivity and/or lability of many of the proposed intermediates which often precludes the usual equilibrium, calorimetric or thermokinetic measurements.

Recently, we have explored the utility of gas-phase ion/molecule reactions in a flowing afterglow apparatus as a means to obtain thermochemical information for organometallic intermediates in model catalytic cycles. The key advantage of gas-phase ion experiments in the present context is the ability to create reactive (ionic) species in the absence of the complicating effects of solvent coordination and ion pairing. For example, we have succeeded in generating and characterizing several previously unknown hydroxycarbonyl complexes (metallocarboxylic acids) related to base-catalysed water–gas shift cycles,[15,16] as well as an extensive series of iron acyl anions involved in nucleophilic addition reactions of $Fe(CO)_5$.[17,18] We have also recently described an experimental protocol for examining hydride transfer reactions of $Fe(CO)_5$ and for obtaining thermochemical information for a prototype iron formyl complex $(CO)_4FeCHO^-$.[19] We have now extended these procedures to the group 6 hexacarbonyls, $M(CO)_6$, M = Cr, Mo, W, and present here the results of our determination of their hydride binding energies along with a discussion of the relative stabilities of the corresponding anionic formyl complexes.

* Author to whom correspondence should be addressed.

EXPERIMENTAL

All measurements were carried out at room temperature using a conventional flowing afterglow apparatus that has been documented previously.[16] Briefly, the system consists of an electron impact ion source, a meter-long helium flow reactor and a quadrupole mass spectrometer detector located behind a 0.5 mm ion-sampling orifice in a stainless steel nose-cone. Primary reagent ions formed at the source are rapidly thermalized by collisions with the helium buffer gas (P(He) = 0.4 torr) and are carried through the reactor with a bulk flow velocity of *ca* 9000 m s^{-1}, as determined by a high capacity Roots blower and a mass-flow controller. Ion/molecule reactions are initiated by the addition of pure, gaseous reagents through fixed inlets located at various positions along the flow tube, or through a moveable neutral gas injector.

Rate coefficients for bimolecular reactions are determined from semi-log plots of the decay of the reactant ion signal versus the distance between the sampling orifice and the moveable injector position with constant neutral flow rate.[20,21] Sulphur hexafluoride is added to the reactor through an upstream inlet ($P(SF_6) < 1 \times 10^{-3}$ torr) during kinetic determinations involving metal carbonyls in order to minimize diffusional variations in the plasma by establishing SF_6^- (*m/z* 146) as a constant, massive negative charge carrier.[17,22] Primary product distributions for reactions in the flow tube are determined by extrapolation of the normalized product ion yields to neutral reagent flow rate or zero reaction time.[23] Neutral products of gas-phase ion/molecule reactions are not detected directly and their structures are inferred.

Most of the hydride donor anions employed in this study were generated from the corresponding neutral conjugate acids by proton transfer to either OH^- or NH_2^-. These primary reagent ions were, in turn, produced by electron impact on an N_2O/CH_4 mixture (1 : 2) and anhydrous NH_3, respectively. The pentavalent silicon hydride ion, $Et_3SiH_2^-$, was produced from direct addition of H^- to triethylsilane.[24] The hydride ion was generated by electron impact on either NH_3 or CH_4.

The group 6 metal carbonyls are of insufficient volatility to permit reliable measurement of their head-vapour flow rates into the reactor, thereby precluding kinetics measurements with these substrates. In order to maximize the concentration of the metal carbonyls in the reactor, a helium-flow inlet was employed. It consists of a 50 cm^3 round-bottomed flask containing the solid sample, which is attached via 1/4 in stainless steel tubing to a high-conductance on/off valve directly mounted to the flow tube at a position 55 cm from the nose-cone. A slow stream of purified helium is passed over the sample (*ca* 5 STP cm^3 s^{-1}) to facilitate sample transport through the valve, and gentle heating ($T < 90°C$) is occasionally used to increase the sample vapour pressure.

The gases used were obtained from commercial suppliers and had the following purities: He (99.995%), NH_3 (anhydrous, 99.99%), N_2O (99.0%), CH_4 (99.0%), 1-butene (99.0%). The metal carbonyls and the liquid samples were also obtained commercially and were used without further purification, except for degassing just prior to use.

RESULTS

In order to provide a proper background for the new results concerning the group 6 metal carbonyls, we first present a general discussion of gas-phase hydride affinities, followed by a review of the earlier results for $Fe(CO)_5$.

Hydride affinities

The hydride affinity of a neutral compound, *HA*(X), is defined as the gas-phase enthalpy of dissociation of the corresponding hydrogen-bearing negative ion, HX^-, to free hydride and neutral X [eq. (1)].[25]

$$HX^- \xrightarrow{\Delta H(1)} H^- + X \qquad (1)$$

$$HA(X) = \Delta H(1) = \Delta H_f(H^-) + \Delta H_f(X) - \Delta H_f(HX^-).$$

Hydride affinities are established for numerous atoms and molecules, and the known values span a range from 8 kcal mol^{-1} for X = CO to 169 kcal mol^{-1} for $X = C_2$.[26] These data are readily calculated from known heats of formation for the neutral compound X and the corresponding anion HX^-. Heats of formation for negative ions are available from gas-phase acidity[25] and electron affinity measurements,[27] as well as from mass spectrometric appearance potential data.[28] For example, the gas-phase acidity of methanol ($D[CH_3O^-—H^+]$) is well established at 381.6 kcal mol^{-1},[29] from which $\Delta H_f[CH_3O^-, g] = -32.3$ kcal mol^{-1} may be derived. Combining this with $\Delta H_f[H^-, g] = 34.7$ kcal mol^{-1} [25] and $\Delta H_f[CH_2O, g] = -26.0$ kcal mol^{-1} [30] yields a hydride affinity for formaldehyde, $HA(CH_2O)$, of 41.0 kcal mol^{-1}. Similarly, the gas-phase acidity and heat of formation of CH_3CH_2CN may be combined with the heat of formation for $CH_2{=}CHCN$ to derive $HA(CH_2{=}CHCN) = 56.3$ kcal mol^{-1}.[26]

A representative listing of hydride affinities for several compounds is provided in Table 1. In general, simple aliphatic aldehydes and ketones have hydride affinities in the 38–45 kcal mol^{-1} range, while α,β-unsaturated nitriles and carbonyl compounds have somewhat higher values (55–60 kcal mol^{-1}). The boranes[31] and unsaturated compounds possessing strongly electronegative substituents occupy the high-affinity end of the scale, while the silanes[24] and low-energy, unsaturated molecules such as CO and benzene occupy the low-affinity end.

When the appropriate reference thermochemical data are not available for a particular anion HX^-, the hydride affinity of a stable molecule X can occasionally be determined experimentally from the outcome of gas-phase hydride transfer reactions. By operating on the reasonable assumption that an ion/molecule reaction in the gas phase will occur at an observable rate only if the enthalpy change is zero or negative,[32] one may infer a hydride affinity ordering for a series of compounds by noting the allowed directions of bimolecular hydride transfer. This so-called "affinity bracketing" approach is well-established for electron,[27] proton[25] and other ion transfers,[33] and it requires that the exothermic bracketing reactions are not impeded in any way by special kinetic factors such as steric effects, spin-problems, etc. While, in principle, the analysis of hydride transfer equilibria is possible, the authors are not aware of any reports of the successful identification and assay of a hydride transfer equilibrium involving negative ions and neutral compounds. This is probably because hydride transfer is usually an inefficient reaction and most neutral hydride acceptors are susceptible to competing side-reactions with hydride donor anions such as proton or electron transfer. A bracketing approach is required for the metal carbonyls since hydride transfer generally represents only a minor channel in their reactions with most hydride donor anions.

Table 1. Hydride affinities[a]

Compound (X)	Anion (HX^-)	HA(X) (kcal mol^{-1})
$(CF_3)_2CO$	$(CF_3)_2CHO^-$	88.6
BH_3	BH_4^-	74.2
BEt_3	$HBEt_3^-$	69.4
CS_2	HCS_2^-	67.3
$CH_2{=}C{=}O$	CH_2CHO^-	62.8
CF_3COCH_3	$CF_3(CH_3)CHO^-$	62.4
$CH_2{=}CHCHO$	CH_3CHCHO^-	61.9
$CH_2{=}CHCOCH_3$	$CH_3CHCOCH_3^-$	58.4
O_2	HO_2^-	58.0
$CH_2{=}CHCN$	CH_3CHCN^-	56.3
$CH_2{=}C(CH_3)CN$	$(CH_3)_2CCN^-$	55.3
CO_2	HCO_2^-	51.6
$CH_2{=}CHPh$	CH_3CHPh^-	48.9
$CH_2{=}C(CH_3)Ph$	$(CH_3)_2CPh^-$	47.4
PhCHO	$PhCH_2O^-$	45.6
n-C_4H_9CHO	n-$C_5H_{11}O^-$	42.4
$CH_2{=}O$	CH_3O^-	41.0
CH_3CHO	$CH_3CH_2O^-$	39.5
$(CH_3)_2CO$	$(CH_3)_2CHO^-$	38.3
$CH_3N{=}CH_2$	$(CH_3)_2N^-$	26.1
C_6H_6	c-$C_6H_7^-$	21.5
CO	HCO^-	8.0

[a] Taken from ref. 26.

$Fe(CO)_5$

In a preliminary account we described hydride affinity bracketing experiments involving $Fe(CO)_5$.[19] The results are briefly reviewed here. Iron pentacarbonyl reacts with a wide variety of negative ions in the gas phase under flowing afterglow conditions. Nucleophilic addition with accompanying decarbonylation usually predominates, and the kinetics, mechanisms and thermochemistry of these reactions have been described by us in detail.[17,18] Slow hydride transfer to $Fe(CO)_5$ yielding an $[M+H^-]$ product ion at m/z 197 is observed with $(CH_3)_2\bar{C}CN$, HCO_2^-, $Ph\bar{C}HCH_3$, $CH_2{=}CH\bar{C}HCH_3$ and almost all primary and secondary aliphatic alkoxides [eq. (2)].

$$HX^- + Fe(CO)_5 \longrightarrow (CO)_4FeCHO^- + X. \quad (2)$$

Only traces of this product are observed with $CH_3\bar{C}HCN$ and it is completely absent from the mixture of product ions formed with $CH_3\bar{C}HCOCH_3$.

The $[M+H^-]$ product ion is believed to be the iron formyl complex, $(CO)_4FeCHO^-$, which results from H^- transfer to a CO ligand (see Structure 1). Supporting evidence for this ion structure

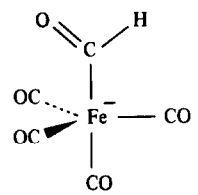

Structure 1.

assignment has been presented earlier.[34] The ion is substitutionally inert in the gas-phase, as are all other 18-electron metal anion complexes we have examined previously in our laboratory.[35] Furthermore, it fails to undergo any other conceivable "neutral switching" type reactions that would be

characteristic of an electrostatically-bonded cluster ion.[36] Dedieu and Nakamura have examined this ion computationally at a high level of theory and concluded that direct H^- addition to an axial CO is strongly exothermic and occurs without activation.[37,38]

Hydride transfer from $(CO)_4FeCHO^-$ does not occur with any of the neutral acceptor compounds we have examined; even those for which H^- transfer is calculated to be exothermic (*vide infra*). Thus, no reaction occurs at all with $CH_2{=}CHCN$ and $CH_2{=}CHCOCH_3$, and only slow (termolecular) addition takes place with BEt_3. We have previously proposed kinetic arguments for this behaviour in terms of the unfavourable charge localization requirements expected for heterolytic cleavage of the C—H bond in $(CO)_4FeCHO^-$.[34] Since the negative charge in the iron formyl ion complex is mainly delocalized over the metal and oxygen atoms,[37-39] hydride-acceptor molecules are not likely to associate with the hydrogen during the short time-span of a gas-phase ion/molecule collision. That is, the hydrogen in $(CO)_4FeCHO^-$ is not particularly "hydridic" in a kinetic sense. In contrast, when the acyl ligand involves an electronegative (lone-pair bearing) heteroatom such as in $(CO)_4FeC(O)F^-$ or $(CO)_4FeC(O)Cl^-$, exothermic ion transfer reactions with neutral acceptor molecules are readily observed.[34]

Complete product distribution and kinetics measurements were performed for several of the hydride transfer reactions in order to more clearly define the H^--transfer threshold. In all cases in which hydride transfer occurs [eq. (2)], it represents only a minor channel (5–13%) compared to the total adduct formation and addition/decarbonylation (70–100%). The efficiency of the hydride transfer channel, as given by $k_{(2)}/k_{collision}$,[40] decreases from 0.01 for $PhC\bar{H}CH_3$ to $\leqslant 0.0002$ for $CH_3C\bar{H}COCH_3$. From these results and the reference hydride affinities listed in Table 1 we assign a final value to $HA(Fe(CO)_5)$ of 56 ± 4 kcal mol^{-1}. Combining this with the known heats of formation for H^- (34.7 kcal mol^{-1}) and $Fe(CO)_5$ (-173.0 ± 1.5 kcal mol^{-1})[30] yields $\Delta H_f[(CO)_4FeCHO^-, g] = -194\pm4$ kcal mol^{-1}. The two iron–formyl bond strengths $D[(CO)_4Fe{-}CHO^-]$ and $D[(CO)_4Fe^-{-}CHO]$ are derived from $HA(Fe(CO)_5)$ and other thermochemical data according to eqs (3) and (4).

$$D[(CO)_4Fe{-}CHO^-] = HA(Fe(CO)_5) - HA(CO) + D[(CO)_4Fe{-}CO] \quad (3)$$

$$D[(CO)_4Fe^-{-}CHO] = D[(CO)_4Fe{-}CHO^-] - EA(Fe(CO)_4) + EA(HCO). \quad (4)$$

Using the values $HA(CO) = 8.0$ kcal mol^{-1},[41] $D[(CO)_4Fe{-}CO] = 41.5$ kcal mol^{-1},[42] $EA(Fe(CO)_4) = 55.3$ kcal mol^{-1}[43] and $EA(HCO) = 7.2$ kcal mol^{-1}[41] from the recent literature, we calculate $D[(CO)_4Fe{-}CHO^-] = 90\pm5$ kcal mol^{-1} and $D[(CO)_4Fe^-{-}CHO] = 41\pm5$ kcal mol^{-1}.

$M(CO)_6$, M = Cr, Mo, W

The results for the group 6 metal carbonyls are described collectively here since their behaviour in reactions with almost all of the negative ions we examined was found to be identical. Because of its greater volatility and smaller number of natural abundance metal isotopes compared to $Mo(CO)_6$ and $W(CO)_6$, $Cr(CO)_6$ was most easily studied and its reactions were investigated in the greatest detail. The major reaction occurring with primary alkoxide ions is nucleophilic addition followed by loss of two and three CO ligands from the metal ion product [eq. (5)].

$$RCH_2O^- + Cr(CO)_6 \longrightarrow \begin{cases} (CO)_4CrOCH_2R^- + 2CO \\ (CO)_3CrOCH_2R^- + 3CO \\ (CO)_5CrCHO^- + RCHO. \end{cases} \quad (5)$$

Hydride transfer yielding the chromium formyl ion (m/z 221) is observed with $CH_3CH_2CH_2O^-$, $CH_3CH_2O^-$ and CH_3O^-, but not with $PhCH_2O^-$ or $(CH_3)_3CCH_2O^-$. The delocalized carbanions shown below react mainly by adduct formation, with varying amounts (20–50%) of monodecarbonylation products also appearing for all but $CH_3C\bar{H}COCH_3$ [eq. (6)].

$$R^- + Cr(CO)_6 \longrightarrow \begin{cases} (CO)_5CrR^- + CO \\ (CO)_5CrC(O)R^-. \end{cases} \quad (6)$$

$R^- = CH_3C\bar{H}COCH_3$, $CH_3C\bar{H}CN$, $(CH_3)_2C\bar{C}N$, $PhC\bar{H}CH_3$, $PhC\bar{(CH_3)}_2$.

Hydride transfer, dissociative electron transfer and adduct formation occur with the cyclohexadienyl anion [eq. (7)].

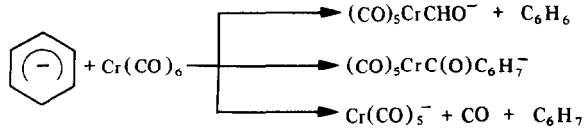

(7)

The potent hydride donor anion $Et_3SiH_2^-$ (formed by direct addition of H^- to Et_3SiH)[24] produces a

quantitative yield of the chromium formyl [eq. (8)].

$$Et_3SiH_2^- + Cr(CO)_6 \longrightarrow Et_3SiH + (CO)_5CrCHO^- \quad (8)$$

As with $(CO)_4FeCHO^-$, bimolecular hydride transfer from $(CO)_5CrCHO^-$ to acceptor molecules is not observed, regardless of their hydride affinities. Thus, no reaction occurs at all between $(CO)_5CrCHO^-$ and either $CH_3COCH{=}CH_2$ (HA = 58.4 kcal mol^{-1}) or $CH_2{=}C(CH_3)Ph$ (HA = 47.4 kcal mol^{-1}). We adopt the same kinetic arguments used for $(CO)_4FeCHO^-$ to rationalize this behaviour and attribute the non-reactivity of $(CO)_5CrCHO^-$ to its extensive charge delocalization.

From the occurrence of hydride transfer to $Cr(CO)_6$ from CH_3O^- ($HA(CH_2O)$ = 41.0 kcal mol^{-1}) but not from $PhCH_2O^-$ (HA(PhCHO) = 45.6 kcal mol^{-1}), we assign a final value to $HA(Cr(CO)_6)$ of 44 ± 4 kcal mol^{-1}. The conservative error limits reflect the uncertainty in the reference thermochemical data and the fact that the hydride affinity bracket could not be established from both forward and reverse reactions. Combining $HA(Cr(CO)_6)$ with $\Delta H_f[Cr(CO)_6, g]$ = −217.1 ± 0.5 kcal mol^{-1} [30] and $\Delta H_f[H^-, g]$ yields $\Delta H_f[(CO)_5CrCHO^-, g]$ = −226 ± 4 kcal mol^{-1}. From an equation analogous to (3) and $D[(CO)_5Cr{-}CO]$ = 36.8 kcal mol^{-1} [42] we further calculate $D[(CO)_5Cr{-}CHO^-]$ = 73 ± 5 kcal mol^{-1}. The electron affinity of $Cr(CO)_5$ has recently been estimated to be ⩾ 48 kcal mol^{-1},[44] from which an upper limit for $D[(CO)_5Cr^-{-}CHO]$ of ⩽ 32 kcal mol^{-1} can be calculated using an equation analogous to (4).

The same general reactivity patterns are found for $Mo(CO)_6$ and $W(CO)_6$. Addition with loss of two and three CO ligands represents the main reactions with alkoxides, and adduct formation along with minor amounts of monodecarbonylation occur with carbanions. Hydride transfer to $Mo(CO)_6$ and $W(CO)_6$ is observed with CH_3O^- and c-$C_6H_7^-$, but not with $PhCH_2O^-$, $PhC^-(CH_3)_2$ or PhC^-HCH_3. The same hydride affinity as for $Cr(CO)_6$ (44 ± 4 kcal mol^{-1}) is deduced from these results. The resulting heats of formation for the formyl ions are: $\Delta H_f[(CO)_5MoCHO^-, g]$ = −228 ± 4 kcal mol^{-1} and $\Delta H_f[(CO)_5WCHO^-, g]$ = −221 ± 4 kcal mol^{-1}, using heats of formation for $Mo(CO)_6$ and $W(CO)_6$ of −219.0 ± 0.4 and −211.4 ± 0.6 kcal mol^{-1}, respectively.[45] From the CO-dissociation energies, $D[(CO)_5Mo{-}CO]$ = 40.5 kcal mol^{-1} [42] and $D[(CO)_5W{-}CO]$ = 46.0 kcal mol^{-1},[42] the heterolytic metal–formyl bond strengths $D[(CO)_5Mo{-}CHO^-]$ = 77 ± 5 kcal mol^{-1} and $D[(CO)_5W{-}CHO^-]$ = 82 ± 5 kcal mol^{-1} are derived. Finally, from estimated lower limits for $EA(Mo(CO)_5)$ and $EA(W(CO)_5)$ of 46 kcal mol^{-1},[44] we calculate $D[(CO)_5Mo^-{-}CHO] \leqslant 38$ kcal mol^{-1} and $D[(CO)_5W^-{-}CHO] \leqslant 43$ kcal mol^{-1}.

DISCUSSION

A summary of hydride affinities, homolytic and heterolytic metal–carbon bond strengths and related thermochemical data is provided in Table 2. Several qualitative and quantitative conclusions may be derived from the absolute and relative magnitudes of the hydride affinities. First of all, it is worthwhile to point out that the hydride affinities of the metal carbonyls are substantially less than the hydride affinities of boranes[31] [eq. (9)].

$$BH_4^- + Fe(CO)_5 \xrightarrow{\Delta H = 18\,\text{kcal mol}^{-1}} (CO)_4FeCHO^- + BH_3 \quad (9)$$

This is significant because alkali borohydride reagents such as LiR_3BH and $K(RO)_3BH$ normally function as good hydride donors with neutral metal carbonyls in solution,[11,46–48] despite the fact that the underlying (gas-phase) energetics for H^- transfer is unfavourable. The same may be said for the borohydride reduction of organic carbonyl compounds since they too have hydride affinities that are significantly less than the boranes.[26]

The obvious implication is that the solvent and alkali metal counter-ion make significant contributions to the mechanisms and the overall thermodynamics of the borohydride reduction reactions in solution. In principle, synchronous boron–oxygen and carbon–hydrogen bond formation in the nascent formyl ion could also mediate the otherwise endothermic hydride transfer. However, this type of (concerted) mechanism has been shown to be insignificant in the reductions of organic carbonyl compounds.[49] Wigfield has emphasized the importance of hydrogen-bonding solvents in the borohydride reductions of organic ketones[50] and it is likely that they could also facilitate reduction of metal carbonyls. Furthermore, in their original report of the synthesis of iron formylates with borohydride reagents, Winter *et al.* demonstrated strong ion-pairing between the alkali cation and the formyl oxygen.[48] Continued mechanistic studies of solvent and counter-ion effects would clearly be of value for further optimizing borohydride-based syntheses of anionic metal formyls.

The relative ordering of the hydride binding energies for the four compounds parallels their relative

Table 2. Thermochemical data for transition-metal formyl anions derived from gas-phase hydride transfer reactions[a]

$M(CO)_n$	HA^b	$\Delta H_f[(CO)_{n-1}MCHO^-, g]^c$	$D[(CO)_{n-1}M—CO]^d$	$D[(CO)_{n-1}M—CHO^-]$	$D[(CO)_{n-1}M^-—CHO]$
$Fe(CO)_5$	56±4	−194±4	41.5	90±5	41±5
$Cr(CO)_6$	44±4	−226±4	36.8	73±5	⩽ 32
$Mo(CO)_6$	44±4	−228±4	40.5	77±5	⩽ 38
$W(CO)_6$	44±4	−221±4	46.0	82±5	⩽ 43

[a] In units of kcal mol^{-1}.
[b] Bracketed hydride affinity as defined in eq. (1).
[c] Based on heats of formation for metal carbonyls given in ref. 45.
[d] Taken from ref. 42.

reactivities towards nucleophilic addition in solutions. For example, on a per-carbonyl basis, benzyl magnesium chloride reacts with $Fe(CO)_5$ to form the acylate complex roughly three to five times faster than with the group 6 hexacarbonyls, and the spread among the rates measured for $Cr(CO)_6$, $Mo(CO)_6$ and $W(CO)_6$ is relatively small [eq. (10)].[51]

$$M(CO)_n + PhCH_2MgCl \longrightarrow (CO)_{n-1}\bar{M}—\overset{\overset{O}{\|}}{C}—CH_2Ph \cdot MgCl^+. \quad (10)$$

Similar reactivity differences are found in reactions of these compounds with alkyllithium reagents,[52] amines,[53] azide ion[54] and other nucleophiles.[2,6]

Darensbourg[51,52] and Algelici[55] have developed useful empirical correlations between the relative reactivity of a metal-coordinated CO (and other ligands) towards nucleophilic attack and its spectroscopically determined C—O stretching force constant (k_{CO}). In general, large k_{CO} values correlate with relatively rapid rates of nucleophilic addition, while smaller k_{CO} values are characteristic of the less reactive compounds. The group 6 hexacarbonyls have nearly identical k_{CO} values (*ca* 16.5 mdyn $Å^{-1}$), whereas k_{CO} for the axial CO in $Fe(CO)_5$ is somewhat larger 17.0 mdyn $Å^{-1}$).[51,52] Both the relative rates of reaction (10) and the gas-phase hydride binding energies of the four metal carbonyls exhibit this same pattern.

The underlying basis for the force constant/reactivity correlation is generally believed to be the direct connection between k_{CO} and the magnitude of the partial positive charge on the carbon of the CO ligand ($^+\delta_c$), i.e. the larger the C—O force constant, the greater the positive charge on carbon and accordingly, the greater its (kinetic) electrophilicity. However, in a recent publication Angelici correctly points out that the relative reactivities of the metal carbonyls may, in fact, be determined by thermodynamic factors as opposed to purely kinetic factors.[55] Several examples were cited in which the equilibrium constants for nucleophilic addition follow the k_{CO} ordering for a series of compounds whereas the rates do not.

The apparent correlation between the hydride affinities of the metal carbonyls and their k_{CO} values is consistent with this latter interpretation, although the basis for such a relationship is not obvious. That is, the hydride affinities are determined by the *differences* in energy between the metal carbonyl and formyl complexes, and ground-state properties of the metal carbonyls such as k_{CO} or $^+\delta_c$ cannot, by themselves, account for the variations. Never-

theless, on the strength of the apparent success of the correlation between k_{CO} and $HA(M(CO)_n)$ exhibited so far, we might venture the predictions that $Ni(CO)_4$ (k_{CO} = 17.2 mdyn Å^{-1})[52] will have a greater hydride affinity than $Fe(CO)_5$, while $CpMn(CO)_3$ (k_{CO} = 15.6 mdyn Å^{-1}) will have a lower hydride affinity than the group 6 metal carbonyls.

Dedieu and Nakamura carried out extensive *ab initio* SCF calculations on the hypothetical gas-phase reaction between H^- and $Fe(CO)_5$.[37,38] From a detailed analysis of the electronic structure of the product formyl ion, $(CO)_4FeCHO^-$, they concluded that the vacant d_{z^2} orbital on iron plays a key role in stabilizing the formyl ligand resulting from hydride attack on an axial CO. For a series of related compounds, as the energy of d_{z^2} decreases, the extent of the stabilizing interaction increases and a greater total H^- binding energy results. Accordingly, at the level of theory employed by Dedieu and Nakamura, $Fe(CO)_5$ and $Ru(CO)_5$ have d_{z^2} energies of 0.243 and 0.176 eV, and calculated hydride affinities of 69 and 76 kcal mol^{-1}, respectively.[38]

For the most part, this model satisfactorily accounts for the experimental results of the present study. The analogous d_{z^2} acceptor orbital in $Cr(CO)_6$ ($6e_g$)[56] is expected to be somewhat higher in energy than the one in $Fe(CO)_5$ since 3*d* orbitals are generally higher-lying in the early transition metals, and the crystal field splitting is larger for octahedral vs trigonal bipyramidal coordination. Therefore, a lower hydride affinity for $Cr(CO)_6$ compared to $Fe(CO)_5$ is expected. Moreover, while the valence *d*-orbitals in metal carbonyls generally decrease in energy down a metal triad due to decreased interelectronic repulsion, the greater σ-interaction between the carbonyls and the relatively diffuse $4d\sigma$ and $5d\sigma$ orbitals compared to $3d\sigma$ raises the energy of the empty $d\sigma^*$ ($6e_g$) orbital to a greater extent.[57] In view of these opposing effects, one might predict that the d_{z^2} energy levels in $Cr(CO)_6$, $Mo(CO)_6$ and $W(CO)_6$ would not differ greatly and, therefore, that the hydride affinities should be similar. Extended Hückel calculations yield d_{z^2} orbital energies for $Fe(CO)_5$, $Cr(CO)_6$, $Mo(CO)_6$ and $W(CO)_6$ of −3, −1, −0.8 and 0.9 eV, respectively.[58] While these estimates are undoubtedly crude and strongly parameter dependent, they are generally consistent with the qualitative picture described above as well as with the experimental differences in hydride affinity between $Fe(CO)_5$ and the group 6 hexacarbonyls.

Inasmuch as the presence of a vacant, low-lying *d*-orbital is a prerequisite for a strong nucleophile binding in a metal carbonyl, one might anticipate relatively weak hydride binding by $Ni(CO)_4$ since the metal *d*-orbitals are fully occupied.† However, this contradicts the empirical prediction made earlier of a high hydride affinity for $Ni(CO)_4$ based on its large C—O force constant. It is noteworthy that although nickel acylates have been known for some time in solution, they are generally less stable than analogous iron acylates and are extremely prone to polymerization, decarbonylation and degradation by oxygen.[2,60] Moreover, $(CO)_3NiCHO^-$ is presently unknown. Therefore, hydride affinity measurements with $Ni(CO)_4$ would be of particular interest and experiments along these lines are currently in progress.

CO *insertion into* M—H *bonds*

The thermochemical data in Table 2 can be used to evaluate the gas-phase energetics for (migratory) insertion of CO into an M—H bond [eq. (11)].[61]

$$L_nMH + CO \longrightarrow L_nM{-}\overset{\overset{O}{\|}}{C}{-}H. \qquad (11)$$

Reaction (11) is usually thermodynamically unfavourable. Indeed, the vast majority of known metal formyl complexes are thermally unstable with respect to decarbonylation.[11,62,63] Notable exceptions are the early transition-metal hydrides[64,65] and actinohydrides[66,67] which produce η^2-formyl products from CO-insertion, and the interesting rhodium porphyrin hydride complex RhOEP(H) (OEP = octaethylporphyrin) described by Wayland *et al.*[68,69]

Calculation of CO-insertion energies requires thermodynamic information for the corresponding metal hydrides. For the iron system [eq. (12)] this can be obtained from recent studies of $(CO)_4FeH_2$.

$$(CO)_4FeH^- + CO \longrightarrow (CO)_4FeCHO^-. \qquad (12)$$

Thus, from an appropriate thermochemical cycle an expression for $\Delta H(12)$ in terms of the acidity and H_2-dissociation energy of $(CO)_4FeH_2$ can be derived [eq. (13)].

$$\Delta H(12) = D[(CO)_4Fe{-}H_2] - D[(CO)_4FeH^-{-}H^+] + D[H^+{-}H^-] - HA(Fe(CO)_5) - D[(CO)_4Fe{-}CO]. \qquad (13)$$

† While a vacant 4*s* orbital is present in $Ni(CO)_4$ which may, in principle, act in a similar capacity as the d_{z^2} orbital in $Fe(CO)_5$, it would not be expected to mix as well with the formyl ligand (higher energy; less efficient overlap) and would therefore provide less stabilization. For a pertinent discussion of this point, see ref. 59.

Pearson and Mauermann have measured the activation energy for H_2-dissociation from $(CO)_4FeH_2$ in aqueous methanol to be 26 ± 2 kcal mol^{-1}.[70] This is likely to be very close to the actual bond energy since Sweany has shown that H_2 oxidatively adds to $Fe(CO)_4$ in frozen matrices with little or no activation energy.[71] Stevens and Beauchamp bracketed the gas-phase acidity of $(CO)_4FeH_2$ ($D(CO)_4FeH^-$—H^+) at 319 ± 5 kcal mol^{-1} from ion/molecule reactions in an ICR.[72] Combining these two bond energies with $D[H^+—H^-] = 400.4$ kcal mol^{-1}[25] and values for the remaining terms from Table 2 yields a final estimate for $\Delta H(12)$ of 10 ± 7 kcal mol^{-1}. Therefore, CO-insertion into the FeH bond in $(CO)_4FeH^-$ is moderately endothermic. From an estimated entropy change for eq. (12) of -35 eu (based on standard statistical formulae), $\Delta G(12)$ is computed to be 21 kcal mol^{-1} at room temperature and one atmosphere pressure.

In a previous study we obtained estimates of the CO-insertion energies for a large series of $(CO)_4FeX^-$ complexes, where X represented different alkyl, aryl and heteroatom-containing ligands.[17] It was found that the enthalpies of CO-insertion generally followed the basicity of the ligand X^- and that insertion was unfavourable ($\Delta H > 0$) for all but the most weakly basic of ligands such as Cl^-, Br^- and I^-. Thus, the present result for $X^- = H^-$ is but one example of a more general situation for this particular system.

Analogous data for evaluating the heats of formation for the group 6 metal hydrides [$(CO)_5MH^-$, M = Cr, Mo, W] are not presently available. However, we can make use of a semi-quantitative analytical approach to CO-insertion energetics developed by Wayland[69] to derive estimates for the energy of reaction (14).

$$(CO)_5MH^- + CO \longrightarrow (CO)_5M—\overset{\overset{O}{\|}}{C}—H \qquad M = Cr, Mo, W. \qquad (14)$$

The enthalpy of CO-insertion into a generalized M—H bond [eq. (15)] may be expressed in terms of the separate bond energy contributions shown in eq. (16), where (M—H), (M—C) and (C—H) are the homolytic metal–hydrogen, metal–carbon and carbon–hydrogen bond strengths in the reactant hydride and product formyl, and (C≡O) − (C=O) is roughly equivalent to the π-bond energy in carbon monoxide.

$$M—H + CO \longrightarrow M—CHO \qquad (15)$$

$$\Delta H(15) = (M—H) - (M—C) + (C{\equiv}O) - (C{=}O) - (C—H). \qquad (16)$$

Wayland derived an approximation for the last three terms of -16 kcal mol^{-1} from thermochemical data for organic carbonyl compounds and concluded that eq. (15) will be exothermic only when the metal–hydrogen bond strength in the hydride does not exceed the metal–carbon bond strength in the formyl by more than 16 kcal mol^{-1}.[69]

The appropriate homolytic bond energies are available for the iron formyl system which allow us to check the performance of eq. (16). Using $D[(CO)_4Fe^-—CHO] = 41$ kcal mol^{-1} from Table 2 and $D[(CO)_4Fe^-—H] = 69$ kcal mol^{-1} derived from the aforementioned data for $(CO)_4FeH_2$[70–72] along with the -16 kcal mol^{-1} approximation for the last three terms, yields a final insertion enthalpy of 12 kcal mol^{-1}. This is in good agreement with the value of 10 ± 7 kcal mol^{-1} derived from our hydride affinity measurements. We therefore conclude that eq. (16) can provide reasonably accurate estimates for the CO-insertion enthalpies.

For the group 6 metal formyl ion complexes we have estimated upper limits for the metal–carbon bond strengths ($D[(CO)_5M^-—CHO]$) of 32, 38 and 43 kcal mol^{-1} for M = Cr, Mo and W, respectively (Table 2). Use of these data with eq. (16) leads to the conclusion that the metal–hydrogen bond strengths in the $(CO)_5MH^-$ ions would have to be less than 48, 54 and 59 kcal mol^{-1} for Cr, Mo, and W, respectively, in order for eq. (14) to become exothermic. Considering the range of known M—H bond energies in mononuclear metal hydrides, (60–70 kcal mol^{-1}),[73–75] bond strengths as low as this are unlikely. For example, $(CO)_5MnH$ and $(CO)_5FeH^+$ are isoelectronic with $(CO)_5CrH^-$ and have homolytic M—H bond energies of 60 and 72 kcal mol^{-1}, respectively.[76,77] Furthermore, the mean M—H bond strengths in H_2MoCp_2 and H_2WCp_2 are 60 and 73 kcal mol^{-1}[78] and the Mo—H bond energy in $HMo(CO)_3Cp$ has recently been measured to be 66 kcal mol^{-1}.[79] We therefore conclude that reaction (14) is likely to be endothermic for all three metals. Gas-phase experiments to establish better thermochemical data for $(CO)_5MH^-$ ions are currently in progress.

Acknowledgements—The authors wish to thank Profs A. Dedieu and T. Ziegler for helpful discussions. The National Science Foundation (CHE-8502515) is gratefully acknowledged for their support of this research and R.R.S. thanks the Alfred P. Sloan Foundation for a fellowship.

REFERENCES

1. C. Masters, *Adv. Organomet. Chem.* 1979, **17**, 61.
2. J. P. Collman, L. S. Hegedus, J. R. Norton and

R. G. Finke, *Principles and Applications of Organotransition Metal Chemistry*. University Science Books, Mill Valley, CA (1987).
3. E. L. Muetterties and J. Stein, *Chem. Rev.* 1979, **79**, 479.
4. G. W. Parshall, *Homogeneous Catalysis*. Wiley, New York (1981).
5. D. R. Fahey, *J. Am. Chem. Soc.* 1981, **103**, 136.
6. P. C. Ford and A. Rokicki, *Adv. Organomet. Chem.* 1987, **28**, 139.
7. D. J. Darensbourg and R. A. Kudaroski, *Adv. Organomet. Chem.* 1983, **22**, 129.
8. F. R. Hartley and S. Patai, (Eds), *The Chemistry of the Metal–Carbon Bond*. Wiley, New York (1982).
9. R. Eisenberg and D. E. Hendricksen, *Adv. Catalysis* 1979, **28**, 79.
10. H. Alper, *Transition Metals in Organic Synthesis*. Academic Press, New York (1976).
11. J. A. Gladysz, *Adv. Organomet. Chem.* 1982, **20**, 1 and refs therein.
12. D. W. Slocum and W. R. Moser (Eds), Catalytic transition metal hydrides, *Ann. N.Y. Acad. Sci.* 1983, 415.
13. H. D. Kaesz and R. B. Saillant, *Chem. Rev.* 1972, **72**, 231.
14. J. R. Norton, in *Inorganic Reactions and Methods*. Verlag Chemie, Weinheim (1987).
15. K. R. Lane, L. Sallans and R. R. Squires, *Inorg. Chem.* 1984, **23**, 1959.
16. K. R. Lane, R. E. Lee, L. Sallans and R. R. Squires, *J. Am. Chem. Soc.* 1984, **106**, 5767.
17. K. R. Lane, L. Sallans and R. R. Squires, *J. Am. Chem. Soc.* 1986, **108**, 4368.
18. K. R. Lane and R. R. Squires, *J. Am. Chem. Soc.* 1986, **108**, 7187.
19. K. R. Lane, L. Sallans and R. R. Squires, *Organometallics* 1985, **3**, 408.
20. E. E. Ferguson, F. C. Fehsenfeld and A. L. Schmeltekopf, *Adv. Atom. Mol. Phys.* 1969, **5**, 1.
21. D. Smith and N. G. Adams, in *Gas Phase Ion Chemistry* (Edited by M. T. Bowers), Chap. 1. Academic Press, New York (1979).
22. G. E. Streit and T. W. Newton, *J. Chem. Phys.* 1980, **73**, 3178.
23. N. G. Adams and D. Smith, *J. Phys. B.* 1976, **9**, 1439.
24. D. J. Hajdasz and R. R. Squires, *J. Am. Chem. Soc.* 1976, **108**, 3139.
25. J. E. Bartmess and R. T. McIver Jr, in *Gas Phase Ion Chemistry* (Edited by M. T. Bowers), Chap. 11. Academic Press, New York (1979).
26. R. R. Squires, in *Structure/Reactivity and Thermochemistry of Ions* (Edited by P. Ausloos and S. G. Lias), p. 373. D. Reidel, Dordrecht (1987).
27. B. K. Janousek and J. I. Brauman, in *Gas Phase Ion Chemistry* (Edited by M. T. Bowers), Chap. 10. Academic Press, New York (1979).
28. J. G. Dillard, *Chem. Rev.* 1973, **73**, 589.
29. M. Meot-Ner and L. W. Sieck, *J. Phys. Chem.* 1986, **90**, 6687.
30. J. B. Pedley and J. Rylance, Sussex NPL computer analysed thermochemical data, University of Sussex, U.K. (1977).
31. D. B. Workman and R. R. Squires, *Inorg. Chem.*, in press.
32. M. S. B. Munson, *J. Am. Chem. Soc.* 1965, **87**, 2332.
33. J. W. Larson and T. B. McMahon, *J. Am. Chem. Soc.* 1985, **107**, 766.
34. K. R. Lane, L. Sallans and R. R. Squires, *J. Am. Chem. Soc.* 1985, **107**, 5369.
35. K. R. Lane, Ph.D. Dissertation, Purdue University (1986).
36. D. K. Bohme, in *Ionic Processes in the Gas Phase* (Edited by M. A. A. Ferriera). D. Reidel, Dordrecht (1984).
37. S. Nakamura and A. Dedieu, *Theor. Chim. Acta.* 1982, **61**, 587.
38. A. Dedieu and S. Nakamura, *Nouv. J. Chim.* 1984, **8**, 317.
39. G. Blyholder, K. Zhao and M. Lawless, *Organometallics* 1985, **4**, 1371.
40. T. Su and M. T. Bowers, in *Gas Phase Ion Chemistry* (Edited by M. T. Bowers), Chap. 3. Academic Press, New York (1979).
41. K. K. Murray, T. M. Miller, D. G. Leopold and W. C. Lineberger, *J. Chem. Phys.* 1986, **84**, 2520.
42. K. E. Lewis, D. M. Golden and G. P. Smith, *J. Am. Chem. Soc.* 1984, **106**, 3905.
43. P. C. Engelking and W. C. Lineberger, *J. Am. Chem. Soc.* 1979, **101**, 5569.
44. D. G. Leopold, K. K. Murray and W. C. Lineberger, private communication of unpublished results.
45. J. A. Connor, *Topics Curr. Chem.* 1977, **71**, 71.
46. C. P. Casey and S. M. Neumann, *J. Am. Chem. Soc.* 1976, **98**, 5395.
47. J. A. Gladysz and J. C. Selover, *Tet. Lett.* 1978, 319.
48. S. R. Winter, G. W. Cornett and E. A. Thompson, *J. Organomet. Chem.* 1977, **133**, 339.
49. O. Eisenstein, H. B. Schlegel and M. M. Kayser, *J. Org. Chem.* 1982, **47**, 2886 and refs therein.
50. D. C. Wigfield, *Tetrahedron* 1979, **35**, 449.
51. M. Y. Darensbourg, H. L. Conder, D. J. Darensbourg and C. Hasday, *J. Am. Chem. Soc.* 1973, **95**, 5919.
52. D. J. Darensbourg and M. Y. Darensbourg, *Inorg. Chem.* 1970, **9**, 1691.
53. R. J. Angelici, *Acc. Chem. Res.* 1972, **5**, 335.
54. H. Werner, W. Beck and H. Engelmann, *Inorg. Chim. Acta.* 1969, **3**, 331.
55. R. C. Bush and R. J. Angelici, *J. Am. Chem. Soc.* 1986, **108**, 2735 and refs therein.
56. J. B. Johnson and W. G. Klemperer, *J. Am. Chem. Soc.* 1977, **99**, 7132.
57. T. Ziegler, V. Tschinke and C. Ursenbach, *J. Am. Chem. Soc.* 1987, **109**, 4825.
58. A. Dedieu, private communication.
59. A. Dedieu and S. Nakamura, in *Quantum Chemistry. The Challenge of Transition Metals and Coordination Chemistry* (Edited by A. Veillard). D. Reidel, Dordrecht (1986).
60. J. K. Simunic and A. R. Pinhaus, *Organometallics* 1987, **6**, 1358 and refs therein.

61. A. Wojcicki, *Adv. Organomet. Chem.* 1973, **11**, 87.
62. C. P. Casey and S. M. Neumann, *Adv. Chem. Ser.* 1979, **173**, 131.
63. C. P. Casey, S. M. Neumann, M. A. Andrews and D. R. McAlister, *Pure Appl. Chem.* 1980, **52**, 625.
64. P. T. Wolczanski and J. E. Bercaw, *Acc. Chem. Res.* 1980, **13**, 121.
65. C. Floriani, *Pure Appl. Chem.* 1983, **55**, 1.
66. P. J. Fagan, K. G. Moloy and T. J. Marks, *J. Am. Chem. Soc.* 1981, **103**, 6959.
67. K. G. Moloy and T. J. Marks, *J. Am. Chem. Soc.* 1984, **106**, 7051.
68. B. B. Wayland and B. A. Woods, *J. Chem. Soc., Chem. Commun.* 1981, 700.
69. M. D. Farnos, B. A. Woods and B. B. Wayland, *J. Am. Chem. Soc.* 1986, **108**, 3659.
70. R. G. Pearson and H. Mauermann, *J. Am. Chem. Soc.* 1982, **104**, 500.
71. R. L. Sweany, *J. Am. Chem. Soc.* 1981, **103**, 2410.
72. A. E. Stevens and J. L. Beauchamp, unpublished results.
73. R. G. Pearson, *Chem. Rev.* 1985, **85**, 41.
74. J. Halpern, *Inorg. Chim. Acta.* 1985, **100**, 41.
75. J. A. M. Simoes and J. L. Beauchamp, *Chem. Rev.* submitted for publication.
76. A. E. Stevens and J. S. Beauchamp, *J. Am. Chem. Soc.* 1981, **103**, 190.
77. J. A. M. Simoes, J. C. Schultz and J. L. Beauchamp, *Organometallics* 1985, **4**, 1238.
78. J. C. G. Calado, A. R. Dias, J. A. M. Simoes and M. A. V. Ribiero da Silva, *J. Organomet. Chem.* 1979, **174**, 77.
79. C. D. Hoff, *J. Organomet. Chem.* 1985, **282**, 201.

Polyhedron Vol. 7, No. 16/17, pp. 1619–1622, 1988
Printed in Great Britain

0277–5387/88 $3.00+.00
© 1988 Pergamon Press plc

APPLICATION OF TIME-RESOLVED PHOTOACOUSTIC CALORIMETRY TO Cr—L BOND ENTHALPIES IN $Cr(CO)_5$—L

GILBERT K. YANG, VERONICA VAIDA* and KEVIN S. PETERS*

Department of Chemistry and Biochemistry, University of Colorado, Boulder, Colorado 80309-0215, U.S.A.

Abstract—Using time-resolved photoacoustic calorimetry, the Cr—L bond enthalpies in $Cr(CO)_5$—L for a variety of ligands have been measured. Also, the enthalpy and entropy of activation for the displacement of heptane in $Cr(CO)_5$(heptane) by pyridine and 2-picoline have been determined.

Understanding the reactivity and selectivity of organotransition metal complexes is predicated upon the availability of energetic information such as metal–ligand bond strengths. Most of the energetic information available for transition metal complexes consists of average metal–ligand bond strengths derived from measured enthalpies of formation of mononuclear complexes.[1–4] Recently, as bond dissociation energies for removal of the first ligand could be measured in a few instances,[5–9] it was found that they are considerably different from the average values. These results underscore the importance of obtaining a data base of specific metal–ligand bond energies to be used in studying reactivity.

We have developed one approach aimed at obtaining specific bond energies for transition metal complexes in solution, which is time-resolved photoacoustic calorimetry. In this paper we will discuss measured metal–ligand bond enthalpies for $Cr(CO)_5L$ as well as a study of steric effects on the activation parameters and the enthalpy of ligand substitution in $Cr(CO)_5$(heptane) by substituted pyridines. Steric interactions between ligand and metal play a significant role in the stabilities of organometallic complexes and in controlling the rates of ligand substitution reactions.

EXPERIMENTAL

The technique of time-resolved photoacoustic calorimetry has been described recently[10] and will not be discussed in detail. In those studies,[10] the response of a transducer to an acoustic wave was investigated by modelling the experiment with a point source of heat and a point detector. The results established that the acoustic wave gives rise to a unique waveform for transients with lifetimes of 50 ns to 50 μs for a 1 MHz transducer. The experimental information obtained in the time-resolved photoacoustic experiment is the experimental waveform, $C_{exp}(t)$, which is the convolution of a time-dependent heat source $E(t)$ and the transducer response function $T(t)$. The deconvolution procedure has been described.[10] It involves calculating a heat wave assuming a set of parameters: τ_k, the transients decay lifetime and ϕ_k, which represents the fraction of the photon energy that is released as heat during the decay of the transient k. A calculated waveform $C_{calc}(t)$ is then generated and compared with the experimental $C_{exp}(t)$ by evaluation of the sum of the residuals. The best values for the fitting parameters ϕ_k and τ_k are obtained by minimizing the residuals.

In the present study, time-resolved photoacoustic calorimetry is employed to obtain the kinetics and enthalpies for the ligand substitution reactions occurring when $Cr(CO)_6$ is photolysed in heptane solutions of various ligands. The kinetic information is obtained from τ_k as $k = (1/\tau_k)[L]$. To obtain bond enthalpies, ΔH, from the measured heat of reaction ϕ_k, the reaction quantum yield, QY, must be available. This than leads to

$$\Delta H = (1-\phi)E_{h\nu}/QY$$

where $E_{h\nu}$ is the photon energy.

The experiments reported here were performed

* Authors to whom correspondence should be addressed.

in helium purged heptane solutions of $Cr(CO)_6$ (10^{-4} M) with 0.02–0.40 M added ligand which were irradiated with < 20 μJ per pulse at 337.1 nm from a nitrogen laser. Arrhenius studies were performed over a 34°C temperature range between 9.3 and 43.3°C with the sample held in a constant temperature block maintained to within ± 0.1°C.

RESULTS AND DISCUSSION

Ligand substitution reactions for the group VI metal hexacarbonyls have been extensively studied.[11-22] For $M(CO)_6$ (M = Cr, Mo, W), the mechanism for the reaction is thought to involve the dissociation of a CO to form $M(CO)_5$ which coordinates to a solvent molecule, S, which in turn is followed by ligand, L, displacement of S.

$$M(CO)_6 + S \rightarrow M(CO)_5S + CO \quad \Delta H_1$$

$$M(CO)_5S + L \rightarrow M(CO)_5\text{—}L + S \quad \Delta H_2.$$

To obtain a direct measure of the $Cr(CO)_5$—L bond energy from the photoacoustic amplitude associated with the photochemical ligand substitution reaction one relies on the extensive mechanistic information available for this reaction. The initial photodissociation of CO and the ensuing solvent coordination to $Cr(CO)_5$ were shown[15] to occur in less than 25 ps following photolysis of $Cr(CO)_6$. The quantum yield for the photochemical substitution of a carbonyl ligand is 0.67 in cyclohexane solutions.[14]

With this information, the results of the photoacoustic calorimetry experiment,[8] namely ϕ_1 (the heat released in less than 50 ns), ϕ_2 (the heat released on longer timescales) and τ (the lifetime associated with process ϕ_2), can be interpreted to give ΔH_1, ΔH_2 and k. The results obtained are presented in Table 1. As indicated, the replacement of bound CO in $Cr(CO)_6$ by heptane is endothermic by 27 kcal mol^{-1}. In interpreting this value, it is informative to consider results of matrix isolation studies[22] which indicated that large energies are involved in coordination of $Cr(CO)_5$ with "inert" molecules. In going from neon to the more interactive methane matrix, the relative stabilization of the ground and excited state of $Cr(CO)_5$ corresponds to a 12.6 kcal mol^{-1} energy increase. The Cr—CO bond strength of 27 kcal mol^{-1} for $Cr(CO)_6$ in heptane solution measured by photoacoustic calorimetry,[8] can be compared with the gas phase bond dissociation energy of $Cr(CO)_6$ of 36.8 kcal mol^{-1}.[6] Assuming a small differential heat of solution between the reactants and products,[16] one obtains a 9.8 kcal mol^{-1} interaction energy between the coordinated heptane and $Cr(CO)_5$, consistent with the matrix isolation studies.

To examine the role that steric effects play in ligand–metal interactions we have studied the substitution of heptane from $Cr(CO)_5$(heptane) with a series of substituted and unsubstituted pyridines: pyridine, 2-methyl-pyridine (picoline) and 2,6-dimethyl-pyridine (lutidine). From the photoacoustic calorimetry experiment, we obtained the enthalpy and rate constant (ΔH_2, k) for the displacement of the coordinated heptane molecule by an incoming pyridine ligand. These results are summarized in Table 2.

The enthalpies of displacement of heptane, ΔH_2, by all three ligands are exothermic and decrease in magnitude by approximately 2.3 kcal mol^{-1} as the ligand becomes successively methyl substituted. This is not surprising due to the increasing steric hindrance about the coordinating nitrogen atom afforded by the methyl groups. However, as observed by PES studies,[23] methyl substitution

Table 1. $Cr(CO)_6 \xrightarrow[\Delta H_1]{\text{heptane}} Cr(CO)_5 \xrightarrow[\Delta H_2]{k[L]} Cr(CO)_5L$

L	ΔH_1 (kcal mol)	ΔH_2 (kcal mol^{-1})	k (10^7 L/mol s)[a]
THF	27.2 ± 1.2[b]	-12.4 ± 1.2[a]	11.8
2,2-Dimethyl-THF	27.1	−10.8	5.3
Ethanol	26.5	−13.8	3.6
Acetone	27.3	−13.5	15.9
Acetonitrile	26.8	−18.2	26.1
N(*n*-Bu)$_3$	27.3	−12.2	1.2
P(*n*-Bu)$_3$	26.3	−21.6	—
1-Hexene	27.2	−12.2	3.0
Tetramethylethylene	27.2	−9.6	2.6

[a] Errors given are 1σ.
[b] $\pm 50\%$.

Table 2. $Cr(CO)_5(heptane) \xrightarrow[\Delta H_2]{k[L]} Cr(CO)_5L$

L	$-\Delta H_2$ (kcal mol^{-1})	$\Delta H^{\ddagger}$ (kcal mol^{-1})	$\Delta S^{\ddagger}$ (eu)	IP (ev)[a]
Pyridine	20.1±0.4[b]	5.1±0.4	−3.2±1.4	9.32
2-Picoline	17.8±1.6	7.3±0.8	2.6±2.8	9.02
2,6-Lutidine	15.5±1.6	—	—	8.85

[a] Ionization potentials ref. 23.
[b] Errors given as 1σ.

actually raises the lone pair orbital energy on the nitrogen (see Table 2) which might be expected to increase the donating ability of the ligand and thus increase the metal–ligand enthalpy. Therefore, the 2.3 kcal mol^{-1} estimate for the interaction of a methyl group with the $Cr(CO)_5$ fragment must be a lower bound for the actual steric effect produced.

From the temperature dependence of the second order rate constants, k, determined between 9.3 and 43.3°C, Arrhenius plots yield $\Delta H^{\ddagger}$ and $\Delta S^{\ddagger}$ for the displacement of the coordinated heptane for pyridine or picoline. These data are presented in Table 2 and the Arrhenius plot for pyridine is shown in Fig. 1.

The enthalpy of activation is small for both ligands but is slightly larger for the more hindered picoline. The heptane–Cr bond strength is approximately 10 kcal mol^{-1}. Since the enthalpy barrier for the substitution process is 5.2±0.4 kcal mol^{-1} for pyridine, the transition state must be associative in the incoming ligand. With the more sterically demanding picoline, $\Delta H^{\ddagger}$ would then be expected to be larger than for pyridine. The entropy of activation for both reactions is close to 0 eu. It is suggestive of a transition state which entails a high degree of heptane–Cr bond lengthening concurrent with the association of the incoming ligand.

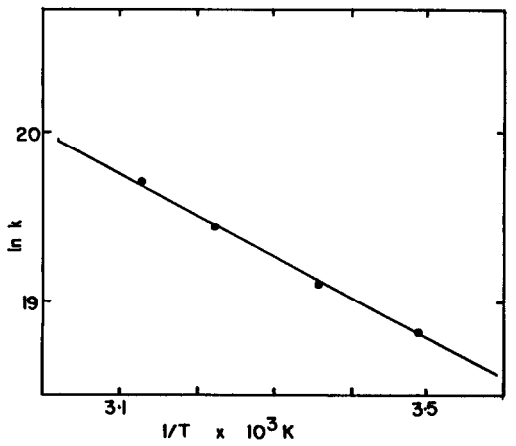

Fig. 1. Plot of $\ln k$ vs $1/T$ for $Cr(CO)_5(heptane) \xrightarrow{k[L]} Cr(CO)_5L$, L = pyridine.

Acknowledgement—Financial support from the NSF (CHE-8607697) is gratefully acknowledged.

REFERENCES

1. J. Connor, *Transition Metal Clusters* (Edited by B. Johnson), Chap. 5. J. Wiley, New York (1980).
2. J. Halpern, *Acc. Chem. Res.* 1982, **15**, 238.
3. J. Connor, *Curr. Topics Chem.* 1977, **71**, 71.
4. (a) E. Muetterties, T. Rhodin, E. Band, C. Brucher and W. Pretzer, *Chem. Rev.* 1979, **79**, 91; (b) M. Nakashima and A. Adamson, *J. Phys. Chem.* 1982, **86**, 2905.
5. P. C. Engelking and W. C. Lineberger, *J. Am. Chem. Soc.* 1979, **101**, 5569.
6. (a) D. F. McMillen, K. E. Lewis, G. P. Smith and D. M. Golden, *J. Phys. Chem.* 1982, **86**, 709; (b) K. E. Lewis, D. M. Golden and G. P. Smith, *J. Am. Chem. Soc.* 1984, **106**, 3095.
7. M. Bernstein, J. D. Simon and K. S. Peters, *Chem. Phys. Lett.* 1983, **100**, 241.
8. G. K. Yang, K. S. Peters and V. Vaida, *Chem. Phys. Lett.* 1986, **125**, 566.
9. G. P. Smith, *Polyhedron* 1988, **7**, 1605.
10. (a) L. J. Rothberg, J. D. Simon and K. S. Peters, *J. Am. Chem. Soc.* 1983, **105**, 3464; (b) J. Rudzki, J. L. Goodman and K. S. Peters, *J. Am. Chem. Soc.* 1985, **107**, 7849.
11. J. D. Atwood, *Inorganic and Organometallic Reactions*, Chap. 4. Brooks/Cole Pub. Co. (1985).
12. J. Kelly, D. Bent, H. Hermann, D. Schulte-Frohlinde and E. von Gustorf, *J. Organomet. Chem.* 1974, **69**, 259.
13. M. Wovkulich and J. Atwood, *J. Organomet. Chem.* 1980, **184**, 77.
14. J. Nasielski and A. Colas, *J. Organomet. Chem.* 1975, **101**, 215.
15. J. D. Simon and K. S. Peters, *Chem. Phys. Lett.* 1983, **98**, 53.
16. M. Nakashima and A. W. Adamson, *J. Phys. Chem.* 1982, **86**, 2905.

17. R. Perutz and J. Turner, *J. Am. Chem. Soc.* 1975, **97**, 4791.
18. J. E. Pardue and G. R. Dobson, *Inorg. Chim. Acta* 1976, **20**, 207.
19. (a) R. J. Angelici and J. R. Graham, *J. Am. Chem. Soc.* 1966, **88**, 3658; (b) J. R. Graham and R. J. Angelici, *Inorg. Chem.* 1967, **6**, 2082.
20. K. M. Al-Kathumi and L. A. P. Kare-Maguire, *J. Inorg. Nucl. Chem.* 1972, **34**, 3759.
21. K. S. Peters, *Pure Appl. Chem.* 1986, **58**, 1263.
22. R. N. Perutz and J. J. Turner, *J. Am. Chem. Soc.* 1975, **97**, 4791.
23. K. Watanave, T. Nakayama and J. Mottl, *J. Quant. Spectros. Radiat. Transfer* 1962, **2**, 369.

Polyhedron Vol. 7, No. 16/17, pp. 1625–1637, 1988
Printed in Great Britain

0277–5387/88 $3.00+.00
© 1988 Pergamon Press plc

A THEORETICAL STUDY OF METAL–LIGAND BOND STRENGTHS (M—L: L = OH, OCH_3, SH, NH_2, PH_2, CH_3, SiH_3, CN AND H) IN THE EARLY TRANSITION METAL SYSTEMS Cl_3ML (M = Ti, Zr AND Hf) AND LATE TRANSITION METAL SYSTEMS $LCo(CO)_4$

TOM ZIEGLER,* VINCENZO TSCHINKE and LOUIS VERSLUIS

Department of Chemistry, University of Calgary, Calgary, Alberta, Canada

and

EVERT JAN BAERENDS and WALTER RAVENEK

Scheikundig Laboratorium, Vrije Universiteit, 1081 HV Amsterdam, The Netherlands

Abstract—The strength of metal–ligand bonds (M—L: L = OH, OCH_3, SH, NH_2, PH_2, CN, CH_3, SiH_3 and H) in the early transition metal systems Cl_3ML (M = Ti, Zr and Hf) and late transition metal systems $LCo(CO)_4$ have been calculated by a non-local density functional method. For the early transition metal systems the Ti—L bond in Cl_3TiL was found to be quite polar, in particular for OCH_3, OH and NH_2. The order of the D(Ti—L) bond strength was calculated to be OH(453) > OCH_3(427) > CN(410) > NH_2(365) > SH(283) > CH_3(268) > H(251) > SiH_3(211) > PH_2(191), where the numbers in parentheses are the bond energies in kJ mol^{-1}. The corresponding bond energies of the Cl_3ZrL systems were calculated to be between 25 kJ mol^{-1} and 50 kJ mol^{-1} higher. An additional increase in the M—L bond energy of 10 kJ mol^{-1} to 20 kJ mol^{-1} was calculated in going from M = Zr to M = Hf. The M—L bonds in the late transition metal systems $LCo(CO)_4$ were calculated to be weaker and less polar than the corresponding bonds in Cl_3TiL. The order for the bond strengths in $LCo(CO)_4$ was calculated to be CN(304) > OH(232) > H(230) > SiH_3(212) > SH(169) > CH_3(160) > NH_2(146) > PH_2(145). The quite different order of stability for the M—L bond strength in early and late transition metal systems was analysed in terms of electronic and steric factors.

The way in which metal–ligand bond energies of early transition metals and *f*-block elements differ from those of middle to late transition metals, or metal–ligand bond energies of 3*d* and 4*f* elements differ from those of their heavier congeners, has been the subject of many experimental[1] as well as a few theoretical[2] studies over the past decade.

The thermochemistry[1a] of transition metal complexes is, however, still a relatively underdeveloped area and nowhere is the dearth of reliable data on metal–ligand and metal–metal bond energies felt stronger than in the field of organo-transition metal chemistry. In this field the lack of data often preclude an accurate assessment of the energetics in elementary reaction steps involving bond-making and bond-breaking.

We shall present here calculations on the D(M—L) bond strength in the Cl_3ML model systems of the early transition metals M = Ti, Zr and Hf, as well as the $LM(CO)_4$ model system with the late transition metal M = Co, for a number of rudimentary ligands L = H, CH_3, SiH_3, OH, SH, OCH_3, NH_2, PH_2 and CN. The choice of model systems should enable us to determine how D(M—L) is governed by the electronegativity of the central ligand-atom in the early transition metal complexes Cl_3M—L through the triad M = Ti, Zr, Hf, as well as in the late transition metal complexes $LCo(CO)_4$.

All calculations have been based on the density functional method due to Becke[3] and the HFS–

* Author to whom correspondence should be addressed.

LCAO program system by Baerends *et al.*[4] The bond energies were evaluated by the Generalized Transition State method[5] or its relativistic extension.[6] Becke's method[3] has previously been applied to calculations on metal–metal bond energies[7] in binuclear metal complexes and metal dimers as well as to the calculation of metal–carbonyl bond energies[8] in $M(CO)_m$ systems and metal–hydrogen or metal–methyl bond energies[9] in $RM(CO)_m^{n+}$ and MR^{n+} ($R = H, CH_3$; $n = 0, 1$). The bond energies calculated by Becke's method are in considerably better agreement with experiment (± 5 kcal) than bond energies calculated by the better known Hartree–Fock–Slater or $X\alpha$ density functional method which considerably overestimates M—M[7,10] and M—L[11] bond energies.

The present investigation is an outgrowth of our previous study[9] on the relative strengths of the metal–hydrogen and metal–methyl bond energies in complexes of middle to late transition metals. We were able in this study, by decomposing the M—H and M—CH_3 bond energies into contributions from steric factors and π- or σ-bonding interactions as well as contributions from relativistic effects, to illustrate that methyl has a weaker bond to middle and late transition metals than hydrogen as a result of stronger repulsive steric interactions. We shall apply here the same decomposition scheme to the Cl_3M—L and $LCo(CO)_4$ systems. Such an analysis should enable us to investigate, in detail, the trend in steric factors and π- or σ-bonding interactions for various ligands of the Ti—L bond. It should further allow us to assess whether this trend is significantly changed through the triad M = Ti, Zr, Hf or in going to the electron-rich late transition metal center of cobalt. Of particular interest to us is the relative M—H and M—CH_3 bond strengths in the electron-poor Cl_3MR (M = H, CH_3) systems, as well as the degree to which π-bonding interactions, due to donation from occupied ligand orbitals to π-type virtual orbitals on the metal center, are enhanced in going from the electron-rich cobalt atom to the electron-poor group 4 metals.

COMPUTATIONAL DETAILS

The Hartree–Fock–Slater (HFS) or $X\alpha$ scheme[12] is by far the most widely used density functional method in chemistry. It has, however, become apparent[13] that the lack of correlation between electrons of different spins, and in particular the purely local representation of the exchange potential, in many instances leads to calculated values for bond energies in considerable disagreement with experimental data. Fortunately, recent advances in density functional theory, which in many ways parallels the development of post-HFS methods, have lead to remedies for the lack of correlation between electrons of different spins[14] as well as non-local correction to the HFS-exchange energy. The energy expression employed in the present set of calculations takes on the form

$$E_{BS} = E_{HFS} + E_C + E_X^{NL} \tag{1}$$

where E_{HFS} is the original statistical energy expression for the HFS-method. The first correction term E_C proposed by Stoll *et al.*[14] represents the correlation between electrons of different spins, whereas the second correction term E_X^{NL}, due to Becke,[3] represents a non-local correction to the local HFS-exchange energy E_X. All calculations presented here were based on the LCAO–HFS program system due to Baerends *et al.*,[4] or its relativistic extension due to Snijders *et al.*,[15] with minor modifications to allow for Becke's non-local exchange correction as well as the correlation between electrons of different spins in the formulation by Stoll *et al.*, based on Vosko's parametrization[16] from electron gas data. The SCF-part of the calculation, as well as the optimization of geometrical parameters, included, of the two corrections in eq. (1), only E_C corresponding to the correlation between electrons of different spins. The wave functions generated from this type of SCF-calculation were used to calculate Becke's non-local exchange correction E_X^{NL} at the optimized or assumed geometries, in order to evaluate E_{BS} of eq. (1). Bond energies were evaluated by the Generalized Transition State method[5] or its relativistic extension.[6]

A double ζ-STO basis[17] was employed for the *ns* and *np* shells of the main group elements augmented with a single 3*d* STO function, except for hydrogen where a 2*p* STO was used as polarization. The *ns*, *np*, *nd*, $(n+1)s$, and $(n+1)p$ shells of the transition metals were represented by a triple ζ-STO basis.[17] Electrons in shells of lower energy were considered as core and treated by the frozen-core approximation according to the procedure due to Baerends *et al.*[4] The total molecular electron density was fitted in each SCF-iteration by an auxiliary basis[18] of *s*, *p*, *d*, *f* and *g* STOs, centered on the different atoms, in order to represent the Coulomb and exchange potentials accurately.

In the transition metal systems, standard bond distances were assumed for the OH, OCH_3, SH, NH_2, PH_2, CH_3, CN and SiH_3 ligands, with HCH and HSiH bond angles of 109°, and HNH or HPN angles of 120°. Geometrical parameters for the $Co(CO)_4$ fragment were those of the $Co(CO)_4$-framework in $HCo(CO)_4$.[19] Standard M—Cl bond distances were adopted for the MCl_3 fragments (M = Ti, Zr, and Hf) with a ClMCl bond angle of

109°. The M—L distances and angles were separately optimized from a three point parabolic fit.

THE M—L BOND STRENGTH IN Cl_3ML WITH M = Ti, Zr, Hf AND L = H, CH_3, SiH_3, OH, SH, OCH_3, NH_2, PH_2 AND CN

The bonding in Cl_3ML can be conveniently analysed in terms of the frontier orbitals[20] on the ligand L and the metal fragment MCl_3. The frontier orbitals on MCl_3 consist of the three σ-nonbonding metal-based d-orbitals $1a_1$ (**1a**) and $1e_x$,$1e_y$ (**1b**) as well as the two σ-antibonding metal-based d-orbitals $2e_x$,$2e_y$ (**1c**) of somewhat higher energy. Orbital energies for the five frontier orbitals of MCl_3 are shown to the left in Fig. 1. The ground-state configuration of MCl_3 was found to be $(1a_1)^1$ for M = Ti, Zr and Hf. Thus, the MCl_3 fragment has one singly occupied orbital **1a** available for electron pairing as well as two sets, **1b** and **1c**, of empty orbitals suitable for a donor–acceptor interaction with occupied orbitals on L. One should not be led to think from Fig. 1 that the effective charge on the metal center in MCl_3 is +3. Firstly, the $2e$ σ-antibonding orbital **1c** will have a bonding counterpart of lower energy (not shown in Fig. 1) with some d-participation. Secondly, there will be some participation from the d-orbitals shown in **1a** and **1b** to chlorine based π-type orbitals. In an actual Mulliken population analysis on $TiCl_3$ we found a charge of +0.48 on the metal.

The CH_3 and SiH_3 ligands of C_{3v} symmetry have a $(2a_1)^1(1e)^4$ groundstate configuration (**2a**), the OH and SH ligands of $C_{\infty v}$ symmetry and OCH_3 or C_{3v} symmetry have a $(2a_2)^2(1e)^3$ configuration (**2b**) in effective C_{3v} symmetry. The NH_2 and PH_2 ligands of C_{2v} symmetry have a $(2a_1)^2(1b_1)^2(1b_2)^1$ configuration (**2c**), whereas CN of $C_{\infty v}$ symmetry has a $(\sigma)^1(\pi)^4$ configuration (**2d**). We finally have the hydrogen atom with the $(1s)^1$ configuration. The

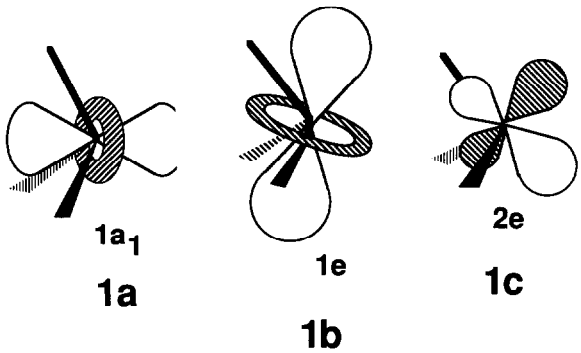

Structure 1.

frontier orbital energies for the ligands are shown to the right in Fig. 1.

It follows from our discussion, so far, that all ligands have one singly occupied orbital available for an electron pairing σ-interaction with $1a_1$ (**1a**) of MCl_3. All ligands, except hydrogen, have in addition occupied orbitals suitable for donor–acceptor interactions with the two pairs of empty orbitals, (**1b**) and (**1c**), on MCl_3.

The $Cl_3M—XH_3$ systems were found to prefer a staggered conformation (**3a**) where the electron pairing σ-interaction (**3b**) involve $1a_1$ of MCl_3 and $2a_1$ of XH_3, whereas the donor–acceptor interactions (**3c**) involves the two e-sets **1b** and **1c** on MCl_3 and the e orbitals on XH_3.

The $Cl_3M—OH$, $Cl_3M—OCH_3$, and $Cl_3M—SH$ model systems were found to prefer conformation **4a** of C_s point group symmetry in which the angle α had a value of 110° in the case of OH and OCH_3, with a value of 101° in the case of SH. The conformation of C_{3v} symmetry with α = 180° was, however, for the different metals and ligands less than 30 kJ mol^{-1} higher in energy. The electron pairing σ-interaction in **4a** is primarily between $1a_1$ on MCl_3

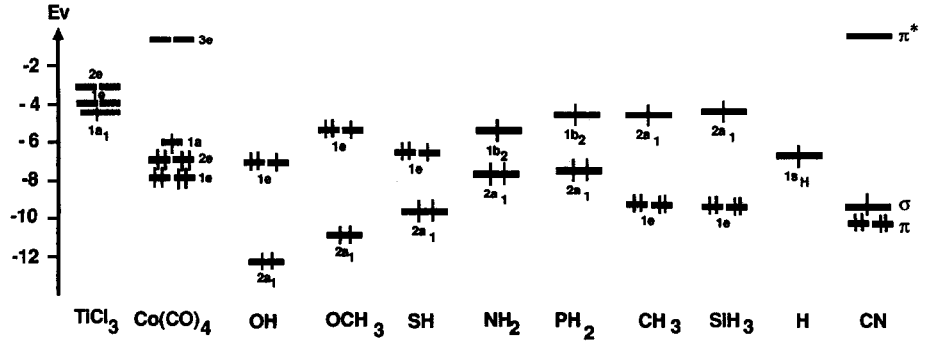

Fig. 1. Energies for the frontier orbitals of the two metal fragments $TiCl_3$ and $Co(CO)_4$ as well as the ligands L = OH, OCH_3, SH, NH_2, PH_2, H, CH_3, SiH_3, CN and H.

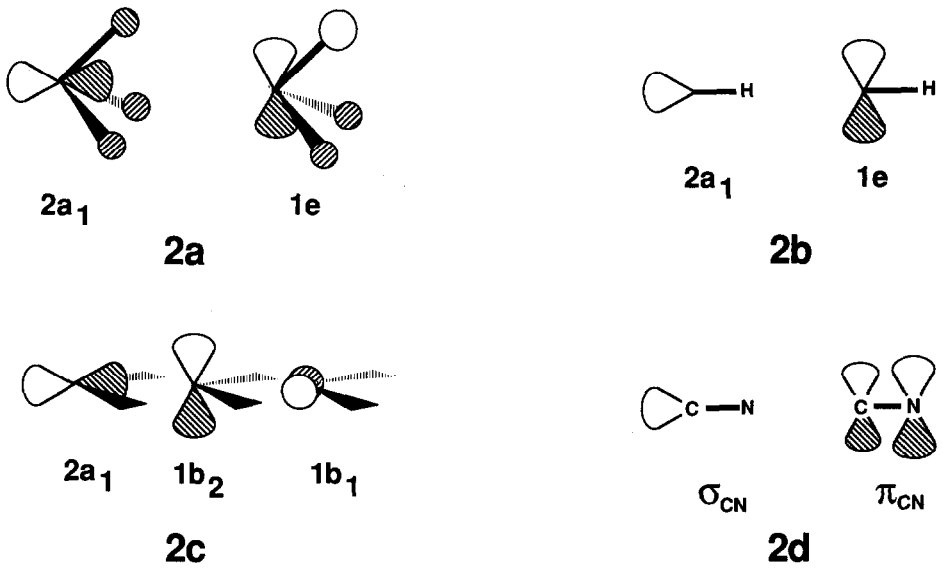

Structure 2.

and the singly occupied $1e$ orbital on the ligand (**4b**), whereas the donor–acceptor interactions are between the MCl_3 *e*-pairs (**1b**,**1c**) and the fully occupied $2a_1$ and $1e$ ligand orbitals (**4c**).

There are many possible conformations for $Cl_3M—NH_2$ and $Cl_3M—PH_2$ corresponding to different choices of the angle θ in **5a**. We found the preferred geometry to have M and XH_2 in a coplanar conformation ($\theta = 180°$) as shown in **5b**. In conformation **5b** of C_s symmetry the singly occupied $1a_1$ orbital on MCl_3 will interact with the doubly occupied $2a_1$ orbital of XH_2 (**5c**), whereas the empty *e*-type orbitals on MCl_3 interacts (**5d**) with the singly occupied $1b_2$ orbital on XH_2. We shall, in order to facilitate the discussion of the bonding in Cl_3MXH_2 of conformation **5b**, promote XH_2 from the $(2a_1)^2(1b_1)^2(1b_2)^1$ groundstate configuration to the "valence configuration" $(2a_1)^1(1b_1)^2(1b_2)^2$. The interaction in **5c** is in this way between two singly occupied orbitals and the interaction in **5b** between empty MCl_3 orbitals and the fully occupied $1b_2$ orbital. The energy ΔE_{prep} required to promote XH_2 from the groundstate configuration to the valance configuration $(2a_1)^1(1b_1)^2(1b_2)^2$, with the XH_2 framework kept constant, was 134 kJ mol^{-1} and 237 kJ mol^{-1} for X = N and X = P, respectively. The bond energy D(M—L) is defined with respect to the groundstate of MCl_3 and L for all ligands L. The electronic promotion of NH_2 and PH_2 will not influence the calculated values for D(M—NH_2) and D(M—PH_2) since ΔE_{prep} will be taken properly into account [see eq. (2) below]. The promotion will, however, make the discussion of the bonding in the Cl_3M—L systems more uniform.

We finally have Cl_3M—H of C_{3v} symmetry with the single bonding interaction **6a** as well as Cl_3M—CN, also, of C_{3v}-symmetry, with the electron pairing σ-interaction **6b** and the donor–acceptor interactions **6c**.

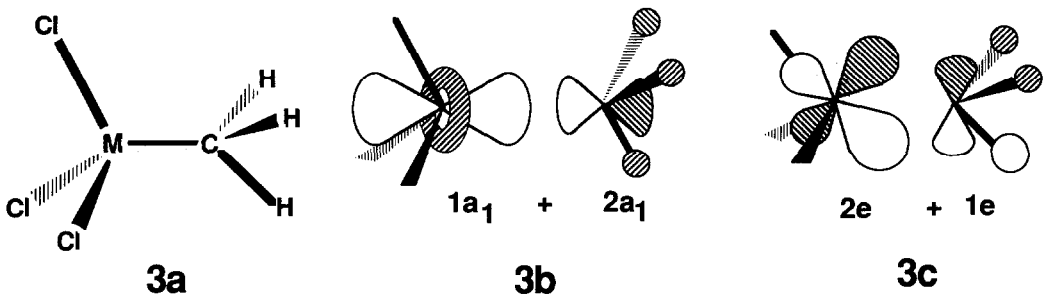

Structure 3.

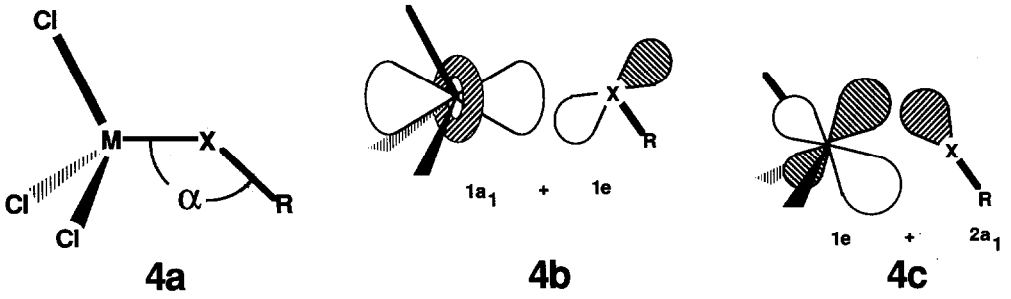

Structure 4.

We have, in accordance with the bonding analysis presented here for Cl_3M—L, decomposed the D(M—L) bonding energy as

$$D(\text{M—L}) = -[\Delta E_{\text{prep}} + \Delta E^0 + \Delta E_\sigma + \Delta E_{\text{DA}} + \Delta E_{\text{Rel}}], \quad (2)$$

by considering the formation of Cl_3M—L from Cl_3M and L in a sequence of steps. The term ΔE_{prep} of eq. (1) represents the energy required in the first step to prepare the ligand L before the formation of Cl_3M—L. That is, the ligand framework is deformed to the conformation it will have in Cl_3M—L and, if required, promoted from its electronic groundstate to its electronic valence configuration. We have for all ligands except CH_3 assumed the same geometry of L in Cl_3M—L as in the free state. However, CH_3 has been deformed from its planar equilibrium geometry with an HCH angle of 120° to the trigonal conformation with an HCH angle of 109°. The energy required to deform CH_3 amounts to 25 kJ mol^{-1} and ΔE_{prep} will as a consequence have the contribution $-\Delta E_{\text{prep}} = -25$ kJ mol^{-1} to D(M—L) in the Cl_3M—CH_3 systems. The only two ligands for which an electronic promotion was required were NH_2 and PH_2. These two ligands were, as already mentioned, promoted from $(2a_1)^2(1b_1)^2(1b_2)^1$ (**2c**) to $(2a_1)^1(1b_1)^2(1b_2)^2$. The contributions to D(M—L) from the promotions were $-\Delta E_{\text{prep}} = -134$ kJ mol^{-1} and $-\Delta E_{\text{prep}} = -237$ kJ mol^{-1} for NH_2 and PH_2, respectively. The MCl_3 fragment and the prepared ligand are, in the second step, placed in the positions they will take up in the combined complex Cl_3M—L, while the electrons are confined to the orbitals they occupy in the separate fragments. The energy contribution to D(M—L) from this step, $-\Delta E^0$, is negative and destabilizing, since it involves interactions between

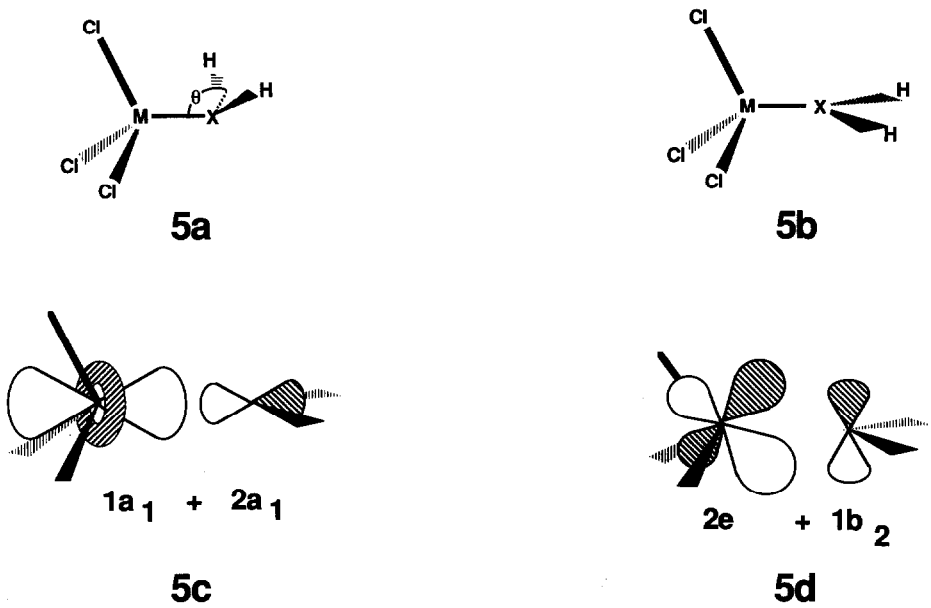

Structure 5.

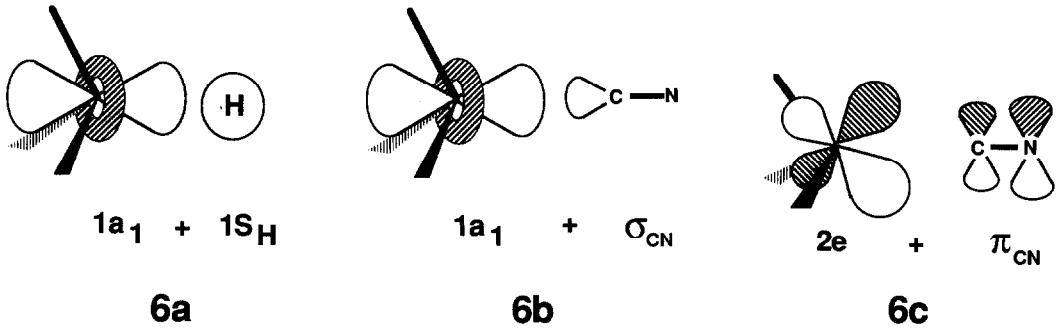

Structure 6.

fully occupied orbitals on L and Cl_3M as well as interactions between a fully occupied orbital on one fragment and a singly occupied orbital on the other fragment. The term $-\Delta E^0$, which we will refer to as the steric interaction energy, includes in addition, the stabilizing electrostatic interaction $-\Delta E_{el}$ between L and Cl_3M.

We allow in the third step the two single electrons on L and Cl_3M to pair up into a bonding orbital (**3b**, **4b**, **5c**, **6a** and **6b**) while restraining any electron density from flowing into the two sets (**1b** and **1c**) of empty *e*-type orbitals on Cl_3M. That is, we carry out a SCF-calculation in which **1b** and **1c** are excluded. The energy contribution to D(M—L) from the third step, which essentially represents the formation of a σ-bond, is referred to as $-\Delta E_\sigma$ in eq. (1).

In the last step we carry out a full SCF-calculation, thus allowing for the flow of density into the empty *e*-type orbitals (**1b** and **1c**) on Cl_3M from occupied ligand orbitals. The contribution to D(M—L) from the donor–acceptor interactions **3c**, **4c**, **5d** and **6c** is referred to as $-\Delta E_{DA}$ in eq. (1). We finally have as a separate term in eq. (1) the contributions from relativistic effects, $-\Delta E_{Rel}$. Relativistic effects are only of importance for heavy elements and have as a consequence only been evaluated for systems containing hafnium.

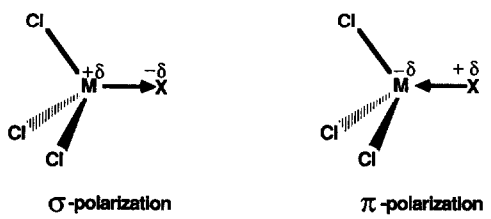

Structure 7.

The calculated D(M—L) bond energies are displayed in Table 1 and a decomposition of D(M—L) according to eq. (1) is given for the Cl_3Ti—L systems in Table 2. It follows from Table 2 that the electron-pairing σ-interactions **3b**, **4b**, **5c**, **6a** and **6b**, with the contribution $-\Delta E_\sigma$, are more important for the strength of the Cl_3M—L bond than the donor–acceptor interactions **3c**, **4c**, **5d** and **6c**, with the contribution $-\Delta E_{DA}$. The bonds formed in the σ-interactions **3b**, **4b**, **5c**, **6a** and **6b** are in most cases strongly polar (**7a**) as one might expect from the difference in electronegativity between the three metals Ti, Zr and Hf on the one side and the coordinating atoms of L on the other side. We have, from a population analysis of the σ-bonding orbitals **3b**, **4b**, **5c**, **6a** and **6b** in Cl_3M—L, calculated δ of **7a** as; 0.71(L = OH), 0.69(L = OCH_3), 0.54(L = SH), 0.52(L = CN), 0.50(L = NH_2), 0.40(L = CH_3), 0.35(L = PH_2) and 0.20(L = H), respectively.

The ligands L = OH, OCH_3, with the coordinating atoms of the highest electronegativity and

Table 1. Calculated D(M—L) bond energies (kJ mol^{-1}) and optimized R(M—L) bond distances (Å) in Cl_3ML

	D(M—L)			R(M—L)[a]		
	M			M		
L	Ti	Zr	Hf	Ti	Zr	Hf
H	250.7	297.2	313.5	1.70	1.82	1.80
CH_3	267.5	309.5	326.6	2.13	2.26	2.25
SiH_3	210.9	239.5	272.2	2.63	2.78	2.79
OH	453.2	527.2	535.9	1.83	1.95	1.97
OCH_3	426.9	484.5	506.6	1.86	1.99	2.01
SH	293.3	347.9	360.1	2.28	2.47	2.47
NH_2	364.7	420.6	439.1	1.87	2.01	2.04
PH_2	190.6	225.6	233.9	2.24	2.48	2.47
CN	410.4	457.6	477.9	2.06	2.21	2.23

[a] Optimized from a quadratic fit through three energy points corresponding to three different M—L distances.

Table 2. Decomposition of D(Ti—L) in Cl_3M—L. All energies in kJ mol^{-1}

L	$-\Delta E^0$	$-\Delta E_{el}$[a]	$-\Delta E_\sigma$	$-\Delta E_{DA}$	$-\Delta E_{prep}$	D(M—L)[b]
H	−44.9	176.7	290.6	5.0	—	250.7
CH_3	−115.7	341.1	396.8	11.4	−25	267.5
SiH_3	−91.9	294.1	273.9	28.9	—	210.9
OH	−330.9	372.9	669.4	114.7	—	453.2
OCH_3	−302.5	400.5	606.1	123.2	—	426.9
SH	−229.7	433.5	412.5	100.5	—	283.3
NH_2	−149.2	300.4	540.2	108.1	−134.4	364.7
PH_2	−94.0	244.2	391.5	129.7	−236.9	190.6
CN	−91.4	269.7	463.5	38.3	—	410.4

[a] The electrostatic interaction energy ΔE_{el} is included in the steric interaction energy ΔE^0.

[b] The total bonding energy is according to eq. (2) given as $D(\text{M—L}) = -[-\Delta E^0 + \Delta E_\sigma + \Delta E_{DA} + \Delta E^0 + \Delta E_{prep}]$. The individual terms are defined in the text.

the most polar Cl_3M—L bond, have the largest D(M—L) bond energies and strongest σ-interactions **4b** (Tables 1 and 2). The ligand L = SiH_3, with the coordinating atom of the lowest electronegativity and the least polar M—L bond, has a modest D(M—L) bond energy and the weakest σ-bonding interaction (**3b**) (see $-\Delta E_\sigma$ of Table 2). For the series of ligands NH_2, SH, CH_3 and H, one finds in Tables 1 and 2 that $-\Delta E_\sigma$ and D(M—L) follow the order of the electronegativity of the coordinating atoms, with SH > NH_2 > CH_3 > H. Both the polarity and strength of the M—CN bonds (Tables 1 and 2) seem out of line with the position of carbon in the electronegativity series, and D(M—CN) is in fact closer to D(M—OCH_3) than to D(M—CH_3). This irregularity illustrates, however, merely the well known fact, that the singly occupied σ_{CN} sp-hybrid orbital of CN has a larger $2s$ composition than the singly occupied $2a_1$ orbital **1a** of CH_3, and thus a lower energy (Fig. 1) as well as a larger orbital electronegativity. The D(M—PH_2) bond energy in Cl_3M—PH_2 is, in spite of a large contribution $-\Delta E_\sigma$ from the σ-bonding interaction **5c**, rather low due to the required promotion energy ΔE_{prep}.

The contribution $-\Delta E_{DA}$ to D(M—L) from the donor–acceptor interactions **3c**, **4c**, **5d** and **6c** is relatively modest (Table 2). It is essentially negligible for the ligands H, CH_3, SiH_3 and CN without non-bonding donor lone pairs and amounts to $\sim$ 100 kJ mol^{-1} for the ligands OH, SH, NH_2, PH_2 and OCH_3 with available non-bonding donor lone pairs. The charge donated in the donor–acceptor interaction **7b** is less than 0.25 for all ligands involved.

The steric interaction energy $-\Delta E^0$ includes the stabilizing electrostatic interaction ΔE_{el} between Cl_3M and L, as well as the repulsive two orbital four electron interactions between occupied orbitals on Cl_3M and L and two orbital three electron interactions between a fully occupied orbital on one fragment and a singly occupied orbital on the other fragment. Each of the ligands L, with the exception of H, have fully occupied orbitals of the same symmetry as the singly occupied orbital on MCl_3. These orbitals are, as it is shown for CH_3 in **8**, involved in three electron two orbital interactions which significantly contribute to the steric interaction energy $-\Delta E^0$. Interactions such as **8** will be reduced as we allow, in the third step of our analysis, for the polar σ-interactions **3b**, **4b**, **5c**, **6a** and **6b**. This is so since $1a_1$ of Cl_3M, depending on the polarity (**7a**) of the Cl_3M—L bond, to a larger or smaller degree will be vacated. The stabilizing reduction of repulsive interactions such as **8** by transfer of charge from $1a_1$ (**1a**) in (**3b**, **4b**, **5c** and **6b**) is in our decompo-

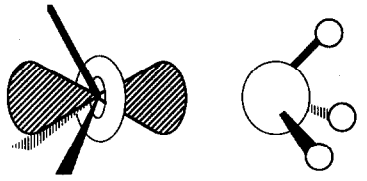

8

Structure 8.

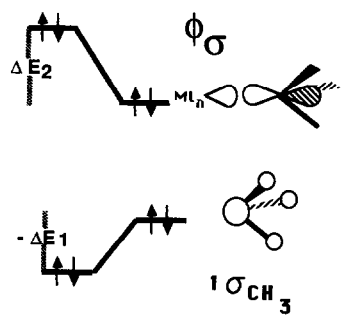

Fig. 2. Schematic representation of the repulsive interaction between the σ-bonding orbital ϕ_σ of $Cl_3M—CH_3$ and the fully occupied 1σ orbital of CH_3.

sition scheme part of $-\Delta E_\sigma$, and of considerable importance for all ligands except hydrogen. The fact that $-\Delta E_\sigma$ for L = CH_3 is larger than $-\Delta E_\sigma$ for L = H by 100 kJ mol^{-1} (Table 2) can in part be attributed to the stabilizing reduction of the repulsive interaction in **8**.

We might illustrate this important point further, in perhaps more familiar terms, by referring to Fig. 2. In Fig. 2 are shown to the left in schematic form **3b**, **4b**, **5c**, **6a** and **6b** from the interaction between the singly occupied metal-fragment orbital σ_{MX} and the singly occupied $2\sigma_L$ ligand orbital. The result of the interaction between σ_{MX} and $2\sigma_L$ is the bonding σ-orbital.

$$\phi_\sigma = C_1\sigma_{MX} + C_2(2\sigma_L). \quad (3)$$

All ligands with the exception of H have, as already mentioned, a fully occupied orbital $1\sigma_L$ of relatively low energy which can interact with σ_{MX} and thus ϕ_σ of eq. (2). The $1\sigma_L$ orbital is for L = CH_3, NH_2, OCH_3 and OH largely a $2s$ orbital on the central ligand atom and for L = SiH_3, PH_2 and SH the corresponding $3s$ orbital. The interaction between $1\sigma_L$ and ϕ_σ of eq. (3) depends, since $1\sigma_L$ and $2\sigma_L$ has zero overlap and thus to a first approximation zero interaction, on C_1 and the overlap $\langle 1\sigma_L|\sigma_{MX}\rangle$. The interaction between $1\sigma_L$ and ϕ_σ will, as shown to the right in Fig. 2, lead to a stabilization of $1\sigma_L$ by $-\Delta E_1(\Delta E_1$ positive) and a destabilization of ϕ_σ by $\Delta E_2(\Delta E_2$ positive). The total destabilization of Cl_3M will be $\Delta E_2 - \Delta E_1$, and it can readily be shown that

$$\Delta E_2 - \Delta E_1 \propto [C_1\langle 1\sigma_L|\sigma_{MX}\rangle]^2. \quad (4)$$

It is clear from eq. (4) that a polarization of the M—L bond in XM—L, which will diminish C_1, has the effect of reducing the destabilization $\Delta E_2 - \Delta E_1$.

Hydrogen does not have a fully occupied $1\sigma_L$ orbital and the M—H bond does as a consequence not suffer a destabilization of the type illustrated in Fig. 2. We have in a previous study[9] shown that the destabilization $\Delta E_2 - \Delta E_1$, in part, is responsible for the relatively unpolar M—CH_3 bond of middle to late transition metals, where $[C_1]^2 \sim 1/2$, being weaker than the corresponding M—H bonds. We find in the present set of calculations the polar M—CH_3 bonds in $Cl_3M—CH_3$ to be at a par in strength with the corresponding M—H bonds, and attribute this to a reduction of C_1 and $\Delta E_2 - \Delta E_1$ in M—CH_3 as a result of the polarity in **7a**. We do not on the other hand find any significant enhancement in the M—CH_3 bond strength of the $Cl_3M—CH_3$ systems from the donor–acceptor interactions **3c**, **4c**, **5d** and **6c** (see $-\Delta E_{DA}$ of Table 2).

It is clear from Table 1 that zirconium, and even more so hafnium, form stronger M—L bonds to the ligands under investigation than titanium in the $Cl_3M—L$ systems. The calculated increase in D(M—L) down the triad M = Ti, Zr and Hf is primarily caused by a corresponding increase in the overlap between $1a_1$ (**1a**) of Cl_3M and the singly occupied ligand orbital on L in the interactions **3b**, **4b**, **5c**, **6a** and **6b**. Thus, the overlaps in **3b** were calculated as 0.36, 0.41 and 0.43 for M = Ti, Zr and Hf, respectively. The contribution $-\Delta E_{rel}$ from relativistic effects to D(M—L) is rather modest. The largest contribution from $-\Delta E_{rel}$ was 8 kJ mol^{-1} in the case of L = OH and the smallest contribution was 2 kJ mol^{-1} in the case of L = SiH_3.

There are few thermochemical data available for M—L bonds involving group 4 metals. Of the ligands under consideration data[1a] are, to our knowledge, only available for L = CR_3, NR_2 and OR (R = alkyl). For these ligands the mean bond energy E(M—L) is known for the homoleptic $M(CR_3)_4$, $M(NR_2)$, and $M(OR)_4$ systems with M = Ti, Zr and HF. The experimental mean bond energies E(M—L) exhibit the same trends as the calculated D(M—L) bond energies of $Cl_3M—L$ with an increase down the triad, E(Hf—L) > E(Zr—L) ≫ E(Ti—L), as well as an increase with the electronegativity of the coordinating atom on the ligand, E(M—OR) > E(M—NR_2) > E(M—CR_3). Group 4 metals are known[21] to form several complexes involving M—L bonds with L = SiR_3, PR_2, and SR ligands. The corresponding D(M—L) bond energies have, however, not been determined experimentally. We find, perhaps not surprisingly, that the M—L bonds of L = SiH_3, PH_2, and SH are weaker and less polar than the M—L bonds of the homologous ligands L = CH_3, NH_2, and SH (Table 1).

Comparative experimental data on M—H and M—CH_3 bond energies of early transition metals are not available. It has, however, been asserted[22] that the M—H and M—CH_3 bond strengths of

early transition metals are quite similar, in contrast to systems involving middle to late transition metals where the M—CH_3 bonds are weaker than the corresponding M—H bonds. We find, indeed, D(M—H) and D(M—CH_3) to be quite similar in the Cl_3M—H and Cl_3M—CH_3 systems, respectively. It follows further from our analysis that the polarity of the M—CH_3 bond in Cl_3MCH_3 considerably enhances the M—CH_3 bond strength by reducing the repulsive interaction shown in Fig. 2.

We shall now in the next section turn to a study of M—L bond energies in the late transition metal complexes $LCo(CO)_4$.

THE M—L BOND STRENGTH IN $LCo(CO)_4$ WITH L = H, CH_3, SiH_3, OH, SH, NH_2, PH_2 AND CN

The geometry of the $Co(CO)_4$ framework in $LCo(CO)_4$ was adopted from the experimentally[19] determined structure of $HCo(CO)_4$ where the $Co(CO)_4$ fragment has a C_{3v} point-group symmetry (**9a**) with an CO_{eq}—Co—CO_{eq} angle θ of 98°. The d^9 radical $Co(CO)_4$ of conformation **9a** has the unpaired electron residing in a $1a_1d(z^2)$ metal-based orbital (**9b**). The two sets of metal-based d-orbitals of e-symmetry, $1e$ (**9c**) and $2e$ (**9d**), are fully occupied and can thus not accept electron density from the lone-pairs of L. Empty e-type acceptor orbitals on $Co(CO)_4$ are, however, available (**9e**). The set of e-type acceptor orbitals of lowest energy is $3e$ (**9e**). The $3e$ orbitals are made up of an out-of-phase combination between a (d,p)-hydride on the metal and the π^*_{CO} orbital on the CO ligands.

The orientation of the ligand L in $LCo(CO)_4$ with respect to the three-fold axis of the metal fragment $Co(CO)_4$ is the same as the orientation of L in Cl_3ML with respect to the three-fold axis of Cl_3M for L = H (**10a**), L = CN (**10b**), L = OH, SH (**10c**), and L = CH_3, SiH_3 (**10d**). The bonding in $LCo(CO)_4$ for L = H, OH, CN, SH, CH_3, and SiH_3 can as a consequence be readily understood in terms of σ-interactions reminiscent of **3b**, **4a**, **6a** and **6b**, where the $1a_1$ orbital of Cl_3M (**1a**) is replaced by the $1a_1$ orbital **9b** of $Co(CO)_4$, as well as a π-donor–acceptor interaction similar to **3c**, **4b** and **6c** where the two e-pairs, **1b** and **1c**, of Cl_3M are replaced by the empty $3e$ (**9d**) acceptor orbitals of $Co(CO)_4$.

The coordination mode (**11a**) in $LCo(CO)_4$ for L = NH_2 and PH_2 is somewhat different from that (**5a**) of the same two ligands in Cl_3ML. That is, θ of **11a** is nearly 109° whereas the same angle in **5a** was found to be 180°. It is as a consequence the partly filled $1b_2$ orbital (**2c**) of XH_2 (X = N, P) that is involved in the σ-bond (**11b**) to $Co(CO)_4$ and the fully occupied $2a_1$ orbital that is involved in the donor–acceptor interaction (**11c**) with $3e$ of $Co(CO)_4$.

The σ-bond in $LCo(CO)_4$ is considerably less polar than in Cl_3ML. This is primarily so because

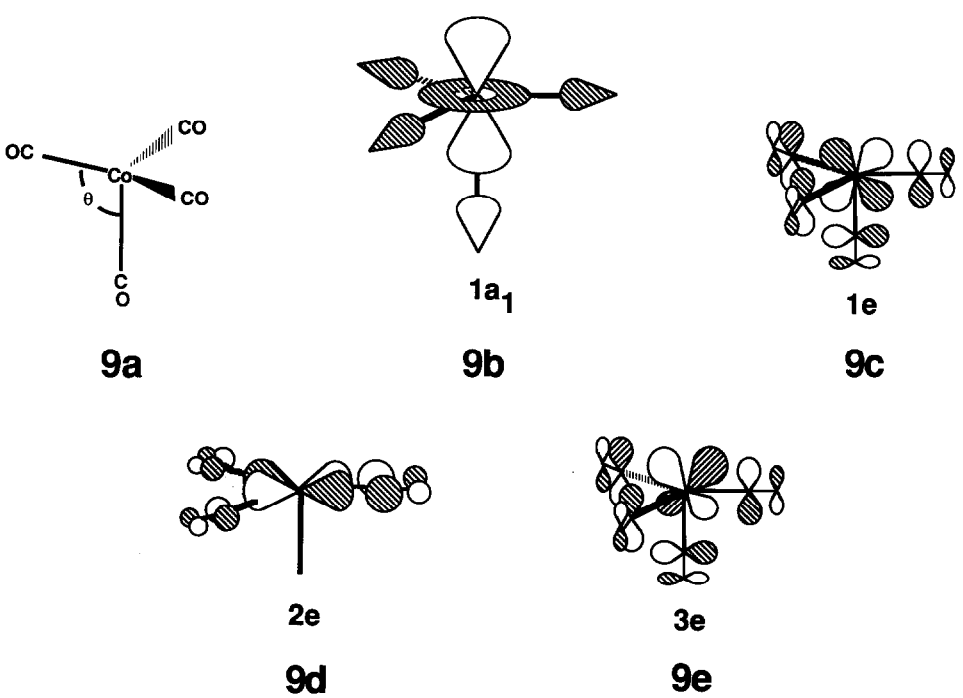

Structure 9.

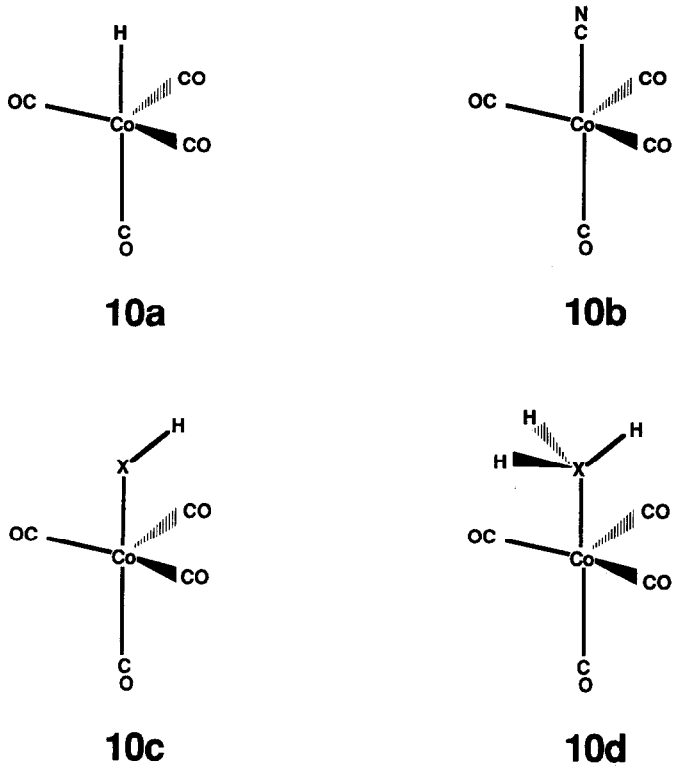

Structure 10.

cobalt is more electronegative than the group 4 metals Ti, Zr and Hf, and the $1a_1$ frontier orbital **9b** on $Co(CO)_4$ is as a consequence of lower energy than the frontier orbital $1a_1$ (**1a**) of Cl_3M (see Fig. 1). We have from a population analysis of the σ-bonding orbitals in $LCo(CO)_4$ calculated δ of **12a** as, 0.40(OH), 0.36(NH_2), 0.26(CN), 0.16(SH), 0.06(PH_2), 0.05(CH_3), 0.04(H) and $-0.27(SiH_3)$. The polarity δ in the donor–acceptor interactions (**12b**) was calculated to be less than 0.10 for all ligands involved.

It should be clear from the discussion of the bonding in $LCo(CO)_4$ that the D(Co—L) bond energy can be decomposed in a manner completely similar to that given for the M—L bond energy of Cl_3ML in eq. (1). Such a decomposition is presented in

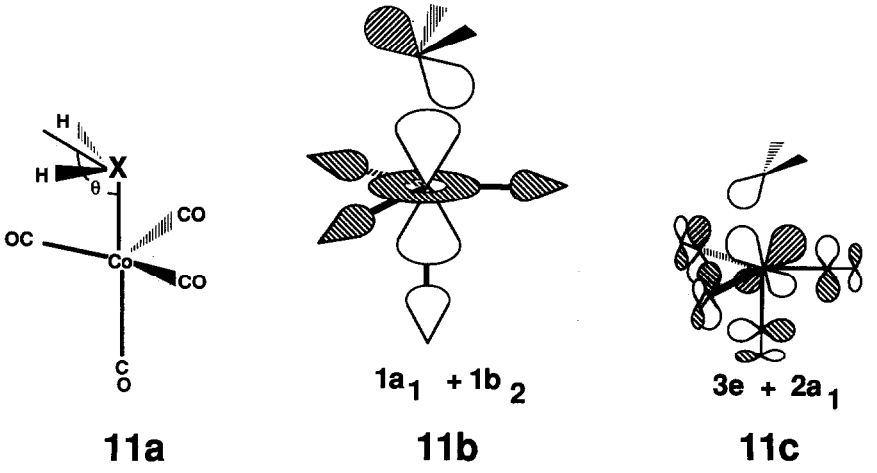

Structure 11.

12a **12b**

Structure 12.

Table 3, where D(Co—L) has been broken down into the contributions from $-\Delta E_{prep}$, $-\Delta E^0$, $-\Delta E_\sigma$ and $-\Delta E_{DA}$.

It follows from Tables 2 and 3 that the M—H bond strengths in the late transition metal complex $HCo(CO)_4$ and the early transition metal complex Cl_3MH are quite similar. This is perhaps not too surprising, since H is a simple one orbital ligand without additional occupied orbitals involved in donor–acceptor interactions, or two orbital four electron repulsive interactions, for which the strength as we shall see, might depend strongly on the *d*-electron count at the metal center.

For ligands other than H we had in the Cl_3ML systems favorable donor–acceptor interactions (**3c**, **4b** and **6c**) from occupied ligand orbitals to the two empty *e*-sets (**1b** and **1c**). In $Co(CO)_4$ the metal-based *d*-orbitals of *e* symmetry (**9c**, **9d**) are fully occupied and the corresponding interactions between occupied ligand orbitals and either 1*e* (**9c**) or 2*e* (**9d**) are as a consequence repulsive. For L = OH and SH we have strong destabilizing (negative) contributions to the steric interaction energy ΔE^0 from **13a** and **13b** at Co—XH (X = O, S) distances similar to the Ti—XH distances optimized for Cl_3TiXH. The Co—XH equilibrium bond distances in $Co(CO)_4XH$ are as a consequence, in order to reduce the repulsive interactions **13a** and **13b**, considerably elongated compared to the corresponding Ti—XH bond distances in Cl_3TiXH. In fact, the total steric interaction energy $-\Delta E^0$ of the $XHCo(CO)_4$ systems, at the equilibrium distance, is as a result of the increase in the bond distances less repulsive than the total steric interaction energy in Cl_3MXH. The relatively long M—XH bond in $XHCo(CO)_4$ will, however, in conjunction with a less polar bond, result in a weakening of the σ-interaction compared to the σ-interaction in Cl_3TiXH. It follows from Tables 2 and 3 that $-\Delta E^0$ and $-\Delta E_\sigma$ combined can account for the trend D(Ti—L) > D(Co—L) with respect to L = OH and SH. The relative magnitude of D(Co—L) and D(Ti—L) is, however, also to some degree influenced by the donor–acceptor interaction between occupied orbitals on L and empty *e*-type orbitals on the metal center (see $-\Delta E_{DA}$ of Tables 3 and 3). Thus, $TiCl_3$ with acceptor orbitals (**1b** and **1c**) of relatively low energy (Fig. 1) has a stronger donor–acceptor interaction ΔE_{DA} than $Co(CO)_4$ with 3*e* acceptor orbitals (**9e**) of relatively high energy.

For L = NH_2 and PH_2 we find as well, that the two ligands form stronger bonds to the early transition metal fragment $TiCl_3$ than the late transition metal fragment, i.e. D(Ti—L) > D(Co—L) for L = NH_2 and PH_2: Again, occupied orbitals on NH_2 and PH_2 are interacting repulsively (**14a** and **14b**) with the occupied metal-based *d*-orbitals of *e*-symmetry causing an elongation of the Co—L bond, and in conjunction with a less polar bond, a weakening of the σ-interaction. The donor–acceptor interactions are in addition, as expected, weaker in $LCo(CO)_4$ than in Cl_3TiL for L = NH_2 and PH_2 (see $-\Delta E_{DA}$ of Tables 2 and 3).

The CN ligand, too, has a pair of occupied

Table 3. Decomposition of D(Co—L) in $LCo(CO)_4$. All energies in kJ mol^{-1}.

L	$-\Delta E^0$	$-\Delta E_{el}$[a]	$-\Delta E_\sigma$	$-\Delta E_{DA}$	$-\Delta E_{prep}$	D(Co—L)[b]	D(M—L)[c]
H	−111	258	341	—	—	230	1.55
CH_3	−210	303	366	29	−25	160	2.11
SiH_3	−168.1	237.1	331.4	48.3	—	211.6	2.73
OH	−198.3	168.6	366.6	64.1	—	232.4	2.09
SH	−141.7	169.1	257.6	53.0	—	168.9	2.49
NH_2	−302.9	329	389.4	59.0	—	145.5	2.09
PH_2	−261.6	323	362.1	45.1	—	145.5	2.43
CN	−248.1	277.6	472.6	78.8	—	304.3	2.04

[a] The electrostatic interaction energy ΔE_{el} is included in the steric interaction energy ΔE^0.

[b] The total bonding energy is according to eq. (1) given as $D(M—L) = -[\Delta E^0 + \Delta E_\sigma + \Delta E_{DA} + \Delta E^0 + \Delta E_{prep}]$. The individual terms are defined in the text.

[c] Calculated M—L bond distance in Å.

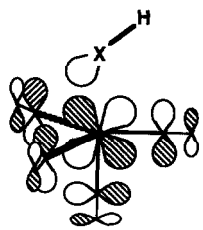

1e - $2a_1$

13a

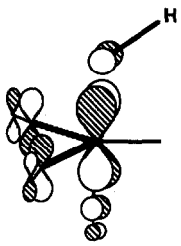

1e - e

13b

Structure 13.

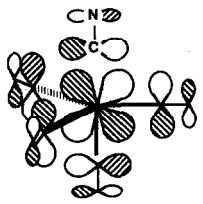

1e + π^*_{CN}

15a

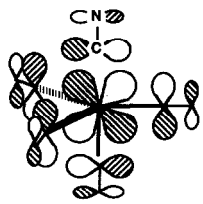

1e + π^*_{CN}

15b

Structure 15.

orbitals, π_{CN} of **2d**, which will interact repulsively with 1*e* (**9c**) of $Co(CO)_4$. The π_{CN} orbitals are, however, polarized towards the nitrogen end of CN and will for this reason not intereact too strongly with 1*e* in **15a**. Further, the empty π^*_{CN} orbitals will interact stabilizing (**15b**) with 1*e* and contribute significantly to $-\Delta E_{DA}$. The stabilization in **15b**, and the modest destabilization in **15a**, makes it possible for CN to maintain a Co—CN distance, and thus a σ-interaction, that is quite similar to that of the Ti—CN bond in Cl_3Ti—CN.

Ungvary[24] has measured the *D*(Co—H) bond energy in $HCo(CO)_4$ to be 238 kJ mol^{-1}, in fair agreement with our theoretical value of 230 kJ mol^{-1}. Experimental *D*(Co—L) bond energies for $Co(CO)_4L$ with L = OH, SH, NH_2, CN and PH_2 are not available. Bryndza, Bercraw and co-workers[1d] have, however, measured the relative *D*(M—L) bond strengths in the electron rich d^6 $Cp^*(PMe_3)_2RuL$ and d^8 (DPPE)MePtL (DPPE = $Ph_2PCH_2CH_2PPh_2$) systems for L = OH, SH, H, CN and NR_2. They find, in agreement with our calculations on the d^8 model systems $LCo(CO)_4$, the order for the bond strengths to be *D*(M—CN) > *D*(M—OH) > *D*(M—H) > *D*(M—SH) > *D*(M—NHPh).

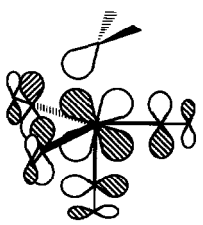

1e - $2a_1$

14a

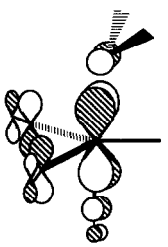

1e - $1b_1$

14b

Structure 14.

Methyl follows the trend of the other many-electron ligands in that the M—CH_3 bond strength is reduced in $CH_3Co(CO)_4$ compared to Cl_3TiCH_3. We find as a consequence that the M—H bond in the late transition complex $HCo(CO)_4$ is stronger than the corresponding M—CH_3 bond. This is in contrast to the early transition complexes Cl_3TiR (R = H, CH_3) where the M—H and M—CH_3 bonds were similar in strength. There are two reasons for the weaker M—CH_3 bond in $CH_3Co(CO)_4$ compared with Cl_3TiCH_3. Firstly, the *e*-type metal based *d*-orbitals (**9c** and **9d**) on $Co(CO)_4$ are occupied and will as a consequence interact repulsively with the occupied 1*e* (**2a**) orbitals on CH_3, whereas the 1*e* orbital on CH_3 will interact by stabilizing the corresponding 1*e* (**1b**) and 2*e* (**1c**) orbitals on Cl_3Ti, since the two *e*-sets (**1b** and **1c**) are vacant. Secondly, the Ti—CH_3 bond is more polar than the Co—CH_3 bond and the repulsive interaction between $1a_1$ of CH_3 (**8**) and the singly occupied $1a_1$ orbital of $TiCl_3$ (**1a**) will as a consequence, according to eq. (4), be reduced more than the corresponding interaction between $1a_1$ of CH_3 (**8**) and $1a_1$ of $Co(CO)_4$ (**9b**).

The silyl ligand seems not to follow the general trend among the many electron ligands, in that *D*(M—SiH_3) is quite similar for $SiH_3Co(CO)_4$ and Cl_3TiSiH_3. We have not analysed the factors behind this exception in any detail. It follows, however, from Tables 2 and 3, that $SiH_3Co(CO)_4$, in comparison with Cl_3TiSiH_3, has more favorable bonding interactions ($-\Delta E_\sigma$ and $-\Delta E_{DA}$) as well as a more repulsive steric interaction ($-\Delta E^0$).

CONCLUDING REMARKS

We have here, with the aid of calculations based on density functional theory,[3] compared M—L bond strengths in the early transition metal complexes Cl_3ML (M = Ti, Zr and Hf) with the cor-

responding M—L bond strengths in the late transition metal complexes $LCo(CO)_4$ for L = H, CH_3, SiH_3, H, CN, OH, OCH_3, SH, NH_2 and PH_2. We have, in agreement with the few available experimental data,[23] found that all ligands except hydrogen form stronger bonds to the early transition metal Ti than to the late transition metal Co. The reason for this trend is not so much due to the fact, that early transition metals have several vacant *d*-orbitals available for donation from occupied ligand orbitals, as it is due to the fact that the same *d*-orbitals in late transition metals are occupied and thus involved in repulsive interactions with the occupied ligand orbitals. The conclusion drawn here from calculations on the model systems Cl_3ML and $LCo(CO)_4$ with respect to the relative strength of the M—L bond in early and late transition metals should be relatively general. Thus, most fragments of early transition metals, like $TiCl_3$, have several vacant *d*-orbitals whereas late transition fragments, like $Co(CO)_4$ have most *d*-orbitals occupied.

We have further found that the M—L bond strength in Cl_3ML, for a given ligand L, increases down the triad M = Ti, Zr and Hf. The increase in bond energy is associated with a corresponding increase in the overlaps for the σ-interactions **3b**, **4b**, **5c**, **6a** and **6b**. The finding here that the M—L bond strength is strongest for the heavier congener within a triad seems to be quite general for a M—L bond with a predominant σ-component.[1a,9]

Acknowledgements—This investigation was supported by the National Sciences and Engineering Research Council of Canada (NSERC). We thank the SARA computing center in Amsterdam and the University of Calgary for access to their Cyber-205 installations.

REFERENCES

1. (a) J. A. Connor, *Top. Curr. Chem.* 1977, **71**, 71; (b) R. G. Pearson, *Chem. Rev.* 1985, **85**, 41; (c) J. L. Beauchamp, *Chem. Rev.*, in press; (d) H. E. Bryndza, L. K. Fong, R. A. Peciello, W. Tam and J. E. Bercaw, *J. Am. Chem. Soc.* 1987, **109**, 1444; (e) J. W. Bruno, T. J. Marks and L. R. Morss, *J. Am. Chem. Soc.* 1983, **105**, 6824.
2. (a) T. Ziegler, V. Tschinke and L. Versluis, *NATO ASI* 1986, Series C **176**, 189, and references therein; (b) P. J. Hay and C. M. Rohlfing, *NATO ASI* 1986, Series C **176**, 135.
3. A. Becke, *J. Chem. Phys.* 1986, **84**, 4524.
4. E. J. Baerends, D. E. Ellis and P. Ros, *Chem. Phys.* 1973, **71**, 71.
5. T. Ziegler and A. Rauk, *Theory. Chim. Acta.* 1977, **46**, 1.
6. T. Ziegler, J. G. Snijders and E. J. Baerends, *J. Chem. Phys.* 1981, **74**, 1271.
7. T. Ziegler, V. Tschinke and A. Becke, *Polyhedron* 1987, **6**, 685.
8. T. Ziegler, V. Tschinke and C. Ursenbach, *J. Am. Chem. Soc.* 1987, **109**, 4825.
9. T. Ziegler, V. Tschinke and A. Becke, *J. Am. Chem. Soc.* 1987, **109**, 1351.
10. (a) T. Ziegler, *J. Am. Chem. Soc.* 1983, **105**, 7543; (b) T. Ziegler, *J. Am. Chem. Soc.* 1984, **106**, 5901.
11. (a) E. J. Baerends and A. Rozendaal, *NATO ASI* 1986, Series C **176**, 159; (b) N. Rosch, H. Jorg and B. I. Dunlap, *NATO ASI* 1986, Series C **176**, 159.
12. J. C. Slater, *Adv. Quantum. Chem.* 1972, **6**, 1.
13. (a) R. M. Dreizler and J. da Providencia (eds), *Density Functional Methods in Physics*. Plenum, New York (1985); (b) J. Avery and J. P. Dahl (eds), *Local Density Approximations in Quantum Chemistry and Solid State Physics*. Plenum, New York (1984); (c) R. M. Erdahl and V. H. Smith, Jr (eds), *Density Matrices and Density Functionals*. D. Reidel, Dordrecht (1987).
14. H. Stoll, E. Golka and H. Preuss, *Theory. Chim. Acta.* 1980, **55**, 29.
15. J. G. Snijders, E. J. Baerends and P. Ros, *Molec. Phys.* 1979, **38**, 1909.
16. S. H. Vosko, L. Wilk and M. Nusair, *Can. J. Phys.* 1980, **58**, 1200.
17. (a) J. G. Snijders, E. J. Baerends and P. Vernooijs, *At. Nucl. Data Tables* 1982, **26**, 483; (b) P. Vernooijs, J. G. Snijders and E. J. Baerends, Slater Type Basis Functions for the Whole Periodic System. Internal Report, Free University, Amsterdam, The Netherlands (1981).
18. J. Krijn and E. J. Baerends, Fit Functions in the HFS-method. Internal Report (in Dutch), Free University, Amsterdam, The Netherlands (1984).
19. R. G. Teller and P. Bau, *Struct. Bonding (Berlin)* 1981, **38**, 1909.
20. T. A. Albright, J. K. Burdett and M. H. Wangbo, *Orbital Interactions in Chemistry*. Wiley, New York (1985), and references therein.
21. (a) D. M. Roddick, B. D. Santasiero and J. Bercaw, *J. Am. Chem. Soc.* 1985, **107**, 4670; (d) D. J. Cardin, M. F. Lappert, C. L. Raston and P. L. Riley, *Comprehensive Organometallic Chemistry* (Edited by G. Wilkinson). Pergamon Press, New York (1982).
22. R. H. Crabtree, *Chem. Rev.* 1985, **85**, 245.
23. (a) M. L. Mandich, L. F. Halle and J. L. Beauchamp, *J. Am. Chem. Soc.* 1984, **106**, 4403; (b) P. B. Armentrout, L. F. Halle and J. L. Beauchamp, *J. Am. Chem. Soc.* 1981, **103**, 6501; (c) J. A. Connor, M. T. Zafarani-Moattar, J. Bickerton, N. I. Saied, S. Suradi, R. Carson, G. A. Al Takhin and H. A. Skinner, *Organometallics* 1982, **1**, 1166.
24. F. Ungvary, *J. Organomet. Chem.* 1972, **36**, 363.

Polyhedron Vol. 7, No. 18, pp. 1639–1665, 1988
Printed in Great Britain

0277–5387/88 $3.00+.00
Pergamon Press plc

POLYHEDRON REPORT NUMBER 24

ADVANCES IN VANADIUM, NIOBIUM AND TANTALUM CARBONYLS

S. C. SRIVASTAVA* and A. K. SHRIMAL

Department of Chemistry, University of Gorakhpur, Gorakhpur, U.P., India

CONTENTS

ABBREVIATIONS 1639

1. INTRODUCTION 1639

2. BINARY CARBONYLS 1640
   2.1. Chemical synthesis and structure 1640
   2.2. Synthesis in CO and inert gas matrices 1641
   2.3. Ionic species 1641

3. SUBSTITUTION REACTIONS 1642
   3.1. Complexes with group 5 donors 1643
   3.2. Complexes with arene donors 1644

4. CARBONYL HYDRIDES 1645

5. CARBONYL HALIDES 1646

6. METHYL, SILYL, STANNYL AND PLUMBYL DERIVATIVES 1647

7. Mn, Cu, Au AND Hg BONDED DERIVATIVES 1647

8. ALKENYL AND ACYL DERIVATIVES 1648

9. CYCLOPENTADIENYL DERIVATIVES 1649
   9.1. Cp bonded mono- and polynuclear metal carbonyls 1649
   9.2. Derivatives containing group 5, 6 and hydrocarbon ligands 1651
   9.3. Derivatives containing M—H and M—H—M′ bonds 1654
   9.4. Mixed metal carbonyls 1656
   9.5. Carbonyl halides and their derivatives 1657
   9.6. Alkyl, alkenyl, silyl, germyl, stannyl and plumbyl derivatives 1658

REFERENCES 1659

ABBREVIATIONS

dppm = $Ph_2PCH_2PPh_2$, dpam = $Ph_2AsCH_2AsPh_2$, dpsm = $Ph_2SbCH_2SbPh_2$, dppe = $Ph_2P(CH_2)_2PPh_2$, dppp = $Ph_2P(CH_2)_3PPh_2$, dppb = $Ph_2P(CH_2)_4PPh_2$, dmpe = $Me_2P(CH_2)_2PMe_2$, diars = *o*-$C_6H_4(AsMe_2)_2$, pab = *o*-$C_6H_4(AsPh_2)PPh_2$, dpase = $Ph_2As(CH_2)_2AsPh_2$, arphos = $Ph_2P(CH_2)_2AsPh_2$, dmdepe = $Me_2P(CH_2)_2PEt_2$, dmdppe = $Me_2P(CH_2)_2PPr^i_2$, triphos = $PPh(CH_2CH_2PPh_2)_2$, tetraphos = $(Ph_2PCH_2CH_2PPhCH_2)_2$, Cp = η^5-C_5H_5.

1. INTRODUCTION

In spite of the chemical synthesis of $V(CO)_6$ in 1959,[1] the carbonyl chemistry of group 5 metals (M) has not received a great deal of attention. Although, it is still not possible to synthesize the

* Author to whom correspondence should be addressed.

analogues ($Nb(CO)_6$ and $Ta(CO)_6$), several of their derivatives have already come into existence. Numerous review articles describing different aspects of metal carbonyls have been published[2-5] in the last 20 years but no review article dealing specially with the chemistry of group 5 metal carbonyls has appeared. Connelly[6a] and Labinger,[6b] in their comprehensive reviews, attempted to cover almost all the aspects of the organometallic chemistry of vanadium, niobium and tantalum but the carbonyl chemistry of these metals did not get the particular attention it deserved. This situation has prompted us to write the present article.

It covers almost all the classes of known derivatives in which at least one direct M—CO bond is present; derivatives which do not involve a M—CO bond but in which M is bonded to any other metal carbonyl moiety, e.g. $[CpVCo_3(CO)_9]$, $[Cp_2HNb(\mu\text{-}C_5H_4)Fe(CO)_2]$, $[(MeC_5H_4)_2V_2S_4Fe(CO)_3]$ and $[(MeC_5H_4)_2V_2S_4Fe(CO)_3Pt(Ph_3P)_2]$, have been excluded.

2. BINARY CARBONYLS

Of the binary carbonyls, only $V(CO)_6$ has been synthesized by conventional methods; other known species, viz. $M(CO)_n$ (M = V, n = 1–5; M = Ta, n = 1–6) and $V_2(CO)_{12}$ exist in inert gas matrices at low temperatures.

2.1. *Chemical synthesis and structure*

$V(CO)_6$ is synthesized as a blue or green–black highly volatile air-sensitive crystalline solid by the reductive carbonylation[1,7-21] of vanadium(III) chloride or acetylacetonate and subsequent acidification (Scheme 1). It can also be obtained[21] by the action of CO on (η^6-toluene)$_2$V.

Numerous structural tools, including IR,[1,21-23] magnetic susceptibility measurements,[1,19,20,22,24] ESR,[21,25-29] PES,[30] CD,[31] electron diffraction[32] and X-ray[20,33] unambiguously established it as a monomer, thus eliminating the controversy, which arose following its first synthesis,[1] regarding its monomeric or dimeric nature. It is isomorphous with $Cr(CO)_6$. A tetragonal distortion from pure O_h symmetry has been established by its ESR spectrum[26,28] supported by a crystal study.[33] The values of crystal field splittings have been obtained[26] as $\Delta_1 \leqslant 36{,}200\ cm^{-1}$ and $\Delta_2 \leqslant 1880\ cm^{-1}$ (Δ_1 and Δ_2 are defined elsewhere).[26] The value of Δ_1 found in this way is in good agreement with the values of Δ observed for other strong field complexes, e.g. $Cr(CO)_6$ ($\Delta = 34{,}150\ cm^{-1}$).[22]

The mean V—C bond dissociation energy, the heat of formation of $V(CO)_6$ vapour and the low ionization potential, suggests the ready formation of $[V(CO)_6]^+$ in its positive ion mass spectrum.[34]

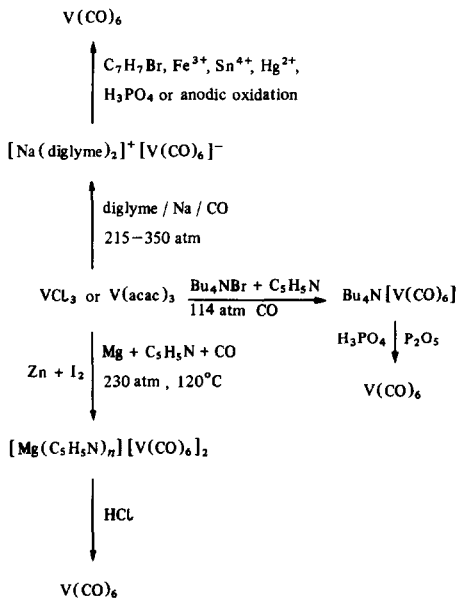

Scheme 1. Synthetic routes to $V(CO)_6$.

The negative ion mass spectrum, which is unique for mononuclear binary carbonyls in showing a parent ion $[V(CO)_6]^-$, has also been recorded.[35]

The electronic spectrum of $V(CO)_6$ has been measured in a variety of media, viz. in a CO matrix at 10 K[36,37] in the gas phase,[23] in the solid state and in cyclohexane solution.[28] In the spectra the weak, lower energy *d–d* absorptions and the stronger, higher energy charge-transfer transitions are poorly resolved. By curve fitting procedures aided by MCD measurements in nitrogen or argon matrices at 5 K, spectral assignments have been made.[31] The appropriate energy level diagrams were derived from MO calculations.[38,39]

2.2. *Synthesis in* CO *and inert gas matrices*

$V(CO)_6$ in a CO matrix is obtained[40,41] when vanadium atoms are cocondensed with pure CO at a ratio of $V:CO \simeq 1:10^5$ concentration at 6.12 K. The IR spectrum consists essentially of an intense CO absorption at 1970 cm^{-1} with weaker, high frequency shoulders at 1976 and 1984 cm^{-1}. The similarity of the spectrum to that of chemically synthesized $V(CO)_6$ suggests that the V/CO reaction provides a direct and efficient route[41] to pure $V(CO)_6$.

In the matrices of CO with argon, krypton or xenon $V(CO)_n$ ($n = 1$–6) species are formed.[40–42] The structures of these species have been deduced on the basis of IR measurements.[42] Discrepancies are often revealed by comparing the structures of the species deduced on the basis of IR measurements with those predicted by various MO calculations.[43–46] Presently $Nb(CO)_n$ are not known but $Ta(CO)_n$ ($n = 1$–6) are formed[47] in an argon matrix at 4.2 K. A band at 2725 Å in the electronic spectrum has been attributed to $Ta(CO)_6$.

As regards dimers, spectroscopic evidence[40–42] has been presented only for the formation of $V_2(CO)_{12}$, the existence of which has been proved at increased vanadium concentration (> 1%). On the basis of IR measurements it has been suggested that the molecule has an inversion centre and is more likely to be structurally similar to the double CO bridged structure $V_2(\mu\text{-}CO)_2(CO)_{10}$. It should be noted that $V_2(\mu\text{-}CO)_2(CO)_{10}$ is not formed by $V(CO)_6$ dimerization.

2.3. *Ionic species*

$[V(CO)_6]^+$, an extremely unstable 16 electron species, is the only known carbonyl cation of group 5 metals. It was generated electrochemically[48] at low temperatures but decomposed irreversibly with loss of CO at −78°C. Chemical generation has not been successful so far.

$[M(CO)_6]^-$ and $[M(CO)_5]^{3-}$ (M = V, Nb and Ta) are well known anions and are isolated in the form of salts with a variety of cations. The existence of both $V(CO)_6$ and $[V(CO)_6]^-$ has led to investigations of the redox properties of both species by chemical and electrochemical methods.[48] Polarography or cyclic voltammetry at platinum shows that the oxidation of $[V(CO)_6]^-$ to $V(CO)_6$ is fully reversible in dichloromethane or acetone[48,49] but that the reduction of $V(CO)_6$ is only reversible in dichloromethane.[48] It has also been noted that a reaction does not occur at the liquid–liquid interface when immiscible solutions of aqueous copper sulphate and $[NBu_4][V(CO)_6]$ in dichloromethane or dichloroethane are kept in contact, but on passing a direct current across the boundary a layer of copper is deposited.[50]

Na^+, Tl^+, Mg^{2+}, NH_4^+, NBu_4^+ and $[SiH_3 \cdot 2NMe_3]^+$ salts of $[V(CO)_6]^-$ were obtained[8,12,14,16,51,52] by the reductive carbonylation of vanadium(III) halides or acetylacetonate in suitable solvents, viz. diglyme or pyridine, but the salts containing VL_6^{2+}, $V(L⁀L)_3^{2+}$ and VL_4^{2+} cations can be recovered[53–55] by the disproportionation of $V(CO)_6$ in the presence of suitable Lewis bases L or L⁀L (L = Me_2CO, Me_2O, Me_2SO, MeOH, AcPh, AcH, BzH, $BzNH_2$, $PhNH_2$, PhCN, MeCN, Ph_3PO, Ph_3AsO, EtOAc, C_4H_9NO, $(C_6H_{11})_2CO$, BzOEt, $Ph_3P{:}CH_2$, $Ph_3P{:}NH$, $HCONMe_2$, THF, dioxane, α- and ν-picoline; L⁀L = *o*-phen, *o*- and *p*-$C_6H_4(NH_2)_2$, 2,2′-bipy, $Ph_2P(CH_2)_2PPh_2$, $PhNH(CH_2)_2NHPh$).

$[V(CO)_3(diars)_2][V(CO)_6]$, in which both the cation and anion are metal carbonyl species, has been obtained[56] by refluxing $V(CO)_6$ and diars in hexane. The cation exhibits two carbonyl bands at 2073 and 1957 cm^{-1} and the anion at 1855 cm^{-1} in dichloromethane.

In arenes, $V(CO)_6$ reacts to give $[V(CO)_4(arene)]^+[V(CO)_6]^-$ (arene = $C_6H_3Me_3$-1,3,5; $C_6H_2Me_4$-1,2,4,5; C_6Me_6) under mild conditions (~ 35° in absence of light).[48,57,58] $[V(arene)_2]^+$ salts are recovered[57,59] when heptane solutions of $V(CO)_6$ and $(arene)_2V$ are allowed to react. In

the preparation of $[V(C_6H_3Me_3)_2]^+[V(CO)_6]^-$, high pressure carbonylation[59,60] of $(C_6H_3Me_3)_2V$ in mesitylene has been used. $V(CO)_6$ oxidizes $(C_5H_5)_2M$ (M = V, Co) to yield[10,61,62] the corresponding complexes $[(C_5H_5)_2V(CO)_2][V(CO)_6]$ and $[(C_5H_5)_2Co][V(CO)_6]$. Cycloheptatriene when heated with $V(CO)_6$ yields[63,64] $[V(\eta^6\text{-}C_7H_8)(\eta\text{-}C_7H_7)][V(CO)_6]$ together with a small amount of $(\eta\text{-}C_7H_7)V(CO)_3$ (*vide infra*). Reaction of $V(CO)_6$ with the alkene $(Me_2N)_2C_2(NMe_2)_2$ yields[65] $[(Me_2N)_2C_2(NMe_2)_2][V(CO)_6]_2$. In contrast, $[Na(diglyme)_2][V(CO)_6]$ causes reductive dimerization[66] of the 1,3-dithiolium cation to 2,2′-bis(1,3-dithiolyl).

Sodium salts of $[Nb(CO)_6]^-$ and $[Ta(CO)_6]^-$ have been obtained[67] as bright yellow solids by aqueous NaOH treatment of the products resulting from reductive carbonylation of M_2Cl_{10} (M = Nb, Ta) followed by extraction with ether and recrystallization from THF, or by the treatment[68] of appropriate chlorides with high pressure $CO/Fe(CO)_5$ in $MeOCH_2CH_2OCH_2CH_2OMe$ in the presence of a Na/K alloy. Light sensitive salts containing $[(PPh_3)_2N]^+$, $[Ph_4As]^+$ and $[Ni(o\text{-}phen)_3]^{2+}$ cations have also been recovered.[20,67–69]

The IR and Raman spectra of $[V(CO)_6]^-$ have been studied[70–72] in detail; 12 of the 13 fundamental vibrations have been assigned and the C—O stretching force constant (k_{CO}: 14.95 mdynes $Å^{-1}$) calculated.[72,73] The NMR spectra of $[V(CO)_6]^-$ salts are relatively uninformative.[74–76]

A crystal structure study[77] confirmed the expected octahedral structure of $[V(CO)_6]^-$ in $[(PPh_3)_2N][V(VO)_6]$. A similar study of $[V(THF)_4][V(CO)_6]_2$ shows[78] the coordination of four oxygen atoms in the THF molecules around the V^{2+} ion in a planar array (**I**). The axial positions of the octahedron are occupied by the oxygen atoms of the two CO molecules of $[V(CO)_6]^-$. It is probably the first known compound with a linear M—C—O—M carbonyl bridge between the two transition metal atoms. The distance V—O(CO), 2.079 Å is shorter than the V—O(THF) distance, 2.170 Å. The IR spectra of a few isocarbonyl bridged species $[V(B)_4][(O\text{—}C)V(CO)_5]_2$ (B = Et_2O, THF, CH_3COCH_3 and C_5H_5N) in dichloromethane exhibited[79] four terminally bonded CO and one isocarbonyl bridged band (1678–1684 cm^{-1}).

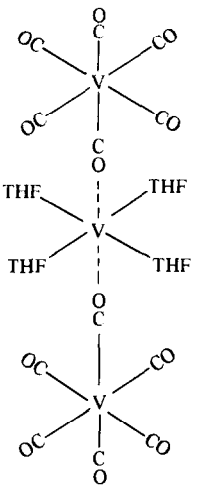

(**I**)

The super reduced trianions, $[M(CO)_5]^{3-}$, of all the three metals in which the metals exist in their lowest formal states have been obtained[80,81] by the alkali metal reduction of $M(CO)_6$ in liquid ammonia (M = V, alkali metal = Na, K, Rb or Cs; M = Nb, Ta, alkali metal = Na or Cs).

3. SUBSTITUTION REACTIONS

Mono- and polydentate group 5 ligands, especially *t*-phosphines and phosphinoalkanes, displace one to four CO molecules from $V(CO)_6$. In no case could complete CO displacement be achieved. These derivatives have also been obtained by the oxidation of the corresponding anions. A few dinuclear neutral derivatives were also prepared by the anion oxidation. Analogous neutral niobium and tantalum derivatives have not been synthesized. In addition to group 5 ligands, CO displacement reactions using some arenes have also been studied.

3.1. *Complexes with group 5 donors*

(a) *Mononuclear.* Except for the cationic complex $[V(CO)_3(diars)_2][V(CO)_6]$,[56] which at one time was erroneously formulated as $V(CO)_4(diars)_2$,[82] all the other known complexes are either neutral or anionic.

Barring $V(CO)_5(NO)$, which was first synthesized[54] in 1961 as a highly unstable diamagnetic red–violet solid by bubbling NO into a cyclohexane solution of $V(CO)_6$ at 0°C, $V(CO)_5L$ derivatives have only come into existence after 1980. Even $V(CO)_5NO$ itself has been synthesized in 1982 by an alternative route[83] (the reaction of NOCl with $[V(CO)_6]^-$ at −78°C). Other isolated derivatives[17,84–86] are $V(CO)_5(Ph_3P)$ and $V(CO)_5(Ph_3As)$. The former has been obtained[17,84,85] as an olive green paramagnetic (μ_{eff} = 1.87 BM) solid in 80% yield by the treatment of Ph_3P with $V(CO)_6$ in dichloromethane at −70°C. It is unstable at room temperature even under nitrogen. A more convenient route for the synthesis of $V(CO)_5L$ is by $C_7H_7BF_4$ oxidation[17,86] of the appropriate $[V(CO)_5L]^-$. IR spectra of the derivatives exhibit[84] only two CO bands (L = Ph_3P, ν_{CO}: 2050m and 1930vs; L = Ph_3As, ν_{CO}: 2051m and 1934s cm^{-1}) while three are expected for C_{4v} symmetry.

A few more derivatives in which L = Me_3P, $MePh_2P$, $(OMe)_3P$, $(i\text{-}Pr)_3P$ and $(n\text{-}Bu)_3P$ have not actually been isolated but are known[79,85] in solution only.

The derivatives $V(CO)_4(L_2$ or L⁀L) are easier to obtain than $V(CO)_5L$. In fact, a number of these derivatives had been described[87] in 1966, much earlier than the synthesis of monosubstitution products. $V(CO)_4(Ph_3P)_2$, for which a *trans* structure was proposed on the basis of a single CO band at 1845 cm^{-1} in its IR spectrum, was first prepared[88] as orange, air-sensitive, paramagnetic solid (m.p. 142°C) in 1961. Other monodentate ligands which yield disubstitution products are Et_3P,[89] Ph_3P,[87–89] Pr_3P,[89] Ph_2HP,[89] PhH_2P,[89] $(OMe)_3P$,[85] Ph_3As[87] and Ph_3Sb.[87] $V(CO)_4(L⁀L)$ derivatives are obtained by the $C_7H_7BF_4$ oxidation of $[V(CO)_4(L⁀L)]^-$. The expected *cis*-configurations of $V(CO)_4(L⁀L)$ (L⁀L = $o\text{-}C_6H_4(PPh_2)_2$,[86] $Ph_2P(CH_2)_nPPh_2$ (n = 1–4)[55,86,90] and $Ph_2PCH_2CH_2AsPh_2$)[86] have been inferred on the basis of IR measurements. Olefin phosphine ligands, (2-allylphenyl)diphenylphosphine and (2-*cis*-propenylphenyl)diphenylphosphine react with $V(CO)_6$ to yield[91] *cis* disubstitution products by coordinating through one phosphorus and one double bond.

Displacement of three or four CO groups has been achieved very rarely. Except for $V(CO)_3\{(OMe)_3P\}_3$, the formation of which has been inferred[85] on the basis of a parent ion peak at m/e = 508 in the mass spectrum of a sample of $V(CO)_4\{(OMe)_3P\}_2$ kept overnight under nitrogen or *in vacuo*, only $V(CO)_3(MeC(CH_2PPh_2)_3)$ has been synthesized.[55]

The only known tetrasubstitution product is the dark red *trans*-$V(CO)_2(Ph_2PCH_2CH_2PPh_2)_2$ which has been obtained[55] by the direct action of excess ligand on $V(CO)_6$ at 120°C.

A number of mono- or polydentate P/As ligand-containing nitrosyl carbonyls $V(CO)_{5-n}(NO)(L_n$ or polydentate) (n = 1, L = Ph_3P,[83,88,92] $(OMe)_3P$,[83] Me_2HP,[83] dppm;[83] n = 2, L = Me_3P,[83,93] Me_2HP,[83] $(OMe)_3P$;[83] polydentate = dppm,[83] dppe,[83,94] dppp,[83,94] dmpe,[83] diars,[83] pab;[83] n = 3, polydentate = $MeC(CH_2PPh_2)_3$[83]) have been isolated by two general methods, viz. by the action of ligands on $V(CO)_5(NO)$ or by the nitrosylation of an acetonitrile solution of $[V(CO)_4L_2$ or $(L⁀L)]^-$ at 0°C in the presence of $NOBF_4$, NOCl or $[Co(NO)_2X]_2$.

The structure of $V(CO)_3(NO)(Me_3P)_2$ has been determined by an X-ray study.[93] The molecule has a pseudo-octahedral structure with CO groups in meridional and the phosphine ligands in *cis* positions.

(b) *Dinuclear.* A variety of dinuclear complexes, viz. $[\{V(CO)_5\}_2(\mu\text{-}L⁀L)]$, $[V(CO)_4(\mu\text{-}ER_2)]_2$, $[(CO)_4V(\mu\text{-}ER_2)_2V(CO)_3L]$ and $[V(CO)_3L(\mu\text{-}ER_2)]_2$ are known. The nature of the peculiar yellow diamagnetic $[V(CO)_4(C_6H_{11})_3P]_2$, reported by Hieber *et al.*,[89] has not been thoroughly investigated.

$[\{V(CO)_5\}_2(\mu\text{-}L⁀L)]$ (L⁀L = $p\text{-}C_6H_4(PPh_2)_2$) is obtained[86] by $C_7H_7BF_4$ oxidation of $\{V(CO)_5\}_2(\mu\text{-}L⁀L)]^{2-}$. Other phosphine and arsine ligands e.g. PH_3,[89] PhH_2P,[89] Ph_2HP,[89] Me_2HP[95] and Ph_2EEPh_2[96] (E = P and As) react with $V(CO)_6$ in solution to give ER_2 bridged centrosymmetric bi-octahedral $[V(CO)_4(\mu\text{-}ER_2)]_2$ (R = H, Me or Ph) with evolution of CO and H_2; the E—E bond cleaves during complexation.

Smooth and stepwise CO displacement in $[V(CO)_4(\mu\text{-}PMe_2)]_2$ proceeds to give[97] $[(CO)_4V(\mu\text{-}PMe_2)_2V(CO)_3L]$ and $[V(CO)_3L(\mu\text{-}PMe_2)]_2$ (L = Me_3P, Bu_3P, Ph_2MeP, Me_2HP, $(OMe)_3P$, $(OPh)_3P$, Me_3As and Me_2HAs) when phosphine and arsine ligands are used.

On irradiating a THF solution of $Et_4N[V(CO)_6]$ and the tripod ligand, $\{Ph_2P(CH_2CH_2PPh_2)_2\}$,

with UV light and passing the content through a silica gel column, orange crystals of *fac*-$[V(CO)_3(PhPCH_2CH_2PPh_2)_2]_2$ are obtained.[98]

A diphosphine bridged nitrosyl carbonyl, $[\{V(CO)_4(NO)\}_2(\mu\text{-}Ph_2PPPh_2)]$, is recovered[96] in place of $V(CO)_3(NO)(Ph_2PPPh_2)$ when Ph_2PPPh_2 reacts with $V(CO)_5(NO)$. A product of uncertain nuclearity $V(CO)_2(NO)$(1.5 diars) is also known.[83]

(c) *Anionic complexes.* Vanadium forms a number of diamagnetic anions $[V(CO)_5L]^-$ [54,85,88,91,98–111] (L = NH_3, C_5H_5N, MeCN, *ter*-BuCN, PhCN, $C_6H_{11}CN$, Bu_3P, Ph_3P, $(OMe)_3P$, Ph_3EtP, *p*-$(ClC_6H_4)_3P$, PF_3, (2-allylphenyl)diphenylphosphine, *cis*-(propenylphenyl)diphenylphosphine, Et_3As, Ph_3As, $(OEt)_3As$, Me_2PhAs, Ph_3Sb, $(EtO)_3Sb$, Et_3Bi, 2-MeTHF, P_2Cy_4, dppm, dppe, dpase, arphos, triphos, As_2Ph_4, Sb_2Ph_4), $[V(CO)_4(L_2$ or L⁀L)$]^-$ [56,98,104–106,109,111–117] (L = PF_3, 2-MeTHF; L⁀L = dppm, dppe, dmpe, arphos, dpase, diars, ferrocene-1,1′-bis(diphenylarsine), triphos, tetraphos) and $[V(CO)_3(L⁀L⁀L)]^-$ [95,104,114] (L⁀L⁀L = triphos, tetraphos) when a mixture of ligands and a $[V(CO)_6]^-$ salt is irradiated with UV light at ambient temperature. Analogous niobium and tantalum complexes, $[M(CO)_5L]^-$ (M = Nb,[106,112,113] L = Et_3P, Ph_3P, $(OMe)_3P$, $(NEt_2)_3P$, dppm, dppe, dppp, dppb, arphos; M = Ta,[102,113] L = C_5H_5N, Ph_3P), $[M(CO)_4(L⁀L)]^-$ (M = Nb,[106,113] L⁀L = dppm, dppe, dppp, dppb, arphos, *cis*-$Ph_2PCH{=}CHPPh_2$; M = Ta,[106] L⁀L = dppe) and $[Nb(CO)_3(PF_3)_3]^-$ [113] are also known. Vanadium complexes are also obtained by Na/Hg reduction of $V(CO)_4(L_2$ or L⁀L) or by NH_3 displacement in $[V(CO)_5(NH_3)]^-$. A dianion, $[V(CO)_5(CN)]^{2-}$, is formed[99] when CN^- is used as a ligand. In the presence of 2,2′-bipyridine, yellow diamagnetic $[V(CO)_4(CN)(\mu\text{-}CN)]_2^{4-}$ may be isolated[99] as the $[NEt_4]^+$ salt. Unusual $[V(CO)_3(dppe)]_2E$ (E = S, Se and Te) derivatives are obtained[100] by the treatment of $[V(CO)_4(dppe)]^-$ with acidic solutions of the appropriate Na_2EO_3 or $S_3N_3Cl_3$ (for S only). The dicarbonyl anion, $[Ta(CO)_2(dmpe)_2]^-$ has not been isolated but its formation has been inferred on the basis of IR and NMR data.[101]

The diamagnetic dinuclear anions $[\{M(CO)_{6-n}\}_2(\mu\text{-}L⁀L)_n]^{2n-}$ (n = 1, L⁀L = P_2Ph_4, $Ph_2PC{\equiv}CPPh_2$, P_2Cy_4, dppe, dpase, arphos, *p*-$C_6H_4(PPh_2)_2$, *trans*-$Ph_2PCH{=}CHPPh_2$; n = 2, L⁀L = P_2Ph_4, As_2Ph_4, dpase) are known[86,105,110,116,118,119] for M = vanadium; the diphosphine and diarsine ligands which cleave into two bridging diphenylphosphido and diphenylarsenido ligands in the neutral derivatives remain intact in the anions. A polymeric anion $[(CO)_4V(\mu\text{-tetraphos})V(CO)_4]_n^{2n-}$ is also known.[114]

3.2. *Complexes with arene donors*

Neutral arene carbonyls are known only for vanadium, although they are of extremely rare occurrence. The formation of green paramagnetic $(\eta^6\text{-}C_6Ph_6)V(CO)_3$ in 2% yield has been claimed[120] when Ph_2C_2 trimerizes during its reaction with $V(CO)_6$ in hexane at 40°C. $(\eta^6\text{-}C_6H_6)_2V_2(CO)_4$ (**II**), of which the crystal structure has been examined,[121] and ill-defined $(\eta^6\text{-}C_6H_6)(\eta^4\text{-}C_5H_6)V(CO)$, prepared[122] by the reaction of C_6H_6 with $(\eta^6\text{-}C_6H_6)_2V$ under 30 atm/150°C of CO, are the other known derivatives. In addition, the neutral compound, $(\eta^6\text{-}C_6H_6)V(CO)_4$, has been suspected[123] to be the precursor to the cation $[(\eta^6\text{-}C_6H_6)V(CO)_4]^+$.

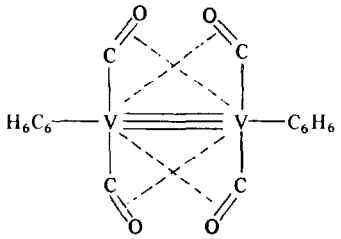

(II)

$[(\eta^6\text{-arene})M(CO)_4]^+$ is the most studied class for which the derivatives are known for all the three metals. Less air-sensitive PF_6^- and BPh_4^- salts of vanadium derivatives (compared to Cl^-, Br^- and $[V(CO)_6]^-$) have been recovered[57,123] by metathetical reactions with $NaBPh_4$ or NH_4PF_6 in THF. $Al_2Br_6Cl^-$ salts of isostructural $[(\eta^6\text{-arene})M(CO)_4]^+$ (M = Nb, Ta; arene = C_6H_6Me,

$C_6H_4Me_2$-*p*, $C_6H_3Me_3$-1,3,5, $C_6H_2Me_4$-1,2,4,5 and C_6Me_6) have been obtained[124,125] by halide displacement in $[M_2(CO)_8Cl_3]^-$ with arenes in the presence of $AlBr_3$.

Reduction of $[(\eta^6\text{-arene})V(CO)_4]^+[V(CO)_6]^-$ in THF with $NaBH_4$ affords[126] the moderately air-stable cyclohexadienyls, $(\eta^5\text{-}C_6H_{7-n}Me_n)V(CO)_4$ ($n = 0$, 2–4 or 6); hydride attack occurs at an unsubstituted carbon atom of the arene ring.

Eighteen electron $[(\eta^6\text{-mesitylene})V(CO)_3]^-$ is the solitary known arene containing anion.[127] It has been prepared by the following route:

$$[(\eta^6\text{-mesitylene})V(CO)_4]PF_6 \xrightarrow[\text{THF, 0°C}]{\text{NaI}} (\eta^6\text{-mesitylene})V(CO)_3I$$

$$\downarrow \text{NaBH}_4$$

$$[(Bu^n_4N)][(\eta^6\text{-mesitylene})V(CO)_3] \xleftarrow[[Bu^n_4N]Br]{\text{NaOH}} (\eta^6\text{-mesitylene})V(CO)_3H$$

The derivatives containing tropenium and substituted tropenium cations, e.g. $(\eta^7\text{-}C_7H_7)V(CO)_3$ (obtained[63,64] in low yield) together with $[(\eta^6\text{-}C_7H_8)(\eta^7\text{-}C_7H_7)V][V(CO)_6]$ and a number of $(\eta^7\text{-}C_7H_6R)V(CO)_3$ (R = Me, Ph, COOEt, OMe and OPr^n) have also been synthesized.[128] ν_{CO} values vary with the nature of R but mass spectroscopy shows little dependence of the ionization potential on the substituent.

In $(\eta^7\text{-}C_7H_7)V(CO)_3$ the seven-membered ring is symmetrically bound to the $V(CO)_3$ group.[129] The most important metal–ring interaction, which leads to $M \rightarrow \pi^*$ ligand electron transfer, involves the d_{xy} and $d_{x^2-y^2}$ orbitals of vanadium and the e_2 π-orbitals of the cycloheptatrienyl group.[130] A detailed NMR study at temperatures from 30 to −79°C showed[131,132] the doublet in the spectrum to arise from the $^{51}V—^1H$ coupling with $J(^{51}V—^1H)$ *ca* 3 Hz.

4. CARBONYL HYDRIDES

The existence of $HV(CO)_6$ was first indicated during a potentiometric study[133] of the reaction of $KV(CO)_6$ with H_3PO_4. Recent reports[134,135] show the instability of $HV(CO)_6$; a stoichiometric amount of water promotes its ionic dissociation to $[H_3O]^+[V(CO)_6]^-$. $HNb(CO)_6$ is still unknown. The formation of $HTa(CO)_6$, as a highly volatile liquid in the reaction of CO/H_2 with Ta_2O_5 has been claimed.[136]

Anionic $[HM(CO)_5]^{2-}$ derivatives of all the three metals have been isolated[137] as air-sensitive highly coloured (V—bright yellow; Nb—orange; Ta—orange–red) solids when the appropriate $[M(CO)_5]^{3-}$ anions reacted with EtOH in liquid NH_3 at −70°C, followed by the addition of NEt_4BH_4. The ^1H NMR spectrum[137] of $Na_2[HTa(CO)_5]$ exhibits a sharp singlet at −2.23 ppm. The ^{93}Nb NMR spectrum of $Na_2[HNb(CO)_5]$ exhibits[137] a sharp hydride signal at −1.89 ppm, and that of the monoprotonated vanadium analogue shows a well resolved octet ($J_{V—H} = 27.6$ Hz) centred at −4.76 ppm due to the coupling of vanadium to hydrogen.

Phosphine ligands, especially of the chelating type, stabilize neutral carbonyl hydrides, $HV(CO)_5L$ ($L = Ph_3P$),[133] $HV(CO)_4(L⁀)$ [L⁀L = dmpe,[56,90,138] dppm,[139,140] dppe,[134,139] dppp,[139] arphos,[140] diars[56,138] and triphos[139,141] (acting as bidentate)], $HV(CO)_3$(terdentate) (terdentate = $P(CH_2CH_2PPh_2)_3$[141] and $[Ph_2PCH_2CH_2PPhCH_2]_2$[141] containing four phosphorus atoms but acting as a terdentate ligand) and $HM(CO)_2(dmpe)_2$ (M = Nb, Ta) are known.[101,142,143] $HV(CO)_4(L⁀L)$ and $HV(CO)_3$(terdentate) are obtained by the reaction of $V(CO)_4(L⁀L)$ or $V(CO)_3$(terdentate) with H_2O, *t*-BuCl/hexane or $Ph_4AsHCl_2 \cdot 2H_2O$/benzene or by eluting, with solvents like THF, THF–heptane or THF–toluene mixtures, from a silica gel column. $HV(CO)_3\{P(CH_2CH_2PPh_2)_3\}$ prepared in this way has a *cis* structure while $HV(CO)_3\{(Ph_2PCH_2CH_2PPhCH_2)_2\}$ attained a *trans* structure. UV irradiation of these two compounds affords $HV(CO)_2$(quadridentate) in which all the four phosphorus atoms coordinate to vanadium atoms. $HM(CO)_2(dmpe)_2$ (M = Nb, Ta) derivatives have been obtained[142,143] by the high pressure carbonylation of $H_5M(dmpe)_2$ in hydrocarbon solvents. The tantalum derivative can also be prepared[101] by acidifying $Ta(CO)_2(dmpe)_2$. Similar acidification of $[V(CO)_4(diars)]^-$ with excess anhydrous HX (X = Cl, Br, I) in HF generates[138] a polyhydrido vanadium carbonyl, $H_3V(CO)_3(diars)$.

X-ray data[144,145] of $HV(CO)_4(dppe)$ and $HTa(CO)_2(dmpe)_2$ are available. In the former the

hydride ligand occupies one edge of a pseudo-octahedron and is positioned between one phosphorus atom and one CO group[145] while the latter has a monocapped octahedral structure[144] in which the hydride is presumed to be the capping ligand (**III**).

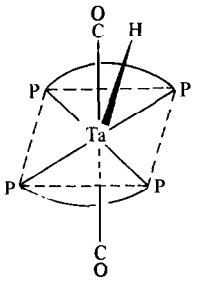

(III)

A dinuclear derivative $[HV(CO)_4(\mu\text{-}Ph_2PCH_2CH_2PPhCH_2)]_2$, which is obtained[141] by *t*-BuCl/H_2O treatment of $(Et_4N)_{2n}[\{V(CO)_4\}_{2n}(\mu\text{-}(Ph_2PCH_2CH_2PPhCH_2)_2)_n]$, has also been reported.

Orange–yellow (η^6-mesitylene)$V(CO)_3H$ is the only known[127] arene substituted metal carbonyl hydride. It has been obtained by treatment of (η^6-mesitylene)$V(CO)_3$ with $NaBH_4$.

5. CARBONYL HALIDES

$M(CO)_mX_n$ (M = V, Nb, Ta; X = halogen) and mononuclear anions are not known, but halogen bridged dinuclear complexes $[M_2(CO)_8X_3]^-$ (M = Nb,[62,125,146] X = Cl, Br, I; M = Ta,[125,146] X = Cl) have been isolated in the form of $[H(THF)_2]^+$ and $[N(Ph_3P)_2]^+$ salts by the direct action of a pentane solution of elemental halogen (for bromo or iodo) or $PhICl_2$ (for chloro) on $NaM(CO)_6$ at temperatures ranging from −60 to −78°C. Niobium derivatives have also been synthesized by the action of appropriate halides, viz. $FeCl_3$, $CuCl_2$, CuCl, AgCl, $HgCl_2$, CuBr and CuI on $NaNb(CO)_6$.

The anions have approximately C_{2v} symmetry[125] with C_{4v} structure of $M(CO)_4$ moiety. The crystal structure of $[H(THF)_2][Nb_2(CO)_8Cl_3]$ shows that the two niobium atoms are bridged through three chlorides located at the vertices of an approximately equilateral triangle on a plane perpendicular to the Nb—Nb bond dividing the complex into two identical halves with each niobium atom bonded through four CO groups[125] (Nb···Nb (non-bonding), 3.631 Å; ∠Cl—Nb—Cl, 76.8° (mean); ∠Nb—Cl—Nb, 88.3° (mean); Nb—C, 2.05 Å), Structure (**IV**).

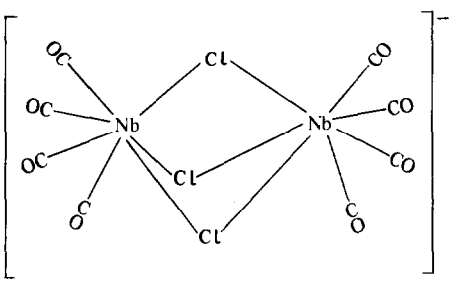

(IV)

Phosphine ligands, when present, stabilize neutral carbonyl halides and, in fact, a variety of derivatives, viz. $V(CO)_4(L\frown L)I$ (L⌒L = dppe,[90] diars[56]), $Ta(CO)_3(Me_3P)_3X$[147] (X = Cl, Br, I) and $M(CO)_2(L\frown L)_2X$ (M = V, L⌒L = diars,[148] X = Cl; M = Nb, L⌒L = dmpe,[149,150] X = Cl, Br; M = Ta, L⌒L = dmpe,[101,151,152] dmdepe,[152] dmdppe,[152] X = Cl, Br, I) have been reported. They attain a hepta-coordinated structure with one or two bidentate group 5 ligands and in this respect they exhibit a close resemblance to molybdenum or tungsten halocarbonyls.[153–155]

$M(CO)_2(L\frown L)_2X$ complexes have a monocapped trigonal prismatic structure[101] and exist in two

isomeric forms, *cis* and *trans*, with respect to the labelled ends of bidentate phosphines which occupy the capped quadrilateral face, Structure (V). Halotricarbonyls containing three Me_3P molecules, which are air-sensitive red to orange solids, are known[147] for tantalum only. An X-ray study[147] of the chloro derivative showed it to have a capped trigonal prismatic structure. The only known vanadium halotricarbonyl is (η^6-mesitylene)$V(CO)_3I$ which is a dark green solid.[127]

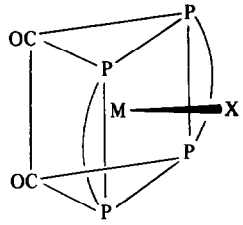

(V)

6. METHYL, SILYL, STANNYL AND PLUMBYL DERIVATIVES

Except for the moderately air stable $CH_3V(CO)_4$(diars), which has been obtained[56] by the treatment of CH_3I with $[Et_4N][V(CO)_4$(diars)] in THF at $-78°C$; σ-bonded alkyl metal carbonyls are not known to date.

Very little work has been done on silyl derivatives also. Only $SiH_3V(CO)_6$, which probably has a face capped octahedral structure[51] with the SiH_3 group occupying the capping position (although the possibility of a lower symmetry structure such as a face capped trigonal prism or edge capped octahedron has not been entirely ruled out), has been obtained[51] by the treatment of iodosilane with $TlV(CO)_6$ or diglyme free $NaV(CO)_6$ in ether or *in vacuo* at 0°C.

Germyl bonded derivatives have not yet been described but both electrically neutral and anionic tin and lead counterparts $EM(CO)_6$ (M = V, E = Et_3Sn,[156] Ph_3Sn,[90,115,156,157] Ph_3Pb;[156] M = Nb, E = Ph_3Sn;[115,157] M = Ta, E = Ph_3Sn[115,157]) $[EV(CO)_5]^{2-}$ (E = Ph_3Sn,[80,156] Ph_3Pb[156]), $[E_2V(CO)_5]^-$ (E = Ph_3Sn,[80,107,158] Ph_3Pb[107,158]) and $[EE'V(CO)_5]^-$ (E = Ph_3Sn, E′ = Me_3Sn,[158] $(C_6H_{11})_3Sn$[158]) are well known.

A crystal structure study[158] of $[(Ph_3Sn)_2V(CO)_5]^{2-}$ indicates that the vanadium atom is hepta-coordinated with five CO and two Ph_3Sn ligands, Structure (VI).

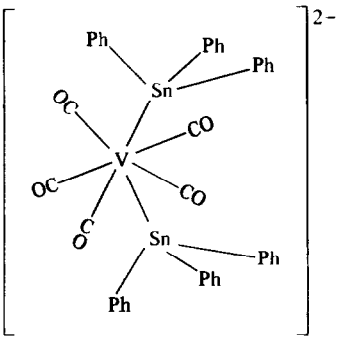

(VI)

Several $EM(CO)_5L$ (M = V, Nb, Ta, E = Ph_3Sn,[112,115,156,157] L = Ph_3P; M = V, E = Ph_3Sn,[115,157] L = Bu_3P; E = Ph_3Pb,[156] L = Ph_3P; M = Ta, E = Ph_3Sn,[115,157] L = $(OPh)_3P$) and $(Ph_3Sn)M(CO)_4(L{-}L)$ (M = V, L—L = dppe,[90,112,157] dmpe,[56,112] diars,[56,112] triphos;[112] M = Nb, Ta, L—L = dppe[112,157]) derivatives have also been synthesized. The triphos complex reacts with MeI to give[112] ionic $[(Ph_3Sn)V(CO)_4\{MeC(CH_2PPh_2)_2(CH_2PPh_2Me)\}]I$.

7. Mn, Cu, Au AND Hg BONDED DERIVATIVES

Anionic $[M(CO)_{6-n}L_n]^-$ derivatives are an excellent source of materials to synthesize a number of metal–metal bonded derivatives.

Although $(CO)_5MnV(CO)_6$ is still unknown, red–brown$(CO)_5MnV(CO)_4$(diars) has been prepared[56] by the action of $Mn(CO)_5Br$ on $[Et_4N][V(CO)_4(diars)]$ in THF at $-78°C$. Its less symmetrical structure was indicated[56] by the appearance of five CO bands at 1978, 1954, 1876, 1863 and 1843 cm^{-1} (in THF) in its IR spectrum. Work has not been carried out on Mn—Nb or Mn—Ta bonded carbonyls.

The Cu—V bonded derivatives, $(L⌒L)_2CuV(CO)_6$ (L⌒L = *o*-phen or 2,2′-bipy)[159] and $MeAs\{C_6H_4(AsMe_2)\}_2CuV(CO)_6$[82] have also been synthesized. $(Ph_3PAu)M(CO)_6$ complexes are known for all the three metals,[82,115,156,157,160] but the crystal structure of only the vanadium compound has been determined.[160] In its structure, the vanadium atom is seven-coordinated and in a capped octahedral environment, the gold atom is in the capping position, and the CO groups are on the capped and uncapped faces (V—Au, 2.69 Å; V—CO(capped), 2.00 Å and V—CO(uncapped), 1.93 Å).

The eight-coordinate complex $(Ph_3PAu)_3V(CO)_5$, prepared by the action of Ph_3PAuCl on $[V(CO)_5]^{3-}$, has a structure in which the vanadium atom is bonded to a novel terdentate $Au_3(Ph_3P)_3$ ligand in such a way that the vanadium and three gold atoms form a slightly distorted tetrahedral cluster.[161] The analogous niobium compound has not been prepared, but the tantalum complex is known.[137]

A few mercury bonded $EM(CO)_6$ (M = V,[157] E = EtHg; M = Nb,[157,162] E = EtHg, $CH_2=CHCH_2Hg$; M = Ta,[157,162] E = MeHg, EtHg, PhHg) and $EM(CO)_5L$ (M^{157} = V, Nb, Ta; E = EtHg, L = Ph_3P) derivatives have also been reported, but they are more thermally sensitive and have been isolated at temperatures between -10 to $-60°C$.

8. ALKENYL AND ACYL DERIVATIVES

A considerable amount of work has been done on the synthesis and structural study of η^3-hydrocarbon bonded vanadium carbonyls; analogous niobium and tantalum derivatives are still unknown. A number of allyl, substituted allyl and cycloalkenyl derivatives have been synthesized[163,164] using $[V(CO)_6]^-$ and $HV(CO)_6$ as key reagents. The former, after reaction with allyl or substituted allyl chlorides in ether under UV irradiation, gives $(\eta^3\text{-}C_3H_4X)V(CO)_5$ (X = H, 2-Cl,. 3-Cl, 2-Me and 3-Me). Thus C_3Ph_3Br reacts[164] with $Na[V(CO)_6]$ in MeCN to give $(\eta^3\text{-}C_3Ph_3)V(CO)_5$. Originally, the ionic compound, $[(C_3Ph_3)][V(CO)_6]$ is formed, which subsequently loses a CO molecule to give $(\eta^3\text{-}C_3Ph_3)V(CO)_5$. Similar (cycloalkenyl)$V(CO)_5$ derivatives are obtained[165] using 3-halocycloalkenes. $HV(CO)_6$ reacts with 1,3-butadiene or a substituted butadiene under UV irradiation[163] to give $(\eta^3\text{-}C_3H_3XX')V(CO)_5$ (X = H, X′ = Me; X = X′ = Me). In a similar way 1,3-cycloalkadienes yield[165] different (cycloalkenyl)$V(CO)_5$ derivatives. These derivatives exhibit[164] three to six IR active CO bands depending upon the distortion of $V(CO)_5$ moiety.

$(\eta^3\text{-}C_3H_4X)V(CO)_4L$ (X = H, 2-Me, 3-Me, L = Et_3P, Ph_3P; X = 2-Cl, 3-Cl, L = Et_3P) and $(\eta^3\text{-}C_3Ph_3)V(CO)_4(Et_3P)$ derivatives are formed[164] when appropriate phosphines react with $(\eta^3\text{-}C_3H_4X)V(CO)_5$ or $(\eta^3\text{-}C_3Ph_3)V(CO)_5$. ^1H and ^{13}C NMR studies[164] indicate η^3-allyl bonding in these derivatives. A single crystal X-ray diffraction study[166] on $(\eta^3\text{-}C_3H_5)V(CO)_4(Ph_3P)$ confirms this mode of bonding. An identical type of bonding has been suggested[165] in (cycloalkenyl)$V(CO)_4L$ (L = Et_3P, Ph_3P) derivatives.

$(\eta^3\text{-}C_3H_4X)V(CO)_3(L⌒L)$ (X = H, 2-Me, 3-Me, L⌒L = dppe,[167] arphos,[111] diars;[56,111,167] X = 3-Ph, L⌒L = dppe,[167] arphos[111]) and $(\eta^3\text{-}C_3H_3XX')V(CO)_3(L⌒L)$ (X = X′ = Me, L⌒L = dppm,[111] arphos[111,140]) derivatives have been obtained by alternative routes, viz. by the action of $[V(CO)_4(L⌒L)]^-$ on XC_3H_4Cl or the action of 2-methyl-1,3-butadiene on $HV(CO)_4(L⌒L)$ under UV irradiation. They exhibit[167] three to four CO bands in the region 1806–1945 cm^{-1}.

X-ray studies of $(\eta^3\text{-}C_3H_5)V(CO)_3$(dppe)[168] and $(\eta^3\text{-}MeC_3H_4)V(CO)_3$(diars)[169] are available. In both derivatives the central vanadium atom is coordinated pseudooctahedrally with the CO groups in meridional positions when considering the $\eta^3\text{-}C_3H_5$ or $\eta^3\text{-}MeC_3H_4$ as a monodentate ligand. The distances from the vanadium to the terminal carbon atoms of the allyl group are significantly greater than to the central carbon atom. The carbon and hydrogen atoms of the allyl groups are not coplanar.

The synthesis of a few (cycloalkenyl)$V(CO)_3(L⌒L)$ (L⌒L = dppm, dppe, arphos) derivatives has been reported.[165] Attempts to prepare the products directly from $[NEt_4][V(CO)_4(L⌒L)]$ (L⌒L = dppe or arphos) and C_3Ph_3Br gave low yields[164] of unusual acyl complexes ($\eta^2\text{-}H_2C_3Ph_3$

CO)V(CO)$_3$(L⁀L). The X-ray crystal structure[170] of the arphos complex revealed hydrogenation of the three-membered ring and a side-on bonded acyl group *cis* to the arphos. Other acyl derivatives, (η^2-RCO)V(CO)$_3$(L⁀L) (L⁀L = dppm, dppe, dppp, arphos, diars, dpase) have been prepared[148] by the photochemical reaction of V(CO)$_4$(L⁀L) with various substituted benzoyl chlorides and cyclopropane carbonyl chloride.

9. CYCLOPENTADIENYL DERIVATIVES

9.1. Cp *bonded mono- and polynuclear metal carbonyls*

Several mono- through tetranuclear derivatives of group 5 metal carbonyls, in which the metals are bonded through one to four unsubstituted, substituted and fused ring cyclopentadienyls, viz. (η^5-ring)M(CO)$_4$ (M = V, η^5-ring = Cp,[171-177] C_5Me_5,[178] MeC_5H_4,[179] BuC_5H_4,[180] $MeCOC_5H_4$,[181,182] $EtCOC_5H_4$,[183] $MeCO(Me)C_5H_3$,[183] $EtCO(Et)C_5H_3$,[183] 2,3,4,5-Me_4C_5H,[175] C_6H_7,[126] (C_6H_{7-n})(CH_3)$_n$,[126] C_9H_7,[184] 3-BuC_9H_6,[175] C_5H_5BR (R = Me, Ph),[185] fluorenyl;[177] M = Nb, Ta, η^5-ring = Cp,[172,174,176,186-190] MeC_5H_4[172]), [CpM(CO)$_3$]$^{2-}$ (M = V,[191,192] Nb,[193] Ta[193]), (η^5-ring)$_2$V(CO) (η^5-ring = Cp,[171,194,195] C_5Me_5[196,197]), [Cp$_2$V(CO)]$^-$,[198] [(η^5-ring)$_2$V(CO)$_2$]$^+$ (η^5-ring = Cp,[61,171,194,196,199] C_5Me_5[197,200]), Cp$_3$Nb(CO),[186] Cp$^*_2$V$_2$(CO)$_x$ (Cp* = azulene,[201] $C_{10}H_5Me_3$,[201] x = 8; Cp* = Cp,[202-205] C_5Me_5,[178] x = 5, Cp* = fulvalene,[206] x = 2), (C_5Me_5)$_2$V(μ-OC)V(CO)$_5$,[207] Cp$_3$M$_3$(CO)$_x$ (M = V,[208] x = 9; M = Nb,[209] x = 7) and Cp$_4$V$_4$(CO)$_4$,[208] have been reported. Vanadium derivatives are more numerous than those of niobium and tantalum.

(a) *Mononuclear.* CpM(CO)$_4$ (M = V, Nb and Ta), Cp$_2$V(CO) and Cp$_3$Nb(CO) are the known derivatives of this class.

All CpM(CO)$_4$ complexes are orange–red solids (m.p. V, 139°C; Nb, 144–146°C; Ta, 171–173°C) which dissolve in most organic solvents. Niobium and tantalum complexes are more thermally and oxidatively stable than the vanadium analogues whose solution is fairly stable in nitrogen but gradually decomposes in air. The appearance of two IR active bands in the C—O region (ν_{CO}: M = V, 1982, 1890 cm^{-1}, M = Nb, 2000, 1901 cm^{-1} and M = Ta, 2020, 1900 cm^{-1} in CS_2) is attributed[174,176] to the A_1+E modes of C_{4v} symmetry. The Raman spectrum of the vanadium compound exhibits[181] an additional C—O band at 1950 cm^{-1} (in Nujol) due to the B_1 mode. Three very strong bands at 624, 601 and 502 cm^{-1} are assigned to δ(V—C—O) and two bands at 490sh and 428m cm^{-1} are assigned to ν(V—CO).[210] The C—O force constants of CpV(CO)$_4$ defined by (VII) (k, 15.56, k_s, 0.31 and k_d, 0.48 mdynes Å^{-1}, calculated from ν_{CO} in cyclohexane) are comparable to those of similar π-bonded metal carbonyls. Almost identical results have been obtained[181] for (η^5-$CH_3COC_3H_4$)V(CO)$_4$.

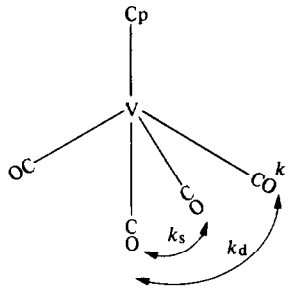

(VII)

Mass spectral data have been presented[211-214] only for CpV(CO)$_4$. The spectrum shows the parent ion and the sequential loss of the CO groups, and allows an estimate of 8.2±0.3 eV for IP_1.[214]

X-ray data are available for CpM(CO)$_4$ (M = V[215] and Nb[216]) which confirm their sandwich structures. The ^{1}H NMR spectrum of CpNb(CO)$_4$ exhibits[172] a broad doublet (~ 18 Hz separation). In the case of CpV(CO)$_4$ and CpTa(CO)$_4$ sharp peaks for Cp ring protons are obtained.

The 17 electron compound, Cp$_2$V(CO), which is an intermediate in the preparation of CpV(CO)$_4$, has been isolated[171,194] as a deep brown, very air-sensitive, solid. Its low ν_{CO} value (1881 cm^{-1}) is

quite comparable to bent bis(cyclopentadienyl) systems of a d^2–d^4 configuration.[171,194] The crystal structure of its η^5-C_5Me_5 analogue has been reported.[196] A structural change from a sandwich structure of Cp_2V to a bent arrangement occurs when the CO is bonded to a vanadium atom. A derivative, $Cp(\eta^5\text{-}C_5H_4Ph)V(CO)$, which contains two different cyclopentadienyl ligands, is also known.[199,217] It has been prepared by the carbonylation of $Cp_2V(Ph)$ followed by Ph migration to a Cp ligand.

$Cp_3Nb(CO)$, which is isolated[186] in the preparation of $CpNb(CO)_4$ in 32% yield during NaHg reduction and subsequent carbonylation of Cp_2NbCl_2, has been shown to have a peculiar structure. Its ^1H NMR spectrum exhibits singlet absorptions at 4.4 and 6.2 ppm whose integration suggested two η^5-C_5H_5 and one η^1-C_5H_5 ligand.[186]

The known anionic $[CpM(CO)_3]^{2-}$ (M = V,[191,192,218] Nb[193] and Ta[219]) and $[Cp_2V(CO)]^-$,[198] and cationic $[Cp_2M(CO)_2]^+$ (M = V[61,171,194,199] and Nb[219]) and $[Cp(\eta^5\text{-}C_5H_4Ph)V(CO)_2]^+$,[199,217] complexes are also mononuclear. The dianions exhibit[191,220] two C—O stretching bands in the ranges 1742–1748 and 1619–1645 cm^{-1}. The monoanion, which is unstable at room temperature, has been generated electrochemically.[198] $[Cp(\eta^5\text{-}C_5H_4Ph)V(CO)_2]I_2$ in which vanadium is bonded to two different cyclopentadienyl rings, has been obtained[199,217] as a maroon–orange crystalline diamagnetic solid by treating a toluene solution of $Cp(\eta^5\text{-}C_5H_4Ph)V(CO)$ with an excess of iodine under CO.

(b) *Dinuclear.* $Cp_2V_2(CO)_5$[111,203–205,221] and $(\eta^5\text{-}C_5Me_5)_2V(\mu\text{-}OC)V(CO)_5$[207] are the only known derivatives of this class. Niobium and tantalum do not form dinuclear carbonyls. The appearance of five CO stretching bands in the region 1828–2006 cm^{-1} in the IR spectrum of $Cp_2V_2(CO)_5$ indicates its low symmetry; the low energy absorptions are associated with the semi-bridging CO. Out of the five, there are three terminal CO groups of a completely conventional type and two intermediate between strictly terminal or bridging.[222] Its crystal structure[24,222,223] shows a metal–metal bond which is probably of the order $1 < n < 3$. Two of the CO groups on one vanadium atom are slightly non-linear ($\angle VCO = 169°$) and their carbon atoms lie 2.40 and 2.44 Å from the second vanadium, i.e. close enough to suggest that these are weak but real C—V (second) bonding interactions.

The structure of paramagnetic $(\eta^5\text{-}C_5Me_5)_2V(\mu\text{-}CO)V(CO)_5$ (μ_{eff} = 2.68 BM) shows a linear V—O—C—V moiety with V—O = 2.075 Å, C—O = 1.167 Å and V—C = 1.899 Å. Of the five CO stretching bands (ν_{CO}: 2032, 1945, 1890, 1857 and 1708 cm^{-1} in THF) in its IR spectrum, the band at 1708 cm^{-1} has been assigned to the *iso*-carbonyl bridge.[207]

(c) *Tri- and tetranuclear.* $Cp_3M_3(CO)_x$ (M = V,[208] $x = 9$; M = Nb,[209] $x = 7$) and $Cp_4V_4(CO)_4$[208] are the only known derivatives of this class.

The vanadium complexes are the side products of the thermal disproportionation of $Cp_2V_2(CO)_5$ in THF. Structural parameters are not available for the two derivatives and therefore they have been characterized by mass spectral measurements.[208] Both derivatives exhibit[208] two C—O stretching bands almost at the same frequencies (ν_{CO}: trimer, 2041m and 2014vs; tetramer, 2035s and 2012vs cm^{-1} in CCl_4).

$Cp_3Nb_3(CO)_7$ has a very unusual structure (**VIII**) in which the mode of bonding of one CO is quite different from the rest. Its crystal structure[209] indicates the extreme bond lengthening for the six electron donor carbonyl, (μ_3-η^2-CO), a distance somewhat between C—O and C=O. The C—O stretching frequency for this non-rigid CO is 1330 cm^{-1}, the lowest metal carbonyl stretch yet

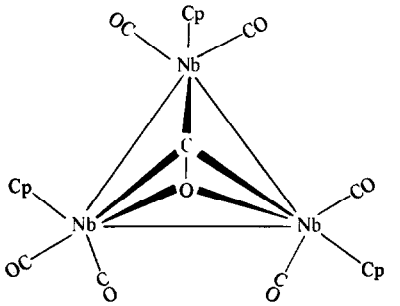

(VIII)

reported. Isotopic labelling[209] also confirms this fact. Two different ring environments in the molecule indicate some fluxional process which does not disrupt the bonding[224] of μ_3-η^2-CO.

9.2. *Derivatives containing group* 5, 6 *and hydrocarbon ligands*

(a) *Complexes with group* 5 *and* 6 *donors.* Substitution reactions of $CpV(CO)_4$ occur fairly readily, but it is difficult to displace all the CO molecules by other ligands. Numerous mono- and bidentate ligands displace CO to give $CpV(CO)_3L$ (L = CH_3CN,[225,226] CD_3CN,[226] PH_3,[203,227,228] Ph_3P,[203,221,225,229–233] Et_3P,[203,225,229,234] Et_2PhP,[203,221] PF_3,[104] Bu_3P,[203,221] Pr^i_3P,[203] Me_2ClP,[235] Ph_2MeP,[203,225,229,231,236] $(OPh)_3P$,[203,225,229,231] $(OCH_2)_3CMeP$,[203,225,229] $(NMe_2)_3P$,[229] Et_3As,[108] Ph_3As,[108,203,236] $(OEt)_3As$,[108] Ph_3Sb,[108,236] $(OEt)_3Sb$,[108] Et_3Bi,[108] CS,[225] THF,[205] P_2Me_4,[110,118] P_2Ph_4,[118] P_2Cy_4,[110,118] Me_2NPMe_2,[225] As_2Ph_4,[236] Sb_2Ph_4,[110,118] dppm,[114,236] dppp,[114] dpsm,[236] triphos,[114] *o*-$C_6H_4(AsPh_2)(SbPh_2)$[236]) and $CpV(CO)_2(L_2$ or L⁀L) (L = PH_3,[203] PF_3,[104,203] Me_3P,[237] Bu_3P,[203] Ph_3P,[203] Et_2PhP,[203] Ph_2MeP,[104] Et_3Bi,[108] CS,[225] $NC_5H_4CN{=}NCMePh$;[238] L⁀L = dppm,[114,236] dppe,[105,114,229,239] dppp,[114] diars,[105] dpae,[105,236] arphos,[105] *o*-$C_6H_4(AsPh_2)(SbPh_2)$,[236] $Ph_2PCH{=}CHPPh_2$,[240] triphos[98,240]) when irradiated with UV light or refluxed in THF or toluene. In several cases, bidentate ligands, e.g. diphosphines, diarsines, distibines, diphenylphosphino- and diphenylstibinomethanes behave[114,236] as monodentates in their reactions. A kinetic study[241] of the reaction: $CpV(CO)_4 + L \rightarrow CpV(CO)_3L$ indicates that the reaction proceeds according to the first-order law; the rate is independent of ligand concentration and type. Reactions with $CpM(CO)_4$ (M = Nb, Ta) are relatively less well studied; the known mono- and disubstitution products are $CpM(CO)_3L$ (M = Nb, L = Ph_3P,[242,243] Cy_3P,[244] Ph_3As,[242,243] Ph_3Sb,[242,243] THF;[118] M = Ta, L = Ph_3P[245]) and $CpM(CO)_2(L_2$ or L⁀L) (M = Nb, L = Ph_3P,[243,246] L⁀L = dmpe,[247–249] $Ph_2P(CH_2)_nPPh_2$ (n = 1–5); M = Ta, L = Ph_3P,[245] L⁀L = dmpe[249]). $Cp^*M(CO)_4$ (M = V,[184] $Cp^* = \eta^5$-C_9H_7; M = Nb,[172] $Cp^* = \eta^5$-MeC_5H_4; M = Ta,[250] $Cp^* = \eta^5$-C_5Me_5) behave similarly in ligand substitution reactions by giving mono- and disubstitution products. $Cp_2V_2(CO)_5$, in addition to $Cp_2V_2(CO)_4L$ (L = Bu_3P, Ph_3P, PH_3, Pr^i_3P, Ph_3As), also yields[203,221] mono- and disubstitution products.

Derivatives containing a single CO group occur rarely; $CpV(CO)(NO)_2$[192,205,251,252] and $CpV(CO)\{PPh(CH_2CH_2CH_2PPh_2)_2\}$[253] are the only known derivatives. The former was obtained by using $MeC_6H_6SO_2NMeNO$,[192] $[Co(NO)_2Br]_2$[252] or even free NO[251] as the nitrosylating agent. The triphos derivative, which at one time was thought to be $CpV(CO)_2$(triphos) containing a *trans* ligand,[98] was actually found to be $CpV(CO)\{PPh(CH_2CH_2PPh_2)_2\}$.

$MeN(PF_2)_2$[254] and PhEH[255,256] (E = S and Se) displace all the CO groups to yield $CpV\{MeN(PF_2)_2\}_2$ and $[CpV(EPh)_2]_2$, respectively. Heteronuclear complexes, $[Cp_3Cr_3(\mu^3\text{-}S)_4]$—MCp (M = V and Nb), containing tetrahedral metallic skeletons are obtained[257] when $(CpCrCSMe_3)_2S$ reacts with the appropriate $CpM(CO)_4$.

Bidentate ligands ($Ph_2PC{\equiv}CPPh_2$,[116] *trans*-$Ph_2PCH{=}CHPPh_2$,[116] R_2PPR_2 (R = Me or Cy),[110] dppm,[236] dpam[236] and dpsm[236]) also give stable (L⁀L) bridged dinuclear $[CpV(CO)_3]_2(\mu$-L⁀L) and $[CpV(CO)_2]_2(\mu$-L⁀L$)_2$. When $(Ph_2PCH_2)_3CMe$ and $Ph_2P(CH_2)_3PPh_2$ are used as ligands, binuclear unsymmetrical $[CpV(CO)_3\{PPh_2CH_2C(Me)(CH_2PPh)_2\}V(CO)_2Cp]$ and a polymeric complex *cis*-$[CpV(CO)_2\{Ph_2P(CH_2)_3PPh_2\}]_n$ are recovered.[114,239] Presently, group 5 ligand bridged niobium and tantalum derivatives are not known, but sulphur donors like H_2S and MeSH react with $CpNb(CO)_3$(THF) (obtained by UV irradiation of $CpNb(CO)_4$ in THF) to yield[258] $[CpNb(CO)_2]_2(\mu$-S$)_2$ (**IX**), $[CpNb(CO)_2]_2(\mu$-S$)_3$ (**X**) and $[CpNb(CO)_2]_2(\mu$-SMe$)_2$ (**XI**). The vanadium analogue of (**XI**)

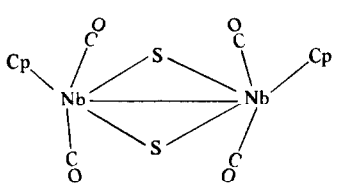

(**IX**)

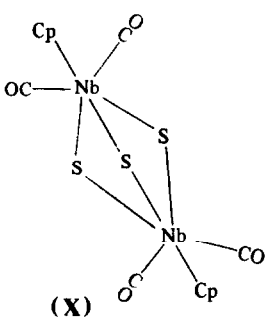

(**X**)

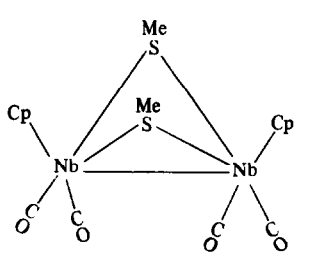

(**XI**)

together with a non-carbonyl product $Cp_2V_2(SMe)_4$ has been prepared[259] by irradiating a mixture of $CpV(CO)_4$ and Me_2S_2 for four days in THF.

$CpM(CO)_3L$ derivatives exhibit two or three CO bands in the range 1830–1975 cm^{-1} depending upon the nature of the ligand. Only two CO absorptions appear for the corresponding dicarbonyls, the magnitude of the frequencies depends upon the ring substituents and the nature of the entering ligands. The shielding of ^{51}V chemical shifts has been studied[237,260,261] in $CpV(CO)_3L$ and $CpV(CO)_2L_2$ derivatives containing a range of phosphine ligands. It decreases with decreasing ligand strength and increasing spatial requirements for the ligands. Qualitative MO calculations[262] of the former also suggest that the ^{51}V NMR chemical shift parameter should correlate with the π-acceptor abilities of L. Based on the observed τ values the ligands may be arranged in a sequence of their π-acceptor ability.

Crystal structural studies are rather limited. X-ray data are available for only $CpV(CO)\{PPh(CH_2CH_2PPh_2)_2\}$,[253] $CpV(CO)_2\{Ph_2P(CH_2)_2PPh_2\}$,[263] $CpV(CO)_3(As_2Ph_4)$[236] and $Cp_2V_2(CO)_4(Ph_3P)$.[222] In the monocarbonyl complex the vanadium atom is centred between the two best planes spanned by the cyclopentadienyl ring and three phosphorus atoms plus the CO ligand while, in the dicarbonyl compound, the vanadium atom is centred between the two best planes spanning the cyclopentadienyl ring atoms, the CO carbon and the phosphinoethane phosphorus atoms, respectively. The V—P distances are longer and the P—V—P bond angle smaller than in most corresponding compounds throughout the periodic table.

Although the crystal structure of any niobium or tantalum derivatives is not available, $^{31}P(^1H)$ and $^{13}C(^1H)$ NMR studies have been applied[258] for structural assignments. On this basis the structures of $(\eta^5\text{-}C_5Me_5)Ta(CO)_2(L_2$ or L⁀L) (L = Me_3P; L⁀L = dmpe) have been assigned as four-legged piano stool type. The resonance in the spectrum of the dmpe product is a doublet ($^2J_{PC}$ = 17 and 4 Hz) which indicates a static structure with the CO ligands *cis*.

(i) *Cations*

Both electrochemical and chemical oxidation have been used for cation formation. The cations $[CpV(CO)_3L]^+$ (L = Ph_3P, Ph_2MeP, Et_3P, $(NMe_2)_3P$, $(OPh)_3P$, $\{(OCH_2)_3CMe\}P$) and $[CpV(CO)_2(L⁀L)]^+$ (L⁀L = dppe) have been generated[229] in cyclic voltammetric studies of $CpV(CO)_3L$ or $CpV(CO)_2(L⁀L)$ in CH_2Cl_2 and MeCN in which the neutral species are oxidized at a platinum electrode. $[CpV(CO)_3(Ph_3P)]^+$ has also been obtained[229] by the oxidation of $CpV(CO)_3(Ph_3P)$ with $NOPF_6$ in a mixture of toluene and methanol.

(ii) *Anions*

Only CN^- containing anions $[CpV(CO)_3(CN)]^-$, $[CpV(CO)_2(CN)_2]^{2-}$ and $[CpV(CO)_2(CN)]_2^{4-}$ have been synthesized.[203,264] The former two are isolated as their sodium salts when $CpV(CO)_4$ is treated[203] with NaCN in methanol followed by chromatographic separation. $K[CpV(CO)_3CN]$ is prepared[264] by the treatment of $CpV(CO)_4$ with $K[N(SiMe_3)_2]$ in benzene; $K_2[CpV(CO)_2(CN)_2]$ is not obtained by this method. The dinuclear CO bridged anion, $[CpV(CO)_2(CN)]_2^{4-}$ is isolated[264] as its NMe_4^+ salt when a mixture of NMe_4CN and $[NMe_4]_2[CpV(CO)_3]$ is irradiated with UV light in CH_3CN.

(iii) $[(Cp \text{ or } Cp^*)_2M(CO)L]^n$ ($n = 0$ *and* $+1$)

Derivatives $(Cp \text{ or } Cp^*)_2M(CO)L$ ($Cp = \eta^5\text{-}C_5H_5$, M = V, L = SMe,[194] SPh,[194] M = Nb, L = SH[265]; $Cp^* = \eta^5\text{-}C_5Me_5$, M = V, L = CN,[196] $SC_6H_4Me\text{-}p$[196]), in which two cyclopentadienyl rings are bonded to a single metal atom, have been obtained by the carbonylation of (Cp or $Cp^*)_2ML$. The X-ray study of $Cp_2Nb(CO)(SH)$ indicates[265] its structure to have a wedge-shaped configuration of the Cp rings essentially analogous to those in $Cp_2Nb(CO)H$. The presence of the large mercapto ligand increases the angle between the Cp rings to 45°. Similar carbonylation of $[Cp_2V]^+$ in the presence of L (L = C_5H_5N, Et_3P, Bu_3P) yields[171] $[Cp_2V(CO)L]^+$ which are isolated as their BPh_4^- salt.

(b) *Complexes with hydrocarbon donors.* Hydrocarbon ligands e.g. dienes, trienes, tetraenes and acetylenes, which act as π-donors, react with $CpM(CO)_4$ (M = V, Nb and Ta) to yield a variety of

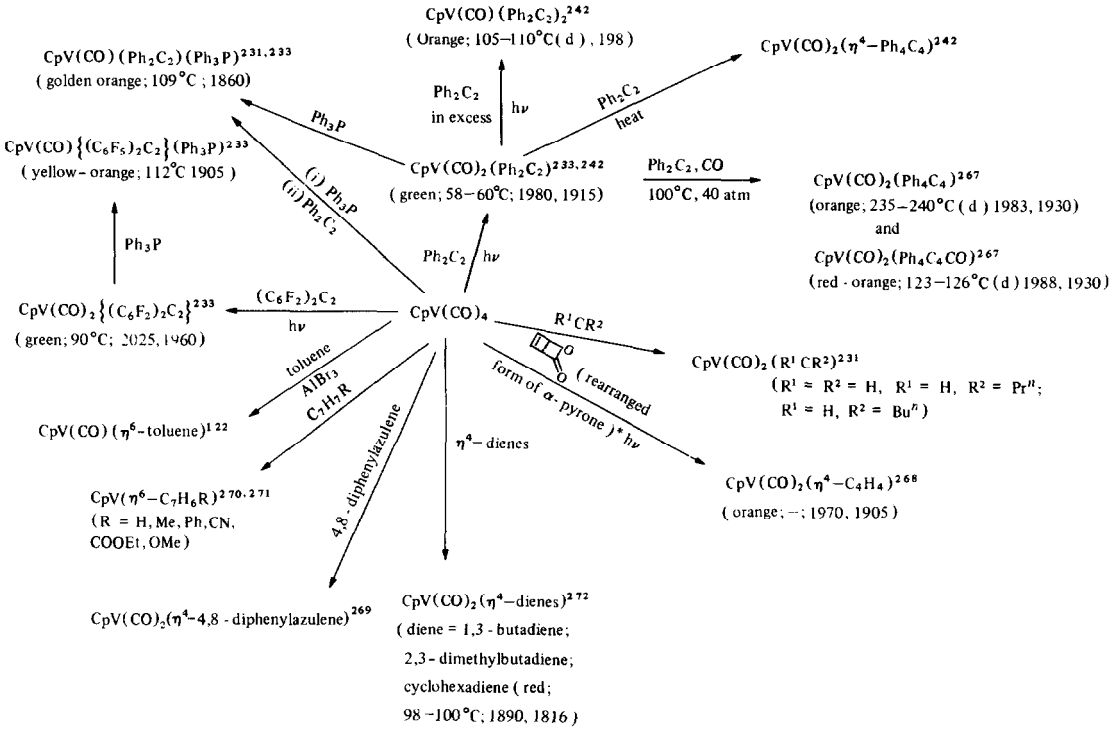

Scheme 2. Reactions of $CpV(CO)_4$ with hydrocarbon donors. * gives $(\eta^4\text{-}C_5H_4(CO)Me)V(CO)_2(\eta^4\text{-}C_4H_4)$[268] when reacted with the analogous $(\eta^5\text{-}C_5H_4(CO)Me)V(CO)_4$. Colour, melting point and ν_{CO} (cm^{-1}) of the products are given in parentheses.

products. $Cp_2V_2(CO)_5$ also yields[266] similar derivatives with acetylenes to those obtained when $CpV(CO)_4$ reacts with acetylenes. Since, to a considerable extent, the reactions of $CpV(CO)_4$ differ from those of the niobium and tantalum analogues, separate schemes (Schemes 2 and 3) have been used to describe their reactions. The principal points of difference of the two schemes are in the very thoroughly investigated reactions of Ph_2C_2 under varying conditions.

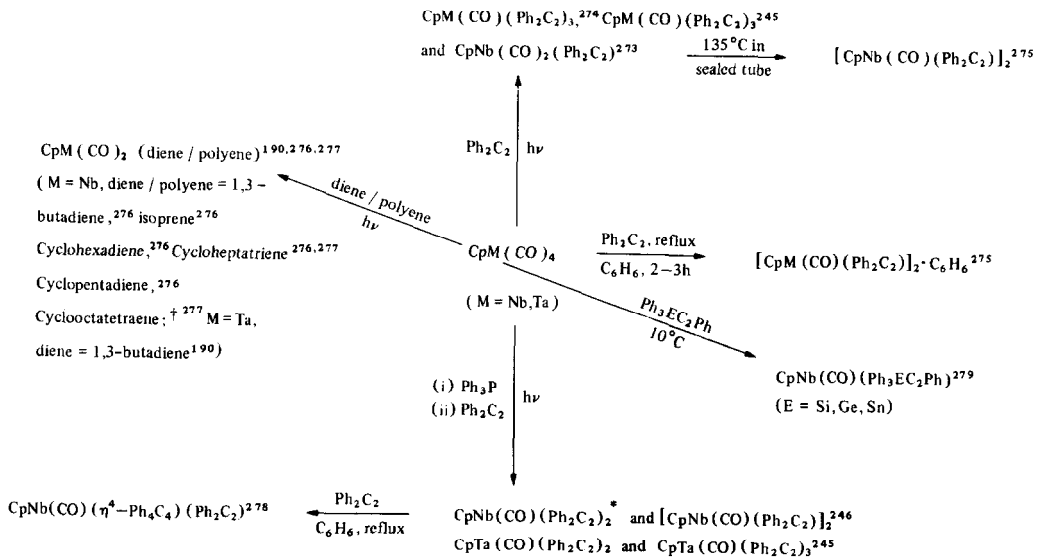

Scheme 3. Reactions of $CpNb(CO)_4$ and $CpTa(CO)_4$ with hydrocarbon donors. $*(\eta^5\text{-}MeC_5H_4)Nb(CO)(Ph_2C_2)$ is formed[172] when $(\eta^5\text{-}MeC_5H_4)Nb(CO)_4$ is used.† Excess cyclooctatetraene gives $CpNb(CO)(C_8H_8)$[277] (not isolated pure).

In the reactions with $CpV(CO)_4$, diphenylacetylene gives[242,267] tetraphenylcyclobutadiene, or in the presence of CO, tetraphenylcyclobutadienone derivatives. The tendency is extremely small for niobium and is practically unknown for the tantalum analogue.

In $CpNb(CO)(Ph_2C_2)(\eta\text{-}Ph_4C_4)$, the Nb atom has an 18 electron configurate and is coordinated to a η^5-Cp and η^4-Ph_4C_4 ligand, the triple bond of Ph_2C_2 and the CO group.[278,280] The Ph_4C_4 ring is planar to within 0.02 Å and makes an angle of 48° with the Cp ring. The spatial arrangement of Ph_2C_2 and the η-Ph_4C_4 ligand is favourable for cyclization into hexaphenylbenzene which is formed upon thermal decomposition of the complex.[280]

The crystal structures of a few more mononuclear, $CpV(CO)_2(\eta^4\text{-}Ph_4C_4)$,[281] $CpNb(CO)(Ph_2C_2)_2$[282–284] and $CpNb(CO)(Ph_3GeC{\equiv}CPh)$[285] derivatives have also been examined.

Bridged dinuclear $[CpM(CO)(Ph_2C_2)]_2$ (M = Nb and Ta) are obtained when Ph_2C_2 reacts with the appropriate $CpM(CO)_4$, but the analogous vanadium derivatives are not known. In the structure of the niobium derivative[284,286,287] **(XII)**, two Ph_2C_2 ligands are bridged between two Nb—Nb bonded niobium atoms. $MeOOCC{\equiv}CCOOMe$ also forms[288] similar acetylene bridged niobium derivatives.

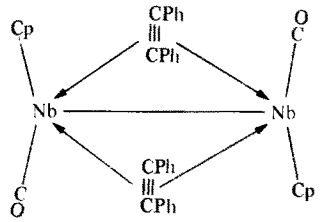

(XII)

9.3. *Derivatives containing* M—H *and* M—H—M′ *bonds*

Like simple vanadium carbonyl hydrides, Cp bonded vanadium hydrocarbonyls are also rare; only two anions $[CpV(CO)_3H]^-$[202,236] and $[Cp(CO)_3V(\mu\text{-}H)V(CO)_3Cp]^-$,[226] and a cation $[CpV(CO)_3(Ph_3P)H]^+$[244] have been reported so far.

Niobium and tantalum derivatives are more numerous and a variety of these, viz. $[CpM(CO)_3H]^-$[193,289] (M = Nb, Ta), $[CpNb(CO)_2(L{\frown}L)H]^+$[248,249,290] (L⁀L = dmpe, dppe), Cp*M(CO)(L_2 or L⁀L)H_2[258,291] (Cp* = Cp, M = Nb, L = Ph_3P; Cp* = η^5-C_5Me_5, M = Ta, L = Me_3P, L⁀L = dmpe), $Cp_2^*M(CO)H$[219,292–297] (Cp* = Cp, η^5-C_5H_4Me, M = Nb, Ta), $[Cp_2Nb(CO)H_2]^+$[219] and $Cp_2(CO)Nb(\mu\text{-}H)M(CO)_3Cp$[298] (M = V, Nb, Ta) have been reported. Cp_2MH_3 (M = Nb and Ta) and Cp_2NbBH_4 are the key reagents for their synthesis, although in a few cases $[CpM(CO)_3]^{2-}$ (M = Nb and Ta), CpNb(CO)(L_2 or L⁀L) (L = Ph_3P, L⁀L = dmpe, dppe) and Cp*Ta $(Me_3P)_2H_4$ have also been used.

Two general methods have been employed to synthesize these derivatives. The reactions involve:

(i) the carbonylation of Cp_2MH_3 or Cp_2NbBH_4 using CO or a binary substituted metal carbonyl moiety and

(ii) the protonation of $[CpM(CO)_3]^{2-}$ or $CpM(CO)_xL_y$ (L = a P^{III} ligand) with the help of water or acids.

It has been observed that the presence of a phosphine ligand facilitates protonation. $CpV(CO)_4$ cannot be protonated at all but $CpV(CO)_3(Ph_3P)$ and $CpNb(CO)_2(L{\frown}L)$ (L⁀L = dmpe, dppe) are protonated at the metal atom by HCl or CF_3COOH. In addition, cyclopentadiene, in its reaction with $CpNb(CO)_2(Ph_3P)_2$ under UV irradiation also proved to be a source for carbonyl hydride synthesis.[291]

As regards structural features, the hydrogen is either terminally bonded through a group 5 metal atom or is bridged between two metal atoms. Additional metal–metal bonding is an important but not an essential feature of the dinuclear derivatives. X-ray studies of some of these complexes indicated that the distance between the metal atoms allows significant metal–metal interaction.

Among mononuclear derivatives, the crystal structure of only $CpNb(CO)(Ph_3P)_2H_2$ is known.[291] In this molecule, the central niobium atom is positioned above the flat Cp ring which is parallel to

a plane above the niobium atom going through both the phosphorus atoms and the carbon atom of the CO group. The Ph_3P ligands are in the *trans* position and a vacant plane in the coordination sphere of the niobium atom probably belongs to the hydrogen atoms, Structure **(XIII)**.

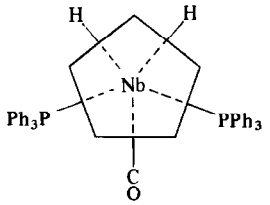

(XIII)

Except for $Cp_2(CO)Nb(\mu\text{-}H)M(CO)_5$[299] (M = Mo, W) the other dinuclear derivatives have been characterized by X-ray studies.[298–304] These studies clearly indicate the presence or absence of metal–metal bonds, e.g. in $Cp_2(CO)Nb(\mu\text{-}H)Fe(CO)_4$ **(XIV)**,[292] $Cp_2(CO)Ta(\mu\text{-}H)Mn_2(CO)_9$ **(XV)**,[303] $[Cp_2(CO)Nb(\mu\text{-}H)Nb(CO)Cp_2]^+[Mn(CO)_5]^-$ **(XVI)**[302] and $Cp_2(CO)Nb(\mu\text{-}H)Zn(BH_4)_2$ **(XVII)**[304] the metal–metal bond distances are significantly shorter than the sum of the covalent radii of the appropriate metal atoms, while in $Cp_2(CO)Nb(\mu\text{-}H)Ni(CO)_3$ **(XVIII)**[300] the Nb · · · Ni distance is 0.25 Å longer indicating a practically non-bonding interaction. This is also the case with $Cp_2(CO)Nb(\mu\text{-}H)Mo(CO)_4(\mu\text{-}H)Nb(CO)Cp_2$ **(XIX)**[300] in which direct Nb—Mo bonding is probably absent.

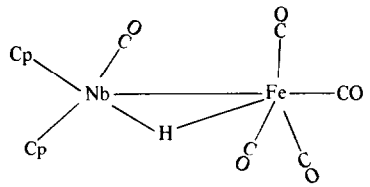

(XIV)

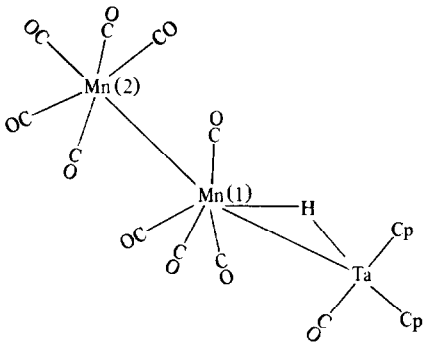

(XV)

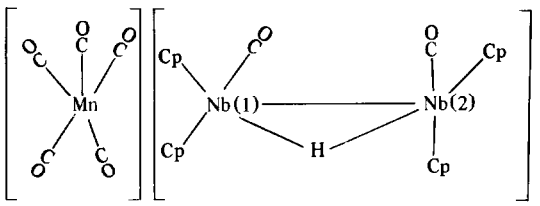

(XVI)

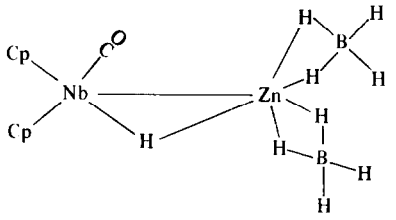

(XVII)

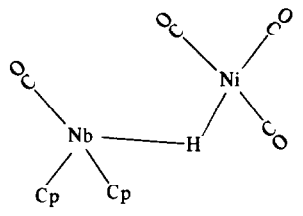

(XVIII)

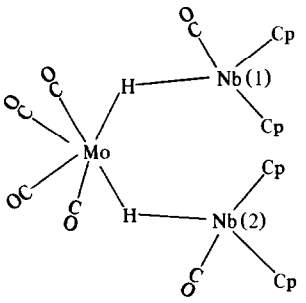

(XIX)

9.4. *Mixed metal carbonyls*

The known carbonyls of this class are $Cp_2(CO)Nb(\mu\text{-}CO)Mn(CO)_4$,[300,305] $Cp_2MM'(CO)_3Cp$ (M = V,[306] M = Cr; M = Nb,[307,308] M′ = Mo, W), $Cp_2(CO)Nb(\mu\text{-}CO)Co(CO)_3$,[309] $[H_2CpVOs_3(CO)_{13}]^{2-}$ [310] and $Cp_3VW(\mu\text{-}CR)(CO)_2$.[311]

$Cp_2(CO)Nb(\mu\text{-}CO)Mn(CO)_4$, which is obtained as one of the products of the reaction between $Mn_2(CO)_{10}$ and Cp_2NbBH_4/Et_3N, has the structure (**XX**) in which $Cp_2(CO)Nb$ and $Mn(CO)_5$ fragments are linked through the Mn—Nb bond in such a way that the bis-C_5H_5 fragments have an eclipsed conformation with a wedge angle of 44.2° and a distorted octahedral environment about the manganese atom.[300–305]

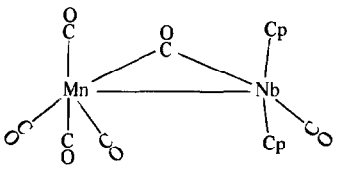

(**XX**)

$Cp_2MM'(CO)_3Cp$, in which M = V and M′ = Cr, has been obtained[306] by the reaction of $[CpCr(CO)_3]_2$ with Cp_2V; analogous niobium derivatives have been obtained from the reaction[307,308] between Cp_2NbH_4 and $[CpM'(CO)_3]_2$ (M = Mo and W). The crystal structure of only the molybdenum compound has been determined.[308] In its structure (**XXI**), a wedge link sandwich Cp_2Nb is linked with a Mo(CO)Cp fragment by a direct Nb—Mo bond and two bridging CO groups, one non-symmetrically bonded through the carbon atom only and the other σ-bonded to molybdenum and π-bonded to niobium.

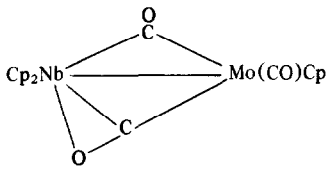

(**XXI**)

$Cp_2(CO)Nb(\mu\text{-}CO)Co(CO)_3$, which is the product[309] of the reaction between Cp_2NbH_3 and $Co_2(CO)_8$, has a structure (**XXII**) in which the Co—Nb bond is supplemented by a semibridged CO. Analogous η^5-$C_5H_4CMe_3$ ring-containing niobium and tantalum derivatives have been obtained[312] in a similar way, but they have different CO patterns. These derivatives with an excess of $Co_2(CO)_8$ give[312] oxymethylidynetricobalt nonacarbonyl, $(\eta^5\text{-}C_5H_4CMe_3)_2M(CO)OC\cdot Co_3(CO)_9$.

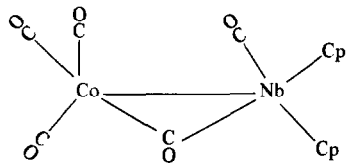

(**XXII**)

The anionic tetrametallic complex, $[H_2CpVOs_3(CO)_{13}]^{2-}$ (**XXIII**), which is a hydrido osmium carbonyl complex, has been prepared[310] by the action of $[CpV(CO)_3]^{2+}$ on $H_2Os_3(CO)_{10}$ in THF below −78°C.

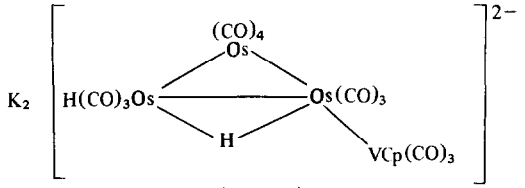

(**XXIII**)

Recently, V—W bonded black, paramagnetic, $Cp_3VW(\mu\text{-}CR)(CO)_2$ (R = Me or C_6H_4Me-4) has been synthesized[311] by the reaction of Cp_2V with $CpW(\equiv CR)(CO)_2$ in light petroleum at 0°C. The crystal structure[311] of the C_6H_4Me-4 product shows that the ligand is bonded between vanadium and tungsten in such a way that one of the two CO ligands on tungsten semibridges the V—W bond (**XXIV**).

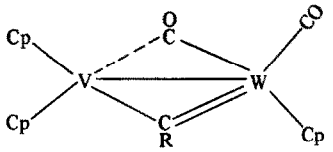

(XXIV)

9.5. *Carbonyl halides and their derivatives*

The synthesis and structural studies of $CpM(CO)_3X_2$, $[CpM(CO)_3X]^-$, $Cp^*M(CO)_2LX_2$, $CpM(CO)(L_2$ or L⁀L)X_2 and (Cp or $Cp^*)_2M(CO)X$ are described in this section. It is noteworthy that niobium and tantalum derivatives have received more attention than their vanadium analogues.

$CpV(CO)_4$, when oxidized with elemental halogen, gives[277] $CpVX_n$ (X = I, $n = 2$; X = Cl, Br, $n = 3$) at ordinary temperatures but $CpV(CO)_3X$ (X = Cl, Br, I) derivatives are obtained[302] when a solution of $[(PPh_3)_2N]^+X^-$ and $CpV(CO)_4$ is irradiated with UV light. The bromo derivative has been obtained in 74% yield by the action[226] of benzyl bromide on $[CpV(CO)_3H]^-$. The halogen dependence of ^{51}V shielding has also been studied.[313]

Bis(Cp) and bis(η^5-C_5Me_5) bonded neutral (Cp or $C_5Me_5)_2V(CO)I$ have been synthesized[194,196] by the carbonylation of (Cp or $C_5Me_5)_2VI$; the method failed to yield the chloro analogue under identical conditions.

$CpM(CO)_3X_2$ (M = Nb, X = Cl,[314] I[277]; M = Ta, X = Cl[314]) derivatives have been obtained by the carbonylation[314] of $CpMCl_4$ in the presence of $Al/HgCl_2$. Niobium derivatives are obtained in better yield (~ 65%) than tantalum (< 10%). $CpNb(CO)_3I_2$, in which CO is very loosely bound to niobium is obtained[277] by the action of iodine on $CpNb(CO)_4$. Upon prolonged evacuation, $CpNb(CO)_3I_2$ gives a CO-free product which reversibly reacts with CO to give[277] a different product, possibly bridged dimeric $[CpNb(CO)_2I_2]$.

$Cp_2M(CO)X$ (M = Nb, Ta, X = Cl,[315] Br[316]) are obtained when Cp_2MX_2 is carbonylated in the presence of reducing agents such as Na/Hg,[186] Zn,[219] K or *t*-BuMgCl.[317] Carbonylation of Cp_2NbCl or the action of HCl on $Cp_2NbH(CO)$ at −78°C results in the formation of $Cp_2Nb(CO)Cl$. An analogous MeCp derivative has been obtained[318] by $(OMe)_3P$ displacement from $(MeCp)_2Nb\{(OMe)_3P\}Cl$ by CO.

Other octacoordinated halocarbonyls of niobium and tantalum have been stabilized in a number of ways. Ligand-induced reductive-elimination of Me_3SiCl by CO (3.5 atm)/THF in (η^5-C_5Me_5)$Ta(SiMe_3)Cl_3$ stabilizes (η^5-C_5Me_5)$Ta(CO)_2(THF)Cl_2$.[319] Mono- or bidentate *t*-phosphines also stabilize the carbonylation products of $CpMCl_4$ by yielding $CpM(CO)(L_2$ or L⁀L)Cl_2 (M = Nb. L = Et_3P,[150] L⁀L = dmpe;[248,249] M = Ta, L = Me_3P,[150] Et_3P,[150] Ph_3P[150] and Me_2PhP[150]). Analogous dmpe containing niobium compounds have been isolated[249] by the action of benzyl bromide or MeI on $CpNb(CO)_2$(dmpe).

Crystal data are not available except for $[CpTa(CO)(PMe_2Ph)_2Cl_2]$ in which the molecule shows[150] approximate mirror symmetry with the P···P vector normal to the mirror plane and a distorted octahedral coordination pattern of tantalum. It can be more easily visualized as derived from a four-legged piano stool structure (**XXV**).

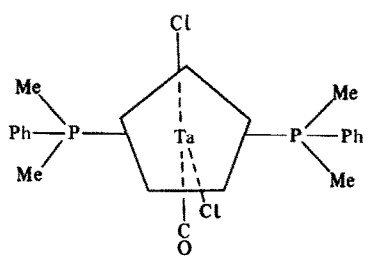

(XXV)

Halocarbonyl hydrides are of extremely rare occurrence; the only known examples [(η^5-C_5Me_5)Ta(CO)$_x$(Me_3P)$_{3-x}$HCl] ($x = 1$ and 2), are isolated[258] as a mixture when [(η^5-C_5Me_5)Ta(Me_3P)$_2H_3$Cl] reacts with CO at 0°C.

9.6. *Alkyl, alkenyl, silyl, germyl, stannyl and plumbyl derivatives*

Although some ER_2 bridged [Cp*M(CO)$_3$(ER_2)]$_2$ (Cp* = η^5-C_5H_4Bu, M = V, Ta, E = Si, R = allyl; Cp* = η^5-$C_5H_3Et_2$, M = V, E = Sn, R = $C_{12}H_{25}$; Cp* = fluorenyl, M = V, E = Pb, R = xylyl) derivatives have been mentioned in the patent literature,[320] systematic work in this area has only been done recently. In addition to the above, derivatives of the following types are presently known.

(i) [CpM(CO)$_3$R]$^-$ and [CpM(CO)$_{3-n}$(EX_3)$_n$]$^{p-}$.
(ii) Cp_2M(CO)(alkyl, acyl, alkenyl, chloroalkylstannyl or trichlorostannyl).

(i) [CpM(CO)$_3$R]$^-$ *and* [CpM(CO)$_{3-n}$(EX_3)$_n$]$^{p-}$. Alkyl bonded, [CpM(CO)$_3$R]$^-$ (R = CH_3 and n-C_8H_{17}) derivatives, are known[226] only for M = V, and have been prepared by the action of an appropriate alkyl halide on [CpV(CO)$_3$]$^{2-}$ in THF or HMPA, and isolated in the form of their [N(PPh_3)$_2$]$^+$ salts.

The only known silyl derivative[156] is the NEt_4^+ salt of the anion [CpV(CO)$_3$($SiPh_3$)]$^-$. Structurally similar [CpV(CO)$_3$($GeCl_3$)]$^-$ has been isolated[321] by irradiating a mixture of $CpV(CO)_4$ and [$AsPh_4$][$GeCl_3$] solutions with UV light. The appropriate [CpM(CO)$_3$H]$^-$ anion is used as starting material for the preparation of [CpM(CO)$_3$($GePh_3$)]$^-$ (M = V[156] and Nb[322]); the trialkyltin analogues[322] [CpNb(CO)$_3$(SnR_3)]$^-$ (R = $PhCH_2$, Et). [CpV(CO)$_3$($SnCl_3$)]$^-$ has been obtained[321] in a way similar to its germanium analogue, but in this case further CO displacement, to give a mixture of *cis*- and *trans*-[CpV(CO)$_3$($SnCl_3$)$_2$]$^{2-}$, has also been achieved.[323] Use of the reaction of $SnPh_3Cl$ with [CpV(CO)$_3$]$^{2-}$ has been made[156,191,193] to obtain the $SnPh_3$ analogue. Similar niobium and tantalum derivatives have also been synthesized.[193,322] The crystal structure[324] of the niobium complex shows that the three CO ligands and tin atom span a tetragonal plane parallel to the Cp ring, with a greatly distorted tetrahedral environment of tin (∠Nb—Sn—Ph, 116.8° and Ph—Sn—Ph, 101.3°).

The plumbyl–tantalum bonded monoanion, [CpTa(CO)$_3$(PbX_3)]$^-$ is not known, although the analogous vanadium (X = Ph[156]) and niobium (X = Ph[193] and Et[322]) derivatives have been synthesized.

(ii) Cp_2M(CO)(*alkyl, acyl, alkenyl, chloroalkylstannyl or trichlorostannyl*). Cp_2V(CO)(alkyl) derivatives probably do not exist. The acyl derivatives, Cp_2V(CO)(COR) (R = Me, $PhCH_2$), which are the carbonylation products of Cp_2VR in heptane or toluene, have been isolated.[199,217] The ν_{CO}(acyl) are at lower wavenumbers (1605–1615 cm^{-1}) and might arise due to intramolecular interaction between the methyl and the acyl group [**XXVI**(a) and (b)].

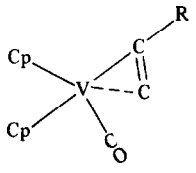

(**XXVI a**)

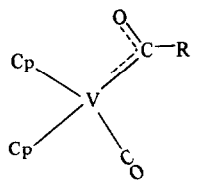

(**XXVI b**)

Well characterized Cp_2M(CO)(alkyl) compounds are known[186,294,325–328] for M = Nb and Ta. They are the carbonylation products of Cp_2MRH, Cp_2MR_2 (M = Nb, R = Me,[186,325,326] Et[328] and $PhCH_2$;[326] M = Ta, R = Me,[327] Et,[294] Pr,[317] Bu,[317] pent[317] and cyclopent[317]) or Cp_2TaH(olefin) (olefin = C_3H_6, C_4H_8, C_5H_{10} and C_5H_8). In the last case migration of hydrogen from the metal atom to olefin takes place to give[317] the corresponding alkyl compound. A unique method for the preparation of $Cp_2Nb(CO)(CH_3)$ is by the action of CH_3MgBr on $Cp_2Nb(CO)Cl$; the reaction of $LiCH_3$ on the above chlorocarbonyl has not been found to be reproducible.[326]

Alkenyl derivatives of niobium have been reported.[328] Thus $Cp_2\overline{Nb(CO)(RC{=}CR'H)}$ and $Cp_2\overline{Nb(CO)(R'C{=}CRH)}$ (R = R′ = Me; R = R′ = Pr; R = Me, R′ = Pr^i; R = Me, R′ = Pr^n) have been prepared[328] by the action of RC≡CR′ on Cp_2NbH_3, followed by the carbonylation of the products. Hydrogen from the metal atom migrates to one carbon atom of the alkyne in these reactions [see eq. (1)].

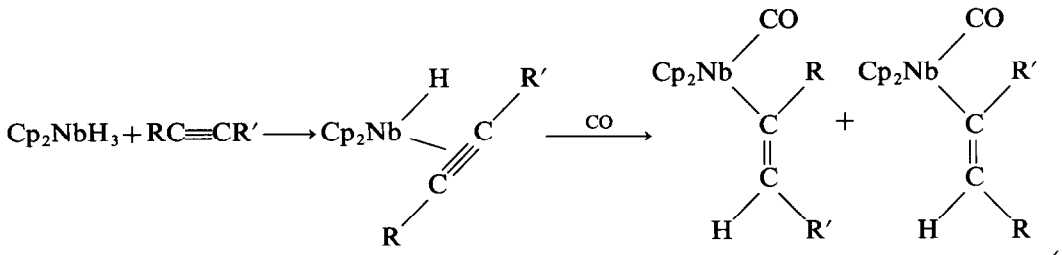

(1)

$Cp_2M(CO)(SnX_3)$ are known[296] for only M = Nb. $Cp_2Nb(CO)(SnR_xCl_{3-x})$ (R = Ph, x = 1–3; R = Et, x = 2) and $(\eta^5\text{-}MeC_5H_4)_2Nb(CO)(SnCl_3)$ are obtained[296] by the action of the appropriate Ph_xSnCl_{4-x}, Et_2SnCl_2 or $SnCl_4$ on a THF solution of (Cp or $\eta^5\text{-}MeC_5H_4)_2Nb(CO)H$ in the presence of pyridine. Treatment of $Cp_2Nb(CO)(SnPh_3)$ with HCl yields $Cp_2Nb(CO)(SnCl_3)$, its NMR spectrum exhibits[296] two satellites of the singlet Cp protons due to $^1H—^{117}Sn$ and $^1H—^{119}Sn$ spin–spin coupling.

REFERENCES

1. G. Natta, R. Ercoli, F. Calderazzo, A. Alberola, P. Corradini and G. Allegra, *Atti. Accad. naz. Lincei Rc. Classe Sci. Fis. Mat. Nat.* 1959, **27**, 107.
2. E. W. Abel and F. G. A. Stone, *Quart. Rev.* 1969, **23**, 325; 1970, **24**, 498.
3. S. C. Tripathi, S. C. Srivastava and R. P. Mani, *J. Sci. Ind. Res.* 1974, **33**, 570.
4. S. C. Tripathi, S. C. Srivastava, R. P. Mani and A. K. Shrimal, *Inorg. Chim. Acta* 1975, **15**, 249; 1976, **17**, 257.
5. E. Band and E. L. Muetterties, *Chem. Rev.* 1978, **78**, 639.
6. (a) N. G. Connelly, *Comprehensive Organometallic Chemistry* (Edited by G. Wilkinson, E. W. Abel and F. G. A. Stone), Vol. 3, p. 647. Pergamon Press, Oxford (1982); (b) J. A. Labinger, *Comprehensive Organometallic Chemistry*, (Edited by G. Wilkinson, E. W. Abel and F. G. A. Stone), Vol. 3, p. 705. Pergamon Press, Oxford (1982).
7. R. Ercoli, F. Calderazzo and A. Alberola, *J. Am. Chem. Soc.* 1960, **82**, 2966.
8. F. Calderazzo and R. Ercoli, *Chim. Ind. Milan* 1962, **44**, 990.
9. R. L. Pruett and J. E. Wyman, *U.S.P.* 1962, 3 053 629; *Chem. Abstr.* 1963, **58**, 273.
10. F. Calderazzo and S. Bacciarelli, *Inorg. Chem.* 1963, **2**, 721.
11. R. P. M. Werner and H. E. Podall, *Chem. Ind. Lond.* 1961, **80**, 144.
12. R. P. M. Werner and H. E. Podall, *Fr.P.* 1963, 1 322 168; *Chem. Abstr.* 1964, **60**, 3015a.
13. R. P. M. Werner, *U.S.P.* 1966, 3 254 953; *Chem. Abstr.* 1966, **65**, 8961g.
14. J. E. Wyman, *U.S.P.* 1966, 3 232 699; *Chem. Abstr.* 1966, **64**, 12242h.
15. R. P. M. Werner, *U.S.P.* 1966, 3 236 755; *Chem. Abstr.* 1966, **64**, 15395f.
16. G. Silvestri, S. Gambino, M. Guaina and R. Ercoli, *J. Chem. Soc., Dalton Trans.* 1972, 2558.
17. J. E. Ellis, R. A. Faltynek, G. L. Ruchfort, R. E. Stevens and G. A. Zank, *Inorg. Chem.* 1980, **19**, 1082.
18. J. E. Wyman, *U.S.P.* 1959, 2 998 301; *Chem. Abstr.* 1962, **56**, 2154d.
19. F. Calderazzo, R. Cini and R. Ercoli, *Chem. Ind. Lond.* 1960, **79**, 934.
20. F. Calderazzo, R. Cini, P. Corradini, R. Ercoli and G. Natta, *Chem. Ind. Lond.* 1960, **79**, 500.
21. R. L. Pruett and J. E. Wyman, *Chem. Ind. Lond.* 1960, **79**, 119.
22. H. J. Keller, P. Lauberau and D. Nothe, *Z. Naturforsch.* 1969, **24B**, 257.
23. H. Haas and R. K. Sheline, *J. Am. Chem. Soc.* 1966, **88**, 3219.
24. J. C. Bernier and O. Kahn, *Chem. Phys. Lett.* 1973, **19**, 414.
25. G. Bonera and A. Rigamanti, *Ric. Sci. Rend. Sez.* 1963, **3A**, 213.
26. D. W. Pratt and R. J. Myers, *J. Am. Chem. Soc.* 1967, **89**, 6470.
27. D. W. Pratt, *U.S. At. Energy Comm.* 1967, UCRL-17406; *Chem. Abstr.* 1968, **69**, 14737g.
28. K. A. Rubinson, *J. Am. Chem. Soc.* 1976, **98**, 5188.
29. J. R. Morton and K. F. Preston, *Organometallics* 1984, **3**, 1386.
30. S. Evans, J. C. Green, A. F. Orchard, T. Sauto and D. W. Turner, *Chem. Phys. Lett.* 1969, **4**, 361.

31. T. J. Barton, R. Grinter and A. J. Thomson, *J. Chem. Soc., Dalton Trans.* 1978, 608.
32. D. J. Schmidling, *J. Mol. Struct.* 1975, **1**, 24.
33. S. Bellard, K. A. Rubinson and G. M. Sheldrick, *Acta Cryst.* 1979, **B35**, 271.
34. D. R. Bindinosti and N. C. McIntyre, *Can. J. Chem.* 1967, **45**, 641.
35. R. E. Sullivan, M. S. Lupin and R. W. Kiser, *J. Chem. Soc., Chem. Commun.* 1969, 655.
36. T. C. DeVore and H. F. Frazen, *Inorg. Chem.* 1976, **15**, 1318.
37. A. B. P. Lever and G. A. Ozin, *Inorg. Chem.* 1977, **16**, 2012.
38. N. A. Beach and H. B. Gray, *J. Am. Chem. Soc.* 1968, **90**, 5713.
39. K. G. Caulton and R. F. Fenske, *Inorg. Chem.* 1968, **7**, 1273.
40. T. A. Ford and G. A. Ozin, *Mol. Spectrosc. Dense Phases, Proc. Eur. Congr. Mol. Spect.* 1975, **12**, 389.
41. T. A. Ford, H. Huber, W. Klotzbuecher, M. Moskovits and G. A. Ozin, *Inorg. Chem.* 1976, **15**, 1666.
42. L. Hanlan, H. Huber and G. A. Ozin, *Inorg. Chem.* 1976, **15**, 2592.
43. D. A. Pensak and R. J. Mckinney, *Inorg. Chem.* 1979, **18**, 3407.
44. J. Demuynck, A. Strich and A. Veillard, *N.J. Chim.* 1977, **1**, 217.
45. J. K. Burdett, *J. Chem. Soc., Faraday Trans.* 1974, 1599.
46. R. Hoffmann and M. Elian, *Inorg. Chem.* 1975, **14**, 1058.
47. R. L. Dekock, *Inorg. Chem.* 1971, **10**, 1205.
48. A. M. Bond and R. Colton, *Inorg. Chem.* 1976, **15**, 2036.
49. C. J. Pickett and D. Pletcher, *J. Organomet. Chem.* 1975, **102**, 327.
50. M. Guainazzi, G. Silvestri and G. Serravalle, *J. Chem. Soc., Chem. Commun.* 1975, 200.
51. J. S. Allinson, B. J. Aylett and H. M. Colquhon, *J. Organomet. Chem.* 1976, **112**, C7.
52. H. Behrens and K. Lutz, *Z. Anorg. Allg. Chem.* 1967, **184**, 354.
53. W. Hieber, E. Winter and E. Schubert, *Z. Anorg. Allg. Chem.* 1963, **319**, 285.
54. W. Hieber, J. Peterhans and E. Winter, *Chem. Ber.* 1961, **94**, 2572.
55. H. Behrens and K. Lutz, *Z. Anorg. Allg. Chem.* 1968, **356**, 225.
56. J. E. Ellis and R. A. Faltynek, *J. Organomet. Chem.* 1975, **93**, 205.
57. F. Calderazzo, *Inorg. Chem.* 1965, **4**, 223; 1964, **3**, 1207.
58. F. Calderazzo, G. Pampaloni, D. Vitali and P. F. Zanazzi, *J. Chem. Soc., Dalton Trans.* 1982, 1983.
59. F. Calderazzo and R. Cini, *J. Chem. Soc.* 1965, 818.
60. F. Calderazzo, *Inorg. Chem.* 1964, **3**, 810.
61. G. Fachinetti and C. Floriani, *J. Chem. Soc., Chem. Commun.* 1975, 578.
62. F. Calderazzo and G. Pampaloni, *J. Chem. Soc., Chem. Commun.* 1984, 1249.
63. R. P. M. Werner and S. A. Manastyrskyj, *J. Am. Chem. Soc.* 1961, **83**, 2023.
64. F. Calderazzo and P. L. Calvi, *Chim. Ind. Milan* 1962, **44**, 1217.
65. R. B. King, *Inorg. Chem.* 1965, **4**, 1518.
66. A. R. Siedle and R. B. Johannsen, *J. Org. Chem.* 1975, **40**, 2002.
67. F. Calderazzo, G. Pampaloni and G. Pelizzi, *Congr. Naz. Chim. Inorg.* 1982, **15**, 117.
68. J. E. Ellis and A. Davison, *Inorg. Synth.* 1976, **16**, 68.
69. F. Calderazzo, G. Pampaloni and G. Pelizzi, *J. Organomet. Chem.* 1982, **233**, C41.
70. W. Beck and R. E. Nitzschmann, *Z. Naturforsch.* 1962, **17B**, 577.
71. R. W. Cattrall and R. J. H. Clark, *J. Organomet. Chem.* 1966, **6**, 167.
72. E. W. Abel, R. A. N. McLean, S. P. Tyfield, P. S. Braterman, A. P. Walker and P. J. Hendra, *J. Mol. Spect.* 1969, **30**, 29.
73. G. R. Dobson, *Inorg. Chem.* 1965, **4**, 1673.
74. P. C. Lauterbur and R. B. King, *J. Am. Chem. Soc.* 1966, **87**, 3266.
75. G. M. Bodner and L. J. Todd, *Inorg. Chem.* 1974, **13**, 1335.
76. T. Nakano, *Bull. Chem. Soc. Japan* 1977, **50**, 661.
77. R. D. Wilson and R. Bau, *J. Am. Chem. Soc.* 1974, **96**, 7601.
78. M. Schneider and E. Weiss, *J. Organomet. Chem.* 1976, **121**, 365.
79. T. G. Richmond, Qi-Zhen Shi, W. C. Trogler and F. Basolo, *J. Am. Chem. Soc.* 1984, **106**, 76.
80. J. E. Ellis, K. L. Fjare and T. G. Hay, *J. Am. Chem. Soc.* 1981, **103**, 6100.
81. G. F. P. Warnock, J. Sprague, K. L. Fjare and J. E. Ellis, *J. Am. Chem. Soc.* 1983, **105**, 672.
82. A. S. Kasenally, R. S. Nyholm, R. J. O'Brien and M. H. B. Stiddard, *Nature* 1961, 204.
83. J. Schiemann, E. Weiss, F. Naumann and D. Rehder, *J. Organomet. Chem.* 1982, **232**, 219.
84. Qi-Zhem Shi, T. C. Richmond, W. C. Trogler and F. Basolo, *J. Am. Chem. Soc.* 1982, **104**, 4032.
85. Qi-Zhem Shi, T. C. Richmond, W. C. Trogler and F. Basolo, *J. Am. Chem. Soc.* 1984, **106**, 71.
86. K. Ihmels and D. Rehder, *J. Organomet. Chem.* 1981, **218**, C54.
87. R. P. M. Werner, *U.S.P.* 1966, 3247 233; *Chem. Abstr.* 1966, **65**, 5489d.
88. R. P. M. Werner, *Z. Naturforsch.* 1961, **16B**, 477.
89. W. Hieber and E. Winter, *Chem. Ber.* 1964, **97**, 1037.
90. A. Davison and J. E. Ellis, *J. Organomet. Chem.* 1972, **36**, 131.

91. L. V. Interrante and G. V. Nelson, *J. Organomet. Chem.* 1970, **25**, 153.
92. R. P. M. Werner, *U.S.P.* 1966, 3 294 828; *Chem. Abstr.* 1967, **66**, 57446s.
93. J. Schiemann and E. Weiss, *J. Organomet. Chem.* 1982, **232**, 229.
94. F. Naumann, D. Rehder and V. Pank, *Inorg. Chim. Acta* 1984, **84**, 117.
95. H. Vahrenkamp, *Chem. Ber.* 1978, **111**, 3472.
96. W. Hieber and R. Kummer, *Z. Naturforsch.* 1965, **20B**, 271.
97. T. Madach and H. Vahrenkamp, *Chem. Ber.* 1981, **114**, 513.
98. I. Mueller and D. Rehder, *J. Organomet. Chem.* 1977, **139**, 293.
99. D. Rehder, *J. Organomet. Chem.* 1972, **37**, 303.
100. J. Schiemann, P. Huebener and E. Weiss, *Angew. Chem.* 1983, **95**, 1021.
101. S. Datta and S. S. Wreford, *Inorg. Chem.* 1977, **16**, 1134.
102. M. S. Wrighton, D. I. Handeli and D. J. Morse, *Inorg. Chem.* 1976, **15**, 434.
103. J. E. Ellis and K. J. Fjare, *J. Organomet. Chem.* 1981, **214**, C33.
104. H. Schmidt and D. Rehder, *Transition Met. Chem.* 1980, **5**, 214.
105. W. R. W. Roose, D. Rehder, H. Lueder and K. H. Theopold, *J. Organomet. Chem.* 1978, **157**, 311.
106. A. Davison and J. E. Ellis, *J. Organomet. Chem.* 1971, **31**, 239.
107. J. E. Ellis and M. C. Palazzotto, *J. Am. Chem. Soc.* 1976, **98**, 8264.
108. R. Talay and D. Rehder, *Chem. Ber.* 1978, **111**, 1978.
109. J. D. Black, M. J. Boylan, P. S. Braterman and A. Fullarton, *J. Chem. Soc., Dalton Trans.* 1980, 1651.
110. H. Baumgarten, H. Johannsen and D. Rehder, *Chem. Ber.* 1979, **112**, 2650.
111. U. Franke and E. Weiss, *J. Organomet. Chem.* 1978, **153**, 39.
112. J. E. Ellis and R. A. Faltynek, *Inorg. Chem.* 1976, **15**, 3168.
113. H. C. Bechthold and D. Rehder, *J. Organomet. Chem.* 1982, **233**, 215.
114. D. Rehder, L. Dahlenburg and I. Mueller, *J. Organomet. Chem.* 1976, **122**, 53.
115. A. Davison and J. E. Ellis, *J. Organomet. Chem.* 1970, **23**, C1.
116. H. C. Bechthold and D. Rehder, *J. Organomet. Chem.* 1979, **172**, 331.
117. G. Muehlbach, B. Rausch and D. Rehder, *J. Organomet. Chem.* 1981, **205**, 343.
118. D. Rehder, *J. Organomet. Chem.* 1977, **137**, C25.
119. T. Kawamura, S. Enoki, S. Hayashida and T. Yonezawa, *Bull. Chem. Soc. Japan* 1982, **55**, 3417.
120. M. Schneider and E. Weiss, *J. Organomet. Chem.* 1976, **114**, C43.
121. J. D. Atwood, T. S. Janik, J. L. Atwood and R. D. Rogers, *Synth. React. Inorg. Met-Org. Chem.* 1980, **10**, 397.
122. Ethyl Corp., *U.S.P.* 1968, 3361 779; *Chem. Abstr.* 1968, **68**, 95983.
123. Ethyl Corp., *U.S.P.* 1964, 3130 214; *Chem. Abstr.* 1964, **61**, 4397.
124. F. Calderazzo, G. Pampaloni and M. Castellani, *Congr. Naz. Chim. Inorg.* 1983, **16**, 11.
125. F. Calderazzo, G. Pampaloni, M. Castellani and P. F. Zanazzi, *J. Chem. Soc., Dalton Trans.* 1985, 1989.
126. F. Calderazzo, *Inorg. Chem.* 1966, **5**, 429.
127. A. Davison and D. L. Reger, *J. Organomet. Chem.* 1970, **23**, 491.
128. J. Müller and W. Goll, *J. Organomet. Chem.* 1974, **71**, 257.
129. G. Allegra and G. Perega, *Ric. Sci. Rend. Sez.* 1961, **1**, 362.
130. D. W. Clark and K. D. Warren, *J. Organomet. Chem.* 1978, **162**, 83.
131. G. M. Whitesides and H. L. Mitchell, *J. Am. Chem. Soc.* 1969, **91**, 2245.
132. H. P. Fritz and C. G. Kreiter, *Chem. Ber.* 1964, **97**, 1398.
133. W. Hieber, E. Winter and E. Schubert, *Chem. Ber.* 1962, **95**, 3070.
134. F. Calderazzo, G. Pampaloni and D. Vitali, *Gazz. Chim. Ital.* 1981, **111**, 455.
135. F. Calderazzo, *Ann. N.Y. Acad. Sci.* 1983, **415**, 37.
136. P. D. Torgashev and Tr. Novocherkassk, *Politekh. Inst.* 1973, **268**, 74.
137. G. F. P. Warnock and J. E. Ellis, *J. Am. Chem. Soc.* 1984, **106**, 5016.
138. J. E. Ellis, R. A. Faltynek and S. G. Hentges, *J. Am. Chem. Soc.* 1977, **99**, 626.
139. U. Puttfarcken and D. Rehder, *J. Organomet. Chem.* 1978, **157**, 321.
140. U. Franke and E. Weiss, *J. Organomet. Chem.* 1978, **152**, C19.
141. U. P. Arcken and D. Rehder, *J. Organomet. Chem.* 1980, **185**, 219.
142. R. R. Schrock, *J. Organomet. Chem.* 1976, **121**, 373.
143. F. N. Tebbe, *J. Am. Chem. Soc.* 1973, **95**, 5823.
144. P. Meakin, L. J. Guggenberger, F. N. Tebbe and J. P. Jesson, *Inorg. Chem.* 1974, **13**, 1025.
145. T. Greiser, U. Puttfarcken and D. Rehder, *Transition Met. Chem.* 1979, **4**, 168.
146. F. Calderazzo, G. Pampaloni and P. F. Zanazzi, *J. Chem. Soc., Chem. Commun.* 1982, 1304.
147. M. F. Leutkens, Jr, D. J. Santure, J. C. Huffman and A. P. Sattebberger, *J. Chem. Soc., Chem. Commun.* 1985, 552.
148. J. Schiemann and E. Weiss, *J. Organomet. Chem.* 1983, **255**, 179.
149. R. J. Burt and G. J. Leigh, *J. Organomet. Chem.* 1978, **148**, C19.

150. R. J. Burt, G. J. Leigh and D. L. Hughes, *J. Chem. Soc., Dalton Trans.* 1981, 792.
151. T. J. McNeese, S. S. Wreford and B. M. Foxman, *J. Chem. Soc., Chem. Commun.* 1978, 500.
152. L. D. Brown, S. Datta, J. K. Kouba, L. K. Smith and S. S. Wreford, *Inorg. Chem.* 1978, **17**, 729.
153. S. C. Tripathi, S. C. Srivastava and R. P. Mani, *J. Organomet. Chem.* 1976, **105**, 239.
154. S. C. Tripathi, S. C. Srivastava and A. K. Shrimal, *Inorg. Chim. Acta* 1976, **18**, 231.
155. S. C. Tripathi, S. C. Srivastava and D. P. Pandey, *Transition Met. Chem.* 1977, **2**, 52.
156. R. Talay and D. Rehder, *J. Organomet. Chem.* 1984, **262**, 25.
157. A. Davison and J. E. Ellis, *J. Organomet. Chem.* 1972, **36**, 113.
158. J. E. Ellis, T. G. Hayes and R. E. Stevens, *J. Organomet. Chem.* 1981, **216**, 191.
159. R. Hackett and A. R. Manning, *J. Chem. Soc., Dalton Trans.* 1975, 1606.
160. M. G. B. Drew, *Acta Cryst.* 1982, **B38**, 254.
161. J. E. Ellis, *J. Am. Chem. Soc.* 1981, **103**, 6106.
162. K. A. Kelbys and M. Dubeck, *Inorg. Chem.* 1964, **3**, 1646; *U.S.P.* 1967, 3 296 288; *Chem. Abstr.* 1967, **66**, 115804v.
163. M. Schneider and E. Weiss, *J. Organomet. Chem.* 1974, **73**, C7.
164. M. Schneider and E. Weiss, *J. Organomet. Chem.* 1976, **121**, 345.
165. U. Franke and E. Weiss, *J. Organomet. Chem.* 1980, **193**, 329.
166. M. Schneider and E. Weiss, *J. Organomet. Chem.* 1976, **121**, 189.
167. U. Franke and E. Weiss, *J. Organomet. Chem.* 1976, **121**, 355.
168. U. Franke and E. Weiss, *J. Organomet. Chem.* 1977, **139**, 305.
169. U. Franke and E. Weiss, *J. Organomet. Chem.* 1979, **168**, 311.
170. U. Franke and E. Weiss, *J. Organomet. Chem.* 1979, **165**, 329.
171. G. Fachinetti, S. D. Nero and C. Floriani, *J. Chem. Soc., Dalton Trans.* 1976, 1046.
172. K. N. Anisimov, N. E. Kolobova and A. A. Pasynskii, *Izv. Akad. Nauk. SSSR, Ser. Khim.* 1969, 2238.
173. R. B. King and F. G. A. Stone, *Inorg. Synth.* 1963, 99.
174. R. P. M. Werner, A. H. Filbery and S. A. Manastyrskyj, *Inorg. Chem.* 1964, **3**, 298.
175. R. P. M. Werner and S. A. Manastyrskyj, *U.S.P.* 1964, 3144 472; *Chem. Abstr.* 1965, **62**, 1688e.
176. R. P. M. Werner and S. A. Manastyrskyj, *Fr.P.* 1963, 1345 821; *Chem. Abstr.* 1964, **60**, 13270f.
177. T. H. Pearson and J. K. Presswood, *U.S.P.* 1962, 3028 404; *Chem. Abstr.* 1962, **57**, 5956g.
178. W. A. Herrmann and W. Kalcher, *Chem. Ber.* 1982, **115**, 3886.
179. K. Hoffmann and W. Weiss, *J. Organomet. Chem.* 1977, **131**, 273.
180. Ethyl Corp., *U.S.P.* 1959, 2916 503; *Chem. Abstr.* 1960, **54**, 5693.
181. J. R. Durig, A. L. Marston, R. B. King and L. W. Houk, *J. Organomet. Chem.* 1969, **16**, 425.
182. E. O. Fischer and K. Plesske, *Chem. Ber.* 1960, **93**, 1006.
183. D. E. Bublitz and K. L. Rinehart, Jr, *Org. React.* 1969, **17**, 75.
184. R. M. Kowaleski, D. O. Kipp, K. J. Stauffer, P. N. Swepston and F. Basolo, *Inorg. Chem.* 1985, **24**, 3750.
185. G. E. Herberich, W. Boreleth, B. Hessner, W. Koch, E. Raabe and D. Schmitz, *J. Organomet. Chem.* 1984, **265**, 225.
186. S. Fredericks and J. L. Thomas, *J. Am. Chem. Soc.* 1978, **100**, 350.
187. W. A. Herrmann and H. Biersack, *Chem. Ber.* 1979, **112**, 3942.
188. W. A. Herrmann and H. Biersack, *J. Organomet. Chem.* 1980, **191**, 397.
189. R. B. King, *Z. Naturforsch.* 1963, **18B**, 157.
190. R. P. M. Werner, *U.S.P.* 1969, 3 474 017; *Chem. Abstr.* 1970, **72**, 43878w.
191. J. E. Ellis, R. A. Faltynek and S. G. Hentges, *J. Organomet. Chem.* 1976, **120**, 389.
192. M. Herberhold, R. Klein and P. D. Smith, *Angew. Chem.* 1979, **91**, 241.
193. K. M. Pfahl and J. E. Ellis, *Organometallics* 1984, **3**, 230.
194. F. Calderazzo, G. Fachinetti and C. Floriani, *J. Am. Chem. Soc.* 1974, **96**, 3695.
195. M. Pasquali, C. Floriani and C. Guastini, *Inorg. Chem.* 1980, **19**, 3847.
196. S. Gambarotta, C. Floriani, A. Chiesi-Villa and C. Gaastini, *Inorg. Chem.* 1984, **23**, 1739.
197. S. Gambarotta and S. S. Strologo, *Congr. Naz. Chim. Inorg.* 1982, **15**, 59.
198. N. E. Murr, C. Molse, M. Riveccie and J. Tiroufiet, *Inorg. Chim. Acta* 1979, **32**, 189.
199. G. Fachinetti, S. Del Nero and C. Floriani, *J. Chem. Soc., Dalton Trans.* 1976, 203.
200. J. L. Robbins, *Energy Res. Abstr.* 1981, **6**, 20854; *Chem. Abstr.* 1982, **96**, 6846j.
201. Ref. 196, cited in ref. 6(a) of this article, E. Priebe, Thesis, Tech. Hochschule München (1963).
202. R. J. Kinney, W. D. Jones and R. G. Bergaman, *J. Am. Chem. Soc.* 1978, **100**, 635.
203. E. O. Fischer and R. J. Schneider, *Chem. Ber.* 1977, **103**, 3684.
204. W. A. Herrmann and J. Plank, *Chem. Ber.* 1979, **112**, 392.
205. L. N. Lewis and K. G. Caulton, *Inorg. Chem.* 1980, **19**, 1840.
206. J. C. Smart and B. L. Pinsky, *J. Am. Chem. Soc.* 1980, **102**, 1009.

207. J. H. Osborne, A. L. Rheingold and W. C. Trogler, *J. Am. Chem. Soc.* 1985, **107**, 6292.
208. W. A. Herrmann, J. Plank and B. Reiter, *J. Organomet. Chem.* 1978, **164**, C25.
209. W. A. Herrmann, M. L. Ziegler, K. Weidenhanmer and H. Biersack, *Angew. Chem.* 1979, **91**, 1026.
210. D. J. Parker, *J. Chem. Soc. A* 1970, 1382.
211. M. R. Blake, J. L. Garnett, I. K. Gregor and S. B. Wild, *Org. Mass Spect.* 1978, **13**, 20.
212. J. Mueller and K. Fenderl, *Chem. Ber.* 1970, **103**, 3141.
213. R. B. King, *J. Am. Chem. Soc.* 1968, **90**, 1417.
214. R. E. Winters and R. W. Kiser, *J. Organomet. Chem.* 1965, **4**, 190.
215. J. B. Wilford, A. Whitla and H. M. Powell, *J. Organomet. Chem.* 1967, **8**, 495.
216. W. A. Herrmann, W. Kalcher, H. Biersack, I. Bernal and M. Gresswick, *Chem. Ber.* 1981, **114**, 3558.
217. G. Fachinetti and C. Floriani, *J. Chem. Soc., Chem. Commun.* 1974, 516.
218. J. E. Ellis, *J. Organomet. Chem.* 1975, **86**, 1.
219. E. E. H. Otto and H. H. Brintzinger, *J. Organomet. Chem.* 1978, **148**, 29.
220. D. Rehder, *Z. Naturforsch* 1976, **31B**, 273.
221. E. O. Fischer and R. J. J. Schneider, *Angew. Chem. Int. Ed. Engl.* 1967, **6**, 569.
222. F. A. Cotton, L. Kruczynskii and B. A. Frenz, *J. Organomet. Chem.* 1978, **160**, 93.
223. J. C. Huffmann, L. N. Lewis and K. G. Caulton, *Inorg. Chem.* 1980, **19**, 2755.
224. L. N. Lewis and K. G. Caulton, *Inorg. Chem.* 1980, **19**, 3201.
225. S. Rajan, *Indian J. Chem.* 1977, **15A**, 920.
226. R. J. Kinney, W. D. Jones and R. G. Bergman, *J. Am. Chem. Soc.* 1978, **100**, 7902.
227. E. O. Fischer, E. Louis, W. Bathelt and J. Mueller, *Chem. Ber.* 1969, **102**, 2547.
228. E. O. Fischer, E. Louis and R. J. J. Schneider, *Angew. Chem. Int. Ed. Engl.* 1968, 7, 136.
229. N. G. Connelly and M. D. Kitchen, *J. Chem. Soc., Dalton Trans.* 1976, 2165.
230. W. Strohmeier and H. Blumenthal, *Z. Naturforsch.* 1967, **22B**, 1351.
231. R. Tsumura and N. Hagihara, *Bull. Chem. Soc. Japan* 1965, **38**, 1901.
232. D. G. Alway and K. W. Bernett, *Inorg. Chem.* 1980, **19**, 779.
233. D. F. Foust and M. D. Rausch, *J. Organomet. Chem.* 1982, **238**, 321.
234. J. Nieman, J. H. Teuben, J. C. Huffman and K. G. Caulton, *J. Organomet. Chem.* 1983, **255**, 193.
235. E. Schaedel and H. Vahrenkamp, *Chem. Ber.* 1974, **107**, 3850.
236. R. Borowski, D. Rehder and K. V. Deuten, *J. Organomet. Chem.* 1981, **220**, 45.
237. D. Rehder, *J. Mag. Res.* 1977, **25**, 177.
238. H. Brunner and W. A. Herrmann, *Z. Naturforsch.* 1973, **28B**, 606.
239. H. Behrens and H. Brandl, *Z. Naturforsch.* 1967, **22B**, 1353.
240. R. B. King, P. N. Kapoor and R. N. Kapoor, *Inorg. Chem.* 1971, **10**, 1841.
241. G. C. Faber and R. J. Angelici, *Inorg. Chem.* 1970, **9**, 1586.
242. A. N. Nesmeyanov, K. N. Anisimov, N. K. Kolobova and A. A. Pasynskii, *Dokl. Akad. Nauk. SSSR* 1968, **182**, 112.
243. A. N. Nesmeyanov, K. N. Anisimov, N. E. Kolobova and A. A. Pasynskii, *Izv. Akad. Nauk. SSSR, Ser. Khim.* 1966, 2231.
244. B. V. Lokshin, A. A. Pasynskii, N. E. Kolobova and K. N. Anisimov, *J. Organomet. Chem.* 1977, **55**, 315.
245. A. A. Pasynskii, K. N. Anisimov, N. E. Kolobova and A. N. Nesmeyanov, *Izv. Akad. Nauk. SSSR, Ser. Khim.* 1969, 183.
246. A. N. Nesmeyanov, K. N. Anisimov, N. E. Kolobova and A. A. Pasynskii, *Izv. Akad. Nauk. SSSR, Ser. Khim.* 1968, 2814.
247. H. C. Bechthold and D. Rehder, *J. Organomet. Chem.* 1981, **206**, 305.
248. M. J. Bunker, M. L. H. Green, C. Couldwell and K. Prout, *J. Organomet. Chem.* 1980, **192**, C6.
249. M. J. Bunker and M. L. H. Green, *J. Chem. Soc., Dalton Trans.* 1981, 85.
250. J. M. Mayer and J. E. Bercaw, *J. Am. Chem. Soc.* 1982, **104**, 2157.
251. E. O. Fischer, R. J. Schneider and J. Mueller, *J. Organomet. Chem.* 1968, **14**, P4.
252. F. Naumann and D. Rehder, *J. Organomet. Chem.* 1981, **204**, 411.
253. K. V. Deuten, D. Rehder and W. Roose, *J. Organomet. Chem.* 1981, **214**, 71.
254. R. B. King and K. N. Chen, *Inorg. Chim. Acta* 1977, **23**, L19.
255. A. A. Pasynskii, I. L. Eremenko, V. M. Novotortsev, Yu. V. Rakitin, O. G. Ellert and V. T. Kalinnikov, *Izv. Akad. Nauk, SSSR, Ser. Khim.* 1976, 1900.
256. A. A. Pasynskii, I. L. Eremenko, B. Orazsaknatov, V. M. Navotorotsev and O. G. Ellert, *Inorg. Chim. Acta* 1980, **39**, 91.
257. A. A. Pasynskii, I. L. Eremenko, B. Orazsakhatov, V. T. Kalinnikov and G. G. Aleksandrov, *J. Organomet. Chem.* 1981, **216**, 211.
258. W. A. Herrmann, H. Biersack, M. L. Ziegler and B. Balbach, *J. Organomet. Chem.* 1982, **206**, C33.
259. F. Y. Petillon, J. L. LeQuere and J. E. Guerchais, *Inorg. Chim. Acta* 1979, **37**, L453.

260. D. Rehder, W. L. Dorn and J. Schmidt, *Transition Met. Chem.* 1976, **1**, 233.
261. D. Rehder, *J. Mag. Res.* 1980, **38**, 419.
262. D. Rehder, W. L. Dorn and J. Schmidt, *Transition Met. Chem.* 1976, **1**, 74.
263. D. Rehder, I. Mueller and J. Kopf, *J. Inorg. Nucl. Chem.* 1978, **40**, 1013.
264. D. Rehder, *Z. Naturforsch.* 1976, **31B**, 273.
265. N. I. Kirillova, A. I. Gusev, A. A. Pasynskii and Yu. T. Struchkov, *Zh. Strukt. Khim.* 1973, **14**, 868.
266. L. N. Lewis and K. G. Caulton, *J. Organomet. Chem.* 1983, **252**, 57.
267. A. A. Pasynskii, K. N. Anisimov, N. E. Kolobova and A. N. Nesmeyanov, *Dokl. Akad. Nauk. SSSR*, 1969, **185**, 610.
268. M. D. Rausch and A. V. Grossi, *J. Chem. Soc., Chem. Commun.* 1978, 401.
269. Ethyl Corp., *U.S.P.* 1962, 3 064 023; *Chem. Abstr.* 1963, **58**, 9135.
270. R. B. King, *Organometallic Syntheses*, Vol. 1, p. 140. Academic Press, New York (1965).
271. J. Müller and B. Mertschenk, *J. Organomet. Chem.* 1972, **34**, 165.
272. E. O. Fischer, H. P. Kögler and P. Kuzel, *Chem. Ber.* 1960, **93**, 3006.
273. A. N. Nesmeyanov, K. N. Anisimov, N. E. Kolobova and A. A. Pasynskii, *Izv. Akad. Nauk. SSSR, Ser. Khim.* 1966, 774.
274. A. N. Nesmeyanov, K. N. Anisimov, N. E. Kolobova and A. A. Pasynskii, *Izv. Akad. Nauk. SSSR, Ser. Khim.* 1969, 100.
275. A. N. Nesmeyanov, K. N. Anisimov, N. E. Kolobova and A. A. Pasynskii, *Dokl. Akad. Nauk. SSSR* 1968, **181**, 1142.
276. A. N. Nesmeyanov, K. N. Anisimov, N. E. Kolobova and A. A. Pasynskii, *Izv. Akad. Nauk. SSSR, Ser. Khim.* 1970, 727.
277. R. B. King and C. D. Hoff, *J. Organomet. Chem.* 1982, **225**, 245.
278. A. N. Nesmeyanov, A. I. Gusev, A. A. Pasynskii, K. N. Anisimov, N. E. Kolobova and Yu. T. Struchkov, *J. Chem. Soc., Chem. Commun.* 1969, 739.
279. A. N. Nesmeyanov, N. E. Kolobova, A. B. Antonova, K. N. Anisimov and O. M. Khitrova, *Izv. Akad. Nauk. SSSR, Ser. Khim.* 1974, 859.
280. A. I. Gusev and Yu. T. Struchkov, *Zh. Strukt. Khim.* 1969, **10**, 515.
281. A. I. Gusev, G. G. Aleksandrov and Yu. T. Struchkov, *Zh. Strukt. Khim.* 1969, **10**, 655.
282. A. N. Nesmeyanov, A. I. Gusev, A. A. Pasynskii, K. N. Anisimov, N. E. Kolobova and Yu. T. Struchkov, *J. Chem. Soc., Chem. Commun.* 1969, 277.
283. A. I. Gusev and Yu. T. Struchkov, *Zh. Strukt. Khim.* 1969, **10**, 294.
284. G. G. Aleksandrov, A. I. Gusev and Yu. T. Struchkov, *Zh. Strukt. Khim.* 1968, **9**, 333.
285. N. I. Kirillova, N. E. Kolobova, A. I. Gusev, A. B. Antonova, Yu. T. Anisimov and O. M. Khitrova, *Zh. Strukt. Khim.* 1974, **15**, 651.
286. A. I. Gusev and Yu. T. Struchkov, *Zh. Strukt. Khim.* 1969, **10**, 107.
287. A. N. Nesmeyanov, A. I. Gusev, A. A. Pasynskii, K. N. Anisimov, N. E. Kolobova and Yu. T. Struchkov, *J. Chem. Soc., Chem. Commun.* 1968, 1365.
288. A. I. Gusev, N. I. Kirillova and Yu. T. Struchkov, *Zh. Strukt. Khim.* 1970, **11**, 62.
289. U. Puttfarcken and D. Rehder, *J. Organomet. Chem.* 1980, **185**, 219.
290. M. J. Bunker, A. de Cian, M. L. H. Green, J. J. E. Moreau and N. Siganporia, *J. Chem. Soc., Dalton Trans.* 1980, 2155.
291. N. I. Kirillova, A. I. Gusev, A. A. Pasynskii and Yu. T. Struchkov, *Zh. Strukt. Khim.* 1974, **15**, 288.
292. J. A. Labinger, K. S. Wong and W. R. Scheidt, *J. Am. Chem. Soc.* 1978, **100**, 3254.
293. G. W. Parshall and F. N. Tebbe, *J. Am. Chem. Soc.* 1971, **93**, 3793.
294. M. E. Eichner, H. G. Alt and M. D. Rausch, *J. Organomet. Chem.* 1984, **264**, 309.
295. F. N. Tebbe, *J. Am. Chem. Soc.* 1973, **95**, 5412.
296. Yu. V. Skripkin, O. G. Volkov, A. A. Pasynskii, A. S. Antsyshkina, S. L. Davydova and S. G. Sakharov, *J. Organomet. Chem.* 1984, **263**, 345.
297. M. L. H. Green and B. Jousseaume, *J. Organomet. Chem.* 1980, **193**, 339.
298. W. A. Herrmann, H. Biersack, B. Balbach and M. Ziegler, *Chem. Ber.* 1984, **117**, 79.
299. K. S. Wong and J. A. Labinger, *J. Am. Chem. Soc.* 1980, **102**, 3652.
300. Yu. V. Skripkin, A. A. Pasynskii, V. T. Kelinnikov, A. S. Anthsyshkina and V. N. Ostrikova, *J. Organomet. Chem.* 1982, **231**, 205.
301. W. A. Herrmann, H. Biersack, B. Balbach and M. Ziegler, *Chem. Ber.* 1984, **117**, 95.
302. S. Baral, J. A. Labinger, W. R. Scheidt and F. J. Timmers, *J. Organomet. Chem.* 1981, **215**, C53.
303. F. J. Timmers, W. R. Scheidt, J. A. Labinger and S. Baral, *J. Organomet. Chem.* 1982, **240**, 153.
304. M. A. Porai-Koshits, A. S. Antsyshkina, A. A. Pasynskii, G. G. Sadikov, Yu. V. Skripkin and V. N. Ostrikova, *Inorg. Chim. Acta* 1979, **34**, L285; *Koord. Khim.* 1979, **5**, 1103.
305. A. A. Pasynskii, A. S. Antsyshkina, Yu. V. Skripkin, V. T. Kalinnikov, V. N. Ostrikova and G. G. Sadikov, *Zh. Neorg. Khim.* 1981, **26**, 2435.

306. A. Miyake, H. Kondo and M. Aoyama, *Angew. Chem. Int. Ed. Engl.* 1969, **8**, 520.
307. A. A. Pasynskii, Yu. V. Skripkin, K. M. Suvorova, O. N. Kuz'micheva and V. T. Kalinnikov, *Izv. Akad. Nauk. SSSR, Ser. Khim.* 1978, 1226.
308. A. A. Pasynskii, Yu. V. Skripkin, I. L. Eremenko, V. T. Kalinnikov, G. G. Aleksandrov, V. G. Andrinov and Yu. T. Struckhov, *J. Organomet. Chem.* 1979, **165**, 49.
309. K. S. Wong, W. R. Scheidt and J. A. Labinger, *Inorg. Chem.* 1979, **18**, 1709.
310. S. Kennedy, J. J. Alexander and S. G. Shore, *J. Organomet. Chem.* 1981, **219**, 385.
311. H. Behrens and F. G. A. Stone, *J. Chem. Soc., Dalton Trans.* 1984, 1605.
312. C. Moise, J. F. Reynoud, J. C. Leblanc and R. Broussier, *J. Organomet. Chem.* 1982, **240**, C15.
313. R. Taley and D. Rehder, *Inorg. Chim. Acta* 1983, **77**, L175.
314. A. M. Cardoso, R. J. H. Clark and S. Moorhouse, *J. Organomet. Chem.* 1980, **186**, 237.
315. D. A. Lemenovskii, T. V. Baukova and V. P. Fedin, *J. Organomet. Chem.* 1977, **132**, C14.
316. L. Acedo, A. Otero and P. Royo, *J. Organomet. Chem.* 1983, **258**, 181.
317. A. H. Klazinga and J. H. Teuben, *J. Organomet. Chem.* 1979, **165**, 31.
318. A. Fakhr, Y. Mugnier, R. Broussier and E. Laviron, *J. Organomet. Chem.* 1983, **255**, C8.
319. J. Arnold and T. Don Tilley, *J. Am. Chem. Soc.* 1985, **107**, 6409.
320. R. D. Gorsich, *U.S.P.* 1969, 3 069 445; *Chem. Abstr.* 1963, **58**, 10237.
321. T. Kruck and W. Molls, *Z. Anorg. Allg. Chem.* 1976, **420**, 159.
322. J. Pforr, F. Naeumann and D. Rehder, *J. Organomet. Chem.* 1983, **258**, 189.
323. T. Kruck and H. Breuer, *Chem. Ber.* 1974, **107**, 263.
324. F. Naeumann, J. Kopf and D. Rehder, *J. Organomet. Chem.* 1984, **267**, 249.
325. E. E. H. Otto and H. H. Brintzinger, *J. Organomet. Chem.* 1979, **170**, 209.
326. R. S. Threlkel and J. E. Bercaw, *J. Am. Chem. Soc.* 1981, **103**, 2650.
327. D. F. Foust and M. D. Rausch, *J. Organomet. Chem.* 1982, **226**, 47.
328. J. A. Labinger and J. Schwartz, *J. Am. Chem. Soc.* 1975, **97**, 1596.

Polyhedron Vol. 7, No. 18, pp. 1667–1672, 1988
Printed in Great Britain

0277–5387/88 $3.00+.00
© 1988 Pergamon Press plc

THE CRYSTAL STRUCTURE OF $[(n\text{-}C_4H_9)_4N]_2Re_2I_8$: THREE-FOLD DISORDER OF THE EFFECTIVELY CUBIC ANION

F. ALBERT COTTON,* LEE M. DANIELS and K. VIDYASAGAR

Department of Chemistry and Laboratory for Molecular Structure and Bonding, Texas A&M University, College Station, TX 77843, U.S.A.

(*Received* 26 *January* 1988; *accepted* 18 *March* 1988)

Abstract—The title compound was prepared by the method of Preetz and Rudzik and its structure determined by single-crystal X-ray diffractometry. It crystallizes in the rhombohedral system, space group $R\bar{3}$ with the following (hexagonal) unit cell dimensions: $a = 12.185(2)$, $c = 30.195(3)$ Å, $V = 3882(2)$ Å^3, $Z = 3$. The set of iodine atoms defines an essentially perfect cube that resides on a crystallographic $\bar{3}$ position. Within this essentially cubic rhombohedron the two Re atoms are disordered over six positions that define an essentially octahedral trigonal antiprism. Pairs of opposite vertices of this octahedron correspond to Re_2^{5+} units which have an internuclear distance of 2.245(3) Å. The Re—I distances are 2.700(3), 2.711(3) and 2.715(2) Å to the six equivalent I atoms and 2.647(3) Å to the other pair. The Re—Re—I angles all lie in the range 104.8(1)–105.9(1)°. The relationship of this structure to those of other octahalo dimetal compounds is discussed.

The $Re_2Cl_8^{2-}$ ion may be regarded historically[1] as the point of departure for the entire field of chemistry involving multiple bonds between metal atoms.[2] More specifically this species (along with the $Mo_2Cl_8^{4-}$ ion) has served as a paradigm for quadruple bonds, and has, therefore, been extensively studied both experimentally and theoretically. It is the most complex inorganic species ever subjected to high-precision *ab initio* molecular orbital calculations.[3,4]

A number of structural studies of compounds containing the $Re_2Cl_8^{2-}$ ion have been reported as well as two concerned with the $Re_2Br_8^{2-}$ ion,[2] but structural work on other $Re_2X_8^{2-}$ species with X = F, I and NCS^- (all have been well known for a long time) has been lacking until recently. Two compounds containing the $Re_2(NCS)_8^{2-}$ ion were structurally characterized in 1987[5] and we now report the structure of a $Re_2I_8^{2-}$ compound. The $Re_2F_8^{2-}$ ion,[6] however, still has not been defined structurally; we are attempting to obtain suitable crystals. The structure of the $Re_2I_8^{2-}$ ion has unique features that justify the separate report and discussion that we present here.

*Author to whom correspondence should be addressed.

EXPERIMENTAL

Preparation

Two methods of preparation have been reported.[7,8] We followed that of Preetz and Rudzik[8] and obtained suitable crystals straightforwardly.

X-ray crystallography

Geometric and intensity data for $[(n\text{-}Bu)_4N]_2Re_2I_8$ were taken with an Enraf–Nonius CAD-4 automated diffractometer using procedures described previously.[9] Pertinent crystallographic data and unit cell parameters are given in Table 1. The crystal was indexed on 25 intense reflections in the range $18.0 < 2\theta < 35.4°$ and the crystal system was found to be trigonal. The Laue symmetry and lattice dimensions were verified by axial photography. Least-squares analysis was used to refine the unit cell dimensions and the orientation matrix.

The intensity data gathered by the ω–2θ technique were reduced by routine procedures. Calculations were carried out using a Micro-Vax II (Micro VMS V4.5) with programs SHELX-76, SHELXS-86 and the commercial package SDP/V, V3.0. Absorption corrections were applied, based

Table 1. Crystal data for $[(n\text{-}C_4H_9)_4N]_2Re_2I_8$

Formula	$Re_2I_8N_2C_{32}H_{72}$
Formula weight	1872.58
Space group	$R\bar{3}$
Syst absences	$-h+k+l=3n$
a (Å)	12.185(2)
b (Å)	12.185(2)
c (Å)	30.195(3)
α (deg)	90
β (deg)	90
γ (deg)	120
V (Å^3)	3882(2)
Z	3
d_{calc} (g cm^{-3})	2.402
Crystal size, mm	0.2 × 0.2 × 0.3
μ(Mo-K$_\alpha$) (cm^{-1})	94.818
Data collection instrument	Enraf–Nonius CAD4
Radiation monochromated in incident beam [λ(Å)]	Mo-K_α, 0.71073
Orientation reflections: number, range (2θ) (deg)	25, $18.00 < 2\theta < 35.40$
Temperature (°C)	20 ± 1
Scan method	ω–2θ
Data collection range, 2θ (deg)	$4 < 2\theta < 50$
No. unique data, total with $F_o^2 > 3\sigma(F_o^2)$	1307, 872
No. parameters refined	56
Transmission factors, %: maximum, minimum	99.99, 56.42
R^a	0.064
$R_w{}^b$	0.069
Quality-of-fit indicator^c	2.331
Largest shift/esd, final cycle	0.24
Largest peak (e Å)	1.788

$^a R = \Sigma\|F_o|-|F_c\|/\Sigma|F_o|$.
$^b R_w = [\Sigma w(|F_o|-|F_c|)^2/\Sigma w|F_o|^2]^{1/2}$; $w = 1/\{\sigma^2(|F_o|)+0.001(|F_o|^2)\}$.
^{c} Quality-of-fit $= [\Sigma w(|F_o|-|F_c|)^2/(N_{observances}-N_{parameters})]^{1/2}$.

on azimuthal scans of several reflections with the diffractometer angle χ near 90°.[10] After equivalent data had been merged, there remained 872 data with $F_o^2 > 3\sigma(F_o^2)$ that were used in the development and refinement of the structure.

The rhenium and iodine atoms were located via Patterson maps. The rhenium atoms were found to reside on 18 general positions that describe octahedra centred at $\bar{3}$ positions (0 0 1/2). The distance along an edge of the octahedron was ~ 1.58 Å, while the distance between opposite vertices was 2.24 Å. These dimensions and the limitation of three molecules per unit cell require each vertex of the octahedron to be occupied by only 1/3 Re. The two crystallographically unique iodine atoms, one on a general six-fold position and the other on the three-fold axis, account for eight iodine atoms of each $[(n\text{-}Bu)_4N]_2Re_2I_8$ formula unit. The subsequent development of the structure was done by an alternating sequence of least-square refinements and difference Fourier maps.

While the atoms of the $Re_2I_8^{2-}$ moiety refined quite steadily, *n*-Bu groups, particularly the disordered one lying along the three-fold axis, gave serious difficulties. Therefore, the atoms of the *n*-Bu groups were refined isotropically and restraints on their interatomic distances were added in least-square refinements. In the final cycle, 56 parameters were refined giving a data : parameter ratio of 15.6, and residuals of $R = 0.064$ and $R_w = 0.069$. In the final difference Fourier map, there were five peaks above 1 e/Å^3. Four of them were ghosts of carbon

Table 2. Positional parameters and their estimated standard deviations for $[(n\text{-}C_4H_9)_4N]_2Re_2I_8$

Atom	x	y	z	B(Å^2)
Re[a]	0.0783(2)	0.0082(2)	0.52182(6)	5.39(7)
I(1)	0.2315(1)	0.2609(1)	0.53466(4)	8.18(6)
I(2)	0.000	0.000	0.60415(8)	9.09(7)
N	0.333	0.667	0.4388(7)	6.3(6)
C(1)	0.390(1)	0.590(1)	0.4246(9)	25(2)[b]
C(2)	0.290(2)	0.468(2)	0.403(1)	22(2)[b]
C(3)	0.343(4)	0.379(2)	0.3957(9)	17(1)[b]
C(4)	0.354(5)	0.361(4)	0.346(1)	23(2)[b]
C(5)	0.333	0.667	0.4879(7)	19(2)[b]
C(6)[c]	0.40(1)	0.8042(8)	0.5044(8)	22(5)[b]
C(7)[c]	0.38(1)	0.803(2)	0.5549(8)	28(7)[b]
C(8)	0.333	0.667	0.5713(9)	33(5)[b]

[a] Site modelled as 1/3 Re.

[b] Atoms refined isotropically. Anisotropically refined atoms are given in the form of the equivalent isotropic displacement parameter defined as:

$$(4/3)[a^2\beta_{11}+b^2\beta_{22}+c^2\beta_{33}+ab(\cos\gamma)\beta_{12}+ac(\cos\beta)\beta_{13}+bc(\cos\alpha)\beta_{23}].$$

[c] Site modelled as 1/3C.

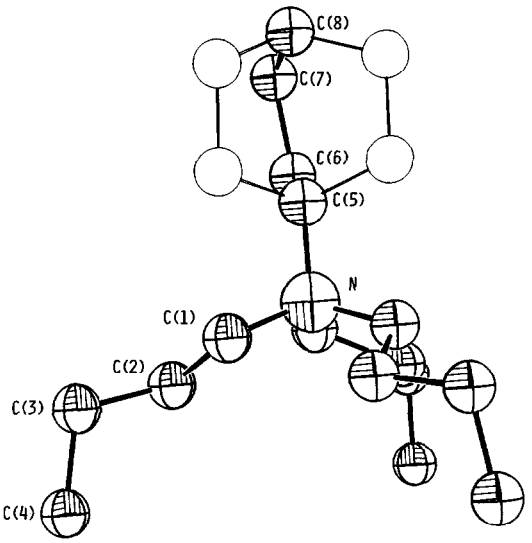

Fig. 1. An ORTEP drawing of the $(n\text{-}Bu)_4N^+$ ion. The carbon atoms have been arbitrarily reduced. Disordered positions of C(6) and C(7) are represented by circles. Unlabelled atoms can be derived from those given. The bond N—C(5) is a crystallographic three-fold axis.

atoms and the fifth one was a ghost of the rhenium atom. Positional parameters are presented in Table 2 and selected bond distances and angles are presented in Table 3.*

RESULTS

The packing in the crystal is rather loose. If the mean atomic volume for the atoms in the $Re_2I_8^{2-}$ ion is taken to be in the range of 20–25 Å^3, then the $(n\text{-}Bu)_4N^+$ ions have at their disposal a mean atomic volume of 30–32 Å^3. Packing forces are, therefore, rather weak and this has two main consequences: (1) the $Re_2I_8^{2-}$ ions are free to adopt an essentially perfect cubic shape that allows systematic disordering of the Re_2 unit within, and (2) the atoms of the $(n\text{-}Bu)_4N^+$ ions have a lot of positional and motional freedom, and are thus difficult to define and refine with precision.

Let us dispose of this latter problem first. Figure 1 shows the model of the $(n\text{-}Bu)_4N^+$ ion that was refined. As shown in Table 2, the N atom refined very cleanly with a realistic thermal parameter, but all of the carbon atoms have large thermal parameters, 17–33 Å^2. Although the 12 carbon atoms, C(1)—C(4) and their symmetry-related sister atoms are ordered, they have much motional freedom (Table 2). The atoms C(5) and C(8) are (or at least could be) on single, well-defined positions, but in fact they too have large thermal parameters. Atoms C(6) and C(7) are very disordered and the three-fold disorder shown in Fig. 1 does not fully describe them. Evidently, the centroid of the $(n\text{-}Bu)_4N^+$ ion, that is, the N atom, is precisely located, but all of the carbon atoms execute large excursions consistent with keeping the N atom fixed.

We turn now to the $Re_2I_8^{2-}$ ion, which is depicted in Fig. 2. The most important dimensions are given in Table 3. Figure 2 is drawn to show all three orientations of the Re_2 unit, but one is emphasized so as to make clear that physically, at any one site at any one time, there is only one well-defined $Re_2I_8^{2-}$ ion, having idealized D_{4h} symmetry. The crystallographic symmetry is $\bar{3}$ and the axis passes through I(2) and I(2)′. The set of eight iodine atoms is thus required to have rhomboidal ($\bar{3}$) symmetry. In fact, it comes so close to having the exact dimensions of a cube that the deviations are negligible from a chemical point of view. The six I(2)—I(1) type distances are 3.674(2) Å and the six I(1)—I(1)′ distances are 3.671(2) Å; these do not differ even in a statistical sense. The three crystallographically distinct types of near-orthogonal I—I—I angles are 89.34(4), 90.62(6) and 90.71(4)°. While there are

* Complete tables of bond distances and angles, anisotropic thermal parameters, structure factors and unit cell packing diagrams are available as supplementary material.

Table 3. Selected bond distances (Å) and angles (deg) for $[(n\text{-}C_4H_9)_4N]_2Re_2I_8$

Distances

Atom 1	Atom 2	Distance	Atom 1	Atom 2	Distance	Atom 1	Atom 2	Distance
Re	Re′	2.245(3)	Re	I(1)′	2.711(3)	Re	I(2)	2.647(3)
Re	I(1)	2.715(2)	Re	I(1)″	2.700(3)			

Angles

Atom 1	Atom 2	Atom 3	Angle	Atom 1	Atom 2	Atom 3	Angle	Atom 1	Atom 2	Atom 3	Angle
Re′	Re	I(1)	104.8(1)	I(1)	Re	I(1)′	85.15(7)	I(1)′	Re	I(2)	149.1(1)
Re′	Re	I(1)′	105.07(9)	I(1)	Re	I(1)″	149.4(1)	I(1)″	Re	I(2)	86.80(6)
Re′	Re	I(1)″	105.70(9)	I(1)	Re	I(2)	86.49(6)				
Re′	Re	I(2)	105.9(1)	I(1)′	Re	I(1)″	85.44(9)				

Numbers in parentheses are estimated standard deviations in the least significant digits.

statistically significant differences here, the variations are, nonetheless, miniscule and physically unimportant.

Because $\bar{3}$ symmetry imposes only a subset of the O_h symmetry elements, the exact alignment of the essentially octahedral set of 1/3 Re units with the essentially cubic set of iodine atoms need not be as regular as that of a true octahedron inscribed within a true cube, and it is not. Again, however, the discrepancies from the highest idealized symmetry are very small. The Re—I distances are of four crystallographically distinct kinds: three of these are effectively equal at the 3σ level, averaging 2.709(5) Å, but the fourth, 2.647(3) Å, is slightly, 0.062(6) Å, different. The Re—Re—I angles lie within the very narrow range of 104.8–105.9°. The Re—Re distance is 2.245(3) Å, which is very similar to those in other Re_2^{6+} compounds.[2]

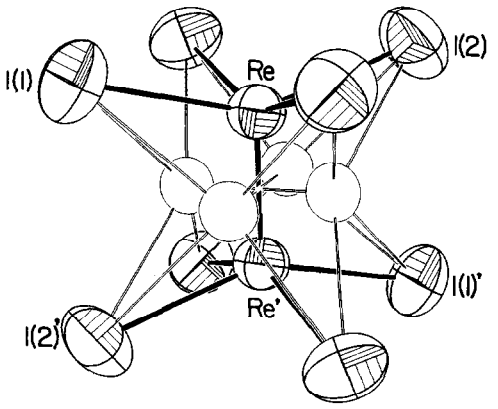

Fig. 2. An ORTEP drawing of the $Re_2I_8^{2-}$ ion. Re represents the rhenium positions with site occupancy of 1/3. Only two of the six fractionally occupied Re positions are represented as ellipsoids, for clarity. The common midpoint of three Re—Re lines is a crystallographic $\bar{3}$ centre. Unlabelled atoms can be derived from those given.

DISCUSSION

Comparison with other iodo species

There are few previously established structures of compounds containing iodine atoms bonded to an Re_2^{6+} unit. One is $Re_2I_4(O_2CC_6H_5)_2$,[11] in which the Re—I bonds are shorter, by about 0.1 Å, than in the $Re_2I_8^{2-}$ ion. There are several possible reasons for this and we have no basis for preferring or dismissing any. Obviously, greater crowding in the $Re_2I_8^{2-}$ could play a role, but so also could the fact that the four iodine atoms may be able to bond more strongly to the $Re_2(O_2CPh)_2^{4+}$ unit than can eight of them to the Re_2^{6+} unit, for electrostatic reasons. Finally, the Re—Re—I angles are very different in the two cases and the hybridization at the Re atoms in the $Re_2I_4(O_2CC_6H_5)_2$ molecule may be better suited for bonding to the iodine atoms.

Another entity which resembles the $Re_2I_8^{2-}$ ion more closely, is found in the molecule $Re_4I_8(CO)_6$.[12] This consists of a central Re_2I_8 unit which is internally rotated by *ca* 40° away from an eclipsed conformation, thereby creating triangular sets of I atoms. Two pyramidal $Re(CO)_3$ groups are attached to two of these I_3 triangles so as to create quasi-octahedral, *fac*-$ReI_3(CO)_3$ units. The Re—Re distance here is 2.279(1) Å, which is 0.034(3) Å longer than that in the $Re_2I_8^{2-}$ ion. It has been proposed[12] that the $Re_4I_8(CO)_6$ molecule may be regarded as consisting of $Re_2I_8^{2-}$ and two $Re(CO)_3^+$

units bound together and that the length of the Re—Re bond is greater than that in more typical $Re_2X_8^{2-}$ species because of the large internal torsion angle. The Re—I distances span a considerable range (those shared with the $Re(CO)_3$ units being *ca* 2.81 Å and the other, 2.64 Å) within which are the ones we have found.

Comparison with other crystal structures

It has been noted and discussed before[2a,13] that the $Re_2X_8^{2-}$ species with X = Cl and Br, as well as their molybdenum counterparts, $Mo_2X_8^{4-}$, have nearly cubic shapes (deviations being *ca* 2%) and that this sets up the possibility of disordered packing in which more than one orientation of the M—M bond may occur. In practically all eclipsed $M_2X_8^{n-}$ (X = Cl, Br) compounds whose structures have been previously reported,[2] some degree of disorder of this type has been found. This has taken the form of a second orientation at *ca* 5 to 40% of the $M_2X_8^{n-}$ sites in the crystal. In all these cases, the environment about the $M_2X_8^{n-}$ ion has been such as to render the three orientations quite distinct in terms of the contacts made by the three pairs of opposite faces of the quasi-cube, with one of them being particularly unfavorable for the MCl_4 faces because of the propinquity of the accompanying cations. Thus, only two orientations occur, and in unequal numbers.

The compound $[(n\text{-}Bu_4)N]_2[Re_2I_8]$ is the first $M_2X_8^{n-}$ compound to have a three-fold disorder, with each orientation equally represented. This occurs in a structure that makes all three orientations crystallographically equivalent. Why does this happen for $[(n\text{-}Bu)_4]_2[Re_2I_8]$ but not for $[(n\text{-}Bu)_4N]_2[Re_2Cl_8]$ or $[(n\text{-}Bu)_4N]_2[Re_2Br_8]$? The latter have monoclinic structures in which there are only two orientations, 74 and 26% occupied for the chloride and 61 and 39% for the bromide. We believe that the large size of the $Re_2I_8^{2-}$ ion sufficiently diminishes the electrostatic forces in the crystal that a much looser packing results. This in turn allows a packing arrangement in which the anion has the freedom to adopt all three orientations. We have already commented on the loose packing in the iodo compound, whereby the volume per formula unit (1294 Å^3) is 11% greater than that (1171 Å^3) in the chloro compound. In the chloro compound the smaller volume available to the cations leads to very precise positioning of all the carbon atoms; it was noted in the original report[13] of the $[(n\text{-}Bu)_4N]_2[Re_2Cl_8]$ structure that it "constitutes one of the rare examples of a well-ordered $[(n\text{-}Bu)_4N]$ structure".

Dimensions of $[Re_2X_8]^{2-}$ *ions*

In Table 4 are listed the important dimensions of the three $Re_2X_8^{2-}$ ions with halogens, now structurally characterized as their Bu_4N^+ salts. The Re—Re distance changes very little, although it is slightly larger in the iodide than in the other two. However, it is not as long in $Re_2I_8^{2-}$ as had been forecast[8,14] (2.27 Å) on the basis of the low $\delta \rightarrow \delta^*$ transition energy. While this prediction seemed a reasonable one at the time, more recent work[15] has shown that in $Mo_2X_4(PMe_3)_4$ compounds $\delta \rightarrow \delta^*$ transition energies are lowered as the halogen changes from Cl to Br to I, without any significant change in the Mo—Mo distance. The rationale of the previous prediction (a simple inverse relation-

Table 4. Comparison of the dimensions of $Re_2X_8^{2-}$ ions with X = Cl, Br and I

	Cl[a]	Br[b]	I[c]
Re—Re (Å)	2.224(1)	2.226(4)	2.245(3)
Re—X (Å)	2.330(2)	2.467(4)	2.694(24)
Re—X (Å) Calc[d]	2.33	2.48	2.67
∠ Re—Re—X (deg.)	103.4(5)	104.6(4)	105.4(3)
Cube edges (Å)[e]	3.30, 3.21, 3.24[f]	3.48, 3.39, 3.42	3.67, 3.67, 3.67
r_{vdw} of X (Å)[g]	1.80	1.95	2.15

[a] $[(n\text{-}Bu)_4N]_2[Re_2Cl_8]$; ref. 13.
[b] For $Cs_2[Re_2Br_8]$; ref. 16.
[c] This work.
[d] Assuming constant r_{Re} of 1.34 and X covalent radii of 0.99, 1.14 and 1.33 for Cl, Br and I.
[e] Max, Min, Av.
[f] Not given in ref. 13; calculated from positional parameters.
[g] van der Waals radius of halogen.

ship presumed between Re—Re distance and $\delta \rightarrow \delta^*$ transition energy) was thus incorrect.

The Re—X distance can be accounted for to within ± 0.01 Å by assuming a fixed covalent radius for Re (1.34 Å) and the standard (Pauling) covalent radii for the halogens. The Re—Re—X angles show a steady increase with increasing size of X, but it is so slight as to be almost negligible. The lengths of the mean cube edges increase in about the same ratios as the Re—X bond lengths, namely, by 5–6% from Cl to Br and by 7–9% from Br to I. These increases are only slightly smaller than the increases in van der Waals radii, viz. 8 and 10%. Thus, on the whole, because the covalent and van der Waals radii increase as they do, the three cubic $Re_2X_8^{2-}$ ions simply increase in size without undue strain or distortion, and without changing the Re—Re bond length as the atomic number of the halogen increases.

Acknowledgements—We thank the National Science Foundation for support and Dr L. R. Falvello for helpful discussions.

REFERENCES

1. F. A. Cotton, N. F. Curtis, C. B. Harris, B. F. G. Johnson, S. J. Lippard, J. T. Mague, W. R. Robinson and J. S. Wood, *Science* 1964, **145**, 1305; F. A. Cotton, *Inorg. Chem.* 1965, **4**, 334.
2. F. A. Cotton and R. A. Walton, *Multiple Bonds Between Metal Atoms*. John Wiley, New York (1982); (b) F. A. Cotton and R. A. Walton, *Struct. Bonding* (Berlin) 1985, **62**, 1; (c) H. W. Huang and D. S. Martin, *Inorg. Chem.* 1985, **24**, 96.
3. P. J. Hay, *J. Am. Chem. Soc.* 1982, **104**, 7007.
4. D. C. Smith and W. A. Goddard III, *J. Am. Chem. Soc.* 1987, **109**, 5580.
5. F. A. Cotton and M. Matusz, *Inorg. Chem.* 1987, **26**, 3468.
6. G. Peters and W. Preetz, *Z. Naturforsch.* 1979, **34b**, 1767.
7. H. D. Glicksman and R. A. Walton, *Inorg. Chem.* 1978, **17**, 3179.
8. W. Preetz and L. Rudzik, *Angew. Chem. Int. Ed. Engl.* 1979, **18**, 150.
9. A. Bino, F. A. Cotton and P. E. Fanwick, *Inorg. Chem.* 1979, **18**, 3558.
10. A. C. T. North, D. C. Phillips and F. S. Mathews, *Acta Crystallograph. Sect. A*; *Cryst. Phys. Diffr. Theor. Crystallograph.* 1968, **24**, 35.
11. W. K. Bratton and F. A. Cotton, *Inorg. Chem.* 1969, **8**, 1299.
12. F. Calderazzo, F. Marchetti, R. Poli, D. Vitali and P. F. Zanazzi, *J. Chem. Soc., Dalton Trans.* 1982, 1665.
13. F. A. Cotton, B. A. Frenz, B. R. Stults and T. R. Webb, *J. Am. Chem. Soc.* 1976, **98**, 2768.
14. W. Preetz, G. Peters and L. Rudzik, *Z. Naturforsch.* 1979, **34b**, 1240.
15. M. D. Hopkins, W. P. Schaefer, M. J. Bronikowski, W. H. Woodruff, V. M. Miskowski, R. F. Dallinger and H. B. Gray, *J. Am. Chem. Soc.* 1987, **109**, 408.
16. F. A. Cotton, B. G. DeBoer and M. Jesemic, *Inorg. Chem.* 1970, **9**, 2143.

Polyhedron Vol. 7, No. 18, pp. 1673–1676, 1988
Printed in Great Britain

0277–5387/88 $3.00+.00
© 1988 Pergamon Press plc

DIAMAGNETIC ANISOTROPY OF QUADRUPLE Mo—Mo BONDS: α-Mo_2Cl_4(DIPHOSPHINE)$_2$ COMPLEXES

F. ALBERT COTTON* and SUSUMU KITAGAWA*†

Department of Chemistry and Laboratory for Molecular Structure and Bonding, Texas A&M University, College Station, TX 77843, U.S.A.

(*Received* 25 *January* 1988; *accepted* 28 *March* 1988)

Abstract—Two components ($\chi_\parallel - \chi'_\perp$ and $\chi_\parallel - \chi''_\perp$) of magnetic anisotropy of Mo—Mo quadruple bonds have been obtained by using the X-ray crystallographic molecular structure and the low temperature ^{1}H NMR spectrum of α-$Mo_2Cl_4[(C_6H_5)_2PCH_2CH_2P(p\text{-}RC_6H_4)_2]_2$ [R = H (dppe), CH_3 (dpdt) and *tert*-C_4H_9 (dpdbp)]. The values of $\chi_\parallel - \chi'_\perp$ and $\chi_\parallel - \chi''_\perp$ for the dpdbp case are $-(8470 \pm 200) \times 10^{-36}$ and $-(5540 \pm 70) \times 10^{-36}$ m^3 molecule^{-1}, respectively, which are several times as large as $\chi_\parallel - \chi_\perp$(Mo—Mo). Through detailed examination of the ^{1}H NMR signals of the ethylene protons, conformational flexing of the chelate rings of α-Mo_2Cl_4(dpdbp)$_2$ has been recognized.

In the overall research effort concerning the behaviour of metal–metal multiple bonds[1,2] studies of compounds containing quadruple bonds between molybdenum atoms have played a major part. An important sub-class of these dimolybdenum compounds are those of composition $Mo_2X_4(diphos)_2$[3] (and their tungsten analogues[4]), where the diphos ligand is 1,2-bis(diphenylphosphino)ethane (dppe), or a derivative thereof. Compounds of this composition exist in two isomeric forms, which have chelating diphos ligands (α) or bridging ones (β). For the dppe compounds, NMR and other solution studies have been severely limited by low solubility, but we have recently reported a considerably more soluble pair of compounds, $Mo_2Cl_4(dpdt)_2$ (where dpdt = 1-diphenylphosphino-2-di(*p*-tolyl) phosphinoethane) and provided extensive NMR data for them.[5] In this way we found that the ethylene hydrogen atoms of α-$Mo_2Cl_4(dpdt)_2$ display a large chemical shift difference between the distal and proximal ones, with the proximal ones being most affected because of their closeness to the centre of the Mo—Mo bond, as shown in Fig. 1. From the previously reported[5] shifts for α-$Mo_2Cl_4(dpdt)_2$ we made an approximate calculation of the diamagnetic anisotropy of the Mo_2^{4+} unit by treating the molecule as if it possessed axial symmetry. This is not strictly true and we now wish to deal with this problem in a more rigorous way.

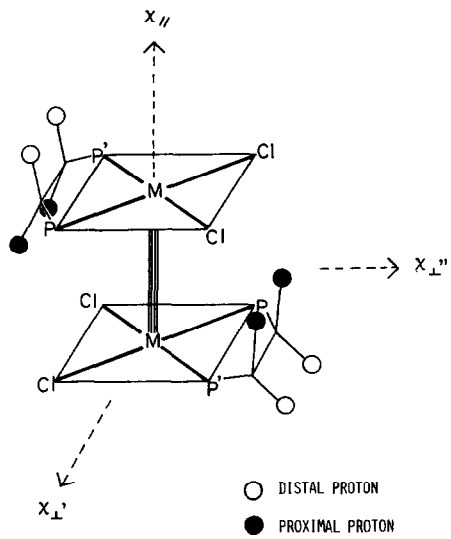

Fig. 1. A schematic drawing of an *anti*-α-$M_2Cl_4(diphos)_2$ molecule showing distal and proximal types of methylene hydrogen atoms and the defined principal components of diamagnetism.

The diamagnetic anisotropy of quadruple and triple bonds between metal atoms has already been the subject of several earlier publications,[6–10] in all of which there have been approximations, ambiguities or non-rigorous assumptions. We believe the present work gives the most rigorous and unambiguous results to date, albeit only for one particular type of complex.

* Authors to whom correspondence should be addressed.
† Permanent address: Department of Chemistry, Kinki University, Kowakae, Higashi-Osaka, 577 Japan.

EXPERIMENTAL

1,2-bis(*p*-ditolylphosphino)ethane (dtpe) was synthesized according to the method reported previously.[5] Found: C, 78.1; P, 13.1; H, 7.2. Calc. for $C_{30}H_{40}P_2$: C, 79.3; P, 13.6; H, 7.1%.

α-$Mo_2Cl_4(dtpe)_2$ was prepared from $K_4Mo_2Cl_8$/dtpe/CH_3OH.[3] CD_2Cl_2 was purchased from Wilmad Co. and used as a solvent for NMR measurements. ^1H NMR spectra were obtained on a Varian XL 400 NMR spectrometer, operating in the Fourier transform mode at $-90°C$. ^1H NMR spectra of α-$Mo_2Cl_4(dpdbp)_2$ and α-$Mo_2Cl_4(dpdt)_2$ were reported previously.[5,11]

RESULTS AND DISCUSSION

A general expression[12] for the effect of diamagnetic anisotropy upon the chemical shift (σ) for a molecule of low symmetry is given in eq. (1)

$$\Delta\sigma_i = 1/3r^3[(\chi_\parallel - \chi'_\perp)(3\cos^2\theta'_\perp - 1) + (\chi_\parallel - \chi''_\perp)(3\cos^2\theta''_\perp - 1)]/4\pi \quad (1)$$

where r is the distance between the centre of the Mo_2 bond and the proton H_i, $\chi_\parallel$ is the longitudinal component of susceptibility (in this case, along the bond direction), $\chi'_\perp$ and $\chi''_\perp$ are the two transverse principal susceptibilities (i.e. perpendicular to the bond), while $\theta'_\perp$ and $\theta''_\perp$ are the angles between r and the appropriate bond perpendicular.

The difference between observed shifts of proximal and distal protons may be expressed by eq. (2), where $G = (3\cos^2\theta - 1)/3r^3$.

$$\Delta\sigma_{distal} - \Delta\sigma_{proximal} = (\chi_\parallel - \chi'_\perp)(G'_{distal} - G'_{proximal})/4\pi + (\chi_\parallel - \chi''_\perp)(G''_{distal} - G''_{proximal})/4\pi. \quad (2)$$

According to eq. (2), there are two unknown parameters, viz. the diamagnetic anisotropy terms, $\chi_\parallel - \chi'_\perp$ and $\chi_\parallel - \chi''_\perp$. To obtain the diamagnetic anisotropy terms, at least two sets of observed shifts of proximal and distal protons are required, and we therefore prepared two unsymmetrical phosphines ($R_2PCH_2CH_2PR'_2$), namely, dpdt[5] and dpdbp.[11] Preliminary work showed that dpdbp is best able to fulfil our requirements, and therefore $Mo_2Cl_4(dpdbp)_2$ became our principal subject of study.

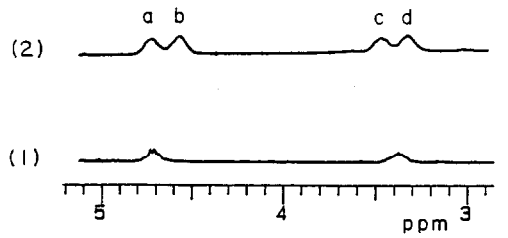

Fig. 2. ^1H NMR spectra in the methylene region for *anti*-α-$Mo_2Cl_4(dpdbp)_2$: (1) at 25°C and (2) at $-80°C$.

Assignment of the ^1H *NMR spectrum of* $Mo_2Cl_4(dpdbp)_2$

Figure 2 shows the ^1H NMR spectrum in the ethylene region of α-*anti*-$Mo_2Cl_4(dpdbp)_2$. The assignments for other regions of the spectrum of this compound have been discussed previously,[11] but the detailed assignment for the four ethylene protons was not previously considered. The large gap between proximal and distal proton chemical shifts is commonly observed for this type of compound, generally in the range of 1.25–1.36 ppm (Table 1). It is interesting that the ethylene protons of dpdbp give four signals at $-90°C$ [Fig. 2(2)]. The downfield (a and b) and upfield (c and d) pairs of signals are those of the proximal and distal protons, respectively. However, Fig. 2(1) shows that the two members of each pair collapse at 25°C, indicating the presence of a signal-averaging dynamic process. In the case of α-$Mo_2Cl_4(dpdt)_2$, no such separation was observed even at $-110°C$.

The dpdbp ligand itself has chemically non-equivalent protons; $(C_6H_5)_2PCH_2$ and $(t\text{-}C_4H_9C_6H_4)_2PCH_2$. While this might suggest that the four signals should be assigned to the proximal and distal protons for each methylene group, such an assignment could not explain the fact that the close pairs collapse to become single signals at 25°C. We therefore conclude that the doubling of the distal and proximal signals at $-90°C$ is associated not with the effect of the substituents* but with different conformations of the ethylene groups.

Close examination of the structure[11] of α-$Mo_2Cl_4(dpdbp)_2$ reveals that the C—C bond vector of the ethylene CH_2CH_2 is not perpendicular to the Mo—Mo bond axis, but is tilted, as shown in Fig. 3. Each of the hydrogen atoms experiences two different regions of diamagnetic anisotropy. In principle, eight signals might have been observed at low temperature, but the distinction based on the differently substituted phosphorus atoms is too small to observe. Therefore, signal a is attributed both to H(1) in A and to H(3) in B. Similarly, signal b is assigned to both H(3) in A and H(1) in B, signal

*In the molecular structure of *anti*-α-$Mo_2Cl_4(dpdbp)_2$,[5] no significant difference between Mo—P and Mo—P′ distances was observed, suggesting that no great chemical shift between the ethylene protons is to be expected. Furthermore, the dpdbp ligand itself shows no difference in chemical shifts between the proton signals for the two methylene groups.

Table 1. Observed ^{1}H NMR shifts of ethylene protons of α-$Mo_2Cl_4(R_2PCH_2CH_2PR'_2)_2$

Ligand	R	R′	δ (ppm) I	δ (ppm) II	Δ[a]	Reference
dppe	C_6H_5	C_6H_5	4.72	3.33	1.39	5[b]
dpdt	C_6H_5	p-$CH_3C_6H_4$	4.68	3.32	1.36	5[b]
dtpe	p-$CH_3C_6H_4$	p-$CH_3C_6H_4$	4.59	3.27	1.32	This work[c]
dpdbp	C_6H_5	p-$tert$-$C_4H_9C_6H_4$	3.33	4.58	1.25	This work[d]
			3.49	4.74	1.25	

[a] The difference between δ_I and δ_{II}.
[b] Observed at −25°C.
[c] Observed at −90°C.
[d] Observed at −80°C.

P = bisphenylphosphino group
P' = bis(tert-butylphenyl)phosphino group

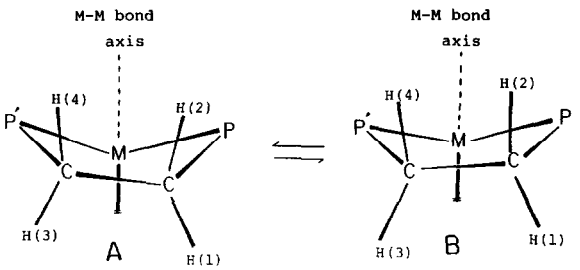

Fig. 3. Schematic diagrams of the conformations of the chelate rings for an α-$M_2X_4(R_2PCH_2CH_2PR')_2$ type molecule.

c to H(2) in A and H(4) in B, and signal d to H(4) in A and H(2) in B. At high temperature the interconversion between structure A and B occurs rapidly, and the pairs of proton signals for A and B configurations are completely averaged to single ones.

Calculation of diamagnetic anisotropy

When the diamagnetic anisotropy of this type of molecule is considered, three coordinate axes need to be chosen. In previous discussions of dimetal compounds, the choice of a principal axis was easily made because the M—M bond axis coincides with the highest symmetry axis C_3 or C_4. For these molecules, which have axial symmetry, the simple McConnell equation,[13] eq. (3), can be employed where θ is the angle between r and axis z.

$$\Delta\sigma = 1/3r^3[(\chi_\parallel - \chi_\perp)(1 - 3\cos^2\theta)]/4\pi. \quad (3)$$

From this equation, the diamagnetic anisotropy of the triple bond system,[7,8,10] $M_2(NMe_2)_6$ (D_{3d} symmetry), has been estimated to be -1784×10^{-36} (M = Mo) and -1960×10^{-36} (M = W) m^3 molecule^{-1}. In our previous work on quadruple bond systems, we estimated the value for α-$Mo_2Cl_4(dppe)_2$ and α-$Mo_2Cl_4(dpdt)_2$ by use of eq. (3). The value obtained for $(\chi - \chi_\perp)$ was -8800×10^{-36} m^3 molecule^{-1}.[5] In this case, the principal axis was taken as the axis perpendicular to the M—M bond direction, which is different from that of triple bond systems, which makes direct comparison difficult. Strictly, α-$Mo_2Cl_4(PP')_2$ has no axial symmetry and the result obtained must be considered as only approximate. In order to assign the conventional principal axis along the M—M bond for the present systems, and to obtain a general diamagnetic anisotropy without approximation, we have turned to the general eqs (1) and (2), with the principal axis (Z axis) taken along the M—M bond (Fig. 3). This selection allows convenient comparison of χ values for the different cases. A choice of X and Y axes is still necessary; we have selected the X axis to coincide with the C_2 axis in α-$Mo_2Cl_4(dpdbp)_2$.

According to eq. (2) two chemical shift differences, Δ and Δ', between the proximal and distal protons are needed. On the basis of the assignment mentioned above, Δ and Δ' for H(2)—H(1) and H(4)—H(3) are obtained, respectively. Both values are accidentally the same, i.e. $\Delta = \Delta' = 1.25$ ppm as shown in Table 1. The geometric factor (G) was calculated from the positions of the ethylene protons, which were obtained by using conventional computer codes in which the geometrical properties of the methylene groups are employed. The resultant G factors are listed in Table 2. From these values, the diamagnetic anisotropies $\chi_\parallel - \chi'_\perp$ and $\chi_\parallel - \chi''_\perp$ are found to be $-(9450 \pm 200) \times 10^{-36}$ and $-(5860 \pm 90) \times 10^{-36}$ m^3 molecule^{-1}, respectively.

There are also X-ray crystal structures available for α-$Mo_2Cl_4(dppe)_2$[14] and α-$Mo_2Cl_4(dpdt)_2$.[5] By employing similar signal assignments (in this case $\Delta = \Delta'$) for the cases of dppe and dpdt, the dia-

Table 2. Geometric factors[a] for proximal [H(1) and H(3)] and distal [H(2) and H(4)] protons of α-$Mo_2Cl_4(PP')_2$

PP′		r (Å)	$\theta'_\perp$(deg)	$\theta''_\perp$(deg)	$G'_\perp$[a]	$G''_\perp$[a]
dppe[b]	H(1)	3.978	108.2	18.2	−3.752	9.046
	H(2)	4.769	103.0	24.4	−2.609	4.567
	H(3)	3.724	74.3	16.2	−5.037	11.401
	H(4)	4.727	75.6	23.0	−2.573	4.986
dpdt[c]	H(1)	3.645	106.1	17.2	−5.299	11.974
	H(2)	4.676	105.2	21.2	−2.588	5.240
	H(3)	3.912	71.9	18.1	−3.961	9.521
	H(4)	4.725	77.9	23.1	−2.741	4.858
dpdbp[d]	H(1)	3.655	105.7	16.2	−5.320	12.056
	H(2)	4.687	104.7	23.0	−2.608	5.076
	H(3)	3.947	72.6	17.4	−3.972	9.393
	H(4)	4.742	78.1	24.3	−2.730	4.660

[a] Unit in $\times 10^{27}$ m^{-3}. The distance of C—H is 1.09 Å and the angle of C—C—H is 109°.
[b] Geometry from ref. 14.
[c] Geometry from ref. 5.
[d] This work.

Table 3. Magnetic anisotropy of quadruple and triple bonds

Compound	$\times 10^{-36}$ (m^3 molecule^{-1}) $\chi_\parallel - \chi'_\perp$[a]	$\chi_\parallel - \chi''_\perp$[a]
α-$Mo_2Cl_4(dppe)_2$	−9340[b]	−6300[c]
α-$Mo_2Cl_4(dpdt)_2$	−8200[b]	−5830[c]
α-$Mo_2Cl_4(dpdbp)_2$	−8470	−5540[d]
$Mo_2(NMe_2)_6$	−1784[e]	
$W_2(NMe_2)_6$	−1960[e]	

[a] $\chi_\parallel$ is a value along the metal–metal bond. $\chi'_\perp$ and $\chi''_\perp$ are values along the axes defined in Fig. 1, respectively.
[b] Error limit, $\pm 200 \times 10^{-36}$ m^3 $molecule^{-1}$.
[c] Error limit, $\pm 70 \times 10^{-36}$ m^3 $molecule^{-1}$.
[d] Error limit, $\pm 90 \times 10^{-36}$ m^3 $molecule^{-1}$.
[e] Reference 8. $\chi_\parallel - \chi_\perp (\chi_\perp = \chi'_\perp = \chi''_\perp)$.

magnetic anisotropies for these molecules are also readily calculated. They are listed in Table 3. The diamagnetic anisotropies are very large: $(\chi_\parallel - \chi'_\perp(Mo\overset{4}{-}Mo))/(\chi_\parallel - \chi_\perp(Mo\overset{3}{-}Mo)) = 4$–5 and $(\chi_\parallel - \chi''_\perp(Mo\overset{4}{-}Mo))/(\chi_\parallel - \chi_\perp(Mo\overset{3}{-}Mo)) \simeq 3$.

It is well known that N=O bonds[15] have the largest diamagnetic anisotropy known among organic compounds, comparable to $|\chi_\parallel - \chi_\perp|$ for $Mo\overset{3}{-}Mo$ bonds but much less than the $|\chi_\parallel - \chi'_{\perp,\perp'}|$ values for $Mo\overset{4}{-}Mo$ bonds. We have pointed out[5] in α-$Mo_2Cl_4(dpdt)_2$ that the ethylene protons experience ring current effects from nearest-neighbour aryl rings, but this effect is only ~ 12% of the whole anisotropy. Consequently, we conclude that the diamagnetic anisotropy of quadruple bonds is the largest among compounds which have so far been synthesized.

Acknowledgements—We thank the National Science Foundation for support and Kinki University for a leave of absence to S.K.

REFERENCES

1. F. A. Cotton and R. A. Walton, *Multiple Bonds Between Metal Atoms*. Wiley, New York (1982).
2. F. A. Cotton and R. A. Walton, *Struct. Bonding (Berlin)* 1985, **62**, 99.
3. S. A. Best, T. J. Smith and R. A. Walton, *Inorg. Chem.* 1978, **17**, 99.
4. F. A. Cotton and T. R. Felthouse, *Inorg. Chem.* 1981, **20**, 3880.
5. F. A. Cotton and S. Kitagawa, *Inorg. Chem.* 1987, **26**, 3463.
6. J. San Filippo, *Inorg. Chem.* 1972, **11**, 3140.
7. M. J. McGlinchey, *Inorg. Chem.* 1980, **19**, 1392.
8. M. J. McGlinchey, R. C. Burns, R. Hofer, S. Top and G. Jaouen, *Organometallics* 1986, **5**, 104.
9. P. Agaskar and F. A. Cotton, *Polyhedron* 1986, **5**, 899.
10. T. P. Blatchford, M. H. Chisholm and J. C. Huffman, *Polyhedron* 1987, **6**, 1677.
11. F. A. Cotton and S. Kitagawa, *Polyhedron* 1988, **7**, 463.
12. R. K. Harris, *Nuclear Magnetic Resonance Spectroscopy*. Longman, U.K. (1986).
13. H. M. McConnell, *J. Chem. Phys.* 1957, **27**, 226.
14. P. A. Agaskar and F. A. Cotton, *Inorg. Chem.* 1986, **25**, 15.
15. R. K. Harris and R. A. Spragg, *J. Mol. Spect.* 1967, **23**, 158.

Polyhedron Vol. 7, No. 18, pp. 1677–1685, 1988
Printed in Great Britain

0277–5387/88 $3.00+.00
© 1988 Pergamon Press plc

CALCULATION OF HETERONUCLEAR SINGLE BOND ENTHALPIES FROM PAULING ELECTRONEGATIVITIES

STEVEN G. BRATSCH

Department of Chemistry, The University of Connecticut, Greater Hartford Campus, 85 Lawler Road, West Hartford, CT 06117, U.S.A.

(*Received* 13 *January* 1988; *accepted* 22 *January* 1988)

Abstract—Modifications to the Pauling method of calculating single bond enthalpies are proposed. First, because bond polarity produces a decrease in equilibrium bond length which strengthens the bond, a correction is made for any deviation in the actual bond length from the covalent radius sum. Secondly, because charge-transfer from a less to a more electronegative atom is exothermic only until electronegativity equalization is achieved, a saturation effect is observed for large electronegativity differences. A correction for the effect is provided. The modified Pauling method is shown to be more accurate than the original Pauling method and valid over the entire range of bond polarity.

The Pauling electronegativity scale[1–3] was developed as a means of calculating heteronuclear single bond enthalpies at 25°C via the equations

$$\Delta H^0_{AB} = \frac{\Delta H^0_{AA} + \Delta H^0_{BB}}{2} + F(X_B - X_A)^2; \quad (1)$$

$$\Delta H^0_{AB} = (\Delta H^0_{AA} \Delta H^0_{BB})^{1/2} + 1.3F(X_B - X_A)^2. \quad (2)$$

In eqs (1) and (2), ΔH^0_{AB} is the A—B single bond enthalpy, ΔH^0_{AA} and ΔH^0_{BB} are the A—A and B—B non-polar covalent single bond enthalpies, respectively, F is the Faraday constant (9.649×10^4 C mol^{-1} = 9.649×10^4 J (V mol^{-1})[4a] and X_A and X_B are the Pauling electronegativities for atoms A and B. Pauling has called the arithmetic mean[1] [eq. (1)] or the geometric mean[2] [eq. (2)] of ΔH^0_{AA} and ΔH^0_{BB} the "normal A—B bond energy" (actually an enthalpy), believed to represent the strength of the hypothetical non-polar covalent A—B bond. The true ΔH^0_{AB} is usually greater than the "normal A—B bond energy", the difference being attributed by Pauling to the resonance of the covalent structure AB with the ionic structure A^+B^- (assuming $X_A < X_B$) and called the "ionic resonance energy". This quantity is approximated in eqs (1) and (2) by the terms involving $(X_B - X_A)$.[2] The problem of negative "ionic resonance energies" is encountered less frequently with eq. (2) than with eq. (1) and therefore eq. (2) is generally believed to be superior.[2] Unfortunately, it is necessary to include the factor 1.3 in eq. (2) in order to keep the Pauling units on the same scale as originally established by eq. (1).[1]

Sanderson,[5] Evans and Huheey[6] and others have developed models of chemical bonding which treat the total bond enthalpy as a weighted sum of covalent and ionic structures. Sanderson[5a] has criticized Pauling's treatment of bond enthalpies by pointing out that the electrons in a bond cannot be both evenly shared all the time and unevenly shared some of the time; that is, the covalent contribution to the total bond enthalpy must decrease as the ionic contribution increases. However, it is possible to reconcile eqs (1) and (2) with more sophisticated chemical bonding models merely by interpretating them differently.

Consider a singly-bonded diatomic molecule AB, with $X_A < X_B$. The A—B bond may be described as polar covalent, the difference in electronegativity between A and B resulting in uneven electron sharing which produces a positive partial charge on atom A ($\delta_A > 0$) and a negative partial charge on atom B ($\delta_B < 0$). The change in enthalpy corresponding to the breaking of the A—B bond may be envisioned as the sum of two steps. In the first step, the A and B nuclei remain fixed at their normal bond length r_{AB} but an appropriate transfer of charge results in the formation of a non-polar covalent AB molecule. In the second step, the non-polar covalent A—B bond is broken. The enthalpy change for step (1) may be called the *discharge enthalpy* and symbolized as $\Delta H^0_{disch.}$, while the

enthalpy change for step (2) may be called the *non-polar covalent bond enthalpy* and symbolized as $\Delta H^0_{cov.}$:

Step/Process	ΔH^0
(1) $A^{\delta+}B^{\delta-} \rightarrow AB$ (non-polar covalent)	ΔH^0_{disch} (3)
(2) AB (non-polar covalent) $\rightarrow A+B$	ΔH^0_{cov} (4)
Sum: $A^{\delta+}B^{\delta-} \rightarrow A+B$	ΔH^0_{AB}. (5)

The discharge enthalpy ΔH^0_{disch} [eq. (3)] corresponds to Pauling's "ionic resonance energy" and the non-polar covalent bond enthalpy ΔH^0_{cov} [eq. (4)] corresponds to Pauling's "normal A—B bond energy". By interpreting the Pauling method of predicting single bond enthalpies at 25°C as the sum of thermochemical steps, it is not necessary to treat the total bond enthalpy as a weight sum of covalent and ionic structures.

However, as discussed by Allred[3] and Matcha,[7] eqs (1) and (2) are unsuccessful for bonds with large electronegativity differences, calculations in error by 50–100% not being unusual. Equations (1) and (2) predict $\Delta H^0_{disch.}$ to increase quadratically with increasing difference in electronegativity, while in reality the discharge enthalpies approach a limiting ("saturation") value when $|X_B - X_A|$ is large. It seems worthwhile to investigate this problem in greater depth, because the Pauling scale of electronegativity is the best-known scale, and eqs (1) and (2) are the best-known simple methods of bond enthalpy estimation.

CALCULATIONS OF NON-POLAR COVALENT HETERONUCLEAR SINGLE BOND ENTHALPY, $\Delta H^0_{cov.}$

It appears that the best method available at present for the calculation of the non-polar covalent heteronuclear single bond enthalpy ΔH^0_{cov} is to take the geometric mean of the non-polar covalent homonuclear single bond enthalpies ΔH^0_{AA} and ΔH^0_{BB}, as done by Pauling[2] [eq. (2)], but to correct for any deviation in the actual bond length r_{AB} from the covalent radius sum $r_A + r_B$:[5a]

$$\Delta H^0_{cov.} = \frac{r_A + r_B}{r_{AB}} (\Delta H^0_{AA} \Delta H^0_{BB})^{1/2}. \quad (6)$$

This correction is necessary because bond polarity produces a decrease in equilibrium bond length which strengthens the bond.[5a,6]

Selected values of homonuclear single bond enthalpies ΔH^0_{AA} are given in Table 1. In many cases, these have been obtained directly from thermochemical data[5a,6,8] for singly-bonded molecules of the elements (H_2, Li_2, Na_2, K_2, Rb_2, Cs_2, Cu_2,

Table 1. Selected atomic properties

A	V_A[a]	r_A[b] (nm)	X_A (= a_A)[c]	b_A[d]	ΔH^0_{AA}[e] (kJ mol^{-1})
H	I	0.0371[f]	2.20	2.18	435.9
Li	I	0.1336	0.98	1.15	102.8
Be	II	0.0887	1.57	1.41	230[g]
B	III	0.0822	2.04	1.46	305[h]
C	IV	0.0772	2.55	1.51	357.4
N	III	0.074[g]	3.04	1.54	170[g]
O	II	0.072[g]	3.44	1.56	160[g]
F	I	0.0709[f]	3.98	1.57	158.0
Na	I	0.1539	0.93	1.07	72.6
Mg	II	0.1373	1.31	1.13	120[g]
Al	III	0.1258	1.61	1.18	180[g]
Si	IV	0.1169	1.90	1.23	227.8
P	III	0.1107	2.19	1.26	199.9
S	II	0.1049	2.58	1.29	266.0
Cl	I	0.0994	3.16	1.33	243.4
K	I	0.1962	0.82	0.95	54.8
Ca	II	0.174	1.00	1.00	100[g]
Cu	I	0.1331	1.90	1.15	192.5
Zn	II	0.1292	1.65	1.17	70[g]
Ga	III	0.1256	1.81	1.18	140[g]
Ge	IV	0.1223	2.01	1.20	188.3
As	III	0.1194	2.18	1.21	177.7
Se	II	0.1167	2.55	1.23	199.7
Br	I	0.1142	2.96	1.24	192.9
Rb	I	0.216	0.82	0.90	49[h]
Sr	II	0.191	0.95	0.96	90[g]
Ag	I	0.1533	1.93	1.07	159.1
Cd	II	0.1493	1.69	1.08	60[g]
In	I	0.1455	1.6[g]	1.10	120[g]
	III	0.1455	1.78	1.10	120[g]
Sn	II	0.1420	1.80	1.11	152.1
	IV	0.1420	1.96	1.11	152.1
Sb	III	0.1389	2.05	1.12	140.7
Te	II	0.1360	2.3[g]	1.14	160[g]
I	I	0.1333	2.66	1.15	151.2
Cs	I	0.235	0.79	0.86	44.8
Ba	II	0.198	0.89	0.94	80[g]
Au	I	0.151[g]	2.54	1.08	217.1
Hg	II	0.150	2.00	1.08	40[g]
Tl	I	0.149	1.62	1.09	100[g]
	III	0.149	2.04	1.09	100[g]
Pb	II	0.148	1.87	1.09	120[g]
	IV	0.148	2.33	1.09	120[g]
Bi	III	0.147	2.02	1.09	110[g]
Po	II	0.146[g]	2.1[g]	1.10	130[g]
At	I	0.145[g]	2.3[g]	1.10	120[g]
Fr	I	0.240[g]	0.8[g]	0.86	40[g]
Ra	II	0.210[g]	0.9[g]	0.91	70[g]

[a] Valence (number of bonds formed).
[b] Covalent radius: ref. 5(a), except as noted.
[c] Inherent electronegativity: ref. 3, except as noted.
[d] Charge coefficient [eq. (20)].
[e] Non-polar covalent single bond enthalpy: ref. 8, except as noted.
[f] Reference 4(b).
[g] Estimated (this work).
[h] References 5(a) and 6.

Ag_2, Au_2, P_4, As_4, Sb_4, S_8, Se_6, F_2, Cl_2, Br_2 and I_2).

Elements not known to exist as singly-bonded molecules must have their homonuclear single bond enthalpies derived by indirect methods. A familiar approach is to assume that a particular *heteronuclear* bond enthalpy remains essentially constant from molecule to molecule and obtain the desired homonuclear bond enthalpy by difference.[1,2,4b] For example, ΔH^0_{BB} can be estimated by assuming that ΔH^0_{BF} is the same in BF_3 and B_2F_4 or that ΔH^0_{BCl} is the same in BCl_3 and B_2Cl_4, ΔH^0_{NN} by assuming that ΔH^0_{NH} is the same in NH_3 and N_2H_4, and ΔH^0_{OO} by assuming that ΔH^0_{OH} is the same in H_2O and H_2O_2.

For crystals of the elements of the carbon family which exhibit the diamond structure (C, Si, Ge and grey Sn), ΔH^0_{AA} may be defined as one half of the sublimation enthalpy.[2,3] Where they are known, ΔH^0_{AA} values for metals are 50–70% of the sublimation enthalpies; this observation allows estimates of ΔH^0_{AA} to be made for Be, Mg, Ca, Sr, Ba, Zn, Cd, Hg, Al, Ga, In, Tl, Pb and Bi which are in good agreement with previous estimates.[5a,6]

Homonuclear single bond enthalpies generally increase across a period, although a notable discontinuity occurs between the carbon and nitrogen families (especially for the earlier members with smaller atoms: N, O and F). This phenomenon is probably connected with the appearance of non-bonding (lone) pairs of electrons on the atoms at this point, although the exact mechanism of the bond weakening effect is not well-understood.[5b] Sanderson[5b] and Evans and Huheey[6] have developed methods of estimating the extent of bond weakening which occasionally lead to very different results. In this work, the fully weakened (i.e. familiar) ΔH^0_{AA} values are listed in Table 1 and used in eq. (6), although this practice may conceivably underestimate ΔH^0_{cov} for some bonds involving elements in the nitrogen, oxygen and halogen families.

PRELIMINARY CALCULATION OF DISCHARGE ENTHALPY, $\Delta H^0_{disch.}$

An "experimental" value for the discharge enthalpy $\Delta H^0_{disch.}$ may be obtained by subtracting the covalent enthalpy [eq. (6)] from the experimental total bond enthalpy ΔH^0_{AB}. The following expression holds for bonds with small electronegativity differences:

$$\Delta H^0_{disch} = F\frac{r_A + r_B}{r_{AB}}(X_B - X_A)^2. \qquad (7)$$

It is noteworthy that application of Sanderson's method[5a] of correcting for the variation of bond strength with equilibrium bond length in both eqs (6) and (7) eliminates the need for data fitting and leads to the restoration of the Faraday constant in the expression for ΔH^0_{disch}.

The "experimental" discharge enthalpies for 100 bonds (corrected for bond length), obtained by subtracting the covalent enthalpies [eq. (6)] from the experimental total bond enthalpies,[2,5,8] are plotted in Fig. 1 against the Pauling electronegativity differences.[3] The bonds considered include 60 typical non-metal–non-metal bonds, and halides of the alkali metals and alkaline earth metals. The upper curve in Fig. 1 corresponds to eq. (7), which is seen to be successful up to about $|X_B - X_A| = 1.5$. Beyond this point, however, ΔH^0_{disch} approaches a limiting ("saturation") value and severely departs from eq. (7).

The mathematical solution to the phenomenon of "saturation" may be found in an equation suggested by Pauling[2] for the degree of ionic character (I_{AB}) in a bond:

$$I_{AB} = 1 - \exp[-(X_B - X_A)^2/4]. \qquad (8)$$

It is debatable whether eq. (8) is a correct expression for the degree of ionic character (see following section). However, it is significant that the leading term in the series expansion of eq. (8) is $(X_B - X_A)^2/4$. For small differences in electronegativity, $4(1 - \exp[-(X_B - X_A)^2/4])$ is approximately equal to $(X_B - X_A)^2$, but for large differences the exponential function approaches a limiting ("saturation") value. Pauling has mentioned that the standard enthalpy of formation of a binary compound AB from A_2 and B_2 (which is essentially its "ionic resonance energy") is roughly proportional to its

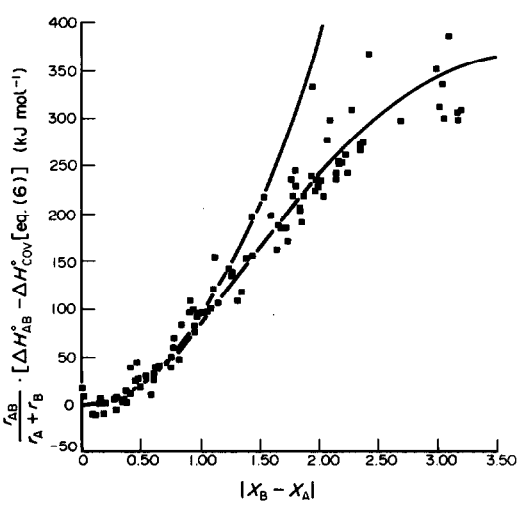

Fig. 1. "Experimental" discharge enthalpy (in kJ mol^{-1}) vs Pauling electronegativity difference.[3] Upper curve: eq. (7). Lower curve: eq. (9).

degree of ionic character as calculated by eq. (8), but surprisingly he has not pursued this idea in the development of his method of bond enthalpy calculation or in the evaluation of his electronegativity scale. Still, it is apparent that eq. (8) provides the necessary correction to the evaluation of $\Delta H^0_{\text{disch}}$.

The following preliminary equation for $\Delta H^0_{\text{disch}}$ may therefore be offered at this point:

$$\Delta H^0_{\text{disch}} = 4F\frac{r_A+r_B}{r_{AB}}(1-\exp[-(X_B-X_A)^2/4]). \quad (9)$$

The lower curve in Fig. 1 corresponds to eq. (9), which is seen to be moderately successful over the entire range of bond polarity. A possible interpretation of the "saturation" effect is offered in the Discussion.

THE DEGREE OF IONIC CHARACTER IN A BOND

In a binary compound of two elements A and B containing only A—B single bonds and $X_A < X_B$, the degree of ionic character (I_{AB}) is related to the partial charges (δ_A and δ_B) by

$$I_{AB} = \delta_A/V_A = -\delta_B/V_B \quad (10)$$

where V_A and V_B are the valences (number of bonds formed) of atoms A and B, respectively. The degree of ionic character in a bond ranges from zero to unity.

When the difference in electronegativity is small, one may view the discharge enthalpy $\Delta H^0_{\text{disch}}$ mainly as the energy needed to overcome the electrostatic attraction of the partial charges produced by uneven electron sharing. In terms of the degree of ionic character, the discharge enthalpy (per mole of bonds) may thus be written on a point charge model as

$$\Delta H^0_{\text{disch}} = \frac{N_A e^2}{4\pi\varepsilon_0}\cdot\frac{V_A V_B I^2_{AB}}{r_{AB}} \quad (11)$$

where N_A is Avogadro's number (6.022×10^{23} mol^{-1}), e is the electronic charge (1.602×10^{-19} C), ε_0 is the permittivity of free space (8.854×10^{-12} C^2 (J m)$^{-1}$ = 8.854×10^{-12} C (V m)$^{-1}$)[4a] and r_{AB} is the bond length.

For small electronegativity differences, Fig. 1 shows that the discharge enthalpy can also be approximated by eq. (7). As $|X_B-X_A|$ approaches zero as a limit, bond shortening due to polarity[5a,6] is negligible, so one can rewrite eq. (7) as

$$\Delta H^0_{\text{disch}} = F(X_B-X_A)^2 = N_A e(X_B-X_A)^2. \quad (12)$$

If eqs (11) and (12) are set equal to one another, rearrangement gives

$$I_{AB} = (4\pi\varepsilon_0/e)^{1/2}[r_{AB}/(V_A V_B)]^{1/2}|X_B-X_A| \quad (13)$$

or

$$I_{AB} = 0.8333[r_{AB}/(V_A V_B)]^{1/2}|X_B-X_A| \quad (14)$$

where r_{AB} is in nm. Unlike eqs (11) and (12), eqs (13) and (14) do not appear to be restricted in their applicability to bonds with small $|X_B-X_A|$.

Equation (14) is probably superior to eq. (8) as an expression for the degree of ionic character in a bond, for two reasons. First, it is dimensionally correct. Secondly and perhaps more importantly, it shows that the degree of ionic character depends not only on the electronegativity difference between two atoms, but also on atomic size; large atoms having a greater capacity for the donation or acceptance of charge.[4c,6] Thus, for example, despite the fact that their electronegativity differences are similar, the degrees of ionic character in gaseous KI and HF are calculated by eq. (14) to be quite different (0.85 and 0.45, respectively), which is consistent with their different physical and chemical properties.

For several of the alkali halide molecules, eq. (14) predicts degrees of ionic character greater than unity. This is physically impossible and merely indicates that one should view such molecules as ion pairs, with $I_{AB} = 1.000$.

CALCULATION OF DISCHARGE ENTHALPY, $\Delta H^0_{\text{disch.}}$ AND TOTAL BOND ENTHALPY, ΔH^0_{AB}

The preliminary expression for the discharge enthalpy $\Delta H^0_{\text{disch.}}$ has been given earlier [eq. (9)]. This expression is found to be satisfactory except for the most ionic of bonds, where it does not take into account the fact that the degree of ionic character in a bond cannot exceed unity. We are now in a position to modify eq. (9) and correct this shortcoming.

Equation (14), the expression for the degree of ionic character, may be rearranged to give

$$\frac{(X_B-X_A)^2}{4} = \frac{0.360 V_A V_B I^2_{AB}}{r_{AB}}. \quad (15)$$

Substitution of this expression for $(X_B-X_A)^2/4$ into eq. (9) gives

$$\Delta H^0_{\text{disch.}} = 4F\frac{r_A+r_B}{r_{AB}}(1-\exp[-0.360 V_A V_B I^2_{AB}/r_{AB}]) \quad (16)$$

where r_{AB} is in nm.

The following general procedure may now be given for the evaluation of the total bond enthalpy (ΔH^0_{AB}).

(1) Calculate the non-polar covalent heteronuclear bond enthalpy (ΔH^0_{cov}) by eq. (6).

(2) Calculate the degree of ionic character (I_{AB}) by eq. (14). If I_{AB} is calculated to be greater than unity, set I_{AB} equal to unity.

(3) Calculate the discharge enthalpy (ΔH^0_{disch}) by eq. (16). [If I_{AB} is less than unity, ΔH^0_{disch} may also be calculated by eq. (9).]

(4) Calculate the total bond enthalpy (ΔH^0_{AB}) as the sum of the non-polar covalent heteronuclear bond enthalpy (ΔH^0_{cov}) and the discharge enthalpy (ΔH^0_{disch}).

Table 2 lists 100 bond enthalpies as determined from thermochemical data,[2,5,8] as calculated by Pauling's method[2] [eq. (2)] and as calculated by the general procedure described above. The bonds considered are those plotted in Fig. 1 (60 typical non-metal–non-metal bonds, and halides of the alkali metals and alkaline earth metals). The average errors associated with Pauling's method are 7.7% for the typical non-metal–non-metal bonds, 76.0% for the metal halides and 35.0% overall. The corresponding average errors for the general procedure described above are 4.4, 4.7 and 4.5%, respectively.

ELECTRONEGATIVITY EQUALIZATION AND PARTIAL CHARGE

Modern electronegativity theory interprets atomic electronegativities such as those listed in Table 1 as pre-bonded, isolated-atom quantities which can be expected to vary in response to their chemical environment. The extent of this variation is indicated by Sanderson's Principle of Electronegativity Equalization:[5a,9] When two or more atoms of different initial electronegativity combine chemically, they become adjusted to the same, intermediate electronegativity within the compound.

A corollary to Sanderson's Principle is that the partial charge acquired by an atom A through chemical combination is related to the change in electronegativity it has experienced in going from its initial, pre-bonded value X_A to its final, equalized value X_{eq}. By assuming a linear variation of electronegativity with charge, one may define two quantities:[4c] the *inherent electronegativity* a_A, which is the familiar pre-bonded X_A value given in electronegativity tables, and the *charge coefficient* b_A, which is the change in electronegativity undergone by an atom accompanying acquisition of unit charge: $b_A = dX_A/d\delta_A$. The following general equations are consistent with these definitions:

$$X_{eq} = \frac{\sum(va/b)+q}{\sum(v/b)}; \qquad (17)$$

$$\delta_A = (X_{eq} - a_A)/b_A. \qquad (18)$$

In eq. (17), v is the number of atoms of each element in the species formula (e.g. for P_4O_6 $v_P = 4$ and $v_O = 6$) and q is the net charge of the species (if it is a polyatomic ion). The latter quantity is not relevant to the present work but is included in eq. (17) for the sake of completeness.

The author[10] has adapted Sanderson's Principle of Electronegativity Equalization to the Pauling scale by assuming that the electronegativity of an atom doubles when it acquires a partial charge of +1 and becomes zero when it acquires a partial charge of −1. This corresponds to defining the charge coefficient b_A in eqs (17) and (18) as equal to X_A (a_A). The set of relative partial charges produced by this adaptation can be made quantitatively useful for the calculation of bond enthalpies by redefining b_A as

$$b_A = 0.588X_A = 0.588a_A. \qquad (19)$$

Degrees of ionic character as calculated by combining eqs (10), (17), (18) and (19) are found to agree reasonably well ($r = 0.903$) with I_{AB} as calculated by eq. (14) for the 100 bonds considered throughout this work.

Even better agreement ($r = 0.954$) can be achieved by defining b_A in terms of the physical dimensions established by eq. (14):

$$b_A = 0.419(r_A)^{-1/2} \qquad (20)$$

where r_A is in nm. This is illustrated in Fig. 2, which plots the degree of ionic character for the 100 bonds considered throughout this work as calculated by eq. (14) against the degree of ionic character as calculated by combining eqs (10), (17), (18) and (20). Figure 2 reveals that the method of bond

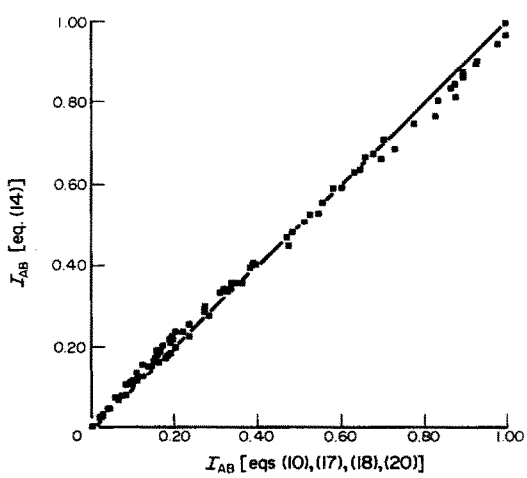

Fig. 2. Degree of ionic character based on electronegativity difference [eq. (14)] vs degree of ionic character based on electronegativity equalization [eqs (10), (17), (18) and (20)].

Table 2. Calculated bond enthalpies (kJ mol^{-1})

Bond	ΔH^0_{AB}[a] (exptl)	Pauling[b] ΔH^0_{AB}	Pauling[b] ±%	r_{AB}[c] (nm)	This work I_{AB}[d]	This work ΔH^0_{cov}[e]	This work ΔH^0_{disch}[f]	This work ΔH^0_{AB}[g]	This work ±%
FH	568.1	660	16.2	0.0918	0.449	309	248	557	−2.0
ClH	432.0	441	2.1	0.1274	0.286	349	85	434	0.5
ClF	255.1	280	9.8	0.163	0.276	205	62	267	4.7
BrH	366.2	362	−1.1	0.1408	0.238	312	56	368	0.5
BrF	284.7	305	7.1	0.176	0.357	184	93	277	−2.7
BrCl	218.9	222	1.4	0.2136	0.077	217	4	221	1.0
IH	298.3	283	−5.1	0.1608	0.154	272	21	293	−1.8
IF	281.5	373	32.5	0.191	0.481	165	146	311	10.5
ICl	210.7	223	5.8	0.2321	0.201	192	23	215	2.0
IBr	177.9	182	2.3	0.2485	0.125	170	9	179	0.6
OH	463.5	457	−1.4	0.0958	0.226	301	140	441	−4.9
OF	191.2	196	2.5	0.1418	0.120	160	27	187	−2.2
OCl	206.1	207	0.4	0.170	0.068	199	8	207	0.4
SH	367.7	359	−2.4	0.133	0.082	364	15	379	3.1
SCl	270.9	297	9.6	0.200	0.153	260	32	292	7.8
SBr	240[h]	245	2.1	0.22[i]	0.105	226	14	240	0.0
SeH	316.6	310	−2.1	0.1460	0.079	311	12	323	2.0
SeCl	251.1	267	6.3	0.213	0.166	224	35	259	3.1
SeBr	236	217	−8.1	0.23[i]	0.116	197	16	213	−9.7
TeH	266.5	265	−0.6	0.1653	0.024	277	1	278	4.3
NH	390.9	361	−7.6	0.1012	0.129	299	69	368	−5.9
NF	278.1	275	−1.1	0.137	0.167	173	81	254	−8.7
NCl	192[j]	205	6.8	0.175[k]	0.024	202	1	203	5.7
PH	321.0	295	−8.1	0.1437	0.002	304	0	304	−5.3
PF	490.1	580	18.3	0.157	0.341	206	246	452	−7.8
PCl	322.2	339	5.2	0.204	0.211	227	83	310	−3.8
PBr	263.2	271	3.0	0.220	0.174	201	54	255	−3.1
PI	215[h]	202	−6.0	0.247	0.112	172	20	192	−10.7
PO	358[j]	375	4.7	0.165	0.173	198	138	336	−6.1
AsH	296.7	278	−6.3	0.1519	0.004	287	0	287	−3.3
AsF	441.7	574	30.0	0.1712	0.358	186	238	424	−4.0
AsCl	309.7	328	5.9	0.2161	0.219	211	83	294	−5.1
AsBr	256	261	2.0	0.233	0.181	186	55	241	−5.9
AsI	191[h]	193	1.0	0.253	0.116	164	22	186	−2.6
AsO	326.2	368	12.8	0.179	0.181	180	135	315	−3.4
SbH	257.0	250	−2.7	0.1707	0.030	255	2	257	0.0
SbF	431[l]	616	42.9	0.190	0.405	165	258	423	−1.9
SbCl	313.7	340	8.4	0.2325	0.257	190	105	295	−6.0
SbBr	264.2	269	1.8	0.251	0.219	166	73	239	−9.5
CH	415.8	410	−1.4	0.1094	0.048	412	12	424	2.0
CF	489	494	1.0	0.132	0.216	267	173	440	−10.0
CCl	326.6	342	4.7	0.177[k]	0.107	294	34	328	0.4
CBr	271	284	4.8	0.194[k]	0.075	259	16	275	1.5
SiH	323.3	326	0.8	0.148[k]	0.048	328	9	337	4.2
SiF	596.6	732	22.7	0.154	0.340	231	311	542	−9.2
SiCl	399.8	435	8.8	0.2019	0.236	252	135	387	−3.2
SiBr	329.7	351	6.5	0.216	0.205	224	101	325	−1.4
SiI	235[h]	258	9.8	0.241	0.155	193	54	247	5.1
SiO	466.2[j]	488	4.7	0.166[k]	0.185	217	196	413	−11.4
GeH	289.4	291	0.6	0.1527	0.031	299	4	303	4.7
GeF	471[l]	659	39.9	0.168	0.336	198	276	474	0.6
GeCl	339.8	380	11.8	0.209	0.219	227	115	342	0.6
GeBr	281.0	304	8.2	0.230	0.190	196	80	276	−1.8
GeI	215.2	222	3.2	0.249	0.135	173	40	213	−1.0
GeO	356.5[j]	430	20.6	0.18[i]	0.179	187	167	354	−0.7
BH	372	368	−1.1	0.119[k]	0.027	366	2	368	−1.1
BF	645.6	692	7.2	0.131	0.338	257	275	532	−17.6

Table 2. (*Cont.*)

Bond	ΔH^0_{AB}[a] (exptl)	Pauling[b] ΔH^0_{AB}	Pauling[b] ±%	r_{AB}[c] (nm)	This work I_{AB}[d]	This work ΔH^0_{cov}[e]	This work ΔH^0_{disch}[f]	This work ΔH^0_{AB}[g]	This work ±%
BCl	443.8	430	−3.1	0.175	0.225	283	108	391	−11.9
BBr	368.0	349	−5.2	0.187	0.191	255	77	332	−9.8
BI	270.7	263	−2.8	0.203	0.134	228	38	266	−1 7
BeF	638.0	919	44.0	0.140	0.531	217	337	554	−13.2
BeCl	463.1	554	19.6	0.177	0.394	251	192	443	−4.3
BeBr	389[l]	453	16.5	0.191	0.358	224	157	381	−2.1
BeI	301[l]	336	11.6	0.212	0.296	195	104	299	−0.7
MgF	514.7	1032	100.5	0.177	0.662	162	378	540	4.9
MgCl	395.7	600	51.6	0.218	0.509	186	241	427	7.9
MgBr	340.5	494	45.1	0.234	0.470	164	205	369	8.3
MgI	266.7	363	36.1	0.257	0.403	142	149	291	9.1
CaF	558.9	1240	121.9	0.210	0.805	147	401	548	−2.0
CaCl	446.5	741	66.0	0.251	0.638	170	289	459	2.8
CaBr	400.1	621	55.2	0.263	0.592	152	261	413	3.2
CaI	332.0	469	41.3	0.288	0.525	131	205	336	1.2
SrF	543.4	1271	133.9	0.220	0.837	142	413	555	2.1
SrCl	446.8	761	70.3	0.267	0.673	161	296	457	2.3
SrBr	399.1	639	60.1	0.282	0.629	143	266	409	2.5
SrI	325.0	483	48.6	0.303	0.555	125	214	339	4.3
BaF	578.0	1310	126.6	0.232	0.877	130	406	536	−7.3
BaCl	474.6	786	65.6	0.282	0.710	147	295	442	−6.9
BaBr	421.4	662	57.1	0.299	0.667	130	265	395	−6.3
BaI	359.8	503	39.8	0.320	0.590	114	217	331	−8.0
LiF	578.2	1256	117.2	0.1564	0.989	167	452	619	7.1
LiCl	476.4	754	58.3	0.2021	0.817	182	309	491	3.1
LiBr	423[l]	633	49.6	0.217	0.769	161	275	436	3.1
LiI	347.3	479	37.9	0.239	0.684	139	218	357	2.8
NaF	477.5	1274	166.8	0.1926	1.000	125	381	506	6.0
NaCl	405.6	757	86.6	0.2361	0.903	143	295	438	8.0
NaBr	362.3	635	75.3	0.2502	0.846	127	266	393	8.5
NaI	293.7	480	63.4	0.2711	0.751	111	215	326	11.0
KF	493.7	1346	172.6	0.217	1.000	115	385	500	1.3
KCl	425.1	802	88.7	0.2667	1.000	128	317	445	4.7
KBr	381.2	677	77.6	0.2821	0.947	113	290	403	5.7
KI	321.6	516	60.5	0.3048	0.846	98	238	336	4.5
RbF	491.3	1341	172.9	0.227	1.000	111	388	499	1.6
RbCl	431.5	796	84.5	0.279	1.000	123	316	439	1.7
RbBr	375.6	672	78.9	0.2945	0.968	109	295	404	7.6
RbI	322.0	511	58.7	0.3177	0.864	95	242	337	4.7
CsF	514.1	1361	164.7	0.2345	1.000	110	395	505	−1.8
CsCl	437.9	809	84.7	0.2906	1.000	120	315	435	−0.7
CsBr	397.1	684	72.2	0.3072	1.000	106	303	409	3.0
CsI	334.8	521	55.6	0.332	0.898	91	250	341	1.9

[a] Experimental bond enthalpy; derived from atomization enthalpies (ΔH^0_{at}) of gaseous binary compounds: ref. 8, except as noted.

[b] Equation (2).

[c] Bond length: ref. 5, except as noted.

[d] Degree of ionic character [eq. (14)]. Upper limit = 1.000 (ion pair).

[e] Non-polar covalent bond enthalpy [eq. (6)].

[f] Discharge enthalpy [eq. (16)].

[g] Sum of eqs (6) and (16).

[h] Reference 2, adjusted to ΔH^0_f(A, g) as given in ref. 8.

[i] Estimated (this work).

[j] Using assumed $\Delta H^0_{vap}(NCl_3, liq)$ and $\Delta H^0_{subl}(P_4O_6, c)$, or from $(\Delta H^0_{at}(SiO_2, c))/4$ and $(\Delta H^0_{at}(GeO_2, c))/4$.

[k] Reference 4(b).

[l] Reference 5.

enthalpy calculation developed in this work is compatible with Sanderson's Principle of Electronegativity Equalization.

DISCUSSION

Matcha[7] has derived an equation for the total bond enthalpy which is similar to the sum of eqs (6) and (9):

$$\Delta H^0_{cov} = (\Delta H^0_{AA}\Delta H^0_{BB})^{1/2} + 4.5F(1-\exp[-0.29(X_B-X_A)^2]). \quad (21)$$

The factors 4.5 and -0.29 arise from data fitting to a number of experimental bond enthalpies. For the 100 bonds listed in Table 2, the average errors associated with eq. (21) are 4.5% for the 60 typical non-metal–non-metal bonds, 7.2% for the 40 metal halides and 5.6% overall.

However, the present work offers the following advantages over Matcha's equation.

(1) The present work provides a new, conceptually simple interpretation of Pauling's original treatment of heteronuclear bonds by introducing the concept of discharge enthalpy [eq. (3)] as a replacement for Pauling's "ionic resonance energy".

(2) By applying Sanderson's method of correcting the total bond enthalpy for any deviation in the actual bond length from the covalent radius sum, the present work offers somewhat greater overall predictive accuracy than Matcha's equation. It also eliminates the need for data fitting and restores the Faraday constant to the equations for the discharge enthalpy [eqs (7), (9) and (16)].

(3) The present work provides a simple, quantitatively useful adaptation of Sanderson's Principle of Electronegativity Equalization to the Pauling electronegativity scale (Fig. 2).

The phenomenon of "saturation", which is exhibited by the discharge enthalpy ΔH^0_{disch} for large differences in electronegativity $|X_B-X_A|$, is illustrated in Fig. 1 and accounted for mathematically by eq. (9). It is due to the fact that, during chemical bond formation, charge-transfer from a less to a more electronegative atom is initially exothermic but increasingly less so as electronegativity equalization is approached.[6,11] As a result, the final transfer of charge needed to achieve equalization is accompanied by only a very small energy change.

The degrees of ionic character I_{AB} calculated by eq. (14) are obviously useful in the calculation of bond enthalpies (cf. Table 2) and from a strictly pragmatic viewpoint it is not important whether or not they are "real". However, this is an intriguing question to consider and the reader is left to his or her own conclusions. It is very interesting that, for the eight alkali halides which are calculated by eq. (14) to have I_{AB} greater than unity, eq. (16) gives better predictions for ΔH^0_{disch} (setting I_{AB} equal to unity) than eq. (9) does. Conversely, for the 12 alkali halides which are calculated by eq. (14) to have I_{AB} less than unity, eq. (16) gives *worse* predictions for ΔH^0_{disch} (setting I_{AB} equal to unity) than eq. (9) does.

The charge coefficient b_A, calculated by eqs (19) or (20), should be interpreted as the change in electronegativity undergone by an atom accompanying acquisition of unit charge *when in the presence of other atoms at normal internuclear distances*. It is related only qualitatively to charge coefficients in the Mulliken electronegativity system which are derived from *isolated-atom* ionization energy–electron affinity curves.[4c,11]

It is pertinent here to discuss average bond "energies" such as those that may be found tabulated in every elementary chemistry textbook. The success of these values in the prediction of total atomization enthalpies for molecules rests on the premise that a particular bond enthalpy remains essentially constant from molecule to molecule; that is, the bond behaves energetically as though it were independent of the remainder of a molecule.[1,2,4b] If the bond length does not change from one molecule to another, eq. (6) predicts a constant non-polar covalent enthalpy, and eqs (14) and (16) predict a constant discharge enthalpy, therefore a constant total bond enthalpy is expected.

A similar conclusion may be reached by the consideration of partial charges calculated in accord with Sanderson's Principle of Electronegativity Equalization. By recognizing that the degree of ionic character in a bond can be interpreted as a measure of the *unevenness* of electron sharing regardless of absolute partial charges, one may write an expression for I_{AB} which is more general than eq. (10):

$$I_{AB} = |\delta_A-\delta_B|/(V_A+V_B). \quad (22)$$

Equation (22) is mathematically equivalent to eq. (10) for a binary compound containing only A—B single bonds, but is also applicable to compounds composed of more than two elements, and to compounds containing homonuclear bonds (such as the O—O bond in H_2O_2).

If one defines the degree of ionic character in a bond by eq. (22) rather than by eq. (10), calculations based on electronegativity equalization reveal that

I_{AB} shows only a small variation from molecule to molecule. For example, δ_C and δ_F calculated by combining eqs (17), (18) and (20) vary from +0.11 and −0.81 in CH_3F to +0.75 and −0.19 in CF_4, yet I_{CF} calculated from eq. (22) only changes from 0.18 to 0.19. It follows that the value of the discharge enthalpy calculated by eq. (16) will show only a small variation from molecule to molecule, leading to a virtually constant value for the total C—F bond enthalpy. The validity of this idea, and of eq. (22) as a general expression for the degree of ionic character in a bond, explains the success of average bond "energies" within the framework of Sanderson's Principle.

For the alkali hydrides, the errors associated with Pauling's method[2] [eq. (2)] are 67 (LiH), 95 (NaH), 122 (KH), 119 (RbH) and 118% (CsH). The method of bond enthalpy calculation developed in this work is somewhat more successful but not satisfactory, the corresponding errors being 49, 59, 77, 77 and 78%, respectively. As Sanderson has pointed out,[5a] a quantitative theory of bonding to very negative hydrogen has not yet been developed. Evans and Huheey[6] have suggested that the problem may be related to the unusual size and diffuse character of the hydride ion, which in terms of the present model must somehow result in a much lower discharge enthalpy than that calculated by eq. (16).

The method of bond enthalpy calculation developed in this work should allow the recalculation of the Pauling electronegativity scale with greatly increased overall accuracy. This will be presented in another paper.

REFERENCES

1. L. Pauling, *J. Am. Chem. Soc.* 1932, **54**, 3570.
2. L. Pauling, *The Nature of the Chemical Bond*, 3rd Edn, Chap. 3. Cornell University Press, Ithaca, NY (1960).
3. A. L. Allred, *J. Inorg. Nucl. Chem.* 1961, **17**, 215.
4. (a) J. E. Huheey, *Inorganic Chemistry*, 3rd Edn, App. C. Harper and Row, New York (1983); (b) J. E. Huheey, *Inorganic Chemistry*, 3rd Edn, App. E. Harper and Row, New York (1983); (c) J. E. Huheey, *Inorganic Chemistry*, 3rd Edn, Chap. 3. Harper and Row, New York (1983).
5. (a) R. T. Sanderson, *Polar Covalence*, Chap. 3. Academic Press, New York (1983); (b) R. T. Sanderson, *Polar Covalence*, Chap. 5. Academic Press, New York (1983).
6. (a) R. S. Evans and J. E. Huheey, *J. Inorg. Nucl. Chem.* 1970, **32**, 373; (b) J. E. Huheey and R. S. Evans, *J. Inorg. Nucl. Chem.* 1970, **32**, 383; (c) R. S. Evans and J. E. Huheey, *J. Inorg. Nucl. Chem.* 1970, **32**, 777.
7. R. L. Matcha, *J. Am. Chem. Soc.* 1983, **105**, 4859.
8. D. D. Wagman, *J. Phys. Chem. Ref. Data* 1982, **11**, Supp 2 (NBS Tables of Chemical Thermodynamic Properties).
9. R. T. Sanderson, *Science* 1951, **114**, 670.
10. (a) S. G. Bratsch, *J. Chem. Educ.* 1984, **61**, 588; (b) S. G. Bratsch, *J. Chem. Educ.* 1985, **62**, 101.
11. R. P. Iczkowski and J. L. Margrave, *J. Am. Chem. Soc.* 1961, **83**, 3547.

Polyhedron Vol. 7, No. 18, pp. 1687–1691, 1988
Printed in Great Britain

0277–5387/88 $3.00+.00
© 1988 Pergamon Press plc

LIGAND FIELD PHOTOCHEMISTRY OF SUBSTITUTIONALLY INERT PENTACYANOFERRATE(II) COMPLEXES

NEYDE YUKIE MURAKAMI IHA,* HENRIQUE EISI TOMA and JAILSON FARIAS DE LIMA

Instituto de Quimica, Universidade de São Paulo, Caixa Postal 20780, São Paulo, SP, Brazil

(*Received* 4 *September* 1987; *accepted* 7 *February* 1988)

Abstract—Ligand field excitation of $[Fe(CN)_5L]^{3-}$ complexes (L = PPh_3, $AsPh_3$, $SbPh_3$, $P(OCH_3)_3$ and CO) leads to photolabilization of L with quantum yields (Φ) around 0.15, except for the carbonyl complex, in this case $\Phi = 0.38$. The results were interpreted in terms of the nature of the low-lying excited states in the series of complexes.

In contrast to the thermal substitution reactions,[1–4] the photosubstitution reactions of pentacyanoferrate(II) complexes, $[Fe(CN)_5]^{3-}$, have been little investigated, particularly in comparison to other related d^6 complexes.[5–8]

The typical chemical deactivation pathway is the labilization of the coordinated ligand L towards substitution by another nucleophile (S), as represented by eq. (1).

$$[Fe(CN)_5L]^{3-} + S \xrightarrow{h\nu} [Fe(CN)_5S]^{3-} + L. \quad (1)$$

Figard and Petersen[9] have reported that the metal-to-ligand charge-transfer (CTTL) excitation of $[Fe(CN)_5L]^{n-}$ complexes with aromatic nitrogen heterocyclic ligands leads essentially to the photosubstitution reaction (1) in aqueous solution. The magnitude of the quantum yields is dependent on whether the LF ($0.1 < \Phi < 1.0$) or CTTL ($\Phi < 0.05$) excited state is the lowest in energy.

The photodissociation of a cyanide ligand was expected to be less favoured than for a neutral ligand, because of the charge separation involved in the process.[10] However, in $[Fe(CN)_5(N—N)]^{3-}$ complexes, where N—N is a bidentate ligand which has a NH_2 group available to enter a vacant coordination site, the photosubstitution of the cyanide ion proceeds with quantum yields comparable to the usual ones for the substitution of L.[11,12] In this case, a ring closure process involving a neighbouring effect in the excited state was observed, yielding a chelate tetracyanoferrate(II) complex, as represented by eq. (2).

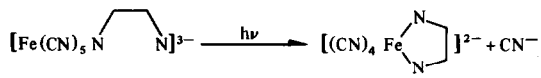

(2)

In the present work, we investigated the ligand field photochemistry of inert $[Fe(CN)_5L]^{3-}$ complexes, where L = PPh_3, $AsPh_3$, $SbPh_3$, $P(OCH_3)_3$ and CO. These complexes do not display MLCT bands in the visible, allowing direct access to the LF excited states. They are also unreactive with respect to thermal substitution processes, favouring the determination of the quantum yields in aqueous solution.

As far as we know, similar photochemical studies involving pentacyanoferrate(II) complexes have only been reported for the $[Fe(CN)_5CO]^{3-}$,[13,14] $[Fe(CN)_5AsO_3H_3]^{3-}$[15] and $[Fe(CN)_5NO]^{2-}$[16,17] derivatives.

EXPERIMENTAL

Materials

Potassium tris(oxalate)ferrate(III) was prepared from reagent grade potassium oxalate and ferric chloride and recrystallized three times as described by Parker.[18] Sodium amminepentacyanoferrate(II) trihydrate was prepared from sodium nitroprusside, as described in the literature.[19] The N-methyl-pyrazinium ion, Mpz^+, was prepared from the reaction of methyl iodide (Aldrich) with pyrazine (Aldrich)

* Author to whom correspondence should be addressed.

in benzene solution and recrystallized from chloroform, according to the method described by Bahner and Norton.[20] The $Na_3Fe(CN)_5L$ [L = PPh_3, $AsPh_3$, $SbPh_3$, $P(OCH_3)_3$] complexes were synthesized and characterized according to the procedures described by Nast and Kruger.[21]

Measurements

The photolysis of the complexes was carried out with a Hanau 90 W St-75 mercury vapour lamp, powered by a Hanau power supply, using a Coleman 12.225 filter, which transmits essentially the 366 and 344 nm emission lines, of relative intensities 100 and 7, respectively. Monochromatic irradiation was carried out using a 200 W Hg(Xe) arc lamp housed in an Oriel Universal Lamp Housing model 6107 and powered by a Model 8500 Universal power supply. The beam was passed through a quartz collimating lens, an Oriel Optic Corp. interference filter (365 nm) and a D. F. Vaconcellos interference filter (400 nm) with a bandpass of 10 nm.

The experiments were performed in the presence of the N-methylpyrazinium ion (Mpz^+) which was the trapping agent for the aquapentacyanoferrate(II) ion, using a 50 mm pathlength quartz cell thermostatted at 25.0°C by a Haake Model FE constant-temperature circulating bath.

The concentrations were adjusted to yield optical densities greater than two in the region of the irradiating wavelength. The solution was continuously stirred during the photolysis in order to ensure homogeneity.

Light intensities were determined by ferrioxalate actinometry before and after each photolysis run. The quantum yields were measured spectrophotometrically by monitoring the appearance of the $[Fe(CN)_5Mpz]^{2+}$ complex at 660 nm. A 10 mm spectrophotometric quartz cell was adapted to a 50 mm photolysis quartz cell, allowing direct measurement of the photolysis product.

At least five determinations were made for each set of conditions and these are reported in Tables 1 and 2. All the values were comparable, within the experimental error. A similar consistency was found for Φ values obtained using different light sources.

A secondary thermal reaction was detected in the case of the $[Fe(CN)_5P(OCH_3)_3]^{3-}$ complex. The effect was minimized by carrying out the quantum yield determinations at a lower temperature (e.g. 15°C) and/or analysing the $[Fe(CN)_5Mpz]^{2-}$ ion after passing it through a BioRad Ag1-X2 (Cl^-) ion exchange column.

Spectral measurements were performed using a Cary 17 spectrophotometer. The contribution from thermal reactions was controlled by using a dark sample prepared in an identical manner.

Table 1. Quantum yields for the photosubstitution reaction of the $[Fe(CN)_5PPh_3]^{3-}$ complex obtained in several experimental conditions

Quantum yields	(% Photolysis)
0.12	(0.25, 0.36, 0.43, 0.48)[a]
0.13	(0.079, 0.123)[b] (0.084, 0.17, 0.25, 0.34, 0.42, 0.50, 0.59, 0.68, 0.76, 0.85, 1.02)[c]
0.14	(0.087, 0.18, 0.34, 0.43, 0.51, 0.60)[d] (0.065, 0.088, 0.13)[e] (0.17, 0.21, 0.26, 0.30, 0.34, 0.39, 0.43, 0.47, 0.51, 0.56, 0.60, 0.64, 0.68, 0.72, 0.77, 0.84, 0.92)[b]
0.15	(0.098)[f] (0.19, 0.24, 0.29, 0.34, 0.39, 0.43, 0.48, 0.53, 0.60, 0.67, 0.78)[e]
0.16	(0.26, 0.32)[f]
0.17	(0.055, 0.17, 0.28, 0.40)[f]
0.18	(0.34, 0.56, 0.63, 0.67)[g]

[a-g] Concentration of the complex, 19.8, 10.6, 10.0, 10.9, 9.86, 9.91, 10.8 mmol, respectively; [a,b,d-g] $[Mpz^+]$ = 1.1 mmol; [c] $[Mpz^+]$ = 2.1 mmol; [a-c,e,g] light source (ORIEL); [a] interference filter (404 nm); [g] Coleman absorption filter; [b,c,e] interference filter (366 nm); [d,f] light source (HANAU), absorption filter; [b] Ionic strength = 0.50 ($LiClO_4$), temperature = 25.0°C.

RESULTS AND DISCUSSION

Spectra

The electronic spectra of an aqueous solution of the pentacyanoferrate(II) complexes show an absorption band of moderate intensity ascribed to the *d–d* transition from the $^1A_1$ ground state to the $^1E(1)$ excited state (Table 3), under C_{4v} symmetry.[22]

Quantum yield determination

The ligand field excitation of aqueous solutions of $[(CN)_5FeL]^{3-}$ complexes led to the typical photochemical reaction described by eq. (3)

$$[(CN)_5FeL]^{3-} + H_2O \xrightarrow{h\nu} [(CN)_5FeH_2O]^{3-} + L. \quad (3)$$

The quantum yield determinations for the photosubstitution of the ligand L were carried out by adding an excess of the N-methylpyra-

Table 2. Quantum yields of the ligand field photolysis of the substitutionally inert $[Fe(CN)_5L]^{3-}$ complexes

L	Quantum yield	(% Photolysis)
PPh_3	0.15±0.03	See Table 1
$AsPh_3$	0.15±0.01	(0.15, 0.24, 0.32, 0.40, 0.46, 0.60)[a]
$SbPh_3$	0.12±0.02	(0.16, 0.25, 0.33, 0.41, 0.49, 0.56, 0.65, 0.68)[b] (0.17, 0.31, 0.42)[c] (0.060, 0.18, 0.43, 0.57, 0.71, 0.85, 0.95, 1.08)[d]
$P(OCH_3)_3$	0.14±0.01	(0.11, 0.23, 0.44, 0.54, 0.67, 0.78)[c] (0.10, 0.18, 0.25, 0.33, 0.39, 0.46, 0.55, 0.63, 0.70)[f] (0.15, 0.43, 0.57, 0.82, 0.90)[g]
CO	0.37±0.01	(0.027, 0.054, 0.061, 0.081, 0.11, 0.12, 0.16)[h] (0.049, 0.073, 0.10, 0.14, 0.16, 0.19)

[a-i] Concentration of the complex, 10.1, 9.94, 9.46, 10.3, 9.57, 10.3, 9.19, 51.0 and 51.0 mmol, respectively; [d,f,g,i] light source (ORIEL), interference filter (366 nm); [a,b,c,e,h] light source (HANAU), absorption filter; [f] temperature = 15.0°C, all other measurements were performed at 25.0°C.

zinium ion[23] in order to trap the photoproduct, $[(CN)_5FeH_2O]^{3-}$, via the fast thermal reaction (4)

$$[(CN)_5FeOH_2]^{3-} + Mpz^+ \xrightarrow{h\nu} [(CN)_5FeMpz]^{2-} + H_2O. \quad (4)$$

The Mpz^+ ion is a suitable trapping agent because of the remarkable thermal and photochemical stability of the $[Fe(CN)_5Mpz]^{2-}$ product.[9] The blue complex also exhibits a high extinction coefficient, which increases the sensitivity of the photometric analysis. The photolysed sample showed continuous spectral changes during the irradiation time, due to the increasing concentration of $[Fe(CN)_5Mpz]^{2-}$ species, as illustrated in Fig. 1. The measured quantum yields are listed in Tables 1 and 2. The extent of photolysis was kept to a minimum, in order to prevent secondary photoreactions and to obtain reliable quantum yields.

Table 3. Ligand field $^1A_1 \rightarrow {}^1E(1)$ transition energies of some pentacyanoferrate(II) complexes

L	$\nu\ ^1A_1 \rightarrow {}^1E(1)$ (cm^{-1})	ε ($M^{-1}\,cm^{-1}$)
CO	33.0	370
$P(OCH_3)_3$	31.3	240
PPh_3	27.8	440
$AsPh_3$	27.4	283
$SbPh_3$	26.7	220

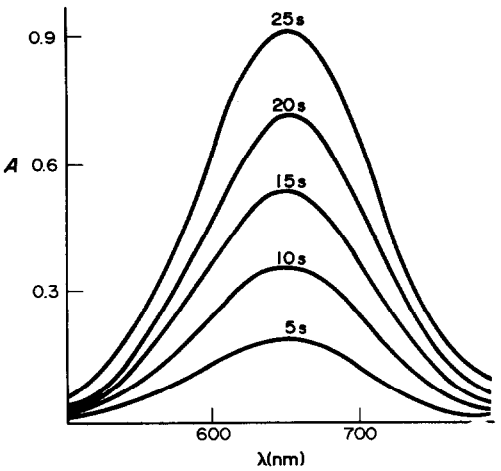

Fig. 1. Spectral change as a function of photolysis time, for the $[(CN)_5FePPh_3]^{3-}$ complex (1.00×10^{-2} M) in the presence of the Mpz^+ ion (1.00×10^{-3} M).

It should be noticed that all the complexes herein studied are much more inert to substitution in comparison to those previously studied.[9] As a consequence, the thermal reaction was not a complicating factor in the determination of the quantum yields for the photoaquation of L, except for the $SbPh_3$ complex, which underwent photoaquation to a small extent.

The effect of several conditions such as irradiation wavelength, concentration of the trap-

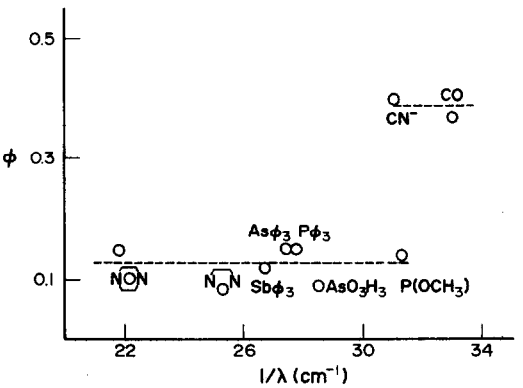

Fig. 2. Photosubstitution quantum yields vs the low energy spin-allowed LF transition wave numbers for $[Fe(CN)_5L]^{3-}$ complexes. Data for L = CN^-, AsO_3H_3, N—N and pyrazine from refs 25, 15, 11 and 9, respectively.

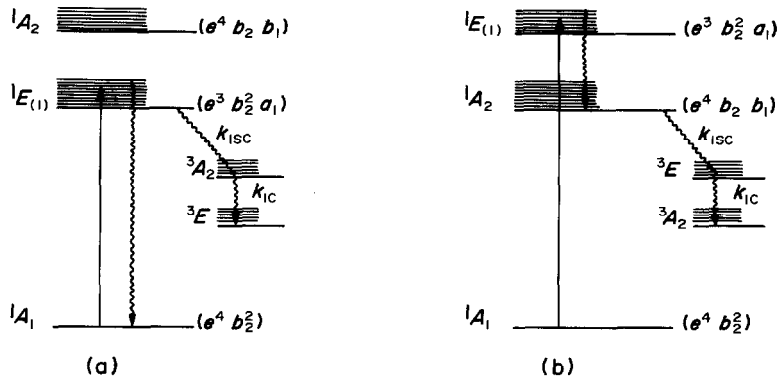

Fig. 3. Energy level diagrams for $[(CN)_5Fe^{II}L]^{3-}$ complexes. (a) LF strength of L < CN^-; (b) LF strength of L > CN^-.

ping agent Mpz^+, and ionic strength, was negligible as one can see for the $[Fe(CN)_5PPh_3]^{3-}$ complex in Table 1. The associative attack by the Mpz^+ ion in excess was ruled out, based on concentration dependence experiments (conditions c and e).

It is noteworthy that the quantum yield for the carbonyl complex is lower than that obtained by Vogler and Kunkely,[13] i.e. $\Phi = 0.9$, but it is in accordance with our previous work using an electrochemical method to monitor the carbonyl substitution.[14] We presume that the difference arises from the contrasting analytical methods employed to detect the photoreaction product. The use of a trapping agent, such as the Mpz^+ ion, improved the accuracy of the quantum yield determination as previously noticed by Figard and Petersen.[9]

In Fig. 2, the quantum yields for the photosubstitution reaction are plotted against the low energy spin allowed LF transition for a large series of ligands. The results indicate that the quantum yields for the photosubstitution reaction, obtained from the ligand field irradiation are quite similar for all the pentacyanoferrate(II) complexes, except for the cyanide and carbonyl ones. The magnitude of these values depends on the intersystem crossing ^{1}LF---^{3}LF efficiency, as well as on the nature of the photoreactive excited state. In general, when the ligand field strength of L is weaker than that of the cyanide ion, the energy levels follow the sequence shown in Fig. 3(a). The photoreactive excited state is the lowest one, namely ^3E. In the case of the carbonylpentacyanoferrate(II) complex, since CO has a ligand field strength stronger than that of CN^-, the ^3E level will be higher in energy than $^3A_2$, as one can see in Fig. 3(b). The rate of the internal conversion process is expected to be relatively fast and the low-lying excited state $^3A_2$,[24] should be responsible for the chemical reaction. The higher quantum yield for the carbonylpentacyanoferrate(II) complex is consistent with an appreciably longer lifetime for the $^3A_2$ excited state, as previously detected by Vera and Zuloaga,[24] leading to a higher photoconversion efficiency.

Acknowledgements—The support of the Fundação de Amparo à Pesquisa do Estado de São Paulo (FAPESP) and of the Conselho Nacional de Desenvolvimento Científico e Tecnológico (CNPq) is gratefully acknowledged.

REFERENCES

1. A. P. Szecsy, S. S. Miller and A. Haim, *Inorg. Chim. Acta* 1978, **28**, 189.
2. P. J. Morando and M. A. Blesa, *J. Chem. Soc., Dalton Trans.* 1982, 2147.
3. A. L. Coelho, H. E. Tomas and J. M. Malin, *Inorg. Chem.* 1983, **22**, 2703.
4. N. Y. Murakami Iha and H. E. Toma, *Rev. Latinoame. Quim.* 1984, **15**, 20.
5. P. C. Ford, *Coord. Chem. Rev.* 1982, **44**, 61.
6. P. C. Ford, D. Wink and J. Dibenedetto, *Prog. Inorg. Chem.* 1983, **30**, 213.
7. V. Balzani and V. Carassiti, *Photochemistry of Coordination Compounds.* Academic Press, London (1970).
8. A. W. Adamson and P. D. Fleishchauer, *Concepts of Inorganic Photochemistry.* Wiley, New York (1975).
9. J. E. Figard and J. D. Petersen, *Inorg. Chem.* 1978, **17**, 1059.
10. G. L. Geoffroy and M. S. Wrighton, *Organometallic Photochemistry.* Academic Press, New York (1979).
11. H. E. Toma and N. Y. Murakami Iha, *Inorg. Chem.* 1982, **21**, 3573.
12. N. Y. Murakami Iha, J. F. de Lima and H. E. Toma, *Proc. An. Meet. Coord. Chem. Jpn* 1984, **34**, 116.
13. A. Vogler and H. Kunkely, *Z. Naturforsch.*, B 1975, **30**, 355.

14. H. E. Toma, N. M. Moroi and N. Y. Murakami Iha, *An. Acad. Brasil. Cienc.* 1982, **54**, 316.
15. J. Legros, *J. Chim. Phys.* 1964, **61**, 923.
16. S. K. Wolfe and J. H. Swinehart, *Inorg. Chem.* 1975, **14**, 1049.
17. T. Jarzynowski, T. Senkowski and Z. Stasicka, *Rocz. Chem.* 1977, **51**, 2299; *Chem. Abstr.* 1978, **88**, 144252y.
18. C. A. Parker, *Proc. R. Soc.*, A 1953, **220**, 104.
19. G. Brauer, *Handbook of Preparative Inorganic Chemistry*, 2nd Edn, Vol. 2, p. 1511. Academic Press, New York (1965).
20. C. T. Bahner and L. L. Norton, *J. Am. Chem. Soc.* 1950, **72**, 2881.
21. R. Nast and K. W. Kruger, *Z. Anorg. Allg. Chem.* 1965, **341**, 189.
22. H. E. Toma, J. M. Malin, E. Giesbrecht and E. Fluck, *Inorg. Chim. Acta* 1975, **14**, 11.
23. H. E. Toma and J. M. Malin, *Inorg. Chem.* 1973, **12**, 1039.
24. L. Vera and F. Zuloaga, *Inorg. Chem.* 1978, **17**, 765.
25. G. Emschwiller and J. Legros, *C. R. Hebd. Seances. Acad. Sci.* 1965, **261**, 1535.

Polyhedron Vol. 7, No. 18, pp. 1693–1703, 1988
Printed in Great Britain

0277–5387/88 $3.00+.00
© 1988 Pergamon Press plc

VARIABLE COORDINATION NUMBERS IN CRYSTALLINE BIS(PENTAMETHYLCYCLOPENTADIENYL)SAMARIUM OXIDE, IODIDE AND ALKOXIDE COMPLEXES

WILLIAM J. EVANS,* DONALD K. DRUMMOND and LAURA A. HUGHES

Department of Chemistry, University of California, Irvine, CA 92717, U.S.A.

and

HONGMING ZHANG and JERRY L. ATWOOD*

Department of Chemistry, University of Alabama, University, AL 35486, U.S.A.

(*Received* 12 *October* 1987; *accepted after revision* 22 *February* 1988)

Abstract—Three crystallographically characterized organosamarium complexes containing formally x-coordinate trivalent samarium have been recrystallized under appropriate conditions to give formally $x+1$-coordinate species. The structures of these complexes have been determined and are compared with the x-coordinate structures. The implications of this structural flexibility on the steric factors which are very important in organolanthanide reactivity are discussed. Recrystallization of the seven-coordinate dihydroindenoindene diolate complex $[(C_5Me_5)_2Sm]_2O_2C_{16}H_{10}$ (**1**) from THF gives the eight-coordinate solvate $[(C_5Me_5)_2Sm(THF)]_2O_2C_{16}H_{10}$ (**2**) which crystallizes as a THF solvate in the space group $P2_1/n$ with $a = 10.811(4)$, $b = 13.878(4)$, $c = 25.114(7)$ Å, $\beta = 98.77(7)°$ and $D_{calc.} = 1.15$ g cm^{-3} for $Z = 2$. Least-squares refinement on the basis of 2208 observed reflections led to a final R value of 0.049. In **2**, two $(C_5Me_5)_2Sm$ bent metallocene units are coordinated to the $O_2C_{16}H_{10}$ framework via Sm—O bonds of 2.099(9) Å. Each Sm centre is also ligated by a THF molecule with a Sm—O distance of 2.490(9) Å. Both **1** and **2** have similar $O_2C_{16}H_{10}$ units but **2** has larger average Sm—C distances (2.75(2) vs 2.70(3) Å) and a smaller (ring centroid)—Sm—(ring centroid) angle (132.9 vs 139.8°). Recrystallization of $[(C_5Me_5)_2Sm]_2(\mu\text{-O})$ (**3**) from toluene in the presence of $CNCMe_3$ forms $[(C_5Me_5)_2Sm(CNCMe_3)]_2(\mu\text{-O})$ (**4**) which crystallizes in the space group $P2_1/c$ with $a = 27.265(10)$, $b = 13.946(5)$, $c = 15.505(5)$ Å, $\beta = 101.25(3)°$ and $D_{calc.} = 1.28$ g cm^{-3} for $Z = 4$. Least-squares refinement on the basis of 8275 observed reflections led to a final R value of 0.064. Like **3**, **4** has short Sm—O distances, 2.101(7) Å, and a nearly linear (174.3(4)°) Sm—O—Sm angle. **4** has a larger Sm—C(ring) average (2.80(1) vs 2.73(1) Å) and a smaller (ring centroid)—Sm—(ring centroid) angle (133.5 vs 137.2°). Recrystallization of $(C_5Me_5)_2SmI(THF)$ (**5**) in the presence of one equivalent of 1,5-pentamethylenetetrazole ($C_6H_{10}N_4$) gives the complex $(C_5Me_5)_2SmI(C_6H_{10}N_4)$ (**6**) which crystallizes in space group $P2_1/a$ with $a = 15.969(10)$, $b = 10.741(10)$, $c = 17.768(7)$ Å, $\beta = 108.81(4)°$ and $D_{calc.} = 1.58$ g cm^{-3} for $Z = 4$. Least-squares refinement on the basis of 3327 observed reflections led to a final R value of 0.061. In addition to the attachments of the two C_5Me_5 rings and the iodide ligand to Sm, two of the nitrogen atoms of the tetrazole ligand are oriented towards the metal at distances of 2.539(14) and 2.812(18) Å. The Sm—C(ring) average (2.73(2) Å) in **6** is the same as that in **5** and the Sm—I distance is larger (3.100(2) vs 3.048(2) Å).

The limited radial extension of the 4*f* valence orbitals of trivalent lanthanide ions[1,2] causes the chemistry of their complexes to be dominated more by electrostatic and steric effects than by orbital factors.[3–8] The importance of steric factors in organolanthanide chemistry has led to efforts to correlate the structural data with observed bonding modes of ligands[9] and with the stability[10–14] and

* Authors to whom correspondence should be addressed.

reactivity[7,8] of these complexes. These correlations have been made from crystallographic data on the organolanthanide species which crystallize from solution.

It has been possible to make these correlations, because in general, a given organolanthanide complex has an optimum steric environment. Hence, a given metal with a specific set of ligands will prefer to crystallize with a specific coordination number. For example, the "$(C_5Me_5)_2SmCl$" system prefers to be eight-coordinate and has been shown to achieve eight-coordination in a number of ways.[15,16] No seven-coordinate $(C_5Me_5)_2SmCl$ or nine-coordinate $(C_5Me_5)_2SmCl(THF)_2$ complexes have crystallized from solution and, on the basis of previous organolanthanide chemistry[3-8] and current structural generalizations,[9-14] this is unlikely. Eight-coordinate complexes apparently give the best balance between the size of Sm^{3+} and the size of the $(C_5Me_5)_2Cl$ ligand set and this is what crystallizes from solution.

Obviously, in solution there will be some variation in coordination number, but in general for materials which crystallize from solution, a single coordination number is favoured. Without any clear steric preference, the above correlations[7-14] could not be made.

For C_5H_5 lanthanide complexes, there are almost no cases in which an x-coordinate and an $x+1$-coordinate complex have crystallized involving the same metal ligand combination. A rare case of this phenomena has recently been reported for $(C_5H_5)_2GdBr$[17] which crystallizes in both an eight-coordinate $[(C_5H_5)_2Gd(\mu\text{-Br})]_2$ form and in a nine-coordinate polymeric form (assuming a cyclopentadienyl ring occupies three coordination positions). For C_5Me_5 lanthanide complexes there are a few more cases. For example, crystals of $(C_5Me_5)_2ClY(\mu\text{-Cl})Y(C_5Me_5)_2$ contain both seven- and eight-coordinate yttrium[18] and $(C_5Me_5)_2Lu(\mu\text{-Me})LuMe(C_5Me_5)_2$ is reported to be the same.* In these cases, the balance between the size of the metal and the ligand set may be intermediate between favouring seven and eight coordination and hence both are accessible.

In this paper, we report crystallographic data on three pairs of trivalent bis(pentamethylcyclopentadienyl)samarium complexes in which both an x-coordinate *and* an $x+1$-coordinate complex can be obtained in crystalline form with the same ligand set. This type of structural flexibility is unusual for complexes of this class.

* Unpublished results cited in ref. 6.

EXPERIMENTAL

The complexes described below are extremely air- and moisture-sensitive. Therefore, all syntheses and subsequent manipulations of these compounds were conducted under nitrogen with the rigorous exclusion of air and water using Schlenk, vacuum line and glovebox (Vacuum/Atmospheres HE-553 Dri-Lab) techniques.

Materials

Toluene and THF were distilled from sodium benzophenone ketyl. THF-d_8 and benzene-d_6 were vacuum transferred from sodium benzophenone ketyl. *tert*-Butylisocyanide (Aldrich) was dried over molecular sieves and degassed. 1,5-Pentamethylenetetrazole (Aldrich) was degassed at room temperature. Literature procedures were followed for the preparation of $[(C_5Me_5)_2Sm]_2(O_2C_{16}H_{10})$ (**1**),[19] $[(C_5Me_5)_2Sm]_2(\mu\text{-O})$ (**3**)[20] and $(C_5Me_5)_2SmI(THF)$ (**5**).[15]

Physical measurements

IR spectra were recorded on a Perkin–Elmer 283 spectrometer. ^1H NMR spectra were recorded with a Bruker 250 MHz spectrometer and were referenced to residual aryl protons in C_6D_6 (δ 7.15). Complexometric analyses were obtained as previously described.[21]

$[(C_5Me_5)_2Sm(THF)]_2O_2C_{16}H_{10}$ (2)

By dissolving **1** (90 mg, 0.084 mmol) in THF, **2** is formed quantitatively (by NMR). Cooling a toluene/THF solution of **2** to $-34°C$ yields X-ray quality crystals of **2**. ^1H NMR (C_6D_6) δ 8.99 (s, 1H), 1.53 (s, 30H, C_5Me_5), -2.44 (s, 4H, C_4H_8O), -3.83 (s, 4H, C_4H_8O). IR (KBr) 2900 s, 2850 s, 1600 m, 1475 m, 1440 s, 1375 m, 1285 s, 1170 s, 1150 s, 1120 s, 1070 s, 1020 s, 910 s, 880 w, 850 w, 800 w, 740 s, 680 m cm^{-1}.

$[(C_5Me_5)_2Sm(CNCMe_3)]_2O$ (4)

In the glovebox Me_3CNC (350 mg, 4.21 mmol) was stirred into a saturated toluene solution of **3** (200 mg, 0.233 mmol in about 10 cm^3 toluene). The solution was cooled to $-34°C$ overnight yielding crystals of **4** (195 mg, 80% yield obtained from several recrystallizations). Found: Sm, 29.7. Calc. for $Sm_2C_{50}H_{78}N_2O$: Sm, 29.4%. ^1H NMR (C_6D_6) δ 1.51, (s, 30H, C_5Me_5), -0.70, (s, 9H, C_4H_9NC). IR (KBr) 2900 s br, 2730 m, 2170 m, 1440 m, 1370 m, 1240 w, 1195 s, 1020 w, 840 w, 725 m cm^{-1}.

$(C_5Me_5)_2SmI(C_6H_{10}N_4)$ (**6**)

A concentrated toluene solution containing **5** (320 mg, 0.516 mmol) and 1,5-pentamethylenetetrazole (75 mg, 0.543 mmol) was cooled to −34°C overnight yielding crystals of **6** (320 mg, 90% yield obtained from several recrystallizations). Found: Sm, 21.1. Calc. for $SmIC_{26}H_{40}N_4$: Sm, 21.9%. ^1H NMR (C_6H_6) δ 1.27 (s, 30H, C_5Me_5), 2.81 (m, 2H), 2.57 (m, 2H), 2.02 (m, 2H), 0.60 (m, 2H), −0.01 (m, 2H). IR (KBr) 2960–2840 s, 2730 m, 1950 w, 1480–1300 s, 1260 s, 1200 s, 1150 m, 1110 s, 1075 m, 1020 s, 960 m, 890 m, 860 m, 825 w, 790 w, 720 w cm^{-1}.

X-ray crystallography of $[(C_5Me_5)_2Sm(THF)]_2O_2C_{16}H_{10}$ (**2**)

A single crystal of **2** measuring approximately $0.1 \times 0.2 \times 0.2$ mm was sealed under N_2 in a thin-walled glass capillary. Final lattice parameters as determined from a least-squares refinement of $[(\sin\theta)/\lambda]^2$ values for 15 reflections ($2\theta > 30°$) accurately centred on the diffractometer are given in Table 1. Data were collected on an Enraf–Nonius CAD-4 diffractometer by the $\theta-2\theta$ scan technique as previously described.[22] Data collection parameters are given in Table 1. The intensities were corrected for Lorentz, polarization and absorption effects. For the latter, an empirical method similar to that of Churchill was employed.[23]

The space group of **2** was uniquely defined by systematic absences as $P2_1/n$. The independent samarium atom was located with the aid of the MULTAN 80 direct methods program system.[24] Subsequent difference Fourier maps served to locate all other non-hydrogen atoms. Neutral atom scattering factors for Sm, C, and O were taken from Cromer and Waber.[25] The full-matrix least-squares refinement with isotropic temperature factors using the SHELX program system[26] for all non-hydrogen atoms led to a reliability index of

Table 1. Crystal data for $[(C_5Me_5)_2Sm(THF)]_2O_2C_{16}H_{10}$ (**2**), $[(C_5Me_5)_2Sm(CNCMe_3)]_2(\mu\text{-}O)$ (**4**) and $(C_5Me_5)_2SmI(C_6H_{10}N_4)$ (**6**)

	(2)	(4)	(6)
Formula	$Sm_2C_{64}H_{86}O_4 \cdot THF$	$Sm_2C_{57}H_{86}N_2O$	$SmIC_{26}H_{40}N_4$
fw	1289.4	1117.13	685.93
Space group	$P2_1/n$	$P2_1/c$	$P2_1/a$
a (Å)	10.811(4)	27.265(10)	15.969(10)
b (Å)	13.878(4)	13.946(5)	10.741(10)
c (Å)	25.114(7)	15.505(5)	17.768(7)
β (deg)	98.77(7)	101.25(3)	108.81(4)
V (Å^3)	3723	5783	2885
Z	2	4	4
$D_{calc.}$ (g cm^{-3})	1.15	1.28	1.58
Radiation	Mo-K_α	Mo-K_α	Mo-K_α
μ (cm^{-1})	16.3	20.16	31.20
Min.–Max. trans. coeff.	0.64–0.73	0.655–0.784	0.279–0.528
Max. cryst. dimensions (mm)	$0.1 \times 0.2 \times 0.2$	$0.30 \times 0.46 \times 0.26$	$0.19 \times 0.35 \times 0.53$
Type of scan	$\theta-2\theta$	$\theta-2\theta$	$\theta-2\theta$
Scan width (deg)	$0.8+0.2\tan\theta$	−1.2 in 2θ from $K\alpha_1$ to +1.2 from $K\alpha_2$	−1.2 in 2θ from $K\alpha_1$ to +1.2 from $K\alpha_2$
Scan speed (deg min^{-1})	Variable[22]	4–16 variable	3–40 variable
Standard reflections	800 080 00$\bar{1}$6	3$\bar{1}\bar{1}$ 8$\bar{1}$3 3$\bar{6}$4	$\bar{2}$10 2$\bar{3}\bar{6}$ $\bar{4}$00
Background counting	Moving crystal, moving counter	Evaluated from 96 step peak profile	Evaluated from 96 step peak profile
Data collection range	$2 < 2\theta < 40°$	$4 < 2\theta < 55°$	$0 < 2\theta < 55°$
Total unique data	4347	14174	5590
Unique data with $I \geq 3.0\sigma(I)$	2208	8275	3327
No. of parameters	192 (block refined)	496	289
$R(F)$	0.049	0.064	0.061
$R_w(F)$	0.052	0.097	0.105
GOF	0.5	2.39	3.38
Max. Δ/σ in final cycle	0.1	0.16	0.01

$R = \Sigma||F_o|-|F_c||/\Sigma|F_o| = 0.10$. Conversion to anisotropic thermal parameters for all non-hydrogen atoms except the carbon atoms of the THF ring and additional cycles of refinement gave the final values of $R = 0.049$ and $R_w = 0.052$. The function minimized in the least-squares calculation was $\Sigma w|\Delta F^2|$ with unit weights. In the last stage of refinement no parameters shifted by more than 0.05 of their estimated standard deviation. The final difference Fourier showed the presence of a badly disordered THF of crystallization in the lattice but the positions of these atoms were not refined. No systematic variation of $W(|F_o|-|F_c|)$ vs $|F_o|$ or $(\sin\theta)/\lambda$ was noted. The final values of the positional parameters are given as supplementary material.

X-ray crystallography of $[(C_5Me_5)_2Sm(CNCMe_3)]_2 O \cdot C_7H_8$ **(4)**

General procedures for data collection and reduction have been described previously.[27] A crystal measuring $0.30 \times 0.46 \times 0.26$ mm was sealed under nitrogen in a glass capillary and mounted on a Syntex $P2_1$ diffractometer. Lattice parameters were determined at 24°C from the angular settings of 15 computer-centred reflections with $30 < 2\theta < 35°$.

Data were collected by the $\theta-2\theta$ scan technique in bisecting geometry. The p factor in the expression[28] for the standard deviation of the observed intensities was given a value of 0.05. Relevant crystal and data collection parameters are given in Table 1. During the data collection, the intensities of three standard reflections measured every 100 reflections showed linear decay of 9%; the intensities were corrected for this decay. An absorption correction was applied. Systematic absences (*0k0*, *k* odd; *h0l*, *l* odd) established the space group as $P2_1/c$ (No. 14). Patterson and difference Fourier techniques were used to locate all non-hydrogen atoms. All non-hydrogen atoms except the carbon atoms in the toluene molecule were refined with anisotropic temperature parameters by use of full-matrix least-squares methods. No hydrogen atoms were located. Atomic scattering factors were taken from ref. 25. A final difference map contained no recognizable features. Fractional coordinates are given as supplementary material.

X-ray crystallography of $(C_5Me_5)_2SmI(\eta^2\text{-}C_6H_{10}N_4)$ **(6)**

A single crystal measuring $0.19 \times 0.35 \times 0.53$ mm was handled as described above for **4**. Lattice parameters were determined from 15 computer-centred reflections. Crystal and data collection parameters are given in Table 1. Systematic absences (*h0l*, *h* odd; *0k0*, *k* odd) established the space group as $P2_1/a$ (non-standard setting of $P2_1/c$, No. 14) and an absorption correction was applied. A combination of direct methods (MITHRIL)[29] and difference Fourier techniques provided the locations of all non-hydrogen atoms which were refined with anisotropic temperature parameters by the use of full-matrix least-squares methods. No hydrogen atoms were located. A final difference map contained no recognizable features; its largest peak was of height 2.70 e $Å^{-3}$ at a distance of 0.85 Å from the samarium atom. Fractional coordinates are given as supplementary material.

RESULTS

Dihydroindenoindene diolate complexes

$(C_5Me_5)_2Sm(THF)_2$ reacts with $C_6H_5C{\equiv}CC_6H_5$ to form a black complex of formula $[(C_5Me_5)_2Sm]_2C_2(C_6H_5)_2$ which reacts with CO according to eq. (1).

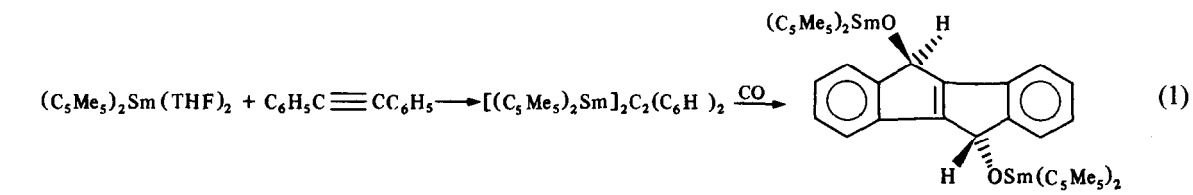

(1)

The product of this remarkable reaction, $[(C_5Me_5)_2Sm]_2(O_2C_{16}H_{10})$ **(1)**, contains a tetracyclic dihydroindenoindene diolate moiety which was identified by X-ray crystallography.[19] The structure of this complex shown in Fig. 1 contains formally seven-coordinate samarium atoms.

Although trivalent samarium attached to two C_5Me_5 rings generally prefers eight coordination, seven coordination for **1** seemed reasonable given the size of the $O_2C_{16}H_{10}$ ligand. Examination of the structure of **1** shown in Fig. 1 supports this contention.

However, **1** can be recrystallized from THF as the THF-disolvate $[(C_5Me_5)_2(THF)Sm]_2(O_2C_{16}H_{10})$ **(2)** in which each samarium atom is eight-coordinate. The structure of **2** presented

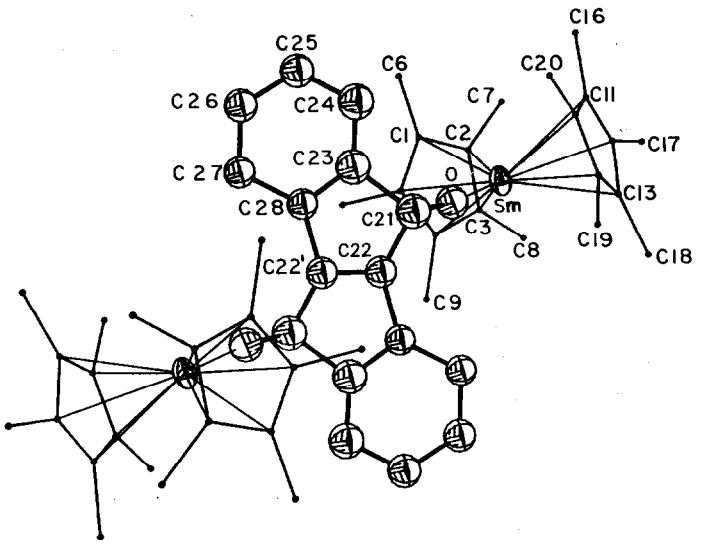

Fig. 1. ORTEP plot of $[(C_5Me_5)_2Sm]_2(O_2C_{16}H_{10})$ (**1**).

in Fig. 2 shows that despite the size of the dihydroindenoindene diolate ligand and the apparent steric congestion in **1**, additional coordination of a molecule of THF is possible.

Both **1** and **2** crystallize in space group $P2_1/n$ with two molecules per unit cell. **2** has a cell volume which is larger by 1230 Å^3 (Table 1). In both structures, the central double bond of the indenoindene unit (C(22)—C(22′) in **1**, C(28)—C(28′) in **2**) resides on an inversion centre. Selected structural features of **1** and **2** are compared in Table 2. Full bond length and angle data are given in the supplementary material.

As expected, the bond lengths in eight-coordinate compound **2** are longer than those in seven-coordinate **1**. Shannon lists eight-coordinate Sm^{3+} as being 0.059 Å larger than seven-coordinate Sm^{3+} in halides and chalcogenide crystal systems.[30] Consistent with this, the Sm—C(ring) average distance in **2** is 0.05 Å larger than that in **1**. The change in the Sm—O(indenoindene) distance is not as great, however: the Sm—O bond in **2** is only 0.019 Å

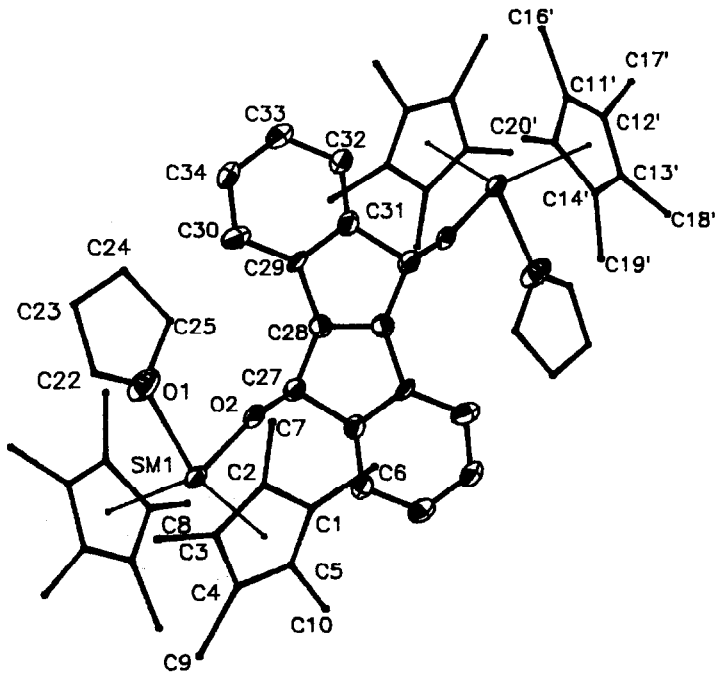

Fig. 2. ORTEP plot of $[(C_5Me_5)_2Sm(THF)]_2(O_2C_{16}H_{10})$ (**2**).

Table 2. Selected bond lengths (Å) and angles (deg) in $[(C_5Me_5)_2Sm]_2(O_2C_{16}H_{10})$ (**1**) and $[(C_5Me_5)_2Sm(THF)]_2(O_2C_{16}H_{10})$ (**2**)

	(**1**)	(**2**)
Coordination number	7	8
Sm—C(ring) average	2.70(3)	2.75(2)
Sm—O(1)(THF)	—	2.490(9)
Sm—O(2)($O_2C_{16}H_{10}$)	2.08(2)	2.099(9)
O(2)—C(27)	1.43(4)	1.45(2)
C(27)—C(28)	1.46(4)	1.49(2)
C(28)—C(28)′	1.25(5)	1.33(2)
(ring centroid)—Sm—(ring centroid)	139.85	132.9
Sm—O(2)—C(27)	173(2)	166.3(7)
O(1)—Sm—O(2)	—	94.0(3)

larger. A similar situation was found in the comparisons of isostructural $(C_5Me_5)_2LnX(THF)$ complexes (Ln = Sm, Y; X = Cl, I), namely that Ln—C(ring) distances followed closely the expected ionic radius changes, but the Ln–(σ bonded ligand) distances did not follow as well.[15]

The 2.490(9) Å Sm—O(THF) distance in **2** is comparable to analogous distances in other $(C_5Me_5)_2SmX(THF)$ systems: $(C_5Me_5)_2SmCl(THF)$,[15] 2.44(2), 2.48(2) Å; $(C_5Me_5)_2SmI(THF)$,[15] 2.45(1) Å; $(C_5Me_5)_2Sm(C_6H_5)(THF)$,[31] 2.511(4) Å; $[(C_5Me_5)_4Sm_2(O_2CCCO)(THF)]_2$,[32] 2.47(1) Å.

The (ring centroid)—Sm—(ring centroid) angle in **1**, 139.85°, decreases to 132.9° in **2** to accommodate the increase in coordination number. The observed value for **2** is within the range of the 131–138° angles observed for trivalent $(C_5Me_5)_2Sm(X)(Y)$ complexes.[33] The Sm—O(2)—C(27) angle is smaller by 7° in **2** than in **1**, but the 166.3(7)° angle is still typical of M—O—C angles of early transition metal, lanthanide and actinide systems.[34] Within the accuracy of the data the structural features of the indenoindene units in **1** and **2** are the same.

Oxo-bridged complexes

The bridged oxo complex, $[(C_5Me_5)_2Sm]_2(\mu\text{-O})$, (**3**), Fig. 3, has been synthesized by reacting 1,2-epoxybutane with $(C_5Me_5)_2Sm(THF)_2$ [eq. (2)].[20]

$$2(C_5Me_5)_2Sm(THF)_2 + CH_2\overset{O}{\diagup\diagdown}CHCH_2CH_3 \rightarrow [(C_5Me_5)_2Sm]_2(\mu\text{-O}) + CH_2{=}CHCH_2CH_3 + 4THF. \quad (2)$$

Complex **3** also forms from a variety of bis(pentamethylcyclopentadienyl) samarium complexes including $(C_5Me_5)_2Sm$,[35] $(C_5Me_5)_2Sm(THF)_2$,[33] $[(C_5Me_5)_2Sm(\mu\text{-H})]_2$,[36] $(C_5Me_5)_2Sm(C_6H_5)(THF)$[31] and $[(C_5Me_5)_2Sm]_2C_2(C_6H_5)_2$[36] when various oxygen-containing substrates are present. The formation of this complex is apparently quite

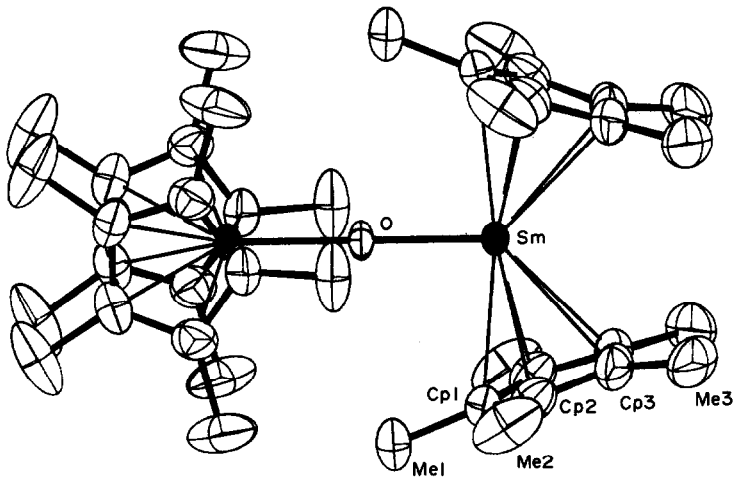

Fig. 3. ORTEP plot of $[(C_5Me_5)_2Sm]_2(\mu\text{-O})$ (**3**).

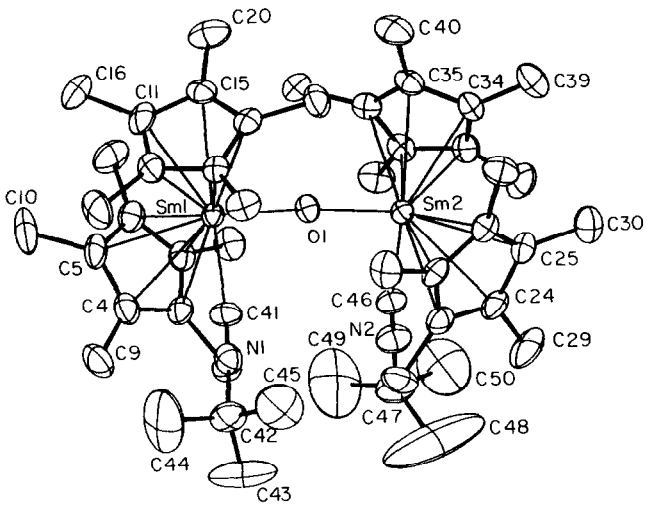

Fig. 4. ORTEP plot of $[(C_5Me_5)_2Sm(CNCMe_3)]_2(\mu\text{-}O)$ (**4**).

favourable and this species is frequently the first to crystallize from solution when it is present in a mixture.

As in complex **1**, the samarium atoms in complex **3** are seven-coordinate. Given the short Sm—O distances and the rigorously linear Sm—O—Sm unit, seven coordination again seemed reasonable. As in complex **1** and in seven-coordinate $(C_5Me_5)_2SmOC_6Me_4H$,[34] the sterically bulky $(C_5Me_5)_2Sm$—O "ligand" might require seven coordination when attached to a trivalent $(C_5Me_5)_2Sm$ unit.

Seven-coordinate **3** has been obtained in a crystalline form from many different systems. However, when **3** is crystallized from toluene containing *tert*-butylisocyanide, the eight-coordinate complex $[(C_5Me_5)_2(Me_3CNC)Sm]_2(\mu\text{-}O)$ **4**, is obtained (Fig. 4). Obviously, the $(C_5Me_5)_2Sm[OSm(C_5Me_5)_2]$ ligand set can still accommodate another ligand around the Sm(III) centre.

The structural features of complexes **3** and **4** are compared in Table 3. The differences in bond distances and angles between **3** and **4** parallel the differences found between **1** and **2**. The Sm—C (ring) average distance is 0.07 Å larger in eight-coordinate **4**, which is consistent with the 0.059 Å larger ionic radius for eight-coordinate Sm^{3+}. In contrast, the Sm—O bond lengths in **4** are only slightly larger, by 0.007–0.021 Å, than those in **3**. The (ring centroid)—Sm—(ring centroid) angle in eight-coordinate **4** is expectedly smaller than that in **3** and is in the normal range.

The most interesting angles in **3** and **4** are the Sm—O—Sm angles. In **3**, this angle is crystallography linear but in **4**, the 174.3(4)° angle is close to but not exactly linear. Considering the

Table 3. Selected bond lengths (Å) and angles (deg) in $[(C_5Me_5)_2Sm]_2(\mu\text{-}O)$ (**3**) and $[(C_5Me_5)_2(Me_3CNC)Sm]_2(\mu\text{-}O)$ (**4**)

	(3)	(4)
Coordination number	7	8
Sm—C(ring) average	2.73(1)	2.80(1)
Sm—O	2.094(1)	2.101(7)
		2.117(7)
Sm—C($CNCMe_3$)	—	2.62(1)
		2.66(1)
C(41)—N(1)	—	1.13(2)
C(46)—N(2)		1.12(2)
(ring centroid)—Sm—(ring centroid)	137.2	133.5
		131.9
Sm—O—Sm	180	174.3(4)
O—Sm—C	—	98.7(4)
		100.7(4)

Table 4. Selected bond lengths (Å) and angles (deg) in $(C_5Me_5)_2SmI(THF)$ (**5**) and $(C_5Me_5)_2SmI(\eta^2\text{-}N_4C_6H_{10})$ (**6**)

	(5)	(6)
Coordination number	8	9
Sm—C(ring) average	2.725(1)	2.73(2)
Sm—I	3.043(2)	3.100(2)
	3.053(2)	
Sm—O	2.45(1)	—
Sm—N	—	2.539(14)
		2.812(18)
(ring centroid)—Sm—(ring centroid)	136	137
	137	
(ring centroid)—Sm—I	106.2 106.1	106.6
	104.7 106.4	104.3

bulk of the $(C_5Me_5)_2Sm$ units and the steric congestion in **3** due to the short Sm—O distances, a linear Sm—O—Sm angle is reasonable. A bent Sm—O—Sm angle would bring the $(C_5Me_5)_2Sm$ units closer together causing more steric crowding. It is therefore interesting that increasing the crowding in this system by adding a $CNCMe_3$ ligand to each samarium atom, bends the Sm—O—Sm angle slightly. As discussed previously,[20] the short M—O distances and linear M—O—M angle in a transition metal complex is usually attributed to metal oxygen π bonding. Considering the limited radial extension of the 4*f* orbitals[1,2] of Sm^{3+} this rationale is not as easy to use for **3** and **4**.

The bonding parameters of the $CNCMe_3$ ligand in **4** are similar to those in $(C_5H_5)_3Pr(CNC_6H_{11})$[37] which has a C—N length of 1.11(1) Å and a CNC angle of 177.8(15)°. The Pr—C(CNR) distance of 2.65(1) Å is within the range of the lengths seen in **4** (2.62(1)–2.66(1) Å). According to Shannon,[30] nine-coordinate Pr^{3+} is 0.047 Å larger than nine-coordinate Sm^{3+} and the radius of Pr^{3+} with a coordination number of 10 should be even higher. Considering radial sizes in this way, the Sm—C (CNR) distance in **4** would be approximately 2.50 Å if it were comparable in length to that in $(C_5H_5)_3Pr(CNC_6H_{11})$. The significantly longer Sm—C bond in **4** suggests that considerable steric crowding exists in this molecule. The ν_{CN} stretching absorption in **4** supports the idea that the isocyanide in **4** is not interacting as strongly with the metal as it is in $(C_5H_5)_3PrCNC_6H_{11}$. For a series of six $(C_5H_5)_3LnCNC_6H_{11}$ complexes (Ln = Pr, Nd, Tb, Ho, Yb and Y),[38] the ν_{CN} stretch varied from 2203–2208 cm^{-1}, 65–70 cm^{-1} higher than the free ligand stretch at 2138 cm^{-1}. In **4**, the ν_{CN} stretch at 2170 cm^{-1} is only 36 cm^{-1} higher than in free $CNCMe_3$ (2134 cm^{-1}).[39]*

Iodide complexes

The iodide complex $(C_5Me_5)_2SmI(THF)$ (**5**)[15] is a good example of an eight-coordinate $(C_5Me_5)_2Sm(X)(Y)$ system. Its structure is typical of a bent metallocene with two additional ligands. The two ring centroids, the iodide and the THF oxygen atom describe a distorted tetrahedron (Table 4). Complex **5** can be formed in a variety of ways and like **3** above seems to be a favoured structure when the constituent ligands, in this case C_5Me_5 and I, are present with Sm(III). However, when $(C_5Me_5)_2SmI(THF)$ is crystallized from toluene in the presence of 1,5-pentamethylenetetrazole, $C_6H_{10}N_4$, a formally nine-coordinate complex $(C_5Me_5)_2SmI(C_6H_{10}N_4)$, complex **6** (Fig. 5), is obtained. Complexes **5** and **6** are compared in Table 4.

Structural comparisons between **5** and **6** differ significantly from those made between **1** and **2** and between **3** and **4**. In other cases, a change in coordination number changed the Sm—C(ring) distances significantly. In contrast, **5** and **6** have indistinguishable Sm—C(ring) distances. For complexes **1**–**4**, the Sm—O distances varied by less than 0.02 Å despite the change in coordination number. In contrast, **6** has a Sm—I distance which is 0.05 Å longer than the one in the lower coordinate **5**. Hence, the parts of the structure responsive to a change in coordination number have switched between **1**–**4** and **5**–**6**.

Examination of the Sm—N distances in **6** shows that one length, Sm—N(2), 2.812(18) Å, is significantly longer than the other, Sm—N(1), 2.539(14) Å. The latter distance is within the range of observed N:→Ln distances in lanthanide com-

*$Nd[N(SiMe_3)_2]_3(CNCMe_3)$ also has a higher ν_{CN}: 2195 cm^{-1}.[40]

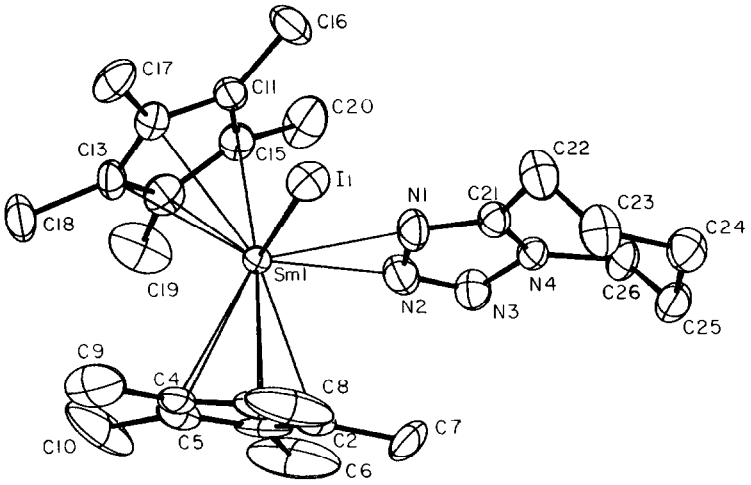

Fig. 5. ORTEP plot of $(C_5Me_5)_2SmI(C_6H_{10}N_4)$ (**6**).

plexes,[41,42] but the former distance is quite long. Similar situations were observed in the other trivalent $(C_5Me_5)_2Sm$ systems in which nine-coordinate Sm^{3+} was found, namely one of the three non-cyclopentadienyl ligand metal distances was quite long.[32,43] The rather long distance between Sm and N(2) in **6** may explain why the Sm—C(ring) distances are not substantially longer than in **5**. Nevertheless, the lengthened Sm—I bond indicates that this complex has made some accommodations for the increased coordination number.

The structural parameters for the pentamethylenetetrazole ligand in **6** are not significantly different from those of other tetrazoles,[44,45] including the ICl adduct of pentamethylenetetrazole $ClIN_4C_6H_{10}$[46] and the silver complex $[Ag(N_4C_6H_{10})_2(NO_3)]_2$.[47]

DISCUSSION

Bis(pentamethylcyclopentadienyl) complexes of trivalent samarium crystallize as seven-, eight-, or nine-coordinate species depending on the particular ligands present. The seven-coordinate complexes $(C_5Me_5)_2SmX$ contain large X ligands, e.g. $X = OC_6Me_4H$,[34] $OSm(C_5Me_5)_2$[20] or $O_2C_{16}H_{10}Sm(C_5Me_5)_2$.[19] Eight-coordinate complexes are more common, i.e. $[(C_5Me_5)_2Sm(\mu\text{-}H)]_2$,[36] $(C_5Me_5)_2Sm(C_6H_5)(THF)$,[31] $[(C_5Me_5)_2(Ph_3PO)Sm]_2(\mu\text{-}OCH{=}CHO)$,[48] $[(C_5Me_5)_4Sm_2(O_2CCCO)(THF)]_2$,[32] $(C_5Me_5)_2SmX(THF)$ (X = Cl, I),[15] $[(C_5Me_5)_2Sm]_2[(\mu,\eta^4\text{-}(PhN)OCCO(NPh)]$,[49] $[(C_5Me_5)_2Sm(\mu\text{-}Cl)]_3$[16] and three of the different Sm^{3+} environments in $(C_5Me_5)_{10}Sm_5Cl_5[Me(OCH_2CH_2)_4OMe]$.[16] Complexes containing the $(C_5Me_5)_2Sm$ unit in which the metal is nine-coordinate are rare and only in $[(C_5Me_5)_4Sm_2(O_2CCCO)(THF)]_2$,[32] $(C_5Me_5)_{10}Sm_5Cl_5[Me(OCH_2CH_2)_4OMe]$[16] and $(C_5Me_5)_2Sm(C_5H_5)$[43] has this been observed. In each of these formally nine-coordinate $(C_5Me_5)_2SmL_3$ systems, at least two of the three "L" donor atoms have been connected in a chelating unit. In the two polymetallic species, nine coordination is found for only one of the samarium atoms in the complex.

Although several coordination numbers are possible for trivalent $(C_5Me_5)_2SmX$ complexes in general, given a specific X ligand, past results suggest that there will be one preferred coordination number. The results presented here indicate that for complexes containing the $(C_5Me_5)_2Sm^{III}$ unit, there is a greater flexibility in coordination number than for previously studied classes of organolanthanides. Complexes **1**–**6** constitute three pairs in which the x-coordinate complex was known to crystallize and seemed to have a reasonably optimum coordination number considering the ligand set, and yet, in each pair, an $x+1$-coordinate complex also could be crystallized from solution. This suggests a greater range of stability for trivalent organolanthanides containing the $(C_5Me_5)_2Sm$ unit than for other metal ligand combinations. This may result due to the relative size of Sm^{3+} to C_5Me_5 ligands. Given that much of organolanthanide chemistry is driven towards steric optimization, this may have important implications for chemical systems which generate products containing the $(C_5Me_5)_2Sm^{III}$ unit.* It is also likely that other lanthanide metal ligand combinations will also strike such a balance in which more than one specific coordination number is favoured.

* For example, reactions of the divalent $(C_5Me_5)Sm$ unit.[8,49]

CONCLUSION

Three structures have been reported which demonstrate that trivalent complexes containing the $(C_5Me_5)_2Sm$ unit can favour more than one coordination number as they crystallize from solution. Similar combinations may be available with other lanthanide systems and may help broaden the range of chemical reactivity available.

Supplementary material. Complete tables of final fractional coordinates, bond distances and angles, thermal parameters (16 pp.), and observed and calculated structure factors (67 pp.) have been deposited with the Cambridge Structural Data File.

Acknowledgements—We thank the National Science Foundation for support of this research and Prof. Robert J. Doedens for help with the crystallography at Irvine.

REFERENCES

1. A. J. Freeman and R. E. Watson, *Phys. Rev.* 1976, **9**, 217; H. M. Crosswhite and A. P. Paszek, personal communication.
2. T. Moeller, in *Comprehensive Inorganic Chemistry* (Edited by J. C. Bailar), Vol. 4, Chap. 44. Pergamon Press, Oxford (1973).
3. T. J. Marks and R. D. Ernst, in *Comprehensive Organometallic Chemistry* (Edited by G. Wilkinson, F. G. A. Stone and E. W. Abel), Chap. 21. Pergamon Press, Oxford (1982).
4. J. H. Forsberg and T. Moeller, in *Gmelin Handbook of Inorganic Chemistry 8th Edn Sc, Y, La–Lu Part D6* (Edited by T. Moeller, U. Kruerke and E. Schleitzer-Rust), p. 137. Springer, Berlin (1983).
5. H. Schumann and W. Genthe, in *Handbook on the Physics and Chemistry of Rare Earths* (Edited by K. A. Gschneidner, Jr and L. Eyring), Vol. 7, Chap. 53 and references therein. Elsevier, Amsterdam (1985).
6. P. L. Watson and G. W. Parshall, *Accts Chem. Res.* 1985, **18**, 51 and refs therein.
7. W. J. Evans, *Adv. Organomet. Chem.* 1985, **24**, 131.
8. W. J. Evans, *Polyhedron* 1987, **6**, 803.
9. K. N. Raymond and C. W. Eigenbrot Jr, *Accts Chem. Res.* 1980, **13**, 276.
10. R. D. Fisher and Li Xing-Fu, *J. Less-common Metals* 1985, **112**, 303.
11. Li Xing-Fu, Xu Ying-Ting, Feng Xi-Zhang and Sun Peng-Nian, *Inorg. Chim. Acta* 1986, **116**, 75.
12. Li Xing-Fu, Feng Xi-Zhang, Xu Ying-Ting, Wang Hai-Tung, Shi Jie, Liu Li and Sun Peng-Nian, *Inorg. Chim. Acta* 1986, **116**, 85.
13. Tang Ber-Lin, Yu Zhi-Hui, Guo Ao-Ling, Sun Peng-Nian, Feng Xi-Zhan, Li Xing-Fu, Zhang Da-Chuan, Zhu Zhan-Yang and Lin Zhen-Jiong, *Polyhedron* 1987, **6**, 647.
14. K. W. Bagnall and Li Xing-Fu, *J. Chem. Soc., Dalton Trans.* 1982, 1365.
15. W. J. Evans, J. W. Grate, K. R. Levan, I. Bloom, T. Peterson, R. J. Doedens, H. Zhang and J. L. Atwood, *Inorg. Chem.* 1986, **25**, 3614.
16. W. J. Evans, D. K. Drummond, J. W. Grate, H. Zhang and J. L. Atwood, *J. Am. Chem. Soc.* 1987, **109**, 3928.
17. W. Lamberts, H. Lueken and U. Elsenhans, *Inorg. Chim. Acta* 1986, **121**, 81.
18. W. J. Evans, T. T. Peterson, M. D. Rausch, W. E. Hunter, H. Zhang and J. L. Atwood, *Organometallics* 1985, **4**, 554.
19. W. J. Evans, L. A. Hughes, D. K. Drummond, H. Zhang and J. L. Atwood, *J. Am. Chem. Soc.* 1986, **108**, 1722.
20. W. J. Evans, J. W. Grate, I. Bloom, W. E. Hunter and J. L. Atwood, *J. Am. Chem. Soc.* 1985, **107**, 405.
21. J. L. Atwood, W. E. Hunter, A. L. Wayda and W. J. Evans, *Inorg. Chem.* 1981, **20**, 4115.
22. J. Holton, M. F. Lappert, D. G. H. Ballard, R. Pearce, J. L. Atwood and W. E. Hunter, *J. Chem. Soc., Dalton Trans.* 1979, 45.
23. M. R. Churchill and F. J. Hollander, *Inorg. Chem.* 1978, **17**, 1957.
24. P. Main, S. J. Fiske, S. E. Hull, L. Lessinger, G. Germain, J-P. Declercq and M. M. Woolfson, *MULTAN 80, A System of Computer Programs for the Automatic Solution of Crystal Structures from X-Ray Diffraction Data* (1980).
25. D. T. Cromer and J. T. Waber, *Acta Cryst.* 1965, **A18**, 104.
26. G. M. Sheldrick, *SHELX, A System of Computer Programs for X-ray Structure Determination* (1976).
27. D. B. Sams and R. J. Doedens, *Inorg. Chem.* 1979, **18**, 153.
28. P. W. R. Corfield, R. J. Doedens and J. A. Ibers, *Inorg. Chem.* 1967, **6**, 197.
29. G. J. Gilmore, *MITHRIL, A Computer Program for the Automatic Solution of Crystal Structures from X-ray Data*, University of Glasgow (1983).
30. R. D. Shannon, *Acta Cryst. Sect. A: Cryst. Phys., Diffraction Theor. Gen. Cryst.* 1976, **A32**, 751.
31. W. J. Evans, I. Bloom, W. E. Hunter and J. L. Atwood, *Organometallics* 1985, **4**, 112.
32. W. J. Evans, J. W. Grate, L. A. Hughes, H. Zhang and J. L. Atwood, *J. Am. Chem. Soc.* 1985, **107**, 3728.
33. W. J. Evans, J. W. Grate, H. W. Choi, I. Bloom, W. E. Hunter and J. L. Atwood, *J. Am. Chem. Soc.* 1985, **107**, 941.
34. W. J. Evans, T. P. Hanusa and K. R. Levan, *Inorg. Chim. Acta* 1985, **110**, 191.
35. W. J. Evans, L. A. Hughes and T. P. Hanusa, *Organometallics* 1986, **5**, 1285.
36. W. J. Evans, I. Bloom, W. E. Hunter and J. L. Atwood, *J. Am. Chem. Soc.* 1983, **105**, 1401.
37. J. H. Burns and W. H. Baldwin, *J. Organomet. Chem.* 1976, **120**, 361.
38. E. O. Fischer and H. Fischer, *J. Organomet. Chem.* 1966, **6**, 141; R. von Ammon, R. D. Fischer and B. Kanellakopulos, *Chem. Ber.* 1971, **104**, 1072.
39. D. Dolphin and A. E. Wick, *Tabulation of Infrared Spectral Data*. Wiley, New York (1977).

40. R. A. Andersen, *Inorg. Chem.* 1979, **18**, 1507.
41. W. J. Evans, J. H. Meadows, W. E. Hunter and J. L. Atwood, *Organometallics* 1983, **2**, 1252.
42. W. J. Evans, T. P. Hanusa, J. H. Meadows, W. E. Hunter and J. L. Atwood, *Organometallics* 1987, **6**, 295.
43. W. J. Evans and T. A. Ulibarri, *J. Am. Chem. Soc.* 1987, **109**, 4292.
44. R. N. Butler, in *Comprehensive Heterocyclic Chemistry* (Edited by A. R. Katritzky and C. W. Rees), Vol. 5, Chap. 4.13. Pergamon Press, Oxford (1984).
45. G. B. Ansell, *J. Chem. Soc., Perkin II* 1973, **2036** and refs therein.
46. N. C. Baenziger, A. D. Nelson, A. Tulinsky, J. H. Bloor and A. I. Popov, *J. Am. Chem. Soc.* 1967, **89**, 6463.
47. R. L. Bodner and A. I. Popov, *Inorg. Chem.* 1972, **11**, 1410.
48. W. J. Evans, J. W. Grate and R. J. Doedens, *J. Am. Chem. Soc.* 1985, **107**, 1671.
49. W. J. Evans and D. K. Drummond, *J. Am. Chem. Soc.* 1986, **108**, 7440.

Polyhedron Vol. 7, No. 18, pp. 1705–1718, 1988
Printed in Great Britain

0277–5387/88 $3.00+.00
© 1988 Pergamon Press plc

TRIGONALLY QUANTIZED LIGAND FIELD POTENTIALS, *d*-ORBITALS AND *d*-ORBITAL ENERGIES

J. R. PERUMAREDDI

Department of Chemistry, Florida Atlantic University, Boca Raton, FL 33431, U.S.A.

(*Received* 20 *January* 1988; *accepted* 4 *March* 1988)

Abstract—The most generalized ligand field potentials for all possible geometries of coordination numbers one to twelve containing a trigonal axis have been derived in trigonal quantization. These potentials have been specialized for idealized geometries and the corresponding trigonally quantized *d*-orbitals and their energies have been derived. The applicability of the potentials and the *d*-orbitals in the study of the systems of idealized as well as slightly deviated trigonal geometries has been described.

The usual ligand field potential that is used in calculating the *d*-orbital energies in cubic symmetry is quantized along the tetragonal axis, i.e. along the four-fold axis of symmetry and the wave functions become the real *d*-orbitals, also tetragonally quantized, i.e. the four-fold axis taken as the *z*-axis. The same orbitals are applicable to any geometry containing a four-fold axis. For geometries containing a three-fold axis of symmetry or trigonal axis, it is convenient to use a ligand field potential quantized along the trigonal axis for calculating the energies of the *d*-orbitals also quantized along the trigonal axis. In fact such a trigonally quantized potential can be obtained for cubic geometries also, since these geometries contain a three-fold axis in which case the *d*-orbitals that are used to calculate the energies are trigonally quantized and not the "regular" *d*-orbitals. Such a set of trigonally quantized cubic *d*-orbitals have been derived quite some time ago[1–4] and employed in calculating the energy levels of many electron configurations in trigonally distorted or substituted cubic geometries.[5–15] It is the purpose of this paper to derive the trigonally quantized ligand field potentials in a number of geometries, to calculate the *d*-orbital energies and to show how the trigonally quantized *d*-orbitals are obtained.

* We shall always use primed notation to imply trigonal and non-primed for tetragonal.

† We will leave out, for simplicity, the θ', ϕ' variables from the spherical harmonics.

LIGAND FIELD POTENTIALS

Other than the trivial one and the linear two-coordinate geometries, which can also be considered as trigonal in that the linear axis of infinite order contains a three-fold rotation, the basic unit for a trigonal geometry is three-coordination, with the three ligand positions making an angle* of θ' with the three-fold axis passing through the centre and the ligand positions separated from each other by $2\pi/3$.

The ligand field potentials for the trivial cases of one- and two-coordination† are

$$V^{LF}_{C_{\infty v}}(1) = ez[\rho_0(r)\sqrt{4\pi}\,Y^0_0 + \rho_2(r)\sqrt{4\pi/5}\,Y^0_2 + \rho_4(r)\sqrt{4\pi/9}\,Y^0_4] \quad (1)$$

$$V^{LF}_{D_{\infty h}}(2) = ez[\rho_0(r)\sqrt{4\pi}\,2Y^0_0 + \rho_2(r)\sqrt{4\pi/5}\,2Y^0_2 + \rho_4(r)\sqrt{4\pi/9}\,2Y^0_4] \quad (2)$$

where e and z are the electronic charge and the effective charge of the ligand, respectively and $\rho_l(r) = r^l_</r^{l+1}_>$, $r_<$ and $r_>$ being the lesser and greater of the electronic radius vector and the metal–ligand bond distance. A ligand field potential in any trigonal geometry quantized along the three-fold rotational axis can have spherical harmonics of order zero or multiples of three. This means for the *d*-orbitals, we are only interested in the Y^0_0, Y^0_2, Y^0_4, and $Y^{\pm 3}_4$ terms in the potential. Thus the most general potential for three-coordination with a tri-

gonal angle θ' and with the x' axis in some general framework is given by

$$V^{LF}_{C_{3v}}(3) = ez\{\rho_0(r)\sqrt{4\pi}(3Y^0_0)+\rho_2(r)\sqrt{4\pi/5}\times(9/2\cos^2\theta'-3/2)Y^0_2+\rho_4(r)\sqrt{4\pi/9}\times(105/8\cos^4\theta'-45/4\cos^2\theta'+9/8)Y^0_4+\rho_4(r)\sqrt{4\pi/9}(\sqrt{35}/4)\sin^3\theta'\cos\theta'\times[-3e^{-3i\phi'}Y^3_4+3e^{3i\phi'}Y^{-3}_4]\}. \quad (3a)$$

The following two special cases are important in obtaining the potentials of all trigonal geometries. The first case is with the x' axis chosen to be in the same plane as the trigonal axis and one of the ligands, i.e. $\phi' = 0$, in which case the potential reduces to

$$V^{LF}_{C_{3v}}(3) = ez[\rho_0(r)\sqrt{4\pi}(3Y^0_0)+\rho_2(r)\sqrt{4\pi/5}\times(9/2\cos^2\theta'-3/2)Y^0_2+\rho_4(r)\sqrt{4\pi/9}\times(105/8\cos^4\theta'-45/4\cos^2\theta'+9/8)Y^0_4+\rho_4(r)\sqrt{4\pi/9}(\sqrt{35}/4)\sin^3\theta'\cos\theta'\times(-Y^3_4+Y^{-3}_4)]. \quad (3b)$$

The second case is when the x' axis bisects two ligand positions, i.e. $\phi' = \pi/3$, in which case the potential becomes

$$V^{LF}_{C_{3v}}(3) = ez[\rho_0(r)\sqrt{4\pi}(3Y^0_0)+\rho_2(r)\sqrt{4\pi/5}\times(9/2\cos^2\theta'-3/2)Y^0_2+\rho_4(r)\sqrt{4\pi/9}\times(105/8\cos^4\theta'-45/4\cos^2\theta'+9/8)Y^0_4+\rho_4(r)\sqrt{4\pi/9}(\sqrt{35}/4)\sin^3\theta'\cos\theta'(-3)\times(-Y^3_4+Y^{-3}_4)]. \quad (3c)$$

It should be noted that the potential in (3b) is also applicable to a situation for trigonal angles of $(\pi-\theta')$ and $\phi' = \pi/3$, and similarly the potential in (3c) is also applicable for trigonal angles of $(\pi-\theta')$ and $\phi' = 0$.

Using the potentials (1), (2), (3b) and (3c) as the building blocks, the potentials for any trigonal geometry can be obtained and the most generalized potentials for trigonal geometries of coordination numbers three to eight are given in Table 1 and for nine to twelve in Table 2. Some comments on the trigonal angles in various geometries are in order here.

The trigonal and tetragonal coordinate systems and the ligand positions in cubic geometries of the octahedron, tetrahedron and cube are depicted in Fig. 1 and the polar angles for the three geometries are given in Table 3. These angles, in particular θ', though not obvious from the figure can be deduced easily from models of an octahedron, tetrahedron or a cube. A time consuming, although useful derivation of these angles is made by utilizing the transformation of the tetragonal coordinates to trigonal coordinates. We will show this derivation using the octahedron as an example.

The trigonal coordinates are related to the tetragonal coordinates by the equation

$$\begin{pmatrix} z' \\ y' \\ x' \end{pmatrix} = \begin{pmatrix} \sqrt{1/3} & \sqrt{1/3} & \sqrt{1/3} \\ 0 & -\sqrt{1/2} & \sqrt{1/2} \\ \sqrt{2/3} & -\sqrt{1/6} & -\sqrt{1/6} \end{pmatrix} \begin{pmatrix} z \\ y \\ x \end{pmatrix}. \quad (4)$$

From the relationships of the cartesian and spherical polar coordinates, it follows that

$$\cos\theta' = \sqrt{1/3}(\cos\theta+\sin\theta\sin\phi+\sin\theta\cos\phi)$$

$$\sin\theta'\sin\phi' = \sqrt{1/2}(-\sin\theta\sin\phi+\sin\theta\cos\phi)$$

$$\sin\theta'\cos\phi' = \sqrt{1/6}(2\cos\theta-\sin\theta\sin\phi-\sin\theta\cos\phi). \quad (5)$$

The polar angles defined along the tetragonal axis for all ligand positions k = 1–6 in an octahedron are listed below.

	Ligand position, k					
	1	2	3	4	5	6
θ	0	$\pi/2$	$\pi/2$	$\pi/2$	$\pi/2$	π
ϕ	0	0	$\pi/2$	π	$3\pi/2$	0.

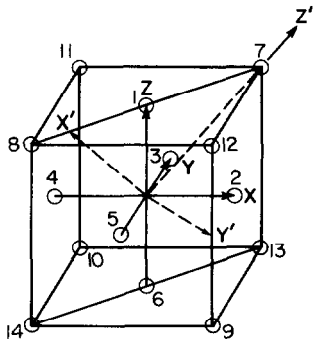

Fig. 1. Cubic geometries, and trigonal and tetragonal coordinate systems. Ligands 1–6, 7–10 and 7–14, respectively, constitute the geometries of the octahedron, tetrahedron and cube. The (z, y, x) and (z', y', x') are the tetragonal and trigonal coordinate systems, respectively.

Table 1. Generalized ligand field potentials in trigonal geometries of coordination numbers three to eight. (The constant *ez* is left out)

Coordination number	Expressions	Idealized geometry	$\rho_0(r)\sqrt{4\pi}\,Y_0^0$	$\rho_2(r)\sqrt{4\pi/5}\,Y_2^0$	$\rho_4(r)\sqrt{4\pi/9}\,Y_4^0$	$\rho_4(r)\sqrt{4\pi/9}\,Y_4^{\pm 3}$
3	3b	Trigonal	3	$\left(\frac{9}{2}\cos^2\theta' - \frac{3}{2}\right)$	$\left(\frac{105}{8}\cos^4\theta' - \frac{45}{4}\cos^2\theta' + \frac{9}{8}\right)$	$\mp\frac{3\sqrt{35}}{4}\sin^3\theta'\cos\theta'$
4	3b+1	Tetrahedron	4	$\left(\frac{9}{2}\cos^2\theta' - \frac{1}{2}\right)$	$\left(\frac{105}{8}\cos^4\theta' - \frac{45}{4}\cos^2\theta' + \frac{17}{8}\right)$	$\mp\frac{3\sqrt{35}}{4}\sin^3\theta'\cos\theta'$
5	3b+2	Trigonal bipyramid	5	$\left(\frac{9}{2}\cos^2\theta' + \frac{1}{2}\right)$	$\left(\frac{105}{8}\cos^4\theta' - \frac{45}{4}\cos^2\theta' + \frac{25}{8}\right)$	$\mp\frac{3\sqrt{35}}{4}\sin^3\theta'\cos\theta'$
6	2(3b)	Octahedron	6	$(9\cos^2\theta' - 3)$	$\left(\frac{105}{4}\cos^4\theta' - \frac{45}{2}\cos^2\theta' + \frac{9}{4}\right)$	$\mp\frac{3\sqrt{35}}{2}\sin^3\theta'\cos\theta'$
6	3b+3c	Trigonal prism	6	$(9\cos^2\theta' - 3)$	$\left(\frac{105}{4}\cos^4\theta' - \frac{45}{2}\cos^2\theta' + \frac{9}{4}\right)$	0
7	3b+3c+1	Monocapped trigonal prism[a]	7	$(9\cos^2\theta' - 2)$	$\left(\frac{105}{4}\cos^4\theta' - \frac{45}{2}\cos^2\theta' + \frac{13}{4}\right)$	0
7	2(3b)+1	Monocapped trigonal antiprism	7	$(9\cos^2\theta' - 2)$	$\left(\frac{105}{4}\cos^4\theta' - \frac{45}{2}\cos^2\theta' + \frac{13}{4}\right)$	$\mp\frac{3\sqrt{35}}{2}\sin^3\theta'\cos\theta'$
8	2(3b)+2	Cube	8	$(9\cos^2\theta' - 1)$	$\left(\frac{105}{4}\cos^4\theta' - \frac{45}{2}\cos^2\theta' + \frac{17}{4}\right)$	$\mp\frac{3\sqrt{35}}{2}\sin^3\theta'\cos\theta'$
8	2(3b)+2	Bicapped trigonal antiprism[b]	8	$(9\cos^2\theta' - 1)$	$\left(\frac{105}{4}\cos^4\theta' - \frac{45}{2}\cos^2\theta' + \frac{17}{4}\right)$	$\mp\frac{3\sqrt{35}}{2}\sin^3\theta'\cos\theta'$
8	3b+3c+2	Bicapped trigonal prism[a]	8	$(9\cos^2\theta' - 1)$	$\left(\frac{105}{4}\cos^4\theta' - \frac{45}{2}\cos^2\theta' + \frac{17}{4}\right)$	0

[a] Capping is on triangular faces.
[b] Capping is on diagonally opposite faces.

Table 2. Generalized ligand field potentials in trigonal geometries of coordination numbers nine to twelve. (The constant ez is left out)

Coordination number	Expressions	Idealized geometry	$\rho_0(r)\sqrt{4\pi}Y_0^0$	$\rho_2(r)\sqrt{4\pi/5}Y_2^0$	$\rho_4(r)\sqrt{4\pi/9}Y_4^0$	$\rho_4(r)\sqrt{4\pi/9}Y_4^{\pm 3}$
9	3b+3c+3b	Tricapped trigonal prism[a]	9	$\left(9\cos^2\theta'_1+\frac{9}{2}\cos^2\theta'_2-\frac{9}{2}\right)$	$\left(\frac{105}{4}\cos^4\theta'_1+\frac{105}{8}\cos^4\theta'_2-\frac{45}{2}\times\cos^2\theta'_1-\frac{45}{4}\cos^2\theta'_2+\frac{27}{8}\right)$	$\mp\frac{3\sqrt{35}}{4}\sin^3\theta'_2\cos\theta'_2$
10	3b+3c+3b+1	Tetracapped trigonal prism[b]	10	$\left(9\cos^2\theta'_1+\frac{9}{2}\cos^2\theta'_2-\frac{7}{2}\right)$	$\left(\frac{105}{4}\cos^4\theta'_1+\frac{105}{8}\cos^4\theta'_2-\frac{45}{2}\times\cos^2\theta'_1-\frac{45}{4}\cos^2\theta'_2+\frac{35}{8}\right)$	$\mp\frac{3\sqrt{35}}{4}\sin^3\theta'_2\cos\theta'_2$
11	3b+3c+3b+2	Pentacapped trigonal prism	11	$\left(9\cos^2\theta'_1+\frac{9}{2}\cos^2\theta'_2-\frac{5}{2}\right)$	$\left(\frac{105}{4}\cos^4\theta'_1+\frac{105}{8}\cos^4\theta'_2-\frac{45}{2}\times\cos^2\theta'_1-\frac{45}{4}\cos^2\theta'_2+\frac{43}{8}\right)$	$\mp\frac{3\sqrt{35}}{4}\sin^3\theta'_2\cos\theta'_2$
12	3b+3c+3b+3c	Icosahedron	12	$[9(\cos^2\theta'_1+\cos^2\theta'_2)-6]$	$\left[\frac{105}{4}(\cos^4\theta'_1+\cos^4\theta'_2)-\frac{45}{2}\times(\cos^2\theta'_1+\cos^2\theta'_2)+\frac{9}{2}\right]$	0

[a] Capping is on square faces.
[b] Capping is on all square faces and one triangular face.

Table 3. Polar angles of the ligand positions along the trigonal axis in regular cubic geometries (β is tetrahedral angle)

Geometry	Ligand position	θ'	ϕ'
Octahedron	1	$\beta/2$	0
	2	$\beta/2$	$2\pi/3$
	3	$\beta/2$	$4\pi/3$
	4	$(\pi-\beta/2)$	$5\pi/3$
	5	$(\pi-\beta/2)$	$\pi/3$
	6	$(\pi-\beta/2)$	π
Tetrahedron	7	0	0
	8	β	0
	9	β	$2\pi/3$
	10	β	$4\pi/3$
Cube	7	0	0
	8	β	0
	9	β	$2\pi/3$
	10	β	$4\pi/3$
	11	$(\pi-\beta)$	$5\pi/3$
	12	$(\pi-\beta)$	$\pi/3$
	13	$(\pi-\beta)$	π
	14	π	0

Substituting these angles for a given ligand position in eq. (5), the corresponding polar angles along the trigonal axis can be determined. Thus, for ligand position 2,

$$\cos\theta' = \sqrt{1/3}, \qquad \theta' = \beta/2$$

where β is tetrahedral angle

$$\sqrt{2/3}\sin\phi' = \sqrt{1/2}, \qquad \phi' = \pi/3 \text{ or } 2\pi/3$$

$$\sqrt{2/3}\cos\phi' = -\sqrt{1/6}, \qquad \phi' = 2\pi/3 \text{ or } 4\pi/3$$

hence $\phi' = 2\pi/3$.

By using these ϕ' angles and leaving θ' as a general angle to allow for obtaining potentials in the case of trigonal distortions the generalized potentials were obtained and are listed in Table 1 for coordination numbers three to eight. It should be noted that the geometries for coordination numbers nine to eleven are trigonal prismatic based with an additional three-coordinate unit inserted at the centre of the trigonal prism and thus require a second general angle θ' for the additional unit.

The 12-coordinate icosahedron geometry can be considered as two interlocking staggered trigonal prisms such that one triangular face of the second prism is in the central plane of the first prism. (See Table 4 for the generalized polar angles.) Such an arrangement will give rise to two trigonal angles θ'_1,

Table 4. Polar angles of the ligand positions along the trigonal axis in a regular icosahedron

Ligand position	θ'^a	ϕ'
1	θ'_1	0
2	θ'_1	$2\pi/3$
3	θ'_1	$4\pi/3$
4	θ'_2	$5\pi/3$
5	θ'_2	$\pi/3$
6	θ'_2	π
7	$(\pi-\theta'_2)$	$4\pi/3$
8	$(\pi-\theta'_2)$	0
9	$(\pi-\theta'_2)$	$2\pi/3$
10	$(\pi-\theta'_1)$	π
11	$(\pi-\theta'_1)$	$5\pi/3$
12	$(\pi-\theta'_1)$	$\pi/3$

[a] $\cos\theta'_1 = \sqrt{[1/3+(2/3\sqrt{5})]}$ and $\cos\theta'_2 = \sqrt{[1/3-(2/3\sqrt{5})]}$ or $\theta'_1 = 37.37°$ and $\theta'_2 = 79.19°$.

and θ'_2, the top and the bottom sets of three ligand positions making angles of θ'_1 and $(\pi-\theta'_1)$, and the middle two sets of three ligand positions making angles of θ'_2 and $(\pi-\theta'_2)$ with the trigonal axis. These angles can be derived as follows. If the edges of the icosahedron are of unit length, the vertices are at $\sqrt{(1+\tau^2)}/2$ from the origin and the distance from the origin to the centre of an edge is $\tau/2$, where $\tau = 2\cos\pi/5$ and $\tau^2-\tau-1=0$.[16] From these distances it can be shown that $\cos\theta = (\tau^2-1)/(1+\tau^2) = \sqrt{1/5}$ and thus $\theta = \cos^{-1}\sqrt{1/5} = 63.44°$, where θ is the angle that five vertices make with the five-fold axis passing through two diagonal vertices of the icosahedron (the other five vertices are at $\pi-\theta$). Since the distance of the C_3 axis from a vertex is $\sqrt{1/3}$, $\cos\theta'_1$ becomes $\sqrt{(3\tau^2-1)}/\sqrt{(3\tau^2+3)}$ or $(\tau+1)/\sqrt{(3\tau^2+3)}$ and from the fact that $\theta'_2 = (\pi-\theta-\theta'_1)$, it can be shown that $\cos\theta'_2 = \sqrt{(3-\tau^2)}/\sqrt{(3\tau^2+3)}$ or $(\tau-1)/\sqrt{(3\tau^2+3)}$. Thus

$$\theta'_1 = \cos^{-1}\sqrt{\frac{3\tau^2-1}{3\tau^2+3}} = \cos^{-1}\sqrt{\frac{\sqrt{5}+2}{3\sqrt{5}}} = 37.37°$$

and

$$\theta'_2 = \cos^{-1}\sqrt{\frac{3-\tau^2}{3\tau^2+3}} = \cos^{-1}\sqrt{\frac{\sqrt{5}-2}{3\sqrt{5}}} = 79.19°.$$

By substituting proper values of θ'_1 and θ'_2 in the generalized potentials, the ligand field potentials for various regular geometries listed in Tables 5 and 6 can be deduced. These potentials fall into three categories. One case is where the $Y^{\pm}_{4}{}^{3}$ terms tend to

Table 5. Regular trigonal geometries of coordination numbers one to eight (β is tetrahedral angle)

Coordination number	Geometry	θ'	Point-group symmetry
1	Linear	0	$C_{\infty v}$
2	Linear	0	$D_{\infty h}$
3	Trigonal planar	$\pi/2$	D_{3h}
3	Trigonal-$\beta/2$[a]	$\beta/2$	C_{3v}
3	Trigonal-β[a]	β	C_{3v}
4	Tetrahedron	β	T_d
4	Trigonal pyramid[b]	$\pi/2$	C_{3v}
5	Trigonal bipyramid	$\pi/2$	D_{3h}
6	Octahedron[c]	$\beta/2$	O_h
6	Trigonal prism[d]	$\beta/2$	D_{3h}
6	Hexagon[b]	$\pi/2$	D_{6h}
7	Monocapped trigonal prism	$\beta/2$	C_{3v}
7	Monocapped trigonal antiprism	$\beta/2$	C_{3v}
7	Hexagonal pyramid[b]	$\pi/2$	C_{6v}
8	Cube	β	O_h
8	Bicapped trigonal prism	$\beta/2$	D_{3h}
8	Bicapped trigonal antiprism	$\beta/2$	D_{3d}
8	Hexagonal bipyramid[b]	$\pi/2$	D_{6h}

[a] These two trigonal cases of $\theta' = \beta/2$ and β are included because of their significance in that they are half the octahedron and a tetrahedron less one ligand, respectively.

[b] The trigonal pyramid, hexagon, hexagonal pyramid and hexagonal bipyramid geometries may also be considered as respectively, trigonally compressed tetrahedron, octahedron, monocapped trigonal antiprism and bicapped trigonal antiprism with the θ' becoming $\pi/2$.

[c] The octahedron is also a trigonal antiprism with $\theta' = \beta/2$ and $(\pi - \beta/2)$.

[d] We shall define a trigonal prism with $\theta' = \beta/2$ and $(\pi - \beta/2)$ as being regular. Any angle different from $\beta/2$ will hence be considered as a distorted trigonal prism.

zero and we will call such a potential cylindrical.* The second case is that of the cubic comprising geometries of the octahedron, tetrahedron, cube and the trigonal case of the half octahedron. The potentials of these cubic geometries are related to each other by a constant factor. The third case of potentials contain non-zero $Y_4^{\pm 3}$ terms and are not related to cubic potentials by a constant factor and hence are called non-cubic potentials. It should be noted that the three regular geometries of non-cubic potentials are cubic based in that the trigonal-β is a tetrahedron but minus the fourth ligand which is along the trigonal axis, and the mono and bicapped

* Cylindrical potentials containing only the Y_0^0, Y_2^0 and Y_4^0 terms also arise in the case of n-polygonal prismoidal ($n > 4$, D_{nh}, D_{nd}, D_n, C_{nv}, C_{nh}, C_n) systems, i.e. pentagonal, hexagonal, etc. prisms and anti-prisms, in addition to planes, pyramids and bipyramids. See, for instance, refs 17–20.

Table 6. Regular trigonal geometries of coordination numbers nine to twelve (β is tetrahedral angle)

Coordination number	Geometry	θ'_1	θ'_2	Point-group symmetry
9	Tricapped trigonal prism	$\beta/2$	$\pi/2$	D_{3h}
10	Tetracapped trigonal prism	$\beta/2$	$\pi/2$	C_{3v}
11	Pentacapped trigonal prism	$\beta/2$	$\pi/2$	D_{3h}
12	Icosahedron	37.37°	79.19°	Y_h

Table 7. Ligand field potentials in regular trigonal geometries—cylindrical potentials. (The constant ez is left out)

Coordination number	Geometry	$\sqrt{4\pi}\rho_0(r)\,Y_0^0$	$\sqrt{4\pi/5}\rho_2(r)Y_2^0$	$\sqrt{4\pi/9}\rho_4(r)Y_4^0$	$\sqrt{4\pi/9}\rho_4(r)Y_4^{\pm 3}$
1	Linear	1	1	1	0
2	Linear	2	2	2	0
3	Trigonal planar	3	−3/2	9/8	0
4	Trigonal pyramid	4	−1/2	17/8	0
5	Trigonal bipyramid	5	1/2	25/8	0
6	Trigonal prism	6	0	−7/3	0
6	Hexagon	6	−3	9/4	0
7	Monocapped trigonal prism	7	1	−4/3	0
7	Hexagonal pyramid	7	−2	13/4	0
8	Bicapped trigonal prism	8	2	−1/3	0
8	Hexagonal bipyramid	8	−1	17/4	0
9	Tricapped trigonal prism	9	−3/2	−29/24	0
10	Tetracapped trigonal prism	10	−1/2	−5/24	0
11	Pentacapped trigonal prism	11	1/2	19/24	0
12	Icosahedron	12	0	0	0

Table 8. Ligand field potentials in regular trigonal geometries—cubic potentials. (The constant ez is left out)

Coordination number	Geometry	$\sqrt{4\pi}\rho_0(r)Y_0^0$	$\sqrt{4\pi/5}\rho_2(r)Y_2^0$	$\sqrt{4\pi/9}\rho_4(r)Y_4^0$	$\sqrt{4\pi/9}\rho_4(r)Y_4^{\pm 3}$
3	Trigonal-$\beta/2$	3	0	−7/6	$\mp\sqrt{70}/6$
4	Tetrahedron	4	0	28/27	$\pm 4\sqrt{70}/27$
6	Octahedron	6	0	−7/3	$\mp\sqrt{70}/3$
8	Cube	8	0	56/27	$\pm 8\sqrt{70}/27$

trigonal antiprisms are octahedron plus one and two ligands, respectively, along the trigonal axis. As we will show later, various distorted forms of cubic geometries with θ' deviating from $\beta/2$ or β and of non-cubic geometries with θ' deviating from $\beta/2$ or β (geometries of non-cubic potentials) and $\pi/2$ (geometries of cylindrical potentials) also belong to this class of non-cubic potentials. The cylindrical, cubic and non-cubic potentials of all regular geometries are listed in Tables 7, 8 and 9.*

Although the ligand field potentials of cubic geometries evaluated along the three-fold axis look somewhat different from the corresponding potentials evaluated along the tetragonal axis, these two potentials are one and the same. Thus, leaving out the Y_0^0 term, the well-known tetragonally quantized octahedral potential

$$V_{O_h}^{LF}(6) = ez\rho_4(r)\sqrt{4\pi/9}(7/2)\{Y_4^0(\theta,\phi) + \sqrt{5/14}[Y_4^4(\theta,\phi)+Y_4^{-4}(\theta,\phi)]\} \quad (6a)$$

$$= ez\rho_4(r)\sqrt{\pi}(35/4) \times (x^4+y^4+z^4-3/5r^4) \quad (6b)$$

can be shown to be equivalent to [by using eq. (4)]:

$$(7/24)[-8z'^4-3x'^4-3y'^4+24y'^2z'^2 + 24z'^2x'^2-6x'^2y'^2+20\sqrt{2}(z'x'^3-3y'^2z'x')] \quad (6c)$$

which is identical to

$$V_{O_h}^{LF}(6) = ez\rho_4(r)\sqrt{4\pi/9}(-7/3) \times [Y_4^0-\sqrt{10/7}(-Y_4^3+Y_4^{-3})], \quad (6d)$$

* Systems having the coordination numbers two, three, five and six (trigonal prism) are well-known. In particular, the five-coordinate trigonal bipyramidal (and distorted trigonal bipyramidal) systems have been extensively studied. See refs 17, 21–24. A discussion on eight coordination, including other possible geometries, can be found in ref. 25.

Table 9. Ligand field potentials in regular trigonal geometries—non-cubic potentials. (The constant ez is left out)

Coordination number	Geometry	$\sqrt{4\pi}\rho_0(r)Y_0^0$	$\sqrt{4\pi/5}\rho_2(r)Y_2^0$	$\sqrt{4\pi/9}\rho_4(r)Y_4^0$	$\sqrt{4\pi/9}\rho_4(r)Y_4^{\pm 3}$
3	Trigonal-β	3	-1	1/27	$\pm 4\sqrt{70}/27$
7	Monocapped trigonal antiprism	7	1	$-4/3$	$\mp\sqrt{70}/3$
8	Bicapped trigonal antiprism	8	2	$-1/3$	$\mp\sqrt{70}/3$

Table 10. Expansions of the products of spherical harmonics of second degree

	Y_0^0	Y_2^0	Y_4^0	$Y_4^{\pm 3*}$
$Y_2^0 \cdot Y_2^0$	$1/2\sqrt{\pi}$	$\sqrt{5/7}\sqrt{\pi}$	$3/7\sqrt{\pi}$	0
$Y_2^{\pm 1*} \cdot Y_2^{\pm 1}$	$1/2\sqrt{\pi}$	$\sqrt{5/14}\sqrt{\pi}$	$-2/7\sqrt{\pi}$	0
$Y_2^{\pm 2*} \cdot Y_2^{\pm 2}$	$1/2\sqrt{\pi}$	$-\sqrt{5/7}\sqrt{\pi}$	$1/14\sqrt{\pi}$	0
$Y_2^{\pm 1*} \cdot Y_2^{\mp 2}$	0	0	0	$\sqrt{5/2}\sqrt{7\pi}$
$Y_2^{\pm 2*} \cdot Y_2^{\mp 1}$	0	0	0	$-\sqrt{5/2}\sqrt{7\pi}$

the octahedral potential evaluated along a trigonal axis.*

d-ORBITAL ENERGIES AND d-ORBITAL WAVE FUNCTIONS

With the potentials of Tables 7–9, and the relevant expansions for the products of spherical harmonics given in Table 10,† the d-orbital energies in a given geometry can be calculated.

*For a symmetry derivation of this potential, see ref. 4.

† These expansions can be obtained either by the application of the $3-j$ symbols[26] or by an algebraic method in a straightforward manner by expressing a product as being equivalent to an appropriate combination of spherical harmonics and insuring that the coefficients of same terms on both sides of the expression must be the same.

‡ The formula for the eigenvalues of a 2×2 secular determinant of two functions ϕ_1 and ϕ_2 with diagonal matrix elements α_1 and α_2, respectively, and of an off-diagonal matrix element β or $-\beta$ is

$$E_\pm = 1/2(\alpha_1+\alpha_2)\pm\sqrt{\{[(\alpha_1-\alpha_2)/2]^2+\beta^2\}}.$$

The corresponding eigenfunctions are given by

$$\Psi_+ = \pm\sqrt{(1-\delta)/2}\phi_1+\sqrt{(1+\delta)/2}\phi_2$$

and

$$\Psi_- = \mp\sqrt{(1+\delta)/2}\phi_1+\sqrt{(1-\delta)/2}\phi_2$$

where $\delta = (\alpha_2-\alpha_1)/\sqrt{[(\alpha_2-\alpha_1)^2+4\beta^2]}$ and the upper signs are for $+\beta$ and the lower signs are for $-\beta$.

Cylindrical potentials

Due to the absence of the $Y_4^{\pm 3}$ terms in the cylindrical potentials, the imaginary d-orbitals, i.e. $Y_2^{\pm 1}$, $Y_2^{\pm 2}$ along with Y_2^0 become pure orbitals or energy levels in the case of these geometries. The imaginary orbitals can still be combined to obtain real forms, of course. The d-orbital energies in geometries with cylindrical potentials are listed in Tables 11 and 12: We have used the usual notation[17] $\langle\rho_l(r)\rangle$ for the matrix element of $\rho_l(r)$, namely, $\langle\rho_l(r)\rangle = ez\int_0^\infty R_{kd}(r)^2(r_<^l/r_>^{l+1})r^2\,dr$ and made the assumption that $\langle\rho_2(r)\rangle = \langle\rho_4(r)\rangle = 6Dq$ where Dq is the octahedral ligand field parameter. Some of these cylindrical potentials and energies are well-known.[17-19]

Cubic potentials

With the octahedral potential, the non-zero matrix elements of the d-orbitals become

$$\langle Y_2^0|V_{O_h}^{LF}(6)|Y_2^0\rangle = -2/3\langle\rho_4(r)\rangle = -4Dq$$

$$\langle Y_2^{\pm 1}|V_{O_h}^{LF}(6)|Y_2^{\pm 1}\rangle = 4/9\langle\rho_4(r)\rangle = 8/3Dq$$

$$\langle Y_2^{\pm 2}|V_{O_h}^{LF}(6)|Y_2^{\pm 2}\rangle = -1/9\langle\rho_4(r)\rangle = -2/3Dq$$

$$\langle Y_2^{\pm 1}|V_{O_h}^{LF}(6)|Y_2^{\mp 2}\rangle = \langle Y_2^{\mp 2}|V_{O_h}^{LF}(6)|Y_2^{\pm 1}\rangle$$

$$= \mp 5\sqrt{2}/9\langle\rho_4(r)\rangle = \mp 10\sqrt{2}/3Dq. \quad (7)$$

The solution of the 2×2 secular determinants‡ of $Y_2^{\pm 1}$ and $Y_2^{\mp 2}$ yields the energies $E_+ = 6Dq$ and

Table 11. d-Orbital energies in geometries of cylindrical potentials. ($x_2 = \langle\rho_2(r)\rangle/7$, $x_4 = \langle\rho_4(r)\rangle/7$)

Coordination number	Geometry	Y_2^0	$Y_2^{\pm 1}$	$Y_2^{\pm 2}$
1	Linear	$2x_2+2x_4$	$x_2-4/3x_4$	$-2x_2+1/3x_4$
2	Linear	$4x_2+4x_4$	$2x_2-8/3x_4$	$-4x_2+2/3x_4$
3	Trigonal planar	$-3x_2+9/4x_4$	$-3/2x_2-3/2x_4$	$3x_2+3/8x_4$
4	Trigonal pyramid	$-x_2+17/4x_4$	$-1/2x_2-17/6x_4$	$x_2+17/24x_4$
5	Trigonal bipyramid	$x_2+25/4x_4$	$1/2x_2-25/6x_4$	$-x_2+25/24x_4$
6	Trigonal prism	$-14/3x_4$	$28/9x_4$	$-7/9x_4$
6	Hexagon	$-6x_2+9/2x_4$	$-3x_2-3x_4$	$6x_2+3/4x_4$
7	Monocapped trigonal prism	$2x_2-8/3x_4$	$x_2+16/9x_4$	$-2x_2-4/9x_4$
7	Hexagonal pyramid	$-4x_2+13/2x_4$	$-2x_2-13/3x_4$	$4x_2+13/12x_4$
8	Bicapped trigonal prism	$4x_2-2/3x_4$	$2x_2+4/9x_4$	$-4x_2-1/9x_4$
8	Hexagonal bipyramid	$-2x_2+17/2x_4$	$-x_2-17/3x_4$	$2x_2+17/12x_4$
9	Tricapped trigonal prism	$-3x_2-29/12x_4$	$-3/2x_2+29/18x_4$	$3x_2-29/72x_4$
10	Tetracapped trigonal prism	$-x_2-5/12x_4$	$-1/2x_2+5/18x_4$	$x_2-5/72x_4$
11	Pentacapped trigonal prism	$x_2+19/12x_4$	$1/2x_2-19/18x_4$	$-x_2+19/72x_4$
12	Icosahedron	0	0	0

Table 12. d-Orbital energies in units of Dq in geometries of cylindrical potentials. ($\langle\rho_2(r)\rangle = \langle\rho_4(r)\rangle = 6Dq$)

Coordination number	Geometry	Y_2^0	$Y_2^{\pm 1}$	$Y_2^{\pm 2}$
1	Linear	$24/7(\sigma^+)$	$-2/7(\pi)$	$-10/7(\delta)$
2	Linear	$48/7(\sigma_g^+)$	$-4/7(\pi_g)$	$-20/7(\delta_g)$
3	Trigonal planar	$-9/14(a_1')$	$-18/7(e'')$	$81/28(e')$
4	Trigonal pyramid	$39/14(a_1)$	$-20/7(e)$	$41/28(e)$
5	Trigonal bipyramid	$87/14(a_1')$	$-22/7(e'')$	$1/28(e')$
6	Trigonal prism	$-4(a_1')$	$8/3(e'')$	$-2/3(e')$
6	Hexagon	$-9/7(a_{1g})$	$-36/7(e_{1g})$	$81/14(e_{2g})$
7	Monocapped trigonal prism	$-4/7(a_1)$	$50/21(e)$	$-44/21(e)$
7	Hexagonal pyramid	$15/7(a_1)$	$-38/7(e_1)$	$61/14(e_2)$
8	Bicapped trigonal prism	$20/7(a_1')$	$44/21(e'')$	$-74/21(e')$
8	Hexagonal bipyramid	$39/7(a_{1g})$	$-40/7(e_{1g})$	$41/14(e_{2g})$
9	Tricapped trigonal prism	$-65/14(a_1')$	$2/21(e'')$	$187/84(e')$
10	Tetracapped trigonal prism	$-17/14(a_1)$	$-4/21(e)$	$67/84(e)$
11	Pentacapped trigonal prism	$31/14(a_1')$	$-10/21(e'')$	$-53/84(e')$
12	Icosahedron[a]	0	0	0

[a] All d-orbitals together transform as h_g representation.

$E_- = -4Dq$. The corresponding wave functions are

$$\Psi_+ = \mp\sqrt{2/3}Y_2^{\pm 1} + \sqrt{1/3}Y_2^{\mp 2} = \sqrt{2/3}d_{\pi'_\pm} + \sqrt{1/3}d_{\delta'_\mp}$$

$$\Psi_- = \mp\sqrt{1/3}Y_2^{\pm 1} - \sqrt{2/3}Y_2^{\mp 2} = \sqrt{1/3}d_{\pi'_\pm} - \sqrt{2/3}d_{\delta'_\mp},$$

where the spherical harmonics refer to the trigonal coordinate system. The orbitals of the $+6Dq$ and $-4Dq$ energy are the e_g set and t_{2g} set, respectively. Thus

$$t_{2ga} = Y_2^0 = d_{\sigma'}$$

$$t_{2g(b_c^c)} = \sqrt{1/3}d_{\pi'_\pm} - \sqrt{2/3}d_{\delta'_\mp}$$

$$e_{g(b_c^a)} = \sqrt{2/3}d_{\pi'_\pm} + \sqrt{1/3}d_{\delta'_\mp}. \quad (8)$$

These are the trigonally quantized cubic d-orbitals.*†

* The symmetry derivation of these orbitals can be found in ref. 4.

† These orbitals when converted to the cartesian forms on a trigonal basis (z', y', x') which are then transformed to the tetragonal coordinates using eq. (4) will yield, within phases, the same trigonal d-orbitals that were employed by others.[2,1] In particular, our t_{2gc} and e_{ga} are related to theirs by a negative phase factor.

Table 13. Symmetry transformation properties of trigonally quantized d-orbitals ($\omega = e^{2\pi i/3}$)

d-Orbital	$C_3(z')$	$C_2(y')$	$C_4(z)$
$d_{\sigma'} = t_{2ga}$	t_{2ga}	t_{2ga}	$-\frac{1}{3}t_{2ga}-\frac{2}{3}\omega^{+1}t_{2gb}-\frac{2}{3}\omega^{-1}t_{2gc}$
$\sqrt{\frac{1}{3}}d_{\pi'_\pm}-\sqrt{\frac{2}{3}}d_{\delta'_\mp}=t_{2g(c)}$	$\omega^{\pm 1}t_{2g(c)}$	$t_{2g(b)}$	$-\frac{2}{3}\omega^{\pm 1}t_{2ga}-\frac{1}{3}t_{2g(b)}+\frac{2}{3}\omega^{\mp 1}t_{2g(c)}$
$\sqrt{\frac{2}{3}}d_{\pi'_\pm}+\sqrt{\frac{1}{3}}d_{\delta'_\mp}=e_{g(b)}$	$\omega^{\pm 1}e_{g(b)}$	$e_{g(a)}$	$e_{g(a)}$

The a, b, c and the a, b notation for the components of t_{2g} and e_g orbitals is determined from the symmetry transformation properties of the orbitals given in Table 13.[13a] Thus, the a component of t_{2g} becomes the a_1 representation and the b, c components become the $e_\pm$ representation on going towards a low symmetry trigonal ligand field (i.e. D_{3d}, D_3, C_{3v} symmetry point groups). Similarly the cubic e_g representation simply transforms into the $e_\pm$ representation of low symmetry trigonal ligand fields.

The ligand field potentials in other cubic geometries, i.e. trigonal $-\beta/2$, tetrahedron and cube, are related to the octahedral potential by a constant factor. Thus

$$V^{LF}_{C_{3v}}(3) = 1/2V^{LF}_{O_h}(6)$$

$$V^{LF}_{T_d}(4) = -4/9V^{LF}_{O_h}(6)$$

and

$$V^{LF}_{O_h}(8) = -8/9V^{LF}_{O_h}(6). \quad (9)$$

This implies that the energies of the orbitals in these geometries will be given by the corresponding constant factor and that the wave functions are just the pure trigonal orbitals. The d-orbital energies of geometries with cubic potentials are summarized in Table 14.

Non-cubic potentials

Since non-cubic potentials are not related to cubic potentials by a proportionality constant, the trigonal based cubic d-orbitals are no longer pure orbitals (i.e. eigenfunctions) with geometries of non-cubic potentials. In other words the cubic d-orbitals mix in these geometries. However, if the mixing is small, it is convenient to utilize these orbitals as zero-order functions.

The energies and wave functions calculated for the regular geometries of non-cubic potentials, namely, the trigonal-β, monocapped trigonal antiprism and bicapped trigonal antiprism are given in Tables 15 and 16. It can be seen that in all these cases, mixing of the cubic d-orbitals is small so that these orbitals are almost pure for these geometries.

Non-cubic potentials can also arise from various distorted geometries, cubic geometries with θ' deviating from $\beta/2$ (trigonal-$\beta/2$ and octahedron) and β (tetrahedron and cube) and non-cubic geometries with θ' deviating from β (trigonal-β), $\beta/2$ (monocapped and bicapped trigonal antiprisms) and $\pi/2$ (trigonal planar, trigonal pyramid, trigonal bipyramid, hexagon, hexagonal pyramid, hexagonal bipyramid, and tricapped, tetracapped and pentacapped trigonal prisms).*† As pointed out above

* In the case of the capped trigonal prisms, the deviation of the second trigonal angle θ'_2 is being considered here. Any deviation of θ'_1 from $\beta/2$ will still result in a cylindrical potential in all these cases of trigonal prismatic-based geometries as in the cases of the trigonal prism, monocapped trigonal prism and bicapped trigonal prism geometries. It is interesting to note that any deviation of either θ'_1 or θ'_2 or of both from the icosahedron angles resulting in a trigonally distorted icosahedron will also give rise to a cylindrical potential.

† Two other forms of distortions also lead to a non-cubic potential. The two forms of distortions which are applicable to geometries of coordination numbers six and above are as follows. One distortion is the elongation or compression of one set of three ligand positions along the trigonal axis independent of the other set of three ligand positions. This occurs in the octahedron, trigonal prism, capped trigonal antiprisms, capped trigonal prisms and icosahedron. Another distortion is the twist of one set of three ligand positions relative to the other set in these same geometries. A more generalized expression for ligand field potential for the basic six-coordinate unit allowing both these distortions simultaneously can be obtained by combining expressions (3b) and (3a) with $\theta' = \theta'_1$ and θ'_2, respectively. This expression specializes for the first case of distortion with $\phi' = \pi/3$ or 0, respectively, for the octahedral based or trigonal prismatic based geometries, and for the second case of distortion with $\theta'_1 = \theta'$ and $\theta'_2 = (\pi - \theta')$. The results obtained in what follows are, in general, applicable to both these distortions also.

Table 14. *d*-Orbital energies in units of Dq in geometries of cubic potentials

Coordination number	Geometry	t_2	e
3	Trigonal-$\beta/2$[a]	−2	3
4	Tetrahedron	16/9	−8/3
6	Octahedron	−4	6
8	Cube	32/9	−16/3

[a] The t_2 set in this case is actually $a_1(t_{2a})$ and e (t_{2b} and t_{2c}) which are degenerate.

Table 15. *d*-Orbital energies in units of Dq in regular geometries of non-cubic potentials. ($\langle\rho_2(r)\rangle = \langle\rho_4(r)\rangle = 6Dq$)

Coordination number	Geometry	a_1	e^-	e^+
3	Trigonal-β	−1.651	−2.059	2.885
7	Monocapped trigonal antiprism	−0.571	−5.076	5.361
8	Bicapped trigonal antiprism	2.857	−6.202	4.773

Table 16. *d*-Orbital wave functions (e representations) in regular geometries of non-cubic potentials. (Only one e representation is given. The other e representation is orthogonal to the one given)

Coordination number	Geometry	$\Psi_+(e)$			
		$t_{2g(c)}$	$e_{g(a,b)}$	$Y_2^{\pm 1}$	$Y_2^{\mp 2}$
3	Trigonal-β	$-\sqrt{(0.9880)}$	$\sqrt{(0.0120)}$	$\pm\sqrt{(0.2346)}$	$\sqrt{(0.7654)}$
7	Monocapped trigonal antiprism	$\sqrt{(0.0027)}$	$\sqrt{(0.9973)}$	$\mp\sqrt{(0.7144)}$	$\sqrt{(0.2856)}$
8	Bicapped trigonal antiprism	$\sqrt{(0.0098)}$	$\sqrt{(0.9902)}$	$\mp\sqrt{(0.7560)}$	$\sqrt{(0.2440)}$

the trigonal-β, and the monocapped and bicapped trigonal antiprism geometries are cubic based and thus are related to the cubic geometries. All the other non-cubic geometries are of the same kind in that they give rise to cylindrical potentials resulting in the original spherical harmonics as the pure orbitals in the absence of a distortion. Choosing the octahedron and tetrahedron as examples of the cubic and cubic-based geometries, and trigonal bipyramid as an example of the cylindrical based geometries, we have calculated the ligand field potentials for varying amounts of distortion. These are listed in Table 17. The corresponding *d*-orbital energies and the wave functions are listed in Tables 18 and 19. In the case of the tetrahedron and octahedron, it can be seen that for small deviations of θ' (near β for tetrahedron and $\beta/2$ for octahedron), mixing of cubic *d*-orbitals is small. Although the cubic *d*-orbitals become purer than the original spherical harmonics for the distorted form of trigonal bipyramid chosen here, for minor deviations of θ' from $\pi/2$ it is expected that the original spherical harmonics will remain pure.*

SUMMARY

The ligand field potentials for a number of geometries containing a three-fold axis of symmetry have been evaluated along the trigonal axis and are categorized into three kinds, cylindrical potentials (no spherical harmonics of non-zero order), cubic potentials (related to each other by a constant factor) and non-cubic potentials (not related to cubic potentials by a constant factor). The energies of the *d*-orbitals defined along the trigonal axis have been

* It should be noted that the distorted form of the trigonal bipyramid ($\theta' = \beta$) chosen here is actually cubic based in that it is a tetrahedron with an extra ligand along the trigonal axis.

Table 17. Ligand field potentials in distorted geometries. (The Y_0^0 term and the constant ez are left out)

Geometry (θ')	$\rho_2(r)\sqrt{4\pi/5}Y_2^0$	$\rho_4(r)\sqrt{4\pi/9}Y_4^0$	$\rho_4(r)\sqrt{4\pi/9}Y_4^{\pm 3}$
Tetrahedron			
π^a	4	4	0
$5\pi/6$	23/8	137/128	$\pm 3\sqrt{105}/64$
$3\pi/4$	7/4	$-7/32$	$\pm 3\sqrt{35}/16$
$(\pi-\beta/2)$	1	$-1/6$	$\pm\sqrt{70}/6$
$2\pi/3$	5/8	17/128	$\pm 9\sqrt{105}/64$
β^b	0	28/27	$\pm 4\sqrt{70}/27$
$\pi/2^c$	$-1/2$	17/8	0
Octahedron			
0^a	6	6	0
$\pi/6^d$	15/4	9/64	$\pm 3\sqrt{105}/32$
$\pi/4^d$	3/2	$-39/16$	$\pm 3\sqrt{35}/8$
$\beta/2^e$	0	$-7/3$	$\mp\sqrt{70}/3$
$\pi/3^f$	$-3/4$	$-111/64$	$\mp 9\sqrt{105}/32$
$\pi/2^g$	-3	9/4	0
Trigonal bipyramid			
β	1	55/27	$\pm 4\sqrt{70}/27$
$\pi/2^h$	1/2	25/8	0

[a] Regular linear geometry.
[b] Regular tetrahedron.
[c] Regular trigonal pyramid.
[d] Elongated octahedron.
[e] Regular octahedron.
[f] Compressed octahedron.
[g] Hexagonal plane.
[h] Regular trigonal bipyramid.

Table 18. d-Orbital energies in units of Dq in distorted geometries. ($\langle\rho_2(r)\rangle = \langle\rho_4(r)\rangle = 6Dq$)

Geometry (θ')	a_1	e^+	e^-
Tetrahedron			
π	13.7143	-1.1429	-5.7143
$5\pi/6$	6.7634	1.3514	-4.7331
$3\pi/4$	2.6250	1.7702	-3.0827
$(\pi-\beta/2)$	1.4286	2.3867	-3.1010
$2\pi/3$	1.2991	2.3091	-2.9586
β^a	1.7778	1.7778	-2.6667
$\pi/2$	2.7857	1.4643	-2.8571
Octahedron			
0	20.5714	-1.7143	-8.5714
$\pi/6$	6.6696	3.3250	-6.6598
$\pi/4$	-1.6071	5.6486	-4.8450
$\beta/2^b$	-4.0000	6.0000	-4.0000
$\pi/3$	-4.2590	5.9440	-3.8144
$\pi/2$	-1.2857	5.7857	-5.1429
Trigonal bipyramid			
β	5.2063	0.8003	-3.4035
$\pi/2^c$	6.2143	0.0357	-3.1429

[a] Regular tetrahedron.
[b] Regular octahedron.
[c] Regular trigonal bipyramid.

Table 19. *d*-Orbital wave functions (*e* representations) in distorted geometries. (Only one *e* representation is given. The other *e* representation is orthogonal to the one given)

Geometry (θ')	$t_{2g}(\zeta)$	$e_g(\zeta)$	$\Psi_+(e)$ $Y_2^{\pm 1}$	$Y_2^{\mp 2}$
Tetrahedron				
π	$\sqrt{(0.3333)}$	$\sqrt{(0.6667)}$	∓ 1	0
$5\pi/6$	$\sqrt{(0.4652)}$	$\sqrt{(0.5348)}$	$\mp\sqrt{(0.9819)}$	$-\sqrt{(0.0181)}$
$3\pi/4$	$\sqrt{(0.3955)}$	$\sqrt{(0.6046)}$	$\mp\sqrt{(0.9959)}$	$-\sqrt{(0.0041)}$
$(\pi-\beta/2)$	$\sqrt{(0.8196)}$	$\sqrt{(0.1804)}$	$\mp\sqrt{(0.7560)}$	$-\sqrt{(0.2440)}$
$2\pi/3$	$\sqrt{(0.9060)}$	$\sqrt{(0.0940)}$	$\mp\sqrt{(0.6397)}$	$-\sqrt{(0.3603)}$
β[a]	1	0	$\mp\sqrt{(0.3333)}$	$-\sqrt{(0.6667)}$
$\pi/2$	$-\sqrt{(0.6667)}$	$\sqrt{(0.3333)}$	0	1
Octahedron				
0	$\sqrt{(0.3333)}$	$\sqrt{(0.6667)}$	∓ 1	0
$\pi/6$	$\sqrt{(0.1891)}$	$\sqrt{(0.8110)}$	$\mp\sqrt{(0.9728)}$	$\sqrt{(0.0272)}$
$\pi/4$	$\sqrt{(0.0465)}$	$\sqrt{(0.9535)}$	$\mp\sqrt{(0.8497)}$	$\sqrt{(0.1503)}$
$\beta/2$[b]	0	1	$\mp\sqrt{(0.6667)}$	$\sqrt{(0.3333)}$
$\pi/3$	$-\sqrt{(0.0020)}$	$\sqrt{(0.9800)}$	$\mp\sqrt{(0.5281)}$	$\sqrt{(0.4719)}$
$\pi/2$	$-\sqrt{(0.6667)}$	$\sqrt{(0.3333)}$	0	1
Trigonal bipyramid				
β	$\sqrt{(0.9833)}$	$\sqrt{(0.0167)}$	$\mp\sqrt{(0.4598)}$	$-\sqrt{(0.5402)}$
$\pi/2$[c]	$-\sqrt{(0.6667)}$	$\sqrt{(0.3333)}$	0	1

[a] Regular tetrahedron.
[b] Regular octahedron.
[c] Regular trigonal bipyramid.

calculated. The original spherical harmonics of the *d*-orbitals are pure wave functions for geometries of cylindrical potentials. The trigonally quantized *d*-orbitals which are the eigenfunctions of cubic geometries have been derived. The *d*-orbital wave functions for regular cubic based and for some trigonally distorted cubic and non-cubic geometries have also been obtained. The original spherical harmonics are the appropriate zero order functions for geometries of cylindrical potentials with small trigonal distortions. Similarly the cubic *d*-orbitals can be used as the appropriate zero order functions for regular cubic based geometries of non-cubic potentials and for trigonally distorted cubic and cubic-based geometries with slight deviations of the trigonal angles.

REFERENCES

1. (a) S. Sugano and Y. Tanabe, *J. Phys. Soc., Japan* 1958, **13**, 880; (b) S. Sugano, Y. Tanabe and H. Kamimura, *Multiplets of Transition-Metal Ions in Crystals*. Academic Press, New York (1970).
2. M. H. L. Pryce and W. A. Runciman, *Disc. Faraday Soc.* 1958, **26**, 34.
3. A. D. Liehr, *J. Phys. Chem.* 1960, **64**, 43.
4. C. J. Ballhausen, *Introduction to Ligand Field Theory*. McGraw-Hill, New York (1962).
5. B. R. McGarvey, *J. Chem. Phys.* 1962, **38**, 388.
6. D. S. McClure, *J. Chem. Phys.* 1962, **36**, 2757.
7. J. S. Griffith, *Mol. Phys.* 1962, **6**, 503.
8. R. M. MacFarlane, *J. Chem. Phys.* 1963, **39**, 3118.
9. H. M. Gladney and J. D. Swalen, *J. Chem. Phys.* 1965, **42**, 1999.
10. J. R. Perumareddi, *J. Phys. Chem.* 1967, **71**, 3144.
11. G. E. Stedman, *J. Chem. Phys.* 1969, **50**, 1461.
12. (a) M. Gerloch, J. Lewis and R. C. Slade, *J. Chem. Soc. A* 1969, 1422; (b) M. Gerloch, J. Lewis, G. G. Phillips and P. M. Quested, *J. Chem. Soc. A* 1970, 1941.
13. (a) J. R. Perumareddi, *Z. Naturforsch.* 1972, **27a**, 1820 (Errata, *ibid.* 1973, **28a**, 1541); (b) J. R. Perumareddi, *Z. Naturforsch.* 1973, **28a**, 1247 (Errata, *ibid.* 1974, **29a**, 364).
14. A. B. P. Lever and B. R. Hollebone, *J. Am. Chem. Soc.* 1972, **94**, 1816.
15. S. Konig and S. Kremer, *Ligand Field Energy Diagrams*. Plenum, New York (1977).
16. A. F. Wells, *The Third Dimension in Chemistry*. Oxford University Press, London (1968).
17. S. T. Spees Jr, J. R. Perumareddi and A. W. Adamson, *J. Phys. Chem.* 1968, **72**, 1822.
18. F. Basolo and R. G. Pearson, *Mechanisms of Inorganic Reactions*. Wiley, New York (1967).
19. (a) R. Krishnamurthy and W. B. Schaap, *J. Chem. Educ.* 1969, **46**, 799: (b) R. Krishnamurthy and W. B. Schaap, *J. Chem. Educ.* 1970, **47**, 433.
20. D. R. Scott and F. A. Matsen, *J. Phys. Chem.* 1968, **72**, 16.

21. (a) J. T. Hougen, G. E. Leroi and T. C. James, *J. Chem. Phys.* 1961, **34**, 1670; (b) C. W. Dekock and D. M. Gruen, *J. Chem. Phys.* 1966, **44**, 4387; (c) C. W. Dekock and D. M. Gruen, *J. Chem. Phys.* 1967, **46**, 1096; (d) C. K. Jorgensen, *Mol. Phys.* 1964, **7**, 417; (e) D. W. Smith, *Inorg. Chim. Acta* 1971, **5**, 231; (f) A. B. P. Lever and B. R. Hollebone, *Inorg. Chem.* 1972, **11**, 2183.
22. (a) E. C. Alyea, D. C. Bradley, R. G. Copperthwaite and K. D. Sales, *J. Chem. Soc., Dalton Trans.* 1973, 185; (b) D. C. Bradley, R. G. Copperthwaite, S. A. Cotton, K. D. Sales and J. F. Gibson, *J. Chem. Soc., Dalton Trans.* 1973, 191; (c) L. G. Vanquickenborne and R. Debuyst, *J. Chem. Soc., Dalton Trans.* 1979, 1150.
23. (a) C. Furlani, *Coord. Chem Rev.* 1968, **3**, 141; (b) R. Morassi, I. Bertini and L. Sacconi, *Coord. Chem. Rev.* 1973, **11**, 343; (c) M. Ciampolini, *Structure and Bonding (Berlin)* 1966, **6**, 52; (d) M. Ciampolini, *Inorg. Chem.* 1966, **5**, 35; (e) M. Ciampolini and N. Nardi, *Inorg. Chem.* 1966, **5**, 41; (f) M. Ciampolini and N. Nardi, *Inorg. Chem.* 1966, **5**, 1150; (g) M. Ciampolini and G. P. Speroni, *Inorg. Chem.* 1966, **5**, 45; (h) G. Dyer and L. M. Venanzi, *J. Chem. Soc. A* 1965, 2771; (i) M. J. Norgett, J. H. M. Thornley and L. M. Venanzi, *J. Chem. Soc. A* 1967, 540; (j) M. J. Norgett, J. H. M. Thornley and L. M. Venanzi, *Coord. Chem. Rev.* 1967, **2**, 99; (k) M. J. Norgett and L. M. Venanzi, *Inorg. Chim. Acta* 1968, **2**, 107; (l) J. S. Wood, *Inorg. Chem.* 1968, **7**, 852; (m) J. S. Wood and P. T. Greene, *Inorg. Chem.* 1969, **8**, 491; (n) J. S. Wood, *J. Chem. Soc. A* 1969, 1582; (o) R. C. Slade, A. A. G. Tomlinson, B. J. Hathaway and D. E. Billig, *J. Chem. Soc. A* 1968, 61; (p) B. J. Hathaway, D. E. Billig, R. J. Dudley, R. J. Fereday and A. A. G. Tomlinson, *J. Chem. Soc. A* 1970, 806; (q) L. Sacconi, *J. Chem. Soc. A* 1970, 248; (r) L. M. Vallarino, V. L. Goedken and J. V. Quagliano, *Inorg. Chem.* 1972, **11**, 1466; (s) I. Bertini, M. Ciampolini, P. Dapparto and D. Gatteschi, *Inorg. Chem.* 1972, **11**, 2254; (t) I. Bertini, M. Ciampolini and D. Gatteschi, *Inorg. Chem.* 1973, **12**, 693; (u) C. A. L. Becker, D. W. Meek and T. M. Dunn, *J. Phys. Chem.* 1968, **72**, 3588; (v) J. A. Varga and C. A. L. Becker, *J. Phys. Chem.* 1972, **76**, 2907; (w) A. Bencini and D. Gatteschi, *J. Phys. Chem.* 1976, **80**, 2126; (x) F. Gomez Beltran and F. Palacio, *J. Phys. Chem.* 1976, **80**, 1373; (y) R. Barbucci, A. Mastroianni and M. J. M. Campbell, *Inorg. Chim. Acta* 1978, **27**, 109; (z) E. Shustorovich, *Inorg. Chem.* 1978, **17**, 2649; (A) R. J. Deeth and M. Gerlock, *Inorg. Chem.* 1984, **23**, 3853.
24. (a) R. A. D. Wentworth, *Coord. Chem. Rev.* 1972/73, **9**, 171; (b) E. Larsen, G. N. LaMar, B. E. Wagner, J. E. Parks and R. H. Holm, *Inorg. Chem.* 1972, **11**, 2652; (c) B. R. Hollebone and J. C. Donini, *Theoret. Chim. Acta* 1975, **39**, 33; (d) J. C. Hempel and M. E. Miller, *J. Chem. Phys.* 1981, **75**, 2959; (e) J. C. Hempel and L. F. Appel, *Inorg. Chem.* 1981, **20**, 3109; (f) P. Comba, A. M. Sargeson, L. M. Engelhardt, J. MacB. Harrowfield, A. H. White, E. Horn and M. R. Snow, *Inorg. Chem.* 1985, **24**, 2325.
25. J. K. Burdett, R. Hoffmann and R. C. Fay, *Inorg. Chem.* 1978, **17**, 2553.
26. M. Rotenberg, R. Bivins, N. Metropolis and J. K. Wooten Jr., *The 3−j and 6−j Symbols.* The Technology Press, MIT, Cambridge, MA (1959).

Polyhedron Vol. 7, No. 18, pp. 1725–1726, 1988
Printed in Great Britain

0277–5387/88 $3.00+.00
© 1988 Pergamon Press plc

THE STRUCTURE OF PBr_4Cl_3

KEITH B. DILLON,* MARTIN P. NISBET and ROGER N. REEVE

Chemistry Department, University of Durham, South Road, Durham DH1 3LE, U.K.

(*Received* 15 *February* 1988; *accepted* 9 *March* 1988)

Abstract—The compound PBr_4Cl_3 has been shown to have the ionic structure $PBr_4^+Cl_3^-$ by means of ^{31}P NMR and Raman spectroscopy. There was no evidence for the formation of mixed bromochlorophosphonium ions. It appears to be a member of a series of derivatives of the PBr_4^+ ion with trihalide or single halide counter-ions.

Several mixed phosphorus(V) halides have been reported from reaction of PCl_3 and bromine under various conditions.[1–9] These include the compound PBr_4Cl_3, which was first described by Prinvault[1] and Michaelis[2] independently in 1872, although nothing was known of its structure. This compound was investigated in more detail by Fialkov and Kuz'menko[3,4] who prepared it from a mixture of PCl_3 and bromine containing 57.42 mol % of PCl_3.[3] The material was recrystallized from CCl_4 and dried in a current of CO_2, giving orange–red crystals of the product. The compound was reported not to conduct in the solid state, but to be a good conductor when molten.[3] It was subsequently shown to be an electrical conductor in polar solvents such as $PhNO_2$ or MeCN, but a non-conductor in C_6H_6, CCl_4 or CS_2.[4] The authors suggested the formulation $[PCl_3Br]^+[Br(Br_2)_n]^-$ for this and a related series of compounds, with $n = 1$ for PBr_4Cl_3.[4] The compound was later prepared by reaction of 40.5 mol % PBr_5 and 59.5 mol % PCl_5 at 313–323 K, according to eq. (1), or by a 3:2 reaction between PCl_5 and PBr_3, eq. (2).[5]

$$6PCl_5 + 4PBr_5 \rightarrow 5PBr_4Cl_3 + 5PCl_3 \quad (1)$$

$$6PCl_5 + 4PBr_3 \rightarrow 3PBr_4Cl_3 + 7PCl_3. \quad (2)$$

Popov *et al.* were unable to reproduce the preparation from PCl_3 and Br_2 in the absence of solvent,[3] obtaining from several attempts a material of composition between $PCl_3Br_{5.1}$ and $PCl_3Br_{5.7}$.[6] Their product lost bromine rapidly to give a yellow powder of composition $PCl_{4.67}Br_{0.33}$, or $P_{12}Cl_{56}Br_4$, which appeared from physical measurements to be a true compound rather than a mixture.[6] Harris and Payne were also unable to reproduce this preparation,[3] obtaining materials which analysed approximately as $PCl_3Br_7 \cdot CCl_4$ and $PCl_3Br_7 \cdot 2CCl_4$.[7] These solids lost CCl_4 and Br_2 on heating, and the possibility of their being CCl_4 solvates of members of the $PCl_3 \cdot nBr_2$ series[4] could not be excluded. The only proposal for the structure of PBr_4Cl_3 was thus $[PCl_3Br]^+Br_3^-$,[4] and there have been no subsequent studies on this compound. We now report the results of an investigation by spectroscopic techniques into its structure.

RESULTS AND DISCUSSION

In view of the difficulties reported[6,7] in the direct preparation from PCl_3 and bromine, the compound was prepared from PCl_5 and PBr_3 in CCl_4.[5] The precipitate which formed was separated and dried *in vacuo*. The product analysed approximately as $PCl_{2.59}Br_{4.21}$, the discrepancies probably being due largely to experimental error, although a small amount of hydrolysis cannot be discounted. There seems little doubt, however, that the main constituent is PBr_4Cl_3, and this was confirmed by the spectroscopic measurements.

The ^{31}P NMR solution spectrum was recorded in 25 oleum, which has been shown by previous work in this group to be an excellent solvent for species containing simple or mixed halogenophosphonium ions.[10] A strong resonance at −85 ppm was discerned, readily assigned to the PBr_4^+ ion.[10] A very weak signal from $PBr_3(OH)^+$ (in equilibrium with unprotonated $POBr_3$)[11] was also apparent at −64 ppm, consistent with the presence of a small amount of hydrolysis. There was no evidence, however, for the formation of mixed bromochlorophosphonium ions such as PCl_3Br^+,

* Author to whom correspondence should be addressed.

the chemical shifts of which are known,[10,12] as suggested by Fialkov and Kuz'menko.[4] This result strongly suggests that the compound should be formulated as $PBr_4^+Cl_3^-$. Confirmation was provided by the Raman spectrum of the solid, which showed in addition to strong bands for the PBr_4^+ ion[13–18] a weak band at 267 cm^{-1}, very similar to the frequency reported (268 cm^{-1}) for the trichloride ion in tetraalkylammonium salts.[19] Hence the ideal structure for the compound PBr_4Cl_3 appears to be $PBr_4^+Cl_3^-$, with any deviations from this composition possibly being due to the presence of free halide rather than trichloride as the counter-ion. The structure may well be similar to that of PBr_7, which has been shown by X-ray crystallography to have the ionic composition $PBr_4^+Br_3^-$.[20]

It is of interest in this connection that Gabes *et al.* prepared the compound PBr_4Cl, and showed by Raman spectroscopy and powder X-ray work that it has the structure $PBr_4^+Cl^-$.[18] Their compound was prepared by recrystallizing from CS_2 the red–brown precipitate obtained from a 4 : 3 reaction of PCl_5 and PBr_3, and then carefully exposing this product to vacuum for several weeks until a yellow powder was left. The product $PBr_4^+Cl^-$ was shown to be isomorphous with $PBr_5(PBr_4^+Br^-)$.[18] It is thus quite possible that their initial red–brown precipitate contained $PBr_4^+Cl_3^-$, with loss of Cl_2 *in vacuo* from the unstable trichloride ion leading to the formation of PBr_4Cl. The mixed phosphorus(V) halide PBr_5ICl has also been prepared from reaction of PBr_5 with ICl, and shown by Raman spectroscopy to have the structure $PBr_4^+BrICl^-$.[16] The structure $PBr_4^+IBr_2^-$ suggested for PBr_6I, prepared by reaction of either PBr_3 (1 : 3) or PBr_5 (1 : 1) with IBr,[21] has similarly been confirmed by solid state ^{31}P NMR spectroscopy.[22] $PBr_4^+Cl_3^-$ is thus one member of a series of derivatives of the PBr_4^+ cation, with either trihalide or single halide as the counter-ion.

EXPERIMENTAL

The compound was prepared from PCl_5 and PBr_3 in CCl_4, as described by Kuz'menko.[5] (Found: P, 6.92; Cl, 20.5; Br, 75.2. PBr_4Cl_3 requires: P, 6.78; Cl, 23.3; Br, 70.0%. The analyses correspond approximately to the composition $PCl_{2.59}Br_{4.21}$.) ^{31}P NMR and Raman spectra were recorded as described in previous papers.[9,11,23] ^{31}P chemical shifts are measured relative to external H_3PO_4, with the downfield (higher frequency) direction taken as positive.

Acknowledgements—We thank the S.E.R.C. for financial support, and Dr P. N. Gates (Royal Holloway and Bedford New College) for assistance with the Raman spectra.

REFERENCES

1. M. Prinvault, *Ber.* 1872, **5**, 323; *Compt. rend.* 1872, **74**, 868.
2. A. Michaelis, *Ber.* 1872, **5**, 411.
3. Ya. A. Fialkov and A. A. Kuz'menko, *J. Gen. Chem. USSR* 1951, **21**, 479.
4. Ya. A. Fialkov and A. A. Kuz'menko, *J. Gen. Chem. USSR* 1952, **22**, 1335.
5. A. A. Kuz'menko, *Ukr. Khim. Zh.* 1952, **18**, 589.
6. A. I. Popov, D. H. Geske and N. C. Baenziger, *J. Am. Chem. Soc.* 1956, **78**, 1793.
7. G. S. Harris and D. S. Payne, *J. Chem. Soc.* 1956, 4613.
8. L. Kolditz and A. Feltz, *Z. Anorg. Allgem. Chem.* 1957, **293**, 286.
9. F. F. Bentley, A. Finch, P. N. Gates, F. J. Ryan and K. B. Dillon, *J. Inorg. Nucl. Chem.* 1974, **36**, 457.
10. K. B. Dillon, M. P. Nisbet and T. C. Waddington, *Polyhedron* 1982, **1**, 123.
11. K. B. Dillon, M. P. Nisbet and T. C. Waddington, *J. Chem. Soc., Dalton Trans.* 1978, 1455.
12. K. B. Dillon, M. P. Nisbet and T. C. Waddington, *J. Chem. Soc., Dalton Trans.* 1979, 1591.
13. H. Gerding and P. C. Nobel, *Rec. Trav. Chim.* 1958, **77**, 472.
14. P. Dhamelincourt and M. Crunelle-Cras, *Bull. Soc. Chim. France* 1970, 2470.
15. P. Dhamelincourt and M. Crunelle-Cras, *Compt. Rend.* 1970, **271B**, 124.
16. P. Dhamelincourt and M. Crunelle-Cras, *Compt. Rend.* 1971, **272B**, 50.
17. W. Gabes and H. Gerding, *Rec. Trav. Chim.* 1971, **90**, 157.
18. W. Gabes, K. Olie and H. Gerding, *Rec. Trav. Chim.* 1972, **91**, 1367.
19. J. C. Evans and G. Y.-S. Lo, *J. Chem. Phys.* 1966, **44**, 3638.
20. G. L. Breneman and R. D. Willett, *Acta Cryst.* 1967, **23**, 467.
21. Ya. A. Fialkov and A. A. Kuz'menko, *J. Gen. Chem. USSR* 1949, **19**, 71.
22. W. Wieker and A.-R. Grimmer, *Z. Naturforsch.* 1967, **22b**, 257.
23. A. Finch, P. N. Gates, F. J. Ryan and F. F. Bentley, *J. Chem. Soc., Dalton Trans.* 1973, 1863.

Polyhedron Vol. 7, No. 18, pp. 1725–1726, 1988
Printed in Great Britain

0277–5387/88 $3.00+.00
© 1988 Pergamon Press plc

THE STRUCTURE OF PBr_4Cl_3

KEITH B. DILLON,* MARTIN P. NISBET and ROGER N. REEVE

Chemistry Department, University of Durham, South Road, Durham DH1 3LE, U.K.

(*Received* 15 *February* 1988; *accepted* 9 *March* 1988)

Abstract—The compound PBr_4Cl_3 has been shown to have the ionic structure $PBr_4^+Cl_3^-$ by means of ^{31}P NMR and Raman spectroscopy. There was no evidence for the formation of mixed bromochlorophosphonium ions. It appears to be a member of a series of derivatives of the PBr_4^+ ion with trihalide or single halide counter-ions.

Several mixed phosphorus(V) halides have been reported from reaction of PCl_3 and bromine under various conditions.[1–9] These include the compound PBr_4Cl_3, which was first described by Prinvault[1] and Michaelis[2] independently in 1872, although nothing was known of its structure. This compound was investigated in more detail by Fialkov and Kuz'menko[3,4] who prepared it from a mixture of PCl_3 and bromine containing 57.42 mol % of PCl_3.[3] The material was recrystallized from CCl_4 and dried in a current of CO_2, giving orange–red crystals of the product. The compound was reported not to conduct in the solid state, but to be a good conductor when molten.[3] It was subsequently shown to be an electrical conductor in polar solvents such as $PhNO_2$ or MeCN, but a non-conductor in C_6H_6, CCl_4 or CS_2.[4] The authors suggested the formulation $[PCl_3Br]^+[Br(Br_2)_n]^-$ for this and a related series of compounds, with $n = 1$ for PBr_4Cl_3.[4] The compound was later prepared by reaction of 40.5 mol % PBr_5 and 59.5 mol % PCl_5 at 313–323 K, according to eq. (1), or by a 3:2 reaction between PCl_5 and PBr_3, eq. (2).[5]

$$6PCl_5 + 4PBr_5 \rightarrow 5PBr_4Cl_3 + 5PCl_3 \quad (1)$$

$$6PCl_5 + 4PBr_3 \rightarrow 3PBr_4Cl_3 + 7PCl_3. \quad (2)$$

Popov *et al.* were unable to reproduce the preparation from PCl_3 and Br_2 in the absence of solvent,[3] obtaining from several attempts a material of composition between $PCl_3Br_{5.1}$ and $PCl_3Br_{5.7}$.[6] Their product lost bromine rapidly to give a yellow powder of composition $PCl_{4.67}Br_{0.33}$, or $P_{12}Cl_{56}Br_4$, which appeared from physical measurements to be a true compound rather than a mixture.[6] Harris and Payne were also unable to reproduce this preparation,[3] obtaining materials which analysed approximately as $PCl_3Br_7 \cdot CCl_4$ and $PCl_3Br_7 \cdot 2CCl_4$.[7] These solids lost CCl_4 and Br_2 on heating, and the possibility of their being CCl_4 solvates of members of the $PCl_3 \cdot nBr_2$ series[4] could not be excluded. The only proposal for the structure of PBr_4Cl_3 was thus $[PCl_3Br]^+Br_3^-$,[4] and there have been no subsequent studies on this compound. We now report the results of an investigation by spectroscopic techniques into its structure.

RESULTS AND DISCUSSION

In view of the difficulties reported[6,7] in the direct preparation from PCl_3 and bromine, the compound was prepared from PCl_5 and PBr_3 in CCl_4.[5] The precipitate which formed was separated and dried *in vacuo*. The product analysed approximately as $PCl_{2.59}Br_{4.21}$, the discrepancies probably being due largely to experimental error, although a small amount of hydrolysis cannot be discounted. There seems little doubt, however, that the main constituent is PBr_4Cl_3, and this was confirmed by the spectroscopic measurements.

The ^{31}P NMR solution spectrum was recorded in 25 oleum, which has been shown by previous work in this group to be an excellent solvent for species containing simple or mixed halogenophosphonium ions.[10] A strong resonance at −85 ppm was discerned, readily assigned to the PBr_4^+ ion.[10] A very weak signal from $PBr_3(OH)^+$ (in equilibrium with unprotonated $POBr_3$)[11] was also apparent at −64 ppm, consistent with the presence of a small amount of hydrolysis. There was no evidence, however, for the formation of mixed bromochlorophosphonium ions such as PCl_3Br^+,

* Author to whom correspondence should be addressed.

the chemical shifts of which are known,[10,12] as suggested by Fialkov and Kuz'menko.[4] This result strongly suggests that the compound should be formulated as $PBr_4^+Cl_3^-$. Confirmation was provided by the Raman spectrum of the solid, which showed in addition to strong bands for the PBr_4^+ ion[13–18] a weak band at 267 cm^{-1}, very similar to the frequency reported (268 cm^{-1}) for the trichloride ion in tetraalkylammonium salts.[19] Hence the ideal structure for the compound PBr_4Cl_3 appears to be $PBr_4^+Cl_3^-$, with any deviations from this composition possibly being due to the presence of free halide rather than trichloride as the counter-ion. The structure may well be similar to that of PBr_7, which has been shown by X-ray crystallography to have the ionic composition $PBr_4^+Br_3^-$.[20]

It is of interest in this connection that Gabes *et al.* prepared the compound PBr_4Cl, and showed by Raman spectroscopy and powder X-ray work that it has the structure $PBr_4^+Cl^-$.[18] Their compound was prepared by recrystallizing from CS_2 the red–brown precipitate obtained from a 4 : 3 reaction of PCl_5 and PBr_3, and then carefully exposing this product to vacuum for several weeks until a yellow powder was left. The product $PBr_4^+Cl^-$ was shown to be isomorphous with $PBr_5(PBr_4^+Br^-)$.[18] It is thus quite possible that their initial red–brown precipitate contained $PBr_4^+Cl_3^-$, with loss of Cl_2 *in vacuo* from the unstable trichloride ion leading to the formation of PBr_4Cl. The mixed phosphorus(V) halide PBr_5ICl has also been prepared from reaction of PBr_5 with ICl, and shown by Raman spectroscopy to have the structure $PBr_4^+BrICl^-$.[16] The structure $PBr_4^+IBr_2^-$ suggested for PBr_6I, prepared by reaction of either PBr_3 (1 : 3) or PBr_5 (1 : 1) with IBr,[21] has similarly been confirmed by solid state ^{31}P NMR spectroscopy.[22] $PBr_4^+Cl_3^-$ is thus one member of a series of derivatives of the PBr_4^+ cation, with either trihalide or single halide as the counter-ion.

EXPERIMENTAL

The compound was prepared from PCl_5 and PBr_3 in CCl_4, as described by Kuz'menko.[5] (Found: P, 6.92; Cl, 20.5; Br, 75.2. PBr_4Cl_3 requires: P, 6.78; Cl, 23.3; Br, 70.0%. The analyses correspond approximately to the composition $PCl_{2.59}Br_{4.21}$.) ^{31}P NMR and Raman spectra were recorded as described in previous papers.[9,11,23] ^{31}P chemical shifts are measured relative to external H_3PO_4, with the downfield (higher frequency) direction taken as positive.

Acknowledgements—We thank the S.E.R.C. for financial support, and Dr P. N. Gates (Royal Holloway and Bedford New College) for assistance with the Raman spectra.

REFERENCES

1. M. Prinvault, *Ber.* 1872, **5**, 323; *Compt. rend.* 1872, **74**, 868.
2. A. Michaelis, *Ber.* 1872, **5**, 411.
3. Ya. A. Fialkov and A. A. Kuz'menko, *J. Gen. Chem. USSR* 1951, **21**, 479.
4. Ya. A. Fialkov and A. A. Kuz'menko, *J. Gen. Chem. USSR* 1952, **22**, 1335.
5. A. A. Kuz'menko, *Ukr. Khim. Zh.* 1952, **18**, 589.
6. A. I. Popov, D. H. Geske and N. C. Baenziger, *J. Am. Chem. Soc.* 1956, **78**, 1793.
7. G. S. Harris and D. S. Payne, *J. Chem. Soc.* 1956, 4613.
8. L. Kolditz and A. Feltz, *Z. Anorg. Allgem. Chem.* 1957, **293**, 286.
9. F. F. Bentley, A. Finch, P. N. Gates, F. J. Ryan and K. B. Dillon, *J. Inorg. Nucl. Chem.* 1974, **36**, 457.
10. K. B. Dillon, M. P. Nisbet and T. C. Waddington, *Polyhedron* 1982, **1**, 123.
11. K. B. Dillon, M. P. Nisbet and T. C. Waddington, *J. Chem. Soc., Dalton Trans.* 1978, 1455.
12. K. B. Dillon, M. P. Nisbet and T. C. Waddington, *J. Chem. Soc., Dalton Trans.* 1979, 1591.
13. H. Gerding and P. C. Nobel, *Rec. Trav. Chim.* 1958, **77**, 472.
14. P. Dhamelincourt and M. Crunelle-Cras, *Bull. Soc. Chim. France* 1970, 2470.
15. P. Dhamelincourt and M. Crunelle-Cras, *Compt. Rend.* 1970, **271B**, 124.
16. P. Dhamelincourt and M. Crunelle-Cras, *Compt. Rend.* 1971, **272B**, 50.
17. W. Gabes and H. Gerding, *Rec. Trav. Chim.* 1971, **90**, 157.
18. W. Gabes, K. Olie and H. Gerding, *Rec. Trav. Chim.* 1972, **91**, 1367.
19. J. C. Evans and G. Y.-S. Lo, *J. Chem. Phys.* 1966, **44**, 3638.
20. G. L. Breneman and R. D. Willett, *Acta Cryst.* 1967, **23**, 467.
21. Ya. A. Fialkov and A. A. Kuz'menko, *J. Gen. Chem. USSR* 1949, **19**, 71.
22. W. Wieker and A.-R. Grimmer, *Z. Naturforsch.* 1967, **22b**, 257.
23. A. Finch, P. N. Gates, F. J. Ryan and F. F. Bentley, *J. Chem. Soc., Dalton Trans.* 1973, 1863.

Polyhedron Vol. 7, No. 18, pp. 1727–1735, 1988
Printed in Great Britain

0277–5387/88 $3.00+.00
© 1988 Pergamon Press plc

COMPLEXES OF RUTHENIUM(III) WITH DIMETHYLSULPHOXIDE—I. $[Ru_2Cl_6(DMSO)_4]$, *FAC* AND *MER* ISOMERS OF $[RuCl_3(DMSO)_3]$: VERSATILE STARTING MATERIALS FOR THE SYNTHESIS OF RUTHENIUM(III) COMPLEXES

UMA CHARAN SARMA, K. P. SARMA* and RAJ K. PODDAR†

Department of Chemistry, North-Eastern Hill University, Bijni Complex, Shillong 793 003, India

(*Received* 15 *July* 1987; *accepted after revision* 9 *March* 1988)

Abstract—Ruthenium(III) complexes with dimethylsulphoxide (DMSO), $[RuCl_3(DMSO)_2]_2$ and $[RuCl_3(DMSO)_3]$ were synthesized and characterized by physical methods. The *fac* and *mer* isomers of $[RuCl_3(DMSO)_3]$, were obtained. The *fac* isomer has all S-bonded DMSO whereas *mer* has both S- and O-bonded DMSO molecules. The above three compounds were reacted with S, P, As, N and O donor ligands leading to partial or complete substitution of DMSO molecules, depending on the reaction conditions and nature of the incoming ligand. S, P and As donor ligands gave complete substitution of DMSO molecules, whereas N and O donor ligands generally gave partial substitution. New compounds prepared and characterized are $[RuCl_3L_2(DMSO)]$ (where L = py, CH_3CN; L_2 = 1,10-phenanthroline, 2,2′-bipyridyl) and $[Ru(acac)(DMSO)_2Cl_2]$.

The ruthenium(II) complex $[RuCl_2(DMSO)_4]$ was reported by James *et al.*[1] A simpler method of preparation was later reported[2] and the complex was used as a precursor for the synthesis of many ruthenium(II) complexes.[3–5] A similar complex of ruthenium(III), viz. $[RuCl_3(DMSO)_3]$ was first reported by Wilkinson's group,[6] using the blue solution of ruthenium(II), however, they[2] later reported the unrepeatability of the reaction. Antonov *et al.*[7] reported its preparation and some physical characteristics. They also reported that all three dimethylsulphoxide molecules are bonded to ruthenium(III) through the oxygen atoms. Most of the physical data reported conform with this composition and the facial structure of the complex. However, the lower magnetic moment value (μ_{eff} = 1.0 BM) and the sharp line ^1H NMR spectrum at room temperature are intriguing. Two reports on other ruthenium(III) complexes with dimethylsulphoxide by Bora and Singh[8,9] describe $[Ru(DMSO)_6]X_3$ (X = Cl, Br or ClO_4) and $M[Ru(DMSO)_2Cl_4]$ (M = Na or Bu_4N). These complexes require further investigation for complete characterization and a thorough study of the dimethylsulphoxide complexes of ruthenium(III) has accordingly been carried out.

EXPERIMENTAL

All the solvents were freshly distilled before use. Ruthenium trichloride trihydrate was obtained from Aurora–Matthey Ltd, Calcutta. The analyses for chloride were carried out by standard methods,[10] after decomposition with a KOH and KNO_3 mixture. Carbon, nitrogen and hydrogen analyses were obtained from the Regional Sophisticated Instrumentation Centre, C.D.R.I., Lucknow. IR spectra were recorded using KBr pellets on a Perkin–Elmer model 297 IR spectrophotometer in the range 4000–600 cm^{-1} and in both KBr and CsI pellets with a Perkin–ELmer 983 IR spectrophotometer in the range 4000–180 cm^{-1}. IR absorption bands are given in Tables 1 and 2. Elec-

*Present address: Guwahati Engineering College, Guwahati, Assam.

†Author to whom correspondence should be addressed.

Table 1. Important IR band positions (in cm^{-1}) and their assignments (in KBr and CsI pellets) of (**1**), (**2**) and (**3**)

1 $[Ru_2Cl_6(DMSO)_4]$	**2** *mer*-$[RuCl_3(DMSO)_3]$	**3** *fac*-$[RuCl_3(DMSO)_3]$	Assignments
1427m, 1410m	1433–1410m–s	1427m, 1413m, 1404m	δ_d(CH)
1317m	1320m	1315m	δ_d(CH)
1298m	1295w	1295m	δ_d(CH)
1110m	1113m, 1093m	1110sh, 1087s, 1065m	$\nu_{S=O}$ (S-bonded)
1028m, 1019m	1032s, 1015m	1037w, 1022m	ρ_r(CH)
—	981vs	—	$\nu_{S=O}$ (O-bonded)
985m, 950m	936vw	975m	ρ_r(CH)
891vs	—	—	$\nu_{S=O}$ (O-bonded)
723w, 683w	725w, 683w	725w, 680w	ν_a(CS)
504m	471br, w	—	ν_{Ru-O}
430m–w	421m-w	422s	ν_{Ru-S} δ_d(CSO)
376w	380w	385m	δ_a(CSO)
335s	340vs, 326s, 313m	343s, 319s	ν_{Ru-Cl}
	288m	279m	ν_{Ru-Cl} (Bridging)
249m–w	—	—	

ν, stretching; ν_a, assymmetric stretching; δ, deformation; δ_d, degenerate deformation; ρ_r, rocking; δ_a, assymmetric deformation.

tronic absorption spectra were recorded in solution on Beckmann 26 and Cary 2300 spectrophotometers in the ranges 800–200 and 1200–200 nm, respectively. The results are given in Table 2. Magnetic susceptibility measurements were carried out using a Faraday balance or a Vibrating Sample Magnetometer EG & G PARC at room temperature (25°C). The ESR spectra were recorded at room and liquid nitrogen temperatures using a Varian E 104 spectrometer. ESR spectra are given in Table 3. ^{1}H NMR spectra were recorded on a Varian EM 390, 90 MHz spectrometer, in deuterated solvent. Conductivity measurements were made on a Systronic Conductivity meter 304 with millimolar solutions in acetonitrile and chloroform. All the melting points are uncorrected.

Preparation of $[Ru_2Cl_6(DMSO)_4]$ (**1**)

Method A. Dimethylsulphoxide (1.5 cm^3) was added to hydrated ruthenium trichloride (0.25 g, 1 mmol) and warmed on a water bath (15–20 min) to get a clear dark red solution. The solution was cooled to room temperature and acetone was added with stirring and a brownish-red coloured compound precipitated out. It was centrifuged and washed 2–3 times with acetone and dried *in vacuo*. Yield, 0.3 g, 75%. This was analysed for $[Ru_2Cl_6(DMSO)_4]$.

Method B. Compound (**1**) could also be obtained by precipitation of hydrated ruthenium trichloride solution in dimethylsulphoxide (at room temperature) with acetone.

Table 2. Important IR and electronic absorption bands of ruthenium(III) complexes containing DMSO

Compound	IR bands (cm^{-1})	Electronic absorption bands in nm (ε) CH_3CN	$CHCl_3$
$[Ru_2Cl_6(DMSO)_4]$	—	455 (11,800) 390 (10,300)	457 (10,400) 380 (10,600)
mer-$[RuCl_3(DMSO)_3]$	—	416 (2900) 385 (3200)	435 (2600) 380 (2900)
fac-$[RuCl_3(DMSO)_3]$	—	468 (140) 405 (585)	—
$[RuCl_3(py)_2(DMSO)]$ (Yellow)	1105s, 1090sh, 1065m, 1015m–s, 423m, 345m, 330m	465 (700) 406 (2200)	470 (740) 408 (2,450)
$[RuCl_3(py)_2(DMSO)]$ (Green)	1105s, 1090s, 1065s, 1015m–s, 426m, 380m, 351m, 330m	—	620 (220) 470 (930) 405 (1620)
$[RuCl_3(phen)(DMSO)]$ (Brown)	1090m–s, 423m, 390m, 323m, 254m	404 (3580) 395 (3770)	404 (4060) 395 (4130)
$[RuCl_3(phen)(DMSO)]$ (Orange)	1090m–s, 430m, 343m, 285m	—	405 (4070) 395 (4280)
$[RuCl_3(CH_3CN)_2(DMSO)]$	2315w, 2280m, 1110s, 1090s, 1020s, 331m	—	—
$[RuCl_3(bipy)(DMSO)]$	1110s, 1015m, 420m, 321m	408 (5140) 404 (4540)	404 (3530) 395 (3700)
$[Ru(acac)(DMSO)_2Cl_2]$	1570m–s, 1510m, 1090s	560 (50)	—

Table 3. ESR spectra of some ruthenium(III) complexes

Serial number	Compound	*g* Values
1	$[Ru_2Cl_6(DMSO)_4]$ (1)	2.37, 2.14, 1.88[a]
2	$[RuCl_3(DMSO)_3]$ (2)	2.41, 2.26, 1.88[a]
3	$[RuCl_3(DMSO)_3]$ (3)	2.42, 1.92[a], 2.40, 1.91[b]
4	$[RuCl_3(CS_2)(PPh_3)_2]$	2.40, 2.16, 1.81[a], 2.25[a]
5	$[RuCl_3(py)_2(DMSO)]$ (Yellow)	2.25[a], 2.5, 2.0, 1.8[c]
6	$[RuCl_3(py)_2(DMSO)]$ (Green)	2.21[a], 2.5, 2.0, 1.8[c]
7	$[RuCl_3(bipy)(DMSO)]$	2.23[a]
8	$[RuCl_3(phen)(DMSO)]$ (Orange)	2.5, 2.12[a]
9	$[RuCl_3(phen)(DMSO)]$ (Brown)	2.27[a]

[a] At room temperature in powder form.

[b] At liquid N_2 temperature in powder form.

[c] At liquid N_2 temperature of frozen $CHCl_3$ solution.

All the room temperature spectra which show only one signal are broad. Two *g* values for (3) and three *g* values for (2) suggest facial and meridional structures with C_{3v} and C_{2v} symmetries, respectively.[22]

Preparation of mer-$[RuCl_3(DMSO)_3]$, *dark orange* (**2**)

Method A. Concentrated HCl (5 cm^3) was added to a solution of hydrated ruthenium trichloride (0.25 g, 1 mmol) in dimethylsulphoxide (1.5 cm^3). The mixture was refluxed on an oil bath (130–140°C) for $1\frac{1}{2}$ h and cooled to room temperature when the compound separated out. This was centrifuged and carefully washed twice with a very small amount (0.1–0.2 cm^3) of ice-cold acetone (acetone soluble) and dried *in vacuo*. Yield, 0.33 g, 80%. The compound was analysed for $[RuCl_3(DMSO)_3]$.

Method B. If the reaction mixture of method A was heated on a water bath for about 4 h instead of refluxing on an oil bath and cooled, (**2**) separated out.

Preparation of fac-$[RuCl_3(DMSO)_3]$, *yellow* (**3**)

Method A. Concentrated HCl (5 cm^3) was added to a solution of hydrated ruthenium trichloride (0.25 g, 1 mmol) in dimethylsulphoxide (1.5 cm^3). The mixture was heated (~ 85°C) for 30 min and the solution was concentrated to 1 cm^3 by heating at *ca* 85°C and then cooled overnight at 10°C. Yellow needle-like crystals separated out. These were concentrated, washed 2–3 times with acetone and dried *in vacuo*. Yield, 0.33 g, 80%. The compound was analysed for $[RuCl_3(DMSO)_3]$.

Method B. (**3**) in powder form could be precipitated out by the addition of acetone with constant stirring to the concentrated solution (1 cm^3) obtained from the reaction as in method A above.

Method C. The mother liquor, obtained after removing (**2**), upon concentration on a water bath to about 1 cm^3 and on the addition of acetone at ice-cold temperature with continuous stirring yielded a small quantity of (**3**).

Reactions of $[Ru_2Cl_6(DMSO)_4]$ (**1**), mer-$[RuCl_3(DMSO)_3]$, *orange isomer* (**2**), *and* fac-$[RuCl_3(DMSO)_3]$, *yellow isomer* (**3**) *with various ligands. General method of reactions*

Compound (**1**), (**2**) or (**3**) (0.2 g) was dissolved in a solvent (20 cm^3), to which a solution of the ligand, L, in the solvent (5–10 cm^3) was added. The reaction mixture was stirred at room temperature, or heated to a higher temperature, for a few hours. A compound separated or was precipitated out with diethyl ether or petroleum ether after concentrating the mother liquor. It was washed successively with the solvent and diethyl ether and dried *in vacuo*. Specific reaction conditions for each ligand and the compounds are given in Table 4.

RESULTS AND DISCUSSION

Complexes of Ru(III) *with chloride and* DMSO

The only ruthenium(III) complex containing chloride and dimethylsulphoxide groups, viz. $[RuCl_3(DMSO)_3]$ was first reported from Wilkinson's group,[6] using the blue solution of ruthenium(II). However, they[2] later reported the unrepeatability of the reaction. Much later, Antonov *et al.*[7] also reported its preparation. We have been able to synthesize two isomers of the formula $[RuCl_3(DMSO)_3]$, and another compound of the formula $[Ru_2Cl_6(DMSO)_4]$. We attempted to prepare $[RuCl_3(DMSO)_3]$ according to Antonov's method but obtained $[Ru_2Cl_6(DMSO)_4]$ only. In fact a closer look at the preparative method of Antonov and compound (**1**) from our method show a close similarity. Normally a reaction carried out at higher temperatures (i.e. refluxing of DMSO) even for a short period (5 min) without using concentrated HCl gives rise to the ruthenium(II) complex, viz. $[RuCl_2(DMSO)_4]$.[2] When the reaction was carried out at a lower temperature (water bath temperature, 70–80°C), the ruthenium(III) complex with dimethylsulphoxide, viz. $[Ru_2Cl_6(DMSO)_4]$ was obtained by us. However, if the reaction was carried out in the presence of conc. HCl, two isomers of the composition $[RuCl_3(DMSO)_3]$ are obtained. If the reaction was carried out at high temperatures (heating in an oil bath, 130–140°C) for $1\frac{1}{2}$ h or at low temperatures (water bath temperature) for 4 h an orange red isomer (**2**) was produced, whereas the reaction at water bath temperature for about 30 min gave a yellow isomer (**3**).

The analytical data (Table 2) of (**1**), (**2**) and (**3**) conform to the compositions $[Ru_2Cl_6(DMSO)_4]$, $[RuCl_3(DMSO)_3]$ and $[RuCl_3(DMSO)_3]$, respectively. The conductivity measurements of these complexes in acetonitrile and nitrobenzene show molar conductance values of the order 7–14 Ω^{-1} cm^2 mol^{-1} which conform to the covalent nature of the chloro groups bonded to ruthenium. Conductivity measurements in water show very high values due to the decomposition of the complexes.

The IR spectra of compounds (**1**), (**2**) and (**3**) throw light on the nature of coordination of DMSO with ruthenium. Important IR bands are given in Table 1 with their most plausible assignments. Compound (**1**) shows absorption bands at 891 and 1120 cm^{-1} assigned to $\nu_{S=O}$ (O-bonded) and $\nu_{S=O}$ (S-bonded) DMSO groups, respectively.[2,7,11] Absorptions at 504 and 430 cm^{-1} could be assigned to ν_{Ru-O} and ν_{Ru-S}, respectively due to O-bonded and S-bonded DMSO.[11–15] Finally a strong band at 335 cm^{-1} could be due to ν_{Ru-Cl} (terminal) and at

Table 4. Conditions for the reactions of **1**, **2** and **3** with various ligands

Compounds reacted	Ligand L	Solvent	Molar ratio Comp : Ligand	Reaction temp. °C (time)	Method of isolation	Composition of the product (colour)
1, 2, 3	PPh_3, $AsPh_3$	CH_3OH	1:1, 1:2, 1:3 or 1:6	R.T. (1 h)	(a)	$[RuCl_3L_2(CH_3OH)]$ (Green)
1	py	CH_3OH	1:10	R.T. (4 h)	(b)	$[RuCl_3(py)_2(DMSO)]$ (Green)
3	py	CH_3OH	1:10	R.T. (4 h)	(a)	$[RuCl_3(py)_2(DMSO)]$ (Yellow)
1, 3	py	CH_3OH	1:10	70–80 (2 h)	(a)	$[RuCl_2(py)_4]$ (Yellow)
1	phen	CH_3OH	1:1	R.T. or 70–80 (2 h)	(a)	$[RuCl_3(phen)(DMSO)]$ (Brown)
2, 3	phen	CH_3OH	1:1	R.T. or 70–80 (2 h)	(a)	$[RuCl_3(phen)(DMSO)]$ (Orange)
2, 3	bipy	CH_3OH	1:1	R.T. (2 h)	(a)	$[RuCl_3(bipy)(DMSO)]$ (Orange)
2, 3	PDA	C_2H_5OH	1:1	80–85 ($\frac{1}{2}$ h)	(b)	$[RuCl_2(PDA)(DMSO)_2]$ (Orange)
2, 3	acacH[a]	$C_6H_5CH_3$	1:10	120–130 (3 h)	(c)	$[RuCl_2(acac)(DMSO)_2]$ (Light brown)
1, 2, 3	CH_3CN	CH_3CN		80–85 (4 h)	(b)	$[RuCl_3(CH_3CN)(DMSO)]$ (Orange)
1, 2, 3	Na(dtc)	CH_3OH	1:3	R.T. (2 h)	(a)	$[Ru(dtc)_3]$ (Dark brown)
1, 2, 3	abt	CH_3OH	1:3	70–80 ($\frac{1}{2}$ h)	(a)	$[Ru(abt)_3]$ (Violet)
2, 3	PPh_3	CS_2	1:2	40–50 ($\frac{1}{2}$ h)	(d)	$[RuCl_3(CS_2)(PPh_3)_2]$ (Dark brown)

[a] Triethylamine (1 cm^3) was also added.

py = pyridine; phen = 1,10-phenanthroline; bipy = 2,2′-bipyridyl; PDA = *o*-phenylenediamine; acacH = acetylacetone; dtc = diethyldithiocarbamate; abt = *o*-aminobenzenethiolate; R.T. = room temperature.

(a) Compound separated after the reaction, washed with the solvent and ether.

(b) Volume of the solution reduced to 5 cm^3 and diethyl ether added to precipitate the compound.

(c) Volume of the solution reduced to 5 cm^3 and petroleum (80–100°C) ether added to precipitate the compound.

(d) Volume of the solution reduced to 5 cm^3 and cooled to room temperature when the compound separated out.

249 cm^{-1} due to ν_{Ru-Cl} (bridging).[16] On the basis of the IR spectrum we may infer that DMSO molecules in compound (**1**) are both O- and S-bonded and that dimerization may take place through chloro-bridges. In compound (**2**) the bands at 1113 and 1093 cm^{-1} of medium intensity may be due to $\nu_{S=O}$ (S-bonded), and a very strong band at 981 cm^{-1} due to $\nu_{S=O}$ (O-bonded).[2,11] ν_{Ru-O} and ν_{Ru-S} are also observed at 471 and 421 cm^{-1}, respectively.[12–15] Comparing the intensities of bands at 981 cm^{-1} and *ca* 1100 cm^{-1} it may be inferred that compound (**2**) has two DMSO molecules which are O-bonded and one which is S-bonded. Compound (**2**) shows bands at 340, 326 and 313 cm^{-1}, which could be assigned to ν_{Ru-Cl}. The number of ν_{Ru-Cl} bands in the spectrum corresponds to a meridional configuration as in $[RhCl_3(DMSO)_3]$.[17] Compound (**3**) seems to be a purely S-bonded isomer, where no strong absorptions between 1000 and 850 cm^{-1} are observed, thereby showing the absence of $\nu_{S=O}$ (O-bonded). Bands around 1100 cm^{-1} are assigned to $\nu_{S=O}$ (S-bonded) and a band at 422 cm^{-1} is due to ν_{Ru-S}.[12–15] In fact, the IR spectral data of (**3**) have an exact resemblance to that of $[NMe_2H_2][RuCl_3(DMSO)_3]^-$ reported by McMillan *et al.*[11] The spectrum of this compound shows bands at 343 and 319 cm^{-1}, which are assigned to ν_{Ru-Cl}. The number and positions of ν_{Ru-Cl} bands conform to the facial configuration of the complex,[18] as in the case of *fac*-$[RuCl_3(py)_3]$.[19] The IR spectra of compounds (**1**), (**2**) and (**3**) in acetonitrile solution are similar to that in the solid state (KBr or CsI medium). There is a

Table 5. Some physical and analytical data of new ruthenium(III) complexes

Compound (colour)	M.P. (°C)	μ_{eff} at R.T. (BM)	Λ_M (Ω^{-1} cm^2 mol^{-1})	Analysis[a] (%) C	H	N	Cl
$[Ru_2Cl_6(DMSO)_4]$ (Brownish red)	160–165	1.1	7[b]	13.2 (13.2)	3.4 (3.3)	—	28.7 (29.3)
mer-$[RuCl_3(DMSO)_3]$ (Dark orange)	135–140	1.9	14[b]	16.6 (16.3)	4.3 (4.1)	—	24.0 (24.1)
fac-$[RuCl_3(DMSO)_3]$ (Yellow)	145–150	1.7	8[b]	16.6 (16.3)	4.2 (4.1)	—	24.6 (24.1)
$[RuCl_3(py)_2(DMSO)]$ (Yellow)	220–225	—	3[b]	32.8 (32.5)	4.1 (3.6)	6.0 (6.3)	—
$[RuCl_3(py)_2(DMSO)]$ (Green)	240[c]	—	20[b]	32.2 (32.5)	3.9 (3.6)	6.1 (6.3)	—
$[RuCl_3(phen)(DMSO)]$ (Orange)	>240	1.8	3[d]	36.2 (36.1)	2.9 (3.0)	5.9 (6.0)	—
$[RuCl_3(bipy)(DMSO)]$ (Orange)	>250	—	6[b]	32.2 (32.6)	3.2 (3.2)	6.3 (6.3)	—
$[Ru(acac)(DMSO)_2Cl_2]$ (Light brown)	215–220		3[b]	25.6 (25.3)	4.8 (4.4)	—	—
$(RuCl_3(CS_2)(PPh_3)_2]$[e] (Dark brown)	180–185[c]	1.8	—	55.2 (54.9)	4.0 (3.7)	—	—
$[Ru(abt)_3]$ (Violet)	—	—	5[d]	46.0 (45.3)	4.2 (4.4)	8.8 (8.8)	—

[a] Calculated values are in parentheses.
[b] In acetonitrile.
[c] Decomposes.
[d] In chloroform.
[e] Ref. 26.

slight deviation (10–20 cm^{-1}) of the bands due to ν_{SO} in acetonitrile solution.

Room temperature magnetic moment values of compounds (**2**) and (**3**) agree with the low spin ruthenium(III) d^5 system.[20] The low value of μ_{eff} for $[Ru_2Cl_6(DMSO)_4]$ may be due to a weak antiferromagnetic interaction of the two ruthenium(III) ions through the bridging chloro groups.[21] Electronic and ESR spectra of (**1**), (**2**) and (**3**) are presented in Tables 2 and 3, respectively.

Reaction of $[Ru_2Cl_6(DMSO)_4]$ (**1**), mer-$[RuCl_3(DMSO)_3]$ (**2**) *and* fac-$[RuCl_3(DMSO)_3]$ (**3**)

Compounds (**1**), (**2**) and (**3**) are soluble in most of the organic solvents, viz. methanol, ethanol, acetonitrile and chloroform. Compound (**2**) is soluble in acetone and benzene also. Hence, these compounds are suitable for carrying out exchange reactions with other ligands in neutral type organic solvents. In water, however, these complexes dissociate.

The reactions of (**1**), (**2**) and (**3**) with various donor ligands can be divided into three categories, viz. (i) where complete substitution of DMSO molecules takes place, (ii) where only one DMSO molecule is coordinated, and (iii) where two DMSO molecules are coordinated. The complete or partial substitution of coordinated DMSO molecules depends on the reaction conditions and the nature of the coordinating molecules, which can be generalized in the following paragraph.

In general, complete substitution of coordinated DMSO molecules takes place, either when the incoming ligand is more strongly coordinating than DMSO or when the reaction is carried out at a higher temperature, generally under refluxing conditions of the solvent. Examples of complete substitution of the DMSO molecules due to the stronger coordinating ability of the ligand is found in the cases of P, As or S donor ligands at room temperature and under refluxing conditions of the solvent. Complete substitution of DMSO takes place even in the cases where there is a nitrogen donor ligand or a nitrogen and sulphur donor chelate, under refluxing conditions of the solvent. Compounds containing one or two DMSO molecules are generally obtained when nitrogen or oxygen donor ligands are treated with (**1**), (**2**) or (**3**) at room temperature conditions. However, in some

cases such compounds are obtained under refluxing conditions of the solvent also.

Phosphorus, arsenic and sulphur donor ligands

Reactions of (1), (2) or (3) with triphenylphosphine or triphenylarsine in varying molar ratios (from 1 : 1 to 1 : 6, complex : PPh_3 or $AsPh_3$) at room temperature or under methanol refluxing conditions resulted in the formation of $[RuCl_3(MPh_3)_2(CH_3OH)]$ (M = P or As) complexes, which are well characterized and reported by Stephenson and Wilkinson.[23] This is due to the stronger coordinating abilities of PPh_3 and $AsPh_3$ compared to DMSO. Even when the complex : MPh_3 ratio was varied, in all the cases only $[RuCl_3(MPh_3)_2(CH_3OH)]$ was obtained and this signified that it is probably the most stable Ru^{III} compound with chloro and MPh_3 groups in a methanol medium.

Reactions of (1), (2) or (3) with the sodium salt of diethyldithiocarbamate at room temperature conditions yielded $[Ru(Et_2NCS)_3]$ which is obtained by the complete substitution of both chloro and DMSO groups from these complexes. The product $[Ru(Et_2NCS_2)_3]$ is well characterized and has been studied earlier.[24,25] Reaction of compound (2) or (3) with carbon disulphide under refluxing conditions did not undergo substitution of DMSO by a thiocarbonyl group or by carbon disulphide, instead the starting materials were recovered. However, when a reaction of (2) or (3) with carbon disulphide was carried out in the presence of triphenylphosphine under refluxing conditions, a dark brown coloured compound separated out which was analysed for $[RuCl_3(PPh_3)_2(CS_2)]$. This compound is the same as that reported by Ruiz *et al.*[26] from the reaction of $[RuCl_3(PPh_3)_2(CH_3OH)]$ with carbon disulphide. Besides all the bands due to triphenylphosphine, it showed an absorption band at 1505 cm^{-1}, assigned to a linearly bonded carbon disulphide group and another band at 332 cm^{-1} assigned to ν_{Ru-Cl}.[26] The magnetic moment of the compound, measured at room temperature (μ_{eff} = 1.8 BM), confirms its behaviour as a low-spin d^5, ruthenium(III) complex.

Reactions of (1), (2) or (3) with *o*-aminobenzenethiol under refluxing methanol conditions gave a completely substituted (both chloro and DMSO groups) compound, viz. ruthenium(*o*-aminobenzenethiol)$_3$. Here, complete substitution may be due to the stronger coordinating ability of the sulphur atom. The IR spectrum of the complex in the region 1100–1000 cm^{-1} shows two weak bands which are due to *o*-aminobenzenethiol and no characteristic band due to O-bonded DMSO is observed between 1000–900 cm^{-1}. This complex could also be prepared by the direct reaction of ruthenium trichloride with *o*-aminobenzenethiol in a suitable solvent.

Oxygen donor ligands

Reactions of compound (2) or (3) with acetylacetone in a weakly basic medium in refluxing toluene gave a compound with the composition, $[RuCl_2(acac)(DMSO)_2]$. The IR spectrum shows two strong bands at 1570 and 1510 cm^{-1} which could be assigned to ν_{CO} of the O-bonded type chelating acetylacetonato groups.[16] The presence of DMSO molecules is characterized by a very strong band at 1090 cm^{-1}. It is evidently due to S-bonded DMSO groups. There is no other band in the region 1000–900 cm^{-1} confirming the absence of any O-bonded DMSO groups. The IR spectra of the compounds obtained from the reactions of (2) and (3) with acetylacetone are superimposable, thereby confirming that the products obtained from the two isomers, viz. (2) having mostly O-bonded DMSO groups and (3) having S-bonded DMSO groups, are one and the same. From the above reactions we may infer that the coordinating behaviour of DMSO in the products depends on the incoming ligand and not on the starting compounds. The non-conducting behaviour of the complex in acetonitrile confirms the formula $[RuCl_2(acac)(DMSO)_2]$, where chloro groups are covalently bonded. Reactions of (1), (2) and (3) were carried out with triphenylphosphine oxide and triphenylarsine oxide separately under room temperature and refluxing methanol conditions. In both cases, no substitution of DMSO molecules took place and the starting materials were recovered.

Nitrogen donor ligands

(a) *Pyridine.* The products obtained from the reactions of (1), (2) or (3) with pyridine are dependent on the reaction conditions and in some cases on the starting compounds. Reactions of (1) and (3), with pyridine at room temperature conditions gave different products in each case whereas reactions of compounds (1), (2) and (3) with pyridine under refluxing conditions of methanol for 2 h gave $[RuCl_2(py)_4]$. Reactions of pyridine with other compounds viz. $RuCl_2(PPh_3)_3$ or $[RuCl_2(MPh_3)_2(CH_3OH)]$ (M = P or As) under similar conditions are reported to give $[RuCl_2(py)_4]$.[26] Here, in addition to the complete substitution of DMSO molecules by pyridine, reduction of ruthenium(III) to ruthenium(II) occurs as well. $[RuCl_2(py)_4]$, obtained as above, has *trans*-

geometry which is reflected by the far-IR and ^1H NMR spectra. The ^1H NMR spectrum shows a doublet at δ 8.6, and two triplets at δ 7.64 and 7.08, which is similar to that reported for *trans*-$[RuCl_2(py)_4]$.[27] The far-IR spectrum is superimposable onto the reported one.[27]

Reactions of compounds (**1**) and (**3**) with pyridine at room temperature yielded products which conform to the composition $[RuCl_3(py)_2(DMSO)]$. The product from compound (**1**) is a green isomer whereas the one from (**3**), is yellow. The very low conductivity values show covalent bonding of chlorides. The IR spectra of both compounds show strong bands around 1100 cm^{-1} which could be assigned to $\nu_{S=O}$ of the S-bonded DMSO group. A band at 1065 cm^{-1} could be due to pyridine or a combination of pyridine and DMSO bands. There was no strong band in the region 1000–900 cm^{-1}, characteristic of O-bonded DMSO groups. A band at 1015 cm^{-1} could be assigned to ρ_r CH of the DMSO group.[2] Characteristic bands due to coordinated pyridine groups were observed in both the complexes. The IR spectrum of the green and yellow isomers shows bands at 426 and 423 cm^{-1}, respectively, which can be assigned to ν_{Ru-S} of the S-bonded DMSO groups. Further, the green isomer shows three bands at 380, 351 and 330 cm^{-1} which may be assigned to ν_{Ru-Cl}. The presence of three absorption bands for ν_{Ru-Cl} indicates that two chloro groups in the complex are arranged in the *trans*-position and the third one is *cis* to these, as in the case of the *mer*-isomer of $[MX_3L_3]$ type systems.[18] The yellow isomer has two absorptions at 345 and 330 cm^{-1} assignable to ν_{Ru-Cl}. The presence of two absorption bands for ν_{Ru-Cl} is indicative that the three chlorides in the complex are arranged in the *cis* form as in the case of the *fac*-isomer of a $[MX_3L_3]$ species.[18]

(b) *2,2′-Bipyridyl.* A reaction of (**2**) or (**3**) with 2,2′-bipyridyl (bipy) at room temperature resulted in the partial substitution of DMSO molecules with the formation of $[RuCl_3(bipy)(DMSO)]$. Both $[RuCl_3(bipy)(DMSO)]$ compounds obtained from (**2**) and (**3**) are identical and their IR spectra are superimposable. The compound is a non-electrolyte. The IR spectrum of the compound shows a strong band at 1110 cm^{-1} which can be assigned to $\nu_{S=O}$ of the S-bonded DMSO groups and a band at 1015 cm^{-1} due to ρ_r CH of the DMSO molecule. In addition, all the characteristic absorption bands due to bipyridine are present. However, no bands of appreciable intensity in the region 1000–900 cm^{-1} are present confirming the absence of O-bonded DMSO groups. A spectrum in the far-IR region shows bands at 420 and 321 cm^{-1} which could be assigned to ν_{Ru-S} and ν_{Ru-Cl}, respectively. An IR spectrum confirms the presence of the S-bonded DMSO molecule.

(c) *1,10-Phenanthroline.* The products obtained from the reaction of compound (**1**) with 1,10-phenanthroline (phen) at room temperature and under methanol refluxing conditions have the same composition $[RuCl_3(phen)(DMSO)]$ and are both brown. The products obtained from the reaction of compound (**2**) or (**3**) with phen under similar conditions also have the same colour (orange–yellow) and composition $[RuCl_3(phen)(DMSO)]$. The brown and orange–yellow compounds may be isomers. The non-ionic nature of the compounds is confirmed by conductivity measurements. IR spectra of both the compounds show strong bands around 1090 cm^{-1} which could be assigned to $\nu_{S=O}$ of the S-bonded DMSO molecule. In the far-IR region, the brown compound shows absorptions at 423, 390, 323 and 254 cm^{-1}. The former band may be due to ν_{Ru-S} whereas the latter ones are probably due to ν_{Ru-Cl}. The orange–yellow compound shows absorptions at 430, 343 and 285 cm^{-1}. Here again, the absorption at 430 cm^{-1} could be due to ν_{Ru-S} whereas the bands at 343 and 285 cm^{-1} may be due to ν_{Ru-Cl}. The presence of three absorption bands due to ν_{Ru-Cl} in the case of the brown compound may be assigned to a structure where two of the chloro groups are *trans* to each other and the third one is *cis* to them, and the presence of two absorption bands due to ν_{Ru-Cl} in the case of the orange–yellow compound may be due to the presence of all three chloro groups being in the *cis* position.[18] (Similar to the green and yellow isomers of $[RuCl_3(py)_2(DMSO)]$.) The magnetic moment of the orange–yellow compound in powder form at room temperature has $\mu_{eff} = 1.9$ BM, a value expected for low-spin d^5 ruthenium(III) complexes.

(d) *o-Phenylenediamine.* Reaction of (**2**) or (**3**) with *o*-phenylenediamine (PDA), under refluxing conditions of methanol gave an orange compound having the composition, $[RuCl_2(PDA)(DMSO)_2]$. It is diamagnetic and has IR absorptions at 1065 cm^{-1}, assignable to $\nu_{S=O}$ of the S-bonded type DMSO. This compound is reported by Evans *et al*[2] by the reaction of PDA with $RuCl_2(DMSO)_4$.

(e) *Acetonitrile.* Reaction of (**1**), (**2**) or (**3**) with acetonitrile (as solvent) under refluxing conditions gave in all cases a compound of the composition, $[RuCl_3(CH_3CN)_2(DMSO)]$. The products obtained from all these compounds were the same and were confirmed by superimposable IR and visible spectra, melting points and the analytical data. Here, complete substitution of the DMSO molecules does not take place probably because of the weak coordinating ability of acetonitrile compared to DMSO. The conductivity measurements of the

complex show very low conductance values, thereby confirming the presence of all covalently bonded chloro groups. IR absorption bands at 2315 and 2280 cm^{-1} could be assigned to ν_{CN} of the coordinated CH_3CN molecules preferably in the *cis* position.[28] Two bands around 1100 cm^{-1} can be assigned to $\nu_{S=O}$ of the S-bonded DMSO group. There are no bands of appreciable intensity in the region 1000–900 cm^{-1} which may be due to O-bonded DMSO, but a band at 331 cm^{-1} is observed, which could be assigned to ν_{Ru-Cl} in the complex.

Acknowledgements—One of the authors (U.C.S.) thanks the U.G.C., New Delhi for the award of a teacher fellowship under the faculty improvement programme. We thank R.S.I.C., NEHU for obtaining the IR, UV and visible spectra and NMR spectra. We thank R.S.I.C., C.D.R.I., Lucknow for obtaining the analytical data, and to I.A.C.S., Calcutta and T.I.F.R., Bombay for obtaining room temperature magnetic measurements. We also thank Prof. J. Subramanian of NEHU, Shillong for the EPR spectra and discussions on it.

REFERENCES

1. B. R. James, E. Ochiai and G. L. Rempel, *Inorg. Nucl. Chem. Lett.* 1971, **7**, 781.
2. I. P. Evans, A. Spencer and G. Wilkinson, *J. Chem. Soc., Dalton Trans.* 1973, 204.
3. H. A. Hudali, J. V. Kingston and H. A. Tayim, *Inorg. Chem.* 1979, **18**, 1391.
4. B. Taqui Khan and A. Mehmood, *J. Inorg. Nucl. Chem.* 1978, **40**, 1938.
5. V. Ravinder, P. Lingaiah and K. Veera Reddy, *Inorg. Chim. Acta* 1984, **81**, 35.
6. J. D. Gilbert, D. Rose and G. Wilkinson, *J. Chem. Soc. A.* 1970, 2765.
7. P. G. Antonov, Y. N. Kukushkin, V. I. Konnov and B. I. Ionin, *Russ. J. Inorg. Chem.* 1978, **23**, 245.
8. T. Bora and M. N. Singh, *J. Inorg. Nucl. Chem.* 1976, **38**, 1815.
9. T. Bora and M. M. Singh, *Trans. Met. Chem.* 1978, **3**, 27.
10. A. I. Vogel, *Inorganic Quantitative Analysis*, 3rd Edn. ELBS & Longman, London (1961).
11. R. S. McMillan, A. Mercer, B. R. James and J. Trotter, *J. Chem. Soc., Dalton Trans.* 1975, 1006.
12. Yu N. Kukushkin, N. V. Ivannikova and K. A. Kokhryakov, *Zhur. Neorg. Khim.* 1970, **15**, 3062.
13. B. B. Wayland and R. F. Schramm, *Inorg. Chem.* 1969, **8**, 971.
14. B. F. G. Johnson and R. A. Walton, *Spectrochim. Acta* 1966, **22**, 1853.
15. J. H. Price, A. N. Williamson, R. F. Schramm and B. B. Wayland, *Inorg. Chem.* 1972, **11**, 1280.
16. K. Nakamoto, *Infrared and Raman Spectra of Inorganic and Coordination Compounds*, 3rd Edn. Wiley Interscience, New York (1978).
17. V. I. Sokol and M. A. Porai-Koshits, *Koord. Khim.* 1975, **4**, 576.
18. J. Chatt, G. J. Leigh and D. M. P. Mingos, *J. Chem. Soc. A* 1969, 1674.
19. J. Lewis, F. E. Mabbs and R. A. Walton, *J. Chem. Soc. A* 1967, 1366.
20. E. A. Seddon and K. R. Seddon, *The Chemistry of Ruthenium*. Elsevier, Amsterdam (1984).
21. J. E. Fergusson, J. D. Kurran and S. Seevaratnam, *J. Chem. Soc.* 1965, 2627.
22. A. Hudson and M. J. Kennedy, *J. Chem. Soc. A* 1969, 1116.
23. T. A. Stephenson and G. Wilkinson, *J. Inorg. Nucl. Chem.* 1966, **28**, 945.
24. D. J. Duffy and L. H. Pignolet, *Inorg. Chem.* 1974, **13**, 2405.
25. R. E. Desimone, *J. Am. Chem. Soc.* 1973, **95**, 6238.
26. L. Ruiz Ramirez, T. A. Stephenson and E. S. Switkes, *J. Chem. Soc., Dalton Trans.* 1973, 1770.
27. D. W. Raichart and H. Taube, *Inorg. Chem.* 1972, **11**, 999.
28. R. K. Poddar and U. Agarwala, *J. Inorg. Nucl. Chem.* 1973, **35**, 3769.

Polyhedron Vol. 7, No. 18, pp. 1737–1743, 1988
Printed in Great Britain

0277–5387/88 $3.00+.00
© 1988 Pergamon Press plc

COMPLEXES OF RUTHENIUM(III) AND -(II) WITH DIMETHYLSULPHOXIDE—II. $[RuBr_3(Me_2SO)_3]$ AND $[RuBr_2(Me_2SO)_3]$: VERSATILE STARTING MATERIALS FOR THE SYNTHESES OF RUTHENIUM BROMO COMPLEXES

UMA CHARAN SARMA and RAJ K. PODDAR*

Department of Chemistry, North-Eastern Hill University, Bijni Complex, Shillong 793 003, India

(*Received* 27 *November* 1987; *accepted after revision* 9 *March* 1988)

Abstract—The ruthenium(III) and -(II) complexes $[RuBr_3(Me_2SO)_3]$ and $[RuBr_2(Me_2SO)_3]$ have been synthesized and characterized using physical methods. $[RuBr_3(Me_2SO)_3]$ is the first example of a ruthenium complex where all three Me_2SO molecules are O-bonded whereas $RuBr_2(Me_2SO)_3$ has all Me_2SO molecules S-bonded. Reactions of $RuBr_3(Me_2SO)_3$ with various monodentate and bidentate ligands containing S, P, As, N and O-donor atoms have been carried out leading to partial or complete substitution of the Me_2SO molecules.

A ruthenium(II) chloride complex with dimethylsuphoxide (Me_2SO), viz. $[RuCl_2(Me_2SO)_4]$ has been studied for its physical and chemical behaviour. It has been used as a precursor for the synthesis of many Ru(II) complexes.[1–5] Similar work on ruthenium(III) complexes, viz. $[RuCl_3(Me_2SO)_3]$ and $[Ru_2Cl_6(Me_2SO)_4]$ has also been attempted.[2,6–8] In comparison to the chloride complexes mentioned above, work on their bromide analogues is relatively sparse and only $[RuBr_2(Me_2SO)_4]$ is known.[1,9–11] No report is available on Ru(III) complexes with bromide and Me_2SO groups. $[RuBr_2(Me_2SO)_4]$ has been used as a precursor for the synthesis of some Ru(II) bromide compounds of the type, $[RuBr_2(Me_2SO)_3L]$ (L = PPh_3, PBu_3, $P(OBu)_3$, $AsPh_3$), $[RuBr_2(Me_2SO)_2(diphos)]$ and $[RuBr_2L_4]$ (L = py or CH_3CN).[12]

The synthesis of complexes containing bromide as one of their ligands involves one of the following methods: (i) preparation of $RuBr_3$ from ruthenium oxide and treating with the ligand;[1,10] (ii) generating $RuBr_3$ *in situ* using $RuCl_3$ and LiBr/HBr and treating with the ligand;[13–15] (iii) metathesis of the chloride to bromide using KBr/HBr[16–19] or (iv) substitution of a ligand L in a bromide complex viz. $[RuBr_3L_2(MeOH)]$ or $[RuBr_3L_3]$ (L = PPh_3 or $AsPh_3$) by other ligands.[9,20]

Out of the above mentioned four methods, methods (iii) and (iv) are the most frequently used. To substitute PPh_3 or $AsPh_3$ completely by weak donor ligands in $[RuBr_3L_3]$ or $[RuBr_3L_2(MeOH)]$ (L = PPh_3 or $AsPh_3$) is not very successful. Hence, we have synthesized and characterized a complex, $[RuBr_3(Me_2SO)_3]$, which is used as a precursor for the synthesis of ruthenium(III) bromide complexes by substituting Me_2SO. Substitution of Me_2SO in this complex may be partial or complete depending on the reaction conditions used.

The new ruthenium(II) complex $RuBr_2(Me_2SO)_3$ also reported here, could be used as a molecular oxygen oxidative catalyst[21] or as a precursor for the synthesis of ruthenium(II) bromide complexes[12] as $[RuBr_2(Me_2SO)_4]$.

EXPERIMENTAL

All the solvents were distilled before use. Ruthenium trichloride trihydrate was obtained from Auroro–Matthey Ltd, Calcutta. The analyses for bromides were carried out by standard methods[22] after decomposition with a KOH and KNO_3 mixture. Carbon, hydrogen and nitrogen analyses were obtained from the Regional Sophisticated Instumentation Centre, C.D.R.I., Lucknow. Physical measurements viz. IR, UV–vis. and ESR (room temperature and liquid nitrogen temperature) spectra, magnetic and conductivity measurements were carried out as reported earlier.[8]

* Author to whom correspondence should be addressed.

(1) *Preparation of* $RuBr_3(Me_2SO)_3$

Hydrated ruthenium trichloride (0.25 g, 1 mmol) was dissolved in concentrated HBr (5 cm^3), to which LiBr (1 g) was added. The mixture was warmed on a water bath to get a clear solution. The solution was centrifuged and dimethylsulphoxide (1.5 cm^3) was added to the clear solution and refluxed in an oil bath (130–140°C) for 5 min (longer refluxation results in the separation of an insoluble compound). Dark violet crystals separated out. The product was cooled, centrifuged and the compound was washed 2–3 times with water followed by ethanol and dried *in vacuo*. It was analysed for $RuBr_3(Me_2SO)_3$, yield: 0.45 g (80%).

(2) *Preparation of* $RuBr_2(Me_2SO)_3$

Hydrated ruthenium trichloride (0.25 g, 1 mmol) was dissolved in ethanol (20 cm^3), to which LiBr (1 g) was added and refluxed for 30 min. To the clear solution, dimethyl sulphoxide (1.5 cm^3) was added and refluxed for another 2 h. The solution was concentrated to a small volume (5 cm^3) on a water bath and cooled to 0°C. A yellow compound separated out. The mother liquor, on concentration and on the addition of acetone gave further amounts of the yellow compound. The compound was washed 2–3 times with ethanol, then with ether and dried *in vacuo*. It was analysed for $RuBr_2(Me_2SO)_3$, yield: 0.35 g (75%).

Reaction of $RuBr_3(Me_2SO)_3$

(i) *With triphenylphosphine and triphenylarsine.* To a solution of $RuBr_3(Me_2SO)_3$ (0.3 g, 0.5 mmol) in ethanol (10 cm^3), triphenylphosphine or triphenylarsine (0.4–0.5 g, 1.5 mmol) in ethanol (10 cm^3) was added and stirred at room temperature for 3 h. A dark purple compound separated out which was centrifuged, washed with a little ethanol and then with ether and dried *in vacuo*. The compound was analysed for $[RuBr_3(MPh_3)_2(Me_2SO)]$ (M = P or As). A reaction similar to the above was carried out but the solvent was refluxed and $RuBr_3(MPh_3)_3$ (M = P or As) was obtained.

(ii) *With pyridine.* (a) To a clear solution of $RuBr_3(Me_2SO)_3$ (0.3 g) in toluene (10 cm^3), pyridine (0.5 cm^3) was added and stirred at room temperature for 1 h. The solution was cooled to 0°C for 2–3 h, when a violet compound separated out. It was centrifuged, washed with ether and dried *in vacuo*. The compound was analysed for $[RuBr_3(py)(Me_2SO)_2]$.

(b) A reaction similar to (a) using methanol as the solvent was carried out but the solution was refluxed for 1 h. Light brown crystals separated out and were collected as in (a). These were analysed for $[RuBr_3(py)_3]$.

(iii) *With 2-methyl pyridine.* 2-Methyl pyridine (0.5 cm^3) was added to $RuBr_3(Me_2SO)_3$ (0.3 g) and the mixture was warmed on a water bath for 30 min to get a clear solution. This was cooled and diethyl ether was added to precipitate a green compound which was centrifuged, washed with ether and dried *in vacuo* and was analysed for $[RuBr_3(C_6H_7N)(Me_2SO)_2]$.

(iv) *With 2,2′-bipyridyl* (bipy). $RuBr_3(Me_2SO)_3$ (0.3 g, 0.5 mmol) was dissolved in ethanol (20 cm^3), to which 2,2′-bipyridyl (0.1 g, 0.6 mmol) was added and refluxed on a water bath for 10 min. The solution was concentrated to a small volume (~ 5 cm^3) and a crystalline compound separated out. This was centrifuged, washed first with ethanol and then with diethyl ether and dried *in vacuo* and was analysed for $[RuBr_3(bipy)(Me_2SO)]$.

(v) *With o-phenylenediamine* (PDA). (a) To a clear solution of $RuBr_3(Me_2SO)_3$ (0.3 g, 0.5 mmol) in toluene (10 cm^3), *o*-phenylenediamine (0.12 g, 1 mmol) was added. The mixture was warmed on a water bath for 10 min and a reddish brown compound separated, which was centrifuged, washed with an ethanol–ether mixture and dried *in vacuo*. This was analysed for $[RuBr_2(PDA)(Me_2SO)_2]$.

(b) A reaction similar to (a) was carried out by taking $RuBr_3(Me_2SO)_3$ and PDA in a molar ratio of 1 : 1. A dark red compound separated out which was soluble in most of the organic solvents. This was washed carefully with a small quantity of ethanol and dried *in vacuo*. It was analysed for $[RuBr_2(PDA)_2(Me_2SO)_2]Br$.

(vi) *With sodium diethyl dithiocarbamate.* (a) To a clear solution of $RuBr_3(Me_2SO)_3$ (0.3 g, 0.5 mmol) in toluene (15 cm^3) sodium diethyldithiocarbamate (0.12 g, 0.5 mmol) was added and the mixture was refluxed on an oil bath for 30 min (110–115°C). The solution was cooled, centrifuged and concentrated to a small volume (~ 5 cm^3) on a water bath. Petroleum ether (60–100°C) was added and a brown complex precipitated. The mixture was cooled to 0°C for 6 h then centrifuged, washed with ether and dried *in vacuo*. The compound was analysed for $[Ru(Et_2NCS_2)(Me_2SO)_2Br_2]$.

(b) A reaction similar to (a) was carried out by refluxing $RuBr_3(Me_2SO)_3$ and sodium diethyldithiocarbamate in the molar ratio 1 : 3 for 2 h. The compound obtained was analysed for $[Ru(Et_2NCS_2)_3]$.

(vii) *With carbon disulphide and triphenylphosphine.* To a clear solution of $RuBr_3(Me_2SO)_3$ (0.3 g, 0.5 mmol) in carbon disulphide (20 cm^3), triphenylphosphine (0.4 g, 1.5 mmol) was added

and refluxed for 1 h. Dark reddish brown crystals separated which were cooled, centrifuged, washed with ether and dried *in vacuo*. The compound was analysed for $[RuBr_2(CS_2)(PPh_3)_3]Br$.

(viii) *With acetylacetone* (acacH). A solution of $RuBr_3(Me_2SO)_3$ (0.3 g) was made in toluene (20 cm^3). Acetylacetone (0.5 cm^3) and triethylamine (0.5 cm^3) were added to the solution and refluxed on an oil bath for 2 h. The solution was cooled, filtered and concentrated slowly to *ca* 2 cm^3. Light petroleum ether (40–60°C) was added to precipitate a purple compound. This was centrifuged, washed with ether and dried *in vacuo*. The compound was analysed for $Ru(acac)_3$.

The products of the substitution reactions of $RuBr_3(Me_2SO)_3$, described in (i)–(viii) are obtained in good yields (70–80%).

RESULTS AND DISCUSSION

We report here two new complexes $[RuBr_2(Me_2SO)_3]$ and $[RuBr_3(Me_2SO)_3]$.

The analytical data (Table 1) of the yellow diamagnetic compound obtained by the reaction of ruthenium trichloride with lithium bromide and dimethylsulphoxide in ethanol medium conforms to the composition $[RuBr_2(Me_2SO)_3]$, a d^6 low spin ruthenium(II) complex. The IR spectrum shows a strong absorption band at 1097 cm^{-1} which could be assigned to $\nu_{S=O}$ (S-bonded).[2] Bands at 423 and 245 cm^{-1} may be assigned to ν_{Ru-S}[23–24] and ν_{Ru-Br},[25] respectively. There is no strong absorption in the region 1000–900 cm^{-1}, indicative of the absence of any O-bonded Me_2SO groups. The ^1H NMR spectrum of a freshly prepared solution of $[RuBr_2(Me_2SO)_3]$ in $(CD_3)_2SO$ shows a sharp signal at δ 3.3 which is δ 0.7 downfield from free Me_2SO (δ 2.6) and indicative of S-bonded Me_2SO groups.[2,26] The other signal observed is at δ 2.6 which could be due to the residual protons of $(CD_3)_2SO$. There are no signals in the range δ 2.6–3.3 indicative of the absence of O-bonded Me_2SO groups. The signal at δ 3.3 is a sharp singlet which is indicative that all three Me_2SO groups are in equivalent positions[26] which is only possible if the structure is trigonal bipyramidal with the three Me_2SO groups in equatorial positions and the two bromides in axial positions. The ^1H NMR spectrum of $[RuBr_2(Me_2SO)_3]$

Table 1. Some analytical and physical data of some new ruthenium(III) and ruthenium(II) bromo–Me_2SO complexes

Compounds (Colour)	M.p. (°C)	Analysis[a] (%) C	H	N	Br	Conductance (Ω^{-1} cm^2 mol^{-1})	μ_{eff} at RT(BM)
$RuBr_2(Me_2SO)_3$	220–225	14.3	3.5	—	31.8	8[b]	D
(Yellow)		(14.5)	(3.6)		(32.3)		
$RuBr_3(Me_2SO)_3$	250	12.4	3.0	—	40.8	5[b]	2.1
(Dark violet)		(12.5)	(3.1)		(41.7)		
$RuBr_3(py)_3$		31.1	3.0	7.0	41.1	3[c]	—
(Light brown)		(31.1)	(2.6)	(7.3)	(41.5)		
$[RuBr_3(py)(Me_2SO)_2]$	140	19.0	3.0	2.3	—	—	2.0
(Violet)		(18.8)	(3.0)	(2.4)			
$[RuBr_3(Me\text{-}py)(Me_2SO)_2]$	180–185	19.5	3.0	2.4	—	—	1.92
(Green)		(19.4)	(3.1)	(2.3)			
$[Ru(bipy)(Me_2SO)Br_3]$	240	25.2	2.5	4.5	—	10[b]	—
(Dark brown)		(25.0)	(2.4)	(4.9)			
$[RuBr_2(PDA)_2(Me_2SO)_2]Br$	190–195	27.2	3.8	7.6	—	128[b]	
(Reddish brown)		(27.0)	(3.9)	(7.8)			
$[RuBr_2(PDA)(Me_2SO)_2]$	200–205	22.9	4.0	5.1		6	D
(Light pink)		(22.8)	(3.8)	(5.3)			
$[Ru(Et_2NCS_2)(Me_2SO)_2Br_2]$	250	18.7	3.4	2.7		2.5[b]	
(Brown)		(19.1)	(3.9)	(2.5)			
$[RuBr_2(CS_2)(PPh_3)_3]Br$	195–200	54.7	3.7	—		112[b]	1.65
(Reddish brown)		(54.9)	(3.7)			80[c]	

py = pyridine; phen = 1,10-phenanthroline; bipy = 2,2′-bipyridyl; PDA = *o*-phenylenediamine; Me_2SO = dimethylsulphoxide; Me-py = 2-methylpyridine; Et_2NCS_2 = diethyldithiocarbamate.

[a] Calculated values are in parentheses.

[b] In acetonitrile.

[c] In chloroform.

D = diamagnetic.

in $(CD_3)_2SO$, after keeping the solution for 100 h at room temperature or by warming on a water bath for 3 h, does not show any change with respect to the spectrum of a freshly prepared solution. The intensity of the signal at δ 3.3 is practically unchanged. This shows that an exchange of $(CH_3)_2SO$ molecules coordinated to the metal, by the solvent $(CD_3)_2SO$ molecules, does not take place under the conditions mentioned above.

Some preliminary reactions have been carried out to examine the potentiality of $[RuBr_2(Me_2SO)_3]$ as a precursor for the syntheses of ruthenium(II) bromide complexes. Reactions carried out at room temperature in methanol, result in partial or complete substitution of Me_2SO groups. Reaction of $[RuBr_2(Me_2SO)_3]$ with PPh_3 at room temperature caused complete substitution presumably giving $[RuBr_2(PPh_3)_4]$. The IR spectrum clearly shows the presence of PPh_3 and the absence of any Me_2SO group. Reaction of $[RuBr_2(Me_2SO)_3]$ with ligands like pyridine, 1,10-phenanthroline and 2,2′-bipyridyl at room temperature gave partial substitution forming $[RuBr_2L_2(Me_2SO)_2]$ ($L_2 = (py)_2$, 1,10-phenanthroline, 2,2′-bipyridyl, etc). The IR spectra of these compounds clearly show the presence of the S-bonded Me_2SO molecules. Either one or two strong absorption bands in the region 1080–1060 cm^{-1} are observed for these complexes which can be assigned to $\nu_{S=O}$ of the S-bonded Me_2SO group. We feel that $[RuBr_2(Me_2SO)_3]$ has a stronger potentiality as a precursor for the syntheses of ruthenium(II) bromide complexes. The only other ruthenium(II) bromide complex reported as a precursor is $[RuBr_2(Me_2SO)_4]$.[12]

The analytical data (Table 1) for the dark violet compound obtained by treating ruthenium trichloride with dimethylsulphoxide in the presence of lithium bromide and hydrogen bromide conform to the composition $[RuBr_3(Me_2SO)_3]$. It shows a very low molar conductance (5 Ω^{-1} cm^2 mol^{-1}) in acetonitrile suggesting covalently bonded bromide. The IR spectrum of the compound throws light on the nature of coordination of Me_2SO to ruthenium, there is a band of medium intensity at 1030 cm^{-1} and a strong band at 970 cm^{-1}. The former can be assigned to ρ_r(CH) whereas the latter may be assigned to $\nu_{S=O}$ (O-bonded) of the Me_2SO groups.[2] Bands at 468 and 295 cm^{-1} in the far-IR region may be assigned to ν_{Ru-O}[23,24] and ν_{Ru-Br},[25] respectively. The room temperature magnetic moment value of the complex (μ_{eff}) is 2.1 BM, confirming the presence of a low-spin d^5 ruthenium(III) system. The room temperature ESR measurement of the compound in the powder form shows a broad signal at $g = 2.2$. A frozen solution ESR in dichloromethane at liquid nitrogen temperature also shows a broad signal at $g = 2.12$ which means that the symmetry around ruthenium(III) is close to cubic, which is possible if one assumes that the O-bonded Me_2SO groups and the bromides have similar ligand fields. With these data, it is not possible to assign a facial or a meridional geometry to the complex. It is inferred that $[RuBr_3(Me_2SO)_3]$ is the first example of a ruthenium complex containing bromide and dimethylsulphoxide groups having all three O-bonded Me_2SO groups. Other known compounds, viz. two isomers of $[RuBr_2(Me_2SO)_4]$, have either completely S-bonded[9] or both S- and O-bonded[10] Me_2SO groups.

Reactions of $RuBr_3(Me_2SO)_3$ *with phosphorus and arsenic donor ligands*

Reaction of $RuBr_3(Me_2SO)_3$ with triphenylphosphine or triphenylarsine gave either complete or partial substitution of dimethylsulphoxide depending on the reaction conditions. Reactions at room temperature resulted in the formation of $[RuBr_3(MPh_3)_2(Me_2SO)]$ (M = P or As) whereas in refluxing ethanol completely substituted complexes, viz. $[RuBr_3(MPh_3)_3]$ were formed. The IR spectra of $[RuBr_3(MPh_3)_3]$ (M = P or As) shows absorption band characteristics of PPh_3 or $AsPh_3$ but no S- or O-bonded Me_2SO was observed. For $[RuBr_3(MPh_3)_2(Me_2SO)]$ all the bands due to PPh_3 or $AsPh_3$ and one band of medium intensity at 975 cm^{-1} which could be assigned to $\nu_{S=O}$ of the O-bonded Me_2SO group[9] were observed. Similar compounds are reported by the reaction of $[RuBr_3(MPh_3)_2(MeOH)]$ (M = P or As) with dimethylsulphoxide.[9]

Reactions of $RuBr_3(Me_2SO)_3$ *with sulphur and oxygen donor ligands*

Reaction of $RuBr_3(Me_2SO)_3$ with sodium diethyl dithiocarbamate ($NaEt_2NCS_2$) in the molar ratio 1:1 resulted in the partial substitution of Me_2SO leading to the formation of a non-electrolyte complex $[RuBr_2(Et_2NCS_2)(Me_2SO)_2]$ ($\Lambda_M = 2.5$ Ω^{-1} cm^2 mol^{-1}). However, a reaction with a molar ratio of 1:3 resulted in the complete substitution of Me_2SO and bromide leading to $[Ru(Et_2NCS_2)_3]$.[27,28] The IR spectrum of $[RuBr_2(Et_2NCS_2)(Me_2SO)_2]$ shows strong bands at 1080 and 1530 cm^{-1}, in addition to all the other bands due to diethyl dithiocarbamate. The former may be assigned to $\nu_{S=O}$ (S-bonded) of the Me_2SO group and the later one to ν_{CN} of a chelating diethyl dithiocarbamate group. ν_{CN} for the unidentate diethyl dithiocarbamate group is generally observed at a

lower frequency (1470 cm^{-1}).[29] Hence, $[RuBr_2(Et_2NCS_2)(Me_2SO)_2]$ is expected to be six-coordinate having a chelating diethyl dithiocarbamato group.

A reaction of $RuBr_3(Me_2SO)_3$ with PPh_3 in carbon disulphide medium resulted in the formation of $[RuBr_2(CS_2)(PPh_3)_3]Br$. However, CS_2 did not react or coordinate to the metal if PPh_3 was not used and the starting compound was isolated instead. The compound, $[RuBr_2(CS_2)(PPh_3)_3]Br$ shows a molar conductance of 112 Ω^{-1} cm^2 mol^{-1} in acetonitrile which is close to the 1 : 1 electrolytic behaviour of the compound. The IR spectrum shows a band of strong intensity at 1510 cm^{-1} besides bands due to PPh_3. The absorption at 1510 cm^{-1} may be assigned to a linearly bonded CS_2 group to the metal.[9] The μ_{eff} of the complex at room temperature is 1.65 BM, which is close to the value for one unpaired electron in low spin d^5 octahedral complexes of Ru(III).

A reaction of $[RuBr_3(Me_2SO)_3]$ with acetylacetone resulted in the complete substitution of the bromide and Me_2SO groups leading to the formation of $Ru(acac)_3$. In this case no partial substitution product could be isolated as in the case of the chloride analogues, reported earlier.[8] $Ru(acac)_3$ shows IR absorptions at 1560 and 1515 cm^{-1} which are characteristics of the chelating O-bonded acetylacetonato group, assigned to $\nu_{C=O}$ and $\nu_{C=C}$, respectively.[25] This is the same compound as reported by Endo *et al.*[30] An attempt to substitute Me_2SO in $[RuBr_3(Me_2SO)_3]$ with $OPPh_3$ was unsuccessful and $RuBr_3(Me_2SO)_3$ was recovered after the reaction.

Reactions of $RuBr_3(Me_2SO)_3$ *with nitrogen donor ligands*

(a) *Pyridine.* Reactions of $RuBr_3(Me_2SO)_3$ with pyridine at room temperature yields a dark violet compound of the composition $[RuBr_3(py)(Me_2SO)_2]$ where only one Me_2SO molecule is substituted by pyridine. The IR spectrum shows a band at 965 cm^{-1} which could be assigned to $\nu_{S=O}$ (O-bonded) and a band at 447 cm^{-1} may be due to ν_{Ru-O}. Besides these, characteristic bands due to pyridine are also observed and the ones at 292 and 245 cm^{-1} may be assigned to ν_{Ru-Br}. The room temperature magnetic moment value, μ_{eff}, is 2.0 BM, thereby confirming the oxidation state of ruthenium as 3+. Dimethylsulphoxide groups in $[RuBr_3(py)(Me_2SO)_2]$ are O-bonded as in the parent compound.

Complete substitution of Me_2SO molecules takes place when stronger reaction conditions are employed, leading to the formation of a brown crystalline compound of the composition $[RuBr_3(py)_3]$. The IR spectrum of the compound shows the presence of pyridine. The room temperature ESR spectrum of the compound in powder form shows three signals corresponding to g values of 2.65, 2.0 and 1.85 which suggests a rhombic geometry around ruthenium(III). If, one presumes a meridional type of structure for $RuBr_3(py)_3$ with C_{2v} symmetry, the three g values can be explained.[8,31]

(b) *2-Methyl pyridine.* A reaction of $RuBr_3(Me_2SO)_3$ with 2-methyl pyridine on slight warming gave a dark green compound of the composition, $[RuBr_3(2\text{-}Me\text{-}py)(Me_2SO)_2]$. The IR spectrum of the compound shows strong bands at 990 and 970 cm^{-1} characteristic of the $\nu_{S=O}$ (O-bonded) of the Me_2SO groups. A band at 478 cm^{-1} may be due to ν_{Ru-O}. The room temperature magnetic moment value, μ_{eff}, is 1.92 BM, thereby confirming the oxidation state of ruthenium as 3+. The partially substituted product obtained with 2-methyl pyridine is similar to that from the pyridine reaction. Attempts to obtain the completely substituted product were unsuccessful.

(c) *2,2′-Bipyridyl* (bipy). A reaction of $RuBr_3(Me_2SO)_3$ with 2,2′-bipyridyl (1 : 1 ratio) resulted in a partially substituted complex of the composition $[Ru(bipy)(Me_2SO)Br_3]$. Conductivity measurements in acetonitrile show negligible molar conductance thereby confirming the covalent bonding of all the bromides. The IR spectrum shows a strong band at 970 cm^{-1} assigned to $\nu_{S=O}$ of the O-bonded Me_2SO groups. All the bands due to bipyridyl are also present. Besides these, weak bands at 479 and 458 cm^{-1} may be due to ν_{Ru-O} and bands at 292 and 275 cm^{-1} due to ν_{Ru-Br}. Room temperature ESR measurements of the powdered sample show a broad signal at $g = 2.19$, which is indicative of one unpaired electron in a low-spin d^5 ruthenium(III) complex.

(d) *o-Phenylenediamine* (PDA). Reaction of $RuBr_3(Me_2SO)_3$ with *o*-phenylenediamine (PDA) in a molar ratio of 1 : 1 resulted in the formation of a reddish brown compound of the composition, $[RuBr_2(PDA)_2(Me_2SO)_2]Br$. The conductance measurement in acetonitrile shows a molar conductance value of 128 Ω^{-1} cm^2 mol^{-1}, thereby confirming the 1 : 1 electrolytic nature of the complex. The IR spectrum shows one strong band at 1120 cm^{-1} besides all the other bands due to *o*-phenylenediamine, which may be assigned to $\nu_{S=O}$ of S-bonded Me_2SO groups. The ESR spectrum of the complex in the powder form at room temperature shows a broad signal at $g = 2.60$ which may confirm the 3+ nature of ruthenium in this complex.

When a reaction of $RuBr_3(Me_2SO)_3$ with PDA in the molar ratio of 1 : 2 was carried out, reduction of ruthenium(III) to ruthenium(II) took place lead-

ing to the formation of a diamagnetic complex of the composition $[RuBr_2(PDA)(Me_2SO)_2]$. The low molar conductance value (6 Ω^{-1} cm^2 mol^{-1}) in acetonitrile confirms the covalent nature of the complex. The IR spectrum shows a strong band at 1130 cm^{-1} which may be assigned to $\nu_{S=O}$ (S-bonded). There is no band of appreciable intensity in the region 1000–900 cm^{-1} which confirms the absence of O-bonded Me_2SO groups. The ^1H NMR spectrum of $[RuBr_2(PDA)(Me_2SO)_2]$ in $(CD_3)_2SO$ shows two broad singlets at δ 7.4 and 7.2, one singlet at δ 6.2 and a sharp singlet at δ 3.3. The signals at δ 7.4 and 7.2 may be assigned as due to the *o*- and *p*-protons in *o*-phenylenediamine.[32] The signals at δ 6.2 may be due to the four protons attached to the two nitrogen atoms of the amino groups. In the case, where the *o*-amino groups are not bonded, the aromatic amino protons are expected to be in the range δ 3.6–4.7.[32] However, due to coordination of the nitrogen atoms to the metal, the electron density around the nitrogen is reduced, thereby decreasing shielding of the protons at the nitrogen atoms and leading to a signal at a lower field, i.e. at a higher δ value (δ 6.2). The ratio of proton area under the curve at δ 6.2 and under the curve at δ 7.4 and 7.2 (combined) is 1 : 1, which confirms that the number of amino protons and aromatic protons is the same, i.e. four in each case. The signal at δ 3.3 is indicative of the S-bonded Me_2SO groups. The ratio of the protons under δ 3.3 and 6.2 is 3 : 1 confirming the presence of 12 protons of two Me_2SO groups (S-bonded). The presence of a singlet for two Me_2SO groups at δ 3.3 is indicative of the presence of six methyl protons on each Me_2SO in equivalent environments. Hence a structure with the two S-bonded Me_2SO groups in *trans*-positions, the two bromo groups in *cis*-positions and the two amino groups of PDA in *cis*-positions is most probable.

Electronic spectra

Electronic spectral data of new ruthenium(III) complexes are given in Table 2. The spectra show similar features in chloroform and acetonitrile solutions. Generally, all ruthenium(III) complexes have two absorptions around 400 and 500 nm with molar extinction coefficients of the order 10^3. The high value of ε for all these complexes is suggestive of a greater contribution due to charge-transfer rather than *d–d* transitions. In some cases, one band at a

Table 2. Important IR and electronic absorption bands of ruthenium(III) and ruthenium(II) complexes containing Me_2SO and other ligands

Compounds	IR bands (cm^{-1})	Electronic absorption bands λ_{max} in nm (ε_{max}) CH_3CN	$CHCl_3$
$[RuBr_2(Me_2SO)_3]$	1097s, 1030m 423m, 247w	365 (330) 220 (37000)	
$[RuBr_3(Me_2SO)_3]$	1030m–s, 970s, 468m, 295w	602 (1150) 520 (2900) 490 (2500) 395 (950)	620 (1200) 540 (2300) 500 (2150) 395 (800)
$[RuBr_3(py)(Me_2SO)_2]$	965m, 447w, 292w, 245w	—	588 (1270) 526 (1700) 476 (2900) 400 (950)
$[RuBr_3(Me\text{-}py)(Me_2SO)_2]$	990s, 970s, 478	440 (990)	—
$[RuBr_3(bipy)(Me_2SO)]$	970s, 479m–s, 458, 292w, 275w	570 (700) 500 (2500) 425 (1800)	575 (1050) 500 (2600) 481 (2750) 420 sh
$[RuBr_2(PDA)(Me_2SO)_2]$	1130s	—	—
$[RuBr_2(PDA)_2(Me_2SO)_2]Br$	1120s	—	495
$[Ru(Et_2NCS_2)(Me_2SO)_2Br_2]$	1080s, 1530m–s	—	465 (1350)
$[Ru(CS_2)(PPh_3)_3Br_2]Br$	1510m–s	656 (210) 485 (2850)	510 (3900) 390 (1850)

lower frequency with a slightly lower ε value is also observed, viz. for $[RuBr_3(bipy)(Me_2SO)]$ at 570 nm ($\varepsilon = 700$) and for $[Ru(CS_2)(PPh_3)_3Br_2]Br$ at 656 nm ($\varepsilon = 210$). These bands may have more *d–d* character (transitions from the $^2T_2$ to $^2A_2$, $^2T_1$ or $^2T_2$ types) than charge-transfer character. Electronic absorption bands for these ruthenium(III) complexes are similar to other ruthenium(III) complexes.[18,33] All the ruthenium(III) complexes described in Table 2 have six coordination around ruthenium(III). However, the symmetry is lowered considerably from O_h due to the presence of two or three different types of ligands, both monodentate and bidentate ones. Absorption bands with a high value of ε for such low symmetry ruthenium(III) complexes, can not be assigned to *d–d* transitions alone, which may be obscured by charge-transfer transitions in these regions.[33] The electronic spectrum of $[RuBr_2(Me_2SO)_3]$ in acetonitrile shows one band at 365 nm with $\varepsilon = 330$. If the complex is assumed to have a trigonal bipyrimidal geometry, it will have D_{3h} symmetry. Due to a lowering in the symmetry the absorption bands due to *d–d* transitions are expected to have slightly higher ε values (10^2), thus the band at 365 nm can be assigned to one of the *d–d* transitions ($^1A_1$ to $^1A_2$, ^1E or $^1B_2$).[34] The other band at 220 nm is due to charge-transfer only.

Acknowledgements—One of the authors (U.C.S.) thanks the U.G.C., New Delhi for the award of a teacher fellowship under the faculty improvement programme. We thank RSIC, NEHU for obtaining IR spectra, UV and visible spectra and ^1H NMR spectra. We thank RSIC, CDRI, Lucknow for obtaining analytical data and IACS, Calcutta for obtaining room temperature magnetic measurements. We also thank Prof. J. Subramanian of NEHU, Shillong for the EPR spectra (both at room temperature and at liquid nitrogen temperature) and discussions on it.

REFERENCES

1. B. R. James, E. Ochiai and G. L. Rempel, *Inorg. Nucl. Chem. Lett.* 1971, **7**, 781.
2. I. P. Evans, A. Spencer and G. Wilkinson, *J. Chem. Soc., Dalton Trans.* 1973, 204.
3. B. Taqui Khan and A. Mehmood, *J. Inorg. Nucl. Chem.* 1978, **40**, 1938.
4. H. A. Hudali, J. V. Kingston and H. A. Tayim, *Inorg. Chem.* 1979, **18**, 1391.
5. V. Ravindar, P. Lingaiah and K. Veera Reddy, *Inorg. Chim. Acta* 1984, **87**, 35.
6. J. D. Gilbert, D. Rose and G. Wilkinson, *J. Chem. Soc. A* 1970, 2765.
7. P. G. Antonov, Y. N. Kukushkin, V. I. Konnov and B. I. Ionin, *Russ. J. Inorg. Chem.* 1978, **23**, 245.
8. U. C. Sarma, K. P. Sarma and R. K. Poddar, *Polyhedron* 1988, **7**, 1727.
9. L. Ruiz-Ramirez, T. A. Stephenson and E. S. Switkes, *J. Chem. Soc., Dalton Trans.* 1973, 1770.
10. T. Bora and M. M. Singh, *Trans. Met. Chem.* 1978, **3**, 27.
11. J. D. Oliver and D. P. Riley, *Inorg. Chem.* 1984, **23**, 156.
12. D. P. Riley, *Inorg. Chim. Acta* 1985, **99**, 5.
13. T. A. Stephenson and G. Wilkinson, *J. Inorg. Nucl. Chem.* 1966, **28**, 945.
14. A. D. Allen and C. V. Senoff, *Can. J. Chem.* 1967, **45**, 1337.
15. K. Natarajan, R. K. Poddar and U. Agarawala, *J. Inorg. Nucl. Chem.* 1977, **39**, 431.
16. J. A. Broomhead and L. A. P. Kane-Magwire, *J. Chem. Soc. A* 1967, 546.
17. J. Chatt, G. J. Leigh, D. M. P. Mingos and R. J. Paske, *J. Chem. Soc. A* 1968, 2636.
18. J. Chatt, G. J. Leigh and D. M. P. Mingos, *J. Chem. Soc. A* 1969, 1674.
19. D. L. Key, L. F. Larkworthy and J. E. Salmon, *J. Chem. Soc. A* 1971, 2583.
20. K. Natarajan and U. Agarawala, *Bull. Chem. Soc. Japan* 1976, **49**, 2877.
21. D. P. Riley, *Inorg. Chem.* 1983, **22**, 1965.
22. A. I. Vogel, *Inorg. Quant. Anal.* 3rd Edn. ELBS & Longman, London (1961).
23. B. B. Wayland and R. F. Schramm, *Inorg. Chem.* 1969, **8**, 971.
24. J. H. Price, A. N. Williamson, R. F. Schramm and B. B. Wayland, *Inorg. Chem.* 1972, **11**, 1280.
25. K. Nakamoto, *Infrared and Raman Spectra of Inorganic and Coordination Compounds*, 3rd Edn. Wiley Insterscience, New York (1977).
26. R. S. McMillan, A. Mercer, B. R. James and J. Trotter, *J. Chem. Soc., Dalton Trans.* 1975, 1006.
27. D. J. Duffy and L. H. Pignolet, *Inorg. Chem.* 1974, **13**, 2405.
28. R. E. Desiomone, *J. Am. Chem. Soc.* 1973, **95**, 6238.
29. C. O'Connor, J. D. Gilbert and G. Wilkinson, *J. Chem. Soc. A* 1969, 84.
30. A. Endo, M. Watanabe, S. Hayashi, K. Shimizer and G. P. Sato, *Bull. Chem. Soc. Japan* 1978, **51**, 800.
31. A. Hudson and M. J. Kennedy, *J. Chem. Soc. A* 1969, 1116.
32. J. R. Dyer, *Application of Absorption Spectroscopy of Organic Compounds*, pp. 93, 110. Prentice–Hall (1978).
33. A. B. P. Lever, *Inorganic Electronic Spectroscopy*, 2nd Edn, p. 453. Elsevier (1984).
34. R. K. Poddar and U. Agarwala, *J. Inorg. Nucl. Chem.* 1973, **35**, 567.

Polyhedron Vol. 7, No. 18, pp. 1745–1749, 1988
Printed in Great Britain

0277–5387/88 $3.00+.00
© 1988 Pergamon Press plc

COPPER(II) CARBOXYLATES AND THEIR 3-PYRIDYLCARBINOL ADDUCTS

M. MELNÍK,* Ľ. MACÁŠKOVÁ and J. MROZIŃSKI†

Department of Inorganic Chemistry, Slovak Technical University, 812 37 Bratislava, Czechoslovakia

(*Received* 8 *December* 1987; *accepted* 9 *March* 1988)

Abstract—New 3-pyridylcarbinol adducts of copper(II) acetate, salicylate, acetylsalicylate and flufenamate, as well as copper(II) flufenamate monohydrate were prepared. The magnetic and spectroscopic properties of copper(II) flufenamate monohydrate indicate the presence of copper(II) dimers structurally similar to those in copper(II) acetate monohydrate. 3-Pyridylcarbinol adducts of copper(II) acetate and copper(II) flufenamate possess octahedral stereochemistry. While 3-pyridylcarbinol adducts of copper(II) salicylate and copper(II) flufenamate possess pentahedral stereochemistry, similar to that found in copper(II) salicylate dihydrate.

Copper(II) carboxylates with nitrogen donor ligands have attracted increasing interest in recent years. This interest largely derives from the discovery that the carboxylate groups possess a pronounced tendency to serve as a bridge between copper(II) atoms with a nitrogen donor ligand in the terminal position.[1] Copper(II) carboxylates with 3-pyridylcarbinol as the ligand have not been studied. This is the aim of the present work. In a study of the donor properties of the 3-pyridylcarbinol, its adducts of copper(II) acetate, copper(II) salicylate, copper(II) acetylsalicylate and copper(II) flufenamate as well as copper(II) flufenamate monohydrate and copper(II) salicylate dihydrate have been prepared. Magnetic and spectroscopic investigations on the compounds are reported herein.

EXPERIMENTAL

Preparations

Copper(II) flufenamate monohydrate was prepared in the following way. To the aqueous solution of copper(II) sulphate (1.59 g, 0.01 mol), the aqueous solution of the sodium salt of [N-(α,α,α-trifluoro-*m*-tolyl)anthranilic acid] (flufenamic acid) (6.06 g, 0.02 mol) of pH adjusted to five with free flufenamic acid was added and stirred at room temperature for about 6 h. The reaction mixture formed a precipitate which was filtered off to yield 4.5 g of copper(II) flufenamate monohydrate as light green microcrystals.

Copper(II) salicylate dihydrate was obtained by drying copper(II) salicylate tetrahydrate[2] at 363 K.

The copper(II) carboxylate compounds of composition $CuX_2(pycar)_2$, where X = acetate, salicylate, acetylsalicylate or flufenamate; and pycar = 3-pyridylcarbinol; were prepared by treating 3-pyridylcarbinol (2.18 g, 0.02 mol) with copper(II) acetate (1.82 g, 0.01 mol); copper(II) salicylate (3.40 g, 0.01 mol); copper(II) acetylsalicylate (4.22 g, 0.01 mol) or copper(II) flufenamate (6.24 g, 0.01 mol) in hot methanol solution. The solutions were left to stand at room temperature. The fine blue microcrystals that precipitated were filtered off (70% yield), washed with cold methanol and dried at room temperature. The crude products were recrystallized from methanol to give a yield of 50%. The elemental analyses are given in Table 1.

Spectral studies

Electronic spectra in the region 1.0–2.8 μm^{-1} were measured with a Perkin–Elmer 450 spec-

* Author to whom correspondence should be addressed.
† Present address: Institute of Chemistry, Wroclaw University, 50 383 Wroclaw, Poland.

Table 1. Elemental analysis

Compound[a]	Calc. (%) Cu	C	H	N	Found (%) Cu	C	H	N
$Cu(ac)_2(pycar)_2$	15.9	48.1	5.0	7.0	15.9	47.9	5.0	7.1
$Cu(sal)_2 \cdot 2H_2O$	17.0	45.0	3.8	—	16.9	45.0	3.8	—
$Cu(sal)_2(pycar)_2$	10.7	52.4	4.1	4.7	10.6	52.1	4.0	4.6
$Cu(acsal)_2(pycar)_2$	9.9	56.3	4.4	4.4	9.9	56.4	4.5	4.4
$Cu(flu)_2 \cdot H_2O$	9.9	52.4	3.1	4.4	9.8	52.6	3.2	4.4
$Cu(flu)_2(pycar)_2$	7.5	57.1	3.8	6.7	7.6	57.0	3.9	6.7

[a] ac, acetate; sal, salicylate; acsal, acetylsalicylate; pycar, 3-pyridylcarbinol.

trophotometer using the Nujol suspension technique. EPR spectra of the powdered samples were run on a Varian Model E 4 spectrometer at 163 K.

Magnetic susceptibility measurements

The magnetic susceptibilities of powdered samples were determined at different temperatures on a Gouy balance (Newport Instruments Ltd), standardized with mercury tetrathiocyanatocobaltate(II).[3] Diamagnetic corrections were calculated from Pascal's constants.[4] The effective magnetic moments were calculated using the expression $\mu_{eff} = 2.83 (\chi_M^{corr} \times T)^{1/2}$.

RESULTS AND DISCUSSION

The electronic absorption spectrum of $Cu(flu)_2 \cdot H_2O$ shows a band with a maximum at 1.49 μm^{-1} (band I) and a shoulder at 2.78 μm^{-1} (band II). Band I can be assigned to *d–d* transitions and band (II) should be the characteristic bridging system antiferromagnetic interaction.[5]

The EPR spectra obtained for the compound at 293 and 77 K are presented in Fig. 1. The absorption feature of the powder at room temperature [Fig. 1(a)] shows the absorptions at low and high field (H_{z1} and H_{z2}, respectively) and the asymmetric absorption near 4.5 kG ($H_{\perp 2}$). One absorption is missing ($H_{\perp 1}$) because $D > h\nu$ at the X-band frequency used. The spectra can be interpreted using a spin Hamiltonian for axial symmetry,

$$H = g_{\parallel}\beta H_z S_z + g_{\perp}\beta(H_x S_x + H_y S_y) + D(S_z^2 - 2/3)$$

where $S = 1$ for the thermally accessible triplet state and the other symbols have their usual meanings. The observed values at 293 K are: $g_{\perp} = 2.086$, $g_{\parallel} = 2.400$ and $|D| = 0.327\ cm^{-1}$.

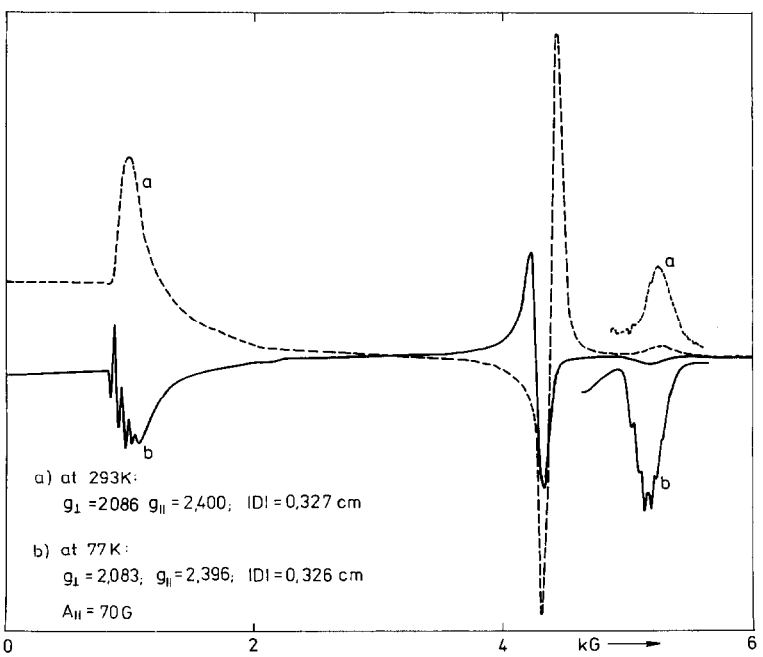

Fig. 1. X-band EPR spectra of $Cu(flu)_2 \cdot H_2O$ at (a) 293 K and (b) 77 K.

Table 2. Spectral data

Compound	Electronic spectra [ν_{max} (μm^{-1})]		EPR spectra[a] $g_\perp$	$g_\parallel$	g_{av}
$Cu(ac)_2(pycar)_2$	1.55		2.057	2.274	2.132
$Cu(sal)_2 \cdot 2H_2O$	1.35		2.089	2.373	2.188
$Cu(sal)_2(pycar)_2$	1.35sh[b]	1.62	2.050	2.298	2.136
$Cu(acsal)_2(pycar)_2$	1.37sh	1.58	2.041	2.298	2.130
$Cu(flu)_2(pycar)_2$	1.50	2.38sh	2.056	2.327	2.162

[a] At 163 K.
[b] sh, shoulder.

The low temperature powder spectrum [Fig. 1(b)] shows better resolution with some copper hyperfine structure appearing on H_{z1} and a clearly resolved seven-line pattern on H_{z2}. The observed hyperfine structure is consistent with coupling to two copper nuclei of spin $I = 3/2$. The observed values at 77 K are: $g_\perp = 2.083$, $g_\parallel = 2.396$, $|D| = 0.326\ cm^{-1}$ and $A_\parallel = 70$ G.

These values are comparable to those reported for other familiar copper(II) carboxylato compounds.[1] The $|D|$ value of about 0.3 cm^{-1} is large compared to magnetic quantities ($\sim$ 3000 G), but is small compared to vibrational frequencies. At room temperature nearly 40% of the dimers are in the thermally-populated triplet state. Therefore interdimer dipolar couplings may also be expected to be significant at room temperature.

Table 3. Magnetic data for $Cu(flu)_2 \cdot H_2O$

T (K)	$(-\Delta \times 10^6 = 229\ cm^3\ mol^{-1})$ $\chi_M^{corr} \times 10^6$	μ_{eff} (BM)	K_{eq}
82	395	0.51	0.0567
90	467	0.58	0.0746
106	580	0.61	0.0832
116	626	0.76	0.1353
125	639	0.80	0.1522
135	679	0.86	0.1802
146	705	0.91	0.2062
157	732	0.96	0.2349
168	758	1.01	0.2667
177	765	1.04	0.2874
188	778	1.08	0.3171
206	791	1.14	0.3666
216	804	1.18	0.4033
227	806	1.21	0.4331
241	818	1.26	0.4875
251	824	1.29	0.5232
263	818	1.31	0.5485
279	818	1.35	0.6031
290	798	1.36	0.6176

The molar susceptibilities corrected for diamagnetism and the magnetic moments for the compound are reported at various temperatures in Table 2. It was found that the effective magnetic moment decreases systematically by lowering the

Table 4. Magnetic data of $Cu(ac)_2(pycar)_2$

T (K)	$(-\Delta \times 10^6 = 151\ cm^3\ mol^{-1})$ $\chi_M^{corr} \times 10^6$	μ_{eff} (BM)
4.2	102000	1.85
5	95900	1.96
6	81600	1.98
7	66700	1.93
8	58800	1.94
9	50200	1.90
10	44600	1.89
12	36400	1.87
14	30500	1.85
16	26600	1.84
20	21200	1.83
30	14000	1.83
40	10600	1.84
50	8430	1.84
60	7010	1.83
70	6000	1.83
80	5180	1.82
90	4630	1.83
100	4190	1.83
110	3790	1.83
120	3660	1.83
130	3180	1.82
140	2970	1.82
150	2760	1.82
160	2570	1.82
170	2420	1.82
180	2300	1.82
200	2060	1.81
220	1840	1.80
240	1670	1.79
260	1540	1.79
280	1420	1.78
290	1350	1.77

temperature, from 1.36 BM at 290 K to 0.51 BM at 82 K. The temperature-susceptibility data can be described by the equation:

$$\chi_M^{corr} = \frac{Ng^2\beta^2}{3kT}\left[1+\frac{1}{3}\exp\left(\frac{-2J}{kT}\right)\right]^{-1} + N\alpha$$

where $-2J$ is the energy separation between a singlet and a triplet level, and $N\alpha$ was taken as 60×10^{-6} cm^3 mol^{-1}. We have selected the apparent g_{av} value from the EPR spectrum. The energy separation between the two spin states of the compound, $-2J = 318\ (\pm10)$ cm^{-1} was observed.

By treating the magnetic data of $Cu(flu)_2\cdot H_2O$ in the manner described by Hatfield *et al*[6] we have calculated equilibrium constants for the singlet $\rightleftharpoons$ triplet equilibrium at various temperatures. The plots of $-\ln K_{eq}$ vs T^{-1} and $RT\ln K_{eq}$ vs T yielded almost straight lines. The slopes of the lines were used to calculate ΔH and ΔS for the compound. The value of $\Delta H = 305(\pm10)$ cm^{-1} obtained in this way agrees well with the value of $-2J$.

The value of entropy change 2.0 e.u. is in good agreement with the value 2.2 e.u. expected for a

Table 5. Magnetic data

T (K)	$\chi_M^{corr}\times10^6$	μ_{eff} (BM)	T (K)	$\chi_M^{corr}\times10^6$	μ_{eff} (BM)
$Cu(sal)_2\cdot2H_2O$ ($-\Delta\times10^6 = 136$ cm^3 mol^{-1})			$Cu(sal)_2(pycar)_2$ ($-\Delta\times10^6 = 244$ cm^3 mol^{-1})		
82	5130	1.83	80	4898	1.74
98	4280	1.83	95	4068	1.75
115	3600	1.82	115	3318	1.74
133	3100	1.82	130	2915	1.74
143	2840	1.80	145	2600	1.75
153	2700	1.82	155	2425	1.74
164	2490	1.81	165	2272	1.74
176	2220	1.77	175	2137	1.735
190	2110	1.79	190	1910	1.74
210	1930	1.79	210	1769	1.735
216	1880	1.80	240	1542	1.72
240	1680	1.80	255	1449	1.715
251	1610	1.80	270	1367	1.715
270	1510	1.81	280	1317	1.71
282	1450	1.80	295	1248	1.71
295	1390	1.81			
$Cu(acsal)_2(pycar)_2$ ($-\Delta\times10^6 = 278$ cm^3 mol^{-1})			$Cu(flu)_2(pycar)_2$ ($-\Delta\times10^6 = 397$ cm^3 mol^{-1})		
82	5600	1.92	80	5630	1.86
100	4540	1.91	90	5060	1.87
117	3930	1.92	100	4570	1.88
137	3340	1.91	115	3990	1.89
149	3040	1.90	125	3600	1.87
160	2750	1.88	150	3070	1.89
169	2520	1.85	170	2730	1.90
181	2400	1.86	185	2490	1.90
190	2290	1.87	200	2290	1.90
208	2090	1.87	210	2200	1.91
220	1970	1.86	230	2000	1.90
231	1900	1.87	250	1810	1.89
244	1780	1.87	275	1660	1.90
253	1730	1.87	285	1570	1.88
262	1670	1.87	295	1520	1.88
272	1620	1.88			
282	1570	1.88			
294	1510	1.88			

Table 6.

Compound	Curie constant C (c.g.s.u.)	Weis constant θ (K)	Error
$Cu(ac)_2(pycar)_2$	0.395 (4)	4.8 (2)	1.44×10^{-4}
$Cu(sal)_2 \cdot 2H_2O$	0.400 (4)	3.0 (1)	2.33×10^{-8}
$Cu(sal)_2(pycar)_2$	0.360 (3)	6.5 (2)	5.32×10^{-8}
$Cu(acsal)_2(pycar)_2$	0.431 (4)	6.0 (2)	4.60×10^{-8}
$Cu(flu)_2(pycar)_2$	0.450 (4)	3.4 (1)	1.78×10^{-7}

singlet–triplet equilibrium, calculated from $R \ln 3$, where 3 is the degeneracy ratio assuming that the only contribution is that from the electronic entropy.

From the above observation it may be suggested that $Cu(flu)_2 \cdot H_2O$ has a binuclear structure similar to that of copper(II) acetate monohydrate.[7] Copper(II) atoms in the structural units of $Cu_2(flu)_4(H_2O)_2$ are bridged in pairs by carboxylic groups of the flufenamate anion, while the molecules of water are bonded through oxygen atoms in axial positions.

The solid state electronic spectrum of $Cu(sal)_2 \cdot 2H_2O$ exhibits a broad ligand field band with a maximum at 1.35 μm^{-1}. The EPR spectrum of the powdered sample is of an axial type[8] with values of the g factor given in Table 3. Magnetic susceptibility measurements of a polycrystalline sample of $Cu(sal)_2 \cdot 2H_2O$ between 82–295 K obey the Curie–Weiss law

$$\chi_M^{corr} = C/(T-\Theta)$$

where $C = Ng^2\beta^2S(S+1)/3k$ with $S = 1/2$.

The μ_{eff} value of $CuX_2(pycar)_2$, (X = ac or acsal), is slightly dependent on temperature (Tables 4 and 5). The compounds possess small positive Weiss constants (Table 6). Apart from $Cu(flu)_2 \cdot H_2O$, all the compounds studied have only very weak magnetic interactions. The spectral and magnetic behaviours of copper(II) salicylate dihydrate correspond well with the crystal structure data.[9]

X-ray analysis of $Cu(sal)_2 \cdot 2H_2O$ shows[9] that the complex contains infinite chains parallel to b, in which one of the salicylate ligands acts as a bridge between the Cu atoms. The copper(II) atom is coordinated by four oxygen atoms in a basal plane ($Cu—O_{eq}$ distances range from 1.93 to 2.01 Å) and by an oxygen atom (Cu—O = 2.26 Å) in an apical position. The above mentioned magnetic interaction operates through the bridged atoms in the infinite chains.

The magnetic and spectroscopic properties of pyridylcarbinol adducts of copper(II) salicylate and copper(II) acetylsalicylate are comparable to those of copper(II) salicylate dihydrate. On the other hand, the d–d transitions of $Cu(ac)_2(pycar)_2$ and $Cu(flu)_2(pycar)_2$ (Table 3) indicate a pseudo-octahedral coordination around the copper(II) atoms.

REFERENCES

1. M. Melník, *Coord. Chem. Rev.* 1981, **36**, 1; 1982, **42**, 259 and refs therein.
2. M. Inoue, M. Kishita and M. Kubo, *Acta Cryst.* 1963, **16**, 699.
3. B. N. Figgis and R. S. Nyholm, *J. Chem. Soc.* 1958, 4190.
4. A. Earnshaw, *Introduction to Magnetochemistry*. Academic Press, London (1968).
5. L. Dubicki and R. L. Martin, *Inorg. Chem.* 1966, **5**, 2203.
6. W. E. Hatfield, T. S. Piper and V. Klabunde, *Inorg. Chem.* 1963, **2**, 629.
7. J. N. van Niekerk and F. R. L. Schoening, *Acta Cryst.* 1953, **6**, 227.
8. B. J. Hathaway and D. E. Billing, *Coord. Chem. Rev.* 1970, **3**, 143.
9. S. Jagner, R. G. Hazell and H. P. Larsen, *Acta Cryst., Sect. B* 1976, **32**, 548.

Polyhedron Vol. 7, No. 18, pp. 1751–1757, 1988
Printed in Great Britain

0277–5387/88 $3.00+.00
Pergamon Press plc

CHARACTERIZATION AND REACTIVITY OF SOME ELECTROCHEMICALLY GENERATED PRODUCTS OF $Rh_2(\mu\text{-dppp})_2(\mu\text{-CO})Cl_2$ (dppp = 2-(DIPHENYLPHOSPHINO)PYRIDINE)

CLIFTON WOODS† and LOUIS J. TORTORELLI

Department of Chemistry, University of Tennessee, Knoxville, TN 37996-1600, U.S.A.

(*Received* 22 *October* 1987; *accepted after revision* 10 *March* 1988)

Abstract—The reaction of the dirhodium(I) complex $Rh_2(\mu\text{-dppp})_2(\mu\text{-CO})Cl_2$, **1**, (dppp = 2-(diphenylphosphino)pyridine) with Cl^- in the presence of CO leads to the monomeric species $Rh(dppp)_2(CO)Cl$ and $Rh(CO)_2Cl_2^-$. In the absence of CO no chemical reaction occurs. Electrochemical oxidation of **1** in the presence of Cl^- at +0.90 V (vs SCE) affords a new dirhodium(II) complex $Rh_2(\mu\text{-dppp})_2(CO)Cl_4$, **4**, whose fluxional behaviour at room temperature is demonstrated using variable temperature ^{31}P NMR. The ^{31}P NMR is interpreted with the aid of the complex containing ^{13}CO. Complex **4** reacts with CO to produce $Rh_2(\mu\text{-dppp})_2(CO)_2Cl_4$, **5**, and with $(CH_3)_3CNC$ (*t*-BuNC) to form $Rh_2(\mu\text{-dppp})_2(t\text{-BuNC})_2Cl_4$, **6**. Complex **6** appears to partially dissociate to give $[Rh_2(\mu\text{-dppp})_2(\mu\text{-Cl})(t\text{-BuNC})_2Cl_2]Cl$. When the equilibrium mixture is treated with NH_4PF_6 the equilibrium is driven in the direction of the ionic species and the complex $[Rh_2(\mu\text{-dppp})_2(\mu\text{-Cl})(t\text{-BuNC})_2Cl_2]PF_6$ is isolated.

The recent interest in dirhodium complexes as potential catalytic agents has encouraged us to investigate factors affecting the nature and the chemical and electrochemical reactivities of some dirhodium complexes with and without metal–metal bonds. Several bridging ligands have been shown to form the dirhodium framework illustrated by **I** such that metal–metal distances can range from those in the metal–metal bond range to those in a range consistent with no metal–metal bond. One of the most widely studied of these ligands is bis(diphenylphosphino)methane (dppm).

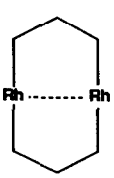

I

The ligand 2-(diphenylphosphino)pyridine (dppp) can accommodate the dirhodium framework of **I**; however, because its bite size is smaller than that of dppm, dppp cannot accommodate as wide a range of metal–metal distances. In fact the small bite size of dppp favours metal–metal distances in the metal–metal single bond range. Thus, where many Rh(I)—Rh(I) dppm complexes contain no formal Rh—Rh bond, Rh(I)—Rh(I) dppp complexes are generally found to contain metal–metal bonds.

We have been investigating the formation and loss of metal–metal bonds in dirhodium complexes during electrochemical processes. We have found that electrochemical oxidation of Rh(I)—Rh(I) species that contain no metal–metal bond to a Rh(II)—Rh(II) species results in the formation of a metal–metal single bond.[1,2] The complex $Rh_2(\mu\text{-dppp})_2(\mu\text{-CO})Cl_2$, **1**, is a formal Rh(I)—Rh(I) complex that contains a metal–metal bond. We have shown that a two-electron electrochemical oxidation of **1** in CH_2Cl_2 containing excess chloride and tetra-*n*-butylammonium nitrate (TBAN) as the supporting electrolyte affords the Rh(II)—Rh(II) species $Rh_2(dppp)_2(\mu\text{-}NO_3)(CO)Cl_3$, **2**, in which the metal–metal bond is retained and the metal centres acquire a higher coordination number.[3] In this paper we report results of additional studies of chemical and electrochemical processes involving **1** and its oxidation products.

† Author to whom correspondence should be addressed.

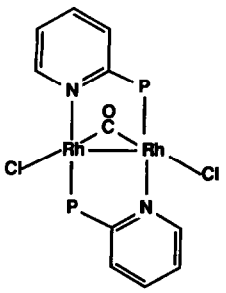

1

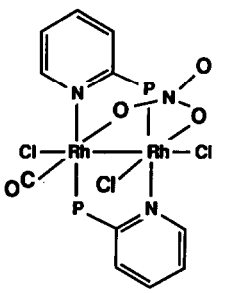

2

EXPERIMENTAL

Materials

Literature procedures were used to prepare dppp[4] and $Rh_2(\mu\text{-dppp})(\mu\text{-CO})Cl_2$.[5] Tetra-*n*-butylammonium hexafluorophosphate (TBAH) was prepared by the metathesis of KPF_6 and tetra-*n*-butylammonium iodide (TBAI) and recrystallized several times from acetone/water and dried *in vacuo*. Tetra-*n*-butylammonium chloride (TBAC) was purchased from Aldrich and purified by three recrystallizations from acetone/diethyl ether followed by drying overnight *in vacuo* at 70°C.

$Rh_2(\mu\text{-dppp})_2(CO)(\mu\text{-Cl})Cl_3 \cdot (CH_3)_2CO$ (4)

Method 1. 50 cm^3 of a CH_2Cl_2 solution of **1** (120 mg, 0.144 mmol) containing 0.1 M TBAH and TBAC (201 mg, 0.722 mmol) was oxidized at +0.90 V. After oxidation the solution was stripped to dryness on a rotary evaporator and the residue was stirred in acetone overnight. The desired product occurred as a brown residue and was filtered and dried *in vacuo*. Yield 80%.

Method 2. Excess Cl_2 was bubbled through a constantly stirred solution of 100 mg (0.120 mmol) of **1** in 125 cm^3 of CH_2Cl_2 at −77°C. The solution was allowed to reach room temperature and was stirred for an additional 1 h. The resulting solution was stripped to dryness. After stirring the residue in acetone the desired product was filtered and dried *in vacuo*. Yield 80%.

UV–vis [λ_{max}, nm(ε)]: 705 (137); 497 (683); 363 (7587); 304 (6015); 163 (17,880). IR (Nujol mull): ν(CO), 2044, 1805, 1715 cm^{-1} (acetone of crystallization). Found: C, 47.6; H, 3.9; N, 3.2; Cl, 14.6. Calc. for $C_{38}H_{34}Cl_4N_2O_2P_2Rh_2$: C, 47.5; H, 3.6; N, 2.9; Cl, 14.8%.

$Rh_2(\mu\text{-dppp})_2(CO)_2Cl_4 \cdot 0.5CH_2Cl_2$ (5)

While stirring 50 cm^3 of a CH_2Cl_2 solution containing 96.4 mg (0.104 mmol) of $Rh_2(\mu\text{-dppp})_2(CO)Cl_4$, CO was bubbled through the solution for 10 min during which time the colour of the solution changed from brown to orange. The volume was reduced to *ca* 20 cm^3 using a rotary evaporator and an orange solid precipitated upon the addition of diethyl ether. Recrystallization from CH_2Cl_2/ether afforded a crystalline orange solid in 90% yield.

UV–vis [λ_{max}, nm(ε)]: 460 (3000); 415 (8400); 325 (8800); 264 (23,600). Found: C, 45.4; H, 3.2; N, 2.8; Cl, 17.9. Calc. for $C_{36.5}H_{29}Cl_5N_2O_2Rh_2$: C, 45.1; H, 3.0; N, 2.9; Cl, 18.2%.

$Rh_2(\mu\text{-dppp})_2(t\text{-BuNC})_2Cl_4$ (6)

To a 100 cm^3 CH_2Cl_2 solution containing 0.11 mmol of **4**, 95 mg (1.13 mmol) of *t*-BuNC was added dropwise as the colour changed from brown to orange. After stirring for 1 h the volume of the solution was reduced to *ca* 50 cm^3 on a rotary evaporator. An orange solid was obtained upon addition of a 1:1 diethyl ether/hexanes solution. The same product is obtained when **5** is used instead of **4**. Yield 70%. Found: C, 49.6; H, 5.0; N, 5.7; Cl, 12.3. Calc. for $C_{44}H_{46}Cl_4N_4P_2Rh_2$: C, 50.8; H, 4.5; N, 5.4; Cl, 13.6%.

$[Rh_2(\mu\text{-dppp})_2(\mu\text{-Cl})(t\text{-BuNC})_2Cl_2]PF_6$ (7)

To 150 cm^3 of a 4:1 CH_2Cl_2/CH_3OH solution of **6** (55.2 mg, 0.053 mmol), NH_4PF_6 (22 mg, 0.13 mmol) in 20 cm^3 of methanol was added. After stirring for 1 h the volume of the orange solution was reduced to *ca* 40 cm^3. A yellow–orange solid was obtained upon addition of a 1:1 diethyl ether/hexanes solution. Found: C, 45.6; H, 4.4. Calc. for $C_{44}H_{46}Cl_3F_6N_4P_3Rh_2$: C, 46.0; H, 4.0%.

Physical measurements

Infrared (IR) spectra were recorded on a Perkin–Elmer 180 spectrophotometer or a Digilab FTS-20 C/V Fourier transform spectrometer. Proton-decoupled ^{31}P NMR spectra were recorded on a JEOL FX90Q Fourier transform spectrometer at 36.21 MHz with 85% H_3PO_4 as the external reference. Unless otherwise noted all NMR spectra were obtained at ambient temperature.

Electrochemistry

All cyclic voltammetry, coulometry, and controlled potential electrolysis experiments were performed with the BAS-100 Electrochemical Analyser. The working electrode for cyclic voltammetry was a platinum-inlay electrode (Beck-

man) and the auxiliary electrode was a 2.76 cm^2 platinum grid. All bulk electrolysis experiments were performed in a conventional H-cell where the working electrode was a 25 cm^2 platinum grid and the auxiliary electrode was a carbon rod. In all cases the reference electrode was a saturated calomel electrode (SCE). All solutions used in the electrochemical experiments were degassed with argon.

RESULTS AND DISCUSSION

When a brown solution of **1** is treated with TBAC and bubbled with CO the solution immediately turns yellow. If the volume is reduced on a rotary evaporator or if the solution is bubbled with Ar, the colour of the solution turns to brown–yellow and the ^{31}P NMR spectrum exhibits resonance lines centred at 43.4 ppm which are attributed to **1** and a doublet centred at 29.6 ppm with a splitting of 126.9 Hz. When the solution is again bubbled with CO it returns to a yellow colour and the ^{31}P NMR peaks due to **1** disappear and only the doublet at 29.6 ppm remains. The IR spectrum of the yellow solution exhibits IR peaks at 2069 and 1991 cm^{-1}. The ^{31}P NMR data and the IR data are consistent with the presence of the monomer $Rh(dppp)_2(CO)Cl$[6] and the anion $Rh(CO)_2Cl_2^-$.[7] The reaction is outlined in eq. (1) (phenyl groups of dppp have been omitted) and is consistent with the observation that addition of either CO or Cl^- alone does not afford the products shown in eq. (1).

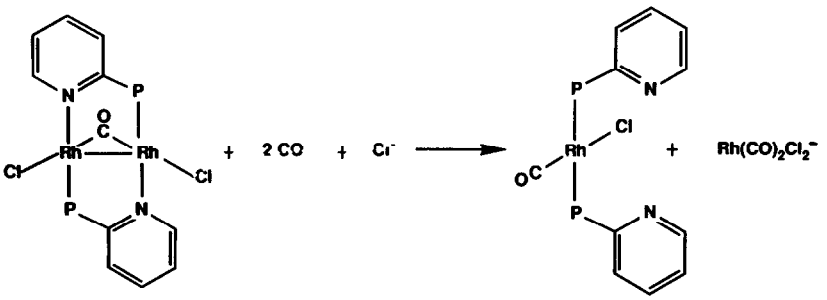

(1)

1

This reaction is somewhat interesting in light of the fact that the dppm complex analogous to **1** affords the face-to-face dimer **3** when treated with CO.[8] Besides possible electronic factors, one factor which almost certainly plays a role in establishing these differences is the difference in bite sizes of the two ligands and the metal–metal distances they can accommodate. If by the addition of a CO molecule **1** were to form a face-to-face complex similar to **3**, the small bite size of the dppp ligand would favour a metal–metal separation in the metal–metal bond range. The existence of a metal–metal bond in such a structure for a dppp Rh(I)—Rh(I) species would result in the metal centres being 17-electron paramagnetic centres and less stable than the corresponding d^8 square planar 16-electron metal centres in **3**. Therefore, as illustrated in eq. (1), the breakdown of such a dimer into monomeric species is favoured over the conversion of the bridging CO to a terminal CO with concomitant addition of CO or Cl^- to form the dinuclear species analogous to **3**.

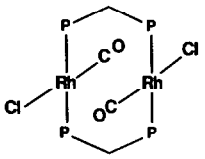

3

Electrochemistry

The cyclic voltammogram of **1** in CH_2Cl_2/TBAH shown in Fig. 1 exhibits two irreversible oxidation waves with E_{p1} at +0.97 V and E_{p2} at 1.36 V. Controlled-potential coulometry at potentials slightly positive of E_{p2} indicates that two electrons are transferred per dinuclear species and suggests that each irreversible oxidation is a one-electron process. An associated cathodic response occurs at −0.057 V on the voltammetric time scale during the reverse scan. Though a two-electron controlled-potential electrolysis has not afforded an isolable oxidation product, the results do indicate that the oxidation product formed on the voltammetric time scale undergoes a follow-up transformation during electrolysis. These data suggest that a reactive Rh(II)—Rh(II) species is initially formed during the electrolysis. The propensity of Rh(II) to acquire a higher coordination number than that favoured for Rh(I) is likely responsible, in part, for the follow-up chemical process. It has been previously shown that when TBAN is the supporting electrolyte, a similar two-electron oxidation of **1** results in the addition of a terminal Cl^- and a bridging NO_3^- to acquire the desired higher coordination number.

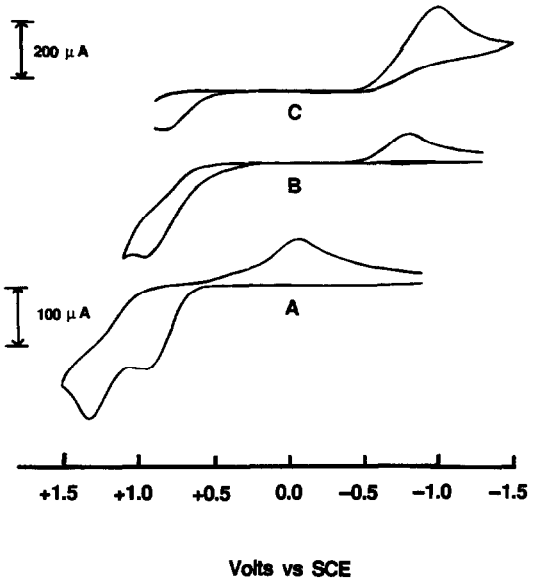

Fig. 1. Cyclic voltammogram of $Rh_2(\mu\text{-dppp})_2(\mu\text{-CO})Cl_2$ in (A) CH_2Cl_2/TBAH; (B) CH_2Cl_2/TBAH/Cl^- before oxidation at +0.90 V; (C) CH_2Cl_2/TBAH/Cl^- after oxidation at +0.90 V.

When free Cl^- was not present in the nitrate medium some of the starting material served as the source of the additional Cl^- found in the oxidation product.[3]

The cyclic voltammetric behaviour of **1** in CH_2Cl_2/TBAH/Cl^- is illustrated in Fig. 1(b). An irreversible oxidation occurs at +0.90 V, just before the onset of the oxidation wave for Cl^-. The cathodic response occurs at −0.80 V. These results indicate that the oxidation product formed on the voltammetric time scale in the presence of Cl^- is more stable toward reduction than that formed in the absence of Cl^-. Controlled-potential oxidation at +0.90 V involves a transfer of two electrons per dinuclear unit and thus involves the formation of a Rh(II)—Rh(II) species. The cyclic voltammogram of the oxidized solution exhibits an irreversible reduction wave at −0.98 V and an associated anodic response at +0.84 V.

The electrochemical oxidation product obtained from the CH_2Cl_2/TBAH/Cl^- medium exhibits an IR band (Nujol mull) at 2044 cm^{-1} which indicates the presence of a terminal CO. When the product is isolated from acetone it gives a strong IR band at 2044 cm^{-1} and a weak band at 1805 cm^{-1}. The product containing C-13 enriched CO exhibits ν(CO) values of 1998 cm^{-1} when isolated from CH_2Cl_2 and ν(CO) values of 1998(s) and 1765(w) cm^{-1} and an acetone band at 1715 cm^{-1} when isolated from acetone. These data indicate that in acetone a small amount of product contains a bridging CO.

At 25°C the ^{31}P NMR spectrum of the oxidation product exhibits the broad peak shown in Fig. 2(a). When the temperature is lowered to 0°C four peaks are apparent [Fig. 2(b)]. Further splitting of these four peaks is observed at −25°C [Fig. 2(c)]. The spectrum at −25°C is interpreted as that resulting from two phosphorus atoms in different environments with chemical shifts of 29.7 and 23.2 ppm. The phosphorus atom giving rise to the low-field resonance exhibits a one-bond Rh (^{103}Rh, $I = 1/2$; 100%) coupling of 117.2 Hz and a two-bond Rh coupling of 14.7 Hz. The phosphorus atom giving rise to the high-field resonance exhibits a one-bond Rh coupling of 109.9 Hz and a two-bond Rh coupling of 12.2 Hz.

The analytical data of the oxidation product of **1** isolated from CH_2Cl_2 resulted in the formulation of the product as $Rh_2(\mu\text{-dppp})_2(CO)Cl_4$, **4**. Based on the low-temperature ^{31}P NMR, IR, and analytical data **4** is assigned the structure shown in Scheme 1. The bridging Cl^- is postulated on the basis of an electron count of 18 for each metal centre.

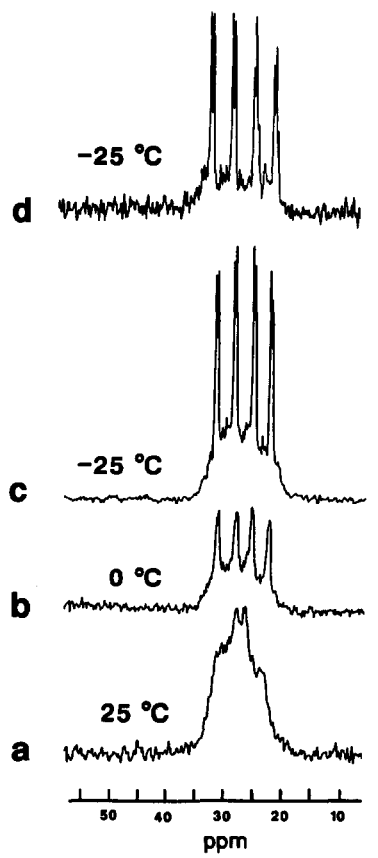

Fig. 2. ^{31}P NMR spectrum of $Rh_2(\mu\text{-dppp})_2(\mu\text{-Cl})(CO)Cl_3$.

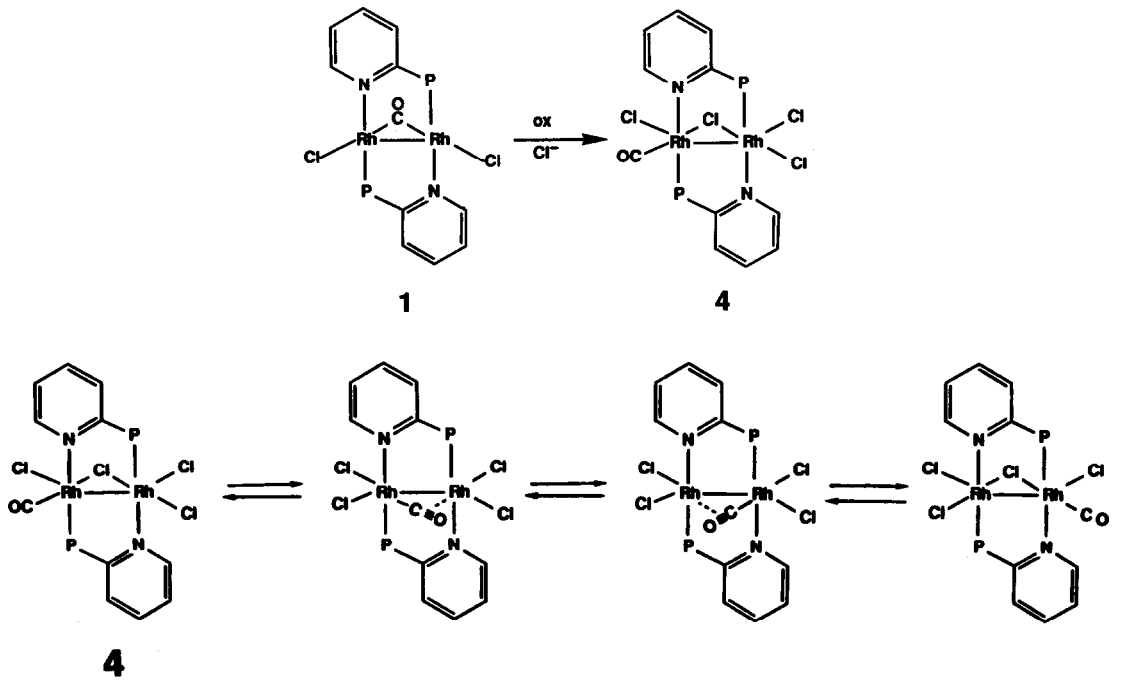

Scheme 1.

The variable-temperature ^{31}P NMR spectra shown in Fig. 2 indicate that **4** is fluxional and the weak IR peak attributable to a bridging CO in acetone suggests that the fluxional process involves a bridging CO. We suggest that a feasible fluxional behaviour is described by the interconversion outlined in Scheme 1. The initial bridging CO species is postulated to be one with a semi-bridging CO. This is based on the fact that in this mode the CO is a four-electron donor and thus the 18-electron configuration at each metal centre is maintained, and the metal–metal bond is also maintained. A symmetrically bridged CO would act as a two-electron donor and would require the loss of the metal–metal bond, a process which is not favoured for the dppp ligand though the symmetrically-bridged CO species might be a transient species formed in the interconversion of the two semi-bridged CO species shown in Scheme 1. The ^{31}P NMR spectrum of **4** in 1,2-dichloroethane at 75°C exhibits two major lines centred at 27.6 ppm that appear to be the components of a doublet compared to that shown in Fig. 2(a) at 25°C. The signal-to-noise ratio for the spectrum in 1,2-dichloroethane was less than ideal due to limitations of solubility. At high temperatures the spectrum is approaching that of two phosphorus atoms in equivalent averaged environments and exhibiting rhodium–phosphorus coupling (*ca* 124.5 Hz at 75°C). The peak separation is well within the range of the rhodium–phosphorus coupling expected for these types of species.

Without the C-13 enriched species it was not possible to unequivocally assign the phosphorus resonances. Figure 2(d) clearly indicates that in **4** the phosphorus atom bonded to rhodium containing the CO gives rise to the resonance at 23.2 ppm. The pseudo-triplet results from the fact that the coupling constant $^2J_{P\_C}$ is 12.2 Hz which is the same as $^2J_{P\_Rh}$. Similar experiments have shown that the phosphorus atom bonded to the CO-containing Rh in the analogous nitrato-bridged complex exhibits a resonance at 33.0 ppm.[3] Since the chemical shifts for the phosphorus atom bonded to the rhodium atoms containing two Cl^- are close for **4** (29.7 ppm) and **2** (28.7 ppm), it is clear that the electronic environment of the CO-bonded rhodium atom is much more susceptible to the structural and electronic requirements of the bridging chloro and nitrato ligands, probably because of variations in the extent of backbonding with the π^* orbitals of CO.

Reaction of **4** *with* CO *and* *t*-BuNC

A new complex is isolated from a CH_2Cl_2 solution of **4** that has been bubbled with CO. This product exhibits strong and medium IR bands at 2066 and 2039 cm^{-1}, respectively, which indicate the presence of terminal CO molecules. The ^{31}P NMR spectrum of the product exhibits a doublet at 22.4 ppm with $J_{Rh\_P} = 109.9$ Hz. The spin system is AA'XX', thus the long-range couplings must be

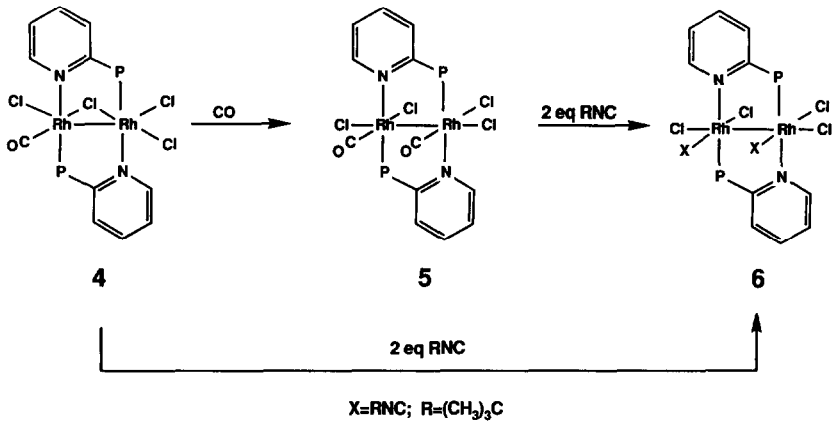

Scheme 2.

such that the pattern appears as that of a simple AX system. The CO addition product is formulated as $Rh_2(\mu\text{-dppp})_2(CO)_2Cl_4$, **5** (Scheme 2). Complex **5** is stable in the solid and solution whereas the dppm analogue loses a molecule of CO if it is not kept under an atmosphere of CO.[2]

Treatment of **4** or **5** with *t*-BuNC as outlined in Scheme 2 affords a product that exhibits a weak IR band at 2218 cm^{-1} and a strong band at 2189 cm^{-1} which have been assigned to ν(NC) of the complex $Rh_2(\mu\text{-dppp})_2(t\text{-BuNC})_2Cl_4$, **6**. The ^{31}P NMR spectrum of **6** is more complex than the simple doublet observed for **5**. Though the spectrum of **6** is symmetrical, each component of the doublet is split into several lines. This difference indicates that the long-range couplings for the AA'XX' systems are much more prominent for **6** than for **5**. This undoubtedly results, in part, from the different electronic environments of the metal centres due to differences in the bonding properties of the CO and *t*-BuNC ligands. The more complex spectrum for **6** may also result in part from averaged coupling of two or more species in equilibrium. Variable temperature experiments do show that the relative intensities of the ^{31}P NMR lines of **6** vary slightly with temperature.

Some Cl^- is detected in a CH_2Cl_2 solution of **6** with a chloride ion selective electrode. This result is interpreted to mean that the non-ionic dinuclear species **6** is in equilibrium with a dirhodium cation and a Cl^-. Addition of NH_4PF_6 in methanol to a CH_2Cl_2 solution of **6** gives a product whose IR spectrum contains a strong band at 2189 cm^{-1} and a weak shoulder at 2225 cm^{-1} in addition to PF_6^- bands at 839 and 557 cm^{-1}. The ^{31}P NMR spectrum of this product is more like that of **5** than **6** since it exhibits a simple doublet at 25.3 ppm with a splitting of 113.0 Hz. The product is formulated as **7** and its formation is summarized in Scheme 3.

The tendency of **6** to dissociate might be related to the short Rh—Rh bond distance and subsequent steric interactions resulting from the proximity of the *t*-BuNC ligands. This interaction can be reduced by twisting the dppp ligands such that when viewing **6** down the Rh—Rh bond axis the groups around the two rhodium atoms are in a slightly staggered conformation similar to that observed for **1**[5] and **2**.[3] Further reduction of this interaction can be achieved through dissociation to form the chloro-bridged dirhodium cation. In the cation the two planes containing the P—Rh—N axes are tilted such that they intersect at the bridging Cl rather than being in an approximate parallel orientation. Thus, formation of the cation should allow the *t*-

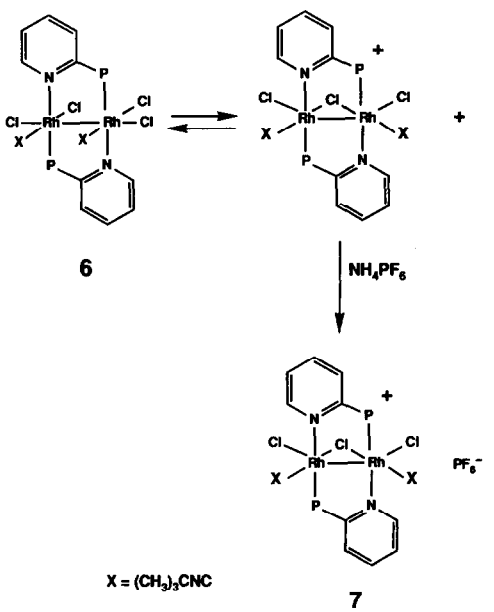

Scheme 3.

BuNC ligands to be further tilted away from each other such that a less sterically hindered species is formed. The extent of dissociation of **6** is apparently small due to the coordinating ability of Cl^- and the non-ionizing power of CH_2Cl_2. Thus, a stoichiometric amount of the chloro-bridged dirhodium cation is not obtained until the Cl^- is precipitated with NH_4^+ and replaced with the non-coordinating anion PF_6^- (Scheme 3).

CONCLUSIONS

This study clearly indicates that the tendency of dirhodium complexes to undergo the formation or cleavage of metal–metal bonds during electrochemical processes depends in part on structural constraints such as the ability of the bridging ligands to accommodate the required metal–metal distances. However, electronic properties of the ligands such as sigma donor and pi acceptor ability also play major roles in determining whether electrochemically generated dirhodium products will exist with or without metal–metal bonds.

Acknowledgements—The authors wish to thank the National Science Foundation for support of this work and Johnson Matthey, Inc. for a generous loan of rhodium trichloride.

REFERENCES

1. D. R. Womack, P. D. Enlow and C. Woods, *Inorg. Chem.* 1983, **22**, 2653.
2. L. J. Tortorelli, P. W. Tinsley, C. Woods and C. J. Janke, *Polyhedron* 1988, **7**, 315.
3. L. J. Tortorelli, C. A. Tucker and C. Woods, *Inorg. Chem.* 1986, **25**, 3534.
4. F. G. Mann and J. Watson, *J. Org. Chem.* 1948, **13**, 502.
5. A. L. Balch, R. R. Guimerans, J. Linehan and F. E. Wood, *Inorg. Chem.* 1985, **24**, 2021.
6. J. P. Farr, M. M. Olmstead and A. L. Balch, *J. Am. Chem. Soc.* 1980, **102**, 6654.
7. J. P. Farr, M. M. Olmstead, F. E. Wood and A. L. Balch, *J. Am. Chem. Soc.* 1983, **105**, 792.
8. M. Cowie and S. K. Dwight, *Inorg. Chem.* 1980, **19**, 2500.

Polyhedron Vol. 7, No. 18, pp. 1759–1765, 1988
Printed in Great Britain

0277–5387/88 $3.00+.00
© 1988 Pergamon Press plc

AN X-RAY CRYSTAL AND ELECTRONIC STRUCTURAL INVESTIGATION OF THE INTERSTITIAL PHOSPHIDE CLUSTER $[Os_6(CO)_{18}PCl]$

STEPHEN B. COLBRAN, CATHERINE E. HOUSECROFT,* BRIAN F. G. JOHNSON, JACK LEWIS,* STEVEN M. OWEN and PAUL R. RAITHBY

University Chemical Laboratory, Lensfield Road, Cambridge CB2 1EW, U.K.

(*Received* 21 *January* 1988; *accepted* 15 *March* 1988)

Abstract—The molecular structure of $[Os_6(CO)_{18}PCl]$ is presented. The phosphorus atom is interstitially sited within a distorted trigonal prismatic array of osmium atoms. The chlorine atom bridges one edge of a triangular face of the Os_6 cage. A comparison is made between the structures of $[Os_6(CO)_{18}PCl]$ and its parent compound, $[Os_6(CO)_{18}P]^-$. By using the model compounds $[Ru_6(CO)_{18}P]^-$ and $Ru_6(CO)_{18}PCl$, the Fenske–Hall quantum chemical technique is used to investigate the mode of bonding of the phosphorus atom in $[Os_6(CO)_{18}P]^-$. In $Ru_6(CO)_{18}PCl$, the interaction of the tangential orbital of the chlorine atom with the ruthenium–ruthenium antibonding LUMO of $[Ru_6(CO)_{18}P]^-$ is the primary interfragment interaction; this results in $Ru_6(CO)_{18}PCl$, and by analogy $[Os_6(CO)_{18}PCl]$, being a 92 electron cluster in contrast to $[Os_6(CO)_{18}P]^-$ which is a 90 electron cluster.

Transition metal clusters containing interstitial atoms are becoming an increasingly well known class of compound. Whilst carbon is by far the most commonly exemplified interstitial atom,[1,2] other types of metal encapsulated atoms are now known.[3] New types of compound present new problems in bonding descriptions and, not surprisingly, considerable interest has been generated by the bonding within transition metal clusters containing interstitial main-group atoms, either in general terms[4–6] or for specific cluster compounds.[7] Compounds containing naked phosphorus atoms have been surveyed,[8] but recently, the first example of a phosphide-containing trigonal prismatic array of metal atoms was reported.[3d] This cluster compound, $[Os_6(CO)_{18}P]^-$ (**I**), contains a D_{3h}-Os_6P cluster core. The chloro-derivative, $[Os_6(CO)_{18}PCl]$ (**II**), has now been synthesized and a single crystal X-ray diffraction study has established that the basic trigonal prismatic framework is preserved, but is significantly perturbed by the presence of the bridging chlorine ligand. The bonding in each of the clusters (**I**) and (**II**) has been investigated by using the Fenske–Hall quantum chemical technique with the model compounds $[Ru_6(CO)_{18}P]^-$ (**Ia**), and $Ru_6(CO)_{18}PCl$ (**IIa**). A notable feature in (**IIa**) is the localized nature of the M—μCl—M bonding. The change from a 90 electron cluster in (**Ia**) to a 92 electron cluster in (**IIa**) is rationalized by the stabilization and occupancy in (**IIa**) of a hitherto unoccupied orbital which possesses the correct symmetry to interact with a *p*-orbital on the chlorine atom.

EXPERIMENTAL

Spectra

IR spectra were obtained using a Perkin–Elmer 983 spectrophotometer. NMR spectra were obtained using a Bruker AM400 spectrometer and ^{31}P chemical shifts were relative to $P(OMe)_3$, downfield shifts being at positive δ. FAB mass spectra were recorded on a MS902 instrument.

Preparation of $[Os_6(CO)_{18}PCl]$ (**II**)

$FeCl_3$ (35 mg, 0.215 mmol) was added to a solution of $[PPN][Os_6(CO)_{18}P]$ (70 mg, 0.031 mmol) in THF at room temperature. The solution was heated to reflux under a nitrogen atmosphere for 45 min.

* Authors to whom correspondence should be addressed.

After the solution had cooled to room temperature, 2 vol. equiv. of water were added. The precipitate which resulted was filtered through a celite plug and was washed with cold water. The product was extracted with dichloromethane and dried with anhydrous magnesium sulphate. After filtration and evaporation of the solvent from the filtrate, the product was isolated as a yellow powder in 88% yield. (**II**): IR (ν_{CO}, cm^{-1}) 2116w, 2089w, 2073vs, 2064s, 2038s, 2019w, 2006w, 1976w; FAB—MS *m/e* 1712 (P^+); ^{31}P NMR (C_6D_6) δ 413.85.

Crystal structure determination of $[Os_6(CO)_{18}PCl]$ **(II)**

Orange crystals were obtained by slow evaporation of a CH_2Cl_2 solution of (**II**).

Crystal data—(**II**)

$C_{18}ClO_{18}Os_6P$, $M = 1711.81$, triclinic, $a = 9.141(1)$, $b = 10.329(1)$ $c = 17.396(1)$ Å, $\alpha = 91.57(1)$, $\beta = 91.02(1)$, $\gamma = 114.70(1)°$, $U = 1491.0$ Å^3 (from 2θ values of 50 centred reflections), $T = 291$ K, graphite monochromated Mo-K_α radiation, $\lambda = 0.71069$ Å, space group $P\bar{1}$ (No. 2), $Z = 2$, $D_c = 3.83$ g cm^{-3}, $F(000) = 1480$. Orange, multifaceted block; crystal dimensions (distances of faces from centre): 0.186 (001, 00$\bar{1}$) × 0.165 (011, 0$\bar{1}\bar{1}$) × 0.144 (01$\bar{1}$, 0$\bar{1}$1) × 0.129 (10$\bar{1}$, $\bar{1}$01) × 0.095 (1$\bar{1}$0, $\bar{1}$10) × 0.171 (101, $\bar{1}$0$\bar{1}$) mm; μ(Mo-K_α) = 256.76 cm^{-1}.

Data collection and processing

Stoe–Siemens AED diffractometer, 24 step ω/θ scan mode, scan range $5.0 \leqslant 2\theta \leqslant 50.0°$ ($+h$, $\pm k$, $\pm l$), scan width 0.05° per step, scan time 0.5–2.0 s per step. 5608 reflections measured, numerical absorption correction applied (transmission factors range 0.0494–0.0043) averaged to give 5250 unique reflections (merging $R = 0.031$), 4470 with $F > 4\sigma(F)$ used in refinement. Three standard reflections showed no significant variation in intensity throughout the data collection.

Structure analysis and refinement

Direct methods (Os atoms) followed by Fourier difference syntheses. Full-matrix least-squares refinement with Os, P, Cl, and O anisotropic. The weighting scheme, $w = 1.00/[\sigma^2(F) + 0.0012(F_0)^2]$, with $\sigma(F_0)$ from counting statistics, gave reasonable agreement analyses. A final Fourier difference map showed residual electron density peaks of *ca* 2.76 e Å^{-3} close to the Os atom positions, but no other regions of significant electron density. Final $R = 0.051$ and $R' = 0.051$. The structure was solved and refined using SHELX 76[9] implemented on the University of Cambridge IBM 3084Q computer. Neutral atom scattering factors were taken from ref. 10. Selected bond distances and angles are listed in Tables 1 and 2.*

Table 1. Selected bond distance in (**II**) Å

Os(1)—Os(2)	3.176(1)	Os(1)—P	2.281(4)
Os(1)—Os(5)	2.954(1)	Os(2)—P	2.280(4)
Os(1)—Os(4)	2.945(1)	Os(3)—P	2.310(4)
Os(2)—Os(3)	2.952(1)	Os(4)—P	2.441(4)
Os(2)—Os(6)	2.957(1)	Os(5)—P	2.432(3)
Os(3)—Os(6)	2.911(1)	Os(6)—P	2.312(4)
Os(4)—Os(6)	3.003(1)	Os(4)—Cl	2.497(4)
Os(3)—Os(5)	3.013(1)	Os(5)—Cl	2.432(4)

Fenske–Hall calculations

Fenske–Hall quantum chemical calculations[11] were carried out by using $[Ru_6(CO)_{18}P]^-$ and $Ru_6(CO)_{18}PCl$ to model $[Os_6(CO)_{18}P]^-$ and $[Os_6(CO)_{18}PCl]$, respectively. The structure of $[Ru_6(CO)_{18}P]^-$ was idealized to D_{3h} symmetry. All C—O bonds were set at 1.15 Å and Ru—CO bonds were 1.90 Å. In $[Ru_6(CO)_{18}P]^-$, intra-triangle Ru—Ru = 2.93 Å and inter-triangle Ru—Ru = 3.14 Å. All Ru—P = 2.31 Å. The atomic numbering is shown in Scheme 1. The geometry of $Ru_6(CO)_{18}PCl$ was based on the crystallographically determined structure, idealized to C_s symmetry with the mirror plane passing through Ru(1), P and Cl, (see Scheme 1 for atomic

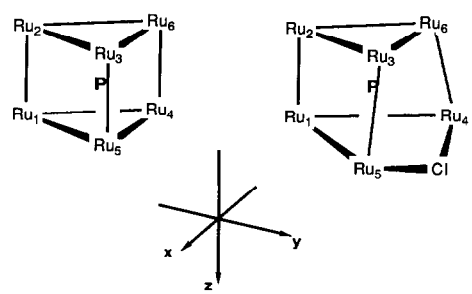

Scheme 1.

* Atomic coordinates, displacement factor coefficients, full lists of bond lengths and angles and lists of F_o/F_c values have been deposited as supplementary data with the Editor, from whom copies are available on request. Atomic coordinates have also been deposited with the Cambridge Crystallographic Data Centre.

Table 2. Selected bond angles in (II) (°)

Os(4)—Os(1)—Os(2)	87.2(1)	Os(1)—P—Os(2)	88.3(2)
Os(5)—Os(1)—Os(2)	86.8(1)	Os(1)—P—Os(3)	139.4(2)
Os(5)—Os(1)—Os(4)	78.3(1)	Os(3)—P—Os(2)	80.1(1)
Os(3)—Os(2)—Os(1)	89.2(1)	Os(1)—P—Os(4)	77.1(1)
Os(6)—Os(2)—Os(1)	88.7(1)	Os(4)—P—Os(2)	126.9(2)
Os(6)—Os(2)—Os(3)	59.0(1)	Os(3)—P—Os(4)	139.6(2)
Os(5)—Os(3)—Os(2)	89.9(1)	Os(1)—P—Os(5)	77.5(1)
Os(6)—Os(3)—Os(2)	60.6(1)	Os(5)—P—Os(2)	126.8(2)
Os(6)—Os(3)—Os(5)	97.6(1)	Os(4)—P—Os(5)	99.6(1)
Os(6)—Os(4)—Os(1)	92.3(1)	Os(6)—P—Os(2)	80.2(1)
Os(3)—Os(5)—Os(1)	92.4(1)	Os(6)—P—Os(4)	78.3(1)
Os(3)—Os(6)—Os(2)	60.4(1)	Os(5)—P—Os(3)	78.8(1)
Os(4)—Os(6)—Os(2)	90.2(1)	Os(1)—P—Os(6)	138.2(2)
Os(4)—Os(6)—Os(3)	97.9(1)	Os(3)—P—Os(6)	78.1(1)
Os(4)—Cl—Os(5)	96.2(2)	Os(5)—P—Os(6)	140.1(2)

numbering and axis system). The two ruthenium triangles were coparallel. Bond distances were Ru(1)—Ru(4) = 3.05, Ru(1)—Ru(2) = 3.04, Ru(2)—Ru(3) = 2.82, Ru(3)—Ru(6) = 2.91, Ru(1)—P = 2.21, Ru(2)—P = 2.25, Ru(4)—P = 2.51 Å. All C—O bonds were set at 1.15 Å and Ru—CO bonds were 1.90 Å. The Fenske–Hall calculations employed single-ζ Slater functions for the 1*s* and 2*s* functions of Cl, O and C. The exponents were obtained by curve fitting the double-ζ functions of Clementi[12] while maintaining orthogonal functions; the double-ζ functions were used directly for the 2*p* orbitals. An exponent of 1.16 was used for hydrogen. Functions for P were as previously described.[3f,*] The Ru functions[13] were chosen for the +1 oxidation state and were augmented by 5*s* and 5*p* functions with exponents of 2.20.

RESULTS AND DISCUSSION

Molecular structure of (II)

The molecular structure of (II) is shown in Fig. 1(a), and the structure of the core is shown in Fig. 1(b). It is based on a trigonal prism of osmium atoms in which one of the basal edges has been significantly lengthened, indeed *broken*, by the presence of a bridging chlorine atom. The average intra-triangle unbridged Os—Os length of 2.944(5) Å compares favourably with an average of 2.930(5) Å found in (I) and with the average of 2.932(5) Å for the unbridged basal bonds in $Os_6(CO)_{18}P(AuPPh_3)$.[3d] The metal edge which is bridged by the chlorine atom is substantially longer, (3.724(2) Å). The inter-osmium triangle bond lengths in (II) average 3.064(2) Å, 0.076 Å shorter than the corresponding average for (I).[3d] However, whereas in (I) the two triangles of the Os_6-prism are parallel, those in (II) are tilted apart; the inter-triangle distance Os(1)—Os(2) which lies on the side of the prism *remote* from the μ-Cl is longer than the remaining two prism sides, viz. Os(3)—Os(5) and Os(4)—Os(6). The bridging chlorine atom is therefore responsible for two deformations of the trigonal prismatic metal framework. A direct consequence is that the interstitial phosphorus, which in (I) is symmetrically bonded to all six osmium atoms, interacts with the metal atoms in (II) with Os—P separations varying from 2.280(4) to 2.441(4) Å.

The Cl atom is bonded almost symmetrically between Os(4) and Os(5) and the average Os—μCl distance of 2.502(5) Å is slightly, but not significantly, longer than other reported Os—μCl bond lengths.[14–17] The chlorine atom lies 0.66 Å below the plane containing Os(1), Os(4) and Os(5). The carbonyl ligand arrangement is not unusual. None of the osmium–carbonyl vectors varies significantly from linearity, and each Os—C—O vector is an extension of either an Os—Os or a μCl—Os bond vector.

* For the calculations reported here, 3*d* orbitals were not included in the basis set for phosphorus. We have however carried out test calculations in which we generated a set of 3*d* orbitals for P with exponents varying in the range 1.8–2.2. The rôle of the 3*d* orbitals on phosphorus in binding the interstitial atom to the hexa-metal cage in $[Ru_6(CO)_{18}P]^-$ was found to be a small one. Primary metal–phosphorus bonding involved the 3*s* and 3*p* AOs, and we are therefore justified in using the smaller basis set of valence orbitals as previously reported.[3f]

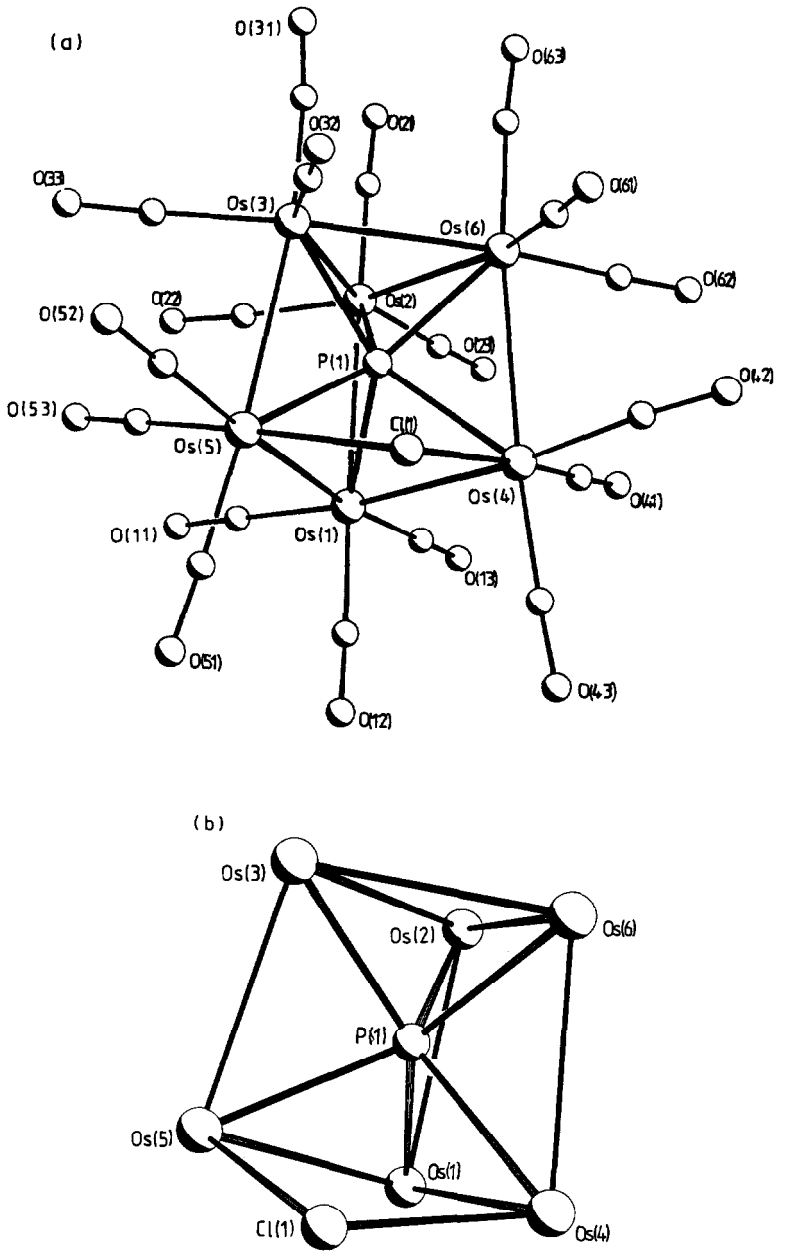

Fig. 1. (a) Molecular structure of $[Os_6(CO)_{18}PCl]$ (**II**); (b) the structure of the Os_6PCl core of (**II**), showing the atom numbering scheme.

Electronic structure of (**Ia**)

In order to understand the rôle played by the chlorine atom in (**II**), both in deforming the metal framework and in allowing the trigonal prismatic phosphide cluster to accommodate 92 instead of 90 electrons, we shall begin by examining the bonding in (**I**), modelled by the hypothetical ruthenium analogue, (**Ia**). Since our prime interest in this paper is in the chloro-derivative, (**II**), only the salient features of (**Ia**) will be presented; the bonding in the trigonal prismatic cluster $Ru_6(CO)_{18}C^{2-}$ has previously been investigated and contrasted with the bonding in octahedral $Ru_6(CO)_{18}C^{2+}$.[6]

We have chosen to examine the bonding in (**Ia**) in terms of the interactions of a phosphorus atom with two eclipsed ruthenium triangles, i.e. two $Ru_3(CO)_9$ fragments. The correlation between fragment MOs is shown in Fig. 2. Remembering that the two $Ru_3(CO)_9$ units are equivalent, the reader should note that, although only one is represented in Fig. 2, both are contributing equally. The highest

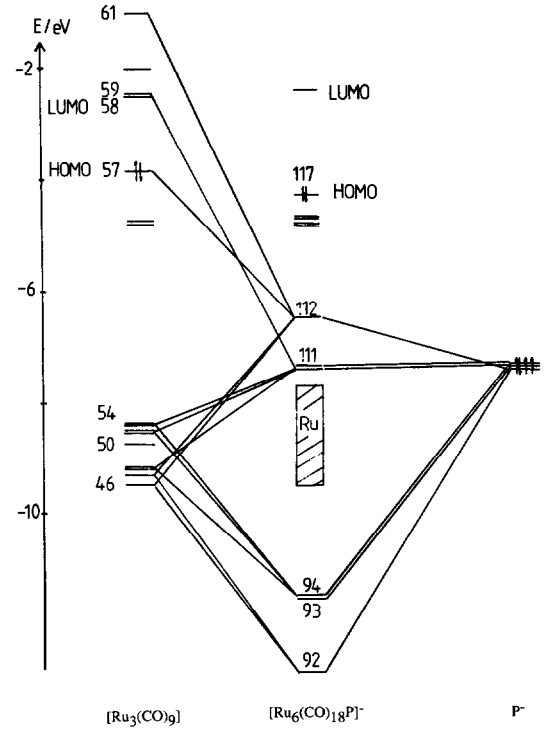

Fig. 2. Molecular orbital correlation diagram for the formation of $[Ru_6(CO)_{18}P]^-$ from two $[Ru_3(CO)_9]$ fragments and P^-. Fragment MO energies are taken from the Fock matrix.[18] For clarity, single correlation lines are used to indicate contributions made by the degenerate pairs of MOs 48/49, 51/52, 53/54 and 58/59 to the degenerate pairs of MOs 93/94 and 110/111 in $[Ru_6(CO)_{18}P]^-$.

filled MOs (113–117) of (**Ia**) are involved solely in metal–metal interactions. The 3*s* orbital of the P atom is low-lying and remains largely localized on phosphorus in the complex. There are six filled MOs (MOs 92–94 and 110–112) in (**Ia**) which contain significant phosphorus 3*p* character. 72% of the total phosphorus character in (**Ia**) is located in MOs 92–94. These three orbitals, schematically represented in Fig. 3, are strongly Ru—P bonding. This fact is borne out by the total atom–atom Mulliken overlap populations (Table 3) for Ru—Ru and Ru—P interactions, although it should be noted that Mulliken overlap populations for metal–main group interactions will usually be larger than for metal–metal interactions. Despite this cautionary note, the interstitial P atom clearly has an important rôle to play in holding the Ru_6P core together. Hoffmann *et al*[6] have pointed out that in the octahedral carbide cluster $Ru_6(CO)_{18}C^{2+}$, the introduction of a carbon atom into the Ru_6 cage redistributes electron density from metal–metal to metal–carbon bonds. The same effect is seen in (**Ia**).

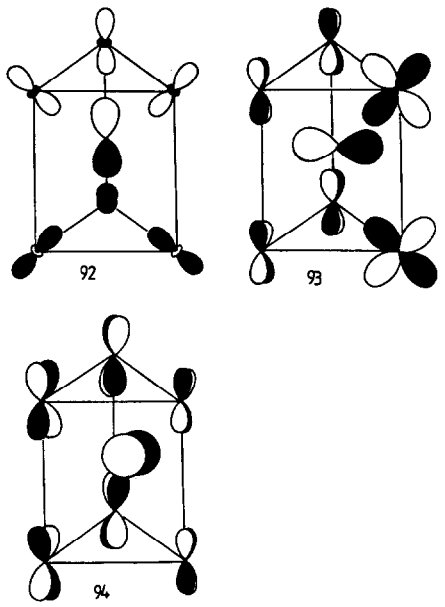

Fig. 3. Schematic representations of MOs 92, 93 and 94 in (**IIa**), the major cluster-P bonding MOs.

Electronic structure of (**IIa**)

When the chlorine atom is introduced into (**Ia**) to form (**IIa**), the cluster bonding is not greatly perturbed. The bonding of the chlorine atom in (**IIa**) is localized in much the same way as the bonding of a bridging hydrogen atom to a transition metal cluster. Obviously though, for a chlorine atom, the availability of 3*p* and 3*s* atomic orbitals allows a greater number of symmetry combinations with cluster fragment MOs than would be available to a hydrogen atom. The 3*s* orbital of the chlorine atom does not participate in the bonding to the cluster, being 97% localized in MO 19 of (**IIa**). The $3p_z$ orbital of the chlorine atom, (see Scheme 1 for axis definition), contributes little to cluster bonding, being of the wrong symmetry to interact well with the available cluster fragment MOs. MOs 93–98 of (**IIa**) together contain about 88% of the total Cl 3*p* character and 73% of the P 3*p* character. These orbitals are shown in Fig. 4. Note that MOs 95

Table 3. Atomic Mulliken overlap populations in (**Ia**)

Bond type	Mulliken overlap population per bond
Inter-triangle Ru—Ru	+0.034
Intra-triangle Ru—Ru	+0.069
Ru—P	+0.192

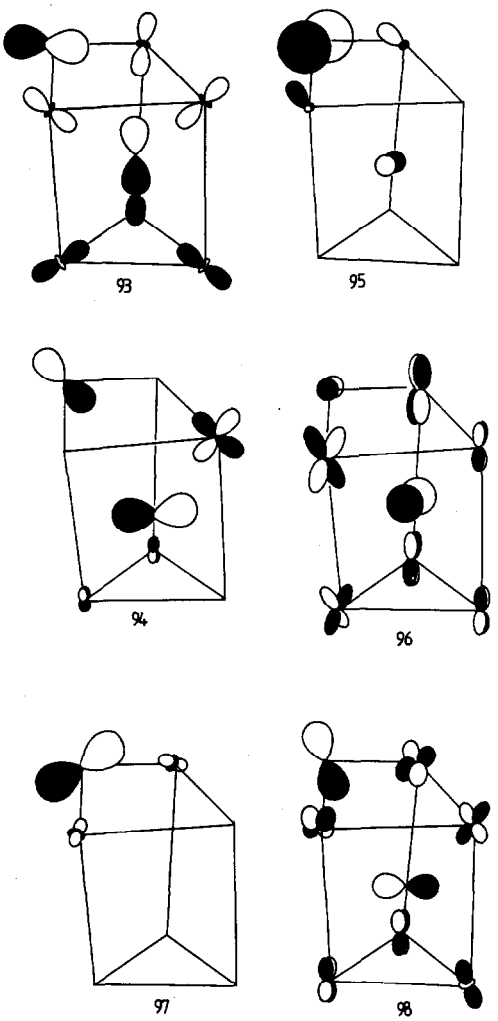

Fig. 4. Schematic representations of MOs 93–98 in (**Ia**), the major cluster-P and cluster-Cl bonding MOs.

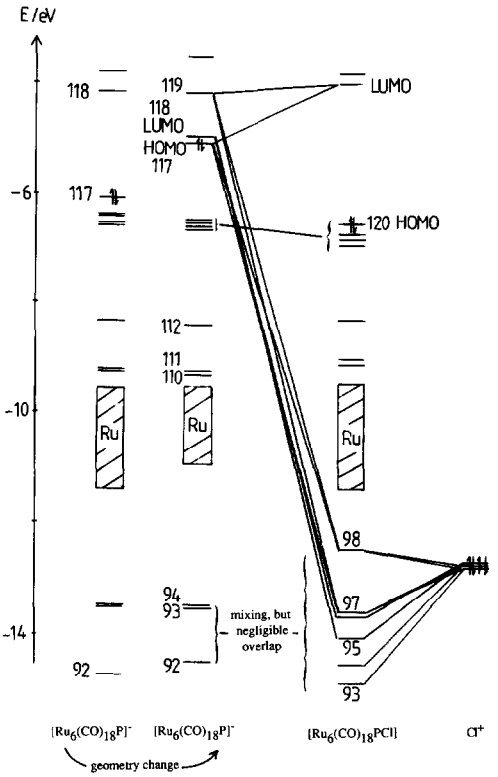

Fig. 5. Molecular orbital correlation diagram (i) comparing the energies of MOs in $[Ru_6(CO)_{18}P]^-$ (**Ia**) with those in the fragment $[Ru_6(CO)_{18}P]^-$ in a geometry taken from complex (**IIa**), and (ii) for the formation of $Ru_6(CO)_{18}PCl$ from $[Ru_6(CO)_{18}P]^-$ and Cl^+. Fragment MO energies are taken from the Fock matrix.[18]

and 97 are well described as Ru—Cl—Ru 3c–2e bonding orbitals. Despite the fact that phosphorus and chlorine contributions occur in the same MOs in (**IIa**), the interaction between the two main group atoms is negligible. This is consistent with the relatively large distance between the two atoms.

The left hand side of Fig. 5 compares the energies of the MOs in $[Ru_6(CO)_{18}P]^-$ as its framework is deformed from that in (**Ia**) to one ready to accommodate the chlorine atom in (**IIa**). Perturbation is minimal. The destabilization of the HOMO (MO 117, Fig. 6) corresponds to a decrease in metal–metal bonding character as the metal–metal edge is opened up; similarly, the stabilization of the lowest-lying unoccupied MOs is concomitant with a decrease in metal–metal antibonding character. The LUMO (MO 118) is shown in Fig. 6.

The right hand side of Fig. 5 correlates the molecular orbitals of the $[Ru_6(CO)_{18}P]^-$ fragment with the atomic orbitals of Cl^+; Table 4 lists the Mulliken overlap populations for the inter-fragment interactions. The first observation is that, compared to (**Ia**), (**IIa**) exhibits one less occupied MO above the group of metal-containing orbitals. The HOMO of $[Ru_6(CO)_{18}P]^-$ interacts with the $3p_y$ orbital, and to a lesser extent with the $3p_z$ AO of the chlorine

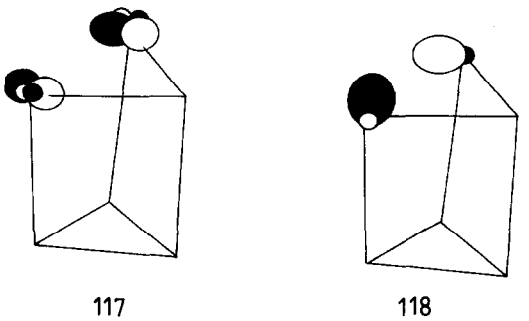

Fig. 6. Schematic representation of the HOMO (MO 117) and LUMO (MO 118) of the $[Ru_6(CO)_{18}P]^-$ fragment in a geometry as found in (**IIa**).

Table 4. Mulliken overlap populations between the fragments $[Ru_6(CO)_{18}P]^-$ and Cl^+ in (**IIa**)

MO in $[Ru_6(CO)_{18}P]^-$	MO in Cl^+ $2(p_x)$	$3(p_y)$	$4(p_z)$
119	—	0.025	—
118(LUMO)	0.181	—	—
117(HOMO)	—	0.080	0.009

atom. The MOs in (**IIa**) which are generated by these interactions also contain contributions from the cluster fragment MO 119. The Mulliken overlap population of fragment MOs 119 and 3 is, however, small, accounting for only 8% of the total $[Ru_6(CO)_{18}P]^-$—$[Cl]^+$ overlap population. Most of the character of MO 119 is carried across to the unoccupied MO 121 in (**IIa**). The second observation in the molecular orbital pattern of (**IIa**) is the presence of one less high-lying unoccupied metal–metal antibonding MO compared to (**Ia**). This is consistent with the interaction of the tangential $3p_x$ atomic orbital on the chlorine atom with, and consequential stabilization of, the LUMO of the $[Ru_6(CO)_{18}P]^-$ fragment; the LUMO is antibonding between Ru(4) and Ru(5). This interaction generates MO 95 in (**IIa**), i.e. a cluster *bonding* orbital. Thus, the cluster electron count is increased by two electrons from 90 to 92 electrons. The prominant rôle of the tangential AO of the chlorine bridging atom has previously been emphasized.[19]

Acknowledgements—We thank the S.E.R.C. (to S. M. O. and S.B.C.) for their support. The Royal Society is acknowledged for a 1983 Research Fellowship (to C.E.H.).

REFERENCES

1. J. S. Bradley, *Adv. Organomet. Chem.* 1983, **22**, 1.
2. E. L. Muetterties, *Prog. Inorg. Chem.* 1981, **28**, 203.
3. See for example: (a) D. E. Fjare and W. L. Gladfelter, *Inorg. Chem.* 1981, **20**, 3532; (b) M. L. Blohm and W. L. Gladfelter, *Organometallics* 1985, **4**, 45; (c) C. K. Schauer and D. F. Shriver, *193rd A.C.S. National Meeting*, INORG 256, Denver, U.S.A., April (1987); (d) S. B. Colbran, C. M. Hay, B. F. G. Johnson, F. J. Lahoz, J. Lewis and P. R. Raithby, *J. Chem. Soc., Chem. Commun.* 1986, 1766; (e) T. P. Fehlner and N. P. Rath, *J. Am. Chem. Soc.* 1987, **109**, 5273; (f) C. E. Housecroft and A. L. Rheingold, *Organometallics* 1987, **6**, 1332; (g) C. E. Housecroft, *Polyhedron* 1987, **6**, 1935 and refs therein.
4. J. W. Lauher, *J. Am. Chem. Soc.* 1978, **100**, 5305.
5. A. J. Stone, *Mol. Phys.* 1980, **41**, 1339; A. J. Stone, *Inorg. Chem.* 1981, **20**, 563; A. J. Stone, *Polyhedron* 1984, **3**, 1299.
6. S. D. Wijeyesekera and R. Hoffmann, *Organometallics* 1984, **3**, 950.
7. See for example: T. P. Fehlner, C. E. Housecroft, W. R. Scheidt and K. S. Wong, *Organometallics* 1983, **2**, 825; J. S. Bradley and S. Harris, *Organometallics* 1984, **3**, 1086; S. D. Wijeyesekera, R. Hoffmann and C. N. Wilker, *Organometallics* 1984, **3**, 962; P. Brint, K. O'Cuill and T. R. Spalding, *Polyhedron* 1986, **5**, 1791.
8. M. Di Vaira, P. Stoppioni and M. Peruzzini, *Polyhedron* 1987, **6**, 351.
9. G. M. Sheldrick, SHELX 76, Crystal structure Solving Package. University of Cambridge (1976).
10. *International Tables for X-Ray Crystallography*, Vol. IV. Kynoch Press (1974).
11. M. B. Hall and R. F. Fenske, *Inorg. Chem.* 1972, **11**, 768.
12. E. Clementi, *J. Chem. Phys.* 1964, **40**, 1944.
13. J. W. Richardson, M. J. Blackman and J. F. Ranochak, *J. Chem. Phys.* 1973, **58**, 3010.
14. M. A. Gallop, B. F. G. Johnson, J. Lewis and P. R. Raithby, *J. Chem. Soc., Chem. Commun.* 1986, 706.
15. R. D. Adams, I. T. Horváth and B. E. Segmüller, *Organometallics* 1982, **1**, 1537.
16. M. R. Churchill and R. A. Lashewycz, *Inorg. Chem.* 1979, **18**, 1926.
17. F. W. B. Einstein, T. Jones and K. G. Tyers, *Acta Cryst.* 1982, **B38**, 1272.
18. N. M. Kostic and R. F. Fenske, *Organometallics* 1982, **1**, 974.
19. C. E. Housecroft and S. M. Owen, *Organometallics*, in press.

Polyhedron Vol. 7, No. 18, pp. 1767–1771, 1988
Printed in Great Britain

0277–5387/88 $3.00+.00
© 1988 Pergamon Press plc

OXO-MOLYBDENUM(IV) AND TUNGSTEN(IV) COMPLEXES WITH PHOSPHINE AND ISOCYANIDE LIGANDS

ERNESTO CARMONA,* AGUSTIN GALINDO, CHRISTIAN GUILLE-PHOTIN and LUIS SANCHEZ

Departamento de Química Inorgánica e Instituto de Ciencias de Materiales, Universidad de Sevilla-CSIC, 41071 Sevilla, Spain

(*Received* 23 *November* 1987; *accepted* 15 *March* 1988)

Abstract—The complexes $[MOCl_2(dmpe)(PMe_3)]$ and $[MOCl_2(dmpe)_2]Cl$ (M = Mo, W; dmpe = $Me_2PCH_2CH_2PMe_2$) have been prepared by reaction of the oxo compounds $[MOCl_2(PMe_3)_3]$ with equivalent amounts of the dmpe ligand under appropriate conditions. The dark blue tungsten species $[WOCl_2(dmpe)(PMe_3)]$ forms only slowly but reacts readily with more dmpe to afford $[WOCl(dmpe)_2]Cl$. This prevents isolation of the former in a pure form. The related isocyanide derivatives $[MOCl_2(CNR)(PMe_3)_2]$, (M = Mo; R = CMe_3 and C_6H_{11}; M = W, R = CMe_3) have been obtained similarly by reaction of the $[MOCl_2(PMe_3)_3]$ complexes with the stoichiometric amount of the isocyanide ligand, but attempts to prepare the carbonyl analogues, $[MOCl_2(CO)(PMe_3)_2]$, have proved unsuccessful. The new compounds have been characterized by analytical and spectroscopic methods (IR, ^1H, ^{13}C and ^{31}P NMR spectroscopy).

In the past few years, the preparation and reactions of a number of oxotrimethylphosphine complexes of Mo(IV) and W(IV), have been extensively studied in this laboratory.[1–4] As part of our continuing interest in this type of chemistry, we have now examined the substitution of the coordinated PMe_3 by dmpe (dmpe = $Me_2PCH_2CH_2PMe_2$) and isocyanide ligands. We report herein the synthesis and properties of new oxo-molybdenum(IV) and tungsten(IV) complexes of composition $[MOCl_2(dmpe)(PMe_3)]$, $[MOCl(dmpe)_2]Cl$ and $[MOCl_2(CNR)(PMe_3)_2]$. While our work was in progress, the compounds $[MoOCl(dmpe)_2]Cl$[5a] and $[WOCl_2(CNCMe_3)(PMePh_2)_2]$[5b] were reported.

RESULTS AND DISCUSSION

(a) 1,2-*bis*(*dimethylphosphino*)*ethane derivatives*

Tetrahydrofuran solutions of the complex $[MoOCl_2(PMe_3)_3]$ react with dmpe in a stepwise manner with substitution of the PMe_3 ligands and initial formation of blue $[MoOCl_2(dmpe)(PMe_3)]$ and then pink–purple $[MoOCl(dmpe)_2]Cl$ complexes, as shown in eqs (1) and (2).

$$MoOCl_2(PMe_3)_3 + dmpe \rightarrow MoOCl_2(dmpe)(PMe_3) + 2PMe_3 \quad (1)$$

$$MoOCl_2(PMe_3)_3 + 2dmpe \rightarrow [MoOCl(dmpe)_2]Cl + 3PMe_3. \quad (2)$$

Analogous reactions are observed for the tungsten system, although the mixing of equimolar amounts of $[WOCl_2(PMe_3)_3]$ and dmpe, produces an incomplete reaction which yields a mixture of the starting material, the desired products, $[WOCl_2(dmpe)(PMe_3)]$, and the fully substituted, $[WOCl(dmpe)_2]Cl$, after 14 h of stirring at room temperature. Addition of 2 mmol of dmpe to 1 mmol of $[WOCl_2(PMe_3)_3]$, produces only $[WOCl(dmpe)_2]Cl$. The facility with which the mono-dmpe complex, $[WOCl_2(dmpe)(PMe_3)]$, reacts with more dmpe, has precluded its isolation in a pure, analytical form, although full characterization has, however, been accomplished by spectroscopic methods.

The ^1H NMR spectra of the dmpe derivatives are

*Author to whom correspondence should be addressed.

very complex and provide little information with regards to their structure. An unequivocal proposal can however be made based on ^{31}P and ^{13}C NMR studies. Thus, the $^{31}P\{^1H\}$ NMR spectra of the $[MOCl_2(dmpe)(PMe_3)]$ complexes correspond to essentially first-order AMX spin systems, as shown in Fig. 1 for the molybdenum derivative, from which the chemical shifts and coupling constants collected in Table 1 can be computed. The three phosphorus nuclei give three doublets of doublets, centred at 36.1 and 31.0 (dmpe) and 8.0 ppm (PMe_3) for M = Mo, and 21.3 and 15.4 (dmpe) and −19.5 ppm (PMe_3) for the tungsten analogue. From the values of $^2J(P_A—P_X)$ (*ca* 200 MHz), it is clear that the PMe_3 ligand is *trans* to one of the phosphorus nuclei of the dmpe group. This and other data collected in Table 1 are in accord with structure **A** for these complexes.

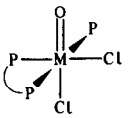

A

This bis-dmpe derivatives, $[MOCl(dmpe)_2]Cl$, are the main products of the reactions of the trimethylphosphine complexes $[MOCl_2(PMe_3)_3]$ with dmpe in a 1:2 molar ratio, and can be isolated as pink–purple crystalline solids by crystallization from CH_2Cl_2. Formulation of these complexes as 1:1 electrolytes follows analytical and conductivity data[6] (see Experimental). On the other hand, the appearance of a singlet in the $^{31}P\{^1H\}$ NMR spectrum, together with other data recorded in Table 1, are in agreement with structure **B** for these complexes. This type of cation, $[MOCl(P—P)_2]^+$, has been previously characterized by X-ray diffraction methods in related dppe complexes[7,8] (dppe = $Ph_2PCH_2CH_2PPh_2$).

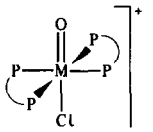

B

(b) *Isocyanide complexes*

Toluene or benzene solutions of $[MOCl_2(PMe_3)_3]$ complexes, interact with isocyanides, CNR, to afford the corresponding monoisocyanide derivatives, $[MOCl_2(CNR)(PMe_3)_2]$, (M = Mo, R = CMe_3, C_6H_{11}; M = W, R = CMe_3) as shown in eq. (3).

$$MOCl_2(PMe_3)_3 + CNR \rightarrow MOCl_2(CNR)(PMe_3)_2 + PMe_3. \quad (3)$$

The substitution reaction takes place readily for the molybdenum complex and can be monitored by IR spectroscopy, following the appearance of a characteristic absorption in the range 2150–2100 cm^{-1} due to the coordinated isocyanide ligand. A similar value of 2130 cm^{-1} has been found for the C—N stretching frequency of the coordinated CNR ligand in the related complex $[WOCl_2(CNCMe_3)$

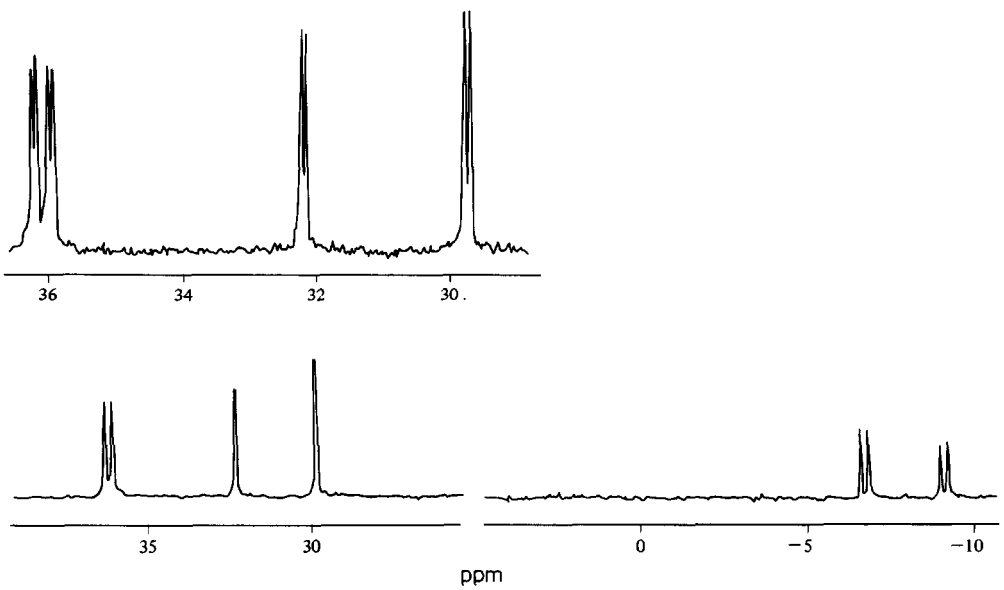

Fig. 1. $^{31}P\{^1H\}$ NMR spectrum ($CDCl_3$) of $MoOCl_2(dmpe)(PMe_3)$.

Table 1. Selected NMR data for the new oxo complexes

	$^1H^a$			$^{31}P\{^1H\}^b$			$^{13}C\{^1H\}^c$	
	PMe_3	dmpe	CNR	PMe_3	dmpe	PMe_3	dmpe	CNR
$MoOCl_2(dmpe)(PMe_3)$	1.59 d (9.1)	2.00 br s (CH_2) 1.67 d (PMe_2) (9.8) 1.46 d (PMe_2) (7.8)		8.00 dd (198.5) (5.3)	36.11 dd (PMe_2) (19.7) (5.3) 31.02 dd (PMe_2) (198.5) (19.7)	16.01 d (24.3)	31.24 dd (CH_2) (29.2) (10.4) 26.79 dd (CH_2) (28.5) (8.8) 15.85 d (PMe_2) (20.8) 14.00 d (PMe_2) (19.4) 11.14 d (PMe_2) (25.6)	
$WOCl_2(dmpe)(PMe_3)$				−19.53 dd (198.0) (5.1)	21.35 dd (PMe_2) (198.0) (19.0) 15.41 dd (PMe_2) (19.0) (5.1)			
$[MoOCl(dmpe)_2]Cl$		2.10 br s (CH_2) 1.81 br s (PMe_2) 1.75 br s (PMe_2)			29.80 s		30.28 pst (CH_2) (9.9) 18.46 br s (PMe_2) 15.89 m (PMe_2)	
$[WOCl(dmpe)_2]Cl$		2.06 pst (CH_2) (6.8) 1.84 pst (PMe_2) (3.6) 1.75 pst (PMe_2) (4.2)			17.96 s (J_{PW} = 313.1)		31.27 pst (CH_2) (10.1) 16.25 br s (PMe_2) 14.89 pst (PMe_2) (16.3)	
$MoOCl_2(CNCMe_3)(PMe_3)_2$	1.62 pst (4.1)		1.59 s	−6.75 s		14.85 pst (13.0)		58.71 s ($\underline{C}Me_3$) 30.47 s ($\underline{C}\underline{Me}_3$)
$WOCl_2(CNCMe_3)(PMe_3)_2$	1.67 pst (4.2)		1.54 s	−18.92 s (J_{PW} = 342.3)		15.60 pst (14.6)		59.43 s ($\underline{C}Me_3$) 31.35 s ($\underline{C}\underline{Me}_3$)
$MoOCl_2(CNC_6H_{11})(PMe_3)_2$	1.64 pst (4.2)		4.35 m 2.04 m 1.79 m 1.50 m	−6.75 s		14.90 pst (12.8)		55.76 s (C_6H_{11}) 32.81 s (C_6H_{11}) 24.82 s (C_6H_{11}) 23.03 s (C_6H_{11})

Coupling constants in Hz. [a] In parentheses J(H—P). [b] In parentheses J(P—P). [c] In parentheses J(C—P). (pst = pseudotriplet).

$(PMePh_2)_2]$.[5b] For the molybdenum compound the reaction is complete after stirring at room temperature for 1–2 h, but the tungsten system requires longer reaction times (5–6 h) and temperatures of around 60°C for completion. The new compounds prepared have been isolated as crystalline materials, of moderate stability to air in the solid state, but very sensitive in solution. As found for other related oxo complexes,[2,9–11] $[MoOCl_2(CNCMe_3)(PMe_3)_2]$ exists in two isomers, blue and green, with apparently the same ligand distribution and spectroscopic properties.

The presence of an isocyanide ligand in the molecule of the complexes is clearly inferred by the appearance of a characteristic absorption in the region 2150–2100 cm^{-1}, as well as by the observation of the corresponding ^1H and ^{13}C NMR resonances. On the other hand,the phosphine ligands give rise to a ^{31}P singlet, in the region −19 to −6 ppm, and to a virtually coupled triplet in the ^1H NMR spectrum. From these and other data, and by similarity with the structures found for other $MOCl_2L_3$ complexes, which have *cis*-chloride ligands,[10–11] structure **C** can be proposed for these oxo-isocyanide derivatives of molybdenum and tungsten.

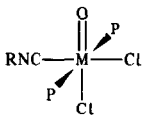

C

We have also attempted to prepare the carbonyl compounds $[MOCl_2(CO)(PMe_3)_2]$, by a route similar to that described above for the analogous isocyanide derivatives. The reaction of $[MOCl_2(PMe_3)_3]$ with CO, under a variety of experimental conditions (temperatures from 20 to 60°C, CO pressure of 1–5 atm) provided only unreacted starting material and decomposition products.

EXPERIMENTAL

Microanalyses were carried out by Pascher Microanalytical Laboratory, Bonn, Germany. IR spectra were recorded as Nujol mulls on Perkin–Elmer Models 577 and 684 instruments. ^1H, ^{13}C and ^{31}P NMR spectra were run on a Varian XL-200 instrument. ^{31}P NMR shifts are referenced to external 85% H_3PO_4. Conductivity measurements were carried out in acetonitrile solutions (*ca* 5×10^{-3} M) at 20°C.

All preparations and operations were carried out under oxygen-free nitrogen or argon, following the conventional Schlenk techniques. Solvents were dried by standard techniques and degassed before use. The compounds $[MOCl_2(PMe_3)_3]$ (M = Mo, W) were prepared according to the literature procedures[1,2] and so were the CNR[12] and PMe_3[13] ligands.

Preparation of $[MOCl_2(dmpe)PMe_3]$, (M = Mo, W)

To a stirred solution of $[MoOCl_2(PMe_3)_3]$ (0.41 g, *ca* 1 mmol) in 35 cm^3 of THF was added a stoichiometric amount of dmpe (0.2 cm^3, *ca* 1 mmol). The resulting solution was stirred at room temperature for 1–2 h. The solvent was evaporated under reduced pressure and the residue extracted with 20 cm^3 of a 1:1 mixture of THF : CH_2Cl_2. After centrifugation and cooling at −35°C dark blue crystals were collected, washed with Et_2O and dried *in vacuo*. Yield 85%. Found: C, 26.3; H, 6.0. Calc. for $C_9H_{25}P_3Cl_2OMo$: C, 26.5; 6.1%. IR (Nujol mull) bands at: 1410, 1295, 1280, 960, 950, 930, 900, 840 cm^{-1}. As indicated above (see Results and Discussion), we have been unable to isolate the tungsten complex $[WOCl_2(dmpe)(PMe_3)]$, in pure form, due to the facility with which it reacts with more dmpe to provide the bis-dmpe compound $[WOCl(dmpe)_2]Cl$. The mono-dmpe derivative can however be fully characterized by NMR studies (Table 1).

Preparation of $[MOCl(dmpe)_2]Cl$, (M = Mo, W)

1,2-bis (dimethylphosphine)ethane (0.2 cm^3 *ca* 1 mmol) was added to a solution of $[MoOCl_2(dmpe)(PMe_3)]$ (0.4 g *ca* 1 mmol) in 35 cm^3 of THF and the reaction mixture was stirred at room temperature for 2–3 h. When the reaction was complete a light red solution and a pink–purple finely divided solid resulted. This suspension was evaporated to dryness and the residue extracted with 20 cm^3 of CH_2Cl_2; further centrifugation and cooling at −35°C overnight produced the desired product as purple crystals in 70% yield. IR (Nujol mull) bands at: 1430, 1290, 1280, 950, 940, 900, 750, 720 cm^{-1}. Conductivity, $\Lambda_M = 110$ ohm^{-1} cm^2 mol^{-1}.

The complex $[WOCl(dmpe)_2]Cl$, was also similarly obtained as pink crystals in *ca* 72% yield. Found: C, 25.1; H, 5.7. Calc. for $C_{12}H_{32}P_4ClOW$: C, 25.3; H, 5.6%. IR (Nujol mull) bands at: 1430, 1290, 1285, 1150, 1060, 1000, 955, 940, 905, 850, 805, 755, 715, 650, cm^{-1}. Conductivity, $\Lambda_M = 108$ ohm^{-1} cm^2 mol^{-1}.

Synthesis of $MOCl_2(PMe_3)_2(CNR)$ *complexes* (M = Mo, R = CMe_3, C_6H_{11}; M = W, R = CMe_3)

t-Butylisocyanide (0.1 cm^3, *ca* 1 mmol) was added to a solution of $[MoOCl_2(PMe_3)_3]$ in benzene or toluene (40 cm^3), the reaction stirred for 1–2 h at room temperature and centrifuged. The resulting solution was evaporated almost to dryness and the residue extracted with Et_2O. A blue solid was separated by filtration from a green solution which was then evaporated to dryness. Crystallization of the residue from a 1:1 mixture of CH_2Cl_2:Et_2O, at −35°C afforded green crystals which were collected, washed with petroleum ether and dried *in vacuo*. Yield 65%.

The residual blue solid was dissolved in 30 cm^3 of CH_2Cl_2: Et_2O (1:1), the volume reduced *in vacuo* and the solution cooled at −35°C to give the blue complex in *ca* 20% yield.

Both green and blue isomers of $[MoOCl_2(PMe_3)_2(CNCMe_3)]$ have identical stoichiometry and spectral properties. Found: C, 31.6; H, 6.4. Calc. for $C_{11}H_{18}NP_2Cl_2OMo$: C, 31.6; H, 6.4%. IR (Nujol mull) bands at: 2120 (CNR), 1280, 1190, 955, 940, 815, 725 cm^{-1}.

Blue crystals of $[MoOCl_2(PMe_3)_2(CNC_6H_{11})]$ and pale violet crystals of $[WOCl_2(PMe_3)_2(CNCMe_3)]$ have been obtained by the same procedure in similar yields. Longer reaction times (*ca* 6 h) and higher temperatures (60°C) are however required for the tungsten complex.

$[MoOCl_2(PMe_3)_2(CNC_6H_{11})]$. IR (Nujol mull) bands at: 2150 (CNR), 1365, 1280, 1125, 950 cm^{-1}.

$[WOCl_2(PMe_3)_2(CNCMe_3)]$. Found: C, 26.2; H, 5.43. Calc. for $C_{11}H_{18}NP_2Cl_2OW$: C, 26.5; H, 5.4%. IR (Nujol mull) bands at: 2110 (CNR), 1415, 1285, 1200, 950, 860 cm^{-1}.

Acknowledgements—We are grateful to the Comisión Asesora de Investigación Científica y Técnica for support of this work, C.G-P. thanks the University of Marseille for leave of absence.

REFERENCES

1. E. Carmona, L. Sánchez, M. L. Poveda, R. A. Jones and J. G. Hefner, *Polyhedron* 1983, **2**, 797.
2. E. Carmona, A. Galindo, L. Sánchez, A. J. Nielson and G. Wilkinson, *Polyhedron* 1984, **3**, 347.
3. E. Carmona, A. Galindo, E. Gutierrez-Puebla, A. Monge and C. Puerta, *Inorg. Chem.* 1986, **25**, 3804.
4. E. Carmona, A. Galindo, C. Guille-Photin, R. Laï, A. Monge, C. Ruiz and L. Sánchez, *Inorg. Chem.* 1988, **27**, 488.
5. (a) L. K. Fong, F. R. Foz, B. M. Foxman and N. P. Cooper, *Inorg. Chem.* 1986, **25**, 1880; (b) F. M. Su, C. Cooper, S. J. Geib, A. L. Rheingold and J. M. Mayer, *J. Am. Chem. Soc.* 1986, **108**, 3545.
6. W. J. Geary, *Coord. Chem. Rev.* 1977, **7**, 81.
7. V. C. Adams, U. A. Gregory and B. T. Kilbourn, *J. Chem. Soc., Chem. Commun.* 1970, 1400.
8. M. W. Bishop, J. Chatt, J. R. Dilworh, M. B. Hursthouse and M. Montevalli, *J. Chem. Soc., Dalton Trans.* 1979, 1603.
9. A. V. Butcher and J. Chatt, *J. Chem. Soc. (A)* 1970, 2652.
10. L. Manojlovic-Muir, *J. Chem. Soc. (A)* 1971, 2796.
11. L. Manojlovic-Muir and K. W. Muir, *J. Chem. Soc., Dalton Trans.* 1972, 686.
12. G. W. Gokel, R. P. Widera and W. P. Weber, *Org. Synth.* 1976, **55**, 96.
13. W. Wolfsberger and H. Schmidbaur, *Synth. React. Inorg. Metal-Org. Chem.* 1977, **110**, 2382.

Polyhedron Vol. 7, No. 18, pp. 1773–1779, 1988
Printed in Great Britain

0277–5387/88 $3.00+.00
© 1988 Pergamon Press plc

FLUOROSILICATE EQUILIBRIA IN ACID SOLUTION

LIBERATO CIAVATTA,* MAURO IULIANO and RAFFAELLA PORTO

Dipartimento di Chimica dell'Università, Via Mezzocannone, 4, 80134 Napoli, Italy

(*Received* 22 *February* 1988; *accepted* 15 *March* 1988)

Abstract—The reaction between silicic acid and the fluoride ion in aqueous solution has been investigated at 25°C in a 3 m $(Li)ClO_4$ medium, by potentiometric methods employing a fluoride ion-selective electrode to observe the free hydrogen fluoride concentration. The acidity varied between 0.3 and 3 m, while the concentration of silicic acid was maintained below 2.5×10^{-3} m which is thought to be the saturation level of amorphous silica.

The experimental data have been explained in terms of $Si(OH)_3F$, SiF_4, SiF_6^{2-}, $HSiF_6^-$ and a minor species to which the composition $Si(OH)_2F^+$ has been tentatively assigned.

The reactions that occur between the fluoride ion and silicic acid in aqueous solution are poorly understood. The only species whose identity is well established from Raman and NMR spectroscopy[1] as well as potentiometric evidence[2] is SiF_6^{2-}. On the other hand, there are no definitive conclusions on equilibria involving the intermediate species of the type $Si(OH)_tF_n^{4-t-n}$ which may be formed. These are of considerable interest if a detailed and complete discription is to be made in naturally occurring systems, such as geothermal brines, where both the F^- ion and $Si(OH)_4$ are usually present.

Busey *et al.*[2] investigated the fluorosilicate equilibria in the acidity range 10^{-2}–10^{-6} m. Under these conditions, in addition to SiF_6^{2-}, a minor species, whose composition could not be uniquely defined, seems to be present in a small amount. The intermediate complexes are more conveniently examined by extending the acidity range to values higher than 10^{-2} m. In fact, the general reaction scheme

$$Si(OH)_4 + nHF \leftrightarrows Si(OH)_tF_n^{4-t-n} + pH^+ + sH_2O \quad (1)$$

clearly indicates that an acidity increase quenches the formation of SiF_6^{2-} and favours complexes bearing less than six fluoride ions which are produced with $p = 0$.

The aim of this investigation was that of studying the fluorosilicate equilibria at 25°C in the acidity range 0.3–3 m.

METHOD

The method consisted of the determination of the hydrogen fluoride concentration, a, using a fluoride ion-selective electrode (EF), in a series of solutions containing silicon(IV) and hydrofluoric acid in various amounts. To minimize the variation in the activity coefficients, the solutions were maintained at 3 m ClO_4^-, by adding $LiClO_4$. This salt, instead of $NaClO_4$, was chosen because of the premature precipitation of Na_2SiF_6 if a large excess of Na^+ is present. 3 m $LiClO_4$ was used as the reference state and consequently the activity coefficient of a reacting species is defined as tending to unity as the composition of the test solution approaches this pure salt solution.

The test solutions (TS) had the general composition B m Si(IV), A m F^-, H m H^+, $2B$ m Na^+, $(3-H-2B)$ m Li^+, 3 m ClO_4^- = TS.† The silicon

*Author to whom correspondence should be addressed.

† Symbols:

- a concentration of HF.
- A total fluoride ion concentration.
- B total Si(IV) concentration.
- $\beta_{p,n}$ equilibrium constant for the formation of $Si(OH)_tF_n^{4-n-t}$, eq. (1).
- h concentration of H^+.
- H analytical concentration excess of H^+, $= [ClO_4^-]-[Li^+]-[Na^+]$.
- K_n conditional constant for all species with n F^-, eq. (7).
- Z average number of fluoride ions bound per silicon(IV), $= (A-a-[F^-]-2[HF_2^-])/B$.

Concentrations and equilibrium constants are expressed in molal units.

concentration was varied from 0.65×10^{-3} to 2.5×10^{-3} m, which we believe is below the saturation level of amorphous silica. The H values were in the range 0.3–3 m. Under these conditions the F^- and HF_2^- ions attain negligible concentrations[3] compared to those of other fluoride-bearing species, so that Z could be calculated without knowledge of their exact concentrations.

The a values in TS were determined with cell(I)

$$-\text{EF/TS, Q}\cdot\text{QH}_2\text{(s)/Au}^+ \qquad \text{(I)}$$

where EF and $Q\cdot QH_2$ stand for the fluoride ion-selective electrode and quinhydrone, respectively. The EMF of cell(I) can be expressed at 25°C by

$$E = E_0' + 0.05916 \log (a\gamma_{HF}) + E_q \qquad (2)$$

in which E_0' is a constant, γ_{HF} is the activity coefficient of HF and E_q is a correction term for the basicity of *p*-benzoquinone.[4] In each experiment, carried out as by potentiometric titration, H was kept constant while Z was varied. Since $B < 0.01$ H, the composition of TS did not change sensibly to cause variations in γ_{HF} and E_q. Consequently, a could be calculated from eq. (3)

$$E = E_0 + 0.05916 \log a \qquad (3)$$

where $E_0 = E_0(H)$ includes γ_{HF} and E_q.

Each titration was divided into two parts. In the first, E_0 was determined in the absence of $Si^{(IV)}$. Under the chosen experimental conditions $[F^-]$ and $[HF_2^-]$ are negligible so that reliable E_0 values could be calculated by putting $a = A$ in eq. (3). E_0 values which are constant to within 0.1 mV were obtained in the A range from 10^{-4} to 4×10^{-3} m.

In the second part silicic acid was added and the complex formation was followed by increasing the A/B ratio. In a few instances the A/B ratio was decreased by adding $Si(OH)_4$ to the HF solutions. The coincidental nature of the data obtained in the forward and backward titrations served as the criterion for true equilibrium. With E_0 being known, a could be deduced from eq. (3) and the average number of fluoride ions bound per $Si^{(IV)}$, Z, could be obtained, neglecting $[F^-]$ and $[HF_2^-]$, as $Z = (A-a)/B$. The $Z(\log a, B)_H$ data form the basis of the following treatment.

EXPERIMENTAL

Materials and analysis

A freshly prepared silicic acid solution was employed for each experiment and no attempt was made to store stock solutions. The silicon source was "sodium metasilicate" $Na_2SiO_3\cdot 9H_2O$. The salt, dissolved in the minimum amount of water, was added in portions under vigorous stirring to an acidic medium with an H^+ excess. Prior to the addition of silicate the weight of the acid medium was about 90% of the final one. The resulting clear solution was immediately employed for the EMF measurements. Solutions after leaving for a few hours gave coinciding data within 0.2 mV. On the other hand, systematic deviations were observed with samples stored for two days.

$Na_2SiO_3\cdot 9H_2O$, Baker p.a., was used without purification. It was kept in a desiccator filled with the $Na_2SiO_3\cdot 9H_2O$ so that the vapour pressure remained constant and the silicate composition did not vary appreciably. The percentage of Na^+ was determined acidimetrically with standardized HCl. The amount of $Si^{(IV)}$ was established gravimetrically using silica insolubilization by repeated acid treatment. The analyses agreed to within 0.2%.

Lithium fluoride, lithium perchlorate and perchloric acid were prepared and analysed as described in previous publications.[5,6] The quinhydrone, Merck p.a., was recrystallized from water and dried over conc. H_2SO_4. No $Fe^{(III)}$ or Cl^- ions could be detected in the final product.

Details of the EMF measurements

The potentiometric titration was performed by immersing cell (I) in a silicone oil thermostat maintained at 25.00 ± 0.02°C. The fluoride electrode and apparatus were the same as described in a previous paper.[7] The EMF values were measured within ± 0.1 mV with a Keithly 195 system DMM multimeter. To measure the potential of the membrane electrode a preamplifier Analog Device 309 K was used. The constancy of the potential was reached 10 min after the addition of reagents and remained unchanged for several hours within 0.1 mV.

DATA AND CALCULATIONS

The $Z(\log a, B)_H$ data are collected in Table 1 and are graphically represented in Fig. 1. As this shows, the Z values for increasing a tend to six and the points, for a different B but the same H value, form a single curve. This means that we are dealing with mononuclear silicon complexes $Si(OH)_t F_n^{4-t-b}$ with $n \leqslant 6$. In order to assess the t, n and $\beta_{p,n}$ values of the predominating complexes, the data were processed as follows. Firstly, the number of F^- bound per $Si^{(IV)}$ and the conditional constants K_n were determined by considering separately data for a given H. Then, by examining the dependence of K_n on H the values of t and preliminary $\beta_{p,n}$ values were calculated. Finally, the equilibrium constants were

$H = 0.3$ m, $Z(-\log a, B \times 10^3)$

(a) 0.170 (3.100, 2.431); 0.192 (3.043, 2.421); 0.219 (2.988, 2.410); 0.261 (2.909, 2.391); 0.323 (2.838, 2.369); 0.411 (2.767, 2.341); 0.561 (2.691, 2.301); 0.745 (2.637, 2.260); 0.972 (2.591, 2.216); 1.25 (2.554, 2.168); 1.60 (2.514, 2.110); 2.03 (2.476, 2.046); 2.44 (2.444, 1.987); 2.93 (2.410, 1.922); 3.57 (2.368, 1.840); 4.03 (2.334, 1.782); 4.43 (2.302, 1.731); 4.84 (2.267, 1.677); 5.14 (2.229, 1.631); 5.37 (2.197, 1.593); 5.55 (2.162, 1.555); 5.75 (2.108, 1.500); 5.86 (2.054, 1.446); 5.93 (2.008, 1.397); 5.98 (1.952, 1.334); 5.85 (2.040, 1.653).

(b) 0.232 (2.980, 1.296); 0.294 (2.879, 1.284); 0.359 (2.814, 1.275); 0.410 (2.770, 1.267); 0.511 (2.721, 1.257); 0.604 (2.681, 1.247); 0.844 (2.618, 1.227); 1.25 (2.554, 1.199); 1.79 (2.498, 1.168); 2.68 (2.431, 1.120); 3.48 (2.377, 1.080); 4.28 (2.322, 1.039); 4.92 (2.265, 1.001); 5.41 (2.201, 0.963); 5.66 (2.143, 0.932); 5.80 (2.106, 0.911); 5.91 (2.027, 0.865); 5.42 (2.182, 1.382); 4.46 (2.290, 1.905); 2.91 (2.399, 2.992).

$H = 1.0$ m, $Z(-\log a, B \times 10^3)$

(a) 0.448 (2.716, 1.897); 0.595 (2.608, 1.882); 0.801 (2.552, 1.867); 1.09 (2.493, 1.849); 1.43 (2.444, 1.830); 1.78 (2.396, 1.810); 2.39 (2.344, 1.780); 3.01 (2.295, 1.749); 3.65 (2.244, 1.718); 4.36 (2.190, 1.682); 4.71 (2.136, 1.656); 5.13 (2.080, 1.626); 5.45 (2.018, 1.594); 5.63 (1.959, 1.565); 5.64 (1.915, 1.544); 5.80 (1.855, 1.508); 5.92 (1.798, 1.471); 6.01 (1.751, 1.437).

(b) 0.295 (2.880, 1.346); 0.404 (2.732, 1.337); 0.539 (2.669, 1.330); 0.797 (2.559, 1.317); 1.04 (2.507, 1.308); 1.47 (2.441, 1.294); 1.87 (2.384, 1.280); 2.48 (2.341, 1.264); 3.36 (2.267, 1.239); 4.15 (2.203, 1.215); 4.73 (2.131, 1.191); 5.21 (2.062, 1.167); 5.52 (2.023, 1.153).

$H = 3.0$ m, $Z(-\log a, B \times 10^3)$

0.248 (3.065, 1.866); 0.313 (2.956, 1.859); 0.372 (2.863, 1.852); 0.452 (2.769, 1.843); 0.538 (2.694, 1.834); 0.683 (2.603, 1.820); 0.876 (2.520, 1.804); 1.21 (2.432, 1.780); 1.55 (2.375, 1.760); 2.07 (2.306, 1.730); 2.52 (2.258, 1.705); 3.02 (2.209, 1.678); 3.64 (2.145, 1.642); 4.27 (2.071, 1.601); 4.64 (2.015, 1.570); 5.05 (1.942, 1.529); 5.37 (1.868, 1.484); 5.55 (1.810, 1.447).

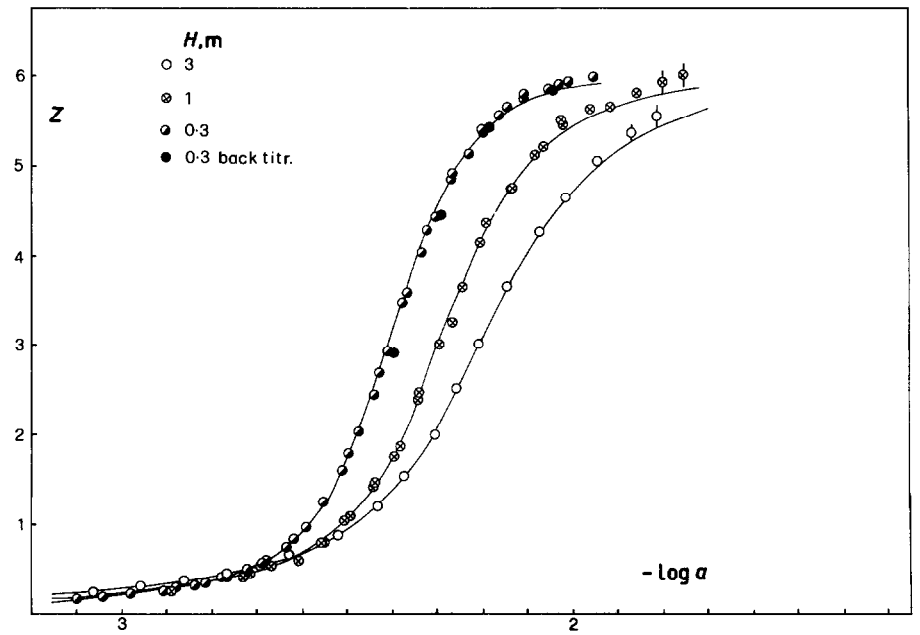

Fig. 1. Z, the average number of fluoride ions bound per silicon(IV), as a function of $\log a$, at three acidities. The experimental uncertainty is shown when it is significantly larger than the symbol used. The curves were calculated using the equilibrium constants of Table 3.

refined using numerical methods based on the principle of least-squares.

Treatment of data at constant H

In this section we consider data for every H value separately. If only mononuclear complexes are formed we may express Z as in eq. (4)

$$Z = \Sigma n\beta_{p,n}\Gamma_{p,n}h^{-p}a^n/(1+\Sigma\beta_{p,n}\Gamma_{p,n}h^{-p}a^n) \quad (4)$$

where n and p, $=n+t-4$, are integers, $\beta_{p,n}$ is the equilibrium constant for the formation of $Si(OH)_tF_n^{4-n-t}$, eq. (1) and $\Gamma_{p,n}$ stands for

$$\Gamma_{p,n} = \gamma_{HF}^{n}\gamma_{Si(OH)_4}\gamma_{H}^{-p}\gamma_{t,n}^{-1} \quad (5)$$

where γ is the activity coefficient. At a given H level, since $B < 0.01$ H, $\Gamma_{p,n}$ by good approximation is constant and furthermore, h must be very close to H. As a consequence, eq. (4) can be written as follows:

$$Z = \Sigma nK_n a^n/(1+\Sigma K_n a^n) \quad (6)$$

where

$$K_n = K_n(H) = \Sigma\beta_{p,n}\Gamma_{p,n}H^{-p}. \quad (7)$$

To determine n and K_n the experimental data were compared with model functions representing various hypotheses. Acceptable agreement was observed by assuming three complexes with $n = 1$, 4 and 6. The essential steps of the curve-fitting procedure are briefly described. Firstly, the P function, eq. (8), was constructed

$$\log P = \int_0^a Z\,\mathrm{d}\log a = \int_0^{a_0} Z\,\mathrm{d}\log a + \int_{a_0}^{a} Z\,\mathrm{d}\log a = \log(1+\Sigma K_n a^n) \quad (8)$$

where a_0 represents the lowest measured a value. $\int_{a_0}^{a} Z\,\mathrm{d}\log a$ was evaluated by the trapezoid rule, while the residual integral was found by extrapolation of the plot antilog ($\int_{a_0}^{a} Z\,\mathrm{d}\log a$) against a which was linear for the lowest three or four points.

Secondly, the $\log\{(P-1)/a\}(\log a)$ data were confronted with the normalized form $Y(\log u)_L$, eqs. (9)–(11), corresponding to the presence of complexes with $n = 1$, 4 and 6

$$Y = \log\{(P-1)/a\} - \log K_1 = \log(1+Lu^3+u^5) \quad (9)$$

$$\log u = \log a + (1/5)\log(K_6/K_1) \quad (10)$$

$$L = K_4K_1^{-2/5}K_6^{-3/5}. \quad (11)$$

The conditional constants given in Table 2 were computed, using eqs. (9)–(11), from the differences $Y-\log(P-1)+\log a$, $\log u-\log a$ and L which were read off at the position of best agreement.

More direct evidence for the presence of species with $n = 4$, instead of 3 or 5, was afforded by comparison of the data in the form of $\log\{[P(Z-1)+1]/a^6\}$ versus $\log a$, with the family of theoretical functions $F_N(\log w)$, eqs. (12) and (13), and calculated with $N = 3$, 4 and 5

$$F_N = \log(1+((N-1)/5)w^{(N-6)}) \quad (12)$$

$$K_NK_6^{-1}a^{(N-6)} = w^{(N-6)}. \quad (13)$$

The comparison of data at $H = 3$ m is shown in Fig. 2. Clearly, a good fit is observed only with $N = 4$, while systematic trends are produced by neighbours. The position of best agreement gave the K_4 and K_6 constants in Table 2.

Evaluation of the most probable t

To determine t we examined the dependence of K_n on H, according to eq. (7). The correct interpretation of the data requires the knowledge of how $\Gamma_{p,n}$ varies when Li^+ is replaced by H^+. Medium effects were estimated by the specific interaction theory.[8] For unchanged ionic strength and ClO_4^- molality, the activity coefficient of positively charged ions can be taken as constant. Activity coefficients for anions and for neutral molecules vary in the extent to which interactions with Li^+ and H^+ differ. Owing to the similarities of H^+ and Li^+, we postulated constant activity coefficients for anions and neutral species. Thus, $\Gamma_{p,n}$ equals unity in the medium scale.

As Table 2 indicates, K_4 within the limits of esti-

Table 2. Survey of the conditional K_n constants

H, m	$\log K_1$	$\log K_4$		$\log K_6$	
		eqs (9–11)	eqs (12, 13)	eqs (9–11)	eqs (12, 13)
0.3	2.45±0.02	9.46±0.1	9.48±0.1	14.65±0.03	14.60±0.05
1.0	2.52±0.03	9.39±0.1	9.30±0.1	13.97±0.03	14.00±0.05
3.0	2.59±0.02	9.40±0.1	9.37±0.1	13.44±0.03	13.45±0.05

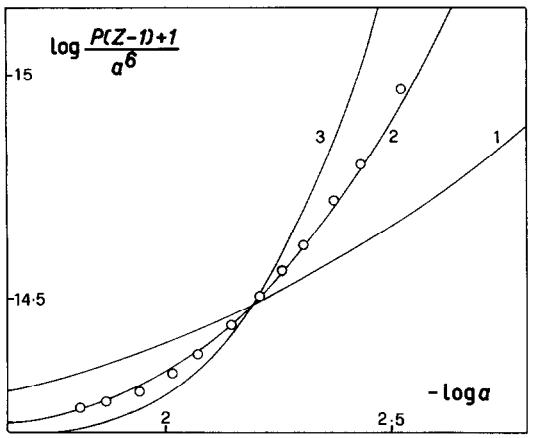

Fig. 2. Measurements at 3 m H^+. Comparison of $\log\{[P(Z-1)+1]/a^6\}$ versus $\log a$ with the family of model curves, eqs (12) and (13), calculated for $6-N=1$, 2 and 3.

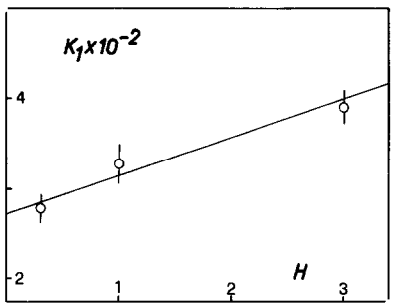

Fig. 3. K_1 as a function of H. The straight line represents $270+43H$.

mated error, does not depend on H, which means that SiF_4 is present. The average K_4 was taken as the preliminary $\beta_{0,4}$ value (Table 3).

On the other hand, K_1 varies slightly with H, hence species with $p \neq 0$ are also formed. The plot of K_1 versus H (Fig. 3) can be well approximated by a straight line, indicating the presence of $Si(OH)_3F$ and $Si(OH)_2F^+$. The $\beta_{0,1}$ and $\beta_{-1,1}$ values, evaluated from the intercept and slope of the best line drawn through the points, are given in Table 3.

The variation of K_6 with H was explained by the presence of $HSiF_6^-$ and SiF_6^{2-}. The validity of this hypothesis is demonstrated by the linear dependence of K_6H with H^{-1}, shown in Fig. 4. The $\beta_{1,6}$ and $\beta_{2,6}$ constants are listed in Table 3.

Refinement of the equilibrium constants

The equilibrium constants were refined by numerical procedures founded on the principles of least-squares, proposed by Sillén.[9] The computation consisted of minimizing the sum.

$$U = \Sigma(1-Z_c/Z)^2, \qquad (14)$$

in which Z_c indicates a value calculated with a given set of $\beta_{p,n}$. The results are given in Table 3. The constants are seen to differ insignificantly from those found graphically.

As a quantitative measure of the agreement between experimental data and the proposed model we considered the distribution of the deviations $(1-Z_c/Z)$. From a total of 95 data points, 59 showed an average positive deviation of 1.8%, whilst 36 showed a negative deviation of 2.1%. No systematic trend was observed in the H and Z functions.

CONCLUSION

The main result of the present investigation can be summarized by stating that in solutions where $0.3 \leqslant H \leqslant 3$ m the predominating fluorosilicate complexes are $Si(OH)_3F$, SiF_4, $HSiF_6^-$ and SiF_6^{2-}. The minor species, $Si(OH)_2F^+$ is tentatively suggested on the basis of small changes of K_1 with H. We feel that the assignment of such a complex calls for more detailed information about the medium effects caused by the substitution of $LiClO_4$ with $HClO_4$ on the variation of activity coefficients of neutral species ($Si(OH)_3F$ and HF).

Figure 5 illustrates the distribution of fluorosilicates as a function of the hydrofluoric acid concentration at different acidity levels. Clearly, if $Si(OH)_2F^+$ exists, it amounts to only 2% of the total $Si^{(IV)}$ at 1 m H^+. It is evident that the acidity promotes displacement of the curves representing SiF_6^{2-} and $HSiF_6^-$ so that room is left for intermediate species.

Table 3. Survey of equilibrium constants

	$\log\beta_{0,1}$	$\log\beta_{-1,1}$	$\log\beta_{0,4}$	$\log\beta_{1,6}$	$\log\beta_{2,6}$
Graphical	2.43±0.03	1.63±0.15	9.43±0.1	13.88±0.05	13.23±0.1
Least-squares (3σ)	2.40+0.01	1.66±0.10	9.35±0.03	13.88±0.03	13.23±0.06

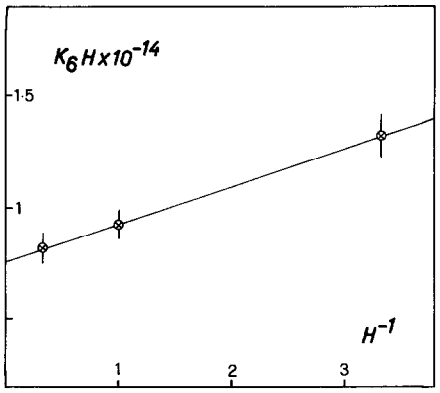

Fig. 4. K_6H as a function of H^{-1}. The line was calculated with $K_6H = 0.76 \times 10^{14} + 0.17 \times 10^{14} H^{-1}$.

COMPARISON WITH OTHER DATA

From the data of Busey *et al.*[2] at 25°C in 1 m NaCl, we calculate, using an equilibrium constant of $10^{2.89}$ for $H^+ + F^- \rightleftarrows HF$, $\log \beta_{2,6} = 12.4$ which, on account of medium differences, compares well with our 13.23. At the highest acidity studied by these authors, i.e. 10^{-2} m, SiF_4 is present in small amounts and explains its escape of detection. Also $Si(OH)_3F$ accounts for less than 12% of the total $Si^{(IV)}$. Owing to the difficulties of uniquely defining the composition of minor complexes, Busey *et al.* assigned the formula $Si(OH)_2F_2$ to this component.

Borodin and Kim Zao employed the ^{19}F NMR method to investigate Li_2SiF_6—$HClO_4$[10] as well as HF—SiO_2—$HClO_4$[11] solutions. The species SiF_4 and SiF_5^- were postulated. From the constants proposed by these authors we derived $\log \beta_{2,6} = 11.6$ and $\log \beta_{0,4} = 7.60$. The discrepancies of the constants in Table 3 are explainable in terms of the different ionic media and also from the neglect of $HSiF_6^-$ and $Si(OH)_3F$ species which are important components in the strongly acidic media employed by Borodin and Kim Zao.

Plakhotnik and Kotlyar[12] have determined the solubility of K_2SiF_6 as a function of the HCl concentration in a 0.4 M (Li)Cl medium. The data were explained with SiF_5^-. However, according to our findings, relatively high concentrations of $Si(OH)_4$, $[Si(OH)_3F]$ and SiF_4 would also be produced. The limited number of data points, six, makes the recalculation arduous.

There have been several reports on the solubility equilibria of amorphous silica in concentrated H_2SiF_6. Kleboth[13] measured the solubility of "precipitated" silicic acid as a function of H_2SiF_6 and $HClO_4$ concentration at 25°C in 4 M $LiClO_4$. From data at the highest concentrations of these components, where the main species are SiF_4 and $HSiF_6^-$, we evaluate for $SiO_2(s) + 2H^+ + 2HSiF_6^- \rightleftarrows 3SiF_4 + 2H_2O$ a constant of $10^{-2.5 \mp 0.3}$ which agrees fairly well with $10^{-2.4}$, obtainable from the data of Table 3, and the solubility of SiO_2, $\sim 10^{-2.7}$ m. On the contrary, the solubility determinations by Thomsen[14] and Ryss and Plakhotnik[15] indicate values which are three times greater than those predictable from our results. Plausible explanations are either the presence of additional complexes in concentrated H_2SiF_6 solutions, or highly active silica involved in the heterogeneous equilibria. The authors furnish no information on the composition or properties of the solid phase, thus making the comparison difficult.

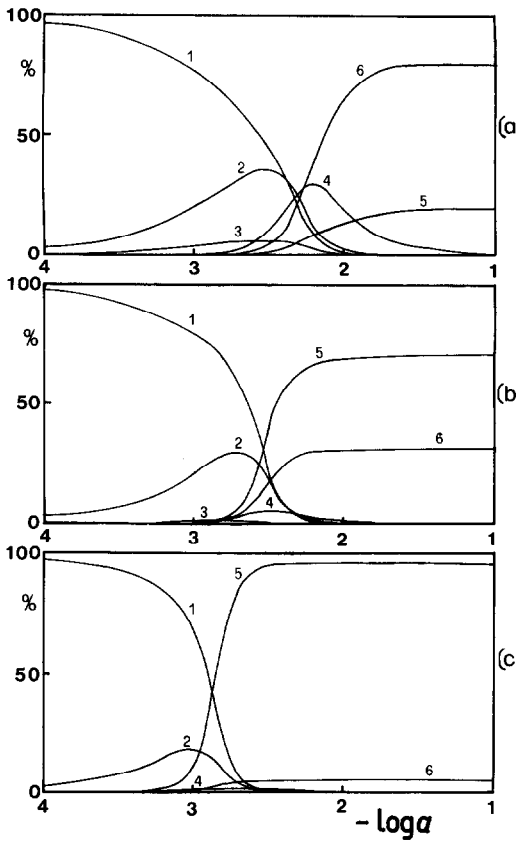

Fig. 5. Distribution of fluorosilicates as a function of the free hydrofluoric acid concentration. Results are shown for the following three acidities: (a) 1 m H^+ (b) 0.1 m H^+ and (c) 0.01 m H^+. (1) $Si(OH)_4$; (2) $Si(OH)_3F$; (3) $Si(OH)_2F^+$; (4) SiF_4; (5) SiF_6^{2-}; (6) $HSiF_6^-$.

Acknowledgement—This work was financially supported by Ministero della Pubblica Istruzione, Rome.

REFERENCES

1. P. A. W. Dean and D. F. Evans, *J. Chem. Soc., A* 1967, 698.

2. R. H. Busey, E. Schwartz and R. E. Mesmer, *Inorg. Chem.* 1980, **19**, 758.
3. L. Ciavatta, *Arkiv Kemi* 1963, **21**, 129.
4. G. Biedermann, *Acta Chem. Scand.* 1956, **10**, 1340.
5. L. Ciavatta, R. De Capua and R. Palombari, *J. Inorg. Nucl. Chem.* 1981, **43**, 1305.
6. L. Ciavatta, M. Iuliano and R. Porto, *Polyhedron* 1987, **6**, 1283.
7. L. Ciavatta and A. Pirozzi, *Polyhedron* 1983, **2**, 769.
8. L. Ciavatta, *Annal. Chim. (Rome)* 1980, **70**, 551.
9. L. G. Sillén, *Acta Chem. Scand.* 1962, **16**, 159.
10. P. M. Borodin and N. Kim Zao, *Russ. J. Inorg. Chem.* 1971, **16**, 1720.
11. P. M. Borodin and N. Kim Zao, *Russ. J. Inorg. Chem.* 1972, **17**, 959.
12. V. N. Plakhotnik and T. N. Kotlyar, *Russ. J. Phys. Chem.* 1976, **50**, 723.
13. K. Kleboth, *Monatsh Chem.* 1968, **99**, 1177.
14. S. M. Thomsen, *J. Am. Chem. Soc.* 1952, **74**, 1690.
15. I. G. Ryss and V. N. Plakhotnik, *Russ. J. Inorg. Chem.* 1970, **15**, 1742.

Polyhedron Vol. 7, No. 18, pp. 1781–1783, 1988
Printed in Great Britain

0277–5387/88 $3.00+.00
© 1988 Pergamon Press plc

COMMUNICATION

BENZOTRIAZOLATO COMPLEXES OF RUTHENIUM, OSMIUM, AND IRIDIUM: X-RAY CRYSTAL STRUCTURE OF (BENZOTRIAZOLE-BENZOTRIAZOLATO) CARBONYL(HYDRIDO)BIS(TRIPHENYLPHOSPHINE)OSMIUM(II)

BRUCE G. OLBY and STEPHEN D. ROBINSON*

Department of Chemistry, King's College, Strand, London WC2R 2LS, U.K.

and

MICHAEL B. HURSTHOUSE* and RICHARD L. SHORT

Department of Chemistry, Queen Mary College, Mile End Road, London E1 4NS, U.K.

(*Received* 18 *April* 1988; *accepted* 21 *April* 1988)

Abstract—The synthesis and characterization of new benzotriazole (btaH) complexes M(bta----H—bta)$_2$(btaH)(PPh$_3$) (N^2 and N^3-btaH linkage isomers), M(bta----H—bta)H(CO)(PPh$_3$)$_2$ (M = Ru or Os) and IrH$_2$(bta----H—bta)(PPh$_3$)$_2$, in which the H-bonded benzotriazolate anion–benzotriazole pair (bta----H—bta) functions as a novel N,N′-chelate ligand, are reported. The stereochemistry of the osmium complex Os(bta----H—bta)H(CO)(PPh$_3$)$_2$ and the nature of the bta----H—bta moiety therein have been confirmed by an X-ray crystal structure determination.

Benzotriazole (**I**) and its conjugate base, the benzotriazolate anion are formally cyclic analogues of 1,3-diphenyltriazene and the 1,3-diphenyltriazenide anion, respectively. However, by virtue of its cyclic nature, the benzotriazolate anion is unable to adopt the N^1N^3-chelate bonding mode encountered in many 1,3-diaryltriazenido complexes.[1] Speculation that the benzotriazolate anion might choose instead to bond in an η^3 fashion through all three nitrogen atoms when called upon to function as a four electron donor prompted us to attempt the synthesis of some benzotriazolato analogues of known platinum metal 1,3-diaryltriazenido chelates.[2,3] The first results of this work which centre upon the characterization of a new H-bonded benzotriazolate–benzotriazole composite ligand (**II**) are described in this communication.

Treatment of the complexes MCl$_2$(PPh$_3$)$_3$ with excess benzotriazole and triethylamine in boiling benzene (M = Ru) or toluene (M = Os) in each case affords a mixture of linkage isomers [M(bta---H—bta)$_2$(N^2-btaH)(PPh$_3$)] (**IIIa**) and [M(bta---H—bta)$_2$(N^3-btaH)(PPh$_3$)] (**IIIb**) as yellow or orange, air-stable crystals from dichloromethane/methanol. In the case of ruthenium the same isomer mixture can be obtained by treatment of RuH$_2$(PPh$_3$)$_4$ with benzotriazole in boiling benzene. Similar reactions of the dihydridocarbonyl complexes [MH$_2$(CO)(PPh$_3$)$_3$] with benzotriazole in boiling benzene (M = Ru) or toluene (M = Os) afford products of the form [M(bta---H—bta)H(CO)(PPh$_3$)$_2$] (**IVa/b**) as white air-stable microcrystalline solids. Finally, treatment of *mer*-IrH$_3$(PPh$_3$)$_3$ with benzotriazole in refluxing toluene yields [IrH$_2$(bta---H—bta)(PPh$_3$)$_2$ (**V**) as white air-stable crystals.

The stoichiometry and stereochemistry of the complexes have been determined in each case by elemental analysis (C, H, N) and by spectroscopic methods (IR and ^{1}H, ^{13}C and ^{31}P{^{1}H} NMR), the latter also established the asymmetric nature of the bta---H—bta moiety (**II**) and the presence of

* Authors to whom correspondence should be addressed.

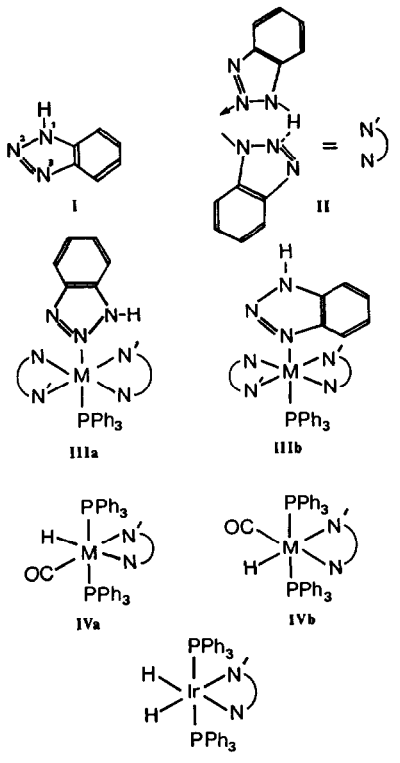

Scheme 1.

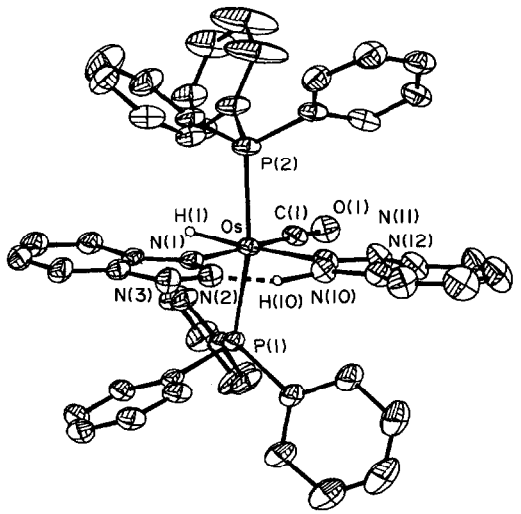

Fig. 1. The structure of Os(bta---H—bta)H(CO)$(PPh_3)_2$. Important bond lengths and angles are Os—P(1) 2.354(3), Os—P(2) 2.353(4), Os—C(1) 1.825(6), Os—N(1) 2.160(5), Os—N(11) 2.176(7), Os—H(1) 1.60(Fixed), N(10)—H(10) 1.265(66), N(2)---H(10) 1.474(76) Å.

the H-bonding interaction. Thus the high field ^{1}H NMR spectrum of the iridium complex $[IrH_2$(bta---H—bta)$(PPh_3)_2]$ displays two almost identical hydride signals [δH −18.84 (t of d), ^2J(PH) 16 Hz, ^2J(HH) 6 Hz, and δH −20.13 (t of d), ^2J(PH) 16 Hz, ^2J(HH) 6 Hz] indicative of a *cis* pair of hydride ligands in very similar environments, coupled to each other, and each in turn coupled to a pair of mutually equivalent ^{31}P nuclei. The H-bonded proton of the bta---H—bta ligand is thought to give rise to the broad signal which appears at δ 19.3.

In the case of the ruthenium and osmium complexes [M(bta---H—bta)H(CO)$(PPh_3)_2$] stereochemistry (**IVb**) was preferred over (**IVa**) because the former places the small hydride ligand adjacent to the more sterically demanding side of the bta---H—bta moiety. In order to confirm this assignment and to provide further information concerning the structure of the new H-bonded bta---H—bta chelating group an X-ray diffraction study has been performed on a crystal of the osmium complex [Os(bta---H—bta)H(CO)$(PPh_3)_2$].* A diagram of the structure, together with some important geometry parameters, is given in Fig. 1. All the structural assumptions made above are confirmed. The geometry of the N—H---N intramolecular link between the btaH and bta ligands is of particular interest. The strong H-bonding interaction is clearly asymmetric but results in a significant lengthening of the formal N–H σ bond.

*Crystal Data: $C_{49}H_{40}N_6O_1Os_1P_2$, $M = 981.042$, triclinic, $a = 10.059(4)$, $b = 11.876(1)$, $c = 20.629(3)$ Å, $\alpha = 74.57(1)$, $\beta = 83.08(2)$, $\gamma = 65.96(2)°$, $u = 2169$ Å^3, $Z = 2$, $D_c = 1.5016$ g cm^{-3}, space group $P\bar{1}$, Mo-K_α radiation, $\lambda = 0.71069$ Å, μ(Mo-K_α) = 29.1 cm^{-1}. Intensity data collected on an Enraf–Nonius CAD4 diffractometer, ω–2θ scan mode;[4] 8048 data recorded, 7608 unique, 6535 observed [$I > 1.5\sigma(I)$], empirical absorption correction. Structure solution by standard heavy atom methods, refinement by full-matrix least-squares. Non-hydrogen atoms anisotropic, all hydrogens freely isotropic, Os—H distance fixed at 1.60 Å for stable refinement. Final $R = 0.032$, $R_w = 0.0034$, 692 parameters, unit weights. Tables of atomic positional and displacement parameters, full lists of bond lengths and angles and F_o/F_c values have been deposited as supplementary material with the Editor, from whom copies are available on request. Atomic coordinates have also been deposited with the Cambridge Crystallographic Data Centre.

REFERENCES

1. For reviews of triazene and benzotriazole coordination chemistry see D. S. Moore and S. D. Robin-

son, *Adv. Inorg. Chem. Radiochem.* 1986, **30**, 1; *Adv. Inorg. Chem.* 1988, **32**, in press.
2. S. D. Robinson and M. F. Uttley, *J. Chem. Soc., Chem. Commun.* 1971, 1315.
3. K. R. Laing, S. D. Robinson and M. F. Uttley, *J. Chem. Soc., Dalton Trans.* 1974, 1205.
4. R. A. Jones, M. B. Hursthouse, K. M. A. Malik and G. Wilkinson, *J. Am. Chem. Soc.* 1979, **101**, 4128.

Polyhedron Vol. 7, No. 18, pp. 1785–1788, 1988
Printed in Great Britain

0277–5387/88 $3.00+.00
© 1988 Pergamon Press plc

COMMUNICATION

REACTION OF OXYGEN WITH A BINUCLEAR COBALT(II) HEXAPHOSPHINE COMPLEX. SINGLE-CRYSTAL X-RAY STRUCTURE OF AN EXTENDED CHAIN COBALT(II) HEXAPHOSPHINE OXIDE SYSTEM

SUZANNE E. SAUM and FREDRIC R. ASKHAM

Department of Chemistry, Washington University, St. Louis, MO 63130, U.S.A.

and

FRANK R. FRONCZEK and GEORGE G. STANLEY*

Department of Chemistry, Louisiana State University, Baton Rouge, LA 70803-1804, U.S.A.

(*Received* 22 *February* 1988; *accepted* 27 *April* 1988)

Abstract—Molecular oxygen reacts rapidly with $Co_2Cl_{4-x}(eHTP)^{x+}$ [$x = 0$ or 2; eHTP = $(Et_2PCH_2CH_2)_2PCH_2P(CH_2CH_2PEt_2)_2$] in dry acetonitrile to produce in approximately 66% yield the fully-oxygenated phosphine oxide eHTP (eHTP=O) Co(II) complex $[Co(eHTP{=}O)^{2+}][CoCl_4^{2-}]$. The X-ray structure on this novel system shows an extended chain system in which the monomeric repeating unit has an octahedral Co(II) centre. The eHTP=O ligand is adopting an unusual conformation with the phosphine oxide groups P(2)—P(1)—P(3) (P(1) is one of the internal phosphorus atoms) forming a P(1)—P(2) chelate to the metal atom while P(3) bridges to another $Co(eHTP{=}O)^{2+}$ monomer unit making up the extended chain, instead of acting as an independent bis chelating group. The third unique coordination site on the cobalt centre is occupied by a phosphine oxide group from the other half of the eHTP=O ligand which bridges over to the cobalt centre forming a facial set of three P=O donor ligands. This mixed bridging/chelating conformation gives rise to fused seven- and nine-membered ring systems with a Co—Co separation of 7.613(0) Å between symmetry related cobalt sites on the extended chain. This structure is the first reported for a $Co(R_3P{=}O)_6^{n+}$ (R = alkyl, phenyl) system.

Our investigations into the coordination chemistry of the hexaphosphine ligand, $(Et_2PCH_2CH_2)_2PCH_2P(CH_2CH_2PEt_2)_2$, eHTP, have demonstrated that it is a powerful binucleating agent for transition metal centres and we have characterized a number of dimer systems that exhibit a variety of coordination numbers, geometries and rotational conformations.[1–5] These structural and conformational studies have allowed us to gain a firmer understanding of the coordination properties and preferences of eHTP. The next stage in our investigations is to study the reactivities of M_2(eHTP) dimers to see if bimetallic cooperative effects can be observed and extended to catalytic cycles. The simple cobalt(II) dimer, $Co_2Cl_{4-x}(eHTP)^{x+}$ ($x = 0$ or 2), was the first eHTP complex characterized[1] and now we would like to report on its clean reaction with molecular oxygen to produce the first crystallographically characterized cobalt peralkylphosphine oxide complex.

Two equivalents of $CoCl_2$ react quantitatively

* Author to whom correspondence should be addressed.

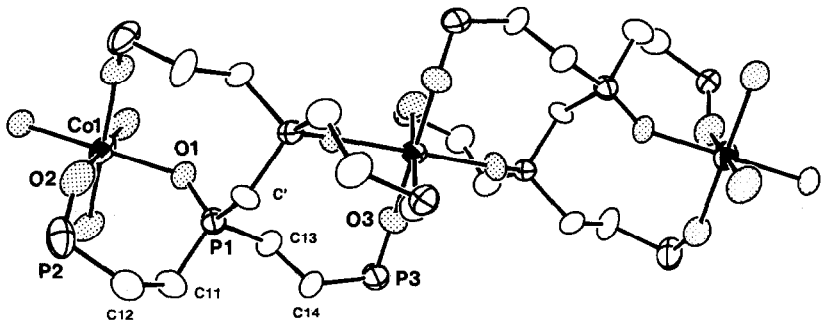

Fig. 1. ORTEP plot of a portion of the extended chain structure that is made up of $Co(eHTP{=}O)^{2+}$ repeating units. Thermal ellipsoids are shown at the 50% probability level. The cobalt atom lies on an inversion centre and a two-fold rotation axis passes through the central methylene group (C′) of the eHTP=O ligand. The ethyl groups on the terminal phosphorus atoms have been omitted for clarity.

with eHTP to produce either the red–brown five-coordinate dimer, $Co_2Cl_4(eHTP)$ or the blue–green four-coordinate tetrahedral complex, $Co_2Cl_2(eHTP)^{2+}$ depending on the solvent used.[1] Both of these compounds react rapidly with molecular oxygen in dry acetonitrile (distilled from CaH_2 under N_2) to produce blue paramagnetic solutions. Column chromatography allows the isolation of two species: a minor blue component representing *ca* 33% yield and a major blue species in *ca* 66% yield.* A single-crystal X-ray structure determination† on the major component revealed the presence of a Co(II) hexaphosphine oxide complex, $[Co(eHTP{=}O)^{2+}][CoCl_4^{2-}]$, where eHTP=O stands for the fully oxygenated eHTP ligand. An ORTEP plot of a portion of the extended chain cation species is shown in Fig. 1 and selected bond distances and angles are listed in Table 1.

The cationic Co(1) centre sits on a crystallographic inversion centre and has six phosphine oxide ligands from eHTP=O coordinated in a slightly distorted octahedral environment. The maximum distortion from octahedral geometry in the cobalt coordination sphere is the O(1)—Co(1)—O(2) angle of 85.6(2)°. The Co—O bond distances are quite uniform and lie in the 2.10–2.12 Å range. The eHTP=O ligand lies on a crystallographic two-fold rotation axis that passes through the central methylene bridge. The eHTP=O ligand is adopting an unusual conformation in which the phosphine oxide groups P(2)—P(1)—P(3), instead of acting as an independent bis chelating group to one Co atom, span the two cobalt centres to give a P(1)—P(2) chelate to one metal atom while P(3) bridges to the other metal centre. This gives rise to fused seven- and nine-membered ring systems for the $Co_2(eHTP{=}O)$ moiety. This is directly related to the conformation seen for the Cr(III) dimer *mer,mer*-$Cr_2Cl_6(eHTP)$.[4] The principal difference between the chromium dimer and this cobalt system, apart from the presence of P=O groups, is that the eHTP ligand in *mer,mer*-$Cr_2Cl_6(eHTP)$ adopts a planar *meridional* coordination geometry about the metal centres, while here the eHTP=O ligand is in a *facial* configuration.

The extended chain structure shown in Fig. 1 is made up of monomeric $Co(eHTP{=}O)^{2+}$ repeating units. Three of the facial P=O coordination sites

* A fibrous cellulose column was used and packed in THF solvent. The crude complex was applied in acetonitrile solution and precipitated onto the top of the column by addition of THF. A minor blue band was eluted with a 1:3 mixture of methanol/THF. Elution of the main blue fraction was performed with a 2:3:5 methanol/THF/acetonitrile mixture. X-ray quality crystals of the major blue component were obtained by very slow evaporation of an acetonitrile solution. Satisfactory elemental analysis was obtained for the BPh_4^- salt.

† X-ray data was collected on an Enraf–Nonius CAD4 diffractometer at room temperature using Cu-K_α radiation and a graphite crystal monochromator by $\theta/2\theta$ scan technique using variable speed scanning rates. Data reduction included corrections for background, Lorentz and polarization effects, as well as an empirical absorption correction (μ(Cu-K_α) = 119.24 cm^{-1}) based on ψ scans of reflections near $\chi = 90°$. Monoclinic $C2/c$ space group: $a = 16.960(2)$, $b = 19.480(1)$, $c = 14.457(1)$ Å, $\beta = 122.68(2)°$, $V = 4020(2)$ Å^3, $Z = 4$. The structure was solved by a combination of Patterson and Direct Methods techniques and refined to $R = 0.049$ and $R_w = 0.071$ based on 1538 unique data with $F_o^2 > 3\sigma(F_o^2)$. Atomic coordinates, bond lengths and angles, and thermal parameters have been deposited at the Cambridge Crystallographic Data Centre. See Notice to Authors, Issue No. 1, 1988.

Table 1. Selected bond distances (Å) and angles (deg) for $[Co(eHTP{=}O)^{2+}]$ $[CoCl_4^{2-}]$

Co(1)—Co(1)	7.613(0)	P(2)—C(12)	1.807(8)
Co(1)—O(1)	2.105(4)	P(2)—O(2)	1.511(6)
Co(1)—O(2)	2.105(5)	P(2)—C(21)	1.91(2)
Co(1)—O(3)	2.123(5)	P(2)—C(23)	1.809(9)
Co(2)—C(11)	2.292(2)	P(3)—O(3)	1.503(5)
Co(2)—C(12)	2.248(2)	P(3)—C(14)	1.800(7)
P(1)—O(1)	1.495(4)	P(3)—C(31)	1.771(9)
P(1)—C′	1.794(5)	P(3)—C(33)	1.88(1)
P(1)—C(11)	1.796(7)	C(11)—C(12)	1.56(1)
P(1)—C(13)	1.792(7)	C(13)—C(14)	1.52(1)
O(1)—Co(1)—O(1)	180.(0)	O(3)—P(3)—C(14)	111.5(3)
O(1)—Co(1)—O(2)	94.4(2)	O(3)—P(3)—C(31)	114.5(5)
O(1)—Co(1)—O(2)	85.6(2)	O(3)—P(3)—C(33)	115.3(4)
O(1)—Co(1)—O(3)	91.2(2)	Co(1)—O(1)—P(1)	138.4(3)
O(1)—Co(1)—O(3)	88.8(2)	Co(1)—O(2)—P(2)	137.8(3)
O(2)—Co(1)—O(2)	180.(0)	Co(1)—O(3)—P(3)	138.7(3)
O(2)—Co(1)—O(3)	91.6(2)	P(1)—C′—P(1)	116.9(5)
O(2)—Co(1)—O(3)	88.4(2)	P(1)—C(11)—C(12)	118.5(5)
O(3)—Co(1)—O(3)	180.(0)	P(2)—C(12)—C(11)	116.2(6)
O(1)—P(1)—C′	112.3(3)	P(1)—C(13)—C(14)	117.4(5)
O(1)—P(1)—C(11)	116.4(3)	P(3)—C(14)—C(13)	112.8(5)
O(1)—P(1)—C(13)	110.2(3)		

Numbers in parentheses are estimated standard deviations in the least significant digits.

on Co(1) are from one eHTP=O ligand while the other three octahedral sites are occupied by the P=O groups from the other "empty" half of an adjacent $Co(eHTP{=}O)^{2+}$ molecule. The chains have a helical twist making them chiral, but both right- and left-handed chains exist in the unit cell. The Co(1)—Co(1) separation is 7.613(0) Å making this the largest M—M separation yet observed for an open-mode eHTP type system. The $CoCl_4^{2-}$ counterion lies on a crystallographic two-fold axis with a Co(1)—Co(2) separation of 7.5535(7) Å. While there are a number of $Co(R_3P{=}O)_x^{2+}$ complexes known, with coordination numbers of four, five and six,[6] we were quite surprised to find that this is the first crystal structure of a peralkylphosphine oxide cobalt system, or, for that matter, any $M(R_3P{=}O)_6^{n+}$ compound except for $Cu[Ph_2P(O)CH_2P(O)Ph_2]_3^{2+}$.[7] There are, however, a few related phosphate (PO_4^{3-}),[8] phosphonato $[(RO)_2PO]$,[9] phosphinamide $[Ph_2P(O)(N)]$[10] and alkylphosphoramide $[(NR_2)_2P(O)OP(O)(NR_2)_2]$[11] structures known in transition metal systems.

After seeing the X-ray structure we suspected that the eHTP ligand could be simply dissociating in solution to be directly oxidized by O_2. While we knew that eHTP was air-sensitive, we had never actually exposed it to O_2 to see how fast and to what level it would be oxidized. Preliminary studies demonstrate that while eHTP does indeed react with O_2 it is *not* a particularly fast reaction and that after four days it has only been *partially* oxidized. This can be contrasted with the oxidation of $Co_2Cl_2(eHTP)^{2+}$ which is complete after a few hours. This points to a metal mediated oxygen transfer reaction, similar to that seen by Hanzlik in the Co(II) catalysed oxidation of electron-rich phosphines such as Bu_3P.[12] Yet, there are differences between Hanzlik's $Co(acac)_2$ system and $Co_2Cl_2(eHTP)^{2+}$: most notable is the production of significant (20–30%) amounts of $(BuO)Bu_2P{=}O$ and other oxidation products with $Co(acac)_2$ which result from free-radical pathways.

Our reaction, on the other hand, appears to be extremely clean and this may result from the fact that we are starting with a binuclear system that can readily form the μ-peroxide bridged dimer that Hanzlik proposed in his mechanism. The ready availability of a second metal centre in $Co_2Cl_2(eHTP)^{2+}$ could significantly reduce the presence of mononuclear Co—O—O$^{\cdot}$ species that can start competing in radical processes. It should be pointed out, however, that the stoichiometric oxidation of $CoCl_2(PEt_3)_2$ to produce $CoCl_2(O{=}PEt_3)_2$ is believed *not* to proceed through

any binuclear intermediates and is not affected by radical traps.[13] Further reactivity and solution studies in this system will be reported in a future full paper.

Acknowledgement—We would like to thank the National Science Foundation (Grant CHE-8613089) for generous support of this research.

REFERENCES

1. F. R. Askham, E. C. Marques and G. G. Stanley, *J. Am. Chem. Soc.* 1985, **107**, 7423.
2. S. A. Laneman and G. G. Stanley, *Inorg. Chem.* 1987, **26**, 1177.
3. S. E. Saum and G. G. Stanley, *Polyhedron* 1987, **6**, 1803.
4. F. R. Askham, A. W. Maverick and G. G. Stanley, *Inorg. Chem.* 1987, **26**, 3963.
5. S. E. Saum, F. R. Askham, F. R. Fronczek and G. G. Stanley, *Organometallics* 1988, **7**, 1409.
6. (a) M. W. G. de Bolster and R. J. F. Jans, *Z. Anorg. Allg. Chem.* 1982, **488**, 207; (b) M. W. G. de Bolster, C. Boutkan, T. A. van der Knaap and L. van Zweeden, *Z. Anorg. Allg. Chem.* 1978, **443**, 269; (c) C. M. Mikulski, J. S. Skryantz, N. M. Karayannis, L. L. Pytlewski and L. S. Gelfand, *Inorg. Chim. Acta* 1978, **27**, 69; (d) N. M. Karayannis, C. M. Milulski, M. J. Strocko, L. L. Pytlewski and M. M. Labes, *Inorg. Chim. Acta* 1974, **8**, 91; (e) N. M. Karayannis, E. E. Bradshaw, L. L. Pytlewski and M. M. Labes, *J. Inorg. Nucl. Chem.* 1970, **32**, 1079; (f) L. Sacconi and R. Morassi, *J. Chem. Soc. A* 1970, 575; (g) N. S. Angerman and R. B. Jordan, *Inorg. Chem.* 1969, **8**, 2579; (h) N. M. Karayannis, C. Owens, L. L. Pytlewski and M. M. Labes, *J. Inorg. Nucl. Chem.* 1969, **31**, 2767.
7. K. B. Yatsimirskii, Y. T. Struchkov, A. S. Batsanov and E. I. Sinyavskaya, *Koord. Khim.* 1985, **11**, 826.
8. (a) R. Cini, M. Sabat, M. Sundaralingam, M. C. Burla, A. Nunzi, G. Polidori and P. F. Zanazzi, *J. Biomol. Struc. Dynam.* 1983, **1**, 633; (b) M. Sabat, R. Cini, T. Haromy and M. Sundaralingam, *Biochemistry* 1985, **24**, 7827.
9. (a) V. Harder, E. Dubler and H. Werner, *J. Organomet. Chem.* 1974, **71**, 427; (b) P. T. Miller, P. G. Lenhert and M. D. Joesten, *Inorg. Chem.* 1973, **12**, 218.
10. E. E. Castellano, G. Oliva, J. Zukerman-Schpector, G. Vicentini and L. R. F. de Carvalho, *Inorg. Chim. Acta* 1985, **109**, 33.
11. M. D. Joesten, M. S. Hussain and P. G. Lenhert, *Inorg. Chem.* 1970, **9**, 151.
12. R. P. Hanzlik and D. Williamson, *J. Am. Chem. Soc.* 1976, **98**, 6370.
13. D. D. Schmidt and J. T. Yoke, *J. Am. Chem. Soc.* 1971, **93**, 637.

Polyhedron Vol. 7, No. 18, p. 1789, 1988
Pergamon Press plc. Printed in Great Britain

BOOK REVIEW

Gmelin Handbook of Inorganic Chemistry, Cu–organocopper Compounds. Cu–copper/System No. 60. Published by Gmelin Institute for Inorganic Chemistry of the Max Planck Society for the Advancement of Science, 8th Edn. Springer, Berlin, 1987. ISBN 3-540-93559-2, viii + 244 pp., DM 1189.

The organocopper compounds are finding increasing use in organic synthesis. The mononuclear compounds carrying one carbon-bonded ligand were listed in Vols 1 (1985), 2 (1983), and 3 (1986), and mononuclear compounds carrying two or more organic ligands, as well as all dinuclear to octanuclear and polymeric compounds were covered in Vol. 4 (1987). In all, some 3000 compounds are listed.

This volume provides the index to these previous four parts. The first 108 pages comprise an empirical formula index for the compounds, then the individual ligands are indexed in 136 pages. This will greatly enhance the accessibility of the work to chemists who wish to use organocopper reagents.

PROF A. G. DAVIES

Department of Chemistry
University College London
20 Gordon Street
London WC1H 0AJ, U.K.

Polyhedron Vol. 7, No. 19/20, p. 1791, 1988
Pergamon Press plc. Printed in Great Britain

FOREWORD

It is an honour and a pleasure to contribute this foreword to the special issue honouring our Editor-in-Chief on his retirement from the chair of Inorganic Chemistry at Imperial College, a position which he has held with such great distinction for 32 years including the time since it was established as the Edward Frankland Chair in 1978. During this period of continuous creativity in research he has received many awards and honours both nationally (FRS, 1965; Knighthood, 1976) and internationally, but pride of place must surely go to the award of the Nobel Prize for Chemistry which he shared with Professor E. O. Fischer in 1973.

When I sought his permission over a year ago to proceed with this special issue he demurred vehemently on the grounds that it was inappropriate for him as Editor-in-Chief to approve of such action and "in any case he did not hold with such nonsense"—typical Geoff! However, the relentless pressure from members of the Editorial Board and from his many former co-workers in favour of this special issue proved to be irresistible and we decided on this one occasion to over-ride our Editor-in-Chief. The list of Geoffrey's publications at the end of the issue is truly impressive both in the scope and originality of the research covering transition metal chemistry in general and organometallic chemistry in particular, but it would be premature to assess his contributions to inorganic chemistry at this stage because he is continuing with unabated vigour to devote himself to research in what we trust will be a long and fruitful "retirement". Another remarkable feature of the list is the number of eminent inorganic chemists who are featured as co-authors by virtue of studying for their Ph.D. degrees or doing postdoctoral research under Geoff's guidance, and it is a wonderful tribute to the great man that so many have been able to contribute original papers at rather short notice to this special issue. I am indebted to Professor Malcolm Green for his invaluable help in organizing this "Festschrift".

In choosing a title for this special issue, we could think of none more apposite than his favourite greeting to his research co-workers—"What's new, then?" It typifies his constant quest for the novel and exciting results which are his hallmark.

Finally, I would like to express my own appreciation of Geoff's leadership as Editor-in-Chief of *Polyhedron* which carried us triumphantly through the initial turbulent times to our present steady progress as one of the leading international journals covering inorganic chemistry.

DON BRADLEY
EXECUTIVE EDITOR

Polyhedron Vol. 7, No. 19/20, pp. 1793–1799, 1988
Printed in Great Britain

0277–5387/88 $3.00+.00
© 1988 Pergamon Press plc

STRUCTURE OF THE DINUCLEAR COMPOUND $[Mo_2(C_5H_5)_2(CO)_4(\mu\text{-}Ph_2PCH_2PPh_2)]$ IN THE CRYSTAL AND IN SOLUTION*

KAZI A. AZAM, ANTONY J. DEEMING† and MARK S. B. FELIX

Department of Chemistry, University College London, 20 Gordon Street, London WC1H 0AJ, U.K.

and

PAUL A. BATES and MICHAEL B. HURSTHOUSE†

Department of Chemistry, Queen Mary College, Mile End Road, London E1 4NS, U.K.

Abstract—The synthesis of $[Mo_2(\eta\text{-}C_5H_5)_2(CO)_4(\mu\text{-dppm})]$ (**1**) (dppm = $Ph_2PCH_2PPh_2$) from the parent hexacarbonyl, its spectra, and X-ray structure are reported. The Mo—Mo bond [3.327(1) Å] is significantly longer than in known related compounds such as the corresponding $^tBuPHCH_2PH^tBu$ compound [3.2109(4) Å] or the parent hexacarbonyl [3.235(1) Å]. The previously reported $^tBuPHCH_2PH^tBu$ compound and the dppm compound (**1**) have different conformations about the Mo—Mo bond in the crystal, having *gauche* and *anti* arrangements of the cyclopentadienyl ligands, respectively. Compound (**1**) exists in solution in these two rotameric forms in equilibrium, interconverting rapidly enough above room temperature to give NMR coalescence. The equilibrium between these rotamers was studied by variable temperature ^1H and ^{31}P NMR spectroscopy.

The molybdenum complex $[Mo_2(\eta\text{-}C_5H_5)_2(CO)_6]$ has only terminal CO ligands both in the solid[1,2] and in solution.[2,3] The crystal contains the *anti* rotamer (A) (Fig. 1) with the cyclopentadienyls remote from each other. This is also present in solution but the IR spectrum contains more than the expected three IR-active ν(CO) absorptions and the presence of a second rotamer accounts for extra absorptions. This minor rotamer is in higher concentration in solvents of high dielectric constant and at higher temperature. Its geometry was not unambiguously established but it is probably rotamer (C) rather than (B) or (D) (Fig. 1) based on the expected stabilities of these isomers. The conversion of (A) to (C) is via (B) so that (B) is accessible but of higher energy than the other two forms. The totally eclipsed rotamer (D) is presumed to be the least stable and there is no evidence for its existence.

Stelzer *et al.* have synthesized the substituted derivatives $[Mo_2(\eta\text{-}C_5H_5)_2(CO)_4(\text{diphosphine})]$ by the addition of the diphosphine to $[Mo(\eta\text{-}C_5H_5)_2(CO)_4]$, where the diphosphine is either $Me_2PCH_2PMe_2$ or various related ligands with one or two secondary phosphorus atoms.[4] A configuration related to that of (C) (Fig. 1) is found in the crystal structure of $[Mo_2(\eta\text{-}C_5H_5)_2(CO)_4(\mu\text{-}^tBuPHCH_2PH^tBu)]$.[4] This is only one of two observed isomers of this compound but this isomerism derives from the different possible configurations at phosphorus rather than from rotation about the Mo—Mo bond as with the parent hexacarbonyl. When the phosphorus atoms do not have different possible configurations, isomers are not found. Thus $[Mo_2(\eta\text{-}C_5H_5)_2(CO)_4(\mu\text{-}Me_2PCH_2PMe_2)]$ exists in a single isomeric form.[4] The IR spectra of all these related diphosphine compounds previously described[4] contain only two ν(CO) absorptions in solution consistent with only one rotameric form.

We now describe the synthesis, structure and spectroscopy of the compound $[Mo_2(\eta\text{-}C_5H_5)_2(CO)_4(\mu\text{-dppm})]$ (dppm = $Ph_2PCH_2PPh_2$), which appears not to have been reported before. Rota-

*We wish to dedicate this paper to Professor Sir Geoffery Wilkinson on the occasion of his retirement in appreciation of his pioneering work on cyclopentadienyl and tertiary phosphine ligands.

† Authors to whom correspondence should be addressed.

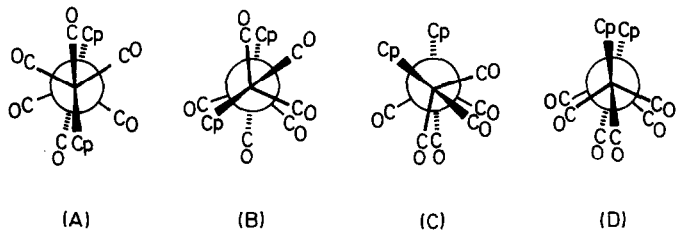

Fig. 1. Rotamers of $[Mo_2(\eta\text{-}C_5H_5)_2(CO)_6]$.

mers are present in solution and the single isomer found in the crystal does not correspond with that observed in the crystal structure of the 'BuPHCH$_2$PHBu' analogue.

RESULTS AND DISCUSSION

Preparation and spectroscopic analysis of $[Mo_2(\eta\text{-}C_5H_5)_2(CO)_4(dppm)]$ **(1)**

The direct reaction between $[Mo_2(\eta\text{-}C_5H_5)_2(CO)_6]$ and tertiary phosphines is quite complex, giving simple substitution products in a few cases (PPh_3, PCy_3 or $P(OR)_3$) but commonly giving the salts $[Mo(\eta\text{-}C_5H_5)(CO)_2L_2][Mo(C_5H_5)(CO)_3]$.[5,6] A better procedure is to add the tertiary phosphines to the decarbonylated compound $[Mo_2(\eta\text{-}C_5H_5)_2(CO)_4]$ and this occurs usually without cleavage of the Mo—Mo bond.[4,7,8] We have synthesized $[Mo_2(\eta\text{-}C_5H_5)_2(CO)_4(\mu\text{-dppm})]$ **(1)** in this way by adding dppm to a solution of the tetracarbonyl prepared *in situ* from the hexacarbonyl. The IR spectrum of **(1)** contains four ν(CO) absorptions [ν(CO) (CH_2Cl_2) 1913(s), 1872(vs), 1835(sh), 1817(s) cm^{-1}] unlike the spectrum of the $Me_2PCH_2PMe_2$ analogue which gives two absorptions [ν(CO) (CH_2Cl_2) 1850, 1805 cm^{-1}] as do the whole series of diphosphine complexes synthesized by Stelzer *et al.*[4] Since there are obviously structural differences, we have determined the single crystal X-ray structure of compound **(1)** to confirm that dppm is bridging and to establish the rotameric form in the crystal.

X-ray structure of $[Mo_2(\eta\text{-}C_5H_5)_2(CO)_4(dppm)]$ **(1)**

Addition of heptane to a solution of **(1)** in dichloromethane gave deep red–brown crystals suitable for X-ray structure determination. The molecular structure is shown in Fig. 2 and selected bond lengths and angles are given in Table 1. The mol-

Table 1. Selected bond lengths (Å) and angles (°) for the compound $[Mo_2(C_5H_5)_2(CO)_4(dppm)]$ **(1)**

Mo(1)—Mo(2)	3.327(1)	P(1)—Mo(1)	2.430(3)
C(1)—Mo(1)	1.939(6)	C(2)—Mo(1)	1.946(6)
C(30)—Mo(1)	2.358(6)	C(31)—Mo(1)	2.421(6)
C(32)—Mo(1)	2.380(6)	C(33)—Mo(1)	2.323(6)
C(34)—Mo(1)	2.304(6)	P(2)—Mo(2)	2.445(3)
C(35)—Mo(2)	2.352(6)	C(36)—Mo(2)	2.426(6)
C(37)—Mo(2)	2.370(6)	C(38)—Mo(2)	2.311(6)
C(39)—Mo(2)	2.296(6)	C(5)—P(1)	1.856(5)
C(6)—P(1)	1.841(5)	C(12)—P(1)	1.834(6)
C(5)—P(2)	1.832(5)	C(18)—P(2)	1.853(5)
C(24)—P(2)	1.848(5)	C(1)—O(1)	1.157(6)
C(2)—O(2)	1.170(6)	C(3)—O(3)	1.156(6)
C(4)—O(4)	1.150(5)		
P(1)—Mo(1)—Mo(2)	79.6(1)	C(1)—Mo(1)—Mo(2)	129.9(2)
C(1)—Mo(1)—P(1)	79.3(2)	C(2)—Mo(1)—Mo(2)	68.1(2)
C(2)—Mo(1)—P(1)	110.6(2)	C(2)—Mo(1)—C(1)	77.9(3)
P(2)—Mo(2)—Mo(1)	79.7(1)	C(3)—Mo(2)—Mo(1)	123.8(2)
C(3)—Mo(2)—P(2)	79.3(2)	C(4)—Mo(2)—Mo(1)	67.5(2)
C(4)—Mo(2)—P(2)	117.5(2)	C(4)—Mo(2)—C(3)	77.7(3)
C(5)—P(1)—Mo(1)	121.4(2)	C(5)—P(2)—Mo(2)	115.3(2)

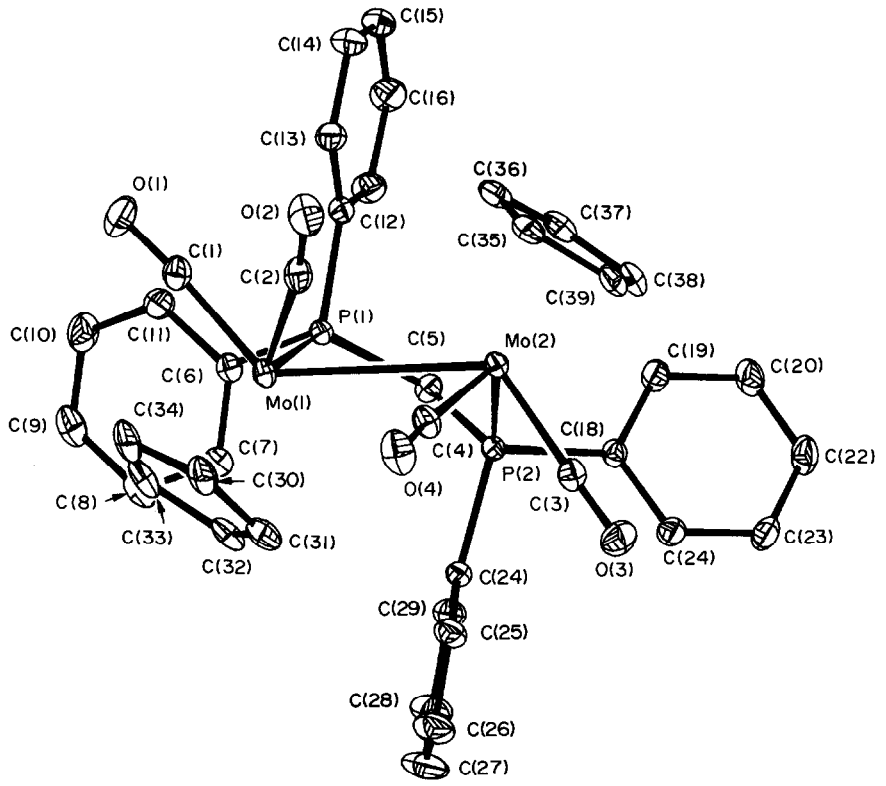

Fig. 2. Molecular structure of $[Mo_2(\eta\text{-}C_5H_5)_2(CO)_4(\mu\text{-dppm})]$ (**1**).

ecule has approximate (non-crystallographic) C_2 symmetry and the isolated molecule would contain equivalent C_5H_5 ligands, equivalent P atoms and equivalent CH_2 protons. There is a Mo—Mo bond [3.327 Å] but this is rather longer than in other related dimolybdenum compounds (see below).

The structure of a closely related diphosphine complex, $[Mo_2(C_5H_5)_2(CO)_4(^tBuPHCH_2PHBu^t)]$ (**2**), has been determined previously.[4] This molecule has crystallographic C_2 molecular symmetry but a different rotamer from that of (**1**) is found. Figure 3 compares the crystal structures of compounds (**1**) and (**2**), showing projections perpendicular to the Mo—Mo direction to emphasize their conformational differences. In each compound there is a considerable P—Mo—Mo—P torsional angle [42.9° for (**1**) and 54.4(2)° for (**2**)] and similar chiral five-membered Mo_2P_2C rings are found in each but with a rather greater deviation from planarity in (**2**).

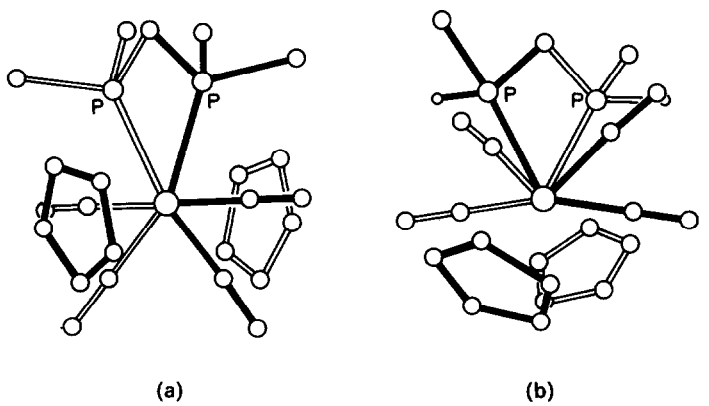

Fig. 3. A comparison of the rotamers in the solid state found for (a) $[Mo_2(C_5H_5)_2(CO)_4(dppm)]$ (**1**) and for (b) $[Mo_2(C_5H_5)_2(CO)_4(^tBuPHCH_2PH^tBu)]$[4] (**2**) viewed along the Mo—Mo direction. The phosphines are shown with a single atom for each substituent at phosphorus. The front Mo atom has filled bonds and the rear Mo atom (obscured) has open bonds.

The geometries of these Mo_2P_2C rings are different from the normal envelope structure (with a carbon flap) normally found when the P—M—M—P torsional angle is close to zero.[9] The main difference between (**1**) and (**2**) (Fig. 3) is in the rotameric form found in each case. In (**1**) the cyclopentadienyl ligands are *anti* to each other whereas in (**2**) they are *gauche*. The *anti* and *gauche* isomers are interconvertable by rotation about the Mo—Mo bond. Thus an anticlockwise rotation of the front Mo coordination sphere of (**1**) (Fig. 3) by approximately 90° about the Mo—Mo bond with respect to the rear Mo atom, requiring an inversion of the puckered five-membered Mo_2P_2C ring, would produce a geometry like that of (**2**). The *anti* and *gauche* forms are both chiral and there is another pair of isomers that are enantiomeric with those shown in Fig. 3, but note that rotation about the Mo—Mo bond does not allow enantiomerization.

It is not clear to us why the different diphosphines give different rotamers in the crystal. The Mo—Mo distance in (**1**) [3.327(1) Å] is longer than that in (**2**) [3.2109(4) Å][4] which is close to that in $[Mo_2(C_5H_5)_2(CO)_6]$ [3.235(1) Å].[1,2] Probably the lengthening in (**1**) compared to (**2**) is because secondary phosphines have been replaced by tertiary phosphines and the associated increase in crowding more than compensates for not having a ^{t}Bu substituent in (**1**). The dppm ligand is therefore the bulkiest diphosphine studied and repulsive interligand forces lead to the Mo—Mo bond lengthening. Assuming that steric pressure is the cause of the Mo—Mo bond length increase, clearly crowding could also have a major effect on rotamer stabilities, but it is not easy to assess this with confidence. Certainly there are quite small energy differences between the rotamers of compound (**1**) in solution so that any theoretical argument for structural preferences is difficult.

Rotameric forms of $[Mo_2(\eta\text{-}C_5H_5)_2(CO)_4(dppm)]$ (**1**) *in solution*

Compound (**1**) has approximate C_2 molecular symmetry in the crystal and the P atoms would be expected to be equivalent in solution. However, two $^{31}P\{^1H\}$ NMR singlets of unequal intensity are observed for dichloromethane solutions at room temperature and below (Fig. 4). We assume that the more intense signal, the one that becomes increasingly predominant at lower temperatures, belongs to the *anti* isomer. At −90°C the other (*gauche*) isomer accounts for only 3% of the material, rising to 30% at −10°C. This assumes that the form found in the crystal is that which predominates in solution. From the temperature-variation of isomer

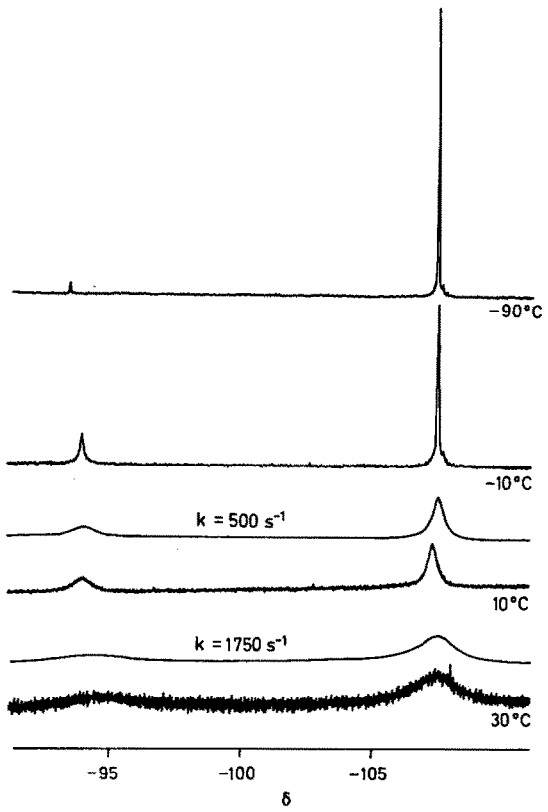

Fig. 4. $^{31}P\{^1H\}$ NMR spectra of $[Mo_2(C_5H_5)_2(CO)_4$ (dppm)] in CD_2Cl_2/CH_2Cl_2 mixtures at different temperatures. Spectra simulated with the given rates for *gauche* to *anti* conversion are shown above the spectra for 10 and 30°C. Chemical shifts relative to $P(OMe)_3$.

concentrations illustrated in Fig. 5, we derived $\Delta H^0 = (12.6 \pm 0.4)$ kJ mol^{-1} (FTNMR spectra recorded with time-delays of 5 and 20 s gave essentially the same relative intensities so we believe that the compositions obtained by the integration given in

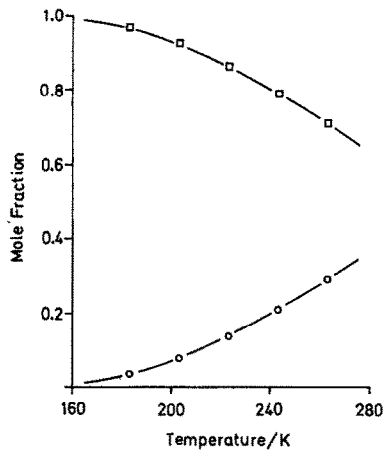

Fig. 5. Dependence of the composition of compound (**1**) in CD_2Cl_2/CH_2Cl_2 mixtures with temperature. □ corresponds to (**1a**) and ○ to (**1b**).

Fig. 5 are reliable). The corresponding value for ΔH^0 for the *anti–gauche* equilibrium for $[Mo_2(\eta\text{-}C_5H_5)_2(CO)_6]$ is much lower (1.8 ± 0.4 kJ mol^{-1}),[3] while for other diphosphines it must have a higher value (with the *gauche* form the more stable) since this is the only isomer observed.[4]

The ^{31}P NMR signals for (1) begin to broaden at -10°C and are very broad at 30°C. Figure 4 shows two computer-simulated spectra[10] at these higher temperatures but we have not examined a sufficiently wide temperature range to obtain full activation parameters. Instead we can just quote $\Delta G^{\ddagger}_{263} = (54.6 \pm 0.8)$ kJ mol^{-1} and $\Delta G^{\ddagger}_{303} = (55.4 \pm 0.8)$ kJ mol^{-1} for the *gauche* to *anti* process. These values compare with $\Delta G^{\ddagger} = (63 \pm 3)$ kJ mol^{-1} for the corresponding rotational barrier in the unsubstituted parent molecule $[Mo_2(\eta\text{-}C_5H_5)_2(CO)_6]$.[3] The rotational barrier is not increased by the need to invert the puckered Mo_2P_2C ring in (1).

^{1}H NMR spectra support the conclusions from ^{31}P NMR. At -60°C the major (*anti*) isomer has signals at δ 5.22 (s, C_5H_5) and 4.34 (t, CH_2) and the minor (*gauche*) isomer at δ 4.49 (s, C_5H_5) and 5.11 (t, CH_2). The proportion of the minor isomer increases with temperature, coalescence occurs at around 10°C and two signals (apart from the Ph signals) are observed at δ 4.80 (C_5H_5) and 4.71 (CH_2) at 53°C. At this temperature the isomers are in similar abundance as judged from the frequencies of the coalesced signals.

Since the IR spectrum of $[Mo_2(C_5H_5)_2(CO)_4(Me_2PCH_2PMe_2)]$ (which exists as only one isomer) exhibits only two ν(CO) absorptions at 1855 and 1805 cm^{-1} (CH_2Cl_2),[4] our observation of four absorptions for (1) at 1913(s), 1872(vs), 1835(sh) and 1817(s) cm^{-1} (CH_2Cl_2) seem to confirm the presence of isomers. For example, we considered assigning the absorptions at 1872 and 1817 cm^{-1} to the *anti* and those at 1913 and 1835 cm^{-1} to the *gauche* isomer. However, the solid spectrum (KBr or Nujol) and those in various solvents (Fig. 6) all contain the same four absorptions. If the above assignments were correct, the solid sample would have to be a mixture of *anti* and *gauche* crystals and we must have selected just one (the *anti*) for structure determination. This interpretation is incorrect since a single well-formed crystal known to contain one isomer gave the same IR (Nujol) spectrum as that of a microcrystalline sample. Therefore the four absorptions correspond to one isomer but this requires the *anti* and *gauche* isomers to have indistinguishable spectra, or the spectrum to be totally dominated by that of the major isomer.

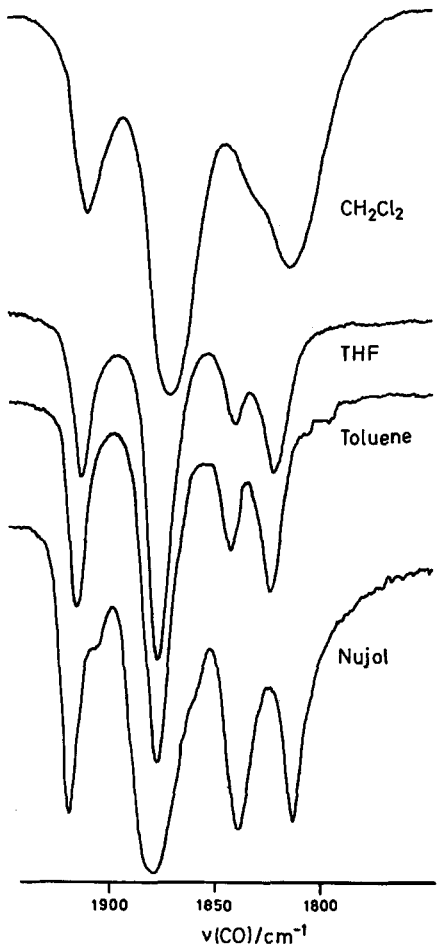

Fig. 6. IR spectra of (1).

We propose the conformation changes in Fig. 7 for the conversion of *anti* to *gauche* rotamers

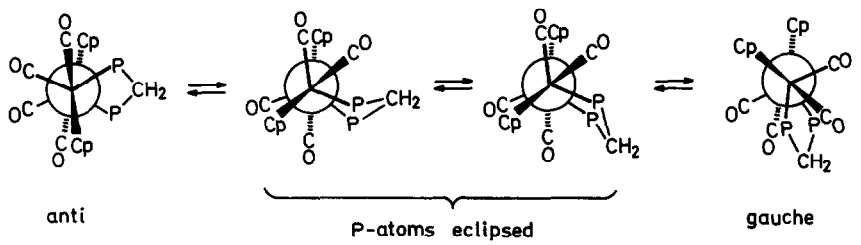

Fig. 7. Proposed isomers of (1) showing how they may be interconverted by rotation about the Mo—Mo bond with inversion of the five-membered Mo_2P_2C ring. There is a second pair of isomers enantiomeric with these.

(corresponding to the crystal structures of compounds (**1**) and (**2**), respectively). A rotamer with eclipsed phosphorus atoms corresponding to (B) (Fig. 1) is a required intermediate. The two representations of this intermediate shown with the envelope flaps in different directions are exactly the same isomer (rotation of one molecule will allow its superimposition on the other). The interconversion of these species by flapping of the CH_2 group will exchange the non-equivalent cyclopentadienyl ligands and methylene hydrogen atoms. This will require very little energy and is unlikely to add much to the overall activation energy in the *anti* to *gauche* conversion.

EXPERIMENTAL

Synthesis of $[Mo_2(\eta\text{-}C_5H_5)_2(CO)_4(dppm)]$

This was prepared essentially the same as other related diphosphine complexes[4] except that the tetracarbonyl was prepared *in situ* from the hexacarbonyl and was not isolated. $[Mo_2(C_5H_5)_2(CO)_6]$ (0.511 g) was heated for 39 h under nitrogen in sodium-dried toluene (50 cm^3) to give a dark red solution containing about 70% $[Mo_2(C_5H_5)_2(CO)_4]$. The solution was cooled and treated with $Ph_2PCH_2PPh_2$ (dppm) (0.442 g) in toluene (10 cm^3). The solution was stirred for 1 h and filtered through silica gel to remove some red–black residues and the product was isolated by crystallization as a dark red–brown solid (0.32 g) from a dichloromethane–heptane mixture. The surface of the solid appears red–brown but clear maroon–red solutions in dichloromethane were obtained. Crystals suitable for the X-ray study were obtained by the addition of hexane to a concentrated dichloromethane solution and allowing this mixture to stand for 60 h. Of the three or four suitable crystals obtained, one was chosen for the X-ray study and another for an IR spectrum. IR [ν(CO)]: (Nujol) 1920(s), 1880(vs), 1840(s), 1814(s); (KBr) 1913(s), 1873(vs), 1837(s), 1815(s); (toluene) 1917(s), 1878(vs), 1844(ms), 1825(s); ($CHCl_3$) 1915(s), 1874(vs), 1835(sh), 1816(s); (CH_2Cl_2) 1913(s), 1872(vs), 1835(sh), 1817(s); (THF) 1915(s), 1878(vs), 1842(ms), 1823(s) cm^{-1}.

Crystallographic studies

Crystal data. $C_{39}H_{32}Mo_2O_4P_2$, $M = 818.51$, monoclinic, space group $P2_1/n$, $a = 17.529(3)$, $b = 18.189(6)$, $c = 10.815(2)$ Å, $\beta = 98.03(1)°$, $U = 3414(1)$ $Å^3$, $Z = 4$, $D_c = 1.592$ g cm^{-3}, $\lambda = 0.71069$ Å, $F(000) = 1648$, μ(Mo-K_α) = 8.5 cm^{-1}, crystal size $0.76 \times 0.45 \times 0.45$ mm.

Data collection. Unit cell parameters and intensity data were obtained by previously detailed procedures,[11] using a CAD4 diffractometer operating in the ω–2θ scan mode with graphite-monochromated Mo-K_α radiation. A total of 5984 unique reflections were collected ($3 \leqslant 2\theta \leqslant 50°$). The segment of reciprocal space scanned was (h) -20 to 20, (k) 0 to 21, (l) 0 to 12. The reflection intensities were corrected for absorption using the azimuthal-scan method;[12] maximum transmission factor 1.00, minimum value 0.93.

Solution structure and refinement. The structure was solved by routine heavy-atom methods (SHELX-86[13]) and refined by full-matrix least-squares (SHELX-76[14]). All non-hydrogen atoms were refined anisotropically. Phenyl and ethyl hydrogen atoms were allowed to ride on the carbon atoms to which they are attached (C—H 0.96 Å). Group isotropic temperature factors for these hydrogen atoms were allowed to refine. Hydrogen atoms of the cyclopentadienyl rings were not included in the model. The final residuals R and R_w were 0.028 and 0.032, respectively for the 5096 data for which $F_o > 6\sigma(F_o)$. The function minimized was $\Sigma_w(|F_o| - |F_c|)^2$ with the weight, w, being defined as $1/[\sigma^2(F_o) + 0.00008F_o^2]$. Atomic scattering factors and anomalous scattering parameters were taken from refs 15 and 16, respectively. All computations were made on a DEC VAX-11/750 computer. Final atomic coordinates, tables of thermal parameters, full tables of bond lengths and angles, selected intramolecular non-bonded distances, and listings of observed and calculated structure factors have been deposited with the Editor as supplementary material. The atomic coordinates have also been deposited with the Cambridge Crystallographic Data Centre.

Acknowledgements—We thank the S.E.R.C. for support of the X-ray work, and the British Council for Research Fellowship and Jahangirnagar University for leave of absence (for K.A.A.).

REFERENCES

1. F. C. Wilson and D. P. Shoemaker, *J. Chem. Phys.* 1957, **27**, 809.
2. R. D. Adams, D. M. Collins and F. A. Cotton, *Inorg. Chem.* 1974, **13**, 1086.
3. R. D. Adams and F. A. Cotton, *Inorg. Chim. Acta* 1973, **7**, 153.
4. D. J. Brauer, G. Hasselkuss and O. Stelzer, *J. Organomet. Chem.* 1987, **321**, 339.
5. R. J. Haines, R. S. Nyholm and M. B. H. Stiddard, *J. Chem. Soc.* (*A*) 1968, 43.
6. R. B. King and P. N. Kapoor, *J. Organomet. Chem.* 1969, **18**, 357.

7. R. J. Klinger, W. M. Butler and M. D. Curtis, *J. Am. Chem. Soc.* 1975, **97**, 3535.
8. M. D. Curtis and R. D. Klinger, *J. Organomet. Chem.* 1978, **161**, 23.
9. R. J. Puddephatt, *Chem. Soc. Rev.* 1983, **12**, 99.
10. D. A. Kleier and G. Binsch, DNMR3 program for calculating line-shapes for exchanging systems. University of Notre Dame, Indiana (1969).
11. M. B. Hursthouse, R. A. Jones, K. M. A. Malik and G. Wilkinson, *J. Am. Chem. Soc.* 1979, **101**, 4128.
12. A. C. T. North, D. C. Phillips and F. S. Mathews, *Acta Cryst. Sect. A* 1968, **24**, 351.
13. G. M. Sheldrick, SHELX-86 Program for Crystal Structure Solution. University of Göttingen (1986).
14. G. M. Sheldrick, SHELX-76 Program for Crystal Structure Determination and Refinement (1976).
15. D. T. Cromer and J. B. Mann, *Acta Cryst. Sect. A* 1968, **24**, 321.
16. D. T. Cromer and D. Liberman, *J. Chem. Phys.* 1970, **53**, 1891.

Polyhedron Vol. 7, No. 19/20, pp. 1801–1806, 1988
Printed in Great Britain

0277–5387/88 $3.00+.00
© 1988 Pergamon Press plc

THE TRIS(HEXASULPHIDO)PLATINATE(IV) ION: SEVEN-MEMBERED CHELATE RINGS

REIJO SILLANPAA

Department of Chemistry, University of Turku, 20500 Turku, Finland

and

PETER S. CARTWRIGHT and R. D. GILLARD*

Department of Chemistry, University College, P.O. Box 78, Cardiff CF1 1XL, Wales, U.K.

and

JUSSI VALKONEN

Department of Chemistry, University of Jyvaskyla, 41000, Jyvaskyla, Finland

Abstract—$[(C_6H_5)_4P]_2[Pt(S_6)_3]$ was isolated from solutions of $[N(C_2H_5)_4]_2PtS_{17}$ or $(NH_4)_2[PtS_{17}]\cdot 2H_2O$ in acetone and characterized by determining its crystal structure: its unique anion contains three seven-membered chelate rings.

Free sulphur occurs in many areas and has been known since ancient times, for example in the destruction of Sodom and Gomorrah by brimstone and the use of sulphur as a fumigant by the Egyptians. Gunpowder, discovered by Bacon in 1245, containing sulphur, charcoal and saltpetre mixed in the weight ratio 20:15:75, was the only ammunition propellant used until the 1850s. Some 90% of sulphur is converted into sulphuric acid. Sulphur and sulphuric acid have been detected in the atmosphere of Venus, and metallic and superconducting polymers $(SN)_x$ are being studied.

Base metal sulphides, the main carriers of precious metal minerals in hydrous silicate deposits, form part of the Merensky Reef: platinum group metals concentrate[1] at the periphery of interstitial sulphides. Metal sulphides play an important role in industrial (hydrodesulphurization of fossil fuels) and enzymic (nitrogen fixation and electron transfer) catalysis. The S_5^{2-} ion is believed to be the favoured species during the sulphur rich stages of the discharge of the sodium–sulphur battery, which is of much current industrial interest.

Polysulphide complexes

Recent interest concerning polysulphides and their solutions follows the pioneering work by the great German coordination chemist K. A. Hofmann. He reported the syntheses[2] of $(NH_4)CuS_4$, $(NH_4)AuS_3$, $(NH_4)_3[IrS_{15}]$, $(NH_4)_2[PdS_{11}]\cdot 1/2H_2O$ and $(NH_4)_2[PtS_{15}]\cdot 2H_2O$. The structure of the pentekaidekakissulphidoplatinate(IV) ion in $(NH_4)_2[PtS_{15}]$ was determined[3] by Jones and Katz, who showed the octahedral coordination of three bidentate pentasulphido (S_5^{2-}) ligands around the central Pt^{IV}, confirming a suggestion[4] by Sidgwick. Wickenden and Krause reported[5] improved syntheses of platinum and palladium compounds and prepared rhodium polysulphides. They prepared $[NPr_4]_2[PtS_{10}]$, following degradation of $(NH_4)_2[PtS_{15}]$ with cyanide,[6] and Krause reported[6] a new polysulphido complex of rhodium, $(NH_4)_3[RhS_{15}]$, followed by a detailed summary[7] of the preparation of $(NH_4)_2[PtS_{15}]$, $(NH_4)_3[RhS_{15}]$, $(NPr_4)_2[PtS_{10}]$ and $(NH_4)_2[PdS_{11}]\cdot 2H_2O$ together with its crystal structure.[8] The palladium ions are linked by S_6^{2-} chains, with no individual $[PdS_{11}]^{2-}$ groups; some absences of sulphur in the structure account for the stoichiometry.

*Author to whom correspondence should be addressed.

Gillard and Wimmer resolved[9] $[Pt(S_5)_3]^2$ by forming diastereoisomers with optically active $[RuLL_3]^{2+}$ (LL = bpy or phen), a rare case of purely inorganic optical activity and the first such compound with a third row transition element. This $[PtS_{15}]^{2-}$ ion shows (using[10] ^{195}Pt NMR spectroscopy) two conformations (both all chair, one C_1 and one C_3) separated by an energy barrier of 50.5 kJ mol^{-1}.

Use of non-aqueous solvents has given many interesting polysulphides. Muller has produced several complexes such as the novel $[(C_2H_5)_4N]_3[Cu_3S_{18}]$,[11] with a central Cu_3S_3 ring and three outer CuS_6 groups, $(PPh_4)_2[Ag_2(S_6)_2]$,[12] the 10-membered ring systems $(PPh_4)[AgS_9]$, $[(PPh_3)_2N][AgS_9]$,[13] and $(PPh_4)[AuS_9]$,[14] which show the remarkable catenating properties of sulphur. $(PPh_4)_4[Ag_2S_{20}]\cdot S_8$ and $(PPh_4)_4[Cu_2S_{20}]$ (which contain bridging S_8^{2-} ligands) have also been synthesized[15,16] together with $(PPh_4)_2[Au_2S_8]$,[14] a 10-membered highly symmetrical ring system with the Au^I adopting a preferred linear coordination, and[14] various $[Cu_4S_x]^{2-}$ anions (x = 13–15).

However, although the S_6^{2-} ion is well enough known, as in $[enH_2](S_6)$,[17] and although a few such compounds as "$\{H[Rh(DMG)_2S_6]\}_n$"[18] and [2,8]$[NH_4]_2[PdS_{11}]\cdot 1/2H_2O$ contain it as a ligand with transition metals, seven-membered rings, like chelate rings $[MS_6]^{(n-2)+}$ containing M^{n+} ions are rare. They include[19] $[Zn(S_6)_2]^{2-}$. There seems to be no previous case where M is a transition metal ion.

We report here the first example of a most unusual structure, a compound of the octahedral homoleptic tris(hexasulphido)platinate(IV) ion $(PPh_4)_2[Pt(S_6)_3]$, containing three such seven-membered rings.

RESULTS AND DISCUSSION

The desired product was obtained unexpectedly. When, in our first experiments, the *tetraethylammonium* salt[20] $[N(C_2H_5)_4]_2[Pt(S_{17})]$ was dissolved in acetone and Ph_4PBr was added, over two months a few, very small, red crystals appeared, which were in fact a salt of the $Pt(S_6)_3^{2-}$ ion. We repeated the preparation using the *ammonium* salt[20] and describe this in detail.

A solution (initially 12.3 mmolar) of the known compound $(NH_4)_2[PtS_{17}]\cdot 2H_2O$ in acetone on treating with successive aliquots of $[PPh_4]Br$ (up to a final 10% molar excess), and allowing to crystallize over a total of five days gave successive crops of $[PPh_4]_2[Pt(S_6)_3]$ and $[PPh_4]_2[Pt(S_5)_3]$ (this a known compound[21,22]), in a total mole ratio of 2:1. Most (78%) of the initial platinum was recovered.

This almost certainly represented the slow dismutation

$$3[PtS_{17}]^{2-} \rightarrow 2[PtS_{18}]^{2-} + [PtS_{15}]^{2-}$$

rather than a mere separation of a mixture for the following reasons:

(a) Most (78%) of the initial platinum is recovered, so we are not simply concentrating one minor component of a mixture.

(b) We have used various conditions in mixing tetraphenylphosphonium bromide with salts of $[PtS_{17}]$ in acetone. If it were really a matter of exceeding the solubility product of the two-thirds of the platinum now present as $[PPh_4]_2[PtS_{18}]$, we would expect approximately similar yields of this salt in about the same time. This was not found; we have obtained either very few crystals or a large number of them.

(c) All samples of $(NH_4)_2[PtS_{17}]\cdot 2H_2O$ have[20] the same solubility in water and the same X-ray powder pattern, strongly suggesting that it is a single compound.

(d) We made two salts of $[PtS_{17}]^{2-}$, the ammonium salt dihydrate and the tetraethylammonium salt, the anions of which have[20] very similar properties (such as molar extinction coefficients).

(e) The *ammonium* salt of $[PtS_{17}]^{2-}$, the starting compound, is[20] strongly optically active. We have never obtained good enough crystals for single crystal work, but clearly, the space group must be acentric. We recovered 78% of the original platinum, as *tetraphenylphosphonium* salts, both having known space groups, both centric. There has therefore been *some* chemical change in the solution, viz. racemization (at least).

(f) Let us assume that our starting compound is, in fact, a mixture of 2 mol $(NH_4)_2[PtS_{18}]\cdot 2H_2O$ and 1 mol $(NH_4)_2[PtS_{15}]\cdot 2H_2O$. The latter exists in two crystalline forms,[3,23] both of known centric structures, so the observed optical activity of the $[PtS_{17}]^{2-}$ salt[20] cannot come from either known form of $(NH_4)_2[PtS_{15}]\cdot 2H_2O$. Indeed, we have never seen any spontaneous optical activity in the $[PtS_{15}]^{2-}$ salts, so, unless there was a very unusual co-crystallization of optically spontaneously resolved $(NH_4)_2[PtS_{15}]\cdot 2H_2O$ enforced by spontaneously resolved $(NH_4)_2[PtS_{18}]\cdot 2H_2O$, the observed optical activity for $(NH_4)_2[PtS_{17}]\cdot 2H_2O$ would have to derive entirely from its $[PtS_{18}]^{2-}$ content (two-thirds). This would not be inconsistent with the fact that the circular dichroism of $[PtS_{17}]^{2-}$ is quite distinct[20] from that of $[PtS_{15}]^{2-}$.

So, assuming we are dissolving a mixture of resolved $[PtS_{18}]^{2-}$ (2 mol) and racemic $[PtS_{15}]^{2-}$ (1

mol) in acetone, the *first* crystals are obtained within a day and are *racemic* $[PtS_{18}]^{2-}$. The racemization of resolved $[PtS_{15}]^{2-}$ in acetone is rather slow. So, either the $[PtS_{18}]^{2-}$ racemizes faster than its congener, or it was not there at all.

(g) The equilibrium solubilities of the ammonium salts $(NH_4)_2[PtS_n]\cdot H_2O$[20] are, at 18.4°C, for $n = 15$, 1.5%, and for $n = 17$, 0.14%. Even if, for $n = 18$, the ammonium salt was insoluble, the apparent solubility of a mixture of $2/3n = 18$, $1/3n = 15$ would be 0.5% and not the 0.14% observed.

(h) If the $(NH_4)_2[PtS_{17}]\cdot 2H_2O$ really were a mixture containing one-third $(NH_4)_2[PtS_{15}]\cdot 2H_2O$, then the X-ray powder photographs should reveal its presence. We routinely used this method to describe the tris-pentasulphido salt, and the powder photographs of both its dimorphs are well known.[23] There is no indication[20] of either in any sample of $(NH_4)_2[PtS_{17}]\cdot 2H_2O$.

The strongest lines in the powder photographs of Forms (**A**) and (**B**) of $(NH_4)_2[PtS_{15}]\cdot 2H_2O$ are (with relative intensities), respectively: 7.114 (80:11$\bar{1}$); 6.950 (100:111); 6.455 (70:002); 7.073 (80:11$\bar{2}$); 6.692 (100:004); 6.499 (70:202), for the reflections indicated. There is no *d*-spacing higher than 8.35 in either. For $(NH_4)_2[PtS_{17}]\cdot 2H_2O$, there is a total absence of the pattern corresponding to these lines: there are strong lines at 8.51 and 3.06 with no counterpart at all in either form of the PtS_{15}^{2-} salts. A very strong line at 6.42 in the $[PtS_{17}]^{2-}$ salt might correspond with the lines at 6.455 and 6.499 of Forms (**A**) and (**B**) of $[PtS_{15}]^{2-}$, but the even stronger lines at 6.950 [Form (**A**)] and 6.692 [Form (**B**)] would then be even more apparent, and there is no intensity at all in this region for $[PtS_{17}]^{2-}$, which has, as its three strongest lines, *d*-spacings of 8.51(s), 6.42(vs) and 3.06(s). None of these belong to either form of $(NH_4)_2[PtS_{15}]\cdot 2H_2O$ which is therefore absent. $(NH_4)_2[PtS_{17}]\cdot 2H_2O$ is a single compound in the solid state.

(i) Dismutation $xS_n^{2-} \rightleftharpoons yS_m^{2-} + zS_p^{2-}$ is common enough (though not well known in chelated compounds). For example, by dissolving K_2S_5 in a solution of sulphur and (crypt-2.2.2) in 1,2-diaminoethane (en), both $[K(cryst\text{-}2,2,2)]_2S_7\cdot en$ and $[K(cryst\text{-}2.2.2)]S_6$ may be crystallized.[17] The mechanism of formation[24] of $[ReS_9]^-$ (in $[Bu_4N][Re(S_4)_2S]$) from Li_2S_5 in THF is presumably not dissimilar. We commonly obtained[21,22] salts of $[Pt(S_5)_3]^{2-}$ from non-pentasulphide factors.

Despite these arguments, we are aware of the difficulty of proving a negative. We hope to settle the question of the persistence on dissolution of $(NH_4)_2[PtS_{17}]\cdot 2H_2O$ as an individual compound, by further measurements of optical activity, including that of $[PtS_{18}]^{2-}$ (not yet available optically active), and of ^{195}Pt resonance.

For $[PPh_4]_2[PtS_{18}]$, the subject of the present paper, the molecular structure consists of Ph_4P^+ cations and $Pt(S_6)_3^{2-}$ anions. The structural parameters of the cation are normal. The anion is shown in Fig. 1; selected bond length and angles are given in Table 1. The S_6^{2-} ligands are coordinated to the platinum(IV) ion and are all bidentate, forming three seven-membered rings. The Pt—S bond distances are of the same order as in $Pt(S_5)_3^{2-}$ compounds,[23] but the values of the chelate S—Pt—S angles in $Pt(S_6)$ units are very large, from 98.4(2) to 100.7(2)° compared to the values[3,23] of 90.9–92.8(2)° for the corresponding S—Pt—S angles in the PtS_5^{3-} units of $(NH_4)_2Pt(S_5)_3\cdot 2H_2O$, and in the other known tris-pentasulphido metallate, $(NH_4)_3[Rh(S_5)_3]\cdot 2H_2O$.[26]

The Pt^{IV} ion is on a C_2-axis. This symmetry axis also goes through the midpoint of the S(9)—S(9^i) bond. Therefore, two of the three seven-membered rings are equivalent. The torsion angles of PtS_6 (S = 1–6) and (S = 7–7^i) rings vary from −35.7(4) to 100.8(4)° and from −46.3(4) to 107.5(4)°, respectively. In cycloheptasulphur (δ-form), the ring torsion angles are in the range 1.1–107.5°.

Chelated S_6^{2-} ligands also occur in $[Hg(S_6)_2]^{2-}$[26] $[Zn(S_6)_2]^{2-}$ and $[Mn(S_5)(S_6)]^{2-}$ ions; (the existence of this last heteroleptic species with both S_5^{2-} and S_6^{2-} as ligands on the same metal of course serves as precedent[19] to our formulation of $[PtS_{17}]^{2-}$ as $[Pt(S_6)_2(S_5)]^{2-}$). The conformation of MS_6 (M = metal ion) rings seems to be different in each

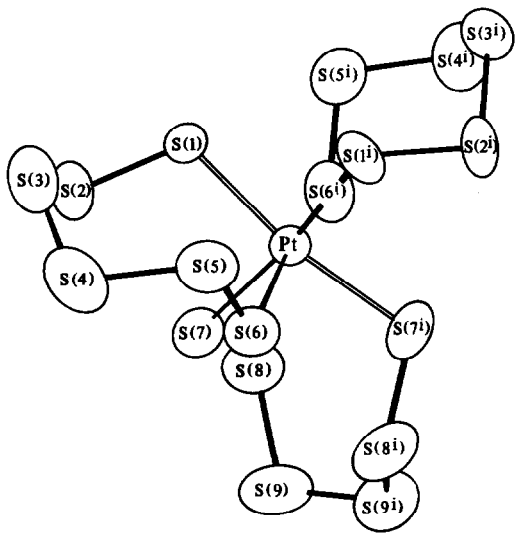

Fig. 1. The structure of $Pt(S_6)_3^{2-}$. The Pt—S and S—S distances range from 235.0(7) to 236.6(7) pm and from 194.8(10) to 205.4(10) pm, respectively. The S—S—S angles range from 104.6(5) to 108.7(5)°.

Table 1. Bond distances (pm) and bond angles (°) of the $Pt(S_6)_3^{2-}$ anion

Pt—S(1)	238.4(6)	S(1)—S(2)	201.4(9)
Pt—S(1^i)	238.4(6)	S(2)—S(3)	205.4(10)
Pt—S(6)	235.0(7)	S(3)—S(4)	196.6(11)
Pt—S(6^i)	235.0(7)	S(4)—S(5)	205.1(11)
Pt—S(7)	238.6(7)	S(5)—S(6)	194.8(10)
Pt—S(7^i)	238.6(7)	S(7)—S(8)	202.8(11)
		S(8)—S(9)	204.1(11)
		S(9)—S(9^i)	199.3(11)
S(1)—Pt—S(1^i)	83.6(2)	Pt—S(1)—S(2)	110.9(3)
S(1)—Pt—S(6)	100.7(2)	S(1)—S(2)—S(3)	107.3(4)
S(1)—Pt—S(6^i)	87.2(2)	S(2)—S(3)—S(4)	108.7(5)
S(1)—Pt—S(7)	89.6(2)	S(3)—S(4)—S(5)	106.9(4)
S(1)—Pt—S(7^i)	169.0(2)	S(4)—S(5)—S(6)	104.6(5)
S(6)—Pt—S(6^i)	169.4(3)	S(5)—S(6)—Pt	114.0(4)
S(6)—Pt—S(7)	85.5(2)	Pt—S(7)—S(8)	109.5(4)
S(6)—Pt—S(7^i)	87.6(2)	S(7)—S(8)—S(9)	105.3(5)
S(7)—Pt—S(1^i)	169.0(2)	S(8)—S(9)—S(9^i)	107.9(5)
S(7)—Pt—S(6^i)	87.6(2)	S(9)—S(9^i)—S(7^i)	105.3(5)
S(7)—Pt—S(7^i)	98.4(2)	S(8^i)—S(7^i)—Pt	109.5(4)
S(1^i)—Pt—S(6^i)	100.7(2)		
S(1^i)—Pt—S(7^i)	89.6(2)		
S(6^i)—Pt—S(7^i)	85.5(2)		

Symmetry code: i = $1-x$, y, $0.5-z$.

known case. These seven-membered rings are clearly rather flexible and the particular metal ion and packing forces may cause the ring to have a certain conformation.

The bond angles at the metal ions for other *independent* anions in $[MS_n(S_6)_x]^{n-}$ are as follows: M = Mn[27]—115.8 and 120.9° (cf. 108.3 and 108.1° for the six-membered MnS_5 rings in the same ions); Hg[28]—117.0 and 113.9°.

These tris seven-membered rings are probably unique, and the three large intra-chelate angles at a six-coordinated ion are without precedent, certainly with so simple a ligand. A unique large (positive) trigonal distortion is present, because the intra-ring angles at the metal ion are so much greater than 90°. All the many known tris cases have angles of 93° or less—chiefly because the ligating atoms are usually nitrogen and oxygen—and most have angles less than 91°. Among the largest positive trigonal distortions are those for $[M(S_5)_3]^{n-}$ where intra-ring angles at M are, for M = Pt,[23] $n = 2$; 90.9(2); 92.6(2) and 92.8(2), and for M = Rh,[26] $n = 3$; 92.7, 92.4, and 93.1. Indeed, as these increasingly large intra-ring angles become accessible, the isomeric trigonal pyramidal tris-chelate structures at the metal, minimizing non-bonded repulsions, may be within range, for chelating S_n^{2-}, with $n > 7$.

The formation of a particular metal polysulphide is strongly dependent on the metal ion. Thus, platinum(II) forms known chelates with S_4^{2-} (as in $(R_3P)_2PtS_4$ recently studied by Chatt and Mingos[27,28] and by others[29]) and S_5^{2-}, whereas the known palladium(II) species are PdS_{11}^{2-}, containing no chelate rings at all and $[(C_2H_5)_4N)_2][Pd(S_4)_2]$.[30]

It is at present rare that a particular metal ion forms a set of homoleptic polysulphides with a range of S_n^{2-} ions, although Zn^{2+} does, forming tetrahedral $Zn(S_n)_2^{2-}$ ions with $n = 4$, 5 and 6;[19] and our present work shows that it is possible to make octahedral $Pt(S_n)_3^{2-}$ ions when $n = 5$ or 6: maybe other ions with $n = 4$ or 7 could be prepared.

EXPERIMENTAL

Preparation of bis-tetraphenylphosphonium(V) *oktokaidekakissulphidoplatinate*(IV)

(a) Bistetraethylammonium heptakaidekakis-sulphidoplatinate(IV), $[N(C_2H_5)_4][PtS_{17}]$ (30 mg) made by a known method[20] in acetone (5 cm^3) was treated with tetraphenylphosphonium bromide (6 mg) in acetone (1 cm^3). The solution was kept in a refrigerator for two weeks when small, red crystals of $[PPh_4]_2[PtS_{18}]$ had formed which were removed

by filtration. Crystallographic work (data collection) was carried out with this sample.

(b) Diammonium heptakaidekakissulphidoplatinate(IV) dihydrate (32 mg) made by a known method[20] was kept for five years, then treated with acetone (3 cm^3). A small insoluble residue (2 mg) was removed by centrifugation. The resulting filtrate (0.037 mmol) was treated with $(PPh_4)Br$ (11 mg, 0.26 mmol) and the mixture kept in a refrigerator for 24 h, to give red $(Ph_4P)_2[PtS_{18}]$ (16 mg). This was separated by decanting, washed with methanol, then ether and identified by measurement of the unit cell (X-ray).

To the supernatant, further Ph_4PBr (12 mg, 0.029 mmol) in acetone (3 cm^3) was added. After 24 h in a refrigerator, this solution yielded a further crop of $(PPh_4)_2[PtS_{18}]$, identified by its similarity to the first compound under the microscope and by measurement of the unit cell of one crystal.

To the supernatant, further Ph_4PBr (11 mg, 0.026 mmol) in acetone (2 cm^3) was added. The solution was kept for three days at ambient temperature then overnight in a refrigerator, when red crystals of $[Ph_4P]_2[PtS_{15}]$ (11 mg) separated. These were identified by their unit cell as being the same as those found earlier[21] for a characterized sample of the compound made by the metathesis, in DMF,

$$(NH_4)_2[PtS_{15}] + 2PPh_4Br \rightarrow [PPh_4]_2[PtS_{15}] + 2NH_4Br.$$

Although the quality of the new crystals was not quite as good as those we obtained from DMF, we have collected and analysed a new data set which clearly establishes that this third crop of crystals is indeed bis-tetraphenylphosphonium pentakaidekakissulphidoplatinate(IV), $[PPh_4]_2[PtS_{15}]$.

The total amount of tetraphenylphosphonium bromide added represents a small excess (*ca* 10%) above that required for the reaction:

$$2[PPh_4]Br + [NH_4]_2[PtS_{17}] \rightarrow \text{“}(PPh_4)_2[PtS_{17}]\text{”} + 2NH_4Br.$$

X-ray measurements

Single-crystal X-ray measurements were carried out with an Enraf–Nonius CAD 4 diffractometer using Mo-K_α radiation. The data obtained were corrected for Lorentz and polarization effects.

Crystal data

$(Ph_4P)_2Pt(S_6)_3$; $M_r = 1450.95$; space group $C2/c$; $a = 1143.0(2)$, $b = 2410.4(4)$, $c = 2066.3(4)$ pm; $\beta = 92.56(2)°$; $Z = 4$; $V = 5.6872$ nm^3; $D_c = 1.69$ g cm^{-3}; $\mu(\text{Mo-K}_\infty) = 34.7$ cm^{-1} and $T = 296$ K.

Two check reflections showed no loss of intensity. Of 2807 independent reflections, 1443 having $I > 2.5\sigma(I)$ were accepted as observed. The structure was solved by direct methods, which gave positional parameters for the Pt and S atoms. The factors for atomic scattering and for corrections of anomalous dispersion for heavy atoms were taken from *International Tables*.[31] The structure was refined with Pt and P atoms having anisotropic and C and H atoms isotropic temperature factors, respectively. Phenyl groups were refined as rigid units. An empirical absorption correction was applied. The C—H hydrogen positions were calculated assuming the C—H distances to be 96 pm.

The refinements led to final $R = 0.055$ and $R_w = 0.052$, where $R = \Sigma\Delta/\Sigma F_o$, $R_w = \Sigma\sqrt{w}\Delta/\Sigma\sqrt{w}F_o$, $\Delta = F_o - F_c$ and $w = 1.46/[\sigma^2(F_o) + 0.000800F_o^2]$.*

Crystallographic calculations were performed with the SHELX-76 program.[32]

* Atomic coordinates, displacement factor coefficients, full lists of bond lengths and angles and lists of F_o/F_c values have been deposited as supplementary data with the Editor, from whom copies are available on request. Atomic coordinates have also been deposited with the Cambridge Crystallographic Data Centre.

REFERENCES

1. C. G. Ballhaus and E. F. Stumpfi, *Contrib. Mineral. Petrol.* 1986, **94**, 193.
2. (a) K. A. Hofmann and F. Hochtlen, *Chem. Ber.* 1903, **36**, 3090; (b) K. A. Hofmann and F. Hochtlen, *Chem. Ber.* 1904, **37**, 245. (Hofmann also discovered, *inter alia*, the compound [Pt(iso-mesityloxide)Cl_2] (“Zeise's second compound”) cf. G. W. Parshall and G. Wilkinson, *Inorg. Chem.* 1962, **4**, 986, and platinum blue, cf. R. D. Gillard and G. Wilkinson, *J. Chem. Soc.* 1964, 2835.)
3. (a) P. E. Jones and L. Katz, *J. Chem. Soc., Chem. Commun.* 1967, 842; (b) P. E. Jones and L. Katz, *Acta Cryst.* 1969, **B25**, 745.
4. N. V. Sidgwick, *The Chemical Elements and Their Compounds*, p. 1622. Oxford University Press, Oxford (1950).
5. A. E. Wickenden and R. A. Krause, *Inorg. Chem.* 1969, **8**, 779.
6. R. A. Krause, *Inorg. Nucl. Chem. Lett.* 1971, **7**, 973.
7. R. A. Krause, A. Wickenden-Kozlowski and J. L. Cronin, *Inorg. Synth.* 1982, **21**, 12.
8. P. S. Haradem, J. L. Cronin, R. A. Krause and L. Katz, *Inorg. Chem. Acta* 1977, **25**, 173.
9. R. D. Gillard and F. L. Wimmer, *J. Chem. Soc., Chem. Commun.* 1978, 936.

10. F. G. Riddell, R. D. Gillard and F. L. Wimmer, *J. Chem. Soc., Chem. Commun.* 1982, 332.
11. A. Muller and U. Schimanski, *Inorg. Chim. Acta* 1983, **77**, L187.
12. A. Muller, E. Krickemeyer, M. Zimmermann, M. Romer, H. Bogge, M. Penk and K. Schmitz, *Inorg. Chim. Acta* 1984, **90**, L69.
13. A. Muller, M. Romer, H. Bogge, E. Krickemeyer and M. Zimmermann, *Z. Anorg. Allg. Chem.* 1986, **69**, 534.
14. A. Muller, M. Romer, H. Bogge, E. Krickemeyer and K. Schmitz, *Inorg. Chim. Acta* 1984, **85**, L39. $[AsPh_4][AuS_9]$ was first made by G. Marbach and J. Strahle, *Angew. Chem. Int. Ed. Engl.* 1984, **23**, 246.
15. A. Muller, M. Romer, H. Bogge, E. Krickemeyer, F. W. Baumann and K. Schmitz, *Inorg. Chim. Acta* 1984, **89**, L7.
16. A. Muller, F. W. Baumann, H. Bogge, M. Romer, E. Krickemeyer and K. Schmitz, *Angew. Chem. Int. Ed. Engl.* 1984, **23**, 632.
17. P. Bottcher and H. Buchkremer-Hermanns, *Z. Naturforsch.* 1987, **42b**, 272.
18. L. Malatesta and F. Turner, *Gazz. Chim. Ital.* 1942, **72**, 489.
19. D. Coucouvanis, P. R. Patil, M. G. Kanatzidis, B. Detering and N. C. Baenziger, *Inorg. Chem.* 1985, **24**, 24.
20. R. D. Gillard, F. L. Wimmer and J. P. G. Richards, *J. Chem. Soc., Dalton Trans.* 1985, 253.
21. P. S. Cartwright, Ph.D. thesis, University of Wales (University College, Cardiff) (1987).
22. P. S. Cartwright, R. D. Gillard, E. R. J. Sillanpaa and J. Valkonen, to be published.
23. E. H. M. Evans, J. P. G. Richards, R. D. Gillard and F. L. Wimmer, *Nouv. J. Chim.* 1986, **10**, 783.
24. F. A. Cotton, P. A. Kibala and M. Matusz, *Polyhedron* 1988, **7**, 83.
25. P. S. Cartwright, R. D. Gillard, E. R. J. Sillanpaa and J. Valkonen, *Polyhedron* 1987, **6**, 1775.
26. A. Muller, J. Schmimanski and U. Schinanski, *Angew. Chem. Int. Ed. Engl.* 1984, **23**, 159.
27. C. E. Briant, M. J. Calhorda, T. S. A. Hor, N. D. Howells and D. M. P. Mingos, *J. Chem. Soc., Dalton Trans.* 1983, 1325.
28. J. Chatt and D. M. P. Mingos, *J. Chem. Soc. A.* 1970, 1243.
29. M. Schmidt and G. G. Hoffman, *Z. Naturforsch.* 1979, **34b**, 451.
30. A. Muller, E. Kirckemeyer, H. Bogge, W. Clegg and G. M. Sheldrick, *Angew. Chem. Int. Ed.* 1983, **22**, 1006.
31. *International Tables for X-ray Crystallography*, Vol. 4. Kynoch Press, Birmingham (1974).
32. G. M. Sheldrick, SHELX 76, University of Cambridge (1976).

Polyhedron Vol. 7, No. 19/20, pp. 1807–1811, 1988
Printed in Great Britain

0277–5387/88 $3.00+.00
© 1988 Pergamon Press plc

FORMATION OF A NEW MACROCYCLIC CHAIN POLYMER CONTAINING THORIUM(IV) AND MERCURY(II): STRUCTURE OF $[Hg_2Th(C_4H_6NO)_4(NO_3)_4]_n$

DAVID M. L. GOODGAME,* DAVID J. WILLIAMS and RICHARD E. P. WINPENNY

Chemistry Department, Imperial College of Science and Technology, London SW7 2AY, U.K.

Abstract—Reaction of $Hg(C_4H_6NO)_2$ (where C_4H_6NO is the anion of 2-pyrrolidinone) with thorium nitrate in methanol yields a polymeric heterometallic complex, $[Hg_2Th(C_4H_6NO)_4(NO_3)_4]_n$ which has been characterized by X-ray diffraction. The crystals are monoclinic, $P2_1/c$, $a = 10.020(5)$, $b = 19.421(10)$, $c = 14.615(6)$ Å, $\beta = 94.97(4)°$, $Z = 4$. The structure was refined on 2570 reflections to $R = 0.047$. The compound has a polymeric chain structure with the links of the chain comprising 16-membered macrocycles, formed by two thorium, two mercury, four oxygen, four carbon and four nitrogen atoms. Each thorium atom is 10-coordinate with a distorted bicapped square antiprismatic array of oxygen atoms (four from 2-pyrrolidinone anions, four from two bidentate nitrates and two from two unidentate nitrates).

Our investigations of the binucleating capabilities of the anion of 2-pyrrolidinone (**I**) have produced several new and unusual structural types. Several of these form novel heterometallic polymeric chain structures, often with alternating metal centres aligned along the chain direction. All feature a mercury atom bound to the deprotonated ring nitrogen and a second, "harder", metal bound to the exocyclic oxygen atom.

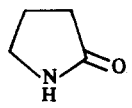

I

These compounds can be formed both with first and second row transition metals, e.g. copper(II),[1] cobalt(II)[2] and silver(I);[3] also with lanthanides.[4] Extending this work, we have explored the reactions of the $Hg(C_4H_6NO)_2$ unit with some actinides, to see if their higher oxidation states and preference for very high coordination numbers would lead to further new, or related, structural types. This has resulted in the formation of the first mercury (II)/thorium(IV) polymer, $[Hg_2Th(C_4H_6NO)_4(NO_3)_4]_n$ (**A**), the structure of which has been determined by X-ray diffraction methods.

* Author to whom correspondence should be addressed.

EXPERIMENTAL

Preparation

$Hg(C_4H_6NO)_2$ (1 mmol) (prepared as described previously[2]) was dissolved in methanol (20 cm^3) and thorium nitrate (0.2 mmol) was added. Immediately, a white precipitate formed which was removed by filtration. The colourless filtrate was allowed to evaporate at room temperature, being filtered whenever a precipitate formed. After 7–10 days small, rhombic crystals suitable for X-ray analysis were obtained. Found: C, 15.8; H, 1.9; N, 8.6. Calc. for $Hg_2Th(C_4H_6NO)_4(NO_3)_4$: C, 15.8; H, 2.0; N, 9.2%.

X-ray study

$[Hg_2Th(C_4H_6NO)_4(NO_3)_4]_n$ crystallizes as small, colourless rhomboids. The crystal data are: monoclinic, $a = 10.020(5)$, $b = 19.421(10)$, $c = 14.615(6)$ Å, $\beta = 94.97(4)°$, $V = 2821$ Å^3, space group $P2_1/c$, $Z = 4$, $Mr = 1217.6$, $D_c = 2.88$ g cm^{-3}, μ(Cu-K_α) = 381 cm^{-1}. Refined unit cell parameters for a crystal of approximate dimensions $0.32 \times 0.05 \times 0.03$ mm were obtained by centring 18 reflections on a Nicolet R3m diffractometer. 3208 independent reflections ($\theta \leqslant 58°$) were measured with graphite monochromated Cu-K_α radiation

using the omega-scan measurement routine. Of these, 2570 had $|F_o| > 3\sigma(|F_o|)$ and were considered observed. Lorentz, polarization and a numerical absorption correction (face-indexed crystal) were applied.

The structure was solved by the heavy-atom method, which revealed the position of the thorium atom. The remaining non-hydrogen atoms were located from subsequent ΔF maps. The hydrogen atom positions were idealized (C—H = 0.96 Å), assigned isotropic thermal parameters, $U(H) = 1.2U_{eq}(C)$, and allowed to ride on their parent carbon atoms. One of the nitrate anions was severely disordered and was thus idealized and refined as a rigid body. The non-hydrogen atoms were refined anisotropically. Refinement was by block-cascade full matrix least-squares to $R = 0.047$, $R_w = 0.048$ ($w^{-1} = \sigma^2(F) + 0.001F^2$).

Computations were carried out on an Eclipse S140 computer using the SHELXTL program system.[5] Scattering factors were taken from ref. 6. Important bond lengths and angles are listed in Table 1.

RESULTS AND DISCUSSION

The X-ray structural analysis confirms that (**A**) has the stoichiometry $Hg_2Th(C_4H_6NO)_4(NO_3)_4$, and shows that a polymeric chain structure is formed.

A view of the thorium environment is shown in Fig. 1. As expected, the thorium ion has a high coordination number, namely 10. The donor atoms are all oxygens, four from four 2-pyrrolidinone anions, four from two bidentate nitrate anions and two from two monodentate nitrates.

The coordination geometry adopted by the ThO_{10} unit (Fig. 2) is best described as a distorted bicapped square antiprism. This geometry has been found for $K_4[Th(C_2O_4)_4]\cdot 4H_2O$[7] and the triclinic form of $K_4[U(C_2O_4)_4]\cdot 4H_2O$,[8] but is in contrast to the tetradecahedron adopted by thorium in $ThNi_2(S_2C_2O_2)_4\cdot 6H_2O$.[9] One plane of the square antiprism comprises O(2), O(3), O(51) and O(81), capped by O(52); the other comprises O(1), O(4), O(61) and O(71), capped by O(62). The O(52)—Th—O(62) angle is 171.4(4)° [cf. 174.7

Table 1. Bond lengths (Å) and angles (°) for (**A**) with e.s.d.'s in parentheses

Hg(1)—N(2)	2.036(12)	Hg(1)—N(4a)	2.012(12)
Hg(2)—N(3)	2.025(11)	Hg(2)—N(1a)	2.019(11)
Th—O(1)	2.302(11)	Th—O(2)	2.309(11)
Th—O(3)	2.336(12)	Th—O(4)	2.392(11)
Th—O(51)	2.615(13)	Th—O(52)	2.704(13)
Th—O(61)	2.588(12)	Th—O(62)	2.699(11)
Th—O(71)	2.495(14)	Th—O(81)	2.463(13)
N(2)—Hg(1)—N(4a)	177.0(6)	N(3)—Hg(2)—N(1a)	179.5(7)
O(1)—Th—O(2)	145.3(4)	O(1)—Th—O(3)	141.5(4)
O(2)—Th—O(3)	73.1(4)	O(1)—Th—O(4)	72.7(4)
O(2)—Th—O(4)	141.8(4)	O(3)—Th—O(4)	69.4(4)
O(1)—Th—O(51)	70.1(4)	O(2)—Th—O(51)	117.8(4)
O(3)—Th—O(51)	90.4(4)	O(4)—Th—O(51)	70.1(4)
O(1)—Th—O(52)	113.6(4)	O(2)—Th—O(52)	71.2(4)
O(3)—Th—O(52)	67.8(4)	O(4)—Th—O(52)	100.6(4)
O(51)—Th—O(52)	47.5(4)	O(1)—Th—O(61)	115.0(4)
O(2)—Th—O(61)	74.9(4)	O(3)—Th—O(61)	68.5(4)
O(4)—Th—O(61)	84.7(4)	O(51)—Th—O(61)	151.8(4)
O(52)—Th—O(61)	130.4(4)	O(1)—Th—O(62)	67.8(4)
O(2)—Th—O(62)	112.9(4)	O(3)—Th—O(62)	105.6(4)
O(4)—Th—O(62)	71.4(4)	O(51)—Th—O(62)	129.3(4)
O(52)—Th—O(62)	171.4(4)	O(61)—Th—O(62)	47.1(4)
O(1)—Th—O(71)	74.4(5)	O(2)—Th—O(71)	75.6(5)
O(3)—Th—O(71)	138.8(5)	O(4)—Th—O(71)	131.6(4)
O(51)—Th—O(71)	128.1(5)	O(52)—Th—O(71)	124.9(4)
O(61)—Th—O(71)	78.1(5)	O(62)—Th—O(71)	63.7(4)
O(1)—Th—O(81)	72.6(4)	O(2)—Th—O(81)	80.0(4)
O(3)—Th—O(81)	130.6(4)	O(4)—Th—O(81)	131.3(4)
O(51)—Th—O(81)	66.7(4)	O(52)—Th—O(81)	64.6(5)
O(61)—Th—O(81)	141.4(4)	O(62)—Th—O(81)	123.1(4)
O(71)—Th—O(81)	67.4(5)		

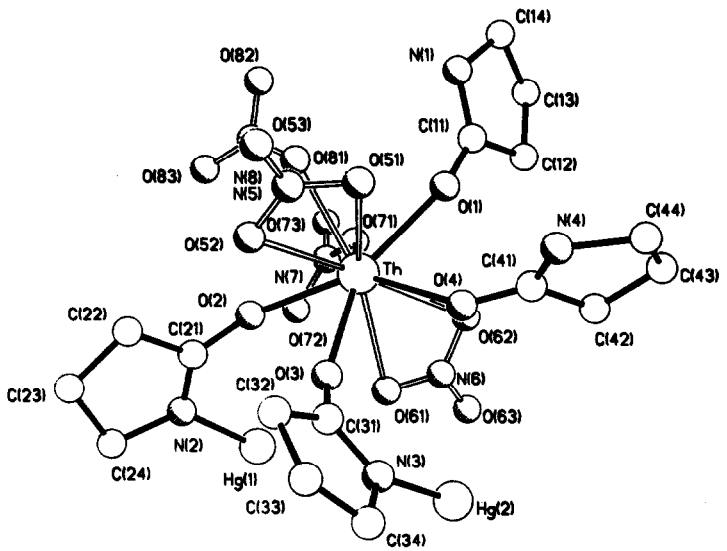

Fig. 1. The thorium environment in $Hg_2Th(C_4H_6NO)_4(NO_3)_4$, showing the crystallographic numbering scheme.

and 174.5° for the corresponding angle in $K_4[M(C_2O_4)_4]\cdot 4H_2O$ (M = Th[7] or U[8])].

One marked difference between (A) and the above oxalato complexes is the effect of the small "bite" of the bidentate nitrate groups. Both capping oxygen atoms, O(52) and O(62) respectively, come from such a nitrate. This results in an appreciable reduction of one of the pyramid angles in each case [O(51)—Th—O(52) 47.5(4)° and O(61)—Th—O(62) 47.1(4)°] compared with angles of 62–66°, mean 64.0°, in $K_4[Th(C_2O_4)_4]\cdot 4H_2O$.[7] Most of the other pyramid angles in (A) show a concomitant increase [64.6(4)–71.4(4)°].

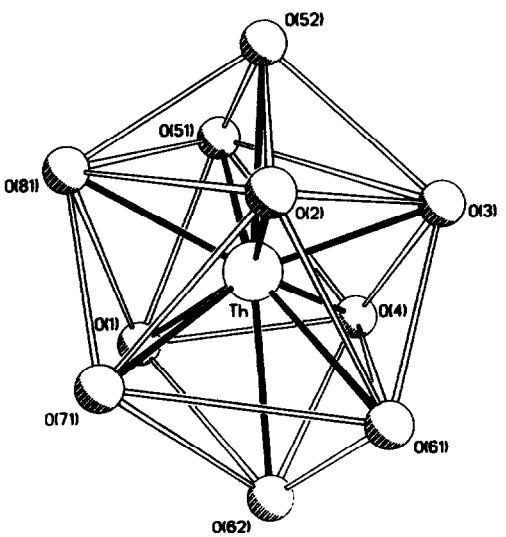

Fig. 2. The distorted bicapped square antiprismatic coordination geometry about thorium.

The Th—O bond lengths fall into three groups. Those from thorium to the oxygen atoms of the 2-pyrrolidinone anions are noticeably the shortest (2.30(1)–2.39(1) Å). There is also a difference between the Th—O bonds involving oxygen atoms of the monodentate and bidentate nitrates—the monodentate being noticeably shorter (2.46(1) and 2.50(1) Å) compared with those to the bidentate nitrates (2.58(1) and 2.70(1) Å). A similar difference in Th—O bond lengths between carbonyl oxygens and nitrate oxygens as donors has been observed elsewhere.[10]

The two inequivalent mercury atoms form strong, essentially linear (177.0(6) and 179.5(7)°) bonds to ring nitrogen atoms. The bond distances (see Table 1) are unexceptional and are similar to those reported previously.[1–4]

These interactions, coupled with the coordination of the pyrrolidinone oxygen atoms to the Th centres, result in the formation of a heterobimetallic chain polymer the links of which comprise 16-membered macrocycles. The constituent atoms of these macrocycles are two Th, two Hg, four N, four O, and four C. The polymeric component of the structure is shown in Fig. 3, the nitrate anions having been omitted for clarity.

There is cross-linking of the polymer chains via mercury–nitrate interactions (see Fig. 4). The shortest of these contacts (2.75 Å) is between O(82), an oxygen in one of the monodentate nitrates in one chain, and Hg(2) in the next. Other, weaker interchain Hg···O contacts occur between Hg(1) and O(72), 2.92 Å, and O(73), 2.98 Å; also between Hg(2) and O(81), 2.96 Å. These structure-stabilizing

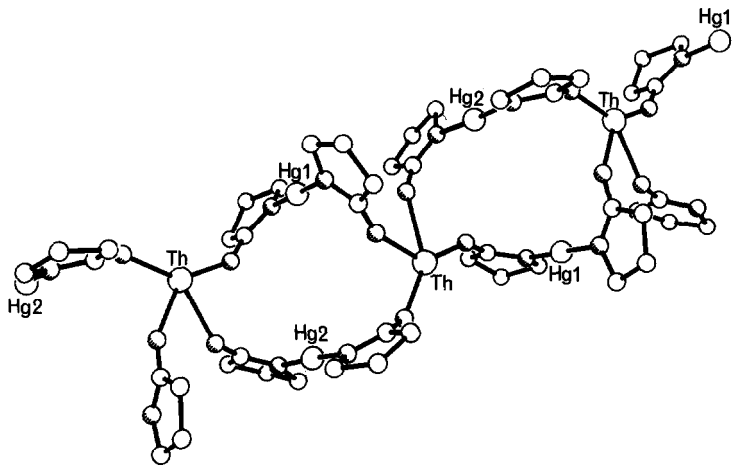

Fig. 3. Part of the polymeric chain structure of (A) showing the interlocking 16-membered rings. The NO_3 groups have been omitted for clarity.

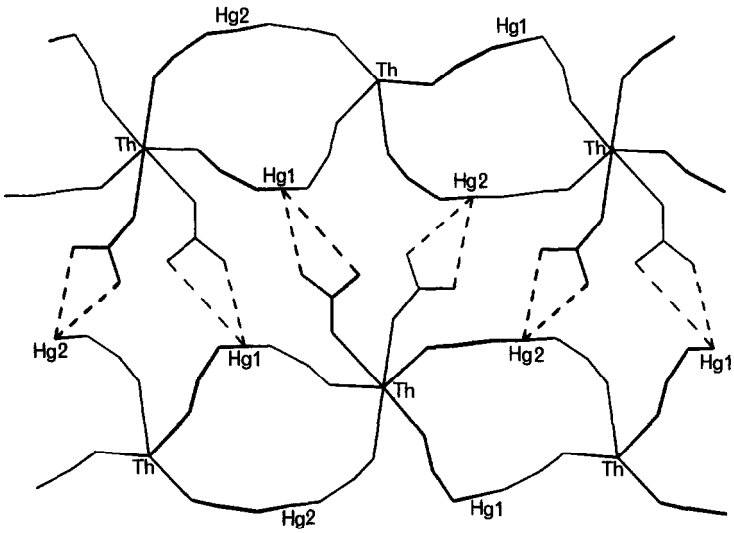

Fig. 4. Inter-chain linking by Hg···O(nitrate) interactions (for clarity, only atoms comprising the macrocycles and the relevant nitrates are shown).

interactions are more important here than in any of the related bimetallic polymers we have reported previously.[1–4] The only similar interaction occurred in a mercury–europium complex[4] and there the shortest contact distance was 2.95 Å.

There are clear similarities between the polymeric array formed by (**A**) and that adopted by the lanthanide complexes $[Hg_2Ln(C_4H_6O)_4(NO_3)_3]_n$, Ln = La–Eu (**B**). In both cases the polymeric chains consist of 16-membered macrocycles, though there are subtle differences between the conformations of these macrocycles. In (**A**) the N—Hg—N units in opposite sides of each macrocycle are approximately co-directional, whereas in (**B**) they are opposed.[4] Furthermore, whilst the intra-annular Th—Th distance (7.6 Å) is the same as the Eu—Eu distance in (**B**), the corresponding Hg···Hg distance is noticeably longer in (**A**) [5.21 cf. 4.45 Å in (**B**)].

The increase in charge and coordination number on changing from Eu^{III} to Th^{IV} has only resulted in more nitrate anions coordinating, and this appears to have mitigated against any dramatic change in the polymer structure. Clearly, a less coordinating anion is required if more 2-pyrrolidinone units are to be coordinated to an *f*-block metal centre. Work in this direction is underway.

Acknowledgement—We thank the SERC for funds for the diffractometer and for a Research Studentship (to R.E.P.W.).

REFERENCES

1. D. M. L. Goodgame, D. J. Williams and R. E. P. Winpenny, *Angew. Chem. Int. Ed. Engl.* 1987, **26**, 1044.
2. D. M. L. Goodgame, D. J. Williams and R. E. P. Winpenny, *Angew. Chem. Int. Ed. Engl.* 1988, **27**, 261.
3. D. M. L. Goodgame, D. J. Williams and R. E. P. Winpenny, *Polyhedron* 1988, **7**, 1299.
4. D. M. L. Goodgame, D. J. Williams and R. E. P. Winpenny, *J. Chem. Soc., Chem. Commun.* 1988, 437.
5. G. M. Sheldrick, SHELXTL. An Integrated System for Solving, Refining and Displaying Crystal Structures from Diffraction Data, Revision 4.1. University of Göttingen, F.R.G. (1983).
6. *International Tables for X-ray Crystallography*, Vol. IV, pp. 99–143. Kynoch Press, Birmingham, U.K. (1974).
7. M. N. Akhtar and A. J. Smith, *Acta Cryst., Sect. B* 1975, **31**, 1361.
8. M. C. Favas, D. L. Kepert, J. M. Patrick and A. H. White, *J. Chem. Soc., Dalton Trans.* 1983, 571.
9. J. C. Trombe, A. Gleizes and J. Galy, *Nouv. J. Chim.* 1985, **9**, 55.
10. A. G. N. Al-Daher, K. W. Bagnall, E. Forsellini, F. Benetollo and G. Bombieri, *J. Chem. Soc., Dalton Trans.* 1986, 615.

Polyhedron Vol. 7, No. 19/20, pp. 1813–1817, 1988
Printed in Great Britain

0277–5387/88 $3.00+.00
© 1988 Pergamon Press plc

METAL CLUSTER TOPOLOGY—IX.† MERCURY VERTICES IN TRANSITION METAL CLUSTERS AND ALKALI METAL AMALGAMS‡

R. B. KING

Department of Chemistry, University of Georgia, Athens, GA 30602, U.S.A.

Abstract—Mercury vertices in metal clusters use a seven-orbital spd^5 bonding manifold with linear *sp* hybrids for strong primary bonding and $d\pi \rightarrow p\pi^*$ and/or $d\sigma \rightarrow p\sigma^*$ interactions for weaker secondary bonding. Transition metal clusters containing mercury vertices can be classified into two types: two-dimensional clusters in which the mercury atoms form a polygon such as a triangle in $[HgOs_3(CO)_{11}]_3$ or a square in $[HgMn(CO)_2C_5H_4Me]_4$ and three-dimensional clusters in which the mercury atoms form a polyhedron such as an octahedron in $Hg_6[Rh(PMe_3)_3]_4$ or a tricapped trigonal prism in $Hg_9[Co(CO)_3]_6$. The structures of such clusters consist of a mercury polygon or polyhedron having secondary Hg—Hg interactions inside a transition metal macropolygon or macropolyhedron with M—Hg—M edges having primary Hg—M interactions. These clusters thus all exhibit edge-localized chemical bonding topology. Alkali metal amalgam structures are constructed from mercury quadrilaterals of which the prototypical species is square Hg_4^{6-}, found in discrete units in the structure of Na_3Hg_2. This homonuclear mercury cluster anion may be regarded as a globally delocalized two-dimensional planar polygonal aromatic system with an aromatic sextet like benzene but with no σ-bonding between adjacent mercury atoms in the Hg_4^{6-} square.

A characteristic property of metal carbonyls, which was recognized in the very early days of the development of their chemistry, is their reactivity towards mercury and its compounds to form transition metal–mercury derivatives, which in general are relatively stable towards air and water. Early discoveries of this type include the formation of *cis*-$Fe(CO)_4(HgCl)_2$ from $Fe(CO)_5$ and $HgCl_2$[2] and the formation of $Hg[Co(CO)_4]_2$ from $Co_2(CO)_8$ and elemental mercury.[3] Mercury derivatives of metal carbonyls such as $Hg[Mn(CO)_5]_2$, $Hg[Co(CO)_4]_2$, $Hg[Mo(CO)_3C_5H_5]_2$ and $Hg[Fe(CO)_2C_5H_5]_2$ are frequent by-products from the preparation of metal carbonyl anions by the treatment of binuclear metal carbonyl derivatives with sodium amalgam.[4]

Structural studies on mercury metal carbonyl derivatives such as $Hg[Mn(CO)_5]_2$,[5,6] $Hg[Co(CO)_4]_2$,[7] $Hg[Co(CO)_3PEt_3]_2$[8] and $Hg[Fe(CO)_2(NO)PEt_3]_2$[9] indicate linear M—Hg—M units containing two-coordinate mercury atoms. This area of transition metal chemistry thus appeared to be relatively uninteresting until the seminal discovery by Wilkinson and co-workers[10] of the sodium amalgam reduction of $[(Me_3P)_4Rh]Cl$ or $(Me_3P)_3RhCl$ to give high yields of the high nuclearity transition metal–mercury cluster $Hg_6[Rh(PMe_3)_3]_4$, which was shown by X-ray diffraction to consist of an Hg_6 octahedron with four tetrahedrally related faces capped by rhodium atoms. This paper surveys the currently known types of such high nuclearity transition metal–mercury clusters with the objective of relating their skeletal bonding to previously discussed[11–14] graph-theory derived models for metal cluster bonding topology. An important conclusion from this study is that almost all of the complicated transition metal–mercury cluster structures can be derived from simple edge-localized bonding models with two-coordinate mercury vertices. The ideas developed in this study of transition metal–mercury clusters also provide some insight into the chemical bonding topology of alkali metal amalgams, which are important as reducing agents in metal carbonyl chemistry and other areas of transition metal chemistry. Thus Wilkinson[15] as well as Hieber[16] and

† For part VIII, see ref. 1.

‡ This paper is dedicated to Sir Geoffrey Wilkinson, F.R.S., in recognition of his many contributions to organometallic and inorganic chemistry.

(*Received* 18 *April* 1988).

their co-workers were pioneers in such applications of alkali metal amalgams for the preparation of metal carbonyl anions from neutral metal carbonyl dimers.

MERCURY VERTICES

The position of mercury to the right of gold in the periodic table suggests that mercury vertices will have some similar properties to gold vertices[14] in metal clusters. Thus two of the outer *p* orbitals in both mercury and gold can be shifted to such high energies that they no longer participate in the primary chemical bonding.[17,18] This manifests itself structurally in d^{10} Au^{I} and Hg^{II} as two linear *sp* hybrid orbitals superimposed on a spherically symmetrical filled *d*-orbital manifold thereby leading to a cylindrical spd^5 seven-orbital primary bonding manifold, which requires 14 electrons for filling. This limitation of the primary bonding of mercury vertices to two linear *sp* hybrids prevents the construction of stable polyhedra containing exclusively mercury vertices. However, transition metal cluster macropolyhedra can be constructed in which the edges are nearly linear M—Hg—M units rather than simple M—M bonds. Thus the $Hg_6[Rh(PMe_3)_3]_4$ cluster[10] can be interpreted as an Rh_4 macrotetrahedron with six Rh—Hg—Rh edges.

The empty *p* orbitals not in the spd^5 cylindrical bonding manifold of the d^{10} Hg^{II} can participate in secondary $d\pi \rightarrow p\pi^*$ or $d\sigma \rightarrow d\sigma^*$ bonding similar to that suggested by Dedieu and Hoffmann[19] for isoelectronic d^{10} Pt^0 complexes and by a previous paper of this series[14] to account for the peripheral Au—Au bonding distances in centred gold clusters. The mercury–mercury interactions within the mercury polygons and polyhedra in the transition metal–mercury clusters consist exclusively of such secondary bonding since the mercury *sp* hybrid orbitals are used for primary bonding to transition metals in the M—Hg—M edges of the transition metal macropolyhedra.

The mercury–mercury distances in polynuclear mercury derivatives (Table 1) provide an excellent indication as to the nature of the mercury–mercury interactions. In Hg_2^{2+} derivatives as well as similar derivatives of longer linear mercury chains (e.g. Hg_3^{2+}, Hg_4^{2+}) the mercury–mercury distances fall in the range 2.4–2.7 Å indicative of strong primary covalent bonding arising from overlap of linear *sp* hybrid orbitals.[20–22] In cases where the primary mercury bonding is diverted to other atoms, such as transition metal atoms in transition metal–mercury clusters, the mercury–mercury distances increase to the range 2.9–3.2 Å indicating the presence of only secondary mercury–mercury bonding.

Table 1. Mercury–mercury bond distances

Compound	Hg—Hg (Å)
Hg metal	3.00, 3.47
Hg_2F_2	2.43
Hg_2Cl_2	2.45
Hg_2Br_2	2.50
Hg_2I_2	2.69
$Hg_3(AsF_6)_2$	2.552(4)
$Hg_3(AlCl_4)_2$	2.56
$Hg_4(AsF_6)_2$	2.70 (inner), 2.57 (outer)
$Hg_{2.85}AsF_6$	2.64(1)
$[HgOs_3(CO)_{11}]_3$	3.122(3), 3.082(3), 3.097(3)
$[HgMn(CO)_2C_5H_4Me]_4$	2.888(2)
$Hg_6[Rh(PMe_3)_3]_4$	3.131(3)–3.149(3)
$Hg_9[Co(CO)_3]_6$	3.094 (av., trig.–trig.), 3.151 (av., trig.–sq.)
$Na_3Hg_2(Hg_4^{6-})$	2.99
NaHg	3.05, 3.05, 3.22
KHg	3.02, 3.04, 3.36
$NaHg_2$	2.90, 3.23
KHg_2	3.00, 3.02, 3.08

Transition metal clusters containing mercury vertices can be classified into two types: two-dimensional clusters (Fig. 1) in which the mercury atoms form a polygon such as a triangle in $[HgOs_3(CO)_{11}]_3$[23] or a square in $[HgMn(CO)_2C_5H_4Me]_4$[24] and three-dimensional clusters (Fig. 2) in which the mercury atoms form a polyhedron

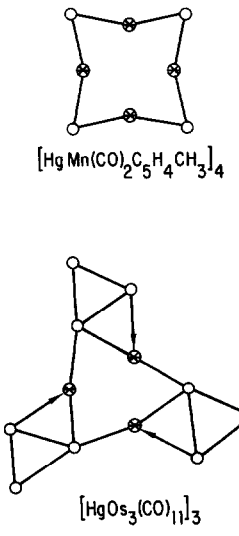

Fig. 1. Transition metal mercury clusters containing mercury polygons. Mercury vertices are starred, mercury–mercury bonds and external groups (carbonyl and cyclopentadienyl) are omitted, and transition metal → mercury dative bonds are indicated by arrows.

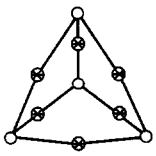

$Hg_6[Rh(PMe_3)_3]_4$

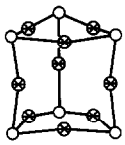

$Hg_9[Co(CO)_3]_6$

Fig. 2. Transition metal mercury clusters containing mercury polyhedra. Mercury vertices are starred and mercury–mercury bonds and external groups (carbonyl and trimethylphosphine) are omitted.

such as an octahedron in $Hg_6[Rh(PMe_3)_3]_4$[10] or a tricapped trigonal prism in $Hg_9[Co(CO)_3]_6$.[25] Transition metal clusters containing mercury polygons arise from bifunctional transition metal fragments such as $Fe(CO)_4$ and $CpMn(CO)_2$ leading to degree two vertices in the large transition metal macropolygon. Transition metal clusters containing mercury polyhedra arise from trifunctional transition metal fragments such as $Co(CO)_3$ and $Rh(PR_3)_3$ leading to degree three vertices in the large transition metal macropolyhedron. The graph of the polygon or polyhedron formed by the mercury vertices is thus the line graph[26] of the graph of the polygon or polyhedron formed by the transition metal vertices.

MERCURY POLYGONS

Combinations of difunctional transition metal vertices with mercury vertices leads to clusters with equal numbers of transition metal and mercury vertices consisting of a mercury polygon within a transition metal macropolygon (Fig. 1). The bond angles at the transition metal vertices determine the sizes of the polygons with squares apparently being preferred. A structurally characterized cluster of this type is $[HgMn(CO)_2C_5H_4Me]_4$.[24] The difunctional $Mn(CO)_2C_5H_4Me$ vertices have the favoured 18-electron rare gas configuration for the manganese atom and are derived from the corresponding $CpMn(CO)_3$ system through a formal oxidative addition reaction. The Mn—Hg—Mn edges of the Mn_4 macrosquare in $[HgMn(CO)_2C_5H_4Me]_4$ are bent inwards towards the centre of the square in accord with secondary mercury–mercury bonding leading to 2.888(2) Hg—Hg bond distances. A similar structure (Fig. 1) can be postulated for the long-known[2,27] but insoluble $[HgFe(CO)_4]_4$ on the basis of its similar IR spectrum to the structurally characterized[28] $[CdFe(CO)_4]_4 \cdot 2Me_2CO$.

A structure containing a mercury triangle (Fig. 1) is found in the "heteronuclear raft cluster"[23] $[HgOs_3(CO)_{11}]_3$. In this case the difunctional transition metal vertex is the $Os(CO)_3$ vertex of an $Os_3(CO)_{11}$ triangle. The Os—Hg bond lengths in the Os—Hg—Os edges of the Os_3 macrotriangle fall in the range 2.71–2.76 Å. In addition there is one 2.98–3.05 Å dative bond from an $Os(CO)_4$ vertex of each $Os_3(CO)_{11}$ triangle to a mercury atom as indicated by arrows in Fig. 1. Such dative bonds from osmium atoms to other types of acceptor atoms have been found in structurally characterized complexes.[29–31] The Hg—Hg distances of 3.08–3.13 Å in the mercury triangle of $[HgOs_3(CO)_{11}]_3$ are significantly longer than those in the mercury square of $[HgMn(CO)_2C_5H_4Me]_4$ suggestive of weaker mercury–mercury secondary bonding possibly because of the *trans* influence of the Os → Hg dative bond. The Os → Hg dative bond as well as the Os—Os bonds in the $Os_3(CO)_{11}$ triangles perturb the external bond angles at the $Os(CO)_3$ vertices so that a mercury triangle is found in $[HgOs_3(CO)_{11}]_3$ in contrast to the mercury square in $[HgMn(CO)_2C_5H_4Me]_4$ discussed above. In $[HgOs_3(CO)_{11}]_3$ all of the osmium atoms have the favoured 18-electron rare-gas configuration and the mercury atoms have the 14-electron configuration corresponding to a filled cylindrical spd^5 seven-orbital manifold.

MERCURY POLYHEDRA

Combination of trifunctional transition metal vertices with mercury vertices leads to clusters having a mercury polyhedron within a transition metal macropolyhedron (Fig. 2). The known examples of such clusters have trifunctional transition metal vertices of the type ML_3 (M = Co, Rh, Ir; L = CO, R_3P). The number of mercury atoms in such clusters is equal to the number of edges in the transition metal macropolyhedron. If this macropolyhedron has m vertices all of degree three implied by the trifunctionality of the transition metal units at the vertices, then there are $(3/2)m$ edges and such clusters have the overall stoichiometry $[Hg_3(ML_3)_2]_x$ where x is even. The properties of the first three clusters of this homologous series, for which both the mercury polyhedron and the transition metal macropolyhedron are readily recognizable polyhedra, are listed in Table 2. In addition to the hypothetical cluster $[Hg_3(ML_3)_2]_4$ having O_h skel-

Table 2. Smallest possible skeletons for clusters of the type $[Hg_3(ML_3)_2]_x$ consisting of a mercury polyhedron inside a transition metal macropolyhedron

		Mercury polyhedron				Transition metal macropolyhedron				
x	Skeletal symmetry	Type	v	e	f	Type	v	e	f	Example
2	T_d	Octahedron	6	12	8	Tetrahedron	4	6	4	$Hg_6[Rh(PMe_3)_3]_4$
3	D_{3h}	Tricapped trigonal prism	9	21	14	Trigonal prism	6	9	5	$Hg_9[Co(CO)_3]_6$
4	O_h	Cuboctahedron	12	24	14	Cube	8	12	6	

etal symmetry consisting of a mercury cuboctahedron inside a transition metal macrocube, a less symmetrical isomeric cluster $[Hg_3(ML_3)_2]_4$ having C_{2v} skeletal symmetry is also possible in which the macropolyhedron is the eight-vertex cuneane polyhedron, namely the dual[32] of the bicapped tetrahedron.[12] The Wilkinson cluster[10] $Hg_6[Rh(PMe_3)_3]_4$ with a mercury octahedron inside a rhodium macrotetrahedron and the Burlitch cluster[25] $Hg_9[Co(CO)_3]_6$ with a mercury tricapped trigonal prism inside a cobalt trigonal macroprism (Fig. 2) represent the first two members of this homologous series. In both of these clusters all of the transition metal atoms have the favoured 18-electron rare-gas configuration and all of the mercury atoms have the 14-electron configuration corresponding to a full cylindrical spd^5 seven-orbital manifold. The linear *sp* primary mercury bonding is used for the M—Hg—M edges of the transition metal macropolyhedra leaving only secondary bonding for the edges of the mercury polyhedra in accord with the 3.06–3.15 Å Hg—Hg distances in these polyhedra.

ALKALI METAL AMALGAMS

Several alkali metal amalgams have been structurally characterized including the sodium amalgams[33] $NaHg_2$, NaHg and Na_3Hg_2, and the potassium amalgams[34] KHg_2 and KHg. The most highly reduced of these species, namely Na_3Hg_2, has been shown[33,35] to contain discrete 2.99 Å square planar Hg_4^{6-} clusters which are *not* isoelectronic with other square planar post-transition element clusters[36–38] such as Bi_4^{2-},[39] Se_4^{2+}[40] and Te_4^{2+}.[41] In gold coloured NaHg[33] slightly distorted 3.05 × 3.22 Å Hg_4 rectangles are fused into a zigzag ribbon whereas in the likewise gold coloured KHg,[34] slightly distorted (93.6 rather than 90°) 3.03 Å Hg_4 squares are linked by 3.36 Å Hg—Hg bonds. More complicated networks of mercury rectangles and parallelograms are present in $NaHg_2$ and KHg_2. Thus the prototypical building blocks for alkali metal amalgams are derived from the Hg_4^{6-} squares found in Na_3Hg_2.

The mercury atoms in Hg_4^{6-} can be considered to have seven-orbital spd^5 cylindrical bonding manifolds. Six of these seven orbitals, namely the *s* orbital and the five *d* orbitals, are external orbitals, whereas the single *p* orbital is an internal orbital. A neutral mercury atom with six external orbitals is a zero skeletal electron donor[42–44] so that the Hg_4^{6-} anion has six skeletal electrons. Since the overlap of the external *p* orbitals in Hg_4^{6-} has the topology of the square, the Hg_4^{6-} anion has a π-bonding network similar to a planar aromatic hydrocarbon such as the cyclobutadiene dianion or benzene. Furthermore, the six skeletal electrons of Hg_4^{6-} can all be π-electrons so that Hg_4^{6-} is an $4k+2$ electron aromatic system with a π-electron network analogous to that of benzene. *However, Hg_4^{6-} has neither the electrons nor the orbitals for any* Hg—Hg σ-*bonding*. Thus the Hg_4^{6-} anion is a unique example of a two-dimensional aromatic system without any σ-bonding. Thus the eight-electron difference in the skeletal electron counts of the square clusters Bi_4^{2-} and Hg_4^{6-} relate to the presence of σ-bonding in the Bi_4^{2-} square but the absence of σ-bonding in the Hg_4^{6-} square.

In a number of areas of chemistry, including metal carbonyl chemistry, amalgamation of alkali metals is often used to facilitate their use as strong reducing agents. The presence of mercury anions, such as Hg_4^{6-}, in alkali metal amalgams indicates that mercury in the form of clusters can be an electron sink so that the reducing action of alkali metal amalgams can be viewed as analogous to that of alkali metal naphthalenides or alkali metal graphite intercalation compounds.[45] Recent electrochemical studies[46,47] indicate that similar mercury cluster anions are present in "quaternary ammonium amalgams" although difficulties in obtaining crystals from these air- and moisture-sensitive systems have precluded their definitive structural characterization.

Acknowledgement—I am indebted to the U.S. Office of Naval Research for partial support of this work.

REFERENCES

1. R. B. King, *J. Mol. Struct. Theochem*, in press.
2. H. Hock and H. Stuhlmann, *Chem. Ber.* 1928, **61**, 2097.
3. W. Hieber and U. Teller, *Z. Anorg. Allgem. Chem.* 1942, **249**, 43.
4. R. B. King, *J. Inorg. Nucl. Chem.* 1963, **25**, 1296.
5. W. Clegg and P. J. Wheatley, *J. Chem. Soc. A* 1971, 3572.
6. M. L. Katcher and G. L. Simon, *Inorg. Chem.* 1972, **11**, 1651.
7. G. M. Sheldrick and R. N. F. Simpson, *J. Chem. Soc. A*, 1968, 1005.
8. R. F. Bryan and A. R. Manning, *J. Chem. Soc., Chem. Commun.* 1968, 1316.
9. F. S. Stephens, *J. Chem. Soc., Dalton Trans.* 1972, 2257.
10. R. A. Jones, F. M. Real, G. Wilkinson, A. M. R. Galas and M. B. Hursthouse, *J. Chem. Soc., Dalton Trans.* 1981, 126.
11. R. B. King and D. H. Rouvray, *J. Am. Chem. Soc.* 1977, **99**, 7834.
12. R. B. King, in *Chemical Applications of Topology and Graph Theory* (Edited by R. B. King), pp. 99–123. Elsevier, Amsterdam (1983).
13. R. B. King, in *Molecular Structure and Energetics* (Edited by J. F. Liebman and A. Greenberg), Vol. 1, pp. 123–148. VCH Publishers, Deerfield Beach, Florida (1986).
14. R. B. King, *Inorg. Chim. Acta* 1986, **116**, 109.
15. T. S. Piper and G. Wilkinson, *J. Inorg. Nucl. Chem.* 1956, **3**, 104.
16. W. Hieber and G. Wagner, *Z. Naturforsch.* 1958, **13b**, 339.
17. R. S. Nyholm, *Proc. Chem. Soc.* 1961, 273.
18. P. Pyykkö and J.-P. Desclaux, *Acc. Chem. Res.* 1979, **12**, 276.
19. A. Dedieu and R. Hoffmann, *J. Am. Chem. Soc.* 1978, **100**, 2074.
20. D. Grdenić, *Quart. Revs.* 1965, **19**, 303.
21. H. L. Roberts, *Adv. Inorg. Chem. Radiochem.* 1968, **11**, 309.
22. R. J. Gillespie and J. Passmore, *Adv. Inorg. Chem. Radiochem.* 1975, **17**, 49.
23. M. Fajardo, H. D. Holden, B. F. G. Johnson, J. Lewis and P. R. Raithby, *J. Chem. Soc., Chem. Commun.* 1984, 24.
24. W. Gäde and E. Weiss, *Angew. Chem. Int. Ed. Engl.* 1981, **20**, 803.
25. J. M. Ragosta and J. M. Burlitch, *J. Chem. Soc., Chem. Commun.* 1985, 1187.
26. N. L. Biggs, *Algebraic Graph Theory*, p. 17. Cambridge University Press, London (1974).
27. H. Hock and H. Stuhlmann, *Chem. Ber.* 1929, **62**, 431.
28. R. D. Ernst, T. J. Marks and J. A. Ibers, *J. Am. Chem. Soc.* 1977, **99**, 2090.
29. F. W. B. Einstein, R. K. Pomeroy, P. Rushman and A. C. Willis, *J. Chem. Soc., Chem. Commun.* 1983, 854.
30. F. W. B. Einstein, T. Jones and R. K. Pomeroy, *J. Am. Chem. Soc.* 1984, **106**, 2707.
31. L. R. Martin, F. W. B. Einstein and R. K. Pomeroy, *Organometallics* 1988, **7**, 294.
32. B. Grünbaum, *Convex Polytopes*, pp. 46–48. Interscience, New York (1967).
33. J. W. Nielsen and N. C. Baenziger, *Acta. Cryst.* 1954, **7**, 277.
34. E. J. Duwell and N. C. Baenziger, *Acta. Cryst.* 1955, **8**, 705.
35. J. D. Corbett, *Inorg. Nucl. Chem. Lett.* 1969, **5**, 81.
36. J. D. Corbett, *Prog. Inorg. Chem.* 1976, **21**, 129.
37. J. D. Corbett, *Chem. Rev.* 1985, **85**, 383.
38. C. Glidewell, *Inorg. Nucl. Chem. Lett.* 1975, **11**, 761.
39. A. Cisar and J. D. Corbett, *Inorg. Chem.* 1977, **16**, 2482.
40. I. D. Brown, D. B. Crump and R. J. Gillespie, *Inorg. Chem.* 1971, **10**, 2319.
41. T. W. Couch, D. A. Lokken and J. D. Corbett, *Inorg. Chem.* 1972, **11**, 357.
42. R. B. King, *Inorg. Chim. Acta* 1982, **57**, 79.
43. R. B. King, in *The Physics and Chemistry of Small Clusters* (Edited by P. Jena, B. K. Rao and S. N. Khanna), pp. 79–82. Plenum Press, New York (1987).
44. R. B. King, *J. Phys. Chem.*, in press.
45. R. Csuk, B. I. Glänzer and A. Fürstner, *Adv. Organometal. Chem.* 1988, **28**, 85.
46. E. Garcia, A. H. Cowley and A. J. Bard, *J. Am. Chem. Soc.* 1986, **108**, 6082.
47. E. Kariv-Miller and V. Svetličić, *J. Electroanal. Chem.* 1986, **205**, 319.

Polyhedron Vol. 7, No. 19/20, pp. 1819–1826, 1988
Printed in Great Britain

0277–5387/88 $3.00+.00
© 1988 Pergamon Press plc

STUDIES ON MONOVALENT η-BUTADIENE DERIVATIVES OF NIOBIUM AND TANTALUM*

PAUL R. BROWN, MALCOLM L. H. GREEN† and PHILIP M. HARE

Inorganic Chemistry Laboratory, South Parks Road, Oxford OX1 3QR, U.K.

and

JUDITH A. BANDY

Chemical Crystallography Laboratory, 9 Parks Road, Oxford OX1 3PD, U.K.

Abstract—The synthesis of [*trans*-Nb(dmpe)$_2$(η-C_4H_6)H], [M(η^3-1-MeC_3H_4)(η-C_4H_6)$_2$], M = Nb or Ta, and [Nb(dmpe)(η^3-1-MeC_3H_4)(η-C_4H_6)] is described. The crystal structure of [*trans*-Nb(dmpe)$_2$(η-C_4H_6)H] has been determined. Variable temperature NMR studies and spin magnetization transfer experiments provide evidence for fluxional processes in these compounds.

Low valent derivatives of niobium and tantalum are rare. The earliest examples of zero-valent derivatives were [M(η-arene)$_2$] and [M(dmpe)$_3$], M = Nb or Ta, dmpe = bis-1,2(dimethylphosphino)ethane, prepared by metal vapour synthesis techniques.[1,2] Here we describe further studies on the synthesis and chemistry of low valent derivatives of niobium and tantalum. A preliminary communication of part of this work has been published.[3]

RESULTS AND DISCUSSION

Treatment of the known compound [Nb(η-C_4H_6)(dmpe)$_2$Cl][4] in tetrahydrofuran with an excess of $LiAlH_4$ gave orange crystals of [Nb(η-C_4H_6)(dmpe)$_2$H] (**1**) (*vide infra*). The analytical, and spectral data for the new compounds described in this work are given in Table 1. The NMR data will be discussed only where interpretation is not straightforward.

Large needle crystals of (**1**), suitable for X-ray diffraction studies were obtained by slow sublimation at 80°C and 10^{-5} torr. The crystal structure of (**1**) is shown in Fig. 1,[5] with selected bond lengths and angles given in Table 2. The niobium atom, P(1) and P(4) lie on a crystallographic mirror plane such that the pair of dmpe ligands occupy two alternative orientations in the equational plane, i.e. that shown in Fig. 1 and its mirror image, each having half occupancy. This disorder is similar to that observed in [M(dmpe)$_3$] (M = Nb and Ta) complexes.[1] The mirror plane also bisects the butadiene ligand. The hydride on niobium was not located by electron density syntheses but it is thought to occupy the vacant coordination site opposite the butadiene ligand (Fig. 2).

The "bite" angles of the dmpe ligands in (**1**) are 79.2 and 78.2°, these are slightly larger than

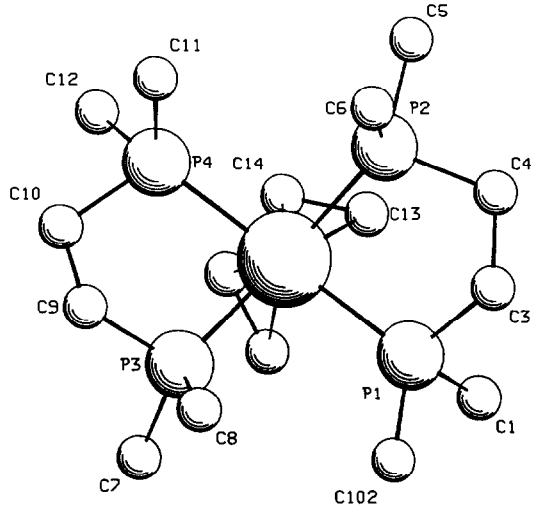

Fig. 1. Molecular structure of (**1**) with atom labels.

* Dedicated to Professor Sir Geoffrey Wilkinson, F.R.S. in appreciation of his pioneering contributions to organotransition metal chemistry and, in particular for his inspiring guidance as my Ph.D supervisor (M.L.H.G.).

† Author to whom correspondence should be addressed.

Table 1. NMR spectroscopic data

Compound, colour	NMR data[a] $^1H^b$	$^{13}C^b$
1[c] Orange	3.81 [2 H, m (11 lines), internal =*CH*—], 1.22 [4 H, br, PCH_2], 1.15 [12 H, d, J_{PH} 7, PCH_3], 1.05 [4 H, br, PCH_2], 0.98 [12 H, d, J_{PH} 7, PCH_3], 0.49 [2 H, m (15 lines), *exo* $=CH_2$], −1.29 [2 H, 8 lines, *endo* $=CH_2$], −2.13 [1 H, quin, J_{PH} 47, *Nb—H*]	63.4 [d, J_{CH} 162, =*CH*—], 37.6 [t, J_{CH} 150, $=CH_2$], 33.4 [t, J_{CH} 126, CH_2—*P*], 25.8 [q, J_{CH} 128, CH_3—*P*], 16.9 [q, J_{CH} 125, CH_3—*P*][d]
2[e] Purple	5.70 [2 H, m (10 lines), H_e and H_k], 5.61 [1 H, m complex, H_j], 5.37 [1 H, m (6 lines), H_p], 3.84 [1 H, d of t, $J_{ab}J_{bd}$ 11.9, J_{bc} 8.3, H_b], 3.62 [1 H, t, $J_{no}J_{op}$ 7.4, H_o], 3.57 [1 H, m (4 lines), J_{fg} 7.0, J_{ef} 7.4, H_f], 3.32 [1 H, m (4 lines) J_{lm} 7.5, J_{kl} 7.8, H_l], 3.16 [1 H, t, $J_{hi}J_{ij}$ 6.8, H_i], 2.97 [1 H, d of q J_{aMe} 6.3, J_{ab} 11.9, H_a], 1.64 [1 H, d, J_{bc} 11.9, H_c], 1.36 [1 H, d, J_{bd} 8.3, H_d], 1.16 [3 H, d, J_{aMe} 6.3, H_{Me}], 0.38 [1 H, t, $J_{lm}J_{km}$ 7.5, H_m], 0.12 [1 H, t, $J_{ig}J_{jg}$ 7.0, H_g], −0.36 [1 H, d of d, J_{he} 6.8, J_{hf} 11.9, H_h], −0.47 [1 H, d of d, J_{no} 7.4, J_{np} 11.0, H_n][f]	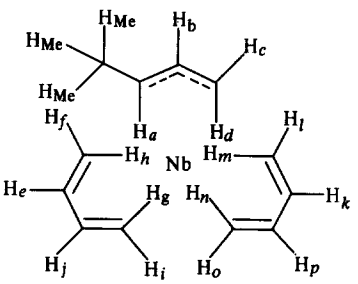
3[g] Orange	5.78 [2 H, m (complex)], 5.65 [1 H, m (complex)], 5.40 [1 H, m (complex)], 4.29 [1 H, d of t], 3.31 [1 H, m (6 lines), 2.73 [1 H, m (complex)], 2.57 [1 H, m (complex)], 2.24 [1 H, m (complex)], 2.14 [1 H, m (complex)], 1.82 [1 H, m (2 lines)], 1.75 [1 H, doublet], 0.99 [3 H, doublet], 0.40 [1 H, m (complex)], 0.25 [1 H, m (complex)], −0.32 [1 H, m (complex)], −0.46 [1 H, m (complex)][f]	
4[h] Orange 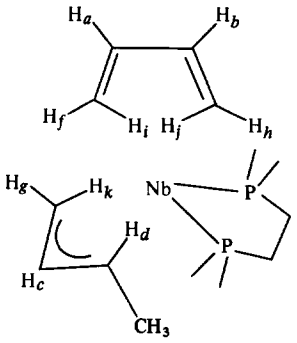	4.58 [1 H, q, J_{HH} 6, H_a], 4.43 [1 H, q, J_{HH} 6, H_b], 4.33 [1 H, dd, J_{HH} 3 and 6, H_c], 3.81 [1 H, q, J_{HH} 6, H_d], 1.86 [3 H, d, J_{PH} 6, PCH_3], 1.06 [3 H, d, J_{HH} 6, C—CH_3], 1.06 [3 H, d, J_{PH} 6, PCH_3], 1.05 [3 H, d, J_{PH} 7, PCH_3], 0.95 [3 H, d, J_{PH} 5, PCH_3], 0.75 [3 H, d, J_{PH} 7, PCH_3], 0.5–1.0 [5 H, broad resonances of PCH_2 and H_f, H_h, H_g], −0.15 [1 H, m, H_i], −0.79 [1 H, q, J_{HH} 8, H_j], −1.78 [1 H, dt, J_{HH} 11 and 4, H_k] ^{31}P NMR.[i] 30.00 [broad s].	104.5 [d, J_{CH} 158, —*CH*=], 97.4 [d, J_{CH} 163, —*CH*=], 92.8 [d, J_{CH} 149, —CH=], 81.8 [d, J_{CH} 158, —CH=], 56.8 [t, J_{CH} 161, $=CH_2$], 48.9 [t, J_{CH} 159, $=CH_2$], 46.2 [t, J_{CH} 159, $=CH_2$], 31.6 [ddt, J_{CP} 22, 22, J_{CH} 127, CH_2P], 29.8 [ddt, J_{CP} 25, 25, J_{CH} 127, CH_2P], 19.2 [q, J_{CH} 125, CH_3—C], 19.1 [dq, J_{CP} 23, J_{CH} 126, PCH_3], 17.5 [dq, J_{CP} 23, J_{CH} 126, PCH_3], 15.6 [dq, J_{CP} 23, J_{CH} 126, PCH_3], 14.2 [dmc, J_{CH} 126, PCH_3]

[a] Given as: chemical shift δ (ppm) [relative intensity, multiplicity, J in Hz, *assignment*].
[b] In [$^2H_6$]-benzene, at room temperature unless otherwise stated.
[c] Found (reqd): C, 42.3(42.8); H, 8.5(8.7)%. *M/e*: 448, [P^+].
[d] In [$^2H_8$]-toluene, 400 MHz, room temperature.
[e] *M/e*: 256.0550 [256.052 (0.002)].
[f] 300 MHz.
[g] *M/e*: 344.0967 [344.096 (0.002)].
[h] *M/e*: 352 [P^+].
[i] [$^2H_6$]-benzene, 101.2 MHz, room temperature.

Table 2. Selected bond lengths (Å) and angles (°) for (1)

Nb(1)—P(1)	2.538(2)	P(1)—C(1)	1.837(8)
Nb(1)—P(2)	2.569(4)	P(1)—C(102)	1.842(10)
Nb(1)—P(3)	2.538(4)	P(1)—C(202)	1.843(10)
Nb(1)—P(4)	2.526(2)	P(1)—C(3)	1.876(9)
		P(2)—C(4)	1.871(9)
C(3)—C(4)	1.532(10)	P(2)—C(5)	1.843(9)
C(9)—C(10)	1.518(9)	P(2)—C(6)	1.838(9)
C(13)—C(14)	1.371(10)	P(3)—C(7)	1.845(9)
C(14′)—C(14)	1.496(16)	P(3)—C(8)	1.836(9)
		P(3)—C(9)	1.859(8)
Nb(1)—C(13)	2.391(6)	P(4)—C(10)	1.874(9)
Nb(1)—C(14)	2.300(6)	P(4)—C(11)	1.839(9)
		P(4)—C(12)	1.837(8)
P(1)—Nb(1)—P(2)	79.22(11)	C(13)—C(14)—C(14′)	114.8(5)
P(3)—Nb(1)—P(4)	78.18(9)		
C(1)—P(1)—C(102)	96.9(29)	C(7)—P(3)—C(8)	103.5(23)
C(1)—P(1)—C(202)	105.5(23)	C(7)—P(3)—C(9)	107.0(17)
C(1)—P(1)—C(3)	97.4(28)	C(8)—P(3)—C(9)	87.7(14)
C(102)—P(1)—C(3)	112.7(16)		
C(202)—P(1)—C(3)	88.6(22)		
C(4)—P(2)—C(5)	96.3(16)	C(10)—P(4)—C(11)	100.4(14)
C(4)—P(2)—C(6)	104.1(16)	C(10)—P(4)—C(12)	91.6(19)
C(5)—P(2)—C(6)	94.9(13)	C(11)—P(4)—C(12)	104.0(12)
P(1)—C(3)—C(4)	114.4(14)	P(3)—C(9)—C(10)	112.3(11)
C(3)—C(4)—P(2)	108.6(15)	C(9)—C(10)—P(4)	112.2(11)

Primes denote atoms generated by mirror plane $(-x, y, z)$.

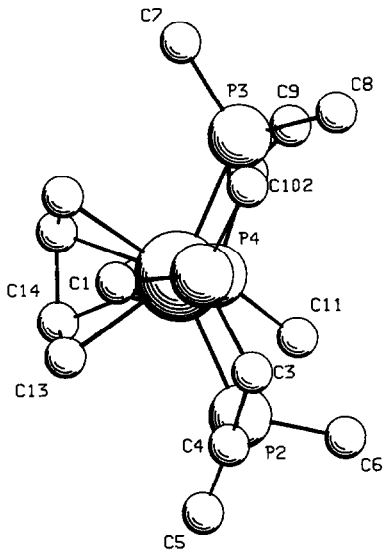

Fig. 2. Structure of (1) orthogonal to Fig. 1 showing hydride cavity.

observed in [Nb(dmpe)$_3$] [74.6(2)°]; which may be considered more sterically crowded. Also, there may be disorder of the dmpe backbones as previously described,[1] but the overlapping dmpe ligands made this difficult to resolve.

The Nb—P distances range from 2.526 to 2.538 Å {cf. 2.526(3) Å in [Nb(dmpe)$_3$]} and the four phosphorus atoms form an approximate plane. For the butadiene ligand the niobium to terminal-carbon distances are longer than to the internal-carbons (by 0.091 Å). The terminal–internal C—C bond is 0.125 Å shorter than that between the two internal carbons indicating the (η^4-1 : 2, 3 : 4) bonding character for the butadiene. This is unusual for early transition metal butadiene complexes such as [Hf(η-C$_4$H$_6$)$_2$(dmpe)][6] which tend to adopt the alternative (1,4-η^2) or metallacyclo-3-pentene structure, and is indicative of the butadiene ligand in (1) acting more as an electron donor than acceptor. The butadiene ligand is also essentially planar and approximately parallel to the plane defined by the four phosphorus atoms.

The variable temperature solution NMR data of (1) indicates that the molecule is fluxional at room temperature but on cooling to −85°C adopts the conformation found in the crystalline state. In particular, the observation of an Nb—H resonance at δ −2.1 [J(P—H) = 47 Hz] in the room temperature ^{1}H NMR spectrum of (1) indicates that the ^{31}P nuclei are magnetically equivalent. Since the buta-

diene ligand also appears as three 2-hydrogen multiplets at this temperature, it is likely that rapid rotation of the η-butadiene ligand about the niobium–ligand axis is occurring at room temperature.

On cooling to -85°C the ^{1}H NMR spectrum becomes markedly different. The hydride signal became a broad, featureless band. The internal hydrogens of the butadiene are observed at δ 3.6 and 4.2, which suggests that butadiene rotation is slow on the NMR timescale at this temperature. However, the resonances due to the terminal vinyllic hydrogens were not readily distinguished because the region δ 0–2 shows several overlapping broad resonances. The two large doublets due to the dmpe methyl hydrogens have also collapsed into this broad signal. This is most likely due to the process of flexing of the methylene backbone in the dmpe ligands being in the regime of intermediate exchange.

The variable temperature ^{31}P{^{1}H} NMR spectrum of (**1**) (Fig. 3) exhibits several interesting features. At -106°C the spectrum consists of two broad resonances in the ratio 3:1. At -70°C the two bands coalesce to a single broad resonance

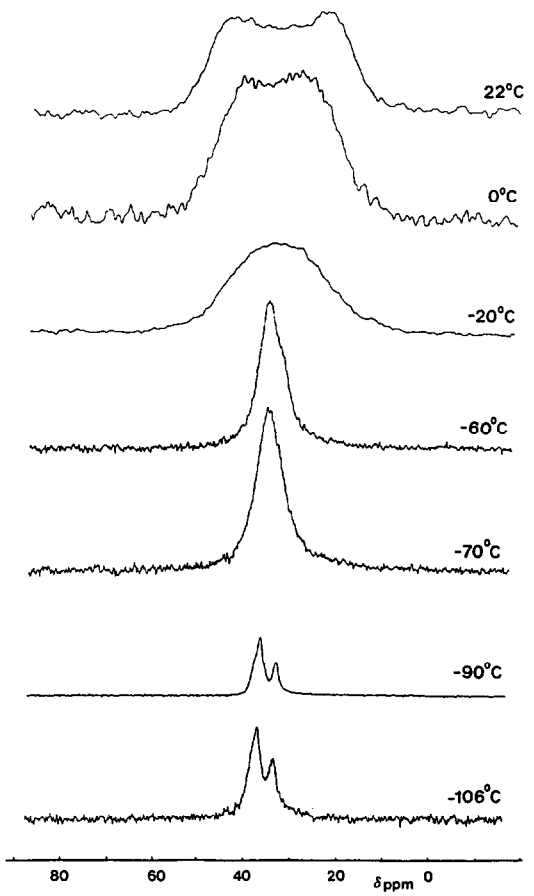

Fig. 3. Variable temperature 101.26 MHz ^{31}P{^{1}H} NMR spectra of (**1**) in [$^2H_8$]-toluene.

($\omega_{1/2}$ = 64 Hz). On further warming to 0°C the resonance broadens further ($\omega_{1/2}$ = 271 Hz), and then apparently separates into two equal components with the separation between the maxima being 190 Hz at room temperature. The doublet appearance of the room temperature spectrum is attributed to partial collapse of the ^{31}P—^{97}Nb quadrupole coupling. Differential broadening of the spectral lines of spin-1/2 nuclei coupled to quadrupolar nuclei (^{97}Nb; $I = 9/2$) is observed when the spin–lattice relaxation time (T_1) of the latter is comparable to $(J)^{-1}$ (where J = quadrupole coupling constant). As the temperature is lowered the T_1 of quadrupolar nuclei generally *decreases* sharply and at low temperatures (typically < -70°C) line-broadening effects on spin-1/2 nuclei due to quadrupolar coupling are removed. The activation energy for the fluxional process leading to coalescence of the ^{31}P nuclei at -80°C is estimated to be $\Delta G^{\ddagger} = 36$ kJ mol^{-1}. We assume this process to be rotation of the butadiene ligand.

Hydrogen-1 spin magnetization transfer experiments on (**1**) show no evidence for intramolecular hydrogen exchange processes. However, ^{1}H and ^{2}H NMR spectra of the orange crystals formed from [Nb(η-C_4H_6)(dmpe)$_2$Cl] and $LiAlD_4$, namely [Nb(η-C_4H_6)(dmpe)$_2$D], (**1**-[^{2}H]) indicate statistical scrambling of deuterium into the terminal *exo* and *endo* sites of the butadiene ligand. There was no deuterium incorporation into the internal hydrogen sites. A similar hydrogen scrambling has been observed in the compound [NbH(η-C_2D_4)(dmpe)$_2$].[7] We note that the crystal structure of (**1**) shows that the butadiene and the hydride ligands are mutually *trans*, and therefore substantial rearrangement must occur to enable intramolecular scrambling.

Co-condensation of niobium or tantalum atoms with an excess of buta-1,3-diene gives, after sublimation, highly sensitive purple or orange crystals of [Nb(η-1-MeC_3H_4)(η-C_4H_6)$_2$] (**2**) or [Ta(η-1-MeC_3H_4)(η-C_4H_6)$_2$] (**3**), respectively. Compounds (**2**) and (**3**) are electron-rich[8] formally 16-electron compounds. In the light of the recently established occurrence of agostic bonding in other formally 16-electron η-methylallyl compounds[9,10] we studied their dynamic NMR spectra to attempt to establish whether agostic bonds were present.

The ^{1}H NMR spectrum of (**2**) is highly complex and despite extensive double resonance experiments only partial assignment is possible. The spectra clearly corresponded to the presence of two η-butadiene groups and a η-1-methylallyl group in (**2**) but do not allow distinction between possible conformers arising from the relative dispositions of the ligands (see Scheme 1). The ^{1}H NMR spectrum of

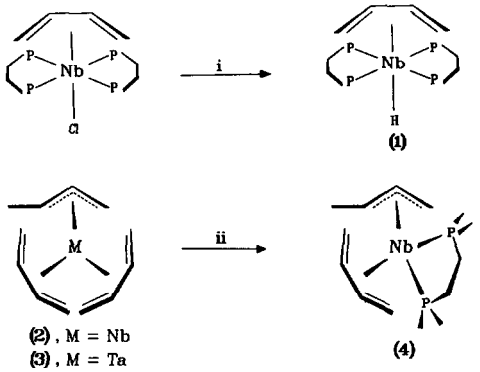

Scheme 1. (i) $LiAlH_4$ in THF, room temperature, 85% and (ii) dmpe in pentane, −10°C, 25%.

(2) in [$^2H_8$]-tetrahydrofuran at room temperature and at −120°C showed no significant differences.

Of particular interest was the band in the room temperature ^{13}C NMR spectrum of (2) assigned to the 1-methyl group, which occurs as a binomial quartet with J(C—H) = 124 Hz. This coupling constant is consistent with either a normal methyl group, or, with a fluxional agostic methyl group.[10] No resolvable change in the coupling constant is observed on cooling to −85°C. Further, there was no evidence for the presence of other conformers of (2). However, the linewidths of the resonances other than that of the 1-methyl group were very temperature dependent. On warming from −85°C the spectrum of (2) changes markedly. The signals became very broad, indeed at −60°C they flattened into the baseline, and then the spectrum sharpens again as the temperature approaches room temperature. Since no other conformers of (2) were readily detected at low temperatures, we attribute the dramatic variations in the linewidths to a combination of changes in the molecular symmetry and the consequent unpredictable quadrupolar relaxation times of the ^{97}Nb nucleus.

A spin saturation transfer experiment on (2) at 45°C shows that all of the hydrogens on the terminal carbons of all three ligands undergo exchange ($\Delta G^{\ddagger}$ 95 ± 5 kJ mol^{-1}). This process is expected to proceed via an equilibrium between [Nb(η-C_3H_5Me)(η-C_4H_6)$_2$] and the unobserved 18-electron hydride [NbH(η-C_4H_6)$_3$].

The room temperature ^1H NMR spectrum of the tantalum analogue (3) was very similar to that observed for (2). The detailed analysis of the spectra was complicated by the appearance of a minor low symmetry isomer at low temperatures. Spin saturation transfer experiments at 50°C showed that the hydrogens of the methyl group are exchanging with all the terminal hydrogens in both the major and minor isomers. The complexity of the spectrum precluded quantitative measurements but the data suggests that the rates of exchange between isomers and hydrogen migration rates must be comparable.

In conclusion, it was not possible to confirm the suspected presence of agostic methyl groups in (2) and (3) due to the complexity of their NMR spectra arising from low symmetry and fluxional behaviour.

Treatment of (2) with dmpe gave the bright orange oily solid [Nb(η-C_3H_4Me)(η-C_4H_6)(dmpe)] (4). The low resolution mass spectrum of (4) showed a parent ion peak at M/e = 352 corresponding to $NbC_{14}H_{29}P_2$. The NMR data may be interpreted in terms of a formally 16-electron structure for (4) shown in the Scheme 1. The connectivity of the signals was established by the use of a ^1H—^1H COSY two-dimensional NMR spectrum. This showed the bands assigned to H_a, H_b, H_f, H_i, H_j and H_h (Table 1) comprise a butadiene ligand at chemical shifts typical for their respective environments. The vinylic hydrogens of the 1-methylallyl group may be assigned to the bands H_c, H_d, H_g and H_k, with the methyl group appearing as a doublet at δ 1.06. Doublets assignable to the dmpe methyl hydrogens are observed at δ 1.85, 0.95 and 0.75, the fourth overlapping with the resonance of the methyl of the 1-methylallyl group. The fully coupled ^{13}C NMR spectrum showed a binomial quartet (J_{CH} = 125 Hz) for the 1-methyl group. ^1H magnetization transfer experiments on (4) at 45°C showed no observable transfer.

The new reactions and proposed structures for the new compounds (1)–(4) are shown in Scheme 1.

EXPERIMENTAL

All preparations, manipulations and reactions were carried out under an inert atmosphere of dinitrogen (< 10 ppm oxygen, < 20 ppm water) using standard Schlenk tube and vacuum-line techniques, or in a dry box. Dinitrogen was purified by passage through a column containing BTS catalyst and 5 Å molecular sieves.

All solvents were thoroughly deoxygenated before use by repeated evacuation followed by admission of dinitrogen. Solvents were pre-dried over activated molecular sieves and then distilled from potassium (tetrahydrofuran, THF), sodium (toluene), sodium–potassium alloy [light petroleum (b.p. 40–60°C throughout), diethyl ether] or phosphorus pentoxide (dichloromethane), under an inert atmosphere of dinitrogen before use. Methanol was dried over activated molecular sieves and deoxygenated before use. Deuterated solvents for NMR samples were stored in Rotaflo ampoules over activated molecular sieves and transferred by

vacuum distillation. Celite 545 filtration aid (Koch–Light) was dried in an oven at 80°C before use.

IR spectra were recorded as Nujol mulls between CsI plates on a Perkin–Elmer 1510 FT interferometer. Hydrogen-1 NMR spectra were determined at 300 and 500 MHz using Bruker WH-300 and AM-500 spectrometers, respectively. Carbon-13 and ^{31}P NMR spectra were determined at 62.89 and 101.26 MHz, respectively, using a Bruker AM-250 spectrometer. Spectra were referenced internally using the residual solvent (^1H) and solvent (^{13}C) resonances relative to tetramethylsilane ($\delta = 0$ ppm), or externally using trimethylphosphate [$P(O)(OMe)_3$] in D_2O (^{31}P). All chemical shifts are quoted in δ (ppm) and coupling constants are in Hertz (Hz).

Metal vapour synthesis experiments were carried out using the apparatus described elsewhere.[11]

Bis[*bis*-1,2(*dimethylphosphino*)*ethane*](η-*buta*-1,3-*diene*)*hydridoniobium* (**1**)

The compound [$NbCl(\eta$-$C_4H_6)(dmpe)_2$] (100 mg, 0.21 mmol), prepared as described,[4] in THF (30 cm^3) was treated with a suspension of $LiAlH_4$ (10 mg, 0.26 mmol) in THF (30 cm^3) with stirring. No immediate colour change was observed but after stirring for 12 h the initially orange solution darkened. The reaction mixture was filtered and solvent was removed from the filtrate under reduced pressure. The solid residue was extracted with petroleum ether (b.p. 60–80°C, 70 cm^3) giving a yellow–orange solution and a large quantity of off-white powder. The solution was filtered and reduced to 30 cm^3. Cooling to −25°C produced orange needle crystals which were isolated and dried *in vacuo*. Yield, 80 mg, 85%. Further purification was achieved by fractional sublimation at 10^{-4} torr and 80°C. After 12 h excellent needle crystals had grown on the sides of the sublimation tube.

[*Bis*-1,2(*dimethylphosphino*)*ethane*](η-*buta*-1,3-*diene*) *deuterioniobium* (**1-[^{2}H]**)

This was prepared from [$NbCl(\eta$-$C_4H_6)(dmpe)_2$] (0.12 g, 0.25 mmol) in a manner identical to that for (**1**) except using $LiAlD_4$. The product was recrystallized from petroleum ether (b.p. 40–60°C, 10 cm^3). Yield, 40 mg, 35%.

Bis(η-*butadiene*)(η-1-*methylallyl*)*niobium* (**2**)

Niobium atoms (*ca* 1 g, 10.7 mmol), generated from *ca* 6 g ingots of the metal at a power of 1.9 kW (5.9 kV at 320 mA), were co-condensed over 4 h with an excess of the co-reactant (90 cm^3 of a mixture of 15% tetrahydrofuran and 85% buta-1,3-diene). During the co-condensation, the matrix was orange. On warming, the matrix melted and became purple. After melting the reaction mixture was extracted from the apparatus with cooled tetrahydrofuran (300 cm^3 at −78°C). The extract was intensely purple and contained a quantity of unreacted metal. The product mixture was maintained at −78°C and rapidly transferred to a vacuum line. The volatile components were then removed under reduced pressure with the mixture initially remaining at −78°C. After approximately 30 min the majority of the excess butadiene had been removed and the mixture was allowed to warm slowly whilst the volatile components were still being removed. In this way the polymerization of the excess butadiene in the extract could be kept to a minimum. After approximately 2 h all of the more volatile components had been removed giving an intensely coloured rubbery material. To this solid was added petroleum ether (60–80°C, 200 cm^3) and the mixture left for 3 h at room temperature to slowly extract the organometallic product. A purple extract was filtered through Celite from pale grey polymeric material. The clear filtrate was reduced in volume to *ca* 50 cm^3 by removal of the solvent under reduced pressure. The residue was sublimed onto a liquid dinitrogen cooled probe at 40°C and 10^{-4} torr. The deep purple sublimate was extracted with petroleum ether (b.p. 30–40°C, 50 cm^3) and the extract was concentrated (to 10 cm^3) and cooled to −30°C for 12 h giving a purple microcrystalline solid. The supernatant was decanted from the solid which was washed with petroleum ether (b.p. 30–40°C, 2 × 5 cm^3) at −30°C and dried *in vacuo*. Yield, *ca* 1 g. It was found (^1H NMR) that the product still contained a small quantity of impurity which could be removed by resublimation *in vacuo* at 40°C.

Bis(η-*butadiene*)(η-1-*methylallyl*)*tantalum* (**3**)

Tantalum atoms (*ca* 2 g, 11.1 mmol) were generated from a *ca* 9 g ingot of the metal at a power of 1.7 kW (5 kV at 340 mA) and co-condensed over 4 h with an excess of the co-reactant (90 cm^3 of a mixture of 15% tetrahyrofuran and 85% buta-1,3-diene). During the co-condensation the matrix was orange. On warming, the matrix melted and remained deep orange. The isolation followed the same procedure as for the niobium analogue except that the tantalum compound required a temperature of 70°C for the sublimation. Yield, *ca* 0.6 g.

Bis-1,2(*dimethylphosphino*)*ethane*(η-*butadiene*)(η-1-*methylallyl*)*niobium* (**4**)

The compound [Nb(dmpe)(η-C_4H_6)(η-1-Me C_3H_4)] (400 mg, 1.6 mmol) in pentane (60 cm^3) at -10°C was treated with dmpe (0.35 g, 2.3 mmol) in pentane (50 cm^3) at -10°C, in a dropwise manner. The initially deep red–purple solution became deep red. The solvent was removed under reduced pressure to give a dark red–orange oil. This was sublimed at 10^{-5} torr and 60°C giving an oily orange solid. Attempts to recrystallize this material from pentane at -78°C did not effect any increase in purity, due to extremely high solubility. Yield *ca* 100 mg.

Crystal data

$C_{16}H_{37}NbP_4$, $M = 448.3$, orthorhombic, $a = 13.246(2)$, $b = 13.336(2)$, $c = 13.057(9)$ Å, $U = 2306.5$ Å^3, space group $Cmc2_1$, $Z = 4$, $D_c = 1.29$ Mgm^{-3}, $F(000) = 936$, λ(Mo-K_α) = 0.70930, μ(Mo-K_α) = 7.69 cm^{-1}, crystal dimensions $0.9 \times 0.15 \times 0.16$ mm.

Data collection and processing

The crystal was sealed under nitrogen in a Lindemann glass capillary and mounted on an Enraf–Nonius CAD4 diffractometer. Cell dimensions were obtained by least-squares methods from the positions of 25 carefully centred reflections. Data collection used ω–2θ scan mode with ω-scan width $(0.9 \pm 0.35 \tan\theta)°$ and scan speed range 0.84–6.71° min^{-1}. 4988 reflections measured ($1 < \theta < 30°$), 1823 unique [merging $R = 0.017$ after Lp and absorption corrections[12] (max., min. correction 1.07, 1.01)] giving 1327 observed [$I > 3\sigma(I)$].

Structure analysis and refinement

Solution by heavy atom method and direct methods on the difference structure using DIRDIF[13] in $Cmc2_1$ to yield Nb and P positions. The structure was developed slowly by difference Fourier methods resulting in the location of all carbon atoms. P(1) and P(4) were placed on the mirror plane, with Nb(1), to avoid ill-conditioned matrices. Refinement was by full-matrix least-squares with all non-hydrogen atoms anisotropic. The geometry of the dmpe ligands was restrained[14] to aid convergence. The carbon atoms of these ligands have relatively large thermal vibration parameters indicating there may be disorder as observed in a number of other dmpe complexes. Attempts to resolve this disorder for all carbons, except C(102) : C(202) gave a poorer fit to the observed electron density than the unresolved anisotropic model which was retained. No hydrogens were located. During the latter stages of refinement corrections were made for isotropic extinction[15] and anomalous dispersion[16] and reflections were assigned weights[17] according to $w = 1/\Sigma A_r T_r(X)$ where $n = 3$, $A_r = 5.87$, -2.48, and 4.19, T_r is the polynomial function and X is the function $|F_o|/|F_{omax}|$. At convergence $R = 0.033$, $R_w = 0.035$.

All calculations were performed on the VAX 11/750 computer of the Chemical Crystallography Laboratory with the CRYSTALS package.[18] Atomic scattering factors were taken from *International Tables*.[19] Atomic coordinates, mean planes, anisotropic thermal vibration parameters and observed and calculated structures factors have been deposited as supplementary material.

$$R = \Sigma(|F_o| - |F_c|)/\Sigma|F_o|,$$

$$R_w = \{\Sigma w(|F_o| - |F_c|)^2/\Sigma w|F_o|^2\}^{1/2}.$$

Acknowledgements—We wish to thank British Petroleum plc for a scholarship (to P.M.H.) and the Science and Education Research Council for a grant (to P.R.B.)

REFERENCES

1. F. G. N. Cloke, P. J. Fyne, V. C. Gibson, M. L. H. Green, M. J. Ledoux, R. N. Perutz, A. Dix, A. Gourdon and K. Prout, *J. Organomet. Chem.* 1984, **277**, 61.
2. F. G. N. Cloke and M. L. H. Green, *J. Chem. Soc., Dalton Trans.* 1981, 1938.
3. P. R. Brown, F. G. N. Cloke and M. L. H. Green, *J. Chem. Soc., Chem. Commun.* 1980, 1126.
4. S. S. Wreford and J. F. Whitney, *Inorg. Chem.* 1981, **20**, 373.
5. E. K. Davies, CHEMGRAF User Manual, Chemical Crystallography Laboratory, University of Oxford (1983).
6. S. S. Wreford and J. F. Whitney, *Inorg. Chem.* 1981, **20**, 3918.
7. R. R. Schrock, *J. Organomet. Chem.* 1976, **121**, 373.
8. J. C. Green and R. R. Watson, personal communication.
9. M. Brookhart and M. L. H. Green, *J. Organomet. Chem.* 1983, **250**, 395.
10. M. Brookhart, M. L. H. Green and L-L. Wong, *Prog. Inorg. Chem.* 1988, in press.
11. M. L. H. Green and D.O'Hare, *ACS Symp. Ser.* 1987, **333**, 260.
12. A. C. T. North, D. C. Phillips and F. S. Mathews, *Acta Cryst.* 1968, **A24**, 351.
13. P. T. Beurskens, W. P. Bosman, H. M. Doesburg, R. O. Gould, Th. E. M. Van den Hark, P. A. J. Prick, J. H. Noordik, G. Beurskens, V. Parthasarathi, H. J. Bruins-Slot and R. C. Haltiwanger, DIRDIF, 1984,

Crystallography Laboratory, Toernooiveld, 6525 ED Nijmegen, Netherlands (1984).
14. J. T. Waser, *Acta Cryst.* 1963, **16**, 1091; J. S. Rollett, *Crystallographic Computing* (Edited by F. R. Ahmed), p. 169. Munksgaard, Copenhagen (1969).
15. A. C. Larson, *Acta Cryst.* 1967, **23**, 664.
16. *International Tables for X-ray Crystallography*, Vol. IV, p. 149. Kynoch Press, Birmingham (1974).
17. J. R. Carruthers and D. J. Watkin, *Acta Cryst.* 1979, **A35**, 698; E. Prince, *Mathematical Techniques in Crystallography*, Springer, New York (1982).
18. D. J. Watkin, J. R. Carruthers and P. W. Betteridge, CRYSTALS User Guide, Chemical Crystallography Laboratory, University of Oxford (1985).
19. *International Tables for X-ray Crystallography*, Vol. IV, p. 99. Kynoch Press, Birmingham (1974).

Polyhedron Vol. 7, No. 19/20, pp. 1827–1829, 1988
Printed in Great Britain

0277–5387/88 $3.00+.00
Pergamon Press plc

HOMOGENEOUS DEUTERIATION OF ALKENES USING [RhCl(4*R*,5*R*-DIOP)] CATALYSTS

MUAMMER GÜNGÖR, FRED H. JARDINE* and J. DENIS WHEATLEY

Department of Physical Sciences, North East London Polytechnic, Romford Road, London E15 4LZ, U.K.

Abstract—Mass spectrometric analyses of the products from the homogeneous deuteriation of alkenes using the [RhCl(4*R*,5*R*-DIOP)] catalyst have shown that considerable quantities of polydeuteriated products are obtained. These products arise from the decomposition of the intermediate rhodium(III) alkyl complex [RhDCl(alkyl)(DIOP)] before the second atom of deuterium can be transferred to the alkyl ligand. Its decomposition by β-hydride abstraction brings about both polydeuteriation and scrambled addition of deuterium to the alkene. The yields of specifically deuteriated products are inferior to those obtained from Wilkinson-type catalysts. The best yields of dideuteroproducts are obtained from substituted alkenes that chelate to the catalyst and thereby stabilize the intermediate alkyl.

The deuteriation of alkene substrates, homogeneously catalysed by [$RhX(PAr_3)_3$] complexes, has recently been investigated. It was shown that the ability of the intermediate rhodium(III) monodeuteroalkyl to receive the second atom of deuterium from rhodium before β-hydride decomposition took place was important in minimizing both polydeuteriation (the incorporation of more than two atoms at the deuterium/alkene bond) and scrambled addition of deuterium (the incorporation of deuterium elsewhere than at the site of the original alkene bond). Stability could be conferred both electronically and sterically. Electron-withdrawing ligands stabilized, and steric crowding destabilized secondary alkyl complexes. However, alk-1-enes gave the best yields of dideuteroproducts when [$RhI(PPh_3)_3$] was the catalyst since in these cases the more stable 1-alkyl intermediate was formed.[1]

Generally the [RhCl(DIOP)] system has been ignored in mechanistic studies of homogeneous, asymmetric hydrogenation although cationic rhodium–DIOP complexes have been extensively investigated.[2] In fact the two systems give virtually identical optical yields under similar conditions.[2,3] Accordingly, the catalytic deuteriation of a range of alkene substrates was investigated using the more accessible neutral complex. Previously it had been reported that isotope exchange occurred in the deuteriation of α-acetamidocinnamic acid[4] but not in the deuteriation of α-benzoylaminocinnamic acid.[5]

*Author to whom correspondence should be addressed.

RESULTS AND DISCUSSION

The relative participation of the dihydride and alkene routes in the asymmetric hydrogenation of prochiral alkenes has attracted much comment.[2] As both routes share a common alkyldeuteriorhodium(III) intermediate, which is the source of non-specific deuteriation, the actual route followed is of little consequence here.

Deuteriation of cyclooctene catalysed by [RhCl(4*R*,5*R*-DIOP)] brought about extensive polydeuteriation. Cyclooctane isotopomers containing up to seven atoms of deuterium were found amongst the products (Table 1). If the reaction was stopped before completion *ca* 27% d_1-cyclooctene could be detected in the reaction mixture. Further, the rapid appearance of HD and H_2 in the gas phase indicated that the intermediate cyclooctyl complexes were decomposing more rapidly by β-hydride abstraction than by transfer of the second atom of deuterium to form cyclooctane.

Similar polydeuteriation and production of HD and H_2 was observed in the catalytic deuteriation of cyclohexene. When [$RhCl(PPh_3)_3$] was used as the catalyst in this reaction only $C_6H_{10}D_2$ was formed.

It has been observed previously in the [$RhCl(PPh_3)_3$] system that for extensive polydeuteriation to occur there must be rotation about either the carbon–carbon or rhodium–carbon bonds of the alkyl complex.[1] This seems to be the case in the [RhCl(4*R*,5*R*-DIOP)] system, since in both catalyses only d_2-norbornane can be formed from bicyclo[2.2.1]hept-2-ene. Rotation about the

Table 1. Yields of deuteriated alkanes from [RhCl(4*R*,5*R*-DIOP)] catalysed reactions

Alkene	Solvent	Alkane isotopomer d_0	d_1	d_2	d_3	d_4	d_5	d_6	d_7
Cyclohexene[a]	Toluene			76.3	18.7	4.5	0.5		
2-Cyclohexen-1-one	Toluene			93.7	6.3				
Cyclooctene[a]	Toluene	7.5	22.2	35.2	19.4	10.2	3.9	1.2	0.4
Norbornene	Toluene			100.0					
Dihydropyran	*o*-Xylene			87.6	9.5	2.9			
3,4-dihydro-2-methoxy-2*H*-pyran	Benzene			98.7	1.3				
Allylbenzene[a]	Toluene			89.4	8.5	2.1			
Allyl phenyl ether[a]	Toluene			90.9	7.1	2.0			
Hept-1-ene	Toluene	1.4	9.2	75.6	7.8	2.8	0.9		
Hex-1-ene[b]	Toluene			68.6	19.2	7.3	3.3	1.6	
5-Hexen-2-one[b]	Benzene			98.0	2.0				
Methyl 2-crotonate	Benzene			71.2	18.8	8.8	1.2		
2-Methylpent-1-ene	Benzene			94.5	3.8	1.1	0.6		
Oct-1-ene[a]	Benzene	3.6	12.6	60.8	14.0	5.8	2.3	0.9	

Catalyst [{RhCl(C_8H_{14})$_2$}$_2$] (0.1 mmol) + 4*R*,5*R*-DIOP (2 mmol).
Alkene 60 mmol; [a] 30 mmol; [b] 35 mmol.
Total solution volume 80 cm^3.
Temperature 297 K.

carbon–carbon bond of the alkyl cannot occur because of the fused ring system, and rotation about the rhodium–carbon bond is to no avail since β-hydride abstraction from a bridgehead carbon contravenes Bredt's rule.

In the Diop system, it is not possible to increase the stability of the intermediate alkyl complex by exchanging the ligands bound to rhodium for others, the only way a more stable alkyl intermediate can be obtained is by incorporating a functional group in the alkene chain that is capable of chelating to rhodium. This has two beneficial effects on the stability of the intermediate alkyl. First it hinders rotation about both the carbon–carbon and rhodium–carbon bonds and second it occupies an additional coordination site on rhodium that might otherwise be available to receive the abstracted hydrido or deuterio ligand and thereby allow the alkyl ligand to revert to an alkene.

The behaviour of alkene hydrocarbons and similar substituted alkenes can now be rationalized. If the substituted alkene does not form a chelated complex then similar, high yields of polydeuteriated species are obtained from it and its hydrocarbon analogue (cf. allyl benzene and allyl phenyl ether in Table 1). If, however, chelation does occur then less extensive polydeuteriation takes place than in the case of the corresponding hydrocarbon (cf. hex-1-ene and 5-hexen-2-one).

The highest yield of dideuterioproduct from a hydrocarbon substrate was obtained from 2-methylpent-1-ene. In this case deuterioisomerization is unlikely to occur since it would require the formation of the tertiary 2-alkyl complex. However, as some d_4- and d_5-alkanes are obtained, the unfavoured tertiary alkyl intermediate must be formed if only infrequently. The excess deuterium is not incorporated in the terminal CH_2D group as experiments using methyl 2-crotonate demonstrate that the thermodynamically favoured Saytzeff β-hydride elimination occurs. Carbon-13 NMR can be used to locate the deuterium atoms in the saturated ester. Triplets at 18.6 and 35.7 ppm indicate the presence of deuterium at C-2 and C-3, but there is no deuterium in the methyl groups since these give singlets at 13.6 and 51.2 ppm. The fifth atom of deuterium in the d_5-product is presumably in a CD_2 group and undetectable because of the long relaxation time involved.

Not all substituted alkenes undergo deuteriation but some such as ethyl 3-aminocrotonate give rise to HD and H_2 in the gas phase.

In general [RhCl(4*R*,5*R*-DIOP)] is a far inferior deuteriation catalyst than [RhCl(PPh_3)$_3$]. It gives lower yields of specifically deuteriated products and requires longer reaction times.

EXPERIMENTAI

Hydrated rhodium trichloride (Johnson Matthey) was used without purification. Deuterium (BDH, 99.5%) was dried by passing it through a tower containing dry silica gel before admission to the apparatus. The apparatus used to deuteriate

alkenes at sub-atmospheric pressure has been described previously.[6]

The alkenes (Aldrich) were dried and freed from hydroperoxides by distillation from sodium at atmospheric pressure. Where this method of purification would have brought about decomposition, they were freed from hydroperoxides by passing them down a column of activated alumina and collecting them in a reservoir by displacement of nitrogen. In both cases they were admitted to the deuteriation apparatus without coming into contact with air.

After deuteriation the catalyst was removed from the reaction mixture by passing it down a column of activated alumina. This minimizes post-deuteriation reactions that may cause erroneous results. The deuteriated products were partially separated from the effluent by fractional distillation. Aliquots of the distillate were analysed using an AEI MS10 or MS902 mass spectrometer. The ionizing voltage was 70 eV. The product yields were calculated from the parent ion peaks after making due allowance for other species of the same molecular mass.

A.R. grade benzene, toluene and 2-xylene were dried over sodium, and degassed in the deuteriation apparatus. Chlorotris(triphenylphosphine) rhodium(I)[7] and $[\{RhCl(C_8H_{14})_2\}_2]$[8] were prepared according to directions given in the literature. The catalyst [RhCl(4*R*,5*R*-DIOP)] was prepared *in situ* from one equivalent of the latter complex by allowing it to react with two equivalents of 4*R*,5*R*-DIOP in the deuteriation vessel.

4R,5R - O - *isopropylidene* - 2,3 - *dihydro* - 1,4-*bis* (*diphenylphosphino*)*butane*

This compound was prepared from diethyl *R,R*-tartrate by the following modifications of procedures given in the literature. The intermediates diethyl-2,3,*O*-isopropylidene-*R,R*-tartrate,[9] and 2,3-*O*-isopropylidene-*R,R*-threitol[10] were prepared according to directions given in the literature. The latter was converted to 1,4-ditosyl-2,3-*O*-isopropylidene-*R,R*-threitol by either of the following methods.

(a) A solution of 2,3-*O*-isopropylidene-*R,R*-threitol (8.4 g) in dry pyridine (55 cm^3) was cooled to −15°C. *Para*-toluenesulphonyl chloride (21 g) was added quickly to the solution in successive small portions. **SAFETY NOTE**:—the addition in one portion is dangerous because of the exothermic reaction. The mixture was shaken until homogeneous and stored at 0°C for 12 h. The crystals of pyridinium chloride were filtered off. The product was precipitated by slow addition of water (90 cm^3) over 1–2 h at 0°C. The crude product was filtered off, washed with a little ethanol and twice recrystallized from ethanol. M.p. 88–89°C (lit. 91–92°C). Found: C, 53.6; H, 5.8. Required: C, 53.6, H, 5.6%.

(b) Small pieces of sodium (1 g) and 2,3-*O*-isopropylidene-*R,R*-threitol (6 g) were mixed in a flask fitted with a reflux condenser. When the reaction rate slowed, dry diethyl ether (50 cm^3) was added and the reaction was allowed to proceed to completion. To this solution *p*-toluenesulphonyl chloride (15 g) was added quickly in small portions. The rate of addition was adjusted so that the mixture refluxed gently. The mixture was stirred for 1 h and the diethyl ether distilled off. The residue was added to water (80 cm^3), and the product allowed to precipitate over a period of 2 h. The crude product was filtered off, washed with a little ethanol and twice recrystallized from ethanol. M.p. 91–92°C. Found: C, 53.5, H, 5.2%.

4*R*,5*R*-DIOP was prepared from the ditosyl compound by Kagan's method.[11]

REFERENCES

1. M. Güngör, F. H. Jardine and J. D. Wheatley, *J. Chem. Soc., Dalton Trans.* 1988, in press.
2. F. H. Jardine in *The Chemistry of the Metal–Carbon Bond* (Edited by F. R. Hartley), Vol. 4, pp. 733–818. Wiley, Chichester (1987).
3. R. Glaser, S. Geresh and J. Blumenfeld, *J. Organomet. Chem.* 1976, **112**, 355.
4. J. M. Brown and D. Parker, *J. Org. Chem.* 1982, **47**, 2772.
5. M. D. Fryzuk and B. Bosnich, *J. Am. Chem. Soc.* 1977, **99**, 6262.
6. F. H. Jardine, Ph.D. Thesis, University of London (1967).
7. J. A. Osborn, F. H. Jardine, G. Wilkinson and J. F. Young, *J. Chem. Soc. (A)*, 1966, 1711.
8. L. Porri, A. Lionetti, G. Allegra and A. Immirzi, *J. Chem. Soc., Chem. Commun.* 1965, 336.
9. M. Carmak and C. J. Kelley, *J. Org. Chem.* 1968, **33**, 2171.
10. P. W. Feit, *J. Med. Chem.* 1974, **7**, 14.
11. H. B. Kagan and Tuan Phat Dang, *J. Am. Chem. Soc.* 1972, **94**, 6429.

Polyhedron Vol. 7, No. 19/20, pp. 1831–1840, 1988
Printed in Great Britain

0277–5387/88 $3.00+.00
© 1988 Pergamon Press plc

ZERO VALENT MOLYBDENUM AND TUNGSTEN ETHYLENE ISOCYANIDE COMPLEXES: SYNTHESIS AND STRUCTURAL PROPERTIES*

ERNESTO CARMONA,† AGUSTIN GALINDO and JOSE M. MARIN

Departamento de Química Inorgánica-Instituto de Ciencia de Materiales, Facultad de Química, Universidad de Sevilla-CSIC, Apartado 553, 41071 Sevilla, Spain

and

ENRIQUE GUTIERREZ, ANGELES MONGE and CARIDAD RUIZ

Instituto de Química Inorgánica Elhúyar y Departamento de Química Inorgánica, Universidad Complutense de Madrid-CSIC, 28040 Madrid, Spain

Abstract—Compounds of composition *trans,mer*-$[M(C_2H_4)_2(CNR)(PMe_3)_3]$ (**1**) and *trans,trans,trans*-$[M(C_2H_4)_2(CNR)_2(PMe_3)_2]$ (**2**) for various combinations of M = Mo, W and R = $CHMe_2$, CMe_3 and C_6H_{11}, have been obtained by the stepwise reaction of *trans*-$[M(C_2H_4)_2(PMe_3)_4]$ with the corresponding isocyanide. Compounds **2** can also be obtained by treatment of **1** with CNR, a reaction that allows the synthesis of the mixed isocyanide *trans,trans*-$[Mo(C_2H_4)_2(CNCMe_3)(CNC_6H_{11})(PMe_3)_2]$ (**2g**). A similar reaction, starting with *trans,mer*-$[M(C_2H_4)_2(CO)(PMe_3)_3]$, produces the mixed isocyanide–carbonyl derivatives *trans,trans*-$[M(C_2H_4)_2(CNR)(CO)(PMe_3)_2]$ (**3**). X-ray structural studies on complexes **2b** and **3b** (M = Mo, R = CMe_3) have been carried out. Both compounds are monoclinic, $P_{2_1/n}$, but while the structure of **3b** has been refined to a conventional *R* value of 0.034 by using 2976 observed reflections (unit cell constants: $a = 10.972(3)$, $b = 18.923(4)$, $c = 10.544(3)$ Å; $\beta = 98.89(2)°$) extensive disorder problems have prevented anisotropic refinement of **2b**, and a final isotropic *R* value of 0.097 has been obtained. For compound **3b**, the Mo—C bond distances are 1.959(5) (Mo—CO), 2.137(4) (Mo—CNR) and 2.283(9) Å (av. Mo—C_2H_4).

The field of isocyanide complexes of transition metals has considerably developed over the past few years.[1] A number of studies aimed at the synthesis of new species,[2] their structural characterization[3] and the ascertaining of their bonding capability, in particular the comparison of their σ-donor and π-acceptor properties with those of carbonyl and carbene ligands,[4] has been reported recently. Earlier studies on molybdenum and tungsten isocyanide chemistry allowed the preparation of mixed phosphine–isocyanide complexes, e.g. *trans*-$[M(CNR)_2(dppe)_2]$[5a] (dppe = $Ph_2CH_2CH_2PPh_2$) and $[M(CNR)_n(PMe_2Ph)_{6-n}]$[5b] ($n = 2$, 3, 4), and of phosphine–carbonyl–isocyanide compounds $[Mo(CO)_2(CNR)_2(PR'_3)_2]$.[6] Using the ethylene complexes *trans*-$[M(C_2H_4)_2(PMe_3)_4]$[7] as starting materials, we have now enlarged the range of complexes of this type. Herein we report the synthesis of the mixed ethylene–isocyanide–phosphine compounds *trans,mer*-$[M(C_2H_4)_2(CNR)(PMe_3)_3]$ (**1**) and *trans,trans,trans*-$[M(C_2H_4)_2(CNR)_2(PMe_3)_2]$ (**2**), as well as that of the mixed ethylene–carbonyl–isocyanide–phosphine species, *trans,trans*-$[M(C_2H_4)_2(CO)(CNR)(PMe_3)_2]$ (**3**). The reactions studied are shown in Scheme 1 and spectroscopic data for the new compounds in Tables 1 and 2. X-ray structural analyses on two of these complexes, **2b** and **3b** (M = Mo, R = CMe_3), are also reported.

* Dedicated to Professor Sir Geoffrey Wilkinson on the occasion of his retirement.

† Author to whom correspondence should be addressed.

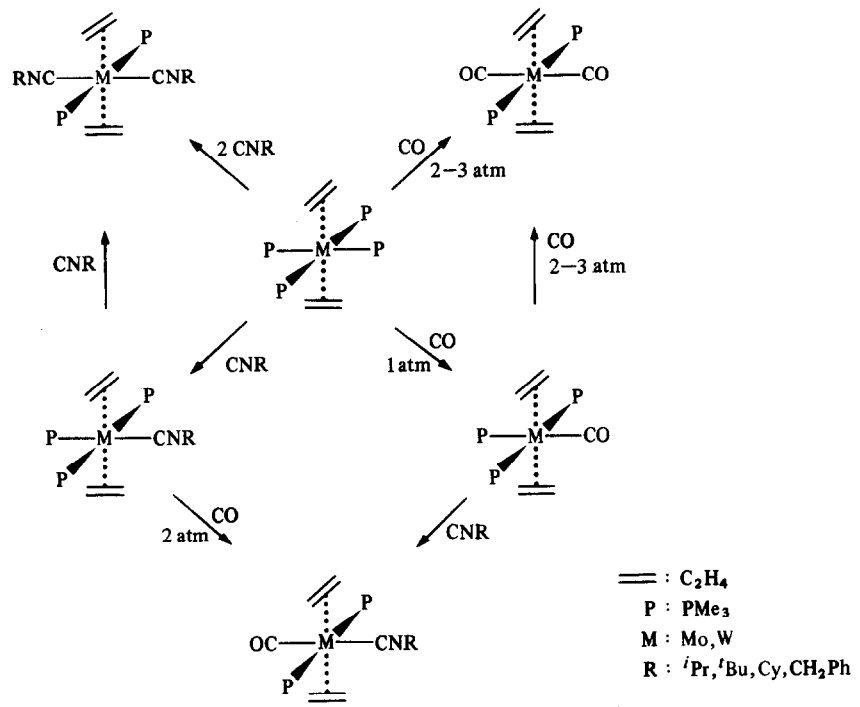

Scheme 1.

RESULTS AND DISCUSSION

Compounds of composition trans,mer-$[M(C_2H_4)_2(CNR)(PMe_3)_2]$ (**1**)

The ethylene complexes *trans*-$[M(C_2H_4)_2(PMe_3)_4]$ (M = Mo, W) have been shown to undergo a facile substitution of one of the coordinated PMe_3 groups by carbon monoxide, with formation[7] of the carbonyl derivatives *trans,mer*-$[M(C_2H_4)_2(CO)(PMe_3)_3]$. A similar reaction has now been found to take place with isocyanides. Low temperature addition of an alkyl isocyanide, CNR, to petroleum ether solutions of *trans*-$[M(C_2H_4)_2(PMe_3)_4]$ produces compounds of composition $[M(C_2H_4)_2(CNR)(PMe_3)_3]$ (**1**), (M = Mo; R = $CHMe_2$, **1a**, CMe_3, **1b**. M = W; R = CMe_3, **1c**), as shown in eq. (1).

$$[M(C_2H_4)_2(PMe_3)_4] + CNR \rightarrow [M(C_2H_4)_2(CNR)(PMe_3)_3] + PMe_3 \quad (1)$$

Other combinations of M = Mo, W and R = $CHMe_2$, CMe_3, C_6H_{11} have been attempted, and although the reactions seem to proceed similarly, only in the above cases have crystalline products been isolated. Compounds **1** are air-sensitive solids, very soluble in common organic solvents from which they can only be crystallized in very concentrated solutions. Their IR spectra display a strong, broad absorption in the range 1990–1960 cm^{-1}, which can be attributed to ν_{CN} of the coordinated isocyanide ligand. This value is lower by *ca* 150–180 cm^{-1} than that of the free ligands, and this suggests an appreciable π-bonding interaction with the metal centre. The shift to low frequency is not however so pronounced as in the compounds *trans*-$[M(CNR)_2(dppe)_2]$[5a] and *trans*-$[M(CNR)_2(PMe_2Ph)_4]$[5b] ($\Delta\nu \simeq 215$–385), but it is much higher than that found in the related carbon dioxide complexes, *trans,mer*-$[Mo(CO_2)_2(CNR)(PMe_3)_3]$ which display values[8] of ν_{CN} very similar to those of the free isocyanide ligands (e.g. 2100 cm^{-1} for R = CMe_3, $\Delta\nu \simeq 35$ cm^{-1}). This is in accord with a larger contribution of resonance structure **II** in compounds **1** than in the

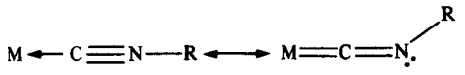

I **II**

CO_2 derivatives, which can, in turn, be interpreted in terms of a higher electron density at the metal centre in the "$Mo(C_2H_4)_2(PMe_3)_3$" core than in the "$Mo(CO_2)_2(PMe_3)_3$" core, in agreement with the strong π-acceptor capability attributed to the side-on coordinated carbon dioxide ligand.[9]

Table 1. ^1H and $^{31}P\{^1H\}$ NMR data for $[M(C_2H_4)_2(CNR)(L)(PMe_3)_2]$ complexes (L = PMe_3, **1**; CNR, **2**; CO, **3**)

	Complex M	R	$^1H^a$ C_2H_4	$PMe_3{}^b$	R[c] (alkyl group)			$^{31}P(^1H)^a$ (ppm)
1a	Mo	$CHMe_2$	1.4 br 1.7 br	0.9 d (5) 1.1 t (2)	1.0 d 3.5 h	CH_3 CH	2.0 d −5.0 t	$^2J_{PP}$ = 22 Hz
1b	Mo	CMe_3	1.2 br 1.4 br	0.9 d (5) 1.0 t (2)	1.1 s	CH_3	1.6 d −3.2 t	$^2J_{PP}$ = 22 Hz
1c	W	CMe_3	1.5 br	1.0 d (5) 1.2 t (3)	1.1 s	CH_3	−35.3 d −36.6 t	$^2J_{PP}$ = 14 Hz $^1J_{PW}$ = 241 Hz
2a	Mo	$CHMe_2$	2.0 t[d]	1.4 t (3)	1.2 d 3.6 h	CH_3 CH	4.1 s	$^1J_{PW}$ = 215 Hz
2b	Mo	CMe_3	1.8 br	1.2 t (3)	1.2 s	CH_3	3.5 s	
2c	Mo	C_6H_{11}	1.8 br	1.2 t (3)	1.5 br 3.6 br	C_6H_{11} C_6H_{11}	4.6 s	
2d	W	CMe_3	1.4 br 1.6 br	1.2 t (3)	1.1 d 3.6 h	CH_3 CH	−32.5 s	$^1J_{PW}$ = 244 Hz
2e	W	C_6H_{11}	1.6 br	1.4 t (3)	1.5 br 3.4 br	C_6H_{11} C_6H_{11}	−30.8 s	$^1J_{PW}$ = 245 Hz
2f	W	$CHMe_2$	1.5 br	1.4 t (3)	1.1 d 3.6 h	CH_3 CH	−31.1 s	$^1J_{PW}$ = 244 Hz
2g	Mo	CMe_3 C_6H_{11}	1.6 br	1.1 t (3)	1.1 s 1.5 br 3.2 br	CH_3 C_6H_{11} C_6H_{11}	4.0 s	
3a	Mo	$CHMe_2$	2.0 t[d]	1.2 t (3)	0.9 d 3.2 h	CH_3 CH	2.6 s	
3b	Mo	CMe_3	1.8 br	1.0 t (3)	0.9 s	CH_3	2.6 s	
3c	Mo	C_6H_{11}	1.9 br	1.0 t (3)	2.9 br	C_6H_{11}	2.8 s	
3d	Mo	$CH_2C_6H_5$	1.9 br	1.0 t (3)	3.9 s 7 m	CH_2 Ph	2.9 s	
3e	W	CMe_3	1.4 br	1.1 t (3)	0.9 s	CH_3	−31.4 s	$^1J_{PW}$ = 241 Hz
3f	W	C_6H_{11}	1.7 br	1.2 t (3)	3.2 br	C_6H_{11}	−31.0 s	$^1J_{PW}$ = 240 Hz

s = singlet, d = doublet, t = triplet, h = heptet, br = broad, m = multiplet.
[a] Recorded in C_6D_6 at 20°C.
[b] In parentheses $^2J_{HP}$ and $^2J_{HPapp}$ in Hz.
[c] $^3J_{HH} \simeq 7$ Hz in all cases.
[d] At 35°C (60 MHz), $^3J_{HP}$ = 5 Hz.

The meridional distribution of the PMe_3 ligands in the molecules **1**, is suggested by the appearance of a doublet (δ 0.9–1.0) and a virtually coupled triplet (δ 1.0–1.2), of relative intensity 1:2 in the ^1H NMR spectra, and by the observation of AX_2 patterns (see Table 1) in the $^{31}P\{^1H\}$NMR spectra (for instance, $\delta P_a = 5.0$, t; $\delta P_X = 2.0$, d; $^2J_{P_AP_X} = 22$ Hz, data for **1a**, M = Mo, R = $CHCMe_3$). The *trans,mer* configuration, **III**, proposed for this complex, is also consistent with ^{13}C NMR data (Table 2): a doublet and a triplet are again observed for the PMe_3 ligands, two broad unresolved resonances for the olefinic carbon atoms and a doublet of triplets for the metal-bonded carbon atom of the isocyanide ligand (for instance for **1b**, M = Mo, R = CMe_3: δ 190.9 ppm, $^2J_{CP_A} = 40.3$, $^2J_{CP_X} = 10.7$ Hz).

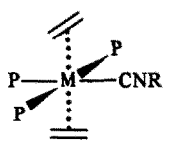

III

Table 2. $^{13}C\{^1H\}$ NMR data for $[M(C_2H_4)_2(CNR)(L)(PMe_3)_2]$ complexes (L = PMe_3, **1**; CNR, **2**; CO, **3**)

Complex					R[a]					
	M	R	$P(CH_3)_3$[b]	C_2H_4	CH_3	CH_2	CH	C	CNR[b]	CO[b]
1a	Mo	$CHMe_2$	17.5 t (8) 18.5 d (12)	27.8 br 30.9 br	24.6		47.4		n.o.	
1b	Mo	CMe_3	17.6 t (8) 19.0 d (13)	27.5 br 30.1 br	31.4			53.9	190.9 dt (10.7 *cis*) (40.3 *trans*)	
2a	Mo	$CHMe_2$	16.8 t (8)	30.4 br	24.6		47.0		194.0 t (10)	
2b	Mo	CMe_3	16.6 s,br	30.3 br	31.5			54.2	191.3 t (10)	
2c	Mo	C_6H_{11}	16.9 t	30.2 br		23.1 25.3 34.2	53.2		191.2 t (10)	
2d	W	CMe_3	15.9 t (11)	20.7 br 22.0 br	31.6			54.5	186.2 t (7)	
2e	W	C_6H_{11}	16.3 t (11)	20.8 br 21.8 br		23.3 25.4 34.5	53.7		186.5 t (7)	
2g	Mo	CMe_3 C_6H_{11}	16.7 t (8)	30.2 br	31.5	23.1 25.3 34.2	53.1	54.2	191.2 t (10) 191.3 t (10)	
3a	Mo	$CHMe_2$	16.9 t (9)	32 br	24.0		47		173.8 br	224.3 (10)
3b	Mo	CMe_3	16.5 t (9)	31.5 br	30.4			54.4	172.1 br	224.4 t (9)
3c	Mo	C_6H_{11}	16.5 t (9)	31.5 br		22.7 24.8 33.0	52.4		172.9 br	224.3 t (10)
3d	Mo	$CH_2C_6H_5$	16.6 t (9)	31.8 br		46.5	126.3 127.9 128.6 135		178.8 br	223.6 t (9)
3e	W	CMe_3	15.9 t (12)	19–25 br	30.5			54.6	163.8 t	216.2 t
3f	W	C_6H_{11}	16.0 t (12)	19.7 br 27.2 br		22.7 24.5 33.2	52.6		164.4 t (8)	216.0 t (6)

Recorded in C_6D_6 at 20°C. d = doublet, t = triplet, dt = doublet of triplets, br = broad, n.o. = not observed.
[a] Singlets.
[b] In parentheses $^2J_{CP}$.

Synthesis and properties of compounds trans,trans,trans-$[M(C_2H_4)_2(CNR)_2(PMe_3)_2]$ (**2**). *X-ray structural determination of* **2b** (M = Mo, R = CMe_3)

Complexes *trans,trans,trans*-$[M(C_2H_4)_2(CNR)_2(PMe_3)_2]$ (**2**) are best obtained by the reaction of the ethylene derivatives, *trans*-$[M(C_2H_4)_2(PMe_3)_4]$ with an excess of the isocyanide (*ca* 2.5 equiv.), at room temperature in petroleum ether solutions, according to eq. (2).

$$[M(C_2H_4)_2(PMe_3)_4] + 2CNR \rightarrow [M(C_2H_4)_2(CNR)_2(PMe_3)_2] + 2PMe_3 \quad (2)$$

In this way, compounds of the above composition for M = Mo, R = $CHMe_2$ (**2a**); CMe_3 (**2b**); C_6H_{11} (**2c**), and M = W, R = CMe_3 (**2d**), C_6H_{11} (**2e**) and $CHMe_2$ (**2f**), have been isolated in good yields. Compounds **2** have physical and spectroscopic properties similar to those of **1**. They are air sensitive, particularly in solution, and very soluble in non-polar solvents. Their IR spectra display an intense and very broad absorption centred in the region 1950–1910 cm^{-1}, due to the coordinated isocyanide ligands. Compounds of composition $Mo(CO)_2(CNR)_2(PR'_3)_2$ have been found to exist[6] as a single isomer, with *trans* phosphines and *cis*

carbonyl and alkyl isocyanide ligands. Chemical or electrochemical oxidation of these species is followed by a rapid isomerization to the all *trans* cations, but re-reduction produces the original isomers. For the analogous aryl isocyanide derivatives, a mixture of isomers is generally observed.[6] Interestingly, compounds **2** seem to exist as single isomers with *trans* phosphine, ethylene and isocyanide ligands, and this is clearly inferred from spectroscopic data (Tables 1 and 2) and from an X-ray study carried out on complex **2b** (M = Mo, R = CMe_3). The ^1H NMR spectra of complexes **2** show, in addition to signals due to the coordinated CNR groups, a virtually coupled triplet for the PMe_3 ligands and a broad, unresolved signal for the ethylene protons, indicating restricted rotation around the M–olefin bond axis. For compound **2a** rotation is rapid at room temperature and a triplet is observed at δ 1.8 ppm ($^3J_{HP}$ = 5 Hz). While ^{31}P NMR data do not provide useful information on the geometrical distribution of the PMe_3 ligands in these complexes, additional evidence for the *trans* arrangement of the two RNC and the two PMe_3 groups comes from ^{13}C NMR studies. In addition to the resonances associated with the phosphine and ethylene groups, which are listed in Table 2, a triplet is observed at δ 191–194 ppm due to the metal-bonded carbon atom of the CNR ligands. This and the values of *ca* 7–10 Hz found for the carbon to phosphorus coupling constant in these complexes, which are typical of *cis* C—P coupling,[10] are clearly indicative of an all *trans* distribution of the ethylene, isocyanide and phosphine groups, as shown in **IV**. To further confirm this proposal, an

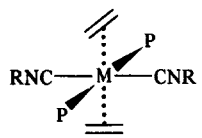

IV

X-ray study of the molybdenum complex, **2b** has been undertaken. The structure has been resolved by Patterson and Fourier techniques (see Experimental), but due to extensive disorder problems it could not be refined anisotropically. Nevertheless, the positions of all but the ethylene atoms could be fixed without ambiguity, although the values obtained for the bond distances and angles should be regarded and used with caution when attempting to establish precise comparisons. The molecule is centrosymmetric, with the molybdenum atom at the (0,0,0) inversion centre, coordinated to two mutually *trans* phosphines, at a Mo—P distance of 2.450(6) Å (av.), to two *trans* isocyanide ligands, with a Mo—C separation of 2.04(3) Å (av.), and to two *trans* ethylene groups whose location cannot be precisely determined, as already indicated. By comparison with the structures found for other related ethylene complexes, e.g. *trans*-[$M(C_2H_4)_2(PMe_3)_4$],[7] *trans-mer*-[$Mo(C_2H_4)_2(CO)(PMe_3)_3$][7] and *trans,trans*-[$Mo(C_2H_4)_2(CO)(CNCMe_3)(PMe_3)_2$] (*vide infra*), a *trans*, mutually perpendicular distribution can be proposed for the ethylene ligands, as shown schematically in **IV**.

Compounds **2** can also be obtained by the reactions of precursors **1** with the corresponding isocyanide [eq. (3)]

$$[M(C_2H_4)_2(CNR)(PMe_3)_3] + CNR \rightarrow [M(C_2H_4)_2(CNR)_2(PMe_3)_2] + PMe_3. \quad (3)$$

If the second isocyanide, CNR′, is different from the one already coordinated, mixed complexes [$Mo(C_2H_4)_2(CNR)(CNR')(PMe_3)_2$] can be obtained. As an example of species of this type, the compound [$Mo(C_2H_4)_2(CNCMe_3)(CNC_6H_{11})(PMe_3)_2$] (**2g**) has been obtained. For **2g** a singlet at 4.0 ppm is observed in the $^{31}P\{^1H\}$ NMR spectrum, and two triplets at 191.2 and 191.3 ppm (Mo—*C*NR) in the $^{13}C\{^1H\}$ NMR spectrum ($^2J_{CP}$ = 10 Hz), in excellent agreement with a structure of type **IV**.

Compounds trans,trans-[$M(C_2H_4)_2(CO)(CNR)(PMe_3)_2$] (**3**). *Preparation and properties and the molecular structure of* **3b** (M = Mo, R = CMe_3)

Previous work from this laboratory[7b] has shown that the complexes *trans,mer*-[$M(C_2H_4)_2(CO)(PMe_3)_3$] react with carbon monoxide under pressure (2–3 atm), with formation of the bis(carbonyl) derivatives *trans,trans,trans*-[$M(C_2H_4)_2(CO)_2(PMe_3)_2$]. A similar reaction with the isoelectronic isocyanide ligand provides the mixed carbonyl–isocyanide derivatives, *trans,trans*-[$M(C_2H_4)_2(CO)(CNR)(PMe_3)_2$] (M = Mo, R = $CHMe_2$, **3a**; CMe_3, **3b**; C_6H_{11}, **3c**; $CH_2C_6H_5$, **3d**. M = W, R = CMe_3, **3e**; C_6H_{11}, **3f**), as depicted in eq. (4).

$$[M(C_2H_4)_2(CO)(PMe_3)_3] + CNR \rightarrow [M(C_2H_4)_2(CO)(CNR)(PMe_3)_2] + PMe_3. \quad (4)$$

Compounds **3** are pale-yellow or white–yellowish crystalline materials, somewhat more stable in air than **1** and **2**, and also very soluble in common organic solvents. Preparation of these derivatives can also be achieved from compounds **1** and CO under pressure [eq. (5)], but yields are generally lower than those obtained following the route speci-

fied in eq. (4).

$$[M(C_2H_4)_2(CNR)(PMe_3)_3]+CO \rightarrow [M(C_2H_4)_2(CO)(CNR)(PMe_3)_2]+PMe_3. \quad (5)$$

The formation of all these compounds and their interconversion reactions are summarized in Scheme 1.

Examination of the IR spectra of complexes **3** shows that they all display a strong absorption in the region 1870–1830 cm^{-1}, due to ν_{CO} of the carbon monoxide ligand, and a second intense band at 2110–2070 cm^{-1} associated with the isocyanide ligand which occupies a position *trans* with respect to the carbonyl. The former appears almost at the same frequency as that in the complexes, *trans,mer*-$[M(C_2H_4)_2(CO)(PMe_3)_3]$ (1870, M = Mo; 1855 cm^{-1}, M = W), and this seems to indicate that the major role in the withdrawing of π-electron density from the metal centre in these compounds is being played by the carbonyl ligand, with little participation of the isocyanide group, which would, at best, behave as a very weak π-acid ligand. This is in agreement with the previous observations by other workers,[4a] who have found that the bonding of the CNR ligand in carbonyl isocyanide carbene complexes of tungsten is dominated by the σ component, with the CNR ligand acting as a stronger Lewis base than CO and as a much weaker π-acid. Also in accord with this, is the high value found for ν_{CN} in these complexes, with very low shifts with respect to the free ligands ($\Delta\nu \simeq 80$ cm^{-1}), as compared with shifts of *ca* 150–200 cm^{-1} found for compounds **1** and **2**. It is clear from these arguments, that the M—CNR bond in **3** is predominantly σ in character, with little or no contribution of π-back donation, i.e. with a larger contribution of resonance structure **I**, and this is also substantiated by the long Mo—CNR bond distance found for complex **3b** and by the almost linear C—N—C angle of the coordinated isocyanide ligand (see below) in this complex.

The all *trans* structure proposed for compounds **3** is supported by NMR data (Tables 1 and 2). Thus, they all exhibit a singlet in the $^{31}P\{^1H\}$ NMR spectrum and a triplet in the ^1H NMR spectrum for the coordinated phosphine ligands. The ^{13}C resonance of the carbonyl ligand appears also as a triplet ($^2J_{PC}$ = 6–10 Hz) while the metal bonded carbon atom of the isocyanide group provides a broad, unresolved signal in the molybdenum derivatives and a triplet ($^2J_{CP}$ = 8 Hz) in the tungsten compounds. This is clearly in agreement with structure **V**.

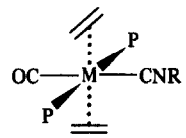

V

Figure 1 shows an ORTEP illustration of complex **3b**, relevant bond distances and angles are col-

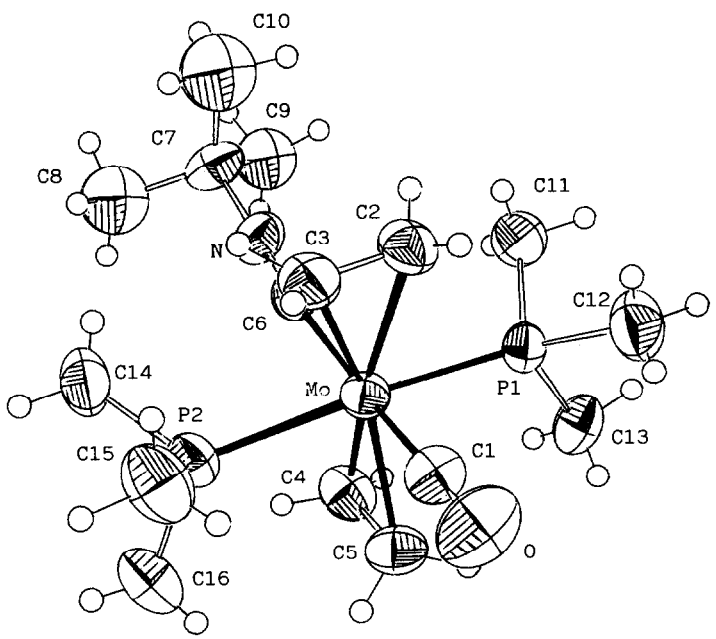

Fig. 1. Molecular structure and atom labelling scheme for *trans,trans*-$[Mo(C_2H_4)_2(CO)(CNCMe_3)(PMe_3)_2]$ (**3b**).

lected in Table 3. The complex is essentially octahedral, with the ethylene ligands mutually perpendicular, each eclipsing the *trans* P—Mo—P or C—Mo—C vectors of the plane perpendicular to the Mo—C_2H_4 bond axis. This orientation, first predicted by Osborn in the complex *trans*-[$Mo(C_2H_4)_2(dppe)_2$][11] and then supported by theoretical calculations,[12] is similar to that found in other related ethylene complexes.[7] The Mo—C and the C—C bond distances for the Mo—C_2H_4 units average 2.283(9) and 1.412(5) Å, respectively, and compare well with the values found[7] in *trans*-[$Mo(C_2H_4)_2(PMe_3)_4$] and *trans,mer*-[$Mo(C_2H_4)_2(CO)(PMe_3)_3$]. The strong interaction between the metal centre and the carbonyl group, previously alluded to, is also shown by the short Mo—C (carbonyl) distance of 1.959(5) Å, which is shorter by *ca* 0.18 Å than the Mo—C (isocyanide) bond length. The latter distance of 2.137(4) Å, is appreciably longer than that found in [$Mo(\eta^6\text{-}C_6H_5P(Me)C_6H_5)(CNCMe_3)(PMePh_2)_2$][3b] (1.984(13) Å) and in *trans,mer*-[$Mo(CO_2)_2(CNR)(PMe_3)_3$][8] (2.07(2) Å, R = $CHMe_2$; 2.03(1) Å, R = $CH_2C_6H_5$). Finally, the C_6—N—C_7 bond angle

Table 3. Selected bond distances (Å) and angles (°) for *trans,trans*-[$Mo(C_2H_4)_2(CO)(CNCMe_3)(PMe_3)_2$] (**3b**)

Bond distances			
Mo—P(1)	2.486(1)	O—C(1)	1.167(6)
Mo—P(2)	2.470(2)	N—C(6)	1.153(6)
Mo—C(1)	1.959(5)	N—C(7)	1.441(6)
Mo—C(2)	2.262(5)	C(2)—C(3)	1.416(7)
Mo—C(3)	2.264(5)	C(4)—C(5)	1.407(7)
Mo—C(4)	2.294(5)		
Mo—C(5)	2.310(5)		
Mo—C(6)	2.137(4)		
Angles			
P(1)—Mo—P(2)	171.1(1)	C(3)—Mo—C(4)	155.4(2)
P(1)—Mo—C(1)	92.9(2)	C(3)—Mo—C(5)	153.4(2)
P(1)—Mo—C(2)	76.4(1)	C(3)—Mo—C(6)	82.5(2)
P(1)—Mo—C(3)	112.9(1)	C(4)—Mo—C(5)	35.6(2)
P(1)—Mo—C(4)	85.7(1)	C(4)—Mo—C(6)	82.2(2)
P(1)—Mo—C(5)	86.4(1)	C(5)—Mo—C(6)	117.7(2)
P(1)—Mo—C(6)	88.3(1)		
P(2)—Mo—C(1)	91.2(2)	Mo—P(1)—C(11)	116.4(2)
P(2)—Mo—C(2)	111.5(1)	Mo—P(1)—C(12)	117.3(2)
P(2)—Mo—C(3)	75.1(1)	Mo—P(1)—C(13)	121.2(2)
P(2)—Mo—C(4)	85.6(1)	C(11)—P(1)—C(12)	101.6(3)
P(2)—Mo—C(5)	87.3(1)	C(11)—P(1)—C(13)	98.6(2)
P(2)—Mo—C(6)	89.1(1)	C(12)—P(1)—C(13)	98.0(3)
C(1)—Mo—C(2)	88.8(2)		
C(1)—Mo—C(3)	87.5(2)	Mo—P(2)—C(14)	116.7(2)
C(1)—Mo—C(4)	108.3(2)	Mo—P(2)—C(15)	117.8(2)
C(1)—Mo—C(5)	72.7(2)	Mo—P(2)—C(16)	120.1(2)
C(1)—Mo—C(6)	169.5(2)	C(14)—P(2)—C(15)	100.8(3)
C(2)—Mo—C(3)	36.5(2)	C(14)—P(2)—C(16)	98.7(3)
C(2)—Mo—C(4)	155.9(2)	C(15)—P(2)—C(16)	99.0(3)
C(2)—Mo—C(5)	154.2(2)		
C(2)—Mo—C(6)	81.4(2)	C(6)—N—C(7)	176.1(5)
		Mo—C(1)—O	178.9(5)
		Mo—C(2)—C(3)	71.8(3)
		Mo—C(3)—C(2)	71.7(3)
		Mo—C(4)—C(5)	72.8(3)
		Mo—C(5)—C(4)	71.6(3)
		Mo—C(6)—N	174.2(4)

of 176.1(5)°, almost linear, is in accord with the considerations outlined above concerning the contribution of resonance form **II** to the total structure of these complexes.

EXPERIMENTAL

Microanalyses were carried out by Pascher Microanalytical Laboratory, Germany. IR spectra were recorded on a Perkin–Elmer model 684 instrument. ^{1}H, ^{31}P and ^{13}C NMR spectra were run on a Varian XL-200 instrument. ^{31}P NMR shifts were measured with respect to external 85% H_3PO_4. ^{1}H and ^{13}C NMR spectra were referenced using the ^{1}H and ^{13}C resonance, respectively, of the solvent as an internal standard but are reported with respect to $SiMe_4$.

All preparations and other operations were carried out under oxygen-free nitrogen, following conventional Schlenk techniques. Solvents were dried and degassed before use. The petroleum ether used had b.p. 40–60°C. The compounds, *trans*-$[M(C_2H_4)_2(PMe_3)_4]$ and *trans,mer*-$[M(C_2H_4)_2(CO)(PMe_3)_3]$[7] and the ligand PMe_3[13] were prepared by published methods. Isocyanides were from commercial sources or prepared by standard methods.[14]

Synthesis of trans,mer-$[M(C_2H_4)_2(CNR)(PMe_3)_3]$ *complexes*, (**1**)

Into a solution of *trans*-$[M(C_2H_4)_2(PMe_3)_4]$ (1 mmol), in petroleum ether (50 cm^3), at −20°C, the corresponding isocyanide (1 mmol) is added. The reaction mixture is stirred and allowed to reach room temperature in about 20 min. The stirring is continued for another 4–5 h and the solvent then removed *in vacuo*. The yellow residue is extracted with petroleum ether (15–20 cm^3), centrifuged and concentrated. Very concentrated solutions are required to crystallize these complexes. Upon cooling at −20°C yellow crystals of the desired compounds are obtained. Yields 70–75%. Complex **1a** (M = Mo, R = $CHMe_2$): IR (Nujol): ν_{CN} 1960 s, br cm^{-1}. Complex **1b** (M = Mo, R = CMe_3): IR (Nujol): ν_{CN} 1990 s, br cm^{-1}. Found: C, 46.4; H, 9.4. Calc. for $C_{18}H_{44}P_3NMo$: C, 46.6; H, 9.5. Complex **1c** (M = W, R = CMe_3): IR (Nujol): ν_{CN} 1990 s, br cm^{-1}.

Synthesis of trans,trans,trans-$[M(C_2H_4)_2(CNR)_2(PMe_3)_2]$ *complexes*, (**2**)

A solution of *trans*-$[M(C_2H_4)_2(PMe_3)_4]$ (*ca* 1 mmol) in 20–25 cm^3 of petroleum ether is treated with an excess (1:2.5) of the isocyanide, CNR (R = $CHMe_2$, CMe_3, C_6H_{11}), at room temperature with stirring. After 15–20 h (or *ca* 30 h for M = W) the resulting solution is evaporated to dryness. Extraction with 20 cm^3 of petroleum ether and centrifugation gives a yellow solution, which upon concentration and cooling at −20°C provides yellow crystals of the corresponding complexes. Yields are between 70% (complexes **2c** and **2e**) and 85% (complex **2a**). Complex **2a** (M = Mo, R = $CHMe_2$): IR (Nujol): ν_{CN} 1930 s (very broad) cm^{-1}. Found: C, 48.4; H, 8.9. Calc. for $C_{18}H_{40}P_2N_2Mo$: C, 48.9; H, 9.1. Complex **2b** (M = Mo, R = CMe_3): IR (Nujol): ν_{CN} 1930 s (very broad) cm^{-1}. Found: C, 51.4; H, 9.6. Calc. for $C_{20}H_{44}P_2N_2Mo$: C, 51.1; H, 9.4. Complex **2c** (M = Mo, R = C_6H_{11}): IR (Nujol): ν_{CN} 1950 s (very broad) cm^{-1}. Found: C, 55.2; H, 9.3. Calc. for $C_{24}H_{48}P_2N_2Mo$: C, 55.2; H, 9.2. Complex **2d** (M = W, R = CMe_3): IR (Nujol): ν_{CN} 1930 s (very broad) cm^{-1}. Found: C, 43.1; H, 8.1. Calc. for $C_{20}H_{44}P_2N_2W$: C, 43.0; H, 7.9. Complex **2e** (M = W, R = C_6H_{11}): IR (Nujol): ν_{CN} 1940 s (very broad) cm^{-1}. Found: C, 47.5; H, 7.9. Calc. for $C_{24}H_{48}P_2N_2W$: C, 47.2; H, 7.9. Complex **2f** (M = W, R = $CHMe_2$): IR (Nujol): ν_{CN} 1910 s (very broad) cm^{-1}.

Preparation of trans,trans-$[Mo(C_2H_4)_2(CNCMe_3)(CNC_6H_{11})(PMe_3)_2]$ (**2g**)

Complex **1b** (0.46 g, 1 mmol), dissolved in petroleum ether (25 cm^3), is reacted with a two-fold excess of CNC_6H_{11} (2 mmol) at room temperature for 20 h. The resulting solution is evaporated to dryness and the residue extracted with 20 cm^3 of petroleum ether. Centrifugation, partial evaporation of the solvent and cooling at −20°C affords yellow crystals of the compounds. Yield 68%. IR (Nujol): ν_{CN} 1950 s (very broad) cm^{-1}. Found: C, 52.6; H, 9.1. Calc. for $C_{22}H_{46}P_2N_2Mo$: C, 53.2; H, 9.3.

Synthesis of trans,trans-$[M(C_2H_4)_2(CO)(CNR)(PMe_3)_2]$ *complexes*, (**3**)

An excess of the isocyanide (2 mmol) is added to a solution of the complexes, *trans*-$[M(C_2H_4)_2(CO)(PMe_3)_3]$ (M = Mo, W) (*ca* 1 mmol) in petroleum ether (25 cm^3). The mixture is stirred at room temperature for 16–20 h (for the tungsten compounds 30–35 h are required). The volatile materials are removed by pumping *in vacuo* and the residue extracted with petroleum ether (20 cm^3). The solution is centrifuged, concentrated and cooled at −20°C. White or white–yellowish crystals are obtained in 80–90% yield (complex **3d** in 65% yield). Complexes **3** can also be obtained by reac-

tion of compounds **1** with CO under pressure (3–4 atm), but the yields are generally lower and the reaction times longer. Complex **3a** (M = Mo, R = $CHMe_2$): IR (Nujol): ν_{CN} 2070 s, ν_{CO} 1840 s cm^{-1}. Found: C, 45.9; H, 8.3. Calc. for $C_{15}H_{33}P_2NOMo$: C, 44.9; H, 8.2. Complex **3b** (M = Mo, R = CMe_3): IR (Nujol): ν_{CN} 2100 s, ν_{CO} 1830 cm^{-1}. Found: C, 46.4; H, 8.6. Calc. for $C_{16}H_{35}P_2NOMo$: C, 46.3; H, 8.4. Complex **3c** (M = Mo, R = C_6H_{11}): IR (Nujol): ν_{CN} 2120 s, ν_{CO} 1870 s cm^{-1}. Found: C, 48.9; H, 8.6. Calc. for $C_{18}H_{37}P_2NOMo$: C, 49.0; H, 8.4. Complex **3d** (M = Mo, R = $CH_2C_6H_5$): IR (Nujol): ν_{CN} 2110 s, ν_{CO} 1840 s cm^{-1}. Found: C, 51.1; H, 7.4. Calc. for $C_{19}H_{33}P_2NOMo$: C, 50.8; H, 7.4. Complex **3e** (M = W, R = CMe_3): IR (Nujol): ν_{CN} 2100 s, ν_{CO} 1870 s cm^{-1}. Found: C, 38.3; H, 7.2. Calc. for $C_{16}H_{35}P_2NOW$: C, 38.2; H, 7.0. Complex **3f** (M = W, R = C_6H_{11}): IR (Nujol): ν_{CN} 2110 s, ν_{CO} 1850 s cm^{-1}. Found: C, 40.8; H, 7.1. Calc. for $C_{18}H_{37}P_2NOW$: C, 40.8; H, 7.0.

Crystallographic studies

Yellow prismatic single crystals of *trans,trans,trans*-$[Mo(C_2H_4)_2(CNCMe_3)_2(PMe_3)_2]$ (**2b**) and *trans,trans,trans*-$[Mo(C_2H_4)_2(CO)(CNCMe_3)(PMe_3)_2]$ (**3b**) were introduced into a Lyndeman capillaries, sealed in an N_2 atmosphere and mounted on a Nonius CAD-4 diffractometer.

Crystal data. Compound **2b**: $C_{20}H_{44}P_2N_2Mo$, $M = 470.47$, monoclinic, space group $P2_1/n$, $a = 11.182(4)$, $b = 13.210(9)$, $c = 10.312(3)$ Å, $\beta = 116.44(3)°$, $U = 1364.1$ Å^3, $Z = 2$, $D_c = 1.14$ g cm^{-3}, μ(Mo-K_α) = 5.9 cm^{-1}, λ(Mo-K_α) = 0.71069 Å.

Crystal data. Compound **3b**: $C_{16}H_{35}P_2NOMo$, $M = 415.35$, monoclinic, space group $P2_1/n$, $a = 10.972(3)$, $b = 18.923(4)$, $c = 10.544(3)$ Å, $\beta = 98.89(2)°$, $U = 2189.2$ Å^3, $Z = 4$, $D_c = 1.28$ g cm^{-3}, μ(Mo-K_α) = 7.38 cm^{-1}, λ(Mo-K_α) = 0.71069 Å.

Data collection. Unit cell dimensions were determined by least-squares refinement of the observed setting angles of 25 accurately centred reflections. Intensity data collection employed the ω-2θ scan technique. Measured data: compound **2b**, 2392 reflections and compound **3b**, 3798 reflections ($2\theta \leqslant 50°$). The data were corrected for Lorentz and polarization effects. Scattering factors for neutral atoms and anomalous dispersion corrections for Mo and P were taken from *International Tables for X-ray Crystallography*.[15]

Structure solution and refinements. Compound **2b**: The structure was solved by conventional Patterson and Fourier techniques, but due to extensive disorder problems it could not be refined anisotropically. Because of this, after checking the space group again, the refinement has been carried out in an isotropic mode. An empirical absorption correction[16] was applied using unit weights. The final residual R value was 0.097. Nevertheless, the position of all, but the ethylene atoms, could be fixed with clarity, although the values obtained for their bond distances and angles should be regarded with some caution in order to establish precise comparisons. Compound **3b**: The structure was solved by conventional Patterson and Fourier techniques. An empirical absorption correction,[16] applied at the end of the isotropic refinement using unit weights, led to a conventional R value of 0.060. After mixed full matrix least-squares refinement with isotropic thermal parameters for C(8), C(9) and C(10), minimizing $\Sigma\omega(|F_o| - |F_c|)^2$ gave an R value of 0.047. A difference synthesis calculated with reflections having a $\sin\theta/\lambda < 0.5$ Å^{-1} showed all H atoms as the highest peaks of the map. Final refinement with fixed isotropic temperature factors for H atoms and unit weights led to $R = 0.034$. Most of the calculations were performed with XRAY80.[17]

For both complexes bond distances and angles, final atomic coordinates, tables of thermal parameters and listing of observed and calculated structure factors have been deposited with the Editor as supplementary material.*

Acknowledgement—We are grateful to the Comisión Asesora de Investigación Científica y Técnica for support of this work (E.C. and E.G.).

REFERENCES

1. P. M. Treichel, *Adv. Organomet. Chem.* 1973, **11**, 21; E. Singleton and H. Oosthuizen, *Adv. Organomet. Chem.* 1983, **22**, 209; Y. Yamamoto, *Coord. Chem. Rev.* 1980, **32**, 193.
2. L. B. Kool, M. D. Rausch, M. Herberhold, H. G. Alt, V. Thewalt and B. Honold, *Organometallics* 1986, **4**, 2465; L. B. Anderson, T. J. Barder, F. A. Cotton, K. R. Dumbar, L. R. Falvello and R. A. Walton, *Inorg. Chem.* 1986, **25**, 3629.
3. (a) W. D. Jones, G. P. Foster and J. M. Putinas, *Inorg. Chem.* 1987, **26**, 2120; (b) R. L. Luck, R. H. Morris and J. F. Sawyer, *Organometallics* 1984, **3**, 247.
4. (a) M. P. Guy, J. T. Guy and D. W. Bennett, *Organometallics* 1986, **5**, 1696; (b) D. B. Beach, R. Bartoncello, G. Granozzi and W. L. Jolly, *Organometallics* 1985, **4**, 311.
5. (a) J. Chatt, C. M. Elson, A. J. L. Pombeiro, R. L.

*Atomic coordinates have also been deposited with the Cambridge Crystallographic Data Centre.

Richards and G. H. D. Royston, *J. Chem. Soc., Dalton Trans.* 1978, 165; (b) A. J. L. Pombeiro, J. Chatt and R. L. Richards, *J. Organometal. Chem.* 1980, **190**, 297.
6. J. C. Deaton and R. A. Walton, *J. Organometal. Chem.* 1981, **219**, 187; K. A. Conner and R. A. Walton, *Inorg. Chem.* 1986, **25**, 4422.
7. (a) E. Carmona, J. M. Marín, M. L. Poveda, J. L. Atwood and R. D. Rogers, *J. Am. Chem. Soc.* 1983, **105**, 3014; (b) E. Carmona, A. Galindo, M. L. Poveda and R. D. Rogers, *Inorg. Chem.* 1985, **24**, 4033.
8. R. Alvarez, E. Carmona, J. M. Marín, M. L. Poveda, E. Gutiérrez-Puebla and A. Monge, *J. Am. Chem. Soc.* 1986, **108**, 2286.
9. C. Mealli, R. Hoffmann and A. Stockis, *Inorg. Chem.* 1984, **23**, 56; S. Sakaki, K. Kitaura and K. Morokuma, *Inorg. Chem.* 1982, **21**, 760.
10. B. E. Mann and B. F. Taylor, *^{13}C NMR Data for Organometallic Compounds* (Edited by P. M. Maitlis, F. G. A. Stone and R. West), p. 23. Academic Press, New York (1981).
11. J. W. Byrne, H. U. Blaser and J. A. Osborn, *J. Am. Chem. Soc.* 1975, **97**, 3871.
12. T. A. Albright, R. Hoffmann, J. C. Thibeault and D. L. Thorn, *J. Am. Chem. Soc.* 1979, **101**, 3801; C. Bachman, J. Demynck and A. Veillard, *J. Am. Chem. Soc.* 1978, **100**, 2366.
13. W. Wolfsberger and H. Schmidbaur, *Synth. React. Inorg. Met. Org. Chem.* 1974, **4**, 149.
14. G. W. Gokel, R. P. Widera and W. P. Weber, *Org. Synth.* 1976, **55**, 96.
15. *International Tables for X-ray Crystallography*, Vol. IV, pp. 72–98. Kynoch Press, Birmingham (1974).
16. N. Walker and D. Stuart, *Acta Cryst.* 1983, **A39**, 158.
17. J. M. Stewart, The XRAY80 System. Computer Science Center, University of Maryland, College Park (1985).

Polyhedron Vol. 7, No. 19/20, pp. 1841–1853, 1988
Printed in Great Britain

0277–5387/88 $3.00+.00
© 1988 Pergamon Press plc

PREPARATION OF BIS AND TRIS(ARYLIMIDO) COMPLEXES OF RHENIUM(VII), INCLUDING BIS(ARYLIMIDO) NEOPENTYLIDENE COMPLEXES, CANDIDATES AS OLEFIN METATHESIS CATALYSTS

ANDREW D. HORTON and RICHARD R. SCHROCK*

Department of Chemistry 6-331, Massachusetts Institute of Technology, Cambridge, MA 02139, U.S.A.

Abstract—The reaction between $ReO_3(OSiMe_3)$ and 3 equiv. of ArNCO (Ar = 2,6-$C_6H_3^iPr_2$) yields mixtures of $(ArN)_3Re—O—Re(O)(NAr)_2$ (**1**), $Re(NAr)_3(OSiMe_3)$ (**2a**), and what is proposed to be $Re(O)(NAr)_2(OSiMe_3)$ (**3**). Conditions can be altered in order to yield **1** or **2a** in satisfactory yield, but **3** has not been prepared in pure form. Analogous reactions between $ReO_3(OSiMe_3)$ and 3 equiv. of Ar'NCO (Ar' = 2,6-$C_6H_3Me_2$) yield $(Ar'N)_3Re—O—Re(NAr')_3$ (**4**) and $Re(NAr')_3(OSiMe_3)$ (**2b**), while those between $ReO_3(OSiMe_3)$ and 3 equiv. of Ar''NCO (Ar'' = 2,6-$C_6H_3Cl_2$) yield only $Re(NAr'')_3(OSiMe_3)$ (**2c**). Complexes of the type $Re(NR)_3(CH_2{}^tBu)$ (R = Ar, Ar', Ar'') have been prepared straightforwardly. Complexes of the type $Re(NR)_2Cl_3(py)$ (**6**) can be prepared by treating tris(imido) complexes **2** with 3 equiv. of pyHCl. These can be alkylated to give mononeopentyl bis(imido) derivatives, $Re(NR)_2(CH_2{}^tBu)Cl_2$ (**8**), in high yield. Dehydrohalogenation of $Re(NAr)_2(CH_2{}^tBu)Cl_2$ yields $Re(NAr)_2(CH{}^tBu)Cl$, from which several monoalkoxide derivatives have been prepared (OR = $OCH(CF_3)_2$, $OCMe(CF_3)_2$, or O-2,6-$C_6H_3{}^iPr_2$). Dehydrohalogenation of $Re(NAr')_2(CH_2{}^tBu)Cl_2$ or $Re(NAr'')_2(CH_2{}^tBu)Cl_2$ did not yield neopentylidene complexes analogous to $Re(NAr)_2(CH{}^tBu)Cl_2$. None of the neopentylidene complexes showed any well-defined metathesis activity, even with norbornene.

We recently discovered that a bulky imido ligand will stabilize high oxidation state molybdenum and tungsten alkylidene complexes of the type $M(CH{}^tBu)(NAr)(OR)_2$ (Ar = 2,6-$C_6H_3{}^iPr_2$; OR = $OCMe_3$, $OCMe_2(CF_3)$, etc.).[1] A dianionic ligand is required in order to form a four-coordinate complex in which the metal is in its highest possible oxidation state ("d^0"), a type of complex that we now feel is the most desirable for forming intermediate metallacyclobutane or metallacyclobutadiene complexes in Group 6 olefin[2] or acetylene[3] metathesis systems, respectively. Bulky imido ligands should continue to be successful relative to oxo ligands or unhindered imido ligands because if a metal centre of low coordination number is electrophilic enough to react with an olefin, then it should also strongly coordinate an oxo or a sterically accessible imido nitrogen atom (if no other good donors are present) to form complexes that contain bridging oxo or imido[4] ligands [eq. (1)].

X = O or small NR ligand (1)

It is not surprising that the alkoxide ligands in $M(CH{}^tBu)(NAr)(OR)_2$ complexes also must be bulky in order to avoid formation of dimers, for example, $[V(N\text{-}p\text{-}C_6H_4Me)(O\text{-}2,6\text{-}C_6H_3Me_2)_2Cl]_2$.[5] The tactic is to use ligands that are large enough to prevent formation of complexes containing bridging ligands and slow down or prevent intermolecular decomposition reactions, but still not so large as to prevent access to the metal by relatively small molecules.

We feel that the principles of olefin and acetylene metathesis by "d^0" metal complexes should extend to rhenium(VII). Several years ago[6] we developed an entry into Re^{VII} *t*-butylimido chemistry based on $Re(N{}^tBu)_3(OSiMe_3)$[4b] as a starting material. We

*Author to whom correspondence should be addressed.

found that we could prepare a large number and variety of new molecules, including relatively attractive target molecules such as $Re(N^tBu)_2(CH^tBu)(CH_2{}^tBu)$. However, several features of the chemistry limited their usefulness, among them the high solubility and often thermal and hydrolytic instability of *t*-butylimido derivatives, and the fact that *t*-butylamine generated as a product of protonation reactions often remained firmly bound to the metal. The ultimate disappointment was that species such as $Re(N^tBu)_2(CH^tBu)(CH_2{}^tBu)$ do not react readily with olefins.[7]

We sought an entry into rhenium(VII) *arylimido* chemistry in the belief that arylimido ligands might significantly increase the electrophilicity of the metal to the point where it would react with olefins. Unfortunately, reactions designed to prepare $Re(NAr)_3(OSiMe_3)$ (where Ar = 2,6-$C_6H_3{}^iPr_2$), i.e. procedures involving $ArNHSiMe_3$ analogous to that used to prepare $Re(N^tBu)_3(OSiMe_3)$,[4b] gave a mixture of products, none of which could be isolated or identified.[8] Attempts to exchange *t*-butylimido by NAr in $Re(N^tBu)_3(OSiMe_3)$ and related derivatives looked promising,[8] but the procedures were tedious and circuitous. In searching for a new, general entry into rhenium arylimido chemistry we settled on reactions between an isocyanate and a metal oxide [eq. (2)], a type of reaction that is a known route to several imido complexes,[4a] although the generality of the reaction has not been fully explored. In this paper we report high yield routes to Re^{VII} complexes containing two or three arylimido ligands of the type N-2,6-$C_6H_3{}^iPr_2$(NAr), N-2,6-$C_6H_3Me_2$ (NAr′), or N-2,6-$C_6H_3Cl_2$ (NAr″). Some of these results were reported in the form of a preliminary communication.[9]

$$M{=}O + ArNCO \rightarrow M{=}NAr + CO_2. \quad (2)$$

RESULTS AND DISCUSSION

$Re_2O_2(NAr)_5$ can be prepared in 27% isolated yield as shown in eq. (3). An ^1H NMR spectrum of **1** shows that methyl groups in the three imido ligands on one metal are equivalent while pairs of methyl groups in each of the two equivalent imido ligands on the second metal are diastereotopic.

$$ReO_3(OSiMe_3) + 3ArNCO \xrightarrow[\text{reflux}]{\text{toluene}} 1/2(ArN)_3Re{-}O{-}Re(O)(NAr)_2. \quad (3)$$

1 (27%)

A Re=O stretch can be observed in the IR spectrum of **1** at 903 cm^{-1}. There is no reason to believe that **1** is not an oxo-bridged species as shown in which the two ends of the molecule can freely rotate on the NMR time scale. We have not been able to replace the last terminal oxo ligand in **1**, presumably because of steric congestion about the metal (cf. **4** below). It should be noted that the electron count on each Re exceeds 18 if π electrons from the terminal oxo and all imido ligands are included. Therefore we cannot be certain that all Re—N—C_{ipso} angles are of the order of 170° or greater in the solid state, as would be the case if an imido ligand fully donates its π electron pair to the metal. However, if both "bent" and "linear" imido ligands are present in **1**, they must interconvert rapidly on the NMR time scale.

NMR examination of the crude mixture obtained in the reaction shown in eq. (3) reveals that **1** comprises only ~ 60% of the diamagnetic product mixture. Approximately 30% of the crude mixture has been identified as $Re(NAr)_3(OSiMe_3)$ (**2a**), while ~ 10% of the mixture is what we speculate to be $Re(O)(NAr)_2(OSiMe_3)$ (**3**). The fraction of **2a** in the crude mixture can be increased to 65% (20% **1**, 15% **3**) by employing $Me_3SiOSiMe_3$ as the reaction solvent, and red crystalline **2a** can be isolated in 46% yield in this manner [eq. (4)]. For this reason we suspect that $ReOSiMe_3$ species are in equilibrium with Re—O—Re species and $Me_3SiOSiMe_3$, a type of reaction that has been observed when DMF is added to a solution of $ReO_3(OSiMe_3)$ in ether or $MeSiOSiMe_3$ [eq. (5)].[10]

$$ReO_3(OSiMe_3) + 3ArNCO \xrightarrow[\text{reflux}]{Me_3SiOSiMe_3} Re(NAr)_3(OSiMe_3) \quad (4)$$

2a (46%)

$$2ReO_3(OSiMe_3) + 2DMF \underset{}{\overset{\text{25°C in ether or } Me_3SiOSiMe_3}{\rightleftharpoons}} Re_2O_7(DMF)_2 + Me_3SiOSiMe_3. \quad (5)$$

Therefore running the reaction in $Me_3SiOSiMe_3$ maximizes the amount of **2a** by minimizing the formation of Re—O—Re species. It is important to note that once **2a** is formed it does *not* lose $Me_3SiOSiMe_3$ in refluxing toluene to give as yet unknown $(ArN)_3Re{-}O{-}Re(NAr)_3$ (cf. **4** below). Therefore only $ReO_x(NAr)_{3-x}(OSiMe_3)$ complexes where $x = 1$, 2 or 3 could be involved in equilibria analogous to that shown in eq. (5).

If the reaction is carried out in toluene (70°, 20 h) or in $Me_3SiOSiMe_3$ (with shorter reflux times), the crude reaction mixture contains only ~ 20% of **2a**; ~80% of the mixture consists of a complex that cannot be isolated, but which NMR and IR evidence suggests is $Re(O)(NAr)_2(OSiMe_3)$ (**3**). Therefore we propose that the reaction between

$ReO_3(OSiMe_3)$ and ArNCO proceeds stepwise as shown in eq. (6), and that one or more of the intermediate $ReO_x(NAr)_{3-x}(OSiMe_3)$ complexes decomposes to Re—O—Re species, which can then react further with ArNCO to give **1**. If less than 3 equiv. of ArNCO are used in reactions of this type, then relatively complicated mixtures result. It seems plausible that species such as $ReO_2(NAr)(OSiMe_3)$, $Re_2O_3(NAr)_4$, or $Re_2O_4(NAr)_3$ are formed under these conditions, in addition to varying amounts of **1**, **2a**, or **3**. Initial studies of reactions between $ArNHSiMe_3$ and $ReO_3(OSiMe_3)$[8] were discouraging perhaps because similar multiple equilibria and reaction stages gave rise to complex mixtures.

$$ReO_3(OSiMe_3) \xrightarrow{ArNCO} Re(O)_2(NAr)(OSiMe_3) \xrightarrow{ArNCO} \underset{\mathbf{3}}{Re(O)(NAr)_2(OSiMe_3)} \xrightarrow{ArNCO} \underset{\mathbf{2a}}{Re(NAr)_3(OSiMe_3)}. \quad (6)$$

Reactions between $ReO_3(OSiMe_3)$ and Ar′NCO (Ar′ = N-2,6-$C_6H_3Me_2$) or Ar″NCO (Ar″ = N-2,6-$C_6H_3Cl_2$) proceed more cleanly than those involving ArNCO. In refluxing toluene **4** [eq. (7)] is formed in high yield and can be isolated in 65% yield.

$$ReO_3(OSiMe_3) + 3Ar'NCO \xrightarrow[\text{reflux}]{\text{toluene}} \underset{\mathbf{4}\ (65\%)}{1/2(Ar'N)_3Re—O—Re(NAr')_3}. \quad (7)$$

Evidently the NAr′ ligand is small enough so that bimolecular elimination of $Me_3SiOSiMe_3$ in $ReO_x(NAr')_{3-x}(OSiMe_3)$ complexes to give Re—O—Re complexes is more facile than in the case of NAr complexes, and ultimately complete replacement of all terminal oxo ligands is now sterically possible. NMR examination of the crude reaction mixture shows that only one other diamagnetic product, $Re(NAr')_3(OSiMe_3)$ (**2b**), is present in ~ 10% relative yield. It is virtually the only product of an analogous reaction that is carried out in $Me_3SiOSiMe_3$ [eq. (8); only traces of **4** are observed]. As with **2a**, **2b** does not decompose to **4** in refluxing toluene, nor does **4** yield **2b** upon being refluxed in $Me_3SiOSiMe_3$. The reaction between Ar″NCO and $ReO_3(OSiMe_3)$ in refluxing xylene yields only $Re(NAr'')_3(OSiMe_3)$ [**2c**; eq. (9)], isolated in 79% yield; there is no evidence (by NMR examination of the crude mixture) for formation of any species analogous to **1** or **3**.

$$ReO_3(OSiMe_3) + 3Ar'NCO \xrightarrow[\text{reflux}]{Me_3SiOSiMe_3} \underset{\mathbf{2b}\ (82\%)}{Re(NAr')_3(OSiMe_3)} \quad (8)$$

$$ReO_3(OSiMe_3) + 3Ar''NCO \xrightarrow[\text{reflux 48 h}]{\text{xylene}} \underset{\mathbf{2c}\ (79\%)}{Re(NAr'')_3(OSiMe_3)}. \quad (9)$$

Note that **2c** shows no tendency to eliminate $Me_3SiOSiMe_3$ to form $Re_2(O)(NAr'')_6$.

It is not yet clear how electronic and steric differences determine the course of reactions of this general nature. What is clear is that the isocyanate route appears to have some general utility for forming Re^{VII} complexes that contain bulky imido ligands.

Neopentyl derivatives of the tris(imido) complexes can be prepared straightforwardly and isolated in high yield as red–purple crystals [eq. (10)]. Note that preparation of **5a** requires the lithium reagent; presumably the trimethylsiloxide cannot be substituted by the less reactive Grignard reagent.

$Re(NR)_3(OSiMe_3) + {}^tBuCH_2MgCl$ or

2a (R = Ar)
2b (R = Ar′)
2c (R = Ar″)

$$LiCH_2{}^tBu \xrightarrow[-40°C]{\text{ether}} \underset{\begin{array}{l}\mathbf{5a}\ (R = Ar;\ 77\%)\\ \mathbf{5b}\ (R = Ar';\ 80\%)\\ \mathbf{5c}\ (R = Ar'';\ 73\%)\end{array}}{Re(NR)_3(CH_2{}^tBu)}. \quad (10)$$

In the case of the formation of **5b** and **5c** the Grignard is required; use of the lithium reagent produces what are believed to be reduced rhenium complexes; they will be reported elsewhere. An alternative preparation of the NAr′ derivative starts with $Re(NAr')_3Cl$ (see later). NMR spectra of these presumably pseudotetrahedral molecules are unexceptional. This series of complexes was prepared in order to examine how they react with HCl (see later); **5b** and **5c** are important precursors.

The reaction between **1** and pyridinium chloride yields **6a** [eq. (11)] in ~ 80% isolated yield as green crystals. We propose that **6a** is octahedral with imido ligands *cis* to one another in order to minimize competition between the π bonds. However only at −60° are the two arylimido ligands inequivalent (pairs of methyl groups in each are diastereotopic) as a result of the pyridine binding to the metal, most likely in a position *trans* to one of the imido ligands.

At normal temperatures the imido and pyridine resonances are broad, we presume as a result of reversible loss of pyridine to give $Re(NAr)_2Cl_3$. **6a** is an 18 electron complex if one of the imido ligands (presumably a bent one[4a]) does not donate its electron pair to the metal. It seems more likely that pyridine would bind *trans* to the bent imido ligand, as the linear imido ligand should be more *trans* labilizing. The feasibility of **6a** as a starting material increases substantially as a result of its isolation in ~75% yield *overall* from $ReO_3(OSiMe_3)$ upon addition of pyridinium chloride to the *crude* product (containing **2** and **3** and probably traces of related oxo/imido complexes) of the reaction between $ReO_3(OSiMe_3)$ and ArNCO in refluxing toluene [eq. (3)]. An analogous two-step reaction sequence leads to **6b** [eq. (12)] while the reaction between $Re(NAr'')_3(OSiMe_3)$ (available in high yield) and pyridinium chloride yields **6c** [eq. (13)]. NMR spectra of **6b** and **6c** suggest that they are entirely analogous to **6a**.

$$Re_2O_2(NAr)_5 \xrightarrow[CH_2Cl_2]{6\ \text{pyridineHCl}} 2\ \text{[Cl, ArN, py, Re, ArN, Cl, Cl]} \quad (11)$$

6a

$$ReO_3(OSiMe_3) \xrightarrow[2.3\ \text{equiv. pyHCl}/CH_2Cl_2]{1.3\ \text{equiv. Ar'NCO/toluene}} Re(NAr')_2Cl_3(py) \quad (12)$$

6b (62%)

$$Re(NAr'')_3(OSiMe_3) \xrightarrow{3\ \text{equiv. pyHCl}/CH_2Cl_2} Re(NAr'')_2Cl_3(py). \quad (13)$$

6c (79%)

If 3 equiv. of gaseous anhydrous HCl (in dichloromethane) are added to the crude product mixture (in dichloromethane) obtained in the reaction shown in eq. (7), than an insoluble material is obtained that reacts with 3 equiv. of pyridine to give **6b**, and with 3 equiv. of triethylamine to give **7** [eq. (14)] in good overall yield from $ReO_3(OSiMe_3)$. On the basis of these reactions we speculate that the insoluble green material is $[Ar'NH_3][Re(NAr')_2Cl_4]$. We propose that **7** is a monomeric pseudo-tetrahedral complex on the basis of its high solubility in pentane.

$$[Ar'NH_3][Re(NAr')_2Cl_4] \xrightarrow[-3Et_3NHCl]{+3Et_3N\ \text{in}\ CH_2Cl_2} Re(NAr')_3Cl \quad (14)$$

7 [67% vs $ReO_3(OSiMe_3)$].

Key compounds in the quest for neopentylidene complexes are of the type $Re(NR)_2(CH_2{}^tBu)Cl_2$. The NAr′ and NAr″ derivatives are readily available from the $Re(NR)_3(CH_2{}^tBu)$ complexes as shown in eq. (15). The analogous reaction of $Re(NAr)_3(CH_2{}^tBu)$ with gaseous HCl yielded several products in what is evidently a relatively non-specific reaction, at least in our hands so far. However, $Re(NAr)_2(CH_2{}^tBu)Cl_2$ can be prepared in good yield by alkylating $Re(NAr)_2Cl_3(py)$ [eq. (16)]. (Addition of 1 equiv. of $^tBuCH_2MgCl$ to $Re(NAr)_2Cl_3(py)$ does not yield **8a** cleanly or in high yield; it is not a suitable preparative method.) Similar selective alkylation reactions involving $Re(NAr')_2Cl_3(py)$ or $Re(NAr'')_2Cl_3(py)$ have not yet been successful, but the routes shown in eq. (15) are satisfactory because of the ready availability of $Re(NAr')_3(CH_2{}^tBu)$ and $Re(NAr'')_3(CH_2{}^tBu)$.

$$Re(NR)_3(CH_2{}^tBu) \xrightarrow[-RNH_3Cl]{3HCl\,(gas)-78°C} Re(NR)_2(CH_2{}^tBu)Cl_2 \quad (15)$$

8b (R = Ar′; 75%)
8c (R = Ar″; 78%)

$$Re(NAr)_2Cl_3(py) \xrightarrow[CH_2Cl_2]{Zn(CH_2{}^tBu)_2/Et_4NCl} Re(NAr)_2(CH_2{}^tBu)Cl_2 \quad (16)$$

8a (72%).

Thus **8a–c** are all available on a relatively large scale (10 g). Unlike $Re(N^tBu)_2(CH_2{}^tBu)Cl_2$, which decomposes over a period of several hours in the solid state at 25°C,[6] **8a–c** are all stable in the solid state in the absence of air and moisture for months. NMR data suggest that their structures are analogous; for example, only one kind of imido ligand is present and the isopropyl methyl groups are diastereotopic. One possible structure that is consistent with these data is a trigonal bipyramidal species in which the imido ligands are located in equatorial positions and the neopentyl ligand is located in an axial position. However a recent report of the unusual structure of $Re(N^tBu)_2(O\text{-}C_6H_4Me)Cl_2$,[11] a tetragonal pyramid containing a *bent* axial imido ligand with the *shortest* Re═N bond length, suggests that predictions concerning the structure of **8a–c**, and indeed other imido complexes we have prepared here, are dangerous, even though the

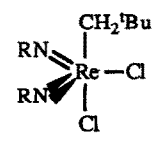

8 (R = Ar, Ar′, Ar″)

imido ligands are equivalent (as they are in $Re(N^tBu)_2(O\text{-}C_6H_4Me)Cl_2$[11]) on the NMR time scale.

The alkylation shown in eq. (16) is very sensitive to the amount of dineopentylzinc that is used. If ~ 1.7 equiv. of dineopentylzinc is used then the reaction proceeds in high yield to give **9a** [eq. (17)]. The mechanism of the reaction may involve dehydrohalogenation of $Re(NAr)_2(CH_2{}^tBu)_2Cl$ by pyridine (see below). A similar reaction of the NAr′ derivative gives $Re(NAr')_2(CH^tBu)(CH_2{}^tBu)$ (**9b**). Preliminary experiments show that other alkylation reactions (e.g. with Me or CH_2Ph groups) lead to complexes of the type $Re(NAr)_2R_3$. Similar behaviour was observed for the analogous *t*-butylimido complexes.[6] So far, $Re(NAr'')(CH^tBu)(CH_2{}^tBu)$ has not yet been prepared pure by an analogous route.

$$Re(NAr)_2Cl_3(py) \xrightarrow{1.7Zn(CH_2{}^tBu)_2/Et_4NCl\text{ in }CH_2Cl_2} Re(NAr)_2(CH^tBu)(CH_2{}^tBu). \quad (17)$$

9a

It is possible to cleanly dehydrohalogenate $Re(NAr)_2(CH_2{}^tBu)Cl_2$ to give red **10** [eq. (18)] virtually quantitatively. Although **10** is very soluble in pentane, it can be isolated from it in ~75% yield. We have tried a wide variety of other bases (among them pyridine, 2,4-lutidine, triethylamine or $Ph_3P{=}CHMe$), solvents and temperatures, but so far we have not been able to discover other conditions that give a good yield of **10**. It would appear, therefore, that HCl must be removed effectively from the system, perhaps in order to prevent a destructive reprotonation reaction. Details of the NMR spectra of **10** are discussed later along with those of related neopentylidene complexes.

$$Re(NAr)_2(CH_2{}^tBu)Cl_2 \xrightarrow{DBU\text{ in ether at }-20°C} Re(NAr)_2(CH^tBu)Cl. \quad (18)$$

10

Unfortunately, analogous dehydrohalogenation reactions starting with $Re(NAr')_2(CH_2{}^tBu)Cl_2$ or $Re(NAr'')_2(CH_2{}^tBu)Cl_2$ so far have not been successful. Reactions carried out in C_6D_6 and examined by ^1H NMR showed the only significant products to be those shown in eq. (19) in approximately a 1:1 ratio. The [DBUH][Re(NAr′)(C′Bu)Cl_3] and [DBUH][Re(NAr″)(C′Bu)Cl_3] complexes appear to be analogous to isolated [DBUH][Re(NAr)(C′Bu)Cl_3];[12] all resonances for [DBUH][Re(NAr′)(C′Bu)Cl_3] and [DBUH][Re(NAr″)(C′Bu)Cl_3] are analogous to those observed for [DBUH][Re(NAr)(C′Bu)Cl_3], and an alkylidyne C_α resonance has been observed in the ^{13}C NMR spectrum of [DBUH][Re(NAr′)(C′Bu)Cl_3] at 313.7 ppm (cf. 314.7 ppm in [DBUH][Re(NAr)(C′Bu)Cl_3][12]). We could only speculate on the mechanism of this disproportionation reaction. The important point is that disproportionation does not take place with the sterically more bulky NAr analogues.

$$Re(NR)_2(CH_2{}^tBu)Cl_2 \xrightarrow[C_6D_6\text{ at }\sim 5°C,\ -0.5\,[DBUH]Cl]{+DBU} 0.5\,Re(NR)_3(CH_2{}^tBu) + 0.5\,[DBUH][Re(NR)(C^tBu)Cl_3]. \quad (19)$$

10 sometimes is contaminated to a significant extent by pseudo-tetrahedral $Re(O)(NAr)_2(CH_2{}^tBu)$ (**11**). **11** may be prepared in good yield and in multigram quantities as shown in eq. (20).

$$Re(NAr)_2(CH^tBu)Cl \xrightarrow[-Me_4NCl]{Me_4NOH/MeOH} Re(O)(NAr)_2(CH_2{}^tBu). \quad (20)$$

11

We propose that the reaction proceeds via intermediate $Re(NAr)_2(CH^tBu)(OH)$ followed by a proton shift from oxygen to carbon. It is interesting to note that $Re(NAr)_2(CH^tBu)Cl$ reacts only slowly with 1 equiv. of water in ether at 25°C (~ 50% of **11** formed after 2 h). $Re(NAr)_2(CH_2{}^tBu)Cl_2$ also reacts with Me_4NOH under similar conditions, but a mixture of products is formed that does not include a substantial amount of **11**. Therefore we believe that DBU dehydrohalogenates $Re(NAr)_2(CH_2{}^tBu)Cl_2$ to give **10**, and completely reacts with traces of water to give the hydroxide ion that then reacts with **10** to give **11**. NMR spectra of **11** show that the imido ligands are equivalent on the NMR time scale, and two sets of diastereotopic methyl groups are present. At this stage we are assuming that **11** is a pseudo-tetrahedral monomer in which one of the imido ligands is bent, and the other is linear. So far attempts to form **11** by treating $Re(NAr)_3(CH_2{}^tBu)$ with water have only produced it in low yield in an apparently complex messy reaction.

Treating $Re(NAr)_2(CH^tBu)Cl$ with alkoxides yields complexes **12a–c** virtually quantitatively [eq. (21)]. Complexes **12** are all red or orange and highly soluble in pentane, so soluble, in fact, that only **12a** and **12c** have been isolated as nicely crystalline samples suitable for elemental analysis. However, on the basis of NMR spectra there is no doubt that

12b is correctly formulated.

$$Re(NAr)_2(CH^tBu)Cl \xrightarrow[\text{ether, } -40°C]{LiOR} Re(NAr)_2(CH^tBu)(OR) \quad (21)$$

12a; OR = $OCH(CF_3)_2$
12b; OR = $OCMe(CF_3)_2$
12c; OR = O-2,6-$C_6H_3{}^iPr_2$.

Selected NMR data for all neopentylidene complexes are collected in Table 1. The values for δH_α, δC_α and J_{CH}(Hz) are all similar to the respective values in $Re(N^tBu)_2(CH^tBu)(CH_2{}^tBu)$[6] (11.95 ppm in toluene d_8, 262.2 ppm in C_6D_6, J_{CH} = 134 Hz). Resonances for H_α and C_α were found to shift downfield in complexes of the type M(NAr)$(CH^tBu)(OR)_2$ (M = Mo or W) as OR became electron-withdrawing.[1] Therefore we had expected δH_α and δC_α for the complexes containing the NAr ligand to reflect to a greater extent the greater electron-withdrawing ability of the phenyl substituent versus that for the *t*-butyl group in the analogous N^tBu complexes. The most important features of the NMR spectra for all neopentylidene complexes are the inequivalent imido ligands and diastereotopic pairs of methyl groups in each. Inequivalent imido ligands also were observed in $Re(N^tBu)_2(CHCMe_3)(CH_2CMe_3)$.[6] The phenomenon in each case could be ascribed to orientation of the neopentylidene ligand so that the α proton lies in a N—Re—C plane and points towards or away from one of the imido ligands, see Fig. 1. Again an X-ray study is required. In these complexes if each imido ligand donates its π electron pair the metal electron count is brought up to 18.

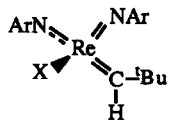

Fig. 1.

Qualitative olefin metathesis experiments

We summarize the results of several tests for metathesis activity in Table 2. In short there was no evidence for metathesis, even when norbornene was employed. The sporadic polymerization activity in the case of norbornene must be ascribed to impurities. These results prove incorrect our hypothesis that aryl imido complexes could be active even though *t*-butylimido analogues are not. We suspect that electronic saturation at the metal centre in these complexes is the primary obstacle to their reaction with olefins. So far attempts to synthesize potentially more reactive analogous alkylidene complexes with less bulky, poorer electron donating imido ligands has been hindered by decomposition reactions; we presume at this stage that decomposition is the result of intermolecular reactions that are now more favourable because of the relatively unhindered nature of the coordination sphere.

The complexes described here have proven to be useful as facile entries into monoarylimido rhenium chemistry, and a monoimido neopentylidyne complex now has been shown to be an active acetylene metathesis catalyst.[13] Therefore we presume that our continued search for a well-characterized Re^{VII} olefin metathesis catalyst ultimately will be successful, although what the nature of that species might be is still in doubt.

EXPERIMENTAL

General experimental procedures may be found elsewhere.[14] NMR chemical shifts are reported relative to TMS. Expected intensities, multiplicities and coupling constants are usually omitted. The NMR solvent is C_6D_6 and the temperature ~25°C unless otherwise specified. DBU (1,8-diazabicyclo [5.4.0]undec-7-ene) was purchased commercially and distilled before use. $ReO_3(OSiMe_3)$[15] and OCN-2,6-$C_6H_3{}^iPr_2$[16] were prepared by literature

Table 1. Selected NMR data for complexes of the type $Re(NR)_2(CH^tBu)X$

NR	X	δ H_α (ppm)	δ C_α (ppm)	J_{CH}(Hz)
2,6-$C_6H_3{}^iPr_2$	CH_2CMe_3	12.28	269.0	139
2,6-$C_6H_3{}^iPr_2$	Cl	12.27	269.4	136
2,6-$C_6H_3{}^iPr_2$	$OCH(CF_3)_2$	11.88	260.5	137
2,6-$C_6H_3{}^iPr_2$	$OCMe(CF_3)_2$	11.56	256.4	139
2,6-$C_6H_3{}^iPr_2$	O-2,6-$C_6H_3{}^iPr_2$	11.25	256.7	146
2,6-$C_6H_3Me_2$	CH_2CMe_3	12.24	270.5	137

Table 2. Results of tests for olefin metathesis activity[a]

Compound	Olefin (equiv.)	Solvent	Time/temp	Method
12a	20 *cis*-2-pentene	Toluene	3 days/25°C	GLC
10, 12c	10 *cis*-2-pentene	C_6D_6	1 day/25°C	NMR
9a, 10, 12a, 12b, 12c	20 norbornene[b]	C_6D_6	18 h/25°C	NMR

[a] Sample size 10–15 mg.

[b] Some polymer (< 50%) was observed sporadically; such experiments could not be repeated and starting material was not consumed.

methods. Other arylisocyanates were purchased commercially.

$Re_2O_2(N\text{-}2,6\text{-}C_6H_3{}^iPr_2)_5$ (**1**)

2,6-Diisopropylphenylisocyanate (1.00 g, 4.93 mmol) was added to a toluene (30 cm^3) solution of $ReO_3(OSiMe_3)$ (0.50 g, 1.55 mmol). The mixture rapidly turned orange and was refluxed for 5 h. An intermediate olive–brown colour was observed which turned to an intense red–orange colour after 30 min. The solvent was removed *in vacuo* and the residue extracted with pentane (200 cm^3). The extract was filtered, concentrated and cooled to 0°C to give dark red crystals (0.27 g, 27%). The analytical sample was recrystallized from a mixture of dichloromethane and pentane: ^1H NMR δ 7.05 (d, 10, H_m), 6.90 (m, 5, H_p), 3.83 (sept, 4, C*H*Me_2), 3.71 (sept, 6, C*H*Me_2), 1.20, 1.19, 1.17 (d, 12, 12, 36, CH*Me*$_2$); ^{13}C NMR δ 152.6 and 151.9 (C_{ipso}), 144.3 and 142.4 (C_o), 128.1 and 127.2 (C_p), 122.6 and 122.4 (C_m), 29.0 and 28.8 (*C*HMe_2), 23.7 (CH*Me*$_2$); IR (Nujol) 903 cm^{-1} (Re=O). Found: C, 56.6; H, 7.1; N, 5.8. Calc. for $Re_2C_{60}H_{85}N_2O_2$: C, 56.3; H, 6.7; N, 5.5%.

$Re(N\text{-}2,6\text{-}C_6H_3{}^iPr_2)_3(OSiMe_3)$ (**2a**)

ArNCO (7.88 g, 38.3 mmol) was added to a solution of $ReO_3(OSiMe_3)$ (4.0 g, 12.32 mmol) in $(Me_3Si)_2O$ (400 cm^3). The initial olive–orange solution became intense orange after refluxing the reaction mixture for 18 h. Removing the solvent *in vacuo* afforded an oily orange residue that upon extraction with pentane (200 cm^3) left behind dark red crystals of $Re_2O_2(NAr)_5$ (0.35 g). Concentrating and cooling the pentane extract gave 4.56 g (four crops, 46%) of $Re(NAr)_3(OSiMe_3)$ as red crystals. Contamination of the product with $Re_2O_2(NAr)_5$ can be avoided by extracting the product into a minimal amount of pentane and slowly recrystallizing it at −30°C: ^1H NMR δ 7.06 (d, 6, H_m), 6.92 (t, 3, H_p), 3.59 (sept, 6, C*H*Me_2), 1.13 (d, 36, CH*Me*$_2$), 0.40 (s, 9, $OSiMe_3$); ^{13}C NMR δ 152.3 (C_{ipso}), 141.2 (C_o), 125.8 (C_p), 122.0 (C_m), 28.4 (*C*HMe_2), 23.9 (CH*Me*$_2$), 1.9 ($OSiMe_3$). Found: C, 58.2; H, 7.6; N, 5.1. Calc. for $ReC_{39}H_6N_3OSi$: C, 58.5; H, 7.5; N, 5.2%.

Although the ^1H NMR spectrum of the crude product mixture showed it to contain $Re(NAr)_3(OSiMe_3)$, $Re_2O_2(NAr)_5$, and $Re(O)(NAr)_2(OSiMe_3)$ (see below) in the approximate ratio 65:20:15, the extremely high solubility of $Re(NAr)_3(OSiMe_3)$ prevented its recovery in higher yield.

$Re(N\text{-}2,6\text{-}C_6H_3Me_2)_3(OSiMe_3)$ (**2b**)

Ar′NCO (7.05 g, 48.0 mmol) was added to a solution of $ReO_3(OSiMe)_3$ (5.0 g, 15.1 mmol) in $(Me_3Si)_2O$ (250 cm^3) and the mixture was heated to reflux for 18 h. Dichloromethane (60 cm^3) was added to the intense orange solution to dissolve some orange precipitate. Filtration of the solution through Celite and concentration of the filtrate *in vacuo* gave orange microcrystals of the product (8.0 g, 82%). Traces of $Re_2(O)(NAr')_6$ are removed when a sample is recrystallized slowly at −30°C from a mixture of dichloromethane and pentane: ^1H NMR δ 6.89 (d, 6, H_m), 6.70 (t, 3, H_p), 2.31 (s, 18, Me), 0.30 (s, 9, $OSiMe_3$); ^{13}C NMR δ 155.4 (C_{ipso}), 131.8 (C_o), 127.7 (C_m), 125.6 (C_p), 18.7 (Me), 1.7 ($OSiMe_3$). Found: C, 51.2; H, 5.8; N, 6.1. Calc. for $ReC_{27}H_{36}N_3OSi$: C, 51.2; H, 5.7; N, 6.6%.

$Re(N\text{-}2,6\text{-}C_6H_3Cl_2)_3(OSiMe_3)$ (**2c**)

Ar″NCO (9.45 g, 50.8 mmol) was added as a solid to a solution of $ReO_3(OSiMe_3)$ (5.46 g, 16.9 mmol) in xylene (300 cm^3). Upon refluxing the reaction mixture for several hours the initial brown colour changed to an intense orange. After 48 h the reaction mixture was cooled and the solvent was removed *in vacuo*, leaving a red microcrystalline solid. The solid was redissolved in a mixture of dichloromethane (200 cm^3) and pentane (150 cm^3) and the solution filtered through Celite. Con-

centrating and cooling the filtrate *in vacuo* gave 11.1 g (two crops, 79%) of red crystalline product that was essentially pure (by ^{1}H NMR): ^{1}H NMR δ 6.83 (d, 6, H_m), 6.08 (t, 3, H_p), 0.40 (s, 9, $OSiMe_3$); ^{13}C NMR δ 151.3 (C_{ipso}), 130.0 (C_o), 127.7 (C_m), 125.9 (C_p), 1.7 ($OSiMe_3$). Found: C, 33.6; H, 2.7; N, 5.4; Cl, 27.8. Calc. for $ReC_{21}H_{18}Cl_6N_3OSi$: C, 33.4; H, 2.7; N, 5.6; Cl, 28.2%.

Observation of Re(O)(N-2,6-$C_6H_3{}^iPr_2)_2(OSiMe_3)$ (**3**)

Treatment of $ReO_3(OSiMe_3)$ with 2 equiv. of ArNCO *either* in toluene at 70°C (2–20 h) *or* in $(Me_3Si)_2O$ over the temperature range 45–100°C (for various time periods) in *closed systems* gave, in each case, a mixture of the desired product and $Re(NAr)_3(OSiMe_3)$. The best reaction $ReO_3(OSiMe_3)$ (0.10 g, 0.31 mmol) plus ArNCO (0.128 g, 0.62 mmol), d_8-toluene (2 cm^3), 70°C, 20 h] gave an 85:15% mixture of $Re(O)(NAr)_2(OSiMe_3)$ and $Re(NAr)_3(OSiMe_3)$. The best ratio in $(Me_3Si)_2O$ was 80:20% [100°C, 1 h or 85°C, 2 h]; lower temperatures gave more of the minor product as well as unreacted ArNCO. The very high solubility of the two products in pentane prevented their separation by fractional crystallization. ^{1}H NMR δ 7.01 (d, 4, H_m), 6.89 (t, 2, H_p), 3.66 (sept, 4, $CHMe_2$), 1.17 and 1.15 (each a d, 2, $CHMe_2$), 0.20 (s, 9, $OSiMe_3$).

$Re_2(O)$(N-2,6-$C_6H_3Me_2)_6$ (**4**)

Ar′NCO (1.46 g, 9.93 mmol) was added to a solution of $ReO_3(OSiMe_3)$ (1.0 g, 3.09 mmol) in xylene (50 cm^3). An intense red–orange colour resulted upon heating the reaction mixture to reflux temperature for 48 h. The solvent was removed *in vacuo* and the residue was extracted with pentane (300 cm^3). The extract was filtered through Celite, cooled and concentrated *in vacuo* to give a red microcrystalline solid (1.1 g, 64%). Large red crystals were obtained by recrystallization from pentane: ^{1}H NMR δ 6.85 (d, 12, H_m), 6.66 (t, 6, H_p), 2.34 (s, 36, Me); ^{13}C NMR δ 155.6 (C_{ipso}), 131.9 (C_o), 127.6 (C_m), 125.9 (C_p), 18.6 (Me). Found: C, 52.3; H, 5.0. Calc. for $Re_2C_{48}H_{54}N_6O$: C, 52.2; H, 4.9%.

The ^{1}H NMR spectrum of the crude reaction mixture (after the initial extraction with pentane) showed it to contain ~10% $Re(NAr')_3(OSiMe_3)$ (see above) and several other minor products. The proportion of additional products increased slightly when toluene was used as the reaction medium. Using 2 equiv. of Ar′NCO in refluxing toluene gave a large number of complexes in low yield and virtually none of the above major product.

Re(N-2,6-$C_6H_3{}^iP_2)_3(CH_2{}^tBu)$ (**5a**)

$LiCH_2{}^tBu$ (0.227 g, 2.92 mmol) was added to a solution of $Re(NAr)_3(OSiMe_3)$ (1.80 g, 2.25 mmol) in ether (20 cm^3) at −40°C. The mixture was allowed to warm to 25°C over a period of 15 min. After stirring the reaction mixture for 2 h, the solvent was removed *in vacuo*. The oily residue was extracted with pentane (50 cm^3) and the extract filtered through Celite. The filtrate was taken to dryness *in vacuo* and the residue was dissolved in pentane (2 cm^3). Red crystals (three crops, 1.35 g, 77%) of product were obtained upon cooling the solution to −30°C: ^{1}H NMR δ 7.06 (m, 9, H_{aryl}), 3.89 (sept, 6, $CHMe_2$), 3.85 (s, 2, CH_2CMe_3), 1.23 (s, 9, CH_2CMe_3), 1.20 (d, 36, $CHMe_2$); ^{13}C NMR δ 153.1 (C_{ipso}), 142.4 (C_o), 126.5 (C_p), 122.5 (C_m), 51.6 (CH_2CMe_3), 35.1 (CH_2CMe_3), 33.1 (CH_2CMe_3), 28.2 ($CHMe_2$), 23.6 ($CHMe_2$). Found: C, 63.3; H, 8.1; N, 5.2. Calc. for $ReC_{41}H_{62}N_3$: C, 62.9; H, 8.0; N, 5.4%.

Re(N-2,6-$C_6H_3Me_2)_3(CH_2{}^tBu)$ (**5b**)

$^tBuCH_2MgCl$ (9.0 cm^3 of 0.6 M solution in ether, 5.40 mmol) was added to a solution of $Re(NAr')_3Cl$ (3.06 g, 5.29 mmol) in ether (150 cm^3) at −40°C. A precipitate of $MgCl_2$ was formed after stirring for several hours at 25°C. After 48 h, the mixture was filtered through Celite to remove $MgCl_2$ and the filtrate was reduced to dryness. The red oily residue was extracted with pentane (300 cm^3) and the extract was filtered through Celite. Concentrating and cooling the extract gave red crystals of the product (three crops, 2.58 g, 80%). The analytical sample was prepared by recrystallization from pentane: ^{1}H NMR δ 6.91 (d, 6, H_m), 6.81 (t, 3, H_p), 3.87 (s, 2, CH_2CMe_3), 2.36 (s, 18, Me), 1.18 (s, 9, CH_2CMe_3); ^{13}C NMR δ 156.3 (C_{ipso}), 132.0 (C_o), 128.1 (C_p), 125.7 (C_m), 48.8 (CH_2CMe_3), 34.6 (CH_2CMe_3), 33.4 (CH_2CMe_3), 19.3 (Me). Found: C, 56.9; H, 6.1. Calc. for $ReC_{29}H_{38}N_3$: C, 56.6; H, 6.2%.

The product also may be obtained in virtually quantitative yield by treating $Re(NAr')_3(OSiMe_3)$ with $^tBuCH_2MgCl$ in ether at 25°C.

Re(N-2,6-$C_6H_3Cl_2)_3(CH_2{}^tBu)$ (**5c**)

$^tBuCH_2MgCl$ (3.7 cm^3 of 2.1 M solution in ether, 7.77 mmol) was added to a suspension of $Re(NAr'')_3(OSiMe_3)$ (5.0 g, 6.62 mmol) in ether (400 cm^3) at −40°C. The solution turned a darker red colour on warming to 25°C over 30 min. After stirring the solution for 2 h, the volume was reduced to 250 cm^3 *in vacuo* and pentane (100 cm^3)

was added. Magnesium salts were removed by filtration through Celite and the solution was reduced to dryness *in vacuo*. The red oily residue was dissolved in a mixture of dichloromethane (50 cm^3) and pentane (300 cm^3). The solution was filtered through Celite and concentrated to give fine purple crystals (two crops, 3.35 g, 73%): ^1H NMR δ 6.84 (d, 6, H_m), 6.18 (t, 3, H_p), 4.46 (s, 2, CH_2CMe_3), 1.29 (s, 9, CH_2CMe_3); ^{13}C NMR δ 152.2 (C_{ipso}), 129.7 (C_o), 128.1 (C_m), 126.0 (C_p), 57.2 (CH_2CMe_3), 35.3 (CH_2CMe_3), 33.2 (CH_2CMe_3). Found: C, 37.3; H, 3.0; Cl, 28.4. Calc. for $ReC_{23}H_{20}N_3Cl_6$: C, 37.5; H, 2.4; Cl, 28.2%.

$Re(N\text{-}2,6\text{-}C_6H_3{}^iPr_2)_2Cl_3(py)$ (6a)

A mixture of $ReO_3(OSiMe_3)$ (4.1 g, 12.7 mmol) and 2,6-diisopropylphenylisocyanate (7.75 g, 38.2 mmol) was heated in refluxing toluene for 5 h. The solvent was removed *in vacuo*, the crude residue redissolved in dichloromethane (200 cm^3), and pyridine · HCl (4.84 g, 41.9 mmol) added as a solid while stirring the solution. The colour changed immediately to dark green. After 1 h, pentane (150 cm^3) was added and a white precipitate, containing excess pyridine · HCl, was removed by filtration through Celite. Upon concentration of the filtrate and cooling it to −20°C, dark green crystals (two crops, 6.95 g, 76%) were obtained. The analytical sample was recrystallized from a mixture of dichloromethane and pentane: ^1H NMR (CD_2Cl_2, −60°C) δ 9.18 (d, 2, py H_o), 7.93 (t, 1, py H_p), 7.49 (t, 2, py H_m), 7.30 and 7.24 (each a d, 2, imido H_m), 7.03 and 7.02 (each a t, 1, imido H_p), 3.86 and 3.14 (each a sept, 2, $CHMe_2$), 1.05 and 0.87 (each a d, 12, $CHMe_2$); ^1H NMR (CD_2Cl_2) δ 9.24 (d, 2, py H_o), 7.96 (t, 1, py H_p), 7.52 (t, 2, py H_m), 7.30 (d, 4, imido H_m), 7.05 (t, 2, imido H_p), 3.80 and 3.45 (each br, 2, $CHMe_2$), 1.05 (br, 24, $CHMe_2$); ^{13}C NMR δ 151.6 (py C_o), 138.3 (py C_p), 132.5 (imido C_m), 124.1 (py C_m), 123.3 (imido C_p), 28.2 ($CHMe_2$), 25.6 ($CHMe_2$). Found: C, 47.7; H, 5.1; N, 5.7. Calc. for $ReC_{29}H_{39}Cl_3N_3$: C, 48.2; H, 5.4; N, 5.8%.

The reaction between isolated $Re_2O_2(N\text{-}2,6\text{-}C_6H_3{}^iPr_2)_5$ and pyridine · HCl under similar conditions gave **2** in 80% yield.

$Re(N\text{-}2,6\text{-}C_6H_3Me_2)_2Cl_3(py)$ (6b)

A mixture of $ReO_3(OSiMe_3)$ (10.3 g, 31.9 mmol) and Ar′NCO (14.1 g, 95.9 mmol) in toluene (250 cm^3) was heated to reflux for 24 h. The solvent was then removed *in vacuo*. The crude residue was redissolved in dichloromethane (150 cm^3) and pyridine hydrochloride (10.7 g, 92.5 mmol) was added. The solution's colour changed rapidly from red to dark green. After 2 h, pentane (100 cm^3) was added and the reaction volume was concentrated to 200 cm^3 *in vacuo*. The mixture was filtered through Celite and reduced to dryness *in vacuo*. The crude residue was extracted with boiling benzene (400 cm^3) and the extract was filtered, leaving 5.8 g of a dirty green precipitate containing pyridine hydrochloride and $Ar'NH_3Cl$ in a *ca* 3:2 ratio. Concentrating and cooling the filtrate gave green crystals (12.0 g, 62%). Large green crystals were prepared for elemental analysis by slow recrystallization from a mixture of dichloromethane and pentane: ^1H NMR (CD_2Cl_2, −30°C) δ 9.32 (d, 2, py, H_o), 7.96 (t, 1, py H_p), 7.50 (t, 2, py H_m), 7.22 and 7.14 (each a d, 2 imido H_p), 6.93 and 6.90 (each a t, 1, imido H_p), 2.76 and 2.24 (each a s, 6, Me); ^1H NMR (CD_2Cl_2, 25°C) δ 9.35 (d, 2, py H_o), 7.98 (t, 1, py H_p), 7.52 (t, 2, py H_m), 7.20 (d, 4, imido H_m), 6.92 (t, 2, imido H_p), 2.77 and 2.32 (each v br, 6, Me); ^{13}C NMR (CD_2Cl_2, 25°C) δ 154.4 (v br, imido C_{ipso}), 152.0 (py C_o), 140.0, 137.7 (v br, imido C_o), 139.8 (py C_p), 128.4 (imido C_m), 125.1 (py C_m), 17.9 (Me). Found: C, 41.0; H, 3.9; Cl, 17.5. Calc. for $ReC_{21}H_{23}Cl_3N_3$: C, 41.3; H, 3.8; Cl, 17.4%.

The product also was obtained in 70% recovered yield by treating $Re(NAr')_3Cl$ (see below) with 2 equiv. of pyridine hydrochloride in dichloromethane at −20°C in an analogous fashion, and in > 70% yield by treating $[Ar'NH_3][Re(NAr')_2Cl_4]$ (see below) with excess pyridine in dichloromethane at −20°C. (The $Ar'NH_3Cl$ remains in solution after crystallization of the organometallic product in the latter preparation.)

$Re(N\text{-}2,6\text{-}C_6H_3Cl_2)_2Cl_3(py)$ (6c)

Pyridinium hydrochloride (0.45 g, 3.93 mmol) was added to a solution of red $Re(NAr'')_3(OSiMe_3)$ (1.0 g, 1.31mmol) in dichloromethane (30 cm^3) at −40°C. After 5 min the now dark green solution was warmed to 25°C over a period of 1.5 h. Pentane (50 cm^3) was added and a green microcrystalline solid was filtered off. The green solid was extracted with benzene (100 cm^3) at 50°C. The extract was filtered through Celite and pentane (100 cm^3) was added to the filtrate. Concentrating and cooling the filtrate *in vacuo* gave green crystals of product (0.72 g, 79%). An analytical sample was prepared by recrystallization from a mixture of dichloromethane and pentane: ^1H NMR (CD_2Cl_2, −20°C) δ 9.34 (d, 2, py H_o), 7.94 (t, 2, py H_o), 7.51 and 7.45 (each a d, 2, imido H_m), 7.08 and 7.05 (each a t, 1, imido H_p); ^{13}C NMR (CD_2Cl_2) δ 152.5 (py C_o), 139.5 (py C_p), 135.6 and 134.1 (imido C_o), 134.3

and 133.6 (imido C_p), 129.0 (imido C_m), 124.9 (py C_m). The imido C_{ipso} resonance was not observed due to the low solubility of the complex in CD_2Cl_2. Found: C, 29.0; H, 2.0; N, 5.5; Cl, 35.7. Calc. for $ReC_{17}H_{11}Cl_7N_3$: C, 29.5; H, 1.6; N, 6.1; Cl, 35.9%.

$Re(N\text{-}2,6\text{-}C_6H_3Me_2)_3Cl$ (7)

A solution of $ReO_3(OSiMe_3)$ (3.0 g, 9.28 mmol) and Ar′NCO (4.09 g, 27.8 mmol) in toluene (100 cm^3) was heated to reflux for 24 h. The solvent was removed *in vacuo* and the residue was redissolved in dichloromethane (50 cm^3). The solution was cooled to −78°C in a Schlenk flask and HCl gas (excess) added by syringe through a rubber septum. The initial red colour of the solution changed to green as the solution was warmed to 25°C over 30 min. After 2 h, 6.8 g of a dirty green precipitate was collected and washed with dichloromethane. The precipitate is believed to consist primarily of $[Ar'NH_3][Re(NAr')_2Cl_4]$ on the basis of its reactions, although the > 100% theoretical yield by weight indicates that other products are also present. "$[Ar'NH_3][Re(NAr')_2Cl_4]$" is virtually insoluble in all common solvents with which it does not react. IR (Nujol) cm^{-1} 3120 (v br, N—H).

"$[ArNH_3][Re(NAr')_2Cl_4]$" (3.0 g) was suspended in dichloromethane (100 cm^3) at −20°C. NEt_3 (2.0 cm^3, 14.4 mmol) was added and the mixture was warmed to 25°C over 30 min to give an intense red solution as the dark solid dissolved. The solvent was removed *in vacuo* and the residue extracted with pentane. The extract was filtered through Celite and the filtrate was reduced to dryness *in vacuo*. Red crystals of the product [two crops, 1.60 g, 67% based on $ReO_3(OSiMe_3)$] were obtained from pentane: ^1H NMR δ 6.82 (d, 6, H_m), 6.69 (t, 3, H_p), 2.26 (s, 18, Me); ^{13}C NMR δ 155.4 (C_{ipso}), 132.4 (C_o), 127.8 (C_m), 127.2 (C_p), 18.6 (Me). Found: C, 50.2; H, 4.8; Cl, 6.3. Calc. for $ReC_{24}H_{27}ClN_3$: C, 49.8; H, 4.7; Cl, 6.1%.

$Re(N\text{-}2,6\text{-}C_6H_3{}^iPr_2)_2(CH_2{}^tBu)Cl_2$ (**8a**)

A solution of $Zn(CH_2{}^tBu)_2$ (1.15 g, 5.54 mmol) in pentane (30 cm^3) at −20°C was added to a stirred solution of $Re(N\text{-}2,6\text{-}C_6H_3{}^iPr_2)_2Cl_3(py)$ (6.15 g, 8.52 mmol) in dichloromethane (200 cm^3) at −20°C. Upon warming the reaction mixture to 25°C over 15 min a red–orange solution was obtained, to which NEt_4Cl (0.917 g, 5.54 mmol) was added. After 30 min, pentane (60 cm^3) was added and the precipitate of $[Et_4N][ZnCl_3]$ and excess NEt_4Cl was removed by filtration through Celite. The solvent was removed from the filtrate and the residue was redissolved in dichloromethane (5 cm^3). Pentane (100 cm^3) was added and the solution was filtered through Celite. The solution was concentrated and cooled to give red crystals (two crops, 4.16 g, 72%): ^1H NMR δ 6.87 (s, 6, phenyl), 4.00 (s, 2, CH_2CMe_3), 3.61 (sept, 4, $CHMe_2$), 1.17 (s, 9, CH_2CMe_3), 1.14 and 0.99 (each a d, 12, $CHMe_2$); ^{13}C NMR δ 151.2 (C_{ipso}), 147.8 (C_o), 132.3 (C_p), 123.7 (C_m), 67.4 (CH_2CMe_3), 36.7 (CH_2CMe_3), 34.5 (CH_2CMe_3), 28.9 ($CHMe_2$), 25.5 and 23.1 ($CHMe_2$). Found: C, 51.2; H, 6.6; N, 4.1. Calc. for $ReC_{29}H_{45}Cl_2N_2$: C, 51.3; H, 6.7; N, 4.1%.

$Re(N\text{-}2,6\text{-}C_6H_3Me_2)_2(CH_2{}^tBu)Cl_2$ (**8b**)

A solution of $Re(NAr)_3(CH_2{}^tBu)$ (1.15 g, 1.87 mmol) in a mixture of dichloromethane (10 cm^3) and pentane (400 cm^3) was cooled to −78°C in a Schlenk flask. HCl gas (148 cm^3, 6.6 mmol) was added by syringe through a septum to give an immediate white precipitate of $ArNH_3Cl$. The reaction was kept at −78°C for 20 min, then warmed to 25°C over 45 min. Dichloromethane (50 cm^3) was added to dissolve some of the orange precipitate and the solution was filtered through Celite. Concentrating and cooling the solution gave orange crystals (two crops, 0.79 g, 75%) of product. The analytical sample was prepared by crystallization from a mixture of dichloromethane and pentane. ^1H NMR δ 6.59 (m, 6, H_{aryl}), 3.92 (s, 2, CH_2CMe_3), 2.31 (s, 12, Me), 1.10 (s, 9, CH_2CMe_3); ^{13}C NMR δ 154.2 (C_{ipso}), 137.8 (C_o), 132.0 (C_p), 128.3 (C_m), 69.5 (CH_2CMe_3), 37.0 (CH_2CMe_3), 34.3 (CH_2CMe_3), 18.7 (imido Me). Found: C, 44.7; H, 5.4; N, 5.5; Cl, 12.8. Calc. for $ReC_{21}H_{29}Cl_2N_2$: C, 44.5; H, 5.2; N, 4.9; Cl, 12.5%.

$Re(N\text{-}2,6\text{-}C_6H_3Cl_2)_2(CH_2{}^tBu)Cl_2$ (**8c**)

A solution of $Re(NAr'')_3(CH_2{}^tBu)$ (1.50 g, 2.04 mmol) in a mixture of dichloromethane (80 cm^3) and ether (300 cm^3) was cooled to −78°C in a Schlenk flask. HCl gas (137 cm^3, 6.1 mmol) was added by syringe through a septum. The mixture was maintained at −78°C for 20 min as the solution colour slowly changed from red to red–green. The solution was warmed to 25°C over a period of 45 min and filtered through Celite. The filtrate was concentrated and cooled to give a red microcrystalline solid. The solid was filtered off and recrystallized from a mixture of ether and pentane to yield 1.04 g (two crops, 78%): ^1H NMR δ 6.54 (d, 4, H_m), 6.07 (t, 2, H_p), 4.57 (s, 2, CH_2CMe_3), 1.12 (s, 9, CH_2CMe_3); ^{13}C NMR δ 150.4 (C_{ipso}), 134.1 (C_o), 133.2 (C_p), 128.3 (C_m), 77.3 (CH_2CMe_3), 38.1

(CH_2CMe_3), 33.9 ($CH_2C\mathit{Me}_3$). Found: C, 31.4; H, 2.8; N, 4.5; Cl, 32.5. Calc. for $ReC_{17}H_{17}Cl_6N_2$: C, 31.5; H, 2.6; N, 4.3; Cl, 32.8%.

Re(N-2,6-$C_6H_3{}^i Pr_2$)$_2$(CH^{t}Bu)($CH_2{}^t$Bu) (**9a**)

A solution of $Zn(CH_2{}^t Bu)_2$ (0.99 g, 4.77 mmol) in pentane (20 cm^3, −20°C) was added to a solution of $Re(NAr)_2Cl_3(py)$ (2.0 g, 2.77 mmol) in dichloromethane (20 cm^3, −20°C). The reaction was warmed to 25°C and stirred for 2 h. The red–green solution immediately changed to an intense yellow colour upon the addition of solid NEt_4Cl (0.79 g, 4.77 mmol). After 30 min the mixture was filtered through Celite and the filtrate was taken to dryness *in vacuo*. The residue was extracted with pentane (50 cm^3), and the extract was filtered through Celite and again taken to dryness. The resulting yellow solid (1.70 g, 90%) was pure according to its ^{1}H NMR spectrum; it was too soluble in pentane to obtain an analytical sample on this scale: ^{1}H NMR δ 12.28 (s, 1, C*H*CMe$_3$), 7.06–7.03 (m, 6, H$_{aryl}$), 3.84 and 3.62 (each a sept, 2, C*H*Me$_2$), 3.20 (m, 2, C*H*$_2$CMe$_3$), 1.30 (s, 9, CHC*Me*$_3$), 1.30, 1.22, 1.21 and 1.11 (each a d, 6, CH*Me*$_2$), 1.20 (CH$_2$C*Me*$_3$); ^{13}C NMR δ 269.0 (d, J_{CH} = 139, *C*HCMe$_3$), 153.2 and 152.7 (C$_{ipso}$), 142.7 and 141.6 (C$_o$), 126.3 and 125.7 (C$_p$), 122.9 and 122.8 (C$_m$), 47.1 (CH*C*Me$_3$), 44.8 (*C*H$_2$CMe$_3$), 33.6 (CH$_2$*C*Me$_3$), 33.5 (CHC*Me*$_3$), 32.2 (CH$_2$C*Me*$_3$), 29.1 and 28.8 (*C*HMe$_2$), 23.9, 23.3, 23.2 and 22.9 (CH*Me*$_2$).

Re(N-2,6-$C_6H_3Me_2$)$_2$(CH^{t}Bu)($CH_2{}^t$Bu) (**9b**)

A solution of $Zn(CH_2{}^t Bu)_2$ (0.62 g, 2.99 mmol) in pentane (10 cm^3, −40°C) was added to a solution of $Re(NAr')_2Cl_3(py)$ (1.0 g, 1.64 mmol) in dichloromethane (−40°C). A dirty red–green solution was formed rapidly upon warming the mixture to 25°C over a period of 15 min. A bright red–yellow solution was formed instantly when NEt_4Cl (0.50 g, 3.02 mmol) was added. The solution was filtered through Celite after 1 h, and the filtrate was taken to dryness *in vacuo*. Careful crystallization of the residue from pentane (2 cm^3) gave large red crystals (0.60 g, 65%): ^{1}H NMR δ 12.24 (s, 1, C*H*CMe$_3$), 6.96–6.83 (m, 6, H$_{aryl}$), 3.23 (m, 2, C*H*$_2$CMe$_3$), 2.37 and 2.23 (each a s, 6, Me), 1.24 (s, 9, CHC*Me*$_3$), 1.13 (s, 9, CH$_2$C*Me*$_3$); ^{13}C NMR δ 270.5 (d, J_{CH} = 137, *C*HCMe$_3$), 156.1 and 155.9 (C$_{ipso}$), 133.5 and 131.4 (C$_o$), 128.1 (C$_m$), 125.7 and 124.8 (C$_p$), 46.1 (CH*C*Me$_3$), 41.2 (*C*H$_2$CMe$_3$), 33.6 (CHC*Me*$_3$), 33.3 (CH$_2$*C*Me$_3$), 32.1 (CH$_2$C*Me*$_3$), 19.6 (imido Me). Found: C, 55.3; H, 7.1. Calc. for $ReC_{26}H_{39}N_2$: C, 55.2; H, 6.9%.

Re(N-2,6-$C_6H_3{}^i Pr_2$)$_2$(CH^{t}Bu)Cl (**10**)

An ether (5 cm^3) solution of DBU (1,8-diazabicyclo[5.4.0]undec-7-ene, 0.70 g, 4.6 mmol) at −20°C was added to a solution of Re(N-2,6-$C_6H_3{}^i Pr_2$)$_2$($CH_2{}^t$Bu)Cl$_2$ (3.0 g, 4.42 mmol) in ether (50 cm^3) at −20°C. The mixture was allowed to warm to 25°C over a period of 15 min to give a bright red solution and a white precipitate of DBU·HCl. After 2 h, the solution was filtered through Celite and all the solvent removed from the filtrate *in vacuo*. The residue was extracted with pentane (50 cm^3) and the extract was filtered through Celite. The solvent was removed from the filtrate *in vacuo* to give a microcrystalline solid that was shown by ^{1}H NMR to be an essentially pure product. Recrystallization from minimal pentane gave red crystals (four crops, 2.09 g, 74%): ^{1}H NMR δ 12.27 (s, 1, C*H*CMe$_3$), 7.04–6.98 (m, 6, phenyl), 3.70, 3.58 (each a sept, 2, C*H*Me$_2$), 1.25 (s, 9, CHC*Me*$_3$), 1.25, 1.20, 1.04 (d, 6, 12, 6, CH*Me*$_2$); ^{13}C NMR δ 269.4 (d, J_{CH} = 125, *C*HCMe$_3$), 153.5 and 151.8 (C$_{ipso}$), 142.9 and 142.3 (C$_o$), 127.6 and 127.3 (C$_p$), 123.1 and 122.8 (C$_m$), 47.2 (CH*C*Me$_3$), 32.3 (CHC*Me*$_3$), 29.4 and 28.6 (*C*HMe$_2$), 23.9, 23.4, 23.0 and 22.7 (CH*Me*$_2$). Found: C, 54.1; H, 6.9; N, 4.3. Calc. for $ReC_{29}H_{44}ClN_2$: C, 54.2; H, 6.9; N, 4.4%.

Re(O)(N-2,6-$C_6H_3{}^i Pr_2$)$_2$($CH_2{}^t$Bu) (**11**)

Me_4NOH (0.264 cm^3 of a 1.86 M solution in methanol, 0.491 mmol) was added to a solution of Re(N-2,6-$C_6H_3{}^i Pr_2$)$_2$(CH^{t}Bu)Cl (0.30 g, 0.468 mmol) in THF (15 cm^3) at 25°C. The solution changed immediately from red to bright orange and a white precipitate of Me_4NCl formed. The solution was stirred for 15 min and filtered through Celite. The filtrate was reduced to dryness *in vacuo*, the residue extracted with pentane (10 cm^3) and the mixture filtered through Celite. Removal of the solvent *in vacuo* gave an orange solid that was virtually pure by ^{1}H NMR. A sample was prepared for analysis by recrystallization from minimal pentane: ^{1}H NMR δ 7.10–6.88 (m, 6, phenyl), 3.77 (sept, 4, C*H*Me$_2$), 3.58 (s, 2, C*H*$_2$CMe$_3$), 1.19 and 1.17 (each a d, 12, CH*Me*$_2$), 1.18 (s, 9, CH$_2$C*Me*$_3$); ^{13}C NMR δ 152.7 (C$_{ipso}$), 143.2 (C$_o$), 128.2 (C$_p$), 122.9 (C$_m$), 53.6 (*C*H$_2{}^t$Bu), 33.9 (CH$_2$*C*Me$_3$), 32.8 (CH$_2$C*Me*$_3$), 28.7 (*C*HMe$_2$), 23.8 and 23.1 (CH*Me*$_2$). IR (Nujol) cm^{-1} 907 (Re=O). Found: C, 55.8; H, 7.3. Calc. for $ReC_{29}H_{45}N_2O$: C, 55.8; H, 7.3%.

Re(N-2,6-$C_6H_3{}^iPr_2)_2$(CH^{t}Bu)[OCH$(CF_3)_2$] (**12a**)

A solution of LiOCH$(CF_3)_2$ (0.325 g, 1.87 mmol) in ether (3 cm^3) that had been cooled to −40°C was added to a −40°C solution of Re_2(N-2,6-$C_6H_3{}^iPr_2)_2$(CH^{t}Bu)Cl (1.0 g, 1.56 mmol) in ether (3 cm^3). Upon warming the solution to 25°C over a period of 15 min a cloudy precipitate formed and the colour changed from red to orange. After 3 h LiCl was removed by filtration through Celite, the solvent was removed *in vacuo* and the crude residue was extracted with pentane (5 cm^3). The ^{1}H NMR spectrum of the product after removal of pentane suggested that essentially only one compound was present in high yield. Crystallization of the oily residue from pentane (1 cm^3) yielded highly pentane-soluble red crystals (0.55 g, 46%). The analytical sample was obtained as large red crystals by very slow recrystalization from pentane (0.5 cm^3) at −40°C: ^{1}H NMR δ 11.88 (s, 1, C*H*CMe$_3$), 7.12–6.99 (m, 6, phenyl), 4.73 (sept, 1, J_{HF} = 6.0, OC*H*$(CF_3)_2$), 3.57 and 3.49 (each a sept, 2, C*H*Me$_2$), 1.26, 1.20, 1.15 and 1.02 (each a d, 6, CH*Me*$_2$), 1.14 (s, 9, CHC*Me*$_3$); ^{13}C NMR δ 260.5 (d, J_{CH} = 137, *C*HCMe$_3$), 153.2 and 151.5 (C_{ipso}), 143.4 and 142.0 (C_o), 127.8 and 127.0 (C_p), 123.5 (q, J_{CF} = 285, OCH$(CF_3)_2$), 123.1 and 122.6 (C_m), 92.1 (d, sept, J_{CH} = 147, J_{CF} = 30, O*C*H$(CF_3)_2$), 47.3 (CH*C*Me$_3$), 33.0 (CHC*Me*$_3$), 29.4 and 28.5 (*C*HMe$_2$), 23.7, 23.6, 22.7 and 22.6 (CH*Me*$_2$). Found: C, 49.8; H, 6.1. Calc. for $ReC_{32}H_{45}F_6ON_2$: C, 49.7; H, 5.9%.

Re(N-2,6-$C_6H_3{}^iPr_2)_2$ (CH^{t}Bu)[OCMe$(CF_3)_2$] (**12b**)

Re(NAr)$_2$(CHCMe$_3$)Cl (0.50 g, 0.78 mmol) was treated with LiOCMe$(CF_3)_2$ (0.150 g, 0.80 mmol) in ether as in the preparation of **5a** above. The ^{1}H NMR spectrum of the crude solid showed that the product was formed essentially quantitatively, although Re(O)(NAr)$_2$(CH$_2$CMe$_3$) was present as a trace contaminant. The product was too soluble to obtain analytically pure material on this scale. In only one case very slow recrystallization of the crude product from pentane gave 0.10 g (16%) of red crystals whose ^{1}H NMR spectrum did not show the trace impurity: ^{1}H NMR δ 11.56 (s, 1, C*H*CMe$_3$), 7.06–6.97 (m, 6, phenyl), 3.64 and 3.45 (each a sept, 2, C*H*Me$_2$), 1.38 (s, 3, OC*Me*$(CF_3)_2$), 1.28, 1.21, 1.19 and 1.00 (each a d, 6, CH*Me*$_2$), 1.22 (s, 9, CHC*Me*$_3$); ^{13}C NMR δ 256.4 (d, J_{CH} = 139, *C*HCMe$_3$), 153.2 and 151.4 (C_{ipso}), 143.3 and 142.5 (C_o), 127.6 and 127.1 (C_p), 124.5 (q, J_{CF} = 289, OCMe(*C*F$_3)_2$), 123.2 and 122.6 (C_m), 79.6 (sept, J_{CF} = 28, O*C*Me$(CF_3)_2$), 47.1 (CH*C*Me$_3$), 33.2 (CHC*Me*$_3$), 29.2 and 28.4 (*C*HMe$_2$), 23.9, 23.5, 22.8 and 22.5 (CH*Me*$_2$), 19.9 (OC*Me*$(CF_3)_2$).

Re(N-2,6-$C_6H_3{}^iPr_2)_2$(CH^{t}Bu)(O-2,6-$C_6H_3{}^iPr_2$) (**12c**)

Re(N-2,6-$C_6H_3{}^iPr_2)_2$(CH^{t}Bu)Cl (0.35 g, 0.55 mmol) was treated with Li(O-2,6-$C_6H_3{}^iPr_2$) (0.144 g, 0.56 mmol) in ether and the reaction mixture worked up as in the preparation of **5a** above. The ^{1}H NMR spectrum of the crude solid showed the product yield to be essentially quantitative. Recrystallization from pentane (3 cm^3) gave a 63% yield of orange crystals (0.27 g): ^{1}H NMR δ 11.25 (s, 1, C*H*CMe$_3$), 7.12–6.93 (m, 9, phenyl), 4.05 (sept, 2, phenoxide C*H*Me$_2$), 3.79 (sept, 4, imido C*H*Me$_2$), 1.39 and 1.35 (each a d, 6, phenoxide CH*Me*$_2$), 1.27, 1.26, 1.24 and 1.05 (each a d, 6, imido CH*Me*$_2$), 1.01 (s, 9, CHC*Me*$_3$); ^{13}C NMR δ 256.7 (d, J_{CH} = 146, *C*HCMe$_3$), 167.4 (phenoxide C_{ipso}), 153.4 and 152.4 (imido C_{ipso}), 143.0 and 142.4 (imido C_o), 137.7 (phenoxide C_o), 127.1 and 126.6 (imido C_p), 123.2 (imido C_m), 122.7 (phenoxide C_m), 122.3 (phenoxide C_p), 46.5 (CH*C*Me$_3$), 32.5 (CHC*Me*$_3$), 29.1 and 28.3 (imido *C*HMe$_2$), 27.1 (phenoxide *C*HMe$_2$), 24.1, 24.0, 23.3 and 23.0 (imido CH*Me*$_2$), 23.6 (phenoxide CH*Me*$_2$). Found: C, 63.3; H, 7.9; N, 3.6. Calc. for $ReC_{41}H_{61}N_2O$: C, 62.8; H, 7.8; N, 3.6%.

REFERENCES

1. (a) C. J. Schaverien, J. C. Dewan and R. R. Schrock, *J. Am. Chem. Soc.* 1986, **108**, 2771; (b) J. S. Murdzek and R. R. Schrock, *Organometallics* 1987, **6**, 1373; (c) R. R. Schrock, R. DePue, J. Feldman, C. J. Schaverien, J. C. Dewan and A. H. Liu, *J. Am. Chem. Soc.* 1988, **110**, 1423.
2. (a) K. J. Ivin, *Olefin Metathesis*. Academic Press, London (1983); (b) R. H, Grubbs, in *Comprehensive Organometallic Chemistry*, (Edited by G. Wilkinson, F. G. A. Stone and E. W. Abel), Vol. 8. Pergamon Press (1982); (c) V. Dragutan, A. T. Balaban and M. Dimonie, *Olefin Metathesis and Ring-opening Polymerization of Cyclo-olefins*, 2nd Edn. Wiley-Interscience, New York (1985); (d) R. R. Schrock, *J. Organometal. Chem.* 1986, **300**, 249; (e) J. Kress, A. Aguero and J. A. Osborn, *J. Mol. Catal.* 1986, **36**, 1.
3. R. R. Schrock, *Acc. Chem. Res.* 1986, **19**, 342.
4. (a) W. A. Nugent and B. L. Haymore, *Coord. Chem. Rev.* 1980, **31**, 123; (b) W. A. Nugent, *Inorg. Chem.* 1983, **22**, 965, and refs therein.
5. D. D. Devore, J. D. Lichtenhan, F. Takusagawa, and E. Maata, *J. Am. Chem. Soc.* 1987, **109**, 7408.
6. D. S. Edwards, L. V. Biondi, J. W. Ziller, M. R. Churchill and R. R. Schrock, *Organometallics* 1983, **2**, 1505.

7. D. S. Edwards, Ph.D. Thesis. Massachusetts Institute of Technology (1983).
8. J. H. Freudenberger, Ph.D. Thesis. Massachusetts Institute of Technology (1986).
9. A. D. Horton, R. R. Schrock and J. H. Freudenberger, *Organometallics* 1987, **6**, 893.
10. C. Ringel and G. Boden, *Zeit. Anorg. Allg. Chem.* 1972, **393**, 65.
11. C. J. Longley, P. D. Savage, G. Wilkinson, B. Hussain and M. B. Hursthouse, *Polyhedron* 1988, **7**, 1079.
12. A. D. Horton, unpublished results. [DBUH][Re(NAr)(C'Bu)Cl_3] will be reported elsewhere.
13. R. R. Schrock, I. A. Weinstock, A. H. Horton, M. H. Schofield and A. H. Liu, *J. Am. Chem. Soc.* 1988, **110**, 1423.
14. J. Okuda, R. C. Murray, J. C. Dewan and R. R. Schrock, *Organometallics* 1986, **5**, 1681.
15. M. Schmidt and H. Schmidbaur, *Chem. Ber.* 1959, **92**, 2667.
16. A.-G. Farbenfabriken Bayer, Fr. Demande 2,000,746; *Chem. Abstr.* 1970, **72**, 111012m.

Polyhedron Vol. 7, No. 19/20, pp. 1855–1859, 1988
Printed in Great Britain

0277–5387/88 $3.00+.00
© 1988 Pergamon Press plc

TRIMETHYLPLATINUM(IV) COMPLEXES OF THE DIMETHYLDITHIOARSINATE(V) ANION: PREPARATION AND MOLECULAR STRUCTURE OF THE DINUCLEAR $[(PtMe_3)_2(Me_2AsS_2)_2]$ AND ITS SELECTIVE FISSION TO MONONUCLEAR $[PtMe_3(Me_2AsS_2)L]$ (L = PPh_3, PPh_2Me, py) COMPLEXES

EDWARD W. ABEL* and MICHAEL A. BECKETT

Department of Chemistry, University of Exeter, Exeter EX4 4QD, U.K.

and

PAUL A. BATES and MICHAEL B. HURSTHOUSE*

Department of Chemistry, Queen Mary College, Mile End Road, London E1 4NS, U.K.

Abstract—Sodium dimethyldithioarsinate(V) undergoes metathesis with the tetrameric trimethylplatinum chloride to yield the binuclear complex $[(PtMe_3)_2(Me_2AsS_2)_2]$ in which the two arsenic atoms are *cis* relative to the four-membered Pt_2S_2 ring. Pyridine and phosphines(L) break down the sulphur bridged dimer to form mononuclear complexes $[PtMe_3(Me_2AsS_2)L]$, in which the dimethyldithioarsinate(V) ligand retains its chelate role. Neither the binuclear nor mononuclear complexes show any detectable fluxionality. An X-ray diffraction study of $[(PtMe_3)_2(Me_2AsS_2)_2]$ is reported.

As part of our continuing research programme on the types of fluxionality encountered in the coordination complexes of the trimethylplatinum(IV) moiety,[1,2] we have synthesized a series of complexes incorporating the dimethyldithioarsinate(V) ligand, Fig. 1(a). Of specific interest to us was the possibility that we would encounter a stereochemical non-rigidity involving rotation of the Me_2AsS_2 ligand relative to the equatorial PtMe groups, as observed for some other bidentate sulphur ligands.[3] A d^6 isoelectronic and isostructural complex of rhenium(I) $[Re(CO)_3(Me_2AsS_2)py]$ has been previously reported.[4]

RESULTS AND DISCUSSION

Preparation and characterization of complexes

The tetrameric trimethylplatinum(IV) chloride undergoes reaction readily with the dimethyldithioarsinate(V) anion in tetrahydrofuran suspension.

$$[\{PtMe_3Cl\}_4] + 4Na \cdot Me_2AsS_2 \cdot 2H_2O \rightarrow 2[(PtMe_3)_2(Me_2AsS_2)_2] + 4NaCl + 8H_2O. \quad (1)$$

The dinuclear product has been characterized by

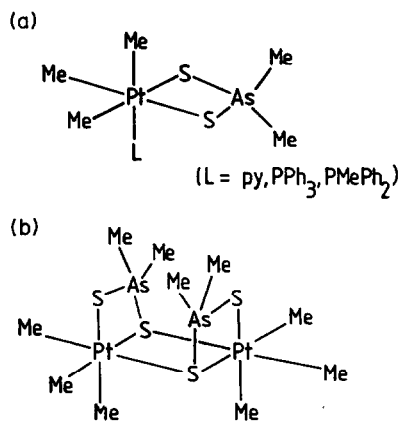

Fig. 1. Schematic structures illustrating (a) the complexes $[(PtMe_3)(Me_2AsS_2)L]$ (L = py, PPh_2, $PMePh_2$) and (b) the binuclear complex $[(PtMe_3)_2(Me_2AsS_2)_2]$.

* Authors to whom correspondence should be addressed.

Table 1. Platinum(IV) complexes of dimethyldithioarsinate(V)

Complex	Yield (%)	Melting point[a] (°C)	Analysis[b] (%) C	H	N
$[(PtMe_3)_2(Me_2AsS_2)_2]$	55	170° (dec)[c]	14.7(14.7)	3.7(3.7)	—
$[(PtMe_3)(Me_2AsS_2)(py)]$	53	108–110	24.6(24.6)	4.1(4.1)	2.9(2.9)
$[(PtMe_3)(Me_2AsS_2)(PPh_2Me)]$	66	134–135	35.5(35.5)	4.7(4.6)	—
$[(PtMe_3)(Me_2AsS_2)(PPh_3)]$	72	151	41.2(41.1)	4.5(4.5)	—

[a] Colourless, crystalline solids unless indicated.
[b] Calculated values in parentheses.
[c] Yellow, crystalline solid.

elemental analysis, multi-element NMR spectroscopy and by a single crystal X-ray diffraction study; its structure is indicated schematically in Fig. 1(b). The complex was isolated as air-stable pale yellow crystals soluble in common organic solvents. Reaction of this sulphur-bridged dimer with neutral donor ligands L held two possibilities, (a) the formation of mononuclear complexes, $[PtMe_3(Me_2AsS_2)L]$ in which the ligand L brings about the fission of bridging Pt—S bonds only, and (b) the formation of mononuclear complexes $[PtMe_3(Me_2AsS_2)L_2]$ in which the ligand L, in addition to dimer fission, displaces one of the sulphur ligand atoms to give the Me_2AsS_2 ligand a monodentate pseudo halide role.

In all cases investigated, the dimethyldithioarsinate(V) anion retained its bidentate function, and bridge fission reactions were selectively dependent upon the nature of ligand L.

$$[(PtMe_3)_2(Me_2AsS_2)_2] + 2L \rightarrow 2[PtMe_3(Me_2AsS_2)L] \quad (L = py, PPh_3, PMePh_2). \quad (2)$$

Triphenylarsine and dialkyl sulphides, such as dibenzyl sulphide, did not bring about fission of the dimer even after prolonged heating under reflux. The mononuclear complexes obtained from pyridine and the phosphines were fully characterized by elemental analysis and multi-element NMR spectroscopy. They are all air-stable, white, crystalline solids which are very soluble in common organic solvents (Table 1).

Molecular structure of $[(PtMe_3)_2(Me_2AsS_2)_2]$

Table 2 records the interatomic distances and angles for this complex. The structure is illustrated in Fig. 2 where the platinum atoms are octahedrally coordinated by three *fac* methyl groups and three *fac* sulphur atoms. The molecule has a C_2 rotation axis and the arsenic centres of the two dimethyldithioarsenate(V) moieties are *cis* relative to the four-membered Pt_2S_2 ring. Such a *cis* configuration permits maximum relief from steric interactions of the ten methyl groups in the molecule. The Pt···Pt non-bonding distance of 3.726 Å is a little shorter than those of 3.790 and 3.740 Å reported,[5,6] respectively for comparable bromide bridged complexes $[(PtBrMe_3)_2dmas]$ and $[(PtBrMe_3)_2(Se_2Me_2)]$. Bridging Pt—S—Pt bond angles are 94.3°, and Pt—S bridging and non-bridging bond lengths are remarkably similar at *ca* 2.54 Å. This latter value is slightly larger than those observed[7] in $[(PtClMe_3)_2(SCH_2SCH_2SCH_2)]$ of *ca* 2.46 Å. The configuration about each platinum atom does show a moderate distortion from octahedral, with 82.8(2)° (S—Pt—S) to 94.6(4)° (C—Pt—S) for "right angles" and 169.2(3)–175.6(3)° (C—Pt—S) for "linear" arrays. There is also a notable distortion from tetrahedral geometry about arsenic in the Me_2AsS_2 group with S—As—S and C—As—C angles at 103.7(2) and 104.1(5)° respectively, and

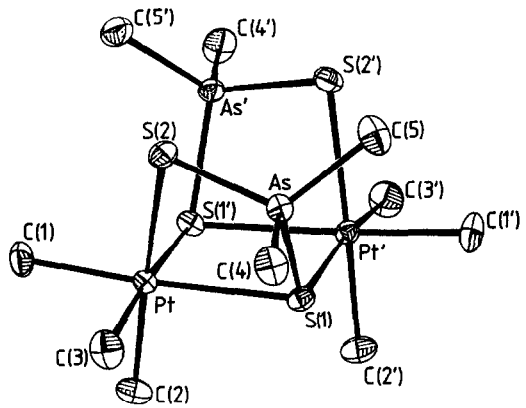

Fig. 2. The molecular structure of $[(PeMe_3)_2(Me_2AsS_2)_2]$ with atom labelling.

Table 2. Interatomic distances and angles for $[(PtMe_3)_2(Me_2AsS_2)_2]$ (with ESDs in parentheses)

(i) Bond angles (deg.)			
S(1′)—Pt—S(1)	85.6(2)	S(2)—Pt—S(1)	82.8(2)
C(1)—Pt—S(1)	175.6(3)	C(1)—Pt—S(1′)	92.9(4)
C(1)—Pt—S(2)	93.4(4)		
C(2)—Pt—S(1)	94.2(4)	C(2)—Pt—S(1′)	84.5(4)
C(2)—Pt—S(2)	174.8(3)	C(2)—Pt—C(1)	89.7(5)
		C(3)—Pt—S(1)	94.6(4)
C(3)—Pt—S(1′)	169.2(3)	C(3)—Pt—S(2)	91.1(4)
C(3)—Pt—C(1)	87.7(5)	C(3)—Pt—C(2)	84.7(5)
S(2)—As—S(1)	103.7(2)		
C(4)—As—S(1)	107.5(4)	C(4)—As—S(2)	111.2(4)
		C(5)—As—S(1)	112.4(4)
C(5)—As—S(2)	117.8(4)	C(5)—As—C(4)	104.1(5)
Pt—S(1)—Pt(′)	94.3(2)	As—S(1)—Pt(′)	110.9(2)
As—S(1)—Pt	84.3(2)	As—S(2)—Pt	85.1(2)
(ii) Bond lengths (Å)			
S(1′)—Pt	2.523(5)	S(1)—Pt	2.558(5)
C(1)—Pt	2.037(11)	S(2)—Pt	2.549(5)
C(3)—Pt	2.058(11)	C(2)—Pt	2.065(10)
S(2)—As	2.132(4)	S(1)—As	2.164(4)
C(5)—As	1.911(11)	C(4)—As	1.952(10)

Symmetry operation (′) = $-x, y, 1.5-z$.

C(5)—As—S angles larger than tetrahedral at 112.4(4) and 117.8(4)°. As—S bond lengths of 2.132(4) and 2.164(4) Å are notably shorter than those observed[5] for a bond order of one in $[(PtBrMe_3)_2dmas]$ (*ca* 2.32 Å), confirming multiple bonding character in these As—S bonds.

NMR studies

Data for the binuclear species and the three mononuclear products are recorded in Table 3. The ^1H spectrum of the sulphur bridged dimer has five signals of equal intensity in accord with its structure. The three highest field signals are coupled to ^{195}Pt and values for $^2J(^{195}Pt—C—H)$ allows the methyl groups with the smaller coupling (71.8 Hz) to be assigned[8,9] as *trans* to the non-bridging sulphur atoms and the larger $^2J(^{195}Pt—C—H)$ couplings at 74.0 and 75.5 Hz are associated with the Pt—Me groups *trans* to the bridging sulphur atoms. The two methyl groups on each arsenic give rise to separate signals in the ^1H and ^{13}C spectra but neither $^4J(^{195}Pt—S—As—C—^1H)$ nor $^3J(^{195}Pt—S—As—^{13}C)$ were detected for the As—Me resonances.

The structure of the ligand adduct complexes (L = py, PPh_3, $PMePh_2$) illustrated in Fig. 1(a) is consistent with the NMR data presented in Table 3. The following discussion of the NMR spectra for $[PtMe_3(Me_2AsS_2)PPh_3]$ could be equally applicable to the other mononuclear species. The ^1H spectrum, in addition to the signals of the aromatic protons of the PPh_3 ligand, consisted of four signals of relative intensity 2:1:1:1. The two higher field signals are coupled to ^{195}Pt and are assigned to the two identical equatorial and the unique axial Pt—Me groups. The $^2J(Pt—C—H)$ coupling constant for the two equatorial PtMe groups of 71.6 Hz is characteristic of groups *trans* to sulphur atoms[8,9] and the much smaller $^2J(Pt—C—H)$ of 60.8 Hz is indicative of the PtMe *trans* to a phosphorus donor ligand.[10] The two other resonances at δ 0.94 and 1.94 result from the non-equivalent As—Me groups. A small $^4J(^{31}P—Pt—S—As—^{13}C)$ coupling is observed for one of the AsMe groups in the ^{13}C spectrum of the complex.

A variable temperature NMR study up to the onset (60°C) of irreversible spectral changes due to decomposition gave no indications of any type of fluxionality in this complex.

Table 3. NMR parameters for $Me_2AsS_2^-$ complexes of trimethylplatinum(IV)[a]

Complex	Data
$[(PtMe_3)_2(Me_2AsS_2)_2]$	$\delta(^1H)$: 1.53 (3H), ^2J(PtH) 74.0 Hz, PtMe; 1.06 (3H), ^2J(PtH) 71.8 Hz, PtMe; 0.92 (3H), ^2J(PtH) 75.5 Hz, PtMe; 2.36 (3H), AsMe; 2.19 (3H) AsMe. $\delta(^{13}C)$: 9.33, ^1J(PtC) 674.7 Hz, PtMe; 7.63, ^1J(PtC) 669.2 Hz, PtMe; 4.70, ^1J(PtC) 666.2 Hz, PtMe; 30.05, AsMe; 31.94, AsMe.
$[PtMe_3(Me_2AsS_2)PPh_3]$	$\delta(^1H)$: 0.91 (6H), ^2J(PtH) 71.6 Hz, ^3J(PH) 7.1 Hz, PtMe *trans* S; 1.81 (3H), ^2J(PtH) 60.8 Hz, ^3J(PH) 7.9 Hz, PtMe *trans* P; 0.94 (3H), AsMe; 1.94 (3H), AsMe; 7.1–7.8 (15H), PPh. $\delta(^{13}C)$: 4.75, ^1J(PtC) 649.0 Hz, ^2J(PC) 2.5 Hz, PtMe *trans* S; 15.4, ^1J(PtC) 554.3 Hz, ^2J(PC) 130.4 Hz, PtMe *trans* P; 29.78, AsMe; 31.58, ^4J(PC) 3.0 Hz, AsMe; 127.6–135.5, PPh. $\delta(^{31}P)$: −0.92, ^1J(PPt) 966.8 Hz.
$[PtMe_3(Me_2AsS_2)PPh_2Me]$	$\delta(^1H)$: 0.75 (6H), ^2J(PtH) 72.3 Hz, ^3J(PH) 7.4 Hz, PtMe *trans* S; 1.66 (3H), ^2J(PtH) 59.2 Hz, ^3J(PH) 8.2 Hz, PtMe *trans* P; 2.23 (3H), ^3J(PtH) 9.8 Hz, ^2J(PH) 8.1 Hz, PMe; 2.03 (3H), AsMe; 1.36 (3H), AsMe; 7.4–7.6 (10H), PPh. $\delta(^{13}C)$: 13.75, ^1J(PtC) 540.2 Hz, ^2J(PC) 135.4 Hz, PtMe *trans* P; 3.58, ^1J(PtC) 644.5 Hz, ^2J(PC) 2.8 Hz, PtMe *trans* S; 10.78, ^2J(PtC) 11.3 Hz, ^1J(PC) 26.9 Hz, PMe; 31.41, AsMe; 30.92, ^4J(PC) 3.6 Hz, AsMe; 127.7–133.3, PPh. $\delta(^{31}P)$: −18.55, ^1J(PtP) 1069.4 Hz.
$[PtMe_3(Me_2AsS_2)py]$	$\delta(^1H)$: 0.93 (6H), ^2J(PtH) 72.6 Hz, PtMe *trans* S; 1.61 (3H), ^2J(PtH) 72.1 Hz, PtMe *trans* N; 1.42 (3H), AsMe; 1.95 (3H), AsMe; 7.3–9.2 (5H), py. $\delta(^{13}C)$: −8.02, ^1J(PtC) 667.5 Hz, PtMe *trans* N; 5.71, ^1J(PtC) 695.7 Hz, PtMe *trans* S; 29.70, AsMe; 31.16, AsMe; 124.75, 137.21, 151.69, py.

[a] All data recorded at room temperature in $CDCl_3$ solution. Chemical shifts (δ) are given in ppm to high frequency (low field) of $SiMe_4$ for ^1H and ^{13}C, and of 85% H_3PO_4 [Ξ40 480 730 Hz] for ^{31}P.

EXPERIMENTAL

Materials and preparations

Reactions were performed under standard Schlenk conditions under nitrogen, and all solvents were distilled from the appropriate drying agent ($CHCl_3$, CaH_2; 60–80°C light petroleum, Na benzophenoneketyl) under nitrogen immediately before use. Sodium dimethyldithioarsinate(V) was prepared by a literature method,[11] and the tetrameric trimethylplatinum halides were prepared by established routines.[12–14] The preparation of $[(PtMe_3)_2(Me_2AsS_2)_2]$ is described below and its reactions with donor ligands is exemplified for L = PPh_3.

Preparation of $[(PtMe_3)_2(Me_2AsS_2)_2]$. The tetrameric trimethylplatinum(IV) chloride (0.877 g, 0.80 mmol) and $Na \cdot Me_2AsS_2 \cdot 2H_2O$ (0.728 g, 3.2 mmol) were heated together in THF (10 cm^3) under reflux for 0.5 h. The mixture was then filtered to remove sodium chloride and the filtrate pumped to dryness. The residue was redissolved in dry chloroform (10 cm^3), layered with light petroleum (20 cm^3) and allowed to crystallize overnight at −20°C. The product was obtained as pale yellow crystals (0.710 g, 55%).

Preparation of $[PtMe_3(Me_2AsS_2)PPh_3]$. The dinuclear $[(PtMe_3)_2(Me_2AsS_2)_2]$ (0.215 g, 0.25 mmol) and PPh_3 (0.140 g, 0.52 mmol) were stirred together in $CHCl_3$ (5 cm^3) for 0.25 h at room temperature. Light petroleum (25 cm^3) was added to the solution, which was then stored at −20°C to crystallize. The product was obtained as a white crystalline solid (0.252 g, 72%).

Crystallographic studies

Crystal data. $C_{10}H_{30}As_2Pt_2S_4$, $M = 818.610$, monoclinic, space group $C2/c$, $a = 14.597(3)$, $b = 12.058(3)$, $c = 11.815(2)$ Å, $\beta = 94.95(2)°$, $U = 2071.7(8)$ $Å^3$, $Z = 4$, $D_c = 2.625$ g cm^{-3}, $F(000) = 1504$, $\lambda = 0.71069$ Å, μ(Mo-K_α) = 171.7 cm^{-1}, crystal size (0.68 × 0.43 × 0.25 mm).

Data collection. Unit cell parameters and intensity data were obtained by following previously detailed procedures,[15] using a CAD4 diffractometer operating in the ω–2θ scan mode, with graphite monochromated Mo-K_α radiation. A total of 1824

unique reflections were collected ($3 < 2\theta < 50°$). The segment of reciprocal space scanned was; (h) $0 \rightarrow 17$, (k) $0 \rightarrow 14$, (l) $-14 \rightarrow 14$. The reflection intensities were corrected for absorption, using the azimuthal-scan method;[16] maximum transmission factor 1.00, minimum value 0.59.

Structure solution and refinement. The structure was solved by the application of routine heavy-atom methods (SHELX-86[17]), and refined by full-matrix least-squares (SHELX-76[18]). All non-hydrogen atoms were refined anisotropically, and methyl hydrogen atoms placed into calculation positions (C—H 0.96 Å; $U = 0.10$ Å^2). The final residuals R and R_w were 0.029 and 0.031, respectively for the 97 variables and 1606 data for which $F_o > 6\sigma(F_o)$. The function minimized was $\Sigma_w(|F_o| - |F_c|)^2$ with the weight, w, being defined as $1/[\sigma^2(F_o) + 0.0005F_o^2]$.*

Atomic scattering factors and anomalous scattering parameters were taken from refs 19 and 20, respectively. All computations were made on a DEC VAX-11/750 computer.

NMR studies

^{1}H and ^{13}C experiments were performed on a Brüker AM250 instrument at 250 and 62.8 MHz, respectively. ^{31}P{^{1}H} were recorded on a JeolFX 90Q at 36 MHz. Samples were in $CDCl_3$ solutions for ambient temperature spectra, and variable temperature ^{1}H spectra were recorded in toluene-d_8 solution.

* Atomic positional and thermal parameters and lists of F_o/F_c values have been deposited as Supplementary Data with the Editor, from whom copies are available on request. Atomic coordinates have also been deposited with the Cambridge Crystallographic Data Centre.

REFERENCES

1. E. W. Abel, S. K. Bhargava and K. G. Orrell, *Prog. Inorg. Chem.* 1984, **32**, 1.
2. E. W. Abel, T. P. J. Coston, K. G. Orrell, V. Sik and D. Stephenson, *J. Mag. Res.* 1986, **70**, 34.
3. E. W. Abel, M. Z. A. Chowdhury, K. G. Orrell and V. Sik, *J. Organometal. Chem.* 1983, **258**, 109.
4. E. Lindner and H. M. Ebinger, *J. Organometal. Chem.* 1974, **66**, 103.
5. E. W. Abel, M. A. Beckett, P. A. Bates and M. B. Hursthouse, *J. Organometal. Chem.* 1987, **325**, 261.
6. E. W. Abel, A. R. Khan, K. Kite, K. G. Orrell and V. Sik, *J. Chem. Soc., Chem. Commun.* 1979, 713.
7. E. W. Abel, M. Booth, K. G. Orrell, G. M. Pring and T. S. Cameron, *J. Chem. Soc., Chem. Commun.* 1981, 29.
8. E. W. Abel, K. G. Orrell and A. W. G. Platt, *J. Chem. Soc., Dalton Trans.* 1983, 2345.
9. E. W. Abel, A. R. Khan, K. Kite, K. G. Orrell and V. Sik, *J. Chem. Soc., Dalton Trans.* 1980, 1169.
10. J. D. Ruddick and B. L. Shaw, *J. Chem. Soc. A*, 1969, 2964.
11. A. T. Casey, N. S. Hom, D. J. Mackey and R. L. Martin, *Aust. J. Chem.* 1970, **32**, 1117.
12. J. C. Baldwin and W. C. Kaska, *Inorg. Chem.* 1975, **14**, 2020.
13. D. E. Clegg and J. R. Hall, *Spectrochim. Acta* 1965, **21**, 357.
14. D. E. Clegg and J. R. Hall, *J. Organometal. Chem.* 1970, **22**, 491.
15. M. B. Hursthouse, R. A. Jones, K. M. A. Malik and G. Wilkinson, *J. Am. Chem. Soc.* 1979, **101**, 4128.
16. A. C. T. North, D. C. Phillips and F. S. Mathews, *Acta Cryst., Sect. A.* 1968, **24**, 351.
17. G. M. Sheldrick, SHELX-86 Program for Crystal Structure Solution. University of Göttingen (1986).
18. G. M. Sheldrick, SHELX-76 Program for Crystal Structure Determination and Refinement. University of Cambridge (1976).
19. D. T. Cromer and J. B. Mann, *Acta Cryst., Sect. A.* 1968, **24**, 321.
20. D. T. Cromer and D. Liberman, *J. Chem. Phys.* 1970, **53**, 1891.

Polyhedron Vol. 7, No. 19/20, pp. 1861–1867, 1988
Printed in Great Britain

0277–5387/88 $3.00+.00
Pergamon Press plc

METALLO-MESOGENS AND LIQUID CRYSTALS WITH A HEART OF GOLD

HARRY ADAMS, NEIL A. BAILEY, DUNCAN W. BRUCE, RUPINDER DHILLON, DAVID A. DUNMUR, SUSAN E. HUNT, ELENA LALINDE, ANDREW A. MAGGS, ROBERT ORR, PETER STYRING, MICHAEL S. WRAGG and PETER M. MAITLIS*

Department of Chemistry, The University, Sheffield S3 7HF, U.K.

Abstract—Metallo-mesogens (molecular coordination complexes which show liquid crystalline properties) of various types have been made and characterized, including $[MCl_2(XC_6H_4C_6H_4CN)_2]$, (M = Pd and Pt; X = *n*-alkyl and *n*-alkyloxy), $[Rh(CO)_2Cl(XC_6H_4C_6H_4CN)]$, $[Ag(ROC_6H_4CH{=}CHC_5H_4N)_2]^+Y^-$, $[AuCl(ROC_6H_4CH{=}CHC_5H_4N)]$, $[M'(ROC_6H_4CS_2)_2]_n$ (M' = Zn, Ni, Pd) and $[Au(ROC_6H_4CS_2)X_2]$ (X = Cl, Br). Most of these molecules are rod-like, with rigid central cores containing the metal and the ligating atoms, and flexible *n*-alkyl or -alkyloxy tails extending out along the molecular axes. They show the typical behaviour of thermotropic mesogens. The behaviour of the complexes can parallel that of the ligands (when they are also mesogenic), but transitions generally occur at rather higher temperatures. Many of these complexes exhibit unusual and useful optical properties; for example the palladium complexes (**1**) show a high birefringence.

Liquid crystalline (mesogenic) compounds can be differentiated into thermotropic,[1] which change phase on heating, and lyotropic,[2] which undergo phase changes on the addition of solvent, usually water.

The characteristics of thermotropic organic materials are, at least in part, well-understood; the systematic synthetic work of Gray and his collaborators especially has done much to allow some rules to be defined. Thus we know that in order to obtain rod-like mesogens it is necessary to have elongated molecules, containing a rigid core, a flexible tail and a polarizable function. An important requirement is for reasonably strong anisotropic dispersion forces between the molecules, of the order of 1–5 kJ mol^{-1}. If the intermolecular forces are too strong, or if they are too weak, no mesogenic phases will appear even if the molecular geometry is right. It is possible to predict with fair accuracy what molecular groupings favour the nematic phase (which shows orientational order, Fig. 1) over smectic phases (which show translational order, Fig. 2), and sometimes even what types of smectic will be favoured.

In 1985 we became interested in the effects of introducing metal ions into organic liquid crystals. Some studies on metallo-mesogens (metal-containing liquid crystals), for example, bis(*p*-alkylphenyldithiolate)nickel and -platinum complexes,[3] *ortho*-palladated azobenzenes,[4] as well as some metal-containing β-diketonates,[5] carboxylates[6] and

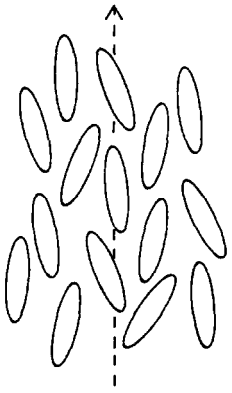

Fig. 1. Diagrammatic representation of molecules in a nematic phase.

With all good wishes to Sir Geoffrey Wilkinson on his 67th birthday.

* Author to whom correspondence should be addressed.
(*Received* 5 *May* 1988).

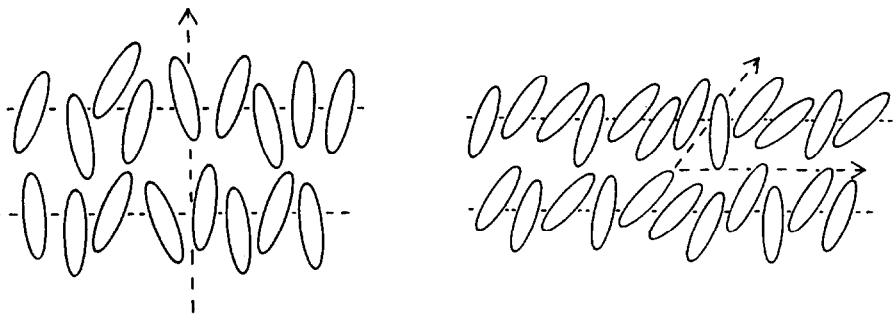

Fig. 2. Diagrammatic representations of molecules in two types of smectic phase.

phthalocyanines,[7] had already started, mainly by workers in France and Italy.

Why put a metal into a liquid crystal? Although metals often represent the points of reactivity (i.e. weakness) in coordination complexes, there is the intrinsic interest, for example, of the effect of new geometries on mesogenic properties. Further, choice of the correct metal ion can introduce colour and paramagnetism, and other unusual and useful optical or electronic properties may result. This short article reviews some of our findings to date in the area of metallo-mesogens.

NITRILE COMPLEXES

Our first complexes were based on some of the Gray 4-alkyl- and 4-alkyloxy-4′-cyanobiphenyl (A and B, respectively*) mesogens as ligands.

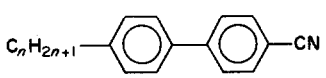

(A)

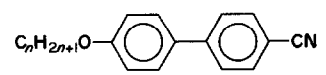

(B)

The nitrile in the 4′-position of a biphenyl is especially useful since it increases the liquid crystalline range by increasing the molecular polarizability without increasing the molecular breadth. We reasoned that complexing a metal via the terminal nitrile function would minimally perturb both the rod-like geometry and the intermolecular forces and thus give the best chance of retaining liquid crystal character in the resultant complex.

The bis(4-alkyl- or -alkyloxy-4′-cyanobiphenyl) dichloropalladium and -platinum complexes [(**1A**)/(**1B**)] and [(**2A**)/(**2B**)] were made by a simple displacement of benzonitrile (palladium) or by direct reaction (platinum),[8–10]

$$[PdCl_2(PhCN)_2] + 2RCN \rightarrow [PdCl_2(RCN)_2] + 2PhCN \quad (1)$$

$$1/n[PtCl_2]_n + 2RCN \rightarrow [PtCl_2(RCN)_2]. \quad (2)$$

X-ray crystal structures showed that (**1**) and (**2**) had the expected *trans*-arrangements of the cyanobiphenyl ligands and that the complexes, as well as the ligands on which they were based, had the desired rod-like shapes.[10,11] Many of them showed mesogenic behaviour.

Thus the platinum complexes mirrored the thermal behaviour of the free ligands quite well but at temperatures 100–150°C higher. For example, the 4-pentyl-4′-cyanobiphenyl complex, $[PtCl_2(4\text{-}C_5H_{11}C_6H_4C_6H_4CN)_2]$ showed a K–N (crystal to nematic) transition at 189°C and a N–I (nematic to isotropic liquid) at 204°C, compared with K–N at 24°C and N–I at 35°C for the free ligand itself. Similarly the 4-nonyloxy-4′-cyanobiphenyl complex, $[PtCl_2(4\text{-}C_9H_{19}OC_6H_4C_6H_4CN)_2]$, showed K–$S_A$ (smectic A) at 167°C, S_A–N at 187°C, and N–I at 209°C, while phase transitions occurred at 64°C (K–S_A), 77°C (S_A–N) and 80°C (N–I) in the free ligand.

However the palladium analogue of the latter, $[PdCl_2(4\text{-}C_9H_{19}OC_6H_4CN)_2]$, showed two smectic phases (K–S_C at 119°C, S_C–S_A at 122°C, and S_A–I at 146°C) but no nematic phase. Further, the

* A nomenclature has been proposed in the liquid crystal literature for these compounds as ligands in complexes. Thus (A) is termed *n*-CB, where *n* is the number of carbon atoms of the alkyl chain and CB stands for cyanobiphenyl, and (B) is *n*-OCB, for the analogous alkyloxycyanobiphenyls. A further series, based on the 4-alkyl-4′-cyanobicyclohexyls (C) is termed CCH-*n*.

palladium complexes formed from the 4-alkyl-4′-cyanobiphenyls showed no thermodynamically stable (= enantiotropic) mesophases at all. However, monotropic (= thermodynamically unstable) nematic phases were found on cooling the melts.

In many areas of chemistry the properties of interest are exhibited by pure single substances. However, although it is necessary to have very pure materials to show the mesophase changes reproducibly, there are substantial advantages to be gained if they are not single compounds. Thus mixtures of related materials will show lower crystallization temperatures, which can enhance the temperature ranges of liquid crystalline mesophases and extend them to lower temperatures, a most desirable feature. Further, stable mesophases can sometimes be generated in mixtures even though the individual components do not show them. For example we found that a mixture containing the 4-propyl- and the 4-pentyl-4′-cyanobicyclohexyl palladium complexes, (**1C**) showed a stable nematic range (of *ca* 6°C), whereas neither $[PdCl_2(C_3H_7C_6H_{10}C_6H_{10}CN)_2]$ nor $[PdCl_2(C_5H_{11}C_6H_{10}C_6H_{10}CN)_2]$ individually showed an enantiotropic phase.[10]

The reason for the differences between the alkylcyanobiphenylpalladium and -platinum complexes [(**1A**), (**2A**)] is not yet understood. The X-ray structures of the 4-pentylcyanobiphenyl complexes of the two metals show that they are isomorphous and isostructural, with very similar molecular parameters, including very long intermolecular M···M (8.31 Å Pd, and 8.42 Å Pt) and M···Cl (> 6 Å) distances (Fig. 3).[10,11] Thus the contrast appears not to be due to their solid state structures. Furthermore, the difference is not immediately apparent either from their enthalpies and entropies of melting which, overall (K–I), are 39.7 kJ mol^{-1} (Pd) and 42.8 kJ mol^{-1} (Pt) and 102 J K^{-1} mol^{-1} (Pd) and 91.5 J K^{-1} mol^{-1} (Pt), respectively. One possibility is that the anomalous behaviour of the Pd complexes (**1A**) is a consequence of the greater reactivity of Pd^{II} complexes by comparison with their Pt^{II} analogues, and that ligand labilization occurs preferentially.

A problem with the nitrile ligands (A, B and C)

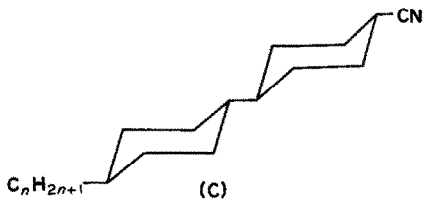

is that they bind rather weakly to the metals. Thus, many of the complexes decompose either just before or just after melting. For example, the rhodium(I) complex of (**B**), *cis*-$[RhCl(CO)_2(4\text{-}C_9H_{19}OC_6H_4C_6H_4CN)]$, (**3**), shows a nematic range of only 2°C (79–81°C) before it decomposes on clearing.[8,9]

DITHIOBENZOATE COMPLEXES

We have therefore synthesized other complexes using ligands which are expected to bind more

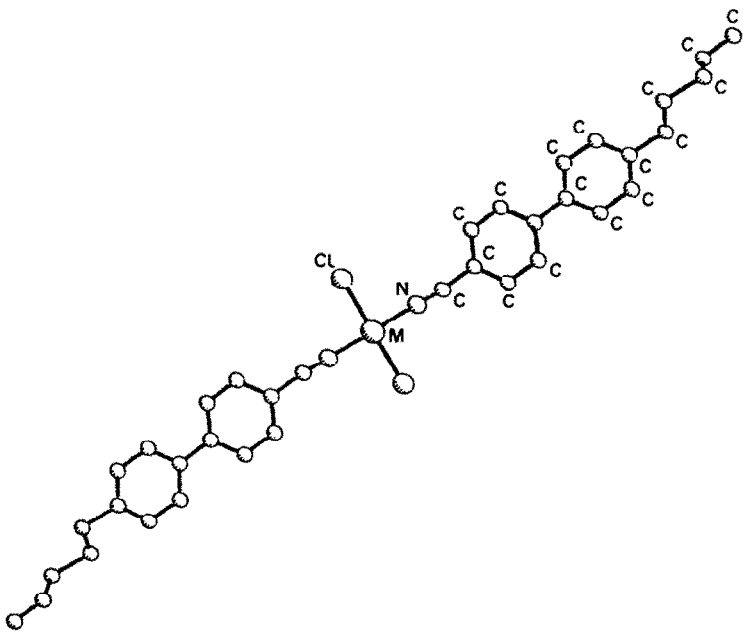

Fig. 3. Structure of $[(C_5H_{11}C_6H_4C_6H_4CN)_2MCl_2]$ (M = Pd or Pt).

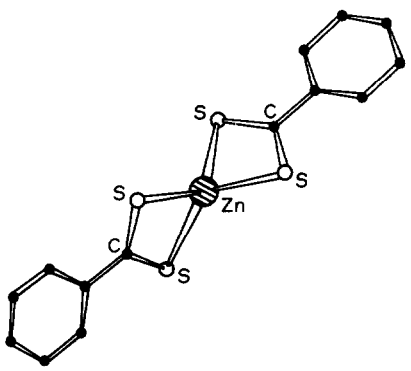

Fig. 4. Structure of $[Zn(S_2CPh)_2]$ (ref. 12).

strongly. The first were based on sulphur ligands, the bis(*p*-alkyloxydithiobenzoates) of zinc, nickel and palladium. Structures of model complexes, for example $[Zn(S_2CPh)_2]$, (Fig. 4)[12] suggested that, with the addition of *p*-alkyl or -alkyloxy chains, the appropriate rod-like molecules should result. Using the 4-*n*-alkyloxy(dithiobenzoates), (D), we were able to make mesogenic $[M(C_nH_{2n+1}OC_6H_4CS_2)_2]$ [(**4**) M = Zn; (**5**) M = Ni; and (**6**) M = Pd; n = 4–10]. For example, the 4-*n*-octyloxy(dithiobenzoate) complexes showed a nematic phase for Zn (K—148° → N; N—180° → I), while the nickel and the palladium analogues showed both nematic and (as yet unidentified) smectic phases (Pd: K—100°C → S_1; S_1—110°C → S_2; S_2—230°C → N; N—334°C → I; dec. Ni: K—158°C → S(?); S(?)—177°C → N; N—245°C → I; dec).

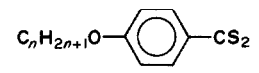

(D)

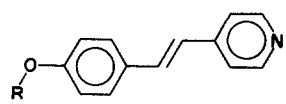

(E)

Since the parent complex, $[Pd(C_6H_4CS_2)_2]$ was itself weakly associated into trimers in the crystal,[13] we anticipated that the mesogenic complexes we had made would also show some intermolecular association in the solid. In fact the X-ray structure of $[Pd(C_8H_{17}OC_5H_4CS_2)_2]$ (Fig. 5) showed it to be weakly associated to dimers (Pd—S intramolecular, 2.29–2.35 Å, intermolecular, $\geqslant$ 3.38 Å).[11]

To our surprise, an X-ray structure determination of the zinc complex showed it to be *dinuclear*,[11] with an eight-membered Zn—S—C—S—Zn—S—C—S ring (Fig. 6) with Zn—S "intermolecular", 2.41 Å, being of the same order as Zn—S "intramolecular", 2.33–2.77 Å.

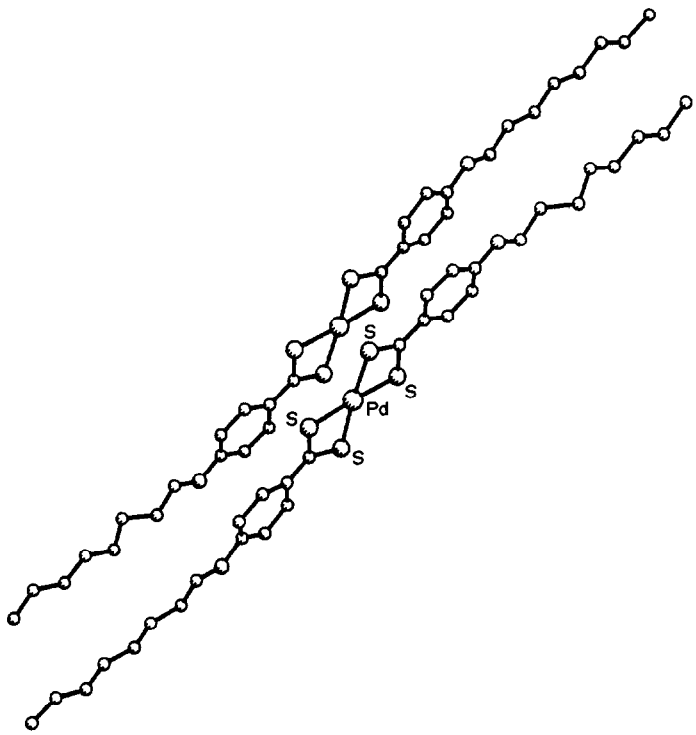

Fig. 5. Structure of $[Pd(S_2CC_6H_4—O—C_8H_{17})_2]$.

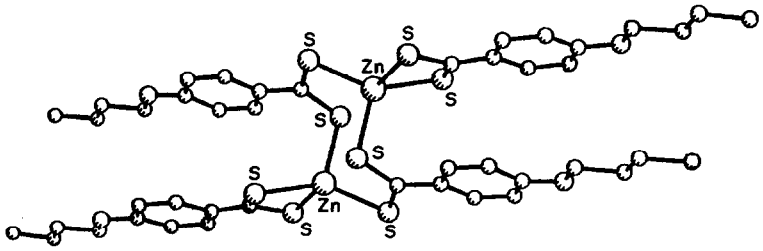

Fig. 6. Structure of $[\{Zn(S_2CC_6H_4OC_4H_9)_2\}_2]$.

However, the complex is monomeric in toluene solution (by osmometry) suggesting that, although the bonds are short, the forces holding the dimer together are rather weak.

STILBAZOLE COMPLEXES

In order to further optimize intermolecular van der Waals forces, without strong M···M or M···X bonds, we also examined *p*-substituted pyridines as ligands. These ligands were again based on mesogenic compounds, in this case, the 4-alkyloxy-4′-stilbazoles, ($ROC_6H_4CH{=}CHC_5H_4N$, E).[14] Of the numerous complexes to have been prepared with these ligands, the bis-stilbazole silver(I) complexes are especially interesting. Thus reaction of $AgBF_4$ with the appropriate stilbazole gave $[Ag(ROC_6H_4CH{=}CHC_5H_4N)_2]^+BF_4^-$ (**7**).[15] For R = *n*-C_8H_{17} this showed two smectic phases, at present still unidentified, between 170 and 270°C and between 270 and 300°C. However the most interesting development was when the BF_4 was exchanged for dodecyl sulphate to give $[Ag(ROC_6H_4CH{=}CHC_5H_4N)_2]^+[n\text{-}C_{12}H_{25}OSO_3]^-$ (**8**).

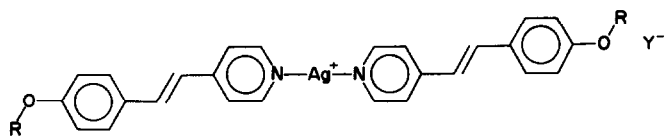

(7, Y = BF_4; 8, Y = $C_{12}H_{25}OSO_3$)

For R = *n*-C_8H_{17}, (**8**) showed a smectic B phase between 144 and 164°C when it changed into a lamellar phase up to the transition, to the isotropic liquid at 177°C.[15] When complex (**8**) was made with a longer, alkyloxy chain (R = $C_{11}H_{23}$), the crystalline form melted to an (unidentified) smectic phase, which then changed into a smectic C phase at 95°C, another smectic phase at 100°C, and a lamellar phase at 128°C, before clearing to the isotropic liquid at 193°C. These novel complexes show mesophases characteristic of both lyotropic and thermotropic liquid crystals, and the temperature ranges can easily be adjusted with some simple molecular engineering. It is also interesting that technologically useful phases such as smectic C are predictably accessible.

GOLD COMPLEXES

Gold can also be introduced into a liquid crystal. Our first complex, of Au^I with one of the stilbazole ligands, $[n\text{-}C_8H_{17}OC_6H_4CH{=}CHC_5H_4N\text{-}Au\text{-}Cl]$ (**9**) showed a mesophase between 120 and 200°C

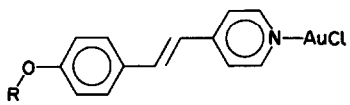

(9)

before decomposing.[9] A well-behaved series of gold complexes is represented by the alkyloxydithiobenzoates of gold(III), $[ROC_6H_4CS_2AuCl_2]$ (**10**) which all show a smectic A phase in the range 150–200°C.[16]

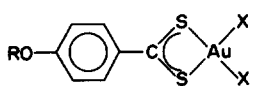

(10)

POTENTIAL APPLICATIONS

So far our work in Sheffield has concentrated on synthesizing the mesogenic complexes, and determining their structures and phase behaviour. How-

ever, the use of such complexes in devices is an intriguing possibility and some measurements to this end have been made.

By virtue of their rod-like shapes, thermotropic liquid crystals show two refractive indices, one parallel to the molecular axis, $n_{\parallel}$, and one perpendicular to it, $n_{\perp}$. The difference between them, Δn, is the birefringence; amongst other factors, the contrast and angle of view of a liquid crystalline display depend on Δn. We have found that the birefringence of, for example, 4-*n*-pentyl-4′-cyanobiphenyl is enhanced if its palladium chloride complex is added.

In another case, $PdCl_2$ complexes have been made of a mixture of $ROC_6H_4C_6H_4CN$, where $R = C_2H_5$, C_4H_9 and C_6H_{13}. The resulting mixture shows a nematic phase between 100 and 142°C on heating, which can be supercooled to 20°C (where it is stable for a few hours before crystallization occurs). An aligned sample of the mixture shows a birefringence, Δn of 0.4–0.5 at 100°C, which is twice as large as for most liquid crystalline materials.[17]

It is also found that the 4-*n*-alkyloxy(dithiobenzoates), $[M(C_8H_{17}OC_6H_4CS_2)_2]$ [(**5**), M = Ni; and (**6**), M = Pd] are highly dichroic,[17] since the extinction coefficient of light along the molecular axis is very much larger than that in a perpendicular direction. This property allows them to be used in guest–host displays. For example, the purple nickel complex is the guest in a cell containing, as host, an organic liquid crystalline compound. In the absence of an electric field, the molecules are aligned perpendicular to the direction of the light, but when the field is applied they align themselves parallel to it. Thus in the absence of the field the cell is coloured purple, but when the field is applied it becomes colourless.

CONCLUSIONS

Although the study of metallo-mesogens is still in its infancy and we are only now beginning to define the questions we need to ask, some conclusions can be drawn. The work our group and others have carried out has shown that coordination complexes can be thermotropic mesogens. Many metals have been used as part of the central rigid core, and it seems certain that many others can also be used. The metal–ligand bond clearly represents a weak link in some of the complexes, as indicated by the tendency for irreversible decomposition at temperatures close to the transition into the isotropic. For this reason the more useful complexes are likely to involve less reactive metal centres, e.g. Pt^{II} compared with Pd^{II}. Not surprisingly, it also appears that complexes with bidentate chelating ligands are likely to be more successful than monodentate ones, for similar reasons.

We initially anticipated that the most stringent requirement would be geometric, and that marked deviations from rod-like linear complexes would not be tolerated. This appears not to be the case. Thus, while we have a number of examples of successful mesogenic complexes which are virtually linear, for example the cations of (**7**), (**8**) and (**9**), *trans*-square planar geometries as in (**1**), (**2**) and (**6**) are well-tolerated, and even five-coordination (at least in the solid state) seems to be allowed, as in the dinuclear zinc complex (**4**). A number of *ortho*-palladated complexes containing quite extended flat areas are also reported to show ordered smectic and nematic mesophases.[4,18] Thus the range of potential new molecules to be investigated is really very large. If, as we anticipate, we can control the phases and the transition temperatures by suitable molecular design, then this promises to develop into a very exciting new area of science.

Acknowledgements—We acknowledge support from the EC Twinning, the Anglo-Spanish Accion Integrada, the SERC, the Royal Society, and the University of Sheffield, gifts of chemicals from BDH and Unilever Research, and loans of platinum metal salts from Johnson Matthey.

REFERENCES

1. G. W. Gray (Ed.), *Thermotropic Liquid Crystals*. Wiley, Chichester (1987).
2. G. J. T. Tiddy, *Phys. Reports, Rev. Sect. Phys. Lett.* 1980, **57**, 1; H. F. Eiche (Ed.), *Mod. Trends Colloid Sci. Chem. Biol., Int. Symp. Colloid and Surface Sci.*, p. 148. Birkhauser Verlag, Basel (1984).
3. U. T. Mueller-Westerhoff, A. Nazzal, R. J. Cox and A. M. Giroud, *Mol. Cryst. Liq. Cryst.* 1980, **56**, 249; M. Veber, R. Fugnitto and H. Strzelecka, *Mol. Cryst. Liq. Cryst.* 1983, **96**, 221.
4. M. Ghedini, M. Longeri and R. Bartolino, *Mol. Cryst. Liq. Cryst.* 1982, **84**, 207; M. Ghedini, S. Licoccia, S. Armentano and R. Bartolino, *Mol. Cryst. Liq. Cryst.* 1984, **108**, 269.
5. A. M. Godquin-Giroud and J. Billard, *Mol. Cryst. Liq. Cryst.* 1983, **97**, 287; K. Ohta, A. Ishii, I. Yamamoto and K. Matsuzaki, *J. Chem. Soc., Chem. Commun.* 1984, 1099.
6. M. Takeochi, N. Watanabe and B. Tamamushi, *Colloid Polymer Sci.* 1978, **256**, 588; A. M. Godquin-Giroud, J. C. Marchon, D. Guillon and A. Skoulios, *J. Phys. Lett.* 1984, **45**, L681.
7. C. Piechocki, J. Simon, A. Skoulios, D. Guillon and P. Weber, *J. Am. Chem. Soc.* 1982, **104**, 5245.
8. P. M. Maitlis, D. W. Bruce and D. A. Dunmur, PCT Int. Appl. WO 87 02,693 (7 May 1987; GB Appl. 85/26,462, 26 Oct. 1985); *Chem. Abstr.* 1987, **107**, 145374n.

9. D. W. Bruce, E. Lalinde, P. Styring, D. A. Dunmur and P. M. Maitlis, *J. Chem. Soc., Chem. Commun.* 1986, 581.
10. H. Adams, N. A. Bailey, D. W. Bruce, D. A. Dunmur, E. Lalinde, M. Marcos, C. Ridgway, A. J. Smith, P. Styring and P. M. Maitlis, *Liq. Cryst.* 1987, **2**, 381; D. W. Bruce and A. A. Maggs, unpublished results.
11. H. Adams and N. A. Bailey, unpublished results.
12. M. Bonamico, G. Dessy, V. Fares and L. Scaramuzza, *J. Chem. Soc., Dalton Trans.* 1972, 2515.
13. M. Bonamico, G. Dessy, V. Fares and L. Scaramuzza, *J. Chem. Soc., Dalton Trans.* 1972, 2250.
14. D. W. Bruce, D. A. Dunmur, E. Lalinde, P. M. Maitlis and P. Styring, *Liq. Cryst.* 1988, **3**, 385.
15. D. W. Bruce, D. A. Dunmur, E. Lalinde, P. M. Maitlis and P. Styring, *Nature* 1986, **323**, 791.
16. D. W. Bruce, D. A. Dunmur, E. Lalinde, P. M. Maitlis and P. Styring, unpublished results.
17. D. A. Dunmur, P. Styring, S. Hunt and R. Orr, unpublished results.
18. J. Barbera, P. Espinet, E. Lalinde, M. Marcos and J. L. Serrano, *Liq. Cryst.* 1987, **2**, 833.

Polyhedron Vol. 7, No. 19/20, pp. 1869–1874, 1988
Printed in Great Britain

0277–5387/88 $3.00+.00
© 1988 Pergamon Press plc

AN ESR STUDY OF MANGANESE(II) IONS IN COMPLEXES OF BIURET

MARGARET GOODGAME,* IZHAR HUSSAIN and J. NIGEL OKEY

Chemistry Department, Imperial College of Science and Technology, London SW7 2AY, U.K.

Abstract—ESR spectra have been measured, at X- and Q-band, of manganese(II) ions doped at a nominal 1% in the lattices of $M(biuret)_2Cl_2$ (M = Zn, Cd, Co, Ni) and $M(biuret)_2Br_2$ (M = Zn, Co, Ni). The cadmium complex, which has a chloride-bridged chain structure, gives completely different spectra from the zinc chloro-complex which contains chelating biuret molecules and monodentate chloride ions. The cobalt and nickel complexes closely resemble the zinc complexes. Values of the zero-field splitting parameters D and λ are reported for all the compounds.

The biuret molecule can adopt either the *cis* or the *trans* configuration (**1a** and **b**). In solid biuret the

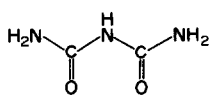

(Ia)

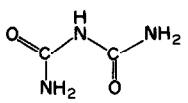

(Ib)

trans arrangement, with intramolecular hydrogen-bonding, is favoured,[1] but when biuret acts as a ligand the *cis* arrangement, which permits chelation, may be expected to dominate. Chelation by biuret has indeed been shown, in the X-ray crystal structure of $Zn(biuret)_2Cl_2$[2] with the metal ion surrounded by four oxygen atoms and two chloride ions. In the corresponding cadmium complex, however, the ligand adopts the monodentate, *trans* configuration and the metal ion octahedron is completed by bridging chloride ions, giving a CdO_2Cl_4 chromophore.[3] We have measured the ESR spectra of manganese ions doped into both these complexes, and show that this technique can readily distinguish between the two structural types.

EXPERIMENTAL

Preparation of complexes

Commercially available biuret was purified by recrystallization from ethanol. Metal salts were used without further purification.

* Author to whom correspondence should be addressed.

$M(Mn)(biuret)_2X_2$, (M = Mn, Co *and* Ni; X = Cl *or* Br, M = Cd; X = Cl)

These were prepared by previously reported methods.[4]

$Zn(Mn)(biuret)_2Cl_2$

Zinc chloride (0.68 g, 0.005 mol) and manganese(II) chloride (0.01 g, 0.00005 mol) were dissolved in water (20 cm^3) and one drop of conc. HCl was added to prevent partial hydrolysis. It was then mixed with a warm solution of biuret (1.03 g, 0.02 mol) in water (50 cm^3), refluxed for 1 h and allowed to evaporate at room temperature. The white precipitate thus formed was refluxed in ethyl acetate to eliminate the excess of ligand. The compound was filtered off, washed with ethyl acetate and dried *in vacuo* over P_2O_5.

$Zn(Mn)(biuret)_2Br_2$

This was prepared by a method similar to that for the analogous chloride complex. Analyses for C, H and N (Imperial College Microanalytical Laboratory) were satisfactory for all compounds.

X-band ESR spectra were obtained using a Varian E12 spectrometer. Q-band spectra were obtained with a Bruker ER 200 D-SRC spectrometer and an ER 078 15 in. electromagnet. All samples had a nominal doping of 1% and were measured as polycrystalline solids.

RESULTS AND DISCUSSION

At X-band, $Zn(Mn)(biuret)_2Cl_2$ gave an extremely complicated spectrum (Fig. 1) with considerable overlapping of transitions throughout the magnetic field range, and detailed interpretation was difficult.

The better resolved Q-band spectrum (Fig. 2) was therefore used to calculate the zero-field splitting parameters D and λ ($= E/D$) in the Spin Hamiltonian, eq. (1).

$$\mathcal{H} = g\beta B \cdot S + D(Sz^2 - 35/12) + E(Sx^2 - Sy^2). \quad (1)$$

The observed resonance fields fitted very well with those calculated, using the programme ESRS,[5] by exact diagonalization of the matrix derived from eq. (1) with $g_{iso} = 2.00$. The results are given in Table 1. The 6–5 transition in the Z direction coincides with a broad absorption due to oxygen and could not be identified with certainty even after purging with nitrogen. This transition is expected to be weak.

The D and λ values obtained from the Q-band spectra were then used to simulate the X-band spectra using the program SHAPE 9,[6] good agreement being obtained (Fig. 1).

The spectra of $Cd(Mn)(biuret)_2Cl_2$ at both the X- and Q-band differ considerably from those of the zinc analogue, with the strongest bands at each frequency occurring in the $g_{eff} = 2$ region. This indicates a much lower D value, and the Q-band spectrum agreed well with the transitions calculated for $D = 0.087$, $\lambda = 0.03$ (Table 2). These figures are consistent with the values previously found[7] for manganese(II) ions in the chloride-bridged polymer $Cd(pyridine)_2Cl_2$, for which $D = 0.125$, $\lambda = 0.02$. It is expected that the D value would decrease when the pyridine is replaced by biuret, since the oxygen

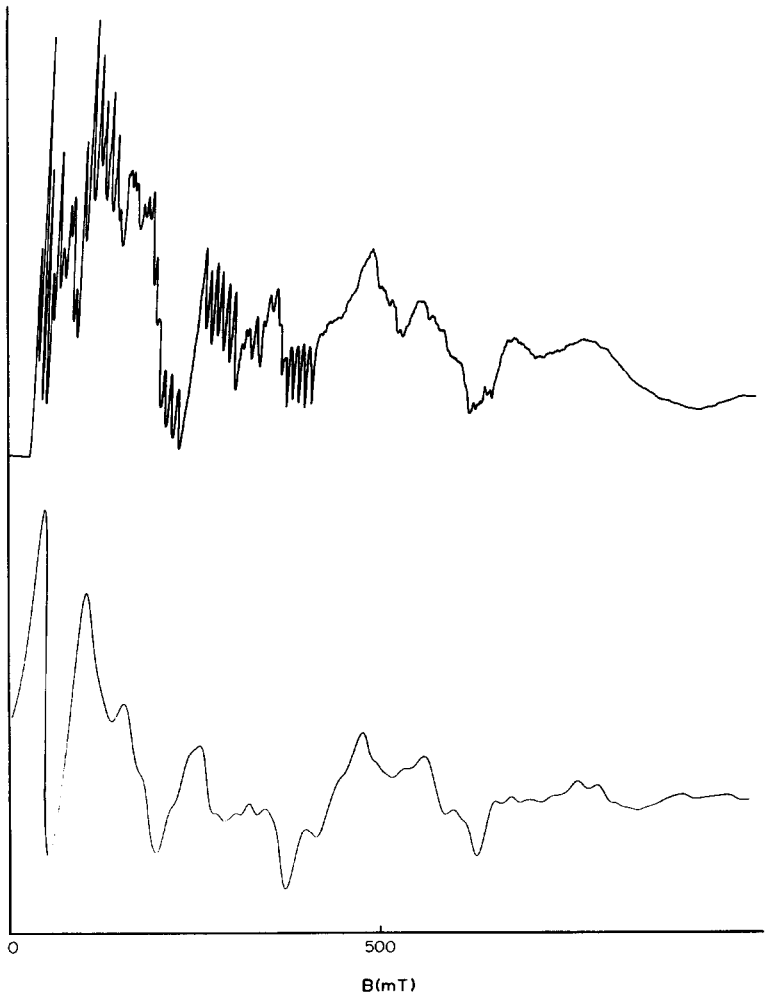

Fig. 1. X-band ESR spectrum of $Zn(Mn)(biuret)_2Cl_2$ and simulated spectrum for $D = 0.192$ cm^{-1}, $\lambda = 0.082$.

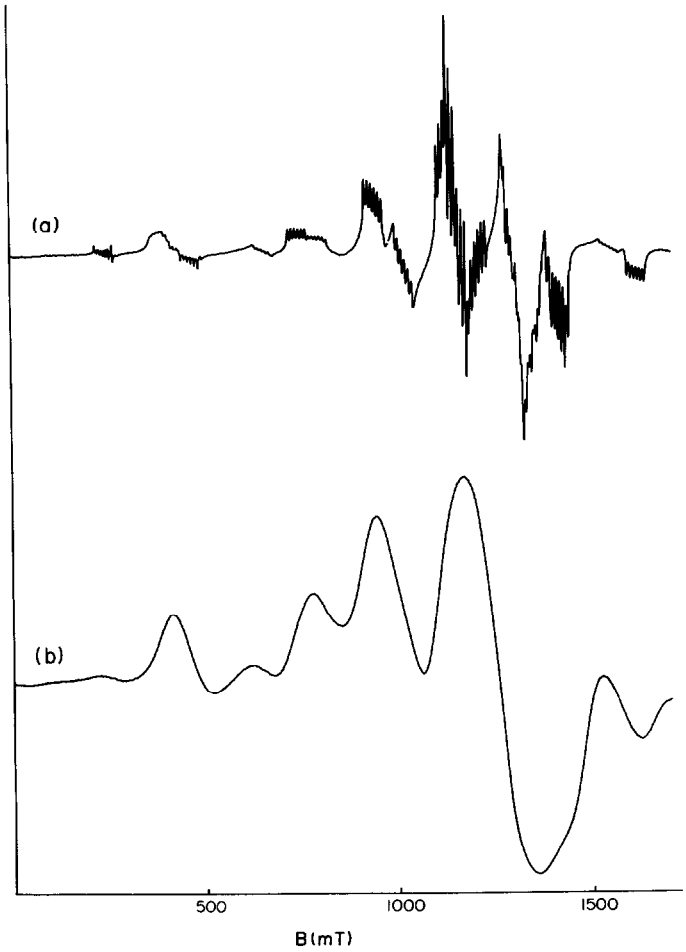

Fig. 2. Q-band ESR spectra of; (a) $Zn(Mn)(biuret)_2Cl_2$ and (b) $Mn(biuret)_2Cl_2$.

donor is closer to chloride in the spectrochemical series, and thus produces less distortion along the principal axis even though the Cd—O distance (2.34 Å) is very similar to the Cd—N distance in the pyridine complex (2.35 Å). The λ value, which is a measure of distortion within the chloride-bridged chain, remains fairly small. Indeed, the value of E in the Spin Hamiltonian is very similar for the two compounds, although the Cd—Cl distances are not quite equal in the biuret complex.

Spectra were also obtained for manganese ions doped into $M(biuret)_2Cl_2$ (M = Co and Ni) and for the pure manganese compound $Mn(biuret)_2Cl_2$. This last case had been studied previously,[8] the spectrum being interpreted using $D = 0.17$ cm^{-1} and $\lambda = 0.167$. However, these figures were obtained essentially from the X-band spectrum, very few transitions being seen at the Q-band. An improved spectrum at the Q-band now permits the observation that this compound is in fact very similar to its zinc analogue (Fig. 2), and although the resolution is necessarily poor, we suggest that $D = ca\ 0.19$ cm^{-1} and $\lambda = ca\ 0.08$. The cobalt and nickel complexes are also similar; that of cobalt gave excellent resolution, but the spectrum of the nickel complex was of poorer quality. Results for all these compounds are collected in Table 3.

With bromide as the anion, and zinc, cobalt and nickel as the host metal ions, the X-band spectra were much simpler in form (Fig. 3), with the main intensity near $g_{eff} = 6$, indicating a much higher value of D and a low but finite λ. Best fits to the Q-band spectra were obtained with D in the range 0.49–0.50 cm^{-1} and $\lambda = 0.015$ (Table 4). Simulation of the X-band spectra using these parameters gave a good fit, though many of the calculated transitions were beyond the range of the spectrometer and some of the Z transitions, which are expected to be very weak, were not seen. Observed and calculated field values are given in Table 5.

Table 1. Q-band ESR spectrum (mT) of $Zn(Mn)(biuret)_2Cl_2$

Observed (ν = 33.870 GHz)	Calculated for $D = 0.192\ cm^{-1}$, $\lambda = 0.082$ B	T.P.[a]	Field direction	Levels[b]
246 W				
250 W				
390 W	390.3	5.34	Z	2–1
424 W	425.1	0.49	$\theta = 23°$, $\phi = 00°$	5–2
470 W/M	470.9	0.64	$\theta = 27°$, $\phi = 90°$	5–2
657 W	658.9	1.44	$\theta = 55°$, $\phi = 00°$	4–2
747 M	746.9	3.53	Y	6–5
	753.8	1.27	$\theta = 61°$, $\phi = 90°$	4–2
800 W	799.4	8.36	Z	3–2
943 M/S	941.0	6.35	Y	5–4
	952.2	3.38	X	6–5
1020 M/S	1020.0	6.27	X	5–4
1131 S	1131.7	8.30	X	4–3
1157 S	1158.6	8.21	Y	4–3
1209 S	1208.7	9.16	Z	4–3
1297 S	1297.8	8.87	X	3–2
1413 M/S	1413.3	8.58	Y	3–2
1547 W	1547.5	6.89	X	2–1
1620 M	1619.3	7.90	Z	5–4
1739 W	1738.7	6.53	Y	2–1
	2032.8	4.77	Z	6–5

[a] T.P. = transition probability.
[b] Levels are labelled 1–6 in order of decreasing energy.

Table 2. Q-band ESR spectrum (mT) of $Cd(Mn)(biuret)_2Cl_2$

Observed (ν = 34.000 GHz)	Calculated for $D = 0.087\ cm^{-1}$, $\lambda = 0.03$ B	T.P.	Field direction	Levels
366.0 VW				
427.0 W	427.9	0.03	$\theta = 30°$, $\phi = 00°$	5–2
433.0 W	432.6	0.05	$\theta = 32°$, $\phi = 90°$	5–2
608–670 W/M	633.5	0.22	$\theta = 66°$, $\phi = 00°$	4–2
	645.9	0.24	$\theta = 66°$, $\phi = 90°$	4–2
703.6 W	702.1	0.10	$\theta = 13°$, $\phi = 00°$	5–3
	703.7	0.14	$\theta = 15°$, $\phi = 90°$	5–3
841.9 W	841.9	5.05	Z	2–1
1015.8 M	1019.8	4.27	Y	6–5
	1028.2	8.05	Z	3–2
1054.6 M	1054.0	4.24	X	6–5
1105.3 M/S	1106.4	7.31	Y	5–4
1123.1 M/S	1121.9	7.29	X	5–4
1199.9 S	1199.5	8.85	X	4–3
1201.1 S	1201.3	8.84	Y	4–3
1215.0 S	1214.5	9.01	Z	4–3
1287.9 S	1288.4	8.52	X	3–2
1308.2 S	1306.2	8.48	Y	3–2
1390.2 M	1390.3	5.80	X	2–1
1402.2 M	1400.9	7.97	Z	5–4
1427.3 M	1423.0	5.75	Y	2–1
1588.3 W	1587.3	4.96	Z	6–5

Table 3. *Zfs* parameter of Mn^{II} in biuret complexes

Complex	D (cm^{-1})	λ
$Co(biuret)_2Cl_2$	0.191	0.083
$Co(biuret)_2Br_2$	0.491	0.015
$Ni(biuret)_2Cl_2$	0.194	0.083
$Ni(biuret)_2Br_2$	0.499	0.015
$Zn(biuret)_2Cl_2$	0.192	0.082
$Zn(biuret)_2Br_2$	0.491	0.015
$Cd(biuret)_2Cl_2$	0.087	0.030

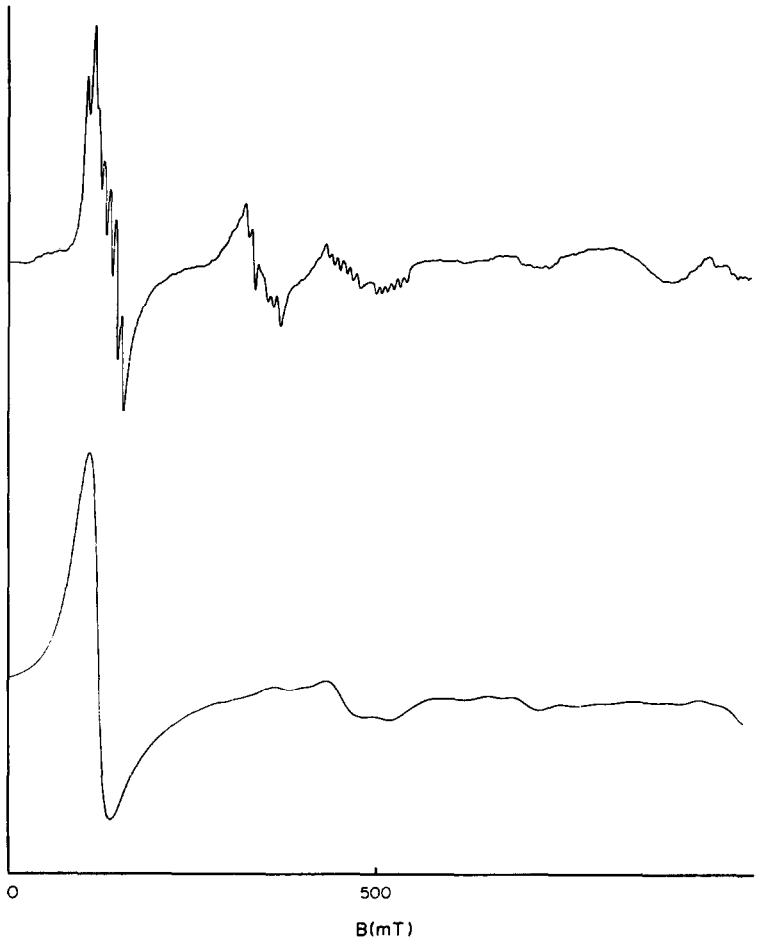

Fig. 3. X-band ESR spectrum of $Zn(Mn)(biuret)_2Br_2$ and simulated spectrum for $D = 0.491$ cm^{-1}, $\lambda = 0.015$.

Table 4. Q-band ESR spectrum (mT) of $Zn(Mn)(biuret)_2Br_2$

Observed (ν = 33.870 GHz)	Calculated for $D = 0.491\ cm^{-1}$, $\lambda = 0.015$ B	T.P.	Field direction	Levels
Region	66.7	1.33	$\theta = 48°, \phi = 90°$	6–3
42–106 M	69.9	1.02	$\theta = 44°, \phi = 00°$	6–3
513 M	513.2	2.02	Y	6–5
581 M	583.8	2.01	X	6–5
	645.0	1.24	$\theta = 20°, \phi = 00°$	4–3
690 VS	688.0	3.66	Y	5–4
	691.4	3.71	X	5–4
Broad / Centre *ca* 840	831.4	3.78	$\theta = 12°, \phi = 90°$	5–3
	855.6	4.16	$\theta = 10°, \phi = 00°$	5–3
1065 M/S	1064.1	6.12	X	4–3
1108 M/S	1108.8	6.01	Y	4–3
1209 S	1208.0	9.23	Z	5–3
1260–1330 W	1282.2	7.49	$\theta = 10°, \phi = 00°$	5–3
	1313.1	7.22	$\theta = 11°, \phi = 90°$	5–3
Region of overlap 1680–1830 M/S	1708.0	7.86	$\theta = 66°, \phi = 00°$	3–2
	1772.1	7.74	$\theta = 67°, \phi = 90°$	3–2
	1779.4	6.12	$\theta = 32°, \phi = 00°$	4–3
	1812.8	6.09	$\theta = 34°, \phi = 90°$	4–3

Table 5. X-band ESR spectrum (mT) of $Zn(Mn)(biuret)_2Br_2$

Observed (ν = 9.528 GHz)	Calculated for $D = 0.491\ cm^{-1}$, $\lambda = 0.015$ B	T.P.	Field direction	Levels
111 S	109.4	1.08	Y	6–5
	113.6	0.04	Z	4–3
121 S	124.0	1.09	X	6–5
343 M	342.7	7.18	Z	6–5
454 W/M	453.4	6.34	X	4–3
521 W/M	522.1	5.95	Y	4–3
ca 710 W	709.1	6.34	Z	6–5
	937.9	0.02	Z	4–3
	1165.1	0.02	Z	4–3

Acknowledgements—We thank the Government of Pakistan for a Scholarship and the University of Baluchistan for leave of absence (to I.H.). We thank Dr J. F. Gibson for the use of computer programs.

REFERENCES

1. E. W. Hughes, H. L. Yakel and H. C. Freeman, *Acta Cryst.* 1961, **14**, 345.
2. M. Nardelli, G. Fava and G. Giraldi, *Acta Cryst.* 1963, **16**, 343.
3. L. Cavalca, M. Nardelli and G. Fava, *Acta Cryst.* 1960, **13**, 594.
4. A. W. McLellan and G. A. Melson, *J. Chem. Soc.* (*A*) 1967, 137.
5. D. Vivian and J. F. Gibson, *J. Chem. Soc., Faraday Trans. II* 1975, 1640.
6. J. F. Gibson and G. M. Lack, unpublished work.
7. M. Goodgame and J. N. Okey, *Inorg. Chim. Acta* 1985, **103**, 67.
8. R. D. Dowsing, J. F. Gibson, M. Goodgame and P. J. Hayward, *J. Chem. Soc.* (*A*) 1970, 1133.

Polyhedron Vol. 7, No. 19/20, pp. 1875–1879, 1988
Printed in Great Britain

0277–5387/88 $3.00+.00
© 1988 Pergamon Press plc

POLYPHOSPHORUS LIGANDS—V.* THE SYNTHESIS, PHOSPHORUS-31 NMR SPECTRA AND CONFORMATIONS OF THE POLYKIS(DIPHENYLPHOSPHINO) BENZENES $(Ph_2P)_nC_6H_{6-n}$ $(n = 1–4)$

H. CHRISTINA E. McFARLANE and WILLIAM McFARLANE†

Department of Chemistry, City of London Polytechnic, Jewry Street, London EC3N 2EY, U.K.

Abstract—All isomers of $(Ph_2P)_nC_6H_{6-n}$ $(n = 1–4)$ have been prepared by the reaction between the corresponding isomer of $C_6H_{6-n}F_n$ and Ph_2PNa in liquid ammonia. In many cases their phosphorus-31 NMR spectra are structurally diagnostic, with $\delta(^{31}P)$ having values characteristic of the stereochemical environment of the Ph_2P unit, and the couplings $^3J(PP)$ being conformationally dependent and lying in the range 35–154 Hz, while $^4J(PP)$ and $^5J(PP)$ are much smaller.

Di- and polyorganophosphorus compounds are important as chelating ligands for the stabilization of transition metals in lower oxidation states and the conferment of special geometries and/or coordination numbers.[2] Most of the ligands used in this way have relatively flexible backbones, e.g. $R_2P(CH_2)_nPR_2$, and therefore are able to exercise only a limited degree of constraining influence upon the geometry of the resulting complex.

A notable exception to this generalization is 1,2-bis(diphenylphosphino) benzene (**2**) in which the two phosphorus atoms have a fixed spatial separation of *ca* 3.3 Å, but which has been relatively seldom used to make chelated transition metal complexes,[3] probably because most methods available for its synthesis are multi-step and/or low-yielding.[3,4] Recently however, we have shown[5] that the reaction between Ph_2PNa and the readily available 1,2-difluorobenzene in liquid ammonia provides a convenient single-step route to (**2**), in marked contrast to reactions based upon other 1,2-dihalobenzenes. In the present paper we extend the scope of this type of reaction to provide straightforward methods of preparing the new tris- and tetrakis(diphenylphosphino) benzenes (**5–10**) from the corresponding tri- and tetrafluorobenzenes in moderate to high yield. The method is also satisfactory as a route to the known (**1**),[6] (**3**)[7] and (**4**),[8] although in these cases it offers no particular advantages over the more conventional use of chloro- or bromobenzenes.

With the exception of (**7**) these polyphosphines should be capable of forming chelate complexes and should also give rise to bi- and polymetallic species in which the rigidity of the ligand backbone may impose important constraints upon the metal–metal interactions. Attempts to make the two remaining members of this series, pentakis- and hexakis (diphenylphosphino) benzene, by the same route have not yet been successful.

RESULTS AND DISCUSSION

In all cases the preparation was conducted by reacting a THF solution of the corresponding fluorobenzene with a small stoichiometric excess of *ca* 1 M Ph_2PNa in liquid ammonia according to eq. (1), and the products were isolated as air-stable solids by recrystallization from methanol–chloroform. Elemental and mass spectral analyses and melting points are in Table 1.

$$n\,Ph_2PNa + C_6H_{6-n}F_n \xrightarrow{\text{liq. NH}_3} (Ph_2P)_nC_6H_{6-n} + n\,NaF. \quad (1)$$

The ^{31}P NMR spectra of the unseparated reaction mixtures showed that crude yields were in the range 35–80%, and it was possible to isolate these amounts of product in a sufficiently pure state for further reactions, e.g. with sulphur, selenium or a

* For part IV see ref. 1.

† Author to whom correspondence should be addressed.

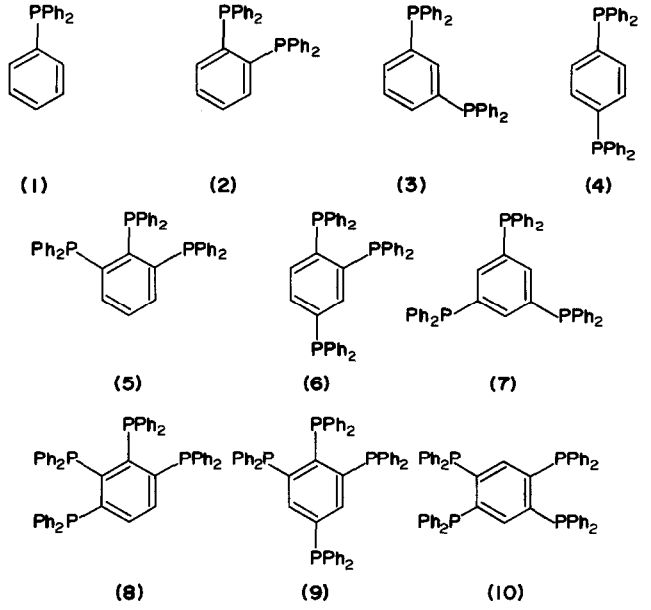

metal substrate. However, the three trisubstituted derivatives were accompanied by substantial amounts of gummy material which did not contain phosphorus and which was very difficult to separate; for these the yields of analytically pure product were therefore much lower.

The ^{31}P NMR spectra of the reaction mixtures also revealed the presence of species in which only some of the fluorine atoms had been replaced by Ph_2P-groups, and this was confirmed by the corresponding ^{19}F NMR spectra. In particular it was possible to isolate (**11**) as a white solid (m.p. 165–167°C; $\delta(^{19}F) = -95.0$, $\delta(^{31}P_2) = -20.4$, $\delta(^{31}P_3) = -9.3$ ppm; $^3J(PP) = 172.0$, $^3J(PF) = 15.9$, $^4J(PF) = 6.1$ Hz) from the reaction of Ph_2PNa with 1,2,3-trifluorobenzene, and the NMR spectra of the reaction mixture from Ph_2PNa and 1,3,5-trifluorobenzene showed the presence of (**12**) ($\delta(^{19}F) = -111.4$, $\delta(^{31}P) = -5.5$ ppm; $^4J(PF) = 5.7$ Hz) and (**13**) ($\delta(^{19}F) = -110.0$, $\delta(^{31}P) = -5.9$ ppm; $^4J(PF) = 4.6$ Hz). More surprisingly, substantial amounts of (**6**) were obtained in the preparation of (**8**) from 1,2,3,4-tetrafluorobenzene. That is, a fluorine atom in the 2- or 3-position had been replaced by a proton, presumably from the solvent, suggesting that benzyne-type intermediates may be involved in these reactions.

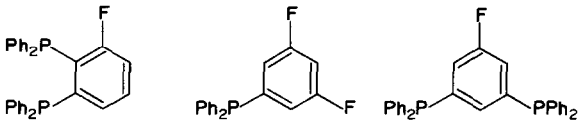

Table 1. Analytical and other data for the new polyphosphorus compounds

Compound	M.p. (°C)	%C Calc.	%C Found	%H Calc.	%H Found	%P Calc.	%P Found	RMM[a] Calc.	RMM[a] Found	Colour
(**5**) 1,2,3-$(Ph_2P)_3C_6H_3$	210–212	80.0	79.2	5.2	5.2	14.7	14.5	630	630	White
(**6**) 1,2,4-$(Ph_2P)_3C_6H_3$	142–144	80.0	79.4	5.3	5.3	14.7	14.4	630	630	White
(**7**) 1,3,5-$(Ph_2P)_3C_6H_3$[b]	110–111	80.0	78.7	5.3	5.3	14.7	14.4	630	630	White
(**8**) 1,2,3,4-$(Ph_2P)_4C_6H_2$	235–239	79.6	78.6	5.2	5.5	15.2	14.9	814	814	Yellow
(**9**) 1,2,3,5-$(Ph_2P)_4C_6H_2$	191–192	79.6	79.0	5.2	5.1	15.2	14.9	814	814	Pale yellow
(**10**) 1,2,4,5-$(Ph_2P)_4C_6H_2$	271–273	79.6	78.9	5.2	5.04	15.2	15.2	814	814	White

[a] Determined mass spectrometrically, molecular ion m^+.

[b] This material was very difficult to purify and the quoted m.p. is probably too low. A similar situation has been reported[7] for 1,3-$(Ph_2P)_2C_6H_4$.

Table 2. ^{31}P NMR parameters of polykis(diphenylphosphino) benzenes

Compound	Spin system	δ (ppm)[a]	J(PP) (Hz)
(1) Ph_3P	A	−6.0	[b]
(2) 1,2-$(Ph_2P)_2C_6H_4$	A_2	−13.3	145[c]
(3) 1,3-$(Ph_2P)_2C_6H_4$	A_2	−5.7	[d]
(4) 1,4-$(Ph_2P)_2C_6H_4$	A_2	−6.1	[d]
(5) 1,2,3-$(Ph_2P)_3C_6H_3$	A_2B	-12.7^A; -8.9^B	97.5
(6) 1,2,4-$(Ph_2P)_3C_6H_3$	ABX	13.4^A; -14.9^B; -6.7^X	153.8 (AB), < 3 (AX,BX)
(7) 1,3,5-$(Ph_2P)_3C_6H_3$	A_3	−5.4	[d]
(8) 1,2,3,4-$(Ph_2P)_4C_6H_2$	AA′XX′ [e]	-2.5^A; -13.5^X	81.0 (AX), 4.7 (AX′) 35.3 (AA′), −0.3 (XX′)
(9) 1,2,3,5-$(Ph_2P)_4C_6H_2$	A_2BX	-12.7^A; -9.3^B; -6.0^X	93 (AB), < 3 (AX,BX)
(10) 1,2,4,5-$(Ph_2P)_4C_6H_2$	A_4	−14.2	[d]

[a] ±0.1 ppm to high frequency of 85% H_3PO_4.
[b] Not available.
[c] Determined by ^{13}C-{^{31}P,^1H} experiment.
[d] Not determined.
[e] A,A′ = $P_{2,3}$; X,X′ = $P_{1,4}$.

The ^{31}P NMR parameters are given in Table 2, and for (5), (6), (8) and (9) are associated with spin systems that give characteristic spectra whose appearance was of material assistance in recognizing their presence in the reaction mixture. The AA′XX′ spectrum of (8) is shown in Fig. 1 together with a spectral simulation based upon the iterative fitting of all 24 observed lines. In the case of (2) the equivalence of the two phosphorus nuclei prevents the measurement of ^3J(PP) from the phosphorus

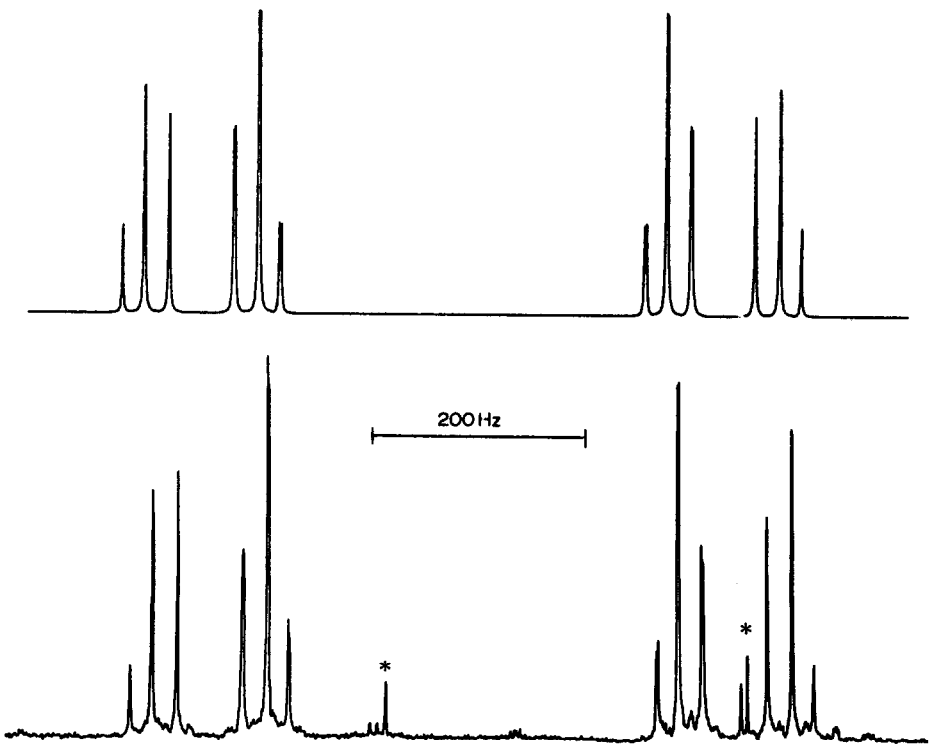

Fig. 1. Experimental (lower trace) and simulated (upper trace) ^{31}P spectra at 36.2 MHz of the AA′BB′ spin systems of 1,2,3,4-$(Ph_2P)_4C_6H_2$. The peaks marked with an asterisk arise from impurities.

spectrum, and this parameter was determined by an indirect ^{13}C-$\{^{31}P, ^{1}H\}$ method.[9,10] This was feasible because the presence of ^{13}C at 1.1% natural abundance introduces magnetic inequivalence between the two phosphorus nuclei and so gives sets of AA'X spin systems. In particular, the *ortho*-^{13}C nuclei of the phenyl groups give deceptively simple triplets with $^{2}J(PC) + {}^{5}J(PC) = N(PC) = 16.2$ Hz. In these circumstances there are also very weak (intensity *ca* 0.002) outer lines in both the ^{13}C and the ^{31}P spectra whose positions can give the magnitude of $^{3}J(PP)$. The ^{13}C-$\{^{31}P\}$ spin tickling experiments (with full proton decoupling) illustrated in Fig. 2 were used to determine the positions of these outermost lines in the ^{31}P spectrum and hence show that $^{3}J(PP)$ has a magnitude of 145 Hz and is of the same sign as $N(PC)$[10], i.e. positive.

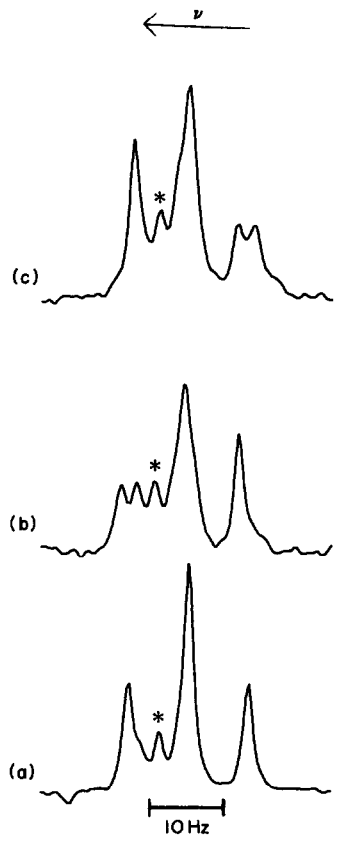

Fig. 2. ^{13}C-$\{^{31}P,H\}$ spin tickling experiments on the AA'X spin system provided by the *ortho*-^{13}C resonances of the phenyl groups of 1,2-$(Ph_2P)_2C_6H_4$. (a) ^{31}P irradiation set off-resonance. (b) With irradiation of a low-transition moment ^{31}P line at *high* frequency: the central and *high* frequency parts of the ^{13}C pseudo triplet are perturbed. (c) With irradiation of a low-transition moment ^{31}P line at *low* frequency: the central and *low* frequency parts of the ^{13}C pseudo triplet are perturbed. The line marked with an asterisk is not part of the spin system and remains unaffected throughout.

It appears that the chemical shift variations are almost entirely steric in origin since $\delta(^{31}P)$ is virtually identical at -5.7 ± 0.3 ppm in (**1**), (**3**), (**4**) and (**7**) which are the four species without adjacent (and therefore potentially interfering) diphenylphosphino groups. Furthermore, the isolated diphenylphosphino groups in (**6**) and (**9**) also have $\delta(^{31}P)$ in this range. The presence of a *single* adjacent diphenylphosphino group changes $\delta(^{31}P)$ to *ca* -13 ppm in (**2**), $(5)_A$, $(6)_{A,B}$, $(8)_X$, $(9)_A$, and (**10**). If this was an electronic effect, it would be expected to be of an additive nature so that *two* adjacent diphenylphosphine groups would reduce $\delta(^{31}P)$ even further, to say -20 ppm, whereas in fact $\delta(^{31}P)$ is *ca* -9 ppm for the "central" Ph_2P units of (**5**) and (**9**), thus confirming the dominance of a steric factor. In (**8**) the even greater steric compression (*vide infra*) leads to an additional increase in $\delta(^{31}P)$ to -2.5 ppm for the two central Ph_2P units. It is difficult to quantify these effects further since the molecules will respond to steric compression in two ways: (a) by rotations about the bonds between the phosphorus atoms and the skeletal aromatic ring so as to alter the relative orientations of the electron lone pairs on phosphorus, and (b) by changes in the degree of propeller twist of the phenyl groups. Both of these can be expected to affect $\delta(^{31}P)$. However, the foregoing discussion shows that there is a consistent pattern, and further that each kind of Ph_2P unit is in a particular kind of conformational environment in view of the narrowness of the chemical shift ranges for each type. It will be noticed that in (**11**) the electronegative fluorine substituent has significantly perturbed these chemical shift patterns.

It is evident that $^{4}J(PP)$ and $^{5}J(PP)$ are small in these molecules and they will not be discussed; however, $^{3}J(PP)$ is large and shows a sterically-determined pattern of wide variation that supports the conclusions drawn from the chemical shifts. It is striking that the three types of vicinal phosphorus–phosphorus coupling in these molecules lie in separate ranges: terminal–terminal, 145–154 Hz [(**2**), (**6**), probably (**10**)]; terminal–central, 81–98 Hz [(**5**), (**8**), (**9**)]; and central–central, 35 Hz [(**8**)]. This can be understood in terms of the electron lone pair orientations on the phosphorus atoms. There is evidence[10,11] that for P^{III} large positive values of $^{3}J(PP)$ occur when the lone pairs are directed approximately towards one another, and small values occur when the lone pair directions are opposed. Molecular models show that there are no steric constraints upon the former situation in (**2**), (**6**) and (**10**), and these do have a large $^{3}J(PP)$. However, in (**5**), (**8**) and (**9**) interactions of the phenyl groups on different phosphorus atoms will

destabilize conformations which have the lone pairs of a central phosphorus atom close to the central molecular plane. Hence, there will be reduced lone pair–lone pair interaction and ^3J(PP) should be smaller, as indeed is the case. This constraint should be greatest in (**8**) in which ^3J(PP) for the central–terminal interaction is significantly smaller than in (**5**) and (**9**). Finally, in (**8**), not only will the lone pairs of the central phosphorus atoms be directed away from the central molecular plane, but steric compression involving the phenyl groups will direct them towards opposite sides of this plane so that they are effectively opposed, and the corresponding central–central ^3J(PP) is much smaller at 35 Hz.

Thus the ^{31}P chemical shifts and the values of ^3J(PP) are consistent with the following pattern local conformations for the different types of phosphorus atom. (a) Isolated—relatively free rotation; (b) terminal—lone pairs directed towards adjacent Ph_2P group and close to central molecular plane; (c) central—directed out of central molecular plane.

EXPERIMENTAL

^{19}F and ^{31}P NMR spectra were recorded at 84.7 and 36.2 MHz, respectively with full proton decoupling on a JEOL FX90Q multinuclear Fourier transform spectrometer using solutions in dichloromethane (plus 10% C_6D_6 to provide a field frequency lock) at 22°C. The ^{13}C-{^{31}P,^{1}H} experiments were performed on the same instrument but with time-sharing of the ^{31}P irradiation and the ^{13}C receiver to reduce electronic interference.

Aromatic fluorocarbons were obtained from Fluorochem Ltd and were used as supplied. Manipulations were performed under an atmosphere of dry ammonia or dry nitrogen. All the syntheses were performed similarly and a typical one is described.

1,2,4,5-*tetrakis*(*diphenylphosphino*) *benzene* (**10**)

Triphenylphosphine (131 g, 0.5 mol) in dry THF (200 cm^3) was added with stirring over 1 h to a solution of sodium (23 g, 1.0 mol) in anhydrous liquid ammonia (1000 cm^3). Dry ammonium chloride (26.8 g, 0.5 mol) was then added in small portions and after the mixture had been stirred for a further hour a solution of 1,2,4,5-tetrafluorobenzene (18 g, 0.12 mol) in dry THF (50 cm^3) was added over 0.5 h. Toluene (200 cm^3) was added, the ammonia was allowed to evaporate overnight and the mixture was then refluxed until no more ammonia vapour could be detected (*ca* 1 h). The remaining solvents were removed under vacuum and the resulting oil was treated with methanol to yield the product which was recrystallized from methanol–chloroform as white crystals. Yield 62 g, 38%.

Acknowledgements—We thank the SERC for support, and Mr B. Saunderson for elemental microanalyses and mass spectra. We also wish to express our gratitude to Sir Geoffrey Wilkinson who was the originator of our collaboration.

REFERENCES

1. J. L. Bookham, W. McFarlane and I. J. Colquhoun, *J. Chem. Soc., Dalton Trans.* 1988, 503.
2. C. A. McAuliffe and W. Levason, *Phosphine, Arsine and Stibine Complexes of the Transition Elements*. Elsevier, Amsterdam (1979).
3. N. K. Roberts and S. B. Wild, *J. Am. Chem. Soc.* 1981, **20**, 1900; T. Talay and D. Rehder, *Z. Naturforsch. B, Anorg. Chem. Org. Chem.* 1981, **36**, 451.
4. R. L. Wife, J. J. M. Snel and A. B. van Oort, *Eur. Pat. Appl. EP* 1986, **183**, 290: *Chem Abstr.* 1986, **105**, 97692z; C. Charrier, W. Chodkiewiez and P. Codiot, *Bull. Soc. Chim. Fr.* 1966, 1002; F. A. Hart, *J. Chem. Soc.* 1960, 3324; E. P. Kyba, M. C. Kerby and S. P. Rines, *Organometallics* 1986, **5**, 1189.
5. H. C. E. McFarlane and W. McFarlane, *Polyhedron* 1983, **2**, 303.
6. A. Michaelis and L. Gleichmann, *Chem. Ber.* 1882, **15**, 801.
7. H. Zorn, H. Schindlbauer and H. Hogen, *Chem. Ber.* 1965, **98**, 2431; R. A. Baldwin and M. T. Chang, *J. Org. Chem.* 1967, **32**, 1572.
8. D. L. Herring, *J. Org. Chem.* 1961, **26**, 3998; H. Zom, H. Schindlbauer and H. Hagen, *Monatsh. Chem.* 1964, **95**, 422.
9. I. J. Colquhoun and W. McFarlane, *J. Mag. Res.* 1978, **31**, 63.
10. I. J. Colquhoun and W. McFarlane, *J. Chem. Soc., Dalton Trans.* 1982, 1915.
11. J. L. Bookham, W. McFarlane, I. J. Colquhoun and M. Thornton-Pett, *J. Organomet. Chem.*, in press.

Polyhedron Vol. 7, No. 19/20, pp. 1881–1889, 1988
Printed in Great Britain

0277–5387/88 $3.00+.00
© 1988 Pergamon Press plc

COMPLEXES OF WATER-SOLUBLE HEXADENTATE SCHIFF BASE LIGANDS WITH A NUMBER OF METAL IONS

DENNIS F. EVANS* and DAVID A. JAKUBOVIC

Inorganic Chemistry Laboratories, Imperial College, London SW7 2AY, U.K.

Abstract—Complexes of Al^{III}, In^{III}, Sc^{III}, Tl^{III}, Ni^{II}, Zn^{II} and Cd^{II} with hexadentate Schiff base ligands have been characterized in aqueous solution, normally by ^1H NMR spectroscopy. They were obtained by the condensation of salicylaldehyde-5-sulphonate with polyamines in the presence of the metal ions. Values of pM are reported for a number of these systems.

Recently we reported some new water-soluble hexadentate Schiff base ligands and their use as sequestrating agents for Fe^{III} and Ga^{III}.[1] The resulting highly water-soluble complexes were shown to have pM values (where $pM = -\log_{10}[\text{metal ion}]_{free}$), at physiological pH, similar to those of related hydroxamic acid siderophore complexes and considerably greater than those of the complexes derived from N,N,N′,N′-ethylenediaminetetraacetic acid (edta), N,N,N′,N′,N″-diethylenetriaminepentaacetic acid (dtpa) or transferrin.[1]

Allied to the long established interest in both natural and synthetic chelating agents for Fe^{III} with respect to certain biomedical applications,[2] there is now a growing interest in the aqueous coordination chemistry of Al^{III} in biological systems.[3]

Recent work has been concerned with the use of siderophores, and siderophore models, as sequestrating agents for Al^{III}[4] and also In^{III} (for use as radiopharmaceuticals).[5] Accordingly, we describe the use of these water-soluble hexadentate Schiff bases as ligands for Al^{III}, In^{III} and, to further explore their versatility, the trivalent metal ions Tl^{III} and Sc^{III}, and also the divalent cations Zn^{II}, Ni^{II} and Cd^{II}.

In studying the stability of the various Schiff base complexes with Al^{III}, In^{III}, Ni^{II} and Zn^{II} we have determined pM values at appropriate pHs. pM values are of more practical significance than stability constants since they express the effective binding strength of a ligand at a particular pH. One can therefore directly compare the efficiency of different ligands in sequestrating a metal ion under the same conditions.

As reported previously[1] the Schiff bases are partially hydrolysed in aqueous solution and so their isolation was not performed, but instead stoichiometric amounts of the aldehyde and the desired polyamine were used to generate the ligands *in situ*. Template reactions are thus, to some extent, involved in the formation of the complexes (see Figs 1, 2 and 3).

EXPERIMENTAL

The materials used were prepared as described elsewhere[1] and all gave satisfactory analyses.

^1H NMR spectra were recorded on Bruker WM250FT (250 MHz) and Jeol GSX270 (270 MHz) spectrometers, with the 2D ^1H NMR correlated shift (COSY) spectrum recorded on a Bruker AM500 (500 MHz) spectrometer. UV–vis. spectra were recorded on a Shimadzu UV-160 spectrometer.

Competition reactions between the Schiff base ligands and the various metal ion complexes of edta, dtpa and iminodiacetic acid (ida) were performed as described previously.[1] For the Ni^{II} systems the reactions were followed spectrophotometrically with absorbance measurements made at two different wavelengths, one of which was the appropriate λ_{max} for the Ni^{II} Schiff base complexes (ranging from 840–915 nm). The reactions were followed by ^1H NMR for the Al^{III}, In^{III} and Zn^{II} systems. As a modification to the reported method[1] the solutions were allowed to equilibrate in aqueous solution, at 25°C and the desired pH,

* Author to whom correspondence should be addressed.

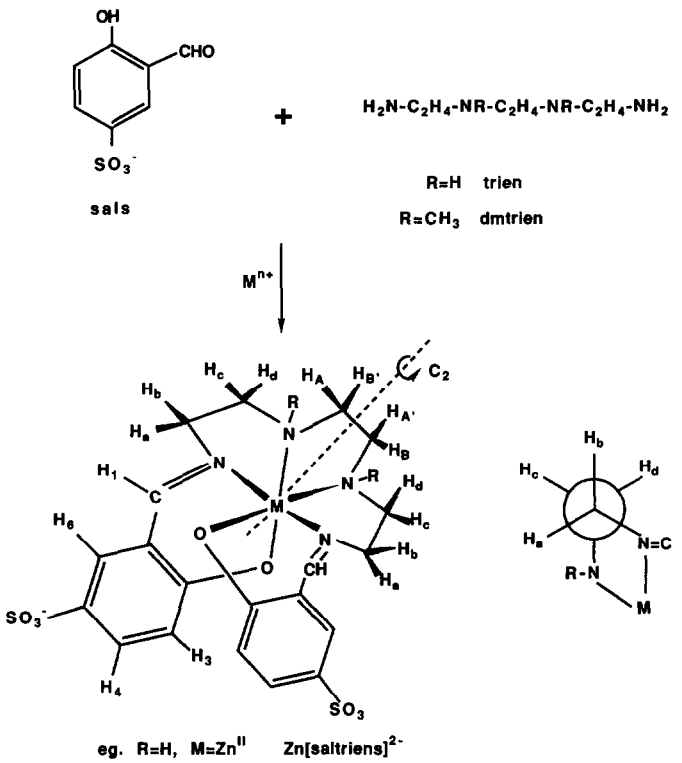
OH
CHO
SO3-
sals
+
H2N-C2H4-NR-C2H4-NR-C2H4-NH2
R=H trien
R=CH3 dmtrien
Mn+
eg. R=H, M=ZnII Zn[saltriens]2-

Fig. 1.

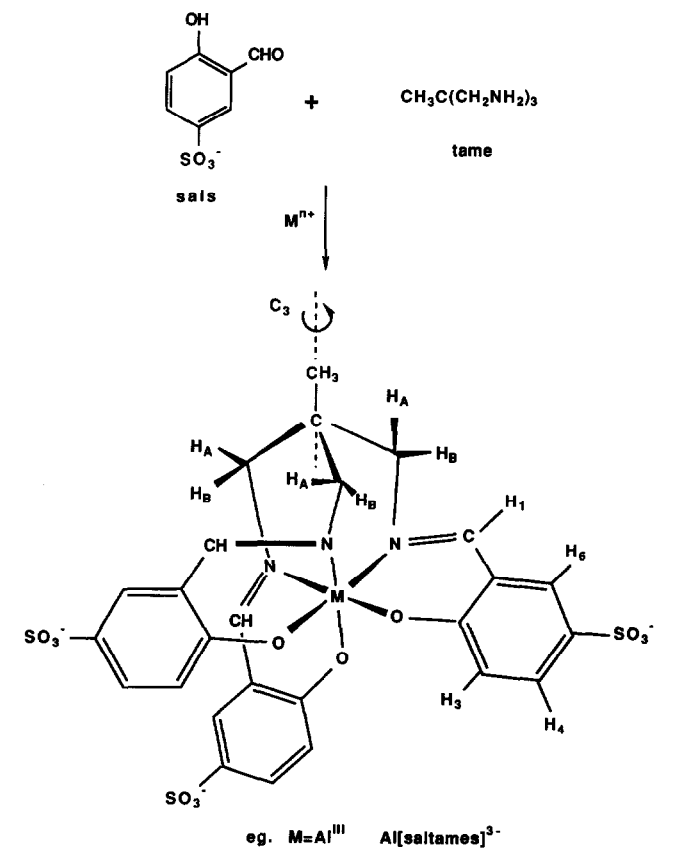
OH
CHO
SO3-
sals
+
CH3C(CH2NH2)3
tame
Mn+
eg. M=AlIII Al[saltames]3-

Fig. 2.

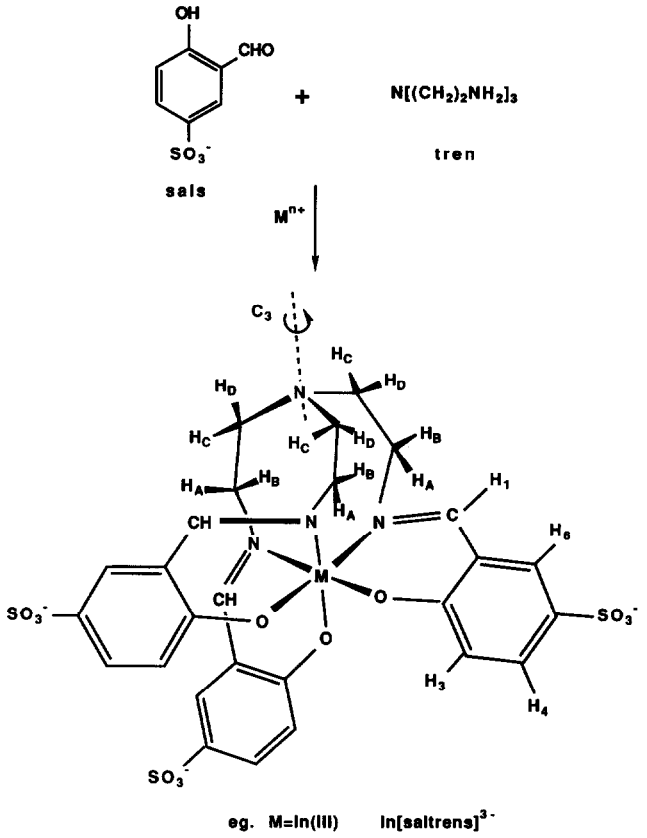

Fig. 3.

and then rapidly evaporated to dryness. An aliquot was placed in an ampoule on a blackened aluminium plate, with good thermal contact ensured by the use of grease, inside a vacuum desiccator. The system was then evacuated and gently warmed with a tungsten lamp, with the sample becoming dry within a few minutes. The dry mixtures were then redissolved in D_2O and the ^1H NMR spectra recorded immediately, before the solutions could re-equilibrate. This was possible since all the reactions required at least 24 h, in H_2O, to attain equilibrium.

The In^{III}–saltrens system ida, even at high concentrations, did not compete with the Schiff base, whereas edta, even at low concentrations, bound the In^{III} too efficiently. Therefore an accurate pM value could not be obtained for $In[saltrens]^{3-}$.

RESULTS AND DISCUSSION

^1H *NMR spectra of the complexes*

The ^1H NMR spectrum of $Al[saltames]^{3-}$ shows an AB pair of doublets and a singlet, in the alkyl region (see Fig. 4 and Table 1). This is consistent with a rigid structure as shown in Fig. 2 and is similar to the spectrum reported for $Ga[saltames]^{3-}$.[1] This structure has also been found by X-ray diffraction of the related solid, unsulphonated, complex Ga^{III}5-MeOsaltame.[6]

In contrast the spectrum of $In[saltames]^{3-}$ shows only two singlets in the alkyl region (see Fig. 5 and Table 1) which would result from fluxional behaviour with H_A and H_B becoming equivalent. Similar spectra are observed for the analogous Sc^{III}, Zn^{II}, Cd^{II} and Tl^{III} complexes. $Cd[saltames]^{4-}$ shows $Cd^{111,113}$ satellites on the methylene proton (H_1), while for $Tl[saltames]^{3-}$ a very large $Tl^{203,205}$ splitting of H_1, and a smaller splitting of the H_{AB} resonance is observed (see Fig. 6 and Table 1). The large splitting of the H_1 resonance is presumably due to the dihedral angle of the Tl^{III}—N=C—H group being close to 180°. Small splittings are also seen for the resonances of the aromatic protons which are more distant from the $Tl^{203,205}$ centre.

The presence of these $Cd^{111,113}$ and $Tl^{203,205}$ splittings shows that the non-rigid complexes are not experiencing intermolecular exchange on an NMR timescale.

The ^1H NMR spectra of all the new saltriens

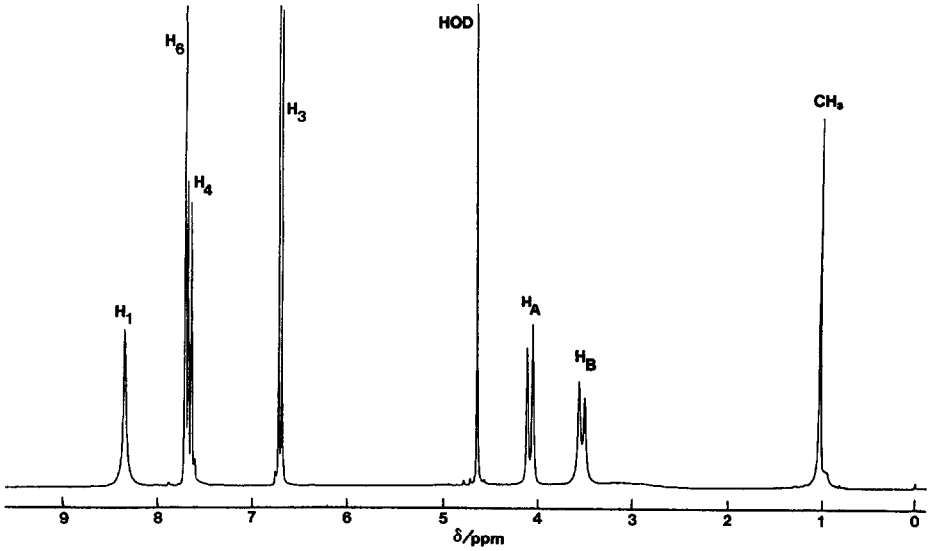

Fig. 4. ^{1}H NMR spectrum (250 MHz) of Al^{III} saltames in D_2O.

Table 1. ^{1}H NMR data for the seltames complexes, in D_2O

Saltames complex	δ (ppm) H_1	H_3	H_4	H_6	H_A	H_B	CH_3
Al^{III}	8.39	6.77	7.79	7.84	4.05	3.53	1.17
Ga^{III}	8.39	6.74	7.69	7.74	4.18	3.65	1.14
In^{III}	8.46	6.96	7.76	7.81	3.96(2H)		1.18
Tl^{III}	8.34	6.92	7.70	7.70	4.08(2H)		1.12
	J_{Tl-H_1} = 480 Hz		J_{Tl-H_3} = 22 Hz		$J_{Tl-H_{AB}}$ = 190 Hz		
Sc^{III}	8.31	6.86	7.80	7.85	3.59(2H)		1.09
Zn^{II}	8.25	6.73	7.59	7.66	3.71(2H)		1.07
Cd^{II}	8.22	6.78	7.55	7.61	3.72(2H)		1.03
	J_{Cd-H_1} = 25.7 Hz						

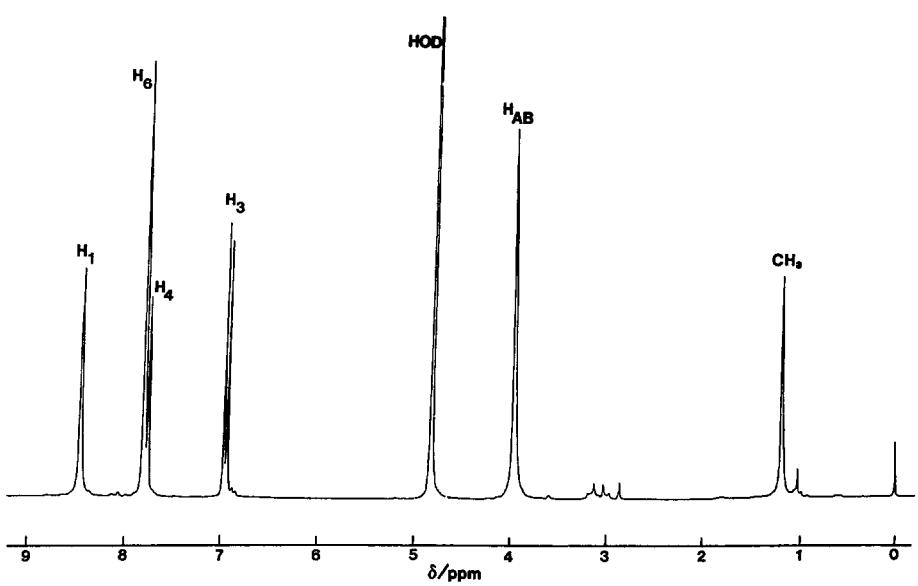

Fig. 5. ^{1}H NMR spectrum (250 MHz) of In^{III} saltames in D_2O.

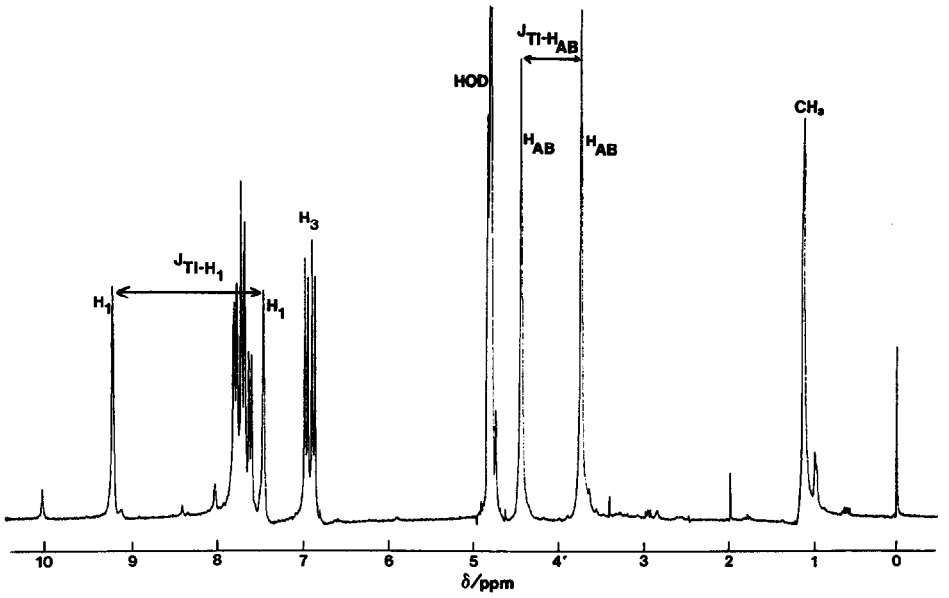

Fig. 6. ^{1}H NMR spectrum (270 MHz) of Tl^{III} saltames in D_2O.

complexes are similar to those of the Ga[saltriens]$^-$ reported elsewhere.[1] The alkyl regions show six multiplets assignable to H_A, H_B, H_a, H_b, H_c and H_d, with overlap of two of these in some cases (see Table 2 and Fig. 1). The spectrum of Zn[saltriens]$^{2-}$ has the best separation of the six multiplets and a 2D ^{1}H NMR correlated shift (COSY) spectrum of this complex was performed, see Fig. 7. From this spectrum it is possible to unambiguously assign the resonances of $H_AH_{A'}$ and $H_BH_{B'}$, since they are only coupled to each other. On the basis of chemical shifts and relative line widths and shapes it is possible to make a tentative assignment for H_a, H_b, H_c and H_d (see Figs 1 and 7).

Cadmium[111,113] satellites are observed on the H_1 resonance of the Cd[saltriens]$^{2-}$ spectrum and large $Tl^{203,205}$ splittings are seen in the Tl[saltriens]$^-$ spectrum (see Table 2).

The spectra are consistent with rigid structures, for all of the saltriens complexes, of the type shown in Fig. 1. This structure has also been found by X-ray diffraction, of the solid, for the related unsulphonated complex Ni^{II} saltrien.[7]

The ^{1}H NMR spectrum of Ga[saldmtriens]$^-$ is

Table 2. ^{1}H NMR data for the saltriens complexes, in D_2O

Saltriens complex	H_1	H_3	H_4	H_6	δ (ppm) {H_A,H_B,H_a,H_b,H_c,H_d}					
Al^{III}	8.62	6.87	7.77	7.84	3.98(2H)		3.35	3.08	2.87	2.72
Ga^{III}	8.66	6.86	7.74	7.82	3.97(2H)		3.40	3.11	2.95	2.78
In^{III}	8.54	6.71	7.61	7.72	3.89(2H)		3.38	3.19	2.98	2.87
Tl^{III}	8.23	6.12	7.37	7.60				[a]		
	J_{Tl-H_1} = 540 Hz		J_{Tl-H_3} = 25 Hz							
Sc^{III}	8.27	6.23	7.36	7.67	4.15	3.74	3.39	3.19	2.83	2.71
Zn^{II}	8.34	6.36	7.35	7.60	3.80	3.59	3.13	2.93	2.77	2.57
Cd^{II}	8.42	6.16	7.29	7.64	3.93	3.56	3.11(2H)		2.92	2.70
	J_{Cd-H_1} = 33.6 Hz									

[a] Due to $Tl^{203,205}$ splitting of the multiplets a complex pattern is observed in this region which was not assigned.

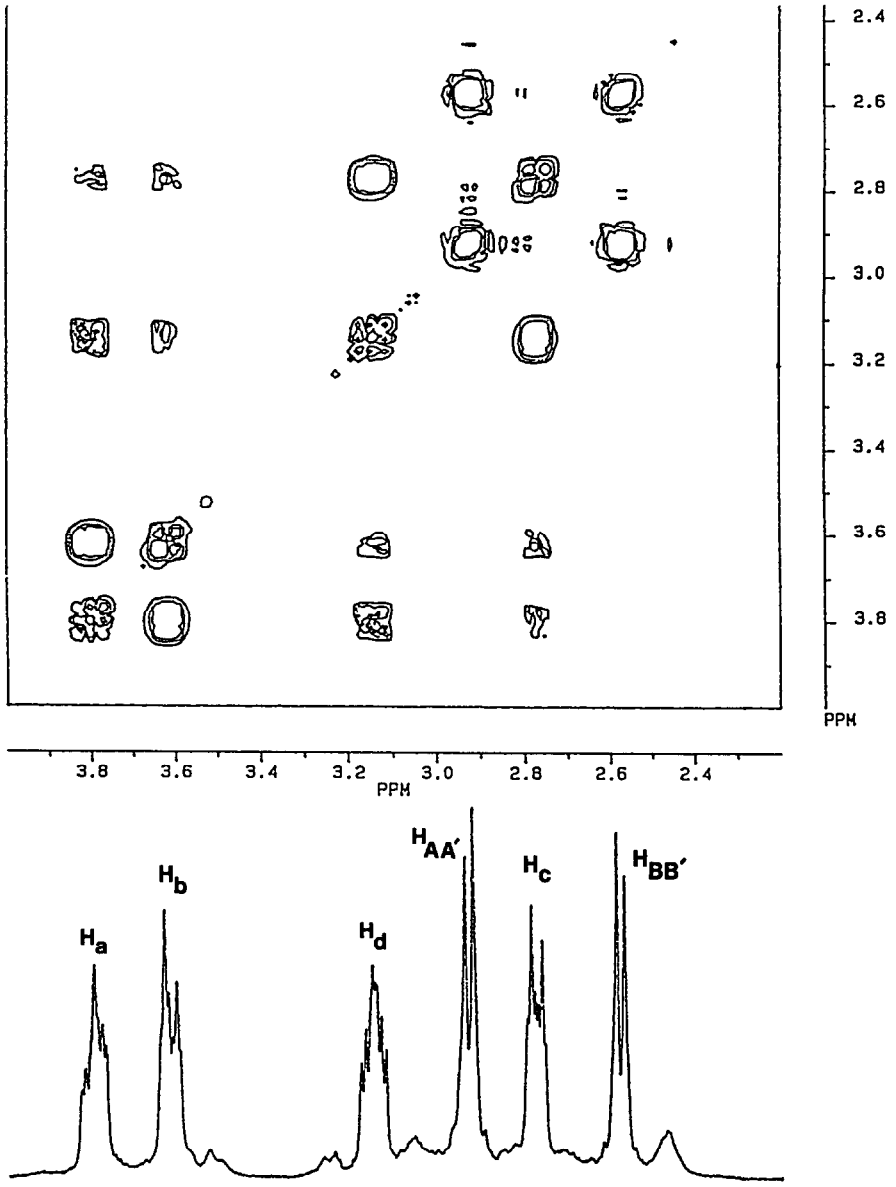

Fig. 7. 2D ^{1}H NMR correlated shift (COSY) spectrum (500 MHz) of Zn^{II} saltriens in D_2O.

similar to that of the saltriens complexes but with an extra singlet due to the methyl groups present on the amine backbone.[1] However, the spectrum of In[saldmtriens]$^-$ contains only four resonances in the alkyl region, see Fig. 8. One can be assigned to the methyl groups, $\delta = 2.43$ (6H), and the other three arise from H_{AB}; $\delta = 3.11$ (4H), H_{ab}; $\delta = 4.01$ (4H) and H_{cd}; $\delta = 3.14$ (4H), indicating that the complex is fluxional. A spectrum run on a solution containing a 100% excess of saldmtriens, with respect to In^{III}, showed separate resonances for the free hexadentate ligand. This confirms that intramolecular, rather than intermolecular, exchange is involved. The presence of separate resonances for free sals or free dmtrien is not sufficient to exclude intermolecular exchange since exchange between the different species present in an aqueous solution of the ligand has been shown to be slow on an NMR timescale.[1]

It can be seen that the saltames complexes of the smaller group III cations, Al^{III} and Ga^{III} are rigid on an NMR timescale whereas the larger group III cations In^{III} and Tl^{III} give rise to fluxional structures. Similar behaviour is found with saldmtriens, with the Ga^{III} complex being rigid, and the In^{III} complex fluxional on an NMR timescale. Related results

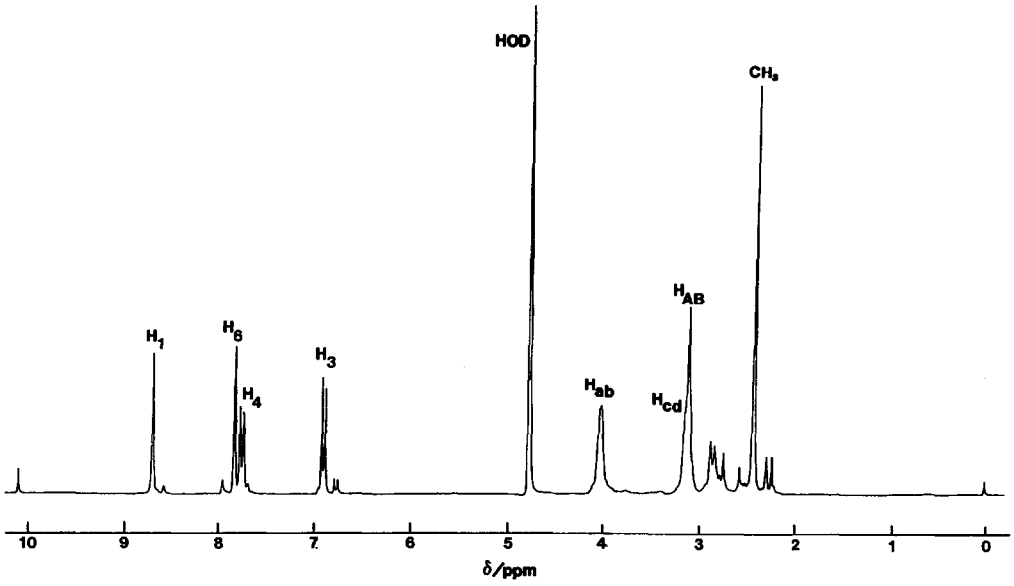

Fig. 8. ^{1}H NMR spectrum (250 MHz) in In^{III} saldmtriens in D_2O.

have recently been reported for the Al^{III}, Ga^{III}, In^{III} and Tl^{III} complexes of 8-hydroxyquinoline,[8] and can be largely attributed to the increasing ionic size going down group III (cf. also ref. 9). In contrast the saltriens ligand produces rigid complexes with all of the group III cations, and also Cd^{II}, Zn^{II} and Sc^{III}. The fact that In[saldmtriens]$^-$ is fluxional may be due to steric hindrance caused by the extra methyl groups present on the amine backbone.

The ^{1}H NMR spectrum of In[saltrens]$^{3-}$ has four multiplets in the alkyl region, see Fig. 9 and Table 3. This is consistent with a rigid structure as shown in Fig. 3 with each of the protons H_A, H_B, H_C and H_D producing a separate multiplet. This solution contained a 20% excess of the ligand and the ^{1}H NMR spectrum shows separate H_1 resonances for all the species present, in equilibrium, in the partially hydrolysed system. This confirms that there is no intermolecular exchange on an NMR timescale.

The spectrum of Sc[saltrens]$^{3-}$ is similar, but with two of the multiplets overlapping (see Table 3), and is also consistent with a rigid structure as shown in Fig. 3. This structure has been found by X-ray diffraction for the related solid, unsulphonated, complex Fe^{III}4-Clsaltren.[10]

In comparison, the spectrum of Cd[saltrens]$^{4-}$ has only two multiplets in the alkyl region. The presence of $Cd^{111,113}$ satellites on the H_1 resonance proves that there is no intermolecular exchange on an NMR timescale and that the complex must be fluxional (see Table 3).

pM values of the complexes

The values of pM obtained in this work are given in Table 4, together with data from the literature for edta and dtpa complexes. The trends can be interpreted qualitatively in terms of the relative "hardness" or "softness" of the ligands and of the metal ions, and also the ability of the ligands to accommodate a metal ion of a particular size.

Thus with saltames, pM increases markedly in going from Al^{III} to Ga^{III} (with both values being appreciably higher than with edta or dtpa), but

Table 3. ^{1}H NMR data for the saltrens complexes, in D_2O

Saltrens complex	δ (ppm)							
	H_1	H_3	H_4	H_6	$\{H_A,H_B,H_C,H_D\}$			
In^{III}	8.44	6.47	7.62	7.70	3.80	3.42	3.13	2.92
Sc^{III}	8.31	6.39	7.66	7.80	3.98	3.42	3.02(2H)	
Cd^{II}	8.31	6.62	7.53	7.59	3.56(2H)		2.77(2H)	
	J_{Cd-H_1} = 32.2 Hz							

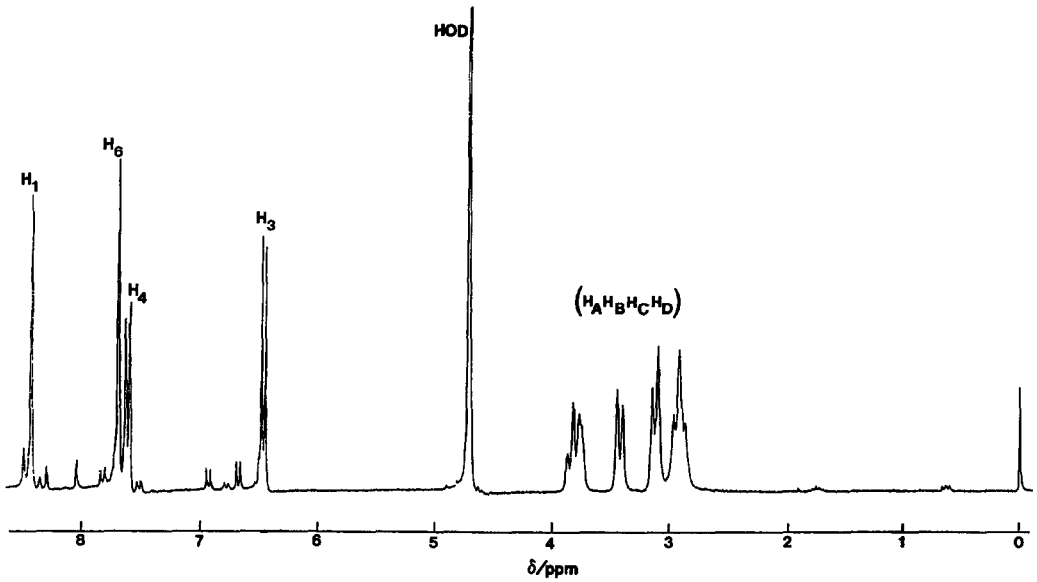

Fig. 9. ^{1}H NMR spectrum (270 MHz) of In^{III} saltrens in D_2O.

drops considerably for In^{III}. With edta and dtpa pM reaches a maximum at In^{III}. The fact that edta and dtpa are good ligands for a wide variety of metal ions shows that they possess considerable flexibility. It seems likely that the low pM value for In[saltames]$^{3-}$ arises from the difficulty of accommodating the relatively large In^{III} cation in the "cavity" of this tripod-like ligand. Although an accurate value of pM for In[saltrens]$^{3-}$ could not be obtained, it is certainly larger than for In[saltames]$^{3-}$, which is consistent with the additional CH_2 units, in the amine backbone, giving a larger

Table 4. pM values for the saltriens, saltames, saltrens, edta and dtpa complexes of Al^{III}, Ga^{III}, In^{III}, Ni^{II} and Zn^{II}

Metal ion	Ionic radius[a]	pH	pM[b] saltriens	saltames	saltrens	edta	dtpa
Al^{III}	0.50	7.40	15.9_0[c]	16.9_3[c]		15.89[d]	15.55[e]
Ga^{III}	0.62	7.50[f]	24.5_4[g]	24.6_4[g]		20.04[h]	22.58[i]
In^{III}	0.81	7.40	[j]	17.0_7[k]	$\geqslant 17.9$[k] $\leqslant 21.8$[k]	23.40[i]	25.55[i]
Ni^{II}	0.70	10.00	21.5_5[l]	19.6_9[l]	18.1_0[l]	19.06[d]	20.59[m]
Zn^{II}	0.74	10.00	17.2_3[n]	14.1_0[n]		17.00[d]	18.67[m]

[a] Reference 11.

[b] $pM = \log_{10}[M^{n+}]_{free}$, at 25°C, where $[ligand]_{total}/[M^{n+}]_{total} = 10$.

[c] $[ligand]_{total} = 0.03$ M.

[d] Reference 12.

[e] Reference 13.

[f] pH refers to the original pH of the aqueous solution, equilibrium was attained in the D_2O solution.[1]

[g] $[ligand]_{total} = 0.004$ M.[1]

[h] Calculated from refs 12 and 14.

[i] Reference 15.

[j] Due to slow precipitation a pM value could not be obtained; for the same reason pM values of the Tl^{III} complexes are not reported.

[k] $[ligand]_{total} = 0.005$ M.

[l] $[ligand]_{total} = 0.135$ M.

[m] Reference 16.

[n] $[ligand]_{total} = 0.026$ M.

"cavity". In contrast, for Ni^{II} and Fe^{III},[1] saltrens is a poorer ligand than saltames.

Saltriens has an N_4O_2 donor set, and should be a "softer" ligand than saltames (N_3O_3), and also more flexible as a consequence of its linear structure. In agreement with this, for the "softer" divalent ions Ni^{II} and Zn^{II}, the pM values for saltriens are considerably higher than for saltames. The difference is particularly marked for Zn^{II}, which may reflect the larger radius of this ion.

Acknowledgements—We thank Mr R. N. Sheppard for his help in running the ^1H NMR spectra and also the S.E.R.C. for a maintenance grant (to D.A.J.).

REFERENCES

1. D. F. Evans and D. A. Jakubovic, *J. Chem. Soc., Dalton Trans.*, in press.
2. A. E. Martell, W. F. Anderson and D. G. Badman, *Development of Iron Chelators for Clinical Use.* Elsevier/North-Holland, New York (1986); K. N. Raymond, W. R. Harris, C. J. Carrano and F. L. Weitl, *ACS Symp. Ser.* 1980, **140**, 313.
3. T. L. Macdonald and R. B. Martin, *Trends Biochem. Sci.* 1988, **13**, 15.
4. W. O. Nelson, T. B. Karpishin, S. J. Rettigand and C. Orvig, *Inorg. Chem.* 1988, **27**, 1045.
5. S. M. Moerlein, M. J. Welch, K. N. Raymond and F. L. Weitl, *J. Nucl. Med.* 1981, **22**, 710.
6. M. A. Green, M. J. Welch and J. C. Huffman, *J. Am. Chem. Soc.* 1984, **106**, 3689.
7. P. D. Cradwick, M. E. Cradwick, G. G. Dobson, D. Hall and T. N. Waters, *Acta Cryst.* 1972, **B28**, 45.
8. P. Addy, D. F. Evans and R. S. Sheppard, *Inorg. Chim. Acta* 1987, **127**, L19.
9. R. H. Holm, in *Dynamic Nuclear Magnetic Resonance Spectroscopy*, p. 336. Academic Press, New York (1975).
10. D. F. Cook, D. Cummins and E. D. McKenzie, *J. Chem. Soc., Dalton Trans.* 1976, 1369.
11. L. Pauling, *The Nature of the Chemical Bond*, 3rd edn. Cornell University Press, Ithaca (1980).
12. G. Schwarzenbach, R. Gutt and G. Anderegg, *Helv. Chim. Acta* 1954, **37**, 937.
13. D. A. Aikens and F. J. Bahbah, *Anal. Chem.* 1967, **39**, 646.
14. K. Saito and H. Terry, *J. Chem. Soc.* 1956, 4701.
15. E. Bottari and G. Anderegg, *Helv. Chim. Acta* 1967, **50**, 2349.
16. G. Anderegg, P. Nageli, F. Muller and G. Schwarzenbach, *Helv. Chim. Acta* 1959, **42**, 827.

Polyhedron Vol. 7, No. 19/20, pp. 1891–1899, 1988
Printed in Great Britain

0277–5387/88 $3.00+.00
© 1988 Pergamon Press plc

CONTRASTING REACTIONS OF ETHYLENE WITH $Os_3\{\mu\text{-}H,\mu\text{-}O{=}C(Me)\}(CO)_{10}$, GIVING AN ETHYLENE ADDUCT, OR A BIS-μ-ACYL COMPLEX. CRYSTAL AND MOLECULAR STRUCTURE OF $Os_3\{1,2\text{-}\mu\text{-}H,1,2\text{-}\mu\text{-}O{=}C(Me)\}\{1\text{-}\eta^2\text{-}CH_2{=}CH_2\}(CO)_9$*

YEA-JER CHEN, CAROLYN B. KNOBLER and HERBERT D. KAESZ†

Department of Chemistry and Biochemistry, University of California,
Los Angeles, CA 90024-1569, U.S.A.

Abstract—Bubbling ethylene at atmospheric pressure through a solution of $Os_3\{\mu\text{-}H,\mu\text{-}O{=}C(Me)\}(CO)_{10}$ (**1**) in octane at 105–110°C gives the complex $Os_3\{1,2\text{-}\mu\text{-}H,1,2\text{-}\mu\text{-}O{=}C(Me)\}\{1\text{-}\eta^2\text{-}CH_2{=}CH_2\}(CO)_9$ (**2**) in 61% yield. By contrast, the bis-acyl complex $Os_3\{\mu\text{-}O{=}C(Me),\mu\text{-}O{=}C(Et)\}(CO)_{10}$ (**3**) is obtained in the reaction of **1** with ethylene and CO (68 : 1 mol ratio) at 167 atm and 140°C; an equilibrium mixture of isomers **3a** (vicinal) and **3b** (geminal) is obtained in which the latter predominates. Complexes **3a** and **3b** show an IR absorption at 1516 cm^{-1}, characteristic of the bridging acyl group; ^{13}C NMR for the carbon atom of this group is shifted significantly to low field, δ = 287.9 ppm.

The crystal and molecular structure of **2** have been determined at 25°C using a Huber four circle diffractometer with graphite-monochromated Mo-K_α radiation. Complex **2** crystallizes in the monoclinic space group $P2_1/c$; cell dimensions, a = 14.423(2), b = 15.119(3), c = 17.200(3) Å, and β = 95.921(5)°; calculated density = 3.19 g cm^{-3}. A total of 3947 unique reflections with $I > 3\sigma(I_0)$ were used in the refinement; final discrepancy indices, R = 0.075 and R_w = 0.087. The location of each of the six Os atoms was determined by the Patterson method. All other non-hydrogen atoms were then located by difference maps. The crystal consists of discrete molecules of complex **2** with two independent molecules in the asymmetric unit. The complex consists of three groups arrayed in a triangle, [Os(1 or 4)(η^2-$CH_2{=}CH_2$)$(CO)_2$], [Os(2 or 5)$(CO)_3$] and [Os(3 or 6)$(CO)_4$], with normal metal–metal separations, Os—Os: (1)–(2) and (4)–(5) = 2.907(2) and 2.909(2) Å, (1)–(3) and (4)–(6) = 2.841(2) and 2.837(2) Å, (2)–(3) and (5)–(6) = 2.872(2) and 2.869(2) Å. A hydrogen atom and an acyl group are seen to be bridging between two of the atoms, Os(1) and Os(2) [or Os(4) and Os(5)]. It is noteworthy that the ethylene is observed to be η^2-coordinated to the same metal atom to which the oxygen of the bridging acyl group is also coordinated. The bridging hydrogen atom was located but its position not refined, Os(1)—H(1) and Os(4)—H(2) = 1.70 and 1.66 Å; Os(2)—H(1) and Os(5)—H(2) = 1.70 and 1.92 Å.

In earlier work of this group, the reaction of ethylene with the edge double-bridged trinuclear complexes $Ru_3\{\mu\text{-}H,\mu\text{-}O{=}C(R)\}(CO)_{10}$, (R = Me, Et, Ph, or NMe_2) was observed at ambient temperature and pressure to yield exclusively the geminal dinuclear bis-acyl complexes, $Ru_2\{\mu\text{-}O{=}C(Et),\mu\text{-}O{=}C(R)\}(CO)_6$ (along with 1/3 mol of $Ru_3(CO)_{12}$).[2] Further work[3] showed these to be the *kinetic* products of this reaction. Interpretation of these observations in terms of the reactivity of the trinuclear starting materials required knowledge of the initial point of substitution. From other studies on the starting complexes involving ^{13}CO exchange and reactions with phosphorus ligands,[4] the initial entry of the ethylene was assumed to be on the metal to which the oxygen atom of the bridging acyl group was bonded. We return to this point in the Discussion.

By contrast, in the analogous reactions for osmium, trinuclear bis-acyl complexes are obtained which are found as an equilibrium mixture of the

* Taken in part from the dissertation of Yea-Jer Chen, see ref. 1.

† Author to whom correspondence should be addressed.

vic and *gem* isomers (the latter predominating).[3] No evidence of the kinetic path is thus available from this product distribution. Previously, Johnson, Lewis and co-workers had obtained the simple adduct $Os_3\{1,2\text{-}\mu\text{-}H,1,2\text{-}\mu\text{-}S(Me)\}\{3\text{-}\eta^2\text{-}CH_2{=}CH_2\}(CO)_9$ by reaction of ethylene with $Os_3\{\mu\text{-}H,\mu\text{-}S(Me)\}(CO)_{10}$ at 40°C.[5] With the parent carbonyl $Os_3(CO)_{12}$, no reaction with ethylene is observed until 126°C, whereupon the dehydrogenation product $Os_3\{\mu\text{-}H\}_2\{\mu\text{-}\eta^3\text{-}CCH_2\}(CO)_9$ is obtained.[6] The ethylene adducts $Os_3(CO)_{11}(C_2H_4)$,[7a] and $Os_3\{\mu\text{-}H,\mu\text{-}Cl\}(CO)_9(C_2H_4)$,[7b] have been obtained by substitution of easily displaced ligands ($CH_3C{\equiv}N$, or Me_3N, respectively, introduced into the cluster by prior reaction with Me_3NO.

Against this background we learned of studies by Basset and co-workers,[8] in which a simple adduct is obtained in the reaction of ethylene with $Os_3\{\mu\text{-}H,\mu\text{-}O(Ph)\}(CO)_{10}$ at *ca* 100°C and ambient pressure. We were thus encouraged to investigate the hydrido/acyl-bridged complex, $Os_3\{\mu\text{-}H,\mu\text{-}O{=}C(Me)\}(CO)_{10}$ (**1**) under the same reaction conditions, obtaining the results reported below. An account of the reaction of **1** with ethylene and CO under higher pressure is also reported here; a preliminary account of the latter work has appeared.[3a] Related triosmium alkene complexes derived from hydrogenation of hexafluorobut-2-yne[9] or coordinated vinyl acetate[10] have also been reported; structural parameters are compared with the results in the present work.

RESULTS

The reactions described in this work are summarized in Scheme 1.

Preparation of $Os_3\{\mu\text{-}H,\mu\text{-}O{=}C(Me)\}(CO)_{10}$ (1)

Earlier we reported the use of RLi in the preparation of **1**.[11] We have since found that the Grignard reagent is preferred to avoid dialkylation products obtained with the more active RLi reagent.[3] The alkylation of **1** with the Grignard reagent may be followed by titration. The first anion produced easily loses CO during the metathesis step with [PPN][Cl], $[PPN]^+ = [(PPh_3)_2N]^+$. The acyl-bridged anion which is thus obtained is acidified at 0°C to produce complex **1** in 60% yield. Some starting material (3% of $Os_3(CO)_{12}$) is recovered. Some of the reaction products remain at the top of the silica gel chromatography column and can not be removed even with CH_2Cl_2 or acetone.

Spectroscopic features of $Os_3\{\mu\text{-}H,\mu\text{-}O{=}C(Me)\}\{\eta^2\text{-}CH_2{=}CH_2\}(CO)_9$ (2)

An AA′BB′ pattern is observed in the ^1H NMR for the coordinated ethylene,[12] see Fig. 1. This is due to the chirality of the metal cluster complex giving diastereotopic hydrogen atoms for the coordinated and very likely free rotating ethylene, as similarly observed for $Os_3\{\mu\text{-}H,\mu\text{-}Cl\}(CO)_9(C_2H_4)$,[7b] or for $Os_3\{\mu\text{-}H\}(OPh)(\eta^2\text{-}C_2H_4)(CO)_{10}$.[8]

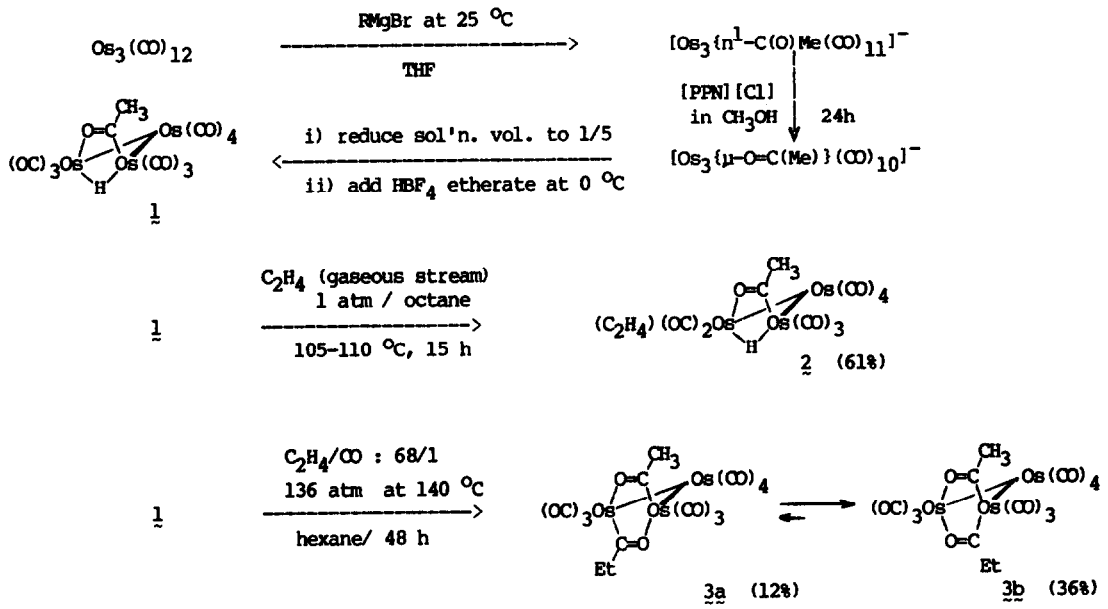

Scheme 1. Summary of the transformations observed in this work.

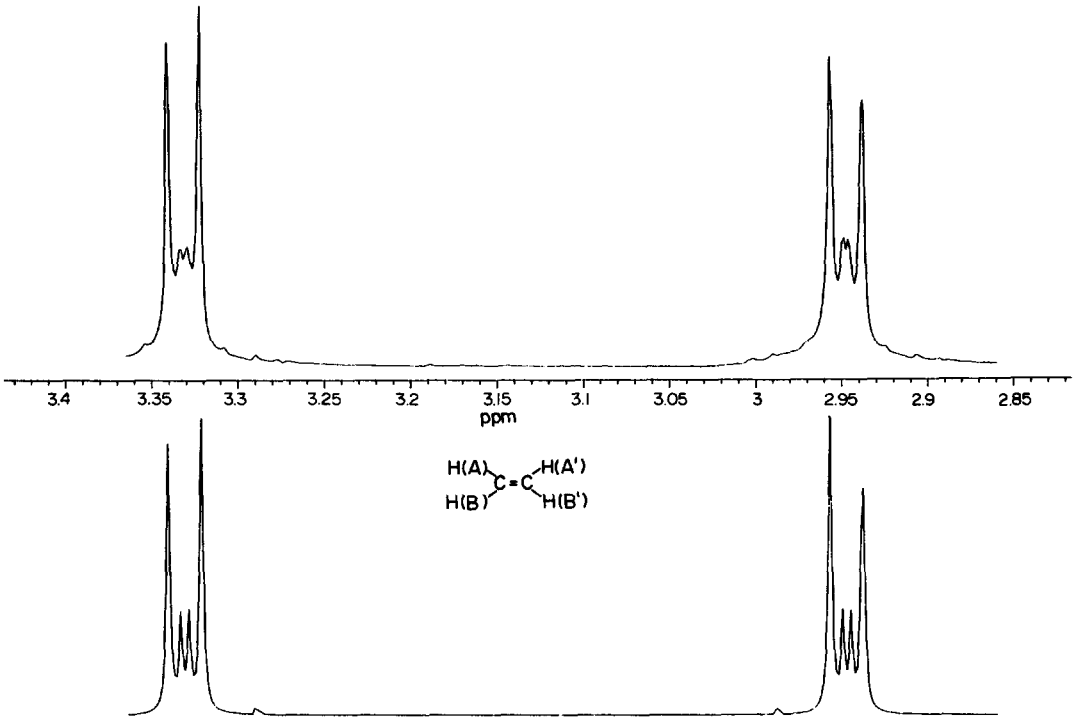

Fig. 1. ^1H NMR for coordinated ethylene. Top scan, observed spectrum, at 500 MHz. Lower scan, calculated spectrum for the AA'BB' multiplet, using PANIC NMR Simulation/Iteration software on the Bruker AM-500. Chemical shifts: $\delta(A) = \delta(A') = 3.331$ ppm; $\delta(B) = \delta(B') = 2.947$ ppm. Coupling constants: $J(A{-}B) = J(A'{-}B') = 0.216$ Hz; $J(AB') = J(BA') = 9.538$ Hz; $J(A{-}A') = J(B{-}B') = 9.544$ Hz.

Preparation and spectroscopic features of vic- *and* gem-$Os_3\{\mu\text{-}O{=}C(Me),\mu\text{-}O{=}C(Et)\}(CO)_{10}$ (**3a** *and* **3b**)

The reaction shown at the bottom of Scheme 1 yields a mixture of two products which could not be separated on the usual chromatography columns. The presence of the mixture of compounds is deduced from the complexity of the IR absorptions in the carbonyl region (see below) whose separate absorptions can be assigned by comparison with *vic* and *gem* isomers, where R is the same in both μ-O=C(R) groups, and where the *vic* isomer is separately synthesized by the double alkylation reaction.[3]

EXPERIMENTAL

Solvents and reagents were purchased and, except for specific instances described below, used as received; triosmium dodecacarbonyl and bis(triphenylphosphine) iminium chloride ([PPN][Cl]), (Strem); MeMgBr (3.0 M in diethyl ether, Aldrich); HBF_4 etherate (Aldrich); *n*-octane (Alfa). Tetrahydrofuran was dried by refluxing over potassium benzophenone ketyl and freshly distilled under nitrogen. Although the cluster complexes were generally air stable, reactions, filtrations and recrystallizations were routinely carried out under a purified nitrogen atmosphere using Schlenkware techniques.[13] Chromatographic separations and handling of neutral complexes can be carried out in air if exposure is limited to a few hours. All chromatographic separations were carried out on a 20×2 cm column of 60-mesh silica gel (EM Reagents) or 60–100-mesh Florisil (Baker). Petroleum ether, boiling range 35–60°C, and methylene chloride (Mallinckrodt) were used without further purification in chromatographic separations.

Carbonyl IR spectra were recorded on a Nicolet MX-1 FT–IR spectrometer. NMR spectra were recorded on Bruker AM-500, Bruker WP-200 and JEOL FX-90 FT NMR spectrometers. ^1H and ^{13}C NMR were calibrated against internal tetramethylsilane (TMS), unless otherwise noted. Elemental analyses were carried out by Schwartzkopf Microanalytical Laboratories.

Preparation of $Os_3\{\mu\text{-}H,\mu\text{-}O{=}C(Me)\}(CO)_{10}$ (**1**)

A quantity of $Os_3(CO)_{12}$ (0.500 g, 0.552 mmol) was dissolved in 500 cm^3 dry, freshly distilled THF

at 25°C and titrated with a 2.0 M solution of MeMgBr in THF until the 2068 cm^{-1} peak of the starting material disappeared. The addition of the Grignard reagent was accomplished over a 10 min period.

Following alkylation, a solution of one equivalent of bis-triphenylphosphineimminium chloride, [PPN]Cl, (316.8 mg, in 1–2 cm^3 of CH_3OH) was added and the resulting solution stirred for 24 h. The solvent was then removed at 25°C *in vacuo* to give a final solution volume of 100 cm^3. This was cooled to 0°C and titrated with a solution of HBF_4 in Et_2O. A peak at 2109 cm^{-1} was seen to grow in the IR spectrum. The titration was continued by one or two drops at a time, monitoring the growth of the 2109 cm^{-1} peak in the IR. The titration was stopped when the 2109 cm^{-1} peak is no longer observed to grow.

The solution was warmed to 25°C and solvent removed *in vacuo* leading to an oily residue. This was treated successively with 5 cm^3 of CH_2Cl_2 followed by 20 cm^3 of petroleum ether. A white precipitate was formed. The mixture was filtered in air (Whatman Filter paper No. 4), and the filtrate reduced in volume to 5 cm^3. This was transferred by means of a syringe onto a silica gel chromatography column. Eluting first with petroleum ether gave a faint yellow band: 15 mg (3%) $Os_3(CO)_{12}$ (unreacted starting material). Continuing with petroleum ether next gave a yellow band, $Os_3\{\mu\text{-H},\mu\text{-O=C(Me)}\}(CO)_{10}$[11] (301 mg, 60% yield). No further materials could be eluted from the column, even using more polar solvents such as CH_2Cl_2 or acetone.

Preparation of $Os_3\{\mu\text{-H},\mu\text{-O=CMe}\}\{\eta^2\text{-CH}_2\text{=CH}_2\}(CO)_9$ (**2**)

A solution of **1** (100 mg in 100 cm^3 octane) was heated to 105–110°C under nitrogen, and then treated with ethylene by bubbling the gas through the solution at a rate of approximately 10 cm^3 min^{-1} at 1 atm pressure. No reflux condenser was used, but at this rate, very little solvent was swept out of the flask. The reaction was followed by IR and stopped after no further changes were observed in the absorption pattern (i.e. *ca* 15 h). The flow of C_2H_4 was increased to sweep solvent out of the flask over a period of 1 h. A yellow powder remained as a residue. This was allowed to cool to room temperature, taken up in 4 cm^3 petroleum ether, and the resulting solution placed at the top of a column of Florisil. Elution with petroleum ether gave two yellow bands. The first is unreacted starting material, **1** (32 mg), closely followed by a second band which is complex **2** (62 mg, 61% yield). Found: C, 17.91; H, 1.23. Calc. C, 17.45; H, 0.89%.

For **2**. IR (cm^{-1}) in hexane: 2102m, 2060s, 2026s, 2012s, 2002w, 1995m, 1982m, 1965m in C_2Cl_4: 1493vw (μ-acyl). ^1H NMR in $CDCl_3$, δ (ppm): 3.33(2), 2.94(2) (AA'BB', coordinated $CH_2\text{=}CH_2$),[12] see Fig. 1; 2.14(3), μ-O=CCH_3; −13.90(1), Os—H—Os.

Autoclave reaction of $Os_3\{\mu\text{-H},\mu\text{-O=CMe}\}(CO)_{10}$, **1**, *with ethylene and* CO

This reaction was carried out in a 100 cm^3 stainless steel autoclave by placing the solvent and reagents in a glass-liner. Only a small amount of solvent was usually found to have transferred outside the liner. Only those materials remaining in the glass liner were removed for characterization. In cases where a significant amount of liquid was found outside the glass liner, IR spectra were taken before this liquid was added to the materials in the glass liner.

A quantity of **1** (0.150 g, 0.165 mmol) was dissolved in 50 cm^3 of hexane in the glass liner of a 100 cm^3 autoclave and the tube placed into the autoclave. The solvent was saturated with CO at 1 atm by bubbling the gas through the solution for 1 min. The autoclave was sealed and pressurized with ethylene to 1000 psi. The solution was then heated to 140°C and, under continuous shaking, maintained at this temperature for 48 h. The autoclave was then permitted to cool to room temperature, the gases vented and the solution contained in the autoclave transferred to a Schlenk flask. An IR spectrum of this solution indicated that about 50% of the starting material was still present together with new bands. The mixture was placed on a column of silica gel and eluted with petroleum ether. Two yellow bands were obtained. The first consisted of $Os_3\{\mu\text{-O-C(Me)},\mu\text{-O=C(Et)}\}(CO)_{10}$ (**3a**+**3b**, 0.072 g, 46% yield), closely followed by unreacted starting material (0.035 g).

IR (cm^{-1}) for **3a** in hexane: 2101w, 2068s, 2046m, 2015s, 2003m, 1996m, 1981m: 1516vw (μ-acyl); for **3b** in hexane: 2101w, 2068s, 2046m, 2015s, 2003m, 1987m, 1975m: 1516vw (μ-acyl) (these have been separately assigned by the selection of peaks in the overall spectrum, by comparison with the spectra of $Os_3\{\mu\text{-O=C(Et)}\}_2(CO)_{10}$, for which the *vic* isomer could separately be obtained using the double alkylation/oxidation route).[3]

Crystal structure determination

Yellow, air and X-ray stable, single crystals of **2** were grown by slow evaporation of a hexane solu-

Table 1. Crystal and intensity collection data for $Os_3\{\mu\text{-}H,\mu\text{-}O{=}CMe\}\{\eta^2\text{-}CH_2{=}CH_2\}(CO)_9$ (2)

Formula	$C_{13}H_8O_{10}Os_3$
Formula wt.	894
a (Å)	14.423(2)
b (Å)	15.119(3)
c (Å)	17.200(3)
β (°)	95.921(5)
V (Å^3)	3731(2)
Z	8
ρ(calc) (g cm^{-3})	3.19
Space group	$P2_1/c$
Temp. (°C)	25
Radiation source, λ (Å)	Mo-K_α (0.71069)
Scan rate (° min^{-1})	3
2θ limits (θ)	0–50
Take off angle (°)	4.0
Observations	$+h, +k, \pm l$
Total observed data	7118
No. unique ($I_0 > 3\sigma I_0$)	3947
Final No. variables	444
Goodness of fit[a]	2.40
R[b]	0.075
R_w[c]	0.087

[a] GOF $= [\sigma w(|F_o|-|F_c|)^2/(N_o-N_v)]^{1/2}$ where $w = 1/[\sigma(|F_o|)]^2$.
[b] $R = \Sigma[|F_o|-|F_c|]/|F_o|$.
[c] $R_w = [\Sigma w(|F_o|-|F_c|)^2/\Sigma w|F_o|^2]^{1/2}$.

tion. One crystal was glued to the tip of a glass fibre and mounted on a Huber four-circle automated diffractometer. The crystal was then centred on the diffractometer equipped with a scintillation counter, graphite monochromator, modified at U.C.L.A. by Dr C. E. Strouse for operation under control of a VAX 11/750 computer.

The 2θ, ω, χ, and ϕ settings of the Mo-K_α peaks of 30 reflections (2θ = 9–21° were determined. These values were used in a least-squares refinement of cell and orientation parameters. The refined unit cell parameters and specifics related to collection and refinement of data are given in Table 1.

The intensities of three standard reflections, (5,0,2), (0,3,2), (4,2,$\bar{6}$) were recorded after every 97 intensity measurements throughout the data collection to monitor crystal and diffractometer stability. The variations in the standards were random showing deviations from the respective mean values of less than 1.6%. A survey of the complete data set revealed systematic absences for reflections (0,k,0), k = odd and (h,0,l) for l = odd, uniquely defining $P2_1/c$ as the space group.

Reflections having $I < 3\sigma(I)$ (3171) were considered to be unobserved and omitted from the refinement. Reflections were corrected for Lorentz and polarization effects and converted to $|F_o|$ and $\sigma(|F_o|)$ by means of the CARESS program (see below).

Solution and refinement of the structure

All calculations were performed on a VAX 11/750 computer (Chemistry Department of UCLA). Programs used for the structure determination consist in all cases of local modifications by Dr C. E. Strouse and his research group. Functions and programs employed are given as follows: data reduction, CARESS, programs for control of the Huber diffractometer originally written by R. W. Broach (University of Wisconsin) and P. Coppens, P. Becker, and R. H. Blessing (SUNY, Buffalo); Patterson and Fourier programs, adapted from algorithms in MULTAN78, P. Main (University of York, U.K.); full-matrix least-squares and error analysis, ORFLS and ORFE, W. R. Busing, K. O. Martin and H. A. Levy (Oak Ridge National Laboratory); absorption correction, ABSN, P. Coppens; least-squares planes, MGTL, P. Gantzel and K. N. Trueblood; thermal ellipsoid plot program, ORTEP II, C. K. Johnson (Oak Ridge National Laboratory); structure factor table listing, PUBLIST, E. Hoel. Scattering factors for neutral osmium, oxygen and carbon atoms were taken from Table 2.2A of the *International Tables*,[14] while those for hydrogen were from Stewart *et al.*[15] Both real (f') and imaginary (f'') components of anomalous dispersion were included for osmium using the values in Table 2.3.1. of ref. 14. The function minimized during least-squares refinement and the discrepancy indices are given in Table 1.

Reasonable positions for the metal atoms were obtained by the Patterson method. Full-matrix least-squares refinement on the metals with isotropic temperature factors followed by difference Fourier syntheses in each case revealed the positions of other atoms and, after further refinement, the positions of all non-hydrogen atoms. The data were also corrected for the effects of absorption, see Table 1. Least-squares refinement first with anisotropic thermal parameters for all the metal atoms and then, with anisotropic thermal parameters for all non-hydrogen atoms, afforded the R factors shown in Table 1.

At this stage, it was possible to locate all hydride atoms as follows. The position of the hydride hydrogen was found on a difference electron density map. Neither the positions nor the temperature factors were refined for hydrogen atoms; these parameters however, were used in the calculation of the final structure factors. The atomic positional and thermal

Table 2. Selected interatomic distances (Å) for $Os_3\{1,2\text{-}\mu\text{-H},1,2\text{-}\mu\text{-O=C(Me)}\}\{1\text{-}\eta^2\text{-CH}_2\text{=CH}_2\}(CO)_9$ (2)

Molecule A		Molecule B	
Metal–metal			
Os(1)—Os(2)	2.907(2)	Os(4)—Os(5)	2.909(2)
Os(1)—Os(3)	2.841(2)	Os(4)—Os(6)	2.837(2)
Os(2)—Os(3)	2.872(2)	Os(5)—Os(6)	2.869(2)
Metal–ligand atom			
Os(1)—C(11)	1.832(36)	Os(4)—C(41)	1.846(39)
Os(1)—C(12)	1.934(47)	Os(4)—C(42)	1.820(46)
Os(2)—C(21)	1.890(43)	Os(5)—C(51)	1.811(38)
Os(2)—C(22)	1.971(39)	Os(5)—C(52)	2.114(51)
Os(2)—C(23)	1.971(49)	Os(5)—C(53)	1.892(45)
Os(3)—C(31)	2.025(52)	Os(6)—C(61)	1.938(33)
Os(3)—C(32)	1.958(35)	Os(6)—C(62)	1.979(40)
Os(3)—C(33)	1.851(44)	Os(6)—C(63)	1.936(43)
Os(3)—C(34)	1.892(52)	Os(6)—C(64)	1.902(42)
Os(1)—C(5)	2.282(37)	Os(4)—C(7)	2.254(60)
Os(1)—C(6)	2.313(49)	Os(4)—C(8)	2.147(56)
C(5)—C(6)	1.335(66)	C(7)—C(8)	1.325(78)
Os(1)—H(1)	1.705	Os(4)—H(2)	1.660
Os(2)—H(1)	1.699	Os(5)—H(2)	1.923
Carbonyl groups			
C(11)—O(11)	1.197(40)	C(41)—O(41)	1.168(41)
C(12)—O(12)	1.162(45)	C(42)—O(42)	1.173(44)
C(21)—O(21)	1.175(45)	C(51)—O(51)	1.205(41)
C(22)—O(22)	1.043(41)	C(52)—O(52)	1.042(49)
C(23)—O(23)	1.079(48)	C(53)—O(53)	1.172(45)
C(31)—O(31)	1.119(50)	C(61)—O(61)	1.136(37)
C(32)—O(32)	1.158(38)	C(62)—O(62)	1.143(41)
C(33)—O(33)	1.182(46)	C(63)—O(63)	1.120(46)
C(34)—O(34)	1.175(52)	C(64)—O(64)	1.161(45)
Bridging acyl groups			
O(1)—Os(1)	2.141(21)	O(2)—Os(4)	2.107(24)
O(1)—C(1)	1.230(39)	O(2)—C(2)	1.243(44)
C(1)—Os(2)	2.113(37)	C(2)—Os(5)	2.170(39)
C(1)—C(3)	1.545(48)	C(2)—C(4)	1.483(48)

parameters as well as observed and calculated structure factors have been deposited.* Selected interatomic distances and angles are given in Tables 2 and 3, respectively.

* Supplementary material available. A table containing final positional and thermal parameters and a listing of observed and calculated structure factors (18 pp.) has been deposited with the Editor, from whom copies are available on request. Atomic coordinates have also been deposited with the Cambridge Crystallographic Data Centre.

RESULTS AND DISCUSSION

Overall structure

The crystal consists of discrete molecular units of $Os_3\{\mu\text{-H},\mu\text{-O=CMe}\}\{\eta^2\text{-CH}_2\text{=CH}_2\}(CO)_9$ in the monoclinic space group $P2_1/c$ with eight molecules per unit cell. There are two independent molecules in the crystallographic asymmetric unit, referred to here as molecules A and B. Atom numbers in the discussion are those shown for A, see Fig. 2. The structure is that of the parent $Os_3\{1,2\text{-}\mu\text{-H},1,2\text{-}\mu\text{-O=C(Me)}\}(CO)_{10}$ with an *equatorial* (CO) group on Os(1) substituted by an $\eta^2\text{-CH}_2\text{=CH}_2$. The

Table 3. Bond angles (°) for $Os_3\{1,2$-μ-H,1,2-μ-O=C(Me)$\}\{1$-η^2-CH_2=$CH_2\}(CO)_9$ (2)

Molecule A		Molecule B	
		cis	
C(11)—Os(1)—C(12)	87.26(149)	C(41)—Os(4)—C(42)	86.55(188)
C(11)—Os(1)—C(5)	95.03(164)	C(41)—Os(4)—C(7)	93.36(205)
C(12)—Os(1)—O(1)	95.54(119)	C(42)—Os(4)—O(2)	93.20(151)
O(1)—Os(1)—C(5)	82.53(136)	O(2)—Os(4)—C(7)	84.79(166)
C(21)—Os(2)—C(22)	92.64(202)	C(51)—Os(5)—C(52)	90.34(157)
C(21)—Os(2)—C(23)	96.75(188)	C(51)—Os(5)—C(53)	97.28(189)
C(21)—Os(2)—C(1)	95.25(159)	C(51)—Os(5)—C(2)	97.24(157)
C(22)—Os(2)—C(23)	93.06(199)	C(52)—Os(5)—C(53)	91.91(175)
C(23)—Os(2)—C(1)	86.29(181)	C(53)—Os(5)—C(2)	88.45(176)
C(31)—Os(3)—C(33)	92.07(170)	C(61)—Os(6)—C(63)	94.75(134)
C(31)—Os(3)—C(34)	88.14(205)	C(61)—Os(6)—C(64)	90.61(160)
C(32)—Os(3)—C(33)	94.48(153)	C(62)—Os(6)—C(63)	91.25(146)
C(32)—Os(3)—C(34)	92.57(183)	C(62)—Os(6)—C(64)	89.24(172)
C(33)—Os(3)—C(34)	103.44(168)	C(63)—Os(6)—C(64)	100.04(141)
		trans	
C(11)—Os(1)—O(1)	176.87(131)	C(41)—Os(4)—O(2)	177.81(129)
C(22)—Os(2)—C(1)	171.90(193)	C(52)—Os(5)—C(2)	172.31(154)
C(31)—Os(3)—C(32)	173.06(153)	C(61)—Os(6)—C(62)	173.93(142)
		Os—C—O (terminal)	
Os(1)—C(11)—O(11)	166.88(336)	Os(4)—C(41)—O(41)	166.88(412)
Os(1)—C(12)—O(12)	176.67(311)	Os(4)—C(42)—O(42)	176.35(399)
Os(2)—C(21)—O(21)	171.77(361)	Os(5)—C(51)—O(51)	174.11(319)
Os(2)—C(22)—O(22)	168.71(469)	Os(5)—C(52)—O(52)	172.26(485)
Os(2)—C(23)—O(23)	177.02(488)	Os(5)—C(53)—O(53)	177.20(397)
Os(3)—C(31)—O(31)	175.86(485)	Os(6)—C(61)—O(61)	176.01(303)
Os(3)—C(32)—O(32)	176.04(310)	Os(6)—C(62)—O(62)	175.81(354)
Os(3)—C(33)—O(33)	170.94(315)	Os(6)—C(63)—O(63)	177.86(331)
Os(3)—C(34)—O(34)	167.58(404)	Os(6)—C(64)—O(64)	176.30(387)
		Bridging acyl groups	
C(1)—O(1)—Os(1)	111.84(214)	C(2)—O(2)—Os(4)	111.44(225)
O(1)—C(1)—C(3)	120.62(334)	O(2)—C(2)—C(4)	121.53(364)
O(1)—C(1)—Os(2)	114.56(240)	O(2)—C(2)—Os(5)	114.14(259)
C(3)—C(1)—Os(2)	124.76(261)	C(4)—C(2)—Os(5)	124.33(299)

overall geometry and interligand angles resemble those reported for $Ru_3\{1,2$-μ-H,1,2-μ-O=C$(NMe_2)\}\{1$-P$(OPh)_3\}(CO)_9$.[4a] Approximately octahedral coordination can be discerned around each of the osmium metal atoms in **2** as indicated by the bond angle data grouped for *cis* or *trans* positioned atoms in Table 4.

Coordination of the ethylene

The position of ethylene, substituted on the metal atom to which the oxygen of the acyl group is also coordinated, is that observed for a number of substituted related edge double-bridged derivatives.[4] By contrast, the ethylene in the adduct $Os_3\{1,2$-μ-H,1,2-μ-S(Me)$\}\{3$-η^2-CH_2=$CH_2\}(CO)_9$ is bonded *away* from the double-bridged edge,[5] occupying the vacant coordination position created in the conversion of the face-bridged μ_3-S(Me) group of the parent complex to the edge-bridged μ-S(Me) group in the product. The significance of the position of ethylene in **2** is taken up again in the Conclusion.

The carbon–carbon separation in the coordinated ethylene in the two independent molecules of the unit cell (Tables 2 and 4) is not shifted significantly away from the value of the carbon to carbon double bond of 1.337(5) Å in ethylene itself,[15] and is shorter than that observed in com-

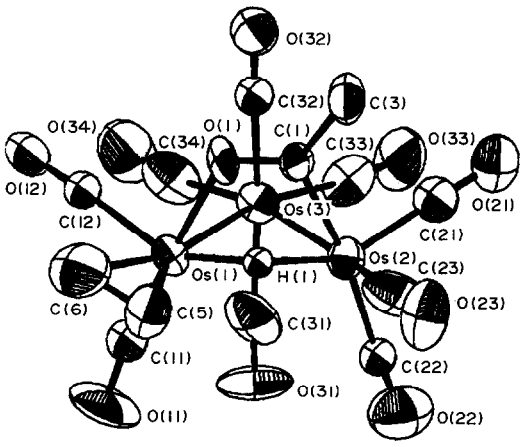

Fig. 2. ORTEP Projection of $Os_3\{1,2\text{-}\mu\text{-}H,1,2\text{-}\mu\text{-}O{=}C(Me)\}\{1\text{-}\eta^2\text{-}CH_2{=}CH_2\}(CO)_9$, (**2**), hydrogen atoms bonded to carbon atoms are omitted for clarity. The numbering scheme is shown for Molecule A; for the numbering of equivalent atoms in Molecule B, see Table 3. Atom H(1) and its equivalent H(2) in Molecule B, was located but not refined. Thermal ellipsoids are at 50% probability; those for C(22) and C(12) are isotropic, due to unreasonable anisotropic parameters obtained in refinement.

Table 4. Comparison of C=C and M—C separations (Å) for coordinated ethylene in $Os_3\{1,2\text{-}\mu\text{-}H,1,2\text{-}\mu\text{-}O{=}C(Me)\}\{1\text{-}\eta^2\text{-}CH_2{=}CH_2\}(CO)_9$ (**2**) and related derivatives

Complex	C=C	Os—C
2	1.335(66)	2.282(37)
		2.313(49)
	1.325(78)	2.254(69)
		2.147(56)
A	1.42[a]	2.23(4)[a]
B	1.489(21)	2.171(14)
		2.120(15)
C	1.40(3)	2.098(21)
		2.147(2)
D	1.46(6)	2.24(3)
		2.16(4)
E	1.531(1)	2.158(22)
		2.17(3)

A = $Os_3\{1,2\text{-}\mu\text{-}H,1,2\text{-}\mu\text{-}S(Me)\}\{3\text{-}\eta^2\text{-}CH_2{=}CH_2\}(CO)_9$,[5a] [a] The C=C separation was fixed at 1.42 Å and the Os—C distances were constrained to be equal in refining a disordered position for the ethylene group.

B = $[Os_3\{trans\text{-}CF_3(H)C{=}C(H)CF_3\}(Br)(CO)_{10}]^-$.[9]

C = $[Os_3\{trans\text{-}CF_3(H)C{=}C(H)CF_3\}\{\mu\text{-}Br\}(CO)_9]^-$.[9]

D = $Os_3\{trans\text{-}CF_3(H)C{=}C(H)CF_3\}\{\mu\text{-}H,\mu\text{-}Br\}(CO)_9$.[9]

E = $Os_3\{CH_2{=}CH{-}O{-}C(O)CH_3\}(CO)_{10}$.[10]

parison derivatives shown in Table 4; the Os—C separations are correspondingly higher.

Metal–metal separations

The metal–metal separations shown in Table 3 do not depart to any significant extent from the mean metal separation of 2.8771(27) Å found for $Os_3(CO)_{12}$,[16] or for like single bonded separations in other polynuclear complexes.[5a,9,10,17]

Bridging acyl group

The average C—O separation in the two bridging acyl groups is 1.24(4) Å (Table 2), close to 1.20 Å expected for a C=O double bond;[15] by comparison, the value for a C—O single bond is 1.43 Å. Moreover the Os—C separations, Os(2)—C(1) = 2.113(37) Å and Os(5)—C(2) = 2.170(39) Å are also close to 2.113 Å expected for an Os—C(sp^2) single bond;[3b,15] that observed for an Os—C(carbene) bond is 1.99(2) Å.[19] Despite lack of structural evidence for some carbene character in the bridge bond, i.e. Os(1)—O—C=(Me)Os(2), the ^{13}C resonance for the O—*C*(Me) carbon atom is shifted significantly downfield, to δ = 287.9 ppm.

CONCLUSIONS

Implications of the structure of **2**

No comparable ethylene adduct has as yet been observed for an edge double-bridged ruthenium complex, whose reaction with ethylene to form exclusively *gem*,bis-acyl dinuclear complexes is much more rapid, Scheme 2.[2] We see the triosmium system with greater barrier to reactivity, serving as a slow motion camera to catch intermediates not isolatable in the ruthenium system.

We suggest that the structure of **2** indicates the position of initial substitution of ethylene on the edge double-bridged parent molecule. We then surmize that hydrogen migration to such a coordinated olefin would create an ethyl group at the same metal atom site, as indicated for intermediate **I** in Scheme 2. Only the *gem* product is obtained in the ruthenium system. We thus deduce that a reductive elimination of the R group with the carbon of a bridging carbonyl (leading to the *gem* product) is greatly favoured over the migration of the R group to a carbonyl group terminally bonded to the same metal atom (which would give the *vic* product, not observed). Thus a key element in the reactivity of metal cluster complexes as compared to that of mononuclear complexes is suggested, namely, that a process *equivalent* to the classic

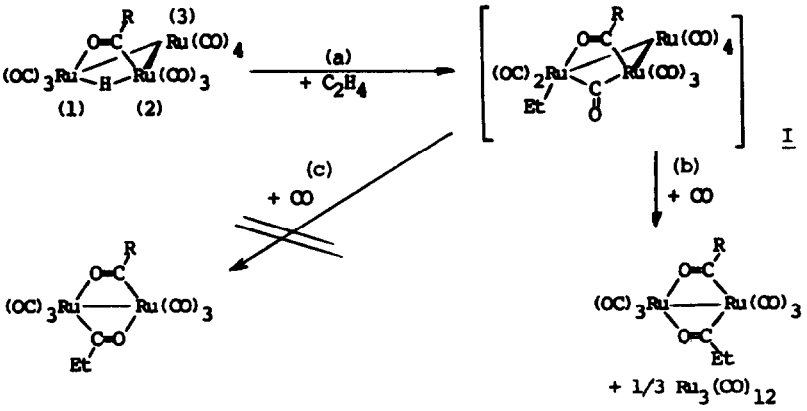

Scheme 2. Implications of the structure of **2** for the reaction pathway in the formation of *gem*-bis(acyl)diruthenium complexes (cf. ref. 2b).

migration reaction on mono-nuclear complexes can be achieved on metal cluster complexes by the *reductive elimination* of a *sigma*-bonded group with a bridging ligand.

Acknowledgement—This work was supported by National Science Foundation Grant CHE-84-05517.

REFERENCES

1. Yea-Jer Chen, dissertation. U.C.L.A. (1986).
2. (a) C. E. Kampe, N. M. Boag and H. D. Kaesz, *J. Am. Chem. Soc.* 1983, **105**, 2896; (b) C. E. Kampe, N. M. Boag and H. D. Kaesz, *J. Mol. Catal.* 1983, **21**, 279.
3. (a) C. M. Jensen, Y.-J. Chen and H. D. Kaesz, *J. Am. Chem. Soc.* 1984, **106**, 4046; (b) C. M. Jensen, Y.-J. Chen, C. B. Knobler and H. D. Kaesz, *New J. Chem.* 1988, **1**, in press.
4. (a) A. Mayr, Y.-C. Lin, N. M. Boag, C. E. Kampe, C. B. Knobler and H. D. Kaesz, *Inorg. Chem.* 1984, **23**, 4640; C. E. Kampe and H. D. Kaesz, *Inorg. Chem.* 1984, **23**, 4646.
5. (a) B. F. G. Johnson, J. Lewis, D. A. Pippard and P. R. Raithby, *Acta Cryst.* 1980, **B36**, 703; (b) B. F. G. Johnson, J. Lewis, D. A. Pippard and P. R. Raithby, *J. Chem. Soc., Chem. Commun.* 1978, 551; (c) B. F. G. Johnson, J. Lewis and D. A. Pippard, *J. Organomet. Chem.* 1981, **213**, 249.
6. (a) A. J. Deeming and M. Underhill, *J. Chem. Soc., Dalton Trans.* 1974, 1415; (b) *cf.* A. P. Humphries and H. D. Kaesz, *Prog. Inorg. Chem.* 1979, **25**, 145.
7. (a) B. F. G. Johnson, J. Lewis and D. A. Pippard, *J. Organomet. Chem.* 1978, **145**, C4; (b) E. J. Ditzel, B. E. Hanson, B. F. G. Johnson and J. Lewis, *J. Chem. Soc., Dalton Trans.* 1987, 1285.
8. (a) B. Besson, A. Choplin, L. D'Ornelas and J. M. Basset, *J. Chem. Soc., Chem. Commun.* 1982, 843; (b) A. Choplin, B. Besson, L. D'Ornelas, R. Sanchez-Delgado and J. M. Basset, *J. Am. Chem. Soc.* 1988, **110**, 2783.
9. Z. Dawoodi, M. J. Mays, P. R. Raithby, K. Henrick, W. Clegg and G. Weber, *J. Organomet. Chem.* 1983, **249**, 149.
10. E. Boyar, A. J. Deeming, I. P. Rothwell, K. Hendrick and M. McPartlin, *J. Chem. Soc., Dalton Trans.* 1986, 1437.
11. A. Mayr, Y.-C. Lin, N. M. Boag and H. D. Kaesz, *Inorg. Chem.* 1982, **21**, 1704.
12. R. Benn, *Org. Mag. Res.* 1983, **21**, 723.
13. D. F. Shriver and M. A. Drezdzon, *The Manipulation of Air-sensitive Compounds*, 2nd edn. McGraw-Hill, New York (1986).
14. *International Tables for X-ray Crystallography*, Vol. IV. Kynoch Press, Birmingham, U.K. (1975).
15. R. F. Stewart, E. R. Davidson and W. T. Simpson, *J. Chem. Phys.* 1965, **42**, 3175.
16. *Interatomic Distances Supplement*, Special Publication No. 18. The Chemical Society, London (1965).
17. M. R. Churchill and B. G. de Boer, *Inorg. Chem.* 1977, **16**, 878.
18. M. I. Bruce, Index of Structures Determined by Diffraction Methods in *Comprehensive Organometallic Chemistry* (Edited by G. Wilkinson, F. G. A. Stone and E. W. Abel), Vol. 9, p. 1392. Pergamon Press, Oxford (1982).
19. C. M. Jensen, C. B. Knobler and H. D. Kaesz, *J. Am. Chem. Soc.* 1984, **106**, 5926.

Polyhedron Vol. 7, No. 19/20, pp. 1901–1908, 1988
Printed in Great Britain

0277–5387/88 $3.00+.00
© 1988 Pergamon Press plc

POTENTIAL SOURCES OF THE ELECTRONIC MATERIALS GaP AND AlAs. SYNTHESIS AND X-RAY STRUCTURES OF $[t\text{-}Bu_2Ga(\mu\text{-}(C_5H_9)PH)]_2$ AND $[Et_2Al(\mu\text{-}t\text{-}Bu_2As)]_2$ (C_5H_9 = CYCLOPENTYL)

DUANE E. HEATON, RICHARD A. JONES,* KENNETH B. KIDD, ALAN H. COWLEY* and CHRISTINE M. NUNN

Department of Chemistry, The University of Texas at Austin, Austin, TX 78712, U.S.A.

Abstract—Reaction of $GaCl_3$ with *t*-BuLi (2 equiv.) and Li-(C_5H_9)PH in THF at −78°C gives colourless crystalline $[t\text{-}Bu_2Ga(\mu\text{-}(C_5H_9)PH)]_2$ (**1**) in 80% yield (C_5H_9 = cyclopentyl). Reaction of Et_3Al with $t\text{-}Bu_2AsH$ at 220°C gives the aluminium arsenide dimer, $[Et_2Al(\mu\text{-}t\text{-}Bu_2As)]_2$ (**2**) (63%). The X-ray structures of both (**1**) and (**2**) have been determined. They are both dimeric with bridging phosphido or arsenido groups and terminal alkyls. The coordination geometry of the Ga or Al atoms is roughly tetrahedral in each case. For compound (**1**) ^{31}P NMR data indicate the presence of both the *syn* and *anti* isomers in solution (relative ratios 1 : 2.5). In the solid state only the *anti* isomer is observed. Crystal data for (**1**): $C_{26}H_{56}Ga_2P_2$, $M = 570.12$, monoclinic, $C2/m$ (No. 12), $a = 16.736(3)$, $b = 11.586(1)$, $c = 8.413(2)$ Å, $\beta = 104.62(1)°$, $U = 1578.6(5)$ Å^3, $D_c = 1.20$ g cm^{-3}, $Z = 2$, μ(Mo-K_α) = 18.11 cm^{-1}. Refinement of 1054 reflections ($I > 3\sigma(I)$) out of 1447 unique observed reflections ($3° \leqslant 2\theta \leqslant 50°$) gave R and R_w values of 0.0503 and 0.0565, respectively. Data/parameter ratio = 12.85, highest peak in final difference Fourier = 0.604 e Å^{-3}. Crystal data for (**2**): $C_{24}H_{56}Al_2As_2$, $M = 434.29$, monoclinic, $P2_1/n$ (No. 14), $a = 8.907(1)$, $b = 11.691(1)$, $c = 14.735(3)$ Å, $\beta = 90.25(1)°$, $U = 1534.4(5)$ Å^3, $D_c = 1.88$ g cm^{-3}, $Z = 4$, μ(Mo-K_α) = 44.47 cm^{-1}. Refinement of 1165 reflections ($I > 3\sigma(I)$) out of 2700 unique observed reflections ($3° \leqslant 2\theta \leqslant 50°$) gave R and R_w values of 0.0523 and 0.0600, respectively. Data/parameter ratio = 9.173, highest peak in the final difference Fourier = 0.439 e Å^{-3}.

There is currently considerable interest in the chemistry of compounds which contain combinations of group 13 and 15 elements since they may serve as useful precursors to compound semiconductors such as GaAs and InP.[1] The pioneering studies of Coates[2] and Beachley[3] established that compounds of formula $[Me_2MEPh_2]_2$ (M = Al, Ga, In; E = P, As) and $[Me_2MER'_2]_3$ (M = Ga, In; E = P, R′ = Me, Et; and E = As, R′ = Me) may be prepared by the thermal reaction of Me_3M with R_2EH. More recent studies have shown that compounds of similar composition are also dimers or trimers depending on the steric demands of the substituents. Thus $[(Me_3SiCH_2)_2AsGaPh_2]_2$,[4] $[(Me_3SiCH_2)_2InPPh_2]_2$[5] and $\{[(Me_3SiCH_2)_2As]_2GaBr\}_2$[6] are dimers while $[Et_2MPEt_2]_3$ (M = Ga, In)[7] are trinuclear. For the heavier group 15 element Sb, both dimeric and trimeric species such as $[(t\text{-}Bu_2Sb)(Cl)In(\mu\text{-}t\text{-}Bu_2Sb)]_2$[8] and $[Cl_2Ga(t\text{-}Bu_2Sb)]_3$[9] have been described. Additionally, the X-ray structures of the novel binary compounds $Ga[As(mes)_2]_3$[10] (mes = mesityl), and $[Ga(As(CH_2SiMe_3)_2)_3]_2$[11] have recently been reported by Wells and coworkers.

We recently reported the use of the dinuclear complexes $[Me_2Ga(\mu\text{-}t\text{-}Bu_2As)]_2$ and $[Me_2In(\mu\text{-}t\text{-}Bu_2P)]_2$ for the organometallic chemical vapour deposition (OMCVD) of thin films of GaAs and InP, respectively.[12] These compounds and other analogues of the type $[Me_2M(\mu\text{-}t\text{-}Bu_2E)]_2$ (M = Al, Ga, In; E = P, As) offer advantages over the currently employed OMCVD processes which typically employ mixtures of group 13 alkyls (e.g. Me_3Ga, Me_3In) with a group 15 source, such as AsH_3 or $AsMe_3$ [e.g. eq. (1)][13]

$$Me_3Ga + AsH_3 \rightarrow GaAs + 3CH_4. \quad (1)$$

* Authors to whom correspondence should be addressed.

They have increased stability towards air and moisture, are hydrocarbon soluble, not appreciably toxic, and are sufficiently volatile for OMCVD processes. In addition, grown films of GaAs and InP were remarkably free of carbon as an impurity which suggested a novel, facile decomposition route for the elimination of the hydrocarbon fragments.[12] This is currently under investigation.

In order to assess the effect of different alkyl or aryl substituents in the precursor compounds on the nature of the grown films, we have undertaken the synthesis of a variety of new 13/15 compounds. We report here the synthesis, characterization and X-ray structures of two such species, $[t\text{-}Bu_2Ga(\mu\text{-}(C_5H_9)PH)]_2$ (**1**) and $[Et_2Al(\mu\text{-}t\text{-}Bu_2As)]_2$ (**2**). Details of their use as precursors for OMCVD processes will be described in another paper. To our knowledge complex **1** is the first example of a dinuclear primary phosphido (RPH^-) complex of gallium. In this case a plausible low temperature pathway for loss of hydrocarbon might be the expulsion of the small cyclic hydrocarbon cyclopentane. In addition, **2** is the first structurally characterized aluminium arsenide complex.

RESULTS AND DISCUSSION

Synthesis and structure of $[t\text{-}Bu_2Ga(\mu\text{-}(C_5H_9)PH)]_2$ (1)

The reaction of $GaCl_3$ with two equivalents of *t*-BuLi and one equivalent of the monolithiated phosphide $Li(C_5H_9)PH$ in THF at $-78°C$ results in the formation of $[t\text{-}Bu_2Ga(\mu\text{-}(C_5H_9)PH)]_2$ (**1**). The compound may be isolated in 80% yield as colourless prisms by crystallization from toluene at $-35°C$. It is relatively air stable in the solid state for short periods of time but decomposes rapidly in solution when exposed to the atmosphere. IR spectroscopic data confirms the presence of P—H units with a weak ν_{P-H} absorption at 2310 cm^{-1}. The ^1H NMR spectrum is relatively uninformative as it consists of numerous overlapping multiplets for the $(C_5H_9)PH$, $(C_5H_9)PH$ and *t-Bu*Ga protons. The $^{31}P\{^1H\}$ NMR spectrum in C_6D_6 at 35°C shows two singlets at δ −90.3 and −94.5 (relative areas 2.5:1). These signals are split by the $(C_5H_9)PH$ protons in the coupled ^{31}P NMR spectrum. We assign the two signals to the presence of both *syn* and *anti* isomers in solution (see Scheme 1). An alternative interpretation of the data is that the signals are due to the presence of monomeric and dimeric species. However, we feel that this is less likely since the $^1J_{P-H}$ coupling constants of both signals are virtually identical and a significant difference would be expected in these couplings for a bridging phosphide as opposed to a terminal phosphide. In addition, the chemical shifts of both signals are to high field and consistent with phosphido groups bridging two metals which are non-bonding. A monomeric species such as $t\text{-}Bu_2Ga[P(C_5H_9)H]$ could have the phosphido group behaving as a three or one electron donor. The ^{31}P NMR chemical shift of a phosphido group acting as a terminal three-electron donor would be expected to be shifted downfield. A monomeric six-electron species resulting from the one-electron donor phosphido case is likely to be highly coloured as found for $Ga(t\text{-}Bu_2P)_3$.[14]

In the solid state **1** crystallizes only in the *anti* form. Presumably this form minimizes the steric interactions between cyclopentyl groups. The complex crystallizes in the monoclinic space group $C2/m$ with two dimeric molecules in the unit cell. A view of the molecule is shown in Fig. 1, and bond lengths and angles are given in Table 1. There is a crystallographically imposed two-fold axis of rotation which passes through both Ga atoms and a mirror plane which contains the P atoms and the C(5) atoms of the cyclopentyl groups. Thus the central Ga_2P_2 core is planar, and there is a roughly tetrahedral coordination geometry about the Ga atoms (P—Ga—P′ = 81.76(3)°, P—Ga—C(1) = 110.65(9)°, P—Ga—C(1)′ = 113.10(9)°, C(1)—Ga—C(1)′ = 121.0(2)°). The Ga—Ga distance (3.71 Å) is too long to be considered a bonding interaction. The Ga—P distance (2.451(1) Å) is slightly shorter than that of other phosphido-bridged gallium dimers which we recently described (*ca* 2.48 Å).[14] This may be due to the electronic effects of replacing one alkyl group on phosphorus with an H atom as well as the decreased sterics of using a primary phosphide as opposed to the secondary phosphides used in other complexes. The Ga—C(1) distance (2.011(3) Å) is comparable to that of the Ga—alkyl bonds in the complexes $[R_2Ga(\mu\text{-}P(t\text{-}Bu)_2)]_2$ (R = *n*-Bu, Me) (*ca* 2.02 Å).[14] All other structural parameters of the molecule fall within normal limits.

Synthesis and structure of $[Et_2Al(\mu\text{-}t\text{-}Bu_2As)]_2$ (2)

We recently described the reaction of $t\text{-}Bu_2AsH$ with MMe_3 (M = Al, Ga, In) which produces the dimeric arsenido species $[Me_2M(\mu\text{-}t\text{-}Bu_2As)]_2$.[15] In order to explore the potential of this synthetic route we examined the reaction of Et_3Al with $t\text{-}Bu_2AsH$. The analogous ethyl derivative $[Et_2Al(\mu\text{-}t\text{-}Bu_2As)]_2$ (**2**) is produced in good yield. The isolation and characterization of **2** should permit a comparison of the effects of changing from Me to Et in the substituents on Al in an OMCVD process to pro-

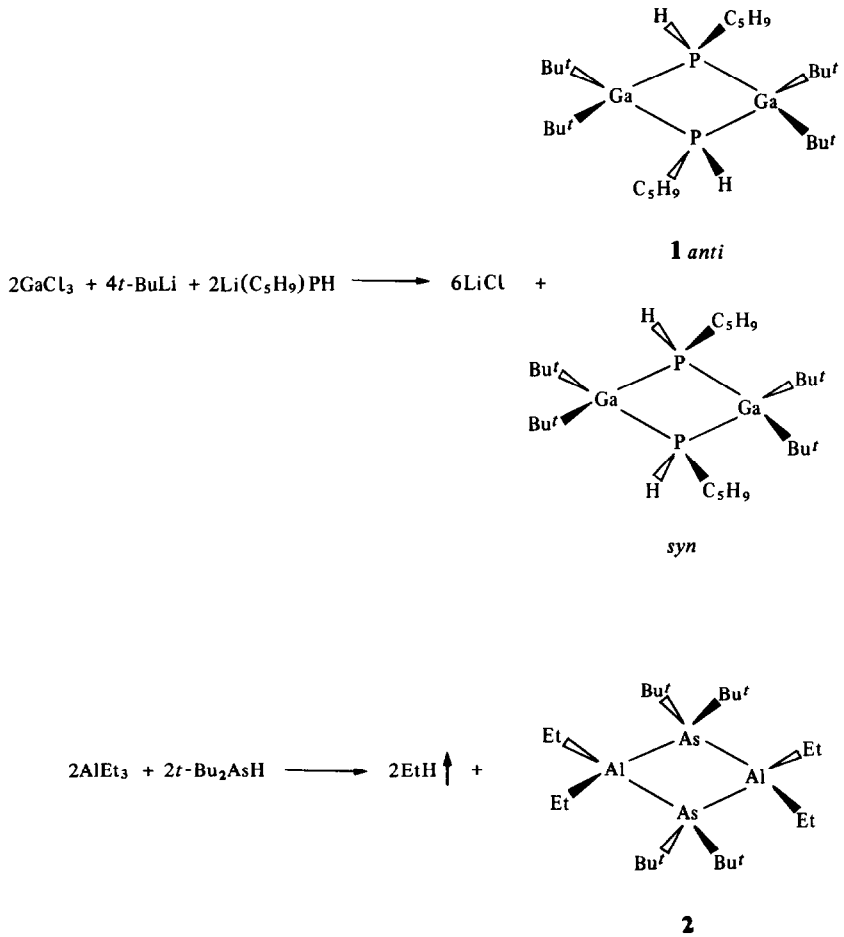

Scheme 1.

duce the compound semiconductor AlAs. The results of these studies will be published separately.

Spectroscopic data for **2** is in accord with the solid state structure as determined by X-ray crystallography. Thus the ^{1}H NMR spectrum contains peaks which may be assigned to Et groups [δ 1.42(t), 0.60(q)] as well as a *t*-Bu unit [δ 1.40(s)].

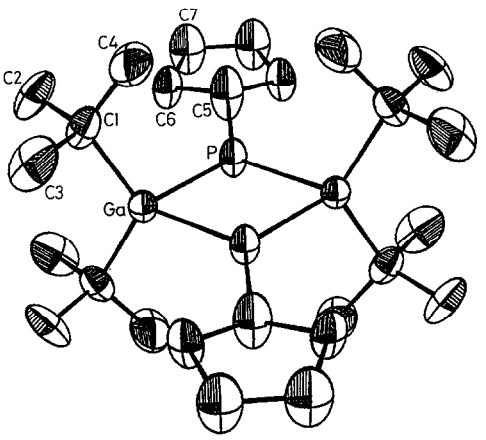

Fig. 1. ORTEP view of complex **1**.

The compound crystallizes in the monoclinic space group $P2_1/n$ with four molecules per unit cell. The molecule sits on an inversion centre at the mid points of the Al—Al and As—As vectors. A view of the compound is shown in Fig. 2, and bond lengths and angles are given in Table 2. To our knowledge **2** is the first structurally characterized aluminium–arsenido complex and so the Al—As distance of 2.571(2) Å is without precedent. The Al—C(41) and Al—C(31) distances of 1.985(5) and 1.999(5) Å, respectively may be considered normal. As in complex **1** the Al atoms have roughly tetrahedral coordination geometry, and the Al—Al distance is considered to be non-bonding (3.77 Å).

EXPERIMENTAL

All manipulations were performed under dry, oxygen-free N_2, under vacuum using standard vacuum line techniques, or in a Vacuum Atmospheres dry box under argon. Microanalyses were con-

Table 1. Bond lengths (Å) and angles (°) for complex **1**

Bond distances

Atom 1	Atom 2	Distance	Atom 1	Atom 2	Distance
Ga	P	2.451(1)	C(1)	C(4)	1.540(5)
Ga	C(1)	2.011(3)	C(5)	C(6)	1.513(4)
P	C(5)	1.743(4)	C(6)	C(7)	1.532(4)
C(1)	C(2)	1.554(4)	C(7)	C(7)′	1.468(7)
C(1)	C(3)	1.561(4)			

Bond angles

Atom 1	Atom 2	Atom 3	Angle	Atom 1	Atom 2	Atom 3	Angle
P	Ga	P′	81.76(3)	Ga	C(1)	C(4)	112.1(2)
P	Ga	C(1)	110.65(9)	C(2)	C(1)	C(3)	108.0(3)
P	Ga	C(1)	113.10(9)	C(2)	C(1)	C(4)	107.4(3)
C(1)	Ga	C(1)′	121.0(2)	C(3)	C(1)	C(4)	110.4(3)
Ga	P	Ga′	98.24(3)	P	C(5)	C(6)	119.3(3)
Ga	P	C(5)	128.00(8)	C(6)	C(5)	C(6)′	108.6(4)
Ga	C(1)	C(2)	109.8(2)	C(5)	C(6)	C(7)	104.6(3)
Ga	C(1)	C(3)	108.9(2)	C(6)	C(7)	C(7)′	108.9(2)

Numbers in parentheses are estimated standard deviations in the least significant digits.

ducted by the Schwarzkopf Microanalytical Laboratory, Woodside, NY. Pentane and THF were distilled from sodium benzophenone ketyl under N_2. Toluene was distilled from sodium under N_2. C_6D_6 was initially dried over 4 Å molecular sieves, stirred over Na/K alloy overnight, and the vacuum transferred to a storage vessel and stored under Na/K alloy. Instruments: IR, Perkin–Elmer 1330, Digilab FTS-40; NMR, GE QE-300 (^1H, ^{31}P); MS, Bell & Howell CEC 21-491, 70 eV. IR spectra were run as Nujol mulls by using NaCl discs or in solution (matched KBr cells). NMR spectra were recorded in C_6D_6 at ambient temperature unless otherwise stated and are in ppm referenced to Me_4Si (δ 0.0, ^1H) and 85% H_3PO_4(aq.) (δ 0.0, ^{31}P). Melting points were determined on an Electrothermal Melting Point apparatus in sealed capillaries under nitrogen (1 atm) and are uncorrected. Et_3Al was purchased as 20% Et_3Al in benzene from the Ethyl Corporation and used as received. $GaCl_3$ was purchased from Johnson Matthey Inc. and was used as received. $Li(C_5H_9)PH$* and t-Bu_2AsH[17] were prepared as previously described. Satisfactory elemental analyses (C, H) were obtained on both compounds.

Synthesis of $[t\text{-}Bu_2Ga(\mu\text{-}(C_5H_9)PH)]_2$ (**1**)

t-BuLi (8.8 cm^3 of a 2.5 M pentane solution, 22 mmol) was added dropwise to a solution of $GaCl_3$ (1.90 g, 11 mmol) in THF (80 cm^3) at −78°C. The solution became yellow during the addition and upon warming to room temperature it was colourless. The solution was stirred (7 h) and then cooled (−78°C). To it was added $Li(C_5H_9)PH$ (21.5 cm^3 of a 0.51 M THF solution, 11 mmol) dropwise via

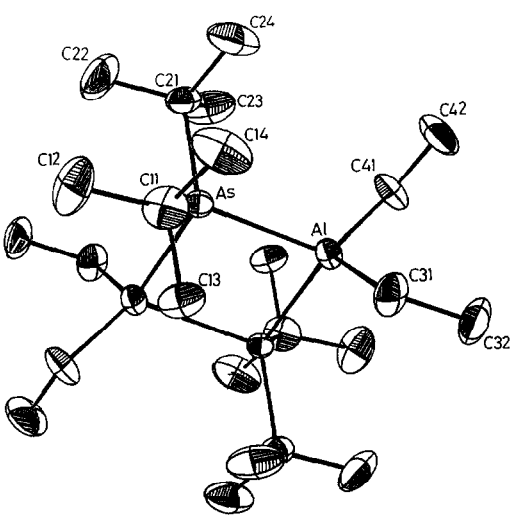

Fig. 2. ORTEP view of complex **2**.

* $Li(C_5H_9)PH$ was prepared from $(C_5H_9)PH_2$ in a manner analogous to the synthesis of Li-t-Bu_2P.[16]

Table 2. Bond lengths (Å) and angles (°) for complex **2**

Bond distances

Atom 1	Atom 2	Distance	Atom 1	Atom 2	Distance
As	Al	2.571(2)	C(11)	C(13)	1.572(9)
As	Al	2.562(2)	C(11)	C(14)	1.528(10)
As	C(11)	2.049(6)	C(21)	C(22)	1.542(10)
As	C(21)	2.033(6)	C(21)	C(23)	1.553(10)
Al	C(31)	1.999(5)	C(21)	C(24)	1.546(10)
Al	C(41)	1.985(5)	C(31)	C(32)	1.521(9)
C(11)	C(12)	1.532(10)	C(41)	C(42)	1.510(9)

Bond angles

Atom 1	Atom 2	Atom 3	Angle	Atom 1	Atom 2	Atom 3	Angle
Al	As	Al′	94.54(4)	As	C(11)	C(13)	103.6(4)
Al	As	C(11)	113.3(2)	As	C(11)	C(14)	110.4(5)
Al	As	C(21)	113.5(2)	C(12)	C(11)	C(13)	110.5(6)
Al	As	C(11)	112.8(2)	C(12)	C(11)	C(14)	111.5(7)
Al	As	C(21)	113.3(2)	C(13)	C(11)	C(14)	109.7(6)
C(11)	As	C(21)	108.9(3)	As	C(21)	C(22)	111.1(5)
As	Al	As′	85.46(4)	As	C(21)	C(23)	105.2(5)
As	Al	C(31)	111.7(2)	As	C(21)	C(24)	110.2(5)
As	Al	C(41)	116.9(2)	C(22)	C(21)	C(23)	109.6(6)
As	Al	C(31)	116.5(2)	C(22)	C(21)	C(24)	111.7(7)
As	Al	C(41)	112.7(2)	C(23)	C(21)	C(24)	108.8(6)
C(31)	Al	C(41)	111.5(3)	Al	C(31)	C(32)	113.0(5)
As	C(11)	C(12)	110.9(5)	Al	C(41)	C(42)	113.6(5)

Numbers in parentheses are estimated standard deviations in the least significant digits.

syringe. The solution was warmed to room temperature (1 h) and stirred (13 h). Volatile materials were removed *in vacuo*, and the residue extracted with toluene (2×40 cm^3). The combined, filtered extracts were concentrated *in vacuo* (60 cm^3) and cooled (−35°C) to produce colourless crystals of **1**. They were collected and dried *in vacuo*. The supernatant was further concentrated and cooled to yield additional amounts of **1**. Yield: 2.48 g, 80% based on Ga. M.p. 202–206°C (dec.). IR (Nujol mull, NaCl plates): 2310 w, 1445 m, 1360 m (cm^{-1}). ^{1}H NMR (300.152 MHz): δ 1.45 (br.mult., μ-(C_5H_9)P*H*, *t*-*Bu*Ga). ^{31}P NMR (121.503 MHz): δ −90.3 (br.dd, $^1J_{P—H}$ = 176 Hz, $^2J_{P—H}$ = 105 Hz, μ-(C_5H_9)*P*H), −94.5 (br.dd, $^1J_{P—H}$ = 178 Hz, $^2J_{P—H}$ = 106 Hz, μ-(C_5H_9)*P*H). ^{21}P{^{1}H} NMR (121.503 MHz): δ −90.3 (s, μ-(C_5H_9)*P*H), −94.5 (s, μ-(C_5H_9)*P*H).

Synthesis of [$Et_2Al(\mu$-*t*-$Bu_2As)]_2$ (**2**)

Et_3Al (0.14 cm^3, 0.12 g, 1.05 mmol) was syringed into a Schlenk flask (100 cm^3) containing *t*-Bu_2AsH (0.2 cm^3, 0.2 g, 1.05 mmol) and a magnetic follower. The stirred mixture was heated to 220°C (12 h). Upon cooling to room temperature, the reaction mixture solidified. Toluene (20 cm^3) was added and the mixture gently heated until all of the solid material had dissolved. The solution was cooled (−20°C) to give colourless crystals of **2**. The supernatant solution was decanted off and the crystals washed with pentane (2×30 cm^3), and dried *in vacuo*. Yield: 0.18 g, 63% based on Al. M.p. 278–280°C (dec.). IR: 1410 w, 1365 m, 1160 br, 1020 w, 975 w, 950 w, 620 br, 585 w, 530 w (cm^{-1}). ^{1}H NMR (300.152 MHz): δ 1.42 (t, 12H, CH_3), 1.40 (s, 36H, μ-t-Bu_2As), 0.60 (q, 8H, $AlCH_2$). ^{13}C{^{1}H} NMR (75.466 MHz): δ 4.10 (br.s, CH_2CH_3), 9.82 (s, CH_2CH_3), 33.82 (s, $C(CH_3)_3$), 39.11 (s, $C(CH_3)_3$).

X-ray experimental data

Details of crystal data and a summary of intensity data collection parameters for **1** and **2** are given in Table 3. Data were collected on an Enraf–Nonius

Table 3. Crystal data and collection parameters for complexes **1** and **2**

	1	**2**
Description of crystal		
Colour	clear	clear
Habit	prism	prism
Max. crystal dimension (mm)	0.20 × 0.40 × 0.20	0.40 × 0.35 × 0.25
Unit cell		
Crystal system	monoclinic	monoclinic
Space group	*C*2/*m* (no. 12)	$P2_1/n$ (no. 14)
Unit cell parameters:		
a (Å)	16.736(3)	8.907(1)
b (Å)	11.586(1)	11.691(1)
c (Å)	8.413(2)	14.735(3)
α (°)	90	90
β (°)	104.62(1)	90.25(1)
γ (°)	90	90
U (Å^3)	1578.6(5)	1534.4(5)
Molecules per unit cell	2	4
Formula	$C_{26}H_{56}Ga_2P_2$	$C_{24}H_{56}Al_2As_2$
Molecular weight (g mol^{-1})	570.12	434.29
Calculated density (g cm^{-3})	1.20	1.88
μ(Mo-K_α) calc. (cm^{-1})	18.11	44.47
Data collection		
Radiation (Å)	Mo-K_α (0.71073)	Mo-K_α (0.71073)
Scan technique	$\theta/2\theta$	$\theta/2\theta$
Scan width (°)	0.8 + 0.35 (tan θ)	0.8 + 0.35 (tan θ)
Range of indices *h*,*k*,*l*	+19, +13, ±10	+10, +13, ±17
2θ range (°)	3 to 50	3 to 50
No. reflections measured	1447	2700
Standard reflections:		
intensity	640, 603	505, 541
orientation	1002, 1003	0010, 0010
Decay of standards	4.2%	27.4%
Min. % transmission	75.20	81.60
Max. % transmission	99.92	99.82
Average % transmission	86.50	90.59
Agreement factor for averaged reflections intensity	0.013	0.026
Structure determination		
No. reflections used ($I > 3\sigma(I)$)	1054	1165
No. parameters varied	82	127
Data/parameter ratio	12.85	9.173
Shift to error ratio	0.004	0.018
E.s.d. of an observation of unit weight	6.24	4.59
R^a	0.0503	0.0523
$R_w{}^b$	0.0565	0.0600

[a] $R = \Sigma(|F_o| - |F_c|)/\Sigma|F_o|$.
[b] $R_w = [\Sigma\omega(|F_o| - |F_c|)^2/\Sigma\omega(|F_o|)^2]^{1/2}$.

CAD-4 diffractometer at 23±2°C using graphite monochromated Mo-K_α radiation. All calculations were performed on a PDP 11/44 computer using the Enraf–Nonius software package "SDP-PLUS".[18] For each structure, the data were corrected for Lorentz and polarization effects. The structures were solved by direct methods (MULTAN)[19] and successive cycles of difference Fourier maps followed by least-squares refinement. Scattering factors were taken from ref. 20.

(1). Crystals suitable for X-ray diffraction were grown by cooling a toluene solution (−35°C). The crystals were mounted in thin walled glass capillaries and sealed under nitrogen. Unit cell parameters were obtained by centring 25 reflections having 2θ values between 24–30°. Examination of the diffraction symmetry and no systematic absences indicated a choice of the monoclinic space groups, Cm, $C2$, $C2/m$. The space group $C2/m$ (No. 12) was chosen to be the correct one on the basis of successful refinement of the structure. Data were collected in the $+h+k\pm l$ quadrant between 2θ values of 3–50°. The check reflections indicated a 4.2% decrease in intensity over the course of data collection, and hence an anisotropic correction was applied. A ψ scan of four reflections having χ values between 80–90° showed a minimum transmission of 75.20% and a maximum transmission of 99.92%. An empirical absorption correction was applied (Program EAC). The observed structure factors of equivalent reflections were averaged, with an agreement factor of 0.013 for intensity. Hydrogen atoms were not located, but their contributions were included in the final refinements. Data with intensities less than $3\sigma(I)$ were excluded, and a non-Poisson contribution weighting scheme with an experimental instability factor of P set at 0.05 was used in the final stages of refinement.* The atoms were refined to final values of 0.0503 and 0.0565 for R and R_w, respectively. The maximum peak in the final difference Fourier map had a height of 0.604 e Å^{-3} and was located 1.203 Å from C(5).

(2). Crystals suitable for X-ray diffraction were grown by cooling a toluene solution (−35°C). The crystals were mounted in thin walled glass capillaries and sealed under nitrogen. Unit cell parameters were obtained by centring 25 reflections having 2θ values between 24–30°. The monoclinic space group $P2_1/n$ (No. 14) was uniquely determined by the systematic absences $0k0$, $k=2n+1$, $h01$, $h+1=2n+1$. Data were collected in the $+h+k\pm l$ quadrant between 2θ values for 3–50°. The check reflections indicated a 27.4% decrease in intensity over the course of data collection, and hence an anisotropic correction was applied. A ψ scan of four reflections having χ values between 80–90° showed a minimum transmission of 81.60% and a maximum transmission of 99.82%. An empirical absorption correction was applied. The observed structure factors of equivalent reflections were averaged, with an agreement factor of 0.026 for intensity. Hydrogen atoms were not located, but their contributions were included in the final refinements. Data with intensities less than $3\sigma(I)$ and $(\sin\theta)/\lambda$ less than 0.10 were excluded, and a non-Poisson contribution weighting scheme with an experimental instability factor of P set at 0.08 was used in the final stages of refinement.* The atoms were refined to final values of 0.0523 and 0.0600 for R and R_w respectively. The maximum peak in the final difference Fourier map had a height of 0.439 e Å^{-3} and was located 1.066 Å from C(13).†

Acknowledgements—We thank the Robert A. Welch Foundation, the National Science Foundation and the Texas Advanced Technology Research Program for support. R.A.J. thanks the Alfred P. Sloan foundation for a fellowship (1985–1989).

* P is used in the calculation of $\sigma(I)$ to downweight intense reflections in the least-squares refinement. The function minimized was $\Sigma\omega(|F_o|-|F_c|)^2$, where $\omega = 4(F_o)^2/[\Sigma(F_o)^2]^2$, where $[\Sigma(F_o)^2]^2 = [S^2(C+R^2B)+\{P(|F_o|)^2\}^2]/(L_p)^2$, where S is the scan rate, C is the total integrated peak count, R is the ratio of scan time to background counting time, B is the total background count and L_p is the Lorentz polarization factor.

† Tables of atomic positional and thermal parameters and observed and calculated structure factors for **1** and **2** have been deposited as supplementary material with the Editor, from whom copies are available on request. Atomic coordinates have also been submitted to the Cambridge Crystallographic Data Centre.

REFERENCES

1. See for example: (a) D. C. Bradley, M. M. Faktor, M. Scott and E. A. D. White, *J. Cryst. Growth* 1986, **75**, 101; (b) F. Maury, A. E. Hammadi and G. Constant, *J. Cryst. Growth* 1968, **68**, 88.
2. G. E. Coates and J. Graham, *J. Chem. Soc.* 1963, 223.
3. O. T. Beachley and G. E. Coates, *J. Chem. Soc.* 1965, 3241.
4. R. L. Wells, A. P. Purdy, A. T. McPhail and C. G. Pitt, *J. Organomet. Chem.* 1986, **308**, 281.
5. O. T. Beachley, J. P. Kopasz, H. Zhang, W. E. Hunter and J. L. Atwood, *J. Organomet. Chem.* 1987, **325**, 69.
6. A. P. Purdy, R. L. Wells, A. T. McPhail and C. G. Pitt, *Organometallics* 1987, **6**, 2099.
7. F. Maury, M. Combes, G. Constant, R. Carles and

J. B. Renucci, *J. de Phys.* 1982, **45**, C1-347; F. Maury and G. Constant, *Polyhedron* 1984, **3**, 581.
8. A. R. Barron, A. H. Cowley, R. A. Jones, C. M. Nunn and D. L. Westmoreland, *Polyhedron* 1988, **7**, 77.
9. A. H. Cowley, R. A. Jones, K. B. Kidd, C. M. Nunn and D. L. Westmoreland, *J. Organomet. Chem.* 1988, **341**, C1.
10. C. G. Pitt, K. T. Higa, A. T. McPhail and R. L. Wells, *Inorg. Chem.* 1986, **25**, 2483.
11. R. L. Wells, A. P. Purdy, K. T. Higa, A. T. McPhail and C. G. Pitt, *J. Organomet. Chem.* 1987, **325**, C7.
12. A. H. Cowley, B. L. Benac, J. G. Ekerdt, R. A. Jones, K. B. Kidd, J. Y. Lee and J. E. Miller, *J. Am. Chem. Soc.* accepted for publication.
13. H. M. Manasevit, *Appl. Phys. Lett.* 1968, **12**, 156; see also T. Nakanisi, *J. Cryst. Growth* 1984, **68**, 282.
14. A. M. Arif, B. L. Benac, A. H. Cowley, R. Geerts, R. A. Jones, K. B. Kidd, J. M. Power and S. T. Schwab, *J. Chem. Soc., Chem. Commun.* 1986, 1543.
15. A. M. Arif, B. L. Benac, A. H. Cowley, R. A. Jones, K. B. Kidd and C. M. Nunn, *New J. Chem.*, accepted for publication.
16. K. Issleib and F. Krech, *J. Organomet. Chem.* 1968, **13**, 283. For $(C_5H_9)PH_2$ see G. M. Kosolapoff and L. Maier, *Organic Phosphorus Compounds*, Vol. 1, p. 4. Wiley, New York (1972).
17. A. Tzschach and W. Deylig, *Z. Anorg. Allg. Chem.* 1956, **336**, 36.
18. *SDP Plus*, 4th edn. B. A. Frenz and Associates, College Station, TX (1981).
19. G. Germain, P. Main and M. M. Wolfson, *Acta. Cryst. Sect. A, Cryst. Phys., Diffr. Theor. Gen. Cryst.* 1971, **A27**, 368.
20. *International Tables for X-Ray Crystallography*, Vol. 4. Kynoch Press, Birmingham, U.K. (1974).

Polyhedron Vol. 7, No. 19/20, pp. 1909–1910, 1988
Printed in Great Britain

0277–5387/88 $3.00+.00
© 1988 Pergamon Press plc

SYNTHESIS AND STRUCTURE OF $[Pb(\mu\text{-P-}t\text{-Bu}_2)P\text{-}t\text{-Bu}_2]_2$. A PERPHOSPHIDO LEAD(II) DIMER

ALAN H. COWLEY,* DEAN M. GIOLANDO, RICHARD A. JONES,* CHRISTINE M. NUNN and JOHN M. POWER

Department of Chemistry, The University of Texas at Austin, Austin, TX 78712, U.S.A.

Abstract—The reaction of $PbCl_2$ with $Li[P\text{-}t\text{-}Bu_2]$ affords the dimeric Pb(II) compound, $[Pb(\mu\text{-P-}t\text{-Bu}_2)P\text{-}t\text{-Bu}_2]_2$ (**1**). The structure of **1** was established by X-ray crystallography. Compound **1** reacts with MeLi to afford the "ate" complex, $[Pb(P\text{-}t\text{-Bu}_2)_2Me]Li$.

The phosphorus ligand chemistry of Pb(II) is not well developed[1] and, in fact, only three compounds with Pb(II)—P bonds have been structurally characterized.[2,3] Interestingly, homoleptic phosphides of empirical composition $Pb(PR_2)_2$ were not known previously. We report the preparation and X-ray crystal structure of $[Pb(\mu\text{-P-}t\text{-Bu}_2)P\text{-}t\text{-Bu}_2]_2$ (**1**), the first example of this type of compound.

A THF solution of $Li[P\text{-}t\text{-Bu}_2]$ (4.8 cm^3, 0.9 M) was added dropwise via a syringe to a stirred solution of $PbCl_2$ (0.6 g, 2.15 mmol) in THF (80 cm^3) at −78°C. The resulting deep red reaction mixture was stirred for 12 h at ambient temperature. After filtration to eliminate a small amount of Pb metal, the THF was removed *in vacuo* from the reaction mixture and the resulting residue was dissolved in hexane (100 cm^3). After concentration and cooling of this solution to −30°C, red–black crystals of **1** were isolated in 88% yield. Crystals of **1** are moderately light-sensitive.

The $^{31}P\{^1H\}$ NMR spectrum of **1** exhibits resonances of equal intensity at δ 65.3 and 90.8,† thus implying a dimeric structure with two bridging and two terminal $t\text{-Bu}_2P$ moieties. As has been proposed for the analogous Sn compound,[1a] the lower field resonance is assigned to the bridging ligands. The ^1H and $^{13}C\{^1H\}$ NMR data are also consistent with a dimeric formulation.

The foregoing structure assignment was confirmed by an X-ray analysis.‡ Individual molecules of **1** reside on a centre of symmetry (Fig. 1) and there are no particularly short intermolecular contacts. As evidenced by the sum of bond angles (302.32(8)°), the geometry at each Pb atom is pyramidal thus implying the presence of a stereochemically active lone pair. A similar comment can be made about the geometry of the terminal phosphido groups (sum of bond angles at P(1) = 308.6(4)°). The conformation about the Pb—P(1) bond is one in which repulsion between the lead and phosphorus lone pairs is minimized. The adoption of a mutually *trans* arrangement of terminal phosphido groups is presumably a consequence of steric bulk. However, it should be noted that the less sterically encumbered compound, $[Sn(\mu\text{-}NMe_2)NMe_2]_2$, possesses a similar structure.[4] Within experimental error, the average Pb—P bond length in **1** (2.796(4) Å) is the same as those in $[Li(THF)\{Pb(P\text{-}t\text{-}Bu_2)_3\}]$[2] and in diphenylphos-

To Professor Sir Geoffrey Wilkinson in recognition of his many outstanding contributions to inorganic and organometallic chemistry.

* Authors to whom correspondence should be addressed.

† ^1H NMR (300 MHz, C_6D_6, TMS ext.) δ 1.45 (d, 36H, $^3J_{PH}$ = 11.9 Hz, *t*-Bu terminal), δ 1.54 (m, unresolved virtual coupling, 36H, *t*-Bu bridge). $^{13}C\{^1H\}$ NMR (75.5 MHz, C_6D_6, TMS ext.) δ 34.73 (s, Me bridge), δ 36.8 (d, $^2J_{PC}$ = 12.6 Hz, Me terminal). $^{31}P\{^1H\}$ NMR (121.5 MHz, C_6D_6, 85% H_3PO_4 ext.) δ 65.3 (s, ^{207}Pb satellites, $^1J_{PbP}$ = 2452 Hz, P bridge), δ 90.8 (s, ^{207}Pb satellites, $^1J_{PbP}$ = 1100 Hz).

‡ Crystal data for **1**: $C_{32}H_{72}P_4Pb_2$, M = 995.2, monoclinic, $P2/n$ (No. 14), a = 12.107(3), b = 11.738(2), c = 15.540(5) Å, β = 111.09(2)°, V = 2060.5 $Å^3$, Z = 2, D_c = 1.60 g cm^{-3}, μ(Mo-K_α) = 83.9 cm^{-1}. Crystal growth: red–black single crystals of **1** were grown by cooling a saturated hexane solution to −30°C for one week.

Intensity data: Enraf–Nonius CAD 4 diffractometer at 23 ± 2°C, ω–2θ scan mode within the range $3 \leqslant 2\theta \leqslant 55°$. The structure was solved by Patterson and Fourier methods by which all non-hydrogen atoms were located and refined anisotropically. Full-matrix least-squares refinement of 3072 reflections [$I > 3\sigma(I)$] from a total of 4727 unique measured reflections gave final R and R_w values of 0.0399 and 0.0508, respectively.

Atomic coordinates, bond lengths and angles and thermal parameters have been deposited at the Cambridge Crystallographic Data Centre. See notice to Authors.

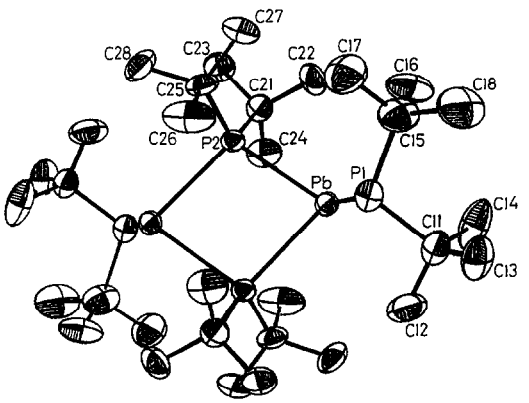

Fig. 1. View (ORTEP) of **1** showing the atom numbering scheme. Key bond lengths (Å) and angles (°): Pb—P(1) 2.781(4), Pb—P(2) 2.812(3), P(2)—Pb—P(2)′ 79.84(8), P(2)—Pb—P(1) 115.17(8), P(2)—Pb—P(1) 107.31(9), Pb—P(2)—Pb′ 100.16(8).

phinomethanide complexes of Pb(II).[3] The intra-ring Pb—P bond lengths (2.812(3) Å) are slightly longer than the terminal Pb—P bond lengths (2.781(4) Å) but this difference is close to the limit of statistical significance. The Pb···Pb distance within the Pb_2P_2 rhombus exceeds 4.3 Å hence metal–metal interaction is precluded.

A similar structure to **1** has been postulated for the analogous Sn(II) compound, $[Sn(\mu\text{-P-}t\text{-Bu}_2)P\text{-}t\text{-Bu}_2]_2$ on the basis of heteronuclear NMR data.[1a] Interestingly, the amido-substituted Sn(II) and Pb(II) compounds, $[M\{N(SiMe_3)_2\}_2]$ (M = Sn, Pb), adopt monomeric structures in both the solid and vapour states.[5]

Preliminary studies have been made of the reactivity of **1**. For example, **1** reacts readily with MeLi to afford the novel "ate" complex, $[Pb(P\text{-}t\text{-Bu}_2)_2Me]Li$. This compound and other reactions of **1** will be described in a subsequent full paper.

Acknowledgements—We are grateful to the National Science Foundation, the Robert A. Welch Foundation and the Texas Advanced Technology Research Program for financial support.

REFERENCES

1. (a) W.-W. du Mont and H.-J. Kroth, *Angew. Chem. Int. Ed. Engl.* 1977, **16**, 792; (b) W.-W. du Mont and B. Z. Neudert, *Z. Anorg. Allg. Chem.* 1978 **441**, 86; (c) P. A. W. Dean, D. D. Phillips and L. Polensek, *Can. J. Chem.* 1983, **61**, 1795.
2. A. M. Arif, A. H. Cowley, R. A. Jones and J. M. Power, *J. Chem. Soc., Chem. Commun.* 1986, 1446.
3. A. L. Balch and D. E. Oram, *Organometallics* 1986, **5**, 2159; A. L. Balch and D. E. Oram, *Inorg. Chem.* 1987, **26**, 1906; A. L. Balch and D. E. Oram, *Phosphorus Sulfur* 1987, **30**, 101.
4. M. M. Olmstead and P. P. Power, *Inorg. Chem.* 1984, **23**, 413.
5. T. Fjeldberg, H. Hope, M. F. Lappert, P. P. Power and A. J. Thorne, *J. Chem. Soc., Chem. Commun.* 1983, 639.

Polyhedron Vol. 7, No. 19/20, pp. 1911–1918, 1988
Printed in Great Britain

0277–5387/88 $3.00+.00
© 1988 Pergamon Press plc

IRON–SULPHUR DIMERS WITH BIDENTATE PHENOLATE–THIOLATE TERMINAL LIGANDS

P. BEARDWOOD and J. F. GIBSON*

Department of Chemistry, Imperial College of Science and Technology, London SW7 2AY, U.K.

Abstract—$[Fe_2S_2L_2]^{2-}$ complexes **1–4** having phenolate–thiolate terminal coordination by the ligands **L1–L4** have been prepared and studied by a range of physical methods. Their electronic spectra show strong absorption in the region 390–420 nm attributable to O → Fe charge-transfer. ^{1}H NMR for **1–4** demonstrates the diagnostic pattern of dipolar broadened resonances with negative isotropic shifts for α-methylene and *meta* protons and positive shifts for *ortho* and *para* protons. ^{57}Fe Mössbauer spectra of the solid complexes display quadrupole doublets with large splittings (0.68–0.99 mm s^{-1}) typical of chelated $[2Fe—2S]^{2+}$ and isomer shifts (0.28–0.31 mm s^{-1}) only slightly raised from those for $[Fe_2S_2(SR)_4]^{2-}$. First reduction processes occur at potentials in the range −1.35 to −1.47 V and are more reversible than those for $[Fe_2S_2(OAr)_4]^{2-}$. On chemical reduction, **1** and **3** give EPR signals having $g_{av} = 1.929$ and 1.928, respectively, attributable to the corresponding trianions. Reduced **2** and **4**, however, more readily give the $g_{av} \simeq 1.92$ type signals characteristic of solvent-induced modification of the coordination. The effectiveness of phenolate coordination in decreasing g_2 and g_3 for $[2Fe—2S]^+$ suggests that the low g values of the Rieske proteins result from oxygenous ligation.

$[Fe_2S_2(SR)_4]^{2-/3-}$ complexes are well known as analogues of $[2Fe—2S]^{2+/1+}$ ferredoxin centres, displaying many coincident physical and chemical properties. The Rieske-type [2Fe—2S] proteins have anomalous spectroscopic and redox properties which demonstrate a departure from the established tetra-thiolate coordination of [2Fe—2S] centres in ferredoxins. In recent years, [2Fe—2S] complexes coordinated terminally by bis-phenolate,[1–3] bis-pyrrolate,[2] carboxylate–thiolate,[4] benzimidazolate–thiolate, benzimidazolate–phenolate or bis-benzimidazolate[5] ligands have been synthesized and studied by a range of physical methods, for comparison with the Rieske proteins. Here, seeking further to map out the effects of the many possible combinations and geometrical arrangements of the biologically relevant coordinating groups, we investigate $[Fe_2S_2L_2]^{2-/3-}$ complexes, **1–4**, having bidentate phenolate–thiolate ligands (L = **L1–L4**).

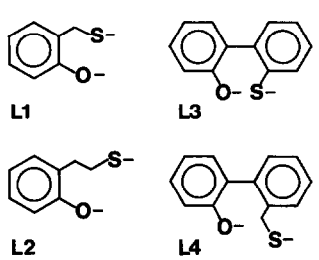

EXPERIMENTAL

Ligand synthesis

Ligand H_2**L1** was prepared from 2-hydroxybenzylalcohol diacetate[6] by reaction with NaHS in methanol according to the procedure of Hayashi and Oka[7] for 2,2′-dihydroxydibenzyldisulphide, followed by reduction with lithium aluminium hydride in ether to give 70% of 2-hydroxybenzylmercaptan after vacuum distillation. ^{1}H NMR ($CDCl_3$) δ 1.88 (t, SH), 3.76 (d, CH_2), 5.87 (s, OH), 6.75–7.25 (m, C_6H_4).

* Author to whom correspondence should be addressed.

H_2**L2**, 2-(2-hydroxyphenyl)ethylmercaptan, was prepared from 2-(2-hydroxyphenyl)ethanol[8] by a similar procedure to that used by Givens and Hamilton[9] when starting from 2,3-dihydrobenzofuran.

H_2**L3**, 2-mercapto-2′-hydroxybiphenyl was obtained from 2-hydroxybiphenyl by the method of Hanson and Kemp.[10]

H_2**L4** was prepared from 2-methylol-2′-hydroxybiphenyl[11] by reaction with HCl in EtOH, removal of the solvent and subsequent reaction with thiourea in DMSO followed by hydrolysis with aqueous NaOH, all at room temperature. After acidification and extraction with ether the crude product was chromatographed on a column of silica using 2 : 1 ether : hexanes solvent to give 30% of 2-mercaptomethyl-2′-hydroxybiphenyl. ^{1}H NMR ($CDCl_3$) δ 1.68 (t, SH), 3.57 (d, CH_2), 4.80 (s, OH), 6.9–7.5 (m, $C_{12}H_8$).

Iron–sulphur dimer synthesis

$[Et_4N]^+$ or $[Ph_4As]^+$ salts of the $[Fe_2S_2L_2]^{2-}$ complexes were formed from $[Fe_2S_2Cl_4]^{2-}$ by exchange of chloride for the deprotonated ligand L = **L1**–**L4** in an aprotic solvent. The formation of $[Et_4N]_2[Fe_2S_2(\mathbf{L3})_2]$ serves as an example. All manipulations were performed in an atmosphere of dinitrogen using deoxygenated solvents.

$[Et_4N]_2[Fe_2S_2(\mathbf{L3})_2]$: 404 mg (2 mmol) of 2-mercapto-2′-hydroxybiphenyl were deprotonated in 2–3 cm^3 of MeOH using 4 mmol of NaOMe (formed *in situ* from 96 mg of granular NaH). After removal of the solvent *in vacuo* the sodium salt of the ligand was dissolved in 40 cm^3 of dimethylformamide (DMF—Aldrich HPLC grade) and added to 578 mg (1 mmol) of $[Et_4N]_2[Fe_2S_2Cl_4]$[12] in 30 cm^3 DMF. The solution was stirred for 1 h at room temperature and then filtered through Celite 521 filter agent (Aldrich) and 150 cm^3 of ether (Na dried) were added with stirring. One hour later the product was filtered from the solution, redissolved in 100 cm^3 of warm DMF, filtered through Celite, and treated with 150 cm^3 of ether. After standing overnight the solid was filtered from the solution, washed well with ether and dried to give 695 mg (83%) of product. Found: C, 57.3; H, 6.5; N, 3.3. Calc. for $C_{40}H_{56}N_2S_4O_2Fe_2$: C, 57.4; H, 6.7; N, 3.3%.

The reaction was also carried out by deprotonating the ligand directly with excess NaH in DMF, or in tetrahydrofuran with addition to the $[Fe_2S_2Cl_4]^{2-}$ in MeCN. In the latter case the product came out of solution during the reaction and was recrystallized twice from DMF–Et_2O. For **L1** and **L2** the sodium salts of the ligands are less soluble in DMF and were added partly in suspension. Complexes **2** and **4** are more soluble in DMF and thus correspondingly less solvent was used in their preparation and recrystallization.

Although the complexes may possibly crystallize from solution with the ligands in a specific geometrical arrangement, when dissolved they are expected, very rapidly, to attain an equilibrium distribution between the isomers, due to the facile ligand exchange typical of these types of complexes. The complexes are converted quantitatively into $[Fe_2S_2(SAr)_4]^{2-}$ by an excess of thiophenol, as judged by optical spectrophotometry.

Reductions of the iron–sulphur dimers were carried out as described previously[13] using *ca* 1.1 equivalents of monosodium acenaphthylenide in DMF or *N*-methylpyrrolidinone (NMP) with subsequent rapid transfer of samples of the solutions to EPR tubes for immediate freezing in liquid nitrogen.

Physical measurements

Electronic absorption spectra were measured using 1 mm silica cells on a Perkin–Elmer 551 spectrophotometer and a Philips PU8740 spectrophotometer.

^{1}H NMR spectra of the complexes in 99.9% d_6-dimethylsulphoxide (DMSO—Aldrich) dried over molecular sieves were obtained at 25–30°C using a JEOL FX90Q at 90 MHz and Bruker WM250 at 250 MHz.

Mössbauer measurements were made on *ca* 100 mg samples of powder in 19 mm diameter nylon containers at 77 K in zero field using a *ca* 10 mCi ^{57}Co/Rh source and Cryophysics MS103 instrumentation calibrated using iron metal at 298 K.

EPR spectra of frozen solutions in 5 mm diameter silica tubes at 77 K in a finger dewar were measured on a Varian E12 instrument for which the frequency was calibrated using an Elliott Bros. WM 16 wavemeter and the field using a Varian NMR gaussmeter. The pure solvents normally crystallized on freezing to give an opaque sample unless nBu$_4$NClO$_4$ was added (0.1 M for DMF, 0.2 M for NMP) in which case they froze in a vitreous state. Yields of reduced species were measured by double integration of their EPR spectra in comparison to a 3 mM Cu–ethylenediaminetetra–acetate standard which usually was measured in the same EPR tube. EPR simulations were calculated using the program EPRPOW originally written by White and Belford[14] and modified by one of the authors.[15]

A PAR 174A polarographic analyser and a Metrohm rapid dropping mercury electrode (RDME) operating at 6 drops s^{-1} were used to perform electrochemical measurements on *ca* 1–2 mM solutions of the complexes in DMF containing

0.1 M nBuN$_4$ClO$_4$ supporting electrolyte. A Pt counter electrode was contained in a compartment separated from the bulk solution by a coarse frit and a Ag/AgCl reference electrode contacted the solution, via an aqueous KCl bridge with a fibre junction, to a 0.1 M nBuN$_4$ClO$_4$ DMF bridge terminating in a Vycor porous plug.

RESULTS AND DISCUSSION

Electronic spectra

Figure 1 shows the electronic absorption spectra for **1** and **3** in DMF. The main features of these spectra and of those for **2** and **4** are listed in Table 1. The spectra show similarities in having strong absorption in the region 390–420 nm attributable to ArO → Fe charge-transfer, as found for $[Fe_2S_2(OAr)_4]^{2-}$ at around 404–417 nm,[1-3] for $[Fe(2,3,5,6\text{-tetramethylphenolate})_4]^-$ at 422 nm[16] and for $[Fe_4S_4(OAr)_4]^{2-}$ at around 410–425 nm.[17] Charge-transfer transitions originating from the bridging and thiolate sulphurs are considered to give rise to the absorption at longer wavelengths.

^{1}H *NMR*

NMR spectra of the protons in thiolate and phenolate ligands coordinating $[2Fe—2S]^{2+}$ show isotropic shifts arising from hyperfine contact interactions as a result of Fe–ligand antiparallel spin transfer.[18,19] The chemical shifts (δ) of the dipolar broadened resonances for $[Ph_4As]^+$ salts (or $[Et_4N]^+$ salts where marked) of **1–4** in d_6-DMSO are given in Table 1 and show the typical pattern of positive isotropic magnetic shifts for protons *para* or *ortho* to the coordinating chalcogenide, negative shifts for *meta* protons and very broad downfield peaks for methylene protons adjacent to coordinated sulphur.

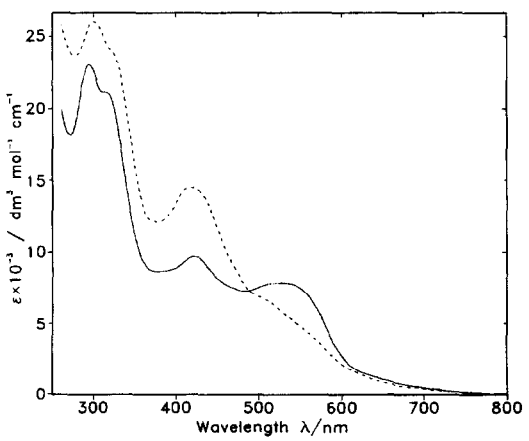

Fig. 1. Electronic absorption spectra of **1** (——) and **3** (– – –) in DMF.

Resonances for protons *meta* to a coordinating oxygen have been found in the range −9.3 to −11.3 ppm for $[2Fe—2S]^{2+}$ complexes.[1-3,5] The assignments at −8.44 ppm for **1** and −12.09 ppm for **4** are thus, respectively, rather extreme. The splitting of the resonances at *ca* −10.6 ppm for **1** and **2** is attributable to geometric isomerism and is of a similar magnitude to that found[5] for $[Fe_2S_2(2\text{-}(2\text{-phenolate})benzimidazolate)_2]^{2-}$. Peaks for *para* phenoxide protons have been reported in the range −0.62 to −2.92 ppm and for *ortho* protons at −2.3 to −2.85 ppm,[1-3,5] making the assignments given here unexceptional. Complex **3** shows only a small spread in the chemical shifts for protons *meta* to oxygen or sulphur and the assignments given in Table 1 are made on the basis of the resonance positions for $[Fe_2S_2(2,2'\text{-biphenolate})_2]^{2-}$ at −9.31 and −9.61 ppm[2] and for $[Fe_2S_2(2,2'\text{-bi(thiophenolate)})_2]^{2-}$ at −8.75 and −8.93 ppm (authors unpublished results).

The methylene resonance for **1** at −50 ppm and the corresponding feature for **2** at −42 ppm are lower than those found in $[Fe_2S_2(SEt)_4]^{2-}$ at −32 ppm,[20] in $[Fe_2S_2(S_2—o\text{-xylyl})_2]^{2-}$ at −39.6 ppm[18] or for $[Fe_2S_2(\text{thiosalicylate})_2]^{2-}$ at −33 ppm.[4] For **4**, two broad low-field features are observed at −45 and −33 ppm in an approximate intensity ratio of 4 : 3. Molecular models show that although ligands **L2–L4** potentially can each bridge across the [2Fe—2S] unit with thiolate coordinated to one iron and phenolate to the other, this is the least strained, and thus the most feasible, for **L4**. It is possible, then, that the resonance at −45 ppm in **4** has a similar origin to those observed for **1** and **2**, with each iron coordinated by phenolate and thiolate from the same ligand, whilst the −33 ppm resonance is due to a geometric isomer having one iron ligated by two thiolates and the other by two phenolates. The ratio of the observed intensities for the two resonances would imply the latter arrangement to be slightly favoured thermodynamically. If this is a valid explanation of the low-field part of the spectrum for **4** it is peculiar that no corresponding diversity is apparent in the isotropically shifted ring resonances. It is, however, not surprising that this inhomogeneity of the coordination in **4** is not manifest in the other methods of physical characterization since both the Mössbauer isomer shift and the first electrochemical reduction potential appear to vary little between phenolate–thiolate and bis-thiolate coordination, while the features in the electronic spectrum of **4** are broad and poorly resolved.

Table 1. Spectroscopic and electrochemical parameters for **1–4**

		1	2	3	4
Electronic absorption		294 [23]	294 [21]	299 [26]	295 [28]
λ (nm) [$\varepsilon \times 10^{-3}$		316 sh [21]	318 sh [18]	325 ap sh [24]	
($dm^3\ mol^{-1}\ cm^{-1}$)]		420 [9.7]	390 [11.0]	416 [14.5]	390 ap sh br [11.3]
			455 ap w sh br		
		515–530 br [7.9]	505 ap w sh br	505 ap w sh [6.9]	525 ap sh br [5.9]
			550 ap w sh br	550 ap w sh br	
^{1}H NMR δ(ppm)					
	CH_2	−50 br	−42 br		−33 br, −45 br
w.r.t. O	*o*	−2.2 ap	−2.9 ap		
	m	−8.44	−9.56	−9.15	−10.85
	m	−10.70 & −10.49	−10.51 & −10.69	−9.43	−12.09
	p	−3.1	−2.11	−2.64	−1.63
w.r.t. S	*o*			−3.9 ap br	
	m			−8.70	−6.60[a]
	m			−8.93	−7.53[a]
	p			−3.08	
^{57}Fe Mössbauer (mm s^{-1} w.r.t. Fe)					
One doublet fit	δ	0.28	0.31	0.29	0.29
	ΔE_Q	0.99	0.77	0.95	0.68
	Γ	0.14	0.31	0.25	0.15
Two doublet fit	δ		0.32, 0.30	0.29, 0.29	0.31, 0.29
	ΔE_Q		1.03, 0.60	1.12, 0.77	0.81, 0.63
	Γ		0.22, 0.25	0.19, 0.19	0.16, 0.14
area ratio			0.38 : 0.42	0.49 : 0.51	0.39 : 0.61
Electrochemical $E_{1/2}$ (V)					
First reduction		−1.44	−1.44	−1.35	−1.47
Second reduction			−1.76	−1.83	−1.76
EPR, reduced in DMF–nBu$_4$NClO$_4$					
g_1		2.018	2.023	2.031	2.021
g_2		1.898	1.930	1.903	1.886
g_3		1.872	1.857	1.849	1.842
g_{av}		1.929	1.937	1.928	1.916
WL_1, WG_1		0.53, 0.43		2.00, 0.40	
WL_2, WG_2		0.52, 1.56		2.15, 0.90	
WL_3, WG_3		3.14, 1.88		1.97, 2.89	

sh = shoulder, br = broad, ap = approximately, w = weak, WL = half-width Lorentzian (mT), WG = half-width Gaussian.

[a] for $[Et_4N]^+$ salt.

^{57}Fe *Mössbauer*

Isomer shift (δ), quadrupole splittings (ΔE_Q) and linewidth (Γ) parameters from the fitting of ^{57}Fe Mössbauer spectra of solid samples of the $[Et_4N]^+$ salts of **1–4** are reported in Table 1. For **2** and **3**, which have relatively large linewidths when fitted with a single quadrupole doublet, and for **4**, parameters are given also for improved fits using two doublets for which the intensity ratio was allowed to float. Although the validity of this increase in the number of fitting parameters is doubtful, such multiplicity could arise from geometric isomerism or from inequivalence of the two irons[13] leading to broadening and slight asymmetry in the two lines. Linewidths in the range 0.25–0.30 mm s^{-1} are, however, not unusual in these types of compounds.[1,13,18,21] Figure 2 shows spectra for **1** and **3** fitted by one and two doublets, respectively.

The isomer shifts of **1**, **2** and **4** are only raised slightly from the value of 0.28 mm s^{-1} found for $[Fe_2S_2(SPh)_4]^{2-}$ and $[Fe_2S_2(S_2$—*o*-xylyl$)_2]^{2-}$[18] in contrast to $\delta = 0.35$ mm s^{-1} for $[Fe_2S_2$(2,2′-biphenolate$)_2]^{2-}$[2] and $\delta = 0.37$ mm s^{-1} for $[Fe_2S_2(OPh)_4]^{2-}$.[1]

For the *Thermus thermophilus* Rieske protein the

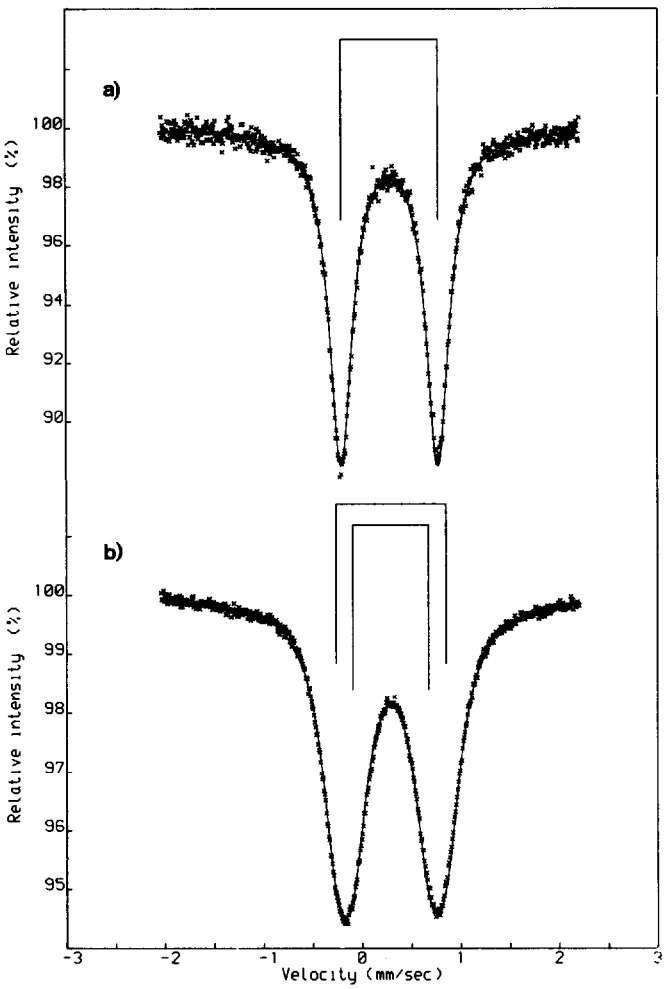

Fig. 2. ^{57}Fe Mössbauer spectra at 77 K and zero field for (a) **1** fitted by one doublet and (b) **3** fitted by two doublets.

iron sites are differentiated by unsymmetrical coordination having (1) $\delta = 0.24$ mm s^{-1} and (2) $\delta = 0.28$ (pH 10) or 0.32 mm s^{-1} (pH 7.8).[22] However, given the relative insensitivity of the isomer shifts of [2Fe—2S]$^{2+}$ complexes to changes in the terminal ligation and the variability found in isomer shift amongst tetra-cysteinyl coordinated [2Fe—2S]$^{2+}$ ferredoxins (δ = *ca* 0.2–0.3) the parameter is of limited utility in making structural comparisons. For the same reasons it is not surprising that we are unable confidently to resolve in the Mössbauer spectra of **4** the geometric isomers involving ligand coordination across the FeS_2Fe bridge indicated by ^{1}H NMR.

The relatively large ΔE_Q values observed for **1** and **3** seem characteristic of coordination by inflexible tight chelate rings since large splittings are also found for $[Fe_2S_2L_2]^{2-}$ L = 2,2′-biphenolate (ΔE_Q = 1.02 mm s^{-1}),[2] L = thiosalicylate (ΔE_Q = 1.09 mm s^{-1}) and L = dimethyl-2,2′-methylenebis(benzimidazolate) (ΔE_Q = 0.92 mm s^{-1}) (authors unpublished results) in comparison to ΔE_Q = 0.32–0.49 mm s^{-1} for coordination by monodentate SPh, OPh or pyrrolate or the more flexible chelate S_2—*o*-xylyl.[1,2,18]

Electrochemistry

DC polarography of the complexes in DMF shows two reduction waves at a RDME having half-wave potentials ($E_{1/2}$) with respect to a saturated calomel electrode as given in Table 1. For **1** the second wave is a composite of two poorly resolved reductions at *ca* −1.9 and −2.02 V and cannot be ascribed to a straightforward 3−/4− couple. The potentials for the first reductions, attributable to [2Fe—2S]$^{2+/1+}$, are very similar for **1**, **2** and **4** being intermediate between the corresponding values for $[Fe_2S_2(S_2$—*o*-xylyl$)_2]^{2-/3-}$ (−1.51 V)[4] and $[Fe_2S_2(OAr)_4]^{2-/3-}$ (*ca* −1.35 V).[3]

$E_{1/2}$ for **3** is consistent with the values for

$[Fe_2S_2(2,2'\text{-biphenolate})_2]^{2-/3-}$ and $[Fe_2S_2(2,2'\text{-bi(thiophenolate))}_2]^{2-/3-}$ of -1.36 and -1.35 V, respectively. These values are peculiarly coincident in view of the *ca* 200 mV increase in $E_{1/2}$ on going from tetra-coordination by monodentate thiophenolates to phenolates, and possibly reflect anomalous electronic properties for these ligands, apparent also in the EPR of their $[2Fe—2S]^+$ complexes.

The mid-point potentials of the cathodic and anodic current extrema observed for the 2−/3− couples of **1–4** by cyclic voltammetry at a glassy carbon electrode are in good agreement with the $E_{1/2}$ values measured using the RDME. For **1** the anodic peak current is around 90% of the cathodic peak current such that its first reduction process is the most reversible amongst the four complexes. The observation of an anodic feature in the 2−/3− cyclic voltammograms of all the complexes contrasts with the lack of such a feature for the monodentate ligated $[Fe_2S_2(XR)_4]^{2-/3-}$ (XR = OPh, SPh or SEt) complexes[1,3,23] and is probably a consequence of the chelate-stabilized coordination in **1–4** since the $[Fe_2S_2(S—o\text{-xylyl})_2]^{2-/3-}$ and $[Fe_2S_2(2,2'\text{-bi(thiophenolate)}_2]^{2-/3-}$ couples are close to reversible. This effect will be at its strongest in **1** for which the chelate ring is six-membered and results in the increased stability of $[Fe_2S_2(\mathbf{L1})_2]^{3-}$. However, little or no second cathodic peak is observed for **1**, in keeping with the anomalous behaviour at the RDME, but scanning to potentials more negative than -1.7 V leads to a small anodic feature at -0.97 V on the reverse scan due to a decomposition product with E_{mid} *ca* -1.0 V. Similar features are seen for **2** and **4**, for **3** at -0.76 V and for $[Fe_2S_2(SPh)_4]^{2-}$ at -0.74 V.[23] **2** and **4** show well-developed cathodic second reduction peaks at -1.90 and -1.92 V, respectively, but essentially no corresponding anodic peaks.

EPR

Before describing the EPR spectra for reduced **1–4** we will summarize briefly the somewhat unusual behaviour of $[2Fe—2S]^+$ complexes.

$[Fe_2S_2(SR)_4]^{3-}$ ferredoxins and inorganic complexes have EPR spectra characterized by average g values (g_{av}) of *ca* 1.96. When RS^- is a monodentate ligand (e.g. EtS^- or $p\text{-}C_6H_4S^-$, Y = Cl, H or Me) radically different EPR lineshapes are obtained if the solvent freezes as a glass.[24] In vitreous NMP these have $g_{av} = 1.91$–1.92 whilst in vitreous DMF $g_{av} \simeq 1.93$, though the latter type of lineshape transforms into the former on annealing the sample. We have interpreted this behaviour as resulting from a chemical modification of $[Fe_2S_2(SR)_4]^{3-}$ in the glassy solvent state involving substitutional or additional coordination, possibly by solvent.[24] For reduced $[Fe_2S_2(OAr)_4]^{2-}$ we obtained approximately axial spectra having $g_{av} = 1.92$, independent of the solvent or its state.[3] For this spectrum, the spectra of the modified $[Fe_2S_2(SR)_4]^{3-}$ having $g_{av} \simeq 1.91$–1.92 and for the Rieske-type proteins Bertrand *et al.*[25] have shown there to be a strong correlation between the lowest g values (g_2 and g_3) and their splitting (g_2–g_3), which may be understood in terms of a variable weak distortion at the Fe^{2+} ion in a coordination environment having a large inequivalence between the bridging-sulphur and terminal ligands.

For complex **1** reduction proceeds quantitatively to give nearly axial spectra which although sharper for the glassy solvent containing $n\text{Bu}_4\text{NClO}_4$ than for pure frozen solvent have g values essentially independent of the solvent with $g_{av} = 1.929$ (see Table 1 where the presence of linewidth data indicates that the g values result from a simulation). Figure 3 shows typical spectra for reduced **1** and **3** in glassy DMF together with calculated lineshapes. The $g_{av} = 1.928$ spectrum of reduced **3**, representing *ca* 60% yield, is also observed in pure DMF or NMP solvents. However, in glassy NMP a new sharper lineshape is observed, having g values of 2.023, 1.904 and 1.865 ($g_{av} = 1.931$), which dominates the spectrum for low concentrations of **3** but which at high concentrations is present as a minority subspectrum superimposed upon a lineshape of the type in Fig. 3(b). In our experience NMP is a more potent agent than DMF for effecting the $g = 1.92$ type modification to $[Fe_2S_2(SR)_4]^{3-}$

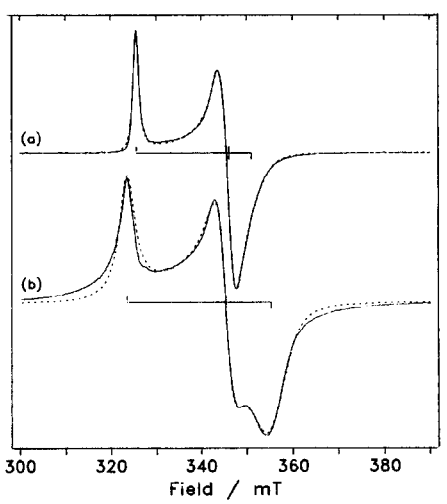

Fig. 3. EPR spectra at 9.20 GHz and 77 K of (a) $[Fe_2S_2(\mathbf{L1})_2]^{3-}$ (reduced **1**) and (b) $[Fe_2S_2(\mathbf{L3})_2]^{3-}$ (reduced **3**) in DMF containing $n\text{Bu}_4\text{NClO}_4$, together with simulated spectra (dashed lines).

described above.[24] However, although the general sharpening of the spectrum for **3** reduced in 0.2 M nBu$_4$NClO$_4$–NMP and the shift of g_1 from 2.030 to 2.023 are typical of the $g = 1.92$ type modification, the values of g_2 and g_3 change very little and g_{av} remains *ca* 1.93.

Whilst the near coincidence of g_{av} for reduced **1** and **3** could properly reflect the similarity of their coordination environments, the anomalous EPR from the use of the symmetrical 2,2′-chalcogenide-substituted biphenyls should be noted. Thus the EPR for $[Fe_2S_2(2,2'\text{-bi(thiophenolate)})_2]^{3-}$ has $g_{av} = 1.951$, rather lower than the range 1.956–1.959 for other $[Fe_2S_2(SR)_4]^{3-}$ complexes,[24] whilst reduced $[Fe_2S_2(2,2'\text{-biphenolate})_2]^{2-}$ has g values of 2.021, 1.901 and 1.858 with $g_{av} = 1.927$, rather higher than 1.920 for other phenolates[3] and in fact very similar to reduced **3**.

In keeping with the information afforded by cyclic voltammetry **1** is the most stable of the four complexes on reduction, having a half-life in excess of 5 min in NMP at room temperature, although this is reduced to *ca* 2–3 min in DMF. This stability is comparable to or better than that for $[Fe_2S_2(S_2\text{—}o\text{-xylyl})_2]^{3-}$ but is low compared to the half-life of *ca* 30 min for $[Fe_2S_2(\text{thiosalicylate})_3]^{3-}$ or 1 h for $[Fe_2S_2(2\text{-(2-phenolate)benzimidazolate})_2]^{3-}$. Reduced **3**, and in particular reduced **2** and **4** are rather less stable with EPR signals measured at 77 K decaying to only a few per cent if samples are held at room temperature for 2–3 min.

On reduction in glassy DMF, **4** shows a well-formed EPR spectrum with g values of 2.021, 1.886 and 1.842 ($g_{av} = 1.916$) in around 60% yield. A very similar spectrum is observed using pure NMP or NMP–nBu$_4$NClO$_4$ glass. The lineshape and g values for this signal closely match those for reduced $[Fe_2S_2(SEt)_4]^{2-}$ in glassy NMP (2.021, 1.895 and 1.849, $g_{av} = 1.922$) for which there is the $g = 1.92$ type modification to the coordination. These g values fit well to the plot of g_2 and g_3 against $(g_2 - g_3)$ for the $g \simeq 1.92$ [2Fe—2S]$^+$ group[25] which includes reduced $[Fe_2S_2(OAr)_4]^{2-}$. Although it is possible that on reduction **4** has undergone some chemical modification involving solvent, of the sort indicated for $[Fe_2S_2(SR)_4]^{3-}$, an alternative explanation is that the ligands have rearranged to coordinate across the FeS_2Fe unit (as suggested by NMR to occur in part before reduction) with two oxygens bound to the Fe^{2+} and two sulphurs to Fe^{3+}, which we believe would lead to a $g \simeq 1.92$ type EPR signal.

For **4**, reduced in pure DMF, there is a complication to the resulting spectrum with the appearance of additional features at $g = 2.004$ and 1.947. The spectra for reduced **2** are intermediate between the cases for **1**, **3** and **4**. Although in glassy NMP a straightforward $\mathbf{g} \simeq 1.92$ type signal is observed ($g = 2.021$, 1.889 and 1.844, $g_{av} = 1.918$), in pure NMP the spectrum is complicated by an additional small feature at $g = 1.931$. This latter signal is predominant in glassy DMF where the spectrum has g values of 2.023, 1.930 and 1.857, $g_{av} = 1.937$.

As judged by their solvent independency and by differences in both g values and lineshape, from the $g \simeq 1.92$ type we assign the spectra of reduced **1** and **3** in Fig. 3(a) and (b) to $[Fe_2S_2(\mathbf{L1})_2]^{3-}$ and $[Fe_2S_2(\mathbf{L3})_2]^{3-}$, respectively, unaffected by solvent modifications. The intermediate case of reduced **2** is more complicated but the spectrum reported in Table 1 likely results from a straightforward reduction. On the other hand the spectra for this complex in NMP and the spectra for reduced **4** of the $g \simeq 1.92$ type are readily assigned to species in which either the ligands have rearranged to provide bis-phenolate coordination at the Fe^{2+} or solvent modification of the coordination sphere has occurred owing to the decreased chelating ability of **L2** and **L4**.

In our original report of the EPR spectra for reduced $[Fe_2S_2(OAr)_4]^{2-}$ with $g_{av} = 1.920$ we were reluctant to make a firm assignment to a trianion formed by straightforward reduction because of the possibility of subsequent solvent modifications to the terminal ligation.[3] However, given the assignments made here for phenolate–thiolate coordination in $[Fe_2S_2L_2]^{3-}$ L = **L1** or **L3** to spectra with $g_{av} = 1.928$–1.929, it does appear that phenolate is very effective in lowering g_2 and g_3 for [2Fe—2S]$^+$ and that the spectrum observed for reduced $[Fe_2S_2(OAr)_4]^{2-}$ does correspond to simple one-electron reduction to the trianion. $[Fe_2S_2(2\text{-(2-phenolate)benzimidazolate})_2]^{3-}$ fits very well into the g_2, g_3 vs $(g_2 - g_3)$ plot for the $g \simeq 1.92$ group,[25] further demonstrating the ability of phenolate to decrease g_2 and g_3 in comparison to $g_{av} = 1.94$ for coordination entirely by benzimidazolate. For carboxylate–thiolate coordination of [2Fe—2S]$^+$, $g_{av} = 1.924$–1.931,[4] similar to the effects of phenolate–thiolate reported here. Thus, our previous observations are confirmed, that coordination by an oxygenous ligand, in addition to the nitrogenous coordination indicated by ENDOR and ESEEM,[26] is necessary to bring the lowest g values of the Rieske proteins into the range $g_{av} \simeq 1.90$–1.92 observed.[25]

Acknowledgements—We would like to thank Sue Johnson for running 250 MHz NMR spectra. We are also very grateful to Mr W. G. Marshall and to Dr B. W. Fitzsimmons of Birkbeck college for measuring and fitting the Mössbauer spectra. This work was supported by SERC grant GR/E 5469.6.

REFERENCES

1. W. E. Cleland and B. A. Averill, *Inorg. Chem.* 1984, **23**, 4192.
2. D. Coucouvanis, A. Salifoglou, M. G. Kanatzidis, A. Simopoulos and V. Papaefthymiou, *J. Am. Chem. Soc.* 1984, **106**, 6081.
3. P. Beardwood and J. F. Gibson, *J. Chem. Soc., Chem. Commun.* 1985, 102.
4. P. Beardwood and J. F. Gibson, *J. Chem. Soc., Chem. Commun.* 1985, 1345.
5. P. Beardwood and J. F. Gibson, *J. Chem. Soc., Chem. Commun.* 1986, 490.
6. R. Grice and L. N. Owen, *J. Chem. Soc.* 1963, 1947.
7. H. Hayashi and S. Oka, *Bull. Inst. Chem. Res., Kyoto Univ.* 1974, **52**, 514.
8. N. Minami and S. Kijima, *Chem. Pharm. Bull.* 1979, **27**, 816.
9. E. N. Givens and L. A. Hamilton, *J. Org. Chem.* 1967, **32**, 2857.
10. G. Hanson and D. S. Kemp, *J. Org. Chem.* 1981, **46**, 5441.
11. W. F. Baitinger, P. von R. Schleyer and K. Mislow, *J. Am. Chem. Soc.* 1965, **87**, 3168.
12. Y. Do, E. D. Simhon and R. H. Holm, *Inorg. Chem.* 1983, **22**, 3809.
13. P. Beardwood, J. F. Gibson, C. E. Johnson and J. D. Rush, *J. Chem. Soc., Dalton Trans.* 1982, 2015.
14. L. K. White and R. L. Belford, *J. Am. Chem. Soc.* 1976, **98**, 4428.
15. P. Beardwood, Ph.D. thesis. University of London (1983).
16. S. A. Koch and M. Millar, *J. Am. Chem. Soc.* 1982, **104**, 5255.
17. W. E. Cleland, D. A. Holtman, M. Sabat, J. A. Ibers, G. C. DeFotis and B. A. Averill, *J. Am. Chem. Soc.* 1983, **105**, 6021.
18. W. O. Gillum, R. B. Frankel, S. Foner and R. H. Holm, *Inorg. Chem.* 1976, **15**, 1095.
19. J. G. Reynolds and R. H. Holm, *Inorg. Chem.* 1980, **19**, 3257.
20. K. S. Hagen, A. D. Watson and R. H. Holm, *J. Am. Chem. Soc.* 1983, **105**, 3905.
21. J. A. Fee, K. L. Findling, T. Yoshida, R. Hille, G. E. Tarr, D. O. Hearshen, W. R. Dunham, E. P. Day, T. A. Kent and E. Münck, *J. Biol. Chem.* 1984, **259**, 124.
22. D. Kuila and J. A. Fee, *J. Biol. Chem.* 1986, **261**, 2768.
23. J. Cambray, R. W. Lane, A. G. Wedd, R. W. Johnson and R. H. Holm, *Inorg. Chem.* 1977, **16**, 2565.
24. P. Beardwood and J. F. Gibson, *J. Chem. Soc., Dalton Trans.* 1983, 737.
25. P. Bertrand, B. Guigliarelli, J-P. Gayda, P. Beardwood and J. F. Gibson, *Biochim. Biophys. Acta* 1985, **831**, 261.
26. J. F. Cline, B. M. Hoffman, W. B. Mims, E. LaHaie, D. P. Ballou and J. A. Fee, *J. Biol. Chem.* 1985, **260**, 3251; J. Telser, B. M. Hoffman, R. LoBrutto, T. Ohnishi, A-L. Tsai, D. Simpkin and G. Palmer, *FEBS Lett.* 1987, **214**, 117.

Polyhedron Vol. 7, No. 19/20, pp. 1919–1924, 1988
Printed in Great Britain

0277–5387/88 $3.00+.00
© 1988 Pergamon Press plc

COMPLEXES OF THE PLATINUM METALS—XXXIV.* SYNTHESIS AND CHARACTERIZATION OF SOME BINUCLEAR RUTHENIUM(I/I) TRIAZENIDO COMPLEXES: X-RAY CRYSTAL STRUCTURE OF TETRACARBONYLBIS (μ-1,3-DI-*p*-TOLYLTRIAZENIDO)BIS(*p*-TOLUIDINE) DIRUTHENIUM(I/I)

STEPHEN F. COLSON and STEPHEN D. ROBINSON†

Department of Chemistry, King's College, Strand, London WC2R 2LS, U.K.

and

MAJID MOTEVALLI and MICHAEL B. HURSTHOUSE

Department of Chemistry, Queen Mary College, Mile End Road, London E1 4NS, U.K.

Abstract—The ruthenium(I) triazenido complexes $[Ru(ArNNNAr)(CO)_3]_2$ (Ar = *p*-C_6H_4Me or *p*-C_6H_4Cl) have been prepared by heating $Ru_3(CO)_{12}$ with free triazene in benzene under a carbon monoxide atmosphere, and by heating $[Ru(O_2CMe)(CO)_2]_n$ with free triazene and triethylamine in acetonitrile under carbon monoxide. Reactions of the diruthenium(I/I) triazenido complexes with PPh_3, $P(OMe)_3$ or ArNNNHAr (Ar = *p*-C_6H_4Cl) afford axial substitution products of the general form $[Ru(ArNNNAr)(CO)_2L]_2$. However, with ArNNNHAr (Ar = *p*-C_6H_4Me) cleavage of triazene to generate axial *p*-toluidine ligands occurs. The structure of the *p*-toluidine adduct, $[Ru(ArNNNAr)(CO)_2(NH_2Ar)]_2$ has been determined by X-ray diffraction methods. The compound crystallizes in space group $P\bar{1}$ with $a = 11.350(1)$, $b = 20.582(4)$, $c = 10.371(5)$ Å, $\alpha = 100.75(4)$, $\beta = 104.30(3)$, $\gamma = 84.40(1)°$; $U = 2303.89$ Å^3 and $Z = 2$.

The synthesis of the carboxylates $[Ru(O_2CR)(CO)_2]_n$ and $[Ru(O_2CR)(CO)_2L]_2$ (R = H, Me, Et, $^nC_9H_{19}$; L = CO, PPh_3, $AsPh_3$, py, MeCN) in 1969[2] marked a significant milestone in the development of ruthenium(I) chemistry. In the intervening years these carboxylate derivatives have been extensively studied[3–9] and a number of analogous metal–metal bonded diruthenium(I/I) complexes with other bridging ligands including mercaptobenzothiazolate[10] and pyrazolate[11] anions have been characterized. However, although there is a marked similarity between the structural chemistry of polynuclear metal carboxylates[12] and triazenides,[13] binuclear ruthenium(I) triazenido complexes of the form $[Ru(ArNNNAr)(CO)_3]_2$ do not appear to have been described. We now report the synthesis and axial substitution reactions of some compounds of this type, and the molecular structure of one example $[Ru(ArNNNAr)(CO)_2(NH_2Ar)]_2$ (Ar = *p*-C_6H_4Me).

EXPERIMENTAL

General

Hydrated ruthenium trichloride was supplied by Johnson Matthey plc, 1,3-diaryltriazenes were prepared by a standard literature procedure.[14] Reactions were performed under a nitrogen atmosphere but products were worked up in the open laboratory. IR spectra were recorded on a Perkin–Elmer 983G spectrometer using samples mulled in Nujol between CsI plates. Proton NMR spectra were recorded in $CDCl_3$ solution on a Bruker WM-250 spectrometer at 250.13 MHz and are referenced to internal TMS. Phosphorus-31 spectra were recorded in $CDCl_3$ solution on a Bruker HFX-90 spectrometer at 36.43 MHz and are referenced to external 85%

Dedicated to Professor Sir Geoffrey Wilkinson in recognition of his outstanding achievements in the field of organometallic chemistry.

* For part XXXIII, see ref. 1.

† Author to whom correspondence should be addressed.

Table 1. Melting points[a] and analytical data[b]

Complex	Ar	M.p. (°C)	C	H	N
$Ru_2(ArNNNAr)_2(CO)_6$	*p*-C_6H_4Me	180–184	50.0(49.8)	3.4(3.4)	10.4(10.2)
$Ru_2(ArNNNAr)_2(CO)_6$	*p*-C_6H_4Cl	206–209	39.7(40.0)	1.6(1.8)	9.1(9.3)
$Ru_2(ArNNNAr)_2(CO)_4(ArNH_2)_2$	*p*-C_6H_4Me	202–205	56.2(55.9)	4.6(4.3)	11.4(12.7)
$Ru_2(ArNNNAr)_2(CO)_4(ArNNNHAr)_2$	*p*-C_6H_4Cl	212-214	45.4(45.3)	2.2(2.5)	11.9(12.2)
$Ru_2(ArNNNAr)_2(CO)_4(PPh_3)_2$	*p*-C_6H_4Me	216–220	63.4(63.4)	4.4(4.5)	6.4(6.5)
$Ru_2(ArNNNAr)_2(CO)_4(PPh_3)_2$	*p*-C_6H_4Cl	247–250	56.3(56.1)	3.3(3.4)	6.0(6.1)
$Ru_2(ArNNNAr)_2(CO)_4\{P(OMe)_3\}_2$	*p*-C_6H_4Me	194–197	45.1(45.1)	4.5(4.6)	8.3(8.3)
$Ru_2(ArNNNAr)_2(CO)_4\{P(OMe)_3\}_2$	*p*-C_6H_4Cl	204–207	37.0(37.4)	3.0(3.1)	7.5(7.7)

[a] M.p. taken in sealed tubes under nitrogen.
[b] Calculated figures in parentheses.

H_3PO_4. Melting points were taken in sealed tubes under nitrogen. Microanalysis were performed in the microanalytical laboratories at King's College and University College London. Melting points and analytical data are collected in Table 1.

*Synthesis of hexacarbonylbis(μ-1,3-di-*p*-tolyltriazenido)diruthenium*(I/I)

(a) *From triruthenium dodecarbonyl.* Triruthenium dodecacarbonyl (0.20 g, 0.31 mmol) was added to a solution of 1,3-di-*p*-tolyltriazene (0.2 g, 0.89 mmol) in benzene (20 cm^3) and the mixture was heated under reflux in a carbon monoxide atmosphere for 18 h. After cooling, the dark solution was filtered and the filtrate evaporated under reduced pressure to leave an oil which solidified on trituration with ethanol. The solid was crystallized from dichloromethane–ethanol then washed with ethanol and dried *in vacuo* to afford *orange microcrystals* (0.12 g, 47%).

(b) *From* catena-*acetatodicarbonylruthenium. Catena*-acetatodicarbonylruthenium (0.25 g, 0.59 mmol) and triethylamine (1 g, 10 mmol) were added to a solution of 1,3-di-*p*-tolyltriazene (0.5 g, 2.23 mmol) in acetonitrile (15 cm^3) and the mixture heated under reflux in a carbon monoxide atmosphere for 3 h. The dark solution was allowed to stand under a carbon monoxide atmosphere for 12 h after which time the product was collected by filtration. Crystallization from dichloromethane–ethanol followed by washing with ethanol and drying *in vacuo* afforded *orange microcrystals* (0.21 g, 43.5%).

*Synthesis of hexacarbonylbis(μ-1,3-di-*p*-chlorophenyltriazenido)diruthenium*(I/I)

Method (a) gave orange–yellow microcrystals (77.5%). Synthesis by method (b) gave orange–yellow microcrystals (69%).

*Synthesis of tetracarbonylbis(triphenylphosphine) bis(μ-1,3-di-*p*-tolyltriazenido)diruthenium*(I/I)

Hexacarbonylbis(μ-1,3-di-*p*-tolyltriazenido)diruthenium (0.1 g, 0.12 mmol) was added to a solution of triphenylphosphine (0.15 g, 0.57 mmol) in benzene (15 cm^3) and the mixture was heated under reflux for 1 h. After cooling, the orange solution was filtered and the filtrate evaporated under reduced pressure, the residual oil was then triturated in ethanol to give a solid.

Crystallization from dichloromethane–ethanol followed by washing with ethanol and drying *in vacuo* afforded *bright orange microcrystals* (0.11 g, 71%).

*Synthesis of tetracarbonylbis(triphenylphosphine) bis(μ-1,3-di-*p*-chlorophenyltriazenido)diruthenium*(I/I)

Using the same method as above gave bright orange microcrystals (75%).

*Synthesis of tetracarbonylbis(trimethylphosphite) bis(μ-1,3-di-*p*-tolyltriazenido)diruthenium*(I/I)

Hexacarbonylbis(μ-1,3-di-*p*-tolyltriazenido)diruthenium (0.15 g, 0.2 mmol) was added to a solution of trimethylphosphite (0.1 g, 0.81 mmol) in benzene (15 cm^3) and the mixture heated under reflux for 1 h. After cooling, the orange solution was filtered and the filtrate evaporated under reduced pressure. The resulting oil was triturated in ethanol to produce a solid which after crystallization from dichloromethane–ethanol, washing with ethanol and drying *in vacuo* afforded *orange–yellow microcrystals* (0.15 g, 74.5%).

Synthesis of tetracarbonylbis(trimethylphosphite) bis(μ - 1,3 - di - p - chlorophenyltriazenido)diruthenium(I/I)

Using the same method as above gave orange microcrystals (54%).

Synthesis of tetracarbonylbis(μ-1,3-di-p-tolyltriazenido)bis(p-toluidine)diruthenium(I/I)

Triruthenium dodecacarbonyl (0.3 g, 0.47 mmol) was added to a solution of 1,3-di-*p*-tolyltriazene (0.5 g, 2.2 mmol) in benzene (15 cm^3) and the mixture heated under reflux for 18 h. After cooling, the orange–red solution was filtered and the filtrate evaporated under reduced pressure. The residual oil was triturated in ethanol to produce a solid which after crystallization from dichloromethane–ethanol, washing with ethanol and drying *in vacuo* afforded *orange–brown crystals* (0.21 g, 43%).

Synthesis of tetracarbonylbis(μ-1,3-di-p-chlorophenyltriazenido)bis(1,3-di-p-chlorophenyltriazene) diruthenium(I/I)

Triruthenium dodecacarbonyl (0.2 g, 0.31 mmol) was added to a solution of 1,3-di-*p*-chlorophenyltriazene (0.5 g, 1.89 mmol) in benzene (20 cm^3) and the mixture heated under reflux for 18 h. After cooling, the orange–red solution was filtered and the filtrate evaporated under reduced pressure. The residual oil was triturated to give a solid which after crystallization from dichloromethane–methanol and drying *in vacuo* afforded *deep red crystals* (0.19 g, 44.5%).

X-ray crystal structure of $[Ru(ArNNNAr)(CO)_2(NH_2Ar)]_2$ (Ar = *p*-C_6H_4Me)

Crystal data. $C_{46}H_{46}N_8O_4Ru_2$, $M = 977.06$. Triclinic, $a = 11.350(1)$, $b = 20.582(4)$, $c = 10.371(5)$ Å, $\alpha = 100.75(4)$, $\beta = 104.30(3)$, $\gamma = 84.40(1)°$, $U = 2303.89$ Å^3. Space group $P\bar{1}$, $Z = 2$, $D_c = 1.41$ g cm^{-3}, $F(000) = 996.06$, μ(Mo-K_α) = 6.90 cm^{-1}.

Data collection. Intensity data were recorded on a Nonius CAD4 diffractometer in a standard manner using Mo-K_α radiation, graphite monochromatized, (Mo-K_α) = 0.71069 Å and a $\omega/2\theta$ scan mode with $1.5 < \theta < 25$.[15] A total of 8844 reflections were recorded, of which 8110 were unique (merging $R = 0.04$) and 6958 satisfied the condition $I > 1.5\sigma(I)$.

Structure solution and refinement. The structure was solved via the heavy atom method and refined by least squares, with non-hydrogen atoms anisotropic and hydrogens inserted in idealized positions with group μ_{iso} values. The final R values are $R = 0.0395$, $R_g = 0.0485$.

RESULTS AND DISCUSSION

The new binuclear ruthenium(I/I) triazenido complexes $[Ru(ArNNNAr)(CO)_3]_2$ have been prepared from $Ru_3(CO)_{12}$ and free 1,3-diaryltriazenes in a reaction which parallels that used in the original synthesis of the binuclear ruthenium(I/I) carboxylates.[2] They can also be obtained by treatment of the latter species with free triazenes in the presence of excess triethylamine, and were isolated as orange–yellow air-stable microcrystals. The IR and ^1H NMR data (Table 2) recorded for these products, in particular the presence of four strong ν(CO) stretches in the region 2100–2000 cm^{-1}, (ref. 7) are entirely consistent with the highly symmetrical structure (**I**). Unlike their carboxylate analogues which spontaneously lose carbon monoxide to form O-bridged polymers $[Ru(O_2CR)(CO)_2]_n$ the triazenido products, $[Ru(ArNNNAr)(CO)_3]_2$, are stable with respect to carbon monoxide dissociation at normal temperature and pressure. This difference in behaviour presumably reflects stronger Lewis basicity of the triazenide ligand relative to the carboxylate ligand, resulting in higher electron density on the metal centre and consequently a greater degree of synergic d_π–p_π bonding from metal t_{2g} to carbonyl π^* orbitals in the triazenido complexes. Support for this hypothesis is provided by the ν(CO) values recorded which are on average 30–35 cm^{-1} lower for the triazenido complexes than they are for the corresponding acetate.[2] Similar reluctance to lose axial carbonyl ligands has recently been reported for the closely related pyrazolato-bridged diruthenium(I/I) species $[Ru(pyrazolate)(CO)_3]_2$,[11] which display ν(CO) frequencies virtually identical to those recorded for the triazenido complexes.

However, carbonyl ligands are readily lost from the complexes $[Ru(ArNNNAr)(CO)_3]_2$ on treatment with P-donor ligands to give axial substitution products, $[Ru(ArNNNAr)(CO)_2L]_2$ [L = PPh_3, $P(OMe)_3$]. The $^{31}P\{^1H\}$ NMR spectra of these complexes each show a singlet consistent with the proposed axial disubstituted structure (**II**). The ^1H NMR spectra of the $P(OMe)_3$ substituted complexes each contain a three-line pattern characteristic of the $A_nA'_n$ part of an $A_nA'_nXX'$ spectrum[16] and thus provide a further example of virtual coupling between $P(OMe)_3$ ligands across a binuclear metal centre.[17]

When a large excess of di-*p*-chlorophenyl triazene was allowed to react with $Ru_3(CO)_{12}$, the isolated

Table 2. Spectroscopic data

Complex	Ar	Infrared spectra[a] ν(CO) (cm^{-1})			Nuclear magnetic resonance spectra[b] δH(aromatic) (ppm)			δH(methyl) (ppm)		δP (ppm)
$Ru_2(ArNNNAr)_2(CO)_6$	*p*-C_6H_4Me	2089(s)	2062(s)	2024(s)	7.16(s)	7.05(d)	—	—	2.31(s)	—
$Ru_2(ArNNNAr)_2(CO)_6$	*p*-C_6H_4Cl	2093(s)	2067(s)	2029(s)	7.25(d)	7.15(d)	—	—	—	—
$Ru_2(ArNNNAr)_2(CO)_4(ArNH_2)_2$	*p*-C_6H_4Me	2093(m)	2073(s)	2036(s)	7.27(d)	7.21(d)	6.95(d)[c]	6.43(d)[c]	2.31(s)	2.22(s)[d]	—
		1979(s)	1958(s)	1936(s)							
$Ru_2(ArNNNAr)_2(CO)_4(ArNNNHAr)_2$	*p*-C_6H_4Cl	2070(s)	2011(s)	—	—	7.35(d)	7.23(d)	7.13(d)	6.94(d)	—	—	—
$Ru(ArNNNAr)_2(CO)_4(PPh_3)_2$	*p*-C_6H_4Me	2015(sh)	1989(s)	1951(s)	—	7.16(m)	7.06(m)	6.69(d)	6.61(d)	2.24(s)	—	25.23(s)
$Ru(ArNNNAr)_2(CO)_4(PPh_3)_2$	*p*-C_6H_4Cl	2018(sh)	1988(m)	1951(s)	—	7.21(m)	7.10(m)	6.81(m)	6.46(d)	—	—	25.47(s)
$Ru_2(ArNNNAr)_2(CO)_4\{P(OMe)_3\}_2$	*p*-C_6H_4Me	2028(m)	1997(s)	1963(s)	—	6.99(d)	6.91(d)	—	—	3.43(t)	2.30(s)	129.8(s)
$Ru_2(ArNNNAr)_2(CO)_4\{P(OMe)_3\}$	*p*-C_6H_4Cl	2031(sh)	2001(s)	1965(s)	—	7.08(d)	6.90(d)	—	—	3.45(t)	—	128.7(s)

[a] IR spectra: s = strong, m = medium, sh = shoulder.
[b] NMR spectra: δ values relative to TMS (^1H) or 85% H_3PO_4 (^{31}P), s = singlet, d = doublet, t = triplet, m = multiplet.
[c] Half integral intensity of resonances at 7.27 and 7.21 ppm.
[d] Half integral intensity of resonance at 2.31 ppm.

product gave analytical and spectroscopic data consistent with the formation of a bis(triazene) axial substitution complex [Ru(ArNNNAr)$(CO)_2$(ArNNNHAr)$]_2$ (Ar = *p*-C_6H_4Cl) formally analogous to the recently reported[7,8] carboxylic acid adduct [Ru$(O_2CPh)(CO)_2(PhCO_2H)]_2$. The ^1H NMR data, which indicate the presence of *p*-C_6H_4Cl groups in two different environments (ratio 1 : 1), are consistent with the proposed structure (**III**) if we assume that the A_2B_2 patterns arising from the aromatic protons in the two *p*-C_6H_4Cl groups of the axial triazene ligands are identical. This situation could be coincidental or might indicate the occurrence of a labile fluxional N(1), N(3) interchange at the axial positions. However, in a similar synthesis involving excess 1,3-di-*p*-tolyltriazene cleavage of triazene molecules and coordination of *p*-toluidine fragments leading to formation of the axial substitution product, [Ru(ArNNNAr)$(CO)_2(NH_2Ar)]_2$ (Ar = *p*-C_6H_4Me) occurs. Fragmentation of 1,3-diaryltriazenes under acid conditions with concomitant coordination of the ArN_2^+ moiety is well-known, and has been used as an efficient route to certain aryldiazo complexes.[18] However, to the best of our knowledge there has been no previously reported example involving coordination of the amine, NH_2Ar, fragment formed in such reactions. The axial N-donor ligands in the complexes [Ru(ArNNNAr)$(CO)_2$(ArNNNHAr)$]_2$ (Ar = *p*-C_6H_4Cl) and [Ru(ArNNNAr)$(CO)_2(NH_2Ar)]_2$ (Ar = *p*-C_6H_4Me) are readily displaced by carbon monoxide, triphenylphosphine and trimethylphosphite to yield products of the form [Ru(ArNNNAr)$(CO)_2L]_2$ (L = CO, PPh_3 and $P(OMe)_3$, respectively).

In order to characterize the binuclear triazenido-bridged diruthenium(I/I) structure and to confirm the nature of the axial *p*-toluidine ligands an X-ray diffraction study was performed on a crystal of [Ru(ArNNNAr)$(CO)_2(NH_2Ar)]_2$ (Ar = *p*-C_6H_4Me). The molecular structure is shown in Fig. 1, selected bond lengths and bond angles are given in Table 3. The structure is similar in general form to those previously determined for related carboxylato-bridged diruthenium(I/I) complexes. The two ruthenium atoms are linked by a Ru—Ru bond and a *cis* pair of bridging triazenide ligands. The coordination sphere about each ruthenium is completed by a pair of terminal carbonyl ligands in the equatorial sites and a *p*-toluidine ligand in the axial position. The coordination geometry about each ruthenium centre is essentially octahedral with bond angles subtended at ruthenium by *cis* ligand pairs ranging from 80.5° [∠ Ru(2)—Ru(1)—N(1)] to 97.4° [∠ N(7)—Ru(1)—C(1)]. The N—Ru—Ru—N axis is approximately linear with

Table 3. Selected bond lengths and bond angles for $C_{46}H_{46}N_8O_4Ru_2$

Bond lengths (Å)			
Ru(2)—Ru(1)	2.665	N(1)—Ru(1)	2.159(6)
N(6)—Ru(1)	2.150(5)	N(7)—Ru(1)	2.332(6)
C(1)—Ru(1)	1.844(7)	C(2)—Ru(1)	1.853(7)
N(3)—Ru(2)	2.162(6)	N(4)—Ru(2)	2.143(5)
N(8)—Ru(2)	2.286(5)	C(3)—Ru(2)	1.861(7)
C(4)—Ru(2)	1.858(6)	N(2)—N(1)	1.294(5)
C(11)—N(1)	1.445(5)	N(3)—N(2)	1.300(6)
C(31)—N(3)	1.437(5)	N(5)—N(4)	1.296(5)
C(41)—N(4)	1.444(5)	N(6)—N(5)	1.293(5)
C(61)—N(6)	1.446(5)	C(21)—N(7)	1.421(6)
C(51)—N(8)	1.430(6)	C(1)—O(11)	1.140(7)
C(2)—O(21)	1.141(8)	C(3)—O(31)	1.143(8)
C(4)—O(41)	1.140(7)		
Bond angles (°)			
N(1)—Ru(1)—Ru(2)	80.5(2)	N(6)—Ru(1)—Ru(2)	82.6(2)
N(6)—Ru(1)—N(1)	87.8(2)	N(7)—Ru(1)—Ru(2)	166.0(1)
N(7)—Ru(1)—N(1)	89.8(2)	N(7)—Ru(1)—N(6)	86.9(2)
C(1)—Ru(1)—Ru(2)	92.6(2)	C(1)—Ru(1)—N(1)	89.0(3)
C(1)—Ru(1)—N(6)	174.6(2)	C(1)—Ru(1)—N(7)	97.4(3)
C(2)—Ru(1)—Ru(2)	93.5(2)	C(2)—Ru(1)—N(1)	172.5(2)
C(2)—Ru(1)—N(6)	96.0(3)	C(2)—Ru(1)—N(7)	96.9(3)
C(2)—Ru(1)—C(1)	86.8(3)	N(3)—Ru(2)—Ru(1)	83.7(2)
N(4)—Ru(2)—Ru(1)	80.7(2)	N(4)—Ru(2)—N(3)	86.7(2)
N(8)—Ru(2)—Ru(1)	168.4(1)	N(8)—Ru(2)—N(3)	89.3(2)
N(8)—Ru(2)—N(4)	89.7(2)	C(3)—Ru(2)—Ru(1)	92.5(2)
C(3)—Ru(2)—N(3)	174.9(2)	C(3)—Ru(2)—N(4)	89.4(3)
C(3)—Ru(2)—N(8)	94.0(3)	C(4)—Ru(2)—Ru(1)	94.3(2)
C(4)—Ru(2)—N(3)	94.1(3)	C(4)—Ru(2)—N(4)	174.8(1)
C(4)—Ru(2)—N(8)	95.4(3)	C(4)—Ru(2)—C(3)	89.5(3)
N(2)—N(1)—Ru(1)	126.7(4)	C(11)—N(1)—Ru(1)	119.3(3)
C(11)—N(1)—N(2)	110.2(4)	N(3)—N(2)—N(1)	116.1(4)
N(2)—N(3)—Ru(2)	123.5(3)	C(31)—N(3)—Ru(2)	124.9(3)
C(31)—N(3)—N(2)	110.4(4)	N(5)—N(4)—Ru(2)	126.7(3)
C(41)—N(4)—Ru(2)	120.5(3)	C(41)—N(4)—N(5)	110.7(4)
N(6)—N(5)—N(4)	115.6(4)	N(5)—N(6)—Ru(1)	123.6(3)
C(61)—N(6)—Ru(1)	124.2(3)	C(61)—N(6)—N(5)	110.1(4)
C(21)—N(7)—Ru(1)	122.3(4)	C(51)—N(8)—Ru(2)	117.9(4)
O(11)—C(1)—Ru(1)	178.2(6)	O(21)—C(2)—Ru(1)	176.3(4)
O(31)—C(3)—Ru(2)	179.3(4)	O(41)—C(4)—Ru(2)	177.0(4)
C(22)—C(21)—N(7)	119.8(4)	C(26)—C(21)—N(7)	120.2(4)
C(52)—C(51)—N(8)	119.1(3)	C(56)—C(51)—N(8)	120.8(4)

∠N(7)—Ru(1)—Ru(2) and ∠N(8)—Ru(2)—Ru(1) equal to 166.0 and 168.4°, respectively. The ruthenium–ruthenium distance (2.665(1) Å) is typical for Ru—Ru bond lengths in complexes of the general form $Ru_2(bridge)_2(CO)_4L_2$ which range from a rather exceptional 3.056(1) Å in $[Ru\{Si(Me)_2CH_2PPh_2\}(CO)_3]_2$[19] to a more usual 2.630(2) Å in $[Ru_2(O_2CBu^{sec})_2(CO)_4(sec\text{-}BuCO_2H)]_2$[7,8] and is similar to the values recorded for a number of binuclear diruthenium(I/I) carboxylates including $[Ru(O_2CPr)(CO)_2(PBu^i_3)]_2$ (2.728(1) Å),[5] $[Ru_2(O_2CC_6H_4F\text{-}4)_2(CO)_5(H_2O)]$ (2.649(2) Å),[7] $[Ru(O_2CPh)(CO)_2(PhCO_2H)]_2$ (2.637(2) Å)[7,8] and $[Ru_2(O_2CBu^{sec})_2(CO)_4(sec\text{-}BuCO_2H)]_2$ (2.630(2) Å).[7,8] Bond lengths and bond angles associated with the bridging triazenide ligands have values similar to those found in other triazenido-bridged complexes.[13] Likewise, the Ru—C and C—O bond lengths found for the carbonyl ligands in the triazenido-bridged com-

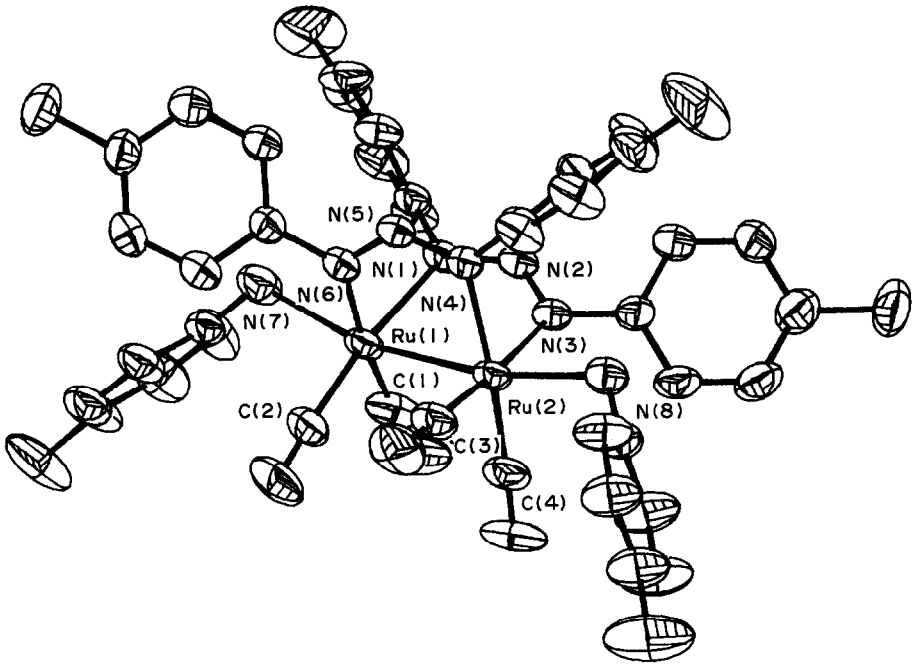

Fig. 1. General view of $[Ru(ArNNNAr)(CO)_2(NH_2Ar)]_2$ (Ar = p-C_6H_4Me) showing the atom labelling scheme. Atoms are represented by their thermal ellipsoids at the 50% probability level. Hydrogen atoms have been omitted for clarity.

plex are very similar to those recorded for related carboxylato-bridged diruthenium(I/I) complexes.[7,8] Finally, the relatively long Ru—N distances [2.332(6) and 2.286(5) Å] found for the axial p-toluidine groups are in keeping with the ease with which these ligands are replaced.

Acknowledgements—We thank Johnson Matthey plc for a generous loan of ruthenium trichloride and SERC for support of the X-ray work.

REFERENCES

1. P. A. Harding, S. D. Robinson and K. Henrick, *J. Chem. Soc., Dalton Trans.* 1988, 415.
2. G. R. Crooks, B. F. G. Johnson, J. Lewis, I. G. Williams and G. Gamlen, *J. Chem. Soc.* (*A*) 1969, 2761.
3. B. F. G. Johnson, R. D. Johnston, J. Lewis and I. G. Williams, *J. Chem. Soc.* (*A*) 1971, 689.
4. B. R. James and G. L. Rempel, *Chem. Ind.* 1971, 1036.
5. H. Schumann, J. Opitz and J. Pickardt, *J. Organomet. Chem.* 1977, **128**, 253.
6. G. Süss-Fink, G. Herrmann, P. Morys, J. Ellermann and A. Veit, *J. Organomet. Chem.* 1985, **284**, 263.
7. M. Rotem, Y. Shvo, I. Goldberg and U. Shmueli, *J. Organomet. Chem.* 1986, **314**, 185.
8. M. Rotem, Y. Shvo, I. Goldberg and U. Shmueli, *Organometallics* 1984, **3**, 1758.
9. M. Bianchi, P. Frediani, U. Matteoli, G. Menchi, F. Piacenti and G. Petrucci, *J. Organomet. Chem.* 1983, **259**, 207 and refs therein.
10. S. Jeannin, Y. Jeannin and G. Lavigne, *Trans. Metal Chem.* 1976, **1**, 186.
11. J. A. Cabeza, C. Landazuri, L. A. Oro, A. Tiripicchio and M. Tiripicchio-Camellini, *J. Organomet. Chem.* 1987, **322**, C16.
12. J. Catterick and P. Thornton, *Adv. Inorg. Chem. Radiochem.* 1977, **20**, 291.
13. D. S. Moore and S. D. Robinson, *Adv. Inorg. Chem. Radiochem.* 1986, **30**, 1.
14. A. Vogel, *Textbook of Practical Organic Chemistry*, 4th Edn, p. 720. Longman, London (1978).
15. R. A. Jones, M. B. Hursthouse, K. M. A. Malik and G. Wilkinson, *J. Am. Chem. Soc.* 1979, **101**, 4128.
16. R. K. Harris, *Can. J. Chem.* 1964, **42**, 2275.
17. E. B. Boyar and S. D. Robinson, *Inorg. Chim. Acta* 1982, **64**, L193.
18. K. R. Laing, S. D. Robinson and M. F. Uttley, *J. Chem. Soc., Dalton Trans.* 1973, 2713.
19. M. J. Auburn, R. D. Holmes-Smith, S. R. Stobart, M. J. Zaworotko, T. S. Cameron and A. Kumari, *J. Chem. Soc., Chem. Commun.* 1983, 1523.

Polyhedron Vol. 7, No. 19/20, pp. 1925–1930, 1988
Printed in Great Britain

0277–5387/88 $3.00+.00
© 1988 Pergamon Press plc

ORGANOMETALLIC PLATINUM SULPHUR NITROGEN COMPLEXES

PAUL F. KELLY, ALEXANDRA M. Z. SLAWIN, DAVID J. WILLIAMS and J. DEREK WOOLLINS*

Department of Chemistry, Imperial College of Science and Technology, South Kensington, London SW7 2AY, U.K.

Abstract—A new route to mixed ligand complexes containing the disulphur dinitrido ligand has been developed. Reaction of $[Me_2Sn(S_2N_2)]_2$ (**1**) with $Pt(COD)Br_2$ gives $Pt(COD)(S_2N_2)$ (**2**) which undergoes further reaction with 1,1′-bis(diphenylphosphino)ferrocene (Fdpp) to give $Pt(Fdpp)(S_2N_2)$ (**3**). The X-ray crystal structures of **2** and **3** are reported. In **3** the Cp rings are staggered by 40° with respect to each other and are inclined by 57° relative to the plane of the PtS_2N_2 ring.

Metal complexes containing sulphur–nitrogen ligands have been known for a number of years. For example, reaction of anhydrous nickel chloride with S_4N_4 gives a mixture of $Ni(S_2N_2H)_2$, $Ni(S_2N_2H)(S_3N)$ and $Ni(S_3N)_2$ which were first separated and studied by T. S. Piper[1] (one of Prof. Wilkinson's earliest students) and have subsequently been investigated in more detail.[2–4] Currently, we are interested in developing rational, high yield, synthetic routes to M—S—N complexes. Recently,[5–7] we have prepared complexes of the type $Pt(S_2N_2)(PR_3)_2$ and $[Pt(S_2N_2H)(PR_3)_2]X$ ($X = Cl^-$, BF_4^- PF_6^-) starting from *cis*-$PtCl_2(PR_3)_2$. Here we report the synthesis of the first example of an organometallic platinum sulphur–nitrogen compound, $Pt(COD)(S_2N_2)$ (**2**). The usefulness of **2** as an intermediate in the preparation of other mixed ligand complexes is illustrated by the formation of a complex containing the ferrocene based ligand 1,1′-bis(diphenylphosphino)ferrocene (Fdpp), $Pt\{(Ph_2PC_5H_4)_2Fe\}(S_2N_2)$ (**3**). The X-ray structures of **2** and **3** are reported.

EXPERIMENTAL

General reaction conditions and spectroscopic measurements are as reported previously.[6] $[Me_2Sn(S_2N_2)]_2$ (**1**) was prepared as described in the literature.[8] $Pt(COD)Br_2$ was prepared by treating a CH_2Cl_2 solution of $Pt(COD)Cl_2$[9] with KBr with stirring for 48 h followed by filtration to remove KCl.

$Pt(COD)(S_2N_2)$ (2)

A mixture of $Pt(COD)Br_2$ (96 mg, 2.1×10^{-4} mol) and $[Me_2Sn(S_2N_2)]_2$ (50 mg, 1×10^{-4} mol) in CH_2Cl_2 (20 cm^3) was stirred for 2 h, then treated with $[^nBu_4N]OH$ (0.25 cm^3 of 1 M solution in MeOH, 2.5×10^{-4} mol). After stirring for a further 15 min the solvent was removed *in vacuo* and the resulting yellow solid washed with water (50 cm^3), then filtered and dried. The residue was extracted into CH_2Cl_2 (10 cm^3) and, after filtration to remove the small amount of white solid present, the crude product was obtained by addition of hexane (50 cm^3) to the solution. Pure (**2**) was obtained as well-formed orange crystals by slow diffusion of hexane into a CH_2Cl_2 solution of the crude product.

Micro-analysis, Found: C, 24.3; H, 2.9; N, 7.0. Calc.: C, 24.3; H, 3.1; N, 7.1%. Mass spec.: *m/e* 395 (M^+), 349 (M^+—NS). IR: 1032(s) (ν[N—S]), 690(s) (ν[N—S]), 481(m) (ν[Pt—N]) and 364 cm^{-1} (ν[Pt—S]/δ[N—S]).

$Pt\{(Ph_2PC_5H_4)_2Fe\}(S_2N_2)$ (3)

A solution of crude (**2**), prepared on the above scale, in CH_2Cl_2 (30 cm^3) was treated with $(Ph_2PC_5H_4)_2Fe$ (0.115 g, 2.1×10^{-4} mol) and the resulting orange solution stirred for 1 h. After this time the volume of the solvent was reduced *in vacuo* to ≈ 10 cm^3 and the product precipitated by

* Author to whom correspondence should be addressed.

addition of hexane (50 cm^3). After filtration from the pale yellow solution the solid was dried *in vacuo* then redissolved in CH_2Cl_2 and crystallized by slow hexane diffusion. The resulting well-formed bright orange crystals of (**3**) were stored under Et_2O to avoid desolvation.

IR: 1048(s) (ν[N—S]), 365(w) (δ[N—S]), 355 cm^{-1} (w) (ν[Pt—S]). Other bands are obscured by the Fdpp ligand vibrations. ^{31}P NMR: δ 20.9 ($^1J(^{195}Pt—^{31}P)$ 2903) and 9.4 ppm (^1J 3008 Hz) $^2J(^{31}P—^{31}P)$ 24 Hz.

Crystal data (**2**). $C_8H_{12}N_2S_2Pt$, $M = 395.4$, monoclinic, $a = 16.251(4)$, $b = 6.514(3)$, $c = 19.747(7)$ Å, $\beta = 91.89(3)°$, $U = 2089$ $Å^3$, space group $I2/a$ (body centred cell used because C face centred cell had $\beta = 139.79(2)°$), $Z = 8$, $D_c = 2.51$ g cm^{-3}. Orange, air-stable prisms, dimensions $0.20 \times 0.27 \times 0.40$ mm, μ(Cu-K_α) = 287 cm^{-1}, $\bar{\lambda} = 1.54178$ Å, $F(000) = 1471$.

Crystal data (**3**). $C_{34}H_{28}N_2S_2P_2FePt \cdot (CH_2Cl_2)_{0.7}$, $M = 901.1$, triclinic, $a = 11.103(2)$, $b = 12.009(3)$, $c = 16.913(4)$ Å, $\alpha = 93.37(2)$, $\beta = 108.40(2)$, $\gamma = 113.67(2)°$, $U = 1915$ $Å^3$, space group $P\bar{1}$, $Z = 2$, $D_c = 1.56$ g cm^{-3}. Orange rods, dimensions $0.17 \times 0.20 \times 0.43$ mm, μ(Cu-K_α) = 128 cm^{-1}, $\bar{\lambda} = 1.54178$ Å, $F(000) = 883$.

Data collection and processing

Nicolet R3m diffractometer, ω-scan method, [$2\theta \leqslant 116°$ for (**2**) and 100° for (**3**)], graphite monochromated Cu-K_α radiation; 1381 and 3925 independent measured reflections of which 1324 and 3721 for (**2**) and (**3**) were observed [$|F_o| > 3\sigma(|F_o|)$]. The data were corrected for Lorentz and polarization factors, empirical absorption corrections based on 400 and 374 azimuthal measurements for (**2**) and (**3**) were applied. The maximum and minimum transmission factors for (**2**) and (**3**) were 0.078, 0.006 and 0.97, 0.385, respectively.

Structure analysis and refinement

In both cases the structures were solved by the heavy atom method and all the non-hydrogen atoms refined anisotropically. In (**2**) the hydrogen atoms on C(1), C(2), C(5) and C(6) were idealized and fixed; the remaining hydrogen atoms in (**2**) and (**3**) were also idealized (C—H = 0.96 Å), assigned isotropic thermal parameters $U(H) = 1.2\ U_{eq}(C)$ and allowed to ride on their parent carbons. In (**3**) there is included CH_2Cl_2 solvent. This is disordered and occupies several partial occupancy, partially overlapping sites. Refinement was by block-cascade full-matrix least-squares to $R = 0.086$ and 0.062, ($R = \Sigma[|F_o| - |F_c|]/\Sigma|F_o|$), $R_w = 0.088$ and 0.066 for **2** and **3**, respectively ($w^{-1} = \sigma^2(F) + 0.0005F^2$ for **2** and $0.003F^2$ for **3**). The maximum and minimum residual electron densities in the final ΔF maps were 2.57 and −2.89 $eÅ^{-3}$ for (**2**) and 2.54 and −2.09 $eÅ^{-3}$ for (**3**). The mean and maximum shifts/error in the final refinement cycle were 0.000 and 0.002 for (**2**) and 0.021 and 0.089 for (**3**), respectively. The somewhat high value of the R factor in **2** reflects poor crystal quality and the significant thermal anisotropy both in the S_2N_2 and COD ligands. Computations were carried out on an Eclipse S140 computer using the *SHELXTL* program system[10] and published scattering factors.[11]

RESULTS AND DISCUSSION

In previous work we have prepared mixed ligand M—S—N complexes via complexes of the type ML_2Cl_2 (M = Pt and Pd, L = phosphine,[6] azobenzene[12]). An alternative and potentially more versatile strategy, is to initially prepare a sulphur–nitrogen complex with a labile *trans* ligand.

Treatment of $Pt(COD)Br_2$ with the dimeric tin complex $[Me_2Sn(S_2N_2)]_2$ (**1**), in the molar ratio 2 : 1, results in the formation of a salt of the novel cation $[Pt(COD)(S_2N_2H)]^+$ which can be converted to **2** by deprotonation with [^{n}Bu$_4$N]OH [eq. (1)]. The formation of the protonated species is consistent with our previous observation[6] that complexes of the type *cis*-$PtCl_2(PR_3)_2$ react with (**1**) to give $[Pt(S_2N_2H)(PR_3)_2][Me_2SnCl_3]$ by picking up HCl from the solvent (CH_2Cl_2), and in turn react with $[NH_4]PF_6$ to give the corresponding PF_6^- salts. If the product of the reaction of $Pt(COD)Br_2$ with **1** is treated with $[NH_4]PF_6$ the resulting salt can be readily crystallized as thin orange needles, the mass spectrum of which clearly shows the presence of $[Pt(COD)(S_2N_2H)]^+$ (*m/e* 396). However, microanalysis of these crystals suggests the presence of a mixed salt, possibly containing Cl^- as well as PF_6^-, and thus to avoid these complications we have found that it is simpler to treat the initial mixture with [^{n}Bu$_4$N]OH in order to obtain the deprotonated species, **2**.

$$2Pt(COD)Br_2 + \underset{(\mathbf{1})}{[Me_2(S_2N_2)]_2} \xrightarrow{CH_2Cl_2} 2[Pt(COD)(S_2N_2H)]^+[Me_2SnCl_3]^- \xrightarrow{[Bu_4N]OH} \underset{(\mathbf{2})}{Pt(COD)(S_2N_2)}. \quad (1)$$

The above method results in samples of **2** which

are contaminated with small amounts of impurities, presumably including [^{n}Bu$_4$N][Me$_2$SnCl$_3$], which are difficult to remove. The most effective method of purification is slow hexane diffusion into the crude solution, which readily yields large, well-formed crystals of **2**; however, as the reaction with Fdpp shows, the impurities present do not hinder substitution reactions in which the COD is displaced and thus it is not strictly necessary to purify **2** before using it to prepare derivatives.

In contrast to complexes of the type Pt(S$_2$N$_2$)(PR$_3$)$_2$, which we have prepared from the corresponding dichloro species using a variety of reagents, the reaction of **1** with Pt(COD)Br$_2$ is the only viable route to **2**. Attempts to prepare **2** from Pt(COD)Cl$_2$ via reaction with Na(S$_3$N$_3$) or S$_4$N$_4$H$_4$/dbu invariably fail, presumably due to the lability of the COD ligand. These observations re-emphasize the usefulness of **1** as a synthetic reagent. Furthermore, surprisingly, in reactions using **1** we have found Pt(COD)Br$_2$ to give better results than Pt(COD)Cl$_2$.

Reactions of **2** with Ph$_2$(C$_5$H$_4$)$_2$Fe (Fdpp) proceeds smoothly with the expected elimination of COD to give **3** [eq. (2)] thus illustrating the potential usefulness of **2**.

$$\underset{(2)}{\text{Pt(COD)(S}_2\text{N}_2\text{)}} + \text{Fdpp} \rightarrow \underset{(3)}{\text{Pt(Fdpp)(S}_2\text{N}_2\text{)}} + \text{COD.} \quad (2)$$

^{31}P-{^{1}H} NMR of the crude reaction reveals (**3**) to be the sole phosphorus containing product. The spectrum of (**3**) is typical[13–15] of Pt(PR$_3$)$_2$(S$_2$N$_2$) complexes, with the ratio of the $^1J(^{195}\text{Pt}—^{31}\text{P})$ coupling constants being 1.04. From preliminary results it appears that in this case, **3** may also be prepared by reaction of Pt(Fdpp)Cl$_2$ with S$_4$N$_4$H$_4$/dbu using a method similar to that previously reported.[16] However, **2** will doubtless prove to be an important synthetic reagent in metalla–sulphur–nitrogen chemistry. Preliminary results indicate that the Pt(S$_2$N$_2$)(CN)$_2^{2-}$ anion may be prepared from **2** by displacement reactions using CN$^-$.

The X-ray structures of **2** and **3** are shown in Figs 1 and 2 with bond distances and angles in Tables 1 and 2. Both compounds have the expected square planar geometry around platinum. In **3** the geometry around platinum and within the PtS$_2$N$_2$ is not significantly different from that observed[13] for Pt(PPh$_3$)$_2$(S$_2$N$_2$). The most noticeable difference between the structures of **2** and **3** is in the Pt—S (2.234(5) and 2.284(4) Å) bond lengths although the Pt—N distances (2.015(19) and 2.034(7) Å) are not significantly different. **2** with the carbon *trans* to sulphur thus appears to enhance the σ-donor/π-acceptor ability of the sulphur atom in the S$_2$N$_2^{2-}$ ligand. The bond lengths and angles within the metallacycle which follow the now established pattern with two short and one long S—N bonds, are not significantly different from **2** and **3** and are in good agreement with those reported for related complexes.[17] In **3** the two Cp rings are almost coplanar (dihedral angle 4.4°) and are inclined to the PtS$_2$N$_2$ plane by 57°. The Cp rings are staggered by 40° with respect to each other [Fig. 2(b)] as is the case in Pt(Fdpp)Cl$_2$.[18]

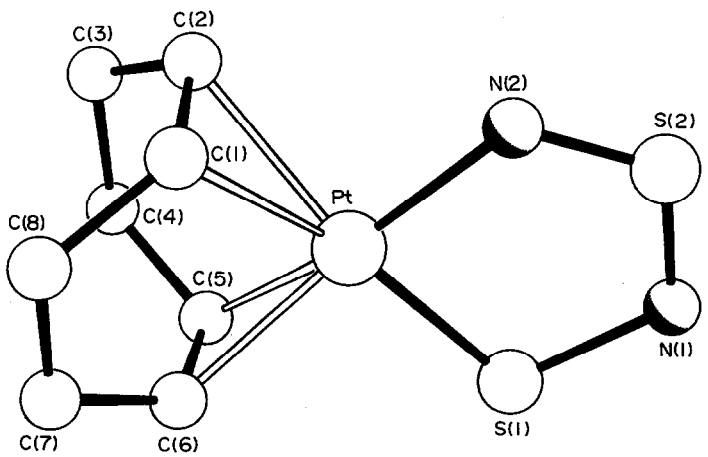

Fig. 1. The X-ray crystal structure of Pt(COD)(S$_2$N$_2$) (**2**).

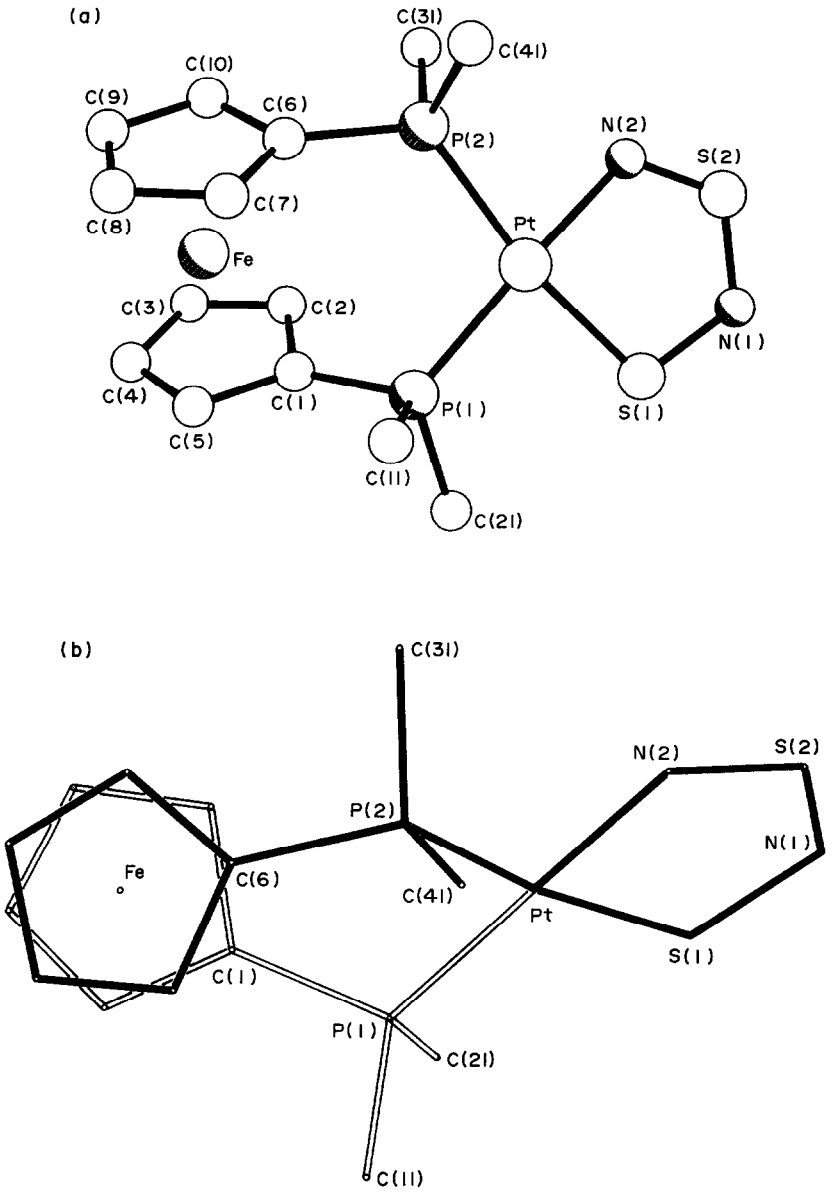

Fig. 2. (a) The X-ray crystal structure of Pt(Fdpp)(S_2N_2) (**3**), the phenyl rings have been omitted for clarity. (b) **3** viewed normal to the C(6)—C(10) Cp ring.

Table 1. Bond distances (Å) and angles (°) in **2**

Pt—S(1)	2.234(5)	Pt—N(2)	2.015(19)
Pt—C(1)	2.220(18)	Pt—C(2)	2.223(21)
Pt—C(5)	2.166(21)	Pt—C(6)	2.196(21)
S(1)—N(1)	1.708(20)	N(1)—S(2)	1.535(21)
S(2)—N(2)	1.537(17)		
S(1)—Pt—N(2)	87.5(5)	Pt—S(1)—N(1)	104.9(7)
S(1)—N(1)—S(2)	114.9(12)	N(1)—S(2)—N(2)	116.4(11)
Pt—N(2)—S(2)	116.3(11)		

Table 2. Bond distances (Å) and angles (°) in **3**

Pt—S(1)	2.284(4)	Pt—N(2)	2.034(7)
Pt—P(1)	2.270(2)	Pt—P(2)	2.307(3)
S(1)—N(1)	1.671(9)	N(1)—S(2)	1.571(11)
S(2)—N(2)	1.519(11)	Fe—C(1)	2.019(13)
Fe—C(2)	2.030(17)	Fe—C(3)	2.063(17)
Fe—C(4)	2.066(12)	Fe—C(5)	2.026(10)
Fe—C(6)	2.002(9)	Fe—C(7)	2.032(13)
Fe—C(8)	2.073(18)	Fe—C(9)	2.046(16)
Fe—C(10)	2.052(12)	C(1)—C(2)	1.480(18)
C(1)—C(5)	1.442(16)	C(1)—P(1)	1.781(12)
C(2)—C(3)	1.432(20)	C(3)—C(4)	1.421(21)
C(4)—C(5)	1.407(19)	C(6)—C(7)	1.439(17)
C(6)—C(10)	1.424(18)	C(6)—P(2)	1.818(12)
C(7)—C(8)	1.409(18)	C(8)—C(9)	1.414(24)
C(9)—C(10)	1.416(19)	P(1)—C(11)	1.806(14)
P(1)—C(21)	1.868(13)	P(2)—C(31)	1.803(11)
P(2)—C(41)	1.828(11)		
S(1)—Pt—N(2)	86.4(3)	S(1)—Pt—P(1)'	90.3(1)
N(2)—Pt—P(1)	176.3(3)	S(1)—Pt—P(2)	170.1(1)
N(2)—Pt—P(2)	83.8(3)	P(1)—Pt—P(2)	99.6(1)
Pt—S(1)—N(1)	104.5(4)	S(1)—N(1)—S(2)	116.3(8)
N(1)—S(2)—N(2)	115.2(5)	Pt—N(2)—S(2)	117.5(5)
C(2)—C(1)—C(5)	106.0(10)	C(2)—C(1)—P(1)	122.1(8)
C(5)—C(1)—P(1)	131.8(9)	C(1)—C(2)—C(3)	106.5(11)
C(2)—C(3)—C(4)	109.8(13)	C(3)—C(4)—C(5)	107.7(11)
C(1)—C(5)—C(4)	110.0(11)	C(7)—C(6)—C(10)	106.3(10)
C(7)—C(6)—P(2)	127.5(9)	C(10)—C(6)—P(2)	126.3(10)
C(6)—C(7)—C(8)	109.4(11)	C(7)—C(8)—C(9)	106.9(12)
C(8)—C(9)—C(10)	109.2(12)	C(6)—C(10)—C(9)	108.1(12)
Pt—P(1)—C(1)	114.5(3)	Pt—P(1)—C(11)	114.9(3)
C(1)—P(1)—C(11)	106.7(6)	Pt—P(1)—C(21)	114.5(4)
C(1)—P(1)—C(21)	101.8(5)	C(11)—P(1)—C(21)	102.9(6)
P(1)—C(11)—C(12)	123.7(9)	P(1)—C(11)—C(16)	118.8(8)
Pt—P(2)—C(6)	122.0(3)	Pt—P(2)—C(31)	111.0(5)
		Pt—P(2)—C(41)	113.0(4)

There are no significant intermolecular interactions in either **2** or **3**, the shortest N···S and S···S contacts being > 4.1 Å in **2**; those in **3** are even greater.

Acknowledgement—We are grateful to Johnson Matthey for loans of K_2PtCl_4.

REFERENCES

1. T. S. Piper, *J. Am. Chem. Soc.* 1958, **80**, 30.
2. J. D. Woollins, R. Grinter, M. K. Johnson and A. J. Thomson, *J. Chem. Soc., Dalton Trans.* 1980, 1910.
3. D. B. Powell and J. D. Woollins, *Spectrochim. Acta* 1980, **A36**, 447.
4. R. Grinter and J. D. Woollins, *Inorg. Chim. Acta* 1980, **39**, 193.
5. R. Jones, P. F. Kelly, C. P. Warrens, D. J. Williams and J. D. Woollins, *J. Chem. Soc., Chem. Commun.* 1986, 711.
6. R. Jones, C. P. Warrens, D. J. Williams and J. D. Woollins, *J. Chem. Soc., Dalton Trans.* 1987, 907.
7. P. F. Kelly and J. D. Woollins, *Polyhedron* 1986, **5**, 607.
8. C. P. Warrens and J. D. Woollins, *Inorg. Synth*, accepted for publication.
9. M. C. Clark and L. E. Manzer, *J. Organomet. Chem.* 1973, **59**, 411.
10. G. M. Sheldrick, *SHELXTL, An Integrated System for Solving, Refining and Displaying Crystal Structures from Diffraction Data.* University of Gottingen, Gottingen, FRG (1978). Revision 4.1 (August 1983).
11. *International Tables for X-ray Crystallography*, Vol. 4, pp. 99–149. Kynoch Press, Birmingham (1974).
12. R. Jones, T. P. Purcell, D. J. Williams and J. D. Woollins, *Polyhedron* 1988, **7**, 647.
13. R. Jones, P. F. Kelly, D. J. Williams and J. D. Woollins, *Polyhedron* 1985, **4**, 1947.

14. P. A. Bates, M. B. Hursthouse, P. F. Kelly and J. D. Woollins, *J. Chem. Soc., Dalton Trans.* 1986, 267.
15. P. F. Kelly and J. D. Woollins, *J. Chem. Soc., Dalton Trans.* 1988, 1053.
16. R. Jones, P. F. Kelly, D. J. Williams and J. D. Woollins, *Polyhedron* 1987, **6**, 1541.
17. R. Jones, P. F. Kelly, D. J. Williams and J. D. Woollins, *J. Chem. Soc., Dalton Trans.* 1988, 803.
18. D. A. Clemente, G. Pilloni, B. Corrain, B. Longata and M. C. Tiripicchio, *Inorg. Chim. Acta* 1986, **115**, L9.

Polyhedron Vol. 7, No. 19/20, pp. 1931–1938, 1988
Printed in Great Britain

0277–5387/88 $3.00+.00
© 1988 Pergamon Press plc

THE FORMATION OF AMINE AND AMIDE COMPLEXES IN THE REACTIONS BETWEEN [Mo(NO){HB(3,5-$Me_2C_3N_2H)_3$}X_2] (X = Cl OR I) AND SATURATED CYCLIC AMINES. THE MOLECULAR STRUCTURES OF [Mo(NO){HB(3,5-$Me_2C_3N_2H)_3$}I(NHC_5H_{10})] AND [Mo(NO){HB(3,5-$Me_2C_3N_2H)_3$}I(NC_4H_8)]

NAJAT ALOBAIDI, THOMAS A. HAMOR, CHRISTOPHER J. JONES,* JON A. McCLEVERTY and KEITH PAXTON

Department of Chemistry, University of Birmingham, PO Box 363, Birmingham B15 2TT, U.K.

and

ANDREW J. HOWES and MICHAEL B. HURSTHOUSE

Department of Chemistry, Queen Mary College, University of London, Mile End Road, London E1 4NS, U.K.

Abstract—The coordinatively unsaturated complex, [Mo(NO){HB(3,5-$Me_2C_3N_2H)_3$}I_2] reacted with pyrrolidine or piperidine to produce both the amine complexes, [Mo(NO){HB(3,5-$Me_2C_3N_2H)_3$}I(NHC_nH_{2n})] ($n = 4$ or 5) and the amide complexes, [Mo(NO){HB(3,5-$Me_2C_3N_2H)_3$}I(NC_nH_{2n})]. Amine complexes could be obtained from similar reactions with [Mo(NO){HB(3,5-$Me_2C_3N_2H)_3$}Cl_2] if NaH was present. The molecular structures of [Mo(NO){HB(3,5-$Me_2C_3N_2H)_3$}I(NHC_5H_{10})] and [Mo(NO){HB(3,5-$Me_2C_3N_2H)_3$}I(NC_4H_8)] were determined and the Mo—N(amine) bond distance of 2.241(6) Å in the former was found to be substantially longer than the Mo—N(amide) distance of 1.937(5) Å in the latter.

The formally 16-electron complexes [Mo(NO)LX_2] (L = hydrotris(3,5-dimethylpyrazol-1-yl)borate, X = Cl or I) undergo substitution reactions with primary amines[1–3] to give the amide derivatives, [Mo(NO)LX(NHR)] (R = alkyl or aryl).[1–4] These reactions proceed according to eq. (1) in which a second molecule of amine is present to consume the HX liberated.

$$[Mo(NO)LX_2] + 2RNH_2 \rightarrow [Mo(NO)LX(NHR)] + RNH_3^+ + X^- \quad (1)$$

Although both the reactants and products in eq. (1) are diamagnetic, paramagnetic intermediates may be detected during the reactions of [Mo(NO)LI_2] with amines or alcohols.[5,6] One of these intermediates appears to be the 17-electron complex [Mo(NO)LI_2]$^-$ which has been isolated[6] in the form of the air-sensitive compound, [Mo(NO)$LI_2Li(OEt_2)_2$]. Under the reaction conditions normally used to prepare monoamide complexes, no free amide, RNH^-, would be present and it seems likely that their formation might also involve the amine complexes, [Mo(NO)$LI(NH_2R)$] or [Mo(NO)$LI(NH_2R)]^+$, as intermediates. The former complex would be a paramagnetic 17-electron compound while the latter would be diamagnetic. As yet no example of an amine complex of the type [Mo(NO)$LI(NH_2R)$] or [Mo(NO)$LI(NH_2R)]^+$ has been reported. Consequently no definitive comment on the chemical properties of such species has been possible. However, it is known that when both halide ligands in [Mo(NO)LX_2] are replaced by neutral nitrogen ligands, air-stable 17-electron complexes such as [Mo(NO)L$(MeCN)_2]^+$ and [Mo(NO)L$(Pyridine)_2]^+$ are obtained.[7,8]

It has been shown[9] that [Mo(NO)LCl_2] reacts with the cyclic secondary amines HNC_nH_{2n} ($n = 4$,

* Author to whom correspondence should be addressed.

5) to give the expected diamagnetic amide derivatives [Mo(NO)LCl(NC$_n$H$_{2n}$)]. We have now found that a similar reaction between [Mo(NO)LI$_2$] and these secondary amines affords not only the analogous 16-electron amide complexes but also the 17-electron amine complexes [Mo(NO)LI(NHC$_n$H$_{2n}$)].

EXPERIMENTAL

Synthetic studies

All reagents were used as supplied. [Mo(NO){HB(3,5-Me$_2$C$_3$N$_2$H)$_3$}I$_2$] and [Mo(NO){HB(3,5-Me$_2$C$_3$N$_2$H)$_3$}Cl$_2$] were prepared according to previously described methods.[10,11] Silica gel 60 (70–230 mesh) was used as the stationary phase for column chromatography with dichloromethane as eluant. All reactions were carried out under nitrogen but purification procedures were carried out in air. Elemental analyses were carried out by the Microanalytical Laboratory, University of Birmingham.

IR spectra were recorded using a PE 297 spectrometer with samples as KBr discs. 400 MHz ^{1}H NMR spectra were obtained from solutions in $CDCl_3$ using a Bruker WH400 spectrometer of the SERC high field NMR service at Warwick University. ESR spectra were obtained from fluid solutions in CH_2Cl_2 using a Hilger–Watts Microspin X-band spectrometer with a 100 MHz modulation (iodo complexes); *g*-values were obtained from frequency measurements with a proton resonance head. Diphenylpicryl–hydrazine was used as the reference. Cyclic voltammetric measurements were made using a Hitek PPR 1 waveform generator and DT 2101 potentiostat or a PAR 174A polarograph. Solutions in MeCN or CH_2Cl_2 were *ca* 10^{-3} mol dm^{-3} in the complex and 0.2 mol dm^{-3} in [Bu^{n}N]BF$_4$ as the base electrolyte. A Pt bead test electrode was used with an SCE reference electrode and ferrocene as internal standard. Potentials are quoted relative to the SCE and under these conditions E_f for the oxidation of ferrocene was found to be 0.42 V with $\Delta E_p = 80$ mV in MeCN and 0.58 V with $\Delta E_p = 100$ mV in CH_2Cl_2. The number of electrons associated with electrode processes was estimated by comparison with [Mo(NO)LCl$_2$].

[Mo(NO){HB(3,5-Me$_2$C$_3$N$_2$H)$_3$}I{HNC$_5$H$_{10}$}] (I)

A solution of [Mo(NO){HB(3,5-Me$_2$C$_3$N$_2$H)$_3$}I$_2$] (1.0 g, 1.5 mmol) and piperidine (1 cm^3, 8 mmol) in dichloromethane (60 cm^3) containing sodium hydride (200 mg) was refluxed for one day. After this time the reaction mixture was filtered and the solvent removed from the filtrate by evaporation under reduced pressure. The residue was purified by column chromatography which afforded firstly a red band containing [Mo(NO){HB(3,5-Me$_2$C$_3$N$_2$H)$_3$}I{NC$_5$H$_{10}$}] (200 mg, 21%) followed by a second green band containing the *complex* (340 mg, 36%). Further purification of the reaction products could be effected by recrystallization from CH_2Cl_2–hexane mixtures. Found: C, 37.2; H, 5.0; N, 17.2. C$_{20}$H$_{33}$N$_8$BMoOI requires: C, 36.7; H, 5.0; N, 18.0%.

[Mo(NO){HB(3,5-Me$_2$C$_3$N$_2$H)$_3$}I{HNC$_4$H$_8$}]

This material was prepared in an identical manner to its piperidinate analogue using pyrrolidine (5 cm^3, 35 mmol) and [Mo(NO){HB(3,5-Me$_2$C$_3$N$_2$H)$_3$}I$_2$] (1.2 g, 1.8 mmol). The first red band from the chromatography column contained [Mo(NO){HB(3,5-Me$_2$C$_3$N$_2$H)$_3$}I{NC$_4$H$_8$}] (400 mg, 33%). Further elution of the column afforded a green band containing the *complex* (320 mg, 29%). Found: C, 37.8; H, 5.2; N, 17.5. C$_{19}$H$_{31}$N$_8$BMoOI requires: C; 37.8; H, 5.2; N, 17.6%.

[Mo(NO){HB(3,5-Me$_2$C$_3$N$_2$H)$_3$}I{NC$_4$H$_8$}] (II)

A solution [Mo(NO){HB(3,5-Me$_2$C$_3$N$_2$H)$_3$}I$_2$] (1.0 g, 1.5 mmol) and pyrrolidine (10 cm^3, 80 mmol) in dichloromethane (60 cm^3) was stirred at room temperature for one day. After this time the reaction mixture was filtered and the solvent removed from the filtrate by evaporation under reduced pressure. The residue was purified by column chromatography which afforded firstly a red band containing the *complex* (460 mg, 50%) followed by a second green band containing [Mo(NO){HB(3,5-Me$_2$C$_3$N$_2$H)$_3$}I{HNC$_4$H$_8$}] (160 mg, 18%). Further purification of the reaction products could be effected by recrystallization from CH_2Cl_2–hexane mixtures. Found: C, 37.4; H, 4.8; N, 17.7. C$_{19}$H$_{30}$N$_8$BMoOI requires: C, 36.8; H, 4.8; N, 18.1%.

[Mo(NO){HB(3,5-Me$_2$C$_3$N$_2$H)$_3$}I{NC$_5$H$_{10}$}]

This material was prepared in an identical manner to its pyrrolidinate analogue using piperidine (10 cm^3, 70 mmol) in place of pyrrolidine. The *complex* was obtained as the first red band from the chromatography column (480 mg, 52%). Further elution of the column afforded a green band containing [Mo(NO){HB(3,5-Me$_2$C$_3$N$_2$H)$_3$}I{HNC$_5$H$_{10}$}] (200 mg, 21%). Found: C, 38.1; H, 5.3; N, 17.8. C$_{20}$H$_{32}$N$_8$BMoOI requires: C, 37.9; H, 5.0; N, 17.7%.

$[Mo(NO)\{HB(3,5\text{-}Me_2C_3N_2H)_3\}Cl\{HNC_4H_8\}]$

A solution of $[Mo(NO)\{HB(3,5\text{-}Me_2C_3N_2H)_3\}Cl_2]$ (1.0 g, 2 mmol) and pyrrolidine (2 cm^3, 16 mmol) in dichloromethane (60 cm^3) containing sodium hydride (200 mg) was refluxed for two days. After this time the reaction mixture was filtered and the solvent removed from the filtrate by evaporation under reduced pressure. The residue was purified by column chromatography which afforded firstly a red band containing $[Mo(NO)\{HB(3,5\text{-}Me_2C_3N_2H)_3\}Cl\{NC_4H_8\}]$ (120 mg, 11%) followed by a second green band containing the *complex* (400 mg, 37%). Further purification of the reaction products could be effected by recrystallization from CH_2Cl_2–hexane mixtures. Found: C, 48.6; H, 6.9; N, 17.9. $C_{19}H_{31}N_8BClMoO \cdot C_6H_{14}$ requires: C, 48.8; H, 7.3; N, 18.2%.

$[Mo(NO)\{HB(3,5\text{-}Me_2C_3N_2H)_3\}Cl\{HNC_5H_{10}\}]$

This material was prepared in an identical manner to its pyrrolidinate analogue using piperidine (3 cm^3, 21 mmol) in place of pyrrolidine. The first red band from the chromatography column contained $[Mo(NO)\{HB(3,5\text{-}Me_2C_3N_2H)_3\}Cl\{NC_5H_{10}\}]$ (200 mg, 18%). Further elution of the column afforded a green band containing the *complex* (420 mg, 38%). Found: C, 39.4; H, 6.0; N, 17.7. $C_{20}H_{33}N_8BClMoO \cdot CH_2Cl_2$ requires: C, 40.1; H, 5.6; N, 17.8%.

Structural studies

X-ray cystallographic analyses of $[Mo(NO)LI\{HN(CH_2)_5\}]$ (**I**) (at Birmingham) and $[Mo(NO)LI\{N(CH_2)_4\}]$ (**II**) (at Queen Mary College).

Crystal data. (**I**): $C_{20}H_{33}BIMoN_8O$, $M_r = 635.2$, monoclinic, $P2_1/c$, $a = 8.654(3)$, $b = 15.046(5)$, $c = 20.202(5)$ Å, $\beta = 100.05(5)°$, $V = 2590$ Å^3, $Z = 4$, $D_c = 1.63$ g cm^{-3}, $F(000) = 1268$ μ(Mo-K_α), ($\lambda = 0.71069$ Å) = 1.723 mm^{-1}. (**II**): $C_{19}H_{30}BIMoN_8O$, $M_r = 602.2$, monoclinic, $P2_1/a$, $a = 20.558(2)$, $b = 14.171(2)$, $c = 8.568(1)$ Å, $\beta = 97.60(1)°$, $C = 2474$ Å^3, $Z = 4$, $D_c = 1.66$ g cm^{-3}, $F(000) = 1232$ μ(Mo-K_α) = 1.802 mm^{-1}. Intensities for both complexes were measured with an Enraf–Nonius CAD-4 diffractometer using monochromated Mo-K_α radiation up to $\theta = 25°$. 4555 reflections (compound **I**), 4675 reflections (compound **II**) were measured and 2864 having $F > 5\sigma(F)$ (compound **I**), 3502 having $F > 3\sigma(F)$ (compound **II**) were used in the analyses. Both structures were determined by Patterson and Fourier methods and refined by least squares using weights $w = 1/[\sigma_2(F_c) + 0.0007F^2]$ (compound **I**)[12,13] and unit weights (compound **II**).[14,15] Non-hydrogen atoms were allowed to vibrate anisotropically. In compound **I** most hydrogen atoms could be located from a difference map and were included in calculated positions "riding" on their respective carbon atoms. The initially unexpected hydrogen atom bonded to the nitrogen atom of the piperidine ring then appeared in a difference map as a peak of 0.22 e Å^{-3}, the largest peak, apart from two, close to molybdenum and two, close to iodine. Coordinates and an isotropic thermal parameter for this hydrogen atom were included in the final cycles of least-squares refinement. At convergence the thermal parameter U was 0.075 Å^2 and geometrical parameters H—N = 0.88(8) Å, angles H—N—C 94(6) and 112(6)°, torsion angles H—N—C—C 60(8) and −48(8)° were as expected for an *axially* bound hydrogen atom. The final values of R and $R_w = 0.040$ and 0.049, respectively for 2864 reflections. In compound **II** all hydrogen positions were located and refined with isotropic thermal parameters. Final $R = 0.0265$ for 3502 reflections.

RESULTS

Synthetic studies

The diiodide complex, $[Mo(NO)LI_2]$, reacted with an excess of pyrrolidine or piperidine to produce mixtures of red and green compounds which could be separated by column chromatography. The red compounds were diamagnetic and were shown to be the amide complexes $[Mo(NO)LI\{NC_nH_{2n}\}]$ ($n = 4$ and 5) on the basis of elemental analyses and IR, ^{1}H NMR and mass spectral data. In the case where $n = 4$ this formulation was confirmed by the single crystal X-ray diffraction study described below. The IR spectra of $[Mo(NO)LI\{NC_nH_{2n}\}]$ contained bands attributable to the ligand L including ν_{BH} at 2550 cm^{-1}. In addition ν_{NO} was observed at 1645 ($n = 4$) and 1650 ($n = 5$) cm^{-1} in accord with the formulation of these complexes as monoamides.[1] Both compounds exhibited molecular ions, $[M]^+$, in their mass spectra at $m/z = 622$ ($n = 4$) and 636 ($n = 5$) (^{98}Mo, ^{11}B, ^{127}I). In addition ions attributable to $[M—(I)]^+$ and $[M—(NO)]^+$ were observed.

The ^{1}H NMR spectrum of $[Mo(NO)LI\{NC_4H_8\}]$ was similar to that of its chloro analogue[9] and contained four distinctive multiplets, each of relative intensity one, at $\delta_{TMS} = 5.06$, 4.19, 3.78 and 2.29 ppm attributable to the α-methylene protons in the pyrrolidinate ligand. Two signals of relative intensity two, attributable to the β-methylene protons

were observed at $\delta_{TMS} = 1.98$ and 1.73 ppm. The pyrazolyl 4-H protons in L appeared as three singlets of relative intensity one at $\delta_{TMS} = 5.85$, 5.84 and 5.80 ppm, while the pyrazolyl methyl signals appeared as six singlets of relative intensity three, at $\delta_{TMS} = 2.70$, 2.43, 2.40, 2.33, 2.32 and 2.11 ppm. The ^{1}H NMR spectrum of [Mo(NO)LI{NC_5H_{10}}] similarly exhibited four multiplets each of relative intensity one, at $\delta_{TMS} = 4.69$, 4.54, 3.66 and 3.10 ppm attributable to the α-methylene protons in the piperidinate ligand. The remaining piperidinate protons appeared as multiplets at $\delta_{TMS} = 1.95$, 1.85, 1.60 and 1.28 ppm in the intensity ratio 1 : 1 : 2 : 2. The pyrazolyl 4-H protons in L appeared as three singlets of relative intensity one, at $\delta_{TMS} = 5.85$, 5.84 and 5.75 ppm, while the pyrazolyl methyl signals appeared as six singlets at $\delta_{TMS} = 2.69$, 2.49, 2.43, 2.40, 2.34 and 2.30 ppm each of relative intensity three.

The green compounds were found to be paramagnetic. Their IR spectra contained bands attributable to L including ν_{BH} at 2550 cm^{-1}. Both exhibited relatively low nitrosyl stretching frequencies ($\nu_{NO} = 1625$ ($n = 4$) and 1620 ($n = 5$) cm^{-1}) suggesting that they were 17-electron species. This was confirmed by the single crystal X-ray diffraction study of [Mo(NO)LI(HNC_5H_{10})] (*vide infra*) which showed that the complex contained an amine ligand. In accord with this formulation bands attributable to ν_{NH} were observed at 3225 cm^{-1} in the IR spectra of the green complexes. Their mass spectra did not contain molecular ions although ions were observed at $m/z = 552$ (^{98}Mo, ^{11}B, ^{127}I) attributable to [Mo(NO)LI]$^+$ formed by loss of the amine ligand. Both compounds exhibited ESR spectra in CH_2Cl_2 solution at room temperature. These contained signals at $g = 1.9989$, $A_{\langle Mo\rangle} = 4.89$ mT ($n = 4$) and $g = 1.9905$, $A_{\langle Mo\rangle} = 4.89$ mT ($n = 5$). These hyperfine coupling constants (to ^{95}Mo, 15.9%, and ^{97}Mo, 9.6%, both $I = 5/2$) are similar to those observed for the other 17-electron complexes containing the {Mo(NO)L}$^+$ core.[7,16]

In an attempt to stimulate deprotonation and thus suppress the formation of amine complexes, NaH was added to the reaction mixtures. To our surprise this had the reverse effect and instead increased the yields of the amine complexes. Thus it appears that sodium hydride functions as a reducing agent rather than a base in these reactions. The previously reported[9] reactions between [Mo(NO)Cl_2] and pyrrolidine or piperidine afforded only the amide complexes, [Mo(NO)LCl{NC_nH_{2n}}] ($n = 4$ and 5). However, when these reactions were carried out in the presence of NaH we found that paramagnetic green complexes could also be obtained. Thus it would appear that, although chloride is unable to effect the reduction required to form the chloro-amine complexes, these can be obtained in the presence of an added reductant such as NaH. The IR spectra of these compounds are similar to those of the iodo–amine complexes described above and contained bands attributable to the presence of the ligand L. The amine ligands gave rise to ν_{NH} at 3300 cm^{-1}. The only significant difference between these spectra and those of the iodo–amine complexes is that the nitrosyl stretching frequencies are lower ($\nu_{NO} = 1585$ ($n = 4$) and 1600 ($n = 5$) cm^{-1}). This is in accord with the general trend for chloro complexes containing the {Mo(NO)L} moiety to exhibit slightly lower NO values than their iodo counterparts.[1] The mass spectrum of [Mo(NO)LCl{HNC_5H_{10}}] contained a weak molecular ion at $m/z = 545$ (^{98}Mo, ^{11}B, ^{35}Cl) but the most intense ion was at $m/z = 476$ possibly due to the fragment [Mo(NO)LCl(NH_2)]$^+$. An ion was also present at $m/z = 460$ attributable to [Mo(NO)LCl]$^+$ formed by the loss of the amine ligand. In the case of [Mo(NO)LCl{HNC_4H_8}] no molecular ion was observed but again an ion attributable to [Mo(NO)LCl]$^+$ was present.

Electrochemical studies

The electrochemical properties of the 17-electron amine complexes, [Mo(NO)LX{HNC_nH_{2n}}] were investigated using cyclic voltammetry. Due to their limited stability in acetonitrile the iodo complexes were studied in CH_2Cl_2 solution. All the complexes exhibited irreversible reduction processes with $E_p^c = -1.50$ (X = I, $n = 4$), -1.68 (X = I, $n = 5$), -1.08 (X = Cl, $n = 4$) and -1.04 (X = Cl, $n = 5$). The irreversible nature of these processes may be associated with the presence of the amine proton since it is found that, whilst the secondary amide complexes, [Mo(NO)LCl{NC_nH_{2n}}], exhibit reversible reduction behaviour,[12] the primary amide analogues [Mo(NO)LCl(NHR)] (R = alkyl) do not.[13] The amine complexes also exhibited anodic one-electron processes in the region 0–1 V. In the case of the chloro complexes these were chemically reversible on the cyclic voltammetry timescale with $E_f = 0.10$ V, $\Delta E_p = 60$ mV ($n = 4$) and $E_f = 0.16$ V, $\Delta E_p = 80$ mV ($n = 5$), but this was not the case for the iodo complexes which exhibited only irreversible processes.

Cyclic voltammetry of the amide complexes, [Mo(NO)LI{NC_nH_{2n}}], revealed no anodic processes in the region 0–1.2 V but irreversible reduction processes were observed at $E_p^c = -1.29$ ($n = 4$) and -1.28 ($n = 5$) V. These observations are in accord with previous findings in that iodo complexes with reduction potentials more cathodic

than *ca* −1 V tend to dissociate iodide after reduction and exhibit irreversible behaviour.[6] This contrasts with the chemically reversible reduction behaviour found in the cyclic voltammograms of the chloro analogues [Mo(NO)LCl{NC_nH_{2n}}].[9]

The green amine complexes appear to be air-stable in the solid state, at least for periods of a few weeks, but they are slowly oxidized to the amide complexes in solution. The oxidation of the amine complexes with iodine was also investigated and it was found that both the chloro and the iodo–amine complexes could be oxidized to their corresponding 16-electron amide complexes. In contrast, the treatment of [Mo(NO)LI(NC_nH_{2n})] with sodium naphthalenide in the presence of excess HNC_nH_{2n} did not afford the corresponding amine complexes but eventually led to decomposition of the starting complex. However, treatment of [Mo(NO)LI(NC_5H_{10})] with NaH in the presence of excess piperidine did afford some of the green amine complex (17% yield).

Structural studies

Selected bond lengths and angles are given in Table 1. The structures of the molecules are illustrated in Figs 1 and 2. In the pyrrolide complex, **II**, the coordination geometry agrees well with that of analogous amido complexes, e.g. [{Mo(NO)Cl}$_2${$N(CH_2)_2N(CH_2)_2$}][9] and [Mo(NO)LI(NHEt)].[2] Thus the Mo—N(amide) length, 1.937(5) Å, compares well with values of 1.942 and 1.959 Å for the corresponding bonds in these two complexes. The Mo—N(pyrazolyl) bond lengths also follow the pattern found previously, the bond *trans* to the halogen atom, 2.174(5) Å, being significantly shorter than those *trans* to the nitrosyl and amide substituents. The Mo—N(nitrosyl) bond, 1.778(5) Å, is by far the shortest Mo–ligand distance and compares with values of 1.804 Å in

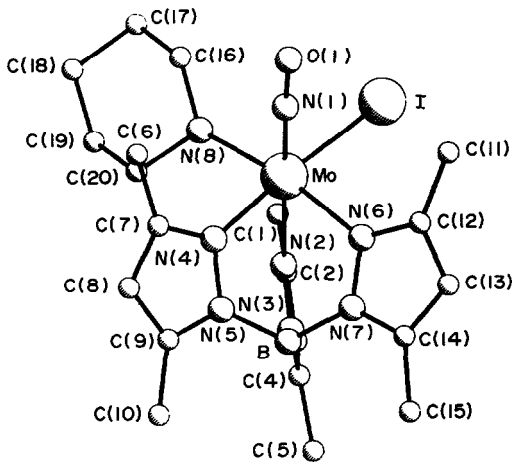

Fig. 1. The molecular structure of **I** showing the atom numbering; H atoms are omitted for clarity.

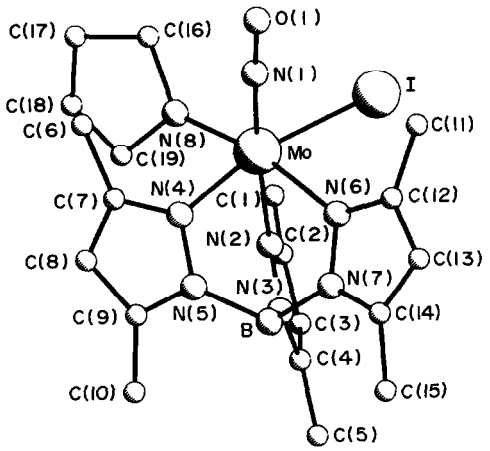

Fig. 2. The molecular structure of **II** showing the atom numbering; H atoms are omitted for clarity.

Table 1. Selected bond lengths and angles

	(I)	(II)
Mo—N(1)	1.774(6)	1.778(5)
Mo—N(2)	2.302(5)	2.246(5)
Mo—N(4)	2.151(5)	2.174(5)
Mo—N(6)	2.175(5)	2.251(5)
Mo—N(8)	2.241(6)	1.937(5)
Mo—I	2.831(1)	2.792(1)
N(1)—Mo—N(2)	179.3(2)	174.8(1)
N(1)—Mo—N(4)	95.3(2)	100.5(2)
N(1)—Mo—N(6)	94.8(2)	93.8(2)
N(1)—Mo—N(8)	94.2(2)	92.8(2)
N(1)—Mo—I	88.2(2)	86.6(2)
N(2)—Mo—N(4)	85.4(2)	84.5(2)
N(2)—Mo—N(6)	85.5(2)	85.4(2)
N(2)—Mo—N(8)	85.5(2)	88.8(2)
N(2)—Mo—I	91.2(1)	88.2(2)
N(4)—Mo—N(6)	81.9(2)	79.6(2)
N(4)—Mo—N(8)	93.8(2)	89.5(2)
N(4)—Mo—I	175.9(1)	168.2(1)
N(6)—Mo—N(8)	170.3(3)	168.1(1)
N(6)—Mo—I	95.7(1)	90.6(2)
N(8)—Mo—I	88.1(2)	99.7(2)
Mo—N(1)—O(1)	176.7(5)	174.8(3)
Mo—N(8)—C(16)	117.5(4)	126.2(4)
Mo—N(8)—C(20)[a]	118.0(5)	127.2(4)
C(16)—N(8)—C(20)[a]	110.3(5)	106.1(5)
H(N8)—N(8)—C(16)	94(6)	
H(N8)—N(8)—C(20)	112(6)	
H(N8)—N(8)—Mo	102(7)	

[a] C(19) in compound **II**.

$[\{Mo(NO)LCl\}_2\{N(CH_2)_2C(CH_2)_2\}]$ and 1.752 Å in [Mo(NO)LI(NHEt)].

The metal–ligand distances in the piperidine complex, **I**, agree reasonably well with those in **II**, with the exception of the Mo—N(8) bond which is longer by 0.3 Å and the Mo—N(pyrazolyl) bond *trans* to this bond which is shorter by 0.076 Å than the corresponding bonds in **II**. These differences are a manifestation of the difference in chemistry at N(8). In (**II**), N(8) is an amido nitrogen atom and the Mo—N(8) distance, 1.937(5) Å, is as expected for a bond of this type, and is indicative of $p\pi$–$d\pi$ donation from the ligand to the metal. In **I**, where N(8) is in the amino form, bonded to two carbon atoms, a hydrogen atom and the molybdenum, the Mo—N(8) distance, 2.241(6) Å, indicates little or no π contribution to the bonding. This conclusion is supported by the lengths of the Mo—N(pyrazolyl) bonds *trans* to Mo—N(8). In **I**, the *trans* bond is relatively short and is similar in length to the Mo—N(pyrazolyl) bonds in **I** and **II** which are *trans* to Mo—I bonds which also do not involve significant π interactions. A further manifestation of the different natures of N(8) in the two complexes is the essentially tetrahedral disposition of bonds in **I** compared with the nearly planar geometry at N(8) in **II**. Thus Mo and H(N8) are bonded respectively, equatorially and axially to the chair-shaped piperidine ring as shown in Fig. 3.

Steric energy calculations[17] show that in both complexes the N(8) ligand is in an orientation close to the calculated energy minimum. In the case of **I**, rotation of the amine ligand about the Mo—N(8) bond is prevented by non-bonding interactions between the C(6) methyl hydrogens of L and a hydrogen on each of the α-methylene carbons of the amine ligand. In the case of **II**, distortion of the Mo—N(8)—pyrrolidide ring centroid angle from the energy minimum value of 170° leads to large steric interactions. In one direction these increase by 76 kJ mol^{-1} within 20° and in the other by 36 kJ mol^{-1}. It thus appears that, in this molecule, a synergy exists between the steric and electronic demands for a near planar stereochemistry at N(8). In the former case this geometry minimizes steric interactions while in the latter it maximizes the overlap of orbitals involved in the $p\pi \rightarrow d\pi$ donation from nitrogen to molybdenum.

The bond angles at molybdenum indicate a slightly distorted octahedral six-coordination in both complexes. The maximum angular deviation from ideal octahedral is 9.7° in **I** and 11.9° in **II**, with mean deviations of 4.3 and 5.6°, respectively.

DISCUSSION

The isolation of amine complexes from the reactions of $[Mo(NO)LI_2]$ with these cyclic secondary amine reagents warrants some comment, in view of our failure to observe such species in the products obtained from reactions involving primary amines. The sterically demanding nature of L suggested that

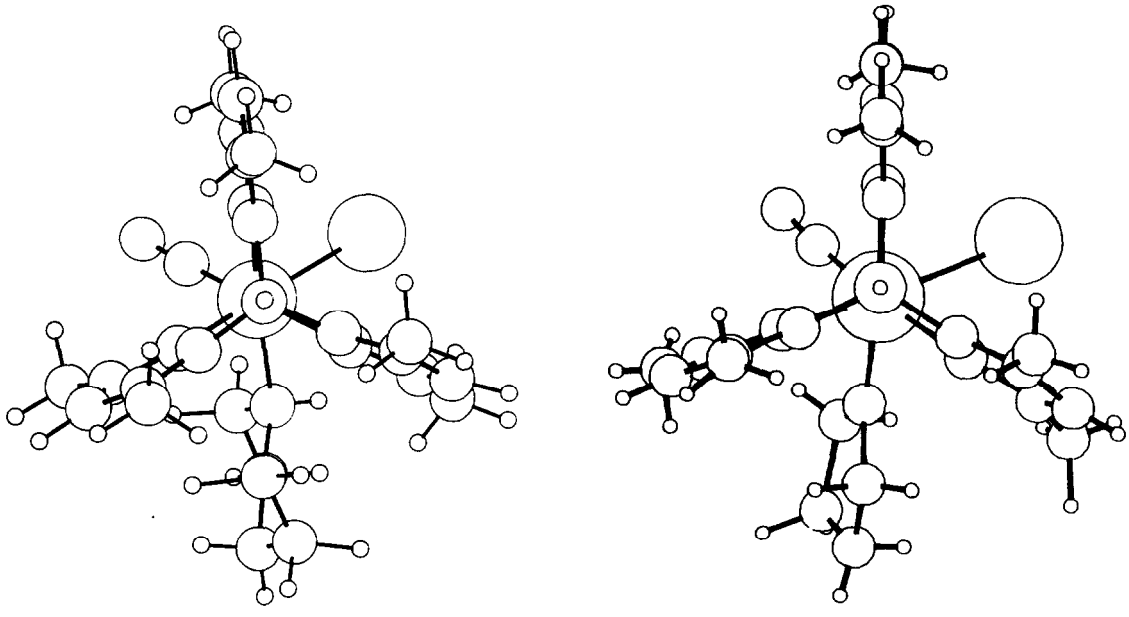

I II

Fig. 3. The molecular structures of **I** and **II** showing the differing geometries of the amine and amide ligands

steric factors might be responsible for these differences in behaviour. The amine proton in **I** is surrounded by atoms in close non-bonded contact (iodide at 3.125 Å and two pyrazolyl-5-methyl protons at 2.184 and 2.696 Å) and the steric energy calculations[17] have shown that the piperidine ligand in this complex is not free to rotate about the Mo—N(piperidine) bond. Thus the amine proton will not be able to adopt a position which would be readily accessible to approaching nucleophiles. The hypothetical amino-bonded $EtNH_2$ complex was also modelled and there was found to be little restriction to the rotation of this ligand about the Mo—N(ethylamine) bond. Thus in the case of this primary amine there appears to be no substantial steric energy barrier to the movement of an amine proton into a location amenable to attack by a nucleophile. In the case of the piperidine complex this will not be the case and kinetic control of the oxidation can arise because of the steric inaccessibility of the amine proton.

It may be concluded that $[Mo(NO)LX_2]$ (X = Cl or I) can react with amines AmH to produce amine complexes. A first step in this process could be the simple substitution of halide to give $[Mo(NO)LX(AmH)]^+$ as shown in eq. (2).

$$[Mo(NO)LX_2]+AmH \rightarrow [Mo(NO)LX(AmH)]^+ + X^- \quad (2)$$

This complex may then undergo deprotonation to a 16-electron amide complex according to eq. (3).

$$[Mo(NO)LX(AmH)]^+ + AmH \rightarrow [Mo(NO)LX(Am)] + AmH_2^+ \quad (3)$$

When a cyclic secondary amine is used in place of a primary amine this deprotonation becomes subject to kinetic control. In the case where X = I the iodide liberated in reaction (2) may function as a reducing agent, as shown in eq. (4),

$$[Mo(NO)LI(AmH)]^+ + I^- \rightarrow [Mo(NO)LI(AmH)] + \tfrac{1}{2}I_2, \quad (4)$$

so that a mixture of amide and amine complexes can arise. When X = Cl, amide complexes are normally formed by deprotonation but, if a reducing agent is added in the form of NaH the neutral 17-electron amine complexes $[Mo(NO)LCl\{HNC_nH_{2n}\}]$ may again be isolated in addition to the amide derivatives.

In the case of reactions involving $[Mo(NO)LI_2]$ the nature of the substitution is further complicated by the presence of displaced I^-. This gives rise to the possibility of an alternative reaction pathway involving labilization of I^- by the reduction of $[Mo(NO)LI_2]$.[5,6] Thus substitution reactions involving 17-electron molybdenum centres, and which may or may not involve the prior coordination of a solvent molecule, can occur as shown in eqs (5)–(8).

$$[Mo(NO)LI_2]+I^- \rightarrow [Mo(NO)LI_2]+\tfrac{1}{2}I_2 \quad (5)$$

$$[Mo(NO)LI_2]^- + Solvent \rightarrow [Mo(NO)LI(Solvent)]+I^- \quad (6)$$

$$[Mo(NO)LI(Solvent)]+AmH \rightarrow [Mo(NO)LI(AmH)]+Solvent \quad (7)$$

$$[Mo(NO)LI_2]^- + AmH \rightarrow [Mo(NO)LI(AmH)]+I^-. \quad (8)$$

Oxidation of the 17-electron amine complex by iodine could then lead to the 16-electron amide complex according to eq. (9)

$$[Mo(NO)LI(AmH)]+\tfrac{1}{2}I_2 \rightarrow [Mo(NO)LI(Am)]+HI, \quad (9)$$

which has been demonstrated chemically.

The isolation of the 17-electron monoamine derivatives described here extends the range of known species containing the $\{Mo(NO)\}^z$ ($z = +1$ or $+2$) moiety. When two anionic ligands such as halide, alkoxide or organo-amide are bound to this fragment, air-stable, diamagnetic, formally 16-electron complexes result.[1] However, when one halide and one neutral amine ligand are present a paramagnetic 17-electron complex results; although this is fairly easily oxidized. A similar situation is found in the case of $[Mo(NO)LI(3,5\text{-}Me_2C_3N_2H_2)]$ which contains halide and neutral dimethylpyrazole ligands and is isolated as a 17-electron complex.[18] When two neutral nitrogen donors such as pyridine are present a 17-electron complex is formed which is not readily oxidized.[7,16]

Acknowledgements—We are grateful to the S.E.R.C. and Mustansirigh University of Iraq for financial support (to A.J.H. and N.AlO., respectively), to Dr J. K. Brown for ESR measurements and to Mr T. Green for technical assistance.

REFERENCES

1. J. A. McCleverty, *Chem. Soc. Rev.* 1983, **12**, 331.
2. J. A. McCleverty, A. E. Rae, I. Wolochowicz, N. A. Bailey and J. M. A. Smith, *J. Chem. Soc., Dalton Trans.* 1982, 429.
3. J. A. McCleverty, G. Denti, S. J. Reynolds, A. S. Drane, N. ElMurr, A. E. Rae, N. A. Bailey, H. Adams and J. M. A. Smith, *J. Chem. Soc., Dalton Trans.* 1983, 81.

4. C. J. Jones, J. A. McCleverty, B. D. Neaves, S. J. Reynolds, H. Adams, N. A. Bailey and G. Denti, *J. Chem. Soc., Dalton Trans.* 1986, 733.
5. J. A. McCleverty and N. El Murr, *J. Chem. Soc., Chem. Comm.* 1981, 960.
6. T. N. Briggs, C. J. Jones, J. A. McCleverty, B. D. Neaves, N. ElMurr and H. M. Colquhoun, *J. Chem. Soc., Dalton Trans.* 1985, 1249.
7. G. Denti, M. Ghedini, J. A. McCleverty, H. Adams and N. A. Bailey, *Trans. Metal Chem.* 1982, 7, 222.
8. N. AlObaidi, K. P. Brown, A. J. Edwards, S. A. Hollins, C. J. Jones, J. A. McCleverty and B. D. Neaves, *J. Chem. Soc., Chem. Commun.* 1984, 690.
9. N. AlObaidi, T. A. Hamor, C. J. Jones, J. A. McCleverty and K. Paxton, *J. Chem. Soc., Dalton Trans.* 1987, 2653.
10. S. J. Reynolds, C. F. Smith, C. J. Jones, J. A. McCleverty, D. C. Bower and J. L. Templeton, *Inorg. Synth.* 1985, **23**, 4.
11. J. A. McCleverty, D. Seddon, N. A. Bailey and N. J. Walker, *J. Chem. Soc., Dalton Trans.* 1976, 898.
12. G. M. Sheldrick, *SHELX, Program for Crystal Structure Determination.* University of Cambridge (1978).
13. W. D. S. Motherwell, *PLUTO, Program for Plotting Molecular and Crystal Structures, Report.* "Cambridge Crystallographic Files", University of Manchester Regional Computer Centre, Manchester (1981).
14. G. M. Sheldrick, *SHELX 80 Computer Program.* Gottingen (1980).
15. E. K. Davies, *SNOOPI from CHEMGRAF Computer Program.* Oxford (1983).
16. N AlObaidi, A. J. Edwards, C. J. Jones, J. A. McCleverty, B. D. Neaves, F. E. Mabbs and D. Collison, submitted to *J. Chem. Soc., Dalton Trans.*
17. S. Motherwell, Energy minimization computer program EENY2. Cambridge; J. D. J. Backer-Dirks, Ph.D. thesis, University of London (1982).
18. N. AlObaidi, A. J. Edwards, C. J. Jones, K. F. Khallow and J. A. McCleverty, manuscript in preparation.

Polyhedron Vol. 7, No. 19/20, pp. 1939–1943, 1988
Printed in Great Britain

0277–5387/88 $3.00+.00
© 1988 Pergamon Press plc

KINETICS OF ASSOCIATIVE REACTIONS OF $Ru_3(CO)_{10}(\mu$-dppm)*

BIMLA AMBWANI, SUDHIR K. CHAWLA and ANTHONY J. POË†

J. Tuzo Wilson Laboratories, Erindale Campus of the University of Toronto, Mississauga, Ontario, Canada L5L 1C6

Abstract—The kinetics of reactions of some more basic P-donor ligands with $Ru_3(CO)_{10}(\mu$-dppm) have been studied and shown to include an associative term. Electronic and steric effects due to different attacking nucleophiles can be separated. The sensitivity of $Ru_3(CO)_{10}(\mu$-dppm) to the basicity of the nucleophiles is slightly greater than that of $Ru_3(CO)_{12}$ but the former is considerably more susceptible to steric effects. The intrinsic susceptibility of $Ru_3(CO)_{10}(\mu$-dppm) to nucleophilic attack is defined and shown to be similar to that of $Ru_3(CO)_{12}$. Activation parameters show, however, that this is due to the combination of a much more favourable activation enthalpy balanced by a much more unfavourable activation entropy. The implications of these results are discussed.

Associative reactions of P-donor nucleophiles with metal carbonyl clusters are now known to be very common.[1] Their rates depend systematically on the electronic and steric nature of the nucleophiles in ways that can be expressed quantitatively by electronic and steric profiles.[2,3] Standard reactivities of the clusters can also be estimated so that a given carbonyl cluster can be quantitatively characterized quite precisely by the systematic kinetics of its associative reactions. These associative reactions can in general lead to substitution and/or fragmentation of the cluster by paths that can be designated, respectively, as S_N2 and F_N2 in nature.[4–6] The relative proportions of these S_N2 and F_N2 processes are, of course, dependent on the detailed natures of the cluster and the nucleophiles[4–6] so that the consequences of nucleophilic attack can provide another way of characterizing a cluster's reactivity.[3] The quantitative effect of substituents in the cluster on its reactivity characteristics must also be expected to vary with the nature of the substituents. We have studied the kinetics of reactions of some more nucleophilic P-donor ligands with $Ru_3(CO)_{10}(\mu$-dppm) in order to determine the substituent effect of the bridging dppm on the susceptibility of the Ru_3 cluster towards nucleophilic attack.

EXPERIMENTAL AND RESULTS

The cluster $Ru_3(CO)_{10}(\mu$-dppm) was prepared, and the P-donor ligands were obtained and treated, exactly as described elsewhere.[2,7] Benzene (BDH, Analar) was chosen as the solvent for solubility reasons and was dried over molecular sieves. Procedures for the kinetic studies have also been described.[7]

Spectroscopic changes during reactions

Reactions were monitored by following the spectroscopic changes as a function of time. Reactions in solutions that had been deoxygenated by bubbling argon showed the same spectroscopic changes and rates as were found without deoxygenation.

At very low concentrations of reacting nucleophiles the changes in the UV–vis. spectra throughout the reactions resemble those observed for reactions with weaker nucleophiles.[7] Thus, reaction with 0.001 M $P(OEt)_3$ leads to an increase in the absorption at 420 nm, the maximum of the band due to $Ru_3(CO)_{10}(\mu$-dppm), and a slight shift to a new maximum at 430 nm with an extinction coefficient *ca* 10% higher. An isosbestic region is evident at *ca* 405 nm. As $[P(OEt)_3]$ is increased the increase in absorbance at 420 nm throughout the reaction decreases until, by $[P(OEt)_3] = 0.01$ M, it has become a decrease *ca* 10%, with an isosbestic point showing at 445 nm. Further increase of $[P(OEt)_3]$ leads to a still more pronounced decrease

*dppm = bisdiphenylphosphinomethane, $Ph_2PCH_2PPh_2$.
† Author to whom correspondence should be addressed.

in absorbance, a shift of the isosbestic point to higher wavelengths, and eventually a complete disappearance of the isosbestic point. These initial spectroscopic changes are followed by further decreases in absorbance over the 300–500 nm range but at rates much slower than those of the initial changes. The rates of reaction were therefore followed by monitoring increases of absorbance at low values of $[P(OEt)_3]$, and decreases at high $[P(OEt)_3]$ with there being a range of values of $[P(OEt)_3]$ where the absorbance changes were too small for rates to be measured accurately.

The UV–vis. changes that occur during reaction with P—*n*-Bu_3 are similar except that the total decrease in absorbance over the course of the reaction is more pronounced. Thus, even with 0.002 M P—*n*-Bu_3 the new maximum at *ca* 445 nm has 10% lower intensity than the initial band at 420 nm. There is an isosbestic point at 442 nm which is lost after *ca* 90% reaction due to a relatively slow further reaction. By $[P—n\text{-}Bu_3] = 0.008$ M the isosbestic point has moved to 485 nm and by $\geqslant 0.01$ M it has disappeared, the total decrease in absorbance becoming steadily greater as $[P—n\text{-}Bu_3]$ is increased still further. The kinetics of the reactions were therefore monitored by following the decreasing absorbance at 420 nm. At higher temperatures and higher values of $[P—n\text{-}Bu_3]$ the reactions were sufficiently fast to require use of the "time-drive" mode of the spectrophotometer but, for slower reactions, the spectra were repetitively scanned from 380–480 nm.

Reaction with $P(OPh)_3$ leads to very small absorbance changes at *ca* 420 nm until $[P(OPh)_3]$ is quite high, but under these conditions subsequent reactions complicate the kinetic analysis. Reactions were therefore followed by observing the decrease in intensity of the CO stretching band at 2080 cm^{-1} observable in benzene and due to the $Ru_3(CO)_{10}$ (dppm) cluster.

Reaction with etpb$\{P(OCH_2)_3CEt\}$ leads simply to a 30% growth in absorbance at 420 nm followed by a much slower decrease in absorbance so that the kinetics were easily monitored at this wavelength.

Reactions with $PPhEt_2$ exhibit rather similar spectroscopic changes to those shown with P—*n*-Bu_3, the final absorbance decreasing with increasing $[PPhEt_2]$. The kinetics were followed simply by monitoring the decrease in absorbance at 420 nm.

The kinetic results are summarized in Table 1, and activation parameters for reactions of $Ru_3(CO)_{10}(\mu$-dppm) with $P(OEt)_3$ and P—*n*-Bu_3, and for some reactions of other relevant Ru_3 clusters, are given in Table 2.

Changes in the IR spectra during reaction in 1,2-dichloroethane and with low concentrations of the nucleophiles lead to spectra that are virtually identical with those observed after reaction with PPh_3, viz. $\nu(CO) = ca$ 2060(m), 2000(s), 1985(vs) and 1950(m) cm^{-1}.[7] After reactions at higher concentrations of P—*n*-Bu_3 (0.08 M) the product spectra show bands at 2052(m), 1980(s) and 1944(vs) cm^{-1}, characteristic in this solvent of independently prepared $Ru(CO)_4$(P—*n*-Bu_3), and 1883 cm^{-1},

Table 1. Rate constants for reactions of $Ru_3(CO)_{10}(\mu$-dppm) in benzene with P-donor ligands, L

L	T (°C)	N^a	[L] (M)	10^4k_1 (s^{-1})^b	10^3k_2 (M^{-1} s^{-1})	$\sigma(k_{obs})$ (%)^c
P—*n*-Bu_3	40.5	18	0.0021–0.115	1.63±0.08^d	10.4±0.5^d	11.9
	40.5	12	0.104–1.15	0.47±0.94	9.86±0.48	10.9
	50.3	6	0.057–0.573	7.34±1.45	17.9±1.3	10.2
	59.0	5	0.115–0.573	17.8±3.4	23.7±1.6	6.6
$P(OEt)_3$	31.0	13	0.088–0.878	1.28±0.25	2.87±0.12	7.7
	40.6	10	0.165–2.25	−0.78±0.51	5.46±0.16	7.0
	40.8	8	0.00098–0.098	1.50±0.05	6.00±0.33	8.3
	49.9	12	0.088–0.527	11.7±1.6	7.43±0.72	12.2
$PPhEt_2$	41.6	10	0.0317–0.476	1.01±0.11	3.57±0.16	9.7
PPh_2Et[e]	40.6	7	0.0122–0.220	1.73±0.04	0.15±0.05	4.6
$P(OPh)_3$	40.6	8	0.200–1.44	1.07±0.12	0.16±0.02	11.1
etpb	40.6	17	0.00425–0.0511	1.18±0.14	118±11	15.4

[a] Number of individual determinations of k_{obs}; $k_{obs} = k_1 + k_2$ [L].

[b] Values of 10^4k_1 obtained[7] from reaction with PPh_3 are: 31.0°C, 0.5 s^{-1}; 40.6°C, 1.8 s^{-1}; 50.0°C, 6.7 s^{-1}; 59°C, 20 s^{-1}.

[c] Probable error of an individual determination of k_{obs}.

[d] Uncertainties here and below are standard deviations.

[e] Data from ref. 7.

Table 2. Kinetic parameters[a] for associative reactions of some Ru_3 clusters with P-donor ligands, L

Cluster	L	$\Delta H_2^{\ddagger}$ (kcal mol^{-1})	$\Delta S_2^{\ddagger}$ (cal K^{-1} mol^{-1})	$10^4 k_2$ (40.0°C)	Reference
$Ru_3(CO)_{10}$(dppm)	P—*n*-Bu_3	9.16±0.86	−38.5±2.9	9.59±0.07	This work
$Ru_3(CO)_{10}$(dppm)	$P(OEt)_3$	10.29±0.79	−36.3±3.2	5.28±0.50	This work
$Ru_3(CO)_{12}$	P—*n*-Bu_3	12.07±0.19	−27.5±0.6	27.3±0.7	8
$Ru_3(CO)_{12}$	$P(OEt)_3$	14.46±0.10	−21.9±0.3	8.82±0.09	8
$Ru_3(CO)_{10}$(P—*n*-$Bu_3)_2$	P—*n*-Bu_3	17.3±2.2	−18.9±7.3	4.3±2.0	5

[a] The activation parameters for reactions of $Ru_3(CO)_{10}(\mu$-dppm) were estimated from data in Table 1 by a linear least squares analysis of the dependence of $\ln(k_2/T)$ on $1/T$. Each value of $\ln(k_2/T)$ was weighted according to the inverse of its variance, the variance being estimated from the standard deviation of k_2.

characteristic of $Ru(CO)_3$(P—*n*-$Bu_3)_2$. Reactions with higher concentrations of etpb lead to the same spectra as with lower concentrations, whereas reactions with higher concentrations of $P(OEt)_3$ and $P(OPh)_3$ lead to complex spectra that have not been assigned. However, reactions with $P(OPh)_3$ in benzene lead to an observable growth of a sharp band at 2060 cm^{-1}, any other bands at lower frequencies being obscured by the solvent. The final intensity of the band at 2060 cm^{-1} decreases with increasing $[P(OPh)_3]$.

DISCUSSION

The products of the reactions at low concentrations of nucleophiles are clearly the substituted clusters $Ru_3(CO)_9(\mu$-dppm)L in which the entering ligand has displaced a CO from the unsubstituted $Ru(CO)_4$ moiety in the cluster.[7,9] However, when L = P—*n*-Bu_3, higher concentrations clearly lead to fragmentation and formation of mononuclear products. Little fragmentation occurs with etpb. The outcome of reactions with higher concentrations of $P(OEt)_3$ and $P(OPh)_3$ is not so clear although some fragmentation appears to be occurring. Reaction with $PPhEt_2$, however, is similar to that with P—*n*-Bu_3, with substantial amounts of fragmentation occurring at higher concentrations of the nucleophile.

The kinetic data show excellent agreement (Table 1) with eq. (1) over values of [L] that vary by up to a factor of 100 in some cases.

$$k_{obs} = k_1 + k_2[L]. \quad (1)$$

No systematic deviations were apparent and the precision of individual values of k_{obs} is quite good in view of the wide range of concentrations generally used. The values of k_1 are in reasonable agreement with the values of k_{obs} obtained[7] from reactions with PPh_3, (which does not show a k_2 [L] term) especially when the large contributions of the k_2 [L] terms to k_{obs} are considered. The values of k_2 remain essentially the same even when concentrations of L are increased, in some cases, to very high values. The reaction path governed by k_2 can be concluded to involve associative attack at the cluster. This is most probably directed at the initially unsubstituted Ru atom since the product, at least for etpb, is $Ru_3(CO)_9(\mu$-dppm)L with one P-donor atom attached to each Ru in the cluster.

The contribution of electronic and steric effects to the second order rate constants can be separated by procedures described elsewhere.[2,3,10] A plot of $\log k_2$ against the value of pK_a for L[11] is shown in Fig. 1 where the straight line drawn is that corresponding to a hypothetical nucleophile with a Tolman cone angle[12] of 130°. This is very close to those for $P(OPh)_3$ (128°) and P—*n*-Bu_3 (132°) the rates for which have been adjusted slightly to allow for the steric effect over this range of cone angles (see below). The gradient (0.19) of the straight line can therefore be taken as the value of β, the electronic discrimination parameter,[2,3,8] since it corresponds to the dependence of $\log k_2$ on pK_a for ligands of the same size. This electronic dependence is assumed to be linear in pK_a on the grounds that this is found to be true for all associative reactions of metal carbonyls, mononuclear as well as polynuclear, in cases where steric effects are unimportant.[2,3,13]

The steric profile can then be obtained by adjusting all the values of $\log k_2$ according to the electronic parameter, β, to what they would have been if the nucleophiles all had the same standard pK_a of −4, i.e. by calculating $\log k_2^0 = \log k_2 - \beta(pK_a + 4)$. (The choice of this hypothetical nucleophile is made for reasons which will be described below.) Values of $\log k_2^0$ are then plotted against the cone angles, θ, of the nucleophiles to give the steric profile shown in Fig. 2. Also plotted in Fig. 2 is the steric profile

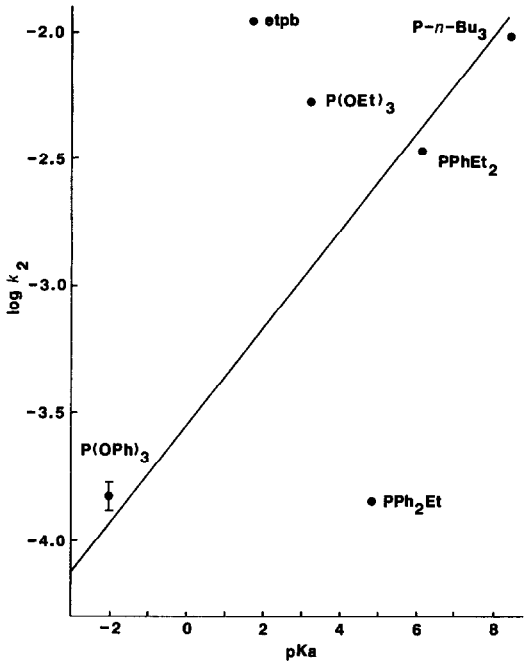

Fig. 1. Dependence of k_2 for associative reactions of $Ru_3(CO)_{10}(\mu$-dppm) on the basicity of the attacking nucleophile. The straight line is drawn between data for $P(OPh)_3$ (cone angle = 128°) and P—*n*-Bu_3 (cone angle = 132°) adjusted according to the steric profile in Fig. 2 to what they would have been if their cone angles were both 130°. The gradient of this line gives a value for the electronic discrimination parameter, β, of 0.19.

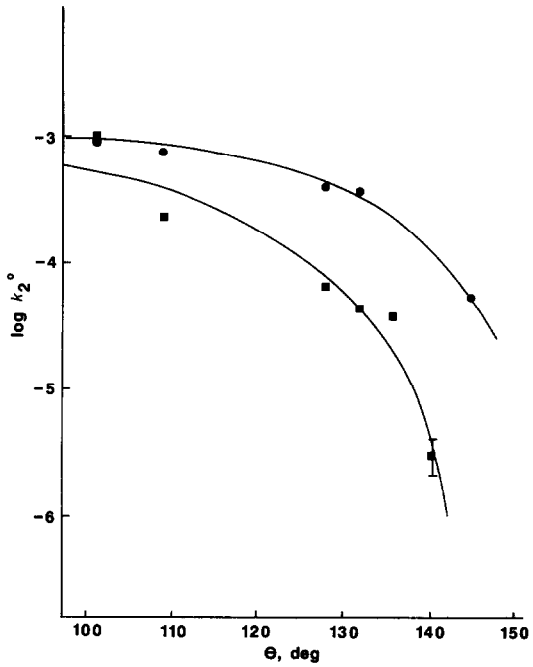

Fig. 2. Dependence of $\log k_2^0 = \log k_2 - \beta(pK_a + 4)$ on the nucleophile cone angle, θ, for associative reactions of $Ru_3(CO)_{10}(\mu$-dppm) (■) and $Ru_3(CO)_{12}$ (●). $\beta = 0.19$ for $Ru_3(CO)_{10}(\mu$-dppm) and 0.15 for $Ru_3(CO)_{12}$.

for $Ru_3(CO)_{12}$ which was obtained in exactly the same way from data already published.[8] The forms of the steric profiles are identical, and show that the $\log k_2^0$ values decrease systematically with increasing cone angle. When the cone angles are sufficiently small the dependence on θ disappears, i.e. the steric profile becomes essentially horizontal at low values of θ when the steric effect is negligible.*

The steric profiles suggest that the electronically adjusted values of $\log k_2$, $\log k_2^0$, become virtually the same for both clusters at low values of θ* and this shows that the susceptibility of the two clusters towards nucleophilic attack by the standard nucleophile with $pK_a = -4$ is approximately the same in the absence of steric effects due to the nucleophiles. It is important to note that the shape of the steric profiles does not depend on the pK_a chosen for the standard nucleophile but the relative positions of the profiles on the vertical axis do change a little, because of the small differences in the values of β. A low value of pK_a for the standard nucleophile was chosen so that the standard reactivity towards nucleophilic attack corresponds to that for a hypothetical very weak nucleophile (one weaker than any known P-donor nucleophile). This standard reactivity will therefore be a better measure of the intrinsic susceptibility of the cluster towards nucleophilic attack because the contribution of the nucleophile to the bonding in the transition state will be relatively small and the rate will depend much more on the energetic changes due to rearrangement of the cluster on going to the transition state. If a stronger nucleophile had been chosen as the standard then $Ru_3(CO)_{12}$, because of its slightly smaller value of β, would have been relatively less susceptible to nucleophilic attack than $Ru_3(CO)_{10}$(dppm), but if an even more weakly basic nucleophile had been chosen then $Ru_3(CO)_{12}$ would have been slightly more susceptible. This ambiguity in the estimation of intrinsic susceptibilities to nucleophilic attack is an inevitable consequence of the impossibility, in principle, of distinguishing exactly the energetic contribution of one participant in a bimolecular event from that of the other participant. The fact remains, however, that the intrinsic susceptibilities of the two clusters to nucleophilic attack must be very similar.

* Steric profiles are generally smooth curves, approaching the horizontal at low θ,[2,3,10] of the type shown by $Ru_3(CO)_{12}$ in Fig. 2. We have, therefore, drawn a similar curve through the data for $Ru_3(CO)_{10}(\mu$-dppm), assuming that the deviations for L = etpb and $P(OEt)_3$ are consistent with normally expected scatter,[2,3] rather than drawing a straight line through data for all the nucleophiles apart from PPh_2Et.

The values of β for the two clusters show that the presence of the dppm substituent increases the sensitivity of the cluster to the basicity of the attacking nucleophile. The steric profiles show that dppm has a very pronounced effect on the sensitivity of the rates to the size of the nucleophile. This effect is sufficiently large that no k_2 term is detectable[7] for attack by PPh_3, the cone angle for which is 145°.[12]

The higher value of β for $Ru_3(CO)_{10}$(dppm) suggests that the extent of bond making in the transition states is slightly greater than in reactions of $Ru_3(CO)_{12}$.[3,8] The activation parameters for corresponding reactions of the two clusters are, however, quite different (Table 2); the activation enthalpies are appreciably lower for $Ru_3(CO)_{10}$(dppm) and the activation entropies are considerably more negative. This does not imply that bond making is much greater in reactions of $Ru_3(CO)_{10}$(dppm) since that would conflict with the relatively small difference suggested by the β-values. It suggests rather that the enthalpy change involved in adjusting the cluster to the approach of the nucleophiles is significantly lower, the enthalpy decrease caused by bond making being similar for reactions of the two clusters with a given nucleophile. This means that the similar intrinsic reactivities of the two clusters arises from a balance between a more favourable enthalpy of adjustment of $Ru_3(CO)_{10}$(dppm), balanced by an equally unfavourable entropic effect. The more favourable enthalpy may be related, at least in part, to the release of steric strain[14] caused by the bridging dppm ligand as the cluster opens up to allow approach of the nucleophile.[2-4,8] It is this opening up of the cluster that allows for the possibility that nucleophilic attack will lead to fragmentation (an F_N2 process) as well as, or instead of, substitution (an S_N2 process), and the quantitative balance between these processes will be discussed elsewhere. An additional contribution to the lower enthalpies for reactions of $Ru_3(CO)_{10}$(dppm) might be the greater ease of Ru—CO bond breaking in this complex.[7] However, this is unlikely to be the only contribution because it might be expected to lead to a more positive value of $\Delta S^{\ddagger}_2$ whereas the more negative values actually observed could be explained by rather precise atomic movements in the cluster that are required during the formation of the transition state. The presence of the relatively basic dppm substituent would tend to increase the electron density on the cluster and might therefore be expected to decrease its electrophilicity. That this is not the case suggests that major electronic effects of substituents are operative in the transition states, a conclusion that has also been reached for S_N1 reactions of some substituted Ir_4 clusters.[1,15] On the other hand, the two quite large and rather basic substituents in $Ru_3(CO)_{10}(P—n\text{-}Bu_3)_2$ do inhibit associative attack (Table 2) as shown by the much higher value of the activation enthalpy. We believe that this is probably due more to steric then electronic effects.

These various considerations show how kinetic data for associative reactions of metal carbonyl clusters can provide unique characterization of the clusters, and can be analysed in some detail to explore the factors involved. This potentially quite general approach merits fuller investigation.

Acknowledgement—We thank the Natural Science and Engineering Research Council, Ottawa, for support.

REFERENCES

1. A. J. Poë, in *Metal Clusters* (Edited by M. Moskovits), Chap. 4. Wiley-Interscience, New York (1986).
2. K. Dahlinger, F. Falcone and A. J. Poë, *Inorg. Chem.* 1986, **25**, 2654.
3. A. J. Poë, *Pure App. Chem.* 1988, **60**, 1209; N. M. J. Brodie, L. Chen and A. J. Poë, *Intl. J. Chem. Kinet.* 1988, **20**, 467.
4. A. J. Poë and V. C. Sekhar, *Inorg. Chem.* 1985, **24**, 4376.
5. N. M. J. Brodie, A. J. Poë and V. C. Sekhar, *J. Chem. Soc., Chem. Commun.* 1985, 1090.
6. N. M. J. Brodie and A. J. Poë, *Inorg. Chem.* 1988, **27**, in press.
7. B. Ambwani, S. K. Chawla and A. J. Poë, *Inorg. Chem.* 1985, **24**, 2635; B. Ambwani, S. K. Chawla and A. J. Poë, *Inorg. Chim. Acta* 1987, **133**, 93.
8. A. J. Poë and M. V. Twigg, *J. Chem. Soc., Dalton Trans.* 1974, 1860.
9. D. F. Foster, J. Harrison, B. S. Nicholls and A. K. Smith, *J. Organomet. Chem.* 1985, **295**, 99.
10. M. N. Golovin, M. M. Rahman, J. E. Belmonte and W. P. Giering, *Organometallics* 1985, **4**, 1981.
11. M. M. Rahman, H. Y. Liu, A. Prock and W. P. Giering, *Organometallics* 1987, **6**, 650.
12. C. A. Tolman, *Chem. Rev.* 1977, **77**, 313.
13. F. Basolo and R. G. Pearson, *Mechanisms of Inorganic Reactions*, 2nd Edn, Chap. 7. Wiley, New York (1967); F. Basolo, *Inorg. Chim. Acta* 1985, **100**, 33 and refs therein.
14. A. W. Coleman, D. F. Jones, P. H. Dixneuf, C. Brisson, J. J. Bonnet and G. Lavigne, *Inorg. Chem.* 1984, **23**, 952.
15. D. C. Sonnenberger and J. D. Atwood, *J. Am. Chem. Soc.* 1982, **104**, 2113; D. C. Sonnenberger and J. D. Atwood, *Organometallics* 1982, **1**, 694.

Polyhedron Vol. 7, No. 19/20, pp. 1945–1951, 1988
Printed in Great Britain

0277–5387/88 $3.00+.00
© 1988 Pergamon Press plc

NAPHTHOQUINODIMETHANE COMPLEXES OF RUTHENIUM(0)*

NIGEL J. SIMPSON and DAVID J. COLE-HAMILTON†

Chemistry Department, University of St. Andrews, St. Andrews, Fife KY16 9ST, Scotland, U.K.

Abstract—Reactions of $[RuCl_2L_4]$ (L = PMe_3, PMe_2Ph or $PMePh_2$) with 2-lithiomethyl-1-methylnaphthalene or 2-lithiomethyl-3-methylnaphthalene lead to $[Ru(CH_2C_{10}H_6CH_2)L_3]$ which contain coordinated 1,2- or 2,3-naphthoquinodimethane moieties. Spectroscopic studies confirm these formulations and suggest significant localization of the double bonds, at least for the 1,2-naphthoquinodimethane fragment. For L = PMe_3 and 2-lithiomethyl-1-methylnaphthalene formation of the 1,2-naphthoquinodimethane complex is accompanied by the formation of $[Ru(CH_2C_{10}H_6CH_2)(PMe_3)_4]$ in which the organic moiety acts as a dialkyl, two-electron donor. Surprisingly for L = PMe_2Ph and 2-lithiomethyl-3-methylnaphthalene, the naphthoquinodimethane is not formed but the major product, although not isolated in a pure state, appears to be $[Ru(CH_2C_6H_{10}CH_3)Cl(PMe_2Ph)_3]$ in which the organic group is coordinated in an η^3 (allyl) mode. Plausible mechanisms, which account for the various products formed in these reactions are presented.

The stabilization of otherwise unstable organic compounds by coordination to transition elements is an area of particular interest, especially if the organic moiety can be released and undergo subsequent reactions. Perhaps the most spectacular early success in this area was the stabilization of cyclobutadiene by bonding to iron(0) and its subsequent release by oxidation.[1,2] More recently, a number of reports has appeared on the stabilization by coordination of *o*-quinodimethane,[3–9] which, although not stable itself, is an important intermediate in a range of organic synthetic reactions.[10] We[11] and others[12] have also reported that *o*-quinodimethane can be released from ruthenium or cobalt complexes by oxidation or ligand displacement and trapped by e.g. MeOOCC≡CCOOMe.

Most of the reported syntheses of *o*-quinodimethane complexes involve deprotonation[4,6] (or oxidation)[9] of hexamethylbenzene metal complexes, or reactions of *o*-bis(bromomethyl)benzene[3,5] or *o*-bis(chloromethyl)benzene derivatives.[8] Since these types of precursor are not always readily available for more complex aromatic systems, complexes of more elaborate analogues of *o*-quinodimethane have not been prepared.

In contrast we have reported that *o*-quinodimethane complexes of ruthenium[7] can be obtained directly from *o*-xylene by deprotonation with BuLi·TMED (TMED = 1,2-bis(dimethylamino)ethane) and reaction of the resulting lithium salt with, for example $[RuCl_2(PMe_3)_4]$. Since *o*-dimethylaromatic compounds are often readily available this reaction should be of more general applicability. Octamethylnaphthalene complexes of ruthenium(II) have been described,[13] but despite the fact that they have been reduced, deprotonation does not appear to have been attempted.

We now report the preparation of a series of 2,3-naphthoquinodimethane (**1**), and 1,2-naphthoquinodimethane (**2**) complexes prepared from 2,3-dimethylnaphthalene and 1,2-dimethylnaphthalene, respectively. A preliminary account of some of these results has appeared.[14]

RESULTS

Preparation of o-naphthoquinodimethane complexes of ruthenium

Reactions of a large excess of 2-lithiomethyl-3-methylnaphthalene·TMED with $[RuCl_2L_4]$ or of a large excess of 2-lithiomethyl-1-methylnaphthalene·TMED‡ with $[RuCl_2L_4]$ (L = PPh_2Me,

* Dedicated to Sir Geoffrey Wilkinson, on the occasion of his retirement from Imperial College, London.

† Author to whom correspondence should be addressed.

‡ It has been suggested[15] that this is the product obtained from the reaction of 1,2-dimethylnaphthalene with BuLi·TMED.

PMe_2Ph, or PMe_3) in diethyl ether leads to orange solutions for the 1,2-dimethylnaphthalene reactions and red solutions for the 2,3-dimethylnaphthalene reactions, from which compounds analysing as $[Ru(CH_2C_6H_{10}CH_2)L_3]$ may be isolated in reasonable yield.

Although the major product isolated from the reaction of $[RuCl_2(PMe_3)_4]$ with 2-lithiomethyl-1-methylnaphthalene is the expected 1,2-naphthoquinodimethane complex, a second product, which analyses as $[Ru(CH_2C_{10}H_6CH_2)(PMe_3)_4]$ is also produced.

Somewhat surprisingly, the expected naphthoquinodimethane complex is not obtained from reaction of $[RuCl_2(PMe_2Ph)_4]$ with 2-lithiomethyl-3-methylnaphthalene but instead the major product appears, from spectroscopic studies (see below), to contain an intact $(CH_2C_{10}H_6CH_3)$ group bound in an η^3-allyl fashion.

We have attempted to interconvert $[Ru(CH_2C_{10}H_6CH_2)(PMe_3)_n]$ ($n = 3$ or 4) by refluxing the former with excess PMe_3 or by treating the latter with S_8 (a well known phosphine scavanger), photolysis or by extensive reflux in the absence of added phosphine, but in none of the cases is the interconversion achieved.

Spectroscopic properties

The ^1H and ^{31}P NMR spectra (Tables 1 and 2) of the 2,3-naphthoquinodimethane complexes are very similar to those of their *o*-quinodimethane analogues[7] with doublets of doublets being observed near δ 0 and 2 for the *endo* and *exo* methylene protons, respectively, pseudo doublets with some intensity between the lines arising from the $A_nXX'A'_n$ spin system of the methyl groups of the two symmetry related phosphines, and a doublet from the methyl group(s) of the unique phosphine. For $[Ru(CH_2C_{10}H_6CH_2)(PMe_3)_3]$, the resonances from the aromatic protons confirm that a plane of symmetry runs through the naphthalene ring. As for the related *o*-quinodimethane complexes,[7] J_{PP} in the ^{31}P NMR spectrum is small (< 11 Hz) con-

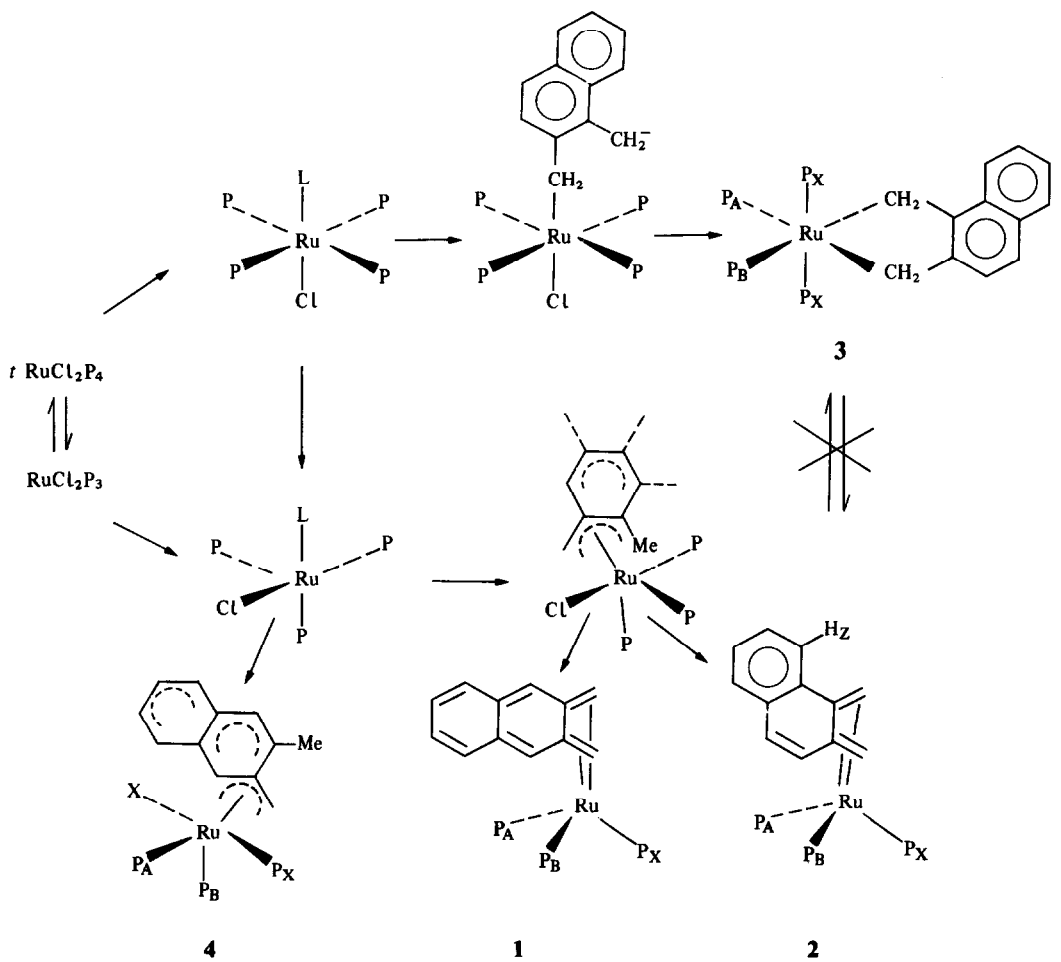

Scheme 1. Proposed mechanism for formation of compounds with structures **1–4**, L = $(CH_2C_{10}H_6CH_3)^-$.

Table 1. High field ^1H NMR data for new ruthenium complexes[a]

Complex	P_AMe $\delta(J_{PH})$	P_BMe $\delta(J_{PH})$	P_XMe $\delta(J_{PH})$	CH_{exo} $\delta(J_{PH})$	CH_{endo} $\delta(J_{PH})$	$J_{H_{exo}H_{endo}}$
$[Ru(2,3\text{-}CH_2C_{10}H_6CH_2)(PMePh_2)_3]$[b]	1.5 pd(4.1)[c]		2.2 d(7.8)	1.7 dd(5.5)	0.7 dd(4.5)	4.5
$[Ru(2,3\text{-}CH_2C_{10}H_6CH_2)(PMe_3)_3]$[d]	0.9 pd(6)[c]		1.4 d(8)	2.3 dd(8)	0.5 dd(5)	6
$[Ru(1,2\text{-}CH_2C_{10}H_6CH_2)(PMePh_2)_3]$[e]	0.9 d(6)	1.35 d(6)	1.55 d(6)	2.55 m 2.0 m	0.4 bm[2H]	
$[Ru(1,2\text{-}CH_2C_{10}H_6CH_2)(PMe_2Ph)_3]$	0.94 d(6) 0.99 d(6)	1.03 d(6) 1.16 d(6)	1.75 d(7)[6H]	2.35 bm[2H]	−0.4 bm[2H]	
$[Ru(1,2\text{-}CH_2C_{10}H_6CH_2)(PMe_3)_3]$	0.7 d(6)	1.0 d(6)	1.5 d(8)	2.7 m 2.0 m	−0.2 bm[2H]	
$[Ru(1,2\text{-}CH_2C_{10}H_6CH_2)(PMe_3)_4]$	1.4 d(5)	1.3 d(5)	0.9 pt(5)[c]	1.9 dd(5,11)[f]	2.45 ddt(4,9.5,9.5)[f]	

[a] Chemical shifts (δ) in ppm to high frequency of $SiMe_4$, coupling constants in Hz; measured in C_6D_6 at 298 K using C_6D_5H (δ 7.3) as internal reference; s = singlet, d = doublet, t = triplet, m = multiplet, p = pseudo (see text); for assignments, see Scheme 1.

[b] Measured in CH_2Cl_2 at 298 K using $CHDCl_2$ (δ 5.3) as internal standard.

[c] $J_{PH}+J_{PH'}$.

[d] Phenyl resonances, 7.8s (2H); 7.5 (AA'BB') (4H).

[e] Me assignments complicated by impurities.

[f] The two hydrogen atoms of each methylene group are equivalent.

Table 2. ^{31}P NMR data for new ruthenium complexes[a]

Complex	δP_A	δP_B	δP_X	$J(P_AP_X)$	$J(P_BP_X)$	$J(P_AP_B)$
$[Ru(2,3\text{-}CH_2C_{10}H_6CH_2)(PMePh_2)_3]$	19.5 d		41.4 t	4.0		
$[Ru(2,3\text{-}CH_2C_{10}H_6CH_2)(PMe_3)_3]$	0.16 d		28.5 t	10.7		
$[Ru(1,2\text{-}CH_2C_{10}H_6CH_2)(PMePh_2)_3]$	15.6 d	20.3 d	30.2 s	0	0	24.2
$[Ru(1,2\text{-}CH_2C_{10}H_6CH_2)(PMe_2Ph)_3]$	2.7 dd	4.1 dd	20.1 t	3.5	3.9	29.6
$[Ru(1,2\text{-}CH_2C_{10}H_6CH_2)(PMe_3)_3]$	−9.8 dd	−6.3 dd	8.0 t	8.0	7.7	32.3
$[Ru(1,2\text{-}CH_2C_{10}H_6CH_2)(PMe_3)_4]$	−20.7 dt	−14.8 dt	−6.15 t	26.5	25.1	13.8
$[Ru(CH_2C_6H_{10}CH_3)X(PMe_2Ph)_3]$	11.5 d	10.8 d	6.1 t	12.3	13.2	0

[a] Chemical shifts in ppm to high frequency of external 85% H_3PO_4, coupling contents in Hz; measured in C_6D_6 at 298 K; for assignments, see Scheme 1.

firming that the P—Ru—P angle is close to 100°. The rather larger value observed for the PMe_3 complex than for others containing bulkier phosphines may suggest a slightly smaller angle on account of reduced steric interaction. These compounds have structure **1**. For the 1,2-naphthoquinodimethane complexes, the lack of a plane of symmetry in the molecules means that more complex spectra are observed with separate doublets from the methyl groups on each phosphine and separate resonances showing coupling to several nuclei from the methylene hydrogen atoms. For L = PMe_2Ph, six doublet resonances are observed from the methyl groups since each pair is diastereotopic (no plane of symmetry runs through any of the phosphorus atoms).

In the ^{31}P spectra, separate resonances are observed for each phosphorus atom and the coupling constants are all small as expected for structure **2**.

The spectra of $[Ru(CH_2C_{10}H_6CH_2)(PMe_3)_4]$ show that it has structure **3**. Most indicative is the ^{31}P NMR spectrum which shows three resonances from the three distinct types of phosphorus atom, all with the couplings expected for *cis* phosphorus atoms in an octahedral complex. Two methylene resonances are observed at δ 1.88 and 2.43, the same region as that observed for the methylene protons in *o*-xylylidene complexes of e.g. platinum.[16,17] The methyl groups of the mutually *trans* phosphines resonate as a pseudotriplet ($A_9XX'A'_9$ with large J_{XX}), whilst doublets are observed from the other phosphine methyl groups.

Surprisingly, the product obtained from $[RuCl_2(PMe_2Ph)_4]$ and 2-lithiomethyl-3-methylnaphthalene · TMED is not the expected naphthoquinodimethane complex. Unfortunately, the complex has not been obtained in an analytically pure form, but resonances in the δ 3–6 region of the ^1H NMR spectrum are similar to those of the η^3 bound *o*-methylbenzyl ligand[18] in $[Rh(o\text{-}CH_2C_6H_4CH_3)(PPh_3)_2]$ although the multiplicities suggest more coupling to phosphorus. The ^{31}P NMR spectrum shows that there are three phosphine ligands in mutually *cis* positions. On this basis, we very tentatively assign the compound as **4** with X being either chloride or a σ bonded $o\text{-}CH_2C_{10}H_6CH_3$ ligand (it is not hydride). Microanalysis of an impure sample shows the presence of Cl so we favour Cl^- as the sixth ligand.

DISCUSSION

X-ray studies have shown[7] that there is significant bond localization in the *o*-quinodimethane group of $[Ru(CH_2C_6H_4CH_2)(PMe_2Ph)_3]$. The larger resonance energy of naphthalenes, which is presumably lost (especially for the 2,3-naphthoquinodimethane) if similar bond localization occurs in $\eta^2:\eta^2$ bonded *o*-naphthoquinodimethane complexes, makes it somewhat surprising that these complexes form so readily. However the spectroscopic data clearly show that this type of bonding does occur.

Although none of the complexes has given crystals of sufficient quality for X-ray structure determination so that a direct indication of the extent of bond localization is not possible, ^1H NMR studies do suggest that this localization does occur. Thus the phenyl region of the ^1H NMR spectrum of $[Ru(1,2\text{-}CH_2C_{10}H_6CH_2)(PMe_3)_4]$, in which the organic moiety is bound as a simple dialkyl so that localization is not expected, is similar to that of the parent 1,2-dimethylnaphthalene. In contrast the phenyl region for $[Ru(1,2\text{-}CH_2C_{10}H_6CH_2)(PMe_3)_3]$ in which $\eta^2:\eta^2$ bonding occurs, is quite different with one proton resonating at very low field (δ 8.35). The phenyl region of the spectrum of this compound is very similar to that of 1,2-naphthoquinone (low field resonance at δ 8.05),[19] in which the bonding is forced to be as in the localized bonding picture for **2**. The low field resonance then arises from proton Z. We therefore conclude that

significant bond localization does occur at least for the 1,2-naphthoquinodimethane complexes.

UV spectra

The UV spectra of $[Ru(2,3\text{-}CH_2C_{10}H_6CH_2)L_3]$ (L = $PMePh_2$ or PMe_3) show strong absorptions near 510 nm, which account for the dark red colour of the complexes. These absorptions are close to the position of the major absorption observed for matrix isolated 2,3-naphthoquinodimethane (541 nm),[20] suggesting again that significant delocalization occurs in the bound 2,3-naphthoquinodimethane complexes.

Mechanistic interpretation

The exact mechanism by which these complexes form is unclear, but since all attempts to interconvert $[Ru(CH_2C_{10}H_6CH_2)(PMe_3)_n]$ (n = 3 or 4) have failed, neither is on the reaction pathway to the other. It seems therefore that the loss of phosphine must occur at an early stage in the reaction but probably after alkylation of at least one Ru—Cl bond since we have shown[7] previously that loss of a phosphine from $[RuCl_2(PMe_3)_4]$ would allow alkylation by Grignard reagents, but that this reaction is not observed. For L = PMe_2Ph or $PMePh_2$, the phosphines are more labile, phosphine loss from the dihalides is known to be facile,[21] and alkylation by Grignard reagents is observed.[7]

The scheme affords a rational explanation for the formation of the various different observed products; which is supported by the following observations:

(i) We have shown that removal of a hydride from a methyl group α to a coordinated allyl moiety is facile in low valent ruthenium phosphine complexes.[22] In the case of the reaction involving PMe_2Ph and 2-lithiomethyl-3-methylnaphthalene, it may be that a marked preference for forming the allyl complex with the unsubstituted ring carbon atom (**4**) precludes the further deprotonation of the other methyl group.

(ii) $[RuCl_2(PMe_3)_4]$ has *trans* stereochemistry and attempts to isomerize it to *cis*, even under very forcing conditions, have not been successful.

It is probable, therefore that alkylation occurs *trans* to Cl^-. This will have two important consequences: firstly, the high *trans* effect of the alkyl ligand will labilize the remaining chloride and secondly the methyl group on the napthalene will become more acidic than that in 1,2-dimethylnaphthalene and hence be readily deprotonated by 2-lithiomethyl-1-methylnaphthalene·TMED. The formed anion clearly must attack the metal in a position *cis* to the bound methylene group and the lability of the Cl^- ligand will allow the formation of $[Ru(CH_2C_{10}H_6CH_2)(PMe_3)_4]$.

Unfortunately it is not clear why certain products are preferred for different combinations of L and dimethylnaphthalene.

EXPERIMENTAL

Microanalyses were carried out by St Andrews University laboratories. NMR spectra were recorded on Bruker WP-80, AM-300 and Varian CFT-20 spectrometers. All solvents were thoroughly dried by distillation from sodium benzophenone ketyl and degassed before use. The light petroleum had a boiling range of 40–60°C. All manipulations were carried out under dry oxygen-free nitrogen using standard Schlenk-line and catheter tubing techniques. The compounds $[RuCl_2(PPh_3)_3]$,[23] $[RuCl_2(PMePh_2)_4]$,[24] $[RuCl_2(PMe_2Ph)_4]$[21] and $[RuCl_2(PMe_3)_4]$[25] were prepared by standard literature methods.

Preparation of lithium reagents

To a stirred solution of BuLi in hexane (6 cm^3, 9.6×10^{-3} mol, 1.6 M) cooled to 0°C was added TMED (3.0 cm^3, 19.8×10^{-3} mol). After 15 min the appropriate dimethylnaphthalene (1.56 g, 10×10^{-3} mol) in petroleum (40 cm^3) was added and the mixture stirred for a further 15 min before removing the ice bath and allowing the mixture to react for 24 h. The petroleum was removed by filtration and the lithium salt dissolved in diethyl ether (40 cm^3) ready for use. Assuming 100% conversion, the concentration of lithium reagent is 0.24 mol dm^{-3}.

Tris(methyldiphenylphosphine) (2-α,3-α′:η⁴-o-naphthoquinodimethane) ruthenium(0)

The complex $[RuCl_2(PPh_2Me)_4]$ (1.0 g, 1.028×10^{-3} mol) was stirred with a solution of 2-lithiomethyl-3-methyl naphthalene·TMED (40 cm^3, 0.24 mol dm^{-3}) in diethyl ether (40 cm^3). After 24 h, water (20 cm^3) was added to the red solution and after stirring for 30 min, the ether was decanted, dried over anhydrous sodium sulphate, and the ether removed *in vacuo*. Excess 2,3-dimethylnaphthalene and free $PMePh_2$ were removed by sublimation at 120°C onto a cold finger (−78°C). The resulting red gum was dissolved in the minimum amount of diethyl ether. After filtration and cooling to −30°C for several days, the product separated as red crystals, which were collected and dried *in vacuo*. Yield 0.35 (40%). Found: C, 70.7;

H, 7.0; P, 10.5. $C_{51}H_{49}P_3Ru$ requires: C, 71.6; H, 5.8; P, 10.9%.

The following complexes were similarly prepared, but with the work-up after the sublimation step as shown.

Tris(dimethylphenylphosphine) (1-α,2-α′:η^4-o-*naphthoquinodimethane*) *ruthenium*(0)

From $[RuCl_2(PMe_2Ph)_4]$ (0.75 g, 1.035×10^{-3} mol) and 2-lithiomethyl-1-methylnaphthalene·TMED (40 cm^3, 0.24 mol dm^{-3}). The orange gum was dissolved in diethyl ether (2 cm^3) and filtered into light petroleum (40 cm^3) precooled to −78°C. The yellow–orange precipitate was collected by filtration and dried *in vacuo*. However, ^{31}P NMR showed the product to contain *ca* 10% impurities. Yield 0.26 g (38%).

Tris(trimethylphosphine)(1-α,2-α′:η^4-o-*naphthoquinodimethane*) *ruthenium*(0)

From $[RuCl_2(PMe_3)_4]$ (0.55 g, 1.155×10^{-3} mol) and 2-lithiomethyl-1-methylnaphthalene·TMED (40 cm^3, 0.24 mol dm^{-3}) in diethyl ether (40 cm^3). The yellow gum was extracted with light petroleum (40 cm^3) to leave a yellow powder which was recrystallized from toluene and light petroleum, and identified as $[Ru(CH_2C_{10}H_6CH_2)(PMe_3)_4]$. Yield 0.07 g (11%). Found: C, 51.8; H, 8.2. $C_{24}H_{46}P_4Ru$ requires; C, 51.5; H, 8.3%.

The yellow petroleum solution was reduced in volume to 5 cm^3 and on cooling to −30°C gave yellow crystals which were collected and dried *in vacuo* and identified as $[Ru(CH_2C_{10}H_6CH_2)(PMe_3)_3]$. Yield 0.13 g (24%). Found: C, 52.3; H, 8.0. $C_{21}H_{37}P_3Ru$ requires: C, 52.5; H, 7.7%.

Tris(trimethylphosphine)(2-α,3-α′:η^4-o-*naphthoquinodimethane*) *ruthenium*(0)

From $[RuCl_2(PMe_3)_4]$ (0.55 g, 1.155×10^{-3} mol) and 2-lithiomethyl-3-methylnaphthalene·TMED (40 cm^3, 0.24 mol dm^{-3}). The red–brown solid was washed with light petroleum and dried *in vacuo*. Yield 0.22 g (40%). Found: C, 51.8; H, 7.5. $C_{21}H_{37}P_3Ru$ requires: C, 52.5; H, 7.7%.

Tris(methyldiphenylphosphine) (1-α,2-α′:η^4-o-*naphthoquinodimethane*) *ruthenium*(0)

From $[RuCl_2(PMePh_2)_4]$ (1.00 g, 1.028×10^{-3} mol) and 2-lithiomethyl-1-methylnaphthalene·TMED (40 cm^3, 0.24 mol dm^{-3}). The orange gum was dissolved in diethyl ether (1 cm^3) and syphoned into light petroleum (40 cm^3) precooled to −78°C. The resulting yellow solid which was collected and dried *in vacuo* was contaminated with $[H_2Ru(PPh_2Me)_4]$[26] (up to 20%) which could not be removed by further recrystallization. Yield 0.35 g.

Reaction of $[RuCl_2(PMe_2Ph)_4]$ *with* 2-CH_2-3-Me-$C_{10}H_6$

Reaction as above—from $[RuCl_2(PMe_2Ph)_4]$ (0.75 g, 1.035×10^{-3} mol) and 2-lithiomethyl-3-methylnaphthalene·TMED (40 cm^3, 0.24 mol dm^{-3}). The red–orange gum was extracted with hot petroleum (40 cm^3). After concentration a brown solid was formed. It could not be further purified but was tentatively assigned as $[Ru(\eta^3\text{-}CH_2C_{10}H_6Me)Cl(PMe_2Ph)_3]$ from its spectroscopic properties. ^1H NMR (C_6D_6) δ 6.5–8 m (Ph); 6.25 bt ($J = 7$ Hz) [1H]; 5.45 d ($J = 7.5$ Hz) [1H]; 4.0 q ($J = 9$ Hz) [1H]; 2.42 dd ($J = 6$, 6.5 Hz); 0.6–2.2 very complex series of doublets.

Acknowledgements—We thank the SERC for a studentship (NJS) and a grant to purchase the high field NMR spectrometer. We are also indebted to Johnson Matthey plc for generous loans of ruthenium salts.

REFERENCES

1. G. F. Emerson, L. Watts and R. Pettit, *J. Am. Chem. Soc.* 1965, **87**, 131.
2. L. Watts, J. D. Fitzpatrick and R. Pettit, *J. Am. Chem. Soc.* 1965, **87**, 3253.
3. W. Roth and J. D. Meier, *Tetrahedron Lett.* 1967, 2053.
4. M. A. Bennett, I. J. McMahon and T. W. Turney, *Angew. Chem. Int. Edn. Engl.* 1982, **21**, 379.
5. W. H. Hersch, F. J. Hollander and R. G. Bergman, *J. Am. Chem. Soc.* 1983, **105**, 5834.
6. J. W. Hull and W. L. Gladfelter, *Organometallics* 1982, **1**, 1716.
7. S. D. Chappell, D. J. Cole-Hamilton, A. M. R. Galas and M. B. Hursthouse, *J. Chem. Soc., Dalton Trans.* 1982, 1867.
8. J-M. Grosselin, H. Le Bozec, C. Moinet, L. Toupet and P. H. Dixneuf, *J. Am. Chem. Soc.* 1985, **107**, 2809.
9. D. Astruc, *Acc. Chem. Res.* 1986, **19**, 377.
10. W. Oppoltzer, *Angew. Chem. Int. Edn. Engl.* 1977, **16**, 10 and refs therein.
11. C. L. Skerratt, S. D. Chappell, R. D. Bowen, R. C. Storr and D. J. Cole-Hamilton, *Polyhedron* 1986, **5**, 1035.
12. W. H. Hersh and R. G. Bergman, *J. Am. Chem. Soc.* 1983, **105**, 5846.
13. J. W. Hull and W. L. Gladfelter, *Organometallics* 1984, **3**, 605.
14. W. Faulkner, D. S. Barratt, D. C. Cupertino and D. J. Cole-Hamilton, *Polyhedron* 1985, **4**, 1993.

15. E. Dunkelblum and H. Hart, *J. Org. Chem.* 1979, **44**, 3482.
16. S. D. Chappell and D. J. Cole-Hamilton, *J. Chem. Soc., Dalton Trans.* 1983, 1051.
17. M. F. Lappert, T. R. Martin, C. L. Raston, B. W. Skelton and A. H. White, *J. Chem. Soc., Dalton Trans.* 1982, 1959.
18. S. D. Chappell, D. J. Cole-Hamilton, A. M. R. Galas, M. B. Hursthouse and N. P. C. Walker, *Polyhedron* 1985, **4**, 121.
19. Aldrich library of NMR spectra.
20. M. Gisin and J. Wirz, *Helv. Chim. Acta.* 1976, **59**, 2273.
21. P. W. Armit, A. S. F. Boyd and T. A. Stephenson, *J. Chem. Soc., Dalton Trans.* 1975, 1663.
22. D. J. Cole-Hamilton and G. Wilkinson, *Nouveau J. Chim.* 1977, **1**, 141.
23. T. A. Stephenson and G. Wilkinson, *J. Inorg. Nucl. Chem.* 1966, **28**, 945.
24. P. W. Armit and T. A. Stephenson, *J. Organometallic Chem.* 1973, **57**, C80.
25. R. A. Jones, F. Mayor Real, G. Wilkinson, A. M. R. Galas, M. B. Hursthouse and K. M. A. Malik, *J. Chem. Soc., Dalton Trans.* 1980, 511.
26. P. Meakin, E. L. Muetterties and J. P. Jesson, *J. Am. Chem. Soc.* 1973, **95**, 75.

Polyhedron Vol. 7, No. 19/20, pp. 1953–1964, 1988
Printed in Great Britain

0277–5387/88 $3.00+.00
© 1988 Pergamon Press plc

SYNTHESIS AND SPECTROSCOPIC CHARACTERISTICS OF TRIMETHYLSILYLMETHYLPLATINUM(II) COMPLEXES WITH η^2 ALKENE, NITROGEN AND PHOSPHORUS AND SULPHUR DONOR LIGANDS

S. KATHERINE THOMSON and G. BRENT YOUNG*

Inorganic Chemistry Laboratories, Imperial College of Science and Technology, London SW7 2AY, U.K.

Abstract—Various complexes *cis*-L_2PtR_2 (L = py, PMe_3, PEt_3, PMe_2Ph, $PMePh_2$, PPh_3, L_2 = bipy, Me_2bipy, bipym, bipyz, Me_4phen, Ph_2phen, dppm, dppe, dppf, R = CH_2SiMe_3) have been synthesized by displacement of the diene from (cod)PtR_2 or (nbd)PtR_2 or by sulphide replacement in $[(dms)PtR_2]_n$. [TerpyPtR]BF_4 has been synthesized via (cod)Pt(R)(X), (X = Cl, I). The complexes have been characterized by IR, ^1H, ^{13}C NMR and, where appropriate, ^{31}P NMR and electronic spectroscopy. Trimethylsilylmethyl exerts a weaker *trans*-influence than neopentyl which, on NMR evidence, has the stronger Pt—C bond.

There is continued activity in evaluation of the rearrangement mechanistics of organo-transition metals as a route to greater understanding of their role in metal-mediated transformations of hydrocarbons. Common labilizing pathways for many alkylmetals feature hydrogen transfers, most often from a β-carbon site. This feature, early recognized by Wilkinson and a few others, led to rapid development in alkyl transition metal chemistry using "β-elimination stabilized" ligands.[1] When this option is restricted, activation of more remote C—H bonds may occur.[2] Again, the earlier examples were characterized by Wilkinson and co-workers. Neopentyl metals, for example, particularly low-valent derivatives of the later *d*-block, have been observed widely to undergo such cyclizations to form metallacyclobutanes.[3] The mechanistics have been elucidated elegantly for dineopentylplatinum(II).[3a] Trimethylsilylmethyl metals may also undergo γ-C-H transfer,[3,4] but, impressionistically, they are more inert.[3] Other than a few thermochemical studies which document the thermodynamic differences in M—C bond strengths between $M(CH_2CMe_3)_n$ and $M(CH_2SiMe_3)_n$[4]—which doubtless contribute to the rearrangement mechanistics where M—C homolysis is important—there has been little attempt to quantify and understand the kinetic effect of silicon on these intramolecular hydrogen transfers for *d*-block elements. An example in *f*-block chemistry has appeared.[5] In parallel with our comparative studies of aromatic C—H activation in $L_2Pt(CH_2CMe_2Ph)_2$[6] and $L_2Pt(CH_2SiMe_2Ph)_2$,[7] we have now synthesized a wide variety of complexes, $L_2Pt(CH_2SiMe_3)_2$, for comparison with analogous neopentyl derivatives.[3a] Here we present some notable characteristics. A few of these complexes have been reported previously.[8] In these cases, we present synthetic improvements and new spectroscopic data.

EXPERIMENTAL

General and instrumental

Elemental analyses were performed by Imperial College Microanalytical Laboratories. NMR spectra were recorded on Brüker WM 250 (^1H 250.13 MHz, ^{13}C 62.9 MHz) and Jeol FX 90 Q (^1H 89.55 MHz, ^{31}P 36.21 MHz) spectrometers. IR data were collected on a Perkin–Elmer 683 instrument as 4% KBr dispersions and electronic spectra were recorded on a Shimadzu UV-160 spectrometer.

All reactions were carried out under argon, using standard anaerobic techniques.[9] The apparatus was thoroughly flame-dried prior to use, and solvents were distilled from sodium under nitrogen. Diethyl ether and *n*-hexane were distilled from sodium–benzophenone.

* Author to whom correspondence should be addressed.

Chloromethyltrimethylsilane, 1,5-cyclooctadiene (cod), bicyclo[2.2.1]hepta-2,5-diene (nbd), dimethyl sulphide (dms), 2,2′-bipyridyl (bipy), 4,4′-dimethyl-2,2′-bipyridyl (Me_2bipy), 2,2′-bipyrazyl (bipyz), 1,10-phenanthroline (phen), 4,7-diphenyl-1,10-phenanthroline (Ph_2phen), 3,4,7,8-tetramethyl-1,10-phenanthroline (Me_4phen), 2,2′:6,2″ terpyridyl (terpy), silver tetrafluoroborate, triphenylphosphine, bis(diphenylphosphino)methane (dppm), 1,2-bis(diphenylphosphino)ethane (dppe), 1,1′-bis(diphenylphosphino)ferrocene (dppf), toluene-d_8 and benzene-d_6 were all used as supplied by the Aldrich Chemical Company. 2,2′-Bipyrimidyl (bipym) was obtained from Lancaster Synthesis. Trimethylphosphine, triethylphosphine, diphenylmethylphosphine and dimethylphenylphosphine were used as supplied by Strem Chemicals. Pyridine (py) was supplied by Rose Chemicals and distilled from sodium hydroxide under nitrogen prior to use. Dichloro(1,5-cyclooctadiene) platinum(II), dichloro(bicyclo[2.2.1]hepta - 2,5 - diene)platinum(II) and *cis*-dichlorobis(dimethylsulphide)platinum(II) were prepared using published methods.[10–12]

Preparation of chloromagnesiomethyltrimethylsilane

A solution of chloromethyltrimethylsilane (5.0 g, 41.0 mmol) in Et_2O (40 cm^3) was added dropwise to a suspension of magnesium shot (5.0 g, 206.0 mmol) in diethyl ether (10 cm^3) previously activated by the introduction of 1,2-dibromoethane (0.25 cm^3). After 2 h stirring at ambient temperature the resulting solution of $Mg(CH_2SiMe_3)Cl$ was filtered off. (Yield, 100%.)

Preparation of bis(trimethylsilylmethyl)(1,5-cyclooctadiene)platinum(II)

A solution of $Mg(CH_2SiMe_3)Cl$ (30.0 cm^3, 24.6 mmol) was added dropwise at −78°C to a stirred suspension of (cod)$PtCl_2$ (3.0 g, 8.02 mmol) in diethyl ether (20 cm^3). The mixture was allowed to reach ambient temperature and stirred for 15 h. On cooling to −20°C, saturated aqueous ammonium chloride (15 cm^3) was added dropwise with stirring. The ether fraction, after separation, was dried over $MgSO_4$ and concentrated *in vacuo* to yield large colourless crystals of the product. (Yield, 2.87 g, 75%.) IR: 2999w, 2994s, 2992sh, 2885s, 2855sh, 1520w, 1475w, 1474sh, 1450w, 1435m, 1405wb, 1365w, 1340m, 1310w, 1305sh, 1285wb, 1255sh, 1235s, 1180w, 1160w, 1085w, 1075w, 1010mb, 990w, 980w, 950m, 840sb, 820sb, 785sh, 760m, 745m, 712m, 675s, 605w, 535wb, 460wb, 270w, 265m, 260w, 255w, 235m, 230m, 215s, 210s.

Preparation of chloro(trimethylsilylmethyl)(1,5-cyclooctadiene)platinum(II)

A solution of 0.42 M HCl in Et_2O (1.05 cm^3, 0.42 mmol) was added dropwise to a stirred solution of (cod)$Pt(CH_2SiMe_3)_2$ (0.20 g, 0.42 mmol) in diethyl ether (20 cm^3) at −78°C. The mixture was allowed to warm to ambient temperature and stirred for 24 h. The solvent was removed *in vacuo* to yield colourless crystals of the product. (Yield, 0.16 g, 89%.) IR: 2945s, 2889m, 2843s, 2700w, 1546w, 1475m, 1454w, 1436m, 1428m, 1408m, 1362m, 1344m, 1317w, 1262s, 1245s, 1183m, 1097sb, 1041s, 1023s, 987m, 960m, 902w, 865s, 828s, 803sb, 776sb, 768m, 747w, 715m, 683m, 615w, 540w, 479m, 432w, 392mb, 313m, 277w.

Preparation of iodo(trimethylsilylmethyl)(1,5-cyclooctadiene)platinum(II)

(cod)$Pt(CH_2SiMe_3)Cl$ (0.30 g, 0.70 mmol) was dissolved with KI (0.83 g, 5.0 mmol) in acetone (20 cm^3) and stirred for 24 h. The acetone was removed *in vacuo* and the residue extracted into Et_2O (40 cm^3). The solution was filtered, concentrated and cooled to −25°C to yield pale yellow plates which were washed with cold hexane (2 cm^3). (Yield, 0.28 g, 74%.) IR: 3031w, 3006m, 2946m, 2923m, 2887m, 2872m, 2835w, 1481w, 1451w, 1428m, 1404w, 1386w, 1374m, 1340m, 1317w, 1292w, 1251m, 1240s, 1181w, 1090w, 1075w, 1045m, 1002m, 987m, 961m, 902m, 876w, 838sh, 821s, 794m, 760m, 752w, 721m, 695w, 682m, 612w, 567w, 533w, 471w, 428w, 264w, 243m, 240m, 229m.

Preparation of bis(trimethylsilylmethyl)(bicyclo[2.2.1]hepta-2,5-diene)platinum(II)

To a stirred suspension of (nbd)$PtCl_2$ (1.36 g, 3.8 mmol) in diethyl ether (20 cm^3) was added dropwise at −78°C a solution of $Mg(CH_2SiMe_3)Cl$ (13.9 cm^3, 11.4 mmol). The mixture was allowed to reach ambient temperature and stirred for 15 h, then cooled to −20°C and saturated aqueous NH_4Cl (10 cm^3) added dropwise. The ether layer was separated and dried over $MgSO_4$ and concentrated *in vacuo*. The cream-coloured crystalline product was further recrystallized from a mixture of Et_2O–hexane. (Yield, 1.21 g, 69%.) IR: 3004w, 2948s, 2896m, 2850m, 2835m, 2789m, 1433m, 1410w, 1369w, 1357w, 1308m, 1251m, 1240s, 1188m, 1154w, 1100w, 1098w, 1008m, 989m, 960m, 934m, 924w, 886m, 850s, 827s, 757sh, 749m, 715m, 676m, 612w, 535w, 488w, 285w, 250m, 244m, 237s, 230s.

Preparation of [*bis*(*trimethylsilylmethyl*)(*dimethylsulphide*)*platinum*(II)]$_n$ ($n = 2$ *or* 3)

To a stirred suspension of $(dms)_2PtCl_2$ (1.5 g, 3.84 mmol) in diethyl ether (10 cm^3) at −78°C was added dropwise a solution of $Mg(CH_2SiMe_3)Cl$ (14.0 cm^3, 11.5 mmol). The mixture was stirred at ambient temperature for 2 h, then cooled to −20°C and saturated aqueous NH_4Cl (10 cm^3) added. The ethereal layer was filtered onto $MgSO_4$ and activated charcoal, then after filtration, concentrated *in vacuo* and cooled to −25°C, yielding a white solid. (Yield, 1.82 g, 55%.) IR: 2998m, 2946m, 2916m, 2895m, 2842m, 1458w, 1425w, 1413w, 1358w, 1262s, 1239s, 1096sbr, 1026s, 985s, 947w, 853s, 823s, 800s, 770m, 747m, 715m, 679s, 609w, 545w, 453w, 408w, 283w, 275w, 266w, 261m, 256m, 252s, 245s, 230s, 224s.

Preparation of bis(*trimethylsilylmethyl*)(2,2′-*bipyridyl*)*platinum*(II)

[(dms)Pt$(CH_2SiMe_3)_2]_n$ ($n = 2$ or 3) (0.10 g) was dissolved together with 2,2′-bipyridyl (0.04 g, 0.24 mmol) in dry deoxygenated toluene (5 cm^3) and the solution kept at room temperature for two days. Any excess free ligand was removed by extraction with aqueous ferrous sulphate solution. The organic phase was then dried over $MgSO_4$ and concentrated *in vacuo*, then cooled to −25°C. The deep red crystals formed were filtered off and washed with cold *n*-hexane. (Yield, 0.11 g, 85%.) IR: 2942m, 2868m, 2829m, 1599w, 1468m, 1445m, 1306w, 1262m, 1237m, 1097mbr, 1011mbr, 955w, 849s, 821sbr, 757m, 745s, 728m, 712m, 672m, 555w, 254m, 248s, 240s, 229s.

Bis(*trimethylsilylmethyl*)(4,4′-*dimethyl*-2,2′-*bipyridyl*)*platinum*(II)

This was prepared according to the above procedure. Product: orange–red crystals from ether. (Yield, 87%.) IR: 2946m, 2869m, 2829m, 1616m, 1553w, 1480w, 1446w, 1414w, 1298w, 1261w, 1233m, 1098wbr, 1018mbr, 973w, 955w, 928w, 888w, 855s, 826s, 774w, 742w, 715w, 672m, 600w, 550w, 517w, 425w, 332w, 295w, 280w, 257w, 245w, 239m, 234m, 230s, 224m.

Preparation of bis(*trimethylsilylmethyl*)(2,2′-*bipyrimidyl*)*platinum*(II)

(cod)Pt$(CH_2SiMe_3)_2$ (0.20 g, 0.42 mmol) was dissolved together with 2,2′-bipyrimidine (0.18 g, 0.84 mmol) in dry deoxygenated toluene (10 cm^3). The solution was heated to 60°C for 14 days, then any excess free ligand removed by extraction with aqueous ferrous sulphate solution. The remaining organic phase was then concentrated, *n*-hexane (2 cm^3) added and the mixture cooled. The claret crystals collected were washed with cold hexane. (Yield, 0.19 g, 86%.) IR: 3083w, 3042w, 2946m, 2877m, 2839m, 2729m, 1627wbr, 1572m, 1547m, 1450w, 1405s, 1367w, 1332w, 1260sh, 1233m, 1199w, 1145w, 1110w, 1102w, 1076w, 1013m, 1000w, 956w, 854s, 826s, 815sh, 775m, 753s, 710w, 681m, 676m, 663m, 638w, 610w, 563w, 487w, 440w, 341w, 270w, 257w.

Bis(*trimethylsilylmethyl*)(1,10 - *phenanthroline*)*platinum*(II)

Product: red crystals from hot toluene. (Yield, 83%.) IR: 3057w, 2954m, 2940m, 2889w, 2868m, 2859m, 2824m, 1627w, 1578w, 1423w, 1415m, 1365m, 1338w, 1251m, 1236m, 1219m, 1202m, 1144w, 985m, 965m, 952w, 944m, 907w, 851s, 839s, 765m, 745m, 734w, 720m, 674m, 611w, 555w, 508w, 490w, 454w, 429w, 278w, 253w.

Bis(*trimethylsilylmethyl*)(4,7 - *diphenyl* - 1,10 - *phenanthroline*)*platinum*(II)

Product: large red crystals from toluene. (Yield, 92%.) IR: 3058w, 3030w, 2948m, 2861m, 2840m, 2725w, 1617w, 1592w, 1556w, 1494w, 1447w, 1435w, 1422m, 1415m, 1395w, 1362w, 1260w, 1249m, 1236m, 1077wb, 1020m, 1003m, 962w, 949w, 907w, 854s, 824s, 764s, 748m, 736m, 717w, 701s, 676m, 632w, 585w, 548w, 465w, 407w, 255w, 246m, 238s.

Bis(*trimethylsilylmethyl*)(3,4,7,8 - *tetramethyl* - 1,10 - *phenanthroline*)*platinum*(II)

Product: orange needles from toluene. (Yield, 86%.) IR: 2946m, 2888w, 2853m, 2835m, 1610w, 1579w, 1514w, 1425m, 1390w, 1263w, 1235m, 1093w, 1012w, 947w, 918w, 850s, 818s, 773w, 747w, 722w, 711w, 674m, 609w, 567w, 329w.

Preparation of bis(*trimethylsilylmethyl*)(2,2′-*bipyrazyl*)*platinum*(II)

(nbd)Pt$(CH_2SiMe_3)_2$ (0.20 g, 0.43 mmol) and 2,2′-bipyrazyl (0.07 g, 0.43 mmol) were dissolved together in toluene (10 cm^3) in a grease-free sealed vessel, and the solution maintained at ambient temperature for 28 days. The purple product was recrystallized from toluene–hexane. (Yield, 0.20 g, 88%.) IR: 3093w, 3058w, 2944m, 2878m, 2836m, 1635wb, 1580m, 1575m, 1469m, 1464m,

1407m, 1400m, 1368w, 1304w, 1261s, 1252s, 1237s, 1176m, 1166m, 1100mb, 1070m, 1034m, 1019m, 977wsh, 950w, 931w, 852s, 834s, 805sh, 765w, 713m, 679m, 623w, 558w, 395w, 267w, 252m.

Preparation of trimethylsilylmethyl(2,2′:6′,2″-terpyridyl)platinum(II) *tetrafluoroborate*

(cod)Pt(I)(CH_2SiMe_3) (0.20 g, 0.39 mmol) was dissolved together with 2,2′:6′,2″-terpyridyl (0.09 g, 0.39 mmol) in acetone (15 cm^3) and the mixture stirred for 40 h to yield an orange solution. $AgBF_4$ (0.08 g, 0.39 mmol) in acetone (10 cm^3) was added via a cannula and the solution filtered to yield an orange–yellow solution. On concentration *in vacuo*, bright yellow–orange needles were formed. (Yield, 0.18 g, 76%.) IR: 3116w, 3090w, 3075w, 2955m, 2890w, 2853w, 1610m, 1599m, 1573w, 1472m, 1452m, 1401w, 1315w, 1289w, 1261m, 1239m, 1188w, 1169w, 1142s, 1098s, 967w, 950w, 853m, 829m, 800m, 774m, 750w, 729w, 682w, 521w, 258w, 254w, 246w, 238s, 230w, 223m.

Preparation of cis-*bis(pyridine)bis(trimethylsilylmethyl)platinum*(II)

(cod)Pt(CH_2SiMe_3)$_2$ (0.20 g, 0.42 mmol) was dissolved in neat pyridine (5 cm^3) and heated to 60°C for three days. The excess pyridine was removed *in vacuo* and the resulting oily solid recrystallized from ether–hexane to yield off-white crystals of the product. (Yield, 77%.) IR: 3077w, 2942s, 2887m, 2868m, 2823s, 2712w, 1971w, 1915w, 1600m, 1572w, 1479m, 1446s, 1402w, 1359w, 1348w, 1235s, 1205w, 1149w, 1067m, 1045w, 1005m, 974w, 964w, 874s, 854s, 823s, 756s, 746m, 719m, 694s, 683m, 667m, 636w, 607w, 558w, 277w, 238m, 227s.

Preparation of cis-*bis(trimethylsilylmethyl)bis(trimethylphosphine)platinum*(II)

To a solution of (cod)Pt(CH_2SiMe_3)$_2$ (0.20 g, 0.42 mmol) in dry deoxygenated toluene (5 cm^3) was added PMe_3 (0.09 cm^3, 0.86 mmol) via a syringe and the solution was heated to 60°C for 14 days. The solvent was then removed *in vacuo* and *n*-hexane (2 cm^3) added to the resultant colourless oil. Cooling to −25°C produced large colourless crystals of the product. (Yield, 0.22 g, 100%.) IR: 2946m, 2913m, 2880m, 1633vw, 1421w, 1301w, 1284m, 1262m, 1246m, 1235s, 1097mbr, 1022mbr, 963s, 943s, 850s, 821s, 771w, 742w, 723m, 708m, 671m, 522w, 383w, 359w, 283w, 259w, 251w, 246m, 242m, 235s, 230s, 225s.

Prepared according to the same procedure were:

cis - *Bis(trimethylsilylmethyl)bis(triethylphosphine) platinum*(II)

Product: large colourless crystals from toluene. (Yield, 95%.) IR: 2964s, 2947s, 2936s, 2918m, 2893m, 1732w, 1633w, 1455m, 1433m, 1405w, 1381w, 1248m, 1235s, 1099w, 1032s, 993w, 950w, 849s, 821s, 755s, 718s, 672m, 624w, 514w, 410w, 371w, 334w, 245m, 234s.

cis - *Bis(trimethylsilylmethyl)bis(dimethylphenylphosphine)platinum*(II)

Product: large colourless crystals from CH_2Cl_2/MeOH. (Yield, 82%.) IR: 3071w, 2982m, 2943m, 2922m, 2915m, 2884m, 1437m, 1421w, 1411w, 1310w, 1294w, 1282w, 1275w, 1262m, 1246m, 1234m, 1100m, 1072w, 1052w, 1029w, 1001w, 902s, 850s, 823s, 772w, 746m, 739m, 723w, 706m, 538w, 501w, 488w, 450w, 432w, 417w, 409m, 395w, 313w, 304w, 294w, 286w, 264m, 257s, 248s, 240s, 230s, 224s.

cis - *Bis(trimethylsilylmethyl)bis(diphenylmethylphosphine)platinum*(II)

Product: colourless crystals from *n*-hexane. (Yield, 88%.) IR: 3075w, 3057w, 2983w, 2944m, 2920m, 2887m, 1963w, 1884w, 1588w, 1573w, 1483w, 1436s, 1420w, 1370w, 1329w, 1307w, 1279w, 1248m, 1238m, 1231m, 1193w, 1156w, 1096m, 1077w, 1028w, 1013w, 1000w, 960m, 914w, 894s, 884s, 875s, 851s, 820s, 750s, 738s, 730s, 698s, 674m, 618w, 605w, 525m, 513s, 484m, 433m, 416m, 362w, 266w, 246w, 242m, 237m, 232s, 227s.

cis - *Bis(trimethylsilylmethyl)bis(triphenylphosphine)platinum*(II)

Product: colourless crystals from toluene. (Yield, 84%.) IR: 3441w, 3055m, 3002m, 2938m, 2879m, 1746w, 1587w, 1484m, 1478m, 1438m, 1433m, 1313w, 1262w, 1249m, 1236m, 1182w, 1159w, 1119w, 1098m, 1091w, 1028w, 999w, 956w, 850s, 825s, 751s, 741m, 720m, 706s, 693sh, 619w, 540s, 524s, 512s, 491m, 464w, 453w, 432w, 421w, 281w, 268m, 251m, 243m, 237s, 230s, 225s.

Bis(trimethylsilylmethyl)[bis(diphenylphosphino)methane]platinum(II)

Product: colourless crystals from toluene–*n*-hexane. (Yield, 83%.) IR: 3058w, 3005w, 2945m, 2875m, 2862m, 2836m, 1587w, 1572w, 1482m,

1436s, 1384w, 1360w, 1329w, 1309w, 1277w, 1249s, 1238s, 1185w, 1098m, 1084m, 1028w, 1000w, 970w, 935w, 849s, 822s, 765m, 753s, 737s, 724s, 702s, 692m, 674sh, 618w, 607w, 541m, 502s, 477m, 443w, 420w, 358w, 302w, 278w, 268w, 262w, 252m, 248m, 243m, 238s, 230s, 225s.

Bis(trimethylsilylmethyl)[1,2-bis(diphenylphosphino)ethane]platinum(II)

Product: colourless crystals from toluene. (Yield, 85%.) IR: 3445w, 3058m, 2942m, 2886m, 2855m, 1966w, 1900w, 1825w, 1589w, 1573w, 1483m, 1436s, 1407m, 1310w, 1262s, 1249m, 1236s, 1186w, 1101s, 1027sh, 948s, 857s, 846s, 821s, 747s, 713m, 694s, 681m, 675m, 653w, 604w, 533s, 482m, 469w, 436w, 400w, 356w, 301w, 290w, 254w, 246w, 239m, 233m, 230s.

Preparation of bis(trimethylsilylmethyl)[1,1′-bis(diphenylphosphino)ferrocene]platinum(II)

(nbd)Pt(CH_2SiMe_3)$_2$ (0.20 g, 0.43 mmol) was dissolved together with dppf (0.23 g, 0.43 mmol) in dry deoxygenated toluene (10 cm^3) and the solution maintained at 60°C for 20 days. The solvent was then removed *in vacuo* and the orange solid recrystallized from toluene (2 cm^3) to yield orange crystals of the product. (Yield, 0.38 g, 96%.) IR: 3051m, 2942m, 2897m, 1970w, 1618w, 1587w, 1571w, 1480m, 1434s, 1384w, 1367w, 1308w, 1261m, 1250m, 1236s, 1194w, 1181w, 1165m, 1097s, 1070w, 1058w, 1038m, 1026m, 1000w, 959w, 850s, 824s, 744s, 719m, 694s, 641w, 619w, 608w, 550s, 527m, 514s, 492s, 477w, 468m, 459w, 449w, 439m, 348w, 278w, 270w, 260w, 247m, 238m, 233s, 224m.

RESULTS AND DISCUSSION

Synthesis of L_2PtR_2

Where L_2 = 1,5-cyclooctadiene the complex could be prepared in 75% yield as a colourless crystalline solid by reaction of the Grignard reagent with (cod)$PtCl_2$. This is a considerable improvement on the method previously reported.[8b] The related new derivative, bis(trimethylsilylmethyl)(bicyclo-[2.2.1]-hepta-2,5-diene)platinum(II) was prepared analogously. Treatment of (dms)$_2PtCl_2$ with trimethylsilylmethyl magnesium chloride resulted in the formation of $[(\mu\text{-dms})Pt(CH_2SiMe_3)_2]_n$. Our spectroscopic observations (and those previously published[8b]) do not allow distinction between dimeric and trimeric structures.

Subsequent replacement of the diene or dimethylsulphide ligands with a series of nitrogen donor ligands yielded highly coloured crystalline products, air-inert as solids. The displacement reaction with the diene complexes is generally complete in 14–30 days at 60°C; nbd is more labile than cod. Dms is replaced by 2,2′-bipyridyl and 4,4′-dimethyl-2,2′-bipyridyl in two days at room temperature and is clearly the most labile of the three. Deoxygenated solutions of these compounds in benzene and other hydrocarbon solvents are inert for indefinite periods.

Reaction of the diene complexes with a series of phosphines yielded colourless, highly crystalline solids in almost quantitative yields. The ligand metathesis was generally complete within 14 days. These air-inert compounds do not decompose in deoxygenated hydrocarbon and chlorocarbon solvents.

Colours and elemental compositions of all these complexes are detailed in Table 1.

Spectroscopic characteristics

For numbering conventions employed, in accord with those previously used,[6] see Fig. 1.

(a) *Electronic spectroscopy*. The electronic spectra of complexes L_2PtR_2 (L_2 = N-donor ligand, R = trimethylsilylmethyl) were recorded as freshly prepared toluene solutions. They are characterized by two absorptions, λ_1 and λ_2, attributable to $d\pi$–π^* metal–ligand charge transfer (MLCT) transitions.[13] The use of these bands in the analysis of the relative electronic effects of bidentate, heteroaromatic N-donor ligands has been well documented. As the very intense π–π^* transitions of the ligand often obscure the higher energy MLCT absorption λ_2, the lower energy band, λ_1, which reflects the energy difference between the metal ($d\pi$) HOMO and the (π^*) LUMO of the ligand, frequently features in comparisons within a series of such complexes.

The energy of λ_1 increases in the order: bipyz < bipym < Ph_2phen < bipy < Me_2bipy < terpy < Me_4phen. This is in full agreement with previous observations.[6,14–16] MLCT transitions in complexes of this type occur at lower energies where the heteroaromatic ligands have electronegative ring atoms or substituents.[17] Proposedly, this arises from a lowering of the LUMO on the ligand, thus reducing the $d\pi$–π^* energy gap. This explanation clearly accounts for the complexes of 2,2′-bipyrazyl and 2,2′-bipyrimidyl. An opposite effect can be invoked for the Me_2bipy complex; electron releasing substituents should raise the energy of the LUMO relative to that of bipy.

As noted elsewhere, coordinated Ph_2phen exhibits a lower energy absorption than phen, consistent with increased conjugation in the aromatic ligand.

Table 1. Physical data for $L_2Pt(CH_2SiMe_3)_2$

Compound	Analytical data[a] C	H	N	Colour
(cod)Pt(Cl)(CH_2SiMe_3)	33.6(33.8)	5.4(5.4)	—	Colourless
(cod)Pt(I)(CH_2SiMe_3)	27.7(28.0)	4.4(4.1)	—	Pale yellow
(nbd)Pt(CH_2SiMe_3)$_2$	39.1(39.0)	6.6(6.5)	—	Cream
(bipy)Pt(CH_2SiMe_3)$_2$	41.0(41.1)	5.3(5.7)	5.1(5.3)	Red
(Me_2bipy)Pt(CH_2SiMe_3)$_2$	43.3(43.4)	6.3(6.2)	4.8(5.1)	Orange–red
(bipym)Pt(CH_2SiMe_3)$_2$	36.2(36.4)	5.3(5.3)	10.3(10.6)	Wine red
(phen)Pt(CH_2SiMe_3)$_2$	43.4(43.7)	5.5(5.5)	5.1(5.1)	Deep red
(Ph_2phen)Pt(CH_2SiMe_3)$_2$	54.9(54.7)	5.6(5.5)	3.8(4.0)	Deep red
(Me_4phen)Pt(CH_2SiMe_3)$_2$	47.2(47.6)	6.0(6.3)	4.4(4.6)	Orange
(bipyz)Pt(CH_2SiMe_3)$_2$	36.7(36.4)	5.3(5.3)	10.7(10.6)	Deep purple
[(terpy)PtCH_2SiMe_3]BF_4	37.4(37.8)	4.0(3.8)	6.3(7.0)	Orange–yellow
(py)$_2$Pt(CH_2SiMe_3)$_2$	40.6(41.0)	6.2(6.1)	4.7(5.3)	Cream
(Me_3P)$_2$Pt(CH_2SiMe_3)$_2$	32.2(32.2)	7.6(7.7)	—	Colourless
(Et_3P)$_2$Pt(CH_2SiMe_3)$_2$	39.5(39.6)	8.8(8.6)	—	Colourless
(Me_2PhP)$_2$Pt(CH_2SiMe_3)-	44.5(44.6)	6.9(6.9)	—	Colourless
($MePh_2P$)$_2$Pt(CH_2SiMe_3)$_2$	53.2(53.0)	6.2(6.3)	—	Colourless
(Ph_3P)$_2$Pt(CH_2SiMe_3)$_2$	59.3(59.7)	5.9(5.9)	—	Colourless
(dppm)Pt(CH_2SiMe_3)$_2$	52.9(52.6)	5.9(5.8)	—	Colourless
(dppe)Pt(CH_2SiMe_3)$_2$	53.6(53.2)	6.1(6.0)	—	Colourless
(dppf)Pt(CH_2SiMe_3)$_2$	54.2(54.6)	5.0(5.5)	—	Yellow

[a] Calculated values in parentheses.

The MLCT transition for bipy occurs at lower energy than that for phen, however, and so the extent of conjugation is not the only factor governing the energies of these transitions.

(b) *NMR spectroscopy.*

(i) ^{1}H *NMR.* Common features of all these spectra are the characteristic singlet near 0 ppm (δ) for the $Si(CH_3)_3$ hydrogens, and the 1:4:1 "triplet" for the methylene hydrogens, as a result of spin–spin coupling to ^{195}Pt ($I = \frac{1}{2}$, 34% abundant). ^2J(Pt—H) is generally of the order of 90–94 Hz in all the dialkyl complexes. Replacement of one R group by halide causes a reduction of 15–20 Hz. ^2J(Pt—H) associated with the coordinated diene protons are 73 and 35 Hz for those *trans* to Cl and R, respectively.

A distinctive feature of the ^{1}H spectra of these complexes is the broadening of the ^{195}Pt satellites

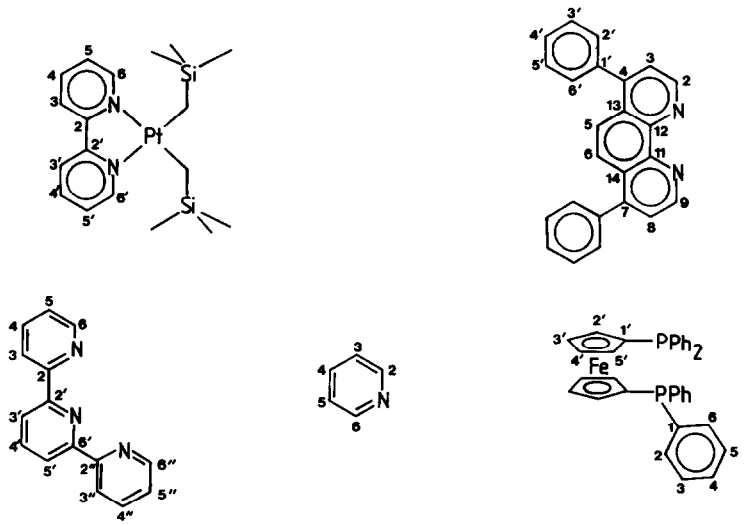

Fig. 1.

Table 2. ^{1}H NMR characteristics of LPtRX (R = CH_2SiMe_3)

Complex L	Complex X	δ ^{1}H ppm $CH_2Si(CH_3)_3$ (J_{Pt-H}) CH_2	CH_3	δ ^{1}H ancillary ligand(s) L (J_{Pt-H}) [Assignment]
cod	R[a]	1.14(93.6 Hz)	0.31	1.34–1.89m [CH_2], 4.46(41.5 Hz) [CH]
cod	Cl[a]	1.35(76.4 Hz)	0.39	1.33–1.84m [CH_2], 3.96(73.0 Hz) [CH *trans* to Cl], 5.29(34.6 Hz) [CH *trans* to R]
cod	I[b]	1.47(76.9 Hz)	0.10	1.94–2.45m [CH_2], 4.67(74.2 Hz) [CH *trans* to I], 5.44(39.8 Hz) [CH *trans* to R]
nbd	R[a]	1.27(102.7 Hz)	0.29	1.0t [CH_2], 3.27m [CH], 4.52m (40.6 Hz) [CH=CH]
bipy	R[c]	1.28(89.7 Hz)	0.35	6.44m [H_5] ($J_{H_5-H_4}$ = 5.7 Hz), ($J_{H_5-H_3}$ = 1.3 Hz), 6.66d [H_3] ($J_{H_3-H_4}$ = 8.0 Hz), 7.00m [H_4], 9.09(27.5 Hz) [H_6] ($J_{H_6-H_5}$ = 5.0 Hz)
Me_2bipy	R[c]	1.23(81.6 Hz)	0.37	1.54 [CH_3], 6.32dd [H_5], 6.74 [H_3], 8.98dd [H_6] ($J_{H_6-H_5}$ = 5.7 Hz)
bipym	R[a]	1.45(91.6 Hz)	0.46	6.05t [H_5], 8.28dd [H_4], 8.99(21.4 Hz) [H_6] ($J_{H_4-H_5 = H_5-H_6}$ = 5.7 Hz)
phen	R[c]	1.45(90.1 Hz)	0.36	6.72m [$H_{3,8}$] ($J_{3(8)-2(9)}$ = 5.1 Hz), 6.87s [$H_{5,6}$], 7.44dd [$H_{4,7}$] ($J_{4(7)-3(8)}$ = 8.0 Hz), 9.32dd [$H_{2,9}$] ($J_{2(9)-4(7)}$ = 1.2 Hz)
Ph_2phen	R[c]	1.57(90.8 Hz)	0.47	6.83d [$H_{3,8}$] ($J_{3(8)-2(9)}$ = 5.4 Hz), 7.05–7.17m [Ph], 7.31 [$H_{5,6}$], 9.46d (23.0 Hz) [$H_{2,9}$]
Me_4phen	R[a]	1.60(90.2 Hz)	0.58	1.71, 1.88 [CH_3], 7.36 [$H_{5,6}$], 9.30(23.1 Hz) [$H_{2,9}$]
bipyz	R[a]	1.75(90.8 Hz)	0.42	7.92d [H_5], ($J_{H_5-H_6}$ = 2.9 Hz), 8.12 [H_3], 8.92(20.2 Hz) [H_6]
$(py)_2$	R	0.77(89.2 Hz)	0.19	6.25m [H_3], 6.74m [H_4] ($J_{H_4-H_{3(5)}}$ = 7.6 Hz), ($J_{H_4-H_2}$ = 1.6 Hz), 8.32m (20.9 Hz) [H_2] ($J_{H_2-H_3}$ = 6.4 Hz)
terpy	BF_4[d]	0.91(77.7 Hz)	0.01	7.97(11.4 Hz) [$H_{5,5''}$], 8.51(15.7 Hz) [$H_{4,4''}$], 8.59–8.65 obs [$H_{3,3'',3',4',5'}$], 9.06(52.8 Hz) [$H_{6,6''}$]
$(PMe_3)_2$	R[c]	0.36(72.9 Hz)	0.19	0.86m (20.4 Hz) [CH_3] ($^2J_{P-H}$ = 7.6 Hz)
$(PEt_3)_2$	R[c]	0.64(73.0 Hz)	0.33	0.77–0.88 [CH_3], 1.44–1.53m [CH_2]
$(PMe_2Ph)_2$	R[b]	0.50(76.2 Hz)	0.03	1.32m (19.9 Hz) [CH_3] ($^2J_{P-H}$ = 7.6 Hz), 7.43–7.55m [$H_{3,4}$], 7.65–7.74m [H_2]
$(PPh_2Me)_2$	R[a]	1.06(78.6 Hz)	0.36	1.55m (19.7 Hz) [Me] ($^2J_{P-H}$ = 7.0 Hz), 7.01–7.05m [$H_{3,4}$], 7.47–7.54m [H_2]
$(PPh_3)_2$	R[a]	1.14m	0.38	6.94m [$H_{3,4}$], 7.57–7.65m [H_2]
dppm	R[b]	0.93(85.6 Hz)	−0.25	4.21m [CH_2] ($^2J_{P-H}$ = 18.4 Hz), 7.25–7.43m [$H_{3,4}$], 7.51–7.59m [H_2]
dppe	R[b]	0.72(82.5 Hz)	−0.36	2.12m [CH_2], 7.36–7.39 [$H_{3,4}$], 7.55–7.62m [H_2]
dppf	R[c]	0.95br	0.15	3.77 [$H_{3',4'}$], 4.10 [$H_{2',5'}$], 7.05m [$H_{3,4}$], 7.83br [H_2]

[a] Run in benzene-d_6.
[b] Run in chloroform-d_1.
[c] Run in toluene-d_8.
[d] Run in acetone-d_6.

of the methylene resonance upon coordination of nitrogen donor ligands. This phenomenon appears to be a general feature of alkylplatinum complexes of this type and is attributed[14,15] to quadrupolar relaxation of ^{195}Pt by ^{15}N. A similar effect has been noted previously in the ^{1}H spectra of MeHgI complexes where efficient relaxation of ^{199}Hg by ^{127}I broadens the satellite peaks to the extent that they cannot be resolved.[18] Slight broadening of the central methylene resonance is sometimes discernible

Table 3. ^{31}P NMR characteristics of $LPtR_2$ (R = $CH_2Si(CH_3)_3$)

Complex L	δ ^{31}P[a] ppm	$J_{Pt—P}$
$(Me_3P)_2$[b]	−26.31	1945.1 Hz
$(Et_3P)_2$[b]	5.13	1987.1 Hz
$(PhMe_2P)_2$[c]	−14.78	1989.4 Hz
$(Ph_2MeP)_2$[c]	2.81	1998.2 Hz
$(Ph_3P)_2$[c]	24.98	2004.9 Hz
dppm[c]	−42.38	1575.1 Hz
dppe[c]	43.61	1938.4 Hz
dppf[b]	19.55	2020.4 Hz

[a] Referenced to external H_3PO_4/D_2O 85%.
[b] Run in benzene-d_6.
[c] Run in chloroform-d_1.

Table 4. Ring contributions for $L_2Pt(CH_2Si(CH_3)_3)_2$

Compound L_2	δP (ppm)	δF[a] (ppm)	Δ (ppm)	ΔR (ppm)	Chelate ring size
dppm	−42.4	−22.7	−19.7	−50.6	4
dppe	43.6	−13.2	56.8	25.9	5
dppf	91.6	−17.1	36.7	5.8	7
$(Ph_2MeP)_2$	2.8	−28.1	30.9	0.0	—

[a] Free phosphine chemical shifts obtained from ref. 15.

for these complexes, due, presumably to enhancement of ^1H relaxation by ^{15}N but this is clearly a less significant effect.

(ii) ^{31}P *NMR*. The ^{31}P NMR spectra show the expected 1:4:1 "triplet" as a result of spin–spin coupling of ^{31}P to ^{195}Pt. ^1J(Pt—P) coupling constants are generally in the range 1940–2000 Hz, typical for *cis*-bis(phosphine)platinum(II) complexes.

As has been previously noted for complexes with different alkyl groups,[19] ^1J(Pt—P) for (dppm)PtR_2 has an appreciably lower value. This reduction originates from the angular constraints around P and Pt due to the four-membered ring.[19a]

A ring contribution, Δ_R, to the chemical shift results upon coordination of phosphorus nuclei in chelate rings, with the magnitude and direction of this shift dependent on ring substitution and size. The value of $\Delta_R = \Delta - \Delta_R^0$ has been measured for L_2PtMe_2 (L_2 = dppm, dppe, dppp, dppb) where Δ is the change in shift upon coordination and Δ_R^0 is a standard ring contribution.[20] Comparison with the values obtained for the trimethylsilylmethyl complexes (Table 4) shows them to be in accord with these findings. We have noted similar trends for related silylmethylplatinum complexes.[14]

A further notable aspect which emerges from these ^{31}P spectra is that the magnitude of ^1J(Pt—P) is consistently greater (by *ca* 300 Hz) than for neopentyl analogues (see Section iv).

(iii) ^{13}C *NMR*. All the compounds have been characterized by $^{13}C\{^1H\}$ NMR. Assignments are in accord with those discussed elsewhere, particularly in related bis(ethenyldimethylsilylmethyl)[14] and bis(phenyldimethylsilylmethyl)[15] complexes. Variation of the N-donor ligands produces little change in the chemical shifts or ^3J(Pt—C) values for the trimethylsilylmethyl group, an indication of the similar electronic and steric environments conferred by this series of ancillary ligands. From these spectra it emerges that ^1J(Pt—C) is uniformly *smaller* than in comparable neopentyl complexes (*vide infra*).

(iv) *General implications*. Compared with analogous neopentylplatinum(II) derivatives with diene,[3a] N-donor[16] and P-donor[3a] ligands, trimethylsilylmethylplatinum(II) complexes exhibit several notable characteristics. First of all, ^1J(Pt—C) for the η^1-alkyl is significantly lower (by 170–180 Hz) for trimethylsilylmethyl. This trend is paralleled in ^1H NMR spectra by decreased ^2J(Pt—H) in the neopentyl case. On the other hand, ^1J(Pt—C) for the diene ligand in, for example, (cod)$Pt(CH_2SiMe_3)_2$ is correspondingly larger than for (cod)$Pt(CH_2CMe_3)_2$ (Fig. 2). The same trend is evident in $^2J(Pt—H_{methine})$ values for the η^2-alkene. For phosphine complexes, for instance triethylphosphine (Fig. 3), the reduction (178 Hz) in ^1J(Pt—C) for $(Et_3P)_2Pt(CH_2SiMe_3)_2$* is matched by an increase in ^1J(Pt—P) of 349 Hz, which is in the typical range for analogues for which comparative data are available. The extent of change in ^1J(Pt—C) and ^1J(Pt—P) is comparable (*ca* 23%).

We have noted closely similar trends in comparisons of neophylplatinum complexes with sila-neophyl-[15] and (related) sila-neohexenylplatinum[14] analogues. Based on the assumption of Fermi contact dominance of ^1J magnitudes,[23] we ascribe the variations to greater attraction by the carbon than by the silicon containing ligand for the platinum 6*s* orbitals. This, in turn, is as a result of deployment of greater 2*s* character in the Pt—C bond by a ligating carbon with a more electronegative alkyl

* Sample of $(Et_3P)_2Pt(CH_2CMe_3)_2$ prepared according to Whitesides *et al.*[3a]

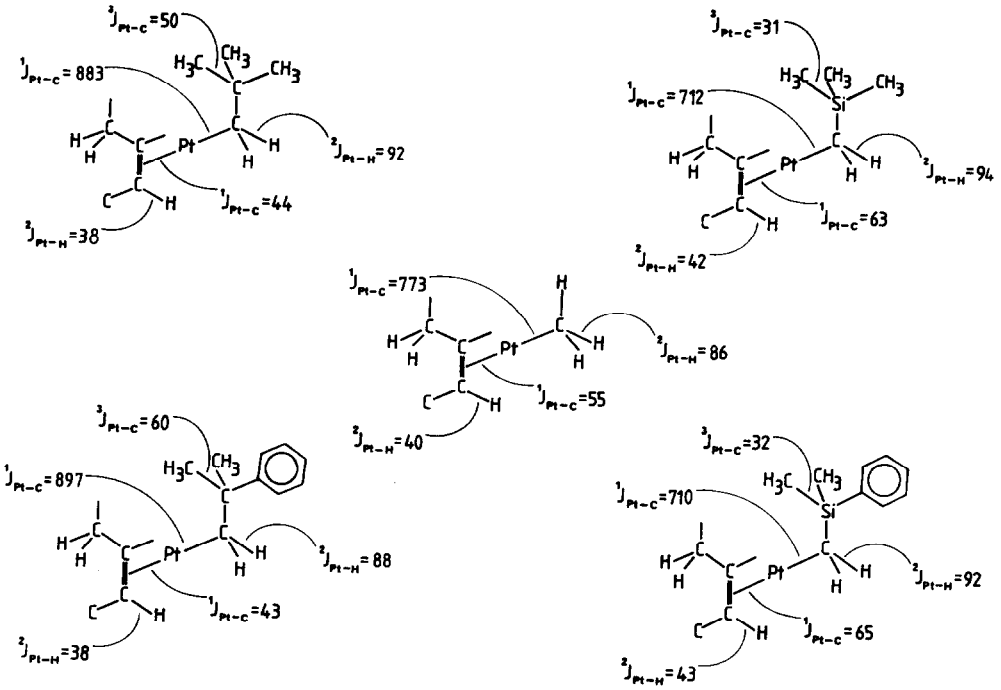

Fig. 2.

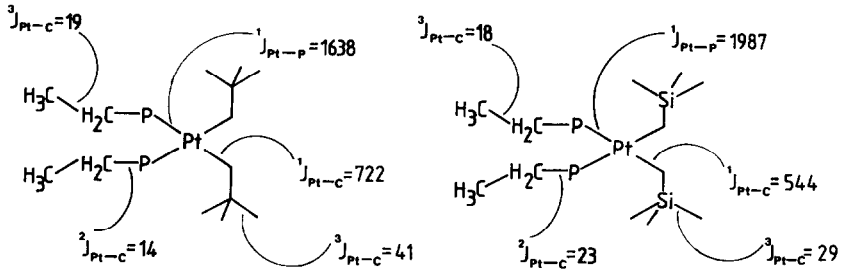

Fig. 3.

Table 5. ^{13}C NMR characteristics of LPtRX (R = $CH_2Si(CH_3)_3$)

Complex L	Complex X	δ ^{13}C ppm $CH_2Si(CH_3)_3$ (J_{Pt-C}) CH_2	CH_3	δ ^{13}C ancillary ligand(s) L (J_{Pt-C}) [Assignment]
cod	R[a]	13.89(712.4 Hz)	3.58(31.0 Hz)	29.99 [CH_2], 97.53(62.8 Hz) [CH]
cod	Cl[b]	16.39(529.0 Hz)	255(16.5 Hz)	28.15(22.1 Hz), 31.92(22.8 Hz) [CH_2], 83.47(215.9 Hz), 111.12(35.2 Hz) [CH]
cod	I[b]	12.64(570.0 Hz)	3.51(17.0 Hz)	28.72(18.0 Hz), 31.28(21.0 Hz) [CH_2], 89.31(181.0 Hz), 109.21(39.0 Hz) [CH]
nbd	R[b]	16.88(754.0 Hz)	3.22(33.0 Hz)	48.79(41.0 Hz) [CH), 72.85(51.0 Hz) [CH_2], 84.84(54.0 Hz) [CH=CH]
bipy	R[a]	−6.27(793.4 Hz)	3.29(36.4 Hz)	121.86(10.8 Hz) [C_5], 126.12(20.1 Hz) [C_3], 134.65 [C_4], 147.26(32.8 Hz) [C_6], 156.17 [C_2]
Me_2bipy	R[a]	−7.44(747.5 Hz)	3.37(36.2 Hz)	21.10 [CH_3], 122.72(11.6 Hz) [C_5], 127.01(20.5 Hz) [C_3], 146.36 [C_4], 146.85(33.2 Hz) [C_6], 156.19 [C_2]
bipym	R[a]	−7.00(762.2 Hz)	3.22(36.2 Hz)	123.07(16.0 Hz) [C_5], 152.52(28.8 Hz) [C_6], 155.29 [C_4], 162.90 [C_2]

(*continued*)

Table 5 (*continued*)

Complex L	X	δ ^{13}C ppm $CH_2Si(CH_3)_3$ (J_{Pt-C}) CH_2	CH_3	δ ^{13}C ancillary ligand(s) L (J_{Pt-C}) [Assignment]
phen	R[a]	−7.59(754.0 Hz)	3.34(36.6 Hz)	125.18(20.5 Hz) [$C_{3,8}$], 126.51 [$C_{5,6}$], 130.50 [$C_{13,14}$], 134.09 [$C_{4,7}$], 147.0(33.4 Hz) [$C_{2,9}$], 148.38 [$C_{11,12}$]
Ph_2phen	R[a]	−6.97(747.7 Hz)	3.51(35.7 Hz)	124.7 [$C_{4'}$], 125.88(20.9 Hz) [$C_{3,8}$], [$C_{5,6}$ obs], 128.91 [$C_{3'}$], 129.21 [$C_{2'}$], 137.82 [$C_{4,7}$], 146.62(33.3 Hz) [$C_{2,9}$], 147.23 [$C_{1'}$], 148.91 [$C_{11,12}$]
Me_4phen	R[a]	−7.96(749.1 Hz)	3.52(36.4 Hz)	14.37, 16.96 [CH_3], 122.50 [$C_{5,6}$], [$C_{13,14}$ obs], 133.27(20.0 Hz) [$C_{3,8}$], 140.70 [$C_{4,7}$], 147.17 [$C_{11,12}$], 148.30(33.9 Hz) [$C_{2,9}$]
terpy	BF_4[c]	4.89(733.0 Hz)	2.48(18.1 Hz)	125.05 [$C_{3,3'}$], 126.60(30.2 Hz) [$C_{5,5''}$], 129.57(43.9 Hz) [$C_{6,6''}$], 141.51 [$C_{4'}$], 142.51 [$C_{4,4''}$], 153.01(31.2 Hz) [$C_{3',5'}$], 153.34 [$C_{2,2''}$], 161.17 [$C_{2',6'}$]
bipyz	R[a]	−3.92(708.7 Hz)	3.08(35.0 Hz)	139.85(29.8 Hz) [C_6], 144.37(9.2 Hz) [C_5], 149.17 [C_2], 149.23 [C_3]
$(py)_2$	R[d]	−11.22(749.1 Hz)	2.86(37.6 Hz)	124.75 [$C_{3,5}$], 134.71 [C_4], 150.90(14.9 Hz) [$C_{2,6}$]
$(PMe_3)_2$	R[b]	6.35(528.2 Hz) ($J_{P-C_{cis}}$ = 7.7 Hz) ($J_{P-C_{trans}}$ = 94.1 Hz)	3.98(29.8 Hz)	17.56(29.2 Hz) [CH_3] (J_{P-C} = 30.5 Hz)
$(PEt_3)_2$	R[b]	5.80(544.5 Hz) ($J_{P-C_{cis}}$ = 8.1 Hz) ($J_{P-C_{trans}}$ obs)	4.36(28.7 Hz)	18.31(18.1 Hz) [CH_3], 17.00(22.5 Hz) [CH_2] (J_{P-C} = 27.9 Hz)
$(PMe_2Ph)_2$	R[b]	6.45(538.3 Hz) ($J_{P-C_{cis}}$ = 7.5 Hz) ($J_{P-C_{trans}}$ = 93.2 Hz)	4.00(29.2 Hz)	15.24(27.5 Hz) [CH_3] (J_{P-C} = 31.5 Hz), 128.0 [C_3] (J_{P-C} = 8.9 Hz), 129.26 [C_4], 131.04(16.1 Hz) [C_2] (J_{P-C} = 10.9 Hz), 139.10(16.9 Hz) [C_1] (J_{P-C} = 43.6 Hz)
$(PMePh_2)_2$	R[b]	7.41(552.9 Hz) ($J_{P-C_{cis}}$ = 7.1 Hz) ($J_{P-C_{trans}}$ = 91.5 Hz)	3.95(29.3 Hz)	14.63(23.0 Hz) [CH_3] (J_{P-C} = 31.6 Hz), 127.86(14.4 Hz) [C_3] (J_{P-C} = 8.8 Hz), 129.19 [C_4], 132.99(14.5 Hz) [C_2] (J_{P-C} = 10.7 Hz), 136.43(18.7 Hz) [C_1] (J_{P-C} = 44.3 Hz)
$(PPh_3)_2$	R[b]	8.53 ($J_{P-C_{cis}}$ = 6.7 Hz) ($J_{P-C_{trans}}$ = 91.6 Hz)	4.04(28.9 Hz)	127.39(8.6 Hz) [C_3] (J_{P-C} = 8.7 Hz), 129.16 [C_4], 133.90(18.5 Hz) [C_1] (J_{P-C} = 43.9 Hz), 134.84(10.8 Hz) [C_2] (J_{P-C} = 10.9 Hz)
dppm	R[b]	5.41(572 6 Hz) ($J_{P-C_{cis}}$ = 6.7 Hz) ($J_{P-C_{trans}}$ = 94.1 Hz)	3.75(30.6 Hz)	49.09(11.4 Hz) [CH_2] (J_{P-C} = 51.2 Hz), 128.49(10.9 Hz) [C_3] (J_{P-C} = 9.9 Hz), 130.20 [C_4], 132.80(19.2 Hz) [C_2] (J_{P-C} = 30.0 Hz), 133.00(12.6 Hz) [C_2] (J_{P-C} = 12.6 Hz)
dppe	R[b]	1.94(551.1 Hz) ($J_{P-C_{cis}}$ = 5.5 Hz) ($J_{P-C_{trans}}$ = 89.3 Hz)	3.58(28.9 Hz)	28.10m [CH_2], 128.30 [C_3] (J_{P-C} = 9.7 Hz), 130.10 [C_4], 133.03 (25.5 Hz) [C_1], (J_{P-C} = 40.2 Hz), 133.57 [C_2] (J_{P-C} = 11.0 Hz)
dppf	R[d]	8.53(568.0 Hz) ($J_{P-C_{cis}}$ = 7.3 Hz) ($J_{P-C_{trans}}$ = 93.7 Hz)	4.58(28.5 Hz)	72.19 [$C_{3',4'}$], 75.28 [$C_{2',5'}$] (J_{C-P} = 8.8 Hz), 79.46 [$C_{1'}$] (J_{P-C} = 47.8 Hz), 127.82 [C_3], 130.09 [C_4], [C_1 obs], 135.70(11.7 Hz) [C_2] (J_{P-C} = 11.2 Hz)

[a] Run in benzene-d_6
[b] Run in chloroform-d_1.
[c] Run in acetone-d_6.
[d] Run in toluene-d_8.

Table 6. ^{13}C NMR characteristics of nitrogen donor ligands

Ligand	δ ^{13}C ppm [Assignments]
2,2′-bipyridine[a]	156.8 [C_2], 149.65 [C_6], 137.40 [C_4], 124.15 [C_3], 121.34 [C_5]
2,2′-bipyrimidine[a]	161.0 [C_2], 156.7 [C_4, C_6], 120.3 [C_5]
1,10-phenanthroline[b]	150.1 [C_2, C_9], 146.1 [C_{11}, C_{12}], 135.9 [C_4, C_7], 128.5 [C_{13}, C_{14}], 126.4 [C_6, C_5], 122.9 [C_3, C_8]
4,7-diphenyl-1,10-phenanthroline[c]	149.8 [C_2, C_9], 148.4 [C_{11}, C_{12}], 138.0 [C_4, C_7], 126.4 (C_{13}, C_{14}], 128.4 [C_5, C_6], 123.4 [C_3, C_8], 146.8, 129.5, 128.5, 123.9 [C_6H_5]

[a] From ref. 21.
[b] From ref. 22.
[c] From ref. 6.

Table 7. First MLCT absorption λ_1 for L_2PtR_2[a]

Complex	λ_{max} (nm)
bipyPtR_2	516.0
Me_2bipyPtR_2	507.5
bipymPtR_2	539.5
bipyzPtR_2	564.0
phenPtR_2	511.0
Ph_2phenPtR_2	519.0
Me_4phenPtR_2	480.0
[terpyPtR]BF_4	482.0

[a] Measured in toluene.

(as opposed to silaalkyl) substituent, in accord with isovalent hybridization.[14,24]

A corollary is that trimethylsilylmethyl appears to exert a lesser (bond-weakening) *trans*-influence than does neopentyl. Ancillary ligand dissociation is often a prerequisite for thermolytic rearrangements in complexes of this type. Such a ground state energetic difference may have a kinetic influence on lability and contribute (in part at least) to the readier reactivity of neopentyl (and neophyl[6]) complexes relative to their silicon analogues.[15] We shall report in due course on our mechanistic observations. An apparent paradox in these ^1J data, however, is the implication that the neopentyl–platinum bond is stronger than that in the trimethylsilylmethyl–platinum complexes, which contradicts previous thermochemical indications.[4,5] We are also investigating this aspect.

REFERENCES

1. For reviews, see (a) R. R. Schrock and G. W. Parshall, *Chem. Rev.* 1976, **76**, 243; (b) P. J. Davison, M. F. Lappert and R. Pearce, *Chem. Rev.* 1976, **76**, 219; (c) M. C. Baird, *J. Organomet. Chem.* 1974, **64**, 289; (d) P. S. Brateman and R. J. Cross, *Chem. Soc. Rev.* 1973, **2**, 271; See also, for example, (e) G. M. Whitesides, J. F. Gaasch and E. R. Stedronsky, *J. Am. Chem. Soc.* 1972, **94**, 5258; (f) R. G. Nuzzo, T. J. McCarthy and G. M. Whitesides, *J. Am. Chem. Soc.* 1981, **103**, 3396; (g) S. Komiya, Y. Morimoto, A. Yamamoto and T. Yamamoto, *Organometallics* 1982, **1**, 1528.
2. See, for example, (a) S. D. Chapell and D. J. Cole-Hamilton, *Polyhedron* 1982, **1**, 739; (b) I. P. Rothwell, *Polyhedron* 1985, **4**, 2; (c) J. C. Calabrese, M. C. Colton, T. Hershovitz, U. Kablunde, G. W. Parshall, D. L. Thorn and T. H. Tulip, *Annu. N.Y. Acad. Sci.* 1983, **415**, 302; (d) G. B. Young, in *Inorganic Reactions and Methods* (Edited by J. J. Zuckerman). Springer, Berlin, in press.
3. (a) P. Foley, R. DiCosimo and G. M. Whitesides, *J. Am. Chem. Soc.* 1980, **102**, 6713; (b) R. A. Andersen, R. A. Jones and G. Wilkinson, *J. Chem. Soc., Dalton Trans.* 1978, 446; (c) P. Diversi, G. Ingrosso, A. Lucherini and D. Fasse, *J. Chem. Soc., Chem. Commun.* 1982, 945; (d) T. H. Tulip and D. L. Thorn, *J. Am. Chem. Soc.* 1981, **103**, 2448; (e) J. W. Bruno, T. J. Marks and V. W. Day, *J. Organomet. Chem.* 1983, **250**, 237.
4. (a) J. C. Baldwin, M. F. Lappert, J. B. Pedley and J. S. Pollard, *J. Chem. Soc., Dalton Trans.* 1972, 1943; (b) J. C. Baldwin, M. F. Lappert, J. B. Pedley and J. A. Treverton, *J. Chem. Soc. (A)* 1967, 1980; (c) I. E. Gümrükcüoglü, J. Jeffery, M. F. Lappert, J. B. Pedley and A. K. Rai, *J. Organomet. Chem.*, in press.
5. J. W. Bruno, T. J. Marks and L. R. Morss, *J. Am. Chem. Soc.* 1983, **105**, 6824.
6. (a) D. C. Griffiths and G. B. Young, *Polyhedron* 1983, **2**, 1095; (b) D. C. Griffiths and G. B. Young, *Organometallics*, in press.
7. B. Ankianiec, D. J. Wilkes and G. B. Young, unpublished results.
8. (a) M. M. Truelock, D.Phil. thesis, University of Sussex (1971); (b) B. Wozniak, J. D. Ruddick and G. Wilkinson, *J. Chem. Soc. (A)* 1971, 3116.
9. D. F. Shriver, *The Manipulation of Air Sensitive Compounds*. McGraw-Hill, New York (1969).
10. J. X. McDermott, J. F. White and G. M. Whitesides, *J. Am. Chem. Soc.* 1976, **98**, 6521.

11. C. R. Kistner, J. H. Hutchinson, J. R. Doyle and J. C. Storlie, *Inorg. Chem.* 1963, **2**, 1255.
12. E. G. Cox, H. Saerger and W. Wardlaw, *J. Chem. Soc.* 1934, 182.
13. N. Chaudhury and R. J. Puddephatt, *J. Organomet. Chem.* 1975, **84**, 105.
14. R. D. Kelly and G. B. Young, *Polyhedron*, in press.
15. B. Ankianiec and G. B. Young, *Polyhedron*, in press.
16. V. Christou and G. B. Young, to be published.
17. R. R. Rumininski and J. D. Petersen, *Inorg. Chem.* 1982, **21**, 3706; V. F. Sutcliffe and G. B. Young, *Polyhedron* 1984, **3**, 87.
18. D. N. Ford, P. R. Wells and P. C. Lauterbur, *J. Chem. Soc., Chem. Commun.* 1967, 616.
19. (a) P. S. Braterman, R. J. Cross, L. Manjlović-Muir, K. W. Muir and G. B. Young, *J. Organomet. Chem.* 1975, **84**, C40; (b) T. G. Appleton, M. A. Bennett and I. B. Tompkins, *J. Chem. Soc., Dalton Trans.* 1976, 439; (c) M. Bochman, G. Wilkinson and G. B. Young, *J. Chem. Soc., Dalton Trans.* 1980, 1879.
20. P. E. Garrou, *Chem. Rev.* 1981, **81**, 229.
21. C. A. Overton and J. A. Connor, *Polyhedron* 1982, **1**, 53.
22. A. Könnecke, E. Lipmann, J. Mlochowski and W. Sliwa, *Org. Mag. Res.* 1979, **12**, 696.
23. P. S. Pregosin, *Annu. Rep. NMR Spectrosc.* 1986, **17**, 285; A. Pidcock, *A.C.S. Adv. Chem. Ser.* 1982, **196**, 1 and refs cited in both.
24. H. A. Bent, *Chem. Rev.* 1961, **61**, 275.

Polyhedron Vol. 7, No. 19/20, pp. 1965–1972, 1988
Printed in Great Britain

0277–5387/88 $3.00+.00
© 1988 Pergamon Press plc

SUBSTITUTION REACTIONS OF THE 17-ELECTRON COMPLEX $\{\eta^5\text{-}C_5H_5Cr(CO)_3\}$

N. A. COOLEY, P. T. F. MacCONNACHIE and M. C. BAIRD†

Department of Chemistry, Queen's University, Kingston, Canada K7L 3N6

Abstract—The compound $[\eta^5\text{-}C_5H_5Cr(CO)_3]_2$ (**I**) has a very weak metal–metal bond, and dissociates in solution at room temperature to generate the substitution-labile, 17-electron species $\{\eta^5\text{-}C_5H_5Cr(CO)_3\}$ (**II**). The latter reacts with monodentate tertiary phosphines to form substitution compounds of the type $\{\eta^5\text{-}C_5H_5Cr(CO)_2L\}$, and with several bidentate phosphines to form products of disproportionation, $[\eta^5\text{-}C_5H_5Cr(CO)_2(diphos)][\eta^5\text{-}C_5H_5Cr(CO)_3]$.

Although organotransition metal chemistry has long been dominated by compounds containing closed-shell electron configurations and obeying the 18-electron rule,[1] increasing evidence has appeared in recent years for the existence of 17-electron organotransition metal compounds. A common approach to the synthesis of such species involves photolysis of a variety of dimeric compounds containing metal–metal bonds and formation of the corresponding 17-electron monomeric compounds.[2]

In contrast to most bimetallic organometallic compounds, however, the compound $[\eta^5\text{-}C_5H_5Cr(CO)_3]_2$ (**I**) is known to have a very long metal–metal bond,[3a] and the apparent weakness[3b] of this bond has been shown to result in partial (thermal) dissociation to the paramagnetic monomer $\{\eta^5\text{-}C_5H_5Cr(CO)_3\}$ (**II**) on sublimation and dissolution [eq. (1)].[4] (Henceforth, to distinguish in the text 17-electron species from closed-shell compounds of similar structures, the chemical formulae of the former will be enclosed in brace brackets.)

$$\underset{\mathbf{I}}{[\eta^5\text{-}C_5H_5Cr(CO)_3]_2} \rightleftharpoons 2\underset{\mathbf{II}}{\{\eta^5\text{-}C_5H_5Cr(CO)_3\}}. \quad (1)$$

Very recently, equilibrium constant data and thermodynamic parameters for this homolytic dissociation have been reported.[4c]

In a recent study of the possible involvement of a radical mechanism[5] in the hydrogenation of conjugated dienes by the hydride, $\eta^5\text{-}C_5H_5Cr(CO)_3H$, we observed coalescence of the cyclopentadienyl resonance of this hydride with the cyclopentadienyl resonance of **I**, which is a product of the hydrogenation reaction.[6] To rationalize this unprecedented phenomenon, we proposed a mechanism in which the exchange process actually involved a direct interaction between $\eta^5\text{-}C_5H_5Cr(CO)_3H$ and the radical-like $\{\eta^5\text{-}C_5H_5Cr(CO)_3\}$ (**II**), present in solution in equilibrium with **I**, as in eq. (2).

$$\eta^5\text{-}C_5H_5Cr(CO)_3H + \{\eta^5\text{-}C_5H_5Cr^*(CO)_3\} \rightleftharpoons [\eta^5\text{-}C_5H_5Cr(CO)_3\cdots H\cdots Cr^*(CO)_3(\eta^5\text{-}C_5H_5)] \rightleftharpoons \{\eta^5\text{-}C_5H_5Cr(CO)_3\} + \eta^5\text{-}C_5H_5Cr^*(CO)_3H. \quad (2)$$

This type of atom abstraction reaction implies great reactivity of the monomer **II**, and it therefore seemed possible that the dissociative process, represented by eq. (1), is sufficiently facile that the chemistry of **I** might more generally reflect the reactivity of **II**. On the basis of preliminary studies designed to test the validity of this hypothesis, we have earlier reported that **I** does indeed take part in a variety of atom abstraction and ligand substitution reactions typical of metal-centred radicals,[6] therefore presumably involving **II** as the reactive species. We now report details of the substitution reactions of **I** with ^{13}CO-labelled CO and with a variety of mono- and bidentate tertiary phosphines. Similar observations have been made elsewhere.[4c]

EXPERIMENTAL

IR spectra were recorded on a Bruker IFS-85 FT IR spectrophotometer. ^1H, $^{13}C\{^1H\}$ and $^{31}P\{^1H\}$ solution NMR spectra were recorded on a Bruker AM 400 spectrometer, while CP–MAS $^{13}C\{^1H\}$

† Author to whom correspondence should be addressed.

were run on a Bruker CXP 200 NMR spectrometer. Chemical shifts are reported in δ (ppm) relative to an internal standard of tetramethylsilane for ^{1}H and ^{13}C, external phosphoric acid for ^{31}P, with positive shifts being downfield of the reference. IR and NMR data are presented in Tables 1–3. Magnetic susceptibilities were determined in the solid state using a Johnson Matthey Magnetic Susceptibility Balance, in solution by NMR spectroscopy using the Evan's method,[7] and are presented in Table 4.

All reactions were carried out in an atmosphere of purified nitrogen using dried, de-aerated solvents. Elemental analyses were carried out by Canadian Microanalytical Service Ltd, New Westminster, British Columbia.

Synthetic procedures

The compound, η^5-$C_5H_5Cr(CO)_3H$, was synthesized by a modification of the literature procedure.[8] A suspension of $Na[\eta^5$-$C_5H_5Cr(CO)_3]$[8,9] (10.5 g) in hexanes (200 cm^3) was treated with 3 cm^3 of glacial acetic acid (10% excess) dissolved in 25 cm^3 of hexanes. The mixture was stirred for 2 h at 0°C, and then filtered through Celite to give a dark yellow solution of the hydride. Removal of the solvent under reduced pressure followed by sublimation at 50°C gave pure products in overall yields of 50–70%. The dimer, $[\eta^5$-$C_5H_5Cr(CO)_3]_2$ (**I**), was prepared by treating a known amount of η^5-$C_5H_5Cr(CO)_3H$, prepared as above, with a two-fold excess of isoprene. The solution was stirred for 2 h, after which the solvent was removed to leave solid, impure **I**, which could be sublimed at 80°C to give pure **I** in up to 70% yields.

The hydride, η^5-$C_5H_5Cr(CO)_2(PPh_3)H$, was prepared by refluxing a solution of η^5-$C_5H_5Cr(CO)_3H$ (2.00 g, 0.01 mol) and PPh_3 (2.50 g, 0.01 mol) in 50 cm^3 of hexanes for 1 h. On cooling, a yellow precipitate formed which, on recrystallization from 3:4 ethyl ether–hexanes at −40°C, formed 3.47 g of the product in 83% yield. Found: C, 69.0; H, 4.9. Calc. for $C_{25}H_{21}CrO_2P$: C, 68.9; H, 4.9%.

Substitution reactions

With ^{13}CO. A solution of **I** (0.400 g, 1 mmol) and THF (40 cm^3) in a 75 cm^3 Schlenk tube was stirred under an atmosphere of ^{13}CO (91.7 atm % enriched) for 5 h. The atmosphere was then replenished, and the solution was stirred overnight to give a solution of **I** enriched to about 66% (by IR spectroscopy). Isolation of the product and analysis

Table 1. IR data

Compound	ν_{CO}
$[\eta^5$-$C_5H_5Cr(CO)_3]_2$	2010(m), 1946(vs), 1920(vs), 1905(s),[a] 2005(s), 1946(vs), 1919(vs), 1901(m)[b]
$Na[\eta^5$-$C_5H_5Cr(CO)_3]$	1897(vs), 1795(vs, br)[b]
η^5-$C_5H_5Cr(CO)_3H$	2018(s), 1946(s), 1936(vs),[c] 2010(s), 1922(vs, br)[b]
η^5-$C_5H_5Cr(CO)_2(PPh_3)H$	1932(vs), 1866(s), 1853(sh)[a]
$\{\eta^5$-$C_5H_5Cr(CO)_2(PEt_3)\}$	1924(s), 1805(m, br)[c]
$\{\eta^5$-$C_5H_5Cr(CO)_2(PBu_3)\}$	1921(s), 1803(m, br)[c]
$\{\eta^5$-$C_5H_5Cr(CO)_2(PCy_3)\}$	1919(s), 1802(m, br)[c]
$\{\eta^5$-$C_5H_5Cr(CO)_2(PPh_3)\}$	1920(s), 1800(m, br)[c]
$\{\eta^5$-$C_5H_5Cr(CO)_2(PMe_2Ph)\}$	1925(s), 1807(m, br)[c]
$\{\eta^5$-$C_5H_5Cr(CO)_2(PEt_2Ph)\}$	1923(s), 1807(m, br)[c]
$\{[\eta^5$-$C_5H_5Cr(CO)_2]_2(\mu$-dppb$)\}$	1915(s), 1806(m, br)[b]
$\{[\eta^5$-$C_5H_5Cr(CO)_2]_2(\mu$-dpph$)\}$	1915(s), 1795(m, br)[b]
$[\eta^5$-$C_5H_5Cr(CO)_2$(dppm)$][\eta^5$-$C_5H_5Cr(CO)_3]$	1976(s), 1920(m, br), 1890(s), 1773(vs, br), 1751(s, br)[d]
$[\eta^5$-$C_5H_5Cr(CO)_2$(dppe)$][\eta^5$-$C_5H_5Cr(CO)_3]$	1969(s), 1913(m), 1889(vs), 1773(s, br), 1751(s, br)[d]
$[\eta^5$-$C_5H_5Cr(CO)_2$(dppb)$][\eta^5$-$C_5H_5Cr(CO)_3]$	1960(w), 1889(vs), 1771(s,br)[d]

[a] Toluene.
[b] THF.
[c] Hexanes.
[d] CH_2Cl_2.

Table 2. ^1H NMR data

Compound	δH (ppm)
$[\eta^5\text{-}C_5H_5Cr(CO)_3]_2$	5.41(br)[a]
$\eta^5\text{-}C_5H_5Cr(CO)_3H$	3.84(s, 5H, Cp), −5.70(s, 1H, Cr—H)[a]
$\eta^5\text{-}C_5H_5Cr(CO)_2(PPh_3)H$	7.0–7.5(m, 15H, Ph), 4.22(d, J_{PH} = 1.2, 5H, Cp), −5.21(d, J_{PH} = 80 Hz, 1H, Cr—H)[a]
$[\eta^5\text{-}C_5H_5Cr(CO)_2(dppm)][\eta^5\text{-}C_5H_5Cr(CO)_3]$	7.3–7.7(m, 20H, Ph), 4.75(s, 5H, Cp), 4.59(t, J_{PH} = 2 Hz, 5H, Cp), 1.53(s, 2H, CH_2)[b]
$[\eta^5\text{-}C_5H_5Cr(CO)_2(dppe)][\eta^5\text{-}C_5H_5Cr(CO)_3]$	7.2–7.7(m, 20H, Ph), 4.59(s, 5H, Cp), 4.53(s, 5H, Cp), 3.30(br s, 2H, CH_2), 2.92(br s, 2H, CH_2)[b]
$[\eta^5\text{-}C_5H_5Cr(CO)_2(dppb)][\eta^5\text{-}C_5H_5Cr(CO)_3]$	7.5–7.6(m, 20H, Ph), 4.56(s, 5H, Cp), 4.52(s, 5H, Cp), 2.74(br s, 4H, CH_2), 1.46(br s, 4H, CH_2)[b]

[a] Toluene-d_8.
[b] CD_2Cl_2.

Table 3. $^{13}C\{^1H\}$ and $^{31}P\{^1H\}$ NMR data[a]

Compound	δ_C	δ_P
$[\eta^5\text{-}C_5H_5Cr(CO)_2(dppm)][\eta^5\text{-}C_5H_5Cr(CO)_3]$	248.3(CO), 128–134(m, Ph), 91.9(s, Cp), 82.6(s, Cp), 44.2(d, J_{CP} = 9 Hz, CH_2)	29.9
$[\eta^5\text{-}C_5H_5Cr(CO)_2(dppe)][\eta^5\text{-}C_5H_5Cr(CO)_3]$	246.8(CO), 129–133(m, Ph), 92.4(s, Cp), 82.6(s, Cp), 29.1(t, J_{CP} = 5 Hz, CH_2)	57.4
$[\eta^5\text{-}C_5H_5Cr(CO)_2(dppb)][\eta^5\text{-}C_5H_5Cr(CO)_3]$	246.9(CO), 128–133(m, Ph), 93.1(s, Cp), 82.6(s, Cp), 34.4(t, CH_2P), 26.3(s, CH_2)	71.7

[a] CD_2Cl_2.

Table 4. Magnetic moments

Compound	Magnetic moment[a]
$\{\eta^5\text{-}C_5H_5Cr(CO)_2(PEt_3)\}$	1.86 BM[b]
$\{\eta^5\text{-}C_5H_5Cr(CO)_2(PBu_3)\}$	1.96 BM[c]
$\{\eta^5\text{-}C_5H_5Cr(CO)_2(PCy_3)\}$	1.92 BM[b,d]
$\{\eta^5\text{-}C_5H_5Cr(CO)_2(PPh_3)\}$	1.83 BM[b,e]
$\{\eta^5\text{-}C_5H_5Cr(CO)_2(PMe_2Ph)\}$	1.80 BM[b]
$\{\eta^5\text{-}C_5H_5Cr(CO)_2(PEt_2Ph)\}$	1.88 BM[c]
$\{[\eta^5\text{-}C_5H_5Cr(CO)_2]_2(\mu\text{-dpph})\}$	1.3 BM[c]

[a] All corrected for diamagnetic ligand contributions.
[b] Benzene-d_6.
[c] Toluene-d_8.
[d] 1.81 BM in the solid state.
[e] 1.85 BM in the solid state.

by mass spectrometry confirmed the extent of enrichment.

A CP–MAS ^{13}C NMR spectrum was obtained by packing about 300 mg of the complex into a 7 mm sapphire spinner; the sample was sealed with Kel-F or Delrin caps and placed in a solid state Doty Scientific probe. Spectra were obtained at room temperature under conditions of high power decoupling and a spinning rate of 2 kHz.

With triethylphosphine (PEt_3). A stirred solution of **I** (0.100 g, 0.25 mmol) in 25 cm^3 benzene was treated with PEt_3 (6.7×10^{-2} cm^3, 0.5 mmol). The colour of the solution changed from dark green to dark orange within 5 min, at which time the IR spectrum indicated that no starting material remained. The solvent was removed under reduced pressure to give a green residue, which was

extracted in turn with hexanes to give an orange solution of $\{\eta^5\text{-}C_5H_5Cr(CO)_2(PEt_3)\}$. Removal of the solvent gave a dark yellow solid which slowly turned green on standing and thus could not be purified satisfactorily. It was therefore characterized by its IR spectroscopic properties (Table 1) and magnetic moment (Table 4).

Similar procedures were followed to prepare analogues of tri-*n*-butylphosphine (PBu_3), dimethylphenylphosphine (PMe_2Ph) and diethylphenylphosphine (PEt_2Ph). All the products were yellow oils or solids which were found to turn muddy green on standing, and which therefore could not be purified. All were characterized by their IR spectra and magnetic properties (Tables 1 and 4).

With tricyclohexylphosphine (PCy_3). A solution of **I** (0.200 g, 0.5 mmol) and PCy_3 (0.28 g, 1.0 mmol) in 25 cm^3 of ethanol was refluxed for 1 h. On cooling, yellow crystals of $\{\eta^5\text{-}C_5H_5Cr(CO)_2(PCy_3)\}$ separated, and were collected by filtration and washed with cold ethanol. The complex of PCy_3 was somewhat more robust than the compounds mentioned above, but no satisfactory elemental analyses could be obtained. Found: C, 64.8; H, 8.7. Calc. for $C_{25}H_{38}CrO_2P$: C, 66.2; H, 8.4%. The compound was characterized by its IR spectrum and magnetic properties.

With triphenylphosphine (PPh_3). This compound was prepared in quantitative yield in the same way as was the PCy_3 complex, and essentially as in the literature.[10] It was recrystallized from toluene–hexanes (1:2) and characterized by its IR spectrum and magnetic properties. An X-ray quality crystal was grown at −40°C by layer diffusion of 2:1 hexanes–ethyl ether into a saturated solution of the complex in ethyl ether. The product was obtained as orange–yellow crystals, and was characterized unambiguously by X-ray crystallography (see below). It can also be prepared by reacting $\eta^5\text{-}C_5H_5Cr(CO)_2(PPh_3)H$ with isoprene.

With bis(diphenylphosphino)methane (*dppm*). A solution of **I** (0.400 g, 1.0 mmol) and dppm (0.400 g, 1.04 mmol) in benzene (20 cm^3) was stirred for 30 h, after which time orange needle-like crystals of $[\eta^5\text{-}C_5H_5Cr(CO)_2(dppm)][\eta^5\text{-}C_5H_5Cr(CO)_3]\cdot 2C_6H_6$ had formed in 87% yield. Found: C, 67.9; H, 5.3. Calc. for $C_{52}H_{44}Cr_2O_5P_2$: C, 68.3; H, 4.8%. The synthesis of this compound requires about 6 h in THF, the product remaining in solution.

With 1,2-bis(diphenylphosphino)ethane (*dppe*). The compound $[\eta^5\text{-}C_5H_5Cr(CO)_2(dppe)][\eta^5\text{-}C_5H_5Cr(CO)_3]$ was synthesized via the procedure described for the dppm analogue. Found: C, 62.7; H, 4.5. Calc. for $C_{41}H_{34}Cr_2O_5P_2$: C, 63.7; H, 4.0%.

With 1,4-bis(diphenylphosphino)butane (*dppb*). A solution of **I** (0.55 g, 1.37 mmol) and dppb (0.58 g, 1.37 mmol) in 65 cm^3 THF was stirred at room temperature for 9 h. The solution was then concentrated to 30 cm^3 and cooled to −30°C overnight. The resulting yellow solid was collected by filtration, washed with cold hexanes and dried to give $[\eta^5\text{-}C_5H_5Cr(CO)_2(dppb)][\eta^5\text{-}C_5H_5Cr(CO)_3]\cdot 2THF$ in 40% yield. Found: C, 63.8; H, 5.5. Calc. for $C_{51}H_{54}Cr_2O_7P_2$: C, 64.8; H, 5.8%.

No further solids precipitated from the filtrate over 120 h, and the solvent was removed under reduced pressure to give a green residue which was extracted with ethyl ether. The IR spectrum of the yellow–green solution exhibited ν_{CO} at 1986 (m), 1920 (vs), 1801 (s, br) and 1726 (w) cm^{-1}. The ether was removed under reduced pressure, and the residue was dissolved in benzene-d_6 and examined for paramagnetism by the Evan's method (see below).

With 1,6-bis(diphenylphosphino)hexane (*dpph*). A solution of **I** (100 mg, 0.25 mmol) and dpph (119 mg, 0.26 mmol) in THF (35 cm^3) was stirred at room temperature for 2 h. After this time, the ν_{CO} of **I** had disappeared, and had been replaced by ν_{CO} at 1915 (vs) and 1795 (s, br) cm^{-1}. The solvent was removed to give a greenish solid which could not be purified.

Magnetic susceptibility measurements on those compounds, prepared as above, which were expected to be paramagnetic were carried out in benzene-d_6 or toluene-d_8 solution using, where possible, samples which appeared by IR spectroscopy to be pure of other carbonyl-containing species. In some cases, where the solution chemistry had been well-defined by IR spectroscopy, the paramagnetic species were generated *in situ* by addition of phosphine to a solution of **I**. In all cases, susceptibility shifts of 18–25 Hz were obtained, giving rise to the magnetic moments listed in Table 4.

RESULTS AND DISCUSSION

The dimer, $[\eta^5\text{-}C_5H_5Cr(CO)_3]_2$ (**I**), has been previously prepared in 37% yield by oxidizing the carbonylate complex $Na[\eta^5\text{-}C_5H_5Cr(CO)_3]$ with tropylium bromide.[9] Although the synthetic procedure utilized here involves two stages from the carbonylate anion, i.e. protonation followed by treatment of the hydride $\eta^5\text{-}C_5H_5Cr(CO)_3H$ with isoprene, the overall yields are generally higher. Thus, the protonation reaction is presumably near quantitative, as is the conversion of the hydride to **I** (by IR spectroscopy). Isolated yields in each of the two steps are routinely 70%. We note that conversion of the hydride to **I** may well involve a radical

pair mechanism, as the olefinic by-products are various mono-olefins.[5]

As has been shown previously,[4] compound **I** dissociates spontaneously in solution at room temperature to form the monomeric, 17-electron, substitution-labile compound $\{\eta^5\text{-}C_5H_5Cr(CO)_3\}$ (**II**) [eq. (1)]. Exchange between monomer and dimer is rapid on the NMR time scale above about $-20°C$, below which temperature separate Cp resonances of the *anti* and *gauche* rotamers of **I** may be observed.[3a] Line shape analyses of the Cp resonances of the two rotamers in the region of their coalescence temperature resulted in the following activation parameters for *anti–gauche* exchange: $\Delta H^{\ddagger} = 55 \pm 2$ kJ mol^{-1}, $\Delta S^{\ddagger} = 20 \pm 8$ J K^{-1} mol^{-1}, $\Delta G^{\ddagger}_{298} = 51 \pm 3$ kJ mol^{-1}.[3a]

Although it was originally believed that *gauche–anti* interconversion involves restricted rotation about the chromium–chromium bond of **I**, it was also recognized that this bond is very weak and that a dissociation–recombination process might well pertain.[3a] We find that the Cp resonance of **I** broadens significantly and shifts to lower field above $-20°C$, the chemical shift and line width at 80°C being δ 9.6 and 560 Hz, respectively. (See Table 2 for room temperature data.)

These observations are consistent with the exchange of eq. (1) if one makes the very reasonable assumptions that the Cp resonance of **II** is very broad and lies to low field.[11] We have carried out a line shape analysis in the temperature range 30–80°C, utilizing an established procedure for the analysis of the NMR spectra of systems in which diamagnetic and paramagnetic species are undergoing rapid exchange.[12] Following this approach, we have found the following activation parameters for the exchange process of eq. (1): $\Delta H^{\ddagger} = 58 \pm 1.4$ kJ mol^{-1}, $\Delta S^{\ddagger} = 16 \pm 4$ J K^{-1} mol^{-1}, $\Delta G^{\ddagger}_{298} = 51.9 \pm 0.2$ kJ mol^{-1}. These data are identical, within experimental error, with the published activation data for the *anti–gauche* interconversion,[3a] suggesting a common mechanism which almost certainly involves homolysis as in eq. (1). Thus the hypothesis that the chemistry of **I** may generally reflect the reactivity of **II** gains further support.

Consistent with this conclusion, treatment of solutions of **I** with ^{13}CO results in enrichment of the dimer [eq. (3)], an observation made elsewhere.[4c]

$$\mathbf{I} + {}^{13}CO \rightarrow (\eta^5\text{-}C_5H_5Cr)_2({}^{13}CO)_x({}^{12}CO)_{6-x}. \quad (3)$$

The IR spectrum of the mixture of isotopomers of **I** formed on exposure of **I** to 1 atm of ^{13}CO for several hours suggested enrichment to the extent of about 66%, an estimate confirmed by mass spectrometry. Although no attempt to effect quantitative ^{13}CO substitution was made, it is clear that CO substitution is facile, as anticipated.[2] In view of the very significant broadening of the Cp resonance of **I** in the ^1H NMR spectrum, a result of exchange with paramagnetic **II**, we expected resonances of the $^{13}CO\{^1H\}$ NMR solution spectrum of the enriched **I** to be broadened so that it is unobservable. This was as found.

In contrast, as **I** exists in the solid state solely as the diamagnetic dimer,[3a] the NMR spectrum of the solid, enriched material should be and is well-resolved. While the CP–MAS ^{13}C NMR spectrum is complicated by an extensive pattern of spinning side bands, the result of a significant degree of chemical shift anisotropy, six carbonyl carbon resonances may be resolved at $\approx \delta$ 245. Although the individual molecules of **I** in the crystal lattice are crystallographically centrosymmetric[3a] and hence might be expected to contain (as in solution) only two carbonyl environments, analysis of the X-ray data shows that all six carbonyl groups of the molecule in the crystalline material are in fact non-equivalent, thus explaining the NMR findings.

Treatment of solutions of **I** with a variety of tertiary phosphines L was found to result in both the facile formation of compounds of the stoichiometry $\{\eta^5\text{-}C_5H_5Cr(CO)_2L\}$ [eq. (4)] and in disproportionation [eq. (5)], depending on the nature of L.

$$[\eta^5\text{-}C_5H_5Cr(CO)_3]_2 + 2L \rightarrow 2\{\eta^5\text{-}C_5H_5Cr(CO)_2L\} \quad (4)$$

$$[\eta^2\text{-}C_5H_5Cr(CO)_3]_2 + 2L \rightarrow [\eta^5\text{-}C_5H_5Cr(CO)_2L_2]^+ + [\eta^5\text{-}C_5H_5Cr(CO)_3]^-. \quad (5)$$

Isolation and purification of the products of eq. (4) were generally not possible, as most of the products were thermally very labile at room temperature. Only the PPh_3 compound was sufficiently robust that it could be isolated and purified, and it was identified unambiguously by X-ray crystallography. The structure of this compound and a discussion of the important structural features have been reported in a preliminary communication[6] and thus all pertinent data are available.*

As anticipated, the compound $\{\eta^5\text{-}C_5H_5Cr(CO)_2(PPh_3)\}$ assumes a "piano-stool" structure, isostructural with the 18-electron manganese

* Tables of bond lengths, bond angles, atomic coordinates, thermal parameters and observed and calculated structure factors are available as "Supplementary Material" of ref. 6. The information is also available from the Cambridge Crystallographic Data Centre.

analogue η^5-$C_5H_5Mn(CO)_2(PPh_3)$.[6a] A subtle, albeit very important difference between the two compounds lies in the observation that, while the OC—Mn—CO bond angle is approximately normal, at $\approx 92°$, the OC—Cr—CO bond angle is 80.9°. Thus it seemed likely that the electron "hole" of the chromium compound is largely localized between the carbonyl groups, a hypothesis which has received support in subsequent single crystal ESR studies.[13]

In accord with the presence of two mutually *cis* carbonyl groups, the IR spectrum of $\{\eta^5$-$C_5H_5Cr(CO)_2(PPh_3)\}$ exhibits two ν_{CO}, as shown in Fig. 1. Identification of the other substitution compounds as having the stoichiometry $\{\eta^5$-$C_5H_5Cr(CO)_2L\}$ was made possible by the fact that they all have similar absorptions, as shown in Table 1. As we had failed in attempts to grow crystals of the other derivatives, we have been unable to ascertain if small ($\approx 81°$) OC—Cr—CO bond angles are a general feature of these compounds, and we looked to the relative intensities of the ν_{CO} of these compounds as an approximate measure of the bond angles.[14]

This approach has been applied to a variety of metal carbonyl compounds, and in particular to a series of iron complexes of the type η^5-$C_5H_5Fe(CO)_2X$,[15] where very reasonable OC—Fe—CO bond angles of 93–97° have been estimated. Interestingly, all compounds of the type $\{\eta^5$-$C_5H_5Cr(CO)_2L\}$ exhibit a pattern of intensities as shown in Fig. 1, suggesting that all assume bond angles similar to that of the PPh_3 analogue. However, as may also be noted from Fig. 1, the ν_{CO} at lower frequency is significantly broader than is the high frequency band, and bond angle calculations utilizing the ratios of integrated intensities for all compounds of the type $\{\eta^5$-$C_5H_5Cr(CO)_2L\}$ suggest that all have OC—Cr—CO bond angles of about 95°, a conclusion inconsistent with the known structure of $\{\eta^5$-$C_5H_5Cr(CO)_2(PPh_3)\}$ and therefore untenable.

Interestingly, if the ratios of peak heights are utilized in the bond angle calculations, acute bond angles in the range 78–84° are obtained, in satisfactory agreement with the crystal structure. We do not know the reason for the broadening of the low frequency band of these chromium compounds, which we find does not occur in the IR spectra of either η^5-$C_5H_5Mn(CO)_2(PPh_3)$ or of compounds of the type η^5-$C_5H_5Fe(CO)_2X$. However, in view of the great similarities in the ν_{CO} of all the 17-electron compounds reported here, we feel confident that all have rather acute OC—Cr—CO bond angles.

Although all of the compounds $\{\eta^5$-$C_5H_5Cr(CO)_2L\}$ exhibited resonances in the ^1H NMR spectra, the resonances were invariably broad, featureless bands, many of them shifted out of the usual region δ 0–10. Thus, the NMR data cannot yet be unequivocally assigned in most cases, and the spectra certainly do not aid in structural elucidation. Further discussions will not be merited until specific deuteration studies, currently underway, make unambiguous assignments possible.

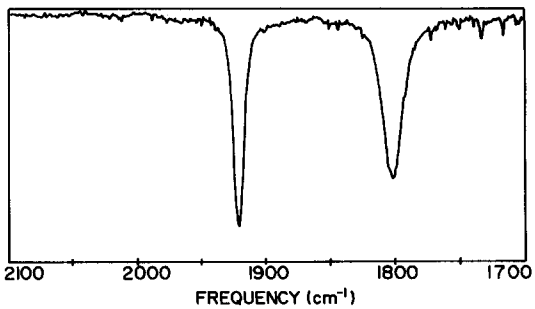

Fig. 1. IR spectrum of the carbonyl stretching region of $\{\eta^5$-$C_5H_5Cr(CO)_2(PPh_3)\}$ (toluene).

All of the 17-electron compounds were characterized by magnetic susceptibility measurements, $\{\eta^5$-$C_5H_5Cr(CO)_2(PCy_3)\}$ and $\{\eta^5$-$C_5H_5Cr(CO)_2(PPh_3)\}$ in the solid state, the others (pure by IR spectroscopy) in solution. The magnetic moments determined are listed in Table 4, and it can be seen that all are consistent with the presence of one unpaired electron in each compound.

Interestingly, the ease of formation of the compounds $\{\eta^5$-$C_5H_5Cr(CO)_2L\}$ appears to decrease as the steric requirements of L increase. Thus formation of the complexes $\{\eta^5$-$C_5H_5Cr(CO)_2L\}$ ($L = PEt_3$, PBu_3, PMe_2Ph, PEt_2Ph) from **I** all occurred within a few minutes in benzene solution at room temperature, while formation of the corresponding complexes of the much larger ligands PCy_3 and PPh_3 required heating. This qualitative observation is being substantiated by kinetic studies of substitution reactions of **I** with tertiary phosphines, currently underway. Thus the substitution reactions are found to be associative,[16] the rate constants decreasing with increasing steric requirements of the incoming phosphine, as is generally true of CO substitution reactions of 17-electron compounds.[2]

Reactions of **I** with the diphosphines, dppm, dppe and, to a significant extent, dppb, proceeded as in eq. (5), to give products of disproportionation. In all cases, diamagnetic, yellow, crystalline products of the stoichiometry $[\eta^5$-$C_5H_5Cr(CO)_2(diphos)][\eta^5$-$C_5H_5Cr(CO)_3]$ were obtained and characterized by elemental analyses and spectroscopic properties (Tables 1–3). In particular, the IR spectra of the dppm and dppe complexes exhibited ν_{CO} at $\approx$ 1970

(s) and $\approx$ 1915 (m, br) cm^{-1}, as expected by analogy with similar complexes of molybdenum,[17] as well as two strong ν_{CO} at $\approx$ 1890 and 1773 cm^{-1}, attributable to the $[\eta^3\text{-}C_5H_5Cr(CO)_3]^-$ carbonylate anion (see Table 1 to compare with data for $Na[\eta^5\text{-}C_5H_5Cr(CO)_3]$). The cations of these complexes presumably contain chelating diphosphines and mutually *cis* carbonyl groups; the relative ratios of the intensities of the ν_{CO} of the cations are consistent with OC—Cr—CO bond angles of $< 90°$, as anticipated for this geometry.*

In contrast, while the IR spectrum of the dppb complex exhibited the ν_{CO} of the carbonylate anion, the only ν_{CO} to be attributed to the cation was a weak absorption at 1960 cm^{-1}. There was no second absorption at a frequency above 2000 cm^{-1}, and thus it would seem that a second band may overlap with the higher frequency absorption of the anion at $\approx$ 1889 cm^{-1}. Similar patterns of ν_{CO} have been reported for complexes of the type "*trans*"-$[\eta^5\text{-}C_5H_5Mo(CO)_2L_2]^+$, where the OC—Mo—CO bond angles are $\gg 90°$.*[18] This conclusion would require the dppb ligand to span mutually "*trans*" positions, which could be reasonable as it would involve a "bite angle" of as little as 114°,* or it may be that the cation is actually dimeric, with two dppb molecules bridging two $[\eta^5\text{-}C_5H_5Cr\{$"*trans*"-$(CO)_2\}]^+$ moieties.

The ^1H, $^{13}C\{^1H\}$ and $^{31}P\{^1H\}$ solution NMR spectra (Tables 2 and 3) may all be assigned on the basis of the structures suggested, and although the carbonyl resonances of the cations could not be observed, presumably because spin–spin coupling to ^{31}P resulted in multiplet resonances, resonances at $\approx \delta$ 247 can be assigned to $[\eta^5\text{-}C_5H_5Cr(CO)_3]^-$.[19] For each compound, there are two Cp resonances in both the ^1H and the $^{13}C\{^1H\}$ spectra, with the observation of spin–spin coupling to ^{31}P facilitating assignments in some cases.

In the case of the reaction of **I** with dppb, examination of the filtrate after the ionic product of disproportionation had been isolated revealed ν_{CO} at 1915 and 1806 cm^{-1}, characteristic of a complex of the type $\{\eta^5\text{-}C_5H_5Cr(CO)_2L\}$. Similar absorptions were not observed for the reactions of dppm and dppe, and it would seem that dppb is unique among the three diphosphines in that it forms a product of CO substitution, as well as a product of disproportionation. The presumed 17-electron species exhibited solubility and thermal instability properties analogous to those of the other compounds of the type $\{\eta^5\text{-}C_5H_5Cr(CO)_2L\}$, extracting into ether to give, on solvent removal, a greenish solid. An NMR spectrum of the clearly impure solid exhibited broadened resonances, while a magnetic susceptibility measurement on a solution showed unequivocally that the material was paramagnetic.

Interestingly, reaction of **I** with an equimolar amount of dpph in THF resulted only in CO substitution. Thus the IR spectrum of the reaction solution exhibited ν_{CO} only at 1915 (vs) and 1795 (s, br) cm^{-1}, there being no absorptions attributable to products of disproportionation. Again the compound was too unstable to purify satisfactorily, but addition of 0.5 equivalents of **I** to a solution containing 100 mg of the material in THF resulted in no reaction. If the dpph compound contained a "dangling" diphosphine, i.e. had the structure $\{\eta^5\text{-}C_5H_5Cr(CO)_2[Ph_2P(CH_2)_6PPh_2]\}$, then it would be anticipated that the uncoordinated phosphorus would react further. Instead, and consistent with the stoichiometries of the reactants initially combined, the dpph must bridge two $[\eta^5\text{-}C_5H_5Cr(CO)_2]$ moieties. Presumably the 17-electron dppb compound, discussed above, is similar.

A magnetic moment measurement of the dpph compound in solution in toluene-d_8 showed that the compound has a magnetic moment of $\approx$ 1.3 BM per chromium. This suggests that pairs of chromium atoms are weakly coupled in solution, as has been reported for the compound $[\eta^5\text{-}C_5H_5Cr(CO)_2\{P(OMe)_3\}]_2$, which is dimeric in the solid state, but partially dissociated in solution.[20]

Acknowledgements—We thank Queen's University (scholarship to P.T.F.M.) and the Natural Sciences and Engineering Research Council (operating grant to M.C.B.) for financial support.

REFERENCES

1. F. A. Cotton and G. Wilkinson, *Advanced Inorganic Chemistry*, 4th Edn, p. 1050. Wiley Interscience, New York (1980).
2. (a) T. J. Meyer and J. V. Caspar, *Chem. Rev.* 1985, **85**, 187; (b) T. L. Brown, *Annu. N. Y. Acad. Sci.* 1980, **333**, 80; (c) M. C. Baird, *Chem. Rev.*, in press.
3. (a) R. D. Adams, D. E. Collins and F. A. Cotton, *J. Am. Chem. Soc.* 1974, **96**, 749; (b) J. T. Landrum and C. D. Hoff, *J. Organomet. Chem.* 1985, **282**, 215.
4. (a) H. J. Keller, *Z. Naturforsch.* 1968, **23b**, 133; (b) T. Madach and H. Vahrenkamp, *Z. Naturforsch.*

*A perusal of many published crystal structures of molybdenum complexes of the type $\eta^5\text{-}C_5H_5Mo(CO)_{4-n}L_n$[18] shows that *cis* OC—Mo—CO, OC—Mo—L and L—Mo—L bond angles generally lie in the range 73–82°, although they can be as large as 87°. The corresponding "*trans*" bond angles vary between 114 and 143°.

1978, **33b**, 1301; (c) S. J. McLain, *J. Am. Chem. Soc.* 1988, **110**, 643.
5. B. Wassink, M. J. Thomas, S. C. Wright, D. J. Gillis and M. C. Baird, *J. Am. Chem. Soc.* 1987, **109**, 1995.
6. N. A. Cooley, K. A. Watson, S. Fortier and M. C. Baird, *Organometallics* 1986, **5**, 2563.
7. D. F. Evans, *J. Chem. Soc.* 1959, 2005.
8. E. O. Fischer, *Inorg. Synth.* 1963, **VII**, 136.
9. R. B. King and F. G. A. Stone, *Inorg. Synth.* 1963, **VII**, 104.
10. P. Hackett, P. S. O'Neill and A. R. Manning, *J. Chem. Soc., Dalton Trans.* 1974, 1625.
11. M. F. Rettig, in *NMR of Paramagnetic Molecules* (Edited by G. N. LaMar, W. D. Horrocks and R. H. Holm), p. 217. Academic Press, New York (1973).
12. (a) D. J. Williams and R. W. Kreilick, *J. Am. Chem. Soc.* 1968, **90**, 2775; (b) D. J. Williams and R. W. Kreilick, *J. Am. Chem. Soc.* 1967, **89**, 3408; (c) R. W. Kreilick and S. I. Weissman, *J. Am. Chem. Soc.* 1966, **88**, 2645; (d) R. W. Kreilick, in *NMR of Paramagnetic Molecules* (Edited by G. N. LaMar, W. D. Horrocks and R. H. Holm), p. 595. Academic Press, New York (1973).
13. (a) J. R. Morton, K. F. Preston, N. A. Cooley, M. C. Baird, P. J. Krusic and S. J. McLain, *J. Chem. Soc., Faraday Trans. 1*, 1987, **83**, 3535; (b) N. A. Cooley, M. C. Baird, J. R. Morton, K. F. Preston and Y. Le Page, *J. Mag. Res.* 1988, **76**, 325.
14. F. A. Cotton and G. Wilkinson, *Advanced Inorganic Chemistry*, 4th Edn, pp. 1073–1075. Wiley Interscience, New York (1980).
15. J. Dalton, I. Paul and F. G. A. Stone, *J. Chem. Soc., Dalton Trans.* 1974, 1625.
16. C. Watkins and M. C. Baird, unpublished results.
17. (a) A. R. Manning, *J. Chem. Soc. A*, 1967, 1984; (b) R. J. Haines, R. S. Nyholm and M. H. B. Stiddard, *J. Chem. Soc. A*, 1968, 43; (c) R. J. Haines and C. R. Nolte, *J. Organomet. Chem.* 1970, **24**, 725; (d) R. J. Haines, A. L. Du Preez and I. L. Marais, *J. Organomet. Chem.* 1971, **28**, 97.
18. See, for instance, (a) M. J. Albright, M. D. Glick and J. P. Oliver, *J. Organomet. Chem.* 1978, **161**, 221; (b) R. H. Fenn and J. H. Cross, *J. Chem. Soc. A* 1971, 3312; (c) M. A. Bush, A. D. U. Hardy, L. Manojlovis-Muir and G. A. Sim, *J. Chem. Soc. A* 1971, 1003; (d) J. H. Cross and R. H. Fenn, *J. Chem. Soc. A* 1970, 3019.
19. G. M. Bodner, *Inorg. Chem.* 1974, **13**, 2563.
20. L.-Y. Goh, M. J. D'Aniello, S. Slater, E. L. Muetterties, I. Tavanaiepour, M. I. Chang, M. F. Fredrich and V. W. Day, *Inorg. Chem.* 1979, **18**, 192.

Polyhedron Vol. 7, No. 19/20, pp. 1973–1979, 1988
Printed in Great Britain

0277–5387/88 $3.00+.00
© 1988 Pergamon Press plc

SURFACE-ENHANCED RAMAN SPECTROSCOPY (SERS) OF LIGANDS AND THEIR COMPLEXES ON SILVER SOLS—I. MALTOL, TROPOLONE AND THEIR COMPLEXES WITH GROUP VIII AND GROUP VI METALS

SARAH J. GREAVES and WILLIAM P. GRIFFITH*

Inorganic Chemistry Laboratories, Imperial College, London SW7 2AY, U.K.

Abstract—New complexes of the form *trans*-$OsO_2(malt)_2$, *trans*-$UO_2(malt)_2$ and *cis*-$MoO_2(malt)_2$, $M(malt)_3$ and $[M'(malt)(PPh_3)_2]^+$ (Hmalt = maltol, M = Ru, Rh, M′ = Pd, Pt) are reported together with their vibrational, ^1H and ^{13}C NMR and mass spectra. SER spectra from Ag sols of maltol, $Ru(malt)_3$, tropolone and $Rh(trop)_3$ (Htrop = tropolone) are reported, and the possible nature of the adsorbed species responsible for the enhanced spectra is briefly discussed.

We have recently reported the preparation, vibrational and NMR spectra of second and third row Group VIII and VI complexes of the "non-innocent" O,O′ donor ligands, catechol (Hcat),[1,2] catecholamines[3] and tropolone (Htrop).[4] We report here an extension of this work to the heterocyclic ligand maltol (Hmalt, 3-hydroxy-2-methyl pyran-4-one, $C_6H_6O_3$; Fig. 1). Also, as part of a study of the application of Surface-Enhanced Raman Spectroscopy (SERS) on silver colloids for the study of coordination complexes in solution,[5] we report the SER spectra of $Ru(malt)_3$, $Rh(trop)_3$ and their parent ligands. It is known that certain species adsorbed on silver or gold surfaces[6] or colloids[7] may give Raman spectra of greatly enhanced intensity; conventional Raman spectroscopy of solutions normally requires concentrations exceeding 0.5 M, but SER spectra can be obtained at solute concentrations of 10^{-4} M or lower. Although there have been a number of studies of organic molecules adsorbed on silver sols,[8] there has been only one on coordination complexes containing organic ring ligands.[9]

RESULTS AND DISCUSSION

(a) *Maltol and its complexes*

Like tropolone (Htrop, $C_7H_6O_2$), maltol possesses a ketonic oxygen atom *ortho* to a hydroxy group, albeit in a heteronuclear ring system; this hydroxy group readily deprotonates ($pK_a = 8.67$[10]) and a number of complexes of the monoanion functioning as an O,O′ chelate with the first row elements and the lanthanides have been reported.[11] The only X-ray crystal structure of a maltolato complex, $Al(malt)_3$,[12] shows the ligand to function as an O,O′ donor, and that the rings retain planarity in the complex. We find that, like catechol, catecholamines and tropolone, maltol forms stable complexes with ruthenium, osmium, rhodium, palladium, platinum, molybdenum and uranium, often analogous to the corresponding trop complexes.[4] The only known complexes of maltol with second and third row transition elements to have been reported are $M(malt)_2$ (M = Pd, Pt) and $UO_2(malt)_2 \cdot 3H_2O$.[13]

We have prepared $Ru(malt)_3$ and $Rh(malt)_3$ from reaction of the appropriate metal trichlorides with maltol under basic conditions. The oxo complex $OsO_2(malt)_2$ was prepared from $K_2[OsO_2(OH)_4]$ and maltol, using a method similar to that giving the catecholato[2] and tropolonato[4] analogues; however, reaction of $[OsCl_6]^{3-}$ with maltol under basic

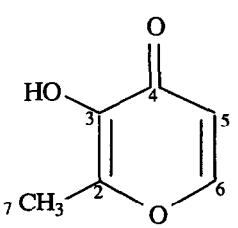

Fig. 1. Maltol, with the carbon atoms numbered.

* Author to whom correspondence should be addressed.

conditions did not give the expected $Os(malt)_3$. The substituted complex $[Pd(PPh_3)_2(malt)]^+$ was prepared using the method developed by Gandolfi *et al.* for the corresponding catecholamines,[14] and $[Pt(PPh_3)_2(malt)]^+$ was prepared via $[Pt(PPh_3)_2O_2]$. The molybdenum complex $MoO_2(malt)_2$ was made from ammonium molybdate and maltol, and reaction of uranyl sulphate with maltol in water–methanol gave red crystals of $UO_2(malt)_2 \cdot CH_3OH$. Reactions of tungstates with maltol failed to give any pure products.

Vibrational spectra of the complexes. The IR spectra of a number of maltolato complexes have been assigned;[11,15] in Table 1 we follow the assignments of Kushch *et al.*[15] for $Pt(malt)_2$. As expected, the ν(OH) mode for maltol at 3350 cm^{-1} is missing for all the complexes. The ν(C=O) band at 1650 cm^{-1} in maltol[15] is shifted to a lower wavenumber by 25–55 cm^{-1} in our complexes. The bands at 1610 and 1550 cm^{-1}, which probably arise from mixed ν(C=C) and ν(C=O) modes,[11,15] are also shifted to lower wavenumbers on coordination (similar effects are also observed in catecholato[2] and tropolonato[4] complexes). The strong IR bands near 850 cm^{-1} in $OsO_2(malt)_2$ and near 925 cm^{-1} in $UO_2(malt)_2 \cdot CH_3OH$, not present in the Raman, are assigned to the asymmetric stretch $\nu_{as}(MO_2)$ of a *trans* O=M=O grouping, while the strong Raman bands in these complexes at 890 and 846 cm^{-1}, respectively, are assigned to $\nu_s(MO_2)$; in accordance with *trans* geometry these bands are very weak in the IR. For $MoO_2(malt)_2$, two IR bands are present near 940 and 905 cm^{-1}, and these are also observed, with reversed intensity, in the Raman spectra. These we assign to $\nu_s(MoO_2)$ and $\nu_{as}(MoO_2)$, respectively; similar bands were observed for *cis*-$MoO_2(trop)_2$.[4]

^{1}H and ^{13}C NMR spectra. The ^{1}H NMR spectra of those complexes soluble enough for spectral measurement (Table 1) are similar to that reported and assigned for $Pd(malt)_2$;[16] the methyl protons (C-7) give a singlet near δ 2.43 (all δ values are quoted in ppm to the low field side of $Si(CH_3)_4$ and the doublets near 6.57 and 7.7 are assigned to the protons in the five and six positions, respectively.

The ^{13}C NMR spectrum of maltol in C^2HCl_3 has been assigned by Kingsbury *et al*;[17] ^{13}C NMR data for maltol and those complexes sufficiently soluble in C^2HCl_3, $C^2H_2Cl_2$ or d_6-DMSO are given in Table 2. In the ^{13}C NMR spectra of catecholato,[1,2] catecholamine[3] and tropolonato[4] complexes it is found that the C atoms adjacent to the O-donor atoms (C-3 and C-4 in the case of maltol) normally shift downfield by some 10 ppm relative to their positions in the free ligand. Comparable shifts to lower field are indeed observed here for C-3 and C-4, but the shift for C-2 is unexpected.

Mass spectra. We have determined the mass spectra of $M(malt)_3$, (M = Fe, Ru, Rh), $Pd(malt)_2$, $MoO_2(malt)_2$ and $UO_2(malt)_2 \cdot MeOH$ using both electron impact (EI+) and fast-atom bombardment (FAB+) conditions where appropriate. The fragmentation patterns observed for the $M(malt)_3$ complexes are similar to those reported for $M'(trop)_3$ (M' = Al, Ga, In, Sc, Cr, Fe) by Charalambous,[18] by us for $M(trop)_3$ (M = Ru, Os, Rh, Ir)[4] and by Orvig for $Al(malt)_3$.[12] $[M(malt)_3]^+$ is observed and peaks characteristic of the products of step-wise ligand loss, as well as peaks suggesting fragmentation of coordinated maltol were observed in the spectra. The spectra of the oxo-maltolato complexes also indicated the successive loss of maltolato ligands.

Cyclic voltammetry. We have studied the electrochemical behaviour of several maltolato complexes using cyclic voltammetry. The most interesting and conclusive results were obtained from $Ru(malt)_3$ using both aqueous solutions of KCl and dichloromethane solutions of $^nBu_4NPF_6$ as supporting electrolytes. The voltammogram of $Ru(malt)_3$ at a Pt working electrode in 0.2 M $^nBu_4NPF_6$ in CH_2Cl_2 is shown in Fig. 2. There are two waves, representing two reversible one-electron steps; (oxidation: E_p^{ox} +0.48; E_p^{red} +0.38; reduction: E_p^{red} −1.35; E_p^{ox} −1.26 V). These results are similar to those of Tocher *et al.*,[19] for $Ru(acac)_3$ under comparable conditions.

(b) *SERS of maltolate and tropolonate species*

The mechanism of the SERS effect is still very much a matter of debate;[20] our intention here is to show that the technique is applicable to ligands of the complexes reported here, without, at this stage, attempting to make rigorous assignments of the spectra.

In Fig. 3(a)–(c) we give normal and SER spectra of maltolate and $Ru(malt)_3$ and in Fig. 4(a)–(d) the corresponding spectra of tropolonate and $Rh(trop)_3$ (we were unable to record the conventional Raman spectrum of $Ru(malt)_3$ because of its dark colour). The SER spectra were obtained at a pH of the sol (9.4) at which the monoanions of maltol (pK_a 8.67[10]) and tropolone (pK_a 6.42[21]) are likely to be the major species present in the bulk solution. In all cases, considerable SERS enhancement was obtained (enhancement factors of 10^4–10^5).

It is generally agreed that enhancement in the relative intensity of a SERS band compared to its intensity in a conventional Raman spectrum indicates that the vibrational mode corresponding to that band is intimately connected with the attachment of the adsorbed molecule to the metal

Table 1. Analytical and spectroscopic data for maltolato complexes

Compound	Analyses[a] C	Analyses[a] H	Vibrational spectra[b] (cm^{-1}) ν(C=O)	ν(C=O)+ν(C=C)		$\nu_s(MO_2)$	$\nu_{as}(MO_2)$	^{1}H NMR data[c] (ppm) CH_3	H-5	H-6	$J_{(5,6)}$ (Hz)
Maltol	—	—	1650	1610	1550			2.37	6.39d	7.63d	3.6
$Fe(malt)_3$	50.1	3.4	1600	1575	1500						
	(50.1)	(3.5)									
$Ru(malt)_3$	44.7	3.0	1600	1565							
	(45.4)	(3.2)									
trans-$OsO_2(malt)_2$	30.5	2.1	1610	1565	1540	890	855, 835		[d]		
	(30.5)	(2.1)				(891)					
$Rh(malt)_3$	44.5	3.1	1595	1550				2.54	6.73d	7.67d	5.0
	(45.2)	(3.2)									
$Pd(malt)_2$	40.1	2.8	1600	1565	1535			2.43	6.57m	7.70d	3.7
	(40.4)	(2.8)									
$[Pd(PPh_3)_2(malt)]BPh_4$	73.2	4.8	1595	1585	1540			2.50	6.50d	[e]	5.1
	(73.7)	(5.2)									
$[Pt(PPh_3)_2(malt)]BPh_4$[f]	56.8	4.0	1600	1575	1540			2.51	6.57d	[e]	4.8
	(57.3)	(4.0)									
cis-$MoO_2(malt)_2$	38.1	2.6	1625	1575	1510	940	905	2.53	6.62d	7.97d	3.5[g]
	(38.1)	(2.7)				(934, 924)	(904)				
trans-$UO_2(malt)_2 \cdot CH_3OH$	27.9	2.4	1605	1575	1545	850, 830	925	2.66	6.92d	8.42d	5.3[h]
	(28.3)	(2.6)				(846)					

[a] Calculated values in parentheses.
[b] Raman data in parentheses.
[c] Recorded at 90 MHz in C^2HCl_3. All NMR data quoted to low field of $Si(CH_3)_4$.
[d] Insufficiently soluble.
[e] Obscured by phenyl resonances.
[f] P = 4.2 (4.0)%.
[g] Recorded in $C^2H_2Cl_2$.
[h] Recorded in d_6-DMSO.

Table 2. ^{13}C NMR data for maltolato complexes

Compound	Chemical shift (ppm) C-2	C-3	C-4	C-5	C-6	C-7
Maltol[a]	148.9	142.6	172.1	113.2	154.3	13.8
Maltolate	152.6	150.0	178.4	111.3	150.7	13.4
$Rh(malt)_3$	160.6	155.8	186.9	111.9	151.2	14.8
		155.5	186.8	111.8		
$Pd(malt)_2$	159.7	155.6	185.6	111.5	151.7	14.1
		155.4	185.2	111.4		
$[Pd(PPh_3)_2(malt)]^+$	164(m)	158.3	[b]	112.1	153.2	14.6
$[Pt(PPh_3)_2(malt)]^+$	164(m)	158.7	[b]	112.7	153.9	13.9
cis-$[MoO_2(malt)_2]$[c]	155.1	153.3	178.3	111.5	156.6	15.1
trans-$[UO_2(malt)_2]$[d]	158.2	154.7	184.8	112.9	156.1	14.1

All spectra recorded at 250 MHz in C^2HCl_3; chemical shifts quoted to low field of $Si(CH_3)_4$.

[a] Reference 17.

[b] Not located.

[c] Recorded in $C^2H_2Cl_2$.

[d] Recorded in d_6-DMSO.

surface.[22] For maltolate, though there are no published assignments of its Raman spectrum, we tentatively assign the bands at 1609 and 1559 cm^{-1} to ν(C═O) and ν(C═C); the former is substantially enhanced and shifted to 1597 cm^{-1} in the SER spectrum, while the similarly enhanced latter band moves to 1555 cm^{-1} in the SER spectrum. This may indicate that the anion is attached to the Ag surface via one or both oxygen atoms adjacent to C-3 and C-4, with some attachment also by the (C-5 to C-6) double bond.

For tropolonate [Fig. 4(a), with its SER spectrum in 4(b)] the situation is clearer; the anion is planar and has C_{2v} symmetry, and the Raman spectrum

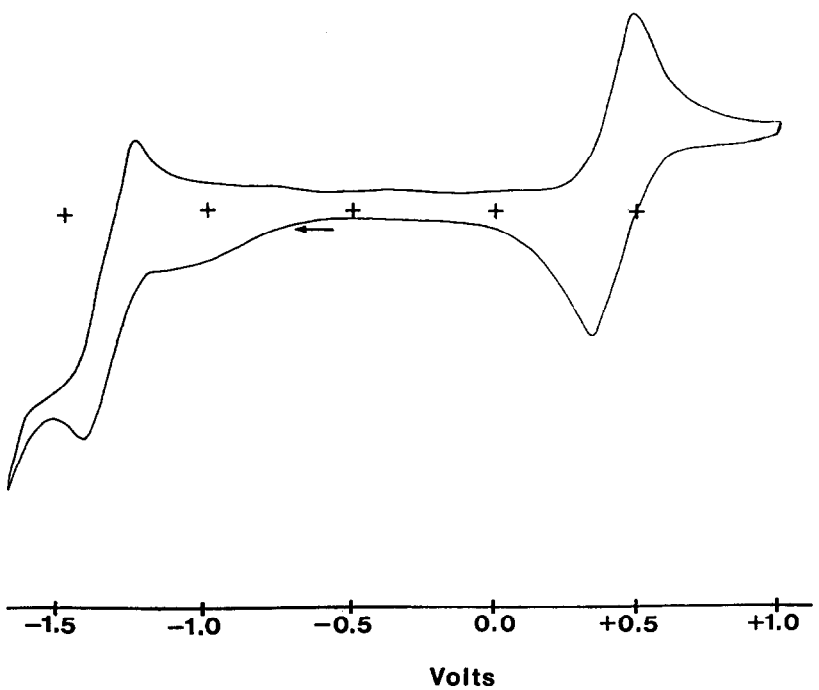

Fig. 2. Cyclic voltammogram of 1×10^{-3} M $Ru(malt)_3$ in a 0.2 M solution of $^nBu_4NPF_6$ in dichloromethane, using a platinum working electrode, silver reference electrode and measured at a scan speed of 100 mV s^{-1}.

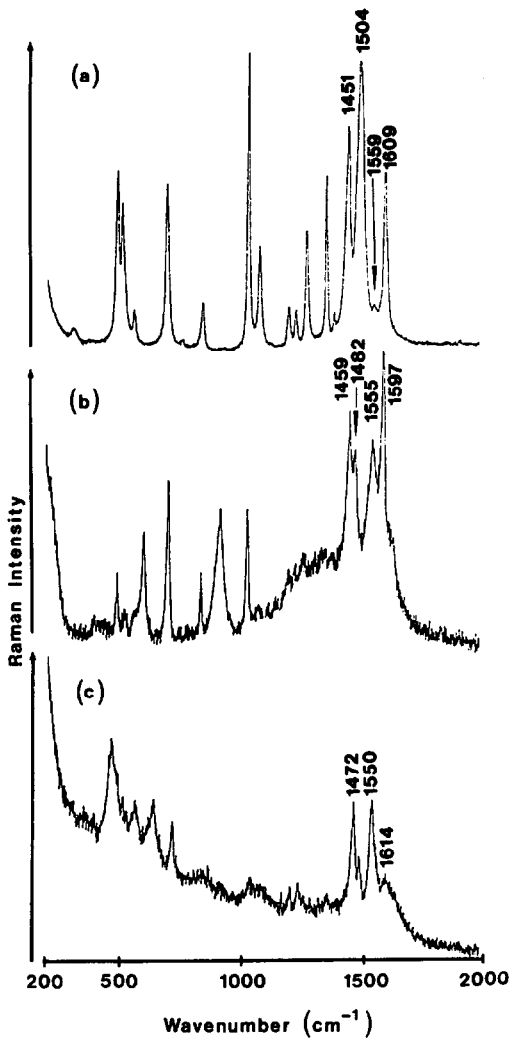

Fig. 3. (a) Conventional Raman spectrum of a 1 M solution of maltol in concentrated aqueous KOH (pH 13.4). (b) SER spectrum of maltol (1×10^{-4} M) on silver sol. (c) SER spectrum of $Ru(malt)_3$ (1×10^{-3} M) on silver sol.

of tropolone has been studied and assigned.[23] The ν(C═O) mode for tropolone has been assigned, using the IR spectrum of the ^{18}O-substituted compound, to a band at 1343 cm^{-1};[24] this is not enhanced in the SER spectrum. There is, however, strong enhancement of bands at 1593 and 1426 cm^{-1}; in tropolone the former has been assigned to a combination of ν(C═C) and ν(C═O), and the latter to a totally symmetric ring stretch. It thus seems possible that the major interaction between tropolonate and the silver surface involves the ring to a greater extent than the oxygen donor atoms; it may be the case that, as has been deduced for the SER spectrum of benzoate,[25] the ring lies parallel with or tilted towards the metal surface. For $Rh(trop)_3$, the most enhanced band occurs at 1435 cm^{-1}, suggesting that at least one of the coordinated ligands is tilted towards the silver plane.

EXPERIMENTAL

The complexes $Fe(malt)_3$[11] and $Pd(malt)_2$[16] were made by the literature methods.

Tris(maltolato) ruthenium (III), $Ru(malt)_3$

Ruthenium trichloride (0.26 g, 1 mmol) was dissolved in an aqueous solution of sodium acetate (0.93 g, 7 mmol, in 20 cm^3); the solution was warmed gently and maltol (0.65 g, 5 mmol) added. The black mixture was refluxed for 3 h, during which it became red and deposited a red solid which was filtered off and dried *in vacuo*. The filtrate was reduced in volume, yielding further crops of red product. Yield 45%.

*Bis(maltolato)*trans*(dioxo) osmium* (VI), $OsO_2(malt)_2$

An aqueous solution of potassium osmate (0.187 g, 0.5 mmol, in 15 cm^3) was filtered into a solution of maltol (0.13 g, 1 mmol) in ethanol (10 cm^3). The resultant green–brown solution was left to stand for 2 h, after which a fine brown precipitate was filtered off and dried *in vacuo*. Yield 25%.

Tris(maltolato) rhodium (III), $Rh(malt)_3$

Rhodium trichloride (0.15 g, 0.5 mmol) was added to a solution of sodium acetate (0.3 g, 2 mmol) in water (15 cm^3). The aqueous solution was heated gently while maltol (0.31 g, 2.5 mmol) was added with stirring, and the reaction mixture refluxed for 12 h, during which time it changed from red to orange and a yellow solid was deposited. The solid was filtered off and dried *in vacuo*. Yield 35%.

Bis(triphenylphosphine)mono(maltolato) palladium (II) *tetraphenylboronate*, $[(PPh_3)_2Pd(malt)]BPh_4$

A modification of the method for the preparation of Pd(II) catecholamine complexes, as developed by Gandolfi *et al.* was used.[14] All manipulations were carried out in an inert atmosphere and all solvents were degassed before use. To a suspension of maltol (0.07 g, 0.5 mmol) in toluene (5 cm^3), was added a methanolic solution of potassium hydroxide (0.033 g, 6 mmol, in 5 cm^3). The toluene–methanol solution was added to a solution of *cis*-$[PdCl_2(PPh_3)_2]$ (0.35 g, 0.5 mmol) in toluene (10 cm^3). The orange solution was stirred at ambient temperature for 1 h, after which it was filtered and

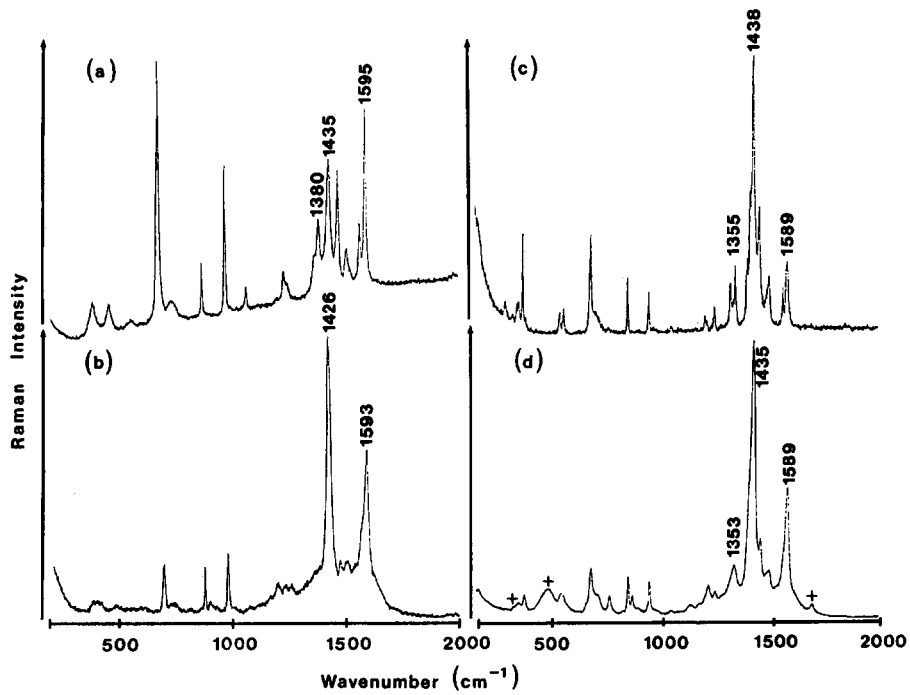

Fig. 4. (a) Conventional Raman spectrum of a 2 M aqueous solution of Na(trop) (pH 11.4). (b) SER spectrum of tropolone (1×10^{-4} M) on silver sol. (c) Conventional Raman spectrum of $Rh(trop)_3$ (KBr disc). (d) SER spectrum of an acetone solution of $Rh(trop)_3$ on silver sol (overall concentration of $Rh(trop)_3$ *ca* 1×10^{-3} M). + denotes bands due to acetone.

a solution of $Na(BPh_4)$ (0.17 g, 0.5 mmol) in ethanol (5 cm^3) was added to the filtrate, upon which yellow crystals readily precipitated. These were filtered off in air and dried *in vacuo*. Yield 55%.

Bis(triphenylphosphine)mono(maltolato) platinum (II) *tetraphenylboronate*, $[(PPh_3)_2Pt(malt)]BPh_4$

This was prepared via the intermediates $Pt(PPh_3)_4$ and $Pt(PPh_3)_2(O_2)$ using an adaptation of the route to $Pt(PPh_3)_2(cat)$.[26] All manipulations were carried out under nitrogen, and all solvents were degassed before use. A solution of maltol (0.12 g, 1 mmol) in ethanol (5 cm^3) was added to a solution of $[Pt(PPh_3)_2(O_2)]$ (0.8 g, 1 mmol) in toluene (10 cm^3) cooled in an ice-water bath. The yellow solution was stirred for 1 h, after which $Na(BPh_4)$ (0.34 g, 1 mmol) in ethanol (10 cm^3) was added. A fine yellow solid precipitated, which was filtered off in air and dried in a stream of nitrogen. Yield 40%.

*Bis(maltolato)*cis(*dioxo*) *molybdenum* (VI), $MoO_2(malt)_2$

The method used was similar to that described for the preparation of $MoO_2(trop)_2$.[4] A solution of maltol (0.25 g, 2 mmol) in ethanol (10 cm^3) was mixed with an aqueous solution of ammonium molybdate (0.19 g, 1 mmol, in 10 cm^3). A precipitate formed at once, and after 1 h the yellow crystalline product was filtered off and dried *in vacuo*. Yield 65%.

*Bis(maltolato)*trans(*dioxo*) *uranium* (VI), $UO_2(malt)_2 \cdot CH_3OH$

Uranyl sulphate trihydrate (0.42 g, 1 mmol) was dissolved in methanol (20 cm^3) and mixed with a solution of maltol (0.25 g, 2 mmol) in methanol–water (15 cm^3, 2:1). The colour of the solution changed at once from yellow to red, and on standing, the solution yielded orange crystals, which were filtered off and dried *in vacuo*. Yield 40%.

SERS samples

Silver colloids were prepared from aqueous solutions of silver nitrate and sodium borohydride as described by Creighton *et al.*[7] (λ_{max} = 392 nm, pH *ca* 9.2–9.4). Samples for SERS were freshly prepared and run within 2 h of preparation. They were made up as follows:

Maltol/maltolate. An aqueous 0.002 M solution of maltol was added to silver sol in order to give an

overall substrate concentration of 1×10^{-4} M. Slow aggregation of the colloid resulted.

$Ru(malt)_3$. A 0.002 M aqueous solution of $Ru(malt)_3$ was added to silver sol, giving a resultant $Ru(malt)_3$ concentration of 1×10^{-4} M. Aggregation was very slow, with the sample reaching the red intermediate stage of aggregation after several hours.

Tropolone/tropolonate. Addition of 0.002 M aqueous tropolone solution to silver sol to achieve a final tropolone concentration of 1×10^{-4} M resulted in very rapid aggregation, with the sample turning blue within a few minutes.

$Rh(trop)_3$. Because of the negligible water solubility of this complex, a 0.01 M solution of $Rh(trop)_3$ in acetone was added to silver sol so as to give a resultant $Rh(trop)_3$ concentration of *ca* 1×10^{-3} M. Aggregation was slow, but the sample reached the blue stage after several hours.

All Raman spectra were measured at 150 mW using the 5145 A line of an Innova 70 CRL argon ion laser with a Spex Ramalog V instrument and Spex Datamate data acquisition unit. Solution samples were run in unsealed capillary tubes. IR spectra were measured on a Perkin–Elmer 1720 Fourier transform spectrometer. ^1H NMR spectra were measured on a JEOL FX 90Q Fourier-transform spectrometer, and ^{13}C NMR spectra on a Bruker WM250 Fourier-transform spectrometer. Cyclic voltammograms were measured with an Oxford Electrodes PVSU potentiostat and Houston Instruments Omnigraphic 2000 recorder. Mass spectra were run by the Organic Mass Spectroscopy Laboratory, Imperial College. Microanalyses were carried out by Mr K. I. Jones of the Microanalytical department, Imperial College.

Acknowledgements—We thank Miss Sue Johnson for the ^{13}C NMR spectra, and Dr Eric Waite and Dr Judy Challis for mass spectra. One of us (S.J.G.) thanks the S.E.R.C. for a grant. We acknowledge loans of platinum metals from Johnson Matthey Ltd.

REFERENCES

1. A. J. Nielson and W. P. Griffith, *J. Chem. Soc., Dalton Trans.* 1978, 1501.
2. W. P. Griffith, C. A. Pumphrey and T. A. Rainey, *J. Chem. Soc., Dalton Trans.* 1986, 1125.
3. A. M. El-Hendawy, W. P. Griffith and C. A. Pumphrey, *J. Chem. Soc., Dalton Trans.* 1988, 1817.
4. W. P. Griffith, C. A. Pumphrey and A. C. Skapski, *Polyhedron* 1987, **6**, 891.
5. S. J. Greaves and W. P. Griffith, *J. Raman Spec.*, in press.
6. M. Fleischmann, P. J. Hendra and A. J. McQuillan, *Chem. Phys. Lett.* 1974, **26**, 163.
7. J. A. Creighton, C. G. Blatchford and M. G. Albrecht, *J. Chem. Soc., Faraday Trans. 2* 1979, **75**, 790.
8. M. Kerker, O. Siiman, L. A. Bumm and D. S. Wang, *Appl. Optics* 1980, **19**, 3253; M. Kim and K. Itoh, *J. Phys. Chem.* 1987, **91**, 126; H. Yamada, H. Nagata and H. Teranishi, *J. Phys. Chem.* 1986, **90**, 2384; T. H. Joo, M. S. Kim and K. Kim, *J. Mol. Struct.* 1987, **160**, 81.
9. K. Kneipp, H. Kneipp and E. Dinjus, *Chem. Phys. Lett.* 1986, **126**, 69.
10. C. Gerard and R. P. Hugel, *J. Chem. Res.* M 1980, 3927; N. K. Dutt and U. M. Sharma, *J. Inorg. Nucl. Chem.* 1975, **37**, 1801.
11. C. Gerard, *Bull. Soc. Chim. France* 1979, **I**, 451.
12. M. M. Finnegan, S. J. Rettig and C. Orvig, *J. Am. Chem. Soc.* 1986, **108**, 5033; M. M. Finnegan, T. G. Lutz, W. O. Nelson, A. E. Smith and C. Orvig, *Inorg. Chem.* 1987, **26**, 2171.
13. C. Chiacchierini, J. Havel and L. Sommer, *Coll. Czech. Chem. Commun.* 1968, **33**, 4240.
14. O. Gandolfi and J. Blum, *Inorg. Chim. Acta* 1983, **80**, 103.
15. S. D. Kushch, E. N. Izakovich, O. S. Roshchunkina, V. M. Nichvoloda and M. L. Khidekel, *Bull. Acad. Sci. USSR. Div. Chem. Sci.* 1981, 681.
16. H. Morita, H. Sakurai, S. Shimomura and S. Kawaguchi, *Trans. Met. Chem.* 1977, **2**, 210.
17. C. A. Kingsbury, M. Clifton and J. H. Looker, *J. Org. Chem.* 1976, **41**, 2777.
18. J. Charalambous, *Inorg. Chim. Acta* 1976, **18**, 241.
19. J. H. Tocher and J. P. Fackler, *Inorg. Chim. Acta* 1985, **102**, 211.
20. S. Efrima, *Mod. Aspects Electrochem.* 1985, **16**, 253; C. Murray, *Adv. Laser Spect.* 1986, **3**, 49; M. Kerker, *Phys. Chem. Colloids Macromol., Proc. Int. Symp.* 1984, pp. 59–66 (1987).
21. Y. Oka, M. Umehara and T. Nozoe, *Nippon Kagaku Zasshi* 1962, **83**, 1197.
22. M. Moskovits and J. S. Suh, *J. Phys. Chem.* 1984, **88**, 1293.
23. Y. Ikegami, *Bull. Chem. Soc. Japan* 1963, **36**, 1118; R. L. Redington and T. E. Redington, *J. Mol. Spectrosc.* 1979, **78**, 229.
24. H. Junge, *Spectrochim. Acta* 1968, **24A**, 1957.
25. M. Paganonne, B. Fornari and G. Mattei, *Spectrochim. Acta* 1987, **43A**, 621.
26. S. Muto, K. Tasaka and Y. Kamiya, *Bull. Chem. Soc. Japan* 1977, **50**, 2493.

Polyhedron Vol. 7, No. 19/20, pp. 1981–1989, 1988
Printed in Great Britain

0277–5387/88 $3.00+.00
© 1988 Pergamon Press plc

ALKENE–GLYCOL INTERCONVERSION WITH TECHNETIUM AND RHENIUM OXO COMPLEXES

RONALD M. PEARLSTEIN and ALAN DAVISON*

Department of Chemistry, Massachusetts Institute of Technology, Cambridge, MA 02139, U.S.A.

Abstract—The trioxotechnetium(VII) complexes $TcO_3Cl(AA)$ (AA = phen, bpy, 5-NO_2-phen, 3,4,7,8-Me_4-phen) cleanly oxidize olefins (C_2R_4) in solution at 22°C, forming in high yields the corresponding oxotechnetium(V) diolate complexes, $TcOCl(OCR_2CR_2O)(AA)$. The complexes have been characterized by ^1H NMR, IR, elemental analysis, and fast atom bombardment mass spectrometry. The free diols isolated by hydrolysis of these diolate complexes with HCl were shown by capillary gas chromatography to represent *syn* addition of the two hydroxyl groups across the double bond. The related rhenium complex, $ReOCl(OCH_2CH_2O)$(phen) undergoes the reverse reaction when thermalized, releasing ethylene and producing ReO_3Cl(phen).

All of the transition metal species known to effect the *cis*-dihydroxylation of olefins (i.e. OsO_4, RuO_4 and MnO_4^-) are tetrahedral tetraoxides.[1] Although alkaline permanganate is capable of oxidizing alkenes to *cis*-1,2-diols, the reaction conditions must be carefully controlled to prevent over-oxidation.[2] No such activity has been demonstrated with the heavier group seven species pertechnetate (TcO_4^-) and perrhenate (ReO_4^-). A few examples of the reverse reaction, the conversion of a coordinated vicinal diolate into an olefin, have been reported with the third row elements tungsten[3] and rhenium.[4] This paper describes the oxidation of olefins to the corresponding diolates with the trioxotechnetium(VII) complexes $TcO_3Cl(AA)$ (AA = phen, bpy, Me_4-phen, NO_2-phen) and the thermal decomposition of the oxorhenium(V) diolate ReOCl(phen)(eg) (eg = 1,2-ethanediolate) into ReO_3Cl(phen) and ethylene.

EXPERIMENTAL

Instrumentation

Fourier transform IR spectra were measured from 4800 to 400 cm^{-1} on an IBM IR/30S spectrometer with DTGS detector and 2 cm^{-1} bandwidth. ^1H NMR spectra were recorded at 250 MHz on a Bruker WM-250, or at 300 MHz on a Varian XL-300.

Fast atom bombardment mass spectra were measured on samples dissolved in a 3-nitrobenzyl alcohol matrix using a MAT 731 mass spectrometer operating at an accelerating voltage of 8 kV. The source was equipped with an Ion Tech B11N FAB gun producing a beam with 6–8 keV xenon neutrals.

UV and visible absorption spectra were recorded on a Hewlett Packard 8451A photodiode array spectrophotometer. Elemental analyses were performed by Atlantic Microlab Inc., Norcross, GA.

Gas chromatography was performed using a HP-5890A capillary gas chromatograph equipped with a flame ionization detector. Separation of diols was performed with a 28.5 m long, 0.317 mm ID J&W fused silica column supporting a 0.25 μ film of DB-5 (5% phenylmethyl silicone). The temperature programmer held the column at 50°C for 4 min then ramped at 8° min^{-1} to a maximum temperature of 250°C.

Syntheses

Caution! ^{99}Tc is a β^- emitter ($t_{1/2} = 2.1 \times 10^5$ y). All manipulations of solutions and solids were performed in a laboratory approved for the handling of radioisotopes using precautions outlined elsewhere.[5]

All solvents were of at least reagent grade and were used as received unless otherwise noted. Dichloromethane, preserved with 70 ppm of isopentene, was stirred overnight with concentrated H_2SO_4, washed with saturated aqueous Na_2CO_3,

* Author to whom correspondence should be addressed.

and predried over anhydrous $CaCl_2$. It was then distilled under N_2 from P_4O_{10} and stored in the dark under N_2. Water was passed through a Barnstead Ultrapure ion-exchange column and distilled using a Corning AG-1 glass still. TcO_3Cl(phen) and TcO_3Cl(bpy) were prepared by the method of Davison *et al.*[6] $(Ph_4As)[ReOCl_4]$ was prepared by the method of Cotton and Lippard.[7] Styrene (Aldrich, 99+%, stabilized with 10–15 ppm ^{t}Bu–catechol) was vacuum distilled (b.p. 45–48°C) using a vacuum insulated, glass bead packed column. Dibutyl fumarate was prepared by condensation of ^{n}BuOH (Mallinckrodt) with fumaryl chloride (Aldrich, 95%) in Et_2O using pyridine to scavenge generated HCl.

Preparation of $TcO_3Cl(5\text{-}NO_2\text{-}phen)$

To 0.109 g 5-nitro-1,10-phenanthroline (G. F. Smith) was added 10 cm^3 MeOH. The ligand was dissolved by gentle heating and the resulting solution cooled to ambient temperature before adding 0.5 cm^3 of 0.385 M $(NH_4)[TcO_4]$ (0.193 mmol). The solution was stirred and 1.5 cm^3 concentrated HCl was added dropwise. An olive-green precipitate formed almost immediately. After cooling the reaction mixture to −20°C, the product was collected on a medium porosity fritted glass funnel. After washing well with MeOH, the product was dried *in vacuo* overnight. Yield: 77.90 mg, 99%. Found: C, 35.8; H, 1.94; Cl, 8.8; N, 10.6. Calc. for $C_{12}H_7ClN_3O_5Tc$: C, 35.4; H, 1.7; Cl, 10.3; N, 10.3%. IR (KBr): 3057 cm^{-1} (w), 3086(w), 1535(s), 1516(s), 1489(w), 1456(w), 1430(m), 1419(m), 1386(m), 1354(m), 1330(s), 1297(w), 1254(w), 1222(w), 1202(w), 1180(w), 1149(w), 1119(w), 899(vs), 872(s), 839(m), 824(m), 756(m), 737(w), 721(m), 654(w). FABMS(+): *m/z* 373 $(M+H-Cl)^+$, 357 $(M+H-Cl-O)^+$, 340 $(M-Cl-2O)^+$.

Preparation of $TcO_3Cl(3,4,7,8\text{-}Me_4\text{-}phen)$

0.109 g of 3,4,7,8-tetramethyl-1,10-phenanthroline (G. F. Smith) was dissolved in 15 cm^3 EtOH. To the resulting solution was added 0.5 cm^3 of 0.3 M $(NH_4)[TcO_4]$ followed by 1.5 cm^3 of concentrated HCl. A white precipitate (presumably Me_4-phen·HCl) formed immediately and became yellow after stirring overnight. The mixture was filtered on a fritted glass funnel and rinsed well with MeOH, EtOH and acetone, then dried *in vacuo* overnight. Yield: 32.66 mg, 52%. IR (KBr): νTc=O 892 cm^{-1}(s), 874(m).

Reaction of TcO_3Cl(AA) *with alkenes in* CH_2Cl_2

Preparation of TcOCl(DL-4,5-*octanediolate*)(*phen*). Into a 50 cm^3 Erlenmeyer flask was added 0.38 g of *trans*-4-octene (3.39 mmol), 40 cm^3 of purified CH_2Cl_2, and 76.67 mg of chlorotrioxo(1,10-phenanthroline)technetium(VII) (0.212 mmol). The resulting yellow slurry was magnetically stirred vigorously for approximately 30 min. The reaction mixture became a homogeneous green solution which was filtered through a medium porosity fritted glass disc. After adding 20 cm^3 of *n*-heptane to the filtrate, the solution was concentrated by rotary evaporation until precipitation commenced. Further precipitation was effected by chilling to −20°C. The green microscrystalline precipitate was isolated on a medium porosity fritted glass funnel and rinsed with *n*-heptane and *n*-hexane, then dried *in vacuo* overnight. Yield: 72.01 mg, 72%. Found: C, 50.0; H, 5.1; Cl,. 7.4; N, 5.9. Calc. for $C_{20}H_{24}ClN_2O_3Tc$: C, 50.6; H, 5.1; Cl, 7.5; N, 5.9%. IR (KBr): 3052 cm^{-1}(w), 2957(w), 2929(w), 2902(w), 2870(w), 1518(w), 1464(w), 1457(w), 1425(m), 1413(w), 1223(w), 1069(w), 990(w), 944(s), 911(w), 873(w), 856(m), 779(w), 739(w), 725(s), 693(w), 680(w), 662(w), 649(w). ^{1}H NMR ($CDCl_3$): δ 10.39 (dd, integral = 8), 10.17 (dd, 5), 9.01 (m, 12), 8.42 (dd, 12), 8.33 (m, 11), 7.94 (m, 13), 7.90 (s, 20), 7.63 (m, 12), 5.77 (m, 7), 5.02 (q, 4), 4.78 (q, 4), 4.19 (m, 7), 2.6–0.7 (^{n}Pr multiplets, 165). UV–vis (CH_2Cl_2): λmax(ε) 270 nm(29,700 l mol^{-1} cm^{-1}), 320(sh), 440(3,000), 640(46), 820(41). FABMS(+): *m/z* [ion, abundance]: 913 $[(2M-Cl)^+$, 3.4%], 894 $[(2M+O-2Cl)^+$, 9.4%], 474 $[M^+$, 5.6%], 439 $[(M-Cl)^+$, 100%], 330 $[(M-octanediolate)^+$, 60%], 327 $[(M-Cl-octene)^+$, 52%].

Preparation of TcOCl(meso-4,5-*octanediolate*)(*phen*). Using the procedure above but reacting 78.68 mg of TcO_3Cl(phen) (0.217 mmol) and 0.42 g of *cis*-4-octene. Yield: 64.0 mg, 70%. IR (KBr): νTc=O 951 cm^{-1}. ^{1}H NMR ($CDCl_3$): δ 10.33 (dd, integral = 18), 10.24(d, 10), 8.99(dd, 32), 8.42(dd, 33), 8.33(dd, 34), 7.95(m, 30), 7.89(s, 64), 7.7–7.5(overlapping multiplets, 29), 5.98(m, 19), 5.36(m, 32), 4.82(m, 11), 2.4–0.6(^{n}Pr multiplets, ~ 640). FABMS(+): *m/z* 439 $(M-Cl)^+$.

Preparation of TcOCl(DL-4,5-*octanediolate*)(5-NO_2-*phen*). Using the procedure above but reacting 23.78 mg of $TcO_3Cl(5\text{-}NO_2\text{-phen})$ (0.058 mmol) and 0.25 g of *cis*-4-octene. Yield: 18.6 mg, 61%. Found: C, 46.3; H, 4.5; Cl, 6.7; N, 8.1. Calc. for $C_{20}H_{23}ClN_3O_5Tc$: C, 46.2; H, 4.5; Cl, 6.8; N, 8.1%. IR (KBr): νTc=O 956 cm^{-1}. ^{1}H NMR ($CDCl_3$): δ 10.60(m, integral = 6), 10.37(m, 4), 9.2(overlapping multiplets, 21), 8.86(m, 9), 8.63(d,

6), 8.54(m, 4), 8.1(m, 11), 7.8(m, 11), 5.76(m, 8), 4.96(m, 4), 4.72(m, 4), 4.18(m, 8), 2.6–0.6(ⁿPr multiplets, ~ 136). UV–vis (CH_2Cl_2): λmax(ε) 234 nm(27,000 1 mol^{-1} cm^{-1}), 276(32,000), 305(sh), 315(sh), 330(sh), 474(3,300). FABMS(+): *m/z* 484 $(M-Cl)^+$.

Preparation of TcOCl(meso-*dibutyltartrate*)(*phen*). Using the procedure above but reacting 61.34 mg of TcO_3Cl(phen) (0.169 mmol) and 0.26 g of dibutyl maleate (Aldrich, 90%). Yield: 61.18 mg, 61%. IR (KBr): νTc=O 953 cm^{-1}, νC=O 1740 cm^{-1}. ^1H NMR ($CDCl_3$): δ 10.28(m, integral = 5), 10.08(dd, 8), 9.48(m, 8), 8.95(td, 5), 8.51(dd, 13), 8.37(m, 13), 7.97(overlapping multiplets, 38), 7.64(m, 14), 6.7(methine, 5), 6.0–5.5(methine, 21), 4.5–3.8(α-methylene, 56), 1.9–1.1(methylene, 110), 1.1–0.7(methyl, 60). FABMS (+): *m/z* [ion, abundance]: 555 $[(M-Cl)^+$, 100%], 460 $[(M-(C_4H_9)_2O)^+$, 8%], 425 $[(M-Cl-(C_4H_9)_2O)^+$, 36%], 327 $[(M-Cl-C_{12}H_{20}O_4)^+$, 5%].

Preparation of TcOCl(DL-*dibutyltartrate*)(*phen*). Using the procedure above but reacting 32.64 mg of TcO_3Cl(phen) (0.090 mmol) and 0.23 g dibutyl fumarate. Yield: 21.94 mg, 41%. IR (KBr): νTc=O 960 cm^{-1}, νC=O 1739 cm^{-1}. ^1H NMR ($CDCl_3$): δ 10.15(dd, integral = 10), 10.04(dd, 15), 9.47(dd, 15), 8.91(dd, 10), 8.47(dd, 24), 8.34(m, 24), 7.94(m, 25), 7.90(s, 46), 7.63(m, 28), 6.61(d, 11), 5.49(d, 11), (AB q: $\delta_A = 5.63$, $\delta_B = 5.53$, $J_{AB} = 7.7$ Hz, integral = 24), 4.5–3.8 (α methylene, 97), 2.0–1.1(methylene, 217), 1.1–0.5 (methyl, 126).

Preparation of TcOCl(DL-5,6-*decanediolate*)(3,4,7,8-Me_4-*phen*). Using the procedure above but reacting 13.75 mg of TcO_3Cl(3,4,7,8-Me_4-phen) (0.033 mmol) and *trans*-5-decene. Yield: 11.5 mg, 63%. IR (KBr): νTc=O 939 cm^{-1}. ^1H NMR ($CDCl_3$): δ 10.07(s, integral = 9), 9.88(s, 6), 8.98(s, 3), 8.74(s, 3), 8.70(s, 9), 8.14(s, 3), 7.98(s, 23), 5.74(m, 8), 5.02(m, 3), 4.79(m, 3), 4.20(m, 7), 2.9–2.3(methyl singlets, 150), 2.3–0.7 (ⁿBu multiplets, 200).

Reaction of TcO_3Cl(AA) *with alkenes in acetone*

Preparation of TcOCl(*phenyl*-1,2-*ethanediolate*)(*phen*). To 1 cm^3 styrene combined with 1 cm^3 acetone was added 50.66 mg of chlorotrioxo(1,10-phenenthroline)technetium(V) (0.140 mmol). After 20 min, 15 cm^3 CH_2Cl_2 was added to the resulting yellow–green slurry to dissolve the product. The solution was filtered through paper then concentrated by evaporation. To the filtrate was added hexane until precipitation was incipient. After chilling to −20°C, a precipitate formed which was filtered in a fritted glass funnel and washed with hexane. The product was dried *in vacuo* overnight yielding 48.05 mg, 74% of the green microscrystalline product. Found: C, 51.1; H, 3.5; Cl, 7.7; N, 6.0. Calc. for $C_{20}H_{16}ClN_2O_3Tc$: C, 51.5; H, 3.5; Cl, 7.6; N, 6.0%. IR (KBr): 3056 cm^{-1}(w), 2903(w), 2845(w), 1629(w), 1605(w), 1579(w), 1520(m), 1490(w), 1452(w), 1429(s), 1305(w), 1226(w), 1142(w), 1110(w), 1082(w), 1025(w), 1013(m), 999(m), 948(s), 916(m), 873(w), 856(m), 847(s), 806(w), 761(w), 740(w), 724(s), 703(m), 685(m), 649(m), 631(w), 595(w), 586(w), 575(w), 508(w), 445(w). ^1H NMR ($CDCl_3$): δ 10.42, 10.40 (2 overlapping dd, integral = 11), 10.14(d, 4), 9.13(m, 11), 9.06(dd, 4), 8.86(d, 3), 9.0–8.3(m, 30), 8.1–7.8(m, 49), 7.8–7.6(m, 13), 7.55–7.3(m, 28), 7.20(s, 36), 6.9(dd, 5), 6.42(dd, 3), 6.21(dd, 7), 6.0(2 overlapping dd, 4), 5.85(dd, 5), 5.74(dd, 4), 5.48(2 overlapping dd, 8), 5.09(dd, 3), 4.86(dd, 3), 4.31(t, 4). FABMS(+): *m/z* [ion, abundance]: 467 $[(M+H)^+$, 3%], 431 $[(M-Cl)^+$, 100%], 330 $[(M+H-$styrenediolate$)^+$, 41%], 327 $[(M+H-Cl-$styrene$)^+$, 16%].

Preparation of TcOCl(1,2-*cyclohexanediolate*)(*bpy*). Using the procedure above but by reacting 13.29 mg of TcO_3Cl(bpy) (0.039 mmol) and cyclohexene (MC/B). Yield: 5.0 mg, 30%. IR (KBr): νTc=O 949 cm^{-1}. FABMS(+): *m/z* [ion, abundance]: 420 $[M^+$, 3%], 385 $[(M-Cl)^+$, 100%].

Preparation of TcOCl(*phenyl*-1,2-*ethanediolate*)(*bpy*). Using the procedure above but by reacting 9.14 mg of TcO_3Cl(bpy) (0.027 mmol) and distilled styrene. Yield: 5.07 mg, 42%. IR (KBr): νTc=O 952 cm^{-1}. FABMS(+): *m/z* [ion, abundance]: 849 $[(2M-Cl)^+$, 3%], 830 $[(2M-2Cl+O)^+$, 0.4%], 443 $[(M+H)^+$, 4%], 407 $[(M-Cl)^+$, 100%], 306 $[(M-$styrenediolate$)^+$, 45%], 303 $[(M-Cl-$styrene$)^+$, 26%], 287 $[(M-Cl-$styrene$-O)^+$, 39%].

Preparation of TcOCl(DL-*diphenyl*-1,2-*ethanediolate*)(*phen*). Using the procedure above but by reacting 24.66 mg of TcO_3Cl(phen) (0.068 mmol) and *trans*-stilbene (Aldrich, 96%). Yield: 18.19 mg, 49%. IR (KBr): νTc=O 947 cm^{-1}. ^1H NMR ($CDCl_3$): δ 10.5(d), 9.3(d), 8.5(d), 7.9(m), 7.6–6.6 (overlapping multiplets), 6.7(d), 5.2(d).

Preparation of TcOCl(meso-*diphenyl*-1,2-*ethanediolate*)(*phen*). Using the procedure above but by reacting 28.54 mg of TcO_3Cl(phen) (0.079 mmol) and *cis*-stilbene (Aldrich 97%). Yield: 16.65 mg, 39%. Found: C, 56.5; H, 4.0; Cl, 6.5. Calc. for $C_{26}H_{20}ClN_2O_3Tc$: C, 57.5; H, 3.7; Cl, 6.5%. FABMS(+): *m/z* [ion, abundance]: 543 $[(M+H)^+$, 4%], 507 $[(M-Cl)^+$, 100%], 330 $[(M-$stilbenediol$)^+$, 82%], 327 $[(M-Cl-$stilbene$)^+$, 16%], 543 $[(M-Cl-$stilbene$-O)^+$, 66%]. ^1H NMR ($CDCl_3$): δ 10.24(dd, 1H), 9.14(dd, 1H), 8.45(overlapping multiplets, 2H), 7.93(overlapping multiplets, 3H), 7.70(dd, 1H), 7.45(d, $J = 6.1$ Hz,

1H), 7.3–6.9(overlapping multiplets, ~ 10H), 6.62(d, $J = 6.2$ Hz, 1H).

Preparation of TcOCl(DL-5,6-*decanediolate*)(*phen*). Using the procedure above but by reacting 46.2 mg of TcO_3Cl(phen) (0.127 mmol) and 5-decene (Aldrich, 99+%). Yield: 49.1 mg, 77%. Found: C, 52.4; H, 5.6; Cl, 7.1; N, 5.6. Calc. for $C_{22}H_{28}ClN_2O_3Tc$: C, 52.5; H, 5.7; Cl, 7.0; N, 5.6%. IR (KBr): νTc=O 948 cm^{-1}. ^1H NMR ($CDCl_3$): δ 10.38(dd, integral = 6), 10.18(dd, 3), 9.02(dd, 10), 8.41(dd, 10), 8.33(dd, 10), 7.95(m, 10), 7.89(s, 18), 7.63(m, 12), 5.78(m, 6), 5.04(q,3), 4.78(q, 3), 4.20(m, 7), 2.5–0.7 (^{n}Bu multiplets, 180). UV–vis (CH_2Cl_2): λmax(ε) 270 nm(32,100 dm^3 mol^{-1} cm^{-1}), 444(3000), 628(70), 810(60). FABMS(+): *m/z* [ion, abundance]: 503 [$(M+H)^+$, 0.6%], 467 [$(M-Cl)^+$, 100%], 409 [$(M+Cl-C_4H_{10})^+$, 1%], 330 [(M−decanediolate)$^+$, 27%], 327 [(M−Cl−decene)$^+$, 10%].

Reaction of TcO_3Cl(AA) *with gaseous alkenes*

Preparation of TcOCl(*eg*)(*phen*). To 18 cm^3 of CH_2Cl_2 in a 20 cm^3 disposable vial was added 34.59 mg of chlorotrioxo(1,10-phenanthroline)technetium(VII) (0.095 mmol). Ethylene (Matheson, C.P. grade) was gently bubbled through the solution for approximately 1 h, periodically adding dichloromethane to compensate for evaporative losses, until the solution became clear green. Heptane was added and the solution was concentrated under vacuum until a green microcrystalline precipitate appeared. Yield: 28.33 mg, 76%.

The product is spectroscopically identical to the crystallographically characterized material prepared by the reaction of $[TcOCl_4]^-$ with $HOCH_2CH_2OH$ and phen.[8]

Preparation of TcOCl(1,1-*dimethyl*-1,2-*ethanediolate*)(*phen*). Into a 100 cm^3 round bottomed flask with a side-arm and stopcock was added 20 cm^3 of acetone and 29.58 mg of chlorotrioxo(1,10-phenanthroline)technetium(VII) (0.082 mmol). The flask was then sealed with a latex balloon and isobutylene (Matheson, C.P.) was admitted through the side-arm. The balloon was filled and deflated twice to purge the air trapped in the system. The balloon was once again filled and the solution stirred rapidly. The dissolution of isobutylene in the acetone solution was enhanced by chilling the flask in a salt–ice–water bath until the balloon had completely collapsed. The solution was stirred at ambient temperature for two additional hours, by which time the solution had become clear green. The solvent was removed at reduced pressure and the residue was recrystallized from CH_2Cl_2–hexane. IR (KBr): νTc=O 948 cm^{-1}. ^1H NMR ($(CD_3)_2CO$): δ 10.29 (dd), 10.11 (dd), 8.95 (dd), 8.80 (dd), 8.70 (dd), 8.19 (m), 7.85 (m), (AB: $\delta_A = 5.80$, $\delta_B = 5.53$, $J = 11.0$ Hz), (AB q: $\delta_A = 4.91$, $\delta_B = 4.78$, $J_{AB} = 10.5$ Hz), 1.53 (s), 1.29 (s), 1.17 (s), 1.05 (s). FABMS(+): *m/z* 383 $(M-Cl)^+$.

Preparation of TcOCl(*vinyl*-1,2-*ethanediolate*)(*phen*). Using the procedure above, but substituting 1,3-butadiene (Matheson, C.P.) for the isobutylene, 8.42 mg of TcO_3Cl(phen) (0.023 mmol) was converted to the corresponding diolate complex. IR (KBr): νTc=O 951 cm^{-1}. ^1H NMR ($CDCl_3$): δ 10.5–7.5(aromatic protons, integral = 69), 6.6–4.1(olefinic and aliphatic protons, integral = 47). Ratio of aromatic to others, 8:5.4; calc. for TcOCl(vinyl-1,2-ethenediolate)(phen), 8:6. FABMS(+): *m/z* 381 $(M-Cl)^+$.

One pot reaction from pertechnetate

Preparation of TcOCl(DL-4,5-*octanediolate*)(*phen*). To 20 cm^3 of anhydrous EtOH in a 50 cm^3 Erlenmeyer flask was dissolved 0.28 g of 1,10-phenanthroline monohydrate (1.41 mmol) followed by 0.5 cm^3 of 0.42 M $(NH_4)[TcO_4]$ (0.21 mmol). To the stirred solution was added 3 cm^3 of conc. HCl. After 1 min, 0.6 g of *trans*-4-octene was added followed by sufficient CH_2Cl_2 and water to form two phases. The green organic layer was separated and the aqueous layer was discarded. The organic layer was washed with two portions of dilute HCl, then dried over anhydrous Na_2SO_4. After filtration, the solvent was removed at reduced pressure leaving small green crystals suspended in a colourless oil. The product was isolated by adding Et_2O, then filtering on a fritted glass funnel. The product was washed with additional Et_2O and dried *in vacuo* overnight. Yield: 40.16 mg, 40%.

Hydrolysis reactions

Preparation of 4,5-*octanediols*. Into a stirred mixture of 30 cm^3 of Et_2O and 10 cm^3 of conc. HCl in a 100 cm^3 Erlenmeyer flask was added 57.41 mg chlorooxo(DL-4,5-octanediolato)(1,10-phenanthroline)technetium(V) (0.121 mmol). The colour rapidly changed from green to bright yellow. The yellow solid was removed by filtration through paper. The precipitate was determined to be $TcOCl_3$(phen) by its IR spectrum, νTc=O 978 cm^{-1} (lit. 977 cm^{-1}). The two phases of the filtrate were separated, saving the organic layer then drying it with $MgSO_4$.* The drying agent was removed by filtration and the filtrate was evaporated to a colourless oil. Yield ~ 7 mg, 40%. A similar

* Other drying agents, such as Na_2SO_4 or K_2CO_3 were subsequently determined to be preferable.

hydrolysis reaction was performed for the *meso* isomer.

Preparation of phenyl-1,2-ethanediol. Hydrolysis was carried out as above, but reacting 15.36 mg of TcOCl(OCHPhCH$_2$O)(phen) (0.033 mmol). The product was purified by vacuum sublimation at 100°C. ^{1}H NMR ($CDCl_3$): δ 7.37 (m, 5H), 4.84 (dd, 1H), 3.76 (dd, 1H), 3.68 (dd, 1H), 2.5 (broad, ~ 1H), 1.26 (s, ~ 1H). EIMS(+) 20°C, 30 eV; *m/z* [ion, abundance]: 138 [$(M)^+$, 39%], 120 [$(M-H_2O)^+$, 4%], 107 [$(M-CH_2OH)^+$, 100%], 91 [$(C_7H_7)^+$, 5%], 79 [$(C_6H_7)^+$, 45%].

Preparation of ReOCl(*eg*)(*phen*). To 35.05 mg of $(Ph_4As)[ReOCl_4]$ (0.048 mmol) in a disposable vial was added 1.5 cm^3 of MeOH and 0.5 cm^3 of 1,2-ethanediol (Fisher). The resulting blue solution was stirred for 5 min before adding 41 mg of crystalline 1,10-phenanthroline monohydrate (Baker, 0.207 mmol) with vigorous stirring. The solution immediately became red–brown and a precipitate gradually formed. The solid (17.29 mg, 75%) was collected on a medium porosity fritted glass funnel and rinsed with methanol and hexanes, then dried *in vacuo* at room temperature. The product is slightly soluble in CH_2Cl_2. IR (KBr): 3050 cm^{-1}(w), 2914(w), 2845(m), 1631(w), 1574(w), 1516(w), 1489(w), 1454(w), 1429(m), 1414(w), 1326(w), 1250(w), 1226(w), 1210(w), 1061(w), 1021(s), 963(vs), 907(s), 875(w), 851(s), 829(w), 781(w), 740(w), 719(s), 656(m), 651(m), 617(s), 541(m), 514(w), 508(w). ^{1}H NMR ($CDCl_3$): δ 9.42(dd, 1H), 8.90(dd, 1H), 8.39(dd, 1H), 7.97(m, 1H), (AB q: $\delta_A = 8.04$, $\delta_B = 7.89$, $J_{AB} = 9.17$ Hz, 2H), 7.72(dd, 1H), 7.63(m, 1H), 5.67(m, 1H), 5.11(m, 1H), 4.68(m, 1H), 4.27(m, 1H). FABMS(+): *m/z* [ion, abundance]: 478 [$(M)^+$, 55%], 443 [$(M-Cl)^+$, 100%], 418 [$(M-OCH_2CH_2O)^+$, 30%], 415 [$(M-Cl-C_2H_4)^+$, 60%], 399 [$(M-Cl-C_2H_4-O)^+$, 30%].

Thermolysis of ReOCl(*eg*)(*phen*)

Preparation of ReO_3Cl(*phen*). Chloro(1,2-ethanediolato)oxo(1,10 - phenanthroline)rhenium(V) (26.0 mg, 0.054 mmol) was placed in a 25 cm^3 round-bottom flask. The system was carefully evacuated to ~ 0.2 torr and then heated in an oil bath to 160°C for 1 h. No reaction was evident. On subsequent heating to 220°C while remaining under vacuum, the red–brown colour faded within 5 min. The resulting off-white powder was cooled under vacuum and reweighed (22.3 mg). Mechanical losses in transfer make accurate weight-loss determination impossible at this scale. IR (KBr): 3058 cm^{-1}(w), 1629(w), 1583(w), 1520(m), 1494(w), 1428(m), 1412(w), 1314(w), 1224(w), 1203(w), 1144(w), 1111(w), 942(s), 922(s), 910(s), 873(m), 851(s), 776(w), 743(m), 722(s), 653(w), 509(w), 492(w), 430(w), 419(w). FABMS(+): *m/z* 415 $(M-Cl)^+$.

RESULTS AND DISCUSSION

Slurries of $TcO_3Cl(AA)$ (AA = phen, bpy, Me_4-phen, NO_2-phen) in acetone or dichloromethane react with a wide variety of olefins (C_2R_4) to form the corresponding technetium(V) diolates, TcOCl(OCR_2CR_2O)(AA) [eq. (1)].

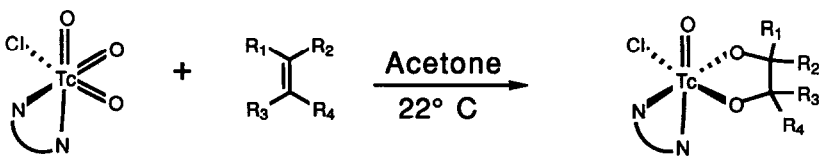

(1)

The isolated yields of the diolate products, summarized in Table 1, are generally greater than 70%. Variations in the yield depend strongly on the scale of the reaction, since mechanical losses in manipulations are significant. The choice of olefin, however, does not seem to alter the per cent conversion. The one pot reaction involving TcO_3Cl(phen) generated *in situ* has a comparable productivity based on pertechnetate, since the starting material is generally isolated in yields of less than 80%.

The different chelating aromatic diamine ligands 1,10-phenanthroline, 2,2′-bipyridine, 5-nitro-1,10-phenanthroline, and 2,3,7,8-tetramethyl-1,10-phenanthroline were studied in order to investigate the possibility of manipulating the reaction with subtle inductive changes in the trioxotechnetium complexes. The inductive effect of these ligands on the reduction potential of metals is well known because the tris-chelate complexes of iron are commonly used as redox indicators. No qualitative differences in the reactivity of $TcO_3Cl(AA)$ as a function of AA were noted. The nitro-phenanthroline ligand, however, does induce changes in the spectral and solubility properties of the complexes. The complex $TcO_3Cl(5\text{-}NO_2\text{-phen})$ is produced in nearly quantitative yields due to its extreme insolubility in the reaction mixture. This trioxotechnetium starting material is olive-green,

Table 1. Isolated yields of diolates from Tc mediated oxidation of olefins

Olefin	Yield (%)	Scale (mmol)
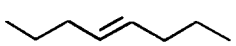	72	0.212
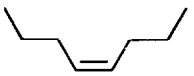	70	0.217
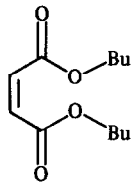	61	0.169
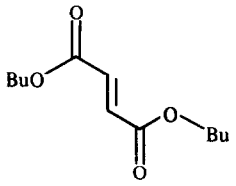	41	0.090
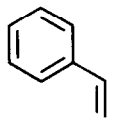	42 74	0.027 0.140
	30	0.039
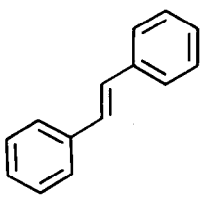	49	0.068
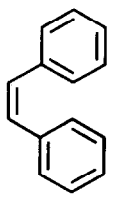	39	0.079
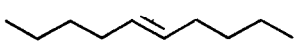	77	0.127
	76	0.095

quite unlike all of the others which are pale yellow. Furthermore, when this species is reacted with alkenes, the resulting technetium(V) diolate complexes are red–brown rather than the usual bright yellow–green.

Although perrhenyl chloride has been shown to oxidize olefins with the major product being the corresponding chlorohydrin,[9] no significant conversion was detected from the reaction of chlorotrioxo(1,10-phenanthroline)rhenium(VII) with olefins, even after prolonged refluxing. Conversely, the Re^{V} diolate complex ReOCl(eg)(phen) is converted to ReO_3Cl(phen) on heating *in vacuo*, whereas the technetium(V) diolates have no such reactivity.

The oxidative cleavage reaction of the osmate (VI) esters of diols has long been assumed to regenerate OsO_4 as the catalytically active species.[10] However, recent evidence suggests that an osmium(VIII) oxyhalide complex may also be involved in some cases. Myers *et al.*[11] noted that the rate of O_2 oxidized, Cu cocatalysed, Os catalysed, diol formation depends directly on the halide : Os ratio up to values of 5 : 1. The absence of OsO_4 in the distillates of these reactions gives further evidence for halide coordination since the oxyhalides are expected to be significantly less volatile. The technetium system validates this hypothesis being the first example of an isolated oxyhalide with which *cis*-dihydroxylation of olefins has been demonstrated.

The mechanism generally proposed[9] for the metal mediated vicinal dihydroxylation reactions involves a concerted [3+2] cycloaddition [eq. (2)]. Arguing that transition metals are more electropositive than oxygen; Sharpless *et al.* suggest[12] that alkenes, being weak nucleophiles, might be bonded to the metal atom in the first step of these reactions [eq. (3)]. The fact that OsO_4 preferentially reacts with more nucleophilic alkenes further supports this hypothesis. The direct attack at the metal, however, seems unlikely for the trioxotechnetium complexes, which are coordinatively saturated octahedral complexes.

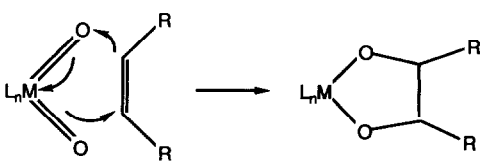

(2)

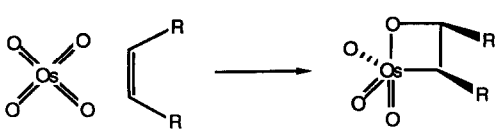

(3)

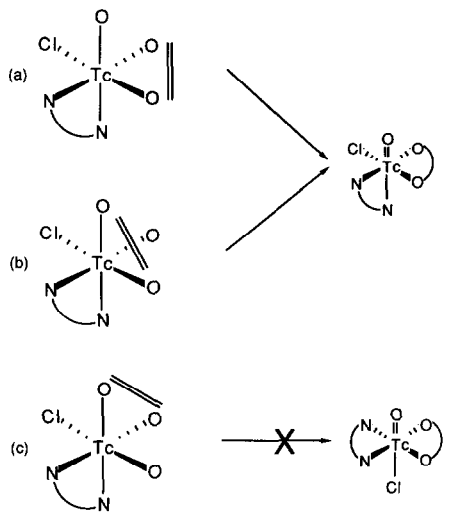

Scheme 1. Potential paths for [3+2] addition.

Scheme 1 shows the three possible paths through which an alkene can approach two of the oxo ligands in the cycloaddition reaction. Note that the two oxo ligands *cis* to the coordinated chloride in the $TcO_3Cl(AA)$ starting material are equivalent by virtue of a mirror plane passing through the *trans* oxo and the chloride, and bisecting the bidentate aromatic amine. In the case of a symmetric alkene (e.g. ethylene), paths (a) and (b) are degenerate, each yielding one of the enantiomers of the asymmetric centre at the technetium atom. Path (c) would yield a complex with mutually *trans* oxo and chloride ligands. Since all of the spectral evidence suggests that only *cis* complexes are formed, path (c) must therefore not contribute appreciably to the formation of products.

When substituted alkenes are used, the possibility of geometric isomers arises. Proton NMR spectroscopy therefore becomes extremely useful in analysing the technetium(V) diolate complexes. Although oxotechnetium(V) complexes are effectively closed-shell and diamagnetic,[13] appreciable position dependent variations in chemical shifts can be induced[14] by the ring currents associated with the multiple bonding to the oxo ligand. Circulation of electrons about the aromatic amine ligands presumably adds to this local magnetic field anisotropy. All of the spectra indicate that the substituents on the ethanediolate backbone are diastereotopic with the distinctive splitting patterns being well separated due to the combined ring currents. Furthermore, since the protons α to the nitrogen donors of the aromatic amine ligands are most shifted, often to > 10 ppm, and are therefore far removed from the other signals, the number of these resonances is indicative of the number of isomers in solution.

The analysis is straightforward for a 1,2-disubstituted alkene, e.g. *trans*-4-octene. The proton NMR spectrum of DL-TcOCl(OCHPrCHPrO)(phen) (Fig. 1) clearly shows two resonances for one of the α protons on the phenanthroline ligand at 10.4 and 10.2 ppm with relative intensities of ~2:1 indicating a non-statistical mixture of the two isomers. There is also a 2:1 ratio of intensities of the resonances for the methine protons of the octanediolate backbone. The major isomer has resonances at 5.8 and 4.2 ppm and the minor isomer has resonances at 5.0 and 4.7 ppm. Since the largest shifts from the average value for the methine protons occur in the major isomer, it might be deduced that the alkyl groups are preferentially going to the lesser shifting region of space which is presumably also a less sterically crowded area. The two possible isomers are shown in Scheme 2.

The NMR spectra indicate that the oxidation reaction is completely stereospecific since *cis* and *trans* alkenes give totally different products. In order to determine the stereochemistry of addition, the octanediolate derivatives were hydrolysed by treating them with concentrated aqueous HCl yielding free diols and $TcOCl_3(phen)$. Gas chromatographic retention times were compared to those of authentic samples of *meso*- and DL-4,5-octanediol which were prepared by osmium tetroxide oxidation of *cis*- and *trans*-4-octene, respectively. The reaction of $TcO_3Cl(phen)$ with *cis*-4-octene gives only the *meso* diol whereas a similar reaction with *trans*-4-octene gives 80% of the DL and 20% of the *meso* isomers. Some racemization may have occurred during the latter hydrolysis reaction.

The technetium centred oxidation of olefins and the rhenium centred reduction of diols are conceptually the forward and reverse reactions of the equilibrium shown below in eq. (4).

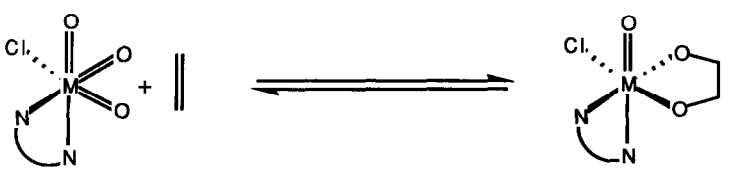

(4)

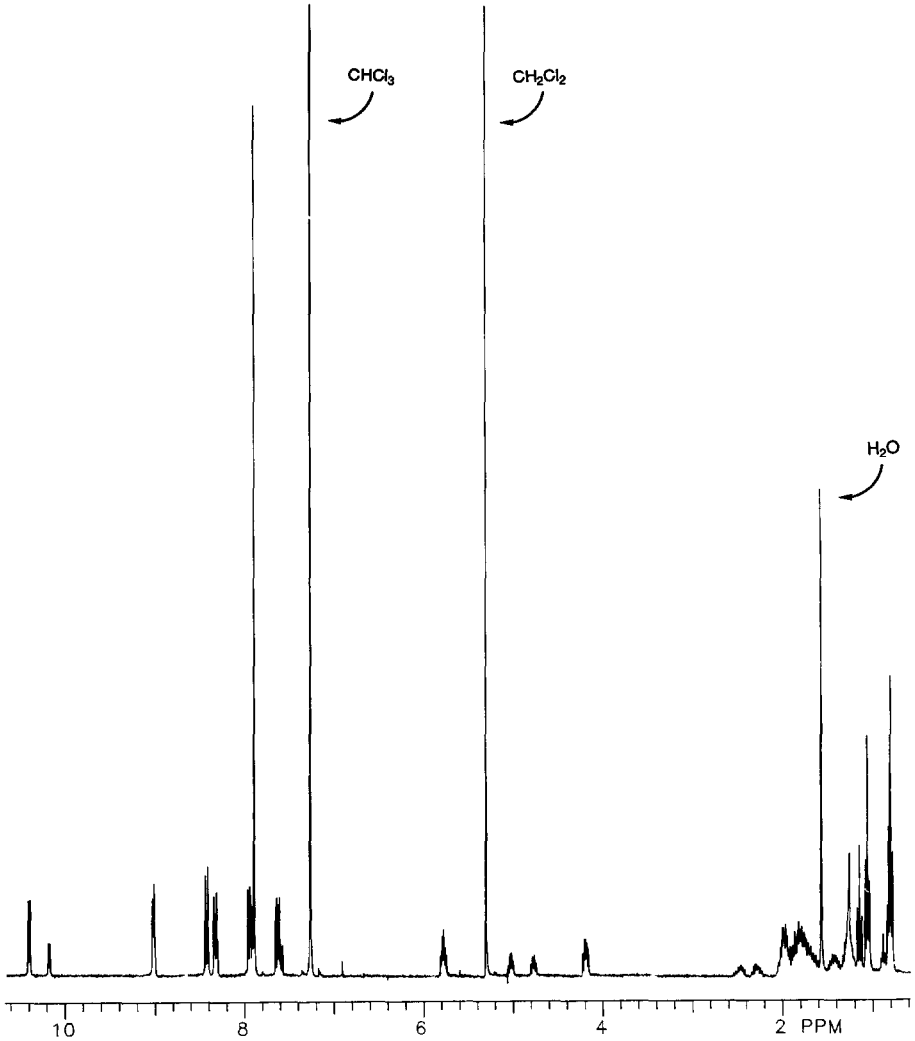

Fig. 1. Proton NMR spectrum of TcOCl(DL-4,5-octanediolate)(phen).

The direction of the reaction is governed primarily by the oxidation/reduction potentials of the central metals in their +5 and +7 oxidation states. These results are therefore consistent with the usual periodic trends for second and third row transition metals having similar environments in which the third row elements are more easily oxidized and the second row elements are more easily reduced.

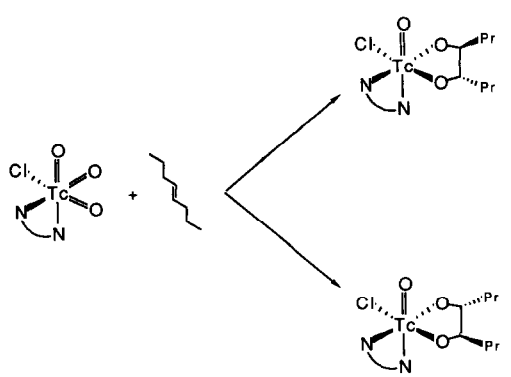

Scheme 2. The origin of two isomers from the oxidation of *trans*-4-octene.

Although the stoichiometric oxidation of alkenes with technetium is not likely to be commercially feasible due to the radioactivity of this element, this reaction provides the basis for investigating catalytic oxidation of alkenes to diols using the group 7 metals. Furthermore, the reactions discussed here give significant new insights into the already well utilized reactions of osmium tetroxide and permanganate.

Acknowledgements—This paper is dedicated to Prof. Sir Geoffrey Wilkinson, FRS. The authors also wish to thank K. B. Sharpless and E. N. Jacobsen for their advice and assistance. Analytical support was provided by: C. E. Costello, C. Zeng and E. Takach.

REFERENCES

1. K. B. Sharpless and K. Akashi, *J. Am. Chem. Soc.* 1976, **98**, 1986 and refs 1–3 therein.
2. A. H. Haines, *Methods for the Oxidation of Organic Compounds*, Section 3.2. Academic Press, London (1985).
3. S. F. Pederson, R. R. Schrock, M. R. Churchill and H. J. Wassermann, *J. Am. Chem. Soc.* 1982, **104**, 6808.
4. W. A. Herrmann, D. Marz, E. Herdtweck, A. Schafer, W. Wagner and H. J. Kneuper, *Angew. Chem. Int. Ed. Engl.* 1987, **26**, 462.
5. (a) A. Davison, C. Orvig, H. S. Trop, M. Sohn, B. V. DePamphilis and A. G. Jones, *Inorg. Chem.* 1980, **19**, 1988; (b) F. A. Cotton, A. Davison, V. W. Day, L. D. Gage and H. S. Trop, *Inorg. Chem.* 1979, **18**, 3024.
6. A. Davison, A. G. Jones and M. J. Abrams, *Inorg. Chem.* 1981, **20**, 4300.
7. F. A. Cotton and S. J. Lippard, *Inorg. Chem.* 1966, **5**, 9.
8. R. M. Pearlstein, C. J. L. Lock, R. Faggiani, C. E. Costello, C. Zeng, A. G. Jones and A. Davison, *Inorg. Chem.* 1988, **27**, 2409.
9. A. Y. Teranishi, Ph.D. thesis, Massachusetts Institute of Technology (1973).
10. M. Schroder, *Chem. Rev.* 1980, **80**, 187.
11. R. S. Myers, R. C. Michaelson and R. G. Austin, *Prep. Am. Chem. Soc., Div. Pet. Chem.* 1987, **32**, 227.
12. K. B. Sharpless, A. Y. Teranishi and J. Backvall, *J. Am. Chem. Soc.* 1977, **99**, 3120.
13. A. Davison and A. G. Jones, *Int. J. Appl. Radiat. Isotopes* 1982, **33**, 875.
14. P. H. Fackler, M. E. Kastner and M. J. Clarke, *Inorg. Chem.* 1984, **23**, 3968.

Polyhedron Vol. 7, No. 19/20, pp. 1991–1999, 1988
Printed in Great Britain

0277–5387/88 $3.00+.00
© 1988 Pergamon Press plc

THE TUNGSTEN–TUNGSTEN TRIPLE BOND—XVI.* BIS(CYCLOPENTADIENYL)- AND BIS(INDENYL)TETRADIMETHYLAMIDODITUNGSTEN (W≡W)

MALCOLM H. CHISHOLM,† MARK J. HAMPDEN-SMITH, JOHN C. HUFFMAN, JAMES D. MARTIN and KARLHEINZ A. STAHL

Department of Chemistry and Molecular Structure Center, Indiana University, Bloomington, IN 47405, U.S.A.

and

KANDASAMY G. MOODLEY

Department of Chemistry, University of Durban-Westville, P/B 54001, Durban, South Africa

Abstract—From the reaction between 1,2-$W_2Cl_2(NMe_2)_4$ and NaCp (Cp = C_5H_5) (two equiv.) in toluene, a yellow–orange, hydrocarbon-soluble, crystalline solid of formula $W_2Cp_2(NMe_2)_4$ has been obtained. NMR data are consistent with a *gauche* 1,2-$W_2R_2(NMe_2)_4$ molecule having a W—W triple bond and restricted rotations about the W—N bonds. The NMR data, however, do not uniquely define the nature of the Cp—W bonding beyond the fact that there are five time-averaged equivalent carbon and hydrogen atoms. No crystals suitable for an X-ray study were obtained. The related reaction involving 1,2-$W_2Cl_2(NMe_2)_4$ and LiC_9H_7 (C_9H_7 = indenyl) (two equiv.) gave an orange, hydrocarbon-soluble, crystalline compound. The NMR data are indicative of a *gauche* 1,2-$W_2R_2(NMe_2)_4$ molecule in solution having a virtual C_2 axis of symmetry and restricted rotations about the W—N bonds. An X-ray study revealed the presence of the *gauche* rotamer and that the indenyl–metal bonding was η^3-C_9H_7. Pertinent bond distances (Å) and angles (°) for 1,2-$W_2(\eta^3$-$C_9H_7)_2(NMe_2)_4$ are W—W = 2.334(1), W—N = 1.96(1) (av.), and W-η^3-C_3(indenyl) = 2.36(1)–2.54(1), W—W—N = 102(1) (av.) and W—W—C(η^3-C_3(indenyl)) = 91–117°. The reaction between 1,2-$W_2Cp_2(NMe_2)_4$ and EtCOOCOEt (> four equiv.) proceeds in hydrocarbon solvents to give the compound $W_2Cp_2(NMe_2)(O_2CEt)_3$ and Me_2NCOEt (three equiv.) in contrast to other 1,2-$W_2R_2(NMe_2)_4$ compounds which yield either $W_2(O_2CEt)_4$ when R contains β-hydrogen atoms or $W_2R_2(O_2CEt)_4$ compounds. The molecular structure of $W_2Cp_2(NMe_2)(O_2CEt)_3$ can be viewed as two fused four-legged piano-stools sharing an edge, μ-NMe_2 and μ-η^1-O_2CEt, with a pair of bridging O_2CEt ligands spanning a W—W bond of distance 2.78 Å. The Cp ligands form W-η^5-C_5H_5 bonds roughly trans to the W—W axis.

We have been systematically investigating the chemistry of compounds containing a central $(M{\equiv}M)^{6+}$ moiety, where M = Mo and W, with respect to their coordination chemistry, electronic structures and reactivity.[2] The first members of this now extensive class of compounds were prepared by Wilkinson *et al.*: $M_2[CH_2Si(CH_3)_3]_6$.[3,4] Much of the work in this laboratory has involved the use of attendant π-donor ligands such as OR, NMe_2, SR and more recently PR_2.[5] We are interested in comparing the relative π-donor properties of these ligands towards the $(M{\equiv}M)^{6+}$ centre and to investigate the π-donor strengths of η^n-C_n π-ligands relative to those of dimethylamido ligands.

For compounds of formula 1,2-$M_2X_2(NMe_2)_4$

* For part XV, see ref. 1.

† Author to whom correspondence should be addressed.

there is no need for the X ligand to act as a π-donor as in the case where X = alkyl or aryl. However, if X = NMe_2, then three NMe_2 ligands at each metal centre compete equally for the use of two metal–ligand π-acceptor orbitals d_{xy} and $d_{x^2-y^2}$ (when the M—M axis is defined as the z axis). Conceivably, if X is a better π-donor than the NMe_2 ligand, then an alternate structure might be found. The remaining nitrogen atoms could become pyramidal or move to bridging positions at the expense of M—M bonding. An analogous type of behaviour is exhibited by the phosphido ligand in certain compounds of formula $M_2(PR_2)_2(NMe_2)_4$ that exist in either bridged (μ-PR_2) or terminal pyramidal forms.[6]

A prototypical η^5-C_n π-ligand is the ubiquitous Cp ligand (Cp = C_5H_5). For a compound of formula 1,2-$M_2Cp_2(NMe_2)_4$ we envisaged one of three scenarios. (1) The π-donating order, $NMe_2^- > Cp^-$ so that 1,2-$M_2Cp_2(NMe_2)_4$ compounds would contain an η^1-C_5H_5 ligand and therefore be analogues of the extensive class of 1,2-$M_2R_2(NMe_2)_4$ compounds where R = σ-alkyl,[7] -benzyl[8] or -aryl.[8] (2) $NMe_2^- \sim C_5H_5^-$ as a four electron donor leading to a situation in which an η^3-C_5H_5 ligand and two NMe_2 ligands compete for use of metal $d_{x^2-y^2}$ and d_{xy} orbitals. Here the relative M—N distances for a series of 1,2-$M_2X_2(NMe_2)_4$ can be a useful measure of the relative electron releasing ability of X versus NMe_2, $\sigma^2+\pi^2$. (3) $C_5H_5^- > NMe_2^-$ in which case the use of all six Cp π-electrons could enforce a new structural type such as $(\eta^5$-$C_5H_5)_2M_2(\mu$-$NMe_2)_2(NMe_2)_2$ or even $(\eta^5$-$C_5H_5)_2M_2(\mu$-$NMe_2)_4$.*

In this paper we describe our initial investigations that were prompted by the above considerations.

RESULTS AND DISCUSSION

Syntheses and NMR studies

The reactions between 1,2-$W_2Cl_2(NMe_2)_4$ compounds and NaCp (two equiv.) proceeded according to the stoichiometry shown in eq. (1).

$$1,2\text{-}W_2Cl_2(NMe_2)_4 + 2NaCp \xrightarrow[\text{toluene}]{23^\circ C} 1,2\text{-}W_2Cp_2(NMe_2)_4 + 2NaCl. \quad (1)$$

The compound 1,2-$W_2Cp_2(NMe_2)_4$ was obtained as an air-sensitive, orange, hydrocarbon-soluble, crystalline solid. This compound displayed variable temperature NMR behaviour (^1H and ^{13}C) typical of *gauche* 1,2-$M_2R_2(NMe_2)_4$ compounds.[7,8] Most significantly, at low temperature, rotations about the M—N bonds were frozen out on the NMR time scale and gave rise to two sets of signals assignable to proximal and distal NMe groups. The sizable chemical shift separation (see Experimental) was indicative of the maintenance of the central $(M{\equiv}M)^{6+}$ moiety unbridged by NMe_2 ligands. However, the resonances associated with the Cp carbons and protons were indicative of only one type of CH moiety. No coupling to ^{183}W, $I = \frac{1}{2}$, 14.5% natural abundance was seen in either the ^1H or ^{13}C NMR spectra.[10] Thus even at the low temperature limit in toluene-d_8 the C_5H_5 ligand was undergoing a rapid "whizzing" of some unspecified type. The NMR data do not allow us to deduce the intimate mode of η^n-C_5H_5 bonding.

Cognisant of the now well defined indenyl effect,[11] we were determined to attempt the synthesis of 1,2-$W_2(C_9H_7)_2(NMe_2)_4$ and this was achieved according to the reaction shown in eq. (2).

$$1,2\text{-}W_2Cl_2(NMe_2)_4 + 2NaC_9H_7 \xrightarrow[Et_2O]{0^\circ C} 1,2\text{-}W_2(C_9H_7)_2(NMe_2)_4 + 2NaCl. \quad (2)$$

The indenyl compound was also an air-sensitive, hydrocarbon-soluble, orange, crystalline solid and displayed variable temperature NMR spectra typical of a *gauche* 1,2-$M_2R_2(NMe_2)_4$ compound, see Fig. 1. However, the presence of the virtual C_2 axis of symmetry was now apparent on the indenyl protons and carbon resonances and one carbon atom showed coupling to ^{183}W, $J_{^{183}W-^{13}C} = 8$ Hz. The coupling is rather small for a W—C σ bond in compounds of formula $W_2R_2(NMe_2)_4$ where R = alkyl, benzyl or aryl.[7,8] For the latter $^1J_{^{183}W-^{13}C}$ is *ca* 100 Hz. Furthermore, on lowering the temperature of a toluene-d_8 solution of $W_2(C_9H_7)_2(NMe_2)_4$, the central indenyl proton of the five-membered ring (H_3) showed a very marked shift to lower field from 7.9 ppm at 105°C to 8.7 ppm at −80°C (see Fig. 1). In contrast, the other protons of the five-membered carbon ring (H_2 and H_4) moved upfield by approximately the same amount over the same temperature range. The chemical shifts of the aromatic protons of the six-membered carbon ring were noticeably temperature independent, and therefore unlikely to be involved in bonding to the metal centre. This led us to believe that the indenyl ligand might well be π-bonded through the five-membered ring and that some process is occurring at low temperature which results in greater shielding of the H_3 nucleus. Unusually

* Related d^2–d^2 $Cp_2M_2(\mu$-$X)_4$ compounds are known[9b] for M = Nb and Ta, X = halide,[9a] and d^3–d^3 $Cp_2Mo_2(\mu$-$Cl)_2$.

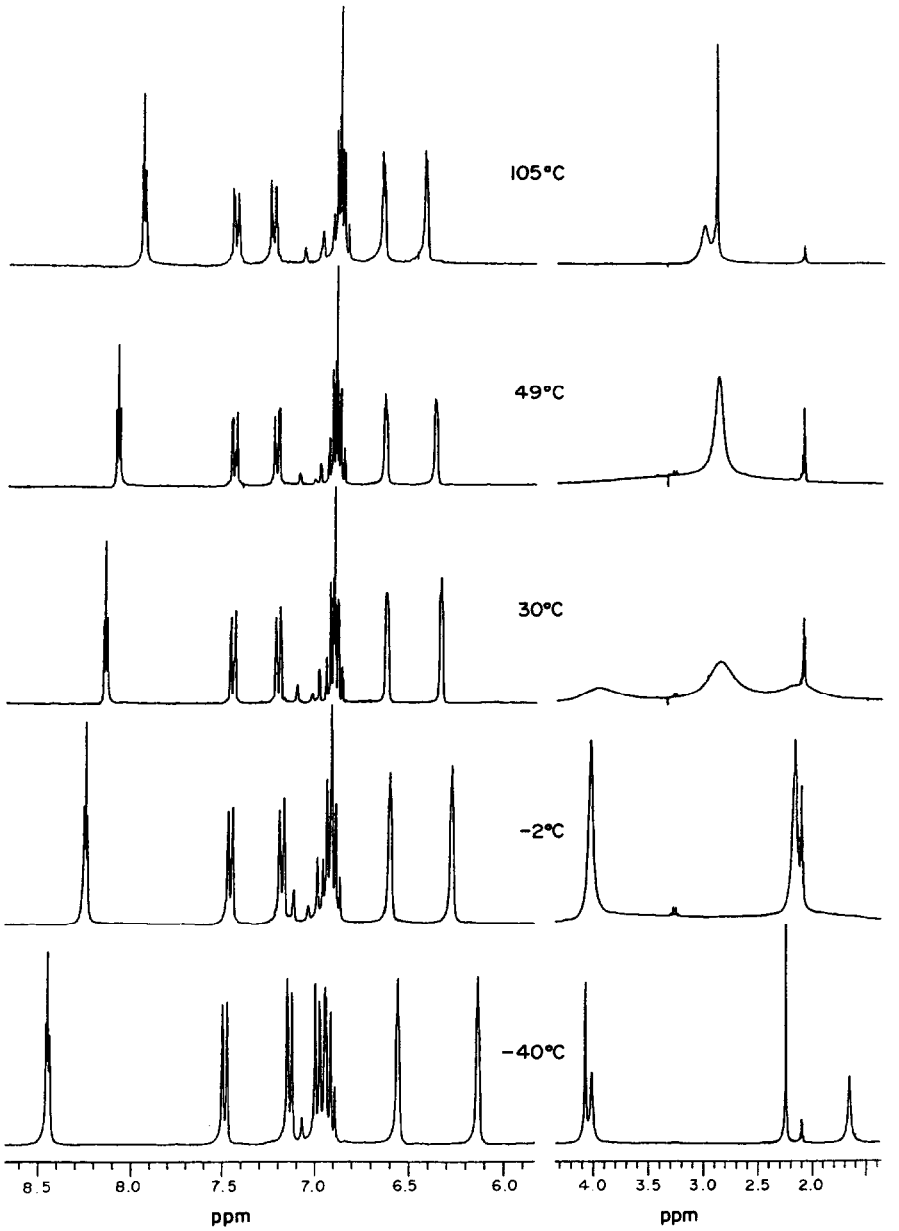

Fig. 1. Variable temperature (300 MHz) ^{1}H NMR spectra for W_2(indenyl)$_2$(NMe$_2$)$_4$ showing the two characteristic pairs of proximal and distal NMe resonances of a *gauche* rotamer. Above 30 and 80°C, respectively, rotation about the N—Me bonds is rapid to give two time-averaged N—Me signals.

large downfield chemical shifts in the ^{1}H NMR spectra have previously been associated with close proximity to the large diamagnetic anisotropy due to metal–metal triple bonds.

One further chemical comparison was made for the 1,2-$W_2R_2(NMe_2)_4$ compounds for R = Cp versus alkyl, benzyl and aryl. This involved the reaction with propionic anhydride. The 1,2-dialkyl compounds have previously been shown to react according to either eq. (3) or (4) depending upon the nature of R.[12,13]

$$1,2\text{-}W_2R_2(NMe_2)_4 + 4EtOOCOEt \xrightarrow[\text{hexane}]{22^\circ C} W_2(O_2CEt)_4 + 4Me_2NCOEt + \text{alkene} + \text{alkane} \quad (3)$$

(R = β-hydrogen containing alkyl)

$$1,2\text{-}W_2R_2(NMe_2)_4 + 4EtOOCOEt \xrightarrow[\text{hexane}]{22^\circ C} 1,2\text{-}W_2R_2(O_2CEt)_4 + 4Me_2NCOEt \quad (4)$$

(R = benzyl, aryl and non-β-hydrogen alkyl).

The reaction between 1,2-$W_2Cp_2(NMe_2)_4$ and EtOOCOEt proceeded differently to both of the above [eqs (3) and (4)] in as much as only three equiv. of EtCOOCOEt were consumed even when excess propionic anhydride was present. The product in these reactions had the formula $Cp_2W_2(NMe_2)(O_2CEt)_3$. Again this was suggestive of the role of the Cp ligand as a η^n type ligand ($n > 1$), though from the NMR data a structure for the new compound could not be unambiguously formulated.

Solid state and molecular structures

Despite several examinations of crystals of 1,2-$M_2Cp_2(NMe_2)_4$ samples, no crystal proved suitable for a detailed single crystal X-ray study.

1,2-$W_2(C_9H_7)_2(NMe_2)_4$. An ORTEP drawing of the *gauche* 1,2-$W_2(C_9H_7)_2(NMe_2)_4$ molecule is given in Fig. 2. The molecule has virtual C_2 symmetry but in the space group $P\bar{1}$ no crystallographic symmetry is imposed. Thus, with one unique molecule in the unit cell we obtain bonding parameters for two independent indenyl–tungsten moieties.

Selected bond distances and bond angles are given in Tables 1 and 2. The W—W distance of 2.334(1) Å is well within the range expected for an unbridged $(W{\equiv}W)^{6+}$ moiety with the M—M MO valence configuration $\sigma^2\pi^4$. The W—N distances span a range 1.955(10)–1.975(9) Å and are essentially the same as those in $W_2(NMe_2)_6$ and $W_2R_2(NMe_2)_4$ compounds. The bonding to the indenyl ligand is distinctly of the η^3-indenyl mode.

Table 1. Selected bond distances (Å) for the W_2(indenyl)$_2(NMe_2)_4$ molecule

A	B	Distance
W(1)	W(2)	2.3344(8)
W(1)	N(3)	1.975(9)
W(1)	N(6)	1.966(10)
W(1)	C(10)	2.513(11)
W(1)	C(11)	2.361(11)
W(1)	C(12)	2.414(12)
W(2)	N(18)	1.955(10)
W(2)	N(21)	1.965(10)
W(2)	C(25)	2.542(11)
W(2)	C(26)	2.392(12)
W(2)	C(27)	2.443(12)
C(10)	C(11)	1.439(17)
C(11)	C(12)	1.417(18)
C(25)	C(26)	1.420(19)
C(26)	C(27)	1.457(20)

For both W—C_9H_7 moieties there are short W—C bond distances W(1)—C(11) = 2.36(1) Å and W(2)—C(26) = 2.39(1) Å. These are distinctly too long to be considered simple W—C σ-bonds for which we would expect distances in the range 2.14–2.21 Å depending upon the hybridization at carbon, sp^2 versus sp^3, respectively.[7,8] In addition to the short W—C indenyl distance, each ring has two other W—C distances that are within π-bonding range, namely W(1)—C(10) = 2.51(1) Å, W(1)—C(12) = 2.41(1) Å and W(2)—C(25) = 2.54(1) Å, W(2)—C(27) = 2.44(1) Å. The other W—C

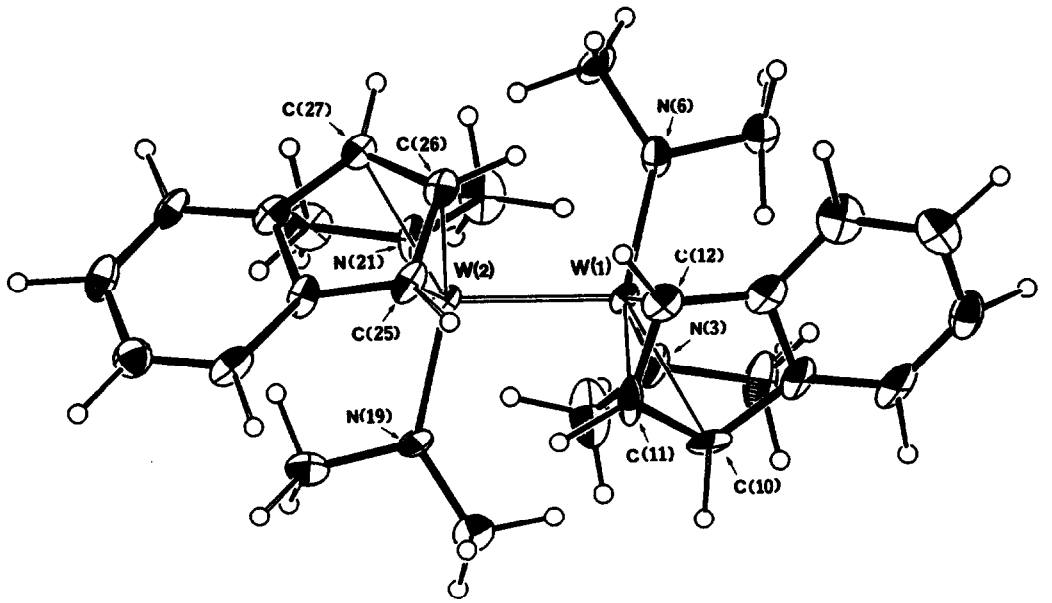

Fig. 2. An ORTEP drawing of the $W_2(C_9H_7)_2(NMe_4)_4$ molecule giving the atom number scheme used in the Tables.

Table 2. Selected bond angles (°) for the W_2(indenyl)$_2(NMe_2)_4$ molecule

A	B	C	Angle
W(2)	W(1)	N(3)	102.61(27)
W(2)	W(1)	N(6)	102.1(3)
W(2)	W(1)	C(10)	117.03(27)
W(2)	W(1)	C(11)	92.5(3)
W(2)	W(1)	C(12)	101.6(3)
N(3)	W(1)	N(6)	106.2(4)
N(3)	W(1)	C(10)	86.1(4)
N(3)	W(1)	C(11)	114.7(4)
N(3)	W(1)	C(12)	140.9(4)
N(6)	W(1)	C(10)	135.4(4)
N(6)	W(1)	C(11)	132.7(4)
N(6)	W(1)	C(12)	98.2(4)
C(10)	W(1)	C(11)	34.2(4)
C(10)	W(1)	C(12)	55.5(4)
C(11)	W(1)	C(12)	34.5(4)
W(1)	W(2)	N(18)	102.7(3)
W(1)	W(2)	N(21)	101.5(3)
W(1)	W(2)	C(25)	116.4(3)
W(1)	W(2)	C(26)	92.0(3)
W(1)	W(2)	C(27)	102.0(3)
N(18)	W(2)	N(21)	106.0(4)
N(18)	W(2)	C(25)	135.5(4)
N(18)	W(2)	C(26)	132.6(5)
N(18)	W(2)	C(27)	97.5(4)
N(21)	W(2)	C(25)	87.1(4)
N(21)	W(2)	C(26)	115.0(5)
N(21)	W(2)	C(27)	142.0(4)
C(25)	W(2)	C(26)	33.3(4)
C(25)	W(2)	C(27)	55.6(4)
C(26)	W(2)	C(27)	35.0(5)

distances to the carbon atoms that are common to both the C_5 and C_6 membered rings are W(1)—C(9) = 2.85(1) Å, W(1)—C(13) = 2.81(1) Å and W(2)—C(24) = 2.87(1) Å, W(2)—C(28) = 2.81(1) Å and are clearly not important with respect to indenyl–tungsten bonding.

$Cp_2W_2(\mu\text{-}NMe_2)(\mu\text{-}OC(O)Et)(O_2CEt)_2$. An ORTEP drawing depicting the structure of this unusual molecule is given in Fig. 3. Since the structure is not germane to the arguments presented concerning the bonding in $(M{\equiv}M)^{6+}$ containing compounds, full discussion of the bonding and full presentation of the structural parameters are not given here but are available from the Editor, Queen Mary College or from the principal investigator upon request. Atomic positional parameters have been deposited with the Cambridge Crystallographic Data Centre.

Pertinent to the considerations at hand are the presence of two η^5-C_5H_5 ligands. These have controlled both the coordination chemistry of the dinuclear compound and the reaction stoichiometry. The compounds of formula $W_2R_2(O_2CEt)_4$ where $R = CH_2CMe_3$ or CH_2Ph, for example, have M—M bonds of distance *ca* 2.20 Å with M—M valence configurations $\pi^4\delta^2$. There are axially aligned alkyl ligands, R—M—M—R, and four O_2CEt ligands that span the M—M bond in the typical paddle-wheel manner for $M_2(O_2CR)_4$ compounds.

The present molecule can be viewed as an example of two four-legged piano-stools joined along a common edge by the μ-NMe_2 and μ-η^1-OC(O)Et

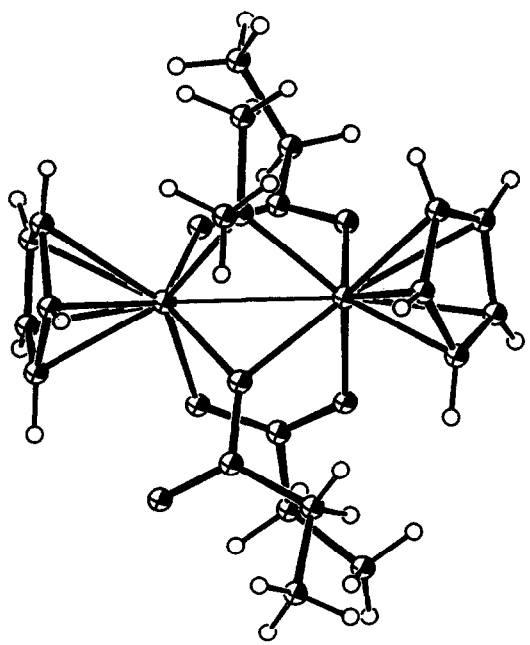

Fig. 3. An ORTEP drawing of the $W_2(Cp)_2(NMe_2)(O_2CEt)_3$ molecule. The W—η^5-C_5 distances span the range 2.14–2.38 Å.

ligands. The other legs of the piano-stool are W—O bonds to O_2CEt ligands that span the W—W bond. Each $(\eta^5\text{-}C_5H_5)WO_3N$ moiety has 17 valence electrons: $W^{III} = d^3$, $Cp^- = 6e$, and each O and N ligand donates 2e for a total of 8e ($d^3 + 6e + 8e = 17e$). The combination of two 17 valence electron metal fragments would be expected to yield a M—M single bond and the distance of 2.78 Å is indeed within the range of d^1–d^1 M—M single bonds supported by alkoxide ligands.[14] Obviously, the M—M bonding is not so simple in the present compound, but a W—W single bond is consistent with both the M—M distance and simple reasoning based on electron counting.

Concluding remarks

While the nature of the Cp—W bonding in 1,2-$W_2Cp_2(NMe_2)_4$ compounds still has some degree of ambiguity it seems reasonable to suppose that in the ground state it is similar to that seen in the indenyl compound. It is unlikely that the indenyl ligand would be η^3-C_9H_7 and the Cp ligand η^1-C_5H_5, for example. Furthermore, the present structure shows a very marked preference for the η^3-mode and the indenyl ligand is known to easily slip from $\eta^5 \rightarrow \eta^3$. The influence of the η^n-C_5H_5 moiety at the W_2^{6+} centre is clearly seen in the reaction between $W_2Cp_2(NMe_2)_4$ and propionic anhydride. The formation of $(\eta^5\text{-}C_5H_5)_2W_2(\mu\text{-}NMe_2)(\mu\text{-}\eta^1\text{-}OC(O)Et)(O_2CEt)_2$ even in the presence of excess EtCOOCOEt suggests that once the μ-NMe_2 ligand is formed it is inert to further attack. A similar result was seen in CO_2 insertion involving $Cr(NEt_2)_3$ that gave $[Cr(O_2CNEt_2)_2(\mu\text{-}NEt_2)]_2$.[15]

With respect to the η^3-C_9H_7 to —W bonding in 1,2-$W_2(C_9H_7)_2(NMe_2)_4$ we conclude that the carbocyclic ring can compete fairly effectively with the NMe_2^- ligands as $\sigma^2 + \pi^2$ donors. The shortness of the W—N bonds and the length of the W—C bond distances in the η^3-C_3—W moiety leads us to propose that the relative donor strength ($\sigma^2 + \pi^2$) is probably in the order $NMe_2 > \eta^3$-C_9H_7. As with other σ–π donating ligands there is an interplay between relative orbital energetics and metal–ligand bond distances.

Further studies are planned to probe these matters.

EXPERIMENTAL

General procedures and spectroscopic instrumentation

Our general experimental techniques have been previously described in detail.[7,8] All manipulations were carried out under an atmosphere of dry nitrogen and solvents were dried and distilled from sodium benzophenone ketyl prior to use. $W_2Cl_2(NMe_2)_4$, NaCp and LiC_7H_9 were prepared by the literature methods.[16,17] ^1H and ^{13}C NMR spectra were recorded on Nicolet NT360, Varian XL300 and Bruker AM500 NMR instruments. Variable temperature ^1H NMR spectra were recorded at 300 MHz, and free energies of activation for restricted rotation about W—N bonds were calculated from coalescence temperatures, T_c.[18] ^1H NMR spectra of $W_2(C_7H_9)_2(NMe_2)_4$ were examined over a temperature range of +105 to −80°C in toluene-d_8 and −60 to −120°C in a 70:30 solution of freon-12:toluene-d_8. Temperatures were calibrated using ethylene glycol and methanol as standards. The numbering scheme for the indenyl ligand of $W_2(indenyl)_2(NMe_2)_4$ is given in the diagram below.

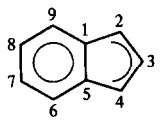

In the ^1H NMR spectrum the two isolated three- and four-proton spin systems were identified by a 2D chemical shift correlated experiment (COSY) at 500.13 MHz (512W (8 scans) × 128 Matrix). A 2D ^{13}C–^1H heteronuclear chemical shift correlated experiment (HETCOR) was carried out to determine which carbon nuclei were directly bonded to each individual proton. Assignments were made as follows. The low field chemical shifts of both the ^{13}C and ^1H NMR resonances labelled C_3 multiplicity of resonance H_3 (doublet of doublets), are consistent with the assignment of C_3 and H_3 to the central tertiary carbon and proton nuclei of the five-membered ring of the indenyl ligand. H_2 and H_4 can then be assigned (from the COSY experiment) and then C_2 and C_4 (from the HETCOR experiment). H_6 and H_9 of the six-membered ring can be assigned from the single large three-bond proton–proton coupling constants (to H_7 and H_8, respectively), and therefore the corresponding carbon nuclei. The quaternary carbon nuclei, C_1 and C_5 were identified from a proton-coupled ^{13}C experiment.

IR spectra were measured on a Perkin–Elmer 283 spectrophotometer.

Synthesis of 1,2-$W_2Cp_2(NMe_2)_4$

$W_2Cl_2(NMe_2)_4$ (3.40 g, 5.53 mmol) was placed in a 100 cm^3 Schlenk flask together with a Teflon-coated magnetic stir bar. Toluene (30 cm^3) was

added, and the solution was stirred vigorously while NaC_5H_5 (1.00 g, 11.35 mmol) was added in small amounts from a solids addition tube. The reaction mixture was stirred for 12 h at room temperature and then filtered through a celite bed on a fine-porosity frit. The celite bed was washed twice with 20 cm^3 toluene. Removal of solvent *in vacuo* yielded an orange–red crystalline product (3.33 g, 90%). Single crystals were obtained by slow cooling of a hot (50°C) hexane solution of the compound.

Found: C, 32.2; H, 5.1; N, 8.4. Calc. for $W_2C_{18}H_{34}N_4$: C, 32.1; H, 5.1; N, 8.3%.

IR data (CsI plates, Nujol mull) cm^{-1}: 2800(vs), 2750(s), 1400(m), 1233(s), 1138(s), 1125(m), 1035(s), 1010(s), 960(vs), 940(vs), 820(2), 795(vs), 765(vs), 598(vw), 545(s), 345(s), 305(m).

^1H NMR data (−80°C, toluene-d_8): C_5H_5, 6.21 ppm, s, 5H; NMe_2, 4.42 ppm, s, 3H; 4.09 ppm, s, 3H; 2.61 ppm, s, 3H; 2.53 ppm, s, 3H.

^{13}C NMR data (−40°C, toluene-d_8): C_5H_5, 104.7 ppm; NMe_2, 62.2, 60.7, 54.6, 52.8 ppm. Amide rotational barriers: by ^1H, 360 MHz, 30°C, $\Delta G^{\ddagger} = 13.4$ kcal mol^{-1}; by ^1H, 360 MHz, 90°C, $\Delta G^{\ddagger} = 16.1$ kcal mol^{-1}; by ^1H, 300 MHz, 25°C, $\Delta G^{\ddagger} = 13.3$ kcal mol^{-1}; by ^{13}C, 300 MHz, 25°C, $\Delta G^{\ddagger} = 13.3$ kcal mol^{-1}. Mass spectrum: $m/e = 674$ $[\{W_2(C_5H_5)_2(NMe_2)_4\}^+]$ (674.2).

Synthesis of 1,2-$W_2(C_9H_7)_2(NMe_2)_4$

Indenyl lithium, C_7H_9Li (0.35 g, 2.87 mmol), was placed in a 100 cm^3 Schlenk flask together with a Teflon-coated, magnetic stir bar. Diethyl ether (50 cm^3) was added and the solution cooled to 0°C. $W_2Cl_2(NMe_2)_4$ (0.86 g, 1.4 mmol) was added in small amounts from a solids addition tube. After 1 h the ice bath was removed and the reaction mixture was stirred at room temperature for 10 h. Diethyl ether was removed *in vacuo*. The residue was extracted with small volumes of hexane (total volume 80 cm^3). Hexane was removed under vacuum and the residue was dissolved in 1 cm^3 toluene. Cooling of the toluene solution to 5°C afforded single crystals (200 mg). The total yield of crystalline material was 580 mg (53.7%).

Found: C, 40.2; H, 4.8; N, 6.9. Calc. for $W_2C_{26}H_{38}N_4$: C, 40.3; H, 4.9; N, 7.2%.

IR data (KBr pellet) cm^{-1}: 3038(w), 3000(br, vw), 2950(vw), 2835(s), 2805(s), 2758(s), 1594(w), 1445(ms), 1420(sh), 1414(m), 1324(s), 1238(s), 1213(w), 1137(m), 1115(m), 1040(ms), 1025(w), 1000(w), 956(s), 940(vs), 804(s), 778(s), 743(s), 735(s), 545(m), 443(w), 393(vw), 349(w).

^1H NMR data: C_7H_9 (23°C, 500.13 MHz): H_2, 6.35 ppm, d, 1H, $J_{2-3} = 3.5$ Hz; H_3, 8.20 ppm, t, 1H, $J_{3-4} = 3.2$ Hz; H_4, 6.64 ppm, d, 1H; H_6, 7.22 ppm, m, 1H, $J_{6-7} = 6.6$ Hz; H_7, 6.93 ppm, m, 1H, $J_{7-8} = 5.8$ Hz; H_8, 6.92 ppm, m, 1H, $J_{8-9} = 5.8$ Hz; $H_9 = 7.42$ ppm, m, 1H: NMe_2 (−80°C, 300 MHz) 4.14 ppm, s, 6H; 3.96 ppm, s 6H; 2.34 ppm, s, 6H; 1.68 ppm, s, 6H: Amide rotational barriers: ^1H NMR, 300 MHz, $T_c = 49$°C, 14.4 kcal mol^{-1}; $T_c = -2$°C, 11.9 kcal mol^{-1}.

^{13}C NMR (23°C, 125.7 MHz): C_1, 138.5 ppm; C_2, 92.4 ppm, $^1J_{C-H} = 168$ Hz, $^2J_{C-H} = 8$ Hz; C_3, 113.2 ppm, $^1J_{C-H} = 170$ Hz, $^2J_{C-H} = 7$ Hz, $J_{C-W} = 8$ Hz; $C_4 = 92.1$ ppm, $^1J_{C-H} = 169$ Hz, $^2J_{C-H} = 7$ Hz; $C_5 = 136.3$ ppm; $C_6 = 122.4$ ppm, $^1J_{C-H} = 158$ Hz, $^2J_{C-H} = 8$ Hz; $C_7 = 123.6$, $^1J_{C-H} = 157$ Hz, $^2J_{C-H} = 8$ Hz; $C_8 = 121.9$, $^1J_{C-H} = 158$, $^2J_{C-H} = 7$ Hz; $C_9 = 121.3$, $^1J_{C-H} = 158$ Hz, $^2J_{C-H} = 7$ Hz.

Reaction of $W_2Cp_2(NMe_2)_4$ *with propionic anhydride*

$W_2(C_5H_5)_2(NMe_2)_4$ (0.350 g, 0.52 mmol) was placed in a 30 cm^3 Schlenk flask together with a Teflon-coated magnetic stir bar. Toluene was added and the red solution cooled to 0°C. Propionic anhydride (0.3 cm^3, 0.3 g, 2.3 mmol) was added from a 0.5 cm^3 syringe. There was an immediate colour change from red to dark brown. The reaction mixture was stirred for 1 h at 0°C after which the solvent was removed *in vacuo* to afford an oily, dark brown solid. This was extracted with hexane (20 cm^3) and filtered through celite on a fine-porosity frit. Hexane was removed *in vacuo* to give a brown powder (yield 0.250 g, 63%). Single crystals were grown by cooling a hexane solution to −20°C for 12 h.

IR data (Nujol mull between CsI plates) cm^{-1}: 1690(s), 1540(s), 1340(m), 1300(m), 1260(w), 1162(w), 1090(m), 1075(m), 1112(m), 980(m), 926(m), 895(m), 800(m), 765(w), 365(vw), 270(vw).

^1H NMR data (22°C, benzene-d_6): C_5H_5, 5.09 ppm, s, 10H; —CH_2—CH_3, 2.50 ppm, q, 2H; 2.39 ppm, q, 2H; 1.63 ppm, q, 2H: NMe_2, 2.20 ppm, s, 3H; 1.99 ppm, s, 3H; —CH_2—CH_3, 0.99 ppm, t, 3H; 0.89 ppm, t, 3H; 0.82 ppm, t, 3H.

Mass spectrum: $m/e = 761$ $[\{W_2(C_5H_5)_2(EtCOO)_3(NMe_2)\}^+]$.

Crystallographic studies

General operating procedures and listings of programs have been given previously.[19] A summary of crystallographic data is given in Table 3.

$W_2(C_9H_7)_2(NMe_2)_4$. A suitable crystal was located and transferred to the goniostat using standard inert atmosphere handling techniques employed by the Indiana University Molecular

Table 3. Summary of crystal data

	I	II
Empirical formula	$W_2C_{26}H_{38}N_4$	$W_2C_{21}H_{31}NO_6$
Colour of crystal	orange	black
Crystal dimensions (mm)	$0.15 \times 0.12 \times 0.12$	$0.80 \times 0.70 \times 0.80$
Space group	$P\bar{1}$	$P\bar{1}$
Cell dimensions		
Temperature (°C)	−155	−155
a (Å)	10.840(2)	14.890(5)
b (Å)	13.455(3)	17.576(6)
c (Å)	9.437(1)	8.854(3)
α (deg)	95.22(1)	95.43(2)
β (deg)	99.00(1)	103.90(2)
γ (deg)	105.25(1)	93.63(2)
Z (molecules/cell)	2	4
Volume (Å^3)	1298.92	2230.49
Calculated density (g cm^{-3})	1.980	2.267
Wavelength (Å)	0.71069	0.71069
Molecular weight	774.31	761.18
Linear absorption coefficient (cm^{-1})	90.606	105.653
Detector to sample distance (cm)	22.5	22.5
Sample to source distance (cm)	23.5	23.5
Average omega scan width at half height	0.25	0.25
Scan speed (deg min^{-1})	6.0	4.0
Scan width (deg + dispersion)	1.6	2.0
Individual background (s)	8	8
Aperture size (mm)	3.0×4.0	3.0×4.0
Two-theta range (°)	6–45	6–45
Total number of reflections collected	3667	5972
Number of unique intensities	3406	5851
Number of $F > 2.33\sigma(F)$	3194	
Number of $F > 3.00\sigma(F)$		5558
$R(F)$	0.0445	0.0616
$R_w(F)$	0.0477	0.0624
Goodness of fit for last cycle	1.632	1.508
Maximum δ/σ for last cycle	0.25	0.05

I = $W_2(C_9H_7)_2(NMe_2)_4$. **II** = $W_2Cp_2(NMe_2)(O_2CEt)_3$.

Structure Center and cooled to −155°C for characterization and data collection.

A systematic search of a limited hemisphere of reciprocal space located a set of diffraction maxima with no symmetry or systematic absences, indicating a triclinic space group. Subsequent solution and refinement of the structure confirmed the centrosymmetric choice, $P\bar{1}$.

Data were collected in the usual manner using a continuous θ–2θ scan with fixed backgrounds. Data were reduced to a unique set of intensities and associated sigmas in the usual manner. The structure was solved by a combination of Patterson techniques and Fourier techniques. All hydrogen atoms were clearly visible in a difference Fourier synthesis phased on the non-hydrogen parameters. All hydrogen atoms were refined isotropically and non-hydrogen atoms anisotropically in the final cycles.

No absorption correction was needed, based on an examination of ψ scans of several reflections near $\chi = 90°$. A final difference Fourier was featureless, with the largest peak being 0.75 e Å^{-1}.

$W_2Cp_2(NMe_2)(O_2CEt)_3$. A suitable crystal was located and transferred to the goniostat using standard inert atmosphere handling techniques employed by the Indiana University Molecular Structure Center and cooled to −155°C for characterization and data collection.

A systematic search of a limited hemisphere of reciprocal space located a set of diffraction maxima with no symmetry or systematic absences, indicating a triclinic space group. Subsequent solution

and refinement of the structure confirmed the centrosymmetric choice, $P\bar{1}$.

Data were collected in the usual manner using a continuous θ–2θ scan with fixed backgrounds. Data were reduced to a unique set of intensities and associated sigmas in the usual manner. The structure was solved by a combination of direct methods (MULTAN78) and Fourier techniques. Two independent molecules were located in the asymmetric cell. It was not possible to locate experimentally the hydrogen positions, so they were included as fixed atom contributors in the final cycles.

Data were corrected for absorption. A final difference Fourier indicated numerous peaks of intensity 0.9–1.8 e $Å^{-3}$ in the vicinity of the four W atoms, but was otherwise featureless.

Crystallographic materials Atomic positional parameters have been deposited with the Director, Cambridge Crystallographic Data Centre. Full details have been deposited with the Editor, Queen Mary College.

Acknowledgements—We thank the National Science Foundation for support. K.G.M. thanks the South African CSIR for financial support and the University of Durban-Westville for sabbatical leave and K.A.S. thanks NATO for a fellowship.

REFERENCES

1. M. H. Chisholm, B. W. Eichhorn, K. Folting and J. C. Huffman, *Inorg. Chim. Acta* 1988, **144**, 193.
2. M. H. Chisholm, *Angew. Chem. Intl. Ed. Engl.* 1986, **25**, 21.
3. F. Huq, W. Mowat, A. Shortland, A. C. Skapski and G. Wilkinson, *J. Chem. Soc., Chem. Commun.* 1971, 1079.
4. M. H. Chisholm, F. A. Cotton, M. W. Extine and B. R. Stults, *Inorg. Chem.* 1976, **15**, 2252.
5. W. E. Buhro, M. H. Chisholm, K. Folting and J. C. Huffman, *J. Am. Chem. Soc.* 1987, **109**, 905.
6. W. E. Buhro, M. H. Chisholm, J. C. Huffman and J. D. Martin, *J. Am. Chem. Soc.*, in press.
7. M. H. Chisholm, D. A. Haitko, K. Folting and J. C. Huffman, *J. Am. Chem. Soc.* 1981, **103**, 4046.
8. M. J. Chetcuti, M. H. Chisholm, K. Folting, D. A. Haitko, J. C. Huffman and J. Janos, *J. Am. Chem. Soc.* 1983, **105**, 1163.
9. (a) C. Ting, N. C. Baenziger and L. Messerle, *J. Chem. Soc., Chem. Commun.*, in press; (b) M. L. H. Green, A. Izquierdo, J. J. M. Polo, V. S. B. Mtetwa and K. Prout, *J. Chem. Soc., Chem. Commun.* 1983, 538.
10. H. Christina, E. McFarlane, W. McFarlane and D. S. Rycroft, *J. Chem. Soc., Dalton Trans.* 1976, 1616.
11. F. Basolo, *Inorg. Chim. Acta* 1985, **100**, 33.
12. M. H. Chisholm, D. L. Clark, J. C. Huffman, W. G. Van Der Sluys, E. M. Kober, D. L. Lichtenberger and B. E. Bursten, *J. Am. Chem. Soc.* 1987, **109**, 6796.
13. M. H. Chisholm, H. T. Chiu and J. C. Huffman, *Polyhedron* 1984, **6**, 759.
14. M. H. Chisholm, *Polyhedron* 1983, **2**, 681.
15. M. H. Chisholm, F. A. Cotton, M. W. Extine and D. C. Rideout, *Inorg. Chem.* 1978, **17**, 3536.
16. M. Akiyama, M. H. Chisholm, F. A. Cotton, M. W. Extine and C. A. Murillo, *Inorg. Chem.* 1977, **16**, 2407.
17. O. Meth-Cohn and S. Gronowitz, *J. Chem. Soc., Chem. Commun.* 1966, 81.
18. J. Sandstrom, *Dynamic NMR Spectroscopy*, pp. 79 and 109. Academic Press, New York (1982).
19. M. H. Chisholm, K. Folting, J. C. Huffman and C. C. Kirkpatrick, *Inorg. Chem.* 1984, **23**, 1021.

Polyhedron Vol. 7, No. 19/20, pp. 2001–2008, 1988
Printed in Great Britain

0277–5387/88 $3.00+.00
© 1988 Pergamon Press plc

A SQUARE-PLANAR OXO-ALKYL OF MANGANESE(III). SYNTHESIS AND X-RAY CRYSTAL STRUCTURE OF $\{Li_2[MnOMe_3] \cdot 2Li_2(Meacac) \cdot tmed\}_2$

ROBERT J. MORRIS and GREGORY S. GIROLAMI*

School of Chemical Sciences, The University of Illinois at Urbana-Champaign, Urbana, Illinois 61801, U.S.A.

Abstract—Alkylation of $Mn(acac)_3$ (acac = 2,4-pentanedionato) with five equiv. of methyllithium in diethyl ether, followed by addition of N,N,N′,N′-tetramethylethylenediamine (tmed), gives the deep red manganese(III) oxo-alkyl $[MnOMe_3^{2-}]$, which has been isolated as a lithium double salt with the 4-methyl-2-penten-2,4-diolate (Meacac) dianion. Overall, the molecular formula is $\{Li_2[MnOMe_3] \cdot 2Li_2(Meacac) \cdot tmed\}_2$. Six lithium atoms and six oxygen atoms form a hexagonal prismatic core which is capped on each hexagonal face by $Li_3(Meacac)_2 \cdot tmed$ groups. Two of the oxygen atoms of the Li_6O_6 core are part of two square-planar $[MnOMe_3^{2-}]$ centres that are slightly distorted tetrahedrally; this is a rare coordination geometry since manganese(III) is known to adopt a square-planar configuration in only one other case. The oxo group of the $[MnOMe_3^{2-}]$ unit is bonded to four lithium atoms, and there are Li···H—C interactions with two of the methyl groups on manganese. Important bond distances and angles involving the $[MnOMe_3^{2-}]$ unit are: Mn—C = 2.040(8) Å (*trans* to O), Mn—C = 2.133(8) Å (*trans* to C), Mn—O = 1.913(4) Å, O—Li = 1.91(2) Å, C—Mn—C = 88.2(3)° (*cis*), C—Mn—C = 149.1(3)° (*trans*), C—Mn—O = 98.6(2)° (*cis*), C—Mn—O = 152.5(3)° (*trans*). Crystal data for $C_{42}H_{90}N_4O_{10}Li_{12}Mn_2$ at −100°C: monoclinic, space group $P2_1/n$, $a = 10.616(3)$, $b = 18.189(4)$, $c = 14.973(4)$ Å, $\beta = 95.06(2)°$, $V = 2880(2)$ Å^3, $Z = 2$, $R_F = 0.037$, $R_{wF} = 0.042$ for 2084 data and 317 variables. The present compound is the first oxo-alkyl of manganese and only the third σ-organomanganese(III) complex of any kind.

Alkyl complexes of the transition elements were for many years thought to be inherently unstable due to the supposed weakness of the metal–carbon bond. This view was overturned by the discovery of whole classes of thermally robust transition metal peralkyls in the 1970s.[1–4] Perhaps most notable among these was the isolation by Shortland and Wilkinson of hexamethyltungsten,[5] which convincingly demonstrated that alkyl groups are in fact capable of stabilizing transition metal compounds even without the assistance of strong π-bonding ligands such as the cyclopentadienyl anion, carbon monoxide, or tertiary phosphines.

Oxo-alkyls constitute a particularly interesting class of organometallic molecules, in part because some are known to be catalytic precursors for the metathesis of alkenes.[6–8] Most of the known representatives involve third-row transition elements, and of these, rhenium forms the largest number of oxo-alkyls, as shown in a series of remarkable investigations over the past decade.[9–14] It is interesting to note that even though the first oxo-alkyl to be described was $VO(CH_2SiMe_3)_3$,[15] today there are very few other monomeric first-row examples.[16,17] We now report the synthesis and characterization of the first oxo-alkyl of manganese: $[MnOMe_3^{2-}]$. This compound is also notable for the presence of a hexagonal prismatic Li_6O_6 core, and a lithium atom coordinated by two diolate ligands in a square-planar array.

RESULTS AND DISCUSSION

We have recently described the synthesis of the remarkable permethyl manganese(III) anion, $[Li(tmed)]_2[MnMe_5]$ (**1**), which is prepared by alkylation of $Mn(acac)_3$ (acac = 2,4-pentanedionate) with eight equiv. of methyllithium.[18] This species is only the second known σ-organo-

* Author to whom correspondence should be addressed.

manganese(III) species; the interesting trigonal bipyramidal complex $Mn(2,4,6\text{-}C_6H_2Me_3)Br_2(PMe_3)_2$ (**2**) has been described previously.[19] The large excess of methyllithium is necessary for the isolation of pure $[Li(tmed)]_2[MnMe_5]$, since acac is retained in the product if fewer equivalents are used. We felt it was of interest to characterize the nature of the organometallic intermediates present during the synthesis of **1**.

The reaction of $Mn(acac)_3$ with only five equiv. of methyllithium in diethyl ether yields a dark orange solution and variable amounts of an off-white precipitate. Filtration of the solution followed by addition of N,N,N′,N′-tetramethylethylenediamine, tmed, results in the formation of dark red octahedra of a new species, **3**. Microanalytical data for **3** are consistent with the unusual stoichiometry $Li_6MnOMe_5(acac)_2 \cdot tmed$, and the IR spectrum contains a strong band at 1609 cm^{-1} that indicates the presence of acac (or acac-like) groups.[20] The complex is EPR silent. Magnetic susceptibility data in solution are consistent with a high-spin d^4 configuration for the manganese(III) centres.

The X-ray crystal structure analysis revealed that **3** is a lithium double salt whose molecular formula is best written $\{Li_2[MnOMe_3] \cdot 2Li_2(OCMe{=}CHCMe_2O) \cdot tmed\}_2$ (Figs 1–3). Crystal data are given in Table 1, while selected bond distances and angles are presented with estimated standard deviations in Table 2. Single crystals of **3** are composed of large clusters that contain 12 lithium and two manganese atoms; each cluster resides on a crystallographic inversion centre. The structure may be broken down into three parts; the $[MnOMe_3^{2-}]$ units, the "Li_6O_6" hexagonal prismatic core and the $Li_3(OCMe{=}CHCMe_2O)_2$ (tmed) caps. These will be discussed in turn.

The $[MnOMe_3^{2-}]$ *units*

The manganese(III) centres in **3** are four-coordinate and are surrounded by three methyl groups and an oxo ligand (Fig. 1). The geometry about the manganese atom may be described as a tetrahedrally-distorted square-plane or as a severely flattened tetrahedron: the "*trans*" C—Mn—C and C—Mn—O angles are 149.0(2) and 152.5(2)°, respectively. The "*cis*" C—Mn—O angles of 98.6(1)° are slightly larger than the "*cis*" C—Mn—C angles of 88.2(2)°, but all are near the 90° value for an ideal square plane.

The Mn—C distances fall into two sets: the Mn—C distances to the two methyl groups *trans* to each other are 2.114(4) Å, while the Mn—C distance to the methyl group *trans* to the oxo ligand is 2.041(5) Å. This 0.07 Å difference is most reasonably ascribed to the strong *trans* influence of the methyl groups. These distances may be compared with the 2.089(8) Å Mn—C distance in the manganese(III) aryl $Mn(2,4,6\text{-}C_6H_2Me_3)Br_2(PMe_3)_2$ (**2**).[19]

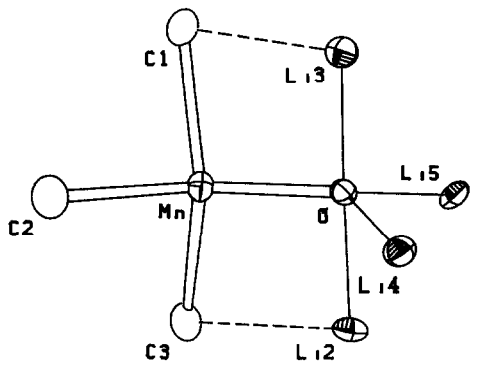

Fig. 1. Structure of the $[MnOMe_3^{2-}]$ unit and associated lithium atoms.

The Mn—O distance of 1.912(3) Å is rather long and indicates that there is little if any π-bonding present. For comparison, other manganese(III) oxo complexes in which the oxo ligand bridges between two or three metal centres typically exhibit Mn—O distances of 1.80–1.85 Å.[21–23] The oxygen atom is surrounded by four lithium atoms at distances of 1.87–1.92 Å, and these Li—O interactions are undoubtedly responsible for the lack of π-bonding between the oxo ligand and the manganese centre. If one includes the lithium atoms, the coordination environment about the oxo group is approximately trigonal bipyramidal, with atoms Li(2) and Li(3)

Table 1. Crystal data for **3** at −100°C

Space group: $P2_1/n$	$V = 2880(2)$ Å^3
$a = 10.616(3)$ Å	$Z = 2$
$b = 18.189(4)$ Å	Mol. wt = 1004.37
$c = 14.973(4)$ Å	$d_{calc} = 1.158$ g cm^{-3}
$\beta = 95.06(2)°$	$\mu_{calc} = 4.67$ cm^{-1}
$\alpha = \gamma = 90°$	Size = 0.3 × 0.3 × 0.4 mm

Diffractometer: Enraf–Nonius CAD4
Radiation: Mo-$K_{\bar{\alpha}}$, $\bar{\lambda} = 0.71073$ Å
Monochromator: graphite crystal, $2\theta = 12°$
Scan range, type: $2.0 \leqslant 2\theta \leqslant 41.0°$, ω/θ
Scan speed, width: 2–8° min^{-1},
$\Delta\omega = 1.50(1.00 + 0.35 \tan\theta)°$
Reflections: 3294, 2881 unique, 2084 with $I > 2.58\sigma(I)$

$R_F = 0.037$	Variables = 317
$R_{wF} = 0.042$	p factor = 0.020

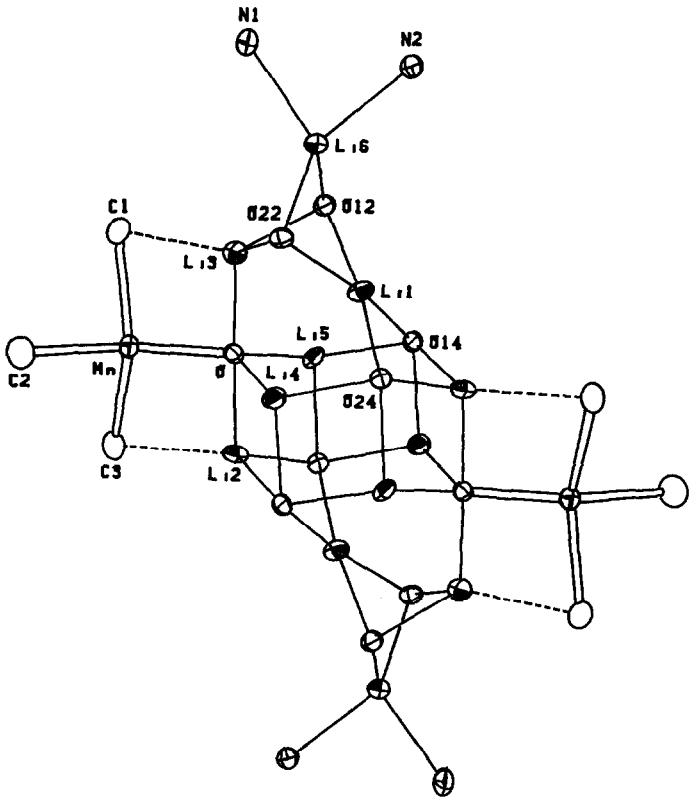

Fig. 2. Structure of **3** showing the cluster geometry. The carbon backbones of the Meacac groups that connect O(12) to O(14) and O(22) to O(24) have been omitted for clarity, as have the carbon atoms of the tmed ligands.

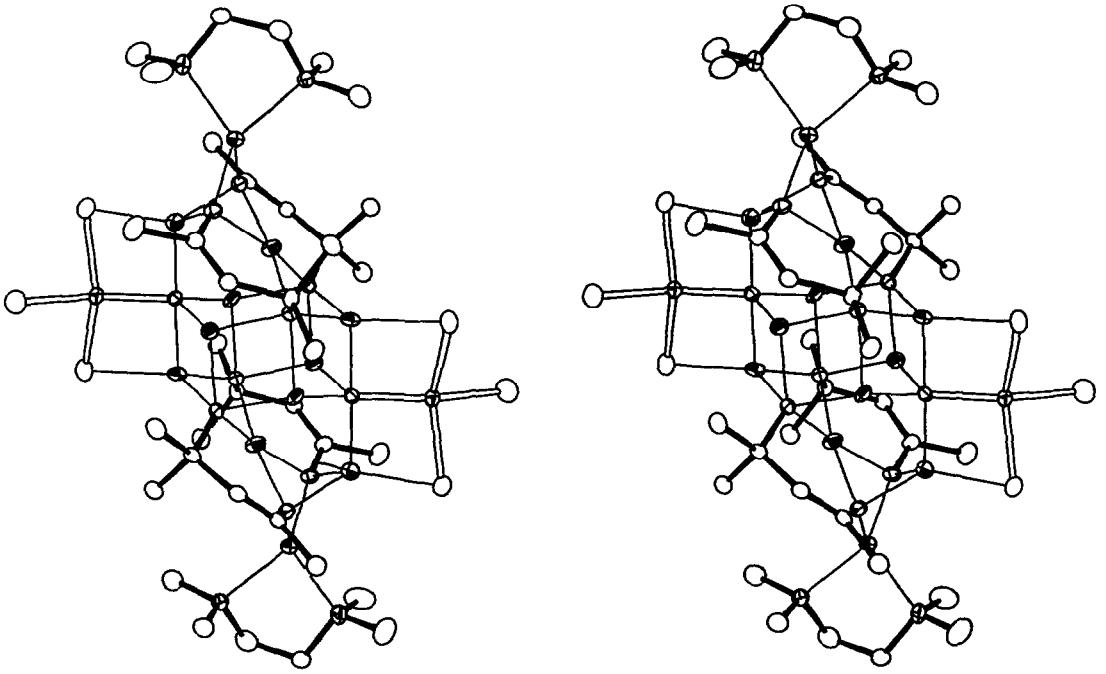

Fig. 3. Stereoview of the complete structure of **3**.

Table 2. Selected distances (Å) and angles (°) for **3** with ESDs in parentheses

(A) The $[MnOMe_3^{2-}]$ unit

Distances

Mn—C(1)	2.122(4)	O—Li(3)	1.869(7)
Mn—C(2)	2.041(5)	O—Li(4)	1.918(7)
Mn—C(3)	2.106(4)	O—Li(5)	1.914(7)
Mn—O	1.912(3)	C(1)···Li(3)	2.245(8)
O—Li(2)	1.918(7)	C(3)···Li(2)	2.355(8)

Angles

C(1)—Mn—C(2)	88.1(2)	Mn—O—Li(4)	119.9(2)
C(2)—Mn—C(3)	88.2(2)	Mn—O—Li(5)	132.6(2)
C(1)—Mn—C(3)	149.0(2)	Li(2)—O—Li(3)	177.1(3)
C(1)—Mn—O	98.4(1)	Li(2)—O—Li(4)	79.2(3)
C(3)—Mn—O	98.9(1)	Li(2)—O—Li(5)	77.7(3)
C(2)—Mn—O	152.5(2)	Li(3)—O—Li(4)	102.2(3)
Mn—O—Li(2)	92.3(2)	Li(3)—O—Li(5)	99.4(3)
Mn—O—Li(3)	89.2(2)	Li(4)—O—Li(5)	103.8(3)

(B) The "Li_6O_6" hexagonal prism[a]

Distances

Li(2)—O(14)	1.953(7)	Li(4)—O(24)	1.958(7)
Li(2)—O(24)	1.895(7)	Li(5)—O(14)	1.942(7)
Li(4)—O(14)	1.995(7)	Li(5)—O(24)	2.027(7)

Angles

Li(2)—O(14)—Li(4)	76.5(3)	Li(5)—O(24)—Li(1)	131.8(3)
Li(2)—O(14)—Li(5)	126.5(3)	O—Li(2)—O(14)	102.9(3)
Li(4)—O(14)—Li(5)	80.0(3)	O—Li(2)—O(24)	105.6(3)
Li(2)—O(24)—Li(4)	126.0(3)	O(14)—Li(2)—O(24)	94.9(3)
Li(2)—O(24)—Li(5)	75.5(3)	O—Li(4)—O(14)	101.3(3)
Li(4)—O(24)—Li(5)	78.9(3)	O—Li(4)—O(24)	119.2(4)
Li(2)—O(14)—Li(1)	79.6(3)	O(14)—Li(4)—O(24)	100.6(3)
Li(4)—O(14)—Li(1)	131.9(3)	O—Li(5)—O(14)	119.0(4)
Li(5)—O(14)—Li(1)	81.7(3)	O—Li(5)—O(24)	100.8(3)
Li(2)—O(24)—Li(1)	81.9(3)	O(14)—Li(5)—O(24)	100.0(3)
Li(4)—O(24)—Li(1)	81.1(3)		

(C) The $Li_3(Meacac)_2 \cdot$ tmed caps[a]

Distances

Li(1)—O(14)	2.014(7)	Li(6)—O(12)	1.912(7)
Li(1)—O(24)	1.978(7)	Li(6)—O(22)	1.941(7)
Li(1)—O(12)	2.016(7)	Li(6)—N(1)	2.153(8)
Li(1)—O(22)	2.098(7)	Li(6)—N(2)	2.177(8)
Li(3)—O(12)	1.938(7)	C(12)—O(12)	1.343(5)
Li(3)—O(22)	1.939(7)	C(24)—O(24)	1.422(4)

Angles

O(12)—Li(1)—O(14)	95.7(3)	Li(3)—O(12)—Li(6)	84.4(3)
O(22)—Li(1)—O(24)	95.4(3)	Li(1)—O(22)—Li(3)	72.2(3)
O(12)—Li(1)—O(22)	77.4(3)	Li(1)—O(22)—Li(6)	86.0(3)
O(14)—Li(1)—O(24)	90.4(3)	Li(3)—O(22)—Li(6)	83.6(3)
O(12)—Li(1)—O(24)	171.2(4)	O(12)—Li(6)—O(22)	83.8(3)
O(22)—Li(1)—O(14)	166.8(4)	O(12)—Li(6)—N(1)	128.3(4)
O—Li(3)—O(12)	113.1(4)	O(12)—Li(6)—N(2)	114.0(3)
O—Li(3)—O(22)	108.5(4)	O(22)—Li(6)—N(1)	117.7(4)
O(12)—Li(3)—O(22)	83.1(3)	O(22)—Li(6)—N(2)	134.7(4)
Li(1)—O(12)—Li(3)	74.1(3)	N(1)—Li(6)—N(2)	84.7(3)
Li(1)—O(12)—Li(6)	89.2(3)		

[a] Some pertinent distances and angles appear earlier in the table.

occupying the axial positions. Although the chemical source of the oxo ligand has not been determined, it most likely arises from trace hydrolysis or the presence of LiOH in the methyllithium stock solution.

There are two short Li···C contacts that involve the methyl groups on manganese. The C(1)—Li(3) and C(3)—Li(2) distances of 2.25 and 2.36 Å, respectively, are well within the 2.60 Å sum of the van der Waals radius of a methyl group and the ionic radius of a lithium atom.[24] In fact, the Li—C distances in methyllithium itself have been determined from powder diffraction data to be 2.31 Å within a tetrahedral unit and 2.36 Å between tetrahedral units;[25] more recent studies show that other alkyllithium complexes have Li—C bond distances that are typically 2.23–2.27 Å.[26–28] Furthermore, the calculated H···Li distances to the hydrogen atoms H(1b) and H(1c) on carbon C(1) are rather short at 2.09 Å. Accordingly, the Li···HC interactions in **3** are quite strong and undoubtedly influence the structure and stability of the $[MnOMe_3^{2-}]$ unit.

The square-planar geometry about manganese is very unusual, and only one other example has been reported: the Mn^{III} dithiolato complex $[PPh_4][Mn(S_2C_6H_3Me)_2]$.[29] Although this species and **3** are similar in that they both are high-spin ($S = 2$), the dithiolato complex is not tetrahedrally distorted and by contrast is essentially flat. Square-planar geometries, while exceedingly rare for manganese(III), are more commonly observed for isoelectronic chromium(II).[30,31] The d^4 electronic configuration half fills the four low-lying *d*-orbitals characteristic of square-planar ligand arrays.

It is interesting to note that the four-coordinate d^4 iron(IV) alkyl Fe(norbornyl)$_4$ is *not* square-planar but adopts a *diamagnetic* tetrahedral geometry instead.[32] In this case, the four *d*-electrons exactly fill the *E* orbitals under tetrahedral symmetry. The large ligand field splitting present in Fe(norbornyl)$_4$ is a consequence of the strong-field nature of alkyl groups and the high oxidation state of the iron centre. It is possible that the tetrahedral distortion observed in the d^4 manganese oxo-alkyl **3** is also a consequence of a high ligand–field splitting; presumably, if the ligand–field splitting were only slightly larger, the $[MnOMe_3^{2-}]$ unit would be tetrahedral and low-spin.

The "Li_6O_6" *hexagonal prismatic core*

Six lithium atoms, two oxo groups from the $[MnOMe_3^{2-}]$ units, and four oxygen atoms from the OCMe=CHCMe$_2$O diolate ligands (see below) are connected together in the centre of the structure to form a Li_6O_6 hexagonal prismatic core (Fig. 2). The hexagonal faces are not exactly planar but instead adopt chair conformations.

The Li—O distances within the hexagonal prism are reasonably regular; they vary from 1.87 to 2.03 Å and average 1.94 Å. The four Li—O distances involving the oxo ligand appear to be slightly shorter at 1.90 Å than the remaining six Li—O distances, which average 1.96 Å. This difference, if real, probably reflects a partial negative charge on the Mn—O oxygen atom that is higher than the charge on the ene-diolate oxygens. Lithium–oxygen distances in $[LiL_x^+]$ species, where L is a Lewis base such as $OPPh_3$ or tetrahydrofuran, are typically 1.97 Å,[28] whereas in Li_2O the distance is 2.00 Å.[33]

All of the lithium centres in the Li_6O_6 core are bonded to three oxygen atoms to give pyramidal coordination geometries. The O—Li—O angles vary from 94.9(3) to 119.2(4)° and average 104.9°. In addition, Li(2) interacts with methyl group C(3) as described above to give a roughly tetrahedral O_3C environment. The ene-diolate oxygen atoms that form the Li_6O_6 core all possess square-pyramidal geometries, with "*cis*" and "*trans*" Li—O—Li angles across the square base that average 79.4 and 129.0°, respectively.

The $Li_2(Meacac)_2 \cdot$ tmed *caps*

Capping each hexagonal face of the hexagonal bipyramid is a tri-lithium unit in which the three lithium atoms adopt very different coordination geometries (Fig. 3). One of these lithium sites, Li(3), is bonded to three oxygen atoms in a pyramidal arrangement, and is also interacting with methyl group C(1) on manganese. As for Li(2) discussed above, this Li···C interaction completes a tetrahedral O_3C coordination environment. A second lithium site, Li(6), possesses a tetrahedral O_2N_2 coordination environment; the Li—N distances to the bound tmed ligand average 2.17 Å.

The third lithium atom, Li(1), adopts an unusual square-planar geometry. It is surrounded by two chelating diolate ligands with relatively long Li—O distances that average 2.03 Å. The *cis* and *trans* O—Li—O angles average 89.7 and 169.0°, respectively. Square-planar lithium centres are rare but have been observed in Li(acac), which adopts a structure with square-planar $[Li(acac)_2^-]$ anions and tetrahedral Li^+ cations.[34]

The 4-methyl-2-penten-2,4-diolate (Meacac) ligands that chelate the square-planar lithium centres have localized C=C double bonds of 1.338 Å [C(12)—C(13) and C(22)—C(23)] in the carbon backbone; the remaining C—C bond lengths are all between 1.50 and 1.53 Å. The C—O single bond distances are, however, significantly different: the

Scheme 1.

C(sp^2)—O bonds average 1.344 Å while the C(sp^3)—O bonds average 1.438 Å. It has been noted that single bonds adjacent to multiple bonds tend to be 0.03 Å shorter than single bonds in saturated compounds,[35] but this effect is not sufficient to account for the observed 0.09 Å difference. Instead, there must be some partial double-bond character to the C(sp^2)—O bond as indicated by the resonance structures in Scheme 1.

The Meacac ligands arise from the C-alkylation of 2,4-pentanedionate anions at a carbonyl carbon. This contrasts sharply with the well-known regiochemistry of the C-alkylation of pentanedionate anions with alkyl halides (R^+); these reactions occur exclusively at the methine carbon atom.[36] Whereas addition of alkyllithium and related reagents to carbonyl functionalities (ketones, esters, etc.) is a fundamental carbon–carbon bond-forming reaction, nucleophilic attack of R^- on pentanedionate anions is rare as expected from charge considerations. The only example of such a transformation in the literature is the reaction between $AlMe_2(acac)$ and $AlMe_3$, which yields a bridging 4-methyl-2-penten-2,4-diolate ligand:[37,38]

$$Me_2Al(acac) + AlMe_3 \rightarrow Me_2Al{-}OCMe{=}CHCMe_2O{-}AlMe_2.$$

The Li(1)···Li(3) separation in the tri-lithium caps of 2.38(1) Å is the shortest such distance in the entire structure, although the Li(2)···Li(5) and Li(2)···Li(4) contacts within the hexagonal prism of 2.40(1) and 2.44(1) Å, respectively, are only slightly longer. We do not consider that these distances are short enough to be chemically significant; for comparison, the Li···Li separations in alkyllithium species are typically 2.45–2.60 Å.[25–28] Recently, Li···Li separations as short as 2.20(1) Å have been reported,[39] although the high unweighted *R*-factor (13.5%) combined with the relatively poor X-ray scattering power of lithium suggest that the reported uncertainty in this distance is underestimated significantly. In any case, the Li···Li separations in **3** are largely dictated by the distances and angles to the oxygen atoms to which they are attached.

CONCLUSIONS

The reaction of $Mn(acac)_3$ with five equiv. of methyllithium has produced the first manganese oxo-alkyl species [$MnOMe_3^{2-}$], which in addition is only the third σ-organomanganese(III) compound of any kind. The coordination geometry around the manganese centre is best described as a square-planar array which exhibits a slight tetrahedral distortion. The [$MnOMe_3^{2-}$] unit is part of an unusual Li—O cluster whose framework consists of 12 lithium and 10 oxygen atoms. Four 4-methyl-2-penten-2,4-diolate (Meacac) dianions are present that are the result of methylation of 2,4-pentanedionate anions at a carbonyl carbon. The main feature of the Li—O cluster array is a Li_6O_6 hexagonal prismatic core which is capped on each hexagonal face by $Li_3(Meacac)_2 \cdot$ tmed groups. The most interesting of the lithium atom environments in these caps is a square-planar coordination geometry formed by two chelating Meacac dianions.

The isolation of the present compound adds to the small but growing class of high-valent manganese alkyl complexes.[18,19,40] The existence of these species suggests that while the high-valent manganese species studied to date invariably react with organic substrates via electron transfer, i.e. radical pathways,[41–46] there is a significant chemistry of organic groups bound directly to a tri- or tetravalent manganese centre.

EXPERIMENTAL

All operations were carried out in vacuum or under argon. Diethyl ether was distilled under nitrogen from sodium–benzophenone immediately before use. Tris(2,4-pentanedionato)manganese(III), $Mn(acac)_3$, was prepared by a literature route.[47] Methyllithium (Aldrich) was filtered before use, and N,N,N′,N′-tetramethylethylenediamine (Aldrich) was distilled from sodium.

Microanalyses were performed by Mr Josef Nemeth and Mr Thomas McCarthy of the University of Illinois Microanalytical Laboratory. The IR spectra were recorded on a Perkin–Elmer 599B IR spectrometer as Nujol mulls. The ^1H NMR data were obtained on a General Electric QE-300 spectrometer at 300 MHz. The X-band EPR experiments were performed on a Varian E-9 instrument using frozen toluene solutions at −196°C. Magnetic moments were determined by a modification of Evans' method.[48] Melting points were measured on a Thomas–Hoover Unimelt apparatus in closed capillaries under argon.

$\{Li_2[MnOMe_3]\cdot 2Li_2(OCMe{=}CHCMe_2O)\cdot tmed\}_2$

To a cold (0°C) suspension of $Mn(acac)_3$ (0.57 g, 1.6 mmol) in diethyl ether (50 cm^3) was added methyllithium (5.1 cm^3 of a 1.63 M solution in diethyl ether, 8.3 mmol) dropwise over 10 min. The solution turned yellow initially and then orange upon completion of the addition. After being stirred for 20 min, the mixture was warmed to room temperature and stirred for 2 h to give a dark orange–red solution and a small amount of off-white precipitate. To the twice-filtered orange–red solution was added N,N,N′,N′-tetramethylethylenediamine (0.96 g, 8.3 mmol), which caused the solution to become darker red. Cooling to −20° gave dark red prisms. Two additional crops were obtained from the supernatant. (Note: the yield of this procedure varies and is apparently dependent on the amount of hydroxide impurity present during the synthesis.) Yield: 0.28 g (35%). M.p. 165°C(dec.). Magnetic moment (toluene, 25°C): 4.9 μ_B per Mn.

IR(cm^{-1}): 2789m, 1609s, 1367s, 1349s, 1291w, 1229m, 1219m, 1160s, 1131w, 1038w, 1021w, 972m, 949s, 899w, 819w, 799w, 743m, 644m, 619m, 569s, 539s, 501s, 464s, 429s.

Crystallographic studies[49]

Single crystals of the complex, grown from diethyl ether, were sealed in thin-walled glass capillaries under argon. Preliminary photographs yielded rough cell dimensions, and a suitable crystal was transferred to the diffractometer. Standard peak search and automatic indexing procedures, followed by least-squares refinement using 25 reflections yielded the cell dimensions given in Table 1.

Data were collected in one quadrant of reciprocal space ($\pm h, +k, -l$) using measurement parameters listed in Table 1. The crystal was loose in the capillary, and recentring was performed after nearly every orientation test (400 reflections/test). However, no other problems were encountered during data collection and there was no change in the appearance of the sample during the experiment. Systematic absences for $h0l$, $h+l \neq 2n$ and $0k0$, $k \neq 2n$ were consistent only with space group $P2_1/n$. The measured intensities were reduced to structure factor amplitudes and their ESDs by correction for background, scan speed, and Lorentz and polarization effects. While corrections for crystal decay were unnecessary, absorption corrections were applied, and the maximum and minimum transmission factors were 0.881 and 0.818. Systematically absent reflections were deleted, and symmetry equivalent reflections were averaged to yield the set of unique data. Only those data with $I > 2.58\sigma(I)$ were used in the least-squares refinement.

The structure was solved using direct methods by Patterson (SHELX-86) and weighted difference Fourier methods. The positions of the manganese atoms were deduced from a vector map, and a partial structure expansion gave positions for the carbon and oxygen atoms adjacent to manganese. Subsequent least-squares difference Fourier calculations revealed positions for the remaining non-hydrogen atoms. The quantity minimized by the least-squares program was $\Sigma w(|F_o|-|F_c|)^2$, where $w = 1.33/(\sigma(F_o)^2+(pF_o)^2)$. The analytical approximations to the scattering factors were used, and all structure factors were corrected for both the real and imaginary components of anomalous dispersion. In the final cycle of least-squares, all non-hydrogen atoms were independently refined with anisotropic thermal coefficients, and a group isotropic thermal parameter was varied for the hydrogen atoms, which were fixed in "idealized" positions with C—H = 0.95 Å. Successful convergence was indicated by the maximum shift/error of 0.007 in the last cycle. Final refinement parameters are given in Table 1. The final difference Fourier map had no significant features. A final analysis of variance between observed and calculated structure factors showed a slight dependence on $\sin\theta$.

Acknowledgements—We thank the National Science Foundation, the Office of Naval Research under their Young Investigator Award Program, and Lubrizol for a Fellowship to R.J.M. G.S.G. is the recipient of an A. P. Sloan Research Fellowship (1988–1990). We also thank Dr Scott Wilson, Charlotte Stern and Connie Odle of the University of Illinois X-ray Crystallographic Laboratory for the crystal structure determination.

REFERENCES

1. G. Wilkinson, *Science* 1974, **185**, 109.
2. G. Wilkinson, *Pure Appl. Chem.* 1972, **30**, 627.
3. R. R. Schrock and G. W. Parshall, *Chem. Rev.* 1976, **76**, 243.
4. P. J. Davidson, M. F. Lappert and R. Pearce, *Chem. Rev.* 1976, **76**, 219.
5. A. J. Shortland and G. Wilkinson, *J. Chem. Soc., Dalton Trans.* 1973, 872.
6. J. H. Wengrovius and R. R. Schrock, *Organometallics* 1982, **1**, 148.
7. R. H. A. Bosma, G. C. N. Van der Aardweg and J. C. Mol, *J. Organomet. Chem.* 1983, **255**, 159.

8. J. Kress, M. Wesolek, J. P. LeNy and J. A. Osborn, *J. Chem. Soc., Chem. Commun.* 1981, 1039.
9. K. Mertis, D. H. Williamson and G. Wilkinson, *J. Chem. Soc., Dalton Trans.* 1975, 607.
10. K. Mertis and G. Wilkinson, *J. Chem. Soc., Dalton Trans.* 1976, 1488.
11. P. Stavropoulos, P. G. Edwards, G. Wilkinson, M. Motevalli, K. M. A. Malik and M. B. Hursthouse, *J. Chem. Soc., Dalton Trans.* 1985, 2167.
12. P. Stavropoulos, P. G. Edwards, T. Behling, G. Wilkinson, M. Motevalli and M. B. Hursthouse, *J. Chem. Soc., Dalton Trans.* 1987, 169.
13. P. D. Savage, G. Wilkinson, M. Motevalli and M. B. Hursthouse, *J. Chem. Soc., Dalton Trans.* 1988, 669.
14. I. R. Beattie and P. J. Jones, *Inorg. Chem.* 1979, **18**, 2318.
15. W. Mowat, A. Shortland, G. Yagupsky, N. J. Hill, M. Yagupsky and G. Wilkinson, *J. Chem. Soc., Dalton Trans.* 1972, 533.
16. K. H. Thiele, B. Adler, H. Grahlert and A. Lachowicz, *Z. Anorg. Allg. Chem.* 1974, **403**, 279.
17. A. Lachowicz and K. H. Thiele, *Z. Anorg. Allg. Chem.* 1977, 431, 88.
18. R. J. Morris and G. S. Girolami, *J. Am. Chem. Soc.*, in press.
19. R. J. Morris and G. S. Girolami, *Organometallics* 1987, **6**, 1815.
20. K. Nakamoto, *Infrared and Raman Spectra of Inorganic and Coordination Compounds*, 3rd Edn, p. 249. Wiley, New York (1978).
21. J. B. Vincent, H.-R. Chang, K. Folting, J. C. Huffman, G. Christou and D. N. Hendrickson, *J. Am. Chem. Soc.* 1987, **109**, 5703.
22. K. Wieghardt, V. Bossek, L. Zsolnai, G. Huttner, G. Blondin, J.-J. Girerd and F. Babonneau, *J. Chem. Soc., Chem. Commun.* 1987, 651.
23. K. S. Hagen, W. H. Armstrong and H. Hope, *Inorg. Chem.* 1988, **27**, 969.
24. L. Pauling, *The Nature of the Chemical Bond*, 3rd Edn. Cornell University Press, Ithaca, NY (1960).
25. E. Weiss and G. Hencken, *J. Organomet. Chem.* 1970, **21**, 265.
26. H. Köster, D. Thoennes and E. Weiss, *J. Organomet. Chem.* 1978, **160**, 1.
27. H. Dietrich, *J. Organomet. Chem.* 1981, **205**, 291.
28. W. N. Setzer and P. von Rague Schleyer, *Adv. Organomet. Chem.* 1985, **24**, 353.
29. G. Henkel, K. Greiwe and B. Krebs, *Angew. Chem., Int. Ed. Engl.* 1985, **24**, 117.
30. A. R. Hermes, R. J. Morris and G. S. Girolami, *Organometallics*, in press.
31. L. F. Larkworthy, K. B. Nolan and P. O'Brien, *Comprehensive Coordination Chemistry* (Edited by G. Wilkinson, R. D. Gillard and J. A. McCleverty), Chap. 35, Table 41. Pergamon Press, New York (1987).
32. B. K. Bower and H. G. Tennant, *J. Am. Chem. Soc.* 1972, **94**, 2512.
33. J. M. Bijvoet and A. Karssen, *Rec. Trav. Chim. Pays-Bas*, 1924, **43**, 680.
34. F. A. Schroder and H. P. Weber, *Acta Cryst. Sect. B.* 1975, **31**, 1745.
35. L. S. Bartell, *J. Chem. Ed.* 1968, **45**, 754.
36. A. W. Johnson, E. Markham and R. Price, *Org. Synth.* 1962, **42**, 75.
37. S. Pasynkiewicz and K. Dowbor, *J. Organomet. Chem.* 1974, **78**, 49.
38. W. R. Kroll and W. Naegele, *J. Organomet. Chem.* 1969, **19**, 439.
39. D. Barr, W. Clegg, S. M. Hodgson, R. E. Mulvey, D. Reed, R. Snaith and D. S. Wright, *J. Chem. Soc., Chem. Commun.* 1988, 367.
40. C. G. Howard, G. S. Girolami, G. Wilkinson, M. Thornton-Pett and M. B. Hursthouse, *J. Chem. Soc., Chem. Commun.* 1983, 1163.
41. J. A. Smegal, B. C. Schardt and C. L. Hill, *J. Am. Chem. Soc.* 1983, **105**, 3510.
42. J. A. Smegal and C. L. Hill, *J. Am. Chem. Soc.* 1983, **105**, 3515.
43. J. T. Groves, W. J. Kruper and R. L. Haushalter, *J. Am. Chem. Soc.* 1980, **102**, 6375.
44. D. Mansuy, J.-F. Bartoli and M. Momenteau, *Tetrahedron Lett.* 1982, **23**, 2781.
45. M. Perree-Fauvet and A. Gaudemer, *J. Chem. Soc., Chem. Commun.* 1981, 874.
46. B. R. Cook, T. J. Reinert and K. S. Suslick, *J. Am. Chem. Soc.* 1986, **108**, 7281.
47. M. N. Bhattacharjee, M. K. Choudhuri and D. T. Khathing, *J. Chem. Soc., Dalton Trans.* 1982, 669.
48. D. F. Evans, G. V. Fazakerley and R. F. Phillips, *J. Chem. Soc. A* 1971, 1931.
49. For a full description of the crystallographic procedure, see J. A. Jensen, S. R. Wilson and G. S. Girolami, *J. Am. Chem. Soc.* 1988, **110**, 4977.

Polyhedron Vol. 7, No. 19/20, pp. 2009–2014, 1988
Printed in Great Britain

0277–5387/88 $3.00+.00
© 1988 Pergamon Press plc

THE SELECTIVE OLIGOMERIZATION OF BUTENES BY NICKEL-BASED CATALYSTS*

STEPHEN J. BROWN, ANTHONY F. MASTERS† and MILAN VENDER

Department of Inorganic Chemistry, University of Sydney, NSW 2006, Australia

Abstract—The compounds Ni(sacsac)P($L^1L^2L^3$)X (sacsac = pentane-2,5-dithionato, L^j = alkyl or aryl, X = halogen) catalyse the oligomerization and isomerization of *n*-butenes at room temperature under autogeneous pressure. The oligomerization proceeds with high selectivity for dimers. The concentration of butene as a function of time is described by $\ln(\text{butene}) = A\exp(Bt)+C$. The product selectivity and the parameters *A*, *B* and *C* are controlled by the choice of phosphine ligand.

Olefin oligomerization is a pivotal process in the catalytic production of fuels and speciality chemicals from low molecular weight olefins. A number of 16-electron nickel complexes generate extremely active olefin oligomerization catalysts when activated by a suitable co-catalyst. These catalysts are commonly of the Ziegler–Natta type and have been extensively investigated.[1–4] Several processes have been commercialized including Shell's higher olefin process[5] and the Dimersol™[6] process.

Many catalytic systems are prepared by "activating" organonickel compounds with strong Lewis acids and enzyme-like activity has been reported in one case.[7] It has been observed that the ligands bonded to the catalyst exhibit product-directing effects.[2,3] Hence, synthetic flexibility in the ligands present on the catalyst precursor is important in obtaining optimum product distribution. Keim[8–11] and others[12,13] have proposed that the use of chelating ligands in nickel-based systems can be remarkably effective in this regard.

Air-stable 16-electron nickel complexes of the general formula Ni(R^2—R^1sacR^3sac)X($PL^1L^2L^3$) (R = alkyl or aryl, X = halide, L = alkyl or aryl, sacsac$^-$ = $C_5H_7S_2^-$ = dithioacetylacetonate anion = pentane-2,5-dithionate anion) (**I**) when activated by a suitable co-catalyst under mild conditions form extremely active olefin oligomerization and isomerization catalysts.[14,15]

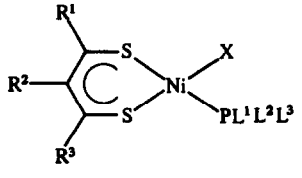

I

We have investigated the kinetics and product distribution of a series of reactions between butenes and catalysts derived from **I** ($R^1 = R^3 = CH_3$, R^2 = H) but with differing phosphine ligands. An empirical mathematical model has been developed for the reaction (excluding the initial period) which can predict the activity of the catalyst to a high degree of accuracy. Butenes are convenient substrates for kinetic study because reaction rates are manageable unlike the much more highly active lower olefins. A preliminary account of this work has appeared.[16]

RESULTS AND DISCUSSION

The catalyst system based on (**I**) and Et_2AlCl is extremely active and selective in the oligomerization of butenes. This catalyst system has also been shown to be a very active double bond shift olefin isomerization catalyst.[14] Skeletal isomerization is not accommodated by the conventional mechanism.[3] Thus, *n*-butenes are rapidly isomerized as well as oligomerized, and similar results are obtained when starting with any of the *n*-butenes, since the thermodynamic equilibrium mixture of *n*-butenes is rapidly and completely established at the start of the reaction. Similarly, the isomerization of 1-octene is extremely rapid. The isomerization of 1-hexene is too rapid to measure by these techniques even at −78°C.[17] The composition of the oligomerization products can be controlled by varying the substituents on the coordinated phosphine as illustrated in Fig. 1.

For the limited range of phosphines used in the

* Dedicated to Professor Sir Geoffrey Wilkinson on the occasion of his retirement.

† Author to whom correspondence should be addressed.

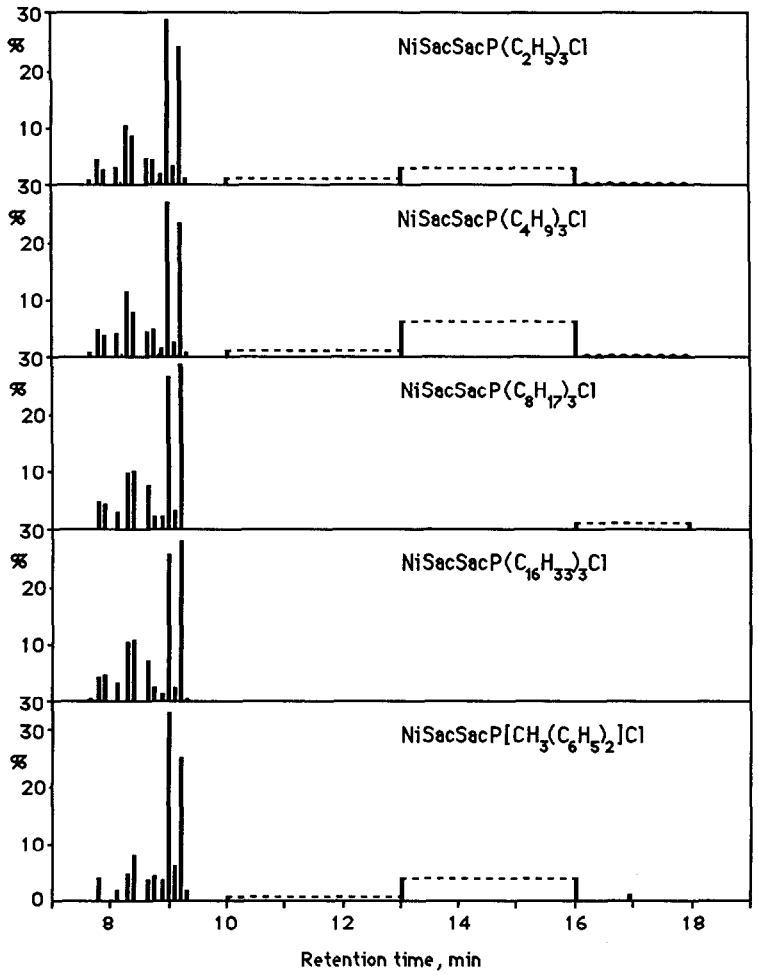

Fig. 1. The relative content of individual components in the final reaction mixtures for catalysts generated from the various Ni(sacsac)(PR_3)Cl derivatives. Peaks with 7.5 < retention time (RT) < 9.5 min correspond to C_8 olefins, peaks with 10 < RT < 13 min correspond to C_{12} olefins, peaks with 13 < RT < 16 min correspond to C_{16} olefins, and peaks with 16 < RT < 20 min correspond to C_{20} olefins.

present investigation, the most significant difference in the product distributions seems to be the higher dimer selectivity for the long chain phosphines. These differences probably reflect steric effects, but within the octene isomers the differences are less striking. The range of substituents examined is limited, however, there appears to be a difference in the octene isomer distribution between catalysts with aliphatic and aromatic substituents.

For all catalysts tested, the butene concentration varied non-linearly with time, and was found empirically to obey the relationship

$$\ln(m_b) = A\exp(Bt) + C \qquad (1)$$

where m_b is the mass of residual butene, and A, B and C are empirical constants specific to individual catalysts. This behaviour is illustrated in Fig. 2 for the catalyst derived from Ni(sacsac)(PEt_3)Cl. After an initial period during which the data systematically deviate from the line, the regression is followed closely.

All experiments showed the same behaviour with values of the index of determination reaching or exceeding 0.99. However, in all cases, the systematic deviation from linearity was observed in the initial stages of the experiment. This initial period can be as long as 30–45 min in some cases. During this initial period, the reaction rate is higher than expected from the regression.

Some caution should attend interpretation of the data for this initial period. The precision of the data obtained during this period is somewhat low due to the rapid, presumably highly exothermic reaction(s) and the time lag in the response of the measuring system. Data is least reliable during the first 15 min of the reaction. Thus, the catalytic behaviour during

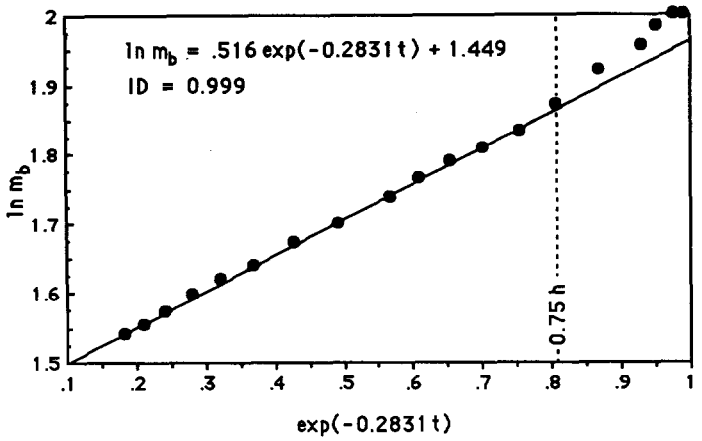

Fig. 2. Typical pattern of the correlation of experimental data. The points represent the experimental data, the solid line is obtained from the regression analysis. The catalyst is derived from Ni(sacsac)(PEt_3)Cl/Et_2AlCl.

this period can be interpreted only qualitatively. Nevertheless, the catalytic behaviour during the bulk of the experiment can be described with high precision.

Dumas and Hsu[18] have examined the kinetics of butadiene polymerization catalysed by homogeneous nickel-based species. They showed that the behaviour described by eq. (1) is consistent with (i) "instantaneous" activation of, (ii) a single catalytic species, (iii) the oligomerization reaction being first order in both substrate and catalyst [eq. (2)], and (iv) the disappearance of the active form of the catalyst being first order in catalyst [eq. (3)].

$$\frac{\partial m_b}{\partial t} = -k_b m_b m_c \tag{2}$$

$$\frac{\partial m_c}{\partial t} = -k_c m_c \tag{3}$$

where m_b and m_c are the masses of residual butene and catalyst, respectively, and k_b and k_c are the oligomerization and catalyst disappearance rate constants, respectively. These assumptions lead to the expression

$$\ln\left(\frac{m_b}{(m_b)_0}\right) = \frac{k_b}{k_c}(m_c)_0[\exp(-k_c t) - 1] \tag{4}$$

which is of the form of eq. (1) with $(m_b)_0$ and $(m_c)_0$ being the initial amounts of butene and catalyst, respectively. Values for k_b and k_c can be extracted from the experimental data by an iterative process maximizing the index of determination. These data are included in Table 1. The magnitude of k_b is clearly dependent on the nature of the phosphine substituent, consistent with the substituent dependence of propylene oligomerization.[14,15] However, the values of k_c are much less sensitive to the nature of the phosphine, particularly for the trialkylphosphine derivatives. Table 1 also illustrates that the initial amount of butene calculated from the regression data agrees well with the measured amount. Thus, in spite of the initial deviations, the regression function yields experimentally meaningful data.

This model also provides estimates of the rate of butene conversion (amount of reacted butene per

Table 1. Parameters from the regression data

Catalyst precursor	k_c (h^{-1})	k_b ($g^{-1}\,h^{-1}$)	$(m_b)_0$ (g) Actual	$(m_b)_0$ (g) Calculated
Ni(sacsac)($P(C_2H_5)_3$)Cl	0.285±0.002	10.8±1.9		7.30±0.01
Ni(sacsac)($P(C_4H_9)_3$)Cl	0.365±0.047	12.6±0.1		7.27±0.40
Ni(sacsac)($P(C_8H_{17})_3$)Cl	0.382±0.021	6.8±0.9	7.50±0.05	7.17±0.53
Ni(sacsac)($P(C_{16}H_{33})_3$)Cl	0.306±0.113	2.9±0.5		7.50±0.01
Ni(sacsac)($PCH_3(C_6H_5)_2$)Cl	0.163±0.053	2.0±0.5		7.55±0.18

Table 2. Comparison of the initial conversion rates

Catalyst precursor	Initial conversion rate (h^{-1})[a] Initial data	Extrapolation of regression data
Ni(sacsac)($P(C_2H_5)_3$)Cl	2100±1100	485±85
Ni(sacsac)($P(C_4H_9)_3$)Cl	5800±2200	700±38
Ni(sacsac)($P(C_8H_{17})_3$)Cl	2200±200	519±78
Ni(sacsac)($P(C_{16}H_{33})_3$)Cl	2500±900	362±62
Ni(sacsac)($PCH_3(C_6H_5)_2$)Cl	640±100	115±29

[a]The dimension of this parameter is mol butene (mol catalyst)$^{-1}$ h^{-1}.

unit time per unit amount of catalyst), the turnover frequency, for the different catalyst systems. The turnover frequency will be time dependent, so different catalysts are best compared on the basis of their initial turnover frequencies which can be determined as the product of k_b and the initial amount of butene in the liquid phase, $(m_b)_0$. This procedure gives initial turnover frequencies extrapolated from data obtained in the advanced stages of the experiment.

Alternatively, the amount of residual butene as a function of time during the initial period can be represented by a polynomial in time.

$$m_b = a+bt+ct^2+dt^3+\cdots. \quad (5)$$

Evaluation of the differential at time zero also leads to estimates of the initial turnover frequency. A comparison of the initial turnover frequencies obtained by the two methods is presented in Table 2. The lower precision of the data obtained during the initial period, and the necessary qualitative interpretation of this data, notwithstanding the data of Table 2, are consistent with the higher reaction rates obtained during the initial period.

Equations (1) and (4) also imply that the maximum fractional butene conversion (i.e. at infinite time), $(C_b)_\infty$, will be given by

$$(C_b)_\infty = 1-\exp\left[\frac{k_b}{k_c}(m_c)_0\right] \quad (6)$$

which will be maximized for large amounts of catalyst, or catalysts for which k_c is small. A direct assessment of this prediction is not possible in the present series of experiments which have been terminated after 6 h. However, our preliminary experiments over long reaction times ranging from 1 to 48 h exhibited the same pattern of regression.[16] High conversions were possible and seemed to approach a limiting value for a particular catalyst concentration.

The representation of the data by eq. (1) as applied to the main reaction period is excellent. The value of the index of determination was at least 0.99, and the differences between the actual and calculated initial amounts of butene are within the limits of error.

The parallel between our empirical mathematical description of the process and the kinetic conversion model of Dumas and Hsu is encouraging and consistent with the expectation that the rate-determining step in the oligomerization is either reaction of a molecule of butene with an activated catalyst, or reaction of a second molecule of butene with a supposed nickel–butyl intermediate. The systematic deviation of our data from the regression during the initial period may be consistent with the initial formation of a highly active catalyst which changes into a less active but more stable form, as described in a more general formulation of the model of Dumas and Hsu. However, the precision of the initial data does not allow for quantification of such a postulate nor for estimations of the reaction order nor rate constants.

These catalyst systems are quite stable and have functioned for several days under the present conditions.[16] However, the parallel with the model of Dumas and Hsu implies a slow catalyst deactivation step. Interestingly, the implied deactivation rates are not very dependent on the nature of the phosphine. We have shown previously[16] that the catalyst can be deactivated by CO (either present initially or added after catalyst activation) or H_2O, both of which may be present in the feed. Alternatively, catalyst solubility in the changing medium or competition from the accompanying isomerizations may be important in this regard. The catalyst is also deactivated by added phosphine.[17] Thus, any phosphine liberated from the nickel centre may further inhibit the remaining catalyst. There is, however, no direct relationship between k_b and k_c. Thus, it may be possible to select substituents which give

an optimum combination of catalyst stability and activity. Clearly, an extended range of phosphine substituent types will be required to quantify any influence of the phosphine on k_b and k_c.

Kinetic data allow only a limited insight into the detailed nature of the catalytic active site(s). The present investigation and those into catalytic propylene[19] and ethylene[20] oligomerization indicate that the catalytic system is quite complex. The co-catalyst also appears to have a non-trivial role. Thus, the detection of two equivalents of octenes per equivalent of Et_2AlCl (present in large excess) during hexene isomerization is consistent not only with a bimetallic nickel–aluminium intermediate, but also with a catalyst/co-catalyst equilibrium.[17] Studies in this area are continuing.

EXPERIMENTAL

All manipulations were carried out in an inert atmosphere of argon or butenes using standard vacuum manifold techniques.[21] Solvents were AR grade and were dried and distilled under argon before use. Diethylaluminiumchloride (Merck) was used as received. The compounds Ni(sacsac)$(PR_3)Cl$ were prepared from Ni(sacsac)$_2$[22] and $NiCl_2(PR_3)_2$[23] by the method previously reported,[24] and their identities confirmed by NMR spectroscopy and FABMS. *trans*-2-Butene (Matheson technical grade) was used as received. Gas chromatographic analysis of the *trans*-2-butene showed it to contain small amounts of 1- and *cis*-2-butenes and no other impurities. Gas chromatograhic analyses were performed on an SGE 25m QC2/BP1 0.25 mm capillary column using a Hewlett Packard 5890A gas chromatograph equipped with an FID and a Hewlett Packard 3393A integrator. The butene dimers were individually resolved and their identities established as reported previously.[25]

Butenes were oligomerized in batch experiments in a magnetically stirred stainless steel tubular reactor system at 22 ± 2°C. The volume of the reactor was 81.3 ± 0.1 cm^3, and the average liquid volume was 21.2 cm^3. The reactor was connected to a calibrated manometer and equipped with a calibrated thermocouple. Pressure and temperature measurements were accurate to ±0.2 kPa and ±0.1°C, respectively. The density of the liquid reaction mixture as a function of the amount of dissolved butene, and the relationship between the vapour pressure, temperature and amount of butene in the liquid phase were calibrated separately.

The weighed reactor was evacuated and charged with butenes (7.50 ± 0.05 g, 0.134 mol) at -5°C, and a solution of the nickel catalyst precursor [$(3.50\pm0.01)\times10^{-5}$ mol in 10.0 ± 0.1 cm^3 of dry deoxygenated chlorobenzene] was injected into the reactor through a septum and the reactor reweighed. The reactor temperature and pressure were allowed to stabilize at 22 ± 2°C and neat diethylaluminiumchloride (0.20 ± 0.05 cm^3, 1.59×10^{-3} mol, Ni:Al ratio 1:45.5) added by injection. The reactor temperature and pressure were monitored for the duration of the reaction. The reaction temperature rose gradually by 2–3°C during this period. After 6 h, the reaction was stopped by the injection of 2 cm^3 of distilled water, the reactor was weighed, excess butenes released and the reactor reweighed. The liquid products were separated from water and analysed by gas chromatography. Solvent chlorobenzene was used as an internal standard, after calibration of the chlorobenzene GC response with standard mixtures of chlorobenzene and 1-octene. Time/temperature/pressure data were evaluated in terms of the mass of residual butene as a function of time, based on the correlation of the liquid phase butene concentration with temperature and pressure in this system. Data were analysed using the program Statview for the Apple Macintosh™ computer. No butene oligomerization was detected using either the nickel or aluminium precursors alone under these conditions.

Acknowledgements—We thank the National Energy Research Development and Demonstration Council, the Australian Research Grants Scheme, the Potter Foundation and the University of Sydney Research Grants Scheme for generous financial support, Dr A. L. Chaffee, CSIRO Division of Energy Technology for assistance with product analyses and Mr L. Hicks, University of Wollongong, for obtaining the FABMS data.

REFERENCES

1. G. Lefebvre and Y. Chauvin, *Aspects of Homogeneous Catalysis* (Edited by Rento Ugo), Vol. 1, Chap. 3, p. 107. D. Reidel, Dordrecht (1970).
2. P. W. Jolly and G. Wilke, *The Organic Chemistry of Nickel*, Vol. 2. Academic Press, New York (1975).
3. B. Bogdanović, *Adv. Organomet. Chem.* 1979, **17**, 105.
4. G. Hentici-Olivé and S. Olivé, *Trans. Met. Chem.* 1976, **1**, 109.
5. E. R. Freitas and C. R. Gum, *Chem. Engng Prog.* 1979, **75**, 73.
6. Y. Chauvin, J. F. Gaillard, D. V. Quang and J. W. Andrews, *Chem. Ind. (London)* 1974, 375.
7. B. Bogdanović, B. Spliethoff and G. Wilke, *Angew. Chem. Int. Ed. Engl.* 1980, **19**, 622.
8. A. Behr, V. Falbe, U. Freudenberg and W. Keim, *Israel J. Chem.* 1986, **27**, 277.
9. W. Keim, A. Behr, B. Gruber, B. Hoffman, F. H.

Kowaldt, U. Kurschner, B. Limbacker and F. P. Sistig, *Organometallics* 1986, **5**, 2356.
10. W. Keim, R. Appel, S. Gruppe and F. Knoch, *Angew. Chem. Int. Ed. Engl.* 1987, **26**, 1012.
11. W. Keim, R. Appel, A. Storeck, C. Krüger and R. Goddard, *Angew. Chem. Int. Ed. Engl.* 1981, **20**, 116.
12. R. B. A. Pardy and I. Tkatchenko, *J. Chem. Soc., Chem. Commun.* 1981, 49.
13. D. L. Beach and J. J. Harrison, U.S. Pat. 4310716. Gulf Research and Development Company (1982).
14. K. J. Cavell and A. F. Masters, *J. Chem. Res.* 1983, 72.
15. A. F. Masters and K. J. Cavell, U.S. Pat. 4533651. C.S.I.R.O. (1985).
16. V. W. L. Chin, A. F. Masters, M. Vender and R. J. Tyler, *Studies in Surface Science and Catalysis* (Edited by D. M. Bibby, C. D. Chang, R. F. Howe and S. Yurchak), Vol. 36, p. 421. Elsevier, Amsterdam (1988).
17. L. M. Clutterbuck, BSc(Hons) Thes. University of Sydney (1987).
18. C. Dumas and C. C. Hsu, *Chem. Engng Commun.* 1983, **24**, 37.
19. S. J. Brown, L. M. Clutterbuck, A. F. Masters, J. I. Sachinides, P. A. Tregloan and M. Vender, *Appl. Catal.*, submitted.
20. S. J. Brown, D. J. Byrum, A. F. Masters and M. Vender, unpublished results.
21. D. F. Shriver, *The Manipulation of Air-Sensitive Compounds*. McGraw-Hill, New York (1969).
22. C. G. Barraclough, R. L. Martin and I. M. Stewart, *Aust. J. Chem.* 1969, **22**, 891.
23. H. Itatani and J. C. Bailar Jr, *J. Am. Chem. Soc.* 1967, **89**, 1600.
24. J. P. Fackler Jr and A. F. Masters, *Inorg. Chim. Acta* 1980, **39**, 111.
25. A. L. Chaffee, K. J. Cavell, A. F. Masters and R. J. Western, *I&EC Res.* 1987, **26**, 1822.

Polyhedron Vol. 7, No. 19/20, pp. 2023–2025, 1988
Printed in Great Britain

0277–5387/88 $3.00+.00
© 1988 Pergamon Press plc

POLYLITHIUM COMPOUNDS: A NEW GENERAL HIGH YIELD SYNTHESIS FOR 1,1-DILITHIO COMPOUNDS

HAJIMU KAWA, BOBBY C. MANLEY and RICHARD J. LAGOW*

Department of Chemistry, University of Texas, Austin, TX 78712, U.S.A.

Abstract—The synthesis of dilithio compounds such as 1,1-dilithioneopentane, (trimethylsilyl)dilithiomethane and bis(trimethylsilyl)dilithiomethane are reported in 88, 97 and 95% yield, respectively. A new general synthesis by thermal rearrangement is developed in this manuscript. Additional characteristics of the reaction chemistry are discussed.

We report the development of a very general high yield synthesis for *gem* 1,1-dilithio compounds. Polylithium organic compounds are of current interest[1–3] while *gem* dilithio compounds are very unusual new reagents and of interest from a structural and theoretical point of view.[4–5]

In 1982, our research group[1] modified and refined a Karl Ziegler pyrolysis and thermal rearrangement of methyllithium generating a high yield synthesis for dilithiomethane. This synthesis made dilithiomethane an accessible reagent and added polylithium chemistry to the repertoire of conventional organic synthetic chemists.

Recently we have established that the Kawa–Lagow modified Ziegler synthesis is a very general and broadly applicable synthetic method. The method can be modified so that synthesis of higher 1,1-dilithio compounds such as 1,1-dilithioneopentane, (trimethylsilyl)dilithiomethane and bis(trimethylsilyl)dilithiomethane are possible in 88, 97 and 95% yield, respectively, see eqs (1), (2) and (3).

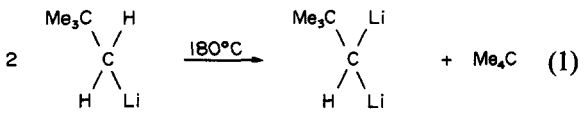

(1)

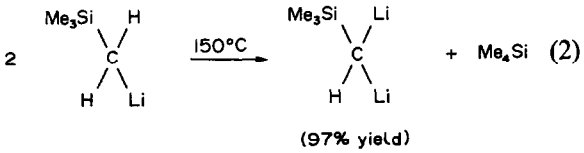

(2)

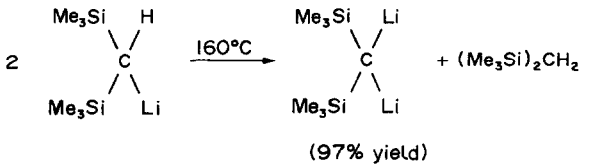

(3)

One of the most commonly observed modes of thermal decomposition of organolithium compounds is the elimination of lithium hydride, leading to alkenes.

$$RCH_2CH_2Li \xrightarrow{\Delta} RCH{=}CH_2 + LiH. \quad (4)$$

This is a widely observed phenomenon in the chemistry of organolithium compounds.

None of the above monolithium compounds have hydrogen at the β-position, therefore they cannot eliminate LiH in the normal manner. Neopentyllithium was found to rearrange at 180°C under an inert atmosphere into the light coloured yellowish solid 1,1-dilithioneopentane and neopentane in yields of 88 and 94%, respectively. Neopentane was collected in a −78°C trap during the reaction, and was found to be > 95% pure by GLC analysis.

The new 1,1-dilithio compounds were converted into their 1,1-dideuterio compound analogues for spectroscopic studies. Quantitative deuteration was achieved by reaction with MeOD at −78°C. A mass spectral data comparison of these compounds with the undeuterated compounds is summarized in Table 1. In each case, the base peak $(p—CH_3)^+$ indicates the existence of two deuterium atoms on the parent molecule. The fragmentation patterns were also compared with authentic samples prepared by the reaction of corresponding 1,1-diiodo compounds with Zn/CH_3CO_2D.

To Geoffrey Wilkinson: our best regards to a very creative chemist.

*Author to whom correspondence should be addressed.

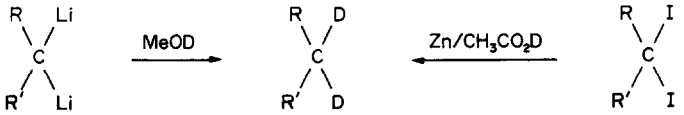

(5)

Dilithiomethane is known to react with chlorotrimethylsilane at 150°C (two days) to give bis (trimethylsilyl)methane in 87% yield.[6] However, none of the new dilithio compounds reacted with chlorotrimethylsilane even at higher temperatures (180°C). The tert-butyl or trimethylsilane groups made the formation of new C—C or C—Si bonds difficult as was expected; for such sterically bulky groups are not easily accommodated around one carbon. The 1,1-dilithio compounds were found to have high proton affinities but very low nucleophilicity. For example, 1,1-dilithioneopentane reacted with dimethylsulphate at room temperature to give a mixture of neopentane (17%), 2,2-dimethylbutane (74%) and 2,2,3-trimethylbutane (9%).

$$Me_3CCHLi_2 \xrightarrow{(MeO)_2SO_2} Me_4C + Me_3CCH_2Me + Me_3CCHMe_2. \quad (6)$$

Proton abstraction predominantly occurred instead of methylation. Quite surprisingly, acyl halides did not react with any of these 1,1-dilithio compounds, including dilithiomethane.

Dilithiomethane decomposes into lithium carbide and tetralithiopropyne at 250°C.[2]

$$(CH_2Li_2)_n \xrightarrow{\Delta} (C_2Li_2)_n + (C_3Li_4)_n + LiH. \quad (7)$$
$$(80\%) \quad (20\%)$$

1,1-Dilithiopentane began to decompose at much lower temperatures (200°C). For example, pyrolysis of this compound at 210°C for 15 min gave a mixture of lithium acetylide (75%) and $(C_3Li_4)_n$ (25%). (Characterization by hydrolysis and flash vaporization mass spectroscopy.)

Maercker *et al.* recently reported the synthesis of 1,1-dilithioethane[7] by the reaction of 1,1-bis(chloromercurio)ethane with lithium:

$$CH_3CH(HgCl)_2 \xrightarrow{Li} CH_3CHLi_2.$$

Though this reaction seems to be applicable to other 1,1-dilithio compounds, the biggest disadvantage is that the products are usually contaminated with inorganic salts and metal amalgam, which cannot be easily removed. The Kawa–Lagow modified Ziegler procedure is very generally applicable to systems in which the organolithium compounds do not have any hydrogens at the β-position.* In spite of this limitation, our method provides a ready source of very pure 1,1-dilithio compounds, which will enable us to do important structural studies. Bulky groups are effective in preventing polymerization, thus giving these 1,1-dilithio com-

Table 1. The mass spectra of 1,1-dideuterio compounds

Compound	Molecular weight	*m/e* (Relative intensity)
Me_4C[a]	72	15(5), 27(15), 29(39), 39(13), 41(42), 57(100), 58(4)
Me_3CCHD_2	74	15(4), 17(1), 27(6), 28(5), 29(11), 30(7), 31(3), 39(13), 40(7), 41(28), 42(20), 43(12), 57(31), 58(10), 59(100), 60(3)
Me_4Si[a]	88	29(7), 42(4), 43(17), 44(4), 45(14), 73(100), 74(8), 88(1)
Me_3SiCHD_2	90	42(1), 43(8), 44(3), 45(11), 46(6), 47(5), 73(32), 74(8), 75(100), 76(8), 77(4)
$(Me_3Si)_2CH_2$[b]	160	43(14), 45(13), 59(11), 73(32), 85(2), 129(5), 145(100)
$(Me_2Si)_2CD_2$	162	43(10), 44(5), 45(7), 59(5), 73(30), 85(1), 131(6), 147(100), 148(16), 149(5)

[a] J. G. Grasselli and W. M. Ritchey, *Atlas of Spectral Data and Physical Constants for Organic Compounds.* CRC Press.

[b] D. R. Rimmel, C. A. Wilkie and F. Ramon, *J. Org. Chem.* 1972, **37**, 2665.

* It should be noted that facile leaving groups (i.e. triphenylmethyl) should also be avoided at the β-position. An elimination of alkyllithium might take place in such cases.

pounds considerable volatility.* Crystal structures are now in progress. Also, the trimethylsilyl group increases the solubility of the compound in organic solvents over simple polylithium compounds such as $(H_2CLi_2)_n$.†

EXPERIMENTAL

The following experiments were carried out under an extremely dry and oxygen-free argon atmosphere. The usual vacuum/Schlenk line technique was used for the isolation of extremely air/moisture-sensitive organolithium compounds.

Neopentyllithium

Bis(neopentyl)mercury (4.78 g, 14 mmol) and lithium shavings (2.00 g) were mixed in 100 cm^3 of *n*-hexane. The mixture was stirred for three days at room temperature. The resultant lithium amalgam and excess lithium were separated by filtration. The filtrate was evaporated to dryness, giving a slightly yellow crude neopentyllithium, which was then purified by sublimation at 130°C *in vacuo* (10^{-5} torr). Yield: 2.00 g (92%); ^{1}H NMR: (C_6D_6); 1.13 (9H), −0.68 (2H) ppm.

(Trimethylsilyl)methyllithium and bis(trimethylsilyl)methyllithium

(Trimethylsilyl)methyllithium was obtained by the same procedure as above in a yield of 78%. Sublimed at 100°C (10^{-5} torr). ^{1}H NMR (C_6D_6); 0.17 (9H), −2.07 (2H) ppm. Diethyl ether was used as a solvent in the above reaction to give an 80% yield of bis(trimethylsilyl)methyllithium from the corresponding mercury compound. Sublimation occurred at 100°C (10^{-5} torr). ^{1}H NMR (C_6D_6); δ 0.13 (18H), −2.50 (1H) ppm.

1,1-*Dilithioneopentane*

Neopentyllithium (390 mg, 5 mmol) was placed in a small distillation apparatus and heated to 180°C for 12 h under argon. A light yellow solid was obtained and a volatile compound was collected in a receiver cooled to −78°C during the reaction. The system was then evacuated and the volatile compound was transferred through the vacuum line to a −196°C trap. Exactly 170 mg of a volatile compound was isolated which was identified as 95% pure neopentane by GLC analysis using a 10 m × 1/4 in. Durapak phenyl isocyanate on Porasil C column (94% yield). Isobutane was the only other product. The light yellow compound (205 mg) was isolated and was carefully hydrolysed with MeOD at −78°C. The reaction mixture was fractionated under vacuum using a −78 and a −196°C trap (excess MeOD was collected in the −78°C trap). The phenyl isocyanate column was used for the quantitative analysis. The yield of 1,1-dilithioneopentane (88%) was calculated based on the amount of 1,1-dideuterioneopentane obtained and the amount of neopentyllithium used. Major impurities were C_2D_2 and C_3D_4.

Similarly, (trimethylsilyl)methyllithium (420 mg) was pyrolysed at 150°C for 12 h, resulting in a white solid (220 mg) and tetramethylsilane (192 mg, 98% pure). Deuterolysis of the white solid gave a mixture of Me_3SiCHD_2 (97%) and C_2D_2 (3%).

By the same procedure as above, bis(trimethylsilyl)dilithiomethane was obtained as a white solid in 95% yield by the pyrolysis of bis(trimethylsilyl)methyllithium at 160°C for 12 h. Photoacoustic IR spectra of mono- and bis(trimethylsilyl)dilithiomethanes showed characteristic patterns for trimethylsilylated compounds; 2903, 1253, 870 and 705 cm^{-1} were observed for (trimethylsilyl)dilithiomethane and 2903, 1257, 1057, 849 and 691 cm^{-1} were observed for bis(trimethylsilyl)dilithiomethane.

Acknowledgements—We are grateful to the National Science Foundation (CHE-8521390) and the Robert A. Welch Foundation (F-700) for support of this work.

REFERENCES

1. J. W. Chinn Jr., J. A. Gurak and R. J. Lagow, *J. Am. Chem. Soc.* 1982, **104**, 2637.
2. L. A. Shimp, J. A. Morrison, J. A. Gurak, J. W. Chinn Jr. and R. J. Lagow, *J. Am. Chem. Soc.* 1981, **103**, 5951.
3. F. J. Landro, J. A. Gurak, J. W. Chinn Jr. and R. J. Lagow, *J. Organomet. Chem.* 1983, **249**, 1.
4. J. B. Collins, J. D. Gill, E. D. Jemmis, Y. Apeloig, P. v. R. Schleyer, R. Seeger and J. A. Pople, *J. Am. Chem. Soc.* 1976, **98**, 5419.
5. E. D. Jemmis, P. v. R. Schleyer and J. A. Pople, *J. Organomet. Chem.* 1978, **154**, 327.
6. P. Krohmer and J. Goubeau, *Chem. Ber.* 1971, **104**, 1347.
7. A. Maercker, M. Theis, A. J. Kos and P. V. R. Schleyer, *Angew. Chem. Int. Ed. Engl.* 1983, **22**, 733.

* All three 1,1-dilithio compounds were analysed with normal mass spectra without using the flash vaporization technique. Though a detailed study of their fragmentation patterns is underway, the parent peak of 1,1-dilithioneopentane was observed at $m/e = 57$ (Me_3C^+) and the parent peaks of both trimethylsilylated dilithiomethanes were observed at $m/e = 73$ (Me_3Si^+).

† Bis(trimethylsilyl)dilithiomethane was the most soluble compound in organic solvents. ^{1}H NMR spectra in C_6D_6 contained a singlet at 0.09 ppm.

Polyhedron Vol. 7, No. 19/20, pp. 2027–2030, 1988
Printed in Great Britain

0277–5387/88 $3.00+.00
© 1988 Pergamon Press plc

CHLORINATION OF HALF-SANDWICH CARBONYL COMPLEXES: THE SQUARE-PYRAMIDAL CATION $[(\eta^6\text{-}C_6Et_6)Mo(CO)_3Cl]^+$ *

W. A. HERRMANN,† W. R. THIEL and E. HERDTWECK

Anorganisch-chemisches Institut der Technischen Universität München,
Lichtenbergstraße 4, D-8046 Garching/München, F.R.G.

Abstract—The molybdenum(0) half-sandwich complex tricarbonyl(η^6-hexaethylbenzene) molybdenum (**1**) undergoes clean oxidation upon treatment with elemental chlorine in methylene chloride–carbon tetrachloride solution or with phenyliodo dichloride, $(C_6H_5)ICl_2$, in methylene chloride solution to yield the ionic complex **2** of net composition $(C_6Et_6)Mo_2(CO)_3Cl_7$ (Et = C_2H_5). This compound was established by a single-crystal X-ray diffraction study to contain the square-pyramidal, diamagnetic d^4-molybdenum(II) cation $[(\eta^6\text{-}C_6Et_6)Mo(CO)_3Cl]^+$ and a hexachloromolybdate(V) counter anion of expected octahedral geometry (d^1; paramagnetic). The crystals are monoclinic, space group $P2_1/n$, with four molecules in a unit cell of dimensions a = 15.770(3), b = 19.172(5), c = 10.415(5) Å and β = 106.40(2)°. The structure was solved by the heavy-atom method and refined by full-matrix least-squares calculations to R_w = 0.037 for 1810 observed data. All molybdenum-to-carbon distances are significantly longer in the ionic compound **2** than in the neutral precursor species **1**.

Oxidation including chlorination of low-valent organometallic half-sandwich carbonyl complexes often not only entails carbonyl substitution but also extensive decomposition. In the context of our work on high-valent organometal oxides[1,2] we became interested in halogenated derivatives that might prove useful for subsequent hydrolysis reactions to yield finally oxo derivatives.[3] Since the half-sandwich rhenium(VII) oxide of formula $(\eta^5\text{-}C_5Me_5)ReO_3$ (Me = CH_3) is an extraordinarily stable compound, there is no reason to assume that the isoelectronic derivatives $(\eta^6\text{-}C_6R_6)MO_3$ of molybdenum and tungsten, on the one hand, and $(\eta^4\text{-}C_4R_4)MO_3$ of osmium on the other hand should not be accessible.[2] However, first attempts of direct oxidation of the molybdenum(0) compound **1** by means of hydrogen peroxide and *t*-butyl hydroperoxide were unsuccessful, thus sharply contrasting the observations made for the isoelectronic rhenium compound $(\eta^5\text{-}C_5Me_5)Re(CO)_3$.[1,2,4] We therefore undertook oxidation reactions using chlorine to check whether **1** can be oxidized cleanly at all.

Treatment of **1** in methylene chloride solution with excess chlorine dissolved in carbon tetrachloride immediately produces the red–brown compound **2** according to Scheme 1 in 81% yield after recrystallization. We have also found phenyliodo dichloride, $(C_6H_5)ICl_2$,[5] to be a clean chlorination reagent for **1** to give the same product **2**.

The IR spectra of this product exhibit three carbonyl stretching vibrations (νCO) that are significantly shifted to higher wavenumbers (2083, 2037, 2003 cm^{-1}; KBr) with respect to the precursor compound **1** (1955, 1875 cm^{-1}), thus indicating the cationic nature of the metal carbonyl species in question. At the same time a band at 340 cm^{-1} attributable to MoCl entities is observed. The NMR spectra did not yield an unambiguous structural assignment nor could a total elemental analysis (showing the net composition $C_{21}H_{30}Cl_7Mo_2O_3$) provide an idea of the structure although

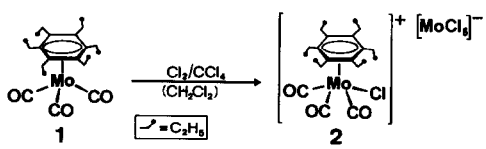

Scheme 1.

* Dedicated to Sir Geoffrey Wilkinson FRS on the occasion of his 65th birthday.

† Author to whom correspondence should be addressed.

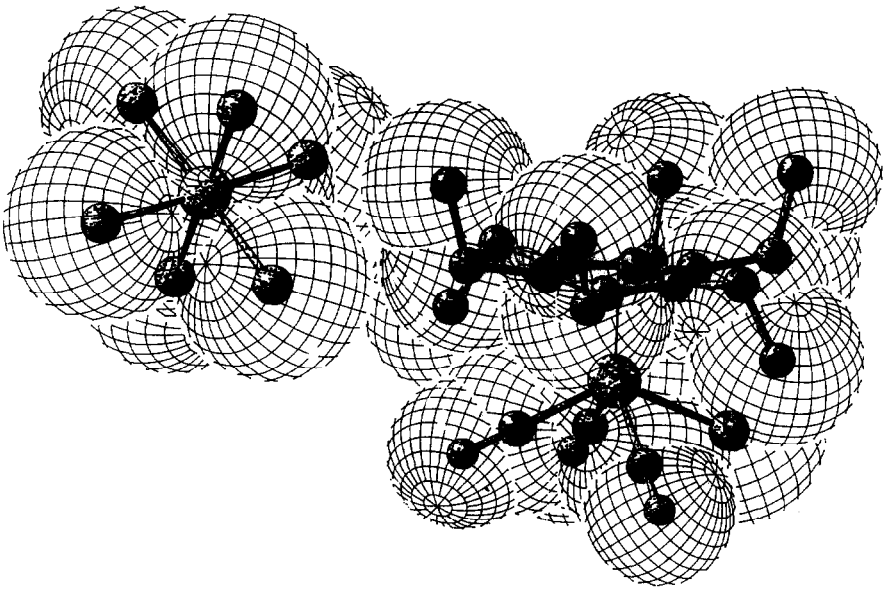

Fig. 1. SCHAKAL drawing of compound **2**'s molecular structure in the crystal. A space-filling model drawing is superimposed. A numbering scheme has been omitted for better clarity.

the low solubility in most organic solvents indicated the ionic nature of the compound. Hence an X-ray structural study was inevitable.

Compound **2** crystallizes from methylene chloride at −25°C in the monoclinic space group $P2_1/n$ with unit cell dimensions $a = 15.770(3)$, $b = 19.172(5)$, $c = 10.411(5)$ Å and $\beta = 106.40(2)°$.* Important bond lengths and angles are listed in Table 1. As can be seen from the SCHAKAL drawing depicted in Fig. 1, the compound consists of the molybdenum(II) cation $[(\eta^6\text{-}C_6Et_6)Mo(CO)_3Cl]^+$ and a hexachloromolybdate(V) anion $[MoCl_6]^-$ in a 1:1 ratio. The half-sandwich cation has a square-pyramidal overall geometry if one considers the π-bonded hexaethylbenzene system to adopt just one coordination site. The basal set of ligands is formed by the three original carbon monoxide groups plus an extra chlorine ligand. Two ring-bonded ethyl groups in 1- and 4-positions are directed towards the metal atom while the other four ethyl groups are oriented in the opposite way. This contrasts with the structure of the starting compound **1** in which every second ethyl group is oriented towards the $Mo(CO)_3$ moiety.[6] Due to the oxidation state all metal-to-carbon distances of the cation of **2** are significantly longer than those in the precursor compound **1** (Table 1).

The hexachloromolybdate(V) anion shows a near perfect octahedral geometry (Table 1) and typical molybdenum chloride bond distances expected for the oxidation state V (Table 2).

The novel compound **2** reported here combines a d^4-Mo^{II} cation (18 electron system) with a d^1-Mo^{V} anion. While the metal of the half-sandwich cation seems to adopt a low-spin electronic state resulting in diamagnetism, the anion is paramagnetic. This was proven by an ESR spectrum (recorded in methylene chloride solution at 296 K) that gave a $\langle g \rangle$ value of 1.980 and a hyperfine splitting $\langle A \rangle$ of 45.7×10^{-4} cm^{-1}.

EXPERIMENTAL

General procedures and materials

The starting compound **1** was synthesized from hexacarbonylmolybdenum and hexaethylbenzene in dibutyl ether at 120°C in 85% yield.[9] Phenyliodo dichloride was prepared from phenyliodide and chlorine in 80% yield according to a published procedure.[6] ^{1}H and ^{13}C NMR spectra were recorded on a JEOL 270 MHz spectrometer, the IR spectra on a NICOLET Fourier-Transform Infrared spectrometer 5-DX.

* Further details of the crystal structure determination can be obtained from the Fachinformationszentrum Energie, Physik, Mathematik, D-7514 Eggenstein-Leopoldshafen 2, F.R.G., by quoting the depository number CSD 53099, the name of the authors and the journal citation.

Table 1. Selected bond distances (Å) and angles (°) of the ionic compound **2**

Atom 1	Atom 2	Distance	Atom 1	Atom 2	Distance
Mo(1)	Cl	2.471(2)	Mo(2)	Cl(1)	2.313(2)
Mo(1)	C(1)	1.84(1)	Mo(2)	Cl(2)	2.299(2)
Mo(1)	C(2)	2.06(2)	Mo(2)	Cl(3)	2.318(2)
Mo(1)	C(3)	2.06(1)	Mo(2)	Cl(4)	2.315(3)
Mo(1)	C(11)	2.398(7)	Mo(2)	Cl(5)	2.324(2)
Mo(1)	C(12)	2.376(8)	Mo(2)	Cl(6)	2.304(2)
Mo(1)	C(13)	2.470(8)			
Mo(1)	C(14)	2.430(8)	Mo C(ring) from 2.362 to 2.402		
Mo(1)	C(15)	2.34(1)	Mo C(O) from 1.818 to 1.828		
Mo(1)	C(16)	2.441(7)			
O(1)	C(1)	1.243(9)			
O(2)	C(2)	1.126(8)			
O(3)	C(3)	1.116(8)			

Atom 1	Atom 2	Atom 3	Angle	Atom 1	Atom 2	Atom 3	Angle
Cl	Mo(1)	C(1)	71.7(4)	Cl(1)	Mo(2)	Cl(2)	90.54(8)
Cl	Mo(1)	C(2)	132.9(3)	Cl(1)	Mo(2)	Cl(3)	90.83(9)
Cl	Mo(1)	C(3)	76.1(3)	Cl(1)	Mo(2)	Cl(4)	88.79(9)
Cl	Mo(1)	Cz[a]	113.5	Cl(1)	Mo(2)	Cl(5)	90.1(1)
C(1)	Mo(1)	C(2)	80.0(4)	Cl(1)	Mo(2)	Cl(6)	178.78(9)
C(1)	Mo(1)	C(3)	104.8(5)	Cl(2)	Mo(2)	Cl(3)	90.10(9)
C(1)	Mo(1)	Cz[a]	127.1	Cl(2)	Mo(2)	Cl(4)	178.9(2)
C(2)	Mo(1)	C(3)	75.8(4)	Cl(2)	Mo(2)	Cl(5)	90.18(9)
C(2)	Mo(1)	Cz[a]	113.6	Cl(2)	Mo(2)	Cl(6)	89.49(9)
C(3)	Mo(1)	Cz[a]	128.0	Cl(3)	Mo(2)	Cl(4)	88.91(9)
				Cl(3)	Mo(2)	Cl(5)	179.0(2)
Mo(1)	C(1)	O(1)	174(2)	Cl(3)	Mo(2)	Cl(6)	90.39(9)
Mo(1)	C(2)	O(2)	178(2)	Cl(4)	Mo(2)	Cl(5)	90.8(1)
Mo(1)	C(3)	O(3)	177(2)	Cl(4)	Mo(2)	Cl(6)	91.2(1)
				Cl(5)	Mo(2)	Cl(6)	88.64(9)

[a] Cz marks the centre of the hexaethylbenzene ligand.

Preparation of [*tricarbonylchloro*(η^6-*hexaethylbenzene*)*molybdenum*(II)]*hexachloromolybdate*(V) (**2**)

Method A. A solution of 1.30 g (3.04 mmol) of **1** in 30 cm^3 dry methylene chloride was treated with 3 cm^3 of a solution of chlorine in carbon tetrachloride (3.36 M). A red–brown colour developed immediately indicating the formation of compound **2**. The solvents were stripped off *in vacuo*, and the remaining residue was washed four times with 50 cm^3 of *n*-hexane after the removal of each solvent. The solid material was then extracted with 30 cm^3 of methylene chloride with subsequent filtration of the resulting extract (G3 glass frit). The filtrate was

Table 2. Comparison of some Mo—Cl distances (Å)

Compound	Oxidation state	*d*(Mo—Cl)	Ref.
$[MoCl_6]^-$	Mo^V	2.31[a]	This work
$[MoCl_6]^-$	Mo^V	2.31[a]	7
$[MoCl_6]^{3-}$	Mo^{III}	2.45[a]	8
$[(\eta^6\text{-}C_6Et_6)Mo(CO)_3Cl]^+$	Mo^{II}	2.471	This work

[a] These distances are mean values.

carefully superlayered with 30 cm^3 of *n*-hexane and slowly cooled down to −25°C. After several hours large, red–brown, air- and water-sensitive crystals had formed. Yield: 950 mg (81%).

Method B. 3.16 g (11.50 mmol) of phenyliodo dichloride were added to a solution of 2.80 g (6.57 mmol) of **1** in 40 cm^3 dry methylene chloride. A red–brown colour developed immediately. After 15 min of stirring the solvent was stripped off *in vacuo*. Work-up of the product is analogous to method A (see above).

Elemental analysis. Found: C, 32.9; H, 3.9; Cl, 29.3; Mo, 25.3; O, 7.8. Calc. for $C_{21}H_{30}Cl_7Mo_2O_3$: C, 32.7; H, 3.9; Cl, 32.2; Mo, 24.9; O, 6.2%. The deviations of the chlorine and oxygen values are most likely due to partial hydrolysis reactions.

Spectroscopic data. IR (cm^{-1}, KBr): 2980–2900 m [νCH]; 2083 vs, 2037 vs, 2003 vs [νCO]; 1614 w [ν(CEt=CEt)]; 1454 m [δCC]; 340 m [νMoCl]. EI–MS (70 eV): *m/e* 246 ($[C_6Et_6]^+$, rel. int. 62%), base line at *m/e* 231 ($C_{17}H_{27}$). ^{1}H NMR (270 MHz, CD_2Cl_2, +20°C): δCH_3 1.55 [br, 18H], δCH_2 2.72 ppm [br, 12H]. ^{13}C NMR (67.80 MHz, CD_2Cl_2, +20°C): δCH_3 21.9, δCH_2 26.4, $\delta C_6(C_2H_5)_6$ 137.8, δCO 210.5 ppm.

X-ray structure of compound **2**

Red–brown monoclinic crystals grown from dichloromethane–*n*-hexane at −25°C. Space group $P2_1/n$: $a = 15.770(3)$, $b = 19.172(5)$, $c = 10.411(5)$ Å and $\beta = 106.40(2)°$ refined from 32 high angle reflections; $Z = 4$; $F_{000} = 1532$; d(calc.) = 1.695 g cm^{-3}; $\mu = 14.6$ cm^{-1}; $T = 24 \pm 1$°C; CAD4 (Enraf–Nonius), Mo-K_α radiation, graphite monochromator; ω-scan, $2.0° < \Theta < 22.5°$, $h(-16/16)$; $k(0/20)$; $l(0/11)$, t(max) = 60 s; number of recorded data: 4305, 1777 weak ($I < 0.0$) suppressed, 2369 independent reflections of which 559 ($I < 3\sigma(I)$) were excluded from refinement. The structure was solved by Patterson method and Difference Fourier techniques. All non-hydrogen atoms were refined anisotropically, hydrogen atoms were calculated from ideal positions included in structure factor calculations but were not refined; 298 parameter full-matrix least-squares, $R = \Sigma||F_o| - |F_c||/\Sigma|F_o| = 0.052$, $R_w = [\Sigma w(|F_o| - |F_c|)^2/\Sigma wF_o^2]^{1/2} = 0.037$, GOF = $[\Sigma w(|F_o| - |F_c|)^2/(NO\text{-}NV)]^{1/2} = 2.922$. For all calculations the program system STRUX-II[10] was employed.

Acknowledgements—This work was supported by the Deutsche Forschungsgemeinschaft and the Fonds der Chemischen Industrie. Dr U. Küsthardt is acknowledged for the recording of the ESR spectrum.

REFERENCES

1. W. A. Herrmann, E. Herdtweck, M. Flöel, J. Kulpe, U. Küsthardt and J. Okuda, *Polyhedron* 1987, **6**, 1165.
2. Recent reviews: (a) W. A. Herrmann, *Angew. Chem.* 1988, **100**, in press; W. A. Herrmann, *Angew. Chem. Int. Ed. Engl.* 1988, **27**, in press; (b) W. A. Herrmann, *Comm. Inorg. Chem.* 1988, **7**, 73.
3. W. A. Herrmann, W. R. Thiel and E. Herdtweck, *J. Organomet. Chem.* 1988, in press.
4. (a) W. A. Herrmann, E. Voss and M. Flöel, *J. Organomet. Chem.* 1985, **297**, C5; (b) Structure: E. Herdtweck, J. Okuda and W. A. Herrmann, *Inorg. Chem.* 1988, **27**, 1254.
5. B. S. Garvey Jr, L. F. Halley and C. F. H. Allen, *J. Am. Chem. Soc.* 1937, **59**, 1827.
6. D. J. Iverson, G. Hunter, J. F. Blount, J. R. Damewood Jr. and K. Mislow, *J. Am. Chem. Soc.* 1981, **103**, 6073; Compounds analogous with **2**: M. H. B. Stiddard and R. E. Townsend, *J. Chem. Soc.* (*A*) 1969, 2355.
7. U. Müller, E. Conradi, U. Patt-Siebel, I. Schmidt, A. Khabou and K. Dehnicke, *Z. Anorg. Allg. Chem.* 1988, in press.
8. A. Herbowski and T. Lis, *Polyhedron* 1985, **4**, 127.
9. G. Brauer, *Handbuch der Präparativen Anorganischen Chemie*, Vol. 3, 3rd edn, p. 2020. Enke-Verlag, Stuttgart (1981).
10. R. E. Schmidt, M. Birkhahn, W. Massa, P. Kiprof and E. Herdtweck, *STRUX-II, Programmsystem zur Verarbeitung von Röntgendaten*. Universität Marburg (1980) and Technische Universität München (1985/1987).

Polyhedron Vol. 7, No. 19/20, pp. 2031–2033, 1988
Printed in Great Britain

0277–5387/88 $3.00+.00
© 1988 Pergamon Press plc

$RuH_2[P(C_6H_5)_2(p\text{-}C_6H_4CH_3)]_3$: AN UNEXPECTEDLY STABLE AND UNREACTIVE 16-ELECTRON RUTHENIUM DIHYDRIDE*

THERESE ARLIGUIE and BRUNO CHAUDRET†

Laboratoire de Chimie de Coordination du CNRS, Unité n° 8241 liée par Convention à l'Université Paul Sabatier et á l'Institut National Polytechnique, 205, route de Narbonne, 31077 Toulouse Cedex, France

and

ROBERT H. MORRIS

Department of Chemistry and the Scarborough Campus, University of Toronto, 80 St George St, Toronto, Ontario, M55 1A1, Canada

Abstract—The title complex is obtained either by daylight exposure in benzene or dissolution in acetone of $RuH_2(\eta^2\text{-}H_2)(PPh_2tol)_3$ [$PPh_2tol = P(C_6H_5)_2(p\text{-}C_6H_5CH_3)$] or by sodium borohydride reduction of $RuCl_2(PPh_2tol)_3$ after evaporation to dryness. It is fluxional and does not react with hydrogen to give the initial $RuH_2(\eta^2\text{-}H_2)(PPh_2tol)_3$.

Mononuclear polyhydride phosphine transition metal complexes have been known for a long time[1] but still play an important role in modern inorganic chemistry. They are usually stable, electronically saturated complexes. These species can lose ligands after thermal or photochemical activation, and generate coordinatively and electronically unsaturated species. The 16- (or less) electron species thus obtained are considered to be reactive intermediates and react readily with a variety of ligands including hydrocarbons in some cases.

Two good examples are "$ReH_5(PR_3)_2$" obtained either by photochemical loss of PR_3 from $ReH_5(PR_3)_3$[2] or loss of H_2 from $ReH_7(P_3)_2$ and "$RuH_4(PR_3)_2$" ($R = c\text{-}C_6H_{11}$, $i\text{-}C_3H_7$)[3] obtained by dissociation of one bulky phosphine ligand from $RuH_2(\eta^2\text{-}H_2)(PR_3)_3$ in solution. These latter species are so reactive that they undergo a rapid H/D exchange at room temperature between the alkyl protons of the phosphines and an aromatic deuterated solvent.

"Tetrahydride" phosphine complexes of ruthenium[4] and iron[5] have been known since the 70s but only recently reformulated as the molecular hydrogen derivatives, $MH_2(\eta^2\text{-}H_2)(PR_3)_3$[6] (M = Fe, $PR_3 = PEt_2Ph$; M = Ru, $PR_3 = PPh_3$[6] or PCy_3).[7] The iron complex was shown to lose H_2 reversibly to give a red 16-electron species, $FeH_2(PR_3)_3$, which may react with N_2 for example.[5] Similarly, the dihydrogen ligand in $RuH_2(\eta^2\text{-}H_2)(PR_3)_3$ is readily replaced by N_2, CO and PR_3,[8] and shows a high reactivity towards olefins and weak acids.[9] In the case of ruthenium, no 16-electron species could be isolated. However, Linn and Halpern have reported the existence of $RuH_2(PPh_3)_3$ in a paper dealing with the catalytic properties of $RuH_2(\eta^2\text{-}H_2)(PPh_3)_3$, but found that this unstable complex readily disproportionated to $RuH_2(PPh_3)_4$ and $RuH_2(PPh_3)_2(L?)_2$.[10]

For some years, we have been interested in the preparation and chemical properties of ruthenium "polyhydrides",[3,11] which in fact are actually molecular hydrogen derivatives.[7] An interesting class of compounds are dinuclear species $Ru_2H_4(\eta^2\text{-}H_2)(PR_3)_4$ ($R = C_6H_5$, $c\text{-}C_6H_{11}$, $i\text{-}C_3H_7$) which appeared to be the first dinuclear molecular hydrogen derivatives.[7] James and co-workers actually reported a similar complex, $Ru_2H_3(\mu\text{-}H)(\mu\text{-}Cl)_2(Ptol_3)_4$, in 1985 which has been reformulated as $Ru_2H(H_2)(\mu\text{-}H)(\mu\text{-}Cl)_2(Ptol_3)_4$.[12] The only complex in the series of complexes, $Ru_2H_4(\eta^2\text{-}H_2)(PR_3)_4$, which is not fluxional at all temperatures is the triphenylphosphine one.[11a] Unfortunately it is not soluble enough at low temperature to obtain good T_1 data to verify the existence of an H—H inter-

* Dedicated to Professor Sir Geoffrey Wilkinson on the occasion of his retirement.

† Author to whom correspondence should be addressed.

Table 1. Some spectroscopic data for compounds 1–3.

Complex	IR νRu—H (cm^{-1})	^{1}H NMR (ppm) δMe	δH	^{31}P NMR
$RuH_2(\eta^2\text{-}H_2)(PPh_2tol)_3$ (1)	1968, 2010	300 K: 2.14 200 K: 2.31	−6.9 br ($w_{1/2}$ 39 Hz) −6.8 br ($w_{1/2}$ 203 Hz)	57.41
$RuH_2(PPh_2tol)_4$ (2)	1900 br	2.16	−9.95 q (35 Hz)	49.4 t, 40.6 t J_{PP} 26.5 Hz
$RuH_2(PPh_2tol)_3$ (3)	1930	2.22	−17.1 q (25.8 Hz)	58.26 br

action.[13] In order to gain solubility, we attempted the preparation of a similar complex with a slightly modified phosphine, i.e. using *p*-tolyldiphenylphosphine. The astonishing results of this modification are described hereafter.

The procedure chosen for the preparation of the desired compounds was that used for the synthesis of $RuH_6(P(c\text{-}C_6H_{11})_3)_2$[3b] and $Ru_2H_4(\eta^2\text{-}H_2)(PR_3)_4$ ($R = c\text{-}C_6H_{11}$, $i\text{-}C_3H_7$), i.e. hydrogenation of $Ru(C_8H_{10})(C_8H_{12})$ in the presence of two equivalents of *p*-tolyldiphenyl phosphine (PPh_2tol) in hexane. However, the reaction at 25°C produced a white precipitate of $RuH_2(\eta^2\text{-}H_2)(PPh_2tol)_3$ (1) whereas at temperatures below 20°C, $RuH_2(PPh_2tol)_4$ (2) was found to be the major product. Bubbling hydrogen into a hexane solution of (2) leads to conversion into (1). No evidence was found for the presence of a hexahydride or a dinuclear complex. (1) and (2) give the expected spectroscopic properties similar to the corresponding PPh_3 complexes (see Table 1). In particular, (1) shows a broad peak at −6.9 ppm ($w_{1/2}$ 39 Hz) in ^{1}H NMR spectrum which broadens considerably at low temperature ($w_{1/2}$ 203 Hz). These are properties which are characteristic of such dihydrogen complexes.[6]

A more conventional route for the preparation of (1) was attempted, viz. the one normally used for $RuH_2(\eta^2\text{-}H_2)(PPh_3)_3$.[8] However, the reduction of $RuCl_2(PPh_2tol)_3$ by $NaBH_4$ in toluene–methanol produced a pink solution. Evaporation to dryness led to the intensification of the red colour while recrystallization from toluene–hexane afforded red microcrystals analysing for $RuH_2(PPh_2tol)_3$ (3).* The complex shows a high field quartet at δ −17.1 ppm (J_{PH} 25.8 Hz) as expected for a fluxional hydride tris-phosphine derivative. The spectrum remains unchanged down to 193 K (the proton coupled phosphorus spectrum shows a triplet).

The same complex, 3, could be obtained from 1 by exposure to daylight under argon in benzene. Dihydrogen loss from $FeH_4(PEt_2Ph)_3$ had been observed by Aresta to yield the 16-electron complex, $FeH_2(PEt_2Ph)_3$, not characterized by NMR.[5] This dihydride reacted readily at 0°C with H_2 or N_2 to give $FeH_4(PEt_2Ph)_3$ and $FeH_2N_2(PEt_2Ph)_3$, respectively. In our case, it was most surprising to see that 3 did not react with hydrogen in toluene. Linn and Halpern have studied the catalytic properties of $RuH_2(\eta^2\text{-}H_2)(PPh_3)_3$ and have shown that the complex reacts stoichiometrically with cyclohexanone according to eq. (1):[10]

$$RuH_4(PPh_3)_3 + C_6H_{10}O \rightarrow RuH_2(PPh_3)_3L + C_6H_{11}OH \quad (1)$$

$$L = C_6H_{10}O \text{ or } C_6H_{11}OH.$$

We observed the immediate reaction of 1 with ketones (acetone or cyclohexanone) to give 3. That the complex is not $RuH_2(PPh_2tol)_3L$ can be demonstrated by comparison with an authentic sample of 3 prepared from Ru(COD)(COT) without adjunction of any polar solvent. Furthermore the hydride chemical shift and coupling constant reported for $RuH_2(PPh_3)_3L$ by Linn and Halpern[10]

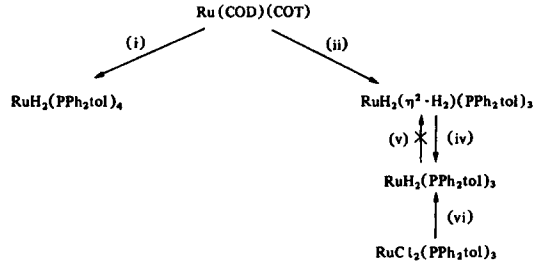

Scheme 1. Preparation of the 16-electron dihydride $RuH_2(PPh_2tol)_3$. (i) H_2 (1 atm), $T < 20$°C, hexane; (ii) H_2 (1 atm), 25°C, hexane; (iii) H_2 (1 atm), hexane; (iv) daylight exposure in benzene or dissolution in acetone; (v) H_2 (1 atm) in toluene or cyclohexanone: no reaction; (vi) $NaBH_4$, toluene–methanol.

*Microanalytical data. Found: C, 72.2; H, 5.9. Expected: C, 72.2; H, 6.0%.

do not correspond to those found for **3** whereas the spectroscopic data of **1** and **2** are very similar to those of $RuH_2(\eta^2\text{-}H_2)(PPh_3)_3$ and $RuH_2(PPh_3)_4$, respectively. No colour change and thus most probably no reaction was observed between **3** and H_2 in ketones even under pressure. Perhaps the most extraordinary result is that an acetone solution of **3** is air-stable.

3 slowly catalysed the hydrogenation of cyclohexanone at 80°C (25 bar H_2), whereas in acetone a yellow solution was obtained showing a νCO band by IR at 1930 cm^{-1}. This absorption can be attributed to $RuH_2(CO)(PPh_2tol)_3$ which is produced by the well-known decarbonylation of acetone by such complexes.[14] However, the carbonyl product was not further characterized.

Finally, **3** is indefinitely stable in benzene even when warmed to 80°C and shows neither any sign of a H–D exchange reaction in C_6D_6 (unlike $RuH_2(\eta^2\text{-}H_2)(PR_3)_3$) nor any sign of dimerization.

To conclude, we show in this note that a very slight modification in a phosphine ligand (CH_3 for H) induces a completely different chemistry of the complexes afforded. We have successfully isolated the first 16-electron hydridophosphine ruthenium complex which is unexpectedly stable and in particular does not react with H_2 whereas the saturated species $RuH_2(PPh_2tol)_4$ (**2**) does. The only proposal we can formulate to explain this behaviour is the existence of an agostic interaction between a phenyl proton and the metal, similar to what is known for $RuCl_2(PPh_3)_3$,[15] even though the complex is fluxional at all temperatures. Unfortunately, we were unable to grow crystals suitable for X-ray diffraction.

REFERENCES

1. G. G. Hlatky and R. H. Crabtree, *Coord. Chem. Rev.* 1985, **65**, 1.
2. (a) M. A. Green, J. C. Huffman and K. G. Caulton, *J. Am. Chem. Soc.* 1981, **103**, 695; (b) M. A. Green, J. C. Huffman, K. G. Caulton, W. K. Rybak and J. J. Ziolkowski, *J. Organomet. Chem.* 1981, **218**, C39.
3. (a) B. Chaudret, *J. Organomet. Chem.* 1984, **268**, C33; (b) B. Chaudret and R. Poilblanc, *Organometallics* 1985, **4**, 1722.
4. W. H. Knoth, *J. Am. Chem. Soc.* 1972, **94**, 103.
5. M. Aresta, P. Giannoccaro, M. Rossi and A. Sacco, *Inorg. Chim. Acta.* 1971, **5**, 115.
6. R. H. Crabtree and D. G. Hamilton, *J. Am. Chem. Soc.* 1986, **108**, 3124.
7. T. Arliguie, B. Chaudret, R. H. Morris and A. Sella, *Inorg. Chem.* 1988, **27**, 598.
8. R. O. Harris, N. K. Hota, L. Sadavoy and J. M. C. Yuen, *J. Organomet. Chem.* 1973, **54**, 259.
9. D. J. Cole-Hamilton and G. Wilkinson, *Nouv. J. Chim.* 1977, **1**, 141.
10. D. E. Linn and J. Halpern, *J. Am. Chem. Soc.* 1987, **109**, 2969.
11. (a) B. Chaudret, J. Devillers and R. Poilblanc, *Organometallics* 1985, **4**, 1727; (b) T. Arliguie and B. Chaudret, *J. Chem. Soc., Chem. Commun.* 1986, 985; (c) T. Arliguie, B. Chaudret, J. Devilliers and R. Poilblanc, *Compte-Rendus Sc. Hebd. Acad. Sc., Série II* 1987, **305**, 1523.
12. C. Hampton, T. W. Dekleva, B. R. James and W. R. Cullent, *Inorg. Chim. Acta* 1988, in press.
13. R. H. Crabtree, M. Lavin and L. Bonneviot, *J. Am. Chem. Soc.* 1986, **108**, 4032.
14. P. S. Hallman, B. R. McGarvey and G. Wilkinson, *J. Chem. Soc. (A)* 1968, 3143.
15. S. J. La Placa and J. A. Ibers, *Inorg. Chem.* 1965, **4**, 778.

Polyhedron Vol. 7, No. 19/20, pp. 2035–2038, 1988
Printed in Great Britain

0277–5387/88 $3.00+.00
© 1988 Pergamon Press plc

SYNTHETIC AND FLUXIONAL BEHAVIOUR OF M(1,5 CYCLOOCTADIENE)(TRIPOD)$^+BF_4^-$ (M = Rh, Ir; TRIPOD = $HC(PPh_2)_3$)

H. EL-AMOURI, A. A. BAHSOUN and J. A. OSBORN*

Laboratoire de Chimie des Métaux de Transition et de Catalyse, UA au CNRS n° 424, Institut Le Bel, Université Louis Pasteur, 4 rue Blaise Pascal, 67000 Strasbourg, France

Abstract—The complexes M(1,5 cyclooctadiene)$(HC(PPh_2)_3)^+BF_4^-$ (M = Rh, Ir) have been synthesized and characterized. The ^{31}P and ^1H NMR spectra show that in the ground-state structure the tripod ligand forms a bidentate chelate with the metal, the third phosphorus atom remaining uncoordinated. However, VTNMR studies show a rapid exchange process to be occurring at room temperature causing equilibration of all the phosphorus nuclei as well as the vinylic and methylenic protons of the diene ligand. An associative intramolecular exchange mechanism is proposed.

Phosphine complexes of Rh^I have attracted much interest since the discovery of the properties of $Rh(PPh_3)_3Cl$ now nearly 25 years ago.[1] The use of the tridentate phosphine ligand, $HC(PPh_2)_3$, (tripod), was originally aimed at the stabilization of triangular arrays of metal atoms[2] but it became clear with time that the coordination properties of this tripod ligand were quite varied. Hence, compounds have been isolated with a single metal coordinated to one [e.g. $Fe(CO)_4$(tripod)],[3] two (e.g. $Fe(CO)_3$(tripod)),[4] and, surprisingly, all three [$(\pi$-$C_5Me_5)Fe(tripod)^+$][5] phosphorus donor atoms. This variable coordination behaviour can be exploited to construct mixed metal complexes by use of the pendant non-coordinating phosphorus donor in, for example, $Fe(CO)_3$(tripod) to complex a second metal e.g. formation of $RhFe(CO)_5$(tripod)$^+$.[4]

In this paper we describe the synthesis of the compounds M(1,5 cyclooctadiene)(tripod)$^+$, (M = Rh, Ir) and their structures. Variable temperature NMR observations show these molecules to be fluxional in solution. The reactivity, catalytic properties and use of these molecules in the construction of mixed bimetallic complexes will be presented elsewhere.

RESULTS AND DISCUSSION

(a) *Structure of* M(1,5 COD)$(HC(PPh_3)_2)^+BF_4^-$ (M = Rh, Ir)

Treatment of $Rh(COD)_2^+BF_4^-$ (**1**)[6] with one equiv. of $HC(PPh_2)_3$ in CH_2Cl_2 yields the orange crystalline $Rh(COD)(HC(PPh_2)_3)^+BF_4^-$ in high yield. The analogous Ir compound **2** can be prepared in an identical manner. The analytical, ^1H and ^{31}P NMR data of **1** and **2** are collected together in the Experimental.

The ^{31}P NMR spectrum of **1** at 203 K [$(CD_3)_2CO/(CH_3)_2CO$] shows a doublet of doublets at δ −20.3 ppm ($^1J_{P(1)—Rh}$ = 130 Hz, $^1J_{P(1)—P(2)}$ = 19 Hz; relative intensity = 2) and a resonance as a doublet of triplets at δ −23.2 ppm ($^2J_{P(1)—P(2)}$ = 19 Hz, relative intensity = 1; $^3J_{Rh—P}$ = 3 Hz). The ^1H NMR spectrum of the bound 1,5 cyclooctadiene ligand at low temperature (195 K) in CD_2Cl_2 shows two signals both for the vinylic protons (δ 5.20, 5.07) and for the methylenic protons (δ 2.38, 2.27). These results indicate that **1** has the structure shown in Fig. 1.

The iridium analogue **2** shows similar low temperature spectra with, in particular, two ^{31}P resonances at δ −24.5 (triplet, $^2J_{P(1)—P(2)}$ = 16 Hz, relative intensity = 1) and at δ −30.3 ppm (doublet, $^2J_{P(1)—P(2)}$ = 16 Hz, relative intensity = 2) at 190 K in $(CD_3)_2CO/CD_2Cl_2$. Hence **2** is isostructural with **1**. However we note that the ^1H NMR spectrum is invariant from 298 to 200 K (the solubility limit) and consists of only one resonance for both vinylic [δ 4.9 ppm (s)] and methylenic [δ 2.2 ppm (s)] protons. This behaviour is discussed below.

(b) *Variable temperature behaviour of* **1** *and* **2**

When the temperature is raised from 203 to 324 K all resonances in the ^{31}P NMR spectrum of **1** broaden and eventually (~ 300 K) yield a single resonance in the form of a doublet ($^1J_{P—Rh}$ = 89

* Author to whom correspondence should be addressed.

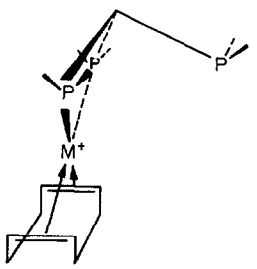

Fig. 1. Structure of $M(COD)[HC(PPh_2)_3]^+BF_4^-$, M = Rh, Ir.

Hz) (Fig. 2). Thus at room temperature all these phosphorus nucleii become equivalent on the NMR time scale, the value of $^1J_{P-Rh}$ being the weighted average of the three J_{P-Rh} values (130, 130 and 3 Hz) found at low temperature. It can be seen that the average resonance position shifts with temperature (*ca* +0.03 ppm K^{-1}) and only an approximate coalescence temperature can be determined i.e. $T_c \sim 255°$. Using the line broadening at 233 K, a rate constant $k = 40\ s^{-1}$ may be calculated at this temperature yielding $\Delta G^{\ddagger} = 11.8$ kcal mol^{-1} assuming the usual expressions for an intramolecular process.

The ^1H NMR spectrum also shows changes, as the temperature is increased coalescence occurs in $CDCl_3$ at *ca* $T = 240$ K for the vinylic protons

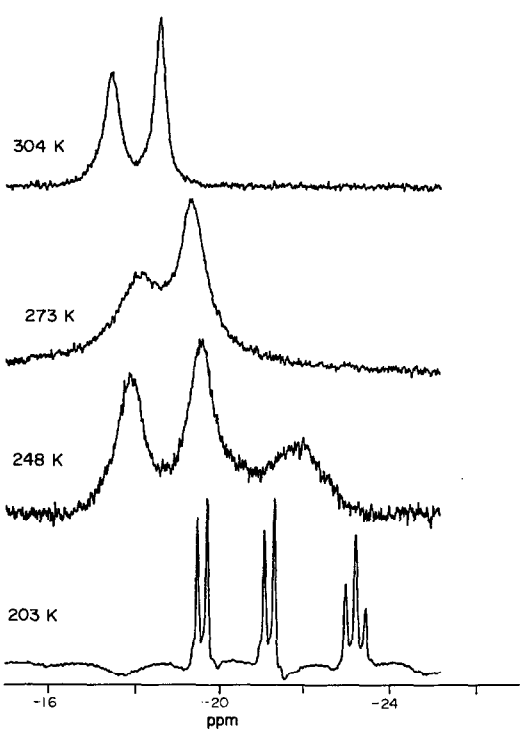

Fig. 2. Variable temperature $^{31}P\{^1H\}$ NMR spectra for the cationic complex $Rh(COD)[HC(PPh_2)_3]^+$, $(CD_3)_2CO$ solution, 81 MHz.

and at $T = 233$ K for the methylenic sets. From this data $\Delta G^{\ddagger} = 11.7$ kcal mol^{-1}.

The ^{31}P NMR of **2** shows similar behaviour to that of **1**, the coalescence of the AA'X spectrum however now occurs at a much lower temperature ($T_c \sim 219$ K). A sharp singlet is observed at the mean position at room temperature. As noted above, the limiting spectrum for the ^1H NMR of **2** was not obtained even at 200 K, but given the value of T_c for the phosphorus spectrum, it can be estimated that the coalescence temperature for both vinylic and methylenic protons would be well below 200 K, assuming that the same process is responsible for the temperature dependence in both spectra.

(c) *Mechanism of the exchange process*

Two overall observations can be made for the exchange process. Firstly, the ^{31}P data indicate the process to be intramolecular, the J_{Rh-P} coupling being preserved and averaged at high temperature. Secondly, observations on **1** show that the inner and outer vinylic and methylene protons on the cyclooctadiene ligand are equilibrated at high temperature. However, our data does not allow us to specify whether these two events occur at exactly the same rate although the activation energies are clearly very similar.

Previous studies on square planar Rh^I and Ir^I complexes involving intermolecular phosphine exchange show that the major pathway is associative.[7] For example, detailed studies by Vrieze and co-workers on the complexes M(diene)LCl (L = PPh_3, $AsPh_3$; diene = norbornadiene, 1,5 cyclooctadiene, M = Rh and diene = 1,5 cyclooctadiene, M = Ir) show that exchange with free PPh_3 or $AsPh_3$ occurs in solution via the association of a phosphine or arsine ligand. Interestingly in this case, also, equilibration of the vinylic protons on the diene ligand was observed during phosphine exchange. The pentacoordinate intermediate formed is generally thought to be of trigonal pyramidal (TBP) geometry.

An associative mechanism of this type can be proposed here, the uncoordinated P_3 binding in the TBP intermediate Y, with either P_1 (or P_2) occupying the axial site (Fig. 3). Departure of P_2 causes exchange of P_3 with P_2 with concomitant equilibration of the inner (i) or outer (o) vinylic protons as well as the corresponding methylenic sets. With P_2 in the axial site, P_3 exchange occurs with P_1, and the diene sets are again equilibrated. Hence, in this mechanism the exchange rate for P_3 sites (k_3) is twice that of P_1 or P_2 but equal to that of vinyl (or methylenic) proton exchange (k_0).

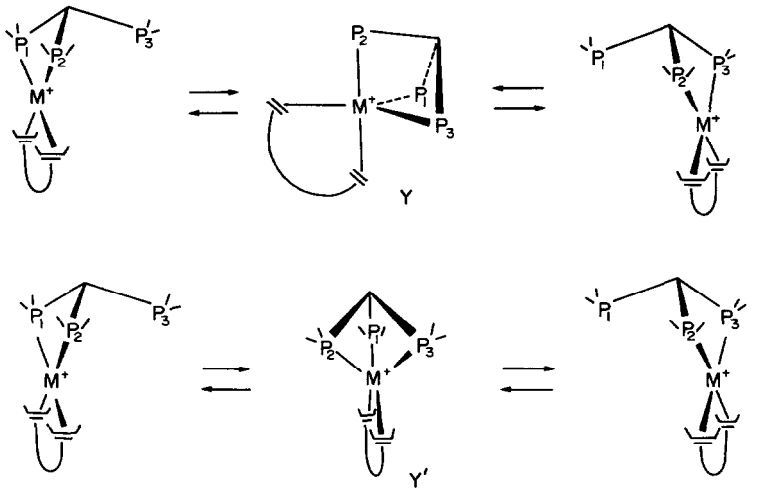

Fig. 3. Proposed mechanism of the intramolecular phosphine exchange process.

However, in view of the existence of the symmetric coordination of the tripod in (π-C_5Me_5)Fe(tripod)$^+$, conceptually a closely related but less classical intermediate Y′ (Fig. 3) could be involved. Here the entering P_3 would form a quasi-capped structure, which by a 60° rotation about the tripod three-fold axis would allow exchange to take place. The result is, however, identical to the classical mechanism above, with $k_3 = k_0$.

Two other events are worth discussion. During the lifetime of the intermediate Y (or Y′), (a) rapid rotation of the tripod ligand takes place thereby equilibrating the three P nucleii before dissociation occurs; in this case it can be shown that $k_3 = 4/3k_0$; or secondly (b) rapid rotation of the diene ligand occurs; here $k_3 = k_0$. The precision of our data, unfortunately, do not allow us to distinguish between these possibilities.

Finally we note that the exchange process is more rapid for the iridium complex **2** than for **1**. This was also observed by Vrieze in the intermolecular phosphine exchange studies and undoubtedly results from the greater stability of pentacoordination in iridium(I) chemistry.

EXPERIMENTAL

The experiments were carried out on high vacuum line or in a nitrogen filled glove box. Solvents were dried prior to use by conventional distillation under nitrogen.

IR spectra were recorded on a Perkin–Elmer 597 IR spectrophotometer as a Nujol mull. NMR spectra were obtained in the F.T. mode, using a Bruker SY 200 (^{1}H, ^{31}P); chemical shifts are relative to Me_4Si(^{1}H) or 85% H_3PO_4(^{31}P); data are presented as proton decoupled with downfield chemical shifts as positive.

Elemental analyses were performed by the Service Central d'Analyses of the CNRS.

Synthesis of Rh(COD)[HC(PPh_2)$_3$]$^+BF_4^-$ (1)

A solution of HC(PPh_2)$_3$ (0.58 g, 1.02 mmol), in CH_2Cl_2 (4 cm^3) was added in a dropwise fashion for 10 min to a well stirred solution of $Rh(COD)_2^+$ BF_4^+ (0.406 g, 1 mmol) in CH_2Cl_2 (6 cm^3). The orange solution was concentrated to half volume and addition of ether yields an orange product which was filtered and recrystallized from dichloromethane–ether (0.77 g, 90%). Found: C, 62.3; H, 5.1; P, 10.7; Rh, 11.3. Calc. for $C_{45}H_{43}P_3F_4$ BRh: C, 62.3; H, 5.0; P, 10.7; Rh, 11.9%. ^{1}H NMR (CD_2Cl_2, T 195 K): δ 7.5–6.8 ppm (m, 30H, H arom.); 5.7 ppm (q, 1H, methine); 5.20 ppm (2H) and 5.07 ppm (2H) (—HC=CH—); 2.38 ppm (4H) and 2.27 ppm (4H) (—CH_2—CH_2—). ^{31}P{^{1}H} NMR, [$(CD_3)_2CO$/$(CH_3)_2CO$; T 203 K]: δ −20.3 ppm (dd, 2P, ^1J(Rh—P) = 130 Hz, ^2J(P—P) = 19 Hz); −23.2 ppm (dt, 1P, ^2J(Rh—P) = 3 Hz, ^2J(P—P) = 19 Hz).

Synthesis of Ir(COD)[HC(PPh_2)$_3$]$^+BF_4^-$ (2)

Using an identical procedure described above for the synthesis of **1**, the reaction of $Ir(COD)_2^+BF_4^-$ with HC(PPh_2)$_3$ affords the new complex Ir(COD)[HC(PPh_2)$_3$]$^+BF_4^-$ (**2**) (yield 75%). Found: C, 57.2; H, 4.1; P, 10.3. Calc. for $C_{45}H_{43}$ P_3F_4BIr: C, 56.5; H, 4.5; P, 9.7%. ^{1}H NMR (CD_2Cl_2, T 298 K): δ 7.4 ppm (m, 30H, H arom.); 5.6 ppm (q, 1H, methine); 4.9 ppm (s, 4H, —HC

=CH—); 2.2 ppm (s, 8H, —CH_2—CH_2—). $^{31}P\{^1H\}$ NMR, [$(CD_3)_2CO/CH_2Cl_2$, *T* 190 K]: δ −24.5 ppm (t, 1P); −30.4 ppm (d, 2P, ^2J(P—P) = 16 Hz).

Acknowledgement—We thank Patrick Maltèse (Ingénieur CNRS) for technical assistance in the NMR measurements.

REFERENCES

1. J. A. Osborn, F. H. Jardine, J. F. Young and G. Wilkinson, *J. Chem. Soc. (A)* 1966, 1711.
2. A. A. Arduini, A. A. Bahsoun, J. A. Osborn and C. Voelker, *Angew. Chem.* 1980, **92**, 1050; A. A. Arduini, A. A. Bahsoun, J. A. Osborn and C. Voelker, *Angew. Chem. Int. Ed. Engl.* 1980, **19**, 1024.
3. (a) A. A. Bahsoun, J. A. Osborn and P. H. Bird, to be published; (b) J. T. Mague and S. E. Dessens, *J. Organomet. Chem.* 1984, **262**, 347.
4. A. A. Bahsoun, J. A. Osborn, P. H. Bird, D. Nucciarone and A. Y. Peters, *J. Chem. Soc., Chem. Commun.* 1984, 72.
5. J. D. Goodrich and J. P. Selegue, *Organometallics* 1985, **4**, 798.
6. (a) R. R. Schrock and J. A. Osborn, *J. Am. Chem. Soc.* 1971, **93**, 3089; (b) T. G. Schenck, J. M. Downes, C. R. C. Milne, P. B. Mackenzie, H. Boucher, J. Wehlan and B. Bosnich, *Inorg. Chem.* 1985, **24**, 2334.
7. H. C. Volger, K. Vrieze and A. P. Praat, *J. Organomet. Chem.* 1968, **14**, 429.

Polyhedron Vol. 7, No. 19/20, pp. 2039–2048, 1988
Printed in Great Britain

0277–5387/88 $3.00+.00
© 1988 Pergamon Press plc

REDOX REACTIONS INVOLVING HEXACARBONYLVANADIUM(0) AND COMPOUNDS CONTAINING ELEMENT–HALIDE, ELEMENT–HYDROGEN AND ELEMENT–CARBON BONDS. SYNTHESIS, AND CRYSTAL AND MOLECULAR STRUCTURE OF $Ph_3PbV(CO)_6$

FAUSTO CALDERAZZO* and GUIDO PAMPALONI

Dipartimento di Chimica e Chimica Industriale, Sezione di Chimica Inorganica, Università di Pisa, Via Risorgimento 35, I-56100 Pisa, Italy

and

GIANCARLO PELIZZI and FRANCESCA VITALI

Istituto di Chimica Generale e Centro C.N.R. di Strutturistica Diffrattometrica, Università di Parma, Viale delle Scienze, I-43100 Parma, Italy

Abstract—Hexacarbonylvanadium, $V(CO)_6$, was found to promote ECl (E = Ph, $PhCH_2$, Ph_3C, and Ph_2P) bond fission to give VCl_3 and E—E coupling products. For E = Ph_3Sn and Ph_3Pb, the derivatives E—$V(CO)_6$ were isolated in 76 and 60% yields, respectively. The dark red $Ph_3PbV(CO)_6$ was studied by X-ray diffraction methods. Crystal data: space group $P2_1/a$; $M = 657.5$; $a = 13.175(8)$; $b = 29.222(16)$; $c = 12.395(6)$ Å; $\beta = 89.28(3)°$; $U = 4772(4)$ Å^3; $D_c = 1.830$ g cm^{-3}; $F(000) = 2496$; μ(Mo-K_α) = 75.13 cm^{-1}. The vanadium atom is seven-coordinated with the donor atoms arranged in a distorted capped octahedral environment, the lead atom occupying the capping position. With Ph_3SnH, $V(CO)_6$ gives the heptacoordinated derivative $Ph_3SnV(CO)_6$. Hexacarbonylvanadium(0) was found to promote electron transfer and cleavage of the C—R bond of $CpCo(\eta^4$-C_5H_5-R) derivatives (Cp = η^5-cyclopentadienyl; R = H, $PhCH_2$), with the formation of $[CoCp_2][V(CO)_6]$.

Hexacarbonylvanadium(0), $V(CO)_6$, is a peculiar compound as far as both the physical and the chemical properties are concerned.[1] Being a 17-electron species of low-spin d^5 vanadium, it is a long-lived radical which easily undergoes one-electron reduction to the closed shell, 18-electron hexacarbonylvanadate(−I) anion, $[V(CO)_6]^-$, a typical reaction being the disproportionation in the presence of Lewis bases[2] or arenes,[3] see eqs (1) and (2).

$$3V(CO)_6 + nB \rightarrow [VB_n][V(CO)_6]_2 + 6CO \quad (1)$$

$$2V(CO)_6 + \text{arene} \rightarrow [V(\eta^6\text{-arene})(CO)_4][V(CO)_6] + 2CO. \quad (2)$$

The reaction of $V(CO)_6$ with cycloheptatriene which affords both $V(\eta^6$-$C_7H_7)(CO)_3$ and $[V(C_7H_7)(C_7H_8)][V(CO)_6]$;[4] the formation of $[V(\eta^6$-arene$)_2][V(CO)_6]$ and of $[(Me_2N)_2C{=}C(NMe_2)_2][V(CO)_6]_2$ by reaction of $V(CO)_6$ with $V(\eta^6$-arene$)_2$[5] or $(Me_2N)_2C{=}C(NMe_2)_2$,[6] respectively; the oxidative carbonylation[7] of VCp_2 promoted by $V(CO)_6$ to give $[VCp_2(CO)_2][V(CO)_6]$, are all examples of reactions whose driving force is probably connected with the attainment of the closed shell configuration of $[V(CO)_6]^-$. Recently, it has been shown that the electron transfer process within the $V(CO)_6/[V(CO)_6]^-$ couple can involve binary and substituted metal carbonyl anions,[8] metallocenes such as $CoCp_2$[8] and protonated nitrogen base adducts of the general formula $BH[V(CO)_6]$.[9] On the other hand, being a zero-valent vanadium systems, $V(CO)_6$ can also behave as a reducing agent towards bis-cyclopentadienyl derivatives of Ni^{II} and Mn^{II} [eqs (3) and (4)].[8]

* Author to whom correspondence should be addressed.

$$NiCp_2 + 2V(CO)_6 \rightarrow Ni(CO)_4 + 2CpV(CO)_4 \quad (3)$$

$$MnCp_2 + V(CO)_6 + CO \rightarrow CpMn(CO)_3 + CpV(CO)_4. \quad (4)$$

The results reported in this paper show further examples of $V(CO)_6$ behaving as a reductant of compounds containing element–chlorine (element = C, P, Sn, Pb), element–hydrogen (element = C, Sn, Cl, Br) or carbon–carbon bonds. Isolation of the corresponding oxidized vanadium derivatives, vanadium(III) halides or heptacoordinated carbonyl compounds, has been possible in some cases. The crystal and molecular structure of $Ph_3Pb—V(CO)_6$ is also reported.

EXPERIMENTAL

Unless otherwise stated, all the operations were carried out under an atmosphere of prepurified nitrogen or argon and under rigorous exclusion of light. Solvents were carefully dried by conventional methods prior to use. $Na[V(CO)_6]$,[10] $V(CO)_6$,[11] Ph_3PbCl,[12] $(OC)_4V(\mu\text{-}PPh_2)_2V(CO)_4$,[13] $CpCo(\eta^4\text{-}C_5H_5R)$, R = H,[14] CH_2Ph,[15] were prepared according to the literature. The rest were commercial products purified prior to use (Ph_2PCl, Ph_3CCl, $PhCH_2Cl$, PhCl) or used without further purification (Ph_3SnH, Ph_3SnCl, bis(triphenylphosphine)iminium chloride, PPNCl).

IR spectra were recorded with a Perkin–Elmer model 283 instrument equipped with a grating in solution, Nujol or halocarbon mulls under exclusion of air and moisture. Gas chromatographic analyses were performed with a Dani model 3200 instrument.

Reaction of $V(CO)_6$ *with* ECl, E = Ph, $PhCH_2$, Ph_3C, Ph_2P

A solution of Ph_3CCl (0.79 g, 2.8 mmol) in *n*-heptane (30 cm^3) was treated with $V(CO)_6$ (0.2 g, 0.9 mmol) at room temperature. Immediate reaction with evolution of gas (CO by gas chromatography) was observed. After 10 min stirring at room temperature, no $V(CO)_6$ was left in solution (IR). The solvent was removed *in vacuo* at room temperature and the residue extracted with toluene (30 cm^3). The violet–brown VCl_3 was separated from the orange solution by filtration, dried *in vacuo* (0.14 g, 98% yield) and identified from its analytical data (Cl, V). The orange solution was evaporated to dryness *in vacuo* at room temperature, the yellow residue was washed with cold *n*-heptane (5 cm^3) and dried *in vacuo* affording 0.60 g (92% yield) of C_2Ph_6 identified from its IR spectrum and elemental analysis.

By operating in a similar way, the following compounds were formed, together with VCl_3: diphenyl (80% with respect to PhCl, reaction time 48 h); dibenzyl (81% with respect to $PhCH_2Cl$, reaction time 12 h).

In the case of Ph_2PCl, a transient blue colour was observed upon adding $V(CO)_6$ (0.13 g, 0.6 mmol) to a solution of Ph_2PCl (0.39 g, 1.8 mmol) in *n*-heptane (30 cm^3), followed by precipitation of VCl_3. After 15 h stirring at room temperature, usual work-up gave an 87% yield of P_2Ph_4.

For $E = Ph_3C$ and Ph_2P, the use of stoichiometries of ECl: $V(CO)_6$ lower than three led to residual $V(CO)_6$ in solution as detected by IR spectra in the carbonyl stretching region.

Reaction of $(OC)_4V(\mu\text{-}PPh_2)_2V(CO)_4$ *with* Ph_2PCl

A suspension of $(OC)_4V(\mu\text{-}PPh_2)_2V(CO)_4$ (0.25 g, 0.37 mmol) in *n*-heptane (30 cm^3) was treated with Ph_2PCl (0.53 g, 2.4 mmol). The blue–green suspension was refluxed for 4 h and a violet precipitate was obtained. The suspension was filtered while hot producing a violet solid [VCl_3 (V and Cl analyses), 0.1 g, 86% yield] and a colourless solution which, on partial evaporation of the solvent and cooling at about −78°C, afforded 0.5 g (91% yield) of P_2Ph_4 identified by comparison of its IR spectrum (Nujol) with that of an authentic sample.

Reaction of $V(CO)_6$ *with* ECl, E = Ph_3Sn, Ph_3Pb

A suspension of Ph_3PbCl (1.72 g, 3.6 mmol) in *n*-heptane (50 cm^3) was treated at room temperature with $V(CO)_6$ (0.27 g, 1.2 mmol). After 4 h the IR spectrum of the solution showed absorptions attributable to $Ph_3PbV(CO)_6$ (*vide infra*). After 24 h stirring at room temperature, the resulting red suspension was filtered. The insoluble violet–brown solid (mainly VCl_3) was washed with boiling toluene, dried *in vacuo* at room temperature and was found to contain 99% of the chloride used in the reaction. The red *n*-heptane solution was partially evaporated to about 10 cm^3 *in vacuo* at room temperature and cooled to about −30°C overnight. The mixed metal complex, $Ph_3PbV(CO)_6$ (0.36 g, 60%), was obtained as red crystals which were stable in air for short periods of time. Found: C, 43.1; H, 2.7. Calc. for $C_{24}H_{15}O_6PbV$: C, 43.9; H, 2.3%. IR spectrum (Nujol mull): 3060w, 2071s, 2024m-w, 1983m-w, 1957sh, 1942sh, 1911vs, 1520m-w, 1430m, 1260w, 995m-w, 800m-w, 722m-s, 690m, 605s and 435m-w cm^{-1}; (*n*-heptane): 2064s, 2006m, 1974sh, 1959sh and 1940vs cm^{-1}.

By operating in a similar way using Ph_3SnCl, the following products were obtained: $Ph_3SnV(CO)_6$;[16] 76% [$\tilde{\nu}_{CO}$ (*n*-heptane): 2069s, 2014m, 1976sh, 1960sh and 1937vs cm^{-1}]; VCl_3, 97% yield (Cl and V analyses).

$Ph_3PbV(CO)_6$; *X-ray data collection and refinement*

A suitable crystal of dimensions $0.18 \times 0.47 \times 0.56$ mm was selected and mounted under a nitrogen atmosphere in a Lindemann glass capillary. The subsequent diffraction experiment was carried out at room temperature on a Siemens AED single crystal computer-controlled diffractometer. A monoclinic symmetry was identified after a search of some intense, low-angle reflections. The setting angles of 30 carefully centred reflections were used to determine accurate cell parameters and their standard deviations were determined by a least-squares fit.

Crystal data: $M = 657.5$; $a = 13.175(8)$; $b = 29.222(16)$; $c = 12.395(6)$ Å, $\beta = 89.28(3)°$; $U = 4772(4)$ $Å^3$; $Z = 8$; $D_c = 1.830$ g cm^{-3}; $F(000) = 2496$; Mo-K_α radiation ($\lambda = 0.71069$ Å); μ(Mo-K_α) = 75.13 cm^{-1}.

One quadrant of data ($\pm h$, $+k$, $+l$) was collected by the θ–2θ scan technique with Mo-K_α radiation. During the data collection the extinctions $h0l$, h = odd, and $0k0$, k = odd, were observed, which uniquely determined the space group as $P2_1/a$. The 2749 unique reflections satisfying the condition $I > 2\sigma(I)$ were retained from a total of 7221 reflections measured within the limits $5.0 < 2\theta < 47.0°$. The intensity of a standard reflection was measured every 50 reflections and remained essentially constant during the entire experiment. The reflection profiles were analysed following the method of Lehmann and Larsen[17] and the intensity data were corrected for Lorentz and polarization factors. Corrections for absorption and extinction effects were applied during the refinement according to the empirical method of Walker and Stuart.[18]

The structure determination showed the presence of two independent molecules per asymmetric unit. The coordinates of the two lead atoms were determined by a three-dimensional Patterson map and the position of the remaining non-hydrogen atoms were estimated from subsequent difference Fourier syntheses. Refinement was by full-matrix least-squares techniques minimizing the function $\Sigma w(|F_o| - |F_c|)^2$. With the lead and vanadium refined anisotropically and the other atoms isotropically, the conventional R index converged to 0.0532. This value dropped further to 0.0511 ($R_w = 0.0610$) after a few cycles in which anisotropic thermal parameters were assigned to all atoms except those of the carbonyl groups. Attempts to treat anisotropically these groups too did not result in any significant improvement of the R indices and led to physically unrealistic thermal motion for some atoms. The phenyl groups were refined as rigid bodies of D_{6h} symmetry. Due to the large numbers of parameters to be refined, the atoms were divided into two groups which were alternatively allowed to vary. The hydrogen atoms were ignored. The data-to-variable ratio was 7.1 : 1. A weighting scheme of the type $w = 0.5218/[\sigma^2(F_o) + 0.002045F_o^2]$ was applied in the final stages of the refinement. A low-angle reflection ($\bar{1}$ 2 1) due to a wrong measurement was omitted from the last cycle. Inspection of the last difference Fourier map revealed two other large peaks, 1.25 and 1.07 e $Å^{-3}$ in height, near two oxygen atoms of the carbonyl groups, possibly indicating a slight disordered situation; however attempts to correct for disorder by locating alternative positions with fractional occupancies were unsuccessful.

Neutral atomic scattering factors were used for lead and vanadium and the remaining atoms were taken from the *International Tables for X-Ray Crystallography*[19] and *SHELX*-76,[2] respectively. Real and imaginary anomalous dispersion corrections to the atomic scattering factors were included. Selected bond distances and angles are in Table 1. The supplementary material (final value of the fractional coordinates, observed and calculated structure factors, thermal parameters and a complete list of bond distances and angles) have been deposited with the Editor. Computation was performed on a GOULD-SEL 32/77 computer by using the *SHELX*-76 suite of programs. Other crystallographic computer programs used have been cited elsewhere.[21]

Reaction of ECl, E = Ph_3Sn, Ph_3Pb, *with* $Na[V(CO)_6]$ *in* THF

A solution of Ph_3PbCl (0.83 g, 1.7 mmol) in THF (50 cm^3) was treated at 0°C with $Na[V(CO)_6]$ (0.42 g, 1.7 mmol). After 6 h stirring at room temperature, the suspension was filtered and the filtrate was evaporated to dryness *in vacuo* at room temperature. The yellow residue was treated with *n*-heptane (50 cm^3) obtaining, after stirring at room temperature for 1 h, a red solution and some yellow solid. The solid was decanted and identified as Ph_3PbCl (IR). The volume of the filtrate was reduced to 20 cm^3 and the resulting suspension was filtered. After further evaporation and cooling to about −78°C, the wine-red filtrate afforded $Ph_3PbV(CO)_6$ (IR and CO analyses) as a dark red precipitate which was decanted from the mother

Table 1. Selected bond distances (Å) and angles (°) in $(C_6H_5)_3PbV(CO)_6$

	Molecule A	Molecule B
Pb—V	2.955(5)	2.936(5)
Pb—C(1)	2.24(1)	2.25(1)
Pb—C(7)	2.24(1)	2.21(1)
Pb—C(13)	2.19(2)	2.19(2)
V—C(19)	1.98(3)	2.03(3)
V—C(20)	1.88(3)	1.91(3)
V—C(21)	1.94(3)	1.83(4)
V—C(22)	1.87(3)	1.96(3)
V—C(23)	1.90(3)	1.89(3)
V—C(24)	1.94(2)	1.88(3)
V—Pb—C(1)	113.1(4)	111.6(4)
V—Pb—C(7)	112.8(4)	114.8(4)
V—Pb—C(13)	112.0(4)	111.2(4)
C(1)—Pb—C(7)	103.1(6)	102.7(5)
C(1)—Pb—C(13)	109.9(6)	111.0(7)
C(7)—Pb—C(13)	105.1(6)	105.1(6)
Pb—V—C(19)	141.0(8)	138.8(10)
Pb—V—C(20)	119.0(10)	120.2(11)
Pb—V—C(21)	120.8(8)	122.8(10)
Pb—V—C(22)	64.0(10)	67.9(8)
Pb—V—C(23)	69.4(10)	69.1(10)
Pb—V—C(24)	70.4(8)	69.7(8)
C(19)—V—C(20)	80.5(12)	84.2(14)
C(19)—V—C(21)	85.8(13)	82.5(15)
C(19)—V—C(22)	154.5(13)	153.3(13)
C(19)—V—C(23)	82.2(12)	83.2(13)
C(19)—V—C(24)	87.6(11)	84.5(13)
C(20)—V—C(21)	97.6(14)	95.7(16)
C(20)—V—C(22)	80.0(14)	79.1(13)
C(20)—V—C(23)	81.1(13)	83.1(14)
C(20)—V—C(24)	168.0(12)	168.7(14)
C(21)—V—C(22)	80.6(13)	78.6(14)
C(21)—V—C(23)	167.9(13)	165.7(14)
C(21)—V—C(24)	82.2(12)	81.8(14)
C(22)—V—C(23)	110.7(14)	115.0(13)
C(22)—V—C(24)	111.7(12)	111.0(11)
C(23)—V—C(24)	96.6(12)	96.6(13)
V—C(19)—O(19)	176(2)	175(3)
V—C(20)—O(20)	166(3)	176(3)
V—C(21)—O(21)	174(3)	176(3)
V—C(22)—O(22)	163(3)	172(2)
V—C(23)—O(23)	170(3)	170(2)
V—C(24)—O(24)	178(2)	172(3)

liquor and dried *in vacuo* at room temperature (0.60 g, 53% yield). The compound is moderately soluble in *n*-heptane and very soluble in toluene and dichloromethane. Donor solvents such as acetone and THF cause heterolytic cleavage of the Pb—V bond. The behaviour in THF is reported in detail. The compound (0.05 g, 0.85 mmol) was dissolved in THF (5 cm^3) and the IR spectrum of the solution, recorded immediately after mixing the reagents, showed weak absorptions attributable to the starting material and a strong absorption at 1851 cm^{-1} typical of the $[V(CO)_6]^-$ anion. The absorptions due to the starting material had completely disappeared after 10 min. Evaporation of the solvent *in vacuo* at room temperature, gave a red solid which was identified as $Ph_3PbV(CO)_6$ from its IR spectrum in *n*-heptane.

A solution of PPNCl (0.11 g, 0.2 mmol) in CH_2Cl_2 (10 cm^3) was treated with $Ph_3PbV(CO)_6$ (0.12 g, 0.18 mmol). The IR spectrum of the resulting yellow solution in the carbonyl stretching region showed a strong absorption at 1853 cm^{-1} attributable to the $[V(CO)_6]^-$ anion. Evaporation of the solvent and extraction with hot toluene (25 cm^3) separated $PPN[V(CO)_6]$[22] (0.13 g, 97% yield) from a colourless solution which, on evaporation of the solvent, afforded Ph_3PbCl (0.07 g, 86% yield).

By operating in a similar way, the compound $Ph_3SnV(CO)_6$ was isolated in 41% yield. A band at 1851 cm^{-1} due to the $[V(CO)_6]^-$ anion was present as the only carbonyl absorption immediately after the compound was dissolved in THF.

Reaction of $V(CO)_6$ *with* $CpCo(\eta^4\text{-}C_5H_5\text{-}R)$, R = H, CH_2Ph

(a) R = H. A solution of $CpCo(\eta^4\text{-}C_5H_6)$ (0.15 g, 0.8 mmol) in *n*-heptane (25 cm^3) was treated at room temperature with $V(CO)_6$ (0.14 g, 0.6 mmol). *Immediate* reaction with evolution of dihydrogen (99% with respect to vanadium) was observed. After 2 h stirring at room temperature, the solid which separated out was filtered, washed with *n*-heptane and dried *in vacuo* at room temperature affording 0.21 g (86% yield) of violet $[CoCp_2][V(CO)_6]$[8] (IR (Nujol) and C, H analysis).

(b) R = CH_2Ph. Using the same method as in (a) above, dibenzyl and $[CoCp_2][V(CO)_6]$ were obtained, after several hours, in 90 and 74% yields, respectively (the progress of the reaction was evidenced by the precipitation of the violet hexacarbonylvanadate salt).

Reaction of Ph_3SnH *with* $V(CO)_6$

A suspension of Ph_3SnH (0.29 g, 0.8 mmol) in *n*-heptane (25 cm^3) was treated at room temperature with $V(CO)_6$ (0.17 g, 0.8 mmol). After 7 days, the gas phase was found to contain dihydrogen (30% with respect to vanadium) and carbon monoxide. An IR spectrum of the yellow solution showed the presence of unreacted $V(CO)_6$ and $Ph_3SnV(CO)_6$. The reaction mixture was filtered and the solvent partially removed *in vacuo* at room temperature affording, on cooling at *ca* −30°C, yellow–orange

crystals of $Ph_3SnV(CO)_6$ (15% yield, IR (*n*-heptane)[16] and C, H analysis).

Reaction of $V(CO)_6$ *with* HX, X = Cl, Br

A solution of $V(CO)_6$ (0.14 g, 0.64 mmol) in *n*-heptane (30 cm^3) was treated at *ca* −78°C with 2.0 mmol of hydrogen chloride introduced into the cold solution through a rubber stopper. When the temperature was around −40°C, vigorous evolution of gas (carbon monoxide and dihydrogen by gas chromatography) and precipitation of a violet–brown solid were observed. The suspension was filtered at room temperature and the solid (0.1 g, 96% yield) identified as VCl_3 from its chloride content.

By operating in a similar way, an 88% yield of VBr_3 (Br and V analyses) was obtained.

RESULTS AND DISCUSSION

E—Cl *derivatives*

When $V(CO)_6$, dissolved in *n*-heptane,* was treated at room temperature with organyl chlorides, ECl, such as PhCl, $PhCH_2Cl$, Ph_3CCl and Ph_2PCl for some hours, VCl_3 and E—E coupling products were formed in high yields (≥ 80%) according to the stoichiometry reported in eq. (5). While the reaction of triphenylmethylchloride with $V(CO)_6$ is fast, in the other cases the reactions require more than 10 h to go to completion.

$$V(CO)_6 + 3ECl \rightarrow VCl_3 + 3/2E—E + 6CO \quad (5)$$

E = Ph, $PhCH_2$, Ph_3C and Ph_2P.

The reaction of diphenylchlorophosphine with $V(CO)_6$ deserves some comment. It is known[23] that P_2Ph_4 promptly reacts with hexacarbonylvanadium(0) to give the blue–green phosphido bridged dimer $(OC)_4V(\mu\text{-}PPh_2)_2V(CO)_4$ (**1**). The observation that P_2Ph_4 is obtained in high yields and that a transient blue colour appears during reaction (5), suggested the intermediacy of **1**. In order to test this hypothesis, **1** was reacted with Ph_2PCl and shown to be converted to the products of eq. (6).

$$(OC)_4V(\mu\text{-}PPh_2)_2V(CO)_4 + 6Ph_2PCl \rightarrow 2VCl_3 + 4Ph_4P_2 + 8CO. \quad (6)$$

Reaction (5) corresponds to the exhaustive chlorination of vanadium to VCl_3. The alternative pathway leading to VCl_3 and $EV(CO)_6$ has not been observed, probably due to the E—V bonds being unstable. As a matter of fact, no heptacoordinated hexacarbonyl derivative containing vanadium–carbon or vanadium–PR_2 (terminal) bonds is known. On the contrary, several examples (*vide infra*) of such compounds containing vanadium–heavy metal bonds (e.g. V—Au, V—Tl) have been reported. It was therefore of interest to investigate the reactions of Ph_3SnCl or Ph_3PbCl with $V(CO)_6$.

The reaction of ECl (E = Ph_3Sn, Ph_3Pb) with $V(CO)_6$ gives yields of the heptacoordinate derivative E—$V(CO)_6$ as high as 70%. Since the chloride initially introduced as E—Cl in the reaction mixture was found as VCl_3, it is reasonable to assume that the $Ph_3EV(CO)_6$ derivatives are formed according to the stoichiometry of eq. (7).

$$4V(CO)_6 + 3ECl \rightarrow 3E—V(CO)_6 + VCl_3 + 6CO \quad (7)$$

E = Ph_3Sn, Ph_3Pb.

While the compound containing the Sn—V bond has been known since 1964,[24] $Ph_3PbV(CO)_6$ is new and adds to the restricted family of heptacoordinated hexacarbonyl derivatives containing a M—V bond: $EtHgV(CO)_6$,[16] $Ph_3PAuV(CO)_6$,[16,24,25] $TlV(CO)_6$,[26] $H_3SiV(CO)_6$.[27]

The IR spectra (*n*-heptane) of E—$V(CO)_6$ (E = Ph_3Sn, Ph_3Pb) in the carbonyl stretching region are similar in both number of bands and wavenumber values to that of $Ph_3PAuV(CO)_6$,[16] whose solid-state structure was shown to be a monocapped octahedron with the gold atom occupying the capping position.[25] A similar structure for E—$V(CO)_6$ was therefore to be expected. However, in view of the still limited number of crystallographically established heptacoordinated hexacarbonyl derivatives of vanadium, it was decided to carry out an X-ray investigation of $Ph_3PbV(CO)_6$. It has been found that in the asymmetric unit there are two crystallographically independent $Ph_3PbV(CO)_6$ molecules, both of which occupy the general position in the group space $P2_1/a$. The two molecules are approximately related by pseudosymmetry elements, namely screw axes and glides, which cause disappearance or weakening of the $00l$, with $l = 2n+1$, and $0kl$, with $l = 2n+1$, reflections as well as reinforcement of the $h00$, with $h = 4n$, reflections. These symmetry elements are drawn in Fig. 1, which shows the molecular packing, the corresponding equivalent positions being as follows: $1/4+x, y, 1/2-z$; $1/4-x, 1/2-y, 1/2+z$; $1/4-x, y, 1/2+z$; $1/4+x, 1/2+y, 1/2-z$. An ORTEP diagram of one of these

* These reactions were carried out in saturated hydrocarbon solution in order to avoid secondary redox processes occurring in the presence of O- or N-Lewis bases[2] or aromatic compounds.[3]

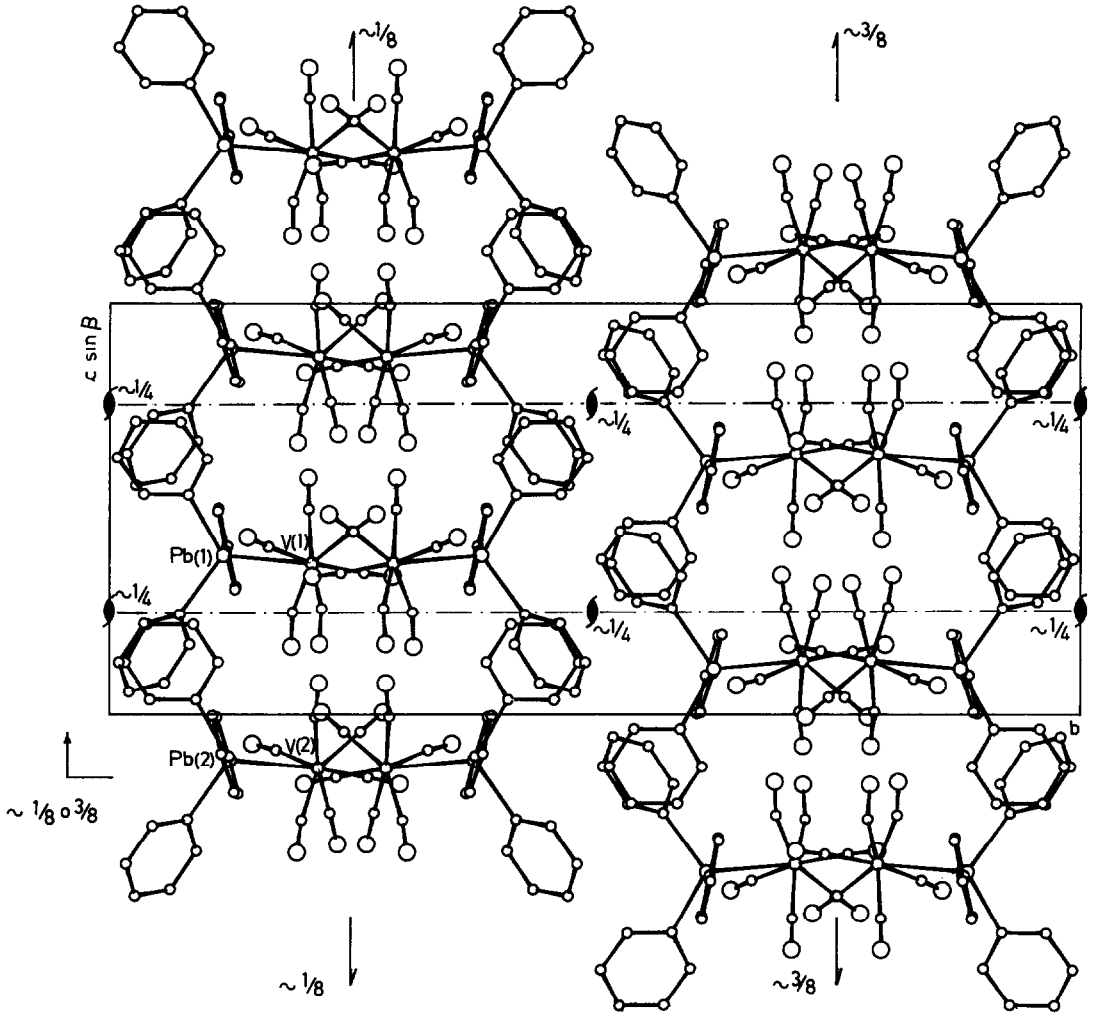

Fig. 1. Projection of the structure of $(C_6H_5)_3PbV(CO)_6$ along [100] showing the molecular packing and the pseudosymmetry elements.

molecules, which adopt essentially the same conformation and show only trivial structural differences, is represented in Fig. 2 along with the numbering scheme used. In both molecules the lead atom is four-coordinated to vanadium and three phenyl carbon atoms. The coordination polyhedron is a slightly distorted tetrahedron with the V—Pb—C angles (mean 112.6°) significantly larger than the C—Pb—C angles (mean 106.1°). As far as the Pb—V bond is concerned, it is worth pointing out that, to the best of our knowledge, the values of 2.955(5) and 2.936(5) Å found here are unique, having no precedents in the crystallographic literature. The average Pb—V bond length of 2.945 Å is shorter than the sum of the atomic radii (1.750 and 1.311 Å, respectively) for the elements in the corresponding metals.[28] On the other hand, by considering half of the Pb—Pb bond distance[29] [av. 2.844(4) Å] in Pb_2Ph_6 and the above mentioned vanadium radius in the metal, one would predict a lead–vanadium distance of 2.733 Å, which is considerably shorter than that observed in $Ph_3PbV(CO)_6$. This suggests that the metal–metal bond in this system should be rather weak. This is consistent with the chemical properties of $Ph_3PbV(CO)_6$, *vide infra*.

The Pb—C bond distances lie in the range 2.19(2)–2.25(1) Å and compare well with those found in other triphenyllead(IV) derivatives. Some typical values are 2.25–2.29 Å in *cis*-$Pt(PPh_3)_2(PbPh_3)Ph$,[30] 2.13–2.19 Å in $Ph_3Pb—GePh_3$,[31] and 2.217–2.224 Å in $Ph_6Pb_2Si_2Ph_6$.[31] The mean value of 2.22 Å practically coincides with the sum of the Pauling's covalent radii (2.23 Å).[32]

The seven-coordinated vanadium atom has the geometry of a distorted capped octahedron. The

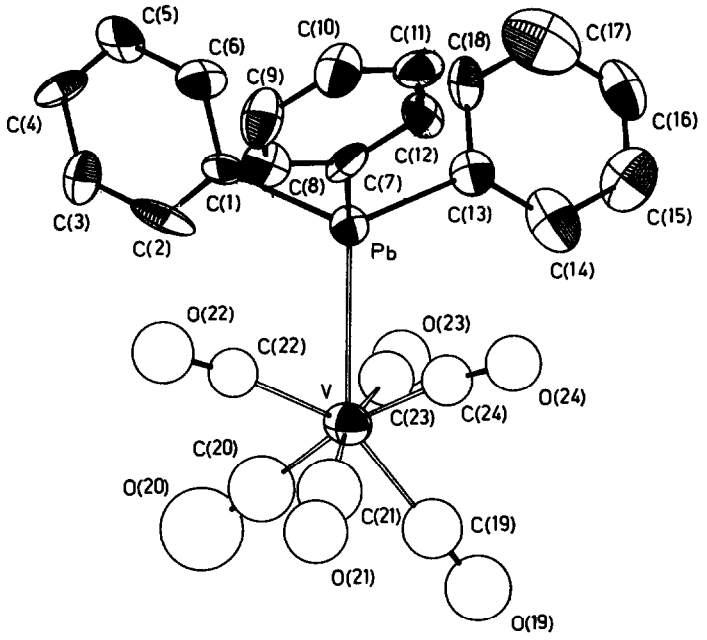

Fig. 2. An ORTEP view of one of the two independent molecules of $(C_6H_5)_3PbV(CO)_6$ with the numbering scheme used. Thermal ellipsoids are drawn to enclose 40% of the probability distribution. Anisotropic parameters were used only for shaded atoms.

lead atom occupies the unique capping position, three of the carbonyl carbon atoms [C(22), C(23) and C(24)] defining the capped face. In the present compound, the angles subtended at vanadium by the capping ligand and the carbon atoms at the capped face range from 64.0(10) to 70.4(8)°, while those subtended at vanadium by the capping ligand and the atoms in the uncapped face range between 119.0(10) and 141.0(8)°. Other angles (mean) are: $C_{capped\ face}$–V—$C_{capped\ face}$, 106.9°; $C_{uncapped\ face}$–V—$C_{uncapped\ face}$, 87.7°; ($C_{capped\ face}$–V—$C_{uncapped\ face}$)$_{cis}$, 82.0° and ($C_{cappd\ face}$–V—$C_{uncapped\ face}$)$_{trans}$, 163°C. The two triangular faces are at an angle of about 12° to each other. The V—C bond distances span a wide range, 1.83(4)—2.03(3) Å, but the spread does not seem to be real and can be related to the low degree of reliability usually shown by the structural parameters involving light atoms in structures containing atoms as heavy as lead. Nevertheless, if we simply average the distances, we get a value of 1.92 Å, which is very similar to the values found in $Ph_3PAuV(CO)_6$,[25] 1.932(33)–2.002(17) Å, and in the octahedral hexacarbonylvanadate(−I) salts of PPN^+, 1.931(9) Å,[22] $[V(CN—Bu^t)_6]^+$, 1.868(17)–1.922(18) Å,[33] $[V(CO)_4(1,2,4,5\text{-}C_6H_2Me_4)]^+$, 1.88(2)–1.95(3) Å,[3c] $[C_5H_5NH]^+$, 1.934(9)–1.926(14) Å,[9] $[(Ph_3P)_3Cu]^+$, 1.933(7)–1.963(7) Å.[34]

The molecular packing is mainly determined by van der Waals interactions. Short intermolecular contacts (*ca* 2.8 Å) occur between the oxygen atoms of carbonyl groups of symmetry independent molecules.

The IR spectra of $Ph_3PbV(CO)_6$ in *n*-heptane solution shows five badly resolved bands. If the solid-state structure persists in solution (and there are no reasons to think the contrary) the carbonyl groups' arrangement of C_{3v} symmetry should give rise to four stretching vibrations ($2A_1+2E$). Removal of degeneracy is, of course, possible.

Compounds such as E—$V(CO)_6$ (E = Ph_3Sn,[16] Tl[26]) have been reported to undergo heterolytic cleavage of the E—V bond in the presence of donor solvents such as THF or diethyl ether affording $[V(CO)_6]^-$ and presumably solvated E^+ species. In the case of $Ph_3SnV(CO)_6$, the reaction was described to be reversible[16] on removing the solvent, see eq. (8).

$$E—V(CO)_6 \rightleftarrows E^+ + [V(CO)_6]^- . \qquad (8)$$

As far as reaction (8) is concerned, the enthalpic contributions are related to the processes reported in eqs (8a)–(8f). Of them, the rupture of the metal–element bond [eq. (8b)], and the electron capture to $[V(CO)_6]^-$ [eq. (8d)] appear to be the most important ones in the case of the hexacarbonylvanadate anions.

$$E—V(CO)_{6(solv)} \rightarrow E—V(CO)_{6(g)} \qquad (8a)$$

$$E—V(CO)_{6(g)} \rightarrow E_{(g)} + V(CO)_{6(g)} \quad (8b)$$

$$E_{(g)} \rightarrow E^+_{(g)} + e^- \quad (8c)$$

$$[V(CO)_6]_{(g)} + e^- \rightarrow [V(CO)_6]^-_{(g)} \quad (8d)$$

$$E^+_{(g)} \rightarrow E^+_{(solv)} \quad (8e)$$

$$[V(CO)_6]^-_{(g)} \rightarrow [V(CO)_6]^-_{(solv)}. \quad (8f)$$

Our lead derivative, which shows a particularly long lead–vanadium bond distance, as noted earlier, makes no exception. $Ph_3PbV(CO)_6$ dissolves in THF with the formation of $[V(CO)_6]^-$ as established by the IR absorption at 1851 cm^{-1} typical of the complexed anion. We assume the counterion to be $[PbPh_3(THF)]^+$, although we have no direct evidence of its existence and attempts to precipitate it with bulky anions such as $[BPh_4]^-$ failed. Mention of $[ER_3]^+$ (E = Sn, Pb) derivatives in aqueous solution exists in the literature;[35] however, only tin(IV) cationic compounds of the formula $[Me_3SnL_2]^+$ (L = H_2O, 4-NH_2-pyridine, dimethylsulphoxide) appear to have been isolated.[36]

We have qualitatively observed that the rate of the heterolytic cleavage of the E—V bond depends on the nature of E: if E = Ph_3Sn, the Sn—V bond cleavage is simultaneous with the dissolution in THF. On the contrary, the corresponding lead compound requires several minutes to be heterolytically cleaved. In both cases, reactions appear to go to completion in neat THF. On the other hand, removal of the solvent gives the metal–metal bonded species. This feature suggested to us the possibility of preparing the lead compound by an alternative route from $Na[V(CO)_6]$ and Ph_3PbCl, both soluble in THF, see eq. (9). The THF solution of the two reagents presumably contains the solvated species Na^+ and $[V(CO)_6]^-$, in addition to Ph_3PbCl. Removal of the solvent gives the expected metal–metal bonded species, the driving force in this case being the lattice energy corresponding to the formation of NaCl.

$$ECl + Na[V(CO)_6] \xrightarrow[(2)\ n\text{-heptane}]{(1)\ THF} E—V(CO)_6 + NaCl \quad (9)$$

$$E = Ph_3Sn,\ Ph_3Pb.$$

Cleavage of the Pb—V bond occurs also in dichloromethane solution in the presence of the appropriate ligand for $[PbPh_3]^+$, e.g. Cl^-, see eq. (10).

$$Ph_3PbV(CO)_6 + PPNCl \rightarrow Ph_3PbCl + PPN[V(CO)_6]. \quad (10)$$

To summarize, this section on the reactions of ECl derivatives with $V(CO)_6$ has shown that, independent on the nature of E, electron-transfer from vanadium(0) to ECl takes place with formation of VCl_3. However, two different stoichiometries have been found, namely those of eqs (5) and (7), corresponding to the formation of the E—E coupling products or of the E—V bond containing compounds, respectively. A rationale for this different behaviour can perhaps be found by considering the reactions of Ph_3E—Cl {with E varying within the same group from carbon [reaction of type (5)], to tin and lead [reaction of type (7)]}. It is quite evident that the deciding factor in these cases is the strength of the E—E vs the E—V bonds. The formation of mixed metal complexes containing non-transition and transition elements will be the subject of a forthcoming paper.[37]

E—H *derivatives*

Cleavage of the E—H bonds promoted by $V(CO)_6$ has been reported earlier. Hieber and Winter[13] described the reaction of Ph_2PH with $V(CO)_6$ to give the bis(diphenylphosphido) bridged dimer **1**. Moreover, earlier studies from these laboratories had established that N—H (from some protonated nitrogen cases)[9] and O—H (from H_3O^+)[11] bonds can be cleaved via H_2 splitting, according to eqs (11) and (12), respectively:

$$[2\text{-Br-}C_5H_4NH][V(CO)_6] \rightarrow 2\text{-Br-}C_5H_4N + 1/2H_2 + V(CO)_6 \quad (11)$$

$$[H_3O][V(CO)_6] \rightarrow H_2O + 1/2H_2 + V(CO)_6. \quad (12)$$

In view of these precedents, it was of interest to explore further the electron-transfer ability of $V(CO)_6$ for C—H, N—H and H—X (X = halogen) bonds.*

An example of C—H bond cleavage is represented by the reaction of $V(CO)_6$ with some derivatives of cobalt(I) of the formula $CpCo(\eta^4\text{-}C_5H_5R)$. The latter are known to react with oxidizing agents in a manner which depends on the nature of the R group.[14,38,39]

We have found that the reaction of $CpCo(\eta^4\text{-}C_5H_5R)$, R = H, CH_2Ph, with $V(CO)_6$ proceeds via an electron transfer to $V(CO)_6$, resulting in the hexacarbonylvanadate salt reported in eqs (13) and (14):

$$CpCo(\eta^4\text{-}C_5H_5H) + V(CO)_6 \rightarrow [CoCp_2][V(CO)_6] + 1/2H_2 \quad (13)$$

* Triphenylmethane was found to react with $V(CO)_6$ under mild conditions to give hexaphenylethane. This reaction is slow and the fate of vanadium was not established: pyrophoric vanadium containing materials separated out from the reaction mixture.

$$CpCo(\eta^4\text{-}C_5H_5CH_2Ph) + V(CO)_6 \rightarrow [CoCp_2][V(CO)_6] + 1/2(CH_2Ph)_2. \quad (14)$$

In view of the fact that electron-transfer processes to $V(CO)_6$ from metal complexes containing carbocyclic ligands ($V(\eta^6\text{-arene})_2$,[5] $CoCp_2$[8]) are well established in the literature, we believe that the first step of the reaction is the formation of the unstable salt-like species $[CpCo(\eta^4\text{-}C_5H_5R)][V(CO)_6]$, followed by cleavage of the C—R bond and electron redistribution within the cobalt system. It is interesting to note that the reaction of the unsubstituted product $CpCo(\eta^4\text{-}C_5H_5H)$ is much faster, substantially diffusion-controlled, than the benzyl derivative. This may suggest that the cleavage of the C—H bond in the former compound may occur via migration of the hydrogen atom to the metal. This mechanism would be highly improbable in the case of the substituted compound, which has an *exo* conformation.[15]

The tin derivative Ph_3SnH reacts with $V(CO)_6$ giving $Ph_3SnV(CO)_6$ according to eq. (15). This reaction is very slow and gives low yields of the final product.*

$$V(CO)_6 + Ph_3SnH \rightarrow Ph_3SnV(CO)_6 + 1/2H_2. \quad (15)$$

Hexacarbonylvanadium(0) reacts promptly with H—X (X = halogen) to give dihydrogen. It has been found that if *n*-heptane solutions of $V(CO)_6$ are treated with hydrogen halides at temperatures as low as −40°C, VX_3, CO and dihydrogen are rapidly and quantitatively formed according to eq. (16).

$$V(CO)_6 + 3HX \rightarrow VX_3 + 3/2H_2 + 6CO \quad (16)$$

$$X = Cl, Br.$$

This reaction appears to be the only method available to prepare vanadium(III) halides at low temperature.[41]

Acknowledgements—The authors wish to thank the Consiglio Nazionale delle Ricerche (CNR, Roma) and the Ministero della Pubblica Istruzione (MPI) for financial support.

REFERENCES

1. F. Calderazzo and G. Pampaloni, *J. Organomet. Chem.* 1986, **303**, 111 and refs therein.
2. W. Hieber, J. Peterhans and E. Winter, *Chem. Ber.* 1961, **94**, 2572; W. Hieber, E. Winter and E. Schubert, *Chem. Ber.* 1962, **95**, 3070; H. Behrens and H. Lutz, *Z. Anorg. Allg. Chem.* 1967, **354**, 184; T. Richmond, Q. Z. Shi, W. C. Trogler and F. Basolo, *J. Am. Chem. Soc.* 1983, **106**, 76.
3. (a) F. Calderazzo, *Inorg. Chem.* 1964, **3**, 1207; (b) F. Calderazzo, *Inorg. Chem.* 1965, **4**, 223; (c) F. Calderazzo, G. Pampaloni, D. Vitali and P. F. Zanazzi, *J. Chem. Soc., Dalton Trans.* 1982, 1993.
4. F. Calderazzo and P. L. Calvi, *Chim. Ind. (Milan)* 1962, **44**, 1217.
5. F. Calderazzo and R. Cini, *J. Chem. Soc.* 1965, 818.
6. R. B. King, *Inorg. Chem.* 1965, **4**, 1518.
7. F. Calderazzo and S. Bacciarelli, *Inorg. Chem.* 1963, **2**, 721.
8. F. Calderazzo, G. Pampaloni and P. F. Zanazzi, *Chem. Ber.* 1986, **119**, 2796.
9. F. Calderazzo, M. Lanfranchi, G. Pampaloni and G. Pelizzi, *J. Organomet. Chem.* 1985, **296**, 1; F. Calderazzo, G. Pampaloni, G. Pelizzi and F. Vitali, *Organometallics* 1988, 7, 1083.
10. F. Calderazzo and G. Pampaloni, *J. Organomet. Chem.* 1983, **250**, C33.
11. F. Calderazzo, G. Pampaloni and D. Vitali, *Gazz. Chim. Ital.* 1981, **111**, 455.
12. L. C. Willemsens and G. J. M. van der Kerk, *J. Organomet. Chem.* 1968, **15**, 117.
13. W. Hieber and E. Winter, *Chem. Ber.* 1964, **97**, 1037.
14. M. L. H. Green, R. Pratt and G. Wilkinson, *J. Chem. Soc.* 1959, 3753.
15. G. E. Herberich and E. Bauer, *J. Organomet. Chem.* 1969, **16**, 301.
16. A. Davison and J. E. Ellis, *J. Organomet. Chem.* 1972, **36**, 113.
17. M. S. Lehmann and K. F. Larsen, *Acta Cryst.* 1974, **30A**, 580.
18. N. Walker and D. Stuart, *Acta Cryst.* 1983, **39A**, 158.
19. *International Tables for X-ray Crystallography*, Vol. 4. The Kynoch Press, Birmingham (1974).
20. G. M. Sheldrick, *SHELX-76, Program for Crystal Structure Determination.* University of Cambridge (1976).
21. D. Delledonne, G. Pelizzi and C. Pelizzi, *Acta Cryst.* 1987, **43C**, 1502.
22. R. D. Wilson and R. Bau, *J. Am. Chem. Soc.* 1974, **96**, 7601.
23. W. Hieber and R. Kummer, *Z. Naturforsch.* 1965, **20B**, 271.
24. A. S. Kasenally, R. S. Nyholm, R. J. O'Brien and M. H. B. Stiddard, *Nature* 1964, **204**, 871.
25. M. G. B. Drew, *Acta Cryst.* 1982, **38B**, 254.
26. S. E. Pedersen and W. R. Robinson, *Inorg. Chem.* 1975, **14**, 2365.
27. J. S. Allison, B. J. Aylett and M. H. Colquhoun, *J. Organomet. Chem.* 1976, **112**, C7.
28. Physical and Chemical Tables, in *International Tables for X-ray Crystallography* (Edited by C. H. MacGillavry and G. D. Rieck), Vol. 3, p. 278. The Kynoch Press, Birmingham (1962).

* Diphenylamine reacts with $V(CO)_6$ giving N_2Ph_4 and unidentified vanadium containing solids. It is to be noted that the disproportionation reaction of $V(CO)_6$ with diphenylamine is not observed under our reaction conditions, which is in agreement with the low basicity of the amine ($pK_a = 0.8$[40]).

29. H. Preut and F. Huber, *Z. Anorg. Allg. Chem.* 1976, **419**, 92.
30. B. Crociani, M. Nicolini, D. A. Clemente and G. Bandoli, *J. Organomet. Chem.* 1973, **49**, 249.
31. N. Kleiner and M. Dräger, *J. Organomet. Chem.* 1984, **270**, 151.
32. L. Pauling, *The Nature of the Chemical Bond*, 3rd Edn. Cornell University Press, Ithaca (1959).
33. L. D. Silverman, P. W. R. Corfield and S. J. Lippard, *Inorg. Chem.* 1981, **20**, 3106.
34. G. Doyle, K. A. Eriksen and D. Van Engen, *Organometallics* 1985, **4**, 2201.
35. R. S. Tobias, *Organomet. Chem. Rev.* 1966, **1**, 93; R. S. Tobias, *Am. Chem. Soc. Symp. Ser.* 1978, **82**, 130.
36. (a) G. Bähr and S. Pawlenko, Methoden zur Herstellung und Umwandlung von Organo-Zinn-Verbindungen, in *Methoden der Organischen Chemie* (Houben Weil) (Edited by E. Müller and O. Bayer), Vol. 13/6, p. 181. Georg Thieme Verlag, Stuttgart (1978); (b) G. Bähr and F. Langer, Methoden zur Herstellung und Umwandlung von Organo-Blei-Verbindungen, in *Methoden der Organischen Chemie* (Houben Weil) (Edited by E. Müller and O. Bayer), Vol. 13/7, p. 84. Georg Thieme Verlag, Stuttgart (1978).
37. F. Calderazzo and F. Ungari, manuscript in preparation.
38. (a) J. E. Sheatz, *J. Organomet. Chem. Library* 1979, **7**, 461; (b) G. E. Herberich and G. Greiß, *J. Organomet. Chem.* 1971, **27**, 113.
39. T. Dahl and C. Moberg, *Acta Chem. Scand.* 1973, **27**, 728.
40. *CRC Handbook of Chemistry and Physics* (Edited by R. C. Weast and M. J. Astle), p. D161. CRC Press Inc., Boca Raton, Florida (1979).
41. G. Brauer, *Handbook of Preparative Inorganic Chemistry*, pp. 1252–1262. Academic Press, New York (1965).

Polyhedron Vol. 7, No. 19/20, pp. 2049–2051, 1988
Printed in Great Britain

0277–5387/88 $3.00+.00
© 1988 Pergamon Press plc

THE SYNTHESIS AND X-RAY CRYSTAL STRUCTURE OF A TETRANUCLEAR SPIROCYCLIC TUNGSTEN COMPLEX WITH TWO METAL–METAL TRIPLE BONDS

DONALD C. BRADLEY,* HELEN M. DAWES, MICHAEL B. HURSTHOUSE* and HAROLD R. POWELL†

Department of Chemistry, Queen Mary College, Mile End Road, London E1 4NS, U.K.

Abstract—The remarkable tetratungsten species $C[W_2\{N(SiMe_3)Si(Me_2)CH_2\}_2\{N(SiMe_3)SiMe_2\}]_2$ (**1**) was isolated in small yield from the reaction of WCl_4 with Na/Hg (one equivalent) in 1,2-dimethoxyethane (dme) followed by treatment with $Li[N(SiMe_3)_2]$ (three equivalents) and was characterized by single crystal X-ray diffraction. The "W"-shaped molecule contains a unique spiro-carbon bonded to two tungstens and two silicons, and the W≡W bond lengths are 2.281 and 2.282(2) Å.

The chemistry of transition metal dialkylamides has developed over the last three decades to include examples of most of the *d*-block elements. The use of the bulky bis-trimethylsilylamide ligand has allowed the isolation of a number of three coordinate complexes with the formula ML_3, where $L = N(SiMe_3)_2$.[1] These are all examples of propellor shaped molecules, with the planes of the SiN_2 fragments inclined to the perpendicular of the N_3 plane. Although compounds such as $MClL_3$ (M = Zr, Hf),[2,3] $RhL(PPh_3)_2$ and $Ru(H)L(PPh_3)_2$[4] have been reported, to date no homoleptic trivalent complex of any of the second or third row transition metals has been prepared.

Reaction between the reduction product formed by WCl_4 and Na/Hg in dimethoxyethane[5] with $LiN(SiMe_3)_2$ gave a dark brown solution from which a small quantity of crystalline **1** was isolated. An X-ray crystal structure determination revealed that **1** had the molecular structure shown in Figs 1 and 2. The molecule consists of two tungsten dimeric units, each with three bridging silylamidomethyleneido ligands, bound in a 1,1,2 fashion. Each of these units reacted further, eliminating the elements of methane to form a spiro ring junction at C(6). The two ditungsten units are joined by C(6) giving the whole molecule a "W"-shaped backbone.

Molybdenum and tungsten are well known for their tendency to form metal–metal triple bonds in their +3 oxidation state, especially in their compounds with dialkylamido ligands[6] and a number of cyclometallation reactions involving either the hexamethyldisilylamide ligand[7,9] or metal–metal multiply bonded dimers have also been reported.[10]

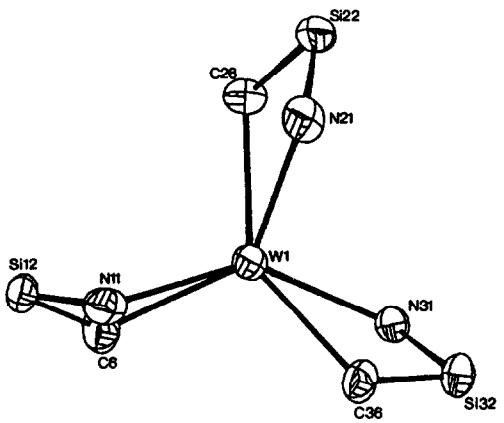

Fig. 1. The structure of **1**, 50% probability thermal ellipsoids. Principal bond lengths (Å) for **1**:

W(1)—W(2)	2.282(2)	W(3)—W(4)	2.281(3)
W(1)—N(11)	1.954(17)	W(4)—N(41)	1.934(14)
W(1)—N(21)	1.962(14)	W(4)—N(61)	1.962(13)
W(1)—C(36)	2.083(19)	W(4)—C(56)	2.120(21)
W(2)—N(31)	1.995(16)	W(3)—N(51)	1.997(15)
W(2)—C(26)	2.107(17)	W(3)—C(66)	2.078(17)
W(2)—C(6)	2.108(16)	W(3)—C(6)	2.113(14)

non-bonded distance W(2)—(3) 3.467(4) Å.

* Authors to whom correspondence should be addressed.
† Present address: School of Chemistry, Polytechnic of North London, Holloway Road, London N7 8DB, U.K.

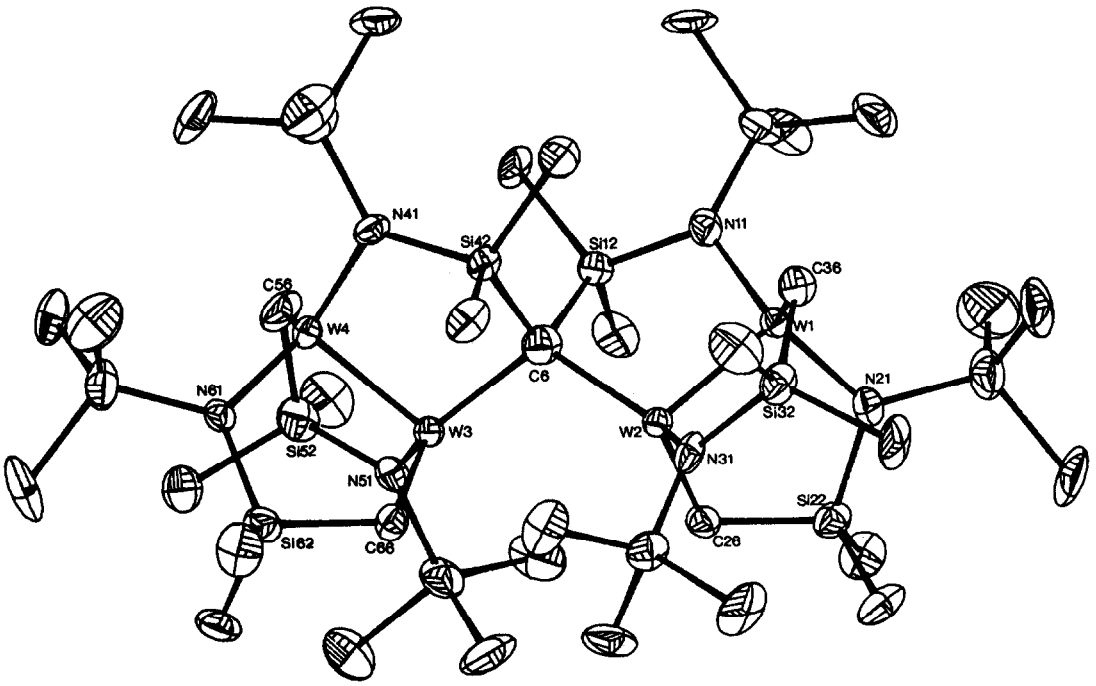

Fig. 2. Line drawing of **1**. Key: N = $N(SiMe_3)_2$, Si = $SiMe_2$.

However, the formation of compound **1** is quite unprecedented and its mechanism remains obscure. We have attempted to synthesize compound **1** by alternative routes, but so far without success.

The tungsten–tungsten bond distances are consistent with those expected for triple bonds, and are not affected greatly by the presence of three bridging ligands.[6] The two ends of each dimer are virtually eclipsed (Fig. 3); as the triple bond has cylindrical symmetry, this would not be expected to have any effect either. As noted for other tungsten alkylamido species, the W—N interactions may be regarded as double bonds.[11]

Crystal Data for **1**: $C_{35}H_{98}N_6Si_{12}W_4$, M = 1675.63, monoclinic, a = 18.129(6), b = 19.406(7), c = 18.851(5) Å, β = 102.78(3)°, V = 6467.44 Å^3, space group $P21/n$ (alternative setting of $P21/c$, no. 14), Z = 4, D_c = 1.72 g cm^{-3}, μ(Mo-K_α) = 70.24 cm^{-1}, $F(000)$ = 3256, R = 0.0518 and R_w = 0.0439 for 5373 reflections corrected for absorption with $I/\sigma(I) > 3$.*

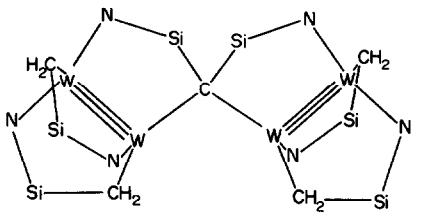

Fig. 3. View along W(1)—W(2); W(3)—W(4) dimer and all exocyclic atoms are omitted to aid clarity. 50% probability thermal ellipsoids.

Acknowledgement—H. R. Powell thanks the S.E.R.C. for a Research Studentship.

REFERENCES

1. D. C. Bradley, P. G. Eller, M. B. Hursthouse and D. W. Meek, *Coord. Chem. Rev.* 1977, **24**, 1.
2. R. A. Andersen, *Inorg. Chem.* 1979, **18**, 2928.
3. C. Airoldi, D. C. Bradley and H. Chudzynska, *Proc. 18th Int. Conf. Coord. Chem.* Sao Paulo, 1977, 207; C. Airoldi, D. C. Bradley, H. Chudzynska, M. B. Hursthouse, K. M. Abdul Malik and P. Raithby, *J. Chem. Soc., Dalton Trans.* 1980, 2010.
4. B. Cetinkaya, M. F. Lappert and S. Torroni, *J. Chem. Soc., Chem. Commun.* 1979, 843.
5. M. A. Schaeffer-King and R. E. McCarley, *Inorg. Chem.* 1977, **12**, 1972.
6. F. A. Cotton and R. A. Walton (Eds), *Multiple Bonds*

* Atomic coordinates, displacement factor coefficients, full lists of bond lengths and angles and lists of F_o/F_c values have been deposited as supplementary data with the Editor, from whom copies are available on request. Atomic coordinates have also been deposited with the Cambridge Crystallographic Data Centre.

between Metal Atoms, and refs therein. Wiley, New York (1982).
7. C. Bennett and D. C. Bradley, *J. Chem. Soc., Chem. Commun.* 1974, 29.
8. R. P. Planalp and R. A. Andersen, *Organometallics* 1983, **2**, 1675, and refs therein.
9. A. Dormond, A. A. El Bouadili and C. Moise, *J. Chem. Soc., Chem. Commun.* 1985, 914 and refs therein.
10. M. Bochmann, G. Wilkinson, A. M. R. Galas and M. B. Hursthouse, *J. Chem. Soc., Dalton Trans.* 1980, 1797.
11. K. H. Ahmed, M. H. Chisholm, K. Folting and J. C. Huffman, *J. Chem. Soc., Chem. Commun.* 1985, 152.
12. M. B. Hursthouse, R. A. Jones, K. M. A. Malik and G. Wilkinson, *J. Am. Chem. Soc.* 1979, **101**, 4128.
13. DIFABS, N. Walker and D. Stuart, *Acta Cryst. Sect A.* 1983, **39**, 158.

Polyhedron Vol. 7, No. 19/20, pp. 2053–2082, 1988
Printed in Great Britain

0277–5387/88 $3.00+.00
© 1988 Pergamon Press plc

HALIDE, HYDRIDE, ALKYL, OXO AND RELATED DERIVATIVES OF BIS(PENTAMETHYLCYCLOPENTADIENYL)TUNGSTEN(IV)

GERARD PARKIN and JOHN E. BERCAW†

A. A. Noyes Laboratory of Chemical Physics, California Institute of Technology, Pasadena, CA 91125, U.S.A.

Abstract—A "wet" entry into permethyltungstenocene chemistry is provided by $Cp^*_2WCl_2$ ($Cp^* = \eta^5$-C_5Me_5), prepared by reduction of $Cp^*WCl_4(PMe_3)$ with Mg followed by metathesis with MCp^* (M = Li, K). $Cp^*_2WCl_2$ may be converted to a variety of other permethyltungstenocene derivatives and thus, $Cp^*_2WH_2$, $Cp^*_2W(H)Cl$. $Cp^*_2W(CH_3)_2$, $Cp^*_2W(CH_3)Cl$, $Cp^*_2W(CH_3)H$, $Cp^*_2W(CH_2C_6H_5)H$, $Cp^*_2W(\eta^2$-$CH_2O)$ and $Cp^*_2W{=}O$ have been isolated. The dihydride derivative, $Cp^*_2WH_2$, is readily protonated to give $[Cp^*_2WH_3]^+$. The protonation occurs by attack at *both* the W—H bonds (and not the d^2 tungsten centre), forming an η^3-trihydrogen species, $[Cp^*_2W(\eta^3$-$H_3)]^+$, prior to collapsing to the trihydride cation, $[Cp^*_2WH_3]^+$. The central and lateral hydride ligands of $[Cp^*_2WH_3]^+$ exchange sites by an intramolecular mechanism in preference to a deprotonation/protonation mechanism. The oxo ligand of $Cp^*_2W{=}O$ undergoes facile isotopic exchange with $H_2{}^{18}O$ and $H_2{}^{17}O$. $Cp^*_2W{=}O$ is oxidized by $H_2O_{2(aq)}$ and by O_2 to give (η^5-C_5Me_5)(η^1-C_5Me_5)$W(=O)_2$ and (η^5-C_5Me_5)$W(=O)_2(OC_5Me_5)$, respectively. (η^5-C_5Me_5)(η^1-C_5Me_5)$W(=O)_2$ possesses both *penta*hapto and *mono*hapto pentamethylcyclopentadienyl ligands which exchange on the NMR timescale with $\Delta G^\ddagger = 10(1)$ kcal mol^{-1} at -60°C. (η^5-C_5Me_5)$W(=O)_2(OC_5Me_5)$ is formed by insertion of an oxygen atom from dioxygen into the W—C_5Me_5 bond. The two oxo ligands of (η^5-C_5Me_5)(η^1-C_5Me_5)$W(=O)_2$ and (η^5-C_5Me_5)$W(=O)_2(OC_5Me_5)$ exhibit a strong *trans* influence, resulting in a coordination geometry of the pentamethylcyclopentadienyl ligand which is more properly described as (η^1,η^4-C_5Me_5). The oxo ligand of $Cp^*_2W{=}O$ may be abstracted by a variety of reagents. Thus, both H_2 and Me_2SiH reduce $Cp^*_2W{=}O$ to $Cp^*_2WH_2$, and Me_3SiCl converts $Cp^*_2W{=}O$ to $Cp^*_2WCl_2$. In contrast, the reaction between $Cp^*_2W{=}O$ and CH_3I gives the oxo-methyl cation, $[Cp^*_2W(=O)CH_3][I]$, which is deprotonated by KH to give initially the *tetra*hapto-coordinated η^4-1,2,3,4-tetramethylfulvene complex, $Cp^*(\eta^4$-$C_5Me_4{=}CH_2)W(=O)(CH_3)$, which subsequently isomerizes to *dihapto*-coordinated *exo*-methylene tautomer, $Cp^*(\eta^2$-$CH_2{=}C_5Me_4)W(=O)(CH_3)$.

The group 6 "bent metallocene" derivatives, Cp_2MX_2 and Cp_2ML ($Cp = \eta^5$-C_5H_5; M = Mo, W; X = halide, hydride, alkyl, etc.; L = CO, PR_3, etc.), first reported by Wilkinson, Green, McCleverty and Pratt in 1961,[1] have been amongst the most important compounds in the development of synthetic, mechanistic, structural and theoretical organotransition metal chemistry. For example, structural studies provided experimental evidence to test the validity of the various molecular orbital descriptions for bent metallocene derivatives.[2] In addition, the tungstenocene system has exhibited a wealth of chemistry which has provided information on many fundamental transformations including: (i) the first example of the photochemical reductive elimination of dihydrogen, (ii) the insertion of $[Cp_2W]$ into sp^3 C—H bonds (i.e. alkane activation), (iii) the first evidence for α-H elimination for $[Cp_2W{-}CH_3]^+$, (iv) ring opening of a tungstenacyclobutane derivative to give an alkylidene–olefin intermediate, which subsequently led to proposal of the Green–Rooney mechanism for olefin polymerization, and (v) the development of rules for predicting the regioselectivity of nucleophilic addition to organometallic cations.[3]

Our research group has had a long-standing interest in studying fundamental organometallic

† Author to whom correspondence should be addressed.

transformations including α and β migratory insertion/elimination, reductive elimination/oxidative addition and sigma bond metathesis. In this regard the permethylmetallocene derivatives of scandium, titanium, zirconium, hafnium, niobium and tantalum have proven to be particularly well-suited to structural and mechanistic studies due to their enhanced solubilities, stabilities and crystallizabilities, as compared with the (η^5-C_5H_5) analogues.[4] Moreover, the steric bulk of their (η^5-C_5Me_5) ligands inhibits bimolecular decomposition pathways, thus allowing isolation of compounds such as $Cp^*_2Ta(=CH_2)H$[4h] ($Cp^* = \eta^5$-C_5Me_5), the first isolable example of an alkylidene hydride derivative. In order to extend our mechanistic studies at "bent permethylmetallocene" centres to the less electropositive transition elements to the right of the Periodic Table, we have long sought a convenient synthetic route to the permethyltungstenocene system. In view of the extensive chemistry of the unsubstituted [(η^5-$C_5H_5)_2W$] system leading to the formation of dimers via intermolecular attack at the C—H bonds of the (η^5-C_5H_5) ligands of other metal centres,[5] we again anticipated a substantial increase in stability for the (η^5-C_5Me_5) analogue. Although the tungstenocene system has been known for more than 25 years, corresponding synthetic approaches to permethyltungstenocene derivatives have been uniformly unsuccessful, and the only previously reported synthesis of $Cp^*_2WH_2$ is the recently described metal vapour synthesis method involving co-condensation of Cp*H with W atoms.[6] Herein we describe a conventional synthesis of $Cp^*_2WCl_2$ and the synthesis, structure and reaction chemistry of other derivatives of permethyltungstenocene derived therefrom.

RESULTS AND DISCUSSION

Halide, hydride, alkyl and formaldehyde derivatives of permethyltungstenocene

(1) *Synthetic studies.* $Cp^*_2WCl_2$ is synthesized in *ca* 30% yield from $Cp^*WCl_4(PMe_3)$[7] by a two-step process involving (i) reduction by Mg (0.5 equivalent) followed by (ii) reaction with either LiCp* or KCp*. This approach is also successful for the mixed-ring derivative (η^5-C_5Me_5)(η^5-$C_5Me_4CH_2CH_2CH_3$)WCl_2.

$$Cp^*WCl_4(PMe_3) \xrightarrow{0.5\,Mg/THF} \{Cp^*WCl_3(PMe_3)(MgCl_2)_{0.5}\} \xrightarrow[(M = Li, K)]{MCp^*/C_6H_5CH_3/145°C} Cp^*_2WCl_2.$$

$Cp^*_2WCl_2$ provides an entry to a variety of other permethyltungstenocene derivatives (Scheme 1). For example, the reaction of $Cp^*_2WCl_2$ with $LiAlH_4$ generates $Cp^*_2WH_2$ in which $Cp^*_2W(H)Cl$ is observed as an intermediate. A more convenient synthesis of $Cp^*_2W(H)Cl$ is the reduction of $Cp^*_2WCl_2$ by Na(Hg) in THF. The origin of the hydride ligand is uncertain, but it is likely that it

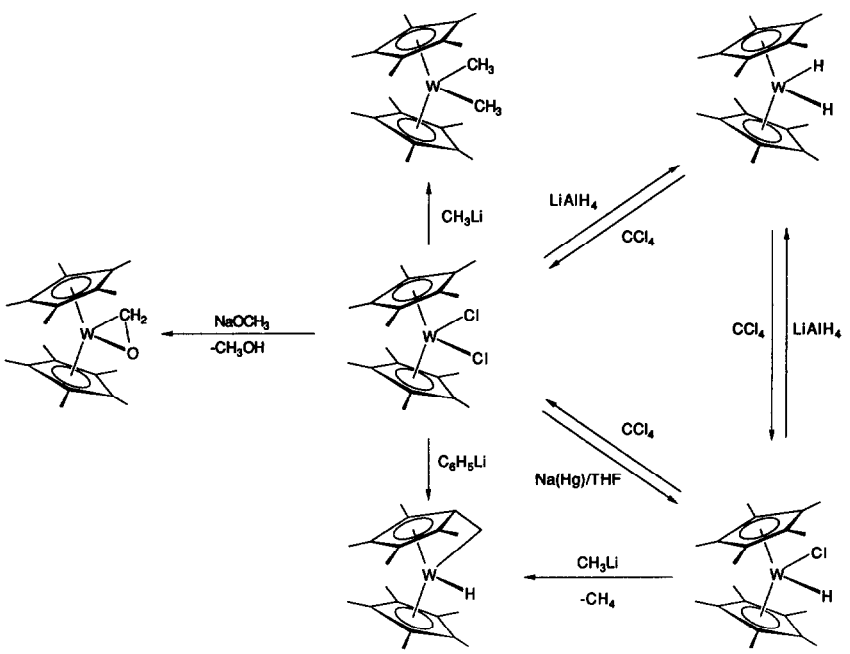

Scheme 1. Syntheses of permethyltungstenocene derivatives from $Cp^*_2WCl_2$.

arises by abstraction from the solvent.† The dimethyl derivative, $Cp^*_2W(CH_3)_2$, is isolated from the reaction of $Cp^*_2WCl_2$ with CH_3Li in toluene at 80°C. In contrast, the reaction of $Cp^*_2WCl_2$ with $NaOCH_3$ gives the η^2-formaldehyde derivative, $Cp^*_2W(\eta^2\text{-}CH_2O)$. This reaction occurs with elimination of methanol and, thus, may proceed via the dimethoxy derivative, $[Cp^*_2W(OCH_3)_2]$, followed by 1,3-elimination of CH_3OH.‡

$$Cp^*_2WCl_2 \xrightarrow{NaOCH_3} [Cp^*_2W(OCH_3)_2] \xrightarrow{-CH_3OH} Cp^*_2W(\eta^2\text{-}CH_2O).$$

Other η^2-formaldehyde derivatives of tungsten, namely $W(PMe_3)_4(\eta^2\text{-}CH_2O)H_2$[9] and $W(\eta^4\text{-}C_4H_6)(\eta^2\text{-}CH_2O)(PMe_3)_3$,[10] as well as the molybdenocene derivative, $Cp_2Mo(\eta^2\text{-}CH_2O)$,[11] have recently been reported.

The metallated derivative, $Cp^*(\eta^5,\eta^1\text{-}C_5Me_4CH_2)WH$,§ is formed by the reaction of $Cp^*_2WCl_2$ with C_6H_5Li. The simple metathesis produce (very sterically crowded) $Cp^*_2W(C_6H_5)_2$, is not obtained nor is it observed as an intermediate; rather, as evidenced by the formation of biphenyl, phenyllithium appears to act as a reducing agent. $Cp^*(\eta^5,\eta^1\text{-}C_5Me_4CH_2)WH$ is also obtained by the reaction of the hydrido-chloride derivative, $Cp^*_2W(H)Cl$, with CH_3Li at 110°C. The latter reaction is observed to proceed via elimination of methane from the initial metathesis product, $Cp^*_2W(CH_3)H$, by ^1H NMR spectroscopy.

$$Cp^*_2W(H)Cl \xrightarrow{CH_3Li/110°C} [Cp^*_2W(CH_3)H] \xrightarrow{-CH_4} Cp^*(\eta^5,\eta^1\text{-}C_5Me_4CH_2)WH.$$

The W^{IV} compound $Cp^*(\eta^5,\eta^1\text{-}C_5Me_4CH_2)WH$ is not as reactive as the analogous Ta^V compound, $Cp^*(\eta^5,\eta^1\text{-}C_5Me_4CH_2)TaH_2$, which is an effective source of the 16-electron intermediate, $[Cp^*_2Ta\text{—}H]$.[12] It does, however, react with H_2 (4 atm) to give $Cp^*_2WH_2$ at 220°C.

$$Cp^*(\eta^5,\eta^1\text{-}C_5Me_4CH_2)WH + H_2 \longrightarrow Cp^*_2WH_2.$$

$Cp^*_2WH_2$ is converted sequentially to the hydrido-chloride, $Cp^*_2W(H)Cl$, and the dichloride derivative, $Cp^*_2WCl_2$ upon treatment with CCl_4. Furthermore, $Cp^*_2WCl_2$ and $Cp^*_2WH_2$ react at 220°C to form $Cp^*_2W(H)Cl$ as an equilibrium mixture.

$$Cp^*_2WH_2 + Cp^*_2WCl_2 \rightleftharpoons 2Cp^*_2W(H)Cl \quad K_{eq} \approx 21(1) \text{ at } 220°C.$$

The methyl–chloride derivative, $Cp^*_2W(CH_3)Cl$, is conveniently obtained by selected cleavage of one of the W—CH_3 bonds of $Cp^*_2W(CH_3)_2$ upon treatment with one equivalent of HCl, generated *in situ* by the reaction of Me_3SiCl (one equivalent) with H_2O (0.5 equivalent). $Cp^*_2W(CH_3)Cl$ is another useful precursor to permethyltungstenocene derivatives and exhibits a variety of reaction pathways as shown in Scheme 2. Simple substitution reactions occur with CH_3Li and $LiAlH_4$ to give $Cp^*_2(CH_3)_2$ and $Cp^*_2W(CH_3)H$, respectively. In contrast to these metathesis reactions, the reaction of $Cp^*_2W(CH_3)Cl$ with C_6H_5Li does not give $Cp^*_2W(CH_3)(C_6H_5)$ but rather $Cp^*_2W(CH_2C_6H_5)H$. A plausible reaction sequence would involve nucleophilic attack by LiC_6H_5 at the methylidene ligand of an intermediate cation, $[Cp^*_2W(=CH_2)H]^+$, generated by α-H elimination from the intermediate $[Cp^*_2W\text{—}CH_3]^+$, e.g.

$$Cp^*_2W(CH_3)Cl \xrightarrow{-Cl^-} [Cp^*_2W\text{—}CH_3]^+ \rightleftharpoons [Cp^*_2W(=CH_2)H]^+ \xrightarrow[-Li^+]{C_6H_5Li} Cp^*_2W(CH_2C_6H_5)H.$$

A similar mechanism has been proposed for the formation of $[Cp_2W(CH_2PR_3)H][PF_6]$ from $[Cp_2W(CH_3)(PR_3)][PF_6]$.[13] The mechanism of this reaction is to be contrasted with the reaction of $Cp^*_2W(CH_3)Cl$ with $LiAlH_4$ to give $Cp^*_2W(CH_3)H$. For this latter reaction, a similar mechanism may have, in principle, occurred since the product of a direct metathesis mechanism and that of an α-H elimination mechanism are identical. However, the reaction of $Cp^*_2W(CH_3)Cl$ with $LiAlD_4$ provides $Cp^*_2W(CH_3)D$, in support of the direct metathesis reaction. A further reaction pathway is demonstrated by the reaction of $Cp^*_2W(CH_3)Cl$ with $LiCH_2PMe_2$ in which dehydrohalogenation occurs, but the overall result is that of deprotonation of one of the Cp* methyl groups, and not [W—CH_3], to give $Cp^*(\eta^5,\eta^1\text{-}C_5Me_4CH_2)W(CH_3)$. The reaction of $Cp^*_2W(CH_3)Cl$ with other organolithium reagents lead to complex mixtures. For example, CH_2CH_3MgBr or Me_3CLi gives *inter alia* $Cp^*_2W(CH_3)H$ with the elimination of olefin.

† Smaller quantities of $Cp^*(\eta^5,\eta^1\text{-}C_5Me_4CH_2)WH$ are also formed by this reduction but $Cp^*_2W(H)Cl$ may be readily separated by crystallization from pentane.

‡ The formation of η^2-thioaldehyde and η^2-imine complexes by 1,3-elimination of CH_4 from $Cp_2Zr(SCH_2R)(CH_3)$[8a] and from $Cp^*Ta(NMe_2)(CH_3)_3$[8b] have been observed.

§ $Cp^*(\eta^5,\eta^1\text{-}C_5Me_4CH_2)WH$ and $Cp^*\{\eta^5,\eta^1,\eta^1\text{-}C_5Me_3(CH_2)_2\}W$ have been prepared previously by photolytic elimination of H_2 from $Cp^*_2WH_2$.[6]

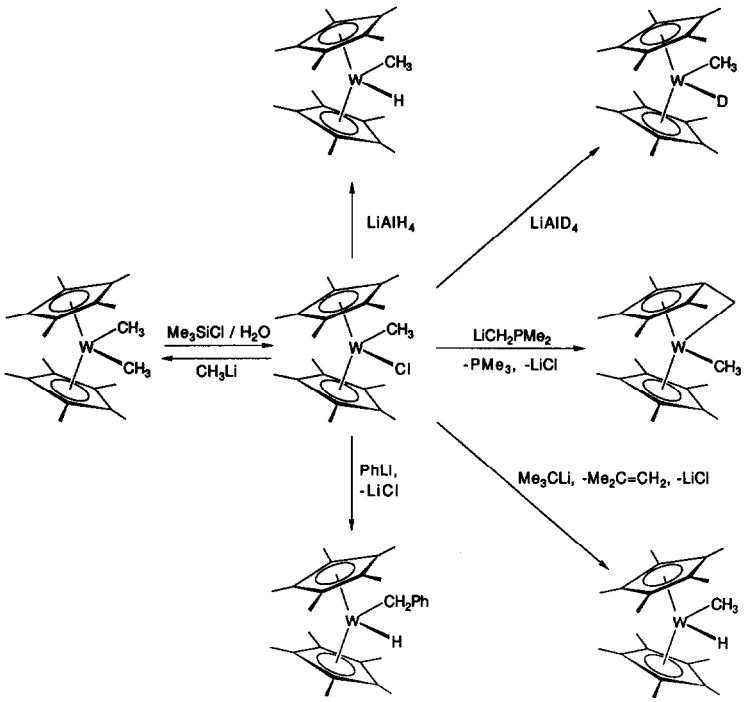

Scheme 2. Synthesis and reaction chemistry of $Cp_2^*W(CH_3)Cl$.

(2) *The mechanism of the protonation of* $Cp_2^*WH_2$: *evidence for a trihydrogen species.* The tungstenocene derivative, Cp_2WH_2, has previously been shown to react with a variety of electrophiles,[14] e.g. BX_3 (X = F, Cl),[15] H^+,[1a] and R_3Al.[16] Similarly, the dihydride, $Cp_2^*WH_2$, is readily protonated by a variety of acids including $HBF_4 \cdot Et_2O$, $HCl_{(aq)}$ and $[Me_3NH][BPh_4]$ to give the trihydride cation, $[Cp_2^*WH_3]^+$.

$$Cp_2^*WH_2 + HX \longrightarrow [Cp_2^*WH_3][X] \, (X = Cl, BF_4, BPh_4).$$

The $[Cp_2^*WH_3]^+$ cation is characterized by two resonances in the ^1H NMR spectrum in D_2O at δ −4.50 (doublet) and δ −5.42 (triplet) corresponding to the central and lateral protons, respectively. The small $^2J_{H-H}$ coupling constant, *ca* 3 Hz, is indicative that the species is formally a trihydride, not a dihydrogen–hydride derivative, $[Cp_2^*W(\eta^2\text{-}H_2)H]^+$. Interestingly, the central hydride ligand exhibits an 11 Hz greater $^1J_{W-H}$ coupling constant ($^1J_{W-H}$ = 66 Hz) than the lateral hydride ligands ($^1J_{W-H}$ = 57 Hz), possibly reflecting a greater a_1 (and thus greater tungsten 6*s*) contribution in the bonding to the central hydride ligand. The trihydride derivative is readily deprotonated by $KOH_{(aq)}$ to regenerate $Cp_2^*WH_2$.

$$[Cp_2^*WH_3]^+ + KOH_{(aq)} \longrightarrow Cp_2^*WH_2 + H_2O + K^+.$$

Some rather unexpected features of this protonation/deprotonation mechanism are revealed by examining the stereochemistry of D^+ addition to $Cp_2^*WH_2$. Treatment of a suspension of $Cp_2^*WH_2$ in D_2O with a solution of DCl/D_2O affords, as the kinetic product, the isotopomer with the deuterium predominantly occupying the *central* position, $[Cp_2^*W(H)(D)(H)]^+$ (*ca* 90%, 1 min), and a much smaller fraction of the laterally deuterated isotopomer, $[Cp_2^*W(H)(H)(D)]^+$ (*ca* 10%, 1 min). Subsequent exchange of the lateral and central hydride ligands occurs over a period of several hours, accompanied by further incorporation of deuterium from excess DCl/D_2O (*vide infra*).

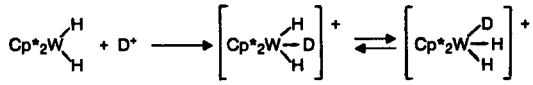

The relatively small doublet ($^2J_{H-H}$ = 3 Hz) attributable to the central hydrogen of $[Cp_2^*W(H)(H)(D)]^+$ initially observed in the ^1H NMR spectrum (resonance H_2O in Fig. 1) is particularly indicative of the strong preference for central protonation. Possible pathways for the protonation of $Cp_2^*WH_2$ with D^+ are shown in Scheme 3. Pathways (a) and (b) involve direct protonation at the tungsten centre in the lateral and central positions, respectively. On the basis of *ground* state orbital control arguments, an electrophile would be

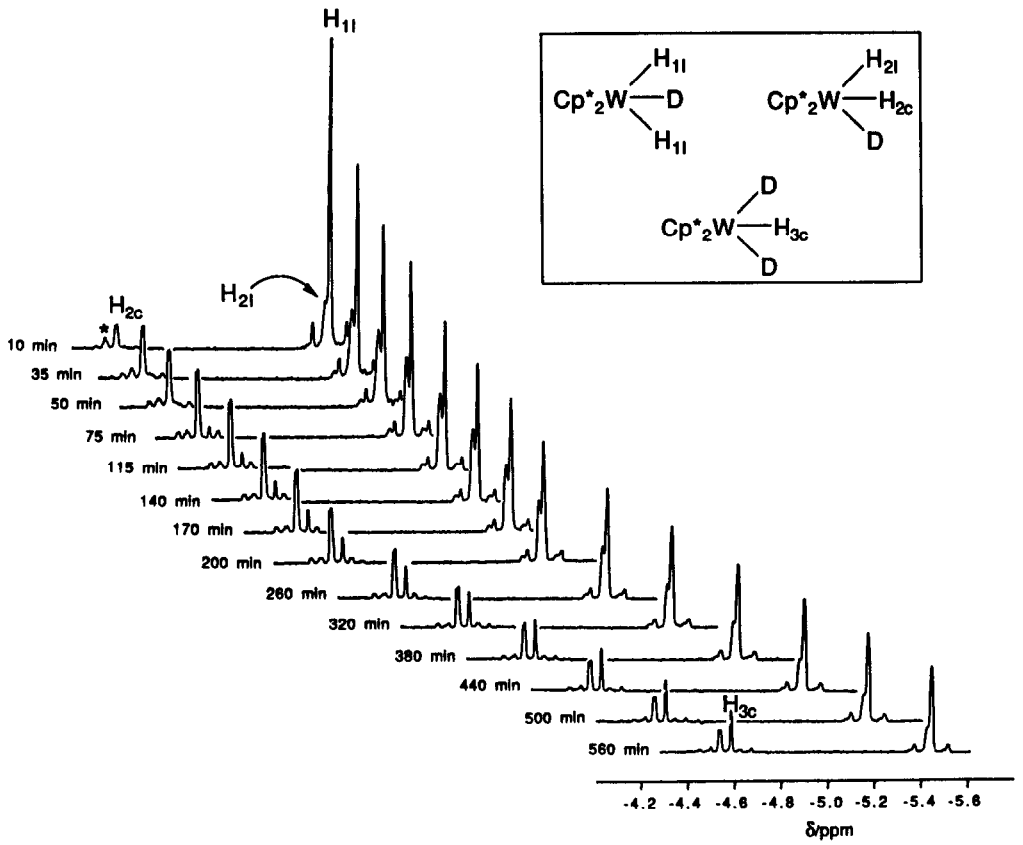

Fig. 1. Evolution of the hydride region of the ^{1}H NMR spectrum for the product of $Cp_2^*WH_2$ with DCl in D_2O (* denotes central hydride of $[Cp_2^*WH_3]^+$).

predicted to attack *initially* the HOMO. The first bonding description of the bent metallocene system was provided by Dahl and Ballhausen[17] in which it was implied that the lone pair of electrons on the metal centre of Cp_2WH_2 resided in an orbital which is directed between the two hydrogen ligands. If this proposal is correct, the observed stereochemistry of the deuteration reaction would be consistent with orbital-controlled electrophilic attack at the HOMO of $Cp_2^*WH_2$. However, the Ballhausen–Dahl description has been questioned. On the basis of the CH_3—Re—CH_3 bond angle in a related derivative, $(\eta^5\text{-}C_5H_5)(\eta^4\text{-}C_5H_5Me)Re(CH_3)_2$, Alcock suggested that, in fact, the lone pair resides in an orbital lateral to the methyl ligands.[18] This suggestion has been overwhelmingly supported by (i) structural studies by Green *et al.* on a series of d^0, d^1 and d^2 Cp_2MX_2 derivatives, which showed that the X—M—X bond angle *decreases* across the series, thus suggesting that the additional d electrons occupy an orbital which lies *laterally* to the two X ligands,[2] (ii) single crystal electron paramagnetic studies on Cp_2VS_5 and $(\eta^5\text{-}C_5H_4CH_3)_2VCl_2$, which indicate that the unpaired electron occupies a lateral orbital[19] and (iii) a combined molecular orbital/photoelectron spectroscopy study.[20] Thus, Green *et al.*[2] proposed a new bonding description for Cp_2MX_2 which comprised elements of both the Ballhausen–Dahl and Alcock models and also resembled the Brintzinger[21] description. Additional support for a lateral HOMO is provided by the calculations of Lauher and Hoffmann[22] and Dahl *et al.*;[23] the validity of their description is underscored by the observation that the H—Mo—H bond angle of 75.5(3)° in Cp_2MoH_2, as determined by neutron diffraction,[24] is very close to that predicted ($\approx$ 78°) for a d^2 molecule.[19] The conclusions of these quantitative studies are summarized in a qualitative MO diagram for $Cp_2^*WH_2$, shown in Fig. 2.† The $2a_1$ HOMO is a tungsten-localized lateral orbital that interacts minimally with the two hydride ligands. Thus, protonation following orbital control would be expected to proceed by path (a) (Scheme 3), giving the lateral d_1-isotopomer, $[Cp_2^*W(H)(H)(D)]^+$. However, observation of the central d_1-isotopomer, $[Cp_2^*W(H)(D)(H)]^+$, which arises by attack along

† Based on the results of refs 22 and 23.

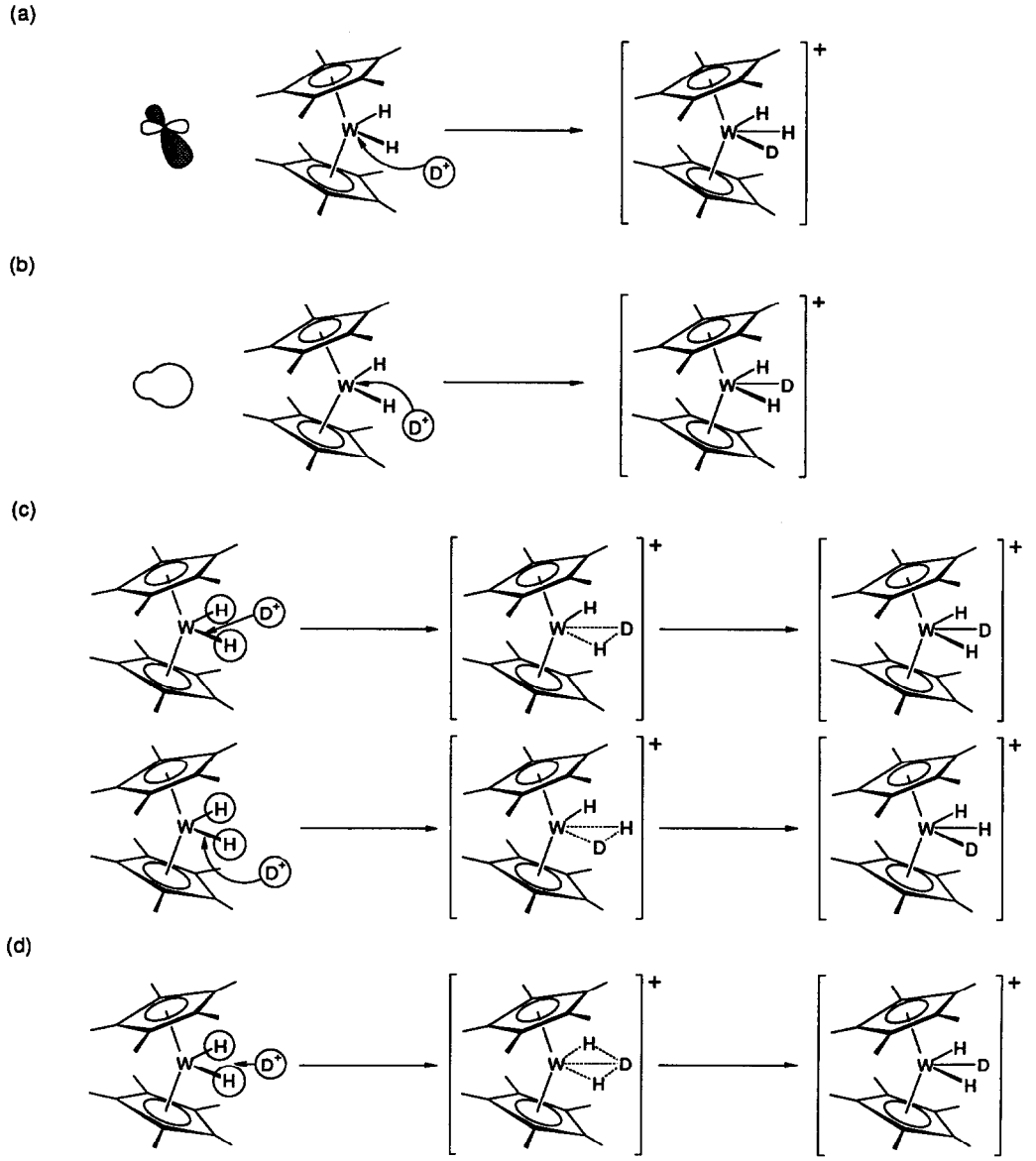

Scheme 3. Possible pathways for protonation of $Cp^*_2WH_2$. (a) Electrophilic attack at a lateral, metal-based, orbital. (b) Electrophilic attack at a central, metal-based, orbital. (c) Central and lateral electrophilic attack at one of the hydride ligands. (d) Central electrophilic attack at both the hydride ligands.

the pseudo-C_2 axis, signals a more subtle situation. There is no occupied, metal-based central orbital in Fig. 2, which therefore rules out path (b) (Scheme 3) as a dominant mechanistic pathway.

Whereas one might be tempted to once again question the conclusions concerning the spatial disposition of the lone pair orbital for $Cp^*_2WH_2$, the alternative protonation pathways [Scheme 3(c) and 3(d)] should be first considered. Protonation at one or both of the hydride ligands is likely, particularly if they are sites of higher negative charge than the tungsten centre. Thus, protonation is subject to charge control (i.e. at $W—H^{\delta-}$) rather than orbital control (at the HOMO).† Protonation of a tungsten–hydrogen bond of $Cp^*_2WH_2$ would initially generate the dihydrogen–hydride cation, $[Cp^*_2W(\eta^2\text{-}H_2)H]^+$, which subsequently collapses to the trihydride cation. Protonation of a Re—H bond for the d^0 complex $Re(PR_3)_2H_7$ has been discussed

† Theoretical calculations have demonstrated that the protonation of $[CpFe(CO)_2]_2(\mu\text{-}CO)(\mu\text{-}CH_2)$ at the methylene ligand and not the Fe—Fe bond is charge and not orbital controlled.[25]

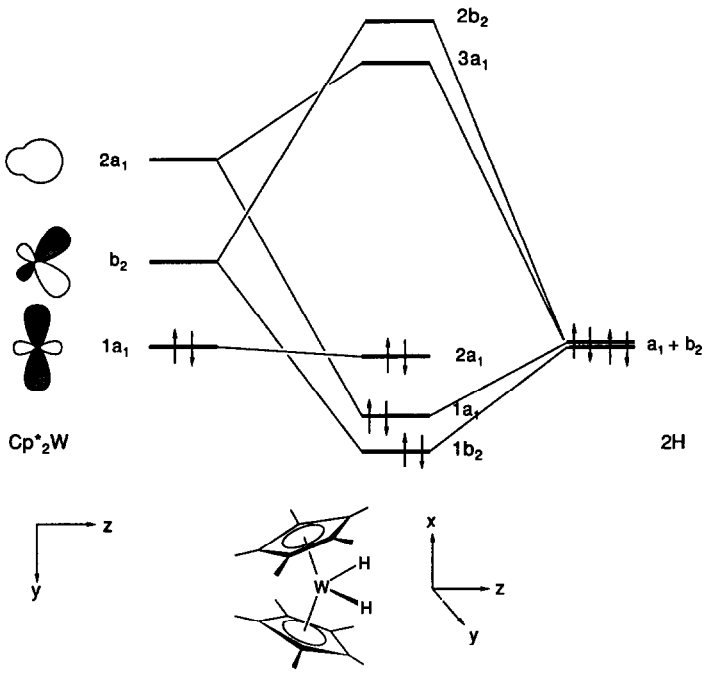

Fig. 2. A qualitative MO diagram for $Cp_2^*WH_2$.

recently.[26]† Moreover, a sequence closely analogous to that proposed for $Cp_2^*WH_2$ has been recently reported for the protonation/deprotonation of $(\eta^5\text{-}C_5H_5)(Me_2PCH_2CH_2PMe_2)RuH$; protonation occurs at the Ru—H bond (rather than at the d^6 metal centre) to afford $[(\eta^5\text{-}C_5H_5)(Me_2PCH_2CH_2PMe_2)Ru(\eta^2\text{-}H_2)]^+$, which subsequently equilibrates with $[(\eta^5\text{-}C_5H_5)(Me_2PCH_2CH_2PMe_2)RuH_2]^+$.[27]‡

Selective protonation of a single W—H bond of $Cp_2^*WH_2$ from the "inside" of the H—W—H angle, rather than from a lateral position could possibly be strongly preferred; however, the factors distating such a preference are not obvious. Alternately, it could be argued that the preferentially central protonation is a consequence of the proton initially interacting with *both* hydride ligands [Scheme 3(d)], producing the trihydrogen cation $[Cp_2^*W(\eta^3\text{-}H_3)]^+$, which subsequently collapses to the trihydride cation. The rather acute (*ca* 75°) H—W—H angle simultaneously offers both hydrides to electrophilic attack. In this regard, a trihydrogen adduct has recently been invoked to account for the unusual NMR behaviour for $[(\eta^5\text{-}C_5H_5)(PMe_3)IrH_3]^+$.[28] An equivalent molecular orbital picture is that attack occurs at the second highest occupied molecular orbital (SHOMO), that of $1a_1$ symmetry (Fig. 2). Thus, in view of the extensive structural, spectroscopic and theoretical studies cited above, pathway (d) (Scheme 3) appears to best reconcile the stereochemical preferences for central protonation of $Cp_2^*WH_2$.§

The kinetic product $[Cp_2^*W(H)(D)(H)]^+$ undergoes subsequent rearrangement to the lateral d_1-isotopomer $[Cp_2^*W(H)(H)(D)]^+$, and further exchange with the solvent (DCl/D_2O) resulting in the formation of d_2, and d_3 derivatives (Fig. 1). Examination of the time evolution of the ^1H NMR spectra for this mixture reveals that conversion of the central d_1-isotopomer, $[Cp_2^*W(H)(D)(H)]^+$, to the lateral d_1-isotopomer, $[Cp_2^*W(H)(H)(D)]^+$ occurs much faster than deuterium incorporation from DCl/D_2O. Since $[Cp_2^*WH_3]^+$ may be cleanly deprotonated to Cp_2WH_2 by $KOH_{(aq)}$, a possible mechanism for the isomerization process would be deprotonation of the central position¶ of $[Cp_2^*W(H)(D)(H)]^+$ generating $Cp_2^*WH_2$, followed

† An alternative explanation is that protonation occurs at the d^2 metal centre of the dihydrogen derivative, $Re(PR_3)_2(\eta^2\text{-}H_2)H_5$, with which $Re(PR_3)_2H_7$ may be in equilibrium.

‡ It was also shown that deprotonation of the dihydrogen derivative, $[CpRu(dmpe)(\eta^2\text{-}H_2)]^+$, is faster than that for the dihydride, $[CpRu(dmpe)H_2]^+$, as expected by the principle of microscopic reversibility.

§ We note that the product obtained from Cp_2WH_2 and R_3Al is also the result of attack at the central position; however, there is no evidence that this is the kinetic product of the reaction (ref. 16).

¶ Deprotonation from the central position is favoured over the lateral position according to the principle of microscopic reversibility.

by addition of D^+ at the lateral position.†

$$[Cp^*_2W(H)(D)(H)]^+ \rightleftharpoons [Cp^*_2WH_2] + D^+ \rightleftharpoons [Cp^*_2W(H)(H)(D)]^+.$$

It is important to recognize, however, that the observed build up of $[Cp^*_2W(H)(H)(D)]^+$ is *inconsistent* with this mechanism, since (i) the rate of conversion of $[Cp^*_2W(H)(D)(H)]^+$ to $[Cp^*_2W(H)(H)(D)]^+$ involves deprotonation of the central position and reprotonation *laterally*, whereas the subsequent conversion of $[Cp^*_2W(H)(H)(D)]^+$ to the d^2-isotopomer, $[Cp^*_2W(H)(D)(D)]^+$ involves deprotonation from the central position and reprotonation *centrally*; the latter must be much faster to account for the initial predominance of $[Cp^*_2W(H)(D)(H)]^+$, and (ii) the large pool of deuterium virtually assures addition of D^+ rather than H^+ to any $Cp^*_2W(X)Y$ (X, Y = H, D). Moreover, the normal, substantial k_H/k_D expected for deprotonation[29] further contributes to the faster conversion of $[Cp^*_2W(H)(H)(D)]^+$ to $[Cp^*_2W(H)(D)(D)]^+$, relative to its formation from $[Cp^*_2W(H)(D)(H)]^+$. The data shown in Fig. 1 clearly show that $[Cp^*_2W(H)(H)(D)]^+$ does, in fact, build up in concentration, and does so substantially faster than the overall conversion of the d_1-isotopomer $[Cp^*_2WH_2D]^+$ to the d_2-isotopomer, $[Cp^*_2WHD_2]^+$, and the d_3-isotopomer, $[Cp^*_2WD_3]^+$, the latter two resulting in an overall decrease in the total intensity of the hydride resonances in the ^1H NMR spectrum.

An additional pathway for the direct *intramolecular* interconversion of the two d_1-isotopomers which does not involve a deprotonation mechanism, is clearly required to accommodate the observed build up of $[Cp^*_2W(H)(H)(D)]^+$.

$$[Cp^*_2W(H)(D)(H)]^+ \rightleftharpoons [Cp^*_2W(H)(H)(D)]^+.$$

A kinetic analysis of these rate data reveals that the intramolecular exchange process for $[Cp^*_2W(H)(D)(H)]^+ \rightarrow [Cp^*_2W(H)(H)(D)]^+$ is approximately an order of magnitude faster than deprotonation.‡ A possible direct pathway for the intramolecular exchange would involve pseudorotation out of the equatorial plane of the bent sandwich structure; however, we are unaware of a precedent for such a process. More likely mechanisms, shown in Scheme 4, include (i) intermediacy of a dihydrogen adduct which rotates, (ii) the intermediacy of a (closed) trihydrogen§ adduct which rotates, and (iii) migration of the hydride ligand to the Cp* ligand to give an η^4-diene intermediate, $[Cp^*(\eta^4\text{-}C_5Me_5H)WHD]^+$, a "Tarzan" type swing over the deuterium, followed by return to the metal centre. Hydride and alkyl group migrations to and from cyclopentadienyl (and arene) ligands have previously been observed and postulated for other reactions.[31] Our data do not allow a distinction between these possibilities.

Syntheses and reactivity of the oxo derivatives $Cp^*_2W{=}O$, $(\eta^5\text{-}C_5Me_5)(\eta^1\text{-}C_5Me_5)W(=O)_2$, $Cp^*W(=O)_2(OCp^*)$ *and* $Cp^*W(\eta^2\text{-}O_2)(=O)(CH_3)$

In view of the increasing interest in organometallic compounds containing oxo and peroxo ligands,[32] we have explored the reactivity of some of these permethyltungstenocene derivatives with reagents such as water, hydrogen peroxide and dioxygen. Some of this work has been communicated.[33]

(1) *Mono-oxo tungsten derivatives: oxo transfer reactions from tungsten and evidence for* 1,2*-addition and elimination processes.* Access to oxo-derivatives of permethyltungstenocene is provided by the reaction of $Cp^*_2WCl_2$ with $KOH_{(aq)}$ in THF which gives $Cp^*_2W{=}O$ as a deep-green crystalline material (Scheme 5) or, alternatively, by the reaction of $Cp^*_2W(\eta^2\text{-}CH_2O)$ with H_2O.

$$Cp^*_2W(\eta^2\text{-}CH_2O) + H_2O \longrightarrow Cp^*_2W{=}O + CH_3OH.$$

$Cp^*_2W{=}O$ is a member of a relatively rare class of oxo-derivatives in which the metal centre is closed-shell (18-electron) in the absence of oxygen lone-pair donation.¶ We propose to denote these as "class b" M=O derivatives in order to distinguish them from the more common "class a" ($M{=}O \leftrightarrow M^-{\equiv}O^+$) derivatives, for which lone-pair donation from oxygen to the metal centre imparts triple $M^-{\equiv}O^+$ bond character, and hence a stronger bond, obtains. Therefore, it appeared reasonable to consider the possibility that the oxo ligand in $Cp^*_2W{=}O$ could be more weakly bound

† Protonation at the central site is clearly favoured, however, protonation at the lateral site may occur, albeit at a much slower rate.

‡ Data were fit using the program "GEAR" [T. Beukelman, J. Chesick, R. J. McKinney and F. J. Weigert, PC Version 1.31 (1987)] and the approximate rate constants obtained are: $[Cp^*_2W(H)(D)(H)]^+ \rightarrow [Cp^*_2WH_2] + D^+$, $k \approx 1.2 \times 10^{-3}$ s^{-1}; $[Cp^*_2W(H)(D)(H)]^+ \rightarrow [Cp^*_2W(H)(H)(D)]^+$, $k \approx 1 \times 10^{-2}$ s^{-1}.

§ Closed trihydrogen species have been studied theoretically to account for the observed exchange processes in bis-dihydrogen complexes.[30]

¶ Other 18-electron oxo-derivatives include $Cp^*_2Ta(=O)R$ (R=H, CH_3), $Cp_2Nb(=O)(CH_3)$, $Cp_2M{=}O$ (M=Mo, W) and $Cp^*Re(=O)_3$.

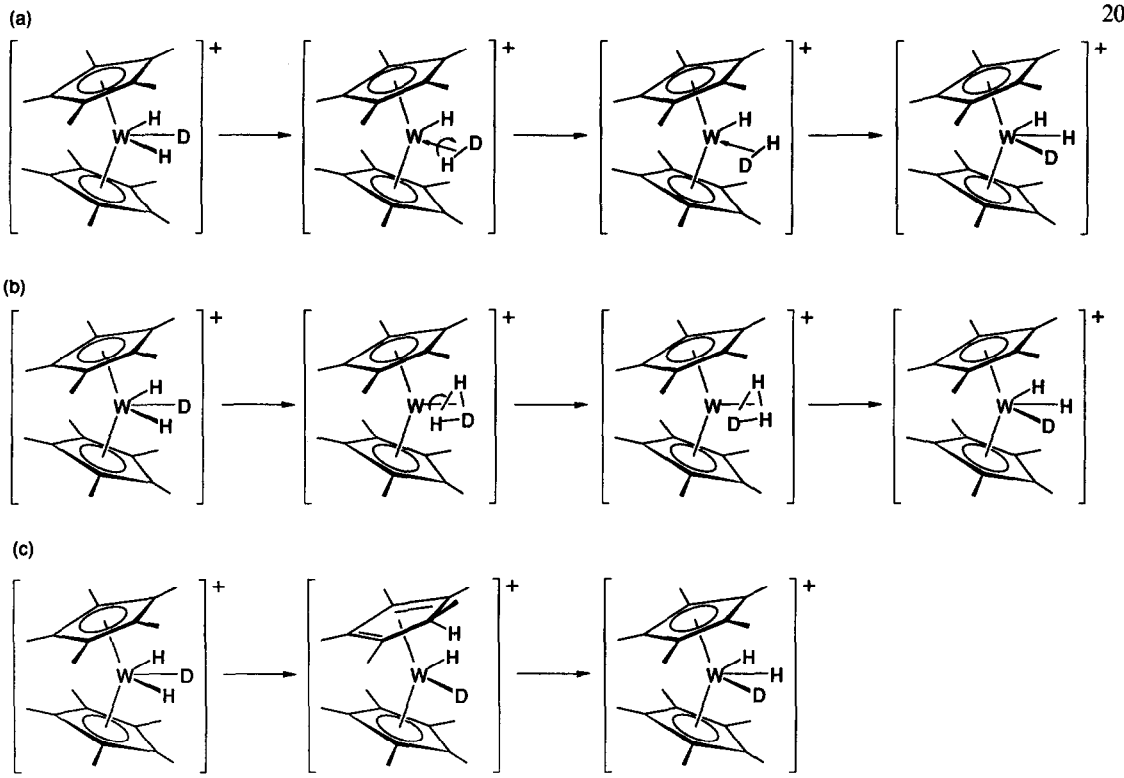

Scheme 4. Possible intramolecular exchange mechanisms for the rearrangement central d_1-$[Cp_2^*W(H)(D)(H)]^+ \rightarrow$ lateral d_1-$[Cp_2^*W(H)(H)(D)]^+$. (a) Exchange via an η^2-dihydrogen intermediate. (b) Exchange via an η^3-trihydrogen intermediate. (c) Exchange via H (or D) migration to the Cp* ligand.

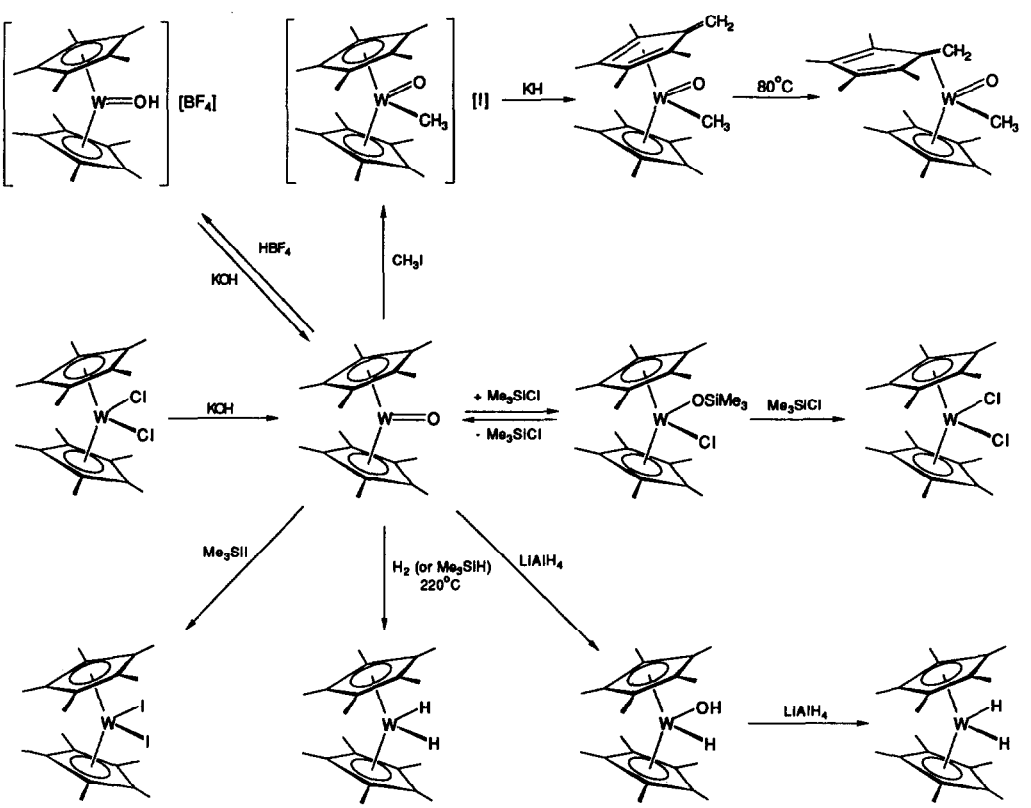

Scheme 5. Synthesis and reaction chemistry of $Cp_2^*W{=}O$.

than other tungsten oxo ligands and, thus, exceptionally reactive.

The comparatively weak W=O bond is evident from both its spectroscopic features and its chemical reactivity. Thus, $Cp_2^*W{=}O$ is characterized by a strong $\nu(W{=}O)$ in its IR spectrum at 860 cm^{-1} (820 cm^{-1} for $Cp_2^*W{=}^{18}O$) compared with $\nu(M{\equiv}O) \approx 930$–$1000\ cm^{-1}$ for class a. An illustrative comparison of $\nu(M{-}O)$ stretching frequencies is that the 14-electron, class a, derivative, CH_3ReO_3,[34] shows absorptions at 999 and 960 cm^{-1}, almost 100 cm^{-1} higher than those of the 18-electron, class b, derivative, Cp^*ReO_3 (909 and 878 cm^{-1}).[35]

The high reactivity of the oxo ligand in $Cp_2^*W{=}O$ is demonstrated by the oxygen exchange reaction with labelled H_2^*O. A solution of $Cp_2^*W{=}^{18}O$ in pentane undergoes facile isotopic exchange with $H_2{}^{16}O$ giving $Cp_2^*W{=}^{16}O$ within 1 h at room temperature (IR spectroscopy). This reaction presumably proceeds via the dihydroxy derivative, $[Cp_2^*W(^{16}OH)(^{18}OH)]$, which may be envisaged to be formed by the overall 1,2-addition† of the $H^{16}O{-}H$ bond across the $W{=}^{18}O$ double bond. The microscopic chemical reverse, i.e. 1,2-elimination of $H_2{}^{18}O$ from this symmetric intermediate, allows exchange of oxygen atoms to occur.

$$Cp_2^*W{=}^{18}O + H_2{}^{16}O \rightleftharpoons [Cp_2^*W(^{18}OH)(^{16}OH)] \rightleftharpoons Cp_2^*W{=}^{16}O + H_2{}^{18}O.$$

Similarly, treatment of $Cp_2^*W{=}^{16}O$ with excess $H_2{}^{17}O$ (*ca* 50% enriched) results in the formation of $Cp_2^*W{=}^{17}O$ as monitored by ^{17}O NMR spectroscopy (δ 760 ppm in C_6D_6 relative to external $H_2{}^{17}O$).‡ The kinetics of this exchange in THF solution at 25°C have been measured and the second-order rate constant for oxygen exchange is approximately $2(1) \times 10^{-4}\ s^{-1}\ M^{-1}$, larger than representative values reported for anionic and cationic complexes in aqueous solutions.§

Similarly, the isoelectronic, d^0, oxo-derivative, $Cp_2^*Ta(=O)H$, which is a class b oxo-derivative, ($\nu(Ta{=}O) = 850\ cm^{-1}$), undergoes rapid exchange of oxygen atoms with labelled $H_2{}^*O$. For this example, the hydride ligand acts as a second probe to study the exchange reaction. Thus, the isotopomer, $Cp_2^*Ta(=^{18}O)H$, was treated with $D_2{}^{16}O$ and the exchange process was monitored by IR spectroscopy. The results clearly demonstrate that exchange of the oxo ligand occurred for the exclusion of the hydride ligand. This is consistent with the mechanism outlined for the exchange reaction of $Cp_2^*W{=}O$ with H_2O in which a reaction occurs only at the M=O double bond, possibly in a concerted manner.

$$Cp_2^*Ta(=^{18}O)H + D_2{}^{16}O \rightleftharpoons [Cp_2^*Ta(^{18}OD)(^{16}OD)H] \rightleftharpoons Cp_2^*Ta(=^{16}O)H + D^{18}OH.$$

The observation of no exchange of deuterium into the tantalum hydride position has two implications: (i) the reaction does not involve an initial α-H migration from Ta to oxygen to generate a 16-electron, $[Cp_2^*Ta{-}OH]$, intermediate which reacts with H_2O by oxidative addition [Scheme 6, steps (c) and (d)], since this mechanism would ultimately lead to the exchange of the tantalum hydride for deuterium. We have noted previously that the α-H migration for $(\eta^5\text{-}C_5Me_5)(\eta^5\text{-}C_5Me_4Ph)Ta(=O)H$ is much slower (as yet unobserved) than that for the methylidene hydride derivative, $(\eta^5\text{-}C_5Me_5)(\eta^5\text{-}C_5Me_4Ph)Ta(=CH_2)H$.[38] Accordingly, treatment of $Cp_2^*Ta(=CH_2)H$ with D_2O gives $Cp_2^*Ta(=O)D$ and CH_3D (via oxidative addition of DO—D to $[Cp_2^*TaCH_3]$), and *not* $Cp_2^*Ta(=O)H$ and CH_2D_2. (ii) The dihydroxy–hydride intermediate, $[Cp_2^*Ta(^{18}OD)(^{16}OD)H]$, loses water by a 1,2-elimination pathway [Scheme 6, step (b)] and *not* by reductive elimination. Reductive elimination would generate $[Cp_2^*Ta{-}^{18}OD]$ from which α-D elimination would result in exchange of the tantalum hydride for deuterium. The 1,2-addition/elimination reactions involving HO—H and [Ta=O] are likely encouraged by interaction of the hydrogen with a lone electron pair of the oxo ligand, at least in the early stages of the reaction. Moreover, the 1,2-elimination pathway ensures that the tungsten centre will remain as 18-electron, d^0, throughout the process and does not necessitate the formation

† The terms 1,2-addition and 1,2-elimination are not meant to imply a concerted mechanism, but are only intended to indicate the overall transformation.

‡ Published data on ^{17}O chemical shifts are thus far limited so that no firm conclusions can be presently drawn regarding the ^{17}O chemical shifts for the different classes (a and b) of oxo ligands. For reference, ^{17}O chemical shifts for some other oxo (terminal and bridging) derivatives are given in ref. 36.

§ We are not aware of similar measurements of the rates for oxygen exchange in other *neutral* oxo compounds; however, the ^{18}O exchange kinetics for ionic complexes *in aqueous solution* have been reviewed. Typical second-order rate constants ($\approx$ 25°C, corrected for $[H_2O]$) include: $[ReO_4]^-$, $10^{-8}\ s^{-1}\ M^{-1}$; *trans*-$[Re(en)_2O_2]^+$, $10^{-6}\ s^{-1}\ M^{-1}$; $[WO_4]^{2-}$, $10^{-2}\ s^{-1}\ M^{-1}$. It should be noted that for all these examples the rate laws are complex, and the rates are very pH dependent.[37]

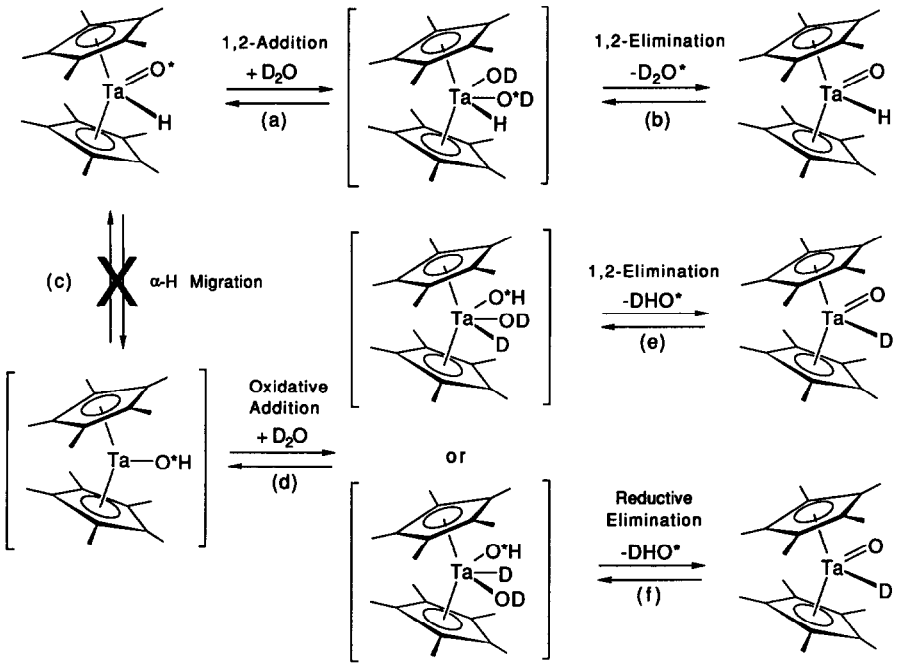

Scheme 6. Possible mechanisms for the exchange of the oxo ligand in $Cp_2^*Ta(=^{18}O)H$ with D_2O.

of the high energy 16-electron, d^2, intermediate, $[Cp_2^*Ta—OH]$. A reaction which follows the same pathway, i.e. 1,2-addition/elimination, is the hydrolysis of $Cp_2^*Ta(=NC_6H_5)H$ with D_2O, which gives $Cp_2^*Ta(=O)H$, not $Cp_2^*Ta(=O)D$ (^1H NMR spectroscopy).

$$Cp_2^*Ta(=NC_6H_5)H + D_2O \longrightarrow Cp_2^*Ta(=O)H + C_6H_5ND_2.$$

An observation of relevance to these oxo exchange reactions is provided by the reaction of $Cp_2^*W=O$ with Me_3SiCl. The initial product is $Cp_2^*W(OSiMe_3)Cl$ which is formed via a 1,2-addition of the Si—Cl bond across the W=O double bond.

$$Cp_2^*W=O + Me_3SiCl \rightleftharpoons Cp_2^*W(OSiMe_3)Cl \longrightarrow 0.5Cp_2^*W=O + 0.5Cp_2^*WCl_2 + 0.5(Me_3Si)_2O.$$

$Cp_2^*W(OSiMe_3)Cl$ reacts further with Me_3SiCl giving $Cp_2^*WCl_2$ and $(Me_3Si)_2O$. Furthermore, the 1,2-addition of a Si—Cl bond across the W=O double bond is reversible, as for the reaction of $Cp_2^*W=O$ with $H_2{}^*O$. Thus, the reaction of $Cp_2^*W=O$ with Me_3SiCl (are equivalent) gives initially an equilibrium mixture with $Cp_2^*W(OSiMe_3)Cl$ which subsequently decomposes with the elimination of $(Me_3Si)_2O$ to form $Cp_2^*WCl_2$ (0.5 equivalent) and $Cp_2^*W=O$ (0.5 equivalent).† In a similar fashion, the reaction of $Cp_2^*W=O$ with Me_3SiI can be used to prepare $Cp_2^*WI_2$.

The exceptional reactivity of $Cp_2^*W=O$ is also illustrated by its reduction to $Cp_2^*WH_2$ by either H_2 or Me_3SiH, although the conditions are rather forcing (*ca* 200°C). This reduction can be achieved more readily by reaction with $LiAlH_4$, in which the hydroxy–hydride derivative, $Cp_2^*W(H)(OH)$, may be isolated as the first-formed product. This reduction of $Cp_2^*W=O$ to the hydroxy hydride derivative, $Cp_2^*W(OH)H$ illustrates the similarity of this W=O double bond with the C=O double bond in ketones and aldehydes. Further similarities are that (i) both dihydroxy derivatives, $[Cp_2^*W(OH)_2]$ and $[R_2C(OH)_2]$, are unstable with respect to elimination of water and formation of the X=O (X = Cp_2^*W, R_2C) double bond, and (ii) as for ketones and aldehydes, $Cp_2^*W=O$ reacts with the glycol, $(CH_2OH)_2$ to form the glycolate, $Cp_2^*W(\eta^2\text{-}O,O—OCH_2CH_2O)$.‡

† This reaction is somewhat more complicated, since variable, small quantities, of a silicon product (at present unidentified, but possibly Me_6Si_2), other than $(Me_3Si)_2O$ are formed.

‡ $Cp_2^*W(OCH_2CH_2O)$ has not been isolated and has only been characterized by ^1H NMR data (in C_6D_6): δ 1.83 (s, Cp*), δ 3.07 (—OCH_2CH_2O—).

In addition to these reactions which result in oxygen atom transfer from tungsten, $Cp^*_2W{=}O$ has also proved to be a valuable starting material for other oxo derivatives of (pentamethylcyclopentadienyl)tungsten as illustrated in Scheme 5. $Cp^*_2W{=}O$ reacts with HBF_4 to generate the ionic species $[Cp^*_2W{=}OH][BF_4]$. The reaction is reversible and treatment with KOH regenerates $Cp^*_2W{=}O$. $Cp^*_2W{=}O$ also reacts with MeI to give an ionic derivative, $[Cp^*_2W(=O)CH_3][I]$, which is characterized by $\nu(W{=}O) = 868\ cm^{-1}$, similar to that of $Cp^*_2W{=}O$ ($\nu(W{=}O) = 860\ cm^{-1}$). However, it is interesting to note that in contrast to the reactions of $Cp^*_2W{=}O$ with Me_3SiCl and HBF_4, nucleophilic attack at CH_3I occurs by the d^2 tungsten centre, not the oxygen ligand. In addition, this reaction with CH_3I is not reversible. Thus, the d_3-derivative, $[Cp^*_2W(=O)CD_3][I]$, does not undergo exchange of methyl groups when treated with CH_3I.

$$[Cp^*_2W(=O)CD_3][I] + CH_3I \not\rightarrow [Cp^*_2W(=O)CH_3][I] + CD_3I.$$

Furthermore, the isoelectronic tantalum derivative, $Cp^*_2Ta(=O)H$, does not react under similar conditions with MeI since the metal centre is d^0 and no longer nucleophilic.[39]

A suspension of $[Cp^*_2W(=O)CH_3][I]$ in THF is readily deprotonated by KH. The initial product is the η^4-1,2,3,4-tetramethylfulvene derivative, $Cp^*(\eta^4\text{-}C_5Me_4{=}CH_2)W(=O)(CH_3)$, obtained by deprotonation of the methyl group of the Cp* ligand as opposed to the W—CH_3 group. The uncoordinated *exo*-$(CH_3C)_4C{=}CH_2$ double bond of the η^4-1,2,3,4-tetramethylfulvene ligand is characterized by a strong absorption at 1600 cm^{-1} in the IR spectrum and resonances in the ^{13}C NMR spectrum at δ 163.0 and 102.2 ppm, assignable to $\eta^4\text{-}(CH_3C)_4C{=}CH_2$ and $\eta^4\text{-}(CH_3C)_4C{=}CH_2$, respectively, only slightly shifted from the free ligand values of δ 155.4 and 109.8, respectively. This η^4-derivative undergoes isomerization to the η^2-*exo*-$CH_2{=}C_5Me_4$ derivative, $Cp^*(\eta^2\text{-}CH_2{=}C_5Me_4)W(=O)(CH_3)$, at 80°C. An analogous η^2-*exo*-$CH_2{=}C_5Me_4$ derivative, $Pd(\eta^2\text{-}CH_2{=}C_5Me_4)(PMe_3)_2$, has recently been reported and its X-ray crystal structure determined.[40] The ^{13}C NMR data for $Cp^*(\eta^2\text{-}CH_2{=}C_5Me_4)W(=O)CH_3$ provide strong evidence for η^2-coordination of the tetramethylfulvene ligand: the resonances assignable to the $(\eta^2\text{-}CH_2{=}C_5Me_4)$ ligand of $Pd(\eta^2\text{-}CH_2{=}C_5Me_4)(PMe_3)_2$ and $Cp^*(\eta^2\text{-}CH_2{=}C_5Me_4)W(=O)CH_3$ are similar (Table 2) and are significantly different from both the η^4-derivative, $Cp^*(\eta^4\text{-}C_5Me_4{=}CH_2)W(=O)CH_3$ and the free ligand, $C_5Me_4{=}CH_2$. Notably, the $\{CH_2{=}C_5Me_4\}$ methylene carbon atom is observed at δ 40.1 (in C_6D_6) for $Cp^*(\eta^2\text{-}CH_2{=}C_5Me_4)W(=O)CH_3$ and at 35.8–43.6 (in $(CD_3)_2CO$) for $Pd(\eta^2\text{-}CH_2{=}C_5Me_4)L_2$ (L = PMe_3, PEt_3, P $(OMe)_3$], whereas for the η^4-derivative, $Cp^*(\eta^4\text{-}C_5Me_4{=}CH_2)W(=O)(CH_3)$, and the free ligand, $CH_2{=}C_5Me_4$, the methylene carbon atom is observed to be approximately 60 ppm to lower field at δ 102.2 and 109.8 (in C_6D_6), respectively. Furthermore, the uncoordinated ring carbon atoms, $\{(MeC)_4C{=}CH_2\}$, of $Cp^*(\eta^2\text{-}CH_2{=}C_5Me_4)W(=O)CH_3$, δ 129.7–135.2, are only slightly shifted from the values of the free ligand, δ 123.7–138.7.

Deprotonation of the d_3-isotopomer, $[Cp^*_2W(=O)CD_3][I]$, gives $Cp^*(\eta^4\text{-}C_5Me_4{=}CH_2)W(=O)CD_3$ and upon heating, $Cp^*(\eta^2\text{-}CH_2{=}C_5Me_4)W(=O)CD_3$, providing evidence that the reaction does not proceed via initial deprotonation of the W—CH_3 group followed by a rearrangement.

(2) *Dioxo derivatives: the formation of η^1-pentamethylcyclopentadienyl derivative.* The dioxo derivative, $(\eta^5\text{-}C_5Me_5)(\eta^1\text{-}C_5Me_5)W(=O)_2$, is obtained by the reaction of $Cp^*_2W{=}O$ with the oxo-transfer reagents, $H_2O_{2(aq)}$ or Me_3CO_2H (Scheme 7). $(\eta^5\text{-}C_5Me_5)(\eta^1\text{-}C_5Me_5)W(=O)_2$ is also formed by the reaction of $Cp^*_2WH_2$ with $H_2O_{2(aq)}$.

$$Cp^*_2WH_2 \xrightarrow{H_2O_{2(aq)}} (\eta^5\text{-}C_5Me_5)(\eta^1\text{-}C_5Me_5)W(=O)_2.$$

Interestingly, this compound does not react with excess H_2O_2 to give the peroxo derivative, $(\eta^5\text{-}C_5Me_5)(\eta^1\text{-}C_5Me_5)W(=O)(\eta^2\text{-}O_2)$, in contrast to the reaction of $Cp^*W(=O)_2CH_3$ with H_2O_2 which gives $Cp^*W(=O)(\eta^2\text{-}O_2)CH_3$.[41] $(\eta^5\text{-}C_5Me_5)(\eta^1\text{-}C_5Me_5)W(=O)_2$ has been structurally characterized by X-ray diffraction techniques (Fig. 3).[47]

Although compounds of the type $(\eta^5\text{-}C_5R_5)W(=O)_2(R')$ have recently been characterized by X-ray diffraction,[43] the principal interest in the structure of $(\eta^5\text{-}C_5Me_5)(\eta^1\text{-}C_5Me_5)W(=O)_2$ arises from the bonding modes of the pentamethylcyclopentadienyl ligands. In particular, one of these ligands adopts a *monohapto*, $(\eta^1\text{-}C_5Me_5)$, bonding mode. Where *monohapto* bonding modes are now common for C_5H_5 ligands,[44] the η^1-bonding mode of one of the pentamethylcyclopentadienyl ligands in $(\eta^5\text{-}C_5Me_5)(\eta^1\text{-}C_5Me_5)W(=O)_2$ represents the first example of a transition metal-coordinated η^1-Cp* ligand. The other pentamethylcyclopentadienyl ligand, while being bonded in a *pentahapto*, $(\eta^5\text{-}C_5Me_5)$, manner is, however, asymmetric with the ligand being displaced in the direction of the oxo ligands so that the structure is more aptly described as $(\eta^1,\eta^4\text{-}C_5Me_5)(\eta^1\text{-}C_5Me_5)W(=O)_2$ (*vide infra*).

Table 1. ^{1}H NMR data[a]

Assignment	δ (ppm)	Coupling (Hz)
$Cp^*_2WCl_2$		
η^5-$C_5(CH_3)_5$	1.68	s
$Cp^*_2WI_2$		
η^5-$C_5(CH_3)_5$	1.97	s
$Cp^*(\eta^5$-$C_5Me_4CH_2CH_2CH_3)WCl_2$		
η^5-$C_5(CH_3)_5$	1.70	s
η^5-$C_5(CH_3)_4(CH_2CH_2CH_3)$		
2(CH_3)	1.80	s
2(CH_3)	1.69	s
η^5-$C_5(CH_3)_4(CH_2CH_2CH_3)$	1.96	m
η^5-$C_5(CH_3)_4(CH_2CH_2CH_3)$	1.34	m
η^5-$C_5(CH_3)_4(CH_2CH_2CH_3)$	0.83	t, $^3J_{H-H} = 7.3$
$Cp^*_2W(H)Cl$		
η^5-$C_5(CH_3)_5$	1.81	s
W—*H*	−11.91	s, $^1J_{W-H} = 97$
$Cp^*_2W(\eta^2$-$CH_2O)$		
η^5-$C_5(CH_3)_5$	1.72	s
η^2-CH_2O	2.01	s[b]
$Cp^*(\eta^5,\eta^1$-$C_5Me_4CH_2)WH$		
η^5-$C_5(CH_3)_5$	1.86	s
η^5,η^1-$C_5(CH_3)_4CH_2$		
1(CH_3)	2.21	d, $J_{H-W(H)} = 3$
1(CH_3)	2.01	s
1(CH_3)	1.59	s
1(CH_3)	1.52	s
η^5,η^1-$C_5(CH_3)_4CH_2$		
1H	3.50	t, $^2J_{H-H} = 2$
1H	3.13	m
W—*H*	−11.94	s (broad), $^1J_{W-H} = 93$
$Cp^*_2W(CH_3)_2$		
η^5-$C_5(CH_3)_5$	1.51	s
$W(CH_3)_2$	−0.54	s
$Cp^*_2W(CH_3)Cl$		
η^5-$C_5(CH_3)_5$	1.60	s
W—CH_3	−0.09	s
$Cp^*_2W(CH_3)H$		
η^5-$C_5(CH_3)_5$	1.76	s
W—CH_3	−0.16	s
W—*H*	−10.86	s, $^1J_{W-H} = 105$
$Cp^*_2W(CH_2C_6H_5)(H)$		
η^5-$C_5(CH_3)_5$	1.72	s
W—CH_2Ph	2.32	s
W—$CH_2C_6H_5$		
1H(*para*)	7.07	t, $^3J_{H-H} = 7.5$
2H(*meta*)	7.25	t, $^3J_{H-H} = 7.5$
2H(*ortho*)	7.49	d, $^3J_{H-H} = 7.5$
W—*H*	−11.09	s, $^1J_{W-H} = 100$

(*continued*)

Table 1 (*continued*)

	Assignment	δ (ppm)	Coupling (Hz)
$Cp^*(\eta^5,\eta^1\text{-}C_5Me_4CH_2)W(CH_3)$			
	$\eta^5\text{-}C_5(CH_3)_5$	1.65	s
	$\eta^5,\eta^1\text{-}C_5(CH_3)_4CH_2$		
	$1(CH_3)$	1.68	s
	$1(CH_3)$	1.64	s
	$1(CH_3)$	1.56	s
	$1(CH_3)$	1.52	s
	$\eta^5,\eta^1\text{-}C_5(CH_3)_4CH_2$		
	1H	3.39	d, $^2J_{H-H} = 2$
	1H	2.59	d, $^2J_{H-H} = 2$
	$W—CH_3$	−0.63	s
$[Cp_2^*WH_3][BF_4]$			
D_2O	$\eta^5\text{-}C_5(CH_3)_5$	2.03	s
	1 W—*H* (central)	−4.50	t, $^2J_{H-H} = 3$, $^1J_{W-H} = 66$
	2 W—*H* (lateral)	−5.42	d, $^2J_{H-H} = 3$, $^1J_{W-H} = 57$
$(CD_3)_2CO$	$\eta^5\text{-}C_5(CH_3)_5$	2.25	s
	1 W—*H* (central)	−4.21	t, $^2J_{H-H} = 3$, $^1J_{W-H} = 66$
	2 W—*H* (lateral)	−5.19	d, $^2J_{H-H} = 3$, $^1J_{W-H} = 57$
Isotopic shifts:			
	W—*H* of $[Cp_2^*W(H)(H)(H)]^+$	−4.21	t, $^2J_{H-H} = 3$
	W—*H* of $[Cp_2^*W(H)(H)(D)]^+$	−4.25	d, $^2J_{H-H} = 3$
	W—*H* of $[Cp_2^*W(D)(H)(D)]^+$	−4.30	s
$[Cp_2^*WH_3][BPh_4]$			
$CDCl_3$	$\eta^5\text{-}C_5(CH_3)_5$	2.09	s
	1 W—*H* (central)	−4.20	t, $^2J_{H-H} = 3$, $^1J_{W-H} = 69$
	2 W—*H* (lateral)	−5.34	d, $^2J_{H-H} = 3$, $^1J_{W-H} = 57$
	$[BPh_4]$		
	ortho	7.43	s (broad)
	meta	7.03	t, $^3J_{H-H} = 7$
	para	6.88	t, $^3J_{H-H} = 7$
$Cp_2^*W{=}O$			
	$\eta^5\text{-}C_5(CH_3)_5$	1.87	s
$[Cp_2^*W(=O)(CH_3)][I]$			
D_2O	$\eta^5\text{-}C_5(CH_3)_5$	1.94	s
	$W—CH_3$	0.94	s
$CDCl_3$	$\eta^5\text{-}C_5(CH_3)_5$	2.13	s
	$W—CH_3$	1.07	s
$Cp_2^*W(OH)H$			
	$\eta^5\text{-}C_5(CH_3)_5$	1.81	s
	W—*H*	−11.08	s, $^2J_{W-H} = 114$
	W—O*H*[c]		
$[Cp_2^*W(=OH)][BF_4]$			
D_2O	$\eta^5\text{-}C_5(CH_3)_5$	1.88	s
	W=O*H*[c]		
$Cp_2^*W(OSiMe_3)Cl$			
	$\eta^5\text{-}C_5(CH_3)_5$	1.71	s
	$W—OSi(CH_3)_3$	0.45	s
$(\eta^1\text{-}C_5Me_5)(\eta^5\text{-}C_5Me_5)W(=O)_2$			
C_6D_6, 25°C	$\eta^5\text{-}C_5(CH_3)_5$	1.80	s

(*continued*)

Table 1 (*continued*)

	Assignment	δ (ppm)	Coupling (Hz)
C_7D_8, 25°C	η^5-$C_5(CH_3)_5$	1.80	s
C_7D_8, −90°C	η^5-$C_5(CH_3)_5$	1.52	s
	η^1-$C_5(CH_3)_5$		
	$1(CH_3)$	2.56	s
	$2(CH_3)$	2.00	s
	$2(CH_3)$	1.92	s
$(\eta^5$-$C_5Me_5)W(=O)_2(OC_5Me_5)$			
	η^5-$C_5(CH_3)_5$	1.85	s
	η^1-$C_5(CH_3)_5$		
	$1(CH_3)$	1.40	s
	$2(CH_3)$	1.62	q, partially resolved, $^5J_{C-H} = 1$
	$2(CH_3)$	1.78	q, partially resolved, $^5J_{C-H} = 1$
$Cp^*W(\eta^4$-$C_5Me_4{=}CH_2)W(=O)(CH_3)$			
	η^5-$C_5(CH_3)_5$	1.57	s
	η^4-$C_5(CH_3)_4{=}CH_2$	2.83	s
		2.59	s
		1.47	s
		1.55	s
	η^4-$C_5(CH_3)_4{=}CH_2$	4.54	s
		4.40	s
	$W-CH_3$	1.44	s[d]
$Cp^*W(\eta^2$-$C_5Me_4{=}CH_2)W(=O)(CH_3)$			
	η^5-$C_5(CH_3)_5$	1.56	s
	η^4-$C_5(CH_3)_4{=}CH_2$	2.55	s
		2.33	s
		1.97	s
		0.89	s
	η^2-$C_5(CH_3)_4{=}CH_2$	3.48	d, $^2J_{H-H} = 9$
		1.57	d,[e] $^2J_{H-H} = 9$
	$W-CH_3$	0.60	s[d]

[a] In C_6D_6 unless specified otherwise.
[b] Assignment tentative.
[c] Not located.
[d] Identified by preparation of the d_3-methyl derivative.
[e] Located by irradiation at δ 3.48 ppm.

Interestingly, at room temperature the resonances due to the Cp* ligands of $(\eta^5$-$C_5Me_5)(\eta^1$-$C_5Me_5)W(=O)_2$ are equivalent in the ^1H NMR spectrum. However, cooling to −90°C freezes out the solid-state structure. The data accumulated from the ^1H NMR variable temperature experiments are shown in Fig. 4. The studies suggest that the exchange process proceeds via η^1–η^5 ligand exchange and that 1,2-sigmatropic shifts of the η^1-C_5Me_5 ligand do not occur on a significantly faster timescale. An approximate barrier for this rearrangement process is 10(1) kcal mol^{-1} at −60°C.

The IR spectrum of $(\eta^5$-$C_5Me_5)(\eta^1$-$C_5Me_5)W(=O)_2$ is characterized by two W=O stretches, $\nu(WO_2)_{sym} = 895\ cm^{-1}$ and $\nu(WO_2)_{asym} = 935\ cm^{-1}$ [Fig. 5(a)]. The IR spectrum of the isotopomer. $(\eta^5$-$C_5Me_5)(\eta^1$-$C_5Me_5)W(=^{18}O)(=^{16}O)$ [Fig. 5(b)] shows two bands assigned to the W=O vibrations with $\nu(W^{16}O^{18}O)_{sym} = 860\ cm^{-1}$ and $\nu(W^{16}O^{18}O)_{asym} = 920\ cm^{-1}$. The difference in the symmetric and asymmetric stretches of the $(\eta^5$-$C_5Me_5)(\eta^1$-$C_5Me_5)W(=^{18}O)(=^{16}O)$ and $(\eta^5$-$C_5Me_5)(\eta^1$-$C_5Me_5)W(=^{16}O)_2$ isotopomers are $\Delta\nu_{sym} = 35\ cm^{-1}$ and $\Delta\nu_{asym} = 15\ cm^{-1}$. This difference of the shifts of the symmetric and asym-

Table 2. ^{13}C NMR data[a]

Assignment	δ (ppm)	Coupling (Hz)
$Cp^*_2WCl_2$		
η^5-$C_5(CH_3)_5$	11.6	q, $^1J_{C-H} = 128$
η^5-$C_5(CH_3)_5$	105.1	s
$Cp^*(\eta^5$-$C_5Me_4CH_2CH_2CH_3)WCl_2$		
η^5-$C_5(CH_3)_5$	11.4	q, $^1J_{C-H} = 128$
η^5-$C_5(CH_3)_5$	105.3	s
η^5-$C_5(CH_3)_4(CH_2CH_2CH_3)$		
2C	11.7	q, $^1J_{C-H} = 128$
2C	11.8	q, $^1J_{C-H} = 128$
η^5-$C_5(CH_3)_4(CH_2CH_2CH_3)$		
2C	103.8	s
1C	106.2	s
2C	107.6	s
η^5-$C_5(CH_3)_4(CH_2CH_2CH_3)$		
1C	24.4	t, $^1J_{C-H} = 126$
1C	28.6	t, $^1J_{C-H} = 130$
η^5-$C_5(CH_3)_4(CH_2CH_2CH_3)$	14.7	q, $^1J_{C-H} = 126$
$Cp^*_2W(H)Cl$		
η^5-$C_5(CH_3)_5$	12.1	q, $^1J_{C-H} = 127$
η^5-$C_5(CH_3)_5$	97.7	s
$Cp^*_2W(\eta^2$-$CH_2O)$		
η^5-$C_5(CH_3)_5$	11.3	q, $^1J_{C-H} = 127$
η^5-$C_5(CH_3)_5$	95.9	s
η^2-CH_2O	45.3	t, $^1J_{C-H} = 159$
$Cp^*(\eta^5,\eta^1$-$C_5Me_4CH_2)WH$		
η^5-$C_5(CH_3)_5$	12.2	
η^5-$C_5(CH_3)_5$	92.2	
η^5,η^1-$C_5(CH_3)_4CH_2$		
1(CH_3)	9.3	
1(CH_3)	10.0	
1(CH_3)	12.6	
1(CH_3)	15.1	
η^5,η^1-$C_5(CH_3)_4CH_2$		
1C	86.1	
1C	87.9	
1C	91.8	
1C	96.8	
1C	109.4	
η^5,η^1-$C_5(CH_3)_4CH_2$	36.1	
$Cp^*_2W(CH_3)_2$		
η^5-$C_5(CH_3)_5$	10.2	q, $^1J_{C-H} = 127$
η^5-$C_5(CH_3)_5$	93.6	s
$W(CH_3)_2$	−6.9	q, $^1J_{C-H} = 123$ $^1J_{W-C} = 76$
$Cp^*_2W(CH_3)Cl$		
η^5-$C_5(CH_3)_5$	10.8	q, $^1J_{C-H} = 127$
η^5-$C_5(CH_3)_5$	99.3	s
W—CH_3	−8.3	q, $^1J_{C-H} = 125$
$Cp^*_2W(CH_3)H$		
η^5-$C_5(CH_3)_5$	11.2	q, $^1J_{C-H} = 127$
η^5-$C_5(CH_3)_5$	91.9	s

(*continued*)

Table 2 (*continued*)

	Assignment	δ (ppm)	Coupling (Hz)
	W—CH_3	−22.1	dq, $^1J_{C-H}$(q) = 123, $^2J_{C-W(H)}$(d) = 7, $^1J_{W-C}$ = 67
$Cp^*_2W(CH_2C_6H_5)(H)$			
	η^5-$C_5(CH_3)_5$	11.4	q, $^1J_{C-H}$ = 127
	η^5-$C_5(CH_3)_5$	92.9	s
	W—CH_2Ph	4.2	t, $^1J_{C-H}$ = 122
	W—$CH_2C_6H_5$		
	1C(*ipso*)	153.5	s
	2C(*ortho*)	126.7	dd, $^1J_{C-H}$ = 156, $^4J_{C-H}$ = 7
	2C(*meta*)	134.0	d, $^1J_{C-H}$ = 155
	1C(*para*)	122.7	dt, $^1J_{C-H}$(d) = 160, $^3J_{C-H}$(t) = 8
$[Cp^*_2WH_3][X]$[b]			
	η^5-$C_5(CH_3)_5$	10.3	q, $^1J_{C-H}$ = 129
	η^5-$C_5(CH_3)_5$	102.2	s
$Cp^*_2W{=}O$			
	η^5-$C_5(CH_3)_5$	13.6	q, $^1J_{C-H}$ = 127
	η^5-$C_5(CH_3)_5$	107.6	s
$[Cp^*_2W(=O)(CH_3)][I]$			
$CDCl_3$	η^5-$C_5(CH_3)_5$	11.4	q, $^1J_{C-H}$ = 127
	η^5-$C_5(CH_3)_5$	121.8	s
	W—CH_3	17.9	q, $^1J_{C-H}$ = 134
$Cp^*_2W(OH)H$			
	η^5-$C_5(CH_3)_5$	11.3	q, $^1J_{C-H}$ = 127
	η^5-$C_5(CH_3)_5$	93.0	s
$(\eta^1$-$C_5Me_5)(\eta^5$-$C_5Me_5)W(=O)_2$			
C_7D_8, 25°C	η^5-$C_5(CH_3)_5$	12.8	Broad (fluxional)
	η^5-$C_5(CH_3)_5$[c]		
C_7D_8, −90°C	η^5-$C_5(CH_3)_5$	10.1	q
	η^5-$C_5(CH_3)_5$	117.4	s
	η^1-$C_5(CH_3)_5$		
	2C	11.2	q
	2C	12.5	q
	1C	30.5	q
	η^1-$C_5(CH_3)_5$		
	1C	83.3	s
	2C	134.0	s
	2C[d]		
$(\eta^5$-$C_5Me_5)W(=O)_2(OC_5Me_5)$			
	η^5-$C_5(CH_3)_5$	11.0	q, $^1J_{C-H}$ = 127
	η^5-$C_5(CH_3)_5$	118.5	s
	η^1-$C_5(CH_3)_5$		
	1(CH_3)	23.9	q, $^1J_{C-H}$ = 127
	2(CH_3)	10.2	q, $^1J_{C-H}$ = 125
	2(CH_3)	11.4	q, $^1J_{C-H}$ = 125
	η^1-$C_5(CH_3)_5$		
	1C	93.4	s
	2C	134.7	s
	2C	137.3	s

(*continued*)

Table 2 (*continued*)

Assignment	δ (ppm)	Coupling (Hz)
$Cp^*W(\eta^4\text{-}C_5Me_4{=}CH_2)W(=O)(CH_3)$		
$\eta^5\text{-}C_5(CH_3)_5$	8.9	q, $^1J_{C-H} = 128$
$\eta^5\text{-}C_5(CH_3)_5$	112.7	s
$\eta^4\text{-}C_5(CH_3)_4{=}CH_2$	24.6	q, $^1J_{C-H} = 126$
	19.4	q, $^1J_{C-H} = 126$
	13.8	q, $^1J_{C-H} = 128$
	10.2	q, $^1J_{C-H} = 128$
$\eta^4\text{-}C_5(CH_3)_4{=}CH_2$	163.0	s
	144.7	s
	129.8	s
	84.7	s
	62.9	s
$\eta^4\text{-}C_5(CH_3)_4{=}CH_2$	102.2	t, $^1J_{C-H} = 156$
$W{-}CH_3$	15.2	q, $^1J_{C-H} = 125$
$Cp^*W(\eta^2\text{-}C_5Me_4{=}CH_2)W(=O)(CH_3)$		
$\eta^5\text{-}C_5(CH_3)_5$	10.4	q, $^1J_{C-H} = 128$
$\eta^5\text{-}C_5(CH_3)_5$	111.6	s
$\eta^4\text{-}C_5(CH_3)_4{=}CH_2$	11.8	q, $^1J_{C-H} = 126$
	11.2	q, $^1J_{C-H} = 126$
	10.6	q, $^1J_{C-H} = 126$
	9.6	q, $^1J_{C-H} = 126$
$\eta^4\text{-}C_5(CH_3)_4{=}CH_2$	135.2	s
	133.7	s
	129.9	s
	129.7	s
	84.4	s
$\eta^4\text{-}C_5(CH_3)_4{=}CH_2$	40.1	t, $^1J_{C-H} = 149$
$W{-}CH_3$	20.9	q, $^1J_{C-H} = 127$

[a] In C_6D_6 unless specified otherwise.
[b] In dilute $DCl_{(aq)}$.
[c] Not observed due to fluxionality.
[d] Obscured by solvent.

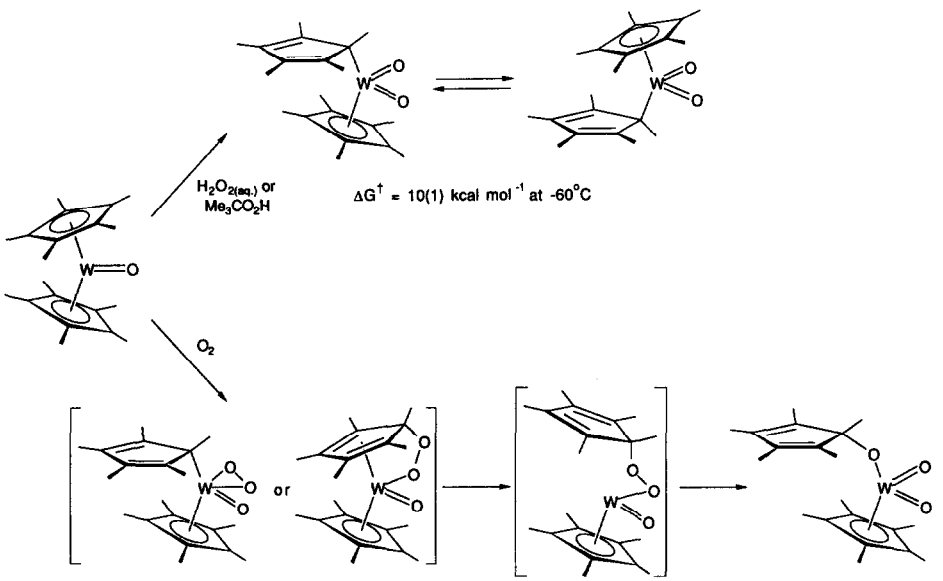

Scheme 7. The formation of dioxo derivatives from $Cp^*_2W{=}O$.

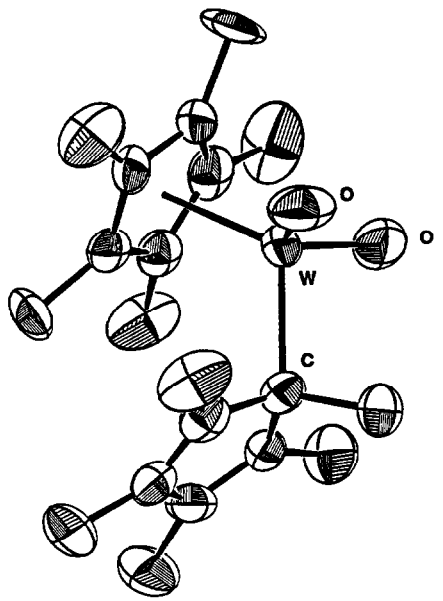

Fig. 3. The molecule structure of $(\eta^5\text{-}C_5Me_5)(\eta^1\text{-}C_5Me_5)W(=O)_2$.

metric vibrations is to be expected because of the different contributions of the tungsten motion to the symmetric and asymmetric vibrations. Essentially, the symmetric stretch corresponds more to the motion of the oxo ligands than does the asymmetric stretch, which has a significant contribution from the motion of the tungsten atom. Thus, the motion of the tungsten atom in the asymmetric vibration diminishes the effect of isotopic substitution of the oxo ligands and results in a shift of only 15 cm^{-1}, compared with 35 cm^{-1} for the symmetric stretch.

The reaction of $Cp_2^*W{=}{}^{18}O$ with $H_2O_{2(aq)}$ results in the formation of an approximately 2:1 mixture of the isotopomers $(\eta^5\text{-}C_5Me_5)(\eta^1\text{-}C_5Me_5)W(=^{18}O)(=^{16}O)$ and $(\eta^5\text{-}C_5Me_5)(\eta^1\text{-}C_5Me_5)W(=^{16}O)_2$. Other studies on the reactions of transition metal derivatives with $H_2O_{2(aq)}$[45] have shown that the products are often η^2-peroxo, $[M]\text{-}(\eta^2\text{-}O_2)$, derivatives obtained via a metathesis reaction. Thus, it was considered that the reaction of $Cp_2^*W{=}O$ with H_2O_2 may have proceeded via an η^2-peroxo intermediate, $[Cp_2^*W(\eta^2\text{-}O_2)]$, which ring-opened to give the dioxo derivative, i.e.

$$Cp_2^*W{=}{}^*O \xrightarrow[-H_2{}^*O]{H_2O_2} [Cp_2^*W(\eta^2\text{-}O_2)] \longrightarrow (\eta^5\text{-}C_5Me_5)(\eta^1\text{-}C_5Me_5)W(=O)_2.$$

If this mechanism were correct, then the product of $Cp_2^*W{=}{}^{18}O$ and $H_2{}^{16}O_{2(aq)}$ would be exclu-

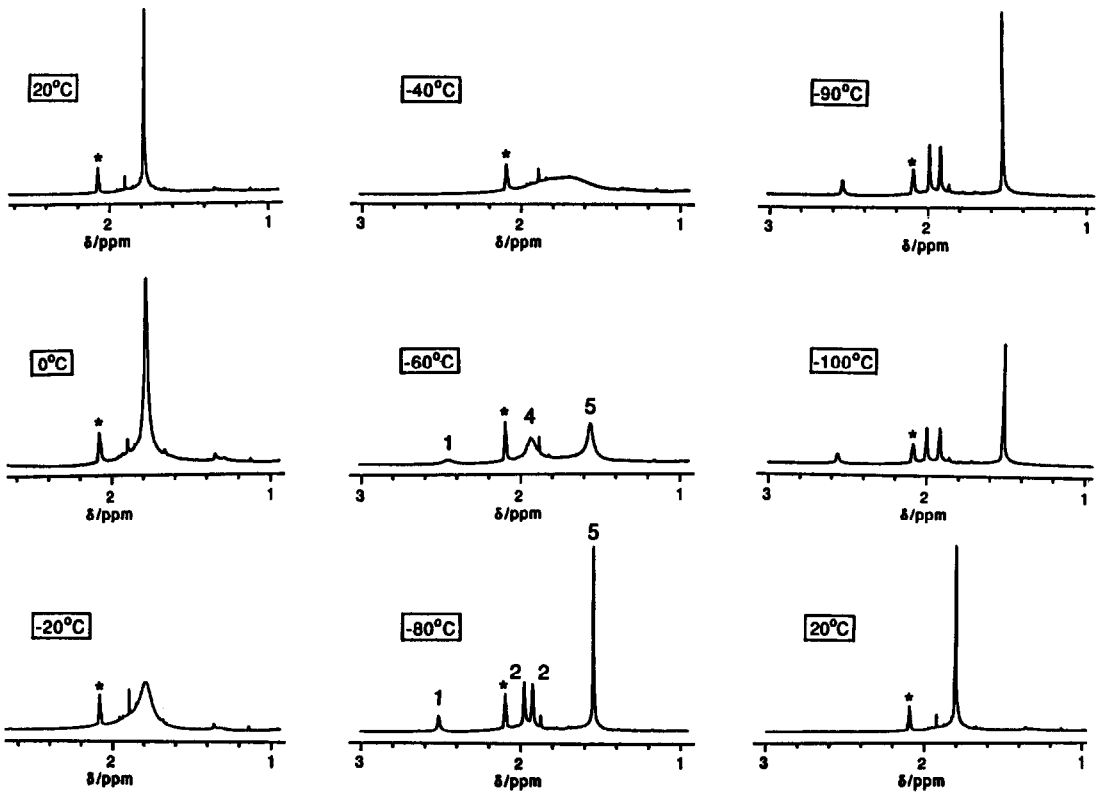

Fig. 4. Variable temperature ^1H NMR spectra of $(\eta^5\text{-}C_5Me_5)(\eta^1\text{-}C_5Me_5)W(=O)_2$ in d_8-toluene (* denotes residual protio solvent; numbers above peaks indicate the respective number of methyl groups).

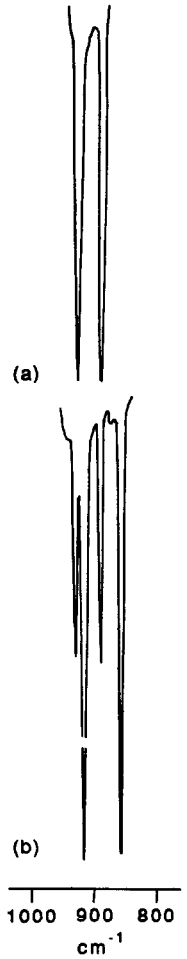

Fig. 5. IR absorptions of the W=O ligands in (a) (η^5-C_5Me_5)(η^1-C_5Me_5)W(=^{16}O)$_2$ and (b) a 2:1 mixture of (η^5-C_5Me_5)(η^1-C_5Me_5)W(=^{16}O)(=^{18}O) and (η^5-C_5Me_5)(η^1-C_5Me_5)W(=^{16}O)$_2$.

sively the isotopomer (η^5-C_5Me_5)(η^1-C_5Me_5)W(=^{16}O)$_2$. However, as described above, the reaction of Cp^*_2W=^{18}O with $H_2{}^{16}O_{2(aq)}$ results in the formation of an approximately 2:1 mixture of the isotopomers (η^5-C_5Me_5)(η^1-C_5Me_5)W(=^{18}O)(=^{16}O) and (η^5-C_5Me_5)(η^1-C_5Me_5)W(=^{16}O)$_2$. The presence of (η^5-C_5Me_5)(η^1-C_5Me_5)W(=^{18}O)(=^{16}O) demonstrates conclusively that the reaction does not proceed via an η^2-peroxo intermediate, Cp^*_2W(η^2-O_2), in which the η^2-peroxo ligand is derived from H_2O_2.

Since Cp^*_2W=O also reacts with Me_3CO_2H to yield (η^5-C_5Me_5)(η^1-C_5Me_5)W(=O)$_2$ (and Me_3COH), a reaction involving Cp^*_2W(OH)(OOR) (R = H, CMe_3), which subsequently eliminates ROH, seems likely. This mechanism would be expected to give only (η^5-C_5Me_5)(η^1-C_5Me_5)W(=^{16}O)(=^{18}O). The origin of *ca* 33% of (η^5-C_5Me_5)(η^1-C_5Me_5)W(=^{16}O)$_2$ may arise from either prior exchange of Cp^*_2W=^{18}O with $H_2{}^{16}O$, or may signal an alternate reaction pathway in which the 2:1 ratio results from decomposition of some intermediate containing three exchangeable oxygen atoms, e.g.

$$Cp^*(\eta^1\text{-}Cp^*)W(^*OH)(OH)(=O) \rightleftharpoons Cp^*(\eta^1\text{-}Cp^*)W(^*OH)(=O)(OH) \rightleftharpoons Cp^*(\eta^1\text{-}Cp^*)W(=^*O)(OH)(OH).$$

We note that (η^5-C_5Me_5)(η^1-C_5Me_5)W(=O)$_2$ does not undergo facile oxygen exchange with labelled $H_2{}^*O$, in contrast to that observed for the mono-oxo derivative, Cp^*_2W=O. Since (η^5-C_5Me_5)(η^1-C_5Me_5)W(=O)$_2$ is a class a oxo derivative, slower exchange is anticipated.

Cp^*_2W=O undergoes a remarkably clean reaction with O_2 to form white, crystalline, Cp^*W(=O)$_2$(OCp*) (Scheme 7). Cp^*W(=O)$_2$(OCp*) has been characterized by an X-ray crystal structure determination and the molecular structure is shown in Fig. 6.[46] In principle, a cyclopentadienyl ligand can bond to a single transition metal centre in a variety of modes, namely η^5-, η^3-,η^1-,η^3,η^2- and η^1,η^4-. In this respect, the bonding between the tungsten atom and the ($\eta^{"5"}$-C_5Me_5) ligand is particularly interesting: while primarily *pentahapto*, η^5-, in character, there is some unmistakable *monohapto*, η^1-, component. Thus, one of the inner-ring carbon atoms, C_α, is displaced from the plane of the other ring atoms, towards W, by about 0.05 Å. This carbon

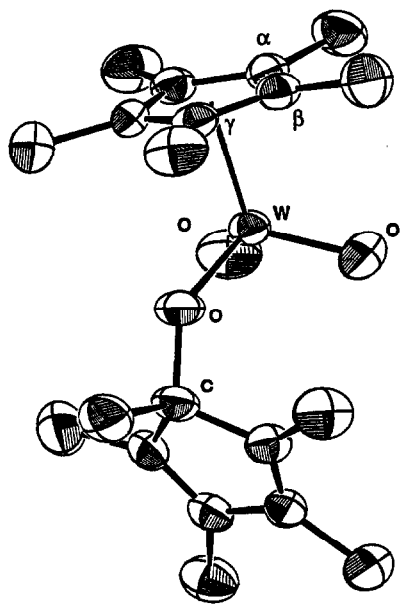

Fig. 6. The molecular structure of ($\eta^{"5"}$-C_5Me_5)W(=O)$_2$(OC_5Me_5).

atom is appreciably pyramidal and the W—C_α distance of 2.334(4) Å is approximately 0.1–0.15 Å shorter than the other W—C distances of this ligand. Indeed, this W—C_α distance is only 0.13 Å longer than the value of 2.20 Å for the W—C distance to the (η^1-C_5Me_5) ligand in (η^5-C_5Me_5)(η^1-C_5Me_5)W(=O)$_2$. There is also considerable localization of the double bonds in the η^{5}-C_5Me_5 η^1 ligand: the C_β—C_γ bonds at 1.396(4) Å, while considerably longer than a pure double bond or the corresponding bonds in the η^1-C_5Me_5 ligand bonded to oxygen, are significantly shorter than the other ring bonds. These observations suggest that the W—(η^5-C_5Me_5) interaction is a mixture of η^5- and η^1-bonding and that the ligand is more aptly described as bonding in an η^1,η^4-fashion.

We note that many of these same features are observed for the (η^5-C_5Me_5) ligand in the structure of the related compound, (η^5-C_5Me_5)(η^1-C_5Me_5)W(=O)$_2$, which differs from (η^5-C_5Me_5)W(=O)$_2$(OC_5Me_5) in that the W atom is directly bonded to the (η^1-C_5Me_5) ligand, rather than being bonded through an oxygen atom. In this complex the W atom is appreciably closer (at about 2.32 Å) to one of the atoms of the (η^5-C_5Me_5) than to the other four, and in each case the ring atom is *trans* to the W—C single bond of the (η^1-C_5Me_5) ligand.

The origin of the asymmetry of the bonding of the (η^5-C_5Me_5) ligand in (η^5-C_5Me_5)(η^1-C_5Me_5)W(=O)$_2$ and (η^5-C_5Me_5)W(=O)$_2$(OC_5Me_5) may be attributed to the strong *trans* influence of two oxo ligands. The ligands *trans* to each oxo ligand may be viewed to be the double bond components of the (η^5-C_5Me_5) ligand. The strong W=O bonding weakens the *trans* tungsten–ligand bonding, and thus lengthening of the bonds to these four carbon atoms results. Other evidence that the oxo ligand exerts a strong *trans* influence is provided by the structures of (η^5-C_5Me_5)Re(=O)Cl_2 and (η^5-C_5Me_5)Re(=O)$(CH_3)_2$.[47] In these examples, the presence of only one oxo ligand results in the lengthening of two Re—ring carbon bonds, so that only one double bond component within the pentamethylcyclopentadienyl ligand obtains. Thus, by extension, the rhenium-(η^5-C_5Me_5) bonding for these structures takes on some η^3,η^2- (i.e. allyl, olefin) character.

The reaction between Cp^*_2W=O and O_2 has been examined by the use of ^{16}O, ^{17}O and ^{18}O labels. Thus, the product of the reaction of $Cp^*_2W=^{18}O$ with $^{16}O_2$ has been studied by IR spectroscopy, and the product of the reaction of $Cp^*_2W=^{17}O$ with $^{16}O_2$ has been studied by ^{17}O NMR spectroscopy. The results show that the oxygen atom which is inserted between the tungsten atom and the Cp* ligand arises from the O_2 rather than the oxo ligand of Cp^*_2W=O. Two potential pathways for the formation of (η^5-C_5Me_5)W(=O)$_2$(OC_5Me_5) involve (i) the formation of an η^2-peroxo intermediate, i.e. (η^5-C_5Me_5)(η^1-C_5Me_5)W(=O)(η^2-O_2), followed by migration of the (η^1-C_5Me_5) ligand to (η^2-O_2), and (ii) attack at both the Cp* ligand and W by O_2 leading to a bridging peroxo species and thus C—O bond formation in the initial stages (Scheme 7). However, the available data does not permit the distinction between these two mechanisms. We note that a potential model for this reaction is the acid-catalysed conversion of Cp^*_2Ta(η^2-O_2)CH_3 to Cp^*_2Ta(=O)OCH_3.[48]

$$Cp^*_2Ta(\eta^2\text{-}O_2)CH_3 \xrightarrow{H^+(catalyst)} Cp^*_2Ta(=O)OCH_3.$$

In order to examine this possibility further, and also to examine the transfer of an oxygen to a methyl group on tungsten, the previously reported oxo–peroxo methyl compound, Cp*W(=O)(η^2-O_2)CH_3,[41] was synthesized by a new procedure involving the oxidation of Cp*W$(CO)_3CH_3$ with $H_2O_{2(aq)}$.

$$Cp^*W(CO)_3CH_3 \xrightarrow{H_2O_{2(aq)}} Cp^*W(=O)(\eta^2\text{-}O_2)CH_3.$$

This compound is analogous to one of the potential intermediates shown in Scheme 7. However, this complex does not *cleanly* undergo a transformation of the type shown and so no firm conclusions regarding the mechanism can be drawn at this time.

The W—OCp* bond in Cp*W(=O)$_2$(OCp*) can be cleaved with Me_3SiCl to give Cp*W(=O)$_2$Cl.[41,43]

$$Cp^*W(=O)_2(OCp^*) \xrightarrow{Me_3SiCl} Cp^*W(=O)_2Cl.$$

Cp*W(=O)$_2$(OCp*) undergoes an acid-catalysed rearrangement to generate the dimer, [Cp*W(=O)$_2$]$_2$O (0.5 equivalent), and the ether, $(C_5Me_5)_2O$, which has been spectroscopically characterized but not isolated. The ether undergoes a further acid-catalysed dehydration to give tetramethylfulvene, $C_5Me_4CH_2$.† This overall process can also be effected photochemically as summarized in Scheme 8.

EXPERIMENTAL

General considerations

All manipulations were performed using a combination of glovebox, high-vacuum or Schlenk tech-

† The organic derivatives $(C_5Me_5)_2O$ and $C_5Me_4CH_2$ have only been spectroscopically characterized and not isolated pure. 1,2,3,4-tetramethylfulvene has been previously reported.[49]

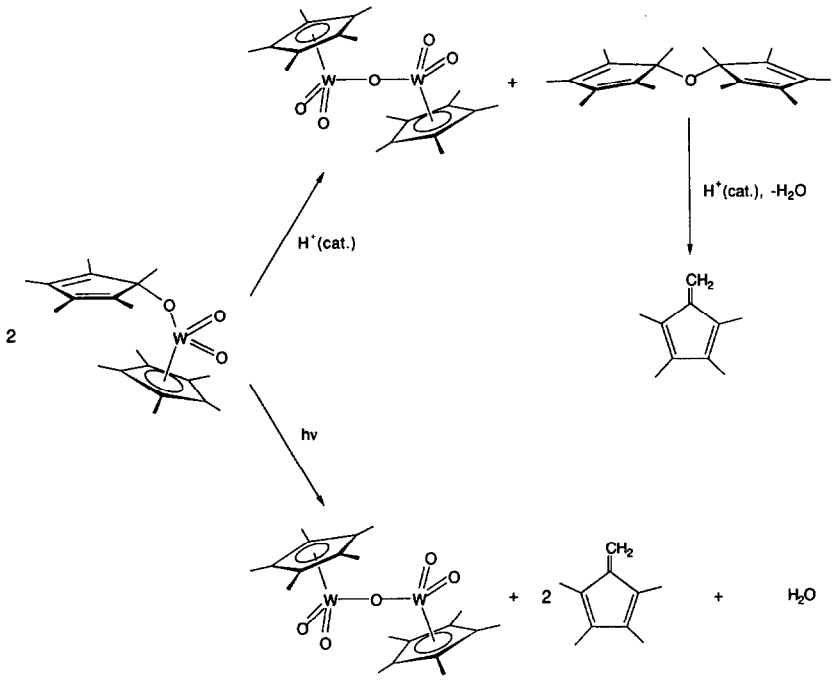

Scheme 8. Acid-catalysed and photochemical conversion of $Cp^*W(=O)_2(OCp^*)$ to $[Cp^*W(=O)_2]_2O$.

niques.[50] Solvents were purified and degassed by standard procedures. C_6D_6 was purified by vacuum transfer from activated molecular sieves (4 Å, Linde) and then from "titanocene".[51]

^1H, ^2H, ^{13}C and ^{17}O NMR spectra were measured on Varian EM-390 (90 MHz), JEOL FX90Q (90 MHz), JEOL GX400Q (400 MHz) and Brucker WM500 (500 MHz) spectrometers and ^1H and ^{13}C NMR data for the compounds are reported in Tables 1 and 2. IR spectra were recorded on a Beckman 4240 spectrophotometer. Elemental analyses and mass spectra were obtained by Mr L. Henling and Mr F. Harvey of the CIT analytical department.

Cp^*WCl_4 and $Cp^*WCl_4(PMe_3)$ were prepared as described previously.[7]

Preparation of $Cp^*_2WCl_2$

(a) *From* $Cp^*WCl_4(PMe_3)$. A mixture of $Cp^*WCl_4(PMe_3)$ (30 g, 55.9 mmol) and Mg (0.68 g, 28.3 mmol) was treated with THF (75 cm^3) at −78°C and stirred as it was allowed to warm to room temperature. A red solution was obtained after *ca* 30 min. The mixture was stirred for a further 12 h after which the solvent was removed under reduced pressure giving a red–orange solid. Cp*Li (10 g, 70.4 mmol) and toluene (*ca* 50 cm^3) were added and the mixture was heated at *ca* 145°C for 4 days. The solvent was removed and the residue was washed with petroleum ether (b.p. 35–60°C, 5 × 100 cm^3). This solid was placed in a Soxhlet extractor and extracted with toluene. The toluene extract was allowed to cool to room temperature overnight forming green crystals which were separated and washed with pentane, giving $Cp^*_2WCl_2$ (3 g). A second crop (0.5 g) was also obtained. The residue in the thimble of the Soxhlet extractor was extracted with CH_2Cl_2. The CH_2Cl_2 was removed from the extract under reduced pressure giving a further quantity of $Cp^*_2WCl_2$ (2.5 g). Total yield $Cp^*_2WCl_2$ 6 g (21%). Elemental analysis (found/calc.): C 46.4 (45.7), H 5.7 (5.7)%. Mass spectrum: $m/e = 526$ for $Cp^*_2W^{184}Cl^{35}Cl^{37}$. IR data (Nujol mull, KBr plates, cm^{-1}): 1490(w,br), 1060(w), 1015(s).

(b) *From* Cp^*WCl_4. A suspension of Cp^*WCl_4 (20 g, 43.4 mmol) in toluene (40 cm^3) was treated with PMe_3 (7 cm^3, *ca* 64 mmol) and stirred for 12 h at room temperature. The solvent was removed under reduced pressure giving $Cp^*(WCl_4(PMe_3)$ as a green powder. Mg (0.54 g, 22.5 mmol) was added and THF (50 cm^3) were added at −78°C. The mixture was stirred as it was allowed to warm to room temperature, giving a red solution which deposited red crystals. The THF was removed under reduced pressure after *ca* 2 h. KCp* (11 g, 62.9 mmol) and toluene (100 cm^3) were added and the mixture was heated at *ca* 145°C in a glass ampoule. Portions of the solvent were removed under vacuum periodically (initially after 2 h). Green crystals could be observed to be present after 16 h. After 2 days the volatile components were removed and the residue

was washed with pentane (5×100 cm^3) and placed in a Soxhlet extractor and extracted with toluene. Green crystals were deposited and were filtered and washed with pentane giving $Cp^*_2WCl_2$ (5 g). A further 800 mg was isolated from the toluene filtrate and 200 mg was isolated by extraction of the residue in the Soxhlet thimble with CH_2Cl_2. Total yield $Cp^*_2WCl_2$, 6 g (26%).

Preparation of $Cp^*(\eta^5\text{-}C_5Me_4CH_2CH_2CH_3)WCl_2$

A suspension of Cp^*WCl_4 (2.1 g, 4.6 mmol) in toluene (10 cm^3) was treated with PMe_3 (0.8 cm^3, *ca* 7.4 mmol) and stirred for 2 h at room temperature. The solvent was removed under reduced pressure giving $Cp^*WCl_4(PMe_3)$ as a green powder. Mg (0.059 g, 2.4 mmol) was added and THF (20 cm^3) added at −78°C. The mixture was stirred as it was allowed to warm to room temperature, giving a red solution which deposited red crystals. The THF was removed under reduced pressure after *ca* 4 h. $Li(C_5Me_4CH_2CH_2CH_3)$ (0.77 g, 4.5 mmol) and toluene (30 cm^3) were added and the mixture was heated at *ca* 145°C in a glass ampoule. Portions of the solvent were removed under vacuum periodically. After 3 days the volatile components were removed and the residue was washed with pentane (4×100 cm^3) extracted into hot toluene and allowed to cool to −78°C. Green crystals were deposited and were filtered and washed with pentane giving $Cp^*(\eta^5\text{-}C_5Me_4CH_2CH_2CH_3)WCl_2$ (250 mg, 10%). Elemental analysis (found/calc.): C 47.4(47.7), H 5.7(6.2)%.

Preparation of $Cp^*_2WH_2$

A mixture of $Cp^*_2WCl_2$ (500 mg, 0.95 mmol) and $LiAlH_4$ (300 mg, 7.9 mmol) was treated with Et_2O (40 cm^3) at −78°C. The mixture was stirred and warmed to room temperature. After 2 h the $Cp^*_2WCl_2$ had dissolved and an orange solution phase was present. The mixture was stirred for a total of 3 days giving a pale yellow solution phase which was cooled to 0°C and slowly treated with Et_2O saturated with H_2O (60 cm^3) and then H_2O (2 cm^3). The mixture was filtered and the solvents removed under reduced pressure. The residue was extracted into pentane and crystallized at −78°C giving yellow needles which were isolated by filtration and dried *in vacuo* giving $Cp^*_2WH_2$ (300 mg, 69%).

When the reaction was hydrolysed after 2 h, the product isolated was a mixture of $Cp^*_2WH_2$ and $Cp^*_2W(H)Cl$. Reduction of $Cp^*_2W(H)Cl$ under similar conditions for 2 days gave $Cp^*_2WH_2$.

Preparation of $Cp^*_2W(H)Cl$

A mixture of $Cp^*_2WCl_2$ (400 mg, 0.76 mmol), Na (100 mg, 4.35 mmol) and Hg (5 cm^3) was treated with THF (20 cm^3) at −78°C. The mixture was stirred and allowed to warm to room temperature. After 18 h the mixture was filtered and the solvent was removed from the filtrate under reduced pressure. The residue was extracted into pentane, concentrated and placed at −78°C giving light brown needles of $Cp^*_2W(H)Cl$ (180 mg, 48%). Elemental analysis (found/calc.): C 49.9 (48.9), H 6.3 (6.3)%. IR data (Nujol mull, KBr plates, cm^{-1}): 2710(w), 1940(m) [W—H], 1065(w), 1020(s).

Preparation of $Cp^*_2W(CH_3)_2$

$Cp^*_2WCl_2$ (2 g, 3.8 mmol) and CH_3Li (400 mg, 18.2 mmol) were treated with toluene (20 cm^3) and heated at 80°C for 2 h giving a red–orange solution. The mixture was filtered and the toluene removed under reduced pressure. The residue was extracted into pentane and cooled to −78°C giving orange needles of $Cp^*_2W(CH_3)_2$ (1.2 g, 65%). Elemental analysis (found/calc.): C 54.4 (54.6), H 7.3 (7.4)%. IR data (Nujol mull, KBr plates, cm^{-1}): 2715(w), 1060(w), 1020(s).

Preparation of $Cp^*_2W(\eta^2\text{-}CH_2O)$

A mixture of $Cp^*_2WCl_2$ (900 mg, 1.7 mmol) and $NaOCH_3$ (400 mg, 7.4 mmol) was heated in toluene (20 cm^3) at 80°C for 2 days giving a red–orange solution. The solvent was removed under reduced pressure and the residue was extracted into pentane and crystallized at −78°C giving brown needles of $Cp^*_2W(\eta^2\text{-}CH_2O)$ (480 mg, 58%). The product was contaminated by small quantities of $Cp^*_2W{=}O$. Elemental analysis (found/calc.): C 51.7 (52.3), H 6.5 (6.6)%.

Preparation of $Cp^*(\eta^5,\eta^1\text{-}C_5Me_4CH_2)WH$

(a) A mixture of $Cp^*_2W(H)Cl$ (180 mg, 0.37 mmol) and CH_3Li (150 mg, 6.8 mmol) were treated with toluene (20 cm^3) and heated at 100°C for 16 h. The solvent was removed under reduced pressure and the residue crystallized from pentane at −78°C giving yellow–orange crystals of $Cp^*(\eta^5,\eta^1\text{-}C_5Me_4CH_2)WH$ (120 mg, 72%). Elemental analysis (found/calc.): C 52.9 (52.9), H 6.4 (6.6)%.

(b) A mixture of $Cp^*_2WCl_2$ (*ca* 15 mg) and CH_3Li (*ca* 10 mg) in C_6D_6 (*ca* 0.5 cm^3) in a NMR tube was heated at 80°C for 1 h and was observed by ^1H NMR spectroscopy to generate $Cp^*(\eta^5,\eta^1\text{-}C_5Me_4CH_2)WH$ via $Cp^*_2W(CH_3)H$.

(c) A mixture of $Cp^*_2WCl_2$ (*ca* 15 mg) and C_6H_5Li (*ca* 10 mg) in C_6D_6 (*ca* 0.5 cm^3) in a NMR tube was heated at 80°C for 4 h and was observed by ^1H NMR spectroscopy to generate $Cp^*(\eta^5,\eta^1\text{-}C_5Me_4CH_2)WH$.

Reaction of $Cp^*(\eta^5,\eta^1\text{-}C_5Me_4CH_2)WH$ *with* H_2

A solution of $Cp^*(\eta^5,\eta^1\text{-}C_5Me_4CH_2)WH$ (*ca* 15 mg) in C_6D_6 (*ca* 0.5 cm^3) was sealed in a NMR tube under H_2 (*ca* 4 atm at 25°C) and heated at 220°C for 24 h. Observation by ^1H NMR spectroscopy demonstrated the formation of $Cp^*_2WH_2$.

Interconversion of $Cp^*_2WH_2$ *and* $Cp^*_2W(H)Cl$

(a) A solution of $Cp^*_2WH_2$ (*ca* 10 mg) in C_6D_6 (*ca* 0.5 cm^3) in a NMR tube was treated with CCl_4 and observed by ^1H NMR spectroscopy to generate sequentially $Cp^*_2W(H)Cl$ and $Cp^*_2WCl_2$, accompanied by the formation of $CHCl_3$.

(b) A solution of $Cp^*_2W(H)Cl$ (*ca* 10 mg) in C_6D_6 (*ca* 0.5 cm^3) in a NMR tube was treated with excess CCl_4 and observed by ^1H NMR spectroscopy to generate, cleanly, $Cp^*_2WCl_2$ and $CHCl_3$ after 30 min at room temperature.

(c) A mixture of $Cp^*_2WH_2$ and $Cp^*_2WCl_2$ (*ca* 1 : 1 molar ratio) in C_6D_6 was heated at 220°C for 1 day to give an equilibrium mixture with $Cp^*_2W(H)Cl$ ($K \approx 21$).

Preparation of $Cp^*_2W(CH_3)Cl$

A stirred solution of $Cp^*_2W(CH_3)_2$ (600 mg, 1.24 mmol) in toluene (20 cm^3) was treated with Me_3SiCl (157×10^{-3} cm^3, 1.68 mmol) and then H_2O (11×10^{-3} cm^3, 0.61 mmol). The solvent was removed under reduced pressure after 1 h at room temperature and the residue was washed with pentane (3×10 cm^3) to give $Cp^*_2W(CH_3)Cl$ as a red–brown crystalline solid (570 mg, 91%). Elemental analysis (found/calc.): C 50.5 (50.0), H 6.6 (6.5)%. IR data (Nujol mull, KBr plates, cm^{-1}): 2710(w), 1060(w), 1020(s).

Reaction of $Cp^*_2W(CH_3)Cl$ *with* CH_3Li; *formation of* $Cp^*_2W(CH_3)_2$

A solution of $Cp^*_2W(CH_3)Cl$ (*ca* 15 mg) in C_6D_6 (*ca* 0.5 cm^3) in a NMR tube was treated with CH_3Li (*ca* 10 mg). The reaction was monitored by ^1H NMR spectroscopy to give $Cp^*_2W(CH_3)_2$ after 30 min at room temperature.

Preparation of $Cp^*_2W(CH_3)H$

A mixture of $Cp^*_2W(CH_3)Cl$ (250 mg, 0.50 mmol) and $LiAlH_4$ (150 mg, 3.95 mmol) was treated with Et_2O at −78°C and the mixture stirred as it was allowed to warm to room temperature. The mixture was stirred for 4 h and cooled to 0°C before adding H_2O (*ca* 2 cm^3) dropwise. The mixture was filtered and the solvent removed under reduced pressure. The residue was extracted into pentane, concentrated and placed at −78°C. The orange crystals which were deposited were a mixture of $Cp^*_2W(CH_3)H$ and $Cp^*_2W(CH_3)_2$ (70 mg, *ca* 30%, ratio *ca* 4 : 1). The solvent was removed from the filtrate under reduced pressure giving $Cp^*_2W(CH_3)H$ (*ca* 30 mg, 13%, <5% $Cp^*_2W(CH_3)_2$). Elemental analysis (found/calc.): C 53.7 (53.6), H 7.2 (7.2)%. IR data (Nujol mull, KBr plates, cm^{-1}): 2715(w), 1900(m) [W—H], 1160(w), 1100(w), 1065(w), 1020(s), 790(w).

The reaction was repeated under similar conditions using $LiAlD_4$ as the reducing agent and D_2O for the hydrolysis. In this case the product of the reaction was identified as $Cp^*_2W(CH_3)D$ by ^1H and ^2H NMR spectroscopy.

Preparation of $Cp^*_2W(CH_2C_6H_5)H$

A mixture of $Cp^*_2W(CH_3)Cl$ (110 mg, 0.22 mmol) and C_6H_5Li (50 mg, 0.60 mmol) was treated with toluene (5 cm^3) and stirred at room temperature for 1 h. The mixture was filtered and the solvent removed under reduced pressure. The residue was extracted into pentane, concentrated and placed at −78°C. The orange crystals which were deposited were a mixture of $Cp^*_2W(CH_3)_2$ and $Cp^*_2W(CH_2Ph)H$ (30 mg, *ca* 50 : 50). The solvent was removed from the filtrate under reduced pressure to give pure $Cp^*_2W(CH_2Ph)H$ (*ca* 70 mg, 59%). Elemental analysis (found/calc.): C 59.0 (59.3), H 6.9 (7.0)%.

Preparation of $Cp^*(\eta^5,\eta^1\text{-}C_5Me_4CH_2)WCH_3$

A solution of $Cp^*_2W(CH_3)Cl$ (*ca* 20 mg) in C_6D_6 (0.5 cm^3) was treated with $LiCH_2PMe_2$ (10 mg). The products were observed by ^1H NMR spectroscopy to be $Cp^*(\eta^5,\eta^1\text{-}C_5Me_4CH_2)W(CH_3)$ and PMe_3 after 18 h at room temperature. The solvent was removed under reduced pressure and the residue was extracted into pentane. The mixture was filtered and the pentane removed from the filtrate under reduced pressure to give a yellow–orange solid, $Cp^*(\eta^5,\eta^1\text{-}C_5Me_4CH_2)W(CH_3)$ (*ca* 15 mg).

Reaction of $Cp^*_2W(CH_3)Cl$ *with* CH_3CH_2MgBr *and* Me_3CLi; *formation of* $Cp^*_2W(CH_3)H$

A solution of $Cp^*_2W(CH_3)Cl$ (*ca* 15 mg) in C_6D_6 (*ca* 0.5 cm^3) was treated with an excess of either CH_3CH_2MgBr or Me_3CLi and the reaction was monitored by ^1H NMR spectroscopy. In each case $Cp^*_2W(CH_3)H$, *inter alia*, was observed to be formed.

Preparation of $[Cp^*_2WH_3][BF_4]$

(a) A solution of $Cp^*_2WH_2$ (30 mg, 0.07 mmol) in Et_2O (5 cm^3) was treated dropwise with a solution of HBF_4 in Et_2O until a white precipitate was formed in a colourless solution. The mixture was filtered and the residue was washed with Et_2O and dried *in vacuo* giving a white powder, $[Cp^*_2WH_3][BF_4]$ (*ca* 30 mg, 84%). Elemental analysis (found/calc.): C 43.7 (44.1), H 6.0 (6.1)%. IR data (Nujol mull, KBr plates, cm^{-1}): 2720(w), 1985(m), [W—H], 1945(m) [W—H], 1800(w,br), 1570(m,br), 1280(w), 1050(s,br), 880(w), 860(w), 825(m), 720(m), 515(w).

(b) A mixture of $Cp^*_2WH_2$ (*ca* 20 mg) and $[Me_3NH][BPh_4]$ (*ca* 30 mg) was treated with $(CD_3)_2CO$ (*ca* 0.5 cm^3). A white solid was deposited which was separated by filtration giving $[Cp^*_2WH_3][BPh_4]$.

(c) A solution of $Cp^*_2WH_2$ (*ca* 20 mg) in Et_2O (*ca* 5 cm^3) was treated with excess $HCl_{(aq)}$ giving a fine white precipitate. The solvents were removed under reduced pressure giving a white solid, $[Cp^*_2WH_3][X]$ (X = Cl or HCl_2).

Protonation of $Cp^*_2WH_2$ *with* D^+

A suspension of $Cp^*_2WH_2$ (*ca* 15 mg) in D_2O (*ca* 0.5 cm^3) in a NMR tube was treated with a solution of DCl in D_2O. The $Cp^*_2WH_2$ dissolved giving a colourless solution. ^1H NMR spectroscopy demonstrated that the D^+ reacted initially at the central position giving d_1-$[Cp^*_2W(H)(D)(H)]^+$. Further exchange processes giving lateral d_1-$[Cp^*_2W(H)(H)(D)]^+$, d_2-$[Cp^*_2WHD_2]^+$ and d_3-$[Cp^*_2WD_3]^+$ occurred over a period of hours.

Deprotonation of $[Cp^*_2WH_3][BF_4]$

A solution of $[Cp^*_2WH_3][BF_4]$ (*ca* 15 mg) in H_2O (1 cm^3) was treated with a solution of $KOH_{(aq)}$ until a yellow precipitate was obtained. The water was removed under reduced pressure and the residue was extracted into pentane. The mixture was filtered and the pentane was removed from the filtrate under reduced pressure giving pure $Cp^*_2WH_2$ (*ca* 10 mg).

Preparation of $Cp^*_2W{=}O$

(a) A stirred suspension of $Cp^*_2WCl_2$ (1.0 g, 1.9 mmol) and KOH (0.27 g, 4.8 mmol) in THF (20 cm^3) was treated with H_2O (5 cm^3). The mixture was stirred for 1 h at room temperature giving a deep green THF solution above the colourless aqueous layer. The solvents were removed under reduced pressure and the residue was extracted into pentane, concentrated and cooled to −78°C giving dark green crystals of $Cp^*_2W{=}O$ (610 mg, 36%). Elemental analysis (found/calc.): C 51.2 (51.1), H 6.4 (6.4)%. ^{17}O NMR data (12 MHz, C_6D_6): δ 760 ppm. IR data (Nujol mull, KBr plates, cm^{-1}): 2710(w), 1060(w), 1025(m), 860(vs) [W=O] {820 $W{=}P^{18}$}.

The isotopically labelled derivative $Cp^*_2W{=}{}^{18}O$ (*ca* 90–95%) was obtained by a modification of the above procedure using $K^{18}OH/H_2{}^{18}O$. $Cp^*_2W{=}{}^{17}O$ was obtained by the exchange of $Cp^*_2W{=}{}^{16}O$ with $H_2{}^{17}O$ (*ca* 45%).

(b) A solution of $Cp^*_2W(\eta^2\text{-}CH_2O)$ (20 mg) in C_6D_6 (0.5 cm^3) was treated with H_2O (excess). The products were observed by ^1H NMR spectroscopy to be $Cp^*_2W{=}O$ and CH_3OH. $Cp^*_2W{=}{}^{17}O$ was also prepared by a large scale modification of this reaction.

Oxo exchange reactions of $Cp^*_2W{=}O$ *with* $H_2{}^*O$

(a) A solution of $Cp^*_2W{=}{}^{18}O$ (30 mg) in pentane (*ca* 5 cm^3) was stirred with excess $H_2{}^{16}O$ for 1 h at room temperature. The solvents were removed and the product was demonstrated to be $Cp^*_2W{=}{}^{16}O$ by IR spectroscopy.

(b) A solution of $Cp^*_2W{=}{}^{16}O$ (*ca* 50 mg) in pentane (5 cm^3) was stirred with excess $H_2{}^{17}O$ (45%) for 3 h at room temperature. The volatile components were removed and the formation of enriched $Cp^*_2W{=}{}^{17}O$ was demonstrated by ^{17}O NMR spectroscopy.

(c) A solution of $Cp^*_2W{=}{}^{17}O$ (*ca* 25 mg) in THF (*ca* 0.5 cm^3) was treated with $H_2{}^{16}O$ (*ca* 10 equivalents). Exchange of the labelled oxygen atoms was observed by ^{17}O NMR spectroscopy (δ 770 ppm in THF relative to external $H_2{}^{17}O$).

Exchange reaction of $Cp^*_2Ta(={}^{18}O)H$ *with* $D_2{}^{16}O$

A solution of $Cp^*_2Ta(={}^{18}O)H$ (50 mg) in pentane (*ca* 10 cm^3) was stirred with D_2O (*ca* 0.1 cm^3) for 3 h at room temperature. The solvents were removed and the product was identified as $Cp^*_2Ta(={}^{16}O)H$ by IR spectroscopy.

Reaction of $Cp^*_2Ta(=NC_6H_5)H$ *with* D_2O; *formation of* $Cp^*_2Ta(=O)H$

A solution of $Cp^*_2Ta(=NC_6H_5)H$ (*ca* 20 mg) in C_6D_6 (*ca* 0.5 cm^3) in a NMR tube was treated with excess D_2O. After 24 h at room temperature the products were observed to be $Cp^*_2Ta(=O)H$ and $PhND_2$ by ^1H NMR spectroscopy.

Reaction of $Cp^*_2W{=}O$ *with* Me_3SiCl; *formation of* $Cp^*_2W(OSiMe_3)Cl$ *and* $Cp^*_2WCl_2$

(a) A solution of $Cp^*_2W{=}O$ (*ca* 10 mg) in C_6D_6 (*ca* 0.5 cm^3) in a NMR tube was treated with excess Me_3SiCl. An immediate reaction occurred and the products $Cp^*_2WCl_2$ and $(Me_3Si)_2O$ were identified by ^1H NMR spectroscopy.

(b) A solution of $Cp^*_2W{=}O$ (*ca* 10 mg) in C_6D_6 (*ca* 0.5 cm^3) in a NMR tube was treated with Me_3SiCl (one equivalent) and was observed by ^1H NMR spectroscopy to generate an equilibrium mixture with $Cp^*_2W(OSiMe_3)Cl$ (*ca* 80% $Cp^*_2W(OSiMe_3)Cl$ initially). Over the period of 36 h, this mixture converted to equimolar amounts of $Cp^*_2W{=}O$ and $Cp^*_2WCl_2$.

Preparation of $Cp^*_2WI_2$

A solution of $Cp^*_2W{=}O$ (50 mg, 0.11 mmol) in toluene (10 cm^3) was treated with Me_3SiI (excess) at room temperature. The solvent was removed after 1 h and the residue washed with pentane (3×10 cm^3) to give a green crystalline solid, $Cp^*_2WI_2$ (50 mg, 67%). Elemental analysis (found/calc.): C 30.3 (33.9), H 4.0 (4.2)%.

Reaction of $Cp^*_2W{=}O$ *with* H_2 *and* Me_2SiH; *formation of* $Cp^*_2WH_2$

A solution of $Cp^*_2W{=}O$ (*ca* 15 mg) in C_6D_6 (*ca* 0.5 cm^3) in a NMR tube was sealed under either H_2 or Me_3SiH and heated at 220°C for *ca* 15 and 6 h, respectively. In each case the product was observed to be $Cp^*_2WH_2$ by ^1H NMR spectroscopy.

Reaction of $Cp^*_2W{=}O$ *with* $LiAlH_4$; *formation of* $Cp^*_2W(OH)H$ *and* $Cp^*_2WH_2$

A mixture of $Cp^*_2W{=}O$ (150 mg, 0.32 mmol) and $LiAlH_4$ (150 mg, 3.95 mmol) was treated with Et_2O (*ca* 20 cm^3) at −78°C. The mixture was stirred as it was allowed to warm to *ca* −20°C. An orange solution was obtained after *ca* 15 min. At this temperature the mixture was treated slowly with Et_2O saturated with H_2O (*ca* 30 cm^3) and then H_2O (1 cm^3). The mixture was filtered and the solvents removed from the filtrate under reduced pressure. The residue was extracted into pentane and crystallized at −78°C giving tan crystals, $Cp^*_2W(OH)H$ (70 mg, 47%). Elemental analysis (found/calc.): C 51.3 (50.9), H 6.7 (6.8)%. ^{17}O NMR data (12 MHz, C_6D_6): δ −110 ppm, $\nu_{1/2} \approx 330$ Hz). IR data (Nujol mull, KBr plates, cm^{-1}): 3600(w) [W—OH], 2715(w), 1905(m) [W—H], 1150(w), 1075(sh), 1060(w), 1025(m), 935(w), 900(w), 790(w). Prolonged reaction times at room temperature produces $Cp^*_2WH_2$.

$Cp^*_2W(OD)D$ was prepared by a similar method using $LiAlD_4$ and D_2O.

Preparation of $[Cp^*_2W(=OH)][BF_4]$

A solution of $Cp^*_2W{=}O$ (120 mg, 0.26 mmol) in Et_2O (10 cm^3) was treated with $HBF_4 \cdot Et_2O$ (excess) at −78°C. The mixture was warmed to room temperature and deposited a white solid which was isolated by filtration and washed with Et_2O giving $[Cp^*_2W{=}OH][BF_4]$ (*ca* 75 mg, 50%). Elemental analysis (found/calc.): C 40.7 (43.0), H 5.3 (5.6)%. IR data (Nujol mull, KBr plates, cm^{-1}): 3340(s,br) [WO—H], 2725(vw), 1285(w), 1210(m), 1050(vs,br), 970(m), 920(m), 875(m), 845(m), 800(vw), 760(w), 720(w), 550(w), 510(m).

Reaction of $[Cp^*_2W(=OH)][BF_4]$ *with* $KOH_{(aq)}$; *formation of* $Cp^*_2W{=}O$

$[Cp^*_2W(=OH)][BF_4]$ (*ca* 50 mg, 0.09 mmol) in THF (5 cm^3) was stirred with excess $KOH_{(aq)}$ for 2 h giving a green solution. The solvents were removed under reduced pressure and the residue was extracted into pentane. The mixture was filtered and the pentane removed under reduced pressure giving a green solid (*ca* 20 mg, 48%) which was identified as $Cp^*_2W{=}O$ by ^1H NMR spectroscopy.

Preparation of $[Cp^*_2W(=O)CH_3][I]$

A solution of $Cp^*_2W{=}O$ (150 mg, 0.32 mmol) in toluene (3 cm^3) was treated with CH_3I (0.2 cm^3, 3.2 mmol) and the mixture was stirred. After *ca* 5 min a yellow microcrystalline deposit started to form. The stirring was continued for 12 h. The mixture was filtered and the solid was washed with pentane (3×2 cm^3) and dried *in vacuo* giving yellow crystals $[Cp^*2W(=O)CH_3][I]$ (150 mg, 77%). $[Cp^*2W(=O)CD_3][I]$ was obtained by a similar procedure using CD_3I. Elemental analysis (found/calc.): C 41.3 (41.2), H 5.4 (5.4)%. IR data (Nujol mull, KBr plates, cm^{-1}): 2715(vw), 1250(vw), 1075 (vw,br), 1020(m), 868(s) [W=O], 790(w), 715(w).

Attempted exchange reaction of $[Cp^*_2W(=O)CD_3][I]$ *with* CH_3I

A solution of $[Cp^*_2W(=O)CD_3][I]$ (*ca* 20 mg) in $CDCl_3$ (*ca* 0.5 cm^3) in a NMR tube was treated with CH_3I (*ca* 10 equivalents). The mixture was heated at 80°C for 18 h. There was no evidence for the formation of the isotopomer, $[Cp^*_2W(=O)CH_3][I]$, by ^1H NMR spectroscopy.

Preparation of $Cp^*(\eta^4\text{-}C_5Me_4{=}CH_2)W(=O)CH_3$

A suspension of $[Cp^*_2W(=O)CH_3][I]$ (*ca* 50 mg, 0.08 mmol) and KH (*ca* 10 mg, 0.25 mmol) in THF (*ca* 5 cm^3) was stirred for 2 h at room temperature giving an orange solution phase. The THF was removed under reduced pressure and the residue was extracted into pentane. The mixture was filtered and the pentane removed under reduced pressure giving orange–red crystals of $Cp^*(\eta^4\text{-}C_5Me_4{=}CH_2)(=O)CH_3$ (*ca* 20 mg, 50%). Elemental analysis (found/calc.): C 52.5 (52.1), H 6.7 (6.6)%. IR data (Nujol mull, KBr plates, cm^{-1}): 3080(w), 2715(w), 1600(s), 1400(m), 1325(w), 1280(w), 1160(m), 1110(vw), 1035(m), 945(vs), 925(w), 845(s), 835(vw), 715(vw), 695(w).

$Cp^*(\eta^4\text{-}C_5Me_4{=}CH_2)W(=O)CD_3$ was obtained by a similar procedure using $[Cp^*_2W(=O)CD_3][I]$ and NaH.

Preparation of $Cp^*(\eta^2\text{-}CH_2{=}C_5Me_4)W(=O)CH_3$

A solution of $Cp^*(\eta^4\text{-}C_5Me_4{=}CH_2)W(=O)CH_3$ (*ca* 25 mg, 0.05 mmol) in C_6D_6 was heated at 80°C for 3 h giving $Cp^*(\eta^2\text{-}CH_2{=}C_5Me_4)(=O)CH_3$ quantitatively as determined by ^1H NMR spectroscopy. The solvent was removed under reduced pressure giving $Cp^*(\eta^2\text{-}CH_2{=}C_5Me_4)W(=O)CH_3$ as a red–orange solid. IR data (Nujol mull, KBr plates, cm^{-1}): 2715(vw), 1505(w), 1410(w), 1175(w), 1020(m), 960(s), 945(m), 795(vw), 715(w).

$Cp^*(\eta^2\text{-}CH_2{=}C_5Me_4)W(=O)CD_3$ was obtained by a similar procedure from $Cp^*(\eta^4\text{-}C_5Me_4{=}CH_2)W(=O)CD_3$.

Preparation of $(\eta^5\text{-}C_5Me_5)(\eta^1\text{-}C_5Me_5)W(=O)_2$

(a) A stirred solution of $Cp^*_2W{=}O$ (200 mg, 0.43 mmol) in pentane (15 cm^3) was treated dropwise with *ca* 30% H_2O_2 (0.1 cm^3, *ca* 1.0 mmol) at room temperature. The green solution became yellow and a pale yellow solid was deposited. After 1 h the volatile components were removed under reduced pressure and the residue was extracted into pentane, concentrated and placed at −78°C giving yellow crystals of $(\eta^5\text{-}C_5Me_5)(\eta^1\text{-}C_5Me_5)W(=O)_2$ (*ca* 180 mg, 87%). Elemental analysis (found/calc.): C 48.8 (49.4), H 5.9 (6.2)%. ^{17}O NMR data (12 MHz, C_6D_6, 25°C): δ 738 ppm. IR data (Nujol mull, KBr plates, cm^{-1}): 2710(w), 1620(w), 1505(w), 1220(m), 1160(w), 1115(w), 1065(sh), 1045(sh), 1025(m), 945(vs) [W=O], 895(vs) [W=O], {920 and 860 for $W^{18}O^{16}O$ isotopomer}, 800(w), 710(w).

(b) A solution of $Cp^*_2W{=}O$ (*ca* 20 mg) in C_6D_6 (0.5 cm^3) was treated with Me_3CO_2H (excess) and observed by ^1H NMR spectroscopy to give $(\eta^5\text{-}C_5Me_5)(\eta^1\text{-}C_5Me_5)W(=O)_2$ after *ca* 5 min at room temperature.

(c) A solution of $Cp^*_2WH_2$ (*ca* 20 mg) in C_6D_6 (0.5 cm^3) was treated with *ca* 30% $H_2O_{2(aq)}$ (excess). $(\eta^2\text{-}C_5Me_5)(\eta^1\text{-}C_5Me_5)W(=O)_2$ was formed immediately, as evidenced by ^1H NMR spectroscopy.

Preparation of $(\eta^5\text{-}C_5Me_5)W(=O)_2(OC_5Me_5)$

A solution of $Cp^*_2W{=}O$ (200 mg, 0.43 mmol) in pentane (10 cm^3) at −78°C was placed under O_2 (1 atm) and was stirred as it was allowed to warm to room temperature. Upon reaching room temperature the initially green solution had become colourless. The solution was concentrated after 30 min and cooled to −78°C giving white (or very pale yellow) crystals of $(\eta^5\text{-}C_5Me_5)W(=O)_2(OC_5Me_5)$ (200 mg, 94%). Elemental analysis (found/calc.): C 47.5 (47.8), H 5.8 (6.0)%. ^{17}O NMR data (12 M Hz, C_6D_6): δ 685 ppm $Cp^*W(=O)_2OCp^*$. IR data (Nujol mull, KBr plates, cm^{-1}): $Cp^*_2W(=^{16}O)_2$ ($^{16}OC_5Me_5$) 2730(w), 1675(w), 1505(m), 1360(m), 1315(vw), 1295(vw), 1260(s), 1140(m), 1065(vs), 1035(s), 1005(vs), 950(vs), 915(vs), 890(vs), 810(m), 800(m), 715(w), 700(s), 600(w), 465(w). $Cp^*_2W(=^{18}O)(=^{16}O)(^{16}OC_5Me_5)$ 2730(w), 1740(vw), 1675(w), 1505(m,sh), 1360(m), 1315(vw), 1295(vw), 1260(s), 1140(m), 1065(vs), 1035(s), 1005(vs), 945(vs), 910(vs), 895(m), 875(vw), 860(vs), 810(m), 800(m), 715(vw), 700(s), 610(w), 465(w).

Preparation of $Cp^*W(\eta^2\text{-}O_2)(=O)CH_3$

A solution of $Cp^*W(CO)_3CH_3$ (300 mg, 0.77 mmol) in $CHCl_3$ (2 cm^3) was treated with $H_2O_{2(aq)}$ (*ca* 0.2 cm^3, 30%, *ca* 2 mmol) and stirred for 24 h at room temperature. The volatile components were removed under reduced pressure and the residue was washed with pentane giving a pale yellow powder of $Cp^*W(\eta^2\text{-}O_2)(=O)CH_3$ (250 mg, 85%).

Reaction of $(\eta^5\text{-}C_5Me_5)W(=O)_2(OC_5Me_5)$ *with* Me_3SiCl; *formation of* $Cp^*W(=O)_2Cl$

A solution of $(\eta^5\text{-}C_5Me_5)W(=O)_2(OC_5Me_5)$ (*ca* 25 mg) in C_6D_6 (*ca* 0.5 cm^3) in a NMR tube was

treated with excess Me_3SiCl. After 8 h at room temperature the product was observed to be quantitatively $Cp^*W(=O)_2Cl$ by ^1H NMR spectroscopy. The product was also characterized by IR spectroscopy.

Acid-catalysed decomposition of $(\eta^5\text{-}C_5Me_5)W(=O)_2(OC_5Me_5)$

A solution of $(\eta^5\text{-}C_5Me_5)W(=O)_2(OC_5Me_5)$ (*ca* 15 mg, 0.03 mmol) in C_6D_6 (*ca* 0.5 cm^3) in a NMR tube was treated with a catalytic quantity of *p*-TsOH (*ca* 0.5 mg, 0.003 mmol). The initial products were observed to be $[Cp^*W(=O)_2]_2O$ and $(C_5Me_5)_2O$ by ^1H NMR and IR spectroscopy. Further reaction resulted in dehydration of $(C_5Me_5)_2O$ to $C_5Me_4{=}CH_2$.

$(C_5Me_5)_2O$. ^1H NMR data (400 MHz, C_6D_6): δ 1.19, s, 1 (CH_3) of $C_5(CH_3)_5$; δ 1.60, q, partially resolved, $^5J_{C-H} = 1$, 2 (CH_3); δ 1.73, q, partially resolved, $^5J_{C-H} = 1$, 2 (CH_3). ^{13}C NMR data (100 MHz, C_6D_6): δ 21.9, q, $^1J_{C-H} = 128$, 1 (CH_3); δ 9.6, q, $^1J_{C-H} = 128$, 2 (CH_3); δ 11.4, q, $^1J_{C-H} = 128$, 2 (CH_3); 84.1, s 1*C*; 132.6, s, 2*C*; 139.9, s, 2*C*. IR data (Nujol mull, KBr plates, cm^{-1}): 1080 [C—O—C] (not separated from $[Cp^*W(=O)_2]_2O$).

$C_5Me_4{=}CH_2$. ^1H NMR data (400 MHz, C_6D_6): δ 1.68, br, 2 (CH_3)$_\alpha$; δ 1.84, q, partially resolved, $^5J_{H-H} = 1$, 2 (CH_3)β; δ 5.33, septet, partially resolved, $^5J_{H-H} = 1$, (CH_2). ^{13}C NMR data (100 MHz, C_6D_6): δ 9.4, q, $^1J_{C-H} = 128.2$ (CH_3); δ 11.1, q, $^1J_{C-H} = 128.2$ (CH_3); δ 109.8, t, $^1J_{C-H} = 157$, (CH_2); δ 155.4, s, $1C_{ipso}$; δ 123.7, s, 2*C*; δ 138.7, s, 2*C*.

Photochemical decomposition of $(\eta^5\text{-}C_5Me_5)W(=O)_2(OC_5Me_5)$

A solution of $(\eta^5\text{-}C_5Me_5)W(=O)_2(OC_5Me_5)$ (*ca* 15 mg) in C_6D_6 (*ca* 0.5 cm^3) in a Pyrex NMR tube was photolysed with a medium pressure mercury lamp for 12 h. The products were observed to be cleanly $[Cp^*W(=O)_2]_2O$ and $C_5Me_4{=}CH_2$ by ^1H NMR spectroscopy.

CONCLUSIONS

A variety of derivatives of permethyltungstenocene, including $Cp^*_2WH_2$, $Cp^*_2W(H)Cl$, $Cp^*_2W(CH_3)_2$, $Cp^*_2W(CH_3)Cl$, $Cp^*_2W(R)H$ (R = CH_3, CH_2Ph), $Cp^*_2W(\eta^2\text{-}CH_2O)$ and $Cp^*_2W{=}O$ have been synthesized starting from $Cp^*_2WCl_2$. The dihydride derivative, $Cp^*_2WH_2$, is readily protonated via attack at the W—H bonds, and not the d^2 tungsten centre, to give $[Cp^*_2WH_3]^+$. An interesting example of charge or SHOMO control, rather than HOMO control, leads to preferentially central protonation, via a trihydrogen ($\eta^3\text{-}H_3$) cation. The central and lateral hydride ligands of $[Cp^*_2WH_3]^+$ exchange sites by an intramolecular mechanism in preference to a deprotonation/protonation mechanism. The oxo derivative, $Cp^*_2W{=}O$, exhibits facile oxo exchange with labelled $H_2{}^*O$ via a 1,2-addition–elimination mechanism. Furthermore, $Cp^*_2W{=}O$ is both easily reduced, e.g. giving $Cp^*_2WH_2$ with either H_2, Me_3SiH or $LiAlH_4$, and easily oxidized giving $[Cp^*_2W(=O)CH_3][I]$ with CH_3I, $(\eta^5\text{-}C_5Me_5)(\eta^1\text{-}C_5Me_5)W(=O)_2$ with H_2O_2 or Me_3CO_2H, and $(\eta^5\text{-}C_5Me_5)W(=O)_2(OC_2Me_5)$ with O_2. This diversity of chemical reactivity of tungsten oxo-derivatives augurs well for their potential relevance to selective catalytic oxidation of hydrocarbons.

Acknowledgements—The authors thank David Wheeler for measuring ^{17}O NMR spectra and Prof. Bruce Bursten for helpful discussions. This work was supported by the National Science Foundation (Grant No. CHE-8600875) and by Shell Companies Foundation, which are gratefully acknowledged. G.P. acknowledges support through a NATO Postdoctoral Fellowship administered through the Science and Engineering Research Council (U.K.).

REFERENCES

1. (a) M. L. H. Green, J. A. McCleverty, L. Pratt and G. Wilkinson, *J. Chem. Soc.* 1961, 4854; (b) R. Davis and L. A. P. Kane-Maguire, *Comprehensive Organometallic Chemistry* (Edited by G. Wilkinson, F. G. A. Stone and E. W. Abel), Vol. 3, pp. 1321–1384 and refs therein. Pergamon Press, New York (1982).
2. (a) J. C. Green, M. L. H. Green and C. K. Prout, *J. Chem. Soc., Chem. Commun.* 1972, 421; (b) K. Prout, T. S. Cameron, R. A. Forder, S. R. Critchley, B. Denton and G. V. Rees, *Acta Cryst., Sect. B*, 1974, **30**, 2290; (c) M. L. H. Green, *Pure Appl. Chem.* 1972, **30**, 373.
3. M. L. H. Green, *Pure Appl. Chem.* 1978, **50**, 27.
4. (a) J. E. Bercaw, *J. Am. Chem. Soc.* 1974, **96**, 5087; (b) J. M. Manriquez, D. R. McAlister, R. D. Sanner and J. E. Bercaw, *J. Am. Chem. Soc.* 1976, **98**, 6733; (c) J. E. Bercaw, *Adv. Chem. Ser.* 1978, **167**, 136; (d) D. R. McAlister, D. K. Erwin and J. E. Bercaw, *J. Am. Chem. Soc.* 1978, **100**, 5966; (e) R. S. Threlkel and J. E. Bercaw, *J. Am. Chem. Soc.* 1981, **103**, 2650; (f) N. M. Doherty and J. E. Bercaw, *J. Am. Chem. Soc.* 1985, **107**, 2670; (g) D. M. Roddick, M. D. Fryzuk, P. F. Seidler, G. L. Hillhouse and J. E. Bercaw, *Organomatallics* 1985, **4**, 97; (h) A. van Asselt, B. J. Burger, V. C. Gibson and J. E. Bercaw, *J. Am. Chem. Soc.* 1986, **108**, 5347; (i) M. E. Thompson, S. M. Baxter, A. R. Bulls, B. J. Burger, M. C. Nolan, B. D. Santarsiero, W. P. Schaefer and J. E.

Bercaw, *J. Am. Chem. Soc.* 1987, **109**, 203; (j) G. Parkin, E. Bunel, B. J. Burger, M. S. Trimmer, A. van Asselt and J. E. Bercaw, *J. Mol. Cat.* 1987, **41**, 21; (k) B. J. Burger, B. D. Santarsiero, M. S. Trimmer and J. E. Bercaw, *J. Am. Chem. Soc.* 1988, **110**, 3134.

5. (a) M. Berry, N. J. Cooper, M. L. H. Green and S. J. Simpson, *J. Chem. Soc., Dalton Trans.* 1980, 29; (b) M. Berry, K. Elmitt and M. L. H. Green, *J. Chem. Soc., Dalton Trans.* 1979, 1950.
6. F. G. N. Cloke, J. C. Green, M. L. H. Green and C. P. Morley, *J. Chem. Soc., Chem. Commun.* 1985, 945.
7. A. H. Liu, R. C. Murray, J. C. Dewan, B. D. Santarsiero and R. R. Schrock, *J. Am. Chem. Soc.* 1987, **109**, 4282.
8. (a) S. L. Buchwald, R. B. Nielsen and J. C. Dewan, *J. Am. Chem. Soc.* 1987, **109**, 1590; (b) J. M. Mayer, C. J. Curtis and J. E. Bercaw, *J. Am. Chem. Soc.* 1983, **105**, 2651.
9. M. L. H. Green, G. Parkin, K. J. Moynihan and K. Prout, *J. Chem. Soc., Chem. Commun.* 1984, 1540.
10. M. L. H. Green and G. Parkin, *J. Chem. Soc., Chem. Commun.* 1986, 90.
11. S. Gambarotta, C. Floriani, A. Chiesi-Villa and C. Guastini, *J. Am. Chem. Soc.* 1985, **107**, 2985.
12. G. Parkin and J. E. Bercaw, unpublished results.
13. (a) J. C. Green, M. L. H. Green and C. P. Morley, *Organometallics* 1985, **4**, 1302; (b) N. J. Cooper and M. L. H. Green, *J. Chem. Soc., Dalton Trans.* 1979, 1121; (c) M. Canestrari and M. L. H. Green, *J. Chem. Soc., Dalton Trans.* 1982, 1789.
14. (a) D. F. Shriver, *Acc. Chem. Res.* 1970, **3**, 231; (b) J. C. Kotz and D. G. Pedrotty, *Organomet. Chem. Rev. A*, 1969, **4**, 479.
15. M. P. Johnson and D. F. Shriver, *J. Am. Chem. Soc.* 1966, **88**, 301.
16. (a) H. Brunner, P. C. Wailes and H. D. Kaesz, *Inorg. Nucl. Chem. Lett.* 1965, **1**, 125; (b) A. Storr and B. S. Thomas, *Can. J. Chem.* 1971, **49**, 2504.
17. J. P. Dahl and C. Ballhausen, *Acta. Chem. Scand.* 1961, **15**, 1333.
18. N. W. Alcock, *J. Chem. Soc. A* 1967, 2001.
19. (a) J. L. Petersen and L. F. Dahl, *J. Am. Chem. Soc.* 1974, **96**, 2248; (b) J. L. Petersen and L. F. Dahl, *J. Am. Chem. Soc.* 1975, **97**, 6416; (c) J. L. Petersen and L. F. Dahl, *J. Am. Chem. Soc.* 1975, **97**, 6422.
20. J. C. Green, S. E. Jackson and B. Higginson, *J. Chem. Soc., Dalton Trans.* 1975, 403.
21. (a) H. H. Brintzinger and L. S. Bartell, *J. Am. Chem. Soc.* 1970, **92**, 1105; (b) H. H. Brintzinger, L. L. Lohr Jr. and K. L. Tang Wong, *J. Am. Chem. Soc.* 1975, **97**, 5146.
22. J. W. Lauher and R. Hoffmann, *J. Am. Chem. Soc.* 1976, **98**, 1729.
23. J. L. Petersen, D. L. Lichtenberger, R. F. Fenske and L. F. Dahl, *J. Am. Chem. Soc.* 1975, **97**, 6433.
24. A. J. Schultz, K. L. Stearley, J. M. Williams, R. Mink and G. D. Stucky, *Inorg. Chem.* 1977, **16**, 3303.
25. B. E. Bursten and R. H. Cayton, *J. Am. Chem. Soc.* 1987, **109**, 6053.
26. X. L. R. Fontaine, E. H. Fowles and B. L. Shaw, *J. Chem. Soc., Chem. Commun.* 1988, 482.
27. M. S. Chinn and D. M. Heinekey, *J. Am. Chem. Soc.* 1987, **109**, 5865.
28. (a) D. M. Heinekey, N. G. Payne and G. K. Schulte, *J. Am. Chem. Soc.* 1988, **110**, 2303; (b) B. Chaudret, private communication.
29. R. P. Bell, *Chem. Soc. Rev.* 1974, **3**, 513.
30. J. K. Burdett, J. R. Phillips, M. R. Pourian, M. Poliakoff, J. J. Turner and R. Upmacis, *Inorg. Chem.* 1987, **26**, 3054.
31. (a) F. W. S. Benfield and M. L. H. Green, *J. Chem. Soc., Dalton Trans.* 1974, 1324; (b) H. E. Bunting, M. L. H. Green and P. A. Newman, *J. Chem. Soc., Dalton Trans.* 1988, 557 and refs therein.
32. (a) H. Mimoun, *Comprehensive Coordination Chemistry* (Edited by G. Wilkinson, R. D. Gillard and J. A. McCleverty), Vol. 6, pp. 317–410. Pergamon Press, New York (1982); (b) F. Bottomley and L. Sutin, *Adv. Organomet. Chem.* 1988, **28**, 339; (c) R. Holm, *Chem. Rev.* 1987, **87**, 1401.
33. G. Parkin and J. E. Bercaw, *J. Am. Chem. Soc.*, submitted.
34. I. R. Beattie and P. Jones, *J. Inorg. Chem.* 1979, **18**, 2318.
35. W. A. Herrmann, R. Serrano and H. Bock, *Angew. Chem. Int. Ed. Engl.* 1984, **23**, 383.
36. (a) M. Filowitz, R. K. C. Ho, W. G. Klemperer and W. Shum, *Inorg. Chem.* 1979, **18**, 93; (b) K. F. Miller and R. A. D. Wentworth, *Inorg. Chem.* 1979, **18**, 984; (c) W. G. Klemperer and W. Shum. *J. Am. Chem. Soc.* 1978, **100**, 4891; (d) C. J. Besecker and W. G. Klemperer, *J. Am. Chem. Soc.* 1980, **102**, 7598; (e) V. W. Day, M. F. Fredrich, M. R. Thompson, W. G. Klemperer, R.-S. Liu and W. Shum, *J. Am. Chem. Soc.* 1981, **103**, 3597; (f) G. L. Hillhouse and J. E. Bercaw, *J. Am. Chem. Soc.* 1984, **106**, 5472.
37. H. Gamsjager and R. K. Murmann, *Advances in Inorganic and Bioinorganic Mechanisms* (Edited by A. G. Sykes), Vol. 2, pp. 317–380. Academic Press, London (1983).
38. (a) A. van Asselt, B. J. Burger, V. C. Gibson and J. E. Bercaw, *J. Am. Chem. Soc.* 1986, **108**, 5347; (b) G. Parkin, E. Bunel, B. J. Burger, M. S. Trimmer, A. van Asselt and J. E. Bercaw, *J. Mol. Cat.* 1987, **41**, 21.
39. G. Parkin and J. E. Bercaw, unpublished results.
40. H. Werner, G. T. Crisp, P. W. Jolly, H.-J. Kraus and C. Kruger, *Organometallics* 1983, **2**, 1369.
41. (a) P. Legzdins, E. C. Phillips, S. J. Rettig, L. Sanchez, J. Trotter and V. C. Yee, *J. Am. Chem. Soc.*, submitted; (b) J. W. Faller and Ma Yinong, *Organometallics* 1988, **7**, 559.
42. G. Parkin, W. P. Schaefer and J. E. Bercaw, manuscript in preparation.
43. (a) P. Legzdins, S. J. Rettig and L. Sanchez, *Organometallics* 1985, **4**, 1470; (b) J. W. Faller and Ma Yinong, *J. Organomet. Chem.*, in press; (c) M. Herberhold, H. Kniesel, L. Haumaier, A. Gieren and C Ruiz-Perez, *Z. Naturforsch, B: Anorg. Chem. Org. Chem.* 1986, **41B**, 1431.

44. J. M. O'Connor and C. P. Casey, *Chem. Rev.* 1987, **87**, 307. η^1-C_5Me_5 derivatives are known in main-group chemistry, e.g. P. Jutzi, *Comm. Inorg. Chem.*, 1987, **6**, 123.
45. (a) B. Bosnich, H. Boucher and C. Marshall, *Inorg. Chem.* 1976, **15**, 634; (b) R. Guilard, J.-M. Latour, C. Lecomte, J.-C. Marchon, J. Protas and D. Ripoll, *Inorg. Chem.* 1978, **17**, 1228.
46. G. Parkin, R. E. Marsh, W. P. Schaefer and J. E. Bercaw, *Inorg. Chem.*, in press.
47. (a) W. A. Herrmann and J. Okuda, *J. Mol. Catal.* 1987, **41**, 109; (b) W. A. Herrmann, E. Herdtweck, M. Floel, J. Kulpe, U. Kusthardt and J. Okuda, *Polyhedron* 1987, **6**, 1165.
48. A. van Asselt, Ph.D. Thesis. California Institute of Technology (1987).
49. A. G. Davies and J. Lusztyk, *J. Chem. Soc., Perkin Trans.* 1981, **2**, 692.
50. (a) J. P. McNally, V. S. Leong and N. J. Cooper, *A.C.S. Symp. Ser.* 1987, **357** 6; (b) B. J. Burger and J. E. Bercaw, *A.C.S. Symp. Ser.* 1987, **357**, 79.
51. R. H. Marvich and H. H. Brintzinger, *J. Am. Chem. Soc.* 1971, **93**, 2046.

Polyhedron Vol. 7, No. 19/20, pp. 2083–2086, 1988
Printed in Great Britain

0277–5387/88 $3.00+.00
© 1988 Pergamon Press plc

INSERTION OF DIPHENYLDIAZOMETHANE INTO $[ZrCp_2(Cl)PR_2]$ ($Cp = \eta$-C_5H_5, $R = SiMe_3$); X-RAY STRUCTURES OF $[ZrCp_2(PR_2)X]$ ($X = Cl$ OR Me) AND $[ZrCp_2(Cl)\{N(CPh_2)NPR_2\}]$*

EVAMARIE HEY and MICHAEL F. LAPPERT†

School of Chemistry and Molecular Sciences, University of Sussex, Brighton BN1 9QJ, U.K.

and

JERRY L. ATWOOD† and SIMON G. BOTT

Department of Chemistry, University of Alabama, University, AL 35486, U.S.A.

Abstract—Treatment of $[ZrCp_2Cl_2]$ or $[ZrCp_2(Cl)Me]$ with $[Li(\mu\text{-}PR_2)(THF)_2]_2$ in appropriate stoichiometry yields $[ZrCp_2(PR_2)X]$ [X = Cl (**1**), X = Me (**2**), or X = PR_2(**3**)] ($Cp = \eta$-C_5H_5, $R = SiMe_3$). Complex (**1**) undergoes a facile 1:1 addition of its $ZrCp_2Cl$ and PR_2 fragments to the terminal nitrogen atom of Ph_2CN_2 to furnish $[ZrCp_2(Cl)\{N(CPh_2)NPR_2\}]$ (**4**). Complexes (**1**) [2.547(6) Å] and (**2**) [2.629(3) Å] have short Zr—P bonds. Crystalline (**4**) has five-coordinate Zr; the η^2-bound ligand is regarded as $\ddot{N}(:CPh_2)NPR_2 \leftrightarrow \ddot{N}(CPh_2)NPR_2$, on the basis of the following bond lengths (Å): Zr—NPR_2, 2.19(2) and 2.22(1); N—CPh_2, 1.37(2).

We have recently reported on metal complexes containing the bis(trimethylsilyl)phosphido ligand $\bar{P}R_2$ ($R = SiMe_3$). Thus, we have discussed (i) and isolation and NMR spectra of $[Li(\mu\text{-}PR_2)(THF)_2]_2$ (**A**), $Li_4(\mu_2\text{-}PR_2)_2(\mu_3\text{-}PR_2)_2(THF)_2$ (**B**) (building on work of Fritz and Hölderich[1]), and $Li(PR_2)(PMDETA)$ (**C**);[2] (ii) $[ZrCp_2(\eta^2\text{-}S_2CPR_2)X]$ [(**D**)(X = Cl) or (**E**) (X = Me) ($Cp = \eta$-C_5H_5)], obtained from carbon disulphide and $[ZrCp_2(PR_2)X]$ [(**1**) (X = Cl) or (**2**) (X = Me)];[3] and (iii) $[ZrCp_2\{P(PR_2)PP(PR_2)P\}]$ (**F**), prepared from white phosphorus and $[Zr(\eta\text{-}C_5H_4R')_2(PR_2)_2]$ (R′ = H) (**3a**).[4] X-ray data were provided for complexes **A**,[2] **B**,[2] **D**,[3] and **F**.[4] Silylphosphines are versatile reagents, as illustrated by Fritz in a review of work up until 1982.[5]

We now describe (a) the behaviour of the bis(trimethylsilyl)phosphidozirconocene(IV) complexes (**1**) and $[Zr(\eta\text{-}C_5H_4SiMe_3)_2(PR_2)_2]$ (**3b**) with diphenyldiazomethane, Scheme 1, including (b) the remarkable 1:1 insertion of the $ZrCp_2(Cl)$ and PR_2 fragments of complex **1** onto the terminal nitrogen atom of $PhCN_2$ to yield $[ZrCp_2(Cl)\{N(CPh_2)NPR_2\}]$ (**4**). Additionally, (c) the X-ray structures of complexes **1** and **2** (Fig. 1) and **4** (Fig. 2) have been elucidated (see also Table 1).

Since our earlier papers,[2–4] two other publications on phosphidozirconocene(IV) complexes have appeared, dealing with (a) $[ZrCp_2(Cl)\{PR(Ar)\}]$ ($Ar = C_6H_2Bu^t_3$-2,4,6) from $[ZrCp_2Cl_2] + Li\{PR(Ar)\}$;[6] (b) $[ZrCp_2(PR_2)_2]$ (**3a**), from $[ZrCp_2Cl_2] + 2Li(PR_2)(THF)_{2.2}$;[7] and (c) $[ZrCp_2(Me)PR_2]$ (**2**), from $[ZrCp_2(Cl)Me] + Li(PR_2)(THF)_{2.2}$.[7] Additionally, (d) the hafnium analogues of **3a** (including X-ray data) and **2** have been described.[7]

Also pertinent to the present study, but related to our diazomethane insertion reaction into the Zr—P bond of complex **1**, and the X-ray data on the product **4**, are the findings of Gambarotta *et al.*, on the reactions of a diazoalkane R'_2CN_2 with a zirconocene(IV) complex $[ZrCp_2R''_2]$ or $ZrCp_2(H)Cl$; X-ray data were provided for the η^2-hydra-

* Dedicated to Professor Sir Geoffrey Wilkinson.

† Authors to whom correspondence should be addressed.

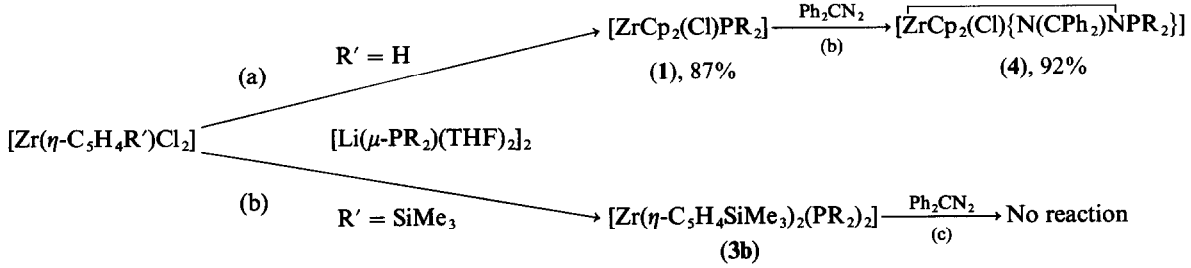

Scheme 1. (a) PhMe, 1 h, 25°C; (b) PhMe, 1 day, 25°C; (c) PhMe, 1 day at 25°C and then 3 h at 100°C. Characterization of compounds **1**, **3b** and **4**. **1** Deep red crystals, m.p. 129°C, subl. *ca* 160°C/10^{-2} mbar; ^{1}H NMR (C_6D_5—CD_3) (δ): 5.95 (d) [J(^{31}P^{1}H), 1.1 Hz], 0.35 (d) [^3J(^{31}P^{1}H), 4.0 Hz]; ^{31}P{^{1}H}: −108.9 ppm. **4** Yellow crystals, m.p. 95–97°C decomp; ^{1}H NMR (C_6D_{12}) (δ): 7.48–7.07 (m), 5.94 (s), 0.22 (d) [J(^{31}P^{1}H), 5.6 Hz]; ^{13}C (δ): 2.14 (d) [^3J(^{31}P^{13}C), 16.3 Hz], 112.5 (s), 131.2 (d) [^4J(^{31}P^{13}C), 6.8 Hz]; ^{31}P{^{1}H}: −24.5 ppm. **3b** Blue crystals, m.p. 146–148°C; ^{1}H NMR (C_6D_6) (δ): 0.545 (d) [J(^{31}P^{1}H), 3.7 Hz], 0.25 (s), 5.89–6.66 (m); ^{31}P{^{1}H} 55.3 ppm. NMR data refer to ambient temperature.

zonato(−1) complexes [ZrCp$_2${N(CR$'_2$)NR″}R″] [R′ = Ph, R″ = Me (**G**); or R′ = CO_2Et, R″ = CH_2Ph (**H**)] and [ZrCp$_2${N(CPh$_2$)NH}Cl] (**I**).[8]

The Zr—P bond in [ZrCp$_2$(PR$_2$)X] is rather short [(**1**) (X = Cl) < (**2**) (X = Me)] and the phosphorus environment is nearer to trigonal planar than pyramidal [e.g. the sum (Σ) of the angles at P in **1** is 344.4° and in **2** is 349.2°]. In [Zr(Cp$_2$(Cl){PR(Ar)}], the Zr—P bond length of 2.541(4) Å was almost identical to that in **1**, with Σ = 359.5°.[6] In [HfCp$_2$(PR$_2$)$_2$], the two phosphorus environments were different: Hf—P(1), 2.553(1) Å and ΣP(**1**), 360°; and Hf—P(2), 2.654(1) Å and ΣP(2), 336°.[7]

The bonding in [ZrCp$_2$(Cl){N(CPh$_2$)NPR$_2$}] (**4**) may be represented as a resonance hybrid of (**4a**)

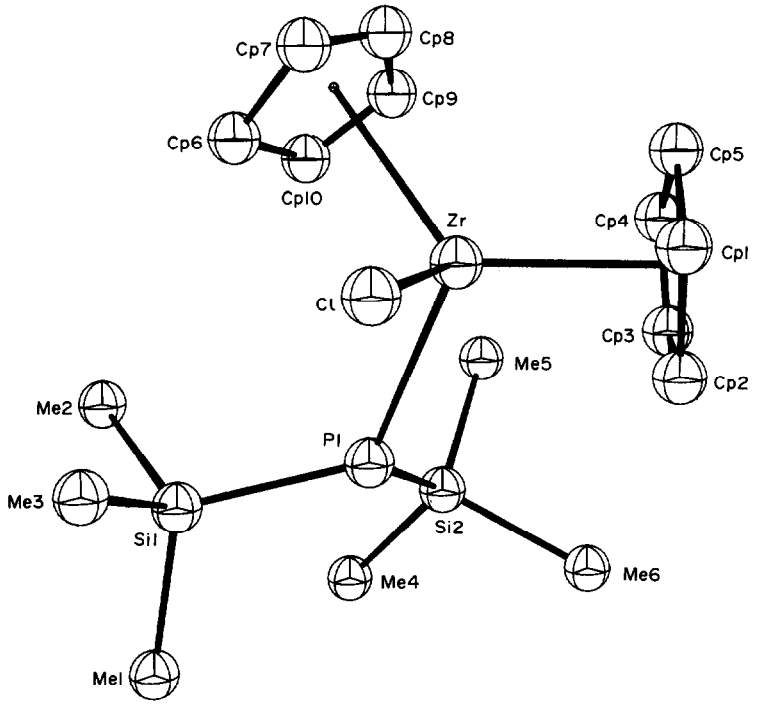

Fig. 1. X-ray structures and atom numbering scheme for [ZrCp$_2${P(SiMe$_3$)$_2$}X] [X = Cl (**1**) or X = Me (**2**)]. Selected bond lengths (Å) and angles (°) for **1** [with **2** in brackets]; Zr—P 2.547(6) [2.629(3)]; Zr—X 2.432(5) [2.35(6)]; Zr—Cen (mean) 2.25 [2.18); Zr—P—Si (mean) 118.8(5) [123.4(1)]; P—Zr—X, 100.6(4) [98(1)]; Si—P—Si′ 106.9(3) [102.4(3)].

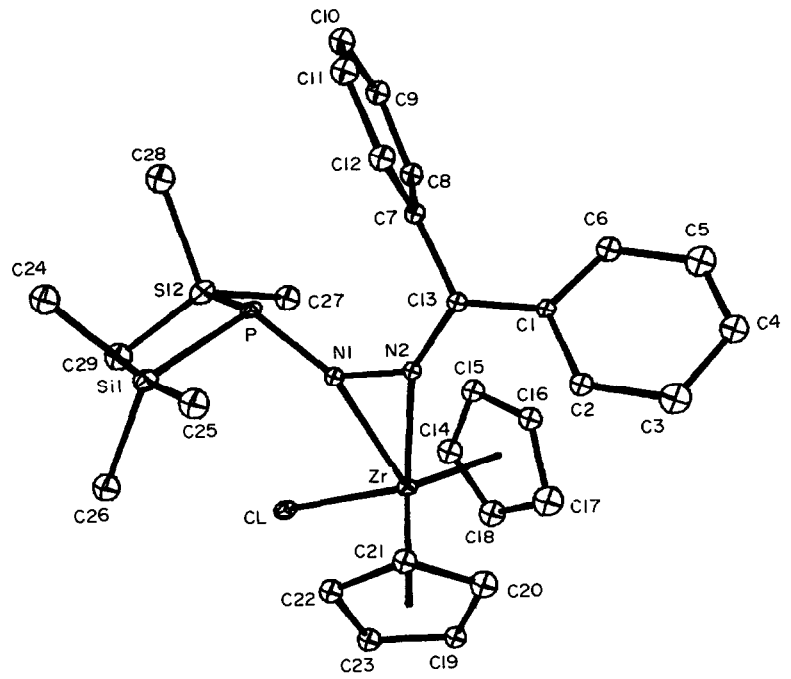

Fig. 2. X-ray structure and atom numbering scheme for $[ZrCp_2(Cl)\{N(CPh_2)NP(SiMe_3)_2\}]$ (**4**). Selected bond lengths (Å) and angles (°): Zr—N(1), 2.19(2); Zr—N(2), 2.22(1); Zr—Cl, 2.490(4); Zr—Cen (mean), 2.24; N(1)—N(2), 1.34(2); N(1)—P, 1.70(2); P—Si, 2.234(7) and 2.249(7); N(2)–C(13), 1.37(2); C(13)—C(1), 1.39(2); C(13)—C(7), 1.47(3); Cl—Zr—N(1), 83.2(3); N(1)—Zr—N(2), 35.3(4); Zr—N(1)—N(2), 73.5(9); Zr—N(2)—C(13), 153(1); N(1)—N(2)—C(13), 131(1); N(2)—C(13)—C(1), 121(2); N(2)—C(13)—C(7), 119(1); C(1)—C(13)—C(7), 120(1). The atoms ZrN(1)N(2)C(13)C(1)C(7) are coplanar; each of N(1), N(2) and C(13) has a nearly trigonal planar environment, whereas P is pyramidal.

Table 1. Crystal data and refinement parameters for compounds **1**, **2** and **4**

Complex	**1**	**2**	**4**
M	434.22	413.82	628.51
Crystal system	Monoclinic	Orthorhombic	Triclinic
a (Å)	27.905(8)	13.663(5)	10.848(8)
b (Å)	9.565(5)	15.730(8)	11.387(8)
c (Å)	16.159(5)	9.861(3)	13.295(9)
α (°)			77.91(5)
β (°)	101.66(2)		84.24(9)
γ (°)			77.73(9)
U (Å^3)	4223	2119	1566
Z	8	4	2
D_c (g cm^{-3})	1.40	1.30	1.34
$F(000)$	2333	1573	3178
Space group	$C2/c$	$Pnma$	$P\bar{1}$
μ(Mo-K_α) (cm^{-1})	8.22	6.91	5.79
2θ limits (°)	1–40	2–40	2–40
Reflections used in refinement $I > 2.5\sigma(I)$	834	1029	1562
R	0.049	0.049	0.074
R'	0.055	0.054	0.082

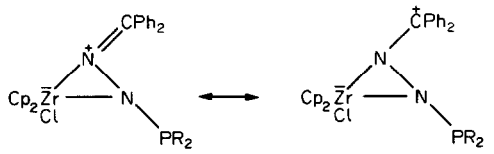

(4a) (4b)

and (**4b**). The canonical form, **4b**, is relatively more important than **4a** than in related complexes **G–I**;[8] e.g. in [$ZrCp_2(Me)\{N(CPh_2)NMe$] (**G**), the Zr—NCP_2 bond was longer [2.283(3) Å] and the N—CPh_2 bond shorter [1.307(4) Å] than in **4**.

Acknowledgements—We thank the Verband der Chemischen Industrie for providing a Liebig–Stipendium for Dr E. Hey, and the S.E.R.C. and N.S.F. for other support.

REFERENCES

1. G. Fritz and W. Hölderich, *Z. Anorg. Allg. Chem.* 1976, **422**, 104; G. Fritz and W. Hölderich, *Z. Anorg. Allg. Chem.* 1975, **417**, 241.
2. E. Hey, P. B. Hitchcock, M. F. Lappert and A. K. Rai, *J. Organomet. Chem.* 1987, **325**, 1.
3. E. Hey, M. F. Lappert, J. L. Atwood and S. G. Bott, *J. Chem. Soc., Chem. Commun.* 1987, 421.
4. E. Hey, M. F. Lappert, J. L. Atwood and S. G. Bott, *J. Chem. Soc., Chem. Commun.* 1987, 597.
5. G. Fritz, *Comments Inorg. Chem.* 1982, **1**, 329.
6. A. M. Arif, A. H. Cowley, C. M. Nunn and M. Pakulski, *J. Chem. Soc., Chem. Commun.* 1987, 994.
7. L. Weber, G. Meine, R. Boese and N. Augart, *Organometallics* 1987, **6**, 2484.
8. S. Gambarotta, C. Floriani, A. Chiesi-Villa and C. Guastini, *Inorg. Chem.* 1983, **22**, 2029.

Polyhedron Vol. 7, No. 19/20, pp. 2087–2089, 1988
Printed in Great Britain

0277–5387/88 $3.00+.00
© 1988 Pergamon Press plc

ISOLATION AND X-RAY CRYSTAL STRUCTURE ANALYSIS OF A HYDRAZINE-CONTAINING RHODIUM CATALYST, $[(MeOH)_2H]^+[RhCl_4(PPh_3)(NHMeNHMe)]^-$

MICHAEL B. HURSTHOUSE* and JOY NEWTON

Department of Chemistry, Queen Mary College, London E1 4NS, U.K.

and

PHILIP R. PAGE* and IVAN VILLAX

Research Laboratories, Hovione Sociedade Quimica Lda., Sete Casas, 2670 Loures, Portugal

Abstract—Reaction of $RhCl(PPh_3)_3$ with N,N′-dimethylhydrazine dihydrochloride in methanol gives the Rh^{III} complex $[(MeOH)_2H]$ $[RhCl_4(PPh_3)(NHMeNHMe)]$ which has been characterized by X-ray crystallography. The complex anion has an octahedral structure with the phosphine and hydrazine ligands mutually *trans*, and is formulated as a rhodium(III) species on the basis of the bond lengths in the structure and its diamagnetism. The compensating cation is a proton which, although not unequivocally identified in the structure, is presumed to be present as a dimethanolium unit, in which the O···O distance is 2.67 Å.

During the course of an extensive investigation of rhodium complexes containing hydrazines, and their potential catalytic properties, we have explored the reaction between Wilkinson's catalyst, $RhCl(PPh_3)_3$ and various hydrazine compounds. By use of the dihydrochloride of 1,2-dimethylhydrazine, we were able to isolate a brick-red product which was found to be a specific catalyst for the hydrogenation of the exocyclic methylene group of 6-demethyl-6-deoxy-6-methylene-5-hydroxytetracycline hydrochloride. The product is α-6-deoxy-5-hydroxytetracycline, also known as doxycycline, which is a wide-spectrum antibacterial agent.

In order to ascertain the identity of the product, we have subjected it to X-ray crystal structure analysis.

RESULTS AND DISCUSSION

The crystal structure comprises a rhodium-containing species of formula $RhCl_4(PPh_3)$ (NHMeNHMe) and two molecules of methanol solvate per complex. A diagram of the asymmetric unit is shown in Fig. 1; selected bond lengths and angles are given in Table 1.

On the basis of magnetic measurements, which show the compound to be diamagnetic, the Rh atom is assigned an oxidation state of (III) and the complex must therefore be anionic. This requires the presence of a compensating cation, and we presume that this is a proton. Whilst this proton could in principle be sited on the non-bonded nitrogen of the hydrazine, making the complex zwitterionic, no evidence for the presence of two hydrogens on this nitrogen could be found. Indeed, the experimental location and refinement of just one hydrogen attached to this nitrogen was achieved quite successfully. We therefore are confident that the proton is associated with the two molecules of methanol found in the asymmetric unit, in which the two hydroxyl oxygens are far closer together than would be likely for normal hydrogen bonding.[1] The dis-

Dedicated to Professor Sir Geoffrey Wilkinson in recognition of his many contributions to inorganic and organometallic chemistry, but especially to the study of homogeneous catalysis.

* Authors to whom correspondence should be addressed.

Table 1. Selected bond lengths (Å) and angles (°)

Bond lengths			
Cl(1)—Rh	2.343(4)	Cl(2)—Rh	2.348(4)
Cl(3)—Rh	2.339(4)	Cl(4)—Rh	2.343(4)
P(1)—Rh	2.282(4)	N(1)—Rh	2.216(8)
C(11)—P(1)	1.824(7)	C(21)—P(1)	1.836(6)
C(31)—P(1)	1.847(6)	C(10)—N(1)	1.458(10)
N(2)—N(1)	1.405(9)	C(20)—N(2)	1.472(10)
C(30)—O(1)	1.438(12)	C(40)—O(2)	1.335(15)
Bond angles			
Cl(2)—Rh—Cl(1)	173.7(1)	Cl(3)—Rh—Cl(1)	87.2(2)
Cl(3)—Rh—Cl(2)	88.9(2)	Cl(4)—Rh—Cl(1)	88.8(2)
Cl(4)—Rh—Cl(2)	94.5(2)	Cl(4)—Rh—Cl(3)	172.5(1)
P(1)—Rh—Cl(1)	96.4(2)	P(1)—Rh—Cl(2)	89.0(2)
P(1)—Rh—Cl(3)	97.5(2)	P(1)—Rh—Cl(4)	89.3(2)
N(1)—Rh—Cl(1)	82.5(3)	N(1)—Rh—Cl(2)	92.6(3)
N(1)—Rh—Cl(3)	90.0(3)	N(1)—Rh—Cl(4)	83.1(3)
N(1)—Rh—P(1)	172.4(2)	C(11)—P(1)—Rh	111.7(3)
C(21)—P(1)—Rh	116.2(2)	C(21)—P(1)—C(11)	104.9(3)
C(31)—P(1)—Rh	117.5(2)	C(31)—P(1)—C(11)	104.2(3)
C(31)—P(1)—C(21)	100.8(3)	C(12)—C(11)—P(1)	120.4(2)
C(16)—C(11)—P(1)	119.6(2)	C(22)—C(21)—P(1)	117.4(2)
C(26)—C(21)—P(1)	122.4(2)	C(32)—C(31)—P(1)	122.7(2)
C(36)—C(31)—P(1)	117.3(2)	C(10)—N(1)—Rh	117.8(6)
N(2)—N(1)—Rh	117.4(5)	N(2)—N(1)—C(10)	114.5(7)
C(20)—N(2)—N(1)	121.4(7)		

tance of 2.67 Å is only slightly greater than distances commonly found in well characterized $[H_5O_2]^+$ ions, 2.60 Å. We thus propose the formation of a "dimethanolium" cation which has not, to our knowledge, been previously identified. Only two hydroxyl hydrogens on the methanol molecules were experimentally located and successfully refined, and the third is thus unidentified. Nevertheless, one of those found connects the two oxygens and is off-centre, the O—H and H···O distances being 1.14 and 1.54 Å, respectively.

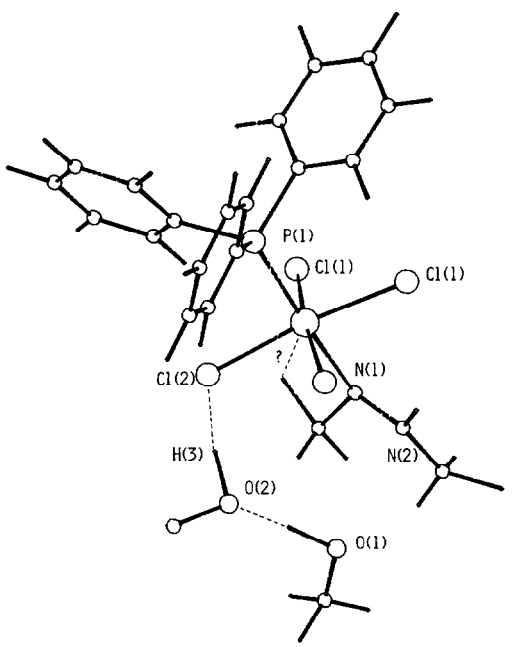

Fig. 1.

The anion contains the four chlorines in one plane, with the phosphine and hydrazine ligands mutually *trans*. The Rh—Cl distances vary slightly, with Rh—Cl(2) being the longest, possibly as a result of hydrogen bonding to a methanol hydrogen [H(3)]. This interaction probably fixes the position of that hydrogen whereas the missing hydrogen on O(1) may be disordered (and therefore less amenable to experimental location) over the two possible positions which, together with H(1) and the methyl carbon, would give pyramidal geometry to O(1). In the structure refinement process we also found that one of the hydrogen atoms of the methyl group attached to the metal-bonded nitrogen of the dimethylhydrazine consistently refined to a position which gave an elongated C—H bond but a short contact of 2.40 Å to the rhodium. However, it is difficult to reconcile this with the presence of an agostic interaction since the metal has a formal 18e configuration. Nevertheless, the presence on the

metal of four electronegative chlorines and a π-accepting phosphine could result in electron deficiency at the metal.

EXPERIMENTAL

Preparation

$RhCl(PPh_3)_3$ (0.5 g) and NHMeNHMe·2HCl (0.215 g) were added to a two-necked flask and pumped for 5–10 min. The flask was filled with N_2 and all further manipulations took place under an N_2 atmosphere. Dry methanol (30 cm^3) was added and the reaction mixture refluxed for 1.5 h to give an orange solution and a small amount of unreacted $RhCl(PPh_3)_3$. The solution was filtered and the volume reduced to about 10 cm^3. On cooling to −30°C, red crystals were deposited, leaving a pale yellow solution. Yield = 0.25 g (72%). Found: C, 41.3; H, 4.7; Cl, 21.1; N, 4.6; P, 4.6; Rh, 16.13. Calc. for $C_{22}H_{32}Cl_4N_2O_2PRh$: C, 41.8; H, 5.1; Cl, 22.4; N, 4.4; P, 4.9; Rh, 16.3%.

X-ray crystallography

The crystal used for X-ray examination was sealed inside a capillary tube in an atmosphere of methanol. X-ray diffraction data were recorded using an Enraf–Nonius CAD4 diffractometer and Ni-filtered Cu-K_α radiation (λ = 1.54178 Å), following standard procedures.[2] Details of the analysis are as follows.

(1) *Crystal data.* $[(MeOH)_2H]^+[RhCl_4(NHMeNHMe)(PPh_3)]^-$, $C_{22}H_{32}Cl_4N_2O_2PRh$, M = 632.17, triclinic, space group $P\bar{1}$, a = 16.430(3), b = 9.848(2), c = 9.850(2) Å, α = 117.79(2), β = 75.99(2), γ = 95.15(2)°, U = 1367.5 $Å^3$, Z = 2, ν(Cu-K_α) = 50.3 cm^{-1}.

(2) *Data collection.* $\omega/2\theta$ scan mode, $3 \leqslant \theta \leqslant 60°$, T = 293 K. 4047 data were recorded of which 3491 were unique and satisfied the condition $I > 1.5\sigma(I)$, and were used in the analysis.

(3) *Structure analysis.* Heavy atom method, full-matrix least-squares. All non-hydrogen atoms were refined with anisotropic thermal parameters, phenyl rings being treated as rigid bodies, with hydrogen atoms included in idealized positions. Some hydrogens of the hydrazine and methanol moieties were located on difference electron-density maps and were successfully refined with individual isotropic thermal parameters, but others proved impossible to locate satisfactorily. The final R value was 0.0393. All calculations were made on a DEC VAX 11/750 computer using standard programs. Final atomic positional and displacement factor coefficients, full lists of bond lengths and angles, and F_o/F_c values have been deposited as supplementary material with the Editor, from whom copies are available on request. Atomic coordinates have also been deposited with the Cambridge Crystallographic Data Centre.

REFERENCES

1. J. Emsley, *Chem. Soc. Quart. Rev.* 1980, **9**, 91.
2. R. A. Jones, M. B. Hursthouse, K. M. A. Malik and G. Wilkinson, *J. Am. Chem. Soc.* 1979, **101**, 4128.

Polyhedron Vol. 7, No. 19/20, pp. 2091–2094, 1988
Printed in Great Britain

0277–5387/88 $3.00+.00
© 1988 Pergamon Press plc

OXIDATION AND HYDROLYSIS OF $(Me_2InPPh_2)_2$: X-RAY STRUCTURE OF $[InMe(OH)(O_2PPh_2)]_4 \cdot (py)_4$ AN In_4O_4 CUBE*

ATTA M. ARIF

Department of Chemistry, University of Utah, Salt Lake City, UT 84112, U.S.A.

and

ANDREW R. BARRON†

Chemical Laboratories, Harvard University, Cambridge, MA 02138, U.S.A.

Abstract—The indium phosphide complex $(Me_2InPPh_2)_2$ can be oxidized with pyridine-N-oxide to give the phosphinate complex $[Me_2In(O_2PPh_2)]_2$, careful hydrolysis of which yields an In_4O_4 cubane cluster $[InMe(OH)(O_2PPh_2)]_4 \cdot (py)_4$ whose structure has been confirmed by X-ray crystallography.

Although compounds featuring bonding between the heavier group 13 and 15 (Ölander numbering) elements, of the general type $R_2MER'_2$ (M = Ga, In; E = P, As, Sb), have been known for 25 years,[1] interest in their chemistry has been recently rekindled[2] due to their possible use as precursors to semiconducting materials such as gallium arsenide and indium phosphide.[3] Previous work has, however, been centred largely on their structural and spectroscopical properties. In an attempt to extend the reaction chemistry of this class of compounds we present here details of the oxidation and hydrolysis of the indium phosphate complex $[Me_2InPPh_2]_2$, and the structural characterization of an In_4O_4 cubane cluster.

The compound $(Me_2InPPh_2)_2$ (**1**) was synthesized by the reaction of Me_2InCl and $(Me_3Si)PPh_2$ in toluene solution at room temperature. Reduction in volume of the solvent followed by cooling (−20°C) yielded colourless crystals in 72% yield.‡ Compound **1** forms a dimer in solution which is not readily cleaved by the addition of Lewis bases.

The addition of a stoichiometric quantity of H_2O to a benzene solution of **1** yields Ph_2PH and MeInO as the only isolatable products. The formation of MeInO, from $InMe_3$, has been proposed to occur via Me_2InOH, however the hydroxide could not be isolated.[4]

Oxidation of **1** with two equivalents of py·O in benzene, yields the previously unreported dimeric phosphinate complex $[Me_2In(O_2PPh_2)]_2$ (**2**)‡ which is spectroscopically similar to the aluminium and gallium derivatives reported by Coates and Mukherjee.[5] Compound **2** may also be prepared by the reaction of $InMe_3$ with HO_2PPh_2.

*Dedicated to Professor Sir Geoffrey Wilkinson, F.R.S.; "onward and upward"!

†Author to whom correspondence should be addressed.

‡Satisfactory elemental analysis was obtained for all new compounds.

1: Yield: 72% isolated. Cryoscopic in benzene. Found: 651. Calc: 659. IR(ν in cm^{-1}, Nujol mull), 3050(w), 2720(w), 1955(w), 1880(w), 1810(w), 1755(w), 1585(w), 1430(s), 1305(m), 1260(m), 1185(w), 1155(w), 1090(m), 1070(m), 1025(s), 1000(m), 740(s), 690(s), 500(m). NMR (δ in ppm, C_6D_6), ^1H 7.39 (m, 4H, P—Ph), 6.95 (m, 6H, P—Ph), 0.17 (s, 6H, In—Me). ^{31}P −56.6(s).

2: Yield: 91% isolated. Cryoscopic in benzene. Found: 730. Calc: 723. IR (ν in cm^{-1}, Nujol mull), 3040(m), 2290(w), 1975(w), 1900(w), 1820(w), 1760(w), 1590(m), 1485(m), 1190(vs), 1185(sh), 1130(vs), 1075(s), 935(m), 790(s), 720(s), 690(s), 620(w), 575(m). NMR (δ in ppm, C_6D_6) ^1H: 8.41 (m, 4H, P—Ph), 7.01 (m, 6H, P—Ph), 0.02 (s, 6H, In—Me). ^{31}P 17.1(s).

3: Yield (based on In): 78% isolated. Cryoscopic in benzene. Found: 1783–1828. Calc: 1929. IR (ν in cm^{-1}, Nujol mull). 3605(m), 2710(w), 1975(w), 1900(w), 1830(w), 1785(w), 1590(m), 1305(m), 1210(w), 1150(sh), 1120(vs), 1065(m), 1030(vs), 1010(vs), 995(s), 740(m), 715(s), 685(vs), 535(m). NMR (δ in ppm, C_6D_6) 8.50 (m, 16H, P—Ph), 8.01 (m, 18H, py), 6.91 (m, 24H, P—Ph), 6.62 (m, 12H, py), 3.37 (s, 4H, OH) −0.17 (s, 12H, In—Me). ^{31}P 26.8(s).

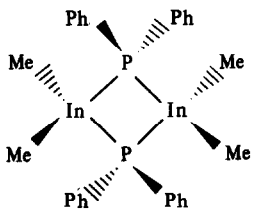

(1)

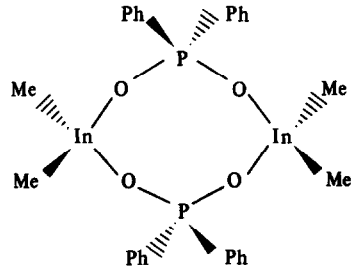

(2)

Structures 1 and 2.

Controlled hydrolysis of **2** in benzene yields a white powder that is only sparingly soluble in benzene. If the hydrolysis is carried out directly on the pyridine containing reaction mixture, (see above) colourless crystals are deposited over a period of a week. Spectroscopic data for the crystals are similar to those of the powder with the exception of peaks due to pyridine.

The ^{1}H NMR and analytical data* were consistent with a formula of $[InMe(OH)(O_2PPh_2)]\cdot(py)_{1.5}$. A consistent molecular weight determination could not, however, be obtained.

X-ray structural analysis† revealed the presence of a tetrameric cluster $[InMe(OH)(O_2PPh_2)]_4(py)_4$ (**3**) containing a distorted cubane core of four indium atoms and four μ_3-OH groups (Fig. 1). The cubane resides on a $\bar{4}$ symmetry site, only 1/4 of the molecule being present in the asymmetric unit.

The pseudo-octahedral coordination sphere at each indium atom is completed by a terminally bonded methyl group and two oxygen atoms from bridging diphenyl phosphinate moieties. The four terminal methyl groups are cited two on each side of the unbridged faces.

The In—OH bond lengths (see Table 1) consist of two long [In—O(1), 2.288(5) Å and In—O(1a), 2.285(6) Å] and a short [In—O(1b), 2.163(6) Å], the latter being *trans* to the methyl group, and joining the faces not bridged by the phosphinate groups. Although the In—O bond distances vary significantly within the core, the angles are essentially constant (see Table 2) [O(1)—In—O(1a), 74.7(2)°, O(1)—In—O(1b), 75.3(2)°, O(1a)—In—O(1b), 75.4(2)°, In—O(1)—In(a), 102.5(2)°, In—O(1)—In(b), 102.6(2)°, In(a)—O(1)—(b), 103.9(2)°].‡

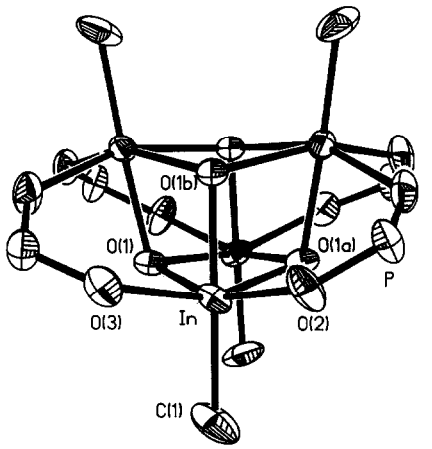

Fig. 1. Perspective view of the core of $[InMe(OH)(O_2PPh_2)]_4(py)_4$ (**3**). All hydrogen atoms, phenyl rings and pyridines have been omitted for clarity.

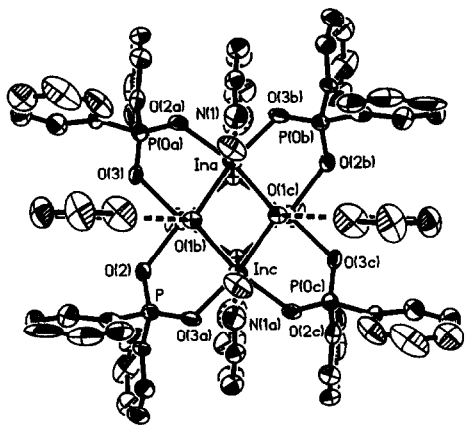

Fig. 2. Molecular structure of $[InMe(OH)(O_2PPh_2)_3]_4(py)_4$ (**3**). Only the pyridines hydrogen bonded to the hydroxy groups are shown. All hydrogens have been omitted for clarity.

* See footnote ‡ on previous page.

† Crystal data for $[InMe(OH)(O_2PPh_2)]_4\cdot(py)_6$ (**3**) ($T = 25$°C): space group $P4/n$, $a = 19.153(6)$, $b = 19.153(6)$, $c = 10.914(3)$ Å, $V = 4003.48$ Å^3, $Z = 2$, Mo-K_α. Of 3579 reflections collected (Syntex $P1$ ambient temperature) 3359 were unique and 1875 with $I > 3\sigma(I)$ were used in the solution and refinement (SPD package). $R = 0.0493$ and $R_w = 0.0512$, GOF = 3.37.

‡ Atomic coordinates, bond lengths and angles have been deposited at the Cambridge Crystallographic data Centre.

Table 1. Bond distances in angstroms

Atom 1	Atom 2	Distance	Atom 1	Atom 2	Distance
In	O(1)	2.288(5)	C(4)	C(5)	1.35(1)
In	O(2)	2.221(3)	C(5)	C(6)	1.32(1)
In	O(3)	2.238(4)	C(6)	C(7)	1.381(9)
In	C(1)	2.149(6)	C(8)	C(9)	1.434(8)
P	C(2)	1.497(3)	C(8)	C(13)	1.37(1)
P	C(2)	1.799(6)	C(9)	C(10)	1.41(1)
P	C(8)	1.820(7)	C(10)	C(11)	1.34(2)
O(1)	H(1)	1.008(5)	C(11)	C(12)	1.33(2)
N(1)	C(14)	1.350(8)	C(12)	C(13)	1.37(1)
N(1)	C(18)	1.338(6)	C(14)	C(15)	1.390(9)
N(1)	H(1)	1.920(3)	C(15)	C(16)	1.36(1)
C(2)	C(3)	1.358(9)	C(16)	C(17)	1.34(1)
C(2)	C(7)	1.386(7)	C(17)	C(18)	1.366(8)
C(3)	C(4)	1.39(1)			

Numbers in parentheses are estimated standard deviations in the least significant digits.

The bond distance between indium and the phosphinate oxygens are within experimental error of each other [In—O(2), 2.221(3) Å and In—O(3), 2.237(4) Å], as are the bonds between oxygen and phosphorus [P—O(2), 1.496(3) Å and P—O(3), 1.504(4)Å], indicating that the charge on the phosphinate is delocalized i.e. O···P···O not O···P—O$^-$.

Of the six pyridines present in the molecule, four are hydrogens bonded to the hydroxy groups. The remaining two are solvents of crystallization, each being disordered about a $\bar{4}$-fold axis. The hydrogen bonded pyridines are orientated almost parallel to the neighbouring phenyl rings of the phosphinates (Fig. 2).

Although cubane structures have been reported for aluminium imides, compound **3** is the first example of a 13/16 cubane, previous examples being adamantane-like in structure.[7]

Table 2. Bond angles in degrees

Atom 1	Atom 2	Atom 3	Angle	Atom 1	Atom 2	Atom 3	Angle
O(1)	In	O(2)	157.1(2)	C(4)	C(5)	C(6)	119.3(8)
O(1)	In	O(3)	92.2(2)	C(5)	C(6)	C(7)	121.5(7)
O(1)	In	C(1)	102.4(2)	C(2)	C(7)	C(6)	120.5(6)
O(2)	In	O(3)	94.9(1)	P	C(8)	C(9)	117.4(7)
O(2)	In	C(1)	97.9(2)	P	C(8)	C(13)	122.4(5)
O(3)	In	C(1)	98.7(2)	C(9)	C(8)	C(13)	120.2(7)
O(2)	P	C(2)	108.1(3)	C(8)	C(9)	C(10)	116.1(9)
O(2)	P	C(8)	109.3(3)	C(9)	C(10)	C(11)	122.0(1)
C(2)	P	C(8)	105.4(3)	C(10)	C(11)	C(12)	119.0(1)
In	O(1)	H(1)	101.6(3)	C(11)	C(12)	C(13)	124.0(1)
C(14)	N(1)	C(18)	115.7(5)	C(8)	C(13)	C(12)	118.5(8)
C(14)	N(1)	H(1)	116.7(3)	N(1)	C(14)	C(15)	124.9(6)
C(18)	N(1)	H(1)	127.6(3)	C(15)	C(14)	C(18)	92.9(5)
In	O(2)	P	132.7(2)	C(14)	C(15)	C(16)	115.4(7)
P	C(2)	C(3)	122.6(4)	C(15)	C(16)	C(17)	121.9(7)
P	C(2)	C(7)	120.5(5)	C(16)	C(17)	C(18)	119.0(7)
C(3)	C(2)	C(7)	116.9(6)	N(1)	C(18)	C(17)	123.1(6)
C(2)	C(3)	C(4)	121.0(6)	C(14)	C(18)	C(17)	90.8(5)
C(3)	C(4)	C(5)	120.6(9)	C(1)	H(1)	N(1)	146.4(3)

Numbers in parentheses are estimated standard deviations in the least significant digits.

We are continuing our investigations into the reaction chemistry of **1** → **3** and to the possibility of sulphur and selenium analogues.

Acknowledgements—Thanks are expressed to the Petroleum Research Fund (administered by the American Chemical Society) and the Milton Foundation for financial support. A. R. Barron is a DuPont Fellow 1987–1988.

REFERENCES

1. G. E. Coates and J Graham, *J. Chem. Soc.* 1963, 233.
2. See for example (a) A. M. Arif, B. L. Benac, A. H. Cowley, R. Geerts, R. A. Jones, K. B. Kidd, J. M. Power and S. T. Schwab, *J. Chem. Soc., Chem. Commun.* 1986, 1543; (b) R. L. Wells, A. P. Purdy, A. T. McPhail and C. G. Pitt, *J. Organomet. Chem.* 1986, **308**, 281; (c) O. T. Beachley Jr, J. P. Koparz, H. Zhang, W. E. Hunter and J. L. Atwood, *J. Organomet. Chem.* 1987, **325**, 69.
3. F. Mauni, *Transformation of Organometallics into Common and Exotic Materials: Design and Activation*; (Edited by R. M. Laine), pp. 195–198. Nijhoff, Boston (1988).
4. H. C. Clark and A. L. Pickard, *J. Organomet. Chem.* 1968, **13**, 61.
5. G. E. Coates and R. N. Mukherjee, *J. Chem. Soc.* 1964, 1295.
6. M. Del Piero, M. Cesari, G. Dozzi and A. Mazzei, *J. Organomet. Chem.* 1977, **129**, 281.
7. B. Krebs, D. Voelker and K. Stiller, *Inorg. Chim. Acta* 1982, **65**, L101.

Polyhedron Vol. 7, No. 19/20, pp. 2095–2101, 1988
Printed in Great Britain

0277–5387/88 $3.00+.00
© 1988 Pergamon Press plc

UNUSUALLY STABLE TRIMETHYLPLATINUM(IV) COMPLEXES WITH AN O_3PtC_3 COORDINATION SPHERE. THE CRYSTAL AND MOLECULAR STRUCTURE OF $\{C_5H_5Co[P(O)(OEt)_2]_3PtMe_3\}$

ALEXIS NETTLE,* MAURICIO VALDERRAMA, RAÚL CONTRERAS and MARIO SCOTTI

Pontificia Universidad Católica de Chile, Facultad de Quimica, Casilla 6177, Santiago, Chile

and

KARL PETERS and HANS GEORG VON SCHNERING

Max-Planck-Institut für Festkörperforschung, Heisenbergstr. 1, D-7000 Stuttgart 80, FRG

and

HELMUT WERNER*

Institut für Anorganische Chemie der Universität Würzburg, Am Hubland, D-8700 Würzburg, F.R.G.

Abstract—The reaction of $[Me_3PtI]_4$ with $\{C_5H_5Co[P(O)(OR)_2]_3\}Na$ (R.= Me, Et) gives the heterometallic dinuclear complexes $\{C_5H_5Co[P(O)(OR)_2]_3PtMe_3\}$ (**3a**: R = Me; **3b**: R = Et) in almost quantitative yield. Compounds **3a**, **3b** are fairly robust and do not react with $[CPh_3]PF_6$ by hydride abstraction. On treatment with HCl in benzene, stable adducts of composition $2\{C_5H_5Co[P(O)(OR)_2]_3PtMe_3\}\cdot 3HCl$ (**4a**, **4b**) are formed which presumably contain two $PtMe_3$ units in different environments. The structure of **3b** has been determined by single-crystal X-ray diffraction studies. **3b** is monoclinic, space group $P2_1/n$ with $a = 1415.6(3)$, $b = 1896.6(5)$, $c = 1148.4(3)$ pm and $\beta = 92.07(2)°$. The structure was solved via Patterson synthesis and refined by least-squares to R and R_w 0.032 for 3355 unique reflections. The platinum atom is octahedrally surrounded by the three P═O oxygen atoms of the phosphonate units and by the carbon atoms of the three methyl groups with Pt—O and Pt—C distances similar to those in $[Me_3Pt(\mu\text{-}OH)]_4$. The structural parameters of the $\{C_5H_5Co[P(O)(OEt)_2]_3\}$ unit in **3b** do not differ from those in other complexes containing this moiety as a tripod ligand.

It is now almost 15 years ago that one of us described the synthesis of unusually stable "super-sandwich" complexes of composition $(C_5H_5)_2Co_3[P(O)(OR)_2]_6$ (**1a, b**).[1] They are obtained in 50% yield by thermolysis of $C_5H_5Co[P(OR)_3]_2$ and almost quantitatively by reaction of cobaltocene with $HP(O)(OR)_2$ (Scheme 1). The structure of the trinuclear compounds consists of a central cobalt(II) ion which is octahedrally coordinated by the oxygen atoms of two $C_5H_5Co[P(O)(OR)_2]_3^-$ fragments.[1] These fragments can be liberated in the protonated form from **1a, b** with acids HX,[2] or more conveniently with NaCN to give the corresponding sodium salts [**2a, b**]Na.[3] Elegant studies, primarily by Kläui *et al.*, demonstrated that the anionic tripod ligands [**2a, b**]$^-$ form a variety of stable complexes with main group as well as transition metals in different oxidation states, and thus in many ways they behave similarly to the cyclopentadienyl anion and its derivatives.[4,5]

The aim of the present study was two-fold.

Dedicated to Professor Sir Geoffrey Wilkinson in honour of his pioneering contributions to organometallic chemistry.

*Authors to whom correspondence should be addressed.

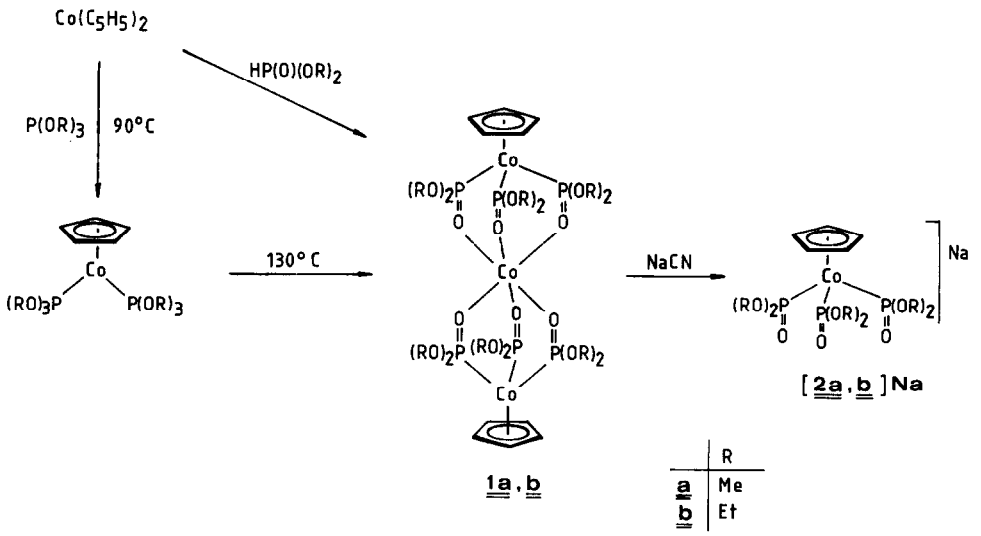

Scheme 1.

Firstly, among the numerous mononuclear trimethylplatinum(IV) complexes there are only a few having the composition $(O)_3PtMe_3$ [(O) = oxygen-donor ligand];[6] and hence we were interested to learn whether the corresponding derivatives with $(O)_3$ = **[2a]**$^-$ and **[2b]**$^-$ can be obtained. They would be analogues of the well known cyclopentadienyl compound $(\pi\text{-}C_5H_5)PtMe_3$.[7,8] Secondly, one of the recent activities of our group was concerned with the chemistry of dimethylmetal complexes $(\pi\text{-}C_nH_n)M(L)Me_2$ ($n = 5$, M = Rh, Ir; $n = 6$, M = Ru, Os; L = PR_3, CO) which react with electrophiles such as $[CPh_3]^+$ to give the ethylene (hydrido)metal cations $[(\pi\text{-}C_nH_n)MH(C_2H_4)(L)]^+$, possibly via $M(=CH_2)CH_3$ intermediates.[9,10] This interesting behaviour which may shed some light on elementary steps of the Fischer–Tropsch (F–T) synthesis,[11] prompted us to address the question as to whether trimethylmetal complexes react similarly to give cationic products containing a $MH(C_2H_4)CH_3$ unit. Such species may also be models for intermediates in the F–T synthesis.[12]

RESULTS AND DISCUSSION

The sodium salts **[2a]**Na and **[2b]**Na react with $[Me_3PtI]_4$ in benzene under reflux to give the title complexes **3a** and **3b** in almost quantitative yield (Scheme 2). **3a** and **3b** form yellow air-stable crystals that are soluble in most organic solvents and only decompose above 250 and 300°C. The IR spectra in the $\nu(CH_3)$ and $\delta(CH_3)$ region (Table 1) are not significantly different from that of the starting material $[Me_3PtI]_4$; indicating that the coordination sphere around the platinum has not changed very much. The P=O stretching fre-

Table 1. IR data of $[Me_3PtI]_4$ and **3a**, **3b** (in KBr)

Complex	$\nu(CH_3)$			$\delta(CH_3)$	
$[Me_3PtI]_4$	2950	2890	2790	1250	1220
3a		2880	2795	1258	1219
3b	2938	2880	2800		1225

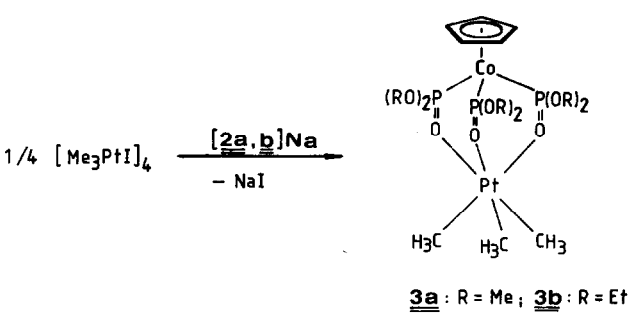

Scheme 2.

quencies of **3a** and **3b** are observed at 1107 and 1121 cm^{-1}, and thus have been shifted to lower frequencies by 53 and 37 cm^{-1} compared with the sodium salts of $[\mathbf{2a}]^-$ and $[\mathbf{2b}]^-$, respectively.[13] The suggested decrease in the P=O bond strength caused by the ligation of the tridentate $C_5H_5Co[P(O)(OR)_2]_3^-$ unit has also been found for **1a, b** and analogous di- and trinuclear complexes.[2,4,13]

The ^1H and ^{31}P NMR spectra of **3a** and **3b** show that in solution the three methyl groups at the platinum and the three phosphonate ligands are equivalent, in agreement with the structure found in the crystalline state. For both compounds, the protons of the $PtMe_3$ fragment give rise to a pseudo-triplet which has almost the same chemical shift (δ *ca* 1.95) and ^{195}Pt–^1H coupling constant (79 Hz) as found for the parent molecule $[Me_3PtI]_4$ (δ 1.8; $J(^{195}Pt^1H) = 78$ Hz).

Various attempts to attack one of the platinum bound methyl groups by $[CPh_3]^+$ and transform it into a CH_2 unit failed. The complexes **3a** and **3b** are surprisingly robust towards hydride abstracting reagents and even after prolonged reaction with $[CPh_3]PF_6$ in CH_2Cl_2 they are unchanged.

Treatment of **3a** and **3b** with concentrated hydrochloric acid in aqueous solution results in the cleavage of the Pt—O bonds and the formation of $[Me_3PtCl]_4$ and the protonated form of the tridentate anions, **[2a]H** and **[2b]H**.[2,3,13] In contrast, the reaction of **3a** and **3b** with a 0.3 M solution of HCl in benzene does not lead to fragmentation of the dinuclear complexes but affords the adducts **4a** and **4b** almost quantitatively. The composition of the yellow air-stable solids is supported by elemental analyses and molecular weight determinations in chloroform. Reaction of **4a** and **4b** with D_2O in $CDCl_3$ regenerates the starting materials.

From the ^1H NMR spectra there is no doubt that the adducts **4a** and **4b** contain two $PtMe_3$ units in different environments, and thus the structure shown in Scheme 3 is tentatively assigned. The two distinct signals (of equal intensity) observed for the $PtMe_3$ protons show ^{195}Pt–^1H coupling constants of 81 and 79 Hz which agree with the values found for $[Me_3PtCl]_4$ (81.7 Hz) and for **3a, b** (79 Hz). We therefore conclude that the methyl groups of one $PtMe_3$ unit in **4a, b** are *trans* to three chlorines and those of the other $PtMe_3$ unit are *trans* to three oxygens of three phosphonate ligands. We note that the chemical shifts of the C_5H_5 and POH signals in the ^1H NMR spectra of **4a, b** are very similar to those of the corresponding C_5H_5 and POH resonances of $\{C_5H_5Co[P(O)(OMe)_2]_3H_2\}PF_6$ [$\delta(C_5H_5)$ 5.40, δ(POH) 11.83; in CD_2Cl_2] and $\{C_5H_5Co[P(O)(OEt)_2]_3H_2\}PF_6$ [$\delta(C_5H_5)$ 5.30, δ(POH) 11.93; in CD_2Cl_2], respectively.[14] This similarity is in agreement with the structural proposal. It is worth mentioning that the octahedral tetramethyl platinum(IV) complexes $[PtMe_4(N—N)]$ (N—N = 2,2′-bipyridyl or 1.10-phenanthroline) react with HCl in CH_2Cl_2/MeOH to give cleavage of one Pt—CH_3 bond with concomitant formation of $[PtMe_3Cl(N—N)]$.[15] The interaction between **3a, b** and HCl is remarkably strong as the adducts do not lose HCl either in vacuum or in ether, acetone, benzene, or chloroform solution.

X-ray crystal structure of **3b**

Various trimethylplatinum(IV) complexes have been investigated by single-crystal X-ray diffraction but to the best of our knowledge no mononuclear representative of the $(O)_3PtMe_3$ type has been studied.[6] The results of the structural analysis of **3b** are summarized in Fig. 1 and Tables 2 and 3. The platinum atom is octahedrally surrounded by the three P=O oxygen atoms of the phosphonate units

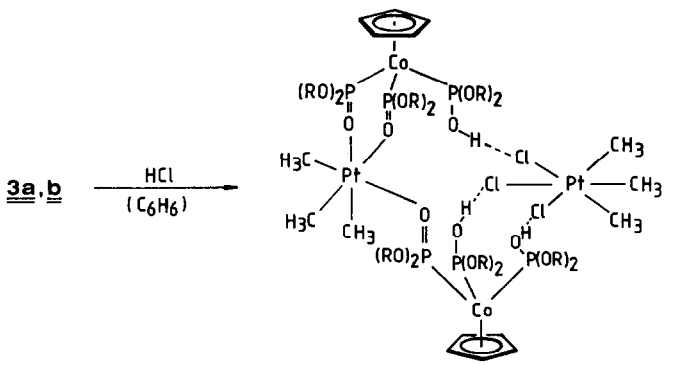

4a: R = Me; **4b**: R = Et

Scheme 3.

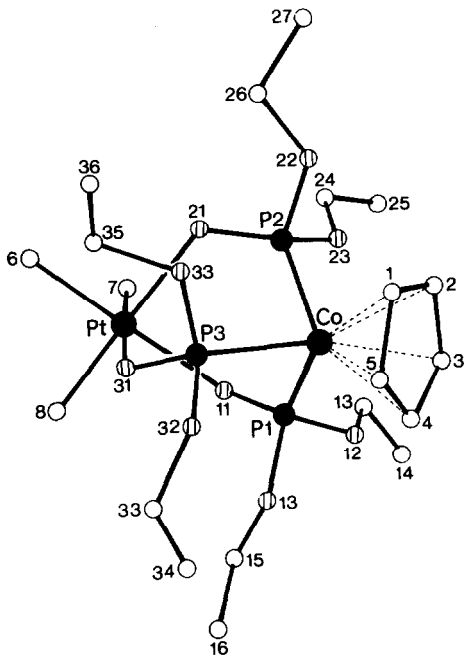

Fig. 1. The molecular structure of **3b**.

and by the carbon atoms of the three methyl groups, and is thus in a very similar coordination sphere as in $[Me_3Pt(\mu\text{-}OH)]_4$.[16] In this tetrameric compound in which the platinum and the oxygen atoms are located at opposite corners of a cube, the Pt—C and Pt—O distances are 204(2) and 222(1) pm, respectively, and only slightly longer than in **3b**. In $(\pi\text{-}C_5H_5)PtMe_3$, the mean value for the Pt—C bond lengths is 211 pm and for the C—Pt—C angles 85.4°.[8] The C—Pt—C angles in **3b** are 89.9(3), 88.3(4) and 90.1(4)°, respectively. We note that the O—Pt—O angles in **3b** (mean value 87.9°) are significantly smaller than the N—Pt—N angles in the related cation $[HC(pz)_3]PtMe_3^+$ (pz = pyrazol-1-yl) (mean value 83.6°),[17] which is probably due to the smaller "bite" of the tridentate $[HC(pz)_3]$ ligand compared with $[\mathbf{2b}]^-$.

The structural parameters of the $\{C_5H_5Co[P(O)(OEt)_2]_3\}$ unit in **3b** are very similar to those of the parent compound **1b**,[1,18] the analogous copper complex $\{C_5H_5Co[P(O)(OEt)_2]_3\}_2Cu$[18] and the recently described sodium salt [**2b**]Na which in the crystalline state forms a trimeric aggregate with two water molecules.[4c] Within the limits of error, no significant deviations from the geometry expected for the $C_5H_5CoP_3$ and $P(O)(OEt)_2$ groups were detected in **3b**. The P=O and P—O(—Et) distances in $\{[\mathbf{2b}]Na\}_3 \cdot 2H_2O$, for example, are 149 and 162 pm (mean values) and compare well with the corresponding bond lengths found in **3b** (see Table 2). The results agree with earlier observations that the metal bound to the anions $[\mathbf{2a}]^-$ and $[\mathbf{2b}]^-$ in the various complexes containing these tripod oxygen ligands has almost no influence on the structure of the $\{C_5H_5Co[P(O)(OR)_2]_3\}$ unit, independent of whether it is a main group or a transition metal element.

EXPERIMENTAL

All reactions were carried out under an atmosphere of purified nitrogen by using Schlenk tube

Table 2. Bond lengths (pm) in **3b**

Pt—C(6)	199.5(9)	Pt—C(7)	199.8(8)
Pt—C(8)	202.0(8)	Pt—O(11)	219.5(4)
Pt—O(21)	219.7(4)	Pt—O(31)	219.6(5)
Co—P(1)	217.3(2)	Co—P(2)	216.3(2)
Co—P(3)	217.0(2)	Co—C(1)	207.0(10)
Co—C(2)	207.1(8)	Co—C(3)	204.4(9)
Co—C(4)	205.3(10)	Co—C(5)	208.4(10)
P(1)—O(11)	150.3(5)	P(1)—O(12)	160.1(5)
P(1)—O(13)	161.2(5)	P(2)—O(21)	150.4(5)
P(2)—O(22)	159.8(6)	P(2)—O(23)	159.9(6)
P(3)—O(31)	151.5(5)	P(3)—O(32)	159.7(6)
P(3)—O(33)	159.1(5)	C(1)—C(2)	133.7(14)
C(1)—C(5)	136.3(15)	C(2)—C(3)	136.7(13)
C(3)—C(4)	136.7(16)	C(4)—C(5)	139.6(19)
O(12)—C(13)	135.3(11)	O(13)—C(15)	139.2(12)
C(13)—C(14)	138.1(14)	C(15)—C(16)	134.9(15)
O(22)—C(26)	132.4(13)	O(23)—C(24)	138.5(12)
C(24)—C(25)	136.0(16)	C(26)—C(27)	133.2(16)
O(32)—C(33)	131.6(10)	O(33)—C(35)	139.0(12)
C(33)—C(34)	139.6(16)	C(35)—C(36)	136.5(14)

Table 3. Bond angles (°) in **3b**

C(6)—Pt—C(7)	89.9(3)	C(6)—Pt—C(8)	88.3(4)
C(7)—Pt—C(8)	90.1(4)	C(6)—Pt—O(11)	178.8(3)
C(7)—Pt—O(11)	91.0(3)	C(8)—Pt—O(11)	92.5(3)
C(6)—Pt—O(21)	91.4(3)	C(7)—Pt—O(21)	91.2(3)
C(8)—Pt—O(21)	178.7(3)	O(11)—Pt—O(21)	87.8(2)
C(6)—Pt—O(31)	91.7(3)	C(7)—Pt—O(31)	178.3(3)
C(8)—Pt—O(31)	90.3(3)	O(11)—Pt—O(31)	87.4(2)
O(21)—Pt—O(31)	88.4(2)	P(1)—Co—P(2)	91.4(1)
P(1)—Co—P(3)	91.2(1)	P(2)—Co—P(3)	91.6(1)
Co—P(1)—O(12)	111.3(2)	Co—P(1)—O(11)	120.1(2)
Co—P(1)—O(13)	106.2(2)	O(11)—P(1)—O(12)	107.8(3)
O(12)—P(1)—O(13)	99.2(3)	O(11)—P(1)—O(13)	110.3(3)
Co—P(2)—O(22)	109.9(2)	Co—P(2)—O(21)	120.8(2)
Co—P(2)—O(23)	105.3(2)	O(21)—P(2)—O(22)	107.3(3)
O(22)—P(2)—O(23)	101.4(3)	O(21)—P(2)—O(23)	110.4(3)
Co—P(3)—O(32)	110.9(2)	Co—P(3)—O(31)	120.5(2)
Co—P(3)—O(33)	106.8(2)	O(31)—P(3)—O(32)	107.4(3)
O(32)—P(3)—O(33)	98.8(3)	O(31)—P(3)—O(33)	110.4(3)
Pt—O(11)—P(1)	125.7(3)	P(1)—O(12)—C(13)	127.0(5)
P(1)—O(13)—C(15)	122.4(6)	O(12)—C(13)—C(14)	119.7(9)
O(13)—C(15)—C(16)	118.7(10)	Pt—O(21)—P(2)	125.0(3)
P(2)—O(22)—C(26)	129.8(6)	P(2)—O(23)—C(24)	124.4(6)
O(23)—C(24)—C(25)	116.4(9)	O(22)—C(26)—C(27)	122.1(11)
Pt—O(31)—P(3)	124.7(3)	P(3)—O(32)—C(33)	131.6(6)
P(3)—O(33)—C(35)	123.5(6)	O(32)—C(33)—C(34)	115.6(9)
O(33)—C(35)—C(36)	118.4(10)		

techniques. The starting materials $[Me_3PtI]_4$,[19] [**2a**]Na and [**2b**]Na,[3] were prepared by published methods. NMR spectra were recorded on a Varian XL-100, and IR spectra on a Perkin–Elmer 567 spectrometer.

Preparation of the complexes $\{C_5H_5Co[P(O)(OR)_2]_3PtMe_3\}$ (**3a, 3b**)

A solution of $[Me_3PtI]_4$ (103 mg, 0.07 mmol) in 20 cm^3 of benzene was treated with a slight excess (0.31 mmol) of [**2a**]Na or [**2b**]Na, and heated for 3 h under reflux. After cooling to room temperature, the solution was filtered (using cellulose as a filter aid) and the solvent was removed *in vacuo*. The light yellow residue was washed with water, dried *in vacuo*, and dissolved in *ca* 5 cm^3 of acetone at 40°C. Cooling the acetone solution to −25°C gave yellow crystals; yield 85% (**3a**) and 90% (**3b**).

3a: m.p. 250°C (dec). Found: C, 24.5; H, 4.6. Calc. for $C_{14}H_{32}CoO_9P_3Pt$: C, 24.3; H, 4.7%. IR (KBr): ν(P=O) 1107, ν(POMe) 1064, 1018 cm^{-1}. ^1H NMR ($CDCl_3$): $\delta(C_5H_5)$ 5.07(s); δ(POMe) 3.7 (virtual quartet), $N = 11$ Hz; $\delta(PtMe_3)$ 1.98 (pseudo triplet), J(PtH) = 79 Hz. ^{31}P NMR ($CDCl_3$): δ 123.3 (slightly broadened singlet).

3b: m.p. 300°C (dec). Found: C, 30.3; H, 5.6. Calc. for $C_{20}H_{44}CoO_9P_3Pt$: C, 31.0; H, 5.7%. IR (KBr): ν(P=O) 1121, ν(POMe) 1076, 1038 cm^{-1}. ^1H NMR ($CDCl_3$): $\delta(C_5H_5)$ 5.05(s); $\delta(POCH_2)$ 4.1(m); $\delta(CH_2CH_3)$ 1.3(t), J(HH) = 7 Hz; $\delta(PtMe_3)$ 1.94 (pseudo triplet), J(PtH) = 79 Hz.

Preparation of the compounds $2\{C_5H_5Co[P(O)(OR)_2]_3PtMe_3\}\cdot 3HCl$ (**4a, 4b**)

A solution of **3a, b** (0.3 mmol) in 2 cm^3 of benzene was treated at room temperature with 8 cm^3 of a 0.3 M solution of HCl in benzene and stirred for 3 h at 25°C. The solvent was removed *in vacuo*, and the oily residue was recrystallized from acetone–ether. After cooling to −25°C yellow, air-stable crystals were obtained; yield 90%.

4a: Found: C, 22.3; H, 4.5; Cl, 6.9; Co, 7.8; Pt, 25.9; mol weight 1372 (osmometric in $CHCl_3$). Calc. for $C_{28}H_{67}Cl_3Co_2O_{18}P_6Pt_2$: C, 22.5; H, 4.5; Cl, 7.1; Co, 7.9; Pt, 26.1%. Mol. weight 1492.1. ^1H NMR ($CDCl_3$): δ(POH) 11.50(s); $\delta(C_5H_5)$ 5.40(s); δ(POMe) 3.75 (virtual quartet), $N = 11$ Hz; $\delta(PtMe_3)$ 1.40 (pseudo triplet), J(PtH) = 81 Hz and 1.28 (pseudo triplet), J(PtH) = 79 Hz.

4b: Found: C, 29.2; H, 5.7; mol weight 1637 (osmometric in $CHCl_3$). Calc. for $C_{40}H_{91}Cl_3Co_2O_{18}P_6Pt_2$: C, 28.9; H, 5.5%. Mol. weight 1660.4.

Table 4. X-ray operations and results

Crystallographic section	
Compound	**3b**
Empirical formula	$C_{20}H_{44}O_9P_3PtCo$
Molecular mass	775.51
a (pm)	1415.6(3)
b (pm)	1896.6(5)
c (pm)	1148.4(3)
β (°)	92.07(2)
V (pm × 10^{-6})	3081.1(9)
Z	4
d (calc.) (g cm^{-3})	1.672
Crystal system	Monoclinic
Space group	$P2_1/n$
Data collection	
Diffractometer	Syntex P3
Radiation	Mo-K_α
Monochromator	Graphite
Crystal size (mm)	0.15 × 1.25 × 0.1
Data collection mode	ω-scan
Theta range (°)	1.75–27.5
Recip. latt. segment	h = 0–18
	k = 0–24
	l = $\overline{14}$–14
No. refl. measd	3527
No. unique refl.	3355
No. refl. $F > 3\sigma(F)$	3303
Lin. abs. coeff. (mm^{-1})	5.498
Abs. correction	ψ-scan
Structural analysis and refinement	
Method of solution	Patterson synthesis
Method of refinement	anisotropic LSQ
	H-positions calculated and refined isotropically
Parameter/F_o ratio	0.093
R, R_w	0.032, 0.032
Program used	SHELXTL

^{1}H NMR ($CDCl_3$): δ(POH) 12.06(s); $\delta(C_5H_5)$ 5.32(s); $\delta(POCH_2)$ 4.09(m); $\delta(CH_2CH_3)$ 1.30(t), J(HH) = 7 Hz; $\delta(PtMe_3)$ 1.38 (pseudo triplet), J(PtH) = 81 Hz and 1.28 (pseudo triplet), J(PtH) = 79 Hz.

X-ray structure analysis of **3b**

The full information for **3b** is summarized in Table 4.*

* Atomic coordinates, displacement factor coefficients, full lists of bond lengths and angles and lists of F_o/F_c values have been deposited as supplementary data with the Editor, from whom copies are available on request. Atomic coordinates have also been deposited with the Cambridge Crystallographic Data Centre.

Acknowledgements—This work was supported by the Stiftung Wolkswagenwerk, the Dirección de Investigación Pontificia Universidad Católica de Chile (DIUC) and the FONDECYT Chile. We thank Mrs Ingrid Keupp, Mrs Marcia Cazanga and Mr Sergio Alegria for technical assistance.

REFERENCES

1. V. Harder, E. Dubler and H. Werner, *J. Organomet. Chem.* 1974, **71**, 427.
2. W. Kläui and H. Werner, *Angew. Chem.* 1976, **88**, 187; W. Kläui and H. Werner, *Angew. Chem. Int. Ed. Engl.* 1976, **15**, 172.
3. W. Kläui, *Z. Naturforsch. B* 1979, **34**, 1403.
4. (a) M. Scotti, M. Valderrama, S. Rojas and W. Kläui, *J. Organomet. Chem.* 1986, **301**, 369; (b) E. M. Holt, W. Kläui and J. J. Zuckerman, *J. Organomet. Chem.* 1987, **335**, 29; (c) W. Kläui, A. Müller, W. Eberspach, R. Boese and I. Goldberg, *J. Am. Chem. Soc.* 1987, **109**, 164.
5. For recent work from other groups see: (a) D. K. Towle, S. J. Landon, T. B. Brill and T. H. Tulip, *Organometallics* 1982, **1**, 295; (b) E. Roman, A. M. Leiva, F. Tapia, J. F. Guzman and A. H. Cowley, Abstracts of papers, p. 671. XVIII. Congreso Latinoamericano de Quimica, Santiago-Chile (1988); (c) A. H. Cowley, personal communication.
6. F. R. Hartley, in *Comprehensive Organometallic Chemistry* (Edited by G. Wilkinson, F. G. A. Stone and E. W. Abel), Vol. 6, Chap. 39, p. 471. Pergamon Press, Oxford (1982).
7. Synthesis: (a) S. D. Robinson and B. L. Shaw, *J. Chem. Soc.* 1965, 1529; (b) H. P. Fritz and K. E. Schwarzhans, *J. Organomet. Chem.* 1966, **5**, 181.
8. Structure: G. W. Adamson, J. C. J. Bart and J. J. Daly, *J. Chem. Soc. (A)* 1971, 2616.
9. (a) H. Kletzin, H. Werner, O. Serhadli and M. L. Ziegler, *Angew. Chem.* 1983, **95**, 49; H. Kletzin, H. Werner, O. Serhadli and M. L. Ziegler, *Angew. Chem. Int. Ed. Engl.* 1983, **22**, 46; (b) H. Werner, H. Kletzin, A. Höhn, W. Paul, W. Knaup, M. L. Ziegler and O. Serhadli, *J. Organomet. Chem.* 1986, **306**, 227; (c) K. Roder and H. Werner, *Angew. Chem.* 1987, **99**, 719; K. Roder and H. Werner, *Angew. Chem. Int. Ed. Engl.* 1987, **26**, 686.
10. For related work in this area see: (a) J. C. Hayes and N. J. Cooper, *J. Am. Chem. Soc.* 1982, **104**, 5570; (b) D. L. Thorn, *Organometallics* 1985, **4**, 192; (c) H. Berke and R. Hoffmann, *J. Am. Chem. Soc.* 1978, **100**, 7224.
11. C. K. Rofer-DePoorter, *Chem. Rev.* 1981, **81**, 447.
12. (a) K. Isobe, D. G. Andrews, B. E. Mann and P. M. Maitlis, *J. Chem. Soc., Chem. Commun.* 1981, 809; (b) I. M. Saez, N. J. Meanwell, A. Nutton, K. Isobe, A. Vazquez de Miguel, D. W. Bruce, S. Okeya, D. G. Andrews, P. R. Ashton, I. R. Johnstone and P. M. Maitlis, *J. Chem. Soc., Dalton Trans.* 1986, 1565.
13. W. Kläui and K. Dehnicke, *Chem. Ber.* 1978, **111**, 451.

14. W. Eberspach, Dissertation Technische Hochschule Aachen (1985).
15. J. E. Hux and R. J. Puddephatt, *Inorg. Chim. Acta* 1985, **100**, 1.
16. T. G. Spiro, D. H. Templeton and A. Zalkin, *Inorg. Chem.* 1986, 7, 2165.
17. P. K. Byers, A. J. Canty, B. W. Skelton and A. H. White, *J. Chem. Soc., Chem. Commun.* 1987, 1093.
18. E. Dubler, L. Linowsky and W. Kläui, *Trans. Met. Chem.* 1979, **4**, 191.
19. D. E. Clegg and S. R. Hall, *Inorg. Synth.* 1967, **10**, 71.

Polyhedron Vol. 7, No. 19/20, pp. 2103–2118, 1988
Pergamon Press plc. Printed in Great Britain

PROFESSOR SIR GEOFFREY WILKINSON, FRS: LIST OF PUBLISHED WORKS TO DATE

1946

Can. J. Research **25B**, 357 (1946). Growth of La^{140} from Ba^{140} (with W. E. Grummitt, J. Gueron and L. Yaffe).

Can. J. Research **25B**, 364 (1946). Yields of Ba^{139}, Ba^{140} in fast and thermal neutron fission of U^{235} and U^{238} (with W. E. Grummitt, J. Gueron and L. Yaffe).

Nature **158**, 163 (1946). Yields of isotopes in U^{235} slow neutron fission (with W. E. Grummitt).

1947

Nature **160**, 864 (1947). A new isotope of tungsten.

1948

Nature **161**, 520 (1948). Yields of isotopes in U^{233} slow neutron fission (with W. E. Grummitt).

Proc. Phys. Soc. London, **60**, 460 (1948). Selk weakening in β-ray measurements (with E. Broda, W. E. Grummitt, J. Gueron and L. Kowarski).

1949

Phys. Rev. **75**, 696 (1949). A new isotope of hafnium (with H. G. Hicks).

Phys. Rev. **75**, 1019 (1949). Radioactive isotopes of Pt and Au.

Phys. Rev. **75**, 1370 (1949). Radioactive isotopes of the rare earths—I. Experimental techniques and thulium isotopes (with H. G. Hicks).

Phys. Rev. **75**, 1687 (1949). Radioactive isotopes of rare earth elements—II. Neodymium (with H. G. Hicks).

J. Chem. Soc. 5360 (1949). Studies of neutron deficient radioactive isotopes.

J. Chem. Soc. 5364 (1949). α-Decay systematics.

J. Chem. Soc. 5366 (1949). The reactions of high energy particles with nuclei.

1950

Phys. Rev. **77**, 314 (1950). Neutron deficient isotopes of rhenium (with H. G. Hicks).

Phys. Rev. **79**, 815 (1950). Radioactive isotopes of rare earth elements—III. Terbium and holmium (with H. G. Hicks).

Phys. Rev. **79**, 1014 (1950). A note on Ti^{202}.

Phys. Rev. **80**, 491 (1950). Radioactive isotopes of rare earth elements—V. Europium (with H. G. Hicks).

Phys. Rev. **80**, 495 (1950). Radioactive isotopes of tantalum and wolfram.

1951

Phys. Rev. **81**, 540 (1951). Radioactive isotopes of rare earth elements—IV. Lutetium, hafnium (with H. G. Hicks).

Nucleonics **9**, 52 (1951). Chemical separation of fission products (with W. E. Grummitt).

National Research Council (Canada) Report 470 (1951). Thermal neutron fission yields of U^{233} and U^{235} (with W. E. Grummitt).

Science **113**, 742 (1951). The preparation and properties of tetrakistrichlorophosphine nickel (with J. W. Irvine, Jr).

J. Am. Chem. Soc. **73**, 5501 (1951). The preparation and properties of tetrakistribromophosphine nickel and tetrakistrifluorophosphine nickel.

J. Am. Chem. Soc. **73**, 5502 (1951). Antimony trichloride substitution compounds with nickel and iron carbonyls.

Nature **168**, 514 (1951). Phosphorus trifluoride–haemoglobin.

1952

J. Am. Chem. Soc. **74**, 2125 (1952). The structure of iron bis-cyclopentadienyl (with M. Rosenblum, M. C. Whiting and R. B. Woodward).

J. Am. Chem. Soc. **74**, 5764 (1952). The heat of formation of ferrocene (with F. A. Cotton).

J. Am. Chem. Soc. **74**, 6146 (1952). The preparation and some properties of ruthenocene and ruthenicinium salts.

J. Am. Chem. Soc. **74**, 6148 (1952). The preparation and some properties of the cobalticinium salts.

J. Am. Chem. Soc. **74**, 6149 (1952). The polarographic chemistry of ferrocene, ruthenocene and the metal hydrocarbon ions (with J. A. Page).

1953

J. Am. Chem. Soc. **75**, 1011 (1953). Bis-cyclopentadienyl derivatives of some transition elements (with P. L. Pauson, J. M. Birmingham and F. A. Cotton).

J. Am. Chem. Soc. **75**, 3586 (1953). Bis-cyclopentadienyl compounds of rhodium(III) and iridium(III) (with F. A. Cotton and R. O. Whipple).

1954

J. Am. Chem. Soc. **76**, 209 (1954). Cyclopentadienyl compounds of chromium, molybdenum and tungsten.

J. Am. Chem. Soc. **76**, 1970 (1954). Bis-cyclopentadienyl compounds of nickel and cobalt (with P. L. Pauson and F. A. Cotton).

J. Am. Chem. Soc. **76**, 2024 (1954). Bis-indenyl derivatives of iron and cobalt (with P. L. Pauson).

J. Am. Chem. Soc. **76**, 4179 (1954). A new preparative method for bis-cyclopentadienyl metal compounds (with J. M. Birmingham and D. Seyferth).

J. Am. Chem. Soc. **76**, 4281 (1954). Bis-cyclopentadienyl compounds of Ti, Zr, V, Nb and Ta (with J. M. Birmingham).

J. Am. Chem. Soc. **76**, 6210 (1954). Cyclopentadienyl compounds of Sc, Y, La, Ce and some lanthanide elements (with J. M. Birmingham).

Chemy Ind. **11**, 307 (1954). Cyclopentadienyl compounds of Mn and Fe (with F. A. Cotton).

Z. Naturforsch. **9b**, 417 (1954). Bis-cyclopentadienyl-Verbindungen von Chrom, Molybdän and Wolfram (with F. A. Cotton).

Z. Naturforsch. **9b**, 446 (1954). Phosphorus tri-pseudo-halogen complexes of nickel(0).

Z. Naturforsch. **9b**, 453 (1954). On the question of octahedral binding in bis-cyclopentadienyl compounds (with F. A. Cotton).

1955

J. Am. Chem. Soc. **77**, 3421 (1955). Cyclopentadienyl rhenium hydride (with J. M. Birmingham).

J. Am. Chem. Soc. **77**, 3689 (1955). Mass spectra of cyclopentadienyl metal compounds—I. Bis-cyclopentadienyl compounds of V, Cr, Fe, Co, Ni, Re and Ru, and manganese and magnesium cyclopentadienides (with L. Friedman and A. P. Irsa).

J. Am. Chem. Soc. **77**, 6519 (1955). Solvent extraction separation of cobalt and nickel with thiocyanate and the preparation of nickel-free cobalt salts (with R. A. Sharp).

J. Inorg. Nucl. Chem. **1**, 165 (1955). Cyclopentadienyl carbon monoxide and related compounds of some transitional metals (with T. S. Piper and F. A. Cotton).

J. Inorg. Nucl. Chem. **1**, 175 (1955). Infrared spectra and structures of cyclopentadienyl–carbon monoxide compounds of V, Mn, Fe, Co, Mo, and W (with F. A. Cotton and A. D. Lichr).

Chemy Ind. 1296 (1955). A chromium methyl compound (with T. S. Piper).

Naturwiss. **42**, 96 (1955). The reduction of bis-cyclopentadienyl compounds (with J. M. Birmingham and A. K. Fischer).

Naturwiss. **42**, 625 (1955). Cyclopentadienyl molybdenum derivatives (with T. S. Piper).

1956

Naturwiss. **43**, 15 (1956). Iron alkyl and aryl compounds (with T. S. Piper).

Naturwiss. **43**, 129 (1956). A silyliron compound; an Fe—Si σ-bond (with T. S. Piper and D. M. Lemal).

J. Inorg. Nucl. Chem. **2**, 32 (1956). Cyclopentadienyl–triethylphosphinecopper(I) and bis-cyclopentadienylmercury(II) (with T. S. Piper).

J. Inorg. Nucl. Chem. **2**, 38 (1956). Cyclopentadienyl–nitric oxide compounds of chromium and manganese (with T. S. Piper).

J. Am. Chem. Soc. **78**, 42 (1956). The cyclopentadienides of scandium, yttrium and some rare earth elements (with J. M. Birmingham).

J. Am. Chem. Soc. **78**, 900 (1956). Cyclopentadienyl–nitric oxide–di-sulfur manganese (with T. S. Piper).

J. Inorg. Nucl. Chem. **2**, 95 (1956). On manganese cyclopentadienide and some chemical reactions of neutral bis-cyclopentadienyl metal compounds (with F. A. Cotton and J. M. Birmingham).

J. Inorg. Nucl. Chem. **2**, 141 (1956). Spectra and structures of metal–carbon monoxide compounds—II. Manganese and rhenium decacarbonyls (with F. A. Cotton and A. Liehr).

J. Inorg. Nucl. Chem. **2**, 149 (1956). Di(π-cyclopentadienyl)titanium(II) (with A. K. Fischer).

J. Inorg. Nucl. Chem. **2**, 246 (1956). π-Cyclopentadienyl compounds of uranium-IV and thorium-IV (with L. T. Reynolds).

J. Inorg. Nucl. Chem. **3**, 104 (1956). Alkyl and aryl derivatives of π-cyclopentadienyl compounds of chromium, molybdenum, tungsten and iron (with T. S. Piper).

Phys. Rev. **101**, 1493 (1956). Nuclear reactions of cobalt with protons from 0- to 100-Mev energy (with R. A. Sharp and R. M. Diamond).

J. Am. Chem. Soc. **78**, 5168 (1956). Heats of combustion and formation of metal carbonyls. I. Chromium, molybdenum and tungsten hexacarbonyl (with F. A. Cotton and A. K. Fischer).

Chemy Ind. 1305 (1956). Some experimental observations on transition metal hydrocarbonyls (with F. A. Cotton).

1957

J. Am. Chem. Soc. **79**, 752 (1957). Infrared spectrum of iron dodecacarbonyl (with F. A. Cotton).

J. Am. Chem. Soc. **79**, 2044 (1957). Heats of combustion and formation... II. Nickel carbonyl (with A. K. Fischer and F. A. Cotton).

Proc. Chem. Soc. 209 (1957). The solubility of potassium and sodium–potassium alloy in certain ethers (with J. L. Down, J. Lewis and B. Moore).

1958

J. Inorg. Nucl. Chem. **6**, 12 (1958). Infra-red spectra of osmium–nitrogen compounds (with J. Lewis).

J. Inorg. Nucl. Chem. **7**, 32 (1958). Infra-red spectra of transition metal–nitric oxide complexes—I. Complexes involving donation from the NO^+ ion (with J. Lewis and R. J. Irving).

J. Inorg. Nucl. Chem. **7**, 38 (1958). Infra-red spectra of transition metal–nitric oxide complexes—II. Complexes involving the NO^- ion (with W. P. Griffith and J. Lewis).

Proc. Chem. Soc. 152 (1958). Cycloheptatriene metal complexes (with E. W. Abel and M. A. Bennett).

J. Inorg. Nucl. Chem. **7**, 295 (1958). Complex cyanides involving metal–metal bonds (with W. P. Griffith).

J. Am. Chem. Soc. **80**, 3149 (1958). Tetracarbonyl halides of rhenium (with E. W. Abel and G. B. Hargreaves).

J. Chem. Soc. 3916 (1958). Biscyclopentadienylrhenium hydride (with M. L. H. Green and L. Pratt).

Nature **182**, 393 (1958). Some complex cyanides of rhenium (with R. Colton and R. D. Peacock).

Nature **182**, 466 (1958). Formation of a transition metal–hydrogen bond in aqueous solution (with W. P. Griffith and L. Pratt).

Chemy Ind. 1205 (1958). An azulene–metal complex (with R. Burton).

J. Chem. Soc. 3993 (1958). Some nitric oxide complexes of iron and copper. [Part III of series] (with W. P. Griffith and J. Lewis).

J. Chem. Soc. 4314 (1958). π-Cyclopentadienylrhenium carbonyl compounds (with M. L. H. Green).

J. Chem. Soc. 4559 (1958). Transition-metal complexes of seven-membered ring systems. I. The cycloheptatriene–metal complexes and related compounds (with E. W. Abel, M. A. Bennett and R. Burton).

Chemy Ind. 1592 (1958). Some new organo-iron complexes (with R. Burton, M. L. H. Green and E. W. Abel).

1959

J. Inorg. Nucl. Chem. **9**, 3 (1959). The Raman and infrared spectra and structure of di-(π cyclopentadienyliron) tetracarbonyl (with F. A. Cotton and H. Stammreich).

J. Inorg. Nucl. Chem. **9**, 86 (1959). Some methylcyclopentadienyl–metal compounds (with L. T. Reynolds).

J. Am. Chem. Soc. **81**, 800 (1959). Heats of combustion. III. Iron pentacarbonyl; the nature of the bonding in metal carbonyls (with F. A. Cotton and A. K. Fischer).

J. Phys. Chem. **63**, 154 (1959). Heats of combustion and formation of bis-benzenechromium (with A. K. Fischer and F. A. Cotton).

J. Inorg. Nucl. Chem. **10**, 23 (1959). The infra-red spectrum and structure of $K_4[Ni(CN)_3CO]_2$ (with W. P. Griffith and F. A. Cotton).

J. Chem. Soc. 833 (1959). Infrared spectra of manganese carbonyl hydride and deuteride (with F. A. Cotton and J. L. Down).

J. Chem. Soc. 872 (1959). Infrared spectra of transition metal–nitric oxide complexes. IV. The pentacyanonitrosyl complexes of chromium and molybdenum (with W. P. Griffith and J. Lewis).

J. Chem. Soc. 1501 (1959). Carbonyl halides of manganese and some related compounds (with E. W. Abel).

J. Chem. Soc. 1629 (1959). An acetylene–cyanide complex of cobalt(III) (with W. P. Griffith).

J. Chem. Soc. 1632 (1959). The preparation of potassium pentacyanonitrosylvanadate(−I) (with W. P. Griffith and J. Lewis).

J. Chem. Soc. 1775 (1959). Studies on transition-metal nitric oxide complexes. V. Nitric oxide complexes of tetrahedral bivalent nickel and some other metals (with W. P. Griffith and J. Lewis).

Proc. Chem. Soc. 61 (1959). Six-membered heterocyclic sandwich compounds of transition metals (with B. Moore).

J. Chem. Soc. 2323 (1959). Substituted carbonyl compounds of chromium, molybdenum, tungsten, and manganese (with E. W. Abel and M. A. Bennett).

J. Chem. Soc. 2484 (1959). The broad-line proton resonance spectrum of iron carbonyl hydride (with E. O. Bishop, J. L. Down, P. R. Emtage and R. E. Richards).

J. Chem. Soc. 2757 (1959). The pentacyanohydride complexes of cobalt(I) and rhodium(I) (with W. P. Griffith).

J. Chem. Soc. 3097 (1959). Molybdenum(II) benzoate (with E. W. Abel and Apar Singh).

J. Chem. Soc. 3178 (1959). Norbornadiene–metal complexes and some related compounds (with E. W. Abel and M. A. Bennett).

J. Chem. Soc. 3684 (1959). The structure of dicyclopentadienyl–tin and –lead (with L. D. Dave and D. F. Evans).

J. Chem. Soc. 3753 (1959). A new type of transition metal–cyclopentadiene compound (with M. L. H. Green and L. Pratt).

J. Chem. Soc. 3767 (1959). The solubility of alkali metals in ethers (with J. L. Down, J. Lewis and B. Moore).

Nature **183**, 1755 (1959). Lowest oxidation states of technetium and rhenium (with R. Colton and W. P. Griffith).

Chemy Ind. 991 (1959). Perfluorolefin–transition metal complexes (with K. F. Watterson).

Chemy Ind. 1067 (1959). Triphenylphosphoniumcyclopentadienylide metal complexes (with E. W. Abel and Apar Singh).

Chemy Ind. 1314 (1959). Halide compounds of rhenium (with R. Colton).

Z. Naturforsch. **14b**, 738 (1959). Some new transition metal π-cyclopentadienyl hydrides (with M. L. H. Green and C. N. Street).

Chemy Ind. 1516 (1959). Some new olefin complexes of Mo(0) and Ru(II) (with M. A. Bennett).

Aspects of the chemistry of carbonyls, cyanides and olefin complexes. (Lecture presented at XVII. Internat. Congress, Munich, September 1959—published in short form in *Angew. Chem.*)

1960

J. Chem. Soc. 71 (1960). Polarographic study of manganese, technetium and rhenium (with R. Colton, J. Dalziel and W. P. Griffith).

J. Chem. Soc. 989 (1960). Spectroscopic studies on some organo–iron complexes (with M. L. H. Green and L. Pratt).

J. Chem. Soc. 1321 (1960). Some π-cyclopentadienyl carbonyls of molybdenum and tungsten (with E. W. Abel and Apar Singh).

J. Chem. Soc. 1374 (1960). Complex cyanides of rhenium (with R. Colton and R. D. Peacock).

Chemy Ind. 319 (1960). Molybdenum(II) carboxylates (with E. Bannister).

Nature **186**, 233 (1960). Some new complexes of rhenium (with R. Colton and R. Levitus).

Chemy Ind. 442 (1960). Reaction of molybdenum carbonyl with various halides; a potassium etherate salt (with E. W. Abel and M. A. Bennett).

J. Chem. Soc. 4121 (1960). Some complex compounds of rhenium (with R. Colton and R. Levitus).

J. Chem. Soc. 4290 (1960). Transition metal complexes of seven-membered ring systems. II. Azulene–metal carbonyls (with R. Burton and L. Pratt).

Chemy Ind. 1083 (1960). Some olefin complexes of cobalt (with G. Winkhaus).

J. Chem. Soc. 5275 (1960). Dialkyldithiocarbamate complexes of Re(III) (with R. Colton and R. Levitus).

Chemy Ind. 1136 (1960). A new catalytic system for the stereospecific polymerisation of acetylene (with M. L. H. Green and M. Nehme).

Proc. Chem. Soc. 311 (1960). π-Cyclohexadienyltricarbonylmanganese (with G. Winkhaus).

Chemy Ind. 1137 (1960). Perfluoro–acetylene–transition metal complexes (with J. L. Boston and D. W. A. Sharp).

Proc. Chem. Soc. 356 (1960). Protonation of transition-metal carbonyl complexes (with A. Davison).

Chemy Ind. 1358 (1960). Fluorocarbon–transition metal complexes (with K. F. Watterson).

1961

J. Chem. Soc. 594 (1961). Transition-metal complexes of seven-membered ring systems. Part III. Cycloheptatrieneiron carbonyl and related compounds (with R. Burton and L. Pratt).

J. Chem. Soc. 602 (1961). Some diolefincobalt carbonyl complexes (with G. Winkhaus).

J. Chem. Soc. 775 (1961). Studies on transition-metal–nitric oxide complexes. Part VI. Platinum, palladium and nickel complexes (with W. P. Griffith and J. Lewis).

J. Chem. Soc. 1418 (1961). Some observations on rhodium olefin complexes (with M. A. Bennett).

J. Chem. Soc. 2037 (1961). Transition metal complexes. Part IV. Proton resonance spectra of cycloheptatriene complexes of Group VI metals (with M. A. Bennett and L. Pratt).

J. Chem. Soc. 2259 (1961). Bis(triphenylphosphine)nickel dinitrosyl (with W. P. Griffith and J. Lewis).

Chemy Ind. 288 (1961). A molecular trihydride of tantalum (with J. A. McCleverty).

Proc. Chem. Soc. 72 (1961). Hydride-ion substitution in metal complexes.

Tetrahedron Lett. 48 (1961). Structures of cycloolefin complexes of transition metals (with D. Jones, G. W. Parshall and L. Pratt).

J. Chem. Soc. 2738 (1961). Transition-metal fluorocarbon complexes. I. Derivatives of perfluoro–olefins (with H. H. Hoehn, L. Pratt and K. F. Watterson).

J. Chem. Soc. 3172 (1961). π-Cyclopentadienyl and cyclopentadiene iron carbonyl complexes (with A. Davison and M. L. H. Green).

Chemy Ind. 553 (1961). Protonation of olefin metal complexes; π-bonded carbonium complex ions (with A. Davison, W. McFarlane and L. Pratt).

J. Chem. Soc. 3807 (1961). π-Cyclohexadienylmanganese tricarbonyl and related compounds (with G. Winkhaus and L. Pratt).

J. Chem. Soc. 4854 (1961). The di-π-cyclopentadienyl hydrides of tantalum, molybdenum and tungsten (with M. L. H. Green, J. A. McCleverty and L. Pratt).

Chemy Ind. 1408 (1961). π-Cyclohexadienyl metal complexes (with D. Jones).

1962

J. Chem. Soc. 1132 (1962). Transition metal fluorocarbon complexes. II. Stabilized fluorocarbanion (with G. W. Parshall).

Chemy Ind. 40 (1962). Complexes of rhenium(V) oxytrichloride (with C. J. L. Lock).

Chemy Ind. 261 (1962). Mesityl oxide complexes of palladium and platinum (with G. W. Parshall).

Chemy Ind. 820 (1962). The stereospecific hydrogenation of cyclooctatetraene iron tricarbonyl (with A. Davison and W. McFarlane).

J. Chem. Soc. 3488 (1962). Transition-metal–fluorocarbon complexes III. Some derivatives of hexafluorobut-2-yne (with J. L. Boston and D. W. A. Sharp).

J. Chem. Soc. 3653 (1962). Formation of metal–hydrogen bonds in the protonation of transition-metal–carbonyl complexes (with A. Davison, W. McFarlane and L. Pratt).

J. Chem. Soc. 4454 (1962). Some sulphide carbonyl complexes of chromium, molybdenum, tungsten and manganese (with H. C. E. Mannerskantz).

J. Chem. Soc. 4458 (1962). π-Cyclohexadienyl compounds of manganese, rhenium, iron, and ruthenium (with D. Jones and L. Pratt).

Inorg. Chem. **1**, 896 (1962). Mesityl oxide complexes of palladium and platinum (with G. W. Parshall).

J. Chem. Soc. 4821 (1962). The protonation of tricarbonylcyclooctatetraeneiron and some related compounds (with A. Davison, W. McFarlane and L. Pratt).

1963

J. Chem. Soc. 1133 (1963). Spectroscopic studies on alkyl and hydrido transition metal carbonyls and π-cyclopentadienyl carbonyls (with A. Davison and J. A. McCleverty).

J. Chem. Soc. 2162 (1963). Cyclo-octatriene and related complexes of iron and cobalt (with W. McFarlane and L. Pratt).

Chemy Ind. 333 (1963). Infrared spectra of *trans*-dioxo complexes of transition metals (with N. P. Johnson and C. J. L. Lock).

J. Chem. Soc. 3163 (1963). Uranium(IV) chloride complexes of 1,2-dimethylthioethane, 1,2-dimethoxyethane, and tetra-P-methylethylenediphosphine (with H. C. E. Mannerskantz and G. W. Parshall).

J. Chem. Soc. 3193 (1963). Triethylenetetramine complexes of cobalt(III) and rhodium(III) (with R. D. Gillard).

J. Chem. Soc. 3468 (1963). Transition-metal fluorocarbon complexes. IV. Hexafluorobut-2-yne complexes of manganese and platinum (with J. L. Boston and S. O. Grim).

J. Chem. Soc. 3594 (1963). Hydrido-complexes of rhodium(III) containing nitrogen ligands (with R. D. Gillard).

J. Chem. Soc. 4096 (1963). Some transition-metal propionyl complexes and a novel ethyl transfer reaction (with J. A. McCleverty).

J. Chem. Soc. 4271 (1963). The co-ordination of ethylene-diaminetetraacetate in complexes of cobalt (III) and rhodium(III) (with R. D. Gillard).

J. Chem. Soc. 5399 (1963). Some quinqueco-ordinated copper(II) complexes (with R. D. Gillard).

J. Am. Chem. Soc. **85**, 1692 (1963). Tin(II) chloride complexes of platinum metals (with A. G. Davies and J. F. Young).

J. Chem. Soc. 5406 (1963). Carboxylic acid complexes of rhenium (with F. Taha).

J. Chem. Soc. 5885 (1963). Adducts of bistrifluoroacetylacetonato copper(II) and the thermochromism of bis-β-diketonatocopper(II) species (with R. D. Gillard).

J. Chem. Soc. 6041 (1963). Hydrogen bonding in

complexes of dimethylglyoxime with cobalt(III) (with R. D. Gillard).

Chemy Ind. 1432 (1963). Tetrakis(trifluoromethyl)cyclopentadienone and some hexafluorobut-2-yne complexes of rhodium (with R. S. Dickson).

1964

J. Chem. Soc. 179 (1964). Interaction of tin(II) chloride with carbonyl-π-cyclopentadienyl complexes of iron, molybdenum, and tungsten (with F. Bonati).

J. Chem. Soc. 524 (1964). Infrared and proton resonance measurements of some stannanes and germane (with P. E. Potter and L. Pratt).

J. Chem. Soc. 870 (1964). Aquation of the trisoxalatorhodate(III) ion (with R. D. Gillard).

J. Chem. Soc. 1054 (1964). Amine, phosphine, arsine, and stibine complexes of rhenium-(III), -(IV), and -(V) (with N. P. Johnson and C. J. L. Lock).

J. Chem. Soc. 1224 (1964). Complexes of rhodium(III) with chlorine and pyridine (with R. D. Gillard).

J. Chem. Soc. 1368 (1964). Absolute configurations of some d^6 complex ions of cobalt, rhodium, iridium and platinum, and of complex ions of chromium(III) (with R. D. Gillard).

J. Chem. Soc. 1640 (1964). Adducts of protonic acids with coordination compounds (with R. D. Gillard).

J. Chem. Soc. 2281 (1964). A nitrido and other complex cyanides of rhenium (V) and (VI) (with C. J. L. Lock).

J. Chem. Soc. 2479 (1964). π-1-Methylcyclohexadienyltricarbonyl manganese (with D. Jones).

J. Chem. Soc. 2538 (1964). Molybdenum(II) carboxylates (with T. A. Stephenson and E. Bannister).

J. Chem. Soc. 2614 (1964). Amine complexes of rhenium(V) (with N. P. Johnson and F. I. M. Taha).

J. Chem. Soc. 2699 (1964). Transition metal fluorocarbon complexes. V. Tetrakis(trifluoromethyl)cyclopentadienone and some related fluorocarbon complexes of rhodium (with R. S. Dickson).

J. Chem. Soc. 2835 (1964). Platinum blue and related complexes (with R. D. Gillard).

J. Chem. Soc. 2838 (1964). Dimeric copper(II) carboxylates (with R. D. Gillard and Miss D. M. Harris).

Chemy Ind. 544 (1964). Carboxylates of palladium, platinum and ruthenium (with S. M. Morehouse, A. R. Powell, J. P. Heffer and T. A. Stephenson).

Platinum Metals Review **8**, 16 (1964). Organometallic compounds of the platinum metals.

Essays in Coordination Chemistry. Experientia Suppl. IX, 233 (1964). Structure and bonding in transition metal complexes of some cyclic unsaturated ligands (with R. Mason).

J. Chem. Soc. 3156 (1964). Dicarbonyl-β-diketonato- and related complexes of rhodium(I) (with F. Bonati).

J. Chem. Soc. 3160 (1964). Configuration of trisdiamine complexes (with J. H. Dunlop and R. D. Gillard).

J. Chem. Soc. 3164 (1964). Infrared spectra of anhydrous complex cyanide acids (with D. F. Evans and D. Jones).

J. Chem. Soc. 3168 (1964). *d–d* transitions in hydridocomplexes. The position of the hydride ion in the spectrochemical series (with J. A. Osborn and R. D. Gillard).

J. Chem. Soc. 4200 (1964). Transition-metal fluorocarbon complexes. VI. Nuclear magnetic resonance studies of perfluoroalkyl compounds of cobalt and rhodium (with J. A. McCleverty).

J. Chem. Soc. 5176 (1964). Complexes of ruthenium, rhodium, iridium, and platinum with tin(II) chloride (with J. F. Young and R. D. Gillard).

J. Chem. Soc. 5189 (1964). The action of reducing agents on pyridine complexes of rhodium(III) (with B. N. Figgis, R. D. Gillard and R. S. Nyholm).

Nature **203**, 1167 (1964). Reaction of tetrafluoroethylene with pentacyanocobaltate ions and with reduced vitamin B_{12} (with M. J. Mays).

Proc. Chem. Soc. 284 (1964). Activation of molecular hydrogen by complexes of rhodium(III) (with R. D. Gillard, J. A. Osborn and P. B. Stockwell).

Proc. Chem. Soc. 401 (1964). A cyclic acetylene complex of hexacarbonyldicobalt, $(CO)_3CoC_6F_6Co(CO)_3$ (with N. A. Bailey, M. R. Churchill, R. Hunt and R. Mason).

1965

J. Chem. Soc. 490 (1965). β-diketone complexes of rhenium (with D. E. Grove, N. P. Johnson and C. J. L. Lock).

J. Chem. Soc. 1900 (1965). Bridge-splitting and replacement reactions of rhodium carbonyl chloride (with D. N. Lawson).

J. Chem. Soc. 1951 (1965). Catalytic approaches to complex compounds of rhodium(III) (with R. D. Gillard and J. A. Osborn).

J. Chem. Soc. 3632 (1965). Carboxylates of palladium, platinum, and rhodium and their adducts (with T. A. Stephenson, S. M. Morehouse, A. R. Powell and J. P. Heffer).

Chem. Commun. 17 (1965). Mild hydroformylation of olefins using rhodium catalysts (with J. A. Osborn and J. F. Young).

J. Chem. Soc. 3890 (1965). The reduction of bistriphenylphosphine tricarbonyl cobalt(I) salts (with J. A. McCleverty and A. Davison).

J. Chem. Soc. 4107 (1965). Polarographic reduction of complexes of rhodium(III) (with R. D. Gillard and J. A. Osborn).

J. Chem. Soc. 5654 (1965). Interaction of fulvenes with octacarbonyldicobalt and dicarbonyl chlororhodium (with J. Altman).

J. Chem. Soc. 6629 (1965). Transition-metal-fluorocarbon complexes. Part VII. Some complexes of cobalt and rhodium with tetrafluoroethylene, chlorotrifluorethylene and hexafluorobut-2-yne (with M. J. Mays).

Chemy Ind. 560 (1965). Homogeneous catalytic hydrogenation and hydroformylation of acetylenic compounds (with F. H. Jardine, J. A. Osborn and J. F. Young).

Chem. Commun. 131 (1965). Hydride intermediates in homogeneous hydrogenation reactions of olefins and acetylenes using rhodium catalysts (with J. F. Young, J. A. Osborn and F. H. Jardine).

Inorg. Chem. **4**, 1270 (1965). Transition metal complexes

derived from octafluorocyclohexa-1,3-diene (with R. H. Hunt).

Nature **208**, 1203 (1965). Homogeneous hydrogenation and hydroformylation using ruthenium complexes (with D. Evans, J. A. Osborn and F. H. Jardine).

1966

J. Chem. Soc. A 52 (1966). Cyano and cyanohydrido complexes of rhodium (with D. N. Lawson and M. J. Mays).

Inorg. Chem. **5**, 20 (1966). Hydrido and carbonylhydrido complexes of iridium containing stannous chloride (with R. Craig Taylor and J. F. Young).

J. Inorg. Nucl. Chem. **28**, 945 (1966). New complexes of ruthenium(II) and (III) with triphenylphosphine, triphenylarsine, trichlorostannate pyridine and other ligands (with T. A. Stephenson).

J. Chem. Soc. A 300 (1966). New diene and carbonyl complexes of ruthenium(II) (with S. D. Robinson).

J. Chem. Soc. A 465 (1966). Products from the reaction of *trans*-oxotrihalogenobis(triphenylphosphine)rhenium(V) with carboxylic acids and related compounds (with G. Rouschias).

J. Chem. Soc. A 1224 (1966). Oxo-complexes of rhenium(V) (with D. E. Grove).

J. Inorg. Nucl. Chem. **28**, 2285 (1966). New ruthenium carboxylate complexes (with T. A. Stephenson).

Chem. Commun. **5**, 129 (1966). Novel addition reactions of chlorotris(triphenylphosphine)rhodium(I) (with C. M. Baird, D. N. Lawson, J. T. Mague and J. A. Osborn).

Chem. Commun. **9**, 267 (1966). Thiocarbonyl complexes of transition metals (with M. C. Baird).

J. Chem. Soc. A 1711 (1966). The preparation and properties of tris(triphenylphosphine)halogenorhodium(I) and some reactions thereof incl. catalytic homogeneous hydrogenation of olefins and acetylenes and their derivatives (with J. A. Osborn, F. H. Jardine and J. F. Young).

J. Chem. Soc. A 1733 (1966). Interaction of tris(triphenylphosphine)chlororhodium(I) with iodomethane, methylallyl and allyl chloride (with D. N. Lawson).

J. Inorg. Nucl. Chem. **28**, 2709 (1966). Dithiocarbamato and trihalogenostannato carbonyl complexes of ruthenium(II) (with J. V. Kingston).

J. Chem. Soc. A 1736 (1966). Tris(triphenylarsine)- and tris(triphenylstibine)chlororhodium(I) complexes and their reactions with hydrogen, olefins and other reagents (with J. T. Mague).

Chem. Commun. 461 (1966). Hydridopentammine- and hydridoaquotetramminerhodium(III) sulphates (with J. A. Osborn and A. R. Powell).

Chem. Commun. **15**, 514 (1966). Bis(triphenylphosphine) (carbon disulphide) platinum (with M. C. Baird).

Chem. Commun. 569 (1966). A polynuclear ruthenium carbonyl hydride (with J. W. S. Jamieson and J. V. Kingston).

1967

J. Chem. Soc. A 270 (1967). Homogeneous catalytic hydrogenation of unsaturated aldehydes to form saturated aldehydes (with F. H. Jardine).

J. Inorg. Nucl. Chem. **29**, 2122 (1967). Acetato complexes of palladium(II) (with T. A. Stephenson).

J. Chem. Soc. A 865 (1967). Carbon disulphide, carbonyl sulphide, alkyl and aryl isothiocyanato and perfluorothioacetone complexes of nickel, palladium, platinum, rhodium and iridium (with M. C. Baird).

J. Chem. Soc. A 982 (1967). The interaction of perfluorobutadiene with iron and cobalt carbonyls (with R. L. Hunt and D. M. Roundhill).

J. Chem. Soc. A 993 (1967). The preparation and reactions of trihalogeno(alkanonitrile)bis(triphenylphosphine) rhenium(III) complexes (with G. Rouschias).

J. Chem. Soc. A 1347 (1967). Addition reactions of tris(triphenylphosphine) chlororhodium(I); hydrido, alkyl, and acyl complexes; carbon monoxide insertion and decarbonylation reactions (with M. C. Baird, J. T. Mague and J. A. Osborn).

J. Chem. Soc. A 1488 (1967). Electron spin resonance spectra of $[Cr(CN)_5(NO)]^{3-}$ (with L. S. Meriwether and S. D. Robinson).

J. Chem. Soc. A 1574 (1967). Further studies on the homogeneous hydrogenation of olefins using tris (triphenylphosphine) halogenorhodium(I) catalysts (with F. H. Jardine and J. A. Osborn).

Chem. Commun. 305 (1967). Specific catalytic homogeneous hydrogenation of terminal olefins using tris(triphenylphosphine)hydridochlororuthenium(II); hydrogen transfer in exchange and isomerisation reactions of olefins (with P. S. Hallman, D. Evans and J. A. Osborn).

J. Inorg. Nucl. Chem. **29**, 133 (1967). Octahedral ruthenium(II) carbonyl complexes with nitrogen, sulphur and tin donor ligands (with J. V. Kingston and J. W. S. Jamieson).

Chem. Commun. **8**, 407 (1967). Bis(triphenylphosphine) carbonatoplatinum(II) (with C. J. Nyman and C. E. Wymore).

J. Chem. Soc. A 2037 (1967). Carbon disulphide complexes of vanadium, iron, cobalt, ruthenium, and iridium; the preparation of *trans*-bis(triphenylphosphine)thiocarbonylhalogenorhodium(I) and -rhodium(III) complexes (with M. C. Baird and G. Hartwell).

1968

J. Chem. Soc. A 348 (1968). The decarbonylation of aldehydes by tris(triphenylphosphine)chlororhodium(I) (with M. C. Baird and C. J. Nyman).

J. Chem. Soc. A 489 (1968). The chemistry of rhenium-nitrile complexes (with G. Rouschias).

J. Chem. Soc. A 506 (1968). Carbonyl, phosphine and arsine complexes of cobalt, palladium, and platinum derived from perfluorobut-2-ene (with M. Roundhill).

J. Chem. Soc. A 561 (1968). Reactions of tris(triphenylphosphine)platinum(0) and tetrakis(triphenylphosphine)palladium(0) with oxygen and carbon dioxide (with C. J. Nyman and C. E. Wymore).

Inorg. Chem. **7**, 542 (1968). Fluorocarbon complexes of rhodium containing triphenylstibine and triphenylarsine (with J. T. Mague).

J. Chem. Soc. A 787 (1968). Interaction of silanes with tris(triphenylphosphine)chlororhodium(I) and other rhodium complexes; hydrosilation reaction of hex-1-

ene using trichlorosilane (with F. de Charentenay and J. A. Osborn).

J. Chem. Soc. A 813 (1968). Cationic π-carbon disulphide complexes of rhodium and iridium. Thiocarbonyl complexes of iridium (with M. Yagupsky).

J. Chem. Soc. A 845 (1968). New complexes derived from the interaction of dicarbonylchlororhodium(I) and tris(triphenylphosphine)chlororhodium(I) with cyclopropane, butadiene, and perfluorobutadiene (with D. M. Roundhill and D. N. Lawson).

J. Chem. Soc. A 849 (1968). The dimerisation of monosubstituted α-hydroxy acetylenes using tris(triphenylphosphine)chlororhodium(I) as catalysts (with H. Singer).

J. Chem. Soc. A 1054 (1968). Further studies on the homogeneous hydrogenation of olefins using tris tertiary phosphine chlororhodium(I) complexes (with S. Montelatici, A. van der Ent and J. A. Osborn).

J. Chem. Soc. A 1801 (1968). The preparation of hydridopentammine- and hydrido-aquotetramminerhodium(III) sulphates and other salts; the formation of alkyl and fluoroalkyl derivatives (with K. Thomas, J. A. Osborn and A. R. Powell).

Chem. Commun. 420 (1968). Homogeneous hydrogenation of α-olefins using hydridocarbonyltris-(triphenylphosphine)rhodium(I) (with C. O'Connor, G. Yagupsky and D. Evans).

J. Chem. Soc. A 2198 (1968). Thiocarbonyl and carbon disulphide complexes of ruthenium (with J. D. Gilbert and M. C. Baird).

J. Chem. Soc. A 2516 (1968). Oxidative addition of hydrogen cyanide, hydrogen sulphide and other acids of triphenylphosphine complexes of iridium(I) and rhodium(I) (with H. Singer).

J. Chem. Soc. A 2660 (1968). Reaction of hydridocarbonyltris(triphenylphosphine)rhodium with carbon monoxide and of the reaction products, hydridodicarbonylbis(triphenylphosphine) and dimeric species with hydrogen (with D. Evans and G. Yagupsky).

J. Chem. Soc. A 2665 (1968). Selective homogeneous hydrogenation of alk-1-enes using hydridocarbonyltris (triphenylphosphine)rhodium(I) as catalyst (with C. O'Connor).

J. Chem. Soc. A 2856 (1968). Chemistry of polynuclear compounds, Part XII. Polynuclear hydridocarbonyls of ruthenium (with B. F. G. Johnson, R. D. Johnston, J. Lewis and B. H. Robinson).

J. Chem. Soc. A 3133 (1968). Hydroformylation of alkenes using rhodium complex catalysts (with D. Evans and J. A. Osborn).

J. Chem. Soc. A 3143 (1968). Preparation and reactions of hydridochlorotris (triphenylphosphine) ruthenium (II) including homogeneous catalytic hydrogenation of alk-1-enes (with P. S. Hallman and B. R. McGarvey).

Bull. Soc. Chim. **12**, 5055 (1968). Homogeneous hydrogenation and hydroformylation of olefins by rhodium triphenylphosphine catalysts.

1969

J. Chem. Soc. A 84 (1969). Unidentate dithiocarbamate complexes of rhodium and iron: dithiocarbamate and xanthate complexes of ruthenium (with C. O'Connor and J. D. Gilbert).

J. Chem. Soc. A 725 (1969). Infrared and nuclear magnetic resonance spectra of hydridocarbonylbis(triphenylphosphine)iridium(I) and related complexes (with G. Yagupsky).

Inorg. Chem. **8**, 1196 (1969). The trioxotrichlororhenate(VII) ion (with D. E. Grove and N. P. Johnson).

Tetrahedron Lett. 1375 (1969). Non-selectivity in the homogeneous hydrogenation of alkenes using chlorobis(triarylphosphine)rhodium(I) catalysts (with C. O'Connor).

J. Chem. Soc. A 1690 (1969). The nature of iridium(IV) iodate (with D. Rose, F. M. Lever and A. R. Powell).

J. Chem. Soc. A 1749 (1969). New complexes of ruthenium(II) with $(PPh_3)_3$ and other ligands (with J. D. Gilbert).

J. Chem. Soc. A 2604 (1969). Oxidative-addition of iodomethane to *trans*-halogenocarbonylbis(triarylPh)RhI and the subsequent isomerisation via methyl transfer to an acetyl complex (with I. C. Douek).

Tetrahedron Lett. 1725 (1969). Catalytic hydroformylation of unsaturated compounds using hydridocarbonyltris$(PPh_3)_3$ rhodium(I) (with C. K. Brown).

J. Chem. Soc. A 2610 (1969). Preparation and properties of hydridocarboxylatotris(triphenylphosphine) ruthenium(II) complexes including homogeneous catalytic hydrogenation of alk-1-enes (with D. Rose, J. D. Gilbert and R. P. Richardson).

Chem. Commun. 825 (1969). Protonation of metal carboxylates; new homogeneous hydrogenation catalysts (with P. Legzdins and G. L. Rempel).

Chem. Commun. 987 (1969). Some novel peroxycarbonate complexes of platinum(II) (with P. J. Hayward, D. M. Blake and C. J. Nyman).

Chem. Commun. 1244 (1969). Intermediates or their analogues in hydroformylation of alkenes catalysed by hydrido carbonyl tris(triphenylphosphine)rhodium(I) (with G. Yagupsky and C. K. Brown).

1970

J. Chem. Soc. A 356 (1970). Substitution reactions of the hydridopentamminerhodium(III) ion (with K. Thomas).

J. Chem. Soc. A 937 (1970). Further studies on hydridocarbonyltris(triphenylphosphine)rhodium(I). Part I. Nature of inactivation of catalytic reactions (with M. Yagupsky, C. K. Brown and G. Yagupsky).

J. Chem. Soc. A 941 (1970). Further studies on hydridocarbonyltris(triphenylphosphine)rhodium(I). Part II. Isomerization of alk-1-ene (with M. Yagupsky).

J. Chem. Soc. A 1392 (1970). Further studies on hydridocarbonyltris(triphenylphosphine)rhodium(I); intermediate species in hydroformylation; rhodium and iridium analogues (with G. Yagupsky and C. K. Brown).

J. Chem. Soc. A 1771 (1970). Oxidative-addition and other reactions of rhodium, iridium and platinum complexes with carbon disulphide, ethyl dithiochloroformate and acids (with D. Commereuc and I. Douek).

J. Chem. Soc. A 1791 (1970). The blue solutions of ruthenium(II) chloride; a cluster anion (with D. Rose).

J. Chem. Soc. A 2753 (1970). Homogeneous hydroformylation of alkenes using hydridocarbonyltris (triphenylphosphine)rhodium(I) as catalyst (with C. K. Brown).

J. Chem. Soc. A 2765 (1970). The preparative use of blue solutions of ruthenium(II), ruthenium(II) and (III) complexes with amines, nitriles, phosphines, . . . (with J. D. Gilbert and D. Rose).

J. Chem. Soc. A 3322 (1970). The protonation of ruthenium and rhodium bridged carboxylates and their use as homogeneous hydrogenation catalysts for unsaturated substances (with P. Legzdins, R. W. Mitchell, G. L. Rempel and J. D. Ruddick).

Chem. Commun. 1369 (1970). Trimethylsilylmethyl compounds of transition metals (with G. Yagupsky, W. Mowat and A. Shortland).

J. Am. Chem. Soc. **92**, 5873 (1970). Some reactions of peroxobis(triphenylphosphine) platinum(II) and analogs with carbon dioxide, carbon disulfide and other unsaturated molecules (with P. J. Hayward, D. M. Blake and C. J. Nyman).

J. Org. Chem. **36**, 3561 (1970). A new ylide from tetrakis(trifluoromethyl)cyclopentadienone and triphenylphosphine (with D. M. Roundhill).

Chem. Commun. 1572 (1970). X-ray crystal structure of diethyldithiocarbamate complexes of rhenium(V) with oxo- and nitrido-ligands (with S. R. Fletcher, J. F. Rowbottom and A. C. Skapski).

1971

J. Chem. Soc. A 850 (1971). Interaction of hydridocarbonyltriphenylphosphine complexes of rhodium and iridium with conjugated dienes and allene (with C. K. Brown, W. Mowat and G. Yagupsky).

J. Chem. Soc. A 3116 (1971). Trimethylsilylmethyl complexes of transition metals with π-bonding ligands (with B. Wozniak and J. D. Ruddick).

J. Chem. Soc. A 3120 (1971). The interaction of hydridocarbonyltris(triphenylphosphine) complexes of iridium(I) and rhodium(I) with alk-1-ynes (with C. K. Brown and D. Georgiou).

J. Chem. Soc. A 3224 (1971). Reactions of the dirhodium cation Rh_2^{4+} with triphenylphosphine and alkali metal carboxylates, dithiocarbamates and other anions (with R. W. Mitchell and J. D. Ruddick).

Chem. Commun 967 (1971). Oxotriruthenium cluster complexes (with F. A. Cotton, J. G. Norman and A. Spencer).

Chem. Commun. 1079 (1971). Structure of hexakis(trimethylsilylmethyl)dimolybdenum (with F. Huq, W. Mowat, A. Shortland and A. C. Skapski).

Chem. Commun. 1477 (1971). Crystal structure of bis-μ-(trimethylsilylmethylidyne) tetrakis(trimethylsilylmethyl)diniobium(V). A new type of carbon bridging group (with F. Huq, W. Mowat and A. C. Skapski).

1972

J. Chem. Soc., Dalton Trans. 533 (1972). Elimination stabilised alkyls: part I, chromium, molybdenum, tungsten and vanadium (with W. Mowat, A. Shortland, G. Yagupsky, N. J. Hill and M. Yagupsky).

J. Chem. Soc., Dalton Trans. 826 (1972). Dithiocarbamate complexes of rhenium(V) and (III) (with J. Rowbottom).

Chem. Commun. 318 (1972). Hexamethyltungsten (with A. Shortland).

J. Chem. Soc., Dalton Trans. 1570 (1972). μ_3-Oxotriruthenium carboxylate complexes (with A. Spencer).

J. Organometal. Chem. **38**, 35 (1972). Neopentyl and related alkyls of chromium(IV) and other transition metals (with W. Mowat).

J. Chem. Soc., Dalton Trans. 1966 (1972). Metal complexes of tris(trimethylsilylmethyl)phosphine, Part 1 (with A. T. T. Hsieh and J. D. Puddick).

Chem. Commun. 922 (1972). Insertion of nitric oxide into tungsten–alkyl bonds; X-ray structure of the eight-coordinate complex tetramethylbis(N-methyl-N-nitrosohydroxylaminato)tungsten(VI) (with S. R. Fletcher, A. Shortland and A. C. Skapski).

1973

J. Chem. Soc., Dalton Trans. 204 (1973). Dichlorotetrakis(dimethylsulphoxide)ruthenium(II) and its use as a source material for some new ruthenium(II) complexes (with I. P. Evans and A. Spencer).

J. Chem. Soc., Dalton Trans. 684 (1973). Dithiocarbamato and carbonyldithiocarbamato complexes of rhenium(I), (III), (IV) and (V) (with J. F. Rowbottom).

J. Chem. Soc., Dalton Trans. 770 (1973). Elimination stabilized alkyls. Part II. Neopentyl and related alkyls of chromium(IV) (with W. Mowat, A. J. Shortland and N. J. Hill).

J. Chem. Soc., Dalton Trans. 786 (1973). Reactions of μ_3-oxotriruthenium carboxylates with π-acid ligands (with A. Spencer).

J. Chem. Soc., Dalton Trans. 846 (1973). Carboxylato triphenylphosphine complexes of ruthenium, cationic triphenylphosphine complexes derived from them, and their behaviour as homogeneous hydrogenation catalysts for alkenes (with R. W. Mitchell and A. Spencer).

J. Chem. Soc., Dalton Trans. 867 (1973). Carbonyl complexes of iron, cobalt and nickel with tris(trimethylsilylmethyl)phosphine (with A. T. T. Hsieh).

J. Chem. Soc., Dalton Trans. 872 (1973). Preparation and properties of hexamethyltungsten (with A. J. Shortland).

J. Chem. Soc., Dalton Trans. 929 (1973). The interactions of hydridocarbonyltris(triphenylphosphine) complexes of iridium(I) and rhodium(I) with organic acids (with C. K. Brown and D. Georgiou).

J. Chem. Soc., Dalton Trans. 946 (1973). Complexes of pyridine-2-thiol with some transition metals (with I. P. Evans).

J. Chem. Soc., Dalton Trans. 1120 (1973). Elimination stabilized alkyls: Part III. Trimethylsilyl methyl and neopentyl alkyls of transition metals (with W. Mowat).

J. Chem. Soc., Dalton Trans. 2565 (1973). μ_3-Oxotrimetal acetate complexes of chromium, manganese, iron, cobalt, rhodium and iridium (with A. Spencer and S. Uemura).

Inorg. Nucl. Chem. Lett. 675 (1973). Eight coordinate dithiocarbamate complexes of rhenium and molybdenum (with J. F. Rowbottom).

J. Organometal. Chem. **52**, C5 (1973). Zinc and alu-

minium trimethylsilylmethyls and their use as alkylating agents (with S. Moorhouse).

Les Prix Nobel En 1973. The long search for stable transition metal alkyls.

1974

J. Chem. Soc., Chem. Commun. 93 (1974). Tetramethyloxorhenium(VI), a paramagnetic d^1 alkyl (with K. Mertis and J. F. Gibson).

J. Chem. Soc., Chem. Commun. 327 (1974). The X-ray structure of the hydrido tris (triphenylphosphine) ruthenium(II) ion, $[RuH(PPh_3)_2(\eta\text{-}Ph\text{-}PPh_2)]^+$ (with J. C. McConway, A. C. Skapski, L. Phillips and R. J. Young).

J. Organometal. Chem. 77, C25 (1974). Trimethyltantalum(V) chelate complexes (with D. H. Williamson and C. Santini-Scampucci).

J. Am. Chem. Soc. **96**, 3842 (1974). The preparation, chemistry and structure of the lithium salt of the octamethyldimolybdate(II) ion (with F. A. Cotton, J. M. Troup, T. R. Webb and D. H. Williamson).

Science **185**, 109 (1974). The long search for stable transition metal alkyls.

J. Chem. Soc., Dalton Trans. 2187 (1974). Bis[(trimethylsilyl)methyl]- and bis(neopentyl)zinc, and tris [(trimethylsilyl)methyl]aluminium–diethyl ether (1/1), their use as alkylating agents in forming niobium and tantalum alkyls (with S. Moorhouse).

1975

J. Chem. Soc., Dalton Trans. 607 (1975). The chemistry of rhenium alkyls. Part I. Synthesis and properties of oxorhenium(VI) methyl and trimethylsilylmethyl compounds (with K. Mertis and D. H. Williamson).

J. Chem. Soc., Dalton Trans. 1093 (1975). The chemistry of rhenium alkyls. Part II. Electron spin resonance and electronic absorption spectra of oxotetraalkylrhenium(VI) (with J. F. Gibson and K. Mertis).

J. Chem. Soc., Dalton Trans. 1100 (1975). Syntheses of carbon monoxide, cyclopentadienyl and related compounds of transition metals containing the η^1 or η^2 dimethylaminomethyl ligand (with C. W. Fong).

J. Organometal. Chem. **22**, C65 (1975). Per methyls of tantalum, tungsten and rhenium: a warning (with K. Mertis and L. Galyer).

J. Organometal. Chem. **85**, C37 (1975). New synthesis of hexamethyltungsten(VI): hexamethylrhenium(VI) and dioxotrimethylrhenium(VII) (with L. Galyer and K. Mertis).

J. Organometal. Chem. **99**, C19 (1975). Trimethylsilylmethyl and methyl compounds of manganese, cobalt and uranium (with R. Andersen, E. Carmona-Guzman, K. Mertis and E. Sigurdson).

J. Organometal. Chem. **100**, 273 (1975). The iron sandwich. A recollection of the first four months.

J. Chem. Soc., Chem. Commun. 497 (1975). The photoelectron spectra of hexamethyltungsten and pentamethyltantalum (with L. Galyer and D. R. Lloyd).

1976

J. Chem. Soc., Dalton Trans. 399 (1976). Further studies on the homogeneous hydroformylation of alkenes using ruthenium complex catalysts (with R. A. Sanchez-Delgado and J. S. Bradley).

J. Chem. Soc., Dalton Trans. 719 (1976). Cationic hydrido and carboxylato triphenylphosphine complexes of ruthenium (with R. J. Young).

J. Chem. Soc., Dalton Trans. 807 (1976). Trimethyltantalum(V) chelate complexes (with C. Santini-Scampucci).

J. Organometal. Chem. **105**, 349 (1976). Adamantylcyclopentadienyldicarbonyliron(II) compounds (with S. Moorhouse).

J. Chem. Soc., Dalton Trans. 1488 (1976). The chemistry of rhenium alkyls. Part III. The synthesis and reactions of hexamethylrhenium(VI), *cis*-dioxotrimethylrhenium(VII) and the octamethylrhenate(VI) ion (with K. Mertis).

J. Chem. Soc., Dalton Trans. 1492 (1976). The chemistry of rhenium alkyls. Part IV. Electron spin resonance spectra of hexamethylrhenium(VI) and the octamethylrhenate(VI) ion (with J. F. Gibson, G. M. Lack and K. Mertis).

J. Chem. Soc., Chem. Commun. 159 (1976). Heat of formation of pentamethyltantalum and hexamethyltungsten (with F. A. Adedeji, J. A. Connor, H. A. Skinner and L. Galyer).

J. Chem. Soc., Dalton Trans. 1995 (1976). π-Arene and π-phenoxo complexes of ruthenium and rhodium (with D. J. Cole-Hamilton and R. J. Young).

J. Chem. Soc., Dalton Trans. 2204 (1976). Neopentyl, neophyl and trimethylsilylmethyl compounds of manganese. Manganese(II) dialkyls; manganese(II) dialkyl amine adducts; tetraalkylmanganate(II) ions and lithium salts; manganese(IV) tetraalkyl (with R. A. Andersen, E. Carmona-Guzman and J. F. Gibson).

Angew. Chem. 692 (1976) [609 (Internat. Edn)]. Tetra-(trimethylsilylmethyl) di-μ_2(trimethylsilylmethylidyne) ditungsten (with R. A. Andersen and A. L. Galyer).

J. Chem. Soc., Dalton Trans. 2235 (1976). New synthesis of hexamethyltungsten(VI). The octamethyltungstate(VI) ion (with A. L. Galyer).

J. Am. Chem. Soc. **98**, 6922 (1976). The synthesis and structure of dilithium octamethyldirhenate(III) (with F. A. Cotton, L. D. Gage, K. Mertis and L. W. Shive).

J. Chem. Soc., Chem. Commun. 858 (1976). Cluster alkyls of rhenium (with K. Mertis and A. F. Masters).

1977

J. Chem. Soc., Dalton Trans. 797 (1977). *Ortho*-metallated triphenylphosphine (2-diphenylphosphinophenyl) and related complexes of ruthenium(II). Part 1. Interaction of hydridochlorotris (triphenylphosphine) ruthenium (II) with methyl and trimethylsilylmethyl alkylating agents (Li, Mg, Zn); hydrido methyl and trimethylsilylmethyl complexes (with D. J. Cole-Hamilton).

J. Chem. Soc., Dalton Trans. 804 (1977). Interaction of diphenyl and other acetylenes with hydridonitrosyltris(triphenylphosphine)ruthenium, hydridocarbonyltris(triphenylphosphine)rhodium and -iridium (with R. A. Sanchez-Delgado).

J. Chem. Soc., Dalton Trans. 809 (1977). Bis(neopentyl)-(trimethylsilylmethyl)- and (neopental)-magnesium (with R. A. Andersen).

J. Chem. Soc., Dalton Trans. 812 (1977). Lithium alkyl anions of uranium(IV) and uranium(V). Addition compounds of uranium(VI)hexa*iso*-propoxide with

lithium, magnesium and aluminium alkyls (with E. R. Sigurdson).

J. Chem. Soc., Dalton Trans. 1546 (1977). The reactions of hydridochloro- and dichlorotris(triphenylphosphine) ruthenium(II) with alkali hydroxides and alkoxides. Hydridohydroxybis(triphenylphosphine)ruthenium(II) monosolvates, their reactions and related compounds (with B. N. Chaudret, D. J. Cole-Hamilton and R. S. Nohr).

J. Chem. Soc., Chem. Commun. 59 (1977). Interaction of alkenes with hydridotriphenylphosphine complexes of ruthenium (with D. J. Cole-Hamilton).

Nouv. J. Chim. 141 (1977). The reactions of dihydridotetrakis(triphenylphosphine)ruthenium(II), tetrakishydridotris(triphenylphosphine)ruthenium and hydrido (η^3-2-diphenylphosphinophenyl) bis (triphenylphosphine)ruthenium(II) with alkenes, dienes, ketones, aldehydes and weak acids (with D. J. Cole-Hamilton).

J. Chem. Soc., Chem. Commun. 283 (1977). Interaction of magnesium dialkyls with binuclear transition metal acetates; crystal structure of bis(trimethylsilylmethyl) bis(trimethylphosphine) bis(μ-trimethylsilylmethyl)dichromium(II) (with R. A. Andersen, R. A. Jones, G. Wilkinson and M. B. Hursthouse).

J. Chem. Soc., Dalton Trans. 1716 (1977). The reactions of tetrahydridotetrakis (methyldiphenylphosphine) molybdenum(IV) and -tungsten(IV) with acids (with E. Carmona-Guzman).

Nouv. J. Chim. 389 (1977). Chemistry of rhenium alkyls. Part V. Cluster alkyls of rhenium(III) and rhenium(IV); dimeric octaalkyl dinitrogen compounds of rhenium(IV); dirhenium(II) tetraallyl (with A. F. Masters, K. Mertis and J. F. Gibson).

Inorg. Chim. Acta **24**, L95 (1977). An O-bonded nitrito nitrosyl Schiff base complex: X-ray molecular structure of [Ru(sal$_2$en)(NO$_2$)(NO)] (with M. A. A. F. de C. T. Carrondó, P. R. Rudolf, A. C. Skapski and J. R. Thornback).

J. Am. Chem. Soc. **99**, 4989 (1977). Preparation and characterization of compounds containing the octamethylditungsten(II) anion and partially chlorinated analogues (with F. A. Cotton, S. Koch, K. Mertis and M. Millar).

J. Chem. Soc., Chem. Commun. 865 (1977). Synthesis and X-ray crystal structure of hexakis(trimethylphosphine)tris-μ-methylidene diruthenium(III) (with R. A. Andersen, R. A. Jones, M. B. Hursthouse and K. M. A. Malik).

1978

J. Chem. Soc., Dalton Trans. 110 (1978). Schiff base complexes of ruthenium(II) (with J. R. Thornback).

J. Chem. Soc., Dalton Trans. 446 (1978). Trimethylsilylmethyl and other alkyls of chromium, molybdenum, ruthenium and rhodium from interaction of magnesium dialkyls with metal–metal bonded binuclear acetates of chromium(II), molybdenum(II), ruthenium(II, III) and rhodium(II) (with R. A. Andersen and R. A. Jones).

J. Chem. Soc., Dalton Trans. 454 (1978). Reactions of dichlorodiphenoxotitanium(IV) (with A. Flamini and D. J. Cole-Hamilton).

J. Chem. Soc., Dalton Trans. 1063 (1978). Neutral, acetate bridged, binuclear alkyls of rhenium(III) (with R. A. Jones).

Nouv. J. Chim. **2**, 137 (1978). Water soluble transition metal phosphine complexes and their use in two phase catalytic reactions of olefins (with A. F. Borowski and D. J. Cole-Hamilton).

J. Chem. Soc., Dalton Trans. 1139 (1978). Alkyl–arene and –cyclooctadiene complexes of molybdenum(II) containing tertiary phosphines (with E. Carmona-Guzman).

J. Chem. Soc., Chem. Commun. 463 (1978). X-ray molecular structure and reactions of bis (styrene) bis(triphenylphosphine)ruthenium(0); the first sixteen-electron ruthenium(0) species (with M. A. A. F. de C. T. Carrondó, B. N. Chaudret, D. J. Cole-Hamilton and A. C. Skapski).

J. Chem. Soc., Dalton Trans. 1403 (1978). Photoelectron spectra of some transition metal alkyls and oxoalkyls (with J. C. Green, D. R. Lloyd, A. L. Galyer and K. Mertis).

J. Chem. Soc., Chem. Commun. 465 (1978). Synthesis and molecular structures of tris(trimethylsilylmethyl) chloro(trimethylphosphine)molybdenum(IV) and η_2-trimethylsilylmethylcarbonylbis (carbonyl) trimethyl phosphinemolybdenum(II)-μ-dichloro-η_2-trimethyl silylmethylcarbonylbis (carbonyl) trimethylphosphinemolybdenum(II) (with E. Carmona Guzman, J. L. Atwood, R. D. Rogers, W. E. Hunter and M. J. Zaworotko).

Acta Chem. Scand. **A32**, 763 (1978). The reactions between bis(styrene)bis(triphenylphosphine)ruthenium(0) and cyclohexene; its relevance to the alkene isomerisation reaction and to the catalytic disproportionation of cyclohexene (with B. N. Chaudret and D. J. Cole-Hamilton).

J. Chem. Soc., Dalton Trans. 1739 (1978). Bis(styrene) bis(triphenylphosphine)ruthenium(0) and its reactions with triphenylphosphine and with alkenes (with B. N. Chaudret and D. J. Cole-Hamilton).

J. Chem. Soc., Chem. Commun. 883 (1978). The reduction of tris(triphenylphosphine)dichlororuthenium(II) in acetonitrile; reformulation of the nature of the product; detection of the first paramagnetic d^8 complex (with D. J. Cole-Hamilton).

1979

J. Chem. Soc., Dalton Trans. 361 (1979). Interaction of trirhenium(III) cluster alkyls with carboxylic acids, β-diketonates and diphenyltriazene (with P. G. Edwards, F. Felix and K. Mertis).

J. Chem. Soc., Dalton Trans. 472 (1979). Synthesis of σ-aryl compounds of molybdenum, rhenium, ruthenium and rhodium from the metal–metal bonded binuclear acetates of Mo^{II}, Re^{III}, $Ru^{II,III}$ and Rh^{II} (with R. A. Jones).

J. Chem. Soc., Dalton Trans. 542 (1979). Schiff-base complexes of rhenium(IV) and rhenium(V) (with A. R. Middleton and A. F. Masters).

J. Chem. Soc., Dalton Trans. 1283 (1979). Reduction of dichlorotris(triphenylphosphine)ruthenium(II) in the presence of acetonitrile, pyridine, 2,2′-bipyridyl and styrene (with D. J. Cole-Hamilton).

J. Chem. Soc., Dalton Trans. 1519 (1979). The crystal structure of $MoMe_2(\eta\text{-}CoH_6)(PPhMe_2)_2$ and $MoMe_2(\eta\text{-}C_6H_5Me)(PPhMe_2)$ (with J. L. Atwood, W. E. Hunter, R. D. Rogers and E. C. Guzman).

J. Am. Chem. Soc. **101**, 4128 (1979). Synthesis and X-ray crystal structures of hexakis(trimethylphosphine)-tris-μ-methylenediruthenium(III) and its mono and dicationic derivatives, hexakis(trimethylphosphine)-μ-methyl-bis-μ-methylene diruthenium(III)tetrafluoroborate and hexakis(trimethylphosphine)-bis-μ-methylene diruthenium(III)bistetrafluoroborate (with M. B. Hursthouse, R. A. Jones and K. M. A. Malik).

J. Chem. Soc., Chem. Commun. 489 (1979). Trimethylphosphine complexes of rhodium(I) and ruthenium (II) (with R. Jones, F. Mayor-Real, M. B. Hursthouse, A. Galas and K. M. A. Malik).

J. Chem. Soc., Chem. Commun. 926 (1979). Interaction of hexamethyltungsten(VI) with trimethylphosphine; X-ray crystal structure of dimethyltetrakistrimethylphosphine tungsten(II) (with R. A. Jones, A. M. R. Galas and M. B. Hursthouse).

J. Chem. Soc., Chem. Commun. 1158 (1979). Interaction of oxotetrachloro rhenium(VI) with alcohols, lithium alkoxides and bis(trimethylsilylamido lithium. X-ray crystal structure of tetramethyoxydio-μ-dimethyoxo-μ-oxodirhenium(VI) (Re—Re) (with P. Edwards, K. M. Malik and M. B. Hursthouse).

J. Chem. Soc., Dalton Trans. 1618 (1979). Reactions of dihydridotetrakis(triphenylphosphine)ruthenium(II) with N, O and S ligands (with R. Obeso Rosete and D. J. Cole-Hamilton).

1980

J. Chem. Soc., Dalton Trans. 55 (1980). Tris(2)pyridylphosphine complexes of ruthenium(II) and rhodium(I) hydroformylation of hex-1-ene by rhodium complexes (with K. Kurtev, R. Ribola, R. Jones and D. J. Cole-Hamilton).

J. Chem. Soc., Dalton Trans. 174 (1980). Interaction of oximes with dichloro-tris(triphenylphosphine)ruthenium(II) (with A. R. Middleton and J. R. Thornback).

J. Chem. Soc., Dalton Trans. 229 (1980). The synthesis and crystal structures of chloro(trimethylphosphine) tris(trimethylsilylmethyl) molybdenum(IV) and di-μ-chlorobis[η^2 - trimethylsilylmethylcarbonylbis(carbonyl)trimethylphosphinemolybdenum(II)] (with E. Carmona Guzman, R. D. Rogers, W. E. Hunter, M. J. Zaworotko and J. L. Atwood).

J. Chem. Soc., Dalton Trans. 334 (1980). Trirhenium(III) cluster alkyls. Synthesis of tertiary phosphine adducts; cleavage to rhenium(I) and (II) dimers; reactions with carbon monoxide, nitric oxide and hydrogen chloride. X-ray structural determination of hexamethylbis (diethylphenylphosphine) - μ - trimethyltriangulotrirhenium(III) and pentakis (trimethylsilylmethyl) - N - trimethylsilylmethyl - N - nitrosohydroxylaminato) - μ - trichlorotriangulortrirhenium(III) (with P. Edwards and K. Mertis).

J. Chem. Soc., Dalton Trans. 467 (1980). The synthesis and crystal structure of hydridoborohydridotetrakis (trimethylphosphine)molybdenum(II) (with J. L. Atwood, W. E. Hunter and E. Carmona Guzman).

J. Chem. Soc., Perkin II 117 (1980). Synthesis and X-ray crystal structure of triphenylmethyltrimethyl-phosphonium tetrafluoroborate (with R. A. Jones, M. B. Hursthouse and K. M. A. Malik).

J. Chem. Soc., Dalton Trans. 511 (1980). Synthesis of trimethylphosphine complexes of rhodium and ruthenium. X-ray crystal structure of tetrakis(trimethylphosphine)rhodium(I)chloride and chlorotris(trimethylphosphine)rhodium(I) (with R. A. Jones, F. Mayor-Real, M. B. Hursthouse, A. M. R. Galas and K. M. A. Malik).

J. Chem. Soc., Dalton Trans. 901 (1980). Preparation and properties of 1-adamantoxides, 2-adamantoxides and 1-adamantylmethoxides of Ti^{IV}, V^{V}, Nb^{IV}, Nb^{V}, Cr^{III}, Mo^{IV}, Mn^{II}, Fe^{III} and Co^{II}. The crystal structure and molecular structure of tetrakis(1-adamantoxo)dimethylamine-molybdenum(IV) (with M. Bochmann, G. B. Young, M. B. Hursthouse and K. M. A. Malik).

J. Chem. Soc., Dalton Trans. 1771 (1980). Further chemistry of hexakis(trimethylphosphine)tris-μ-methylene)diruthenium(III). Synthesis and X-ray crystal structures of bis[tetrakistrimethylphosphinebis(μ-methylene)ruthenium(III)] ruthenium(IV) (Ru—Ru —Ru) bis(tetrafluoroborate), hexakistrimethylphosphine tris(μ-hydroxo)diruthenium(II) tetrafluoroborate and bistrimethylphosphine tricarbonylruthenium(0) (with R. A. Jones, A. M. R. Galas, K. M. A. Malik and M. B. Hursthouse).

J. Chem. Soc., Dalton Trans. 1797 (1980). Synthesis and crystal structure and molecular structure of bis(trimethylsilylmethylidyne)tetrakis(trimethylsilylmethyl) dirhenium (Re—Re) (with M. Bochmann, A. M. R. Galsa, K. M. A. Malik and M. B. Hursthouse).

J. Chem. Soc., Dalton Trans. 1863 (1980). Synthesis and properties of *bis*(t-butyl)methoxides of chromium(III,IV) manganese(II), iron(II), cobalt(II) and copper(I). The crystal and molecular structure of lithium tetrakis[bis(*t*-butyl)methoxo]chromate(III) tetrahydrofuran, tetrakis[bis(*t*-butyl)methoxo]chromate(IV) and lithiumtetrakis[bis(*t*-butyl)methoxo]chromate(IV) and lithiumtetrakis[bis(*t*-butyl)methoxo] ferrate(III)[bis(*t*-butyl)methanol] (with G. B. Young, M. Bochmann, M. B. Hursthouse and K. M. A. Malik).

Inorg. Chim. Acta **44**, L7 (1980). A novel linear O—Re—O—Re—O—Re system: the synthesis and X-ray structure of di-μ-oxobis[NN′-ethylenebis(acetylacetiminato)]oxo-rhenium(V)[NN′ - ethylenebis-(acetylacetiminato)]rhenium(V) perrhenate (with M. A. A. F. de C. T. Carrondo, R. Middleton, A. C. Skapski and A. P. West).

J. Chem. Soc., Dalton Trans. 1879 (1980). Preparation and properties of 1-adamantylmethyl and adamantyl complexes of transition metals (with G. B. Young and M. Bochmann).

J. Chem. Soc., Dalton Trans. 1888 (1980). Interaction of nitric oxide with paramagnetic and diamagnetic alkyls of titanium, zirconium, vanadium, niobium and tantalum (with A. R. Middleton).

J. Chem. Soc., Dalton Trans. 2315 (1980). Synthesis and crystal structure of bis[η^5-cyclopentadientyl tricarbonylmanganese]-η^5-dicyclopentadientyl titanium

(with R. J. Daroda, M. B. Hursthouse, K. M. A. Malik and M. Thornton-Pett).

J. Chem. Soc., Chem. Commun. 408 (1980). Synthesis and crystal structure of hexakistrimethylphosphine dihydrido μ-dihydrido dimolybdenum(II) Mo—Mo (with R. A. Jones, K-W. Chiu, M. B. Hursthouse and A. Galas).

J. Chem. Soc., Dalton Trans. 2467 (1980). Improved syntheses of oxotetrachlororhenium(VI) and trioxochlororhenium(VII). Synthesis of alkoxo and dialkylamido rhenium compounds. The crystal and molecular structures of tetramethoxodioxo-μ-dimethoxo-μ-oxodirhenium(VI), (Re—Re), lithium oxopentaisopropoxorhenate(VI) lithium chloride and *trans* - bistrimethylphosphinetetraphenoxorhenium (VI) (with P. G. Edwards, M. B. Hursthouse and K. M. A. Malik).

J. Chem. Soc., Dalton Trans. 2480 (1980). Trimethylphosphine hydrido and hydroxo complexes of ruthenium multinuclear magnetic resonance studies on hexakistrimethylphosphine - μ - hydrido - μ - hydroxodiruthenium(I). Crystal structures of hexakistrimethylphosphine dihydrido bis(μ-hydrido)diruthenium(II) and hexakistrimethylphosphine tris-μ-hydridodiruthenium(II) tetrafluoroborate (with R. A. Jones, W. McFarlane, I. J. Colquhoun, A. M. R. Galas and M. B. Hursthouse).

J. Chem. Soc., Chem. Commun. 654 (1980). Interaction of hydrogen with hexakis(trimethylsilylmethyl)-(μ-trichloro)triangulo trirhenium(I). The X-ray crystal structure of nonakis(trimethyl)hydrido(μ-hexachlorohexarhenium. New types of rhenium(II) alkyls (with P. G. Edwards, K. Mertis, K. M. Malik and M. B. Hursthouse).

J. Am. Chem. Soc. **102**, 7978 (1980). Reaction of t-butylisocyanide with hexamethyltungsten. Synthesis and X-ray crystal structure of W—N(Bu^t)CMe$_2$(Me)[N(Bu^t)(CMe=CMe$_2$)] (with R. A. Jones, K. W. Chiu, M. B. Hursthouse and A. M. R. Galas).

J. Chem. Soc., Chem. Commun. 1098 (1980). Synthesis of two carbon compounds by homogeneous Fischer–Tropsch type reactions (with R. J. Daroda and J. R. Blackborow).

J. Chem. Soc., Chem. Commun. 1101 (1980). Synthesis of methanol and derived compounds by homogeneous Fischer–Tropsch type reactions (with R. J. Daroda and J. R. Blackborow).

1981

J. Chem. Soc., Dalton Trans. 126 (1981). Further chemistry of trimethylphosphine complexes of rhodium(I): X-ray crystal structures of dodeca(trimethylphosphine)tetrarhodiumhexamercury, $Hg_6Rh(PMe_3)_{12}$, and *trans* - bis(trimethylphosphine) triphenylphosphine chlororhodium(I) (with R. A. Jones, F. Mayor-Real, A. M. R. Galas and M. B. Hursthouse).

J. Chem. Soc., Dalton Trans 191 (1981). Oxo-centred triruthenium formate complexes. Diphosphine adducts of oxo-centred triruthenium acetates (with H. Lehman).

J. Chem. Soc., Dalton Trans. 705 (1981). The interaction of hydrogen with hexakis(trimethylsilylmethyl)(μ-trichloro)triangulotrirhenium(III) its adducts with carbon monoxide, triphenylphosphine and pyridine and with chloropentakis(trimethylsilyl)(μ-trichloro) triangulotrirhenium(III). The X-ray crystal structures of hydridomonakis (trimethylsilylmethyl) (μ-trichloro) (triphenylphosphine) triangulotrirhenium(III) and tris (trimethylsilylmethyl) syn, syn, anti-trichloro [μ-tris (trimethylsilylmethyl)] triangulo trirhenium (with K. Mertis, P. G. Edwards, K. M. A. Malik and M. B. Hursthouse).

J. Chem. Soc., Chem. Commun. 189 (1981). Interaction of alkyl halides with the diironoctacarbonylate anion: the crystal structures of the tetraethylammonium salts of the μ-Acetyl-C^1(Fe^1,Fe^2)O(Fe^1,Fe^3)-nonacarbonyl-triangulotriferrate and μ^2-carbonylnonacarbonyl-μ^3-2,4 - dioxapentylidynetriangulotriferrate anions (with W-K. Wong, A. M. A. Galas, M. Thornton-Pett and M. B. Hursthouse).

J. Chem. Soc., Dalton Trans. 892 (1981). Trimethylphosphine complexes of molybdenum– tungsten, niobium and tantalum. X-ray crystal structures of hexakis (trimethylphosphine)dihydrido-μ-dihydrido dimolybdenum(II) (Mo—Mo) and of tetrahydrido(μ-hydrido)(μ - dimethylphosphine)pentakis(trimethylphosphine)ditungsten(II,IV) (with K. W. Chiu, R. A. Jones, A. M. R. Galas and M. B. Hursthouse).

J. Chem. Soc., Dalton Trans. 1204 (1981). Reactions of hexamethyltungsten(VI) in presence of trimethylphosphine. Synthesis of methyl, ethylidyne, hydrido, alkoxo and other tungsten compounds. X-ray crystal structures of *trans*-methylethylidynetetrakis (trimethylphosphine)tungsten(IV) and trihydrido-phenoxotetrakis(trimethylphosphine)tungsten(IV) (with K. W. Chiu, R. A. Jones, A. M. R. Galas, K. M. A. Malik and M. B. Hursthouse).

J. Chem. Soc., Dalton Trans. 1898 (1981). Further studies on the interaction of nitric oxide with transition metal alkyls (with A. R. Middleton).

J. Chem. Soc., Chem. Commun. 451 (1981). Phenylamido complexes of rhenium(I) and rhenium(III) (with K. W. Chiu and W. K. Wong).

J. Chem. Soc., Dalton Trans. 2088 (1981). Interaction of t-butyl isocyanide with methyl compounds of tungsten, rhenium, zirconium, titanium, and tantalum. The X-ray crystal structures of W—N(Bu^t)CMe$_2$(Me)(NBu^t)[N(Bu^t)CMe=CMe$_2$] and its hydrogen chloride adduct. t-Butyl isocyanide complexes of molybdenum(0), ruthenium(II) and rhodium(I) (with K. W. Chiu, R. A. Jones, A. M. R. Galas and M. B. Hursthouse).

J. Chem. Soc., Dalton Trans. 2496 (1981). Synthesis and crystal structures of tetraethylammonium μ_3-acetyl-C^1(Fe^{1}Fe^2)O(Fe^{1}Fe^3) - nonacarbonyl - triangulo - triferrate and tetraethylammonium μ-carbonyl-nonacarbonyl - μ_3 - 2,4 - dioxapentylidyne - triangulo - triferrate (with W. K. Wong, A. M. A. Galas, M. B. Hursthouse and M. Thornton).

Inorg. Chem. **20**, 3934 (1981). Trimethylsilylmethylidene compounds of Mo and W (with R. A. Andersen, M. H. Chisholm, J. F. Gibson, W. Reichert and I. P. Rothewell).

J. Chem. Soc., Chem. Commun. 1164 (1981). Acetato

complexes of Osmium(II,III) (with D. S. Moore and A. S. Alves).

1982

J. Chem. Soc., Dalton Trans. 663 (1982). Synthesis and X-ray crystal structure of 1,2-dimethyl-4,6-dinitro-3,5-bis(trimethylphosphine) platinum(IV) (with A. R. Middleton, N. P. Walker and M. B. Hursthouse).

Polyhedron **1**, 31 (1982). Synthesis and reactions of phenylimidotrimethylbis (trimethylphosphine) rhenium(V). Synthesis and X-ray crystal structure of bis (trimethylsilylmethyl) oxorhenium(V) - μ - oxo - tetrakis (triomethylphosphine) rhenium(I) (trimethylsilyl methyl) dioxorhenium(V) (Re—Re) (with K. W. Chiu, W. K. Wong, A. M. R. Galas and M. B. Hursthouse).

Polyhedron **1**, 37 (1982). Reactions of phenylimidotrichlorobis (triphenylphosphine) rhenium(V). Reaction with trimethylphosphine and reduction of trimethylphosphine complex to phenylimido complexes of rhenium(I,III). The X-ray crystal structures of phenylamido (dinitrogen) tetrakis (trimethylphosphine) rhenium(I) and phenylamido(buta-1,3-diene)-tetrakis(trimethylphosphine)rhenium(I) (with K. W. Chiu, W. K. Wong, A. M. R. Galas and M. B. Hursthouse).

Coord. Chem. Rev. **43**, 17 (1982). (Sacconi Lecture, Florence), Homogeneous hydrogenation of carbon monoxide (with J. R. Blackborow and R. J. Daroda).

Polyhedron **1**, 83 (1982). Triphenylphosphonium and trimethylphosphonium hexachloroosmates(IV) and their reactions with alkylating agents: methyl and trimethylsilylmethyl osmium compounds; *trans*-dichlorotetrakis(trimethylphosphine)osmium(II); tetrakis (trimethylsilylmethyl) oxoosmium(VI) (with A. S. Alves, D. S. Moore and R. A. Andersen).

Polyhedron **1**, 209 (1982). Convenient syntheses of zero valent 2,2′-bipyridine and related complexes of transition metals (with J. M. Quirk).

Polyhedron **1**, 441 (1982). Trimethyl and diethylphenylphosphine complexes of rhenium(I,III,IV,V) and their reactions. X-ray crystal structures of a bis(η^5-cyclopentadienyl)-ethane-bridged dirhenium(I) compounds obtained from phenylacetylene, tetrakis (diethylphenylphosphine) (dinitrogen) hydridorhenium(I), tetrakis(trimethylphosphine)(η^2 - dimethylphosphinomethyl)rhenium(I) and tetrakis(trimethylphosphine) (iodo)methylrhenium(III) iodide tetramethylphosphonium iodide (with K. W. Chiu, C. G. Howard, H. S. Rzepa, R. N. Sheppard, A. M. R. Galas and M. B. Hursthouse).

Polyhedron **1**, 641 (1982). Synthesis of the hexaphenoxotungstate ion; The X-ray crystal structures of the tetraethylammonium and lithium salts (with J. I. Davies, J. F. Gibson, A. C. Skapski and W. K. Wong).

Polyhedron **1**, 803 (1982). t-Butyl isocyanide complexes of rhenium(I), chromium(0), tungsten(0,I) and platinum(II); X-ray crystal structures of bis(t-butylisocyanide) tris (trimethylphosphine) chlororhenium(I) and tris (t-butylisocyanide) bis(trimethylphosphine) chlororhenium(I) (with K. W. Chiu, C. G. Howard, A. M. R. Galas and M. B. Hursthouse).

J. Chem. Soc., Chem. Commun. 482 (1982). Two-dimensional δ/J resolved ^{31}P NMR spectroscopy of [bis (diphenyl)phosphinomethane] (trimethylphosphine) chlororhodium(I) (with K. W. Chiu, H. S. Rzepa, R. N. Sheppard and W-K. Wong).

Polyhedron **1**, 809 (1982). Bis(diphenylphosphino)methane trimethylphosphine alkyl and η^5-cyclopentadienyl compounds of rhodium(I); $^{31}P\{^1H\}$ two dimensional δ/J resolved and Overhauser effect nuclear magnetic resonance spectroscopy (with K. W. Chiu, H. S. Rzepa, R. N. Sheppard and W. K. Wong).

J. Chem. Soc., Chem. Commun. 1077 (1982). Tertiary phosphine adducts of manganese(II) dialkyls: Synthesis and X-ray crystal structure of bis(trimethylphosphine)bis(trimethylsilylmethyl) bis (μ-trimethylsilylmethyl) dimanganese(II) (with J. I. Davies, C. G. Howard and A. C. Skapski).

Polyhedron **1**, 840 (1982). X-ray crystal structure of the tris(acetato)dioxoosmate(VI) anion (with T. Behling, M. V. Capparelli and A. C. Skapski).

Angew. Chem. 441 (1982). Bis(dinitrogen)- and diethylenemolybdenum(0) complexes (with E. Carmona, J. M. Marin, M. L. Poveda, J. L. Atwood and R. D. Rogers).

Polyhedron **1**, 842 (1982). Electrophilic attacks on μ_3-bridging acetyl in a triiron carbonyl cluster; C—O bond cleavage to give μ_3-ethylidyne and μ-methoxo groups (with W. K. Wong, A. M. R. Galas, M. Thornton-Pett and M. B. Hursthouse).

1983

J. Chem. Soc., Dalton Trans. 1557 (1983). Electrophilic attack on the μ_3-acetyl $C^1(Fe^1Fe^2)O(Fe^1Fe^2)$-(nonacarbonyltriangulo triferrate anion by fluoroboric acid and methylfluorosulphate. Carbon oxygen bond cleavage to give μ_3-ethylidyne and μ-methoxo groups. X-ray crystal structures of $Fe_3(CO)_9(\mu\text{-}H)(\mu_3\text{-}CH_3CO)$, $Fe_3(CO)_9(\mu\text{-}CCH_3)(\mu_3\text{-}OCH_3)$ and $Fe_3(CO)_9(\mu_3\text{-}CCH_3)(\mu_3\text{-}COCH_3)$ (with W. K. Wong, K. W. Chiu, A. M. R. Galas, M. Thornton-Pett and M. B. Hursthouse).

Polyhedron **2**, 803 (1983). Trimethylphosphine complexes of tungsten(0) and (IV). X-ray crystal structures of trimethylphosphine tris(phenylacetylene)tungsten(0); bis (trimethylphosphine) tetrakis (methylisocyanide) tungsten(0), and oxodichlorotris (trimethylphosphine) tungsten(0) (with K. W. Chiu, D. Lyons, M. Thornton-Pett and M. B. Hursthouse).

J. Chem. Soc., Chem. Commun. 476 (1983). Trimethylphosphine hydrides of Mo(II), W(IV) and Re(VII); X-Ray crystal structure of pentakis (trimethylphosphine) dihydro molybdenum(II) (with M. B. Hursthouse, D. Lyons and M. Thornton-Pett).

J. Chem. Soc., Dalton Trans. 2025 (1983). Tertiary phosphine adducts of manganese(II) dialkyls. Part I. Synthesis, properties and structures of alkyl-bridged dimers (with C. G. Howard, M. Thornton-Pett and M. B. Hursthouse).

J. Chem. Soc., Dalton Trans. 2631 (1983). Tertiary phosphine adducts of manganese(II) dialkyls. Part 2. Synthesis, properties and structures of monomeric complexes (with C. G. Howard, G. S. Girolami, M. Thornton-Pett and M. B. Hursthouse).

J. Am. Chem. Soc. **105**, 5944 (1983). Alkyl, hydride and dinitrogen 1,2-bis-(dimethylphosphino)ethane complexes of chromium. Crystal structures of $Cr(CH_3)_2(dmpe)_2$, $CrH_4(dmpe)_2$, and $Cr(N_2)_2(dmpe)_2$ (with G. S. Girolami, J. E. Salt, M. Thornton-Pett and M. B. Hursthouse).

J. Chem. Soc., Chem. Commun. 1163 (1983). Manganese(IV) alkyls. Synthesis and structure of tetramethyl[1,2 - bis(dimethylphosphino)ethane]manganese(IV) (with C. G. Howard, G. S. Girolami, M. Thornton-Pett and M. B. Hursthouse).

J. Am. Chem. Soc. **105**, 6752 (1983). Hydrido, alkyl, and ethylene, 1,2-bis(dimethyl-phosphino)ethane complexes of manganese and the crystal structures of $MnBr_2(dmpe)_2$, $[Mn(AlH_4)(dmpe)_2]_2$ and $MnMe_2(dmpe)_2$ (with G. S. Girolami, M. Thornton-Pett and M. B. Hursthouse).

1984

J. Chem. Soc., Dalton Trans. 305 (1984). Synthesis and reactions of osmium(II) chloro carboxylates. X-ray crystal structure of tetrakis(-*n*-butrato)dichlorodiosmium(III) (with T. Behling, T. A. Stephenson, D. A. Tocher and M. D. Walkinshaw).

Polyhedron **3**, 34 (1984). Mononuclear and dinuclear tertiary phosphine molybdenum complexes. Oxomolybdenum(IV), dinuclear $Mo_2Cl_4L_4$ and related derivatives (with E. Carmona Guzman, A. Galindo, L. Sanches and A. J. Nielson).

J. Chem. Soc., Dalton Trans. 695 (1984). Synthesis, X-ray crystal structure, reactions of pentakis(trimethylphosphine)dihydrido-dimolybdenum(II). The crystal structure of the carbon dioxide insertion product, tetrakis(trimethylphosphine)formato hydrido molybdenum(II) (with D. Lyons, M. Thornton-Pett and M. B. Hursthouse).

Polyhedron **3**, 79 (1984). Interaction of organic azides with methyl compounds of cobalt, rhodium, iridium, ruthenium, and zirconium to give azido 1,3-triazenido complexes. The crystal structures of tris-trimethylphosphineazidodimethylcobalt(III) and bis (carbonyl) trimethylphosphineazidocobalt(I) (with K. W. Chiu, M. Thornton-Pett and M. B. Hursthouse).

J. Am. Chem. Soc. **106**, 2033 (1984). Tertiary phosphine adducts of manganese(II) biscyclopentadienide; magnetic studies and structural characterisation of 'tilted' cyclopentadienyl rings (with C. G. Howard, G. S. Girolami, M. Thornton-Pett and M. B. Hursthouse).

J. Chem. Soc., Dalton Trans. 877 (1984). Trimethylphosphine alkyl and hydrido derivatives of osmium(II). X-ray crystal structure of the metallocycle $Os(CH_2)_2SiMe_2(PMe_3)_4$ (with T. Behling, Gregory S. Girolami, Richard G. Somerville and M. B. Hursthouse).

J. Chem. Soc., Dalton Trans. 1731 (1984). Alkyl, hydrido and related compounds of ruthenium(II) with trimethylphosphine. X-ray crystal structures of hydrido(η^2 - tetrahydridoborato)tetrakis(trimethylphosphine)ruthenium(II), tri-μ-chlorobis[trimethylphosphine)ruthenium(II)]tetrafluoroborate and bis*cis* [methyltetrakis (trimethylphosphine) ruthenium (II)] mercury tetrahydrofuran (1 : 1) (with J. A. Statler, M. Thornton-Pett and M. B. Hursthouse).

J. Chem. Soc., Dalton Trans. 2067 (1984). The preparation and properties of ditertiary phosphine containing complexes of ruthenium(0) (with R. O. Rosete and D. J. Cole-Hamilton).

J. Chem. Soc., Dalton Trans. 2347 (1984). η^5-Cyclopentadienyl and η^5-methylcyclopentadienyl, 1,2 - bis (dimethylphosphino)ethane complexes of titanium(II). The crystal structure of $(C_5H_4Me)_2Ti(dmpe)$ (with G. S. Girolami, M. Thornton-Pett and M. B. Hursthouse).

J. Chem. Soc., Dalton Trans. 2695 (1984). Trioxorhenium(VII)alkoxides, diisopropylamides, and related compounds (with P. Edwards).

Polyhedron **3**, 1025 (1984). Alkyl complexes of palladium(II) with trimethylphosphine and 1,2-bis(dimethylphosphino)ethane ligands (with R. Tooze and K. W. Chiu).

J. Chem. Soc., Dalton Trans. 2789 (1984). 1,2-Bis (dimethylphosphino)ethane alkyl compounds of zirconium(IV) and hafnium(IV). Crystal structures of $Zr(CH_3)_4(dmpe)_2$ and $Zr(CH_2C_6H_5)_4(dmpe)^+$ (with G. S. Girolami, M. Thornton-Pett and M. B. Hursthouse).

Polyhedron **3**, 1083 (1984). Synthesis and X-ray structure of the *trans*-dioxo tetrakis(trimethylphosphine)rhenium(V) cation (with P. G. Edwards, A. C. Skapski and A. M. Z. Slawin).

J. Chem. Soc., Chem. Commun. 799 (1984). Alkyl compounds of diruthenium(III) and diosmium(III). X-ray crystal structure of the first ruthenium peralkyl, hexakis(neopentyl)diruthenium(III) (with R. P. Tooze, M. Motevalli and M. B. Hursthouse).

Polyhedron **3**, 1255 (1984). Alkyl, hydrido and related compounds with trimethylphosphine and bis(1,2-dimethylphosphino)ethane. X-ray crystal structure of *cis*-hydrido ethyltetrakis(trimethylphosphine)ruthenium(II) and ethylene tetrakis(trimethylphosphine) ruthenium(0) (with W. W. Wong, K. W. Chiu, J. A. Statler, M. Motevalli and M. B. Hursthouse).

J. Chem. Soc., Chem. Commun. 1383 (1984). The syntheses and structure of tetra-μ-acetato diruthenium (II,II) bis tetrahydrofuran (with A. J. Lindsay, R. P. Tooze, M. Motevalli and M. B. Hursthouse).

1985

Polyhedron **4**, 603 (1985). Bis(dimethylphosphino) methane complexes of iron and ruthenium (with W. K. Wong, K. W. Chiu, A. J. Howes, M. Motevalli and M. B. Hursthouse).

J. Chem. Soc., Dalton Trans. 587 (1985). Trimethylphosphine polyhydrides of tungsten and ruthenium (with D. Lyons).

J. Chem. Soc., Dalton Trans. 685 (1985). Synthesis and characterisation of 1,2-bis(dimethylphosphino)ethane complexes of chromium(0) and (IV). X-ray crystal structures of *trans*-$Cr(N_2)_2(dmpe)_2$, *cis*-$Cr(CO)_2(dmpe)_2$, $(Ph_2C_2)_2Cr(dmpe)$ and $CrH_4(dmpe)_2$ (with J. E. Salt, G. S. Girolami, M. Motevalli, M. Thornton-Pett and M. B. Hursthouse).

J. Chem. Soc., Dalton Trans. 921 (1985). Alkyl, hy-

dridо and tetrahydroaluminato complexes of manganese with 1,1-bis-(dimethylphosphino)ethane. X-ray crystal structures of $(\mu\text{-}c\text{-}C_6H_{11})_2(C\text{-}C_6H_{11})_2$dmpeMn$_2$, $(dmpe)_2Mn(\mu\text{-}H)_2AlH(\mu H_2)Mn(dmpe)_2^{**}$ and $[Li(Et_2)]_2Li_2\{MnH(C_2H_4)[CH_2(Me)PCH_2CH_2PMe_2]_2\}_2$ (with G. S. Girolami, C. G. Howard, H. M. Dawes, M. Thornton-Pett, M. Motevalli and M. B. Hursthouse).

J. Chem. Soc., Dalton Trans. 931 (1985). Reaction on transition metal carbonylate anions and 1,1,1-tris (halomethyl)ethane. X-ray crystal structures of η^5-cyclopentadienyl - 1 - methylcyclopropylmethyltungsten(II), and tetraethylammonium iodoenna carbonyldodirhenate(0) (with R. Poli, M. Motevalli and M. B. Hursthouse).

J. Chem. Soc., Dalton Trans. 1339 (1985). Synthesis and properties of the divalent 1,2-bis(dimethylphosphino) ethane complexes $MCl_2(dmpe)_2$ and $M(CH_3)_2(dmpe)_2$, M = Ti, V, Cr, Mn or Re. X-ray crystal structures of $MCl(dmpe)_2$, M = Ti, V, Cr, $MnBr_2(dmpe)_2$, "$TiCl_{0.7}Me_{1.3}(dmpe)_2$" and $CrMe_2(dmpe)_2$ (with G. S. Girolami, A. M. R. Galas, M. Thornton-Pett and M. B. Hursthouse).

Polyhedron **4**, 1103 (1985). Synthesis of rhodium(II) pyrazolate complexes. Crystal structure of tetra-μ-3,5-dimethylpyrazolato dirhodium(II) bis-acetonitrile, (Rh—Rh) (with A. R. Barron, M. Motevalli and M. B. Hursthouse).

Polyhedron **4**, 1231 (1985). Bis(dimethylphosphino) methane (dmpe) complexes of iron and chromium. X-ray crystal structures of $FeCr(CO)_6(\mu\text{-dmpm})_2$ and $Fe_2(CO)_4(\mu\text{-dmpm})_2$ (with W. K. Wong, K. W. Chiu, M. Motevalli and M. B. Hursthouse).

J. Chem. Soc., Dalton Trans. 2167 (1985). Oxoalkyls of rhenium(V) and (VI). X-ray crystal structures of $(Me_4ReO)_2Mg(thf)_4$, $[(Me_3SiCH_2)_4ReO]_2Mg(thf)_2$, $Re_2O_3Me_6$ and $Re_2O_3(CH_2SiMe_3)_6$ (with P. Stavropoulos, P. G. Edwards, M. Motevalli, K. M. Abdul Malik and M. B. Hursthouse).

J. Chem. Soc., Chem. Commun. 664 (1985). The synthesis and structure of a new type of bridged hydridoaluminate complex: 1,2; 1,2; 2,3; 2,3-tetra-μ-hydrido - 1,1,1,2,3,3,3 - heptahydrido - 1,1,1,3,3,3 - hexakis(trimethylphosphine) - 1,2 - ditungsten(IV) - 2 - aluminium (with A. R. Barron, M. B. Hursthouse and M. Motevalli).

J. Chem. Soc., Dalton Trans. 2321 (1985). The synthesis, magnetic, electrochemical and spectral properties of diruthenium(II,II)tetra-μ-carboxylates and their adducts. X-ray structures of $Ru_2(O_2CR)_4L_2$, R = Me, L = H_2O, thf, E = Et, L = Me_2CO (with A. J. Lindsay, M. Motevalli and M. B. Hursthouse).

Polyhedron **4**, 1491 (1985). Nitrosation of alkenes by nitric oxide. Crystal structures of bis-(1-nitroso-2-nitro-cyclohexane) and bis-(1-nitroso-2-nitrophenylethane) (with K. W. Chiu, P. D. Savage and D. J. Williams).

J. Chem. Soc., Chem. Commun. 1139 (1985). Synthesis and X-ray structures of the first tetrahedral osmium(IV) compounds, tetrakis(cyclohexyl)osmium(IV) and tetrakis(*o*-methylphenyl)osmium(IV) (with R. P. Tooze, P. Stavropoulos, M. Motevalli and M. B. Hursthouse).

1986

J. Chem. Soc., Dalton Trans. 81 (1986). Transition metal polyhydride anions: a new synthetic route. X-ray crystal structure of $\{[(Me_3P)_3WH_5]^-Li^+\}_4$ (with A. R. Barron, M. B. Hursthouse and M. Motevalli).

J. Chem. Soc., Dalton Trans. 279 (1986). Synthesis and characterisation of tungsten and rhenium alumion–polyhydrides; X-ray crystal structures of $(Me_3)_3H_3W(\mu\text{-}H)_2Al(H)(\mu\text{-}OBu^n)_2Al(H)(\mu\text{-}H)_2WH_3(PMe_3)_3$ and $(Me_3P)_3H_3W(\mu\text{-}H)_2Al(H)(\mu\text{-}H)_2WH_3(PMe_3)_2$ (with A. R. Barron, D. Lyons, M. Motevalli, A. J. Howes and M. B. Hursthouse).

J. Chem. Soc., Dalton Trans. 287 (1986). Tertiary phosphine aluminohydride complexes of ruthenium(II) and osmium (with A. R. Barron).

J. Chem. Soc., Dalton Trans. 1141 (1986). Reactions of bis(dinitrogen)bis[1,2 - bis(dimethylphosphino) ethane]chromium(0) and bis(carbonyl)bis[1,2-bis(dimethylphosphino)ethane]chromium(0) with acids and oxidizing agents. X-ray crystal structure of *trans*-$Cr^{II}(O_2CCF_3)_2(dmpe)_2$, *trans*-$[Cr^{II}(NCR)_2(dmpe)_2](CF_3CO_2)_2$, (R = Me, Et), *trans*-$[Cr^{III}Cl_2(dmpe)_2](BPh_4)\cdot CH_2Cl_2$, *trans*-$[Cr^{I}(CO)_2(dmpe)_2](PB_4)$ and $[Cr^0H(CO)_2(dmpe)_2](BPh_4)$ (with J. E. Salt, M. Motevalli and M. B. Hursthouse).

J. Chem. Soc., Dalton Trans. 1329 (1986). Tertiary phosphine aluminohydride complexes of chromium-, molybdenum- and tungsten(II) (with A. R. Barron and J. E. Salt).

J. Chem. Soc., Chem. Commun. 433 (1986). The synthesis and structure of the unusual polymeric compounds $\{Na_3[Ru_2(\mu\text{-}O_2CR)_4]\cdot 6H_2O\}_n$ (with A. J. Lindsay, M. Motevalli and M. B. Hursthouse).

J. Chem. Soc., Dalton Trans. 2017 (1986). Bis(η^5-cyclopentadienyl)(η^2-acetonitrile)molybdenum(II): the first structurally characterized complex containing a η^2-nitrile ligand (with T. C. Wright, M. Motevalli and M. B. Hursthouse).

J. Chem. Soc., Dalton Trans. 2711 (1986). Alkyl compounds of ruthenium(III and V) and osmium(III). Structures of hexakis(trimethylsilylmethyl)- and hexakis (neopentyl)diruthenium(III), hexakis(trimethylsilylmethyl)dioxodiruthenium(V) and hexakis(neopentyl) bis(η^3-allyl)diosmium(III) (with R. P. Tooze, M. Motevalli and M. B. Hursthouse).

Polyhedron **5**, 1625 (1986). Note on the hydrogenation of imines by rhodium phosphine complexes (with C. J. Longley and T. J. Goodwin).

Polyhedron **5**, 1833 (1986). Tertiary phosphine borohydrido complexes of chromium, tungsten and rhenium. Crystal structures of *trans*-hydrido(η^2-tetrahydroborato) bis[1,2 - bis (dimethylphosphino) ethane] chromium(II) (with A. R. Barron, J. E. Salt, M. Motevalli and M. B. Hursthouse).

Polyhedron **5**, 1897 (1986). Transition-metal aluminohydride complexes (with A. R. Barron).

J. Chem. Soc., Chem. Commun. 1398 (1986). Synthesis and X-ray structure of a chromium(VI) aryl, $(Bu^tN)_2$

$Cr(2,4,6\text{-}Me_3C_6H_2)_2$ (with M. B. Hursthouse, M. Motevalli and A. C. Sullivan).

1987

J. Chem. Soc., Dalton Trans. 169 (1987). Oxoaryls of rhenium(V), (VI) and osmium(VI). X-ray crystal structure of dioxodimesitylrhenium(VI), oxotetramesitylrhenium(VI) and dioxodimesitylosmium(VI) (with P. Stavropoulos, P. G. Edwards, T. Behling, M. Motevalli and M. B. Hursthouse).

J. Chem. Soc., Dalton Trans. 557 (1987). The synthesis and X-ray crystal structures of homoleptic tetrahedral aryls of osmium(IV) and of cyclohexyls of osmium, ruthenium and chromium(IV) (with P. Stavropoulos, P. D. Savage, R. P. Tooze, B. Hussain, M. Motevalli and M. B. Hursthouse).

J. Chem. Soc., Dalton Trans. 837 (1987). Reactions of aluminopolyhydride complexes of tungsten. X-ray crystal structures of $[(Me_3P)_3H_3W(\mu\text{-}H)_2AlCl(\mu\text{-}N{=}CHEt)]_2$, $[(Me_3P)_2WH_5]Li(Me_3P)_3WH_2I(SiMe_3)$ and $(Me_3P)_3H_2W(\mu\text{-}H)_3AlCl_2NMe_3$ (with A. R. Barron, M. Motevalli and M. B. Hursthouse).

Acta. Cryst. C. **C43**, 214 (1987). Crystal structure of hydridochloro (carbonyl) tris (diphenylmethylphosphine)ruthenium(II) $[RuHCl(CO)(PPh_2Me)_3]$ (with M. Motevalli, M. B. Hursthouse and A. R. Barron).

J. Chem. Soc., Dalton Trans. 2723 (1987). Reactions of tetra - μ - carboxylatodiruthenium(II,II) compounds. X-ray crystal structures of $Ru_2(\mu\text{-}O_2CR)_4(thf)_2$, $Ru_2(\mu\text{-}O_2CR)_4(NO)_2$, R = Et, CF_3 and $\{Na_3[Ru_2(\mu\text{-}O_2CO_4]\cdot 6H_2O\}_n^+$ (with A. J. Lindsay, M. Motevalli and M. B. Hursthouse).

Polyhedron **6**, 1081 (1987). Oxo methyls of molybdenum(V), tungsten(V) and rhenium(V). X-ray crystal structure of $(Me_4WO)_2Mg(thf)_4$ (with P. Stavropoulos, M. Motevalli and M. B. Hursthouse).

Polyhedron **6**, 1089 (1987). Organonitrile complexes of iron and ruthenium(II). X-ray crystal structure of *trans*-$[Fe(NCMe)_2(dmpe)_2](BPh_4)_2$ (with A. R. Barron, M. Motevalli and M. B. Hursthouse).

Polyhedron **6**, 1351 (1987). Synthesis and reaction of *trans*-dicarbonyl bis[1,2-bis(dimethylphosphino)ethane] vanadium(0). X-ray crystal structures of *trans*-$V(CO)_2(dmpe)_2$, $[cis\text{-}V^I(CO)_2(dmpe)_2(CH_3CN)]BP_4$ and *cis*-$V(CO)_2(dmpe)_2(O_2CEt)$ (with F. J. Wells, M. Motevalli and M. B. Hursthouse).

J. Chem. Soc., Dalton Trans. 2947 (1987). The chemistry of chromium–nitrile complexes of 1,2-bis(dimethylphosphino)ethane. X-ray crystal structures of *trans*-$[Cr^{IV}Cl(NEt)(dmpe)_2]CF_3SO_3$, *trans*-$[Cr^{IV}(N{=}CHMe)_2(dmpe)_2](BPh_4)_2$, and *trans*-$[Cr^0(H\cdot MeCN)_2(dmpe)_2](BPh_4)_2$ (with A. R. Barron, J. E. Salt, M. Motevalli and M. B. Hursthouse).

Polyhedron **6**, 1599 (1987). Synthesis and molecular structure of chlorotris(trimethylsilylmethyl)trimethylsilylmethylidyne rhenium(VII) (with P. D. Savage, M. Motevalli and M. B. Hursthouse).

1988

J. Chem. Soc., Chem. Commun. 704 (1988). Facile formation of a rhenium benzyne derivative by ligand induced *ortho*-hydrogen abstraction in a homoleptic rhenium aryl. X-ray crystal structure of $Re(\eta^2\text{-}2\text{-}MeC_6H_3)(2\text{-}MeC_6H_4)_2(PMe_2Ph)_2$ (with J. Arnold, B. Hussain and M. B. Hursthouse).

Polyhedron **7**, 1079 (1988). Alkylimido and oxo aryls of rhenium. X-ray structures of $(Bu^tN)_2ReCl_2(o\text{-}MeC_6H_4)$ and $MO_2(2,6\text{-}Me_6C_6H_3)_2$, M = Re and Os (with C. J. Longley, P. D. Savage, B. Hussain and M. B. Hursthouse).

J. Chem. Soc., Dalton Trans. 53 (1988). Synthesis and reactions of d^0 imido aryl derivatives of chromium, molybdenum and tungsten. Crystal structures of $(Bu^tN)Crmes$, $(Bu^tN)_2Mo(2,6\text{-}xylyl)_2$ and $(Bu^tN)_2Cr(Cmes{=}NBu^t)mes$ (with A. C. Sullivan, M. Motevalli and M. B. Hursthouse).

J. Chem. Soc., Dalton Trans. 219 (1988). Triangulotrirhenium(III) alkyl compounds. The X-ray crystal structures of $Re_3(\mu\text{-}Cl)_{1.5}(\mu\text{-}Me)_{1.5}(CH_2Ph)_6$ and $Re_3(\mu\text{-}Me)_3(CH_2Ph)_6$ (with A. C. C. Wong, P. G. Edwards, M. Motevalli and M. B. Hursthouse).

J. Chem. Soc., Dalton Trans. 669 (1988). The synthesis of homoleptic tetrahedral aryls of rhenium(IV) and ruthenium(IV). The X-ray crystal structures of tetrakis (*o*-methylphenyl)rhenium(IV), oxotetrakis(*o*-methylphenyl)rhenium(VI) and tetrakis(*o*-methylphenyl) rhenium(IV) (with P. D. Savage, G. Wilkinson, M. Motevalli and M. B. Hursthouse).

J. Chem. Soc., Dalton Trans. 1737 (1988). Interaction of bis(cyclopentadienyl)acetonitrile molybdenum(II), tricarbonyl tris(acetonitrile)molybdenum(0) and (μ-tetraacetato)dimolybdenum(II) with electrophilic reagents in acetonitrile. X-ray crystal structures of $[(\eta^5\text{-}C_5H_5)_2Mo^{IV}(MeCN)(HN{=}CHMe)](BF_4)_2$, $[(\eta^5\text{-}C_5H_5)_2Mo^{IV}(PMe_3)_2](BF_4)_2$, $(Mo^0(CO)_2(MeCN)_3(\eta^3\text{-}CH_2CHNH_2)](BF_4)$, and $[Mo_2^{III}(\mu\text{-}O)(MeCN)_{10}](BF_4)_4$ (with B. S. McGilligan, T. C. Wright, M. Motevalli and M. B. Hursthouse).

Polyhedron **7**, 1239 (1988). Hydrogenation of alkenes by diruthenium(II) tetraacetate (with A. J. Lindsay and G. McDermott).

Polyhedron **7**, 1363 (1988). Triangulorhenium(III) alkoxides. X-ray crystal structures of $Re_3(\mu\text{-}Cl)_3(OBu^t)_6$ and $Re_3(\mu\text{-}Cl)(\mu\text{-methoxo})_2(menthoxo)_5$ and of $Re_2(\mu\text{-}Cl)_2(CO)_6(THF)_2$ (with A. C. C. Wong, B. Hussain, M. Motevalli and M. B. Hursthouse).

Polyhedron, in press. 1,2-bis(dimethyl)phosphinoethane complexes of molybdenum and vanadium. X-ray crystal structure of *trans*-$[MoCl(\eta^2\text{-}NCMe)(dmpe)]BPh_4$, *trans*-$[Mo(SPh)_2(dmpe)_2]$, *trans*-$[V(NCMe)_2(dmpe)_2](BPh_4)_2$, *trans*-$[V(CNBu^t)_2(dmpe)_2](PF_6)_2$ (with S. J. Anderson, F. J. Wells, B. Hussain and M. B. Hursthouse).

Polyhedron Vol. 7, No. 21, pp. 2119–2128, 1988
Printed in Great Britain

0277–5387/88 $3.00+.00
© 1988 Pergamon Press plc

MOLECULAR ORBITAL BOND INDEX (MOBI) CALCULATIONS ON SELECTED ORGANOLITHIUM AND LITHIUM 'ATE SPECIES: EVIDENCE FOR Li···H—C THREE-CENTRE INTERACTIONS

DONALD BARR and RONALD SNAITH

University Chemical Laboratory, Lensfield Road, Cambridge CB2 1EW, U.K.

and

ROBERT E. MULVEY and PETER G. PERKINS*

Department of Pure and Applied Chemistry, University of Strathclyde, Glasgow G1 1XL, U.K.

(*Received* 16 *December* 1987; *accepted* 15 *March* 1988)

Abstract—Molecular Orbital Bond Index (MOBI) calculations have been carried out on selected organolithium tetramers and hexamers, and on certain lithium 'ates, all of which had previously been shown to exhibit short Li···HC contacts in their solid-state structures. Species so examined comprised $(MeLi)_4$, $(EtLi)_4$ and their "dimerized" forms (to mimic the further association of these tetramers in the crystal), $(Me_2CHLi)_6$ and $(H_3SiCH_2Li)_6$, [as models for $(c\text{-}C_6H_{11}Li)_6$ and $(Me_3SiCH_2Li)_6$, respectively], and $(LiAlEt_4)_n$ and $(LiBMe_4)_n$, with $n = 1, 2$. The calculational results indicate that the short Li···HC distances observed reflect genuine three-centre interactions between lithium centres and C—H bonds: thus, summed Li···H bond indices (measures of the electron density between the nuclei concerned) contribute significantly (44 → 14%) to the total lithium valency, and concomitant weakening of the indices of involved C—H bonds (0.80–0.90; cf. indices of distant C—H bonds, *ca* 0.95) is observed.

"Agostic" ligands which place C—H bonds near to transition metal centres, thereby forming M···H—C bridging systems, are now well documented and these metal–hydrocarbon interactions have considerable ramifications for the possible activation of involved C—H bonds.[1] In fact, however, the likely occurrence of interactions between *lithium* centres and C—H units was foreseen and remarked upon long before transition metals were found to also show such effects.[2,3] Evidence for these like-interactions is usually found when lithium's coordination number is less than four due to the steric requirements of the attached ligands. Such evidence has to date mainly rested on short Li···(H—C) distances in the crystal structures of certain organolithiums such as $(c\text{-hexylLi})_6$,[4] {Li···C_α 2.184 Å, Li···H_α 2.003 Å, Li···C_β 2.300 Å, Li···H_β 2.09 and 2.33 Å}, and cubanes $(MeLi)_4$[2,5] and $(EtLi)_4$[6] {whose tetrameric units polymerize through inter-cubane interactions with Li···C/Li···H distances of 2.37/2.29 Å and (to methylene unit) 2.53/2.23 Å, respectively, while, within each tetramer, Li—C and Li···H distances are 2.31/2.40 Å and (to methylene unit) 2.30/2.44 Å, respectively}; in these hexamers and (isolated) tetramers, the Li atoms are only three-coordinate (with respect to C atoms). Several lithium 'ate species also exhibit short Li···H contacts in their crystal structures, e.g. in $(LiAlEt_4)_\infty$[7] and in $(LiBMe_4)_\infty$.[8] Other evidence possibly in favour of Li···HC interactions has come from IR spectroscopy, in that, for alkyl- and aryllithiums aliphatic α-CH and aromatic *ortho*-CH stretching modes appear at lower frequencies relative to those in the parent hydrocarbons.[9] Furthermore, several dilithiations are known to proceed regioselectively, the position

*Author to whom correspondence should be addressed.

of the second lithiation being apparently directed by Li···HC interactions within the monolithium species, e.g. for 2,2′-dilithiobiphenyl,[10] 1,8-dilithionaphthalene;[11] in the monolithium precursors of these systems, MNDO calculations implied the presence of interactions between the single lithium and the kinetically activated H atoms, the LUMO coefficients being largest at these atoms, and the corresponding C—H bond lengths being the largest. Such structural, reactivity and calculational studies have recently been combined, and re-inforced by NMR spectroscopy, in a study of the dilithiation of 2-lithio-1-phenylpyrrole, whose crystal structure (and MNDO-optimized one) shows a short Li···*ortho*-phenyl C—H contact; a 2D-HOESY NMR experiment detected this short ^{6}Li—^{1}H distance and a second lithiation was shown to occur at this C—H position.[12] Similar NMR work has revealed unusually short Li···H distances in $(Bu^nLi)_4$ and, linked to MNDO calculations, has supported the proposed mechanism of specific second lithiation of 1-lithionaphthalene through detection of a short Li···H(C_8) contact in a MeLi·1-lithionaphthalene aggregate.[13]

Despite the above accumulated evidence, the extent and electronic importance of Li···HC interactions remains uncertain. For example, it has been pointed out that in $(Me_3SiLi)_6$,[14] Li···H distances are much longer (shortest 2.31 Å, most exceeding 2.5 Å) than those in (*c*-hexylLi)$_6$, yet the two compounds adopt very similar structures. A recent publication in this area concerning the crystal structure of $(Me_3SiCH_2Li)_6$,[15] with Li—C distances of 2.20 and 2.27 Å, and short Li···H ones of 2.0–2.3 Å, concludes that the latter such distances alone do not answer the question regarding Li···H bonding, and calls for IR spectroscopic and theoretical studies to probe this question further. In this paper we respond in part to this by presenting the results of Molecular Orbital Bond Index (MOBI) calculations on many of the organolithiums and lithium 'ates noted above as exhibiting short Li···HC contacts.

EXPERIMENTAL

Theoretical calculations

Molecular Orbital Bond Index (MOBI) calculations were run within a modified INDO–MO–SCF framework, on an ICL 2900 computer and in selected cases, by ground-state SCF followed by configuration interaction methods using a known suite of programs.[16] In this paper we make use of the *bond index* (N.B. not bond *order*) and this is a rotationally invariant quantity and is constructed from the Coulson density matrix

$$B_{AB} = \sum_{\varepsilon A} \sum_{\sigma \varepsilon B} P^2_{\lambda\sigma}.$$

The valency is hence

$$V_A = \sum_B B_{AB}.$$

RESULTS AND DISCUSSION

Molecular Orbital Bond Index (MOBI) studies

Apart from the MNDO optimizations referenced above,[10–13] few MO studies have been applied specifically to the question of Li···HC interactions in known (rather than theoretical) organolithiums, although several have, in passing, remarked on results relevant to them. For example, a PRDDO study on planar $(MeLi)_n$, $n = 4$–6 showed small Li···H atomic overlap populations, though, for more realistic T_d tetramer and D_{3d} hexamer forms, overlap populations were larger despite similar Li···HC distances;[17] such a result in itself implies that Li···H/C distances alone are unlikely to be a good guide to the importance or otherwise of these M–hydrocarbon interactions. In the INDO-based MOBI method used to investigate the electronic structures and thermochemistries of many main-group species,[18] interactions between all orbitals on every atom of the molecule are taken into account, whether or not the atoms are formally contacted and thus "bonded". From these, bond indices B_{IJ},[19] viewed as the covalent contribution to the bond between the nuclei concerned, are computed. These will rarely be integral although in electron-precise molecules of low polarity (e.g. hydrocarbons) they are quasi-integral, and further, indices for formally "non-bonded" interactions will usually be small, but not negligible in terms of the overall picture of bonding within the molecule. It follows that the valency of an individual atom, the sum of all its bond indices, will generally deviate from a simple whole number. Although representations like INDO may suffer from basis set superposition effects,[20] leading to an underestimation of the positive charges on lithium, three-centre Li···H—C interactions nevertheless, involving low polarity C—H bonds, will have some covalent character and overall weakening of C—H bonds, whether brought about by covalent or electrostatic interactions or by some combination of them, will be detectable through a reduction of their bond indices. This has been borne out in many calculations of intrinsic bond energies.[18]

Calculations on selected organolithium systems

The set of organolithium molecules specifically chosen for MOBI studies comprised methyllithium $(MeLi)_4$,[5] ethyllithium $(EtLi)_4$,[6] cyclohexyllithium $(c\text{-}C_6H_{11}Li)_6$,[4] and trimethylsilylmethyllithium $(Me_3SiCH_2Li)_6$.[15] For calculational simplicity $(c\text{-}C_6H_{11}Li)_6$ was treated as $(Me_2CHLi)_6$ and $(Me_3SiCH_2Li)_6$ was treated as $(H_3SiCH_2Li)_6$. All the atomic coordinates inserted into the calculational program were taken directly from the published solid-state structures of the four compounds, determined from X-ray powder (in the case of $(MeLi)_4$ only) or crystalline studies. As the tetrameric compounds exist in the solid state as connected pseudo-cubane units, an attempt was made to ascertain the reason for such association by carrying out additional calculations on $[(MeLi)_4]_2$ and $[(EtLi)_4]_2$, "dimerized" forms of these tetramers.

The pseudo-cubane skeleton of the $(MeLi)_4$/$(EtLi)_4$ tetramers, made up of interpenetrating C_4 and Li_4 tetrahedra, is shown in Fig. 1(a). Each carbon bridges a triangle of metal atoms, so in total there are 12 C—Li bonds in the $(CLi)_4$ electron-deficient core. Formal coordination numbers, even disregarding possible Li···HC contacts or short Li···Li contacts, are six for carbon and three for lithium. The model structures of both $[(MeLi)_4]_2$ and $[(EtLi)_4]_2$, which mimic the way the tetramers pack in their crystal lattices, consist of two such pseudo-cubane units linked together by intermolecular C—Li contacts, which raise the coordination numbers of the participating atoms to seven and four, respectively. Figure 1(b) shows the distorted octahedral arrangement of the six lithium atoms in the $(Me_2CHLi)_6$ and $(H_3SiCH_2Li)_6$ hexameric models. The six organic groups (for clarity only one is shown) sit over six of the eight triangular lithium faces (the remaining larger faces are both unbridged) making a total count of 18 C—Li bonds. The core atoms have equivalent coordination numbers to those of corresponding atoms in the smaller tetramers, due to similar bridge-bonding in each type of cluster.

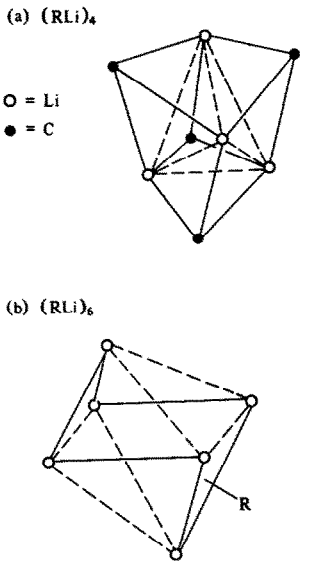

Fig. 1. (a) The pseudo-cubane skeleton of $(RLi)_4$ organolithium tetramers and (b) the distorted octahedral arrangement of the six lithium atoms in $(RLi)_6$ hexamers; the two triangular Li_3 faces unbridged by R groups are marked by broken lines.

Table 1 records mean values of C—Li interatomic distances, valencies and charges for the car-

Table 1. MOBI calculational data on organolithium clusters

Species	C—Li distances (Å)	Carbon valency	Lithium valency	Carbon charge	Lithium charge	C—Li bond[a] indices	I_v[b]
$(MeLi)_4$	2.31	3.54	1.49	−0.38	+0.16	0.26 × 3	51
$[(MeLi)_4]_2$	2.31	3.54	1.48	−0.38	+0.16	0.25 × 3	51
	2.37[c]	3.45	1.63	−0.40	+0.08	0.14 × 1	8
$(EtLi)_4$	2.30	3.46	1.55	−0.23	+0.13	0.21 × 3	42
$[(EtLi)_4]_2$	2.30	3.47	1.53	−0.23	+0.14	0.21 × 3	42
	2.53[c]	3.45	1.56	−0.25	+0.12	0.09 × 1	6
$(Me_2CHLi)_6$	2.23	3.71	1.60	−0.16	+0.10	0.20 × 3	38
$(H_3SiCH_2Li)_6$	2.22	3.59	1.56	−0.35	+0.12	0.20 × 3	39

[a] Each tetramer has 12 such intramolecular C—Li bonds and each hexamer 18 of such. This column presents the mean bond index (×3 for a particular lithium). As expected from the symmetries of the species (reflected in a small range of bond lengths) little variation in the index was observed.

[b] I_v = mean bond index for all such bonds divided by the mean lithium valency, expressed in percentages.

[c] Data found for the C—Li *inter*molecular contacts.

Table 2. MOBI calculational data on Li···H contacts in organolithium clusters

Species	No. of contacts	Mean Li···H distances (Å)	Range of Li···H distances (Å)	Li···H indices	I_v^a
$(MeLi)_4$	6	2.40	2.40	0.05 × 6	21
$[(MeLi)_4]_2$	3	2.40	2.40	0.05 × 6	21
	3[b]	2.29	2.29	0.05 × 9	25
$(EtLi)_4$	2[c]	2.68	2.36–3.00	0.04 × 2	22
	4[d]	2.44	2.05–2.67	0.06 × 4	
$[(EtLi)_4]_2$	2[c]	2.68	2.36–3.00	0.03 × 2	23
	4[d]	2.44	2.05–2.67	0.04 × 4	
	1[e]	2.86	2.86	0.02 × 1	
	2[f]	2.23	2.09–2.38	0.05 × 2	
$(Me_2CHLi)_6$	1[g]	1.98	1.94–2.02	0.07 × 1	14
	2[h]	2.21	2.10–2.33	0.05 × 2	
$(H_3SiCH_2Li)_6$	4[i]	2.19	1.98–2.46	0.05 × 4	20
	1[j]	2.59	2.54–2.71	0.10 × 1	

[a] Mean Li···H index divided by the mean lithium valency, expressed in percentages.
[b] Li···H between $(MeLi)_4$ units.
[c] Li···(methyl)H.
[d] Li···(methylene)H.
[e] Li···(methyl)H between $(EtLi)_4$ units.
[f] Li···(methylene)H between $(EtLi)_4$ units.
[g] Li···α-H.
[h] Li···β-H.
[i] Li···H (on C).
[j] Li···H (on Si).

bon and lithium atoms, and C—Li bond indices (and their contributions to total lithium valencies) for the organolithium species under investigation. The Li···H contacts are dealt with in Table 2, which lists the number of such contacts, their mean lengths and the ranges of lengths, and their calculated bond indices. The final column in this table, I_v values—the total Li···H index divided by the total lithium valency, expressed as a percentage—is worth singling out as it indicates how much of the lithium valency in each system is due to Li···H interactions. Such numbers thus provide a relative measure of the importance of Li···H interactions for cluster stability.

Pondering over the MOBI-determined valencies and charges catalogued in Table 1, columns 3–6, it is seen that typically, by clustering, lithium achieves a valency of around 1.5–1.6 (cf. its "classical" valency of one precisely), whereas carbon, with values of around 3.4–3.7, fails to reach its "classical" valency of four even in these unusually high coordination environments. Indeed, the data on the $[(MeLi)_4]_2$ or $[(EtLi)_4]_2$ "twin" tetramers [Figs 2(a) and (b)] show that the carbon atoms with the highest coordination numbers, those belonging to one unit which are allowed to interact intermolecularly with a lithium from the second unit, have the lower valencies of 3.45, cf. 3.54 or 3.47, respectively, for the carbon atoms belonging solely to one unit. The implication here is that carbon makes progressively somewhat less efficient use of its valency electrons when surrounded by an increased number of neighbours (i.e. formally six or seven in these systems cf. a maximum of four in conventional organics). Charge effects must not be overlooked, however, because those carbons attached to four lithium atoms (through intra- and intermolecular contact) carry a slightly greater negative charge than those attached to only three (see Table 1, column 5), and this could give extra weighting to the ionic term in the overall bonding scheme. Against this, though, is the fact that the affected lithium centres carry lower positive charges themselves (see Table 1, column 6). Furthermore, it is these lithium atoms linking up the tetramers and not those bound within individual cubanes, that register the higher valency (same table, column 4), i.e. the converse of what was observed for the carbon atoms (see above). Thus, irrespective of the magnitude of the covalency in these systems, it can be concluded that the association phenomenon of solids such as $[(MeLi)_4]_\infty$ or $[(EtLi)_4]_\infty$ (whose lithium···carbon intermolecular

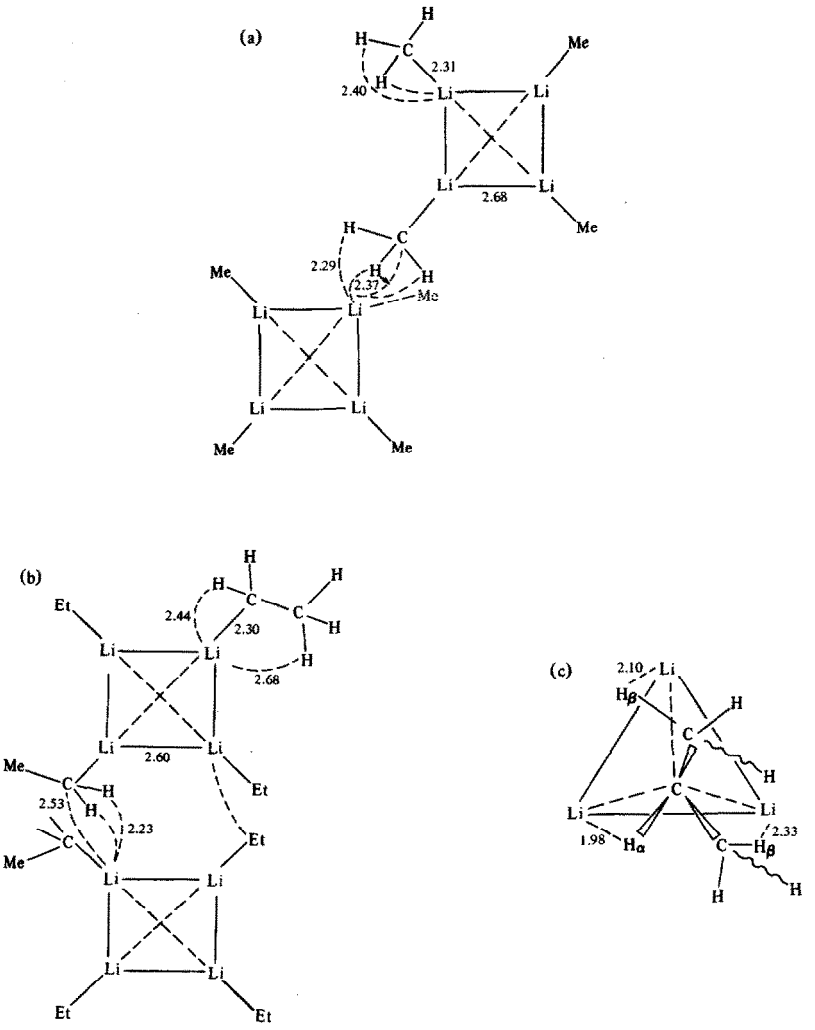

Fig. 2. A plan of the Li···H contacts (with selected interatomic distances in Å) in (a) $[(MeLi)_4]_2$, (b) $[(EtLi)_4]_2$ and (c) one triangular Li_3 face of $(Me_2CHLi)_6$.

association is continuous), derives primarily from the *metal's* desire for high coordination numbers (i.e. to maximize its valency), even though this happens at the expense of some carbon bonding efficiency.

The shortness of the Li···H contacts observed in certain crystal structures can be put into some perspective by comparison with the Li—H *bond* distance in solid lithium hydride, 2.043(1) Å.[21] Bearing this in mind, the yet closer Li···α-H contacts in $(Me_2CHLi)_6$ (mean length, 1.98 Å), our model for $(c\text{-}C_6H_{11}Li)_6$ are remarkable even though as noted earlier, interactions cannot be established on the basis of distance alone. The distances of corresponding contacts in the other organolithiums studied make less of an impact, being generally somewhat longer as can be seen in the mean lengths and ranges of lengths highlighted in columns 3 and 4, respectively of Table 2. It is discernible from the same table that these are not systems with distinct and individual Li···H contacts, since without exception each C—Li structure exhibits three or more per lithium atom. Clearly then, to make a realistic appraisal of their worth, these "interactions" must be considered not just individually but also collectively. Scrutinizing the calculated bond indices (Table 2, column 5) in this way illustrates the inadequacies of making assumptions based on bond length arguments, because although the $(c\text{-}C_6H_{11}Li)$-derived hexamer displays the shortest Li···H lengths (to α-H, mean value 1.98 Å) of all the models examined, the corresponding Li···H indices (mean, 0.07) despite being individually large, do not contribute as much collectively to the total lithium valency (see the I_v values, column 6) as the similar Li···H interactions in other C—Li clusters. Indeed, the I_v value for $(Me_2CHLi)_6$ which takes into account both the Li···α-H and Li···β-H geo-

metrical features [e.g. as in Fig. 2(c)] is the smallest of all the systems studied.

The measured bond indices and their percentage contributions to total lithium valencies I_v (Table 2, columns 5 and 6, respectively) shed light on the key question of this study: does lithium utilize two-electron H—C ligand bond density to help satisfy its valency requirements? The $[(MeLi)_4]_2$ system displays *both* the intra- and intermolecular bonds that are present in the condensed phase tetramer, so the results here should be a more reliable guide than those for the discrete tetramer also examined. It seems significant, therefore, that in the "dimer" the unique, most realistic lithium that connects the two tetrameric units interacts the most, and strongly at that, with nearby protons [Fig. 2(a) shows a plan of these Li···HC contacts], i.e. I_v value 25, cf. 21 in the discrete $(MeLi)_4$ tetramer. Furthermore, although all the C—H distances are equivalent in the calculation (0.98 Å), the corresponding C—H indices differ and in a manner which strengthens the view that Li···H interactions are important in two ways. Thus, the C—H bonds within either one tetrameric unit which are not affected by the lithium atom from the other, have indices of typically 0.86–0.87 (themselves rather weaker than expected for a normal C—H bond, due to internal Li interactions), whereas the C—H bonds involved with lithium atoms drawn from *both* the units are significantly even weaker, index range 0.80–0.81, implying that Li···H—C interactions are not only important in holding each Li_4 cluster together, but also contribute to the mode of coupling of such clusters. The bonding picture in $[(EtLi)_4]_2$—whose Li···HC contacts are shown diagrammatically in Fig. 2(b)—is in accord with that found for $[(MeLi)_4]_2$, in that, although double aggregation now produces a slight weakening of all the Li···H indices *within* the tetramers, the additional intermolecular interactions outweigh this decrease, and consequently the Li···H contribution to the total Li valency increases from 22% in the discrete $(EtLi)_4$ model to 23% in $[(EtLi)_4]_2$. Concomitantly, the C—H bonds influenced by the linking Li atoms weaken [mean index 0.80 cf. C—H bonds not so influenced, mean index, 0.88; cf. in $(EtLi)_4$, mean C—H index, 0.83]. In conclusion, the calculations on these "dimeric" systems certainly support the view that Li···H interactions play a significant part *both* in holding together the respective individual pseudo-cubane units *and* in linking them together.

Results on the hexameric clusters likewise suggest that the observed Li···HC geometrical arrangements represent genuine interactions, although these appear to be rather less important than those in the tetrameric systems. Thus, in $(Me_2CHLi)_6$, each lithium atom has one extremely short contact to an α-H (mean, 1.98 Å) and slightly longer contacts to two β-H's (mean, 2.21 Å) [see Fig. 2(c)] but despite having, as referred to earlier, relatively large individual indices (Table 2, column 5), collectively they account for only 14% of the total Li valency (the smallest found for any C—Li system studied). This, in relative terms, low value, is hardly surprising in view of the small number of Li···H contacts per lithium present (i.e. three) compared to that found in the tetramers (six or nine in the "dimeric" versions). In this instance, although it is clear that these secondary interactions are not as important, it would nevertheless be unwise to dismiss them completely, as 14% is still a considerable contribution. The greater I_v value found for $(H_3SiCH_2Li)_6$, 20% can be accounted for by the larger number of Li···H contacts present (i.e. five, Table 2, column 2), although this still falls short of the lowest recorded for any tetramer studied (21%).

A final feature of these calculations that deserves comment is the notably large contributions made to the lithium valencies by Li···Li indices, arising from the short Li···Li contacts present in these clusters. Many of these contacts are shorter in length (Table 3) than the closest Li···Li separations (3.04 Å)[22] in metallic lithium, a point raised frequently to promote the view that there is extensive electron delocalization in molecular orbitals extending over entire organolithium cluster cages. This gives rise to a significant amount of Li···Li interaction. Although the lithium centres bear partial positive charges, as has been previously pointed out even partial ionic bonds have a covalent component expressible in the bond index, and certainly the magnitude of our I_v values for the Li···Li indices (Table 3) imply an important role for such interactions; thus these values range from 18% for the four distinct Li···Li contacts (per lithium) in $(H_3SiCH_2Li)_6$ to 25% for the three distinct Li···Li contacts (per lithium) in $(MeLi)_4$. Indeed, there is little difference between these I_v values and those found for the Li···H interactions (except in the case of $(Me_2CHLi)_6$, where the Li···H share of the valency is considerably less than the Li···Li share). However, this does not necessarily mean that Li···H and Li···Li interactions contribute equally to the cluster bonding, because in energy terms Li···Li indices may be substantially weaker than Li···H ones. This is given credence by the fact that in metallic lithium, which adopts a body-centred cubic structure, each Li has eight nearest neighbours (i.e. takes part in eight Li···Li bonds), yet the overall bonding is weak, reflected by the metal's softness and its relatively low heat of vapourization.

Table 3. MOBI calculational data on Li···Li contacts in organolithium clusters

Species	Mean Li···Li distances (Å)[a]	Li···Li indices	I_v[b]
$(MeLi)_4$	2.681	0.11 × 3	25
$[(MeLi)_4]_2$	2.681	0.11 × 3	22
$(EtLi)_4$	2.553	0.12 × 3	23
$[(EtLi)_4]_2$	2.553	0.11 × 3	21
$(Me_2CHLi)_6$	2 × 2.397 2 × 2.968	0.10 × 4	24
$(H_3SiCH_2Li)_6$	2 × 2.448 2 × 3.178	0.07 × 4	18

[a] Each tetramer has six similar Li···Li contacts, three for each Li. In hexamers, each Li has two short contacts and two longer (around the "open face"). The value given here is the average of these interactions. The longer "cross ring" contacts have been ignored.

[b] I_v = mean Li···Li index divided by the mean lithium valency, expressed in percentages.

Calculations on the 'ate systems

As alluded to earlier, short Li···HC contacts have also been observed in the crystal structures of some lithium 'ate compounds. Here, we evaluate in turn the results of MOBI calculations on model systems of two such compounds, $(LiAlEt_4)_\infty$[7] and $(LiBMe_4)_\infty$,[8] given in Tables 4, 5 and 6 respectively.

The positive evidence for Li···H interactions that has emerged from the above $(CLi)_{4,6}$ study manifests itself much more markedly in calculations (using actual crystal coordinates) on $(LiAlEt_4)_{1,2}$, the relevant results of which are displayed in Table 4. In the "monomeric" unit [Fig. 3(a)], the conspicuously *individually* large Li···(methylene)H indices (0.11) are in summation apparently responsible for an astonishing 35% of the total lithium valency (1.26), cf. 43% for the total (methylene)C—Li indices; the effect of such interactions is to produce an appreciable weakening of the corresponding methylene C—H bonds (index, 0.82, cf. non-interacting C—H bonds, of distant methylene groups, 0.93). Surprisingly, the shortness of these Li···(methylene)H contacts does not seem to have been previously commented upon (and H atoms were located, rather than their positions calculated). However, these results could be misleading because, in reality, the 'ate is not a discrete molecule but a linear chain structure of alternating lithium and aluminium atoms, bridged by ethyl ligands. Yet, the results in Table 4 for $(LiAlEt_4)_2$ [Fig. 3(b)] are even more emphatic since the Li···H share (I_v) of the whole lithium valency (now 1.52; cf. 1.26 in the "monomer") stays the same (35%) for the "realistic" lithium [i.e. Li_1, sandwiched, as in the crystal structure, between two Al atoms through four

Table 4. MOBI calculational data on $(LiAlEt_4)_{1,2}$ systems

System	$(H_2)C$—Li contacts[a] Total bond index	I_v	Li···$H_2(C)$ contacts[b] No. of contacts	Mean bond index	Total bond index	I_v[c]
$LiAlEt_4$	0.54	43	4	0.11	0.44	35
$(LiAlEt_4)_2$	0.58[d]	38	8	0.06	0.54	35
	0.51[e]	42	4	0.11	0.44	35

[a] Li···(methylene)C, 2.30 Å.

[b] Li···(methylene)H, 2.15 Å.

[c] Total bond index for all such bonds divided by the total lithium valency.

[d] Values for "realistic" Li atom sandwiched between two aluminium atoms through four bridging CH_2 units.

[e] Values for the Li atom linked to one aluminium atom through two bridging CH_2 units.

Table 5. MOBI calculational data on $LiBMe_4$

Atom	Valency	Charge	Contact	Distance (Å)	Index	I_v[a]
Li	1.07	+0.38	C···Li	2.36	0.52	48
B	3.62	+0.17				
C[b]	3.80	−0.16	Li···H_1	2.23	0.12	11
H_1[b]	1.00	+0.06	Li···H_2	2.23	0.12	11
H_2[b]	1.00	+0.06	Li···H_3	2.24	0.13	12
H_3[b]	1.00	+0.05	ΣLi···H	—	0.37	34

[a] The bond index of a particular bond divided by the total lithium valency expressed as a percentage.

[b] These atoms belong to the interacting methyl groups [see Fig. 3(c)].

bridging CH_2 units], even though the corresponding I_v value for the C—Li_1 bonds falls (i.e. 38% cf. 43% for C—Li interactions in the monomer and 42% for "less realistic" C—Li_2 contacts in the dimer). This is due in part to an increased contribution from a second Li···Al contact (2 × 0.10; cf. 1 × 0.11 in the monomer). Again, as in the monomer, the C—H bonds affected by these significant Li···H interactions weaken considerably (index 0.82, cf. non-interacting methylene C—H bonds, 0.93). In conclusion, on the basis of these calculations it is difficult to advocate a case *against* the existence, and indeed importance, of Li···H interactions in this particular molecular structure.

Another 'ate complex highly relevant to the theme of this discussion is $(LiBMe_4)_\infty$. Its structure consists of planar sheets of lithium atoms, which are bridged by the tetramethylboron groups through linear B—CH_3—Li and multi-centre fragments; the geometry of these bridges is such that two types of

Table 6. MOBI calculational data on $(LiBMe_4)_2$[a]

Atom	Valency Isolated dibridge	Charge	Contact	Distance (Å)	Index	I_v[b]
Li_2	1.15	+0.37	Li_2···$C_{2,3}$	2.21	0.25 × 2	44
B_1	3.64	+0.19	Li_2···2H	2.12	0.11 × 2	19
$C_{2,3}$[c]	3.82	−0.21	Li_2···2H	2.11	0.12 × 2	21
2H[c]	1.00	+0.05	ΣLi_2···4H	—	0.46	40
2H[c]	1.00	+0.04				
2H	1.00	+0.06				
	Tribridge to Li_1					
Li_1	1.37	+0.24	Li_1···C_1	2.36	0.19	14
B_2	3.64	+0.18	Li_1···2H	2.23	0.07 × 2	11
C_1[c]	3.86	−0.21	Li_1···H	2.24	0.06	4
3H[c]	1.00	+0.06	ΣLi_1···3H	—	0.20	15
	Dibridge to Li_1					
$C_{5,6}$[c]	3.81	−0.22	Li_1···$C_{5,6}$	2.21	0.20 × 2	29
2H[c]	1.00	+0.04	Li_1···2H	2.12	0.12 × 2	17
2H[c]	1.00	+0.02	Li_1···2H	2.11	0.08 × 2	12
2H	1.00	+0.04	ΣLi_1···4H	—	0.40	29
			Overall			
			Li_1···3C	—	0.59	43
			Li_1···7H	—	0.60	44

[a] For numbering scheme see Fig. 3(d).

[b] Bond index divided by the total lithium valency, expressed as a percentage.

[c] Interacting atoms.

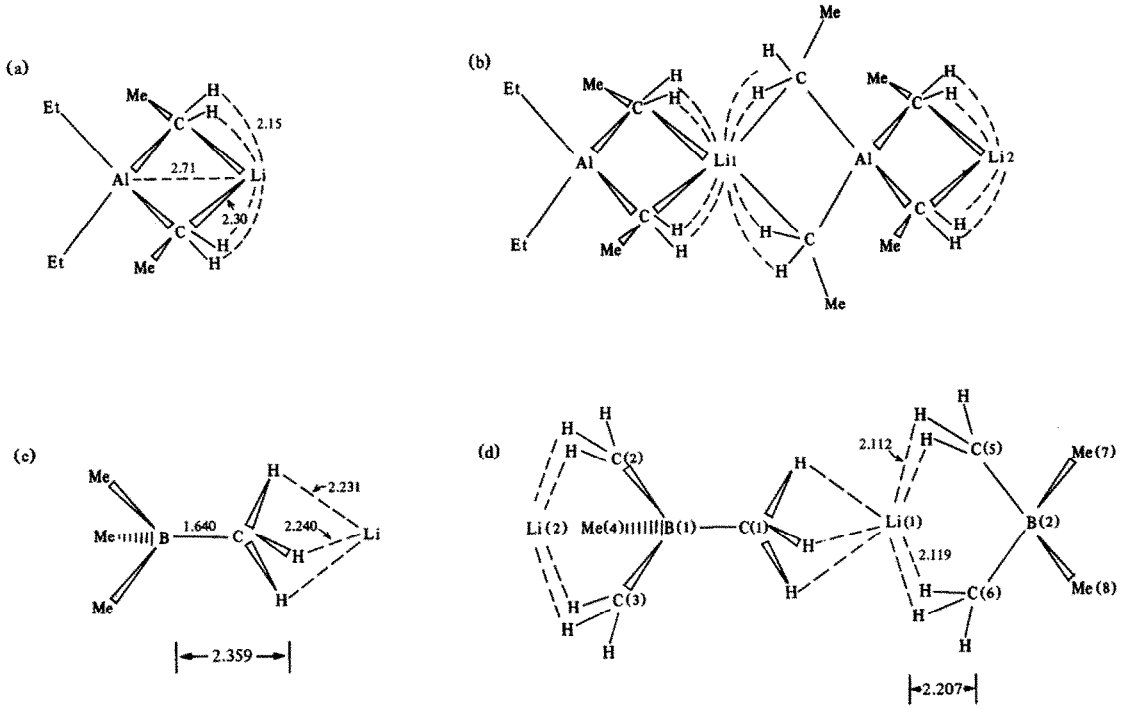

Fig. 3. A plan of the Li···H contacts (with selected interatomic distances in Å) in (a) $(LiAlEt_4)_1$, (b) $(LiAlEt_4)_2$, (c) $(LiBMe_4)_1$ and (d) $(LiBMe_4)_2$.

Li···H···C interactions have been proposed[8] to exist [the two distinct lithium–methyl group environments are shown in Figs 3(c) and 3(d)]. To evaluate this proposition, MOBI calculations were carried out on $(LiBMe_4)_n$ (where $n = 1,2$), using coordinates obtained from a *neutron* diffraction study. Principal results from the study on the monomeric fragment are recorded in Table 5 [this system shows only the effect of the 3H bridge moiety; see Fig. 3(c)]. Li···C and Li···H_3C interactions are strongly implicated by these results, in concord with the earlier report of $(LiBMe_4)_\infty$, as the corresponding bond indices, both collectively and individually, appear to be significant. Moreover, the case for such interactions is consolidated by the observation that the B—(interacting)C bond is substantially weaker (index, 0.67) than the other three B—C bonds present (indices, 0.92 and 0.93). This weakening is not due to an excessively longer bond—indeed, its length (1.640 Å) is actually slightly shorter than that of one of the others (1.654 Å). Similarly, the C—H bonds of the interacting methyl group have smaller indices (mean value, 0.85; mean length, 1.07 Å) than the unaffected ones (mean value, 0.96; mean length, 1.08 Å).

The "dimerized" form, $(LiBMe_4)_2$, was also examined by MOBI calculation and key results are given in Table 6, while Fig. 3(d) shows the numbering scheme used. Thus, Li_1, originally interacting with $C_{(1)}H_3$ ($Li_1···C_1$, 2.36 Å) in a tribridge conformation (mean $Li_1···H$, 2.23 Å) now has further, and indeed closer, contacts with two carbon atoms (5, 6) at 2.21 Å on a second $Me_4B(2)$ unit and with four atoms (two on each carbon, in a double "dibridge" arrangement, mean $Li_1···H$, 2.12 Å); its first coordination therefore now consists of seven H atoms, cf. 10 H in the actual crystal structure where there is a further tribridge to a second CH_3 group. The second lithium atom now added, Li_2, shows only the doubly dibridged interactions to two of the carbon atoms (2, 3) and to four of their attached hydrogen atoms, on B_1 from the original calculation.

Discussion centres first on this "isolated" dibridge; data are shown in the top part of Table 6 and these may be compared with those for the "isolated" tribridge given in Table 5. It is then apparent not only that Li_2 interacts strongly with both CH_2 units, but indeed, that such bonding is apparently even stronger than that noted earlier for the tribridge. Thus the valency of Li_2 here (1.15) is higher than that of the original lithium atom (1.07); further, while indices to the methyl C(2, 3) atoms (2×0.25, 44% of Li_2 valency) are in total, comparable to the single C—Li in the tribridge (0.52, 48%), the four Li···H indices ($2 \times 0.11 + 2 \times 0.12$,

sum 0.46, 40%) are cumulatively greater than the three in the tribridge ($2 \times 0.12+0.13$, sum 0.37, 34%). Numerous significant features noted earlier for the tribridge are also apparent here, notably that the four interacting C—H indices average 0.85 cf. the two non-interacting ones on the same two carbon atoms (2, 3) at 0.95, and the three on the totally uninvolved $C_{(4)}H_3$ group at average, 0.96. Similarly, $B_{(1)}$—C indices vary in an explicable way in that the value to uninvolved C_4 is 0.94, but values to the interacting $C_{2,3}$ atoms in the dibridges are 0.83×2, and to the tribridge C_1, 0.87; although this latter value has increased from that found in the $(LiBMe_4)_1$ calculation (0.67), where this carbon atom (and its three H) was totally providing the covalence requirement of the then single lithium atom, it is still significantly low in this more realistic calculation.

Having made such points, the bonding of the more realistically placed Li_1 atom can now be examined. The first notable feature is the heightened valency of Li_1, 1.37 (cf. 1.07 in the original calculation, 1.15 for Li_2 in this one); in the actual solid structure, where there is further $Li\cdots(CH_3)$ contact, this value can thus be anticipated to rise further to $\sim$ 1.5, which, as pointed out in the section on $(CLi)_{4,6}$ clusters seems a typical value in associated lithium species (indeed such a value reflects the rationale for such association). As expected, interactions to the $C_{(1)}H_3$ unit, particularly to the C_1 atom, weaken (Li_1—C_1, 0.19, 14% of Li_1 valency; to 3H, sum 0.20, 15%) cf. values in the original calculation (0.52, 48%; 0.36, 34%), though they remain significant, a point further emphasized by the weakened $C_{(1)}$—H indices (0.89×2, 0.90) cf. indices within the totally uninvolved $C_{(4)}H_3$ unit on the same B_1 atom, 0.96×3. Very similar comments apply to the Li_1—$C_{(5)}H_2$, $C_{(6)}H_2$ dibridges, with indices to the two C atoms of 0.20×2, sum 0.40, 29% of Li_1 valency (cf. for the dibridges to Li_2 in this same calculation, 0.25×2, 0.50, 44%) and to the 4H atoms of $0.12 \times 2+0.08 \times 2$, sum 0.40, 29% of Li_1 valency (cf. to Li_2, $0.12 \times 2+0.11 \times 2$, 0.46, 40%). Other significant, and now to be expected, features are weakened C—H indices for these dibridges ($C_{5,6}$—four interacting H atoms, mean, 0.87; cf. to two non-interacting H, on same C atoms, 0.96, and the mean index within the totally uninvolved $C_{(7)}H_3$ and $C_{(8)}H_3$ methyl groups, 0.96) and weakened B—C bonds (thus B_2—interacting $C_{5,6}$, 0.83×2; cf. B_2—$C_{7,8}$, 0.92×2).

In conclusion, the calculational results obtained here lend much support to the suggestion made in the structural report of $(LiBMe_4)_\infty$,[8] that lithium$\cdots$alkyl hydrogen interactions, in effect brought about by the strong Lewis acidity of polarized Li centres towards weakly basic alkyl hydrogen atoms, constitute a stereochemically important mechanism for achieving coordinative saturation at lithium centres.

Acknowledgements—We thank the SERC (D.B., R.E.M., R.S.) for financial support and the Royal Society for the award of a 1983 University Research Fellowship (to R.E.M.).

REFERENCES

1. M. Brockhart and M. L. H. Green, *J. Organomet. Chem.* 1983, **250**, 395.
2. E. Weiss and E. A. C. Lucken, *J. Organomet. Chem.* 1964, **2**, 197.
3. G. E. Coates, M. L. H. Green and K. Wade, *Organometallic Compounds: The Main Group Elements*, 3rd Edn, Vol. 1, pp. 35–38. Methuen, London (1967).
4. R. Zerger, W. Rhine and G. Stucky, *J. Am. Chem. Soc.* 1974, **96**, 6048.
5. E. Weiss and G. Hencken, *J. Organomet. Chem.* 1970, **21**, 265.
6. H. Dietrich, *Acta Cryst.* 1963, **16**, 681.
7. R. L. Gerteis, R. E. Dickerson and T. L. Brown, *Inorg. Chem.* 1964, **3**, 872.
8. W. E. Rhine, G. Stucky and S. W. Peterson, *J. Am. Chem. Soc.* 1975, **97**, 6401.
9. E. Maslowsky, *Chem. Soc. Rev.* 1980, **9**, 25; A. N. Rodionov, *Russ. Chem. Rev.* 1973, **42**, 998.
10. U. Schubert, W. Neugebauer and P. v. R. Schleyer, *J. Chem. Soc., Chem. Commun.* 1982, 1184; W. Neugebauer, A. J. Kos and P. v. R. Schleyer, *J. Organomet. Chem.* 1982, **228**, 107.
11. W. Neugebauer, T. Clark and P. v. R. Schleyer, *Chem. Ber.* 1983, **116**, 3283.
12. W. Bauer, G. Müller, R. Pi and P. v. R. Schleyer, *Angew. Chem. Int. Ed. Engl.* 1986, **25**, 1103.
13. W. Bauer, T. Clark and P. v. R. Schleyer, *J. Am. Chem. Soc.* 1987, **109**, 970.
14. W. H. Ilsley, T. F. Schaaf, M. D. Glick and J. P. Oliver, *J. Am. Chem. Soc.* 1980, **102**, 3769.
15. B. Tecle', A. F. M. M. Rahman and J. P. Oliver, *J. Organomet. Chem.* 1986, **317**, 267.
16. D. R. Armstrong, P. G. Perkins and J. J. P. Stewart, *J. Chem. Soc. A* 1971, 3674.
17. G. Graham, S. Richtsmeier and D. A. Dixon, *J. Am. Chem. Soc.* 1980, **102**, 5759.
18. For example, see T. N. Bell, K. A. Perkins and P. G. Perkins, *J. Chem. Soc. Faraday Trans.* 1 1981, 1779; R. E. Mulvey, M. E. O'Neill, K. Wade and R. Snaith, *Polyhedron* 1986, **5**, 1437.
19. D. R. Armstrong, P. G. Perkins and J. J. P. Stewart, *J. Chem. Soc., Dalton Trans.* 1973, 838, 2273.
20. For recent work in this area, see S. M. Bachrach and A. Streitwieser, *J. Am. Chem. Soc.* 1984, **106**, 2283, 5818; K. C. Waterman and A. Streitwieser, *J. Am. Chem. Soc.* 1984, **106**, 3138.
21. E. Zintl and A. Harder, *Z. Phys. Chem. Abt. B* 1935, **28**, 478.
22. A. F. Wells, *Structural Inorganic Chemistry*, 4th Edn. Oxford University Press (1975).

Polyhedron Vol. 7, No. 21, pp. 2129–2133, 1988
Printed in Great Britain

0277–5387/88 $3.00+.00
Pergamon Press plc

THERMODYNAMICS OF METAL–LIGAND BOND FORMATION—XXXVI. FORMATION OF COMPLEX ZINC AND CADMIUM HALIDES IN ACETONITRILE SOLUTION

D. P. GRADDON* and C. S. KHOO

School of Chemistry, University of New South Wales, Kensington 2033, Australia

(*Received* 23 *January* 1987; *accepted* 15 *March* 1988)

Abstract—Thermodynamic data are reported for the reaction of zinc and cadmium halides with halide ions in acetonitrile solution. ZnX_2 forms first ZnX_3^- then ZnX_4^{2-} by successive replacement of solvent molecules in the tetrahedral solvate ZnX_2S_2, except that with ZnI_2 only the first step can be observed. CdX_2 forms in succession $Cd_2X_5^-$, CdX_3^- and CdX_4^{2-}; displacement of the solvent from the probably tetra-solvated CdX_2 occurs early and the CdX_3^- species is probably mono-solvated and tetrahedral.

There have been numerous studies on the formation of complex halides of zinc and cadmium; most have been in aqueous solution and have reported only equilibrium constant data.[1] Agreement between authors is not very good because the successive formation constants are usually small and analysis of the experimental data thus particularly difficult. There have also been a few determinations of complete thermodynamic data for these systems and the most reliable values of thermodynamic constants in aqueous solution are probably those selected by Ahrland,[2] who also reports complete thermodynamic data for the formation of these complex halides in solution in dimethyl sulphoxide.

Our interest in these systems is in the behaviour of zinc and cadmium halides as Lewis acids and we have therefore used acetonitrile as solvent in which it is known that the halides give almost non-conducting solutions.[3] Zinc halides are probably present in acetonitrile solution as the four-coordinate solvates, $ZnX_2(MeCN)_2$ and a chloride of this form has been isolated and shown by crystal structure analysis to be monomeric with tetrahedral geometry.[4] Cadmium iodide has been shown to form a similar solvate in saturated solutions in acetonitrile,[3] but the chloride and bromide probably form five- or six-coordinate solvates as many complex chlorides and bromides are known to be six-coordinate in the solid state. Cadmium chloride however has a very low solubility in acetonitrile and we have not been able to obtain data for this compound.

The reaction of the neutral solvated halides with halide ions leads eventually to the formation of complex halides, MX_4^{2-} as a result of replacement or displacement of solvent molecules by halide ions. This paper reports the determination by calorimetric titration of thermodynamic data for the successive reactions involved in this overall process.

EXPERIMENTAL

Materials

Anhydrous zinc chloride (99.99%) was obtained from BDH, the bromide (99%) from ROC/RIC and the iodide (99%) from Aldrich Chemicals, as were the cadmium halides (99+%). All were used without further purification but the very hygroscopic zinc chloride was heated in a vacuum pistol over phosphorus pentoxide for at least a week before use. Tetrabutylammonium chloride and bromide were obtained from Fluka AG and the iodide from Ega-Chemie; the chloride was pretreated in the same way as the zinc chloride. Acetonitrile for use as solvent was obtained from May and Baker, distilled twice from P_4O_{10} and stored over 4 Å molecular sieves.

Solutions of metal halides were prepared by direct weighing of the halide; the concentrations of the solutions of butylammonium halides were

* Author to whom correspondence should be addressed.

checked by titration with silver nitrate. Solid compounds and acetonitrile solutions were handled at all times under an atmosphere of high purity dry nitrogen.

Calorimetry

Titrations in acetonitrile solution were carried out in a LKB 8700 titration calorimeter, using the previously described technique.[5] Briefly, an acetonitrile solution of the tetrabutylammonium halide was added incrementally to 100 cm^3 of a solution of the metal halide and the heat produced was measured after each addition. Control titrations were carried out to determine the heat of dilution. An enthalpogram was then constructed by plotting the corrected cumulative heat produced against the amount of added base. All titrations were repeated over a wide range of concentrations of the metal halide.

RESULTS AND DISCUSSION

Enthalpograms for zinc chloride and bromide show a linear portion up to a halide ion : zinc ratio of 1 : 1 followed by a curved portion (Fig. 1), consistent with a two-step reaction:

$$ZnX_2 + X^- \rightleftharpoons ZnX_3^- \quad (1)$$

$$ZnX_3^- + X^- \rightleftharpoons ZnX_4^{2-} \quad (2)$$

in which the first step is quantitative ($K > 10^6$ l mol^{-1}) and ΔH_1^0 was obtained from the slope of the straight line portion; the value of ΔH_2^0 was obtained by extrapolation, calculation of K_2 at each point in the second half of the enthalpogram and iterative refinement to produce constant values of K_2. The results are summarized in Table 1, in which the data are the average of five determinations for zinc chloride and ten for zinc bromide over the range of concentrations shown. Quoted uncertainties for ΔH^0 are mean deviations from the average, and for K are the sum of mean deviations from the average in different titrations and the average standard deviation in individual titrations. For zinc bromide these results are close to those previously obtained by the flow calorimetric technique (ΔH_1^0 -21, ΔH_2^0 -15, $\log K_2$ 1.7).[6]

For zinc iodide the enthalpograms are curved throughout (Fig. 2) and correspond to the formation of a 1 : 1 complex only, according to eq. (1); the value of ΔH_1^0 was obtained by extrapolation, followed by calculation of K_1 at each point and iterative refinement of ΔH_1^0 to give consistent values of K_1 throughout the titration. Results summarized in Table 1 are the average of ten determinations over the range of concentrations shown and uncertainties have the same meaning as for the chloride and bromide.

The failure of the reaction of zinc iodide with iodide ions to go beyond the formation of ZnI_3^- is interesting since the ZnI_4^{2-} ion is well established and has been confirmed by crystal structure determination.[7] In the present case the non-observance of ZnI_4^{2-} is probably simply a result of the rather low concentrations used in the calorimetric titration technique. Extrapolation from the values of ΔH_1^0 and ΔH_2^0 for the bromide suggests a value of about -6 kJ mol^{-1} for ΔH_2^0 for formation of ZnI_4^{2-} from ZnI_3^- and if ΔS_2^0 is similar to the other halides (near

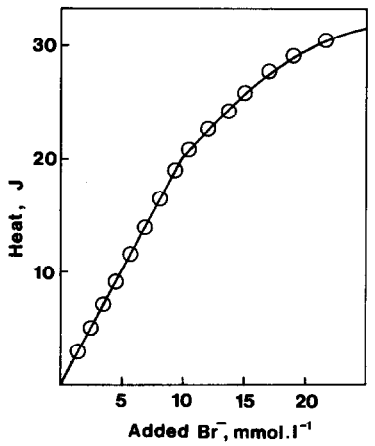

Fig. 1. Calorimetric titration of Br^- into $ZnBr_2$, 9.75 mmol l^{-1}. Points experimental. Curve computed for $\Delta H_1^0 = -20.5$, $\Delta H_2^0 = -15.3$ kJ mol^{-1}, $K_1 = \infty$, $K_2 = 450$ l mol^{-1}.

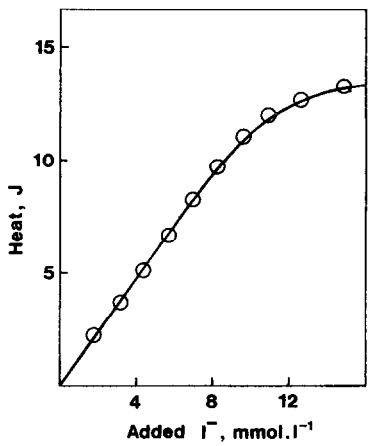

Fig. 2. Calorimetric titration of I^- into ZnI_2, 11.31 mmol l^{-1}. Points experimental. Curve computed for $\Delta H_1^0 =$ 12.7 kJ mol^{-1}, $K_1 = 3060$ l mol^{-1}.

Table 1. Thermodynamic data for the reaction of ZnX_2 with X^- in acetonitrile solution at 30°C according to reactions (1) and (2). Range of ZnX_2 concentrations in mmol l^{-1}, K in mol l^{-1}, ΔH^0, ΔG^0 in kJ mol^{-1}, ΔS^0 in J K^{-1} mol^{-1}

X	Concentration	Reaction	log K	$-\Delta H^0$	$-\Delta G^0$	$-\Delta S^0$
Cl	11.0–21.5	1	> 6	26.4±0.9		
		2	3.34±0.03	21.1±0.8	19.4±0.2	−6±3
Br	9.4–24.9	1	> 6	20.5±1.2		
		2	2.65±0.03	15.3±1.0	15.4±0.2	0±4
I	5.0–18.2	1	3.49±0.02	12.7±0.5	20.2±0.1	25±2

zero) this would lead to a value of about 10 l mol^{-1} for K_2; ZnI_4^{2-} would then be undetectable.

Formation of ZnX_4^{2-} from ZnX_2 in acetonitrile solution involves displacement of coordinated solvent and the alternative routes shown in Scheme 1 may be considered likely.

For the upper route we could expect that ΔH_1^0 would be considerably more negative than ΔH_2^0 and ΔS_2^0 much more positive than ΔS_1^0; for the lower route we can expect near equality of ΔH_1^0 with ΔH_2^0 and ΔS_1^0 with ΔS_2^0. The results in Table 1 clearly support the lower route, but the differences between ΔS_1^0 and ΔS_2^0 suggest that there is additional entropy support for step 1; this may arise from the dispersal of a more highly organized solvation of ZnX_2 than is implied in the simple formula ZnX_2S_2. We conclude that the zinc atom remains four-coordinate throughout the reaction and that five-coordination of ZnX_3^- does not occur to a significant extent, though this has been proposed in other solvents.[8]

Enthalpograms for cadmium bromide are nearly linear throughout the range of bromide ion concentrations up to a Br : Cd ratio of 2 : 1, but there is a distinct inflection at a Br : Cd ratio of 1 : 2 and a small curvature at the end of the titration (Fig. 3). While this small curvature shows that formation of $CdBr_4^{2-}$ is not quite quantitative, the departure from linearity is not enough to allow the accurate determination of an equilibrium constant. The inflection at the beginning of the curve indicates formation of a complex halide ion, $Cd_2Br_5^-$, but again it is not possible to determine complex stability. The enthalpogram gives no evidence for the formation of the 1 : 1 complex ion, $CdBr_3^-$, but since the existence of this species is well documented both in solution[9,10] and in the solid state[11,12] it is assumed that the species also occurs here and that the enthalpograms represent successive formation of three complex halides, most conveniently represented by the three equations:

$$CdX_2 + 1/2X^- \rightleftharpoons 1/2Cd_2X_5^- \quad (3)$$

$$CdX_2 + X^- \rightleftharpoons CdX_3^- \quad (4)$$

$$CdX_2 + 2X^- \rightleftharpoons CdX_4^{2-}. \quad (5)$$

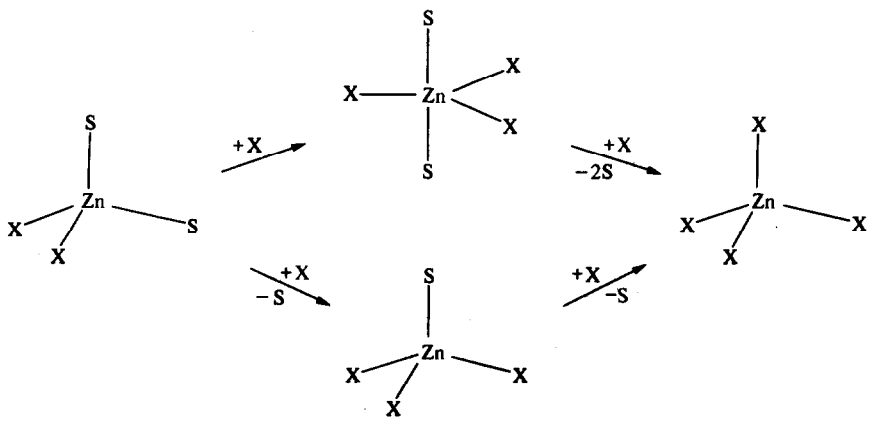

Scheme 1.

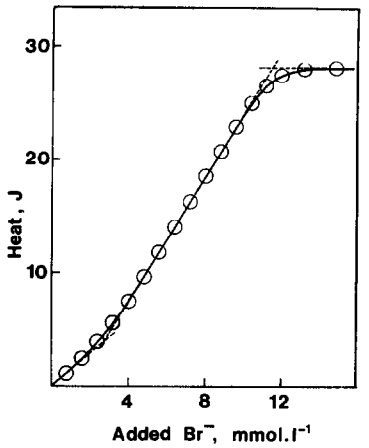

Fig. 3. Calorimetric titration of Br^- into $CdBr_2$, 5.76 mmol l^{-1}. Points and curve experimental.

Table 2. Enthalpies of formation, kJ (g-atom Cd)$^{-1}$, of complex halides from CdX_2 in acetonitrile solution at 30°C. Range of CdX_2 concentrations in mmol l^{-1}

X	Concentration	$-\Delta H^0_{1/2}$	$-\Delta H^0_1$	$-\Delta H^0_{1+2}$
Br	2.0–7.1	7.0±0.4	21.1±0.8	48.8±1.2
I[a]	3.7–7.1	8.2±0.6	20.3±1.0	46.9±1.4

[a] For the reaction $CdI_3^- + I^- \rightleftharpoons CdI_4^{2-}$: $\log K = 3.50 \pm 0.02$ l mol^{-1}; $\Delta H^0 = -26.6 \pm 2.3$ kJ mol^{-1}; $\Delta G^0 = 20.3 \pm 0.1$ kJ mol^{-1}; $\Delta S^0 = -21 \pm 8$ J K^{-1} mol^{-1}.

The enthalpy change for the first of these reactions was obtained by extrapolation of the linear portions of the enthalpogram on either side of the inflection; where the lines intersect the ratio Br : Cd = 1 : 2 (Fig. 3) and the enthalpy change corresponding to the formation of $Cd_2X_5^-$ was read at the intersection. The enthalpy change for the second reaction was read directly from the enthalpogram at the stoichiometry ratio of 1 : 1, but as small deviations from linearity in this region would be obscured by the inflection this is not a very precise value for this enthalpy change. The enthalpy change for the overall reaction, forming CdX_4^{2-} from CdX_2, can be read from the total heat produced at the end of the reaction. The results obtained are summarized in Table 2, in which the values of ΔH^0 are the average of six determinations over the range of cadmium bromide concentrations shown and uncertainties in ΔH^0 are mean deviations.

Enthalpograms for cadmium iodide also showed a slight inflection close to a ratio of I : Cd = 1 : 2 and the upper portion of the enthalpogram is distinctly curved (Fig. 4). This indicates successive formation of $Cd_2I_5^-$, CdI_3^- and CdI_4^{2-}. The curvature of the upper part of the enthalpogram allows calculation of the equilibrium constant for the last step; consistent values of ΔH^0_1 and ΔH^0_2, and of the equilibrium constant, K_2, throughout this part of the titration and over a wide range of cadmium iodide concentrations confirm the existence of this equilibrium. Results summarized in Table 2 are the average of eleven determinations over the range of concentrations shown; uncertainties quoted for $\Delta H^0_{1/2}$, ΔH^0_1 and ΔH^0_{1+2} are mean deviations and uncertainties in K_2 are the sum of the mean deviation from the average in different titrations and the average standard deviation in individual titrations.

The data obtained for cadmium bromide and iodide are very similar, suggesting that the solvation of analogous species is the same throughout and that both halides exist in acetonitrile solution as tetra-solvated linear molecules; this conflicts with the previous observation that a solvate of the form CdI_2S_2 is formed,[3] but that conclusion was reached from solubility equilibria and consequently refers to much higher concentrations. As with the zinc halides, it is possible to consider the desolvation which must accompany halide coordination occurring by several alternative routes:

$$\begin{array}{ccccc} & & CdX_3S_3^- \text{ (six-coordinate)} & & \\ & \nearrow & & \searrow & \\ CdX_2S_4 \text{ (six-coordinate)} & \rightarrow & CdX_3S_2^- \text{ (five-coordinate)} & \rightarrow & CdX_4^{2-} \text{ (four-coordinate).} \\ & \searrow & & \nearrow & \\ & & CdX_3S^- \text{ (four-coordinate)} & & \end{array}$$

With both halides it is found that the enthalpy change is more negative in the second of these steps, implying that desolvation occurs largely in the first step; this is confirmed by the equilibrium data for the formation of CdI_4^{2-} from CdI_3^-, which is entropy resisted as could be expected if no desolvation occurs in this step. We conclude that the reaction proceeds by the lower route with both halides.

The occurrence of the species $Cd_2X_5^-$ in these systems is unexpected. Two possible structures for such a species are shown in Scheme 2. In the first of these the cadmium is only partly desolvated as might be expected in a complex intermediate between CdX_2S_4 and CdX_3S^-, and the very small negative enthalpies of formation are consistent with a structure of this type; but the second based on

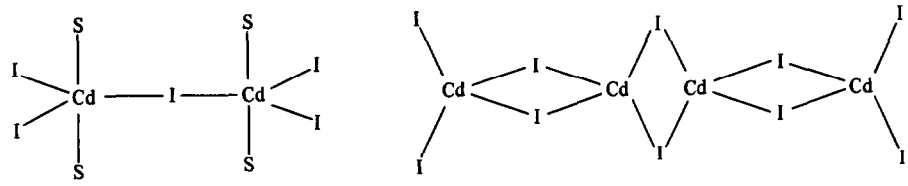

Scheme 2.

tetrahedrally coordinated cadmium atoms surrounded by iodide, seems more likely to form a stable entity. The calorimetric results do not make it possible to distinguish between these structures, although in principle, equilibrium measurements should be able to do so if appropriate to the magnitude of the equilibrium constant.

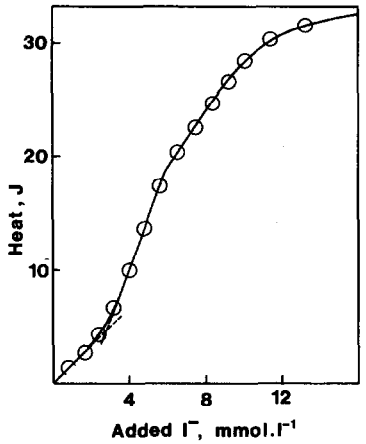

Fig. 4. Calorimetric titration of I^- into CdI_2, 5.86 mmol l^{-1}. Points experimental. Curve computed for $\Delta H^0_{1/2} = -8.2$, $\Delta H^0_1 = 20.3$, $\Delta H^0_2 = -26.6$ kJ (g-atom Cd)$^{-1}$, $K_2 = 3130$ l mol^{-1}.

REFERENCES

1. *Chem. Soc.* Special Publications 1964, **17**; 1971, **25**.
2. S. Ahrland, N. Bjork and R. Portanova, *Acta Chem. Scand.* 1976, **A30**, 270.
3. L. T. Ang and D. P. Graddon, *J. Inorg. Nucl. Chem.* 1976, **38**, 2279.
4. I. V. Isakov and Z. V. Zvenkova, *Dokl. Akad. Nauk. SSSR* 1962, **145**, 1027.
5. D. P. Graddon and K. B. Heng, *Aust. J. Chem.* 1971, **24**, 1781.
6. D. P. Graddon, M. Micheloni and P. Paoletti, *J. Chem. Soc., Dalton Trans.* 1981, 336.
7. P. L. Orioli and H. C. Lip, *Cryst. Struct. Commun.* 1974, **3**, 447.
8. D. F. C. Morris, E. L. Short and D. N. Waters, *J. Inorg. Nucl. Chem.* 1963, **25**, 975; K. Tamura, *J. Phys. Chem.* 1977, **81**, 820.
9. J. E. D. Davies and D. A. Long, *J. Chem. Soc. A* 1968, 2054.
10. M. A. Bredig and E. R. van Artsdalen, *J. Chem. Phys.* 1956, **24**, 478.
11. G. L. McPherson, A. M. McPherson and J. L. Atwood, *J. Phys. Chem. Solids* 1980, **41**, 49J.
12. M. N. Iyer, R. Faggiani and I. D. Brown, *Acta Cryst.* 1977, **B33**, 127.

Polyhedron Vol. 7, No. 21, pp. 2135–2141, 1988
Printed in Great Britain

0277–5387/88 $3.00+.00
© 1988 Pergamon Press plc

THERMODYNAMICS OF TETRAHEDRAL–OCTAHEDRAL CONFIGURATIONAL INTERCONVERSIONS IN Co^{II} COMPLEXES IN NITROMETHANE

YURIKO ABE,* MAKIKO MORIKAWA and MAYUMI KIKUKAWA

Graduate Division of Human Culture and Department of Chemistry,
Nara Women's University, Nara 630, Japan

(*Received* 9 *November* 1987; *accepted* 15 *March* 1988)

Abstract—The visible absorption spectra for $[Co(hmpa)_4](ClO_4)_2$-L-nitromethane systems (L = H_2O, MeOH, EtOH, *n*-PrOH, *i*-PrOH, *n*-BuOH, FA, NMF, DMF, DEF, DMA, DEA or DMSO) have been studied. The results indicate that the configurational interconversions from the tetrahedral $[Co(hmpa)_4]^{2+}$ to the octahedral $[Co(hmpa)_2L_4]^{2+}$ accompanying the ligand substitution reactions occur in nitromethane, except for the DMA and DEA systems. The values of both ΔH and ΔS for the interconversions increase in the following order: H_2O < MeOH < EtOH < *n*-PrOH ~ *n*-BuOH < *i*-PrOH ~ FA ~ NMF ~ DMF ~ DEF ⩽ DMSO. The solvent effects on the interconversions are discussed in terms of the basic and steric nature of the solvents.

Equilibria between configurational isomers of inorganic complexes in non-aqueous solvents are well known.[1] This is especially true for the configurational interconversions between octahedral and tetrahedral or square planar cobalt(II) or nickel(II) complexes which have been extensively studied.[2–12]. In the case of Co^{II} complexes, thermodynamic and spectral data have been obtained for a number of tetrahedral CoL_2X_2 and octahedral CoL_4X_2 equilibria, where L = pyridine or 2-methylpyridine, X = Cl, Br, I, OCN, NCS and SeCN.[3–4] King *et al.* have pointed out that the nature of both L and X has a striking effect on the equilibria.[3] Their results are interpreted in terms of steric and electronic effects. It seems that in all cases, anionic ligands, X^-, play an important role on the configurational equilibria. However, there are few data for the configurational equilibria in Co^{II} complexes, where only the neutral monodentate ligands coordinate to Co^{II} ions.[11]

In the donor solvents such as water, ethanol, dimethyl sulphoxide and N,N-dimethylformamide, solvated Co^{2+} ions are mostly octahedral.[13] On the other hand, the solvated Co^{2+} ion is tetrahedral in hexamethylphosphoric triamide (HMPA).[14–15] Thus, the existence of equilibria between tetrahedral and octahedral solvated Co^{2+} ions, having only the neutral monodentate ligands, would be expected in the mixed media of HMPA and the other solvents. In the present study, we examine the reaction of the tetrahedral $[Co(hmpa)_4]^{2+}$ ion with another donor solvent ligand L, using nitromethane as an inert solvent, where the concentration of L could be arbitrarily varied. The donor solvents used were as follows: water, methanol (MeOH), ethanol (EtOH), *n*-propanol (*n*-PrOH), *i*-propanol (*i*-PrOH), *n*-butanol (*n*-BuOH), formamide (FA), N-methylformamide (NMF), N,N-dimethylformamide (DMF), N,N-diethylformamide (DEF), N,N-dimethylacetamide (DMA), N,N-diethylacetamide (DEA) and dimethyl sulphoxide (DMSO). The solvent effects on the equilibria will be discussed in terms of their basic and steric characteristics.

EXPERIMENTAL

$[Co(hmpa)_4](ClO_4)_2$ was prepared by the method described in the literature.[14–15] The reagent grade tetraethylammonium perchlorate (Et_4NClO_4) was recrystallized from water and was dried *in vacuo* at room temperature. The purifications of HMPA and nitromethane were carried out according to our previous description.[14–15] Water was distilled twice

*Author to whom correspondence should be addressed.

from aqueous $KMnO_4$ solution. The purifications of MeOH, EtOH, *n*-PrOH, *i*-PrOH, *n*-BuOH and FA, and those of NMF, DMF, DEF, DMA, DEA and DMSO were drying over four and five molecular sieves, respectively. They were then distilled at atmospheric pressure and under reduced pressure, respectively.

A stock solution of $[Co(hmpa)_4]^{2+}$ was prepared by weight. Absorption spectra were measured using a Shimazu spectrophotometer UV 210 with a thermostated cell compartment. The ionic strength was adjusted to 0.06 M (mol dm^{-3}) with tetraethylammonium perchlorate.

RESULTS AND DISCUSSION

Absorption spectra for $[Co(hmpa)_4](ClO_4)_2$-L-*nitromethane*

Figure 1 shows the dependence of the absorption spectra of Co^{II} complexes upon the concentration of NMF in nitromethane at $[[Co(hmpa)_4]^{2+}]_0 = 1.0 \times 10^{-3}$ M and $[HMPA]_0 = 0.1$ M, where the symbol, $[\ ]_0$, represents the initial concentration. Figure 2 shows the *n*-PrOH system when $[[Co(hmpa)_4]^{2+}]_0 = 9.5 \times 10^{-4}$ M and $[HMPA]_0 = 0$ M. Essentially similar data were also obtained except for the DMA and DEA systems. The variation of the absorption spectra for the DMA system is shown in Fig. 3. Similar variation in the spectra was seen for the DEA system.

The absorption spectrum at $[L]_0 = 0$ M (Curve 1 in Figs 1, 2 and 3) is due to the tetrahedral $[Co(hmpa)_4]^{2+}$ ion.[14-15] In Figs 1 and 2, the absorbance decreased monotonously without any shift in the peaks upon adding NMF or *n*-PrOH. In general, the absorption bands due to $\nu_3(^4T_1(P) \leftarrow {}^4A_2)$ transitions in tetrahedral Co^{II} complexes appear at 550–700 nm.[13] The molar absorptivities of the peaks are 100–2000 M^{-1} cm^{-1}, but, absorption bands of octahedral Co^{II} complexes, such as $[Co(H_2O)_6]^{2+}$, $[Co(dmso)_6]^{2+}$, $[Co(pyo)_6]^{2+}$ (pyo = pyridine oxide) and $[Co(NH_3)_6]^{2+}$ are observed in the visible region near 500 nm, having far smaller molar absorptivities (5–40 M^{-1} cm^{-1}). These bands allow a fairly clear-cut distinction between tetrahedral and octahedral configurations of Co^{II} complexes.[13] Thus, it is suggested that in all cases, except the DMA and DEA systems, the absorptions at 550–650 nm are due to the tetrahedral $[Co(hmpa)_4]^{2+}$ ion and that the monotonous decreases in the absorptivities are attributed to the formation of octahedral Co^{II} complexes which may show no absorption in this region. Therefore, the equilibria of configurational interconversions between tetrahedral and octahedral Co^{II} complexes occur in the ligand substitution reaction in the H_2O, alcohols, FA, NMF, DMF, DEF and DMSO systems.

Since, in the DMA system, the isosbestic points appear at 555 and 594 nm, it is supposed that the Co^{II} complex equilibrates between tetrahedral

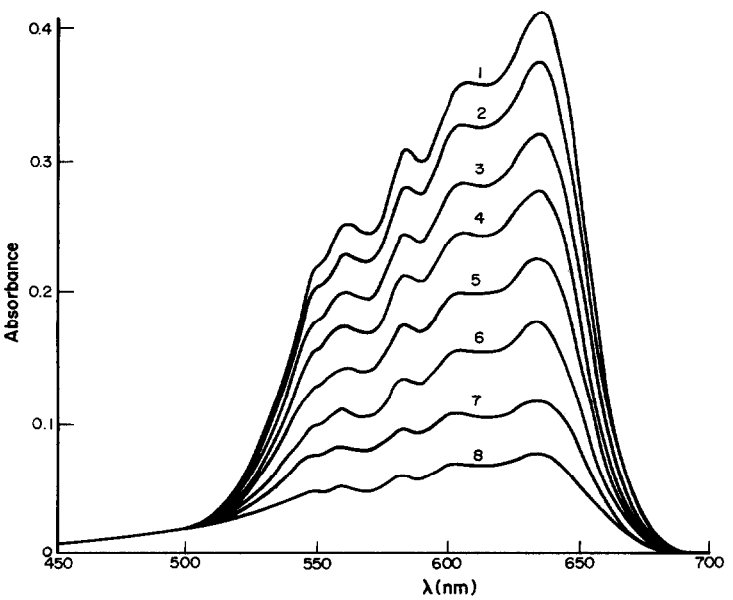

Fig. 1. Absorption spectra of the Co^{II} complex at various concentrations of NMF in nitromethane at $[[Co(hmpa)_4]^{2+}]_0 = 1 \times 10^{-3}$ M, $[HMPA]_0 = 0.1$ M, $I = 0.06$ M and 25°C. $[NMF]_0$: (1) 0 M (2) 0.20 M (3) 0.30 M (4) 0.35 M (5) 0.40 M (6) 0.45 M (7) 0.50 M (8) 0.60 M.

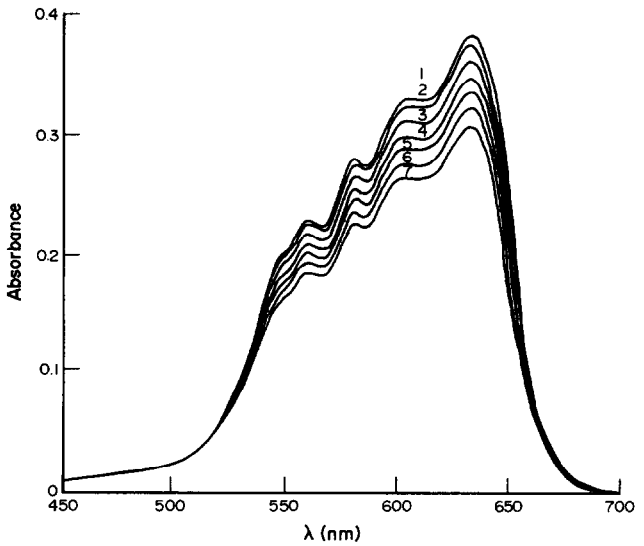

Fig. 2. Absorption spectra of the Co^{II} complex at various concentrations of *n*-PrOH in nitromethane at $[[Co(hmpa)_4]^{2+}]_0 = 9.5 \times 10^{-4}$ M, [HMPA] = 0 M, $I = 0.06$ M and 25°C. $[n\text{-PrOH}]_0$: (1) 0 M (2) 0.4 M (3) 0.5 M (4) 0.6 M (5) 0.7 M (6) 0.8 M (7) 0.9 M.

$[Co(hmpa)_4]^{2+}$ and tetrahedral $[Co(hmpa)_3(dma)]^{2+}$ ions. Above a $[DMA]_0$ of 0.08 M, the spectra exhibit no isosbestic point. An equilibrium between tetrahedral and octahedral configurations in the Co^{II} complexes seems to occur as the second step during substitution.

Determination of the equilibrium constant K

In the case of the H_2O, FA, NMF, DMF, DEF and DMSO systems, it was considered that the first equilibrium holds only when $[L]_0$ is not much larger than $[HMPA]_0$. If tetrahedral $[Co(hmpa)_4]^{2+}$ reacts with x moles of L to form the octahedral $[Co(hmpa)_{6-x}(L)_x]^{2+}$ ion where x should be larger than two, the following relations are established;

$$[Co(hmpa)_4]^{2+} + xL \overset{K}{\rightleftharpoons} [Co(hmpa)_{6-x}(L)_x]^{2+} + (x-2)hmpa \quad (1)$$

$$K = \frac{[[Co(hmpa)_{6-x}(L)_x]^{2+}][hmpa]_{free}^{x-2}}{[[Co(hmpa)_4]^{2+}][L]_{free}^{x}}. \quad (2)$$

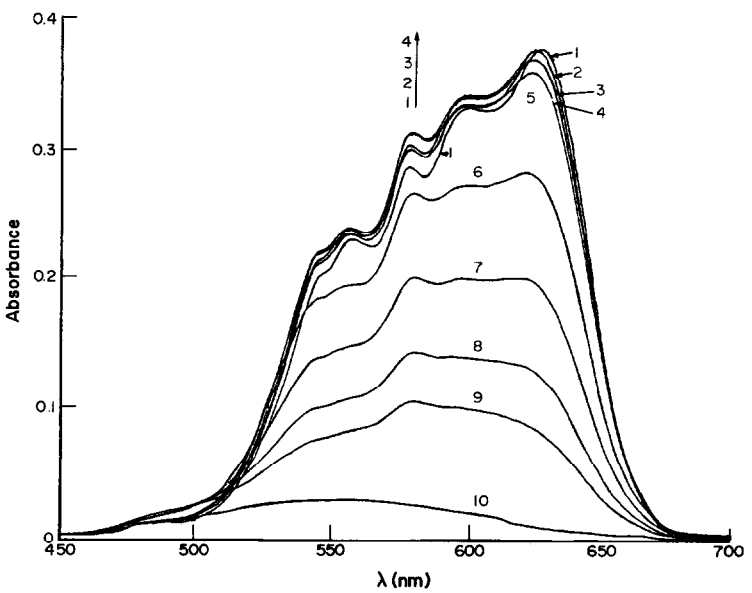

Fig. 3. Absorption spectra of the Co^{II} complex at various concentrations of DMA in nitromethane at $[[Co(hmpa)_4]^{2+}]_0 = 9.5 \times 10^{-4}$ M, $[HMPA]_0 = 0$ M, $I = 0.06$ M and 25°C. $[DMA]_0$: (1) 0 M (2) 0.01 M (3) 0.02 M (4) 0.04 M (5) 0.06 M (6) 0.08 M (7) 0.2 M (8) 0.5 M (9) 0.8 M (10) 9.56 M.

The total absorptivity of the solution, A, is expressed in the following form:

$$A = \varepsilon[Co^{II}] = \varepsilon_1[[Co(hmpa)_4]^{2+}] + \varepsilon_2[[Co(hmpa)_{6-x}(L)_x]^{2+}] \quad (3)$$

in which ε is the apparent absorptivity of all Co^{II} complexes and ε_1 and ε_2 are molar absorptivities of the tetrahedral $[Co(hmpa)_4]^{2+}$ ion and octahedral $[Co(hmpa)_{6-x}(L)_x]^{2+}$ ion, respectively. Since the value of ε_2 seems to be negligibly small compared to that of ε_1 near 600–700 nm, eq. (3) can be reduced to eq. (3′)

$$A = \varepsilon[Co^{II}] = \varepsilon_1[[Co(hmpa)_4]^{2+}]. \quad (3')$$

The total concentration of all Co^{II} complexes is related by eq. (4)

$$[Co^{II}]_0 = [[Co(hmpa)_4]^{2+}] + [[Co(hmpa)_{6-x}(L)_x]^{2+}]. \quad (4)$$

Under the conditions of a large excess of $[L]_0$ and $[HMPA]_0$ as compared with $[Co^{II}]_0$, eqs (5) and (6) hold;

$$[L]_0 = [L]_{free} \quad (5)$$

$$[HMPA]_0 = [hmpa]_{free}. \quad (6)$$

Combining eqs (2)–(6) produces the following equation:

$$\log\left(\frac{\varepsilon_1}{\varepsilon} - 1\right) - 2\log[L]_0 = \log K + (x-2)\log\frac{[L]_0}{[HMPA]_0}. \quad (7)$$

Figure 4 shows the plots at 633 nm for various systems using eq. (7). The plots are straight lines with no deviation from linearity. This indicates that only the one equilibrium accompanies the ligand substitution reactions in the concentration regions of L. The values of $(x-2)$ and $\log K$ can be obtained from the slopes and intercepts of the straight lines, respectively. As shown in Fig. 4, $(x-2)$ is equal to two, namely, $x = 4$ in all cases. Thus, the following equilibrium exists in the ligand substitution reaction:

$$\underset{\text{Tetrahedral}}{[Co(hmpa)_4]^{2+}} + 4L \overset{K}{\rightleftarrows} \underset{\text{Octahedral}}{[Co(hmpa)_2L_4]^{2+}} + 2hmpa. \quad (1')$$

Figure 5 shows the temperature dependence of the absorption spectra for the DMF system. A fairly large temperature dependence of the absorption spectra in Fig. 5 allows us to estimate the thermodynamic parameters of the interconversions between tetrahedral and octahedral configurations. Plots of $\ln K$ vs T^{-1} for various systems conform to

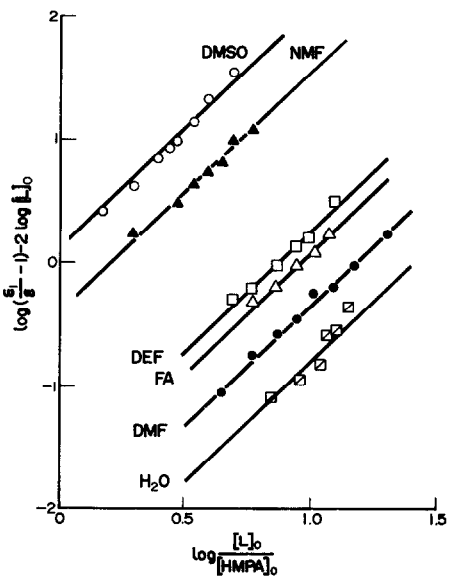

Fig. 4. Plots of $\{\log[(\varepsilon_1/\varepsilon)-1]-2\log[L]_0\}$ vs $\log([L]_0/[HMPA]_0)$ ○: DMSO, ▲: NMF, □: DEF, △: FA, ●: DMF, ⊠: H_2O.

straight lines as shown in Fig. 6, suggesting that only the equilibrium of eq. (1′) exists without a successive reaction. The values of $\log K$ at 25°C, ΔH and ΔS are summarized in Table 1.

In the case of the MeOH, EtOH, *n*-PrOH, *i*-PrOH and *n*-BuOH systems, absorption spectra were obtained under the condition of $[HMPA]_0 = 0$ M. The values of K were calculated by $K = [[Co(hmpa)_2L_4]^{2+}][hmpa]^2_{free}/[[Co(hmpa)_4]^{2+}][L]^4_{free}$, using eqs (3′), (4), (5) and the following eq. (8)

$$[hmpa]_{free} = 2[[Co(hmpa)_2L_4]^{2+}]. \quad (8)$$

The calculated K values for the *n*-PrOH system are given in Table 2. They show a constant value for K. Essentially similar results are obtained in the other systems. They strongly indicate that eq. (1′) holds not only in the H_2O, FA, NMF, DMF, DEF and DMSO systems, but also in the MeOH, EtOH, *n*-PrOH, *i*-PrOH and *n*-BuOH systems. Plotting $\ln K$ vs T^{-1} gave straight lines with no deviation from linearity. The values of $\log K$ at 25°C, ΔH and ΔS are listed in Table 1.

Basic and steric effects of solvent (L)

The configurations of solvated metal ions in HMPA are widely different from those in water or in a number of other donor solvents such as MeOH, DMF and DMSO, in which solvated complex ions are generally octahedral.[13] Solvated ions in HMPA prefer the tetrahedral configurations to the octahedral ones since the HMPA molecule is very bulky

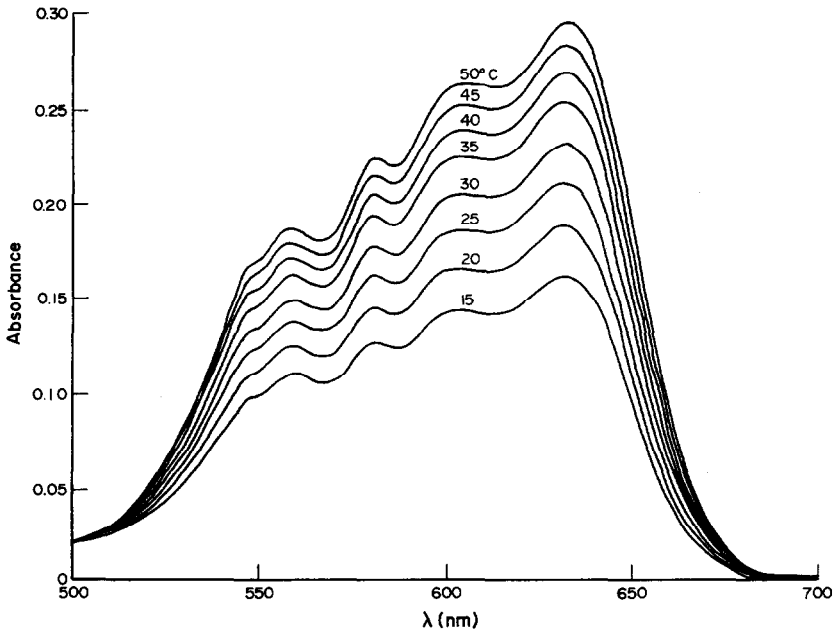

Fig. 5. Temperature dependence of absorption spectra in nitromethane at $[[Co(hmpa)_4]^{2+}]_0 = 1 \times 10^{-3}$ M, $[HMPA]_0 = 0.1$ M, $[DMF]_0 = 1.25$ M and $I = 0.06$ M.

as compared with DMSO or DMF.[14-15] Tetrahedral complexes avoid the steric interaction of HMPA molecules which are more closely packed in the octahedral complexes. In nitromethane, tetrahedral $[Co(hmpa)_4]^{2+}$ reacts with other donor solvents (L) to form the octahedral $[Co(hmpa)_2L_4]^{2+}$ according to eq. (1′). As shown in Table 1, the K value is fairly small in all systems in spite of the large negative values of ΔH. This is due to the large negative values of ΔS since two more molecules are bound to the Co^{II} ion in the course of the configurational change from tetrahedral to octahedral in eq. (1′). Moreover, Table 1 shows that the large variation in $\log K$ from -8.72 to 0.41 is determined not only by the entropy factor but also by the enthalpy factor. The main factors by which the solvent molecules (L) affect the equilibrium of eq. (1′) may be their basic and steric effects. Due to the competitive coordination of the Co^{II} ion between HMPA and the solvent molecules (L), the increase in basicity of the solvents would result in a decrease in ΔH values. On the other hand, increases in the degree of avoiding the steric interaction between the bulky HMPA and the solvents (L) would tend to increase both ΔH and ΔS values.

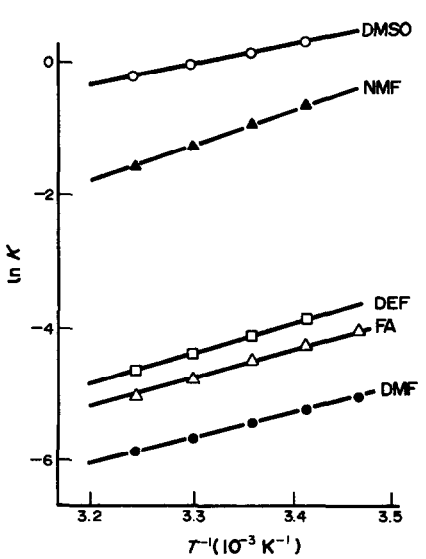

Fig. 6. Plots of $\ln K$ vs T^{-1}. ○: DMSO, ▲: NMF, □: DEF, △: FA, ●: DMF.

Gutmann *et al.* pointed out that the donor strength of HMPA towards Co^{II} in $[Co(hmpa)_4]^{2+}$ is smaller than that expected from its donor number (DN = 38.8) and the coordination centre is not fixed within the tetrahedron formed by the bulky HMPA.[16] Since the H_2O molecule is fairly small compared with the HMPA molecule, the steric interaction between the bulky HMPA and H_2O molecules in octahedral $[Co(hmpa)_2(H_2O)_4]^{2+}$ does not occur. Thus, the donor strength of HMPA in octahedral $[Co(hmpa)_2(H_2O)_4]^{2+}$ exhibits the originally high value. Therefore, the H_2O system has the smallest values of ΔH and ΔS. Moreover, H_2O, MeOH and EtOH have about the same donor num-

Table 1. The values of K(25°C), ΔH and ΔS in nitromethane

Solvents (L)	Donor number	log K	ΔH (kJ mol^{-1})	ΔS (J mol^{-1} K^{-1})
H_2O	18	−2.81	−116	−436
MeOH	19	−6.19	−63	−339
EtOH	20	−7.33	−54	−315
n-PrOH	—	−7.63	−50	−305
i-PrOH	—	−8.72	−30	−273
n-BuOH	—	−7.55	−49	−311
FA	24	−1.92	−33	−149
NMF	—	−1.49	−32	−115
DMF	26.6	−2.31	−30	−147
DEF	30.9	−1.66	−31	−139
DMA	27.8	—	—	—
DEA	32.2	—	—	—
DMSO	29.8	0.41	−18	−59

bers as seen in Table 1.[17] For protic solvents, the large differences in the ΔH and ΔS values are mainly attributed to a steric effect. The increase in the degree of avoiding the steric interaction with increasing size of the protic solvent is expected to be as follows: H_2O < MeOH < EtOH < *n*-PrOH < *n*-BuOH < *i*-PrOH. As a result of this increase, the values of both ΔH and ΔS would increase in the same sequence. Actually, as shown in Fig. 7, the linear relation between ΔH and ΔS holds for protic solvents.

For formamide derivatives, the replacement of hydrogen atoms on amino radicals by methyl or ethyl radicals has little influence on the values of ΔH and ΔS as seen in Table 1. The steric interaction between the bulky HMPA and the formamide derivatives may increase in the following order: FA < NMF < DMF < DEF, which is similar to the order of increasing donor number, FA < DMF < DEF. Thus, the basic and steric effects are cancelled by each other, resulting in similar values of ΔH and ΔS for the formamide derivatives.

Table 2. The values of K at various [*n*-PrOH]$_0$

No.	[*n*-PrOH]$_0$ (M)	K (M^{-2})
1	0	—
2	0.4	4.6×10^{-8}
3	0.5	4.6×10^{-8}
4	0.6	4.8×10^{-8}
5	0.7	4.8×10^{-8}
6	0.8	4.5×10^{-8}
7	0.9	4.6×10^{-8}

Since DMA and DEA correspond to DMF and DEF whose hydrogen atom bonding to the carbon atom is replaced by a methyl radical, respectively, a more steric interaction between the bulky HMPA and DMA or DEA molecules may retard the coordination of DMA or DEA to the Co^{II} ion. Consequently, for the systems of acetamide derivatives, reaction (1′) cannot occur, but the tetrahedral configuration is maintained during the first step in the ligand substitution. In the case of the DMSO system, the reaction of eq. (1′) can hold because the DMSO molecule is smaller than that of DMA or DEA. The fact that the values of ΔH and ΔS for DMSO are larger than those for the formamide derivatives seems to be attributed to a decrease in the strength of bonding of the oxygen atom to the Co^{II} and, accordingly, to an increase in the degree of freedom of motion related to the DMSO molecules in their coordination sphere.

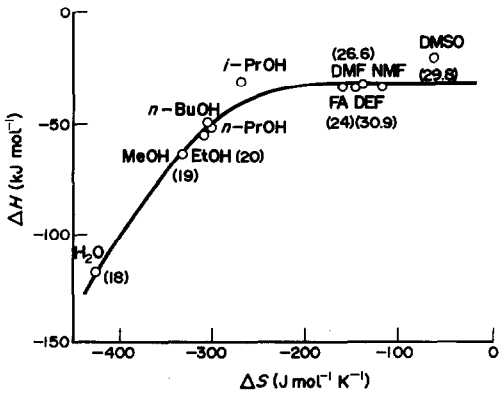

Fig. 7. Relationship between enthalpy changes (ΔHs) and entropy changes (ΔSs).

CONCLUSIONS

It is of interest to compare the obtained interconversions with the following one:[3]

$$\underset{\text{Tetrahedral}}{CoX_2L_2} + 2L \overset{K}{\rightleftharpoons} \underset{\text{Octahedral}}{CoX_2L_4} \quad (9)$$

where L = pyridine or 2-methylpyridine, X = Cl, Br, I, OCN, NSC and SeCN. King *et al.* have pointed out that the large variations in K are mainly attributed to the contribution of the entropy factor and not the enthalpy.[3] There is a loss of rotational entropy as a result of steric hindrance due to formation of the octahedral complex. Moreover, the influence of the anionic ligands, X^-, is interpreted in terms of an electronic effect transmitted to the metal–pyridine. In the other systems, the anionic ligand, X^-, plays an important role in the tetrahedral–octahedral equilibria. However, there are few data for the interconversion equilibria in Co^{II} complexes which are coordinated with only the donor solvents.[11] The equilibrium of eq. (1′) is the first sample of the solvated tetrahedral–octahedral interconversions in solution at room temperature that we have encountered using Co^{II} complexes. The large differences in K are determined not only by the entropy factor but also by enthalpy. The solvent effect on the equilibria is interpreted in terms of their steric and basic nature. Since the H_2O and alcohols have approximately the same donor numbers, the basic effect is nearly constant in these systems. Therefore, in these systems, the values of ΔH and ΔS increase with increasing degree of avoidance of the steric interaction: H_2O < MeOH < EtOH < *n*-PrOH < *n*-BuOH < *i*-PrON. On the other hand, the basic and steric effects are cancelled by each other for the formamide derivatives, resulting in similar values of ΔH and ΔS. Therefore, plotting ΔH vs ΔS shows a linear relationship for the H_2O and alcohols, and nearly constant values for the formamide derivatives, as shown in Fig. 7.

Acknowledgement—The authors wish to express their thanks to Prof. Emeritus Goro Wada of Nara Women's University for his valuable discussion.

REFERENCES

1. F. Basolo and R. G. Pearson, *Mechanisms of Inorganic Reactions*, 2nd Edn. John Wiley, New York (1967).
2. L. I. Katzin, *J. Chem. Phys.* 1961, **35**, 467.
3. H. C. A. King, E. Körös and S. M. Nelson, *J. Chem. Soc.* 1963, 5449; 1964, 4832.
4. S. M. Nelson and T. M. Shepherd, *J. Chem. Soc.* 1965, 3284.
5. L. Sacconi, P. Nannelli and U. Campigli, *Inorg. Chem.* 1965, **4**, 818.
6. D. E. Scaife and K. P. Wood, *Inorg. Chem.* 1967, **6**, 358.
7. R. H. Holm, A. Chakravorty and G. O. Dudek, *J. Am. Chem. Soc.* 1964, **86**, 379.
8. G. W. Everett, Jr. and R. H. Holm, *J. Am. Chem. Soc.* 1965, **87**, 5867.
9. N. Iwasaki, K. Sone and Y. Fukuda, *Z. Anorg. Allg. Chem.* 1975, **412**, 170.
10. J. R. Dickinson, T. R. Griffiths and P. J. Potts, *J. Inorg. Nucl. Chem.* 1975, **37**, 511.
11. T. W. Swaddle and L. Fabes, *Can. J. Chem.* 1980, **58**, 1418.
12. S. Ishiguro, K. Ozutsumi and H. Ohtaki, *Bull. Chem. Soc. Jpn.* 1987, **60**, 531.
13. A. B. P. Lever, *Inorganic Electronic Spectroscopy*, Chap. 9. Elsevier, Amsterdam (1968).
14. Y. Abe and G. Wada, *Bull. Chem. Soc. Jpn.* 1980, **53**, 3547.
15. Y. Abe and G. Wada, *Bull. Chem. Soc. Jpn.* 1981, **54**, 3334.
16. V. Gutmann, A. Weisz and K. Kerber, *Monatsh. Chem.* 1969, **100**, 206.
17. V. Gutmann, *The Donor and Acceptor Approach to Molecular Interactions*, Chap. 2. Plenum Press, New York (1978).

Polyhedron Vol. 7, No. 21, pp. 2143–2148, 1988
Printed in Great Britain

0277–5387/88 $3.00+.00
© 1988 Pergamon Press plc

[BIS(DIMETHYLSULPHOXIDE)PROTIUM][*TRANS*-BISDIMETHYLSULPHOXIDETETRACHLOROIRIDATE(III)]

P. S. CARTWRIGHT and R. D. GILLARD*

Department of Chemistry, University College, P.O. Box 78, Cardiff CF1 1XL, U.K.

E. R. J. SILLANPAA

Department of Chemistry, University of Turku, 20500 Turku, Finland

and

J. VALKONEN

Department of Chemistry, University of Jyvaskyla, Jyvaskyla, Finland

(*Received* 17 *August* 1987; *accepted* 15 *March* 1988)

Abstract—$[(DMSO)_2H]$*trans*-$[IrCl_4(DMSO)_2]$ (DMSO = dimethylsulphoxide) has been structurally characterized. The hydrogen bonded cation $[DMSO—H—DMSO]^+$ has a very short O—H—O bond distance (2.405 Å) which compares well with that in the known rhodium analogue.

The two DMSO ligands are *trans* on iridium and coordinate via the sulphur atoms. Earlier work had assigned the *cis* structure to the anion in this compound.

Chloroiridium complexes can be used as catalysts in organic reductions. For example, Henbest's group[1] found that a solution of "chloroiridic acid, H_2IrCl_6" and trimethylphosphite in aqueous propan-2-ol would reduce a cyclic ketone to give approximately 95% of the axial alcohol (a reaction similar to the Meerwein–Ponndorf–Verley reduction)—equatorial alcohols are generally the products of the reaction of cyclohexanone with most reductants. They also found such catalytic properties if dimethyl sulphoxide (DMSO) was used instead of trimethylphosphite, and isolated two neutral and two acidic chloroiridium–DMSO complexes, *cis*- and *trans*-$IrCl_3(DMSO)_3$ and *cis*- and *trans*-$H[Cl_4Ir(DMSO)_2](DMSO)_2$, respectively. The preparative details for the *cis* and *trans* acids were reported later,[2] when the formulae were written $[H(Me_2SO)_2]^+[IrCl_4(Me_2SO)_2]^-$. The anions in the yellow and pink crystalline compounds obtained were labelled *cis* and *trans*, respectively, initially on the basis of a very small difference in methyl proton chemical shift, which was later supported by other arguments. Several arguments in the catalytic systems based on these acids depend on the assignment of geometric structure; the stereochemical nature of products (and differences between them) was attributed to the structure of the iridium acid.[3] James, Morris and Kvintovics[4] modified the preparation of these acids used to study the reactivity of the hydridoiridium sulphoxide species toward dioxygen. They agreed with Henbest's assignment of *cis* and *trans* isomeric structures (giving further stereochemical argument) but found the "*trans*" isomer to be orange rather than pink and to have a higher melting point (152–154°C cf. 120–122°C), and assumed that there were different crystal modifications.

The protonation of DMSO has attracted attention for other reasons and Kreevoy and Williams[5] measured the IR spectrum of the 1:2 proton:DMSO cation showing that it contained a short strong hydrogen bond.

Potts[6] isolated $(DMSO)_2H[AuCl_4]$ which presumably contains a short strong O—H—O hydrogen bond. The complex $[(DMSO)_2H][RhCl_4(DMSO)_2]$ has been prepared and structurally characterized by James *et al.* having a strong O—H—O hydrogen bond with an O—O distance of 2.42 Å.

* Author to whom correspondence should be addressed.

A compound formulated "$H_2[IrCl_6]\cdot 4DMSO$", made[7] (cf. Henbest's original method) by treatment of H_2IrCl_6 in *iso*-propanol with dimethylsulphoxide, whose IR indicated that DMSO was attached to Ir via S, has not been further studied, although James and his colleagues said that Henbest's and Antonov's protonated chloroiridate complexes "must also contain the $[H(Me_2SO)_2]^+$ cation".

We now report the molecular structure of one of the original iridium complexes, which we prepared whilst looking for an acetonitrile-soluble iridium(III) complex in the course of other work. It turns out, contrary to most earlier suggestions, to be the *trans* isomer which is completely analogous to the known rhodium structure.

EXPERIMENTAL

General

Electronic spectra were measured with a Perkin–Elmer λ 5 spectrophotometer. IR spectra were recorded, as Nujol mulls, on a Perkin–Elmer 783. NMR spectra were run on a Bruker WM360 spectrometer. Thermogravimetric analyses were obtained with a Stanton Redcroft TG 750 balance in a dynamic nitrogen atmosphere at a heating rate of 20°C min^{-1}. Microanalyses (C and H) were performed by the microanalytical laboratory, Department of Chemistry, University College, Cardiff. All solvents were of reagent grade purity. "$IrCl_3\cdot 3H_2O$" was supplied by Johnson Matthey.

Preparation of $[(DMSO)_2H]$*trans*-$[IrCl_4(DMSO)_2]$

$IrCl_3\cdot 3H_2O$ (1.14 g) was dissolved in DMSO (10 cm^3) by heating and the solution filtered. THF (25 cm^3) was added to the filtrate and, after 10 days at room temperature followed by 20 days at 5°C, the resulting yellow–brown crystals (480 mg) were isolated (setting the filtrate aside) and washed twice with THF and ether. THF (15 cm^3) was added to the filtrate, giving a milky solution which cleared when heated. After allowing the solution to stand for 2 days at room temperature diethyl ether (10 cm^3) was added and the solution was stored for 6 weeks in the refrigerator. The yellow crystals (325 mg) which formed were separated and washed with diethyl ether. Found: C, 14.9; H, 3.8. Calc. for $C_8H_{25}S_4O_4Cl_4Ir$: C, 14.9; H, 3.9%. The melting point was 127 ± 2°C. The crystal structure was determined using crystals from the second crop. Table 1 shows the identity of the compound with earlier preparations.

Crystal data

$HIrCl_4\cdot 4DMSO$; $M_r = 647.19$; space group $P2/c$; $a = 920.4(2)$, $b = 1652.1(2)$, $c = 1527.7(2)$ pm; $\beta = 115.43(1)°$; $Z = 4$; $V = 2.0979$ nm^3; $D_c = 2.05$ g cm^{-3}: $D_m = 2.06$ g cm^{-3}; μ(Mo-K_α) = 69.8 cm^{-1} and $T = 296$ K (cf. Table 2).

X-ray measurements

Single-crystal X-ray measurements were carried out with an Enraf-Nonius CAD 4 diffractometer using Mo-K_α radiation. The data obtained were corrected for Lorentz and polarization effects. The intensities of two check reflections showed no loss of intensity. Out of 5199 independent reflections 3726 having $I > 2.5\sigma(I)$ were accepted as observed.

The structure was solved by heavy-atom and direct methods, which gave positional parameters for Ir, S and Cl atoms. The atomic scattering factors and anomalous dispersion correction factors for heavy atoms were taken from *International Tables*.[8] The structure was refined with heavy atoms and hydrogen atoms having anisotropic and isotropic temperature factors, respectively. An empirical absorption correction was applied. The C—H hydrogen positions were calculated assuming

Table 1. Properties of samples of $[(DMSO)_2H][IrCl_4(DMSO)_2]$

Structure	Reference	Colour	M.p. (°C)	NMR solvent	NMR δ	Original formulation
trans	This work	Yellow	127 ± 2	D_2O	3.50, 2.72	—
	Ref. 1	Yellow	125			*cis*
	Ref. 2	Yellow needles	120–122	D_2O	3.52, 2.69	
	Ref. 4	Yellow needles	—	D_2O	3.52, 2.71	*cis*
Other isomer	Ref. 1	Pink	165–170			
	Ref. 2	Orange pink	171.5–172		3.48, 2.69	*trans*
	Ref. 4	Orange needles	152–154	D_2O	3.50, 2.71	

Table 2. Unit cells of $[(DMSO)_2H]$*trans*$[MCl_4(DMSO)_2]$

M.p. (°C)		*a*	*b*	*c*	*β*	*V*	*r*OHO
Rh 120–121[a]	$P2_{1/n}$	9.217(8)	16.50(2)	14.03(1)	100.73(6)°	2170.8 (Å^3)	2.42
Ir 120–122[b]							
127±1[c]	*P*2/*c*	9.204(2)	16.52(1)	15.27(7)	115.43(1)°	2097.9 (Å^3)	2.405

[a] H. B. Henbest and J. Trocha-Grimshaw, *J. Chem. Soc., Perkin I* 1974, 607.
[b] Ref. 2.
[c] This work.

Table 3. Anisotropic temperature factors (Å^2) for $HIrCl_4 \cdot 4DMSO$

	U_{11}	U_{22}	U_{33}	U_{23}	U_{13}	U_{12}
Ir(1)	0.0242(2)	0.0237(2)	0.0244(2)	0.0000(0)	0.0102(1)	0.0000(0)
Ir(2)	0.0230(2)	0.0234(2)	0.0233(2)	0.0000(0)	0.0098(1)	0.0000(0)
Cl(1)	0.0380(8)	0.0822(12)	0.0287(7)	−0.0090(7)	0.0108(6)	−0.0047(8)
Cl(2)	0.0698(16)	0.0303(11)	0.1064(21)	0.0000(0)	0.0550(16)	0.0000(0)
Cl(3)	0.0541(14)	0.0275(10)	0.0652(15)	0.0000(0)	0.0252(12)	0.0000(0)
Cl(4)	0.0364(9)	0.2460(35)	0.0285(8)	0.0215(13)	0.0119(7)	0.0028(13)
Cl(5)	0.1372(30)	0.0268(13)	0.1965(39)	0.0000(0)	0.1400(31)	0.0000(0)
Cl(6)	0.1354(31)	0.0303(14)	0.2925(58)	0.0000(0)	0.1725(39)	0.0000(0)
S(1)	0.0292(7)	0.0408(9)	0.0315(7)	0.0009(6)	0.0137(6)	0.0001(5)
S(2)	0.0260(6)	0.0312(8)	0.0315(7)	0.0010(5)	0.0134(6)	−0.0009(5)
S(3)	0.0504(9)	0.0497(10)	0.0563(10)	−0.0063(8)	0.0292(8)	−0.0018(7)
S(4)	0.0514(9)	0.0488(9)	0.0508(9)	−0.0157(7)	0.0253(8)	−0.0083(7)
O(1)	0.0291(22)	0.1009(41)	0.0402(24)	0.0115(24)	0.0112(19)	0.0070(23)
O(2)	0.0261(20)	0.0850(36)	0.0384(23)	0.0053(21)	0.0100(18)	−0.0034(20)
O(3)	0.0534(26)	0.0515(28)	0.0523(26)	0.0116(22)	0.0184(22)	0.0033(22)
O(4)	0.0702(34)	0.0943(43)	0.0674(34)	−0.0262(31)	0.0298(29)	−0.0389(32)
C(1)	0.0631(50)	0.0849(61)	0.0877(62)	−0.0447(48)	0.0482(48)	−0.0094(42)
C(2)	0.0585(43)	0.0692(52)	0.0872(54)	0.0305(42)	0.0483(42)	0.0018(37)
C(3)	0.0463(36)	0.0451(36)	0.0413(33)	0.0084(27)	0.0259(29)	−0.0004(27)
C(4)	0.0526(39)	0.0369(34)	0.0728(46)	−0.0103(31)	0.0394(36)	0.0009(28)
C(5)	0.0589(43)	0.0438(37)	0.0525(40)	0.0032(32)	0.0018(33)	−0.0005(33)
C(6)	0.0701(51)	0.0587(50)	0.0863(60)	−0.0182(42)	0.0181(45)	−0.0148(42)
C(7)	0.1147(84)	0.0768(65)	0.0809(66)	0.0077(46)	0.0489(63)	−0.0175(55)
C(8)	0.0831(61)	0.1279(87)	0.0662(54)	−0.0153(55)	0.0228(47)	0.0417(61)

The U(iso) values for the H atoms are 0.097(7).

the C—H distance to be 96 pm. The refinements led to final $R = 0.028$ and $R_w = 0.029$, where $R = \Sigma\Delta/\Sigma F_o$, $R_w = \Sigma w\Delta/\Sigma wF_o$, $\Delta = |F_o - F_c|$ and $w = 1.09/[\sigma^2(F_o) + 0.000300F_o^2]$.

Crystallographic calculations were performed with the SHELX-76 program[9] and the figure (Fig. 1) was drawn with ORTEP.[10]* The final positional coordinates of heavy atoms and equivalent isotropic temperature factors are listed in Table 3.

The NMR spectra (Table 1) showed two singlets, of equal intensity, at 3.50 (due to methyl protons of DMSO coordinated to iridium via sulphur atoms) and 2.72 (methyl protons of free DMSO). The first value is consistent with that found for S-bonded DMSO in $RuCl_2(DMSO)_4$.[11]

The IR spectrum of $[(DMSO)_2H]$*trans*-$[IrCl_4(DMSO)_2]$ showed bands at 3540w, 3395w, 1630m, 1296m, 1115s, 1018s, 990w, 970m, 938w, 918w, 720(broad), 495m, 425s, 385s, 335s, 320s, 288m. The broad band from 950–600 cm^{-1} is assigned to the O—H—O stretch. The quite broad

* Atomic coordinates, displacement factor coefficients, full lists of bond lengths and angles and lists of F_o/F_c values have been deposited as supplementary data with the Editor, from whom copies are available on request. Atomic coordinates have also been deposited with the Cambridge Crystallographic Data Centre.

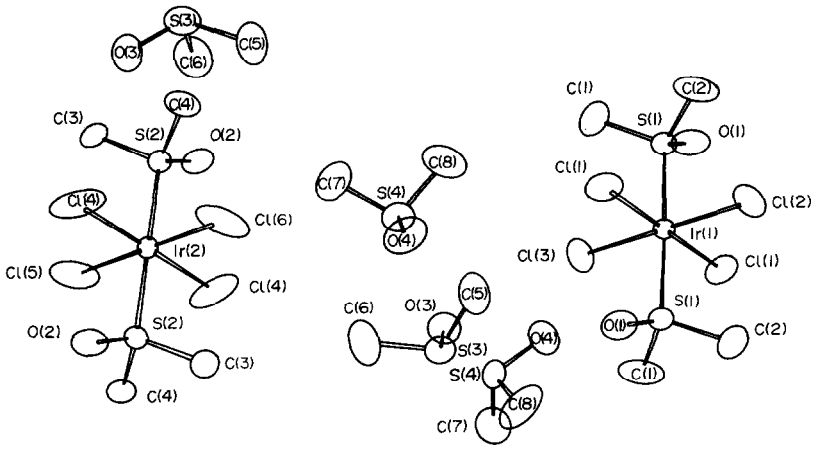

Fig. 1. ORTEP view of the structure of $[(DMSO)_2H][IrCl_4(DMSO)_2]$.

band at *ca* 1120 cm^{-1} is assigned as the S—O stretch from an S-bonded DMSO and the bands at energies less than 350 cm^{-1} are labelled as Ir—Cl vibrations, compared with values for compounds such as $[NMe_4]$*trans*-$[Ir(SMe_2)_2Cl_4]$.[12] Indeed, for both isomers of the iridium acid, $[H(OSMe_2)_2]$ $[IrCl_4(OSMe_2)_2]$ Henbest and his coworkers assign bands from 350 to 250 cm^{-1} as Ir—Cl modes, without any details other than absorption frequencies.

The electronic spectrum shows peaks at: λ(nm), (ε, 1 mol^{-1} cm^{-1}) 453.0(21.2), 377.0(44.1), 335.4(153.0), 295.0(232.5). The two weak peaks at longer wavelength belong to the two spin forbidden transitions $^1A_{1g} \rightarrow {}^3T_{1g} + {}^3T_{2g}$ and the lower wavelength to spin allowed $^1A_{1g} \rightarrow {}^1T_{1g} + {}^1T_{2g}$: the symmetry is of course D_{4h} here but we use labels for O_h, as if the symmetry were that of $IrCl_6^{3-}$. Because there has been some confusion between *cis* and *trans* isomers, we give our electronic spectrum (a very good means of distinguishing) in full (Fig. 2).

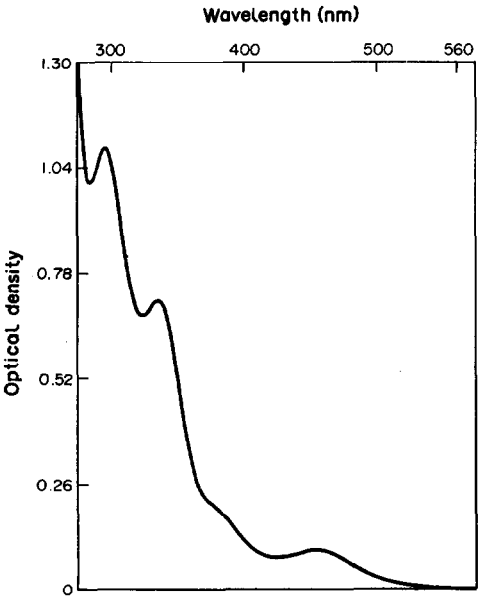

Fig. 2. Electronic absorption spectrum of $[(DMSO)_2H]$ $[IrCl_4(DMSO)_2]$ in water, concentration 4.67×10^{-3} M, measured in 1 cm cell.

Earlier work assigned the two geometric isomers incorrectly, through an argument based on the very slight (δ 0.02) chemical shift difference of methyl protons of coordinated DMSO between the two compounds. The *trans* isomer was thought to resonate at higher field (closer to free DMSO) owing to the greater distance between the methyl group and SO bond of the other coordinated DMSO. (In fact, Antonov[7] assigned the *cis* and *trans* acids correctly, on the basis of their electronic absorption spectra.)

Yellow $[(DMSO)_2H]$*trans*-$[IrCl_4(DMSO)_2]$ (m.p. 125 ± 5°C), prepared here and by others, contains two S-bonded DMSO ligands. There are six pos-

Table 4. Bond distances (pm) of $HIrCl_4 \cdot 4DMSO$

Ir(1)—S(1)	231.3(1)	Ir(2)—S(2)	236.6(1)
Ir(1)—S(1^i)	231.3(1)	Ir(2)—S(2^i)	231.6(1)
Ir(1)—Cl(1)	235.7(1)	Ir(2)—Cl(4)	233.6(1)
Ir(1)—Cl(1^i)	235.7(1)	Ir(2)—Cl(4^{ii})	233.1(1)
Ir(1)—Cl(2)	236.2(2)	Ir(2)—Cl(5)	234.0(3)
Ir(1)—Cl(3)	234.7(2)	Ir(2)—Cl(6)	232.0(3)
S(1)—O(1)	146.8(4)	S(2)—O(2)	147.0(4)
S(1)—C(1)	176.4(6)	S(2)—C(3)	176.9(5)
S(1)—C(2)	176.0(7)	S(2)—C(4)	177.5(6)
S(3)—O(3)	153.7(5)	S(4)—O(4)	154.8(5)
S(3)—C(5)	176.9(7)	S(4)—C(7)	175.6(8)
S(3)—C(6)	178.3(8)	S(4)—C(8)	174.4(8)

Symmetry codes: (i) = $1-x$, y, $0.5-z$; (ii) = $-x$, y, $1.5-z$.

Table 5. Bond angles (°) of $HIrCl_4 \cdot 4DMSO$

S(1)—Ir(1)—S(1^{i})	178.5(1)	S(2)—Ir(2)—S(2^{ii})	179.8(1)
S(1)—Ir(1)—Cl(1)	91.8(1)	S(2)—Ir(2)—Cl(4)	91.9(1)
S(1)—Ir(1)—Cl(1^{i})	88.2(1)	S(2)—Ir(2)—Cl(4^{ii})	88.1(1)
S(1)—Ir(1)—Cl(2)	90.8(1)	S(2)—Ir(2)—Cl(5)	89.9(1)
S(1)—Ir(1)—Cl(3)	89.2(1)	S(2)—Ir(2)—Cl(6)	90.1(1)
S(1^{i})—Ir(1)—Cl(1)	88.2(1)	S(2^{ii})—Ir(2)—Cl(4)	88.1(1)
S(1^{i})—Ir(1)—Cl(1^{i})	91.8(1)	S(2^{ii})—Ir(2)—Cl(4^{ii})	91.9(1)
S(1^{i})—Ir(1)—Cl(2)	90.8(1)	S(2^{ii})—Ir(2)—Cl(5)	89.9(1)
S(1^{i})—Ir(1)—Cl(3)	89.2(1)	S(2^{ii})—Ir(2)—Cl(6)	90.1(1)
Cl(1)—Ir(1)—Cl(1^{i})	179.4(1)	Cl(4)—Ir(2)—Cl(4^{ii})	178.7(1)
Cl(1)—Ir(1)—Cl(2)	89.7(1)	Cl(4)—Ir(2)—Cl(5)	89.4(1)
Cl(1^{i})—Ir(1)—Cl(2^{i})	89.7(1)	Cl(4^{ii})—Ir(2)—Cl(5^{ii})	89.4(1)
Cl(1)—Ir(1)—Cl(3)	90.3(1)	Cl(4)—Ir(2)—Cl(6)	90.6(1)
Cl(1^{i})—Ir(1)—Cl(3)	90.3(1)	Cl(4^{ii})—Ir(2)—Cl(6)	90.6(1)
Cl(2)—Ir(1)—Cl(3)	180.0(1)	Cl(5)—Ir(2)—Cl(6)	180.0(1)
Ir(1)—S(1)—O(1)	116.6(2)	Ir(2)—S(2)—O(2)	117.1(2)
Ir(1)—S(1)—C(1)	111.9(3)	Ir(2)—S(2)—C(3)	111.5(2)
Ir(1)—S(1)—C(2)	112.6(2)	Ir(2)—S(2)—C(4)	111.9(2)
O(1)—S(1)—C(1)	106.9(4)	O(2)—S(2)—C(3)	107.4(3)
O(1)—S(1)—C(2)	107.2(3)	O(2)—S(2)—C(4)	108.2(3)
C(1)—S(1)—C(2)	100.2(4)	C(3)—S(2)—C(4)	99.2(3)
O(3)—S(3)—C(5)	105.5(3)	O(4)—S(4)—C(7)	104.0(4)
O(3)—S(3)—C(6)	105.4(3)	O(4)—S(4)—C(8)	102.2(4)
C(5)—S(3)—C(6)	100.9(4)	C(7)—S(4)—C(8)	100.6(5)

Symmetry codes: (i) = $1-x, y, 0.5-z$; (ii) = $-x, y, 1.5-z$.

sible isomers; both O-bonded, both S-bonded or one O- and one S-bonded—each of these may be *cis* or *trans* forms, and it is one of the two least likely isomers statistically which forms as crystals. The two DMSO molecules per cation are held together by a very short, strong hydrogen bond [bond length O—H—O is 2.405 Å (see Tables 4 and 5 for bond distances and bond angles)].

There are undoubtedly two compounds of composition "H(IrCl$_4$)4DMSO". One (yellow, m.p. 125°C) is described here and is [(DMSO)$_2$H]*trans*-[IrCl$_4$(DMSO)$_2$]. The other (orange or pink, m.p. 154 or 165°C) therefore clearly cannot be the same (which is how it has been formulated). It may be the other geometric isomer, or a linkage isomer, or may contain both features. Evans *et al.* found[11] that [RuCl$_2$(DMSO)$_4$] had both O-bonded and S-bonded ligands. Indeed, the situation is summarized by Goggin:[13] the present-δ value (*ca* 3.50 ppm) suggests S-bonding (and hence the *cis* structure). However, the present situation for the *trans* isomer differs from that he describes "when there are three or more sulphoxide ligands on rhodium(III) or ruthenium(II), a mixed coordination is preferred, and structures with mutually *trans*-S-bonded sulphoxide ligands tend to be avoided." That generalization does not extend to iridium(III).

REFERENCES

1. Y. M. Y. Haddad, H. B. Henbest, J. Husbands and T. R. B. Mitchell, *Proc. Chem. Soc.* 1964, 361.
2. Y. M. Y. Haddad, H. B. Henbest and J. K. Trocha-Grimshaw, *J. Chem. Soc., Perkin I* 1974, 592.
3. Y. M. Y. Haddad, H. B. Henbest, J. Husbands, T. R. B. Mitchell and J. Trocha-Grimshaw, *J. Chem. Soc., Perkin I* 1974, 596.
4. B. R. James, R. H. Morris and P. Kvintovics, *Can. J. Chem.* 1986, **64**, 897.
5. M. M. Kreevoy and J. M. Williams, *J. Am. Chem. Soc.* 1967, **89**, 5499; M. M. Kreevoy, T. Liang and K.-C. Chang, *J. Am. Chem. Soc.* 1977, **99**, 5207.
6. R. A. Potts, *Inorg. Chem.* 1970, **9**, 1284.
7. P. G. Antonov, Y. N. Kukushkin, V. F. Shknedov, L. V. Konovalov and B. I. Ionin, *Koord. Khim.* 1977, **3**, 907: *Chem. Abs.* 1977, **87**, 61901n.
8. *International Tables for X-ray Crystallography*, Vol. 4. Kynoch Press, Birmingham (1974).
9. G. M. Sheldrick, SHELX-76. *Program for Crystal Structure Determination.* University of Cambridge (1987).

10. C. K. Johnson, ORTEP-II. *A Fortran Thermal-ellipsoid Plot Program for Crystal Structure Illustrations. Report ORNL-5138.* Oak Ridge National Laboratory, Tennessee (1976).
11. I. P. Evans, A. Spencer and G. Wilkinson, *J. Chem. Soc., Dalton Trans.* 1973, 204.
12. D. J. Gulliver, W. Levason, K. G. Smith, M. J. Selwood and S. G. Murray, *J. Chem., Soc. Dalton Trans.* 1980, 1872.
13. P. L. Goggin, in *Comprehensive Coordination Chemistry* (Edited by G. Wilkinson, R. D. Gillard and J. A. McCleverty), Vol. 2, p. 489. Pergamon Press, Oxford (1987).

Polyhedron Vol. 7, No. 21, pp. 2149–2153, 1988
Printed in Great Britain

0277–5387/88 $3.00+.00
© 1988 Pergamon Press plc

COMPLEXES OF MANGANESE(II), COBALT(II) AND NICKEL(II) WITH THE KETO FORM OF SOME ANTIPYRINE SCHIFF BASE DERIVATIVES

AHMED M. DONIA* and F. A. EL-SAIED

Department of Chemistry, Faculty of Science, Menoufia University, Shebin El-Kom, Egypt

(*Received* 31 *July* 1987; *accepted after revision* 15 *March* 1988)

Abstract—Manganese, cobalt and nickel complexes of some Schiff base derivatives of antipyrine have been prepared and characterized. Spectroscopic and other studies on these air-stable complexes indicated that the Schiff bases are coordinated through the carbonyl oxygen of the pyrazolone ring, the quinonoid oxygen and the secondary nitrogen. The stereochemistry of the complexes as well as the nature of the bonding of the chloride were discussed.

Antipyrine (2,3-dimethyl-1-phenyl-5-pyrazolone) Structure (I) and its derivatives have a variety of applications including biological,[1] clinical[2] and pharmacological[3,4] areas. Among these we mention their use as antipyretic, analgesic and anti-rheumatic.[4] Antipyrines have also been used as analytical reagents in the estimation of some metal ions.[5–9] The classical coordination chemistry of antipyrine was studied[10–15] and its complexing ability has been modified by the preparation of Schiff base derivatives[6,16] which are important in, for example the fluorimetric estimation of metal ions.[17] However, very little work has been done on the behaviour of these compounds towards the transition metal ions which commonly exist in biological fluids. In the present communication, a number of transition metal complexes of Schiff base derivatives of antipyrine were prepared and characterized by a variety of spectral and analytical methods to clarify the structure as well as the nature of the bonding in these complexes.

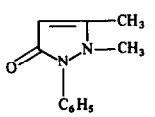

Structure (I).

It has been recently reported that some antipyrine Schiff bases undergo photochromism in the crystalline state.[18] The yellow enolic form gives the orange quinonoid structure upon photo-irradiation ($\lambda_{ex.}$ = 365 nm). In the present study, we show that the quinonoid structure of antipyrine Schiff bases exhibits a higher tendency for metal–complex formation in the solutions compared with the enolic forms. This might be of significance in the specific trapping of the quinonoid structure.

EXPERIMENTAL

Materials

All chemicals were reagent grade. The ligands [HL^1, HL^2 and HL^3] were prepared by condensation of 4-aminoantipyrine and different aldehydes [salicylaldehyde HL^1, 2-hydroxy-1-naphthaldehyde HL^2 and 2,4-dihydroxybenzaldehyde HL^3] in ethanol. The mixture was refluxed for *ca.* 15 min. The precipitate obtained after cooling was collected and purified by crystallization from ethanol.

Preparation of the complexes

The complexes were prepared by the addition of the stoichiometric amounts of the metal chloride salt in absolute ethanol to a hot alcoholic solution of the ligand and sodium acetate, (1 : 1 : 1) molar ratio. A precipitate was formed after 2 h reflux for ligands HL^1 and HL^2 and after 30 min for ligand HL^3. The precipitate was filtered off, washed with ethanol several times and dried over ($CaCl_2/P_4O_{10}$). The complexes are slightly soluble in hot ethanol

*Author to whom correspondence should be addressed.

Table 1. Analytical and conductance data for ligands and their complexes

Compound	Colour	C(%)	H(%)	N(%)	Cl(%)	Λm Ω^{-1} cm^2 mol^{-1}	Electro-lytic nature	Effect of heat[a]
HL^1	Yellow	70.4(70.0)	5.5(5.5)	13.7(13.7)				
$[Mn(HL^1)(H_2O)Cl_2]\cdot H_2O$	Yellow	46.0(46.0)	4.4(4.5)	9.0(8.9)	15.0(15.1)	88	[b]	Decomposes at 250°C
$[Co(HL^1)(H_2O)Cl_2]\cdot H_2O$	Red	45.5(45.6)	4.4(4.4)	9.0(8.9)	15.0(15.0)	55	[b]	Changes to black at 120°C
$[Ni(HL^1)(H_2O)_2Cl]Cl\cdot H_2O$	Yellowish green	43.9(44.0)	4.7(4.7)	8.5(8.6)	14.2(14.5)	155	1:1	Changes to orange at 150°C
HL^2	Greenish yellow	73.7(74.0)	5.5(5.3)	11.7(11.8)				
$[Mn(HL^2)(H_2O)_2Cl]Cl\cdot H_2O$	Yellow	49.2(49.2)	4.7(4.7)	7.7(7.8)	13.3(13.2)	140	1:1	Decomposes at 250°C
$[Co(HL^2)(H_2O)_2Cl]Cl$	Faint yellow	50.5(50.5)	4.4(4.4)	8.0(8.0)	13.5(13.6)	116	1:1	Changes to black at 150°C
$[Ni(HL^2)(H_2O)_3]Cl_2\cdot 4H_2O$	Yellowish green	43.0(43.0)	5.5(5.4)	6.8(6.9)	11.7(11.6)	201	1:2	Changes to orange at 160°C
HL^3	Yellow	67.0(66.9)	5.2(5.3)	12.9(13.0)				
$[Mn(HL^3)(H_2O)Cl_2]\cdot H_2O$	Yellow	44.6(44.6)	4.2(4.3)	8.7(8.7)	14.6(14.7)	1	[b]	Decomposes at 250°C
$[Co(HL^3)(H_2O)Cl_2]\cdot H_2O$	Light green	44.1(44.2)	4.3(4.3)	8.6(8.6)	14.4(14.5)	2.3	[b]	Decomposes at 270°C
$[Ni(HL^3)(H_2O)Cl_2]\cdot 3H_2O$	Yellowish green	41.3(41.2)	4.9(4.8)	7.9(8.0)	13.5(13.5)	0.7	[b]	Changes to orange at 150°C

Calc. analyses in parentheses.

$HL^1 = C_{18}H_{17}O_2N_3$; $HL^2 = C_{22}H_{19}O_2N_3$; $HL^3 = C_{18}H_{17}O_3N_3$.

[a] The change in colour takes place in the solid state.

[b] Non-conducting solutions.

and hot chloroform but they are more soluble in dimethylformamide.

The elemental analysis (C,H,N) were carried out in the National Research Centre—Dokki, Cairo. The chloride was estimated as silver chloride. IR spectra were obtained on a Perkin–Elmer 598 (4000–200 cm^{-1}) IR spectrophotometer using KBr discs. The electronic spectra were carried out in nujol mulls using a Perkin–Elmer 550S spectrophotometer which was calibrated using holmium oxide film. The conductivity measurements were made in dimethylformamide solutions using TACUSSEL conductimetre type CD6N.

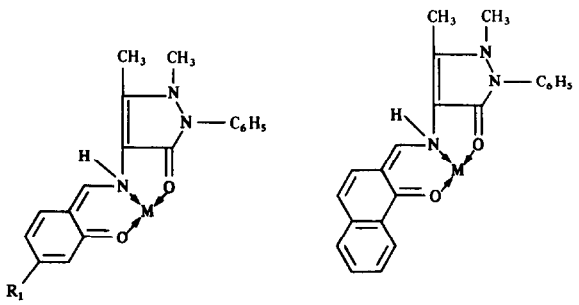

Fig. 1.

RESULTS AND DISCUSSION

The reactions between Mn(II), Co(II) and Ni(II) and Schiff base derivatives of antipyrine give 1 : 1 complexes. These complexes are stable at room temperature and display colour changes (in the solid state) upon heating as shown in Table 1.

Table 1 also shows that some complexes gave non-conducting solutions in DMF which indicates the coordination of the chloride ions but others gave conducting solutions which indicates the non-coordination of the chloride ions.[19,20]

Vibrational spectra

The IR spectra of antipyrine and its derivatives are too complex but a comparison of the spectrum with some previous work[8] has enabled us to assign the more characteristic bands. The observed bands of the ligands and their complexes together with their possible assignments are listed in Table 2.

(a) *4000–2000 cm^{-1}*. In this region the free Schiff bases HL^1 and HL^2 show intramolecular hydrogen bonding (O—H···N) which gives rise to a broad absorption near 3420 cm^{-1},[21] whilst HL^3 shows two absorption bands near 3120 cm^{-1} and 3430 cm^{-1} that are assigned to intramolecular hydrogen bonding (O—H···N)[22] and free νOH, respectively. The band near 3420 cm^{-1} or 3120 cm^{-1} shifts to the region 3330–3200 cm^{-1} in the spectra of the metal complexes as the hydrogen bonding arrangement change N—H due to the enolimine to ketoenamine tautometric conversion[22,23] through the formation of the metal complexes. The lowering of the frequency of νN—H may be attributed to a metal (secondary) nitrogen coordinate bond.[24–26] The spectra of the complexes show an additional broad band near the 3440–3400 cm^{-1} region which was assigned to water molecules.

(b) *2000–300 cm^{-1}*. In this region the free Schiff bases show a very strong absorption band near 1660–1630 cm^{-1} region and a very weak or medium absorption band near 1625–1613 cm^{-1} region which were assigned to νC=O[8] of the pyrazolone ring and νC=N, respectively. The IR spectra of the complexes show a considerable shift ($\sim$ 100 cm^{-1}) of the carbonyl stretching of the pyrazolone ring to a lower frequency, indicating a decrease in the stretching force constant of C=O as a consequence of coordination through its oxygen.[8] The C=N stretching vibration disappears upon metal complexation which favours the ketoenamine tautomer formation. The enolimine to ketoenamine tautometric conversion was confirmed also by the presence of new absorption bands with different intensities in the spectra of the complexes at 3330–3200 cm^{-1}, 1620–1610 cm^{-1} and 1570–1535 cm^{-1} regions that were assigned to coordinated νN—H, δN—H[25] and a metal coordinated carbonyl group stretching,[27] respectively. This can be taken as an evidence for the participation of the carbonyl group of the ketoenamine tautomer in coordination. Consequently the Schiff base reacts with metal ions in its keto form. The band in the region 310–325 cm^{-1} may be associated with metal chloride[28,29] stretching vibrations. A strong evidence regarding the bonding of νM—O[28] of the ligand has been provided by the appearance of an absorption band in the region 450–520 cm^{-1}. The above arguments indicated that the contribution of the structures indicated in Fig. 1 became more significant.

Electronic spectra

The electronic spectral data of the solid complexes are given in Table 2. The electronic spectra of Ni(II) complexes show bands with comparatively

Table 2. IR and electronic spectral data for ligands and their complexes

Compound	νOH	νN—H	νC=O of pyrazolone ring	νC=O of phenyl/ naphthyl ring	νC=N
HL^1	3440(br)		1655(vs)		1625(vw)
$[Mn(HL^1)(H_2O)Cl_2]\cdot H_2O$	3420(br)	3330(m)	1540(m)	1540(m)	
$[Co(HL^1)(H_2O)Cl_2]\cdot H_2O$	3420(br)	3320(m)	1535(m)	1550(sh)	
$[Ni(HL^1)(H_2O)_2Cl]Cl\cdot H_2O$	3420(br)	3320(m)	1540(m)	1550(sh)	
HL^2	3410(br)		1640(vs)		1620(m)
$[Mn(HL^2)(H_2O)_2Cl]Cl\cdot H_2O$	3440(br)	3230(w)	1535(m)	1550(w)	
$[Co(HL^2)(H_2O)_2Cl]Cl$	3400(br)	3200(br)	1555(sh)	1570(m)	
$[Ni(HL^2)(H_2O)_3]Cl_2\cdot 4H_2O$	3400(br)	3280(m)	1540(m)	1550(w)	
HL^3	3120(br) 3430(m)		1630(sh)		1612(s)
$[Mn(HL^3)(H_2O)Cl_2]\cdot H_2O$	3420(br)	3280(m)	1545(s)	1545(s)	
$[Co(HL^3)(H_2O]Cl_2]\cdot H_2O$	3420(br)	3250(s)	1542(s)	1542(s)	
$[Ni(HL^3)(H_2O)Cl_2]\cdot 3H_2O$	3410(br)	3230(w)	1535(m)	1545(sh)	

w = weak, s = strong, v = very, m = medium, br = broad and sh = shoulder.

low intensities around 605–590 nm and 350–340 nm. These bands may be assigned to $^3A_{2g} \rightarrow {}^3T_{1g}$ and $^3A_{2g} \rightarrow {}^3T_{1g}$ (P), respectively in an octahedral geometry.[30]

The electronic spectra of Co(II) complexes show a broad and a weak band around 590–570 nm. This band may be assigned to $^4T_{1g} \rightarrow {}^4T_1$ (P) in an octahedral geometry.[31]

REFERENCES

1. D. G. Craciunescu, *An. R. Acad. Farm.* 1977, **43**, 265.
2. J. Hosler, C. Tschanz, C. E. Hignite and D. L. Azarnoff, *J. Invest. Dermatol.* 1986, **74**, 51.
3. P. J. Meffin, R. L. Williams, T. F. Blaschke and M. Rowland, *J. Pharm. Sci.* 1977, **66**, 135.
4. E. V. Schmidt, T. P. Priskchep and N. A. Chernova, *IZV. Tomsk. Politekhn* In-Ta 1975, 156; M. M. Shoukry, A. Kh. Ghoneim, E. M. Shoukry and M. H. El-Nagdi, *Synth. React. Inorg. Met. Org. Chem.* 1982, **12**, 815.
5. N. L. Olenovich and L. I. Koval Chuk, *Zh. Anal. Khim.* 1975, **28**, 2162.
6. Sh. T. Talipov, A. T. Tashkhodzhaev, L. E. Zel'tser and Kh. Khilkmatov, *Izv. Vyssh. Ucheb. Zaved. Khim. Tekhnol.* 1975, **15**, 1109.
7. A. T. Pilipenko, S. L. Lisichenok and A. I. Volkova, *Ukr. Khim. Zh.* (Russ. Ed.), 1976, **42**, 76.
8. V. V. Savant, P. P. Ramamurthy and C. C. Patel, *J. Less-Common Metals* 1970, **22**, 479.
9. B. Janik and S. Sawicki, *Mikro. Chim. Acta* 1970, 1050.
10. E. Wilke-Dörfurt and O. Schlcephake, *Z. Anorg. Allg. Chem.* 1929, **183**, 301.
11. E. Wilke-Dörfurt and H. G. Mureck, *Z. Anorg. Allg. Chem.* 1930, **184**, 121.
12. R. Rascanu. *Ann. Sci. Univ. Jassy* 1933, **18**, 72.
13. J. V. Dubsky, E. Krametz and J. Trtilek, *Collection Czechoslov. Chem. Commun.* 1935, **7**, 311.
14. J. V. Dubsky, E. Krametz and J. Trtilek, *Collection Czechoslov. Chem. Commun.* 1936, **8**, 141.
15. M. Ragno, *Gazz. Chim. Ital.* 1938, **68**, 741.
16. V. L. Letunov, *Zh. Org. Khim.* 1984, **20**, 162.
17. K. Morishige, *Anal. Chim. Acta* 1980, **121**, 301.
18. E. M. Ebeid, A. M. Donia and F. A. El-Saied. *J. Phys. Chem. Solids* (submitted for publication).
19. A. W. Ainscough and R. A. Plowman. *Austral. J. Chem.* 1970, **23**, 699.
20. M. Massacesi, R. Pinna and G. Ponticelli, *Spectrochim. Acta* 1982, **38A**, 725.
21. K. Morisige, *J. Inorg. Nucl. Chem.* 1978, **40**, 843.
22. R. C. Aggarwal, R. Bala and R. L. Prasad, *Spectrochim. Acta* 1986, **42A**, 725.
23. G. Condorelli, I. Fragala, S. Guiffrida and A. Cassol, *Z. Anorg. Allg. Chem.* 1975, **412**, 251.
24. C. T. Spencer and L. T. Taylor, *Inorg. Chem.* 1971, **11**, 2407.
25. K. Nakamoto, *Infrared and Raman Spectra of Inorganic and Coordination Compounds*, 3rd edn. Wiley-Interscience, New York (1977).
26. W. M. Coleman and L. T. Taylor, *J. Inorg. Nucl. Chem.* 1980, **42**, 683.
27. P. A. Vigato, U. Casellato, S. Tamburini, M. Vidali,

Table 2—*continued*

δN—H	Phenyl ring/ naphthyl ring stretching	νM—O	νM—Cl	Electronic spectra (nm) *d–d* transition	other bands
	1590(s)				
1610(s)	1580(m)	520(m)	318(w)		
1610(s)	1600(sh), 1580(w)	477(m)	325(w)	570(br)	430(sh), 400(w), 370(w)
1610(s)	1600(sh), 1585(w)	477(w)	332(w)	600(w), 340(m)	410(m)
1615(s)		455(m)	325(w)		
1620(m)		452(m)	310(w)	590(w)	485(sh), {406, 380}, 335(m)
1620(s)		460(m)		605(w), 350(m)	420(m)
	1575(m), 1585(m)				
1612(s)	1600(w), 1580(m)	495(m)	327(w)		
1622(s)	1600(m), 1580(m)	473(m)	315(m)	590(m)	490(sh), 400(s)
1610(s)	1585(w)	467(m)	320(w)	590(w)	390(br)

F. Milani and M. M. Musiani, *Inorg. Chim. Acta* 1982, **61**, 89.
28. M. W. G. De Bolster and W. L. Groeneveld, *Rec. Trav. Chim.* 1971, **90**, 477, 687.
29. G. E. Coates and D. Ridley, *J. Chem. Soc.* 1964, 166.
30. A. B. P. Lever, *Inorganic Electronic Spectroscopy*, p. 333. Elsevier, Amsterdam (1968).
31. R. L. Carlin, *Transition Metal Chemistry* (Edited by R. L. Carlin), Vol. 1, p. 320. Marcel Decker, New York (1965).

Polyhedron Vol. 7, No. 21, pp. 2155–2157, 1988
Printed in Great Britain

0277–5387/88 $3.00+.00
© 1988 Pergamon Press plc

COMPLEXING PROPERTIES OF SQUARIC ACID WITH IRON(II), COBALT(II) AND NICKEL(II) IN PROPAN-2-OL

D. I. MAHARAJ and L. A. HALL*

Department of Chemistry, The University of the West Indies, St. Augustine, Trinidad

(*Received* 26 *August* 1987; *accepted after revision* 18 *March* 1988)

Abstract—Reaction of cobalt(II) chloride and nickel(II) bromide with squaric acid in propan-2-ol solution produced the four-coordinate complexes $[Co(OH)(HC_4O_4)]_2$ and $[Ni(OH)(HC_4O_4)]_2 \cdot C_3H_7OH$, respectively. Both metals are tetrahedral and have hydroxyl bridges. The iron(II) complex, however, has the formula $[Fe(HC_4O_4)(OH)(C_3H_7OH)]_2 \cdot C_3H_7OH$ and is five-coordinate.

The formation of four-coordinate cobalt(II) and nickel(II) squarate complexes in propan-2-ol instead of five-coordinate complexes as occurred in the primary alcohol, ethanol[1,2] is apparently due to the steric constraints imposed by the secondary alcohol. However, in spite of these steric constraints the iron(II) squarate prepared from propan-2-ol is five-coordinate. This has been attributed to the predominance of the instability of tetrahedral iron(II) over the steric effects in this case.

EXPERIMENTAL

Chemicals

Squaric acid obtained from the Aldrich Chemical Company, Milwaukee, WI was used as received. The propan-2-ol used was Analar grade from BDH. The iron(II) chloride, nickel(II) chloride and nickel(II) bromide were used in their hydrated form. The iron(II) chloride was feshly prepared from iron filings and AR concentrated hydrochloric acid.

Preparation of the complexes

The pale blue cobalt(II) and yellow–brown iron(II) complexes were prepared by mixing hot degassed solutions of squaric acid (0.15 g, 1.3 mmol) with cobalt(II) chloride-6-water (3.00 g, 12.6 mmol) and iron(II) chloride-4-water (0.26 g, 1.3 mmol), respectively. The yellow–green nickel(II) complex was prepared similarly except that nickel(II) bromide was used instead of the chloride due to its greater solubility in propan-2-ol. Approximately 0.15 g (1.3 mmol) of squaric acid and 0.36 g (1.3 mmol) of nickel(II) bromide-3-water were used in the preparation of the nickel(II) complex. The collection and drying of the complexes were similar to that described previously[1,2] except that the iron(II) complex was vacuum dried for only 5 min since longer drying resulted in oxidation. Yield: iron(II) complex, 0.17 g (50%); cobalt(II) complex, 0.25 g (38%); nickel(II) complex, 0.28 g (36%). Found: C, 37.7; H, 5.0; Fe, 20.6. Calc. for $C_{17}H_{28}O_{13}Fe_2$: C, 37.0; H, 5.1; Fe, 20.2%. Found: C, 24.9; H, 3.0; Co, 30.8. Calc. for $C_8H_4O_{10}Co_2$: C, 25.4; H, 1.06; Co, 31.0%. Found: C, 31.3; H, 3.3; Ni, 26.6. Calc. for $C_{11}H_{12}O_{11}Ni_2$: C, 30.2; H, 2.7; Ni, 26.8%.

Instrumentation

The IR spectra were obtained using a Nicolet 5DX FTIR spectrophotometer and KBr discs. The UV–vis–near IR reflectance spectra were recorded on a Perkin–Elmer 330 spectrophotometer. The room temperature magnetic moments were determined on a Newport magnetic balance using the Gouy method and employing $Hg[Co(SCN)_4]$ as the calibrant. The thermogravimetric analyses were performed on a Du Pont Instruments 1090 thermogravimetric analyser.

Analyses

The carbon and hydrogen analyses were carried out by Huffman Laboratories Inc., Colorado. The

*Author to whom correspondence should be addressed.

iron and nickel determinations were made with a Pye–Unicam SP 9 atomic absorption spectrophotometer while the cobalt was determined by Schwarzkopf Microanalytical Laboratory Inc., New York.

RESULTS AND DISCUSSION

The IR spectra of the three complexes are very similar. The major difference is the weakness of the C=O stretch in the cobalt(II) and iron(II) complexes compared to the C=O stretch in the nickel(II) complex. These stretches appear at around 1800 cm^{-1} in each complex. The O—H stretch in the cobalt(II) complex is narrow and occurs at about 3250 cm^{-1} while the O—H stretch in the nickel(II) complex is broad and extends from 3050 to 3700 cm^{-1}. The O—H stretch in the iron(II) complex is actually a combination of two closely spaced bands at 3300 and 3500 cm^{-1}. These differences in the positions and nature of the O—H stretches are most likely due to the different types of O—H groups present in the three complexes. The band which peaks at about 1500 cm^{-1} in the spectra of the three complexes is assignable to a mixture of C—C and C—O stretchings.[3] The C=C absorption which occurs at about 1620 cm^{-1} in the nickel(II) complex is apparently obscured by the C—C and C—O absorptions in the iron(II) and cobalt(II) complexes. The O—H bending of the hydroxyl bridge[4] in the cobalt(II) complex occurs at 1103 cm^{-1}. The envelope of peaks around 1100 cm^{-1} in the iron(II) complex is due to the coordinated propan-2-ol, the propan-2-ol of crystallization[5,6] and the hydroxyl bridge. The propan-2-ol of crystallization and the hydroxyl bridge in the nickel(II) complex produces an envelope of fewer peaks at about 1100 cm^{-1}. The out-of-plane bonded deformation and additional squarate bands occurred between 500 and 900 cm^{-1} in the spectrum of each complex.[3,7–9] The bridging M—O absorptions[4,10] occur at 396 and 462 cm^{-1} in the iron(II) complex, at about 426 cm^{-1} in the cobalt(II) complex and as a multiplet around 444 cm^{-1} in the nickel(II) complex.

The UV–vis spectrum of the cobalt(II) complex shows an absorption between 13,300 and 17,500 cm^{-1} with a fine structure which is characteristic of tetrahedral cobalt(II).[11] The UV–vis spectrum of the nickel(II) complex has two absorptions at 6100–10,500 cm^{-1} and 10,800–18,200 cm^{-1} which is consistent with tetrahedral nickel(II) while the UV–vis–near IR spectrum of the iron(II) complex shows three absorptions known to be characteristic of five-coordinate iron(II).[11] These occurred between 9100 and 11,800 cm^{-1}, at 20,000 and 30,000 cm^{-1}.

The structures shown in Fig. 1 are proposed.

Two inflections occur in the thermal weight loss curve of the iron(II) complex at about 170 and 290°C and correspond to weight losses of 11 and 27%, respectively. The calculated weight losses for the removal of the propan-2-ol of crystallization followed by the two coordinated propan-2-ol molecules are 10.88 and 32.63%. The propan-2-ol of crystallization is apparently removed first but some decomposition of the complex possibly occurs during removal of the coordinated alcohol molecules. The weight loss curves of the other two complexes are difficult to interpret possibly because the complexes decompose in a complicated manner.

The magnetic moments of the cobalt(II) and nickel(II) complexes are 4.73 and 2.81 BM, respectively which are consistent with tetrahedral cobalt(II) and nickel(II). The magnetic moment of the iron(II) complex is 5.04 BM which is consistent with high-spin five-coordinate iron(II).

It is possible that the propan-2-ol, due to its size and shape, forces the cobalt and nickel to adopt a tetrahedral geometry unlike ethanol which produces five-coordinate complexes and water which produces six-coordinate complexes because the latter solvents do not have the required steric effect. The poor H analysis for the cobalt(II) complex could be explained in terms of the large lattice spaces available for water contamination[1,2,8] due to its tetrahedral geometry and the absence of propan-2-ol of crystallization and coordinated propan-2-ol. It should be noted that these complexes are insoluble in many common solvents and either decompose or undergo changes in geometry in others.

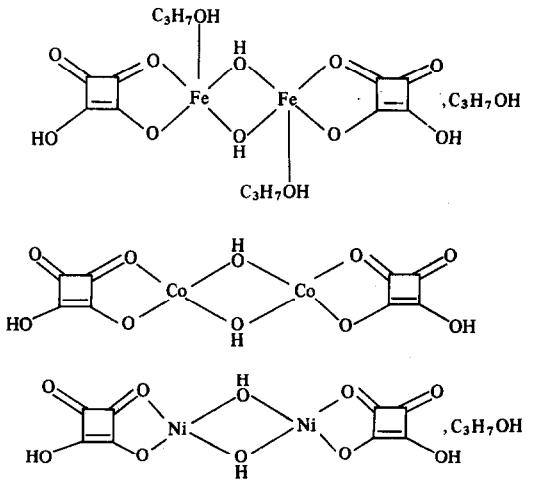

Fig. 1.

Thus, recrystallization has not been possible so far. The quality of the H analyses for the nickel(II) and iron(II) complexes suggests that contamination is negligible in these complexes due to the lack of lattice space caused by the propan-2-ol of crystallization in both complexes and, additionally, coordinated propan-2-ol in the iron(II) complex.

The iron(II) complex is unstable and oxidizes rapidly on exposure to the atmosphere. Prolonged vacuum drying also causes oxidation.

REFERENCES

1. O. St. C. Headley and L. A. Hall, *Polyhedron* 1985, **4**, 1697.
2. O. St. C. Headley and L. A. Hall, *Polyhedron* 1986, **5**, 1829.
3. R. West and H. Y. Niu, *J. Am. Chem. Soc.* 1963, **85**, 2589.
4. J. R. Ferraro, R. Driver, W. Walker and W. Wozniak, *Inorg. Chem.* 1967, **6**, 1586.
5. K. Nakamoto, *Infrared and Raman Spectra of Inorganic and Coordination Compounds*, 3rd Edn, p. 230. Wiley Interscience, New York (1977).
6. G. Socrates, *Infrared Characteristic Group Frequencies*, p. 45. John Wiley, New York (1980).
7. F. G. Baglin and C. B. Rose, *Spectrochim. Acta* 1970, **26A**, 2298.
8. B. C. Gerstein and M. Habenschuss, *J. Appl. Phys.* 1972, **12**, 5155.
9. M. Ito and R. West, *J. Am. Chem. Soc.* 1963, **85**, 1580.
10. D. Adams, *Metal–Ligand and Related Vibrations*, p. 235. Edward Arnold, London (1967).
11. A. B. P. Lever, *Inorganic Electronic Spectroscopy*, 2nd Edn, pp. 376–572. Elsevier, Amsterdam (1984).

Polyhedron Vol. 7, No. 21, pp. 2159–2163, 1988
Printed in Great Britain

0277–5387/88 $3.00+.00
© 1988 Pergamon Press plc

THE REACTIVITY OF $[Os_3(CO)_{10}(C_2Ph_2)]$ TOWARDS PHENYL MERCURY HALIDES

JUAN M. FERNÁNDEZ-G., MARÍA J. ROSALES* and R. A. TOSCANO

Instituto de Química, Universidad Nacional Autónoma de México, Circuito Exterior, Ciudad Universitaria, Coyoacán 04510, México, D. F.

(*Received* 4 *January* 1988; *accepted after revision* 18 *March* 1988)

Abstract—The reaction of $Os_3(CO)_{10}(C_2Ph_2)$ with PhHgCl in benzene yields $[Os_3(CO)_9(\mu_3\text{-}C_2Ph_2)(\mu_2\text{-}Cl)(HgCl)]_2$. The complex has been characterized by the usual spectroscopic methods and by an X-ray crystal structure determination. The compound crystallizes in the triclinic space group $P\bar{1}$, cell dimensions $a = 9.727(3)$, $b = 12.590(4)$, $c = 14.863(7)$ Å, $\alpha = 96.75(3)$, $\beta = 109.02(3)$, $\gamma = 99.58(2)°$, $V = 1667.8(8)$ Å^3, $Z = 1$. The three osmium atoms form a bent arrangement with the diphenyl acetylene and a chloride ion bridging the non-bonded (Os—Os distance of 3.768 Å) osmium–osmium edge, a mercury atom bridges a metal–metal bond and is also bound, in an unsymmetrical fashion to two chlorine atoms which act as bridges to an identical triosmium–mercury unit. A toluene molecule is also present in the asymmetric unit.

The reactivity of cluster compounds containing coordinated alkyne groups has received little attention. One aspect of these compounds that has not been examined is whether the carbon–carbon bond can still behave as an isolated unsaturated bond. One set of reagents that could help to study this, is the set of Seyferth derivatives $PhHgCX_nY_{3-n}$, (X,Y = halogens, n = 1–3), which are halocarbene generators that react with olefins to give cyclopropane.[1,2] Therefore some alkyne clusters were made to react with several halocarbene generators. The reactions were found to yield complexes containing mercury.[3]

One point that has to be taken into consideration is that PhHgX is produced in the generation of the halocarbene. This compound has been reported to react with a transition metal cluster.[4] Other mercury(I) and mercury(II) salts have been observed to react with carbonyl clusters to yield a range of compounds in which mercury atoms either bridge a previously existing metal–metal bond[5] or link several cluster units.[6–8]

In this paper we describe the results of the reaction of a series of alkyne clusters $Os_3(CO)_{10}(C_2R_2)$ with phenyl mercury halides and the crystal structure of one of the products.

RESULTS AND DISCUSSION

The reaction of $Os_3(CO)_{10}(C_2Ph_2)$ with PhHgCl in benzene produced a yellow solution which yielded two products, one of them a light yellow compound, **1**, in a much larger yield than the other one **2**. The spectroscopic information for these and other new compounds reported in this paper are given in Table 1. The information obtained from the IR, ^{1}H NMR and mass spectra suggested a formulation $Os_3(CO)_9HgCl(C_2Ph_2)$. Since these

Table 1

Compound	ν_{CO}[a]	M$^+$
1	2108(w), 2084(s), 2055(vs), 2052(sh), 2012(s), 1986(m)	1241
2	2117(w), 2086(m), 2070(m), 2024(s), 1991(w)	—
3	2109(w), 2083(m), 2068(w), 2057(vs), 2041(w), 2015(s), 1998(m), 1983(w)	1160
4	2098(m), 2069(w), 2029(s), 2012(vs), 1949(m)	1108

[a] In CH_2Cl_2.

* Author to whom correspondence should be addressed.

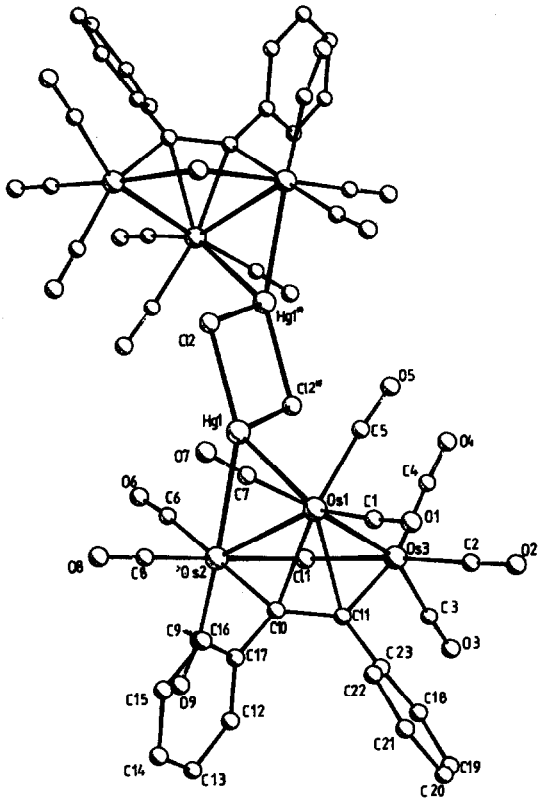

Fig. 1. The molecular structure of **1** with the atomic numbering scheme.

data did not allow an unambiguous proposition of the structure for the complex, an X-ray crystal structure determination was undertaken.

The molecular structure of **1** is shown in Fig. 1. Bond lengths and angles are given in Tables 2 and 3. The complex consists of a centrosymmetric dimer of two tetranuclear Os_3—Hg units linked by two chlorine atoms bridging the two Hg atoms asymmetrically (Hg—Cl distances: 2.387(8) and 2.946(10) Å). Each Os—Os distance is different. Os(1) and Os(3) are separated by 2.824(2) Å while the distance between Os(1) and Os(2) is 3.020(2) Å. Os(2) and Os(3) are not bonded since the distance between them is 3.768 Å. This last edge is bridged by both a chloride and the diphenyl acetylene group. Similar molecular geometries, i.e. a triangle of three osmium atoms with the long (non-bonded) edge spanned by two bridging groups, have been reported for other osmium compounds.[9]

The Hg atom bridges Os(1) and Os(2). The Os—Hg distances (2.830(1) and 2.712(2) Å) are similar to those observed in other mercury containing ruthenium and osmium clusters.[4,7,8]

The metal framework can be described as a spiked-triangle with Os(1), Os(2) and Hg forming the triangle. The dihedral angle between the planes formed by Os(1)—Os(2)—Hg and Os(1)—Os(2)—Os(3) is 106.1°.

The diphenyl acetylene ligand remains in a similar bonding fashion to that in the starting material, $Os_3(CO)_{10}(C_2Ph_2)$.[10] The chloride ligand is bridging the non-bonded Os—Os edge in a symmetrical fashion. Os(2)—Cl(1) and Os(3)—Cl(1) show bond lengths of 2.431(8) and 2.447(6) Å, respectively, not significantly different from those reported in other complexes.[11] The plane passing through Os(2)—Os(3)—Cl(1) forms an angle of 25.9° with the plane formed by Os(1), Os(2) and Os(3).

A similar structure was observed in $[Ru_3(CO)_9(C_6H_9)HgBr]_2$ (C_6H_9 = HC≡CBu).[3] The only significant difference is that in the ruthenium compound, all three ruthenium atoms are bonded in a

Table 2. Bond lengths (Å)

Os(1)—Os(2)	3.020(2)	Os(1)—Os(3)	2.824(2)
Os(1)—Hg	2.830(1)	Os(1)—C(1)	1.901(35)
Os(1)—C(5)	1.919(27)	Os(1)—C(7)	1.933(34)
Os(1)—C(10)	2.272(30)	Os(1)—C(11)	2.378(27)
Os(2)—Hg	2.712(2)	Os(2)—Cl(1)	2.431(8)
Os(2)—C(6)	2.825(23)	Os(2)—C(8)	1.895(31)
Os(2)—C(9)	1.920(38)	Os(2)—C(10)	2.222(27)
Os(3)—Cl(1)	2.447(6)	Os(3)—C(2)	1.937(27)
Os(3)—C(3)	1.924(36)	Os(3)—C(4)	1.993(27)
Os(3)—C(11)	2.125(26)	Hg—Cl(2)	2.387(8)
Hg—Cl(2a)	2.946(10)	Cl(2a)—Hg(a)	2.387(8)
O(1)—C(1)	1.079(42)	O(2)—C(2)	1.088(36)
O(3)—C(3)	1.146(48)	O(4)—C(4)	1.105(32)
O(5)—C(5)	1.103(35)	O(6)—C(6)	1.068(30)
O(7)—C(7)	1.141(43)	O(8)—C(8)	1.144(38)
O(9)—C(9)	1.140(45)	C(10)—C(11)	1.385(42)
C(18)—C(17)	1.490(32)	C(11)—C(23)	1.527(25)

Table 3. Bond angles (deg)

Os(2)—Os(1)—Os(3)	88.2	Os(2)—Os(1)—Hg	55.1
Os(3)—Os(1)—Hg	97.3	Os(2)—Os(1)—C(1)	152.2(10)
Os(3)—Os(1)—C(1)	98.4(13)	Hg—Os(1)—C(1)	151.0(11)
Os(2)—Os(1)—C(5)	120.2(8)	Os(3)—Os(1)—C(5)	82.7(10)
Hg—Os(1)—C(5)	71.2(7)	C(1)—Os(1)—C(5)	86.8(13)
Os(2)—Os(1)—C(7)	92.3(9)	Os(3)—Os(1)—C(7)	172.5(9)
Hg—Os(1)—C(7)	77.4(7)	C(1)—Os(1)—C(7)	88.7(15)
C(5)—Os(1)—C(7)	100.4(13)	Os(2)—Os(1)—C(10)	47.1(7)
Os(3)—Os(1)—C(10)	74.9(10)	Hg—Os(1)—C(10)	102.1(7)
C(1)—Os(1)—C(10)	105.5(13)	C(5)—Os(1)—C(10)	155.7(14)
C(7)—Os(1)—C(10)	100.8(13)	Os(2)—Os(1)—C(11)	70.4(6)
Os(3)—Os(1)—C(11)	47.3(7)	Hg—Os(1)—C(11)	120.2(6)
C(1)—Os(1)—C(11)	88.1(13)	C(5)—Os(1)—C(11)	128.2(12)
C(7)—Os(1)—C(11)	131.0(10)	C(10)—Os(1)—C(11)	34.6(11)
Os(1)—Os(2)—Hg	58.9	Os(1)—Os(2)—Cl(1)	84.5(2)
Hg—Os(2)—Cl(1)	87.1(2)	Os(1)—Os(2)—C(6)	132.6(8)
Hg—Os(2)—C(6)	74.0(8)	Cl(1)—Os(2)—C(6)	88.1(9)
Os(1)—Os(2)—C(8)	95.0(9)	Hg—Os(2)—C(8)	92.7(8)
Cl(1)—Os(2)—C(8)	179.5(8)	C(6)—Os(2)—C(8)	92.2(11)
Os(1)—Os(2)—C(9)	132.6(9)	Hg—Os(2)—C(9)	165.9(10)
Cl(1)—Os(2)—C(9)	86.2(12)	C(6)—Os(2)—C(9)	93.3(12)
C(8)—Os(2)—C(9)	94.2(15)	Os(1)—Os(2)—C(10)	48.5(8)
Hg—Os(2)—C(10)	107.2(8)	Cl(1)—Os(2)—C(10)	89.8(9)
C(6)—Os(2)—C(10)	177.5(14)	C(8)—Os(2)—C(10)	89.9(11)
C(9)—Os(2)—C(10)	85.2(12)	Os(1)—Os(3)—Cl(1)	88.6(2)
Os(1)—Os(3)—C(2)	92.0(10)	Cl(1)—Os(3)—C(2)	176.4(8)
Os(1)—Os(3)—C(3)	158.7(9)	Cl(1)—Os(3)—C(3)	84.1(9)
C(2)—Os(3)—C(3)	94.2(13)	Os(1)—Os(3)—C(4)	106.0(10)
Cl(1)—Os(3)—C(4)	89.7(8)	C(2)—Os(3)—C(4)	93.6(11)
C(3)—Os(3)—C(4)	93.9(13)	Os(1)—Os(3)—C(11)	55.3(8)
Cl(1)—Os(3)—C(11)	87.8(7)	C(2)—Os(3)—C(11)	89.6(11)
C(3)—Os(3)—C(11)	104.4(11)	C(4)—Os(3)—C(11)	161.2(13)
Os(1)—Hg—Os(2)	66.0	Os(1)—Hg—Cl(2)	133.2(2)
Os(2)—Hg—Cl(2)	155.1(2)	Os(1)—Hg—Cl(2a)	116.8(2)
Os(2)—Hg—Cl(2a)	101.3(2)	Cl(2)—Hg—Cl(2a)	84.2(3)
Os(2)—Cl(1)—Os(3)	101.2(3)	Hg—Cl(2)—Hg(a)	95.8(3)
Os(1)—C(1)—O(1)	175.2(33)	Os(3)—C(2)—O(2)	177.1(29)
Os(3)—C(3)—O(3)	177.3(26)	Os(3)—C(4)—O(4)	174.2(29)
Os(1)—C(5)—O(5)	175.4(25)	Os(2)—C(6)—O(6)	174.9(28)
Os(1)—C(7)—O(7)	176.1(24)	Os(2)—C(8)—O(8)	176.9(24)
Os(2)—C(9)—O(9)	171.0(30)	Os(1)—C(10)—Os(2)	84.4(8)
Os(1)—C(10)—C(11)	76.9(17)	Os(2)—C(10)—C(11)	120.2(20)
Os(1)—C(10)—C(17)	131.0(25)	Os(2)—C(10)—C(17)	111.1(18)
C(11)—C(10)—C(17)	124.1(21)	Os(1)—C(11)—Os(3)	77.5(8)
Os(1)—C(11)—C(10)	68.5(17)	Os(3)—C(11)—C(10)	124.8(16)
Os(1)—C(11)—C(23)	125.2(19)	Os(3)—C(11)—C(23)	117.2(17)
C(10)—C(11)—C(23)	117.9(22)		

triangular shape. This difference may be due to the difference in reaction conditions. **1** was obtained in refluxing benzene while the ruthenium cluster was prepared in refluxing THF. In fact, a trial reaction between $Os_3(CO)_{10}(C_2Ph_2)$ and PhHgCl carried out in THF produced a complex different from **1** which has not been as yet characterized. With both Ru and Os complexes, HgX_2 could be also used as the mercury reagent.

Another factor that could be important in explaining this difference is the halide. The preparations of the ruthenium complex were carried out with bromide and iodide.[3,12] However, a brief mention was made in a later paper[13] that the chloride Ru_3Hg complex had been prepared.

In order to observe the influence of the halide on the type of product obtained, $Os_3(CO)_{10}(C_2Ph_2)$ was allowed to react with PhHgBr and PhHgI under

similar reaction conditions to those of PhHgCl. These reactions were much more sensitive towards slight changes in reaction conditions (i.e. concentration). There are, however, two main products in the reaction with PhHgBr. Compound **3**, red, and compound **4**, green, were obtained in approximately equal yields. The spectroscopic information obtained for these complexes (Table 1) is insufficient to allow us to propose a structure for them at this time. Single crystals of **3** and **4** have not yet been obtained.

The reaction between $Os_3(CO)_{10}(C_2Ph_2)$ and PhHgI gave many more products than the previous ones, all of them in very low yields, but a complex with a similar IR spectrum to that of **3** was obtained.

A series of derivatives $Os_3(CO)_{10}(C_2RR')$ (R = Ph, R′ = H or $SiMe_3$, R = R′ = Me, H or EtOOC—C) was also allowed to react with PhHgCl in order to test for substituent effect on the reactivity of the compounds. All the reactions were carried out under the same reaction conditions. The main products of the reactions, from spectroscopic evidence, were all similar. However, there were significant variations in the yields.

The best yield of an equivalent compound to **1** was obtained in the reaction of $Os_3(CO)_{10}(PhC{\equiv}CSiMe_3)$ while the poorest occurred with $Os_3(CO)_{10}(C_2H_2)$. It is then difficult to say at present which effect is the most important in determining the reaction path.

EXPERIMENTAL

None of the compounds reported here are air-sensitive but all reactions were carried out under an atmosphere of dry nitrogen to exclude moisture. All new compounds decompose slowly at room temperature in solution and in the solid state, however they are sufficiently stable to handle for several hours before repurification is required. Products were separated in the air by thin layer chromatography (TLC) with plates coated with 0.5 mm of Merck Kieselgel 60 F_{254}. All solvents were dried over appropriate reagents and distilled prior to use.

IR spectra were recorded on a Nicolet FT-55S between 2150 and 1700 cm^{-1}. Mass spectra were obtained on an AEI MS12 spectrometer with *ca* 70 eV ionizing potential. Tris(perfluoroheptyl)-S-triazine was used as reference. $Os_3(CO)_{10}(C_2Ph_2)$ was prepared by the literature method.[14]

Preparations

All the compounds were prepared by reacting $Os_3(CO)_{10}(C_2Ph_2)$ with a slight excess of the appropriate phenyl mercury halide in refluxing benzene for *ca* 10 h. The solvent was then removed under vacuum. The residue was dissolved in a small volume of dichloromethane and the products isolated by TLC using ethyl acetate–hexane (10:90) as eluant.

Crystal structure determination of $[Os_3(CO)_9(C_2Ph_2)(\mu\text{-Cl})(\mu\text{-HgCl})]_2$, **1**

A single crystal of **1** was obtained by slow evaporation of a toluene–cyclooctane solution. The crystal was mounted on a glass fibre with epoxy resin.

Crystal data and additional data collection parameters are given in Table 4. The intensity data were collected using ω scans with a variable scan speed from 4 to 30 deg min^{-1} and a scan width of 1.0° on a Nicolet R3m diffractometer. Two standard reflections monitored every 100 measurements showed only minor fluctuations during data collection. Data were corrected for Lorentz and polarization effects. An absorption correction based on azimuthal scans was also applied.

The structure was solved by a combination of direct methods and difference Fourier maps. The refinement was carried out by full-matrix least-

Table 4. Summary of crystal data, intensity data collection and structure refinement

Molecular formula	$Os_6Hg_2C_{46}H_{20}O_9Cl_4$
Molecular weight	2400.4
Cryst. dimens (mm)	$0.06 \times 0.14 \times 0.28$
Cryst. syst.	Triclinic
Space group	$P\bar{1}$
Cell dimensions	
a (Å)	9.727(3)
b (Å)	12.590(4)
c (Å)	14.863(7)
α (deg)	96.75(3)
β (deg)	109.02(3)
δ (deg)	99.58(2)°
V (Å^3)	1667.8(8)
ρ_c (g cm^{-1})	2.39 g cm^{-3}
Z	1
$F(000)$	1138
λ (Å)	0.71069 Å
μ(Mo-K_α) (cm^{-1})	160.43
Diffractometer	Nicolet R3m
2θ min (deg)	3
2θ max (deg)	45
No. of reflections measured	4367
No. of unique reflections	3465
$n, F > n\sigma(F)$	3
Converged residuals	
R	0.0722
R_w	0.0705

squares techniques with anisotropic thermal parameters for all but the hydrogen atoms and the carbon atoms of the carbonyl groups. The hydrogen atoms were placed in idealized positions and included in the refinement. The laminar type crystal was not of very good quality and did not allow a better refinement.

The atomic scattering factors were taken from the *International Tables.*[15] The solution and refinement of the structure was carried out using SHELXTL[16] on a Nova 4S computer. Final atomic coordinates and other crystallographic data have been deposited with the Editor and can be obtained from the Cambridge Crystallographic Data Centre.

Acknowledgement—We wish to thank CONACYT for the financial contribution (PCCBCNA-740272) towards a preliminary presentation of this work at the XXIV ICCC Meeting in Athens, Greece.

REFERENCES

1. D. Seyferth and J. Murphy, *J. Organometal. Chem.* 1973, **49**, 117.
2. D. Seyferth, M. E. Gordon, J. Y. P. Mui and J. M. Burlitch, *J. Am. Chem. Soc.* 1967, **89**, 959.
3. J. M. Fernández and M. J. Rosales, to be published.
4. R. Fahmy, K. King, E. Rosenberg, A. Tiripicchio and M. Tiripicchio-Camellini, *J. Am. Chem. Soc.* 1980, **102**, 3636.
5. G. Predieri, A. Tiripicchio, C. Vignali, E. Sappa and P. Braunstein, *J. Chem. Soc., Dalton Trans.* 1986, 1135.
6. Y. Yamamoto, H. Yamazaki and J. Sakurai, *J. Am. Chem. Soc.* 1982, **104**, 2329.
7. M. Fajardo, H. D. Holden, B. F. G. Johnson, J. Lewis and P. R. Raithby, *J. Chem. Soc., Chem. Commun.* 1984, 24.
8. M. P. Gómez-Sal, B. F. G. Johnson, J. Lewis, P. R. Raithby and S. N. A. B. Syed-Mustaffa, *J. Organometal. Chem.* 1984, **272**, C21.
9. M. O. Albers, D. J. Robinson and N. J. Coville, *Coord. Chem. Rev.* 1986, **69**, 127 and refs cited therein.
10. C. Pierpont, *Inorg. Chem.* 1977, **16**, 636.
11. M. A. Gallop, B. F. G. Johnson, J. Lewis and P. R. Raithby, *J. Chem. Soc., Chem. Commun.* 1986, 706.
12. S. Ermer, K. King, K. I. Hardcastle, E. Rosenberg, A. M. Manotti-Lanfredi, A. Tiripicchio and M. Tiripicchio-Camellini, *Inorg. Chem.* 1983, **22**, 1339.
13. E. Rosenberg, D. Ryckman, I. N. Hsu and R. W. Gellert, *Inorg. Chem.* 1986, **25**, 194.
14. M. Tachikawa, J. Shapley and C. Pierpont, *J. Am. Chem. Soc.* 1975, **97**, 7172.
15 *International Tables for X-Ray Crystallography*, Vol. IV, pp. 72–98. Kynoch Press, Birmingham, U.K. (1974).
16. G. M. Sheldrick, SHELXTL *Version 3. An Integrated System for Solving, Refining and Displaying Crystal Structures from Diffraction Data.* University of Göttingen, F.R.G. (1981).

Polyhedron Vol. 7, No. 21, pp. 2165–2169, 1988
Printed in Great Britain

0277–5387/88 $3.00+.00
© 1988 Pergamon Press plc

TIME DIFFERENTIAL PERTURBED ANGULAR CORRELATION (TDPAC) STUDY OF SOME HAFNIUM GLYCOLATE COMPLEXES

ROBERTO SANTOS BARBIÉRI* and STANLEI I. KLEIN

Instituto de Química, Universidade Estadual Paulista "Julio de Mesquita Filho", 14 800, Araraquara, SP, Brazil

and

ANTONIO MARQUES NETTO

Departamento de Química, ICEx, Universidade Federal de Minas Gerais, 31 270 Belo Horizonte, MG, Brazil

(*Received* 17 *September* 1987; *accepted after revision* 14 *April* 1988)

Abstract—Time differential measurements of the 133–482 keV γ–γ angular correlation of ^{181}Ta have been performed in solid hafnium complexes of the type [Hf(glycol)$_4$] (glycol = *p*-chloromandelate, *p*-bromomandelate, β-naphthylglycolate and mandelate). The quadrupolar frequencies (ω_Q) were found to increase within the series. This behaviour was explained by supposing a dissipation of electronic density at the metal level, caused by an increase in intermolecular hydrogen bonding in the complexes throughout the series studied. These results seem to agree with complementary data from IR spectroscopic studies.

The method of perturbed angular correlation (PAC) of nuclear γ-rays is suitable for studying the influence of extranuclear field gradients in the angular correlation of sequentially emitted γ-rays, and as Mössbauer Resonance Spectroscopy it can be a useful tool for the study of local properties in condensed matter. The chemical influences on the angular correlation of γ-rays was discussed in comprehensive reviews mainly by Vargas[1] and Adloff.[2] In the field of solid state inorganic chemistry the method of PAC can provide information similar to that available from Mössbauer but it is important to note that routine Mössbauer nuclei are not good candidates for PAC, whereas due to the lack of favourable transitions, high energy and short mean life times,[3] Mössbauer spectroscopy does not allow accurate information to be gathered on the high coordination complexes typical of the third transition series. Generally PAC experiments have been performed on the cascades emitted by ^{111}Cd and ^{181}Ta which are particularly well adapted nuclei for probing quadrupole coupling in solids. The two techniques are therefore complementary rather than competitive.

Recently PAC has been successfully used in materials science for the detection of certain physical properties of ceramics[4,5] and for probing biological systems, and data relating to flexibility and aggregation of proteins coordinated to ^{111}In have been obtained.[6,7]

Over the past years one of us has been studying several structural and related aspects of hafnium complexes using PAC. For instance, we found that in the DL-mandelate complex[8] the hafnium atoms sit in two slightly different sites. This result was attributed to a dimeric molecular structure as previously suggested by Larsen and Homeier for the compound.[9] Investigation of the neutron irradiated hafnium chelates by ion exchange[10] and TDPAC[11] showed discrepancies which were attributed to the possibility of different chemical environments for the hafnium atoms in the complexes.

These results showed the necessity for additional experiments on hafnium compounds in order to test the differences between *in situ* and conventional analysis.

*Author to whom correspondence should be addressed.

METHOD

Radioactive ^{181}Hf undergoes beta decay to produce the intermediate and excited state of ^{181}Ta (spin = 5/2), which de-excites by sequential emission of two angular correlated, easily observable and distinguishable γ-rays (the 133 and 482 eV "cascade") (Fig. 1).

In a metal complex, the ligands introduce extranuclear fields that can interact with the nuclear moments of the intermediate state and perturb the angular correlation function.[2]

The perturbed angular correlation function is:

$$W(\theta, t) = 1 + A_2 G_2(t) P_2(\cos\theta) + A_4 G_4(t) P_4(\cos\theta) \quad (1)$$

where $P_k(\cos\theta)$ are Legendre polynomials, and A_k are angular correlation coefficients which reflect the unperturbed anisotropy of the emitted radiation and depend only on known nuclear factors. In general, the coefficient A_4 is so much smaller than A_2 that the last term of eq. (1) can be neglected. In fact, all chemical information is contained in the time dependent perturbation coefficient $G_2(t)$. For a static quadrupolar interaction (the electric field gradient, EFG, does not fluctuate with time) in a polycrystalline sample and for the case with spin $I = 5/2$ of the intermediate level, $G_2(t)$ takes the following expression:

$$G_2(t) = s_{2o} + \sum_{n=1}^{3} s_{2n} \cos(\omega_n t)\, e^{-(\delta\omega_n t + 1/2\omega_n^2 \tau_R^2)} \quad (2)$$

where δ is the relative width of the frequency distribution, s_{2o} and s_{2n} are functions of the asymmetry parameter, η of the EFG, ω_n is a function of both η and the quadrupolar frequency ω_Q:

$$\omega_Q = \frac{eQV_{zz}}{40\hbar}. \quad (3)$$

V_{zz} is the principal component of the EFG, Q is the nuclear quadrupole moment and e the electronic charge. Operationally, the analysis of experimental data using eq. (2) yields frequencies from which ω_Q, V_{zz} and η can be derived. These factors are very sensitive probes to explore local symmetry properties in solids. The constant τ_R is the resolution time of the electronic system used in counting the rate of successive photons of a γ–γ cascade.

A layout of the instrumentation used in PAC spectroscopy is shown in Fig. 2 and consists of a conventional fast–slow system. The two detectors, one fixed and the other movable, are 38 × 38 mm NaI(*Tl*) crystals coupled to photomultipliers. The time resolution achieved is typically 2.9 ns FWHM.

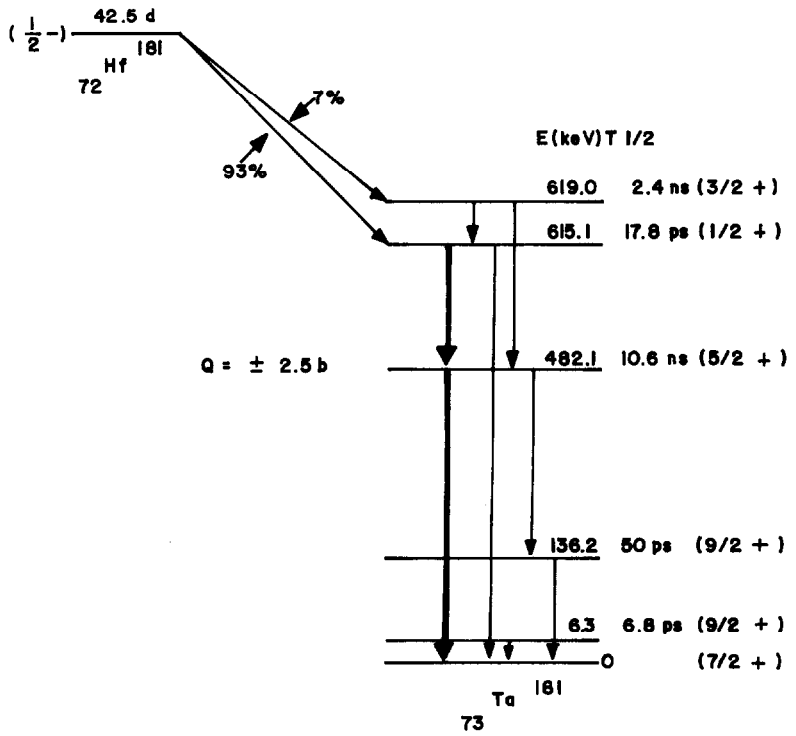

Fig. 1. Disintegration scheme for the decay of ^{181}Hf.

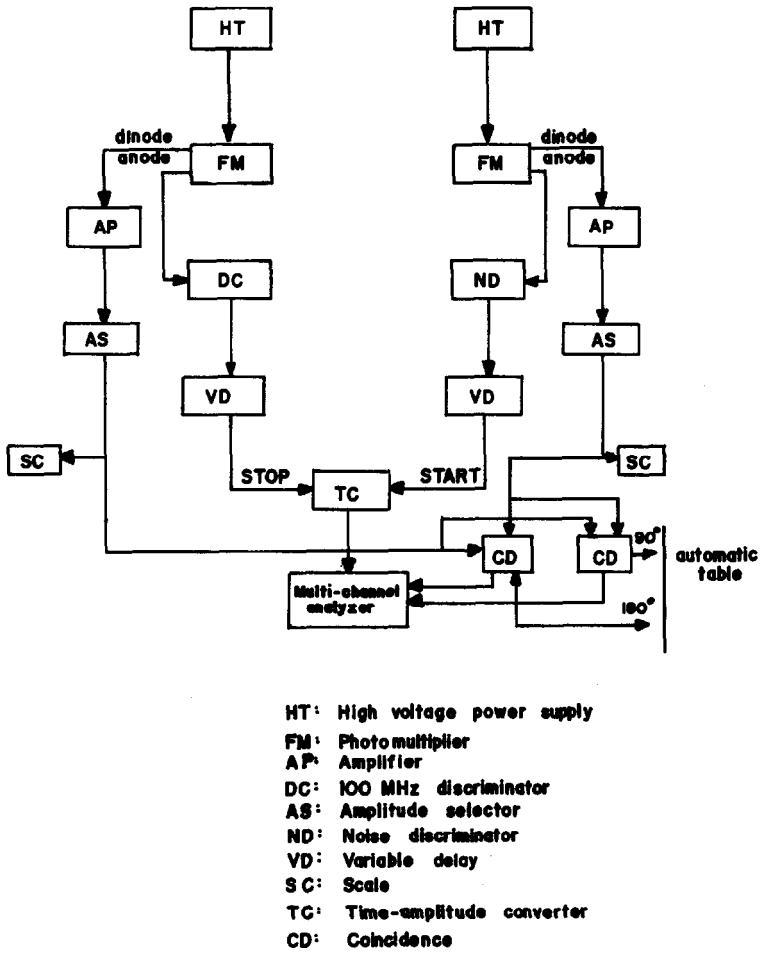

Fig. 2. Block diagram of the electronic system associated with the automatic table.

EXPERIMENTAL

The complexes $[Hf\{O_2CCH(OH)R\}_4]$ (R = *p*-ClC_6H_4, *p*-BrC_6H_4, *β*-$C_{10}H_7$, C_6H_5) were prepared by the method described by Hahn and Joseph[12] and their compositions were defined by microanalysis. The radioactive samples were prepared similarly, but using $HfOCl_2 \cdot 8H_2O$ previously irradiated for 8 h at about 40°C in a nuclear reactor with a thermal neutron flux of 4×10^{12} n cm^{-1} s^{-1}. The IR spectra of the inactive samples (discs, 10^{-6} mol Hf per 0.100 g KBr) were performed on a Perkin–Elmer model 621 spectrometer. The TDPAC measurements were performed at 25°C on polycrystalline samples in aluminium cylinders.

The data were analysed using a computer programme developed by the Grenoble Group and the details of data processing are given elsewhere.[13]

RESULTS AND DISCUSSION

The molecular structures of zirconium and hafnium complexes containing glycolate ligands are difficult to analyse, mainly due to their relative instability in solution, which prevents their immediate recrystallization. However, IR spectroscopic studies on microcrystalline samples showed the possible existence of monomers $[ML_4]$ and dimers $[L_3M(\mu\text{-}L)_2ML_3]$, the latter representing the form M—O(H)C(R)C(O)O—M. The existence of such bridges was inferred by the appearance of bands at 2600, 2300 and 1850 cm^{-1} in the IR spectra of these compounds, which are typical of hydrogen bonds. These bonds should link the alcoholic oxygen of one bridging glycolate and the carboxylic oxygen of the second bridging glycolate.[9]

The IR spectra of the series of hafnium glycolates studied (Fig. 3) showed an increase in the intensities of the bands attributed to these hydrogen bonds, in the order *p*-chloromandelate < *p*-bromomandelate < *β*-naphthylglycolate < mandelate (traces 1–4 in Fig. 3). This suggests that the complex containing the mandelate ligand should have greater dimeric character whereas the one containing *p*-chloromandelate should be monomeric. This observation implies that a rearrangement of the molec-

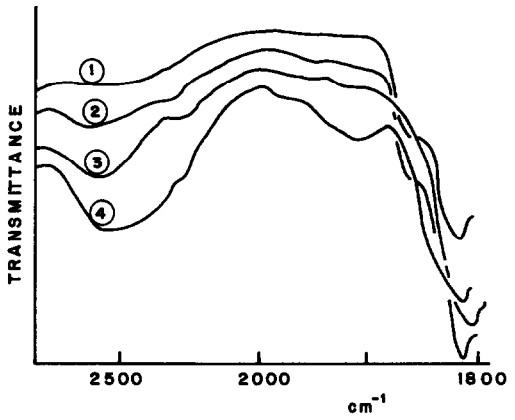

Fig. 3. IR spectra of the hafnium glycolate complexes: (1) *p*-chloromandelate, (2) *p*-bromomandelate, (3) β-naphthylglycolate and (4) mandelate.

ular structure of the complexes throughout the above series exists.

The TDPAC spectra of the tetrakis(DL-glycolate)hafnium(IV) are shown in Fig. 4.

Since the quadrupolar frequency is sensitive to the variations of electronic density at the hafnium nucleus, their values, measured by TDPAC (Table 1), should reflect the change in character suggested by the IR data, and as expected, the values found suggest that ω_Q increases with increasing dimeric character of the complex. The parameter which measures the distribution of these frequencies, δ, also supports the molecular reorganization along the series. Thus, for the compound which is "strictly" monomeric (*p*-chloromandelate) and for the one which is "strictly" dimeric (mandelate), the frequency distributions are lower, whereas for the complexes with intermediate characteristics they are somewhat higher. Within the series which shows hydrogen bonding, a lowering of δ accompanies an increase in ω_Q, indicating an increase in molecular organization following the establishment of well-defined bridges. The reorganization of the hafnium glycolates can be envisaged schematically (see Scheme 1).

Table 1. Quadrupolar interaction frequencies (ω_Q) and frequency distribution factors δ

Complexes	ω_Q (Mrd s^{-1})	δ (%)
[Hf{$O_2CCH(OH)p$-ClC_6H_4}$_4$]	107±1	1.0±0.1
[Hf{$O_2CCH(OH)p$-BrC_6H_4}$_4$]	109±4	2.1±0.3
[Hf{$O_2CCH(OH)\beta$-$C_{10}H_7$}$_4$]	138±4	1.8±0.3
[Hf{$O_2CCH(OH)C_6H_5$}$_4$]	155±3	1.5±0.1

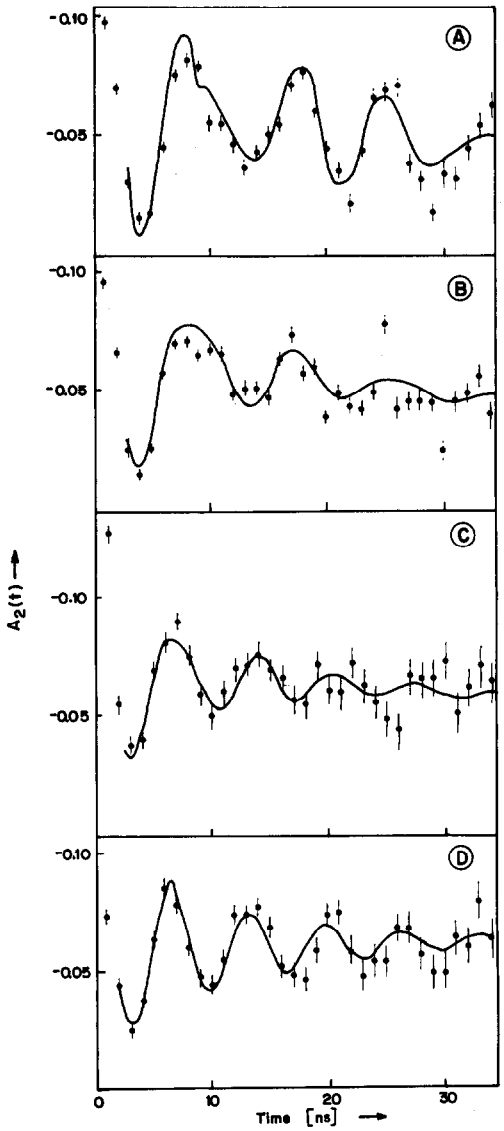

Fig. 4. Perturbation functions $A_2(t) = A_2G_2(t)$ of the hafnium glycolate complexes at 25°C: (A) *p*-chloromandelate; (B) *p*-bromomandelate; (C) β-naphthylglycolate and (D) mandelate.

Studies by TDPAC carried out by Boyer[14,15] in the hafnium(IV) oxide, tetrakis(acetylacetonate)-, tetrakis(N-benzoyl-N-phenyl-hydroxylaminato)-, tetrakis(cupferronate)- and tetrakis(tropolonate)-hafnium(IV) systems showed an inverse relation between ω_Q and increase in the delocalization of electronic charges at the hafnium nucleus. The value of ω_Q was larger for hafnium(IV) oxide and ω_Q decreased in the order indicated above.

From a purely structural viewpoint, the series of hafnium glycolate complexes studied is more homogeneous than that studied by Boyer. In the present case, a dissipation of electronic density at the metal level should increase as the intramolecular hydro-

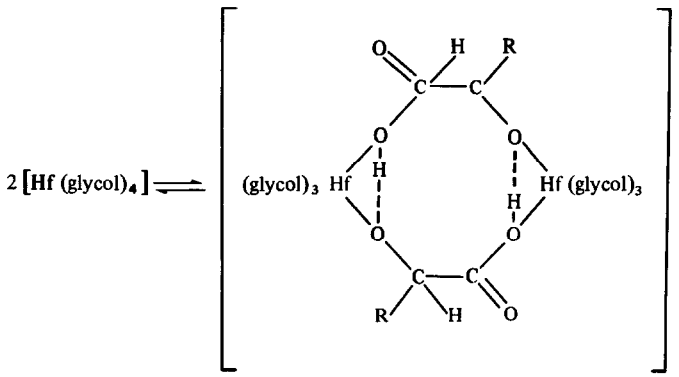

Scheme 1.

gen bridges are organized. The behaviour of the values found for ω_Q in this work are therefore in opposition to the behaviour noted by Boyer. However, it is noteworthy that the EFG in eight-coordinated complexes is very sensitive to lattice distortions[16] and it is possible that within Boyer's series the trend in observed ω_Q values is also being affected by some type of molecular organization.

Acknowledgements—The authors are grateful to CNPq and FINEP for financial support.

REFERENCES

1. J. I. Vargas, *MTP International Review of Science, Radiochemistry, Inorganic Chemistry. Series one* (Edited by A. G. Maddock), Vol. 8, p. 45. Butterworths, London (1972).
2. J. P. Adloff, *Radiochim. Acta* 1978, **25**, 57.
3. P. Boyer, A. Tissier, J. I. Vargas and P. Vuilliet, *Chem. Phys. Lett.* 1972, **14**, 601.
4. A. Baudry, P. Boyer and A. L. Oliveira, *Phys. Lett. A* 1980, **79A**, 345.
5. J. Oliveira, O. O. Damasceno, J. R. F. Ferreira, A. L. Oliveira, J. D. Fabris, P. Boyer and A. Baudry, *Phys. Status Solidi B*, 1978, **90**, K169.
6. C. Haydock, Ph.D. thesis, University of Massachussetts (1982).
7. O. C. Mullins and M. Kaplan, *J. Chem. Phys.* 1983, **79**, 4475.
8. A. Boussaha, A. Marques Netto, J. Ch. Abbe and A. Haessler, *Radiochem. Radioanal. Lett.* 1976, **24**, 43.
9. E. M. Larsen and H. Homeier, *Inorg. Chem.* 1972, **11**, 2687.
10. A. Marques Netto and J. Ch. Abbe, *J. Inorg. Nucl. Chem.* 1975, **37**, 2235.
11. J. Ch. Abbe and A. Marques Netto, *J. Inorg. Nucl. Chem.* 1975, **37**, 2239.
12. R. B. Hahn and P. T. Joseph, *J. Am. Chem. Soc.* 1955, **77**, 4777.
13. J. D. Fabris, J. I. Vargas, A. Marques Netto and A. L. Baudry, *Radiochem. Acta* 1978, **25**, 85.
14. P. Boyer, *Thèse "Docteur Ès-Sciences Physics"*, Université de Grenoble (1971).
15. P. Boyer, A. Tissier and J. I. Vargas, *Inorg. Nucl. Chem. Lett.* 1972, **8**, 813.
16. P. Vuilliet, A. Baudry, P. Boyer and A. Tissier, *Chem. Phys. Lett.* 1978, **55**, 297.

Polyhedron Vol. 7, No. 21, pp. 2171–2173, 1988
Printed in Great Britain

0277-5387/88 $3.00+.00
© 1988 Pergamon Press plc

A SINGLE BOND COVALENT RADIUS FOR Ir^{III}: CRYSTAL AND MOLECULAR STRUCTURE OF *fac*-$Ir(CH_3)_3(PMe_2Ph)_3$

ERIC G. LUNDQUIST, KIRSTEN FOLTING, JOHN C. HUFFMAN and KENNETH G. CAULTON*

Indiana University, Department of Chemistry and Molecular Structure Center, Bloomington, IN 47405, U.S.A.

(*Received* 12 *February* 1988; *accepted after revision* 14 *April* 1988)

Abstract—A low temperature (−145°C) X-ray diffraction structure determination of crystalline *fac*-$Ir(CH_3)_3(PMe_2Ph)_3$ grown from CH_2Cl_2/pentane shows it to contain two independent molecules per unit cell with Ir—C = 2.160(9) and 2.158(9), and Ir—P = 2.3343(24) and 2.3307(26) Å. Angles C—Ir—C are compressed to 83.4(4) and 83.3(4)°, and angles P—Ir—P are expanded to 99.99(8) and 99.83(8)°. An Ir^{III} covalent radius of 1.40 Å can be deduced from these data. Crystallographic data (−145°C): Space group $R3c$ with $a = b = 14.980(4)$, $c = 41.732(12)$ Å and $Z = 12$.

In the course of examining electron transfer, acidolysis and Lewis acids as possible means to increase the reactivity of 18-electron polymethyl compounds,[1,2] we have determined the detailed structural parameters of *fac*-$Ir(CH_3)_3(PMe_2Ph)_3$ by X-ray diffraction at low temperature. This provides benchmark structural data on this compound initially reported by Chatt and Shaw,[3,4] and thereby provides ideal data from which to calculate a single bond covalent radius for Ir^{III}.

EXPERIMENTAL

The compound was synthesized by the method of Chatt and Shaw.[3,4] Crystals suitable for crystallography were obtained by slow diffusion of pentane into a concentrated methylene chloride solution of the trimethyl complex.

Crystallography of fac-$Me_3Ir(PMe_2Ph)_3$

A well-formed prismatic crystal was selected and transferred to the goniostat where it was cooled to −145°C for characterization and data collection. A systematic search of a limited sphere of reciprocal space yielded a set of reflections which showed $\bar{3}m$ symmetry. The reflections were indexed on a rhombohedrally centred hexagonal lattice. The general condition for observed reflections of $hh(-2h)l$ for $l = 3n$, and $h(-h)0l$ for $h+l = 3n$ and $l = 2n$ lead us to the two possible space groups $R3c$ or $R\bar{3}c$. The choice of the non-centrosymmetric space group $R3c$ (No. 161) was confirmed by the subsequent solution and refinement of the structure. Data collection ($6 \leqslant 2\theta \leqslant 45°$) was carried out using the parameters available as supplementary material. A total of 12,594 reflections were collected (including redundancies, systematic space group extinctions and standard reflections). Following the usual data reduction and averaging of equivalent reflections (Friedel pairs were not averaged) a unique set of 2,764 reflections remained. The R for the averaging was 0.053. The data were corrected for absorption using an analytical method based on measured crystal faces.

The structure was solved using a combination of direct methods (MULTAN) and Fourier techniques. Some initial difficulty was encountered due to the fact that the unit cell contains 12 molecules of the Ir-complex, six each of two almost identical molecules. Molecule 1 [Ir(1) through C(11)] and molecule 2 [Ir(12) through C(22)] are both located on a three-fold axis, with the Ir atoms separated by approximately a quarter (0.2483) along the c-axis. The molecules are oriented in the same direction but rotated about 10° with respect to each other. The separation of the molecules by almost exactly $c/4$ causes all reflections with l divisible by four to be much stronger than the rest of the data. However, once the problem was realized,

*Author to whom correspondence should be addressed.

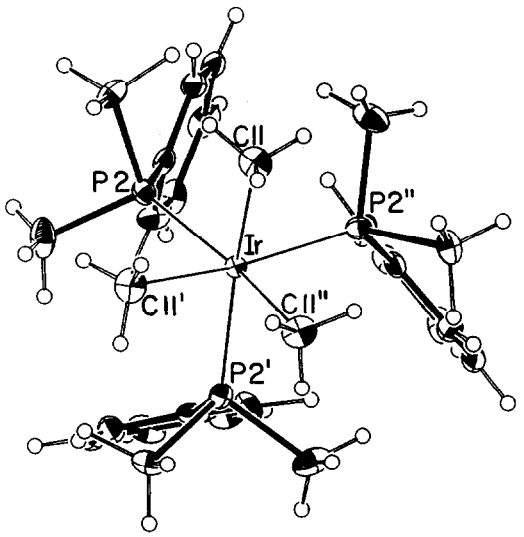

Fig. 1. ORTEP drawing of *fac*-$Ir(CH_3)_3(PMe_2Ph)_3$ ("molecule 1"), showing atom labelling. The view is down the crystallographic C_3 axis.

the structure solution proceeded normally. The hydrogen atoms were evident in a later difference Fourier and were introduced. Using anisotropic thermal parameters for all non-hydrogen atoms, the hydrogen atoms on the C(11) and C(22) methyl groups did not refine properly and were kept fixed in the final cycles of full matrix least-squares refinement; all other hydrogen atoms were refined with individual isotropic thermal parameters. Since this is a non-centrosymmetric space group, both enantiomers were tested. The one reported here refined considerably better ($R = 0.031$) than did its enantiomer, which led to $R = 0.051$. The final difference Fourier was essentially featureless, except for two peaks of about 1.5 $eÅ^{-3}$ in the immediate vinicity of the Ir atoms.

Molecule 1 consists of atoms Ir(1) through C(11) with hydrogens H(1) through H(14); Molecule 2 consists of atoms Ir(12) through C(22) with hydrogens H(15) through H(28). The asymmetric unit of the cell contains only a third of each molecule. The results of the X-ray study are shown in Table 1 and in Figs 1 and 2. Refined C—H distances range from 0.70(11) to 1.17(14) Å. Additional details are available as supplementary material.*

* Supplementary material available. Anisotropic thermal parameters, cell constants, parameters of the data collection and intra-ligand distances have been deposited with the Cambridge Crystallographic Data Centre, University Chemical Laboratory, Lensfield Road, Cambridge CB2 1EW, U.K.

Table 1. Selected bond distances (Å) and angles (deg) for $Me_3Ir(PMe_2Ph)_3$

Ir(1)	P(2)	2.3343(24)
Ir(1)	C(11)	2.160(9)
Ir(12)	P(13)	2.3307(26)
Ir(12)	C(22)	2.158(9)
P(2)	C(3)	1.829(10)
P(2)	C(4)	1.822(9)
P(2)	C(5)	1.853(8)
P(13)	C(14)	1.845(9)
P(13)	C(15)	1.834(9)
P(13)	C(16)	1.853(8)
C(5)	C(6)	1.384(11)
C(5)	C(10)	1.385(11)
C(6)	C(7)	1.375(12)
C(7)	C(8)	1.388(13)
C(8)	C(9)	1.374(12)
C(9)	C(10)	1.393(12)
C(16)	C(17)	1.398(11)
C(16)	C(21)	1.380(12)
C(17)	C(18)	1.406(12)
C(18)	C(19)	1.371(12)
C(19)	C(20)	1.376(13)
C(20)	C(21)	1.378(12)

P(2)	Ir(1)	P(2)′	99.99(8)
P(2)″	Ir(1)	C(11)	91.3(3)
P(2)′	Ir(1)	C(11)	167.01(26)
P(2)	Ir(1)	C(11)	84.21(24)
C(11)	Ir(1)	C(11)′	83.4(4)
P(13)	Ir(12)	P(13)′	99.83(8)
P(13)	Ir(12)	C(22)	84.48(26)
P(13)″	Ir(12)	C(22)	91.27(28)
P(13)′	Ir(12)	C(22)	167.16(25)
C(22)	Ir(12)	C(22)′	83.3(4)
Ir(1)	P(2)	C(3)	115.3(4)
Ir(1)	P(2)	C(4)	115.3(3)
Ir(1)	P(2)	C(5)	124.05(26)
C(3)	P(2)	C(4)	98.6(5)
C(3)	P(2)	C(5)	99.5(4)
C(4)	P(2)	C(5)	100.0(4)
Ir(12)	P(13)	C(14)	116.1(3)
Ir(12)	P(13)	C(15)	115.2(3)
Ir(12)	P(13)	C(16)	123.43(25)
C(14)	P(13)	C(15)	98.5(5)
C(14)	P(13)	C(16)	99.2(4)

RESULTS AND DISCUSSION

$IrMe_3(PMe_2Ph)_3$ crystallizes from CH_2Cl_2/pentane in the hexagonal space group *R3c* with two crystallographically-independent molecules in the unit cell, each possessing a crystallographic three-fold rotational axis of symmetry (Figs 1 and 2). The two molecules show no dimensions which disagree by more than 2σ. Each molecule displays a compression of the C—Ir—C angles by approximately

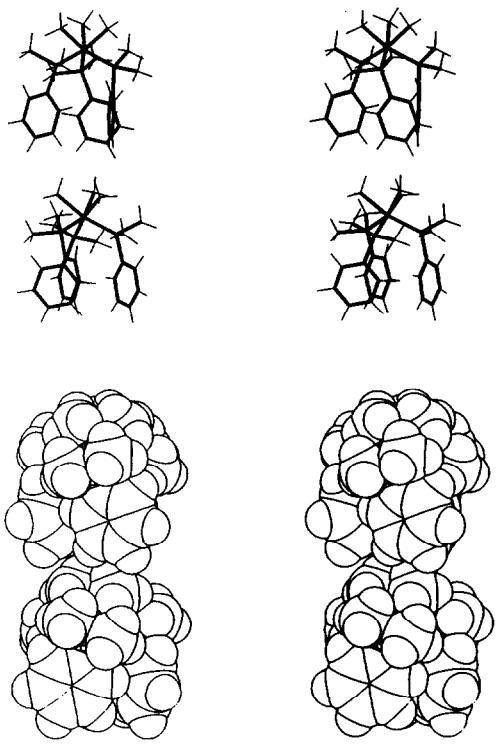

Fig. 2. Stereo stick figure and space-filling drawings of both independent molecules of *fac*-$Ir(CH_3)_3(PMe_2Ph)_3$, showing their relative orientation in the unit cell.

7° below 90°, and an expansion of the P—Ir—P angles by approximately 10° above 90°. Other structural parameters reported here for *fac*-$Me_3Ir(PMe_2Ph)_3$ are extremely similar to those in *fac*-$H_3Ir(PMePh_2)_3$:[5] Ir—P = 2.314(2) Å and ∠ P—Ir—P = 98.55(8)°. A similar statement applies to *fac*-$Cl_3Ir(PMe_2Ph)_3$:[6] Ir—P = 2.285(2)–2.295(2) Å and ∠ P—Ir—P = 100.26(6)–100.75(7)°.

The two molecules possess very similar orientations about the Ir—P bonds. The rotation is such that the phenyl rings point away from the intramolecular $IrMe_3$ moiety, but towards that same group in the second independent molecule (Fig. 2). There is *no* intramolecular face-to-face stacking of phenyl rings. Note that the helicity of the P—C (ipso phenyl) bonds is in the opposite sense in the two independent $IrMe_3(PMe_2Ph)_3$ molecules (Fig. 2). The unit cell of *fac*-$Cl_3Ir(PMe_2Ph)_3$, while not isomorphous with that of the trimethyl compound, also contains two independent molecules of opposite helicity.

fac-$IrMe_3(PMe_2Ph)_3$ furnishes an excellent opportunity to calculate a single bond covalent radius for six-coordinate Ir^{III} since the methyl group is *trans* to neither a strongly σ- nor π-effect ligand. If the methyl carbon radius (0.77 Å) is subtracted from the average Ir—CH_3 distance (2.17 Å), an iridium radius of 1.40 Å results. Twice this value compares well with the unbridged Ir—Ir distance (2.83 Å) in the dimer $[Ir(Tcbiim)(CO)_2P(Et)_3]_2$ (Tcbiim = tetracyanobiimidazole),[7] and thus supports the claim that there is no Ir/Ir multiple bonding in this compound. This covalent radius will also be a useful standard for comparison of Ir/Ir separations in stacked infinite chains of planar iridium compounds.[8]

Acknowledgements—This work was supported in part by the National Science Foundation, grant no. CHE-8707055. We also thank Johnson Matthey Co. for material support and Scott Horn for skilled technical assistance.

REFERENCES

1. D. Alvarez and K. G. Caulton, *Polyhedron* 1988, **7**, 1285.
2. D. E. Westerberg and K. G. Caulton, in preparation.
3. J. Chatt and B. L. Shaw, *J. Chem. Soc. A.* 1966, 1836.
4. B. L. Shaw and A. C. Smithies, *J. Chem. Soc. A.* 1967, 1047.
5. R. Bau, private communication of neutron diffraction results.
6. G. B. Robertson and P. A. Tucker, *Acta Cryst.* 1981, **B37**, 814.
7. P. G. Rasmussen, J. E. Anderson, O. H. Bailey, M. Tamres and J. C. Bayon, *J. Am. Chem. Soc.* 1985, **107**, 279.
8. J. S. Miller and A. J. Epstein, *Prog. Inorg. Chem.* 1976, **10**, 1.

Polyhedron Vol. 7, No. 21, pp. 2175–2181, 1988
Printed in Great Britain

0277-5387/88 $3.00+.00
© 1988 Pergamon Press plc

PREPARATION AND PROPERTIES OF BASIC IRON(III) CARBOXYLATES: REACTIONS OF $FeCl_3$ WITH SOME CARBOXYLIC ACIDS

RAMESH KAPOOR,* BALBIR KUMAR BAHL, PARMINDER KAUR and PRATIBHA KAPOOR*

Department of Chemistry, Panjab University, Chandigarh-160014, India

(*Received* 8 *June* 1987; *accepted after revision* 14 *April* 1988)

Abstract—Anhydrous iron(III) chloride reacts with pure carboxylic acids RCOOH [where R = C_2H_5, n-C_3H_7, CH_2Cl, $CHCl_2$ and CCl_3] at low temperature to yield $Fe_2Cl_5(OOCR)\cdot n$RCOOH [n = 3 when R = C_2H_5 and n-C_3H_7 and n = 2 when R = CH_2Cl, $CHCl_2$ and CCl_3] and $[Fe_3O(OOCR)_6(H_2O)_3][FeCl_4]$ at about 70–80°C. These reactions reveal that no hydrogen chloride is evolved but an acyl chloride is formed. Pyridine combines with $[Fe_3O(OOCR)_6(H_2O)_3][FeCl_4]$ (R = C_2H_5 and n = C_3H_7) to form $[Fe_3O(OOCR)_6(C_5H_5N)_3][FeCl_4]$. Piperidine, on the other hand, reacts with the elimination of piperidinium chloride to form $[Fe_3O(OOCR)_6(H_2O)_3][Fe(NC_5H_{10})_4]$ compounds containing covalently bonded piperidide. Compounds containing polyatomic ligands such as NO_3^- and NCS^- instead of the chloro group in $[Fe_3O(OOCR)_6(H_2O)_3][FeCl_4]$ (R = C_2H_5 and n-C_3H_7) have been prepared. All these compounds have been characterized on the basis of IR, UV–vis., molar conductance, molecular weight and room temperature magnetic susceptibility measurements.

In continuation of our studies of the chemistry of chromium carboxylates,[1–5] we report here the preparation and characterization of some iron(III) carboxylates. Iron(III) chloride is known to react with formic and acetic acids to form $FeCl(OOCH)_2\cdot H_2O$[6–8] and $Fe_3Cl_3(OOCCH_3)_6\cdot CH_3COOH$,[7] respectively. Iron(III) chloride also reacts with sodium acetate to give a trinuclear compound, $[Fe_3O(OOCCH_3)_6(H_2O)_3]Cl\cdot 5H_2O$.[9] Paul *et al.*[10] have recently reported the reaction of anhydrous iron(III) chloride with acetic acid and isolated $FeCl(OH)(OOCCH_3)\cdot(CH_3COOH)\cdot 0.5H_2O$ at room temperature, which has been shown to be monomeric in nitrobenzene but dimeric in acetone. However, Anzenhofer and De Boer[11] have crystallized a basic trinuclear compound, $[Fe_3O(OOCCH_3)_6(H_2O)_3][FeCl_4]\cdot 2CH_3COOH$ from the reaction of $FeCl_3$ with acetic acid. Similar reactions of acetic acid with vanadium(III) and chromium(III) chlorides are reported to give $V_3(OH)(OOCCH_3)_8$[12,13] and $Cr_3(OH)(OOCCH_3)_8$,[12] respectively. Reinvestigations of these reactions have suggested trinuclear formulations, $[V_3O(OOCCH_3)_6(OOCCH_3)_{2/2}(CH_3COOH)_\infty]$[14] and $[Cr_3O(OOCCH_3)_6]Cl$[3] for these compounds on the basis of their IR and magnetic susceptibility measurements. It seems quite likely that reaction of iron(III) chloride with acetic acid may also yield a basic trinuclear complex unlike the product reported in the literature.[10] We have, therefore, reinvestigated the reactions of anhydrous iron(III) chloride with a number of pure carboxylic acids (RCOOH where R = C_2H_5, n-C_3H_7, CH_2Cl, $CHCl_2$ and CCl_3) at different temperatures, and report our results here.

EXPERIMENTAL

Iron(III) chloride (anhydrous, Merck) was treated with an excess of thionyl chloride at room temperature until the reaction ceased. It was then refluxed for 6 h, filtered and washed with dry carbon tetrachloride and dried *in vacuo*.

The carboxylic acids were purified by distillation as described by standard methods.

Reactions of iron(III) chloride with carboxylic acids: at low temperatures

Carboxylic acid (200 mmol) diluted with 50 cm^3 of CH_2Cl_2 was added to iron(III) chloride (40 mmol)

*Authors to whom correspondence should be addressed.

and placed in a bath maintained at about −20°C with constant stirring in a closed system. The temperature was allowed to rise to 0°C when the iron(III) chloride dissolved to give a reddish-brown solution. The solutions were stirred for 3–4 h at 0°C but the pressure remained constant suggesting that no HCl gas had evolved. The solvent was distilled off under vacuum and the product left behind was washed with freshly distilled CCl_4 and finally dried to a constant weight *in vacuo* at room temperature. Compounds **1–5** were isolated by this procedure.

At high temperatures

Carboxylic acid (200 mmol) diluted with 50 cm^3 of CCl_4 was added to iron(III) chloride (30 mmol) at room temperature with constant stirring in a closed system. The contents were refluxed on a water bath for 10–12 h, but again no volatile products were evolved during the course of the reaction. The solvent was distilled off *in vacuo* and the pasty material left behind was dissolved in diethyl ether. Some insoluble material which analysed as iron(II) chloride was removed and the compound precipitated by adding light petroleum ether to the solution. The final product was obtained by keeping it *in vacuo* for 48 h. The solution, on fractionation, distills over a small amount of acetyl chloride (b.p. 52°C). Compounds **6–10** were obtained by this method.

Reactions with pyridine

In a typical experiment, compound **6** (1.75 g, 2 mmol) was dissolved in CH_2Cl_2 (50 cm^3) and a solution of pyridine (0.8 g, 10 mmol) in CH_2Cl_2 was added dropwise with constant stirring. The solution was stirred for 2–3 h and then the solvent was removed *in vacuo*. The concentrate was treated with light petroleum ether, filtered and the residue was washed with fresh petroleum ether and finally dried *in vacuo*. The same procedure was adopted for its complexation with **7**.

Reactions with piperidine

Compound **6** (1.75 g, 2 mmol) was dissolved in CH_2Cl_2 (50 cm^3) and a solution of piperidine (0.85 g, 10 mmol) was added with constant stirring. The dark brown solution was stirred for 2 h and then treated with light petroleum ether to precipitate piperidinium chloride quantitatively. The filtrate was evacuated and the residue was washed with petroleum ether and finally dried *in vacuo*. The reaction with compound **7** was carried out under identical conditions.

Reaction of **6** *with silver nitrate*

Compound **6** (1.75 g, 2 mmol) was dissolved in CH_2Cl_2 (50 cm^3) and dried silver nitrate (1.36 g, 8 mmol) dissolved in the minimum amount of CH_3CN was added dropwise. The solution was stirred for about 3 h and the precipitated AgCl was filtered off. The solvent was removed from the filtrate *in vacuo* giving a reddish-brown sticky solid which on keeping *in vacuo* for a few days gave a fine powdered material.

Reaction of **6** *with potassium thiocyanate*

Compound **6** (1.75 g, 2 mmol) was dissolved in acetone (50 cm^3) and potassium thiocyanate (0.78 g, 8 mmol) solution in acetone was added dropwise. The mixture was stirred for about 48 h. The whole solution was evacuated and the residue was stirred with a large excess of diethyl ether. The mixture was filtered to obtain KCl. The filtrate was evacuated and the complex was dried *in vacuo* to get the thiocyanate complex.

Iron and chlorine were estimated gravimetrically as Fe_2O_3 and AgCl, respectively. Carbon, hydrogen and nitrogen were analysed microanalytically. IR spectra of the compounds were recorded as Nujol and hexachlorobutadiene films in NaCl and CSI plates on a Perkin–Elmer double beam grating spectrophotometer 621. UV–vis. spectra were recorded on a Hitachi 330 spectrophotometer. Thermal analyses were carried out on a MOM Budapest Derivatograph (Type Paulik, Paulik and Erdey). All manipulations were carried out under a dry nitrogen atmosphere in a dry-box.

RESULTS AND DISCUSSION

The interaction of iron(III) chloride with carboxylic acids at low temperatures does not give any stable addition compounds but the partially substituted products **1–5** have been obtained. Even when the contents are refluxed, complete loss of chlorine has not been observed and the solvolysed products **6–10** are obtained. However, we did not observe any evolution of HCl gas. This is in agreement with the earlier observations of Paul *et al.*[10] who recognized the formation of acetyl chloride as one of the reaction products and suggested the following equilibrium:

$$2CH_3COOH \rightleftharpoons H_2O + CH_3CO^+ + CH_3COO^-.$$

During these investigations all volatile materials were trapped and the presence of acid chlorides was confirmed.

Compounds **1–5** are extremely sensitive to moisture. They are soluble in CH_2Cl_2, $CHCl_3$, CH_3NO_2, $C_6H_5NO_2$ and CH_3CN, but insoluble in CCl_4 and light petroleum ether. IR spectra of these compounds have been recorded and band assignments have been made by analogy to the spectrum of the sodium salts of the parent acids.[15,16] Bands at *ca* 1710 and between 1220 and 1270 cm^{-1} may be assigned to ν(C=O), and ν(C—O), respectively, of the coordinated acid.[17] Bands at *ca* 1600 and 1400 cm^{-1} have been assigned to $\nu_a(COO^-)$ and $\nu_s(COO^-)$ stretching modes. The $\Delta\nu(COO^-)$ values of *ca* 200 cm^{-1} are suggestive of the presence of ionic or bridging bidentate carboxylato group.[18,19] The presence of the ionic carboxylato group can be easily ruled out on indirect evidence such as molar conductance data, UV–vis. spectra and the appearance of bands in the far IR region which may be assigned to iron–oxygen stretching modes. Bands at *ca* 370 and 310 cm^{-1} have been assigned to Fe—Cl modes by analogy with the spectrum of $FeCl_4^-$.[20,21] Other bands below 500 cm^{-1} which cannot be attributed to the internal vibrations of the carboxylato group have been assigned to the ν and δ(Fe—O) modes of the Fe—OOCR group.

Compounds **1–5** give lemon–yellow solutions in CH_2Cl_2 and their UV–vis. spectra show intense absorption bands at 240, 310 and 360 nm. These bands suggest the presence of tetrachloroferrate(III) ions in these solutions which are known to show identical absorption peaks in non-aqueous media.[22,23] Molar conductances of their millimolar solutions in nitrobenzene are in the range expected for 1:1 electrolytes.[24] Therefore, in solution they may exist as:

$$Fe_2Cl_5(OOCR)\cdot nRCOOH \longrightarrow [FeCl(OOCR)\cdot nRCOOH][FeCl_4]$$

$$\left.\begin{array}{l} R = CH_3, C_2H_5; n = 3 \\ R = CH_2Cl, CHCl_2 \text{ and } CCl_3; n = 2 \end{array}\right\} \quad \downarrow\uparrow$$

$$[FeCl(OOCR)\cdot nRCOOH]^+ + [FeCl_4]^-$$

Molecular weights in $C_6H_5NO_2$ have been found to be half of their formula weights (Table 1) as expected for 1:1 electrolytes in nitrobenzene.

Compounds **6–10** (Table 1) have been obtained by the reactions of iron(III) chloride with carboxylic acids at the reflux temperature of CCl_4, but no evolution of HCl gas was detected. The reactions may be represented as:

$$2FeCl_3 + 7RCOOH \rightarrow Fe_2Cl_2(OH)_2(OOCR)_2 \cdot RCOOH + 4RCOCl + 2H_2O.$$

IR spectra of these compounds are very similar. They all exhibit a broad medium intensity band in the region 3200–3100 cm^{-1} which is characteristic of ν(O—H···O). However, no bands have been observed in the regions 1600–1800 cm^{-1} and between 1220–1280 cm^{-1} which could be assigned to ν(C=O) and ν(C—O), respectively, of the coordinated carboxylic acid.[17] The $\Delta\nu(COO^-)$ value of *ca* 160 cm^{-1}, as already discussed, may be attributed to the bridging carboxylato group.

Compounds **6–10** are relatively more stable than compounds **1–5**. They are soluble in all polar organic solvents but are insoluble in solvents like CCl_4, n-C_5H_{12} and light petroleum ether. Molecular weights of compounds **6–10**, as determined by measuring the depression of the freezing point of nitrobenzene, correspond to twice their empirical representation, $Fe_2Cl_2(OH)_2(OOCR)_2\cdot RCOOH$. Solutions of **6–10** in CH_2Cl_2 or CH_3CN show absorption maxima at 238, 310 and 360 nm which suggest the presence of $FeCl_4^-$ species in solutions.[22,23] Based on these studies, we propose that compounds **6–10** may be reformulated as: $[Fe_3O(OOCC_2H_5)_6(H_2O)_3][FeCl_4]$ (**6**), $[Fe_3O(OOCC_3H_7)_6(H_2O)_3][FeCl_4]$ (**7**), $[Fe_3O(OOCCH_2Cl)_6(H_2O)_3][FeCl_4]$ (**8**), $[Fe_3O(OOCCHCl_2)_6(H_2O)_3][FeCl_4]$ (**9**) and $[Fe_3O(OOCCl_3)_6(H_2O)_3][FeCl_4]$ (**10**), respectively, by analogy to the known basic trinuclear iron acetate, $[Fe_3O(OOCCH_3)_6(H_2O)_3][FeCl_4]\cdot 2CH_3COOH$.[11] Λ_M^{1000} values in nitrobenzene fall in the range 4.0–8.0 ohm^{-1} (Table 1). These values are much less than expected for 1:1 electrolytes (20–30 $ohm^{-1}\ cm^2\ mol^{-1}$)[24] and suggest that compounds **6–10** are only weakly dissociated in solution.

$$[Fe_3O(OOCR)_6(H_2O)_3][FeCl_4] \rightleftharpoons [Fe_3O(OOCR)_6(H_2O)_3]^+ + [FeCl_4]^-.$$

Pyridine and piperidine complexes of **6** *and* **7**

Reactions of **6** and **7** with pyridine (tertiary nitrogen base) and piperidine (secondary nitrogen base) have been investigated with an aim to understand the nature of different functional groups in these compounds. Reactions of pyridine, which has excellent coordinating properties, were attempted to give products which may be formed by the displacement of coordinated water molecules. On the other hand, reactions of **6** and **7** with piperidine yield entirely different products because it has a replaceable hydrogen atom.

Pyridine combines with **6** and **7**, to replace weakly coordinated water molecules to yield,

Table 1. Analytical results and some physical properties

Compound	Colour	Molar[a] conductance ($ohm^{-1} cm^2 mol^{-1}$)	Magnetic moment (BM)	Molecular weight Calc.	Obs.	Analytical data (%)[b] Fe	Cl	C	H	N
At low temperature										
$C_{12}H_{23}O_8Fe_2Cl_5$ (1)	Reddish-brown viscous liquid	30.0	—	583.9	285	19.1 (19.2)	30.1 (30.4)	24.52 (24.66)	4.12 (3.94)	—
$C_{16}H_{31}O_8Fe_2Cl_5$ (2)	Reddish-brown viscous liquid	28.2	—	639.9	328	17.0 (17.5)	27.5 (27.7)	29.85 (30.00)	5.02 (4.84)	—
$C_6H_6O_6Fe_2Cl_8$ (3)	Brownish-black solid	29.0	4.80	571.3	290	19.4 (19.6)	49.6 (49.6)	12.52 (12.60)	1.79 (1.40)	—
$C_6H_5O_6Fe_2Cl_{11}$ (4)	Brownish-black solid	26.8	4.88	674.6	330	16.4 (16.6)	56.4 (57.8)	10.42 (10.67)	1.60 (0.74)	—
$C_6H_2O_6Fe_2Cl_{14}$ (5)	Brown solid	25.4	4.90	781	400	14.2 (14.3)	62.8 (63.5)	9.04 (9.22)	0.56 (0.26)	—
At high temperature										
$C_9H_{18}O_8Fe_2Cl_2$ (6)	Brown solid	7.0	4.64	436.6	903	24.9 (25.6)	16.0 (16.2)	24.42 (24.73)	4.70 (4.12)	—
$C_{12}H_{24}O_8Fe_2Cl_2$ (7)	Reddish-brown viscous liquid	8.0	—	478.6	972	23.0 (23.3)	14.2 (14.8)	29.90 (30.09)	5.32 (5.01)	—

$C_6H_9O_8Fe_2Cl_5$ (**8**)	Reddish-brown solid	5.6	4.70	497.0	1018	23.2 (22.5)	35.2 (35.7)	14.30 (14.49)	2.32 (1.81)	—
$C_6H_6O_8Fe_2Cl_8$ (**9**)	Reddish-brown solid	4.8	4.64	600.3	1240	17.9 (18.6)	48.3 (47.2)	12.16 (11.99)	1.38 (1.00)	—
$C_6H_3O_8Fe_2Cl_{11}$ (**10**)	Reddish-brown solid	6.0	4.76	703.6	1434	15.2 (15.9)	56.1 (55.4)	11.01 (10.23)	0.86 (0.43)	—
Pyridine, piperidine and polyanion compounds										
$[Fe_3O(OOCC_2H_5)_6(C_5H_5N)_3][FeCl_4]$ (**11**)	Dark brown solid	7.2	4.23	1056.2	1042	20.6 (21.2)	13.0 (13.4)	36.76 (37.49)	4.36 (4.26)	3.60 (3.98)
$[Fe_3O(OOCC_3H_7)_6(C_5H_5N)_3][FeCl_4]$ (**12**)	Dark brown solid	6.5	4.34	1140.2	—	19.2 (19.6)	12.0 (12.4)	40.72 (41.04)	5.46 (5.00)	3.24 (3.68)
$[Fe_3O(OOCC_2H_5)_6(H_2O)_3][Fe(NC_5H_{10})_4]$ (**13**)	Light brown solid	1.0	3.82	1067.4	1030	20.0 (20.9)	—	42.00 (42.72)	6.84 (7.12)	5.10 (5.25)
$[Fe_3O(OOCC_3H_7)_6(H_2O)_3][Fe(NC_5H_{10})_4]$ (**14**)	Light brown solid	1.2	3.92	1151.4	—	19.0 (19.4)	—	44.82 (45.86)	7.92 (7.64)	4.42 (4.86)
$[Fe_3O(OOCC_2H_5)_6(H_2O)_3][Fe(NO_3)_4]$ (**15**)	Reddish-brown solid	9.0	3.73	979.4	960	22.4 (22.8)	—	21.90 (22.05)	3.80 (3.68)	—
$[Fe_3O(OOCC_2H_5)_6(H_2O)_3][Fe(NCS)_4]$ (**16**)	Dark brown solid	30.0	3.70	963.4	982	22.8 (23.2)	—	27.20 (27.40)	4.20 (3.73)	5.24 (5.61)

[a] In $C_6H_5NO_2$ (value for 1:1 electrolytes falls in the range 20–30 $ohm^{-1}\ cm^2\ mol^{-1}$).[24]
[b] Required values are given in parentheses.

$[Fe_3O(OOCC_2H_5)_6(C_5H_5N)_3][FeCl_4]$ (**11**) and $[Fe_3O(OOCC_3H_7)_6(C_5H_5N)_3][FeCl_4]$ (**12**), respectively. They are insoluble in non-polar organic solvents but dissolve in CH_2Cl_2, CH_3CN, CH_3NO_2, $C_6H_5NO_2$ and THF. Molecular weights of **11** and **12** in nitrobenzene agree well with their proposed formulations (Table 1). Their Λ_M^{1000} values in $C_6H_5NO_2$ are less than those expected for 1:1 electrolytes (Table 1) but the small values suggest some dissociation:

$$[Fe_3O(OOCR)_6(C_5H_5N)_3][FeCl_4] \rightleftharpoons [Fe_3O(OOCR)_6(C_5H_5N)_3]^+[FeCl_4]^- \quad (R = C_2H_5,\ n\text{-}C_3H_7).$$

The existence of $FeCl_4^-$ has been confirmed by studying the UV–vis. spectra of **11** and **12** in CH_2Cl_2. They exhibit bands at 240, 310 and 360 nm which are assigned to $FeCl_4^-$.[22,23]

The IR spectra of **11** and **12** are quite complex. Coordinated pyridine causes a slight positive shift of some C⋯C and C⋯N stretching modes.[25,26] Their spectra cannot be interpreted unambiguously due to the presence of vibrational bands of pyridine and the carboxylate group in the same region. However, coordinated pyridine is readily distinguished from the free base by the shifting of the 601 and 403 cm^{-1} bands to 630 and 435 cm^{-1}, respectively. Both **11** and **12** contain all the bands which were present in **6** and **7** without any significant shift, except that the ν(O—H⋯O) and δ(HOH) modes of coordinated water at *ca* 3400 and 1660 cm^{-1} are now missing.

Piperidine combines with **6** and **7** with the elimination of chlorine as the hydrochloride base (recovered quantitatively) and results in the isolation of **13** and **14**, respectively, in which piperidide is coordinated through nitrogen as an amido derivative. These compounds are stable in air and insoluble in non-polar organic solvents but soluble in polar organic solvents. Molecular weights of **13** and **14** in nitrobenzene agree well with their proposed formulations as: $[Fe_3O(OOCC_2H_5)_6(H_2O)_3][Fe(NC_5H_{10})_4]$ (**13**) and $[Fe_3O(OOCC_3H_7)_6(H_2O)_3][Fe(NC_5H_{10})_4]$ (**14**). Their Λ_M^{1000} values in nitrobenzene show that they do not ionize in solution. Their UV–vis. spectra in dichloromethane show no absorption bands at 240, 310 and 360 nm which were assigned to $FeCl_4^-$ species in the parent compounds, **6** and **7**. The covalent nature of the bonded piperidide was confirmed by comparing the IR spectra of **13** and **14** with those of piperidine,[25] piperidinium chloride[27] and lithium piperidide.[10] The ν(NH) band which is observed at 3270 cm^{-1} in piperidine disappears in the spectra of **13** and **14** and is also absent in the compound $LiNC_5H_{10}$.[10] The H—N—C deformation mode[25] is also absent in **13** and **14**. Comparison with the piperidinium chloride spectrum in the region 2600–1900 cm^{-1} rules out the possibility of any $>NH_2^+$ type of structure. The wagging modes of piperidine, which are observed between 1390–1250 cm^{-1}, shift to a higher spectral region in compounds **13** and **14** but cannot be assigned unambiguously to the presence of overlapping bands of the carboxylate ligand. Other bands due to the carboxylato group have been assigned by comparison with the spectra of **6** and **7**. The formation of a new anionic species, $[Fe(NC_5H_{10})_4]^-$ in **13** and **14** has been speculated on the assumption that trinuclear cationic species remain intact, whereas $FeCl_4^-$ is quantitatively converted to tetrapiperididoferrate(III) by elimination of piperidine hydrochloride.

Polyanion compounds of **6**

Silver nitrate and potassium thiocyanate combine with **6** to give the dark brown solids, **15** and **16**, respectively (Table 1). IR spectra of these compounds have been recorded and bands due to the propionato group have been carefully assigned by comparison with the spectrum of **6**. It is not possible to determine on the basis of the IR spectrum alone, the precise nature of the covalent bonding between the metal and nitrate groups in **15**. In the $Fe(NO_3)_4^-$ anion, the nitrate groups may be unidentate or bidentate. The splitting of the ν_4 band suggests that more than one type of coordination exists in $Fe(NO_3)_4^-$.[28] Compound **15** is soluble in polar organic solvents and the Λ_M^{1000} value in $C_6H_5NO_2$ suggests that it is only weakly dissociated. Its molecular weight in nitrobenzene agrees with its proposed formulation. Its UV spectrum in CH_3CN shows a strong absorption at 280 nm. The UV spectrum of $NO^+[Fe(NO_3)_4]^-$ in CH_3CN exhibits a broad, intense band at 275–288 nm.[28] This absorption has been attributed to the transfer of electrons from the nitrate ligand to the metal.

The thiocyanate complex **16** is obtained as a dark brown hygroscopic solid. Its IR spectrum shows ν_1 and ν_2 modes due to ν(C⋮N) and δ(NCS), at 1995 and 470 cm^{-1}, respectively, which suggest that the thiocyanate ligand is bonded through its terminal nitrogen atom.[29,30] Other bands due to the propionate ligand have been assigned. The Λ_M^{1000} value for **16** in $C_6H_5NO_2$ lies in the range expected for 1:1 electrolytes.[24]

Magnetic susceptibilities of a few compounds have been measured at room temperature (Table 1). The μ_{eff} value per iron atom is much less than the normal observed magnetic moment for high-spin iron(III) compounds (5.92 BM).[31] This result suggests that the present compounds, like many

other trinuclear iron(III) carboxylates[9] are antiferromagnetic.

Thermal analysis (TG, DTG and DTA) of **6** which is the most stable of the present compounds has been studied. It begins to lose weight around 70°C and in a single step between 70–320°C loses the entire organic mass. On further heating, it slowly loses weight and around 600°C acquires a constant weight which corresponds to the formation of Fe_2O_3. The total weight loss (64.0%) agrees well with that required for the formation of Fe_2O_3 (63.3%). Due to burning of the organic matter in air the entire process is expressed as a large exotherm.

REFERENCES

1. R. C. Paul, O. B. Baidya, S. K. Gupta and R. Kapoor, *Z. Naturforsch.* 1977, **32b**, 148.
2. R. C. Paul, P. Kapoor, O. B. Baidya and R. Kapoor, *Z. Naturforsch.* 1979, **34b**, 160.
3. R. Kapoor and R. Sharma, *Z. Naturforsch.* 1979, **34b**, 1369.
4. R. Kapoor and R. Sharma, *Z. Naturforsch.* 1982, **38b**, 42.
5. R. Kapoor, R. Sharma and P. Kapoor, *Z. Naturforsch.* 1984, **39b**, 1702.
6. A. Rosenheim and P. Müller, *Z. Anorg. Chem.* 1904, **39**, 186.
7. H. Funk and M. Demmel, *Z. Anorg. Allg. Chem.* 1936, **227**, 94.
8. R. C. Paul, O. B. Baidya, A. J. Kaur, R. D. Sharma and R. Kapoor, *Aust. J. Chem.* 1977, **30**, 1439.
9. G. J. Long, W. T. Robinson, W. P. Tappmeyer and D. L. Bridges, *J. Chem. Soc., Dalton Trans.* 1973, 573.
10. R. C. Paul, R. C. Narula, S. Kaur and S. K. Vasisht, *Transition Met. Chem.* 1976, **1**, 289.
11. K. Anzenhofer and J. J. de Boer, *Rec. Trav. Chim.* 1969, **88**, 286.
12. H. Funk, C. Mueller and A. Paul, *Z. Chem.* 1966, **6**, 227.
13. B. G. Bennett and D. Nicholls, *J. Inorg. Nucl. Chem.* 1972, **34**, 673.
14. B. J. Allin and P. Thornton, *Inorg. Nucl. Chem. Lett.* 1973, **9**, 449.
15. E. Spinner, *J. Chem. Soc.* 1964, 4217.
16. D. Chapman, *J. Chem. Soc.* 1958, 784.
17. J. K. Wilmshurst, *J. Chem. Phys.* 1956, **25**, 1171.
18. N. W. Alcock, V. M. Tracy and T. C. Waddington, *J. Chem. Soc., Dalton Trans.* 1976, 2243.
19. A. I. Grigor'ev, *Russ. J. Inorg. Chem.* 1963, **8**, 409.
20. L. A. Woodward and M. J. Taylor, *J. Chem. Soc.* 1960, 4473.
21. G. M. Bancroft, A. G. Maddock, W. K. Ong and R. H. Prince, *J. Chem. Soc (A)* 1966, 723.
22. T. B. Swanson and V. M. Laurie, *J. Phys. Chem.* 1968, **69**, 244.
23. D. W. Meek and R. S. Drago, *J. Am. Chem. Soc.* 1961, **83**, 4322.
24. W. J. Geary, *Coord. Chem. Rev.* 1971, **7**, 81.
25. N. N. Greenwood and K. Wade, *J. Chem. Soc.* 1960, 1130.
26. N. S. Gill, R. H. Nuttall, D. E. Scaife and D. W. A. Sharp, *J. Inorg. Nucl. Chem.* 1961, **18**, 79.
27. A. Cabana and C. Sandorfy, *Can. J. Chem.* 1962, **40**, 615.
28. C. C. Addison, P. M. Boorman and N. Logan, *J. Chem. Soc.* 1965, 4978.
29. P. S. K. Chia and S. E. Livingstone, *Aust. J. Chem.* 1969, **22**, 1613.
30. A. H. Norbury and A. I. P. Sinha, *Quart. Rev.* 1970, **24**, 69.
31. B. N. Figgis and J. Lewis, *Modern Coordination Chemistry*, p. 406. Wiley-Interscience, New York (1964).

Polyhedron Vol. 7, No. 21, pp. 2183–2187, 1988
Printed in Great Britain

0277–5387/88 $3.00+.00
© 1988 Pergamon Press plc

SYNTHESIS, CHARACTERIZATION AND FUNGITOXICITIES OF METAL CHELATES OF A PENTADENTATE N_3S_2 LIGAND

S. M. M. H. MAJUMDER and M. AKBAR ALI*

Department of Chemistry, University of Chittagong, Chittagong, Bangladesh,

and

F. E. SMITH

Department of Chemistry, Laurentian University, Ontario, Canada

and

M. A. U. MRIDHA

Department of Botany, University of Chittagong, Chittagong, Bangladesh

(*Received* 14 *September* 1987; *accepted after revision* 14 *April* 1988)

Abstract—The Schiff base obtained by reaction of S-methyldithiocarbazate with 2,6-diacetylpyridine behaves as a dinegatively charged pentadentate N_3S_2 chelating agent producing stable crystalline complexes of the general formula, M(SNNNS) (where M = Ni, Cu, Co, Zn and Cd; SNNNS = the dinegative anion of the Schiff base). The complex Fe(SNNNS)Cl was also isolated. Conductivity data and magnetic and spectroscopic evidence support a five-coordinate configuration for the M(SNNNS) complexes and an octahedral configuration for the Fe(SNNNS)Cl complex. Fungitoxicities of the Schiff base and its metal complexes against three plant pathogens viz. *Alternaria solani*, *Curvularia geniculata* and *Colletotrichum capsici* have been studied. The ligand and its complexes display marked antifungal activities against all the test fungi.

Metal complexes of sulphur–nitrogen chelating agents have attracted considerable attention because of their interesting physicochemical properties and pronounced biological activities.[1–3] Although a vast amount of research work on metal complexes of bi-, tri- and tetradentate sulphur–nitrogen chelating agents have been reported, pentadentate ligands and their metal complexes have been less well investigated. Lindoy and Busch[4] attempted to synthesize a pentadentate sulphur–nitrogen chelating agent by reacting 2-aminobenzenethio with 2,6-diacetylpyridine but the reaction did not yield the expected Schiff base. Instead, a thiazolidinethione was obtained. However, these authors found that in the presence of zinc(II) and cadmium(II) ions, the thiadiazolidinethione rearranged producing five-coordinate complexes containing the pentadentate N_3S_2 ligand. The X-ray crystal structure determination of the zinc(II) complex[5] showed that the compound had a five-coordinate structure (**1**).

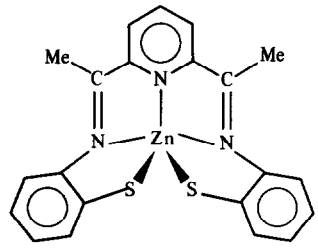

(1)

In this paper we report the synthesis, characterization and antifungal properties of some new nickel(II), copper(II), zinc(II), cadmium(II), iron(III) and cobalt(II) complexes of a pentadentate

* Author to whom correspondence should be addressed.

N_3S_2 ligand formed from S-methyldithiocarbazate and 2,6-diacetylpyridine.

EXPERIMENTAL

Physical measurements

The IR spectra in the range 4000–200 cm^{-1} were measured in KBr discs on a Perkin–Elmer 433 spectrometer. The far-IR spectra in the range 200–50 cm^{-1} were recorded in polystyrene on a Fourier Polytec FIR 30 spectrometer. The ^1H and ^{13}C NMR spectra were recorded by means of Varian T-60 and Bruker-WH 270 FT NMR spectrometer, respectively. The ESR spectrum of the copper(II) complex was obtained with a Varian E-line Century series spectrometer. The mass spectrum of the ligand was obtained by means of a Finnigan 4000 GC/MS spectrometer. Magnetic and conductivity measurements were made as reported before.[6] Microanalyses for C, H and N were obtained from the Canadian Microanalytical Service Ltd.

Preparation of ligand

S-methyldithiocarbazate (1.0 g) dissolved in absolute ethanol (30 cm^3) was added to a solution of 2,6-diacetylpyridine (0.64 g) in the same solvent. The mixture was heated under reflux for 30 min and then left to stand for slow cooling. The yellow crystalline product was filtered off and recrystallized from chloroform to obtain pale yellow crystals of the ligand: m.p. 205°C. Found: C, 41.6; H, 4.7; N, 18.8; $C_{13}H_{17}N_5S_4$ requires: C, 42.2; H, 4.6; N, 18.8%.

Preparation of the complexes, M(SNNNS) (M = Ni, Cu, Co, Zn *and* Cd)

To a filtered solution of the appropriate metal(II) acetate (1 mmol) in methanol (50 cm^3) was added a solution of the Schiff base (1 mmol) in a mixture of acetone and methanol (1 : 1; 50 cm^3). The resulting solution was heated on a hot plate for about 10 min and then left to stand and cool. The product which had formed was filtered off, washed several times with ethanol and dried in a vacuum desiccator over P_4O_{10}.

Preparation of Fe(SNNNS)Cl

The Schiff base (1 mmol) dissolved in a 1 : 1 mixture of acetone and methanol (50 cm^3) was added to a solution of anhydrous ferric chloride (1 mmol) in a mixture of methanol and 2,2-dimethoxypropane (20 cm^3). The mixture was then heated on a hot plate for *ca* 10 min and then left at room temperature for 1 h. The compound which separated out was filtered off, washed with ethanol and dried *in vacuo* over P_4O_{10}.

Antifungal screening experiments

The antifungal activities of the Schiff base and some of its metal complexes were studied against three fungi, viz. *Alternaria, solani, Curvularia geniculata* and *Colletotrichum capsici* at concentrations of 0.005 and 0.01% in a mixture of dimethyl sulphoxide and water. Proper control sets with solvents only were also maintained. The spores of the test fungus were grown on Potato–Dextrose–Agar (PDA) medium. The spore suspension of each of the organisms was prepared separately for different treatments. Six drops of spore suspension from each treatment were placed on two clean slides which were incubated in a moist chamber. After 24 h of incubation at ambient temperature the percentage spore germination was recorded under a microscope and the percentage inhibition was calculated.

RESULTS AND DISCUSSION

The Schiff base, hereinafter abbreviated as H_2SNNNS, was obtained in good yield as a yellow powder. It was sparingly soluble in ethanol but could be dissolved in a mixture of methanol and acetone on heating. Its mass spectrum shows the highest mass peak centred around $m/z = 371$; this corresponds to the monomeric formulation as shown in **IIA**.

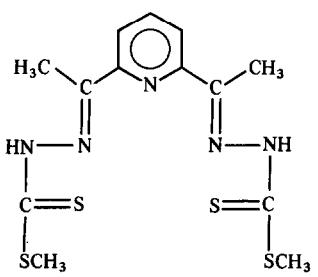

(IIA)

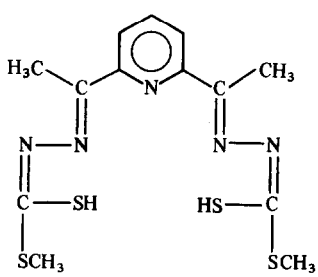

(IIB)

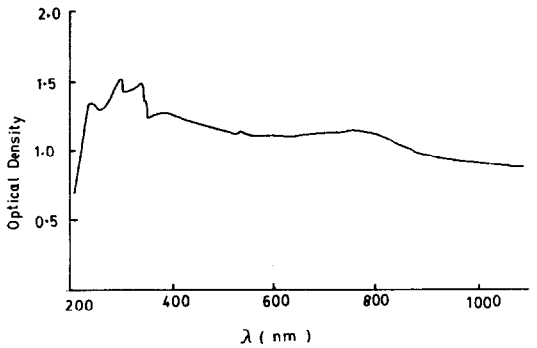

Fig. 1.

The Schiff base (**IIA**) has protons adjacent to the thione groups and consequently, it can remain either as the thione form (**IIA**) or as the thiol form (**IIB**) or as a tautomeric equilibrium mixture of both the thione and thiol forms.

The IR spectrum of the Schiff base does not show *v*S—H at *ca* 2570 cm^{-1} but shows the *v*N—H band at 3220 cm^{-1} indicating that in the solid state it remains in the thione form (**IIA**). Its ^1H NMR spectrum in $(CD_3)_2SO$ shows resonances at 2.69, 2.94, 8.14, 8.18, 8.27 and 8.30 ppm. Of these absorptions, the ones at 2.69 and 2.94 ppm can be ascribed to the $—SCH_3$ and $—CH_3$ (attached to the pyridine ring) protons, respectively. The other peaks between 8.14 and 8.30 ppm may be attributed to the pyridine ring protons. No signal, not even a weak one, at around 4.00 ppm due to the S—H proton[7] could be located in the spectrum. This is an indication that the thiol form (**IIB**) of the Schiff base is presumably not present in DMSO solution.

However, in the presence of metal ions, enethiolization of the Schiff base was found to be greatly enhanced with the concomitant formation of metal complexes of the deprotonated form of the ligand. The complexes which were isolated are shown in Table 1 along with their colours, conductivities, magnetic moments and partial analytical data. The complexes were found to be insoluble in most of the common polar and non-polar organic solvents except for dimethyl sulphoxide, in which conductivity measurements were made. The molar conductance data in Table 1 are consistent with the non-electrolytic natures of the complexes. The ligand, therefore, must be acting as a dinegatively charged species. A comparison of the IR spectrum of the ligand with the spectra of its metal complexes (Table 2) shows that the *v*N—H band of the free ligand at 3220 cm^{-1} is absent in the spectra of metal complexes, confirming that the ligand is deprotonated during complexation with metal ions.

The Schiff base has several potential donor sites, but from the steric point of view, a maximum of five donor atoms can coordinate at any time with a metal ion. Inspection of the IR data in Table 2 reveals that the *v*C=N band of the free ligand at 1620 cm^{-1} is shifted by about 30 cm^{-1} to lower frequencies in the spectra of the complexes, indicating that the azomethine nitrogen atoms are coordinated to the metal ion.[8] The coordination of the azomethine nitrogen atom is also indicated by the shift of the band chiefly assigned to the N—N stretch.[9] In the spectra of the complexes, this band shows a low frequency displacement from 1068 to *ca* 1040 cm^{-1}. In the far-IR region, bands at *ca* 370 and 240 cm^{-1} are assigned to the metal–sulphur[10]

Table 1. Colour, conductivity, magnetic moment and analytical data for the complexes

Compound	Colour	Λ^a (Ohm^{-1} cm^2 mol^{-1})	$\mu_{eff}{}^b$	Analytical data[c] C	H	M
Ni(SNNNS)	Brown	0.4	Diamagnetic	36.0 (36.3)	3.2 (3.7)	13.5 (13.6)
Cu(SNNNS)	Greenish black	3.3	1.74	35.4 (35.9)	3.4 (3.7)	14.6 (14.5)
Zn(SNNNS)	Bright yellow	1.0	Diamagnetic	35.8 (35.8)	3.4 (3.6)	14.9 (15.0)
Cd(SNNNS)	Orange yellow	2.3	Diamagnetic	32.2 (32.3)	3.1 (3.3)	23.1 (23.2)
Fe(SNNNS)Cl	Dark green	10.5	5.93	33.7 (33.8)	3.6 (3.4)	12.0 (12.1)
Co(SNNNS)	Dark green	15.0	1.86	36.4 (36.4)	3.5 (3.5)	12.5 (12.7)

[a] Molar conductance of *ca* 10^{-3} M solutions in dimethyl sulphoxide.
[b] $2.83\sqrt{10^6\chi M.T.}$ (BM).
[c] Calculated values are given in parentheses.

Table 2. IR spectral data for the ligand and its complexes[a]

Compound	νC=N	νN—H	νN—N	νM—N	νM—S	νM—X	Bands due to pyridine
H_2SNNNS	1620m	3220m	1068s	—	—	—	1570s, 1450s, 960s, 630m
Ni(SNNNS)	1590br	—	1055s	240s	370s	—	1465m, 975w
Cu(SNNNS)	1590m,br	—	1035s	260s	390m	—	1560s, 1460w, 958s
Zn(SNNNS)	1590br,m	—	1040s	230s	385m	—	1570m, 950s, 618
Cd(SNNNS)	1588m,br	—	1050s	—	350s	—	1560s, 1450, 950s, 610m
Fe(SNNNS)Cl	1590br	—	1048s	245w	400m	225w	1460w, 960m, 620
Co(SNNNS)	1595br	—	1043s	240w	350w	—	1465sh, 955s, 630m

[a] *ν* denotes stretching frequency; band intensities are denoted by s, m, w and br meaning strong, medium, weak and broad, respectively.

and metal–nitrogen[11,12] stretching frequencies, respectively.

Reaction of the Schiff base with nickel(II) acetate produces a brown compound, Ni(SNNNS), which is diamagnetic in nature. This may seem to suggest a square- or rectangular-planar geometry for the compound. However, its diffuse reflectance electronic spectrum is different from the spectra of nickel(II) complexes of sulphur–nitrogen ligands, for which square-planar structures have been proposed.[13] The electronic spectrum of Ni(SNNNS) displays two broad bands at 15,500 and 19,500 cm^{-1}, which does not show any similarity with the spectra of regular or distorted octahedral nickel(II) complexes.[14] The spectrum, however, resembles those of low-spin five-coordinate nickel(II) species.[15] Based on the foregoing evidences a five-coordinate structure with the Schiff base acting as a pentadentate N_3S_2 ligand is proposed for the Ni(SNNNS) complex. Because of the very low solubility of the compound in almost all non-polar and weakly polar solvents, its molecular weight in solution could not be measured.

The room-temperature magnetic moment (1.74 BM), solid reflectance spectrum with two absorption bands at 7500 and 18700 cm^{-1} and solution ESR spectrum in dimethyl sulphoxide solution with two "*g*" values ($g_{\parallel} = 2.12$ and $g_{\perp} = 2.01$) of the Cu(SNNNS) complex are consistent (while not proving) with five-coordination.

Reaction of anhydrous ferric chloride with the Schiff base produces a brown complex with the empirical formula, Fe(SNNNS)Cl, which behaves as a non-electrolyte in dimethyl sulphoxide (Table 1). This is strong evidence that the chloride ion is coordinated to the iron(III) ion. The presence of νFe—Cl[12] at 245 cm^{-1} in the far-IR spectrum of the complex lends further support in favour of coordination by the chloride ion. The room temperature magnetic moment of Fe(SNNNS)Cl (5.93 BM) suggests that it is a high-spin iron(III) compound. Since the Schiff base behaves as an N_3S_2 pentadentate ligand and there is one chloride coordinated to the iron(III) ion, the subject complex may be assigned an octahedral structure. Its electronic spectrum in Nujol mull (Fig. 1) shows bands at 761, *ca* 510 sh, 385, 299 and 240 nm, of which the band at 761 nm and the shoulder at *ca* 510 nm may be assigned to the $^6A_1 \rightarrow {}^4T_1$ and $^6A_1 \rightarrow {}^4T_2$ transitions, respectively, of octahedral iron(III). The other expected band corresponding to the transition, $^6A_1 \rightarrow {}^4A_1$, ^4E is probably hidden under charge-transfer or intra-ligand transitions.

The reaction of cobalt(II) chloride with H_2SNNNS yields a dark green compound, which on the basis of analytical data may be formulated as Co(SNNNS). Its molar conductance value in dimethyl sulphoxide (Table 1) suggests that it is a non-electrolyte in this solvent. Its IR spectrum does not show the νN—H bands of the free ligand. All these facts seem to indicate that the ligand is coordinated as a dinegatively charged species. The room temperature magnetic moment of 1.86 BM suggests that it is a low-spin cobalt(II) complex. This moment is similar to those shown by other low-spin five-coordinate cobalt(II) complexes.[16] The diffuse reflectance spectrum of Co(SNNNS) shows a band at 500 nm (20,000 cm^{-1}) which does not bear any similarity with spectra of octahedral cobalt(II) complexes. Based on the above evidences, a five-coordinate configuration is tentatively assigned to this complex.

The zinc(II) and cadmium(II) complexes of empirical formulas, M(SNNNS) are non-electrolytes in dimethyl sulphoxide. Their very low solubilities in most of the common polar and non-polar organic solvents suggest that monomeric five-coordinate structures are unlikely. A sulphur-bridged polymeric octahedral structure is suggested for these complexes.

Table 3. Fungicidal screening data for the ligand and some of its metal complexes

Compound	% Inhibition after 24 h Organism *Alternaria solani* Conc. used 0.005%	0.01%	Organism *Curvularia geniculata* Conc. used 0.005%	0.01%	Organism *Colletotrichum capsici* Conc. used 0.005%	0.01%
H_2SNNNS	60	84	59	87	67	79
Cu(SNNNS)	69	75	56	87	60	79
Co(SNNNS)	65	74	50	87	60	79
Fe(SNNNS)Cl	67	75	36	87	66	79
Cd(SNNNS)	66	74	66	85	65	79

Fungitoxicities

Alternaria solani, *Curvularia geniculata* and *Colletotrichum capsici* were employed to study the antifungal properties of the Schiff base as well as some of its metal complexes. The fungicidal screening data in Table 3 suggest that the ligand as well as its complexes display marked toxicities towards all three fungi even at low concentrations.

Acknowledgements—We thank Prof. R. W. Hay of the Department of Chemistry, University of Stirling, U.K., Prof. D. X. West of the Chemistry Department, Illinois State University, U.S.A. and Dr D. J. Phillips of the School of Chemistry, University of New South Wales, Sydney, Australia for their generous help with NMR, ESR and diffuse reflectance spectra, respectively. We also thank the University of Chittagong, Bangladesh and Laurentian University, Sudbury, Ontario, Canada for partial support. One of us (SMMH) thanks the University of Chittagong for a Ph.D. research fellowship.

REFERENCES

1. M. Akbar Ali and S. E. Livingstone, *Coord. Chem. Rev.* 1974, **13**, 101.
2. M. J. M. Campbell, *Coord. Chem. Rev.* 1975, **15**, 279.
3. S. Padhye and G. B. Kauffman, *Coord. Chem. Rev.* 1985, **63**, 127.
4. L. F. Lindoy and D. H. Busch, *J. Chem. Soc., Chem. Commun.* 1972, 683.
5. V. L. Goedjen and G. G. Christopher, *Inorg. Chem.* 1973, **12**, 2316.
6. M. Akbar Ali, D. A. Chowdhury and M. Nazimuddin, *Polyhedron* 1984, **3**, 595.
7. D. Gattegno and A. M. Giuliani, *Tetrahedron* 1974, **30**, 701.
8. J. E. Kovacic, *Spectrochim. Acta* 1967, **23A**, 183.
9. G. R. Burns, *Inorg. Chem.* 1968, **7**, 277.
10. D. M. Adams, *Metal–Ligand and Related Vibrations*, p. 319. Arnold, London (1967); D. M. Adams and J. B. Correll, *J. Chem. Soc. A* 1968, 1299.
11. M. Mohan, P. Sharma and N. K. Jha, *Inorg. Chim. Acta* 1985, **107**, 91.
12. J. R. Ferraro, *Low Frequency Vibrations of Inorganic and Coordination Compounds*. Plenum Press, New York (1971).
13. N. F. Curtis, *Coord. Chem. Rev.* 1968, **3**, 3; H. Kobayashi and B. Korybut-Daskiewicz, *Bull. Chem. Soc. (Japan)* 1972, **45**, 2485; M. Akbar Ali and R. Bose, *Polyhedron* 1984, **3**, 517.
14. A. B. P. Lever, *Inorganic Electronic Spectroscopy*. Elsevier, Amsterdam (1968).
15. G. A. Mair, H. M. Powell and D. E. Henn, *Proc. Chem. Soc.* 1960, 415; M. O. Workman, G. Dyer and W. T. Huntress, *Proc. Chem. Soc.* 1964, 228.
16. G. Dyer and D. W. Meek, *Inorg. Chem.* 1965, **4**, 1398; D. W. Meek, M. O. Workman and T. D. DuBois, *Am. Chem. Soc. 151st Nat. Meet.* (1965).

Polyhedron Vol. 7, No. 21, pp. 2189–2192, 1988
Printed in Great Britain

0277–5387/88 $3.00+.00
© 1988 Pergamon Press plc

HYDROSILYLATION OF 1-VINYLSILATRANE

MOHAMMED NASIM, ARVIND K. SAXENA and LALIT M. PANDE*

Defence Materials & Stores Research & Development Establishment,
Post Box No. 320, Kanpur 208 013, India

(*Received* 15 *September* 1987; *accepted after revision* 14 *April* 1988)

Abstract—Hydrosilylation of 1-vinylsilatrane using Speier's catalyst gave 1,2-addition products of the type $R_2MeSiCH_2CH_2Si(OCH_2CH_2)_3N$, (R = Et, *n*-Pr, *n*-Bu, allyl, Ph, *p*-ClC_6H_4, *p*-FC_6H_4, *p*-tolyl and benzyl) in yields ranging from 75 to 90%.

The 1-alkenylsilatranes undergo free radical as well as photochemical addition to the double bond,[1–3] with the substituents on the alkenyl group dictating the direction of addition. However, in the case of 1-vinylsilatrane the free radical addition is a facile process resulting in the synthesis of 2-substituted-1-ethylsilatrane, especially if perfluoroiodoalkanes are used.[1]

The facile addition of $\rangle$SiH to the double bond, conveniently called hydrosilylation, has been extensively studied[4–7] and has provided synthons. However, in the case of 1-vinylsilatrane the hydrosilylation reactions have not been studied in any great detail. Few references are cited for this addition and for the structures of the silanes related to those containing furyl, thienyl and oligomeric polysiloxane functionalities.[1,8,9]

EXPERIMENTAL

Benzene, isopropanol, diethyl ether, ethyl bromide, *n*-propyl bromide, *n*-butyl bromide, allyl bromide, *p*-bromobenzene, *p*-bromotoluene, *p*-fluorobromobenzene and benzyl chloride (BDH/E. Merck/Fluka/Aldrich–AR) were dried and distilled before use. Chloroplatinic acid (Alfa–AR) for the preparation of Speier's catalyst, magnesium powder (Glaxo–Grignard grade) for the preparation of Grignard reagent and *p*-bromochlorobenzene (Fluka–AR) were used as received.

IR and ^{1}H NMR were recorded on Perkin–Elmer 783 and Jeol FX-90Q spectrophotometers, respectively. Melting points and boiling points are uncorrected. Satisfactory elemental analyses were obtained.

Synthesis of methyldiorganosilanes, methyl bis(p-tolyl)silane

To a stirred suspension of magnesium powder (4.8 g, ~ 200 mmol), in dry diethyl ether (200 cm^3) kept under argon, was added a solution of *p*-bromotoluene (34.2 g, ~ 200 mmol) in diethyl ether (25 cm^3) over 30 min and stirring was continued for an additional 2–3 h. The reaction mixture was cooled (ice–salt mixture) and dichloromethylsilane (11.5 g, ~ 100 mmol) in diethyl ether (25 cm^3) was then added dropwise (30 min). The resulting mixture was allowed to reach room temperature and stirring was continued for 2 h followed by heating under reflux for 1 h. The reaction mixture was then hydrolysed with ammonium chloride and the organic layer separated. The aqueous layer was further extracted with an excess of diethyl ether (2×100 cm^3). The combined organic layers were dried over anhydrous sodium sulphate and the ether was removed by distillation. The residue on vacuum distillation yielded methyl bis(*p*-tolyl)silane (14.0 g, 62%), b.p. 128–130°C/3 mm. (Found: C, 79.5; H, 8.21; Si, 12.4. Calc. for $C_{15}H_{18}Si$: C, 79.6; H, 8.0; Si, 12.4%.) IR: ν(Si—H) 2100 cm^{-1}. ^{1}H NMR (δ, ppm), 0.82, d, 3H (Si—CH_3); 5.17, q, 1H (Si—H); 2.55, s, 6H (Ar—CH_3); 7.38, d, 4H (*m*-Ar—H) and 7.68, d, 4H (*o*-Ar—H).

Similarly other silanes viz. methyl bis(*p*-chlorophenyl)- (13.6 g, 75%), b.p. 129–130°C/0.05 mm. (Found: C, 58.4; H, 4.5; Si, 10.5. Calc. for $C_{13}H_{12}SiCl_2$: C, 58.4; H, 4.5; Si, 10.5%.) IR: ν(Si—H) 2100 cm^{-1}. ^{1}H NMR: (δ, ppm), 0.67, d, 3H (Si—CH_3); 4.98, q, 1H (Si—H); 7.38, m, 4H (*m*-

* Author to whom correspondence should be addressed.

Ar—H) and 7.50, m, 4H (*o*-Ar—H); methyl bis(*p*-fluorophenyl)- (11.6 g, 85%), b.p. 86–87°C/0.1 mm. (Found: C, 66.6; H, 5.2; Si, 12.0. Calc. for $C_{13}H_{12}SiF_2$: C, 66.6; H, 5.2; Si, 12.0%.) IR: ν(Si—H) 2100 cm^{-1}. ^1H NMR: (δ, ppm), 0.74, d, 3H (Si—CH_3); 5.10, q, 1H (Si—H); 7.18, m, 4H (*m*-Ar—H) and 7.64, m, 4H (*o*-Ar—H); methyldiethyl- (11.0 g, 55%), b.p. 76–77°C, ref. 10 77.2–77.6°C; methyl-*n*-dipropyl- (7.2 g, 55%), b.p. 126–127°C, ref. 10 125.9°C/743 mm; methyl-*n*-dibutyl- (10.2 g, 64%), b.p. 172–173°C, ref. 10 172.9°C; methyldiallyl- (16 g, 64%), b.p. 120–123°C, ref. 10 122.5°C/745 mm; methyldiphenyl- (6.7 g, 78%), b.p. 81–82°C/0.1 mm, ref. 10 79°C/0.1 mm and methyldibenzylsilane (13.3 g, 58%), b.p. 137–139°C/3.5 mm, ref. 11 131–140°C/3 mm, were prepared.

Hydrosilylation with 2-methyldiethylsilyl(silatranyl)ethane

To 1-vinylsilatrane (2.0 g, ~ 10 mmol) in benzene (25 cm^3) and Speier's catalyst (4–5 drops), under a dry argon atmosphere, a solution of methyldiethylsilane (1.0 g, ~ 10 mmol) in benzene (25 cm^3) was added over 15 min under reflux. The reaction mixture was stirred under reflux for an additional period of 4–5 h. The solution was then concentrated on a boiling water bath to a volume of 25 cm^3 and petroleum ether (30 cm^3, 60–80°C) was added to precipitate out a white solid product. This was dissolved in chloroform (20 cm^3) and to it petroleum ether (30 cm^3, 60–80°C) was added to afford a white crystalline product, identified as 2-methyldiethylsilyl(silatranyl)ethane (**1**) (1.20 g, 80%), m.p. 79–80°C. (Found: C, 51.3; H, 9.4; N, 4.8; Si, 18.5. Calc. for $C_{13}H_{29}O_3Si_2N$: C, 51.5; H, 9.6; N, 4.6; Si, 18.5%.) ^1H NMR (δ, ppm), 3.75, t 6H (O—CH_2); 2.77, t, 6H (CH_2—N); −0.13, s, 3H (Si—CH_3); 0.35, m, 6H (—CH_2Si—$(CH_2)_2$—); 0.57, m, 2H (Si—CH_2); 0.92, t, 6H (CH_3).

Similarly, hydrosilylation with other methyldiorganosilanes was carried out. The results are summarized in Table 1.

RESULTS AND DISCUSSION

Addition of $\rangle$Si—H compounds to 1-vinylsilatrane have been reported in only a few cases.[8,9] These reactions involve highly substituted silanes viz. furyl- and thienylsilanes and terminal dimethylsilyl (Me_2SiH) containing oligomeric polysiloxanes (M.W. 1000–2000). It has been observed that the ease of addition was dependent upon the number of furyl and/or thienyl groups present in the hydrosilanes.[1] Thus, tri(2-furyl)silane added with greater ease (at room temperature) than dimethyl(2-furyl)silane (needed heating).[8,9] This limited study and the conclusions of reactivity derived from these hydrosilylation reactions of 1-vinylsilatrane are not only surprising but also inconclusive and they prompted us to investigate the addition of silanes containing alkyl, alkenyl and aryl radicals.* In the course of the present study, methyldiethyl-, methyldi-*n*-propyl-, methyldi-*n*-butyl-, methyldiallyl-, methyldiphenyl-, methylbis(*p*-fluorophenyl)-, methylbis(*p*-chlorophenyl)-, methylbis(*p*-tolyl)- and methyldibenzylsilanes were prepared by the Grignard reaction on dichloromethylsilane in yields ranging between 55–85%.

For hydrosilylation, Speier's catalyst was used which was made by dissolving chloroplatinic acid ($H_2PtCl_6 \cdot 6H_2O$) in freshly distilled isopropanol and keeping the solution for six weeks. The reaction between the silanes and 1-vinylsilatrane was carried out in benzene under reflux (4–5 h) and the course of the reaction was followed by observing the disappearance of the $\rangle$Si—H band in the IR at 2100 cm^{-1}. In the case of alkylsilanes the CH=CH_2 band at 1600 cm^{-1} also disappeared. However, when there were aryl substituents on the silanes, the 1600 cm^{-1} absorption band was of no help in monitoring the progress of reaction. The diverse structure of silanes, containing alkyl, alkyl aryl and alkyl allyl, all assist in the facility to give 2-substituted-1-ethylsilatrane in yields ranging between 75–90%. The exclusive formation of 2-substituted-1-ethylsilatrane shows that the steric consideration in the complex formation step, involving platinum and 1-vinylsilatrane, is of paramount importance.

^1H *NMR*

^1H NMR spectra of all hydrosilylated products were obtained in $CDCl_3$ (Table 1). The compounds showed characteristic triplets of —OCH_2 and —NCH_2 protons at δ 3.75±0.02 ppm and δ 2.77±0.02 ppm, respectively. Whereas there was no significant shift change in the —OCH_2 protons of 1-vinylsilatrane and hydrosilylated silatrane, the —NCH_2 protons showed a marked shift from the original value of δ 2.84 ppm.[13] The reason may be attributed to the loss of the π-bonded system in the vinyl groups which in turn reduces the deshielding effect and causes the shift of —NCH_2 protons to a

* After the submission of this work for publication, we discovered a report by Voronkov *et al.* on the hydrometallation (R_3MH, R = Et, EtO and Bu, M = Si, Ge, Sn) of alkenylsilatranes.[12]

Table 1. Proton chemical shifts in ^{1}H NMR spectra of the hydrosilylated compounds of the type $R_2CH_3SiCH_2CH_2Si(OCH_2CH_2)_3N$

Number	Compound (% yield) R	M.p. (°C)	δ (ppm) Si—O—CH_2(*t*) (*J* in Hz)	δ (ppm) N—CH_2(*t*) (*J* in Hz)	$R_2\overset{\alpha''}{C}H_3Si\overset{\alpha'}{C}H_2\overset{\beta'}{C}H_2Si(OCH_2CH_2)_3N$
1	$\overset{\beta}{C}H_3\overset{\alpha}{C}H_2$— (80)	79–80	3.75 (5.56, 5.86)	2.77 (5.86, 5.57)	−0.13, s, 3H (α″) 0.35, m, 6H (α,α′) 0.57, m, 2H (β′) 0.92, t, 6H (β)
2	$\overset{\nu}{C}H_3\overset{\beta}{C}H_2\overset{\alpha}{C}H_2$— (90)	80–81	3.77 (5.86, 5.86)	2.79 (5.86, 5.86)	−0.10, s, 3H (α″) 0.43, m, 6H (α,α′) 0.57, m, 2H (β′) 0.92, t, 6H (ν) 1.45, m, 4H (β)
3	$\overset{\delta}{C}H_3\overset{\nu}{C}H_2\overset{\beta}{C}H_2CH_2$— (89)	81–82	3.75 (5.86, 5.57)	2.77 (5.57, 5.86)	−0.12, s, 3H (α″) 0.42, m, 6H (α,α′) 0.60, m, 2H (β′) 0.84, t, 6H (δ) 1.24, m, 8H (β,ν)
4	$\overset{\nu}{C}H_2{=}\overset{\beta}{C}H{-}\overset{\alpha}{C}H_2$— (86)	49–50	3.75 (5.86, 5.86)	2.78 (5.86, 5.86)	−0.07, s, 3H (α″) 0.35, m, 2H (α′) 0.60, m, 2H (β′) 1.51, m, 4H (α) 4.82, m, 4H (ν) 5.75, m, 2H (β)
5	C_6H_5— (75)	128–129	3.74 (5.86, 5.56)	2.76 (5.56, 5.86)	0.42, m, 2H (β′) 0.54, s, 3H (α″) 1.29, m, 2H (α′) 7.29, m, 6H (*m*,*p*-ArH) 7.54, m, 4H (*o*-ArH)
6	*p*-FC_6H_4— (77)	139–140	3.74 (5.86, 5.57)	2.77 (5.85, 5.57)	0.48, m, 5H (α″,β′) 1.02, m, 2H (α′) 6.99, m, 4H (*m*-ArH) 7.41, m, 4H (*o*-ArH)
7	*p*-ClC_6H_4— (79)	157–158	3.73 (5.86, 5.57)	2.77 (5.57, 5.86)	0.45, m, 2H (β′) 0.47, s, 3H (α″) 1.10, m, 2H (α′) 7.26, m, 4H (*m*-ArH) 7.41, m, 4H (*o*-ArH)
8	*p*-$CH_3C_6H_4$— (82)	165–166	3.73 (5.85, 5.57)	2.77 (5.86, 5.56)	0.41, m, 2H (β′) 0.48, s, 3H (α″) 1.12, m, 2H (α′) 2.32, s, 6H (*p*-CH_3Ar) 7.16, t, 4H (*m*-ArH) 7.43, d, 4H (*o*-ArH)
9	$C_6H_4\overset{\alpha}{C}H_2$— (77)	110–111	3.79 (5.56, 5.86)	2.81 (5.86, 5.57)	−0.17, s, 3H (α″) 0.52, m, 4H (α′,β′) 2.09, s, 4H (α) 7.07, m, 6H (*m*,*p*-ArH) 7.32, m, 4H (*o*-ArH)

higher field. This statement is supported by the fact that the methylene protons of —NCH_2 in ethylsilatrane appear at δ 2.79 ppm.[13]

The disappearance of the $\rangle$Si—H quartet of methyl dialkyl/aryl silanes at δ 3.42–5.20 ppm is accompanied by the marked shift of α''-CH_3 protons towards higher field in all the cases. This is caused by the loss of the deshielding effect and an increase in the shielding by the —CH_2 protons generated as a consequence of addition to the vinyl function.

The methylene protons with alkyl substituents on the adjacent silicon atom, as expected, appear as a multiplet at $\delta \sim 0.58$ ppm and with aryl substituents are shifted upfield to $\delta \sim 1.2$ ppm. Only minor shifts appear with changes of substituents on the aryl functions.

Acknowledgement—Thanks are due to the Director, DMSRDE, Kanpur for permission to publish this work.

REFERENCES

1. M. G. Voronkov, V. M. Dyakov and S. V. Kirpichenko, *J. Organometal. Chem.* 1982, **233**, 20.
2. M. G. Voronkov, M. S. Sorokin and V. M. Dyakov, *Zh. Obshch. Khim.* 1979, **49**, 1285; *Chem. Abs* 1979, **91**, 211473y.
3. M. G. Voronkov, V. M. Dyakov, N. M. Kydyakov and M. V. Sigalov, *Zh. Obshch. Khim.* 1979, **49**, 1525; *Chem. Abs* 1979, **91**, 175431x.
4. D. A. Armitage, *Comprehensive Organometallic Chemistry* (Edited by G. Wilkinson, F. G. A. Stone and E. W. Abel), Vol. 2, p. 115. Pergamon Press, Oxford (1982).
5. E. Lukevics, Z. V. Belyakova, M. G. Pomerantseva and M. G. Voronkov, *Journal of the Organometallic Chemistry Library 5*, p. 1. Elsevier, Amsterdam (1977).
6. John L. Speier, *Advances in Organometallics Chemistry*, Vol. 17, p. 407. Academic Press, New York (1979).
7. Gerald L. Larson, *Journal of Organometallic Chemistry Library 17*, p. 18. Elsevier, Amsterdam (1985).
8. British Patent 1, 321, 616 (1973) to Harold F. G. Patient and R. P. Bush; *Chem. Abs* 1973, **79**, 105741b.
9. M. G. Voronkov, V. M. Dyakov and S. V. Kirpichenko, *J. Organometal. Chem.* 1982, **233**, 101, 109.
10. Vladimír Bažant, Václav Chvalovsk'y and Jiři Rathousky, *Organo-Silicon Compounds*, Vol. 2, Part 1. Academic Press, New York (1965).
11. Vladimír Bažant, Václav Chvalovsk'y and Jiři Rathousky, *Hand Book of Organosilicon Compounds Advances since 1961*, Vol. 3. Marcel Dekker, New York (1973).
12. M. G. Voronkov, S. N. Adamovich, N. M. Kudyakov, S. Yu. Khramtsova, V. I. Rakhlm and R. G. Mirskov Izu, *Akad. Nauk, SSSR, Ser. Khim.* 1986, **2**, 488; *Chem. Abs* 1987, **106**, 18670k.
13. M. G. Voronkov, *Pure Appl. Chem.* 1966, **13**, 35.

Polyhedron Vol. 7, No. 21, pp. 2193–2195, 1988
Printed in Great Britain

0277-5387/88 $3.00+.00
© 1988 Pergamon Press plc

THE OXIDATION OF OCTACYANOTUNGSTATE(IV) BY NITRITE IONS IN ACIDIC MEDIUM

C. ROBERT DENNIS,* A. J. VAN WYK,† S. S. BASSON and J. G. LEIPOLDT

Chemistry Department, University of the Orange Free State, Bloemfontein, 9300 Republic of South Africa

(*Received* 4 *January* 1988; *accepted* 14 *April* 1988)

Abstract—The kinetics of the oxidation of octacyanotungstate(IV) by nitrite ions has been studied in aqueous perchloric acid medium between 0.01 and 0.5 M $HClO_4$. An acid dissociation constant for $HW(CN)_8^{3-}$, $K_a = 0.26 \pm 0.2$ M at 25°C and $I = 1.0$ M, is obtained from the kinetic data.

The redox equilibrium of the ferri/ferrocyanide couple in nitrous acid was reported by Stedman and coworkers. The kinetics of this equilibrium [eq. (1)] were found to be of a complex nature.[1,2]

$$Fe(CN)_6^{3-} + HNO_2 + 2H^+ + H_2O \rightleftharpoons 2H_2Fe(CN)_6^{2-} + HNO_3. \quad (1)$$

The reaction is dependent on the hydrogen ion concentration[3] and is complicated by the reactions:[4]

$$HNO_2 + NO_3^- + H^+ \rightleftharpoons N_2O_4 + H_2O \quad (2)$$

$$N_2O_4 \rightleftharpoons 2NO_2 \quad (3)$$

$$NO_2 + Fe(CN)_6^{3-} \rightarrow 1/2HCN + \text{Intermediate}. \quad (4)$$

The intermediate in eq. (4) is slowly converted to the nitroprusside ion, $[Fe(CN)_5NO]^{2+}$.

The oxidation–reduction equilibrium of the $IrCl_6^{2-/3-}$ couple in nitrous acid has been reported by Ram and Stanbury.[5] A strong product inhibition was observed. The net reaction (similar to that of the $Fe(CN)_6^{3-/4-}$) can be represented by:

$$2IrCl_6^{2-} + HNO_2 + H_2O \rightleftharpoons 2IrCl_6^{3-} + NO_3^- + 3H^+. \quad (5)$$

The oxidation of ferrocyanide[6] and hexachloroiridate(III)[5] was reported by Bates *et al.* and Ram and Stanbury, respectively. Both these reactions were $[H^+]$ dependent and the NO^+/NO pathway has been found to play a prominent role. In the ferrocyanide investigation the $[H^+]$ dependence was attributed to a more reactive protonated ferrocyanide species.

It was previously shown[7–9] that the redox reactions of the $Fe(CN)_6^{3-/4-}$, $W(CN)_8^{3-/4-}$ and $Mo(CN)_8^{3-/4-}$ couples proceed via similar outer-sphere reaction pathways. The kinetic study of the oxidation of $W(CN)_8^{4-}$ by HNO_2 was thus carried out for comparison with the above-mentioned results.

EXPERIMENTAL

Potassium octacyanotungstate(IV)dihydrate, $K_4W(CN)_8 \cdot 2H_2O$, was prepared as described by Leipoldt *et al.*[10] and was used as a primary standard[11] after recrystallization. Stock solutions of sodium nitrite were prepared daily using a Merck "Pro Analisi" reagent. All other reagents used were analytical grade and redistilled water was used throughout.

The kinetics were followed by stopped-flow spectrophotometry at 357 nm using a Durrum D-110 instrument. The temperature of reaction mixtures was controlled to within 0.1°C. Experiments were carried out in perchloric acid medium with $[NO_2^-]$ in excess by a factor of ten relative to $[W(CN)_8^{4-}]$ to obtain pseudo-first-order reaction conditions. Reaction mixtures were maintained at constant ionic strength by the addition of sodium perchlorate.

* Author to whom correspondence should be addressed.
† Present address: Department of Research and Development, ISCOR HQ, Pretoria, Republic of South Africa.

Table 1. Observed rate constants for the oxidation of octacyanotungstate(IV) by nitrite ions where $T = 25.0°C$ and $[H^+] = 0.20$ M $HClO_4$

$10^4[W(CN)_8^{4-}]$ (M)	$10^3[NO_2^-]$ (M)	$10^4[W(CN)_8^{3-}]$ (M)	$I(NaClO_4)$ (M)	k_{obs} (s^{-1})
2.0	4.0		1.0	49.9
3.0	4.0		1.0	51.0
4.0	4.0		1.0	51.5
5.0	4.0		1.0	50.3
4.0	3.0		1.0	38.5
4.0	4.0		1.0	50.9
4.0	5.0		1.0	63.2
4.0	6.0		1.0	76.9
4.0	4.0	1.0	1.0	50.6
4.0	4.0	2.0	1.0	49.9
4.0	4.0	3.0	1.0	51.2
4.0	4.0	4.0	1.0	49.7
4.0	4.0		0.90	48.3
4.0	4.0		0.70	49.4
4.0	4.0		0.50	48.6

RESULTS AND DISCUSSION

The oxidation of octacyanotungstate(IV) by nitrite ions in aqueous acidic medium show first-order kinetics in $[W(CN)_8^{4-}]$ and log/time plots were linear for about two half-lives. The results in Table 1 show that the reaction is linearly dependent on $[NO_2^-]$ and that variation in initial concentration of the product $W(CN)_8^{3-}$ have no significant effect on the reaction rate.

Since the pK_a for HNO_2 is 3.37[12] and the equilibrium constant for reaction (6) is 3×10^{-7} M^{-1},[13] the main N^{III} species under the experimental conditions is HNO_2.

$$HNO_2 + H^+ \rightleftharpoons NO^+ + H_2O. \quad (6)$$

Stedman and coworkers[6] attributed the hydrogen ion dependence of the $Fe(CN)_6^{4-}$–nitrous acid reaction to an equilibrium between two cyano species. From their results a dissociation constant K_a for $H_2Fe(CN)_6^{2-}$ is obtained which is in agreement with values available in the literature.

Kinetic measurements with variation in $[H^+]$ for the reaction between $W(CN)_8^{4-}$ and NO_2^- (Fig. 1) show the hydrogen ion dependence of the reaction. These results clearly show a dissociation constant which, considering the information above, indicates an equilibrium between two cyano species. From the available data an appropriate reaction pathway for the acidity range of this study could be the following:

$$W(CN)_8^{4-} + H^+ \overset{K_a^{-1}}{\rightleftharpoons} HW(CN)_8^{3-} \quad (7)$$

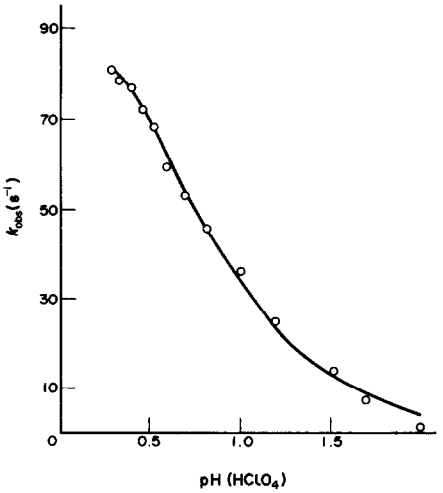

Fig. 1. The hydrogen ion dependence for the oxidation of octacyanotungstate(IV) by nitrite ions. $[W(CN)_8^{4-}] = 4 \times 10^{-4}$ M, $[NO_2^-] = 4 \times 10^{-3}$ M, $I = 1.0$ M ($NaClO_4$) and $T = 25°C$. The solid curve is the computer fit.

$$HW(CN)_8^{3-} + HNO_2 \xrightarrow{k} W(CN)_8^{3-} + NO + H_2O. \quad (8)$$

This reaction mechanism corresponds to the rate law:

$$\frac{-d[W(CN)_8^{4-}]}{dt} = \frac{kK_a^{-1}[H^+]}{1 + K_a^{-1}[H^+]} [W(CN)_8^{4-}][HNO_2]. \quad (9)$$

A non-linear least-squares fit of the data in Fig. 1 to the rate law (9) yields the values $k = (3.1 \pm 0.1) \times 10^4$ M^{-1} s^{-1} and $K_a = 0.26 \pm 0.02$ M at 25°C and $I = 1.0$ M. The value for K_a at an ionic strength of zero was calculated from the Davies equation[14] [eq. (10)] as $K_a = 0.041$ M ($pK_a = 1.39$).

$$\log k = \log k_0 + Z_A Z_B (I^{1/2}/1 + I^{1/2}) + 0.3I. \quad (10)$$

This value is of the same order of magnitude as the value reported for K_{a4} of $H_4W(CN)_8$ ($pK_{a4} = 1.6$) by Samotus and Kosowics-Czajkowska.[15]

Acknowledgements—We thank the South African C.S.I.R. and the research fund of this university for financial support.

REFERENCES

1. K. M. Davies and G. Stedman, *J. Chem. Soc., Chem. Comm.* 1968, 118.
2. J. C. Bates, K. M. Davies and G. Stedman, *J. Chem. Soc., Dalton Trans.* 1974, 2182.
3. J. C. Bates, K. M. Davies and G. Stedman, *J. Chem. Soc., Dalton Trans.* 1974, 246.
4. K. M. Davies and G. Stedman, *J. Chem. Soc., Dalton Trans.* 1974, 2176.
5. M. S. Ram and D. M. Stanbury, *Inorg. Chem.* 1985, **24**, 2954.
6. J. C. Bates, P. Reveco and G. Stedman, *J. Chem. Soc., Dalton Trans.* 1980, 1487.
7. C. R. Dennis, S. S. Basson and J. G. Leipoldt, *Polyhedron* 1983, **2**, 1357.
8. C. R. Dennis, J. G. Leipoldt, S. S. Basson and A. J. van Wyk, *Inorg. Chem.* 1986, **25**, 1268.
9. C. R. Dennis, A. J. van Wyk, S. S. Basson and J. G. Leipoldt, *Inorg. Chem.* 1987, **26**, 270.
10. J. G. Leipoldt, L. D. C. Bok and P. J. Cilliers, *Z. Anorg. Allg. Chem.* 1974, **407**, 350.
11. S. S. Basson, L. D. C. Bok and S. R. Grobler, *Z. Anal. Chem.* 1974, **268**, 287.
12. *Handbook of Chemistry and Physics*, 55th Edn. Chemical Rubber Company, U.S.A. (1974).
13. J. H. Ridd, *Adv. Phys. Org. Chem.* 1978, **16**, 1.
14. C. W. Davies, *Ion Association*, Chap. III. Butterworths, London (1962).
15. A. Samotus and B. Kosowics-Czajkowska, *Rocz. Chem.* 1971, **45**, 1623.

Polyhedron Vol. 7, No. 21, pp. 2197–2200, 1988
Printed in Great Britain

0277–5387/88 $3.00+.00
© 1988 Pergamon Press plc

A NEW SYNTHETIC APPROACH TO MACROCYCLIC COMPLEXES WITH PERIPHERAL SUBSTITUENTS CARRYING CARBOXYL AND ESTER FUNCTIONS

JULITA EILMES

Faculty of Chemistry, Jagiellonian University, Karasia 3, 30-060 Cracow, Poland

(*Received* 29 *February* 1988; *accepted* 14 *April* 1988)

Abstract—The transformations of γ,δ-unsaturated-δ-lactonic substituents of γ,γ'-disubstituted Jäger-type macrocyclic complexes into the new open-chain peripheral substituents are reported. The base-catalysed methanolysis leads to the methyl esters of corresponding δ-ketoacids. The fission of the lactonic rings by alkalies gives rise to the salts of δ-ketoacids. The latter can be easily converted into esters by means of alkyl halides. The new compounds were characterized by elemental analysis, IR, ^{1}H NMR and MS data.

It is well known that the reactivity of the macrocyclic complexes and their coordination behaviour can be controlled by the ligand design. Introducing suitable substituents onto the ligand framework modifies the coordination geometry around the metal centre and influences the metal ion reactivity. This is the most often employed strategy for the preparation of a variety of bioinorganic models.

In our earlier paper[1] the synthesis of disubstituted Jäger-type macrocyclic complexes having γ,δ-unsaturated-δ-lactonic substituents in the *meso* positions has been reported.

Since unsaturated lactones are known for their high reactivity and very rich chemistry[2,3] it is expected that chemical modifications of these substituents will provide an advantageous synthetic method for the preparation of a broad variety of new peripherally substituted macrocyclic complexes.

This paper reports the transformation of γ,δ-unsaturated lactones into the new open-chain substituents by methanolysis and an alkaline hydrolysis of the lactonic rings. The alkylation of the salts of the open-chain δ-ketoacids is also described as an efficient route to various esters.

RESULTS

The methanolysis of the lactonic substituents of the macrocyclic complexes proceded smoothly when compounds **1** and **2** were refluxed in an excess of methanol in the presence of sodium methoxide (see Scheme 1). The complexes **3** and **4** having two methylglutaroyl groups in the *meso* positions were obtained in good yield (80%). The use of sodium or potassium hydroxides as catalysts resulted in a remarkable decrease in the yield (28%).

An alkaline hydrolysis of γ,δ-unsaturated-δ-lactonic rings was accomplished by refluxing the starting compounds **1** and **2** in butanolic potassium hydroxide and led to the formation of the potassium salt of the corresponding δ-ketoacids (compounds **5** and **6**).

Addition of dilute acetic or hydrochloric acid to the aqueous solution of the alkali salt resulted in precipitation of the free acid. This procedure, however, was successfully applied only in the case of product **6**. Salt **5** underwent partial decomposition with the loss of substituents leading to the non-substituted macrocyclic complex.

The potassium salts **5** and **6** were alkylated with the use of methyl and ethyl iodides as well as *p*-bromophenacyl bromide giving corresponding esters in reasonable yields (75–88%). The results suggest that the alkylation procedure can be easily extended to other reactive alkyl halides affording a convenient entry to a broad variety of new peripheral substituents.

DISCUSSION

γ,δ-Unsaturated-δ-lactonic substituents appear to be susceptible to chemical conversions into the new open-chain groups.

It should be noted, however, that the reactivity of the macrocyclic framework itself, imposes some

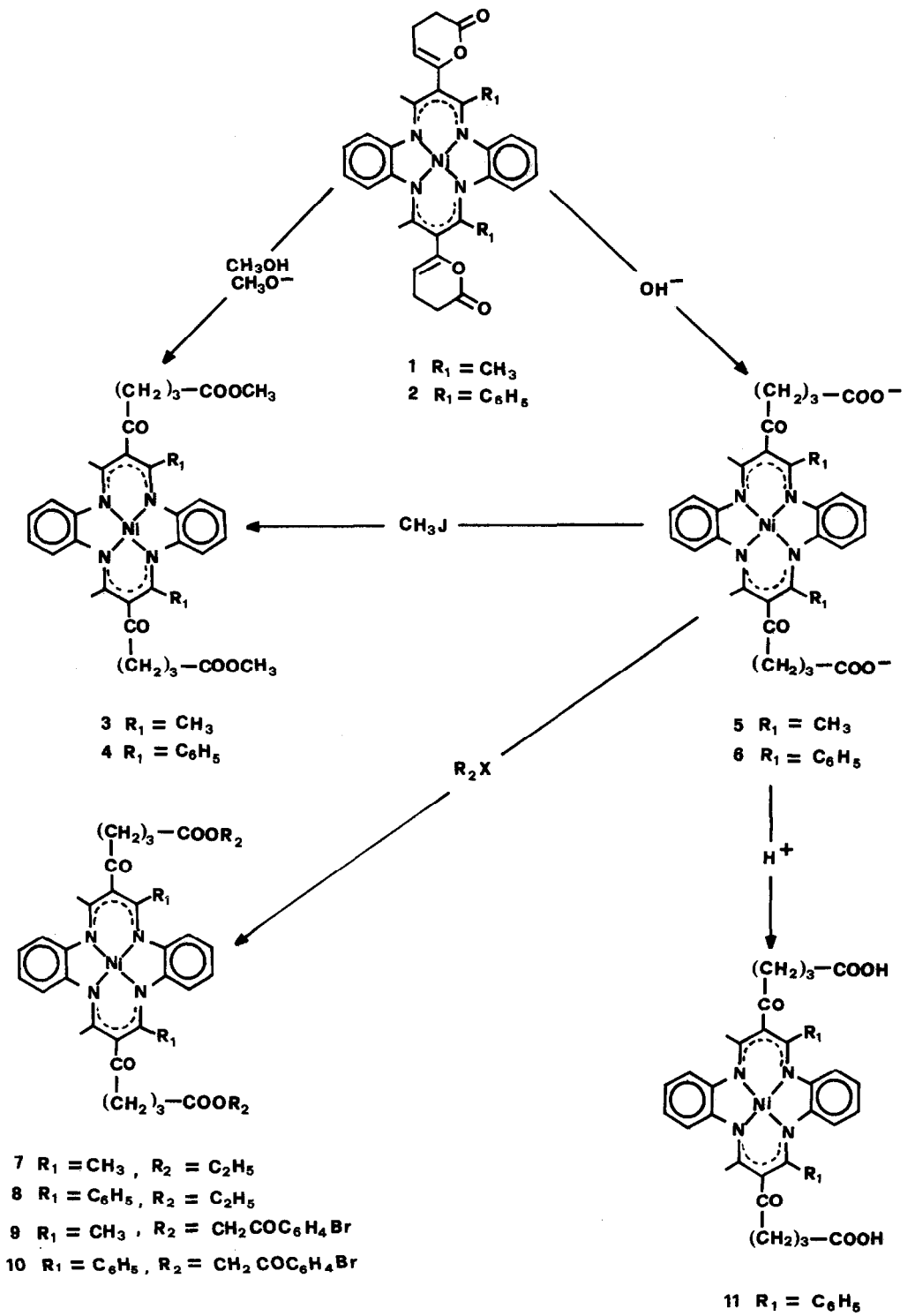

Scheme 1.

restrictions on the experimental conditions. Thus, the procedures involving the base catalysed opening of the lactonic rings have to be applied since the metal complexes of dibenzotetraaza[14]annulene are easily destroyed by aqueous acids.[4,5]

Furthermore, there is a high tendency for hydrolytic deacylation[6,7] which must be taken into account. This tendency is markedly influenced by the nature of the substituents and by the steric conditions on the ligand periphery.

The isolation of a free acid from its alkali salt, **5** by means of the usual procedure was not possible and resulted only in the loss of the γ,γ'-substituents. On the contrary, the same method was successfully applied to product **6**, affording the corresponding acid **11**.

EXPERIMENTAL

Melting points are uncorrected. IR spectra were recorded in Nujol and hexachlorobutadiene on a Zeiss UR-10 spectrometer. ^{1}H NMR spectra were taken on a Tesla BS 567A, 100 MHz instrument. Mass spectra were taken on a Jeol D-100 instrument.

Methanolysis of the γ,δ-unsaturated-δ-lactonic rings

1 g (1.5 mmol) of complex **1** was added to a methanolic solution of sodium methoxide prepared from anhydrous methanol (50 cm^3) and sodium metal (0.23 g, 0.01 mol). The reaction mixture was heated under gentle reflux for 30 min then left at room temperature. A green crystalline material was filtered off, washed carefully with methanol and recrystallized from *n*-butanol.

Products **3** and **4** were synthesized in this manner in 81 and 79% yields, respectively.

3 (*green needles*, m.p. 180°C). Found: C, 61.9; H, 5.9; N, 8.3. Calc. for $C_{34}H_{38}N_4O_6Ni$: C, 62.1; H, 5.8; N, 8.5%. MS: 656 (P^+ ^{58}Ni). IR (cm^{-1}): 1675s (νC=O keto), 1725s (νC=O ester). ^{1}H NMR ($CDCl_3$, δ (ppm)): [1.97(s) —CH_3, 2.0(m) —CH_2—CH_2—CH_2—] 16H, 2.45 (t, 4H) —CO—CH_2—CH_2—CH_2, 2.81 (t, 4H) —CH_2—COO, 3.69 (s, 6H) —$COOCH_3$, 6.63 (b.s., 8H) *o*-C_6H_4.

4 (*brown cubes*, m.p. 175°C). Found: C, 67.5; H, 5.3; N, 7.2%. Calc. for $C_{44}H_{42}N_4O_6Ni$: C, 67.6; H, 5.4; N, 7.2%. MS: 780 (P^+ ^{58}Ni). IR (cm^{-1}): 1670s, (νC=O keto), 1730s (νC=O ester). ^{1}H NMR ($CDCl_3$, δ (ppm)): 1.57 (m, 4H) —CH_2—CH_2—CH_2—, [2.0(m) —CH_2—CH_2—CH_2—, 2.11(s) —CH_3] 14H, 3.62 (s, 6H) —$COOCH_3$, 5.7 (mAA'BB', 4H) *o*-C_6H_4, 6.74 (m, 4H) *o*-C_6H_4, 7.32 (m, 10H) —C_6H_5.

Alkaline hydrolysis of the γ,δ-unsaturated lactonic rings

A reaction mixture consisting of the complex **1** (1 g, 1.5 mmol), potassium hydroxide (1.5 g), *n*-butanol (25 cm^3) was heated under reflux for 30 min. An abundant, green precipitate which appeared after cooling of the reaction mixture was filtered off, washed carefully with *n*-butanol and dried. The potassium salts, **5** and **6**, were obtained in this way in 85% yield. They were subjected to the alkylation procedure without further purification.

5 (*green powder*, m.p. 280°C). IR (cm^{-1}): 1655s (νC=O keto), 1555s (νasym.COO^-). ^{1}H NMR (methanol-d_4, δ (ppm)): [1.98(s) —CH_3, 2.0–2.25 (b.m.) —CO—CH_2—CH_2—] 20H, 2.87 (b.t., 4H) —CH_2—COO, 6.7 (m, AA'BB', 8H), *o*-C_6H_4.

6 (*green powder*, m.p. > 300°C). IR (cm^{-1}): 1660s (νC=O keto), 1555s (νasym.COO^-). ^{1}H NMR (methanol-d_4, δ (ppm)): [1.5–2.0 (b.m.) —CO—CH_2—CH_2—CH_2—, 2.1(s) —CH_3] 18H, 5.7 (m, AA'BB', 4H) *o*-C_6H_4, 6.8 (m, 4H) *o*-C_6H_4, 7.35 (m, 10H) —C_6H_5.

*Reaction of the potassium salt, **5**, with methyl and ethyl iodides*

An appropriate alkyl halide (10 cm^3) was added to a solution of product **5** (0.7 g, 1 mmol) in methanol (5 cm^3). The reaction mixture was allowed to reflux for 2 h, then the solvent and the reagent's excess were distilled off on a rotatory evaporator. A green solid was washed with water, dried and chromatographed on a column of silica gel (0.05–0.2 mm) with use of chloroform as eluent. The main green fraction afforded pure products **3** and **7**, respectively in 85 and 75% yields.

The same procedure was used for the preparation of the products **4** and **8**.

7 (*green powder*, m.p. 100°C). Found: C, 63.1; H, 6.0; N, 8.3. Calc. for $C_{36}H_{42}N_4O_6Ni$: C, 63.1; H, 6.2; N, 8.2%. MS: 684 (P^+ ^{58}Ni). IR (cm^{-1}): 1680s (νC=O keto), 1725s (νC=O ester). ^{1}H NMR ($CDCl_3$, δ (ppm)): 1.25 (t, 6H) —CH_2—CH_3, 2.0 (s, 12H) —CH_3, 2.2 (m, 4H) —CH_2—CH_2—CH_2—, 2.4 (t, 4H) —CO—CH_2—CH_2—CH_2, 2.75 (t, 4H) —CH_2—COO, 4.13 (q, 4H) —CH_2—CH_3, 6.6 (b.s., 8H) *o*-C_6H_4.

8 (*green powder*, m.p. 115°C). Found: C, 68.0; H, 5.5; N, 6.8. Calc. for $C_{46}H_{46}N_4O_6Ni$: C, 68.2; H, 5.7; N, 6.9%. MS: 808 (P^+ ^{58}Ni). IR (cm^{-1}): 1670s (νC=O keto), 1720s (νC=O ester). ^{1}H NMR ($CDCl_3$, δ (ppm)): 1.25 (t, 6H) —CH_2—CH_3, 1.6 (m, 4H) —CH_2—CH_2—CH_2—, 1.9 (m, 8H) —CH_2—CH_2—CH_2, 2.11 (s, 6H) —CH_3, 4.08 (q, 4H) —CH_2—CH_3, 5.70 (m, AA'BB', 4H) *o*-C_6H_4, 6.75 (m, 4H) *o*-C_6H_4, 7.32 (m, 10H) —C_6H_5.

*Reaction of the potassium salt, **5**, with p-bromophenacyl bromide*

p-Bromophenacyl bromide (0.28 g, 1 mmol) was added to a solution of the starting product **5** (0.35 g, 0.5 mmol) in methanol (15 cm^3). The reaction mixture was heated under reflux for 30 min. A green

solid material which precipitated after cooling was filtered off, washed with methanol and water. The crude product was chromatographed on a column of silica gel (0.05–0.2 mm) with the use of chloroform as eluent. The main green fraction gave pure product **9** in 88% yield.

The same procedure was used for the preparation of the product **10**.

9 (*green powder*, m.p. 210°C). Found: C, 56.1; H, 4.1; N, 5.3. Calc. for $C_{48}H_{44}N_4O_8Br_2Ni$: C, 56.3; H, 4.3; N, 5.5%. IR (cm^{-1}): 1675s (νC=O, CO—$(CH_2)_3$—), 1700s (νC=O, CO—C_6H_4Br), 1740s (νC=O ester). ^1H NMR ($CDCl_3$, δ (ppm)): [2.0(s) —CH_3, 2.1(m) —CH_2—CH_2—CH_2] 16H, 2.62 (t, 4H) —CO—CH_2—CH_2—CH_2, 2.89 (t, 4H) —CH_2—COO, 5.3 (s, 4H) —COO—CH_2—CO—, 6.6 (m, 8H) *o*-C_6H_4, 7.7 (m, 8H) *p*-C_6H_4Br.

10 (*green powder*, m.p. 150°C). Found: C, 60.3; H, 4.0; N, 4.4. Calc. for $C_{58}H_{48}N_4O_8Br_2Ni$: C, 60.7; H, 4.2; N, 4.9%. IR (cm^{-1}): 1675s (νC=O, CO—$(CH_2)_3$—), 1700s (νC=O, CO—C_6H_4Br), 1740s (νC=O ester). ^1H NMR ($CDCl_3$, δ (ppm)): 1.6 (m, 4H) —CH_2—CH_2—CH_2—, [2.0(m) —CH_2—CH_2—CH_2—, 2.12(s) —CH_3] 14H, 5.23 (s, 4H) —$COOCH_2$—CO—, 5.7 (m, AA'BB', 4H) *o*-C_6H_4, 6.75 (m, 4H) *o*-C_6H_4, 7.32 (m, 10H) —C_6H_5, 7.7 (m, 8H) *p*-C_6H_4Br.

Isolation of the acid **11**

A solution of salt **6** (1 g, 1.2 mmol) in water (25 cm^3) was acidified to pH 5 with dilute acetic acid. An abundant green precipitate that appeared in solution was filtered off and washed with water. A crude product was recrystallized from aqueous acetone. Yield 0.7 g (77%).

11 (*green powder*, m.p. 130°C). Found: C, 66.9; H, 5.0; N, 7.2. Calc. for $C_{42}H_{38}O_6N_4Ni$: C, 67.0; H, 5.1; N, 7.4%. MS: 752 (P^+ ^{58}Ni). IR (cm^{-1}): 1680s (νC=O keto), 1700s (νC=O carboxyl), 2500–2900m (νO—H). ^1H NMR ($CDCl_3$, δ (ppm)): 1.5 (m, 4H) —CH_2—CH_2—CH_2—, 2.1 (s, 6H) —CH_3, 2.5 (b.t, 4H) —CO—CH_2—CH_2—CH_2, 2.75 (t, 4H) —CH_2—COOH, 5.75 (m, AA'BB', 4H) *o*-C_6H_4, 6.75 (m, 4H) *o*-C_6H_4, 7.3 (m, 10H) —C_6H_5, 9.3 (b.s, 2H) —COOH.

Acknowledgement—This research was supported financially by the Committee of Chemical Sciences of the Polish Academy of Sciences.

REFERENCES

1. J. Eilmes, *Polyhedron* 1987, **6**, 423.
2. H. Kröper, *Methoden der Organischen Chemie (Houben–Weyl)*, Vol. 6, Part 2, p. 561. Georg Thieme Verlag, Stuttgart (1963).
3. Y. S. Rao, *Chem. Rev.* 1964, **64**, 353.
4. E. G. Jäger, *Z. Anorg. Allg. Chem.* 1969, **364**, 177.
5. E. G. Jäger, *Z. Chem.* 1964, **4**, 437.
6. C. J. Hipp and D. H. Busch, *J. Chem. Soc., Chem. Commun.* 1972, 737.
7. D. P. Riley and D. H. Busch, *Inorg. Synth.* 1978, **18**, 41.

Polyhedron Vol. 7, No. 21, pp. 2201–2204, 1988
Printed in Great Britain

0277–5387/88 $3.00+.00
© 1988 Pergamon Press plc

CONVERSION OF DIMOLYBDENUM TETRAACETATE TO $Mo_2Cl_4(Ph_2Ppy)_2$ AND $Mo_2(O_2CCH_3)_2(Ph_2Ppy)_2Cl_2$ [Ph_2Ppy = 2-(DIPHENYLPHOSPHINO)PYRIDINE]

F. ALBERT COTTON* and MAREK MATUSZ

Department of Chemistry and Laboratory for Molecular Structure and Bonding, Texas A&M University, College Station, TX 77843, U.S.A.

(*Received* 26 *March* 1988; *accepted* 9 *May* 1988)

Abstract—Dimolybdenum tetraacetate reacts with $(CH_3)_3SiCl$ and Ph_2Ppy [2-(diphenylphosphino)pyridine] to give green $Mo_2Cl_4(Ph_2Ppy)_2$ which was too insoluble to crystallize or characterize. The reaction of $Mo_2Cl_4(Ph_2Ppy)_2$ with acetic acid has been investigated. $Mo_2(O_2CCH_3)_4$ and $Mo_2(O_2CCH_3)_2(Ph_2Ppy)_2Cl_2$ are the products resulting from total and partial ligand substitution reactions. The molecular structure of $Mo_2(O_2CCH_3)_2(Ph_2Ppy)_2Cl_2$ has been investigated by X-ray crystallography. The crystallographic data are as follows: triclinic space group $P\bar{1}$, $a = 10.789(2)$, $b = 12.414(3)$, $c = 9.888(2)$ Å, $\alpha = 110.48(2)°$, $\beta = 113.86(2)°$, $\gamma = 67.36(3)°$, $V = 1088(1)$ Å^3 and $Z = 1$. The molecule has two *trans* bridging acetate groups, two *trans* 2-diphenylphosphinopyridine ligands arranged in a head-to-tail fashion, and two axial chlorine atoms. The length of the quadruple bond between the molybdenum atoms is 2.1900(3) Å, which makes it the longest one known.

Among all the transition elements forming multiple bonds, molybdenum has been a centre of interest[1] due to the ease of formation and stability during substitution reactions. In this work we began with the objective of extending our knowledge of the series of $Mo_2X_4(LL)_4$ type compounds by studying in more detail, $Mo_2Cl_4(Ph_2Ppy)_2$. However, we soon confirmed the earlier brief note[2] concerning this compound, namely, that it is extremely insoluble and does not lend itself to classical chemical studies. We therefore explored its reactivity and can report in detail the reaction with acetic acid to produce $Mo_2(O_2CCH_3)_2(Ph_2Ppy)_2Cl_2$ as well as the structure and properties of the latter.

EXPERIMENTAL

Preparation of $Mo_2Cl_4(Ph_2Ppy)_2$

Dimolybdenum tetraacetate (0.428 g, 1 mmol), 2-diphenylphosphinopyridine (0.553 g, 2.1 mmol), $(CH_3)_3SiCl$ (0.63 cm^3, 5 mmol) and 15 cm^3 of THF were refluxed for 24 h. During this time a green precipitate of $Mo_2Cl_4(Ph_2Ppy)_2$ was deposited. It was filtered, washed with THF and vacuum dried. The yield was usually better than 90%. $Mo_2Cl_4(Ph_2Ppy)_2$ is virtually insoluble in all common solvents. While it is sparingly soluble in CH_2Cl_2 to give a green solution over a period of several hours this changes colour to red.

Preparation of $Mo_2(O_2CCH_3)_2(Ph_2Ppy)_2Cl_2$

Freshly prepared $Mo_2Cl_4(Ph_2Ppy)_2$ (0.46 g, 0.58 mmol) was suspended in 15 cm^3 of acetic acid. The reaction mixture was stirred and refluxed for 18 h. It was cooled and filtered to give pale yellow crystals (0.13 g) and a red solution. The solution was evaporated to dryness and extracted with CH_2Cl_2. The red CH_2Cl_2 solution was layered with hexane and a crop of green crystals was collected in a few days. Yield 0.2 g (60% based upon recovered Mo). Upon removal from the mother liquor these crystals lose interstitial solvent. Electronic spectrum, CH_2Cl_2 solvent: $\lambda = 580$ nm, $\lambda = 500$ nm (sh). The yellow

* Author to whom correspondence should be addressed.

Table 1. Crystal data for $Mo_2(Ph_2Ppy)_2(OAc)_2Cl_2 \cdot 2CH_2Cl_2$

Formula	$Mo_2Cl_6P_2O_4C_{40}H_{38}$
Formula weight	1077.31
Space group	$P\bar{1}$
Systematic absences	
a (Å)	10.789(2)
b (Å)	12.414(3)
c (Å)	9.888(2)
α (deg.)	110.48(2)
β (deg.)	113.86(2)
γ (deg.)	67.36(3)
V (Å^3)	1088(1)
Z	1
d_{calc} (g cm^{-3})	1.394
Crystal size (mm)	0.5 × 0.3 × 0.3
μ(Mo-K_α) (cm^{-1})	7.945
Data collection instrument	CAD-4S
Radiation (monochromated in incident beam)	Mo-K_α ($\lambda_\alpha^- = 0.71073$ Å)
Orientation reflections, number, range (2θ)	25, $2\theta > 20°$
Temperature (°C)	22
Scan method	ω–2θ
Data col. range (2θ deg)	4, 50
No. unique data, total with $F_o^2 > 3\sigma(F_o^2)$	4767, 4511
Number of parameters refined	253
Trans. factors, max., min.	1.0815, 0.787
R^a	0.0496
R_w^b	0.07401
Quality-of-fit indicator^c	2.47
Largest shift/esd, final cycle	0.03
Largest peak (e Å^{-3})	1.84

[a] $R = \Sigma ||F_o| - |F_c|| / \Sigma |F_o|$.
[b] $R_w = [\Sigma w(|F_o| - |F_c|)^2 / \Sigma w|F_o|^2]^{1/2}$; $w = 1/\sigma^2(|F_o|)$.
[c] Quality-of-fit = $[\Sigma w(|F_o| - |F_c|)^2 / (N_{obs} - N_{parameters})]^{1/2}$.

crystals have been identified as $Mo_2(O_2CCH_3)_4$, by comparison of the IR spectrum with that of an authentic sample.

X-ray crystallography

A red crystal with approximate dimensions 0.5 × 0.3 × 0.3 mm was glued inside a glass capillary filled with a mineral oil–mother liquor mixture (5 : 1). The preliminary search and indexing revealed a triclinic cell. The axial lengths were confirmed with oscillation photographs. Data were processed with procedures routine to our Laboratory.[2] Lorentz and polarization corrections were applied. Three standard reflections monitored after every hour of data collection did not show any significant changes in intensity. An absorption correction was applied based on psi scans with the χ angle near 90°. The structure was solved with the direct methods package of SHELXS-86. Refinement in space group $P\bar{1}$ proceeded routinely.* Pertinent crystallographic data are summarized in Table 1.†

RESULTS AND DISCUSSION

$Mo_2Cl_4(PP)_2$ (where X = Cl, Br, I, PP = diphosphine) have been intensively studied in the past

*Calculations were done on a Micro VAXII with a SDP package software.

†Atomic positional and thermal parameters, full lists of bond lengths and angles and F_o/F_c values have been deposited as supplementary material with the Editor, from whom copies are available on request. Atomic coordinates have also been deposited with the Cambridge Crystallographic Data Centre.

$$Mo_2(O_2CCH_3)_4 \xrightarrow[Ph_2Ppy]{(CH_3)_3SiCl} Mo_2Cl_4(Ph_2Ppy)_2$$

$$\uparrow \qquad\qquad \downarrow CH_3COOH$$

$$Mo_2(O_2CCH_3)_2(Ph_2Ppy)_2Cl_2$$

Scheme 1.

few years. This class of compounds has been used to derive the relationship between metal–metal bond strength and the torsional angle.[3] We decided to study the molecular geometry of $Mo_2Cl_4(Ph_2Ppy)_2$ and compare it with diphosphine complexes. The complex was prepared according to the reaction:

$$Mo_2(O_2CCH_3)_4 + 4(CH_3)_3SiCl + 2Ph_2Ppy \rightarrow Mo_2Cl_4(Ph_2Ppy)_2 + 4(CH_3)_3SiO_2CCH_3.$$

It was isolated in a good yield, as a green microcrystalline powder, but attempts to grow single crystals suitable for X-ray diffraction studies have been futile so far due to the insoluble nature of the compound. CH_2Cl_2 is the only solvent we have found that will dissolve $Mo_2Cl_4(Ph_2Ppy)_2$, but the initially green solution quickly turns red, and no crystalline material could be isolated. We next turned our attention to the reactivity of $Mo_2Cl_4(Ph_2Ppy)_2$. When its suspension in acetic acid is refluxed, the mixture turns red and two products are isolated according to Scheme 1. They are $Mo_2(O_2CCH_3)_4$, which was identified by comparison with an authentic sample and $Mo_2(O_2CCH_3)_2(Ph_2Ppy)_2Cl_2$.

Reactions of $Mo_2X_4(PR_3)_4$ compounds with carboxylic acids have been investigated before[4,5] and the products isolated for monodentate phosphines characteristically have the stoichiometry $Mo_2X_2(O_2CCR')_2(PR_3)_2$. These compounds can also be prepared by a direct reaction of $Mo_2(O_2CCH_3)_4$ with phosphine in the presence of Me_3SiCl.[6,7] Corresponding reactions with bidentate phosphines have not been studied. The stoichiometry and geometry of our compound are novel, but not surprising. With two bridging acetate groups and two phosphinopyridine ligands, which prefer a bridging rather than a dangling mode of coordination, the remaining two chloride ligands are forced into axial positions. We have also investigated the reaction of $Mo_2Cl_4(dppm)_2$ with acetic acid, but we could not isolate any crystalline products. Quite possibly with this bulkier diphosphine there is not enough room for the axial coordination of chloride ions and ionic species are formed.

The molecular structure of $Mo_2(O_2CCH_3)_2(Ph_2Ppy)_2Cl_2$ is shown in Fig. 1 and selected bond distances and angles are presented in Table 2. There are also two interstitial CH_2Cl_2 molecules per dimolybdenum unit; these make normal van der Waals contacts with the dimolybdenum molecule.

The dimolybdenum molecule resides on a crystallographic centre of inversion. The $Mo_2(O_2CCH_3)_2$ portion of the structure has dimensions comparable to those found in $Mo_2(O_2CR)_4$ molecules generally, except for the Mo—Mo distance, which will be discussed below. The rest of the structure shows distortions that are understandable from the unsymmetrical nature of the Ph_2Ppy ligands, which are in a head-to-tail relationship. As can be seen in Fig. 1, the short Mo—N distance with C(14) close to the region of axial coordination, together with the long Mo—P distance and the phenyl groups directed away from the axial region causes a displacement of the axial Cl atoms away from the "linear" axial site by *ca* 16.5°.

It may also be noted that the Mo—Cl distances are quite long in view of the fact that the $Mo_2(O_2CCH_3)_2(Ph_2Ppy)_2^{2+}$ unit to which Cl^- ions are bound is a dication. In the $[Mo_2(O_2CCF_3)_4X_2]^{2-}$ ions,[8] where X = Br and I, the Mo—X distances are 2.88 and 3.18 Å, respectively. Subtracting the pertinent differences in halogen radii, these would

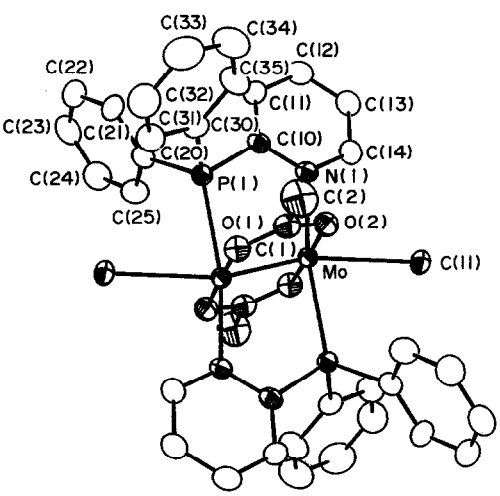

Fig. 1. ORTEP drawing of $Mo_2(O_2CCH_3)_2(Ph_2Ppy)_2Cl_2$ at 50% probability level. Only the unique part of the molecule is labelled.

Table 2. Selected bond distances in angstroms and angles in degrees for $Mo_2(O_2CCH_3)_2(Ph_2PPy)_2Cl_2 \cdot 2CH_2Cl_2$

Atom 1	Atom 2	Distance	Atom 1	Atom 2	Distance	Atom 1	Atom 2	Distance
Mo	Mo	2.1900(3)	Mo	O(2)	2.116(3)	O(2)	C(1)	1.263(4)
Mo	Cl(1)	2.7544(7)	Mo	N(1)	2.240(2)	N(1)	C(10)	1.351(3)
Mo	P(1)	2.5341(7)	P(1)	C(10)	1.844(3)	C(1)	C(2)	1.524(8)
Mo	O(1)	2.110(3)	O(1)	C(1)	1.269(4)			

Atom 1	Atom 2	Atom 3	Angle	Atom 1	Atom 2	Atom 3	Angle	Atom 1	Atom 2	Atom 3	Angle
Mo	Mo	Cl(1)	163.44(2)	Cl(1)	Mo	N(1)	88.94(6)	Mo	O(1)	C(1)	117.3(3)
Mo	Mo	P(1)	84.77(2)	P(1)	Mo	O(1)	86.42(6)	Mo	O(2)	C(1)	118.7(2)
Mo	Mo	O(1)	91.24(5)	P(1)	Mo	O(2)	96.63(6)	Mo	N(1)	C(10)	119.4(2)
Mo	Mo	O(2)	89.64(5)	P(1)	Mo	N(1)	165.72(8)	O(1)	C(1)	O(2)	122.9(4)
Mo	Mo	N(1)	107.54(6)	O(1)	Mo	O(2)	176.90(8)	O(1)	C(1)	C(2)	118.6(3)
Cl(1)	Mo	P(1)	79.12(2)	O(1)	Mo	N(1)	86.1(1)	O(2)	C(1)	C(2)	118.5(3)
Cl(1)	Mo	O(1)	91.54(6)	O(2)	Mo	N(1)	90.8(1)	P(1)	C(10)	N(1)	113.0(2)
Cl(1)	Mo	O(2)	88.46(6)	Mo	P(1)	C(10)	113.4(1)				

Numbers in parentheses are estimatd standard deviations in the least significant digits.

correspond to an Mo—Cl distance of *ca* 2.73 Å. Since in these cases X^- ions are approaching a neutral $Mo_2(O_2CCF_3)_4$ unit, one might have expected a shorter distance in the present case, but we actually find a distance of 2.75 Å.

In spite of the relative weakness of these axial Mo—Cl bonds, the Mo—Mo distance is remarkably long, 2.1900(3) Å. This is longer than any previously reported Mo—Mo quadruple bond distance, although only 0.01–0.02 Å longer than several others.[1]

Acknowledgement—We thank The National Science Foundation for financial support.

REFERENCES

1. (a) F. A. Cotton and R. A. Walton, *Multiple Bonds Between Metal Atoms*. John Wiley, New York (1982); (b) F. A. Cotton, Highlights of recent research on compounds with Mo—Mo bonds, *Polyhedron* 1986, **5**, 3.
2. T. J. Barder, F. A. Cotton, G. L. Powell, S. M. Tetrick and R. A. Walton, *J. Am. Chem. Soc.* 1984, **106**, 1323 (see footnote 34).
3. (a) F. L. Campbell, III, F. A. Cotton and G. L. Powell, *Inorg. Chem.* 1984, **23**, 4222; (b) F. A. Cotton, K. R. Dunbar and M. Matusz, *Inorg. Chem.* 1986, **25**, 3641.
4. J. San Filippo and H. J. Sniadoch, *Inorg. Chem.* 1976, **15**, 2209.
5. J. A. Potenza, R. J. Johnson and J. San Filippo, *Inorg. Chem.* 1976, **15**, 2215.
6. J. D. Arenivar, V. V. Mainz, H. Ruben and R. A. Anderson, *Inorg. Chem.* 1982, **21**, 2649.
7. (a) M. L. H. Green, G. Parkin, J. Bashkin, J. Fail and K. Prout, *J. Chem. Soc., Dalton Trans.* 1982, 2519; (b) F. A. Cotton and G. L. Powell, *Polyhedron* 1985, **4**, 1669.
8. F. A. Cotton and P. E. Fanwick, *Inorg. Chem.* 1983, **22**, 1327.

Polyhedron Vol. 7, No. 21, pp. 2205–2207, 1988
Printed in Great Britain

0277–5387/88 $3.00+.00
© 1988 Pergamon Press plc

A MODEL FOR THE NON-MOLECULAR STRUCTURES OF THE THIOLATES, MSR, OF COPPER AND SILVER

IAN G. DANCE

School of Chemistry, University of New South Wales, PO Box 1, Kensington, NSW 2033, Australia

(*Received* 25 *January* 1988; *accepted* 22 *April* 1988)

Abstract—A model for the unknown crystal structures of copper (and silver) thiolates, MSR, is derived from the known crystal structure of $Cu_8(SCMe_2Et)_4(S_2CSCMe_2Et)_4$ and other derivatives of MSR. The proposed structure is one-dimensionally non-molecular and tubular. Steric pressure between large substituents R contiguous along the chain could be accommodated with simple structural modifications, involving elongated secondary bonds and concomitant change of metal coordination from trigonal towards digonal. This results in either two intertwined infinite helical strands, or stacks of $M_4(SR)_4$ cycles along the chain, both of which are precedented structural functions.

One of the unanswered questions in the structural chemistry of metal thiolates is that of the structures of the insoluble compounds, CuSR, which are presumed to be non-molecular in structure.[1] No researchers in this field have been able to obtain crystals suitable for single crystal diffractometry, and relevant structural data have been obtained only from derivatives which have additional ligands and therefore are structurally molecular as a consequence of the higher ligand/Cu ratios. Crystal structures are known for homoleptic anionic molecular complexes $[Cu(SR)_3]^{2-}$ and $[Cu_4(SR)_6]^{2-}$,[1] for heteroligated phosphine derivatives $Cu_2(SPh)_2(PPh_3)_4$,[2] $Cu_3(SPh)_3(PPh_3)_4$,[3] $Cu_4(SPh)_4(PPh_3)_4$,[4] $Cu_4(SCMe_3)_4(PPh_3)_2$,[5] $Cu_4(SCMe_2Et)_4(dppm)_2$,[6] and for the product $Cu_8(SR)_4(S_2CSR)_4$ (**1**), R = CMe_2Et, of the reaction of CuSR with CS_2.[7] From all of these results it is fairly certain that the local coordination of Cu in CuSR will be digonal or trigonal.[1]

The structure of $AgSCMeEt_2$ is known to be one-dimensionally non-molecular with digonal coordination and doubly-bridging thiolate,[8] and in the case of AgSAr (Ar = C_6H_5, C_6H_4Cl-4) there is good evidence that a two-dimensionally non-molecular layer structure occurs with trigonal Ag coordination and triply-bridging thiolate.[9]

The crystal structure of (**1**) suggests a new one-dimensionally non-molecular model for the structures of compounds MSR, M = Cu, Ag. The purpose of this note is to analyse the structure of (**1**) and present the structural model.

RESULTS

As shown schematically in Fig. 1, the molecule of (**1**) is elongated, with the thiolate SR ligands around the equator, comprising a $Cu_4(SR)_4$ cycle [Cu(1)]. The thiolate ligands are in fact triply-bridging, due to connections to additional copper atoms [Cu(2)] at either end of the molecule. Trigonal coordination at all copper atoms is completed by the

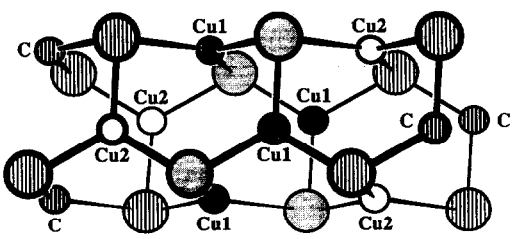

Fig. 1. Schematic representation of the core of the molecular structure of $Cu_8(SCMe_2Et)_4(S_2CSCMe_2Et)_4$ (**1**), with only the S_2C section of each thioxanthate ligand included. The Cu(1) and S atoms of the central $Cu_4(SR)_4$ cycle (shaded grey) are connected through the S atoms to another four Cu(2) atoms (open). Completion of the trigonal coordination at all Cu atoms is by the eight S atoms (vertical stripes) of four thioxanthate ligands at the ends of the molecule.

eight sulphur atoms of the thioxanthate ligands. The thioxanthate ligands terminate the elongated molecule, which has pseudo-S_4 axial symmetry. The constancy of the angles involving Cu, S, C in (1) is an indication of the structural stability of its core.

In this structure the positions of the thioxanthate donor S atoms correspond to the positions of the S atoms of triply-bridging thiolate ligands, translated along the axis of the molecule. If the thioxanthate S atoms are replaced by the donor S atoms of thiolate ligands, and metal atoms are introduced close to the thioxanthate carbon locations, the central $Cu_4(SR)_4$ cyclic portion of (1) is repeated by translation in both directions along the axis. Thus this construction leads to an extended linear chain structure, (2), shown in Fig. 2, in which all M atoms are trigonally coordinated and all thiolate ligands are triply-bridging. The M coordination planes in (2) lie in the faces of a square tube. The M—S—M angles, which are independent of M—S distances, are ideally 120, 90, 90°: in fact at the four independent triply-bridging thiolates in (1) one Cu—S—Cu angle is $120 \pm 0.4°$, one $88 \pm 2°$, and one $73 \pm 2°$. Cyclic moieties which are established in other copper and silver thiolate compounds occur also in (2): M_3S_3 cycles, as in $[Cu_4(SR)_6]^{2-}$, occur in the surface of the tube, and M_4S_4 rings in two different centrosymmetric conformations girdle the tube.

The substituents R project perpendicular to the tube axis, as portrayed in Fig. 2, with conventional stereochemistry at the sulphur atoms. Steric interference between substituents is most likely to occur along the edges of the tube, where substituents which are parallel to each other repeat at *ca* 4 Å for an M—S distance of 2.3 Å. There is precedent for substituents with this proximity, in the pairs of substituents axial to the $M_3(SR)_3$ chairs in the adamantanoid cages $[M_4(SR)_{10}]^{2-}$.[1] In these it is recognized[1] that where such an axial substituent pair occurs the enclosed S—M—S angle is widened from

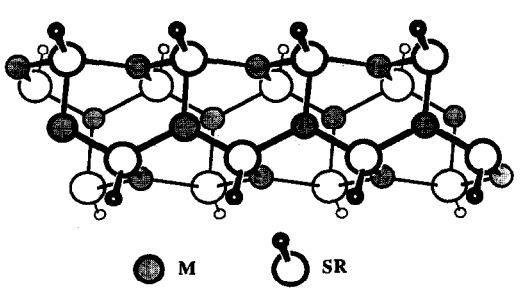

Fig. 2. Four repeat units of the linear chain structure (2). The smallest circles represent the α-carbon atoms of the substituents.

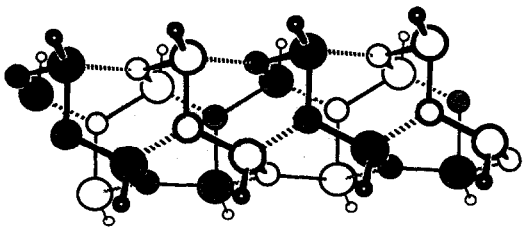

Fig. 3. An elongated modification of structure (2), in which one third of the M—S interactions (marked broken) are lengthened to secondary bonds, such that the primary bonds constitute two interwound strands, one of which is differentiated by grey circles. The S—M—S segments have not been linearized in this diagram.

the normal (tetrahedral) value. Structure (2) allows similar widening of the S—M—S angles along the edges of the tube, beyond 120°, with concomitant closing of the other two S—M—S angles in the faces of the tube. The precedents cited are with ethyl and phenyl groups,[1,10,11] and it is noted that tertiary thiolate ligands could require more than 4–4.5 Å as the repeat distance along the tube edges, as the van der Waals diameter of a methyl group is 3.4 Å. Structure type (2) is able to accommodate steric pressure of this type by elongation of one third of the M—S interactions to secondary bonds, with a concomitant adjustment of M coordination towards digonal stereochemistry.

This structural mechanism for chain elongation can occur in two different ways, shown in Figs 3 and 4. In one modification (see Fig. 3) the primary M—S bonds constitute two infinite strands, which are interwound but unconnected except for the secondary interactions. This arrangement is similar to the one-dimensionally non-molecular structure of crystalline $AgSCMeEt_2$,[8] in which there are two intertwined strands of linear segments but with the strands not connected even by secondary S---Ag bonds. The modification of (2) shown in Fig. 3 could be stretched even further to have non-bonding distances at the broken lines. In the second modification, Fig. 4, the primary bonds constitute $M_4(SR)_4$ cyclic molecules, stacked along the chain. There is precedent for the $Cu_4(SR)_4$ cycle in $Cu_4(SCMe_3)_4(PPh_3)_2$,[5] and for confacially stacked $Ag_4(SR)_4$ cycles in the crystal structure of $Ag_8(SCMeEt_2)_8(PPh_3)_2$.[12] Note that molecular $M_4(SR)_4$ cycles of a different conformation, but still stacked along the chain, could be formed from (2) with a different selection of M—S bonds to be elongated.

DISCUSSION

The analysis here echoes a recurring theme in the chemistry of metal–group 16 derivatives, namely

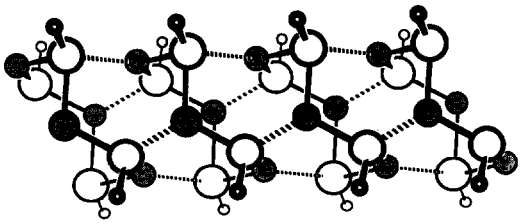

Fig. 4. Another elongated version of structure (**2**), in which one third of the M—S interactions (marked broken) are lengthened to secondary bonds, such that the primary connections constitute $M_4(SR)_4$ cycles. The S—M—S segments have not been linearized.

that the structures of polymetallic molecular aggregates are fragments of non-molecular structures, terminated with additional ligands.[1,13] Thus (**1**) is interpreted as a molecular fragment, capped by terminating hetero-ligands, of a proposed non-molecular structure (**2**). In this case the positions of the S donor atoms of the heteroligands are very close to those of the SR ligands in (**2**), and the C positions of the thioxanthates are close to the M positions of (**2**).

Acknowledgement—The financial support of this research by the Australian Research Grants Scheme is gratefully acknowledged.

REFERENCES

1. I. G. Dance, *Polyhedron* 1986, **5**, 1037.
2. I. G. Dance, P. J. Guerney, A. D. Rae and M. L. Scudder, *Inorg. Chem.* 1983, **22**, 2883.
3. I. G. Dance, L. J. Fitzpatrick and M. L. Scudder, *J. Chem. Soc., Chem. Commun.* 1983, 546.
4. I. G. Dance, L. J. Fitzpatrick and M. L. Scudder, *Inorg. Chem.* 1985, **24**, 2547.
5. I. G. Dance, L. J. Fitzpatrick and M. L. Scudder, to be published.
6. dppm = $Ph_2PCH_2PPh_2$: M. A. Khan, R. Kumar and D. G. Tuck, *Polyhedron* 1988, **7**, 49.
7. R. Chadha, R. Kumar and D. G. Tuck, *J. Chem. Soc., Chem. Commun.* 1986, 188. Atomic coordinates are available from the Cambridge Crystallographic Database.
8. I. G. Dance, L. J. Fitzpatrick, A. D. Rae and M. L. Scudder, *Inorg. Chem.* 1983, **22**, 3785.
9. I. G. Dance and H. R. M. Banda, to be published.
10. K. S. Hagen, D. W. Stephan and R. H. Holm, *Inorg. Chem.* 1982, **21**, 3928.
11. K. S. Hagen and R. H. Holm, *Inorg. Chem.* 1984, **23**, 418.
12. I. G. Dance, L. J. Fitzpatrick, M. L. Scudder and D. C. Craig, *J. Chem. Soc., Chem. Commun.* 1984, 17.
13. I. G. Dance, abstract 09.X-6, Fourteenth Int. Cong. Crystallography (Edited by H. C. Freeman) (August 1987); manuscript in preparation.

Polyhedron Vol. 7, No. 21, pp. 2209–2211, 1988
Printed in Great Britain

0277–5387/88 $3.00+.00
© 1988 Pergamon Press plc

COMMUNICATION

SYNTHESIS AND REACTIVITY OF FUNCTIONALIZED RHENIUM GERMYL COMPLEXES (η^5-C_5H_5)Re(NO)(PPh_3)($GePh_2X$); DYNAMIC EQUILIBRIA WITH GERMYLENE COMPLEX [(η^5-C_5H_5)Re(NO)(PPh_3)(=$GePh_2$)]$^+X^-$

KENNETH E. LEE and J. A. GLADYSZ*

Department of Chemistry, University of Utah, Salt Lake City, UT 84112, U.S.A.

(*Received* 20 *April* 1988; *accepted* 10 *June* 1988)

Abstract—Reaction of $Li^+[(\eta^5\text{-}C_5H_5)Re(NO)(PPh_3)]^-$ with Ph_3GeCl and Ph_2GeCl_2 (THF, −75°C) gives germyl complexes (η^5-C_5H_5)Re(NO)(PPh_3)($GePh_3$) (84%) and (η^5-C_5H_5)Re(NO)(PPh_3)($GePh_2Cl$) (**3**, 82%), respectively. Reaction of **3** and $(CH_3)_3SiOTf$ gives (η^5-C_5H_5)Re(NO)(PPh_3)($GePh_2OTf$) (**4**, 82%). Several properties show the triflate substituent in **4** to be extremely labile. First, reaction of **4** and pyridine to give [(η^5-C_5H_5)Re(NO)(PPh_3)($GePh_2NC_5H_5$)]$^+TfO^-$ (**5**) is complete in < 5 min at −78°C; the pyridine in **5** rapidly exchanges with pyridine-d_5 (CD_2Cl_2, −80°C). Second, the ^{13}C NMR resonances of the diastereotopic germanium phenyl substituents in **4** coalesce upon warming ($\Delta G^{\ddagger}_{268K}$ (CD_2Cl_2) = 12.6±0.2 kcal mol^{-1}). The most likely mechanisms for this dynamic behaviour entail initial triflate dissociation to give the germylene complex [(η^5-C_5H_5)Re(NO)(PPh_3)(=$GePh_2$)]$^+TfO^-$.

Metal complexes of unsaturated silicon, germanium, tin and lead containing ligands have been the focus of much recent attention.[1-2] We have previously demonstrated the ready availability of cationic chiral rhenium alkylidene complexes of the formula [(η^5-C_5H_5)Re(NO)(PPh_3)(=CHR)]$^+X^-$.[3,4] The rhenium fragment (η^5-C_5H_5)Re(NO)(PPh_3)$^+$ is a powerful π donor by virtue of the high-lying *d* orbital HOMO shown in **I** below (Scheme 1),[3d] and hence these alkylidene complexes exhibit some of the highest M=C double bond rotational barriers known (18–21 kcal mol^{-1}).[3a,c,d] Thus, we sought to probe the accessibility of analogous germylene complexes, [(η^5-C_5H_5)Re(NO)(PPh_3)(=GeR_2)]$^+X^-$. Neutral germylene complexes with bulky germanium substituents have been previously synthesized,[1] but cationic germylene complexes remain to our knowledge unknown. In this communication, we report the synthesis of functionalized germyl complexes (η^5-C_5H_5)Re(NO)(PPh_3)(GeR_2X), and dynamic NMR data that suggest facile equilibria with the corresponding germylene complexes.

The rhenium anion $Li^+[(\eta^5\text{-}C_5H_5)Re(NO)PPh_3)]^-$ (**1**) was generated in THF as previously described[5] and treated with germyl chloride Ph_3GeCl (1.5 equiv.) at −75°C (Scheme 1). Work-up gave the triphenylgermyl complex (η^5-C_5H_5)Re(NO)(PPh_3)($GePh_3$) (**2**) in 84% yield.† Next, anion **1** was similarly treated with dichloride Ph_2GeCl_2. The functionalized germyl complex (η^5-C_5H_5)Re(NO)(PPh_3)($GePh_2Cl$) (**3**) was isolated in 82% yield after work-up. Complex **3** and $(CH_3)_3SiOTf$[2a] were in turn reacted in CH_2Cl_2. Work-up gave the germyl complex (η^5-C_5H_5)Re(NO)(PPh_3)($GePh_2OTf$) (**4**) in 82% yield.

Several observations indicated the triflate substituent in germyl complex **4** to be extremely labile. First, addition of pyridine (2.0 equiv.) to **4** gave the pyridinium salt, [(η^5-C_5H_5)Re(NO)(PPh_3)($GePh_2NC_5H_5$)]$^+$ TfO^- (**5**), in 83% yield after

* Author to whom correspondence should be addressed.

† Reaction conditions, work-up procedures and product spectroscopic properties are similar to those recently described for related silyl complexes.[6]

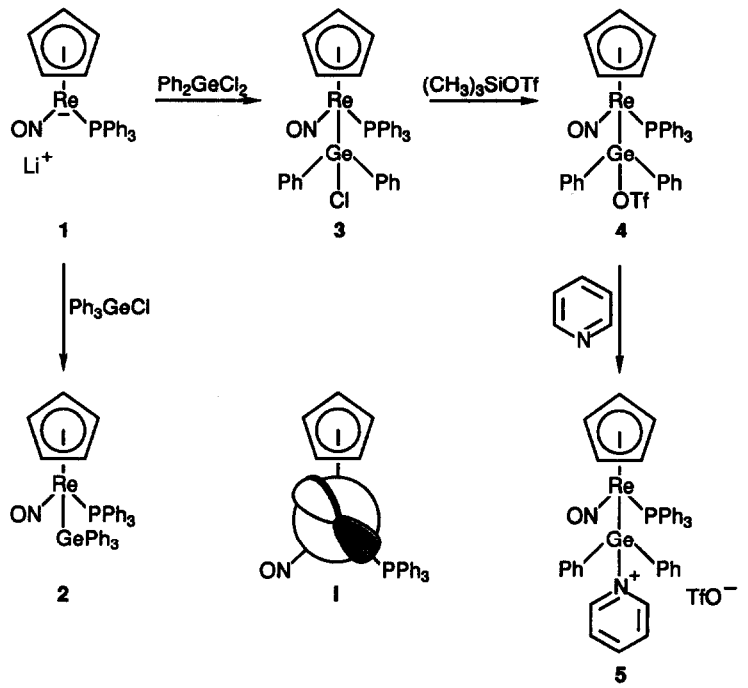

Scheme 1. Synthesis of functionalized germyl complexes.

work-up. We sought to determine the rate law for this transformation, and specifically the order in pyridine. However, reaction was complete in < 5 min at −78°C, as assayed by ^{31}P NMR monitoring. Similarly, pyridinium salt **5** (0.02 M in CD_2Cl_2) was treated with 2.5 equiv. of pyridine-d_5 at −80°C. Equilibration with **5**-d_5 was complete in < 5 min.

Germyl complexes **2**–**5** were characterized by microanalysis and by IR, and ^1H, ^{13}C and ^{31}P NMR spectroscopy, as described in supplementary material furnished to the reviewers.* IR $\nu(CF_3SO_3)$ (KBr, cm^{-1}, s) were noted for **4** (1331, 1234, 1200) and **5** (1271, 1224, 1150, 1045). The high frequency band of **5** was in a typical range for ionic triflates (1280–1270 cm^{-1}), whereas that of **4** was outside the typical range for covalent triflates (1395–1365 cm^{-1}).[7]

Importantly, germyl complexes **3** and **5** exhibited separate ^{13}C NMR resonances for the diastereotopic germanium–phenyl substituents in CD_2Cl_2 at room temperature (two *o*, *m*, *p*, *ipso*). However, triflate-substituted complex **4** showed dynamic behaviour. At lower temperatures, separate phenyl carbon resonances were observed as with **3** and **5**. However, these coalesced to a single set of resonances upon warming. The coalescence temperatures were determined from spectra recorded in 5°C increments, and differed for each type of carbon. Standard treatment of the data for the *ipso* carbons gave $\Delta G^{\ddagger}_{268K}$ (CD_2Cl_2) = 12.6±0.2 kcal mol^{-1} for the process equivalencing the phenyl groups.[8,9] The $\Delta G^{\ddagger}$ significantly increased in the less polar solvent chlorobenzene ($\Delta G^{\ddagger}_{323K}(C_6D_5Cl)$ = 15.3±0.2 kcal mol^{-1}).

What is the mechanism by which the diastereotopic phenyl groups of **4** are equivalenced? One possibility is to invoke the inversion of configuration at rhenium. However, analogous rhenium alkyl, phosphido, bromo and iodo complexes show good configurational stability.[4a,9,10] Hence, we conclude that a net inversion of configuration at germanium must occur. Accordingly, the most probable inversion mechanisms entail triflate anion dissociation to give the germylene complex, $[(\eta^5\text{-}C_5H_5)Re(NO)(PPh_3)(=GePh_2)]^+TfO^-$ (**6**), as shown in Scheme 2.[11] The Re=Ge conformation of **6** depicted is analogous to Re=C conformations found in corresponding alkylidene complexes.[3] Dissociation would be followed by either (1) Re=Ge bond rotation, and addition of triflate anion to the Re=Ge face *anti* to PPh_3, or (2) addition of the triflate anion to the Re=Ge face *syn* to PPh_3, and Re—Ge bond rotation (Scheme 2). Both mechanisms interconvert the diastereotopic phenyl groups, and account for the solvent polarity trend noted above. However, since nucleophiles preferentially attack the corresponding alkylidene complexes on the Re=C face *anti* to the bulky PPh_3 ligand,[3] we view the first possibility as more likely.

Importantly, the $\Delta G^{\ddagger}_{268K}$ (CD_2Cl_2) of 12.6 kcal

* See footnote † on previous page.

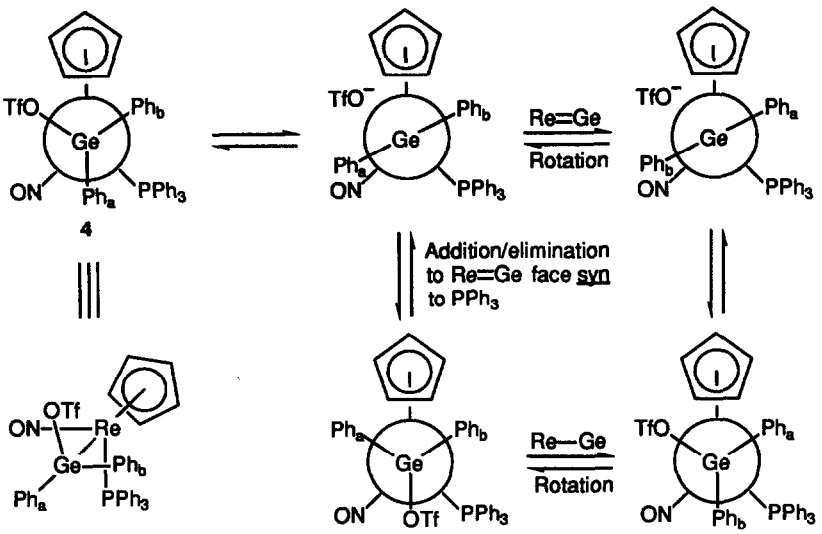

Scheme 2. Possible mechanisms for the equivalencing of diastereotopic phenyl groups Ph_a and Ph_b in germyl complex **4**.

mol^{-1} for the equivalencing of the diastereotopic phenyl groups of germyl complex **4** constitutes the *maximum* ΔG that can separate **4** from germylene complex **6** at 268 K. Since the Re=Ge bond rotational barrier could well contribute to this $\Delta G^{\ddagger}$, the actual ΔG between **4** and **6** may be much less. Hence, appropriate structural variants of **4** have a good chance of being thermodynamically unstable with respect to a germylene complex. Experiments designed to probe this possibility are in progress.

Acknowledgement—We thank the NSF for support of this research.

REFERENCES

1. W. Petz, *Chem. Rev.* 1986, **86**, 1019.
2. See, *inter alia*. (a) D. A. Straus, T. D. Tilley, A. L. Rheingold and S. Geib, *J. Am. Chem. Soc.* 1987, **109**, 5872; (b) C. Zybill and G. Müller, *Angew. Chem. Int. Ed. Engl.* 1987, **26**, 669.
3. (a) W. A. Kiel, G.-Y. Lin, A. G. Constable, F. B. McCormick, C. E. Strouse, O. Eisenstein and J. A. Gladysz, *J. Am. Chem. Soc.* 1982, **104**, 4865; (b) W. A. Kiel, G.-Y. Lin, G. S. Bodner and J. A. Gladysz, *J. Am. Chem. Soc.* 1983, **105**, 4958; (c) W. A. Kiel, W. E. Buhro and J. A. Gladysz, *Organometallics* 1984, **3**, 879; (d) S. Georgiou and J. A. Gladysz, *Tetrahedron* 1986, **42**, 1109; (e) E. J. O'Connor, M. Kobayashi, H. G. Floss and J. A. Gladysz, *J. Am. Chem. Soc.* 1987, **109**, 4837.
4. See also (a) J. H. Merrifield, G.-Y. Lin, W. A. Kiel and J. A. Gladysz, *J. Am. Chem. Soc.* 1983, **105**, 5811; (b) D. R. Senn, A. Wong, A. T. Patton, M. Marsi, C. E. Strouse and J. A. Gladysz, *J. Am. Chem. Soc.* 1988, **110**, in press.
5. (a) G. L. Crocco and J. A. Gladysz, *J. Chem. Soc., Chem. Commun.* 1985, 283; (b) G. L. Crocco and J. A. Gladysz, *J. Am. Chem. Soc.* 1988, **110**, in press.
6. G. L. Crocco, C. S. Young, K. E. Lee and J. A. Gladysz, *Organometallics* 1988, **7**, in press.
7. G. A. Lawrance, *Chem. Rev.* 1986, **86**, 17.
8. J. Sandström, *Dynamic NMR Spectroscopy*. Chap. 7. Academic Press, New York (1982).
9. W. E. Buhro, B. D. Zwick, S. Georgiou, J. P. Hutchinson and J. A. Gladysz, *J. Am. Chem. Soc.* 1988, **110**, 2427.
10. (a) J. H. Merrifield, C. E. Strouse and J. A. Gladysz, *Organometallics* 1982, **1**, 1204; (b) J. H. Merrifield, J. M. Fernández, W. E. Buhro and J. A. Gladysz, *Inorg. Chem.* 1984, **23**, 4022.
11. For other germanium inversion mechanisms, see F. Carré, R. Corriu and M. Leard, *J. Organomet. Chem.* 1970, **24**, 101.

Polyhedron Vol. 7, No. 21, pp. 2213–2216, 1988
Printed in Great Britain

0277–5387/88 $3.00+.00
© 1988 Pergamon Press plc

COMMUNICATION

X-RAY STRUCTURE OF A STERICALLY PROTECTED 1-AZA-3-PHOSPHA-ALLENE

MASAAKI YOSHIFUJI,* TAKASHI NIITSU, KOZO TOYOTA and NAOKI INAMOTO

Department of Chemistry, Faculty of Science, The University of Tokyo, Hongo, Tokyo 113, Japan

and

KEN HIROTSU,* YOSHIHIKO ODAGAKI and TAIICHI HIGUCHI

Department of Chemistry, Faculty of Science, Osaka City University, Sumiyoshi, Osaka 558, Japan

and

SHIGERU NAGASE*

Department of Chemistry, Faculty of Education, Yokohama National University, Hodogaya, Yokohama 240, Japan

(*Received* 11 *April* 1988; *accepted* 4 *July* 1988)

Abstract—Sterically protected 1-phenyl—(**1**) and 1-*t*-butyl—(**2**) 3-(2,4,6-tri-*t*-butylphenyl)-1-aza-3-phospha-allenes were prepared and the X-ray structure was determined for **1**; *ab initio* calculations were carried out for the parent compound, HP=C=NH.

We reported the preparation of 1-phenyl-3-(2,4,6-tri-*t*-butylphenyl)-1-aza-3-phospha-allene[1] as an unusual phosphorus compound stabilized by steric protection (see Scheme 1). The phosphorus atom involved is in a low coordination state and the molecule is of a hetero-cumulene type. However, there have been no reports on the X-ray structures of phosphacumulenes having high field chemical shifts in ^{31}P NMR.[1,2] In order to clarify this important feature, we have been very interested in the basic structure of this particular 1-aza-3-phosphacumulene (**1**).

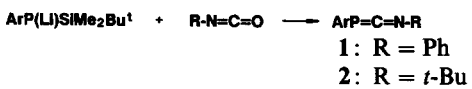

1: R = Ph
2: R = *t*-Bu

(Ar = 2,4,6-$Bu^t_3C_6H_2$)

Scheme 1.

EXPERIMENTAL

Compound **1** was prepared as described before and purified by column chromatography and recrystallization, and was subjected to X-ray analysis. The corresponding 1-alkyl-1-aza-3-phospha-allene (**2**) was obtained, using *t*-butyl isocyanate via the Peterson reaction, in 78% yield after column chromatographic separation (silica gel, pentane, 0°C). **2**: ^1H NMR ($CDCl_3$) 7.37 (d, $^4J_{PH}$ = 1.95 Hz, 2H, aromatic), 1.64 (s, 18H, *o*-Bu^t), 1.30 (s, 9H, *p*-Bu^t)

* Authors to whom correspondence should be addressed.

Table 1. Some physical and spectroscopic data for **1** and **2**

Compound	**1**	**2**
M.p. (°C)	90–92	166–168
IR ν(PCN) (cm^{-1})	1845	1885
^{31}P NMR ($CDCl_3$) δ(P)	−106.2	−101.9
^{13}C NMR ($CDCl_3$) δ(PCN) [$^1J_{PC}$(Hz)]	209.4 [27.4]	192.2 [76.2]
UV (hexane) $\lambda_{MAX}(\varepsilon)$(nm)	202 (73500)	203 (49600)
	257 (45100)	250sh (7200)
	286sh (14500)	291 (9600)
	412 (1410)	376 (490)

and 1.16 (s, 9H, N-Bu^t). Table 1 shows some important physical and spectroscopic data for **1** and **2**.

RESULTS AND DISCUSSION

Figure 1 is an ORTEP[3] drawing of the 1-aza-3-phospha-allene (**1**).* The P, C(1), N and C(2) are coplanar within 0.06 Å. This plane makes an angle of 22.7° with the phenyl group [C(2)—C(7)]. The C(8), P, C(1) and N are also coplanar within 0.06 Å and the interplanar angle between this plane and the former plane is 75.8° with the torsion angle of C(8)—P···N—C(2) = −102.2° (−90°), probably due to the steric repulsion of the phenyl group and one of the methyl groups of the *o*-*t*-butyl group C(24). The distance C(3)···C(24) is 3.762(5) Å and causes the torsion mentioned above. The latter plane (C(8), P, C(1), N) makes an angle of 87.4° with the 2,4,6-tri-*t*-butylphenyl ring. Thus the bulky phenyl group is almost perpendicular to the C(8)—P=C=N π system. The P—C(1) and C(1)—N bond distances are 1.651(3) and 1.209(4) Å, respectively. The bond angle P—C(1)—N is 171.1(2)° and the linearity is distorted in this direction to release the repulsion. The bond angle C(1)—P(1)—C(8) is 99.2(1)°.

The C=N bond lengths are 1.213 and 1.226 Å for bis(*p*-methoxyphenyl)carbodiimide,[6] and 1.204(4) and 1.223(5) Å for di-*p*-tolylcarbodiimide[7] and the carbodiimide systems deviate from a linear arrangement, i.e. the N=C=N bond angles are 169.0 and 170.4°, respectively. The cumulenic π-bond systems have a nearly perpendicular orientation, i.e. the torsion angles, C—N···N—C, are 87.9 and 88.0°, respectively. Karsch *et al.*[8] reported the X-ray structure of 1,3-bis(2,4,6-tri-*t*-butylphenyl)-1,3-diphospha-allene,[9] indicating that the P=C bond lengths are 1.635(8) and 1.630(8) Å with the bond angle for P=C=P of 172.6(5)° and the torsion angle of C—P···P—C being 83.0°. On the other hand, we reported the X-ray structures of some phospha-ethylenes, *E*-(**3**)[10] and *Z*-(**4**)[11] 1-(2,4,6-tri-*t*-butylphenyl)-2-phenyl-1-phospha-ethylenes, indicating that the bond lengths P=C are 1.660(6) Å for **3** and 1.674(2) Å for **4**. The bond length of P=C in ArP=C=CPh_2[12] is 1.625(4) Å with the bond angle P=C=C being 168.0(3)°.

There seems to be some contribution from a canonical form of the type **1A**, from the point of view of X-ray analysis and its ^{31}P NMR high field chemical shifts (see Scheme 2).

The slightly compressed C=N bond length and the elongated P=C bond length as well as deviating from a linear arrangement were confirmed by *ab initio* calculations of HP=C=NH. The calculations were carried out at the Hartree–Fock (HF) level with the split-valence 3-21 G,[13] and polarized 6-31 G(*d*), 6-31 G(*d*,*p*), and 6-31 G(2*d*,*p*) basis sets[14] for HP=C=NH. The optimized geo-

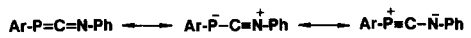

1 **1A** **1B**

Scheme 2.

* Reddish yellow crystal, 0.53 × 0.41 × 0.30 mm, from pentane solution. Crystal data: $C_{25}H_{34}NP$, M = 379.53, triclinic, space group $P\bar{1}$, a = 11.923(3), b = 11.253(2), c = 9.953(2) Å, α = 115.12(2), β = 91.15(2), γ = 75.26(2)°, U = 1163.4(5) Å^3, Z = 2, D_c = 1.08 g cm^{-3}, λ(Mo-K_α) = 0.7107 Å. Intensities of the 4126 reflections measured, of which 2988 were treated as observed in the refinement with ($I > 3\sigma(I)$). The structure was solved by direct methods.[4] The methyl groups on C(18) are disordered. The occupancy factors of two sets of three methyl carbons were refined to be 0.81 and 0.19. The methyl carbons with the lower occupancy are omitted from Fig. 1 for clarity. All H-atoms except for the disordered methyl hydrogens with low occupancy were located in difference syntheses and refined isotropically. Full-matrix least-squares refinement[5] carried out on F, when function minimized was $\Sigma w(|F_o| - |F_c|)^2$, $w = 1.0/[\sigma^2(F_o) + 0.01 \times F_o^2]$, led to convergence at R = 0.042. Fractional coordinates and temperature factors, bond distances and angles, and observed and calculated structure factors have been deposited with the Editor. Coordinates have also been deposited at the Cambridge Crystallographic Data Centre, University Chemical Laboratory, Lensfield, Cambridge, CB2 1EW, U.K.

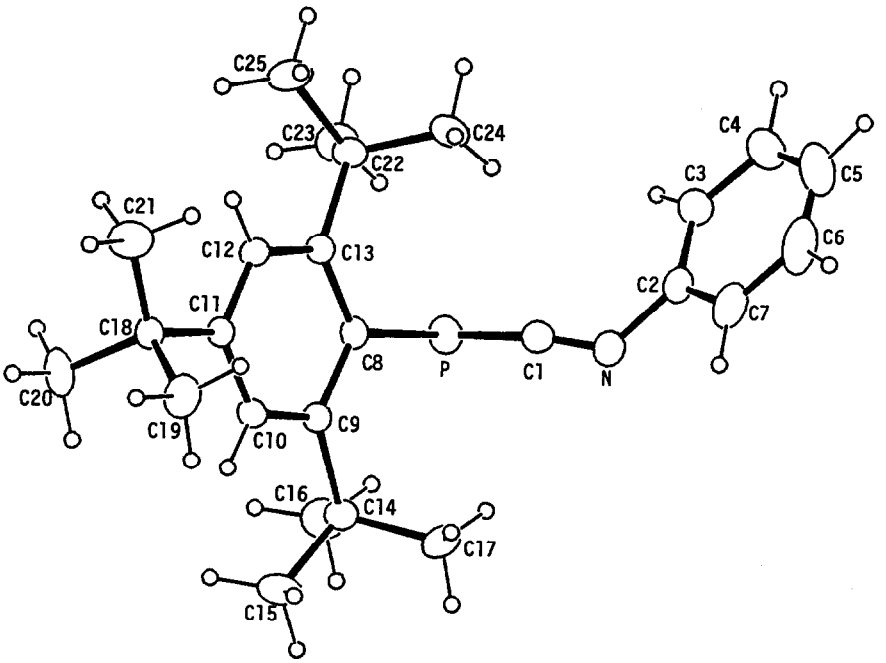

Fig. 1. ORTEP drawing of **1**.

Table 2. Geometries from *ab initio* calculation of HPCNH and X-ray crystallography of **1**

	3–21 G	4–31 G[a]	6–31 G(*d*)	6–31 G(*d,p*)	6–31 G(2*d,p*)	X-ray
Bond length (Å)						
PC	1.787	1.718	1.677	1.677	1.673	1.651
CN	1.153	1.180	1.193	1.192	1.191	1.209
PH[b]	1.435	1.448	1.406	1.408	1.406	
NH	0.983	0.990	1.003	1.002	1.003	
Bond angle (°)						
HPC	90.7	92.3	92.5	92.3	92.3	99.2[b]
PCN	176.7	175.8	174.9	175.0	174.8	171.1
HNC	179.5	140.0	121.9	122.0	120.1	130.5[b]
Dihedral angle (°)						
HPCN	−179.9	138.0	135.1	134.8	133.8	128[b]
HNCP	−4.3	131.6	135.2	135.5	136.5	134[b]
Twist angle (°)						
(H)P···N(H)	179.2	−92.8	−91.2	−91.1	−91.0	−102.2[b]
Atomic charge						
H(P)	−0.074	0.037	−0.029	−0.062	0.034	
P	0.204	−0.009	0.021	0.053	−0.151	
C	0.301	−0.062	0.208	0.217	0.167	
N	−0.879	−0.253	−0.610	−0.546	−0.379	
H(N)	0.448	0.286	0.411	0.338	0.328	
Total energy (au)						
	−431.89719	−433.58831	−434.13943	−434.14623	−434.15545	

[a] Data taken from ref. 13. Atomic charges are at the HF/DZP//4–31 G level.
[b] (H) should read *ipso*-carbon in the X-ray results for **1**.

metries are listed in Table 2 together with the results by Nguyen and Hegarty at the 4–31 G level.[15] The optimized structures are dependent on the basis-set used, and suggest that the contribution of the *d*-orbitals is fairly important in the P=C=N system. The structures optimized at higher levels in total are very similar to that observed for **1** by X-ray analysis. The small differences are probably due to the steric hindrance.

Acknowledgements—This work was supported in part by the Grant-in-Aid for Scientific Research (No. 62540371) from the Ministry of Education, Science and Culture, Japan. The authors thank the Crystallographic Centre, Institute for Protein Research at Osaka University for computer calculation. *Ab initio* calculations were carried out at the Computer Center of the Institute for Molecular Science using the GAUSSIAN 82 program.[16] We thank Shin-Etsu Chemical Co. Ltd, for donating organosilicon compounds and Toyo-Stauffer Chemical Co. Ltd, for organolithium reagents.

REFERENCES

1. M. Yoshifuji, K. Toyota, K. Shibayama and N. Inamoto, *Tetrahedron Lett.* 1984, **25**, 1809.
2. R. Appel and W. Paulen, *Angew. Chem., Int. Ed. Engl.* 1983, **22**, 785.
3. C. K. Johnson, ORTEP, Oak Ridge National Laboratory Report, ORNL-TM-3794. Oak Ridge, TN (1965).
4. G. Germain, P. Main and M. M. Woolfson, *Acta Cryst.* 1970, **B26**, 274.
5. W. R. Busing, K. O. Martin and H. A. Levy, A Fortran Crystallographic Least Squares Program, USAEC Report ORNL-TM-305. Oak Ridge National Laboratory, Oak Ridge, TN (1962).
6. H. Irngartinger and H.-U. Jäger, *Acta Cryst.* 1978, **B34**, 3262.
7. A. T. Vincent and P. J. Wheatley, *J. Chem. Soc., Perkin II* 1972, 687.
8. H. H. Karsch, H.-U. Reisacher and G. Müller, *Angew. Chem., Int. Ed. Engl.* 1984, **23**, 618.
9. M. Yoshifuji, N. Inamoto, K. Hirotsu and T. Higuchi, *J. Chem. Soc., Chem. Commun.* 1985, 1109.
10. M. Yoshifuji, K. Toyota, I. Matsuda, T. Niitsu, N. Inamoto, K. Hirotsu and T. Higuchi, *Tetrahedron* 1988, **44**, 1363.
11. M. Yoshifuji, K. Toyota, N. Inamoto, K. Hirotsu and T. Higuchi, *Tetrahedron Lett.* 1985, **26**, 6443.
12. M. Yoshifuji, K. Toyota, N. Inamoto, K. Hirotsu, T. Higuchi and S. Nagase, *Phosphorus Sulfur* 1985, **25**, 237.
13. M. S. Gordon, J. S. Binkley, J. A. Pople, W. J. Pietro and W. J. Hehre, *J. Am. Chem. Soc.* 1982, **104**, 2797.
14. M. M. Francl, W. J. Pietro, W. J. Hehre, J. S. Binkley, M. S. Gordon, D. J. DeFrees and J. A. Pople, *J. Chem. Phys.* 1982, **77**, 3654; M. J. Frisch, J. A. Pople and J. S. Binkley, *J. Chem. Phys.* 1984, **80**, 3265.
15. M. T. Nguyen and A. F. Hegarty, *J. Chem. Soc., Perkin II* 1985, 2005.
16. J. S. Binkley, M. J. Frisch, D. J. DeFrees, K. Rahgavachari, R. A. Whiteside, H. B. Schlegel, E. M. Fludre and J. A. Pople, GAUSSIAN 82 program. Department of Chemistry, Carnegie-Mellon University, Pittsburgh, PA, U.S.A.

Polyhedron Vol. 7, No. 21, pp. 2217–2219, 1988
Printed in Great Britain

0277-5387/88 $3.00+.00
© 1988 Pergamon Press plc

COMMUNICATION

CONVENIENT, HIGH YIELD SYNTHESES OF $[Nb(O)Cl_3]$, $[Nb(O)Cl_3(CH_3CN)_2]$ AND $[Nb(O)Cl_3(THF)_2]$. FORMATION AND DECOMPOSITION OF INTERMEDIATE ALKOXO (AND SILOXO) DERIVATIVES OF GENERAL FORMULA $[NbCl_4(OR)]_2$ (R = Me, Et, $SiMe_3$)

VERNON C. GIBSON,* TERENCE P. KEE and ALAN SHAW

Department of Chemistry, University Science Laboratories, South Road, Durham DH1 3LE, U.K.

(*Received* 16 *May* 1988; *accepted* 11 *July* 1988)

Abstract—Trimethylsilylaklylethers, Me_3SiOR (R = Me, Et) and hexamethyldisiloxane react with $NbCl_5$ in dichloromethane under ambient conditions to give readily isolable mono-alkoxides, $[NbCl_4(OR)]_2$ (R = Me, **1**; Et, **2**) and the thermally sensitive siloxide $[NbCl_4(OSiMe_3)]_2$ (**3**), respectively. At 80°C in 1,2-dichloroethane, **1–3** undergo efficient conversion to $[Nb(O)Cl_3]$ with elimination of RCl. In acetonitrile solution, the reaction of $NbCl_5$ with $(Me_3Si)_2O$ proceeds smoothly to give $[Nb(O)Cl_3(CH_3CN)_2]$ which is readily converted to $[Nb(O)Cl_3(THF)_2]$ upon dissolution in tetrahydrofuran (THF).

Oxychlorides of general formula $M(O)Cl_3$ are known for all three members of the group 5 triad.[1] While volatile $V(O)Cl_3$ is readily prepared by treatment of V_2O_5 with $SOCl_2$,[2] the heavier congeners have not proved accessible via this method or a similarly mild synthetic procedure. For example, established routes to niobium oxychloride include *inter alia* treatment of the pentahalide with Sb_2O_3 in a stream of gaseous chlorine,[3] the action of molecular oxygen on heated pentahalide,[4] or pyrolysis of the pentachloride diethyl ether adduct.[4]

Recently, we have reported a convenient, mild procedure for the controlled introduction of oxygen atoms into the coordination sphere of the heavier group 6 transition metals.[5] Here, we describe the extension of this methodology to the synthesis of $Nb(O)Cl_3$ via isolable mono-alkoxide intermediates, and the preparation of the solvent-stabilized monomers $[Nb(O)Cl_3(CH_3CN)_2]$ and $[Nb(O)Cl_3(THF)_2]$.

*Author to whom correspondence should be addressed.

EXPERIMENTAL

Solvents and reagents were dried and distilled prior to use, and all manipulations were carried out on a conventional inert gas/vacuum line, or in a dry box under an atmosphere of nitrogen. $(Me_3Si)_2O$ (Aldrich), Me_3SiOMe (Fluka) and Me_3SiOEt (Fluka) were distilled from P_2O_5 or dried over molecular sieves (4 Å) before use. $NbCl_5$ (Aldrich) was used as received. Elemental analyses were provided by the microanalytical service of this department. ^1H NMR spectra were recorded at 250 MHz on a Bruker AM 250 spectrometer. IR spectra (Nujol mulls between KBr or CsI plates) were recorded using Perkin–Elmer 577 and 457 spectrophotometers. Mass spectra were recorded on a VG 7070E mass spectrometer.

Synthesis of $[NbCl_4(OMe)]_2$ (1)

A dichloromethane solution of Me_3SiOMe (1.15 g, 11.1 mmol in 15 cm^3 of CH_2Cl_2) was added dropwise to a suspension of $NbCl_5$ (3 g, 11.1 mmol) in dichloromethane (20 cm^3) at room temperature.

The mixture was stirred for 2 h during which the $NbCl_5$ suspension reacted to give a colourless solution. Filtration, followed by concentration to half volume and cooling to −30°C afforded colourless crystals of $[NbCl_4(OMe)]_2$ (2.60 g, 88%). Found: Nb, 34.8; Cl, 53.2; C, 4.4; H, 0.99. Calc. for CH_3Cl_4NbO: Nb, 35.0; Cl, 53.4; C, 4.5; H, 1.14%. IR data (Nujol mull, cm^{-1}): 1140(w), 1060(s,br), 910(w), 865(w), 775(w), 735(w), 720(w), 595(m), 570(m), 390(m), 350(m). The CI^+ mass spectrum (isobutane carrier gas) gave molecular ions at *m/z* 532 and 215 corresponding to protonated $[NbCl_4(OMe)]_2$ and $Nb(O)Cl_3$, respectively. ^1H NMR (250 MHz, $CDCl_3$): δ 5.17 [singlet, CH_3].

Synthesis of $[NbCl_4(OEt)]_2$ **(2)**

A similar procedure to that described for $[NbCl_4(OMe)]_2$ may be used for the preparation of $[NbCl_4(OEt)]_2$ (yield 90%). Characterizing data: Found: Nb, 33.1; Cl, 50.2; C, 8.7; H, 1.9. Calc. for $C_2H_5Cl_4NbO$: Nb, 33.2; Cl, 50.7; C, 8.6; H, 1.8%. IR data (Nujol mull, cm^{-1}): 1350(m), 1265(m), 1135(sh), 1090(s), 1035(s,br), 945(s), 900(m,br), 835(m,br), 815(m,br), 580(m), 540(w), 490(w), 390(br). ^1H NMR (250 MHz, $CDCl_3$): δ 5.46 [q, $^3J_{HH}$ = 7.0 Hz, CH_2]; δ 1.76 [t, $^3J_{HH}$ = 7.0 Hz, CH_3].

Synthesis of $[Nb(O)Cl_3]$ **(4)**

A 1,2-dichloroethane solution of $(Me_3Si)_2O$ (1.8 g, 11.1 mmol in 15 cm^3 of $C_2H_4Cl_2$) was added to a suspension of $NbCl_5$ (3 g, 11.1 mmol) in dichloroethane (20 cm^3) at room temperature. The mixture was swiftly warmed to 80°C with stirring, and maintained at this temperature for 4.5 h. Dissolution of yellow $NbCl_5$ was accompanied by formation of a white granular precipitate. After cooling to room temperature, the supernatant solution was decanted from the white solid, which was collected, washed with light petroleum ether (b.p. 40–60°C, 2 × 20 cm^3) and dried *in vacuo* to yield 2.03 g (75%) of $Nb(O)Cl_3$. Found: Cl, 49.6; Nb, 43.3. Calc. for Cl_3NbO: Cl, 49.4; Nb, 43.2% (small amounts of residual Me_3SiO may lead to variable microanalytical data). IR data (Nujol mull, cm^{-1}): 780(s,br), ν(Nb—O—Nb).

Synthesis of $[Nb(O)Cl_3(CH_3CN)_2]$ **(5)**

An acetonitrile solution of $(Me_3Si)_2O$ (1.8 g, 11.1 mmol in 15 cm^3 of CH_3CN) was added dropwise at room temperature to a suspension of $NbCl_5$ (3 g, 11.1 mmol) in acetonitrile (20 cm^3). The mixture was stirred at room temperature for 2 h to give a colourless solution which was filtered, concentrated to half volume under reduced pressure and cooled to −30°C. The resultant colourless crystalline product was collected and dried *in vacuo* to yield $[Nb(O)Cl_3(CH_3CN)_2]$ (3.1 g, 95%). Found: C, 15.9; H, 2.1; N, 9.4. Calc. for $C_4H_6Cl_3N_2NbO$: C, 16.1; H, 2.0; N, 9.4%. IR data (Nujol mull, cm^{-1}): 960(s,br), ν(Nb=O).

Synthesis of $[Nb(O)Cl_3(THF)_2]$ **(6)**

Tetrahydrofuran (30 cm^3) was added to $[Nb(O)Cl_3(CH_3CN)_2]$ (0.53 g, 1.78 mmol) at −30°C. The mixture was warmed to room temperature with stirring to afford a colourless solution. After 15 min the mixture was filtered, concentrated to *ca* 5 cm^3 and cooled to −10°C. Addition of cold pentane (10 cm^3, −20°C) gave white crystals of $[Nb(O)Cl_3(THF)_2]$ (0.57 g, 90%). Found: C, 26.1; H, 4.4. Calc. for $C_8H_{16}Cl_3NbO_3$: C, 26.7; H, 4.4%. IR data (Nujol mull, cm^{-1}): 1348(m), 1300(w), 1250(m), 1180(m), 1037(w), 1046(m), 1015(s), 995(s), 960(s), 930(m), 920(m), 860(s,br), 833(s,br), 675(m), 578(w), 365(s,br), 326(s), 250(m).

RESULTS AND DISCUSSION

When niobium pentachloride is treated with equimolar amounts of Me_3SiOR (R = Me, Et, $SiMe_3$) in dichloromethane at room temperature, an immediate reaction ensues leading to dissolution of the starting halide. The resulting colourless or pale yellow solutions give rise to white, crystalline, thermally sensitive compounds of general formula $[NbCl_4(OR)]_2$ (R = Me, **1**; Et, **2**; $SiMe_3$, **3**) [eq. (1)], which are readily isolable for R = Me and Et. It has not proved possible to isolate **3** under ambient conditions without partial decomposition, due to its thermal sensitivity. However, the tantalum analogue of **3** is stable at room temperature and has been fully characterized.[6]

$$2NbCl_5 + 2Me_2SiOR \longrightarrow [NbCl_4(OR)]_2 + 2Me_2SiCl$$
$$(R = Me, \mathbf{1}; Et, \mathbf{2}; SiMe_3, \mathbf{3}). \quad (1)$$

Compounds **1** and **2** have been characterized by microanalysis, IR and NMR spectroscopies (see Experimental), and are formulated as dimeric species on the basis of low resolution CI^+ mass spectrometry (the solution instability of compounds **1**–**3** precluding accurate molecular weight determinations) and by analogy with the known edge-shared bi-octahedral geometry of $NbCl_5$.[7]

However, the available data do not allow us to distinguish unequivocally between alkoxo or halide bridges. Although it has been suggested that phenoxy bridges prevail in $[NbCl_4(OPh)]_2$,[8] this does not appear to be the case for **1** and **2**: IR spectra reveal bands assignable to ν(Nb—O) at 595 and 580 cm^{-1}, respectively, which are consistent with terminal alkoxo groups.[9] The chloro ligands are then presumed to occupy bridging sites. X-ray structural analyses are presently in progress to resolve these details.

The thermal instability of compounds **1–3** arises due to their facile decomposition to $Nb(O)Cl_3$ (**4**) with liberation of RCl [eq. (2)].

$$[NbCl_4(OR)]_2 \xrightarrow{80°C,\ C_2H_4Cl_2} 2Nb(O)Cl_3 + 2RCl$$
$$(R = Me, \mathbf{1}; Et, \mathbf{2}; SiMe_3, \mathbf{3}). \quad (2)$$

Of compounds **1–3**, **3** is the least stable, slowly releasing Me_3SiCl in solution at room temperature to give a white deposit of $Nb(O)Cl_3$. Similar, albeit slower, decomposition occurs in the solid state. The process proceeds swiftly in dichloroethane solution at 80°C affording a good yield of $Nb(O)Cl_3$ with only minor organic contamination due to residual trimethylsiloxy groups (these have not proved troublesome in subsequent transformations). Indeed, the treatment of $NbCl_5$ with $(Me_3Si)_2O$ at an elevated temperature allows the preparation of $[Nb(O)Cl_3]$ directly according to eq. (3). In addition, when $NbCl_5$ is reacted with $(Me_3Si)_2O$ at room temperature in CH_3CN, the previously reported acetonitrile adduct, $[Nb(O)Cl_3(CH_3CN)_2]$[10] (**5**) is obtained in 95% yield [eq. (4)]. This "one-pot", room temperature procedure offers a considerable improvement over the previously available method.[10]

$$NbCl_5 + (Me_3Si)_2O \xrightarrow{80°C,\ C_2H_4Cl_2} [Nb(O)Cl_3] + 2Me_3SiCl \quad (3)$$

$$NbCl_5 + (Me_3Si)_2O \xrightarrow{CH_3CN(s),\ RT,\ 2\,h} [Nb(O)Cl_3(CH_3CN)_2] + 2Me_3SiCl. \quad (4)$$

However, analogous treatment of $NbCl_5$ with $(Me_3Si)_2O$ in THF does not afford $[Nb(O)Cl_3(THF)_2]$ (**6**) cleanly. Instead, **6** is readily isolated in 90% yield by dissolution of **5** in THF [eq. (5)].

$$[Nb(O)Cl_3(CH_3CN)_2] \xrightarrow{THF(s),\ 15\,min} [Nb(O)Cl_3(THF)_2] + 2CH_3CN. \quad (5)$$

In summary, the treatment of $NbCl_5$ with silylated ethers offers convenient, high yield syntheses of mono-alkoxide niobium derivatives, and either base-free or solvent-stabilized $[Nb(O)Cl_3]$. We are particularly interested in utilizing the oxyhalide derivatives as precursors to oxo complexes of niobium. In preliminary investigations, a number of tertiary phosphine and alkoxide niobium oxo derivatives have been prepared which will be reported separately.

Acknowledgements—We thank the S.E.R.C. for a grant (to V.C.G.) and studentships (to T.P.K. and A.S.).

REFERENCES

1. R. A. Walton, *Prog. Inorg. Chem.* 1972, **16**, 135.
2. H. Hecht, G. Jander and H. Schlapmann, *Z. Anorg. Chem.* 1947, **254**, 255.
3. C. Djordijevic and V. Katovic, *J. Inorg. Nucl. Chem.* 1963, **25**, 1099.
4. A. H. Cowley, F. Fairbrother and N. Scott, *J. Less-Common Metals* 1959, **1**, 206.
5. V. C. Gibson, T. P. Kee and A. Shaw, *Polyhedron* 1988, **7**, 579.
6. T. P. Kee and V. C. Gibson, unpublished results.
7. D. L. Kepert, *The Early Transition Metals*. Academic Press, London (1972).
8. K. C. Malhotra, U. K. Banerjee and S. C. Chandry, *S. Ind. Chem. Soc.* 1980, **57**, 868.
9. R. J. H. Clark, *Spectrochim. Acta* 1965, **21**, 955.
10. C. Chavant, J. C. Daran, Y. Jeannin, G. Constant and R. Morancho, *Acta Cryst., Sect. B* 1975, **31**, 1828.

Polyhedron Vol. 7, No. 21, pp. 2221–2223, 1988
Printed in Great Britain

0277–5387/88 $3.00+.00
© 1988 Pergamon Press plc

COMMUNICATION

SYNTHESIS AND X-RAY STRUCTURAL CHARACTERIZATION OF THE SEVEN-COORDINATE NIOBIUM OXO COMPLEX, $[Nb(O)Cl_3(PMe_3)_3]$; THE FIRST TERTIARY PHOSPHINE ADDUCT OF $Nb(O)Cl_3$

VERNON C. GIBSON,* TERENCE P. KEE and ROBERT M. SORRELL

Department of Chemistry, University Science Laboratories, South Road, Durham DH1 3LE, U.K.

and

ALAN P. BASHALL and MARY McPARTLIN*

School of Chemistry, The Polytechnic of North London, London N7 8DB, U.K.

(*Received* 16 *May* 1988; *accepted* 11 *July* 1988)

Abstract—Treatment of $Nb(O)Cl_3$ with three equivalents of trimethylphosphine in dichloromethane affords the seven-coordinate niobium oxo complex, $[Nb(O)Cl_3(PMe_3)_3]$ in 80% yield. The crystals are monoclinic, space group $P2_1/c$ with unit cell parameters $a = 15.250(3)$, $b = 11.131(2)$, $c = 11.673(3)$ Å, $\beta = 93.61(2)°$, $U = 1977.54$ Å^3 and $Z = 4$. The niobium coordination geometry is distorted mono-capped octahedral with the oxo group capping the face defined by the trimethylphosphine ligands.

A diverse array of oxo species are involved in laboratory, industrial and biological oxidation processes,[1] ranging from discrete mononuclear oxo complexes through to high nuclearity polyoxoanions, complex enzymes and extended metal oxide lattices. An interest in delineating the factors surrounding the reactivity of metal-bound oxygen atoms has led us to investigate routes to new oxo complexes of the transition metals. In this respect, the convenient synthetic procedure for the preparation of transition metal oxyhalides exploiting reactions between silyl ethers and metal halides[2] has enabled us to prepare mononuclear oxo complexes of niobium for which very little derivative chemistry has been reported. The solid-state structure of $Nb(O)Cl_3$ has previously been shown to consist of an extended chain of Nb_2Cl_6 units linked by oxo bridges.[3] In an attempt to prepare low nuclearity derivatives, we are investigating its reactivity towards tertiary phosphines since the ability of strong donor ligands to break up oxo and halide bridges is well precedented.[4]

The reaction of $Nb(O)Cl_3$ with three equivalents of trimethylphosphine in dichloromethane solvent leads to dissolution of the sparingly soluble oxyhalide over a period of 3 h to give a translucent yellow–green solution. Upon removal of solvent, a yellow, air-sensitive, microcrystalline solid is obtained which is moderately soluble towards aromatic solvent. Indeed, large yellow prisms are formed upon slow cooling of a saturated toluene solution to −35°C.

Microanalytical and NMR data indicate a trisphosphine adduct of $Nb(O)Cl_3$ with the trimethylphosphine ligands occupying equivalent solution environments: the ^1H NMR spectrum (250 MHz) in $CDCl_3$ gives a doublet at δ 1.43 ($J_{PH} = 8.6$ Hz) due to the phosphine methyl hydrogens while the $^{31}P\{^1H\}$ NMR spectrum shows a singlet at δ

*Authors to whom correspondence should be addressed.

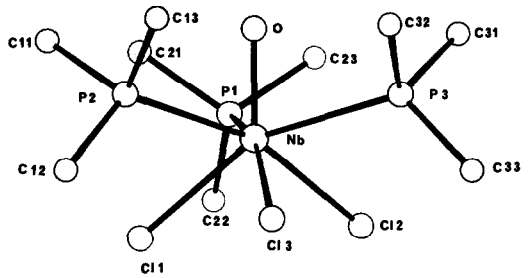

Fig. 1. The molecular structure of $[Nb(O)Cl_3(PMe_3)_3]$ showing the atom labelling; bond lengths (Å): Nb—O 1.781(6), Nb—Cl(1) 2.516(3), Nb—Cl(2) 2.533(3), Nb—Cl(3) 2.505(3), Nb—P(1) 2.642(3), Nb—P(2) 2.633(3), Nb—P(3) 2.645(3); important bond angles (°): O—Nb—Cl(1) 127.8(2), O—Nb—Cl(2) 121.2(2), O—Nb—Cl(3) 126.0(2), O—Nb—P(1) 76.9(2), O—Nb—P(2) 76.4(2), O—Nb—P(3) 76.3(2), Cl(2)—Nb—Cl(1) 90.9(1), Cl(3)—Nb—Cl(1) 88.0(1), Cl(3)—Nb—Cl(2) 92.3(1), P(1)—Nb—Cl(1) 75.3, P(1)—Nb—Cl(2) 161.9(1), P(1)—Nb—Cl(3) 75.8(1), P(2)—Nb—Cl(1) 75.0(1), P(2)—Nb—Cl(2) 73.8(1), P(2)—Nb—Cl(3) 157.6(1), P(2)—Nb—P(1) 112.7(1), P(3)—Nb—Cl(1) 155.9(1), P(3)—Nb—Cl(2) 74.0(1), P(3)—Nb—Cl(3) 74.3(1), P(3)—Nb—P(1) 114.5(1), P(3)—Nb—P(2) 116.9(1).

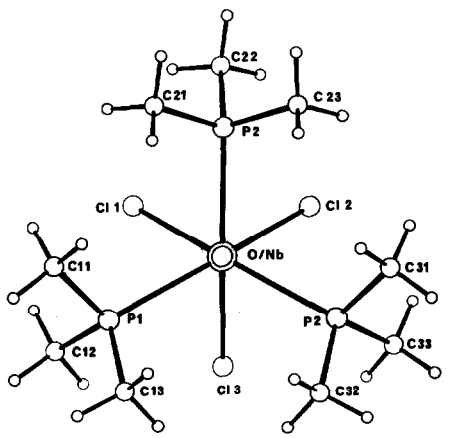

Fig. 2. A view of the molecule down the O—Nb bond showing the virtual C_{3v} symmetry.

−2.64. In addition, a sharp metal oxo stretch is observed at 882 cm^{-1} in the IR spectrum confirming the presence of a terminal oxo ligand.[5]

X-ray structure analysis of $[Nb(O)Cl_3(PMe_3)_3]$* (**1**) shows that the coordination may be described as distorted mono-capped octahedral (Fig. 1) with facial arrangements of chloro and trimethylphosphine ligands, giving the molecule virtual C_{3v} symmetry (Fig. 2). The oxo group is in a site capping the face defined by the phosphine ligands, and lies 1.16 Å above the P(1), P(2), P(3) plane with the niobium atom 0.62 Å below this plane. This coordination is similar to that observed in $NbCl_4(PMe_3)_3$ (**2**),[6] yet very different to the distorted pentagonal bipyramidal arrangement observed in the seven-coordinate oxo-niobium(V) complex $[Nb(O)(CS_2 \cdot NEt_2)_3]$.[7]

The Nb=O bond length of 1.781(6) Å in **1** is considerably longer than the niobium–oxygen distances observed in six-coordinate oxo-niobium(V) complexes (1.67–1.71 Å),[8] and the four-coordinate niobium(V) complex $[Nb(O)(N(SiMe_3)_2)_3]$ (1.699 (2) Å).[9] It is also significantly longer than the Nb=O length of 1.74(1) Å found[7] in the pentagonal bipyramidal tris(diethylthiocarbamato) complex, and presumably arises due to the presence of three highly electron-releasing PMe_3 ligands within the crowded coordination sphere of **1**.

In $[Nb(IV)Cl_4(PMe_3)_3]$ (**2**), a marked lengthening of the three equivalent facial Nb—Cl bonds (mean 2.453(3) Å) compared to that of the face-capping chloro ligand (2.409(4) Å) is observed,[6] and has been interpreted in terms of the strong *trans*-influence of the organophosphine ligand. Interestingly, the mean Nb—Cl bond distance in **1** is 0.065 Å longer than that in the niobium(IV) complex (**2**), the reverse of the trend expected on the basis of oxidation state. This lengthening must be attributed to the presence of the oxo ligand in **1**. Although a *trans*-influence by the oxo group is well established for complexes of the transition series,[10] the mean O—Nb—Cl angle of 125.0° in **1** is too far from linear for this effect to be important in explaining the elongation of the Nb—Cl bond. Furthermore, in **1** the Nb—Cl(2) length (2.533(3) Å), which is significantly longer than the other two Nb—Cl lengths (mean 2.511(3) Å), corresponds to the smallest O—Nb—Cl angle of 121.2°. In earlier work, comparison of the two six-coordinate compounds $NbOCl_3(NCCH_3)_2$ and $NbCl_5(NCH)$, revealed a marked lengthening of the Nb—Cl bonds in the former which was attributed[8] to a "*cis*-influence" of the oxo ligand arising from the strong repulsion between the valence electrons of the Nb=O double bond and the Nb—Cl bond (mean O—Nb—Cl 99.0(3)°).[8a] In the present study

* Crystal data: $C_9H_{27}Cl_3OP_3Nb$, $M = 443.41$, monoclinic, space group $P2_1/c$, $a = 15.250(3)$, $b = 11.131(2)$, $c = 11.673(3)$ Å, $\beta = 93.61(2)°$, $U = 1977.54$ $Å^3$, $F(000) = 904$, $\mu(Mo\text{-}K_\alpha) = 11.32$ cm^{-1}, $Z = 4$, $D_c = 1.490$ g cm^{-3}. Data were collected using a crystal of dimensions 0.56 × 0.35 × 0.16 mm in a sealed Lindemann tube using a Philips OW1100 diffractometer and graphite crystal monochromated Mo-K_α radiation. Weights were applied to the individual reflections as $1/\sigma^2(F_o)$ and refinement converged at $R = 0.0418$ and $R_\omega = 0.0410$.

there is no evidence for such an effect; even the Nb—P bonds, which are very close to the Nb=O group (mean O—Nb—P 76.2(2)° compared to O—Nb—Cl 125.0(2)°), are slightly shorter (mean 2.640(3) Å) than those in the tetrachloro niobium (IV) compound[6] as expected on the basis of formal oxidation state. Therefore, these results appear to be consistent with a non-directional lengthening influence of the oxo ligand on the Nb—Cl bonds of **1**.

The acute O=Nb—P angles (mean 76.5(2)°) lead to a staggered arrangement of PMe_3 ligands with respect to the capping oxo group (as viewed along the P—Nb vector) in order to minimize inter-ligand repulsion (a similar arrangement is also found for the PMe_3 ligands and the capping chlorine atom in $NbCl_4(PMe_3)_3$). Consequently, relatively close O···H contacts result in the range 2.79–2.97 Å.

To our knowledge, **1** represents the first example of a niobium oxo species stabilized by tertiary phosphine ligands. This convenient derivatization of the highly oxo- and chloro-bridged lattice of $Nb(O)Cl_3$ should facilitate the development of both the ancilliary oxo ligand chemistry and the chemistry of niobium-attached oxygen atoms. It will also be of interest to establish the influence of other tertiary-phosphine ligands on the structure of related complexes, since considerable variation has been observed for simple halo-phosphine derivatives of the heavier group 5 elements.[6] Preliminary studies on PEt_3 and PMe_2Ph derivatives suggest that marked structural differences may be anticipated.

Acknowledgement—We thank the S.E.R.C. for financial support.

REFERENCES

1. (a) Proc. Climax 5th Int. Conf. The Chemistry and Uses of Molybdenum, *Polyhderon* 1986, **5**, 1; (b) R. A. Sheldon and J. K. Kochi, *Metal Catalysed Oxidations of Organic Compounds*. Academic Press, New York (1981); (c) C. D. Garner and S. Bristow, *Molybdenum Enzymes* (Edited by T. G. Spiro), p. 345. John Wiley, New York (1985).
2. (a) V. C. Gibson, T. P. Kee and A. Shaw, *Polyhedron* 1988, **7**, 579; (b) V. C. Gibson, T. P. Kee and A. Shaw, *Polyhedron* 1988, **7**, 2217.
3. D. E. Sands, A. Zalkin and R. F. Elson, *Acta Cryst.* 1959, **12**, 21.
4. F. A. Cotton and G. Wilkinson, *Advanced Inorganic Chemistry*, 4th edn. John Wiley, New York (1980).
5. V. Katovic and C. Djordjevic, *Inorg. Chem.* 1970, **9**, 1720.
6. F. A. Cotton, M. P. Diebold and W. J. Roth, *Polyhedron* 1985, **4**, 1103.
7. B. Kamenar and C. K. Prout, *J. Chem. Soc. A* 1970, 2379.
8. See, for example, (a) C. Chavant, J.-C. Daran, Y. Jeannin, G. Constant and R. Morancho, *Acta Cryst., Sect. B* 1975, **31**, 1828; (b) R. Mercier, J. Douglade, J. Amaudrut, J. Sala-Pala and J. E. Guerchais, *J. Organomet. Chem.* 1983, **244**, 145.
9. L. G. Hubert-Pfalzgraf, M. Tsunoda and G. Le Borgne, *J. Chem. Soc., Dalton Trans.* 1988, 533.
10. U. Massi, F. Refosco, F. Tisato, G. Bardoli and M. Nicolini, *J. Chem. Soc., Dalton Trans.* 1986, 1623 and refs cited therein.

Polyhedron Vol. 7, No. 21, pp. 2225–2227, 1988
Printed in Great Britain

0277–5387/88 $3.00+.00
© 1988 Pergamon Press plc

COMMUNICATION

TIN(IV) PORPHYRIN COMPLEXES WITH UNSYMMETRICAL AXIAL LIGATION

DENNIS P. ARNOLD

Department of Chemistry, Queensland Institute of Technology, G.P.O. Box 2434, Brisbane 4001, Australia

(*Received* 22 *February* 1988; *accepted* 18 *July* 1988)

Abstract—Visible absorption and ^{1}H and ^{13}C NMR spectra have been measured for some *meso*-tetraphenyl- and *meso*-tetra(*p*-tolyl)porphyrin complexes of tin(IV) containing axial hydroxo and formato ligands. The unsymmetrical hydroxo/formato complexes allow assessment of *cis* and *trans* influences on NMR chemical shifts and J(Sn—H) and J(Sn—C) values, confirming the strong donor properties of the OH ligand bound to six-coordinate tin(IV).

The tin(IV) complexes of porphyrins are particularly suitable for investigations by NMR spectroscopy of metal–porphyrin bonding. Such complexes are readily prepared, are diamagnetic and have two axial ligands which can be varied systematically to span a wide range of donor strengths. A large number of complexes $Sn(TPP)X_2$ (TPP = 5,10,15,20-tetraphenylporphyrin) with two identical axial ligands has been prepared.[1–5] Studies of the coupling constants ^{4}J(Sn—H) between ^{117}Sn and ^{119}Sn and the pyrrole protons have revealed that for O-bound anionic ligands, the strength of the tin–porphyrin bonding is enhanced by decreasing the basicity of the axial ligands.[1,4,5] Thus a *cis* influence series has been constructed for these complexes, with X ranging from OSO_2CF_3 to OCH_3.

During some of this work, it was apparent that unsymmetrical complexes Sn(TPP)XY were formed in small amounts. Such complexes allow studies of *trans* influences of ligands as well as addressing the question of additivities of *cis* and *trans* influences in Group 14 metalloporphyrins. Because of its proximity to the metal atom, the natural choice of ligand for such studies appears to be OH, but the NMR behaviour of this proton is complicated by fast exchange with traces of water.[1,2] Indeed, OH protons in some metalloporphyrins, e.g. Tl^{III},[6] have not been observed. The next best choice is OCH_3, but rapid hydrolysis interferes. It seemed likely that the formato ligand would be useful, since ^{3}J(Sn—O—C(O)—H) should be large, and offer a sensitive probe of electronic effects of the *trans* ligand, while its steric demand is small. This communication reports ^{1}H and ^{13}C NMR and visible absorption spectra of some complexes (Fig. 1) which illustrate these points.

The formato complexes are prepared by reaction of the versatile starting material $Sn(TPP)(OH)_2$ with either one equivalent or an excess of formic acid in $CHCl_3$. The TPP complexes **1–3** were isolated and fully characterized by microanalysis, absorption spectra and ^{1}H and ^{13}C NMR spectra. For comparison, and to help in assignment of the aryl ring protons, the analogous tetrakis(*p*-tolyl) porphyrin (TTP) complexes were prepared. The hydroxo/formato complex **5** was prepared *in situ* by the redistribution reaction between **4** and **6**. This reaction is slow in $CDCl_3$, equilibrium (*K ca* 36) being reached in some three weeks at *ca* 25°C and

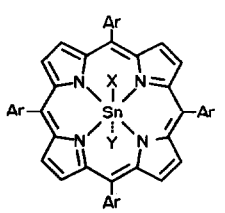

1 Ar = C_6H_5, X = Y = OH
2 Ar = C_6H_5, X = OH, Y = OCOH
3 Ar = C_6H_5, X = Y = OCOH
4 Ar = *p*-tolyl, X = Y = OH
5 Ar = *p*-tolyl, X = OH, Y = OCOH
6 Ar = *p*-tolyl, X = Y = OCOH

Fig. 1.

Table 1. ^{1}H NMR and selected visible absorption spectral data

Compound	Pyrrole β-H δ	Pyrrole β-H ^4J(Sn—H)[a]	Aryl group *ortho*	Aryl group *meta, para*	Axial ligands δ [J(Sn—H)][a]	Visible absorption λ_{max} (nm)($\varepsilon \times 10^{-3}$) Q(1,0)(β)	Q(0,0)(α)	$\varepsilon_\beta/\varepsilon_\alpha$
1	9.14	10.4	8.34	7.8	−7.45 br (*ca* 36)	561(21.8)	600(13.4)	1.63
2	9.20	13.1	8.25,[b] 8.34[c]	7.8	1.81(23.8); −6.9 v.br (OH)	558(22.3)	598(12.1)	1.84
3	9.24	15.3	8.28	7.8	2.65(43.8, 42.0)	556(22.9)	595(10.8)	2.12
4	9.14	10.3	8.21	7.61[d]	−7.46 br	563(21.2)	603(17.0)	1.25
5	9.20	13.1	8.14,[b] 8.21[c]	7.62[d]	1.72(21.4); OH not observed	—[e]	—	—
6	9.26	15.5	8.16	7.63[d]	2.51(39.2, 37.3)	558(20.7)	597(13.6)	1.52

[a] J(^{119}Sn—H), J(^{117}Sn—H) (Hz), or the average if not resolved.
[b] *ortho* proton *cis* to OCOH.
[c] *ortho* proton *cis* to OH.
[d] *meta* protons only; *p*-CH_3 at 2.74 ppm.
[e] Prepared *in situ* from **4** and **6**, not pure.

concentrations of 0.04 M. The opposite reaction, the symmetrization of **2** and **5**, can be observed in ^{1}H and ^{13}C spectra. These reactions are slow enough that the NMR lines for all compounds are sharp at 25°C. Studies of substitutions at tin should be possible without interference from these exchanges. Complexes with weakly nucleophilic anions (e.g. triflate, perchlorate) exhibit more complex behaviour as shown by broad lines in their NMR spectra.[1,4]

^{1}H *NMR spectra* (*Table* 1)

The reported trends[1] in chemical shifts and tin–proton coupling constants for the β-pyrrole protons are followed by this series of compounds. The *cis* influences of the ligands are additive, the data for **2** and **5** being the averages of those for the symmetrical complexes. The effects of the *p*-methyl groups in **4**–**6** on the β-pyrrole protons are minor. The unsymmetrical ligation in **2** and **5** is clearly shown by the *meso*-aryl proton signals. At 300 MHz the lines for the *ortho* protons are sharp, and the protons *cis* to OH and *cis* to OCOH are readily resolved. Aryl group rotation is thus slow in these complexes, although these axial ligands should offer little steric hindrance to such rotation.

The *ortho* protons *cis* to OCOH in **2** and **5** are shifted slightly upfield from their positions in **3** and **6**, respectively, perhaps reflecting the strong *trans* influence of OH, and the assumed lengthening of the Sn—OCOH bond. This effect is more obvious in the OCOH signals. Firstly, ^3J(Sn—H) decreases by almost 50% on changing the *trans* ligand from formate to hydroxide (**3** → **2** and **6** → **5**). Secondly, the strength of OH as an electron donor to Sn^{IV} and the transmission of this effect to the *trans* ligand is shown by an upfield shift of some 0.8 ppm for the formate protons. This is despite the expected *downfield* shift in δ(OCO*H*) caused by any lengthening of the Sn—O bond, which would shift the formate proton farther out in the shielding zone of the aromatic macrocycle. Another possible explanation for these changes is movement of the Sn atom out of the ring plane, or a slight "doming" of the porphyrin. However, the additivities of the *cis* influences for the β-pyrrole protons argue against such phenomena. Structural data could resolve these questions. Lastly, the sensitivity of the axial ligands to *cis* influences is apparent by comparing **2** with **5** and **3** with **6**, where the remote *p*-methyl substituent transmits a donor effect on both δ and ^3J(Sn—H) to the OCO*H* proton.

^{13}C *NMR spectra* (*Table* 2)

Typical seven-line spectra were observed, carbons being assigned by chemical shift comparisons with published data.[2,6] There are discrepancies between the present data for J(Sn—C) and those of Milgrom and Sheppard.[3] The data for **1**–**3**, especially ^3J(Sn—C_β) and ^3J(Sn—C_{meso}), where the *cis* influences of the axial ligands are shown, are internally consistent. For confirmation, the spectrum of Sn(TPP)Cl_2 was also recorded, and its J(Sn—C) values also fit the present data. The ^{13}C data complement the ^{1}H data, with slight downfield shifts and coupling constant increases on changing from OH to OCOH. The non-equivalence of the phenyl ring carbons in **2** is clearly seen, with the *cis* influences being in opposite directions for C-2′ (*ortho*) and C-3′ (*meta*), but the non-additivity exhibited by the corresponding ^{1}H signals in **2** and **5** is not present. The magnitude of this non-

Table 2. ^{13}C NMR data[a] for Sn(TPP)XY complexes

Compound	C-α	C-β	C-*meso*	C-1′	C-2′	C-3′	C-4′	C(OCOH)
1	146.7(8)	132.6(22)	121.3(17)	141.3	135.1	126.9	128.2	
1[b]	146.4(18)	132.5(7)	121.5(12.5)	141.5	135.1(6)	126.9	128.2	
2	147.0(9)	133.0(26)	121.7(19)	140.6	135.1[c]	127.0[c]	128.5	159.7(15)
					134.8[d]	127.2[d]		
3	147.2(8)	133.2(32)	122.1(23)	140.2	134.8	127.2	128.8	159.0(17)
$Sn(TPP)Cl_2$	146.4(9)	132.7(31)	121.2(24)	140.7	134.9	127.1	128.6	
$Sn(TPP)Cl_2$[b]	146.4(−)	132.6(30.5)	121.2(−)	140.7	134.9	127.1	128.5	

[a] Chemical shifts (J(Sn—H) in Hz), relative to the centre line of $CDCl_3$ triplet at 77.0 ppm.
[b] Data from ref. 2.
[c] *ortho* or *meta* carbons *cis* to OH.
[d] *ortho* or *meta* carbons *cis* to formate.

equivalence is less than that in thallium(III) TPP complexes in which the metal atom is out of the porphyrin plane.[7] Perhaps surprising is the small effect of the *trans* ligand on the formate carbon chemical shift. This may be due to the approximate cancellation of the opposing effects discussed above in relation to the ^1H data. However, the *trans* influence of OH is apparent in the data for ^2J(Sn—O—C) for **2** and **3**.

Visible absorption spectra (*Table* 1)

In such spectra, the most sensitive indicator of electronic effects of the axial ligands is the extinction coefficient ratio $\varepsilon_\beta/\varepsilon_\alpha$ for the two major visible bands.[1,8,9] An increase in positive charge on the metal atom causes lowering of the energy of the a_{2u} orbital of the porphyrin which is reflected in a decrease in intensity of the longer wavelength α band, and blue shifts of all bands. In this series of compounds, the expected changes are observed, and the influences are again additive. Another general trend is apparent, viz. that the more electron-rich porphyrin TTP affects $\varepsilon_\beta/\varepsilon_\alpha$ and the wavelengths in a comparable fashion. The very electronegative ligand tetrakis(4-pyridyl)porphyrin and its quaternary salts represent the other extreme, their Sn^{IV} complexes exhibiting $\varepsilon_\beta/\varepsilon_\alpha$ ratios of > 3.5.[10]

EXPERIMENTAL

Spectroscopic methods were as described.[1] ^{13}C NMR spectra were recorded at 75.46 MHz on the Bruker CXP-300 spectrometer, Brisbane NMR Centre, Griffith University. $Sn(TPP)(OH)_2$ and $Sn(TTP)(OH)_2$ were prepared from the chlorin-free porphyrin and $SnCl_2 \cdot 2H_2O$ in pyridine, followed by hydrolysis with ammonia, and column chromatography on neutral alumina (Merck, activity V).[5,11] Formato complexes were prepared by reaction of appropriate amounts of formic acid (Merck, 100%) and the hydroxo complexes in $CHCl_3$ with added anhydrous Na_2SO_4.[5] The products were recrystallized from CH_2Cl_2/hexane by layering or vapour diffusion. Elemental analyses for the new compounds were satisfactory, although the unavoidable presence of minor amounts of symmetrization products in Sn(TPP)(OH)(OCOH) would not be detected by this means. Sn(TTP)(OH)(OCOH) was prepared *in situ* in an NMR tube by dissolving equimolar amounts of Sn(TTP)$(OH)_2$ and Sn(TTP)$(OCOH)_2$ in $CDCl_3$, and standing for four weeks at room temperature.

Acknowledgements—I thank Mr D. Tucker and Mr P. Comino for assistance with the NMR measurements.

REFERENCES

1. D. P. Arnold, *Polyhedron* 1986, **5**, 1957.
2. L. R. Milgrom and R. N. Sheppard, *J. Chem. Soc., Chem. Commun.* 1985, 351.
3. C. Cloutour, C. Debaig-Valade, C. Gacherieu and J.-C. Pommier, *J. Organomet. Chem.* 1985, **269**, 239.
4. D. P. Arnold, unpublished results.
5. D. P. Arnold, *J. Chem. Educ.*, in press.
6. R. J. Abraham, G. H. Barnett and K. M. Smith, *J. Chem. Soc., Perkin Trans. I* 1973, 2142.
7. R. J. Abraham, G. E. Hawkes and K. M. Smith, *J. Chem. Soc., Perkin Trans. II* 1974, 627.
8. M. Gouterman, F. P. Schwarz, P. D. Smith and D. Dolphin, *J. Chem. Phys.* 1973, **59**, 676.
9. J. A. Shelnutt and V. Ortiz, *J. Phys. Chem.* 1985, **89**, 4733.
10. A. Harriman, M. C. Richoux and P. Neta, *J. Phys. Chem.* 1983, **87**, 4957.
11. G. Meyer, M. Hartmann and D. Wöhrle, *Makromol. Chem.* 1975, **176**, 1912.

Polyhedron Vol. 7, No. 21, pp. 2229–2232, 1988
Printed in Great Britain

0277–5387/88 $3.00+.00
© 1988 Pergamon Press plc

COMMUNICATION

A NEW DITOPIC POLYAZA MACROBICYCLIC LIGAND: X-RAY CRYSTALLOGRAPHIC STRUCTURE DETERMINATION

MICHAEL G. B. DREW*

The University, Whiteknights, Reading RG6 2AD, U.K.

and

DEBBIE McDOWELL and JANE NELSON*

The Open University, 40 University Road, Belfast BT7 1SU, U.K.

(*Received* 25 *May* 1988; *accepted* 18 *July* 1988)

Abstract—The N_8 crytand [**1**] was obtained in good yield by a (2+3) Schiff-base condensation of tris(2-amino ethyl)amine with terephthalaldehyde; X-ray crystal structure determination of the disilver(I) cryptate [**2**] reveals distorted tetrahedral coordination for Ag^+ and an internuclear Ag—Ag distance of 6.06 Å.

Since their introduction[1] by Lehn in 1967, cryptating ligands have found many uses particularly in the fields of transport and molecular recognition.[2] Cryptand synthesis, however, has not been a trivial exercise, but one requiring considerable skill and patience; high dilution methods are frequently necessary and yields are often low. The two major strategies for cryptand synthesis explored so far are:

(i) a stepwise process requiring two cyclization reactions each forming two bonds, which generate an intermediate macrocycle. (Overall yields in syntheses of this type are typically around 4%);

(ii) direct macrobicyclization via tripod coupling, which requires formation of at least three bonds in a single condensation step. A recently developed procedure[3] achieves 11% yield for a synthesis of this type without recourse to high dilution conditions.

The synthesis we describe is similar to type (ii) although it requires formation of six rather than three bonds in a single condensation step. This approach has been used by Newkome *et al.*[4] in the condensation of tris(ethanol)amine with 2,6-dichloropyridine to give the resulting diazahexaoxo cryptand in only 2% yield, presumably reflecting the low probability of simultaneous formation of six bonds. Despite the improbability of such an occurrence, however, we have been able to prepare the series of N_8 cryptands[5] [**3**]–[**6**] in good yield by (2+3) Schiff-base condensation of the tripod amine, tris(2-aminoethyl)amine (tren), with the series of dicarbonyls: isopthalaldehyde, diformylpyridine, diformylfuran and diformylthiophene. The same approach has been used recently[7]† by Lehn to prepare, in 70% yield, the new polyaza cryptand [**7**], with an ellipsoidal cavity 15 Å long and approximately 6–7 Å in diameter.

These hexaimino cryptands may be easily hydrogenated to octaamino derivatives, superior in chemical robustness and flexibility to their Schiff-base parents, thus generating a second family of host molecules with polarity appropriate to the

*Authors to whom correspondence should be addressed.

† This paper also reports synthesis of the pyridine-based cage [**4**].

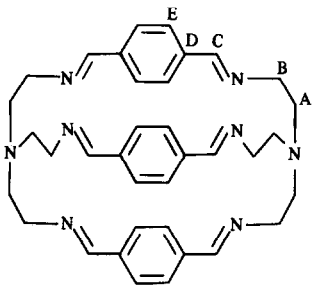

[1]

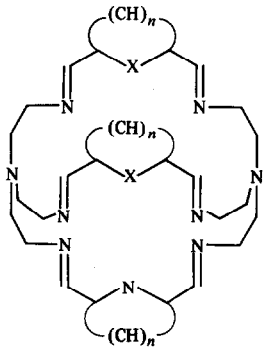

[3] X = CH $n = 3$
[4] X = N $n = 3$
[5] X = O $n = 2$
[6] X = S $n = 2$

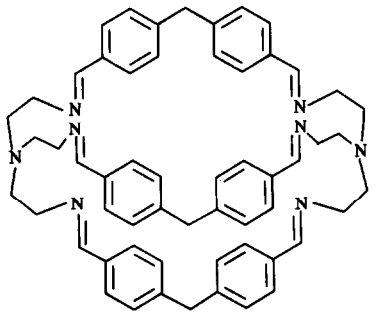

[7]

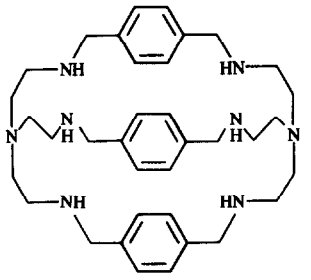

[8]

encapsulation of inorganic ions or polar organic guests. In order to explore further the possibilities for host–guest chemistry in these systems, we are investigating the use of larger dialdehydes than those mentioned in ref. 5. As a first step in this direction we here report the formation of the cryptand [1] by condensation of tren with terephthalaldehyde, the length of the cavity being thereby increased by ~ 1.3 Å relative to that in the cages prepared earlier.[5]

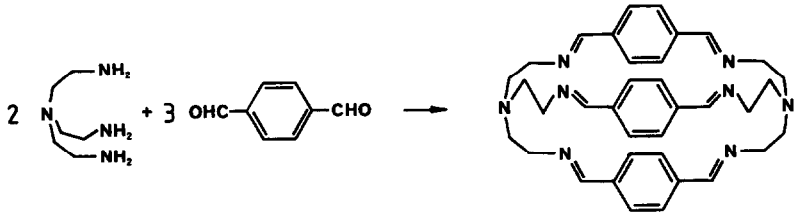

(1)

[1] is formed metal-free (20% yield) by reaction (1) taking place in methanol solution. IR and ^{1}H NMR spectra indicate that it retains H_2O solvate. The disilver cryptate $[Ag_2[1]](CF_3SO_3)_2$[2], is formed in higher yield ($\sim$ 65%) when reaction (1) occurs on an Ag^+ template. The absence of any absorption due to ν_{NH_2} or $\nu_{C=O}$ in the IR spectrum of [1] and [2] together with the presence of a medium–strong absorption around 1640 cm^{-1} due to $\nu_{C=N}$, showed Schiff-base condensation to be complete. Satisfactory elemental analysis together with the observation of parent ion mass spectral peaks at m/e = 586 for [1] and m/e = 951 corresponding to $[Ag_2[1]CF_3SO_3]^+$ in the FAB mass spectrum of [2] confirmed formation of the desired cryptand in reaction (1).

The ^{13}C NMR spectrum of [1] was simple with resonances at 63.49(t), 69.86(t), 154.15(d), 165.59(s) and 194.58(d) (symbol in parentheses indicating the off-resonance multiplicity, respectively, of the methylene carbons A and B, phenyl carbons E, phenyl carbon D and imino carbon C). A weak ^{13}C spectrum (in CD_3CN) for [2] allowed us to note the existence of upfield shifts of around 30–40 ppm in the aromatic and around 13 ppm in the methylene carbon signals strengthening our impression that cryptand conformation is quite different in [1] and [2].

The ^{1}H NMR spectrum of [1] is quite simple in comparison with that observed[5] for [3]. There is just a hint of fluxional behaviour in the slight broadening of the methylene signals and in the fact that the CH_2 α to the bridgehead nitrogen appears as a poorly resolved quintet rather than a triplet.

The aromatic and imino resonances are unsplit however. A high-field singlet (at $\sim$ 2.1 ppm) is attributed to solvated H_2O. It may be the effect of this solvated water which inhibits nitrogen inversion and thus reduces fluxionality in [1] versus [3]. The methylene resonances in [2] appear as sharp triplets; furnishing no evidence for any dynamic process taking place on the NMR time-scale in the disilver cryptate. As in the case of Lehn's cryptand [7], large downfield shifts of both imino and aromatic protons are evident on complexation.

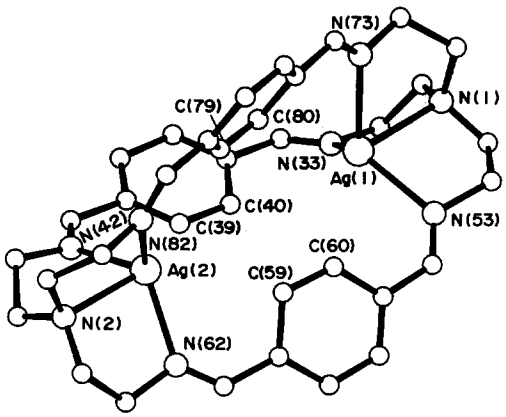

Fig. 1. Structure* of the macrobicyclic hexamine cryptate [2] viewed from the side, and showing the atomic numbering scheme.

An X-ray crystallographic structure determination was carried out on [2]. The structure consists of discrete $[Ag_2L]^{2+}$ cations (Fig. 1) and anions. In the cation, two silver atoms are encapsulated at a distance of 6.06(1) Å apart. Each silver atom is bonded to a bridgehead nitrogen atom [Ag(1)—N(1), 2.42 (2); Ag(2)—N(2), 2.37 (2) Å] and to three methylene nitrogen atoms [Ag—N, 2.27(2)–2.38(2) Å]. The geometry of the silver environment is equivalent to that of a seven-coordinate capped octahedron with the uncapped face removed. Thus, the bridgehead nitrogen atom N_b caps a triangular face of nitrogen atoms N, with N_b—Ag—N angles of 75.4–78.8° and N—Ag—N angles of 110.3–119.1°. However, both silver atoms have close contacts with three hydrogens from the bridging benzene rings (see Fig. 1). These Ag—H distances (using calculated hydrogen atom positions) are from Ag(1) H(40) 2.72, H(60) 2.65, H(80) 2.52 Å and from Ag(2) H(39) 2.37, H(59) 2.32, H(79) 2.26 Å. However, any interaction with the phenyl hydrogens must be minimal, as the 250 MHz ^{1}H NMR spectrum of [2] shows no sign of splitting of the aromatic proton signal. Both the short Ag—H contact and the unusual Ag^+ coordination geometry may result from steric necessity rather than from any weak bonding interaction, although it is interesting that a molecular mechanics calculation using appropriate van der Waals constants[6] for metal and hydrogen atoms led to a minimum energy structure in which the metal–metal

*Crystal data for $[Ag_2L][CF_3SO_3]_2$, $Ag_2C_{38}H_{42}F_6S_2O_6$, M = 1100.2, monoclinic, a = 13.362(9), b = 21.403(21), c = 15.780(14), β = 109.0(1), U = 4265.8 Å^3, $F(000)$ = 2216, d_m = 1.68 g cm^{-3}, d_c = 1.72 g cm^{-3}, Z = 4, Mo-K_α radiation (I = 0.7107 Å), μ(Mo-K_α) = 10.8 cm^{-1}. Space group $P2_1/a$.

7366 independent reflections with 2θ max of 50° were measured on a diffractometer, of which 2993 with $I > 3\sigma(I)$ were used in the calculations. The structure was solved by heavy atom methods and refined [Ag, N, C, S, F, O anisotropic, H isotropic in calculated positions] to R = 0.084 (R_w = 0.091).

Atomic coordinates, displacement factor coefficients, full lists of bond lengths and angles and lists of F_o/F_c values have been deposited as supplementary data with the Editor, from whom copies are available on request. Atomic coordinates have also been deposited with the Cambridge Crystallographic Data Centre.

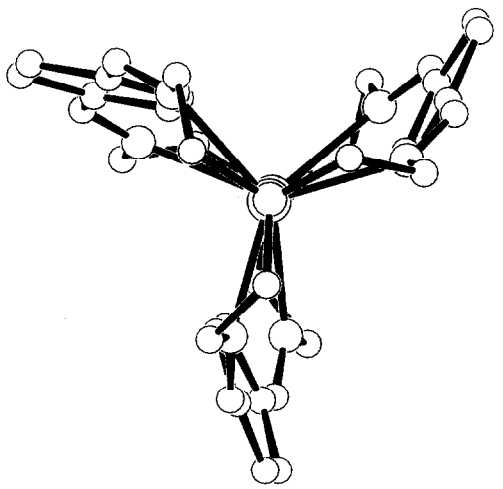

Fig. 2. Structure of [2] viewed along the bridgehead N,N axis.

distance was 7.39 Å. Similarly close Cu···H contacts [i.e. an average of 2.38 Å from Cu(1) and 2.79 Å from Cu(II)] can be estimated from the atomic coordinates[7] for $[Cu_2[7]]^{2+}$, the hydrogen atoms in this case also completing a capped octahedral arrangement around the metal ion.

Figure 2 shows a view of the cation down the N—Ag···Ag—N vector. As observed[7] in the dicopper(I) cryptate of Lehn's macrobicyclic hexaimine [7], the two sets of bridgehead N—C bonds are eclipsed, giving an approximate D_3 symmetry with the N—M···M—N vector axial. The conformation adopted in our disilver cryptate results in a closing up of the potential cavity even at the cost of some loss of planarity (i.e. a mean N=C—C—C torsion angle of 21.30°) in the conjugated phenylene bis methylimino link.

We then modelled the possibility of guest inclusion. Taking the crystal structure of $[Ag_2L]^{2+}$ as a starting point, an atom X at a point intermediate between the two silver atoms would be only 2.62 Å from a phenyl carbon atom and indeed only 3.03 Å from the two silver atoms. Clearly there is no room in this conformation for guest inclusion. However, on energy minimization (assuming normal van der Waals repulsions between Ag and H), X (given parameters appropriate to oxygen) fitted into the cavity with no contacts to the macrocycle of less than 3.0 Å. However, we were unable to fit a diatomic molecule into this cavity without severe distortion of the macrocycle. Our NMR spectral results suggest that the conformation in the free cryptand allows for a larger cavity capable of encapsulating small molecules. An X-ray crystallographic structure determination, which should reveal the size of the cavity in [1] and the siting of the solvated H_2O, is in progress.[8]

We have succeeded in preparing the hydrogenated (octaamine) derivative [8] of [1] by reduction of [2] with $NaBH_4$, and a solid product with a strong mass spectral parent ion peak at $m/z = 498$ results. This octaamine dissolves in dilute aqueous acids, presumably as a result of protonation at the amine nitrogens. So [8] promises, in both its free and its protonated form, to be of value in the recognition and transport of small polar or non-polar molecules.

The cryptand ligands described in this paper are thus likely to be of interest as hosts capable of accommodating:

(a) molecules or ions up to 4–5 Å long;
(b) pairs of metal ions separated by 6–7 Å. Electron transfer or magnetic interaction between such coordinated ions may have unusual properties as the cryptand will not easily accommodate a bridging ligand between the coordination sites and transmission of electronic effects may have to rely on a through-space mechanism.

Although it seems unlikely that [1] or [8] will show any specificity for the coordination of large cations such as Cs^+, Tl^+, UO_2^+, etc., we plan to briefly examine this capacity. The smaller, more nearly spherical cages which we[9] are presently synthesizing show greater promise in this respect.

Acknowledgements—We thank the Dupont Company and the Research Committee of the Open University for a Matched-funds award (to D.McD.). We thank the SERC for FAB mass spectra and for funds for the diffractometer. Thanks are also due to Mr A. W. Johans for assistance with the diffraction measurements.

REFERENCES

1. B. Dietrich, J. M. Lehn and J. P. Sauvage, *Tetrahedron Lett.* 1969, 2885.
2. J. M. Lehn, Supramolecular organic chemistry: From molecular receptors to coreceptors, in *Biomimetic Chemistry* (Edited by Z. Yoshida and N. Ise), p. 163. Elsevier, Amsterdam (1983).
3. B. Dietrich, M. W. Hosseini, J. M. Lehn and R. B. Sessions, *Helv. Chim. Acta.* 1985, **68**, 289.
4. G. R. Newkome, Y. K. Majestic and F. R. Fronczek, *Tetrahedron Lett.* 1981, 3035.
5. D. McDowell and J. Nelson, *Tetrahedron Lett.* 1988, 385.
6. M. G. B. Drew and P. C. Yates, *J. Chem. Soc., Dalton Trans.* 1987, 2563.
7. J. Jazwinski, J. M. Lehn, D. Lilienbaum, R. Ziessel, J. Guilheim and C. Pascard, *J. Chem. Soc., Chem. Commun.* 1987, 1691.
8. M. G. B. Drew, D. McDowell and J. Nelson, to be published.
9. J. Hunter, D. McDowell and J. Nelson, to be published.

Polyhedron Vol. 7, No. 21, pp. 2233–2234, 1988
Printed in Great Britain

0277–5387/88 $3.00+.00
© 1988 Pergamon Press plc

COMMUNICATION

REACTION OF NICKEL(II) β-DIKETONATES WITH HYDROXYLAMINE. SYNTHESIS OF NICKEL(II) COMPLEXES OF MONO-OXIMES OF β-DIKETONES (β-KETOOXIMES)

RONALD BENNETT, CHRISTOS BOLOS,* JOHN CHARALAMBOUS† and JASBIR S. LOTA

Department of Applied Chemistry and Life Sciences, The Polytechnic of North London, Holloway Road, London N7 8DB, U.K.

(*Received* 12 *April* 1988; *accepted* 22 *July* 1988)

Abstract—Nickel(II) acetylacetonate or benzoylacetonate on treatment with hydroxylamine at 0°C give adducts of the type $Ni(\beta\text{-diket})_2(NH_2OH)_2$ which on heating in refluxing ethanol afford β-ketooximato complexes of the type $Ni(\beta\text{-ketox})_2(H_2O)_2$.

Apart from a report describing briefly the preparation of the nickel(II) and copper(II) bischelates derived from benzoylacetaldehyde mono-oxime (**1**; $R^1 = H$, $R^2 = Ph$)[1] no studies of the synthesis, properties and structure of complexes derived from mono-oximes of β-diketones (**1a**) (henceforth referred to as β-ketooximes and abbreviated as β-ketoxH) have been reported. This contrasts with the very extensive interest shown in complexes derived from related ligands e.g. β-diketones and β-ketoimines.[2] As part of our interest in oximic complexes[3] we have investigated the reaction of hydroxylamine with metal β-diketonates and the potential of this reaction for the synthesis of complexes of β-ketooximes. Here we report briefly on reactions involving nickel(II) β-diketonates and on the successful synthesis of nickel(II) β-ketooximates. The synthesis of complexes of β-ketooximes by the direct reaction of β-ketooximes with metal salts is hindered because β-ketooximes (a) exist entirely or predominantly in the cyclic isoxazoline form (**1b**),[4] and (b) readily dehydrate to give isoxazoles.[5]

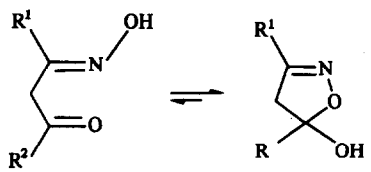

(1a) **(1b)**

Reaction of hydroxylamine with a suspension of nickel(II) complexes of acetylacetone and benzoylacetone in ethanol at *ca* 0°C gave hydroxylamine adducts of the type $Ni(\beta\text{-diket})_2(NH_2OH)_2$.

When suspensions of the adducts $Ni(acac)_2(NH_2OH)_2$ and $Ni(bzac)_2(NH_2OH)_2$ in ethanol were heated under reflux, condensation of hydroxylamine with the keto group occurred resulting in the formation of the nickel(II) β-ketooximato chelates $Ni(acacm)_2(H_2O)_2$ (acacmH = 1; $R^1 = R^2 = Me$) and $Ni(bzacm)_2(H_2O)_2$ (bzacmH = 1; $R^1 = Me$, $R^2 = Ph$), respectively.

The formulation of the β-ketooximato chelates is indicated by their elemental analysis and mass spectra which exhibit intense $[Ni(\beta\text{-ketox})_2]^+$ ions. Furthermore, the complex $Ni(bzacm)_2(H_2O)_2$ on treatment with dilute hydrochloric acid afforded *ca* 2 moles of 3-methyl-5-phenylisoxazole per mole of the complex. The nature of the isooxazole indicates

* On leave from the University of Thessaloniki, Greece.

† Author to whom correspondence should be addressed.

Table 1. Yields and analytical data for the new complexes

	Yield (%)	%C	%H	%N	%Ni
$Ni(acac)_2(NH_2OH)_2$	40	37.6 (37.2)	6.5 (6.2)	9.0 (8.7)	18.2 (18.2)
$Ni(bzac)_2(NH_2OH)_2$	75	53.4 (53.5)	5.7 (5.8)	6.2 (6.2)	13.1 (13.1)
$Ni(acacM)_2(H_2O)_2$	50	37.0 (37.2)	6.4 (6.2)	9.0 (8.7)	17.9 (18.2)
$Ni(bzacM)_2(H_2O)_2$	55	53.2 (53.5)	6.1 (5.8)	6.4 (6.2)	12.9 (13.1)

that the condensation occurred at the carbonyl group which is adjacent to the methyl group.

EXPERIMENTAL

Yields, analytical and other data are given in Table 1.

Action of hydroxylamine on Ni(β-diket)$_2$

Hydroxylamine (25 mmol) and Ni(β-diket)$_2$ (10 mmol) were stirred in anhydrous ethanol at 0°C. After 24 h Ni(β-diket)$_2$(NH$_2$OH)$_2$ was filtered off, washed with ethanol and dried *in vacuo*.

Preparation of Ni(β-ketox)$_2$(H$_2$O)$_2$

A suspension of Ni(β-diket)$_2$(NH$_2$OH)$_2$ (5 mmol) in anhydrous ethanol (50 cm^3) was heated under reflux for 8 h. Filtration gave Ni(β-ketox)$_2$(H$_2$O)$_2$ which was washed with ethanol and dried *in vacuo*. Hydroxylamine (25 mmol) and Ni(β-diket)$_2$ (10 mmol) were stirred in anhydrous ethanol at 0°C. After 24 h Ni(β-diket)$_2$(NH$_2$OH)$_2$ was filtered off, washed with ethanol and dried *in vacuo*.

Acidolysis of Ni(bzacm)$_2$(H$_2$O)$_2$

Ni(bzacm)$_2$(H$_2$O)$_2$ (1.0 g, 2.2 mmol) was stirred with hydrochloric acid (15%, 10 cm^3) for 1 h. The resulting mixture was diluted with water, neutralized and extracted with diethyl ether. After drying the extract ($MgSO_4$), removal of the diethyl ether gave 3-methyl-5-phenyl-isoxazole (0.5 g, 85%), m.p. 65–67°C (ref. 6, 67°C). (Found: C, 75.5; H, 5.8; N, 8.8. Calc. for $C_{10}H_9NO$: C, 75.7; H, 5.7; N, 8.8%); *m/z* 159 (M^+).

REFERENCES

1. R. Uhlemann, *J. Prakt. Chem.* 1963, **21**, 277.
2. F. A. Cotton and G. Wilkinson, *Advanced Inorganic Chemistry*, pp. 139 and 166. Wiley-Interscience, New York (1980).
3. J. Charalambous, K. Henrick, Y. Musa, R. G. Rees and R. N. Whiteley, *Polyhedron* 1987, **6**, 1509 and refs therein.
4. J. Castells and A. Colombo, *Chem. Comm.* 1969, 1062.
5. R. Escale, F. Petrus and J. Verducci, *Bull. Soc. Chim. France* 1974, 725.
6. G. Bianchi and P. Grunanger, *Tetrahedron* 1965, **21**, 817.

Polyhedron Vol. 7, No. 21, pp. 2235–2237, 1988
Printed in Great Britain

0277–5387/88 $3.00+.00
© 1988 Pergamon Press plc

COMMUNICATION

SYNTHESIS AND X-RAY CRYSTAL STRUCTURE OF TRIS(1,2-DIMETHYL-3-HYDROXYPYRID-4-ONATO)IRON(III)

JOHN CHARALAMBOUS, AZITA DODD, MARY McPARTLIN, SIMBA O. C. MATONDO, NAVIN D. PATHIRANA and HAROLD R. POWELL*

The Polytechnic of North London, Holloway Road, London N7 8DB, U.K.

(*Received* 24 *March* 1988; *accepted* 25 *July* 1988)

Abstract—An X-ray crystal structure analysis of the product of the reaction between $FeCl_3$ and three equivalents of 1,2-dimethyl-3-hydroxypyrid-4-one (LH) in alkali shows it to be the tris chelate compound FeL_3; the unexpected solubility in aqueous media appears to be the result of localization of negative charge on the periphery of the molecule. Crystal data: trigonal, space group $P\bar{3}$ (no. 147), $a = b = 16.665(3)$, $c = 6.854(1)$ Å, $U = 1648.49$ Å^3, $Z = 2$, $D_c = 1.383$ g cm^{-3}; 1071 reflections to give $R = 0.0501$ and $R' = 0.0469$.

Currently there is considerable interest in 3-hydroxypyrid-4-ones, especially with regard to their application as agents for the treatment of iron overload, for example in thalassaemic patients.[1–4] Although 1,2-dimethyl-3-hydroxypyrid-4-one (LH) has been shown to complex with iron,[1] and has been investigated with some success in clinical trials,[3] little is known about its coordination chemistry with this metal. We have prepared several complexes derived from these ligands and here we report the X-ray crystallographic structure of tris(1,2-dimethyl-3-hydroxypyrid-4-onato)iron(III) dodecahydrate (see Fig. 1).†

The title compound was prepared from the reaction of 1,2-dimethyl-3-hydroxypyrid-4-one (three equivalents) and iron(III) chloride (one equivalent) in the presence of sodium hydroxide. Suitable crystals were obtained by crystallization from nitromethane/water.

The tris chelate compound $FeL_3 \cdot 12(H_2O)$ (**1**) is isomorphous with the analogous Al^{III} complex reported by Nelson *et al.*[5] The molecule of (**1**) has crystallographic C_3 symmetry and the coordination of the Fe^{III} may be described as distorted octahedral. The bond lengths from the oxygen atoms are unequal, Fe—O(1) being shorter than Fe—O(2) by 0.040(4) Å, and C(3)—O(1) longer than C(4)—O(2) by 0.043(8) Å; this indicates that some ketonic character has been retained in the coordinated ligand. However, both the C—O distances are intermediate between those expected for C—O single and double bonds (*ca* 1.43 and 1.23 Å, respectively).[6] The two carbon–carbon bond distances in the ring adjacent to O(2) [C(3)—C(4) 1.408(7) Å and C(4)—C(5) 1.423(8) Å] are longer than the other bond lengths in the ring which do not differ significantly from each other [1.346–1.382(10) Å]. The ligand rings and substituent atoms are planar to within 0.016 Å. The bond lengths in the aluminium analogue $AlL_3 \cdot 12(H_2O)$ have not been discussed,[5] but a similar pattern of bond lengths is present in the related complex $Zn(OH_2)L_2$.[7] Unlike most formally neutral tris chelate compounds, (**1**) is virtually insoluble in non-polar solvents but readily soluble in water; the

*Author to whom correspondence should be addressed.

†Crystal data for (**1**): $C_{21}H_{24}FeN_3O_6 \cdot 12(H_2O)$, $M = 686.45$, trigonal, space group $P\bar{3}$ (no. 147), $a = b = 16.665(3)$, $c = 6.854(1)$ Å, $U = 1648.49$ Å^3, $F(000) = 730$, μ(Mo-K_α) = 4.84 cm^{-1}, $Z = 2$, $D_c = 1.383$ g cm^{-3}. Data were collected on a Philips PW1100 diffractometer in the θ-range 3–25°, with a scan width of 0.80°, $R = 0.0501$ and $R' = 0.0469$ for 1071 reflections with $I/\sigma(I) > 3.0$.

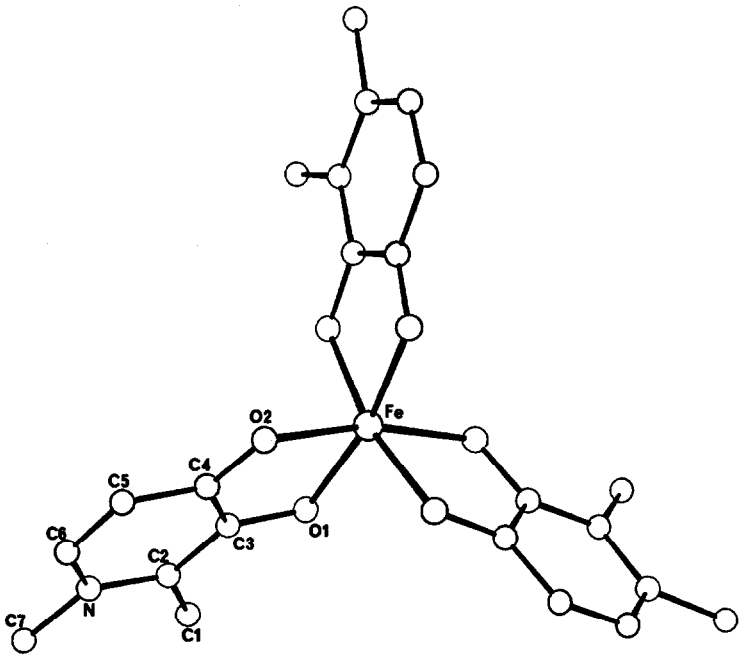

Fig. 1. The structure of the molecule of (1) viewed along the three-fold axis; bond lengths (Å): Fe—O(1) 1.998(4), Fe—O(2) 2.038(4), O(1)—C(3) 1.342(7), O(2)—C(4) 1.299(8), C(1)—C(2) 1.470(7), C(2)—C(3) 1.382(9), C(2)—N 1.364(7), C(3)—C(4) 1.408(7), C(4)—C(5) 1.423(8), C(5)—C(6) 1.346(10), C(6)—N 1.365(7), C(7)—N 1.474(9).

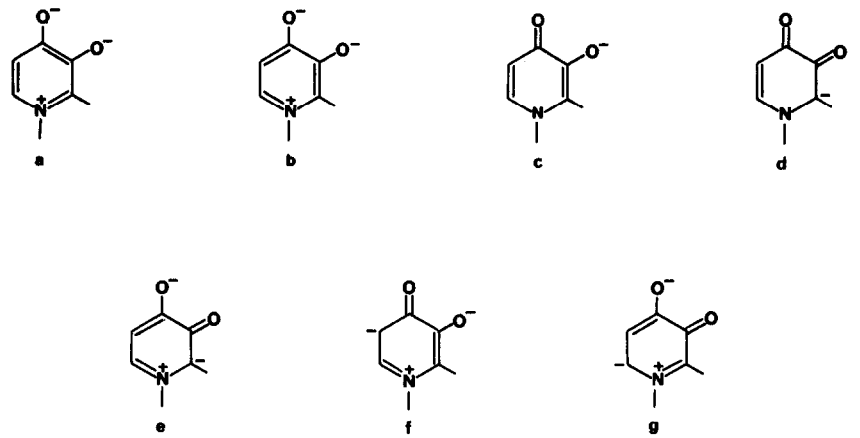

Fig. 2. Possible canonical forms of the ligand L^- in the complex $FeL_3 \cdot 12(H_2O)$.

presence of a large quantity of water of crystallization is also indicative of the molecule having some polar character. These facts are consistent with the canonical forms (**a**) and (**b**) predominating in the molecule (Fig. 2) and are of potential importance in the clinical applications of the ligand.

Acknowledgements—We thank the U.K. Thalassaemia Society for a Research Studentship (S.O.C.M.), and the National Advisory Board (N.D.P.) and Science and Engineering Research Council (H.R.P.) for Research Fellowships.

REFERENCES

1. M. Gyraparaki, J. B. Porter, S. Hurani, M. Streater, R. C. Hider and E. R. Heuhns, *Acta. Haemat.* 1987, **78**, 217.
2. G. J. Kontoghiorghes, L. Sheppard, A. V. Hoffbrand, J. Charalambous, J. Tikerpae and M. J. Pippard, *J. Clin. Path.* 1987, **40**, 404.

3. G. J. Kontoghiorghes, M. A. Aldouri, A. V. Hoffbrand, J. Barr, B. Wonke, T. Kouraclaris and L. Sheppard, *Brit. Med. J.* 1987, **295**, 1509.
4. M. J. Pippard, *Acta. Haemat.* 1987, **78**, 206.
5. W. O. Nelson, S. J. Rettig and C. Orvig, *J. Am. Chem. Soc.* 1987, **109**, 4121.
6. *Tables of Interatomic Distances and Configuration in Molecules and Ions*, p. S.17. Chemistry Society (1958).
7. J. Charalambous, A. Dodd, N. Gwatidzo, M. McPartlin, N. D. Pathirana, H. R. Powell and S. Turner, to be submitted.

Polyhedron Vol. 7, No. 21, pp. 2239–2241, 1988
Printed in Great Britain

0277–5387/88 $3.00+.00
© 1988 Pergamon Press plc

COMMUNICATION

SYNTHESIS AND X-RAY CRYSTAL STRUCTURE OF A DIMOLYBDENUM COMPLEX FEATURING A TRANSVERSE-BRIDGING, FOUR-ELECTRON-DONOR DIBISMUTH LIGAND; $[Mo_2(CO)_4(\eta\text{-}C_5H_4Me)_2(\mu\text{-}\eta^2\text{-}Bi_2)]$

WILLIAM CLEGG, NEVILLE A. COMPTON, R. JOHN ERRINGTON* and NICHOLAS C. NORMAN*

The University of Newcastle upon Tyne, Department of Inorganic Chemistry, Newcastle upon Tyne NE1 7RU, U.K.

(*Received* 15 *July* 1988; *accepted* 25 *July* 1988)

Abstract—Photolysis of the trimolybdenum–bismuth complex, $[Bi\{Mo(CO)_3(\eta\text{-}C_5H_4Me)\}_3]$, in THF solution affords the dimolybdenum–dibismuth complex, $[Mo_2(CO)_4(\eta\text{-}C_5H_4Me)_2(\mu\text{-}\eta^2\text{-}Bi_2)]$, which contains a transverse-bridging, four-electron-donor Bi_2 ligand; the structure has been determined by X-ray crystallography.

One area of inorganic chemistry which has witnessed a rapid growth in the last few years concerns the synthesis of organotransition metal complexes containing atoms or small aggregates of the heavier main group elements. This is particularly noticeable for complexes containing elements of Group V (P, As, Sb, Bi), attested by the number of recent reviews in this field,[1] and probably originating from interest in the multiple bonding and low coordination numbers often associated with these compounds. A subset of this family of complexes comprises those featuring E_2 fragments (E = P, As, Sb, Bi), but whilst a large number of examples are known for phosphorus and arsenic,[1] very few reports exist of compounds containing Sb_2 and Bi_2 units. We are aware of only one structurally characterized example of a di-antimony complex, viz. $[\{W(CO)_5\}_3Sb_2]$,[2] and five such dibismuth complexes, $[\{W(CO)_5\}_3Bi_2]$,[3] $[Bi_2Fe_2Co(CO)_{10}]^-$,[4] $[Bi_2Os_4(CO)_{12}]$,[5] $[Bi_2Co_4(CO)_{11}]^-$[6] and $[W_2(CO)_8(\mu\text{-}\eta^2\text{-}Bi_2)(\mu\text{-}Bi(Me)W(CO)_5)]$.[7] Herein we report the synthesis and structural characterization of the title complex which contains a bridging, four-electron-donor Bi_2 ligand.

As part of a programme aimed at synthesizing new organotransition metal–bismuth complexes, we have synthesized the trimolybdenum complex $[Bi\{Mo(CO)_3(\eta\text{-}C_5H_5)\}_3]$ (**1a**),[8] which gave an interesting and informative electron impact–mass spectrum showing signals consistent with a dimolybdenum–dibismuth complex, $[Mo_2Bi_2(CO)_4(C_5H_5)_2]$ (**2a**),† rather than a trimolybdenum–monobismuth product. This observed rearrangement suggested that **2a** was probably stable enough to be a viable synthetic target and, accordingly, a route to **2a** was sought.

Solution thermolysis of **1a** led only to extensive decomposition but photolysis (THF solution, 100 W medium pressure UV lamp, 40 min) resulted in a rapid colour change from dark red to brown. Subsequent chromatographic work-up (Florisil) afforded two products identified spectroscopically as $[Mo_2(CO)_6(\eta\text{-}C_5H_5)_2]$ (purple fraction, hexane eluant) and $[Mo_2(CO)_4(\eta\text{-}C_5H_5)_2(\mu\text{-}\eta^2\text{-}Bi_2)]$ (**2a**), (yellow–brown fraction, THF eluant)‡ both in

* Authors to whom correspondence should be addressed.

† This formula was confirmed by high resolution mass measurement studies.

‡ Spectroscopic data for **2a**: IR $\nu_{C\equiv O}$ (THF) cm^{-1} 1917s, 1866m; NMR in $(CD_3)_2CO$, ^1H δ 5.21 (s, 5H, C_5H_5), $^{13}C\{^1H\}$ δ 83.1 (s, C_5H_5); EI mass spectrum, M^+ 852. Data for **2b**: IR $\nu_{C\equiv O}$ (THF) cm^{-1} 1913s, 1863m; NMR in CD_2Cl_2, ^1H δ 5.12 (m, 2H, C_5H_4Me), 4.94 (m, 2H, C_5H_4Me), 2.12 (s, 3H, C_5H_4Me), $^{13}C\{^1H\}$ δ 82.8 (s, C_5H_4Me), 81.7 (s, C_5H_4Me), 15.2 (s, C_5H_4Me); EI mass spectrum, M^+ 880. Satisfactory microanalytical data were obtained for both complexes.

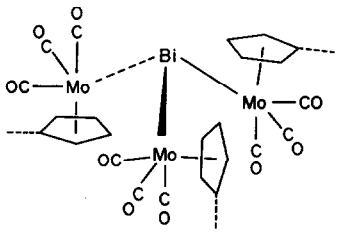

(1a) C_5H_5
(1b) C_5H_4Me

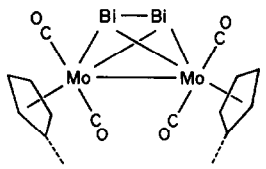

(2a) C_5H_5
(2b) C_6H_4Me

approximately 20% yields although these decrease rapidly if irradiation is prolonged.

Analogous observations were made and results obtained from photolysis of the methylcyclopentadienyl derivative (**1b**). Similar work-up procedures afforded dark yellow–brown **2b**, X-ray quality crystals being obtained from THF–hexane mixtures at −30°C.

Spectroscopic data for **2b*** were in accordance with the formula, $[Mo_2(CO)_4(\eta\text{-}C_5H_4Me)_2(\mu\text{-}\eta^2\text{-}Bi_2)]$, but in order to determine the structure more precisely, an X-ray crystallographic study was undertaken,† the results of which are shown in Fig. 1. The molecule resides on a crystallographic C_2 axis, and comprises a dimolybdenum unit transversely bridged by a dibismuth ligand giving a tetrahedral Mo_2Bi_2 core.‡ Each molybdenum is additionally bonded to a methylcyclopentadienyl and two terminal carbonyl ligands. Electron counting procedures require that the Bi_2 ligand acts as a four electron donor to the Mo—Mo single-bonded dimolybdenum centre in **2b**. Consistent with this, the molybdenum–molybdenum distance (Mo—Mo′ 3.167(2) Å) is in the range normally observed for such bonds. Also, the bismuth–bismuth separation (Bi—Bi′ 2.838(1) Å) is similar to that found in the only other structurally characterized complex containing a $\mu\text{-}\eta^2\text{-}Bi_2$ ligand, viz. $[W_2(CO)_8(\mu\text{-}\eta^2\text{-}Bi_2)(\mu\text{-}Bi(Me)W(CO)_5)]$ (**3**),[7] (Bi—Bi 2.796(1) Å). In all other examles of Bi_2 complexes, this ligand behaves as a formal six-electron donor to at least three metal centres with Bi—Bi separations usually slightly longer than those found in **2b**.[3-6,9]

Another aspect of the structure of **2b** concerns the relative orientations of the $Mo(CO)_2(C_5H_4Me)$ fragments. These are disposed such that the molecule has a C_2 axis (crystallographically exact in this case) as represented in the Newman projection (**A**). This configuration is also found in other $[Mo_2(CO)_4(C_5H_5)_2(\mu\text{-L})]$ complexes where L is either an alkyne (RC≡CR)[10] or phosphinidene (PR)[11] fragment, both of which are isolobal with Bi_2. An alternative configuration has also been observed for both alkyne[12] and phosphinidene[11] complexes, (**B**), in which one of the metal fragments adopts an orientation at approximately 90° to that in **A**. The factors determining which configuration is adopted are subtle[11] but the two forms may be distinguished in solution by their IR spectra, **A** having two CO absorptions and **B** having four.[10-12] IR spectra for **2a,b** reveal that the solid-state structure is maintained in solution.*

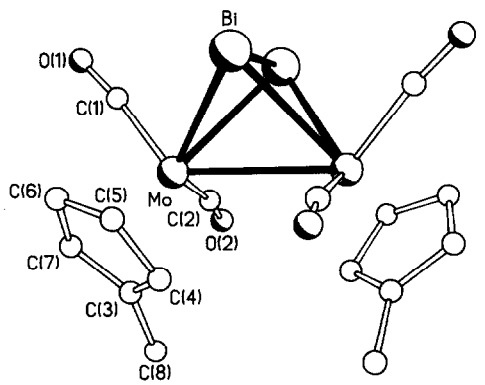

Fig. 1. A diagram of the molecular structure of **2b** showing the atom numbering scheme. Important bond length and angle data include Bi—Mo 2.848(1), Bi—Mo′ 2.985(1), Bi—Bi′ 2.838(1), Mo—Mo′ 3.167(2) Å; Mo—Bi—Bi′ 63.3(1), Bi′—Bi—Mo′ 58.5(1), Mo—Bi—Mo′ 65.7(1)°.

* See footnote ‡ on previous page.

† Crystal data for **2b**: $C_{16}H_{14}Bi_2Mo_2O_4$, $M = 880.1$, trigonal, $a = 8.8996(5)$, $c = 19.944(2)$ Å, $V = 1368.0$ Å^3, $Z = 3$, space group $P3_121$ (distinguished from $P3_221$ by anomalous dispersion effects); $R = 0.027$, $R_w = 0.028$ from 1511 unique observed reflections with $2\theta < 50°$, measured with Mo-K_α radiation ($\lambda = 0.71073$ Å) and corrected for absorption. Atomic coordinates, bond lengths and angles, and thermal parameters have been deposited as supplementary data with the Editor, from whom copies are available on request. Atomic coordinates have also been deposited with the Cambridge Crystallographic Data Centre.

‡ The Bi—Bi and Mo—Mo vectors are not quite perpendicular; the angle between them is 84.9°. This twist is probably due to the steric effect of the adjacent carbonyls.

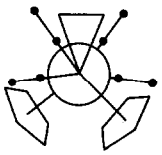

(A)

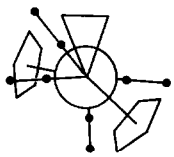

(B)

Finally we note the comparison between **2a,b** and the lighter congeneric complexes $[M_2(CO)_4(\eta\text{-}C_5R_5)_2(\mu\text{-}\eta^2\text{-}E_2)]$ (**4**, M = Mo, R = H, E = P;[13] **5**, M = Mo, R = Me, E = P;[14] **6**, M = Mo, W, R = H, E = As;[15] **7**, M = Mo, R = Me, E = As[16]). Structure determinations carried out on **4**[13] and **6**[15a] reveal that the same, type **A**, configuration is adopted in the solid-state and IR data[13,15b] indicate that this is maintained in solution.

Theoretical, electrochemical and reactivity studies on **2a,b** are in progress and preliminary experiments indicate that the di-antimony analogues are also isolable.[17]

Acknowledgements—We thank the S.E.R.C. for financial support and BP Research (Sunbury) for a CASE Award (N.A.C.). The Research Corporation Trust and Nuffield Foundation are also thanked for additional supporting funds (N.C.N.).

REFERENCES

1. For recent reviews, see O. J. Scherer, *Angew. Chem. Int. Ed. Engl.* 1985, **24**, 924; O. J. Scherer, *Comments Inorg. Chem.* 1987, **6**, 1; W. A. Herrmann, *Angew. Chem. Int. Ed. Engl.* 1986, **25**, 56; M. DiVaira, P. Stoppioni and M. Peruzzini, *Polyhedron* 1987, **6**, 351.
2. G. Huttner, U. Weber, B. Sigwarth and O. Scheidsteger, *Angew. Chem. Int. Ed. Engl.* 1982, **21**, 215.
3. G. Huttner, U. Weber and L. Zsolnai, *Z. Naturforsch.* 1982, **37b**, 707.
4. K. H. Whitmire, K. S. Raguveer, M. R. Churchill, J. C. Fettinger and R. F. See, *J. Am. Chem. Soc.* 1986, **108**, 2778; K. H. Whitmire, M. Shieh, C. B. Lagrone, B. H. Robinson, M. R. Churchill, J. C. Fettinger and R. F. See, *Inorg. Chem.* 1987, **26**, 2798.
5. H. G. Ang, C. M. Hay, B. F. G. Johnson, J. Lewis, P. R. Raithby and A. J. Whitton, *J. Organomet. Chem.* 1987, **330**, C5.
6. S. Martinengo and G. Ciani, *J. Chem. Soc., Chem. Commun.* 1987, 1589.
7. A. M. Arif, A. H. Cowley, N. C. Norman and M. Pakulski, *J. Am. Chem. Soc.* 1985, **107**, 1062; A. M. Arif, A. H. Cowley, N. C. Norman and M. Pakulski, *Inorg. Chem.* 1986, **25**, 4836.
8. W. Clegg, N. A. Compton, R. J. Errington and N. C. Norman, *J. Organomet. Chem.* 1987, **335**, C1; W. Clegg, N. A. Compton, R. J. Errington, N. C. Norman, A. J. Tucker and M. J. Winter, *J. Chem. Soc., Dalton Trans.*, in press.
9. N. C. Norman, *Chem. Soc. Rev.*, in press.
10. J. A. Beck, S. A. R. Knox, R. F. D. Stansfield, F. G. A. Stone and M. J. Winter, *J. Chem. Soc., Dalton Trans.* 1982, 195.
11. A. M. Arif, A. H. Cowley, N. C. Norman, A. G. Orpen and M. Pakulski, *Organometallics* 1988, **7**, 309.
12. W. I. Bailey, M. H. Chisholm, F. A. Cotton and L. A. Rankel, *J. Am. Chem. Soc.* 1978, **100**, 5764.
13. O. J. Scherer, H. Sitzmann and G. Wolmershäuser, *J. Organomet. Chem.* 1984, **268**, C9.
14. O. J. Scherer, H. Sitzmann and G. Wolmershäuser, *Angew. Chem. Int. Ed. Engl.* 1985, **24**, 351.
15. (a) P. J. Sullivan and A. L. Rheingold, *Organometallics* 1982, **1**, 1547; (b) G. Huttner, B. Sigwarth, O. Scheidsteger, L. Zsolnai and O. Orama, *Organometallics* 1985, **4**, 326.
16. I. Bernal, H. Brunner, W. Meier, H. Pfisterer, J. Wachter and M. L. Ziegler, *Angew. Chem. Int. Ed. Engl.* 1984, **23**, 438.
17. N. C. Norman and P. M. Webster, unpublished observations.

Polyhedron Vol. 7, No. 21, pp. 2243–2247, 1988
Pergamon Press plc. Printed in Great Britain

BOOK REVIEWS

Comprehensive Coordination Chemistry. The Synthesis, Reactions, Properties and Applications of Coordination Compounds. Edited by Sir Geoffrey Wilkinson, FRS, Robert D. Gillard and Jon A. McCleverty, Pergamon Press, Oxford, 1987. 7 volumes, 7800 pp., US$ 2450.00. ISBN 0-08-026232-5.

Comprehensive Coordination Chemistry is the latest in a series of major reference works initiated by Pergamon Press some 15 years ago with the publication of *Comprehensive Inorganic Chemistry*. This new treatise comprises 7 volumes which are designed to give readers a contemporary overview of the synthesis, reactions, properties and applications of coordination compounds.

Volume 1. Theory & Background

The first volume deals with the theory and background of coordination chemistry and is presented in 10 chapters. G. B. Kauffman in the first chapter provides a splendid historical survey up to 1930 of the discovery of coordination compounds and the stepwise developments which led to Werner's theory of their constitution. It is interesting to read that as long ago as 1841, "Berzelius viewed metal ammines as conjugated or copulated compounds consisting of ammonia and a conjugate or copula". The complementary and concluding section to Chapter 1 summarizes the perception of J. C. Bailar Jr, Chapter 2 (D. L. Kepert) is devoted to coordination numbers and geometries and provides a comprehensive account of contemporary Valence Shell Electron Pair Repulsion theory (VSEPR theory) and its quantitative application for predicting the stereochemistry of a wide range of coordination compounds. According to T. E. Sloan (Chapter 3), inorganic chemical nomenclature has evolved from the mystical terminology of alchemy into its present day "additive" terminology which enables "a name for a compound to indicate empirical composition, molecular composition, composition and connectivity, and complete qualitative three-dimensional compound structure". Teachers and students will find this account of the nomenclature of coordination compounds according to IUPAC rules and recommendations complemented by the expertise of *Chemical Abstracts* Service, an immensely valuable reference. Polymetallic clusters and cages form the topic of Chapter 4 (I. G. Dance). Although metal clusters containing from three (e.g. $[Re_3Cl_{12}]^{3-}$) up to ~4500 (e.g. ferritin) metal atoms have long been known, the emerging recognition of the underlying principles for rational synthesis of polymetallic clusters together with their widespread occurrence has encouraged the author to designate this as "a new field of coordination chemistry".

The successful resolution of optically active coordination compounds, especially Werner's resolution in 1914 of completely carbon-free coordination compounds, was the *coup de grâce* that finally secured the recognition and acceptance of his coordination theory. Chapter 5 (J. M. Harrowfield) provides an excellent overview of the occurrence of isomerism in coordination chemistry and its relevance to understanding the subtle chemistry underlying some biological and industrial processes. This is followed in Chapter 6 by an excellent account of ligand field theory and its application to the interpretation of the spectra and magnetism of transition metal complexes (B. N. Figgis). A detailed survey of the mechanism of inorganic reactions is presented in Chapter 7 which is sub-divided into five sections: Substitution Reactions (M. L. Tobe), Electron Transfer Reactions (T. J. Meyer and H. Taube), Photochemical Processes (C. Kutal and A. W. Adamson), Reactions of Coordinated Ligands (D. St. C. Black), and Reactions in the Solid State (H. E. LeMay).

The versatile technique of electrochemistry is being applied increasingly to coordination complexes in aqueous and non-aqueous media. Chapter 8 surveys recent developments in three sections: Electrochemistry and Coordination Chemistry (C. J. Pickett), Electrochemical Properties in Aqueous Solutions (D. H. Vaughan) and Electrochemical Properties in Non-aqueous Solutions (C. J. Pickett). In the concluding chapters of Volume 1, D. H. Vaughan in Chapter 9 deals with the quantitative aspects of solvent effects on rates of reactions, redox potentials, and equilibrium constants in analysis in Chapter 10. A detailed Subject Index and Formula Index complete this introductory volume of 613 pages.

The contributions to Volume 1 are written with authority and clarity, and provide the reader with an admirable and critical overview of contemporary chemistry. Although as many as 18 authors have been involved, the editors have achieved a pleasant uniformity of presentation and style which make the volume eminently readable. If the succeeding volumes all achieve the same high standard, this reference work will make a valuable addition for all libraries with a chemistry collection.

Monash University
Australia

R. L. MARTIN

Volume 2. Ligands

The subject of Volume 2 of this immense series is "Ligands". The Book contains over 1000 pages and was

Polyhedron Vol. 7, No. 21, pp. 2243–2247, 1988
Pergamon Press plc. Printed in Great Britain

BOOK REVIEWS

Comprehensive Coordination Chemistry. The Synthesis, Reactions, Properties and Applications of Coordination Compounds. Edited by Sir Geoffrey Wilkinson, FRS, Robert D. Gillard and Jon A. McCleverty, Pergamon Press, Oxford, 1987. 7 volumes, 7800 pp., US$ 2450.00. ISBN 0-08-026232-5.

Comprehensive Coordination Chemistry is the latest in a series of major reference works initiated by Pergamon Press some 15 years ago with the publication of *Comprehensive Inorganic Chemistry*. This new treatise comprises 7 volumes which are designed to give readers a contemporary overview of the synthesis, reactions, properties and applications of coordination compounds.

Volume 1. Theory & Background

The first volume deals with the theory and background of coordination chemistry and is presented in 10 chapters. G. B. Kauffman in the first chapter provides a splendid historical survey up to 1930 of the discovery of coordination compounds and the stepwise developments which led to Werner's theory of their constitution. It is interesting to read that as long ago as 1841, "Berzelius viewed metal ammines as conjugated or copulated compounds consisting of ammonia and a conjugate or copula". The complementary and concluding section to Chapter 1 summarizes the perception of J. C. Bailar Jr, Chapter 2 (D. L. Kepert) is devoted to coordination numbers and geometries and provides a comprehensive account of contemporary Valence Shell Electron Pair Repulsion theory (VSEPR theory) and its quantitative application for predicting the stereochemistry of a wide range of coordination compounds. According to T. E. Sloan (Chapter 3), inorganic chemical nomenclature has evolved from the mystical terminology of alchemy into its present day "additive" terminology which enables "a name for a compound to indicate empirical composition, molecular composition, composition and connectivity, and complete qualitative three-dimensional compound structure". Teachers and students will find this account of the nomenclature of coordination compounds according to IUPAC rules and recommendations complemented by the expertise of *Chemical Abstracts* Service, an immensely valuable reference. Polymetallic clusters and cages form the topic of Chapter 4 (I. G. Dance). Although metal clusters containing from three (e.g. $[Re_3Cl_{12}]^{3-}$) up to ~4500 (e.g. ferritin) metal atoms have long been known, the emerging recognition of the underlying principles for rational synthesis of polymetallic clusters together with their widespread occurrence has encouraged the author to designate this as "a new field of coordination chemistry".

The successful resolution of optically active coordination compounds, especially Werner's resolution in 1914 of completely carbon-free coordination compounds, was the *coup de grâce* that finally secured the recognition and acceptance of his coordination theory. Chapter 5 (J. M. Harrowfield) provides an excellent overview of the occurrence of isomerism in coordination chemistry and its relevance to understanding the subtle chemistry underlying some biological and industrial processes. This is followed in Chapter 6 by an excellent account of ligand field theory and its application to the interpretation of the spectra and magnetism of transition metal complexes (B. N. Figgis). A detailed survey of the mechanism of inorganic reactions is presented in Chapter 7 which is sub-divided into five sections: Substitution Reactions (M. L. Tobe), Electron Transfer Reactions (T. J. Meyer and H. Taube), Photochemical Processes (C. Kutal and A. W. Adamson), Reactions of Coordinated Ligands (D. St. C. Black), and Reactions in the Solid State (H. E. LeMay).

The versatile technique of electrochemistry is being applied increasingly to coordination complexes in aqueous and non-aqueous media. Chapter 8 surveys recent developments in three sections: Electrochemistry and Coordination Chemistry (C. J. Pickett), Electrochemical Properties in Aqueous Solutions (D. H. Vaughan) and Electrochemical Properties in Non-aqueous Solutions (C. J. Pickett). In the concluding chapters of Volume 1, D. H. Vaughan in Chapter 9 deals with the quantitative aspects of solvent effects on rates of reactions, redox potentials, and equilibrium constants in analysis in Chapter 10. A detailed Subject Index and Formula Index complete this introductory volume of 613 pages.

The contributions to Volume 1 are written with authority and clarity, and provide the reader with an admirable and critical overview of contemporary chemistry. Although as many as 18 authors have been involved, the editors have achieved a pleasant uniformity of presentation and style which make the volume eminently readable. If the succeeding volumes all achieve the same high standard, this reference work will make a valuable addition for all libraries with a chemistry collection.

Monash University
Australia

R. L. MARTIN

Volume 2. Ligands

The subject of Volume 2 of this immense series is "Ligands". The Book contains over 1000 pages and was

written by over 40 authors. Included are chapters on such simple ligands and ligand families as Cyanides and Fulminates, Chapter 12.1; Ammonia and Ammines, Chapter 13.1; Nitriles, Chapter 13.7; Water, Hydroxide and Oxide, Chapter 15.1; Dioxygen, Superoxide and Peroxide, Chapter 15.2; Oxyanions, Chapter 15.5; Sulfides, Chapter, 16.1; Metallothio Anions, Chapter 16.3; Halogens as Ligands, Chapter 18; and Hydrogen and Hydrides, Chapter 19. Specific kinds of donor atoms figure in the organization with a section on Group IV Ligands having two chapters, a section on Nitrogen Ligands, containing eight chapters; that on Oxygen Ligands having nine chapters while Sulfur Ligands are treated in six chapters. Separate chapters are devoted to Phosphorus, Arsenic, Antimony and Bismuth Ligands, Chapter 14 and Selenium and Tellurium Ligands, Chapter 17. Many familiar and important classes of organic ligands are treated in separate chapters; these include a variety of topics on nitrogen, oxygen, sulfur and mixed donor ligand systems. Some are as common as Heterocyclic Nitrogen-donor Ligands, Chapter 13.2; Oximes, Guanidines and Related Species, Chapter 13.8; Diketones and Related Ligands, Chapter 15.4; Dithiolenes and Related Species, Chapter 16.5; Schiff Bases as Acyclic Polydentate Ligands, Chapter 20.1; and Amino Acids, Peptides and Proteins, Chapter 20.2. In contrast, some of the chapters may strike readers as a bit specialized; e.g. Mercury as a Ligand, Chapter 11; Sulfurdiimine, Triazenido, Azabutadiene and Triatomic Hetero Anion Ligands, Chapter 13.5; Polypyrazolylborates and Related Ligands, Chapter 13.6; and Bidentate Ligands, Chapter 20.4. The final 20% or so of the book is devoted to a section labelled Multidentate Macrocyclic Ligands. It covers much of the important new chemistry of relatively complicated ligands, Chapter 21.3, Macropolycyclic Ligands, Chapter 21.2, Other Polyaza Macrocycles, while also treating the classic ligands derived, either directly or indirectly, from natural sources, Chapter 21.1, Porphyrins, Hydroporphyrins, Azaporphyrins, Phthalocyanines, Corroles, Corrins and Related Macrocycles, and Chapter 22 Naturally Occurring Ligands. Equally impressive is the array of distinguished authors who have written the chapters making up this volume. The authors are generally highly qualified to write their subjects and, in some cases, uniquely qualified to do so. This compliments the distinction represented by the editors of this collected compendium.

Volume 2 constitutes a useful contribution to the literature of the diverse area of coordination compounds. The chapters tend to be subdivided in logical and useful ways, adding to their value as secondary scientific literature. Most authors have indicated the scope and limitations of their reviews and indicated where more specialized reviews are available. In this manner, excellent literature surveys are presented despite space limitations. The cut-off time for the literature covered varies from chapter to chapter but few papers more recent than 1984 are cited. Although the coverage is comprehensive and often quite thorough, several sections covering highly active fields are so condensed that they are likely to be of interest only to general readers. This is probably inevitable for a publication having such global goals as is true in the present case.

Several aspects of the volume are particularly appealing. The presence of Nomenclature or Appendix sections (13.1, 15.7, 20.1, 21.3) which define abbreviations and acronyms used within a chapter is helpful and could profitably be extended to other chapters. The chapters that routinely reference structures, figures and tables are the most convenient to use. Referencing is generally excellent but the few examples where this is not the case are frustrating (e.g. p. 8, reduction of cyanide; p. 84, Scheme 4; p. 85, Scheme 5; p. 903, Schemes 6 and 7). The use of both footnotes and references within tables can be distracting (e.g. Table 7, p. 309) and we recommend that references be confined to bibliographies in subsequent editions.

A document such as *Comprehensive Coordination Chemistry* should avoid presentations or illustrations that are inconsistent with the pace of the manuscript or which might confuse the reader. We feel that the discussion of the stereochemistry of DMF (p. 491) is inappropriate. Similarly, the structure given for dithiooxamide [p. 800, Structure (**28**)] shows an imino form rather than the typical amino representation.

For the most part, the illustrations are clear and emphasis has obviously been placed on defining stereochemistry where applicable. A few sections are deficient in this respect and occasionally diagrams using mixtures of perspective and wedge shaped bonds are unclear [examples are p. 91, Fig. 23 (also, a phenyl is missing); p. 555, structures *meso*-(**16**), ±(**16**)–(**19**); p. 748, Scheme 1; p. 967, Structures (**11**) and (**12**)]. The use of arrows to indicate dative bonds in structure diagrams is archaic and should be avoided. One author is inconsistent in this respect (Chapter 21.2). In addition, assignment of charge to a ligand without including charge on a metal ion might create confusion as to the net charge of the complex [for examples see p.94, Fig. 25; p. 596 Structures (**1**)–(**3**); p. 491, eq. (19); p. 272, Structure (**15**); p. 59, Structure (**117**); p. 902, Schemes 4 and 5 and Structures (**11**) and (**12**)].

There are a few cases where we feel that the text might be misleading. On p. 8 a misuse of nomenclature occurs. It should be recognized that "bidentate" indicates that two sites of a ligand bind to a single metal ion (when a ligand binds in a monodentate mode to each of two metal ions this is bridging and not "bidentate" chelation). Unfortunate language sometimes appears. For example, on p. 31 the phrasing "bidentate mono(ethylenediamine) complexes" is used. This would seem to imply that the complex is bidentate? The introductory sentences to the two sections beginning on p. 323 seem to be at cross purposes. The first case fails to point out the fact that the actual process is simply binding of the second metal atom to the previously bound superoxo moiety, while the second requires that this fact be taken for granted.

Typographical errors are inevitable in a manuscript of this magnitude and we were pleased by the small number. Errors in diagrams or sections where text and diagrams are inconsistent are more serious. The caption to Fig. 25 on p. 94 claims that the picture shows a tetrahedral spec-

ies; it does not. On p. 596 the diagram shows four structures but uses three structure numbers; it will be claimed that the centre two structures are like two Kekulé structures of benzene. Page 733, Fig. 18 and preceding text: X = N does not work. Page 919, Structure (18), methyl substitutes and cation charge are missing.

Ohio State University **N. STEPHENSON and**
U.S.A. **D. H. BUSCH**

Volume 3. Main Group & Early Transition Elements

The third volume of this colossal work deals with the coordination chemistry of main group and early transition elements including the lanthanides and actinides in 1600(!) pages. Traditionally, typical non-metal elements like B, Si, S, the halogens and noble gases are rarely considered to have a coordination chemistry. At least in the country of this reviewer there appears to exist a psychological and/or language barrier between the camps of main group and transition metal chemists. Chapters 23–30 undertake the heroic attempt to overcome much pride and many prejudices on both sides—after all, it is merely inorganic chemistry. The authors, all of them are experts in their fields, of these chapters are to be congratulated for their excellent presentation of a diverse and complicated material. I am convinced that the members of both camps will enjoy the reading, and many new research ideas will evolve—be it only from the "interdisciplinary" character of this venture.

About 80% of Volume 3 deals with the coordination chemistry of Ti, Zr, Hf, V, Nb, Ta, Cr, Mo, W, the lanthanides and actinides—real metals. The explosive development of the chemistry of molybdenum in all its various oxidation states during the past two to three decades has found its precipitation in seven individual chapters. The vast existing literature on this element has been sifted. A chapter on isopolyanions and heteropolyanions (a fast growing field in coordination chemistry of importance to both fundamental research and industrial application), a chapter on the aqueous solution chemistry of Mo, one chapter covering oxidation states 0, I and II, one with oxidation states III, IV and V and a whole chapter on the chemistry of molybdenum(VI) have been prepared. Each of these is well written and covers recent, exciting developments in Mo chemistry. The final chapter of Volume 3 highlights some special topics of Mo chemistry (bioinorganic aspects, Fe—Mo—S clusters and other clusters, hydride and dihydrogen complexes of Mo).

Within the series of transition elements the review on the coordination chemistry of chromium has probably been one of the most difficult to write. Chromium chemistry has been an active field of research for at least 100 years—just imagine the pile of 1457 Xerox copies of papers, which are referenced in this review.

Most of the literature cited [more than an estimated 80% of a total of 10,500 references(!)] has been published during the 1970s and 1980s; thus the material presented here covers all actual research areas (fundamental and to some degree industrial). An author writing a review of this kind always faces serious problems concerning the choice of topics to be covered; his personal preferences and dislikes will certainly be of influence. In my opinion all authors have done a balanced and excellent job. The editors were very fortunate in picking their authors.

Of course, in a monumental piece of work such as this an assiduous reviewer will always find a topic or a paper of his own that is missing or not cired; this is human, but I do not understand why the coordination chemistry of vanadium(V) has not been dealt with. Surely, there must be some complexes of this element in this particular oxidation state in the literature.

In summary, *Comprehensive Coordination Chemistry* Volume 3 is a masterpiece of the editors and the authors. It will serve as a reference source and spring for new research ideas for many years to come. It is a must for all libraries and should be on the shelf of chemists involved in fundamental and industrial research.

Ruhr-Universität Bochum **K. WIEGHARDT**
F.R.G.

Volume 4. Middle Transition Elements

Volume 4 of this seven-volume series contains treatise on coordination compounds of important middle transition elements from manganese to iridium. Each chapter is really *comprehensive* and will be of great help to the reader of this book. The authors, editors and the publisher deserve our gratitude.

Each chapter begins with a concise introduction and is followed by a description of the coordination compounds of the element in various oxidation states having carbon, oxygen, sulfur, halide, hydrogen and hydride ligands. For most metals the treatise also contains compounds with macrocyclic ligands such as porphyrins and phthalocyanines. Some chapters discuss such relevant topics as photochemical, biological and catalytic properties as well. Extensive and up-to-date references are thorough and quite valuable. The following is the number of references cited in the appropriate chapters for respective elements: Mn (759), Re (639), Fe(III) and higher states (503), Ru (2653), Os (908), Co (1217), Rh (1357), Ir (638), Fe(II) and lower states (1117). Previous handbooks and reviews including Gmelin are appropriately referred to. There are reasonable overlaps with the companion work from the same publisher, *Comprehensive Organometallic Chemistry*, to the extent that both are complementary and can be consulted independently. Presentation of formulae and equations is clear and readable. Thoughtful but not excessive usage of tables is quite appropriate. Subject and formula indices attached at the end make quick consultation of the volume easier. It is unfortunate that the chapter dealing with technetium is not included and iron is placed in two separate chapters in the present volume because of factors beyond the editors' control. However, the editors' decision to publish the materials in the present form is justified to avoid undue delay of the publication of this valuable series.

ies; it does not. On p. 596 the diagram shows four structures but uses three structure numbers; it will be claimed that the centre two structures are like two Kekulé structures of benzene. Page 733, Fig. 18 and preceding text: X = N does not work. Page 919, Structure (18), methyl substitutes and cation charge are missing.

Ohio State University **N. STEPHENSON and**
U.S.A. **D. H. BUSCH**

Volume 3. Main Group & Early Transition Elements

The third volume of this colossal work deals with the coordination chemistry of main group and early transition elements including the lanthanides and actinides in 1600(!) pages. Traditionally, typical non-metal elements like B, Si, S, the halogens and noble gases are rarely considered to have a coordination chemistry. At least in the country of this reviewer there appears to exist a psychological and/or language barrier between the camps of main group and transition metal chemists. Chapters 23–30 undertake the heroic attempt to overcome much pride and many prejudices on both sides—after all, it is merely inorganic chemistry. The authors, all of them are experts in their fields, of these chapters are to be congratulated for their excellent presentation of a diverse and complicated material. I am convinced that the members of both camps will enjoy the reading, and many new research ideas will evolve—be it only from the "interdisciplinary" character of this venture.

About 80% of Volume 3 deals with the coordination chemistry of Ti, Zr, Hf, V, Nb, Ta, Cr, Mo, W, the lanthanides and actinides—real metals. The explosive development of the chemistry of molybdenum in all its various oxidation states during the past two to three decades has found its precipitation in seven individual chapters. The vast existing literature on this element has been sifted. A chapter on isopolyanions and heteropolyanions (a fast growing field in coordination chemistry of importance to both fundamental research and industrial application), a chapter on the aqueous solution chemistry of Mo, one chapter covering oxidation states 0, I and II, one with oxidation states III, IV and V and a whole chapter on the chemistry of molybdenum(VI) have been prepared. Each of these is well written and covers recent, exciting developments in Mo chemistry. The final chapter of Volume 3 highlights some special topics of Mo chemistry (bioinorganic aspects, Fe—Mo—S clusters and other clusters, hydride and dihydrogen complexes of Mo).

Within the series of transition elements the review on the coordination chemistry of chromium has probably been one of the most difficult to write. Chromium chemistry has been an active field of research for at least 100 years—just imagine the pile of 1457 Xerox copies of papers, which are referenced in this review.

Most of the literature cited [more than an estimated 80% of a total of 10,500 references(!)] has been published during the 1970s and 1980s; thus the material presented here covers all actual research areas (fundamental and to some degree industrial). An author writing a review of this kind always faces serious problems concerning the choice of topics to be covered; his personal preferences and dislikes will certainly be of influence. In my opinion all authors have done a balanced and excellent job. The editors were very fortunate in picking their authors.

Of course, in a monumental piece of work such as this an assiduous reviewer will always find a topic or a paper of his own that is missing or not cired; this is human, but I do not understand why the coordination chemistry of vanadium(V) has not been dealt with. Surely, there must be some complexes of this element in this particular oxidation state in the literature.

In summary, *Comprehensive Coordination Chemistry* Volume 3 is a masterpiece of the editors and the authors. It will serve as a reference source and spring for new research ideas for many years to come. It is a must for all libraries and should be on the shelf of chemists involved in fundamental and industrial research.

Ruhr-Universität Bochum **K. WIEGHARDT**
F.R.G.

Volume 4. Middle Transition Elements

Volume 4 of this seven-volume series contains treatise on coordination compounds of important middle transition elements from manganese to iridium. Each chapter is really *comprehensive* and will be of great help to the reader of this book. The authors, editors and the publisher deserve our gratitude.

Each chapter begins with a concise introduction and is followed by a description of the coordination compounds of the element in various oxidation states having carbon, oxygen, sulfur, halide, hydrogen and hydride ligands. For most metals the treatise also contains compounds with macrocyclic ligands such as porphyrins and phthalocyanines. Some chapters discuss such relevant topics as photochemical, biological and catalytic properties as well. Extensive and up-to-date references are thorough and quite valuable. The following is the number of references cited in the appropriate chapters for respective elements: Mn (759), Re (639), Fe(III) and higher states (503), Ru (2653), Os (908), Co (1217), Rh (1357), Ir (638), Fe(II) and lower states (1117). Previous handbooks and reviews including Gmelin are appropriately referred to. There are reasonable overlaps with the companion work from the same publisher, *Comprehensive Organometallic Chemistry*, to the extent that both are complementary and can be consulted independently. Presentation of formulae and equations is clear and readable. Thoughtful but not excessive usage of tables is quite appropriate. Subject and formula indices attached at the end make quick consultation of the volume easier. It is unfortunate that the chapter dealing with technetium is not included and iron is placed in two separate chapters in the present volume because of factors beyond the editors' control. However, the editors' decision to publish the materials in the present form is justified to avoid undue delay of the publication of this valuable series.

ies; it does not. On p. 596 the diagram shows four structures but uses three structure numbers; it will be claimed that the centre two structures are like two Kekulé structures of benzene. Page 733, Fig. 18 and preceding text: X = N does not work. Page 919, Structure (18), methyl substitutes and cation charge are missing.

Ohio State University **N. STEPHENSON and**
U.S.A. **D. H. BUSCH**

Volume 3. Main Group & Early Transition Elements

The third volume of this colossal work deals with the coordination chemistry of main group and early transition elements including the lanthanides and actinides in 1600(!) pages. Traditionally, typical non-metal elements like B, Si, S, the halogens and noble gases are rarely considered to have a coordination chemistry. At least in the country of this reviewer there appears to exist a psychological and/or language barrier between the camps of main group and transition metal chemists. Chapters 23–30 undertake the heroic attempt to overcome much pride and many prejudices on both sides—after all, it is merely inorganic chemistry. The authors, all of them are experts in their fields, of these chapters are to be congratulated for their excellent presentation of a diverse and complicated material. I am convinced that the members of both camps will enjoy the reading, and many new research ideas will evolve—be it only from the "interdisciplinary" character of this venture.

About 80% of Volume 3 deals with the coordination chemistry of Ti, Zr, Hf, V, Nb, Ta, Cr, Mo, W, the lanthanides and actinides—real metals. The explosive development of the chemistry of molybdenum in all its various oxidation states during the past two to three decades has found its precipitation in seven individual chapters. The vast existing literature on this element has been sifted. A chapter on isopolyanions and heteropolyanions (a fast growing field in coordination chemistry of importance to both fundamental research and industrial application), a chapter on the aqueous solution chemistry of Mo, one chapter covering oxidation states 0, I and II, one with oxidation states III, IV and V and a whole chapter on the chemistry of molybdenum(VI) have been prepared. Each of these is well written and covers recent, exciting developments in Mo chemistry. The final chapter of Volume 3 highlights some special topics of Mo chemistry (bioinorganic aspects, Fe—Mo—S clusters and other clusters, hydride and dihydrogen complexes of Mo).

Within the series of transition elements the review on the coordination chemistry of chromium has probably been one of the most difficult to write. Chromium chemistry has been an active field of research for at least 100 years—just imagine the pile of 1457 Xerox copies of papers, which are referenced in this review.

Most of the literature cited [more than an estimated 80% of a total of 10,500 references(!)] has been published during the 1970s and 1980s; thus the material presented here covers all actual research areas (fundamental and to some degree industrial). An author writing a review of this kind always faces serious problems concerning the choice of topics to be covered; his personal preferences and dislikes will certainly be of influence. In my opinion all authors have done a balanced and excellent job. The editors were very fortunate in picking their authors.

Of course, in a monumental piece of work such as this an assiduous reviewer will always find a topic or a paper of his own that is missing or not cired; this is human, but I do not understand why the coordination chemistry of vanadium(V) has not been dealt with. Surely, there must be some complexes of this element in this particular oxidation state in the literature.

In summary, *Comprehensive Coordination Chemistry* Volume 3 is a masterpiece of the editors and the authors. It will serve as a reference source and spring for new research ideas for many years to come. It is a must for all libraries and should be on the shelf of chemists involved in fundamental and industrial research.

Ruhr-Universität Bochum **K. WIEGHARDT**
F.R.G.

Volume 4. Middle Transition Elements

Volume 4 of this seven-volume series contains treatise on coordination compounds of important middle transition elements from manganese to iridium. Each chapter is really *comprehensive* and will be of great help to the reader of this book. The authors, editors and the publisher deserve our gratitude.

Each chapter begins with a concise introduction and is followed by a description of the coordination compounds of the element in various oxidation states having carbon, oxygen, sulfur, halide, hydrogen and hydride ligands. For most metals the treatise also contains compounds with macrocyclic ligands such as porphyrins and phthalocyanines. Some chapters discuss such relevant topics as photochemical, biological and catalytic properties as well. Extensive and up-to-date references are thorough and quite valuable. The following is the number of references cited in the appropriate chapters for respective elements: Mn (759), Re (639), Fe(III) and higher states (503), Ru (2653), Os (908), Co (1217), Rh (1357), Ir (638), Fe(II) and lower states (1117). Previous handbooks and reviews including Gmelin are appropriately referred to. There are reasonable overlaps with the companion work from the same publisher, *Comprehensive Organometallic Chemistry*, to the extent that both are complementary and can be consulted independently. Presentation of formulae and equations is clear and readable. Thoughtful but not excessive usage of tables is quite appropriate. Subject and formula indices attached at the end make quick consultation of the volume easier. It is unfortunate that the chapter dealing with technetium is not included and iron is placed in two separate chapters in the present volume because of factors beyond the editors' control. However, the editors' decision to publish the materials in the present form is justified to avoid undue delay of the publication of this valuable series.

The reviewer highly recommends the purchase of this series by libraries related to chemistry. The present volume attests the high standard of the series.

Tokyo Institute of Technology **A. YAMAMOTO**
Japan

Volume 5. Late Transition Elements

Volume 5 of the seven-volume series of *Comprehensive Coordination Chemistry* contains the following chapters: 50, Nickel by L. Sacconi, F. Mani and A. Bencini (Firenze), pp. 1–347; 51, Palladium by M. J. H. Russell and C. F. J. Barnard (Reading), pp. 1099–1130; 51.8, Palladium(II): Sulfur Donor Complexes by A. T. Hutton (Belfast), pp. 1131–1155; 51.9, Palladium(II): Phosphorous Donor Complexes by A. T. Hutton and C. P. Morley (Belfast), pp. 1157–1170; 52, Platinum by D. M. Roundhill (New Orleans), pp. 351–531; 53, Copper by B. J. Hathaway (Cork), pp. 533–774; 54, Silver by R. J. Lancashire (Kingston, Jamaica), pp. 775–859; 55, Gold by R. J. Puddephatt (London, Ontario), pp. 861–923; 56.1, Zinc and Cadmium by R. H. Prince (Cambridge, U.K.), pp. 925–1045; 56.2, Mercury by K. Brodersen and H. U. Hummel (Erlangen), pp. 1047–1097. The volume is completed by a Subject Index and by a Formula Index.

Each chapter ends with the list of references: the total number of references contained in this volume is 10,728, which corresponds to an average of more than 9.3 papers reviewed per printed page, if multiple references are taken into consideration.

This impressive volume dedicated to late transition elements is arranged under the distinction, which is presumably valid for the whole treatise, that compounds containing a number of metal–carbon bonds equal to or higher than the coordination number of the central metal atom are regarded as organometallics and as such are outside the scope of this volume series. Also binary oxides and sulfides have generally been excluded, which may appear at the first sight unfortunate in view of the present interest in this type of compound. On the other hand, other reference sources are available for these compounds characterized by three-dimensional extended structures. Even with these limitations, this volume covers a huge amount of inorganic chemistry and the authors and editors must be congratulated for their efforts in carrying out and accomplishing such a remarkable work. Scientific papers continue to grow in number every year and, as a consequence, people tend to specialize. This is why a volume series like the one which is now offered in print is very valuable since it gives every interested person the possibility of acquiring reliable knowledge of a specific subject with relatively small effort.

The material in this volume is classified in chapters according to the metal and, within each sub-chapter, according to the oxidation state of the metal and the type of donor atom. However, in several instances, authors have written remarkably good additional sub-chapters on general aspects and theories getting across the oxidation state and ligand type classification. Particularly remarkable from this point of view are the following sub-chapters: 50.5.1. on Electronic Spectra and Spectromagnetic Properties of Nickel(II) Complexes; 53.4.4. on Electronic Properties of Copper(II); 52.9 on Substitution Reactions and Reaction Mechanisms of Platinum(II) Complexes; 56.1.14 on Aspects of the Biological Chemistry of Zinc and Cadmium.

Literature coverage goes as far as 1985 in most cases. In this connection, a word of caution should perhaps be given for those who would like to use this volume as a substitute for the literature survey: these volumes were not meant, I believe, to be exhaustive of the available literature. Thus, failure to find a given compound in this volume and/or in its Formula Index does not necessarily exclude its existence. Acquisition of this volume series does not vanify the literature search either computerized or "manual", or, better, both.

This volume is generally speaking extremely well written and the number of typographical errors is really reduced to a minimum. As a whole this is an outstanding accomplishment and the acquisition of this volume by libraries is certainly a must. As far as can be judged from this Volume, the entire treatise dedicated to Coordination Chemistry appears to be an extremely useful reference work for researchers and teachers.

Università di Pisa **F. CALDERAZZO**
Italy

Volume 6. Applications

It is in a volume entitled "Applications" where the appropriateness of the word "Comprehensive" should receive its most severe test. How are topics to be defined—broadly or narrowly? Which should be included? Are individual chapters to be aimed primarily at specialists in the particular application, in which case complete coverage of the literature is essential; or at those with general knowledge, for whom identification of basic concepts and outstanding problems is more valuable? The editors and authors of this volume, perhaps following Emerson's precept, do not appear to have sought a consistent set of answers to these dilemmas: articles vary widely in approach and depth of coverage. Nonetheless, the majority present well-organized summaries of huge quantities of useful information, and represent, at the minimum, excellent starting points for entering the literature of their respective topics.

The largest section of this volume is entitled "Uses in Synthesis and Catalysis" and contains five articles, three with rather general titles. Two of these, "Stoichiometric Reactions of Coordinated Ligands" and "Lewis Acid Catalysis and the Reactions of Coordinated Ligands" form a nice complementary pair: the first deals primarily with template-type condensation reactions; the second with hydrolysis reactions. A third, "Catalytic Activation of Small Molecules", attempts to cover the whole of this huge topic, with mixed results—a number of areas receive only cursory attention. One problem is the distinction between subjects falling into the scope of this work and those belonging in the companion *Comprehensive Organometallic Chemistry*. For example, hydroformylation and

The reviewer highly recommends the purchase of this series by libraries related to chemistry. The present volume attests the high standard of the series.

Tokyo Institute of Technology **A. YAMAMOTO**
Japan

Volume 5. Late Transition Elements

Volume 5 of the seven-volume series of *Comprehensive Coordination Chemistry* contains the following chapters: 50, Nickel by L. Sacconi, F. Mani and A. Bencini (Firenze), pp. 1–347; 51, Palladium by M. J. H. Russell and C. F. J. Barnard (Reading), pp. 1099–1130; 51.8, Palladium(II): Sulfur Donor Complexes by A. T. Hutton (Belfast), pp. 1131–1155; 51.9, Palladium(II): Phosphorous Donor Complexes by A. T. Hutton and C. P. Morley (Belfast), pp. 1157–1170; 52, Platinum by D. M. Roundhill (New Orleans), pp. 351–531; 53, Copper by B. J. Hathaway (Cork), pp. 533–774; 54, Silver by R. J. Lancashire (Kingston, Jamaica), pp. 775–859; 55, Gold by R. J. Puddephatt (London, Ontario), pp. 861–923; 56.1, Zinc and Cadmium by R. H. Prince (Cambridge, U.K.), pp. 925–1045; 56.2, Mercury by K. Brodersen and H. U. Hummel (Erlangen), pp. 1047–1097. The volume is completed by a Subject Index and by a Formula Index.

Each chapter ends with the list of references: the total number of references contained in this volume is 10,728, which corresponds to an average of more than 9.3 papers reviewed per printed page, if multiple references are taken into consideration.

This impressive volume dedicated to late transition elements is arranged under the distinction, which is presumably valid for the whole treatise, that compounds containing a number of metal–carbon bonds equal to or higher than the coordination number of the central metal atom are regarded as organometallics and as such are outside the scope of this volume series. Also binary oxides and sulfides have generally been excluded, which may appear at the first sight unfortunate in view of the present interest in this type of compound. On the other hand, other reference sources are available for these compounds characterized by three-dimensional extended structures. Even with these limitations, this volume covers a huge amount of inorganic chemistry and the authors and editors must be congratulated for their efforts in carrying out and accomplishing such a remarkable work. Scientific papers continue to grow in number every year and, as a consequence, people tend to specialize. This is why a volume series like the one which is now offered in print is very valuable since it gives every interested person the possibility of acquiring reliable knowledge of a specific subject with relatively small effort.

The material in this volume is classified in chapters according to the metal and, within each sub-chapter, according to the oxidation state of the metal and the type of donor atom. However, in several instances, authors have written remarkably good additional sub-chapters on general aspects and theories getting across the oxidation state and ligand type classification. Particularly remarkable from this point of view are the following sub-chapters: 50.5.1. on Electronic Spectra and Spectromagnetic Properties of Nickel(II) Complexes; 53.4.4. on Electronic Properties of Copper(II); 52.9 on Substitution Reactions and Reaction Mechanisms of Platinum(II) Complexes; 56.1.14 on Aspects of the Biological Chemistry of Zinc and Cadmium.

Literature coverage goes as far as 1985 in most cases. In this connection, a word of caution should perhaps be given for those who would like to use this volume as a substitute for the literature survey: these volumes were not meant, I believe, to be exhaustive of the available literature. Thus, failure to find a given compound in this volume and/or in its Formula Index does not necessarily exclude its existence. Acquisition of this volume series does not vanify the literature search either computerized or "manual", or, better, both.

This volume is generally speaking extremely well written and the number of typographical errors is really reduced to a minimum. As a whole this is an outstanding accomplishment and the acquisition of this volume by libraries is certainly a must. As far as can be judged from this Volume, the entire treatise dedicated to Coordination Chemistry appears to be an extremely useful reference work for researchers and teachers.

Università di Pisa **F. CALDERAZZO**
Italy

Volume 6. Applications

It is in a volume entitled "Applications" where the appropriateness of the word "Comprehensive" should receive its most severe test. How are topics to be defined—broadly or narrowly? Which should be included? Are individual chapters to be aimed primarily at specialists in the particular application, in which case complete coverage of the literature is essential; or at those with general knowledge, for whom identification of basic concepts and outstanding problems is more valuable? The editors and authors of this volume, perhaps following Emerson's precept, do not appear to have sought a consistent set of answers to these dilemmas: articles vary widely in approach and depth of coverage. Nonetheless, the majority present well-organized summaries of huge quantities of useful information, and represent, at the minimum, excellent starting points for entering the literature of their respective topics.

The largest section of this volume is entitled "Uses in Synthesis and Catalysis" and contains five articles, three with rather general titles. Two of these, "Stoichiometric Reactions of Coordinated Ligands" and "Lewis Acid Catalysis and the Reactions of Coordinated Ligands" form a nice complementary pair: the first deals primarily with template-type condensation reactions; the second with hydrolysis reactions. A third, "Catalytic Activation of Small Molecules", attempts to cover the whole of this huge topic, with mixed results—a number of areas receive only cursory attention. One problem is the distinction between subjects falling into the scope of this work and those belonging in the companion *Comprehensive Organometallic Chemistry*. For example, hydroformylation and

The reviewer highly recommends the purchase of this series by libraries related to chemistry. The present volume attests the high standard of the series.

Tokyo Institute of Technology **A. YAMAMOTO**
Japan

Volume 5. Late Transition Elements

Volume 5 of the seven-volume series of *Comprehensive Coordination Chemistry* contains the following chapters: 50, Nickel by L. Sacconi, F. Mani and A. Bencini (Firenze), pp. 1–347; 51, Palladium by M. J. H. Russell and C. F. J. Barnard (Reading), pp. 1099–1130; 51.8, Palladium(II): Sulfur Donor Complexes by A. T. Hutton (Belfast), pp. 1131–1155; 51.9, Palladium(II): Phosphorous Donor Complexes by A. T. Hutton and C. P. Morley (Belfast), pp. 1157–1170; 52, Platinum by D. M. Roundhill (New Orleans), pp. 351–531; 53, Copper by B. J. Hathaway (Cork), pp. 533–774; 54, Silver by R. J. Lancashire (Kingston, Jamaica), pp. 775–859; 55, Gold by R. J. Puddephatt (London, Ontario), pp. 861–923; 56.1, Zinc and Cadmium by R. H. Prince (Cambridge, U.K.), pp. 925–1045; 56.2, Mercury by K. Brodersen and H. U. Hummel (Erlangen), pp. 1047–1097. The volume is completed by a Subject Index and by a Formula Index.

Each chapter ends with the list of references: the total number of references contained in this volume is 10,728, which corresponds to an average of more than 9.3 papers reviewed per printed page, if multiple references are taken into consideration.

This impressive volume dedicated to late transition elements is arranged under the distinction, which is presumably valid for the whole treatise, that compounds containing a number of metal–carbon bonds equal to or higher than the coordination number of the central metal atom are regarded as organometallics and as such are outside the scope of this volume series. Also binary oxides and sulfides have generally been excluded, which may appear at the first sight unfortunate in view of the present interest in this type of compound. On the other hand, other reference sources are available for these compounds characterized by three-dimensional extended structures. Even with these limitations, this volume covers a huge amount of inorganic chemistry and the authors and editors must be congratulated for their efforts in carrying out and accomplishing such a remarkable work. Scientific papers continue to grow in number every year and, as a consequence, people tend to specialize. This is why a volume series like the one which is now offered in print is very valuable since it gives every interested person the possibility of acquiring reliable knowledge of a specific subject with relatively small effort.

The material in this volume is classified in chapters according to the metal and, within each sub-chapter, according to the oxidation state of the metal and the type of donor atom. However, in several instances, authors have written remarkably good additional sub-chapters on general aspects and theories getting across the oxidation state and ligand type classification. Particularly remarkable from this point of view are the following sub-chapters: 50.5.1. on Electronic Spectra and Spectromagnetic Properties of Nickel(II) Complexes; 53.4.4. on Electronic Properties of Copper(II); 52.9 on Substitution Reactions and Reaction Mechanisms of Platinum(II) Complexes; 56.1.14 on Aspects of the Biological Chemistry of Zinc and Cadmium.

Literature coverage goes as far as 1985 in most cases. In this connection, a word of caution should perhaps be given for those who would like to use this volume as a substitute for the literature survey: these volumes were not meant, I believe, to be exhaustive of the available literature. Thus, failure to find a given compound in this volume and/or in its Formula Index does not necessarily exclude its existence. Acquisition of this volume series does not vanify the literature search either computerized or "manual", or, better, both.

This volume is generally speaking extremely well written and the number of typographical errors is really reduced to a minimum. As a whole this is an outstanding accomplishment and the acquisition of this volume by libraries is certainly a must. As far as can be judged from this Volume, the entire treatise dedicated to Coordination Chemistry appears to be an extremely useful reference work for researchers and teachers.

Università di Pisa **F. CALDERAZZO**
Italy

Volume 6. Applications

It is in a volume entitled "Applications" where the appropriateness of the word "Comprehensive" should receive its most severe test. How are topics to be defined—broadly or narrowly? Which should be included? Are individual chapters to be aimed primarily at specialists in the particular application, in which case complete coverage of the literature is essential; or at those with general knowledge, for whom identification of basic concepts and outstanding problems is more valuable? The editors and authors of this volume, perhaps following Emerson's precept, do not appear to have sought a consistent set of answers to these dilemmas: articles vary widely in approach and depth of coverage. Nonetheless, the majority present well-organized summaries of huge quantities of useful information, and represent, at the minimum, excellent starting points for entering the literature of their respective topics.

The largest section of this volume is entitled "Uses in Synthesis and Catalysis" and contains five articles, three with rather general titles. Two of these, "Stoichiometric Reactions of Coordinated Ligands" and "Lewis Acid Catalysis and the Reactions of Coordinated Ligands" form a nice complementary pair: the first deals primarily with template-type condensation reactions; the second with hydrolysis reactions. A third, "Catalytic Activation of Small Molecules", attempts to cover the whole of this huge topic, with mixed results—a number of areas receive only cursory attention. One problem is the distinction between subjects falling into the scope of this work and those belonging in the companion *Comprehensive Organometallic Chemistry*. For example, hydroformylation and

methanol carbonylation using Rh-based catalysts are covered, but the same reactions involving CO are excluded—a rather arbitrary choice. Also within this section are articles on Metal Complexes in Oxidation and Decomposition of Water into its Elements. Both are excellent reviews—thorough, critical, and relatively up-to-date (the former in particular contains an addendum bringing literature coverage up into 1985, considerably later than most of this volume).

The longest single review (over 200 pages, with more than 1500 references!) is on "Coordination Compounds in Biology"; while this may not strictly be an "application" (which implies human intention), it is a first-rate summary of a topic which usually requires an entire book. It is noteworthy that this is not simply an updating of the author's (M. N. Hughes) 1981 monograph, but is a substantially new effort—reorganized, and focused more towards those with a good background in the subject than to the general chemical readership. The impact of this review would be even greater were it not for the fact that work in this field is moving so fast that many of the topics—e.g. calcium biochemistry, electron transfer in proteins—are already woefully out of date. Also in this section ("Biological and Medical Aspects") is an article, Uses in Therapy, on several aspects of the role of metals in treating diseases; targeted radiolabelled complexes are not covered here, though, but rather included in "Applications in the Nuclear Fuel Cycle and Radiopharmacy".

A number of articles address topics which receive relatively little attention from basic researchers. These include: Dyes and Pigments, Photographic Applications, Application to Extractive Metallurgy, and Geochemical and Prebiotic Systems. All should prove useful both to the applied researcher seeking to bring more basic principles to bear on his work, and to the general coordination chemist looking for new "relevant" fields. "Electrochemical Applications" deals primarily with electrodeposition, which fits into the above category, as well as with surface modified electrodes; while "Compounds Exhibiting Unusual Electrical Properties" presents a topic of materials science which is of great current interest. Lastly, "Other Uses of Coordination Compounds" is mainly a compendium of references from *Chemical Abstracts* and lesser-known journals over the period 1974–1981.

In general the articles are well-written and produced, living up to the standards set by the previous *Comprehensive . . . Chemistry* compendia. Few elaborate figures are included, but there is a generous provision of clear line drawings. While there are a few fairly major errors (examples: a reversed application of Le Chatelier's principle on p. 2; incorrect table entries on p. 545 which state, among other inaccuracies, that the typical human body contains 1 g of calcium!), the volume is generally free from excessive typos. A separate volume index is provided but, because of the substantial overlap of coverage with chapters in other volumes, most readers will probably get more use out of the cumulative indices in Volume 7. The only real deficiency, as noted earlier, is the early termination of literature coverage in most chapters—often more than four years before publication. All in all, this is a volume to which practitioners of all aspects of inorganic chemistry will want to have access.

California Institute of Technology **J. A. LABINGER**
U.S.A. **and H. B. GRAY**

Volume 7. Indexes

This Volume provides an Index of Review Articles and Specialist Texts together with Cumulative Subject and Formula Indexes.

Gmelin: Handbook of Inorganic Chemistry. Be—Beryllium (System No. 26—Organoberyllium Compounds). Published by the Gmelin Institute for Inorganic Chemistry of the Max Planck Society for the Advancement of Science, 8th Edn. Springer, Berlin, 1987. ISBN 3-540-93556-8, 247 pp.

This is another volume in the excellent series of Gmelin Handbooks describing the inorganic chemistry of individual elements; in this case organoberyllium compounds.

The treatment covers the literature up until 1986 plus selected references from 1987. It is characteristically comprehensive although, as is pointed out in the preface, the field is both comparatively small and unlikely to expand appreciably in the future.

The main body of data is classified by the number of Be—C bonds per organyl ligand: the first chapter deals with tri- and tetraorganyl beryllates, and mono- and diorganyl compounds and their adducts; subsequent chapters report beryllocarboranes and finally cyclopentadienyl systems. A short section follows on compounds of unknown structure and the text concludes with reports of theoretical studies on hypothetical compounds (the latter being unusually large for beryllium relative to the body of experimental data).

The overall treatment is clear and concise; data on specific compounds are easy to find from the empirical formula and ligand formula indices. However, it is difficult to imagine to whom this text should be recommended. That the chemistry of beryllium is fascinating is indisputable, but the brevity of the paragraph on "Uses" (p. 33) is perhaps as much a reason for the lack of progress as the hazardous nature of the compounds; particularly in such an application-orientated age. The increasing importance of one application, viz. the incorporation of beryllium as a dopant in the Metal–organic Vapour Phase Epitaxy of III–V semiconductors may, however, lead to renewed interest in the near future.

In conclusion, this handbook is an excellent treatment of the subject, and is a fitting tribute to the pioneering work in this field by Prof. Geoffrey Coates.

Department of Chemistry **D. M. FRIGO**
Queen Mary College
London E1 4NS, U.K.

methanol carbonylation using Rh-based catalysts are covered, but the same reactions involving CO are excluded—a rather arbitrary choice. Also within this section are articles on Metal Complexes in Oxidation and Decomposition of Water into its Elements. Both are excellent reviews—thorough, critical, and relatively up-to-date (the former in particular contains an addendum bringing literature coverage up into 1985, considerably later than most of this volume).

The longest single review (over 200 pages, with more than 1500 references!) is on "Coordination Compounds in Biology"; while this may not strictly be an "application" (which implies human intention), it is a first-rate summary of a topic which usually requires an entire book. It is noteworthy that this is not simply an updating of the author's (M. N. Hughes) 1981 monograph, but is a substantially new effort—reorganized, and focused more towards those with a good background in the subject than to the general chemical readership. The impact of this review would be even greater were it not for the fact that work in this field is moving so fast that many of the topics—e.g. calcium biochemistry, electron transfer in proteins—are already woefully out of date. Also in this section ("Biological and Medical Aspects") is an article, Uses in Therapy, on several aspects of the role of metals in treating diseases; targeted radiolabelled complexes are not covered here, though, but rather included in "Applications in the Nuclear Fuel Cycle and Radiopharmacy".

A number of articles address topics which receive relatively little attention from basic researchers. These include: Dyes and Pigments, Photographic Applications, Application to Extractive Metallurgy, and Geochemical and Prebiotic Systems. All should prove useful both to the applied researcher seeking to bring more basic principles to bear on his work, and to the general coordination chemist looking for new "relevant" fields. "Electrochemical Applications" deals primarily with electrodeposition, which fits into the above category, as well as with surface modified electrodes; while "Compounds Exhibiting Unusual Electrical Properties" presents a topic of materials science which is of great current interest. Lastly, "Other Uses of Coordination Compounds" is mainly a compendium of references from *Chemical Abstracts* and lesser-known journals over the period 1974–1981.

In general the articles are well-written and produced, living up to the standards set by the previous *Comprehensive . . . Chemistry* compendia. Few elaborate figures are included, but there is a generous provision of clear line drawings. While there are a few fairly major errors (examples: a reversed application of Le Chatelier's principle on p. 2; incorrect table entries on p. 545 which state, among other inaccuracies, that the typical human body contains 1 g of calcium!), the volume is generally free from excessive typos. A separate volume index is provided but, because of the substantial overlap of coverage with chapters in other volumes, most readers will probably get more use out of the cumulative indices in Volume 7. The only real deficiency, as noted earlier, is the early termination of literature coverage in most chapters—often more than four years before publication. All in all, this is a volume to which practitioners of all aspects of inorganic chemistry will want to have access.

California Institute of Technology **J. A. LABINGER**
U.S.A. **and H. B. GRAY**

Volume 7. Indexes

This Volume provides an Index of Review Articles and Specialist Texts together with Cumulative Subject and Formula Indexes.

Gmelin: Handbook of Inorganic Chemistry. Be—Beryllium (System No. 26—Organoberyllium Compounds). Published by the Gmelin Institute for Inorganic Chemistry of the Max Planck Society for the Advancement of Science, 8th Edn. Springer, Berlin, 1987. ISBN 3-540-93556-8, 247 pp.

This is another volume in the excellent series of Gmelin Handbooks describing the inorganic chemistry of individual elements; in this case organoberyllium compounds.

The treatment covers the literature up until 1986 plus selected references from 1987. It is characteristically comprehensive although, as is pointed out in the preface, the field is both comparatively small and unlikely to expand appreciably in the future.

The main body of data is classified by the number of Be—C bonds per organyl ligand: the first chapter deals with tri- and tetraorganyl beryllates, and mono- and diorganyl compounds and their adducts; subsequent chapters report beryllocarboranes and finally cyclopentadienyl systems. A short section follows on compounds of unknown structure and the text concludes with reports of theoretical studies on hypothetical compounds (the latter being unusually large for beryllium relative to the body of experimental data).

The overall treatment is clear and concise; data on specific compounds are easy to find from the empirical formula and ligand formula indices. However, it is difficult to imagine to whom this text should be recommended. That the chemistry of beryllium is fascinating is indisputable, but the brevity of the paragraph on "Uses" (p. 33) is perhaps as much a reason for the lack of progress as the hazardous nature of the compounds; particularly in such an application-orientated age. The increasing importance of one application, viz. the incorporation of beryllium as a dopant in the Metal–organic Vapour Phase Epitaxy of III–V semiconductors may, however, lead to renewed interest in the near future.

In conclusion, this handbook is an excellent treatment of the subject, and is a fitting tribute to the pioneering work in this field by Prof. Geoffrey Coates.

Department of Chemistry **D. M. FRIGO**
Queen Mary College
London E1 4NS, U.K.

Polyhedron Vol. 7, No. 21, p. 2249, 1988
Pergamon Press plc. Printed in Great Britain

CORRIGENDA

Oxovanadium(IV) and amino acids—I. The system L-alanine+VO^{2+}; a potentiometric and spectroscopic study. J. Costa Pessoa, L. F. Vilas Boas, R. D. Gillard and R. J. Lancashire (*Polyhedron*, Vol. 7, No. 14, pp. 1245–1262, 1988).

(i) On p. 1255 of this paper, in the last complete paragraph, the second sentence should start: "In all cases, the ε (or $\Delta\varepsilon$) values for species MAH, MA, MA_2H_2, MA_2H, $M_2A_2H_{-2}$ and MA_2..." : i.e. the present list of species in this sentence omitted $M_2A_2H_{-2}$.

(ii) The last incomplete paragraph should begin: "Taking β_{111}, β_{110}, β_{122}..."; i.e. the second constant should read β_{110} not, as originally printed, β_{112}.

Polyhedron Vol. 7, No. 22/23, pp. 2251–2253, 1988
Printed in Great Britain

0277–5387/88 $3.00+.00
© 1988 Pergamon Press plc

FOREWORD

The discovery that certain metal alloys have catalytic properties that are far superior to those of their components has been one of the most important developments to occur in the area of heterogeneous catalysis in the last 20 years.[1–6] These catalysts have demonstrated higher activities, greater selectivities and better stabilities than their homonuclear components. Recent studies have shown that some heteronuclear clusters[7–8] and bimetallic mixtures[9–13] exhibit improved catalytic properties in homogeneous phases. Today, a major research effort is being made to develop an understanding of this unusual behaviour.

During the last 25 years, the study of transition metal cluster compounds has also become a focus of considerable attention.[14] These compounds have provided unique opportunities to study the nature of organic transformations at multinuclear metal sites. A wealth of results has already revealed a variety of new and unusual multinuclear ligand activations and rearrangements.[15] Systematic routes for the synthesis of heteronuclear cluster compounds are presently being developed,[16–17] and reports describing remarkable organic transformations by these complexes are now beginning to appear.[18–21]

Due to the importance of catalysis to the petrochemical industry and the recent developments in the study of heteronuclear clusters and multimetallic catalysts, it was decided to convene an international seminar on this topic for the purpose of presenting the latest findings in research, identifying topics of mutual interest to these two areas, formulating current problems and goals, and planning directions for new research. The following topics were the focus of attention:

(1) *Synthesis*

Heteronuclear cluster compounds are generally made by the agglomeration of metal atoms from complexes. These procedures include pyrolysis, redox coupling, bridge-assisted coupling, and coupling promoted by the formation and elimination of small molecules.[16] These techniques are becoming increasingly sophisticated.

Metal alloy catalysts usually have the form of highly dispersed metal on "inert" supports. These clusters are usually much larger than molecular clusters, but their methods of preparation (e.g. impregnation of the supports by solutions of metals containing salts and deposition of molecular clusters) have close similarities and relationships to those of molecular clusters.[22–23]

(2) *Structure*

The physical methods used to study the structure of molecules are vastly different from those used to establish the structure of surfaces.[24–25] Clearly, however, the structures at the reaction sites must be similar both in molecular clusters and on surfaces.[26–27] Studies of the structures of small metal crystallites have now shown that they adopt atomic arrangements that contain five-fold symmetry[28] which is the same as that observed in large molecular clusters[29] and unlike that of macroscopic materials.

X-ray crystallographic analyses of molecular clusters have provided a wealth of detailed information about the nature of the heteronuclear metal–metal bond.[16] NMR spectroscopy which is widely used in the study of molecular complexes is now being applied to the study of the structure and chemistry of surfaces[30] and adsorbates on surfaces.[31–32]

(3) *Reactivity*

The changes in reactivity that have been observed for metal alloys and bimetallic catalysts can be attributed broadly to two influences: geometric and electronic effects.[2]

Electronic effects would result from changes in the electronic structure of a metal atom that are induced by the neighbouring atoms. This effect is frequently referred to as the "ligand effect" both by surface chemists and by solution chemists. While the effect of non-metallic ligands is very important in the chemistry of complexes, it seems to be much less important on surfaces where the ligands are neighbouring metal atoms.[2–4] Heteronuclear metal complexes may provide a unique opportunity to study the electronic influences of neighbouring metal atoms on reactivity. Vahrenkamp has recently reported evidence for stereoselective preference in a hydrogen shift in an alkyne ligand coordinated to a heteronuclear cluster. He attributed the stereoselective induction to an *electronic* effect.[33]

Geometric effects are determined by the structure of the active site. Important factors are: the size

(or nuclearity) of the site (or ensemble) and the nature of its environment (steric effects).[2,6] These factors will be important both in molecular clusters and on the surfaces of alloys. Studies have indicated that the size of the site is very important in catalysis on surfaces.[3] Studies of molecular clusters are showing a variety of small molecule transformations that are based primarily on multinuclear interactions, but to date these studies have been limited to clusters containing very small numbers of metal atoms.[15]

The effects of ion promoters (e.g. halides) and selectivity modifiers[2] (e.g. sulphur) could operate both by electronic and geometric effects. Such effects have been observed in studies of molecular clusters.[34,35]

The most important steps in the catalytic transformations of small molecules are the bond breaking processes that lead to the activation of the reactant and the bond making processes that lead to formation of the products. In metal complexes, ligand elimination to generate a vacant coordination site is frequently a prerequisite to substrate activation. Recently, Atwood has shown that CO dissociation is more facile in mixed Fe/Ru clusters than in the homonuclear species.[36]

The rearrangement of hydrocarbons by surface catalysts can be traced very successfully by combining the results of product formations with those of isotopic labelling experiments.[3] However, details concerning the nature of the bond rearrangement steps, intermediates and the character of the active sites are difficult to establish by these methods. On the other hand, studies of clusters have revealed a great deal about the stability and transformation behaviour of the putative intermediates of hydrocarbon reactions.[15] Studies on alloys and heteronuclear clusters have indicated the importance of cooperative and bifunctional interactions.[19] These effects will promote greater efficiency and selectivity in catalysis.

Studies of multicomponent metal systems under homogeneous conditions have revealed the existence of reactivity enhancements when compared to the reactivity of the individual components.[9,11,37] These enhancement effects are known collectively as **Synergism** and may have a variety of mechanistic origins. For most cases, it has not been established if this synergism is produced by the metal atoms operating in concert or individually in reaction sequences, but regardless of their origin, synergism has been shown to play an important role in the development of more efficient and more selective catalysts.

The seminar was organized by Richard D. Adams of the University of South Carolina, U.S.A. and Wolfgang A. Herrmann of the Technische Universtät München, F.R.G. and was held at the Albertus Magnus College in Königstein, F.R.G. on 7–11 September 1987. The speakers were invited to prepare manuscripts of their presentations for inclusion in this Symposium-in-Print issue of *Polyhedron*. The organizers wish to thank the seminar participants for their generous contributions to this issue and the U.S. National Science Foundation and the Deutsche Forschungsgemeinshaft for their financial support of the meeting.

RICHARD D. ADAMS

REFERENCES

1. (a) J. H. Sinfelt, *Bimetallic Catalysts: Discoveries, Concepts and Applications*. Wiley, NY (1983); (b) J. H. Sinfelt, *Sci. Am.* 1985, **253**, 90.
2. W. M. H. Sachtler, *J. Mol. Catal.* 1984, **25**, 1.
3. V. Ponec, *Adv. Catal.* 1983, **32**, 149.
4. J. H. Sinfelt, *Accts Chem. Res.* 1977, **10**, 15.
5. J. H. Sinfelt, *Catal. Rev.-Sci. Engng* 1974, **9**, 147.
6. L. Guczi, *J. Mol. Catal.* 1984, **25**, 13.
7. T. Venalainen, E. Iiskola, J. Prusiainen, T. A. Pakkanen and T. T. Pakkanen, *J. Mol. Catal.* 1986, **34**, 293.
8. M. Roper, M. Schieren and A. Fumagalli, *J. Mol. Catal.* 1986, **34**, 173.
9. B. D. Dombek, *Organometallics* 1985, **4**, 1707.
10. R. Whyman, *J. Chem. Soc., Chem. Commun.* 1983, 1439.
11. (a) J. F. Knifton, *J. Chem. Soc., Chem. Commun.* 1983, 729; (b) M. Hidai, A. Fukuoka, Y. Koyasu and Y. Uchida, *J. Mol. Catal.* 1986, **35**, 29.
12. R. M. Laine, *J. Org. Chem.* 1980, **45**, 3370.
13. P. C. Ford, R. G. Rinker, R. M. Laine, C. Ungermann, S. A. Landis and S. A. Moya, *J. Am. Chem. Soc.* 1978, **100**, 4595.
14. B. F. G. Johnson (Ed.), *Transition Metal Clusters*. Wiley, Chichester (1980).
15. (a) R. D. Adams and I. T. Horvath, *Prog. Inorg. Chem.* 1985, **33**, 127; H. D. Kaesz, in *Metal Clusters in Catalysis* (Edited by H. Knozinger, B. C. Gates and L. Guczi). Elsevier, Amsterdam (1986).
16. D. A. Roberts and G. L. Geoffroy, in *Comprehensive Organometallic Chemistry* (Edited by G. Wilkinson, F. G. A. Stone and E. W. Abel), Chap. 40. Pergamon Press, Oxford (1982).
17. (a) H. Vahrenkamp, *Phil. Trans. R. Soc. London* 1982, **308A**, 17; (b) A. Ceriotti, F. Demartin, G. Longoni, M. Manassero, M. Marchionna, G. Piva and M. Sansoni, *Angew. Chem. Int. Ed. Engl.* 1985, **24**, 697.
18. J. R. Shapley, C. H. McAteer, M. R. Churchill and H. J. Wasserman, *Organometallics* 1984, **3**, 1595.
19. J. R. Shaplely, J. T. Park, M. R. Churchill, J. W. Ziller and L. R. Beanan, *J. Am. Chem. Soc.* 1984, **106**, 1144.

20. (a) J. T. Park, J. R. Shapley, M. R. Churchill and C. Bueno, *J. Am. Chem. Soc.* 1983, **105**, 6182; (b) J. R. Shapley, J. T. Park, M. R. Churchill, C. Bueno and H. J. Wasserman, *J. Am. Chem. Soc.* 1981, **103**, 7385; (c) L. Busetto, J. C. Jeffrey, R. M. Mills, F. G. A. Stone, M. J. Went and P. Woodward, *J. Chem. Soc., Dalton Trans.* 1983, 101; (d) M. H. Chisholm, D. M. Hoffman and J. C. Huffman, *Chem. Soc. Rev.* 1985, **14**, 69.
21. E. Roland and H. Vahrenkamp, *J. Mol. Catal.* 1983, **21**, 233.
22. (a) J. R. Shapley, S. J. Hardwick, D. S. Foose, M. R. Churchill, C. Bueno and J. P. Hutchinson, *J. Am. Chem. Soc.* 1981, **103**, 7383; (b) A. Choplin, L. Huang, A. Theolier, P. Gallezot, J. M. Basset, U. Siriwardane, S. G. Shore and R. Mathieu, *J. Am. Chem. Soc.* 1986, **108**, 4224.; (c) A. Choplin, L. Huang, J.-M. Basse, R. Mathieu, U. Siriwardane and S. G. Shore, *Organometallics* 1986, **5**, 1547.
23. M. Komiyama, *Catal. Rev.-Sci. Engng* 1985, **27**, 341.
24. J. H. Sinfelt, G. A. Via and F. W. Lytle, *Catal. Rev.-Sci. Engng* 1984, **26**, 81.
25. E. L. Muetterties, T. N. Rhodin, E. Band, C. F. Brucker and W. R. Pretzer, *Chem. Rev.* 1979, **79**, 91.
26. E. L. Muetterties, *Science* 1977, **196**, 839.
27. P. Brun, G. M. Dawkins, M. Green, A. D. Miles, A. G. Orpen and F. G. A. Stone, *J. Chem. Soc., Chem. Commun.* 1982, 926.
28. J. J. Burton, *Catal. Rev.-Sci. Engng* 1974, **9**, 209.
29. D. M. Washececk, E. J. Wucherer, L. F. Dahl, A. Ceriotti, G. Longini, M. Manassero, M. Sansoni and P. Chini, *J. Am. Chem. Soc.* 1979, **101**, 6110.
30. C. A. Fyfe, *Solid State NMR for Chemists.* CRC Press, Guelph (1983).
31. P. J. Toscano and T. J. Marks, *Organometallics* 1986, **5**, 400.
32. P. J. Toscano and T. J. Marks, *J. Am. Chem. Soc.* 1985, **107**, 653,
33. C. Schnering, T. Albiez, W. Bernhardt and H. Vahrenkamp, *Angew. Chem. Int. Ed. Engl.* 1986, **25**, 479.
34. J. L. Zuffa, M. L. Blohm and W. Gladfelter, *J. Am. Chem. Soc.* 1986, **107**, 552.
35. R. D. Adams, J. E. Babin and M. Tasi, *Organometallics* 1986, **6**, 1717.
36. R. Shojaie and J. D. Atwood, *Inorg. Chem.* 1987, **26**, 2199.
37. B. M. Trost and J. M. Tour, *J. Am. Chem. Soc.* 1987, **109**, 5268.

Polyhedron Vol. 7, No. 22/23, pp. 2255–2261, 1988
Printed in Great Britain

0277–5387/88 $3.00+.00
© 1988 Pergamon Press plc

DIRECTED SYNTHESIS OF BIMETALLIC HYDROCARBON BRIDGED COMPOUNDS BY NUCLEOPHILIC ATTACK OF CARBONYL METALATES ON COORDINATED UNSATURATED HYDROCARBONS

WOLFGANG BECK

Institut für Anorganische Chemie, Universität München, Meiserstr. 1, 8000 München 2, F.R.G.

Abstract—The addition of carbonyl metalates (particularly $[Re(CO)_5]^-$) to π-bonded hydrocarbons (olefin, alkyne, allyl, diene, cyclopenta- and hexadiene, trimethylenemethane, cycloheptatriene, benzene and cycloheptatrienyl) in cationic complexes provides a synthesis of new hydrocarbon bridged homo- and heteronuclear complexes.

The addition of nucleophiles to unsaturated hydrocarbons which are π-coordinated to transition metals, is one of the fundamental and particularly well studied reactions in organometallic chemistry.[1,2] These reactions have found many applications in organic synthesis[3] and in industrial processes,[4] such as the Wacker process.[5] A number of theoretical analyses have been made to account for the high degree of regio- and stereoselectivity of these reactions. Rules have been developed for the most favourable positions for nucleophilic attack at the unsaturated hydrocarbon and for the reactivity of different hydrocarbons.[1,6] We have found that addition of carbonyl metalates instead of common nucleophiles to π-coordinated hydrocarbons in cationic complexes gives a series of hydrocarbon bridged bimetallic compounds in a directed way. Most of these complexes are not accessible by other synthetic routes.[7]

RESULTS AND DISCUSSION

Cationic ethylene complexes react with carbonyl metalates to give ethylene bridged homo- and heteronuclear compounds (Scheme 1).[8,9] The possibility of formation of ethylene bridged complexes by this route has been previously mentioned.[10]

$Cp(OC)_3MoCH_2CH_2Mo(CO)_3Cp$ **(1)**

$Cp(OC)_3WCH_2CH_2W(CO)_3Cp$ **(2)**

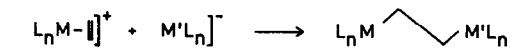

Scheme 1.

$Cp(OC)_3MoCH_2CH_2W(CO)_3Cp$ **(3)**

$Cp(Ph_3P)(OC)_2WCH_2CH_2W(CO)_2(PPh_3)Cp$ **(4)**

$Cp(OC)_3MoCH_2CH_2Re(CO)_5$ **(5)**

$Cp(OC)_3WCH_2CH_2Re(CO)_5$ **(6)**

$(OC)_5MnCH_2CH_2Mn(CO)_5$ **(7)**

$(OC)_5ReCH_2CH_2Re(CO)_5$ **(8)**

$(OC)_5ReCH(Me)CH_2Re(CO)_5$ **(9)**

$(OC)_5MnCH_2CH_2Re(CO)_5$ **(10)**

The heteronuclear complexes **3** and **10** are best prepared from $[Cp(OC)_3Mo]^-$ and $[Cp(OC)_3W(C_2H_4)]^+$ and from $[Mn(CO)_5]^-$ and $[Re(CO)_5(C_2H_4)]^+$, respectively. Cationic complexes $[(OC)_5Re(olefin)]^+$ are readily accessible by reaction of $(OC)_5ReFBF_3$ with olefins under very mild conditions.[9,11,12] The reaction of $[(OC)_5Mn(C_2H_4)]^+$ with $[Re(CO)_5]^-$ results in the formation of a mixture of the homonuclear complexes $(OC)_5MnCH_2CH_2Mn(CO)_5$ and $(OC)_5ReCH_2CH_2Re(CO)_5$. This parallels the preparation of the mixed carbonyl $(OC)_5Mn—Re(CO)_5$ which is only obtained in good yields from $(OC)_5ReX$ (X = Cl, Br) with $[Mn(CO)_5]^-$.[13] In the mixed complexes **5**, **6** and **10** the weaker nucleophiles $[M(CO)_3Cp]^-$ (M = Mo, W) and $[Mn(CO)_5]^-$ can be replaced by $[Re(CO)_5]^-$ to give $(OC)_5ReCH_2CH_2Re(CO)_5$. The order of nucleophilicity has been determined to be $[Re(CO)_5]^- \gg [W(CO)_3Cp]^- > [Mn(CO)_5] > [Mo(CO)_3Cp]^-$.[14]

The thermal stability of the ethylene bridged complexes decreases in the order Re > W > Mo in accordance with the corresponding metal–carbon

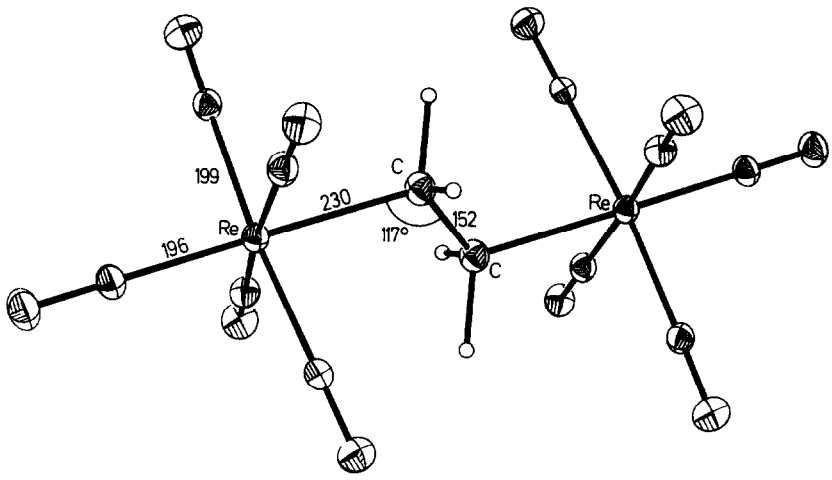

Fig. 1. Molecular structure of $(OC)_5ReCH_2CH_2Re(CO)_5$.

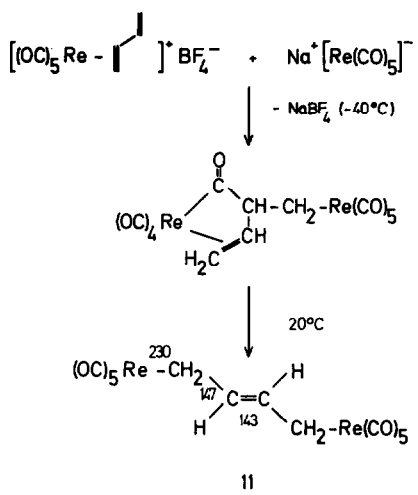

Scheme 2.

bond strength.[15] Thermolysis usually gives ethylene and the metal–metal bonded dimers.

The X-ray structural analysis[9] shows **8** to be a truly dimetallated ethane derivative in the staggered *trans* conformation. The carbon–carbon bond in **8** is almost exactly the same as in ethane.

A further example is the addition of $[Re(CO)_5]^-$ to the coordinated butadiene in $[(OC)_5Re(butadiene)]^+BF_4^-$ which results in the formation of the 2-butene-1,4-diyl bridged complex **11** as the stable product (Scheme 2).[12]

At low temperatures a complex is first formed, which, according to the IR and ^1H NMR spectra, can be formulated as a product of kinetically controlled 1,2-addition with CO insertion and which isomerizes in solution to give **11**. CO insertion or decarbonylation is rare in the case of alkyl and acylcarbonylrhenium complexes. In the case of pentacarbonyl-(2-cyclopropene-1-carbonyl)rhenium,[16] however, decarbonylation already takes place at 20°C, possibly via a similar intermediate as for **11** (Scheme 3).

The reactivity of cationic alkyne η^5-cyclopentadienyl molybdenum[17] and iron[18] complexes has been extensively studied. The addition of $[M(CO)_5]^-$ (M = Mn, Re) or $[CpW(CO)_3]^-$ to the alkyne ligand in $[Cp(OC)(PR_3)(C_2R_2)Mo]^+$ in which the alkyne ligand can be considered as a four electron donor provides a new synthesis of hetero dimetalla tetrahedranes **12** and **13** (Schemes 4 and 5).[19,20] By this method, and using unsymmetrically substituted alkynes, chiral tetrahedral clusters with four different vertices are available in a directed way. Hetero dimetalla tetrahedranes have previously been obtained by other routes.[21]

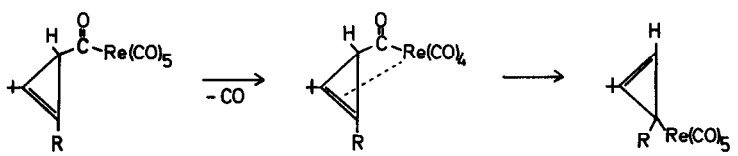

Scheme 3.

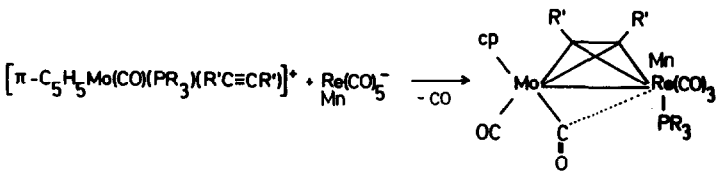

12

	PR_3	R'CCR'	M		PR_3	R'CCR	M
12a	PPh_3	MeCCMe	Mn,Re	d	PEt_3	PhCCPh	Re
b	PPh_3	MeCCPh	Re	e	PMe_2Ph	PhCCPh	Re
c	PPh_3	PhCCPh	Re	f	PPh_3	MeCCnPr	Re

Scheme 4.

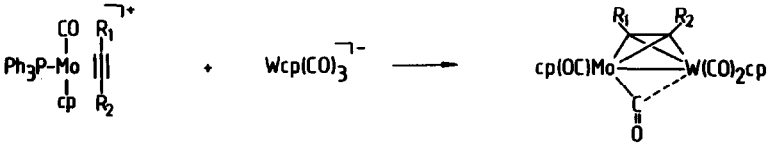

	R_1CCR_2
13a	MeCCPh
b	MeCCEt
c	MeCCMe
d	PhCCPh

13

Scheme 5.

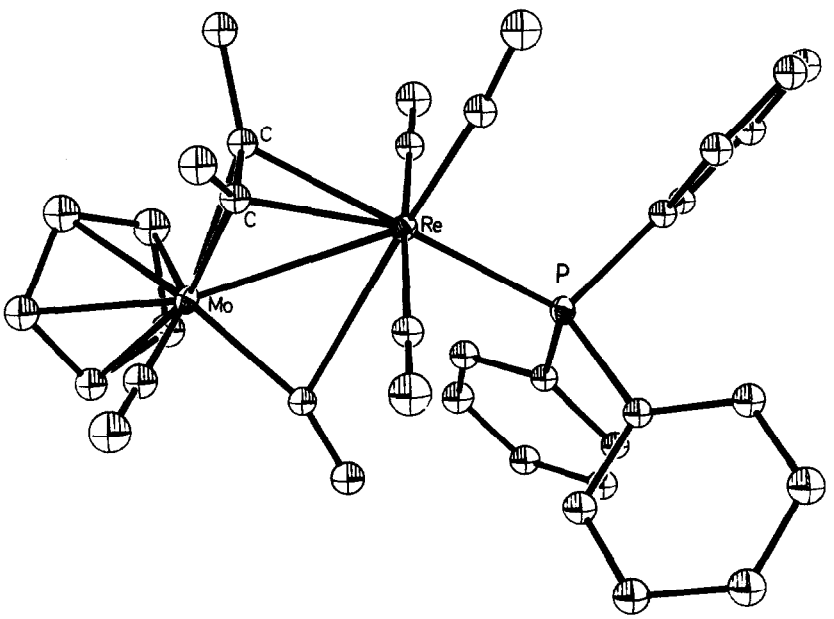

Fig. 2. Molecular structure of $Cp(OC)_2Mo(C_2Me_2)Re(CO)_3PPh_3$.

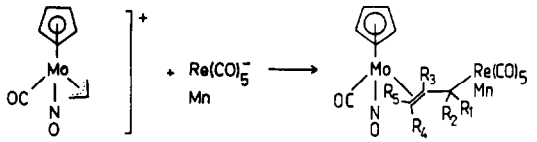

14a $R_1 - R_5 = H$; M = Re
b $R_1 - R_5 = H$; M = Mn
c $R_1, R_2, R_4, R_5 = H$; $R_3 = Me$; M = Re
d $R_1 - R_4 = H$; $R_5 = Me$; M = Re
e $R_1 - R_3 = H$; $R_4, R_5 = Me$; M = Re

Scheme 6.

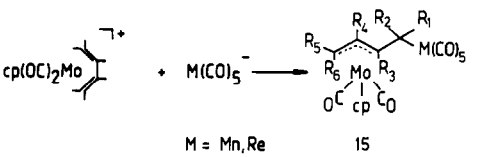

15a $R_1 - R_6 = H$; M = Re
b $R_1 - R_6 = H$; M = Mn
c $R_1 - R_5 = H \cdot R_6 = Me$; M = Re
d $R_1, R_2, R_4, R_5, R_6 = H$; $R_3 = Me$; M = Re
e $R_1, R_2, R_5, R_6 = H$; $R_3, R_4 = Me$; M = Re

Scheme 7.

The nucleophilic attack of $[Re(CO)_5]^-$ or $[Mn(CO)_5]^-$ on the allyl ligand of $[CpMo(CO)(NO)(allyl)]^+$ leads to σ,π-allyl bridged complexes $Cp(OC)(ON)Mo(allyl)M(CO)_5$ (**14**) (M = Re, Mn) (Scheme 6).[22] The crystal structure is consistent with attack of $[Re(CO)_5]^-$ on the allyl group *cis* to NO in the *exo* isomer of the starting allyl complex, as has been previously observed with organic nucleophiles.[23] The stereospecificity of these reactions has been theoretically analysed.[24]

Similarly, the addition of $[Re(CO)_5]^-$ and $[Mn(CO)_5]^-$ to coordinated dienes of cationic molybdenum complexes leads to products which are expected from reactions with organic nucleophiles[25] and from the rules given by Davies, Green and Mingos.[1-3] Attack occurs on the terminal position of the diene to give μ_2-$\eta^3:\eta^1$-complexes[20] as has been confirmed for one example by X-ray structural analysis (Scheme 7).[26]

Also cyclic dienes in cationic molybdenum complexes are attacked by $[Re(CO)_5]^-$ to yield the corresponding σ,π-hydrocarbon bridged compounds **16**. Another σ,π-hydrocarbon bridge **17**[20] (Scheme 8) is formed by addition of $[Re(CO)_5]^-$ to coordinated trimethylenemethane in $[Cp(OC)_2Mo(\eta^4\text{-}C(CH_2)_3)]^+$, the chemistry of which was explored by Green *et al.*[27]

Angelici's group has contributed a further example of this type of reaction.[28] The cycloheptatriene ligand of the cation $[(\eta^6\text{-}C_7H_8)Mn(CO)_3]^+$ adds $[Re(CO)_5]^-$ to give the σ,π-cycloheptadienyl bridged complex **18** which was characterized by X-ray structural determination (Scheme 9).[28]

Recently we also found that coordinated benzene in cationic complexes undergoes nucleophilic attack with $[Re(CO)_5]^-$ to give σ,π-cyclohexadienyl bridged bimetallic compounds **19**, **20** (Scheme 10).[29] **19** shows typical fluxional behaviour in solution. At room temperature only one signal appears for the six protons of the C_6H_6 ring in the ^1H NMR spectrum, whereas at $-70°C$ the expected pattern of the rigid hexadienyl ring is observed.

σ,π-Benzene bridged complexes have recently been obtained by substitution of halide in $[\eta^6$-haloarene $Cr(CO)_3]$ by carbonyl metalates.[30] These complexes may be compared with metalated ferrocenes such as $CpFeC_5H_4ML_n$ ($ML_n = AuPPh_3$, $Fe(CO)_2Cp$).[31]

Cycloheptatrienyl-tricarbonyl complexes $[(\eta^7$-

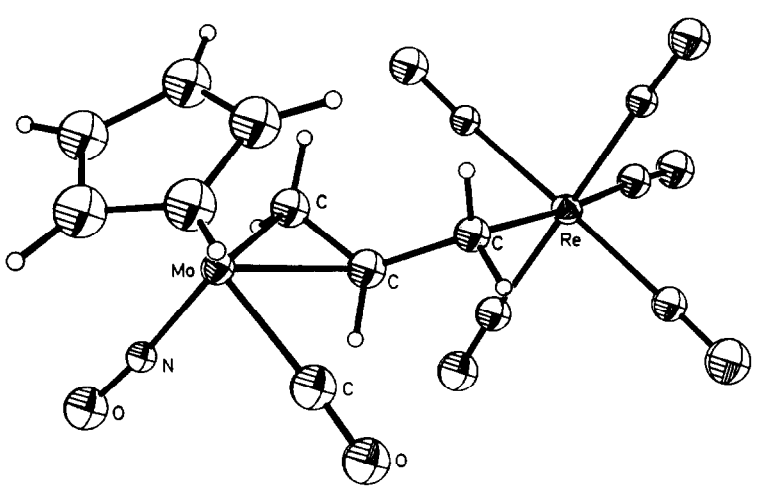

Fig. 3. Molecular structure of $Cp(OC)(ON)Mo(allyl)Re(CO)_5$.

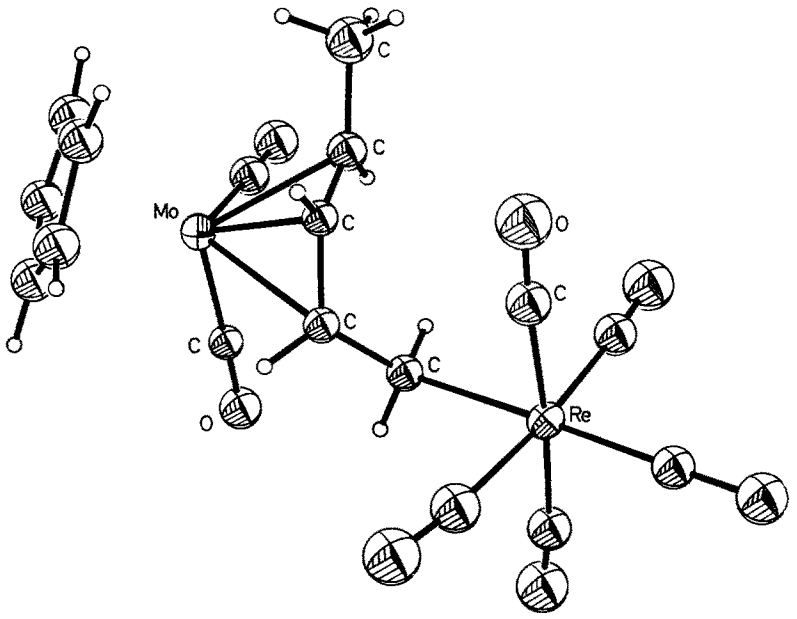

Fig. 4. Molecular structure of $Cp(OC)_2Mo(\mu_2\text{–}\eta^3:\eta^1\text{-}CH_2CHCHCHMe)Re(CO)_5$.

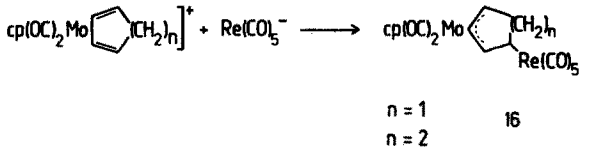

Scheme 8.

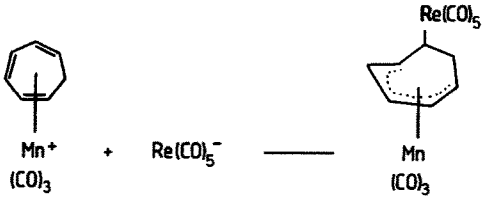

Scheme 9.

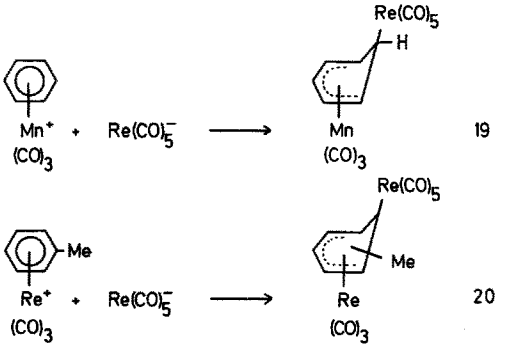

Scheme 10.

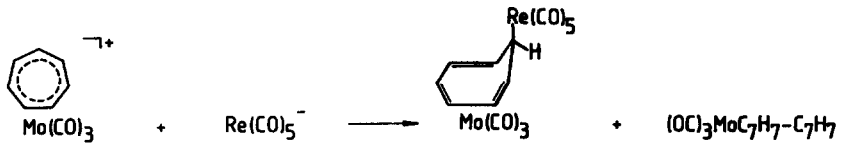

21 22

Scheme 11.

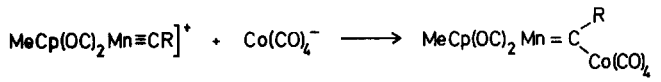

Scheme 12.

$C_7H_7)M(CO)_3]^+$ (M = Cr, Mo, W) undergo with $[(\eta^5\text{-}C_5H_5)(OC)_3M]^-$ (M = Mo, W) and $Mn(CO)_5^-$ the "anomal" reaction;[32] they behave as reducing agents to give μ-(bi-2,4,6-cycloheptatriene-1-yl) bis(tricarbonylmetal) complexes.[8]

Again with $[Re(CO)_5]^-$ it was possible[20] to direct the reaction to attack at the seven membered ring. Besides, the product of electron transfer from $[Re(CO)_5]^-$ to $[C_7H_7Mo(CO)_3]^+$ (**22**) is formed (Scheme 11). The structure of the σ,π-cycloheptatriene bridged compound **21** and that of **22** have been confirmed by X-ray diffraction.[33] **21** shows alternating C—C bond lengths as has been found for the parent complex $\eta^6\text{-}C_7H_8Mo(CO)_3$.[34]

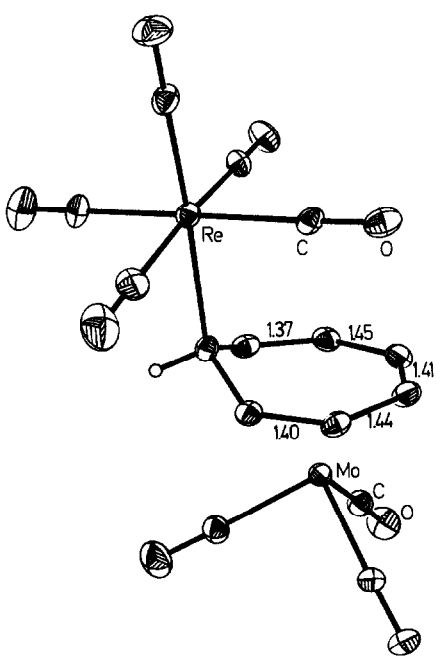

Fig. 5. Molecular structure of $(OC)_3Mo(\mu_2\text{-}\eta^6:\eta^1\text{-}C_7H_7)Re(CO)_5$.

To include the smallest C_1 "unsaturated" hydrocarbon the carbyne ligand in a cationic complex adds $[Co(CO)_4]^-$ to give a bimetallic carbene complex (Scheme 12).[35]

In summary these reactions work particularly well with $[Re(CO)_5]^-$ as the nucleophile, which is certainly due to its relatively strong nucleophilicity and to the formation of the very stable rhenium–carbon bond.[15] Use of other carbonyl metalates has to be studied but they also may give attack at the metal of the cationic complex and formation of metal–metal bonded dimers.[36]

Since there exists a large series of model reactions with organic nucleophiles we believe that attack of organometallic nucleophiles on π-bonded hydrocarbons may be of broader scope for the design of heterometallic hydrocarbon bridged compounds. Work is in progress in our laboratory to extend this chemistry.

Acknowledgements—These studies have been carried out by Dr Bernhard Olgemöller, Dr Klaus Raab, Dr Hans-Joachim Müller, Burkhard Niemer and Dr Wolfgang Sacher. The crystal structures have been determined by Dr Ulrich Nagel, Manfred Steimann and Dr Kurt Polborn. I am deeply indebted to my coworkers for their initiative and their invaluable contributions. Generous support by Deutsche Forschungsgemeinschaft and Fonds der Chemischen Industrie is gratefully acknowledged.

REFERENCES

1. St. G. Davies, M. L. H. Green and D. M. P. Mingos, *Tetrahedron* 1978, **34**, 3047.
2. Reviews: P. L. Pauson, *J. Organomet. Chem.* 1980, **200**, 207; L. A. P. Kane-Maguire, E. D. Honig and D. A. Sweigart, *Chem. Rev.* 1984, **84**, 525; R. C. Bush and R. J. Angelici, *J. Am. Chem. Soc.* 1986,

108, 2735; J. P. Collman, L. S. Hegedus, J. R. Norton and R. G. Finke, *Principles and Applications of Organotransition Metal Chemistry*, University Science Books, Mill Valley (1987); L. S. Hegedus, in *The Chemistry of the Metal–Carbon Bond* (Edited by F. R. Hartley and S. Patai), Vol. 2. Wiley Interscience, New York (1985); J.-E. Bäckvall, J. L. Davidson, St. G. Davies, M. L. H. Green, D. M. P. Mingos, J. A. S. Howell and P. Powell, in *Reactions of Coordinated Ligands* (Edited by P. S. Braterman), Vol. 1. Plenum Press, New York (1986).

3. St. G. Davies, *Organotransition Metal Chemistry: Application to Organic Synthesis*. Pergamon Press, Oxford (1982).
4. e.g. G. W. Parshall, *Homogeneous Catalysis*. Wiley, New York (1980).
5. J. Smidt, W. Hafner, R. Jira, R. Sieber, J. Sedlmeier and A. Sabel, *Angew. Chem.* 1962, **74**, 93.
6. P. Sautet, O. Eisenstein and K. M. Nicholas, *Organometallics* 1987, **6**, 1845 and references therein.
7. Reviews on hydrocarbon bridged complexes: W. A. Herrmann, *Adv. Organomet. Chem.* 1982, **20**, 160; J. Holton, M. F. Lappert, R. Pearce and P. I. W. Yarrow, *Chem. Rev.* 1983, **83**, 135; J. R. Moss and L. G. Scott, *Coord. Chem. Rev.* 1984, **60**, 171; Ch. P. Casey and J. D. Audett, *Chem. Rev.* 1986, **86**, 339.
8. W. Beck and B. Olgemöller, *J. Organomet. Chem.* 1977, **127**, C45; B. Olgemöller and W. Beck, *Chem. Ber.* 1981, **114**, 867.
9. K. Raab, U. Nagel and W. Beck, *Z. Naturforsch. Teil B* 1983, **38**, 1466.
10. J. E. Ellis, *J. Organomet. Chem.* 1975, **86**, 22.
11. K. Raab, B. Olgemöller, K. Schloter and W. Beck, *J. Organomet. Chem.* 1981, **214**, 81.
12. W. Beck, K. Raab, U. Nagel and W. Sacher, *Angew. Chem. Int. Ed. Engl.* 1985, **24**, 505.
13. Th. Kruck, M. Höfler and M. Noack, *Chem. Ber.* 1966, **99**, 1153; S. A. R. Knox, R. J. Hoxmeier and H. D. Kaesz, *Inorg. Chem.* 1971, **10**, 2636.
14. R. E. Dessy, R. L. Pohl and R. B. King, *J. Am. Chem. Soc.* 1966, **88**, 5121.
15. G. Al-Takhin, J. A. Connor and H. A. Skinner, *J. Organomet. Chem.* 1983, **259**, 313; J. Halpern, *Inorg. Chim. Acta* 1985, **100**, 41; G. P. McQuillan, C. D. McKean, C. Long, A. R. Morrisson and I. Torto, *J. Am. Chem. Soc.* 1986, **108**, 863.
16. D. M. DeSimone, P. J. Desrosiers and R. P. Hughes, *J. Am. Chem. Soc.* 1982, **104**, 4842.
17. M. Green, *J. Organomet. Chem.* 1986, **300**, 93; R. G. Beevor, M. Green, A. G. Orpen and I. D. Williams, *J. Chem. Soc., Dalton Trans.* 1987, 1319 and previous publications by Green *et al.* on "Reactions of Coordinated Ligands".
18. D. L. Reger, K. A. Belmore, E. Mintz and P. J. McElligott, *Organometallics* 1984, **3**, 134 and references therein.
19. W. Beck, H.-J. Müller and U. Nagel, *Angew. Chem., Int. Ed. Engl.* 1986, **25**, 734.
20. H.-J. Müller and W. Beck, *J. Organomet. Chem.* 1987, **330**, C13.
21. K. Yasufuku, K. Aoki and H. Yamazaki, *J. Organomet. Chem.* 1975, **84**, C28; B. H. Freeland, J. E. Hux, N. C. Payne and K. G. Tyers, *Inorg. Chem.* 1980, **19**, 693; G. Jaouen, A. Marinetti, J. Y. Saillard, B. G. Sayer and M. J. McClinchey, *Organometallics* 1982, **1**, 225; J. C. Jeffery, J. C. V. Laurie and F. G. A. Stone, *Polyhedron* 1985, **4**, 1135; M. C. Azar, M. J. Chetcuti, Ch. Eigenbrot and K. A. Green, *J. Am. Chem. Soc.* 1985, **107**, 7209; S. D. Jensen, B. H. Robinson and J. Simpson, *Organometallics* 1986, **5**, 1690.
22. H.-J. Müller, U. Nagel and W. Beck, *Organometallics* 1987, **6**, 193.
23. J. W. Faller and K.-H. Chao, *J. Am. Chem. Soc.* 1983, **105**, 3893; *Organometallics* 1984, **3**, 927; W. E. van Arsdale, R. E. K. Winter and J. K. Kochi, *Organometallics* 1986, **5**, 645; *J. Organomet. Chem.* 1985, **296**, 31.
24. B. E. R. Schilling, R. Hoffman and J. W. Faller, *J. Am. Chem. Soc.* 1979, **101**, 592; M. D. Curtis and D. Eisenstein, *Organometallics* 1984, **3**, 887.
25. J. W. Faller, H. H. Murray, D. L. White and K. H. Chao, *Organometallics* 1983, **2**, 400; A. J. Pearson and Md. N. I. Khan, *J. Org. Chem.* 1985, **50**, 5276.
26. M. Steimann, H.-J. Müller and W. Beck, to be published.
27. St. R. Allen, St. G. Barnes, M. Green, G. Moran, L. Trollope, N. W. Murrall, A. J. Welch and D. M. Sharaiha, *J. Chem. Soc., Dalton Trans.* 1984, 1157.
28. R. C. Bush, R. A. Jacobson and R. J. Angelici, *J. Organomet. Chem.* 1987, **323**, C25.
29. B. Niemer and W. Beck, *Chem. Ber.*, in press.
30. J. A. Heppert, Abstracts of 193rd and 194th ACS Meeting 1987, No. 69 and No. 443; J. A. Heppert, M. E. Thomas-Miller, P. N. Swepston and M. W. Extine, *J. Chem. Soc., Chem. Commun.* 1988, 280.
31. Gmelin, *Handbuch der Anorganischen Chemie, Eisenorganische Verbindungen*, Teil A, Ferrocen 5. Springer, Berlin (1980); M. Herberhold and H. Kniesel, *J. Organomet. Chem.* 1987, **334**, 347 and references cited therein.
32. J. D. Munro and P. L. Pauson, *J. Chem. Soc.* 1961, 3484.
33. K. Polborn, H.-J. Müller and W. Beck, to be published.
34. J. D. Dunitz and P. Pauling, *Helv. Chim. Acta* 1960, **43**, 2188.
35. E. O. Fischer, J. K. R. Wanner, G. Müller and J. Riede, *Chem. Ber.* 1985, **118**, 3311.
36. e.g. M. Green, N. C. Norman and A. G. Orpen, *J. Am. Chem. Soc.* 1981, **103**, 1269; P. Härter, H. Pfisterer and M. L. Ziegler, *Angew. Chem., Int. Ed. Engl.* 1986, **25**, 839.

Polyhedron Vol. 7, No. 22/23, pp. 2263–2269, 1988
Printed in Great Britain

0277–5387/88 $3.00+.00
© 1988 Pergamon Press plc

THE REACTIONS OF $Mo_2Ru(CO)_7Cp_2(\mu_3\text{-}S)$ WITH PHENYLACETYLENE AND $Ru(CO)_5$

RICHARD D. ADAMS,* JAMES E. BABIN and MIKLOS TASI

Department of Chemistry, University of South Carolina, Columbia, SC 29208, U.S.A.

Abstract—The reactivity of the heteronuclear cluster complex $Mo_2Ru(CO)_7Cp_2(\mu_3\text{-}S)$ (**1**) toward HC_2Ph was investigated and compared with the reactivity of the homonuclear complexes $Ru_3(CO)_{10}(\mu_3\text{-}S)$ (**2**) and $[Mo(CO)_2Cp]_2$ (**3**). The reaction of **1** with HC_2Ph yielded the new compound $Mo_2Ru(CO)_2Cp_2[\mu_3\text{-}\eta^6\text{-}HCC(Ph)CHC(Ph)CHC(Ph)](\mu_3\text{-}S)$ (**6**), 15%. The compound contains a 1,3,5-triphenyldimetallahexatrienyl ligand formed by the head-to-tail coupling of three HC_2Ph molecules. The C_6-chain bridges one face of the triangular cluster. Three of the carbon atoms of the chain are π-bonded to one molybdenum atom. The other three carbon atoms are π-bonded to the ruthenium atom. The two ends of the chain are σ-bonded to the second molybdenum atom. When treated with CO at 100°C/25 atm, **6** eliminates 1,3,5,triphenylbenzene and reforms **1**. At 125°C under nitrogen, the C_6-chain in **6** is split at the C(3)—C(4) bond to yield the two isomeric products $Mo_2Ru(CO)_2Cp_2[\mu_3\text{-}\eta^3\text{-}HCC(Ph)CH][\mu\text{-}\eta^3\text{-}PhCC(H)CPh](\mu_3\text{-}S)$ (**7**) and $Mo_2Ru(CO)_2Cp_2[\mu_3\text{-}\eta^3\text{-}HCC(Ph)CH][\mu\text{-}\eta^3\text{-}PhCC(Ph)CH](\mu_2\text{-}S)$ (**8**). Both products contain two dimetallaallyl ligands. One bridges the face of the cluster. The other bridges the Mo—Mo edge. Compound **7** is converted into **8** at 125°C. When **1** is treated with Me_3NO and HC_2Ph at 25°C, the compound $Mo_2Ru(CO)_5Cp_2[\mu\text{-}\eta^4\text{-}PhCC(H)CC(H)Ph](\mu_3\text{-}S)$ (**9**) is formed in 11% yield. Compound **9** consists of an open cluster with a PhCC(H)CC(H)Ph ligand that bridges the open edge of the cluster. The four-carbon chain is π-bonded to a molybdenum atom while one carbon serves as the bridging link by bonding to the ruthenium atom. Compound **9** does not appear to be an intermediate en route to **6**. When **1** is treated with $Ru(CO)_5$ at 80°C, two higher nuclearity cluster products $Mo_2Ru_4(CO)_{13}(\mu_4\text{-}\eta^2\text{-}CO)Cp_2(\mu_4\text{-}S)$ (**10**) and $Mo_2Ru_5(CO)_{14}(\mu_4\text{-}\eta^2\text{-}CO)_2Cp_2(\mu_4\text{-}S)$ (**11**) are formed. Compound **10** consists of a square pyramidal Mo_2Ru_4 cluster containing a quadruply bridging sulphido ligand on the square base. An $Ru(CO)_3$ group bridges an Ru—Ru edge of the square base. A dihapto quadruply bridging carbonyl ligand is bonded by its carbon atom to an $MoRu_2$ triangle of the square pyramid and is bonded by its oxygen atom to the $Ru(CO)_3$ group. Compound **11** is similar to **10** but has an additional $Ru(CO)_3$ group bridging the second Ru—Ru basal edge of the cluster and also has a second dihapto quadruply bridging carbonyl ligand. IR spectra show that the two quadruply bridging carbonyl ligands are vibrationally coupled by the appearance of two C—O stretching absorptions at 1419 and 1453 cm^{-1}. When **10** is heated to 80°C, it is converted to an isomer **12** by shifting the quadruply bridged carbonyl ligand to a terminal bonding mode. The cluster is transformed from an edge bridging form in **10** to a face capped form in **12**.

The most important question concerning the design and use of a multimetallic (heteronuclear) catalyst is, "Will it produce reactivity that is different from that of its components?" To answer this question, one must have a knowledge of the reactivity of each of the components to compare with that of the heteronuclear system. Molecular cluster complexes can provide a unique opportunity to make these comparisons, because the details of the reactivity can be established very precisely.

In this study, we have investigated the reactivity of the molybdenum–ruthenium mixed-metal cluster complex $Mo_2Ru(CO)_7Cp_2(\mu_3\text{-}S)$ (**1**) towards phenylacetylene, HC_2Ph. This complex was originally made by Vahrenkamp by a sequence of molyb-

*Author to whom correspondence should be addressed.

$$RuCo_2(CO)_9(\mu_3\text{-}S) \xrightarrow{+\,CpMo(CO)_3AsMe_2} RuCoMo(CO)_8Cp(\mu_3\text{-}S) \xrightarrow{+\,[CpMo(CO)_3]_2} RuMo_2(CO)_7Cp_2(\mu_3\text{-}S) \quad (1)$$

42% 48%

$$Ru_3(CO)_{10}(\mu_3\text{-}S) + [CpMo(CO)_2]_2 \xrightarrow{-2\,CO} Ru_3Mo_2(CO)_{12}Cp_2(\mu_4\text{-}S) \xrightarrow{-2\,Ru} RuMo_2(CO)_7Cp_2(\mu_3\text{-}S) \quad (2)$$

49% overall

denum atom substitutions on the complex $RuCo_2(CO)_{11}(\mu_3\text{-}S)$, eq. (1),[1] and more recently by us through the one step reaction of $Ru_3(CO)_9(\mu_3\text{-}S)$ (**2**) with $[Mo(CO)_2Cp]_2$ (**3**), eq. (2).[2] Compound **1** has been characterized by crystallographic methods and was shown to consist of a triangular cluster of two molybdenum and one ruthenium atoms with a triply bridging sulphido ligand (see Fig. 1).

The reactivity of **2**[3] and **3**[4–8] toward HC_2Ph at 100°C has been reported. Compound **2** forms the substitution product $Ru_3(CO)_9(\mu_3\text{-}HC_2Ph)(\mu_3\text{-}S)$ (**4**) at 100°C when the HC_2Ph/**2** ratio is less than 10. Under these conditions, **4** exhibits no further tendency to add HC_2Ph, eq. (3). Compound **3** is well-known to add one equivalent of alkyne to form the compound $Mo_2(CO)_4Cp_2(\mu\text{-}HC_2Ph)$ (**5**) at 25°C and, at 100°C, **5** will react with a variety of alkynes to yield dimolybdenum products containing alkyne oligomers.

For several years, we have also been investigating the ability of sulphur-containing cluster complexes to undergo enlargement by the addition of small metal carbonyl fragments.[9] $Ru(CO)_5$ is known to lose a CO ligand upon mild heating and the $Ru(CO)_4$ fragments will combine to form clusters (e.g. $Ru_3(CO)_{12}$). We have used $Ru(CO)_5$ recently to assist in the preparation of a variety of new high nuclearity sulphido ruthenium carbonyl cluster complexes.[10,11] Thus, we have also investigated the potential of **1** to undergo cluster enlargement by reactions with $Ru(CO)_5$. Several new higher nuclearity molybdenum–ruthenium cluster complexes have been prepared. Two of these have been found to possess quadruply bridging carbonyl ligands and one of these provides the first example of a molecular complex to contain two quadruply bridging carbonyl ligands.[12] In the second part of this report the structures and properties of these higher nuclearity clusters is described.

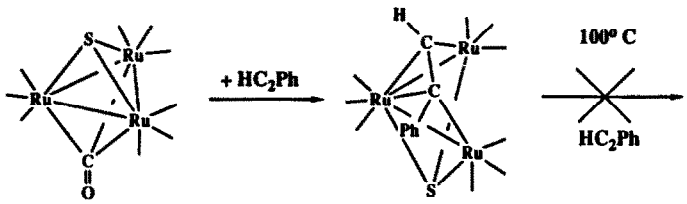

(3)

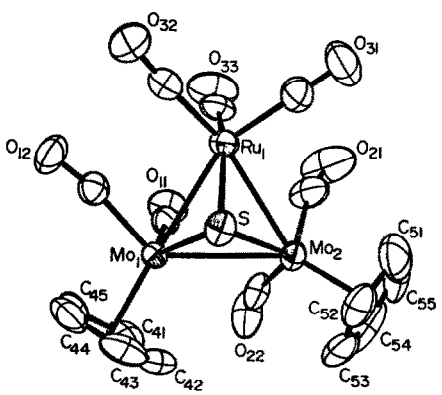

Fig. 1. An ORTEP diagram of $Mo_2Ru(CO)_7Cp_2(\mu_3\text{-}S)$ (**1**).

RESULTS AND DISCUSSION

1. *Reactions of* $Mo_2Ru(CO)_7Cp_2(\mu_3\text{-}S)$ (**1**) *with* HC_2Ph

Two products were isolated from the reaction of **1** with HC_2Ph at 98°C.[13] Both products were formed by the loss of five carbonyl ligands from **1** and the addition of three equivalents of HC_2Ph; thus, they are isomers, but they have significantly different structures as was determined from crystallographic studies. One has the molecular formula $Mo_2Ru(Co)_2Cp_2[\mu_3\text{-}\eta^6\text{-}HCC(Ph)C(H)C(Ph)C(H)C(Ph)](\mu_3\text{-}S)$ (**6**) and was obtained in 15% yield. An ORTEP drawing of its molecular structure is shown in Fig. 2. The molecule consists of a triangular cluster of metal atoms with a triply bridging sulphido ligand. The three alkyne molecules have been joined in a head-to-tail fashion by the formation of carbon–carbon bonds. This resulted in the formation of a 1,3,5-triphenyl-

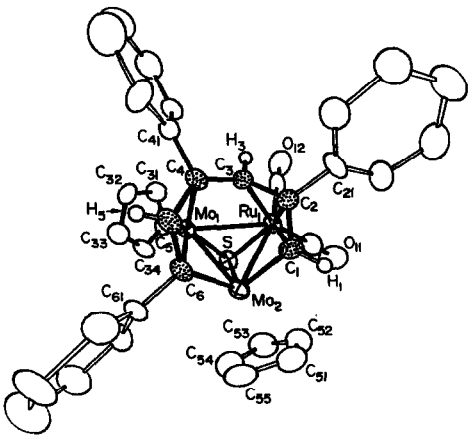

Fig. 2. An ORTEP diagram of $Mo_2Ru(CO)_2Cp_2[\mu_3\text{-}\eta^6\text{-}HCC(Ph)CHC(Ph)CHC(Ph)](\mu_3\text{-}S)$ (**6**).

dimetallahexatrienyl ligand that is coordinated across the face of the cluster that is opposite that of the sulphido ligand. Three of the carbon atoms are π-bonded to the ruthenium atom. The remaining three are π-bonded to one of the molybdenum atoms. The termini of the C_6-chain are σ-bonded to the second molybdenum atom. The C—C bond distances in the C_6-chain all lie in the range 1.42(1)–1.46(1) Å. This indicates that the C—C π-bonding is distributed fairly uniformly across the entire chain. The electron count about the metal atoms is 46, two less than that required by the Effective Atomic Number (EAN) rule. Interestingly, the Mo—Mo metal–metal bond is unusually short, 2.663(1) Å, and is similar to that of the Mo—Mo double bond found in the complex $Mo_2Cp_2[(MeO_2)C_2(CO_2Me)(HC_2H)\{(MeO_2C)C_2(CO_2Me)\}_2]$, 2.618(1) Å.[14] Thus, the shortness of the Mo—Mo bond in **6** could be due to a localization of the unsaturation. The Mo(1)—Ru and Mo(2)—Ru distances are significantly different, 3.031(1) vs 2.775(1) Å. The former is similar to the Mo—Ru distances found in **1**. The shortness of the Mo(2)—Ru bond could be due to bond contraction effects caused by the presence of the bridging carbon atom, C(1). Likewise, the shortness of the Mo—Mo bond in **6** could also be attributed in part to the bridging carbon atom C(6). It seemed reasonable to think that the formation of a carbon–carbon bond between the atoms C(1) and C(6) could be induced and would lead to 1,3,5-triphenylbenzene. This was successfully accomplished by the treatment of **6** with CO (at 100°C/25 atm). A 74% yield of triphenylbenzene was accompanied by the formation of an equivalent amount of **1**. Although this **1** could be converted back into **6** by reaction with HC_2Ph, the process is not catalytic because **6** is not formed from **1** and HC_2Ph under the conditions required for the triphenylbenzene elimination reaction.

The second product obtained from the reaction of **1** and HC_2Ph has the formula $Mo_2Ru(CO)_2Cp_2[\mu_3\text{-}\eta^3\text{-}HCC(Ph)CH][\mu\text{-}\eta^3\text{-}PhCC(H)CPh](\mu_3\text{-}S)$ (**7**) 11%.[13] An ORTEP drawing of its structure is shown in Fig. 3. Compound **7** consists of a triangular cluster of metal atoms with a triply bridging sulphido ligand and two dimetallaallyl ligands. One of these, HCC(Ph)CH, serves as a triply bridging ligand that is π-bonded to the ruthenium atom and each end σ-bonded to a different molybdenum atom. The second dimetallaallyl ligand, PhCC(H)CPh, bridges the Mo—Mo edge of the cluster and is π-bonded to Mo(2) and σ-bonded to Mo(1). It appears that **7** could be formed from **6** simply by a cleavage of the C(3)—C(4) bond in the C_6-chain followed by minor reorganization of the coordination to the metal atoms. Interestingly, the C(3)—C(4) bond was the location of the C—C triple bond of one of the original HC_2Ph molecules. Indeed, when compound **6** was heated to 125°C for 3 h, it was converted to **7** in 57% yield, but in addition another isomer $Mo_2Ru(CO)_2Cp_2[\mu_3\text{-}\eta^3\text{-}HCC(Ph)CH][\mu\text{-}\eta^3\text{-}PhCC(Ph)CH](\mu_3\text{-}S)$ (**8**) was also formed in 38% yield. The structure of **8** is described below. Compound **7** contains 48 valence electrons and is thus saturated according to the EAN rule. However, the Mo(1)—Mo(2) is nearly as short as that in **6**. In this case, the shortness must be due to bond contraction effects caused by the bridging atoms C(4) and C(6). It is believed that the removal of the electronic unsaturation about the Mo—Mo bond in **6** may be the driving force for cleavage of the carbon–carbon bond in the C_6-chain.

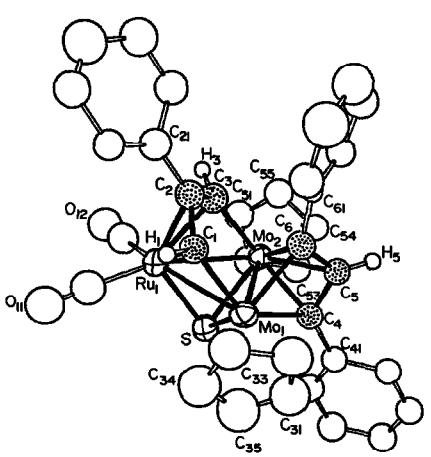

Fig. 3. An ORTEP diagram of $Mo_2Ru(CO)_2Cp_2[\mu\text{-}\eta^3\text{-}PhCC(H)C(Ph)][\mu_3\text{-}\eta^3\text{-}HCC(Ph)CH](\mu_3\text{-}S)$ (**7**).

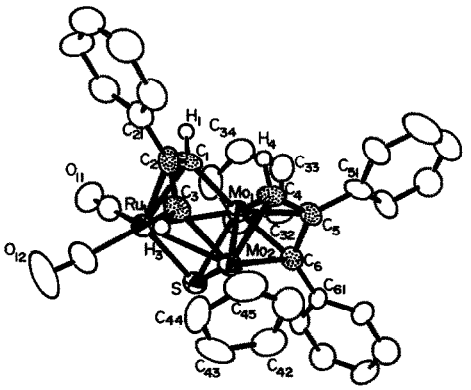

Fig. 4. An ORTEP diagram of $Mo_2Ru(CO)_2Cp_2[\mu\text{-}\eta^3\text{-}HCC(Ph)CPh][\mu_3\text{-}\eta^3\text{-}HCC(Ph)CH](\mu_3\text{-}S)$ (**8**).

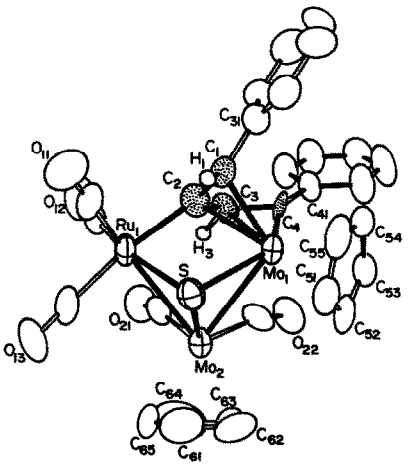

Fig. 5. An ORTEP diagram of $Mo_2Ru(CO)_5Cp_2[\mu\text{-}\eta^4\text{-}PhCC(H)CC(H)Ph](\mu_3\text{-}S)$ (**9**).

The molecular structure of **8** is shown in Fig. 4. The structure is analogous to that of **7** except that the phenyl groups of the edge bridging dimetallaallyl group are located on adjacent carbon atoms, HCC(Ph)C(Ph). It was found that **8** could be obtained in 24% yield by heating **7** to 125°C for 3 h. This remarkable isomerization is believed to occur by a 1,2 interchange of the C(5)—H(5) and C(6)—Ph groups of the edge bridging dimetallaallyl ligand in **7**. The mechanism is believed to involve the formation of a cyclopropenyl ligand by the formation of a carbon–carbon bond between the atoms C(4) and C(6) (see intermediate **A** in Scheme 1). This step links the two phenyl-substituted carbon atoms. After a 60° rotation of the cyclopropenyl ligand to **B**, a cleavage of the carbon–carbon bond between the CH and one CPh group will give **8**. A similar process was proposed by Chisholm to explain an interchange of carbon atoms in a dimetallaallyl ligand on a ditungsten centre.[15] In that case, the interchange was rapid on the NMR timescale. We have no evidence for the existence of 1,2-interchange processes involving the triply bridging HCC(Ph)CH, dimetallaallyl ligand. If the reason for this is due to a higher activation barrier, this could imply an important difference between the basic reactivity of the trinuclear metal site and the dinuclear metal site. Site-sensitivity such as this could have an analogy to the structure–function reactivity relationships that are believed to play an important role in the chemistry of small molecule transformations on metal surfaces.[16]

We have not been able to isolate any products from the reaction of **1** with HC_2Ph at 98°C that contain only one or two equivalents of HC_2Ph. Certainly, such species must have been traversed in the formation of **6**. In an effort to obtain such species, the reaction of **1** with HC_2Ph was performed at 25°C with an initiation by Me_3NO.[17] Under these conditions, a species formed by the addition of two HC_2Ph equivalents was obtained in 11% yield. Its formula $Mo_2Ru(CO)_5Cp_2[\mu\text{-}\eta^4\text{-}PhCC(H)CC(H)Ph](\mu_3\text{-}S)$ (**9**) was established by a crystallographic analysis and an ORTEP drawing of its molecular structure is shown in Fig. 5. This compound consists of an open cluster of three metal atoms. There are only two metal–metal bonds, Mo(1)—Mo(2) = 3.024(2) and Mo(2)—Ru = 3.015(2) Å. There is a PhCC(H)CC(H)Ph ligand that bridges the non-bonded pair of metal atoms Mo(1)···Ru. The four-carbon chain is π-bonded to Mo(1). Carbon C(2) is also bonded

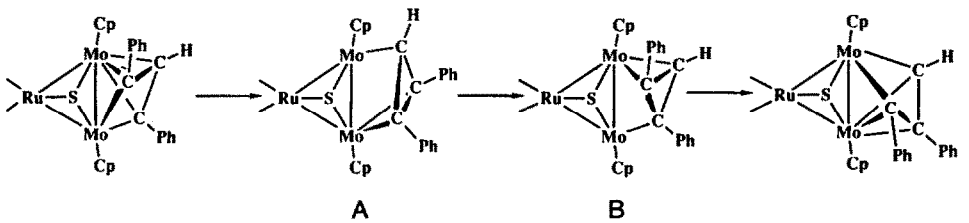

Scheme 1.

to Ru and serves as the bridge. The presence of the two substituents H and Ph on the carbon C(1) requires the occurrence of a substituent shift in the original HC_2Ph molecule. Most likely, this was a hydrogen shift since it has been shown previously that metal clusters can isomerize coordinated terminal alkynes to vinylidene ligands, eq. (4).[18] A coupling of the vinylidene carbon atom to the hydrogen-substituted end of an HC_2Ph molecule should lead directly to the ligand found in **9**. As one might expect, the reaction of **9** with additional HC_2Ph does not lead to **6**, **7** or **8**. Thus, **9** is believed not to be an intermediate in their formation.

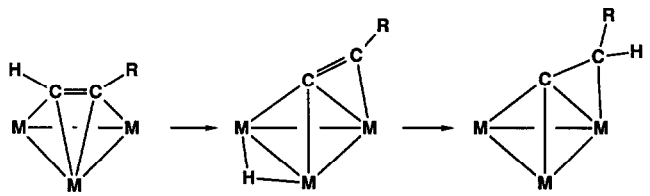

(4)

Our studies have shown that **1** clearly exhibits a greater tendency to oligomerize HC_2Ph than **2**, but is probably less effective than **3**. We believe that the enhanced alkyne oligomerization reactivity of **1** can be attributed to the presence of the dimolybdenum centre in this cluster. However, as shown by the structure of **6**, all the metal atoms participate in the oligomerization process. To our knowledge, there have been no reports that **3** is capable of producing the splitting of alkyne trimers into C_3-groupings. Thus, the reactivity of **1** does have one feature that distinguishes it from **3**. It also seems reasonable to attribute this, at least in part, to the presence of the ruthenium atom since the ruthenium atom is bonded both to the C_6-chain in **6** and to one of the C_3-fragments in **7**. We have not yet obtained products derived from **7** or **8**, but the implications of the trimerization/splitting reaction are very intriguing. If one could incorporate it into a catalytic process, such as hydrogenation, it could provide the basis for the expansion of C_2 functionality to C_3 functionality, e.g. eq. (5).

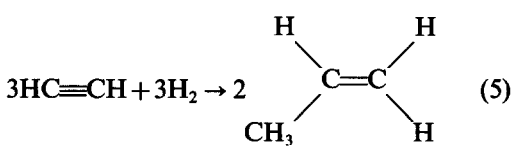

(5)

2. *Reactions of* **1** *with* $Ru(CO)_5$

Two higher nuclearity clusters were obtained from the reaction of **1** with $Ru(CO)_5$, 80°C/1 h. These have been identified as $Mo_2Ru_4(CO)_{13}(\mu_4\text{-}\eta^2\text{-}CO)Cp_2(\mu_4\text{-}S)$ (**10**), 23% yield and $Mo_2Ru_5(CO)_{14}(\mu_4\text{-}\eta^2\text{-}CO)_2Cp_2(\mu_4\text{-}S)$ (**11**), 15% yield. These products are also obtained in very low yields from the synthesis of **1**.[12] Both products were characterized by crystallographic methods. An ORTEP diagram of **10** is shown in Fig. 6.[12] The molecule consists of a square pyramidal cluster of three ruthenium plus two molybdenum atoms. A molybdenum atom occupies the apical position of the pyramid and a quadruply bridging sulphido ligand spans the Ru_3Mo square base. An $Ru(CO)_3$ group bridges an Ru—Ru edge of the pyramid and there is a quadruply bridging CO ligand that lies in the Ru_3Mo fold. The carbon atom is bonded to an $MoRu_2$ triangular face of the pyramid and the oxygen atom is coordinated solely to the edge bridging $Ru(CO)_3$ group. Quadruply bridging carbonyl ligands generally exhibit elongated C—O bonds and reduced C—O stretching frequencies.[19] This is true for this ligand also, C—O = 1.262(8) Å, and $\nu(CO) = 1457\ cm^{-1}$.

An ORTEP drawing of **11** is shown in Fig. 7.[12] The structure of **11** is very similar to **10** except that it contains an additional $Ru(CO)_3$ group that bridges the second Ru—Ru basal edge of the square pyramidal cluster. Most interestingly, there is a quadruply bridging carbonyl ligand lying in this Ru_3Mo fold also. This molecule is the first one ever

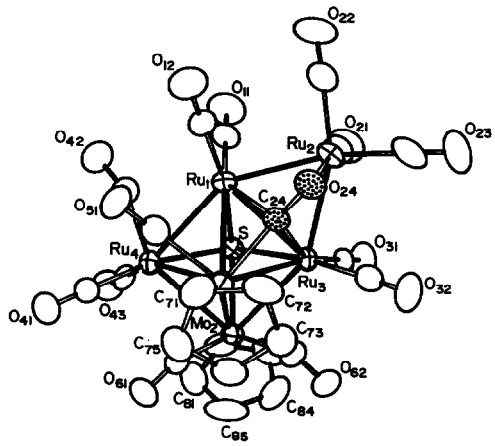

Fig. 6. An ORTEP diagram of $Mo_2Ru_4(CO)_{13}(\mu_4\text{-}\eta^2\text{-}CO)Cp_2(\mu_4\text{-}S)$ (**10**).

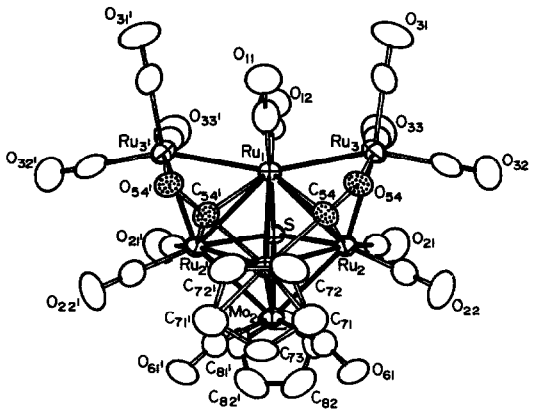

Fig. 7. An ORTEP diagram of $Mo_2Ru_5(CO)_{14}(\mu_4\text{-}\eta^2\text{-}CO)_2Cp_2(\mu_4\text{-}S)$ (**11**).

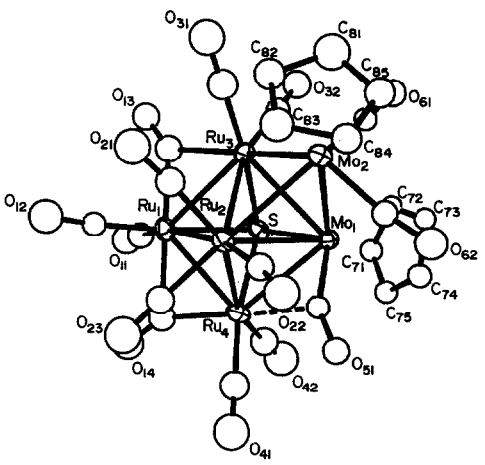

Fig. 8. An ORTEP diagram of $Mo_2Ru_4(CO)_{14}Cp_2(\mu_4\text{-}S)$ (**12**).

prepared that contains two quadruply bridging carbonyl ligands. These ligands are related by a molecular plane of symmetry that passes through the two molybdenum atoms, ruthenium Ru(1), and the sulphido ligand. The CO distance 1.25(1) Å is long, as expected. Most interestingly, however, the CO stretching vibration appears as two absorptions, 1419 and 1453 cm^{-1}, even though the ligands are equivalent. The splitting of the band can be attributed to vibrational coupling that yields symmetric and antisymmetric modes. In accord with the coupling theories that have been applied to CO ligands in mono- and dinuclear metal complexes, the higher frequency absorption should be assigned to the symmetrically coupled mode and the lower frequency to the antisymmetrically coupled mode.[20] The magnitude of the coupling, 34 cm^{-1}, indicates that the coupling is surprisingly large.

The mechanism of formation of **10** has not been established, but we have shown that **11** can be made from **10** in 47% yield by reaction with $Ru(CO)_5$, 80°C/3 h. A plausible mechanism for the formation of **11** would involve the interaction of an $Ru(CO)_4$ fragment with the oxygen atom of the terminally coordinated carbonyl ligand on Mo(1). Metal–oxygen interactions of this type have been structurally characterized for cases where the metal belongs to one of the early groups of the transition series.[18] CO elimination accompanied by metal–metal bond formation is a well-established process. A series of these should lead to **11** directly.

When **10** was refluxed in cyclohexane for 4 h, it was converted to the new compound $Mo_2Ru_4(CO)_{14}Cp_2(\mu_4\text{-}S)$ (**12**) in 46% yield. The molecular structure of **12** is shown in Fig. 8. According to its formula, **12** is an isomer of **10**, but it has a significantly different structure. First, it does not contain a quadruply bridging carbonyl ligand. Second, the cluster consists of a square pyramidal arrangement of four ruthenium and one molybdenum atoms. The sulphido ligand remains as a quadruple bridge across the base of the pyramid. Unlike **10**, a ruthenium atom occupies the apical position of the pyramid and one of the molybdenum atoms has been squeezed out of the main body of the cluster into a capping position on the Mo(1), Ru(2), Ru(3)

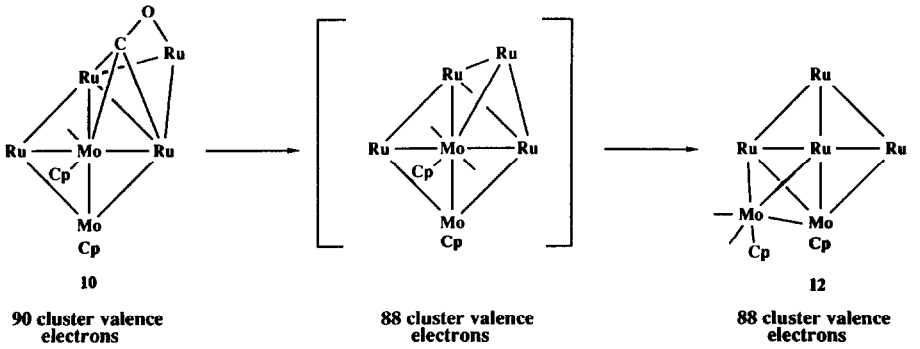

Scheme 2. Isomerization process. All structures obey skeletal electron pair theory.

face. Compound **12** contains 88 electrons and thus obeys the SEP theory.[21] Compound **10**, which has 90 valence electrons, also obeys the SEP theory. The two-electron difference between the electron counts in **10** and **12** is due to the conversion of the four-electron donating quadruply bridging CO ligand in **10** to a two-electron donating ligand in**12**. As a consequence, the cluster must condense, when the quadruply bridging CO ligand is shifted to a terminal position and it does so by converting from an edge bridged cluster, **10**, to a face capped cluster **12**. It is noteworthy, however, that a shift of the edge bridging ruthenium group to the capping site does not yield **12** (see Scheme 2). This ruthenium capped species is a logical intermediate which evidently isomerizes to **12** by interchanging the sites of the capping ruthenium atom with the apical molybdenum atom in the pyramid. It seems premature to propose details for this rearrangement at this time.

Our studies of the reactivity of **1** toward HC_2Ph have revealed some unusual details of a trimerization and ligand splitting process that appears to distinguish it from the reactivity properties of either of the homonuclear metal components. It is believed that unique features of the reactivity of **1** can be attributed to its heteronuclear metal content.

The higher nuclearity clusters have provided at least one interesting ligand ensemble that could have implications for surface phenomena; namely, the existence of quadruply bridging carbonyl ligands that have their carbon atoms coordinated on adjacent trinuclear metal sites. Studies of these systems are continuing.

Acknowledgements—These studies were supported by the U.S. Department of Energy and the National Science Foundation.

REFERENCES

1. F. Richter, E. Roland and H. Vahrenkamp, *Chem. Ber.* 1984, **117**, 2429.
2. R. D. Adams, J. E. Babin and M. Tasi, *Organometallics* 1988, **7**, 219.
3. R. D. Adams, J. E. Babin, M. Tasi and T. Wolfe, *Organometallics* 1987, **6**, 2228.
4. J. A. Beck, S. A. R. Knox, R. F. D. Stansfield, F. G. A. Stone, M. J. Winter and P. Woodward, *J. Chem. Soc., Dalton Trans.* 1982, 195.
5. S. A. R. Knox, R. F. D. Stansfield, F. G. A. Stone, M. J. Winter and P. Woodward, *J. Chem. Soc., Dalton Trans.* 1982, 173.
6. A. M. Boileau, A. G. Orpen, R. F. D. Stansfield and P. Woodward, *J. Chem. Soc., Dalton Trans.* 1982, 187.
7. S. Slater and E. L. Muetterties, *Inorg. Chem.* 1981, **20**, 946.
8. J. S. Bradley, *J. Organomet. Chem.* 1978, **150**, C1.
9. R. D. Adams, *Polyhedron* 1985, **4**, 2003, and references therein.
10. R. D. Adams, J. E. Babin and M. Tasi, *Inorg. Chem.* 1987, **26**, 2807.
11. R. D. Adams, J. E. Babin and M. Tasi, *Organometallics* 1988, 7, 503.
12. R. D. Adams, J. E. Babin and M. Tasi, *Angew. Chem., Int. Ed. Engl.* 1987, **26**, 685.
13. R. D. Adams, J. E. Babin and M. Tasi, *Organometallics* 1987, **6**, 2247.
14. S. A. R. Knox, R. F. D. Stansfield, F. G. A. Stone, M. J. Winter and P. Woodward, *J. Chem. Soc., Chem. Commun.* 1978, 221.
15. M. H. Chisholm, J. A. Heppert and J. C. Huffman, *J. Am. Chem. Soc.* 1984, **106**, 1151.
16. G. A. Somorjai, *Adv. Catal.* 1977, **26**, 1.
17. R. D. Adams, J. E. Babin and M. Tasi, *Organometallics* 1988, **7**, 755.
18. E. Roland and H. Vahrenkamp, *J. Molec. Catal.* 1983, **21**, 233.
19. C. P. Horwitz and D. F. Shriver, *Adv. Organomet. Chem.* 1984, **23**, 219.
20. F. A. Cotton and C. S. Kraihanzel, *J. Am. Chem. Soc.* 1962, **48**, 4432.
21. (a) D. M. P. Mingos, *Accts Chem. Res.* 1984, **17**, 311; (b) K. Wade, in *Transition Metal Clusters* (Edited by B. F. G. Johnson). John Wiley, New York (1980); (c) B. F. G. Johnson and R. E. Benfield, in *Topics in Stereochemistry* (Edited by G. L. Geoffroy), Vol. 12. John Wiley, New York (1981).

Polyhedron Vol. 7, No. 22/23, pp. 2271–2283, 1988
Printed in Great Britain

0277–5387/88 $3.00+.00
© 1988 Pergamon Press plc

ELECTRONIC AND STERIC EFFECTS IN CLOSELY RELATED HETERONUCLEAR CLUSTERS. SELECTIVE PATHWAYS IN SYNTHETIC AND CATALYTIC BIMETALLIC CHEMISTRY

ROBERT BENDER, PIERRE BRAUNSTEIN* and CLAUDE DE MERIC DE BELLEFON

Laboratoire de Chimie de Coordination, UA 416 CNRS, Université Louis Pasteur, 4, rue Blaise Pascal, F-67070 Strasbourg Cédex, France

Abstract—Comparisons are made between closely related heteronuclear clusters whose compositions only differ by the nature of a metal fragment or a ligand. Thus, addition of electrophilic d^{10} metal fragments to the Co_3 face of the tetrahedral ruthenium–cobalt cluster $[RuCo_3(CO)_{12}]^-$ affords new clusters in which the variation of the distance between the Ru capping atom and this face shows that electronic communication takes place between the apices of the trigonal bipyramid. This allows the establishment of the *trans*-influence series: $Cu(PPh_3) < Au(PPh_3) < HgCo(CO)_4 \sim HgRuCo_3(CO)_{12}$. Examples are shown where the different reactivity of Pd(I) and Pt(I) complexes toward Cu(I) and Au(I) complexes lead to completely different clusters despite the isolobal character of the reagent pairs. On the other hand, varying the nature of the phosphine ligands in the 58 electron tetranuclear clusters $[Mo_2Pt_2Cp_2(CO)_6L_2]$ (Cp = η-C_5H_4R; R = H, Me) allows the formation of planar, triangulated clusters with five metal–metal bonds (e.g. L = PEt_3), of a tetrahedral cluster with six metal–metal bonds (L = PCy_3), or of a metalloligated cluster with four metal–metal bonds (L_2 = $Ph_2PCH_2CH_2PPh_2$ (dppe)). Further examples of clusters in which an 18 electron carbonylmetalate fragment behaves as a four electron donor bridging anion are provided with a series of mixed-metal clusters containing the ligand $Ph_2PCH_2PPh_2$ (dppm). Highly regioselective pathways are observed during the synthesis of such clusters, e.g. of core composition $PdPtMn_2$, $PdPtFe_2$ or $PdPtCo_2$. Selective substitution reactions are observed which occur under steric control, illustrating the idea that metal–metal bonds can play an important role in molecular recognition. Finally, mention is made of the promising applications of mixed-metal cluster-derived heterogeneous catalysts for the selective carbonylation of organic nitro derivatives.

During the last decade, research in cluster chemistry has been very active, notably in the directions of (i) the rational synthesis of molecules containing hetero metal–metal bonds, (ii) a better understanding of their bonding and of the relationships between structural and chemical properties, (iii) the study of the selective interactions between clusters and small molecules, e.g. carbon monoxide, unsaturated organic and inorganic fragments, and of the frequently encountered subsequent activation of the latter. This has led to an improved fundamental knowledge of the nature and reactivity of new chemical bonds, in the discovery and mechanistic study of cluster-mediated stoichiometric and catalytic transformations sometimes involving bridging or capping ligands, e.g. μ_n-S, μ_n-PR, not available in mononuclear complexes, and in the design of new homogeneous and heterogeneous catalytic systems.[1–17]

During the course of our studies, we have made extensive use of the ability of bridging groups to stabilize polynuclear complexes. It has become apparent that metal ions and organometallic fragments can behave like bridging ligands and that these similarities may be nicely accounted for by the isolobal analogy concept.[18] A selection of bridging ligands frequently encountered is given in Table 1,

* Author to whom correspondence should be addressed.

Table 1. Examples of μ_2- or μ_3-bridges in di- and polynuclear complexes

Electron donation	Ligand	ML_n
0	H^+	$[CuPPh_3]^+$, $[AuPPh_3]^+$, Hg^{2+}
2	CO	
4	μ-$[PPh_2]^-$ μ-$[Ph_2P—CHY]^-$ μ_3-S $Ph_2PCH_2PPh_2$ η^2-RC≡CR	$[CpMo(CO)_3]^-$, $[Co(CO)_3L]^-$
6	μ_3-Cl^-	$[CpMo(CO)_3]^-$ (see Ref. 19)

together with organometallic fragments ML_n that may display similar bonding capabilities in cluster compounds.

In the following, we shall illustrate these aspects with examples taken from our own work. For experimental details, the reader is invited to consult the corresponding literature references.

DISCUSSION

Comparisons between copper, gold and mercury reagents

The isolobal analogy concept is very powerful in helping to understand the structure of complex molecules and in predicting the possible existence of others.[18a] Thus for example, it has been possible to prepare the series of clusters $[RuCo_3(\mu_3\text{-CuL})(\mu\text{-CO})_3(CO)_9]$ (L = PPh_3) (**1**),[20] $[RuCo_3(\mu_3\text{-AuL})(\mu\text{-CO})_3(CO)_9]$ (**2**),[20,21] $[RuCo_3\{\mu_3\text{-HgCo(CO)}_4\}(\mu\text{-CO})_3(CO)_9]$ (**3**)[22] and $Hg[RuCo_3(\mu\text{-CO})_3(CO)_9]_2$ (**4**)[23] [eq. (1)] in which the d^{10} metal ion Cu(I), Au(I) or Hg(II) is triply bridging the Co_3 face of the tetrahedral precursor cluster $[Co_3Ru(\mu\text{-CO})_3(CO)_9]^-$, like H^+ in $HRuCo_3(\mu\text{-CO})_3(CO)_9$.

$$2K[RuCo_3(CO)_{12}] + HgBr_2 \xrightarrow[-2KBr]{CH_2Cl_2} Hg[RuCo_3(\mu\text{-CO})_3(CO)_9]_2 \quad (1)$$

(4)

The structural characterization of clusters **1**–**4** has enabled us to study the influence of the d^{10} fragment on the distance between the ruthenium cap and the Co_3 plane. In agreement with the bonding scheme previously detailed for these clusters,[20] we have established the *trans*-influence series: $Cu(PPh_3) < Au(PPh_3) < HgCo(CO)_4 \sim HgRuCo_3(CO)_{12}$, which reflects the increase in the distance between the Ru atom and the Co_3 plane in the corresponding clusters, as reported in Table 2.

The diplatinum complex $[Pt_2Cl_2(\mu\text{-dppm})_2]$ (dppm = $Ph_2PCH_2PPh_2$), containing a d^9–d^9 metal–metal bond, has been found to react with the electrophilic reagents $[AuL]^+$ [eq. (2)][24] or $HgCl_2$ [eq. (3)][25] to afford the A-frame clusters $[Pt_2(\mu\text{-AuL})Cl_2(\mu\text{-dppm})_2]^+$ (**5**) or $[Pt_2(\mu\text{-HgCl}_2)(\mu\text{-dppm})_2]$ (**6**), respectively. The bonding of the apex metal fragment in these clusters appears to be predominantly of a_1 symmetry and is reminiscent of that of H^+ in $[Pt_2(\mu\text{-H})Cl_2(\mu\text{-dppm})_2]^+$, obtained by protonation of $[Pt_2Cl_2(\mu\text{-dppm})_2]$.[26]

However, the isolobal analogy cannot provide quantitative kinetic or thermodynamic data. Thus for example, in contrast to the reaction of, for example eq. (2) which afforded an A-frame complex, the dipalladium complex $[Pd_2Cl_2(\mu\text{-dppm})_2]$ was found recently to react with the electrophilic reagent $[Cu(CH_3CN)_4][BF_4]$ in CH_2Cl_2 with formation of the new palladium cluster $[Pd_4(\mu\text{-Cl})_2(\mu\text{-dppm})_4][BF_4]_2$ (**7**)[27] [eq. (4)]. This interesting molecule, which apparently results from the dimerization of the unsaturated cation $[Pd_2(\mu\text{-dppm})_2Cl]^+$, can be prepared quantitatively by the reaction of eq. (5). Its structure clearly shows that palladium–phosphorus bonds have broken and formed, under very mild conditions, in the process. No A-frame Pd_2Cu complex analogous to **5** was detected, probably as a result of both the thermodynamically preferred formation of insoluble CuCl and of the greater Pd—P vs Pt—P bond lability in the precursor complexes. On the other hand, a complex analogous to **7** was not observed in the reaction of $Pd_2(\mu\text{-dppm})_2Cl_2$ with $[Au(PPh_3)]^+$, but instead insertion of gold into a Pd—P bond probably took place. The formation of a triangulo unit of the type $AuPd_2(\mu\text{-dppm})_2$ was supported by $^{31}P\{^1H\}$ NMR spectroscopy.[27] These results emph-

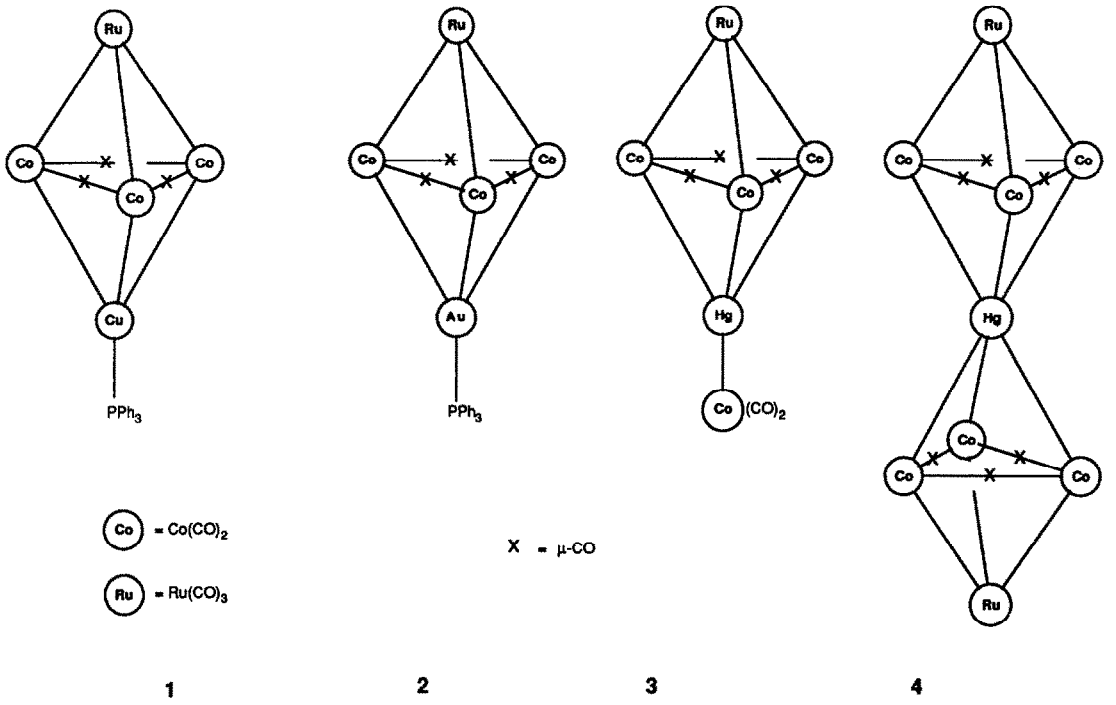

Table 2. Structural change as a function of the d^{10} metal fragment M

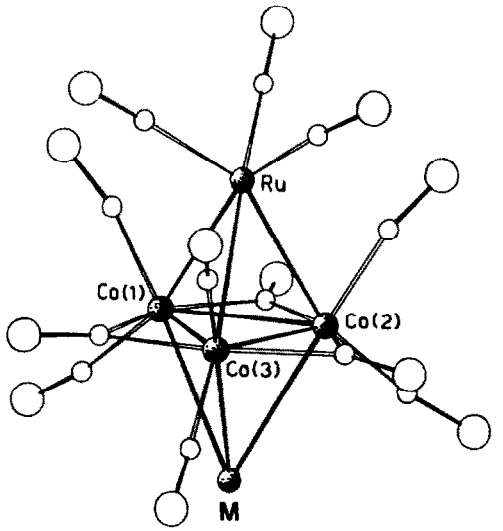

M	Distance Ru—Co_3 plane (Å)
$Cu(PPh_3)$	2.189(2)
$Au(PPh_3)$	2.240(3)
$HgCo(CO)_4$	2.258(5)
$HgRuCo_3(CO)_{12}$	2.254(2)

trans-Influence series:

$Cu(PPh_3) < Au(PPh_3) < HgCo(CO)_4 \simeq HgRuCo_3(CO)_{12}$.

asize the differences in reactivity observed between d^9 complexes of Pd(I) and Pt(I) on the one hand and between the d^{10} ions $[AuL]^+$ and $[CuL]^+$ on the other.

Tetranuclear mixed-metal clusters containing bridging $M(CO)_3(\eta\text{-}C_5H_4R)$ (M = Cr, Mo, W; R = H, Me) *fragments*

The carbonylmetalate anions $[M(CO)_3Cp]^-$ (M = Cr, Mo, W; $Cp = \eta\text{-}C_5H_4R$) classically behave like two electron donors, as in, for example, X—Hg—$M(CO)_3Cp$ or $Hg[M(CO)_3Cp]_2$, like pseudohalides. The first examples of these anions behaving as four electron donors in metal–metal bonded complexes were found with the planar, triangulated clusters $[M_2M'_2Cp_2(CO)_6(PR_3)_2]$ (M = Cr, Mo, W; M′ = Pd, Pt) (Scheme 1).[28]

In these centrosymmetric clusters, the two metalate anions bridge the almost linear $[L—M'—M'—L]^{2+}$ unit through metal–carbonyl and metal–metal interactions. The presence of five metal–metal bonds is consistent with these clusters having 58 electrons and containing two metals which utilize eight valence orbitals only. The arrangement of the bridging carbonyl ligand, one triply bridging the MM'_2 face, two semi-bridging the MM′ edges is reminiscent of that found in the carbonylmetalate anions $[M(CO)_3Cp]^-$ with, of course, a flattening of the $M(CO)_3$ cone since the

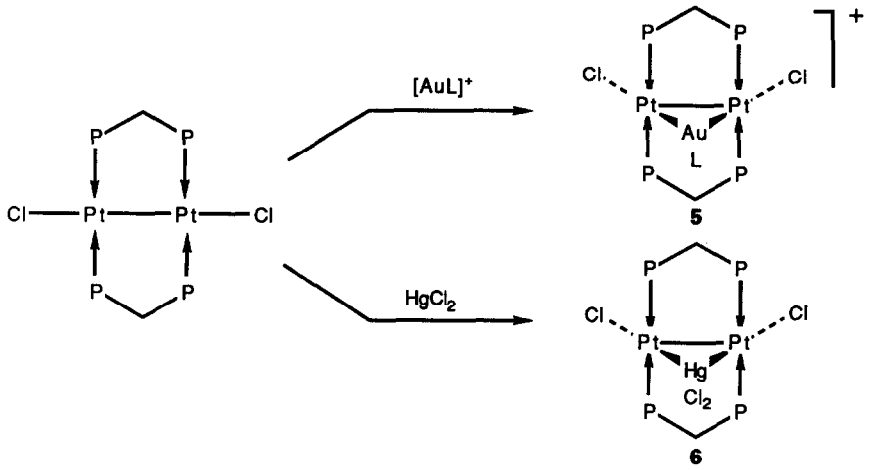

(2)

(3)

M'_2 unit is located within this cone.[28] Considering the isolobal analogy between these four electron donor metalates,[29] allyl anions and phosphido ligands PR_2^- (or between the corresponding three electron donor neutral ligands) the relationships of Scheme 2 result, which involve well characterized complexes.[13,30-32]

In order to evaluate the steric and electronic effects induced by the phosphine ligands on the structure of these unusual clusters, we prepared a series of them, including clusters containing a Pd—Pt bond instead of a Pd—Pd or a Pt—Pt bond. These clusters are listed in Table 3. In some cases, the η-C_5H_4Me ligand was used instead of η-C_5H_5 for crystallization purposes. Slight deviations away from planarity are sometimes observed for the $M_2M'_2$ core (M'_2 = Pd_2, Pt_2, PdPt) but the most dramatic effect is observed in the case of PCy_3 as a ligand. In this case, folding of the cluster wings occurs, producing a structure intermediate between that of a butterfly and of a tetrahedron (Fig. 1).

Thus, the Pt—Pt distance in **8** is elongated to 2.992(1) Å whereas the Mo—Mo distance is now 3.126(1) Å,[33] *ca* 0.11 Å shorter than in

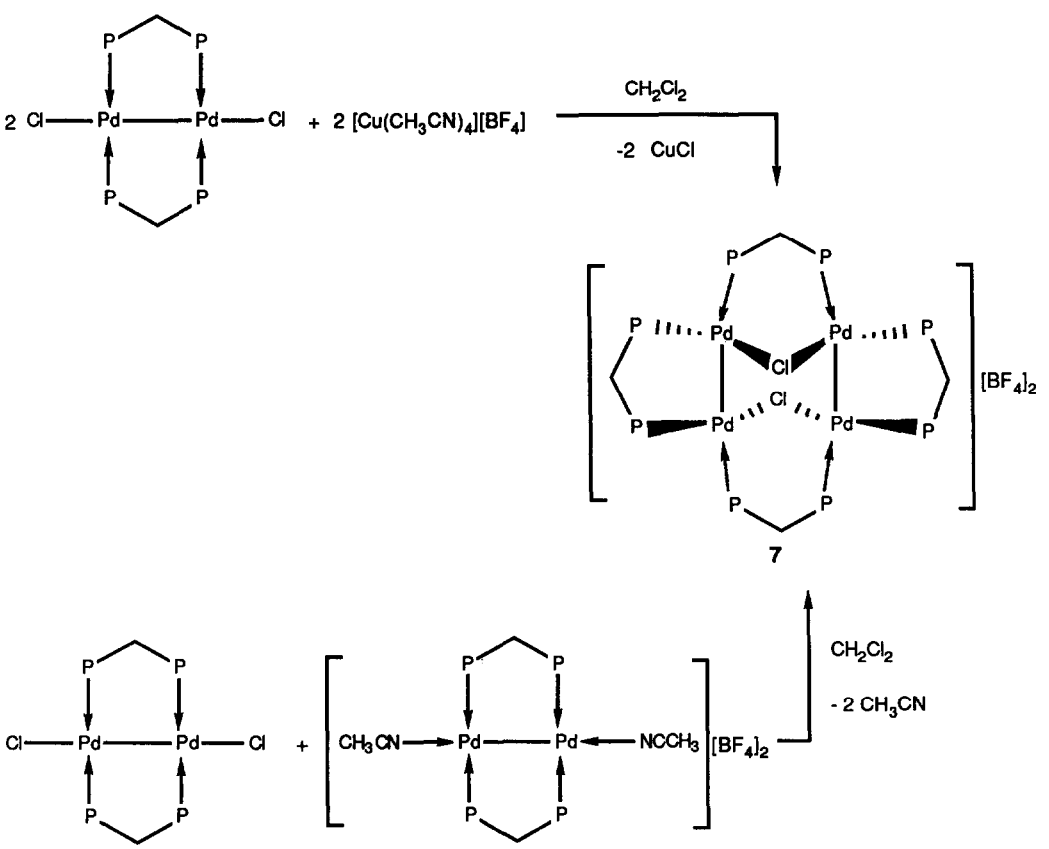

(4)

(5)

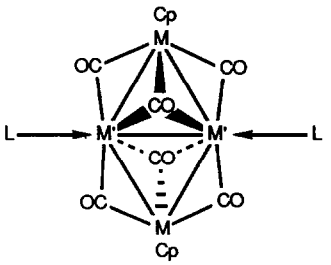

M = Cr, Mo, W

M' = Pd, Pt

L= tertiary phosphine

Scheme 1.

$[Mo(CO)_3Cp]_2$.[34] This would support the description of **9** as a tetrahedral cluster having six metal–metal bonds rather than of a butterfly. A concomitant decrease of the Pt—Pt—P angle is observed (Table 3). The sterically-induced planar to butterfly or tetrahedral rearrangement observed here is particularly remarkable since it occurs within a family of 58 electron clusters which differ only by the nature of the phosphine ligand. This is also relevant to the dynamic behaviour of M_4 clusters in solution[35] (Scheme 3).

Another example where steric factors play a key role is to be found with the cluster $[Mo_2Pt_2Cp_2(CO)_6(dppe)]$ (dppe = $Ph_2PCH_2CH_2PPh_2$) (**10**), which, although also having 58 electrons and containing the same metals as, for example, the planar, triangulated cluster $[Mo_2Pt_2Cp_2(CO)_6(PEt_3)_2]$ (**9**) or the tetrahedral **8**, possesses a metalloligated structure with only four metal–metal bonds.[36]

Going from **8** or **9** to **10** only requires the formal replacement of two monodentate phosphines by a bidentate phosphine. Despite their very similar core composition and identical total number of electrons (58 e), dramatic structural changes have occurred. Clearly, this results from the steric properties of the chelating dppe ligand. In **10** also, the carbonylmetalate fragments may be described as anionic four electron donors towards the $[Pt_2(dppe)]^{2+}$ unit. One of them is bridging the Pt—Pt bond through metal–carbonyl and metal–metal interactions, the metalloligated one through two bridging carbonyls and a metal–metal bond.

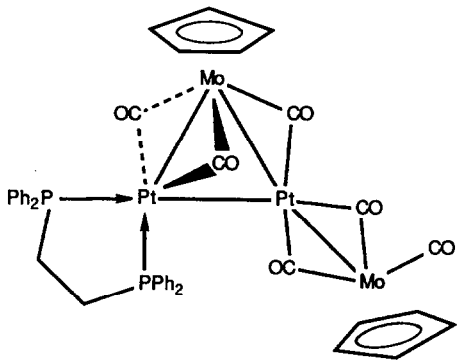

10

Mixed-metal clusters containing the dppm ligand

The diphosphine ligand $Ph_2PCH_2PPh_2$(dppm) has been widely used for the construction and stabilization of di- and polynuclear complexes because of its ability to span metal–metal bonds, thus forming five-membered rings.[37] We have developed

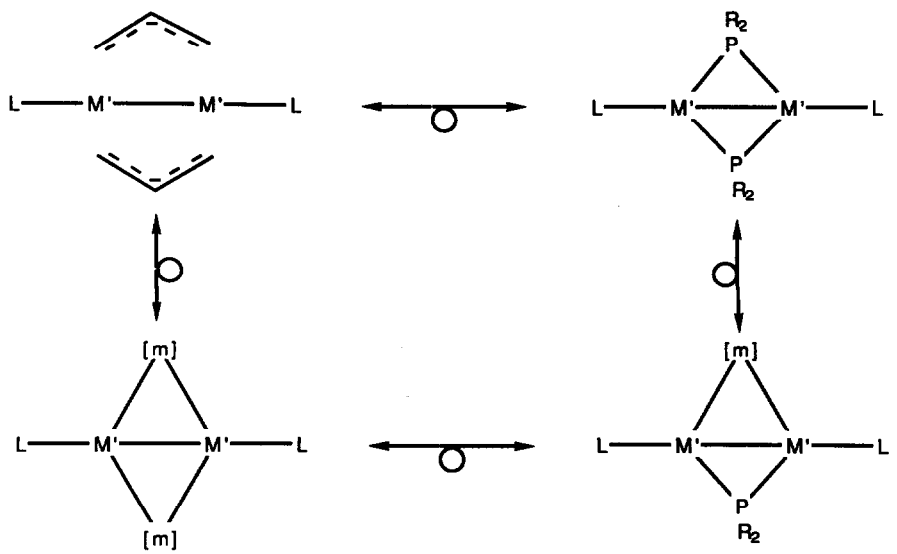

Scheme 2.

Table 3. Comparative structural data for the clusters $[m]_2M'_2L_2$ ([m] = $Mo(CO)_3(\eta\text{-}C_5H_4R)$)

M'_2	R	L	θ (°)	Angle (°) P(1)—M′—M′ P(2)—M′—M′	d_1 d_2 (Å)	d_3 d_6 (Å)	d_4 d_5 (Å)	Ref.
Pd_2	H	PEt_3	0	177.20(4) 177.20(4)	2.582(1) > 4	2.864(1) 2.864(1)	2.827(1) 2.827(1)	28c
Pd_2	Me	PEt_3	0	173.54(8) 173.54(8)	2.592(1) > 4	2.871(1) 2.871(1)	2.811(1) 2.811(1)	33
Pt_2	H	PEt_3[a]	0	173.3(1) 173.3(1)	2.677(1) > 4	2.777(1) 2.777(1)	2.835(2) 2.835(2)	28d
			0	169.7(1) 169.7(1)	2.646(1) > 4	2.793(1) 2.793(1)	2.846(1) 2.846(1)	28d
Pt_2	Me	$PPhMe_2$	0	171.57 171.57	2.652(1) > 4	2.767(1) 2.767(1)	2.828(1) 2.828(1)	33
Pt_2	Me	PPh_2Me	7	171.3(1) 171.7(1)	2.656(1) > 4	2.758(2) 2.779(2)	2.847(2) 2.849(2)	33
Pt_2	Me	PPh_3	0	172.0(1) 172.0(1)	2.654(1) > 4	2.767(1) 2.767(1)	2.844(1) 2.844(1)	33
PdPt[b]	H	PPh_3	13.4	172.67(6) 160.49(6)	2.623(1) > 4	2.804(1) 2.870(1)	2.904(1) 2.838(1)	33
Pt_2	Me	PCy_3	98	140.07(5) 138.73(5)	2.992(1) 3.126(1)	2.755(1) 2.727(1)	2.870(1) 2.884(1)	33

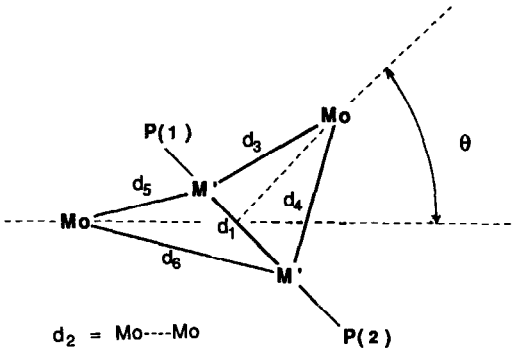

[a] There are two independent molecules in the unit cell.
[b] The Pt atom is bound to P(1).

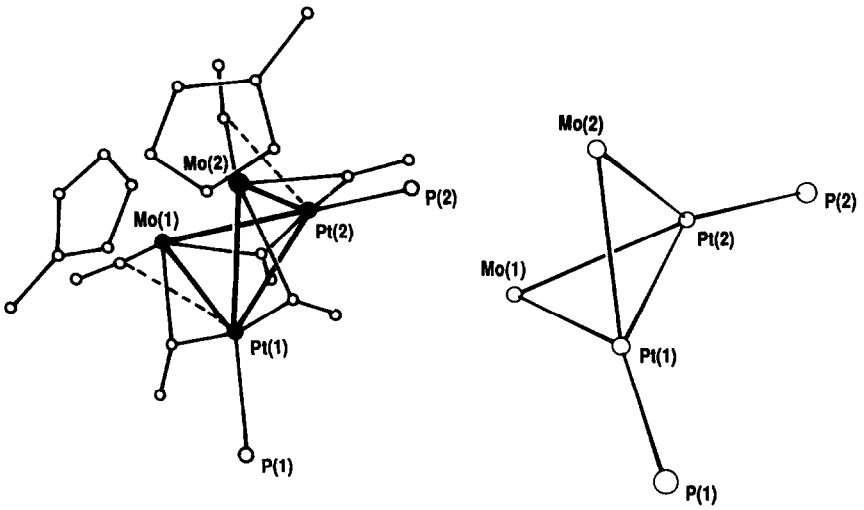

Fig. 1. View of the structure of $[Mo_2Pt_2(\eta\text{-}C_5H_4Me)_2(CO)_6(PCy_3)_2]$ (**8**). For clarity, the phosphine ligands are represented by their phosphorus atom only. Metal–metal distances (Å): Pt(1)—Pt(2): 2.992(1); Pt—Mo: 2.727(1)–2.884(1); Mo(1)—Mo(2): 3.126(1).

two general methods for obtaining mixed-metal clusters containing this ligand. The first one makes use of the carbonylmetalate-induced P → Pt bond lability which converts a chelating dppm ligand into a bridging one, the resulting five-membered ring being more stable than the four-membered one. This is illustrated with the synthesis of **11** and **12** in Scheme 4.[38]

The strengthening role of the μ-dppm ligand is evidenced by the reversible CO fixation under very mild conditions observed with these complexes. This reaction occurs with complete site selectivity since only the M—M bond of **11** or **12**, and no Pt—M bond, is involved in the process.[38] However, this reaction principle does not always lead to the formation of a heteronuclear metal–metal bond. Thus, for example, the reaction of eq. (6) occurs via hydride transfer from Cr or W to Pt, affording the trihydrido A-frame complex $[Pt_2H_3(\mu\text{-dppm})_2]^+$ in high yield.[39]

The second method that we have used for preparing heterometallic complexes containing the dppm ligand involves the reaction of carbonylmetalate anions with dinuclear dppm complexes, as exemplified in Scheme 5.[40] When M′ = Pt, two possible isomers are conceivable, depending on the respective position of Pd and Pt in the product. However, only the isomers drawn in Scheme 5 are formed ($^{31}P\{^1H\}$ NMR evidence) and isolated, showing that the reaction proceeds with complete *regioselectivity*.[40] Formal insertion of the metal carbonyl fragment occurs into the more

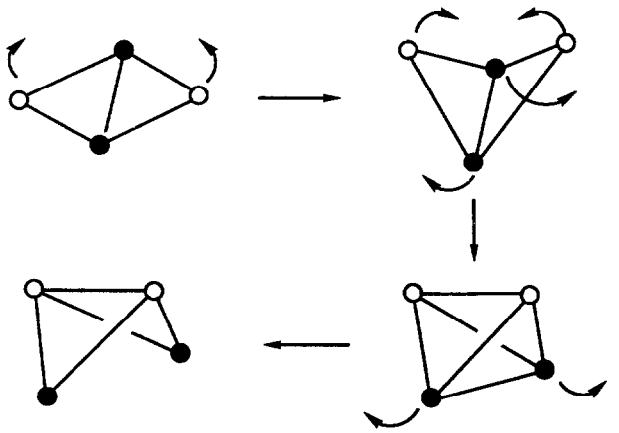

Scheme 3. Planar → butterfly → tetrahedral rearrangement of tetranuclear clusters.

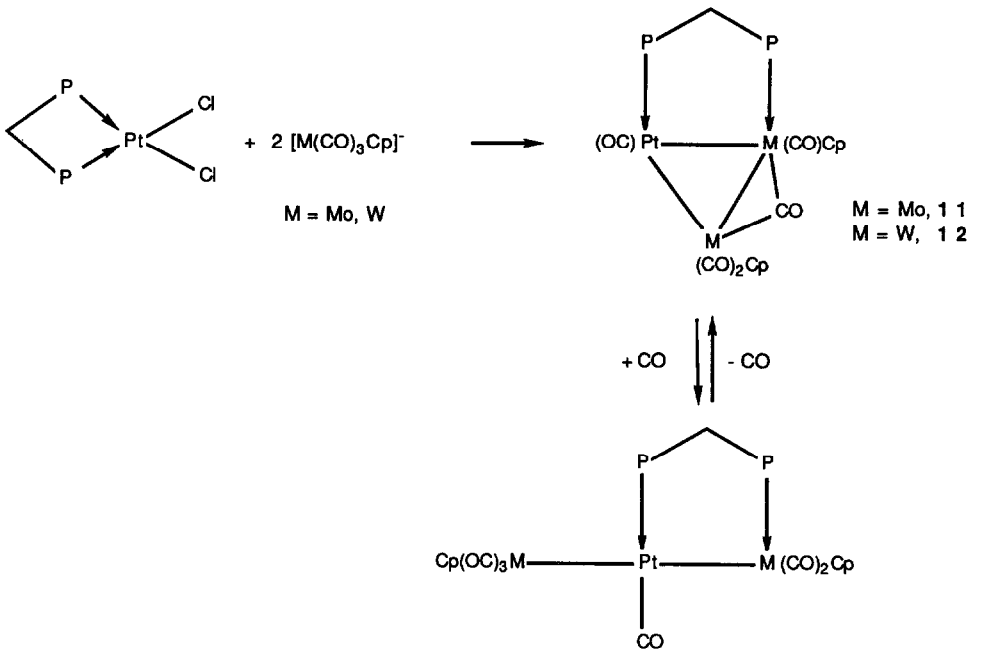

Scheme 4.

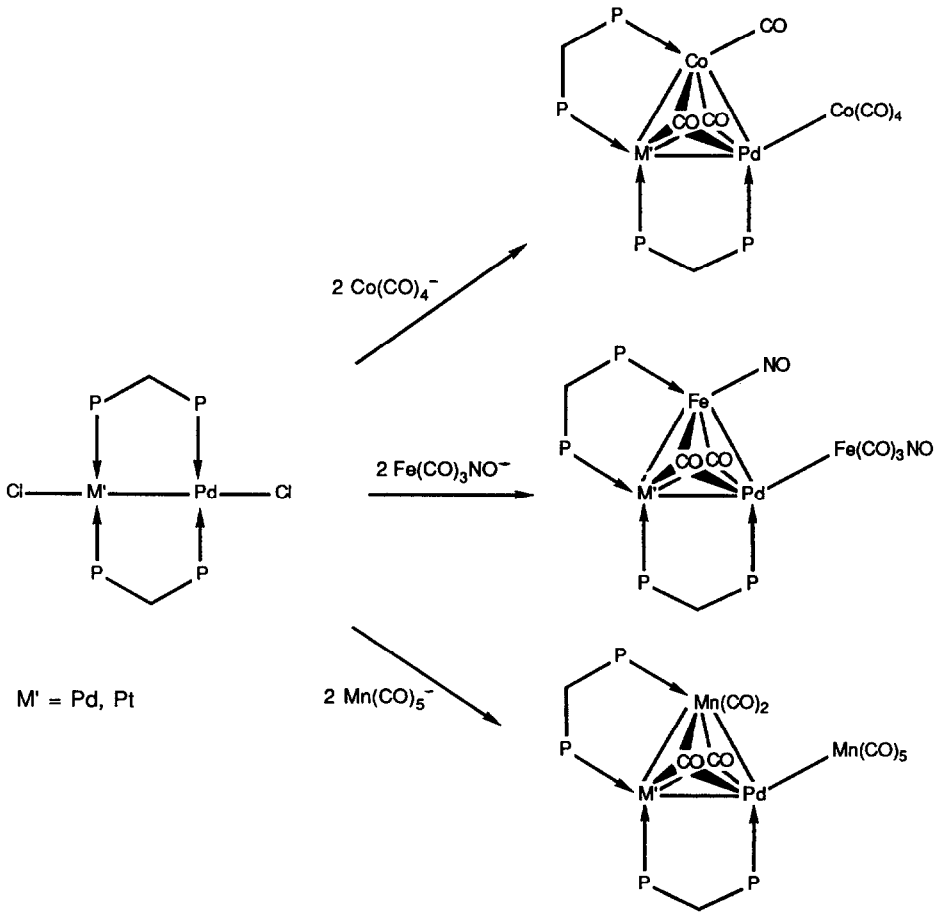

Scheme 5.

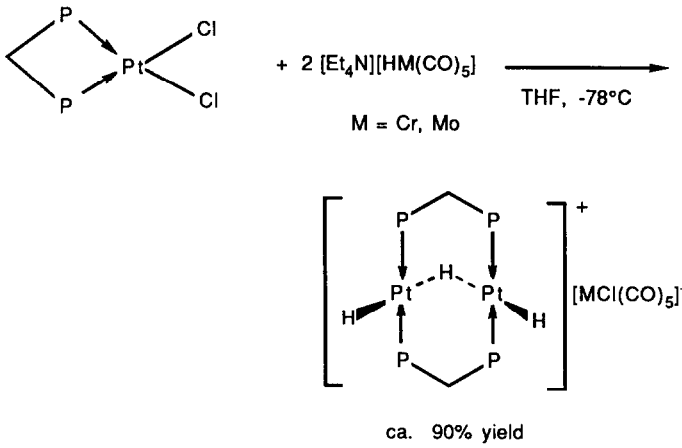

(6)

labile Pd—P bond. However, in the reaction with $[Fe(CO)_4]^{2-}$, both isomers of the product $[PdPtFe(CO)_4(dppm)_2]$ have been identified and the isomerization process is characterized at equilibrium (25°C) by a ratio of *ca* 1 : 1 between the kinetic and thermodynamic isomers [eq. (7)].[41]

The heterotetranuclear clusters shown in Scheme 5 are all characterized by a labile exocyclic metal–metal bond, thus allowing an easy functionalization of the clusters to be achieved. An example is given in eq. (8) where iodide can reversibly replace the $Fe(CO)_3NO^-$ anion.[40c]

Interestingly, these and related monohalide trinuclear clusters may be used as precursors of metalloligated clusters containing four different metal atoms (Scheme 6).[42] In these clusters, the endocyclic metal carbonyl fragment behaves like a four electron donor anionic ligand. This extends our previous findings and emphasizes the relationships between the clusters shown in Scheme 7.

The fact that the anion $[Mo(CO)_3Cp]^-$ does not react with the clusters $[PdMCoX(CO)_3(dppm)_2]$ should be related to the observation that the reaction of eq. (9) does not lead to a tetranuclear cluster either, even in the presence of an excess of carbonylmetalate.[36]

This would be consistent with a steric inhibition resulting from the size of the space delimited by the phenyl groups attached to phosphorus and the ligands of the endocyclic Mo atom. Only the metalate anion having a smaller size can have access to this site: the selective substitution at the Pd centre

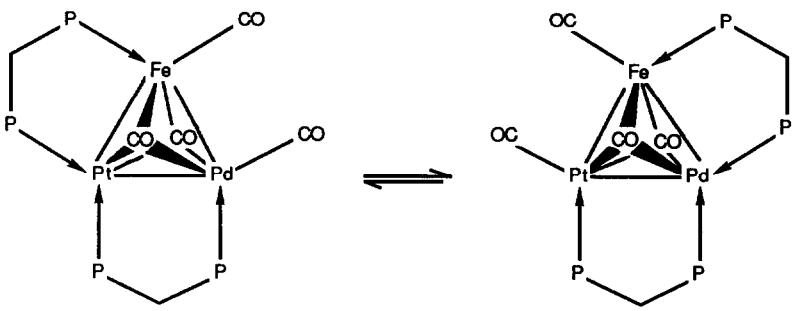

(7)

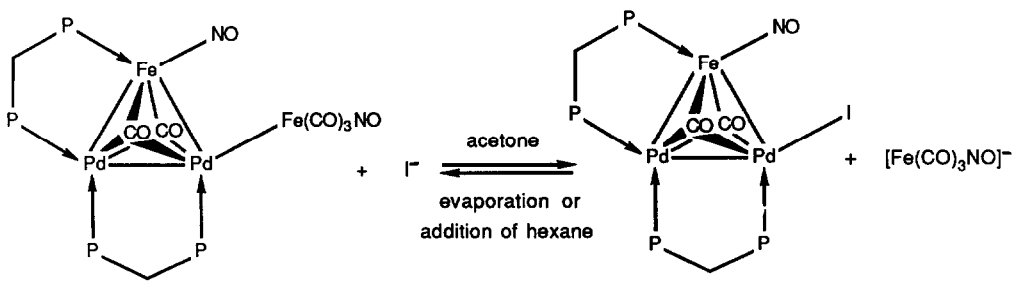

(8)

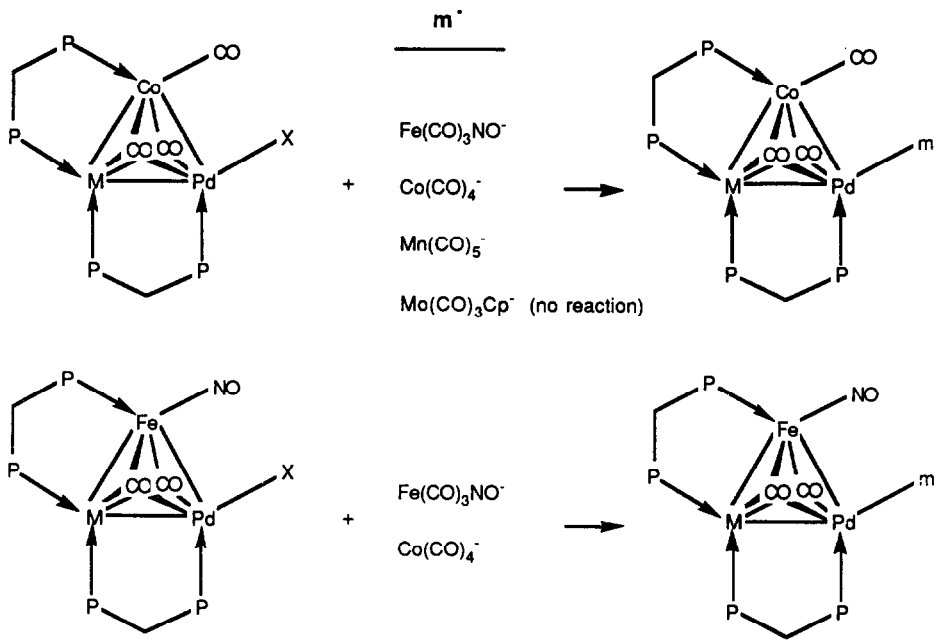

Scheme 6.

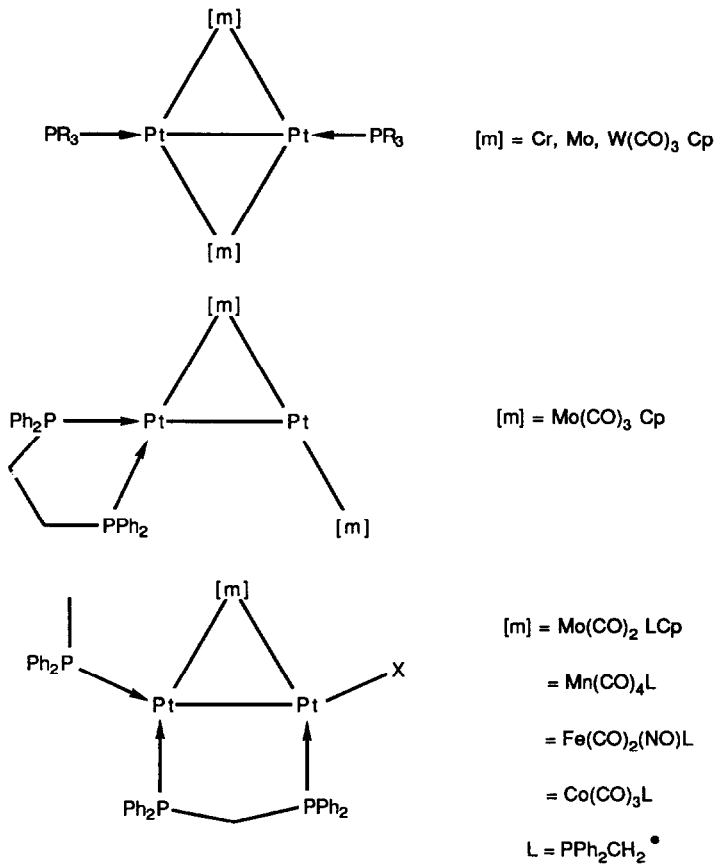

Scheme 7.

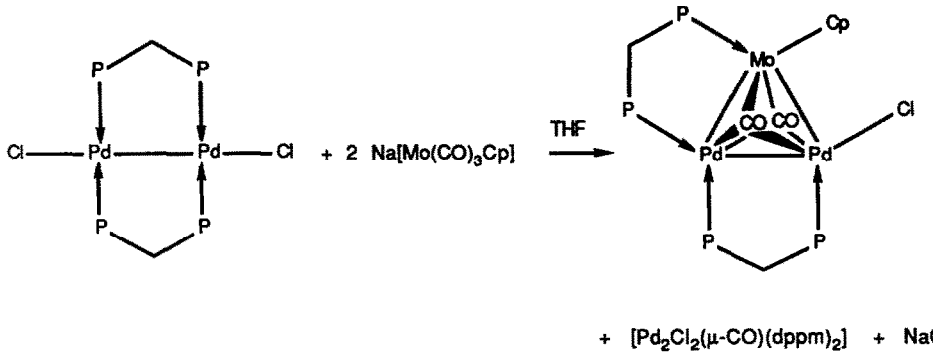

(9)

is governed by steric control (Scheme 8). Therefore, these clusters provide examples showing that metal–metal bonds can play a significant role in molecular recognition, a severe discrimination occurring between the metal carbonylate anions.

Heterometallic clusters in heterogeneous catalysis

The use of mixed-metal cluster compounds in homogeneous and heterogeneous catalysis has been reviewed recently.[1] We have been particularly interested in their application in heterogeneous catalysis, hoping that the catalytic materials resulting from the anchoring and thermal decomposition of mixed-metal clusters onto supports may display improved properties over the conventional catalysts containing the same metals.

The high-yield synthesis of molecular palladium-containing mixed-metal clusters has allowed their evaluation as catalyst precursors for the carbonylation of nitro derivatives into organic isocyanates.[43] The latter constitute a very important class of chemicals, classically made by phosgenation of amines. We have previously reported that the heterogeneous catalyst prepared from the planar, molybdenum–palladium cluster $[Mo_2Pd_2Cp_2(CO)_6(PPh_3)_2]$ converts nitrobenzene into phenylisocyanate [eq. (10)] with a much higher selectivity (80%) than conventional catalysts of these metals under the same conditions.[43]

$$Ph—NO_2 + 3CO \rightarrow Ph—N{=}C{=}O + 2CO_2. \quad (10)$$

More recently, it was found that the beneficial role of mixed-metal clusters as catalyst precursors can be extended to the synthesis of benzoxazolone-2 by carbonylation of *o*-nitrophenol [eq. (11)].[41] Iron–palladium catalysts were chosen for this reaction and a conventional system was compared with catalysts derived from the dppm clusters $[FePd_2(CO)_4(dppm)_2]$ [eq. (7)] or $[Fe_2Pd_2(CO)_5(NO)_2(dppm)_2]$ (Scheme 5, M′ = Pd). In all cases, the support was silica and the reaction conditions comparable. The cluster-derived catalysts led to conversions and selectivities of *ca* 99 and 96%, respectively.[41]

Obviously, there can be a clear advantage to use molecular mixed-metal cluster compounds as catalyst precursors, particularly for "bimetallic-sensitive" reactions. The considerable improvements observed in the reactions of eqs (10) and (11) should be taken as indications of the potential of mixed-metal cluster derived catalysts.[1]

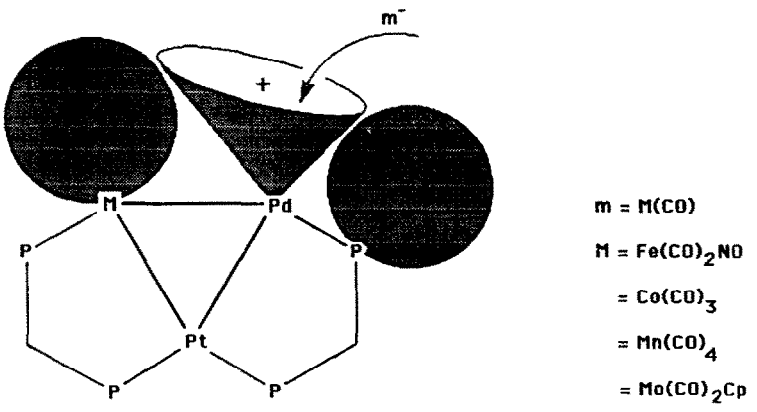

Scheme 8. Selective substitution via steric control. Metal–metal bonds in molecular recognition.

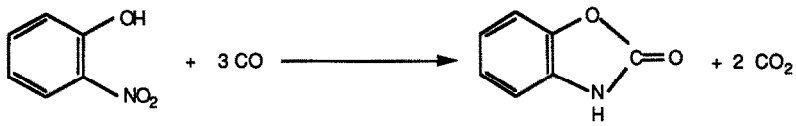

(11)

Acknowledgements—We are grateful to Dr. S.-E. Bouaoud for the drawing of Fig. 1 and to the CNRS, the Université Louis Pasteur, Atochem and Johnson–Matthey Co. Ltd. for support.

REFERENCES

1. P. Braunstein and J. Rosé, in *Stereochemistry of Organometallic and Inorganic Compounds* (Edited by I. Bernal), Vol. 3. Elsevier, Amsterdam (1988).
2. M. H. Chisholm, *New J. Chem.* 1987, **11**, 459.
3. J. Hein, J. C. Jeffery, P. Sherwood and F. G. A. Stone, *J. Chem. Soc., Dalton Trans.* 1987, 2211 and references cited.
4. G. Huttner and K. Knoll, *Angew. Chem., Int. Ed. Engl.* 1987, **26**, 743.
5. P. Braunstein, *Nouv. J. Chim.* 1986, **10**, 365 and references cited.
6. M. H. Chisholm and J. A. Heppert, *Adv. Organomet. Chem.* 1986, **26**, 97.
7. A. J. Deeming, *Adv. Organomet. Chem.* 1986, **26**, 1.
8. B. C. Gates, L. Guczi and H. Knözinger (Eds), *Studies in Surface Science and Catalysis*, Vol. 29: Metal Clusters in Catalysis. Elsevier, Amsterdam (1986).
9. M. D. Vargas and J. N. Nicholls, *Adv. Inorg. Chem. Radiochem.* 1986, **30**, 123.
10. R. D. Adams and I. T. Horvath, *Prog. Inorg. Chem.* 1985, **33**, 127.
11. D. M. P. Mingos and J. C. Hawes, *Struct. Bonding (Berlin)* 1985, **63**, 1.
12. P. R. Raithby and M. J. Rosales, *Adv. Inorg. Chem. Radiochem.* 1985, **29**, 170.
13. E. Sappa, A. Tiripicchio and P. Braunstein, *Coord. Chem. Rev.* 1985, **65**, 219.
14. G. Schmid, *Struct. Bonding (Berlin)* 1985, **62**, 51.
15. H. Vahrenkamp, *Comments Inorg. Chem.* 1985, **4**, 253.
16. B. F. G. Johnson (Ed.), *Polyhedron* 1984, **3**, 1277.
17. F. G. A. Stone, *Angew. Chem., Int. Ed. Engl.* 1984, **23**, 89.
18. (a) R. Hoffmann, *Angew. Chem., Int. Ed. Engl.* 1982, **21**, 711; (b) M. Elian, M. M. L. Chen, D. M. P. Mingos and R. Hoffmann, *Inorg. Chem.* 1976, **15**, 1148; (c) M. Elian and R. Hofmann, *Inorg. Chem.* 1975, **14**, 1058.
19. P. Braunstein, J. Fischer, D. Matt and M. Pfeffer, *J. Am. Chem. Soc.* 1984, **106**, 410.
20. P. Braunstein, J. Rosé, A. Dedieu, Y. Dusausoy, J.-P. Mangeot, A. Tiripicchio and M. Tiripicchio Camellini, *J. Chem. Soc., Dalton Trans.* 1986, 225.
21. P. Braunstein, J. Rosé, Y. Dusausoy and J.-P. Mangeot, *C. R. Hebd. Séances Acad. Sci., Ser. II* 1982, 967.
22. P. Braunstein, J. Rosé, A. Tiripicchio and M. Tiripicchio Camellini, *J. Chem. Soc., Chem. Commun.* 1984, 391.
23. P. Braunstein, J. Rosé, A. Tiripicchio and M. Tiripicchio Camellini, *Angew. Chem., Int. Ed. Engl.* 1985, **24**, 767.
24. G. J. Arsenault, L. Manojlovic-Muir, K. W. Muir, R. J. Puddephatt and I. Treurnicht, *Angew. Chem., Int. Ed. Engl.* 1987, **26**, 86.
25. P. R. Sharp, *Inorg. Chem.* 1986, **25**, 4185.
26. (a) M. P. Brown, R. J. Puddephatt, M. Rashidi and K. R. Seddon, *J. Chem. Soc., Dalton Trans.* 1978, 516; (b) M. C. Grossel, J. R. Batson, R. P. Moulding and K. R. Seddon, *J. Organomet. Chem.* 1986, **304**, 391.
27. P. Braunstein, M. A. Luke, A. Tiripicchio and M. Tiripicchio Camellini, *Angew. Chem., Int. Ed. Engl.* 1987, **26**, 768.
28. (a) R. Bender, P. Braunstein, Y. Dusausoy and J. Protas, *Angew. Chem., Int. Ed. Engl.* 1978, **17**, 596; (b) *J. Organomet. Chem.* 1979, **172**, C51; (c) R. Bender, P. Braunstein, J.-M. Jud and Y. Dusausoy, *Inorg. Chem.* 1983, **22**, 3394; (d) *Ibid.* 1984, **23**, 4489.
29. P. Hofmann and H. R. Schmidt, *Angew. Chem., Int. Ed. Engl.* 1986, **25**, 837.
30. H. Werner and A. Kuhn, *Angew. Chem., Int. Ed. Engl.* 1977, **16**, 412.
31. N. J. Taylor, P. C. Chieh and A. J. Carty, *J. Chem. Soc., Chem. Commun.* 1975, 448.
32. R. Bender, P. Braunstein, B. Metz and P. Lemoine, *Organometallics* 1984, **3**, 381.
33. (a) R. Bender, S.-E. Bouaoud, P. Braunstein, C. de Méric de Bellefon and D. Grandjean, unpublished results; (b) S.-E. Bouaoud, Doctorat ès Sciences Physiques, Université de Rennes, France (1987).
34. R. D. Adams, D. M. Collins and F. A. Cotton, *Inorg. Chem.* 1974, **13**, 1086.
35. (a) A. Moor, P. S. Pregosin, L. M. Venanzi and A. J. Welch, *Inorg. Chim. Acta* 1984, **85**, 103; (b) R. Bender, P. Braunstein and B. T. Heaton, unpublished results.
36. P. Braunstein, J.-M. Jud, Y. Dusausoy and J. Fischer, *Organometallics* 1983, **2**, 180.
37. (a) A. L. Balch, in *Homogeneous Catalysis with Metal Phosphine Complexes* (Edited by L. Pignolet), p. 167. Plenum Press, New York (1983); (b) R. J. Puddephatt, *Chem. Soc. Rev.* 1983, **12**, 99.
38. P. Braunstein, N. Guarino, C. de Méric de Bellefon and J.-L. Richert, *Angew. Chem., Int. Ed. Engl.* 1987, **26**, 88.
39. P. Braunstein and B. Oswald, *J. Organomet. Chem.* 1987, **328**, 229.
40. (a) P. Braunstein, C. de Méric de Bellefon, M. Ries, J. Fischer, S.-E. Bouaoud and D. Grandjean, *Inorg. Chem.* 1988, **27**, 1327; (b) P. Braunstein, C. de Méric de Bellefon and M. Ries, *Inorg. Chem.* 1988, **27**, 1338;

(c) P. Braunstein, C. de Méric de Bellefon, M. Ries and J. Fischer, *Organometallics* 1988, **7**, 332.
41. P. Braunstein, J. Kervennal and J.-L. Richert, *Angew. Chem., Int. Ed. Engl.* 1985, **24**, 768.
42. P. Braunstein, C. de Méric de Bellefon and M. Ries, *J. Organomet. Chem.* 1984, **262**, C14.
43. P. Braunstein, R. Bender and J. Kervennal, *Organometallics* 1982, **1**, 1236.

Polyhedron Vol. 7, No. 22/23, pp. 2285–2295, 1988
Printed in Great Britain

0277–5387/88 $3.00+.00
©1988 Pergamon Press plc.

DIFFERENTIATING METAL SITES IN HOMOPOLYNUCLEAR SYSTEMS VIA INCORPORATION OF π-DONORS: COMPLEXES OF BRIDGING PHOSPHIDOXO ($Ph_2P{=}O$) LIGANDS

DERYN E. FOGG and ARTHUR J. CARTY*

Guelph-Waterloo Centre for Graduate Work in Chemistry, Waterloo Campus, Department of Chemistry, University of Waterloo, Waterloo, Ontario, Canada N2L 3G1

Abstract—An interesting chemistry for polynuclear clusters containing bridging phosphidoxo (μ-$R_2P{=}O$) ligands can be anticipated for the following reasons: (i) the combination of a soft donor (P) and a hard ligand (=O) differentiates metal centres even in homobinuclear systems; (ii) the μ-$R_2P{=}O$ moiety should, like the μ-R_2P group, be capable of bridging both bonding and non-bonding metals; (iii) there is evidence that phosphine oxides exert a labilizing influence on metal–carbonyl bonds. Thus the oxygen end of the μ-phosphidoxo ligand may exercise control over the sites of substitution in polynuclear complexes. A brief review of literature data for μ-$R_2P{=}O$ (R = aryl, alkyl, alkoxy) complexes is given and some synthetic strategies summarized. A facile route to polynuclear carbonyl complexes of iron and ruthenium containing a single μ-$Ph_2P{=}O$ ligand will be described. X-ray analyses of $Ru_2(CO)_6(\mu_2\text{-}\eta^2\text{-}C{\equiv}CBu^t)(\mu\text{-}Ph_2P{=}O)$ (**1**) and $Fe_3(CO)_9(\mu_3\text{-}\eta^2\text{-}C{\equiv}CBu^t)(\mu\text{-}Ph_2P{=}O)$ (**4**) suggest that μ-Ph_2PO ligands may be equally as versatile as their μ-Ph_2P counterparts. A direct comparison of structural parameters for $Ru_2(CO)_6(\mu_2\text{-}\eta^2\text{-}C{\equiv}CBu^t)(\mu\text{-}PPh_2)$ and $Ru_2(CO)_6(\mu_2\text{-}\eta^2\text{-}C{\equiv}CBu^t)(\mu\text{-}Ph_2P{=}O)$ confirms the dramatic effect of the oxo end of the bridge on the hydrocarbyl and the *trans* CO. The directing effect of the oxygen on substitution reactions with PMe_3 is demonstrated. The novel trinuclear vinylidene complex $Fe_3(CO)_9(\mu_3\text{-}\eta^2\text{-}C{=}C(Pr^i)PPh_2)$ as well as the unusual binuclear compound $Fe_2(CO)_6\{\mu\text{-}Me_2C{=}C{=}CH{-}P(=O)Ph_2\}$ containing an allenic phosphine oxide are described.

Two aspects of polynuclear chemistry which continue as the focus of attention are the use of main group bridging ligands to help maintain the structural integrity of a cluster framework and the potential of heterometallic systems for promoting unique types of chemical transformations. One of the most thoroughly investigated main group ligands has been the phosphido bridge on account of its ability to support both strongly bonding and non-interacting metal centres.[1] Although a great deal of interesting chemistry has been accomplished on phosphido bridged complexes, particularly when an activated reaction site such as a μ-η-hydrocarbyl fragment is present, many instances of non-innocent behaviour of the bridge are now known which result in reaction of the M—PR_2 group and bridge cleavage.[2] The established work clearly illustrates that development of a useful chemistry for phosphido-bridged complexes requires that a lower-energy pathway be available in order to forestall activation of the bridge.[1a] While this has traditionally taken the form of an exceptionally reactive ligand, a promising but little-explored alternative is the use of a bridging ligand which combines framework-stabilizing and cluster-activating functions. We hoped to explore this avenue by suitable modification of the phosphido bridge.

A series of bridging $R_2P{=}X$ systems capable of functioning as binucleating groups exists where X = CR'_2, O, S and (rarely) Se (Fig. 1). For example ylid-like complexes have been prepared by carbene insertion into a μ-R_2P bridge,[3] and the [P=O] and [P=S] systems have likewise been obtained by oxygen and sulphur insertion.[4] More specifically, as recent reviews indicate, a substantial number of coordination complexes with [R_2PO] ligands formally derived from secondary phosphine oxides $R_2PH(O)$ or their phosphinous acid counterparts R_2POH are known.[5] There have not, however, to our knowledge been any attempts to relate the

*Author to whom correspondence should be addressed.

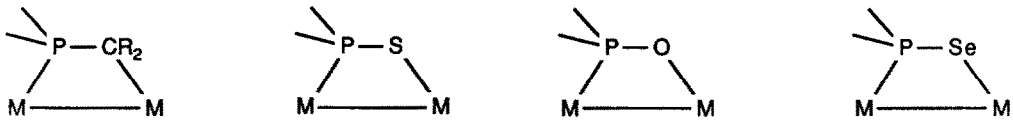

Fig. 1. Some three-electron donor bridging $R_2P{=}X$ ligands.

chemistry of μ-$R_2P{=}O$-bridged systems to that of the corresponding phosphido complexes.

Our interest in developing this comparison stems from the potential ability of an $R_2P{=}O$ unit to stabilize the skeletal framework of a cluster while simultaneously activating it towards substitution reactions. If the remarkable stability evinced by the phosphoryl unit in organic chemistry extends to transition metal complexes, and both ends of the ambidentate ligand are capable of strong metal–ligand binding, the requirement of framework stabilization is satisfied. At the same time, recent evidence suggests that regio- and stereospecific cluster activation may be induced by such a bridging ligand. A powerful labilizing effect is exhibited by the oxygen atom in oxygen-coordinated phosphine oxides, the magnitude of which is virtually unmatched by any other donor (being in fact comparable to that of the hard base Cl^-).[6] Thus the combination of the soft donor phosphorus and the hard oxygen atom results in a markedly different metal environment at either end of the bridge, producing an effectively heterobimetallic species even in a homobinuclear system.

SYNTHETIC STRATEGIES

Several approaches to $[R_2P{=}O]$-bridged systems have been explored, for R = alkyl, aryl, and alkoxy. In surveying this area it is immediately apparent that the practice of naming all of these anions as derivatives of a different phosphorus acid (Table 1) gives rise to unnecessary complexity in nomenclature, inevitably leads to misuse, and obscures the common element of the $P{=}O$ substructure. We propose a generic name for the $R_2P{=}O$ unit in order to remedy these problems. The term phosphidoxo, which will be adopted throughout this work, focusses on the phosphoryl unit without reference to the intricacies of the acid nomenclature. More importantly, it permits these ligands to be treated as a single class, providing an unambiguous description of the anion formally derived from any secondary phosphine oxide (irrespective of the actual parent) just as the term phosphido relates to the anion derived from any secondary phosphine.

Literature approaches to phosphidoxo-bridged systems commonly involve hydrolysis of a chlorophosphine–metal complex, or addition of a secondary phosphine oxide (either directly or generated *in situ* from the halophosphine) to a suitably labile metal complex. This gives in some cases (following dimerization) a centrosymmetric bis(μ-$R_2P{=}O$) structure,[7] but typically results in a monomeric acac-type of compound, which has been extensively employed as a chelating metalloligand (Fig. 2).[5,8] Treatment of the parent phosphine oxide with base before or after coordination to the metal centre gives access to $[R_2P{=}O]$ systems.[5] Reaction of the parent with strong base (i.e. $LiNH_2$, NaH, LiPh, etc.) is reported to give the oxygen-bonded species $M{-}OPR_2$,[9] to which coordination of a second metal fragment can be envisaged. Michaelis–Arbuzov reactions of metal phosphites offer a rational route to phosphidoxo systems.[10] Thus the chelating ligand $(\eta\text{-}C_5H_5)Co[P(O)(OMe)_2]_2[P(OMe)_3]$ is obtained on treatment

Table 1. Nomenclature of oxygen and phosphorus bound ligands

Parent	Name	Derivative	Ligand name
$P(OH)_3$	Phosphorous acid	$M{-}O{-}P(OR)_2$	Phosphito
$HP(OH)_2$	Phosphonous acid	$M{-}P(OR)_2$	Phosphonito
$H_2P{-}OH$	Phosphinous acid	$M{-}O{-}PR_2$	Phosphinito
PH_3	Phosphine	$M{-}PR_2$	Phosphido
$O{=}P(OH)_3$	Phosphoric acid	$M{-}O{-}P(O)(OR)_2$	Phosphato
$O{=}PH(OH)_2$	Phosphonic acid	$M{-}P(O)(OR)_2$	Phosphonato
$O{=}PH_2(OH)$	Phosphinic acid	$M{-}O{-}P(O)R_2$	Phosphinato
$O{=}PH_3$	Phosphine oxide	$M{-}P(O)R_2$	Phosphidyl

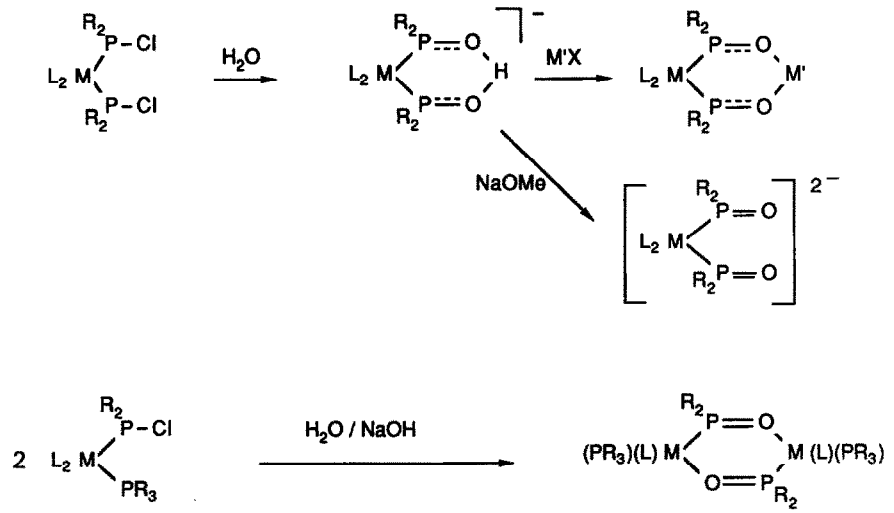

Fig. 2. The synthesis of μ-$R_2P{=}O$ complexes via the hydrolysis of coordinated chlorophosphines.

of $(\eta\text{-}C_5H_5)Co(CO)I_2$ with $P(OMe)_3$. Pyrolysis or reaction with $CoCl_2$ produces a tripod ligand, resulting in $M'L_2$ species, where L is the metalloligand.[11] In a related synthesis the tripod ligand $(\eta\text{-}C_5R_5)M[MeO)_2P{=}O]_3^-$ (M = Co, Rh) is isolated directly by reaction of $[(\eta\text{-}C_5R_5)M\{P(OMe)_3\}_3]^{2+}$ with cyanide or iodide ions,[12] and reacts with a wide variety of metal salts to generate similar $M'L_2$ systems (Fig. 3). M'_2L_2 complexes of low-valent metals have also been reported recently,[13] in an extension of this widely applicable route to homo- and heteronuclear sandwich compounds. Arbuzov rearrangements are also thought to be implicated in the formation of phosphidoxo systems during thermolysis reactions of metal–phosphite complexes.[14] While a number of structurally interesting [P=O]-bridged species have been isolated by this route,[15] conditions are harsh and yields are often low.

Another attractive approach is Werner's preparation of μ-phosphidoxo systems by insertion of oxygen into the phosphido bridge.[4] Unfortunately, the scope of this method may be expected to be limited by the oxygen affinity of the metals involved, and by the tendency of low oxidation state metals to undergo oxidation to their normal valence states. Other strategies which may prove useful are: the cleavage of the P—P bond in diphosphine dioxides (cf. the preparation of $[(CO)_2Ni(PR_2)]_2$[16] from reaction of $Ni(CO)_4$ with Ph_2P—PPh_2); oxidative addition of labile $R_2P(O)$—X groups to metal carbonyls. In the hope of developing a systematic comparison of μ-phosphido and μ-phosphidoxo systems, we adopted the latter route.

μ-Phosphido, μ-acetylide complexes of iron group carbonyls, prepared by oxidative insertion of an $M(CO)_4$ fragment into the P—C bonds of phosphinoalkynes, have been extensively investigated in these laboratories.[17] Synthesis of the phosphidoxo analogues by the same route was undertaken in an effort to access structurally related phosphidoxo species. Treatment of $Ph_2P(O)C{\equiv}CR$ (R = Bu^t, Pr^i) with iron and ruthenium carbonyls afforded the products shown in Fig. 4. No evidence of the monosubstitution product (cf. $[Ru_3(CO)_{11}(Ph_2PC{\equiv}CBu^t)]$)[17] was observed for the phosphine oxides. Instead the binuclear product $Ru_2(CO)_6(Ph_2P{=}O)(C{\equiv}CBu^t)$ (**1**)[18] was isolated

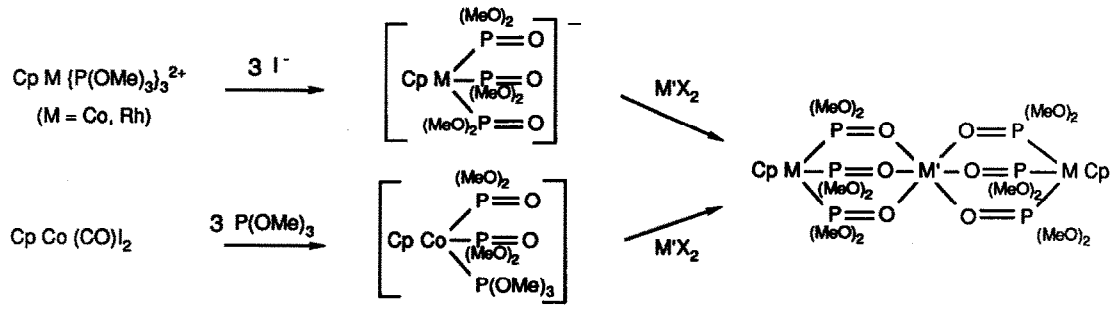

Fig. 3. Michaelis–Arbuzov rearrangement reactions leading to μ-$(MeO)_2P{=}O$ complexes.

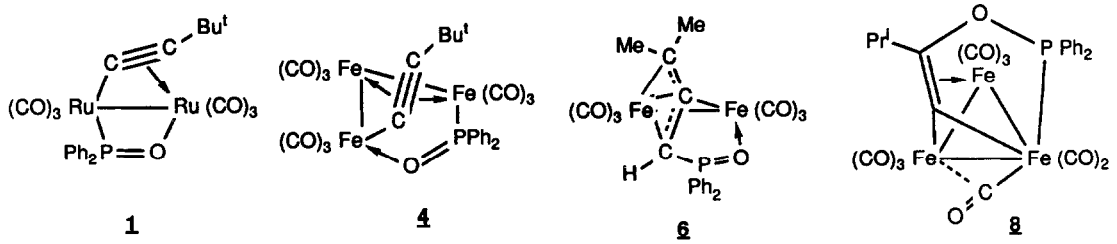

Fig. 4. Some products from the reactions of $Ru_3(CO)_{12}$ and $Fe_2(CO)_9$ with acetylenic phosphine oxides $Ph_2P(=O)C{\equiv}CR$ (R = Pr^i, Bu^t).

in 76% yield after refluxing at 67°C (THF, $Ph_2CO^-Na^+$) for 30 h. (In contrast, a 40% yield of the phosphido-bridged analogue **2** was obtained after heating the monosubstitued cluster at 50°C in THF for 8 h.) Principal spectroscopic characteristics of the phosphidoxo compound are a ^{31}P singlet at 83.2 ppm, well downfield of the phosphine oxide $Ph_2P(O)C{\equiv}CBu^t$ ($\delta = 1.1$ ppm), and a $\nu(P{=}O)$ band in the IR at 985 cm^{-1}, a value 215 cm^{-1} lower than in the free ligand ($\nu(P{=}O)$ 1200 cm^{-1}). Bands in the 990–1075 cm^{-1} region have been assigned to bridging $R_2P{=}O$ groups in other work.[19]

STRUCTURAL FEATURES OF PHOSPHIDOXO COMPLEXES

The X-ray data for $Ru_2(CO)_6(\mu_2\text{-}\eta^2\text{-}C{\equiv}CBu^t)(\mu\text{-}PPh_2)$ (**2**) and $Ru_2(CO)_6(\mu_2\text{-}\eta^2\text{-}C{\equiv}CBu^t)(\mu\text{-}Ph_2PO)$ (**1**) have provided a unique opportunity to examine in detail the influence of a π-donor oxygen atom on the structural parameters for two related molecules. The basic skeletal features are remarkably similar with, in each case, a metal–metal bond between the two $Ru(CO)_3$ units bridged by a $\mu_2\text{-}\eta^2$-acetylide and a three-electron donor phosphorus ligand. The Ru(1)—Ru(2) bond distance in **1** (2.7729(3) Å) is slightly longer than that in **2** (2.7523(3) Å), a reflection in part of the presence of a two-atom $Ph_2P{=}O$ bridge in **1** and a single-atom Ph_2P bridge in **2**. The P—O distance in **1** (1.544(2) Å) compares with reported values of 1.44–1.55 Å in other complexes containing $R_2P{=}O$ ligands.[20] Although the distance in **1** is at the high end of the range of values shown, it is significantly shorter than the typical P—O (phosphite) bond distance of 1.64 Å,[21] and must therefore be considered intermediate between double and single bond values. The Ru(2)—O(7) distance in **1** (2.135(2) Å) compares with a value of 2.29(3) Å in $HRu_2(CO)_3[P(OC_6H_4)(OPh)_2]_2[(PhO)_2P{=}O]$ (**3**), the only other diruthenium (Ru—Ru) complex with an $R_2P{=}O$ bridging ligand.[15b] In the μ_2-acyl complex $Ru_2(CO)_6[\mu_2\text{-}O{=}CCH{=}C(Ph)NEt_2](\mu\text{-}PPh_2)$ the Ru—O bond length of 2.119(3) Å[22] is rather similar to that in **1** and the two values are probably typical of donor–acceptor interactions between ruthenium atoms and bridging sp^2-hybridized oxygen.

Taken as a whole, the above structural features indicate that of the two canonical forms **A** and **B** possible for this complex (Fig. 5), the P^V phosphidoxo representation **A** must be considered more accurate. Comparison of **1** with its phosphido-bridged analogue **2** reveals a number of differences which may be assumed to arise from the π-donor characteristics of the oxygen ligand. A significant shortening of the M(2)–acetylide bonds is apparent (Fig. 6) in **1** where the hard oxygen atom is coordinated to Ru(2), suggesting stronger ruthenium–acetylide bonding as a result of the increased electron density on the metal. Similarly, a considerable decrease (0.08 Å) is seen in the Ru(2)—C(6) bond distance for the carbonyl group *trans* to the oxygen atom in **1**, relative to its counterpart in **2**. The average M(1)—CO bond distance is in contrast approxi-

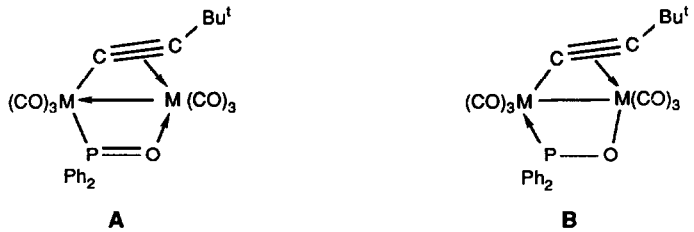

Fig. 5. Contributing canonical forms to the ground state description of $M_2(CO)_6(\mu_2\text{-}\eta^2\text{-}C{\equiv}CBu^t)(\mu\text{-}Ph_2P{=}O)$.

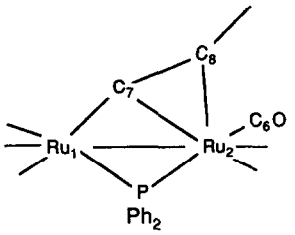

Bond Lengths (Å)		Bond Angles (°)	
Ru(1) - Ru(2)	2.7523(3) A	Ru(1) - P - Ru(2)	72.0(0)
Ru(1) - P	2.3399(8)	Ru(2) - Ru(1) - P	54.0(9)
Ru(1) - C(7)	2.044(3)	Ru(1) - Ru(2) - P	54.0(0)
Ru(2) - P	2.3406(8)	Ru(1) - C(7) - C(8)	158.9(1)
Ru(2) - C(6)	1.955(4)	C(7) - C(8) - C(9)	158.5(2)
Ru(2) - C(7)	2.285(3)		
Ru(2) - C(8)	2.417(3)		
C(7) - C(8)	1.218(4)		

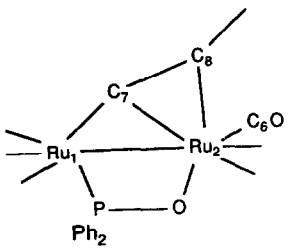

Bond Lengths (Å)		Bond Angles (°)	
Ru(1) - Ru(2)	2.7729(3)	Ru(1) - P - O(7)	106.67(8)
Ru(1) - P	2.3552(9)	Ru(2) - Ru(1) - P	69.31(2)
Ru(1) - C(7)	2.020(3)	Ru(1) - Ru(2) - O(7)	79.14(6)
Ru(2) - O(7)	2.135(2)	Ru(1) - C(7) - C(8)	158.7(2)
Ru(2) - C(6)	1.875(4)	C(7) - C(8) - C(9)	155.9(2)
Ru(2) - C(7)	2.244(3)		
Ru(2) - C(8)	2.338(4)		
P - O(7)	1.544(2)		
C(7) - C(8)	1.220(5)		

Fig. 6. A comparison of X-ray structural parameters for $Ru_2(CO)_6(\mu_2\text{-}\eta^2\text{-}C{\equiv}CBu^t)(\mu\text{-}Ph_2P{=}O)$.

mately the same in **1** as **2**. Metal–carbon bond shortening for CO groups trans to poor π-acceptor ligands is ascribed to a compensating increase in orbital interactions between the metal and the strong π-donor CO.

Reaction of $Ph_2PC{\equiv}CBu^t$ with diiron enneacarbonyl at ambient temperatures gives low yields (*ca* 11%) of **4**, a trinuclear phosphidoxo-bridged species. In this complex the $\{Ph_2P{=}O\}$ ligand bridges an open edge of the Fe_3 triangle. The location of the ν(P=O) band is unchanged relative to **1**, and the P—O bond distance (1.539(2) Å) is virtually identical, indicating that the flexibility of the ligand is sufficient to accommodate the rather substantial increase (*ca* 0.824 Å) in bridging distance without further reduction of the multiple bond character of the phosphidoxo unit. The ^{31}P NMR (δ = 150.5 ppm) provides a clearer indication of the magnitude of the structural change, but the dearth of spectroscopic and crystallographic data for related μ-$Ph_2P{=}O$ compounds precludes correlation of chemical shift with structural form. The X-ray crystal structure shows a μ_3-η^2 acetylide σ-bound to the oxygen-substituted metal. The alkyne triple bond (C(10)—C(11) = 1.287(5) Å) and the bendback angle at C_β are larger than in the μ_2-η^2 acetylide of **1**, as is usual for this coordination mode. Certain notable differences exist between the molecular structures of **4** and its closest phosphido-bridged counterpart **5** (Fig. 7). Most obvious is the symmetrical disposition of the acetylide in the latter, where the hydrocarbyl unit is σ-bonded to the unique metal atom. Unfavourable steric interactions between the acetylide substituent and the bulky Ph_2P group are probably responsible for the sharp deviation from planarity at phosphorus in the Ru(1)—P—Ru(3)—Ru(2) core. In **4**, this interaction is not possible, and an approximately planar five-membered ring is seen. The bendback angle at C_β is *ca* 4° greater in **4** than in **5**, possibly due to steric hindrance resulting from the shorter intermetallic distance bisected by the acetylide in the former. Although no effect of the oxo-ligand on acetylide distortion is likely with this arrangement of the bridge, it should be noted that the *trans* M—C(O) bond shortening seen in **1** is also evident in **4**.

COMPLEXES OF ALLENIC PHOSPHINE OXIDES

Reaction of $Ph_2P(O)C{\equiv}CPr^i$ with $Fe_2(CO)_9$ (12 h, RT) gives quite different products. The major product (*ca* 50% yield) is the binuclear metalloallylic phosphine oxide[23] **6**, a complex closely related to products obtained on reaction of allenes with $Fe_2(CO)_9$.[24] Its crystal structure (Fig. 8) shows a bent σ,π-allyl fragment bridging a strong metal–metal bond (2.6278(5) Å), π-bonded to Fe(1) and σ-bound to Fe(2) at the central carbon C(8). Precedence exists for the asymmetry within the allyl unit (C(7)—C(8) 1.447(3) Å, C(8)—C(9) 1.403 (3)Å), and the structural similarity between **6** and the phosphine-substituted species $Fe_2(CO)_6(\mu\text{-}\eta^1,\eta^3\text{-}C_5F_5PCy_2)$ (**7**)[25] (in which the corresponding allyl distances are 1.447(7) Å and 1.393(7) Å) is noteworthy. In both cases incomplete delocalization can be inferred not only from the C—C bond lengths but from the increased Fe(1)—C(9) bond distances (2.296(3) Å in **6**,

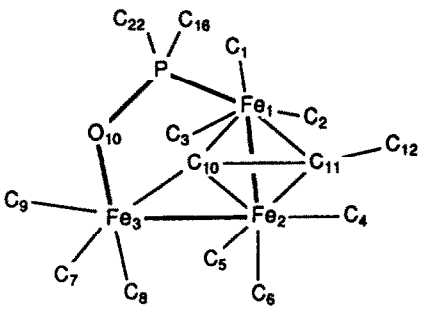

4

Bond Lengths (Å)		Bond Angles (°)	
Fe(1) - Fe(2)	2.6012(6) Å	Fe(1) - P - O(10)	112.62(8)
Fe(2) - Fe(3)	2.6837(6)	P - O(10) - Fe(3)	110.17(6)
Fe(3) - Fe(1)	3.6064(6)	O(10) - Fe(3) - Fe(2)	90.64(6)
Fe(1) - P	2.2692(9)	Fe(3) - Fe(2) - Fe(1)	86.05(1)
Fe(1) - C(10)	1.912(3)	Fe(2) - Fe(1) - P	96.10(2)
Fe(1) - C(11)	2.122(3)	Fe(1) - C(11) - Fe(2)	75.56(9)
Fe(2) - C(10)	1.979(3)	C(10) - C(11) - C(12)	142.1(2)
Fe(2) - C(11)	2.124(3)		
Fe(3) - C(10)	2.155(3)		
Fe(3) - O(10)	1.989(2)		
P - O(10)	1.539(2)		
C(10) - C(11)	1.287(5)		

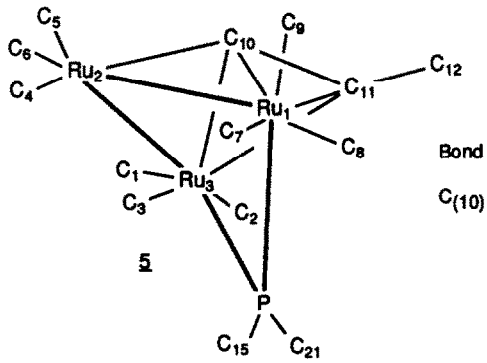

5

Bond Lengths (Å)		Bond Angles (°)	
C(10) - C(11)	1.284(8)	Ru(1) - P - Ru(3)	92.8(0)
		Ru(2) - C(10) - C(11)	154.0(2)
		Ru(1) - C(10) - Ru(3)	100.1(0)
		C(10) - C(11) - C(12)	145.2(3)

Fig. 7. A comparison of structural parameters for $Fe_3(CO)_9(\mu_3\text{-}\eta^2\text{-}C{\equiv}CBu^t)(\mu\text{-}Ph_2P{=}O)$ and $Ru_3(CO)_9(\mu_3\text{-}\eta^2\text{-}C{\equiv}CPr^i)(\mu\text{-}PPh_2)$.

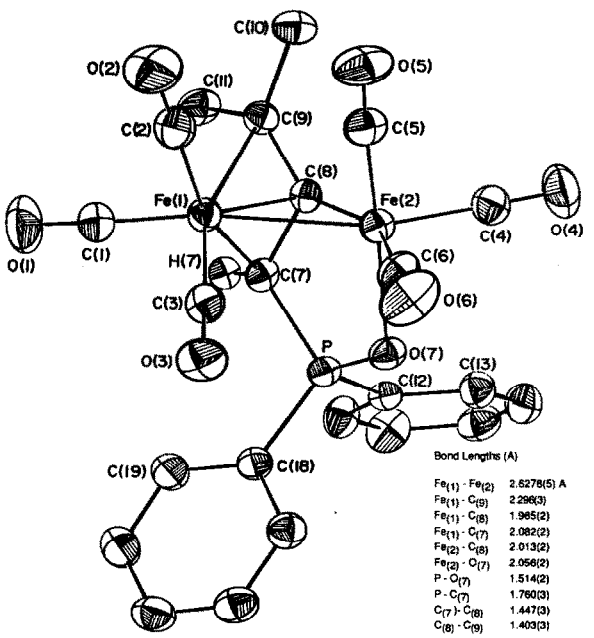

Bond Lengths (A)		Bond Angles (°)	
Fe(1) - Fe(2)	2.6278(5) A	Fe(1) - C(8) - Fe(2)	82.68(6)
Fe(1) - C(9)	2.296(3)	Fe(1) - C(7) - C(8)	64.77(9)
Fe(1) - C(8)	1.965(2)	Fe(1) - C(9) - C(8)	58.38(9)
Fe(1) - C(7)	2.082(2)	Fe(2) - O(7) - P	112.32(4)
Fe(2) - C(8)	2.013(2)	C(7) - P - O(7)	106.9(1)
Fe(2) - O(7)	2.056(2)	C(8) - C(7) - P	114.07(9)
P - O(7)	1.514(2)	C(7) - C(8) - C(9)	114.8(1)
P - C(7)	1.760(3)		
C(7) - C(8)	1.447(3)		
C(8) - C(9)	1.403(3)		

Fig. 8. An ORTEP plot of the structure of $Fe_2(CO)_6(\mu\text{-}Ph_2P(=O)CH{=}C{=}CMe_2)$.

2.121(5) Å in **7**) relative to the Fe(1)—C(7) distances (2.082(2) and 2.083(5) Å, respectively). The angles at C(7) in **6**, are, however, far from tetrahedral (Fe(1)—C(7)—C(8) 64.77(9)°, P—C(7)—C(8) 114.07(9)°) which supports the metallo π-allyl representation. The similarity in structure between **6** and **7** is not confined to the allylic fragment; also notable is the coordinated phosphine in the latter, which bears the same relation to both allyl unit and Fe(2) as the oxygen-bound phosphoryl group in **6**. Retention of the P=O double bond in **6** is indicated by the short bond distance (P—O(7) 1.514(2) Å), in keeping with which a band is observed at 1063 cm^{-1} in the IR spectrum. Formation of this unusual complex as the major reaction product, without P—C activation, is particularly interesting in view of the fact that corresponding systems have not been observed in the phosphido chemistry, in which the iron analogue of **2** is the chief product. Although P—C bond cleavage is facile in phosphinoacetylene systems there is evidence that the propensity of P—C scission drops markedly in the series P—C_{sp} > P—C_{sp^2} > P—C_{sp^3}.[17] In the present case a prior propargylic rearrangement of the C≡C—CHR_2 unit, possibly related to the presence of the P=O unit, presumably yields an allenic phosphine oxide $Ph_2P(O)$—CH=C=CMe_2.

VINYLIDENE CLUSTERS

A trinuclear phosphinitovinylidene is isolated in 15% yield from the same reaction.[26] The ^{31}P spectrum shows a single peak far downfield (*ca* 178 ppm), suggesting a high degree of phosphite character in the P—O bond. The structure of **8**, determined by X-ray diffraction, consists of a closed metal triangle with a μ_3-vinylidene asymmetrically bound to one face; C_α is σ-bound to Fe(1) and Fe(3), and π-bonded to Fe(2) (Fig. 9). Coordination of the phosphoryl oxygen to C_α of the vinylidene forms a five-membered Fe(2)—Fe(3)—P—O(10)—C(11) ring at the expense of the P—O double bond. The resulting phosphinito complex has a typical phosphite P—O bond length of 1.631(2) Å, considerably longer than the value of *ca* 1.54 Å seen in the previous examples. The Fe(3)—P bond distance (2.1954(9) Å) is significantly shorter than its value in the trinuclear iron complex **4** (2.3552(9) Å), where however the Ph_2P=O fragment bridges two metal atoms.

The structure of **8** bears a striking similarity to a vinylidene complex isolated in low yield (*ca* 10%) from solutions of $Ru_3(CO)_9\{\mu_3\text{-}\sigma,\eta^2\text{-}C_2CHMe_2\}(PPh_2)$. The latter is converted in solution to several products including the closed-shell isomer

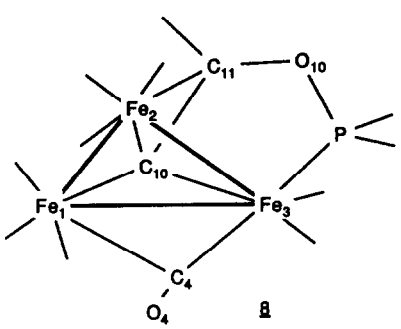

8

Bond Lengths (Å)		Bond Angles (°)	
Fe(1) - Fe(2)	2.6096(8)	Fe(1) - Fe(2) - Fe(3)	59.29(1)
Fe(1) - C(10)	1.853(3)	Fe(2) - Fe(3) - Fe(1)	60.18(1)
Fe(1) - - C(4)	2.291(4)	Fe(3) - Fe(1) - Fe(2)	60.53(1)
Fe(2) - Fe(3)	2.6186(7)	Fe(1) - C(10) - C(11)	146.0(1)
Fe(2) - C(10)	1.982(3)	C(10) - C(11) - O(10)	113.7(1)
Fe(2) - C(11)	2.230(3)	O(10) - P - Fe(3)	108.07(7)
Fe(3) - Fe(1)	2.5862(7)	P - Fe(3) - Fe(2)	92.94(2)
Fe(3) - P	2.1954(9)	Fe(3) - Fe(2) - C(11)	74.3(1)
Fe(3) - C(10)	1.945(3)	Fe(2) - C(11) - O(10)	111.7(1)
Fe(3) - C(4)	1.838(4)	Fe(3) - C(4) - O(4)	155.2(2)
C(10) - C(11)	1.388(5)		
P - O(10)	1.631(2)		
C(11) - O(10)	1.429(4)		

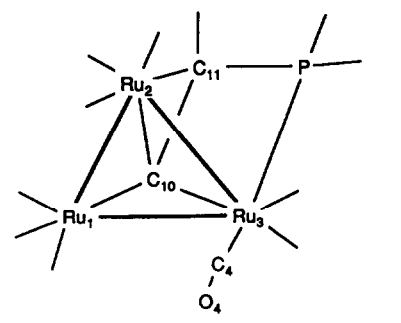

9

Bond Lengths (Å)		Bond Angles (°)	
Ru(1) - Ru(2)	2.8007(6)	Ru(1) - Ru(2) - Ru(3)	63.54(1)
Ru(1) - C(10)	1.921(5)	Ru(2) - Ru(3) - Ru(1)	59.36(1)
Ru(1) - - - C(4)	2.881(7)	Ru(3) - Ru(1) - Ru(2)	57.11(1)
Ru(2) - Ru(3)	2.7332(5)	Ru(1) - C(10) - C(11)	154.58(2)
Ru(2) - C(10)	2.126(5)	C(10) - C(11) - P	93.6(2)
Ru(2) - C(11)	2.340(5)	C(11) - P - Ru(3)	88.5(1)
Ru(3) - Ru(1)	2.9140(6)	P - Ru(3) - Ru(2)	76.91(3)
Ru(3) - P	2.375(1)	Ru(3) - Ru(2) - C(11)	70.6(1)
Ru(3) - C(10)	2.182(5)	Ru(2) - C(11) - O(10)	99.6(1)
Ru(3) - C(4)	1.925(6)	Ru(3) - C(4) - O(4)	167.9(2)
C(10) - C(11)	1.408(7)		
C(11) - P	1.809(5)		

Fig. 9. A comparison of X-ray structural data for $Fe_3(CO)_9\{\mu_3\text{-}\sigma,\sigma,\eta^3\text{-}C{=}CCHMe_2(Ph_2PO)\}$ and $Ru_3(CO)_9\{\mu_3\text{-}\sigma,\sigma,\eta^3\text{-}C{=}CCHMe_2(PPh_2)\}$.

$Ru_3(CO)_9\{\mu_3\text{-}\sigma,\sigma,\eta^3\text{-}C{=}CHMe_2\}(PPh_2)$ (**9**), in which a phosphinovinylidene ligand is coordinated to one face of the M_3 triangle, forming a strained four-membered Ru(2)—Ru(3)—P—C(11) ring.[26] The smaller ring size in **9** relative to **8** results in distortion of the metal triangle, shortening the Ru(2)—Ru(3) bond distance by 0.12 Å relative to the other two sides. This effect is much less pronounced in **8**, in which the metal triangle is virtually equilateral. A correspondingly greater degree of asymmetry is apparent in the M(1)—C(10) vs M(3)—C(10) distances in the iron complex, but in both cases the primary vinylidene interaction involves M(1)—C(10) (1.853(3) Å in **8**, 1.921(5) Å in **9**). The M(3)—C(10) interaction, though weaker, is significant, giving rise to localized electron counts of 17 and 19 electrons for M(1) and M(3), respectively. The high electron density on Fe(1) resulting from a donor–acceptor Fe(3) → Fe(1) bond in **8** is offset by a semibridging interaction between C(4)O and the electron-rich Fe(1) (C(4)—Fe(1) = 2.291(4) Å; C(4)—Fe(3) = 1.838(4) Å; Fe(3)—C(4)—O(4) = 155.2(2)°). The increase in metal–metal bond distance precludes such an interaction in **9** where M = Ru; here C(4)—Ru(1) = 2.881(7) Å, C(4)—Ru(3) = 1.925(6) Å, Ru(3)—C(4)—O(4) = 167.9(2)°. A compensating donor–acceptor bond may exist between Ru(1) and Ru(3), although this is the longest bonding distance in the molecule.

REACTION CHEMISTRY OF PHOSPHIDOXO-BRIDGED COMPLEXES

We were interested in studying the substitution reactions of the phosphidoxo complexes in an attempt to evaluate the directing effect of the donor oxygen atom. The availability of corresponding $Ru_2(\mu\text{-}PPh_2)$ and $Ru_2(\mu\text{-}Ph_2P{=}O)$ complexes provided a unique opportunity to assess the influence of the oxygen atom on the reactivity pattern. A powerful labilizing effect exerted by oxygen-bound phosphine oxides on mononuclear group 6 and 8 metal carbonyls was noted by Darensbourg *et al.*[6] This labilization was ascribed to transition state stabilization, for which the site preference model of Atwood and Brown was invoked as an explanation.[27] Strong donor, non-π-acceptor ligands stabilize the pentacoordinate intermediate formed by loss of one carbonyl group from an octahedral complex, accounting for the labilizing effect. Dissociation occurs *cis* to the labilizing ligand as a consequence of the ground-state strengthening of the *trans* M—CO bond by the donor ligand. Site specificity in Darensbourg's phosphine oxide complexes was not established, but stereoselective substitution at *cis*-carbonyl sites has been claimed for a number of μ-carboxylato[6] and μ-acyl systems.[28] The superior electron releasing (net σ- and π-donor) properties of [P═O] as opposed to [C═O], and the higher energy of the [P═O] π^* orbital, should result in more efficient labilization in the former.

In order to study the influence of the phosphidoxo group on substitution behaviour we have examined the reactions of **1** and **2** with tertiary phosphines. Although $Ru_2(CO)_6(\mu_2\text{-}\eta^2\text{-}C{\equiv}CPh)(\mu\text{-}PPh_2)$ undergoes preferential attack at the hydrocarbyl moiety in reactions with phosphines and phosphites,[29] the bulky t-butylacetylide **2** affords CO substitution products. Thus treatment of **2** with 1 equivalent of PMe_3 at 297 K results in slow evolution of CO and formation of the disubstitution product. Other work in this laboratory has convincingly shown that mono-substituted **2** is more rapidly substituted than **2** itself, hence the disubstituted complex is kinetically favoured with the final product mix being *ca* 50% of the disubstituted and unsubstituted species. In the former the substitution sites, identified on the basis of ^{31}P—$^{13}C(CO)$ coupling constants and ^{31}P 2D-COSY experiments, are *cis* to the σ-bound acetylide carbon and *trans* to the μ-PPh_2 group on M(1) and *cis* to the μ-PPh_2 group, *trans* to the metal–metal bond on M(2).

In sharp contrast the reaction of **1** with PMe_3 in a 1:1 ratio results in substitution of a single CO ligand *cis* to the oxygen atom and *trans* to the metal–metal bond. The reaction is rapid at 297 K and gives exclusively the monosubstitution product **10**, the X-ray structure of which (Fig. 10) confirms the *cis* relationship of the oxo and tertiary phosphine ligands. The acetylide however is now σ-

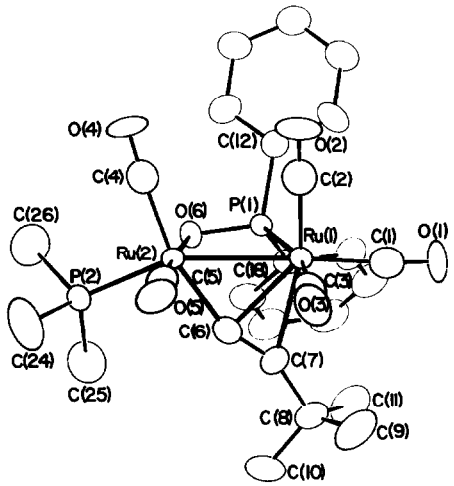

Fig. 10. An ORTEP plot of the structure of $Ru_2(CO)_5(\mu_2\text{-}\eta^2\text{-}C{\equiv}CBu^t)(\mu\text{-}Ph_2P{=}O)(PMe_3)$.

bound to Ru(2) whereas in **1**, Ru(2) interacts in η^2-fashion with the alkynyl group. Since the acetylide is dynamic in **2** and may also be dynamic in **1** the acetylide reversal from **1** to **10** is most interesting. The structure of **10** presumably reflects the greater thermodynamic stability of the isomer in which the σ-bound metal is substituted.

The substitution reaction was monitored by ^{31}P NMR over a 210–300 K range in an effort to elucidate the mechanism. (The rate enhancement conferred by the oxo ligand is illustrated by the fact that the reaction of PMe_3 with **1** begins below 210 K, whereas for the phosphido analogue no substitution is observed below 250 K.) In the spectrum of a 1:1 mixture of **1** and PMe_3 singlets at +83 and −65 ppm due to **1** and free ligand respectively gradually decrease in size as two new singlets (+64, +8 ppm) and two doublets (+83 ppm, $J = 5$ Hz, +4 ppm, $J = 5$ Hz) appear. The latter set of resonances are due to **10**, a fact confirmed by the spectrum of isolated, crystalline **10**. Altlhough the two singlets at +64 and +8 ppm of unknown **11** gradually diminish up to 297 K as the amount of **10** increases, for the first half of the reaction the amount of the intermediate steadily increases relative to both starting complex **1** and product **10**. These results may indicate either of two possibilities. In Path A (Fig. 11) the intermediate **11a** is not directly on the reaction path between **1** and **10**; i.e. a competitive equilibrium exists between **1** and **10**, in which the latter is favoured, and evolution of **11** to **10** occurs via the starting complex **1** (in which case the conversion **1** → **10** dominates at higher temperatures). Also possible (Path B) is the direct conversion **1** → **11b** → **10** with the first step being rate-determining. Possible structures for the intermediates generated by these two pathways are also shown in Fig. 11. That of Path A is derived from **1** by nucleophilic attack on C_α of the acetylide, which produces a zwitterionic two-carbon bridge similar to that in $Fe_2(CO)_6[\mu_2\text{-}\eta^2\text{-}C\{P(OMe)_3\}CPh](\mu\text{-}PPh_2)$.[17] In support of this there is no observable ^{31}P–^{31}P coupling between the phosphido bridge and the phosphine in the intermediate. If this is the structure of **11**, it suggests that the phosphidoxo ligand has increased the susceptibility of the μ_2-η^2-acetylide to nucleophilic attack, since the corresponding phosphido system affords no evidence for competitive attack at the alkynyl carbon atoms. This result would be in accord with the structural data (*vide supra*) which show a greater distortion of the acetylide from linearity in **1** than **2**, implying a stronger Ru(2)—acetylide η^2 interaction in the former. It may be significant that in the triad of complexes $M_2(CO)_6(\mu_2\text{-}\eta^2\text{-}C{\equiv}CBu^t)(\mu\text{-}PPh_2)$ reactivity at C_α

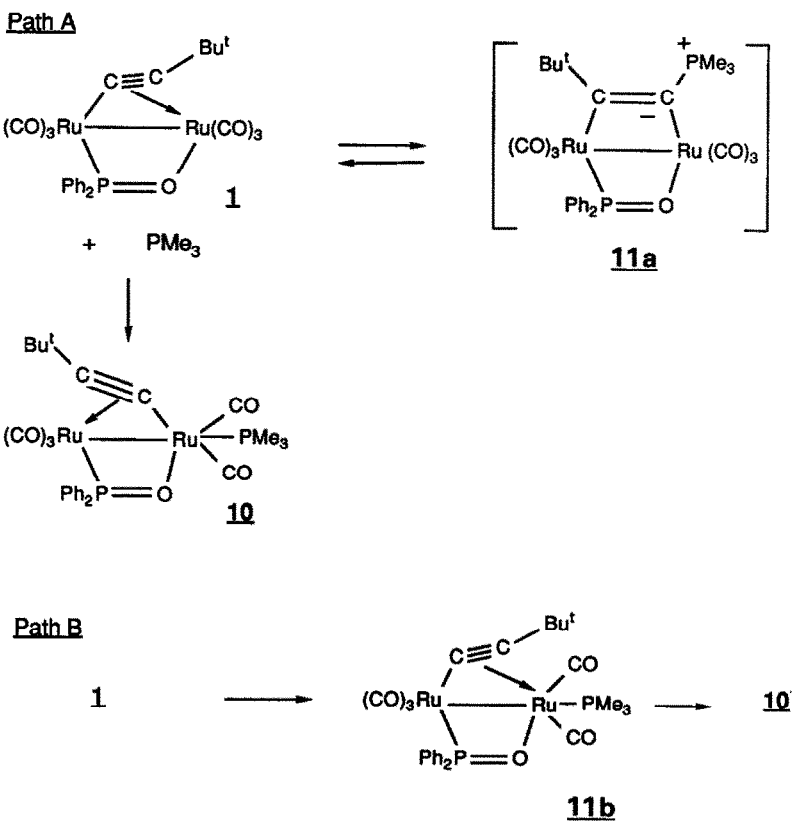

Fig. 11. Possible reaction pathways for $Ru_2(CO)_6(\mu_2\text{-}\eta^2\text{-}C{\equiv}CBu^t)(\mu\text{-}Ph_2P{=}O)$ with PMe_3.

increases down the triad as the M(2)-acetylide π-interaction increases in strength.[30]

The intermediate structure of Path B differs from that of the product **10** in that the acetylide is now π-bound to the substituted atom. This species represents an intermediate stage between CO substitution and acetylide flipping. In this case the rate-determining step is assumed to be CO loss, with the pentacoordinate intermediate being too unstable, or present in too small an amount, to be spectrally observable. Substantial precedence exists for rate-determining dissociation of CO in substitution reactions of carbonyl compounds.

We are currently extending this work to a wider range of nucleophiles to further examine the enhancement of reactivity afforded by π-donor phosphidoxo bridges.

Acknowledgements—We are grateful to the Natural Sciences and Engineering Research Council for financial support of this work in the form of operating grants (to A.J.C.). We are grateful to Stephane Carty for help with the illustrations.

REFERENCES

1. (a) D. Nucciarone, S. A. MacLaughlin, N. J. Taylor and A. J. Carty, *Organometallics* 1988, **7**, 106; (b) A. J. Carty, S. A. MacLaughlin and D. Nucciarone, in *Phosphorus-31 NMR Spectroscopy in Stereochemical Analysis: Organic Compounds and Metal Complexes* (Edited by J. G. Verkade and L. D. Quinn), Chapter 16, pp. 559–615. VCH Publishers, New York (1986).
2. For early examples see: (a) K. Yasufuku and H. Yamazaki, *J. Organomet. Chem.* 1972, **35**, 367; (b) B. L. Barnett and C. Kruger, *Cryst. Struct. Commun.* 1973, **2**, 347; (c) W. F. Smith, N. J. Taylor and A. J. Carty, *J. Chem. Soc., Chem. Commun.* 1976, 896. Recent examples are summarized in: (d) S. Rosenberg, G. L. Geoffroy and A. L. Rheingold, *Organometallics* 1985, **4**, 1184; (e) H. Werner and R. Zolk, *Chem. Ber.* 1987, **120**, 1003.
3. (a) Y.-F. Yu, C.-N. Chau, A. Wojcicki, M. Calligaris, G. Nardin and G. Balducci, *J. Am. Chem. Soc.* 1984, **106**, 3704; (b) Y.-F. Yu, J. Gallucci and A. Wojcicki, *J. Chem. Soc., Chem. Commun.* 1984, 653; (c) Y.-F. Yu, A. Wojcicki, M. Calligaris and G. Nardin, *Organometallics* 1986, **5**, 47; (d) G. L. Geoffroy, S. Rosenberg, P. M. Shulman and R. R. Whittle, *J. Am. Chem. Soc.* 1984, **106**, 1519; (e) G. D. Williams, G. L. Geoffroy, R. R. Whittle and A. L. Rheingold, *J. Am. Chem. Soc.* 1985, **107**, 729; (f) H. Werner and R. Zolk, *Organometallics* 1985, **4**, 601.
4. B. Klingert and H. Werner, *J. Organomet. Chem.* 1983, **252**, C47.
5. (a) W. Walther, *Coord. Chem. Rev.* 1984, **60**, 67; (b) D. M. Roundhill, R. P. Sperline and W. B. Beaulieu, *Coord. Chem. Rev.* 1978, **26**, 263; (c) See also: E. Lindner, F. Bouachir and S. Hoehne, *Chem. Ber.* 1983, **116**, 46 and earlier references therein.
6. D. J. Darensbourg, M. Y. Darensbourg and N. Walker, *Inorg. Chem.* 1981, **20**, 1918.
7. J. Chatt and B. T. Heaton, *J. Chem. Soc. (A)*, 1968, 2745.
8. D. E. Berry, K. A. Beveridge, J. Browning, G. W. Bushnell and K. R. Dixon, *Can. J. Chem.* 1986, **64**, 1903, and references therein.
9. K. Moedritzer, *J. Inorg. Nucl. Chem.* 1961, **22**. 19.
10. T. B. Brill and S. J. Landon, *Chem. Rev.* 1984, **84**, 577.
11. D. K. Towle, S. J. Landon, T. B. Brill and T. H. Tulip, *Organometallics* 1982, **1**, 295.
12. W. Klaui, H. Otto, W. Eberspach and E. Buchholz, *Chem. Ber.* 1982, **115**, 1922.
13. W. Klaui, A. Muller, R. Herbst and E. Egert, *Organometallics* 1987, **6**, 1824.
14. B. B. Wayland and B. A. Woods, *J. Chem. Soc., Chem. Commun.* 1981, 475.
15. (a) J. M. Fernandez, B. F. G. Johnson, J. Lewis and P. R. Raithby, *J. Chem. Soc., Dalton Trans.* 1981, 2250; (b) M. I. Bruce, G. Shaw and F. G. A. Stone, *J. Chem. Soc., Dalton Trans.* 1973, 1667.
16. J. A. Jarvis, R. H. B. Mais, P. G. Owston and D. T. Thompson, *J. Chem. Soc. (A)* 1970, 1867.
17. A. J. Carty, *Adv. Chem. Ser.* 1982, **196**, 163.
18. D. E. Fogg, N. J. Taylor, A. Meyer and A. J. Carty, *Organometallics* 1987, **6**, 2252.
19. (a) H. Werner, personal communication; (b) M. I. Bruce, J. Howard, I. W. Nowell, G. Shaw and P. Woodward, *J. Chem. Soc., Chem. Commun.* 1972, 1041; (c) H. Schmidbaur, A. A. M. Aly and U. Schubert, *Angew. Chem., Int. Ed. Engl.* 1978, **17**, 846; (d) M. C. Cornock, R. O. Gould, C. L. Jones and T. A. Stephenson, *J. Chem. Soc., Dalton Trans.* 1977, 1307.
20. (a) M. Lattman, B. N. Anand, S. S. C. Chu and R. D. Rosenstein, *Organometallics* 1984, **3**, 670; (b) S. Hoehne, E. Lindner and B. Schilling, *J. Organomet. Chem.* 1977, **139**, 315.
21. D. E. C. Corbridge, *The Structural Chemistry of Phosphorus*, p. 7. Elsevier, New York (1974).
22. G. N. Mott, R. Granby, S. A. MacLaughlin, N. J. Taylor and A. J. Carty, *Organometallics* 1983, **2**, 189.
23. D. E. Fogg, W. F. Smith, N. J. Taylor and A. J. Carty, to be published.
24. (a) R. Ben-Shoshan and R. Pettit, *J. Chem. Soc., Chem. Commun.* 1968, 247; (b) R. E. Davis, *J. Chem. Soc., Chem. Commun.* 1968, 248.
25. W. R. Cullen, M. Williams, F. W. B. Einstein and A. C. Willis, *J. Organomet. Chem.* 1978, **155**, 259.
26. D. E. Fogg, S. A. MacLaughlin, K. Kwek, A. A. Cherkas, N. J. Taylor and A. J. Carty, *J. Organomet. Chem.* 1988, in press.
27. (a) J. D. Atwood and T. L. Brown, *J. Am. Chem. Soc.* 1976, **98**, 3160; (b) J. D. Atwood, M. J. Wovkulich and D. C. Sonnenberger, *Accts. Chem. Res.* 1983, **16**, 350.

28. (a) N. Lugan, G. Lavigne and J.-J. Bonnet, *Inorg. Chem.* 1987, **26**, 585; (b) C. E. Kampe and H. D. Kaesz, *Inorg. Chem.* 1984, **23**, 4646.
29. (a) A. J. Carty, G. N. Mott, N. J. Taylor, G. Ferguson, M. A. Khan and P. J. Roberts, *J. Organomet. Chem.* 1978, **149**, 345; (b) Y. S. Wong, H. N. Paik, P. C. Chieh and A. J. Carty, *J. Chem. Soc., Chem. Commun.* 1975, 309.
30. A. A. Cherkas and A. J. Carty, unpublished results.

Note added in proof. Recent ^{13}CO NMR studies have shed further light on the nature of the intermediate **11** in this reaction. Six distinct carbonyl peaks are evident in the ^{13}C spectrum of the ^{13}C-enriched intermediate **11** and integration gives a value of six carbon atoms. Thus it appears that the intermediate illustrated in Fig. 11, Path B is unlikely and an intermediate on the reaction pathway formed by an *associative* process is a more feasible possibility. In this case a vacant coordination site may be generated by temporary decoordination of one end of the P—O bridge or a switch from a μ_2-PO bonding mode to an η^2-PO mode at Ru(1). Further studies on this system are in progress.

Polyhedron Vol. 7, No. 22/23, pp. 2297–2305, 1988
Printed in Great Britain

0277–5387/88 $3.00 + .00
© 1988 Pergamon Press plc

SYNTHETIC AND HIGH FIELD NMR STUDIES OF CHIRAL CLUSTERS

DEBBIE T. CLARK, KAREN A. SUTIN, RICHARD E. PERRIER and MICHAEL J. McGLINCHEY*

Department of Chemistry, McMaster University, Hamilton, Ontario, L8S 4M1, Canada

Abstract—Over the last few years, the development of logical routes to small organometallic clusters has opened the way towards the directed syntheses of chiral clusters. Tetrahedral systems comprised of four chemically different vertices are chiral. However, under the conditions required for catalytic action, clusters of this type generally racemize. The introduction of a chelating unsymmetrical ligand, such as $Ph_2P—CH_2—CH_2—AsPh_2$, renders chiral a $Co_3(CO)_9CR$ cluster but again such systems racemize on the NMR time scale via migration of the arsenic terminus from one cobalt vertex to another. It has been long suspected that cluster vertices such as $CpMo(CO)_2$ could undergo localized rotation and this has now been unequivocally verified using high field NMR spectroscopy at low temperature. Furthermore, it is shown that in solution the predominant rotameric forms of the mixed metal clusters $CpMoCo_2(CO)_8CR$ are not necessarily those found in the solid state. Finally, the syntheses of a series of mixed metal clusters of general formula $CpMo(CO)_2Co_2(CO)_6CR$ in which the apical substituents are derived from natural products, e.g. steroids or terpenes, are described. Treatment of these chiral clusters shows evidence of chiral discrimination in that preferential attack at one of the diastereotopic cobalt atoms is observed.

The development of logical routes to chiral organometallic systems has attracted considerable attention in recent years.[1] One approach, which Vahrenkamp has pioneered, involves the preparation of tetrahedral mixed metal clusters in which each of the four vertices is chemically different. The obtention of the cluster as a single pure enantiomer requires either a spontaneous resolution (which in some fortuitous instances occurs) or a series of diastereomer separations. Moreover, it has been shown that such tetrahedral molecules can undergo racemization not only under the relatively severe conditions required for catalytic action,[2] but also, in some cases, even on the NMR time scale.[3] These situations are exemplified in Scheme 1.

DISCUSSION

Routes to chiral clusters

In an attempt to circumvent the problem of cluster fragmentation, polydentate ligands such as $Ph_2PCH_2CH_2PPh_2$ (diphos) or $(Ph_2P)_3CH$ (triphos) have been used to hold the metallic framework together.[4,5] We attempted to utilize such a strategy to build chiral clusters which would be sufficiently robust to resist fragmentation. For this purpose we synthesized a series of molecules containing the bidentate ligand $Ph_2AsCH_2CH_2PPh_2$ (arphos) which we reasoned would not only stabilize the cluster framework but also impose chirality on the system. The site of complexation of the arphos moiety was established by X-ray crystallography (see Fig. 1) which revealed that two equatorial carbonyl ligands in $Co_3(CO)_9CR$ had been replaced.[6]

In order to detect molecular chirality, the carbynyl capping group contained an isopropyl ester functionality; the potentially diastereotopic methyl groups provide a ready means of following the rate of racemization of such molecules by ^1H or ^{13}C NMR spectroscopy.[7] In fact, the system (arphos) $Co_3(CO)_7CCO_2R$ undergoes rapid racemization via migration of the diphenylarsenido terminus from one cobalt vertex to another, as in Scheme 2. This rearrangement has been fully discussed elsewhere,[6,8] and need not be further amplified here.

* Author to whom correspondence should be addressed.

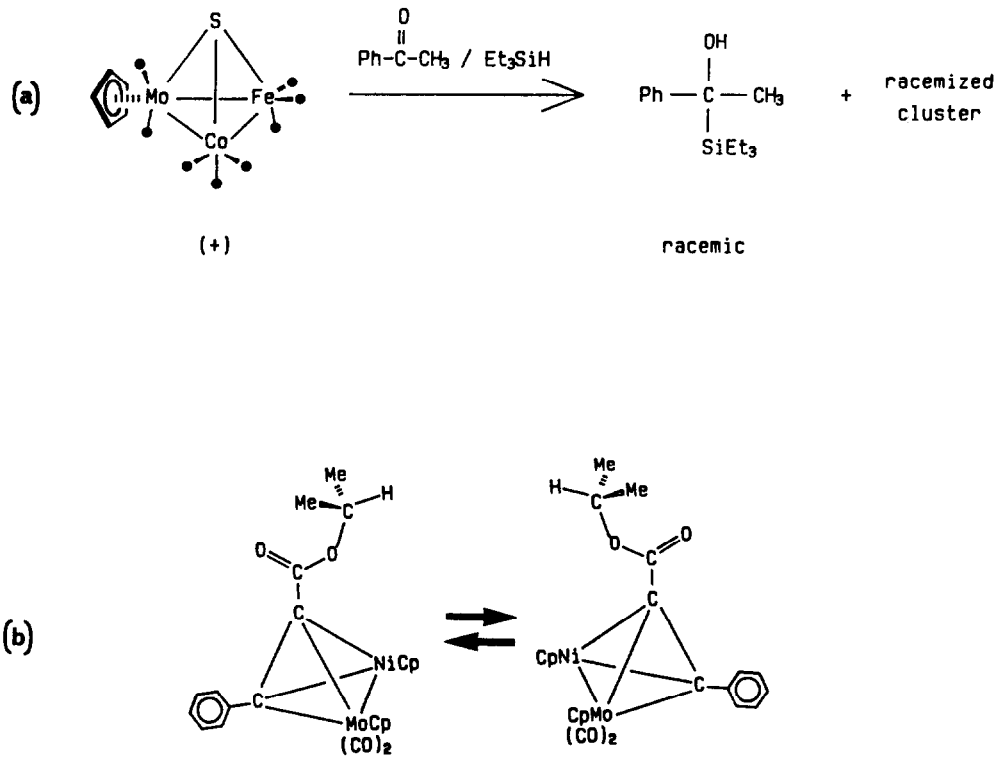

Scheme 1. Racemization of chiral clusters (a) during the hydrosilylation process and (b) on the NMR time scale.

Restricted rotation of (cyclopentadienyl)$M(CO)_2$ *vertices*

An interesting observation which emerged from this study was that in the mixed metal cluster $(C_5Me_5)MoCo_2(CO)_6(arphos)C—CO_2CHMe_2$ (**1**),

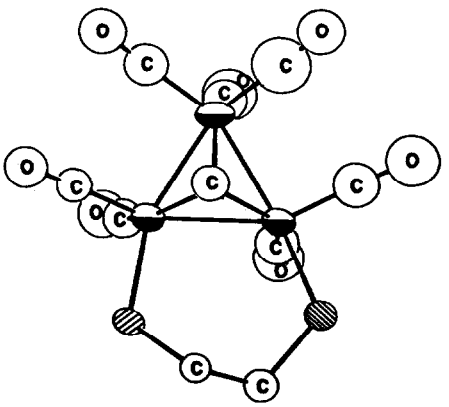

Fig. 1. X-ray crystal structure of $Co_3(CO)_7(arphos)C—CO_2CHMe_2$ with the phenyl rings and the ester functionality removed for clarity; the view is down the pseudo-three-fold axis showing the equatorial orientation of the arphos ligand.

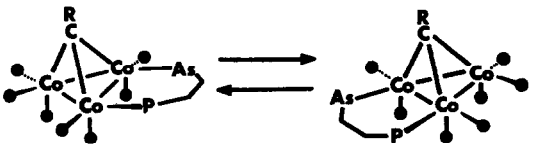

Scheme 2. Interconversion of the enantiomers of $Co_3(CO)_7(arphos)CR$ via migration of the diphenylarsenido terminus.

the molecule not only retained its chirality (as shown by the ^1H NMR non-equivalence of the isopropyl methyls at room temperature) but also showed the presence of numerous diastereomers at low temperature. We suspected that this phenomenon involved different rotameric conformations of the $Cp^*Mo(CO)_2$ vertex. Such a possibility had been suggested by Stone who noted that in $CpWCo_2(CO)_8C—C_6H_4Me$ (**2**), the number of IR bands in the carbonyl stretching region was too large to be attributed to a single isomer.[9,10] Likewise, in $CpMoCo_2(CO)_8C—C_6H_5$ (**3**), it had previously been reported by Vahrenkamp that although in the solid state the cyclopentadienyl group is situated below the trimetallic plane (as in **4a**) there were too many ν_{CO} bands for this single isomer.[11]

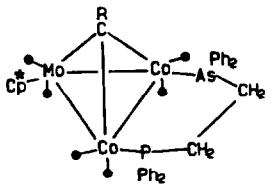

1

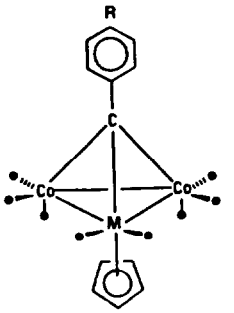

2 M=W ; R=Me
3 M=Mo; R=H

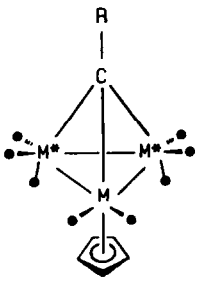

4a

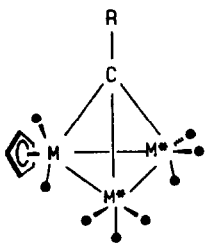

4b

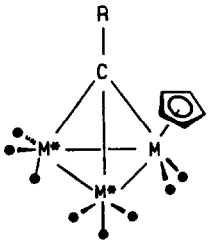

4c

Since that time, the X-ray crystal structures of $CpWFe_2(CO)_9C—C_6H_4Me$,[12] and of $CpFe_3(CO)_8C—OMe$,[13] have been determined. The cyclopentadienyl rings have been shown to adopt orientations **4b** and **4c**, respectively. We, therefore, ran the 125 MHz ^{13}C NMR spectra of the series of complexes $Cp^*MCo_2(CO)_8CR$, (where $Cp^* = C_5H_5$, C_5H_4Me or C_5Me_5 and M = Mo or W) at −90°C. Typical spectra are shown in Fig. 2 and reveal that for the bulky C_5Me_5 substituent the favoured rotamer is **4a**. In contrast, with the sterically less demanding C_5H_5 and C_5H_4Me groups, rotamer **4c** is favoured in dichloromethane solution. These data are in complete accord with the IR spectra of these molecules in the solid state and in solution and show that the favoured rotamers of the pentamethyl complexes are the same in both environments. However, it is apparent that for the unsubstituted cyclopentadienyl (or the monomethyl analogue) the more favoured rotamers are not the same in the solid state and in solution.[14]

Dimetallic complexes derived from natural products

Concomitant with our synthetic and spectroscopic studies on mixed metal clusters, other projects (in collaboration with G. Jaouen and his colleagues) had focussed on detailed NMR investigations of organometallic derivatives of hormonal steroids. Typically, by using several of the recently developed two-dimensional NMR techniques[15] in conjunction with a high field NMR spectrometer (^1H at 500 MHz; ^{13}C at 125 MHz) we had successfully differentiated between the α- and β-isomers of (17β-estradiol)$Cr(CO)_3$, **5a** and **5b**, respectively.[16] Metal carbonyl complexes of hormonal steroids are currently under investigation as reagents to assay hormonal receptor sites.[17] Thus a knowledge of the receptor count is absolutely crucial for the effective treatment of hormonal related cancers. Furthermore, the work of Jaouen and Vessières has established that the estradiol complex in which the tricarbonylchromium moiety is positioned on the α face of the steroid has a much higher relative binding affinity to the receptor site than does the β-isomer. Thus, it was important to develop a quick and straightforward method of distinguishing between the α- and β-diastereomers without having to resort to X-ray crystallography.

In the course of this work it had been clearly established that there existed shielding and

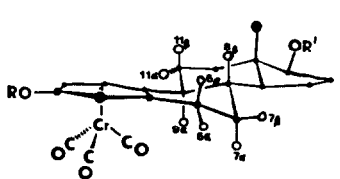

5a

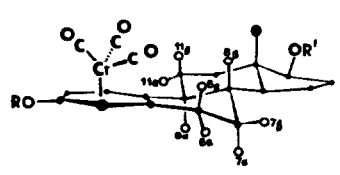

5b

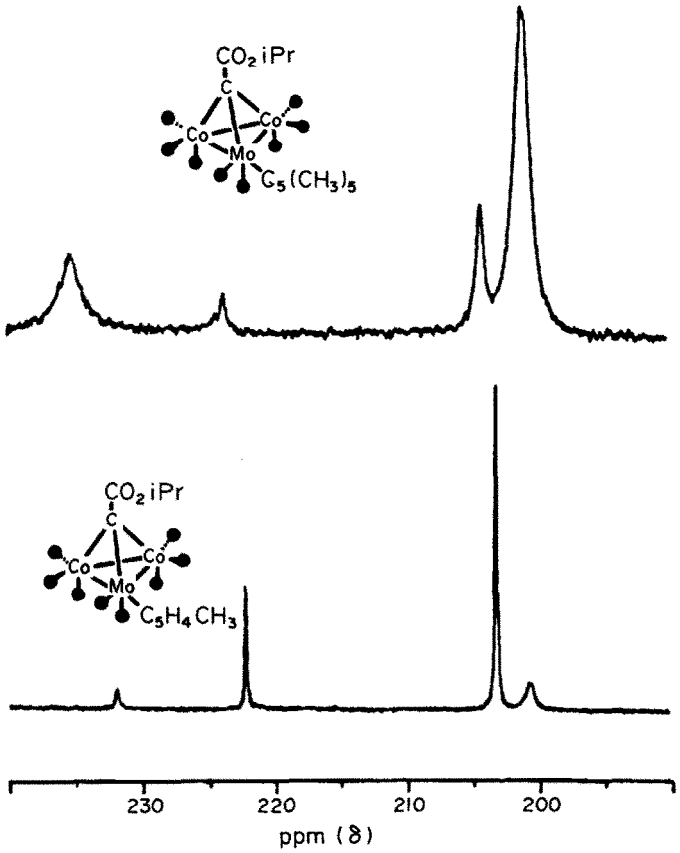

Fig. 2. Section of the 125 MHz ^{13}C NMR spectra of $Cp^*MoCo_2(CO)_8CR$ clusters recorded at −90°C. In the upper spectrum the major rotamer is of the type **4a**; in the lower spectrum the molecule adopts predominantly structure **4c**.

deshielding zones in the vicinity of the metal carbonyl ligands.[18] In particular, protons sited near the plane orthogonal to the carbon–oxygen bond axis are markedly deshielded. This result may surprise those who might have anticipated that any proton positioned near a transition metal would be shielded. These ideas are directly applicable to the characterization of chiral metal clusters. Thus, consonant with the realization that metals can more profitably be attached to the α face of the hormone, we prepared a series of organometallic derivatives of 17α-alkynyl-estradiols. (The simplest alkynyl derivative, viz., 3β-methoxy-17α-ethynyl-estradiol (**6**) is sold commercially as a contraceptive under the name Mestranol.) The high resolution NMR spectra of these dimetalla-tetrahedranes provide much information concerning the conformation adopted by the molecules in solution. To demonstrate the quality of the spectra obtainable, we show (see Fig. 3) the 500 MHz ^1H COSY spectrum of one of the alkyne ligands, **7**. This two-dimensional spectrum is presented as a contour plot in

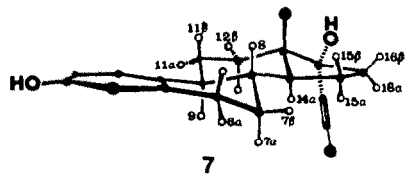

7

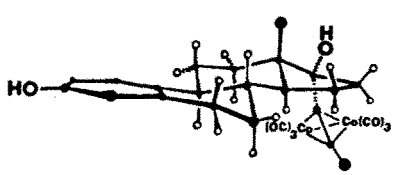

8

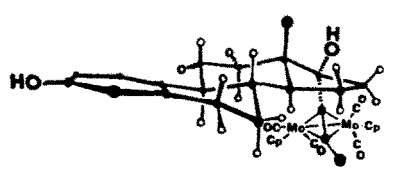

9

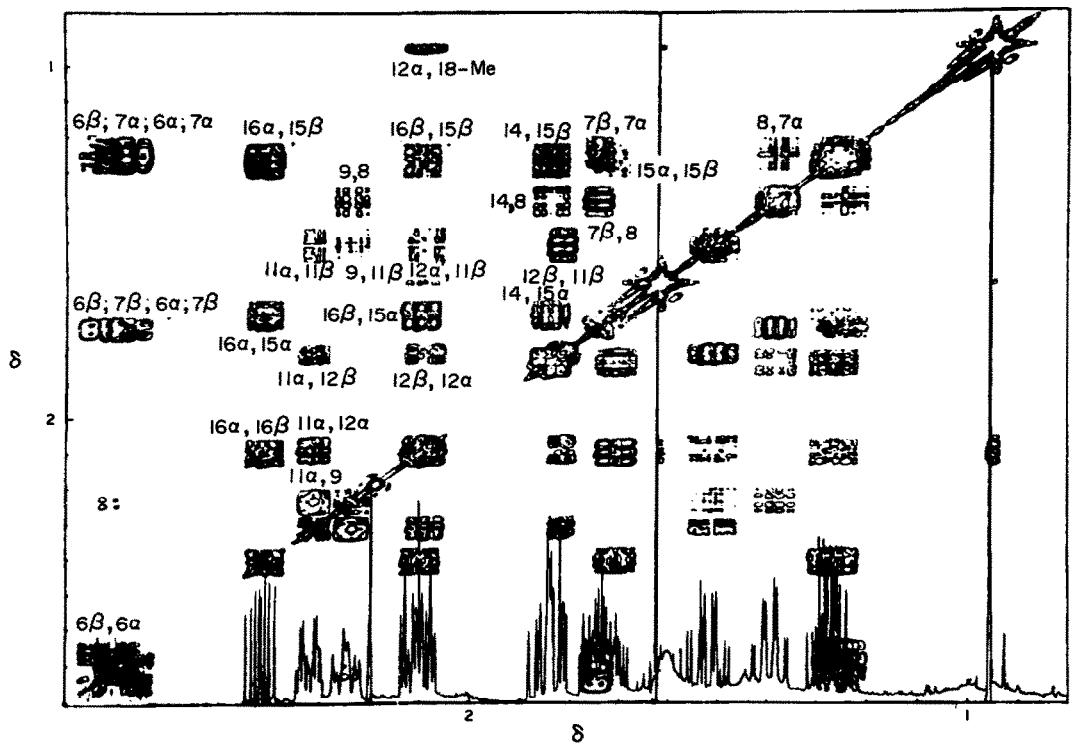

Fig. 3. Two-dimensional 500 MHz ^{1}H NMR spectrum of **7**. Expanded contour plot of the matrix for a COSY experiment. The matrix has been symmetrized.

which the conventional one-dimensional spectrum lies along the diagonal and the off-diagonal contours correlate those protons which are connected via scalar coupling. Thus, it is relatively straightforward to assign every proton resonance in the molecule. These can be confirmed by a ^{1}H–^{13}C shift-correlated NMR spectrum which indicates which protons are directly bonded to a particular carbon. Figure 4 presents such a spectrum for the $Co_2(CO)_6$ cluster derived from **6**.[19]

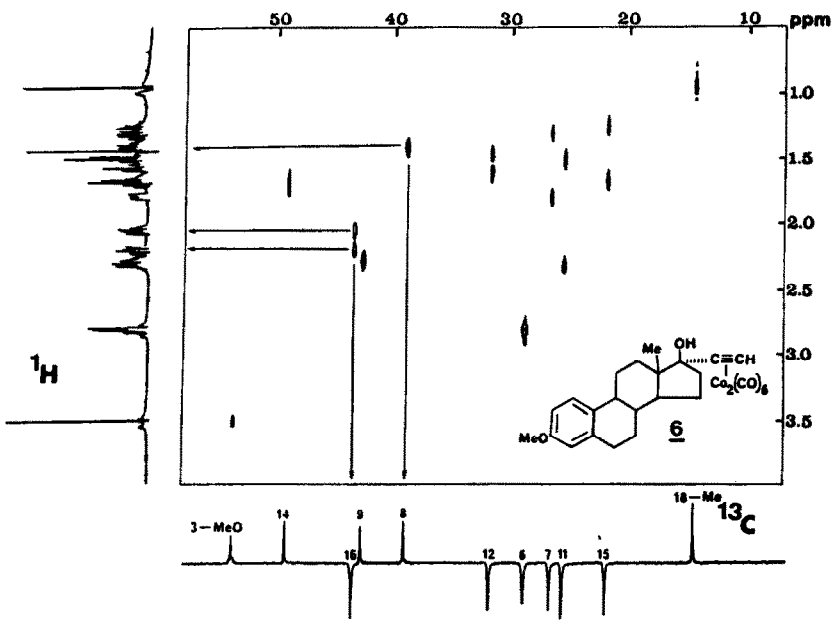

Fig. 4. A partial two-dimensional heteronuclear chemical shift correlated ^{1}H–^{13}C NMR spectrum of (mestranol)$Co_2(CO)_6$. A proton spectrum is projected onto the vertical axis; on the horizontal axis is a ^{13}C spectrum in which CH and CH_3 moieties have positive phase and CH_2 carbons have negative phase.

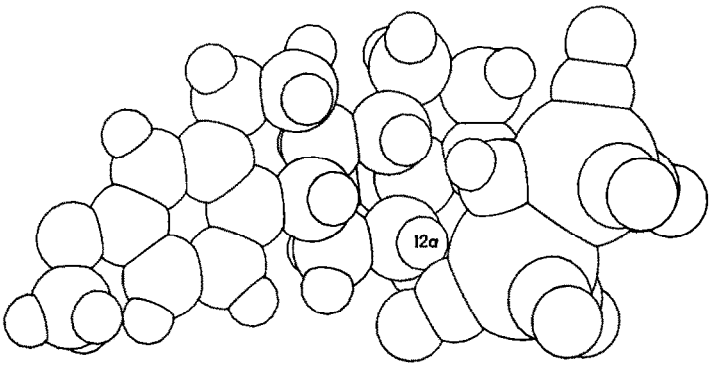

Fig. 5. CHEM-X plot of (mestranol)$Co_2(CO)_6$ showing an orientation which places a cobalt carbonyl ligand proximate to the 12α proton of mestranol; the view is of the α face of the steroidal skeleton.

With these data one can compare the ^1H NMR chemical shifts of the free ligands and of their metal complexes. Typically, we note that the 12α proton in the steroidal portion of **8** has moved dramatically from its resonance position in the free ligand. This can be attributed not merely to loss of the triple bond character of the 17α substituent but also to the proximity of the metal carbonyl ligand. A very convenient method of evaluating possible molecular conformations is to construct the molecules in a modelling program, such as CHEM-X,[20] by melding together crystallographic data from known structures; in this particular case, we took the structures of 17β-estradiol and $(HC{\equiv}CH)Co_2(CO)_6$ and then allowed free rotation about the C-17–cluster bond so as to minimize steric interactions and also place a cobalt carbonyl ligand in close proximity to the 12α proton, as in Fig. 5.

Similarly, one can construct a CHEM-X model (see Fig. 6) of (mestranol)$Mo_2(CO)_4Cp_2$ (**9**), so

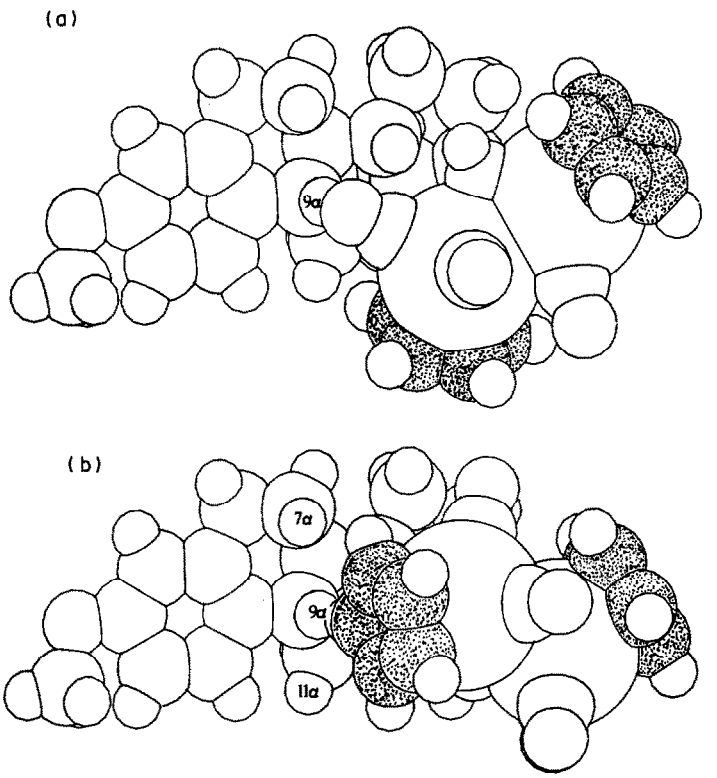

Fig. 6. CHEM-X plots of (mestranol)$Cp_2Mo_2(CO)_4$ showing orientations which (a) place a cyclopentadienyl ligand proximate to the 9α proton of mestranol and (b) position the C_5H_5 group unfavourably close to the B and C rings of the steroid.

as to minimize the steric interactions between the steroid and the cyclopentadienyl groups. As outlined previously, one can use the two-dimensional COSY NMR experiment to identify those protons which are connected by scalar couplings. In a different but related NMR experiment it is possible to generate spectra in which the off-diagonal contours indicate those protons which exhibit nuclear Overhauser enhancements; that is, such protons are not necessarily coupled to each other but they are close neighbours in space. By utilizing this so-called NOESY experiment,[21] it is possible to select a molecular conformation which satisfies all of the steric requirements as well as the nOe data. Figure 6a shows a favourable orientation in which one of the carbon monoxide ligands is proximate to the 9α proton; in contrast, the orientation in Fig. 6b places the C_5H_5 ring directly below the B and C rings of the steroid which would require nOe interactions between one of the cyclopentadienyl rings and the 7α, 9α, 11α, 12α and 14α protons of the steroidal ligand.

In effect, these dimetallic complexes of steroidal alkynes are merely $[R^*C{\equiv}CH](ML_x)_2$ clusters in which the R* group is not only chiral but also of known absolute configuration. Thus, the two metal vertices are diastereotopic and, in principle, should exhibit different chemical reactivity.

Trimetallic complexes derived from natural products

In order to extend these concepts to mixed metal clusters, it was decided to incorporate natural product moieties into some trimetallic systems. Recently, Vahrenkamp has synthesized mixed metal clusters containing the menthyl substituent,[22] as in **10**, and we have extended this to other terpenoid and steroidal fragments, as in **11** and **12**.

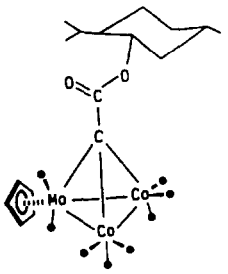

10

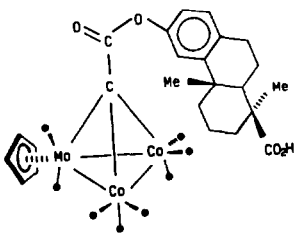

11

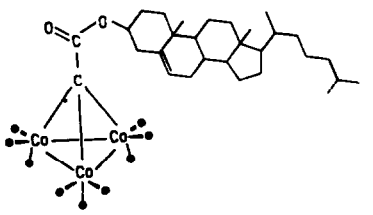

12

Our preliminary reactivity studies have revealed that, although a small reagent such as trimethylphosphite apparently cannot discriminate between the two cobalt centres in **10** and so yields a 50/50 mixture of products **13a** and **13b**, a much bulkier reagent, viz., tricyclohexylphosphine, does exhibit partial discrimination (70/30) as indicated by ^{31}P NMR data for **14a** and **14b**.[23]

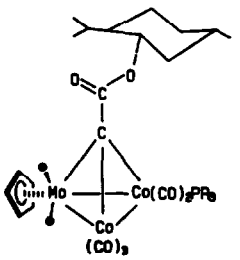

13a R = MeO
14a R = cyclohexyl

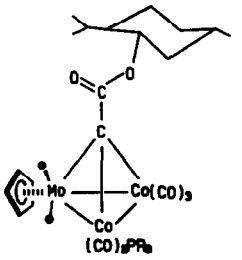

13b R = MeO
14b R = cyclohexyl

Our current activities are focussed towards placing the chiral auxiliary closer to the diastereotopic metal centres. A general route to $Co_3(CO)_9C{-}OR$ clusters has been developed by Patin and colleagues[24] and Scheme 3 shows how we are applying these concepts towards the rational syntheses of chiral clusters of known absolute configuration.

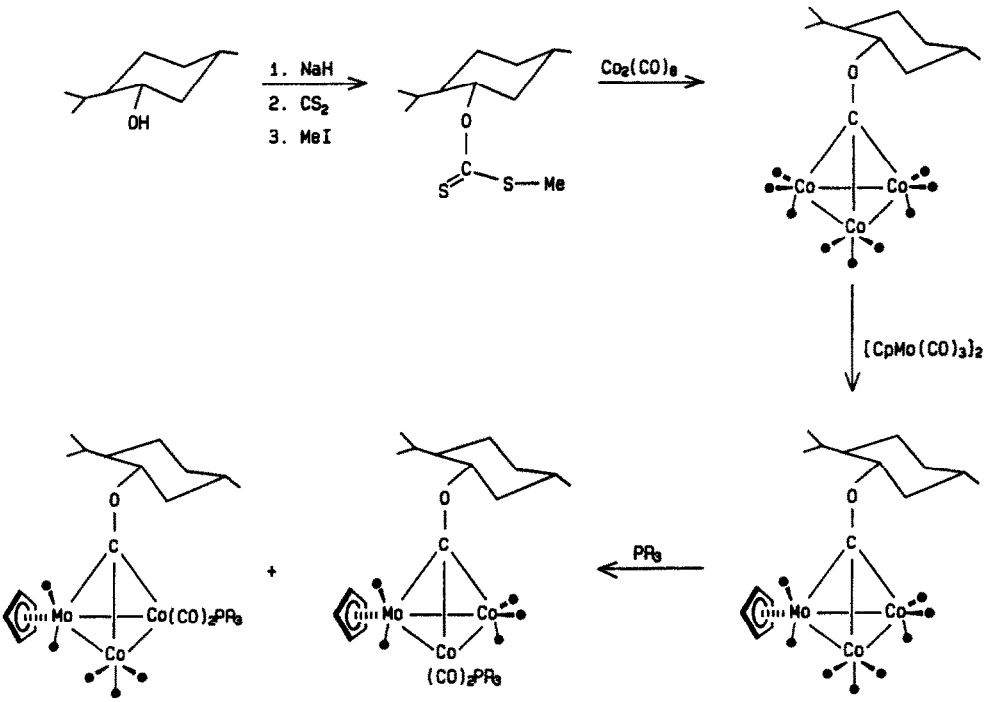

Scheme 3. Synthetic route to $CpMoCo_2(CO)_8C—R^*$ clusters containing a chiral capping group; in this case, R* is derived from (+)-menthol.

Acknowledgements—We thank the donors of the Petroleum Research Fund, administered by the American Chemical Society, for partial support of this research. Financial support from the Natural Sciences and Engineering Research Council of Canada is gratefully acknowledged. K.A.S. and D.T.C. thank NSERC for graduate fellowships.

REFERENCES

1. H. Brunner, *Adv. Organomet. Chem.* 1980, **18**, 151.
2. C. U. Pittman Jr., M. G. Richmond, M. Absi-Halabi, H. Beurich, F. Richter and H. Vahrenkamp, *Angew. Chem. Int. Ed. Engl.* 1982, **21**, 786.
3. G. Jaouen, A. Marinetti, J.-Y. Saillard, B. G. Sayer and M. J. McGlinchey, *Organometallics* 1982, **1**, 225.
4. A. A. Bahsoun, J. A. Osborn, C. Voelker, J. J. Bonnet and G. Lavigne, *Organometallics* 1982, **1**, 1114.
5. D. J. Darensbourg, D. J. Zalewski and T. Delord, *Organometallics* 1984, **3**, 1210.
6. K. A. Sutin, J. W. Kolis, M. Mlekuz, P. Bougeard, B. G. Sayer, M. A. Quilliam, R. Faggiani, C. J. L. Lock, M. J. McGlinchey and G. Jaouen, *Organometallics* 1987, **6**, 439.
7. M. Mlekuz, P. Bougeard, B. G. Sayer, S. Peng, M. J. McGlinchey, A. Marinetti, J.-Y. Saillard, J. Ben Naceur, B. Mentzen and G. Jaouen, *Organometallics* 1985, **4**, 1123.
8. M. F. D'Agostino and M. J. McGlinchey, *Polyhedron* 1988, **7**, 807.
9. M. J. Chetcuti, P. A. M. Chetcuti, J. C. Jeffery, R. M. Mills, P. Mitrprachachon, S. J. Pickering, F. G. A. Stone and P. Woodward, *J. Chem. Soc., Dalton Trans.* 1982, 699.
10. E. Delgado, J. Hein, J. C. Jeffery, A. L. Ratermann, F. G. A. Stone and L. J. Farrugia, *J. Chem. Soc., Dalton Trans.* 1987, 1191.
11. H. Beurich and H. Vahrenkamp, *Angew. Chem. Int. Ed. Engl.* 1978, **17**, 863.
12. L. Busetto, J. C. Jeffery, R. M. Mills, F. G. A. Stone, M. J. Went and P. Woodward, *J. Chem. Soc., Dalton Trans.* 1983, 101.
13. A. A. Aitchison and L. J. Farrugia, *Organometallics* 1987, **6**, 819.
14. K. A. Sutin, B. G. Sayer and M. J. McGlinchey, unpublished results.
15. R. Benn and H. Günther, *Angew. Chem. Int. Ed. Engl.* 1983, **22**, 350.
16. S. Top, G. Jaouen, A. Vessières, J.-P. Abjean, D. Davoust, C. A. Rodger, B. G. Sayer and M. J. McGlinchey, *Organometallics* 1985, **4**, 2143.
17. G. Jaouen, A. Vessières, S. Top, M. Savignac, I. S. Butler and A. A. Ismail, *Organometallics* 1987, **6**, 1985.
18. M. J. McGlinchey, R. C. Burns, R. Hofer, S. Top and G. Jaouen, *Organometallics* 1986, **5**, 104.
19. M. Savignac, G. Jaouen, C. A. Rodger, R. E. Perrier, B. G. Sayer and M. J. McGlinchey, *J. Org. Chem.* 1986, **51**, 2328.
20. CHEM-X, developed and distributed by Chemical Design Ltd, Oxford, U.K. (July 1986 Version).

21. J. Jeener, B. H. Meier, P. Bachmann and R. R. Ernst, *J. Chem. Phys.* 1979, **71**, 4546.
22. R. Blumhofer and H. Vahrenkamp, *Chem. Ber.* 1986, **119**, 683.
23. D. T. Clark, K. A. Sutin and M. J. McGlinchey, *Organometallics*, submitted for publication.
24. G. Mignani, H. Patin and R. Dabard, *J. Organomet. Chem.* 1979, **169**, C19.

Polyhedron Vol. 7, No. 22/23, pp. 2307–2315, 1988
Printed in Great Britain

0277–5387/88 $3.00+.00
© 1988 Pergamon Press plc

ORGANOMETALLIC COMPOUNDS OF THE LANTHANIDES—XL.* RECENT DEVELOPMENTS IN ORGANOLANTHANIDE CHEMISTRY

H. SCHUMANN,† I. ALBRECHT, M. GALLAGHER, E. HAHN, C. JANIAK, C. KOLAX, J. LOEBEL, S. NICKEL and E. PALAMIDIS

Institut für Anorganische und Analytische Chemie, Technische Universität Berlin, D-1000 Berlin 12, F.R.G.

Abstract—Lanthanide trichlorides $LnCl_3$ react with pentamethylcyclopentadienyl alkali metal derivatives with formation of novel compounds of the type $C_5Me_5LnCl_3ML_n$ (M = alkali metal, L = donor solvent like Et_2O, THF, DME). X-ray structural investigations showed that $YbCl_3$ reacts with KC_5Me_5 in THF and DME with formation of $[K(DME)_3][K((C_5Me_5Yb)_3Cl_8K(DME)_2)_2]$. Compounds of the type $Cp_2Ln(\mu\text{-}CH_3)_2LiL_2$ and $[Li(TMED)_2][CpLn(CH_3)_3]$ are useful starting materials for the synthesis of new organolanthanide derivatives with bonds between the lanthanides and other elements. By their reactions with ^{t}BuSH, PhSeH, Ph_2PH, and Ph_2AsH, e.g. the new organolutetium compounds $(C_5Me_5)_2Lu(\mu\text{-}S^tBu)_2Li(THF)_2$, $(C_5H_5)_2Lu(\mu\text{-}SePh)_2Li(THF)_2$, $(C_5H_5)_2Lu(\mu\text{-}PPh_2)_2Li(TMED)$, and $(C_5H_5)_2Lu(\mu\text{-}AsPh_2)_2Li(TMED)$ could be synthesized and characterized by X-ray structural analyses. Dicyclopentadienylsamarium chloride reacts with trimethylsilyl lithium in DME with formation of $[Li(DME)_3][(C_5H_5)_2Sm(SiMe_3)_2]$, whereas in the reaction of $(C_5H_5)_2Sm(\mu\text{-}Cl)_2Na(DME)$ with $LiGeMe_3$ redistribution occurs with formation of hexamethyldigermane and $[Li(DME)_3][(C_5H_5)_3Sm—Cl—Sm(C_5H_5)_3]$. The same anion is formed in the reaction of NaCl with $(C_5H_5)_3Sm$ in DME. Finally LiN_3 reacts with $(C_5H_5)_3Sm$ in DME with formation of the complex $[Li(DME)_3][(C_5H_5)_3Sm—NNN—Sm(C_5H_5)_3]$.

Organometallic compounds of the lanthanide metals are among the very newest organometallic compounds.[1] With the exception of cerium, which forms dicyclooctatetraenylcerium(IV)[2] and europium, samarium and ytterbium, which form cyclopentadienyl and pentamethylcyclopentadienyl lanthanide(II) derivatives,[3] all the other rare earth metals form only organometallic compounds with the metal in the oxidation state Ln^{3+}. Most of them have unsubstituted or substituted cyclopentadienyls bonded to the metal along with hydrogen, halogen, alkyl groups or alkoxides as additional ligands.

Only a few examples of organometallic compounds of the hard Lewis acidic electropositive lanthanide metals with bonds to soft donors such as phosphorus,[4] arsenic[5] and sulphur[6] are known. Organometallic compounds with bonds between the lanthanide metals and metalloids or metals like germanium, tin or even transition metals have been described in the literature, but they are only very poorly characterized. However, such compounds are of particular interest in organic synthesis because of the high reactivity of the probably covalent Ln—X bonds, as well as for several catalytic processes because of the high degree of unsaturation around the large electropositive lanthanide metals.

With respect to catalytic activity, organometallic clusters containing lanthanide metals with or without metal–metal bonds should be even much more interesting. Until now, no systematic research has been done in this field.

PENTAMETHYLCYCLOPENTADIENYL-LANTHANIDE HALIDE CLUSTERS

Lanthanide trichlorides react with pentamethylcyclopentadienylsodium in tetrahydrofuran in the presence of ether or dimethoxyethane with formation of $(C_5Me_5)_2Ln(\mu\text{-}Cl)_2Na(Et_2O)_2$ or $(C_5Me_5)_2Ln(\mu\text{-}Cl)_2Na(DME)_2$,[7] see eq. (1).

* For Part XXXIX, see S. J. Swamy and H. Schumann, *J. Organomet. Chem.*, in press.

† Author to whom correspondence should be addressed.

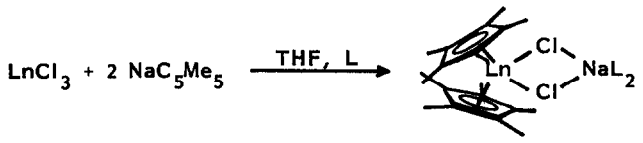

(1)

Ln = Sc, Y, La to Lu (except Pm)
L = Et_2O, DME

The X-ray structural analysis of $(C_5Me_5)_2Pr(\mu\text{-}Cl)_2Na(DME)_2$ shows two slightly different independent molecules per asymmetric unit, both with bridging chlorine atoms between praseodymium and sodium[7] (see Structure 1).

In contrast, compounds of the type $C_5Me_5LnCl_2$ have been only poorly characterized. After the synthesis of the first derivatives of this class, $C_5Me_5NdCl_3Na(Et_2O)_2$[8] and $C_5Me_5YbCl_3Li(THF)$[9] in 1981, we studied the 1 : 1 molar reactions of $PrCl_3$, $YbCl_3$ and $LuCl_3$ with pentamethylcyclopentadienylsodium and -potassium. $PrCl_3$ reacts with NaC_5Me_5 in diethylether with formation of green crystals, the analyses of which agree with the formula $C_5Me_5PrCl_3Na(Et_2O)$. They decompose during some days with loss of NaCl to give $C_5Me_5PrCl_2(Et_2O)$. The lutetium complex $C_5Me_5LuCl_3Na(Et_2O)_2$ could be isolated in a 37% yield from the reaction of $LuCl_3$ with NaC_5Me_5 in ether.

$YbCl_3$ reacts with KC_5Me_5 in THF in the presence of DME with formation of blue crystals, which decompose above 250°C. The X-ray structural analysis proves the complex to be built up from six $C_5Me_5YbCl_2$, four KCl and seven DME units forming a cation–anion pair, $[K(DME)_3]^+[K((C_5Me_5Yb)_3Cl_8K(DME)_2)_2]^-$, see eqs (2)–(4).

In the anion, two clusters each consisting of three $C_5Me_5YbCl_2$ units and one two-fold coordinated KCl unit are connected symmetrically to a central KCl_2^- anion. Thus, the central K atom is surrounded octahedrally by six Cl atoms at a distance of 3.11 Å. This distance corresponds with the K—Cl distances in ionic, crystalline potassium chloride (3.14 Å). The Yb—Cl distances are shorter and have values between 2.62 and 2.94 Å (see Structure 2).

ORGANOLANTHANIDE-SULPHUR, -SELENIUM, -PHOSPHORUS AND -ARSENIC COMPOUNDS

The X-ray structural analyses of some of the few organolanthanide compounds containing transition metals prove that there are no direct lanthanide to transition metal bonds. Thus, in $(C_5Me_5)_2Yb—OC—Co(CO)_3(THF)$[10] for example, the metals are bridged by a carbonyl group, forming a lanthanide–isocarbonyl linkage. On the other hand the first organolanthanide compounds containing the "soft" elements phosphorus or arsenic, $(C_5H_5)_2LnP(t\text{-}C_4H_9)_2$[4] or $Ln[As(t\text{-}C_4H_9)_2]_3$,[5] show real lutetium to phosphorus or lutetium to arsenic bonds, respectively [see eqs (5) and (6)].

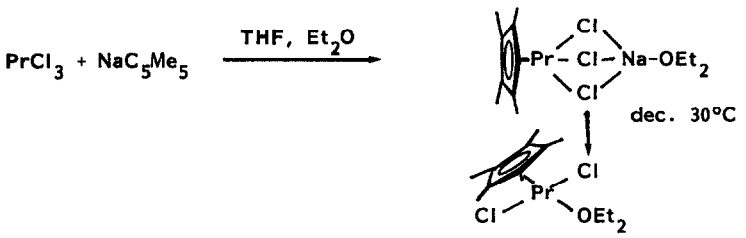

(2)

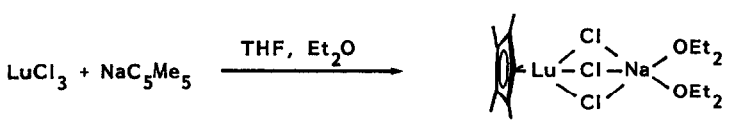

(3)

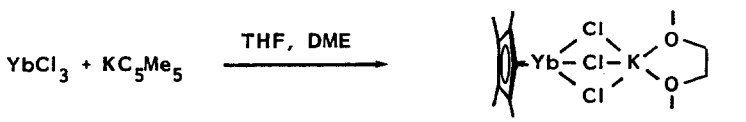

(4)

$K_4(C_5Me_5)_6Yb_6Cl_{16}(DME)_7 \equiv 6\ C_5Me_5YbCl_2 \cdot 4\ KCl \cdot 7\ DME$

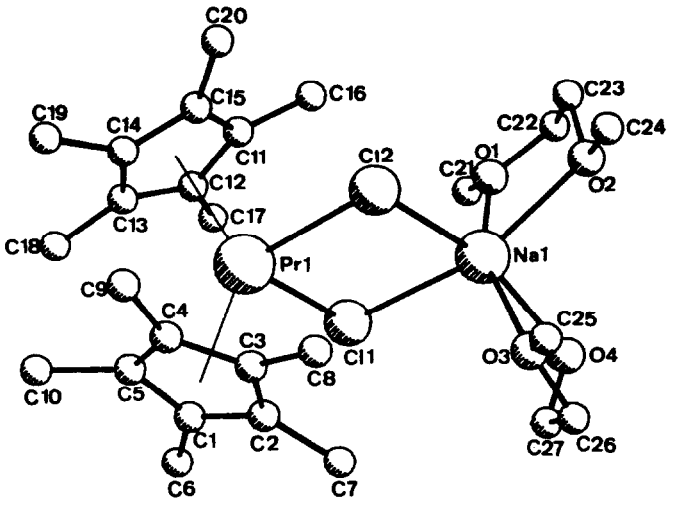

Structure 1.

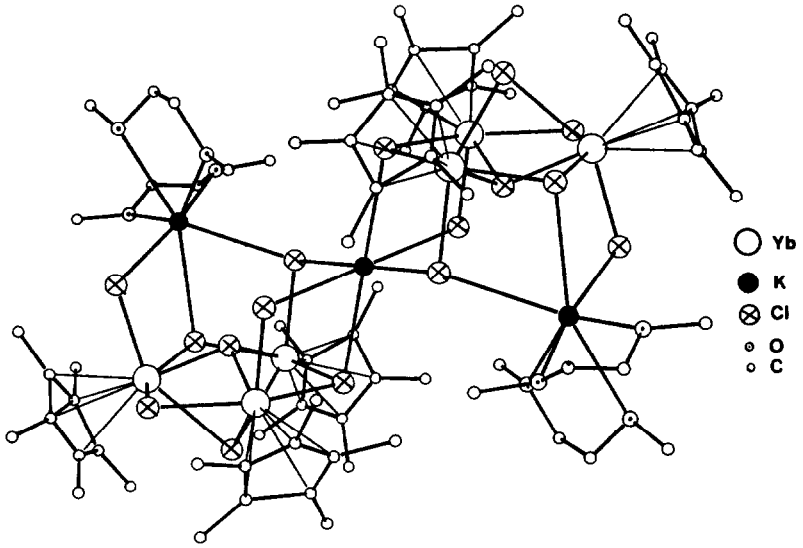

Structure 2. The anion $[K((C_5Me_5Yb)_3Cl_8K(DME)_2)_2]^-$.

$$(C_5H_5)_2LnCl + LiP^tBu_2 \xrightarrow{THF} (C_5H_5)_2Ln{-}P^tBu_2 + LiCl \quad (5)$$

$$LnCl_3 + 3LiAs^tBu_2 \xrightarrow{THF} Ln(As^tBu_2)_3 + 3LiCl. \quad (6)$$

We have now found a simple, versatile route to this interesting class of compounds via the elimination of methane from complexes of formulae shown below by acidic compounds like HSR, HSeR, HPR_2 or $HAsR_2$, see Structure 3.

Bis(pentamethylcyclopentadienyl)lutetiumdi(μ-methyl)bis(tetrahydrofuran)lithium reacts with t-C_4H_9SH in ether at −78°C with formation of $(C_5Me_5)_2Lu(\mu\text{-}SC_4H_9\text{-}t)_2Li(THF)_2$[11] [see eq. (7)]. $[Li(TMED)_2][C_5Me_5Lu(CH_3)_3]$ which exists as an ion pair, reacts with t-C_4H_9SH with formation of a complex, in which the lithium atom is bridged via sulphur to lutetium [see eq. (8)]. The NMR spectrum shows only one signal for the three tert-butyl ligands, proving a rapid exchange between terminal and bridging tert-butylsulphide ligands.

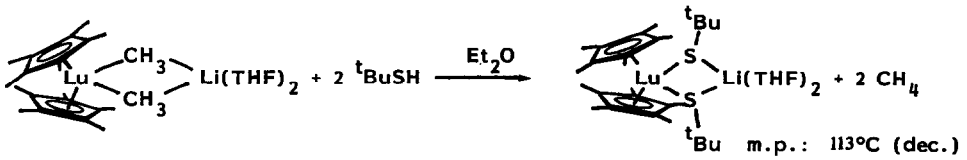

(7)

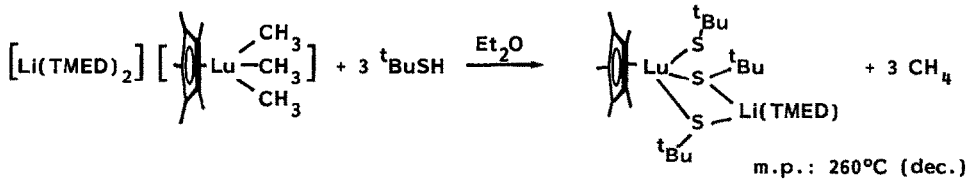

(8)

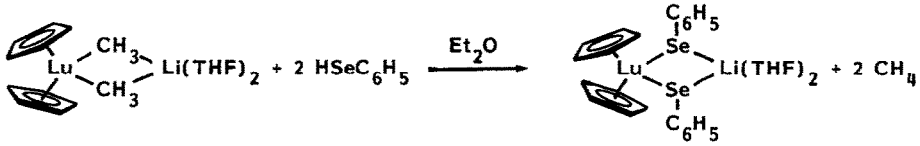

(9)

The X-ray structural analysis of the bis-(cyclopentadienyl)lutetium derivative shows the lutetium atom in a distorted tetrahedral environment consisting of the centroids of two cyclopentadienyl rings and the two bridging sulphur atoms. A dihedral angle of 168.7° is found between the S1—Lu—S2 and S1—Li—S2 planes[11] as shown in Structure 4.

Dicyclopentadienyllutetiumdi(μ-methyl)bis(tetrahydrofuran)lithium reacts with phenylselenol in ether with formation of the first organolanthanide compound containing an Ln—Se bond as shown in eq. (9) The compound darkens on exposure to light with the formation of diphenyldiselenide.

The X-ray structural analysis shows, in analogy to the above sulphur derivative, a folded four-membered ring with the lutetium and the lithium being bridged by two phenylseleno groups as shown in Structure 5. The dihedral angle is 166.5°. In contrast to the sulphur analogue, both phenylseleno groups are on the same site of the ring. The Lu—Se distances (2.80 Å) are the same order of magnitude as the Lu—S distances (2.72 Å).

Diphenylphosphine reacts with $(C_5H_5)_2Lu(\mu\text{-}CH_3)_2Li(THF)_2$ in ether or toluene at room temperature with elimination of methane yielding the dicyclopentadienyllutetium bis(phosphine) compound.[12] The NMR spectroscopic control of the reaction proves the stepwise CH_3 substitution, see eq. (10).

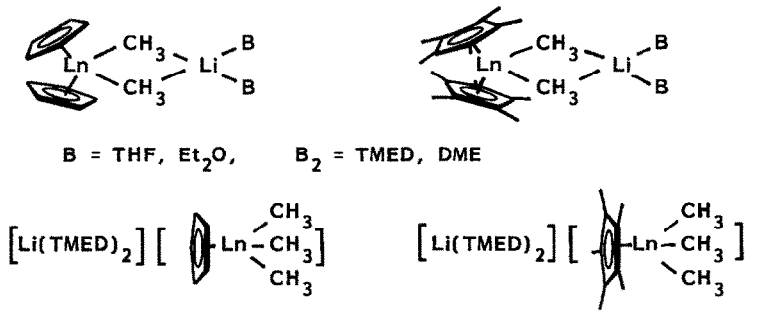

Structure 3.

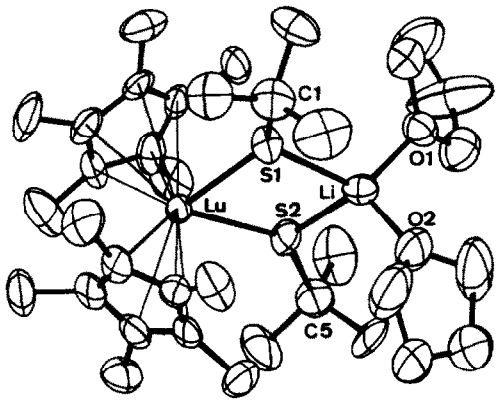

Structure 4.

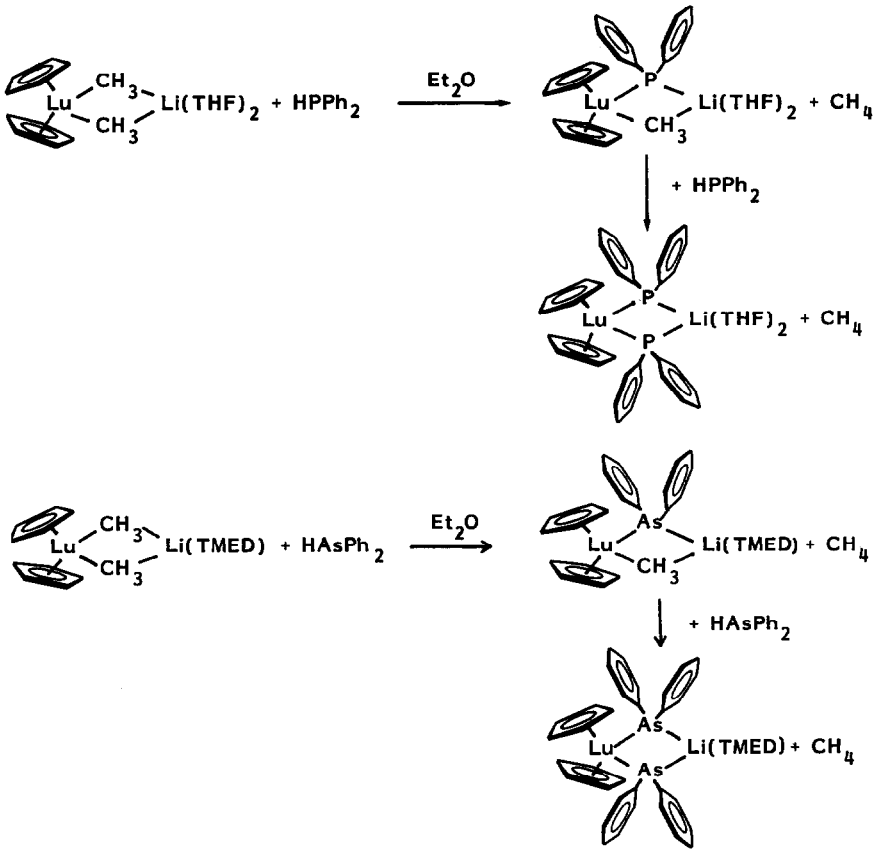

(10)

(11)

$(C_5H_5)_2Lu(\mu\text{-}CH_3)_2Li(TMED)$ reacts similarly, the only difference being that the complex formed contains one molecule of toluene per two organolutetium molecules in the crystal. In both cases, the P1—Lu—P2 and P1—Li—P2 planes form an angle of 148.7° in the four-membered ring system, see Structure 6.

The same method of preparation led to the successful isolation of the analogous arsenic compound. Via the monosubstitution product, monitored by NMR, dicyclopentadienyllutetium bis(diphenylarsino)lithium(tetramethylethylenediamine) is formed as yellow, air-sensitive crystals [see eq. (11)].

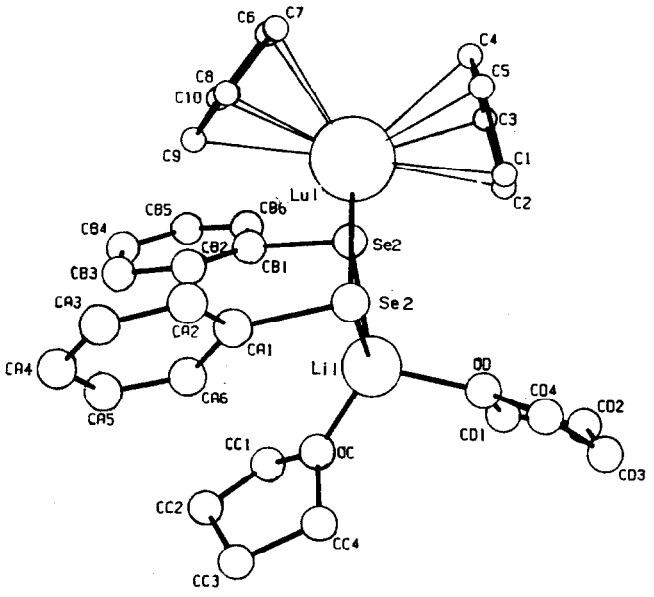

Structure 5.

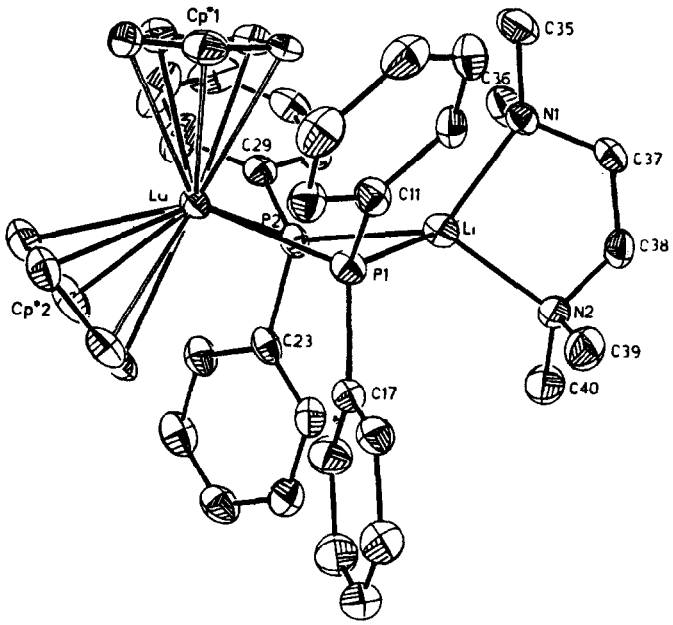

Structure 6.

The X-ray structural analysis shows the same ligation system as in the analogous phosphorus complex with an Lu—As distance of 2.88 Å, an Li—As distance of 2.7 Å, and a dihedral angle of the four-membered ring of 152° (see Structure 7 for details).

ORGANOLANTHANIDE-SILICON AND -GERMANIUM COMPOUNDS

Some years ago we reported the synthesis of the first lanthanide triphenylgermyl and triphenylstannyl complexes of the $Ln(E(C_6H_5)_3)_3$ and $(C_5H_5)_2Ln—E(C_6H_5)_3$ type (E = Ge, Sn) from $LnCl_3$ (Ln = Pr, Nd, Gd, Er) or $(C_5H_5)_2LnCl$ (Ln = Er, Yb) and $LiE(C_6H_5)_3$ (E = Ge, Sn).[13] The purification of these compounds, which contain different amounts of THF, was very difficult and therefore a characterization by X-ray structural analysis was not possible.

However, recently we have been successful in synthesizing the first organometallic compounds with lanthanide to silicon bonds, using the reaction

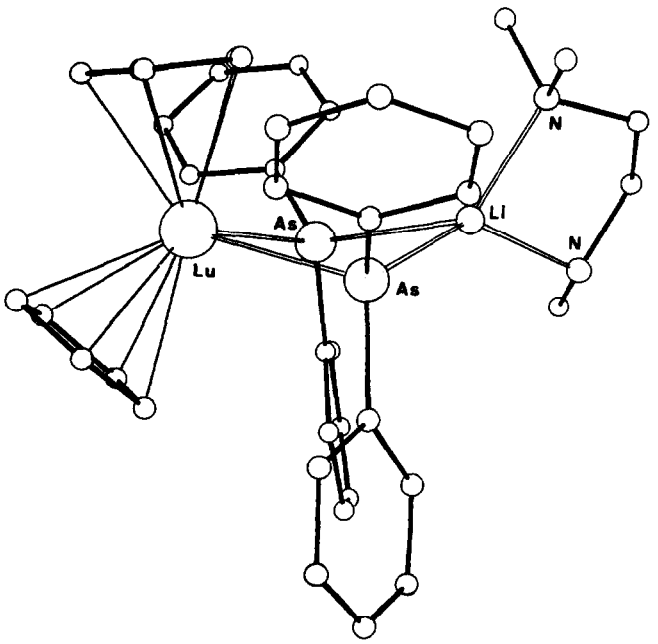

Structure 7.

between dicyclopentadienyllanthanide chlorides and lithiotrimethylsilane in DME at −78°C:[14]

$$(C_5H_5)_2SmCl + 2LiSiMe_3 \rightarrow$$

$$[Li(DME)_3]\left[(C_5H_5)_2Sm(SiMe_3)_2\right] + LiCl \quad (12)$$

yellow, dec.p.: 86°C

$[Li(DME)_3][(C_5H_5)_2Dy(SiMe_3)_2]$
tan, dec.p.: 92°C

$[Li(DME)_3][(C_5H_5)_2Ho(SiMe_3)_2]$
yellow, dec.p.: 68°C

$[Li(DME)_3][(C_5H_5)_2Er(SiMe_3)_2]$
pink, dec.p.: 73°C

$[Li(DME)_3][(C_5H_5)_2Tm(SiMe_3)_2]$
green, dec.p.: 74°C

$[Li(DME)_3][(C_5H_5)_2Lu(SiMe_3)_2]$
colourless, dec.p.: 87°C.

derivative shows a discrete cation–anion pair. At 80 K, the lithium cation is coordinated with three DME ligands resulting in coordination number six for Li. The anion is composed of two cyclopentadienyl and two trimethylsilyl ligands arranged in a distorted tetrahedral fashion around the samarium atom as shown in Structure 8. The Sm—Si distances are 2.88 Å, and the length of the Sm—C bonds varies between 2.582 and 2.637 Å, which is very short in comparison to the Sm—C bonds in other cyclopentadienylsamarium derivatives, indicating a partially covalent bonding in the bonds of the cyclopentadienyl rings to samarium.[14]

Lithiotrimethylgermane does not react with dicyclopentadienyllanthanide chlorides in the same way. $(C_5H_5)_2Sm(\mu\text{-}Cl)_2Na(DME)$ and $LiGe(CH_3)_3$ react in pentane first with the formation of hexamethyldigermane and ligand redistribution at the samarium atom yielding tricyclopentadienylsamarium, which on its turn reacts with chloride ions present in the reaction mixture, to give yellow $[Li(DME)_3][(C_5H_5)_3Sm—Cl—Sm(C_5H_5)_3]$:

$$(C_5H_5)_2Sm(Cl)_2Na(DME) + LiGeMe_3 \rightarrow [Li(DME)_3][(C_5H_5)_2Sm(GeMe_3)_2] \quad (13)$$

$$\rightarrow [Li(DME)_3][(C_5H_5)_3Sm(Cl)Sm(C_5H_5)_3]$$

yellow crystals, dec.p.: 192°C.

$$+ Me_3Ge—GeMe_3.$$

The coloured complexes are extremely sensitive toward moisture and air. They decompose slowly at room temperature, even when kept in an argon atmosphere. The molecular structure of the Sm

We could isolate the same complex, along with other unidentified products, from the reaction of $(C_2H_5)_3SiH$ with $(C_5H_5)_2Sm(\mu\text{-}CH_3)_2Li(DME)$ which was contaminated with $(C_5H_5)_2Sm(\mu\text{-}$

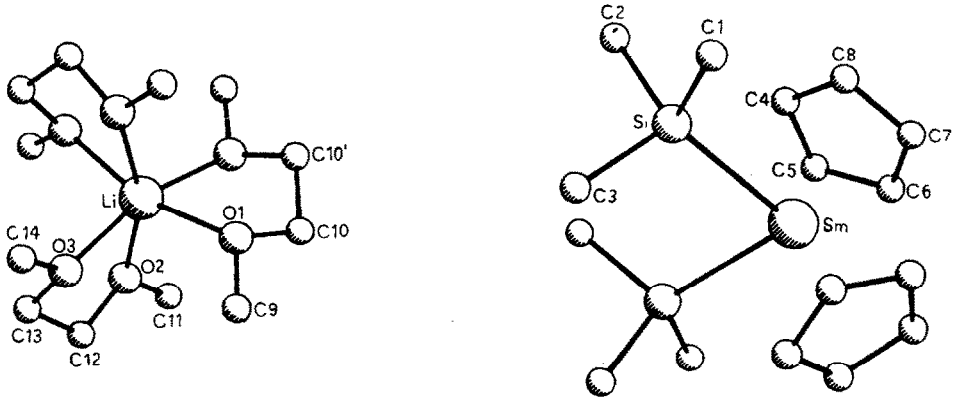

Structure 8.

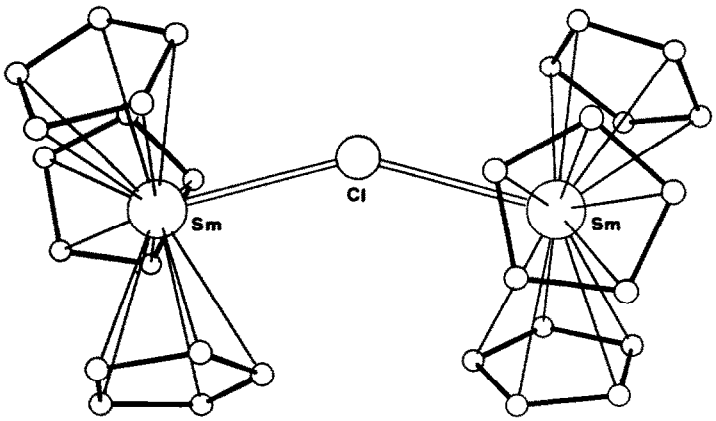

Structure 9. The anion $[(C_5H_5)_3Sm—Cl—Sm(C_5H_5)_3]^-$.

$Cl)_2Li(DME)$. X-ray structural analysis of both samples gave exactly the same result: a cation–anion pair, with the anion formed from two tricyclopentadienylsamarium units bridged by a chlorine atom, as shown in Structure 9. The Sm—Cl—Sm unit is angled by 146.5° and both Sm—Cl distances are 2.82 Å. Some years ago, we found an analogous structural situation in $[Na(THF)_6][(C_5H_5)_3Lu—H—Lu(C_5H_5)_3]$, where a hydrogen atom forms the bridge between two tricyclopentadienyllutetium units.[15]

However, the reaction of $(C_5H_5)_2Sm(\mu\text{-}Cl)_2Na(DME)$ with a four-fold excess of $LiGe(CH_3)_3$ leads to the formation of an organometallic compound containing Ge—Sm bonds. Elemental analyses and NMR spectra indicate a cation–anion pair with two tricyclopentadienylsamarium units now bridged by a trimethylgermanium ion:

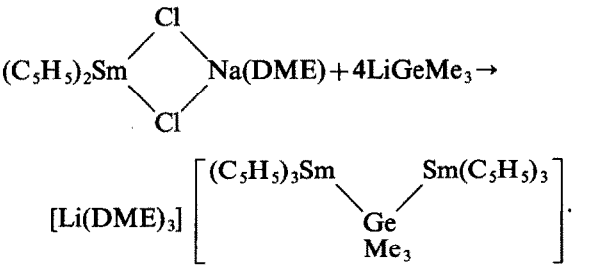

(14)

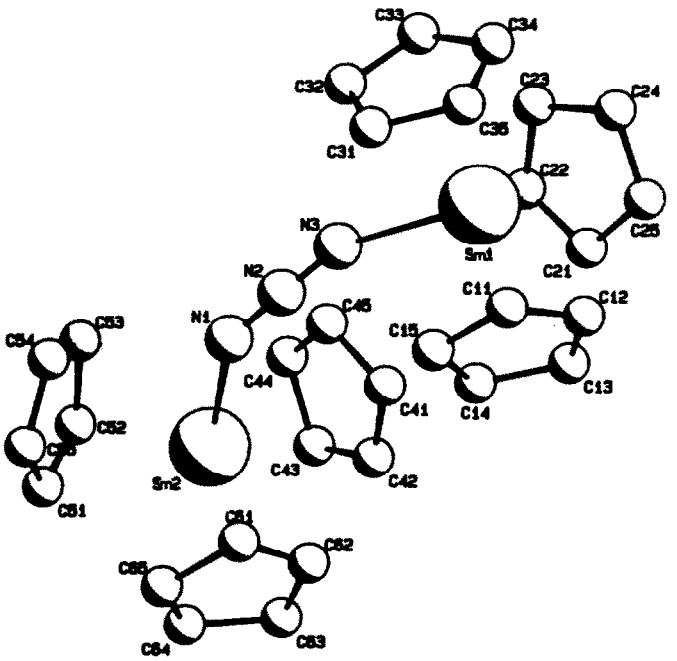

Structure 10. The anion $[(C_5H_5)_3Sm—NNN—Sm(C_5H_5)_3]$.

The apparently high stability of the $[(C_5H_5)_2Sm—Cl—Sm(C_5H_5)_3]^-$ anion, as well as that of the corresponding H bridged ion $[(C_5H_5)_3Lu—H—Lu(C_5H_5)_3]^-$ focused our interest to the synthesis of anions built up from two other tricyclopentadienyllanthanide units bridged by different anions.

First we could demonstrate that both the known complexes of this type, $[Na(THF)_6][(C_5H_5)_3Lu—H—Lu(C_5H_5)_3]$ and $[Li(DME)_3][(C_5H_5)_3Sm—Cl—Sm(C_5H_5)_3]$, can be prepared straight from tricyclopentadienyllutetium and sodium hydride or tricyclopentadienylsamarium and lithium chloride, respectively. Tricyclopentadienylsamarium also reacts with lithium azide in the same manner yielding the corresponding azide-bridged complex:

$$2(C_5H_5)_3Lu + NaH \xrightarrow{THF} [Na(THF)_6][(C_5H_5)_3Lu—H—Lu(C_5H_5)_3] \quad (15)$$

$$2(C_5H_5)_3Sm + LiCl \xrightarrow{DME} [Li(DME)_3][(C_5H_5)_3Sm—Cl—Sm(C_5H_5)_3] \quad (16)$$

$$2(C_5H_5)_3Sm + LiN_3 \xrightarrow{DME} [Li(DME)_3][(C_5H_5)_3Sm—NNN—Sm(C_5H_5)_3]. \quad (17)$$

The X-ray structural analysis of the yellow crystals formed shows again an anion built up from two tricyclopentadienylsamarium units, bridged via a linear N_3^- anion (see Structure 10 for details). The following distances and bonding angles have been determined: Sm(1)—N(3): 2.47 and Sm(2)—N(1): 2.48 Å; N(1)—N(2): 1.13 Å; N(2)—N(3): 1.17 Å; Sm(1)—N(3)—N(2): 151°; Sm(2)—N(1)—N(2): 134°; N(1)—N(2)—N(3): 176°.

Acknowledgements—We thank the Deutsche Forschungsgemeinschaft and the Fonds der Chemischen Industrie for generous support and the TU Berlin for special grants in connection with partnership agreements between the TU Berlin and the M.I.T., Cambridge, MA.

REFERENCES

1. H. Schumann, *Angew. Chem.* 1984, **96**, 475; *Angew. Chem., Int. Ed. Engl.* 1984, **23**, 474.
2. A. Streitwieser, S. A. Kinsley, J. T. Rigsbee, I. L. Fragala, E. Ciliberto and N. Rösch, *J. Am. Chem. Soc.* 1985, **107**, 7786.
3. W. J. Evans, *Polyhedron* 1987, **6**, 803.
4. H. Schumann and G. M. Frisch, *Z. Naturforsch.* 1981, **36b**, 1244.
5. H. Schumann and G. M. Frisch, *Z. Naturforsch.* 1982, **37b**, 168.
6. T. D. Tilley, R. A. Andersen, A. Zalkin and D. H. Templeton, *Inorg. Chem.* 1982, **21**, 2644.
7. H. Schumann, I. Albrecht, J. Loebel, E. Hahn, M. B. Hossain and D. van der Helm, *Organometallics* 1986, **5**, 1296.
8. T. D. Tilley and R. A. Andersen, *Inorg. Chem.* 1981, **20**, 3267.
9. P. L. Watson, J. F. Whitney and R. L. Harlow, *Inorg. Chem.* 1981, **20**, 3271.
10. T. D. Tilley and R. A. Andersen, *J. Chem. Soc., Chem. Commun.* 1981, 985.
11. H. Schumann, I. Albrecht and E. Hahn, *Angew. Chem.* 1985, **97**, 991; *Angew. Chem., Int. Ed. Engl.* 1985, **24**, 985.
12. H. Schumann, E. Palamidis, G. Schmid and R. Boese, *Angew. Chem.* 1986, **98**, 726; *Angew. Chem., Int. Ed. Engl.* 1986, **25**, 718.
13. H. Schumann and M. Cygon, *J. Organomet. Chem.* 1978, **144**, C43.
14. H. Schumann, S. Nickel, E. Hahn and M. J. Heeg, *Organometallics* 1985, **4**, 800.
15. H. Schumann, W. Genthe, E. Hahn, M. B. Hossain and D. van der Helm, *J. Organomet. Chem.* 1986, **299**, 67.

Polyhedron Vol. 7, No. 22/23, pp. 2317–2320, 1988
Printed in Great Britain

0277–5387/88 $3.00+.00
© 1988 Pergamon Press plc

CLUSTER OF CLUSTERS: A NEW SERIES OF HIGH NUCLEARITY Au–Ag CLUSTERS

BOON K. TEO

Department of Chemistry, University of Illinois at Chicago, Chicago, IL 60607, U.S.A.

Abstract—The structure of a novel series of bimetallic Au–Ag clusters containing 25 ($Au_{13}Ag_{12}$), 37 ($Au_{18}Ag_{19}$), and 38 ($Au_{18}Ag_{20}$) metal atoms is discussed. The most interesting structural characteristic of these clusters is that they can be considered as being built from 13-atom centred icosahedral cluster units. Thus, the 25-atom cluster can be considered as two icosahedra sharing a vertex; the 37- and 38-atom clusters as three icosahedra sharing three vertices in a cyclic manner plus one and two capping atoms, respectively. These observations led to the concept of "cluster of clusters". It is predicted that tetrahedral, trigonal-bipyramidal, and pentagonal-bipyramidal arrays of vertex-sharing icosahedra will give rise to nuclearities ($10n+6$) of 46-, 56- and 76-atom clusters, respectively. One exception to the rule is the 127-atom icosahedral cluster which is formed by 12 centred icosahedra sharing 30 corners. Here the icosahedral hole created by the 12 icosahedra is filled with one additional atom. It is suggested that the idea of "cluster of clusters" may provide new pathways to novel high nuclearity supraclusters via vertex-, edge-, and face-sharing and/or close-packing of smaller cluster units as building blocks.

Recently, developments in cluster synthesis[1] have produced many high nuclearity metal clusters with metal arrangements resembling fragments of metallic lattices.[2–12] A special class of metal clusters is the heteronuclear or mixed-metal clusters[10–12] containing more than one type of metals which we shall refer to as "metal alloy clusters".

Advances in gold phosphine chemistry have produced a great number of novel gold-containing clusters.[13–28] Our work in this area focuses on large Au–Ag clusters containing a few dozen metal atoms.[29–31] Unusual optical, electronic and magnetic properties of these and related clusters have been observed.[32–40] In this paper, we will discuss some of our recent results on the structures of these large metal alloy clusters based on the concept of "cluster of clusters".[29–31]

Recently, we reported the structure of a novel 25-atom cluster[29] containing 13 Au and 12 Ag atoms prepared by reducing a mixture (Au : Ag = 1 : 1) of Ph_3PAuCl and $(Ph_3P)_4Ag_4Cl_4$[41] with $NaBH_4$ in ethanol. The metal framework (Fig. 1c) can be considered as two Au-centred Au_7Ag_6 icosahedra sharing one vertex. The cluster can also be viewed as having a metal arrangement of 1(Ag) : 5(Au) : 1(Au) : 5(Ag) : 1(Au) : 5(Ag) : 1(Au) : 5(Au) : 1(Ag). In this respect, the 25-atom cluster is related to $[Au_{13}(PMe_2Ph)_{10}Cl_2]^{3+}$[42] (Fig. 1a) and $[Pt_{19}(CO)_{22}]^{4-}$[43] (Fig. 1b) which has a metal

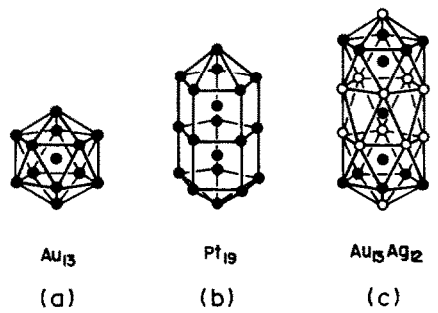

Fig. 1. Metal frameworks of (a) Au_{13}, (b) Pt_{19}, and (c) $Au_{13}Ag_{12}$ clusters.

arrangement of 1 : 5 : 1 : 5 : 1 and 1 : 5 : 1 : 5 : 1 : 5 : 1, respectively. It is worth mentioning that the adjacent metal pentagons in the cationic Au_{13} and $Au_{13}Ag_{12}$ clusters are staggered (hereafter designated as s) with respect to one another, giving rise to icosahedral (or bicapped pentagonal antiprismatic) cages, whereas those in the anionic Pt_{19} cluster are eclipsed (hereafter designated as e), giving rise to bicapped pentagonal prismatic cages.

We also succeeded in isolating and structurally characterizing a novel 38-atom cluster $[(p\text{-}Tol_3P)_{12}Au_{18}Ag_{20}Cl_{14}]$[30] from a similar reaction.

The metal framework of the 38-atom cluster is shown in Fig. 2 (top view) and Fig. 3a (side view). It can be described in a number of ways. The most

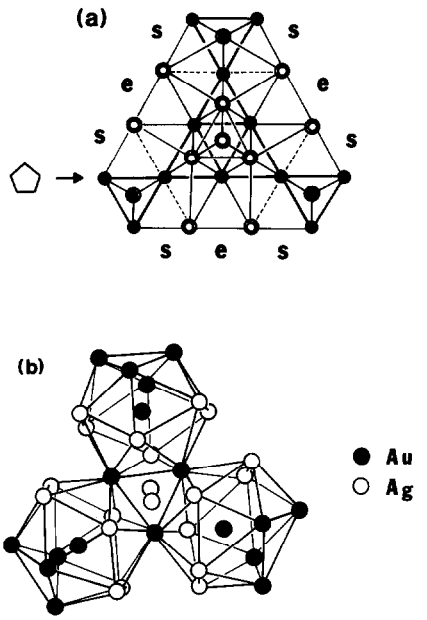

Fig. 2. The metal framework of the 38-atom cluster (p-$Tol_3P)_{12}Au_{18}Ag_{20}Cl_{14}$ (not all metal–metal bonds are shown).

obvious description is based on the close-packing or nearly close-packing of metal atoms. In this description (Fig. 2a), imagine a two-dimensional close-packing of 12 Au atoms (designated as solid circles) resulting in a v_2 triangle (centre) and three v_1 triangles sharing corners. Above and below the three small triangles are six more Au atoms conceptually changing the smaller triangles into trigonal bipyramids. Above and below the central (large) triangle are eight Ag atoms (open circles) arranged in a tetrahedral array, giving rise to a v_2 trigonal bipyramid. On the three edges are 12 Ag atoms, six above and six below the plane of the 12 Au atoms.

A better description is based on the idea of building up a cluster by sharing vertices (corners). In this case, the metal framework (Fig. 2b) can be visualized as three Au-centred Au_7Ag_6 icosahedra sharing three corners in a triangular arrangement, thereby giving rise to a $3 \times 13 - 3 = 36$ metal atom cluster; two more exopolyhedral Ag atoms are added to the top and the bottom Ag_3 triangles along the three-fold axis.

We have also synthesized and structurally characterized a novel 37-atom cluster $[(p\text{-}Tol_3P)_{12}Au_{18}Ag_{19}Br_{11}]^{2+}$.[31] The metal framework is depicted in Fig. 3b (side view). The 37-atom (Fig. 3b) is related to the 38-atom (Fig. 3a) cluster via removal of one of the two Ag^+ ions *exo* to the 36-atom cluster "main frame" which can be approximated as a three- or five-layer structure (Fig. 3).

The most interesting structural characteristic of the clusters mentioned above is that they can be considered as being built up from 13-atom centred icosahedral cluster units (Fig. 4a). If each icosahedron is represented by a sphere, one can envisage close-packing of such close-packed spherical icosahedra to form supraclusters (s_n) as depicted in Fig. 4. Thus, the 25-atom cluster s_2 (Fig. 4b) can be considered as *two* centred icosahedra (13-atom cluster) sharing a vertex. Likewise, the 38- and 37-atom clusters can be considered as *three* centred icosahedra sharing three vertices in a cyclic (triangular) manner (36-atom cluster s_3, Fig. 4c) plus two or one capping atoms, respectively, on the three-fold axes. These observations led to the con-

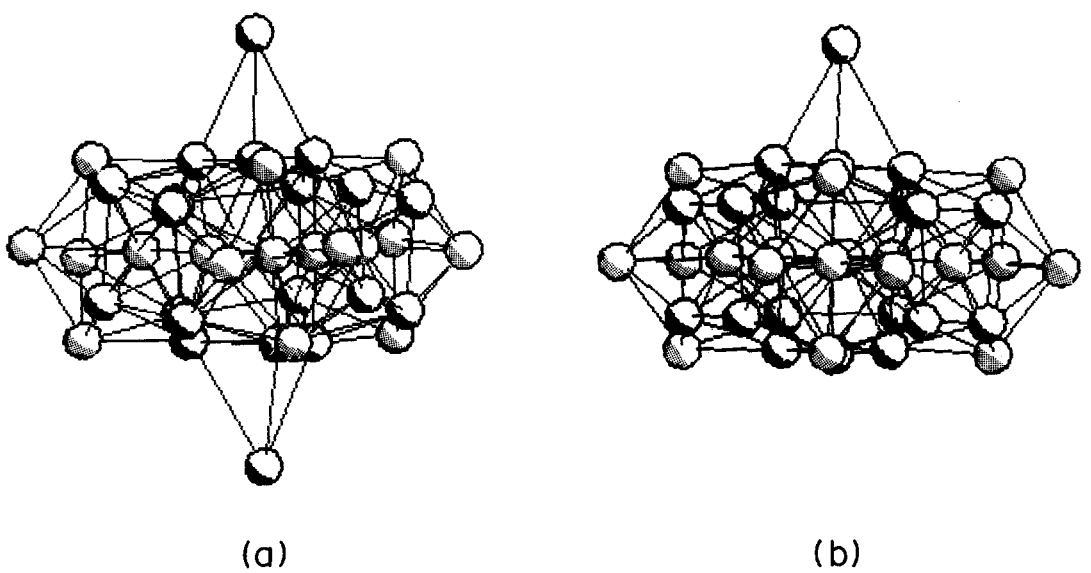

Fig. 3. Side views of the metal framework of (a) 38-atom and (b) 37-atom clusters.

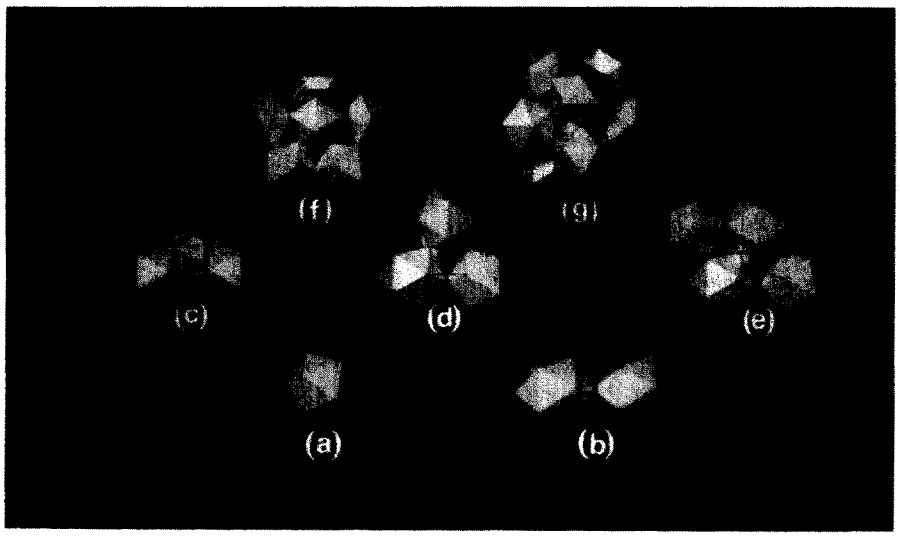

Fig. 4. Supracluster s_n formed by n centred icosahedra (nuclearity in parentheses): (a) s_1 (13); (b) s_2 (25); (c) s_3 (36); (d) s_4 (46); (e) s_5 (56); (f) s_7 (76); (g) s_{12} (127).

cept of "cluster of clusters".[31] It is predicted that tetrahedral (s_4), trigonal-bipyramidal (s_5), and pentagonal-bipyramidal (s_7) arrays of vertex-sharing icosahedra will give rise to nuclearities $(10n+6)$ of 46-, 56- and 76-atom clusters, respectively, as depicted in Fig. 4d–f. One exception to the rule is the 127-atom icosahedral cluster s_{12} (Fig. 4g) which is formed by 12 centred icosahedra sharing 30 corners. Here the icosahedral hole created by the 12 icosahedra is filled with one additional atom.

We are currently engaged in the synthetic and structural investigations of large Au–Ag clusters s_n with $n \geqslant 3$ shown in Fig. 4.

It is suggested that the idea of "cluster of clusters" may provide new pathways to novel high nuclearity superclusters via vertex-, edge-, and face-sharing and/or close-packing of smaller cluster units as building blocks.

Acknowledgements—Acknowledgement is made to the National Science Foundation (CHE-8722339) and the donors of the Petroleum Research Fund (No. 18873-AC3), for partial financial support of this research. I am also grateful to the University of Illinois at Chicago for a Campus Research Board Award. I would also like to acknowledge the important contributions of my present and past co-workers whose names appear in the references.

REFERENCES

1. For reviews on transition metal clusters see e.g.: (a) P. Chini, *Gazz. Chim. Ital.* 1979, **109**, 225; (b) P. Chini, *J. Organomet. Chem.* 1980, **200**, 37; (c) P. Chini, G. Longoni and V. G. Albano, *Adv. Organomet. Chem.* 1976, **14**, 285; (d) B. F. G. Johnson (Ed.), *Transition Metal Clusters*. Wiley-Interscience, Chichester (1980); (e) B. F. G. Johnson and R. E. Benfield, in *Topics in Inorganic and Organometallic Stereochemistry* (Edited by G. Geoffroy). John Wiley, New York (1981); (f) B. K. Teo, *Inorg. Chem.* 1985, **24**, 4209.
2. A. Ceriotti, P. Chini, G. Longoni, D. M. Washecheck, M. A. Murphy and L. F. Dahl, unpublished results.
3. E. G. Mednikov, N. K. Eremenko, Y. L. Slovokhotov and Y. Struchkov, *J. Chem. Soc., Chem. Commun.* 1987, 218.
4. (a) A. Ceriotti, A. Fait, G. Longoni, G. Piro and L. Resconi, *J. Am. Chem. Soc.* 1986, **108**, 5370; (b) A. Ceriotti, A. Fait, G. Longoni, G. Piro, F. Demartin, M. Manassero, N. Masciocchi and M. Sansoni, *J. Am. Chem. Soc.* 1986, **108**, 8091.
5. D. Fenske, J. Ohmer and J. Hachgenei, *Angew. Chem., Int. ed. Engl.* 1985, **24**, 993.
6. S. Martinengo, G. Ciani and A. Sironi, *J. Am. Chem. Soc.* 1980, **102**, 7564.
7. J. L. Vidal, R. C. Schoening and J. M. Troup, *Inorg. Chem.* 1981, **20**, 227.
8. P. F. Jackson, B. F. G. Johnson, J. Lewis, W. J. H. Nelson and M. McPartlin, *J. Chem. Soc., Dalton Trans.* 1982, 2099.
9. C. T. Hayward, J. R. Shapley, M. R. Churchill, C. Bueno and A. L. Rheingold, *J. Am. Chem. Soc.* 1982, **104**, 7347.
10. A. Ceriotti, F. Demartin, G. Longoni, M. Manassero, M. Marchionna, G. Piva and M. Sansoni, *Angew. Chem., Int. ed. Engl.* 1985, **24**, 697.
11. G. Longoni, M. Manassero and M. Sansoni, *J. Chem. Soc.* 1980, **102**, 3242.
12. A. Fumagalli, S. Martinengo and G. Ciani, *J. Chem. Soc., Chem. Commun.* 1983, 1381.
13. For reviews of gold phosphine clusters, see, for example (a) J. J. Steggerda, J. J. Bour and J. W. A. van

der Velden, *Recl. Trav. Chim. Pays-Bas* 1982, **101**, 164; (b) K. P. Hall and D. M. P. Mingos, *Prog. Inorg. Chem.* 1985, 237.
14. (a) R. J. Puddephatt, *The Chemistry of Gold.* Elsevier, Amsterdam (1978); (b) L. Manjojlovic-Muir, K. W. Muir, I. Treurnicht and R. J. Puddephatt, *Inorg. Chem.* 1987, **26**, 2418.
15. (a) L. Malatesta, L. Naldini, G. Simonetta and F. Cariati, *Chem. Commun.* 1965, 212; (b) M. McPartlin and R. Mason, *Chem. Commun.* 1969, 334; (c) F. Cariati and L. Naldini, *Inorg. Chim. Acta* 1971, **5**, 172.
16. B. D. Alexander, P. D. Boyle, B. J. Johnson, J. A. Casalnuovo, S. M. Johnson, A. M. Mueting and L. H. Pignolet, *Inorg. Chem.* 1987, **26**, 2547.
17. P. D. Boyle, B. J. Johnson, B. D. Alexander, J. A. Casalnuovo, P. R. Gannon, S. M. Johnson, E. A. Larka, A. M. Mueting and L. H. Pignolet, *Inorg. Chem.* 1987, **26**, 1346.
18. B. D. Alexander, B. J. Johnson, S. M. Johnson, A. L. Casalnuovo and L. H. Pignolet, *J. Am. Chem. Soc.* 1986, **108**, 4409 and references cited therein.
19. P. D. Boyle, B. J. Johnson, A. Buehler and L. H. Pignolet, *Inorg. Chem.* 1986, **25**, 5.
20. A. L. Casalnuovo, T. Laska, P. V. Nilsson, J. Olofson, L. H. Pignolet, W. Bos, J. J. Bour and J. J. Steggerda, *Inorg. Chem.* 1985, **24**, 182.
21. J. W. Lauher and K. Wald, *J. Am. Chem. Soc.* 1981, **103**, 7648.
22. P. Braunstein, H. Lehner, D. Matt, A. Tiripicchio and M. Tiripicchio-Camellini, *Angew. Chem., Int. ed. Engl.* 1984, **23**, 304 and references cited therein.
23. (a) P. Braunstein, J. Rose, A. M. Manotti-Lanfredi, A. Tiripicchio and E. Sappa, *J. Chem. Soc., Dalton Trans.* 1984, 1843; (b) P. Braunstein and J. Rose, *Gold Bull.* 1985, **18**, 17.
24. B. F. G. Johnson, J. Lewis, W. J. H. Nelson, P. R. Raithby and M. D. Vargas, *J. Chem. Soc., Chem. Commun.* 1983, 608.
25. B. F. G. Johnson, D. A. Kaner, J. Lewis, P. R. Raithby and M. J. Taylor, *Polyhedron* 1982, **1**, 105.
26. L. J. Farrugia, M. J., Freeman, M. Green, A. G. Orpen, F. G. A. Stone and I. D. Salter, *J. Organomet. Chem.* 1983, **249**, 273.
27. A. L. Casalnuovo, L. H. Pignolet, J. W. A. van der Velden, J. J. Bour and J. J. Steggerda, *J. Am. Chem. Soc.* 1983, **105**, 5957.
28. J. W. A. van der Velden, J. J. Bour, W. P. Bosman and J. H. Noordik, *Inorg. Chem.* 1983, **22**, 1913.
29. B. K. Teo and K. Keating, *J. Am. Chem. Soc.* 1984, **106**, 2224.
30. B. K. Teo, M. C. Hong, H. Zhang and D. B. Huang, *J. Chem. Soc., Chem. Commun.* 1988, 204.
31. B. K. Teo, M. C. Hong, H. Zhang and D. B. Huang, *Angew. Chem., Int. Ed. Engl.* 1987, **26**, 897.
32. G. K. Wertheim, J. R. Kwo, B. K. Teo and K. A. Keating, *Solid State Commun.* 1985, **55**, 357.
33. B. K. Teo, F. J. DiSalvo, J. V. Waszczak, G. Longoni and A. Ceriotti, *Inorg. Chem.* 1986, **25**, 2262.
34. B. K. Teo, K. Keating and Y. H. Kao, *J. Am. Chem. Soc.* 1987, **109**, 3494.
35. B. K. Teo and N. J. A. Sloane, *Inorg. Chem.* 1985, **24**, 4545.
36. (a) N. J. A. Sloane and B. K. Teo, *J. Chem. Phys.* 1985, **83**, 6520; (b) B. K. Teo and N. J. A. Sloane, *Inorg. Chem.* 1986, **25**, 2315.
37. (a) B. K. Teo, *Inorg. Chem.* 1984, **23**, 1251; (b) B. K. Teo, G. Longoni and F. R. K. Chung, *Inorg. Chem.* 1984, **23**, 1257.
38. B. K. Teo, *Inorg. Chem.* 1985, **24**, 1627.
39. B. K. Teo, *Inorg. Chem.* 1985, **24**, 4209.
40. B. K. Teo, *J. Chem. Soc., Chem. Commun.* 1983, 1362.
41. B. K. Teo and J. C. Calabrese, *Inorg. Chem.* 1976, **15**, 2467.
42. C. E. Briant, B. R. C. Theobald, J. W. White, L. K. Bell, D. M. P. Mingos and A. J. Welch, *J. Chem. Soc., Chem. Commun.* 1981, 201.
43. D. M. Washecheck, E. J. Wucherer, L. F. Dahl, A. Ceriotti, G. Longoni, M. Manassero, M. Sansoni and P. Chini, *J. Am. Chem. Soc.* 1979, **101**, 6110.

Polyhedron Vol. 7, No. 22/23, pp. 2321–2329, 1988
Printed in Great Britain

0277–5387/88 $3.00+.00
© 1988 Pergamon Press plc

METAL CLUSTERS AND CLUSTER METALS

GÜNTER SCHMID

Institut für Anorganische Chemie der Universität Essen, Universitätsstr. 5–7, D-4300 Essen 1, F.R.G.

Abstract—The desirable aim to create uniform naked metal clusters still fails. On the other hand, there exist many ligand stabilized clusters. If there was any possibility of eliminating the ligand sphere, a wide field of study, naked clusters of the same size, could be opened. Naked clusters with a magic number of metal atoms (full shell clusters) should have a special stability because of their complete outer geometry. Two-shell clusters of the type $M_{55}L_{12}Cl_x$ (M = Au, Rh, L = PPh_3, $x = 6$; M = Rh, Ru, L = $P(t\text{-}Bu)_3$, $x = 20$, M = Pt, L = $As(t\text{-}Bu)_3$, $x = 20$; M = Co, L = PMe_3, $x = 20$) seem to be suited for studying those problems. As can be seen from HRTEM images and from other investigations, they have a cubic close packed structure (ccp) with the outer geometry of a cuboctahedron. The 12 vertices are coordinated by the 12 ligands L, and the chlorine atoms partially fill the gaps between the phosphine or arsine molecules. The nature of the ligands makes the cluster molecules soluble in organic solvents. The transformation into water soluble compounds succeeds if PPh_3 is exchanged by the hydrophilic derivative $Ph_2PC_6H_4SO_3Na \cdot 2H_2O$. So, the cluster $Au_{55}(Ph_2PC_6H_4SO_3Na \cdot 2H_2O)_{12}Cl_6$ can be obtained as a very stable (in contrast to $Au_{55}(PPh_3)_{12}Cl_6$) water soluble compound which is completely dissociated in aqueous solution. Using a 100 kV electron beam, small crystalline areas of probably intact cluster molecules can be imaged by TEM. The giant cluster $Pd_{561}(phen)_{36}O_{190-200}$ (phen = phenanthroline) is obtained by reduction of palladium acetate with H_2 in the presence of appropriate amounts of phen with subsequent oxidation by oxygen. The generation of naked clusters indeed succeeds if the $M_{55}L_{12}Cl_x$ species are degraded in solution by 20 V d.c., using Pt electrodes. The ligand sphere together with the outer shell of metal atoms is eliminated, generating the inner naked M_{13} nuclei. These full-shell particles are metastable and build up novel structures. The structural principle can be described as an aggregation of 13 M_{13} particles, combined in a kind of close packed arrangement. The $(M_{13})_{13}$ superclusters again act as building blocks and form particles $[(M_{13})_{13}]_n$. This construction principle is realized for all metals in this investigation, i.e. Au, Rh, Ru, Pt and Co.

A predominent number of high-nuclearity transition metal clusters consist of close packed structures, either hexagonal or cubic or sometimes of both types. This is obvious as large clusters can be understood as submicroscopic small metal particles. Consequently, clusters are very informative objects to study the properties of aggregation from only a few (up to some hundreds) atoms. Little is known about naked clusters, as it is still a romantic project to generate uniform naked clusters. On the other hand, the physical and chemical properties of naked clusters depend mainly on their size, not only on their structure. Numerous methods to generate naked metal clusters are known,[1] but none is suitable for the formation of particles of the same size.

If at all, those naked clusters should have a special stability which consists of a magic number of metal atoms, because these particles would have a complete outer geometry (full-shell cluster). If a central metal atom is surrounded by 12 others of the same size in a cubic (ccp) or hexagonal close packed (hcp) manner, the first magic number 13 is realized. Forty-two atoms form a second shell around the first 12 atoms, yielding the second magic number 55. Generally, the nth shell consists of $10\ n^2+2$ atoms. Clusters of this type are nothing but cut-outs of typical metal structures. Most of the transition metals crystallize in a ccp or hcp lattice. There are many indications that full-shell clusters are more stable than others. The first evidence for this assumption was given in 1981,

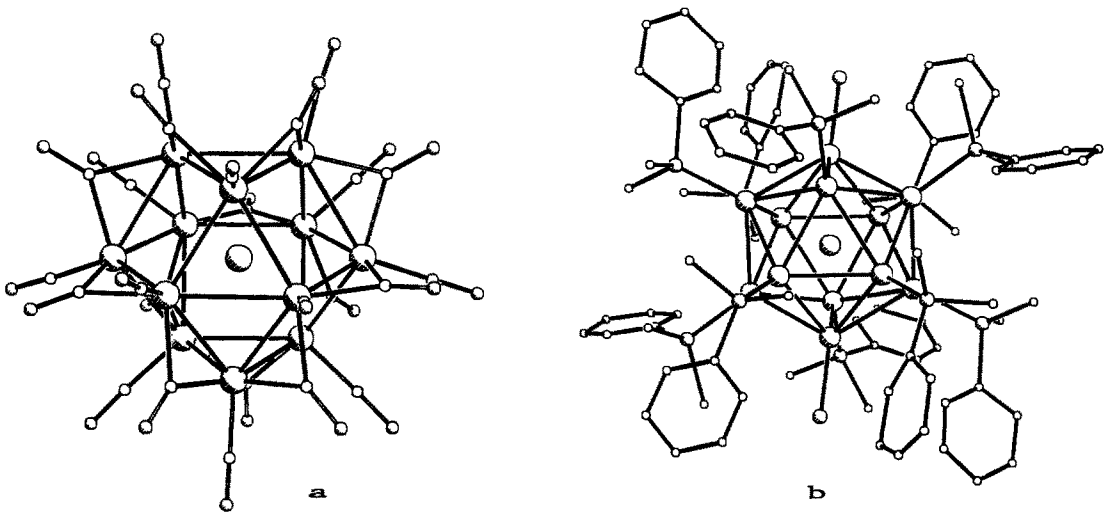

Fig. 1. Examples for 13 atom clusters. (a) An Rh_{13} cluster with hcp structure; (b) an icosahedral Au_{13} cluster.

when a supersaturated atmosphere of xenon gas was adiabatically expanded into a special mass spectrometer.[2] Besides many other xenon clusters those with the magic numbers 13, 55 and 147 showed maxima.

Ligand stabilized clusters with 13 metal atoms have been described in the literature years ago. Two are shown in Fig. 1. The Rh_{13} cluster[3] contains a hcp packed nucleus, but the Au_{13} cluster shows icosahedrally arranged gold atoms.[4] Obviously smaller clusters can exist in the five-fold symmetry, whereas clusters of higher nuclearity have never been observed with an icosahedral structure. An icosahedral packing of atoms of the same size has a lower density than ccp or hcp structures, and a hypothetical high nuclearity icosahedral cluster must collapse sometimes into the dense packed state.

The aim to generate naked clusters of a uniform size might be reached via ligand stabilized full-shell clusters whose ligand shell is subsequently peeled off.

RESULTS

The first two-shell clusters with 55 ccp metal atoms have been synthesized by us some years ago.[5-7] They are formed from simple transition metal complexes L_nMCl_x by reduction with diborane in organic solvents like benzene or tetrahydrofuran, if certain conditions are fulfilled. The most important condition is the choice of the appropriate ligand system. The two-shell clusters of the type $M_{55}L_{12}Cl_x$ ($M = Au$, Rh, $L = PPh_3$, $x = 6$; $M = Rh$, Ru, $L = P(t\text{-}Bu)_3$, $x = 20$; $M = Pt$, $L = As(t\text{-}Bu)_3$, $x = 20$; $M = Co$, $L = PMe_3$, $x = 20$) all contain 12 phosphine or arsine ligands which we believe to be coordinated to the 12 vertices of a cuboctahedron. The diameter of the ligands is so large that the ligand spheres just touch each other to form a good envelope. Gaps which are consequently formed between the ligand spheres are partially occupied by Cl atoms which originate from the starting complexes.

The molecular model in Fig. 2 elucidates the situation. A second important condition for a successful M_{55} cluster synthesis is connected with the use of diborane. B_2H_6 not only reduces the metal complexes, but also binds the excess of the arsine or phosphine ligands L as an adduct H_3B—L. Only if the concentration of L is small enough is there a

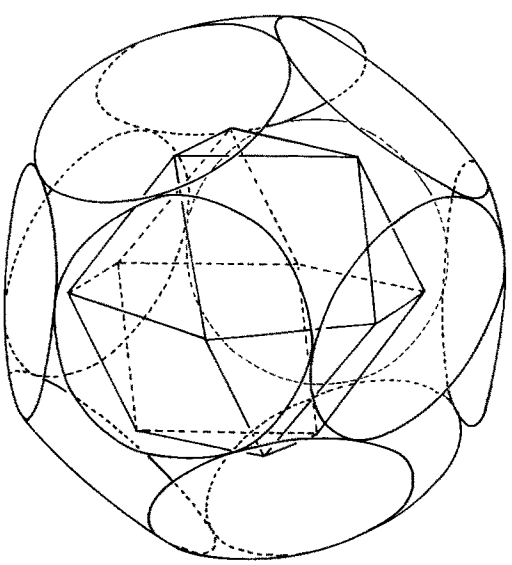

Fig. 2. Model of $Au_{55}(PPh_3)_{12}Cl_6$.

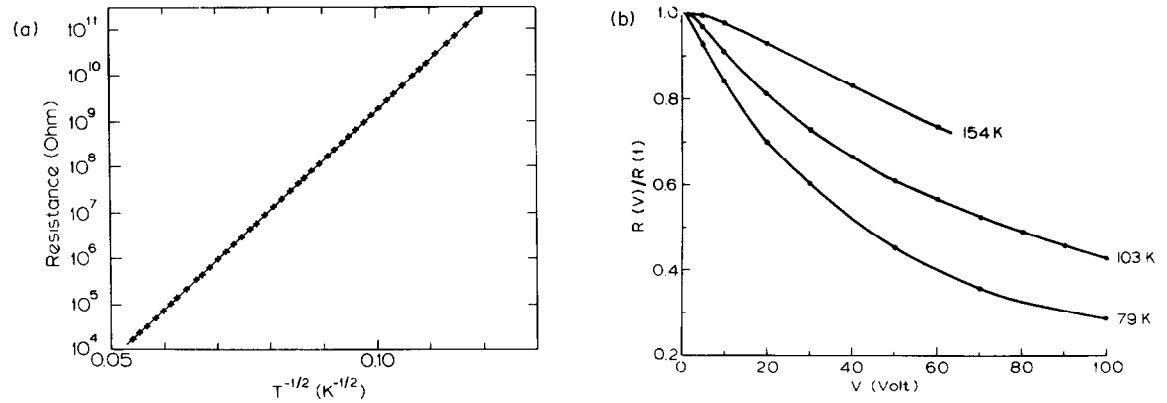

Fig. 3. (a) Logarithm of the resistance of an $Au_{55}(PPh_3)_{12}Cl_6$ pellet plotted against $T^{-1/2}$. (b) Normalized resistance of an $Au_{55}(PPh_3)_{12}Cl_6$ pellet as a function of voltage at different temperatures.

chance to yield large clusters. In the presence of a ligand excess only small clusters and complexes are formed. If one of the conditions mentioned here is not realized, the syntheses fail. The M_{55} clusters have been investigated extensively by NMR spectroscopy,[6,7] magnetic,[8] and conductivity measurements.[9] As an example, one result will be mentioned briefly.

Pellets of $M_{55}L_{12}Cl_x$ clusters can be regarded as a system consisting of very small metal particles in a dielectricum. As is known from similar systems, e.g. dispersed metals in ceramics, they should behave like semiconductors, and indeed they follow the law $R\exp(T_0/T)^{1/2}$ ($T_0 = 5.7 \times 10^4$ K).

The diagram in Fig. 3 shows the relation between the resistance of an $Au_{55}(PPh_3)_{12}Cl_6$ pellet and $T^{-1/2}$, leading to a straight line (a). (b) gives the relation between the normalized resistance and the voltage at different temperatures. The problem in question is how the electrons move from one metal particle to the next. The advantage of our cluster system, compared with ceramics for example, is the uniformity of the cluster size and the cluster distances.

Probably the most informative knowledge at present about structure and behaviour of large clusters comes from High Resolution Transmission Electron Microscopy (HRTEM).[10–14]

Figure 4 shows an image of a Pt_{55} cluster with ccp structure along the [110] direction, compared with the model. The high voltage used to yield that atomic resolution warms the sample up to an unknown temperature (estimated ~ 500°C). Under these conditions the ligand shell is lost and the clus-

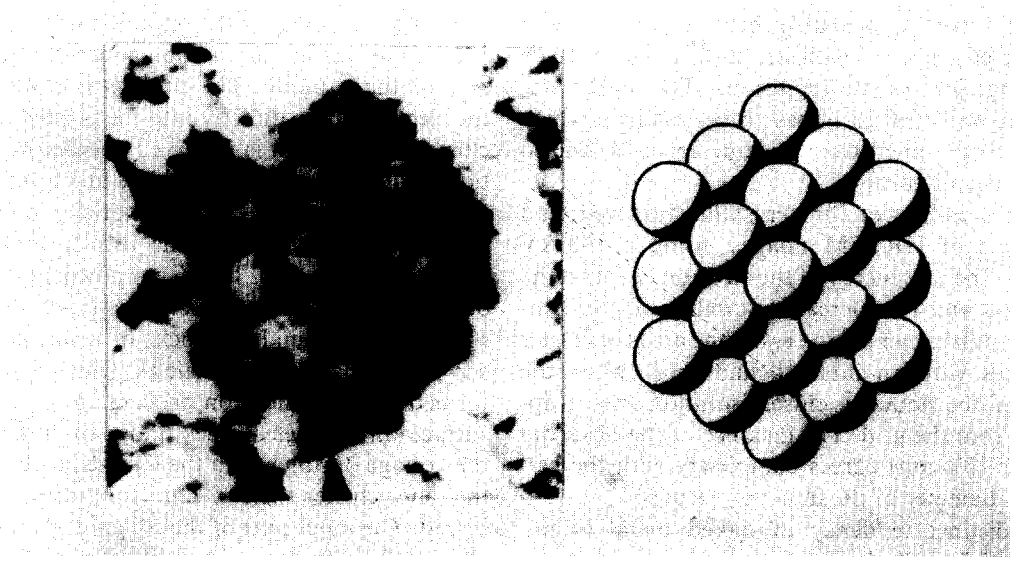

Fig. 4. HRTEM image and model of Pt_{55} in the [110] direction.

ter nuclei rearrange their structure very quickly. Therefore, the observation of ccp or hcp structures is accidental. Though the clusters are in a permanent motion, icosahedral structures can be observed only rarely. The conditions in the microscope lead to evaporation processes, and crystal growth as well as crystal degradation can be observed in atomic steps. M_{55} images have meanwhile been observed from Au_{55},[10] Pt_{55},[14] and Ru_{55}[15] clusters.

Earlier NMR investigations with different M_{55} clusters showed us the ligand shell in solution to be extremely fluxional, e.g. the contact time of PPh_3 with the metal surface in a dichloromethane solution of $Au_{55}(PPh_3)_{12}Cl_6$ is only 3 μs if additional PPh_3 is added. Due to that fluxionality, the ligands can easily be exchanged by others. For example, the mono *para*-sulphonated triphenylphosphane,[16] a water soluble compound, can substitute all the 12 PPh_3 ligands in $Au_{55}(PPh_3)_{12}Cl_6$.[17]

$$\underset{\text{in } CH_2Cl_2}{Au_{55}(PPh_3)_{12}Cl_6} + 12\underset{\text{in } H_2O}{Ph_2PC_6H_4SO_3Na} \rightarrow \underset{\text{in } H_2O}{Au_{55}(Ph_2PC_6H_4SO_3Na)_{12}Cl_6} + \underset{\text{in } CH_2Cl_2}{PPh_3}.$$

If $Au_{55}(PPh_3)_{12}Cl_6$, dissolved in dichloromethane, is treated with an aqueous solution of $Ph_2PC_6H_4SO_3Na$, the ligand exchange occurs quantitatively in a few hours, in the course of which the cluster moves from the organic into the water phase. This is an excellent method of creating water soluble clusters. In aqueous solution $Au_{55}(Ph_2PC_6H_4SO_3Na)_{12}Cl_6$ is completely dissociated into 12 Na^+ and the 12-fold negative anion $[Au_{55}(Ph_2C_6H_4SO_3)_{12}]^{12-}$. These solutions are highly stable compared with those of $Au_{55}(PPh_3)_{12}Cl_6$ in organic solvents, probably because of the high negative charge on the cluster surface, which leads to strong electrostatic repulsions. The higher stability in water raises hopes to get crystals which cannot be obtained from organic solvents, due to the fast decomposition.

The first indication for a crystallization we found by means of HRTEM images, using a 100 kV beam.[17] The low energy of the electron beam on the one hand and the increased stability of the compound on the other led to crystalline areas of cluster molecules with an intact ligand shell, when the water of the aqueous cluster solution was evaporated from the grid. The distance of the observed columns (2.1 nm) agrees completely with the calculated diameter of the intact molecules.

The distinct tendency of naked metal atoms to form full-shell clusters is impressively demonstrated by the synthesis of the giant cluster $Pd_{561}(phen)_{36}O_{190-200}$ in which, of course, the exact number of oxygen atoms is not determined, and also the idealized number of 561 Pd atoms for a five-shell cluster may deviate to a certain extent. However, as can be seen from the half-width of the lines in the X-ray spectra, the number of Pd atoms must be very close to 561, arranged in a ccp structure (diameter calculated in the [111] direction: 24.3 Å, found: 24.3 Å). A very similar compound with another ligand shell was described in 1985,[18] but the authors deduced an icosahedral structure from different measurements. Our Pd_{561} cluster is formed if palladium acetate is reduced by hydrogen in the presence of small amounts of phenanthroline (phen), followed by oxygenation with air. As the model in Fig. 5 shows, 36 phenanthroline ligands fit best with the cuboctahedral surface. There would be no place for one or two more phen groups. The isolation of that cluster occurs by ultracentrifugation from an aqueous solution. After the precipitation, the compound becomes insoluble in water. If the solid material is treated with acetic acid, propionic acid, pyridine or acetonitrile, it becomes soluble again. We believe that, due to a hydrophobic/hydrophobic interaction between the phenanthroline and the hydrophobic end of the polar molecules, their hydrophilic ends show outwards and enable the water solubility. This ligand-rich form of the cluster can be isolated by precipitation from solution. Centrifugation again slips the outer shell off. Using Cl_3CCOOH or F_3CCOOH the outlined effect fails as no hydrophobic/hydrophobic interaction is possible. In Fig. 6 these conditions are shown schematically.

The clusters $M_{55}L_{12}Cl_x$, dissolved in dichloromethane in a U-tube, show the phenomenon of electrophoresis[19] if platinum electrodes dip into water layers, covering the organic phase. Using 20 V d.c., the cluster colour soon concentrates on the side of the cathode. The process is reversible. If the electrodes dip directly into the cluster solution, cluster degradation is observed, leading to a solution of different metal complexes and a black metallic precipitate.[19] The solid material contains new metallic modifications of the investigated metals (Au, Rh, Ru, Pt, Co). The X-ray powder diffraction data clearly prove at least two types of superstructures, the building blocks of which consist of ccp-packed naked M_{13} particles. They are probably formed by a degradation process on the platinum surface on both electrodes under the influence of the voltage during which the ligands, together with the outer cluster shell of 42 metal atoms, are eliminated. The inner part of the original M_{55} cluster is generated as metastable, naked one-shell clusters M_{13}. They are long-lived enough to create the

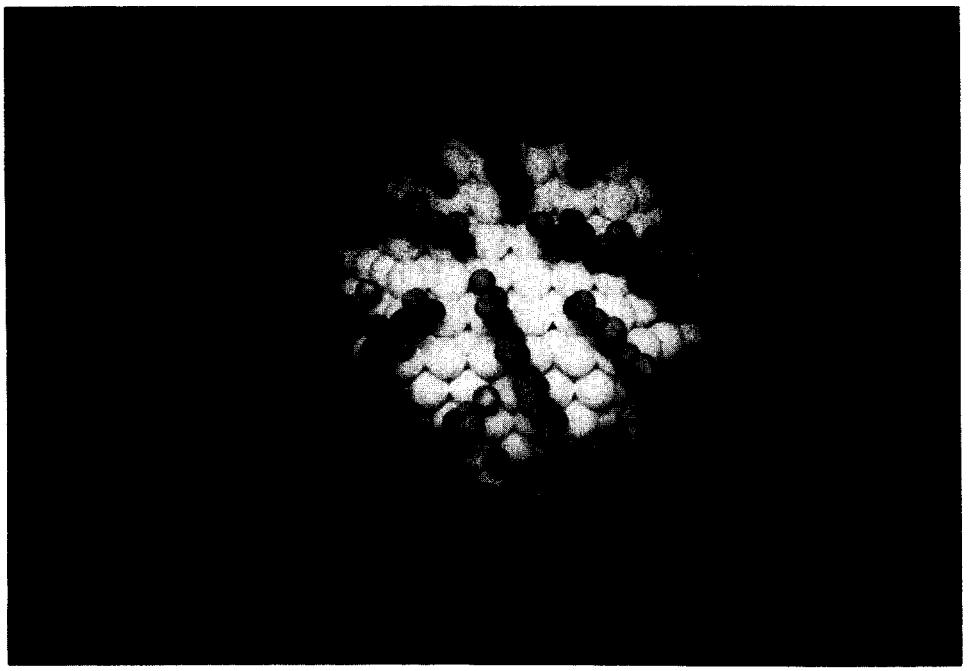

Fig. 5. Model of $Pd_{561}(phen)_{36}$.

observed novel structures. The M_{13} particles behave like individual molecules and aggregate to the first superstructure $(M_{13})_{13}$ as a kind of a "pseudo ccp structure" of M_{13} spheres. Not only M_{13} clusters aggregate via their triangle faces to $(M_{13})_{13}$, but these M_{169} superclusters again behave as building blocks to form a second superstructure $[(M_{13})_{13}]_n$ with $n \geqslant 13$. These very complicated events are best followed by studying Figs 7–10.

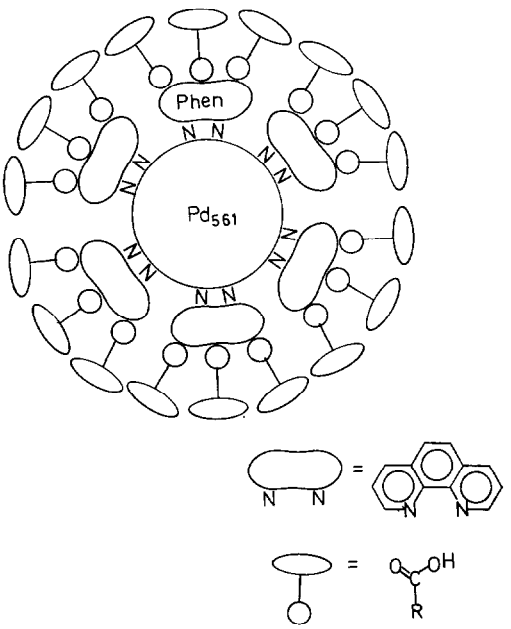

Fig. 6. Schematically drawn situation in $Pd_{561}(phen)_{36}O_{190-200}$ with a second ligand shell of a carbonic acid.

In Fig. 7 the degradation process is shown schematically without ligands. Figure 8 demonstrates the aggregation of the M_{13} clusters up to $(M_{13})_{13}$ via the triangle faces. The growth to larger particles $[(M_{13})_{13}]_n$ up to $n = 13$ is shown in Fig. 9. We believe that n is much larger than 13 because microcrystals, for example of the new gold modification, have diameters of a few nanometers. The series 10(a–d) shows $(M_{13})_{13}$ superclusters, viewed along different directions, to demonstrate the architecture of the superclusters in connection with the observed X-ray reflections. In Fig. 10(a) one of the 13 Ru_{13} ccp clusters is drawn dark to elucidate the structure characteristics. We look along the [111] direction of the marked Ru_{13} cluster and recognize that these rows are not only present in Ru_{13}, but also in the whole supercluster $(Ru_{13})_{13}$ (and of course also in $[(Ru_{13})_{13}]_n$). In Fig. 10(b) two neighbouring Ru_{13} clusters viewed along the [222] direction are darkened. A new periodicity of $3 \times d_{222}$ can be seen (grey shaded atoms). A $7 \times d_{331}$ periodicity is shown in Fig. 10(c), looking along the [331] direction of two Ru_{13} clusters.

Finally in Fig. 10(d), the very important $8 \times d_{200}$ periodicity is demonstrated, looking along the [200] direction of Ru_{13} clusters. This periodicity proves the diameter of 15.2 Å for an $(Ru_{13})_{13}$ cluster which serves again as a building block, otherwise the periodicity would not be explicable. The X-ray data

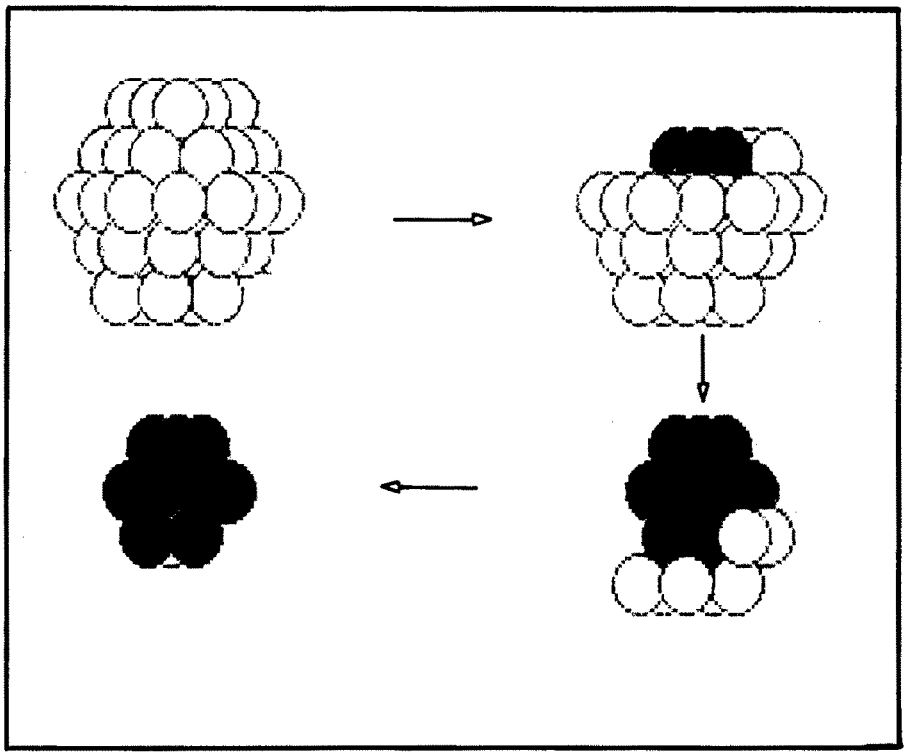

Fig. 7. Degradation of M_{55} to M_{13}. The ligands are omitted for clearness.

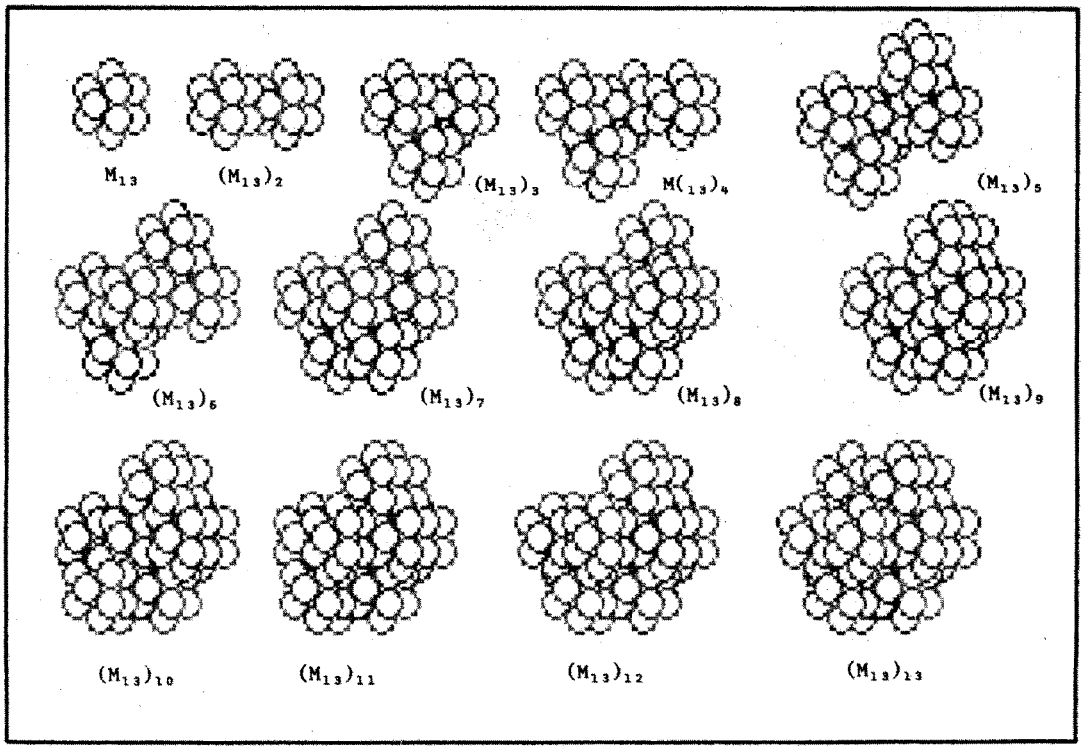

Fig. 8. Formation of an $(M_{13})_{13}$ super cluster from M_{13} clusters.

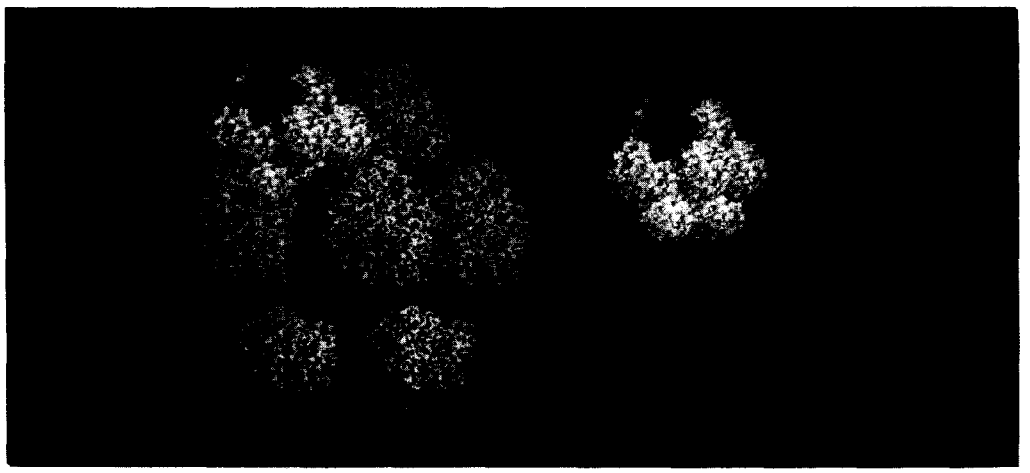

Fig. 9. Formation of an $[(M_{13})_{13}]_{13}$ particle from M_{13} clusters. From the right: an M_{13} cluster forms $(M_{13})_{13}$. Each light grey sphere symbolizes an M_{13} cluster. Thirteen of these $(M_{13})_{13}$ super clusters form the $[(M_{13})_{13}]_{13}$ particle (left). Each large dark grey sphere symbolizes an $(M_{13})_{13}$ building block.

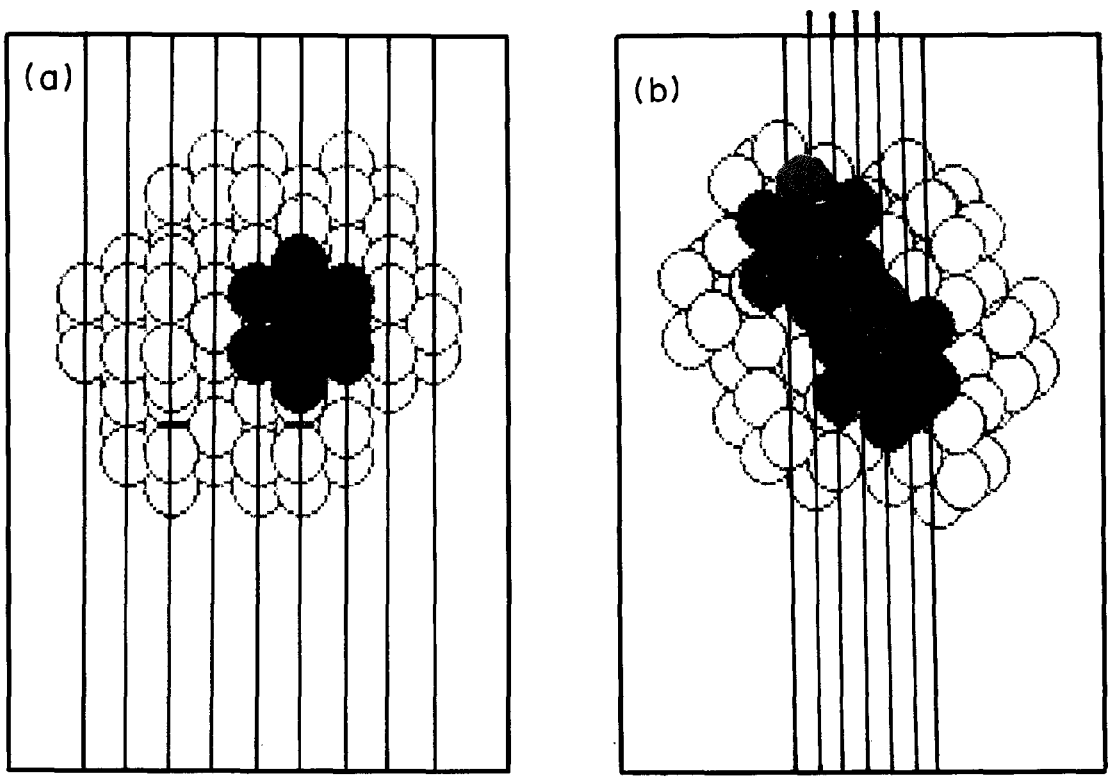

Fig. 10. Different views of an $(M_{13})_{13}$ particle. The data correspond here to M = Ru. (a) Viewed along the [111] direction of the ccp M_{13} clusters. One M_{13} cluster is drawn in black to elucidate the structure principle. X-ray data: $2\theta = 40.25°$, $d_{111} = 2.24$ Å, calculated: 2.196 Å. (b) Viewed along the [222] direction of the M_{13} clusters. The two grey shaded atoms show a new periodicity of the superstructure. It is $3 \times d_{222}$. X-ray data: $2\theta = 27.5°$, $d = 3.24$ Å, calculated: 3.294 Å. (c) Viewed along the [331] direction of the M_{13} clusters. Two M_{13} clusters are drawn in black. The grey shaded atoms show a new periodicity of the superstructure. It is $7 \times d_{331}$. X-ray data: $2\theta = 14.5°$, $d = 6.11$ Å, calculated: 6.108 Å. (d) Viewed along the [200] direction of the M_{13} clusters. A new periodicity is determined by the distance from the first (black) row to the last (black) row. It is $8 \times d_{200}$. X-ray data: $2\theta = 5.8°$, $d = 15.3$ Å, calculated: 15.216 Å.

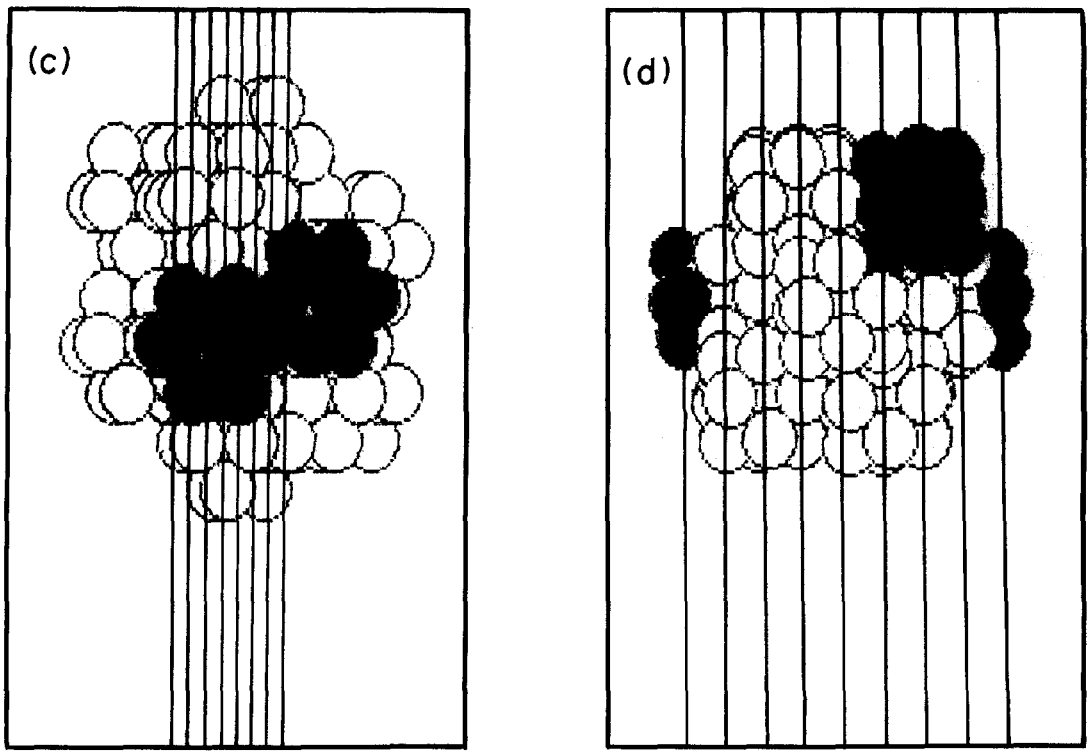

Fig. 10 (continued).

of all other metals prove corresponding structure principles as in the Ru case mentioned above. The Ru case is of special interest, as bulk Ru metal crystallizes in an hcp structure, whereas $[(Ru_{13})_{13}]_n$ consists of ccp Ru_{13} building blocks.

The $[(M_{13})_{13}]_n$ metals are highly sensitive to oxygen besides in the case of gold. Therefore, first investigations on the physical properties are carried out with $[(Au_{13})_{13}]_n$. Here we found that the new kind of gold gives rise to its own Mössbauer contribution.[20] The structure of $[(Au_{13})_{13}]_n$ is transferred into that of normal bulk gold at temperatures between 400 and 500°C. These investigations are just beginning and will be carried out extensively in the near future.

One disadvantage of all these metal samples should be mentioned. They are contaminated with normal metal particles which are also formed during the syntheses. We still do not have a method to avoid that. On the other hand, pure samples are required for many investigations of physical properties.

REFERENCES

1. For a survey of some new results, see: G. Schmid, *Nachr. Chem. Tech. Lab.* 1987, **34**, 249.
2. O. Echt, K. Sattler and E. Recknagel, *Phys. Rev. Lett.* 1981, **47**, 1121.
3. V. G. Albano, A. Ceriotti, P. Chini, G. Cioni, S. Martinengo and M. Anker, *J. Chem. Soc., Chem. Commun.* 1975, 859.
4. C. E. Briant, B. R. C. Theobald, J.-W. White, L. K. Bell, D. M. P. Mingos and A. J. Welch, *J. Chem. Soc., Chem. Commun.* 1981, 201.
5. G. Schmid, R. Pfeil, R. Boese, F. Bandermann, S. Meyer, G. H. M. Calis and J. W. A. van der Velden, *Chem. Ber.* 1981, **114**, 3634.
6. G. Schmid, U. Giebel, W. Huster and A. Schwenk, *Inorg. Chim. Acta* 1984, **85**, 97.
7. G. Schmid and W. Huster, *Z. Naturforsch.* 1986, **41b**, 1028.
8. L. J. de Jongh, NATO Advanced Research Workshop, 3–8 May 1987, Menorca, Spain.
9. M. P. J. van Staveren, H. B. Brom, L. J. de Jongh and G. Schmid, *Solid State Commun.* 1986, **60**, 319.
10. L. R. Wallenberg, J.-O. Bovin and G. Schmid, *Surface Sci.* 1985, **156**, 256.
11. A. K. Patford-Long, D. J. Smith, L. R. Wallenberg and J.-O. Bovin, *J. Cryst. Growth* 1987, **80**, 218.
12. J.-O. Bovin, L. R. Wallenberg and D. J. Smith, *Nature* 1985, **317**, 47.
13. L. R. Wallenberg, J.-O. Bovin and D. J. Smith, *Naturwissenschaften* 1985, **72**, 72.
14. L. R. Wallenberg, J.-O. Bovin, A. K. Petford-Long and D. J. Smith, *Ultramicroscopy* 1986, **20**, 71.
15. J.-O. Malm, J.-O. Bovin, A. Petford-Long, D. J. Smith, G. Schmid and N. Klein, *Angew. Chem.* 1988,

100, 580; J.-O. Malm, J.-O. Bovin, A. Petford-Long, D. J. Smith, G. Schmid and N. Klein, *Angew. Chem., Int. Ed. Engl.* 1988, **27**, 555.
16. European Patent No. 0163233, 1985, Ruhrchemie AG, Oberhausen.
17. G. Schmid, N. Klein, L. Korste, U. Kreibig and D. Schönauer, *Polyhedron* 1988, **7**, 605.
18. M. N. Vorgaftik, V. P. Zagorodnikov, I. P. Stolyarov, I. I. Moiseev, V. A. Likholobov, D. I. Kochubey, A. L. Churilin, V. I. Zaikovsky, K. I. Zamoraev and G. I. Timofeeva, *J. Chem. Soc., Chem. Commun.* 1985, 937.
19. G. Schmid and N. Klein, *Angew. Chem.* 1986, **98**, 910; *Angew. Chem., Int. Ed. Engl.* 1986, **25**, 922.
20. A. H. A. Smit, R. C. Theo and L. J. de Jongh, unpublished results.

Polyhedron Vol. 7, No. 22/23, pp. 2331–2339, 1988
Printed in Great Britain

0277–5387/88 $3.00+.00
© 1988 Pergamon Press plc

HALIDE PROMOTION OF THE FORMATION AND CARBONYLATION OF μ_3-IMIDO LIGANDS. RELEVANCE TO THE HALIDE PROMOTION OF NITROAROMATIC CARBONYLATION CATALYSIS

SUNG HWAN HAN and GREGORY L. GEOFFROY*

Department of Chemistry, The Pennsylvania State University, University Park, PA 16802, U.S.A.

Abstract—The individual reaction steps that are believed to occur during the catalytic carbonylation of nitroaromatics to form isocyanates, carbamates, amines, and ureas are reviewed with focus on stoichiometric organometallic reactions that model the proposed reaction steps. Especially emphasized are recent studies that show how halides dramatically promote both the formation and carbonylation of imido ligands. These results provide insight into the role that halides play in the known halide promoted $Ru_3(CO)_{12}$ catalytic system for the formation of methyl *N*-phenylcarbamate from nitrobenzene, CO, and methanol [S. Cenini *et al.*, *J. Chem. Soc., Chem. Commun.* 1984, 1286].

Imido ligands (NR, nitrenes) attached to late transition metals are suggested intermediates in a number of catalytic reactions involving the carbonylation of nitroaromatics to form a variety of other products (Scheme 1).[1,2]

Such reactions are known to be catalysed by both homogeneous and heterogeneous catalysts, but to our knowledge none have been commercialized, presumably because of poor catalyst selectivities and/or efficiencies. Direct formation of isocyanates from the relatively inexpensive nitro compounds is a potentially important reaction as it avoids the present use of toxic phosgene to prepare these versatile industrial intermediates. Also, important products which now derive by addition of alcohols to preformed isocyanates are carbamates (urethanes) which find pesticide applications. However, isocyanates can be hazardous intermediates, and direct routes to carbamates which avoid their intermediacy would be highly desirable.

Although there has been a good deal of speculation, relatively little is known about the actual mechanisms of catalytic nitroaromatic carbonylation reactions. However, most mechanistic hypotheses have invoked imido ligands at some stage in the process,[1] in part because they are known to readily derive from nitroaromatics (see below).[3] Scheme 2 presents a hypothetical reaction sequence for the formation of imido ligands via the stepwise deoxygenation of nitrobenzene, and Schemes 3–5 outline ways in which these ligands can then be transformed into amines, isocyanates, ureas, and carbamates.

The imido ligand has proven to be a highly flexible species, coordinating to both electron-rich and electron-poor metals in a variety of coordination modes as illustrated in I–V.[4] It is generally known that coordination modes I and II are associated with electron poor, "early" transition metals whereas only modes IV and V[4c] have been seen with the more electron-rich "late" transition metals of the type which efficiently catalyse nitroaromatic carbonylations.[4] However, even though stable Group VIII metal imido complexes have these ligands attached as in IV and V, catalytically significant intermediates could possess the more reactive mononuclear and dinuclear coordination modes I–III.

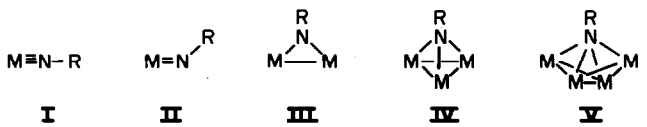

I II III IV V

* Author to whom correspondence should be addressed.

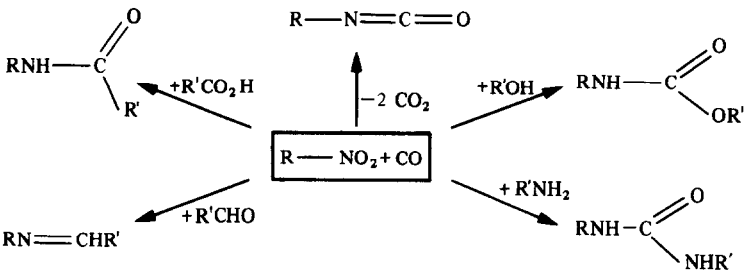

Scheme 1.

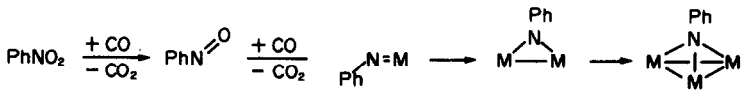

Scheme 2.

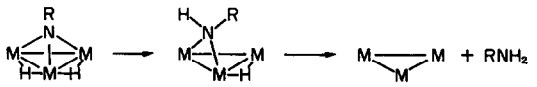

Scheme 3.

One effective way to more thoroughly understand the mechanism of a catalytic system as complex as nitroaromatic carbonylation is by conducting modeling studies using discreet organometallic complexes to test the feasibility of the proposed reaction steps. A few such studies related to this catalysis have been conducted, and the purpose of this article is to review that work, with emphasis on our own research directed at unraveling the reasons for the known promoting effect of halides in this chemistry. This effect is best illustrated by the work of Cenini who showed that halides markedly improve both the selectivity and activity of the $Ru_3(CO)_{12}$ catalytic system for producing carbamates, eq. (1).[1a,h] Chloride ion was a substantially better promoter than bromide or iodide, and under comparable reaction conditions, its presence resulted in an increase in conversion from 36 to 100% and an increase in selectivity for the carbamate from 22.2 to 92.7% over that obtained in its absence.[1a,h]

$$PhNO_2 + CO + CH_3OH \xrightarrow[\substack{[NEt_4]Cl \\ 160\text{–}170^\circ C \\ 82\,atm.}]{Ru_3(CO)_{12}} PhN(H)-C(=O)-OCH_3 \;(92.7\%) \; + PhNH_2 \;(6.5\%) \qquad (1)$$

Eq. (1)

The following paragraphs summarize progress which has been made in modeling the individual reaction steps proposed in Schemes 2–5. We have not attempted to be completely comprehensive, but have tried to cite the most important contributions

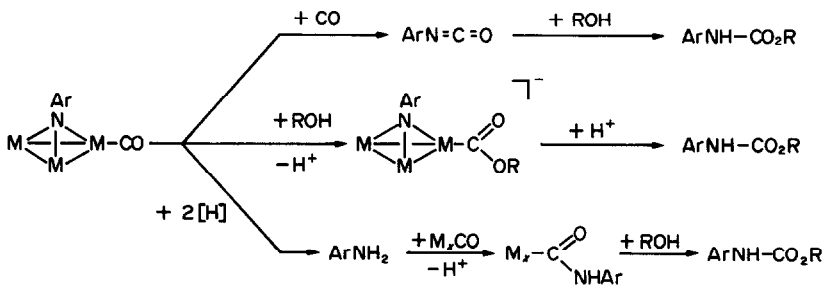

Scheme 4.

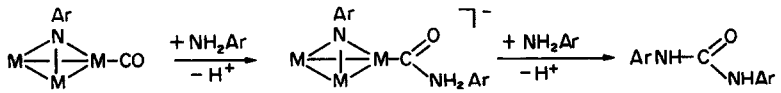

Scheme 5.

in these areas. Details of our own studies have been published elsewhere,[5,6] and this article reviews those results.

MODELING STUDIES

Formation of imido ligands from nitroaromatics

As illustrated by the example in eq. (2),[3a] this is a well-documented reaction, although the yields of the imido products are typically low. In addition to the formation of the Ru_3 imido clusters illustrated in eq. (2),[3] the Fe_3 imido cluster $Fe_3(\mu_3\text{-NPh})_2(CO)_9$ is known to form from the reaction of $Fe_3(CO)_{12}$ with $PhNO_2$.[1c,7] Similarly, the monoimido cluster $[HFe_3(\mu_3\text{-NPh})(CO)_9]^-$ has been reported to form in low yield upon reaction of $[HFe_3(CO)_{11}]^-$ with $PhNO_2$.[1e]

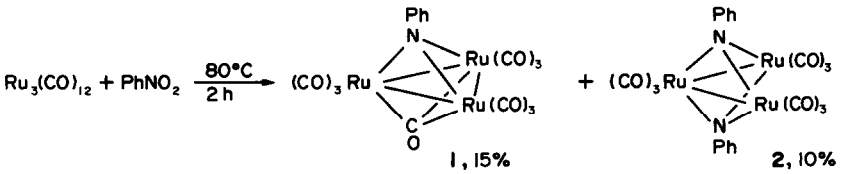

Eq. (2)

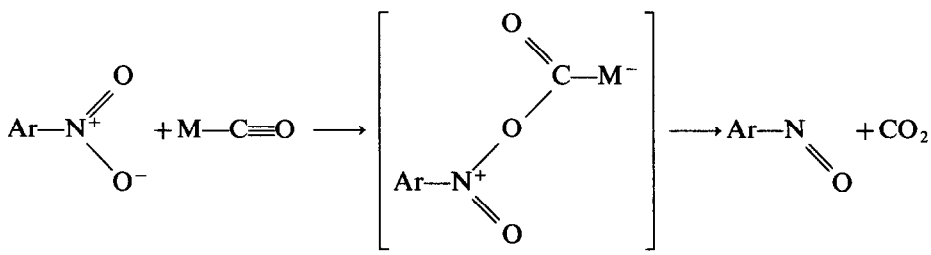

Eq. (3)

Although speculative mechanisms have been presented to explain the reduction of nitroaromatics to imido ligands,[1c,3a] nothing is really known about how this reaction occurs. It is likely that it proceeds via the stepwise deoxygenation of the nitroaromatic to first form a nitroso reagent which then undergoes further deoxygenation to yield the imido ligand (Scheme 2). This assumption is supported by the greatly increased yields of clusters with imido ligands when nitrosoaromatics are used as synthetic reagents (see below). The nitro to nitroso conversion may proceed via nucleophilic attack of the nitroaromatic on a metal carbonyl oxygen, as illustrated in eq. (3). However, this has never been directly proven and is a reaction sequence clearly in need of further study. Nitroaromatics are in general poor nucleophiles, a fact which probably accounts for the relatively low yields of imido clusters in synthetic reactions and the forcing conditions generally needed in the catalytic transformations of nitroaromatics.

In our studies of the effect of halides in nitroaromatic carbonylation, we briefly examined the effect of halide ions on the synthetic reaction of eq. (2) but observed no improvement in yield nor increase in rate.

Formation of imido ligands from nitrosoaromatics

As illustrated in Scheme 2, the formation of imido ligands from nitroaromatics likely proceeds via a stepwise deoxygenation sequence to first form nitrosoaromatics, either coordinated or free. Indeed, Gladfelter has recently shown that imido clusters readily derive from nitrosoaromatics in good to excellent yields, eq. (4).[8] The reaction tolerates a

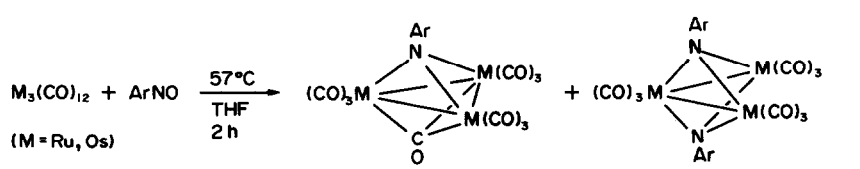

Eq. (4)

diversity of aromatic substituents, and under the conditions given in eq. (4), a 46% yield of **1** (M = Ru, Ar = Ph) was obtained compared to the 15% yield of eq. (2). This reaction was also used to prepare the Os_3 analogs of **1** and **2**, which cannot be prepared by the reaction of nitroaromatics with $Os_3(CO)_{12}$.[8] Interestingly, reaction of PhNO with $Fe_3(CO)_{12}$ gave only trace amounts of $Fe_3(\mu_3\text{-}NPh)_2(CO)_9$,[8] in contrast to the known routes to this product using $PhNO_2$.[1c,3]

We have found that halides significantly promote the formation of imido ligands from nitrosobenzene. As noted in eq. (4), the unpromoted reaction between $Ru_3(CO)_{12}$ and PhNO proceeds slowly at 57°C to give **1** in modest yield.[8] However, in the presence of one equivalent of halide, the reaction occurs *within minutes at 22°C* to give the halide substituted imido clusters **3a–c** in near quantitative yield, eq. (5).[6] Each of these anionic clusters was

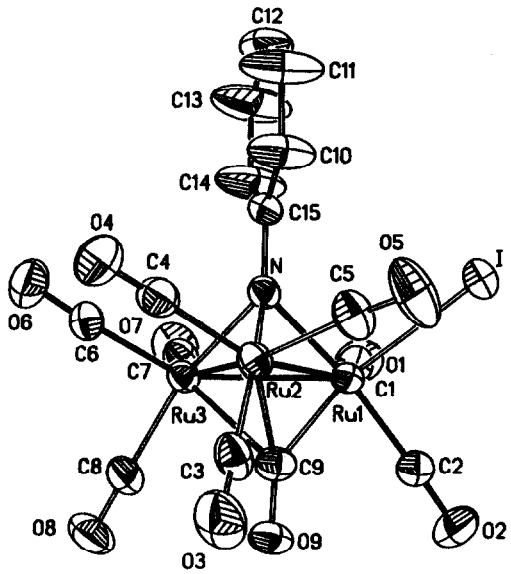

Fig. 1.

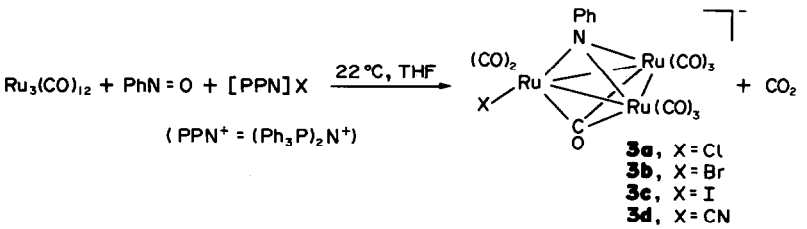

(5)

Eq. (5)

isolated as its PPN^+ salt in high yield, and all were spectroscopically characterized.[6] In addition, cluster **3c** as its $[Na(18\text{-crown-6})]^+$ salt was crystallographically characterized (Fig. 1).[6] Halides are known to react with $Ru_3(CO)_{12}$ to rapidly form the substituted clusters $[Ru_3(\mu_2\text{-}X)(CO)_{10}]^-$, **4a–c**,[9] and we have found that these species in turn react with PhN=O to form **3a–c** with the half-lives given in eq. (6). Note that chloride is superior to iodide as a promoter, exactly as observed by Cenini in his catalytic studies of reaction (1).[1a]

Halides have been demonstrated to be effective promoters for ligand substitution reactions of $Ru_3(CO)_{12}$, and although the mechanism has not been firmly established, clusters **4a–c** may be intermediates in this process.[9] Since the nitrosobenzene to imido conversion likely proceeds via deoxygenation of a *coordinated* PhN=O ligand, we suggest that the halide promotion of the PhN=O reaction is simply a consequence of the halide promotion of substitution of PhN=O for CO. Note that the relative halide promoting ability of the ligand substitution reaction as found by Kaesz[9a] is exactly the same as that observed for reaction (6): $Cl^- > I^-$. Furthermore, we have found that PhN=O reacts within seconds with $Ru_3(CO)_{11}(CH_3CN)$[10] at 22°C to form $Ru_3(\mu_3\text{-}NPh)(CO)_{10}$ in good yield, eq. (7).

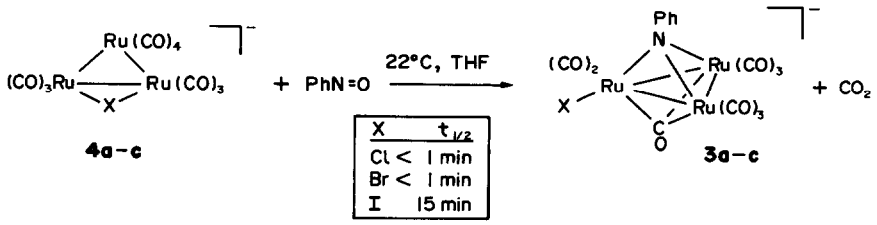

(6)

Eq. (6)

$$Ru_3(CO)_{12} + CH_3CN \xrightarrow[-CO_2,\ -Me_3N]{+Me_3NO} Ru_3(CO)_{11}(CH_3CN) \xrightarrow[-CO_2,\ -CH_3CN]{+PhNO} Ru_3(\mu_3\text{-}NPh)(CO)_{10} \quad (7)$$

1, 51%

Eq. (7)

These various results indicate that the rate-limiting step in the reaction of PhNO with $Ru_3(CO)_{12}$ to form $Ru_3(\mu_3\text{-NPh})(CO)_{10}$ is loss of CO and coordination of the nitroso reagent. Halides apparently promote this process by promoting the ligand substitution reaction. We thus suggest the reaction sequence shown in eq. (8), with the nitroso reagent

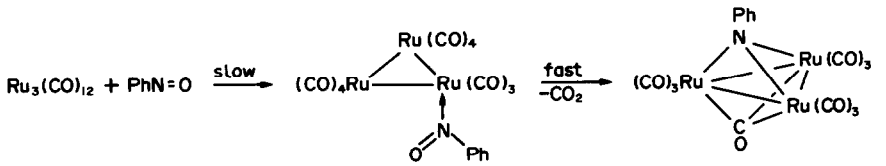

(8)

Eq. (8)

bound to a single Ru atom via the lone pair of electrons on the nitrogen atom. This is a well-established coordination mode for nitroso ligands, as indicated by the molecular structure of $(CO)_5W(Bu^tN{=}O)$ shown in Fig. 2.[11] Exactly how the PhN=O deoxygenation proceeds is not known, but a metathesis-like reaction as illustrated in eq. (9) seems likely.

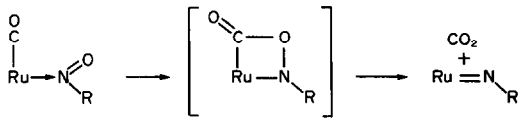

(9)

Eq. (9)

We have recently extended the methodology of eq. (7) to improve the yield of $Os_3(\mu_3\text{-NPh})(CO)_{10}$ to 40% from the 5% yield reported in Ref. 8 and have also prepared heteronuclear FeRu clusters by this route, eqs (10) and (11).[12] This appears to be a general method for introducing imido ligands into metal clusters, and we are currently trying to extend these syntheses to other heteronuclear species and to the Co, Rh and Ir carbonyls.

Stepwise hydrogenation of imido ligands to form amines

Carbonylation of nitroaromatics in the presence of a hydrogen source often leads to the formation of aromatic amines, as illustrated by Calderazzo's catalytic reaction of eq. (12).[1d]

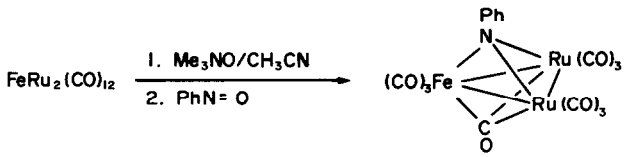

(35%) (10)

Eq. (10)

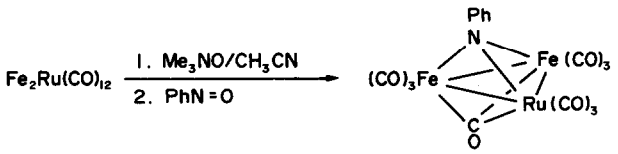

(34%) (11)

Eq. (11)

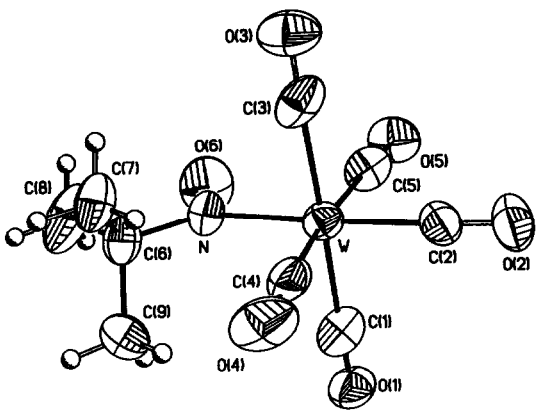

Fig. 2.

$$PhNO_2 + CO/H_2 \xrightarrow[1:1]{Ru_3(CO)_{12},\ 160^\circ C,\ 200\ atm.,\ 6\ h} PhNH_2 + CO_2. \quad (\sim 266\ turnovers/Ru) \qquad (12)$$

Eq. (12)

Diphenylurea is also produced at lower H_2 partial pressures. Aniline has similarly been prepared from $PhNO_2$ using basic $Fe_3(CO)_{12}$ solutions in which the active reducing agent is apparently $[HFe_3(CO)_{11}]^-$.[1c,7] Cluster bound μ_3-NPh ligands have been invoked as key intermediates in both the Ru_3[1d] and Fe_3[1e] chemistry.

This overall reaction has been effectively modeled by Bhaduri and coworkers who demonstrated the

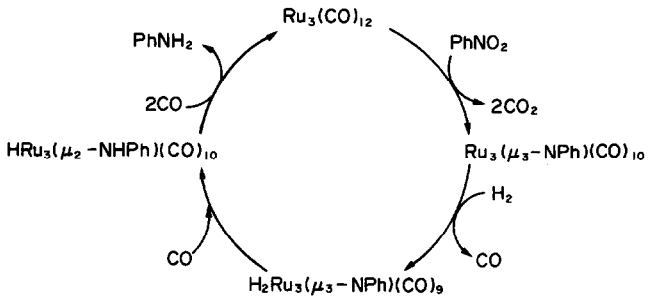

Scheme 6.

reactions shown in eq. (13) and who invoked the overall catalytic cycle shown in Scheme 6, with all the reaction steps now based on known transformations.[1g] The carbonylation of cluster **5** likely proceeds via initial formation of the known amido-hydride cluster **6**, eq. (14),[3a] which then further carbonylates to form the aniline product. The first step in reaction (14) has been firmly established by Vahrenkamp's demonstration that this exact reaction readily occurs when the benzylimido analog of **5** is heated to 135°C under 1 atm CO.[13] in THF solution to give PhN=C=O and $Ru(CO)_5$ under 170 atm of CO at 120°C,[14] although we observed no reaction when lower CO pressures (4 atm, 120°C, 22 h) were used. However, a recent report by Bhaduri and coworkers showed that these carbonylations are markedly solvent dependent and that both **1** and $Ru_3(\mu\text{-NPh})_2(CO)_9$ form PhN=C=O and $Ru_3(CO)_{12}$ when heated at 140°C under 20 atm of CO in CH_3CN solutions.

We have found that addition of one equivalent of halide to THF *solutions of* **1** *dramatically promotes*

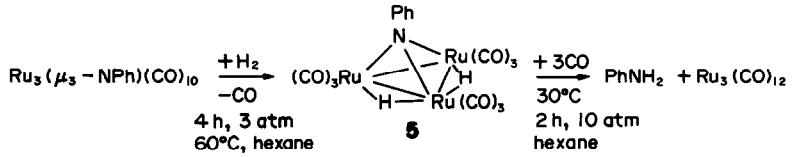

(13)

Eq. (13)

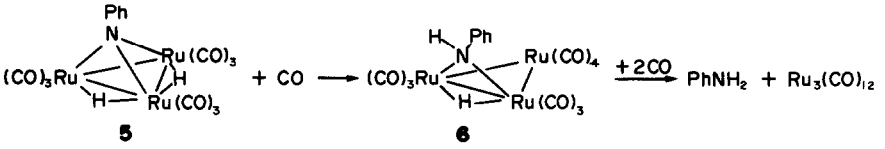

(14)

Eq. (14)

Carbonylation of μ_3-imido ligands to form isocyanates

As Scheme 4 illustrates, isocyanates should readily form by carbonylation of imido ligands. However, this has proven to be a particularly difficult reaction to accomplish, unless promoters are present (see below). The resistance of imido clusters to carbonylation is particularly well illustrated by our high yield recovery of $M_3(\mu_3\text{-NPh})_2(CO)_9$ (M = Fe, Ru) following attempted carbonylation at 120 atm, 150°C for 22 h in THF solution.[5,6] The mono(imido) cluster $Ru_3(\mu_3\text{-NPh})(CO)_{10}$ (**1**) is a bit more reactive, and Gladfelter has shown that it slowly (6.5 h) carbonylates *the carbonylation such that it proceeds rapidly and under far milder conditions (22°C, 1 atm* CO) *than those noted above*. The products of this reaction are PhN=C=O and the known halide-bridged clusters **4a–c** (Scheme 7).[9] IR spectral changes showed that the halide promotion proceeds via the near instantaneous formation of the substituted cluster anions **3a–c**. These can be isolated in high yield from the direct reaction of **1** with halides *in the absence of* CO, and they in turn react with CO to give the observed products. The half-life data given in Scheme 7 show that chloride is clearly the superior promoter, exactly paralleling the promoting order seen in Cenini's catalytic reaction summarized in eq. (1).[1a]

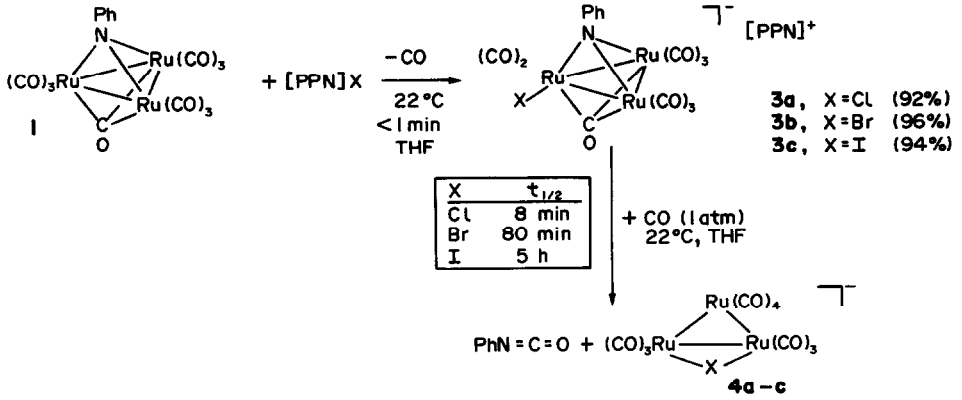

Scheme 7.

Why are halides such effective promoters of the imido carbonylation? The determined crystal structure of **3c** (Fig. 1), gives no insight into why the presence of the halide activates the cluster for this reaction. Indeed, the only notable structural consequence of the halide substitution is a movement of the μ_3-CO ligand closer to Ru(1) and away from Ru(2), but there is little change in Ru—Ru and Ru—N distances as compared to **1**.[3b] However, it is clear that halides must somehow weaken the Ru—N bonds so as to allow the carbonylation to proceed. The observed halide promotion may be a consequence of the increased electron density on the cluster as a result of the halide substitution. This should weaken the N→Ru dative interaction, thereby facilitating the carbonylation. Arguing against this explanation is the observation that cluster **3d** with X = CN^- does not undergo carbonylation under these relatively mild conditions,[6] even though the cluster charge is the same as when X = Cl^-.

We suggest that halides facilitate the carbonylation reaction by assuming a bridging position and displacing a N→Ru bond to form a *di*bridging imido ligand which then undergoes nucleophilic attack on a coordinated CO, eq. (15). Note that there is no change in cluster electron count in the **VI** → **VII** → **VIII** conversion, and these three species may actually be in equilibrium. In support of this suggestion we note that $H_2Os_3(\mu$-RNCO)$(CO)_8(PMe_2Ph)$ (R = Bu^{t}CH=N) has an isocyanate ligand bonded exactly as depicted in **VIII**, and furthermore this latter species was suggested to derive by *reversible* attack of a transient μ_2-imido on a coordinated CO as in the **VII** to **VIII** conversion.[16] Further support for the mechanistic suggestion of eq. (15) comes from our observation

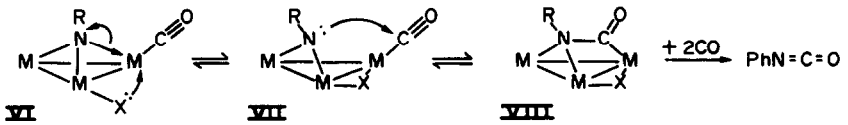

(15)

Eq. (15)

than the CN^- analog of **3** does not readily carbonylate. This may be attributed to the fact that CN^- is not a good bridging ligand and thus is not effective at displacing a PhN→Ru bond.

Formation of carbamates via alkoxycarbonyl intermediates

As illustrated in Scheme 4, the carbamate products of nitroaromatic carbonylation could form via addition of alcohols to isocyanate intermediates, the latter formed by carbonylation of imido ligands. However, as originally suggested by Alper[1b] and illustrated in Scheme 4, carbamates may also form by alkoxide attack on a carbonyl to form an alkoxycarbonyl species which then couples with an imido ligand followed by protonation to yield the carbamate product. Alkoxides are well known to form such alkoxycarbonyl ligands by this reaction with $Ru_3(CO)_{12}$,[17] but stable alkoxycarbonyl compounds do not form with $Fe_3(CO)_{12}$ which was used in Alper's catalysis.[17b] However, we recently showed that a stable methoxycarbonyl cluster **7** results from addition of MeO^- to the imido cluster $Fe_3(\mu_3$-NPh$)_2(CO)_9$, eq. (16).[5] This species was isolated as a red solid and was spectroscopically characterized. As illustrated in eq. (16), methyl *N*-phenylcar-

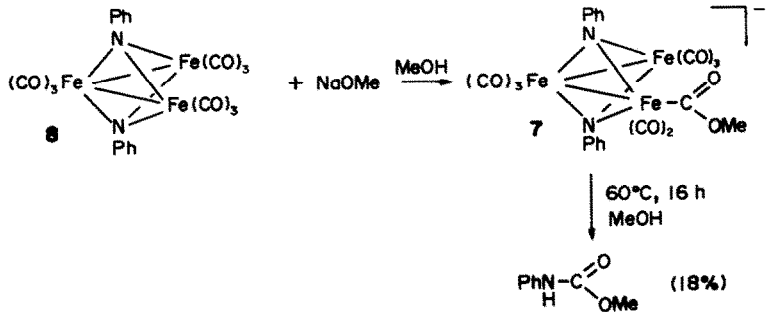

(16)

Eq. (16)

bamate formed when the methoxycarbonyl cluster **7** was heated in methanol solution, although the isolated yield was low. Air- or $[Cp_2Fe]^+$-induced oxidation of methanol solutions of **7** also gave the carbamate, with a significantly higher yield (61%) when $[Cp_2Fe]^+$ was employed.

Methyl *N*-phenylcarbamate also formed in good yield when cluster **8** was subjected to conditions identical to those used by Alper and coworkers[1b] in the $Fe_3(CO)_{12}$ catalysed carbonylation of $PhNO_2$ to produce the carbamate, eq. (17).[5]

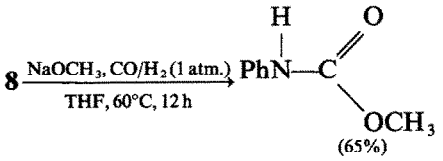

(17)

Eq. (17)

initially generated ureas, as this is a well-established organic transformation.

Formation of ureas by carbamoyl–imido coupling

Ureas are also known to be products of nitroaromatic carbonylation catalysis, and they can form either by addition of amines to isocyanate intermediates, or by a process similar to that discussed above involving formation of a carbamoyl ligand by amine attack on a coordinated CO and then carbamoyl–imido coupling, eq. (18). Although amines are well known to attack metal carbonyls to form carbamoyl ligands, the specific reactions outlined in eq. (18) have never been studied. We did observe that $Fe_3(\mu_3\text{-NPh})_2(CO)_9$, **8**, slowly decomposes over a period of weeks at 22°C or within 5–6 h at 65°C in degassed or N_2 saturated THF solu-

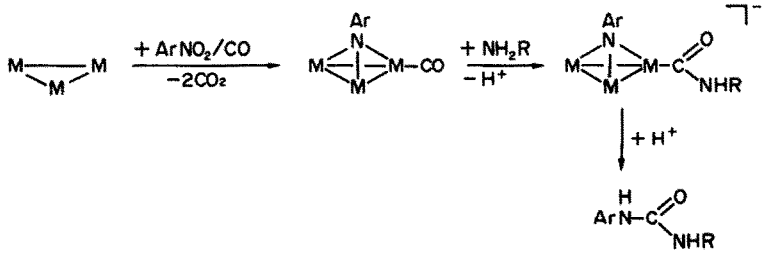

(18)

Eq. (18)

This reaction likely proceeds via the *in situ* formation of methoxycarbonyl cluster **7**, followed by imido–methoxycarbonyl coupling.

The above results show that carbamates can form via coupling of *in situ* generated alkoxycarbonyl and imido ligands and that such a process must be considered as a viable alternative to the addition of alcohol to isocyanate intermediates, the latter formed by carbonylation of imido ligands. As indicated in Scheme 4, carbamates can conceivably form via carbamoyl intermediates. However, there have been no reported attempts to model this chemistry and the facility of these reactions is unknown. Carbamates may also form via alcoholysis of

tions to form diphenylurea in low yield.[5] The yield of diphenylurea increased to 25% upon the addition of 2 equiv. of aniline to the refluxing solutions of **8** while addition of *p*-toluidine gave diphenylurea (7%), tolylphenylurea (17%) and ditolylurea (1%). A control experiment in which *p*-toluidine and diphenylurea were combined in refluxing THF for 12 h in the *absence* of iron containing organometallics showed that diphenylurea did not convert into tolylphenylurea under these conditions. When a mixture of **8** and **8**-d_{10} were refluxed in THF, the isolated diphenylurea consisted of 35% PhNHC{O}NHPh-d_0, 37% PhNHC{O}NHPh-d_5 and 29% PhNHC{O}NHPh-d_{10}, indicating that the

formation of diphenylurea from **8** occurs largely by an *intermolecular* path.

SUMMARY

As the above discussion illustrates, significant progress has been made in modeling many of the reaction steps that are believed to be important in nitroaromatic carbonylation catalysis. Particularly well modeled is the catalytic reduction of $PhNO_2$ to $PhNH_2$ using CO/H_2 and $Ru_3(CO)_{12}$ as catalyst[1d] where all the essential reaction steps have been individually observed (Scheme 6).[1g] Our own research has focussed on trying to understand the reasons why halides promote the formation of carbamates from nitroaromatics,[1a] and as detailed above, we have found that halides significantly promote both the formation of imido ligands from nitrosobenzene and their carbonylation to form isocyanates. Halides appear to promote the former reaction by accelerating the rate at which PhNO substitutes for CO on $Ru_3(CO)_{12}$, and a proposal has been presented in eq. (15) to rationalize the observed halide promotion of the imido carbonylation reaction. However, this latter process needs to be further investigated to develop a more complete understanding of the role of halide. Such studies are currently in progress.

Acknowledgements—The Office of Basic Energy Sciences of the Department of Energy is gratefully acknowledged for supporting this research. We also thank Prof. A. L. Rheingold of the University of Delaware for determining the crystal structures shown in Figs 1 and 2.

REFERENCES

1. (a) S. Cenini, M. Pizzotti, C. Crotti, F. Porta and G. La Monica, *J. Chem. Soc., Chem. Commun.* 1984, 1286; (b) H. Alper and K. E. Hashem, *J. Am. Chem. Soc.* 1981, **103**, 6514; (c) H. des Abbayes and H. Alper, *J. Am. Chem. Soc.* 1977, **99**, 98; (d) F. L'Eplattenier, P. Matthys and F. Calderazzo, *Inorg. Chem.* 1970, **9**, 342; (e) M. A. Andrews and H. D. Kaesz, *J. Am. Chem. Soc.* 1979, **101**, 7254; (f) Z. Dawoodi, M. J. Mays and K. Henrick, *J. Chem. Soc., Dalton Trans.* 1984, 433; (g) S. Bhaduri, K. S. Gopalkrishnan, W. Clegg, P. G. Jones, G. M. Sheldrick and D. Stalke, *J. Chem. Soc., Dalton Trans.* 1984, 1765; (h) S. Cenini, C. Crotti, M. Pizzotti and F. Porta, *J. Org. Chem.* 1988, **53**, 1243.
2. (a) E. Alessio and G. Mestroni, *J. Organomet. Chem.* 1985, **291**, 117; (b) H. A. Dieck, R. M. Laine and R. F. Heck, *J. Org. Chem.* 1975, **40**, 2819; (c) M. Yamashita, K. Mizushima, Y. Watanabe, T. Mitsudo and Y. Takegami, *J. Chem. Soc., Chem. Commun.* 1976, 670; (d) B. K. Nefedov and V. I. Manov-Yuvenskii, *Izv. Akad. Nauk SSSR, Ser. Khim.* 1977, **11**, 2597; (e) B. K. Nefedov, V. I. Manov-Yuvenskii, Kh. O. Koshdurdyev and S. S. Novikov, *Dokl. Akad. Nauk SSSR* 1977, **232**, 1088; (f) B. K. Nefedov, V. I. Manov-Yuvenskii and S. S. Novikov, *Dokl. Akad. Nauk SSSR* 1977, **234**, 1343; (g) B. Elleuch, Y. B. Taarit, J. M. Basset and J. Kervennal, *Angew. Chem., Int. Ed. Engl.* 1982, **21**, 687; (g) F. J. Weigert, *J. Org. Chem.* 1973, **38**, 1316; (h) W. B. Hardy and R. P. Bennett, *Tetrahedron Lett.* 1967, 961; (i) K. Unverferth, R. Hontsch and K. Schwetlick, *J. Prakt. Chem.* 1978, **321**, 928; (j) P. Braunstein, R. Bender and J. Kervennal, *Organometallics* 1982, **1**, 1236 and references therein; (k) P. Braunstein, J. Kervennal and J.-L. Richert, *Angew. Chem., Int. Ed. Engl.* 1985, **24**, 768; (l) A. F. M. Iqbal, *J. Org. Chem.* 1972, **37**, 2791; (m) Y. Watanabe, Y. Tsuji, T. Kondo and R. Takeuchin, *J. Org. Chem.* 1984, **49**, 4451.
3. (a) E. Sappa and L. Milone, *J. Organomet. Chem.* 1973, **61**, 383; (b) S. Bhaduri, K. S. Gopalkrishnan, G. M. Sheldrick, W. Clegg and D. Stalke, *J. Chem. Soc., Dalton Trans.* 1983, 2339.
4. (a) W. A. Nugent and B. L. Haymore, *Coord. Chem. Rev.* 1980, **31**, 123; (b) S. Cenini and G. La Monica, *Inorg. Chim. Acta* 1976, **18**, 279; (c) M. L. Blohm and W. L. Gladfelter, *Organometallics* 1986, **5**, 1049.
5. G. D. Williams, R. R. Whittle, G. L. Geoffroy and A. L. Rheingold, *J. Am. Chem. Soc.* 1987, **109**, 3936.
6. S. H. Han, G. L. Geoffroy and A. L. Rheingold, *Inorg. Chem.* 1987, **26**, 3426.
7. (a) J. M. Landesberg, L. Katz and C. Olsen, *J. Org. Chem.* 1972, **37**, 930; (b) M. Dekker and G. R. Knox, *J. Chem. Soc., Chem. Commun.* 1967, 1243; (c) H. Alper and H.-N. Paik, *Nouv. J. Chim.* 1978, **2**, 245.
8. J. A. Smieja and W. L. Gladfelter, *Inorg. Chem.* 1986, **25**, 2667.
9. (a) G. Lavigne and H. D. Kaesz, *J. Am. Chem. Soc.* 1984, **106**, 4647; (b) G. Lavigne, N. Lugan and J. J. Bonnet, *J. Chem. Soc., Chem. Commun.* 1987, 957.
10. G. A. Foulds, B. F. G. Johnson and J. Lewis, *J. Organomet. Chem.* 1985, **296**, 147.
11. R. Pilato, G. L. Geoffroy and A. L. Rheingold, to be submitted.
12. S. Nyugen, S. H. Han and G. L. Geoffroy, unpublished results.
13. W. Bernhardt, C. von Schnering and H. Vahrenkamp, *Angew. Chem., Int. Ed. Engl.* 1986, **25**, 279.
14. J. A. Smieja, J. E. Gozum and W. L. Gladfelter, *Organometallics* 1987, **6**, 1311.
15. A. Basu, S. Bhaduri and H. Khwaja, *J. Organomet. Chem.* 1987, **319** C28.
16. A. J. Deeming, Y. Fuchita, K. Hardcastle, K. Henrick and M. McPartlin, *J. Chem. Soc., Dalton Trans.* 1986, 2259; See also S. Bhaduri, H. Khwaja and P. G. Jones, *J. Chem. Soc., Chem. Commun.* 1988, 194 for a directly relevant example of imido–carbonyl coupling on a Ru_3 cluster.
17. (a) D. J. Darensbourg, R. Gray and M. Pala, *Organometallics* 1984, **3**, 1928; (b) D. C. Gross and P. C. Ford, *J. Am. Chem. Soc.* 1985, **107**, 585.

Polyhedron Vol. 7, No. 22/23, pp. 2341–2344, 1988
Printed in Great Britain

0277–5387/88 $3.00+.00
© 1988 Pergamon Press plc

NOVEL CATALYTIC APPLICATIONS OF ANIONIC RUTHENIUM CLUSTERS IN ISOCYANATE CHEMISTRY*

GEORG SÜSS-FINK,** GERHARD HERRMANN and GERHARD F. SCHMIDT

Aachen University of Technology, Institute of Inorganic Chemistry, Templergraben 55, D-5100 Aachen, F.R.G.

Abstract—The anionic ruthenium clusters $[HRu_3(CO)_{11}]^-$, $[H_3Ru_4(CO)_{12}]^-$ and $[Ru_3(CO)_{11}]^{2-}$ were found to catalyse novel coupling reactions of alkyl isocyanates. Under the catalytic influence of the appropriate cluster, alkyl isocyanates react with silanes to give *spiro*-pentazadecanetetrons; with hydrogen, carbamylformamides are obtained, and with phenyl acetylene, benzylidene hydantoins. All these catalytic processes involving C—N coupling of isocyanate units lead to new organic compounds, thus demonstrating the unique catalytic potential of anionic ruthenium clusters.

Ever since transition metal clusters have been discussed as catalysts, there has been controversy as to whether or not such clusters can be really useful in catalysis. In the 1970s the chemistry of transition metal clusters set out with the goal to contribute significantly to the development of systematic catalysis, stimulated mainly by Jack Lewis and the late Earl Muetterties.

As oligonuclear species with intermetallic bonds, metal clusters occupy the no-man's-land between mononuclear metal complexes and polynuclear metal surfaces (Fig. 1). Because of this intermediary position between typical homogeneous catalysts and typical heterogeneous catalysts, transition metal clusters have raised expectations that they might provide a new generation of catalysts. The actual success of cluster-mediated catalysis, however, has remained modest. A number of transition metal clusters have been found to catalyse conventional reactions such as hydrogenations and hydroformylations, but *novel* catalytic applications had not been discovered.

It was therefore the aim of our own studies to search for catalytic properties of transition metal clusters which are *unique* for these systems, that is to say: catalytic properties which had not been observed with other catalysts before. This paper reports novel reactions of alkyl isocyanates catalysed by anionic ruthenium clusters which lead to new organic compounds, thus demonstrating the *innovative* catalytic potential of transition metal clusters.

* Dedicated to Professor Sir Jack Lewis on the occasion on his 60th birthday.

** Author to whom correspondence should be addressed.

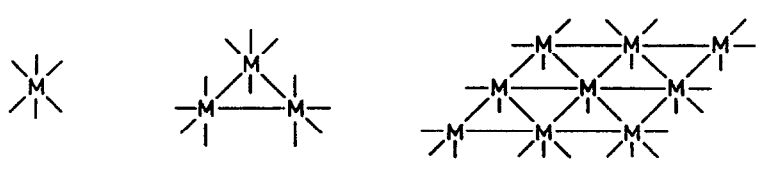

Fig. 1.

I. SILANE-ASSISTED SPIROCYCLIZATION OF ALKYL ISOCYANATES CATALYSED BY $[HRu_3(CO)_{11}]^-$

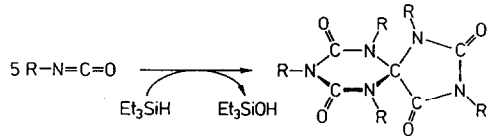

	Ia	Ib	Ic	Id	Ie
R	Me	Et	n-Pr	i-Pr	n-Bu

Tetrahydrofuran, 120°C
Catalyst: $[NEt_4][HRu_3(CO)_{11}]$
Molar ratio:
isocyanate/silane/catalyst 5000 : 1000 : 1.

II. HYDRO-COUPLING OF ALKYL ISOCYANATES CATALYSED BY $[H_3Ru_4(CO)_{12}]^-$

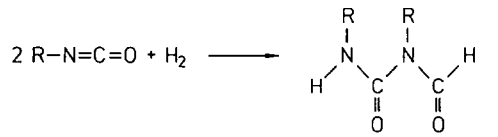

	IIa	IIb	IIc	IId
R	Me	Et	n-Pr	n-Bu

Tetrahydrofuran, 120°C
Catalyst: $[N(PPh_3)_2][H_3Ru_4(CO)_{12}]$
Molar ratio: isocyanate/catalyst 1000 : 1.

III. COUPLING OF ALKYL ISOCYANATES WITH PHENYL ACETYLENE CATALYSED BY $[Ru_3(CO)_{11}]^{2-}$

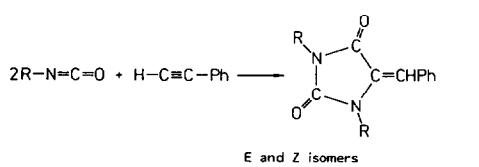

	IIIa	IIIb	IIIc	IIId
R	Me	Et	n-Pr	n-Bu

Tetrahydrofuran, 120°C
Catalyst: $[N(PPh_3)_2]_2[Ru_3(CO)_{11}]$
Molar ratio:
isocyanate/acetylene/catalyst 1000 : 1000 : 1.

The reactions I–III all involve catalytic C—N coupling of two isocyanate units. In reaction I five isocyanate molecules are coupled together to yield the spiroheterocycles **Ia–Ie** (see Structure 1 for the Structure of **Ia**), composed of alternating CO and NR building blocks. One of the five isocyanate molecules must have lost its oxygen atom thus providing the spiro carbon centre of the product; accordingly, one equivalent of Et_3SiOH—derived from Et_3SiH—is detected in the reaction mixture. This reaction provides a surprisingly simple access to a new series of spiroheterocycles, and, to our knowledge, it was the first *unique* catalytic application of a transition metal cluster. In reaction II two isocyanate molecules are combined with uptake of hydrogen to give the carbamyl formamides **IIa–IId**, and in reaction III two isocyanate molecules couple incorporating phenyl acetylene as an olefinic moiety to yield the benzylidene hydantoines **IIIa–IIId**, which can be separated into the two expected *E* and *Z* isomers.

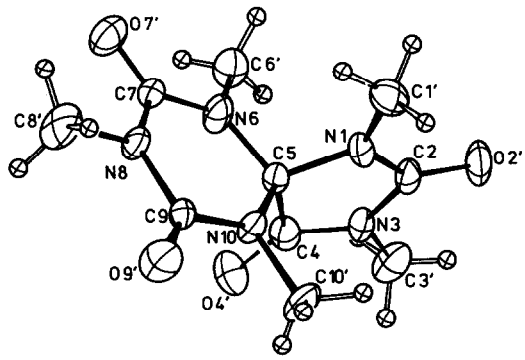

Structure 1. Molecular structure of the spiroheterocycle, **Ia**.

With exception of the known *Z* isomer of **IIIa**, all the organic products of the catalytic reactions I-III are new compounds. They were isolated by chromatography and characterized by spectroscopic and analytical methods. The spirocyclic nature of compounds **Ia–Ie** was revealed by a single-crystal X-ray structure analysis (U. Thewalt, Ulm): as expected, the two rings are almost planar and perpendicular with respect to each other.

The reactions I-III are catalysed by the ruthenium cluster anions $[HRu_3(CO)_{11}]^-$ (**1**), $[H_3Ru_4(CO)_{12}]^-$ (**2**) and $[Ru_3(CO)_{11}]^{2-}$ (**3**), respectively. The question arising is the key question of cluster-mediated catalysis: Does the catalytic reaction proceed through the intermediacy of intact clusters, or does the cluster disintegrate? Under appropriate conditions the cluster anions **1**, **2** and **3** can be interconverted into each other, so that cluster break-down and cluster build-up reactions cannot be excluded during the catalytic processes. However, none of the reactions I–III is catalysed by mononuclear ruthenium complexes which do not form clusters, such as $(Ph_3P)_3RuCl_2$.

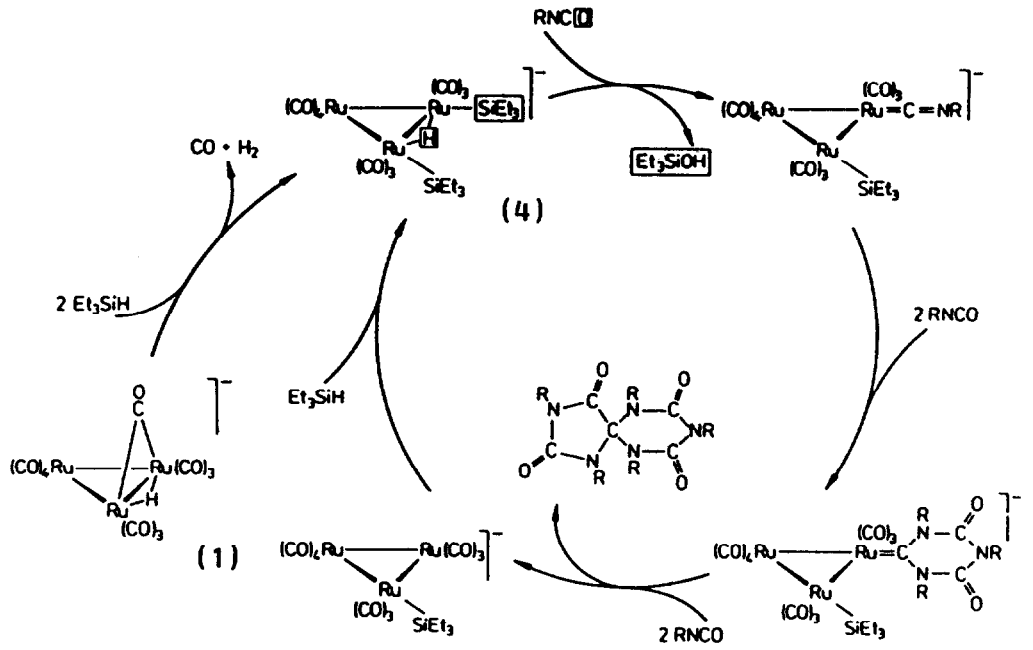

Scheme 1. Proposed mechanism for reaction (I).

For reaction I, (see Scheme 1) the silane-assisted spirocyclization of alkyl isocyanates was found to involve the activation of the silane on the cluster anion as the initial step. Two molecules of Et_3SiH react with **1** under cleavage of the Si—H bond and transfer of two triethylsilyl groups to the metal framework to give the silylated intermediate $[HRu_3(CO)_{10}(SiEt_3)_2]^-$ (**4**). In the further course of the catalytic process, we observed the formation of triethylsilanol suggesting anion **4** (see Structure 2) reacts with isocyanate with elimination of Et_3SiOH; for the resulting cluster anion we assume an isonitrile complex. The isonitrile ligand could then incorporate two isocyanate molecules to build up a six-membered heterocycle coordinated to the cluster in a carbene-like fashion. With two further RNCO molecules the spiroheterocycle is closed and detached from the cluster; the remaining unsaturated cluster fragment reacts with Et_3SiH to go back to the silylated cluster anion **4**, thus closing the catalytic cycle.

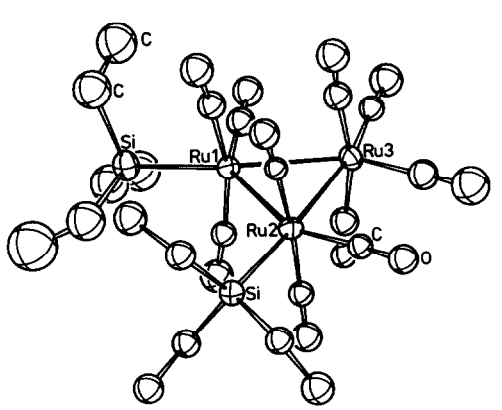

Structure 2. Molecular structure of the silylated cluster anion, **4**.

The silylated cluster anion **4** could be isolated and characterized as the $[N(PPh_3)_2]^+$ salt; the X-ray crystal structure analysis (U. Thewalt, Ulm) reveals that the trinuclear cluster framework has remained intact: anion **4** contains an isosceles Ru_3 triangle with two equatorial triethylsilyl ligands. The position of the hydride ligand as a bridge between the two silyl-substituted Ru atoms was assigned on the basis of the NMR data.

For reaction II, no organometallic intermediate could be detected. After completion of isocyanate hydro-coupling, the tetranuclear cluster anion **2** was found to be unchanged in the solution; it could be recovered in an almost quantitative yield. GC–MS analysis of the reaction mixture revealed the intermediary formation of formamides; these formamides were shown to react with isocyanates to yield the coupling products without catalyst. This means that the hydro-coupling of alkyl isocyanates proceeds by catalytic hydrogenation of the isocyanate to give the formamide, followed by a non-catalytic coupling step of the formamide produced with unreacted isocyanate.

$$R{-}N{=}C{=}O + H_2 \xrightarrow{2} R{-}NH{-}CH{=}O$$

$$R{-}NH{-}CH{=}O + R{-}N{=}C{=}O \rightarrow R{-}NH{-}CO{-}NR{-}CH{=}O.$$

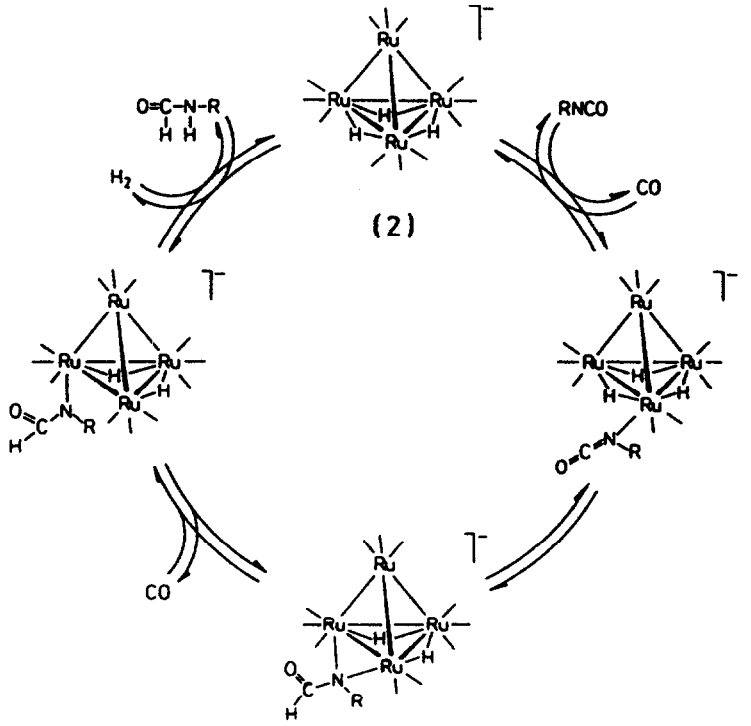

Scheme 2. Proposed mechanism for the catalytic step of reaction (II).

As to the hydrogenation step (see Scheme 2) we propose a catalytic cycle involving exclusively intact Ru_4 cluster anions. We assume that the catalytic process is initiated by the substitution of a CO ligand by an isocyanate molecule. Subsequently, a hydride ligand is transferred from the metal framework to the isocyanate ligand to give a formylamido bridge. This three-electron ligand is then converted into a terminal one-electron ligand by the re-addition of CO; finally it is eliminated by the action of H_2 to yield the formamide, recycling the cluster anion **2**.

As to reaction III, the catalytic coupling of alkyl isocyanates with phenyl acetylene is not yet understood on the basis of a mechanism involving intact cluster anions. Further studies are in progress.

Acknowledgements—This work was supported by the Deutsche Forschungsgemeinschaft, the Fonds der Chemischen Industrie, the Minister für Forschung und Wissenschaft des Landes Nordrhein-Westfalen, the Karl-Winnacker-Stiftung and the Stiftung Volkswagenwerk.

REFERENCES

Parts of this work have been published giving full experimental details:

1. G. Süss-Fink, G. Herrmann and U. Thewalt, *Angew. Chem.* 1983, **95**, 899; *Angew. Chem., Int. Ed. Engl.* 1983, **22**, 880; *Angew. Chem. Suppl.* 1983, 1203.
2. G. Hermann and G. Süss-Fink, *Chem. Ber.* 1985, **118**, 3959.
3. H.-P. Klein, U. Thewalt, G. Herrmann, G. Süss-Fink and C. Moinet, *J. Organomet. Chem.* 1985, **286**, 225.
4. G. Süss-Fink and G. Herrmann, *Angew. Chem.* 1986, **98**, 568; *Angew Chem., Int. Ed. Engl.* 1986, **25**, 570.
5. G. Süss-Fink, G. F. Schmidt and G. Herrmann, *Chem. Ber.* 1987, **120**, 1451.

Polyhedron Vol. 7, No. 22/23, pp. 2345–2349, 1988
Printed in Great Britain

0277–5387/88 $3.00+.00
© 1988 Pergamon Press plc

HETEROSITE REACTIVITY OF COBALT–RHODIUM MIXED-METAL CLUSTERS

ISTVÁN T. HORVÁTH*

Department of Industrial and Engineering Chemistry, Swiss Federal Institute of Technology, ETH-Zentrum, CH-8092 Zürich, Switzerland

Abstract—It has been established that reactions of cobalt–rhodium mixed-metal clusters with nucleophiles such as PEt_3, THF, MeCN and Cl^- occur on the rhodium site, with alkynes on the cobalt site. Several reversible tetranuclear–dinuclear transformations were observed with preferential retainment of the cobalt–rhodium bond.

The application of multimetallic catalysts has attracted much interest since their catalytic activity and/or selectivity often differs significantly from that of the homometallic systems of the constituent metals.[1,2] Although synergism has been observed in various homogeneous catalytic reactions,[2] very little is known of the actual role of the different metals in the catalytic cycle. The synergetic effect is probably due to the presence of a mixed-metal species, which could form from homo- or heteronuclear catalyst precursors. Such species could exhibit novel reactivity compared to the homonuclear analogues.[3] For example, in a mixed-metal dinuclear complex three different coordination sites are available for ligand activation (Scheme 1). Incoming substrates can be activated on sites 1 and 2 (*heterosite ligand activation*), or on site 3 (*heteronuclear ligand activation*). Since the two metals possess different electronic structure and thus different reactivity, facile activation could occur preferentially at one of these sites.

Cobalt–rhodium synergism has been reported for homogeneous catalytic hydrogenation,[4] hydroformylation[5] and hydrocarbonylation.[6] It was suggested by Pino and von Bezard that the synergetic effect, observed in the combined application of $Co_2(CO)_8$ (**1**) and $Rh_4(CO)_{12}$ (**2**) in the hydrocarbonylation of diketene, could arise from the presence of a cobalt–rhodium carbonyl complex.[6] It was later shown by Bor, Pino and coworkers that **1** and **2** are indeed in equilibrium with a new mixed-metal compound, formulated as $CoRh(CO)_7$ (**3**) [eq. (1)].[7]

$$\underset{\mathbf{1}}{2Co_2(CO)_8} + \underset{\mathbf{2}}{Rh_4(CO)_{12}} \rightleftharpoons \underset{\mathbf{3}}{4CoRh(CO)_7} \quad (1)$$

Complex **3** was recently isolated and its formula was established by analytical methods.[8] The proposed structure of $CoRh(CO)_7$ (**3**) contains a distorted tetrahedral $[Co(CO)_4]$ group bonded to a square-planar $[Rh(CO)_3]$ fragment through a Co—Rh bond and two semibridging carbonyl ligands.[8,9] It has also been found that $CoRh(CO)_7$ (**3**) is in equilibrium with two mixed-metal complexes: $CoRh(CO)_8$ (**4**)[8] and $Co_2Rh_2(CO)_{12}$ (**5**)[10] [eqs (2) and (3)].

$$\underset{\mathbf{3}}{CoRh(CO)_7} + CO \rightleftharpoons \underset{\mathbf{4}}{CoRh(CO)_8} \quad (2)$$

$$\underset{\mathbf{3}}{2CoRh(CO)_7} \rightleftharpoons \underset{\mathbf{5}}{Co_2Rh_2(CO)_{12}} + 2CO. \quad (3)$$

* Present address: Exxon Research and Engineering Company, Annandale, NJ 08801, U.S.A.

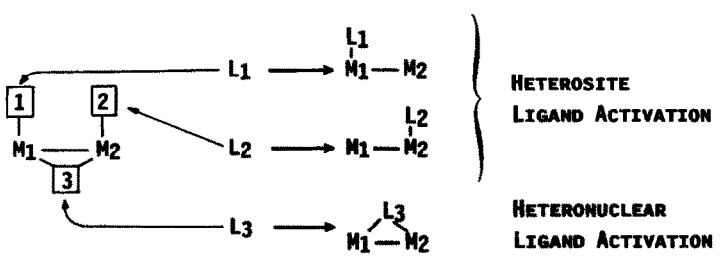

Scheme 1.

In contrast, $CoRh(CO)_5(PEt_3)_2$ (**6**) does not dimerize to give a tetranuclear cluster but easily undergoes reversible or irreversible fragmentation when treated with MeCN and [PPN]Cl, respectively [eqs (4) and (5)].[11]

$$\underset{\mathbf{6}}{CoRh(CO)_5(PEt_3)_2} + MeCN \rightleftharpoons [Rh(CO)(PEt_3)_2(MeCN)]^+[Co(CO)_4]^- \quad (4)$$

$$\underset{\mathbf{6}}{CoRh(CO)_5(PEt_3)_2} + [PPN]Cl \rightarrow ClRh(CO)(PEt_3)_2 + PPN[Co(CO)_4] \quad (5)$$

Furthermore, the reactions of **6** with nucleophiles showed preferential attack at the rhodium site. These results indicated that the reactivity of cobalt–rhodium clusters is strongly influenced by the nature of the ligands present. Therefore, we have undertaken a systematic study to develop a better understanding of the observed ligand dependence.

DISCUSSION

The reaction of $Co_2Rh_2(CO)_{12}$ (**5**) with four equivalents of PEt_3 results in the quantitative formation of $CoRh(CO)_5(PEt_3)_2$ (**6**) (Scheme 2).[12] Compound **6** has been previously isolated and structurally characterized.[11] When the reaction was followed by IR, the formation of three intermediates was observed: $Co_2Rh_2(CO)_{11}(PEt_3)$ (**7**), $Co_2Rh_2(CO)_{10}(PEt_3)_2$ (**8**), and $CoRh(CO)_6(PEt_3)$ (**9**). These compounds were separately isolated and their solution structures were established by spectroscopic methods. The structure of **7** consists of a *closo*-Co_2Rh_2 tetrahedral cluster with two rhodium atoms in the basal plane. There are eight terminal carbonyl ligands and three bridging carbonyl ligands along the basal plane. The PEt_3 ligand is bonded to a rhodium atom, and it probably occupies an axial position as was found for $Co_4(CO)_{11}(PPh_3)$.[13] The structure of $Co_2Rh_2(CO)_{10}(PEt_3)_2$ (**8**) is essentially the same as that of **7**, but each rhodium atom has one PEt_3 ligand; one has it in an axial and the other in an equatorial position. A similar structure was found for $Ir_4(CO)_{10}(PPh_3)_2$.[14] In the reaction of **5** and four equivalents of PEt_3, two moles of free carbon monoxide must be formed which can subsequently react with **7**, **8**, and **9**. It was interesting to see if $Co_2Rh_2(CO)_{11}(PEt_3)$ (**7**), $Co_2Rh_2(CO)_{10}(PEt_3)_2$ (**8**), and $CoRh(CO)_6(PEt_3)$ (**9**) do react with carbon monoxide as previously found for **3** and **5** [eqs (2) and (3)]. Indeed, facile and reversible reactions are observed. **7** reacts with carbon monoxide at atmospheric pressure and room temperature to give an equilibrium mixture of **7**, $CoRh(CO)_7$ (**3**), and $CoRh(CO)_6(PEt_3)$ (**9**) [eq. (6)].

$$\underset{\mathbf{7}}{Co_2Rh_2(CO)_{11}(PEt_3)} + 2CO \rightleftharpoons \underset{\mathbf{3}}{CoRh(CO)_7} + \underset{\mathbf{9}}{CoRh(CO)_6(PEt_3)} \quad (6)$$

Upon purging the equilibrium mixture with N_2, **3** and **9** recombine to give **7** quantitatively. Similarly, $Co_2Rh_2(CO)_{10}(PEt_3)_2$ (**8**) undergoes facile and reversible fragmentation when treated with 1 bar CO at room temperature to give $CoRh(CO)_6(PEt_3)$ (**9**)

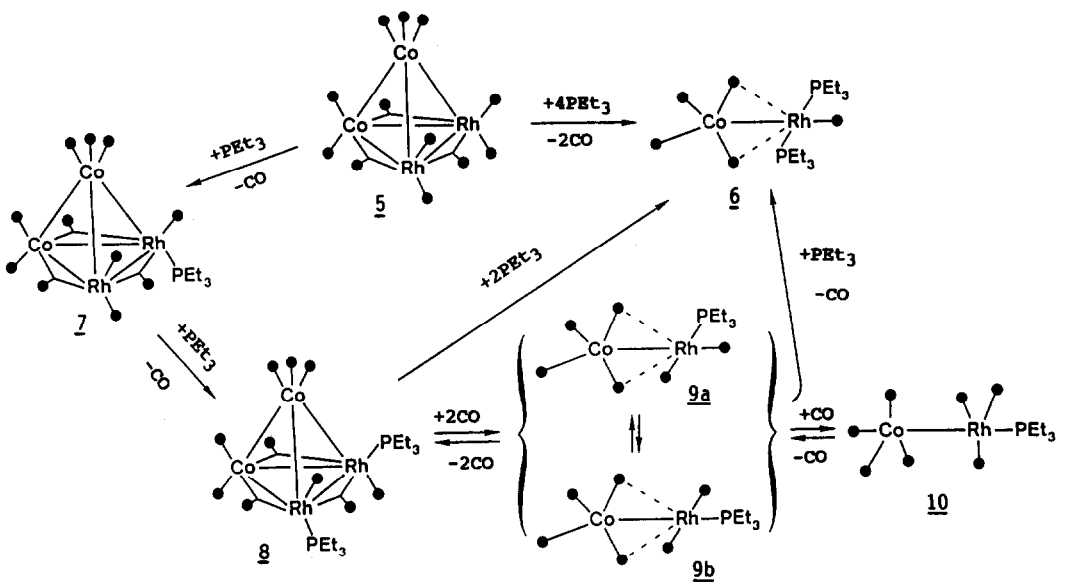

Scheme 2.

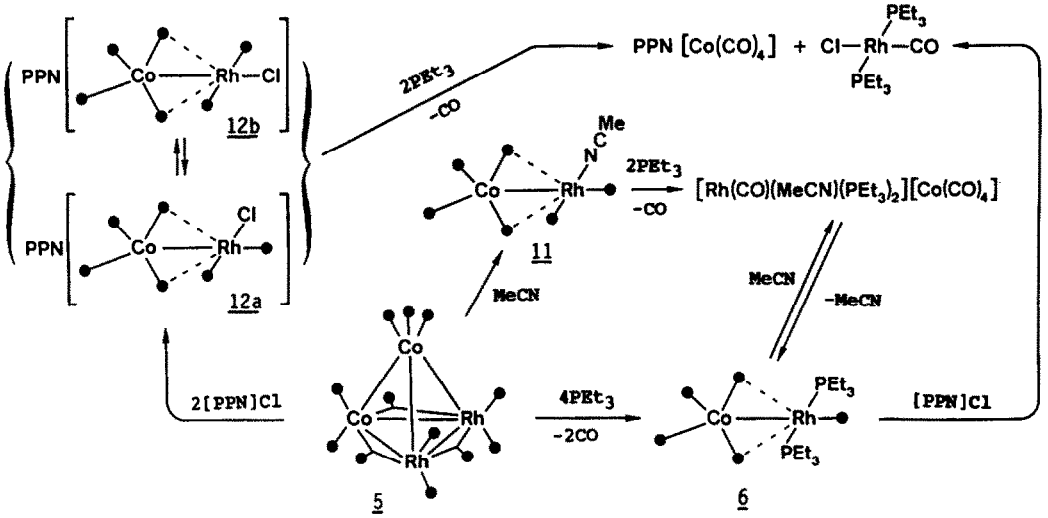

Scheme 3.

(Scheme 2). A structure has been proposed for **9**, in which a distorted tetrahedral $[Co(CO)_4]$ fragment is bonded to a square-planar $[Rh(CO)_2PEt_3]$ group through a Co—Rh bond and two cobalt-bonded semi-bridging carbonyl ligands.[9,12] The presence of two isomers, **9a** and **9b**, having a PEt_3 ligand *cis* and *trans*, respectively, to the $[Co(CO)_4]$ moiety, in solution was postulated. The relative ratio between **9a** and **9b** is 95 : 5. Medium-pressure IR studies have revealed that at higher carbon monoxide pressure $CoRh(CO)_6(PEt_3)_2$ (**9**) is in equilibrium with $CoRh(CO)_7(PEt_3)$ (**10**).[12] IR and NMR observations suggest that **10** is structurally analogous to $Co_2(CO)_7(PEt_3)$,[15] as shown in Scheme 2. The exact metal-site for the carbon monoxide addition to **4**, **8**, and **9** could not be determined. However, it is also believed to occur at the rhodium site(s), since the analogous $Co_2Ir_2(CO)_{12}$ cluster[10] does not react with CO at 15 bar and room temperature within 72 h.[16]

The reactivity of $Co_2Rh_2(CO)_{12}$ (**5**) towards other nucleophiles was also studied.[12] When **5** is dissolved in THF, its dark colour disappears and the solution becomes light orange. The IR spectrum of this solution indicates the transient formation of $CoRh(CO)_6(THF)$, which readily undergoes fragmentation to give an ionic species, probably $[Rh(CO)_2(THF)_2][Co(CO)_4]$.[16] **5** reacts similarly with excess or neat MeCN to give initially $CoRh(CO)_6(MeCN)$ (**11**) (Scheme 3). The solution structure of **11** was studied by IR and ^{13}C NMR, which indicate a structure analogous to **9a**. Although the stability of **11** is higher than that of $CoRh(CO)_6(THF)$, it slowly reacts further with the excess of MeCN to yield $[Rh(CO)_2(MeCN)_2][Co(CO)_4]$.[16] $Co_2Rh_2(CO)_{12}$ (**5**) undergoes irreversible fragmentation when treated with two equivalents of [PPN]Cl or $[N(CH_2Ph)Et_3]Cl$ to give $PPN[CoRh(CO)_6Cl]$ (**12**) and $[N(CH_2Ph)Et_3][CoRh(CO)_6Cl]$, respectively (Scheme 3).[12] An analogous compound, $[N(C_{12}H_{25})Me_3][CoRh(CO)_6Cl]$ has been previously prepared.[17] The solution structure of **12** was established by IR and ^{13}C NMR spectroscopy and is similar to **9**. The presence of two isomers, **12a** and **12b**, having a chloride ligand *cis* and *trans*, respectively, to the $[Co(CO)_4]$ moiety has been found. The relative ratio between these two isomers is 4 : 1.

It has been shown that $CoRh(CO)_5(PEt_3)_2$ (**6**) easily undergoes reversible or irreversible heterolytic cleavage of its metal–metal bond when treated with MeCN and [PPN]Cl [eqs (4) and (5)].[11] It was interesting to see if the same products form in the reaction of **11** and **12** with two equivalents of PEt_3, respectively. Indeed, the addition of PEt_3 to **12** results in the formation of the heteronuclear ion pair $[Rh(CO)(PEt_3)_2(MeCN)]^+[Co(CO)_4]^-$. After the solvent and MeCN are removed, compound **6** is the only product present, in agreement with eq. (4). The reaction of **12** with PEt_3 gives *trans*-$ClRh(CO)(PEt_3)_2$ and $PPN[Co(CO)_4]$, quantitatively (Scheme 3).

$Co_2Rh_2(CO)_{12}$ (**5**) reacts with alkynes via specific insertion into the Co—Co bond to give the butterfly cluster $Co_2Rh_2(CO)_{10}(\mu_4\text{-}\eta^2\text{-}RC_2R')$ [R = R′ = C_6F_5 (**13a**), Ph (**13b**); R = H, R′ = Ph (**13c**); R = Me, R′ = Ph (**13d**)] (Scheme 4).[18] The molecular structure of **13a** was determined crystallographically, and it is very similar to related clusters containing a *closo*-M_4C_2 framework.[19] Upon addition of one equivalent of $F_5C_6C_2C_6F_5$ to **13a** in the presence of CO, highly regiospecific

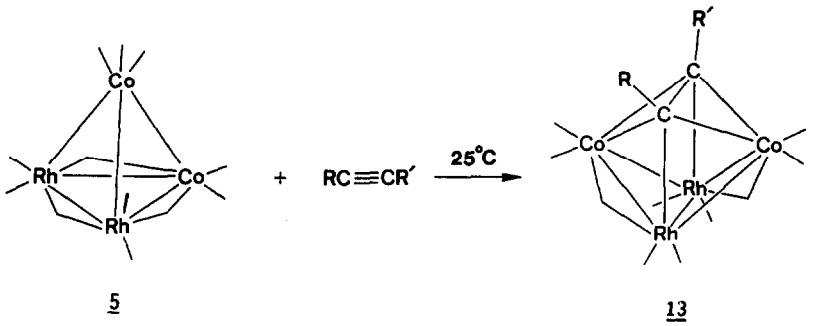

5 13

Scheme 4.

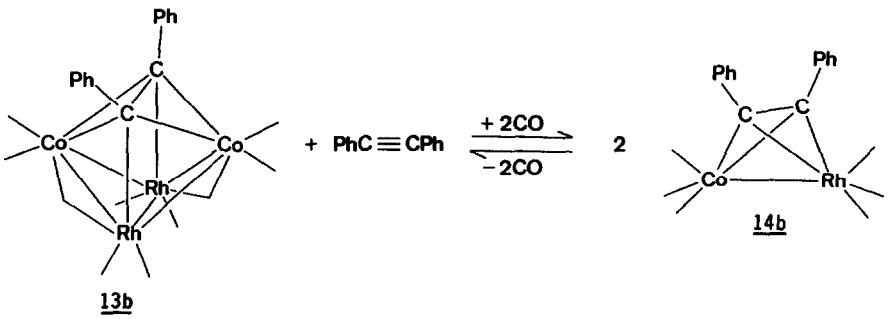

13b 14b

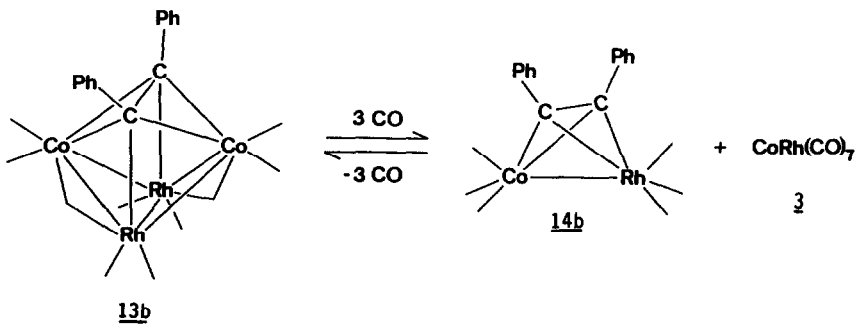

13b 14b 3

Scheme 5.

fragmentation occurs to give $CoRh(CO)_6(\mu\text{-}\eta^2\text{-}F_5C_6C_2C_6F_5)$ (**14a**).

$Co_2Rh_2(CO)_{10}(\mu_4\text{-}\eta^2\text{-}PhC_2Ph)$ (**13b**) reacts similarly with diphenylacetylene and carbon monoxide to yield $CoRh(CO)_6(\mu\text{-}\eta^2\text{-}PhC_2Ph)$ (**14b**) (Scheme 5). Surprisingly, the reaction is fully reversible, such that upon bubbling N_2 into the reaction mixture **14b** reforms quantitatively. Since **13b** does not react with PhC_2Ph in the absence of carbon monoxide, it was assumed that **13b** reacts with CO and then with diphenylacetylene. Indeed, it was found that **13b** easily undergoes reversible fragmentation to give a 1 : 1 mixture of **14b** and $CoRh(CO)_7$ (**3**) at 2 bar CO pressure. In contrast, **13c,d** do not react with the corresponding alkynes in the presence of 1 bar CO at room temperature.[16] These results indicate that the nature of the substituents of the alkyne ligand has an opposite effect on the stability of **13** and **14**. Upon increasing the electronegativity of the substituents, the stability of the tetranuclear clusters decreases and that of the dinuclear complexes increases.

The present study has established that the combination of cobalt and rhodium in mixed-metal carbonyl complexes leads to regiospecific reactivity on rhodium or cobalt. Reactions of cobalt–rhodium mixed-metal clusters with nucleophiles such as PEt_3, THF, MeCN and Cl^- (and probably CO) occur on the rhodium site, with alkynes on the cobalt site. Several tetranuclear–dinuclear transformations are observed with the preferential retainment of the cobalt–rhodium bond. This indi-

cates a higher "resistance" of the Co—Rh bond against metal–metal bond breaking than the Co—Co or Rh—Rh bonds. It is not clear if this is a characteristic feature of the Co_2Rh_2 framework itself, implying stronger Co—Rh bonds, or is a consequence of the attack of the substrates occurring exclusively on a rhodium or a cobalt centre. The facile formation of the coordinately unsaturated compounds $CoRh(CO)_{7-x}L_x$ (L = CO, THF, MeCN, Cl^-, PEt_3) could have an important role in homogeneous catalytic reactions. Studies concerning the mechanism of these reactions and the possible role of the coordinatively unsaturated cobalt–rhodium compounds in homogeneous catalytic hydroformylation are in progress.

Acknowledgements—Professors Piero Pino and György Bor are thanked for their continuous support, helpful discussions, and the scientific freedom I have enjoyed in Zürich. I am grateful to Prof. Giambattista Consiglio, Dr Robert Waymouth and Marc Garland for their helpful discussions. This work was supported by the "Schweizerischer Nationalfonds zur Förderung der wissenschaftlichen Forschung", No. 5.521.330.784/2.

REFERENCES

1. J. H. Sinfelt, *Bimetallic Catalysts: Discoveries, Concepts, and Applications*. John Wiley, New York (1983).
2. P. Braunstein and J. Rose, in *Stereochemistry of Organometallic and Inorganic Compounds* (Edited by I. Bernal), Vol. 3. Elsevier, Amsterdam (in press).
3. W. L. Gladfelter and G. L. Geoffroy, in *Comprehensive Organometallic Chemistry* (Edited by G. Wilkinson, F. G. A. Stone and E. Abel), Chap. 40. Pergamon Press, Elmsford, NY (1982).
4. D. Labroue and R. Poilblanc, *J. Molec. Catal.* 1977, **2**, 329.
5. A. Ceriotti, L. Garlaschelli, G. Longoni, M. C. Malatesta, D. Strumolo, A. Fumagalli and S. Martinengo, *J. Molec. Catal.* 1984, **24**, 309.
6. P. Pino and D. A. von Bezard, Ger Offen 2 807 215, 1978.
7. F. Spindler, G. Bor, U. K. Dietler and P. Pino, *J. Organomet. Chem.* 1981, **213**, 303.
8. I. T. Horváth, G. Bor, M. Garland and P. Pino, *Organometallics* 1986, **5**, 1441.
9. I. T. Horváth and G. Bor, manuscript in preparation.
10. S. Martinengo, P. Chini, V. G. Albano, F. Cariati and T. Salvatori, *J. Organomet. Chem.* 1973, **59**, 379.
11. D. A. Roberts, W. C. Mercer, S. M. Zaharuk, G. L. Geoffroy, C. W. DeBrosse, M. E. Cass and C. G. Pierpont, *J. Am. Chem. Soc.* 1982, **104**, 910; D. A. Roberts, W. C. Mercer, G. L. Geoffroy and C. G. Pierpont, *Inorg. Chem.* 1986, **25**, 1439.
12. I. T. Horváth, *Organometallics* 1986, **5**, 2333.
13. D. J. Darensbourg and M. Incoriva, *Inorg. Chem.* 1981, **20**, 1911.
14. K. Karel and G. Norton, *J. Am. Chem. Soc.* 1974, **96**, 6812.
15. P. Szabó, L. Fekete, G. Bor, Z. Nagy-Magos and L. Markó, *J. Organomet. Chem.* 1968, **12**, 245.
16. I. T. Horváth, unpublished results.
17. F. Joó and H. Alper, *Can. J. Chem.* 1985, **63**, 1157.
18. I. T. Horváth, L. Zsolnai and G. Huttner, *Organometallics* 1986, **5**, 180.
19. L. F. Dahl and D. L. Smith, *J. Am. Chem. Soc.* 1962, **84**, 2450; G. Gervasio, R. Rossetti and P. L. Stanghellini, *Organometallics* 1985, **4**, 1612; E. Sappa, A. Tiripicchio and P. Braunstein, *Chem. Rev.* 1983, **83**, 203.

Polyhedron Vol. 7, No. 22/23, pp. 2351–2367, 1988
Printed in Great Britain

0277–5387/88 $3.00+.00
© 1988 Pergamon Press plc

BIMETALLIC CLUSTER-DERIVED HETEROGENEOUS CATALYSTS—HETERONUCLEAR TWO-SITE ACTIVATION OF CO IN SYNGAS CONVERSION TO OXYGENATES

MASARU ICHIKAWA

Research Institute for Catalysis, Hokkaido University, Sapporo 060, Japan

Abstract—Tailored bimetal catalysts have been prepared by using SiO_2-supported Rh_4Fe_2, Rh_5Fe, Ir_4Fe and Pd_6Fe_6 carbonyl clusters and NaY (or NaX) zeolite-entrapped RhFe and $Rh_{6-x}Ir_x$ ($x = 0$–6) carbonyl clusters as the molecular precursors. They exhibited markedly high activity and selectivities for C_1+C_2 alcohols in a $CO+H_2$ reaction and higher alcohols in olefin hydroformylation. The bimetal cluster-derived catalysts are structurally characterized by EXAFS, Mössbauer and FTIR spectroscopies in terms of their cluster frameworks and metal compositions including their oxidation states in catalysis. Iron promotion is proposed to be associated with the heteronuclear activation of CO with the adjacent Rh—Fe^{3+}, Pd—Fe^{3+} and Ir—Fe^{3+} located at the metal/oxide interfaces to enhance the migratory insertion of CO into M—H and M—alkyl, reflected in the marked increase of C_1+C_2 alcohol formation from CO and H_2.

The chemical modification of solid surfaces, e.g. SiO_2, Al_2O_3, MgO and zeolites by using organometallic clusters as the precursors has been a subject of recent interest,[1] because this gives the possibilities for the sophisticated control of the size of metal ensembles less than 10 Å, and the well-managed metal compositions. This approach will make possible a molecular-level preparation of tailored metal catalysts involving the well-characterized metal centres. In fact, in some cases the cluster-derived heterogeneous catalysts provide the advantages of higher activities and improved selectivities over conventional metal catalysts.[2] In general, the metal particle size (nuclearity), metal compositions of bimetal ensembles including alloys, and geometric environments (steric effect) associated with heteronuclear interaction and molecular-shape controlling by zeolite frameworks, may influence the activities and product selectivities in catalytic reactions, e.g. the $CO+H_2$ reaction and skeletal rearrangements of hydrocarbons.[3]

A number of supported multimetal catalysts have been extensively studied and some of these have been developed for useful industrial processes. For example, they are composed of the combination of: (a) both reduced metals: e.g. Pt+Re and Ni+Cu alloys in petroleum–naphtha reforming; (b) reduced metals and oxides: e.g. $Pt+TiO_2$, Rh+MnO and Cu+ZnO in syngas conversion; (c) both metal oxides (sulphides): e.g., $MoO_3+Bi_2O_3$ and $CoS+MoS_3$ in the selective oxidation of propene and hydrodesulphurization. They also exhibit unique promotions of catalytic performances, improving the stability of catalyst life, which is markedly different from those of the constituent elements. Studies on the origin of the promotion due to the heteronuclear interaction of multimetallic catalysts are of great interest and importance. Moreover, it has been recently demonstrated[4,5] that some additive metal ions exert a significant promotion in CO hydrogenation catalysed on rhodium, in enhancing the yields and unexpectedly increasing the selectivities toward oxygen-containing products such as alcohols. It is of interest to clarify the potential role of positive metal ions on the promoted Rh catalysts in modifying the oxygenate formation. Accordingly, as localized model precursor compounds for the promoted multimetallic catalysts, we have employed some Fe-containing Rh, Pt and Pd bimetal carbonyl clusters to impregnate the well-characterized bimetal ensembles highly dispersed on the metal oxides such as SiO_2 or entrapped inside zeolite supercages to be physically isolated. They are strikingly active catalysts for oxygenate for-

mation consisting mostly of alcohols in $CO+H_2$ and olefin hydroformylation reactions. We report here on the structural characterization and catalytic performance of RhFe, PtFe and PdFe bimetallic carbonyl cluster-derived catalysts. We shall pay some attention to the problems of how the promoter ions affect the decisive steps essential for the oxygenate formation in syngas conversion catalysed on Rh, Pt and Pd. Additionally, the unique promotion of positive ions such as Fe and Mo will be proposed to be associated with the heteronuclear two-site activation of CO in enhancing CO migratory insertion with M—H and M—alkyl bondings to give methanol and higher oxygenates such as ethanol in the catalytic CO hydrogenation. In this connection, the function of an electropositive promoter is discussed in terms of C- and O-bonded CO interaction to promote CO dissociation and/or migratory insertion of CO with the synergic bimetallic compositions, similar in nature to the organometallic adduct formation.[6]

SPECIFIC PROMOTION OF INORGANIC IONS FOR SYNGAS CONVERSION TO ALCOHOLS CATALYSED ON Rh, Ir AND Pd

Among the transition metal catalysts, Rh exhibits a unique catalytic activity of the syngas ($CO+H_2$) reaction to form carbon-two oxygenates such as C_2H_5OH, CH_2CHO and CH_3COOH. On the other hand, the typical Fischer–Tropsch (F–T) catalyst metals such as Fe, Co and Ru strongly dissociate CO (CO = [C]+[O]) and catalyse the preferential formation of methane and higher hydrocarbons in CO hydrogenation. In contrast, the metals at the opposite side of the Periodic Table (Fig. 1), Pt, Ir, Pd, and also including Cu, chemisorb CO non-dissociatively under the prevailing syngas reaction conditions, and catalyse the hydrogenation of chemisorbed CO prefentially to methanol. In this sense, rhodium is characterized by the intermediate catalyst metal in between the F–T metals and methanol synthesis metals. Its catalytic performance is inherently dependent upon the variables, e.g. temperature, CO/H_2 molar ratios and the presence of supports and some metal additives.

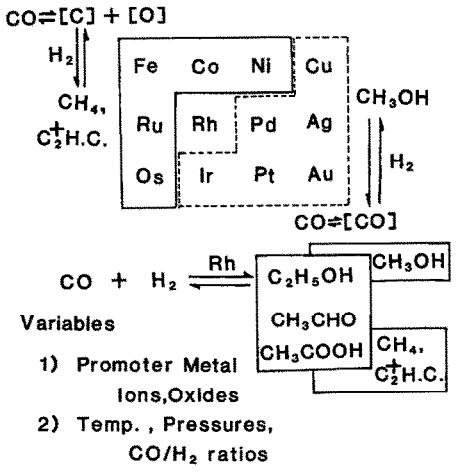

Fig. 1. Characterization of transition metals for CO chemisorption and CO hydrogenation.

In fact, we have recently found[7] that the product selectivities in CO hydrogenation were markedly influenced with the used metal oxide supports. This is illustrated in Table 1, where highly dispersed Rh crystallites, prepared by decomposing $Rh_4(CO)_{12}$ on the oxides of oxophilic elements including La, Nd, Ti, Zr, Nb and Mn, give C_2-oxygenates such as ethanol to a considerable extent. With a second group, including ZnO, MgO and CaO, methanol is almost exclusively formed, while with SiO_2 and γ-Al_2O_3 hydrocarbons are the only reaction product. Moreover, electropositive metal additives also exert a significant promotion in modifying activity and selectivity toward oxygenates in the $CO+H_2$ reaction catalysed on Rh.

As shown in Table 2, by the addition of oxophilic positive ions (e.g. Ti, Mn, and Zr to Rh/SiO_2), the $CO+H_2$ conversion is dramatically enhanced by a factor of 10–100 times compared to Rh alone, but

Table 1. Product selectivities in an atmospheric pressure $CO+H_2$ reaction over $Rh_4(CO)_{12}$-derived catalysts impregnated on various metal oxides

MO_x	T (°C)	CO conv. (%h)	Selectivity (C.E.%) MeOH	C_2—O	H.C.
ZnO	220	1.6	94	+	4
MgO	220	2.6	88	2	7
CaO	230	0.8	92	1	2
La_2O_3	205	3.0	38	43	10
Nd_2O_3	210	3.8	24	47	21
ZrO_2	215	4.4	13	50	36
TiO_2	210	6.0	6	40	51
Nb_2O_5	195	5.8	7	39	51
MnO_2	205	1.2	4	25	63
SiO_2	235	1.7	+	6	92
γ-Al_2O_3	250	8.6	+	+	99

$Rh_4(CO)_{12}/MO_x$, followed by decomposition at 120–200°C in a vacuum and in H_2. C_2—O, mainly EtOH and AcH.

$CO:H_2 = 20:45$ cm Hg in a closed circulating reactor (420 cm^3).

Table 2. Ethylene hydroformylation on Rh, RhFe and Fe carbonyl cluster-derived catalysts

Precursor/SiO_2 (0.5 wt% metal)	Fe/Rh	T.O.F. (mmol/Rh-mmol/min)		Selectivity for oxygenates (mol %)	Selectivity for alcohol (mol %)
		C_2H_6	EtCHO+PrOH		
$Rh_4(CO)_{12}$	0	0.006 (1)[a]	0.002 (1)[a]	28	0
$[FeRh_5(CO)_{16}]^-$	0.20	0.16 (30)	0.13 (61)	45	4
$[FeRh_4(CO)_{15}]^{2-}$	0.25	0.28 (53)	0.20 (96)	42	2
$[Fe_2Rh_4(CO)_{16}]^{2-}$	0.50	0.30 (57)	0.18 (86)	37	3
$Fe_3Rh_2(CO)_{14}C$	1.5	0.22 (41)	0.22 (107)	50	6
$[Fe_3(CO)_{11}]^{2-}$	—	0	0	—	—
$(Rh_4(CO)_{12}+[Fe_3(CO)_{11}]^{2-})/SiO_2$	0.26	0.039 (7)	0.036 (17)	48	0
$Rh_4(CO)_{12}/SiO_2+[Fe_3(CO)_{11}]^{2-}/SiO_2$	0.24	0.003 (0.6)	0.001 (0.6)	27	0

Reaction conditions: 135°C; C_2H_4: CO: H_2 = 20:20:20 cm^3 min^{-1}, 1 atm.
[a] Relative activities.

keeps the C_2-oxygenate selectivities.[4] In contrast, the other class of metal ions such as Fe, Mo and Zn substantially suppress hydrocarbon formation and provide a drastic change of oxygenated products, orienting toward alcohols such as CH_3OH and ethanol.[5] Additionally, when Rh–Ti/SiO_2 was combined with Fe to prepare the three-composite Rh–Ti–Fe/SiO_2 catalyst, it gave substantially higher selectivities toward ethanol with large CO conversions, as shown in Table 3. The cause of these promoter effects is still a challenging subject of research.

For the SiO_2-supported conventional Rh+Fe, Rh+Mo, Ir+Fe and Ir+Mo bimetal catalysts, promotion by Fe and Mo is quite remarkable for enhancing the production of C_1–C_2 alcohols in the CO+H_2 reaction.[8–10] As shown in Fig. 2, the effect of Fe added to Rh/SiO_2 is unexpectedly large and specific.[8,10] Basically the product distribution shifts from a mixture of CH_3CHO and CH_3COOH on Rh/SiO_2 to a mixture of C_2H_5OH and CH_3OH on RhFe/SiO_2. Fe/Rh ratios were below 0.3; the addition of Fe to Rh/SiO_2 did not influence the CO conversion, or the selectivity toward total oxygenates. The ethanol selectivity dramatically increases at the expense of CH_3CHO and CH_3COOH. With a large content of Fe, above Fe/Rh = 0.3 atomic ratio, the yield and selectivity of CH_3OH are not substantially enhanced, even compared with the increase of ethanol. The formation of methane and

Table 3. Performances of catalysts in the CO+H_2 conversion

Rh—M (1:x atom ratio)	CO conv (%)	Selectivity (C.E.%)					STY
		MeOH	AcH	EtOH	C_2—O	CH_4	C_2—O
4.6 wt% Rh	1.1	2	29	8	48	43	9
Rh—Ti(1:1)	12.3	3	3	27	40	47	78
Rh—Mn(1:1)	8.2	1	37	8	58	38	69
Rh—Fe(1:0.3)	2.3	27	1	30	32	38	12
Rh—Mo(1:0.3)	6.9	34	+	17	18	23	20
Rh—Zn(1:0.3)	0.2	89	+	3	5	4	0.2
Rh—Ti—Fe (1:1:0.3)	6.0	7	2	48	53	38	55

C.E. (carbon efficiency) = $iC_j \Big/ \sum_j iC_j \times 100(\%)$, STY (specific time yield) = g dm^{-3} cat/h. Catalysts: $RhCl_3+MCl_x/SiO_2$, H_2 red, 400°C. Reaction conditions: total pressure = 21 atm, CO/H_2 = 0.5 v/v, 250°C, SV = 6000 h^{-1}.

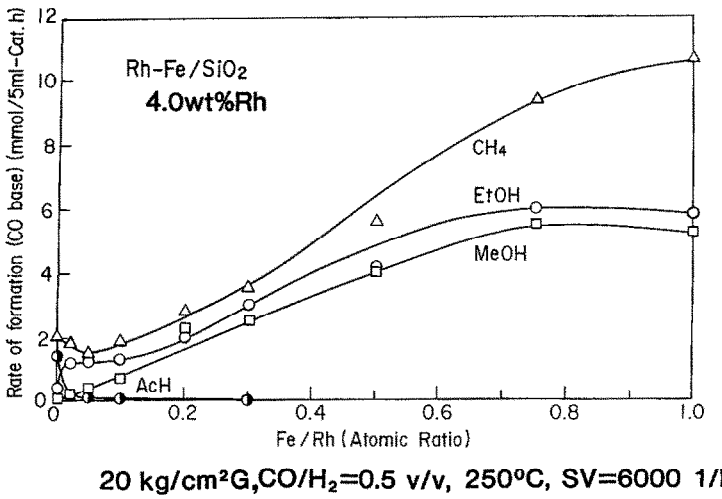

Fig. 2. Dependency of rates of formation (CO base) of products in the $CO+H_2$ reaction on Rh–Fe/SiO_2 by varying the Fe content.

higher hydrocarbons is suppressed by the addition of Fe.

Similarly, by the addition of Fe (or Mo) to Ir/SiO_2 catalysts a dramatic increase of CH_3OH yield[9] was observed, and at the same time, yields of methane were effectively suppressed as shown in Fig. 3. The optimum addition of Fe to Ir/SiO_2 resulted in the substantial improvement of selectivities toward methanol to above 90% selectivity in CO base. Incidentally, it is worth pointing out the problem of the promotion of Fe (or Mo) toward alcohol formation catalysed on the modified Rh and Ir. Generally, Fe and Mo including other typical F–T metals catalyse a preferential production of methane and higher hydrocarbons on their metal crystallites. Nevertheless, they apparently lose

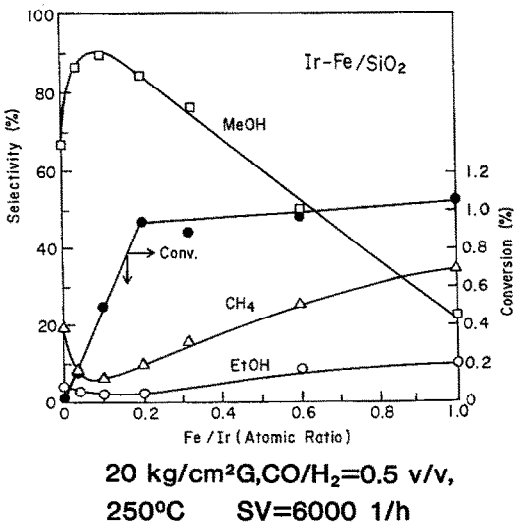

Fig. 3. Product selectivities and CO conversion in the $CO+H_2$ reaction on $Ir–Fe/SiO_2$ vs Fe/Rh atomic ratios; 4.0 wt% Ir loading, 5 cm^3 catalyst charged.

their original catalytic performances when they are combined with Rh and Ir. The resulting multimetal catalysts suppress the hydrocarbons, but rather promote the formation of alcohols. This might be associated with the different oxidation states of promoter elements or ensemble sizes of the constituent metals such as Rh (Ir, Pd and Fe, Mo) in the multimetal catalysts.

ELEMENTARY REACTIONS FOR SYNGAS CONVERSION TO OXYGENATES ON THE PROMOTED Rh

According to our previous ^{13}C-labelling tracer experiments on the promoted $Rh–Ti/SiO_2$, it has been demonstrated[10] that only the methyl carbon in C_2-oxygenates such as CH_3CHO and C_2H_5OH is enriched with the labelled ^{13}C derived from CO dissociation ($2*CO = [C^*]+*CO_2$), as shown in Fig. 4. In contrast, it is obvious that carbonyl fragments (e.g. CHO and CH_2OH) of the C_2-oxygenates were definitively based on the insertion of non-labelled gaseous CO. Similarly, the ^{13}C was not incorporated into the methanol produced on the $Rh–Ti/SiO_2$. Consequently, it appears probable that C_2-oxygenate formation consists of two essential steps, illustrated in Fig. 5. Primarily, CO dissociates (1) to provide surface alkyl groups (e.g. CH_3/CH_2), followed by the CO insertion; (2) with a methyl group to build up C_2-oxygenate in intermediates such as acyl "CH_3CO". This CO insertion competes with the hydrogenation (or H-elimination); (3) of surface alkyl groups, resulting in the formation of methane and higher hydrocarbons. Basically, we can predict that the former elementary step (1), namely CO dissociation, requires larger ensembles of Rh atoms (five or more surface Rh atoms) to activate CO in leading to cleavage of the triple CO

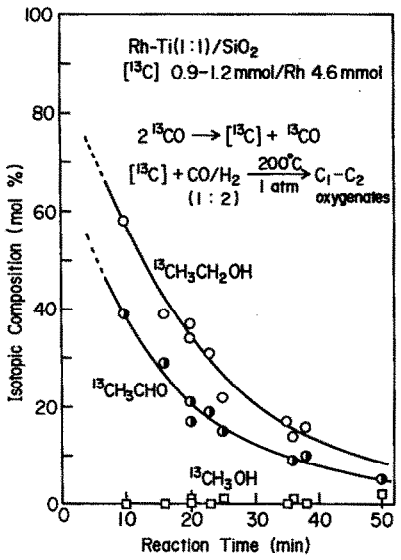

Fig. 4. ^{13}C isotopic composition of MeOH, EtOH and AcH in the reaction of $CO+H_2$ over $Rh–Ti/SiO_2$ labelled with ^{13}C deposited by ^{13}CO dissociation at 200°C.

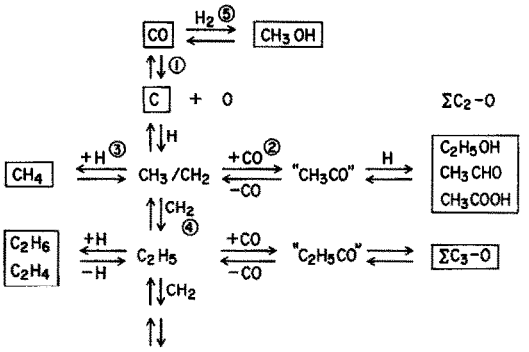

Fig. 5. Elementary steps for syngas conversion to oxygenates and hydrocarbons (see Ref. 8a).

bonds.[11] In the dissociative adsorption of CO, C and O atoms are bonded with different sites, where probably a pair of two contiguous hollow† sites are occupied. While the later migratory CO insertion reaction requires only the isolated Rh ion/atoms, in a manner comparable to the complexes,[12] e.g. $HRh(CO)_2(PPh_3)_2$, which are catalytically active in a homogeneous olefin hydroformylation. In fact, this hydroformylation (OXO) reaction is considered[13] as the common process for the formation of higher aldehydes and alcohols in the $CO+H_2$ reaction.

$$C_nH_{2n}+CO+H_2 = C_{n+1}H_{2n+1}CHO \quad (+C_{n+1}H_{2n+1}CH_2OH).$$

†That is, those adsorption sites which are used by metal atoms when an Rh crystal grows in its vapour ("Freundlich site").

On the other hand, methanol is produced by hydrogenation of non-dissociative CO via a formyl intermediate due to the CO insertion with metal hydride,[14,15] as follows:

$$M—H+CO \rightleftharpoons M—\underset{\underset{O}{\|}}{C}—H$$

$$\xrightleftharpoons{+H_2} M—OCH_3 \xrightleftharpoons{+H_2} CH_3OH \quad (M = Rh, Pt, Pt).$$

Accordingly, it could be imagined that the different mode of promotion due to each promoter ion would be related to how each promoter ion will influence one or two essential steps, e.g. CO dissociation, CO migratory insertion and/or $[CH_2]$ chain-growth for the oxygenate production in the $CO+H_2$ catalysed on the promoted Rh (or Pr, Pd) catalysts.

Based on recent studies,[16] three effects have been discussed in terms of the decoration model of Rh (or Pt, Pd) crystallites with the promoters such as Fe, Mo and Zn including Ti, Mn and Zr, which concentrate at the surface layer of the crystallites and/or interfaces of supporting oxides. We assume either:

1. The overlayer promoter ions stabilize electrodeficient atoms of the catalyst metals (e.g. Rh^+ and Pd^+).
2. The adsorbed ions (or atoms) block sites where CO would dissociate or form bridging bondings.
3. A direct chemical interaction due to the localized two-site activation of CO by the pair of the adjacent Rh (or Pd, Pt) atoms with promoter ions.

LOCATION AND ELECTRONIC STATES OF Fe ATOMS ON THE Fe-PROMOTED Rh CATALYSTS

The nature of the surface carbon monoxide was studied by IR spectroscopy. IR spectra for those of Fe, Mo and Zn promoted Rh are shown in Fig. 6. Two strong bands at 2065 and 1918 cm^{-1} for CO on Rh/SiO_2 are reasonably assigned to the linearly bonded (terminal) carbonyl and bridging carbonyl, respectively. In the absence of the positive promoters, the two bands are of comparable intensity. Interestingly, we found that the bridging CO band intensities were considerably decreased with increasing Fe (Mo, Zn) content, and eventually disappeared by the sufficient addition of Fe,[16] Mo (or Zn)[17] to Rh/SiO_2, while the linear CO band intensities were not affected. This could be explained in terms of a geometric ensemble effect[18] (site iso-

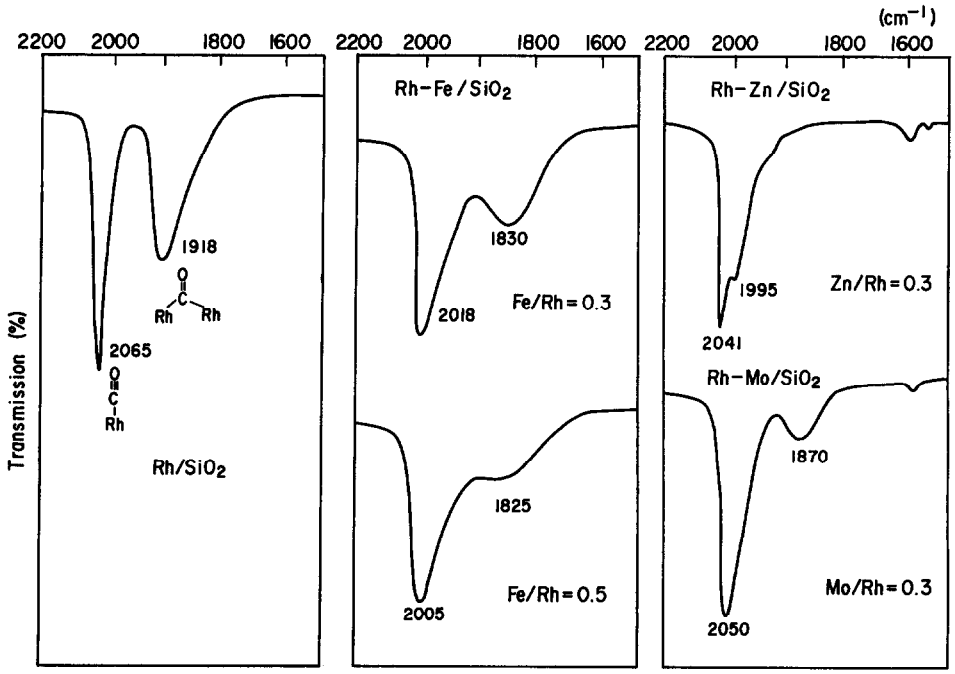

Fig. 6. IR carbonyl spectra in CO chemisorption on Fe-, Mo- and Zn-decorated Rh catalysts. Catalysts: 4.0 wt% Rh loading; CO pressure = 100–600 torr at 25°C in 10 min, replaced with He or *in vacuo*.

lation) due to Fe (Mo or Zn), which plausibly resides at a "hollow site" on the decorated Rh (or Ir) surface. Zn and Fe act as a breaker of the Rh (or Ir) ensemble and prevent the multibonding CO chemisorption. The similar mode of site-blocking to decrease bridged CO on Ru has been recently demonstrated[19] by Basset *et al.* on $Sn(CH_3)_4$-decorated catalysts. Site-blocking of promoter ions is nicely reflected in the marked suppression of CO dissociation, and thus the decrease of methanation on the Zn-, Fe- and Mo-modified Rh catalysts.

Recently, EXAFS studies were performed to get information on the nearest neighbour, the location, and the coordination circumstances around the modifier elements, e.g. Fe, Mo and Zn, in the promoted catalysts.[20] As shown in Fig. 7, Fe—K edge EXAFS provides direct evidence for the Rh—Fe bonding coordination (Rh—Fe: C.N. = 4–5, $R = 2.56$ Å) on the SiO_2-supported RhFe (Fe/Rh = 0.3) catalyst, but there is a small contribution of Fe—O bonding and negligible Fe—Fe bonding. On the other hand, the Rh—K edge (Fig. 8) spectrum shows a main peak of Rh—Rh bonding (C.N. = 9–11) and suggests that Rh exists in a bulk crystal (a closed packing structure) and Fe is concentrated in the surface layer of the RhFe particles. Independently, Mössbauer studies have been performed[21] and show that Fe in $RhFe/SiO_2$ and $IrFe/SiO_2$ preferentially exists in the state of Fe^{3+} (above 75% abundances). A small portion of Fe could be reduced to Fe^0 in the excess addition of Fe to Rh or Ir. These results imply that Fe species (Fe^{3+} and Fe^0) are decorated on Rh and Ir particles (in 20–30 Å sizes), and the mixed ensembles of Rh—Fe^0 lie possibly on the Rh surface and Rh—Fe^{3+} located at the metal–support interface. Fe^{3+} could be associated with the oxygen atoms sharing from the support SiO_2 and may play a role in anchoring Rh(Ir) ensembles to prevent sintering. The local model of the Fe-decorated Rh(Ir) particles, pictorially represented in Fig. 9, consists of two different bimetallic sites which serve not only as a site-blocking of Rh (or Ir) ensembles with Fe^0 but also as an acid-promoted activation of chemisorbed CO, possibly with positive ion, Fe^{3+}.

BIMETALLIC RhFe, PtFe AND PdFe CARBONYL CLUSTERS AS THE LOCALIZED MODEL OF THE PROMOTED MULTIMETALLIC CATALYSTS

The RhFe bimetallic carbonyl clusters having the different Fe/Rh atomic ratios, e.g. $[TMBA]_2$

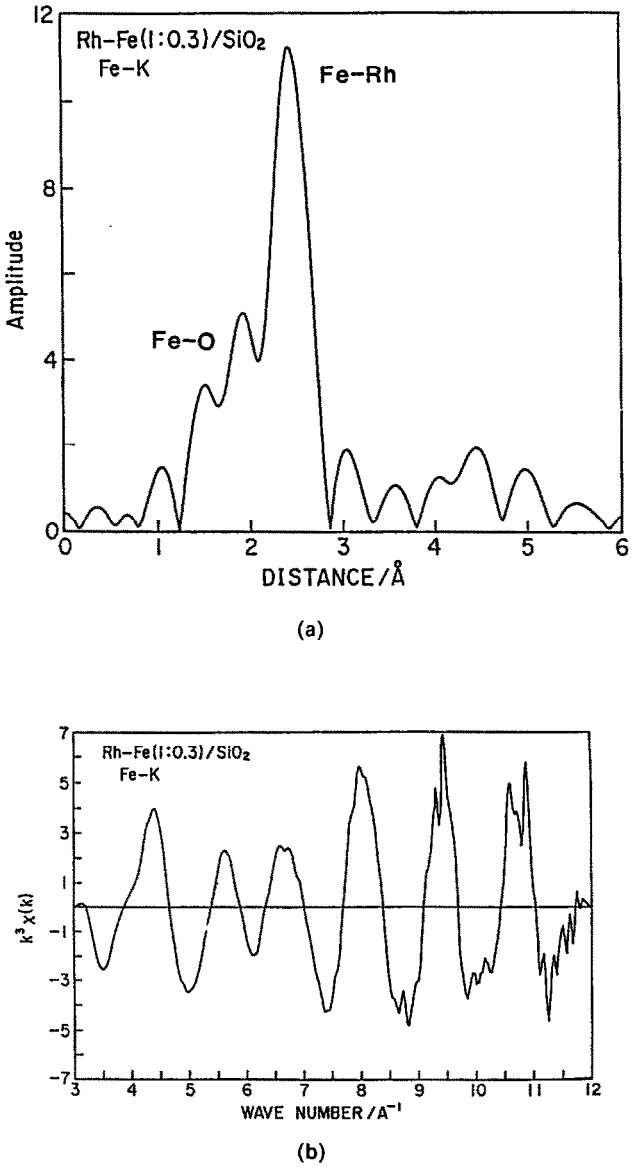

Fig. 7. (a) Fe—K-edge EXAFS oscillation $k^3\chi(k)$ and (b) its Fourier transform of the Rh–Fe/SiO_2 catalyst (Fe/Rh atomic ratio = 0.3, total metal 4.0 wt% loading after H_2 reduction at 400°C).

$[FeRh_5(CO)_{16}]$, $[NMe_4]_2[FeRh_4(CO)_{15}]$, $[TMBA]_2$ $[Fe_2Rh_4(CO)_{16}]$ and $Fe_2Rh_2(CO)_{14}C$ were synthesized according to literature methods.[21] They were employed as molecular precursors (Fig. 10) for the impregnation of well-characterized RhFe bimetal ensembles on SiO_2 support. The general catalyst preparation is as follows.

SiO_2 gel (Davison #57, 10–20 mesh, surface area = 280 $m^2\,g^{-1}$) was impregnated with each carbonyl cluster from a suitable organic solution (THF, acetone, acetonitrile). After removal of the solvent, the impregnated catalysts were oxidized in air at room temperature overnight and reduced in flowing H_2 (1 atm, 60 $cm^3\,min^{-1}$) as the temperature was raised from 200 to 400°C and held at 400°C for 2 h. On the other hand, a sample of a physical mixture of Rh and Fe ensembles was obtained by the impregnation of SiO_2 with a solution of $Rh_4(CO)_{12}$ and $Fe_3(CO)_{12}$ in THF, followed with the similar treatments to prepare the reduced catalysts. The structural properties of the resulting RhFe, Rh and Rh+Fe cluster-derived catalysts have been also determined by means of EXAFS, Mössbauer and FTIR in CO chemisorption. The gas phase hydroformylation of ethylene and propene has been carried out to evaluate the activities of CO inser-

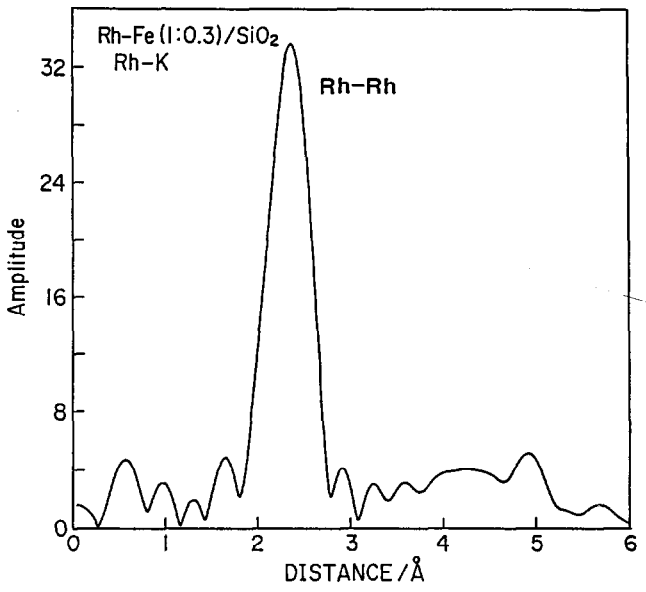

(a)

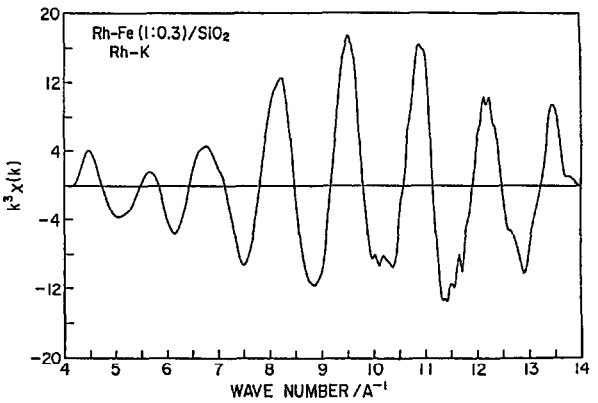

(b)

Fig. 8. (a) Rh—K-edge EXAFS oscillation $k^3\chi(k)$ and (b) its Fourier transform of the Rh–Fe/SiO_2 catalyst (Fe/Rh = 0.3, total metal 4.0 wt% loading after H_2 reduction at 400°C).

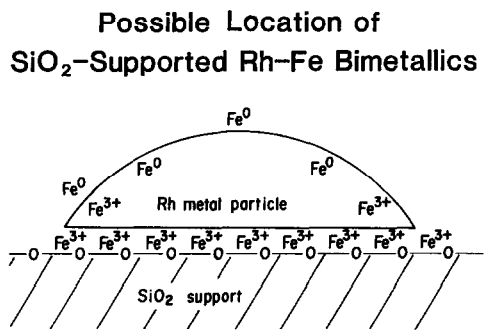

Fig. 9. A pictorial representation of the location of Fe (Fe^0, Fe^{3+}) in the reduced Rh–Fe/SiO_2 catalysts.

tion. This is an essential step for the formation of higher oxygenates and methanol in the $CO+H_2$ reaction, as has been mentioned earlier (Fig. 2).

CATALYTIC PERFORMANCES OF RhFe CARBONYL CLUSTER-DERIVED CATALYSTS IN OLEFIN HYDROFORMYLATION AND THE $CO+H_2$ REACTION

The hydroformylation of ethylene was studied as the test reaction. The results as shown in Table

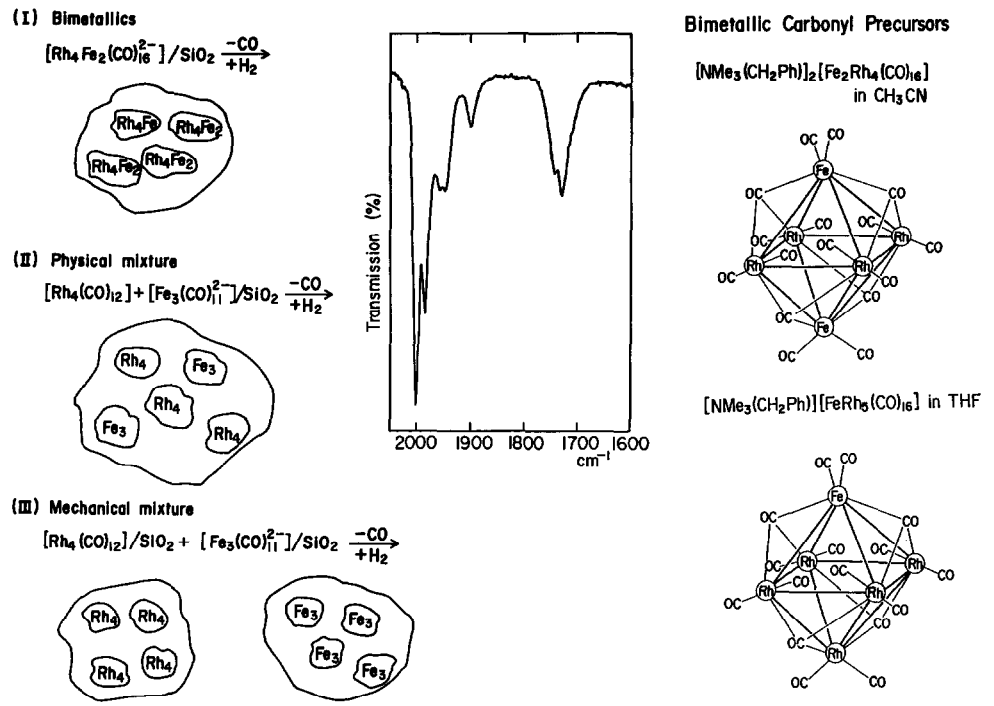

Fig. 10. RhFe bimetallic carbonyl clusters as the localized model precursors for the Fe-promoted Rh catalysts and pictorial representation of the tailored bimetal catalysts consisting of bimetallic $[Rh_4Fe_2]/SiO_2$, a physical mixture of $[Rh_4]+[Fe_3]/SiO_2$ and a mechanical mixture of $[Rh_4]/SiO_2 + [Fe_3]/SiO_2$.

4 substantiated[22] the marked promotion of Fe in enhancing CO insertion and alcohol conversion on the Rh_5Fe, Rh_4Fe, Rh_4Fe_2 and Rh_3Fe_2 carbonyl cluster-derived catalysts. In contrast, the catalysts from $Rh_4(CO)_{12}$ gave a negligible activity for the ethylene hydroformylation but a simple hydrogenation of ethylene to ethane proceeded preferentially. On the catalysts derived from $[Fe_3(CO)_{11}][TMBA]_2$, neither the hydroformylation nor the simple hydrogenation occurred at all under

Table 4a. Catalytic performances of SiO_2-supported RhFe carbonyl cluster-derived catalysts (250°C, $CO/H_2 = 0.5$, SV = 1000 l/l/h, total pressure = 5 kg cm^{-2} G)

Catalyst precursor/SiO_2 (2 wt% metal)	CO conv. (%)	Specific rates of product formation ($\times 10^{-3}$ mmol/min/mmol Rh) [Selectivity in CO base][a]					
		CH_3OH	CH_3CHO	C_2H_5OH[b]	CH_4	C_2^+H.C.	Oxygenate selectivity (%)
$Rh_4(CO)_{12}$	0.5	0.05 [0.4]	0.18 [3]	—	12 [97]	—	3.4
$[FeRh_4(CO)_{15}]^{2-}$	1.5	3.7 [8]	1.4 [6]	1.7 [7]	39 [79]	—	21
$[Fe_2Rh_4(CO)_{16}]^{2+}$	2.4	7.0 [7]	1.3 [3]	13 [33]	45 [56]	—	45
$RhCl_3+FeCl_3$ (Fe/Rh = 0.2; 4 wt% metal)	3.6	1.3 [3]	0.5 [2]	4.7 [20]	36 [75]	—	25

[a] $\%C.E. = \left(iC_j \Big/ \sum_j iC_j\right) \times 100$, where i = number of carbon atoms in a product molecule and C_j = concentration of molecule j.

[b] Including ethyl group in the form of acetate.

Table 4b. Catalytic performances of SiO_2-supported PtFe and PdFe carbonyl cluster-derived catalysts (250°C, $CO/H_2 = 0.5$, SV = 1000 l/l/h, total pressure = 5 kg cm^{-2} G)

Catalyst precursor/SiO_2 (2 wt% metal)	CO conv. (%)	Specific rates of product formation ($\times 10^{-3}$ mmol/min/mmol Pt, Pd) [Selectivity in CO base][a] CH_3OH	CH_4	C_2^+H.C.	CO_2	Oxygenate selectivity (%)
$[Pt_{12}(CO)_{24}]^{2-}$	0.1	4.2 [100]	—	—	—	100
$[Fe_3Pt_3(CO)_{15}]^{2-}$	0.2	13 [100]	—	—	—	100
$[Fe_4Pt(CO)_{16}]^{2-}$	1.7	12 [7]	31 [18]	23 [26]	88 [50]	7
H_2PtCl_6	0.03	1.5 [100]	tr	tr	—	~ 100
$[Fe_6Pd_6(CO)_{24}H]^{3-}$	0.5	20 [79]	5.4 [21]	—	—	79
$[Fe_4Pd(CO)_{16}]^{2-}$	1.1	12 [12]	36 [35]	16 [32]	21 [21]	12
$PdCl_2$	0.03	1.5 [100]	tr	tr	—	~ 100

[a] $\%C.E. = \left(iC_j \Big/ \sum_j iC_j\right) \times 100$, where i = number of carbon atoms in a product molecule and C_j = concentration of molecule j. tr, trace amount.

similar reaction conditions. Interestingly, the hydroformylation activity was dramatically increased on the catalysts derived from Fe-containing Rh carbonyl clusters, e.g. 62, 96, 86 and 107 times larger for the catalysts derived from $FeRh_5$, $FeRh_4$, Fe_2Rh_4 and Fe_3Rh_2 carbonyl clusters, respectively, compared with those on $Rh_4(CO)_{12}$ alone. Propanol as a further hydrogenation product was also obtained on Fe-rich bimetallic carbonyl cluster-derived catalysts, while the $Rh_4(CO)_{12}$-derived one gave only an aldehyde (C_2H_5CHO) as the hydroformylation product.

Similarly, an obvious Fe promotion was observed in the propene hydroformylation. Table 5 shows that rates of hydroformylation were increased on $FeRh_4$, Fe_2Rh_4 and Fe_3Rh_2 carbonyl cluster-derived catalysts by a factor of over 300 times over that on $Rh_4(CO)_{12}$. Moreover, the selectivities toward alcohols (iso- plus n-butanol) were substantially improved on Fe-rich RhFe bimetal cluster

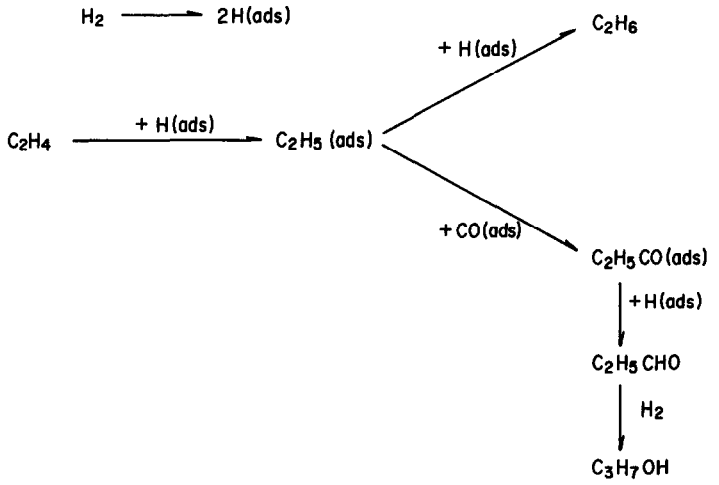

Scheme 1.

Table 5. Propylene hydroformylation on Rh, RhFe and Fe carbonyl cluster-derived catalysts

Precursor/SiO_2 (0.5 wt% metal)	Fe/Rh	T.O.F. (mmol/Rh-mmol/min) C_3H_8	T.O.F. (mmol/Rh-mmol/min) PrCHO+BrOH	Selectivity for oxygenates (mol %)	Selectivity for alcohol (mol %)	Selectivity for n-isomers (mol %)
$Rh_4(CO)_{12}$	0	~0.001	0.0003 (1)[a]	—	—	—
$Rh_4(CO)_{12}$[b]	0	0.027	0.004	13	0	75
$[FeRh_5(CO)_{16}]^-$	0.20	0.078	0.037 (129)	32	46	72
$[FeRh_4(CO)_{15}]^{2-}$	0.25	0.12	0.075 (262)	38	42	74
$[Fe_2Rh_4(CO)_{16}]^{2-}$	0.50	0.13	0.088 (306)	41	44	73
$Fe_3Rh_2(CO)_{14}C$	1.5	0.10	0.084 (294)	45	63	70
$[Fe_3(CO)_{11}]^{2-}$	—	0	0	—	—	—
$(Rh_4(CO)_{12}+[Fe_3(CO)_{11}]^{2-})/SiO_2$	0.26	0.015	0.010 (36)	41	33	78

Reaction conditions: 162°C; $C_3H_6:CO:H_2 = 20:20:20$ cm^3 min^{-1}, 1 atm.
[a] Relative activities.
[b] 4.0 wt% metal.

catalysts, giving the higher (70–75% molar selectivity) normal-alcohols. It is difficult to simply explain such a remarkable enhancement of hydroformylation activity and substantial increase of alcohol selectivities by the addition of products catalysed on the individual Rh and Fe atoms in the catalysts. To rationalize the promotional role of Fe, a physical mixture $[Rh+Fe]/SiO_2$ catalyst was prepared from a THF solution of $Rh_4(CO)_{12}$ and $[TMBA]_2[Fe_3(CO)_{11}]$ (Fe/Rh atomic ratio = 0.26) impregnated on SiO_2. The resulting H_2-reduced catalyst gave much lower activity for the ethylene (and propene) hydroformylation and a negligible alcohol conversion compared to that for $[TMBA]_2[FeRh_4(CO)_{15}]$ (Fe/Rh = 0.25). For comparison, a mechanical mixture of $Rh_4(CO)_{12}/SiO_2$ and $[TMBA]_2[Fe_3(CO)_{11}]/SiO_2$ (Fe/Rh = 0.24) was prepared from the individual clusters, followed by the subsequent hydrogen reduction. The mechanically mixed catalyst ($Rh/SiO_2+Fe/SiO_2$) gave negligible or lower activities for ethylene hydroformylation, and no selectivity toward alcohol products, which is similar to those on the $Rh_4(CO)_{12}$ catalyst. Accordingly, the results suggest that RhFe bimetal carbonyl clusters provide the discrete intact ensemble of RhFe atoms substantially active for the olefin hydroformylation, and for the successive hydrogenation to give higher alcohols. The higher order of the enhancement for the hydroformylation over the simple hydrogenation of olefins on the Fe-containing Rh cluster-derived catalysts, resulted in the appreciable improvement of oxygenate selectivities.

SELECTIVE CO HYDROGENATION TO C_1–C_2 ALCOHOLS ON RhFe, PtFe AND Pd BIMETAL CLUSTER-DERIVED CATALYSTS

Similarly, the PtFe and PdFe bimetal cluster-derived catalysts (0.5–2.0 wt% metal loading) were also prepared by using $[Fe_3Pt_3(CO)_{15}][TMBA]_2$, $[Fe_4Pt(CO)_{15}][TMBA]$, $[HFe_6Pd_6(CO)_{24}][TMBA]_3$ (Fig. 11a,b) and $[Fe_4Pd(CO)_{16}][TMBA]_2$[23] which were impregnated on SiO_3 gel, followed with the H_2 reduction at 400°C. A $CO+H_2$ reaction was conducted at 230–270°C with an open-flow mode stainless-steel reactor (5–10 kg cm^{-2}, $CO/H_2 = 0.5$ v/v, SV = 1000 h^{-1}). The results for the CO hydrogenation on the catalysts derived from RhFe, PtFe and PdFe bimetal carbonyl clusters are exemplified in Table 4.[24] It was of interest to find that the rates of oxygenates consisting mainly of methanol and ethanol were substantially enhanced on the Rh_4Fe_2 and Rh_4Fe carbonyl cluster-derived catalysts, compared with those on the $Rh_4(CO)_{12}$-derived one. Fe promotion for production of C_1–C_2 alcohols is quite remarkable on the Fe-containing Rh bimetal cluster-derived catalysts even compared with the conventional RhFe catalysts from the chlorides. Moreover, the hydrocarbon formation was considerably suppressed on the RhFe cluster-derived catalysts, possibly due to the site-blocking of the RhFe ensembles. This is similar to the conventional Fe (Mo, Zn) decorated Rh mentioned earlier. The Fe promotion toward alcohol synthesis was also observed on the catalysts from the Fe-containing Pt and Pd bimetal carbonyl clusters, where methanol

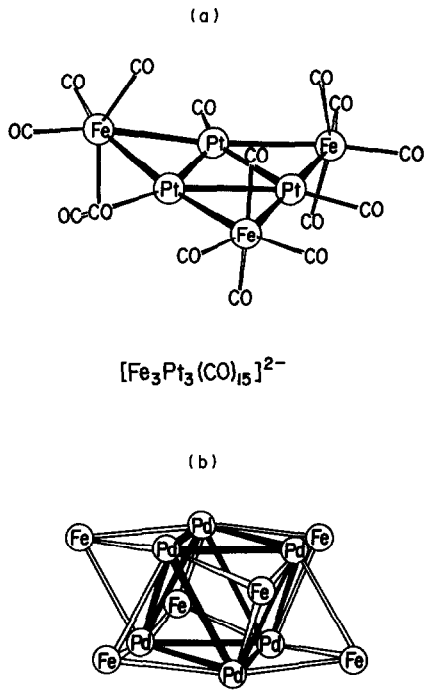

Fig. 11. Structures of Pt_3Fe_3 (a) and Pd_6Fe_6 (b), with the carbonyl ligands omitted; carbonyl clusters as the precursors for the preparation of PtFe and PdFe bimetal cluster-derived catalysts.

yields were strikingly enhanced in higher selectivities (near 100% in CO base). The Fe_4Pt- and Fe_4Pd-derived catalysts gave an appreciable amount of methane and higher hydrocarbons with methanol. This might be explained by the cluster segregation in the catalyst preparation, resulting in the isolated Fe particles active for the typical F–T synthesis of hydrocarbons.

EXAFS, MÖSSBAUER AND IR CHARACTERIZATION OF THE RhFe AND PtFe BIMETAL CLUSTER-DERIVED CATALYSTS

The structure and location of the RhFe and PtFe bimetal carbonyl cluster-derived catalysts have been studied by means of EXAFS, Mössbauer and FTIR in CO chemisorption.[24,25]

The Fourier transform of Rh—K and Fe—K EXAFS on the H_2-reduced samples prepared from SiO_2-supported $[Rh_4Fe_2][TMBA]_2$ (4 wt% Rh) suggest that the RhFe bimetal ensembles are formed in a high dispersion (around 10 Å in size) and have direct Rh—Fe—O bondings (Rh—Rh: C.N. = 7.2, R = 2.65 Å and Rh—Fe: C.N. = 1.8, R = 2.54 Å). A relatively large contribution of Fe—O bonding (Rh—O: C.N. = 3.0, R = 1.99 Å) was obtained, compared with that of Rh—CO (C.N. = less than 1.0, R = 2.03 Å). Mössbauer measurements of the sample gave an absorption band which could be resolved into a singlet and pair of quadrupole doublets (Fig. 12). They were reasonably assigned to Fe^0 and Fe^{3+}, respectively. No band for Fe^{2+} was observed. The results imply that Fe atoms in the Rh_4Fe_2- and Pt_3Fe_3-derived catalysts are mostly in the state of Fe^{3+} (more than 85% abundance after the recoilless-factor correction) even after the H_2 reduction at 400°C. This could be explained in terms of the localized mode of RhFe and PtFe ensembles on silica as shown in Fig. 9, where Fe^{3+} is located in between Rh (or Pt) clusters and the silicon dioxide interface. It seems the electropositive Fe plays a role in anchoring the small ensembles of Rh and Pt atoms and prevents a sintering under the reduction and $CO+H_2$ reaction conditions. It also affects the catalytic performance of Rh, Pt and, possibly, Pd in promoting the activity toward C_1–C_2 alcohols in CO hydrogenation, as mentioned before. On the other hand, the FTIR spectrum was observed in CO

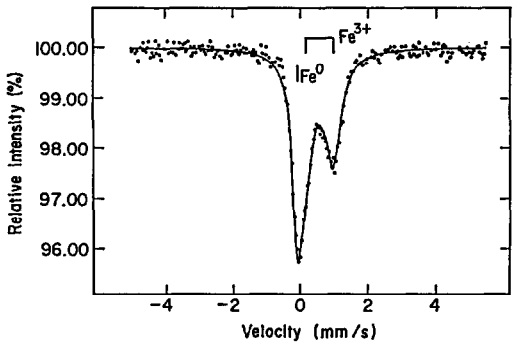

	I.S.(mm/s)	Q.S.(mm/s)	Area(%)
Fe^0	-0.09	—	26
Fe^{3+}	0.55	0.83	73

Fig. 12. ^{57}Fe Mössbauer spectrum of SiO_2-supported $[Rh_4Fe_2(CO)_{16}][NMe_3CH_2Ph]_2$-derived catalysts (4 wt% metal loading, after H_2 reduction at 400°C in 2 h) and the Mössbauer parameters obtained.

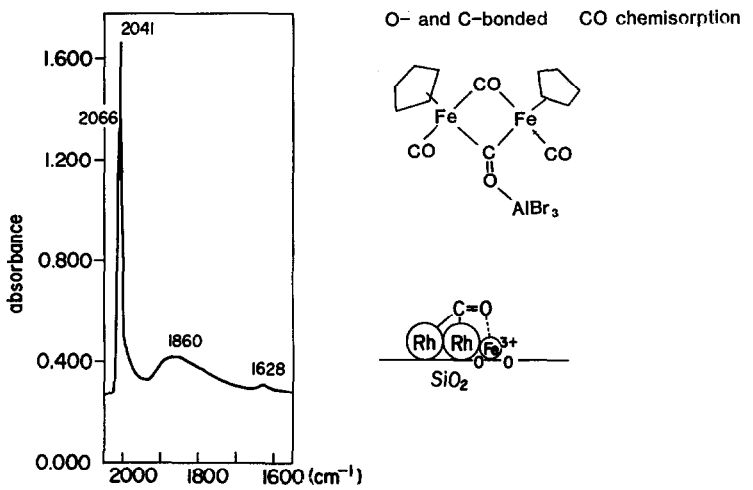

Fig. 13. The IR spectrum in CO chemisorption on the reduced sample of SiO_2-supported $[Rh_4Fe_2(CO)_{16}][NMe_3CH_2Ph]_2$: H_2 reduction at 350°C, 2 h. CO (22 torr) at 25°C.

chemisorption on the H_2-reduced catalyst derived from Rh_4Fe_2/SiO_2 (Fig. 13). In addition to the strong linear CO band at 2058 cm^{-1} and a bridging CO band at 1806 cm^{-1}, comparatively weaker than on the $Rh_4(CO)_{12}$-derived one, it is worthy to note a lower frequency band appearing at 1628 cm^{-1}. This may arise from C- and O-bonded interaction of CO chemisorbed on the adjacent Rh—Fe^{3+} ensemble. In homogeneous organometallic chemistry Shriver *et al.* have suggested that a similar bifunctional activation of CO is observed in the stoichiometric adduct formation between organometallic carbonyl complexes (e.g. $Fe_2(CO)_9$ and $Fe_4(CO)_4Cp_4$) and Lewis acid reagents such as $AlBr_3$ and BF_3, even on the Al_2O_3 surface (Fig. 13), due to C- and O-bonded interactions.[6] Additionally, it has been reported by Burwell and Shriver that such a Lewis acid reagent could greatly enhance the rate of migratory CO insertion with the methyl group of $MeMn(CO)_4$ to make an acetyl complex due to the adduct formation. Accordingly, it is conceivable that Fe^0 atoms act as an inert breaker to divide the Rh (or Pt) ensembles into isolated Rh atoms. On the other hand, an electropositive $Fe(Fe^{3+})$ in the RhFe ensembles has a bifunctional role as a Lewis acid–promoter to enhance CO migratory insertion and to stabilize formyl and acetyl intermediates which are eventually converted into methanol and ethanol in hydrogenation (see Scheme 2).

ZEOLITE-ENTRAPPED $Rh_6(CO)_{16}$ AND BIMETAL RhFe CLUSTERS AS TAILORED METAL CATALYSTS FOR OLEFIN HYDROFORMYLATION

We have recently tried to prepare the well-characterized Rh, Fe and bimetallic RhFe clusters entrapped inside NaY zeolite supercages[26] by means of a "ship-in-bottle synthesis" (Fig. 14). $[Rh_6(CO)_{16}]$/NaY (2 wt% Rh) was synthesized by the reaction of CO/H_2 and Rh^{3+}/NaY, as previously reported.[24] $[HFe_3(CO)_{11}]$/NaY (2–5 wt% Fe) was also prepared in the reaction of NaY with $Fe_2(CO)_9$ at 343 K. $HFe_3(CO)_{11}$, formed on the external zeolite surface, could be extracted as the salts by washing with a tetraglyme solution of bulky alkyl ammonium bromides such as $[(n\text{-}C_6H_{13})_4N]Br$. The bimetallic RhFe carbonyl clusters inside NaY frameworks were prepared by the reaction between $[HFe_3(CO)_{11}]$/NaY and Rh carbonyls such as $Rh_4(CO)_{12}$ *in vacuo* at 373 K. NaY

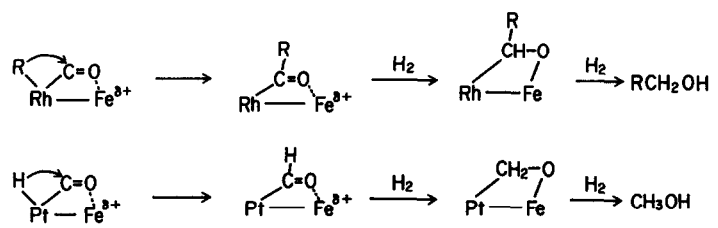

Scheme 2. Two-site interaction of C- and O-bonded CO with Rh and $Fe^{\delta+}$ (Pt and $Fe^{\delta+}$).

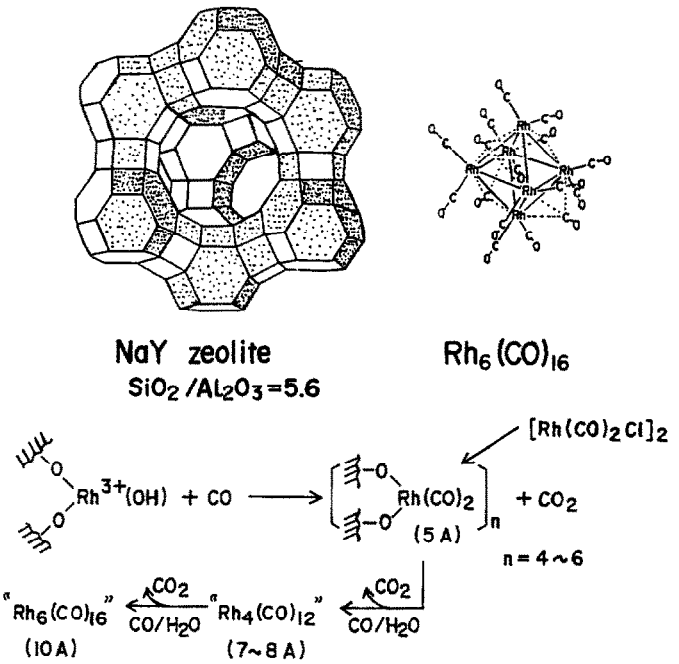

Fig. 14. Zeolite-entrapped Rh_6 carbonyl clusters and preparation by means of a "ship-in-bottle synthesis".

zeolite-entrapped Rh_6 and RhFe bimetallic carbonyl clusters showed the characteristic IR carbonyl spectra in Figs 15 and 16. The band at 1760 cm^{-1} in Fig. 15 is due to the triply bridging CO of $Rh_6(CO)_{16}$ interacting with Al^{3+} (or Na^+) located on the wall of an NaY supercage. As shown in Table 6, the Rh—K-edge EXAFS data on $[Rh_6(CO)_{16}]$/NaY, in comparison with those of $Rh_6(CO)_{16}$ in the crystal, provided direct evidence for the stoichiometric formation of hexanuclear Rh carbonyls inside an NaY supercage, but with a small contribution of Rh—O bonding with the oxide wall. After oxidation of $[Rh_6(CO)_{16}]$/NaY by heating from 293 to 423 K in O_2 to eliminate CO, followed with hydrogen reduction at 473–673 K by flowing H_2, the reduced sample, $[Rh_6]$/NaY, was obtained. The EXAFS analysis for $[Rh_6]$/NaY substantiated the retention of an Rh cluster unit in the reduced

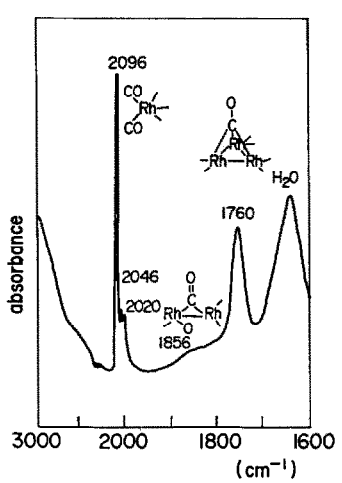

Fig. 15. The IR carbonyl spectrum of $Rh_6(CO)_{16}$ entrapped inside NaY zeolite.

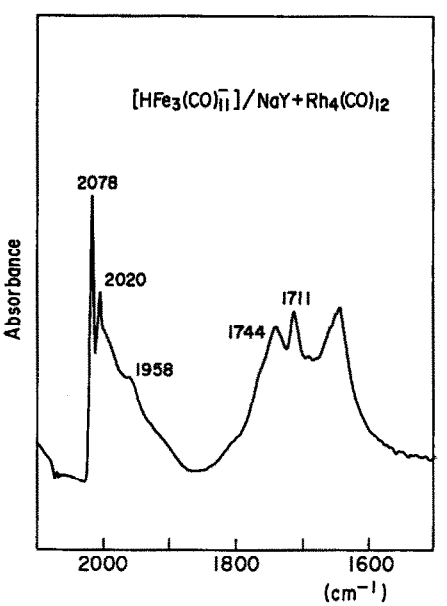

Fig. 16. The IR carbonyl spectrum of the resulting RhFe bimetal carbonyl clusters prepared by the reaction of $[HFe_3(CO)_{11}^{2-}]$/NaY with $Rh_4(CO_{12})$ *in vacuo*.

Table 6. Results of the curve-fitting analysis of EXAFS data for Rh_6 clusters in NaY zeolite

Sample	Rh—*C*O(terminal) C.N.	R (Å)	Rh—*C*O(bridge) C.N.	R (Å)	Rh—O(support) C.N.	R (Å)	Rh—Rh C.N.	R (Å)
$[Rh_6(CO)_{16}]$/NaY	1.5	1.88	1.6	2.15	1.9	2.06	3.1	2.74
$[Rh_6]$/NaY (473 K red.)	—	—	—	—	0.7	2.10	4.6	2.70
$[Rh_6]$/NaY (673 K red.)	—	—	—	—	0.7	2.09	4.6	2.70
$[Rh_6]$/NaY+CO	1.4	1.85	1.4	2.15	0.8	2.03	3.2	2.72
$Rh_6(CO)_{16}$	2.1	1.97	2.0	2.17	—	—	4.0	2.76

state in terms of coordination number and atomic distance (Rh—Rh: C.N. = 4.6, R = 2.7 Å). In CO chemisorption on $[Rh_6]$/NaY the EXAFS data in Table 8 suggest that the Rh ensembles of less than 10 Å size still retain their Rh—Rh frameworks (Rh—Rh: C.N. = 3.2, R = 2.72 Å) and result in the carbonyl clusters which are also partially linked to the zeolite–oxide wall (Rh—O: C.N. = 0.8, R = 2.03 Å). The results suggest that the Rh_6 clusters are accommodated and stabilized inside zeolite frameworks, whatever the treatment and temperature, and without formation of large crystallites on the external zeolite surface. Interestingly, the resulting RhFe bimetal carbonyl clusters, RhFe/NaY, obtained by the reaction of $[HFe_3(CO)_{11}]$/NaY and $Rh_4(CO)_{12}$, gave the IR carbonyl bands (Fig. 16), which considerably resemble those of $[TMBA]_2[Rh_4Fe_2(CO)_{16}]$[23] deposited on NaY from THF solution (2093(s), 2044(w), 1741(m), 1711(m) and 1689(w) cm^{-1}).

An atmospheric pressure hydroformylation of ethylene and propene was conducted on $[Rh_6]$/NaY and RhFe/NaY, and the results are presented in Tables 7 and 8, respectively. Acetaldehyde was catalytically obtained as the hydroformylation product on $[Rh_6]$/NaY. In contrast, it is of interest to find that the bimetallic RhFe/NaY catalyst gave much higher activities and selectivities for the normal-rich alcohol formation rather than $[Rh_6]$/NaY. A simple hydrogenation of olefins was suppressed on the RhFe/NaY, resulting in the marked improvement of oxygenate selectivities. $[HFe_3(CO)_{11}]$/NaY was completely inactive for both hydroformylation and a simple hydrogenation of ethylene and propene under similar reaction conditions. On the other hand, a physical mixture catalyst, $[Rh_6]+[Fe_3]$/NaY, consisting of isolated Rh_6 and Fe_3 entrapped inside zeolite cages, was prepared by the reaction between presynthesized $[Rh_6(CO)_{16}]$/NaY and $Fe_2(CO)_9$ in the presence of water vapour at 343 K. The resulting sample showed the IR carbonyl spectrum apparently consisting of a simple addition between those of $[Rh_6(CO)_{16}]$/NaY and $[HFe_3(CO)_{11}]$/NaY. The reduced sample of the $[Rh_6]+[Fe_3]$/NaY showed activities and selectivities in the ethylene and propene hydroformylation reactions almost the same as those obtained on $[Rh_6]$/NaY as shown in Table 8. Additionally, it was of interest to find that the bimetallic RhFe/NaY (and RhFe/NaX)

Table 7. Hydroformylation of ethylene on $[Rh_6]$/NaY and RhFe/NaY catalysts[a]

Catalyst/NaY	Specific rates of formation[b] (min^{-1}) C_2H_6	$C_2H_5CHO+C_3H_7OH$	Selectivity (mol %) Oxygenates[c]	Alcohol[d]
$[Rh_6]$	0.074	0.022	23	3.8
$[Rh_6]+[Fe_3]$	0.081	0.029	26	2.8
RhFe	0.12	0.068	37	33

[a] Reaction temp., 150°C; flow rate, $C_2H_4:CO:H_2 = 20:20:20$ cm^3 min^{-1}; total pressure, 1 atm.

[b] mmol $mmol_{Rh}^{-1}$ min^{-1}.

[c] $(EtCHO+PrOH)/(C_2H_6+EtCHO+PrOH)\times 100$.

[d] $PrOH/(EtCHO+PrOH)\times 100$.

Table 8. Hydroformylation of propene on $[Rh_6]$/NaY and RhFe/NaY catalysts[a]

Catalyst/NaY	Specific rates of formation[b] (min^{-1})		Selectivity (mol %)		
	C_3H_8	$C_3H_7CHO+C_4H_9OH$	Oxygenates[c]	Alcohol[d]	n-isomers[e]
$[Rh_6]$	0.034	0.0038	10	8	57
$[Rh_6]+[Fe_3]$	0.038	0.0057	13	11	57
RhFe	0.042	0.011	21	73	78

[a] Reaction temp., 175°C; flow rate, $C_3H_6:CO:H_2 = 20:20:20$ cm^3 min^{-1}; total pressure, 1 atm.

[b] mmol $mmol_{Rh}^{-1}$ min^{-1}.

[c] $(PrCHO+BuOH)/(C_3H_8+PrCHO+BuOH)\times 100$.

[d] $BuOH/(PrCHO+BuOH)\times 100$.

[e] (butanal + butanol)/$(PrCHO+BuOH)\times 100$.

samples provided a good yield of oxygenates, consisting mainly of EtOH and MeOH at the expense of decreasing the yields of methane and higher hydrocarbons. With the $[Rh_6]$/NaY and $[Rh_6]+[Fe_3]$/NaY catalysts only CH_3CHO was formed in lower selectivities as the oxygenate product. The results also showed that the adjacent RhFe bimetal ensembles are essential for the promotion of hydroformylation activity in enhancing CO insertion with M—H and M—alkyl groups to make methanol and higher alcohols. The results are similar to those previously proposed on the catalysts derived from SiO_2-supported RhFe and carbon-supported RuCo bimetal carbonyl clusters.[27]

CONCLUSIONS

Fe-containing Rh, Pt and Pd bimetallic carbonyl clusters were employed as the potential precursors to provide highly dispersed bimetallic sites impregnated on SiO_2 and entrapped inside zeolite frameworks. The structural characterization by means of EXAFS, Mössbauer and FTIR spectroscopies suggested that the resulting bimetal cluster-derived catalysts were well behaved in terms of ensemble sizes, metal compositions, and oxidation states (Fe^0 and Fe^{3+}) of the promoter Fe. They are highly active for C_1–C_2 alcohols in the $CO+H_2$ reaction. Fe^0 acts as an inert breaker of the Rh (Pt or Pd) ensembles in forming alloy block sites for bridging CO chemisorption. This results in the effective suppression of CO dissociation. This is reflected in the decrease of hydrocarbon formation in the reaction catalysed on Fe (Mo, Zn) decorated Rh (Pt, Pd) catalysts.

$RhFe^{3+}$ (or $PtFe^{3+}$, possibly $PdFe^{3+}$) pairs impregnated from bimetallic carbonyl clusters on SiO_2 effectively promote the migratory insertion, as judged by the rate enhancement of the olefin hydroformylation. This is reflected in the promotion of C_1–C_2 alcohols on RhFe catalysts and similarly MeOH synthesis on PtFe and PdFe catalysts in the $CO+H_2$ reaction.

NaY(NaX) zeolite-entrapped RhFe bimetallic carbonyl clusters have been prepared by *in situ* synthesis. Compared to $[Rh_6]$/NaY and a physically mixed $[Rh_6]+[Fe_3]$/NaY, RhFe/NaY exhibited a marked increase of the activities and selectivities toward MeOH and EtOH in $CO+H_2$ and toward normal-alcohols in propene hydroformylation.

From the above results, Fe promotion is proposed to be interpreted in terms of C- and O-bonded CO activation to enhance CO insertion with M—H and M—alkyl intermediates on the contiguous heteronuclear $RhFe^{3+}$ ($PtFe^{3+}$, $PdFe^{3+}$ also) pair sites, which are located at the interface between Rh (or Pt, Pd) ensembles and the supporting SiO_2 (and the oxide wall of the zeolite supercages).

Acknowledgements—I am greatly indebted to Atsushi Fukuoka, Takuma Kimura and Rao Ling-fen at The Research Institute for Catalysis, Hokkaido University for their contributions in the related research works on cluster-derived heterogeneous catalysts, and Dr N. Kosugi and Prof. H. Kuroda at Tokyo University for their EXAFS evaluation and discussion. Additionally, I am greatly appreciative of Dr Y. Sakai, Ms M. Tanaka and Prof. T. Tominaga at Tokyo University for their contribution in the Mössbauer measurements and helpful discussion on the data. Finally, I wish to express my thanks to Profs W. M. H. Sachtler and D. F. Shriver at Northwestern University for their helpful and stimulating discussion and collaboration on the promotion roles of inorganic ions and heteronuclear interaction of bimetal clusters.

REFERENCES

1. M. Ichikawa, in *Tailored Metal Catalysts* (Edited by Y. Iwasawa), pp. 183–263. D. Reidel, Dordrecht (1985); B. C. Gates, L. Guczi and H. Knozinger, in *Metal Clusters in Catalysis*, p. 415. Elsevier, Amsterdam (1986) and refs therein; A. Choplin, L. Huang, P. Theolier, P. Gallezot, J. M. Basset, U. Siriwardane, S. G. Shore and R. Mathieu, *J. Am. Chem. Soc.* 1986, **108**, 4224; M. Ichikawa, *J. Catal.* 1979, **56**, 127; **59**, 57; *Homogeneous and Heterogeneous Catalysis* (Edited by Y. I. Yermakov), pp. 819–835. NUV Press, Utrecht (1986); M. Kaminsky, K. J. Yoon, G. L. Geoffroy and M. A. Vannice, *J. Catal.* 1985, **91**, 338.
2. M. Ichikawa, *Chemtech* 1982, **12**, 674; J. Phylips and J. A. Dumesic, *Appl. Catal.* 1984, **9**, 1; J. Zwart and R. Nel, *J. Molec. Catal.* 1985, **30**, 305.
3. J. R. Anderson, *Adv. Catal.* 1973, **23**, 1; G. Maire, in *Metal Clusters in Catalysis* (Edited by B. C. Gates *et al.*), pp. 509–545. Elsevier, Amsterdam (1986); M. Araki and V. Ponec, *J. Catal.* 1981, **57**, 397; W. M. H. Sachtler, *Proc. 8th Int. Congr. Catal.*, Vol. I, p. 151. Berlin (1984).
4. P. C. Ellgen, W. J. Bartley, M. M. Bhasin and T. P. Wilson, *Adv. Chem. Ser.* 1979, **178**, 147; M. Ichikawa, K. Shekizawa, K. Shikakura and M. Kawai, *J. Molec. Catal.* 1981, **11**, 167; M. Ichikawa, T. Fukushima and K. Shikakura, *Proc. 8th Int. Congr. Catal.*, Vol. II, p. 69. Berlin (1984).
5. M. M. Bhasin, W. Bartley, P. C. Ellgen and T. P. Wilson, *J. Catal.* 1978, **54**, 120; T. Fukushima, H. Arakawa and M. Ichikawa, *J. Phys. Chem.* 1985, **89**, 4440.
6. C. P. Hortwitz and D. F. Shriver, *Adv. Organomet. Chem.* 1984, **23**, 219.
7. M. Ichikawa, *Bull. Chem. Soc. Japan* 1978, **51**, 2268; *J. Chem. Soc., Chem. Commun.* 1978, 697.
8. (a) W. M. H. Sachtler and M. Ichikawa, *J. Phys. Chem.* 1986, **90**, 475; (b) J. M. Driessen, E. K. Poels, J. P. Hindermann and V. Ponec, *J. Catal.* 1983, **82**, 26.
9. M. Ichikawa and T. Fukushima, *J. Chem. Soc., Chem. Commun.* 1985, 321; H. Orita, S. Naito and K. Tamaru, *ibid.* 1984, 150.
10. P. Biloen and W. M. H. Sachtler, *Adv. Catal.* 1980, **30**, 165; J. A. Rabo, A. P. Risch and M. L. Poutsma, *J. Catal.* 1978, **53**, 295.
11. O. Roelen, *Chem. Exp. Didak.* 1977, **3**, 119.
12. A. Takeuchi and J. R. Katzer, *J. Phys. Chem.* 1981, **85**, 937; H. Yamazaki, Y. Kobori, S. Naito, T. Onishi and K. Tamaru, *J. Chem. Soc., Faraday Trans.* 1981, **77**, 2913.
13. M. Ichikawa, K. Shikakura and M. Kawai, *Proc. China–Japan–US Symp. Heterogeneous Catal. Rel. Energy. Prob.*, A08J. Dalian (1982).
14. G. Yagupsky, C. K. Brown and G. Wilkinson, *J. Chem. Soc. A* 1970, 1392; R. L. Pruett, *Adv. Organomet. Chem.* 1979, **17**, 1; S. Siegel, *J. Catal.* 1973, **30**, 139.
15. T. Fukushima, Y. Ishii, Y. Onda and M. Ichikawa, *J. Chem. Soc., Chem. Commun.* 1985, 1752.
16. M. Ichikawa and T. Fukushima, *J. Phys. Chem.* 1985, **89**, 1564.
17. M. Ichikawa, A. J. Lang, D. F. Shriver and W. M. H. Sachtler, *J. Am. Chem. Soc.* 1985, **107**, 7216.
18. Y. Soma-Noto and W. M. H. Sachtler, *J. Catal.* 1974, **32**, 315; M. Primet, M. V. Matthieu and W. M. H. Sachtler, *ibid.* 1976, **44**, 324.
19. L.-Y. Hsu, S. G. Shore, L. D'Ornelas, A. Choplin and J.-M. Basset, *Polyhedron* 1988, **7**, 2399.
20. M. Ichikawa, T. Fukushima, T. Yokoyama, N. Kosugi and H. Kuroda, *J. Phys. Chem.* 1985, **90**, 1222.
21. Y. Minai, T. Fukushima, M. Ichikawa and T. Tominaga, *J. Radioanal. Nucl. Chem.* 1984, **87**, 189; J. W. Niemantsverdriet, A. M. van der Kraan and W. N. Delgas, *J. Catal.* 1984, **89**, 138.
22. A. Ceriotti, G. Longoni, R. D. Pergola, B. T. Heaton and D. O. Smith, *J. Chem. Soc., Dalton Trans.* 1983, 1433; J. A. Hriljac, E. M. Holt and D. F. Shrivert, *Inorg. Chem.* 1987, **26**, 2943.
23. G. Longoni, M. Manassero and M. Sansoni, *J. Am. Chem. Soc.*1985, **102**, 3243, 7973.
24. A. Fukuoka, T. Kimura and M. Ichikawa, *J. Chem. Soc., Chem. Commun.* 1988, 428.
25. A. Fukuoka, M. Ichikawa, J. A. Hriljac and D. F. Shriver, *Inorg. Chem.* 1987, **26**, 3643.
26. R. Shannon, J. C. Vedrine, C. Naccache and F. Lefevre, *J. Catal.* 1985, **88**, 43; E. J. Rode and M. E. Davis, *ibid.* 1985, **86**, 574.
27. A. Fukuoka, H. Matsuzaka, H. Hidai and M. Ichikawa, *Chem. Lett.* 1987, 941.

Polyhedron Vol. 7, No. 22/23, pp. 2369–2374, 1988
Printed in Great Britain

0277–5387/88 $3.00+.00
© 1988 Pergamon Press plc

CHEMISTRY OF COBALT–RUTHENIUM MIXED METAL COMPLEXES: CARBONYLATION AND METALLO-SELECTIVE SUBSTITUTION REACTIONS

MASANOBU HIDAI* and HIROYUKI MATSUZAKA

Department of Synthetic Chemistry, Faculty of Engineering, University of Tokyo, Hongo, Bunkyo-ku, Tokyo 113, Japan

Abstract—The reaction of $RuCl_3$ with 4 molar equivalents of $Na[Co(CO)_4]$ gives a mixed cluster $Na[RuCo_3(CO)_{12}]$ in high yield. The cluster readily undergoes a cation exchange by bulky cations such as $[(Ph_3P)_2N]^+$, while protonolysis by phosphoric acid produces $HRuCo_3(CO)_{12}$. The X-ray structure of $[(Ph_3P)_2N][RuCo_3(CO)_{12}]$ shows that the four metals are located at the corners of a tetrahedron. These mixed clusters are very effective for the homologation of methanol compared with $Co_2(CO)_8$. On the other hand, the $Co_2(CO)_8$—$Ru_3(CO)_{12}$ bimetallic catalyst shows remarkably high catalytic activity for hydroformylation of olefins such as cyclohexene compared with $Co_2(CO)_8$ alone. The synergistic effects for cobalt and ruthenium on these carbonylation reactions are discussed. Metallo-selective substitution reactions were observed when $HRuCo_3(CO)_{12}$ was treated with amines or phosphines. The substitution of amines for the carbonyl ligand takes place preferentially at the ruthenium atom whereas the substitution of phosphines occurs exclusively at the cobalt atoms.

Homogeneous multimetallic catalysts have recently been receiving much attention because it is hoped that the cooperativity of different metals during chemical transformations might lead to more selective and efficient reactions and, in some cases, to new types of reactions which are inaccessible through homometallic systems.[1–3] Several years ago we started our study toward this direction. The reaction we first chose was the homologation of methanol to ethanol since interesting reports had appeared which claimed that the selectivity of ethanol was remarkably improved by addition of a small amount of ruthenium iodide[4] or ruthenium carbonyl[5] to cobalt carbonyl. Stimulated by these findings, we found that $[RuCo_3(CO)_{12}]^-$ mixed clusters show notable catalytic activity for the homologation of methanol. Detailed investigation of this reaction led us to discover that the $Co_2(CO)_8$—$Ru_3(CO)_{12}$ bimetallic system shows high catalytic activity for hydroformylation of olefins compared with $Co_2(CO)_8$ or $Ru_3(CO)_{12}$ alone. The synergistic effects for cobalt and ruthenium on these carbonylation reactions are discussed here. During the course of this study, we have recently found metallo-selective substitution reactions by amines or phosphines in $HRuCo_3(CO)_{12}$. To our knowledge, this is one of a few examples in which mixed clusters react with similar substrates at different specific locations.[6]

HOMOLOGATION OF METHANOL BY USING $[RuCo_3(CO)_{12}]^-$ CLUSTERS[7]

The homologation of methanol using the $Co_2(CO)_8$—$RuCl_3$ bimetallic system has been investigated in detail. Methyl iodide was used as a promoter. The influence of the Ru/Co molar ratio on the yields of products is shown in Fig. 1, where various amounts of $RuCl_3 \cdot 3H_2O$ were added to a constant amount of cobalt carbonyl. When only cobalt carbonyl was used as the catalyst, the main C_2 products were acetaldehyde and its dimethyl acetal under the reaction conditions employed (180°C, $CO:H_2$ ratio = 1:2, initial pressure 120 kg cm^{-2} at ambient temperature). Increase of the Ru : Co ratio sharply decreased the yield of total acetaldehyde whereas it remarkably improved the yield of total ethanol. It is of great interest that addition of $RuCl_3$ slightly but notably increases the yield of total C_2 products, i.e. the carbon–carbon bond formation, and the yields of both total ethanol and total C_2 compounds reach a maximum at the Ru : Co ratio

*Author to whom correspondence should be addressed.

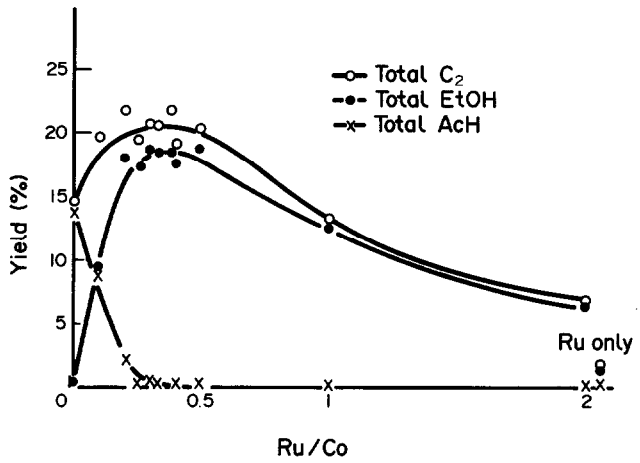

Fig. 1. Effect of the Ru/Co ratio on the methanol homologation catalysed by the $Co_2(CO)_8$—$RuCl_3 \cdot 3H_2O$ system. Yield (%) of total C_2 = AcH(mol) + DMA(mol) + EtOH(mol) + MeOEt(mol) + 2 × Et_2O(mol) + AcOMe(mol)/MeOH added(mol) × 100 (DMA = dimethyl acetal of acetaldehyde). Yield (%) of total EtOH = EtOH(mol) + MeOEt(mol) + 2 × Et_2O(mol)/MeOH added(mol) × 100. Yield (%) of total AcH = AcH(mol) + DMA(mol)/MeOH added(mol) × 100.

of *ca* 1:3. These results suggest that some cobalt–ruthenium mixed clusters such as an $RuCo_3$ cluster are formed under reaction conditions which are effective for the homologation of methanol. This led us to prepare well-defined cobalt–ruthenium mixed clusters.

A reddish brown complex $Na[RuCo_3(CO)_{12}]$ was obtained in high yield by reaction of $RuCl_3 \cdot 3H_2O$ with 4 molar equiv. of $Na[Co(CO)_4]$ in methanol/THF [eq. (1)].

$$RuCl_3 + 4Na[Co(CO)_4] \rightarrow Na[RuCo_3(CO)_{12}] + 3NaCl + 1/2[Co_2(CO)_8]. \quad (1)$$

Protonolysis of the cluster with phosphoric acid gives the hydrido cluster $HRuCo_3(CO)_{12}$ in moderate yield. This hydrido cluster was previously prepared by reaction of $Ru_3(CO)_{12}$ with $Co_2(CO)_8$ in acetone followed by acidification with hydrochloric acid, but the yield was very low.[8] The sodium cation in $Na[RuCo_3(CO)_{12}]$ is readily exchanged by bulky cations such as the bis(triphenylphosphine) imminium ion. X-ray crystallographic analysis of $[(Ph_3P)_2N][RuCo_3(CO)_{12}]$ reveals that the four metal atoms in the anion form a tetrahedron with the apical Ru atom bonded to three terminal carbonyl ligands and three basal Co atoms each bonded to two terminal and two bridging carbonyl ligands.

These cobalt–ruthenium mixed clusters are very effective for the formation of ethanol from methanol and synthesis gas as in the case of the $Co_2(CO)_8$—$RuCl_3$ bimetallic system. The selectivity of total ethanol was improved up to 64% at *ca* 25% conversion of methanol with the methyl iodide/cluster ratio of *ca* 9 at 180°C, while the selectivity was below 5% in the case of $Co_2(CO)_8$ under similar conditions. The study on time dependence of yield and selectivity of the products unequivocally shows that methanol is first converted to acetaldehyde and then hydrogenated to ethanol. These results have led to the conclusion that the synergistic effect for cobalt and ruthenium appears in the first step for formation of acetaldehyde, and the second step for hydrogenation of acetaldehyde to ethanol is probably catalysed by ruthenium complex(es) [eq. (2)].

$$CH_3OH \xrightarrow[Co/Ru]{CO/H_2} CH_3CHO \xrightarrow[Ru]{H_2} CH_3CH_2OH. \quad (2)$$

The synergistic effect might be explained by either cluster catalysis or bimetallic catalysis which, for example, involves dinuclear reductive elimination of acetaldehyde from acetylcobalt and hydridoruthenium complexes. However, from the recovered solution after catalysis, the salt of $[Ru(CO)_3I_3]^-$ was isolated in moderate yield, but no parent cluster. This finding appeared to favour the latter type of explanation. This led us to discover that the $Co_2(CO)_8$—$Ru_3(CO)_{12}$ bimetallic system shows high catalytic activity for hydroformylation of olefins compared with $Co_2(CO)_8$ or $Ru_3(CO)_{12}$ alone, since both processes involve alkyl and acyl complexes as common intermediates.

Table 1. Hydroformylation of cyclohexene by Co–Ru mixed metal calalysts[a]

Run	Catalyst	Ru : Co	Yield of CyCHO (%)[b]	Initial rate (V_0)[c]
1	$Co_2(CO)_8$	—	14	1.0
2[d]	$Ru_3(CO)_{12}$	—	3	0.3
3	$Co_2(CO)_8 + Ru_3(CO)_{12}$	0.34	32	3.6
4	$Co_2(CO)_8 + Ru_3(CO)_{12}$	0.95	52	5.9
5	$Co_2(CO)_8 + Ru_3(CO)_{12}$	3.2	62	8.4
6	$Co_2(CO)_8 + Ru_3(CO)_{12}$	9.9	100[e]	27

[a] Reaction conditions: Co, 0.2 mg atom; cyclohexene, 80 mmol; THF, 10 cm^3; reaction temp., 110°C; reaction time, 4 h; $CO : H_2 = 40 : 40$ kg cm^{-2} (initial pressure at room temp.).

[b] The yield of CyCHO is based on the starting cyclohexene. It includes the 2,4,6-tricyclohexyl-1,3,5-trioxane formed, because the latter quantitatively decomposes to CyCHO under the conditions of our direct GC analysis.

[c] Relative to $Co_2(CO)_8$ alone (Run 1).

[d] Ru, 0.6 mg atom.

[e] Small amount of cyclohexanemethanol formed.

HYDROFORMYLATION OF OLEFINS BY HOMOGENEOUS COBALT–RUTHENIUM BIMETALLIC CATALYST[9]

Table 1 summarizes the results of the hydroformylation of cyclohexene in THF using the $Co_2(CO)_8$—$Ru_3(CO)_{12}$ mixed metal catalyst. The yield of cyclohexanecarbaldehyde with the bimetallic catalyst was considerably higher than would be expected by a simple additive effect based on the values observed for $Co_2(CO)_8$ and $Ru_3(CO)_{12}$, respectively. The initial rate increased as more $Ru_3(CO)_{12}$ was added to $Co_2(CO)_8$. At Ru : Co = 9.9 : 1, the initial rate was 27 times as fast as that with $Co_2(CO)_8$ alone.

Solvent effect on the hydroformylation of cyclohexene catalysed by $Co_2(CO)_8$ or with the $Co_2(CO)_8$—$Ru_3(CO)_{12}$ bimetallic catalyst is shown in Table 2. The initial rate with $Co_2(CO)_8$ alone was almost independent of the nature of the solvent employed. In contrast, the initial rate with the cobalt–ruthenium bimetallic catalyst was remarkably influenced by the nature of the solvent. Interestingly, alcohols such as methanol were the best

Table 2. Solvent effect on the hydroformylation of cyclohexene by the Co—Ru bimetallic catalyst[a]

Run	Solvent	Initial rate (V_0)[b]	Yields of products[c] (%)			
			CyCHO	$CyCH_2OH$	Acetal	Ester
1	pyridine	1.4(0.1)	19(0)	0(0)		
2	hexane	5.4(1.1)	58(12)	1(0)		
3	dioxane	5.8(0.9)	61(11)	1(0)		
4	THF	5.9(1.0)	52(14)	1(0)		
5	benzene	9.1(1.1)	73(12)	2(0)		
6	ethanol	15(1.1)	39(2)	2(0)	$CyCH(OEt)_2$ 54(14)	CyCOOEt 2(1)
7	methanol	19(1.1)	19(0)	1(0)	$CyCH(OMe)_2$ 68(15)	CyCOOMe 5(1)

[a] Reaction conditions: $Co_2(CO)_8$, 0.10 mmol; $Ru_3(CO)_{12}$, 0.067 mmol; cyclohexene, 80 mmol; solvent, 10 mmol; reaction temp., 110°C; reaction time, 4 h; $CO : H_2 = 40 : 40$ kg cm^{-2} (initial pressure at room temp.). Values in parentheses are those catalysed by $Co_2(CO)_8$ (0.10 mmol) alone.

[b] Relative to $Co_2(CO)_8$ in THF.

[c] Yields are based on the starting cyclohexene.

among the solvents investigated. The initial rate with the bimetallic catalyst using an Ru : Co molar ratio of 1:1 in methanol was 19 times faster than that with $Co_2(CO)_8$ alone in THF. In this case, the aldehyde initially formed was mostly converted into its dimethyl acetal.

A synergistic effect for cobalt and ruthenium was also observed for hydroformylation of other olefins such as 1-hexene and styrene. However, rate enhancement was not as great compared with the hydroformylation of cyclohexene. The initial rate of the hydroformylation of 1-hexene in benzene by the bimetallic catalyst using an Ru : Co molar ratio of 1:1 was about three times as fast as that with $Co_2(CO)_8$ alone. However, the normal : iso ratio of the aldehyde formed was essentially the same as in the case of $Co_2(CO)_8$. The hydroformylation of styrene with the same bimetallic catalyst in benzene roughly doubled the initial rate. On the other hand, the initial rate of the hydroformylation of cyclohexene under the same conditions increased about ninefold as shown in Table 2. Thus, it may be concluded that the synergistic effect for cobalt and ruthenium on hydroformylation of olefins occurs in the following order: cyclohexene > 1-hexene > styrene. It is noteworthy that cyclohexene, which is the least reactive substrate in the $Co_2(CO)_8$ catalysed hydroformylation, is as readily hydroformylated as 1-hexene if the bimetallic catalyst is used.

A high pressure IR spectral study of the reaction solution did not show the existence of cobalt–ruthenium hydride(s), although the hydrogenolysis conditions. This observation led us to expect that the synergistic effect for cobalt and ruthenium might be explained by dinuclear reductive elimination of aldehydes from cobalt acyls and ruthenium hydride(s), although the hydrogenolysis step of metal acyl intermediates forming aldehydes is still the subject of controversy. Thus, the reactions between hexanoyl cobalt tetracarbonyl and several kinds of metal carbonyl hydrides including $HCo(CO)_4$, $[HRu(CO)_4]^-$ and $[HRu_3(CO)_{11}]^-$ have been investigated as model reactions. Interestingly, the hydride $[HRu(CO)_4]^-$ reacts much more readily with the acyl cobalt complex at ambient temperature to form hexanal than does $HCo(CO)_4$.[10] This suggests that ruthenium is probably involved in the aldehyde-forming step in the hydroformylation with the bimetallic system. However, Whyman previously proposed from a high pressure IR spectral study that in the hydroformylation of internal olefins catalysed by $Co_2(CO)_8$, initial interaction of the olefin with $HCo(CO)_4$ might be the rate-determining step although hydrogenolysis of an acyl cobalt intermediate is a significant rate-determining step in the case of simple terminal olefins.[11] The fact that the synergistic effect for cobalt and ruthenium is most effectively realized in the case of cyclohexene (*vide infra*) indicates that ruthenium might also be involved in the olefin insertion step. This is compatible with the finding that the synergistic effect for cobalt and ruthenium also appears in the hydroesterification of olefins which does not involve hydrogenolysis of an acyl intermediate.

METALLO-SELECTIVE SUBSTITUTION REACTIONS BY AMINES OR PHOSPHINES IN $HRuCo_3(CO)_{12}$[12]

A mixed-metal cluster $HRuCo_3(CO)_{12}$ (**1**) reacted with trimethylamine N-oxide to give an amine substituted cluster $HRuCo_3(CO)_{11}(NMe_3)$ (**2**) in moderate yield concurrent with evolution of CO_2. A series of amine substituted clusters $HRuCo_3(CO)_{11}L$ (**3**, L = NEt_3; **4**, L = Me_2NPh; **5**, L = p-$H_2NC_6H_4NH_2$; **6**, L = 1,4-cyclohexanediamine) were prepared by direct treatment of cluster **1** with 1 molar equiv. of amines, during which evolution of CO was observed. Even if a large excess of amines was used, only the mono-substituted clusters were obtained. In contrast, cluster **1** reacted with one molar equiv. of triphenylphosphine to give a mono-substituted cluster $HRuCo_3(CO)_{11}(PPh_3)$ (**7**) whereas treatment with 3 molar equiv. of triphenylphosphine produced a disubstituted cluster $HRuCo_3(CO)_{10}(PPh_3)_2$ (**8**). Substitution of amine for the two carbonyl ligands in cluster **1** proceeded only when a bidentate ligand $Me_2NCH_2CH_2NMe_2$ (tmeda) was used (Scheme 1). Interestingly, when the corresponding iron analogue $HFeCo_3(CO)_{12}$ was treated with amines, the protic hydrogen was abstracted by the amines to give ammonium salts $[R_3NH][FeCo_3(CO)_{12}]$.

Substitution of electron-donating amines or phosphines for the carbonyl ligands results in a lower shift of ν(CO) in the IR spectra. The bands due to ν(CO) of amine substituted clusters appear at lower frequencies than those of phosphine substituted clusters. Furthermore, the IR spectra of amine substituted clusters in the ν(CO) region are quite different from those of phosphine substituted clusters. The amine substituted cluster **3** shows one medium peak at 1815 cm^{-1} assigned to bridging carbonyl groups, whereas the phosphine substituted cluster **7** exhibits two medium peaks at 1861 and 1846 cm^{-1} assigned to bridging carbonyl groups. This strongly suggests that the site for the substitution of amines and phosphines in cluster **1** may be different.

^1H NMR spectra of amine substituted clusters **2**–**6** show a broad singlet at −17.1 to −17.4 ppm characteristic of a metal hydride. The line width

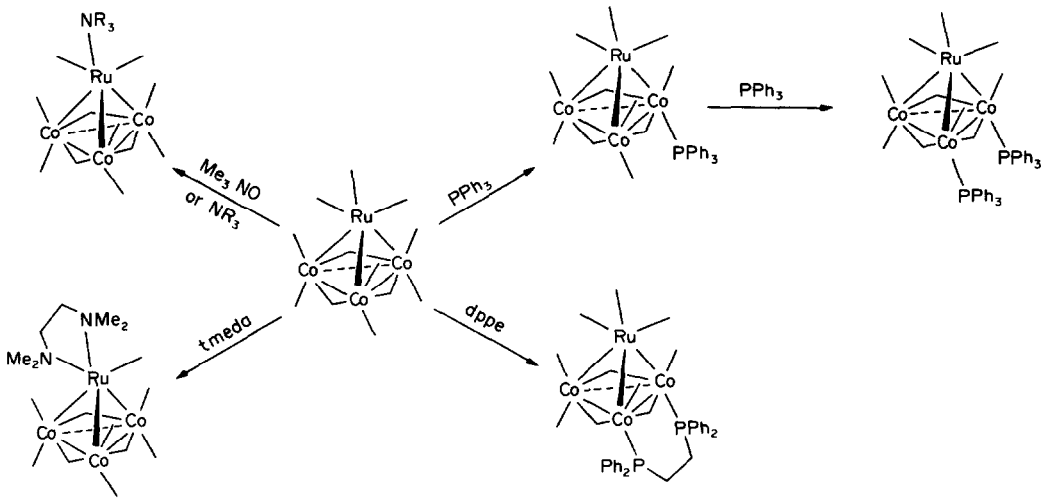

Scheme 1.

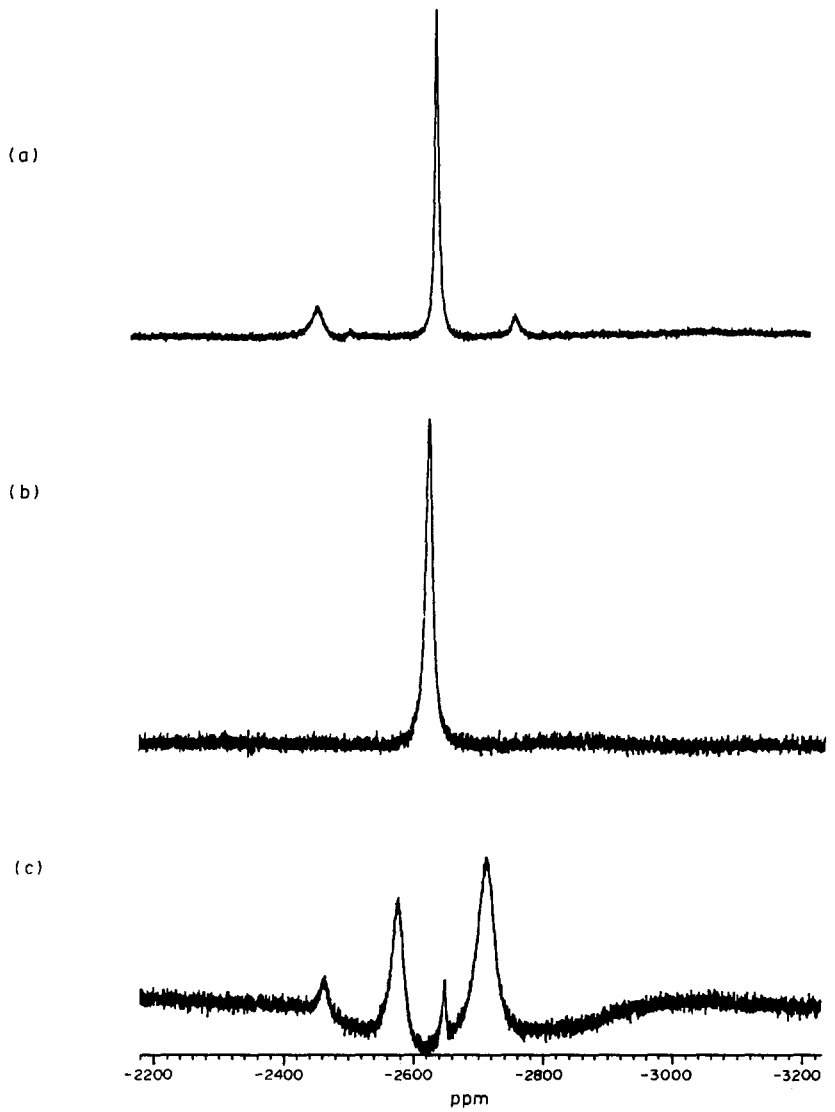

Fig. 2. ^{59}Co NMR spectra of amine or phosphine substituted clusters. (a) $HRuCo_3(CO)_{12}$ (**1**); (b) $HRuCo_3(CO)_{11}(NEt_3)$ (**3**); (c) $HRuCo_3(CO)_{11}(PPh_3)$ (**7**); measured in acetone-d_6 at 27°C by using an aqueous solution of $K_3[Co(CN)_6]$ as an external standard.

becomes narrower as the temperature is lowered. The line broadening is probably caused by the quadrupolar effect of ^{59}Co nuclei and the hydride resonance peak becomes sharp at lower temperatures when the relaxation time T_1 of ^{59}Co nuclei becomes much smaller. On the other hand, ^{59}Co NMR spectra show only one resonance at -2630 to -2649 ppm which is similar to that of the parent cluster **1**. Typical ^{59}Co NMR spectra of clusters **1**, **3**, and **7** are shown in Fig. 2. Although we could not obtain crystals of **2–6** suitable for X-ray structural analysis, the above findings lead to the conclusion that amine substitution takes place at the ruthenium atom and the hydride ligand is probably μ_3-bound to the Co_3 face as in $HFeCo_3(CO)_{12}$ and **1**.[13]

^1H NMR spectra of phosphine substituted clusters **7** and **8** show a broad singlet at -19.4 to -19.9 ppm assigned to the metal hydride. The ^{59}Co NMR spectrum of **7** exhibits two strong peaks at -2574 and -2712 ppm with intensity ratio 1:2. This indicates that the phosphine substitution reaction takes place at the cobalt atom. The existence of a small amount of isomers in solution is supposed by observation of weak peaks as shown in Fig. 2. The X-ray structural analysis of **7** shows that the cluster has a tetrahedral framework and the phosphine ligand is axially coordinated to one of three basal cobalt atoms. The hydride ligand is probably μ_3-bound to the Co_3 face because the Co—Co—C axial carbonyl angles (av. 121.6°) are relatively large. Pursiainen and Pakkanen have recently determined the crystal structure of **8** where each phosphine ligand is axially coordinated to two different cobalt atoms and hydrogen is triply bridged to the Co_3 face.[14]

Bidentate ligands, tmeda and dppe, also show a quite different reactivity toward the substitution for the carbonyl ligands in **1** (Scheme 1). The ^1H NMR spectrum of the tmeda substituted cluster shows only one set of singlets at 2.99 and 2.72 ppm with intensity ratio 4:12, which are assigned to methylene and methyl protons in the coordinated tmeda, respectively. The metal hydride resonance appears at -17.4 ppm as a broad peak. The ^{59}Co NMR spectrum exhibits one resonance at -2649 ppm. These results suggest that tmeda chelates the ruthenium atom and the hydride ligand is probably μ_3-bound to the Co_3 face. On the other hand, Pursiainen and Pakkanen have recently determined the molecular structure of the dppe substituted cluster where dppe is axially coordinated to two different cobalt atoms.[15]

Acknowledgement—The authors wish to thank the Ministry of Education, Japan, for financial support by a Grant-in-Aid for scientific research.

REFERENCES

1. D. A. Roberts and G. L. Geoffroy, *Comprehensive Organometallic Chemistry* (Edited by G. Wilkinson, F. G. A. Stone and E. W. Abel), Vol. 6, pp. 763–877. Pergamon Press, Oxford (1982).
2. W. L. Gladfelter and G. L. Geoffroy, *Adv. Organomet. Chem.* 1980, **18**, 207.
3. P. Braunstein and J. Rose, in *Stereochemistry of Organometallic and Inorganic Compounds* (Edited by I. Bernal), Vol. 3. Elsevier, Amsterdam (in press).
4. D. Butter and T. Haute, U.S. Patent 3285948, 1966.
5. M. Mizoroki, T. Matsumoto and A. Ozaki, *Bull. Chem. Soc. Jpn.* 1979, **52**, 479.
6. J. R. Fox, W. L. Gladfelter, T. G. Wood, J. A. Smegal, T. K. Foreman, G. L. Geoffroy, I. Tavanaiepour, V. W. Day and C. S. Day, *Inorg. Chem.* 1981, **20**, 3214.
7. M. Hidai, M. Orisaku, M. Ue, Y. Koyasu, T. Kodama and Y. Uchida, *Organometallics* 1983, **2**, 292.
8. M. J. Mays and R. N. F. Simpson, *J. Chem. Soc.* (*A*) 1968, 1444.
9. M. Hidai, A. Fukuoka, Y. Koyasu and Y. Uchida, *J. Molec. Catal.* 1986, **35**, 29.
10. Y. Koyasu, A. Fukuoka, Y. Uchida and M. Hidai, *Chem. Lett.* 1985, 1083.
11. R. Whyman, *J. Organomet. Chem.* 1974, **81**, 97.
12. H. Matsuzaka, T. Kodama, Y. Uchida and M. Hidai, *Organometallics*, in press.
13. T. Saito and S. Sawada, *Bull. Chem. Soc. Jpn.* 1985, **58**, 459.
14. J. Pursiainen and T. A. Pakkanen, *J. Organomet. Chem.* 1985, **290**, 85.
15. J. Pursiainen and T. A. Pakkanen, *J. Organomet. Chem.* 1986, **309**, 187.

Polyhedron Vol. 7, No. 22/23, pp. 2375–2381, 1988
Printed in Great Britain

0277–5387/88 $3.00+.00
© 1988 Pergamon Press plc

POLYMERIZATION OF OLEFINS WITH HOMOGENEOUS ZIRCONOCENE/ALUMOXANE CATALYSTS

W. KAMINSKY and R. STEIGER

Institut für Tech. and Makromolecular Chemie, Universität Hamburg, Bundesstrasse 45, 2000 Hamburg 13, F.R.G.

Abstract—The homogeneous Ziegler–Natta catalyst, consisting of zirconocene compounds and methylalumoxane, leads to extremely high polymerization activities. With bis(cyclopentadienyl)zirconium dichloride, polyethylene with activities up to 40×10^6 g PE/g Zr · h is formed. The higher the degree of oligomerization of the alumoxane the more active are the catalysts. The density of polyethylene (LLDPE) can be lowered by using 1-butene or 1-hexene as comonomers. Incorporation of dienes gives EPDM-elastomers. Highly isotactic polypropylene can be prepared by using chiral rac-ethylene bis(tetrahydroindenyl) zirconium dichloride together with methylalumoxane as cocatalyst. The toluene soluble part here consists of less than 0.2 weight per cent. Cyclopentene gives a highly isotactic and insoluble polymer. With the *R* or *S* enantiomers of the catalyst it is also possible to produce optically active oligomers. The side reactions and the mechanism are discussed.

Organometallic complexes formed by zirconocene/methylalumoxane belong to the most active Ziegler–Natta catalysts for olefin polymerization known today.[1–3] Every active site consists of one zirconium atom and between six and 20 aluminum atoms. So a real multimetallic catalyst is given. The structure of the methylalumoxane is not known in detail. It exists in a linear and a cyclic form:

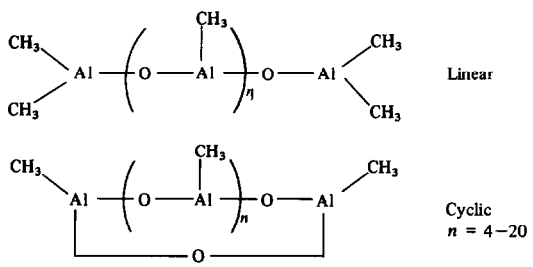

(Structure 1)

By decreasing the number of aluminium atoms per alumoxane molecule, that is decreasing the number of aluminium atoms per active site, a drastic decrease of polymerization activity is observed (Table 1).

The analogous titanium and hafnium compounds also form active catalysts. Especially at temperatures over 50°C, the zirconium catalyst is more stable and active than the titanium or hafnium systems. Of the cocatalysts methylalumoxane is much more effective than the ethylalumoxane or isobutylalumoxane. Assuming that every zirconium atom forms an active complex, one zirconium complex produces about 15,000 polymer chains in 1 h with an average molecular weight of 150,000. The molecular weight distribution of the resulting polyethylene is narrow with $M_w/M_n = 1.6–2.4$.

At temperatures below −20°C the transfer reaction is so slow that the molecular weight is only a function of the polymerization time as is found in living polymer systems. The molecular weight of the polyethylene can be varied over a wide range between 10,000 and 2,000,000 by changing the polymerization temperature between 20 and 100°C and the zirconium concentration. In addition, the molecular weight can be influenced by addition of hydrogen.[4] In contrast to most heterogeneous catalysts, only traces of hydrogen were needed to lower the molecular weight of the polymer.

Natural substances like starch, cellulose and lignin can, due to their free water, form alumoxane analogous structures on addition of trimethylaluminium. After addition of the metal compound, starch grains or cellulose fibres treated in this manner have a considerable polymerization activity when suspended in toluene. By this procedure physical and chemical properties of natural and synthetic polymers can be combined.[5,6]

In the same manner it is possible to cover cellulose, lignin or inorganic materials like $CaCO_3$, $CaSO_4 \cdot 0.5\ H_2O$ or Al_2O_3 with polyethylene or other polyolefins.

Table 1. Polymerization activity of different zirconocene/methylalumoxan catalyst systems in 330 cm^3 toluene at 8 bar ethylene pressure, 5×10^{-3} mol aluminium units and 70°C

Zirconocene (mol)	Cocatalyst	Activity (g PE/g Zr · h)	No. of Al-units per alumoxan
$(10^{-7})Cp_2Zr(CH_3)_2$	Methylalumoxane	1,200,000	8
$(10^{-7})Cp_2Zr(CH_3)_2$	Methylalumoxane	2,600,000	18
$(3 \times 10^{-8})Cp_2ZrCl_2$	Methylalumoxane	8,000,000	18
$(1.5 \times 10^{-6})Cp_2ZrCl_2$	Ethylalumoxane	400,000	16
$(3 \times 10^{-6})Cp_2Zr(CH_3)_2$	Tetraisobutylalumoxane	1,400,000	2

The catalysis can easily produce co- and terpolymers. The density of the polymer can be lowered by using hexene-1 or butene-1 as an additional monomer in copolymerizations. Incorporation of 1 mol% hexene-1 yields a polymer which, in the molten state, has a density lower than 0.95 g cm^{-3}. With 5 mol% incorporated the density is 0.92 g cm^{-3} and decreases to 0.89 g cm^{-3} for 9 mol%, so that LLDPE can be obtained.

Using dienes in addition to propene and ethylene leads to EPDM-elastomers.[7]

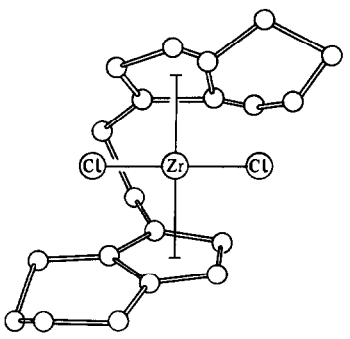

(Structure 2)

Structure of chiral ethylenebis(tetrahydroindenyl) zirconium dichloride.

ISOTACTIC POLYMERIZATION

Bis(cyclopentadienyl)zirconium or titanium IV compounds produce solely atactic polypropylene in polymerizations of propene with activities of 17,000 g/g Zr · h at 20°C. It can be freely chosen to work either in solution or in liquid monomer. At low temperatures mean molecular weights (M_η) of the atactic polypropylenes reach values of 590,000. Increasing polymerization temperatures lead to decreasing values.

^{13}C NMR spectroscopic investigations of the polymers result in nearly ideally atactic samples which are appropriate for blending of elastomers.[8]

By variation of ligands at the zirconium atom it has been attempted to introduce asymmetric centres into the catalyst in order to synthesize isotactic polypropylene also. (Pentamethylcyclopentadienyl)cyclopentadienylzirconiumalkylchloride, a compound consisting of four different ligands, has been applied. But even this highly demanding compound in combination with methylaluminoxane was only able to produce atactic polypropylene.[9] On the other hand it is possible to make high isotactic polypropylene with stereorigid chiral zirconocenes of the kind Brintzinger first synthesized.[10,11] The analogous titanium compounds lead to polypropylene of lower isotacticity.

The CH_2—CH_2 bridge serves as a very stereorigid conformation around the zirconium atom, so that fluctuation among the ligands is not possible. The two indenyl groups are arranged in a chiral array. Ethylene bis(tetrahydroindenyl) zirconium dichloride appears in two isomeric forms (*R* and *S*). The analogous titanium compound can exist in an additional mesomeric form which is not stable in the case of zirconium.

By use of the racemic mixture of ethylene bis(indenyl)zirconium dichloride or ethylene bis(tetrahydroindenyl)zirconium dichloride together with the cocatalyst methylalumoxane in polymerizations of propene, highly isotactic polypropylenes can be produced (Table 2).[12] Polymerization activities of bridged, low soluble bis(indenyl) zirconium dichloride are distinctly greater than those of the corresponding hydrated compounds. This gives evidence for the hypothesis that isotactic polymerizations are dependent on chiral centres which so far have only been generated with heterogeneous catalysts. Working with stable chiral transition metal compounds makes isotactically run polymerizations, even in the homogeneous phase, possible.

The activities referred to the concentration of the transition metal overcome those values which are achieved today with carrier fixed heterogeneous catalysts. In a 1 h polymerization period up to 43,000 kg polypropylene per mole zirconocene can

Table 2. Polymerization of 70 cm^3 propene with 7×10^{-7} mol dm^{-3} rac-$Et(Ind)_2ZrCl_2$ (I) or 8.4×10^{-6} mol dm^{-3} rac-$Et(TH\text{-}Ind)_2ZrCl_2$ (II) and 1.6×10^{-2} mol Al dm^{-3} methylalumoxane in 330 cm^3 toluene

Monomer	Catalyst	T (°C)	Time (min)	Yield (g)	Activity (kgPP/mole Zr · h)
Propene	I	15	629	3.6	1500
	I	21	500	31	16,000
	I	35	120	26.6	43,000
	II	−10	270	4.5	300
	II	15	170	26.7	2900
	II	20	120	31.3	4750
	II	60	90	38.7	7700

be produced at a zirconium concentration of 5×10^{-6} mol dm^{-3}.

Alumoxane concentrations in the range of 3×10^{-2} mol Al dm^{-3} are quite high. For mean molecular weights M_w of 45,000 the growth time of one macromolecule is approximately 3.8 s and the insertion time of a propene molecule is 3.5×10^{-3} s. These calculations are based on the assumption that every zirconium atom forms an active centre. This could be proved in the case of ethylene polymerizations.[13]

Molecular mass distribution M_w/M_n has typical values between 1.9 and 2.6 which are extraordinarily narrow. NMR-spectroscopic investigations show that the atactic amount is smaller than the toluene soluble amount. Typical values lie below 0.2% which are 10-fold smaller than for those polymers which are synthesized by technical heterogeneous catalysts. By varying the polymerization temperature between −10 and 20°C molecular weights can be controlled in the range from 305,000 to 45,000.

In order to investigate the ligand effect when the chiral centre is more remote from the zirconium atom, bis(neomenthylcyclopentadienyl)zirconium dichloride has been synthesized and used as a catalyst component. Bis(neomenthylcyclopentadienyl) zirconium dichloride consists of three chiral C-atoms.

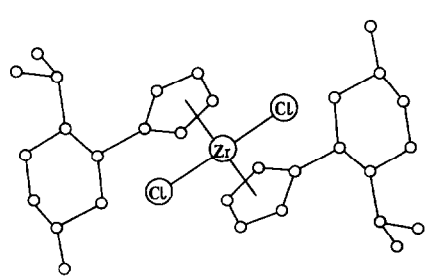

(Structure 3)

Structure of bis(neomenthylcyclopentadianyl)zirconium dichloride.

Together with methylalumoxane as cocatalyst it yields, in polymerizations of propene, stereo block polymers with isotactic sequences of $n = 3$–7. Table 3 shows the polymerization results.[14]

At low temperatures relatively high mean molecular weights are obtained, reaching values of 640,000 at −60°C. A sequence analysis of polymers produced in this way has been carried out with the help of ^{13}C NMR spectroscopy. It becomes obvious that the isotactic sequences at 21 ppm rise with decreasing temperatures.

Furthermore the catalyst system ethylene-bis(indenyl)zirconium dichloride/methylalumoxane allows polymerization of cycloalkanes such as cyclopentene to isotactic polymers.[15] No ring opening takes place and the reaction leads to the following structure:

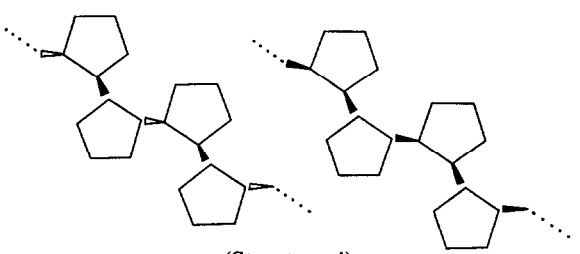

(Structure 4)

The polycyclopentene product is insoluble in aromatic or aliphatic hydrocarbons and highly crystalline with a melting point higher than the decomposition point of 250°C. With the help of optically active binaphtol, it is possible to separate the racemic mixture ethylene(tetrahydroindenyl) zirconium dichloride into the pure enantiomers.[16] Using these enantiomers for the oligomerization of alkenes yields optically active alkanes and alkenes (Table 4). The optical purity of these products is in the range of 70–80%.

MECHANISM

The polymerization of α-olefins, promoted by homogeneous Ziegler–Natta catalysts, occurs sim-

Table 3. Propene polymerization with bis(neomethylcyclopentadienyl)zirconium dichloride/methylalumoxane

I (°C)	Zr (mol)*10^5	P (bar)	Propene (mol)	t (h)	PP (g)	Activity (kp PP/mol Zr · h)	M_η (g mol^{-1})
70	0.36	8.0	0.95	4.0	7.2	530	530[a]
65	0.36	7.2	0.90	5.0	8.0	630	500[a]
60	0.36	6.6	0.95	5.0	50.0	3570	720[a]
50	0.36	5.8	1.0	5.0	46.4	3080	960[a]
40	0.36	4.8	0.93	5.0	38.0	2680	1220[a]
30	0.36	4.0	0.89	5.0	27.2	1950	
20	0.36	3.3	1.07	5.0	22.8	1300	2100[a]
20	0.36	3.3	1.07	5.0	19.3	1100	
20	1.45	4.0	1.52	4.1	72.8	881	1300[a]
0	1.45	2.0	1.43	19.8	77.3	198	16,000
−20	1.45	—	1.00	21.3	26.7	86	82,000
−40	1.45	—	1.43	65.5	42.5	31	360,000
−60	1.45	—	1.43	70.5	3.0	2	643,000

[a] Cryoscopically determined mean molecular weight.

Table 4. Purity and optical rotation of the di- and trimers of 1-butene oligomerization with S—Et(TH Ind)$_2$ZrCl$_2$

Oligomer	Compound	Purity (%)	α^{25}_{589}	α^{25}_{365}
Dimers	3-methylheptane	97	−8.3	−23.4
Trimers	3-methyl-5-ethylnonane	94	−34.1	−102.6

ultaneously with a series of reactions that greatly complicate the kinetic interpretation (Fig. 1).

Concomitant with continued olefin insertion into the metal–carbon bond of a transition metal alumoxane complex, alkyl exchange and hydrogen transfer reactions are observed. By the release of ethene, a dimetallo alkane is formed. In a second step, in the case of some titanium compounds, ethylene from the dimetallo alkane is evolved and two reduced metal atoms remain. Because of the much greater resistance of zirconium to reduction, the dimetallo alkane compounds can be isolated from the system bis(cyclopentadienyl) zirconium dichloride/triethylaluminum. Figure 2 shows the X-ray structure of a zirconium component.

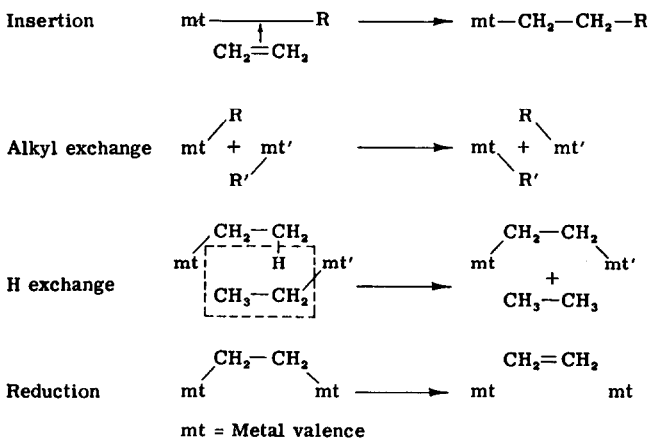

Fig. 1. Reaction with homogeneous Ziegler–Natta catalysts.

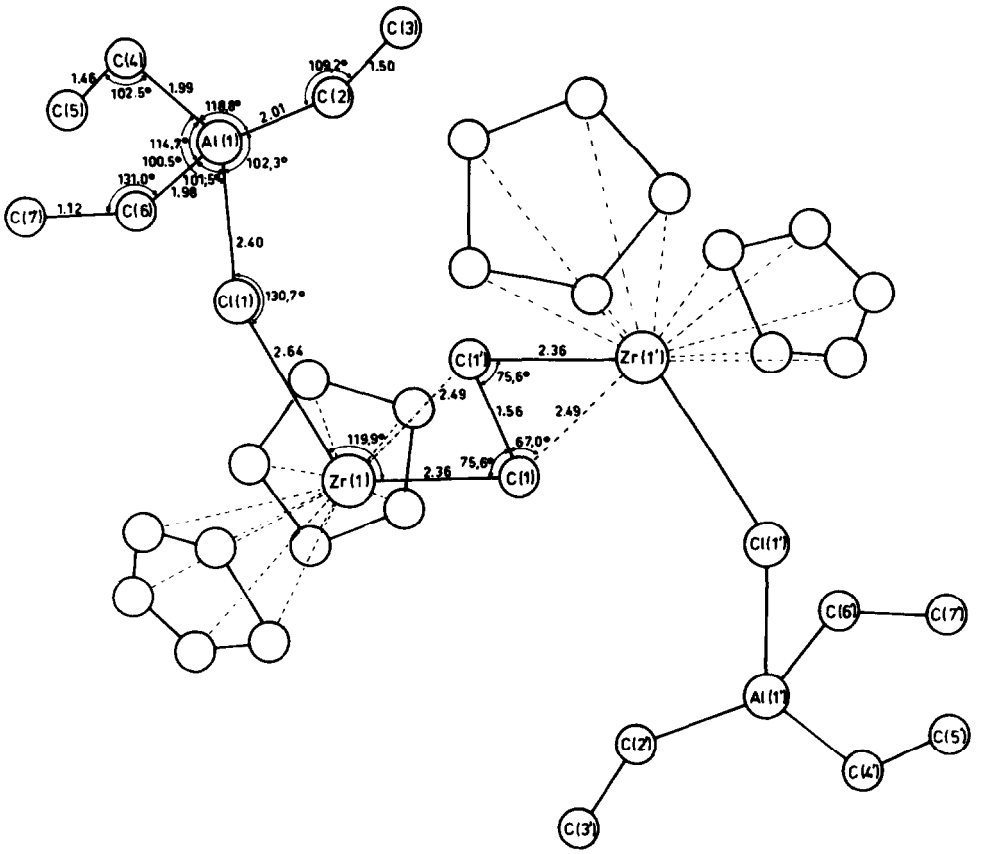

Fig. 2. X-ray structure of 1,2-bis(μ-ethyl-μ-chlorodiethylaluminio(dicyclopentadienyl)zirconio(IV) ethane.

The carbon–carbon angle of the σ-bonded CH_2—CH_2 bridge between the zirconium atoms is only 76°. The β-C atom distance to zirconium is only slightly longer than that of the α-C atom. This is possibly a reason for the easy insertion of ethylene into the zirconium–carbon bond. Other zirconium–aluminum complexes also show the same unusual angle (Fig. 3).[17]

Similar reactions are observed in the catalyst system based on bis(cyclopentadienyl)zirconium dichloride/methylalumoxane. The oligomeric alumoxanes appear as di- and trimers. Together with the zirconocene they form a UV-spectroscopically proved complex (Fig. 4).

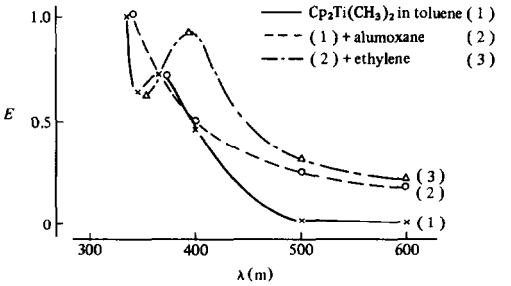

Fig. 4. UV spectroscopic measurements of the catalyst system $Cp_2Ti(CH_3)_2$/methylalumoxane/ethylene. Curve 1: $Cp_2Ti(CH_3)_2$ in toluene. Curve 2: $Cp_2Ti(CH_3)_2$ with alumoxane. Curve 3: $Cp_2Ti(CH_3)_2$ with alumoxane and ethylene.

Fig. 3. X-ray structures of zirconium–aluminum complexes with an angle of the Zr—CH_2—CH bridge of 75.4°.

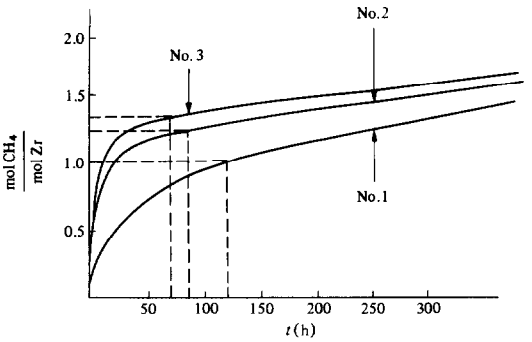

Fig. 5. Methane evolution versus catalyst aging time by 10°C in toluene with the conditions:

No.	Zirconocene (mol dm^{-3})	Alumonoxane (mol dm^{-3})	Al/Zr mol ratio
1	0.057	0.057	1
2	0.057	0.285	5
3	0.043	0.430	10

The cryoscopic molecular weight determination of the used methylaluminoxane gives a value of 1200.

Moreover, methyl exchanges and α-hydrogen transfers are also given. Referring to ^{1}H NMR spectroscopic measurements of the reaction system bis(cyclopentadienyl)zirconium dichloride/methylalumoxane in toluene-d_8 the primary reaction step is the methylation of the zirconium compound by methylalumoxane. Even at −20°C the ligand exchange takes place immediately when the solvated reactants are allowed to have contact.

Quantitative interpretation of dynamic ^{1}H NMR experiments implies that the bis(cyclopentadienyl)zirconium(monomethyl)monochloride reacts with methylalumoxane oligomers to form further complexes. From the beginning of the reaction of bis(cyclopentadienyl)zirconium dichloride/methylalumoxane in toluene, continual methane evolution takes place. So α-hydrogen transfer is an important reaction step in the observed system.

A plot mole CH_4/mole Zr·h allows the determination of the first reaction phase which is characterized by a very vigorous methane evolution. For a molar ratio Al/Zr ⩾ 5 the plot leads to mole CH_4/mole Zr values of one and more (Fig. 5).

One can assume the following reactions steps:

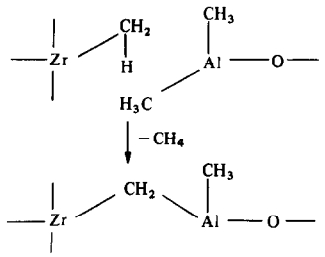

Scheme 1.

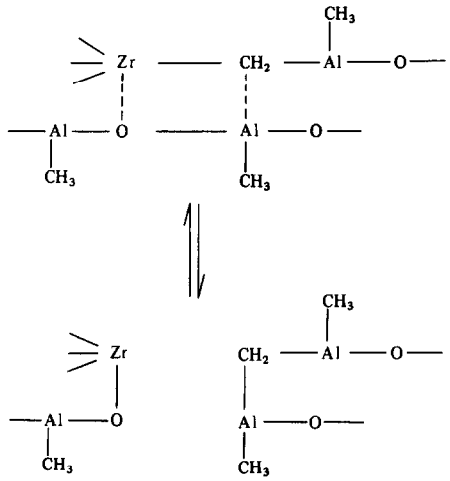

Scheme 2.

Because of exchange as seen by EXAFS measurements Zr—O—Al structures can appear.

The same structure can be given by exchange of halogen ligands without methane evolution.

Through a Zr—O—Al bond, electron density is withdrawn from the zirconium atom. Hence the appearance of an agostic hydrogen bond to the zirconium atom becomes possible as a prestep for β-splitting.[18] If there is ethylene present, it can become bonded by zirconium forming a π-complex. The following figure gives a model for the insertion mechanism (Fig. 6).

This model is in accord with hypotheses where the chain growth in systems of bis(cyclopentadienyl)titanium compounds and aluminiumalkyl halogens is explained by the existence of

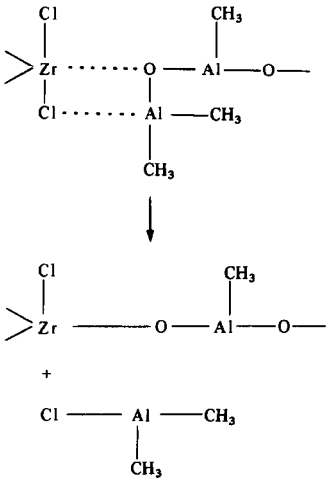

Scheme 3.

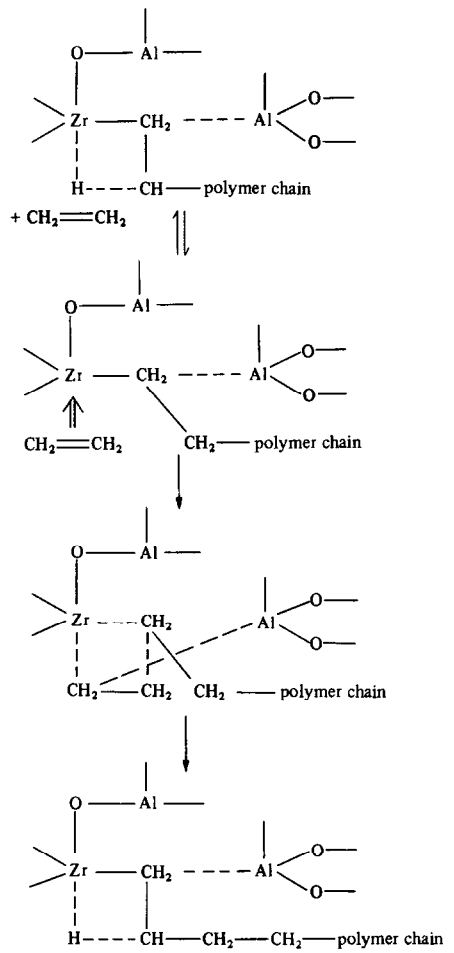

Fig. 6. Possible mechanism for the propene polymerization with a homogeneous catalyst.

electron deficient compounds in penta-coordinated bimetal complexes.[19,20]

Acknowledgements—Acknowledgement is made to the donors of the Deutsche Forschungsgemeinschaft and the Hoechst AG, Frankfurt for support of this research.

REFERENCES

1. H. Sinn, W. Kaminsky, H.-J. Vollmer and R. Woldt, *Angew. Chem., Int. Ed. Engl.* 1980, **19**, 390.
2. H. Sinn and W. Kaminsky, *Adv. Organomet. Chem.* 1980, **18**, 99.
3. W. Kaminsky, in *Transition Metal Catalyzed Polymerization* (Edited by R. P. Quirk), MMI Press, Symposium Series, Vol. 4, p. 225. Harwood Academic Press, New York (1983).
4. W. Kaminsky and H. Lüker, *Makromol. Chem. Rapid Commun.* 1984, **5**, 225.
5. W. Kaminsky, M. Miri, H. Sinn and R. Woldt, *Makromol. Chem. Rapid Commun.* 1983, **4**, 464.
6. J. Dutschke, W. Kaminsky and H. Lüker, in *Polymer Reaction Engineering* (Edited by K. H. Reichert and W. Geiseler), p. 207. Hanser, Munich (1983).
7. W. Kaminsky and M. Miri, *J. Polym. Sci., Polym. Chem. Ed.* 1985, **23**, 2151.
8. P. Pino and R. Mülhaupt, *Angew. Chem.* 1980, **92**, 869.
9. J. A. Ewen, *J. Am. Chem. Soc.* 1984, **106**, 6355.
10. F. R. W. P. Wild, L. Zsolnai, G. Huttner and H. H. Brintzinger, *J. Organomet. Chem.* 1982, **232**, 233.
11. F. R. W. P. Wild, M. Wasiacionek, G. Huttner and H. H. Brintzinger, *J. Organomet. Chem.* 1985, **228**, 63.
12. W. Kaminsky, K. Külper, H. H. Brintzinger and F. R. W. P. Wild, *Angew. Chem.* 1985, **97**, 507.
13. P. J. T. Tait, in *Transition Metals and Organometallics as Catalysts for Olefin Polymerization*, proc. Int. Symp. Hamburg, F.R.G. (Edited by W. Kaminsky and H. Sinn), p. 309. Springer, Berlin (1988).
14. M. Buschermöhle, Dissertation, University of Hamburg (1987).
15. R. Spiehl, Dissertation, University of Hamburg (1987).
16. F. R. W. P. Wild, L. Zsolnai, G. Huttner and H. H. Brintzinger, *J. Organomet. Chem.* 1985, **288**, 63.
17. J. Kopf, H.-J. Vollmer and W. Kaminsky, *Cryst. Struct. Commun.* 1980, **9**, 271.
18. H. Takaya, M. Yamakowa and K. Mashima, *J. Chem. Soc., Chem. Commun.* 1983, 1283.
19. F. Patat and H. Sinn, *Angew. Chem.* 1958, **70**, 496.
20. J. W. Lauher and R. Hoffmann, *J. Am. Chem. Soc.* 1976, **98**, 1729.

Polyhedron Vol. 7, No. 22/23, pp. 2383–2386, 1988
Printed in Great Britain

0277–5387/88 $3.00+.00
© 1988 Pergamon Press plc

FACTORS DETERMINING THE SELECTIVITY OF MULTIMETALLIC CATALYSTS

V. PONEC

Gorlaeus Laboratories, Leiden University, P.O. Box 9502, 2300 RA Leiden, The Netherlands

Abstract—The results relevant for the theory of catalysis and of interest for this Conference, obtained with model alloys (active metal with an inactive one) are reviewed first. It is argued that of the two effects of alloying—ensemble size effect and the electronic (ligand) effect—the first one is more important. Recent results obtained with Pt/Re alloys (two active metals) are briefly summarized and a conclusion is made that the results can be rationalized by ideas reviewed in the first part of this paper.

Three events which took place almost simultaneously in the second half of the sixties influenced dramatically our view on alloys in general and on alloys (or better, bimetallics, multimetallics) in catalysis, in particular. These were:

(1) The evidence has been obtained by UPS and later also by XPS that (i) the rigid band theory is not valid and (ii) in alloys, important features of the UPS spectrum of the alloy components are conserved also in alloys.[1]

The Coherent Potential Approximation Theory, and later some other higher approximations, offered an explanation of the observations and replaced the Rigid Band Theory.[2] Both the theory and the experiment were then at variance with the often made assumptions (RBT of alloys was based on this idea) that electrons are shifted in an alloy from one component to another.[3]

(2) Both the theory and the analysis of the experiments revealed that the chemisorption of the reactants of a catalytic reaction is a rather localized phenomenon involving one or only a few surface metal atoms ("an ensemble" of surface atoms).[4]

(3) Alloys or bimetallic catalysts appeared to be superior to the existing catalysts in various fields of industrial activities; in the first place in the naphtha reforming (high octane gasoline production).[5]

The early development along the lines just described has already been reviewed and analysed[6–10] and, therefore, we can confine ourselves to a short presentation of the main ideas and concentrate attention to the still existing problems. By that, the purpose of this Conference—to initiate new research oriented toward catalysis—will be served in the best way.

ELECTRONIC OR GEOMETRIC EFFECTS OF ALLOYING

Let us mention first the typical results obtained[11] with VIII gr. (i.e. an active) metal—Ib (inactive) metal alloys. A representation of results is shown in Fig. 1. The left part shows how much H_2 is adsorbed per unit surface area of the unsupported Ni/Cu alloys (evaporated films) and the curve reflects the Ni surface content as the function of the bulk Cu concentration. The right part shows the catalytic data. They concern cyclopropane which undergoes two simultaneous reactions: hydrogenolysis (full points) into ethene and methane and addition of H_2-hydrogenation (upper curve). It is typical for Ni/Cu alloys that one reaction is dramatically suppressed (hydrogenolysis) while the rate of another reaction is slightly enhanced (hydrogenation of cyclopropane) or slightly suppressed, in the proportion of the decrease of the Ni surface concentration.[8,12] Analysis[13] of our own and the literature data revealed that quite generally reactions already studied can be subdivided into two classes:

I. Reactions insensitive to alloying, like hydrogenations, dehydrogenations (C—C, C—N, C—O bonds), hydrogen/deuterium exchange in hydrocarbons.

II. Reactions sensitive to alloying (by alloying, the rate is suppressed appreciably more than the surface concentration of the VIII gr. metal), like hydrogenolysis, isomerization, ether formation from alcohols, Fischer–Tropsch synthesis and methanation.

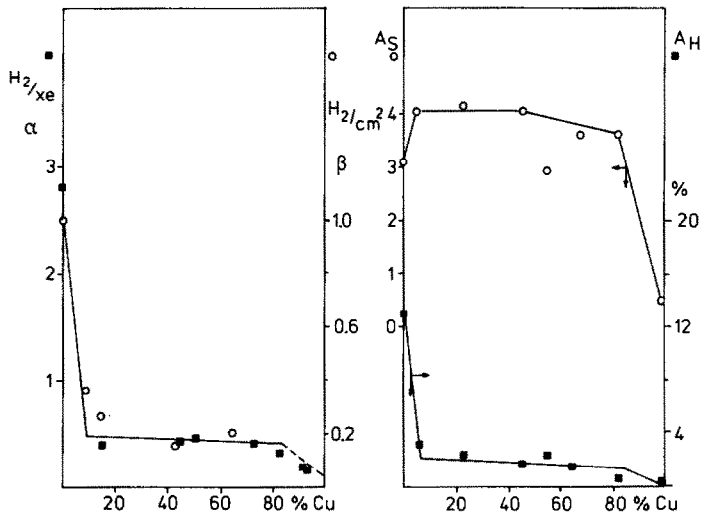

Fig. 1.

From the very start of the studies two reasons have been put forward to explain the pronounced suppression of some rates by alloying.[7,12] (i) Reactions of group II require several contiguous atoms of the VIII gr. metal to be simultaneously available to form chemisorption complexes. The presence of such ensembles is suppressed by alloying ("ensemble" size, or "geometric" effect). (ii) The electronic structure of the VIII gr. metal is modified by alloying, which makes it inactive (less active). This is usually called the "electronic" or "ligand" effect.[14,15]

The solid state physics data[8,14] did not support the idea of sub (ii), but people doubted the results and pointed out that the methods of solid state physics are insensitive to detect small changes caused by alloying and the small changes can still be important in catalysis. Everybody agreed that two methods should be sensitive enough: IR spectra of a good probe molecule and the methods of identification of sites or ensembles by their energetics of adsorption (such as thermal programmed desorption). After some discussion regarding the proper interpretation,[8] one could make a conclusion that these two methods also did not support idea (ii); no pronounced changes in the electronic structure of alloy components have been observed (no pronounced "ligand" effects). Explanation of the alloying effects and of the division of reactions into two groups, based on the idea of ensembles, is now accepted quite widely.

However, two pieces of new criticism appeared recently. Rooney[15] argued that there is no principle reason why the reactions of hydrocarbons should require "an ensemble" and why one single atom should not be sufficient. Burch[16] argues that the reactions of sub (ii), perhaps, do not require several atoms (ensemble) but one atom in a special crystallographic position which is, upon alloying, preferentially occupied by the inactive metal that then causes the dramatic suppression of certain reactions found experimentally. There are already some data which could be used in this place as an answer to this criticism, but it seems to be more useful than the reader of this paper realizes, that there are still debatable points and that new experimental data are still welcome. Professor Gates has actually responded to this challenge (see the Proceedings of this Conference) and his experiments with Os-clusters of varying nuclearity as catalysts and cyclopropane reactions as a probe are very important. They seem to support the idea of ensembles operating in hydrogenolysis, but this might not be the last word on this subject. In particular, more direct evidence of operating ensembles of Pt and Ir is still necessary.

CHARACTERIZATION OF BIMETALLIC CATALYSTS USED IN INDUSTRIAL PRACTICE

The main—in the volume production—application of bimetallic catalysts is the naphtha reforming. From various catalysts used, the Pt–Re combination is the most important one. Under industrial reaction conditions (10–20 bar H_2 pressure, temperature 450–500°C), the catalyst works in a sulphided state. In this state most of Re is present as a sulphide, some zero valent Pt and PtS_x being present next to it. Characterization undertaken in our laboratory employs a test at temperatures round 275°C and one bar total pressure,

with a hydrocarbon/H_2 ratio of 1 : 18, in a continuous flow system. Catalysts had been prepared as 2% wt Pt on Al_2O_3 (γ-alumina), with x% (atomic) of Pt replaced by Re and the catalysts were tested after a reduction *in situ* at 450°C for at least 4 h. The test molecule was 2,2-dimethylbutane (neohexane). The catalysts were tested unsulphided.

Neohexane reaction products supply us with the following pieces of information, as can be seen from Scheme 1. When the attachment of the neohexane molecule to the surface is as the one indicated by "$\alpha\beta$" (2C atoms involved), the main product should be neopentane (plus methane, but methane is "diagnostically" less valuable). On the other hand, the two products isopentane and isobutane, indicate an "$\alpha\gamma$" and "$\alpha\gamma'$" mode of attachment (3C atoms involved). Further, the selectivity to isomerization (3-methylpentane, 2,2-dimethylbutane) can be compared with the selectivity to hydrogenolysis. Some products indicate the presence of multiple reactions (two step hydrogenolysis, or hydrogenolysis combined with isomerization, etc.). If the multiple reactions are really extensive the conclusions about the preferential mode of attachment on the given metal or given alloy would be impossible, in some favourable cases a conclusion on all aspects mentioned above can be made.

Platinum–rhenium alloys offer us the following picture.[17] Rhenium added in small (10–50% Re) amounts to Pt, increases the isomerization selectivity, in spite of the fact that Re alone is a pure hydrogenolysis catalyst. This lack of additivity is an indication that Re and Pt form bimetallic particles. The catalysts in the mentioned low Re content region show a very low selectivity for the formation of the 2C $\alpha\beta$ complexes (see Fig. 2). The Re rich (more than 50% Re) alloys show a very pronounced preference for 2C $\alpha\beta$ complexes. Moreover, Re rich alloys and pure Re show multiple reactions (more than one reaction during one sojourn of a molecule on the surface), which are on pure Re so extensive that neopentane used to evaluate the propensity for 2C $\alpha\beta$ hydrogenolysis (cracking) is cracked down to pieces and the curve shows an apparent maximum.

There are no indications in the IR spectra of the adsorbed CO molecule, used as a probe, that in the

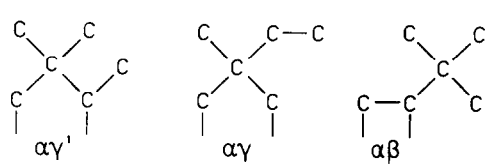

Scheme 1.

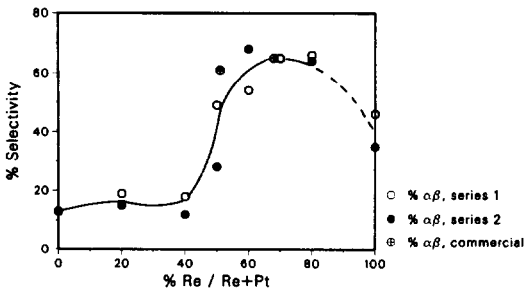

Fig. 2.

Pt/Re alloys (bimetallics) a pronounced ligand effect of alloying occurs,[18] which would change the identity of compounds. Thus, the 3C $\alpha\gamma$ attachment should be induced by the Pt atoms; the 2C $\alpha\beta$ attachment by the Re atoms. If the assumption is correct that the surface composition of the small particles of the alloys (electron microscopy revealed particles of about 1 nm in size) is approximately their overall composition and if all Re present is associated with Pt, the results (of which Fig. 2 is quite representative) indicate that several Re atoms are necessary to induce the 2C $\alpha\beta$ carbon–carbon bond fission.

It is not the subject of this paper, but the reader might be interested in the information on what happens when the surface of Pt/Re bimetallics is poisoned by sulphur, as under industrial conditions. In that case the total activity is suppressed and the isomerization selectivity is markedly increased. The experiments with pyridine poisoning showed that the "surviving" isomerization activity should be ascribed to the acidic (thus non-metallic) centres. Investigations on the identification of acid centres are still running.[19]

CONCLUSIONS

The results obtained with alloys (and bimetallics) revealed that the prevailing effect of alloying (mixing) is the ensemble size effect. However, direct identification of operating ensembles, in particular those of Pt and Ir, is still very desirable.

REFERENCES

1. D. H. Seib and W. E. Spicer, *Phys. Rev. Lett.* 1968, **20**, 1441; J. Hedman *et al.*, *Phys. Scripta* 1971, **4**, 495; S. Hufner, G. K. Wertheim and J. H. Wernick, *Phys. Rev. B* 1973, **10**, 4511; A. Wegner and S. Steinemann, *Helv. Phys. Acta* 1979, **47**, 321; R. J. Weiss and J. J. Marco, *Rev. Modern Phys.* 1958, **30**, 59; C. G. Robbins, H. Claus and P. A. Beck, *J. Appl. Phys.* 1969, **40**, 2269; J. P. Perrier, B. Fissier and R.

Tournier, *Phys. Rev. Lett.* 1970, **24**, 313; E. Vogt, *Phys. States Solids A* 1975, **28**, 11.
2. P. Soven, *Phys. Rev.* 1967, **156**, 809; P. Soven, *Phys. Rev.* 1969, **178**, 1136; B. Velicky, S. Kirkpatrick and H. Ehrenreich, *Phys. Rev.* 1968, **175**, 747; J. Slechta, *J. Phys.* 1976, **F6**, 2081; F. Yonezawa and K. Morigaki, *Prog. Theor. Phys.* (*Japan*) 1973, suppl. 53, 1 (this is only a selection of relevant papers on the subject).
3. N. F. Mott and H. Jones, *Theory and Properties of Metals and Alloys*. Oxford University Press, London (1936); D. A. Dowden, *J. Chem. Soc.* 1950, 242; D. A. Dowden, *Ind. Engng Chem.* 1952, **44**, 977; A. R. Miedema, *J. Less Common Metals* 1973, **32**, 115; *Z. Metal. Kunde* 1978, **69**, 455.
4. P. van der Planck and W. M. H. Sachtler, *Surf. Sci.* 1969, **18**, 62.
5. U.S. Patent, 3. 415 737 (1968); H. E. Kluksdahl, F. G. Ciapetta and D. N. Wallace, *Catal. Rev. Sci. Engng* 1971, **5**, 67.
6. V. Ponec, *Catal. Rev. Sci. Engng* 1975, **11**, 1.
7. W. M. H. Sachtler and R. A. van Santen, *Adv. Catal.* 1977, **26**, 69.
8. V. Ponec, *Adv. Catal.* 1983, **32**, 149.
9. J. H. Sinfelt, *Accts Chem. Res.* 1977, **10**, 15.
10. J. K. A. Clarke, *Chem. Rev.* 1975, **75**, 291.
11. J. M. van Beelen, W. M. H. Sachtler and V. Ponec, *J. Catal.* 1973, **28**, 376.
12. V. Ponec and W. M. H. Sachtler, *J. Catal.* 1972, **24**, 250; (b) J. H. Sinfelt, J. L. Carter and D. C. Yates, *J. Catal.* 1972, **24**, 283.
13. V. Ponec, *Int. J. Quantum Chem.* 1977, **12** (*suppl.*), 1; V. Ponec, *Surf. Sci.* 1979, **80**, 352.
14. For a more detailed review on this subject see: V. Ponec, in *Electronic Structure and Reactivity of Metal Surfaces* (Edited by E. G. Derouane and A. A. Lucas), p. 737. Plenum, New York (1976).
15. J. J. Rooney, *J. Molec. Catal.* 1985, **31**, 147.
16. R. Burch, private communication; R. Burch, *Accts Chem. Res.* 1982, **15**, 24.
17. M. J. P. Botman, Ph.D. Thesis, Leiden University (1987).
18. F. J. C. M. Toolenaar, A. G. T. M. Bastein and V. Ponec, *J. Catal.* 1983, **82**, 35.
19. A. J. den Hartog, unpublished results, Leiden University.

Polyhedron Vol. 7, No. 22/23, pp. 2387–2392, 1988
Printed in Great Britain

0277–5387/88 $3.00+.00
© 1988 Pergamon Press plc

ELEMENTARY STEPS IN THE FORMATION OF BIMETALLIC CATALYSTS DERIVED FROM CARBONYL CLUSTERS

L. GUCZI* and A. BECK

Institute of Isotopes of the Hungarian Academy of Sciences, P.O. Box 77, H-1525 Budapest, Hungary

Abstract—The elementary steps in the surface reactions of the transition metal carbonyl clusters on alumina and silica leading to small metal particles have been investigated. It was established that after the initial interaction with the surface oxygen or hydroxyl groups the carbonyl clusters undergo disruption including metal–metal bond rupture to form monometallic dicarbonyl species which are responsible for highly dispersed metal particles on the alumina surface. In contrast, on the silica surface there are several surface transformations of the original cluster framework including the build-up of a framework with higher nuclearity which ultimately leads to metal particles larger in size than those formed on alumina. The difference is reflected in the catalytic properties of the supported catalysts formed from the carbonyl clusters.

The advantage of using metal carbonyl clusters supported on inert carriers lies in the possibility of modelling supported, highly dispersed metal catalysts.[1] It is generally accepted that the metal particles produced from cluster precursors are smaller than those prepared from inorganic salt solutions by the incipient wetness method.[2] When small bimetallic particles are formed in which two different metals with a large miscibility gap are present, a thermodynamically non-existing composition can be produced.[3] Unfortunately, the strong cluster–support interaction generally causes disruption of the polymetallic cluster framework. Formation and stabilization of small metal aggregates results in an increased metal–support interaction that involves a modified electron interaction between the metal particles and the support. Therefore coalescence of the particles can be retarded.[4]

An important problem that should be addressed is whether in a multimetallic system the different metals are actually included in the same particles or there is only a mixture of the two monometallic particles. Sometimes this can be determined only by chemical reaction although metal segregation during reaction or chemisorption cannot be excluded, either.

So far it has been established that the catalytic activity of a cluster derived catalyst depends mainly upon the atmosphere in which the original cluster-on-support has been decomposed.[5,6] That is, the catalytic activity was always higher when decomposition took place in helium than in hydrogen. Furthermore, the activity was also higher if the decomposition occurred up to 570 K instead of 770 K. In the former case the presence of subcarbonyl species that might influence the active sites, could be observed.[7] It was also found that in addition to the factors of temperature and atmosphere used for decomposition, the nature of support also exerted a predominent role in the generation of metal particles.[8] In this latter case the cluster–support interaction may play a decisive role.

In the heterogeneous catalysis the activity and selectivity of a metal catalyst are controlled by the metal–support interaction. The higher the metal dispersion, the larger the metal–support interaction is. As was indicated earlier, the metal dispersion can be greatly influenced by the cluster–support interaction which is dependent upon the nature of support and the conditions under which the decomposition was carried out. Consequently, by studying the cluster–support interaction, i.e. the elementary surface reaction steps which are strongly related to this interaction, prediction can be made to the activity and selectivity of a metal catalyst produced by surface decomposition of metal carbonyl clusters.

* Author to whom correspondence should be addressed.

CHARACTERISTIC CLUSTER–SUPPORT INTERACTIONS[9–12]

The surfaces of alumina, silica, magnesia and titania contain significant amounts of O^{2-} and OH^- groups which may interact with the metal carbonyl clusters after the initial contact. The main types of these interactions are summarized in Table 1.

(1) Hydrogen bonding between CO groups and hydrogen in the OH^- group is a frequent form of interaction. Such an interaction is typical for the $Fe_3(CO)_{12}/SiO_2$ system immediately after impregnation.

(2) OH^- and O^{2-} are good electron donors. Thus, one CO ligand can be exchanged and oxygen can enter the ligand sphere. However, this bond is weaker than the metal—CO bond. Such interaction can be observed in the $Ru_3(CO)_{12}$/alumina system.

(3) Metal atoms in the cluster framework can be oxidized after the cleavage of the trinuclear cluster by the oxygen in the OH^- group. This is typical for $Ru_3(CO)_{12}$ on alumina.

(4) A hydrido–carbonyl cluster may be formed via oxidation of a CO ligand by a surface hydroxyl group after contacting $Fe_3(CO)_{12}$ with alumina. This interaction was observed also on magnesia support.

(5) Lewis acid–base interactions at a rather frequent type of bonding. These exist when coordinatively unsaturated surface cations, such as Al^+, are bonded to the cluster via an oxygen atom in the carbonyl ligand.

Normally, distinction among the different types of interactions cannot be made. They overlap each other and exist simultaneously. However, they are undoubtedly responsible for the cluster–support interactions which ultimately lead to the metal–support interaction.

ELEMENTARY STEPS IN THE SURFACE TRANSFORMATION OF METAL CLUSTERS

In this part, the cluster–support interactions that control the surface subcarbonyl species in the systems containing $FeRu_2(CO)_{12}$, $Fe_2Ru(CO)_{12}$ and $H_2FeRu_3(CO)_{13}$ supported on silica and alumina are summarized. The results are compared to the interactions revealed in the studies of $Ru_3(CO)_{12}$ deposited on alumina and silica. Finally, the work is complemented with catalytic results.

Interaction of cluster with alumina[13–16]

The behaviour of the four clusters is very similar. In all cases both in hydrogen and in vacuum decomposition, mononuclear species indicated by the CO stretching region measured by FTIR are formed. Monoruthenium dicarbonyl species containing the ruthenium in various oxidation states were identified shortly after impregnation. Its formation is independent of the type of carbonyl clusters, but the relative amount of the ruthenium in different oxidation states depends only on the atmosphere in which the decomposition was carried out.

The first and most important conclusion is that iron–ruthenium bimetallic clusters are decomposed into the identical ruthenium anchored surface species as the ruthenium cluster itself, and no iron subcarbonyl species could be assigned on the surface. These processes are fast even at room temperature.

From an FTIR study the following conclusions can be drawn for the mechanism.[16] The original carbonyl cluster is first physisorbed on hydrated alumina. Due to the strong interaction, the original cluster loses some of the carbonyl ligands.

Table 1. Characteristic cluster interactions with surface O^{2-} and OH^- groups

1. Hydrogen bonding

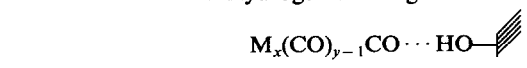

2. Exchange of CO with surface ligands (OH^- and O^{2-})

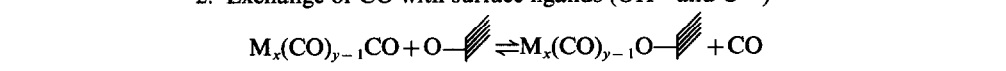

3. Oxidation of metal atoms

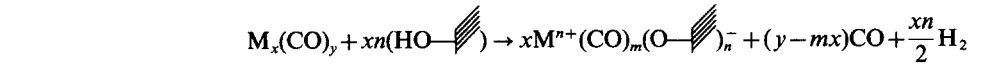

4. Oxidation of CO ligands resulting in hydrido anions

5. Lewis acid–base interaction with unsaturated cation of the surface

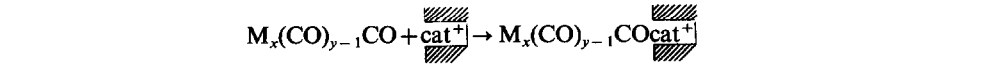

The metal framework is cleaved and via subcarbonyl species such as M—CO···M, $M(CO)_x$, $(HM(CO)_x)^-$, (where $x = 1$–5, M = Fe or Ru) the original cluster molecules are transformed into $Ru_3(CO)_{12}$ and $Fe(CO)_5$. Further decomposition of these species results in anchored $Ru(O)(CO)_2$, $Ru(II)(CO)_2$ and $Ru(III)(CO)_2$ entities as well as Fe^{2+} and Fe^{3+} ions. These products are stable over a wide range of temperature (273–573 K).

Interaction of cluster with silica[17–19]

On the silica surface the cluster–support interaction is weaker than in the case of alumina. In accordance with the milder conditions, individual behaviour of the clusters can be anticipated. Instead, individualities only in their stabilities can be found and an overall consistency in the mechanism of the surface reaction in which they are involved. Their stability decreases in the sequence of

$$H_2FeRu_3(CO)_{13} > Ru_3(CO)_{12} > FeRu_2(CO)_{12} > Fe_2Ru(CO)_{12}.$$

If one compares the decomposition schemes for $H_2FeRu_3(CO)_{13}$ deposited on alumina and silica, an entirely different picture can be seen as indicated in Fig. 1. While for the alumina supported cluster the peaks at 2139, 2074, 2055, 2006 and 1980 cm^{-1} frequencies are dominating the whole spectrum, on silica a more complicated band structure can be identified. The precise assignment of the peaks shows the following. At room temperature both in a vacuum and in hydrogen most of the original molecule (about 70%) stays in the original molecular form. In addition to that, in a vacuum $Fe_2Ru(CO)_{12}$, $Ru_3(CO)_{12}$ and $HRu_3(CO)_{10}(OSi\langle)$ are present in traces, and in hydrogen $H_4FeRu_3(CO)_{12}$ or $H_2Ru_4(CO)_{13}$ and $H_4Ru_4(CO)_{12}$ in 10% and in traces, respectively, can be identified. The $Ru(II)(CO)_2$ and $Ru(O)(CO)_2$ species amount to 10% on silica.

The most characteristic difference between the behaviours of $H_2FeRu_3(CO)_{13}$ supported on alumina and on silica is that on silica the first step of the surface reaction is not necessarily the cleavage of all metal bonds in the framework. The original structure is retained to a large extent. Moreover, by increasing the temperature the next step is not the disrupture of the cluster structure, but after some surface rearrangement expansion of the cluster framework takes place and the collapse of the original structure occurs only at higher temperature. Of course, in the reaction where an iron atom is replaced by ruthenium, the original tetranuclear structure must first collapse, thereby supplying ruthenium atoms to the reaction. Because of the weak interaction, the individual ruthenium atoms are not rigidly anchored to the surface sites, and thus their mobility enables them to be involved in further surface reactions.

FORMATION OF SUPPORTED BIMETALLIC CATALYSTS

As was demonstrated in the previous section, it is a rule that bimetallic clusters are decomposed when they are brought into contact with the surface OH^- or O^{2-} groups. It is valid for iron–ruthenium bimetallic clusters but in the literature several other examples can be found. For instance, clusters like $H_2RhOs_3(CO)_{10}(acac)$ deposited on alumina are decomposed in the presence of a CO atmosphere to form $Rh(I)(CO)_2$ and $HOs_3(CO)_{10}{=}O{-}Si\langle$.[20] Similarly, $H_2FeOs_3(CO)_{13}$ on silica produces $HOs_3(CO)_{10}{=}O{-}Si\langle$ and ferric ions.[21] After full decarbonylation, these species may form bimetallic particles. This is proven by the selectivity changes of the CO hydrogenation.[20] In any case the dispersion is very high, which is ensured by the presence of a highly dispersed iron oxide matrix. The metallic rhodium or osmium particles are embedded into this matrix and the intimate contact between iron oxide and metallic particles may lead to the partial reduction of the iron oxide phase. On the other hand, when bimetallic clusters such as $H_2FeOs_3(CO)_{13}$, $H_2FeRu_3(CO)_{13}$ and $H_2FeCo_3(CO)_{13}$ are deposited on partially hydrated MgO, after decomposition not only kinetic evidence but direct TEM measurements point to the existence of bimetallic particles.[22]

The unique behaviour of the hydroxyl groups and their reactivity toward the bimetallic cluster framework can be proven using supports without hydroxyl groups. Thus, for example, $Fe(CO)_5$ deposited on grafoil (graphite-like material) does not lead to the formation of Fe^{3+} ions but instead zero-valent iron is formed after decomposition.[23] Similarly, the formation of bimetallic particles resulted from $H_2FeRu_3(CO)_{13}$, $Fe_2Ru(CO)_{12}$ and $FeRu_2(CO)_{12}$ supported over CSX-203 graphite carrier, as evidenced by the turnover frequency, TOF. In contrast to that, a mixture of $Fe_3(CO)_{12}$ and $Ru_3(CO)_{12}$ after decomposition leads to metal particles with inhomogeneous distribution on the CSX-203 surface and the TOF value is about one third of that measured on bimetallic particles derived from bimetallic clusters.[24]

The problem arising is, therefore, rather com-

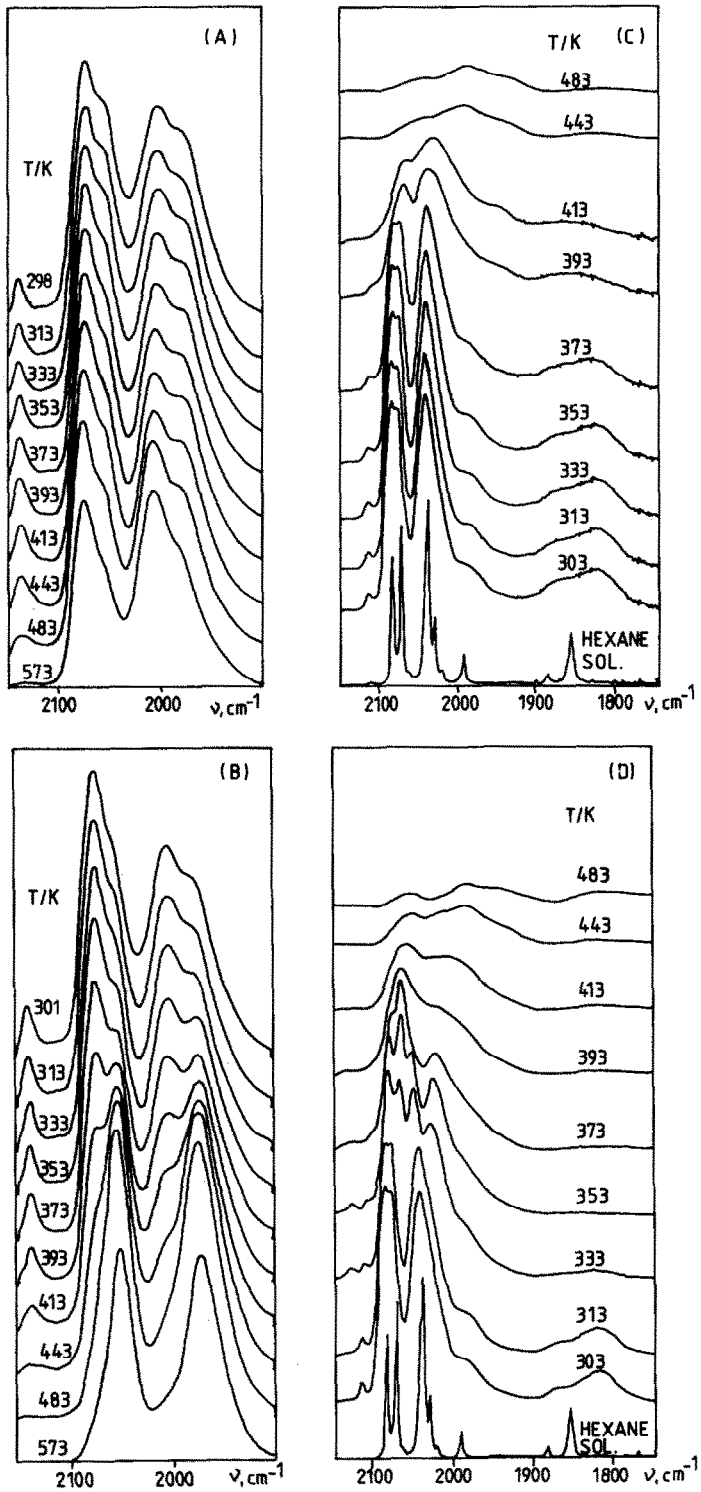

Fig. 1. IR spectra of the systems $H_2FeRu_3(CO)_{13}$ supported on alumina in a vacuum (A) and in hydrogen (B), on silica in a vacuum (C) and in hydrogen (D) during thermal decomposition.

plex: as a rule, the bimetallic cluster may decompose on the support and apparently the more acidic the support is, the greater the decomposition is. On basic or neutral supports (carbon or magnesia, respectively) no reaction takes place between the metallic cluster framework and the surface hydroxyl groups. Consequently, after removal of the carbonyl ligands in a thermal treatment, small metal or bimetallic particles are formed. On the other hand, on acidic supports such as silica and alumina,

the main reaction is always the cleavage of the cluster framework, but reconstruction of the bimetallic particles does not take place in every case. It depends on the extent to which the decomposed cluster is treated, e.g. the temperature of the post-decomposition hydrogenation, the severeness of the thermal treatment, etc. In some instances reconstruction of the bimetallic particles occurs during the catalytic reaction and their presence can be clarified only by the activity and selectivity. Sometimes very sophisticated methods are required to identify the presence of bimetallic particles. The problem is further complicated by the metal particles being extremely small. Thus, methods like XRD or small angle X-ray scattering cannot be utilized (e.g. the iron–ruthenium system bimetallic particles could be identified by means of low temperature and high external field Mössbauer spectroscopy[25]).

Finally, the catalytic activity measured for iron–ruthenium systems[26] is in full agreement with those obtained from decomposition results. As was mentioned earlier, on alumina, due to the strong cluster–support interactions, practically atomically dispersed ruthenium stabilized by carbonyl ligands, and iron are present. These species cannot migrate along the surface. Therefore, after high temperature hydrogenation, small metal and bimetallic particles are formed. Since the above interaction is weaker on a silica surface, surface rearrangement of the starting cluster occurs before decomposition. Thus, on silica smaller metal dispersion can be anticipated. In Table 2 the corresponding catalytic activities are presented in the CO hydrogenation.

It is obvious from Table 2 that

(i) activity is higher on an alumina supported catalyst than on that supported on silica; and

(ii) activity on the bimetallic catalysts prepared from a bimetallic cluster is higher than that formed from a mixture of two monometallic clusters.

Table 2. Catalytic activity of FeRu bimetallic catalysts.

Reaction: $CO+H_2$, flow rate 15 cm^{-3} min^{-1}

Substances	Rate
$Fe+Ru/SiO_2$	1.4
$Fe+Ru/Al_2O_3$	4.5
Fe_3+Ru_3/SiO_2 (773 K)	3.4
(573 K)	12.0
Fe_3+Ru_3/Al_2O_3	12
$FeRu_3/SiO_2$	7
$FeRu_3/Al_2O_3$ (773 K)	25
(573 K)	55

Note: Fe+Ru—inorganic source;
Fe_3+Ru_3—$Fe_3(CO)_{12}+Ru_3(CO)_{12}$;
$FeRu_3$—$H_2FeRu_3(CO)_{13}$.
Rate: $\times 10^8$ mol s^{-1} g_{cat}^{-1}.

The explanation can again be sought in the metal–support interaction: since the catalyst components are randomly distributed when the bimetallic cluster is the precursor, less surface migration is needed to form bimetallic particles using the neighbouring iron and ruthenium atoms. For a mixture the different ensembles are separated and migration, particularly for alumina, is prevented.

CONCLUSION

It can be established that on a hydroxylated acidic surface the main interaction always leads to the cleavage of the cluster framework.

The surface reaction depends upon the reactivity of the support and the conditions under which the thermal treatment is carried out.

The intermediates formed are directly responsible for the state of the metal particle produced.

Surface subcarbonyl species are required to be present for stabilizing the highly dispersed metal particles.

REFERENCES

1. R. Ugo, R. Psaro, G. M. Zanderighi, J. M. Basset, A. Theolier and A. K. Smith, *Fundamental Research in Homogeneous Catalysis* (Edited by M. Tsutsui), Vol. 3, p. 579. Plenum Publ. Co. (1979).
2. L. Guczi, Z. Schay, K. Matusek, I. Bogyay and G. Steffler, *Proc. 7th Int. Congr. Catal.*, Tokyo, Part A, p. 211 (1981).
3. D. F. Ollis, *J. Catal.* 1971, **23**, 131.
4. L. Guczi, Z. Schay, K. Matusek and I. Bogyay, *Appl. Catal.* 1986, **22**, 289.
5. Z. Schay and L. Guczi, *Acta Chim. Acad. Sci. Hung.* 1982, **111**, 607.
6. L. Guczi, Z. Schay and I. Bogyay, *Preparation of Catalysts III* (Edited by G. Poncelet, P. Grange and P. A. Jacobs), p. 451. Elsevier, Amsterdam (1983).
7. L. Guczi and S. Dobos, *Homogeneous and Heterogeneous Catalysis* (Edited by Yu. I. Yermakov and Likholobov), p. 901. VNU Science Press, Utrecht, The Netherlands (1986).
8. Z. Schay and L. Guczi, *Acta Chim. Hung.* 1985, **119**, 105.
9. K. Lázár, K. Matusek, J. Mink, S. Dobos, L. Guczi, A. Vizi-Orosz, L. Markò and W. M. Reiff, *J. Catal.* 1987, **87**, 163.
10. A. Zecchina, E. Guglielminotti, A. Bossi and M. Camia, *J. Catal.* 1982, **74**, 225.
11. F. Hughes, A. K. Smith, B. Taarit and J. M. Basset, *J. Chem. Soc., Chem. Commun.* 1980, 68.

12. J. S. Kristoff and D. F. Schriver, *Inorg. Chem.* 1974, **13**, 499.
13. S. Dobos, I. Böszörmènyi, L. Guczi and J. Mink, *Inorg. Chim. Acta* 1985, **96**, L13.
14. I. Böszörmènyi and L. Guczi, *Inorg. Chim. Acta* 1986, **112**, 5.
15. S. Dobos, I. Böszörmènyi, J. Mink and L. Guczi, *Inorg. Chim. Acta* 1986, **120**, 135.
16. S. Dobos, I. Böszörmènyi, J. Mink and L. Guczi, *Inorg. Chim. Acta* 1986, **120**, 145.
17. Z. Schay, K. Lázár, J. Mink and L. Guczi, *J. Catal.* 1984, **87**, 179.
18. S. Dobos, I. Böszörmènyi, J. Mink and L. Guczi, *Inorg. Chim. Acta* 1987, **134**, 203.
19. S. Dobos, I. Böszörmènyi, J. Mink and L. Guczi, *Inorg. Chim. Acta* 1988, **144**, 37.
20. J. R. Budge, B. F. Lücke, B. C. Gates and J. Toran, *J. Catal.* 1985, **91**, 272.
21. A. Choplin, M. Leconte, J. M. Basset, S. G. Shore and W. L. Hsu, *J. Molec. Catal.* 1983, **21**, 389.
22. A. Choplin, L. Huang, A. Theolier, P. Gallezot and J. M. Basset, *J. Am. Chem. Soc.* 1986, **108**, 4224.
23. J. Phillips and J. A. Dumesic, *Appl. Catal.* 1984, **9**, 1.
24. M. Kaminsky, Ki J. Yoon, G. L. Geoffroy and M. A. Vannice, *J. Catal.* 1985, **91**, 338.
25. K. Làzàr, W. M. Reiff, W. Morke and L. Guczi, *J. Catal.* 1986, **100**, 118.
26. I. Böszörmènyi, S. Dobos, L. Guczi, L. Markó, K. Lázár, W. M. Reiff, Z. Schay, L. Takács and A. Vizi-Orosz, *Proc. 8th Int. Congr. Catal.*, Berlin, Vol. 5, p. 183 (1984).

Polyhedron Vol. 7, No. 22/23, pp. 2393–2398, 1988
Printed in Great Britain

0277–5387/88 $3.00+.00
© 1988 Pergamon Press plc

REDOX REACTIONS ON OXIDES HAVING BLOCK STRUCTURES: HIGH-RESOLUTION TRANSMISSION ELECTRON MICROSCOPY

REGINALD GRUEHN

Institut für Anorganische und Analytische Chemie der Justus-Liebig-Universität Gießen, Heinrich-Buff-Ring 58, D-6300 Gießen, F.R.G.

Abstract—Improved preparative investigations using redox reactions made it possible to prepare oxides which have previously unknown block structures. In this work poor crystallinity or microheterogeneity of solids often prevents or complicates the application of other diffraction methods. Therefore high-resolution transmission electron microscopy was useful for the clarification of structures as in the case of doubling of block size in the system Nb/W/O or in the investigation of metastable oxidation products on $Nb_{12}O_{29}$. In addition the *in situ* reduction of oxides V/Nb/O could be observed within the electron microscope.

When non-specialists hear the term electron microscopy they mostly remember the nice photographs taken with a scanning electron microscope because numerous instruments of this type are used in laboratories in biology, mineralogy, chemistry, physics, medicine and so on. The scanning electron microscope gives information on the surface of solids, of the shape of crystals and sometimes it reveals details which give hints that defects are present. This should be mentioned to avoid certain misunderstanding.

In contrast to this, our main interest is directed to the atomic structure within the volume of a crystal or to materials having a certain degree of crystallinity. For objects of this kind transmission electron microscopy can be a powerful tool[1,2] and structural information will become available if the resolution of the instrument is in the order of atomic distances or at least equal to the size of interesting building units.

METHOD

The resolution of a transmission electron microscope depends on the acceleration voltage and on the spherical aberration constant C_s of the objective lens. Additional instrumental parameters are important too.[1,2] Our microscope, a Philips EM 400 HMG, has a maximum acceleration voltage of 120 kV and is equipped with an LaB_6 cathode. Thus a resolution of 3.0–3.5 Å can be obtained.

Particularly suitable for investigations with high resolution transmission electron microscopy (HRTEM) are crystal structures whose building elements can be projected parallel to a crystallographic axis onto a plane in such a way that at high magnification and with high resolution, structural details can be observed and the contrast is as high as possible. Samples are prepared for microscopy by producing fragments with thin edges, e.g. by mechanical means (crushing in an agate mortar). The crystal pieces are brought onto a copper grid covered with a holey foil and are then orientated with one crystallographic axis parallel to the electron beam using the diffraction mode of the microscope. Now a pile of parallel lattice planes corresponding to a small piece of a crystal is orientated perpendicular to the electron beam of the microscope.[2] The resulting image may under certain imaging conditions look like a projection of the structure but one should keep in mind that the way of image formation is not the same as in a usual microscope. The objective lens combines the beams of the diffraction pattern in a suitable way forming an interference figure. Mathematically this corresponds to a second Fourier transformation within the description of the imaging process. In this respect the electron microscope is used as an interferometer. Only for optimum conditions can one assume that the details of the resulting images correspond in a simple way to the projected structure. It is indispensable that samples must be thin, if possible 50–100 Å thick. The microscope must be defocussed, usually one needs an underfocus near to the so called Scherzer focus.

For the interpretation of the images computer

simulations[3-5] play an important role. In many cases the contrast of the images which depends on the value of defocus and on the thickness of the crystal region cannot be interpreted directly.[4,5] Therefore a sufficient number of simulated images computed for different experimental parameters must be available. During the investigation of oxides having block structures it was found that the correspondence between the image contrast and the details of structure is nearly one to one. Therefore in some special cases it is possible to interpret images of block structures "directly".

Strong limitations come from the high energy of the electron beam. At the highest resolution nearly all organic materials and other sensitive substances are damaged. Only compounds having a high thermal stability and especially high melting inorganic materials can be investigated at atomic resolution. In our laboratory mainly transition metal oxides[1,2,4,6-18] and a few oxyhalides[3] were investigated.

The structural units of the niobium-, tungsten- or vanadium-containing compounds mentioned here can be described as a framework of corner sharing metal–oxygen octahedra. In addition there is a relationship to the perovskite-type structures which now in some cases were detected to be superconductors.[1] A combination of edge sharing and corner sharing octahedra allows us to build up so called block structures having a high variability of composition depending on the size of the building units and on their connections. Figure 1 shows the block structures of $Nb_{12}O_{29}$ (mon.) and $V_3Nb_9O_{29}$ having [3 × 4] blocks which are connected in a different way. Images shown in this paper (Figs 2–6) were always obtained as a projection along the short crystallographic axis.

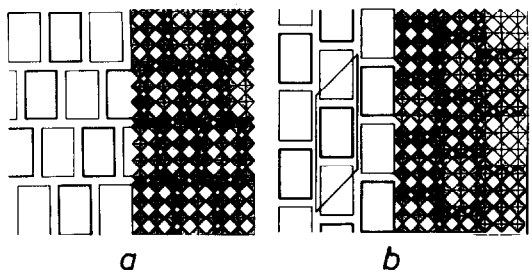

Fig. 1. Ideal structures of monoclinic $Nb_{12}O_{29}$ (a)[21] and $V_3Nb_9O_{29}$ (b)[6] as examples of block structures. The niobium (and V) is surrounded octahedrally by oxygen. The right hand side of the figures shows the idealized octahedra which can be regarded as square-base bipyramids. The direction of view is from an apex down onto the basal plane, so that in projection the apexes appear to be the points of intersection of the base diagonals. Within the blocks the octahedra are interconnected via the apexes in all directions; where the blocks abut against one another, the octahedra are linked with each other along edges. The outlines of the blocks are shown more clearly on the left. The different "heights" of the blocks in the direction of the short *b*-axis (perpendicular to the plane of the figure) are indicated by lines of different thickness. For $V_3Nb_9O_{29}$ (b) the elementary cell is drawn in.

RESULTS

System Nb/W/O

By mixing the oxides Nb_2O_5 and WO_3 and heating them in air (e.g. 1300–1350°C; closed vessels) in the compositions 6 : 1, 7 : 3, 8 : 5 and 9 : 8, phases having simple block structures ([3 × 4], [4 × 4], [4 × 5] and [5 × 5] octahedra) could be found.[19] Experiments using different preparative methods show[7,8] that in the thermodynamically stable system Nb/W/O block structures cannot exceed a maximum block size of [5 × 5] octahedra corresponding to a ratio W/Nb = 0.444. In order to prepare samples with higher W/Nb ratios still having block structures WO_3+NbO_2 was substituted for Nb_2O_5 to an appreciable extent. For the occurring 6 : 1, 7 : 3, 8 : 5 and 9 : 8 phases we were successful in substituting W for Nb in a wide range thus establishing four series of solid solutions.[7] With samples of these "reduced" solid solution series oxidation experiments were performed outside the microscope on a preparative scale.[7,9-12]

By using mild metastable conditions (oxidation temperature for example 700°C instead of 1300°C) oxygen is introduced and corner sharing octahedra are formed. In this process edge sharing octahedra disappear and looking parallel to the short crystallographic axis of such a crystal one can observe a doubling of the block size.

Starting for example with a [3 × 4] block structure having the composition $Nb_{10}W_3O_{33}$ the oxidation leads to the composition $Nb_{10}W_3O_{34}$ ($O/\Sigma M = 2.615$; M = Nb, W). The HRTEM image (Fig. 2) shows that [3 × 4] blocks are still present in the structure but as a new feature [6 × 4] blocks have been formed (2[3 × 4] → [6 × 4]). By counting the different blocks in the region of Fig. 2 one can calculate the structural ratio $O/\Sigma M = 2.611$ that corresponds well with the experimental values.[12] On calculation of the structural $O/\Sigma M$ one must keep in mind that tetrahedral positions disappear when larger blocks are formed[11-12] (see Fig. 4).

In the case of rectangular blocks nature allows both possibilities of "doubling" to be realized as a

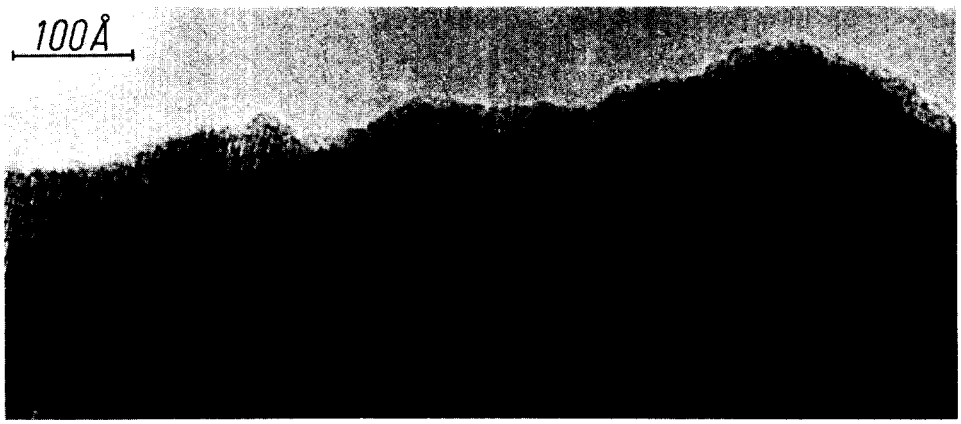

Fig. 2. Transmission electron micrograph[12] of the oxidation product $Nb_{10}W_3O_{34}$ ($O/\Sigma M = 2.615$) built up by rows of [6 × 4] and [3 × 4] blocks.

look at Fig. 3 shows. In this case the oxidation of a sample with [3 × 4] blocks produced an arrangement of [3 × 8] (corresponding to 2[3 × 4] → [3 × 8]) besides [3 × 4] blocks.[12]

It is important to mention that a determination of this structure by X-rays was impossible because of the disorder of these samples. This disorder is also indicated by the selected area diffraction pattern (c in Fig. 4). In spite of only very few rows of [4 × 4] blocks the diffraction spots corresponding to the direction of disorder (recognizable in Fig. 4a) are strongly diffuse.[9,12] A large portion of blocks participated in the doubling during oxidation of this sample (2[4 × 4] → [4 × 8]). This could be achieved due to the higher W-content of the educt and was made possible by the more extended [4 × 4] block solid solution series.

As Fig. 5 shows, the largest blocks can be pro-

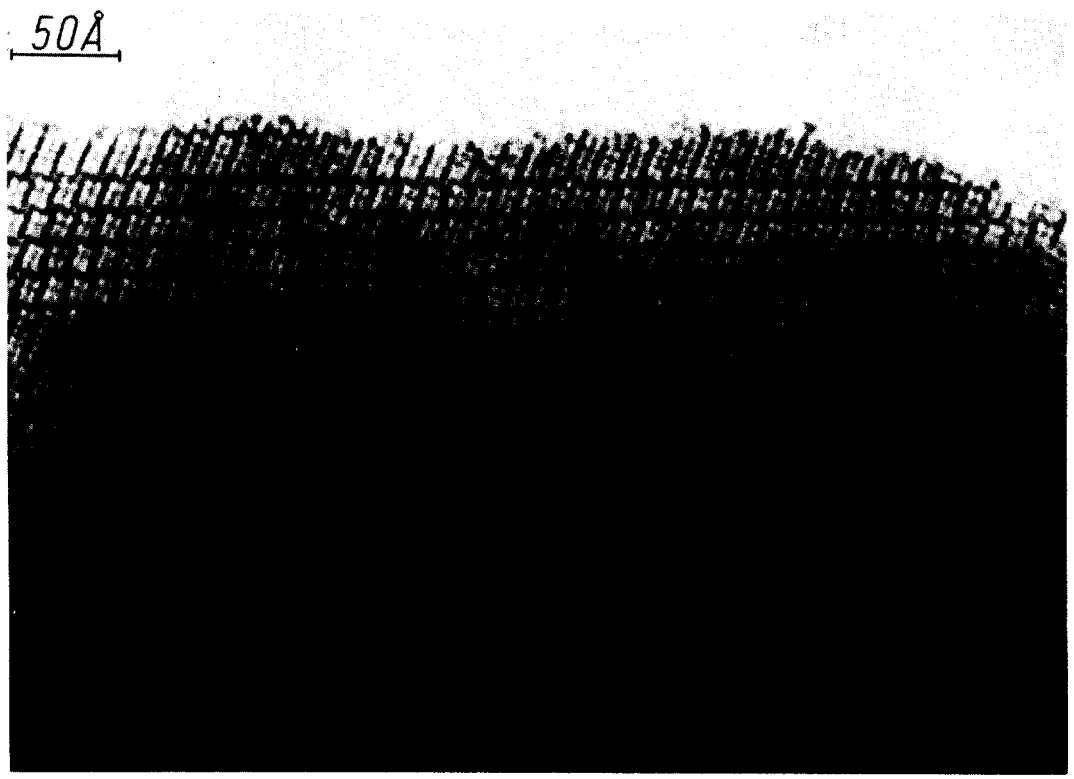

Fig. 3. Transmission electron micrograph[12] of the oxidation product $Nb_{10.4}W_{2.6}O_{33.8}$ ($O/\Sigma M = 2.600$) built up by rows of [3 × 8] and [3 × 4] blocks.

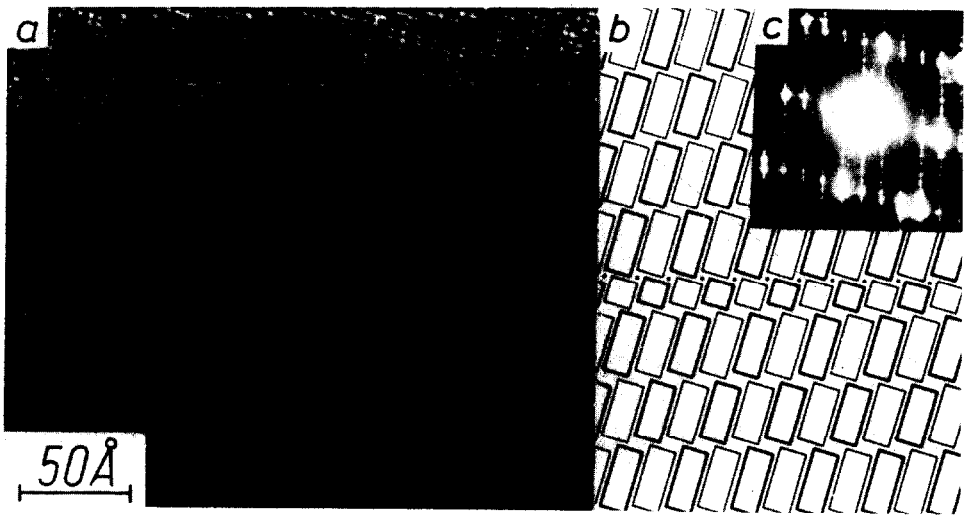

Fig. 4. Transmission electron micrograph (a) of the oxidation product $Nb_{10}W_7O_{46}$ (starting composition $Nb_{10}W_7O_{44}$).[12] The interpretation (b) shows the arrangement of [4 × 8] and (one row) of [4 × 4] blocks. Tetrahedral positions (black dots) disappeared by formation of the larger blocks. (c) Electron diffraction pattern.

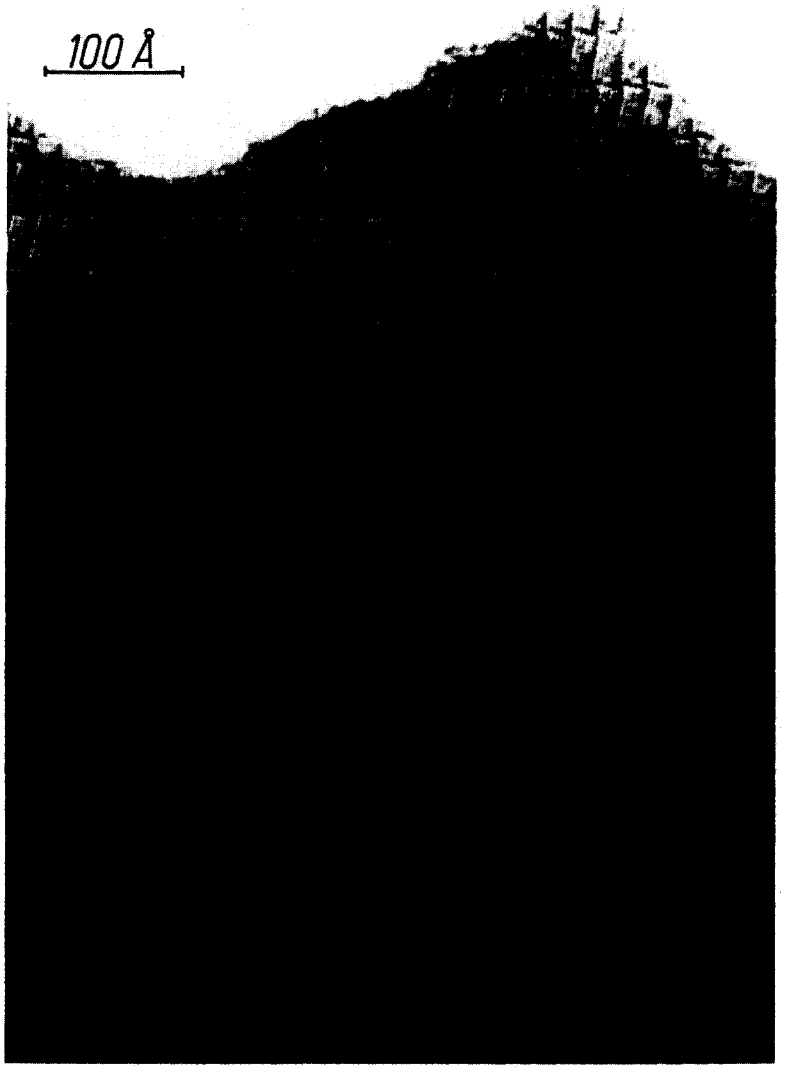

Fig. 5. Transmission electron micrograph[12] of the oxidation product $Nb_{11}W_{15}O_{72.5}$ ($O/\Sigma M = 2.788$) built up by [5 × 10], [5 × 15] and (one row) [5 × 5] blocks.

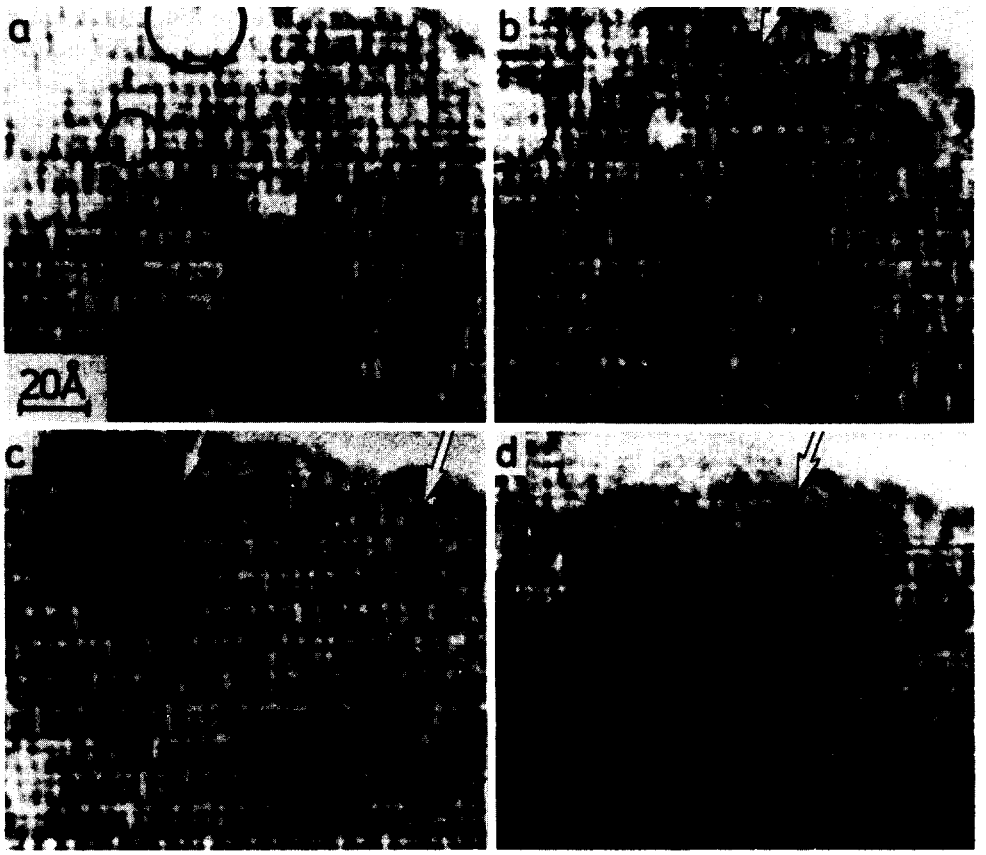

Fig. 6. Transmission electron micrographs of a crystal fragment: increasing irradiation time.[13] Damaged regions are encircled, increasing division of block rows ([3 × 4] → 2[3 × 2]) marked by arrows. (a) Long irradiation at low density. (b) Diaphragm removed for 0.5 s. (c) Like (b) but for 1 s. (d) After further irradiation like in (c).

duced starting with a [5 × 5] block structure. The oxidation of the sample with a composition $Nb_{11}W_{15}O_{69}$ results in a high portion of [5 × 10] blocks (2[5 × 5] → [5 × 10]) but besides this the formation of [5 × 15] block rows[10,12] begins. It seems the formation of the [5 × 15] blocks could not reach the perfect shape.

System V/Nb/O

A previously unknown phase $V_3Nb_9O_{29}$ having the structure shown in Fig. 1b could be found recently.[6] With $V_3Nb_9O_{29}$ ($O/\Sigma M = 2.417$; M = V, Nb), in contrast to the doubling of blocks just mentioned, a division of blocks in two halves could be observed (Figs 6 and 7). This means that corresponding to the division of blocks a reduction occurs connected with the introduction of edge sharing of octahedra. The *in situ* reaction in the electron microscope started when the irradiation was increased by removing the condenser diaphragm for a few seconds.[13,14] The resulting regions of the crystal piece with a block size of [2 × 3] octahedra correspond to the structure of V_6O_{13} (Fig.

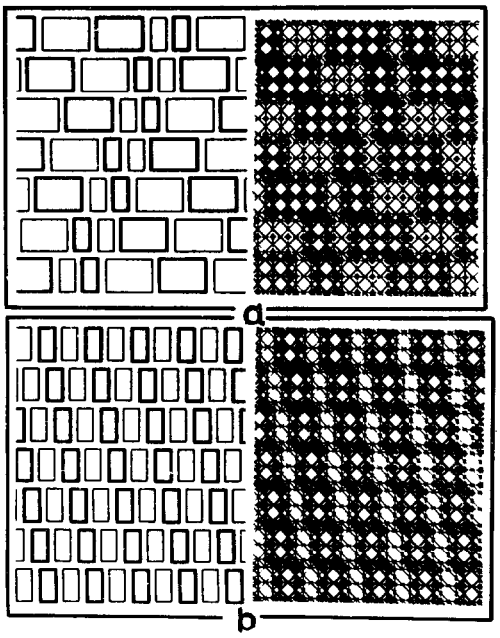

Fig. 7. Interpretation of the change of the crystal structure shown in Fig. 6. (a) $V_3Nb_9O_{29}$ structure with one block row (direction [1 0 2]) divided into [3 × 2] blocks as in Fig. 6b. (b) Idealized structure of V_6O_{13}, the hypothetical end product of the *in situ* reduction.

7b)[20] with O/V = 2.167. A preparative reaction of $V_3Nb_9O_{29}$ with H_2 immediately led to the dioxide phase (V, Nb)O_2 with a rutile structure. As Fig. 6a, b shows, the *in situ* experiments must be performed carefully to avoid the possible damage of the structure (encircled regions).

At the same ratio of O/ΣM = 2.417 but with a lower content of V a solid solution series exists with the structure of $Nb_{12}O_{29}$ (mon.) as shown in Fig. 1a. Crystal pieces of $Nb_{12}O_{29}$ can be investigated by HRTEM without damage; they are practically stable against irradiation.[15]

By oxidation of $Nb_{12}O_{29}$ (mon.) in oxygen or in air two novel structures appear, which can be looked upon as additional modifications of Nb_2O_5.[16,17] In each case ("stage") the oxidation was complete as indicated by the loss of the black–blue colour.

The first stage can be obtained by oxidation at very low temperature. This form was unstable in the electron microscope so that investigations were difficult. The second form was stable against irradiation. Preparative experiments showed that it could not be reduced back to the starting material using H_2. Reduction led to an intermediate oxide or with increasing temperature to NbO_2. The structure appears to be disordered but shows some characteristic features, e.g. rows of narrow blocks with [2 × 4] or [2 × 5] octahedra and tetrahedral positions.[16]

A third form can be prepared by slow oxidation of monoclinic $Nb_{12}O_{29}$ at low oxygen pressure. Again a disordered real structure could be observed by HRTEM but the block size of [3 × 4] octahedra remained nearly unchanged. In contrast to the forms mentioned, rectangular tunnels (like those in $NaNb_{13}O_{33}$, but empty) are now the most characteristic building elements (Fig. 8).[17]

Samples with the monoclinic structure of $Nb_{12}O_{29}$ containing ≈ 5% V were a little more difficult to oxidize. One also obtains two stages similar to the products of the oxidation of $Nb_{12}O_{29}$ (mon.). But the reduction of the first oxidation stage in the EM and of the second stage in a stream of H_2 (550°C) was much easier. It seems to be important that this second stage can be reduced stepwise by the irradiation in the microscope, when the diaphragm is removed for a few seconds. In this reaction, structural elements like those shown in Fig. 8 may be mainly involved. This possibility of a back reaction may for oxidized V-containing samples open a way to observe details of the structural rearrangement that are connected with a reduction.[18]

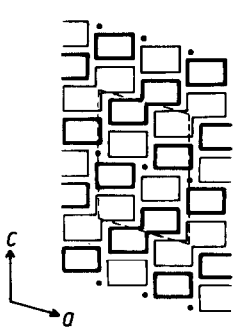

Fig. 8. Model of the averaged structure of the product of the slow oxidation of $Nb_{12}O_{29}$ (mon.) at low oxygen pressure.[17] By oxidation, tetrahedral positions (black dots) and pairs of blocks with a rectangular tunnel have been formed.

Acknowledgements—I wish to thank my coworkers Dr H. Groh, Dr B. Meyer, Dr W. Mertin and Dr B. Reitz for cooperation. We are indebted to the Deutsche Forschungsgemeinschaft and the Fonds der Chemischen Industrie for financial support.

REFERENCES

1. R. Gruehn and R. Roß, *Chem. unserer Zeit* 1987, **21**, 194.
2. R. Gruehn and W. Mertin, *Naturwissenschaften* 1982, **69**, 53.
3. B. Langenbach-Kuttert, R. Roß and R. Gruehn, *Monatsh. Chem.* 1985, **116**, 1275.
4. B. Langenbach-Kuttert, W. Mertin and R. Gruehn, *Z. Naturforsch.* 1985, **40b**, 1651.
5. W. Mertin and B. Langenbach-Kuttert, *Z. Kristallogr.* 1986, **174**, 114.
6. H. Groh, B. Reitz, R. Gruehn and W. Mertin, *Naturwissenschaften* 1982, **69**, 187.
7. H. Groh, B. Meyer and R. Gruehn, *Z. anorg. allg. Chem.* 1983, **497**, 56.
8. F. Wendenburg and J.-H. Müller, unpublished results.
9. H. Groh and R. Gruehn, *Z. anorg. allg. Chem.* 1983, **503**, 165.
10. H. Groh and R. Gruehn, *Z. anorg. allg. Chem.* 1984, **509**, 111.
11. H. Groh and R. Gruehn, *Z. anorg. allg. Chem.* 1985, **529**, 179.
12. H. Groh, Dissertation, Gießen (1984).
13. B. Reitz and R. Gruehn, *Z. anorg. allg. Chem.* 1986, **540/541**, 215.
14. B. Reitz, Dissertation, Gießen (1987).
15. B. Meyer, Dissertation, Gießen (1981).
16. B. Meyer and R. Gruehn, *Z. anorg. allg. Chem.* 1982, **484**, 53.
17. B. Meyer and R. Gruehn, *Z. anorg. allg. Chem.* 1982, **484**, 98.
18. B. Reitz and R. Gruehn, in preparation.
19. R. S. Roth and A. D. Wadsley, *Acta Crystallogr.* 1965, **19**, 26, 32, 38, 42.
20. K. A. Wilhelmi, K. Waltersson and L. Kihlborg, *Acta Chem. Scand.* 1971, **25**, 2675.
21. R. Norin, *Acta Chem. Scand.* 1966, **20**, 871.

Polyhedron Vol. 7, No. 22/23, pp. 2399–2403, 1988
Printed in Great Britain

0277–5387/88 $3.00+.00
© 1988 Pergamon Press plc

METAL–SUPPORT INTERACTION: $(\mu\text{-H})(\mu\text{-OSiEt}_3)\text{Os}_3(\text{CO})_{10}$, A MOLECULAR ANALOGUE OF A SURFACE COMPLEX AND THE COMPUTER MODELLED SURFACE STRUCTURES OF $(\mu\text{-H})(\mu\text{-OSi}\equiv)\text{Os}_3(\text{CO})_{10}$ AND $(\mu\text{-OSi}\equiv)_2\text{Os}_3(\text{CO})_{10}$

LEH-YEH HSU* and SHELDON G. SHORE*

Department of Chemistry, The Ohio State University, Columbus, OH 43210, U.S.A.

and

LINDA D'ORNELAS, AGNES CHOPLIN* and JEAN-MARIE BASSET*

Institut de Recherches sur la Catalyse, Laboratoire Propre du C.N.R.S. Conventionné à l'Université Claude Bernard, Lyon I, 2, Avenue Albert Einstein, 69626 Villeurbanne Cedex, France

Abstract—Metal–support interaction involving the surface complex formed from the reaction of silica with $Os_3(CO)_{12}$ at 150°C has been modelled employing computer graphics and molecular mechanics techniques. This surface complex is generally represented as $(\mu\text{-H})(\mu\text{-OSi}\equiv)\,Os_3(CO)_{10}$ (I), with a surface oxygen bridging two osmium atoms. However, a second arrangement with two surface oxygens bridging the same two osmium atoms, $(\mu\text{-OSi}\equiv)_2Os_3(CO)_{10}$ (II), has also been considered. A computer model has been developed for partially hydroxylated silica surface. Employing structural parameters from model compounds, metal–support interaction of the cluster fragments $(\mu\text{-H})Os_3(CO)_{10}$ and $Os_3(CO)_{10}$ with surface oxygens to form surface complexes I and II was studied using energy minimization techniques and considering non-bonded contacts as a function of dihedral angle. The results clearly indicate that the cluster fragment $Os_3(CO)_{10}$ will not fit on the silica by means of a double oxygen bridge to two osmium atoms to give complex II; however, the $(\mu\text{-H})Os_3(CO)_{10}$ fragment will bind to selected oxygen sites of the silica without steric restraint to form complex I.

The surface complex formed from the reaction of $Os_3(CO)_{12}$ with silica at 150°C has been studied extensively by a variety of experimental techniques.[1–12] Spectroscopic results are consistent with a triangulated osmium core with a single surface oxygen binding the triosmium cluster by bridging two Os atoms,[2–5] $(\mu\text{-H})(\mu\text{-OSi}\equiv)Os_3(CO)_{10}$ (I). A second possible arrangement, $(\mu\text{-OSi}\equiv)_2Os_3(CO)_{10}$ (II), involving two surface oxygen atoms bridging the same two osmium atoms, has also been considered.[9a] However, this possibility is now thought to be more likely on alumina than on silica.[9b] How the triosmium cluster is accommodated on the surface is not discerned by the available experimental data, but is generally represented schematically as in Fig. 1.

We have found it of interest to model the surface complexes I and II to determine if modelling can discriminate between them as to the favoured arrangement, and to gain possible insight as to how the cluster might be accommodated on local sites of a silica surface. A model for partially hydroxylated

*Authors to whom correspondence should be addressed.

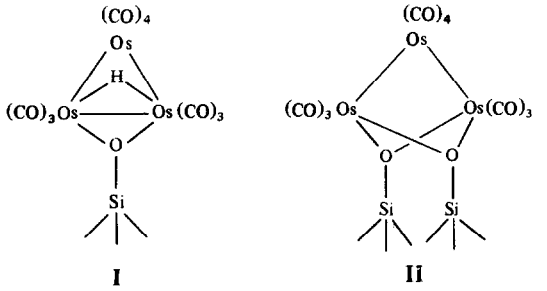

Fig. 1. Representation of (μ-H)(μ-OSi<)$Os_3(CO)_{10}$ (I) and (μ-OSi<)$_2Os_3(CO)_{10}$ (II).

silica using CHEMX* computer graphics and MacroModel† molecular mechanics techniques has been developed. With this model and parameters from the model compounds (μ-H)(μ-$OSiEt_3$)$Os_3(CO)_{10}$[13] and (μ-OMe)$_2Os_3(CO)_{10}$[14] possible structures of the surface complex obtained from the reaction of $Os_3(CO)_{12}$ with silica at 150°C[2-5] were investigated.

RESULTS AND DISCUSSION

A. *Syntheses and structure*

The compounds (μ-H)(μ-$OSiR_3$)$Os_3(CO)_{10}$ [R = Et (III), Ph (IV)] were prepared according to the following reactions.[13]

$$Os_3(CO)_{12} + R_3SiOH \rightarrow (\mu\text{-H})(\mu\text{-OSiR}_3)Os_3(CO)_{10} + 2CO$$

$$Os_3(CO)_{10}(CH_3CN)_2 + R_3SiOH \rightarrow (\mu\text{-H})(\mu\text{-OSiR}_3)Os_3(CO)_{10} + 2CH_3CN.$$

The molecular structure of III was determined from a single crystal X-ray study[13] and is shown in Fig. 2. It has a structure which is like that of (μ-H)(μ-OMe)$Os_3(CO)_{10}$.[15]

Molecular clusters III and IV appear to be good models for the surface complex I.[13] IR spectra in the carbonyl stretching region are virtually identical for both clusters and correspond very well with those of the surface complex, which infers that the cluster fragment bound to the silica surface is (μ-H)$Os_3(CO)_{10}$.

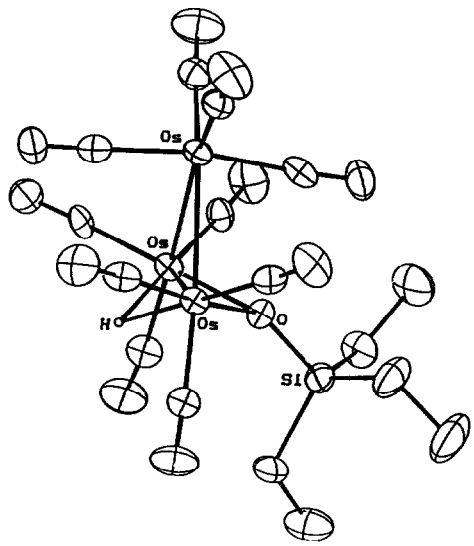

Fig. 2. ORTEP of (μ-H)(μ-$OSiEt_3$)$Os_3(CO)_{10}$, thermal ellipsoids at 50% probability.

B. *Modelling partially hydroxylated silica*

Although hydroxylated silica is amorphous, evidence indicates a structural arrangement which resembles that of β-crystobalite and related crystalline phases.[16] Studies of hydroxylated and partially hydroxylated silica suggest that the surface is heterogeneous and is probably composed of regions of partially hydroxylated (100) and (111) surfaces, with the degree of hydroxylation being a function of the treatment of the silica.[17] Hydroxylation of the (100) surface leads to geminal $Si(OH)_2$ groups,[17,18] which form hydrogen bonded chains through interaction with neighbouring geminal groups.[18b,c] Hydroxylation of the (111) surface gives isolated SiOH groups.[17,18] Dehydroxylation of the (100) surface occurs readily to form siloxane bridges.[18] On the other hand dehydroxylation of the (111) plane is unlikely under the conditions in which the surface bound cluster is formed.[17a,18d] We have modelled, separately, each of these proposed components of the silica surface including defects, edges formed from the intersection of the (100) plane with the (001) plane and the intersection of the (100) with the (111) plane.

Modelling of the local regions on the (100) plane involved first generating, by means of CHEMX, a β-cristobalite lattice consisting of 5 × 5 unit cells along the *b* and *c* axes.[19] Hydrogen atoms were added to these surface oxygens to form geminal silanol groups which were oriented to allow hydro-

* Created by E. K. Davies, Chemical Crystallography Laboratory, Oxford University, and distributed by Chemical Design Ltd., Oxford, England. Graphics facilities of the Interactive Molecular Graphics Center (IMAG Center) of The Ohio State University were employed.

† The 1986 version of MacroModel was provided by Professor Clark Still, Department of Chemistry, Columbia University.

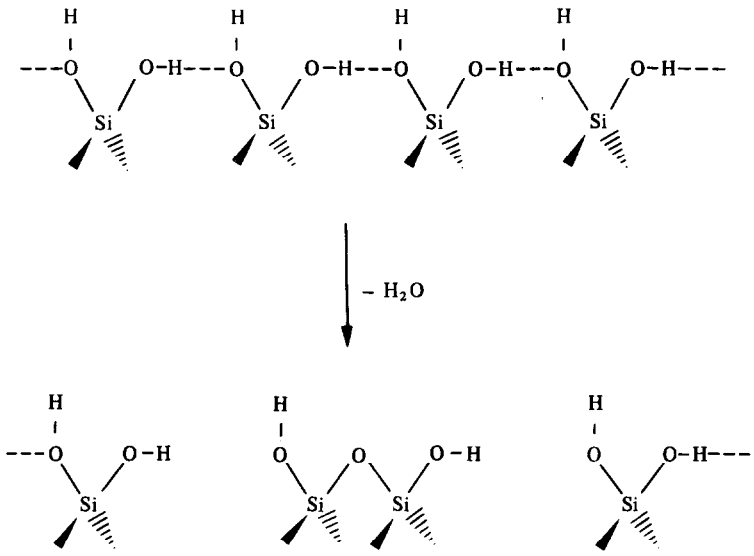

Scheme 1.

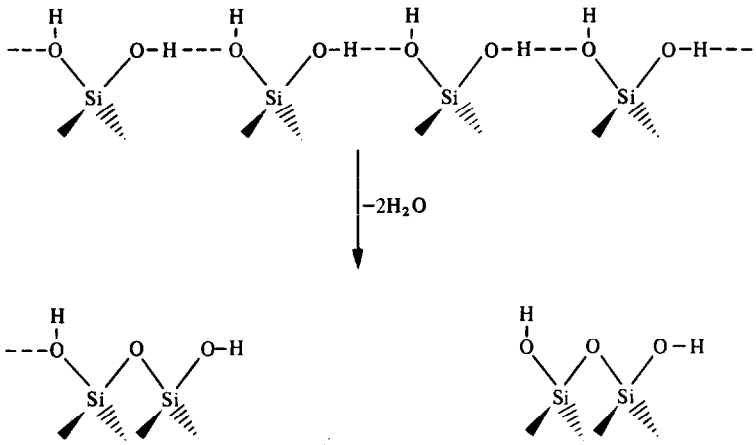

Scheme 2.

gen bonded chains consistent with spectroscopic studies.[18b,c] Molecular mechanics optimization on a subset of the hydrogen atoms residing in the inner 15 unit cells was carried out to give a final arrangement for optimized hydrogen positions (designated local region A). To obtain a model of the (111) plane (designated local region B) a 3 × 3 × 3 lattice was constructed and then a section was removed by cutting through the (111) intercepts thereby exposing the (111) plane. In this case there is no hydrogen bonding between the isolated SiOH units because of the large distance of separation of the SiOH groups (*ca* 4–6 Å).

A partially dehydroxylated local surface region (designated local region C) was derived by removing an H_2O molecule from the centre of the fully hydroxylated (100) surface (Scheme 1) thereby forming an Si—O—Si bridge and then the structure was optimized (see footnote † on p. 2).

Since experimental results suggest a relatively low concentration of geminal $Si(OH)_2$[17b,c] units there is probably a significant concentration of local dehydroxylated surface which contains adjacent siloxane bridges. This region (designated local region D) was constructed by modelling the removal of two H_2O molecules from the fully hydroxylated (100) plane to give two adjacent Si—O—Si bridges (Scheme 2).

C. *Modelling cluster fragments on local regions of the silica surface*

We attempted to generate the surface complexes **I** and **II** by fitting the cluster fragments $(\mu\text{-H})Os_3(CO)_{10}$ and $Os_3(CO)_{10}$ to each of the regions

of surface. For each orientation of the cluster examined the van der Waals non-bonded interaction energy between the cluster and the surface atoms was calculated,* summing from the individual cluster atoms all of the interactions with surface atoms up to 6 Å away. "Short" non-bonded contact distances between cluster atoms and surface atoms were also monitored in order to further evaluate each arrangement. A non-bonded contact is considered to be "short" if it is less than the non-bonded shortest contacts in β-cristobalite,[21] 2.4 Å.

1. *Attempts to fit* $(\mu\text{-H})Os_3(CO)_{10}$ *and* $Os_3(CO)_{10}$ *to the silica surface.* No satisfactory fit was achieved in attempts to place $(\mu\text{-H})Os_3(CO)_{10}$ on an oxygen of the fully hydroxylated (100) plane or an oxygen of the (111) plane. By the same token the fragment would not fit on a vicinal oxygen of an isolated siloxane group (region C). However, a satisfactory fit was achieved on a vicinal oxygen of a siloxane group adjacent to a second siloxane group (region D). These conclusions were reached from results of the following procedures. A hydrogen atom was removed from a silanol group on the type A and B regions and from a silanol of a siloxane bridge of type C and D regions. The fragment $(\mu\text{-H})Os_3(CO)_{10}$ was then fitted to this oxygen, binding it in the same way that the $OSiEt_3$ unit binds this fragment in complex **III**. The $(\mu\text{-H})Os_3(CO)_{10}$ unit was then rotated about the oxygen of the Si—O bond in order to permit selection of an orientation which minimized steric repulsion between the carbonyls and the neighbouring hydroxyl groups. Contact distances were monitored at 3° intervals during rotation of the cluster from 0 to 357° around the oxygen atom. Also the dihedral angle between the Os—O—Os plane and the Si—O bond was varied. This is equivalent to assuming that the bending force constant is small and that the dihedral angle might be opened up in order to provide a better fit to the surface. For the type A, B, and C local regions at the minimum van der Waals interaction energies calculated, 364.1, 151.1 and 47.6 kcal, respectively, there are a number of unreasonably short non-bonded contact distances between the cluster fragment and surface atoms. However, for the type D region (adjacent siloxane groups) at the minimum van der Waals interaction energy obtained, 2.4 kcal, no short contacts between the cluster atoms and surface atoms were observed. Thus the type D region appears to accommodate the cluster fragment $(\mu\text{-H})Os_3(CO)_{10}$. Figure 3 shows this arrangement.

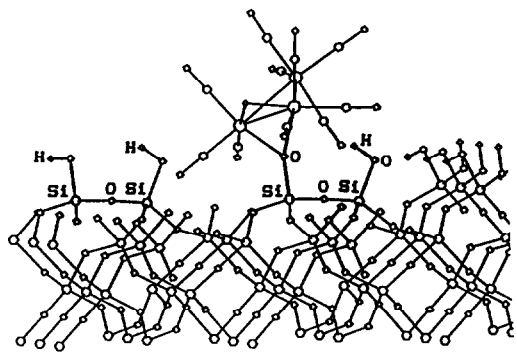

Fig. 3. Optimized model for $(\mu\text{-H})(\mu\text{-OSi}\diagdown\!\!\diagup)Os_3(CO)_{10}$ (I). $(\mu\text{-H})Os_3(CO)_{10}$ bound to a surface oxygen of a local partially hydroxylated region of the (100) plane containing adjacent Si—O—Si bridges. Some $Si(OH)_2$ groups removed to give a clearer view of the Si—O—Si bridges.

No acceptable fit of the fragment $Os_3(CO)_{10}$ was obtained for any of the regions A, B, C and D. In the case of the A surface the minimum van der Waals repulsion energy obtained was 1861.8 kcal and a number of short non-bonded contacts were observed between cluster and surface atoms. For the type B, C and D surfaces the $Os_3(CO)_{10}$ fragment could not be fitted with a double oxygen bridge because of the long distance between available oxygen atoms, 4–6 Å, compared to the observed distance between the bridge oxygen atoms, 2.59 Å, in the model compound $(\mu\text{-OMe})_2Os_3(CO)_{10}$.

2. *Attempts to fit* $(\mu\text{-H})Os_3(CO)_{10}$ *and* $Os_3(CO)_{10}$ *to defect sites.* The cluster fragment $(\mu\text{-H})Os_3(CO)_{10}$ is readily accommodated at the defect sites created by the intersection of the (100) plane with the (001) plane. A minimum van der Waals repulsion energy of -3.6 kcal is calculated and no short contacts between the cluster surface atoms are observed. On the other hand the fragment $Os_3(CO)_{10}$ could not be fitted to this edge and still retain the double bridged arrangement of oxygen atoms.

For the defect site created by the intersection of the (100) and (111) planes the fragment $(\mu\text{-H})Os_3(CO)_{10}$ is not as well accommodated as on the (100), (001) intersection, but the fit is much better than on surfaces A, B and C. The minimum van der Waals repulsion energy is 12.3 kcal and there are but two short contacts of about 2.2 Å. Another defect site which has been suggested[17c] is that which could occur from dehydroxylation at the junction of the (100) and (111) planes. Attempts to fit the $(\mu\text{-H})Os_3(CO)_{10}$ fragment to the vicinal oxygen of the

* The non-bonded atom–atom potential function contained an (exp-6) term and a Coulombic term. The potential parameters (E and R) for H, C, O and Si (Sept. 1986 version) were provided by Professor Norman Allinger,[20] Department of Chemistry, University of Georgia. The values of E and R for Os were estimated as 0.26 and 2.65 respectively.

resulting siloxane group gives a minimum van der Waals repulsion energy of 15.8 kcal and five short contacts from 2.1 to 2.3 Å.

The fragment $Os_3(CO)_{10}$ could not be fitted to any of the defect sites considered and still retain the double bridged arrangement of oxygen atoms.

CONCLUSIONS

The results of this study are in accord with experimental evidence which favours **I** over **II** as the surface complex formed from the reaction of $Os_3(CO)_{12}$ with silica at 150°C.[2-5] Furthermore, favourable or likely sites for attachment of the cluster fragment $(\mu\text{-H})Os_3(CO)_{10}$ have been discerned. It is suggested that the application of these modelling techniques will prove useful in gaining insight into the potential properties of surface substrates in interacting with multimetallic species.

Acknowledgements—Support from NATO to S.G.S. and J.M.B. and support to S.G.S. from the National Science Foundation through Grant No. CHE 84-11630 is gratefully acknowledged.

REFERENCES

1. J. M. Basset and A. Choplin, *J. Molec. Catal.* 1983, **21**, 95.
2. B. Besson, B. Moraweck, A. K. Smith, J. M. Basset, R. Psaro, A. Fusi and R. Ugo, *J. Chem. Soc., Chem. Commun.* 1980, 569.
3. R. Psaro, R. Ugo, B. Besson, A. K. Smith and J. M. Basset, *J. Organomet. Chem.* 1981, **213**, 215.
4. A. K. Smith, B. Besson, J. M. Basset, R. Psaro, A. Fusi and R. Ugo, *J. Organomet. Chem.* 1980, **192**, C31.
5. M. Deeba and B. C. Gates, *J. Catal.* 1981, **67**, 303.
6. B. Besson, A. Choplin, L. D'Ornelas and J. M. Basset, *J. Chem. Soc., Chem Commun.* 1982, 843.
7. J. M. Basset, B. Besson, A. Choplin and A. Theolier, *Phil. Trans. Roy. Soc. Lond.* 1982, **A308**, 115.
8. R. Barth, B. C. Gates, Y. Zhao, H. Knozinger and J. Hulse, *J. Catal.* 1983, **82**, 147.
9. (a) S. L. Cook, J. Evans and G. Neville Greaves, *J. Chem. Soc., Chem. Commun.* 1983, 1287; (b) S. L. Cook, J. Evans, G. S. McNulty and G. Neville Greaves, *J. Chem. Soc., Dalton Trans.* 1986, 7.
10. A. Choplin, M. Leconte and J. M. Basset, *J. Molec. Catal.* 1983, **21**, 2389.
11. M. Beeba, B. J. Streusand, G. L. Schrader and B. C. Gates, *J. Catal.* 1981, **69**, 218.
12. H. Knozinger, Y. Zhao, B. Tesche, R. Barth, R. Epstein, B. C. Gates and J. P. Scott, *Faraday Discuss. Chem. Soc.* 1982, **72**, 54.
13. L. D'Ornelas, A. Choplin, J. M. Basset, L.-Y. Hsu and S. G. Shore, *Nouv. J. Chim.* 1985, **9**, 155.
14. V. Allen, R. Mason and P. B. Hitchcock, *J. Organomet. Chem.* 1977, **140**, 297.
15. M. R. Churchill and H. J. Wasserman, *Inorg. Chem.* 1980, **19**, 2391.
16. (a) I. Krejei and E. Ott, *J. Phys. Chem.* 1931, **35**, 2061; (b) C. Frondel, *The System of Minerology of Dana*, 7th edn., Vol. 3 (*Silica Minerals*), p. 154. Wiley, New York (1962); (c) R. K. Iler, *The Colloid Chemistry of Silica and Silicates*, pp. 242–247. Cornell University Press, Ithaca, NY (1955).
17. (a) C. G. Armistead, A. J. Tyler, F. H. Hambleton, S. A. Mitchell and J. A. Hokey, *J. Phys. Chem.* 1969, **73**, 3947; (b) D. W. Sindorf and G. E. Maciel, *ibid.* 1982, **86**, 5208; (c) D. W. Sindorf and G. E. Maciel, *J. Am. Chem. Soc.* 1983, **105**, 1487.
18. (a) J. B. Peri and A. L. Helmsley, Jr., *J. Phys. Chem.* 1968, **72**, 1926; (b) A. J. van Roosmalen and J. C. Mol, *ibid.* 1978, **82**, 2748; (c) G. Ghiotti, E. Garrone, C. Morterra and C. Boccuzi, *ibid.* 1979, **83**, 2863; (d) D. W. Sindorf and G. E. Maciel, *ibid.* 1983, **87**, 5516.
19. R. W. Wycoff, *Crystal Structure*, Vol. 1, p. 318. Interscience, New York (1963).
20. N. Allinger, *J. Am. Chem. Soc.* 1977, **99**, 8127.

Polyhedron Vol. 7, No. 22/23, pp. 2405–2409, 1988
Printed in Great Britain

0277–5387/88 $3.00+.00
© 1988 Pergamon Press plc

A NEW HIGHLY ACTIVE HYDROTREATING CATALYST PREPARED BY THE DECOMPOSITION OF THIOTUNGSTATONICKELATE AND CHARACTERIZED BY HIGH RESOLUTION ELECTRON MICROSCOPY

W. ELTZNER,* M. BREYSSE,† M. LACROIX, C. LECLERCQ and M. VRINAT

Institut de Recherches sur la Catalyse du C.N.R.S., 2 avenue Albert Einstein, F-69626 Villeurbanne Cédex, France

and

A. MÜLLER† and E. DIEMANN

Faculty of Chemistry, University, D-4800 Bielefeld, F.R.G.

Abstract—The bisthiometalato complex $[Ni(WS_4)_2]^{2-}$ was utilized as a precursor for the preparation of the unsupported mixed nickel tungsten sulphide catalyst. Catalytic activities in hydrotreating model reactions are better for the decomposed complex than for catalysts prepared by conventional methods. HREM and AEM studies show that the structure of the catalyst is highly disordered, and that nickel is well distributed in all particles. The activity loss observed after a catalytic test at 673 K is related to a partial nickel segregation. Better crystallized particles are formed and the position of nickel atoms is mainly restricted to edge positions of the WS_2 crystallites. The decomposed complex is considered as a model for mixed hydrotreating catalysts.

Hydrodesulphurization (HDS) and other catalytical hydrogenation processes on the constituents of fossil oil provide a very active and important field of applied research.[1] The catalysts are based on MoS_2 or WS_2 and their activity can be significantly promoted when Co or Ni is added. This promotion, in the case of HDS catalysis, has been attributed to the presence of the so-called CoMoS phase (rather small but regular "crystallites" of MoS_2 with Co atoms exclusively at their edges[2]‡). The question now arises whether it would be possible to generate more irregular (and, consequently, more active) phases by the thermal decomposition of well defined bisthiometalato complex salts which contain $[Ni(WS_4)_2]^{2-}$ (**1**) (Fig. 1) and were first prepared by us several years ago.[3,4] Different phases were studied by high resolution electron microscopy (HREM).

The thermal decomposition of the Et_4N^+ salt of **1** occurs between 473 and 573 K according to

$$(Et_4N)_2[Ni(WS_4)_2] \xrightarrow{(H_2/H_2S\ \text{atmosphere})} 2Et_3N + Et_2S\ (\text{or}\ Et_2S_2) + H_2S + NiW_2S_{5-6}$$

$$\xrightarrow{(N_2\ \text{atmosphere})} \cdots + NiW_2S_{6-7}.$$

The catalytic properties of the thermally decomposed complex (in the following abbreviated as NiW–EC) were compared with those of NiW sulphides obtained by the homogeneous sulphide pre-

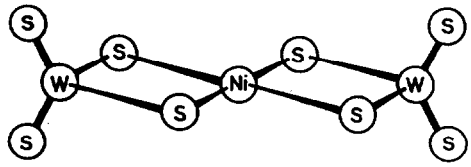

Fig. 1. Structure of the $[Ni(WS_4)_2]^{2-}$ ion.

* Present address: Labofina S.A., Brussels, Belgium.

† Authors to whom correspondence should be addressed.

‡ These represent novel heterometallic inorganic clusters.

cipitation (NiW–HSP),* and with pure WS_2 prepared by the decomposition of $(NH_4)_2WS_4$.[5]

The catalytic activities were determined via the dibenzothiophene hydrodesulphurization reaction performed at atmospheric pressure and the biphenyl (BP) hydrogenation reaction performed at medium pressure. Experimental details concerning these tests are given elsewhere.†

The conditions utilized allow the determination of the properties of the original catalysts. Nevertheless, it can be useful to submit the samples to severe conditions in order to estimate what kind of modifications of the solids can occur and what the influence of these changes on the catalytic activity would be. This was done by means of an "accelerated ageing test" (AAT) in the case of biphenyl conversion experiments: after leaving overnight on stream at 673 K the reaction temperature was decreased to 530 K and the percentage of activity loss was obtained from $\Delta R = (A_b - A_a)/A_b$ at 530 K (where A_b is the BP hydrogenation rate at 530 K before the AAT, and A_a its value at 530 K after the test).

The results given in Tables 1 and 2 show that in both reactions the NiW–EC catalysts have an activity two or three times higher than that of NiW–HSP and of course a much higher activity than pure WS_2 or Ni_3S_2. Activity losses during the AAT are observed for all the NiW samples. This cannot be ascribed to textural modifications since surface areas do not change during the tests but reveal the instability of the mixed phase in a poorly sulphided atmosphere.[9] Moreover, it should be underlined that even after an AAT, the intrinsic activity of the NiW–EC sample is higher than that of the NiW–HSP catalyst. In the case of pure WS_2, very large textural modifications occur and activity losses are here related to decreases in surface areas.[10]

Figure 2 shows HREM micrographs of WS_2, NiW–HSP and NiW–EC samples.‡ In the case of the WS_2 catalyst we find a characteristic disordered "rag" type layer structure which is similar to that observed for MoS_2.[13] Measurements of the number of fringes n and their length l give an average value of the "crystallite" dimensions. The situation is almost similar in the case of the NiW–HSP catalyst and differences are noticeable only in the "crystallite" dimensions. A completely different feature is found in the case of NiW–EC. No well aligned layers are present and the degree of disorder is very high. Short layer "substructures" stick into each other and form areas of strands.

Comparison of HREM examinations before and after the AAT indicate that the variations of the morphological properties are small in the case of WS_2 and NiW–HSP and variations of the crystallite dimensions are within the limits of error. However, the features of the NiW–EC have changed drastically. Measurements of the particle size now give comparable results for NiW–HSP.

Before the AAT, an almost homogeneous composition was found for all analysed areas of NiW–EC (aggregates of "crystallites", "crystallites" with one or more layers). The average atomic composition found by STEM analysis (see earlier) was S = 0.602, Ni = 0.146 and W = 0.252, which gives

---

* Catalysts preparation: a NiW–HSP catalyst with an average atomic composition $r = Ni/(Ni+W) = 0.3$ was prepared by a method similar to the homogeneous sulphide precipitation described by Candia *et al.*[6] A diluted solution (10^{-2} mol l^{-1}) of ammonium tungstate and nickel nitrate was heated at 343 K and vigorously stirred. A solution of $(NH_4)_2S$ was added slowly. The slurry was stirred until complete evaporation and then decomposed in an H_2–H_2S atmosphere at 673 K. Using homogeneous sulphide precipitation to prepare CoMo catalysts, it was found by Mössbauer Emission Spectroscopy that for an atomic concentration of the promotor $r = 0.3$, 23% of the total amount of Co is involved in the CoMoS phase and 77% as Co_9S_8.[7] A similar value can be expected in the case of the NiW system since NiS and CoS have comparable solubility constants in aqueous solution.

† Catalytic activity measurements: the hydrodesulphurization of dibenzothiophene (DBT) was carried out in the vapour phase using a dynamic atmospheric flow microreactor ($p_{H_2} = 10^5$ Pa; $p_{DBT} = 67$ Pa). The hydrogenation of biphenyl (BP) was carried out in the vapour phase using a dynamic high pressure flow microreactor described previously[8] ($p_{H_2} = 22 \times 10^5$ Pa; $p_{BP} = 8 \times 10^2$ Pa; $p_{H_2S} = 4.5 \times 10^2$ Pa). For both reactions, the weight of the catalyst was chosen so that a low conversion was obtained (lower than 15%) and the activities of the different catalysts were compared at about the same conversion. The specific activity was determined at 530 K after 16 h on stream at the pseudo-stationary state. The specific rate A_s was calculated using the following equation:

$$A_s = Q \cdot \tau / m \ (\text{mol s}^{-1}\,\text{g}^{-1})$$

τ is the total conversion, m the weight of the catalyst and Q the flow in mol s^{-1} ($Q_{BP} = 5.7 \times 10^{-8}$ mol s^{-1}; $Q_{DBT} = 1.3 \times 10^{-8}$ mol s^{-1}).

‡ For the high resolution electron microscopy the samples were ultrasonically dispersed in ethanol and the suspension was collected on carbon copper grids (JEM 100 CX employing a UHP polar piece). For the analytical electron microscopy measurements a VG 501 STEM with a LINK Si-Li-Detector and a TN 5500 multichannel analyser were used. This equipment provides information concerning small areas (1–2 nm^2). Quantitative element concentrations were calculated with a "Standardless Metallurgical Thin Film Correction Program" (developed by TRACOR, based on reports by Cliff and Lorimer[11] and Goldstein[12]).

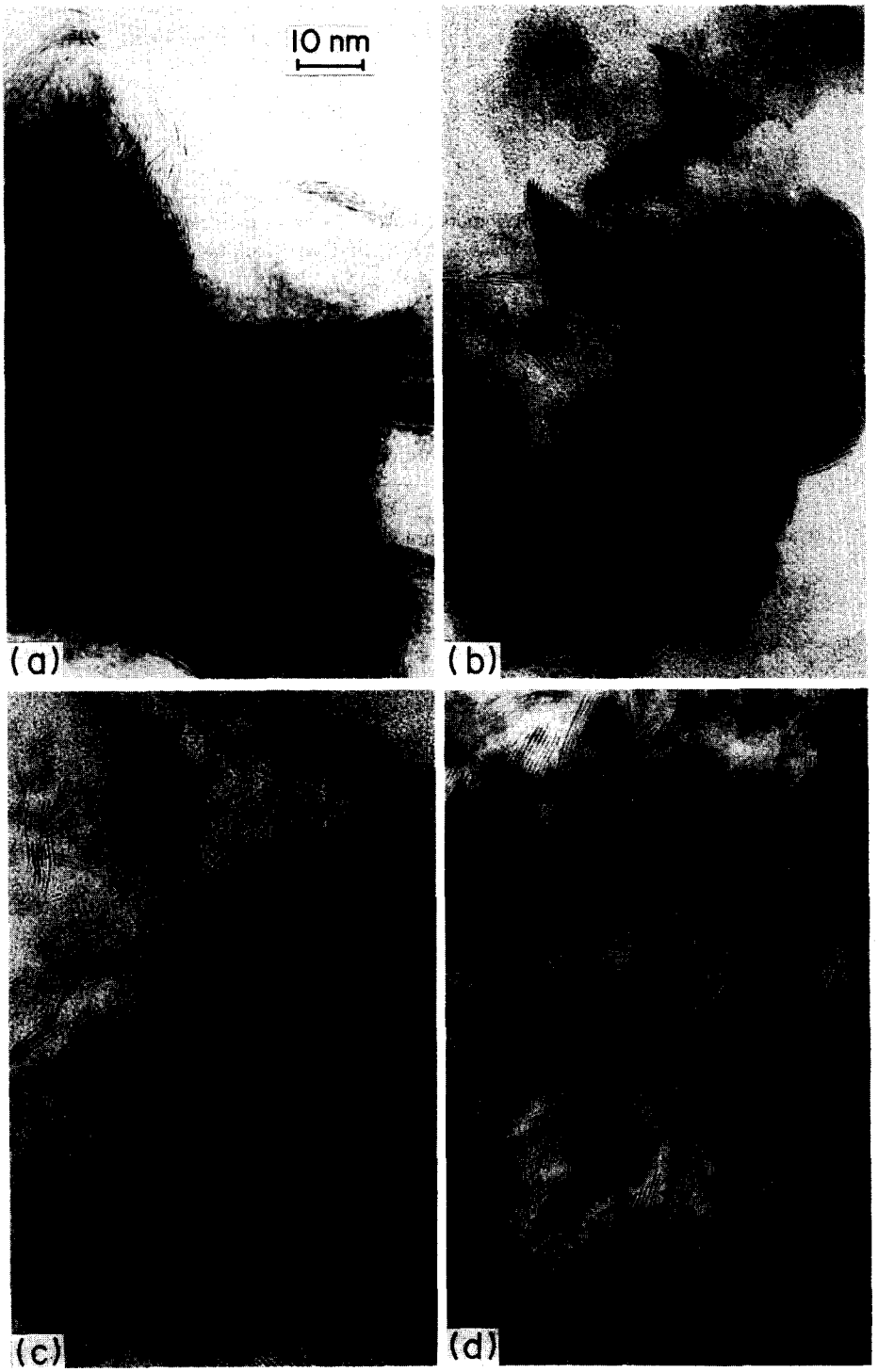

Fig. 2. High resolution electron micrographs for: (a) NiW–EC before AAT (particle size < 2 nm); (b) NiW–EC after AAT (particle size *ca* 4 nm); (c) NiW–HSP (particle size *ca* 5 nm); and (d) WS_2 (particle size *ca* 8 nm).

Table 1. Catalytic activities for biphenyl hydrogenation

Catalyst	S[a] ($m^2 g^{-1}$)	A_s (530 K) (10^{-8} mol $s^{-1} g^{-1}$)	A_i (530 K)[b] (10^{-8} mol $s^{-1} m^{-2}$)	A_i (530 K)[c] (10^{-8} mol $s^{-1} m^{-2}$)	ΔR[d] (%)
WS_2	19.4	3.8	0.2		
Ni_3S_2	10	0.5	0.05		
NiW–HSP 0.3	10	14	1.4	1.0	28
NiW–EC	3	10.2	3.4	2.6	23

[a] Surface areas have been determined by the BET method using argon as inert adsorbant. As the activity for the reaction is directly proportional to the surface areas for WS_2 and NiW sulphides,[9] a direct comparison for all catalysts can be made.

[b] Before AAT.

[c] After AAT.

[d] Loss in intrinsic activity.

Table 2. Catalytic activities for dibenzothiophene hydrodesulphurization

Catalyst	S ($m^2 g^{-1}$)	A_s (530 K) (10^{-8} mol $s^{-1} g^{-1}$)	A_i (530 K) (10^{-8} mol $s^{-1} m^{-2}$)
WS_2	19.4	0.05	0.026
Ni_3S_2	10	0.08	0.008
NiW–HSP 0.3	10	2.1	0.21
NiW–EC	3	1.8	0.6

$r = Ni/(Ni+W) = 0.36$, very close to the nominal composition $r = 0.22$ [Fig. 3(a)]. The sulphur concentration is slightly lower than that found by chemical analysis (STEM: $Ni_{1.16}W_2S_{4.8}$, chemical analysis: NiW_2S_5). After the AAT, the elemental distribution is no longer homogeneous. In Fig. 3(b), three main regions can be distinguished:

- very few particles have kept the same composition as before the test ($r = 0.36$ and a sulphur concentration of 60.2%);
- some particles contain almost only nickel ($r = 1$) and a sulphur concentration corresponding to Ni_3S_2;
- a large number of particles contain less nickel than before the AAT ($0.17 \leqslant r \leqslant 0.24$) and a sulphur concentration of up to 60%.

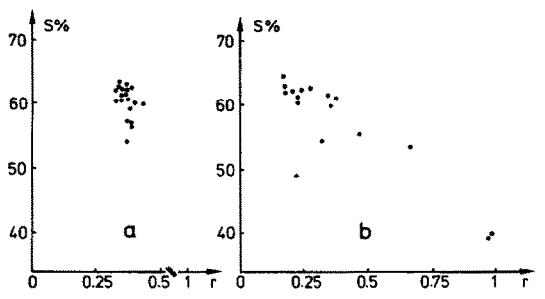

Fig. 3. STEM analytical results for NiW–EC (a) before and (b) after an accelerated ageing test [atomic ratio $r = Ni/(Ni+W)$].

No particles containing only tungsten and sulphur were found.

We conclude from the results that the new, catalytically very active phase NiW–EC has a structure which derives from that of WS_2, with Ni (perhaps in a distorted trigonal prismatic environment) distributed in the layer (uniformly, within the resolution of the experiment). After the AAT, a large number of particles contain less nickel than initially. The comparison of the average composition before and after AAT suggests that the initial catalyst has "lost" nickel and suphur at the same time. As the HREM investigations show that better crystallized particles were formed, it can be assumed that the positions of Ni atoms are now restricted to edge positions of WS_2 crystallites of an increased but almost uniform size, in a similar way as has also been discussed for the "CoMoS" phase.[14]

In order to prove the validity of this hypothesis, the maximum concentration of nickel atoms which can cover the edges was calculated for NiW–EC after the AAT, assuming one nickel atom for each tungsten atom on edge positions. A reasonable agreement is obtained between this calculated value

($r = 0.25$) and the experimental concentration of Ni in the particles given by STEM analysis ($r = 0.2$).

This study shows the potential significance of using this kind of catalyst precursor for a better understanding of mixed hydrotreating catalysts and for the preparation of highly active materials. Actually, the stability of the phase depends drastically on the H_2S partial pressure and conditions can be found in which no segregation occurs, even at 673 K.

Acknowledgements—A.M. and E.D. thank the Minister für Wiss. und Forsch. NRW and the "Fonds der Chemischen Industrie" for financial support.

REFERENCES

1. F. E. Massoth, *Adv. Catal.* 1978, **27**, 265; A. C. Jacobson, in *Surface Properties and Catalysis by Non-Metals* (Edited by J. P. Bonnelle *et al.*), pp. 305–317. Reidel, Dordrecht (1983).
2. H. Topsøe, B. S. Clausen, N. Y. Topsøe, E. Pedersen, W. Neimann, A. Müller, H. Bögge and B. Lengeler, *J. Chem. Soc., Faraday Trans. 1* 1987, **83**, 2157 and references cited therein.
3. A. Müller and E. Diemann, *J. Chem. Soc., Chem. Commun.* 1971, 65.
4. A. Müller, E. Diemann, R. Jostes and H. Bögge, *Angew. Chem.* 1981, **93**, 957; *Angew. Chem., Int. Ed. Engl.* 1981, **20**, 934; A. Müller, *Polyhedron* 1986, **5**, 323.
5. M. Breysse, R. Fréty, M. Lacroix and M. Vrinat, *React. Kinet. Catal. Lett.* 1984, **26**, 92.
6. R. Candia, B. S. Clausen and H. Topsøe, *J. Catal.* 1982, **77**, 564.
7. I. Alstrup, I. Chorkendorff, R. Candia, B. S. Clausen and H. Topsøe, *J. Catal.* 1982, **77**, 397.
8. M. L. Vrinat and L. de Mourgues, *React. Kinet. Catal. Lett.* 1980, **14**, 389.
9. M. Lacroix, M. Vrinat and M. Breysse, *Appl. Catal.* 1986, **21**, 73.
10. R. Fréty, M. Breysse, M. Lacroix and M. Vrinat, *Bull. Soc. Chim. Belg.* 1984, **93**, 663.
11. G. Cliff and G. W. Lorimer, *J. Microsc.* 1975, **103**, 203.
12. J. I. Goldstein, in *SEM 77* (Edited by O. Johari). Chicago (1977).
13. R. R. Chianelli, E. B. Prestridge, T. A. Pecoraro and J. P. de Neufville, *Science* 1979, **203**, 1105.
14. B. S. Clausen, H. Topsøe, R. Candia and B. Lengeler, *ACS Symp.* No. 248.

Polyhedron Vol. 7, No. 22/23, pp. 2421–2427, 1988
Printed in Great Britain

0277–5387/88 $3.00+.00
© 1988 Pergamon Press plc

SUPPORTED METAL CATALYSTS PREPARED FROM BIMETALLIC CLUSTERS: $ReOs_3$ CLUSTERS ON γ-Al_2O_3

A. S. FUNG, P. A. TOOLEY, M. R. McDEVITT and B. C. GATES*

Center for Catalytic Science and Technology, Department of Chemical Engineering, University of Delaware, Newark, Delaware 19716, U.S.A.

and

M. J. KELLEY

E. I. du Pont de Nemours & Company, Wilmington, Delaware 19898, U.S.A.

Abstract—Supported metal catalysts were prepared by the reaction of $H_3ReOs_3(CO)_{13}$ with the surface of γ-Al_2O_3. After treatment of the sample in He or in H_2 followed by treatment in H_2, the Os was present in the metallic state as small crystallites, and Re was present in higher oxidation states, which were controlled by the pretreatment. Re in a high oxidation state (approximately +7), resulting from the former pretreatment, did not affect the catalytic performance of the Os for hydrogenolysis of *n*-butane, but Re in a lower oxidation state (approximately +2 or +3), resulting from the latter pretreatment, doubled the activity of the catalyst and increased its resistance to deactivation. The results point the way to control of the structure and properties of catalysts by manipulation of the surface organometallic chemistry.

Many of the supported metal catalysts used in technology are bimetallics. A second metal may confer advantages of activity, selectivity, and stability on the first, but the reasons for the benefits are often unknown. In alloy-like catalysts, a second metal may dilute the catalytically active metal so that it is isolated in the bimetallic surface, to the detriment of unwanted reactions that are favoured by neighbouring centres of the active metal. When the second metal is in a cationic form, it often stabilizes the catalyst, perhaps by helping to maintain a high dispersion of small crystallites of the active metal on a high surface area support. Many promoters are present on support surfaces as cationic complexes.

Molecular bimetallic clusters are appealing precursors of supported metal catalysts, offering the advantages of stoichiometrically controlled metal compositions, zero-valent metals that are easily activated on a surface, and the absence of ligands such as chloride that would remain on the support surface and act as catalyst modifiers or poisons. There are now well-established patterns of the reactivity of organometallics on metal oxide supports, the reactions including oxidative addition of surface hydroxyl groups reacting with metal clusters, exemplified by $Os_3(CO)_{12}$; nucleophilic attack of hydroxyl groups on carbonyl ligands of metal complexes; and deprotonation of hydrido metal complexes to give surface-bound anions.[1] This latter reaction has proved to be an especially useful synthetic route to well-defined surface organometallics, being applied with basic supports such as MgO and γ-Al_2O_3.[2,3]

The supported metal catalysts formed from mixed-metal clusters on metal oxide surfaces typically lack the molecular structures of the precursors. The structural changes occurring during reduction or other treatments include oxidative fragmentation of the metal clusters to give mononuclear complexes[4] (often strongly bonded to the surface) and reductive processes leading to formation of metallic aggregates, which are common with group 8 metals on metal oxide supports in the presence of hydrogen.

The supported metal catalysts formed from molecular bimetallic clusters on metal oxide support can be classified on the basis of the surface structures (Table 1). The metals may be segregated, and aggregates may form, which may be molecular in nature (clusters) or non-uniform metallic struc-

* Author to whom correspondence should be addressed.

tures (crystallites, which are most typical in industrial supported metal catalysts). When the metals are aggregated into crystallites, the structures may be alloy-like, but not necessarily uniform, as one metal may be concentrated at the outside of the crystallite and constitute most of the metal surface;[5] this is the common situation when both metals are group 8. Alternatively, the metals may be segregated, with at least one present in the form of cationic complexes; this is the typical situation when one of the metals lies to the left of the group 8 metals in the periodic table.

The classes of supported bimetallic catalysts listed in Table 1 have all been demonstrated, but there is a lack of systematic investigations whereby several pairs of metals have been used to prepare families of catalysts that would help identify the structural patterns and provide a basis for determining how to design supported bimetallics. The objective of this research was to investigate a series of supported bimetallic catalysts made from a family of bimetallic clusters including $H_3ReOs_3(CO)_{13}$, $Re_2Pt(CO)_{12}$, and an Os–Pt carbonyl. These metals were chosen because there is literature characterizing the reactivities of mononuclear complexes of each on metal oxide surfaces. Further, the RePt combination is important industrially (for reforming of petroleum distillates), and the structure of the catalyst is a subject of lively debate.[10–13] The Re–Pt pair is also of interest because it includes a group 7 metal, which has a tendency to be present on metal oxide surfaces both as cationic complexes and as metallic crystallites. Here we report the work with the first of these clusters as the precursor of catalysts supported on γ-Al_2O_3, which is a common support for industrial catalysts.

RESULTS AND DISCUSSION

Characterization of initial $ReOs_3$ *supported clusters*

$H_3ReOs_3(CO)_{13}$ and $H_3Re_3(CO)_{12}$ were synthesized according to the literature methods,[14,15] and $Os_3(CO)_{12}$ (Strem) was used without purification. The initial surface species derived from $H_3Re_3(CO)_{12}$ and $Os_3(CO)_{12}$ on γ-Al_2O_3 have been reported previously.[16,17] The supported $ReOs_3$ clusters were prepared by depositing $H_3ReOs_3(CO)_{13}$ on partially dehydroxylated γ-Al_2O_3 (calcined at 500°C) in dry hexanes. A homogeneous orange–yellow solid was formed having an IR spectrum similar to that of the cluster physically mixed with KBr (Fig. 1). The spectrum of the supported species has an intense absorption at 2024 cm^{-1}. Attempts were made to elucidate the strength of the

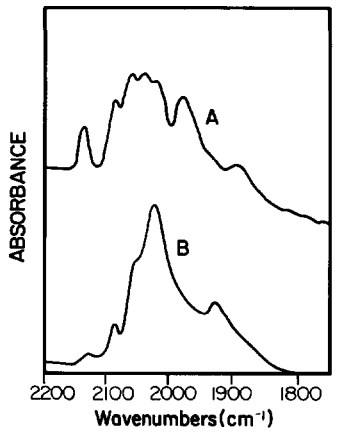

Fig. 1. IR spectra in the carbonyl region of (A) physical mixture of $H_3ReOs_3(CO)_{13}$ with KBr and (B) sample prepared by adsorption of $H_3ReOs_3(CO)_{13}$ from hexanes onto γ-Al_2O_3 under N_2.

cluster–support interaction by washing the sample with organic solvents. Refluxing THF (in which the precursor cluster is soluble) did not extract the $H_3ReOs_3(CO)_{13}$-derived surface species, indicating the absence of physisorbed organometallics. In addition, $NaBPh_4$ in THF was added in an attempt to extract anionic surface species by cation metathesis. An IR spectrum of the extract solution was similar to that of the still uncharacterized ionic cluster $[H_{3-x}ReOs_3(CO)_{13}]_x$ ($x = 1,2$) formed when $NaBPh_4$ in THF came into contact with the precursor cluster. This result is consistent with the suggestion that the cluster framework remains intact on the surface. When the sample was momentarily exposed to a trace of moisture at room temperature, the major absorption at 2024 cm^{-1} was downshifted to 2019 cm^{-1}. The original IR spectrum was restored by evacuating the sample at 50°C (Fig. 2). Evidently the adsorbed donor molecule

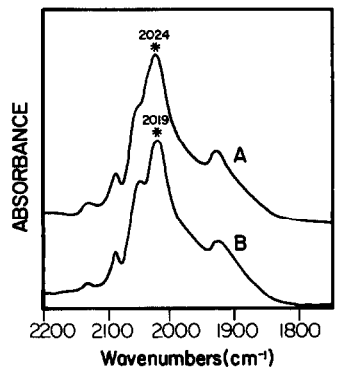

Fig. 2. IR spectra in the carbonyl region of (A) sample prepared by adsorption of $H_3ReOs_3(CO)_{13}$ from hexanes onto γ-Al_2O_3 under N_2 (spectrum obtained following exposure to a trace of moisture) and (B) after evacuation at 50°C for 20 min.

Table 1. Supported bimetallic catalysts; examples illustrating structural types

Structural type	Periodic group of metals	Precursors	Support	Activation conditions	Structure	Reference(s)
I. Alloy-like metals	8–8	$Co_2Rh_2(CO)_{12}$ $Co_3Rh(CO)_{12}$	SiO_2	(1) Initial physisorption (2) 300–350°C, under N_2 or O_2 or vac (3) 350–400°C under H_2	Metallic particle 28 Å "alloy"	6
		$Co_2Rh_2(CO)_{12}$ $Co_3Rh(CO)_{12}$	γ-Al_2O_3	(1) Oxidative decarbonylation (2) 300–350°C under N_2 or O_2 or vac (3) 350–400°C under H_2	Metallic particle 10–15 Å "alloy"	6
		$Rh_2Co_2(CO)_{12}$ $RhCo_3(CO)_{12}$	ZnO	(1) Evacuate at 100°C (2) $C_3H_6:CO:H_2$ = 18 : 18 : 20 cm Hg	Alloy	7
II. Multiple phases, including a metal oxide	8–7B	$NEt_4[Fe_2Mn(CO)_{13}]$ $NEt_4[FeMn(CO)_9]$ $Mn_2Fe(CO)_{14}$	Carbon black (H_2, 950°C, 12 h vac, 300°C, 8 h)	LTR = He, 200°C H_2, 2–5 h	(a) Mn/Fe > 0.5 Separate MnO phase with $(Mn_{1-y}Fe_y)_3O_4$ ($y \ll 1$) (b) Fe/Mn > 2 metallic Fe with $(Fe_{1-x}Mn_x)_3O_4$ ($x < 1$) Possible active phase Fe_2MnO_4	8,9
III. Metal crystallites with neighbouring cationic promoters	8–7B	$H_3ReOs_3(CO)_{13}$	γ-Al_2O_3	(1) He → 400°C H_2 → 400°C (2) H_2 → 400°C H_2, 400°C (see text)	Metallic Os + Re(VII) Metallic Os + Re(II or III)	This work
IV. Intact molecular clusters	8–8	$H_2RuOs_3(CO)_{13}$	γ-Al_2O_3 (200°C, vac)	H_2+CO, 200°C	$Al^+[H_3RuOs_3(CO)_{12}]^-$	3

disturbed the chemical interaction between the surface and the cluster. We conclude that the cluster was chemically bonded, intact, to the Al_2O_3 surface, but the exact nature of the interaction remains to be determined.

Structural evolution of supported clusters under various treatment conditions

Hucul and Brenner's[18] temperature programmed decomposition experiments demonstrated that supported monometallic carbonyl clusters, upon heating, are oxidized by surface hydroxyl groups, forming cationic species with the evolution of H_2 and CO, as depicted in eq. (1):

$$M(CO)_j + n(\sigma\text{-OH}) \xrightarrow{\Delta} (\sigma\text{-O}^-)_n M^{n+} + \left(\frac{n}{2}\right)H_2 + jCO. \quad (1)$$

The average oxidation state of Re in a 0.37 wt% Re/Al_2O_2 sample derived from $Re_2(CO)_{10}$ after activation in He to 600°C was found to be 5.4.[18] In a patent describing the preparation of a Pt–Re/Al_2O_3 catalyst, Antos[19] stated that pyrolysis of rhenium carbonyl complexes on γ-Al_2O_3 under anhydrous hydrogen at 105–400°C provided the best catalytic results when compared with pyrolysis carried out in an inert atmosphere or *in vacuo*. These results imply that the final oxidation state of Re is highly dependent on the gas environment used for activation, but the role of neighbouring metal centres and their influence on the extent of oxidation of Re derived from mixed metal clusters has not been clearly addressed. This is a major issue to be investigated in the present research.

The conditions for activation of the supported $ReOs_3$ catalysts were the following:

(a) The sample was first heated in flowing He from ambient temperature to 400°C, followed by reduction at 400°C in flowing H_2 for 4 h.
(b) Instead of heating initially in He, the sample was treated in flowing H_2 as the temperature was raised from ambient to 400°C, and the sample was then reduced in the flowing H_2 at 400°C for 4 h.

The presumption was that decarbonylated metal centres would be susceptible to oxidation by surface hydroxyl groups when the supported carbonyl complexes were decomposed in the inert atmosphere; whereas in the reducing atmosphere the low valency of the decarbonylated metal centre could possibly be maintained.

The structural changes of the supported mixed-metal cluster and of the monometallic samples prepared from $H_3Re_3(CO)_{12}$ and from $Os_3(CO)_{12}$ for each of the activation procedures were monitored by *in situ* IR spectroscopy in a controlled-environment cell for each of the activation procedures. The metal framework of the $H_3ReOs_3(CO)_{13}$-derived surface species was disrupted at temperatures greater than 100°C, with the subsequent formation of osmium and rhenium subcarbonyl species similar to those obtained by performing the same treatments with the monometallic samples. After the reduction of the bimetallic catalyst at 400°C, no observable absorption was found in the carbonyl region. CO chemisorption at 50°C resulted in the formation of a three-band pattern characteristic of the Os subcarbonyl species $Os(II)(CO)_{2\text{ or }3}(OAl)_3$.[17] No carbonyl band was found for terminal CO on metallic Re or for Re subcarbonyl species.

The observation of the Os subcarbonyl species does not rule out the possibility that metallic Os was present after reduction at 400°C. CO may oxidize highly dispersed Os crystallites on alumina, leading to the formation of Os(II) carbonyl complexes; comparable chemistry of Rh crystallites on alumina is well documented.[20] The lack of a difference in the osmium carbonyl IR spectrum between the bimetallic and the monometallic samples after CO chemisorption indicates the lack of electronic interactions between Re and Os surface species following the activation treatments.

X-ray photoelectron spectroscopy was used to estimate the oxidation states of the supported metals following reduction. The activation experiments were performed in the prechamber of a Physical Electronics AES/XPS instrument (Model 550). The binding energy of Os $4f_{7/2}$ and of Re $4f_{7/2}$ of the treated samples and that of various standards was measured with an operating pressure $< 5 \times 10^{-8}$ Torr. Al $2p = 74.5$ eV was used as the internal reference of the supported samples, and C $1s$ was used to check the internal consistency of the peak assignments.

The Re $4f_{7/2}$ binding energies of Re foil, $[Re(OH)(CO)_3]_4$, ReO_2, and Re_2O_7 were determined and used as the references characterizing the Re $4f_{7/2}$ binding energies for Re(0), Re(I), Re(IV), and Re(VII), respectively. Os foil was not used because of the toxicity of the easily formed OsO_4; instead two reduced alumina-supported Os samples were used as the metallic Os reference; these contained 2.5 and 2.0 wt% Os and were prepared, respectively, from H_2OsCl_6 and $Os_3(CO)_{12}$. The observed binding energies agree with the literature value for alumina-supported Os metal particles.[21]

The binding energies of Os in the mixed-metal

cluster-derived samples after each of the activation procedures (Table 2) indicate that the alumina-supported Os was metallic. The low Os $4f_{7/2}$ binding energy characterizing the sample after He heat-up followed by H_2 reduction is attributed to the presence of oxidic Re(VII) species, leading to the overlap of Os $4f_{7/2}$ and Re $4f_{5/2}$ XP peaks. In addition, transmission electron microscopy showed no discernible particles in either sample; further, the binding energy of bulk Os metal is reported to be 50.6 eV.[22] Therefore, we rule out the possibility of a particle size effect to explain the difference in the Os binding energies of the bimetallic catalysts after the different treatments.

The X-ray photoelectron spectra characterizing Re in the alumina-supported sample prepared from $H_3Re_3(CO)_{12}$ after treatment (a) or treatment (b) showed the existence of highly oxidized Re species, likely Re(VII). However, after treatment (a), with the sample incorporating metallic Os, the binding energy of Re was 41.6 eV, which corresponds to an Re species with the oxidation state in the range of 1–4. The Re $4f_{7/2}$ binding energy of the mixed-metal cluster-derived surface species after treatment (b) was found to be 47.1 eV. These data demonstrate that the final oxidation state of rhenium depends strongly on the atmosphere used for activation and that a wide variation in Re oxidation states can be achieved. Moreover, the presence of neighbouring metallic structures evidently plays a role. Group 8 metal surfaces are known to facilitate hydrogen spillover (whereby H_2 is dissociated on the metal surface and then is transported to neighbouring positions on the support surface);[23] metallic Os can thereby supply the oxidic rhenium with atomic hydrogen, giving a more reducing environment than in the monometallic Re samples. The observed difference in the reducibility of Re in the samples containing Os after treatment (a) or treatment (b) can be explained by either the efficiency of Os in promoting hydrogen spillover or by a stronger Re–alumina interaction when the supported cluster is activated in an inert atmosphere.[24]

Table 2. XP binding energies (eV)

	Os $4f_{7/2}$	Re $4f_{7/2}$	C 1*s*
References			
Re foil	—	40.2	(284.6)
$[Re(OH)(CO)_3]_4$	—	40.2	(284.6)
ReO_2	—	42.5	(284.6)
Re_2O_7	—	46.4	(284.6)
(Precursor/support)			
$Os_3(CO)_{12}/Al_2O_3$[a]	50.7	—	284.4
H_2OsCl_6/Al_2O_3[a]	50.9	—	284.3
$H_3Re_3(CO)_{12}/Al_2O_3$[b,c]	—	42.4, 47.0	284.4
$H_3Re_3(CO)_{12}/Al_2O_3$[a,c]	—	46.7	284.6
$H_3ReOs_3(CO)_{13}/Al_2O_3$[b,c]	49.9	47.1	284.6
$H_3ReOs_3(CO)_{13}/Al_2O_3$[a]	50.6	41.6	284.6

[a] H_2 pre-heat, H_2 reduction at 400°C, 4 h.
[b] He pre-heat, H_2 reduction at 400°C, 4 h.
[c] A mixture of (IV) to (VII) oxidation states.

Catalyst testing

The samples described above were tested as catalysts for *n*-butane hydrogenolysis to determine the influence of the Re oxidation state. Kinetics experiments were done with a standard microflow reactor with an on-line gas chromatograph for periodic product analysis. The activities of the following alumina-supported catalysts were measured at 197°C with an H_2:hydrocarbon ratio of 10:1 (molar) at 1 atm. The catalysts were the monometallic Os, monometallic Re, a mechanical mixture of monometallic Re and monometallic Os, and the bimetallic sample formed from the Re–Os mixed-metal cluster; the catalysts were tested after treatment (a) and after treatment (b). The activity shown in Fig. 3 is normalized to the amount of Os in each sample.

No activity was observed for the monometallic Re sample after either treatment (a) or treatment (b). The lack of activity is associated with the presence of high-valent rhenium in both samples. This

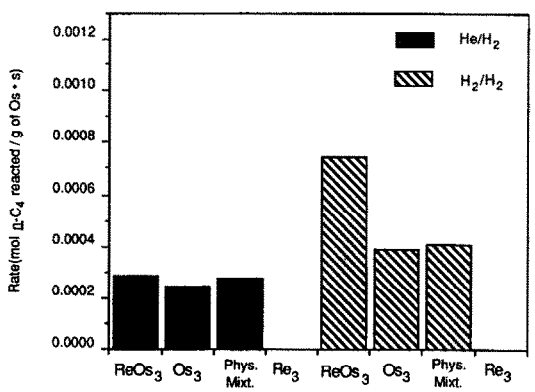

Fig. 3. Comparison of the activity of alumina-supported catalysts ($ReOs_3$: catalyst prepared from $H_3ReOs_3(CO)_{13}$ on γ-Al_2O_3; Os_3: catalyst prepared from $Os_3(CO)_{12}$ on γ-Al_2O_3; Phys. Mixt. = physical mixture of γ-Al_2O_3-supported catalysts prepared from $Os_3(CO)_{12}$ and from $H_3Re_3(CO)_{12}$; Re_3: catalyst prepared from $H_3Re_3(CO)_{12}$ on γ-Al_2O_3 measured at 1 atm, 197°C, H_2:*n*-C_4 = 10:1 (molar) with a feed rate of 5.5 $cm^3\ s^{-1}$ g of catalyst). The metal contents of the catalysts were the following (in wt%): $ReOs_3$: 0.46% Os, 0.14% Re; Os_3: 0.60% Os; Phys. Mixt.: 0.41% Os, 0.13% Re; Re_3: 1.0% Re.

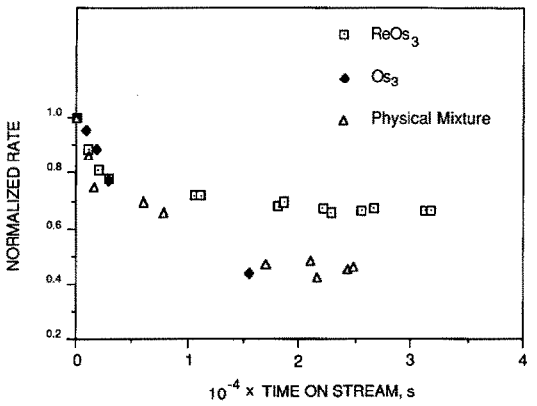

Fig. 4. Decline in activity of Os-containing catalysts in a flow reactor at 1 bar, 177°C, H_2:*n*-C_4 = 10:1 (molar). The labels have the same meanings as stated in the caption of Fig. 3.

observation could also explain why the samples that contained Os had nearly the same activity after treatment (a), since only high-valent rhenium was initially present in the bimetallic samples. On the other hand, after treatment (b), the sample formed from the mixed-metal cluster exhibited a two-fold higher activity and was more selective for methane formation than the monometallic Os and the physical mixture of Re and Os catalysts. This comparison indicates the importance of a reducing atmosphere in the activation and a facilitation of the reduction of Re by closely neighbouring Os, initially present in the precursor state of the bimetallic cluster. The bimetallic cluster may be uniquely valuable as a catalyst precursor because of this facilitation of the reduction.

The stability during catalytic reaction in the flow reactor was also examined for the three Os-containing samples after treatment (b) (Fig. 4). The activities of the samples were monitored at 177°C with an H_2: hydrocarbon ratio of 10:1 (molar) at 1 atm, and the effluent from the reactor was intercepted at various times on stream. The conversion data were normalized to the initial rate obtained at an on stream time of 7 min for a given sample. The sample derived from the mixed-metal cluster achieved a steady state in a shorter time and had higher activity than the others; the samples containing monometallic Os or a physical mixture of monometallic Os and monometallic Re behaved similarly to each other. These data again show the uniqueness of the catalyst prepared from the bimetallic cluster.

CONCLUSIONS

The ReOs catalysts prepared from $H_3ReOs_3(CO)_{13}$ on γ-alumina are examples of Type III catalysts (Table 1). There is a clear distinction in the reducibility of Re and of Os on the support surface, although these metals are near neighbours in the periodic table. Osmium was present in the reduced (metallic) state, independent of the treatment conditions, but rhenium was always present in a higher oxidation state. The catalytic activity of the alumina-supported cluster-derived Re–Os surface species is dominated by the Os. The atmosphere used for catalyst activation and the presence of neighbouring reduced metal allow some control of the oxidation state of the Re. Low-valent Re (but not high-valent Re) helped to stabilize the catalyst and increase its activity for *n*-butane hydrogenolysis. These results illustrate a distinct influence of the second (non-catalytic) metal and the means to control this influence through regulation of the oxidation state, made possible by use of the bimetallic cluster as a catalyst precursor.

The role of the Re is yet to be explained. Perhaps the presence of Re in the neighbourhood of Os could provide extra hydrogenation sites and minimize the rate of deposition of carbonaceous material covering the Os surface. This hypothesis is supported by the observation of increased stability when low-valent rhenium was present in the Re–Os catalyst combined with the known hydrogenation activity of low-valent rhenium in oxidic structures.[25]

Acknowledgement—This work was supported by the National Science Foundation (CBT-8317140).

REFERENCES

1. H. H. Lamb, H. Knözinger and B. C. Gates, *Angew. Chem.*, in press.
2. (a) H. H. Lamb and B. C. Gates, *J. Am. Chem. Soc.* 1986, **108**, 81; (b) A. Choplin, L. Huang, J. M. Basset, R. Mathieu, U. Siriwardane and S. G. Shore, *Organometallics* 1986, **5**, 1547.
3. J. R. Budge, J. P. Scott and B. C. Gates, *J. Chem. Soc., Chem. Commun.* 1983, 342.
4. J. R. Budge, B. F. Lücke and B. C. Gates, *J. Catal.* 1985, **91**, 272.
5. J. H. Sinfelt, G. H. Via, F. W. Lytle and R. B. Greegor, *J. Chem. Phys.* 1981, **75**, 5527.
6. J. R. Anderson, P. S. Elmes, R. F. Howe and D. E. Mainwaring, *J. Catal.* 1977, **50**, 508.
7. M. Ichikawa, *J. Catal.* 1979, **59**, 67.
8. J. Venter, M. Kaminsky, G. L. Geoffroy and M. A. Vannice, *J. Catal.* 1987, **103**, 450.
9. J. Venter, M. Kaminsky, G. L. Geoffroy and M. A. Vannice, *J. Catal.* 1987, **105**, 155.
10. R. J. Bertolacini and R. J. Pellet, in *Catalyst Deactivation* (Edited by B. Delmon and G. F. Froment), *Stud. Surf. Sci. Catal.* 1980, **6**, 72.

11. J. H. Onuferko, D. R. Short and M. Kelley, *J. Appl. Surf. Sci.* 1984, **19**, 227.
12. V. K. Sheen, J. B. Butt and W. M. H. Sachtler, *J. Catal.* 1985, **96**, 371.
13. G. Meitzner, G. H. Via, J. H. Sinfelt and F. W. Lytle, *ACS Petrol. Div. Prepr.* 1987, **32**, 733.
14. J. Knight and M. J. Mays, *J. Chem. Soc., Dalton Trans.* 1972, 1022.
15. M. A. Andrew, S. W. Kirtley and H. D. Kaesz, *Inorg. Synth.* 1977, **17**, 66.
16. P. S. Kirlin, F. A. DeThomas, J. W. Bailey, K. Moller, H. S. Gold, C. Dybowski and B. C. Gates, *Surf. Sci.* 1986, **175**, L707.
17. H. Knözinger and Y. Zhao, *J. Catal.* 1981, **77**, 337.
18. D. A. Hucul and A. Brenner, *J. Phys. Chem.* 1981, **85**, 496.
19. G. J. Antos, U.S. Patent 4,210,524 (1980).
20. H. F. J. van't Blik, J. B. A. van Zon, T. Huizinga, J. C. Vis, D. C. Koningsberger and R. Prins, *J. Am. Chem. Soc.* 1985, **107**, 3139.
21. H. Knözinger, Y. Zhao, B. Tesche, R. Barth, R. Epstein, B. C. Gates and J. P. Scott, *Faraday Discuss. Chem. Soc.* 1981, **72**, 53.
22. A. Berndtsson, R. Nyholm, H. Martensson, R. Nilsson and J. Hedman, *Phys. Stat. Sol. B* 1979, **93**, K103.
23. D. A. Dowden, in *Specialist Periodical Reports—Catalysis* (Edited by D. A. Dowden and C. Kemball), The Chemical Society, London, 1980, **3**, 136.
24. H. C. Yao and M. Shelef, *J. Catal.* 1975, **44**, 392.
25. W. H. Davenport, V. Kollonitsch and C. H. Kline, *Ind. Engng Chem.* 1968, **60**, 10.

Polyhedron Vol. 7, No. 22/23, pp. 2429–2436, 1988
Printed in Great Britain

0277–5387/88 $3.00+.00
© 1988 Pergamon Press plc

WHAT DO WE ACTUALLY KNOW ABOUT REACTION PATHWAYS?

HANS BOCK

Institute of Inorganic Chemistry, Johann Wolfgang Goethe University, Niederurseler Hang, D-6000 Frankfurt (M) 50, F.R.G.

Abstract—Facets of reaction pathways as deduced from a combination of preparative efforts, photoelectron and electron spin resonance spectroscopic detection of intermediates and accompanying hypersurface calculations are presented for the temperature-dependent gas phase pyrolysis of methyl azide under nearly unimolecular conditions and for the two-step single electron transfer reduction of quinones in aprotic solution containing alkaline metal salts. Aspects of molecular dynamics and especially of chemical activation are discussed for medium-sized molecules with many degrees of freedom as well as advantages of additional potentials like ion-pairing in solution or chemisorption on surfaces.

PRESENT STATE OF AFFAIRS

Referring to G. Pimentel's statement "Despite all that is known about reaction behaviour, understanding of it is rather shallow..."[1] and as a "late evening eye-opener lecture", our lack of knowledge about microscopic reaction pathways especially of medium-sized molecules shall be critically reviewed.[2]

Presently, many areas of inorganic chemistry are explored with tremendous speed and success—often even quoted as its "renaissance"—stretching from the novel super-conducting perovskite-type solid materials via astounding new organometallic compounds such as H_3CReO_3[3] or $(RC)_5Fe(P)_5$[4] to the recently discovered ocean of unsaturated main group element compounds like R—N≡Si with a singly coordinated, triply bonded silicon.[5] As concerns molecular physics, intricate beam experiments combined with numerically exact quantum chemical calculations, shed more and more light on the reaction channels of atoms and/or few-atom molecules from the angular dependence of collision cross sections to the energy transfer in the intermediate transition states.[6]

In sharp contrast, so far it remains largely unknown from which directions medium-sized molecules, containing more than five or six atoms and energetically "hot" from preceding collisions, must collide to successfully penetrate each other and form the reaction complex, how their structures change during the energy transfer between them and what role molecular dynamics plays in this process.

In the following, selected examples from work of the Frankfurt group[2] shall illustrate how little we know, and how some progress might be achieved, if proper experiments are designed by the preparative chemist and interesting compounds he is able to synthesize and to handle are selected.

THE GAS PHASE PYROLYSIS OF METHYL AZIDE

Starting from compounds with known structures and studying their thermal (or photochemical) decomposition will avoid the difficulty to solve any collision problem by starting half-way in the overall reaction pathway, and can be advantageous, especially if one of the fragments is a thermodynamically favoured (singlet) "leaving molecule" and if the analysis technique chosen allows the detection and characterization of intermediates. The pyrolysis of methyl azide[2d] will illustrate both the use of real-time photoelectron spectroscopic gas analysis in a flow system[7] and the interpretation of experimental results by hypersurface calculations.[8]

Surprisingly, the potentially dangerous methyl azide, which can explode violently in liquid bulk at room temperature causing harm and damage, in a vacuum system requires "red-glow" temperatures above 720 K (!) to lose N_2 and rearrange via a 1,2-hydrogen shift into the interstellar molecule methane imine $H_2C{=}NH$ (Fig. 1). This intermediate. which rapidly polymerizes in the liquid phase at room temperature, above 770 K expels H_2 in an

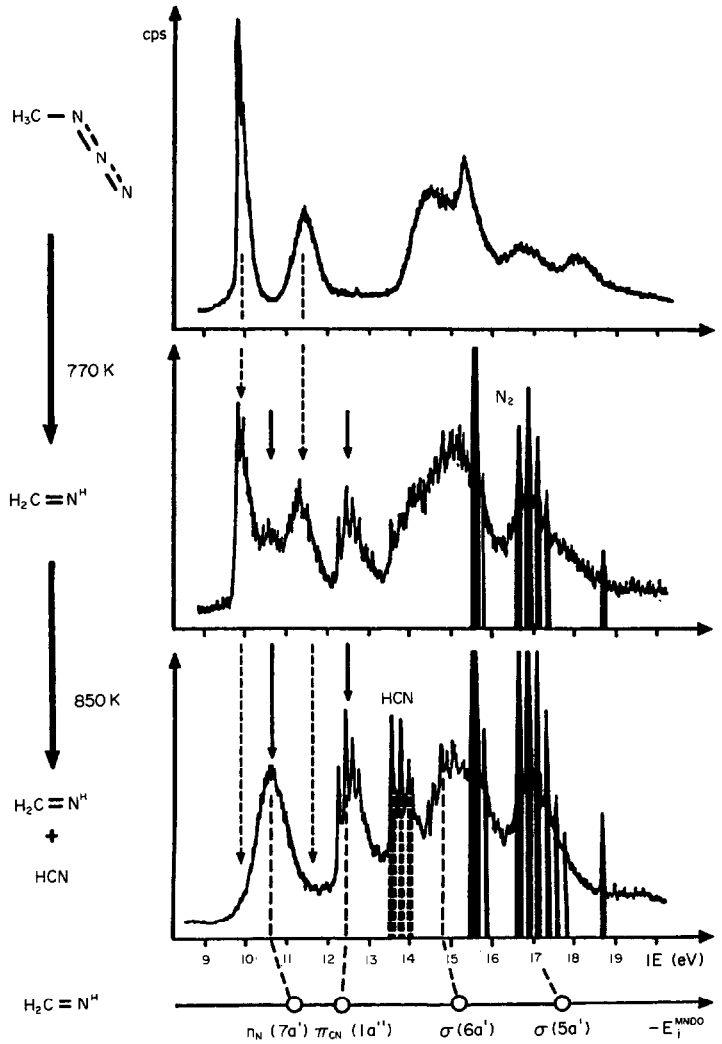

Fig. 1. He(I) PE spectra of methyl azide and its decomposition products at 770 and 850 K. The start of the pyrolysis is recognized by the appearance of the unmistakable N_2 ionization needles (blackened) between 15.5 and 18.7 eV, and complete decomposition by the disappearance of the characteristic azide bands (------→). At 770 K, the ionization pattern of $H_2C{=}NH$ (——→), here assigned by Koopmans correlation with MNDO eigenvalues, starts to emerge. The second thermal reaction pathway to H—C≡N (PE bands between 13.6 and 14.21 eV) and H_2 is populated at temperatures above 820 K.

energetically close second reaction channel and forms the thermodynamically stable end product HCN (Figs 1 and 3A).

All information obtained by PES real-time gas analysis for the first reaction channel is satisfactorily reproduced by a gradient norm MNDO hypersurface calculation (Fig. 2). For the synchronous methyl azide decomposition, a lower barrier is calculated than for the one via a methyl nitrene H_3CN intermediate, elusive under our reaction conditions. The MNDO predicted structural changes show a curved trajectory for the extruded N_2, which appears to be coupled to the formation of the H_2C subunit via a 1,2-hydrogen shift to the imine nitrogen and shortening of the CN bond (Fig. 2).

For the consecutive reaction channel from $H_2C{=}NH$ to H_2 and HCN, a drastic temperature difference is observed by PES depending on whether the gas stream from the $H_3C{-}N_3$ pyrolysis is heated further or whether the cool-trapped liquid $H_2C{=}NH$ is thermally decomposed after reevaporation (Fig. 3A). For $H_2C{=}NH$ formed by unimolecular thermal decomposition of $H_3C{-}N_3$, a "chemical activation" of approximately 340 kJ mol^{-1} is estimated from both literature bond

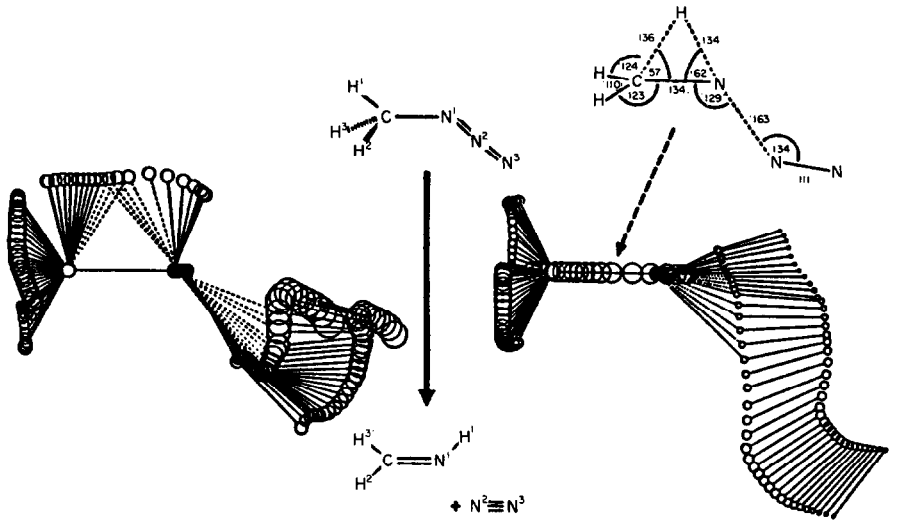

Fig. 2. Stroboscopic representation of geometry changes on an MNDO energy hypersurface for the synchronous $H_3C—N_3$ decomposition; with views onto (left) and in the H^1CN^1 plane (right) as well as the geometry of the saddle point (------→).

enthalpies and the activation energy for the N_2 extrusion (Fig. 3B). Since the excess energy stored in the $H_2C{=}NH$ cannot be dissipated under the nearly unimolecular flow conditions, a small temperature increase leads into the second reaction channel to H_2 and HCN. In contrast, the thermal dehydrogenation of isolated $H_2C{=}NH$ requires that the full activation energy be supplied, resulting in a temperature for the same reaction being higher by more than 500 K (Fig. 3A).

Numerous other molecules have been thermally decomposed in gas flow systems[2,7] by using the advantageous real-time PES analysis method,[7] and the experimental facts have been rationalized by semi-empirical hypersurface calculations. In addition the importance of molecular dynamics, i.e. the $3n$–6 degrees of freedom of non-linear n atomic molecules, is emphasized. Thus the temperature-dependent decomposition channels of S_2N_2[9] (see Scheme 1) can be discussed by assuming for the

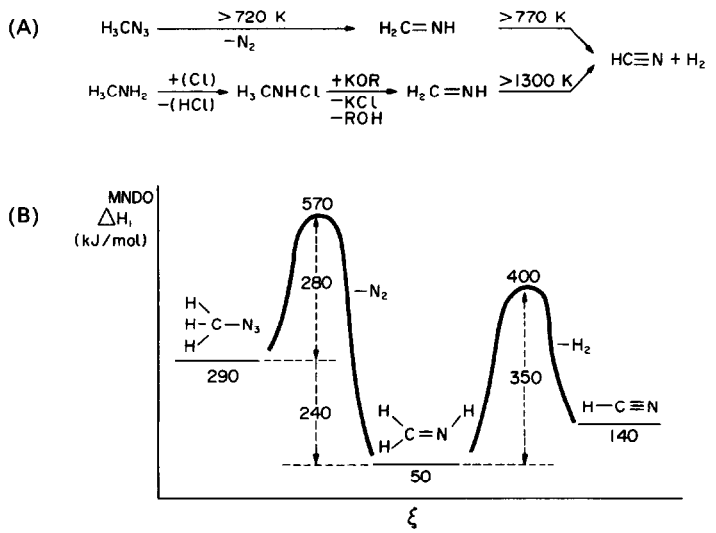

Fig. 3. (A) Decomposition temperature difference for $H_2C{=}NH$ generated in the $H_3C—N_3$ pyrolysis and after reevaporation from a cool-trap, (B) Enthalpy diagram for the N_2 extrusion from $H_3C—N_3$ and for the dehydrogenation of the $H_2C{=}NH$ (see text).

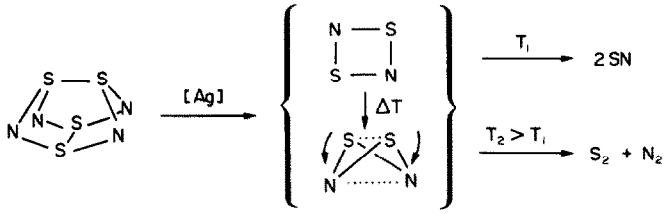

Scheme 1.

formation of N_2 and S_2 at T_2 a vibrationally induced, distorted tetrahedral transition state of S_2N_2.

Summarizing, the generation and identification of short-lived molecules studied by, for example, real-time PES gas analysis, not only allows one to optimize the conditions for the preparation of novel molecules[5,9] and/or for specific decomposition channels,[2,9] but in addition provides a method to study the still largely unknown reaction paths of medium-sized molecules with numerous degrees of freedom. Intermediates detected (Fig. 1), partly isolated in their vibrational ground state and partly "chemically activated" (Fig. 3), are of interest and should, after further investigation by more time-resolved measurement techniques, help to improve the presently still fragmented knowledge of microscopic reaction pathways of common chemical compounds.

ELECTRON TRANSFER AND ION PAIRING IN SOLUTION: THE Li^+ COMPLEXES OF 3,5-BIS(TRIMETHYLSILYL)-*p*-BENZOSEMIQUINONE RADICAL ANION

In solution, solvation of reactants and products plays an important role. Therefore, to obtain some information on the rather complex microscopic pathways of redox reactions, the introduction of dominating "Coulombic potentials" by adding well-chosen counterion salts is as advisable as the extensive removal of perturbing species, especially protons. As an illustration, the two-step reduction of a *p*-benzoquinone derivative by two consecutive one-electron transfer steps to its corresponding dianion under largely aprotic, i.e. water-free, conditions without and with addition of lithium salts will be presented.[10]

Starting out with the reversed electrochemical series[11] for aprotic solvents like DMF established by cyclic voltammetry (cf. Fig. 4), one recognizes that 3,5-bis(trimethylsilyl)-*p*-benzoquinone can be reduced chemically by a large variety of reagents like the hyperoxide radical anion $O_2^{\bullet-}$, the d^1-radical manganate(VI) MnO_4^{2-} or by electron-rich systems like tetrakis(dimethylamino)ethene (Scheme 2). The resulting and rather stable radical cation/radical anion pair can be unequivocally characterized by the partly overlapping ESR signal patterns of both paramagnetic species.[10]

The cyclovoltammogram recorded for 2,5-bis(trimethylsilyl)-*p*-benzoquinone (Fig. 4A) in aprotic DMF solution using tetra(n-butyl)ammonium perchlorate as the conducting salt shows two completely reversible consecutive electron transfer steps.

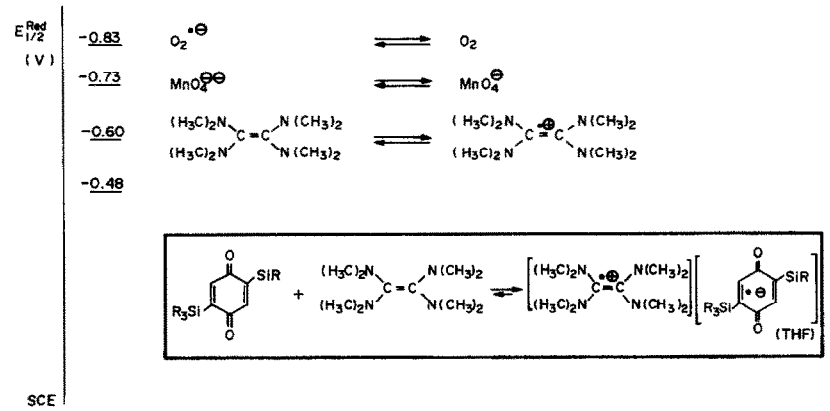

Scheme 2.

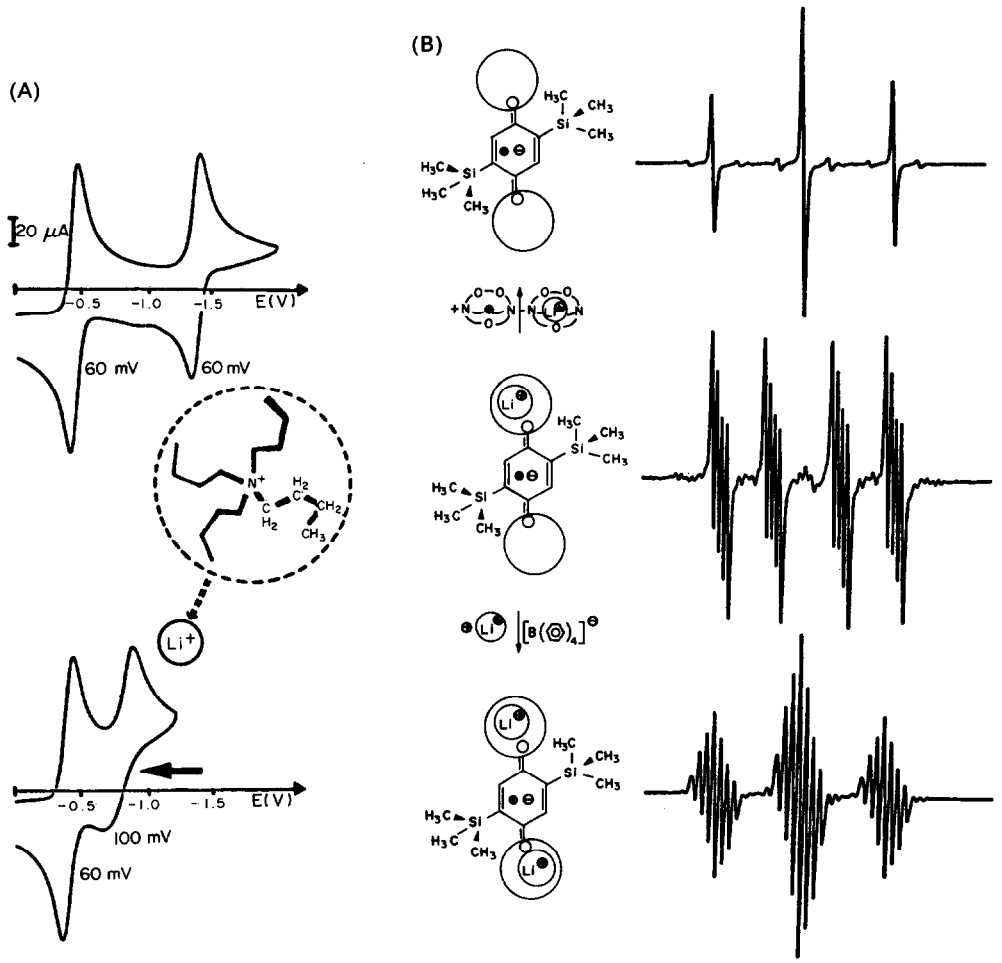

Fig. 4. (A) Cyclovoltammograms for the completely reversible two-step reduction of 2,5-bis(trimethylsilyl)-*p*-benzoquinone to the corresponding hydroquinone dianion in the presence of "innocent" tetraalkylammonium cations as well as the drastic changes inflicted by Li^+ as counter ion. (B) ESR spectra of "naked" 2,5-bis(trimethylsilyl)-*p*-benzoquinone radical anion, generated by lithium metal reduction in the presence of [2.1.1]cryptand, the radical $[M^{\bullet-}Li^+]^{\bullet}$ formed directly on reduction with lithium metal and the triple ion radical cation $[Li^+M^{\bullet-}Li^+]^{\bullet+}$ prepared by adding $Li^+[B(C_6H_5)_4]^-$, thus increasing the Li^+ concentration in the THF solution.

Exchanging the rather large, well-shielded R_4N^+ for the small, strongly solvated Li^+ counter cation shifts the second and now irreversible reduction potential by 0.6 V (!) to more positive values. What has happened?

Radical ion pairs, the formation of which is advantageously screened by cyclic voltammetry, are best characterized subsequently by ESR and ENDOR spectroscopy.[12] The ESR multiplet signal pattern of the 2,5-bis(trimethylsilyl)-*p*-semiquinone radical anion in THF changes with varying concentrations of Li^+ counter cations (Fig. 4B) as follows:[10] reduction using lithium metal in the presence of [2.1.1]cryptand generates the "naked" radical anion $M^{\bullet-}$, for which the ESR 1 : 2 : 1 triplet proves two equivalent ring protons. On reduction with lithium metal without addition of a complexing agent, the ion pair radical $[M^{\bullet-}Li^+]^{\bullet}$ is formed, exhibiting a ^1H doublet of doublets for the no longer equivalent semiquinone hydrogens with all four lines split into a quartet due to the additional coupling by one $^7Li^+$ ($I = 3/2$, natural abundance 92.58%) fixed into one of the two equivalent positions near the carbonyl subunits. Increasing the Li^+ concentration in the THF solution by addition of lithium tetraphenyl borate leads to the triple ion radical cation $[Li^+M^{\bullet-}Li^+]^{\bullet+}$ as deduced from the triplet for the equivalent hydrogens split each into a septet due to the coupling of two $^7Li^+$ cations now covering both available and equivalent positions near the carbonyl subunits of the semiquinone (Fig. 4B).

Both the cyclovoltammetric and the ESR spec-

troscopic results[10] combined convey some insight into the network of equilibria, through which the seemingly straightforward electrochemical two-step reduction of a quinone via its semiquinone radical anion to the corresponding hydroquinone dianion has to pass, if a conducting salt like $Li^+ClO_4^-$ is added to the aprotic solvent (Scheme 3).

The first electron transfer produces the semiquinone radical anion and immediately induces ion pairing to form the ESR spectroscopically detected ion pair radical $[M^{\bullet -}Li^+]^{\bullet}$ (Fig. 4B). In the resulting triple ion radical cation $[Li^{\bullet +}M^{\bullet -}Li^+]^{\bullet +}$, the hydroquinone dianion salt is already preformed, and both the tremendous lowering of the reduction potential as well as its irreversibility become self-explicable.

Altogether, the results of the rather sensitive ESR–ENDOR measurements for a well-chosen example of ion pairing in aprotic solution provide information on essential parts of the microscopic pathway along the two-step reduction. Additional experiments using other counter cations like Na^+, K^+ or $^+Tl(C_6H_5)_2$ yield some insight into the dynamics of the system. For example, K^+ moves within the ESR time scale of 10^{-7} s over the semiquinone radical anion, docking again in the equivalent position on the opposite side.[10] This ion movement can again be simulated by (open shell) MNDO energy hypersurface calculations[10] and leads to a rather satisfying reproduction of the experimental observation. According to the temperature-dependent ESR spectra, the K^+ movement starts at about 220 K, and the activation barrier calculated amounts to approximately 30 kJ mol^{-1}—a result with both biochemical as well as industrial implications!

OUTLOOK: REACTIONS OF GASES CHEMISORBED AT SURFACES

Another prospective method for the preparative chemist to gain some insight into microscopic reaction pathways is by investigations of the rather selective decomposition channels of molecules chemisorbed at the surface of catalytically active solids, i.e. restricted to two-dimensional migration within the additional and usually quite strong surface potential.

For illustration, two examples from our own work based exclusively on the identification of products by real-time PE spectroscopic gas analysis,[7] will be presented: the decarbonylation of isopropyl cyanate at Ni_x clusters on carbon as support[13] and the N_2 split-off from diazo acetic acid ester at Raney nickel[14] or rhenium metal[14] yielding stereoselectively a 90:10 mixture[14] of maleic and fumaric acid diester (Scheme 4).

Whereas the pyrolysis of isopropyl cyanate on quartz wool only starts above 850°C and yields exclusively propene and HNCO, on Ni_x/C_∞ the temperature is lowered by 650°C (!) and the unequivocally identified products are carbon monoxide, methane and acetonitrile.[13] Together with analogous results from other decarbonylations,[13] formation of an isopropyl nitrene on the Ni_x surface is assumed for rationalization, which splits off methane to form the thermodynamically favourable

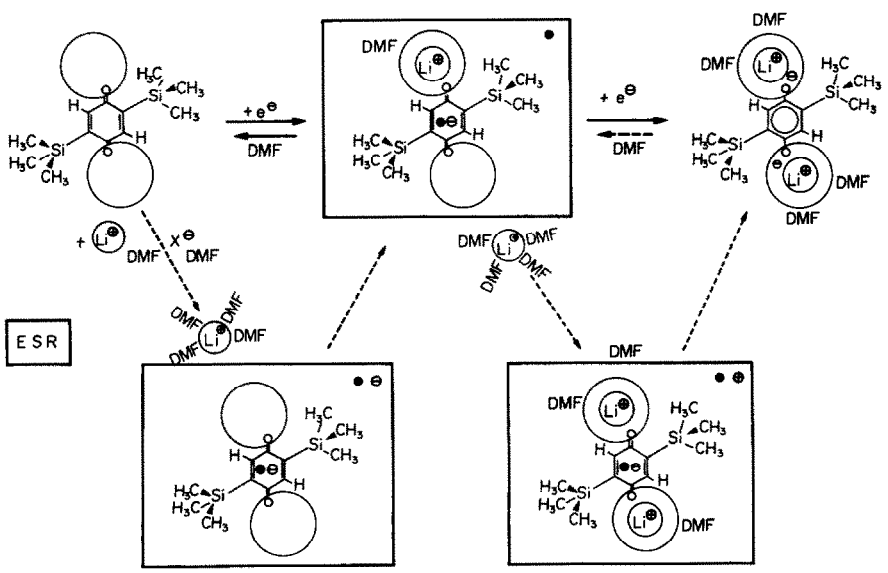

Scheme 3.

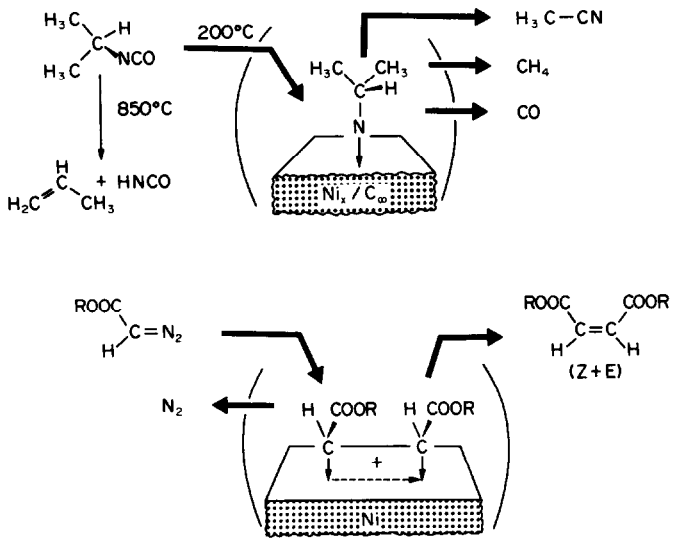

Scheme 4.

acetonitrile. For the diazo acetic methyl ester, thermal fragmentation above 350°C leads to N_2, CO and acetaldehyde,[14] while the Ni- or Re-catalysed N_2 elimination with subsequent dimerization proceeds at temperatures below 100°C. The presence of surface carbene intermediates can be proven by reacting a 50 : 50 mixture of methyl and ethyl esters, which yield each 25% of methyl and ethyl diesters together with 50% of the mixed methyl/ethyl diester.[14] This is further substantiated by the Ni_x/C_∞-catalysed decomposition of 2-diazo-propane $(H_3C)_2C{=}N_2$ to a mixture of propene and tetramethylethene $(H_3C)_2C{=}C(CH_3)_2$.[15] The stereoselectivity of the surface reaction as proven by GC/MC analysis of the isolated reaction mixture is assumed to arise from the final chemidesorption step in which the C=C bond formed by surface carbene dimerization leaves first and the additional, more strongly chemisorbed O centres leave last.[14]

This research report to a predominantly organometallic audience concerned the numerous difficulties in learning more about microscopic reaction pathways of medium-sized, *n* atomic molecules with their rather frightening though fascinating $3n$–6 degrees of freedom. In conclusion, advice for possible contributions from "benches to beams" (i.e. from the preparative chemistry to the molecular physicist) may be forwarded as follows: the detection of intermediates and, if possible their isolation, might be as welcome as the design of additional potentials in solution or the discovery of novel surface reactions. And, in return, the present worldwide effort, especially by groups developing and applying highly time-resolved measurement techniques, hopefully will backfire and stimulate all of us in our respective research areas!

Acknowledgements—The research results reported have been achieved by the coworkers quoted, whose impetus and dedication are emphasized. The University of Frankfurt and the Deutsche Forschungsgemeinschaft provided the instrumentation and sponsored the investigations. Additional support of the Fonds der Chemischen Industrie, the Hoechst AG, the Max Buchner and Herrmann Schlosser Foundations is gratefully acknowledged.

REFERENCES

1. Cf. *Chem. Engng News* 1980, **58**, 14 January, p. 7.
2. For other reviews along these lines, cf. e.g. (a) H. Bock, *Akad. Wiss. Lit. Mainz, Ber. Natwiss.* K1. 1986/2. F. Steiner Verlag, Wiesbaden (1986); (b) H. Bock, B. Solouki, S. Aygen, G. Brähler, R. Dammel, J. Giordan, P. Hänel, H. Herrmann, B. Hierholzer, T. Hirabayashi, D. Jaculi, W. Kaim, U. Lechner-Knoblauch, S. Mohmand, H. Müller, P. Rittmeyer, B. Roth and U. Stein, *Nova Acta Leopoldina, Neue Folge* 1985, **59**, 93f; (c) H. Bock, *L'actualité chim.* 1986, **3**, S. 33f; (d) H. Bock and R. Dammel, *Angew. Chem.* 1987, **99**, 503; *Angew. Chem., Int. Ed. Engl.* 1984, **26**, 489; and literature quoted.
3. Cf. Lecture W. A. Herrmann, this conference.
4. Cf. Lecture O. J. Scherer, this conference.
5. H. Bock and R. Dammel, *Angew. Chem.* 1985, **97**, 128; *Angew. Chem., Int. Ed. Engl.* 1985, **24**, 111.
6. Cf. e.g. the lectures at the EUCHEM Conference "The Use of Synchroton Radiation in Chemistry", Elmau, F.R.G., April (1986).
7. H. Bock and B. Solouki, *Angew. Chem.* 1981, **93**,

425; *Angew. Chem., Int. Ed. Engl.* 1981, **20**, 427 and literature cited.

8. Cf. e.g. H. Bock, R. Dammel and B. Roth, in *Inorganic Rings and Clusters* (Edited by A. G. Cowley), Vol. 232, p. 139. ACS Symposium Series (1983) and literature cited.
9. For recent results, cf. e.g. $H_2C{-}P{=}CH_2$: H. Bock and M. Bankmann, *Angew. Chem.* 1986, **98**, 287; *Angew. Chem., Int. Ed. Engl.* 1986, **25**, 265; $O{=}C{=}C{=}C{=}S$: H. Bock, R. Dammel and D. Jaculi, *J. Am. Chem. Soc.* 1986, **108**, 7844; the prebiotic $H_2C{=}N{-}CH_2{-}CN$: R. Dammel and H. Bock, *Z. Naturforsch.* 1987, **42b**, 810; the nitrile ylides $RC{\equiv}N^+{-}N^-{-}SiR_3$: H. Bock, R. Dammel, S. Fischer and C. Wentrup, *Tetrahedron Lett.* 1987, **28**, 617; or $H_3C{-}B{=}O$: H. Bock, B. Solouki, L. Cederbaum and P. I. Paetzold, unpublished.
10. H. Bock, B. Solouki, P. Rosmus, R. Dammel, P. Hänel, B. Hierholzer, U. Lechner-Knoblauch and H. P. Wolf, in *Organosilicon and Bioorganosilicon Chemistry* (Edited by H. Sakurai), pp. 59–69. E. Horwood, Chichester (1985) cf. also Refs 2a–c.
11. Cf. e.g. H. Bock and D. Jaculi, *Angew. Chem.* 1984, **96**, 298; *Angew. Chem., Int. Ed. Engl.* 1984, **23**, 305; H. Bock and U. Lechner-Knoblauch, *J. Organomet. Chem.* 1985, **294**, 295 or H. Bock, U. Lechner-Knoblauch and P. Hänel, *Chem. Ber.* 1986, **119**, 3749, and literature cited. All measurements are performed under ppm aprotic conditions either in an atmosphere of purified Ar or in vacuum.
12. Cf. e.g. H. Bock, B. Hierholzer, F. Vögtle and G. Hollmann, *Angew. Chem.* 1984, **96**, 74; *Angew. Chem., Int. Ed. Engl.* 1984, **23**, 57 or H. Bock, B. Hierholzer and P. Schmalz, *Angew. Chem.* 1987, **99**, 811; *Angew. Chem., Int. Ed. Engl.* 1987, **26**, 791 as well as literature quoted, especially W. Lubitz, M. Plato, K. Möbius and R. Biehl, *J. Phys. Chem.* 1979, **83**, 3402.
13. H. Bock and O. Breuer, *Angew. Chem.* 1987, **99**, 492; *Angew. Chem., Int. Ed. Engl.* 1987, **26**, 461.
14. Cf. H. Bock and H. P. Wolf, *Angew. Chem.* 1985, **97**, 411; *Angew. Chem., Int. Ed. Engl.* 1985, **24**, 418. For Re catalysis cf. Master Thesis, E. Roth, University of Frankfurt (1986) and for the stereoselectivity detected by GC/MS Thesis, H. P. Wolf, University of Frankfurt (1988).
15. H. Bock, G. Tschmutowa and H. P. Wolf, *J. Chem. Soc., Chem. Commun.* 1986, 1068.

Polyhedron Vol. 7, No. 22/23, pp. 2437–2439, 1988
Printed in Great Britain

0277–5387/88 $3.00+.00
© 1988 Pergamon Press plc

ALLOWED AND FORBIDDEN NATURE OF DIAMOND–SQUARE–DIAMOND DEGENERATE REARRANGEMENTS IN POLYHEDRAL BORANES—A GENERAL TOPOLOGICAL ANALYSIS

D. MICHAEL P. MINGOS* and ROY L. JOHNSTON

Inorganic Chemistry Laboratory, University of Oxford, South Parks Road, Oxford OX1 3QR, U.K.

Abstract—The topological and orbital symmetry constraints governing the intramolecular rearrangements of *closo*-polyhedral borane anions have been analysed. If the diamond–square–diamond rearrangement process occurs through an intermediate of C_{4v} symmetry it corresponds to a pseudo-90° rotation of the polyhedron. For deltahedra such an intermediate is only possible if there are a total of $4p+1$ ($p = 1, 2, \ldots$) boron atoms. These rearrangements are orbitally forbidden and consequently have high activation energies, e.g. $B_5H_5^{2-}$ and $B_9H_9^{2-}$. If the diamond–square–diamond rearrangement proceeds through a C_{2v} or C_s intermediate it corresponds to a pseudo-reflection of the polyhedron and the process is symmetry allowed. Such symmetry allowed processes can occur for $B_8H_8^{2-}$ and $B_{11}H_{22}^{2-}$.

Although Lipscomb[1] first proposed the general diamond–square–diamond (DSD) rearrangement mechanism more than 20 years ago, the topological and orbital symmetry restrictions associated with this mechanism have only been addressed recently. King[2] recognized that a single DSD process could only result in the regeneration of the original deltahedral skeleton if the difference in the sums of the connectivities across the diamond differed by two. He described these as degenerate rearrangements. Only $B_5H_5^{2-}$, $B_8H_8^{2-}$, $B_9H_9^{2-}$ and $B_{11}H_{11}^{2-}$ can rearrange by single DSD rearrangements. Gimarc and Ott[3,4] have used extended Hückel molecular orbital calculations to demonstrate that the single DSD process is Woodward–Hoffmann forbidden in $B_5H_5^{2-}$ and $B_9H_9^{2-}$, and Kleir and Lipscomb[5] have used PRDDO calculations to show that the degenerate DSD rearrangements in $B_8H_8^{2-}$ and $B_{11}H_{11}^{2-}$ have low activation energies because they are symmetry allowed. The purpose of this paper is to demonstrate that these degenerate DSD rearrangements are governed by changes in nodal surfaces governed by the topological features of the DSD process.

Although a degenerate rearrangement recreates the original polyhedral skeleton its orientation in space is different. If the four outer edges of the two faces involved in the DSD process are symmetry equivalent then a single DSD process results in a *pseudo-rotation of the initial polyhedron by 90°*. In contrast if the edges are not symmetry equivalent then the DSD rearrangement results in a *pseudo-reflection* of the initial polyhedron. This topological distinction is readily understood in terms of the local symmetries of the intermediates for the DSD process shown in Fig. 1. If the edges are symmetry equivalent then the intermediate has C_{4v} symmetry with two of the mirror planes coincident with the switch edges.[2] In the lower symmetry intermediates the mirror planes do not coincide with these directions. For reasons which will be developed below, *pseudo-90° rotations* are anticipated to have larger activation energies than *pseudo-reflections*.

Figure 2 gives the "particle in a diamond" energy levels, which are governed by the kinetic energies of the particles.[6] The lowest energy level is not noded. The second function is orthogonal to it and has a higher kinetic energy because it is noded horizontally. The third level, with two thinner triangles separated by a vertical nodal line, has higher kinetic energy because the kinetic energy for vertical motion finds no compensation in the low kinetic energy for horizontal motion. The final function shown is doubly noded and has the highest kinetic energy. Also shown in the figure are the symmetry designations of the functions either with respect to

*Author to whom correspondence should be addressed.

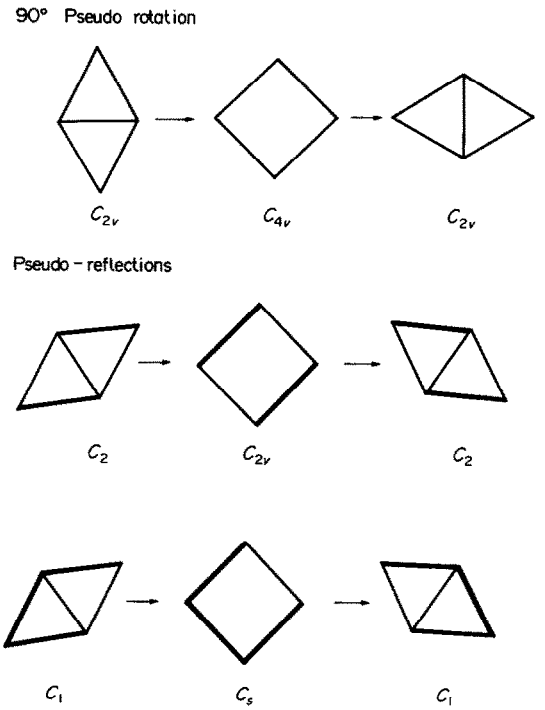

Fig. 1. The definition of the diamond–square–diamond rearrangement process and its symmetry consequences. Particularly noteworthy is the distinction between pseudo-90° rotations and pseudo-reflections.

a two-fold rotation axis perpendicular to the page or a horizontal mirror plane. These symmetry designations follow the same sequence as those noted previously for disrotatory and conrotatory ring closure reactions based on the solutions of a particle in a rectangular box.[6] Effective bonding across the short diagonal requires that the energy levels for the "particle in a diamond" be occupied by four electrons, i.e. the situation is analogous to butadiene ring closures.[7]

The activation energy for the DSD process depends on the ease of reorientation of the nodal surfaces resulting from changes in shape of the diamond. If the edges of the diamond are symmetry equivalent the DSD rearrangement involves the simultaneous compression and expansion along the two mirror plane directions. The "symmetry forbiddenness" of the rearrangement can be ascribed to a rise in kinetic energy as the molecular shape changes so that two of the four electrons become squeezed along one of their directions of motion. Only after the transition state is reached can the squeeze be relieved by the change in nodal surface direction with a concomitant change in preferred direction in motion of the electron pair. It is apparent from Fig. 2 that at the transition state the symmetric (S) and antisymmetric components (A) are

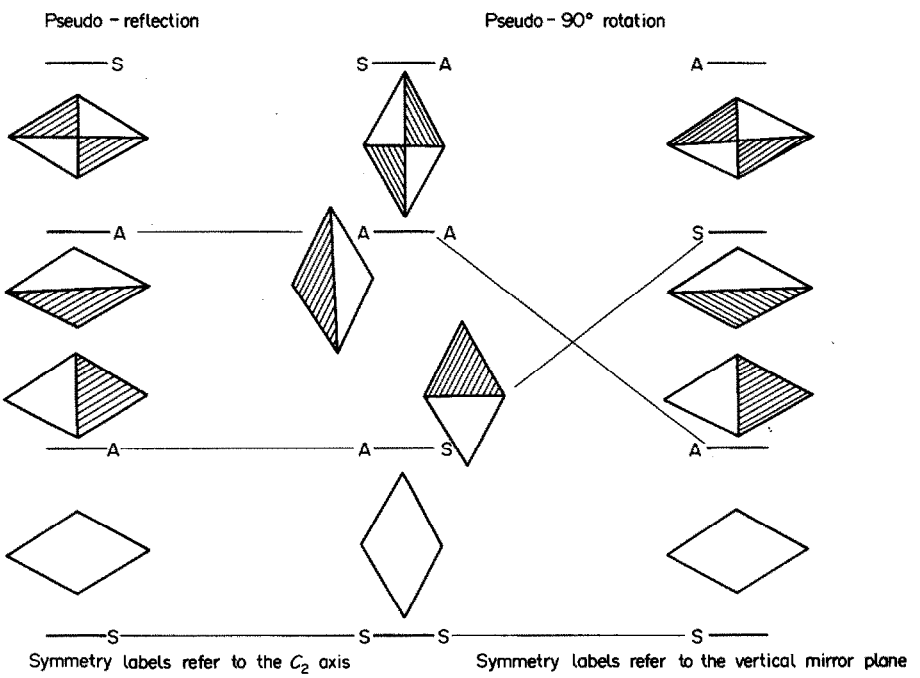

Fig. 2. Molecular orbital correlation diagrams for pseudo-reflections and pseudo-rotation DSD processes.

required to be degenerate for the crossover to occur. Such a C_{4v} transition state with a single square face can only be achieved for a polyhedral borane if the total number of atoms is $4p+1$ ($p = 1, 2, \ldots$), i.e. for a polar polyhedron.[8] This leads to our first conclusion: *Pseudo-90° rotations are symmetry forbidden for* closo-*boranes with* 4p+1 *atoms.* This agrees with Gimarc's conclusions for $B_5H_5^{2-}$ and $B_9H_9^{2-}$.[3,4]

When only the opposite edges of the diamond are equivalent the DSD rearrangement is achieved by combinations of rotations about the C_2 axis. Since the highest occupied orbital and the lowest unoccupied orbital in Fig. 2 are both antisymmetric to C_2 the reorientation of the nodal plane can occur smoothly as the DSD rearrangement proceeds. This leads to our second conclusion: *Pseudo-reflection degenerate rearrangements are symmetry allowed.*

The general topological nature of these arguments makes them equally applicable to a wide range of *closo-* and *nido*-boranes and is consistent with the computed low activation energies for the rearrangements in $B_8H_8^{2-}$ and $B_{11}H_{11}^{2-}$.[5]

Finally we note briefly that double DSD degenerate rearrangements will be symmetry allowed because the nodal lines in the two diamonds are either orthogonal or close to orthogonal.[3,4]

In a recent publication Wales and Stone[9] have an alternative interpretation of the rearrangements in *closo*-borane anions which is based on the tensor surface harmonic theory.

Acknowledgement—The SERC is thanked for financial support.

REFERENCES

1. W. N. Lipscomb, *Science* 1966, **153**, 373.
2. R. B. King, *Inorg. Chim. Acta* 1981, **49**, 237.
3. B. M. Gimarc and J. J. Ott, *Inorg. Chem.* 1986, **25**, 83.
4. B. M. Gimarc and J. J. Ott, *Inorg. Chem.* 1986, **25**, 2708.
5. D. A. Kleir and W. N. Lipscomb, *Inorg. Chem.* 1979, **18**, 1312.
6. L. Salem, *Electrons in Chemical Reactions.* John Wiley, New York (1982).
7. R. B. Woodward and R. Hoffmann, *The Conservation of Orbital Symmetry.* Verlag Chemie, Weinheim (1970).
8. R. L. Johnston and D. M. P. Mingos, *Polyhedron* 1986, **5**, 2059 and references therein.
9. D. J. Wales and A. J. Stone, *Inorg. Chem.* 1987, **25**, 3845.

Polyhedron Vol. 7, No. 22/23, pp. 2441–2450, 1988
Printed in Great Britain

0277–5387/88 $3.00+.00
© 1988 Pergamon Press plc

COOPERATIVE EFFECT BETWEEN TWO METAL CENTRES IN HYDROFORMYLATION: ROUTES TOWARDS HETEROBIMETALLIC CATALYSIS

PHILIPPE KALCK

Laboratoire de Catalyse et de Chimie Fine, Ecole Nationale Supérieure de Chimie, 118 route de Narbonne, 31077 Toulouse Cédex, France

Abstract—The $Rh_2(\mu\text{-}SR)_2(CO)_2L_2$ complexes are good catalyst precursors for the hydroformylation reaction of alkenes under mild conditions; high conversion rates are obtained, but when L is a phosphite or triphenylphosphine ligand no more than 85% of linear aldehyde is obtained for a full selectivity of the conversion of alkenes into the corresponding aldehydes. Introduction of the water-soluble $P(m\text{-}SO_3C_6H_4)_3$ ligand leads to 96% of selectivity in linear aldehyde and solves the problem of catalyst recovery; in this case the CO/H_2 or CO/H_2O couples can be used as feedstock. Various bisphosphine L_2 ligands can be introduced. These include several containing a transition metal centre (Zr, Fe, Ru). The major effect observed is electronic. Extension to heterobimetallic complexes was carried out. Various rhodium–palladium complexes have been synthesized and the first results of hydroformylation show that aldehydes are produced due to the presence of the rhodium centre.

Since the discovery by O. Roelen in 1938 that cobalt can catalyse the reaction of carbon monoxide and hydrogen with an alkene to give an aldehyde [eq. (1)],

$$R\text{—}CH{=}CH_2 + H_2 + CO \xrightarrow{[Co]} R\text{—}CH_2\text{—}CH_2\text{—}CHO + \text{the branched aldehyde} \quad (1)$$

the major challenges to solve were those of chemoselectivity and regioselectivity.[1] Indeed, many side reactions can take place, such as the hydrogenation of the alkene in alkane or aldehyde in alcohol or the isomerization of the terminal reactive carbon–carbon double bond. Similarly for the light olefins and particularly for propene it is essential to enhance the selectivity of linear aldehyde. Since the early work on cobalt, various improvements have been done and although plants are still working with Roelen's process, most of the new units operate with Wilkinson's complex $HRh(CO)(PPh_3)_3$[2,3] (**1**) developed by Union Carbide Corp., Davy Powergas, and Johnson Matthey and Co. Low concentrations of rhodium can be used, the hydrogenation of propene is limited to about 5% and a high linear to branched ratio (92 : 8) is obtained provided that a large excess of triphenylphosphine is introduced.[1] This rhodium complex can work at 50 bar and not be reactivated. However, it is very sensitive to various poisons present in syn-gas such as acetylene and sulphur-containing compounds.[1] The catalytic pathway has been extensively studied and appears to be well understood.[4,5]

The hydroformylation reaction is an elegant way to prepare aldehydes starting from various alkenes. Nevertheless, we observed for various allyl- or propenyl-benzenes issued from the biomass,[6] that isomerization of the terminal alkene (allyl-benzene) occurs as well as the hydrogenation reaction and the formation of the inactive cluster $Rh_4(\mu\text{-}PPh_2)_4(CO)_5(PPh_3)$.[7]

For all these reasons we decided to design a new rhodium system in order to reach high selectivities and reactivities.

Dinuclear rhodium(I) complexes appeared to us as good candidates for catalyst precursors. Sanger showed that A-frame complexes, in which the two rhodium atoms are bridged by two bis(diphenylphosphino)methane ligands, present a low catalytic activity.[8] We explored the dirhodium complexes bridged by two thiolato ligands which present a good flexibility around the two sulphur atoms and which maintain the dinuclear framework. We found that the complex $Rh_2(\mu\text{-S-t-Bu})_2(CO)_2[P(OMe)_3]_2$ (**2**) is highly active for the low pressure

hydroformylation of hex-1-ene.[9] For instance at 5 bar ($H_2/CO = 1:1$) and 80°C the turnover frequency is 32 min^{-1}. After the run, the IR spectra show that only species **2** is present in the solution. A new charge of hex-1-ene is transformed with almost the same rate. Chromatographic analysis of the products obtained after catalysis revealed that the reaction is fully selective in aldehyde (i.e. no trace of hexane or alcohols are detected). Moreover we checked that no isomerization of hex-1-ene occurs under the hydroformylation reaction. Similarly various phosphite ligands can be used.[9,10] However, these catalytic systems give deceiving selectivities in linear aldehyde since, even under optimum conditions, no more than 88% of heptanal for 12% of 2-methylhexanal can be obtained.

It should be noted that complex **2** which contains two sulphur atoms attached to the rhodium centres is a good catalyst precursor and even in the presence of one equivalent of extra mercaptan is still active, although the conversion rate becomes lower.

We have also examined the catalytic activity of the complex $Rh_2(\mu\text{-S-t-Bu})_2(CO)_2(PPh_3)_2$ (**3**) and compared it with that of $HRh(CO)(PPh_3)_3$ (**1**). The kinetic curves are shown in Fig. 1. Complex **1**, which posseses a hydride ligand, starts almost immediately. After 30 min, the reaction rate becomes slow so that 18 h are necessary to convert all the hex-1-ene introduced into the autoclave. Complex **3** presents an induction period of 12 min before the reaction occurs at a moderate rate. After 30 min the quasi-stationnary conditions are obtained and the charge of alkene is fully converted in 50 min. In addition, we have added one equivalent of t-BuSH to complex **1** and registered the kinetic curve.[11] At the beginning it follows approximately that of the hydride **1**. However, after 25 min the rate increases and progressively tends to the curve of **3**. After the catalytic run only complex **3** was found as the rhodium species. This reaction was also followed by IR and ^{31}P NMR spectroscopy under nitrogen and under hydroformylation conditions (hex-1-ene, 2.5 bar of H_2/CO). The spectra recorded during the reaction show unambiguously that the reaction of thiol on **1** slowly and irreversibly affords the di-μ-thiolato dirhodium complex $Rh_2(\mu\text{-S-t-Bu})_2(CO)_2(PPh_3)_2$. Thus the following equation of reaction is obeyed:

$$2HRh(CO)(PPh_3)_3 + 2t\text{-BuSH} \rightarrow Rh_2(\mu\text{-S-t-Bu})_2(CO)_2(PPh_3)_2 + 4PPh_3 + 2H_2. \quad (2)$$

We observed that complex **3**, which is very active for the hydroformylation reaction, is progressively deactivated into the complex $Rh_2(\mu\text{-S-t-Bu})_2(CO)_4$ (**4**), being totally inactive under our conditions. It is necessary to add an excess of triphenylphosphine ligand in order to shift the equilibrium [eq. (3)] and maintain the highest concentration of species **3**:

$$Rh_2(\mu\text{-S-t-Bu})_2(CO)_4 \underset{CO}{\overset{PPh_3}{\rightleftharpoons}} Rh_2(\mu\text{-S-t-Bu})_2(CO)_4(PPh_3)_2 \underset{CO}{\overset{PPh_3}{\rightleftharpoons}} Rh_2(\mu\text{-S-t-Bu})_2(CO)_2(PPh_3)_2. \quad (3)$$

This system of **3** in the presence of an excess of PPh_3 was examined in catalysis.[11] Table 1 lists the results obtained for various P/Rh ratios.

It is interesting to note that for a P/Rh ratio of 11 a turnover frequency of 53 min^{-1} is observed i.e. very near to one cycle per second. With higher quantities of extra ligand the rate decreases while better selectivities in linear aldehyde are obtained, viz. 88%. The nature of the solvent has also been examined.

Table 2 presents selected results showing that polar solvents such as 1,2-dichloroethane favour

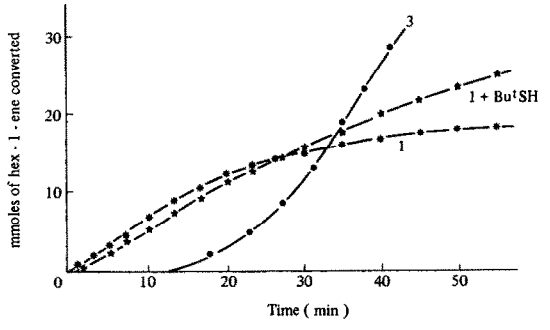

Fig. 1. Conversion of hex-1-ene using the complexes **1**, **1** + t-BuSH and **3**. $P = 5$ bar, $T = 80°C$, 10 cm^3 of hex-1-ene in 30 cm^3 of dimethylformamide, 10^{-4} atm of rhodium, were used.

Table 1. Catalytic activity of $Rh_2(\mu\text{-S-t-Bu})_2(CO)_2(PPh_3)_2 + PPh_3$

P/Rh	R_0 (μ mol·s^{-1})	TO (min^{-1})	n (%)
6	75	41	76
11	98	53	78
26	58	32	88

Hex-1-ene, 40 mmol. Solvent: toluene (25 cm^3). $T = 80°C$, $P = 8$ bar ($CO/H_2 = 1:1$). Rh = 2.2×10^{-4} g atm. R_0 is the initial rate of hydroformylation, TO is the turnover frequency calculated for a dinuclear species.

Table 2. Catalytic activity of $Rh_2(\mu\text{-S-t-Bu})_2(CO)_2(PPh_3)_2 + 10PPh_3$ in various solvents

Solvent	R_0 (μ mol·s^{-1})	TO (min^{-1})	Selectivity in n (%)
Toluene	75	41	76
$C_2H_4Cl_2$	120	65	73
DMF	100	55	76

Conditions as in Table 1.

the reaction whereas polar coordinating solvents such as *N*,*N*-dimethylformamide are slightly less interesting. Turnover rates near to one cycle per second were reached (65 and 55 min^{-1}, respectively).

In order to have an insight into the mechanism of the reaction and thus to propose a catalytic cycle we have carried out numerous spectroscopic investigations on the rhodium complexes **2** and **3** by ^1H, ^{31}P NMR and IR spectroscopy. Even with NMR tubes charged under 3 bar of H_2 and/or CO, with and without hex-1-ene, we did not detect any intermediate species and only observed the presence of the starting rhodium complex and the growing of the C_7 aldehydes.

On the basis of the chemistry of dirhodium or diiridium model complexes (see Ref. 10 and references therein), extended Hückel calculations[10] and very recently *ab initio* calculations[12] for step 2 carried out by A. Dedieu and NMR observations on diiridium complexes under the hydroformylation conditions,[13] we propose a catalytic cycle in which the dinuclear framework is retained for all the steps (Fig. 2). All these steps have been presented and discussed elsewhere.[10] Three important concepts give account of the peculiar path followed by these dinuclear complexes: (i) the flexibility around the sulphur–sulphur axis permits a transfer of an atom or a ligand from one metal centre to the other one; (ii) the σ donation of the various ligands or parts of the molecule on one metal centre; (iii) the back donation on the whole complex. The first concept is related to the mobility necessary in the complex

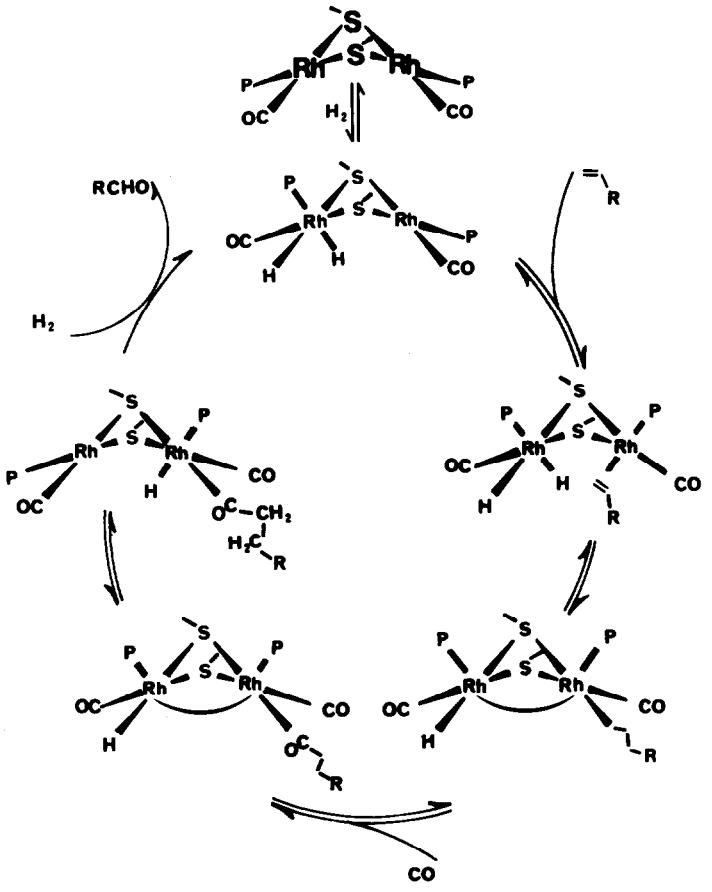

Fig. 2.

for the activated molecules, and the last two concepts concern the electron density on one rhodium atom modulated by each step (oxidative addition, reductive elimination, hydride transfer, CO insertion). In our opinion these three concepts account for the cooperative effect which takes place between the two rhodium centres and which is the driving force of the selectivity and of the rate we observed for the low pressure hydroformylation reaction.

Within a collaboration with the research group of L.A. Oro in Spain we prepared dinuclear rhodium complexes with a mixed bridge, i.e. one tert-butylthiolato group and one pyrazolato ligand.[14] Addition of two aliquots of pyrazole to the di-μ-chloro bis(η^4-1,5-cyclooctadiene)dirhodium gives the complex CODRhCl($C_3H_5N_2H$) which is reacted with CODRh(acac) to afford CODRh(μ-Cl)(μ-pz)COD and acacH.[14] Substitution of the chloro bridge by the S-t-Bu ligand generates the mixed species CODRh(μ-S-t-Bu)(μ-pz)RhCOD where pz is either pyrazolate or benzotriazolate. Bubbling of carbon monoxide through dichloromethane solutions of these two complexes leads to the formation of the tetracarbonyl species $Rh_2(\mu\text{-pz})(\mu\text{-S-t-Bu})(CO)_4$. Addition of two equivalents of trimethyl, triphenylphosphite or triphenylphosphine gives rise to the formation of the disubstituted complexes *cis*-$Rh_2(\mu\text{-pz})(\mu\text{-S-t-Bu})(CO)_2L_2$. We did not observe any dismutation of these heterobridged complexes. Moreover they were slowly formed by mixing the homobridged species $Rh_2(\mu\text{-pz})_2(CO)_2L_2$ and $Rh_2(\mu\text{-S-t-Bu})_2(CO)_2L_2$ as shown by IR and ^{31}P NMR studies.[14] An X-ray crystal structure was carried out on the complex where $L = P(OMe)_3$. The two rhodium atoms, separated by a distance of 3.477(9) Å, are in a distorted square planar environment. The two phosphorus atoms are *trans* to the bridging sulphur atom. The catalytic activity for the low pressure hydroformylation of alkenes is only slightly lower than that presented by $Rh_2(\mu\text{-S-t-Bu})_2(CO)_2[P(OMe)_3]_2$ and greater than that of the corresponding di-μ-pyrazolato complex. Thus, presumably the P—Rh—S—Rh—P framework is responsible for the catalytic activity shown by this family of complexes.

With such active dinuclear rhodium catalysts in our hands it was necessary to take an interest in the recovery of the rhodium complex. This problem can easily be solved for propene since the butanal produced is distilled off. However, for heavy alkenes other solutions must be found. Various methods were published to immobilize complex **1** through phosphine- or amine-containing organic or mineral polymers.[15,16] For instance, if POL indicates such a polymer, the method can be summarized by the following equations:

$$POL + C_2H_5OCH_2Cl\ (+SnCl_2) \rightarrow POL-CH_2Cl + C_2H_5OH$$

$$POL-CH_2Cl + LiPPh_2 \rightarrow POL-CH_2PPh_2 + LiCl$$

$$POL-CH_2PPh_2 + RhH(CO)(PPh_3)_3 \rightarrow (POL-CH_2PPh_2)RhH(CO)(PPh_3)_2 + PPh_3.$$

After the first results published by Rollman who prepared $Rh_2(\mu\text{-Cl})(\mu\text{-SCH}_2\text{POL})(CO)_4$, starting from $Rh_2(\mu\text{-Cl})_2(CO)_4$ and a polyvinyl benzylthiol resin,[17] we developed another method to graft our complexes onto an insoluble support:[18]

$$POL-CH_2Cl \xrightarrow[\text{(ii) NaOH}]{\text{(i) thiourea}} POL-CH_2SH \xrightarrow[\text{THF}]{\text{BuLi}} POL-CH_2SLi$$

$$2POL-CH_2SLi + Rh_2(\mu\text{-Cl})_2(CO)_2L_2 \rightarrow Rh_2(\mu\text{-SCH}_2\text{POL})(CO)_2L_2 + 2LiCl.$$

Our starting material was a chloromethylated styrene macroporous resin reticulated with 4% divinylbenzene. We operated the functionalization in order to have about 2 m. eq. of SLi groups per g of resin so that the sites are dispersed and further reticulation due to the grafting method are reduced. Thus we prepared $Rh_2(\mu\text{-SCH}_2\text{POL})_2(CO)_4$ and by addition of two aliquots of $P(OMe)_3$ the active complex $Rh_2(\mu\text{-SCH}_2\text{POL})_2(CO)_2L_2$. However, catalytic runs showed that the conversion rate is dramatically reduced with regard to the soluble complex **2** (3% in n-hexane, 20% in toluene for 18 h). Moreover, loss of rhodium occurs in the solution and after leaching the recycling does not give any further reactivity even in the presence of a new charge of phosphite ligand. Presumably the hydrogenolysis of one carbon–carbon bond produces the loss of a rhodium complex into the solution. In order to avoid such a bond breaking we started from a poly(styrene-divinylbenzene) resin that we reacted with bromine to prepare POLBr by bromination of the aromatic rings. By a similar method we prepared the $Rh_2(\mu\text{-SPOL})_2(CO)_2L_2$ complexes. The catalytic experiments showed the same results as those obtained when we started from the chloromethylated resin. Thus, in our opinion, the loss of rhodium in the organic phase results from a hydrogenolysis reaction which cleaves either a sulphur–carbon or a carbon–carbon bond.

We preferred another approach to solve the problem of the recovery of rhodium and to investigate biphasic systems. In collaboration with Rhône-Poulenc we used the tris(*m*-sulphophenyl) phosphine ligand, or TPPTS, to hold the rhodium complexes in the aqueous phase. Indeed, after the

first results published by Chatt and coworkers[19] on $Ph_2P(m\text{-}C_6H_4SO_3Na)$, TPPMS, Rhône-Poulenc Industries patented[20–22] the preparation of the TPPTS ligand and its use in the hydroformylation reaction. The species used industrially is mainly the complex $HRh(CO)(TPPTS)_3$ (**5**), analogous to **1**. Similarly TPPMS was shown by Wilkinson and coworkers[23] to give $HRh(CO)(TPPMS)_3$ by exchange of the ligands on **1** and to be active for the hydroformylation of alkenes but with a significant loss of rhodium in the organic phase.

For our part, we prepared the complex **5** starting from **1** by the exchange of the PPh_3 ligand with $P(m\text{-}C_6H_4SO_3Na)_3$ and the complex $Rh_2(\mu\text{-S-t-Bu})_2(CO)_2(TPPTS)_2$ (**6**) by addition of two equivalents of TPPTS to $Rh_2(\mu\text{-S-t-Bu})_2(CO)_4$ in methanol solution. Complex **5** is characterized by a ν_{CO} stretching frequency at 1925 cm^{-1} (m, broad) and a ν_{Rh-H} band at 2002 cm^{-1} (s, broad) in CsBr pellets; on the other hand **6** shows in methanol two ν_{CO} bands at 1986 (vs) and 1954 (s) cm^{-1} and in ^{31}P NMR a doublet centred at 37.7 ppm (D_2O, J_{Rh-P} = 133 Hz). These two complexes were tested in the hydroformylation of hex-1-ene under mild conditions. In Table 3 the results are shown for the same P/Rh ratio.

This table shows that at 5 bar and for 65 h the dinuclear species **6** is 1.5 times faster than the mononuclear precursor **5**. As in the case of the triphenylphosphine complexes **1** and **4**, the kinetic curves start more quickly for **5** than for **6** but after 3 h complex **6** is definitively more active than **5**. After the reaction, the organic phase and the aqueous phase, which contains the rhodium complex, are easily separated by decanting. The last three runs of Table 3 are related to the recycling of the catalyst. The pressure was raised to 8 bar to overcome to a slight extent the transfer phenomena between the two phases which limit the conversion rates. An excess of TPPTS was added to complex **6** (P/Rh = 5) so that we did not observe any formation of $Rh_2(\mu\text{-S-t-Bu})_2(CO)_4$ nor loss of rhodium into the organic phase (0.5 ppm). The three kinetic curves for these experiments are quite the same.

An important feature is also the selectivity of the reaction. Indeed, for all the experiments we observed a full conversion of the alkene into the corresponding aldehydes (> 98%) as well as a very good selectivity in linear aldehyde. Thus the mononuclear precursor led to 93%, the dinuclear complex alone to 88% or in the presence of an excess of ligand (P/Rh = 5) to 96% of the n-aldehyde.

With Rhône-Poulenc Chimie de Base we compared the performances of **5** and **6** for the hydroformylation of propene. Industrial conditions were retained: 50 bar of total pressure, 120°C and a large excess of phosphine ligand. Table 4 summarizes some of our results.

Propene is more soluble in water than hexene, so that the reactions required about 1 h to obtain a complete conversion of propene. Moreover the selectivity in butanal was 100%. Complex **5** gave a turnover frequency of five cycles per minute with a selectivity in butanal of 92% whereas **6** led to higher rates (28 min^{-1}) and slightly higher selectivity in butanal (96%). In these two experiments the P/Rh ratio was kept to 50 so that the organic phase was recovered colourless (loss of rhodium < 0.1 ppm). As expected, the reaction rates are very sensitive to the presence of an excess of phosphorus ligand. The two last runs show that for the same selectivities a P/Rh ratio of 100 decreases the rate; for P/Rh = 10 the turnover frequency reaches 53 min^{-1}.

Thus, using the tris(*m*-sulphophenyl)phosphine ligand, the dinuclear μ-thiolato complex is an excellent catalyst precursor for the selective conversion

Table 3. Catalytic activities of $RhH(CO)(TPPTS)_3$ (**5**) and $Rh_2(\mu\text{-S-t-Bu})_2(CO)_2(TPPTS)_2$ (**6**) for the hydroformylation of hex-1-ene

Precursor	Pressure (bar)	Time (h)	Conversion (%)	n (%)
5	5	65	50	93
6	5	65	72	88
6+4TPPTS	8	17	35	96
Recycling	8	17	35	96
Recycling	8	45	70	96

Hex-1-ene, 40 mmol; solvent H_2O (30 ml). T = 80°C, CO/H_2 = 1:1, Rh = 2×10^{-4} g atm. Selectivity in aldehyde ≃ 98–99%.

Table 4. Catalytic activities of $RhH(CO)(TPPTS)_3$ (**5**) and $Rh_2(\mu\text{-S-t-Bu})_2(CO)_2(TPPTS)_2$ (**6**) for the hydroformylation of propene

Precursor	P/Rh ratio	Turnover frequency (min^{-1})	n (%)
5[a]	50	5	92
6	50	28	96
6	100	14	96
6	10	53	95

[a] Generated from $Rh_2Cl_2(COD)_2$.

Complex **6** or $Rh_2Cl_2(COD)_2$ = 2.5 mmol, propene 0.2 mol. T = 120°C, P = 50 bar, CO/H_2 = 1:1, reaction time 1 h. Selectivity in butanal = 100%.

of an alkene into the corresponding linear aldehyde, and also permits a facile recovery of the catalyst from the aqueous phase.[24]

Moreover, since the catalyst precursor is dissolved in water, we thought it might be interesting to use the solvent itself as the hydrogen source by combining the water–gas-shift reaction with the hydroformylation reaction:

$$CO + H_2O \rightarrow CO_2 + H_2$$

$$RCH{=}CH_2 + 2CO + H_2O \rightarrow RCH_2CH_2CHO + CO_2.$$

These two reactions are usually accomplished with the late transition metal carbonyl complexes either in basic, neutral or acidic conditions.[25]

A preliminary study was undertaken in basic media, since it has been reported in the literature[25] that the most active systems, although they present low kinetic rates, are found in basic conditions. The two complexes **5** and **6** are active, as shown in Table 5.

As previously observed complex **6** is more active than **5**. The selectivity in the corresponding aldehydes is very high (98%) and the selectivities in heptanal are very interesting, particularly for **6**. However, this study was not further pursued since the basic conditions induce the fast oxidation, presumably accelerated by the rhodium complexes, of the TPPTS ligand to give the oxide OTPPTS. Moreover the formation of heavy species through aldolization was observed after long reaction times.

For this reason we studied the catalytic activity of **5** and **6** in neutral and acidic conditions. Since Kaspar *et al.* had shown that the cationic species $[Rh(COD)(TPPMS)_2]^+$, which contains the monosulphonated triphenylphosphine, was an active precursor for the water–gas-shift reaction,[26] our study was extended to the complex $[Rh(COD)(TPPTS)_2]^+$ (**7**). In neutral media, the main results are shown in Table 6.

The selectivity in aldehyde remains interesting but hydrogenation of the alkene was detected (5% with **5** and **7**, less than 3% with **6**). Complex **6** presents good conversion rates, 63% in 15 h, i.e. 28 h^{-1} for the calculated turnover frequency. Similarly the selectivity in linear aldehyde is high: n/(n+iso) = 94.8%.

The following study in acidic medium was restricted to complexes **6** and **7** due to their higher linear to branched selectivities. Several pH values were examined. Table 7 reports the results obtained for the cationic complex **7**, whereas Table 8 lists those obtained with complex **6**.

The most interesting results[27] come from the activity of the dinuclear complex **6**, since (see Table 8) turnover frequencies of 40 h^{-1} were reached for the reaction with an acetic acid/acetate buffer at pH 4.8 instead of 28 h^{-1} at pH 6. The selectivities in linear aldehyde remained almost constant at 95%. The gaseous phase after reaction contained *ca* 20% of H_2 for pHs between 4.2 and 6 but only 2% for a formic buffer.

In order to understand how the water–gas-shift and the hydroformylation catalytic cycles are connected, the overall amounts of hydrogen produced were calculated and compared in the two cases. The results appear in Table 9.

Table 5. Hydroformylation of hex-1-ene with CO/H_2O

Precursor	Conversion (%)	Heptanal (%)
5	20	91.8
6	50	95.8

Precursor 2×10^{-4} mol, P/Rh = 4, NaOH 20 mmol, H_2O 30 cm^3, hex-1-ene 40 mmol. Selectivity in aldehydes 98%.

Table 6. Hydroformylation of hex-1-ene by **5**, **6** and **7** with CO/H_2O in neutral media

Precursor	Conversion into aldehyde (%)	Turnover frequency (h^{-1})	n (%)
7	20	5.3	93.8
5	25	6.6	90
6	53	28	94.8

Rh 10^{-4} g atm, P/Rh = 6, hex-1-ene 40 mmol, H_2O 25 cm^3. T = 80°C, P_{CO} = 8 bar, pH = 6, t = 15 h.

Table 7. Hydroformylation of hex-1-ene in acidic media by $[Rh(COD)(TPPTS)_2]ClO_4$ with CO/H_2O

pH	Conversion into aldehyde (%)	Turnover frequency (h^{-1})	H_2 produced (%)	$\frac{n}{n+i}$ (%)
6	20	5.3	12	93.8
4.8	35	9.3	n.d.	95.8
3.7	60	16	1	95

Rh 10^{-4} g atm, P/Rh = 6, hex-1-ene 40 mmol, H_2O 20 cm^3, acetic or formic buffer 5 cm^3. T = 80°C, P_{CO} = 8 bar, t = 15 h.

Table 8. Hydroformylation of hex-1-ene in acidic media by $Rh_2(\mu\text{-S-t-Bu})_2(CO)_2(TPPTS)_2$ with CO/H_2O

pH	Conversion into aldehyde (%)	Turnover frequency (h^{-1})	H_2 produced (%)	$\frac{n}{n+i}$ (%)
6	53	28	19	94.8
4.8	75	40	21	95.8
4.2	58	31	18	93
3.7	40	21	2	95.5

Conditions as in Table 7.

For a given pH value, the amount of hydrogen in the gas phase was determined for the water–gas-shift reaction alone and for the hydroformylation reaction. The conversion rate of hex-1-ene into the corresponding aldehydes allowed us to calculate the quantities of hydrogen consumed in this reaction and to add them to those analysed in the gas phase. From the last column of Table 9 it appears that the production of hydrogen was four to five times as important as for the WGSR reaction itself. The results indicate that the presence of an alkene increases significantly the production of hydrogen from water. Presumably an $Rh(H)_2$ hydride species is a common intermediate of the two catalytic cycles. In our opinion the hydroformylation reaction utilizes the hydride intermediate complex generated by the water–gas-shift reaction.

Another goal of our research work is to associate two different metals by bridging or assembling ligands, avoiding the presence of a simple metal–metal bond which could easily generate mononuclear fragments during the catalysis, and to study the possible cooperative effect of one metal centre on the other for the carbonylation reactions. The coordination chemistry of M—M′ complexes has been recently reviewed by Geoffroy.[28] In a collaboration with the research group of D. Gervais we developed the synthesis of complexes in which a rhodium atom is combined with an oxophilic metal such as Ti(IV) or Zr(IV)[29] in order to have an interaction between the oxygen atom of the acyl ligand and thus induce new reactivities and/or selectivities in the hydroformylation reaction. Several complexes,[30] for example $Cp_2ZrCl(CH_2PPh_2)$, $Cp_2ZrH(CH_2PPh_2)$, $[Cp_2Zr(CH_2PPh_2)]_2O$ and $Cp_2Ti(CH_2PPh_2)_2$, were added to $Rh_2(\mu\text{-S-t-Bu})_2(CO)_4$ and tested for the hydroformylation of hex-1-ene at 80°C and 5 bar. Little or no activity was observed. However, the complex $Cp_2Zr(CH_2PPh_2)_2$ gave interesting results[31,32] since 95% of the alkene was converted in 2.5 h. As previously, the selectivity in aldehyde was complete, but the selectivity in n-heptanal was only 65%. After the reaction, the complex $Rh_2(\mu\text{-S-t-Bu})_2(CO)_2[\mu\text{-}Cp_2Zr(CH_2PPh_2)_2]$ (**8**) was observed in the solution as revealed by the IR spectra. Complex **8**, prepared by addition of one equivalent of the zirconium diphosphine to $Rh_2(\mu\text{-S-t-Bu})_2(CO)_4$, is active in catalysis, but with a slightly longer induction period than the "tetracarbonyl **4**+ZrP_2" system introduced in the autoclave.[32] Complex **8** was fully characterized by IR, ^1H, ^{31}P and ^{13}C NMR spectra and by an X-ray crystal structure. This structure (Fig. 3) shows that the two phosphorus atoms are symmetrically attached in a cisoid manner to the two rhodium atoms. The Rh_2S_2 core is folded along the S—S line and the two rhodium atoms are almost in a square planar environment. The most striking feature is the pentacoordination around the zirconium atom due to the strong interaction between Zr and the lone pair of one sulphur atom ($d = 2.995$ Å).[29]

This interaction could be responsible for the good catalytic activity shown by complex **8**, so that the modulation of the electronic density on one rhodium centre is given by the zirconium atom with its coordination sphere not only through the phosphorus atoms but also directly by way of this Zr—S interaction.

Similarly the $Rh_2(\mu\text{-S-t-Bu})_2(CO)_2(\widehat{LL})$ complexes have been prepared with $\widehat{LL}$ = 1,3-bis(diphenylphosphino)propane (complex **9**),[31] 1,4-bis(diphenylphosphino) butane (**10**),[31,32] 1,1′-bis(diphenylphosphino)ferrocene[33] (**11**) and 1,1′-bis(diphenylphosphino)ruthenocene (**12**).[33] The X-ray structures of **10** and **11** were determined in collaboration with the H. tom Dieck's laboratory in Hamburg.[34] The overall structure of these two complexes is very similar to that of **8**, except there is no interaction between the iron atom and S.

Table 9. Overall H_2 produced by the WGSR with or without hex-1-ene ($CO+H_2O$, complex **6**)

pH	Hex-1-ene	H_2 (mmol)	Conversion of hex-1-ene into aldehyde (%)	H_2 total (mmol)
6	hex-1-ene	4.8	53	25
6	0	6.3		6.3
4.8	hex-1-ene	5.3	75	35
4.8	0	7.5		7.5

Conditions as in Table 7.

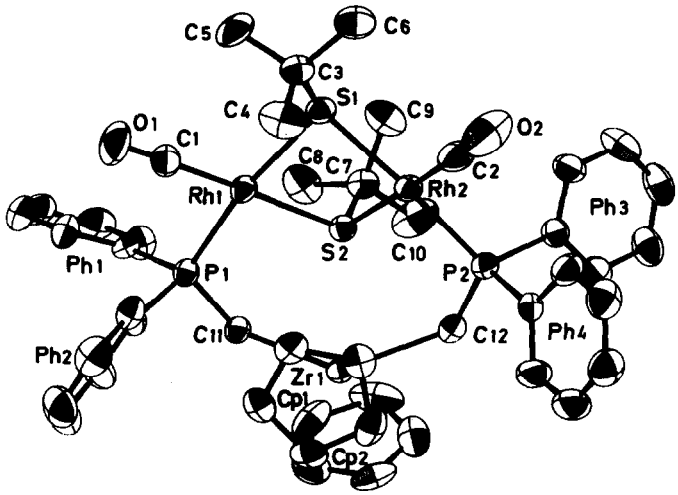

Fig. 3.

The rhodium–rhodium distances are respectively 3.039(1) in **10**, 3.089(1) in **11** and 3.391(1) Å in **8**. The X-ray structure of the ferrocenyldiphosphine complex (Fig. 4) has revealed that one Rh—P bond significantly deviates from the square plane around the rhodium atom so that the two phosphorus atoms are not symmetrical. The ^{31}P NMR spectra recorded at low temperature[34] show that the structure of **11** in solution is the same as in the solid state. Indeed at 240 K two inequivalent phosphorus doublets are detected, and split into doublets by coupling with the more distant rhodium atom (Fig. 5): 28.8 ppm, $^{1}J_{P—Rh} = 155.1$ Hz; 25.1 ppm, $^{1}J_{P'—Rh'} = 150.2$ Hz; $^{3}J_{P—Rh} = {}^{3}J_{P'—Rh} = 4$ Hz. When the temperature is raised, a coalescence occurs at around 288 K and at 312 K only one doublet persists showing that the two Rh—P situations are interchanged in the molecule by rotation of the diphosphinoferrocene ligand.[34] All these complexes or the systems **4**+diphos are active precursors for the low pressure hydroformylation of hex-1-ene. Table 10 presents the results obtained for the four complexes **9**–**12** as well as for the system **4**+1,3-bis(diphenylphosphino)propane, dppp.

The turnover frequencies are calculated after the induction period. The *in situ* reaction of $Rh_2(\mu\text{-S-t-Bu})_2(CO)_4$ (**4**) with an equimolar amount of dppp gives rise to a catalyst with almost the same performance as **11** and **12**, whereas the well-defined complex **9** is slower. Complex **10** shows an important induction period. Analysis of the results of Table 10 as well as the kinetic curves,[34] shows that the activation of dihydrogen and the transfer of one hydrogen atom from one metal centre to the alkene

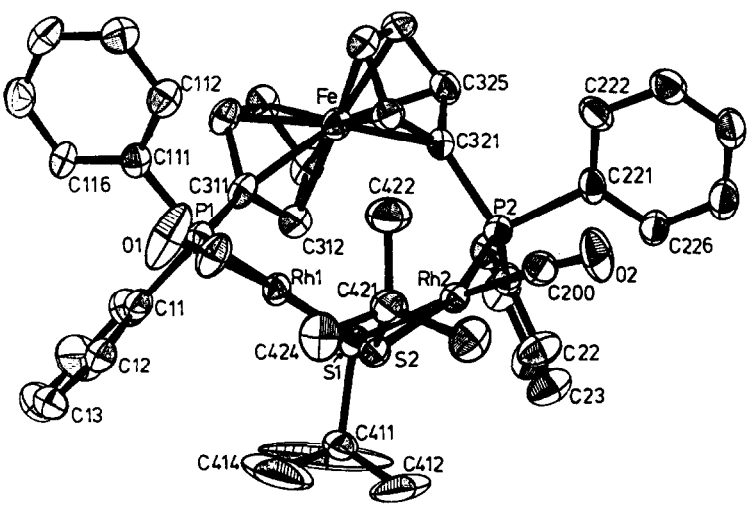

Fig. 4.

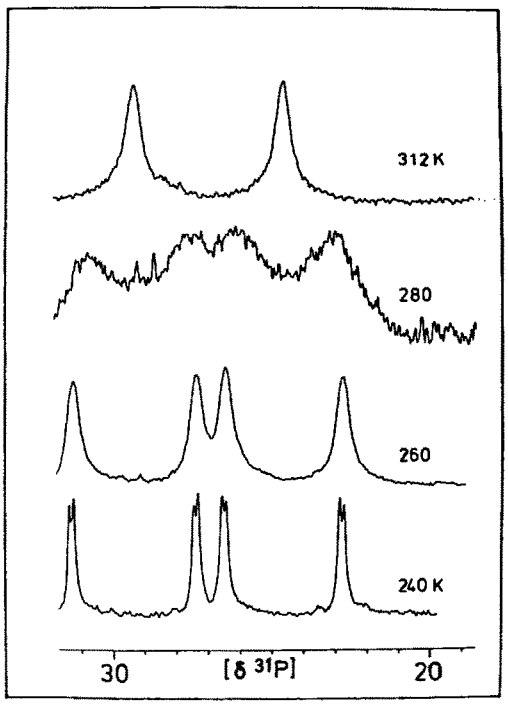

Fig. 5.

coordinated to the second rhodium centre is governed by the flexibility around the S—S axis, and is not rate determining.

Presumably, in connection with the distortion in the Rh—P coordination revealed for complex **11**, the catalytic cycle should involve a step where one, and only one, Rh—P bond is opened in order to facilitate the addition of an alkene or CO ligand. The reclosure of this Rh—P bond is necessary for the other steps of the cycle. Moreover, it is clear that steric parameters of the diphosphine ligands play an important role. In addition, the selectivity in linear aldehyde appears, except for **11**, to be lower than for the monodentate phosphine ligands.

Table 10. Catalytic activity of $Rh_2(\mu\text{-S-t-Bu})_2(CO)_2$ (diphos) complexes

Precursor	Conversion into aldehyde (%)	Time (h)	Turnover frequency (min^{-1})	n (%)
9 (dppp)	97	6	2.3[a]	64
4+dppp	98	5	7.1[b]	69
10 (dppb)	96	8	0.2[a]	70
11 (dppf)	95	5	7.7[b]	83
12 (dppr)	98	5	8.1[b]	73

Rh 2×10^{-4} g atm, hex-1-ene 40 mmol, toluene 25 cm^3. $T = 80°C$, $P = 5$ bar, $CO/H_2 = 1:1$.

[a] Calculated after 60 min.

[b] Calculated after 30 min.

This could be due to the presence of a CO ligand *trans* to the hydride ligand which is transferred to the alkene. It should be mentioned that aldehydes are still selectively obtained and that the metal-containing ligand still exerts an electronic influence on the course of the catalytic cycle followed by the rhodium centres.

We have devoted a great part of our work to use or design of heterobimetallic complexes which would be active in catalysis. Concerning the rhodium–palladium complexes we have encountered numerous problems with regard to disproportionation, inactivity, and very often precipitation of palladium black. However, with the use of L. A. Oro's laboratory we prepared three heterodinuclear complexes [Rh—Pd] which are active in hydroformylation.[35,36] The two chlorine atoms of $dppePdCl_2$ are substituted by two pyrazolate (pz) benzotriazolate (Btz) or azindolate (Az) ligands. The two nitrogen doublets are used to coordinate the rhodium atom of the cationic complex $[Rh(COD)(solvent)_2]ClO_4$. For instance with pyrazole:

$$dppePdCl_2 + 2Kpz \rightarrow dppePd(pz)_2 + 2KCl$$

$$dppePd(pz)_2 + [Rh(COD)(Me_2CO)_2]^+ \rightarrow [dppePd(\mu\text{-pz})_2Rh(COD)]^+ + 2Me_2CO.$$

Carbonylation gives the complex $[dppePd(\mu\text{-pz})_2Rh(CO)_2]ClO_4$. It is necessary to add one equivalent of triphenylphosphine to observe a catalytic activity. Table 11 presents our first results for the hydroformylation of hex-1-ene.

Some decomposition of the pz and Az complexes was observed, but for the benzotriazolate almost no precipitation of metal occurred. The catalytic level remains low (about 3 min^{-1} compared to 1 s^{-1} for **3**) and the selectivity in linear aldehyde is not very high. However, these results encourage us to investigate and extend this series of heterobinuclear complexes.

In conclusion, this study shows that the dinuclear complexes $Rh_2(\mu\text{-SR})_2(CO)_2L_2$ are very active precursors for the selective hydroformylation of

Table 11. Catalytic activity of $[dppePd(\mu\text{-X})_2Rh(CO)(PPh_3)]^+$

X	Conversion in aldehyde % (in 15 h)	Turnover frequency (min^{-1})	n (%)
pz	75	2.7	56
Btz	92	2.9	75
Az	65	1.9	69

alkenes under mild conditions. L can be phosphites and triphenylphosphine or L_2 a diphosphine ligand which can include a transition metal such as Zr, Fe or Ru. Study of the catalytic activity of all these systems has shown that a cooperative effect between the two rhodium centres takes place. The use of the water-soluble ligand $P(m\text{-}SO_3C_6H_4Na)_3$, with either CO/H_2 or CO alone, allows higher selectivities in linear aldehyde. At the same time the problem of catalyst recovery is solved by using biphasic systems.

Acknowledgements—I have the pleasure of thanking my coworkers who have contributed to one or several parts of this study and without whose competence this work would not have been possible: J. M. Frances, P. M. Pfister, T. G. Southern, A. Thorez, P. Escaffre, C. Claver, M. Ridmy, F. Senocq, C. Randrianalimanana, F. Serein-Spirau. I thank also my colleagues for very fruitful collaborations: A. Dedieu (Strasbourg), Prof. D. Gervais and R. Choukroun (Toulouse), Prof. L. A. Oro (Saragossa, Spain) and Prof. H. tom Dieck (Hamburg, F.R.G.). Thanks for financial support are due to the "Délégation générale à la Recherche Scientifique et Technique", the CNRS (GRECO "Oxydes de Carbone"), Atochem, Rhône-Poulenc Recherches and Rhône-Poulenc Chimie de Base. I am indebted to the "Comptoir Lyon-Alemand-Louyot" for a generous gift of rhodium salt.

REFERENCES

1. B. Cornils, in *New Syntheses with Carbon Monoxide* (Edited by J. Falbe), pp. 1–181. Springer, Berlin; Heidelberg, New York (1980).
2. J. A. Osborn, G. Wilkinson and J. F. Young, *J. Chem. Soc., Chem. Commun.* 1965, 17.
3. Johnson Matthey and Co. Ltd (to G. Wilkinson) DE-OS 1 518 236 (1965), DE-OS 2 136 470 (1970/1972), DE-OS 2 034 909 (1971), DE-OS 2 064 471 (1971), DE-OS 2 047 748 (1971), DE-OS 2 055 539 (1971), GB 1 357 735 (1974).
4. (a) F. H. Jardine, *Polyhedron* 1983, **1**, 569; (b) L. Marko, in *Aspects of Homogeneous Catalysis* (Edited by R. Ugo), Vol. 2, pp. 4–10. D. Reidel, Dordrecht (1974).
5. I. Tkatchenko, in *Comprehensive Organometallic Chemistry* (Edited by G. Wilkinson, F. G. A. Stone and E. W. Abel), Vol. 8, pp. 115–157. Pergamon Press, Oxford (1982).
6. J. M. Frances, A. Thorez and Ph. Kalck, *Nouv. J. Chim.* 1984, **8**, 213.
7. J. D. Jamerson, R. L. Pruett, E. Billig and F. A. Fiato, *J. Organomet. Chem.* 1980, **193**, C43.
8. A. R. Sanger, in *Homogeneous Catalysis with Metal-phosphine Complexes* (Edited by L. H. Pignolet), p. 228. Plenum Press, New York (1983).
9. Ph. Kalck, J. M. Frances, P. M. Pfister, T. G. Southern and A. Thorez, *J. Chem. Soc., Chem. Commun.* 1983, 510.
10. A. Dedieu, P. Escaffre, J. M. Frances, Ph. Kalck and A. Thorez, *Nouv. J. Chim.* 1986, **10**, 631.
11. P. Escaffre, A. Thorez, Ph. Kalck, B. Besson, R. Perron and Y. Colleuille, *J. Organomet. Chem.* 1986, **302**, C17.
12. A. Dedieu, personal communication.
13. P. Escaffre, Thèse de Docteur de l'Institut National Polytechnique, Toulouse (1986).
14. C. Claver, Ph. Kalck, M. Ridmy, A. Thorez, L. A. Oro, M. T. Pinillos, M. C. Apreda, F. H. Cano and C. Foces-Foces, *J. Chem. Soc., Dalton Trans.*, in press.
15. C. U. Pittman Jr. and A. Hirao, *J. Org. Chem.* 1978, **43**, 640.
16. M. O. Farrell, C. H. Van Dyke, L. J. Boucher and S. Metlin, *J. Organomet. Chem.* 1979, **169**, 199.
17. L. G. Rollman, *Inorg. Chim. Acta* 1972, **6**, 137.
18. Ph. Kalck, R. Poilblanc, A. Gaset, A. Rovera and R. P. Martin, *Tetrahedron Lett.* 1980, **21**, 459.
19. S. Arhland, J. Chatt, N. R. Davies and A. A. Williams, *J. Chem. Soc.* 1958, 276.
20. Rhône-Poulenc Chimie de Base (to E. G. Kuntz) Fr 75 19407 (29.06.1975).
21. Rhône-Poulenc Chimie de Base (to E. G. Kuntz) Fr 76 12672 (29.04.1976).
22. Rhône-Poulenc Industries (to J. Jenck) Fr 80 05488 (12.03.1980).
23. A. F. Borowski, D. J. Cole-Hamilton and G. Wilkinson, *Nouv. J. Chim.* 1978, **2**, 137.
24. Rhône-Poulenc Chimie de Base (to B. Besson, Ph. Kalck and A. Thorez) EP 85420169-6 (16.10.1984).
25. P. Escaffre, A. Thorez and Ph. Kalck, *J. Molec. Catal.* 1985, **33**, 87.
26. J. Kaspar, R. Spogliarich, G. Mestroni and M. Graziani, *J. Organomet. Chem.* 1981, **208**, C15.
27. P. Escaffre, A. Thorez and Ph. Kalck, *New J. Chem.* 1987, **11**, 601.
28. D. A. Roberts and G. L. Geoffroy, in *Comprehensive Organometallic Chemistry* (Edited by G. Wilkinson, F. G. A. Stone and E. W. Abel), Vol. 6, pp. 763–877. Pergamon Press, Oxford (1982).
29. R. Choukroun, D. Gervais, J. Jaud, Ph. Kalck and F. Senocq, *Organometallics* 1986, **5**, 67 and references quoted therein.
30. F. Senocq, Thèse de Docteur de l'Institut National Polytechnique, Toulouse (1985).
31. F. Senocq, C. Randrianalimanana, A. Thorez, Ph. Kalck, R. Choukroun and D. Gervais, *J. Chem. Soc., Chem. Commun.* 1984, 1376.
32. F. Senocq, C. Randrianalimanana, A. Thorez, Ph. Kalck, R. Choukroun and D. Gervais, *J. Molec. Catal.* 1986, **35**, 213.
33. Ph. Kalck, M. Ridmy and A. Thorez, *C.R. Acad. Sci. Paris, Series II* 1987, **305**, 953.
34. Ph. Kalck, C. Randrianalimanana, M. Ridmy, A. Thorez, H. tom Dieck and J. Ehlers, *Neur. J. Chem.*, in press.
35. M. Ridmy, Thèse de Docteur de l'Institut National Polytechnique, Toulouse (1987).
36. Ph. Kalck, L. A. Oro, M. T. Pinillos, M. Ridmy and A. Thorez, unpublished results.

Polyhedron Vol. 7, No. 22/23, pp. 2451–2463, 1988
Printed in Great Britain

0277-5387/88 $3.00+.00
© 1988 Pergamon Press plc

BIMETALLIC TRANSITION METAL CARBENE COMPLEXES—SOME NOVEL ASPECTS AND DEVELOPMENTS

GERHARD ERKER

Institut für Organische Chemie der Universität Würzburg, Am Hubland, D-8700 Würzburg, F.R.G.

Abstract—Readily available (butadiene)zirconocene and -hafnocene complexes react with various metal carbonyls to form metallacyclic metal oxycarbene complexes. The π-allyl species $Cp_2\overline{MOC[=M'L_n]}(\overline{C_4H_6})$ (M = Zr, Hf) can often be obtained crystalline. The bimetallic carbene complexes exhibit a rather short O—C(carbene) bond distance indicating a pronounced metal acyl complex character. Carbene complex formation between (s-*trans*-η^4-butadiene)zirconocene and $CpCo(CO)_2$ or $CpV(CO)_4$, respectively is reversible. The equilibrium can be shifted towards the carbene complex side by reducing the electron density at the carbene ligand bearing metal or by using the hafnium instead of the zirconium containing butadiene metallocene reagent. Five-membered benzannelated zirconium oxycarbene complexes $Cp_2\overline{ZrOC[=W(CO)_5]}(\overline{C_6H_4})$ were obtained by CC-coupling from thermally generated (1,2-didehydrobenzene)zirconocene and $W(CO)_6$. This carbene complex is an oligomer in the solid state as revealed by X-ray diffraction. Monomeric units are linked together via intermolecular Zr—O≡C—W bonds. This zirconium oxycarbene complex acts as an organometallic Lewis acid in solution. It reversibly coordinates organic carbonyl compounds. Zirconium oxycarbene complexes $Cp_2Zr(OR)$—$OC(Ph)$=$W(CO)_5$ react readily with several non-stabilized phosphorus ylides to produce zirconium enolates $Cp_2Zr(OR)$—$OC(Ph)$=CHR which can be used as carbon nucleophiles in *syn*-selective aldol condensation reactions. The (butadiene)zirconocene derived metallacyclic zirconium oxycarbene complexes $Cp_2\overline{ZrOC[=M(CO)_5]}(\overline{C_4H_6})$ (M = Cr, Mo, W) act as carbon nucleophiles at the Zr-bound substituted π-allyl ligand. Ketones or aldehydes are CC-coupled regioselectively to the allyl-CH_2 terminus to form chiral nine-membered metallacyclic products.

Transition metal carbene complexes make up an increasingly important class of organometallic compounds. The M=CXY functionality seems to play a key role in many catalytic processes.[1] Metal carbene complexes are applied more and more as stoichiometric reagents in organic synthesis.[2]

The majority of heteroatom stabilized carbene complexes are probably prepared by variations of E. O. Fischer's original synthetic route,[3,4] i.e. from a metal carbonyl by adding a nucleophile to the carbon, then an electrophile to the oxygen atom of the M—C≡O-unit (1). There have been several very successful attempts to overcome the few limitations of the Fischer procedure. For example, Lappert has introduced non-nucleophilic carbene complex syntheses having a broad scope, using very electron rich alkenes $(R_2N)_2C$=$C(NR_2)_2$[5] or Vilsmeyer salts[6] $[R_2N(CHCl)]^+Cl^-$ as heteroatom stabilized carbene ligand sources.

It can be advantageous using metal complexes of the oxophilic group 4 transition metals as reagents for the metal carbonyl → metal carbene complex transformation. Forming the strong early transition metal to oxygen bond[7] favourably assists the carbene complex formation. In addition, the bonding features of the M=C(R)—O-unit are markedly affected by attaching a metal substituent with pronounced σ-donor/π-acceptor properties to the carbene oxygen atom. This seems to induce a more pronounced acyl metallate character [$^-$M—C(R)=O^+—] to the carbene complex.

Bercaw has used the $Cp^*_2ZrH_2$ reagent for preparing metal oxycarbene complexes L_nM=C(H)—OZr(H)Cp^*_2 from metal carbonyls L_nM—CO.[8]

This seems principally to be another example of a "nucleophilic" carbene complex synthesis as the carbonyl carbon atom of the educt is attacked by nucleophilic hydride at some time during the reaction. However, here the sequence of nucleophilic and electrophilic reaction steps appears to be reversed as compared to E. O. Fischer's original method[3] for the metal carbonyl → metal carbene complex conversion. This might explain the extended scope of the carbene complex synthesis using the early transition metal hydride reagent [see eq. (2)].

We have recently found a new carbene complex synthesis which may turn out to be a truly "non-nucleophilic" procedure.[9] Very reactive (olefin) metallocene complexes of titanium, zirconium or hafnium are reacted with metal carbonyls to give metallacyclic metal oxycarbene complexes. Formally, this reaction is very similar to the Fischer procedure. However, the reaction path followed here is probably quite different from the usual "nucleophilic" synthesis. The addition of the coordinatively unsaturated reagent is assumed to give a binuclear (η^2-alkene)(μ-CO)-type intermediate, which subsequently forms a carbon–carbon bond between the π-ligand of the reagent and the carbonyl group via a (possibly concerted electrocyclic[10]) ring closure reaction (3).

bound metallocene moiety may create interesting novel chemical features.

SYNTHESES OF METAL OXYCARBENE COMPLEXES

Reactive metal olefin π-complexes are needed as starting materials for the synthesis of heteroatom stabilized carbene complexes according to eq. (3). (Butadiene)zirconocene and -hafnocene have turned out to be very well suited reagents.[11] They are readily available from the reaction of the respective metallocene dihalides with butadiene magnesium.[12] At ambient temperature (butadiene)zirconocene exists as a stable mixture of two geometric isomers which to a first approximation can be described as (η^4-s-*trans*-)- and (η^4-s-*cis*-butadiene)$ZrCp_2$. At equilibrium a *ca* 1 : 1 mixture of these is present. Their mutual interconversion occurs with a moderate rate at ambient temperature ($\Delta G^{\ddagger}(10.5°C) = 22.7$ kcal mol^{-1}). The thermally induced isomerization of the isolable (η^4-C_4H_6)$ZrCp_2$ species probably occurs through a reactive (η^2-butadiene)zirconocene complex.[13] The 18-electron (η^4-s-*trans*-diene)metallocene complex often reacts through the coordinatively unsaturated (η^2-diene)MCp_2 species with which it rapidly equi-

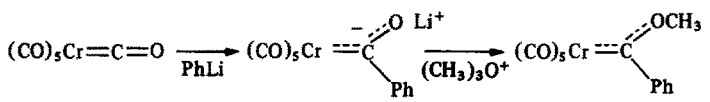

(1)

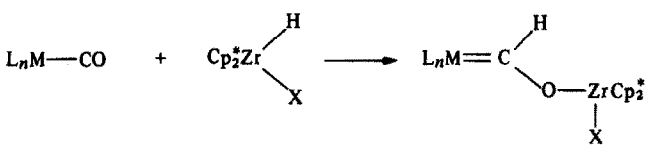

(2)

M = Zr; Nb; Cr; Mo; W; Co; Rh.

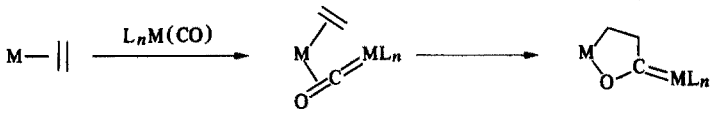

(3)

In this article the formation of several new examples of metal oxycarbene complexes using this method will be discussed. This will be followed by a brief description of several reactions which metallacyclic zirconium oxycarbene complexes undergo. Some of these show that in this combination an interaction of the carbene complex with the O-

librates. The latter is separated by a much higher activation barrier from the (η^4-s-*cis*-diene)metallocene isomer. This complex exhibits a pronounced metal alkyl character. The terminal diene carbon centres possess nucleophilic properties. This complex is best described as a σ,π-type metallacycle.[11,14]

The (butadiene)zirconocene reagent reacts with chromium, molybdenum, or tungsten hexacarbonyl slowly at room temperature.[9] Formation of a new carbon–carbon bond between a CH_2-group of the diene ligand and a carbonyl carbon atom takes place. The reaction of the (butadiene)metallocene reagent with the metal carbonyl is slower than the (s-*cis*- → s-*trans*-diene)$ZrCp_2$ isomerization.[13] Therefore, an ordinary nucleophilic pathway is hard to distinguish from a reaction via the reactive (η^2-butadiene)zirconocene intermediate. In addition, the five-membered metallacyclic bimetallic σ-allyl zirconium oxycarbene complexes are not stable under the reaction conditions (if formed at all). We have isolated the metallacyclic π-allyl metal oxycarbene complexes instead in high yields (see Scheme 1).

The X-ray crystal structure analyses[9,15] have revealed rather unsymmetrically bonded substituted π-allyl ligands at zirconium. For all three bimetallic carbene complexes (Zr, Cr; Zr, Mo; Zr, W) the Zr—C(6) distance is longer than the Zr—C(7) or Zr—C(8) bonds. The incorporation of the carbene-oxygen into the rigid metallacyclic ring system leads to somewhat different bonding parameters as compared to the corresponding acyclic Fischer-type carbene complexes bearing ordinary alkoxy substituents.[4] Most noteworthy is the substantially shorter C(4)—O(4) bond distance of the zirconium oxycarbene complexes. This structural feature indicates a more pronounced acyl metallate character of the $Cp_2\overline{ZrOC[=M(CO)_5]}(C_4H_6)$ complexes. A considerable contribution of the corresponding resonance form B seems to be important for describing the structural properties of the binuclear metallacyclic carbene complexes (see Scheme 2).

The same type of product is obtained by reacting (butadiene)zirconocene with $Fe(CO)_5$. However, here the kinetic situation is slightly different. The formation of the π-allyl zirconium oxycarbene iron complex occurs faster than the (butadiene)$ZrCp_2$ s-*cis*- ⇄ s-*trans*-isomerization. This allows for a mechanistic characterization of the preferred reaction path taken. It is only the (s-*trans*-η^4-butadiene)zirconocene isomer that reacts with the $Fe(CO)_5$ under kinetic control. The more nucleophilic (s-*cis*-η^4-C_4H_6)$ZrCp_2$ complex has turned out to be unreactive towards this metal carbonyl in a direct competition experiment at low temperature. This seems to indicate that a reaction path for the M—CO → M—carbene conversion very different from the usual "nucleophilic" route[3,4,8] is operative here, possibly proceeding through (η^2-butadiene)zirconocene as a reactive intermediate. Similar observations were made for the conversion of the phosphine iron carbonyl complex $Fe(CO)_4PPh_3$ to *trans*-$Cp_2\overline{ZrOC[=Fe(CO)_3PPh_3]}(C_4H_6)$[16] (Scheme 3).

Only a few cobalt carbene complexes have been prepared via the original Fischer route so far.[17] For the conversion of CO-ligands into carbene groups at the (η-cyclopentadienyl)cobalt fragment alternative methods have been applied.[18] The Cp_2Zr(butadiene) reagent very cleanly converts one carbonyl ligand of $CpCo(CO)_2$ to the heteroatom containing the carbene moiety at ambient temperature. The metallacyclic π-allyl zirconium oxycarbene complex $Cp_2\overline{ZrOC[=Co(CO)Cp]}(C_4H_6)$ is obtained as a crystalline product.[19]

However, there is a complication associated with this system. When the crystalline cobalt carbene complex is dissolved, rapid equilibration with the starting materials Cp_2Zr(butadiene) and $CpCo(CO)_2$ is observed by NMR spectroscopy. Initially, only the formation of the (s-*trans*-η^4-butadiene)zirconocene isomer is monitored. Subsequently this rearranges to (s-*cis*-η^4-C_4H_6)$ZrCp_2$

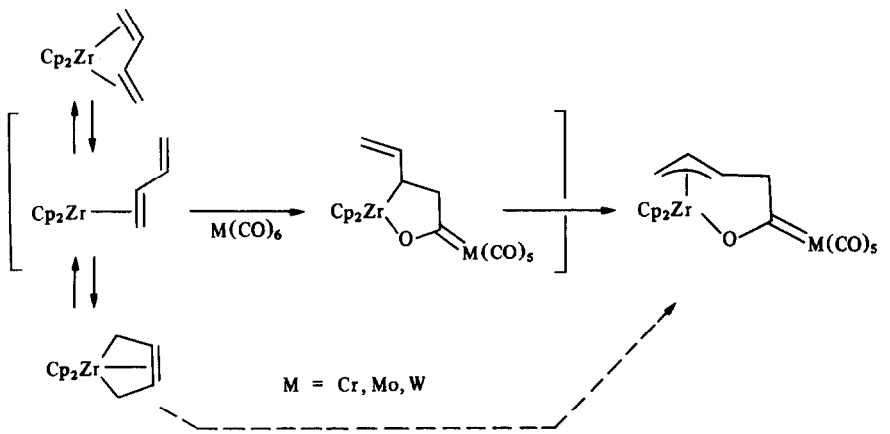

Scheme 1.

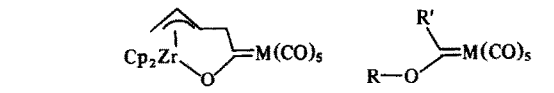

M:	Cr	W	Cr	W
C4—M	2.063(4)	2.198(10)	2.053(1)	2.23(2)
C4—O4	1.254(5)	1.262(11)	1.314(1)	1.35(2)
C4—C5	1.562(8)	1.528(13)	1.511(1)	1.43(3)
M—C3	1.879(5)	2.024(11)		
M—C1	1.887(3)	2.023(7)		
Zr—O4	2.188(3)	2.179(5) Å		

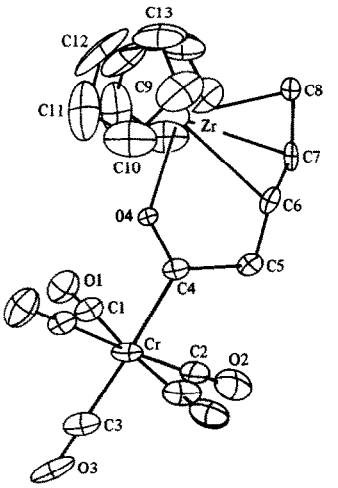

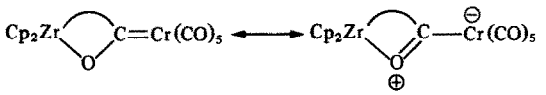

A B

Scheme 2.

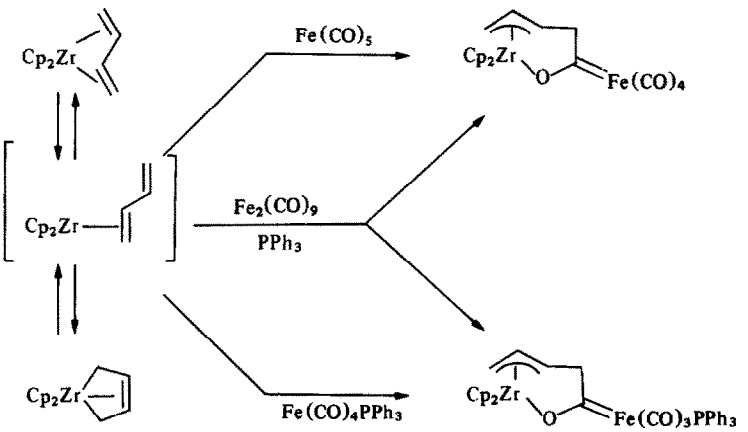

Scheme 3.

(with the known reaction rate) until the 45 : 55 equilibrium of (butadiene)metallocene isomers is reached. Starting from the pure carbene complex $Cp_2ZrOC[=Co(CO)Cp](C_4H_6)$ an equilibrium mixture is obtained in toluene solution at 25°C containing about 85% of the bimetallic complex and 15% of each of its monometallic components. The equilibrium can be shifted to the carbene complex side by attaching electron withdrawing substituents at the cobalt bound Cp-ligand. The zirconium oxycarbene ligand appears to be a stronger σ-donor/weaker π-acceptor than the carbonyl group. Therefore, the carbene complex is less affected by reducing the electron density at cobalt than the metal carbonyl. Consequently, the $(Cp—Cl)Co(CO)_2 + (C_4H_6)ZrCp_2 \rightarrow Cp_2ZrOC[=Co(CO)(CpCl)](C_4H_6)$ equilibrium is shifted to the product side by this substituent effect. For the (Cp—Cl) containing system no starting material has been observed by NMR to be formed when the carbene complex was dissolved in an aromatic hydrocarbon at room temperature[20] (Scheme 4).

Clean formation of the π-allyl zirconium oxycarbene complex takes place when (butadiene)zirconocene is reacted with $CpRh(CO)_2$. In contrast to the analogous (cyclopentadienyl) cobalt complex, there is no sign of equilibration with its monometallic components when $Cp_2ZrOC[=Rh(CO)Cp](C_4H_6)$ is dissolved.

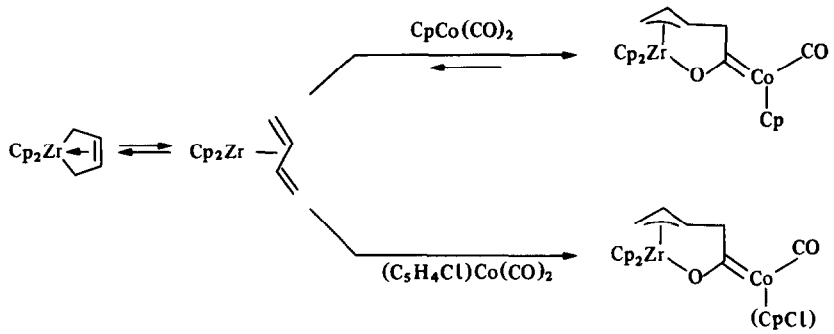

Scheme 4.

The X-ray crystal structure analysis of the zirconium oxycarbene complexes derived from $(ClCp)Co(CO)_2$, $CpCo(CO)_2$ and $CpRh(CO)_2$ all reveal a coplanar arrangement of substituents at the metal carbene moiety. The Rh—C(carbene) bond distance in $Cp_2\overline{ZrOC[=Rh(CO)Cp]}(C_4H_6)$ is 1.925(3) Å. Only one of the two geometrical isomers possible for this structural type has been observed. It is characterized by exhibiting the CO-ligand at rhodium and the carbene oxygen at C(5) in a *Z*-orientation. NMR spectroscopy also shows that there is only one isomer present in solution. Presumably it is the same that has been found in the solid state by X-ray diffraction. Figure 1 shows the molecular structure of $Cp_2\overline{ZrOC[=Rh(CO)Cp]}(C_4H_6)$ as a typical example (the zirconium bound allyl group here shows a disorder often encountered in these complexes).[21]

There have only been very few reports on the preparation of carbene complexes of the elements vanadium[21] or niobium.[22,23] Our new method can be used to prepare such complexes from metal carbonyls of these elements. The complex $CpV(CO)_4$ reacts readily with (s-*trans*-η^4-butadiene)zirconocene to cleanly convert one of the four carbonyl ligands into a zirconium oxycarbene moiety. Crystalline $Cp_2\overline{ZrOC[=V(CO)_3Cp]}(C_4H_6)$ was obtained in good yield[24] (Scheme 5).

This complex appears to be the first example of a vanadium carbene complex that has been characterized by X-ray diffraction. A view of the molecular structure of this π-allyl zirconium oxycarbene complex of vanadium is shown in Fig. 2. In this complex, the V—C(carbene) distance (2.102(3) Å) is substantially longer than the V—C(CO) linkages. Again, the O—C(carbene) bond (1.270(4) Å) is rather short.

In solution $Cp_2\overline{ZrOC[=V(CO)_3Cp]}(C_4H_6)$ rapidly equilibrates with $CpV(CO)_4$ and (s-*trans*-η^4-C_4H_6)$ZrCp_2$. In contrast to the CpCo carbene complex, which also showed such behaviour, the equilibrium here is shifted much further to the side of the starting materials. At 25°C about half of the vanadium carbene complex is decomposed to give (butadiene)zirconocene and $CpV(CO)_4$ at equilibrium. However, this unfavourable situation can

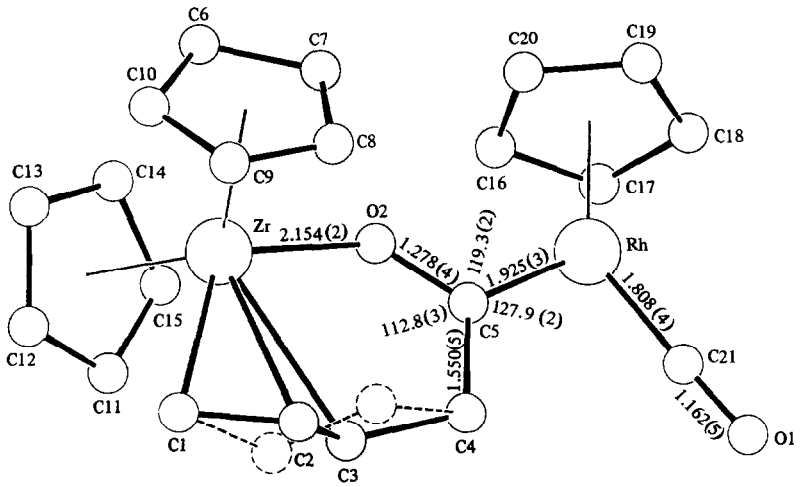

Fig. 1. X-ray crystal structure analysis of $Cp_2\overline{ZrOC[=Rh(CO)Cp]}(C_4H_6)$: molecular geometry with selected bond distances and angles.

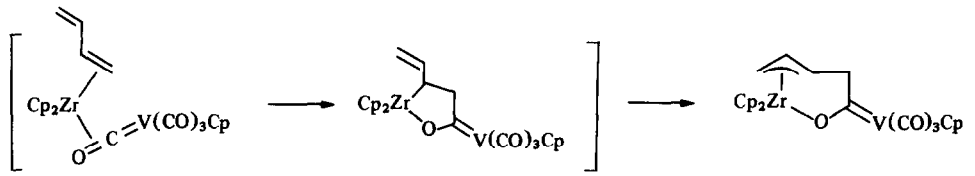

Scheme 5.

readily be changed by employing (s-*trans*-η^4-butadiene)hafnocene as the M—CO converting reagent instead of the zirconium compound. Carbene complex formation takes place rapidly between $CpV(CO)_4$ and Cp_2Hf(butadiene). In solution the equilibrium lies far on the side of the $Cp_2\overline{HfOC[=V(CO)_3Cp](C_4H_6)}$ product. Starting from the pure π-allyl hafnium oxycarbene vanadium complex a slow subsequent rearrangement is observed to occur at room temperature to give the corresponding seven-membered metallacyclic σ-allyl hafnocene isomer. Eventually, a *ca* 1:1 mixture of these two isomeric forms of the bimetallic carbene complex is obtained at 25°C in solution.[24]

Similarly, π-allyl $Cp_2\overline{HfOC[=Nb(CO)_3Cp](C_4H_6)}$ in solution does not notably equilibrate with its monometallic components $Cp_2Hf(C_4H_6)$ and $CpNb(CO)_4$ but with the seven-membered metallacyclic σ-allyl form of the bimetallic carbene complex[25] (Scheme 6).

This method of forming metal oxycarbene complexes is not restricted to using (butadiene)group 4 metallocene complexes as reagents. Several other (diene)- and (olefine)metal complexes have been used as well. Group 6 metal hexacarbonyls have been converted to carbene complexes using (butadiene)$ThCp_2^*$[26] or (ethylene)$TiCp_2^*$. The latter reagent has also been used to prepare carbene complexes from $Mn_2(CO)_{10}$ and $Re_2(CO)_{10}$.[27]

We have used bis(cyclopentadienyl)zirconium and titanium(aryne) complexes as very reactive reagents for the carbene complex synthesis. The $Cp_2M(C_6H_4)$ species can conveniently be generated at *ca* 80°C from the diphenyl metallocene complexes.[28] The (benzyne)zirconocene complex reacts with *cis*- or *trans*-stilbene, respectively, to form the diphenylzirconaindans stereospecifically.[29] The aryne complex is reactive enough to undergo C—H activation reactions with aromatic hydrocarbons[28] or ylides.[30] Recently, $Cp_2Zr(C_6H_4)$ was trapped with PMe_3 to give a stable metallocene aryne complex[31] (Scheme 7).

Thermally generated (η^2-1,2-didehydrobenzene)zirconocene reacts readily with $W(CO)_6$ to form the five-membered metallacyclic benzannelated zirconium oxycarbene complex $Cp_2\overline{ZrOC[=W(CO)_5](C_6H_4)}$. It was shown by a typical labelling experiment, that the (aryne) metallocene intermediate was directly involved in the reaction. Thermolysis of bis(*p*-tolyl)zirconocene (generating the aryne complex intermediate with the methyl label in the 4-position) in the presence of $W(CO)_6$ yielded a mixture of the

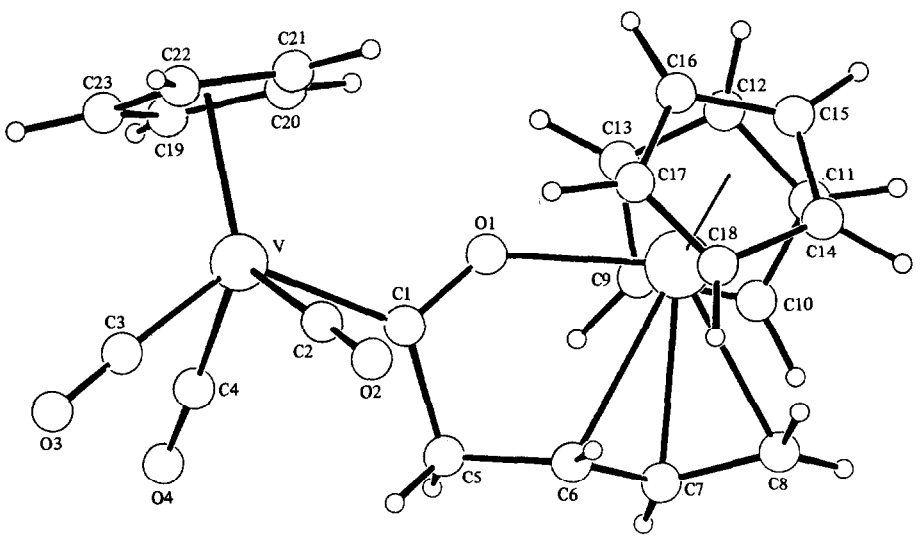

Fig. 2. A view of the molecular structure of $Cp_2\overline{ZrOC[=V(CO)_3Cp](C_4H_6)}$ in the crystal.

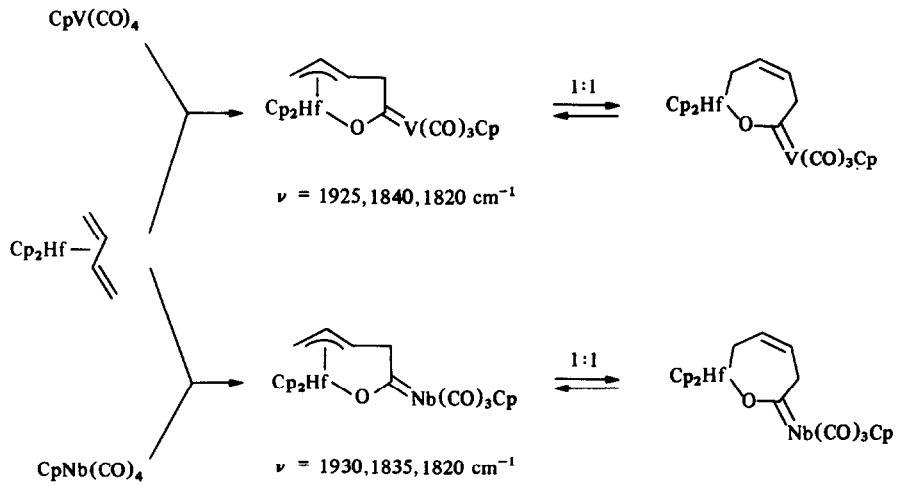

Scheme 6.

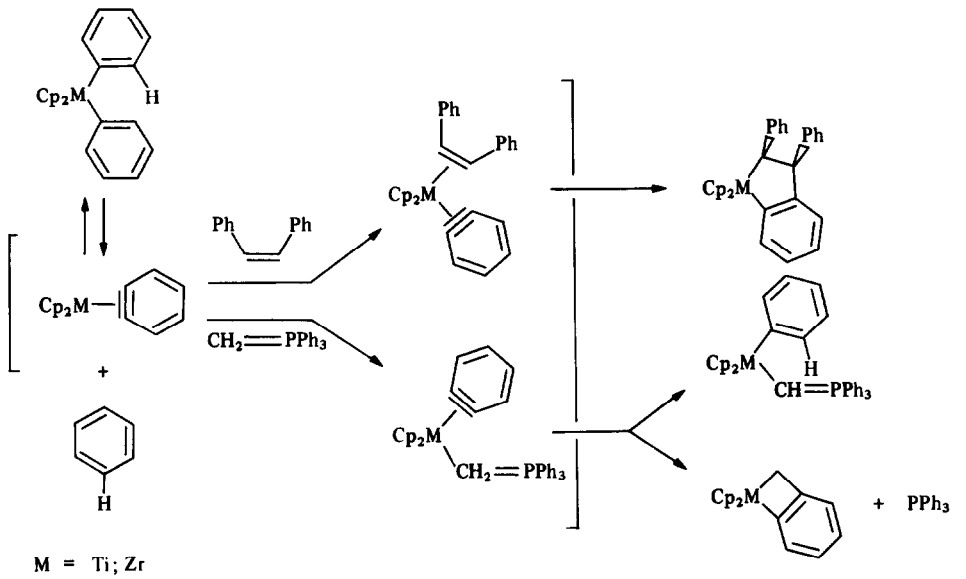

Scheme 7.

expected differently labelled zirconium oxycarbene complexes[32] (Scheme 8).

The X-ray structure attributes a pronounced acyl metallate complex character to $Cp_2\overline{ZrOC[=W(CO)_5]}(C_6H_4)$ In this respect this complex is very similar to the metal oxycarbene complexes prepared from the (butadiene) metallocene reagents. However, the solid state structure of the aryne-derived carbene complex is in a way unique among the many structurally characterized metal oxycarbene complexes. In the crystal, monomeric $Cp_2\overline{ZrOC[=W(CO)_5]}(C_6H_4)$ units are linked together to form oligomeric chains of a helical arrangement (Fig. 3). The "intermolecular" interaction occurs through binding of a W—C≡O oxygen (oriented *trans* to the carbene ligand at tungsten) to the zirconium centre of an adjacent molecule. This analogously coordinates to the next molecular unit by forming the O(26)—Zr(1) bond. Thus formed helical molecular chains made up of monomeric $Cp_2\overline{ZrOC[=W(CO)_5]}(C_6H_4)$ molecular subunits are separated from one another by solvent molecules incorporated into the crystal.[33]

SOME REACTIONS OF THE ZIRCONIUM OXYCARBENE COMPLEXES

The unusual adduct formation, in the solid state, of $Cp_2\overline{ZrOC[=W(CO)_5]}(C_6H_4)$ indicates a pronounced electrophilic character of the zirconium

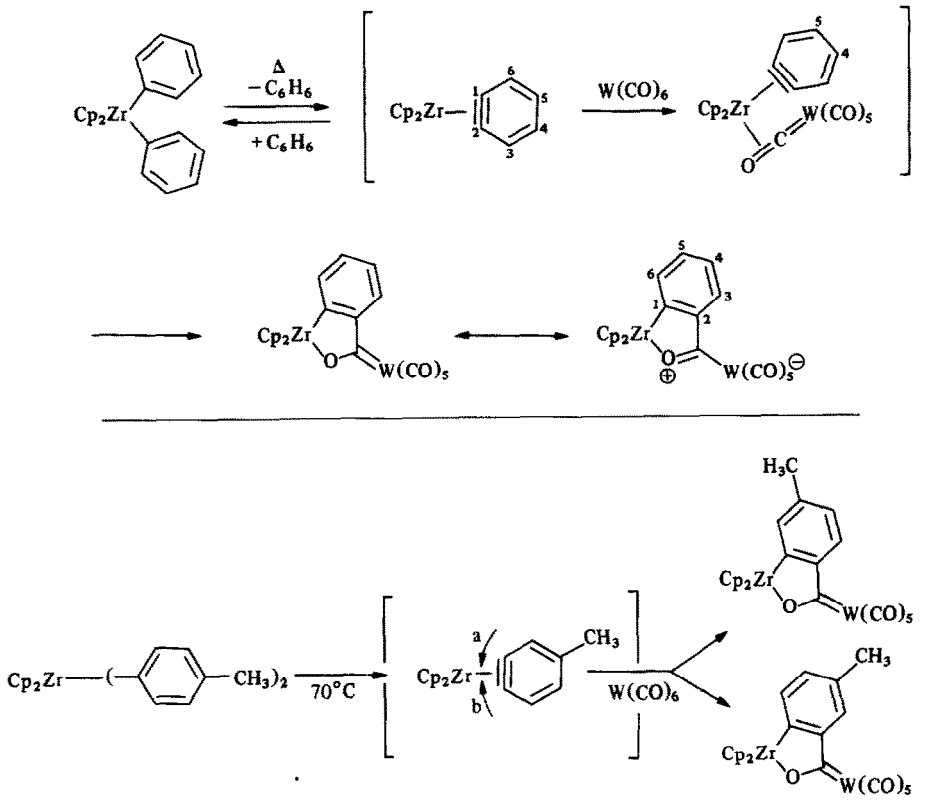

Scheme 8.

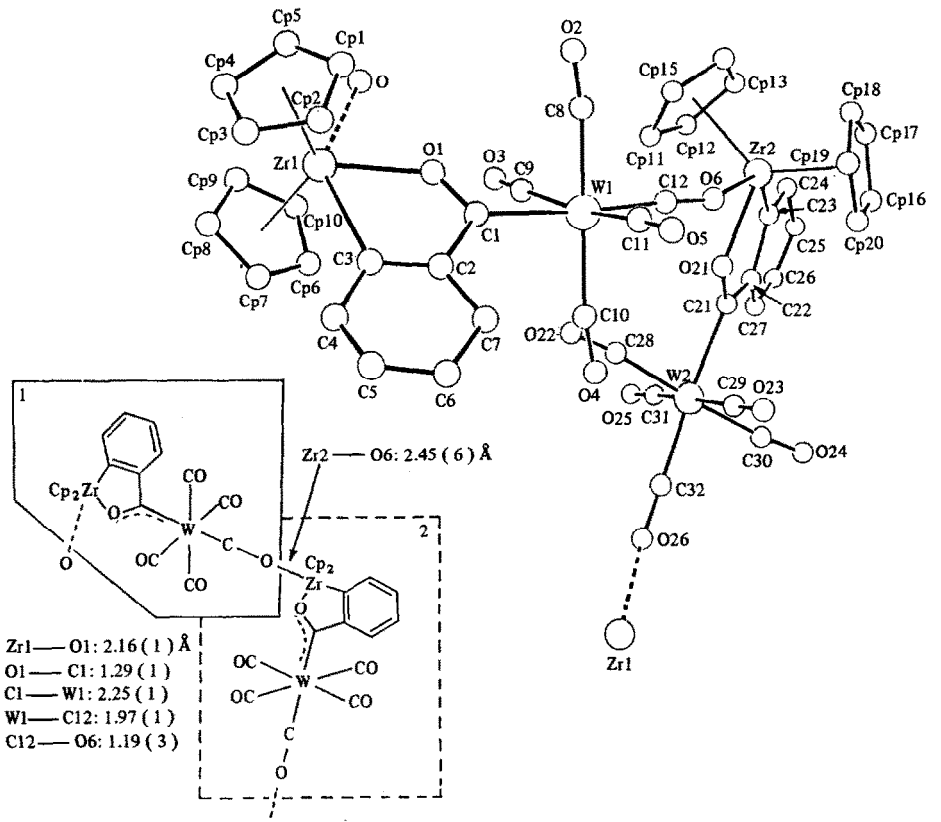

Fig. 3. Asymmetric unit of the $[Cp_2\overline{ZrOC\{=W(CO)_5\}(C_6H_4)}]_x$ complex in the crystal.

centre of 16-electron configuration in this carbene complex. In solution this complex seems to be monomeric. Nevertheless, the zirconium centre in this carbene complex is sufficiently Lewis acidic to allow coordination and activation of organic donor substrates. Not unexpectedly, amines have been shown by NMR to interact (reversibly) with the group 4 transition metal in $Cp_2ZrOC[=W(CO)_5](C_6H_4)$.[25] Moreover, the zirconium oxycarbene complex also adds organic carbonyl compounds. With acetophenone rapidly reversible adduct formation is observed by NMR spectroscopy in solution. IR spectroscopy as well as competition experiments reveal that the metallacyclic carbene complex functions as a weak organometallic Lewis acid.[33] Activation of organic carbonyl compounds by such organometallic Lewis acids suited to carry additional structural and stereochemical information could lead to interesting developments in organic synthesis (Scheme 9).

Reactions at the carbene carbon atom can be of special interest when employed with zirconium oxycarbene complexes. Casey has shown that some Fischer-type carbene complexes react with non-stabilized phosphorus ylides to give enol ethers.[34] Thus, $RHC{=}C(Ph)OCH_3$ was obtained from $(CO)_5W{=}C(Ph)OCH_3$ and $Ph_3P{=}CHR$. The analogous reaction, if carried out starting from a zirconium oxycarbene complex, would have a different quality. There are many indications that ordinary Fischer-type carbene complexes behave as the organometallic analogues of esters, the [M] = C(carbene) unit functioning as an equivalent of the organic carbonyl group functionality. A zirconium oxycarbene complex could then be viewed as an organometallic analogue of a carboxylate, here a zirconium derivative of the carboxylic acid anion.

Applying this analogy to Casey's above cited reaction type, the reaction of a phosphorus ylide with a zirconium oxycarbene complex to give a zirconium enolate would formally be a synthetic equivalent of a carboxylate to enolate anion transformation, a reaction which, of course, cannot be achieved directly by Wittig olefination because of the lacking carbonyl activity of carboxylate salts.

The anticipated reaction sequence can in fact be carried out starting from the aryne-derived carbene complex $Cp_2ZrOC[=W(CO)_5](C_6H_4)$.[35] For practical purposes, the very moisture-sensitive five-membered metallacycle was opened up first by treatment with one equivalent of an alcohol. Reaction of the acyclic zirconium oxycarbene complex with methylene triphenylphosphorane occurred readily at room temperature to give a good yield of the $Cp_2Zr(OR)$–acetophenone enolate. As an efficient carbon nucleophile this was subsequently reacted with benzaldehyde to give the CC-coupled aldol product (Scheme 10).

Some initial studies have been carried out to characterize the reactivity and selectivity of the metal carbene complex → metal enolate transformation. A competition experiment has revealed that $Cp_2Zr(OPh)OC(Ph){=}W(CO)_5$ is slightly less reactive than $(CO)_5W{=}C(Ph)OC_2H_5$ towards $Ph_3P{=}CH_2$. The zirconium oxycarbene complex is much more selective, however. While $(CO)_5W{=}C(Ph)OC_2H_5$ reacts with a 1 : 1 mixture of $Ph_3P{=}CH_2$ and $Ph_3P{=}CHCH_3$ nearly statistically, the $(CO)_5W{=}C(Ph)O[Zr]$ complex reacts by far preferentially with the less substituted phosphorus ylide. The zirconium oxycarbene complex does react with $Ph_3P{=}CH{-}CH_3$ alone to give an 80 : 20 mixture of the $CH_3CH{=}C(Ph){-}O[Zr]$ enolate isomers. In contrast, $(CO)_5W{=}C(Ph)OC_2H_5$ in our hands was completely unselective, yielding a *ca*

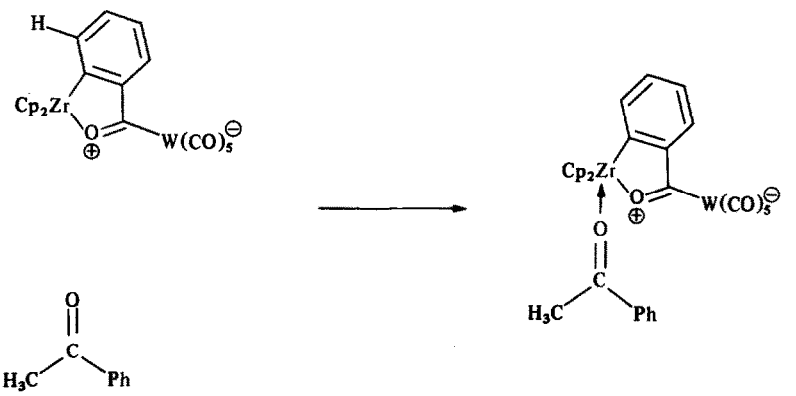

$\nu(C{=}O)$ = 1684 cm^{-1} [CD_2Cl_2]; 1647 cm^{-1}

Scheme 9.

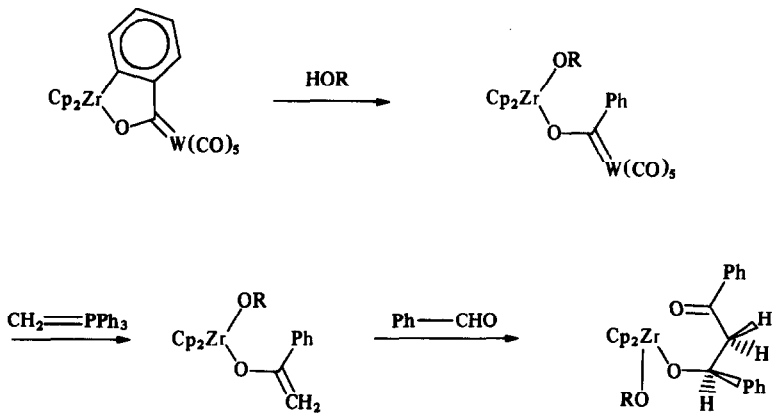

Scheme 10.

1 : 1 mixture of *E*- and *Z*-$CH_3CH{=}C(Ph)OC_2H_5$ upon reaction with the substituted ylide.[35]

Prochiral zirconium enolates have been used as reagents in *syn*-selective aldol condensation reactions.[36] An example studied in some detail using $CH_3CH{=}C(Ph)—O[Zr]$ provided the zirconium aldol product with benzaldehyde [Zr]—O—CHPh—$CH(CH_3)$—COPh with an 85% *syn*-selectivity.[37]

In the bimetallic zirconium oxycarbene complexes the organometallic early transition metal functional group can be used for making a new carbon–carbon bond as well. The (π-allyl)$ZrCp_2$-group in $Cp_2ZrOC[{=}W(CO)_5](C_4H_6)$ undergoes carbon–carbon coupling with added ketones or aldehydes at 50°C. Principally, CC-bond formation could occur at C(1) or C(3) of the substituted allyl chain. Of the two possibilities only coupling of the allyl-CH_2 terminus is observed with the ketones acetone, benzophenone or acetophenone. Only the regioisomeric product having a nine-membered metallacyclic ring-system is formed in each of these examples[38] (Scheme 11).

Surprisingly, the addition of acetone yields a chiral product exhibiting diastereotopic methyl groups at carbon as well as cyclopentadienyl ligands at zirconium in the low temperature limiting NMR spectra obtained at ambient temperature. The addition product of the prochiral reagent acetophenone to the carbene complex is recovered as a mixture of two diastereoisomers. These observations indicate a chiral confor-

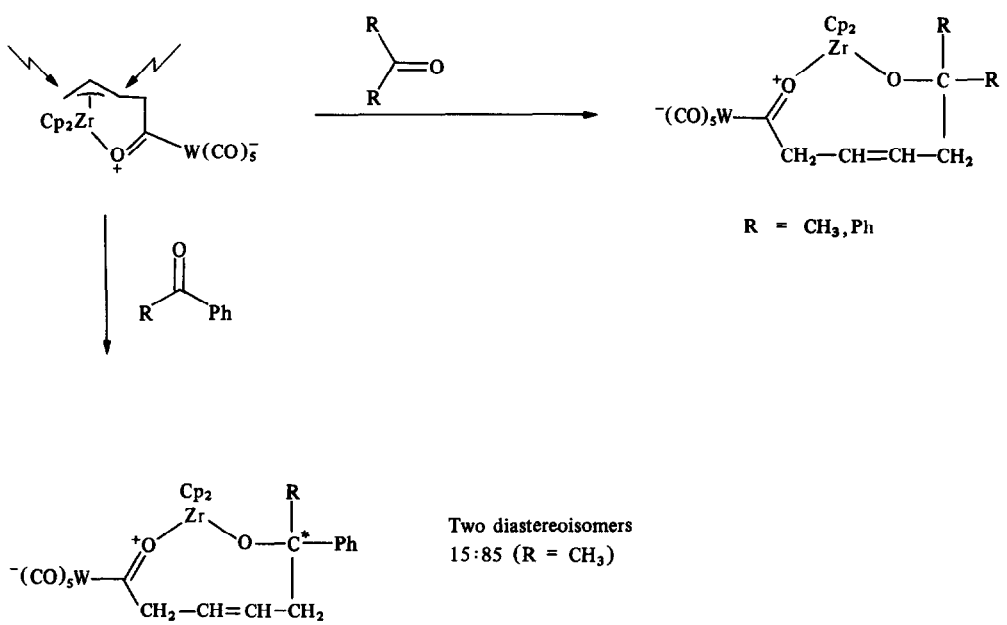

Scheme 11.

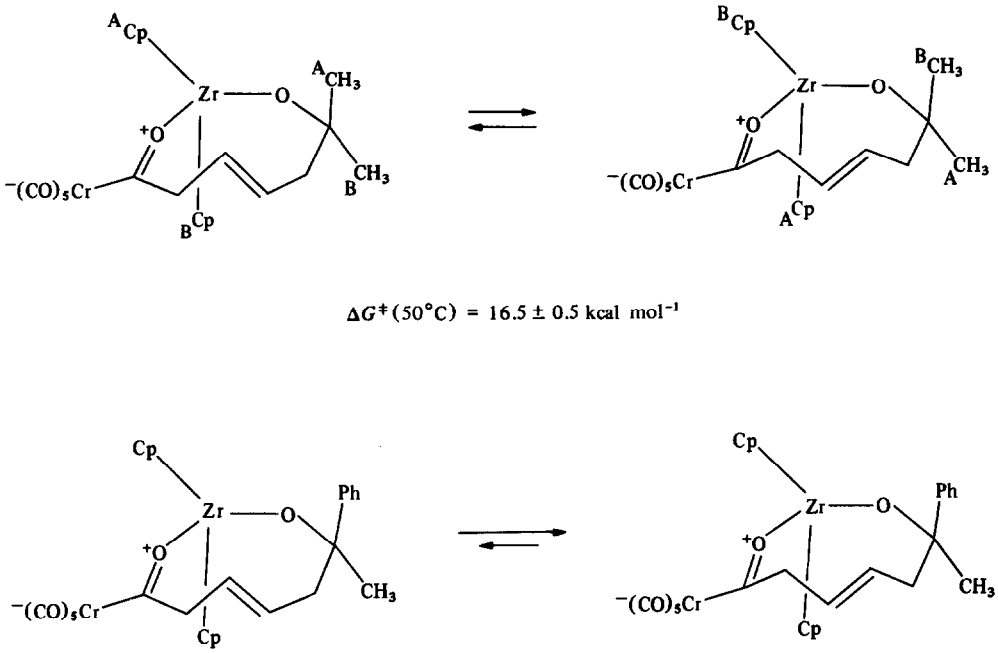

Scheme 12.

mation of the medium size organometallic ring system being favoured. In accord with this interpretation, dynamic behaviour leading to much simpler NMR spectra at high temperatures is observed. Thermally induced equilibration of the $Cp_2\overline{ZrOC[=Cr(CO)_5]}(\overline{C_4H_6})$/acetone adduct isotopomers removing the effects of the conformational chirality element on the NMR spectra has an activation barrier of $\Delta G^{\ddagger} = 16.5$ kcal mol^{-1} at 50°C[38] (Scheme 12).

CONCLUSIONS

In 1984 we reported the first example of a new synthesis of heteroatom-stabilized carbene complexes from metal carbonyls.[9] Treatment of (butadiene)zirconocene with $Cr(CO)_6$ led to the formation of the π-allyl metal oxycarbene complex $Cp_2\overline{ZrOC[=Cr(CO)_5]}(\overline{C_4H_6})$. Up to now many more examples of this reaction type, i.e. the formation of carbene complexes by means of addition of reactive metal olefin complexes to a CO ligand of a metal carbonyl, have become known. Presently, only olefin, aryne or conjugated diene complexes of very electropositive early transition metals or an actinide element have been used as reagents. It is conceivable, however, that this method may not be restricted to such reagents but that sufficiently reactive alkene complexes of the late transition elements could undergo this reaction as well. Car-

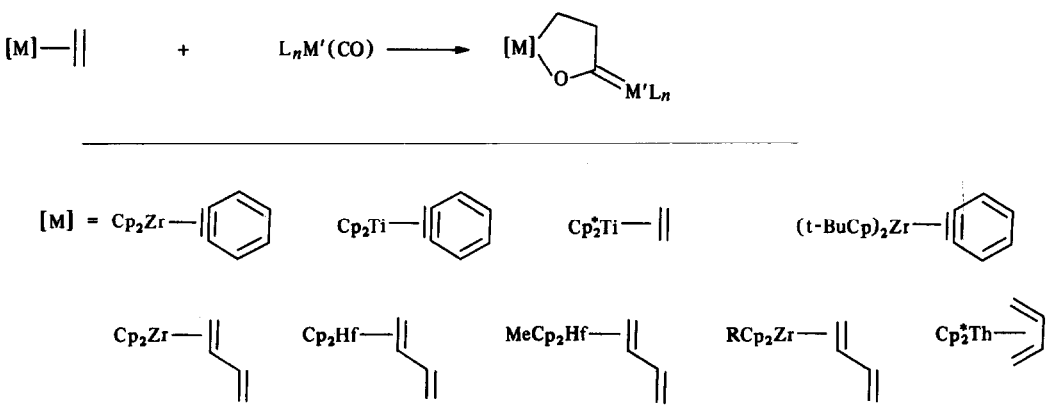

M' = Zr; Hf; V; Nb; Cr; Mo; W; Mn; Re; Fe; Co; Ni; Rh.

Scheme 13.

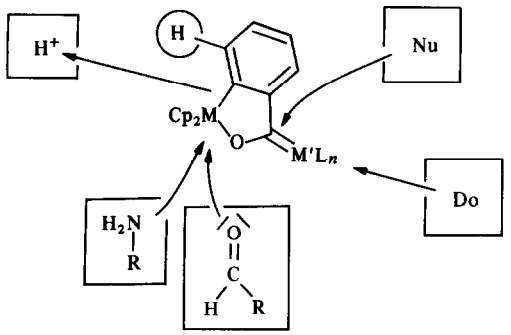

Scheme 14.

bonyl complexes of *d*-block elements ranging from groups 4 to 10 have been converted to carbene complexes using this method.[9,15,16,19–21,24–27,32] This scope should make our procedure a useful complementary method to the presently known variants of E. O. Fischer's original M—CO → M—carbene conversion.

The resulting metallacyclic metal oxycarbene complexes exhibit structural features as well as chemical reactivities somewhat different from the ordinary heteroatom-stabilized Fischer-type carbene complexes. They all appear to be characterized by a shorter O—C(carbene) bond distance, giving these complexes a substantially higher metal acyl character. In some instances this makes the adjacent early transition metal centre very Lewis acidic. This indicates a potential use of similarly structured (possibly chiral) complexes as selective organometallic Lewis acid catalysts. The metallacyclic metal oxycarbene complexes prepared by our method appear to be interesting new types of bimetallic substrates that are characterized by exhibiting a number of distinctively different reaction centres located very close to each other in a simple molecular framework.

Acknowledgements—The majority of work related to the carbene complex synthesis done in my laboratory at the Max Planck Institut für Kohlenforschung in Mülheim a. d. Ruhr and subsequently at the Institut für Organische Chemie der Universität Würzburg was carried out by a small group of very talented coworkers whose names are mentioned in the references. I wish to thank Prof. Dr. Carl Krüger, Prof. Dr. J. L. Petersen, Priv.-Dozent Dr. Reinhard Benn, Dr. Richard Mynott and their coworkers for their valuable collaboration. Generous financial support from the Stiftung Volkswagenwerk, the Deutsche Forschungsgemeinschaft, the Fonds der Chemischen Industrie, the Max Planck Gesellschaft, NATO (Grant No. 04 0346 86), the Fritz-Thyssen-Stiftung, and the Alfried Krupp von Bohlen und Halbach-Stiftung is gratefully acknowledged.

REFERENCES

1. N. Calderon, J. P. Lawrence and E. A. Ofstead, *Adv. Organomet. Chem.* 1979, **17**, 449; T. J. Katz, *Adv. Organomet. Chem.* 1977, **16**, 283; H. W. Turner, R. R. Schrock, J. D. Feldmann and S. J. Holmes, *J. Am. Chem. Soc.* 1983, **105**, 4942.
2. C. P. Casey, in *Transition Metal Organometallics in Organic Synthesis* (Edited by H. Alper), Vol. I, p. 190. Academic Press, New York (1976); F. J. Brown, *Prog. Inorg. Chem.* 1980, **27**, 1; K. H. Dötz, *Angew. Chem.* 1984, **96**, 573.
3. E. O. Fischer and A. Maasböl, *Angew. Chem.* 1964, **76**, 645.
4. K. H. Dötz, H. Fischer, P. Hofmann, F. R. Kreissl, U. Schubert and K. Weiss, *Transition Metal Carbene Complexes*. Verlag Chemie, Weinheim (1983).
5. M. F. Lappert and A. J. Oliver, *J. Chem. Soc., Dalton Trans.* 1974, 65.
6. M. J. Doyle, M. F. Lappert, P. L. Pye and P. Terreros, *J. Chem. Soc., Dalton Trans.* 1984, 2355.
7. J. A. Connor, *Topics Curr. Chem.* 1977, **71**, 71; J. K. Kochi, *Organometallic Mechanisms and Catalysis*. Academic Press, New York (1978).
8. P. T. Wolczanski, R. S. Threlkel and J. E. Bercaw, *J. Am. Chem. Soc.* 1979, **101**, 218; R. S. Threlkel and J. E. Bercaw, *J. Am. Chem. Soc.* 1981, **103**, 2650; P. T. Barger, B. D. Santarsiero, J. Armantrout and J. E. Bercaw, *J. Am. Chem. Soc.* 1984, **106**, 5178; See also: W. Petz, *J. Organomet. Chem.* 1974, **72**, 369.
9. G. Erker, U. Dorf, R. Benn, R.-D. Reinhardt and J. L. Petersen, *J. Am. Chem. Soc.* 1984, **106**, 7649.
10. (a) A. Stockis and R. Hoffmann, *J. Am. Chem. Soc.* 1980, **102**, 2952; (b) G. Erker, K. Engel, U. Dorf, W. E. Hunter and J. L. Atwood, *Angew. Chem.* 1982, **94**, 915; U. Dorf, K. Engel and G. Erker, *Angew. Chem.* 1982, **94**, 916; V. Skibbe and G. Erker, *J. Organomet. Chem.* 1983, **241**, 15; G. Erker, K. Engel, J. L. Atwood and W. E. Hunter, *Angew. Chem.* 1983, **95**, 506; G. Erker and U. Dorf, *Angew. Chem.* 1983, **95**, 800.
11. G. Erker, C. Krüger and G. Müller, *Adv. Organomet. Chem.* 1985, **24**, 1.
12. U. Dorf, K. Engel and G. Erker, *Organometallics* 1983, **2**, 462.
13. G. Erker, J. Wicher, K. Engel, F. Rosenfeldt, W. Dietrich and C. Krüger, *J. Am. Chem. Soc.* 1980, **102**, 6344; G. Erker, J. Wicher, K. Engel and C. Krüger, *Chem. Ber.* 1982, **115**, 3300; G. Erker, K. Engel, C. Krüger and A.-P. Chiang, *Chem. Ber.* 1982, **115**, 3311; G. Erker, K. Engel, C. Krüger and G. Müller, *Organometallics* 1984, **3**, 128.
14. C. Krüger, G. Müller, G. Erker, U. Dorf and K. Engel, *Organometallics* 1985, **3**, 215.
15. U. Dorf, Dissertation, Univ. Bochum (1986); J. L. Petersen, U. Dorf and G. Erker, unpublished results.
16. G. Erker and R. Lecht, *J. Organomet. Chem.* 1986, **311**, 45.
17. E. O. Fischer, F. R. Kreissl, E. Winkler and C. G. Kreiter, *Chem. Ber.* 1972, **105**, 588; D. J.

Darensbourg and M. Y. Darensbourg, *Inorg. Chem.* 1970, **9**, 1691; F. Carre, G. Cerveau, E. Colomer, R. J. P. Corriu and J. C. Young, *J. Organomet. Chem.* 1979, **179**, 215; G. Cerveau, E. Colomer, R. J. P. Corriu and J. C. Young, *J. Organomet. Chem.* 1981, **205**, 31; Y. Yamamoto and H. Yamazaki, *Bull. Chem. Soc. Jpn* 1975, **48**, 3691.

18. P. T. Barger and J. E. Bercaw, *Organometallics* 1984, **3**, 278; D. W. Macomber and R. D. Rogers, *Organometallics* 1985, **4**, 1485; See however: P. T. Barger and J. E. Bercaw, *J. Organomet. Chem.* 1980, **201**, C39.
19. G. Erker, R. Lecht, J. L. Petersen and H. Bönnemann, *Organometallics* 1987, **6**, 1962.
20. G. Erker, R. Lecht, C. Krüger, Y.-H. Tsay and H. Bönnemann, *J. Organomet. Chem.* 1987, **326**, C75.
21. G. Erker, R. Lecht, Y.-H. Tsay and C. Krüger, *Chem. Ber.* 1987, **120**, 1763.
22. A. J. Hartshorn, M. F. Lappert and K. Turner, *J. Chem. Soc., Dalton Trans.* 1978, 348; J. Martin, C. Moise and J. Tirouflet, *C. R. Seanc. Acad. Sci., Ser. 2* 1981, **292**, 1143.
23. R. S. Threlkel and J. E. Bercaw, *J. Am. Chem. Soc.* 1981, **103**, 2650.
24. G. Erker, R. Lecht, R. Schlund, K. Angermund and C. Krüger, *Angew. Chem.* 1987, **99**, 708.
25. R. Lecht, Dissertation, Univ. Würzburg (1987).
26. G. Erker, T. Mühlenbernd, R. Benn and A. Rufinska, *Organometallics* 1986, **5**, 402.
27. K. Mashima, K. Jyodoi, A. Ohyoshi and H. Takaya, *J. Chem. Soc., Chem. Commun.* 1986, 1145.
28. G. Erker, *J. Organomet. Chem.* 1977, **134**, 189; E. G. Berkovich, V. B. Shur, M. E. Vol'pin, B. Lorenz, S. Rummel and M. Wahren, *Chem. Ber.* 1980, **113**, 70, *loc. cit.*
29. G. Erker and K. Kropp, *J. Am. Chem. Soc.* 1979, **101**, 3659; G. Erker and K. Kropp, *J. Organomet. Chem.* 1980, **194**, 45; K. Kropp and G. Erker, *Organometallics* 1982, **1**, 1246.
30. G. Erker, P. Czisch, R. Mynott, Y.-H. Tsay and C. Krüger, *Organometallics* 1985, **4**, 1310; H. J. R. de Boer, O. S. Akkerman, F. Bickelhaupt, G. Erker, P. Czisch, R. Mynott, J. M. Wallis and C. Krüger, *Angew. Chem.* 1986, **98**, 641.
31. S. L. Buchwald, B. T. Watson and J. C. Huffman, *J. Am. Chem. Soc.* 1986, **108**, 7411.
32. G. Erker, U. Dorf, R. Mynott, Y.-H. Tsay and C. Krüger, *Angew. Chem.* 1985, **97**, 572.
33. G. Erker, M. Aulbach and M. T. Ashby, unpublished results.
34. T. J. Burkhardt and C. P. Casey, *J. Am. Chem. Soc.* 1972, **94**, 6543.
35. G. Erker and M. T. Ashby, unpublished results.
36. D. A. Evans and L. R. McGee, *Tetrahedron Lett.* 1980, 3975; J. Yamamoto and K. Maruyama, *Tetrahedron Lett.* 1980, 4607; M. T. Reetz and R. Peter, *Tetrahedron Lett.* 1981, 4691.
37. G. Erker, P. Czisch and R. Mynott, *J. Organomet. Chem.* 1987, **334**, 91; P. Czisch, Dissertation, Univ. Bochum (1986).
38. G. Erker, F. Sosna and J. L. Petersen, unpublished results.

Polyhedron Vol. 7, No. 24, pp. 2465–2471, 1988
Printed in Great Britain

0277–5387/88 $3.00 + .00
© 1988 Pergamon Press plc

INFRARED SPECTRAL, VARIABLE-TEMPERATURE MAGNETIC SUSCEPTIBILITY AND MÖSSBAUER SPECTRAL INVESTIGATIONS ON TRIS(CARBODITHIOATO)IRON(III) COMPLEXES

BALDEV SINGH MANHAS* and SHASHI BALA

Department of Chemistry, Punjabi University, Patiala-147002, India

(*Received* 30 *May* 1986; *accepted after revision* 18 *February* 1988)

Abstract—Two types of iron(III) carbodithioate complexes, (i) normal complexes, $Fe(R_2NCS_2)_3$ with R_2N = 4-methyl-, 4-phenyl-, or 2-methyl-piperazyl, piperidyl and thiomorpholyl and (ii) zwitterionic complexes, $Fe(R_2NCS_2H)_3X_3$ with R_2N = 4-methyl- or 4-phenyl-piperazyl and X = Cl or Br have been synthesized. The complexes have been characterized by elemental analyses, IR spectral studies, variable-temperature magnetic susceptibility and in three cases by variable-temperature Mössbauer spectral studies. All the complexes exhibit the $^2T_2$ (low spin, $S = 1/2$) $\rightleftharpoons$ $^6A_1$ (high spin, $S = 5/2$) spin equilibrium process. The zwitterionic carbodithioate ligands have a weaker ligand field strength than their normal ligand analogues.

In the course of extensive investigations of iron(III) disubstituted dithiocarbamates it has been found[1–13] that whereas most of these compounds have intermediate room-temperature magnetic moments, i.e. varying between the limiting values of 2.0 BM for $^2T_2$ and 5.92 BM for $^6A_1$ spin states, there are a few which are either pure high spin ($^6A_1$ state)[7,10] or pure low-spin ($^2T_2$ state)[8,11,13] species. In this study, iron(III) carbodithioates with the heterocyclic bases —piperidine (Pipd), thiomorpholine (Thim), 2-methylpiperazine (2-MPipz), 1-methylpiperazine (1-MPipz) and 1-phenylpiperazine (1-PPipz), and zwitterions (BH^+X^-) (X = Cl, Br) with the last two of these bases as parent secondary amines—have been investigated to find out which category of electronic structure they correspond to.

EXPERIMENTAL

Materials and methods

The heterocyclic bases were procured, purified and dried as described earlier.[14] Anhydrous ferric chloride and hydrobromic acid from BDH, hydrochloric acid (AR) and carbon disulphide (AR), both from SD, and anhydrous ferric bromide from ICN Pharmaceuticals Inc. were used as obtained. Ethanol (Bengal Chemicals), methanol, acetone, benzene, diethyl ether and chloroform, all from BDH, were purified by the usual methods.

Preparation of ligands

4-MPipzcdtH. 1-Methylpiperazine (5 g, 50.00 mmol) in ethanol (40 cm^3) was cooled to 5°C. To this cooled solution, carbon disulphide (4 g, 53.00 mmol) was added slowly with stirring. A cream coloured solid separated immediately. The solid was filtered, washed with ethanol and diethyl ether and air dried. Found: C, 41.0; H, 6.0; N, 16.1; S, 35.9. Calc. for $C_6H_{12}N_2S_2$: C, 40.9; H, 6.2; N, 15.9; S, 36.4%.

4-MPipzcdtNa·H_2O. To the solid 4-methylpiperazine-1-carbodithioic acid (5 g, 28.40 mmol) was added sodium hydroxide (1.135 g, 28.37 mmol) dissolved in water (40 cm^3). The resulting solution was filtered and the filtrate was evaporated to dryness on a water bath. Found: C, 32.9; H, 6.0; N, 13.0; S, 30.0. Calc. for $C_6H_{13}ON_2S_2Na$: C, 33.3; H, 6.1; N, 13.0; S, 29.6%.

4-PPipzcdtNa·H_2O. 1-Phenylpiperazine (0.5 g, 3.08 mmol) in ethanol (10 cm^3) was cooled to 5°C. To this cooled solution, carbon disulphide (0.235 g, 3.09 mmol) was added slowly with stirring and

*Author to whom correspondence should be addressed.

a white solid separated. This solid was dissolved in a sodium hydroxide solution (0.123 g, 3.07 mmol) in a 50% water–ethanol mixture (20 cm^3). The resulting solution was filtered and this filtrate was used for the preparation of metal complexes of this ligand.

PipdcdtNa·$2H_2O$, ThiMcdtNa·H_2O *and* {2-Mpipz(cdt)$_2$}Na_2·$2H_2O$. For these ligands the white solid obtained after the reaction between the stoichiometric amounts of amine and carbon disulphide was dissolved in a saturated aqueous solution of a stoichiometric amount of sodium hydroxide. The resulting solution was filtered and the filtrate of the ligands, sodium piperidine-N-carbodithioate dihydrate and sodium thiomorpholine-N-carbodithioate monohydrate, was evaporated to dryness on a water bath. However, in the case of disodium 2-methylpiperazine-1,4-dicarbodithioate dihydrate, the solid product was obtained by refrigeration of the filtrate for 3–4 h; the white precipitate was purified by dissolving in methanol, then filtering and precipitating the solid by the addition of dry diethyl ether; the solid was finally filtered under reduced pressure and washed with diethyl ether. Found: C, 32.9; H, 6.5; N, 6.0; S, 29.0. Calc. for $C_6H_{14}O_2NS_2Na$ (PipdcdtNa·$2H_2O$): C, 32.9; H, 6.4; N, 6.4; S. 29.2%. Found: C, 27.0; H, 5.1; N, 6.0; S, 43.6. Calc. for $C_5H_{10}ONS_3Na$(ThiMcdtNa·H_2O): C, 27.4; H, 4.6; N, 6.4; S, 43.8%. Found: C, 25.2; H, 4.1; N, 8.4; S, 38.4. Calc. for $C_7H_{14}N_2S_4O_2Na_2$ ({2-Mpipz(cdt)$_2$}Na_2·$2H_2O$): C, 25.3; H, 4.2; N, 8.4; 38.5%.

Preparation of complexes

Fe(4-MPipzcdt)$_3$. Anhydrous ferric chloride (0.500 g, 3.08 mmol) dissolved in water (5 cm^3) was added with stirring to an aqueous solution (100 cm^3) of sodium 4-methylpiperazine-1-carbodithioate monohydrate (2.00 g, 9.26 mmol). The separated dark brown solid was filtered, washed with water and methanol, and dried in air. The product was recrystallized from dry chloroform and the crystals were dried *in vacuo* over P_4O_{10}. Found; C, 36.6; H, 5.4; N, 14.4; S, 32.8; Fe, 9.7. Calc. for $C_{18}H_{33}N_6S_6Fe$: C, 37.2; H, 5.7; N, 14.4; S, 33.0; Fe, 9.7%.

Fe(Pipdcdt)$_3$, Fe(ThiMcdt)$_3$, Fe$_2${2-MPipz(cdt)$_2$}$_3$ *and* Fe(4-PPipzcdt)$_3$. These complexes were obtained by a method similar to the one described above for Fe(4-MPipzcdt)$_3$, except that for the tris(4-phenylpiperazine-1-carbodithioato)iron(III) complex an aqueous ethanolic solution of the ligand prepared *in situ* was employed. Found: C, 40.0; H, 5.3; N, 5.0; Fe, 10.2. Calc. for $C_{18}H_{30}N_2S_6Fe$(Fe(Pipdcdt)$_3$): C, 40.2; H, 5.6; N, 5.2; Fe, 10.4%. Found: C, 30.6; H, 4.0; N, 6.9; Fe, 9.3. Calc. for $C_{15}H_{24}N_3S_9Fe$(Fe(ThiMcdt)$_3$): C, 30.5; H, 4.1; N, 7.1; Fe, 9.5%. Found: C, 29.0; H, 3.4; N, 9.5; S, 44.0; Fe, 12.9. Calc. for $C_{21}H_{30}N_6S_{12}Fe_2$(Fe$_2${2-MPipz(cdt)$_2$}$_3$): C, 29.2; H, 3.5; N, 9.7; S, 44.5; Fe, 13.0%. Found: C, 52.1; H, 5.3; N, 10.9; S, 25.0; Fe, 6.9. Calc. for $C_{33}H_{39}N_6S_6Fe$ (Fe(4-PPipzcdt)$_3$): C, 51.6; H, 5.1; N, 10.9; S, 25.0; Fe, 7.3%.

Fe(4-MPipzcdtH)$_3$$Cl_3$. Slightly less than the stoichiometric amount of solid 4-methylpiperazine-1-carbodithioic acid (0.500 g, 2.84 mmol) was added in small portions (~ 10 mg), at successive intervals of 0.5 h for a total period of about 25 h, to a continuously stirred ethanolic solution (15 cm^3) of anhydrous ferric chloride (0.162 g, 1.00 mmol) at 30°C. The dark brown solid separated as the solid carbodithioic acid reacted. The solid product was filtered under reduced pressure, washed with ethanol and dry diethyl ether, and finally dried *in vacuo* over P_4O_{10}. Found: C, 30.8; H, 5.2; N, 12.2; S, 27.6; Cl, 15.2; Fe, 8.0. Calc. for $C_{18}H_{36}N_6S_6Cl_3Fe$: C, 31.3; H, 5.2; N, 12.2; S, 27.8; Cl, 15.4; Fe, 8.1%.

Fe(4-MPipzcdtH)$_3$$Br_3$. For the preparation of this compound, the procedure outlined above was employed except that the solution of anhydrous ferric bromide was made using dry acetone. Found: C, 26.6; H, 4.0; N, 10.1; S, 23.0; Br, 29.6; Fe, 6.8. Calc. for $C_{18}H_{36}N_6S_6Br_3Fe$: C, 26.2; H, 4.4; N, 10.2; S, 23.3; Br, 29.1; Fe, 6.8%.

Fe(4-PipzcdtH)$_3$$Cl_3$. Normal tris (4-phenylpiperazine-1-carbodithioato)iron(III) of undefined quantity was dissolved in dry benzene. To this solution, conc. aqueous hydrochloric acid was added dropwise (1–2 drops per time) with stirring at intervals of 25 min. The reaction mixture was continuously stirred and the addition of the acid was continued until there remained a very light green colour in the solution after the precipitate had been allowed to settle down. The dark green precipitate was filtered, washed with dry benzene and then with dry diethyl ether. This reaction and the drying of the product were carried out in a polyethylene bag which had been dried overnight with P_4O_{10}. Found: C, 45.4; H, 4.6; N, 9.2; S, 22.0; Cl, 11.9; Fe, 6.3. Calc. for $C_{33}H_{42}N_6S_6Cl_3Fe$: C, 45.2; H, 4.8; N, 9.6; S, 21.0; Cl, 21.1; Fe, 6.4%.

Fe(4-PPipzcdtH)$_3$$Br_3$. For the preparation of this compound, the procedure outlined above was employed except that instead of hydrochloric acid, hydrobromic acid was used. Found: C, 38.9; H, 4.2; N, 8.1; S, 19.4; Br, 23.8; Fe, 5.5. Calc. for $C_{33}H_{42}N_6S_6Br_3Fe$: C, 39.2; H, 4.2; N, 8.3; S, 19.0; Br, 23.7; Fe, 5.5%.

Elemental analyses

Iron and sulphur in the complexes were determined gravimetrically as Fe_2O_3 and $BaSO_4$. Carbon and hydrogen analyses were performed on an automatic Coleman-33 analyser while nitrogen was estimated by Kjeldahl's method in the departmental microanalytical laboratory. The halogens were estimated by Volhard's method.

Physical measurements

The room temperature magnetic susceptibility of the complexes was measured on a Gouy balance using $Hg[Co(NCS)_4]$ as a calibrant. Variable-temperature (77–300 K) magnetic susceptibilities were obtained using a PAR-155 vibrating sample magnetometer which was calibrated with $Cu(OAC)_2 \cdot H_2O$. IR spectra (KBr pellets) of the complexes and the ligands were recorded on a Pye–Unicam SP3-300 IR spectrophotometer, in the 200–4000 cm^{-1} region. Mössbauer spectral measurements of the complexes were made on a Cryophysics microprocessor controlled Mössbauer spectrometer using a 25 mCi $^{57}Co/Rh$ source.

RESULTS AND DISCUSSION

Two types of iron(III) carbodithioates, with the empirical formulae $Fe(cdt)_3$ and $Fe(cdtH)_3X_3$ deduced from elemental analysis data, are reported. The free dithiocarbamic acids are generally unstable, but the free 4-methylpiperazine-1-carbodithioic acid used in the synthesis of some complexes of the type $Fe(cdtH)_3X_3$ with iron(III) chloride and iron(III) bromide was found to be quite stable. Although free 4-phenylpiperazine-1-carbodithioic acid is unstable, its zwitterionic complexes with iron(III) chloride and iron(III) bromide have been obtained by the following reaction:[15]

$$Fe(4\text{-}PPipzcdt)_3 + 3HX(aq) \xrightarrow{C_6H_6} Fe(4\text{-}PPipzcdtH)_3X_3.$$

IR spectra

The appearance of an additional broad band in the region 3140–3650 cm^{-1}, ascribable to the N—H stretch, in the IR spectra of complexes having chlorides and bromides as counter-anions, and also in free 4-MPipzcdtH as compared to the normal iron and sodium carbodithioates, indicates the existence of 4-MPipzcdt and 4-PPipzcdt ligands as zwitterions in these complexes and in free 4-MPipzcdtH. The $\nu(C{=}N)$ band in the normal and zwitterionic carbodithioates or iron(III) has been observed at higher energies (1428–1485 cm^{-1}) compared to the free ligands (1410–1467 cm^{-1}).[16] The positions of the antisymmetric $\nu_a(SCS)$ and symmetric $\nu_s(SCS)$, stretching modes of the vibrations of the $\rangle NCS_2$ group of carbodithioate ligands (at 942–1031 and 900–973 cm^{-1}, respectively) suggest a chelating bidentate mode of coordination to the metal ion.[17] The simultaneous appearance of two separate metal–sulphur stretching vibrational signals in the complexes (at 310–370 and 260–315 cm^{-1}, respectively) is in consonance with the thermal population in the two spin states ($S = 5/2$ and $S = 1/2$), commonly observed in iron(III) dithiocarbamates.[6]

Magnetic susceptibility studies

The observed room-temperature magnetic moment values (3.4–5.4 μ_B) for the iron(III) carbodithioates under study are intermediate between high-spin ($S = 5/2$) and low-spin ($S = 1/2$) values (5.92 and 2.0 μ_B, respectively), for octahedral iron(III) dithiocarbamates. Variable-temperature (77–300 K) magnetic susceptibility behaviour for these complexes [Fig. 1(a) and (b)] indicates anomalous decreases in magnetic moments as the temperature is lowered to 77 K. These observations suggest that spin-free ($S = 5/2$) and spin-paired ($S = 1/2$) isomers exist in equilibrium with each other.[18] At low temperatures, in some of the complexes [see Fig. 1(a)], the effective Bohr magneton number tends towards a value of 2.0 which is characteristic of a t_{2g}^5 electronic configuration for the $S = 1/2$ ($^2T_{2g}$) spin state. However, it is noticed that in no case is the μ_{eff} value below the spin-only value of 1.73 which is expected for an exchange coupled antiferromagnetic system, even at the lowest temperatures studied. Although, based on the general curvature of the μ_{eff} vs T plots, a lower limit approaching this value does not seem unattainable. For zwitterionic iron(III) carbodithioates and the tris(2-methylpiperazine-1,4-dicarbodithioato)diiron(III) complex, the low temperature limit of magnetic moments is higher than that of the normal iron(III) carbodithioates (e.g. for $Fe(4\text{-}MPipzcdtH)_3Cl_3$, $Fe(4\text{-}MPipzcdtH)_3Br_3$, $Fe(4\text{-}PPipzcdtH)_3Br_3$ and $Fe_2\{2\text{-}MPipz(cdt)_2\}_3$ complexes it is 2.84 (77 K), 3.03 (94 K), 4.72 (89 K) and 2.73 (77 K), respectively). In view of the two distinct, high-spin and low-spin state, IR spectral signals (see IR spectra), the higher μ_{eff} values at low temperatures in these complexes are not indicative of the presence of mixed-spin species of "variable character";[19,20] nor are these μ_{eff} values, because of

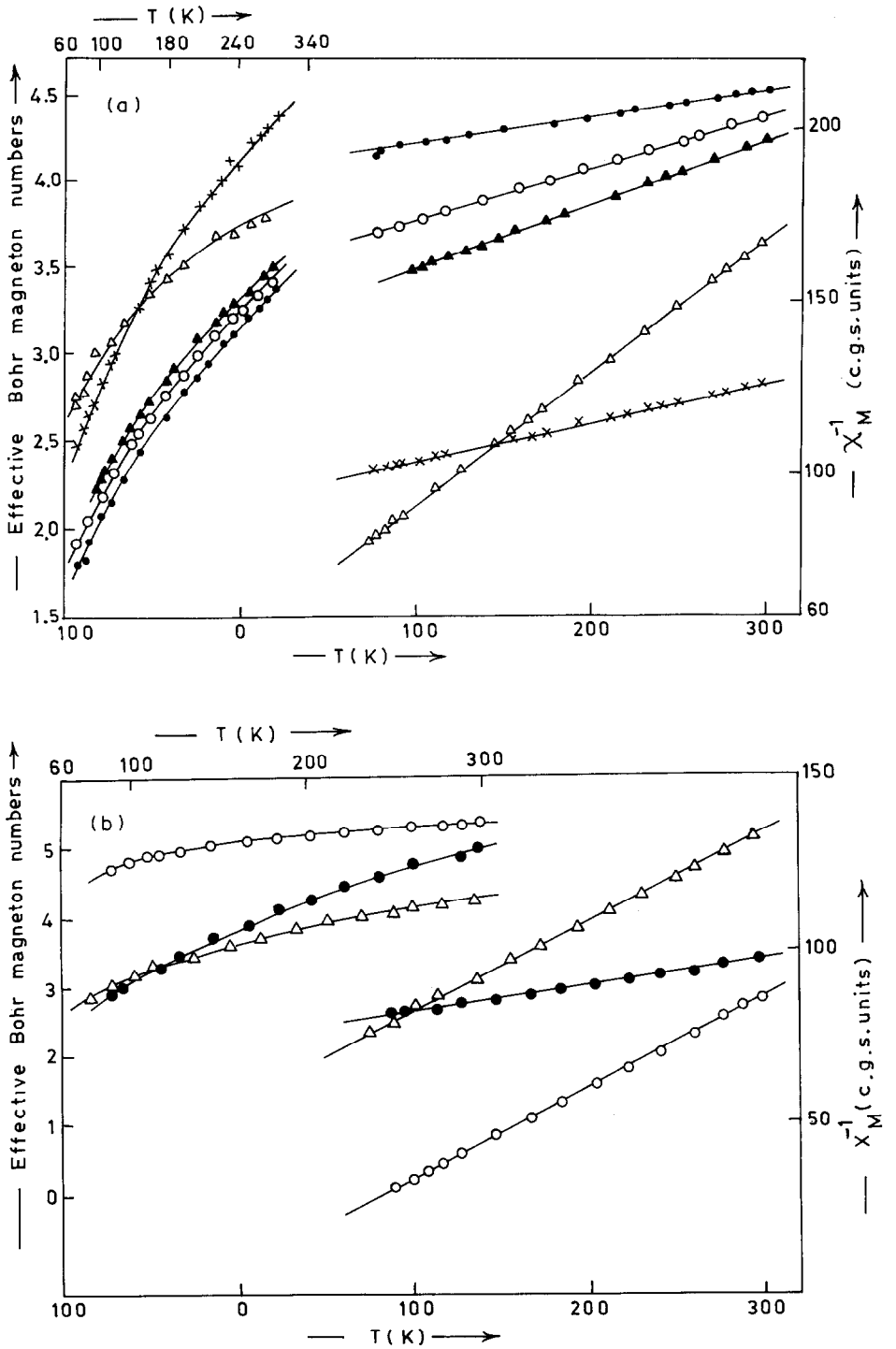

Fig. 1. (a) Variation of molar magnetic susceptibility and effective Bohr magneton numbers of $Fe(ThiMcdt)_3$ (—●—●—●—), $Fe(4\text{-}MPipzcdt)_3$ (—⊙—⊙—⊙—), $Fe(Pipdcdt)_3$ (—▲—▲—▲—), $Fe_2\{2\text{-}MPipz(cdt)_2\}_3$ (—△—△—△—) and $Fe(4\text{-}PPipzcdt)_3$ (—×—×—×—), with temperature. (b) Variation of molar magnetic susceptibility and effective Bohr magneton numbers of $Fe(4\text{-}MPipzcdtH)_3Cl_3$ (—△—△—△—), $Fe(4\text{-}MPipzcdtH)_3Br_3$ (—●—●—●—) and $Fe(4\text{-}PPipzcdtH)_3Br_3$ (—⊙—⊙—⊙—) with temperature.

the ground intermediate-spin state ($S = 3/2$) as suggested by Butcher and Sinn for iron(III) dithiocarbamates,[21] since this spin state is not permitted by the ligand field theory for octahedral geometry.[2,22] These μ_{eff} values may result from the crystal packing effects in these complexes being of a different type to those in other iron(III) carbodithioates, due to the proton–chloride or proton–bromide interactions present in the zwitterionic complexes and the different stoichiometry in $Fe_2\{2\text{-MPipz(cdt)}_2\}_3$. These differences may sterically hinder the achievement of the pure low-spin geometry in these complexes at low temperatures. It is, therefore, suggested that all these iron(III) carbodithioates under study belong to the type of the usual (phase I/phase II) sample of $Fe(Morphcdt)_3 \cdot CH_2Cl_2$[23] and exhibit the doublet–sextet spin equilibrium.

Taking the room temperature values 5.92 and 2.24 for μ_{HS} and μ_{LS}, respectively, the percentages of high-spin isomers (HS) in the normal complexes, $Fe(cdt)_3$, with parent secondary amines 1-MPipz, Pipd, ThiM, 2-MPipz and 1-PPipz, are 22.47, 28.63, 28.63, 32.91 and 49.53, respectively, while for iron(III) complexes with zwitterionic carbodithioates—$Fe(4\text{-MpipzcdtH})_3Cl_3$, $Fe(4\text{-MpipzcdtH})_3Br_3$ and $Fe(4\text{-PPipzcdtH})_3Br_3$—these are 43.72, 67.38 and 80.40, respectively. A higher percentage of the low-spin form (LS) at room temperature for the normal $Fe(cdt)_3$ complexes with 1-MPipz and 1-PPipz as the parent secondary amines as compared to the respective zwitterionic iron(III) complexes, suggests that the normal 4-methylpiperazine-1-carbodithioate and 4-phenylpiperazine-1-carbodithioate ligands have a higher ligand field strength than their zwitterionic carbodithioate ligands.

Mössbauer spectra

Room-temperature and liquid nitrogen-temperature Mössbauer spectral measurements on three of the iron(III) carbodithioates, viz. $Fe(4\text{-Mpipzcdt})_3$, $Fe(Pipdcdt)_3$ and $Fe(4\text{-MPipzcdtH})_3Cl_3$, were made. The Mössbauer parameters, isomer shift δ, quadrupole splitting ΔE_Q and the line width τ (width at half maximum), are listed in Table 1. These complexes display only one signal (one Mössbauer doublet) at room temperature as well as at liquid nitrogen temperatures in their computerized Mössbauer spectra. (Figure 2 shows the Mössbauer spectra for $Fe(4\text{-MPipzcdt})_3$ and $Fe(4\text{-MPipzcdtH})_3Cl_3$ complexes.) The appearance of only one doublet and not a doublet of doublets has been explained on the basis of the existence of a rapid dynamic spin-interconversion between $^6A_{1g}$ and $^2T_{2g}$ states.[24] The Mössbauer spectra offer no direct support for the existence of the $^2T_{2g} \rightleftharpoons {}^6A_{1g}$ spin equilibrium in iron(III) dithiocarbamates which is invoked to explain the anomalous temperature dependence of the magnetic moments. Although the absence of excessive signal broadening or of six-line magnetic hyperfine spectra at low temperatures for the lower moment $Fe(4\text{-MPipzcdt})_3$ and $Fe(Pipdcdt)_3$ complexes indicates that anti-ferromagnetism does not contribute to the observed anomalous magnetic behaviour of these $Fe(cdt)_3$ complexes.[24]

The general trend of the linear decline of the room-temperature isomer shift with the decreasing value of the solid state magnetic moment for six-coordinate iron(III) dithiocarbamates[25,26] is not uniformly observed by the three complexes investigated here by Mössbauer spectroscopy: δ_{298} $Fe(4\text{-MPipzcdt})_3$ ($\mu_{eff}^{rt} = 3.4$) < δ_{298} $Fe(Pipdcdt)_3$ ($\mu_{eff}^{rt} = 3.69$) > δ_{298} $Fe(4\text{-MPipzcdtH})_3Cl_3$ ($\mu_{eff}^{rt} = 4.37$). This indicates that whereas the overall covalence, which is generally considered to increase the amount of low-spin species, is larger for $Fe(4\text{-MPipzcdt})_3$ and $Fe(Pipdcdt)_3$, the effective s-electron density at the iron nucleus, which determines the isomer shift, is higher for $Fe(4\text{-MPipzcdtH})_3Cl_3$. This is understandable in terms of the following arguments. Since the overall covalence is largely

Table 1. Isomer shifts δ^a (mm s^{-1}), quadrupole splitting ΔE_Q (mm s^{-1}) and widths at half maximum τ (mm s^{-1}) for ^{57}Fe in iron(III) complexes

Sr. No.	Compound	δ	ΔE_Q	τ
(1)	$Fe(4\text{-MPipzcdt})_3$	0.39 (298 K)	0.32 (298 K)	0.38 (298 K)
		0.47 (77 K)	0.70 (77 K)	0.38 (77 K)
(2)	$Fe(Pipdcdt)_3$	0.42 (298 K)	0.23 (298 K)	0.35 (298 K)
		0.48 (77 K)	0.73 (77 K)	0.27 (77 K)
(3)	$Fe(4\text{-MPipzcdtH})_3Cl_3$	0.39 (298 K)	0.60 (298 K)	0.49 (298 K)
		0.49 (77 K)	0.80 (77 K)	0.50 (77 K)

[a] δ values are with respect to the iron metal as the standard.

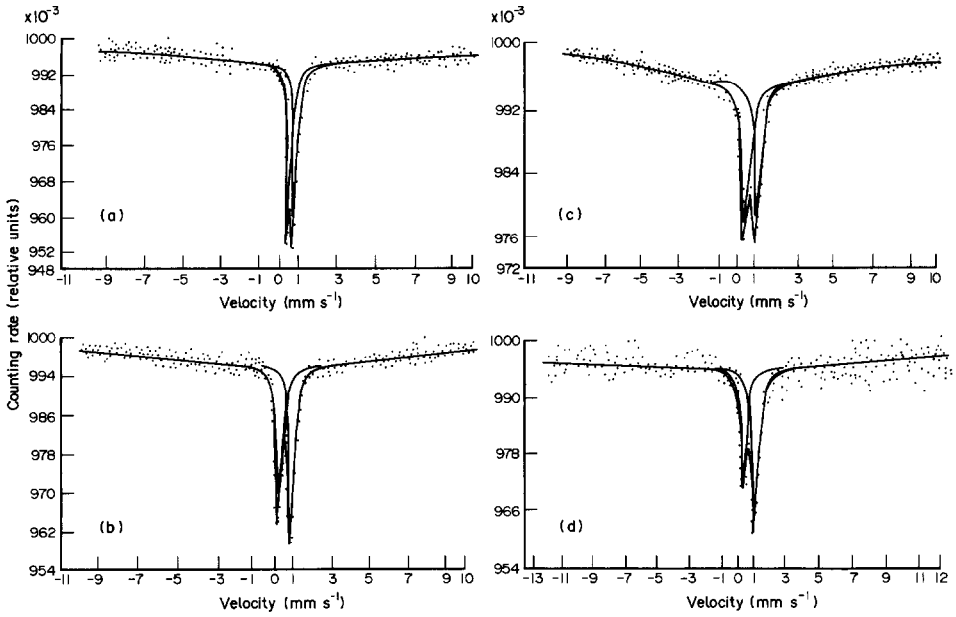

Fig. 2. Mössbauer spectra of Fe(4-MPipzcdt)$_3$. (a) At 298 K. (b) At 77 K and Fe(4-MPipzcdtH)$_3$Cl$_3$. (c) At 298 K. (d) At 77 K.

determined by the stronger $\sigma_{L\rightarrow M}$ and not by the relatively weaker $\pi_{M\rightarrow L}$, and the effective *s*-electron density at the metal nucleus is increased mainly by the $\pi_{M\rightarrow L}$, the zwitterionic complex must have smaller $\sigma_{L\rightarrow M}$ (sulphur → iron σ donation), and larger $\pi_{M\rightarrow L}$ (iron → sulphur π-back donation). These relative values of $\sigma_{L\rightarrow M}$ (lower) and $\pi_{M\rightarrow L}$ (greater) are indeed expected on account of the positive charge on the nitrogen of the NCH_3 group in the zwitterionic complex. At liquid nitrogen temperatures, the measured energy shift δ_{total} ($\delta_{total} = \delta_I + \delta_{SOD}$, δ_I = isomer shift and δ_{SOD} = energy shift due to the second-order Doppler effect) increases (by 0.06, 0.08 and 0.1 mm s^{-1}) with increasing low-spin state population (inferred from the decrease in μ_{eff} value), for all the three complexes. This observation is to some extent in agreement with previous studies on iron(III) dithiocarbamates.[24,27]

The room-temperature quadrupole splitting (Table 1) for the variable-spin iron(III) carbodithioates under study, appears to parallel an increase in the low-spin $^2T_{2g}$ isomer population. The complex Fe(4-MPipzcdtH)$_3$Cl$_3$ is an exception, for which the quadrupole splitting is quite large even though it has a lower low-spin isomer population. In this complex, the greater quadrupole splitting may be attributed to an additional electric field gradient produced at the iron atom, due to the lowering of the symmetry on account of different types of lattice effects arising from the ligands being in the zwitterionic form. At liquid nitrogen temperature the observed increase in the quadrupole splitting values for the three iron(III) carbodithioates is consistent with the values reported in the literature for iron(III) dithiocarbamates,[27,28] observing the high spin ⇌ low spin equilibrium.

Acknowledgements—We thank Prof. Kailash Chandra (University of Roorkee, Roorkee) and Dr F. J. Berry (University of Birmingham, U.K.) for help with the magnetic susceptibility and Mössbauer spectral measurements, respectively. One of us (S.B.) is grateful to the U.G.C., New Dehli, for the award of a fellowship.

REFERENCES

1. D. Coucouvanis, *Prog. Inorg. Chem.* 1970, **11**, 233.
2. D. Coucouvanis, *Prog. Inorg. Chem.* 1979, **26**, 301.
3. R. L. Martin and A. H. White, *Trans. Met. Chem.* 1968, **4**, 113.
4. E. Sinn, *Coord. Chem. Rev.* 1974, **12**, 185.
5. L. Cambi and A. Cagnosso, *Atti. Accad. Naz. Lincei, Cl. Sci. Fis. Mat. Nat. Rend.* 1931, **13**, 809; L. Cambi and L. Szego, *Ber. Dt. Chem. Ges. A* 1931, **64**, 2591.
6. B. Hutchinson, P. Neill, A. Finkelstein and J. Takemoto, *Inorg. Chem.* 1981, **20**, 2000.
7. E. J. Cukauskas, Jr., B. S. Deaver and E. Sinn, *J. Chem. Soc., Chem. Commun.* 1974, 1698.
8. A. H. Ewald, R. L. Martin, E. Sinn and A. H. White, *Inorg. Chem.* 1969, **8**, 1837.

9. H. H. Wickman and C. F. Wagner, *J. Chem. Phys.* 1969, **51**, 435.
10. G. A. Eisman, W. M. Reiff, R. J. Butcher and E. Sinn, *Inorg. Chem.* 1981, **20**, 3484.
11. R. J. Butcher, J. R. Ferraro and E. Sinn, *Inorg. Chem.* 1976, **15**, 2077.
12. K. Ståhl and I. Ymén, *Acta Chim. Scand.* 1983, **A37**, 729.
13. A. G. El A'mma and R. S. Drago, *Inorg. Chem.* 1977, **16**, 2975.
14. B. S. Manhas, A. K. Trikha and M. Singh, *Indian J. Chem.* 1978, **16A**, 431.
15. R. L. Martin and A. H. White, *Inorg. Chem.* 1967, **6**, 712.
16. R. Eisenberg, *Prog. Inorg. Chem.* 1970, **12**, 295.
17. F. Bonati and R. Ugo, *J. Organomet. Chem.* 1967, **10**, 257.
18. L. Cambi and L. Szego, *Ber.* 1933, **66**, 656.
19. G. Harris, *Theor. Chim. Acta.* 1966, **5**, 379.
20. G. Harris-Loew, *J. Chem. Phys.* 1968, **48**, 2191; G. Harris-Loew and R. L. Ake, *J. Chem. Phys.* 1969, **51**, 3143.
21. (a) R. J. Butcher and E. Sinn, *J. Am. Chem. Soc.* 1976, **98**, 5159; (b) R. J. Butcher and E. Sinn, *J. Am. Chem. Soc.* 1976, **98**, 2440; (c) R. J. Butcher, J. R. Ferraro and E. Sinn, *J. Chem. Soc., Chem. Commun.* 1976, 910.
22. (a) J. S. Griffith, *J. Inorg. Nucl. Chem.* 1956, **2**, 1; (b) J. S. Griffith, *J. Inorg. Nucl. Chem.* 1956, **2**, 229.
23. K. Ståhl, *Acta Cryst.* 1983, **B39**, 612.
24. K. R. Kunze, D. L. Perry and L. J. Wilson, *Inorg. Chem.* 1977, **16**, 594.
25. A. Malliaris and V. Papaefthimiou, *Inorg. Chem.* 1982, **21**, 770.
26. R. R. Eley, N. V. Duffy and D. L. Uhrich, *J. Inorg. Nucl. Chem.* 1972, **34**, 3681.
27. R. Rickards, C. E. Johnson and H. A. O. Hill, *J. Chem. Phys.* 1968, **48**, 5231.
28. P. B. Merrithew and P. G. Rasmussen, *Inorg. Chem.* 1972, **11**, 325.

Polyhedron Vol. 7, No. 24, pp. 2473–2476, 1988
Printed in Great Britain

0277–5387/88 $3.00+.00
© 1988 Pergamon Press plc

POTENTIOMETRIC STUDY OF CHLORO COMPLEXES OF SOME DIVALENT TRANSITION METAL CATIONS IN DIMETHYL SULPHOXIDE AT 25°C

HENRYK STRZELECKI* and WACŁAW GRZYBKOWSKI

Department of Physical Chemistry, Technical University of Gdańsk,
80-952 Gdańsk, Poland

(*Received* 1 *March* 1988; *accepted* 14 *April* 1988)

Abstract—Formation of the chloro complexes of manganese(II), cobalt(II), nickel(II), copper(II) and zinc(II) in DMSO has been studied potentiometrically at 25°C. The concentration stability constants for the ionic strength of 0.1 mol kg^{-1} are derived and discussed. The stability of the divalent transition metal cations towards the chloride anion follows the sequence Mn > Co > Ni ≪ Cu > Zn disobeying the Irving–Williams series.

It has been shown recently that the stability constants of the monohalide complexes of divalent transition metal cations in non-aqueous solvents as well as in water follow the sequence[1–4]

$$MnX^+ > CoX^+ > NiX^+ < CuX^+ > ZnX^+$$

which is distinctly opposite to the well-known Irving–Williams series.[5] The sequence seems to be characteristic of the monohalide complexes, while the Irving–Williams series is valid for the complexes involving the O- and N-donor ligands only.

In a previous paper from our laboratory we described a new method of accomplishing the constant ionic strength medium concept in the potentiometric study of complex formation and stability constants of monobromo complexes in N,N-dimethylacetamide were reported.[6] It is the purpose of this paper to study the monochloro complexes of the divalent transition metal cations in DMSO.

EXPERIMENTAL

Dimethylsulphoxide was dried over calcium hydride and then distilled under reduced pressure. Specific conductance of the purified solvent was $2.0–8.0 \times 10^{-8}$ S cm^{-1}.

The DMSO-solvated metal perchlorates were obtained from the corresponding hydrates by dissolving them in anhydrous DMSO, followed by removing any excess of solvent and water under reduced pressure at *ca* 70°C. The crystalline solids were isolated and recrystallized twice from anhydrous DMSO. The final products were used to prepare the stock solutions. The latter were standardized by titration with EDTA.

Tetraethylammonium chloride was recrystallized three times from anhydrous acetonitrile and dried at 80°C *in vacuo*.

The Ag|AgCl|Cl electrodes were made by coating silver and silver chloride on platinum wire.[7] The potential difference for a pair of electrodes in water was smaller than 0.01 mV (V-540 MERATRONIK V-meter was used).

The half-cell solutions were equilibrated with solid AgCl over 24 h before measurements were taken, in order to avoid a dissolution of AgCl on the surface of the Ag|AgCl electrode.

The design of the cell eliminated contact of the half-cell solutions with the atmosphere and also ensured mutual mixing. The preparations of the solutions and further manipulations were performed in a dry-box.

RESULTS AND DISCUSSION

The method applied in the present work consists of the study of the concentration cell

$$Ag|AgX(s)|N(ClO_4)_2(m),\ Et_4NX(m_1)\,\|\,M(ClO_4)_2(m),\ Et_4NX(m_1)|AgX(s)|Ag \quad (1)$$

where $M(ClO_4)_2$ and $N(ClO_4)_2$ are the divalent transition metal perchlorates and X denotes a halide or pseudohalide anion.

*Author to whom correspondence should be addressed.

As shown, the cell consists of two almost identical half-cells, differing only in the cation nature of the salt forming ionic medium. Due to the fact that the transference numbers of the ClO_4 anion are almost the same, the liquid junction potential may be neglected.

The essential assumption underlying the applied method consists of the fact that the divalent transition metal perchlorates behave as effective constant ionic media, i.e. their activity coefficients may be expected to be independent of the nature of the cation.[1,2] It is obvious that the same conclusion is valid for the activity coefficients of the X^- anion. Thus, the electromotive force of the cell is determined directly by the ratio of "free" anion concentrations, X_N and X_M, i.e. is given by the equation

$$E = \frac{RT}{F} \ln \frac{X_N}{X_M}. \tag{2}$$

Assuming that in the half-cell solutions only the monohalide complexes are formed the following system for the equilibria is valid for each of the half-cell solutions

$$Ag + X^- \rightleftharpoons AgX(s) + e^- \tag{3}$$

$$AgX(s) + X^- \rightleftharpoons AgX_2^- \tag{4}$$

$$M^{2+} + X^- \rightleftharpoons MX^+. \tag{5}$$

From the equations arising from the material balances for the half-cell solutions, the equations defining the stability constants of the MX^+ and NX^+ complexes and the formation constants of the AgX_2^- complex, the expression follows

$$E = \frac{RT}{F} \ln \frac{1 + K_2 + Q_1^M[M^{2+}]}{1 + K_2 + Q_1^N[N^{2+}]} \tag{6}$$

where Q_1^M and Q_1^N are the equilibrium concentration quotients related to the stability constants of the MX^+ and NX^+ complexes, i.e. the medium or concentration stability constants. K_2 is the concentration quotient corresponding to the formation of the AgX_2^- complex, and $[M^{2+}]$ and $[N^{2+}]$ are the equilibrium concentrations of the uncomplexed metal cations.

When the concentrations of the metal perchlorates are much higher than the concentration of Et_4NX, $m \gg m_1$, the equilibrium concentration of free metal cations $[M^{2+}]$ and $[N^{2+}]$ may be approximated by the total metal perchlorate concentrations, provided that the association with the ClO_4^- anion is negligible. The latter seems to be a sufficiently good approximation for the divalent transition metal perchlorates in DMSO and DMA solution, as may be inferred from the association constants.[8,9] Thus, eq. (7) follows

$$E = \frac{RT}{F} \ln \frac{1 + K_a + Q_1^M m}{1 + K_2 + Q_1^N m}. \tag{7}$$

As is seen, the electromotive force of the cell [eq. (1)] may be expected to be independent of the Et_4NX concentration and therefore could be determined by the total metal perchlorates concentration and the values of the concentration stability constants, Q_1^M and Q_1^N only.

The results obtained for the $M(ClO_4)_2$–Et_4NBr–DMA (M = Mn, Co, Ni, Cu, Zn) system provided good experimental evidence for the validity of the assumption presented above.[6] The electromotive force of the cells was within the experimental error independent of Et_4NBr concentration, and the data obtained were intrepreted in terms of concentration stability constants.

In the present paper we report the results obtained for the $M(ClO_4)_2$–Et_4NCl–DMSO system for the following pairs of metal perchlorates: Mn–Co, Co–Ni, Cu–Zn, Ni–Zn, Co–Zn, Ni–Cu and Co–Cu. Moreover, the cells containing $Mg(ClO_4)_2$ in one of the half-cells were studied, the measurements being performed for Mn–Mg and Co–Mg pairs only. The latter systems were studied in order to obtain the absolute values of the respective concentration stability constants. Due to the fact that the Mg^{2+} cation may be considered as a coordinatively non-active ion the respective electromotive force equations take the following forms

$$E = \frac{RT}{F} \ln \frac{1 + K_2 + Q_1^M[M^{2+}]}{1 + K_2} \tag{8}$$

and

$$E = \frac{RT}{F} \ln \frac{1 + K_2 + Q_1^M m}{1 + K_2}. \tag{9}$$

The measurements were performed for a constant concentration of the metal perchlorates corresponding to $I = 0.10$ ($m = 0.0333$ mol kg^{-1}) and for a number of different concentrations of Et_4NCl not exceeding 0.0035 mol kg^{-1}.

The results are presented in Table 1. The sign (+ or −) indicates a polarity of the $Ag|AgCl|Cl^-$ electrode for the respective half-cell. The positive sign indicates that the free chloride anion concentration in the given half-cell solution is lower than in the second half-cell. As is seen, the sign of the $Ag|AgCl|Cl^-$ electrode immersed in the solution of $Co(ClO_4)_2$ is positive when the second half-cell contains a solution of $Mg(ClO_4)$. The signs of the electrodes are reversed for the Co–Zn cell. Further inspection of the electrode signs shows that the $Ag|AgCl|Cl^-$ electrode in the $Ag|AgCl|Ni(ClO_4)_2$ (m), Et_4NCl half-cell is always negative. It indicates that the Ni^{2+} cation exhibits the poorest

Table 1. The electromotive force values for the concentration cell (1) for $I = 0.1$ mol kg^{-1} at 25°C

Co–Mg (+) (–)		Mn–Mg (+) (–)		Co–Mn (–) (+)	
m_1	EMF	m_1	EMF	m_1	EMF
0.00063	7.7	0.00061	13.0	0.00061	5.3
0.00080	7.4	0.00094	12.5	0.00094	5.2
0.00110	7.1	0.00120	11.8	0.00120	4.9
0.00140	6.7	0.00200	10.2	0.00200	4.6
0.00173	6.2	0.00260	9.5	0.00260	4.8

	EMF		
	Co–Ni	Zn–Cu	Zn–Ni
m_1	(+) (–)	(–) (+)	(+) (–)
0.000588	2.6	7.5	70.5
0.00115	2.0	12.0	74.0
0.00177	2.1	21.0	78.0
0.00228	1.8	27.5	80.0
0.00280	1.4	31.0	82.0
0.00347	1.0	—	86.0

	Zn–Co	Ni–Cu	Cu–Co
m_1	(+) (–)	(–) (+)	(+) (–)
0.000588	67.5	78.0	75.0
0.00115	71.0	87.5	85.0
0.00177	75.0	98.0	96.0
0.00228	77.0	107.5	105.0
0.00280	81.6	114.0	115.0
0.00347	85.5	—	—

Units: m_1 (mol kg^{-1}), EMF (mV).

ability for complex formation. Moreover, the following sequence of stability towards the chloride anion may be deduced from the electrode signs

$$Mn^{2+} > Co^{2+} > Ni^{2+} \ll Cu^{2+} > Zn^{2+}.$$

Inspection of the data listed in Table 1 shows that the electromotive force of the cells depends on the Et_4NCl concentration. This indicates a failure of the assumptions which lead to eqs (7) and (9). Figure 1 shows the almost linear variation of the electromotive force with increasing concentration of Et_4NCl for the Ni–Cu, Ni–Zn, and Ni–Co cells. The data presented are representative for all the systems studied. The electromotive force increases with increasing concentration of Et_4NCl when one of the half-cells contains $Zn(ClO_4)_2$ or $Cu(ClO_4)_2$. This is also observed for the Cu–Zn cell. For other cells, a slight decrease is always observed. Moreover, the electromotive forces of the Ni–Zn, Ni–Cu, Co–Zn and Co–Cu cells are markedly higher than those of the Mn–Co, Co–Ni, Co–Mg and Mn–Mg cells.

Detailed numerical analysis of the equilibria system, eqs (3)–(5) leads to a conclusion that a decrease in the electromotive force may be expected for this model. However, the predicted slope is somewhat lower than the experimental values. This means that the model assuming formation of the monochloro complex is valid for the solutions containing perchlorates of manganese(II), cobalt(II), and nickel(II) only. Although, eqs (6) or (8), without the assumption that $[M^{2+}] = m$, describe the respective cells.

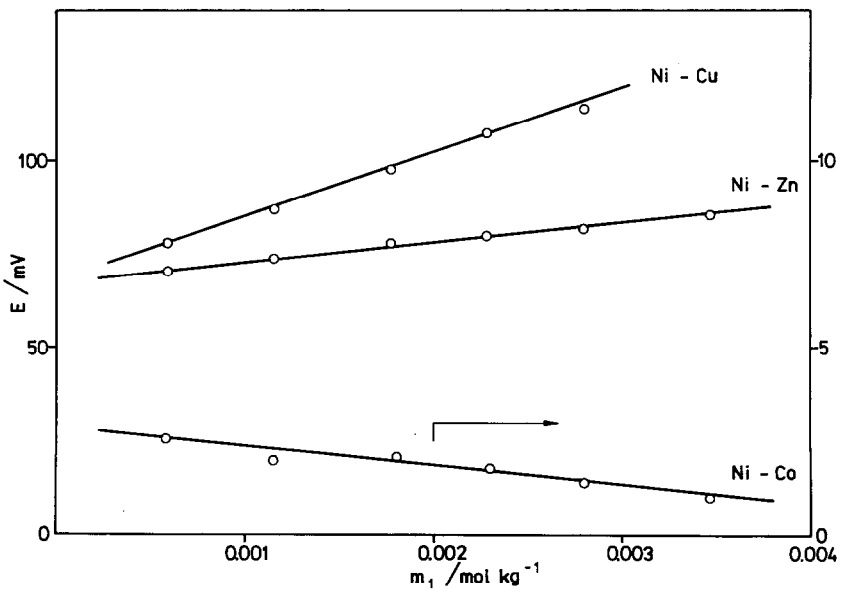

Fig. 1. Dependence of electromotive force of the concentration cell (1) on Et_4NCl concentration (m_1) at 25°C.

Further analysis of the system studied results in the conclusion that an increase in the electromotive force may be expected when formation of a dichloro complex is assumed, even at the lowest values of the $Et_4NCl/M(ClO_4)_2$ ratio, and (10) has been added to the model.

$$M^{2+} + 2X^- \rightleftharpoons MX_2. \qquad (10)$$

Thus, the concentration of the Cl^- anion in the respective half-cell solution is determined by two concentration stability constants of the consecutive chloro complexes, Q_1^M and Q_2^M, only the first factor controls an electromotive force of the half-cell in which a monochloro complex only is formed.

An analysis of the electromotive force values listed in Table 1 shows that the data exhibit mutual agreement. Thus, it is possible to evaluate them in terms of their respective concentration stability constants which are the parameters in eqs (6) and (8), and the respective equation arising from the addition of equilibrium (10) to equilibria (3)–(5). It is obvious that a value for a particular complex should be the same for different cells. Moreover, the stability constants are related to a given ionic strength, i.e. to $I = 0.1$ mol kg^{-1}, which is common for all the half-cell solutions.

The numerical treatment was performed assuming the presence of one or two chloro complexes in the half-cells, in accordance with the observations mentioned above. The calculations were performed using the literature data for the solubility product of AgCl and the instability constants of $AgCl_2^-$ in DMSO.[10]

The resulting values of concentration stability constants are presented in Table 2. As is seen, copper(II) and zinc(II) exhibit higher stability for complex formation than manganese(II), cobalt(II) and nickel(II). The value for the dichloro complex of copper(II) should be considered as an approximation only. Its high uncertainty arises from a drift of the potential of the respective half-cell during the experiments. A similar effect was observed previously for the analogous DMA system,[6] and may be related to the processes involving the reduction of the Cu^{2+} cation. However, the high value of Q_2^{Cu} explains the electrolytic behaviour of copper(II) chloride in DMSO solution reported by Libuś *et al.*[11] The molar conductance of $CuCl_2$ decreases rapidly with increasing concentration of the solute, and amounts to *ca* 7.0 S cm^2 mol^{-1} for the most concentrated solution (0.01 mol dm^{-3}), while the limiting molar conductance of the $Cu(DMSO)_6^{2+} \cdot 2Cl^-$ complex electrolyte has a value of 88.8 S cm^2 mol^{-1}. The pronounced ability of the Zn^{2+} cation for chloro complex formation is a consequence of its natural tendency to be in a tetrahedral environment. The dichloro complex of zinc(II) is the most favoured species in DMSO solution while the monochloro complex exists in a very narrow range.[12] The values obtained for the $CoCl^+$ and $NiCl^+$ complexes compare well with those of 2.78 and 2.47 reported by Libuś on the basis of the spectrophotometric and conductometric measurements.[11]

The data presented in this paper confirm a monotonic decrease in stability from manganese(II) to nickel(II) for the monochloro complexes of the divalent transition metal cations in DMSO solution. Unfortunately, the extremely high stability of the dichloro complex of copper(II) makes derivation of the stability constants for the monochloro complex impossible.

Table 2. The concentration stability constants of the mono- and dichloro complexes of the divalent transition metal cations in DMSO at 25°C ($I = 0.1$ mol kg^{-1})

M^{2+}	log Q_1^M	log Q_2^M
Mn^{2+}	2.83 (±0.05)	—
Co^{2+}	2.60 (±0.05)	—
Ni^{2+}	2.45 (±0.04)	—
Cu^{2+}	—	10.5 (±1.0)
Zn^{2+}	4.08 (±0.05)	9.8 (±0.1)

Acknowledgements—This work was supported by Program C.P.B.P.-01.15, Poland.

REFERENCES

1. W. Libuś, R. Pastewski and T. Sadowska, *J. Chem. Soc., Faraday Trans.* 1982, **78**, 377.
2. W. Grzybkowski and M. Pilarczyk, *J. Chem. Soc., Faraday Trans.* 1986, **82**, 1745.
3. L. R. Solomon, A. M. Bond, J. W. Bixler and D. R. Hallenbeck, *Inorg. Chem.* 1983, **22**, 1644.
4. Z. Libuś and H. Tiałowska, *J. Solution Chem.* 1975, **4**, 1011.
5. H. Irving and R. Williams, *J. Chem. Soc.* 1953, 3192.
6. H. Strzelecki and R. Pastewski, *Bull. Pol. Ac. Chem.* 1987, **35**, 31.
7. J. G. Ives and G. J. Janz, *Reference Electrodes.* Academic Press, New York (1961).
8. W. Libuś, W. Grzybkowski and R. Pastewski, *J. Chem. Soc., Faraday Trans.* 1, 1981, **77**, 147.
9. E. Kamieńska and I. Uruska, *Electrochim. Acta* 1977, **22**, 181.
10. R. Alexander, E. C. F. Ko, Y. C. Mac and A. J. Parker, *J. Am. Chem. Soc.* 1967, **89**, 3703.
11. W. Libuś, M. Pilarczyk and T. Szuchnicka, *Electrochim. Acta* 1980, **25**, 1033.
12. S. Ahrland and N.-O. Björk, *Coord. Chem. Rev.* 1975, **16**, 115.

Polyhedron Vol. 7, No. 24, pp. 2477–2486, 1988
Printed in Great Britain

0277–5387/88 $3.00+.00
© 1988 Pergamon Press plc

THE BEHAVIOUR OF SOME SELENOGLYCOLLIC ACID DERIVATIVES IN AQUEOUS SOLUTIONS AND SPECTROPHOTOMETRIC DETERMINATION OF CONSTANTS OF THE SYSTEM Pd(II)/ETHYLENE-BIS-SELENOGLYCOLLIC ACID

LUIZ R. M. PITOMBO* and ERMELINDO FLUMIGNAN

Departamento de Química Fundamental, Instituto de Química, Universidade de São Paulo, São Paulo, Brazil

(*Received* 4 *March* 1988; *accepted* 14 *April* 1988)

Abstract—Interactions between ethylselenoglycollic, selenoglycollic and ethylene-bis-selenoglycollic acids and some "soft", "borderline" and "hard" metallic ions have been studied. The interactions of $[PdCl_4]^{2-}_{aq}$ with the three ligands were verified conductometrically and spectrophotometrically. The stability constants β_1 and β_2 for the system $[PdCl_4]^{2-}$–ethylene-bis-selenoglycollic acid have been determined at 25°C at ionic strength 3.0 M (NaCl). The stoichiometric ionization constant of the mentioned acid was also studied.

In this paper we report the results of the systematic comparison of organic sulphur and selenium compounds concerning their use as analytical reagents.

In a previous paper in this series,[1] the behaviour of four thioglycollic acid derivatives was studied, using several analytical applications.[2–4]

Taking into account the general purpose of this work, it was decided to extend the studies to three selenoglycollic acid derivatives: ethylselenoglycollic acid ($L_1 = H_5C_2$—Se—CH_2COOH), selenodiglycollic acid (L_2 = HOOC—CH_2—Se—CH_2COOH) and ethylene-bis-selenoglycollic acid (L_3 = HOOC—CH_2—Se—CH_2—CH_2—Se—CH_2—COOH).

EXPERIMENTAL

Apparatus

Absorbance spectra were obtained with a Beckman spectrophotometer model DBG, and a Zeiss spectrophotometer model DMR-10 coupled with a Fluke digital voltimeter model 820 A was used for absorbance measurements. All these were carried out in 1.00 cm silica cells at 25±0.5°C.

For pH measurements, a Metrohm Herisau, model E 448 was used. Conductance measurements were obtained with a conductivity bridge model Metrohm Herisau E 382 and a conductivity cell model Metrohm Herisau EA 608 (0.76 cm^{-1} platinized platinum, at 25±0.5°C). IR spectra were obtained on a Perkin–Elmer model 337. In the determination of the ionization constants of L_3, an Orion Research model 801-A digital potentiometer with combined glass and silver/silver chloride electrodes was used for pH measurements using hydrochloric acid at 3.0 M (NaCl) ionic strength as a reference.[5] All measurements were made at 25±0.5°C at 3.0 M (NaCl) ionic strength.

Reagents

Ethylselenoglycollic acid (L_1). The ethyldiselenide was prepared by the method of Backer and Van Dan,[6] but using Na_2Se_2 obtained *in situ*.[7]

The required acid was prepared by the following procedure. To 30 cm^3 of ethanol, under a nitrogen stream, containing 21.6 g (0.1 mol) of ethyldiselenide, 60 cm^3 of an aqueous solution containing 12 g of NaOH and 9.4 g of $NaBH_4$ were carefully added. The solution was stirred until discolouration occurred. To this cooled solution, 60 cm^3 of aqueous solution of monochloroacetic acid (previously neutralized with Na_2CO_3) was dropwise added. After leaving for 17 h, the solution was

* Author to whom correspondence should be addressed.

acidified with H_2SO_4 (1 M at pH = 2), and extracted with ether over 6 h.

The oily product after the elimination of ether yielded 28.5 g (85.4%). The IR spectrum, in CCl_4, agreed with the literature.[8] The sodium salt was obtained by adding 20% NaOH solution to give pH 6.5, and then adding an excess of acetone (m.p. 194–195°C with decomposition; yield—92.5%). Found: C, 25.0; H, 3.9. Calc.: C, 25.4; H, 3.7%. The salt is hygroscopic.

Selenodiglycollic acid (L_2). The compound was obtained following the general method for the preparation of selenoethers proposed by Klayman[7] (m.p. 107–108°C; literature m.p. 109°C;[9] yield 68%).

IR data (KBr); ν_{COOH} (3.000–2500 cm^{-1}); ν_{CO} (1.716 cm^{-1}); δ_{CH_2} (1.441 cm^{-1}).

The sodium salt was obtained in the same way as above (m.p. 300°C with decomposition; yield 95.5%). Found: C, 20.6; H, 1.7. Calc.: C, 19.9; H, 1.7%.

Ethylene-bis-selenoglycollic acid (L_3). The acid was prepared by the method of Pitombo, Flumignan and Umemura,[10] the yield was 87% (m.p. 152–153°C; literature m.p. 153–154°C).[11]

The sodium salt was prepared by the usual method (m.p. 300°C with decomposition; yield 98%). Found: C, 21.3; H, 2.3. Calc.: C, 20.7; H, 2.3%.

Standard L_1, L_2 and L_3 sodium salts solutions. 0.1 M solutions of L_1, L_2 and L_3 sodium salts were prepared. They were standardized by passage through a resin column in the acid from (Amberlite IR-120) and titration with standard sodium hydroxide solution.

Standard palladium solution. This was prepared from palladium chloride (Riedel-de Haen AG Seelze–Hannover) to contain *ca* 1.20 mg/Pd(II) cm^{-3} in 0.1 M hydrochloric acid. The solution was standardized gravimetrically with dimethylglyoxime.

Solutions of diverse ions. Stock solutions containing *ca* 10 mg cm^{-3} of the metallic ion were prepared from their chlorides or sulphates in water. To prevent hydrolysis, in some experiments 0.1 M hydrochloric or sulphuric acids were used. For lead, acetate was used.

The sodium perchlorate solution for ionic strength control was standardized gravimetrically, by evaporating an aliquot in an oven, first at 80°C and later at 110°C until it reached constant weight. Standard sodium chloride solution was prepared by weighing the correct amount of NaCl. All inorganic chemicals used were of analytical grade.

Isolation of $Pd(L_3)_2$. Solid NaCl was added (to adjust the ionic strength to 3.0 M) to a 50 cm^3 solution containing 0.363 g (3.4 mmol) of Pd(II) at pH 1.0 (hydrochloric acid). To this solution, with continuous stirring, 69 cm^3 of solution containing 2.44 g (7 mmol) of $Na_2(L_3)$ was added. After 48 h in a refrigerator, the yellow crystals formed were filtered off, washed with cold water (yield—2.37 g, 94%; decomposed at 158–168°C). Found: C, 18.7; H, 2.53. Calc. for $(HOOCCH_2SeC_2H_4SeCH_2COOH)_2PdCl_2$: C, 18.3; H, 2.57%. This isolated compound showed a maximum in aqueous solution in the same spectral region as the 2:1 species.

RESULTS AND DISCUSSION

Preliminary studies—visual changes

Due to the lack of information on the behaviour of the three mentioned ligands, visual changes were observed in acidic solutions (0.1 M) of some "soft", "borderline" and "hard" Lewis acids. To one drop of these solutions (500 μg per drop) several drops of an aqueous solution, 2×10^{-2} M of the sodium salt of reagents L_1, L_2 or L_3 were added. To verify the acidity dependence in these interactions, one drop of 70% perchloric acid was added before the addition of the ligand solution.

The perceptible interactions are shown in Table 1. No reactions were observed with any of the ligands with Zn(II), Os(IV) and Rh(III).

More visual changes were observed with these three ligands in comparison with the corresponding sulphur derivatives.[4] Interesting inversions were detected; while the sulphur compounds form precipitates with Hg(II), the selenium species do not; with regards to Ag(I) the reverse was observed (with L_1 and L_2).

In order to obtain more information about the interactions of the three ligands and the metallic ions mentioned above, conductimetric titrations were carried out in "neutral" (salts aqueous solutions) and in acid solutions (within the compatible limits—$[H^+] = 4.0 \times 10^{-2}$ M; $[Me^{n+}] = 1.0 \times 10^{-3}$ M; $[L^{n-}] = 1.0 \times 10^{-2}$ M; $t = 25 \pm 0.5$°C). (See Table 2.)

Although the conductimetric titrations give only preliminary data about complex formation and nothing with relation to chelation phenomena,[14] some considerations arise from the results obtained.

In acid media for almost all "hard" and "borderline" metallic ions studied, the molar ratio (L : M) changed. During the titration in this medium, if it is assumed that the pH could vary within the range 2–3, the species present in the higher percentages is probably monoprotonated for ligand L_1, and diprotonated for ligands L_2 and L_3.[1] Therefore, under these conditions ligand L_1 and L_2 could act

Table 1. Visual changes with ligands L_1, L_2 and L_3[a]

Metallic ion		Ligand L_1	L_2	L_3
Fe(III)		+	+	++
	(H^+)	0	0	0
Co(II)		0	+	0
	(H^+)	0	0	+
Ni(II)		0	+	+
	(H^+)	0	0	0
Cu(II)		+	+	+
	(H^+)	+	+	+
Cd(II)		0	++	0
	(H^+)	0	0	0
Pb(II)		0	+++	++
	(H^+)	0	0	0
Ag(I)		++	++	++
	(H^+)	++	++	0
Hg(II)		0	0	0
	(H^+)	0	0	++
Ru(III)		+	+	++
	(H^+)	0	0	+
Ir(IV)		+	+	+
	(H^+)	+	+	+
Pd(II)		+	+	+
	(H^+)	+	+	+
Pt(IV)		+	+	+
	(H^+)	+	+	+
Pt(IV)*hv*		+	+	++
	(H^+)	+	+	+
Au(III)		++	++	++
	(H^+)	++	++	++

[a](H^+) acidity increased; (0) no change; (+) colour change; (++) precipitation; (+++) precipitate dissolves in excess of ligand; *hv* light from a photo-flood 500 W bulb over a 10 min period (previously filtered by distilled water).

as monodentate and L_3 as bidentate. Further investigations should be run to clarify these considerations.

Taking into account the visual changes, the results again presented a promising selectivity with respect to Pd(II) in an acid medium and undoubted interactions of Pt(IV) with the ligands appeared, although this kind of interaction is scarcely studied.[15] Considering the precipitation as a signal, in acid medium ligands L_1 and L_2 presented fairly good selectivity in respect to silver, and ligand L_3 in respect to mercury.

Aiming at a better understanding of the behaviour of the selenium donor atom in the complexation with Pd(II) it was decided to study their interactions with L_1, L_2 and L_3 and also determine the formal constants for the system Pd(II)/L_3 under the same conditions as the corresponding sulphur compound.[16]

INTERACTIONS OF Pd(II), L_1, L_2 AND L_3

Reactions of Pd(II) *with sodium ethylselenoglycollate*

Conductimetric titrations in the aforementioned conditions, showed only the species with molar ratio 2:1 (L:M).

The changes in the $[PdCl_4]^{2-}_{aq}$ absorption spectra were recorded, after suitable amounts of ligands (molar ratios L:M varied from 0 to 10) were added to 3.02×10^{-5} M palladium solutions (pH = 1.5 ± 0.1; $t = 25\pm0.5$°C; $I = 0.5$ M). In the molar ratio 1:1, the characteristic $[PdCl_4]^{2-}_{aq}$ maximum (278 nm) disappeared and for the molar ratio 2:1, a well defined maximum at 280 nm appeared and remained constant until the ratio reached 10:1. The absorbance values also became constant above a 3:1 ratio, see Fig. 1.

The molar ratio method applied to this system (225, 263, 280 and 285 nm; $[Pd^{2+}] = 3.02\times10^{-5}$ M; pH = 1.5 ± 0.1; $I = 0.5$ M; $t = 25\pm0.5$°C) provided evidence for 1:1, 2:1 and 3:1 composition of the three complexes. The 1:1 and 2:1 species are quite well defined using all the wavelengths mentioned, and the 3:1 species also appeared clearly at 263, 280 and 285 nm.

Reactions of Pd(II) *with sodium selenodiglycollate*

Using conductimetric titrations, under similar conditions as mentioned above, two species (1:1 and 2:1) were found.

Following similar molar ratio variations in the same experimental conditions as above, the 1:1 ratio eliminated the $[PdCl_4]^{2-}_{aq}$ maximum, and above the ratios 5:1 to 10:1, a defined maximum with constant absorbance values was observed at 275 nm, see Fig. 2.

Molar ratios (L:M) ranging from 0:1 to 5:1 at 225, 263, 278 and 285 nm, under the same conditions, indicated the existence of 1:1 and 2:1 complexes.

Reactions of Pd(II) *with sodium ethylene-bis-selenoglycollate*

Two species 1:1 and 2:1 were found using conductometric titrations under the same conditions. The spectral changes were recorded (similar experimental conditions), and with equimolar amounts of ligand and metal, two maxima at 270 and 395 nm appeared. The 395 nm band disappeared and

Table 2. Ligand–metal molar ratios obtained from conductimetry titration[a]

Metallic ions	L_1		L_2		L_3		L_2 Lit. values (ref.)	
	Neutral	Acid	Neutral	Acid	Neutral	Acid		
Fe(III)	0	3:2	0	1:1, 2:1	0	1:1, 2:1		
Co(II)	1:1, 2:1	2:1	+	1:1, 2:1	1:1	2:1	1:1	(12)
Ni(II)	1:1	1:1	1:1	1:1, 2:1	1:1	1:1, 2:1	1:1, 2:1	(12)
Cu(II)	1:1, 2:1	1:1, 2:1	1:1, 2:1	2:1	1:1	1:1	1:1, 2:1	(12)
Zn(II)	1:1, 2:1	2:1	+	2:1	2:1	1:1, 2:1	1:1	(12)
Cd(II)	1:1	+	+	+	1:1	2:1	1:1	(12)
Pb(II)	1:1	+	1:1	3:2	1:1	+	1:1	(12)
Ag(I)	1:1, 2:1	+	1:2	+	1:1, 2:1	+	1:1, 2:1	(13)
Hg(II)	0	2:1	0	1:1, 2:1	0	1:1		
Ru(III)	0	1:1, 2:1	0	1:2, 1:1 2:1	0	1:1		
Ir(IV)	0	+	0	1:1	0	1:1		
Rh(III)	0	1:1, 2:1	0	1:1	0	1:1		
Pt(IV)	0	1:1, 2:1	0	1:1, 2:1	0	1:1, 2:1 3:2		
Pt(IV)*hv*	0	1:1, 2:1	0	1:1, 2:1	0	1:1, 2:1		
Au(III)	0	1:1	0	1:1, 2:1	0	2:1		

[a] (0) difficult to perform in neutral medium; (+) no inflections were detected in the plots. *hv*, same light source as previously mentioned.

the 270 nm maximum was shifted to 310 nm when the ligand to metal ratios were increased, and absorbance values became constant from L:M ratios of 3:1 to 10:1.

The compositions of the complexes were confirmed by the molar ratio method at 265, 270, 310 and 320 nm in similar conditions as above (see Fig. 3).

Ligand 1 with respect to Pd(II), in acid medium probably acts as monodentate forming the species $[PdCl_3L_1]^-_{aq}$, $[PdCl_2(L_1)_2]^0$ and $[PdCl(L_1)_3]^+_{aq}$; ligand 2 also behaves as monodentate and similarly to all thioethers. Ligand 3 behaves as bidentate identical to the sulphur analogues,[16] forming $[PdCl_2(L_3)]^0_{aq}$ and $[Pd(L_3)_2]^{2+}_{aq}$.

The bathochromic trend proposed[17] for selenium palladium complexes was confirmed. While ethylthioglycollic and thiodiglycollic complexes did not present definite maxima within 250–300 nm,[1] the corresponding selenium compounds showed respective maxima at 280 and 275 nm. A similar shift was detected in ligand 3; the sulphur compound presented a maximum at 290 nm[1] and selenium complexes at 310 nm.

L_3 *stoichiometric ionization constants*

Following the method proposed by Speakman,[18] a set of eight solutions was prepared containing L_3 at an analytical concentration of 4.00×10^{-3} M and ionic strength 3 M (NaCl). By using correct 0.101 M NaOH volume additions the C_{NaOH} value ranged from 2.02 to 6.06×10^{-3} M corresponding to 25–76% of hydrogenic ionic concentration. The final volume was 10.00 cm^3.[18] Before each pH measurement at 25 ± 0.5°C, N_2 was bubbled through the solution for 10 min. The pH values ranged from 3.56 to 4.46 (formal pH).

The stoichiometric constants were found by solving the proposed equation,[18] and the linear fit (after least-squares treatments) between x and y values was checked.

$$K_1 = 2.20 \times 10^{-4} \text{ M } (pK_1 = 3.61)$$

$$K_2 = 5.68 \times 10^{-5} \text{ M } (pK_2 = 4.24).$$

It is interesting to note that both pK_1 and pK_2 of ethylene-bis-thioglycollic ($pK_1 = 3.46$; $pK_2 = 4.10$; $I = 2$ M)[19] and ethylene-bis-selenoglycollic acids increase. Regarding the hetero atoms, Suzuki[12] suggested that this order agrees with the decreasing electronegativity and the increasing size of the O, S and Se atoms. Sandell[20] also reported that some alkoxyacetic acids are stronger than the corresponding alkylthio derivatives. It seems that these two factors affect the acid strength of these acids.

On the basis of these values, calculations of α_0, α_1 and α_2 and plotting the relative amounts of the species at different pH values indicate that, in the pH range 1–2 the predominant form present is the diprotonated one and at pH 6 the predominant form is the ligand as a free anion.

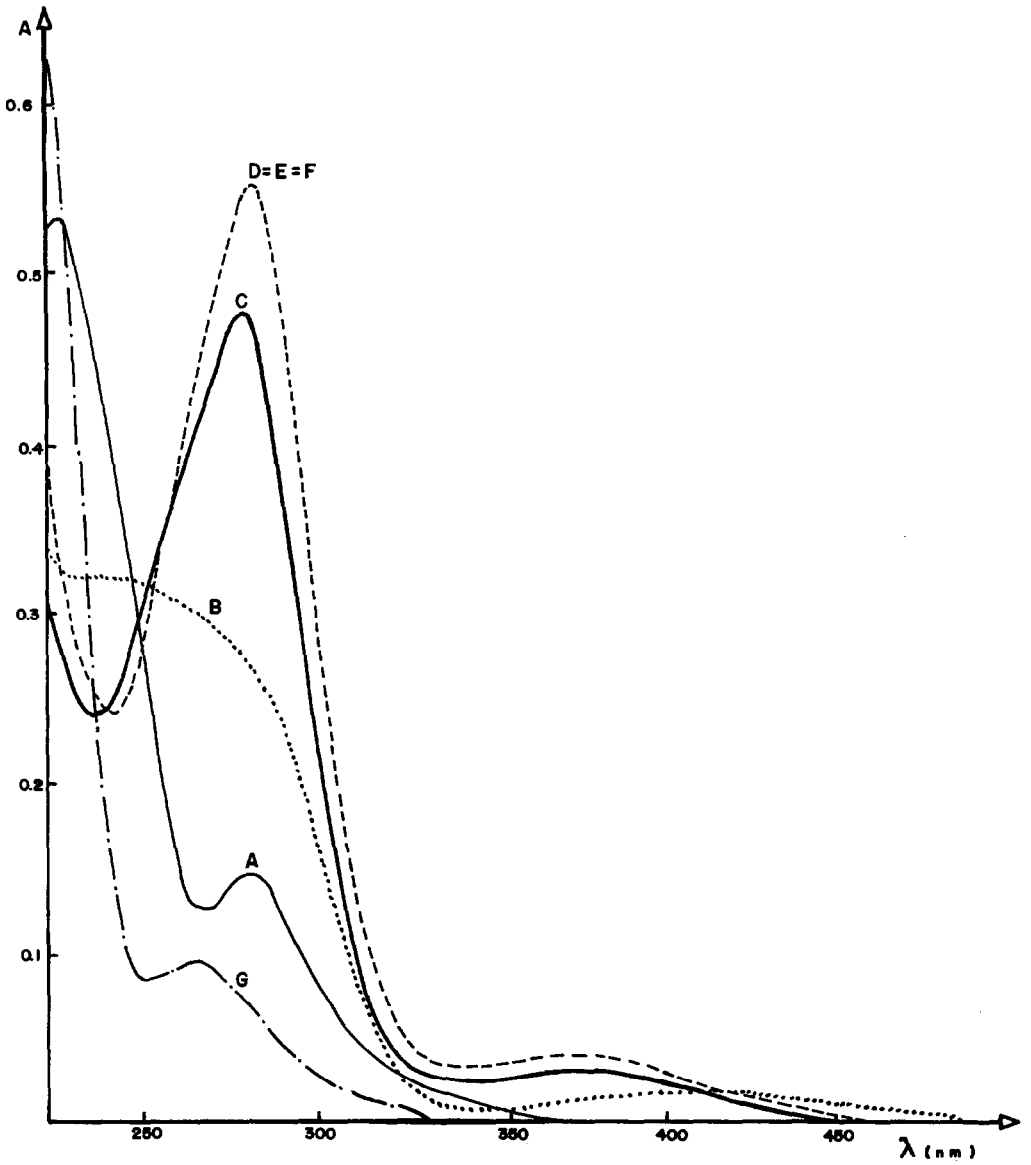

Fig. 1. Absorption spectra for Pd(II)/L_1 system. Values for $C_{Pd(II)}$ and $C_{L_1^-}$, respectively: (A) 3.02×10^{-5} M, no value; (B) 3.02×10^{-5} M, 3.01×10^{-5} M; (C) 3.02×10^{-5} M, 6.03×10^{-5} M; (D) 3.02×10^{-5} M, 9.04×10^{-5} M; (E) 3.02×10^{-5} M, 1.54×10^{-4} M; (F) 3.02×10^{-5} M, 3.01×10^{-4} M; (G) no value, 3.01×10^{-4} M. $I = 0.5$ M ($NaClO_4$), $t = 25\pm0.5$°C. Optical path = 1.00 cm, pH = 1.5 ± 0.1. Measurements against respective reagent blank.

Determination of Pd(II)/L_3 *system constants*

Taking into account the data reported before, the formations of the two species could be represented by

$$[PdCl_4]^{2-}_{aq} + L_{3aq} \overset{\beta_1}{\rightleftharpoons} [PdCl_2L_3]^0_{aq} + 2Cl^-_{aq} \quad (1)$$

$$[PdCl_4]^{2-}_{aq} + 2L_{3aq} \overset{\beta_2}{\rightleftharpoons} [Pd(L_3)_2]^{2+}_{aq} + 4Cl^-_{aq}. \quad (2)$$

To assure only the existence of $[PdCl_4]^{2+}_{aq}$ high chloride concentrations and pH 1 are necessary.[21,22] As pointed out before at this pH the ligand is present as the diprotonated acid.

Thus in equilibrium (1), one L_3 should replace two chloride ions forming a mixed complex (1 : 1 species); probably the ligand will act as bidentate, bonding the metal to the two selenium atoms (five-membered ring). In equilibrium (2), four chloride ions should be replaced by two ligands resulting in the 2 : 1 species.

On the basis of the previous data obtained, it seems that the corresponding solution methods[23,24] will give the more consistent values of $\bar{n}$ and [L] to

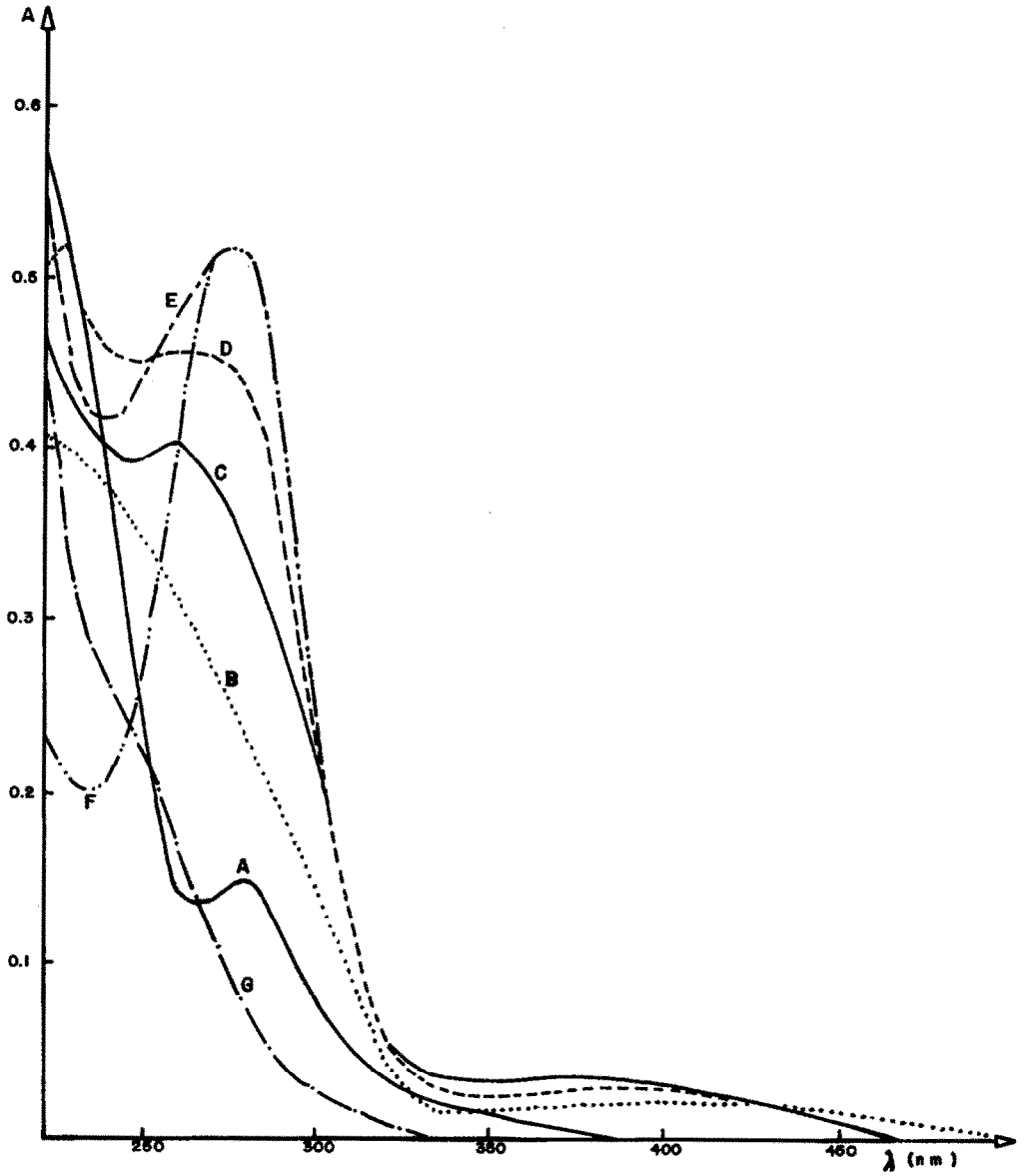

Fig. 2. Absorption spectra for Pd(II)/L_2 system. Values for $C_{Pd(II)}$ and $C_{L_2^{2-}}$, respectively: (A) 3.02×10^{-5} M, no value; (B) 3.02×10^{-5} M, 3.02×10^{-5} M; (C) 3.02×10^{-5} M, 6.04×10^{-5} M; (D) 3.02×10^{-5} M, 9.05×10^{-5} M; (E) 3.02×10^{-5} M, 1.51×10^{-4} M; (F) 3.02×10^{-5} M, 3.02×10^{-4} M; (G) no value, 3.02×10^{-4} M. $I = 0.5$ M ($NaClO_4$), $t = 25\pm0.5$°C. Optical path = 1.00 cm, pH = 1.5 ± 0.1. Measurements against respective reagent blank.

be used in the calculation of constants. The great discrimination between the absorbance values of the metal solutions and the complex solutions, indicated that wavelengths of 300, 310 and 320 nm should be used for the measurements.

Determination at 300 nm

Three sets of nine solutions in 10.0 cm^3 volumetric flasks were prepared. In each set, the palladium concentration was maintained constant and the ligand concentration ranged within the correct limits. Table 3 presents the absorbance values obtained and the respective calculated molar absorptivities.

The three curves (ε/C_{L_2}) obtained were adjusted using the "curve fitting" procedure.[25] This procedure aims to decrease the graphical errors of the C_L values taken from the curves. Thus, for this curve, C_L^e values were estimated for the ε_i chosen in the fitted curve.

On the basis of C_M^I, C_M^{II} and C_M^{III} values and the

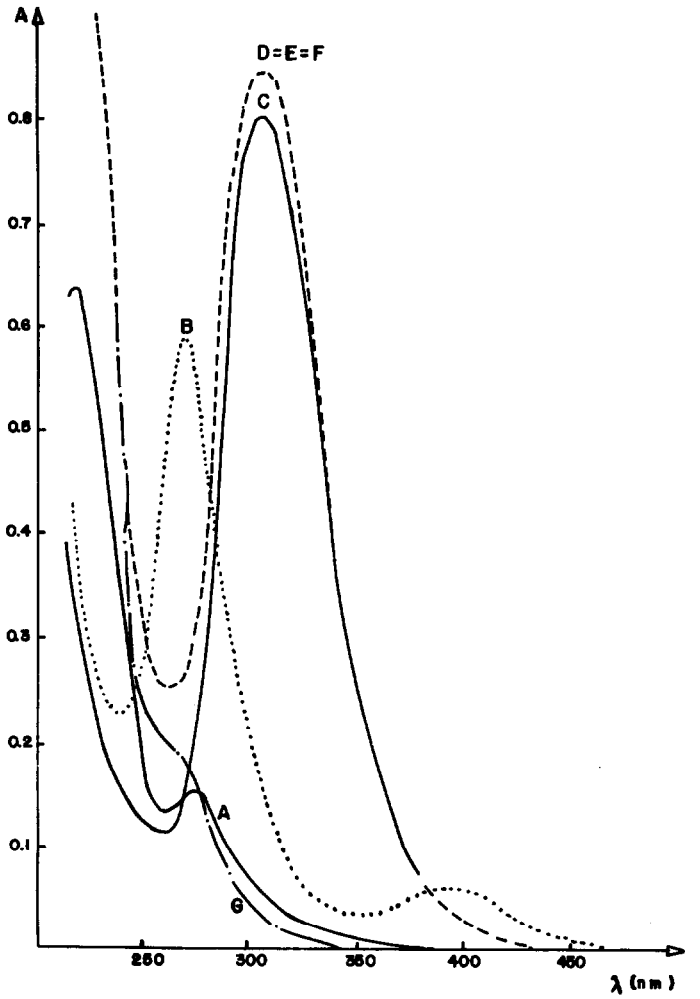

Fig. 3. Absorption spectra for Pd(II)/L_3 system. Values for $C_{Pd(II)}$ and $C_{L_3^{2-}}$, respectively: (A) 3.02×10^{-5} M, no value; (B) 3.02×10^{-5} M, 3.02×10^{-5} M; (C) 3.02×10^{-5} M, 6.04×10^{-5} M; (D) 3.02×10^{-5} M, 9.05×10^{-5} M; (E) 3.02×10^{-5} M, 1.51×10^{-4} M; (F) 3.02×10^{-5} M, 3.02×10^{-4} M; (G) no value, 3.02×10^{-4} M. $I = 0.5$ M (NaCl), $t = 25\pm0.5$°C. Optical path = 1.00 cm, pH = 1.5 ± 0.1. Measurements against respective reagent blank.

Table 3. Absorbance and molar absorptivities of the $[PdCl_4]^{2-}/L_3$ system. $I = 3.0$ M (NaCl), pH = 1.0, $t = (25.0\pm0.5)$°C, $\lambda = 300$ nm, $C_M = [PdCl_4]^{2-}$ concentrations, C_{L_3} = ligand concentrations, ε = molar absorptivity

Solutions	$C_M^I = 3.02\times10^{-5}$ M		$C_M^{II} = 3.42\times10^{-5}$ M		$C_M^{III} = 4.02\times10^{-5}$ M	
	$C_{L_3}\times10^{-5}$ M	$\varepsilon\times10^3$	$C_{L_3}\times10^{-5}$ M	$\varepsilon\times10^3$	$C_{L_3}\times10^{-5}$ M	$\varepsilon\times10^3$
1	0.00	4.64	0.00	4.56	0.00	4.55
2	1.61	5.89	1.61	5.76	1.61	5.60
3	3.02	7.62	3.02	7.05	3.02	6.75
4	4.02	9.11	4.02	8.30	4.02	7.71
5	5.03	10.2	5.03	9.59	5.03	9.99
6	6.04	11.3	6.04	10.6	6.04	9.93
7	7.44	12.3	7.44	11.8	7.44	11.2
8	9.05	13.6	9.05	12.9	9.05	12.3
9	10.7	14.2	10.7	14.0	10.7	13.4

corresponding $C_{L_3}^{el}$, $C_{L_3}^{ell}$ and $C_{L_3}^{elll}$, linear regression was applied and using the general equation $C_L = \bar{n}C_M + [L]$, experimentals $\bar{n}$ ($\bar{n}_{exp}$) and $[L_3]([L_3]_{exp})$ were obtained.

Fronaeus[26] suggested an equation that transforms the experimental $\bar{n}$ into the Leaden function ($F_0(x)$)[27] by an integration process. To ensure a significant contribution of the first species ($\bar{n} < 0.5$), the integration started using a small ligand concentration. In such conditions the equation

$$F_0(x) = \frac{1}{1-\bar{n}}$$

provides the smaller $(F_0(x)_i)$. From $\log F_0(x)_i$ small increments of $\bar{n}$ and $[L_3]$ generated the respective $\Delta \log F_0(x)$. Considering the area beneath the curve as the sum of small triangles and rectangles for the mentioned increments, this area was calculated on a programmable calculator as

$$\log F_0(x) = \tfrac{1}{2}(\bar{n}_2 - \bar{n}_1)(\log[L_3]_2 - \log[L_3]_1) + \bar{n}_1(\log[L_3]_2 - \log[L_3]_1).$$

As the integration curve process successively requires a greater number of $\bar{n}$ and $[L_3]$ values, this was achieved by the normalization of the curve $\bar{n}/[L_3]$. The experimental curve obtained was normalized through the least-squares method following the procedure reported by Neves,[28] and using a programmable calculator to solve the matrix (second approximation). (See Fig. 4.)

The $\bar{n}$ and $[L_3]$ normalized values obtained ($\bar{n}_{norm}$ and $[L_3]_{norm}$) allowed the integration process to be used. These values presented as the calculated $F_0(x)$ and $F_1(x)$ values are shown in Table 4.

The $F_0(x)$ and $F_1(x)$ data were plotted versus $[L_3]$. The $F_1(x)$ subsidiary functions ($F_1(x) = \beta_1 + \beta_2 L_3$) showed a linear relation with $[L_3]$, in the range 2.0–1.9×10^{-7} M, and by applying the linear regression to this ($r^2 = 0.998$) β_1 and β_2 values were generated. The same procedure was performed at 310 and 320 nm.

The β_1 and β_2 values were also determined at 300, 310 and 320 nm using the Rossotti equation[29] and the Irving and Rossotti criteria for $\bar{n}$ values.[30]

$$\frac{\bar{n}}{(1-\bar{n})[L_3]} = \beta_1 + \frac{(2-\bar{n})[L_3]}{(1-\bar{n})}\beta_2.$$

The convenient[30] $\bar{n}$ and $[L_3]$ values (Table 4) were applied to the above equation and via linear regression application to the values obtained ($r^2 = 0.998$) the desired values of β_1 and β_2 were found. The values found are summarized in Table 5.

These equilibrium constants do not include exponential terms for the chloride contribution, as the ion concentration was kept constant (3 M) in all the measurements.

Table 4. Normalized $\bar{n}$ and $[L_3]$ values and $F_0(x)$ and $F_1(x)$ calculated, $\lambda = 300$ nm

$[L]_{norm}$	$\bar{n}_{norm}$	$F_0(x)$	$F_1(x)$
5.00×10^{-8}	0.106	1.12	—
7.00×10^{-8}	0.137	1.17	2.36×10^6
1.00×10^{-7}	0.184	1.23	2.34×10^6
1.25×10^{-7}	0.221	1.29	2.33×10^6
1.50×10^{-7}	0.257	1.35	2.32×10^6
2.00×10^{-7}	0.327	1.47	2.33×10^6
2.50×10^{-7}	0.394	1.54	2.36×10^6
3.00×10^{-7}	0.456	1.72	2.39×10^6
3.50×10^{-7}	0.516	1.85	2.43×10^6
4.00×10^{-7}	0.572	1.99	2.48×10^6
4.50×10^{-7}	0.624	2.14	2.52×10^6
5.00×10^{-7}	0.674	2.29	2.57×10^6
5.50×10^{-7}	0.720	2.44	2.63×10^6
6.00×10^{-7}	0.764	2.61	2.68×10^6
6.50×10^{-7}	0.804	2.78	2.73×10^6
7.00×10^{-7}	0.842	2.95	2.79×10^6
7.50×10^{-7}	0.877	3.13	2.84×10^6
8.00×10^{-7}	0.910	3.32	2.90×10^6
8.50×10^{-7}	0.940	3.51	2.95×10^6
9.00×10^{-7}	0.968	3.70	3.01×10^6
9.50×10^{-7}	0.993	3.91	3.06×10^6
1.00×10^{-6}	1.02	4.11	3.11×10^6
1.10×10^{-6}	1.06	4.54	3.22×10^6
1.20×10^{-6}	1.09	4.99	3.32×10^6
1.30×10^{-6}	1.12	5.45	3.42×10^6
1.40×10^{-6}	1.14	5.32	3.52×10^6
1.50×10^{-6}	1.15	6.41	3.61×10^6
1.60×10^{-6}	1.16	6.91	3.69×10^6
1.70×10^{-6}	1.17	7.41	3.77×10^6
1.80×10^{-6}	1.18	7.43	3.85×10^6
1.90×10^{-6}	1.18	8.46	3.92×10^6
2.00×10^{-6}	1.19	8.99	3.99×10^6
2.10×10^{-6}	1.19	3.52	4.06×10^6
2.20×10^{-6}	1.19	10.1	4.12×10^6
2.30×10^{-6}	1.20	10.6	4.18×10^6
2.40×10^{-6}	1.21	11.2	4.24×10^6
2.50×10^{-6}	1.22	11.7	4.30×10^6

The comparison of β_1 and β_2 values is presented in Table 6.

Ahrland[31] reported that in Ag(I) complexes, with ligands such as R—E—$C_6H_4SO_3^-$ (E = O, S and Se) the first constant values follow the order S ≃ Se ≫ O. Pettit and coworkers[9,32] also reported an extensive study on the Ag(I) interaction with organic ligands such as R—E—$(CH_2)_n$—COOH and E$(CH_2)_n$—COOH (E = O, S, Se and Te) and concluded from the constant values that the stability order of the derivatives follows Te > Se > S ≫ O.

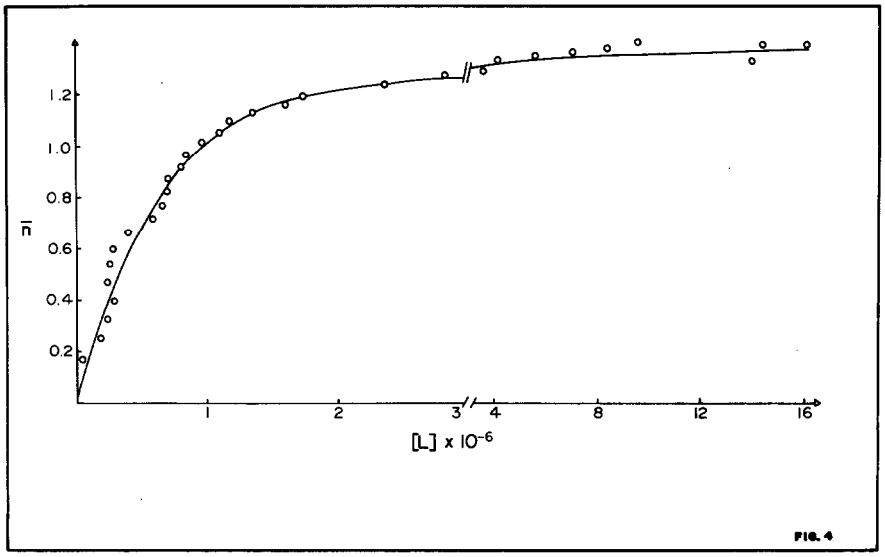

Fig. 4. Formation curve for $[PdCl_4]^{2-}/L_3$ system, $\lambda = 300$ nm. Normalized curve through second approximation matrix calculation. ○—experimental points ($\bar{n}_{exp}$ and $[L]_{exp}$).

Table 5. β_1 and β_2 values for the $[PdCl_4]^{2-}/L_3$ system ($I = 3.0$ M; pH = 1.0; $t = 25°C$)

	Method 1 (Leden)		Method 2 (Rossotti and Rossotti)	
λ (nm)	β_1	β_2	β_1	β_2
300	2.10×10^6 M	9.89×10^{11} M^2	2.21×10^6 M	1.04×10^{12} M^2
310	2.04×10^6 M	8.25×10^{11} M^2	2.01×10^6 M	8.68×10^{11} M^2
320	1.99×10^6 M	8.75×10^{11} M^2	2.21×10^6 M	8.84×10^{11} M^2
Average	$(2.04 \pm 0.06) \times 10^6$ M	$(9.0 \pm 0.8) \times 10^{11}$ M^2	$(2.1 \pm 0.1) \times 10^6$ M	$(9.3 \pm 0.9) \times 10^{11}$ M^2

Table 6

	$[PdCl_4]^{2-}/L_3$(method 1)	$[PdCl_4]^{2-}/^{\text{sulphur}}_{\text{corresponding ligand}}$[16]
β_1 (K_1)	2.04×10^6 M	2.74×10^4M
K_2	4.41×10^5 M	2.68×10^2 M
β_2 ($K_1 K_2$)	9.0×10^{11} M^2	7.34×10^6 M^2

The data presented in Table 6 show a similar trend which is in agreement with the statement that selenium is more "soft" than sulphur[32a,b] and therefore can form stronger bonds with the low-spin d^8 Pd(II) ion.

As Ag(I) (d^{10} ions) showed the same trend, a hypothesis could be formed from the results obtained: for the low-spin d^8 ions, Pd(II), Pt(II) and Au(II) and for the d^{10} ions, Cu(I), Ag(I), Au(I) and Hg(II), the complexes formed with selenium as the donor atom will be stronger than the similar complex containing sulphur.

Acknowledgements—The authors are grateful to Coordenação do Aperfeiçoamento de Pessoal de Nível Superior (CAPES) and the Universidade Federal do Mato Grosso for financial support. We also express our thanks to Dr Eduardo F. A. Neves for extremely valuable suggestions and discussions.

REFERENCES

1. L. R. M. Pitombo and G. Oliveira Neto, *Anal. Chim. Acta* 1975, **75**, 391.
2. L. R. M. Pitombo and G. Oliveira Neto, *Anal. Chim. Acta* 1975, **75**, 401.

3. L. R. M. Pitombo, G. Oliveira Neto and E. Oliveira, *Mikrochim. Acta* 1976, 121.
4. L. R. M. Pitombo and J. M. Cesário, *Rev. Latinoam. Quim.* 1981, **1**, 65.
5. P. Senise and E. F. A. Neves, *J. Inorg. Nucl. Chem.* 1972, **34**, 1915.
6. H. J. Backer and W. Van Dan, *Recl. Trav. Chim. Pay-Bas* 1930, **49**, 479.
7. L. Klayman and T. S. Griffin, *J. Chem. Soc.* 1973, **95**, 197.
8. G. Bergson and A. Delin, *Ank. Kemi* 1961, **18**, 441.
9. D. K. Laing and L. D. Pettit, *J. Chem. Soc., Dalton Trans.* 1975, **21**, 2297.
10. L. R. M. Pitombo, E. Flumignan and I. Umemura, *Rev. Latinoam. Quim.* 1982, **13**, 108.
11. A. Fregda, *Sven. Kem. Tidskr.* 1936, **48**, 91.
12. K. Suzuki and K. Yamasaki, *J. Inorg. Nucl. Chem.* 1966, **28**, 473.
13. K. Suzuki, I. Vakano and K. Yamasaki, *J. Inorg. Nucl. Chem.* 1968, **30**, 545.
14. A. E. Martell and M. Calvin, *Chemistry of Metal Chelate Compounds*, p. 39. Prentice-Hall, Englewood Cliffs, New Jersey (1959).
15. S. G. Murray and F. R. Hartley, *Chem. Rev.* 1981, **81**, 365.
16. L. R. M. Pitombo and E. Oliveira, *Anal. Chim. Acta* 1978, **101**, 177.
17. L. R. M. Pitombo, O. Serra and Y. Iamamoto, *An. Acad. Brasil. Ciênc.* 1982, **52**, 671.
18. J. C. Speakman, *J. Chem. Soc.* 1940, 855.
19. M. Aplincourt and R. Hugel, *J. Inorg. Nucl. Chem.* 1974, **36**, 345.
20. A. Sandell, Inaugural Dissertation, Division of Inorganic Chemistry, Chemistry Centre, University of Lund, Sweden (1971).
21. W. F. Rittner, A. Gulko and G. Schumckler, *Talanta* 1970, **17**, 807.
22. A. Gulko and G. Schumckler, *J. Inorg. Nucl. Chem.* 1972, **35**, 603.
23. J. Bejerrum, *K. Dan. Kidensk, Selsk. Mat. Fys. Medd.* 1944, **4**, 21.
24. W. A. E. McBryde, *Talanta* 1974, **21**, 1979.
25. Hewlett–Packard, HP 97—Manual (1976).
26. S. Fronaeus, *Acta. Chem. Scand.* 1950, **4**, 72.
27. I. Leden, *Z. Phys. Chem.* 1941, **A188**, 160.
28. E. A. Neves, I. G. R. Gutz and R. G. Tavares, *J. Electroanal. Chem.* 1984, **179**, 91.
29. F. J. C. Rossotti and H. S. Rossotti, *Acta Chem. Scand.* 1955, **9**, 1166.
30. H. Irving and H. S. Rossotti, *J. Chem. Soc.* 1953, 3397.
31. S. Ahrland, J. Chatt, A. A. Davies and A. A. Willians, *J. Chem. Soc.* 1958, 264.
32. (a) L. D. Pettit, A. Royston and R. J. Whewell, *J. Chem. Soc. A* 1968, 2009; (b) L. D. Pettit, C. Sherrington and R. J. Whewell, *J. Chem. Soc. A* 1968, 2004; (c) D. Barnes, P. G. Laye and L. D. Pettit, *J. Chem. Soc. A* 1969, 2073.

Polyhedron Vol. 7, No. 24, pp. 2487–2494, 1988
Printed in Great Britain

0277–5387/88 $3.00+.00
© 1988 Pergamon Press plc

THALLIUM INTERACTIONS IN BIOLOGICAL FLUIDS. A POTENTIOMETRIC INVESTIGATION OF DIMETHYLTHALLIUM COMPLEX EQUILIBRIA WITH SOME TYPICAL AMINO ACIDS

MERCEDES GARCIA BUGARIN,* MARIA ESTHER GARCIA* and GUY BERTHON†

INSERM U305, Université Paul Sabatier, 38 rue des Trente-Six Ponts, 31400 Toulouse, France

and

JOSE SERGIO CASAS and JOSE SORDO

Departamento de Quimica Inorganica, Universidad de Santiago de Compostela, 15706 Santiago de Compostela, Spain

(*Received* 9 *March* 1988; *accepted* 14 *April* 1988)

Abstract—This paper concerns dimethylthallium (DMT) complex equilibria with sulphur-containing amino acids, glycine also being considered as a reference for simple amino acids. Formation constants for DMT complexes with L-cysteine (Cys), DL-penicillamine (Pen), N-acetyl-L-cysteine (Acy), N-acetyl-DL-penicillamine (Ape) and glycine (Gly) were determined under physiological conditions using glass electrode potentiometry. It is concluded that, as expected from the HSAB theory, the coordination of DMT by the carboxylate anion is insignificant. Binding of DMT to the amino and thiol groups involves logarithmic stability constants of 1.2 and 2.6, respectively. When these two groups are engaged in the same chelate ring, no additional effect is noted with respect to the sum of their individual contributions.

Thallium is quite a toxic element which may damage a number of essential functions.[1] In this respect, acute accidental poisonings by thallium-containing rodenticides have been reported frequently to occur in many parts of the world.[2] Attention has also been drawn to the potential health hazards that may result from the occurrence of this metal in the environment.[3] Thallium may be emitted as a by-product from various industrial sources such as smelters, coal mines, coal-fired power stations,[4] or cement factories.[5] Its multifarious uses as a catalyst, in alloys, pigments, semiconductors, dyes, even in medicinal depilatory agents[6] also represent many factors for it spreading in the environment. The mode of action of thallium compounds *in vivo* still remains unclear. However, it is generally accepted that Tl^+ substitutes for K^+ in many physiological processes.[2]

Like mercury and lead, inorganic thallium can be biomethylated by anaerobic organisms in sediment.[7] Experimental information concerning its biological transformation is scarce, and the Me_2Tl^+ ion has been the only methylated species detected *in vitro*.[8] Usually, the biomethylation step reduces the toxicity of heavy metals to the microorganisms while increasing mammalian toxicity.[7] Since Me_2Tl^+ is less toxic to bacteria than Tl^+, it should logically be more toxic to mammals.[9] Actually, dimethylthallium does affect erythrocyte production in the bone marrow of mice,[7] but this toxic effect occurs at a level above the LD_{50} for the corresponding inorganic salt, which suggests that the ability of Tl^+ to substitute for K^+ could be lost upon methylation.

Up until now, the only detoxifying drug used in thallium poisoning is dithizone, in spite of its

* On leave from the University of Santiago de Compostela, Spain.

† Author to whom correspondence should be addressed.

important side-effects.[6,10] Its lack of specificity is also an argument in favour of the research of new thallium sequestering agents. Pertinent speciation studies may be very helpful to meet this objective.[6,10] This is indeed the only technique likely to provide knowledge about the ability of various substances to selectively mobilize a given metal ion within the main biofluids.[6,10] However, the development of appropriate simulation models requires that the formation constants of all the possible complexes involved in these biofluids have been properly assessed beforehand. Reliable determinations of this kind usually necessitate long term investigations,[11–13] and it is often advisable to start such investigations with constant estimates that can be temporarily used in preliminary models.[14–16] Corresponding estimations may be based on chemical considerations involving known complex equilibria with simple ligands containing specific donor groups.

Concerning thallium, available complex formation constants relative to Tl^+ are rare[17] and only one reference to dimethylthallium could be found in the literature, concerning equilibria with diketones.[18] As a preliminary study, the present paper reports the potentiometric determination of formation constants for Me_2Tl^+ complexes with a series of amino acids of the typical structures, namely L-cysteine (Cys), DL-penicillamine (Pen), N-acetyl-L-cysteine (Acy), N-acetyl-DL-penicillamine (Ape) and glycine (Gly), under physiological conditions. The dianionic forms of cysteine and penicillamine may *a priori* coordinate dimethylthallium via their $-COO^-$, $-NH_2$ or $-S^-$ donor groups. In contrast, binding to the NH_2 donor group is blocked by the acetyl function in their substituted derivatives. In addition, glycine is used as a reference for simple glycine-like amino acids.

EXPERIMENTAL

Reagents

L-cysteine, N-acetyl-L-cysteine and DL-penicillamine were supplied by Ega-Chemie as biochemical grade products. N-acetyl-DL-penicillamine was purchased from Sigma Chemical Company and glycine was a biochemical Merck product. All these substances were potentiometrically assayed and proved sufficiently reliable so that further purification was not needed. Corresponding stock solutions were stored in the dark under a nitrogen atmosphere. Nevertheless, they had to be frequently renewed, especially for sulphur-containing ligands.

Dimethylthallium chloride was obtained from its hydroxide using hydrochloric acid,[19] this hydroxide being itself obtained by reacting dimethylthallium iodide[20] with silver oxide in water. The stock solution of dimethylthallium chloride was prepared with dilute BDH *pro analysi* hydrochloric acid so as to prevent the hydrolysis of the organometallic cation. The corresponding proton concentration was calculated from direct potentiometric measurements.

Sodium hydroxide stock solutions were prepared by diluting the contents of BDH concentrated volumetric solution vials with freshly boiled double-deionized water, which was saturated with purified nitrogen before use. These solutions were stored under a nitrogen atmosphere. They were systematically checked and proved to be carbonate-free by appropriate Gran titrations[21] against Prolabo R.P. pa potassium hydrogenphthalate.

Pro analysi sodium chloride was purchased from Merck. High quality grade nitrogen was scrubbed through concentrated sodium hydroxide, pyrogallol and ionic background solutions at 37°C.

Experimental conditions

Sodium chloride (0.15 mol dm^{-3}) was chosen as a background electrolyte to maintain the activity coefficients of the reactants constant and to ensure isotonicity with the physiological medium. From the thermodynamic point of view, this salt may appear as far from ideal because of the potential interactions it implies between chloride and metal ions. However, its use may be considered as particularly suitable for physiological applications. Indeed, the influence of the sodium chloride naturally contained in biological fluids is implicitly accounted for by the resulting formation constants, which makes them directly applicable to relevant computer simulation models.

EMF variations in electrochemical cells of the following type

G.E./ligand, Me_2Tl^+,

$NaCl\ 0.15\ mol\ dm^{-3}$//NaCl (satd)/Hg_2Cl_2—Hg

were monitored by means of a Corning Type 113 digital mV-meter equipped with a Beckman glass electrode (Cat. No. S39301) and a Beckman saturated sodium chloride calomel electrode. These electrodes were fitted into an Ingold titration cell system thermostatted at 37 ± 0.02°C by circulating water, in which a constant pressure of purified nitrogen was maintained by bubbling it into the solution. The electrode system was calibrated in the concentration scale as described elsewhere.[22] Under these conditions, the logarithm of the ionic product of water calculated with the help of the ESTA optimizer[23]

was found to be equal to −13.336, the electrode slope being equivalent to its theoretical value.

Initial solutions containing the metal and ligand were made sufficiently acidic so that all the ligand donor groups were significantly protonated at the outset of each titration. Successive aliquots of standard sodium hydroxide were delivered by a Radiometer ABU12 autoburette. Ligand : proton and metal : ligand ratios were varied to a large extent over the set of experiments performed for each system. For both ligand protonation and metal complex formation equilibria, data were recorded over the largest possible pH interval, although a number of experimental points were frequently discarded for the final stability constant calculations, especially within the range where the complexation observed was insignificant. Table 1 summarizes the experimental conditions used.

Calculation procedures

The two-fold approach involving both optimization and simulation steps[22,24,25] was employed throughout. The ESTA[23] and MINIQUAD[26] programs were used to refine the formation constants whose estimates were derived from the related protonation and formation curves. Initial sets of possible complexes were tested on the usual numerical criteria such as sums of squared residuals and *R* factors.[26] However, the final discrimination among those sets which displayed similar numerical fits was based on graphical comparisons between experimental formation curves and their simulated homologues obtained from PSEUDOPLOT[27] and ESTA[23] calculations.

RESULTS

Formation constants resulting from the final MINIQUAD analysis of protonation and metal complex equilibria are reported in Table 2.

Protonation constants

In general, the protonation constants determined in this work are in close agreement with previous values referring to identical experimental conditions.[28,29] They also compare well with other values relative to the same conditions of ionic strength and temperature, but in the presence of $NaClO_4$.[22,30]

Complex formation constants

Me_2Tl^+–*cysteine and* Me_2Tl^+–*penicillamine systems.* Except for a few points for which the average number of ligands bound to each metal ion $\bar{p}$ was found to be superior to two, the experimental formation curves of these two systems generally tended to a maximum value of about one, thus suggesting the predominance of a 1 : 1 metal-to-ligand ratio species. In addition, protonation curves drawn in the presence of the metal indicated that protonated species were likely to form with neutral to slightly basic pH values. Also, if the ability of sulphur to accept electrons from the metal by π bonding[22] is taken into account, polynuclear species should not be *a priori* excluded.

For both systems, the ML and MLH complexes were found to be the main species present under the conditions described in Table 1. Among the other species tested, ML_2 also proved to exist, its presence significantly improving the standard deviations of the first two complexes, and the *S* and *R* parameters as well. Other sets of constants were found, including M_2L and M_2L_3 and their protonated homologues, but all of the involved species were ruled out, either because their constants were made negative during refinement or because they gave unacceptable statistical errors.

The "best" model was therefore considered to mainly consist of ML and MLH, with ML_2 as a minor species. Figures 1 and 2 are shown as an example of the graphical comparisons developed in this study.

Me_2Tl^+–N–*acetylcysteine and* Me_2Tl^+–N–*acetylpenicillamine systems.* For these two systems, the average coordination number was always observed inferior to unity, whatever the metal-to-ligand ratio investigated. Moreover, the examination of the corresponding protonation curves in the presence of the metal indicated that no protonated species was likely to be present. Accordingly, MLH constants turned out to be negative for both ligands. The M_2L constant with Acy and the M_2L_2 one with Ape were also rejected by the optimization programmes. It may be worth mentioning that with Ape, the model formed by ML and M_2L gave rise to smaller *S* and *R* values than ML alone, but this improvement was to a limited extent and the standard deviation affecting the ML constant was made worse. M_2L was thus finally discarded. Taking into account other polynuclear species all the goodness-of-fit parameters systematically deteriorated. For both systems, ML was therefore selected as the only species definitely present in solution.

Me_2Tl^+–*glycine system.* For this system, the protonation curves obtained in the presence of the metal were found to be almost superimposable onto the reference curve, relative to the ligand alone, this being indicative of very poor complexation of Me_2Tl^+ with glycine. This observation was con-

Table 1. Summary of titration data used in formation constant calculations. Initial total concentrations of dimethylthallium (C_M), amino acid (C_L), hydrochloric acid (C_H), pH[a] range investigated. All concentrations are expressed in mmol dm^{-3}

System	C_M	C_L	C_H	pH range
Proton–L-cysteine		4.98	10.08	2.08–11.47
		10.00	20.16	1.81–11.09
		10.00	25.16	1.69–10.96
		20.00	40.32	1.53–11.27
Proton–DL-penicillamine		4.98	10.08	2.08–11.03
		10.00	20.16	1.82–11.29
		10.00	20.16	1.81–11.54
		10.00	25.16	1.70–11.29
		20.00	40.32	1.54–11.48
Proton–N-acetyl-L-cysteine		4.98	10.15	1.98–10.72
		10.00	20.29	1.67–10.85
		10.00	25.32	1.57–10.99
		20.00	20.51	1.66–11.07
Proton–N-acetyl-DL-penicillamine		2.00	2.01	2.63–10.67
		5.00	5.02	2.27–10.06
		5.00	10.05	1.99–11.19
		10.00	10.05	1.99–11.33
		10.02	10.05	1.99–11.06
Proton–glycine		4.98	5.04	2.53–10.81
		4.98	10.05	2.16–10.66
		10.00	10.05	2.32–11.00
		10.00	10.05	2.32–10.72
		10.00	20.13	1.89–10.91
Me_2Tl–L-cysteine	2.00	10.00	20.56	1.80–11.08
	2.00	4.98	10.49	2.06–10.89
	2.50	4.98	10.59	2.06–10.77
	5.00	10.00	21.16	1.78–11.19
	10.00	10.00	22.17	1.75–10.72
	10.00	4.98	12.10	1.99–10.68
Me_2Tl–DL-penicillamine	2.00	10.00	20.56	1.80–11.69
	2.00	4.98	10.49	2.06–11.28
	2.50	4.98	10.59	2.06–11.26
	5.00	10.00	21.16	1.78–11.53
	10.00	10.00	22.17	1.76–11.18
	10.00	4.98	12.10	1.99–10.54
Me_2Tl–N-acetyl-L-cysteine	2.00	10.00	10.53	1.95–10.59
	2.00	4.98	5.48	2.21–10.93
	2.50	4.98	5.58	2.20–10.84
	5.00	10.00	11.13	1.92–10.90
	10.00	10.00	12.14	1.87–10.74
	10.00	4.98	7.09	2.09–10.73
Me_2Tl–N-acetyl-DL-penicillamine	2.00	10.02	10.45	1.98–11.23
	2.00	5.02	5.42	2.25–10.99
	2.50	5.02	5.52	2.24–11.02
	5.00	10.02	11.05	1.95–11.18
	10.00	10.02	12.06	1.91–11.10
	10.00	5.02	7.03	2.13–10.94
Me_2Tl–glycine	5.00	10.00	11.05	2.26–10.98
	10.00	20.00	22.15	2.05–11.34
	10.00	10.00	12.06	2.20–11.38
	20.00	20.00	24.16	1.98–10.94
	10.00	4.98	7.05	2.35–10.82

[a] See text.

Table 2. Formation constants obtained from these studies. The formula of the general complex is $M_qL_pH_r$. S = sum of the squared residuals; R = R factor as defined in ref. 26; n = number of experimental observations taken into account in final calculations (see text)

System	p	q	r	$\log\beta$	±	S	R	n
Proton–L-cysteine	1	0	1	10.068	0.001	5.93E−07	0.0021	278
	1	0	2	17.979	0.002			
	1	0	3	19.796	0.004			
Proton–DL-penicillamine	1	0	1	10.417	0.001	2.38E−07	0.0012	353
	1	0	2	18.144	0.001			
	1	0	3	20.036	0.002			
Proton–N-acetyl-DL-cysteine	1	0	1	9.355	0.002	2.77E−07	0.0024	230
	1	0	2	12.426	0.002			
Proton–N-acetyl-DL-penicillamine	1	0	1	10.037	0.006	9.41E−07	0.0081	155
	1	0	2	13.393	0.009			
Proton–glycine	1	0	1	9.279	0.001	1.05E−07	0.0023	167
	1	0	2	11.647	0.002			
Me_2Tl–L-cysteine	1	1	0	3.621	0.002	5.13E−08	0.0013	211
	1	1	1	11.850	0.006			
	2	1	0	5.349	0.016			
Me_2Tl–DL-penicillamine	1	1	0	3.814	0.002	7.58E−08	0.0017	181
	1	1	1	11.853	0.013			
	2	1	0	5.217	0.086			
Me_2Tl–N-acetyl-L-cysteine	1	1	0	2.622	0.002	2.94E−08	0.0017	94
Me_2Tl–N-acetyl-DL-penicillamine	1	1	0	2.628	0.005	1.53E−07	0.0037	101
Me_2Tl–glycine	1	1	0	1.189	0.011	2.07E−07	0.0028	90

firmed by the shape of the corresponding formation curves whose maximum average coordination numbers were found at around 0.3 only.

DISCUSSION

According to the HSAB principle,[31] bonds formed between hard Lewis acids and hard bases, or between soft acids and soft bases, are expected to be more stable than those which result from hard–soft associations. For elements of variable valence, there is usually a smooth increase in hardness as the formal oxidation state increases.[32] Since the Tl^+ ion is classified as a soft Lewis acid, Tl^{III} formally involved in Me_2Tl^+ would thus be expected to be

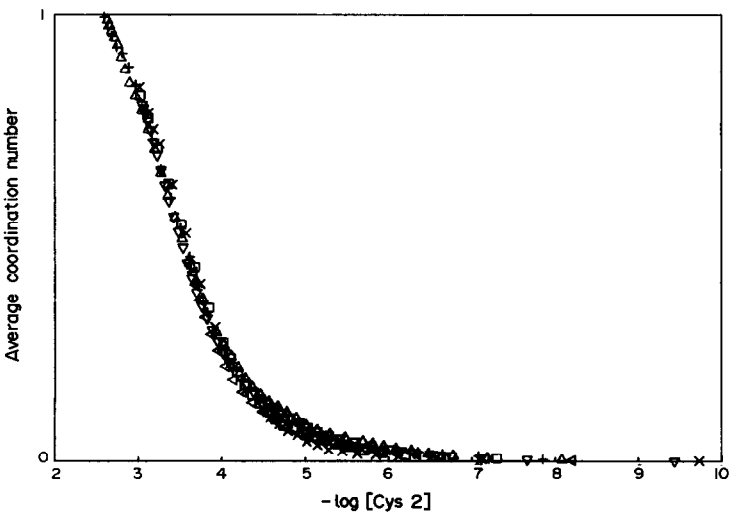

Fig. 1. Experimental formation curves of the Me_2Tl^+–cysteine system (37°C, I = 0.15 mol dm^{-3} NaCl). The following symbols correspond to the respective order of experiments summarized in Table 1: +, ×, □, △, ◁, ▷.

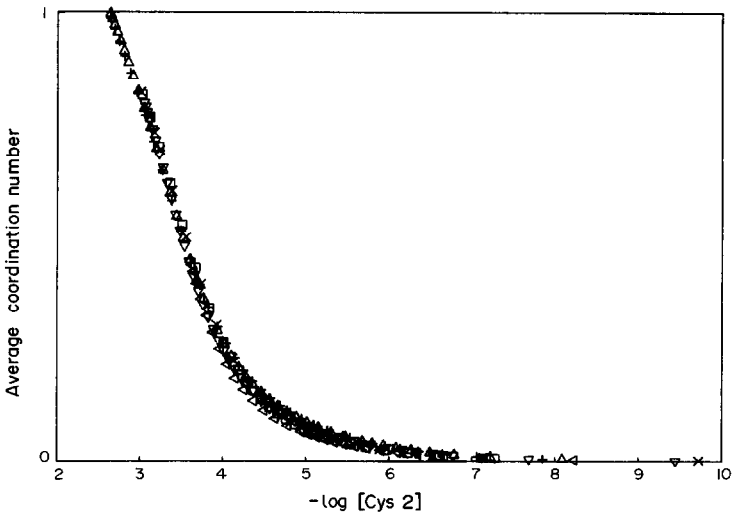

Fig. 2. Formation curves of the Me_2Tl^+–cysteine system, simulated on the basis of the results in Table 2; key to symbols as in Fig. 1.

slightly harder. However, the above rule suffers exceptions at the end of the transition series, where the presence of electrons in the 5*s* and 6*s* orbitals seems to decrease softness by a shielding effect on the outer *d* electrons. In other words, Tl^{III} is actually softer than Tl^{I},[32] which partly explains why the present studies were first devoted to Tl^{III} interactions with sulphur-containing amino acids. It is indeed evident from the above principle that among the potential donors encountered in substances acting as ligands *in vivo*, the sulphur atom is likely to give rise to the strongest bonds with Me_2Tl^+, nitrogen and oxygen following with decreasing affinity order.

Respective contributions of these three donor atoms to the binding of Me_2Tl^+ with the ligands investigated in this study may be estimated from the data in Table 2. With respect to nitrogen and oxygen, the formation constant of the ML complex with glycine shows that the affinity of the organometallic cation for nitrogen is poor, the oxygen binding being presumably insignificant. First of all, no complex was characterized with the zwitterionic form of the amino acid, which means that the oxygen atom cannot coordinate Me_2Tl^+ by itself. Furthermore, the low stability of the ML species suggests that even the possible formation of a chelate ring involving the carboxylate group, as evidenced by NMR,[33] would be of little significance in quantitative terms.

Let us now consider the complexes formed with Acy and Ape. Since (i) the coordination capacity of the nitrogen atom is cancelled by the substitution of the acetyl group and (ii) the oxygen binding has been shown to be quantitatively insignificant—which seems also substantiated by the absence of protonated species in the present case—the ML stability constant should essentially account for the affinity of Me_2Tl^+ for the sulphur anion. While the higher basicity of Pen with respect to Cys may be attributed to the electron-repelling effect of the methyl groups,[34] ML complexes of Me_2Tl^+ with Acy and Ape display equal stabilities. This suggests that the electronic influence of the methyl groups may be compensated for by a correlative solvent effect, the entropy of reaction probably being less positive in the case of Ape than Acy, as was previously observed for other coordination equilibria.[35,36] Such observations are explained by the increased order of the solvent molecules which results from the hydrophobic character of the methyl groups.[37]

If we comparatively examine the stability constants of the complexes formed with Cys and Pen, two remarks are in order: (i) a MLH protonated complex has been shown to exist in both cases and (ii) the stabilities of the ML species are of the same order of magnitude, and they are higher than their homologues with Acy and Ape. In the MLH complexes, the $—S^-$ anion or the $—NH_2$ group may be protonated. Indeed, whereas the most acidic protonation constant of Cys and Pen can be unambiguously ascribed to the carbonyl group,[34] the other two protonation step–stability constants arise from a combination of the two remaining possible microprocesses, i.e. $—S^-$ and $—NH_2$ may be simultaneously protonated to different extents. As far as the MLH formation constants are concerned, the addition of a proton to ML corresponds to increments in stability of 8.24 and 8.04 for Cys and

Pen, respectively. These values compared favourably with the step–stability constants relative to the formation of the diprotonated forms of these ligands (7.91 and 7.74, respectively) which, by comparison with Acy and Ape, would mainly correspond to the protonation of the amino groups. If we assume that the two active sites involved are at a sufficient distance from each other, so that their dissociation process is not affected, it can be inferred from these observations that sulphur is the main coordinating atom in MLH, and that both sulphur and nitrogen donors presumably chelate Me_2Tl^+ in the ML complexes. This appears all the more likely as the ML constants for Cys and Pen are approximately equivalent to the sums of their homologues for Acy and Gly, and for Ape and Gly, respectively.

To conclude, the above discussion suggests that (i) under the present experimental conditions the coordination of Me_2Tl^+ with glycine-like amino acids will involve a logarithmic stability constant of approximately 1.2, (ii) that complexes involving a deprotonated thiol group as the donor centre will display a stability of about 2.6 and (iii) that both sulphur and nitrogen may combine to chelate Me_2Tl^+, but without any apparent additional effect on corresponding stabilities. Although coordination through carboxylate cannot be totally excluded, it appears negligible in quantitative terms.

Acknowledgements—This work was generously supported by the CAYCIT (Spain). The award of scholarships to M.E.G. (by the Ministère des Relations Extérieures de la République Française) and to M.G.B. (by the Xunta de Galicia, Spain) is gratefully acknowledged.

REFERENCES

1. E. Sabbioni and L. Manzo, *Advances in Neurotoxicology* (Edited by L. Manzo), pp. 249–270. Pergamon Press, Oxford (1980).
2. L. Manzo, R. Scelsi, A. Moglia, P. Poggi, E. Alfonsi, R. Pietra, F. Mousty and E. Sabbioni, *Chemical Toxicology and Clinical Chemistry of Metals* (Edited by S. S. Brown and J. Savory), pp. 401–405. Academic Press, London (1983).
3. V. Zitko, *Sci. Total Environ.* 1975, **4**, 185.
4. R. L. Davison, D. F. S. Natusch, J. R. Wallace and C. A. Evans Jr., *Environ. Sci. Technol.* 1974, **8**, 1007.
5. A. Brockhaus, R. Dolgner, U. Ewers, U. Krämer, H. Soddemann and H. Wiegand, *Int. Arch. Occup. Environ. Health* 1981, **48**, 375.
6. D. R. Williams and B. W. Halstead, *J. Toxicol. Clin. Toxicol.* 1982–1983, **19**, 1081.
7. J. M. Morgan, Thesis, University of Mississippi (1980), University of Microfilms Int, London (1982).
8. F. Huber and H. Kirchman, *Inorg. Chim. Acta* 1978, **29**, L249.
9. J. S. Thayer, *J. Organomet. Chem.* 1977, **54**, 662.
10. P. M. May and R. A. Bulman, *Prog. Med. Chem.* 1983, **20**, 225.
11. G. Berthon, M. Piktas and M. J. Blais, *Inorg. Chim. Acta* 1984, **93**, 117.
12. G. Berthon, *Inorg. Chim. Acta* 1983, **79**, 46.
13. G. Berthon, B. Hacht, M. J. Blais and P. M. May, *Inorg. Chim. Acta* 1986, **125**, 219.
14. P. M. May, P. W. Linder and D. R. Williams, *J. Chem. Soc., Dalton Trans.* 1977, 588.
15. G. Berthon, C. Matuchansky and P. M. May, *J. Inorg. Chem.* 1980, **13**, 63.
16. P. M. May, J. M. Slater and G. Berthon, *TEMA-5 Proc.* 1984, 542.
17. (i) *Stability Constants*, Special publication No. 17. The Chemical Society, London (1964); Supplement No. 1, Special publication No. 25. London (1971); (ii) *Stability Constants of Metal–ion Complexes, Part B. Organic Ligands*. IUPAC Chemical Data Series No. 22. Pergamon Press, Oxford (1979); (iii) *Critical Stability Constants, Vol. 1: Amino Acids* (Edited by A. E. Martell and R. M. Smith). Plenum Press, New York (1974); *ibid*, Vol. 5, First supplement (Edited by A. E. Martell and R. M. Smith). Plenum Press, New York (1982).
18. D. F. Martin and W. J. Randall, *J. Inorg. Nucl. Chem.* 1968, **30**, 2909.
19. G. D. Shier and R. S. Drago, *J. Organomet. Chem.* 1966, **5**, 330.
20. H. Gilman and R. G. Jones, *J. Am. Chem. Soc.* 1946, **68**, 517.
21. F. J. C. Rossotti and H. Rossotti, *J. Chem. Educ.* 1965, **42**, 375.
22. G. Berthon, P. M. May and D. R. Williams, *J. Chem. Soc., Dalton Trans.* 1978, 1433.
23. K. Murray and P. M. May, *ESTA Users' Manual*. UWIST, Cardiff (1984).
24. M. J. Blais and G. Berthon, *J. Chem. Soc., Dalton Trans.* 1983, 1803.
25. E. Freijanes and G. Berthon, *Inorg. Chim. Acta* 1986, **124**, 141.
26. A. Sabatini, A. Vacca and P. Gans, *Talanta* 1974, **21**, 53.
27. A. M. Corrie, G. K. R. Makar, M. L. D. Touche and D. R. Williams, *J. Chem. Soc., Dalton Trans.* 1975, 105.
28. A. Cole, C. Furnival, Z. X. Huang, D. C. Jones, P. M. May, G. L. Smith, J. Whittaker and D. R. Williams, *Inorg. Chim. Acta* 1985, **108**, 165.
29. M. J. Willes and D. R. Williams, *Inorg. Chim. Acta* 1983, **80**, L35.
30. T. Alemdaroglu and G. Berthon, *Bioelectrochem. Bioenerg.* 1981, **8**, 49.
31. R. G. Pearson, *Hard and Soft Acids and Bases*. Dowden, Hutchinson & Ross, Stroudsburg (1973).
32. R. G. Pearson, *J. Chem. Educ.* 1968, **45**, 581.

33. Y. B. Yakovlev and V. G. Ushakova, *Russ. J. Inorg. Chem.* 1983, **28**, 1217.
34. A. Gergely and I. Sovago, *Metal Ions in Biological Systems* (Edited by H. Sigel), Vol. 9, pp. 77–102. Marcel Dekker, New York (1979).
35. G. Berthon, *Analytical Calorimetry* (Edited by R. S. Porter and J. F. Johnson), pp. 119–125. Plenum Press, New York (1974).
36. G. Berthon, M. J. Blais and O. Enea, *J. Phys. Chem.* 1977, **81**, 1991.
37. S. Cabani, G. Conti and L. Lepori, *Trans. Faraday Soc.* 1971, **67**, 1933.

Polyhedron Vol. 7, No. 24, pp. 2495–2502, 1988
Printed in Great Britain

0277–5387/88 $3.00+.00
© 1988 Pergamon Press plc

CRYSTAL STRUCTURE AND SPECTROSCOPIC STUDIES OF CATENA-DIAQUA-TRIS-μ-(L-PROLINE)NEODYMIUM(III) TRIPERCHLORATE, $[Nd(L\text{-pro}\cdot H)_3(H_2O)_2](ClO_4)_3$

J. LEGENDZIEWICZ,* T. GŁOWIAK, E. HUSKOWSKA and DAO CONG NGOAN

Institute of Chemistry, University of Wrocław, Wrocław, Poland

(*Received* 26 *October* 1987; *accepted* 3 *May* 1988)

Abstract—The crystal structure of the Nd^{III} L-proline complex $[Nd(C_5H_9O_2N)_3(H_2O)_2](ClO_4)_3$ has been determined. The complex crystallizes in the monoclinic space group $P2_1$, with the following crystal data: $a = 13.379(3)$, $b = 21.912(5)$, $c = 9.870(2)$ Å, $\beta = 91.28(4)°$, $V = 2892.8$ Å^3, $Z = 4$, $M_r = 823.6$, $d_x = 1.89$ g cm^{-3}, $d_m = 1.91$ g cm^{-3}, $\mu(Mo\text{–}K_\alpha) = 21.7$ cm^{-1}. Absorption and laser excited fluorescence spectra of the monocrystal were measured along the crystallographic axis a at 300, 123 and 77 K. The probabilities of f–f transitions were analysed, based on the Judd–Ofelt theory. The significant dependence of intensity on temperature was observed and in such conditions the contribution of possible mechanisms to the hypersensitive transitions was considered. Stark components were determined and energy diagrams for $^4I_{9/2}$ and $^4I_{11/2}$ levels were proposed. Bridging coordination bonds from carboxyl groups of the proline molecules create linear polymers and the hydrogen bonds formed stabilize the crystal structure.

Lanthanide ions are often used as spectroscopic probes in studies of biological systems. Substitution of Ca^{II} by Ln^{III} allows the spectroscopic studies especially of peptide and protein complexes. Since the Ca^{II} ion is attached to aspartate and glutamate residues it is reasonable to explain the bonding mode of lanthanide ions with simple amino acids to understand the more complicated bioinorganic systems. It seems important to explain the influence of the amine group and the other functional groups on the bonding mode of the carboxylate groups. These investigations are important in spectroscopy and in the chemistry of lanthanides as well.

Recently, we have studied the crystal structure and spectroscopy of a series of lanthanide complexes with amino acids.[1–5] All the determined structures are in the dimeric or polymeric forms. The polymer types of these complexes are dependent significantly on the stoichiometric relation of Ln : amino acid (Ln^{3+} : A). Our studies revealed the following results:

—for Ln : A = 1 : 1, the linear polymers are formed,[4]

—for Ln : A = 1 : 2, the dimers or linear polymers are formed,[4,2]

—for Ln : A = 1 : 3, the polymers, in which Ln ions are linked to each other by chains containing four carboxylate bridges and two carboxylate bridges are formed.[1]

In this paper the structure of Ln^{III} complexes with L-proline is discussed on the basis of X-ray crystallographic and spectroscopic results. Since the low temperature spectroscopy studies allow the determination of the site symmetry of the lanthanide ion, spectroscopy measurements were performed at 300, 123 and 77 K. Room temperature absorption spectra were used for the intensity analysis.

EXPERIMENTAL

X-ray measurements

The crystals of the title compound were obtained from an aqueous solution. Two types of crystals were obtained: $[Ln(L\text{-pro}\cdot H)_3(H_2O)_2](ClO_4)_3$ where Ln = La–Nd and $[Ln(L\text{-pro}\cdot H)_2(H_2O)_5](ClO_4)_3$ for heavy lanthanide ions.

* Author to whom correspondence should be addressed.

The lanthanide ion concentrations were determined complexometrically; the concentrations of the other elements by elemental analysis. A rose coloured monocrystal of the Nd^{3+} complex of dimensions $0.3 \times 0.4 \times 0.5$ mm was used for structure determination. Cell parameters were calculated by the least-squares method from the setting angles of 15 reflections with $20 < 2\theta < 29°$. 5260 unique reflections with $4.0 < 2\theta < 60.0°$ were measured on a Syntex $P2_1$ diffractometer with graphite monochromatized Mo-K_α radiation. The index range, h from 0 to 15, k from 0 to 26 and l from -11 to 11. The intensity data were collected at 287 K using a θ–2θ scan, with a variable scan rate 3.0–29.3° min^{-1}. The data were corrected for Lorentz and polarization factors and absorption using the DIFABS procedure[6] which was applied to the isotropically refined data. 5143 reflections with $I > 1.96\sigma(I)$ were used in the analysis.

The structure was solved by Patterson and Fourier methods. Blocked least-squares refinement with anisotropic thermal parameter for non-hydrogen atoms gave final $R = 0.036$ and $R_w = 0.048$. All crystallographic calculations were made on a RC 3600 computer using the XTL program.[7] The atomic scattering factors were taken from *International Tables for X-ray Crystallography* (1974).[8] The final atomic, positional and thermal parameters, lists of F_o/F_c values, have been deposited as supplementary material with the Editor, from whom copies are available on request. Atomic coordinates have also been deposited with the Cambridge Crystallographic Data Centre.

Spectroscopy studies

Absorption spectra of the monocrystals were recorded at 123 and 300 K in the region 11000–42000 cm^{-1} on a Beckman UV spectrophotometer. The lower temperature could not be reached, because the crystal cracked. The oscillator strengths of f–f transitions were estimated by means of integrating the program ICH 30. Judd's parameters were calculated from the following equation

$$P_{exp} = \sum_{\lambda=2,4,6} \tau_\lambda \sigma |\langle f^N_{SLJ} \| U^{(\lambda)} \| f^N_{S'L'J'} \rangle|^2 \times (2J+1)^{-1} \quad (1)$$

where $\langle f^N_{SLJ} \| U^{(\lambda)} \| f^N_{S'L'J'} \rangle$ is the reduced matrix element of the unit tensor operator $U^{(\lambda)}$, τ_λ are the phenomenological parameters estimated from experimental data and σ is the wavenumber in cm^{-1}.[9,10] Fluorescence spectra were measured on a spectrophotometer using a GDM monochromator (Carl–Zeiss–Jena) and a phase-sensitive detection system equipped with a photomultiplier with S-1 response at room and liquid nitrogen temperatures. The excitations were performed for Nd^{3+} on the 488 and 514 nm lines of an argon ILA 120 laser.

Discussion of X-ray data

The crystal is built up from linear polymers as shown in Fig. 1. The Nd ions in the polymeric chains repeat every 4.590 and 5.321 Å. The shorter Nd—Nd distance is bridged by four carboxyl groups from the proline molecules and the longer

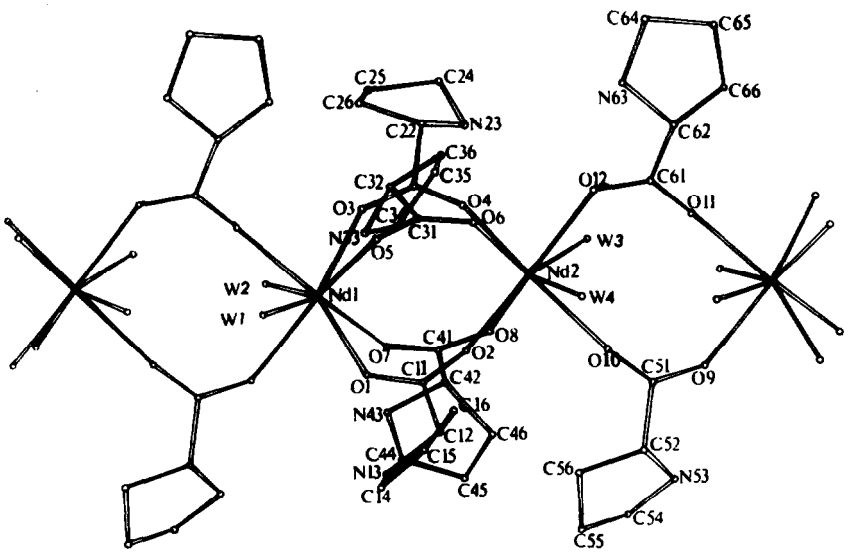

Fig. 1. An ORTEP drawing of structure of the $[Nd(L\text{-pro} \cdot H)_3(H_2O)_2](ClO_4)_3$ compound.

Table 1. Interatomic distances (Å) and angles (deg) within coordination polyhedra with ESDs in parentheses

Nd(1)—O(1)	2.509(8)	Nd(2)—O(2)	2.395(8)
Nd(1)—O(3)	2.405(8)	Nd(2)—O(4)	2.546(7)
Nd(1)—O(5)	2.467(7)	Nd(2)—O(6)	2.353(8)
Nd(1)—O(7)	2.378(8)	Nd(2)—O(8)	2.365(9)
Nd(1)—O(9)	2.418(7)	Nd(2)—O(10^i)	2.401(7)
Nd(1)—O(11)	2.366(7)	Nd(2)—O(12^i)	2.450(7)
Nd(1)—W(1)	2.575(8)	Nd(2)—W(3)	2.506(8)
Nd(1)—W(2)	2.547(8)	Nd(2)—W(4)	2.596(8)
W(1)—O(1)	2.74(1)	O(6)—W(3)	2.97(1)
W(1)—O(3)	3.06(1)	O(6)—O(12^i)	3.34(1)
O(11)—O(3)	3.29(1)	O(4)—O(12^i)	2.99(1)
O(11)—O(5)	3.15(1)	O(4)—W(4)	2.90(1)
W(2)—O(5)	2.85(1)	O(2)—W(4)	3.06(1)
W(2)—O(7)	3.06(1)	O(2)—O(10^i)	3.30(1)
O(9)—O(7)	3.22(1)	O(8)—O(10^i)	3.06(1)
O(9)—O(1)	3.15(1)	O(8)—W(3)	2.96(1)
W(1)—O(11)	2.77(1)	O(6)—O(4)	2.99(1)
O(11)—W(2)	2.96(1)	O(4)—O(2)	3.00(1)
W(2)—O(9)	2.84(1)	O(2)—O(8)	2.91(1)
O(9)—W(1)	3.07(1)	O(8)—O(6)	2.97(1)
O(3)—O(5)	2.89(1)	O(12^i)—W(4)	2.88(1)
O(5)—O(7)	3.11(1)	W(4)—O(10^i)	2.79(1)
O(7)—O(1)	3.05(1)	O(10^i)—W(3)	3.09(1)
O(1)—O(3)	3.05(1)	W(3)—O(12^i)	2.88(1)
W(1)—Nd(1)—W(2)	125.7(3)	O(6)—Nd(2)—O(2)	107.9(3)
O(9)—Nd(1)—O(11)	94.4(3)	O(8)—Nd(2)—O(4)	130.8(3)
O(3)—Nd(1)—O(7)	109.8(3)	O(12^i)—Nd(2)—O(10^i)	98.3(3)
O(1)—Nd(1)—O(5)	132.3(2)	W(3)—Nd(2)—W(4)	122.3(3)

distance is bridged only by two carboxyl groups from proline molecules. Selected bond lengths and angles are given in Table 1. Geometry parameters for the proline molecules have been deposited. The polymeric chains are parallel to the crystallographic *c* axis. The carboxylate oxygen–neodymium distances range from 2.353 to 2.546 Å and the four aqua oxygens have an average bonding distance of 2.556 Å.

The coordination polyhedron around each Nd ion is a distorted dodecahedron (Fig. 2). The oxygen atoms O(1), W(1), W(2), O(5) and O(8), W(3), W(4), O(4) occupy positions A, while atoms O(3), O(9), O(7), O(11) and O(6), O(10^i), O(2), O(12^i) occupy the B positions. The shape characteristics calculated according to Drew[11] for these polyhedra are given in Table 2. As values of Δ show, the polyhedra are distorted in the direction of a square antiprism.

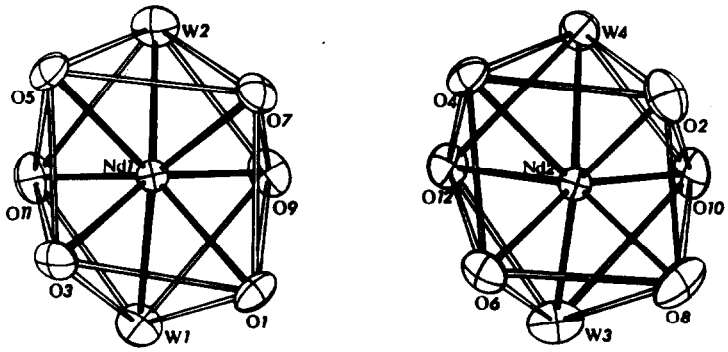

Fig. 2. The coordination polyhedron around each Nd^{3+} ion.

Table 2. The shape characteristics of the coordination polyhedron in $[Nd(L\text{-pro}\cdot H)_3(H_2O)_2](ClO_4)_3$

	Δ_{Dod}	Δ_{SAP}	δ				θ	θ_A	θ_B	γ	ϕ	$1/s$	$\frac{M-A}{M-B}$
Nd(1)	0.035	0.101	16.68	22.75	43.17	37.75	57.96	33.47	74.86	86.79	21.94	1.03	1.06
Nd(2)	0.026	0.073	19.20	17.87	49.54	35.54	57.56	35.80	72.07	80.98	24.69	1.04	1.04

The six proline ligands exhibit a zwitterion form, but with different conformations. In this work, the conformations of the pyrrolidine rings were determined according to Ashida and Kakudo,[12] and Cremer and Pople.[13] For all rings (except proline 6), the results calculated by both methods are in agreement. The phase angle value (ϕ) for the ring of proline 6 (32.9°) shows that the ring may have a conformation of an envelope, but there is no well-defined plane formed by four independent atoms of the ring. The deviation of atoms C(65) and C(61) from the plane formed by C(64), N(63), C(62) show the ring conformation of T, C_2-C_γ-exo. The parameters determined for the conformations of six proline molecules and the torsion angles have been deposited.

In this complex there is evidence for the presence of hydrogen bonds. Bonds of this type connect polymers to perchlorate groups and water oxygen. The distances and angles for hydrogen bonds are given in Table 3.

It is interesting that proline molecules coordinate with Nd ions to form a linear polymer as do glycine molecules in $Nd_2(gly)_6(ClO_4)_6\cdot 9H_2O$.[1] The differences found between these complexes are the coordination mode of the carboxylate groups of the amino acids. In the complex of neodymium with glycine there are the bridged and chelated-bridged modes of carboxylate group bonding, whereas in the title compound there is only the bridged mode.

Discussion of spectroscopic data

Absorption spectra for the neodymium monocrystal are presented in Fig. 3. The experimentally observed intensities of *f–f* transitions in lanthanide ions should include transitions of the magnetic and electric dipole type. The majority of the neodymium bands are of the electric dipole type, so this one will be considered in the intensity analysis. The low temperature spectra exhibit a rich fine structure especially for the hypersensitive transition. The

Table 3. Distances (Å) and angles (deg) for hydrogen bonds with ESDs in parentheses

D—H···A	D···A	H···A	< D—H···A
W(1)—H(1)···O(61^{ii})	2.88(3)	2.03	144
W(1)—H(2)···W(4^{ii})	2.97(1)	2.29	125
W(2)—H(3)···O(33^{iii})	2.96(2)	2.26	133
W(2)—H(4)···O(71^{iv})	3.08(1)	2.38	145
W(3)—H(5)···W(2^{i})	3.03(1)	2.30	177
W(4)—H(7)···O(72)	2.84(2)	2.01	176
W(4)—H(8)···O(62)	2.76(2)	1.97	171
N(13)—H(10)···O(22^{v})	2.93(2)	2.28	122
N(13)—H(11)···O(64^{ii})	3.10(2)	2.37	130
N(23)—H(19)···O(21)	2.97(1)	2.24	128
N(33)—H(28)···O(44^{iii})	2.98(1)	2.50	109
N(33)—H(29)···O(41^{iii})	2.92(1)	2.15	133
N(43)—H(37)···O(32^{iii})	2.96(2)	2.11	141
N(43)—H(38)···O(54^{vi})	2.89(2)	2.07	138
N(53)—H(46)···O(51^{vi})	3.06(2)	2.21	143
N(53)—H(47)···O(33^{iii})	3.19(2)	2.35	142
N(63)—H(55)···O(73^{ii})	3.03(2)	2.09	157
N(63)—H(56)···O(24^{ii})	2.97(2)	2.22	130

Code symmetry: (i) $x, y, 1+z$. (ii) $x, y, -1+z$. (iii) $1-x, -1/2+y, -z$. (iv) $1-x, -1/2+y, 1-z$. (v) $-1+x, y, z$. (vi) $-x, -1/2+y, 1-z$.

oscillator strength values of *f–f* transition are collected in Table 4. The decrease of intensity with temperature decrease was observed for almost all the bands measured. It can be explained if the vibronic mechanism takes place in transitions or the population of the higher components of the Nd^{3+} ground state change with temperature.

According to the vibronic transition theory for lanthanide ions however, such an effect can only be found for hypersensitive transitions.[14,15] Since the contributions of the intensity changes in all the transitions are different, both of the above reasons can be assumed. It is noteworthy that the intensities observed are higher (especially for $^4I_{9/2} \rightarrow {}^4G_{5/2}$, $^2G_{7/2}$) than for the neodymium monocrystal with alanine for which the same bonding mode of the carboxyl group and coordination number were observed.[2] Since the intensity of the hypersensitive bands can be affected by symmetry change, polarizability of ligands or other effects, it is interesting to consider the intensity changes of this bond for different monocrystals of carboxylate, for which the crystal structures have been determined.[1–5]

Unfortunately, up until now only a few crystals are known for which the X-ray structure has been solved and the spectroscopy measured. Moreover, if the composition of the complex with lanthanide ions is changed, the coordination mode of the carboxyl group will also change with the same ligand. This had been observed for two types of glutaric acid complexes[16,17] and now has been seen for complexes with proline in 1 : 3 and 1 : 2 complexes.[18]

As crystallographic data show, monocrystals of the title compound form the same type of polymer as does the glycine complex, however, the bonding mode of the carboxyl group for these two types of compounds is different. The intensity for the $^4I_{9/2} \rightarrow {}^2G_{7/2}$, $^4G_{5/2}$ transition is also different. In our earlier studies we tried to consider the relation between intensity and Ln—O distances, i.e. the covalency effect in mechanisms of hypersensitive transitions. The intensities observed are somewhat lower than for the glutamic acid complex with Nd^{3+}.[3] The mean Ln—O distances for the neodymium compound are 2.458 and 2.451 Å for the I and II positions, respectively. Whereas for Nd^{3+} in the monocrystal with glutamic acid (estimated from crystal data for Pr^{3+}) the distance is 2.50 Å.[5] The Judd parameters calculated from relation (1) are presented in Table 4. The values of τ_4 and τ_6 are comparable with those in other systems but τ_2 changed from one system to another. In this case τ_2 is near to the value for the glutamic acid complex.[3] The low temperature spectra in the region of the $^4I_{9/2} \rightarrow {}^2P_{1/2}$ transition exhibit five components which together with luminescence spectra allowed the preparation of the energy level diagram for the ground and the first excited state of Nd^{3+} (see Table 5) and enabled us to find the site symmetry position of the Nd^{3+} ions (Figs 4 and 5).

The dodecahedron is the most suitable coordination polyhedron for the neodymium compound as is seen from the fitting procedure (Tables 1 and

Table 4. Oscillator strength values of *f–f* transitions of the $[Nd(L\text{-pro}\cdot H)_3(H_2O)_2](ClO_4)_3$ monocrystal; τ_λ parameter values are calculated from Judd's relation

Spectral region (Å)	S', L', J'	P × 10^8	
9090–9300	$^4F_{3/2}$	205.2	225.3
7700–8330	$^4F_{5/2}$, $^2H_{9/2}$	797.4	636.8
7200–7700	$^4S_{3/2}$, $^4F_{7/2}$	989.1	835.5
6580–7040	$^4F_{9/2}$	59.4	51.4
6170–6410	$^2H_{11/2}$	18.0	15.7
5500–6020	$^4G_{5/2}$, $^2G_{7/2}$	1480.6	1397.6; 1251.7; 999.7[a]
4950–5370	$^2K_{13/2}$, $^4G_{7/2}$, $^4G_{9/2}$	726.2	640.4
4460–4950	$^2K_{15/2}$, $^2G_{9/2}$, $^2D^2F_{3/2}$, $^4G_{11/2}$	221.5	233.5
4130–4330	$^2P_{1/2}$, $^2D_{5/2}$	37.6	31.7
3360–3620	$^4D_{3/2}$, $^4D_{5/2}$, $^2I_{11/2}$, $^4D_{1/2}$, $^2L_{15/2}$	924.1	817.2
3190–3360	$^2I_{13/2}$, $^4D_{7/2}$, $^2L_{17/2}$	225.6	258.7
3090–3200	$^2H_{9/2}$	10.9	9.7
2860–2950	$^2D_{5/2}$	35.4	29.3
2500–2620	$^2F_{5/2}$	25.3	22.2
2420–2520	$^2F_{7/2}$	9.6	8.8

[a] At 223, 173 and 123 K, respectively.

$\tau_2 = 5.16 \mp 0.77$; $\tau_4 = 4.97 \mp 0.69$; $\tau_6 = 10.92 \mp 0.99$.

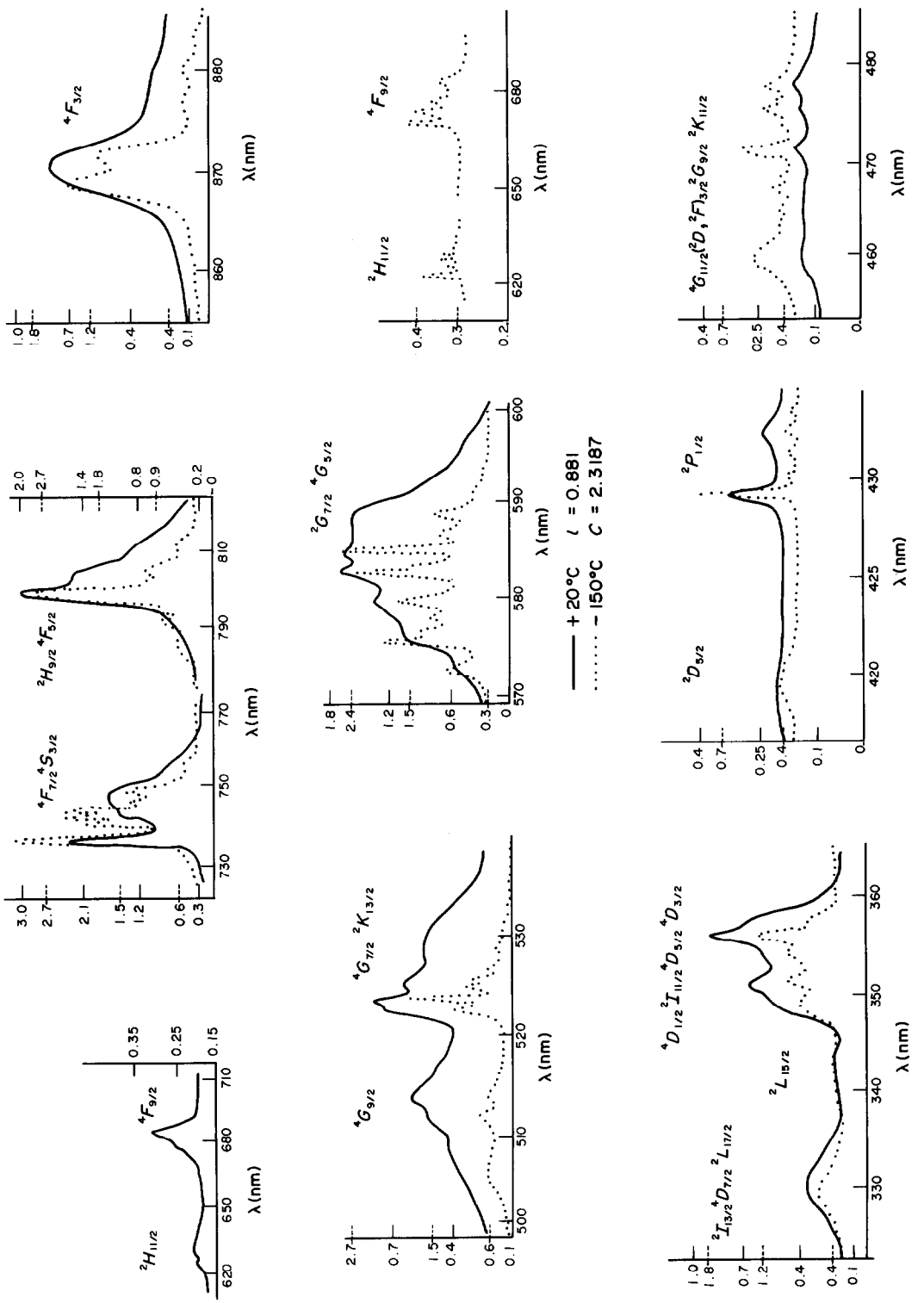

Fig. 3. Absorption spectra of the $[Nd(L\text{-pro}\cdot H)_3(H_2O)_2](ClO_4)_3$ monocrystal at 123 and 300 K.

Table 5. Energy level diagrams for the ground and first excited state of Nd^{3+} in the $[Nd(L\text{-pro}\cdot H)_3(H_2O)_2](ClO_4)_3$

	Observed fluorescence Series I (cm^{-1})	Observed fluorescence Series II (cm^{-1})	Positions of levels (cm^{-1})
	11532	11475	
	11495	11438	37
$^4I_{9/2}$	11425	11365	107
	11357	11300	175
	11213	11157	317
	9574	9516	1958
	9545	9485	1988
	9520	9461	2013
$^4I_{11/2}$	9488	9431	2044
	9444	9386	2088
	9396	9338	2136

Splitting of the $^4F_{3/2} = 58\ cm^{-1}$.

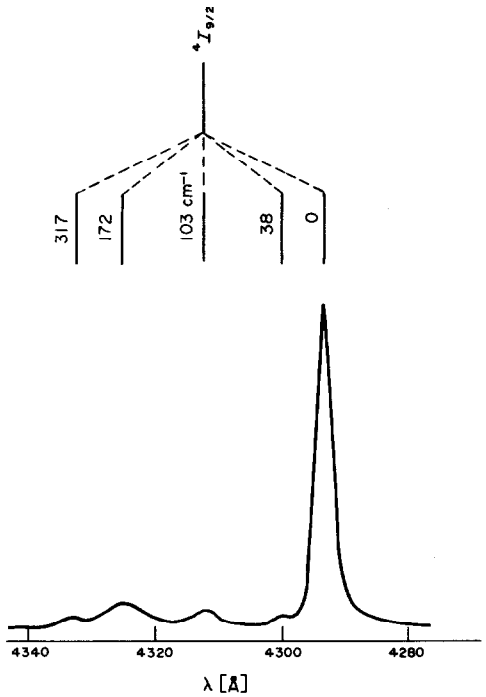

Fig. 5. The $^4I_{9/2} \rightarrow {}^2P_{1/2}$ transition for the title compound.

2). However, some distortion is observed, so the closest point symmetry for the Nd^{3+} ion seems to be C_{2v} because of the water molecule positions. Moreover, different Nd—O distances are observed for positions I and II.

Figure 4 shows the luminescence spectrum for the $[Nd(L\text{-pro}\cdot H)_3(H_2O)_2](ClO_4)_3$ compound at 77 K. Although the Nd^{3+} ion has a great number of absorbing levels in the 11400–40000 cm^{-1} spectral region (see Fig. 3), only the $^4F_{3/2}$ level shows the notable fluorescence in the near IR region. This feature results from the small energy gaps between adjacent successive levels, which can be rapidly depopulated by an efficient non-radiative relaxation process leading to the situation where the population of the $^4F_{3/2}$ level is separated from the next lowest lying level by about 6000 cm^{-1}. So the fluorescence for Nd^{3+} originates totally from the $^4F_{3/2}$ level, which is split into two Stark components in non-cubic systems.

Since the levels $^4I_{9/2}$ and $^4I_{11/2}$ are split into five and six components, respectively, at the elevated temperature we can expect 10 and 12 Stark components for $^4F_{3/2} \rightarrow {}^4I_{9/2}$ and $^4I_{11/2}$ transitions. However, for the $^4F_{3/2} \rightarrow {}^4I_{9/2}$ transition more components were found in the luminescence spectra which could point either to more than one site position of the Nd^{3+} ion in the crystal measured or to the vibronic components in the observed band.

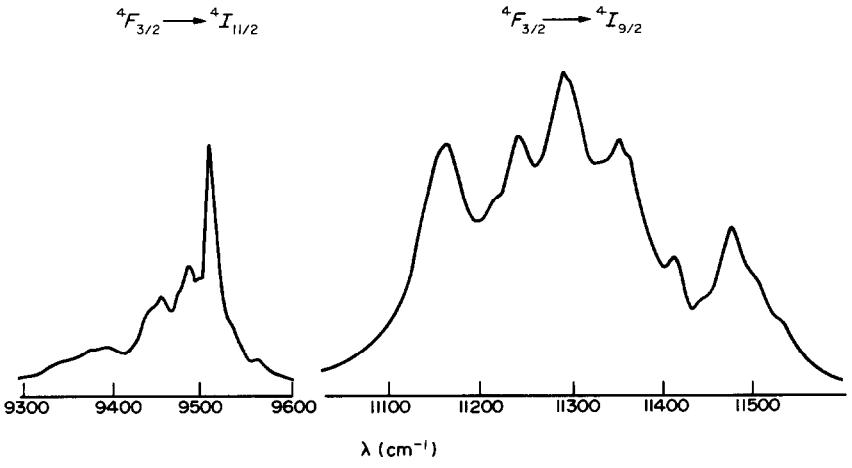

Fig. 4. Luminescence spectrum of $[Nd(L\text{-pro}\cdot H)_3(H_2O)_2](ClO_4)_3$ at 77 K.

Intensity analysis seems to confirm the vibronic mechanism in the intensities observed for the *f–f* transitions in that monocrystal, but as it follows from the X-ray measurements, positions I and II of the Nd^{3+} ion may vary in bond length, and can influence the distortion of the point symmetry as well. On the other hand only five well-resolved components were found in the absorption band at 123 K. The band corresponding to the $^4I_{9/2} \rightarrow {}^2P_{1/2}$ transitions point to one site symmetry at elevated temperatures. Thus, the components found in the luminescence spectra are of the vibronic character, or, at 77 K (i.e. the temperature is lower than that used for measuring the absorption spectra for the $^4I_{9/2} \rightarrow {}^2P_{1/2}$ transition) the phase transformation proceeds, and then Nd occupies more than one symmetry site.

In Table 5 the energy level diagrams of Nd^{3+} ion for the one site symmetry position in the $[Nd(L\text{-pro}\cdot H)_3(H_2O)_2](ClO_4)_3$ monocrystal are presented. The splitting of the $^4I_{9/2}$ and $^4I_{11/2}$ levels is 317 and 178 cm^{-1}, respectively.

REFERENCES

1. J. Legendziewicz, E. Huskowska, A. Waśkowska and Gy. Argay, *Inorg. Chim. Acta* 1984, **92**, 151.
2. J. Legendziewicz, T. Głowiak, E. Huskowska and C. N. Dao, *Rare Earth Spectroscopy* (Edited by B. Jeżowska-Trzabiatowska, J. Legendziewicz and W. Stręk), p. 146. World Scientific Company, Singapore (1985).
3. J. Legendziewicz, E. Huskowska, A. Waśkowska and Gy. Argay, *Inorg. Chim. Acta* 1984, **95**, 57.
4. T. Głowiak, J. Legendziewicz, C. N. Dao and E. Huskowska, in preparation.
5. I. Csoregh, P. Kierkegaard and J. Legendziewicz, *Abstracts of Xth E.C.M.* p. 162. Science Publishing House, Wrocław, Poland (1986).
6. N. Walker and D. Stuart, *Acta Cryst.* 1983, **39A**, 158.
7. Syntex. XTL/XTLE Structure Determination System (1976).
8. *International Tables for X-ray Crystallography*, Vol. IV. Kynoch Press, Birmingham (1974).
9. B. R. Judd, *Phys. Rev.* 1962, **127**, 750.
10. W. F. Carnall, P. R. Fields and K. Rajnak, *J. Phys. Chem.* 1968, **49**, 4429; *ibid*, 1968, **49**, 4450.
11. M. G. B. Drew, *Coord. Chem. Rev.* 1977, **24**, 179.
12. T. Ashida and M. Kakudo, *Bull. Chem. Soc. Japan* 1974, **47**, 1129.
13. P. Cramer and I. A. Pople, *J. Am. Chem. Soc.* 1975, **97**, 1354.
14. B. R. Judd, *Phys. Sci.* 1980, **21**, 543.
15. W. Stręk, *Rare Earth Spectroscopy* (Edited by B. Jeżowska-Trzebiatowska, J. Legendziewicz and W. Stręk), p. 635. World Scientific Company, Singapore (1985).
16. T. Głowiak, C. N. Dao and J. Legendziewicz, *Acta Cryst.* 1986, **42**, 1492.
17. T. Głowiak, J. Legendziewicz, C. N. Dao and E. Huskowska, *J. Less Common Metals* 1987, **134**, 153.
18. J. Legendziewicz, T. Głowiak, E. Huskowska and C. N. Dao, in preparation.

Polyhedron Vol. 7, No. 24, pp. 2503–2508, 1988
Printed in Great Britain

0277–5387/88 $3.00+.00
© 1988 Pergamon Press plc

THIONE COMPLEXES OF GROUP IIB DIHALIDES. X-RAY CRYSTAL STRUCTURE OF $Cd(ETTC)_2I_2$

A. CASTIÑEIRAS,* C. F. VIDAL, R. BASTIDA and A. MACIAS

Departamento de Química Inorgánica, Universidad de Santiago de Compostela, Campus Universitario, E-15706 Santiago de Compostela, Spain

and

W. HILLER

Institut für Anorganische Chemie der Universität Tübingen, Auf der Morgenstelle 18, D-7400 Tübingen, F.R.G.

(*Received* 18 *January* 1988; *accepted* 3 *May* 1988)

Abstract—Complexes having the empirical formulae $M(ETTC)_2X_2$ (M = Zn or Hg, X = Br or I, ETTC = ethylene trithiocarbonate), $Cd(ETTC)_2I_2$ and $Hg(ETTC)X_2$ (X = Cl, Br or I) were obtained by the reaction of zinc, cadmium or mercury dihalides in dichloromethane or ethanol with ETTC. The structures of the compounds were characterized by ^1H NMR and IR spectrometry, conductance measurements and elemental analysis. The X-ray crystal structure of $Cd(ETTC)_2I_2$ has been determined using counter data and refined to an R value of 0.045. The unit cell constants are $a = 1586.3(2)$, $b = 699.7(1)$ and $c = 724.9(3)$ pm, the space group is $Pmn2_1$ and $Z = 2$. Coordination about the cadmium atom is tetrahedral.

It is known that trithiocarbonates exhibit insecticidal and fungicidal activities,[1] but they are also potentially polyfunctional ligands which can be linked to metals through either the terminal sulphur atom or the thiaether sulphur atoms. Ethylene trithiocarbonate (ETTC) is frequently coordinated via the exocyclic sulphur atom.[2–4] Since the halides of group IIB metals are soft Lewis acids,[5] their complexes with ETTC may be expected to be stable and, in principle, to involve coordination through both exo- and endocyclic sulphur atoms.

RESULTS AND DISCUSSION

The analytical data, some physical properties and ^1H NMR data of the ETTC complexes studied are listed in Table 1. All the complexes proved to be non-electrolytes in methyl cyanide,[6] which suggests the formulae ML_2X_2 or MLX_2, though some solvolysis involving partial liberation of the halide ion may take place.

The ^1H NMR spectrum of ETTC in DMSO-d_6 shows a single peak at 4.08 ppm that is retained in all complexes. This indicates that the donor ability and high concentration of the solvent allows the formation of $M(DMSO)_nX_2$ species, with ETTC being displaced from the metal coordination sphere, since in other ETTC–metal complexes the ligand protons are shifted upfield by 0.5 ppm.[3]

Description of the structure of $Cd(ETTC)_2I_2$

The molecular structure and atom labelling scheme are shown in Fig. 1, and selected geometrical features in Table 2.

The CdI_2 moiety is located in the mirror plane bound to a mirror-symmetrical pair of ligand molecules. Each ETTC molecule acts as a monodentate ligand coordinating to a Cd atom via the exocyclic S atom, the two endocyclic S atoms remaining uncoordinated. The structure is built of discrete molecules $Cd(ETTC)_2I_2$.

The coordination polyhedron of Cd is a slightly distorted tetrahedron. The I—Cd—I angle of 112.18(4)° is wider than the regular tetrahedral

* Author to whom correspondence should be addressed.

Table 1. Analytical, melting point, conductance and ^{1}H NMR data for metal complexes

Compound	M.p. (°C)	Found (calc.) (%) C	H	M	Λ_m[a]	δ^1H (ppm)[b]
$Zn(ETTC)_2Br_2$	167	13.8 (14.5)	1.39 (1.62)	13.0 (13.1)	7.2	4.08
$Zn(ETTC)_2I_2$	195	12.0 (12.2)	1.18 (1.36)	11.0 (11.0)	9.7	4.08
$Cd(ETTC)_2I_2$	145	11.1 (11.3)	1.22 (1.26)	17.1 (17.6)	18.3	4.08
$Hg(ETTC)_2Br_2$	157	11.0 (11.4)	1.15 (1.28)	31.0 (31.7)	14.3	4.08
$Hg(ETTC)_2I_2$	116	9.9 (9.9)	1.16 (1.11)	27.5 (27.6)	17.7	4.10
$Hg(ETTC)Cl_2$	165	9.0 (8.8)	1.00 (0.99)	48.5 (49.2)	23.4	4.08
$Hg(ETTC)Br_2$	168	6.9 (7.2)	0.85 (0.81)	39.8 (40.4)	22.6	4.08
$Hg(ETTC)I_2$	117	5.9 (6.1)	0.71 (0.68)	33.0 (33.9)	21.1	4.08

[a] $Ohm^{-1}\,cm^2\,mol^{-1}$, $\sim 10^{-3}$ M in CH_3CN.
[b] In DMSO-d_6.

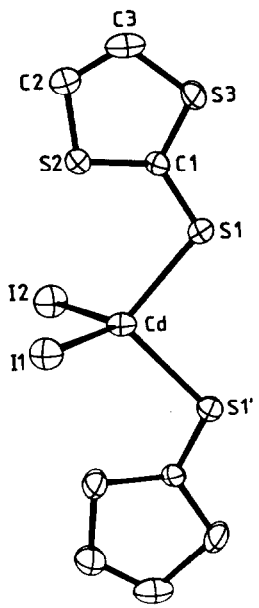

Fig. 1. Molecular structure and labelling scheme for $Cd(ETTC)_2I_2$.

angle due to the repulsion between the I atoms, which causes a decrease in the S—Cd—S angle to 86.23(5)°. The Cd—I bond lengths of 271.0(1) and 271.9(1) pm are slightly shorter than in other CdI_2 complexes, while the Cd—S bond length of 260.9(3) pm is about 4 pm longer than expected for the Cd—S bond lengths of a tetrahedrally coordinated Cd atom.[7] There are no other atoms around the Cd atom at a distance shorter than the sum of the corresponding van der Waals radii.

In the ligand moiety the C atoms are displaced towards the plane through the three S atoms to give a planar structure in which the torsion angles are near to 0 or 180° (Table 2). The bond lengths and angles reflect modification of the electron delocalization within the planar CS_3 group of the free ligand.[8] The exocyclic C(1)—S(1) is somewhat longer than in ETTC (165.2 pm), whereas coordination increases the double bond character of the endocyclic C—S bonds, since they are between 4 and 9 pm shorter than in the free ligand. The C(1)—S bonds nevertheless remain considerably shorter than the C(sp^3)—S bonds.

IR spectra

The assignments of the principal IR ligand bands (Table 3) are based on published data for ETTC.[9,10] The most characteristic frequencies in the IR spectra of the complexes are also given in Table 3.

The interesting bands as regards explanation of the coordination of the ligand to the metal atom are the vibrations of the trithiocarbonate group. The strong band at 1062 cm^{-1}, an out-of-phase combination of νC=S and ν_sSCS coupled to

Table 2. Selected geometrical features of $Cd(ETTC)_2I_2$ (EDSs in parentheses)

Distances (pm)			
Cd—I(1)	271.0(1)	S(2)—C(2)	173.0(8)
Cd—I(2)	271.9(1)	S(3)—C(1)	165.5(6)
Cd—S(1)	260.9(3)	S(3)—C(3)	178.1(9)
S(1)—C(1)	168.5(6)	C(2)—C(3)	148(1)
S(2)—C(1)	166.8(7)		
Angles (deg)			
I(1)—Cd—I(2)	112.18(4)	S(1)—C(1)—S(2)	124.3(4)
I(1)—Cd—S(1)	112.99(5)	S(1)—C(1)—S(3)	119.8(4)
I(2)—Cd—S(1)	111.29(5)	S(2)—C(1)—S(3)	116.0(4)
S(1)—Cd—S(1′)	86.23(5)	S(2)—C(2)—C(3)	112.5(6)
C(1)—S(2)—C(2)	100.3(5)	S(3)—C(3)—C(2)	112.3(6)
C(1)—S(3)—C(3)	98.7(4)		
Torsion angles (deg)			
C(2)—S(2)—C(1)—S(1)	179.92	C(3)—S(3)—C(1)—S(2)	−1.56
C(2)—S(2)—C(1)—S(3)	−0.53	C(1)—S(3)—C(3)—C(2)	3.55
C(1)—S(2)—C(2)—C(3)	2.99	S(2)—C(2)—C(3)—S(3)	−4.28
C(3)—S(3)—C(1)—S(1)	177.86		

δCSS,[10] is split and shifted 10–50 cm^{-1} towards lower frequencies; the strong band near 882 cm^{-1}, which is due to ν_{as}SCS with a small amount of δC=S coupled strongly to ρCH_2,[10] is shifted towards higher frequencies; and the band at 503 cm^{-1}, an in-phase combination of νC=S and ν_sSCS coupled with a small amount of δ_sCSC,[10] decreases considerably in intensity but is shifted between 10–20 cm^{-1} up-spectrum. This behaviour suggests that double bond character is lost by the exocyclic C=S bond and is gained by the endocyclic C—S bonds, especially the C(sp^2)—S bonds. Both these variations are to be expected when there is coordination of ETTC to the metal via the sulphur atom,[2–4] as is shown by the molecular structure found for $Cd(ETTC)_2I_2$. In general, the largest shifts of νC=S (down-spectrum) and ν_{as}SCS (up-spectrum) are observed in the mercury complexes and the smallest in the zinc complexes, in keeping with the softness of the corresponding halides.[11]

The bands observed in the far-IR region, may be attributed to halogen–metal and metal–ligand stretching modes. Specifically, the distorted tetrahedral coordination with C_{2v} symmetry assumed for all the $M(ETTC)_2X_2$ complexes by analogy with $Cd(ETTC)_2I_2$ implies the possibility of two IR MX_2 stretching vibrations, $\nu_s MX(A_1)$ and $\nu_{as}MX(B_1)$, and two IR MS_2 stretching modes, $\nu_s MS(A_1)$ and $\nu_{as}MS(B_1)$.[12] For all the $M(ETTC)_2X_2$ complexes, one of the IR bands that appears is ascribed to the symmetric metal–halogen stretching mode and a lower-frequency band to the antisymmetric mode. The fact that the position of both bands is affected by the mass of the halogen and the νMI/νMBr ratio (0.78 in the Zn complexes and 0.70–0.80 in the Hg complexes), supports these identifications,[13] which are consistent with other recent assignments for these vibrations.[7,14]

Like other $HgLX_2$ complexes,[15,16] the Hg $(ETTC)X_2$ complexes probably have a dimer structure with two halogen bridges. This kind of symmetry implies two mass-dependent IR mercury–halogen stretching modes, ν_tHgX(Bu) and ν_bHgX(Au), and one IR Hg—S stretching mode, νHgS(Bu). In the three complexes studied, the strong band observed between 250–170 cm^{-1} is assigned to the terminal HgX stretching and the band below 170 cm^{-1} to the bridging mode. This assignment implies νHgBr/νHgCl and νHgI/νHgCl ratios of 0.85 and 0.69, respectively and ν_b/ν_t ratios of 0.66, 0.61 and 0.58, all of which are within the range for binuclear complexes with halogen bridging.[12,13]

In all complexes, the νMS modes have been tentatively identified in the 350–290 cm^{-1} region.[14–17] The second νMS band is not observed in the $M(ETTC)_2X_2$ complexes.

EXPERIMENTAL

Commercial ethylene trithiocarbonate was purified by sublimation. Reagent grade metal halides were used as received. ^{1}H NMR spectra referenced to internal tetramethylsilane were obtained at 250 MHz on a Bruker-WM 250 spectrometer. IR spectra were recorded on a Perkin–Elmer 180

Table 3. IR spectral data for ETTC and its metal complexes[a]

Assignments	ETTC[b]	$Zn(ETTC)_2Br_2$	$Zn(ETTC)_2I_2$	$Cd(ETTC)_2I_2$	$Hg(ETTC)_2Br_2$	$Hg(ETTC)_2I_2$	$Hg(ETTC)Cl_2$	$Hg(ETTC)Br_2$	$Hg(ETTC)I_2$
$\nu C{=}S$, $\nu_s SCS$ (ν_6)	1062vs	1050m 1022s,br	1044s 1030vs	1043s 1029s	1025s 1012s	1045s 1030s	1020s 1008s	1022s 1010s	1022s 1012s
$\nu_{as}SCS$ (ν_{18})	882s	915s	918s	917s	923m	916s	931m	928m	929m 920m
$\nu_{as}SCS$ (ν_{19})	832s	833m	833m	835s	839m	839m	840m	836m	831m
$\nu_s CH_2S$ (ν_9)	674m	663m	668m	664m	663m	672m	667m	664m	663m
$\nu_{as}CH_2S$ (ν_{20})	650vw	—	—	—	—	—	—	—	—
$\nu C{=}S$, $\nu_s SCS$ (ν_{10})	503m	521vw	518vw	519vw	513w	519m	522w	520vw	—
CS_3 group def. vib.	478m 383m	478w 385m	472w 383m	480vw 385m	481vw 387m	480w 388m	480w 384m	477w 383m	476w 381m
Ring vib.	454m	454m	456w	458m	456m	459m	455m	454m	452w
νMS	—	293m	300m	325sh	348w?	355w?	328w	322w	308w
$\nu_t MX$	—	247s	195s	165s	212s	150s	248s 244s	212s	172s
	—	225s 210s	170m 152m	142m	175s	138s	—	—	—
$\nu_b MX$	—	—	—	—	—	—	164s	130sh	100s

[a] t and b denote terminal and bridging νMX stretching modes. Abbreviations: s = strong, m = medium, w = weak, v = very, sh = shoulder, br = broad.
[b] Ref. 9.

Table 4. Crystal data for $Cd(ETTC)_2I_2$

Molecular formula	$I_2CdS_6C_6H_8$
Molecular weight	638.72
Crystal class	orthorhombic
Space group	$Pmn2_1$
Lattice constants	$a = 1586.3(2)$ pm
	$b = 699.7(1)$ pm
	$c = 724.9(3)$ pm
Cell volume	$V = 804.6 \times 10^6$ pm^3
Formula units	$Z = 2$
$F(000)$	588
Density	$\rho_x = 2.635$ g cm^{-3}
Coef. abs.	$\mu = 58.72$ cm^{-1}

spectrophotometer in Nujol mulls. Conductivity measurements were carried out using a WTW LF-3 conductimeter with a WTW LT-A cell. Melting points were determined in a Büchi apparatus. Elemental analyses were performed as follows: Zn and Cd by titration against EDTA,[18] Hg by atomic absorption[19] in a Varian Techtron AA-6 spectrophotometer, C and H with a Perkin–Elmer 240 Elemental analyser.

Preparation of $M(ETTC)_2X_2$ *complexes*

Solutions consisting of approximately 2.5 g of ETTC (4 mmol), metal dihalide (2 mmol) and 25 cm^3 of dichloromethane (or dry ethyl alcohol for HgX_2), were refluxed for 12 h and then cooled. The reaction mixtures were evaporated to dryness under reduced pressure. The residues were stirred with 10 cm^3 of carbon tetrachloride and then filtered, and the solid phase was washed with carbon tetrachloride and dried *in vacuo* to give a yellowish powder. Attempts at recrystallization from absolute ethanol only afforded crystals for $Cd(ETTC)_2I_2$.

Preparation of $M(ETTC)X_2$ *complexes*

A solution of 2.5 g of ethylene trithiocarbonate (4 mmol) in 10 cm^3 of dichloromethane was added dropwise with continuous stirring to a solution or suspension of the corresponding mercury dihalide (2 mmol) in the same solvent (10 cm^3) until the metal : ligand molar ratio was 1 : 1, when a solid was precipitated. Stirring was continued for several days, and after filtration the solids were washed with dichloromethane and dried *in vacuo*.

Determination of the crystal structure of $Cd(ETTC)_2I_2$

A yellowish crystal of $Cd(ETTC)_2I_2$ measuring approximately $0.25 \times 0.30 \times 0.10$ mm was selected to collect intensities on a CAD-4 Enraf–Nonius four-circle automatic diffractometer at room temperature using graphite-monochromated Mo–K_α radiation ($\lambda = 0.71073$ Å). The cell constants were determined from the setting angles of 25 reflections (Table 4). 3120 reflections were collected in the range $3 < \theta < 32°$ in the ω–2θ scan mode. Of 2126 symmetry-independent reflections ($R_{int} = 0.028$), 1707 with $I < 3\sigma(I)$ were used in structure determination and refinement. Lp corrections and an empirical absorption correction[20] were applied to the data.

The structure was solved by Patterson and Fourier methods.[21] In the last refinement all atoms were assigned anisotropic temperature parameters. No hydrogens were included. The final refinement converged at $R = 0.045$, $R_w = 0.048$. Computations were performed on a DECMicroVAXII computer.*

Acknowledgements—The authors (A.C. and A.M.) are indebted to the Ministerio de Educación y Ciencia and Xunta de Galicia, respectively, for financial support.

REFERENCES

1. J. T. Bashour, U.S. Patent 2676129 (1954) *Chem. Abstr.* 1954, **48**, 8472h, U.S. Patent 2731487 (1956) *Chem. Abstr.* 1956, **50**, 15583g; H. J. Renner, G. Scheider and J. Weissflog, Ger. (East) Patent 15413 (1958) *Chem. Abstr.* 1960, **54**, 2650f.
2. J. A. Gladysz and W. Avakian, *Synth. React. Inorg. Met.-Org. Chem.* 1975, **5**, 247.
3. A. R. Siedle, *J. Organometal. Chem.* 1976, **120**, 369.
4. M. T. Pereira, M. R. Bermejo, A. Castiñeiras and M. Gayoso, *An. Quím.* 1980, **76B**, 203; *An. Quim.* 1982, **78B**, 152.
5. R. G. Pearson (Ed.) *Hard and Soft Acids and Bases.* Dowden, Hutchinson and Ross, Stroudsburg (1973).
6. J. A. Davies, F. R. Hartley and S. G. Murray, *Inorg. Chim. Acta* 1980, **43**, 69.
7. A. Castiñeiras, A. Arquero, J. R. Masaguer, A. Ruiz-Amil, S. Martinez-Carrera and S. García-Blanco, *Polyhedron* 1985, **4**, 143.
8. B. K. Klewe and H. M. Seip, *Acta Chem. Scand.* 1972, **26**, 1860.
9. P. Klaboe, *Acta Chem. Scand.* 1968, **22**, 1532.
10. G. Borch, L. Henriksen, P. H. Nielsen and P. Klaboe, *Spectrochim. Acta* 1973, **29A**, 1109.

* Atomic coordinates, displacement factor coefficients, full lists of bond lengths and angles and lists of F_o/F_c values have been deposited as supplementary data with the Editor, from whom copies are available on request. Atomic coordinates have also been deposited with the Cambridge Crystallographic Data Centre.

11. P. P. Singh, S. K. Srivastava and A. K. Srivastava, *J. Inorg. Nucl. Chem.* 1980, **42**, 521.
12. J. R. Ferraro, *Low-frequency Vibrations of Inorganic and Coordination Compounds*. Plenum Press, New York (1971).
13. R. J. H. Clark and T. M. Dunn, *J. Chem. Soc.* 1963, 1198.
14. A. Arquero, J. R. Masaguer and A. Castiñeiras, *Z. Anorg. Allg. Chem.* 1985, **531**, 183.
15. W. Hiller, A. Castiñeiras, A. Arquero and J. R. Masaguer, *Acta Cryst.* 1986, **42C**, 151.
16. A. Castiñeiras, A. Arquero, J. R. Masaguer, S. Martinez-Carrera and S. García-Blanco, *Z. Anorg. Allg. Chem.* 1986, **539**, 219.
17. A. Catiñeiras, A. Arquero and J. R. Masaguer, *Transition Met. Chem.* 1984, **9**, 273.
18. E. Merck, *Metodos Complexómetricos de Valoraciones con Titriplex*, 3rd Edn. Darmstadt (1969).
19. M. Lopez-Lamas, F. Bermejo and F. Lopez-Capont, *Agroquímica y Tecnología de alimentos* 1973, **13**, 470.
20. N. Walker and D. Stuart, *Acta Cryst., Sect. A. Found. Crystallogr.* 1983, **A39**, 158.
21. Enraf-Nonius Structure Determination Package. SDP-PLUS, B. A. Frenz and Associates, College Station TX (1981).

Polyhedron Vol. 7, No. 24, pp. 2509–2514, 1988
Printed in Great Britain

0277–5387/88 $3.00+.00
© 1988 Pergamon Press plc

MERCURY–SULPHUR STRETCHING FREQUENCIES, SYNTHESIS AND X-RAY CRYSTAL STRUCTURE OF *CATENA*-μ-(3-DIMETHYLAMMONIO-1-PROPANETHIOLATO)DICHLOROMERCURY(II)

I. CASALS, P. GONZÁLEZ-DUARTE* and J. SOLA

Departament de Química, Unitat de Química Inorgànica, Universitat Autònoma de Barcelona, 08193 Bellaterra, Barcelona, Spain

and

C. MIRAVITLLES and E. MOLINS

Inst. Geologia "Jaume Almera", Martí i Franquès s/n, 08028 Barcelona, Spain

(*Received* 18 *January* 1988; *accepted* 3 *May* 1988)

Abstract—The crystal structure of the title compound has been determined. Crystals of $[HgCl_2\{\mu\text{-}S(CH_2)_3NH(CH_3)_2\}]$ are monoclinic, space group $P2_1/n$, with $a = 10.136(2)$, $b = 6.519(1)$, $c = 15.940(6)$ Å and $\beta = 97.20(3)°$. The structure consists of $(—Hg—S—)_n$ helicoidal chains linked by hydrogen bonding, which give rise to chemically unconnected layers along the $(\bar{2}02)$ planes. Each mercury is tetrahedrally coordinated to two terminal chlorine atoms and two bridging sulphur atoms. Assignments of ν_{as}(SHgS) and ν_s(SHgS) for this complex and its isostructural bromine analogue, and of ν_s(ClHgCl) and ν_s(BrHgBr) from IR and Raman spectroscopy are reported. Comparison of Hg—S frequencies with those reported for closely related compounds as well as correlation with Hg—S bond distances are made.

An important part of our research work on aliphatic γ-mercaptoamine complexes has been devoted to the structural characterization and solution equilibria studies[1–3] of complexes with Zn^{II}, Cd^{II} and Hg^{II} ions. The structures found in solid complexes of 4-mercapto-1-methylpiperidine range in size from discrete units, as with Hg^{II},[4] through dimers, as with Zn^{II},[5,6] Cd^{II}[6] and Hg^{II},[6] to one-dimensional polymeric chains, as with Cd^{II}.[7] Under the same conditions in which the dimers are obtained, the ligand 3-dimethylamino-1-propanethiol gives rise to isostructural polymeric compounds of the formula $[MX_2\{\mu\text{-}S\text{-}(CH_2)_3\text{-}NH(CH_3)_2\}]$ where M = Zn^{II}, Cd^{II} or Hg^{II}; and X = Cl or Br.[8]

The most striking features of these results are the different structures obtained when the same metal ion is coordinated to very similar ligands and the behaviour of Hg^{II} towards a particular ligand when compared with that of Zn^{II} or Cd^{II}. Thus, the molecular structure of bis(1-methylpiperidinium-4-thiolato)mercury(II) perchlorate is the only known example of a mononuclear metal–non chelating γ-mercaptoamine discrete species. This structure together with the synthesis and vibrational spectra of several $[RSHg^{II}]^{2+}(ClO_4)_2$ complexes, where RS denotes a γ-mercaptoamine ligand, have already been published.[4]

In the present work we report the crystal and molecular structure, and vibrational spectra, of the complex *catena*-μ-(3-dimethylammonio-1-propanethiolato)dichloromercury(II). The frequencies corresponding to the S—Hg—S symmetric and asymmetric stretchings are assigned and these values correlated with those given in the literature

* Author to whom correspondence should be addressed.

for simple thiol–Hg^{II} complexes with known structure and different geometries around the metal atom.[9–12]

EXPERIMENTAL

All reagents and solvents were research grade ($\geq 98\%$) and were not further purified. The ligand was obtained according to a previously published procedure,[13] its purity always being $> 95\%$.

Catena-μ-(3-*dimethylammonio*-1-*propanethiolato*) *dichloromercury*(II)

A solution of 3-dimethylamino-1-propanethiol (0.60 g, 5 mmol) in methanol (8 cm^3) and dimethylsulphoxide (2 cm^3), at 50°C, was added slowly with stirring to a solution of $HgCl_2$ (1.35 g, 5 mmol) in the same solvent and at the same temperature. The resultant solution was allowed to cool at room temperature and was stored in the dark. After two weeks pink, prismatic-shaped crystals separated. The crystals were filtered off, washed with cold water and dried *in vacuo*. Recrystallization was not necessary because of the extremely good quality of the crystals obtained. (Found: C, 15.3; N, 3.5; S, 8.0. $C_5H_{13}Cl_2NSHg$ requires C, 15.4; N, 3.6; S, 8.2%.)

This compound is soluble in Me_2SO but practically insoluble in water, methanol, ethanol, acetonitrile and tetrahydrofuran.

Analyses

Microanalyses were performed by one of the authors (I.C.) with a Carlo Erba NA-1500 analyser.

Physical measurements

The IR spectra of the complex and the ligand were recorded from 4000 to 600 cm^{-1} in KBr on a Perkin–Elmer 1710 spectrophotometer and from 600 to 200 cm^{-1} in Nujol mulls between polythene plates on a Perkin–Elmer 983 apparatus.

The Raman spectra were recorded on a Dilor spectrophotometer using 514.5 nm excitation and samples were run as powders in spinning capillary tubes.

CRYSTALLOGRAPHY

Crystal data

A single crystal of dimensions $0.21 \times 0.12 \times 0.08$ was used for X-ray diffraction study. The lattice parameters at 294 K were determined by a least squares fit to the setting parameters of 25 independent reflections on an Enraf–Nonius CAD-4 diffractometer using graphite monochromatized Mo-K_α radiation. $[C_5H_{13}NSCl_2Hg]_n$, $M = 390.7$, monoclinic, space group $P2_1/n$, $a = 10.136(2)$, $b = 6.519(1)$, $c = 15.940(6)$ Å, $\beta = 97.20(3)°$, $D_{calc} = 2.48$ g cm^{-3}, $V = 1044.9$ $Å^3$, $Z = 4$, μ(Mo-K_α) $= 15.4$ mm^{-1}, $\lambda = 0.71069$ Å, $F(000) = 720$.

Intensity data were collected in the range $1 > \Theta > 25°$, $\omega - 2\theta$ scan and $-12 \leqslant h \leqslant 12$, $0 \leqslant k \leqslant 7$, $0 \leqslant l \leqslant 18$. The standard reflection decay was 0.9%. No correction was made for absorption. Of the 1848 independent reflections collected, 1270 unique reflections with $F > 3\sigma(F)$ were considered "observed" and used in the calculations.

Solution and refinement

The application of the straightforward run of the program MULTAN-11/84[14] gave the mercury and one chlorine atom positions. A subsequent difference Fourier synthesis allowed us to locate the remaining non-hydrogen atoms. The structure was refined by the full-matrix least-squares methods on F. Anisotropic thermal parameters for non-hydrogen atoms were used. The hydrogen atoms were introduced in calculated positions and geometrically fixed along the refinement by employing a global isotropic temperature factor. Ninety-two parameters were refined. The refinement converged to $R = 0.079$ and $R_w = 0.080$. The weighting scheme employed was $w = 1/(\sigma^2(F) + 0.000356F^2)$. The maximum shift per ESDs for any parameter was 0.22 and the average shift per ESD, 0.05. The difference Fourier map showed maximum and minimum peak heights of 3 and -3 e $Å^{-3}$, respectively, near the Hg atom (at 0.9 Å).

Atomic scattering factors for the non-hydrogen atoms were taken from Cromer and Mann[15] and those for hydrogen atoms from Steward, Davidson and Simpson.[16] The calculations were performed using the SHELX-76 program.[17] Bond lengths and bond angles are given in Tables 1 and 2, respectively.*

* Atomic coordinates, displacement factor coefficients, full lists of bond lengths and angles and lists of F_o/F_c values have been deposited as supplementary data with the Editor, from whom copies are available on request. Atomic coordinates have also been deposited with the Cambridge Crystallographic Data Centre.

Table 1. Bond lengths (Å) with estimated standard deviations in parentheses

Cl(1)—Hg	2.513(6)
Cl(2)—Hg	2.634(5)
S—Hg	2.464(6)
C(1)—S	1.792(22)
C(3)—N	1.512(28)
C(4)—N	1.463(29)
C(5)—N	1.471(29)
C(2)—C(1)	1.521(21)
C(3)—C(2)	1.526(22)
Hg—S′	2.471(6)
Hg—Hg′	3.861(1)

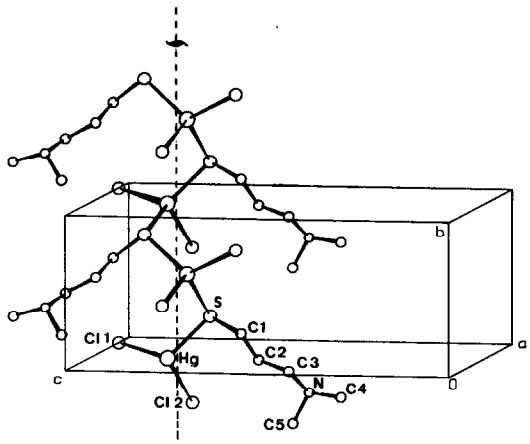

Fig. 1. Part of the chain of $[HgCl_2\{\mu\text{-}S(CH_2)_3NH(CH_3)_2\}]$ showing the two-fold helicoidal axis parallel to *b*. The atom labelling (Tables 1 and 2) is indicated. Arbitrary atomic radii have been drawn.

RESULTS AND DISCUSSION

Description of the structure of $[HgCl_2\{\mu\text{-}S(CH_2)_3NH(CH_3)_2\}]$

The crystal structure of $[HgCl_2\{\mu\text{-}S\text{-}(CH_2)_3NH(CH_3)_2\}]$ consists of infinite parallel spirals of alternating mercury and sulphur atoms (Fig. 1), each mercury atom being coordinated to two bridging sulphur atoms, S and its corresponding symmetry related S′, and to two terminal chlorine atoms, Cl(1) and Cl(2), in a distorted tetrahedra which by corner-sharing gives rise to helices running parallel to *b*.

The most significant bond distances and angles are the following: Hg—S, 2.464(6) Å; Hg—Cl(1), 2.513(6) Å; Hg—Cl(2), 2.634(5) Å; S—Hg—Cl(1), 112.5(2)°; S—Hg—Cl(2), 102.3(2)°; Cl(1)—Hg—Cl(2), 99.0(2)°; S—Hg—S′, 130.2(3)°; the remainder are given in Tables 1 and 2. The coordination tetrahedron around the mercury atom is more distorted than the one found in the isostructural cadmium complex as the dihedral angle formed by the planes ClMCl and SMS indicates, being 86.9 and 88.1° for M = Hg or Cd,[8] respectively. Also, by comparing the $HgCl_2S_2$ unit of this complex with that found in $[Hg(SPr^i)Cl]$,[30] where S—Hg—S and Cl—Hg—Cl angles are respectively 119 and 115°, it can be concluded that in the present case the coordination around mercury is more distorted (actual point group symmetry C_1) and the S—Hg—S angle, 130.2°, departs severely from that of a regular tetrahedron, although the mercury atom is not involved in additional interactions.

Table 2. Bond angles in degrees with estimated standard deviations in parentheses

Cl(2)—Hg—Cl(1)	99.0(2)
S—Hg—Cl(1)	112.5(2)
S—Hg—Cl(2)	102.3(2)
C(4)—N—C(3)	109.2(17)
C(5)—N—C(3)	112.1(19)
C(5)—N—C(4)	111.7(18)
C(2)—C(1)—S	109.6(14)
C(3)—C(2)—C(1)	111.0(17)
C(2)—C(3)—N	109.7(17)
S—Hg—S′	130.2(3)
Cl(1)—Hg—S′	104.1(3)
Cl(2)—Hg—S′	104.0(3)
Hg—S—C(1)	102.4(8)
Hg—S′—Hg′	102.9(2)

Within each infinite $(—Hg—S—)_n$ chain the dihedral angle formed by the planes defined by all mercury and all sulphur atoms, respectively, is 84.2°, which is close to the one found in the isostructural cadmium complex.[8] The shortest Hg···Hg distance is found to be intra-chain and is 3.861(1) Å, which indicates no interaction between these atoms.[18] These chains resemble those of the cinnabar, where Hg—S and the shortest Hg···Hg distances are, respectively, 2.38 and 3.75 Å,[19] the difference being the presence in our case of a two-fold screw axis instead of a three-fold one in the cinnabar.

Each chain is held together laterally by two other chains by means of hydrogen bonding between each ammonium group and Cl(2) atoms, as is shown by the distance Cl(2)···N′ (3.15 Å).[20] Those chains joined through the hydrogen bond give rise to parallel layers of helicoidal axes lying on the $(\bar{2}02)$ planes (Fig. 2). Layers are too wide apart to be chemically interconnected, the shortest inter-layer N—Cl distance being 4.3 Å, Fig. 3.

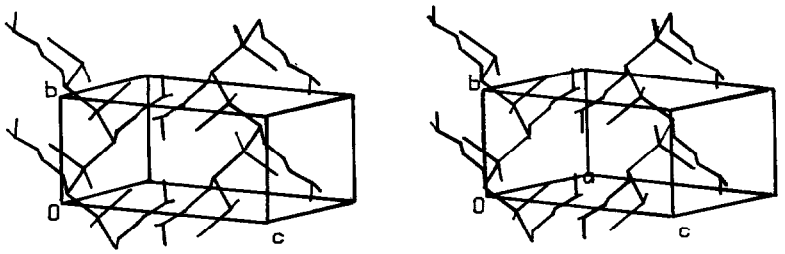

Fig. 2. Stereoview of a layer formed by $[HgCl_2\{\mu\text{-}S(CH_2)_3NH(CH_3)_2\}]$ chains linked by hydrogen bond interactions.

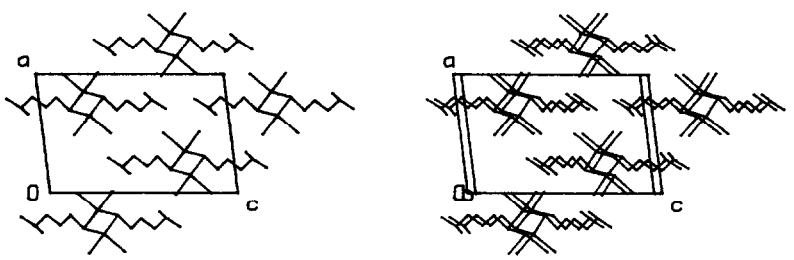

Fig. 3. Stereoview of the unit cell showing the helicoidal chains and the chemically unconnected layers oriented along the $\bar{2}02$ planes.

The Hg—S bond length (2.46 Å) is within the range of previously reported values for mercury thiolate complexes (2.36 Å for $[Hg(SMe)_2]$,[21] 2.45 Å* for $[Hg(SEt)_2]$,[22] 2.59 Å for $[Hg(SBu^t)_2]$,[23] 2.48–2.63 Å for $[Hg(SBu^n)_2]$,[24] 2.54 Å for $[Hg(SC_6H_4Cl)_4]^{2-}$,[25] 2.44–2.71 for $[Hg_2(SMe)_6]^{2-}$[26] and 2.36–2.86 for $[Hg_3(SCH_2CH_2S)_4]^{2-}$[27]), for bis-(1-methylpiperidinium-4-thiolato)mercury(II) perchlorate (2.33 Å),[4] and for mixed ligands $RSHg^{II}Cl$ complexes (2.505,[28] 2.40,[29] 2.56[28] and 2.38–2.54 Å[30]). One of the observed Hg—Cl distances, Hg—Cl(1) 2.51 Å, lies within the range found in the literature for mercury terminal–chlorine bonds, 2.34–2.57 Å.[28–31] The second Hg—Cl distance is longer, Hg—Cl(2) 2.63 Å, which arises from the fact that this chlorine atom is involved in hydrogen bonding, as already indicated.

Vibrational spectra

The IR spectrum of the complex $[HgCl_2\{\mu\text{-}S(CH_2)_3NH(CH_3)_2\}]$ and that of the isomorphous bromine compound,[8] from 4000 to 600 cm^{-1}, are very similar to the spectrum of 3-dimethylamino-1-propanethiol in its zwitterionic form, thus confirming that the amine group is protonated (broad bands at 2460–2480 and 2770–2780 cm^{-1}) and also indicating that weak hydrogen bonding occurs in both cases (shoulder at 2980–3000 cm^{-1}).

Even if the local symmetry of the HgS_2X_2 unit was considered to be C_{2v} all stretching vibrational modes should be IR and Raman active, thus it is unnecessary to take into account degradation of the symmetry to C_1. By comparing the IR (600–200 cm^{-1}) and Raman (600–150 cm^{-1}) spectra of the ligand and both mercury complexes it has been possible to assign the frequencies corresponding to Hg—S and Hg—X (X = Cl or Br) stretching vibrations, Table 3. The bands appearing at 308 and *ca* 270 cm^{-1} (both IR and Raman) have been attributed, respectively, to ν_{as}(Hg—S) and ν_s(Hg—S), and the strong halogen dependent absorptions in the Raman spectra at 233 and 155 cm^{-1} have been assigned to ν_s(Hg—Cl) and ν_s(Hg—Br), respectively.

The comparison between the assignments made in this work with those already reported for the ν(Hg—S) modes in closely related complexes is given in Table 4, where the corresponding Hg—S bond distances have also been included. One significant feature common to many (alkylthiolato)halomercury(II) compounds and bis(alkylthiolato)mercury(II) complexes is the existence of additional weak intermolecular Hg···S or Hg···X interactions,[12,30] which modify the metal

* Misstated as 2.54 Å in ref. 10.

Table 3. Bands (cm^{-1}) assigned to ν(S—Hg), ν(Cl—Hg) and ν(Br—Hg) vibrations

Compound		ν_{as}(Hg—S)	ν_s(Hg—S)	ν(Hg—Cl)	ν(Hg—Br)
$[HgCl_2\{\mu\text{-}S(CH_2)_3NH(CH_3)_2\}]$	IR	308(m)	270(m)	233(m)	
	R	308(w)	272(m)	232(s)	
$[HgBr_2\{\mu\text{-}S(CH_2)_3NH(CH_3)_2\}]$	IR	307(s)	263(m)		
	R	308(w)	268(m)		155(s)

environment and thus reflect in their spectroscopic behaviour. This, together with the facts that some structure determinations do not give accurate interatomic distances[21,22] and that until recently[18] different values for the van der Waals radius of mercury had been proposed make the correlation between structure and vibrational frequencies rather difficult. Despite all this, the data in Table 4 indicate that the absorption frequencies assigned to ν(Hg—S) for $[HgX_2\{\mu\text{-}S(CH_2)_3NH(CH_3)_2\}]$, X = Cl or Br, (308, 270 cm^{-1}) agree well with those expected, as they lie in between those corresponding to "pure" linear (complexes **I** and **III**) and "pure" tetrahedral (complex **IV**) coordinations. In considering complexes **I**–**VI**, the Hg—S bond distances correlate fairly well with ν(Hg—S) frequencies as the additional Hg···S interactions are probably the cause for the lowering of the ν(Hg—S) values in compound **II** and it also seems likely that 2.45 Å is too long for the Hg—S bond distance in complex **III**. The additional contacts involving Hg atoms in compounds **VII** and **VIII** make it difficult to include them in the previous correlation.

The frequencies assigned to the stretching vibrations, ν(Hg—Cl) 233 cm^{-1} and ν(Hg—Br) 155 cm^{-1}, corresponding to terminal Hg—X bonds, are especially intense in the Raman spectra compared with those in the IR spectra.[26] Practically the same absorption frequencies have been assigned to the mercury–halogen stretching modes in $[HgCl_2(PPh_3)_2]$, ν(Hg—Cl) 232 cm^{-1}, $[HgBr_2(PPh_3)_2]$, ν(Hg—Br) 153 cm^{-1},[32] and to those corresponding to the S_2HgCl_2 units in [Hg(SPr^i)Cl], ν(Hg—Cl) 220 cm^{-1}.[30] Hg—Cl distances in these units (2.53 Å) are almost the same as for Hg—Cl(1) in the compound reported here.

Table 4. Selected vibrational frequencies and corresponding Hg—S bond distances for several mercury(II)–thiolate complexes with known structure

	Compound	Geometry around Hg	*d*(Hg—S) (Å)	ν(Hg—S) (cm^{-1})	Reference
I	$[Hg\{SC_5H_9NH(CH_3)\}_2](ClO_4)_2$	Linear	2.33	395(IR) 372(R)	4
II	$[Hg(SMe)_2]$	Essentially linear	2.36	337(IR) 297(R)	12, 21
III	$[Hg(SEt)_2]$	Linear	2.45	405(IR) 394(R)	12, 22
IV	$[Hg(SBu^t)_2]$	Tetrahedral	2.59–2.66	172(IR) 188(R)	12, 23
V	$[HgCl_2\{\mu\text{-}S(CH_2)_3NH(CH_3)_2\}]$	Distorted tetrahedral	2.46	308(IR,R) 270(IR,R)	This work
VI	$(NEt_4)_2[Hg_2(SMe)_6]$	Distorted tetrahedral	2.44–2.47 (Hg—S terminal)	280, 262(IR) 271, 259(R)	26
VII	[Hg(SMe)Cl]	Pseudo-octahedral	2.43	326, 282(IR) 296, 248(R)	28
VIII	[Hg(SPr^i)Cl]	Pseudo-octahedral tetrahedral	2.38 2.54	231(IR) 235(R)	30

ν(Hg—X) values assigned by us have also been proposed for the anions $[Hg_2Cl_6]^{2-}$, 233 cm^{-1} and $[Hg_2Br_6]^{2-}$, 150 cm^{-1},[31] the absorption of the former being associated with the bridging Hg—Cl bonds whose distances (2.56–2.67 Å) are similar to the terminal ones present in our case. Furthermore, thioamide mercury halide complexes show ν(Hg—Cl) and ν(Hg—S) at 230 and 310 cm^{-1}, respectively.[33]

Acknowledgements—P.G. and J.S. thank CIRIT (AR 85/99) and CAICYT (1058/84) for financial support. C.M. and E.M. gratefully acknowledge the grants 603/846 and 603/847 from CSIC and CAICYT. IR (600–200 cm^{-1}) and Raman spectra were measured at "Laboratoire de Chimie de Coordination (Toulouse)" and "Laboratoire de Spectroscopie Infrarouge" de l'Université de Bordeaux 1, France, respectively. We thank Prof. P. Cassoux and C. Sourisseau for their kindness.

REFERENCES

1. J. C. Bayón and P. González-Duarte, *J. Chem. Soc., Dalton Trans.* 1982, 487.
2. (a) J. C. Bayón, P. González-Duarte and J. Vives, *J. Chem. Soc., Dalton Trans.* 1984, 2671; (b) P. González-Duarte and J. Vives, *J. Chem. Soc., Dalton Trans.* 1988, in press.
3. J. C. Bayón, Ph.D. thesis. Universitat Autònoma de Barcelona (1981).
4. H. Barrera, J. C. Bayón, P. González-Duarte, J. Sola, J. M. Viñas, M. C. Briansó, J. L. Briansó and X. Solans, *Polyhedron* 1982, **1**, 647.
5. M. C. Briansó, J. L. Briansó, W. Gaete, J. Ros and C. Suñer, *J. Chem. Soc., Dalton Trans.* 1981, 852.
6. J. C. Bayón, I. Casals, W. Gaete, P. González-Duarte and J. Ros, *Polyhedron* 1982, **1**, 157.
7. J. C. Bayón, M. C. Briansó, J. L. Briansó and P. González-Duarte, *Inorg. Chem.* 1979, **18**, 3478.
8. I. Casals, P. González-Duarte, J. Sola, M. Font-Bardía, J. Solans and X. Solans, *J. Chem. Soc., Dalton Trans.* 1987, 2391.
9. N. Iwasaki, J. Tomooka and K. Toyoda, *Bull. Chem. Soc. Japan* 1974, **47**, 1323.
10. P. Biscarini, L. Fusina and G. D. Nivellini, *J. Chem. Soc., Dalton Trans.* 1974, 2140.
11. P. Biscarini, L. Fusina and G. D. Nivellini, *Spectrochim. Acta* 1980, **36A**, 593.
12. A. J. Canty, R. Kishimoto, G. B. Deacon and G. J. Farquharson, *Inorg. Chim. Acta* 1976, **20**, 161.
13. B. C. Cossar, J. O. Fournier, D. L. Fields and D. D. Reynolds, *J. Org. Chem.* 1962, **27**, 93.
14. P. Main, C. Germain and M. M. Woolfson, MULTAN 11/84. A System of Computer Programs for the Automatic Solution of Crystal Structures from X-Ray Diffraction Data. Universities of York (U.K.) and Louvain (Belgium) (1984).
15. D. T. Cromer and J. B. Mann, *Acta Cryst.* 1968, **A24**, 321.
16. R. F. Steward, E. R. Davidson and W. T. Simpson, *J. Chem. Phys.* 1965, **42**, 3175.
17. G. M. Sheldrick, SHELX76. A Program for Crystal Structure Determination. University of Cambridge, U.K. (1976).
18. A. J. Canty and G. B. Deacon, *Inorg. Chim. Acta* 1980, **45**, L225.
19. K. Aurivillius, *Trans. Royal Inst. Tech. Stockholm* 1972, **290**, 533.
20. G. C. Pimental and A. L. McClelland, *The Hydrogen Bond* (Edited by L. Pauling). W. H. Freeman, San Francisco (1960).
21. D. C. Bradley and N. R. Kunchur, *J. Chem. Phys.* 1964, **40**, 2258.
22. D. C. Bradley and N. R. Kunchur, *Can. J. Chem.* 1965, **43**, 2786.
23. N. R. Kunchur, *Nature* 1964, **204**, 468.
24. C. Stålhandske and F. Zintl, *Acta Cryst.* 1987, **C43**, 863.
25. S. Choudhury, I. G. Dance, P. J. Guerney and A. O. Rae, *Inorg. Chim. Acta* 1983, **70**, 227.
26. G. A. Bowmaker, I. G. Dance, B. C. Dobson and D. A. Rogers, *Aust. J. Chem.* 1984, **37**, 1607.
27. G. Henkel, P. Betz and B. Krebs, *J. Chem. Soc., Chem. Commun.* 1985, 1498.
28. A. J. Canty, C. L. Raston and A. H. White, *Aust. J. Chem.* 1979, **32**, 311.
29. W. J. Kozarek and Q. Fernando, *Inorg. Chem.* 1973, **12**, 2129.
30. P. Biscarini, E. Foresti and G. Pradella, *J. Chem. Soc., Dalton Trans.* 1984, 953.
31. P. G. Goggin, P. King, D. M. McEwan, G. E. Taylor, P. Woodward and M. Sandström, *J. Chem. Soc., Dalton Trans.* 1982, 875.
32. G. B. Deacon and J. H. S. Green, *J. Chem. Soc., Chem. Commun.* 1966, 629.
33. A. Castiñeiras, A. Arquero, J. R. Masaguer, S. Martínez-Carrera and S. García-Blanco, *Z. Anorg. Allg. Chem.* 1986, **539**, 219.

Polyhedron Vol. 7, No. 24, pp. 2515–2520, 1988
Printed in Great Britain

0277–5387/88 $3.00+.00
© 1988 Pergamon Press plc

TETRAKISDIMETHYLAMIDOZIRCONIUM AND ITS DIMETHYLAMIDO LITHIUM ADDUCT: STRUCTURES OF $[Zr(NMe_2)_4]_2$ AND $Zr(NMe_2)_6Li_2(THF)_2$

MALCOLM H. CHISHOLM,* CHARLES E. HAMMOND and JOHN C. HUFFMAN

Department of Chemistry and Molecular Structure Center, Indiana University, Bloomington, IN 47405, U.S.A.

(*Received* 1 *February* 1988; *accepted* 3 *May* 1988)

Abstract—The molecular structure of $[Zr(NMe_2)_4]_2$ has been determined by an X-ray study and shown to involve a central Zr_2N_8 moiety involving the fusing of two trigonal bipyramidal units along a common axial–equatorial edge. The terminal Zr—NMe_2 units have trigonal planar coordination about the nitrogen atoms: Zr—N = 2.050(5) and 2.104(5) Å, and Zr—N (bridge) = 2.224(3) and 2.453(4) Å for equatorial and axial bonds, respectively. The Zr—Zr distance is 3.704(1) Å as expected for a non-M—M bonding bridged compound. In tetrahydrofuran solution, $Zr(NMe_2)_4$ and $LiNMe_2$ react irreversibly giving $Zr(NMe_2)_6Li_2(THF)_2$ which has been isolated and characterized by an X-ray study. The central ZrN_6 octahedral moiety is capped on two opposite faces by Li atoms which are also coordinated to an oxygen atom of a THF molecule. Pertinent distances are: Zr—N = 2.22(7) (av.), N—Li = 2.155(25) (av.) and Li—O = 1.915(10) Å.

Previously we reported our characterization of $Mo(NMe_2)_6Li_2(THF)_2$ formed reversibly in the reaction between $Mo(NMe_2)_4$ and $LiNMe_2$.[1] We speculated that a similar equilibrium might exist between $Zr(NMe_2)_4$ and $LiNMe_2$ and furthermore that the lithio adduct might be responsible for the low yields of $Zr(NMe_2)_4$ sometimes obtained in the reaction between $ZrCl_4$ and $LiNMe_2$ (4 equiv.),[2] given that the adduct $Zr(NMe_2)_6Li_2(THF)_2$ might be reluctant to release the volatile $Zr(NMe_2)_4$ upon heating under vacuum. We herein confirm these predictions and in addition report the molecular structures of $Zr(NMe_2)_4$ and $Zr(NMe_2)_6Li_2(THF)_2$ in the solid state.

Syntheses

$Zr(NMe_2)_4$ was prepared according to the literature method[2] and purified by sublimation, 80–100°C at 10^{-4} mm Hg. Crystals of $[Zr(NMe_2)_4]_2$ were obtained from hexane. The dilithio salt, $Zr(NMe_2)_6Li_2(THF)_2$, was prepared by mixing $Zr(NMe_2)_4$ and $LiNMe_2$ (2 equiv.) and dissolving the mixture in a minimum amount of tetrahydrofuran, followed by crystallization upon cooling to *ca* −15°C. The mixed metal amide is non-volatile and at *ca* 100°C, 10^{-4} mm Hg loses THF yielding a tan-coloured insoluble residue.

Solid-state and molecular structures

A summary of crystal data is given in Table 1.

$[Zr(NMe_2)_4]_2$. In the solid-state the local coordination about each zirconium atom corresponds to a distorted trigonal bipyramid, tbp, and dimerization of the two $Zr(NMe_2)_4$ units occurs by the fusing of the two tbps along a common axial–equatorial edge (see Fig. 1). The Zr_2N_8 moiety is analogous to the Mo_2O_8 moiety in $Mo_2(O\text{-}i\text{-}Pr)_8$ though the M—M distances are very different. Zr-to-Zr = 3.70 Å is consistent with the non-bonding d^0–d^0 interaction while Mo—Mo = 2.48 Å is indicative of a Mo≡Mo bond arising from the d^2–d^2 Mo_2^{8+} centre.[3] Perhaps the most pertinent comparison is with the molecular structure of $[U(NEt_2)_4]_2$ found in the solid-state which also has a fused tbp structure involving the sharing of axial and equatorial edges.[4] Here, the U^{IV} to U^{IV} distance is 4.04 Å, again a non-bonding distance.

* Author to whom correspondence should be addressed.

Table 1. Summary of crystal data

	I	II
Empirical formula	$Zr_2N_8C_{16}H_{48}$	$ZrC_{20}H_{52}N_6O_2Li_2$
Colour of crystal	Colourless	Colourless
Crystal dimensions (mm)	0.25 × 0.25 × 0.25	0.25 × 0.25 × 0.25
Space group	$P2_1/n$	$P2_1/c$
Cell dimensions		
Temperature (°C)	−155	−155
a (Å)	22.069(5)	8.542(2)
b (Å)	14.130(3)	10.694(3)
c (Å)	8.848(2)	15.200(5)
beta ( )	110.24(2)	93.82(1)
Z (Molecules/cell)	4	2
Volume (Å^3)	2588.6	1385.51
Calculated density (g cm^{-3})	1.373	1.232
Wavelength (Å)	0.71069	0.71069
Molecular weight	535.05	513.77
Linear absorption coefficient (cm^{-1})	8.074	4.129
Detector to sample distance (cm)	22.5	22.5
Sample to source distance (cm)	23.5	23.5
Average omega scan width at half height	0.25	0.25
Scan speed (min^{-1})	6.0	6.0
Scan width (° + dispersion)	1.8	1.6
Individual background (s)	6	4
Aperture size (mm)	3.0 × 4.0	3.0 × 4.0
Two-theta range ( )	6–45	6–45
Total number of reflections collected	4493	2114
Number of unique intensities	3400	1822
Number with $F > 0.0$	3125	1681
Number with $F > 2.33\sigma(F)$	2847	1530
$R(F)$	0.0329	0.0472
$R_w(F)$	0.0402	0.0534
Goodness of fit for the last cycle	1.131	1.468
Maximum δ/σ for last cycle	0.05	0.45

I = $[Zr(NMe_2)_4]_2$. II = $Zr(NMe_2)_6Li_2(THF)_2$.

The terminal Zr—N equatorial bonds are shorter than the axial bonds, 2.05 vs 2.10 Å, and in the bridges the equatorial bonds are even shorter relative to their axial counterparts, 2.22 vs 2.45 Å(av.). The terminal M—NC_2 units are planar, which taken together with the relatively short Zr—N bonds, is indicative of a significant degree of Me_2N-to-Zr π-bonding.

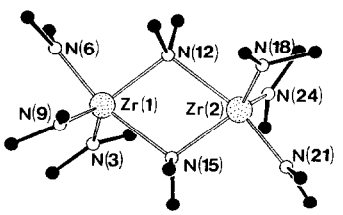

Fig. 1. A ball-and-stick drawing of the $[Zr(NMe_2)_4]_2$ molecule. Hydrogen atoms are omitted for clarity.

$Zr(NMe_2)_4Li_2(THF)_2$. In the solid-state the central ZrN_6 moiety closely approaches an octahedron shape, Zr—N = 2.22 Å(av.), with the lithium atoms capping opposite faces (see Fig. 2). The effect of the Li atoms is to cause a contraction of the N—Zr—N angles from 90 to 85° for nitrogen atoms mutually bonded to the same Li atom. Conversely the other N—Zr—N angles involving *cis* pairs of N atoms bonded to different Li atoms are 95°. In this respect the structure is very similar to that seen for the MoN_6Li_2 moiety in $Mo(NMe_2)_6Li_2(THF)_2$, although the Mo—N distances in the latter are only 2.12 Å(av.), namely 0.1 Å shorter, consistent with expectations based on the covalent radii of Zr^{IV} and Mo^{IV}. By contrast, the Li—N distances in Mo $(NMe_2)_6Li_2(THF)_2$, 2.08 Å(av.) are nearly 0.1 Å

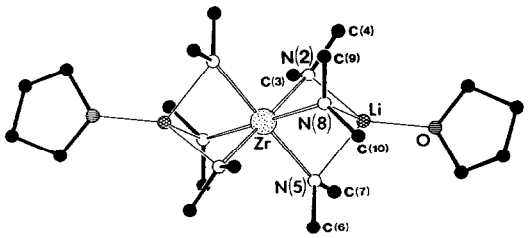

Fig. 2. A ball-and-stick drawing of $Zr(NMe_2)_6Li_2(THF)$. Hydrogen atoms are omitted for clarity.

shorter than those seen in $Zr(NMe_2)_6Li_2(THF)_2$. This implies a greater degree of $Zr(NMe_2)_6^{2-}$ character, relative to the dilithiomolybdenum hexaamide and is consistent with the apparent greater stability of $Zr(NMe_2)_6Li_2(THF)_2$ (if not kinetic inertness) with respect to the elimination of the $M(NMe_2)_4$ species when heated *in vacuo*. Also the $ZrNC_2$ units are nearly planar as evidenced by the sum of the angles at nitrogen, 356°, N(2); 355°, N(5); 357°, N(8) compared with *ca* 346°(av.) for the Mo—NC_2 units in $Mo(NMe_2)_6Li_2(THF)_2$. A final point of note is that the $Zr(NC_2)_6$ moiety can be seen to be only slightly distorted by the face-capping Li atoms from the $W(NC_2)_6$ unit in $W(NMe_2)_6$ that has T_h symmetry.[5,6]

Listings of pertinent bond distances and angles for the molecules $[Zr(NMe_2)_4]_2$ and $Zr(NMe_2)_6Li_2(THF)_2$ are given in Tables 2 and 3, respectively.

Table 2. Selected bond distances (Å) and angles (°) for the $[Zr(NMe_2)_4]_2$ molecule

A	B	Distance
Zr(1)	Zr(2)	3.704(1)
Zr(1)	N(3)	2.054(3)
Zr(1)	N(6)	2.108(3)
Zr(1)	N(9)	2.045(3)
Zr(1)	N(12)	2.224(3)
Zr(1)	N(15)	2.451(3)
Zr(2)	N(12)	2.454(3)
Zr(2)	N(15)	2.224(3)
Zr(2)	N(18)	2.047(3)
Zr(2)	N(21)	2.099(3)
Zr(2)	N(24)	2.054(3)
N	C	1.45(1) (av.)

A	B	C	Angle
N(3)	Zr(1)	N(6)	93.56(14)
N(3)	Zr(1)	N(9)	118.50(14)
N(3)	Zr(1)	N(12)	119.42(13)
N(3)	Zr(1)	N(15)	92.55(12)
N(6)	Zr(1)	N(9)	94.97(14)
N(6)	Zr(1)	N(12)	92.88(13)
N(6)	Zr(1)	N(15)	167.61(12)
N(9)	Zr(1)	N(12)	120.77(13)
N(9)	Zr(1)	N(15)	91.56(12)
N(12)	Zr(1)	N(15)	74.74(11)
N(12)	Zr(2)	N(15)	74.68(11)
N(12)	Zr(2)	N(18)	91.89(13)
N(12)	Zr(2)	N(21)	165.21(12)
N(12)	Zr(2)	N(24)	89.26(13)
N(15)	Zr(2)	N(18)	117.03(13)
N(15)	Zr(2)	N(21)	91.86(13)
N(15)	Zr(2)	N(24)	124.22(13)
N(18)	Zr(2)	N(21)	99.84(14)
N(18)	Zr(2)	N(24)	116.55(14)
N(21)	Zr(2)	N(24)	93.46(14)
Zr(1)	N(12)	Zr(2)	104.59(13)
Zr(1)	N(15)	Zr(2)	104.72(13)

NMR studies

$[Zr(NMe_2)_4]_2$. Previously work by Bradley *et al.*[2,7] had indicated that $[Zr(NMe_2)_4]_n$ showed a degree of oligomerization by a cryoscopic molecular weight determination in benzene, $n = 1.2$, and temperature dependent NMR behaviour. We reasoned that highly concentrated solutions of $Zr(NMe_2)_4$ would, at low temperatures in toluene-d_8, be essentially dimeric and indeed both low temperature ^1H and ^{31}C spectra show two resonances in the integral ratio 3:1 (see Fig. 3). It is not unreasonable to assign these to terminal and bridging NMe_2 groups, respectively, given that the terminal groups are still labile to a pseudo rotational process, a turnstile motion, that causes axial $\rightleftharpoons$equatorial site exchange. This seems quite reasonable and is again analogous to the low temperature spectrum observed for $Mo_2(OPr^i)_8$.[3]

$Zr(NMe_2)_6Li_2(THF)_2$. The spectra for this dilithiozirconium hexaamide show only one NMe_2 and one THF group over a wide temperature range, though the chemical shifts are temperature dependent. The simplest interpretation of this behaviour is that the equilibrium between $Zr(NMe_2)_4$ and $LiNMe_2$ (2 equiv.) favours the adduct and is rapid on the NMR time-scale. This differs from the behaviour of $Mo(NMe_2)_6Li_2(THF)_2$ which, in toluene-d_8, shows NMR spectra consistent with $Mo(NMe_2)_4$ and THF. In addition a precipitate of $LiNMe_2$, is formed in the NMR tube.

Concluding remarks

The previous prediction concerning $Zr(NMe_2)_6Li_2(THF)_2$ has been proven correct and the "salt" is indeed non-volatile, quite probably accounting

Table 3. Selected bond distances (Å) and angles (°) for $Zr(NMe_2)_6Li_2(THF)_2$

A	B	Distance
Zr(1)	N(2)	2.230(4)
Zr(1)	N(5)	2.221(5)
Zr(1)	N(8)	2.216(4)
O(12)	Li(11)	1.915(10)
N(2)	C(3)	1.468(7)
N(2)	C(4)	1.435(8)
N(2)	Li(11)	2.152(11)
N(5)	C(6)	1.475(7)
N(5)	C(7)	1.451(8)
N(5)	Li(11)	2.116(11)
N(8)	C(9)	1.451(8)
N(8)	C(10)	1.463(7)
N(8)	Li(11)	2.196(11)

A	B	C	Angle
N(2)	Zr(1)	N(5)	84.79(17)
N(2)	Zr(1)	N(5)	95.21(17)
N(2)	Zr(1)	N(8)	95.17(16)
N(2)	Zr(1)	N(8)	84.83(16)
N(5)	Zr(1)	N(5)	179.96
N(5)	Zr(1)	N(8)	85.19(17)
N(5)	Zr(1)	N(8)	94.81(17)
N(8)	Zr(1)	N(8)	179.97
Zr(1)	N(2)	C(3)	117.7(3)
Zr(1)	N(2)	C(4)	131.0(4)
Zr(1)	N(2)	Li(11)	75.1(3)
C(3)	N(2)	C(4)	107.4(5)
C(3)	N(2)	Li(11)	128.6(5)
C(4)	N(2)	Li(11)	92.0(4)
Zr(1)	N(5)	C(6)	118.3(4)
Zr(1)	N(5)	C(7)	129.4(4)
Zr(1)	N(5)	Li(11)	76.0(3)
C(6)	N(5)	C(7)	107.2(5)
C(6)	N(5)	Li(11)	129.2(5)
C(7)	N(5)	Li(11)	92.2(4)
Zr(1)	N(8)	C(9)	119.9(4)
Zr(1)	N(8)	C(10)	130.6(4)
Zr(1)	N(8)	Li(11)	74.5(3)
C(9)	N(8)	C(10)	106.8(5)
C(9)	N(8)	Li(11)	126.4(5)
C(10)	N(8)	Li(11)	91.3(4)
O(12)	Li(11)	N(2)	133.7(5)
O(12)	Li(11)	N(5)	121.5(5)
O(12)	Li(11)	N(8)	123.8(5)
N(2)	Li(11)	N(5)	89.4(4)
N(2)	Li(11)	N(8)	87.2(4)
N(5)	Li(11)	N(8)	88.3(4)

for the sometimes low yields obtained in the synthesis of $Zr(NMe_2)_4$ in the reaction between $ZrCl_4$ and $LiNMe_2$. The slow addition of $LiNMe_2$ to a slurry of $ZrCl_4$ is clearly preferred to the inverse addition. The molecular structure of $Zr(NMe_2)_6Li_2(THF)_2$ bears a close resemblance to that of $W(NMe_2)_6$ and in relation to $Mo(NMe_2)_6Li_2(THF)_2$ it appears that the $Zr(NMe_2)_6Li_2(THF)_2$ species is more stable.

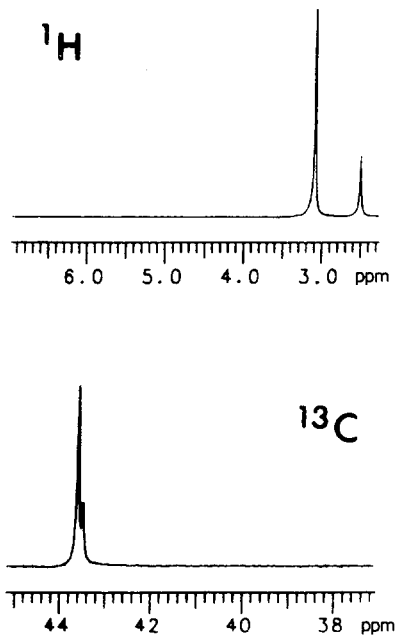

Fig. 3. Low temperature limiting ^{1}H and ^{13}C NMR spectra for $[Zr(NMe_2)_4]_2$ obtained in toluene-d_8 on a Varian XL300 spectrometer.

EXPERIMENTAL

All reactions were carried out using standard inert atmosphere techniques. All solvents were appropriately purified and oxygen free. The ^{1}H and ^{13}C NMR spectra were acquired with a Varian XL300 and referenced to the protio impurity of the methyl group of toluene-d_8. IR spectra were obtained from mineral oil mulls between CsI plates on a Perkin–Elmer 283 IR spectrophotometer. Analyses were carried out by Oneida Research Services, Inc., Whitesboro, NY.

$[Zr(NMe_2)_4]_2$

$[Zr(NMe_2)_4]_2$ was made by the addition of $LiNMe_2$ (7.2 g, 140 mmol) to $ZrCl_4$ (8.2 g, 35 mmol) in THF at 0°C. The product (6.0 g, 65%) was sublimed out of the reaction vessel and was resublimed in an evacuated sealed tube prior to X-ray analysis.

^{1}H NMR data at 24°C, δ (ppm): 2.94. At −80°C: 3.08 (3, NMe_2), 2.48 (1, NMe_2). ^{13}C NMR data at 24°C, δ (ppm): 41.73 (NMe_2). At −80°C: 43.59 (3, NMe_2), 43.47 (1, NMe_2).

$Zr(NMe_2)_6Li_2(THF)_2$

THF (40 cm^3) at 0°C was added to 600 mg (2.24 mmol) $Zr(NMe_2)_4$ and 22.8 mg (44.7 mmol) $LiNMe_2$ until both solids were in solution. Removal of the solvent gave a quantitative recovery of the product. Recrystallization from THF yielded 8.12 mg of crystalline solid. Analysis for $C_{20}H_{52}Li_2N_6O_2Zr$. Found (Calc.): C, 46.8 (46.8); H, 10.4 (10.2); N, 16.3 (16.4). IR data (mineral oil mull, ν cm^{-1}): 2790w, 2770w, 2730w, 1220s, 1131sh, 1119s, 1050s, 1039sh, 930vs, 894sh, 720w, 673w, 505s, 350s, 273m. ^1H NMR data at 25°C, δ (ppm): 3.38 (THF), 3.11 (NMe_2), 1.26 (THF). At −80°C: 3.35 (NMe_2), 1.48 (THF), 0.97 (THF). ^{13}C NMR data at 24°C, δ (ppm): 68.41 (THF), 46.46 (NMe_2), 25.44 (THF). At −60°C: 68.12 (THF), 46.45 (NMe_2), 25.25 (THF).

Thermal decomposition of $Zr(NMe_2)_6Li_2(THF)_2$

The sample (800 mg, 1.56 mmol) was heated *in vacuo* to the sublimation temperature of $Zr(NMe_2)_4$ with no noticeable change in the colourless crystals. Between 100–120°C, at 10^{-4} mm Hg, the trap acquired the solvent and the crystals became white in colour. Continued heating at 120°C made the crystals turn to a tan colour. 525 mg of sample was removed from the flask (some of the residue in the flask was unattainable). The theoretical residue for a compound of formula $Li_2Zr(NMe_2)_6$ was 575 mg.

IR data for the residue from a mineral oil mull between CsI plates, ν (cm^{-}): 2770w, 2750w, 2485w, 2428w, 2417w, (a forest of weak bands between 1900 and 1500), 1251m, 1229m, 1218m, 1200w, 1151m, 1127s, 1118s, 1053sh, 1049m, 949sh, 930sh, 910s, 720w, 578w, 543m, 510m, 493m, 353m, 322m. ^1H NMR data δ (ppm): a multitude of minor resonances between 2–2.4 ppm and an insoluble orange solid at the bottom of the tube.

Crystallographic studies

General operating procedures have been described previously.[8] A summary of crystal data is given in Table 1.

$[Zr(NMe_2)_4]_2$. A suitable crystal was located and transferred to the goniostat using standard inert atmosphere handling techniques and cooled to −155°C for characterization and data collection.

A systematic search of a limited hemisphere of reciprocal space located a set of diffraction maxima with symmetry and systematic absences corresponding to the unique monoclinic space group $P2_1/n$. Subsequent solution and refinement of the structure confirmed this choice. Data were collected in the usual manner using a continuous θ–2θ scan with fixed backgrounds. Data were reduced to a unique set of intensities and associated sigmas in the usual manner.

The structure was solved by a combination of direct methods (MULTAN 78) and Fourier techniques. All hydrogen atoms were clearly visible in a difference Fourier synthesis phased on the non-hydrogen parameters. All hydrogen atoms were refined isotropically and non-hydrogen atoms anisotropically in the final cycles.

A final difference Fourier was featureless, with the largest peak being 0.37 e $Å^{-3}$.

$Zr(NMe_2)_6Li_2(THF)_2$. A suitable crystal was located and transferred to the goniostat using standard inert atmosphere handling techniques and cooled to −155°C for characterization and data collection.

The sample was believed to be isomorphous to $Mo(NMe_2)_6Li_2(THF)_2$ and a search of a limited hemisphere of reciprocal space did, in fact, locate diffraction maxima similar to those found for the Mo analogue. Data were collected in the usual manner using a continuous θ–2θ scan with fixed backgrounds. Data were reduced to a unique set of intensities and associated sigmas in the usual manner. When the coordinates of the Mo analogue were used as starting points for the refinement, convergence was not achieved. Several attempts were made before attempting to solve the structure "from scratch". At this point, the statistics clearly indicated a non-centrosymmetric structure, so the space group was assigned $A2$. A solution was found with no disorder, although there were chemically impossible inequalities present (N—C distances varied from 1.2 to 1.9 Å). Although the refinement converged to $R = 0.062$, it was apparent that a gross error was present.

At this point the crystal was carefully examined on the diffractometer, and it was determined that the A centring was not present. Data were therefore recollected with no reject routine and reprocessed.

The structure was then solved by a combination of direct methods (MULTAN 78) and Fourier techniques. All hydrogen atoms were clearly visible in a difference Fourier synthesis phased on the non-hydrogen parameters. All hydrogen atoms were refined isotropically and non-hydrogen atoms anisotropically in the final cycles. The hydrogen atoms are not well behaved, with distances of up to 1.4 Å, and some H—C—H angles of less than 90°. A final difference Fourier was featureless, with the largest peak being 0.45 e $Å^{-3}$.

The structural characterization of $Mo(NMe_2)_6Li_2(THF)_2$ is currently being re-examined in order

to determine whether or not the space group was correctly assigned.

Atomic positional parameters have been deposited with the Director of the Cambridge Crystallographic Data Centre.

Acknowledgement—We thank the National Science Foundation for support.

REFERENCES

1. M. H. Chisholm, C. E. Hammond and J. C. Huffman, *Polyhedron* 1988, **7**, 399.
2. D. C. Bradley and I. M. Thomas, *J. Chem. Soc.* 1960, 3857.
3. M. H. Chisholm, F. A. Cotton, M. W. Extine and W. W. Reichert, *Inorg. Chem.* 1978, **17**, 2944.
4. J. G. Reynolds, A. Zalkin, D. H. Templeton, N. M. Edelstein and L. K. Templeton, *Inorg. Chem.* 1976, **15**, 2498.
5. D. C. Bradley, M. H. Chisholm, C. E. Heath and M. B. Hursthouse, *J. Chem. Soc., Chem. Commun.* 1969, 1261.
6. M. H. Chisholm, F. A. Cotton, M. W. Extine and B. R. Stults, *J. Am. Chem. Soc.* 1976, **98**, 4477.
7. D. C. Bradley and M. H. Gitlitz, *J. Chem. Soc. A* 1969, 980.
8. M. H. Chisholm, K. Folting, J. C. Huffman and C. C. Kirkpatrick, *Inorg. Chem.* 1984, **23**, 1021.

Note added in proof: The structure of monomeric $Zr(NMe_2)_4$ has recently been reported from gas phase studies: *Inorg. Chem.* 1988, **27**, 2032.

Polyhedron Vol. 7, No. 24, pp. 2521–2530, 1988
Printed in Great Britain

0277–5387/88 $3.00+.00
© 1988 Pergamon Press plc

REACTIONS OF MONOAZADIENES WITH METAL CARBONYL COMPLEXES—III. THERMAL CONVERSION OF N-ALKYL-(*E*)-CROTONALDIMINE WITH $Ru_3(CO)_{12}$ TO σ-N,μ_2-η^3-ALLYL AND μ_2-η^3-AZAALLYL BONDED SIX ELECTRON FRAGMENTS COORDINATED TO A HEXACARBONYL DIRUTHENIUM UNIT. X-RAY SINGLE CRYSTAL STRUCTURE DETERMINATIONS OF $Ru_2(CO)_6\{\sigma\text{-N},\mu_2\text{-}\eta^3\text{-}CH_2CC(H)C(H)=N—C_4H_9\text{-}t\}$ AND $Ru_2(CO)_6\{\mu_2\text{-}\eta^3\text{-}C_2H_5—CC(H)N—C_4H_9\text{-}t\}$*

L. H. POLM, C. J. ELSEVIER,† W. P. MUL and K. VRIEZE

Anorganisch Chemisch Laboratorium, Universiteit van Amsterdam, Nieuwe Achtergracht 166, 1018 WV Amsterdam, The Netherlands

and

M. J. N. CHRISTOPHERSEN, F. MULLER and C. H. STAM

Laboratorium voor Kristallografie, Universiteit van Amsterdam, Nieuwe Achtergracht 166, 1018 WV Amsterdam, The Netherlands

(*Received* 2 *February* 1988; *accepted* 3 *May* 1988)

Abstract—Two complexes $Ru_2(CO)_6L$ that arise from thermal reactions of monoazadienes (*E*)-$CH_3C(H)=C(H)C(H)=NR$ (**1**); (R = *t*-C_4H_9, *i*-C_3H_7, *c*-C_6H_{11}) with $Ru_3(CO)_{12}$ are reported. The bonding of the six-electron donating organic fragments in the complexes $Ru_2(CO)_6\{\sigma\text{-N},\mu_2\text{-}\eta^3\text{-}CH_2CC(H)C(H)=N—C_4H_9\text{-}t\}$ (**4a**) and $Ru_2(CO)_6\{C_2H_5—CC(H)N—C_4H_9\text{-}t\}$ (**5a**) is described on the basis of their X-ray single crystal structure determinations. In compound **4a** the organic ligand is σ-N,μ_2-η^3-coordinated and contains a distorted η^3-allyl fragment bridging the two $Ru(CO)_3$ moieties. Compound **5a** features a μ_2-η^3-azaallyl dianion which bridges the Ru centres in the $Ru_2(CO)_6$ core. Possible pathways for the formation of **4a** and **5a**, involving dehydrogenation and a 1,2-H shift, respectively, are discussed.

The reactivity of conjugated monoazadienes (MAD)‡ towards metal carbonyl compounds, in particular small clusters, has hitherto received limited attention compared to related conjugated systems, e.g. butadienes[2] and 1,4-diaza-1,3-dienes such as R—DAB[3] and R—PyCa.[4] By studying the reactivity of such coordinated unsaturated organic fragments on small metal clusters, one may gain insight into processes that bear relevance to intimate steps of heterogeneous and homogeneous catalytic reactions. Earlier investigations into the coordination chemistry of MAD ligands have revealed the occurrence of several coordination modes e.g. σ-N (2e) in (MAD)$Fe(CO)_4$,[5] η^2-C=C (2e) in (MAD)$Ni(PPh_3)_2$[6] and η^2-C=C, η^2-C=N (4e) in (MAD)$Fe(CO)_3$.[7] In addition to complexes in which the MAD ligand is coordinated as such, C-metallated compounds containing a monoazadienyl (MAD-yl) fragment have been obtained from reactions of MAD ligands with $IrCl(CO)(PPh_3)_2$ to give HIr-

* For Part II, see ref. 1.

† Author to whom correspondence should be addressed.

‡ Abbreviations used: MAD = N-alkyl-monoazadiene, R—N=C(H)—C(H)=C(R^1)R^2; R—DAB = N, N′-dialkyl-1,4-diaza-1,3-butadiene, R—N=C(H)—C(H)=NR; R—PyCa = N-alkyl-pyridine-2-carbaldehyde-imine, C_6H_4N-2-C(H)=N—R.

$Cl(PPh_3)_2\{C_6H_5—C{=}C(H)C(H){=}N—C_3H_7\text{-}i\}$[8] and with $H_2Os_3(CO)_{10}$ yielding $(\mu\text{-}H)_2Os_3(CO)_9\{\mu_2\text{-}\eta^3\text{-}(CH_3)_2C(H)CC(CH_3){=}N—C_6H_5\}$.[9] Recently, we have encountered a rather exotic ligating behaviour of the MAD-yl ligand derived from $(E)\text{-}CH_3—C(H){=}C(H)C(H){=}NR$ (**1**), namely as 7e donating σ-N, σ-C, η^2-C=C, η^2-C=N bonded $CH_3—C{=}C(H)—C(H){=}NR$ fragments coordinated to a linear tetranuclear chain in $Ru_4(CO)_{10}\{\mu_2\text{-}\eta^4\text{-}CH_3—C{=}C(H)C(H){=}N—R\}_2$ (**2**)[10] and to a bent Ru_3 core in $Ru_3(CO)_6\{\mu_2\text{-}\eta^4\text{-}CH_3—C{=}C(H)C(H){=}N—R\}_2$ (**3**)[1] (see Fig. 1). In both complexes two Ru—C—C—C—N heterocycles (which are isolobal with an η^5-bonded cyclopentadienyl moiety) can be discerned. In Fig. 1 it is shown for **2** that two Ru—C—C—C—N heterocycles are present which are η^5-bonded to each Ru atom of the $Ru_2(CO)_4$ entity, while in **3** two such heterocycles are η^5-coordinated to the central Ru atom. From these observations we concluded that compounds **2** and **3** are isolobally related to $(\eta^5\text{-}C_5H_5)_2Ru_2(CO)_4$ and $(\eta^5\text{-}C_5H_5)_2Ru$, respectively. These compounds are formed during thermal reactions of $Ru_3(CO)_{12}$ with the MAD ligand **1** in heptane solution. After completion of the reaction, also other products which contained ligands derived from the parent MAD ligand were isolated. In this paper we wish to report the molecular structure of two major products of the reaction of $Ru_3(CO)_{12}$ with (*E*)-(**1**), together with a discussion of possible pathways of their formation.

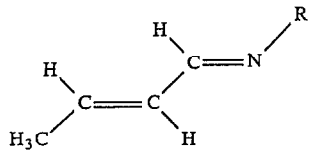

1a; R = t-Bu
1b; R = i-Pr
1c; R = c-Hex

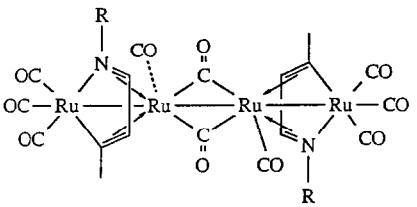

2

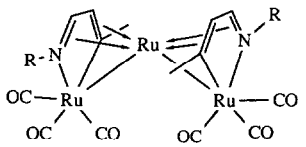

3

Fig. 1. Monoazadienes **1a–1c** and the known products **2** and **3** from their reaction with $Ru_3(CO)_{12}$.

EXPERIMENTAL

Materials and apparatus

NMR spectra were obtained on Bruker WM 250 and AC 100 spectrometers. IR spectra were recorded using a Perkin–Elmer 283 spectrophotometer. Elemental analyses were carried out by the Elemental Analyses section of the Institute for Applied Chemistry, TNO, Zeist, The Netherlands. All preparations were carried out in an atmosphere of purified nitrogen, using carefully dried solvents. Silica gel for column chromatography (Merck, 60 Mesh) was dried and activated before use. $Ru_3(CO)_{12}$ was obtained from Strem Chemicals Ltd. The monoazadienes **1a–1c** were prepared from (*E*)-crotonaldehyde and the relevant primary amine according to standard procedures.[11]

Synthesis of $Ru_2(CO)_6\{\sigma\text{-}N,\mu_2\text{-}\eta^3\text{-}CH_2CC(H)C(H){=}N—C_4H_9\text{-}t\}$ (**4a**) *and* $Ru_2(CO)_6\{\mu_2\text{-}\eta^3\text{-}C_2H_5CC(H)N—C_4H_9\text{-}t\}$ (**5a**)

A solution of $Ru_3(CO)_{12}$ (0.64 g, 1.0 mmol) and monoazadiene (**1a**) (3 mmol) in 50 cm^3 of heptane (b.p. 98.5°C) was stirred at reflux temperature for 20 h. The solution was evaporated to dryness leaving a yellow–orange residue that was purified by column chromatography on silica, using hexane as the eluent. One broad yellow band was obtained, the first part of which contained pure **5a** and the last part contained pure **4a**. This column chromatographic separation was carefully monitored by IR. A small fraction containing a mixture of **4a** and **5a** was discarded. Both compounds were crystallized from hexane (−80°C) yielding yellow crystals of **4a** and **5a**, respectively, both in about 30% yield. Recrystallization from hexane afforded crystals suitable for crystal structure determinations.

Analytical data for **4a**: Found (Calc.): C, 34.10 (34.08); H, 2.68 (2.66); N, 2.48 (2.84). **5a**: Found (Calc.): C, 33.87 (33.94); H, 3.04 (3.05); N, 2.78 (2.83). IR and NMR data are given in Tables 1 and 2.

Table 1. IR data ($\tilde{\nu}$(CO) region (cm^{-1}) solvent hexane)

4a	2076(m)	2042(vs)	2002(s)	1997(s)	1982(m)
4b	2077(m)	2042(vs)	2003(s)	1998(s)	1983(m)
4c	2076(m)	2042(vs)	2003(s)	1997(s)	1983(m)
5a	2075(m)	2042(vs)	2003(s)	1990(s)	1978(m)

Table 2. NMR data of **4a–4c** and **5a**

^{13}C NMR[a]	**4a**	**4b**	**4c**	**5a**
C(7)	176.1	177.2	177.4	106.6
C(8)	67.0	67.0	67.2	139.8
C(9)	199.0[b]	199.0[b]	199.0[b]	31.1
C(10)	54.4	54.1	54.0	17.1
R(N—*C*)	61.2	62.5	70.7	55.3
	31.3	24.1/23.7	34.5/34.2	30.5
			25.7, 25.5,[2] 25.4[7]	
COs	202.6	203.0	203.1	197.2
	200.4	200.8	200.8	
	199.6	199.5	199.6	
	198.4	198.7	198.7	
	193.5	193.9	193.9	
	190.9	191.1	191.1	
^{1}H NMR[c]	**4a**	**4b**	**4c**	**5a**
H(7)	8.06 (d, 2.0, 1)	8.02 (d, 2.0, 1)	8.01 (d, 2.0 1)	6.91 (s, 1)
H(8)	3.44 (d, 2.0, 1)	3.40 (d, 2.0, 1)	3.41 (d, 2.0, 1)	—
H(9)	—	—	—	2.38 (q, 7.5, 2)
H(102)	3.81 (s, 1)	3.82 (s, 1)	3.81 (s, 1)	1.06 (t, 7.5, 3)
H(101)	3.30 (s, 1)	3.32 (s, 1)	3.32 (s, 1)	
R	1.27 (s, 9)	3.56 (sept, 6.4, 1)	3.12 (br, 1)	0.95 (s, 9)
		1.23 (d, 6.4, 3)	1.0–1.8 (br, 10)	
		1.17 (d, 6.4, 3)		

[a] 25.1 MHz, in $CDCl_3$ at 263 K. Diastereotopic pairs separated by solidus (/).

[b] Assigned by means of intensity considerations when compared to the ^{13}CO resonances.

[c] 250.1 MHz, in $CDCl_3$ at 297 K. In parentheses: multiplicity, J(H, H), integral. Numbering as in the molecular structures of **4a** and **5a**.

Synthesis of $Ru_2(CO)_6\{\sigma\text{-N},\mu_2\text{-}\eta^3\text{-}CH_2CC(H)\text{—}C(H)\text{=}NR\}$, (**4b**): R = *i*-$C_3H_7$; (**4c**): R = *c*-$C_6H_{11}$

A solution of $Ru_3(CO)_{12}$ (0.64 g, 1.0 mmol) and monoazadiene **1b** or **1c** (2.5–3 mol) in 50 cm^3 heptane (b.p. 98.5°C) was stirred at reflux temperature for 16–20 h. After cooling to 20°C the orange–red precipitate was collected and worked up as described,[10] producing **2**. The remaining solution was evaporated to dryness, leaving an orange residue that was further purified by column chromatography using hexane as the eluent. A yellow fraction was obtained and crystallization from ethanol at −80°C yielded yellow crystals of **4b** or **4c** in about 30% yield. Analytical data for **4b**: Found (Calc.): C; 32.57 (32.57); H, 2.38 (2.31); N, 2.96 (2.92). **4c**: C, 36.76 (37.0); H, 2.83 (2.91); N, 2.58 (2.70). IR and NMR data are compiled in Tables 1 and 2.

X-ray single crystal structure determinations of {(σ-N,μ_2-η^3-CCC)-2,2-*dimethyl*-3-*azahept*-3,5-*dien*-6,7-*diyl*}*hexacarbonyldiruthenium* [$C_{14}H_{13}NO_6Ru_2$, (**4a**)] *and of* {(μ_2-η^3-NCC)-2,2-*dimethyl*-3-*azahept*-3-*en*-5,5-*diyl*}*hexacarbonyldiruthenium* [$C_{14}H_{15}NO_6Ru_2$ (**5a**)]*

Structure solution and refinement for the compounds was essentially the same as reported for compound **2**.[10]

Crystal data of **4a**. $M_r = 493.40$, monoclinic, $P2_1/a$, $a = 12.277(1)$, $b = 14.638(1)$, $c = 10.069(1)$ Å, $\beta = 102.53(1)°$, $V = 1766.4(3)$ Å^3, $Z = 4$, $D_c = 1.82$ g cm^{-3}, Cu-K_α, $\lambda = 1.5418$ Å, $\mu = 144.5$ cm^{-1}, $T = 295$ K, $R = 0.034$ ($R_w = 0.054$, $w = (5.5 + F_o + 0.016F_o^2)^{-1}$) for 3087 observed reflections [$I > 2.5\sigma(I)$].

Crystal data of **5a**. $M_r = 495.42$, monoclinic,

* Atomic coordinates, displacement factor coefficients, full lists of bond lengths and angles and lists of F_o/F_c values have been deposited as supplementary data with the Editor, from whom copies are available on request. Atomic coordinates have also been deposited with the Cambridge Crystallographic Data Centre.

$P2_1/n$, $a = 13.388(2)$, $b = 15.411(2)$, $c = 8.843(1)$ Å, $\beta = 95.44(2)°$, $V = 1816.3(4)$ Å^3, $Z = 4$, $D_c = 1.81$ g cm^{-3}, Cu-K_α, $\lambda = 1.5418$ Å, $\mu = 140.5$ cm^{-1}, $T = 295$ K, $R = 0.037$ ($R_w = 0.048$, $w = (6.0 + F_o + 0.027F_o^2)^{-1}$) for 1659 observed reflections [$I > 2.5\sigma(I)$].

RESULTS AND DISCUSSION

Molecular structure of **4a**

The molecular geometry of **4a** is shown in Fig. 2 and selected bond distances and angles are given in Table 3.

The organometallic complex consists of a "sawhorse" type $Ru_2(CO)_6$ core, composed of two $Ru(CO)_3$ units held together by a bridging 6e donating σ-N,μ_2-η^3-allyl imine fragment and a Ru—Ru bond distance of 2.7979(6) Å, which falls within the range of 2.70–2.85 Å for single Ru—Ru bonds.[2] The Ru(1)—C and C—O distances within the $Ru(1)(CO)_3$ unit are equal (average Ru(1)—C 1.922(4) Å, C—O 1.139(5) Å). Contrastingly, a rather long Ru(2)—C(6) distance of 1.968(3) Å and a short Ru(2)—C(4) distance of 1.885(3) Å are found in the $Ru(2)(CO)_3$ moiety. These observations can be readily explained by invoking the large *trans*-influence exerted by C(9), which tends to elongate the Ru(2)—C(6) distance, and the comparatively small *trans*-influence of N on the Ru(2)—C(4) distance (see Fig. 2).

The imine N atom is σ-coordinated as is indicated by the normal bond length of 2.167(3) Å for the Ru(2)—N dative bond. The N—C(7) bond distance amounts to 1.290(4) Å and points to a localized double bond.

The carbon atom C(9) is σ-coordinated to Ru(2), the bond distance of 2.065(3) Å for Ru(2)—C(9) being slightly shorter than for normal single Ru—C bonds.[10] The carbon fragment C(8)—C(9)—C(10) exhibits η^3-coordination to Ru(1), as can be inferred from the Ru(1)—C(8), Ru(1)—C(9) and Ru(1)—C(10) bond distances of 2.251(3), 2.100(3) and 2.273(3) Å, respectively. Assuming for convenience Ru(2) as a substituent at C(9), the C(8)—C(9)—C(10) fragment may indeed be considered as a η^3-allyl type ligand that is η^3-coordinated to Ru(1), and of which the substituent [Ru(2)] at the central allyl carbon atom C(9) is bent out of the allyl plane. The angle between the Ru(2)—C(9) vector and the plane defined by the allyl group amounts to 12.2°. This structural {η^3-$CH_2C(M)C(H)R$} coordination entity has also been found in $Fe_2(CO)_7\{\mu_2$-η^3-$C_3H_4\}$,[12,13] where the Fe(2)—C vector makes an angle of 27° with the allyl plane. In both cases, the fact that Ru(2) (or Fe(2), respectively) is out of the plane defined by the η^3-allyl carbon atoms can be attributed to the

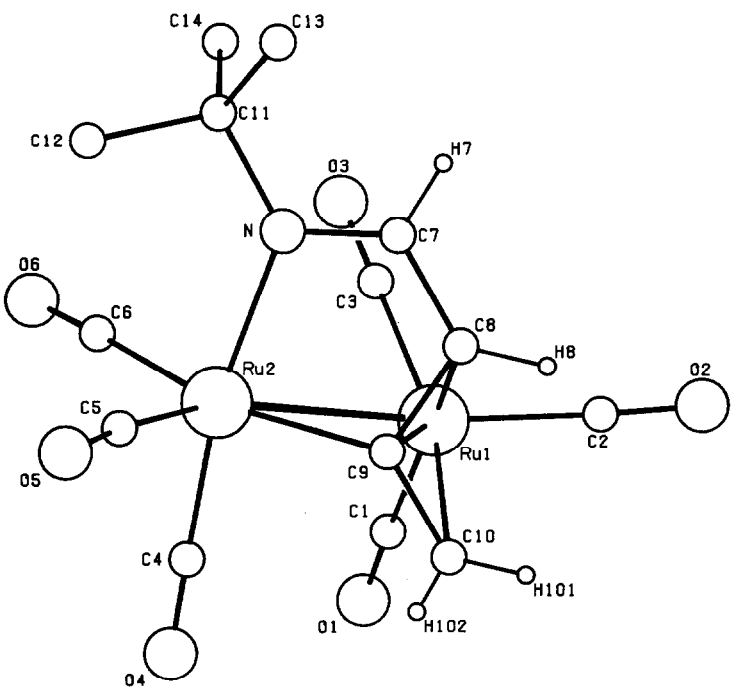

Fig. 2. PLUTO drawing of the molecular structure of **4a** with the adopted numbering scheme. The hydrogen atoms, except at C(7), C(8) and C(10) have been omitted.

Table 3. Relevant bond distances of **4a** in Ångstrom and angles in degrees with e.s.d. in parentheses

Ru(1)—Ru(2)	2.7979(6)	Ru(2)—Ru(1)—C(8)	68.20(11)
Ru(1)—C(1)	1.920(4)	Ru(2)—Ru(1)—C(9)	47.26(10)
Ru(1)—C(2)	1.919(4)	Ru(2)—Ru(1)—C(10)	75.37(12)
Ru(1)—C(3)	1.926(3)	C(2)—Ru(1)—C(8)	94.55(22)
Ru(1)—C(8)	2.251(3)	C(2)—Ru(1)—C(9)	118.63(18)
Ru(1)—C(9)	2.100(3)	C(2)—Ru(1)—C(10)	97.63(20)
Ru(1)—C(10)	2.273(3)	C(8)—Ru(1)—C(9)	38.43(13)
Ru(2)—N	2.167(3)	C(8)—Ru(1)—C(10)	64.13(16)
Ru(2)—C(4)	1.885(3)	C(9)—Ru(1)—C(10)	37.41(14)
Ru(2)—C(5)	1.911(4)	Ru(1)—Ru(2)—N	86.71(10)
Ru(2)—C(6)	1.968(4)	Ru(1)—Ru(2)—C(9)	48.34(10)
Ru(2)—C(9)	2.065(3)	N—Ru(2)—C(4)	170.39(14)
N—C(7)	1.290(4)	N—Ru(2)—C(9)	80.03(17)
N—C(11)	1.518(4)	Ru(2)—N—C(7)	110.3(3)
C(1)—O(1)	1.140(5)	N—C(7)—C(8)	119.8(3)
C(2)—O(2)	1.151(5)	Ru(1)—C(8)—C(7)	113.4(3)
C(3)—O(3)	1.128(4)	Ru(1)—C(8)—C(9)	65.1(3)
C(4)—O(4)	1.131(5)	C(7)—C(8)—C(9)	115.4(3)
C(5)—O(5)	1.128(6)	Ru(1)—C(9)—Ru(2)	84.40(17)
C(6)—O(6)	1.114(5)	Ru(1)—C(9)—C(8)	76.5(3)
C(7)—C(8)	1.437(5)	Ru(1)—C(9)—C(10)	77.9(3)
C(8)—C(9)	1.439(4)	Ru(2)—C(9)—C(8)	108.5(3)
C(9)—C(10)	1.412(5)	Ru(2)—C(9)—C(10)	127.2(3)
C(11)—C(12)	1.555(7)	C(8)—C(9)—C(10)	114.8(3)
C(11)—C(13)	1.531(7)	Ru(1)—C(10)—C(9)	64.7(3)
C(11)—C(14)	1.491(8)	Ru—C—O(av.)	176.3(3)

presence of a metal–metal bond. Similar three-carbon fragments have been reported for e.g. $Cp_2Ru_2(CO)_3(\mu_2\text{-}\eta^3\text{-}C_3H_{4-n}Me_n)$[14] (no Ru—Ru bond) and $Os_3(CO)_{11}(\mu_2\text{-}\eta^3\text{-}C_3H_4)$[15] (no Os—Os bond). In the latter case it has been shown by crystallographic analysis that the Os(2) atom, which is σ-coordinated to the central carbon atom of the allyl group, resides within the plane of the η^3-allyl group which is in turn η^3-coordinated to Os(1), comparable to the situation in compound **4a**.

The carbon–carbon distances C(8)—C(9) and C(9)—C(10) of 1.439(4) and 1.412(5) Å, respectively, indicate extensive electron delocalization over the C(8)—C(9)—C(10) fragment. Taken together with the C(8)—C(9)—C(10) angle of 114.8(3)° and the distances of these atoms to Ru(1) (*vide supra*), this supports its interpretation as a η^3-allyl fragment. The η^3-allyl ligand is slightly distorted because the "substituent" Ru(2) does not reside within the plane of the allyl group.

Molecular structure of **5a**

The molecular geometry of **5a** is shown in Fig. 3 and selected bond distances and angles are given in Table 4.

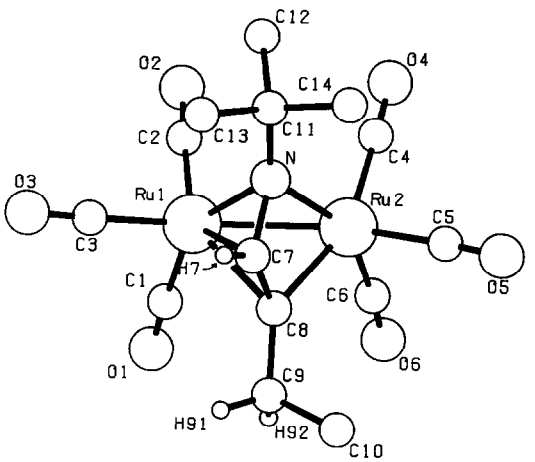

Fig. 3. PLUTO drawing of the molecular structure of **5a** with the adopted numbering scheme. The hydrogen atoms, except at C(7) and C(9) have been omitted.

This diruthenium complex also features the well known $Ru_2(CO)_6$ core, in which the Ru atoms are bridged by a 6e $\mu_2\text{-}\eta^3$-azaallyl ligand. In this molecule the intermetallic distance of 2.649(1) Å points to a rather short formal single Ru—Ru bond, as normally distances of 2.70–2.85 Å are found in com-

Table 4. Relevant bond distances of **5a** in Ångstroms and angles in degrees with e.s.d. in parentheses

Ru(1)—Ru(2)	2.6499(8)	Ru(2)—Ru(1)—N	51.92(13)
Ru(1)—N	2.127(4)	Ru(2)—Ru(1)—C(3)	155.96(21)
Ru(1)—C(1)	1.915(6)	Ru(2)—Ru(1)—C(7)	62.53(19)
Ru(1)—C(2)	1.914(6)	Ru(2)—Ru(1)—C(8)	50.43(17)
Ru(1)—C(3)	1.904(7)	N—Ru(1)—C(3)	105.5(3)
Ru(1)—C(7)	2.240(5)	N—Ru(1)—C(7)	37.40(21)
Ru(1)—C(8)	2.227(6)	N—Ru(1)—C(8)	62.20(22)
Ru(2)—N	2.143(4)	C(3)—Ru(1)—C(7)	94.7(4)
Ru(2)—C(4)	1.935(6)	C(7)—Ru(1)—C(8)	35.09(22)
Ru(2)—C(5)	1.918(6)	Ru(1)—Ru(2)—N	51.36(13)
Ru(2)—C(6)	1.889(6)	Ru(1)—Ru(2)—C(5)	149.62(19)
Ru(2)—C(8)	2.113(5)	Ru(1)—Ru(2)—C(8)	54.34(19)
N—C(7)	1.404(7)	N—Ru(2)—C(8)	63.8(3)
N—C(11)	1.497(7)	Ru(1)—N—Ru(2)	76.72(21)
C(1)—O(1)	1.124(8)	Ru(1)—N—C(7)	75.7(4)
C(2)—O(2)	1.126(8)	Ru(1)—N—C(11)	133.4(3)
C(3)—O(3)	1.151(9)	Ru(2)—N—C(7)	90.0(4)
C(4)—O(4)	1.135(7)	Ru(2)—N—C(11)	135.6(3)
C(5)—O(5)	1.144(8)	C(7)—N—C(11)	124.8(5)
C(6)—O(6)	1.138(8)	Ru(1)—C(7)—N	66.9(4)
C(7)—C(8)	1.347(8)	Ru(1)—C(7)—C(8)	71.9(5)
C(8)—C(9)	1.488(8)	N—C(7)—C(8)	109.8(6)
C(9)—C(10)	1.522(10)	Ru(1)—C(8)—Ru(2)	75.2(3)
C(11)—C(12)	1.526(8)	Ru(1)—C(8)—C(7)	73.0(5)
C(11)—C(13)	1.553(10)	Ru(1)—C(8)—C(9)	129.9(4)
C(11)—C(14)	1.552(9)	Ru(2)—C(8)—C(7)	92.9(5)
		Ru(2)—C(8)—C(9)	136.3(4)
		C(7)—C(8)—C(9)	126.1(6)
		Ru—C—O(av.)	177.3(5)

parable compounds.[2] Similarly, a short Fe—Fe distance (2.453(4) Å) has been observed in the structurally analogous compound $Fe_2(CO)_6\{\mu_2\text{-}\eta^3\text{-}C(CO_2Me)C(CO_2Me)N—C(C_6H_5)=CH_2\}$ (**6**, see Fig. 4).[16] The short intermetallic distance in **5a** can be explained by assuming a bent bond between the metal centres (cf. ref. 17). This conjecture is corroborated by the fact that the normal vectors to the (approximate) planes through Ru(1)—N—C(1)—C(2)—C(8) and Ru(2)—N—C(4)—C(6)—C(8) each make an acute angle of about 34° with the Ru(1)—Ru(2) vector.

A striking aspect of the structure of **5a** is the η^3-azaallyl-type bonding of N—C(7)—C(8) to Ru(1), indicated by the bond distances Ru(1)—N, Ru(1)—C(7) and Ru(1)—C(8) that amount to 2.127(4), 2.240(5) and 2.227(6) Å, respectively. Similar distances, i.e. 2.178(5), 2.159(6) and 2.285(6) Å, respectively, have been found in the only other comparable ruthenium–azaallyl system,

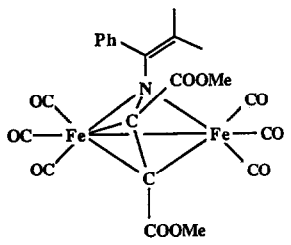

6

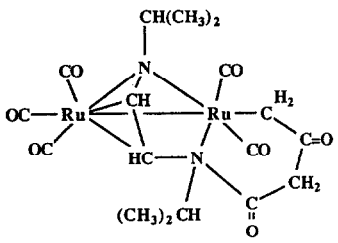

7

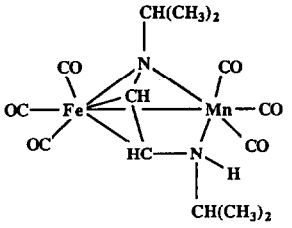

8

Fig. 4. Compounds $M_2(CO)_nL$ which contain a μ_2-η^3-azaallyl fragment L comparable to the N—C(7)—C(8) moiety in **5a**.

$Ru_2(CO)_5\{i\text{-}C_3H_7$—NC(H)C(H)N($C_3H_7$-$i$)C(O)$CH_2C(O)CH_2\}$ (**7**).[18a] The N—C(7) and C(7)—C(8) distances in (**5a**) are 1.404(7) and 1.347(8) Å, respectively, indicating some delocalization in this N—C—C moiety. The N—C(7)—C(8) plane makes an angle of 64.1° with the Ru(1)—Ru(2) vector and the angle N—C(7)—C(8) amounts to 109.8(6)°. All these facts indicate that a bonding description of the 6e MAD-yl ligand to the $Ru_2(CO)_6$ core as η^3-azaallyl to Ru(1) and σ-N, σ-C(8) to Ru(2) is appropriate.

The extent of delocalization within the N—C(7)—C(8) group is not as pronounced as in **7**[18] or $FeMn(CO)_6\{t\text{-}C_4H_9NC(H)C(H)N(H)$—$C_4H_9$-$t\}$ (**8**),[19] (see Fig. 4) where the bond distances within the azaallyl moiety are equal and amount to 1.37 Å in **7** and 1.40 Å in **8**. The distances in the N—C—C moiety in **5a** are comparable to those found in one of the NCC units in $Fe_2(CO)_4\{i\text{-}C_3H_7$—NC(H)C(H)N($i$-$C_3H_7$C(H)$=C(H)CO_2Me\}$.[18e] There, the N—C and C—C distances are 1.427(16) and 1.357(16) Å, respectively, which points to a single N—C bond and a η^2-coordinated C=C double bond. Hence, the coordination of the NCC moiety in **5a** could alternatively be interpreted as symmetric (3e) μ_2-N bridging as for anionic amido groups, σ-coordination of C(8) to Ru(2) and η^2-coordination of a C(7)—C(8) double bond to Ru(1), but we prefer the above description involving η^3-azaallyl bonding. It is further observed that whereas C(9) resides approximately in the plane described by the N—C(7)—C(8) moiety (deviation 0.06 Å, dihedral angle N—C(7)/C(8)—C(9) is 177°), C(11) does not (deviation 0.26 Å, dihedral angle C(11)—N/C(7)—C(8) is 168°). Possibly the steric influence of the $C(CH_3)_3$ group tilts C(11) out of this plane, obviously inducing some rehybridization of the N atom towards sp^3. This may also explain the observed incomplete delocalization within the N—C(7)—C(8) moiety (as evidenced by the unequal N—C(7) and C(7)—C(8) distances, *vide supra*). Another factor influencing the geometry of the NCC unit will be the bridging of C(8) between the Ru atoms (the Ru(2)—C(8) distance of 2.113(5) Å represents a normal Ru—C single bond) and this feature may contribute to the observed difference in the bond lengths of N—C(7) and C(7)—C(8). Again the observation of equal N—C and C—C distances of 1.416(24) and 1.433(31) Å, respectively, in **6** (whose complex is structurally analogous to **5a**, see Fig. 4) would suggest that the latter argument is not valid. It must be borne in mind, however, that in **6** resonance stabilization of the azaallyl fragment with the N-coordinated olefin is achieved. This cannot occur in **5a**.

IR spectra

All complexes exhibit a characteristic pattern of five intense bands in the region of terminal CO stretching frequencies (see Table 1), similar to those observed for $Ru_2(CO)_6L$ (L = R-DAB, R-PyCa) complexes.[20,21]

^{13}C NMR spectra

The data are compiled in Table 2. The numbering of the carbon atoms is as in Figs 2 and 3. The δ-value of 177 ppm for C(7) in **4a–4c** lies within the range normally found for H—^{13}C=N imine carbon atoms in free and σ-N-coordinated mono- and diazadienes.[22] The ^{13}C signals for C(8) and C(10) in **4a–4c** are found between 50–70 ppm, which is indicative of terminal allylic carbon atoms coordinated to a metal atom.[23] The high δ-value for the C(9) carbon in **4a–4c** cannot be readily explained. For $HRu_3(CO)_9\{C_3R_3\}$, the resonance of the central carbon atom in the $\mu_3\eta^3$-coordinated allyl fragment (which is comparable to C(9) in **4a–4c**) has been found at values between 160–200 ppm.[24] In mononuclear (η^3-allyl)metal complexes the resonance of the central carbon atom is usually found at substantially lower frequencies; typically 90–140 ppm.[23]

The intramolecular CO exchange rate in **4a–4c** is slow on the NMR time scale at 2.35 T and 263 K, as is evidenced by six separate resonances for the six CO ligands. Under the same conditions a single signal at 197.2 ppm is observed for all six CO ligands of **5a**. We will report on the dynamic behaviour in solution in the future.

The ^{13}C signal for C(7) in **5a** is found in the same region as the comparable resonance in complexes **7**[18a] and **8**.[19] The resonances of the ethyl group C(9)—C(10) fall within the expected range. The chemical shift of the C(8) atom in **5a** is found at 140 ppm, which is a considerably higher value than has been observed in the analogous diiron compound **6**.[16] There, the C(7) and C(8) resonances were found at 112 and 126 ppm (or *vice versa*) but could not be unambiguously assigned. In view of the present knowledge about comparable Ru complexes, the 112 ppm signal can be attributed to C(7) in **6** (see Fig. 4). It has been suggested[19] that the higher shifts for C(7) and C(8) in the case of **6** compared to **8** can be explained by the presence of strongly electron-withdrawing substituents on the allylic carbon atoms in **6**. This argument cannot hold now, since in **5a** no electron withdrawing substituents at C(7) or C(8) are present and yet δ[C(8)] is even higher than in **6**. On the other hand, the resonance of C(8) is found at a lower frequency than would be expected for such μ_2-coordinated

carbon atoms in μ_2-η^3-allyl groups.[24] The intimate factors determining the chemical shift of C(8) in **5a** are not yet clear.

^{1}H *NMR spectra*

The ^{1}H NMR spectra of **4a–4c** and **5a** in solution (see Table 2; for the numbering see Figs 2 and 3) are in agreement with their structures in the solid state. The proton resonance at *ca* 8.0 ppm for compounds **4a–4c** is characteristic of the imine proton in σ-N-coordinated R′C(*H*)=NR groups as in σ-N,σ-N′ and σ-N,μ_2N′,η^2—C=N′ coordinated R-DAB ligands.[20] It can be attributed to H(7) in **4a–4c**. The resonances at 3.40 and 3.30 ppm are typical for terminal *syn*-protons of η^3-allyl groups and can be assigned to H(8) and H(101), respectively. The vicinal coupling at H(7) of 2 Hz is also present in the 3.40 ppm signal, which must therefore belong to H(8). The coupling between H(7) and H(8) is smaller than one would expect: *ca* 5 Hz based on the observed dihedral angle of 40° between the C(7)—H(7) and C(8)—H(8) bonds in the crystal structure. The signal at 3.80 ppm for **4a–4c** can be assigned to the *anti*-proton H(102), since *anti*-protons are indeed usually found at lower field than *syn*-protons of η^3-allyl groups.[25] The chemical shift difference between the *syn*- and *anti*-protons H(101) and H(102) is not very large. Also the mutual coupling is negligible, as expected for geminal coupling in an η^3-allyl group. We note the diastereotopicity of the N-isopropyl methyl groups.

The ^{1}H NMR spectrum of **5a** is very different from that of **4a** and features (besides the intense singlet at 0.95 ppm due to the *tert*-butyl group) resonances at 1.06 and 2.38 ppm with the simple pattern of an ethyl group (C(9)H_2—C(10)H_3 in Fig. 3) that is attached to a quaternary carbon atom [C(8)]. The singlet at 6.91 ppm can be attributed to H(7) in **5a**, consistent with the observed shift δ 6.64 ppm for the central C*H* in the μ_3-η^3-allyl group in $HRu_3(CO)_9\{\mu_3$-η^3-CH_3—CC(H)C—C_2H_5.[18b]

Reaction pathways

The thermal reactions of the MAD ligands **1b** and **1c** with $Ru_3(CO)_{12}$ at 100°C in heptane proceed readily to give mainly the dehydrogenated complexes **4b** and **4c**, together with substantial amounts of **2b** and **2c**, respectively. On the other hand, when **1a** (R = *t*-Bu) is used under these conditions only small amounts of **2a** (< 10%) could be detected in the reaction mixture after 20 h. Instead of **2a**, the azaallyl complex **5a** was formed in appreciable quantities (see Experimental). Complexes isostructural with **5** seem not to be formed in the case of ligands **1b** (R = *i*-C_3H_7) or **1c** (R = *c*-C_6H_{11}). This deviating reactivity is not understood at the moment.

It appears from HPLC measurements (reversed phase hypersil ODS, MeOH–H_2O: 87/13) performed on the reaction mixtures taken at intervals of 1–2 h, that compounds **2a–2c** and **4a–4c** are the ultimate products. During the reaction of the MAD ligand **1a** with $Ru_3(CO)_{12}$ the concentration of a third compound, **5a**, was found to increase with time. In the case of **1b** and **1c** the HPLC measurements reveal the initial formation of small amounts of at least two other compounds, the concentration of which thereupon declines rapidly with time. Isolation and identification of these unknown compounds presently receives considerable attention in our laboratory.

Apart from the as yet missing azaallyl compounds $Ru_2(CO)_6\{\mu_2$-η^3-C_2H_5—CC(H)N—R$\}$ **5b** (R = *i*-C_3H_7) and **5c** (R = *c*-C_6H_{11}), a possible structure of one of these elusive compounds could be a diruthenium hydride to which a 5e MAD-yl ligand is coordinated, e.g. as in $(\mu$-H$)Ru_2(CO)_6\{\mu_2$-η^3-CH_3—C=C(H)C(H)=N—R$\}$ (**9**). Such a complex (see Fig. 5) would be a candidate as a precursor for **2**[10] and **4**. It could easily arise from the insertion of Ru into the C(9)—H bond of **1**. A precedent for a comparable insertion and the existence of a diruthenium hydride which is isostructural with **9** is available in the case of the known reaction of benzylidene acetone with $Ru(CO)_3(COD)$.[26]

The formation of complexes **4** from **9** is easily conceivable, since it only requires an insertion of Ru(1) into a C—H bond at C(10) in **9** (see Figs 2 and 5) and loss of H_2 from the formed dihydride. Alternatively, elimination of CO from **9** and subsequent dimerization (with loss of 2H) gives the tetranuclear complex **2** (cf. ref. 10). Overall, the formation of **4** from **1** involves dehydrogenation of the MAD ligand. Such dehydrogenation reactions are known, e.g. the formation of pentalene complexes from dihydropentalenes (C_8H_8) and iron carbonyls,[27] or from thermal reactions of $Ru_3(CO)_{12}$

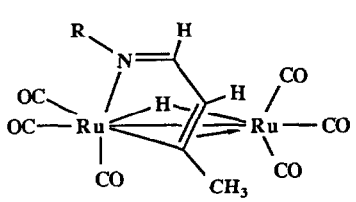

9

Fig. 5. Possible structure of the proposed intermediate hydrido–diruthenium species **9**.

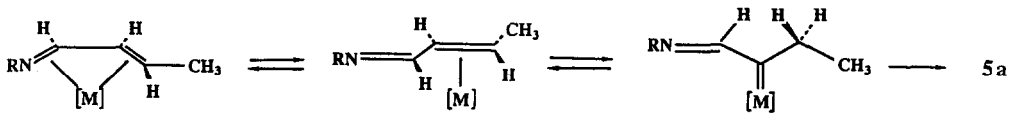

Fig. 6. Proposed 1,2-hydrogen shift in a monoazadiene ligand coordinated to a $Ru_m(CO)_n$ fragment [M].

with butadienes, cyclooctatriene and related reactions involving cyclic polyalkenes and polyenyl compounds.[28] Dehydrogenation has also been observed for the metallated monoazadiene in $(\mu\text{-H})_2Os_3(CO)_9\{\mu_3\text{-}\eta^2\text{-}(CH_3)_2C(H)CC(CH_3)\!=\!N\!-\!C_6H_5\}$, in which case the formation of another type of μ_2-η^3-coordinated allyl group occurred.[9]

Finally, an explanation must be given for the formation of **5a**. First of all it should be mentioned that this azaallyl complex seems to be formed only in the case of R = t-C_4H_9, suggesting that its formation (or lack of conversion) partly depends upon steric factors. There appears to be no straightforward pathway for the conversion of **9** into **5a**. It is also possible that **5a** is formed via an as yet unappreciated route. This may involve the conversion of **1a** via an intermediate where the MAD ligand is η^2-N=C, η^2-C=C coordinated to a ruthenium carbonyl fragment, followed by a 1,2-hydrogen shift from C(8) to C(9) generating formally a carbene C(8) atom (see Figs 3 and 6). Although a similar reaction in isolated species in the gas-phase would be highly endothermic, this 1,2-shift may become favourable when the generated carbenoid is stabilized by metal centres,[29] such as is the case here. This conjecture is supported by the reported 1,2-H shift on a trinuclear osmium cluster, yielding $(\mu\text{-H})_2Os_3(CO)_9\{(CH_3)_2C(H)CC(CH_3)\!=\!N\!-\!C_6H_5\}$, in which a μ_2-carbene ligand has been found.[9] This 1,2-H shift could be relevant for alkyl chain growth and isomerization reactions occurring on metallic surfaces.[30]

Acknowledgements—We wish to express our gratitude to Mr J. M. Ernsting for assistance with NMR measurements. This investigation was supported in part (W.P.M) by the Netherlands Foundation for Chemical Research (SON) with financial aid from the Netherlands Organization for the Advancement of Pure Research (NWO).

REFERENCES

1. W. P. Mul, C. J. Elsevier, K. Vrieze, W. J. J. Smeets and A. L. Spek, *Rec. Trav. Chim. Pays-Bas* 1988, **107**, 297.
2. M. A. Bennett, M. I. Bruce and T. W. Matheson, in *Comprehensive Organometallic Chemistry* (Edited by G. Wilkinson, F. G. A. Stone and E. W. Abel), Vol. 4, p. 691. Pergamon Press, Oxford (1982).
3. G. Van Koten and K. Vrieze, *Adv. Organometal. Chem.* 1982, **21**, 151.
4. L. H. Polm, C. J. Elsevier, G. van Koten, J. M. Ernsting, D. J. Stufkens, K. Vrieze, R. R. Andréa and C. H. Stam, *Organometallics* 1987, **6**, 1096.
5. A. N. Nesmeyanov, L. V. Rybin, N. A. Stelzer, Yu. T. Struchkov, A. S. Batsanov and M. I. Rybinskaya, *J. Organometal. Chem.* 1979, **182**, 399.
6. C. Müller, L. Stamp and H. tom Dieck, *J. Organometal. Chem.* 1986, **308**, 105.
7. A. De Cian and R. Weiss, *Acta. Cryst.* 1972, **B28**, 3264.
8. J. F. Van Baar, K. Vrieze and D. J. Stufkens, *J. Organometal. Chem.* 1975, **97**, 461.
9. R. D. Adams and J. P. Selegue, *Inorg. Chem.* 1980, **19**, 1795.
10. L. H. Polm, W. P. Mul, C. J. Elsevier, K. Vrieze, M. J. N. Christophersen and C. H. Stam, *Organometallics* 1988, **7**, 423.
11. H. C. Barany, E. A. Braude and M. Pianka, *J. Chem. Soc.* 1949, 1898.
12. R. Ben-Shoshan and R. Pettit, *Chem. Commun.* 1968, 247.
13. R. E. Davis, *Chem. Commun.* 1968, 248.
14. R. E. Colborn, A. F. Dyke, S. A. R. Knox, K. A. Mead and P. Woodward, *J. Chem. Soc., Dalton Trans.* 1983, 2099.
15. B. F. G. Johnson, J. Lewis, P. R. Raithby and S. W. Sankey, *J. Organometal. Chem.* 1982, **231**, C65.
16. Y. Nakamura, K. Backmann, H. Heimgartner and H. Schmid, *Helv. Chim. Acta* 1978, **61**, 589.
17. P. S. Braterman, *Struct. Bonding (Berlin)* 1972, **10**, 1.
18. (a) L. H. Polm, G. van Koten, K. Vrieze, C. H. Stam and W. C. J. van Tunen, *J. Chem. Soc., Chem. Commun.* 1983, 1177; (b) M. Evans, M. B. Hursthouse, E. W. Randall, E. Rosenberg, L. Milone and M. Valle, *J. Chem. Soc., Chem. Commun.* 1972, 545; (c) K. Ogawa, A. Torii, H. Kobayashi-Tamura, T. Watanabé, T. Yoshida and S. Otsuka, *J. Chem. Soc., Chem. Commun.* 1971, 991; (d) T. Sielisch and U. Behrens, *J. Organometal. Chem.* 1987, **327**, 85; (e) F. Muller, G. van Koten, K. Vrieze, B. Krijnen and C. H. Stam, *J. Chem. Soc., Chem. Commun.* 1986, 150.
19. J. Keijsper, J. Mul, G. van Koten, K. Vrieze, H. C. Ubbels and C. H. Stam, *Organometallics* 1984, **3**, 1732.
20. L. H. Staal, L. H. Polm, R. W. Balk, G. van Koten, K. Vrieze and A. M. F. Brouwers, *Inorg. Chem.* 1980, **19**, 3343.
21. L. H. Polm, G. van Koten, C. J. Elsevier, K. Vrieze, B. F. K. van Santen and C. H. Stam, *J. Organometal. Chem.* 1986, **304**, 353.

22. L. H. Staal, J. Keijsper, L. H. Polm and K. Vrieze, *J. Organometal. Chem.* 1981, **204**, 101.
23. B. E. Mann, *Adv. Organometal. Chem.* 1974, **12**, 135.
24. S. Aime, L. Milone, D. Osella, M. Valle and E. W. Randall, *Inorg. Chim. Acta* 1976, **20**, 217.
25. M. L. H. Green and P. L. I. Nagy, *Adv. Organometal. Chem.* 1964, **2**, 325.
26. A. J. P. Domingos, B. F. G. Johnson, J. Lewis and G. M. Sheldrick, *J. Chem. Soc., Chem. Commun.* 1973, 912.
27. D. F. Hunt and J. W. Russel, *J. Organometal. Chem.* 1976, **104**, 373.
28. S. A. R. Knox and F. G. A. Stone, *Acc. Chem. Res.* 1974, **7**, 321.
29. H. F. Shaeffer, *Acc. Chem. Res.* 1979, **12**, 288.
30. W. A. Hermann, *Angew. Chem.* 1982, **94**, 118.

Polyhedron Vol. 7, No. 24, pp. 2531–2536, 1988
Printed in Great Britain

0277–5387/88 $3.00+.00
© 1988 Pergamon Press plc

THE PREPARATION AND COORDINATION CHEMISTRY OF 2,2′:6′,2″-TERPYRIDINE MACROCYCLES—VI.* PLANAR HEXADENTATE MACROCYCLES INCORPORATING 2,2′:6′,2″-TERPYRIDINE

EDWIN C. CONSTABLE† and JEREMY M. HOLMES

University Chemical Laboratory, Lensfield Road, Cambridge CB2 1EW, U.K.

(*Received* 24 *March* 1988; *accepted* 3 *May* 1988)

Abstract—The template condensation of 6,6″-bis(α-methylhydrazino)-2,2′:6′,2″-terpyridines L^2 and L^3 with 2,6-pyridinedialdehyde may give a number of different products depending upon the metal ion which is used. In the presence of nickel(II) the products are either the nickel(II) complexes of the 18-membered ring macrocycles L^4 or L^5 or the free macrocycles. The metal ion acts as a transient template and is removed in a chloride ion specific demetallation. The use of dimethyltin(IV) as a template results in the formation of complexes of the ring contracted macrocycles L^6 or L^7.

We have recently described the synthesis, coordination chemistry and properties of a pentadentate macrocycle incorporating a 2,2′:6′,2″-terpyridine moiety (L^1, R = Ph).[2] We have also prepared the unsubstituted macrocyclic ligand (L^1, R = H), and demonstrated the unusual redox properties associated with its complexes.[1] In each case, metal complexes of these ligands could be obtained by template condensation of the appropriate 6,6″-bis(α-methylhydrazino)-2,2′:6′,2″-terpyridine (L^2 or L^3) with ethanedial (glyoxal) in the presence of a metal ion, or by the reaction of the free macrocyclic ligands, prepared by a transient template reaction[3] utilizing dimethyltin(IV), directly with the metal salt. We have now extended these studies to the preparation of potentially hexadentate macrocyclic ligands incorporating the 2,2′:6′,2″-terpyridine functionality. We report herein, the preparation and coordination chemistry of the hexadentate macrocyclic ligands L^4 and L^5, which are obtained by the condensation of L^2 or L^3 with 2,6-pyridinedialdehyde. We also report a novel type of transient template reaction associated with nickel(II).

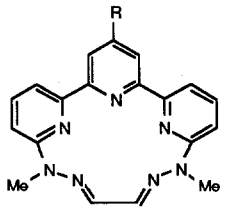

L^1 R = Ph or H

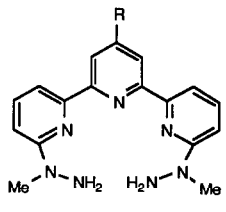

L^2 R = H
L^3 R = Ph

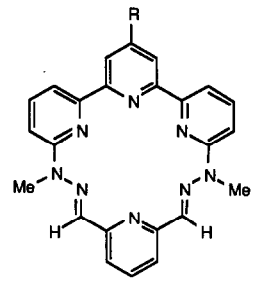

L^4 R = H
L^5 R = Ph

RESULTS AND DISCUSSION

The 6,6″-bis(α-methylhydrazino)-2,2′:6′,2″-terpyridines (L^2 or L^3) were prepared by the literature methods,[1,2] and the condensation with 2,6-pyridinedialdehyde was investigated in the presence of various metal ions. Treatment of a methanolic solu-

* For Part V, see ref. 1.

† Author to whom correspondence should be addressed.

tion of L^2 with nickel(II) acetate led to the formation of a yellow–green solution containing the $[NiL^2(MeOH)_2]^{2+}$ cation; the addition of one mole equivalent of 2,6-pyridinedialdehyde and an excess of hydrochloric acid resulted in the rapid formation of a deep orange solution. The addition of $[NH_4][PF_6]$ to this solution resulted in the deposition of deep red crystals of a material analysing correctly for the metal-free hexadentate macrocyclic salt $[H_2L^4][PF_6]_2$. The phenyl substituted macrocyclic salt $[H_2L^5][PF_6]_2$ was obtained from an exactly analogous reaction utilizing L^3 instead of L^2. The isolated yields of these crystalline products were typically in the region of 65–70%.

The formation of the free ligands in these reactions is somewhat surprising, but was fully confirmed by a range of techniques. The compounds were diamagnetic, and exhibited mass spectra (EI and FAB) fully in accord with the proposed [1+1] metal-free formulations (L^{4+}, m/z 420; L^{5+}, m/z 496). The IR spectra of the compounds did not exhibit any peaks between 1640–2000 cm^{-1}. The salts are readily soluble in solvents such as Me_2CO, MeCN or Me_2SO; an observation which supports their formulation as monomers rather than polymers or oligomers. The ^1H NMR spectra of the compounds were also in accord with the proposed structures. In CD_3COCD_3 solution the ^1H NMR spectra were broad and very poorly resolved, but the addition of a trace of CF_3COOD led to sharp well-resolved spectra. This is probably due to a rapid protonation–deprotonation equilibrium of the hexadentate macrocyclic cations. We have observed similar equilibria in the cations of related pentadentate macrocycles. The aromatic region of a solution of $[H_2L^4][PF_6]_2$ in CD_3COCD_3 containing a trace of CF_3COOD is shown in Fig. 1, and demonstrates the high molecular symmetry (on the NMR time-scale) of the cation. The spectrum clearly illustrates that the two terminal rings are equivalent and give rise to an ABM pattern. The resonances of the "terpyridyl" fragment are shifted from those observed in the related pentadentate ligand $[H_2L^1]^{2+}$, as might be expected from the different interannular angles which must be present. In L^1 the terminal pyridyl rings are "bent" inwards, and the internal interannular N—C(2)—C(2′) angle is 113°, whereas in L^4 and L^5, models suggest an angle of 120°.[2] The ^1H NMR spectrum of $[H_2L^4][PF_6]_2$ also exhibits sharp singlets at δ 4.05 and 8.74, which may be assigned to the *N*-methyl and azomethine protons, respectively. This is a strong indication that the product is the fully aromatic [18]-annulene analogue, rather than a polycyclic derivative related to the product from the reaction of 2,6-diacetylpyridine with 1,2-diaminobenzene.[4]

It was found that the free ligands were only obtained if the reaction solutions were moderately concentrated, and made strongly acidic in hydro-

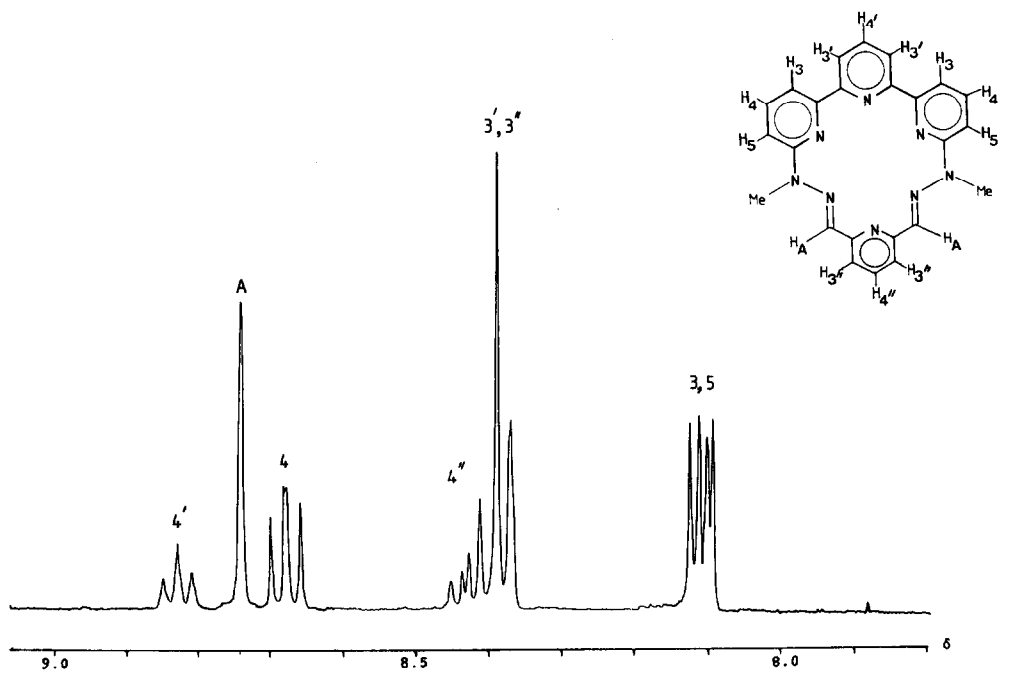

Fig. 1.

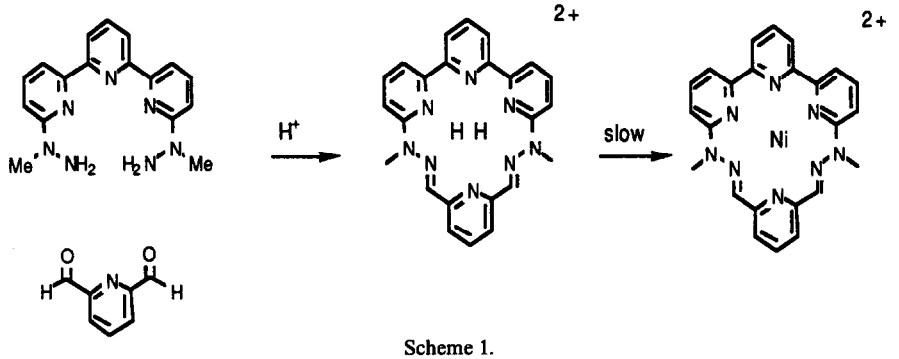

Scheme 1.

chloric acid. In dilute or weakly acidic solution, the products were the yellow nickel(II) complexes $[NiL^4(MeOH)_2][PF_6]_2$ or $[NiL^5(MeOH)_2][PF_6]_2$. The behaviour is compatible with several possible mechanisms. Firstly, the reaction might be specific acid catalysed, with the proton acting as the true template, with slow incorporation of nickel(II) into the macrocyclic product (Scheme 1) or, secondly, the reaction might involve a true transient template effect with a nickel(II) mediated condensation followed by an acid dependent demetallation (Scheme 2). The diamagnetic metal-free products were observed when the isolated complexes $[NiL^2(MeOH)_2][PF_6]_2$ or $[NiL^3(MeOH)_2][PF_6]_2$ (μ_{eff} 3.10 BM) were reacted with methanolic 2,6-pyridinedialdehyde in the presence of hydrochloric acid. The complexes $[NiL^2(MeOH)_2][PF_6]_2$ and $[NiL^3(MeOH)_2][PF_6]_2$ are known not to be labile in acid, and this would argue against the mechanism proposed in Scheme 1. The reaction of L^2 or L^3 with 2,6-pyridinedialdehyde in the presence or absence of acid led to the formation of predominantly polymeric materials. Replacing the hydrochloric acid by an equivalent quantity of HBF_4 or HPF_6, or adding sodium acetate to the hydrochloric acid reaction mixture, led to the formation of *only* the yellow nickel complexes of L^4 or L^5. Similarly, the nickel(II) complexes were only obtained if the hydrochloric acid was replaced by an equivalent quantity of lithium chloride. Incorporation of nickel(II) was rapid when methanolic solutions of $[H_2L^4][PF_6]_2$ or $[H_2L^5][PF_6]_2$ were heated with nickel(II) acetate in the absence of acid. The yellow solutions so obtained gave an orange colouration characteristic of the free macrocycle upon the addition of hydrochloric acid.

We consider that these observations are consistent with a mechanism related to that indicated in Scheme 2, in which the nickel(II) acts as the true template. The formation of polymeric products in the absence of metal ion appears to preclude any mechanism in which the condensation is acid catalysed and nickel(II) is incorporated into the macrocycle late in the reaction scheme. It is also unlikely that the high-spin $[Ni(MeOH)_6]^{2+}$ ion would be incorporated into the macrocycle in a very slow step.

We believe that the key step in the formation of the metal-free macrocyclic ligand is an acid-catalysed chloride ion specific demetallation. This explains why the reaction is specific to hydrochloric acid, and why the metal ion must be present, but it is rather unusual to observe such facile demetallation of marocyclic complexes. When such

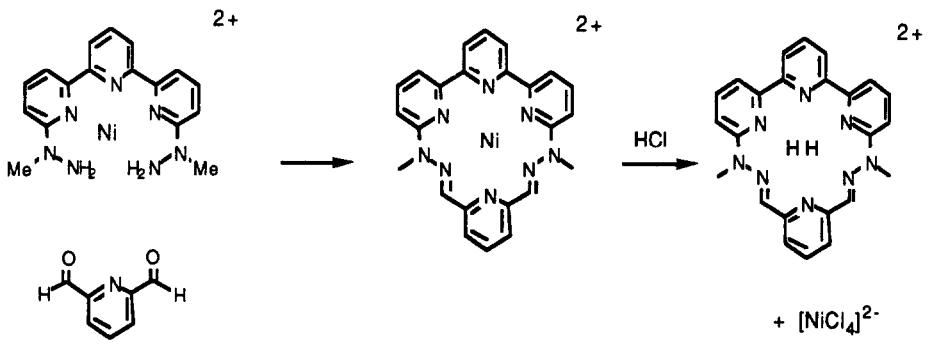

Scheme 2.

demetallation does occur, it may be traced to a mismatch in the coordination requirements of the metal ion and the ligand. We have previously shown the importance of such mismatches in the preparation of free pentadentate macrocycles using dimethyltin(IV) templates, and demonstrated the effect to originate in the diminution in hole size on passing from the open-chain ligand L^2 to the macrocycle L^1 (R = Ph)[2]. Such an effect is not likely to be operative in this case since the macrocycle possesses, if anything, a greater hole size than the open chain precursors. Nelson and co-workers have investigated a number of planar or near-planar, macrocycles incorporating an N_6 donor set in an 18-membered ring.[4] If a planar hexagonal arrangement of the six-donor atoms is assumed, a study of molecular models combined with crystallographic studies on related compounds, suggests that the ligands L^4 and L^5 possess a hole size of the order 2.7 ± 0.1 Å. This would result in the nickel(II) ion ($r = 0.69$ Å) "rattling" in the macrocyclic hole, with a concomitant lowering of the stability constant. The chloride ion specificity of the demetallation offers a clue to the mechanism; the driving force for the loss of metal is the formation of $[NiCl_4]^{2-}$.

We have previously demonstrated the use of dimethyltin(IV) as a transient template in the preparation of the pentadentate ligands L^1 (R = H or Ph),[1,2] and considered that it might also act in this manner for the preparation of the 18-membered ring sexidentate macrocycles L^4 and L^5. The addition of 2,6-pyridinedialdehyde to a yellow methanolic solution of $[Me_2SnL^2]Cl_2$ or $[Me_2SnL^3]Cl_2$ resulted in the formation of orange–yellow solutions from which orange microcrystalline solids were obtained after the addition of ammonium hexafluorophosphate. The IR spectra of these solids were significantly different from those of the complexes, $[Me_2SnL^2]Cl_2$ or $[Me_2SnL^3]Cl_2$ and from those of the expected macrocyclic products, $[H_2L^4][PF_6]_2$ and $[H_2L^5][PF_6]_2$. The most noticeable features in the IR spectra were strong absorptions at 1673 and 3239 cm^{-1}. Elemental analysis suggested the formulations $[Me_2Sn(C_{18}H_{17}N_7)][PF_6]_2$ or $[Me_2Sn(C_{24}H_{23}N_7)][PF_6]_2$, respectively. The mass spectra of the complexes supported this formulation, with the highest mass peaks in the EI spectra being observed at *m/z* 331 ($C_{18}H_{17}N_7$) and *m/z* 409 ($Cl_{24}H_{23}N_7$), respectively. We believe that a metal ion induced rearrangement has occurred to produce the dimethyltin(IV) complexes of the 13-membered ring pentadentate macrocycles L^6 and L^7. We suspect that these macrocycles are not planar, as we have already demonstrated that the bonding cavity in a planar 14-membered ring macrocycle is too

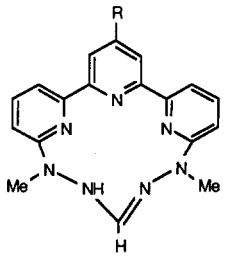

L^6 R = H
L^7 R = Ph

small for dimethyltin(IV). Attempts to characterize the dimethyltin(IV) complexes of these ligands by ^1H NMR spectroscopy was unsuccessful; upon dissolution in CD_3COCD_3, CD_3CN or CD_3SOCD_3 the complexes rapidly demetallated, with the deposition of tin oxides. The resultant solutions gave very broad unresolved spectra. Attempts to recrystallize the complexes $[Me_2SnL^6][PF_6]_2$ or $[Me_2SnL^7][PF_6]_2$ resulted in demetallation and the deposition of tin oxides. The resulting pale yellow solution was found to contain only the starting bis(α-methylhydrazines). Although the free macrocycles may not be obtained from the tin complexes, transmetallation occurs readily upon treatment with other transition metal salts, and we will describe the coordination chemistry of these novel ligands at a later date.[5]

The reaction of either $[H_2L^4][PF_6]_2$ or $[H_2L^5][PF_6]_2$ with methanolic solutions of nickel(II) acetate resulted in the formation of pale yellow solutions from which the complexes $[NiL^4(MeOH)_2][PF_6]_2$ or $[NiL^5(MeOH)_2][PF_6]_2$ could be obtained. These complexes were identical to the nickel complexes obtained from the template reaction in the absence of hydrochloric acid. In the absence of structural data it is not possible to eliminate the possibility of nucleophilic attack on the imine bonds by water or methanol in these complexes. This is known to be a metal-mediated process which occurs in other 18-membered ring hexadentate macrocycles.[4] The IR spectra of the nickel complexes do not exhibit the NH absorptions expected for such aminol products, but this cannot be regarded as conclusive. The complexes are consistently obtained from water or methanol with at least two solvent molecules associated. If the solvent has not attacked the imine bonds, it is tempting to propose that the metal is in a hexagonal bipyramidal environment.

The macrocyclic ligands L^4 and L^5 are expected to have a hole size of 2.7 ± 0.1 Å, and are thus expected to form stable complexes with second row transition elements. The reaction of $[H_2L^4][PF_6]_2$ or $[H_2L^5][PF_6]_2$ with silver(I) acetate in MeCN

results in the formation of pale yellow solutions from which $[AgL^4][PF_6]$ or $[AgL^5][PF_6]$ may be obtained as yellow crystalline solids. The ^1H NMR spectrum of $[AgL^4][PF_6]$ clearly indicates that the ligand is unchanged upon binding to the metal. The spectrum exhibits sharp well-resolved resonances at δ 8.17 (s, 3H, $H_{3'}$ and $H_{4'}$), 8.12 (t, 2H, H_A), 8.03 (t, 1H, $H_{4''}$), 8.00 (t, 2H, H_4), 7.69 (d, 2H, H_3), 7.60 (d, 2H, $H_{3''}$) and 7.42 (d, 2H, H_5). The observation of the resonance for the imine protons (H_A) confirms that the imines have not undergone nucleophilic attack. Treatment of a solution of $[AgL^4][PF_6]$ or $[AgL^5][PF_6]$ with K[SCN] led to the precipitation of $[AgL^4(SCN)]$ or $[AgL^5(SCN)]$; in each case, the observation of an IR absorption at 2085 cm^{-1} suggests that the thiocyanate is S-bonded to the silver.

EXPERIMENTAL

The bis(α-methylhydrazines) L^2 and L^3 were prepared by the literature methods;[1,2] 2,6-pyridinedialdehyde was prepared by the selenium dioxide oxidation of 2,6-pyridinedimethanol (Aldrich).

Electronic spectra were recorded using a Pye–Unicam 8800 spectrophotometer; IR spectra were recorded using Perkin–Elmer 1710 FT or 983 spectrometers with the compound in compressed KBr pellets or in suspension in Nujol. Fast atom bombardment mass spectra were measured using a Kratos MS-50 spectrometer, and were loaded using acetonitrile as solvent with 3-nitrobenzyl alcohol as supporting matrix. NMR spectra were recorded on a Bruker WM250 spectrometer. EPR spectra were recorded using a Varian E109 spectrometer.

Preparation of $[H_2L^4][PF_6]_2$

L^2 (0.405 g, 1.26 mmol) and $Ni(OAc)_2 \cdot 4H_2O$ (0.315 g, 1.26 mmol) were warmed in MeOH (100 cm^3) to give a yellow–green solution; 2,6-pyridinedialdehyde (0.170 g, 1.26 mmol) and concentrated hydrochloric acid (3 drops) were added, and the solution heated to reflux for 1 h. The orange solution so obtained was treated with aqueous $[NH_4][PF_6]$ (0.2 g in 2 cm^3 H_2O), heated to reflux for 5 min, and cooled, whereupon orange–red crystals of $[H_2L^4][PF_6]_2 \cdot 3H_2O$ separated. (Found: C, 37.7; H, 3.7; N, 14.8. Required for $C_{24}H_{28}F_{12}N_8O_3P_2$: C, 37.6; H, 3.6; N, 14.6%. *m/z* 420) (0.63 g, 65%).

Preparation of $[H_2L^5][PF_6]_2$

This was prepared in an analogous manner to $[H_2L^4][PF_6]_2$ replacing L^2 by L^3 (0.500 g, 1.26 mmol). Red crystals of $[H_2L^5][PF_6]_2 \cdot 2H_2O$ were obtained. (Found: C, 43.7; H, 3.6; N, 13.8. Required for $C_{30}H_{30}F_{12}N_8O_2P_2$: C, 43.7; H, 3.6; N, 13.6%. *m/z* 496) (0.72 g, 70%).

Preparation of $[NiL^5(MeOH)_2][PF_6]_2$

Method 1. The above preparation was repeated, substituting aqueous $H[PF_6]$ for the concentrated hydrochloric acid. Yellow microcrystals of the complex $[NiL^5(MeOH)_2][PF_6]_2 \cdot H_2O$ were obtained. (Found: C, 41.4; H, 3.6; N, 12.0; Ni, 6.8. Required for $C_{32}H_{34}F_{12}N_8NiO_3P_2$: C, 41.4; H, 3.7; N, 12.1; Ni, 6.3%.)

Method 2. $[H_2L^5][PF_6]_2 \cdot 2H_2O$ (0.083 g, 0.1 mmol) and $Ni(OAc)_2 \cdot 4H_2O$ (0.025 g, 0.1 mmol) were heated to reflux for 1 h in MeOH (20 cm^3) to give a yellow solution. The solution was treated with $[NH_4][PF_6]$ (0.1 g) and allowed to cool, when the complex separated as a yellow solid, identical in all respects to the material obtained by Method 1.

Preparation of $[Me_2SnL^6][PF_6]_2$

2,6-pyridinedialdehyde (0.014 g, 0.1 mmol) was added to a solution of $[Me_2SnL^2]Cl_2$ (0.047 g, 0.1 mmol) in MeOH (25 cm^3) containing three drops of concentrated hydrochloric acid. The solution was heated to reflux for 2 h, filtered hot and $[NH_4][PF_6]$ (0.06 g) added to the pale orange filtrate. Upon cooling, yellow crystals of $[Me_2SnL^6][PF_6]_2$ separated. (Found: C, 31.5; H, 3.5; N, 12.9. Required for $C_{20}H_{25}F_{12}N_7P_2Sn$: C, 31.1; H, 3.2; N, 12.7%. *m/z* 331) (0.054 g, 70%).

Preparation of $[Me_2SnL^7][PF_6]_2$

This was prepared in an analogous manner to $[Me_2SnL^6][PF_6]_2$ using $[Me_2SnL^3]Cl_2$ (0.047 g, 0.1 mmol). Yellow crystals of $[Me_2SnL^7][PF_6]_2$ were obtained (*m/z* 409).

Preparation of $[AgL^5][PF_6]$

$[H_2L^5][PF_6]_2 \cdot 2H_2O$ (0.041 g, 0.05 mmol) was added to a solution of silver acetate (0.008 g, 0.05 mmol) in MeOH (10 cm^3). The solution was heated to reflux for 1 h, treated with $[NH_4][PF_6]$ (0.2 g) and cooled, when pale yellow needles of $[AgL^5][PF_6]$ separated. Dissolution of these in MeCN, followed by treatment with K[SCN] led to the precipitation of $[AgL^5(SCN)]$. (Found: C, 56.5; H, 3.7; N, 19.2.

Required for $C_{31}H_{24}N_9AgS$: C, 56.2; H, 3.6; N, 19.0%.)

Acknowledgements—We should like to thank the S.E.R.C. for the award of a studentship (JMH) and the Royal Society for a grant towards the cost of a spectrometer.

REFERENCES

1. E. C. Constable, J. M. Holmes and R. C. S. McQueen, *J. Chem. Soc., Dalton Trans.* 1987, 5.
2. E. C. Constable and J. Lewis, *Polyhedron* 1982, **1**, 303; E. C. Constable, J. Lewis, M. C. Liptrot, P. R. Raithby and M. Schroder, *Polyhedron* 1983, **2**, 301; E. C. Constable, J. Lewis, M. C. Liptrot and P. R. Raithby, *J. Chem. Soc., Dalton Trans.* 1984, 2177; E. C. Constable, F. K. Khan, J. Lewis, M. C. Liptrot and P. R. Raithby, *J. Chem. Soc., Dalton Trans.* 1985, 333.
3. L-Y. Chung, E. C. Constable, J. Lewis, P. R. Raithby and M. D. Vargas, *J. Chem. Soc., Chem. Commun.* 1984, 1425.
4. S. M. Nelson, S. G. McFall, M. G. B. Drew and A. H. B. Otuman, *J. Chem. Soc., Chem. Commun.* 1977, 370; M. G. B. Drew, A. H. B. Otuman, S. G. McFall, P. D. A. McIllroy and S. M. Nelson, *J. Chem. Soc., Dalton Trans.* 1977, 438; M. G. B. Drew, F. S. Esho, A. Lavery and S. M. Nelson, *J. Chem. Soc., Dalton Trans.* 1984, 545; M. G. B. Drew, J. Nelson, F. Esho, V. McKee and S. M. Nelson, *J. Chem. Soc., Dalton Trans.* 1982, 1837.
5. E. C. Constable and J. M. Holmes, unpublished results.

Polyhedron Vol. 7, No. 24, pp. 2537–2542, 1988
Printed in Great Britain

0277–5387/88 $3.00+.00
© 1988 Pergamon Press plc

THE REACTIVITY OF CATIONIC [TRIOXO-(1,4,7-TRIAZACYCLONONANE)RHENIUM(VII)] AND OXO-RHENIUM(V) COMPLEXES CONTAINING TRIAZAMACROCYCLES

CHRISTA POMP and KARL WIEGHARDT*

Lehrstuhl für Anorganische Chemie I, Ruhr-Universität, D-4630 Bochum, F.R.G.

(*Received* 7 *April* 1988; *accepted* 3 *May* 1988)

Abstract—The reduction of colourless $[LRe^{VII}O_3]Br$ in an acetone–water mixture (6:1) with zinc amalgam affords green, air-sensitive $[LRe^{V}O_2Br]$ which forms a violet complex $[LReO(\mu\text{-}O)_2ReOBr_2]$ in aqueous solution (L = 1,4,7-triazacyclononane; $C_6H_{15}N_3$). From a similar reduction of $[LReO_3]ReO_4$ the violet neutral complex $[LReO(\mu\text{-}O)_2ReO(ReO_4)_2]$ was obtained. $[LReO_3]^+$ is deprotonated in alkaline solution ($pK_a = 10.3+0.2$, 25°C) and $[(C_6H_{14}N_3)ReO_3]$ was isolated as a yellow solid. The latter amido rhenium(VII) compound reacted in dimethylformamide with R—X (R = CH_3, benzyl; X = Cl), affording at the cyclic amine, N,N′,N″-trisalkylated complexes of the type $[L'ReO_3]X$. The monomeric rhenium(V) complexes $[LReOX_2]X$ (X = Cl, Br, I) were obtained from the reaction of $[n\text{-Butyl}_4N]ReOX_4$ and L in acetonitrile. IR, UV–vis, ^{17}O NMR spectra of these compounds are reported.

Recently we have reported the synthesis and crystal structure of $[LReO_3]Cl$ (Fig. 1)[1] where L represents the cyclic triamine 1,4,7-triazacyclononane (L). This octahedral rhenium(VII) complex is available in excellent yields from the reaction sequence depicted in eqs (1)–(4).

$$Re(CO)_5Br + L \rightarrow [LRe(CO)_3]Br \quad (1)$$

$$[LRe(CO)_3]^+ + NO^+ \rightarrow [LRe(NO)(CO)_2]^{2+} + CO \quad (2)$$

$$[LRe(CO)_3]Br \xrightarrow{5M\ HNO_3} [LReO_3]ReO_4 \quad (3)$$

$$[LRe(NO)(CO)_2]^{2+} \xrightarrow{H_2O_2} [LReO_3]^+. \quad (4)$$

Subsequently we and others have found that eq. (1) represents a general synthetic route to *fac*-tricarbonylrhenium(I) complexes containing tridentate macrocycles[2,3] and the tridentate hydrotris(3,5-dimethylpyrazolyl)borate(1−).[4] But in contrast to $[LRe(CO)_3]^+$ [1,2] the analogous complexes with Me_3[9]aneN$_3$ and [9]aneS$_3$ are quite stable towards nitrosylation with $NOBF_4$; thus, reaction (2) was not observed to occur. $[(Me_3[9]aneN_3)Re(CO)_3]^+$ is extremely stable: neither Br_2, Cl_2 nor hot concentrated nitric acid or 30% H_2O_2 at 90°C led to oxidative decarbonylation reactions.

Reaction (4) is very interesting because this exhaustive oxidative decarbonylation reaction encompasses a change of formal oxidation state at the rhenium centre by six units *without* detectable

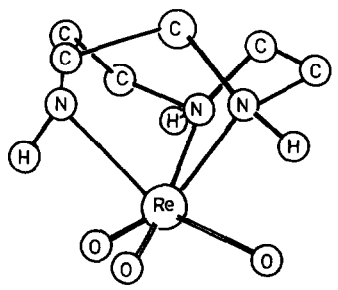

Fig. 1. Schematic representation of the cation in $[LReO_3]Cl$ (methylene H atoms are omitted). Average bond distances [Å] and angles [deg]: Re—O 1.756(5); Re—N 2.197(5); O—Re—O 102.7(4); N—Re—N 76.5(2); O—Re—N 88.9(3); 161.0(4).

* Author to whom correspondence should be addressed.

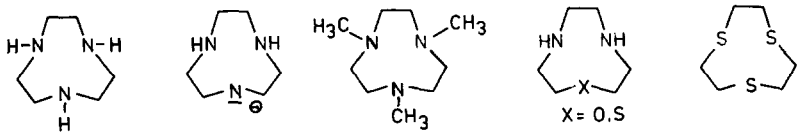

dissociation of the ligand L. This reaction resembles in many respects the chemistry of organometallic $(\eta^5\text{-}Me_5C_5)Re(CO)_3$ with H_2O_2 which yields $(\eta^5\text{-}Me_5C_5)ReO_3$ in excellent yields.[5-7] We have in the past found that the formal substitution of η^5-coordinated $C_5H_5^-$ or $Me_5C_5^-$ ligands in organometallic compounds by tridentate macrocycles leads to similar, but in many instances to thermodynamically and kinetically more stable, octahedral complexes (both ligand-types are 6e donors). They are quite effective blocking groups for three facial coordination sites in an octahedron and the reactivity of (i) the metal centre (redox reactions) (ii) the remaining three coordination sites in LM(X)(Y)(Z) species (substitution and oligomerization reactions), and (iii) the coordinated ligands X, Y, Z may be investigated.[8]

Here we report on the reactivity of $[LReO_3]^+$ towards strong reductants such as zinc amalgam. The rhenium(V)oxo complexes, $[LRe^VO(\mu\text{-}O)_2Re^VOBr_2]$ and $[LRe^VO(\mu\text{-}O)_2Re^VO(Re^{VII}O_4)_2]$ have been obtained. In addition, $[LReO_3]^+$ can be deprotonated in aqueous solution ($pK_a = 10.3+0.2$) at the coordinated amine ligand $C_6H_{15}N_3$ yielding the yellow–orange neutral species $(C_6H_{14}N_3)ReO_3$ which reacts smoothly with alkylhalides, R—X, in dimethylformamide over Na_2CO_3 generating the tris-N-alkylated complexes $[(R_3[9]aneN_3)ReO_3]^+$, which are not available via reactions (1)–(4). Finally, oxo-rhenium(V) complexes containing triazamacrocycles, $[LReOX_2]^+$ (X = Cl, Br, I) were prepared from $[ReOX_4]^-$ species.

EXPERIMENTAL

Materials

The ligand 1,4,7-triazacyclononane (L) and the complexes, $[LReO_3]X$ (X = Cl, Br) and $[LReO_3](ReO_4)$ have been prepared as described previously.[1,9] The monodeprotonated form of the ligand L ($C_6H_{14}N_3^-$) is abbreviated as (tacn-H) throughout this paper.

Synthesis of $(tacn\text{-}H)ReO_3$

To $[LReO_3]Cl$ (0.40 g, 1 mmol) suspended in acetone (20 cm^3) was added concentrated ammonia (3 cm^3). An immediate change of colour to yellow was observed. The suspension was stirred for 30 min at room temperature after which time the yellow microcrystalline precipitate was filtered off, washed with ice-cold NH_3 solution and diethylether. Yield: *ca* 85%. (Found: C, 19.7; H, 3.9; N, 11.4; Re, 51.2. $C_6H_{14}N_3O_3Re$ requires: C, 19.9; H, 3.9; N, 11.6; Re, 51.4%.) IR(KBr disc, cm^{-1}) bands at 840–920 (vs, b) ν(ReO). Mass spectrum: *m/e*: 363 (M^+). UV–vis spectrum in 0.1 M NaOH at 20°C: $\lambda = 303$ nm ($\varepsilon = 3.2 \times 10^3\ M^{-1}\ cm^{-1}$).

Synthesis of $[(Me_3[9]aneN_3)ReO_3]Cl$

To a solution of $[(tacn\text{-}H)ReO_3]$ (0.37 g, 1 mmol) in anhydrous dimethylformamide (DMF) (20 cm^3) was added solid Na_2CO_3 (0.32 g, 3 mmol) and CH_3I (0.43 g, 3 mmol). The suspension was refluxed for 2 h and then the DMF solvent was removed under reduced pressure. The colourless residue was dissolved in water (30 cm^3) and a saturated aqueous NaCl solution (5 cm^3) was added. Colourless crystals precipitated which were filtered off, washed with diethyl ether and air-dried. Yield: *ca* 60%. (Found: C, 25.8; H, 5.0; N, 9.7; Cl, 8.0; Re, 45.3. $C_9H_{21}N_3ClO_3Re$ requires: C, 26.2; H, 5.1; N, 10.2; Cl, 8.6; Re, 45.1%.) IR(KBr, cm^{-1}): 900(s), 920(s) (ν_s and ν_{as}(ReO), respectively). ^1H NMR data (D_2O at 20°C): $\delta = 3.10$–3.51 (m, 12H, $—CH_2—CH_2—$); $\delta = 3.60$ (s, 9H, $—CH_3$). ^{13}C NMR data (D_2O at 20°C): $\delta = 56.06$ (s, $—CH_3$); $\delta = 60.30$ (s, $—CH_2CH_2—$). ^{17}O NMR data (D_2O at 20°C): $\delta = 747$ (s, Re—O).

The perchlorate salt was obtained from an aqueous solution of the chloride salt upon addition of solid $NaClO_4$.

Synthesis of $[(Benzyl)_3[9]aneN_3)ReO_3]Br$

The same reaction conditions as described above for $[(Me_3[9]aneN_3)ReO_3]Cl$ were employed using benzylbromide instead of CH_3I. After removal of the solvent, to the resulting yellow oil water (4 cm^3) and acetone (50 cm^3) were added. The colourless precipitate was filtered off, washed with diethyl ether and air-dried. Yield: 68%. (Found: C, 45.2; H, 4.5; N, 5.9; Br, 11.0; Re, 26.5. $C_{27}H_{33}N_3BrO_3Re$ requires: C, 45.4; H, 4.7; N, 5.9; Br, 11.2;

Re, 26.1%.) IR(KBr, cm^{-1}): 940(s), 910(s) [ν_{as} and ν_s(Re—O)]. ^1H NMR data (DMSO-d_6): $\delta = 3.01$, 3.70 (2m, 12H, —CH_2CH_2—); $\delta = 5.85$ (s, 6H, —CH_2—); $\delta = 7.48$, 7.65 (2m, 15H, —C_6H_5). ^{13}C NMR data (DMSO-d_6): $\delta = 53.28$ (s, —CH_2—CH_2—); $\delta = 66.00$ (s, —CH_2—); $\delta = 128.63$–132.90 (2m, —C_5H_5).

Synthesis of [$LReO_2Br$]

To a deaerated solution of [$LReO_3$]Br (0.45 g, 1 mmol) in an acetone–water mixture (6:1) was added zinc amalgam under an argon atmosphere. The solution was stirred at room temperature for 2 h. The zinc amalgam was removed and the solvent was evaporated under reduced pressure. The green, unstable product was washed three times with ice-cold deaerated methanol (95%) and diethyl ether under an argon atmosphere. Yield: 65%. (Found: C, 15.9; H, 3.6; N, 8.9; Br, 17.8; Re, 42.5. $C_6H_{15}N_3BrO_2Re$ requires: C, 16.9; H, 3.5; N, 9.8; Br, 18.7; Re, 43.6%.) IR(KBr, cm^{-1}): 900(s), 930(s) [ν_{as} and ν_s(Re—O)]. UV–vis spectrum (H_2O): $\lambda = 427$ nm ($\varepsilon = 130\ M^{-1}\ cm^{-1}$), 540 (51).

Synthesis of [$LReO(\mu\text{-}O)_2ReOBr_2$]

The above green material (0.2 g) dissolved in water (50 cm^3) under an argon atmosphere slowly changed colour to red–violet at room temperature. Upon evaporation of the solvent under reduced pressure red–violet crystals were obtained, which were filtered off and washed with diethyl ether. Yield: *ca* 90%. (Found: C, 9.7; H, 2.0; N, 5.8; Br, 21.9; Re, 50.9. $C_6H_{15}N_3Br_2O_4Re_2$ requires: C, 9.9; H, 2.1; N, 5.8; Br, 22.0; Re, 51.3%.) IR(KBr, cm^{-1}): 790(m), 820(m) [ν(Re—O—Re)]; 900(s), [ν(Re=O)]. UV–vis spectrum (H_2O): $\lambda = 554$ nm ($\varepsilon = 685\ M^{-1}\ cm^{-1}$).

Synthesis of [$LReO(\mu\text{-}O)_2ReO(ReO_4)_2$]

Method A. To a solution of [$LReO_3$]ReO_4 (0.62 g, 1 mmol) in an acetone–water mixture (4:1) (50 cm^3) zinc amalgam was added. The solution was refluxed for 1 h under an argon atmosphere. After the zinc amalgam was removed the solution was filtered in the presence of air whereupon the colour changed to red–violet. The volume of the solution was reduced to 10 cm^3. Red–violet, needle-shaped crystals precipitated, which were filtered off, washed with diethyl ether and were stored under argon. Yield: 38%.

Method B. [$LReO_3$]ReO_4 (0.62 g, 1 mmol) was dissolved in a water–THF mixture (1:2) (30 cm^3) and $NaBH_4$ (0.08 g, 2 mmol) was added under an argon atmosphere. The solution was refluxed for 4 h. The work-up was as described above. Yield: 46%. (Found: C, 6.5; H, 1.2; N, 4.6; Re, 69.7. $C_6H_{15}N_3O_{12}Re_4$ requires: C, 6.8; H, 1.4; N, 4.0; Re, 69.9%.) IR(KBr, cm^{-1}) data: 790(s) [ν(Re—O—Re)], 820(s), 890–940(s,b) [ν(Re=O)]. UV–vis spectrum (H_2O): $\lambda = 554$ nm ($\varepsilon = 685\ M^{-1}\ cm^{-1}$).

Synthesis of complexes [$LReOX_2$]X (X = Cl, Br, I)

The compounds [(*n*-But)$_4$N][$ReOX_4$] (X = Cl, Br, I)[10] (1 mmol) dissolved in anhydrous, freshly distilled acetonitrile (100 cm^3) reacted with 1,4,7-triazacyclononane (0.13 g, 1 mmol) at room temperature under an argon atmosphere within 24 h to afford dark-green precipitates of [$LReOX_4$]X·$2CH_3CN$, which were filtered off under argon and washed with anhydrous, deaerated diethyl ether. Yields: 55–65%. When $ReOX_3(PPh_3)_2$[10] compounds were used as starting materials (1 mmol) under identical reaction conditions the same products were obtained in 50–60% yields. Recrystallization of the above acetonitrile containing salts from anhydrous absolute methanol yielded the [$LReOX_2$]X complexes in an analytically pure form.

[$LReOCl_4$]Cl. (Found: C, 16.2; H, 3.2; N, 9.5; Cl, 24.1; Re, 42.1. $C_6H_{15}N_3Cl_5ORe$ requires: C, 16.5; H, 3.5; N, 9.6; Cl, 24.3; Re, 42.5%.) IR(KBr, cm^{-1}): 940(s) [ν(Re=O)]. UV–vis spectrum (CH_3OH): $\lambda = 374$ nm ($\varepsilon = 101\ M^{-1}\ cm^{-1}$), 548 (55).

[$LReOBr_4$]Br. (Found: C, 12.4; H, 2.4; N, 7.3; Br, 41.8; Re, 32.3. $C_6H_{15}N_3Br_5ORe$ requires: C, 12.6; H, 2.6; N, 7.6; Br, 42.0; Re, 32.6%.) IR(KBr, cm^{-1}): 930(s) [ν(Re=O)]. UV–vis spectrum (CH_3OH): $\lambda = 388$ nm ($\varepsilon = 95\ M^{-1}\ cm^{-1}$), 555(47).

[$LReOI_4$]I. (Found: C, 9.9; H, 1.9; N, 5.7; I, 53.2; Re, 25.9. $C_6H_{15}N_3I_5ORe$ requires: C, 10.1; H, 2.1; N, 5.9; I, 53.5; Re, 26.1%.) IR(KBr, cm^{-1}): 925(s) [ν(Re=O)]. UV–vis .spectrum (CH_3OH): $\lambda = 396$ nm ($\varepsilon = 89\ M^{-1}\ cm^{-1}$), 561(50).

Physical measurements

Magnetic susceptibilities of powdered samples were measured by the Faraday method (Sartorius microbalance, Bruker B-E 10C8 research magnet and B-VT 1000 automatic temperature control) in the temperature range 98–293 K. Diamagnetic corrections were applied in the usual manner with use of Pascal's constants.

The NMR spectra were recorded in the FT mode with a Bruker AM-400 spectrometer at a magnetic

field of 9.395 T (^{1}H, ^{13}C, ^{17}O frequencies 400.1, 100.6 and 54.24 MHz, respectively). ^{17}O NMR spectra were obtained from samples in 10 mm diameter tubes at 70°C, and the chemical shifts were measured from the D_2O solvent line. A pulse width of 25 μs provided the 90° tip angle, sweep widths of 50,000–100,000 Hz were used with acquisition times of 0.041–0.026 s, and more than 10^5 transients were obtained for each spectrum.

Electronic spectra were measured on a Perkin–Elmer Lambda 9 spectrophotometer, and the IR spectra were recorded on a Perkin–Elmer 983 spectrophotometer (KBr discs).

RESULTS AND DISCUSSION

Figure 1 shows a schematic representation of the cation $[LReO_3]^+$ in $[LReO_3]Cl$ as has been determined by X-ray crystallography.[1] Coordination of secondary amines to transition metals in high oxidation states (> II) leads in general to a remarkable increase of the acidity of the N—H protons. Thus $[Pt^{IV}L_2]^{4+}$ behaves as a weak acid in aqueous solution and salts of the monodeprotonated form $[Pt^{IV}L(tacn\text{-}H)]^{3+}$ have been isolated.[11] $[FeL_2]^{3+}$ forms the amido complex $[Fe^{III}L(tacn\text{-}H)]^{2+}$ in alkaline aqueous solution ($pK_a = 11.4 + 0.4$ at 25°C).[12] Colourless aqueous solutions of $[LReO_3]X$ are stable for many weeks; no ligand dissociation was observed. Upon addition of sodium hydroxide to such a solution the colour changed to yellow and slowly the neutral species $[(tacn\text{-}H)ReO_3]$ precipitated out (see Structure 1). The acid dissociation constant, K_a, in eq. (5) was determined spectrophotometrically by following the increase in absorbance at 303 nm as a function of pH (0.1 M buffer solutions), or potentiometrically by titration of 10^{-3} M $[LReO_3]Br$ solution with 2 M NaOH at 25°C (the ionic strength was adjusted to 0.1 M with KCl).

$$[LReO_3]^+ \overset{K_a}{\rightleftharpoons} [(tacn\text{-}H)ReO_3] + H^+. \quad (5)$$

Both independent methods afforded a pK_a value of 10.3 ± 0.2 (25°C, $I = 0.1$ M).

In the IR spectrum of $[LReO_3]^+$ the ν_{as}(Re=O) and ν_s(Re=O) stretching modes are observed at 945 and 920 cm^{-1} in agreement with the local C_{3v} symmetry of the ReO_3^+ moiety ($A_1 + E$). For $(tacn\text{-}H)ReO_3$, a broad ν(ReO) multicomponent band in the range 840–920 cm^{-1} is observed. The electronic spectrum of $[LReO_3]^+$ exhibits no absorption above 200 nm whereas for the deprotonated form a strong ligand-to-metal charge-transfer band at $\lambda = 303$ nm ($\varepsilon = 3.2 \times 10^3$ M^{-1} cm^{-1}) is observed.

$[(tacn\text{-}H)ReO_3]$ was found to be a useful starting material for alkylation reactions at the coordinated N-atoms of the cyclic triamine. Thus $[(tacn\text{-}H)ReO_3]$ dissolved in dimethylformamide (DMF) reacts in the presence of Na_2CO_3 readily with alkylhalides such as CH_3I, or benzylbromide to yield the tris-N-alkylated complexes $[(Me_3[9]aneN_3)ReO_3]I$ and $[(Benzyl)_3[9]aneN_3)ReO_3]Br$. These complexes cannot be prepared via the reaction sequence (1)–(4) because the rhenium(I) tricarbonyl complexes are chemically quite inert; they do not react with $[NO]BF_4$, HNO_3 or H_2O_2 even at elevated temperatures and prolonged reaction times.

$$[(tacn\text{-}H)ReO_3] + 3R\text{—}X \xrightarrow[Na_2CO_3]{DMF} [(R_3[9]aneN_3)ReO_3]^+ \quad (6)$$

$$R = CH_3, \quad X = I, Br.$$

^{17}O NMR spectra of these trioxorhenium(VII) compounds have been obtained in aqueous solution. Chemical shifts are summarized in Table 1. ^{17}O NMR data for a number of trioxomolybdenum(VII) and trioxotungsten(VI) complexes with triazacyclononane ligands have been reported recently.[14] Figure 2 shows the ^{17}O NMR spectra of the rhenium(VII) complexes. The spectrum of $[(tacn\text{-}H)ReO_3]$ was obtained in an 0.1 M NaOH solution of $[LReO_3]Br$. Interestingly, only one signal is observed. This indicates that N—H proton exchange of the secondary amine protons of

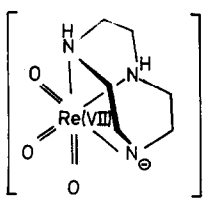

Structure 1.

Table 1. ^{17}O NMR data of LMO_3 complexes (H_2O)

Complex	Chemical shift (δ)	Ref
$[(Me_3[9]aneN_3)ReO_3]Br$	747	This work
$[LReO_3]Br$	728	This work
$[(tacn\text{-}H)ReO_3]$	703	This work
$(\eta^5\text{-}Me_5C_5)ReO_3$	646	13
$LMoO_3$	689	14
$[(Me_3[9]aneN_3)MoO_3]$	576	14
$[(Me_3[9]aneN_3)WO_3]$	560	14
$[LWO_3]$	541	14

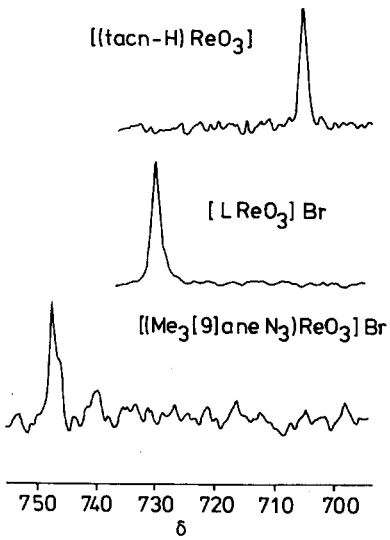

Fig. 2. ^{17}O NMR spectra of trioxorhenium(VII) complexes.

the coordinated tacn-H ligands in solution is fast on the NMR time scale.

The oxygen atoms in $(\eta^5\text{-}Me_5C_5)ReO_3$ are more shielded than those in the corresponding complexes with cyclic triamine ligands (even more than those in $[(tacn\text{-}H)ReO_3]$ which is also a neutral compound). The oxygen atoms in the corresponding $Mo^{VI}O_3$ and $W^{VI}O_3$ compounds are more shielded than those in the rhenium(VII) complexes which is probably due to the lower oxidation state of the Mo and W centres as compared to rhenium(VII). The basicity of the oxygen atoms increases in the sequence $Me_3[9]aneN_3$ < tacn < tacn-H.

As Herrmann and coworkers have in recent years amply demonstrated, $(\eta^5\text{-}Me_5C_5)ReO_3$ is a key compound in organometallic chemistry. Lewis acids as well as Lewis bases induce partial deoxygenation reactions generating a variety of reactive rhenium(V) complexes.[7,15-17] Therefore, it appeared to be interesting to investigate the reactivity of $[LReO_3]^+$ towards reducing agents. $[LReO_3]^+$ does not react with PPh_3, no oxygen transfer has been observed, in contrast in this respect to $(\eta^5\text{-}Me_5C_5)ReO_3$. The reduction of $[LReO_3]Br$ in a water–acetone mixture with zinc amalgam affords an air sensitive, quite unstable, green solid material which analysed as $[LReO_2Br]$. Even when stored under an argon atmosphere this material decomposed within hours. We have not been able to fully characterize this material due to its instability, and its formulation as the monomeric *cis*-dioxorhenium(V) complex is tentative. In the IR spectrum two bands at 900 and 930 cm^{-1} are in agreement with a *cis*-dioxorhenium(V) moiety. The electronic spectrum (H_2O, 5°C) exhibits two absorption maxima at 427 nm ($\varepsilon = 130\ M^{-1}\ cm^{-1}$) and 540(51). This is comparable to some $[LReOBr_2]^+$ complexes described below. The low absorption coefficients are indicative of the monomeric nature of this material (see below). The green compound is diamagnetic. It is noted that monomeric, octahedral *cis*-dioxorhenium(V) compounds have not been described previously.[18]

A green, deaerated aqueous solution of $[LReO_2Br]$ slowly changes colour to purple, and purple crystals precipitate out. Elemental analysis of this material indicated a ratio L : Re : O : Br = 1 : 2 : 4 : 2. In the IR spectrum typical bands of the ligand and one characteristic ν(Re=O) stretching mode at 900 cm^{-1} is observed. In addition, two bands at 790 and 820 cm^{-1} are assigned to ν(Re—O—Re) vibrations,[19] indicating a dimeric structure **A** as is depicted in Structure 2.

When $[LReO_3]ReO_4$ was reduced in a water–acetone mixture with either zinc amalgam or $NaBH_4$, purple crystals also precipitated out with a ratio L : Re = 1 : 4. In the IR a ν(Re=O) band at 900 cm^{-1} is again observed which is very broad (890–940 cm^{-1}) indicating the presence of O-coordinated ReO_4 groups. Bands at 790 and 820 cm^{-1} are again due to a di-μ-oxo-dirhenium(V) bridging unit. Thus we propose structure **B** for this material. Both complexes are diamagnetic and exhibit a strong absorption maximum at 554 nm ($\lambda = 685\ M^{-1}\ cm^{-1}$) in the electronic spectrum. The above structures lack a crystal structure and are therefore proposed on the basis of a similar complex $(\eta^5\text{-}Me_5C_5)_2Re_2O(\mu\text{-}O)_2(ReO_4)_2$,[15] which was prepared by reduction of $(\eta^5\text{-}Me_5C_5)ReO_3$ with PPh_3.

Octahedral oxorhenium(V) complexes are well known.[20] A number of such complexes containing Schiff-base ligands have been described[21] and the organometallic counterparts $(\eta^5\text{-}C_5H_5)ReOX_2$ (X = F, Cl, Br, I) have recently been synthesized.[22] We have found that $[(n\text{-}But)_4N][ReOX_4]$ and $ReOX_3(PPh_3)_2$[10] (X = Cl, Br, I) react with 1,4,7-triazacyclononane in acetonitrile under an argon atmosphere affording the complexes, $[LReOX_2]X \cdot 2CH_3CN$ as dark green microcrystalline ma-

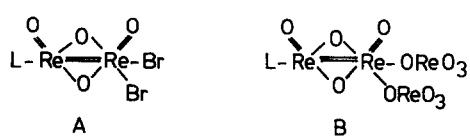

Structure 2.

terials (X = Cl, Br, I). These compounds are quite unstable, they decompose rapidly in the presence of air; they are soluble in polar solvents (H_2O, CH_3OH). Recrystallization from CH_3OH under argon yields the dark green complexes, $[LReOX_2]X$. In the IR spectra one typical ν(Re=O) stretching mode is observed at 940, 930, and 925 cm^{-1} for the chloro, bromo and iodo complex, respectively. All $[LReOX_2]X$ complexes are diamagnetic in agreement with other oxorhenium(V) compounds. In the electronic spectra two absorption maxima of low intensity are observed for each complex[10,23] which are shifted to higher wavelengths on going from the chloro to the bromo and iodo compound. These bands are assigned to *d–d* transitions.

Acknowledgement—We thank the Fonds der Chemischen Industrie for financial support of this work.

REFERENCES

1. K. Wieghardt, C. Pomp, B. Nuber and J. Weiss, *Inorg. Chem.* 1986, **25**, 1659.
2. C. Pomp, S. Drüeke, H.-J. Küppers, K. Wieghardt, C. Krüger, B. Nuber and J. Weiss, *Z. Naturforsch.* 1988, **43b**, 299.
3. P. Hoffmann, A. Steinhoff and R. Mattes, *Z. Naturforsch.* 1987, **42b**, 867.
4. J. A. McCleverty and I. Wolochowicz, *J. Organomet. Chem.* 1979, **169**, 289.
5. W. A. Herrmann, R. Serrano and H. Bock, *Angew. Chem.* 1984, **96**, 364; *Angew. Chem. Int. Ed. Engl.* 1984, **23**, 383.
6. W. A. Herrmann, *J. Organomet. Chem.* 1986, **300**, 111.
7. W. A. Herrmann, E. Herdtweck, M. Flöel, J. Kulpe, U. Küsthardt and J. Okuda, *Polyhedron* 1987, **6**, 1165.
8. P. Chaudhuri and K. Wieghardt, *Prog. Inorg. Chem.* 1987, **35**, 329.
9. (a) T. J. Atkins, J. W. Richman and W. F. Oettle, *Org. Synth.* 1978, **58**, 86; (b) K. Wieghardt, W. Schmidt, B. Nuber and J. Weiss, *Chem. Ber.* 1979, **112**, 2220.
10. (a) T. Lis and B. Jezowska-Trzebiatowska, *Acta Cryst.* 1977, **B33**, 1248; (b) V. Yatirajam and H. Singh, *J. Inorg. Nucl. Chem.* 1975, **37**, 2006; (c) F. A. Cotton and S. J. Lippard, *Inorg. Chem.* 1966, **5**, 9; (d) N. P. Johnson, C. J. L. Lock and G. Wilkinson, *J. Chem. Soc.* 1964, 1054.
11. K. Wieghardt, M. Köppen, W. Swiridoff and J. Weiss, *J. Chem. Soc., Dalton Trans.* 1983, 1869.
12. K. Pohl, K. Wieghardt, W. Kaim and S. Steenken, *Inorg. Chem.* 1988, **27**, 440.
13. (a) U. Küsthardt, A. Schäfer, R. Serrano and W. A. Herrmann, *J. Organomet. Chem.* 1984, **272**, 55; (b) W. A. Herrmann, E. Voss and M. Flöel, *J. Organomet. Chem.* 1985, **297**, C5.
14. P. S. Roy and K. Wieghardt, *Inorg. Chem.* **26**, 1885.
15. W. A. Herrmann, R. Serrano, U. Küsthardt, M. L. Ziegler, E. Guggolz and T. Zahn, *Angew. Chem.* 1984, **96**, 498; *Angew. Chem. Int. Ed. Engl.* 1984, **23**, 515.
16. W. A. Herrmann, R. Serrano, M. L. Ziegler, H. Pfisterer and B. Nuber, *Angew. Chem.* 1985, **97**, 50; *Angew. Chem. Int. Ed. Engl.* 1985, **24**, 50.
17. W. A. Herrmann, R. Serrano, U. Küsthardt, E. Guggolz, B. Nuber and M. L. Ziegler, *J. Organomet. Chem.* 1985, **287**, 329.
18. R. H. Holm, *Chem. Rev.* 1987, **87**, 1401.
19. W. P. Griffith, *J. Chem. Soc. A* 1969, 211.
20. J. E. Ferguson, *Coord. Chem. Rev.* 1966, **1**, 459.
21. (a) U. Mazzi, F. Refosco, F. Tisato, G. Bandoli and M. Nicolini, *J. Chem. Soc., Dalton Trans.* 1986, 1623; (b) U. Mazzi, F. Refosco, G. Bandoli and M. Nicolini, *Trans. Met. Chem.* 1985, **10**, 127; (c) U. Bertolasi, U. Ferretti, G. Gilli, A. Duatti, A. Marchi and L. Magon, *J. Chem. Soc., Dalton Trans* 1987, 613; (d) F. Tisato, F. Refosco, U. Mazzi, G. Bandoli and M. Nicolini, *J. Chem. Soc., Dalton Trans.* 1987, 1693; (e) F. Refosco, F. Tisato, U. Mazzi, G. Bandoli and M. Nicolini, *J. Chem. Soc., Dalton Trans.* 1988, 611.
22. W. A. Herrmann, U. Küsthardt, M. Flöel, J. Kulpe, E. Herdtweck and E. Voss, *J. Organomet. Chem.* 1986, **314**, 151.
23. D. W. Pipes and T. J. Meyer, *Inorg. Chem.* 1986, **25**, 3256.

Polyhedron Vol. 7, No. 24, pp. 2543–2547, 1988
Printed in Great Britain

0277–5387/88 $3.00+.00
© 1988 Pergamon Press plc

A NEW DIRHENIUM COMPLEX WITH AN UNSUPPORTED BRIDGING HYDRIDE LIGAND

RICHARD D. ADAMS* and JONATHAN D. KUHNS

Department of Chemistry, University of South Carolina, Columbia, SC 29208, U.S.A.

(*Received* 22 *April* 1988; *accepted* 9 *May* 1988)

Abstract—The reaction of $Re_2(CO)_8(\mu\text{-}H)_2$ with $CH_2(NMe_2)_2$ in chloroform at 25°C yielded the new compound $Re_2(CO)_8(NHMe_2)(Cl)(\mu\text{-}H)$ (**1**) in 31% yield. Compound **1** was characterized by IR, ^1H NMR and a single-crystal X-ray diffraction analysis. Crystal data: orthorhombic, *Pbca*, $a = 13.787(4)$, $b = 19.884(5)$, $c = 12.296(2)$ Å. Solution by direct methods (MITHRIL), $R = 0.035$ for 1800 reflections. The complex contains two rhenium atoms linked by an unsupported hydride bridge, Re···Re = 3.362(1) Å, Re(1)—H = 1.8(1) Å and Re(2)—H = 2.0(1) Å. A chloride ligand abstracted from the solvent is terminally bonded to Re(1), and a dimethylamine ligand abstracted from the $CH_2(NMe_2)_2$ is coordinated to Re(2). When heated to 68°C, the dimethylamine ligand was eliminated and the chloride ligand became a bridge in the new compound $Re_2(CO)_8(\mu\text{-}H)(\mu\text{-}Cl)$ (**2**), yield 76%.

Although there are a large number of polynuclear metal complexes that contain bridging hydride ligands,[1–3] there are relatively few examples where the hydride ligand is the sole link between the metal atoms, **A**.[4–7]

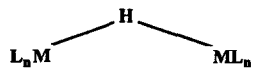

A

In our recent studies we have been investigating the reaction of bis-(dialkylamino)methanes with polynuclear metal carbonyl compounds that contain hydride ligands. We have found that the bis-(dialkylamino)methanes are effective reagents for the introduction of secondary dialkylaminocarbene ligands, $HCNR_2$, into the metal complexes by a carbonyl ligand replacement, eq. (1).[8–11]

$$HM_n(CO)_x + CH_2(NR_2)_2 \xrightarrow[-Me_2NH]{-CO} HM_n(CO)_{x-1}[C(H)NR_2]. \quad (1)$$

It has been presumed that the transformation of bis-(dialkylamino)methane also yields secondary amines, R_2NH, but these have not yet been observed. In this report the reaction of $Re_2(CO)_8(\mu\text{-}H)_2$ with $CH_2(NMe_2)_2$ is described. In contrast to our previous studies, the product of this reaction was found to contain a dimethylamine ligand in a new dirhenium complex that also contains a new example of an unsupported hydride bridge, **A**.

EXPERIMENTAL

General procedures and materials

All reactions were performed under an inert atmosphere of prepurified nitrogen. The solvent $CHCl_3$ was dried by refluxing over P_2O_5 and was distilled just prior to use. The reagents $Re_2(CO)_{10}$, H_2 and $(CH_3)_2NCH_2N(CH_3)_2$ were obtained commercially and were used without further purification. The complex $H_2Re_2(CO)_8$ was prepared by the reported procedure.[12] TLC separations were performed in air on 0.25 mm Kieselgel 60 (UV sensitized) F_{254} (E. Merck) purchased from Bodman Chemicals. IR spectra were recorded on a Nicolet 5 DXB FT IR spectrometer. ^1H NMR spectra were run on the Bruker AM-300 spectrometer operating at 300 MHz. Elemental analyses were performed by Desert Analytics, Tucson, AZ. Mass spectra were obtained on a VG Model 70 SQ spectrometer at 120°C with electron impact ionization at 15 eV.

* Author to whom correspondence should be addressed.

Synthesis of $Re_2Cl(CO)_8(NHMe_2)(\mu\text{-H})$ **(1)**

$H_2Re_2(CO)_8$ (68.3 mg, 0.11 mmol) was allowed to react with (0.08 cm^3, 0.58 mmol) of $CH_2(NMe_2)_2$ in refluxing $CHCl_3$. The reaction was followed by IR for 15 min. The solution changed from pale yellow to colourless after 15 min. The solution was allowed to cool to room temperature and was then concentrated to a volume of 2 cm^3 by a nitrogen purge. The product was separated by TLC (hexane–CH_2Cl_2, 1 : 1). Compound **1** is nearly colourless but was observed just above the base line under UV light. IR (ν(CO) in CH_2Cl_2): 2118(w), 2100(m), 2019(vs), 1962(s) cm^{-1}. ^1H NMR (δ in $CDCl_3$): −13.19(s, 1H), 2.97(d, 6H), J_{H-H} = 6.0 Hz. Mass spectrum for ^{187}Re m/e: $679-28x$, $x = 0-8$ (M^+-8CO). Found: C, 17.9; H, 1.13; N, 2.02%. Calc. for **1**: C, 17.7; H, 1.18; N, 2.07%.

Synthesis of $Re_2(CO)_8(\mu\text{-Cl})(\mu\text{-H})$ **(2)**

37.6 mg (0.056 mmol) of **1** was dissolved in 15 cm^3 of hexane. Under a nitrogen purge the reaction solution was heated to reflux for 10 min. At this time the reaction was complete and was allowed to cool to room temperature. The solution was concentrated to 2 cm^3 under a flow of nitrogen. This solution was then chromatographed by TLC with a hexane–CH_2Cl_2, 1 : 1 solvent mixture. The colourless product **2** was observed (under UV irradiation) as the fastest moving band and yielded 26.6 mg, 76%. For **2**: IR (ν(CO) in CH_2Cl_2) 2105(w), 2029(vs), 2005(m), 1968(s) cm^{-1}. ^1H NMR (δ in $CDCl_3$) −12.72(s, 1H). Mass spectrum for ^{187}Re m/e: $634-28x$, $x = 0-8$ (M^+-8CO).

Crystallographic analyses

Colourless crystals of **1** were obtained by slow evaporation of solvent from a hexane–CH_2Cl_2 solvent mixture at −20°C. The data crystal was mounted in a thin-walled glass capillary. Diffraction measurements were made on a Rigaku AFC6 fully automated four-circle diffractometer using graphite monochromatized Mo-K_α radiation. The unit cell was determined and refined from 25 randomly selected reflections obtained by using the AFC6 automatic search, centre, index and least-squares routines. Crystal data, data collection parameters and results of the analysis are listed in Table 1. All data processing was performed on a Digital Equipment Corp. MICROVAX II computer by using the TEXSAN structure solving program library obtained from the Molecular Structure Corp., College Station, TX. Neutral atom scattering factors were calculated by the standard procedures.[13a] Anomalous dispersion corrections were applied to all non-hydrogen atoms.[13b] Full-matrix least-squares refinements minimized the function:

$$\Sigma w(|F_o|-|F_c|).^2$$

Where

$$w = 1/\sigma(F)^2 = \sigma(F_o^2)/2F_o$$

and

$$\sigma(F_o^2) = [(I_{raw})^2+(PF_o^2)^2]^{1/2}/Lp.$$

Compound **1** crystallized in the orthorhombic crystal system. The space group *Pbca* was identified on the basis of the systematic absences observed during the collection of data. The coordinates of the heavy atoms were obtained by direct methods (MITHRIL). All remaining non-hydrogen atoms were subsequently obtained from a difference Fourier synthesis. All non-hydrogen atoms were refined with anisotropic thermal parameters. The bridging hydride ligand was located in a difference Fourier map and was successfully refined.*

RESULTS AND DISCUSSION

The reaction of $H_2Re_2(CO)_8$ with $CH_2(NMe_2)_2$ in refluxing chloroform yielded the product $Re_2(CO)_8(NHMe_2)Cl(\mu\text{-H})$ **(1)** in 31% yield. Compound **1** was characterized by IR, mass spectral, ^1H NMR, elemental and single-crystal X-ray diffraction analyses. Interatomic distances and angles are listed in Tables 2 and 3, respectively. An ORTEP drawing of the molecular structure of compound **1** is shown in Fig. 1. The molecule contains two rhe-

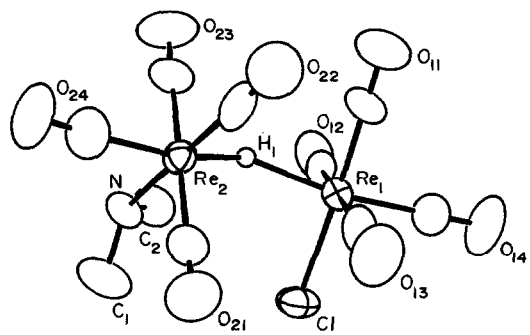

Fig. 1. An ORTEP diagram of $Re_2(CO)_8(NHMe_2)(Cl)(\mu\text{-H})$ **(1)** showing 50% probability thermal ellipsoids.

* Complete tables of bond lengths, angles, positional and thermal parameters for **1** and observed and calculated structure factors for **1** have been deposited as supplementary material with the Editor, from whom copies are available on request. Atomic coordinates have been submitted to the Cambridge Crystallographic Data Centre.

Table 1. Crystallographic data for diffraction study

Compound	1
(A) Crystal data	
Formula	$Re_2ClO_8NC_{10}H_7$
Temperature (±3°C)	23°
Space group	*Pbca*, No. 61
a (Å)	13.787(4)
b (Å)	19.844(5)
c (Å)	12.296(2)
α (deg)	90.0
β (deg)	90.0
γ (deg)	90.0
V (Å^3)	3364(1)
M_r	677.0
Z	8
ρ (g cm^{-3})	2.67
(B) Measurement of intensity data	
Radiation	Mo-K_α (0.71069 Å)
Monochromator	Graphite
Detector aperture (mm)	
horizontal	2.0
vertical	2.0
Crystal faces	100, $\bar{1}$00, 010, 0$\bar{1}$0, 001, 00$\bar{1}$
Crystal size (mm)	0.06, 0.23, 0.22
Crystal orientation direction;	
deg from ϕ axis	[001]; 2.3
Reflections measured	$+h$, $+k$, $+l$
Max 2θ (deg)	46
ω-scan width (deg)	1.1
Scan type	Moving crystal–stationary counter
bkgd (count time at each end of scan)	1/4 scan time
ω-scan rate (deg min^{-1})[a]	4.0
No. data used ($F^2 > 3.0\sigma F^2$)	1800
(C) Treatment of data	
Abs corr.	Analytical
Abs coeff. (cm^{-1})	154.1
Transmission coeff.	
max	0.379
min	0.044
P-factor	0.02
Final residuals	
R_F	0.035
R_{wF}	0.040
Goodness-of-fit	2.15
Largest shift/error value of final cycle	0.09
Largest peak in final diff. Fourier	0.99
No. of variables	202

[a] Rigaku software uses a multiple-scan technique. If the $I/\sigma(I)$ ratio is less than 10.0, a second scan is made and the results are added to the first scan, etc. A maximum of three scans was permitted per reflection.

Table 2. Intramolecular distances for **1**

Atom	Atom	Distance	Atom	Atom	Distance
Re(1)	Re(2)	3.363(1)	Re(2)	C(24)	1.94(2)
Re(1)	C(11)	1.89(1)	Re(2)	C(22)	1.95(2)
Re(1)	C(14)	1.95(2)	Re(2)	C(23)	1.96(2)
Re(1)	H(1)	2.0(1)	Re(2)	C(21)	1.99(2)
Re(1)	C(13)	1.99(2)	Re(2)	N	2.24(1)
Re(1)	C(12)	2.00(2)	N	C(2)	1.46(2)
Re(1)	Cl	2.481(3)	N	C(1)	1.49(2)
Re(2)	H(1)	1.8(1)	O	C(av.)	1.13(2)

Distances are in angstroms. Estimated standard deviations in the least significant figure are given in parentheses.

nium carbonyl fragments that are linked by the bridging hydride ligand, H(1). The Re(1)···Re(2) distance at 3.363(1) Å is much longer than that found in $Re_2(CO)_{10}$, 3.041(1) Å,[14] but is similar to the Re—Re distance 3.392(2) Å found in $Re_2Mn(CO)_{14}(\mu\text{-H})$ which also contains an unsupported hydride bridge between two rhenium atoms.[7] These hydride bridges have been variously described as protonated forms of the metal–metal bonds of the corresponding anions **B**,[15] or as coordination complexes formed by the donation of an M—H bond of one fragment to a vacant site on the metal atom of the second fragment, **C**.[14] These forms are simply limiting extremes of the more general three-centre two-electron bond **D**.[2] However, form **C** would imply an unsymmetrical bonding for the hydride bridge while forms **B** and **D** would imply symmetrical arrangements. The Re—H distances observed in **1** appear to be unequal, Re(2)—H(1) = 1.8(1) Å and Re(1)—H(1) = 2.0(1) Å, but the large standard deviations would preclude this difference as being significant. The Re—H—Re angle of 129(5)° does appear to be significantly nonlinear as observed in other systems.[2,3] The hydride

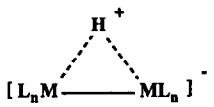

B

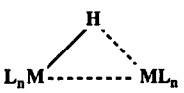

C

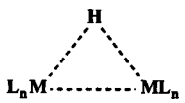

D

Table 3. Intramolecular bond angles for **1**

Atom	Atom	Atom	Angle	Atom	Atom	Atom	Angle
C(11)	Re(1)	C(14)	88.8(7)	C(13)	Re(1)	Cl	88.8(5)
C(11)	Re(1)	H(1)	84(2)	C(12)	Re(1)	Cl	89.0(4)
C(11)	Re(1)	C(13)	93.1(7)	H(1)	Re(2)	C(24)	163(3)
C(11)	Re(1)	C(12)	89.2(7)	H(1)	Re(2)	C(22)	94(3)
C(11)	Re(1)	Cl	177.2(5)	H(1)	Re(2)	C(23)	73(3)
C(14)	Re(1)	H(1)	166(3)	H(1)	Re(2)	C(21)	109(3)
C(14)	Re(1)	C(13)	86.6(6)	H(1)	Re(2)	N	84(3)
C(14)	Re(1)	C(12)	91.2(6)	C(2)	N	C(1)	111(1)
C(14)	Re(1)	Cl	93.3(5)	C(2)	N	Re(2)	117(1)
H(1)	Re(1)	C(13)	106(3)	C(1)	N	Re(2)	113(1)
H(1)	Re(1)	C(12)	77(3)	Re(2)	H(1)	Re(1)	129(5)
H(1)	Re(1)	Cl	94(2)	O	C	Re(av.)	177(2)
C(13)	Re(1)	C(12)	176.8(6)				

Angles are in degrees. Estimated standard deviations in the least significant figure are given in parentheses.

ligand exhibits the characteristic high field NMR shift, $\delta = -13.19$ ppm. Each rhenium atom possesses a pseudo-octahedral coordination geometry with the ligands on one metal atom in a staggered conformational geometry with respect to the other. Each metal has four linear terminal carbonyl ligands with one positioned approximately *trans* to the Re—H bond. Re(2) contains a dimethylamine ligand, Re(2)—N = 2.24(1) Å while Re(1) contains a chloride ligand, Re(1)—Cl = 2.481(3) Å which was evidently abstracted from the $CHCl_3$ solvent. The tendency of metal–hydride complexes to abstract halogen atoms from halogenated hydrocarbons is well-known.[16]

The amine ligand in **1** is labile and was eliminated when **1** was heated to 125°C under a nitrogen purge. The product $Re_2(CO)_8(\mu\text{-H})(\mu\text{-Cl})$ (**2**) was identified by IR, ^1H NMR, and mass spectral (parent ion $m/e = 634$ for ^{187}Re with ions corresponding to the loss of each of eight CO ligands) analyses. It is believed to have the structure **E** with a bridging

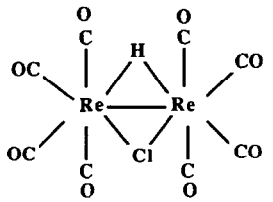

E

chloride ligand serving as a three-electron donor. The hydride ligand in **2** also exhibits the characteristic high-field NMR shift, $\delta = -12.72$ ppm.

Acknowledgements—Acknowledgement is made to the donors of the Petroleum Research Fund, administered by the American Chemical Society, for partial support of this research. The Brüker AM-300 NMR spectrometer was purchased with funds from the National Science Foundation, Grant No. CHE-8411172.

REFERENCES

1. A. P. Humphries and H. D. Kaesz, *Prog. Inorg. Chem.* 1979, **25**, 145.
2. R. Bau, *Struct. Bond.* 1981, **44**, 1.
3. R. Bau, *Transition Metal Hydrides, Adv. Chem. Ser., ACS*, No. 167 (1978).
4. B. Balbach, S. Barol, H. Biersack, W. A. Herrmann, J. A. Labinger, W. R. Scheidt, F. J. Timmers and M. L. Ziegler, *Organometallics* 1988, 7, 325.
5. J. Roziere, J. M. Williams, R. P. Stewart, Jr, J. L. Petersen and L. F. Dahl, *J. Am. Chem. Soc.* 1977, **99**, 4497.
6. K. S. Wong, W. R. Scheidt and J. A. Labinger, *Inorg. Chem.* 1979, **18**, 136.
7. H. D. Kaesz, R. Bau and M. R. Churchill, *J. Am. Chem. Soc.* 1967, **89**, 2775.
8. R. D. Adams, J. E. Babin and H. S. Kim, *J. Am. Chem. Soc.* 1987, **109**, 924.
9. R. D. Adams and J. E. Babin, *Organometallics* 1987, **6**, 1364.
10. R. D. Adams and J. E. Babin, *Organometallics* 1988, **7**, 963.
11. R. D. Adams and J. E. Babin, *Polyhedron* 1988, **7**, 967.
12. M. A. Andrews, S. W. Kirtley and H. D. Kaesz, *Inorg. Chem.* 1977, **16**, 1556.
13. *International Tables for X-ray Crystallography*, Vol. IV. Kynoch Press, Birmingham (1975): (a) Table 2.2B, pp. 99–101, (b) Table 2.3.1, pp. 149–150.
14. M. R. Churchill, K. N. Amoh and H. J. Wasserman, *Inorg. Chem.* 1981, **20**, 1609.
15. M. R. Churchill, *Transition Metal Hydrides, Adv. Chem. Ser., ACS*, No. 167, p. 36 (1978).
16. R. A. Schunn, in *Transition Metal Hydrides* (Edited by E. L. Muetterties). Marcel Dekker, New York (1971).

Polyhedron Vol. 7, No. 24, pp. 2549–2552, 1988
Printed in Great Britain

0277–5387/88 $3.00+.00
© 1988 Pergamon Press plc

THE QUESTION OF TIMESCALE ASSOCIATED WITH THE DETERMINATION OF MOLECULAR STRUCTURES

ROBERT E. BENFIELD*

Chemical Laboratory, University of Kent at Canterbury, Canterbury, CT2 7NH, Kent, U.K.

DARIO BRAGA

Dipartimento di Chimica "G. Ciamician", University of Bologna, Via F. Selmi 2, 40126 Bologna, Italy

and

BRIAN F. G. JOHNSON

University Chemical Laboratory, Lensfield Road, Cambridge, CB2 1EW, U.K.

(*Received* 11 *March* 1988; *accepted* 16 *May* 1988)

Abstract—A critical view of the "timescale" problem arising in spectroscopic and diffraction experiments is presented and a comparison made between the different types of information on dynamic processes obtainable from these methods. X-ray structural data on solids are intrinsically time-averaged over the period of data collection, and therefore contain information on dynamic processes which must be considered when interpreting solid-state NMR spectra. Intramolecular rearrangements in solid $Fe_3(CO)_{12}$ (tri-iron dodecacarbonyl) and $C_{10}H_{10}$ (bullvalene) are discussed as examples.

The development of spectroscopic methods, spanning a wide range of electromagnetic frequencies, has led to enormous advances in our understanding of the structures and reactions of molecules. It has been recognized that each type of spectroscopy delivers structural information averaged over a characteristic *timescale*, so giving a measure of the lifetimes of molecular structures. A wealth of information has been derived about intramolecular rearrangements, intermolecular interactions and reaction pathways, and the activation energies associated with them.

Although the timescale concept was clearly laid out by Muetterties[1] in 1965, we find that much confusion still exists about it. The purpose of this paper is to point out that in the interpretation of X-ray crystallographic data it has been misunderstood, and applied too literally. This has led to inconsistencies in correlating crystallographically-determined molecular structures with dynamic processes demonstrated by NMR, particularly those found in solids using recently-developed magic-angle spinning methods (MASNMR).

Confusion arises because the timescale of the structure determination is sometimes associated with the inverse of the radiation frequency. Although this is clearly erroneous in absorption spectroscopy, where the timescale is related to the frequency *span* of the spectral range, the situation is less clear when diffraction methods are employed; we emphasize the correct approach below.

In a spectroscopic experiment, an absorbing group with a limited lifetime gives a broadened spectral line, as a direct consequence of the Uncertainty Principle. Structurally inequivalent groups undergoing site exchange at a rapid enough rate cannot therefore be distinguished, because their spectral lines are not resolved. Rigorous consideration of the Bloch equations shows that, in the absence of additional broadening arising from short relaxation times, the criterion for coalescence of two equally intense singlet Lorentzian lines is that the appropriately defined jumping rate exceeds $\pi/\sqrt{2}$ times their frequency difference in Hz.[2–5]

* Author to whom correspondence should be addressed.

In NMR spectroscopy, the range of resonance frequencies spanned by a nucleus in different chemical environments is typically only a few parts per million of the operating radio frequency. For example, the ^{13}C NMR lines from terminal and bridging ligands in metal carbonyls have a typical chemical shift difference of 50 ppm. The rate of site exchange required for their coalescence corresponds to an NMR timescale of the order of 10^{-4} s. This of course is much longer than the reciprocal of the operating frequency.

Many dynamic processes take place within the NMR timescale; in these cases spectra corresponding to ground-state structures are not observed, and the molecules are termed "fluxional".[6] As an inorganic example, $Fe_3(CO)_{12}$ in solution shows complete ^{13}C NMR equivalence of all 12 carbonyl ligands even at $-150°C$.[7] Among organic molecules, the classic example of a highly fluxional structure is bullvalene, $C_{10}H_{10}$, which gives a singlet ^1H NMR spectrum in solution above room temperature.[6,8]

In vibrational (IR) spectroscopy, the combination of a higher radiation frequency and a wider spectral range produces a much shorter timescale. In metal carbonyls, the rate of site exchange necessary for loss of resolution of terminal and bridging ligands corresponds to an IR timescale of 10^{-13} s. (In this case, the timescale does approximate to the reciprocal of the operating frequency.) As virtually all molecular rearrangements take much longer than this, IR spectroscopy gives information on the ground-state structures of molecules which are fluxional on the NMR timescale.

However, when a molecular structure is determined by *diffraction methods* such as X-ray (or neutron) crystallography, radiation frequencies absorbed by individual nuclei or bonds are no longer relevant. The "X-ray crystallographic timescale" has instead been erroneously assigned as the inverse of the X-radiation frequency, i.e. about 10^{-18} s, which is also the approximate duration of the photon–atom interaction. This has led to the widespread belief that atomic positions determined by X-ray crystallographic methods are necessarily exact representations of static, ground-state molecular structures; and that crystallography gives an instantaneous structural "space average" quite distinct from the "time average" given by NMR.

This is incorrect. The value of 10^{-18} s is not relevant for an experiment in which radiation is not absorbed, but diffracted in accordance with Bragg's Law. In fact, measurement of the intensity of a single X-ray reflection takes on average 100–500 s implying a "snap shot" of *ca* 10^{20} pictures of the atomic positions. This procedure is repeated thousands of times during data collection, taking up to several days, with the intensities of all reflections containing information on the entire unit cell contents. The average, over space *and* time, of this extremely large number of pictures of the atomic positions (more precisely, of the electron density centroids) represents what can be observed in an X-ray diffraction experiment to determine molecular structure, *with the true X-ray crystallographic timescale corresponding to the period of data collection.* Crystallographic data must therefore contain information on dynamic processes taking place in the solid on a timescale very much longer than 10^{-18} s.

With this idea in mind, solid-state dynamic processes, which are receiving increased attention now that MASNMR is widely available, can be considered more precisely. To obtain a complete picture, information from the spectroscopic and diffraction types of experiment must be carefully interpreted together, instead of separately as has generally been the case.

The significant factor in a diffraction experiment is not the time required for a dynamic process, because all possible kinds of molecular motions (vibrations, librations, rotations and rearrangements) take longer than 10^{-18} s; but the "number of jumps" between consecutive positions occurring during data collection. If this number is small (in general that is to say if the energy barrier is high and/or the Arrhenius pre-exponential factor is small), no trace of the motion will be detected and the atoms will be seen only in their extreme positions. On the other hand, if the energy barrier is low and the pre-exponential factor large, the number of jumps during data collection will be great and the dynamic process will affect the X-ray diffraction observations.

Three types of dynamic effect must be distinguished (see Fig. 1). With a relatively smooth potential energy curve [Fig. 1(a)], substantial electron density from the rearranging atoms will be observed between their ground-state positions. In the extreme example of free rotation of a molecular fragment, diffuse, unresolved features will appear in the electron density maps. If, however, the potential energy barrier for a rapid rearrangement rises steeply to its maximum [Fig. 1(b)], the atoms will spend a much smaller proportion of their time in positions associated with the transition state. X-ray electron density maps appear to show only fixed atoms vibrating around their ground-state positions, and detection of the rearrangement will require analysis of these vibrations. Examples of this type greatly outnumber those of less hindered rearrangements, because of the restrictive effect of crystal packing forces, which prevent structural

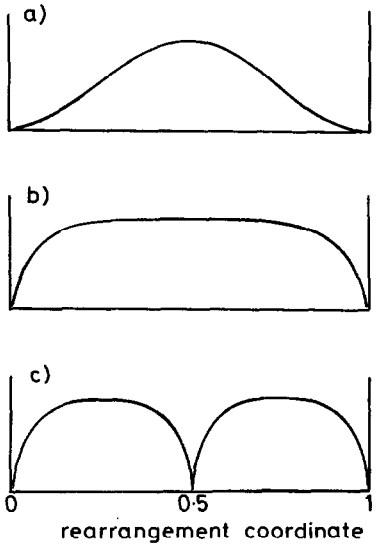

Fig. 1. Three forms of the potential energy profile for rapid molecular rearrangements between equivalent structures in the solid state. (a) Gently rising curve; (b) steeply rising curve; (c) steeply rising curve with steep well in intermediate position.

rearrangements altogether in the majority of solid compounds.

The occurrence of relatively steep wells in the potential energy curve [Fig. 1(c)] will cause significant concentrations of electron density in intermediate positions. The crystal structure will contain fractionally occupied atomic sites. This "dynamic disorder" (time-averaged structure) is particularly feasible in molecules of high symmetry. It will be liable to misinterpretation as a static disorder representing alternative molecular orientations in different unit cells (space averaged structure).

A reliable method to detect solid-state dynamic processes, and distinguish dynamic from static disorder, may be provided by an analysis of the mean-square anisotropic atomic displacement amplitudes ("thermal parameters")[9] obtained from diffraction data. In a carefully executed experiment, these contain real information on atomic vibrations. Methods based on this approach have recently been used to correlate vibrational "soft modes" revealed by crystallographic data with ligand migrational pathways found by NMR for metal carbonyls in solution[10] and in the solid state;[11] and to demonstrate the occurrence of dynamic Jahn–Teller distortions in solid complexes.[12,13] Moreover, X-ray studies on both organic and organometallic species have shown that the temperature-dependence of these thermal parameters also has physical significance and contains information on true atomic motions.[14,15] In this connection, we also mention that *uncorrelated* motions of molecules in unit cells distant from one another, as a consequence of the propagation of thermal waves through the crystal, destroy the exact translational periodicity necessary for Bragg's Law to be obeyed. Information on these molecular motions in the solid state, which cause incoherent diffraction of X-ray intensity, is contained in the thermally diffuse background scattering;[16] this, of course, is not ordinarily studied in crystallographic experiments.

We illustrate the logical consequences of our argument with some examples. Notable solid-state rearrangements occur in the metal carbonyls $Fe_3(CO)_{12}$ and $Co_4(CO)_{12}$. These molecules contain metal clusters enveloped by icosahedra of ligands.[17] Their crystal structures[18,19] are disordered, with half-occupied metal atom sites in 60° steps around the crystallographic symmetry elements which coincide with approximate three-fold molecular axes. These structures are regarded as classic examples of static orientational disorder. In both compounds, however, ^{13}C MASNMR spectra are incompatible with a static structure, the carbonyl ligand equivalence patterns suggesting that the metal clusters actually rotate around the three-fold axes within the ligand polyhedra.[20–23] In recognizing that X-ray diffraction gives crystal structures which are intrinsically time-averaged over a longer period than the NMR spectra, the full significance of the results from the two types of experiment can be appreciated for the first time: if the metal clusters are indeed rotating on the NMR timescale, the crystallographic disorder must be dynamic rather than static.

To investigate this idea, we have made a detailed analysis of the crystallographic thermal parameters of $Fe_3(CO)_{12}$ to characterize the vibrational soft modes of this molecule in the solid state.[11] The results suggest that rotation of the iron triangle does *not* take place. A new proposal for the mechanism of the fluxional behaviour of solid $Fe_3(CO)_{12}$, which accounts for all the features of the crystallographic structure and ^{13}C MASNMR spectra, will be published separately;[11] other disordered metal carbonyl structures are being examined for evidence of solid-state dynamic processes.

In the case of bullvalene, its crystal structure is ordered at room temperature and below,[24–26] with several distinct carbon atomic sites. ^1H broadline NMR indicates that structural rearrangement occurs in the solid above room temperature,[27] and ^{13}C MASNMR demonstrates that fluxionality by the Cope rearrangement renders all carbon atoms equivalent at 85°C.[28] We predict that if the crystal structure of this compound were to be determined

at progressively higher temperatures, the onset of dynamic processes within the X-ray crystallographic timescale would be directly detected by qualitative changes in the atomic thermal parameters, followed by the appearance of dynamic structural disorder.

In summary, we emphasize that the timescale concept associated with spectroscopic methods of molecular structure determination can by no means be applied in the same way to diffraction techniques. Crystallographic structures determined by diffraction methods are intrinsically time-averaged over the period of data collection, as well as space-averaged. Molecular rearrangements suggested by MASNMR must be carefully correlated with crystallographic data on atomic vibrations and disorder to give a full picture of dynamic processes in the solid state.

REFERENCES

1. E. L. Muetterties, *Inorg. Chem.* 1965, **4**, 769.
2. A. Carrington and A. D. McLachlan, *Introduction to Magnetic Resonance*, Chap. 12. Harper and Row, London (1966).
3. A. Allerhand, H. S. Gutowsky, J. Jonas and R. A. Meinzer, *J. Am. Chem. Soc.* 1966, **88**, 3185.
4. F. A. Bovey, *Nuclear Magnetic Resonance Spectroscopy*, Chap. 7. Academic Press, New York (1969).
5. R. G. Bryant, *J. Chem. Educ.* 1983, **60**, 933.
6. W. von E. Doering and W. R. Roth, *Angew. Chem. Int. Ed. Engl.* 1963, **2**, 115.
7. F. A. Cotton and D. L. Hunter, *Inorg. Chim. Acta* 1974, **11**, L9.
8. J. F. M. Oth, K. Müllen, J-M. Gilles and G. Schröder, *Helv. Chim. Acta* 1974, **57**, 1415.
9. B. T. M. Willis and A. W. Pryor, *Thermal Vibrations in Crystallography*. Cambridge University Press, New York (1975).
10. D. Braga and B. T. Heaton, *J. Chem. Soc., Chem. Commun.* 1987, 608.
11. C. E. Anson, R. E. Benfield, A. W. Bott, B. F. G. Johnson, D. Braga and E. A. Marseglia, *J. Chem. Soc., Chem. Commun.* 1988, 889.
12. J. H. Ammeter, H. B. Bürgi, E. Gamp, V. Meyer-Sandrin and W. P. Jensen, *Inorg. Chem.* 1979, **18**, 733.
13. K. Chandrasekhar and H. B. Bürgi, *Acta Cryst. Sect. B.* 1984, **40**, 387.
14. V. Schomaker and K. N. Trueblood, *Acta Cryst. Sect. B* 1968, **24**, 63.
15. P. Seiler and J. D. Dunitz, *Acta Cryst. Sect. B* 1979, **35**, 2020.
16. J. L. Amorós and M. Amorós, *Molecular Crystals, their Transforms and Diffuse Scattering*, Wiley, New York (1968).
17. R. E. Benfield and B. F. G. Johnson, *Transition Met. Chem.* 1981, **6**, 131.
18. F. A. Cotton and J. M. Troup, *J. Am. Chem. Soc.* 1974, **96**, 4155.
19. F. H. Carré, F. A. Cotton and B. A. Frenz, *Inorg. Chem.* 1976, **15**, 381.
20. H. C. Dorn, B. E. Hanson and E. Motell, *Inorg. Chim. Acta.* 1981, **54**, L71.
21. B. E. Hanson, E. C. Lisic, J. T. Petty and G. A. Iannaconne, *Inorg. Chem.* 1986, **25**, 4062.
22. B. E. Hanson and E. C. Lisic, *Inorg. Chem.* 1986, **25**, 715.
23. B. E. Hanson, in *Advances in Dynamic Stereochemistry* (Edited by M. F. Gielen), Vol. 1, p. 89. Freund, London (1985).
24. A. Amit, R. Huber and W. Hoppe, *Acta Cryst. Sect. B.* 1968, **24**, 865.
25. S. M. Johnson, J. S. McKechnie, B. T-S. Lin and I. C. Paul, *J. Am. Chem. Soc.* 1967, **89**, 7123.
26. P. Luger, J. Buschmann, R. K. McMullan, J. R. Ruble, P. Matias and G. A. Jeffrey, *J. Am. Chem. Soc.* 1986, **108**, 7825.
27. J. D. Graham and E. R. Santee, *J. Am. Chem. Soc.* 1966, **88**, 3453.
28. B. H. Meier and W. L. Earl, *J. Am. Chem. Soc.* 1985, **107**, 5553.

Polyhedron Vol. 7, No. 24, pp. 2553–2559, 1988
Printed in Great Britain

0277–5387/88 $3.00+.00
© 1988 Pergamon Press plc

A NEW SYNTHETIC ROUTE TO AMINOPHOSPHINES

D. K. SRIVASTAVA, L. K. KRANNICH* and C. L. WATKINS

Department of Chemistry, University of Alabama at Birmingham, UAB Station, Birmingham, AL 35294, U.S.A.

(*Received* 14 *March* 1988; *accepted* 18 *May* 1988)

Abstract—The reactions of R_2PPR_2 (R = Me, Et, Ph) and $(MeP)_5$ with $Me_{3-n}As(NMe_2)_n$ (n = 1, 2, 3) and of Me_2PPMe_2 with $Me_2AsNR'_2$ (R′ = Et, Pr^n, and Pr^i) were investigated as a function of time at room temperature using ^1H and ^{31}P NMR spectroscopy. For the diphosphine/$Me_2AsNR'_2$ reactions, the NMR spectral data suggest a reaction pathway involving the initial formation of R_2PAsMe_2 and the respective acyclic dialkylaminophosphine, $R_2PNR'_2$. The P—As intermediate then symmetrizes to R_2PPR_2 and $Me_2AsAsMe_2$, the parent aminoarsine is completely consumed, and additional $R_2PNR'_2$ is formed. The relative rate of aminophosphine production is dependent upon the nature of the substituent on the phosphorus and nitrogen atoms. For systems involving $MeAs(NMe_2)_2$ and $As(NMe_2)_3$ as reactants, the intermediates could not be characterized, but the products were the expected aminophosphine and $(MeAs)_5$ or elemental arsenic, respectively. $(MeP)_5$ reacts to give $MeP(NMe_2)_2$ and the expected As—As bonded species. A comparison of the reactivity of these systems with analogous diarsine/aminoarsine systems is discussed. The results of the NMR study were utilized in designing a convenient, high yield, synthetic route to acyclic aminophosphines.

The chemistry of P—P, As—As, P—N, As—N, and As—P bonded compounds has been of continued interest[1–17] with most of the attention being directed towards the chemistry of P—N bonded systems.[5–17] Acyclic aminophosphines have been synthesized by a variety of methods. The most common procedure involves the aminolysis of PCl_3 followed by alkylation with the appropriate Grignard reagent[16] or aluminum alkyl.[17] Alternatively, PCl_3 can be reacted with the appropriate Grignard reagent to give an organohalophosphine, which is then reacted with the desired secondary amine[18–20] or amide.[21] Since the aminehydrochloride by-products are very difficult-to-remove contaminants in these reactions, yields are usually low to moderate. Cleavage of P—C bonds using secondary amines,[22] of Sn—N bonds with halophosphines,[23] and of Si—N bonds with PF_3[24] also serve as routes to particular aminophosphines.

The literature[25–27] establishes that As—As and As—N bonds are more labile than P—P and P—N bonds, respectively. Recently, as part of our NMR investigations of exchange reactions involving As—As, As—N and As—H bonding systems, we noted that Me_2AsNMe_2 reacts with Et_2PPEt_2[28] to give Et_2PNMe_2 and an equilibrium mixture of $Me_2AsAsMe_2$, Et_2PPEt_2 and Me_2AsPEt_2. No other reports have been noted in the literature on the reactivities of aminoarsines towards P—P bonded compounds. In this paper, we report on the generality of the diphosphine/aminoarsine reaction system as a convenient synthetic pathway to acyclic aminophosphines and discuss the extension of this work to $(MeP)_5$/aminoarsine systems. As part of this study, we also determined the effect that substituents on the P, As and N atoms have on the relative rate of acyclic aminophosphine production.

EXPERIMENTAL

Standard high vacuum line techniques and a Vacuum Atmospheres Model HE-13-Drilab equipped with a Model HE-493 Dri-Train were used for storing and handling all compounds. Benzene and petroleum ether (90–110°C) were distilled over calcium hydride and stored over molecular sieves prior to

* Author to whom correspondence should be addressed.

use. Diethyl ether was dried over sodium and distilled before use. Benzene-d_6 and Me_4Si were stored over molecular sieves. Me_2NH (b.p. 7.4°C), Et_2NH (56.3°C), Pr^n_2NH (109°C), and Pr^i_2NH (84°C) were stored over sodium and distilled *in vacuo* prior to use. Me_2AsCl (106°C),[29] $MeAsCl_2$ (61–63°C/50 mm Hg)[30] and $Me_2AsAsMe_2$ (60°C/25 mm Hg)[31] were synthesized by reported methods. Me_2AsNMe_2 (74°C/108 mm Hg), Me_2AsNEt_2 (80.5°C/90 mm Hg), $Me_2AsNPr^n_2$ (107–109°C/84 mm Hg), $Me_2AsNPr^i_2$ (78°C/28 mm Hg), $MeAs(NMe_2)_2$ (63°C/50 mm Hg) and $As(NMe_2)_3$ (55–57°C/10 mm Hg) were synthesized by the aminolysis of the appropriate chloroarsine or $AsCl_3$ and/or by the transamination of Me_2AsNMe_2.[27,32] All the arsines were distilled on a spinning band column prior to use and their purity was checked by ^1H and ^{13}C NMR spectroscopy (see NMR spectral data). Me_2PPMe_2 (38–40°C/16 mm Hg) and Et_2PPEt_2 (84°C/10 mm Hg) were synthesized by the reaction of the appropriate tetraalkylbiphosphine bisulphide with $P(Bu^t)_3$.[33] Ph_2PPPh_2 (m.p. 120°C) was prepared by the reaction of Ph_2PH with Ph_2PCl.[34] $(MeP)_5$ (110–112°C/1 mm Hg) was synthesized by the reduction of $MePCl_2$ using lithium in THF.[35] Me_2PNMe_2 (110°C/720 mm Hg), Me_2PNEt_2 (50°C/33 mm Hg), $Me_2PNPr^n_2$ (172–174°C), $Me_2PNPr^i_2$ (166°C), Et_2PNMe_2 (86°C/146 mm Hg), Ph_2PNMe_2 (123–124°C/0.1 mm Hg) and $MeP(NMe_2)_2$ (141°C) were independently synthesized by the aminolysis of the corresponding chlorophosphines with the appropriate secondary amine in benzene or ether.[9,14–18,36] The purity of all the phosphines was checked by ^1H and ^{31}P NMR spectroscopy.

^1H, ^{13}C and ^{31}P NMR spectra were recorded on a Nicolet 300 MHz multinuclear FT NMR spectrometer operating at 300.1, 75.4 and 121.5 MHz, respectively. The ^1H and ^{13}C chemical shifts were measured with respect to Me_4Si as an internal reference. The ^{31}P chemical shifts were measured with respect to 85% H_3PO_4 as external reference. The reaction mixtures were protected from exposure to light. All NMR tubes were carefully washed in a non-acid media to prevent any possible catalysed exchange.

NMR studies of reactions of aminoarsines with diphosphines

The following diphosphine/aminoarsine reaction systems were studied as neat mixtures (see Table 1 for reactant mole ratios) with constant stirring at 24°C as a function of time: Me_2PPMe_2/Me_2AsNMe_2, $Me_2PPMe_2/MeAs(NMe_2)_2$, $Me_2PPMe_2/As(NMe_2)_3$, Me_2PPMe_2/Me_2AsNEt_2, $Me_2PPMe_2/Me_2AsNPr^n_2$, $Me_2PPMe_2/Me_2AsNPr^i_2$, Et_2PPEt_2/Me_2AsNMe_2, $Et_2PPEt_2/MeAs(NMe_2)_2$, $Et_2PPEt_2/As(NMe_2)_3$, Ph_2PPPh_2/Me_2AsNMe_2, $Ph_2PPPh_2/MeAs(NMe_2)_2$, $Ph_2PPPh_2/As(NMe_2)_3$, $(MeP)_5/Me_2AsNMe_2$, $(MeP)_5/MeAs(NMe_2)_2$ and $(MeP)_5/As(NMe_2)_3$. At specified time intervals, accurately measured aliquots were removed from the mixtures and diluted to a pre-determined solution volume using d_6-benzene as the solvent. Independent NMR experiments indicated that this procedure quenched the reaction. The ^1H NMR spectra were obtained and the spectral integration data were used to follow the course of each reaction and establish the [mol aminophosphine formed]/[mol aminoarsine consumed] ratio at each time interval. Additionally, the ^{31}P NMR data were obtained for intermediate and product identification.

General procedure for the synthesis of dialkylamino phosphines, $R_2PNR'_2$ (R = Me, Et, Ph; R′ = Me, Et, Pr^n, Pr^i) *and* $MeP(NMe_2)_2$

The measured quantity (10 mmol) of the appropriate phosphine [R_2PPR_2 or $(MeP)_5$] was mixed with the required stoichiometric amount of the corresponding aminoarsine at RT (24°C). The neat reaction mixture was then stirred at 100°C and 750 mm Hg for the required reaction time (see Table 1). The products were separated either by fractional distillation at reduced pressure or by filtration (when elemental arsenic is a product) followed by distillation. Table 1 summarizes the data for the studied reaction systems.

NMR spectral data

The following is a list of NMR spectral data (values in ppm) determined independently in our laboratory at RT in benzene-d_6 solution on synthesized compounds that were identified in the reaction mixture.

^1H *spectral data. Reactants*: Me_2AsNMe_2: 0.83 (MeAs) and 2.45 (MeN). Me_2AsNEt_2: 0.88 (MeAs), 0.99 (CH_3CH_2N, t, $^3J_{HH}$ = 7.0 Hz), and 2.83 (CH_3CH_2N, q). $Me_2AsNPr^n_2$: 0.84 ($CH_3CH_2CH_2N$, *t*), 0.89 (MeAs), 1.44 ($CH_3CH_2CH_2N$, m) and 2.74 ($CH_3CH_2CH_2N$, m). $Me_2AsNPr^i_2$: 0.89 (MeAs) 1.08 (Me_2CHN, d, $^3J_{HH}$ = 6.6 Hz), and 3.17 (Me_2CHN, septet). $MeAs(NMe_2)_2$: 0.96 (MeAs) and 2.63 (MeN).[37] $As(NMe_2)_3$: 2.61 (MeN).[38] Me_2PPMe_2: 0.93 (MeP, t, $^2J_{PH}$ = 7.0 Hz).[3,39] Et_2PPEt_2: 1.10 (CH_3CH_2P, m) and 1.46 (CH_3CH_2P, m).[40] Ph_2PPPh_2: 6.96 (m) and 7.55 (m). $(MeP)_5$: 1.3–1.5 (m, bd).[41] *Intermediates*: Me_2PAsMe_2: 0.90 (MeAs, d, $^3J_{PH}$ = 8.1 Hz) and 1.00 (MeP, d, $^2J_{PH}$ = 4.2 Hz).[3] Et_2PAsMe_2: 0.97

Table 1. Phosphine/aminoarsine reaction systems data

Reactants		Reactant mole ratio			Products		Aminophosphine
phosphine	aminoarsine	phosphine : arsine	Reaction period (h)	Intermediate	aminophosphine	arsenic containing	yield (%)
Me_2PPMe_2	Me_2AsNMe_2	1 : 2	47 (s)[a]	Me_2PAsMe_2	Me_2PNMe_2	$Me_2AsAsMe_2$	70
	$MeAs(NMe_2)_2$	1 : 1	0.08 (s)	Unchar	Me_2PNMe_2	$(MeAs)_5$	79
	$As(NMe_2)_3$	3 : 2	22 (s)	Unchar	Me_2PNMe_2	As	79
	Me_2AsNEt_2	1 : 2	0.08 (s)	Unchar	Me_2PNEt_2	$Me_2AsAsMe_2$	80
	$Me_2AsNPr^n_2$	1 : 2	8 (s)	Me_2PAsMe_2	$Me_2PNPr^n_2$	$Me_2AsAsMe_2$	74
	$Me_2AsNPr^i_2$	1 : 2	96 (s)	Me_2PAsMe_2	$Me_2PNPr^i_2$	$Me_2AsAsMe_2$	—
Et_2PPEt_2	Me_2AsNMe_2	1 : 2	7 days (s)	Et_2PAsMe_2	Et_2PNMe_2	$Me_2AsAsMe_2$	88
	$MeAs(NMe_2)_2$	1 : 1	4 (s)	Unchar	Et_2PNMe_2	$(MeAs)_5$	82
	$As(NMe_2)_3$	3 : 2	>>> 10 days (s)	Unchar	Et_2PNMe_2	As	—
Ph_2PPPh_2	Me_2AsNMe_2	1 : 2	8 (s) or 1 (r)	Ph_2PAsMe_2	Ph_2PNMe_2	$Me_2AsAsMe_2$	79
	$MeAs(NMe_2)_2$	1 : 1	No reaction (s) or 6 (r)	Unchar	Ph_2PNMe_2	$(MeAs)_5$	73
	$As(NMe_2)_3$	3 : 2	No reaction (s) 10 (r)	Unchar	Ph_2PNMe_2	As	—
$(MeP)_5$	Me_2AsNMe_2	1 : 10	6 days (s) 20 (r)	Unchar	$MeP(NMe_2)_2$	$Me_2AsAsMe_2$	71
	$MeAs(NMe_2)_2$	1 : 5	10 days (s) 70 (r)	Unchar	$MeP(NMe_2)_2$	$(MeAs)_5$	74
	$As(NMe_2)_3$	3 : 10	No reaction (s) 110 (r)	Unchar	$MeP(NMe_2)_2$	As	78

[a] s—stirred, r—refluxed.

(MeAs, d, $^3J_{PH}$ = 7.9 Hz), 1.03 (CH_3CH_2P, m) and 1.46 (CH_3CH_2P, m).[42] Ph_2PAsMe_2: 0.90 (MeAs, d, $^3J_{PH}$ = 9.2 Hz), 7.07 (Ph_2P, m) and 7.62 (Ph_2P, m). *Products*: $Me_2AsAsMe_2$: 0.96 (MeAs).[3] $(MeAs)_5$: 1.47, 1.52, 1.55.[43] Me_2PNMe_2: 0.92 (MeP, d, $^2J_{PH}$ = 5.1 Hz) and 2.38 (MeN, d, $^3J_{PH}$ = 9.6 Hz).[44,45] Me_2PNEt_2: 0.99 (MeP, d, $^2J_{PH}$ = 6.0 Hz), 0.92 (CH_3CH_2N, t, $^3J_{HH}$ = 7.0 Hz) and 2.82 (CH_3CH_2N, q, d, $^3J_{PH}$ = 9.6 Hz, $^3J_{HH}$ = 7.0 Hz). $Me_2PNPr^n_2$: 0.78 ($CH_3CH_2CH_2N$, t), 1.00 (MeP, d, $^2J_{PH}$ = 6.0 Hz), 1.38 ($CH_3CH_2CH_2N$, m) and 2.74 ($CH_3CH_2CH_2N$, m, $^3J_{PH}$ = 9.6 Hz). $Me_2PNPr^i_2$: 0.97 (MeP, d, $^2J_{PH}$ = 6.2 Hz), 1.05 (Me_2CHN, d), and 3.15 (Me_2CHN, m, $^3J_{PH}$ = 10.1 Hz, $^3J_{HH}$ = 6.7 Hz). Et_2PNMe_2: 1.06 (CH_3CH_2P, m), 1.10–1.45 (CH_3CH_2P, m), and 2.49 (MeN, d, $^3J_{PH}$ = 8.1 Hz). Ph_2PNME_2: 2.50 (MeN, d, $^3J_{PH}$ = 9.6 Hz), 7.13 (Ph_2P, m) and 7.45 (Ph_2P, m).[46] $MeP(NMe_2)_2$: 1.14 (MeP, d, $^2J_{PH}$ = 7.5 Hz) and 2.55 (MeN, d, $^3J_{PH}$ = 9.0 Hz).[45,47]

^{13}C *spectral data.* $MeAsCl_2$: 30.32. Me_2AsCl: 20.25. Me_2AsNMe_2: 9.92 (MeAs) and 41.9 (MeN). Me_2AsNEt_2: 12.1 (MeAs), 15.7 (CH_3CH_2N) and 44.3 (CH_3CH_2N). $Me_2AsNPr^n_2$: 11.7 (MeAs), 12.1 ($CH_3CH_2CH_2N$), 23.4 ($CH_3CH_2CH_2N$) and 53.2 ($CH_3CH_2CH_2N$). $Me_2AsNPr^i_2$: 12.2 (MeAs), 25.0 (Me_2CHN), and 46.5 (Me_2CHN). $MeAs(NMe_2)_2$: 12.5 (MeAs) and 42.2 (MeN). $As(NMe_2)_3$: 39.7 (MeN). $Me_2AsAsMe_2$: 5.96 (MeAs). $(MeAs)_5$: 3.78, 5.23, and 6.81.

^{31}P *spectral data.* Me_2PPMe_2: −58.4.[40] Et_2PPEt_2: −32.7.[40] Ph_2PPPh_2: −14.3.[4] $(MeP)_5$: 17.3 (m).[41] Me_2PAsMe_2: −56.2.[3] Et_2PAsMe_2: −15.7. Ph_2PAsMe_2: −8.3. Me_2PNMe_2: 39.2.[17,44] Me_2PNEt_2: 34.6. $Me_2PNPr^n_2$: 36.1. $Me_2PNPr^i_2$: 7.2. Et_2PNME_2: 63.7.[17] Ph_2PNMe_2: 65.4.[36] $MeP(NMe_2)_2$: 87.2.[36]

RESULTS AND DISCUSSION

The reactions of R_2PPR_2 (R = Me, Et, Ph) with $Me_{3-n}As(NMe_2)_n$ and of Me_2PPMe_2 with $Me_2AsNR'_2$ (R′ = Et, Pr^n, Pr^i) were followed using multinuclear NMR spectroscopy. In the Me_2PPMe_2/ME_2AsNMe_2 (1:2 mol ratio) system, the reaction proceeds very rapidly at RT to consume all the original Me_2PPMe_2 and one-half the original amount of Me_2AsNMe_2 within 5 min. The initial products were identified as Me_2PAsMe_2[3] and Me_2PNMe_2. The ^1H spectrum also indicates the presence of a very low intensity peak assigned to $Me_2AsAsMe_2$. With time, the intensities of the peaks associated with Me_2AsNMe_2 and Me_2PAsMe_2 decrease with a concomitant increase in the intensities of the peaks assigned to Me_2PNMe_2 and $Me_2AsAsMe_2$. The NMR spectra indicate that the reaction goes to completion in 47 h with complete conversion of Me_2AsNMe_2 and Me_2PPMe_2 to Me_2PNMe_2 and $Me_2AsAsMe_2$. A plot of the ratio (mol aminophosphine)/(mol aminoarsine) vs time is given in Fig. 1.

These results suggest that the first step in the reaction pathway is the rapid consumption of all the original Me_2PPMe_2 and one-half of the Me_2AsNMe_2 [eq. (1)]:

$$Me_2PPMe_2 + Me_2AsNMe_2 \rightarrow Me_2PAsMe_2 + Me_2PNMe_2. \quad (1)$$

This reaction probably proceeds through a four-centred intermediate[48] that rapidly undergoes P—P and As—N bond dissociation and P—As and P—N bond formation. The subsequent production of $Me_2AsAsMe_2$ and the remaining stoichiometric amount of Me_2PNMe_2, and the consumption of the remaining half of the aminoarsine are much slower processes. This can occur via either of the following two paths:

Pathway A:

$$Me_2PAsMe_2 + Me_2AsNMe_2 \rightarrow Me_2AsAsMe_2 + Me_2PNMe_2 \quad (2)$$

Pathway B:

$$Me_2PAsMe_2 \rightleftarrows 1/2Me_2PPMe_2 + 1/2Me_2AsAsMe_2. \quad (3)$$

Me_2PPMe_2 formed in (3) then reacts with the remaining Me_2AsNMe_2 according to eq. (1). Based upon the observed very fast rate of consumption of the diphosphine by Me_2AsNMe_2 and our previous work on the reactions of diarsines and aminoarsines,[28] we would expect that Pathway A would be fast. Pathway B assumes symmetrization of the phosphinoarsine [eq. (3)] followed by consumption of the symmetric diphosphine according to eq. (1). We observed previously that the phosphinoarsine symmetrization reaction is quite slow.[42] Since the Me_2PPMe_2/Me_2AsNMe_2 reaction [eq. (1)] is fast, we would not expect to observe, in the NMR spectra, any peaks attributable to the Me_2PPMe_2 produced via eq. (3). This is consistent with the spectral data obtained for the Me_2PPMe_2/Me_2AsNMe_2 system. Although we were unable to unequivocally determine the reaction pathway for the subsequent product ion of aminophosphine, based upon our earlier work, we favour Pathway B.

We assume that this reaction pathway [eqs (1) and (3)] for the Me_2PPMe_2/Me_2AsNMe_2 system is also applicable to the other $R_2PPR_2/Me_2AsNR'_2$

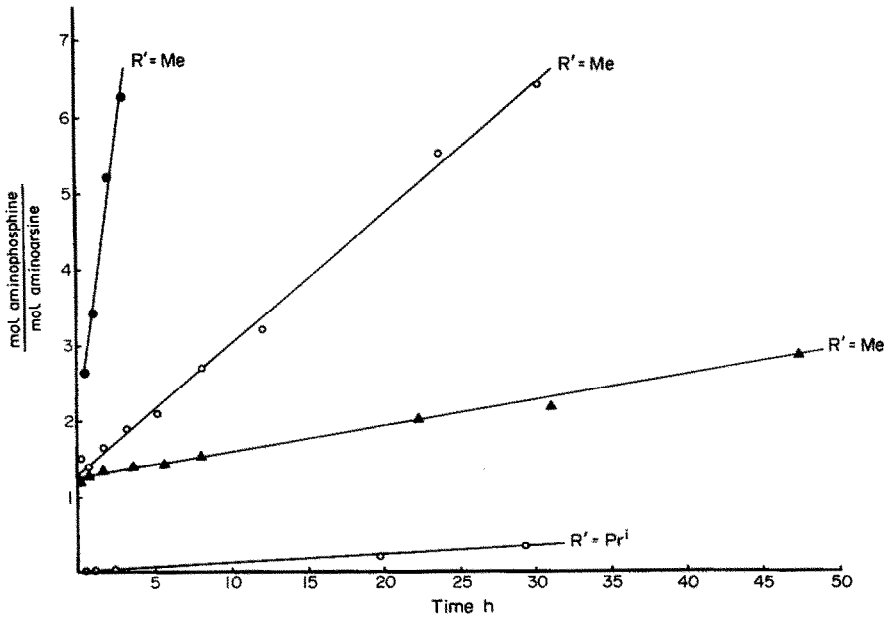

Fig. 1. [Mol aminophosphine]/[mol aminoarsine] as a function of time for the $R_2PPR_2/Me_2AsNR'_2$ reaction systems [○—R = Me, ▲—R = Et, ●—R = Ph].

systems studied, since analogous intermediates and products are observed (see Table 1). Although the reaction period for these systems varied from 5 min to seven days (Table 1), in each case, the predicted aminophosphine was produced quantitatively. In a separate study, no reaction of Me_2PNMe_2 with $Me_2AsAsMe_2$ was observed over an extended period of time at room temperature. Considering the known lability of the As—N and As—As bonds in the analogous R_2AsAsR_2/Me_2AsNMe_2 systems[28] and the P—P bond energy in diphosphines,[3,4,49] the greater strength of the P—N bond is undoubtedly the reason why these reactions go to completion.

The plot of [mol aminophosphine]/[mol aminoarsine] (Fig. 1) suggests that the relative rate of production of aminophosphine depends upon the substituents on the phosphorus and nitrogen atoms. For R_2PPR_2 and a given aminoarsine, the relative rate decreases in the order R = Ph > Me > Et. This is consistent with the previously observed trends in the ease of P—P bond cleavage in diphosphines, which is related to the substituent effects on P—P bond strength.[50]

For the $Me_2PPMe_2/Me_2AsNR'_2$ systems, the relative rate of aminophosphine production (Fig. 1) decreases in the order R′ = Et > Me > Pr^i. Unfortunately, rate data could not be collected for the R′ = Pr^n case, since the neat reaction mixture contained both solid and liquid phases. In the analogous $Me_2AsAsMe_2/Et_2AsNR'_2$ system,[28] substitution of an Et for a Me group dramatically increases the rate of reaction. Assuming that these reactions proceed through a concerted four-centred activated intermediate,[51,48] these data suggest that substitution of an Et for a Me group lowers the energy barrier for As—N bond dissociation and P—N bond formation, and leads to more rapid aminophosphine production. Such Et/Me group substitution should also enhance the P—N bond strength through the $p\pi$–$d\pi$ bonding system in the product aminophosphine. On the other hand, the rate of aminophosphine production is significantly diminished upon substitution of the more bulky Pr^i group. Thus, both substituent steric and electronic effects on the relative rate of aminophosphine production must be considered for the series.

The reaction pathways for the diphosphine/bis(or tris)-aminoarsine systems are more complicated due to the involvement of two or three labile dialkylamino groups on the parent aminoarsine. Furthermore, the chaining, ring closure or crosslinking mechanisms, which ultimately lead to the formation of $(MeAs)_5$[52–54] or elemental arsenic must be considered. Due to the extremely low intensity, multiplet band structure, or absence of peaks assignable in the NMR spectra to condensed P—As bonded intermediates, we do not have sufficient data to elucidate possible reaction pathways in these systems. For either Me_2PPMe_2 or Et_2PPEt_2, the relative rate of production of aminophosphine

decreases in the order $MeAs(NMe_2)_2 > Me_2AsNMe_2 > As(NMe_2)_3$. Comparisons with the Ph_2PPPh_2 reactions could not be made, since the Ph_2PPPh_2 is insoluble in the aminoarsine and refluxing conditions were needed to bring about complete reaction.

The scope of the reactivity of the P—P bond towards $Me_{3-n}As(NMe_2)_n$ was extended to $(MeP)_5$. Here, each reaction yields $MeP(NMe_2)_2$ as the only P—N bonded compound. The arsenic containing products are the expected $Me_2AsAsMe_2$, $(MeAs)_5$ and elemental arsenic. These reactions are all slower than the analogous Me_2PPMe_2 and Et_3PPEt_2 reactions. Heating is required to facilitate complete reaction. Any reaction pathway describing the $(MeP)_5/Me_{3-n}As(NMe_2)_n$ system is further complicated by polyphosphine ring cleavage mechanisms.

The diphosphine/aminoarsine reactions are not as facile as the analogous diarsine/aminoarsine reactions,[28] which may be related to the greater P—P bond strength. Owing to the strength of the P—N bond, all the diphosphine/aminoarsine reactions go to completion, whereas the diarsine/aminoarsine reactions[28] yield equilibrium distributions of reactants and products. In the latter cases, the lability of the As—As and As—N bonds in the reactant and product species facilitates equilibrium redistribution reactions, which preclude utilizing these reaction systems as synthetic pathways to aminoarsines or diarsines.

Since the NMR study suggested that these reactions were suitable as synthetic pathways to aminophosphines, each reaction was scaled-up and carried out in the appropriate mole ratios to establish it as a viable synthetic route to a mono- or bis-aminophosphine. The neat reactions were very straightforward and the pure aminophosphines were isolated in 70–90% yields (Table 1) after distillation of the product mixture. The acyclic aminophosphines, $Me_2AsAsMe_2$ and $(MeAs)_5$ are highly air sensitive, colourless, distillable liquids.

The results of this study indicate conclusively that the reactions of diphosphines and $(MeP)_5$ with aminoarsines are irreversible and give high yields of acyclic aminophosphines. In all cases, the only products are the aminophosphine and the As—As bonded species. These are easily separated and purified by fractional distillation or filtration followed by distillation when elemental arsenic is produced. The added advantage of this synthetic route is the absence of the highly undesirable aminehydrochloride and side reactions that are common in other synthetic routes to the aminophosphines. Thus, this is a very convenient and high yield synthetic route to very pure acyclic aminophosphines.

REFERENCES

1. H. H. Sisler, in *Inorganic Reactions and Methods* (Edited by J. J. Zuckerman), Vol. 7, pp. 17–36 and refs therein. VCH Publishers, Deerfield Beach, Florida (1988).
2. L. K. Krannich, in *Inorganic Reactions and Methods* (Edited by J. J. Zuckerman), Vol. 7, pp. 39–60 and refs therein. VCH Publishers, Deerfield Beach, Florida (1988).
3. A. J. Ashe, III and E. G. Ludwig Jr, *J. Organomet. Chem.* 1986, **303**, 197.
4. A. Belforte, F. Calderazzo, A. Morvillo, G. Pelizzi and D. Vitali, *Inorg. Chem.* 1984, **23**, 1504.
5. A. H. Cowley and R. A. Kemp, *Inorg. Chem.* 1983, **22**, 547.
6. R. R. Ford, M. A. Goodman, R. H. Neilson, A. K. Roy, V. G. Wettermark and P. Wissan-Neilson, *Inorg. Chem.* 1984, **23**, 2063.
7. H. W. Roesky, J. Lucas, M. Noltemeyer and G. M. Sheldrick, *Chem. Ber.* 1984, **117**, 1583.
8. A. B. Burg, *J. Am. Chem. Soc.* 1961, **83**, 2226.
9. R. R. Holmes and R. P. Wagner, *J. Am. Chem. Soc.* 1962, **84**, 357.
10. J. G. Reiss, *Phosphorus Sulfur* 1986, **27**, 93.
11. D. Grec, L. G. Hubert-Pfalzgraf, A. Grand and J. G. Riess, *Inorg. Chem.* 1985, **24**, 4642.
12. J. Febvay, F. Casabianca and J. G. Riess, *Inorg. Chem.* 1985, **24**, 3235.
13. R. T. Paine, *Inorg. Chem.* 1977, **16**, 2996.
14. A. H. Cowley, M. J. S. Dewar, W. R. Jackson and W. B. Jennings, *J. Am. Chem. Soc.* 1970, **92**, 5206.
15. D. Dakternieks and R. DiGiiacomo, *Phosphorus Sulfur* 1985, **24**, 217.
16. A. B. Burg and P. J. Slota, *J. Am. Chem. Soc.* 1958, **80**, 594.
17. L. Maier, *Helv. Chim. Acta* 1964, **47**, 2129.
18. H. J. Kleiner, *Liebigs Annln Chem.* 1974, **5**, 751.
19. G. Ewart, D. S. Payne, A. L. Porte and A. P. Lane, *J. Chem. Soc.* 1962, 3984.
20. E. M. Evleth Jr, LeVern D. Freeman and R. I. Wagner, *J. Org. Chem.* 1962, **27**, 219.
21. T. Cuvigny and H. Normant, *C. R. Acad. Sci.* 1969, **268**, 834.
22. C. G. Barlow and L. F. Nixon, *J. Chem. Soc. A* 1966, 228.
23. E. W. Abel, D. A. Armitage and G. R. Willey, *J. Chem. Soc.* 1965, 57.
24. T. A. George and M. F. Lappert, *J. Chem. Soc. A* 1969, 992.
25. L. K. Krannich, in *Compounds Containing* As—N *Bonds* (Edited by H. H. Sisler), Vol 5. Benchmark Papers in Inorganic Chemistry, Dowden Hutchinson and Ross, Stroudsburg, PA (1976).
26. O. Adler and F. Kober, *Chem. Ztg.* 1976, **100**, 235.
27. F. Kober, *Z. Anorg. Allg. Chem.* 1973, **400**, 285.
28. V. K. Gupta, L. K. Krannich and C. L. Watkins, *Polyhedron* 1987, **6**, 1229.
29. W. Steinkopf and W. Mieg, *Chem. Ber.* 1920, **53**, 1013.

30. W. M. Dehn and B. B. Wilcox, *Am. Chem. J.* 1906, **35**, 1.
31. R. W. Bunsen, *Liebigs Annln Chem.* 1842, **42**, 14.
32. K. Moedritzer, *Chem. Ber.* 1959, **92**, 2637.
33. L. Maier, *J. Inorg. Nucl. Chem.* 1962, **24**, 275.
34. W. Kuchen and H. Buchwald, *Chem. Ber.* 1958, **91**, 2871.
35. W. A. Henderson, M. Epstein and F. S. Seichter, *J. Am. Chem. Soc.* 1963, **85**, 2462.
36. L. Maier, *Helv. Chim. Acta* 1963, **46**, 2667.
37. F. Kober, *Z. Anorg. Allg. Chem.* 1973, **379**, 609.
38. K. Moedritzer, *Inorg. Chem.* 1964, **3**, 609.
39. E. G. Finer and R. K. Harris, *Mol. Phys.* 1967, **12**, 457.
40. S. Aime, R. K. Harris, E. M. McVicker and M. Fild, *J. Chem. Soc.* 1976, 2144.
41. L. R. Smith and J. L. Mills, *J. Am. Chem. Soc.* 1976, **98**, 3852.
42. V. K. Gupta, L. K. Krannich and C. L. Watkins, *Inorg. Chim. Acta.* 1987, **134**, 197.
43. C. L. Watkins, L. K. Krannich and H. H. Sisler, *Inorg. Chem.* 1969, **5**, 385.
44. D. F. Clemens, H. H. Sisler and W. S. Brey Jr, *Inorg. Chem.* 1965, **4**, 1223.
45. A. H. Cowley and R. P. Pinnell, *J. Am. Chem. Soc.* 1965, **87**, 4454.
46. J. F. Nixon and R. Schmutzler, *Spectrochim. Acta.* 1966, **22**, 565.
47. J. R. VanWazer and L. Maier, *J. Am. Chem. Soc.* 1964, **86**, 811.
48. J. C. Lockhart, *Redistribution Reactions*, p. 158. Academic Press, New York (1970).
49. N. N. Grishin, G. M. Bogolyubov and A. A. Petrov, *J. Gen. Chem. U.S.S.R.* (English translation) 1968, **38**, 2595.
50. A. H. Cowley, *Chem. Rev.* 1965, **65**, 617 and refs therein.
51. J. B. Lambert, G. F. Jackson, III and D. C. Mueller, *J. Am. Chem. Soc.* 1970, **92**, 3093.
52. V. K. Gupta, L. K. Krannich and C. L. Watkins, *Inorg. Chim. Acta.* 1987, **126**, 173.
53. A. L. Rheingold, J. E. Lewis and J. M. Bellama, *Inorg. Chem.* 1969, **8**, 385.
54. A. L. Rheingold and J. M. Bellama, *J. Chem. Soc., Chem. Commun.* 1969, 1058.

Polyhedron Vol. 7, No. 24, pp. 2561–2567, 1988
Printed in Great Britain

0277-5387/88 $3.00+.00
© 1988 Pergamon Press plc

THE PREPARATION AND CHARACTERIZATION OF TlClBrI COMPLEXES. X-RAY CRYSTAL STRUCTURE OF CHLOROBROMOIODO-BIS-(TRIPHENYLPHOSPHINE OXIDE)THALLIUM(III)*

M. R. BERMEJO,† A. FERNANDEZ and M. GAYOSO

Departamento de Química Inorgánica, Universidad de Santiago de Compostela, Campus Universitario, E-15706 Santiago de Compostela, Spain

and

A. CASTIÑEIRAS, W. HILLER and J. STRÄHLE

Institut für Anorganische Chemie der Universität Tübingen, Auf der Morgenstelle 18, D-7400 Tübingen, F.R.G.

(*Received* 4 *March* 1988; *accepted* 18 *May* 1988)

Abstract—The complexes $TlClBrI \cdot L_2$ ($L = C_5H_5NO$, 2-, 3-, 4-$CH_3C_5H_4NO$, 4-ClC_5H_4NO, 4-CNC_5H_4NO, 4-$NO_2C_5H_4NO$, 4-$CH_3OC_5H_4NO$, HMPA and $OPPh_3$) have been prepared and characterized by elemental analysis. The solids behave as non-electrolytes in acetonitrile solution and are monomers in benzene. The structure of $TlClBrI(OPPh_3)_2$ has been determined by X-ray crystallography and refined to a conventional R factor of 0.05. This compound crystallizes in the monoclinic space group $P2_1/c$ and $a = 14.742(5)$, $b = 14.418(3)$, $c = 17.234(4)$ Å, $\beta = 107.54(2)°$ and $Z = 4$. The structure consists of neutral monomeric complexes in which the thallium atom shows a five-fold coordination in the form of a distorted trigonal bipyramid, the halogen atoms being located in the equatorial plane. ^1H NMR and vibrational (IR and Raman) spectra of all of these complexes are discussed on the basis of this structure.

Although a great deal of research has been carried out on the coordination chemistry of thallium(III) complexes,[1,2] very little is known about the structure of these compounds. Structural investigations have been carried out through the use of X-ray diffraction techniques and are reported by Baxter *et al.*,[3] Gutierrez *et al.*,[4] Small *et al.*[5] and Glasser.[6]

Recently we have reported the detailed characterization of complexes of the type $TlX_3 \cdot L_2$[7,8] and $TlXX'_2 \cdot L_2$[9–12] following a new and simple synthesis procedure that improves on the one proposed by Cotton *et al.*[1] At the same time we have resolved the structure of some new complexes of the types $TlX_3 \cdot L_2$[13–15] and $TlXX'_2 \cdot L_2$.[16–19]

The stabilization of tetrahalothallates of the form $[TlX_{4-n}X'_n]$[20–22] and of molecular adducts of the $TlXX'_2 \cdot L_n$[11] type are well known, but nothing is known about the chemical stabilization of $TlClBrI \cdot L_n$ type complexes.

We now describe the synthesis and structural characterization of interhalo derivatives of thallium(III) of the type $TlClBrI \cdot L_2$. The ligands used here are ones whose donor atom behaves as hard in Pearson's terminology[23] and are good stabilizers of thallium(III).[24] The selected ligands are: pyridine-N-oxide (C_5H_5NO), 2-, 3- and 4-methylpyridine-N-oxide (2-, 3- and 4-$CH_3C_5H_4NO$), 4-chloropyridine-N-oxide (4-ClC_5H_4NO), 4-cyanopyridine-N-oxide (4-CNC_5H_4NO), 4-nitropyridine-N-oxide (4-$NO_2C_5H_4NO$), 4-methoxypyridine-N-oxide (4-$CH_3OC_5H_4NO$), hexamethylphosphorotriamide (HMPA) and triphenylphosphine oxide ($OPPh_3$).

* Presented in part at the XXIV ICCC, Athens, Greece, 24–29 August, 1986.

† Author to whom correspondence should be addressed.

The complexes with C_5H_5NO, HMPA and $OPPh_3$, although previously known,[10,23,26] have now been prepared by a new procedure for comparison purposes.

EXPERIMENTAL

Merck synthesis grade TlCl, $OPPh_3$ and HMPA (Fluka) were used without further purification. Aromatic amine oxides (Merck, Fluka or Aldrich) were recrystallized from acetone, benzene or 1,2-dichloroethane. IBr (Merck) was resublimed. C, H and N microanalyses were carried out using a Perkin–Elmer 240-B elemental analyser. Thallium was determined using an atomic absorption spectrometer. The molecular weights of these complexes that were sufficiently soluble were measured in benzene with a vapour pressure osmometer and the conductivity data (in acetonitrile) were obtained with a WTW conductivimeter. ^1H NMR spectra were obtained in $CDCl_3$ solvent with TMS as internal reference using a Varian CFT-20 and Bruker WM 250 apparatus. IR spectra were recorded as Nujol mulls or pressed KBr discs on a Perkin–Elmer 180 spectrophotometer with a far-IR accessory, and Raman spectra on a Jarrell-Ash 500 spectrometer (Ar^+ Laser 5415 A).

Preparation of complexes

The complexes were prepared according to the equation:

$$TlCl + 2L \xrightarrow[CH_3CN]{IBr} TlClBrI \cdot L_2.$$

This method has been discussed in detail elsewhere[8] and it improves on the one proposed previously.[1] All the preparative work was performed under an inert atmosphere in a dry box. Once isolated, the compounds were shown to be stable in air.

$TlClBrI(C_5H_5NO)_2$ (**I**). This has been prepared by the same method as described elsewhere.[10]

$TlClBrI(2\text{-}CH_3C_5H_4NO)_2$ (**II**). A solution of 4.4 mmol (0.91 g) of IBr in acetonitrile (25 cm^3) was slowly added to a magnetically stirred suspension of 4.2 mmol (1.0 g) of TlCl and 8.6 mmol (0.94 g) of $2\text{-}CH_3C_5H_4NO$ in the same solvent (30 cm^3). The resulting solution was concentrated *in vacuo* and a yellow solid was precipitated. The compound was recrystallized in CH_3CN as yellow crystals. (Yield: 85%.) Found: C, 21.5; H, 2.1; N, 4.6; Tl, 29.6. Calc. for $C_{12}H_{14}BrClIN_2O_2Tl$: C, 21.7; H, 2.1; N, 4.2; Tl, 30.7%. M.p. 124°C, Λ_M 58 Ohm^{-1} cm^2 mol^{-1}.

$TlClBrI(2\text{-}CH_3C_5H_4NO)_3$ (**III**). To a suspension of 4.2 mmol (1.0 g) of TlCl and 21.6 mmol (2.36 g) of $2\text{-}CH_3C_5H_4NO$ in acetonitrile (50 cm^3), a solution of 4.4 mmol (0.91 g) of IBr in the same solvent (25 cm^3) was added dropwise. A yellow solid was precipitated before the reaction was complete. When the reaction was finished the yellow solid was filtered off and vacuum dried. The compound obtained was $TlClBrI(2\text{-}CH_3C_5H_4NO)_2$, but when the resulting orange solution was concentrated *in vacuo* an orange solid was precipitated. (Yield: 40%.) Found: C, 26.9; H, 2.7; N, 5.2; Tl, 26.2. Calc. for $C_{18}H_{21}BrClIN_3O_3Tl$: C, 27.9; H, 2.7; N, 5.4; Tl, 26.4%. M.p. 105°C, Λ_M 59 Ohm^{-1} cm^2 mol^{-1}.

$TlClBrI(3\text{-}CH_3C_5H_4NO)_2$ (**IV**). The complex was prepared by following the method reported for $TlClBrI(2\text{-}CH_3C_5H_4NO)_2$. (Yield: 79%.) Found: C, 21.3; H, 2.1; N, 4.2; Tl, 29.5. Calc. for $C_{12}H_{14}BrClIN_2O_2Tl$: C, 21.7; H, 2.1; N, 4.2; Tl, 30.7%. M.p. 118°C, Λ_M 63 Ohm^{-1} cm^2 mol^{-1}.

$TlClBrI(4\text{-}CH_3C_5H_4NO)_2$ (**V**). To a suspension of 4.2 mmol (1.0 g) of TlCl and 8.5 mmol (0.93 g) of $4\text{-}CH_3C_5H_4NO$ in acetonitrile (30 cm^3), a solution of 4.3 mmol (0.90 g) of IBr in the same solvent (25 cm^3) was added. The resulting red solution was concentrated *in vacuo* and an oil was obtained. The residual oil was stirred with dry ether to give a yellow solid. (Yield: 75%.) Found: C, 21.5; H, 2.0; N, 3.8; Tl, 29.6. Calc. for $C_{12}H_{14}BrClIN_2O_2Tl$: C, 21.7; H, 2.1; N, 4.2; Tl, 30.7%. M.p. 86°C, Λ_M 59 Ohm^{-1} cm^2 mol^{-1}.

$TlClBrI(4\text{-}ClC_5H_4NO)_2$ (**VI**). A solution of 4.7 mmol (0.96 g) of IBr in CH_3CN was slowly added to a suspension of 4.2 mmol (1.0 g) of TlCl and 8.6 mmol (1.1 g) of $4\text{-}ClC_5H_4NO$ in acetonitrile (50 cm^3). The mixture was stirred for one day and then was warmed to 50°C. The solid obtained was filtered off and the resulting red solution was left at room temperature and then placed in a refrigerator. Orange crystals were obtained. (Yield: 55%.) Found: C, 17.0; H, 1.0; N, 4.2; Tl, 28.1. Calc. for $C_{10}H_8BrClIN_2O_2Tl$: C, 17.0; H, 1.1; N, 4.0; Tl, 29.0%. M.p. 133°C, Λ_M 65 Ohm^{-1} cm^2 mol^{-1}.

$TlClBrI(4\text{-}CNC_5H_4NO)_2$ (**VII**). A solution of 4.5 mmol (0.94 g) of IBr in acetonitrile (25 cm^3) was added dropwise to 4.2 mmol (1.0 g) of TlCl and 8.5 mmol (1.2 g) of $4\text{-}CNC_5H_4NO$ in the same solvent (100 cm^3). The orange solid which precipitated was filtered off, washed with cold acetonitrile and vacuum dried. (Yield: 71%.) Found: C, 21.0; H, 1.1; N, 8.2; Tl, 28.6. Calc. for $C_{12}H_8BrClIN_4O_2Tl$: C, 21.0; H, 1.1; N, 8.2; Tl, 29.7%. M.p. 145°C, Λ_M 66 Ohm^{-1} cm^2 mol^{-1}.

$TlClBrI(4\text{-}NO_2C_5H_4NO)_2$ (**VIII**). The complex has been prepared by following the method reported for compound **IV**. (Yield: 74%.) Found: C, 16.5; H, 1.0; N, 7.4; Tl, 28.4. Calc. for

$C_{10}H_8BrClIN_4O_6Tl$: C, 16.5; H, 1.1; N, 7.7; Tl, 28.1%. M.p. 97°C, Λ_M 80 Ohm^{-1} cm^2 mol^{-1}.

$TlClBrI(4\text{-}CH_3OC_5H_4NO)_2$ **(IX)**. A solution of 4.4 mmol (0.91 g) of IBr in CH_3Cl was added to a suspension of 4.2 mmol (1.0 g) of TlCl and 8.8 mmol (1.1 g) of $4\text{-}CH_3OC_5H_4NO$ in methylene chloride (50 cm^3). The resulting yellow solution was concentrated *in vacuo* and an oil was obtained. The oil was stirred with ether and a yellow powdery solid was formed. The solid was filtered off, washed with cold ether and vacuum dried. (Yield: 70%.) Found: C, 21.7; H, 2.0; N, 4.1; Tl, 30.5. Calc. for $C_{12}H_{14}BrClIN_2O_4Tl$: C, 21.7; H, 2.1; N, 4.2; Tl, 30.7%. M.p. 103°C, Λ_M 70 Ohm^{-1} cm^2 mol^{-1}.

$TlClBrI(HMPA)_2$ **(X)** *and* $TlClBrI(OPPh_3)_2$ **(XI)**. These have been prepared by the method described elsewhere[25,26] and their elemental analyses have produced satisfactory results.

X-ray crystallographic structure determination of XI

A crystal suitable for X-ray studies was selected from the reaction product. The crystal was mounted on a glass fibre and data were collected according to the parameters in Table 1. Lorentz and polarization corrections were applied. An empirical absorption correction was undertaken using DIFABS.[27]

The structure was solved using the Patterson method which revealed the position of the Tl atom. The remaining atoms were located in succeeding difference Fourier syntheses. Hydrogen atoms were not included in the calculations. The structure was refined using full-matrix least-squares where the function minimized was $\Sigma w(|F_o|-|F_c|)^1$ and the weight "w" is defined as $1/\sigma^2(F_o)$. A secondary extinction correction with a final coefficient of 1.5214×10^{-8} was refined in the least-squares.[28]

All calculations were performed on a VAX 11/750 computer using VAXSDP.[29] The scattering factors for all atoms were taken from standard sources.[30] Selected bond distance and angle parameters are given in Table 2, and tables of final positional parameters, anisotropic thermal parameters, complete bond lengths and angles, and lists of observed and calculated structure factors are available as supplementary material.

Table 1. Summary of crystal data and intensity data collection

Formula	$C_{36}H_{30}BrClIO_2P_2Tl$
f_w	1003.22
$F(000)$	1912
Colour	yellowish
Habit	prismatic
Crystal system	monoclinic
Space group	$P2_1/c$
a (Å)	14.742(3)
b (Å)	14.418(3)
c (Å)	17.234(4)
β (°)	107.54(2)
V (Å^3)	3492.8
Z	4
d_{calc} (g cm^{-3})	1.908
Abs coeff. (cm^{-1})	68.8
Crystal dimensions (mm)	$0.40 \times 0.20 \times 0.10$
Diffractometer	Enraf–Nonius CAD4
Radiation	Mo-K_α ($\lambda = 0.71073$ Å)
Monochromator	graphite crystal
Scan type	ω/θ
Scan rate (° min^{-1})	6–10 (in omega)
Maximum 2θ (°)	50
Reflections measured	$+h, +k, \pm l$
Temperature (K)	173
No. of data collected	6014
No. of unique data	5871
Total with $F_o > 3\sigma(F_o)$	4256
Final No. of variables	398
$R = \Sigma(\|F_o\|-\|F_c\|)/\Sigma\|F_o\|^{1/2}$	0.05
$R_w = \|\Sigma w(\|F_o\|-\|F_c\|)^2/\Sigma wF_o^2\|$	0.058
Weighting scheme	$1/\sigma^2(F_o)$
Std error in observation of unit wt (e)	6.26

RESULTS AND DISCUSSION

All compounds were prepared for the molar ratio 1:2, but we have proved that complexes can be obtained with 1:3 stoichiometry as has been mentioned before.[31] The species are yellow crystalline solids, air and light stable, hardly soluble in solvents, with low dielectric constants and millimolar conductivity values below those typical of electrolytes.[32] The compounds are monomers in benzene, as proved by computation of the molecular weight of those soluble in the solvent. Calc. for $TlClBrI(4\text{-}CH_3OC_5H_4NO)_2$: 665. Found: 650. Calc. for $TlClBrI(HMPA)_2$: 800. Found: 815. Calc. for $TlClBrI(OPPh_3)_2$: 1002. Found: 978.

Structure of $TlClBrI(OPPh_3)_2$

$TlClBrI(OPPh_3)_2$ **(XI)** was structurally characterized by X-ray crystallography. The crystal structure is isotypic with $TlBr_3(OPPh_3)_2$,[5] $TlBr_2I(OPPh_3)_2$[16] and $TlBrI_2(OPPh_3)_2$.[17] The asymmetric unit consists of two $OPPh_3$ ligands and one Cl, Br, I and Tl atom. The structure of one unit is shown in Fig. 1 and its stereoscopic view in Fig. 2. The Tl atom is in a distorted trigonal bipyramidal environment. The three equatorial atoms are the Cl, Br and I. Within the limits of error (0.021 Å) the Tl and

Table 2. Selected bond distances (Å) and angles (°)

Tl—I	2.646(0)	P1—C11	1.787(5)
Tl—Br	2.563(1)	P1—C21	1.800(5)
Tl—Cl	2.469(1)	P1—C31	1.797(5)
Tl—O1	2.396(4)	P2—C41	1.793(5)
Tl—O2	2.404(4)	P2—C51	1.798(6)
P1—O1	1.491(4)	P2—C61	1.789(5)
P2—O2	1.485(4)		
I—Tl—Br	123.34(3)	O1—P1—C11	112.5(2)
I—Tl—Cl	116.30(3)	O1—P1—C21	109.9(2)
I—Tl—O1	91.18(9)	O1—P1—C31	112.9(2)
I—Tl—O2	93.03(9)	C11—P1—C21	107.3(2)
Br—Tl—Cl	120.34(3)	C11—P1—C31	106.8(2)
Br—Tl—O1	88.26(9)	C21—P1—C31	107.2(2)
Br—Tl—O2	88.6(1)	O2—P2—C41	110.1(2)
Cl—Tl—O1	89.21(9)	O2—P2—C51	108.3(3)
Cl—Tl—O2	89.9(1)	O2—P2—C61	116.7(2)
O1—Tl—O2	175.7(1)	C41—P2—C51	107.0(2)
Tl—O1—P1	149.0(2)	C41—P2—C61	107.3(2)
Tl—O2—P2	148.5(2)	C51—P2—C61	107.1(2)

halide atoms are coplanar. The axial sites are occupied by two oxygen atoms of the $OPPh_3$ ligands. Bond distances and angles are given in Table 2.

The angles about the Tl atom deviate only slightly from idealized trigonal-bipyramidal geometry. The greatest deviation arises from the O(1)—Tl—O(2) angle (175.7(1)°) even if angular distortions are also observed in the equatorial plane (123.34(3)–116.30(3)°). Although the M—O—P angles may be affected by crystal packing effects,[33] the values of Tl—O—P found in $TlClBrI(OPPh_3)_2$ are similar to those found in the isotypic compounds.

As expected, the Tl—Cl distance of 2.469(1) Å is shorter then in $[TlCl_3(C_5H_5N)_3]\cdot C_5H_5N$,[34] 2.520(6) and 2.498(4) Å, where the coordination around the Tl atom is octahedral; and also shorter than in $(p\text{-}HC_6F_4)_2TlCl(OPPh_3)$[33] which is dimeric with unsymmetrical chlorine bridging (Tl—Cl 2.541(3) Å, Tl—Cl′ 2.936(3) Å). The Tl—Br distance is not significantly different (2.563(1) Å) from those observed in other five-coordinate thallium(III) halide complexes, e.g. 2.580(1) Å in $TlBrI_2(OPPh_3)_2$,[17] average 2.567(1) Å in $TlBr_2I(OPPh_3)_2$ or average 2.549(1) Å in $TlBr_3(C_5H_5NO)_2$[15] but greater than in $TlBr_3(OPPh_3)_2$,[5] average 2.505(2) Å. The Tl—I distance of 2.646(0) Å resembles those observed in simple compounds of thallium(III) containing $OPPh_3$[16,17] coordinated, but is shorter than

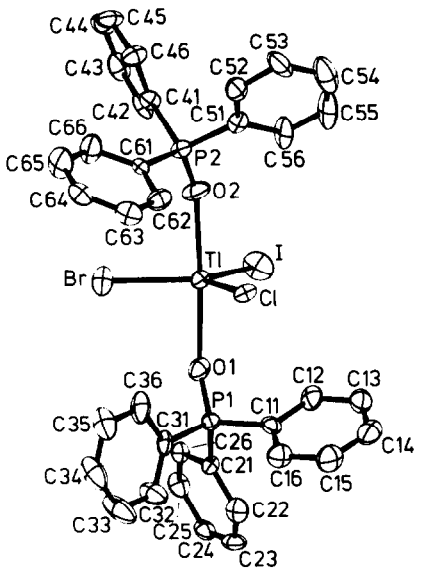

Fig. 1. Structure of $TlClBrI(OPPh_3)_2$, showing 50% probability ellipsoids and atom-labelling scheme.

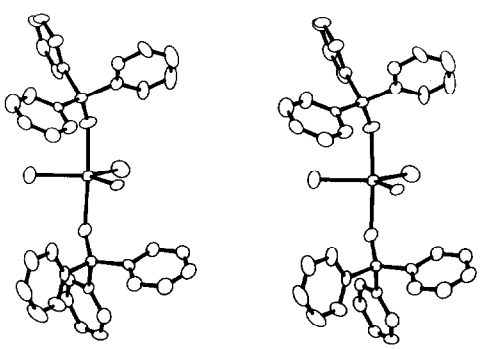

Fig. 2. Stereographic view of $TlClBrI(OPPh_3)_2$.

the average 2.703(0) Å in $TlI_3(3\text{-}CH_3C_5H_4NO)_2$.[13] The variations in some of the thallium–halide distances may be attributed to a distinct electronegativity of the halogen atoms in equatorial positions in conjunction with the different ligand strengths in axial positions.

The Tl—O distances in $TlClBrI(OPPh_3)_2$, (2.396(4), 2.404(4) Å) are similar to those observed in other thallium(III) halide complexes of $OPPh_3$,[5,16,17,33] suggesting comparable bond strengths.

The geometries of the triphenylphosphine oxide ligands in complexes appear to be normal, although, as expected, the P—O distances of 1.491(4) and 1.485(1) Å are a little larger than in the uncoordinated compounds with the orthorhombic modification, 1.46(1) Å[35] or with the monoclinic modification, 1.487(2) Å.[36] The mean C—P—C angles are smaller and the O—P—C angles greater than the ideal tetrahedral angle.

^{1}H *NMR spectra*

The ^{1}H NMR spectra of the ligands and complexes have been assigned using the results known for aromatic amine oxides;[37,38] only the spectrum of $TlClBrI(4\text{-}CNC_5H_4NO)_2$ has not been recorded because it decomposes in $CDCl_3$. These assignments with the chemical displacements [$\Delta(\delta H_\alpha)$, $\Delta(\delta H_\beta)$] and the internal chemical shifts $\Delta\delta$ are presented in Table 3. From the collected data it can be concluded that the ligand molecules occupy equivalent positions in the complexes as has been observed by Williams[39] and which is in agreement with crystallographic data of $TlClBrI(OPPh_3)_2$.

Table 3. Proton chemical shifts (ppm relative to TMS)

Compounds	δH_α	$\Delta(\delta H_\alpha)$	δH_β	$\Delta(\delta H_\beta)$	$\Delta\delta$
C_5H_5NO	8.18		7.27		0.91
I	8.35	0.17	7.46	0.19	0.89
$2\text{-}CH_3C_5H_4NO$	8.26		7.23		1.03
II	8.42	0.16	7.40	0.17	1.02
$3\text{-}CH_3C_5H_4NO$	8.08		7.23		0.85
IV	8.15	0.07	7.27	0.04	0.88
$4\text{-}CH_3C_5H_4NO$	8.06		7.04		1.02
V	8.27	0.21	7.25	0.21	1.02
$4\text{-}ClC_5H_4NO$	8.09		7.21		0.88
VI	8.30	0.21	7.45	0.24	0.85
$4\text{-}CNC_5H_4NO$	8.18		7.47		0.71
VII[a]	—	—	—	—	—
$4\text{-}NO_2C_5H_4NO$	8.30		8.16		0.14
VIII	8.39	0.09	8.26	0.10	0.13
$4\text{-}CH_3OC_5H_4NO$	8.09		6.78		1.31
IX	8.25	0.16	6.94	0.16	1.31

[a] It has not been possible to record this spectrum because it decomposes in Cl_3CD.

Vibrational spectra

The most significant bands in the IR and Raman spectra of the ligands and their complexes are shown in Table 4. The ligand bands have been assigned according to the literature.[40–44]

The position of the ν(NO) and ν(PO) vibration modes in the compounds is shifted towards lower frequencies ($\Delta\nu \simeq 20$–$50\ cm^{-1}$), showing that coordination takes place through the oxygen atom of the N—O and P—O groups. Similar results have been obtained for other complexes with these ligands.[10,11,41,45]

The influence of the inductive character of the ring substituents on the location of the ν(NO) bands in the complexes with pyridine N-oxide and substituted pyridine N-oxides has been the object of analysis. We have studied the existing relationship between the "σ" parameter which measures the inductive capacity of the substituents and the location of the ν(NO) bands in the ligands and complexes. Similarly, the relationship of σ with $\Delta\nu$ has been studied and is plotted in Fig. 3. It can be observed that, as Karayannis *et al.* have shown,[41] the linearity of σ vs ν(NO) and $\Delta\nu$ holds when the complexes are formed.

The bands that appear between 400–50 cm^{-1} containing information concerning the structure of the compounds are ν(TlX) and ν(TlO). The assignments of the ν(TlCl), ν(TlBr) and ν(TlI) vibrations have been accomplished by the method discussed elsewhere[10,11] and taking into account Carty's ideas.[46] The bands appearing at 120–100 cm^{-1} have

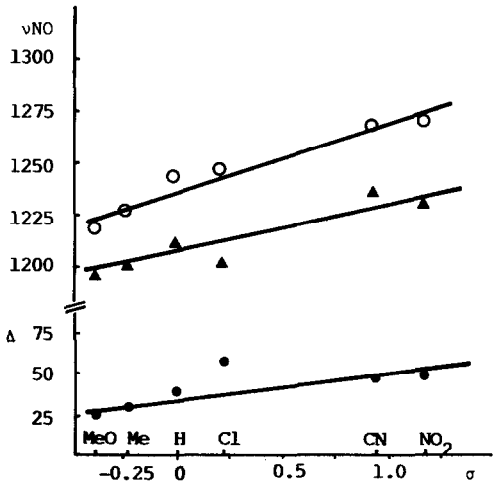

Fig. 3. Correlations of σ with: ν(NO) for the ligands, ○; for the complexes, ▲; and $\Delta\nu$(NO), ●.

Table 4. Most significant (IR and Raman) bands of the ligands and the complexes

Compounds		ν(ZO)	δ(NO)	ν(TlCl)	ν(TlBr)	ν(TlI)	ν(TlO)	Other bands
C_5H_5NO	IR	1243vs	842s	—	—	—	—	515m, 460s, 406w, 254w
	R	1235m	842s	—	—	—	—	515m, 460s, 405w
I	IR	1211vs	827vs	287s	196s	167s	310vs	515m, 457vs, 405w, 120$^+$m
	R	1210s	840m	275vs	200s	170s	322vs	510m, 454m
2-$CH_3C_5H_4NO$	IR	1242vs	855s	—	—	—	—	470s, 454s, 342m, 270w, 230m
	R	1240s	855m	—	—	—	—	470s, 450s, 340m, 235m
II	IR	1198vs	842s	275s	197s	163s	325m	468s, 458s, 342m, 235m, 112$^+$m
	R	1207s	848m	270vs	195s	—	326vs, 230s	468s, 458w
III	IR	1202vs	843s	277s	192s	161s	320s	469s, 458m, 345m, 233m, 115$^+$m
	R	1207s	842m	275s	195s	160s	332vs	470s, 452w
3-$CH_3C_5H_4NO$	IR	1278vs	—	—	—	—	—	492s, 438m, 308s, 203w
	R	1283s	—	—	—	—	—	490w, 445m, 305w
IV	IR	1258vs	—	273s	193s	173s	294s	485s, 439m, 315s, 208w, 105$^+$s
	R	1265vs	—	273vs	198s	180m	305vs	490m, 445w
4-$CH_3C_5H_4NO$	IR	1228vs	852s	—	—	—	—	478s, 465m, 336s, 317w, 222w
	R	1228s	852m	—	—	—	—	475m, 460s, 360s
V	IR	1202vs	830s	288s	193s	163s	285sh	480s, 465m, 330s, 225m, 110m
	R	1203s	830m	275vs	196s	—	338w	474w, 457m, 360m
4-ClC_5H_4NO	IR	1248vs	848s	—	—	—	—	480m, 325m, 275m
	R	1248s	848m	—	—	—	—	480m, 320m, 273m
VI	IR	1201vs	845s	273s	198s	168s	—	472m, 320m, 250w, 109$^+$m
	R	1210s	847m	286vs	200s	170s	373vs	468m, 330sh
4-CNC_5H_4NO	IR	1275vs	845s	—	—	—	—	455m, 410m, 220w
	R	1275s	845s	—	—	—	—	452s, 402w
VII	IR	1237vs	850s	287s	217s	161s	309m	455m, 420m, 230m, 105$^+$s
	R	1245s	860s	272vs	205s	165s	332s, 250m	450s, 400m
4-$NO_2C_5H_4NO$	IR	1273vs	874s	—	—	—	—	455m, 360w, 220w
	R	1273s	884s	—	—	—	—	460s, 375w
VIII	IR	1233vs	868s	280s	195vs	175sh	329m	460s, 365m, 230m, 105$^+$m
	R	1249s	880s	273vs	200s	180m	340w	460s, 410w
4-$CH_3OC_5H_4NO$	IR	1213vs	850s	—	—	—	—	455s, 400s, 310w, 250s
	R	—	858s	—	—	—	—	457s, 400s, 250m
IX	IR	1192vs	845s	282s	200s	165s	305m	455s, 410s, 250s, 114$^+$m
	R	1200w	843s	280s	205s	—	320s	455m, 410s, 250s
HMPA	IR	1208vs	—	—	—	—	—	475s, 376s, 350m, 260w
	R	1205s	—	—	—	—	—	470s, 375s, 345m
X	IR	1188vs	—	293s	202vs	170s	—	475s, 376s, 350m, 260w, 115$^+$m
	R	1188s	—	300s	210vs	176s	320m	475s, 370m, 350w
$OPPh_3$	IR	1187vs	—	—	—	—	—	302vs, 291s, 262m
	R	1185s	—	—	—	—	—	300vs, 291s, 262m
XI	IR	1150vs	—	295vs,br	210s	181s	—	305sh, 256m, 105$^+$s
	R	1155s	—	296s,br	215s	180s	—	256m

been taken as δ(TlX) as it has been suggested.[21,47] The position of the ν(TlO) bands has been placed at 300 cm^{-1} according to the assignments of other papers.[7,9] These assignments are listed in Table 4.

The small number of bands in the vibrational spectra of these complexes and their position may exclude the presence of covalent dimeric or polymeric structures as well as ionic forms.[48,49]

In these spectra we have found three bands which we have assigned as ν(TlC), ν(TlBr) and ν(TlI) (see Table 4) and we have only one band assigned as ν(TlO) except for the $TlClBrI(2\text{-}CH_3C_5H_4NO)_2$ compound.

Complexes of thallium(III) with stoichiometry 1:3 are known, for instance $TlCl_3(C_5H_5N)_3$ and $TlBr_3(C_5H_5N)_3$, which have an octahedral environment around the thallium atom,[34,50] but for $TlClBrI(2\text{-}CH_3C_5H_4NO)_3$ the number, position and intensity of the bands present in its spectrum are very similar to those of $TlClBrI(2\text{-}CH_3C_5H_4NO)_2$. According to these data we suggest a structure for this compound comparable to that

of $TlClBrI \cdot L_2$ compounds with the third ligand molecule occluded in the cell.

Finally we must suggest that the most probable structure for $TlClBrI \cdot L_2$ compounds should be very similar to the one found for $TlClBrI(OPPh_3)_2$.

Acknowledgements—This research was supported by a grant from the Xunta de Galicia. We also thank the Ministerio de Educación y Ciencia for financial support (A.C.).

REFERENCES

1. F. A. Cotton, B. F. G. Johnson and R. M. Wing, *Inorg. Chem.* 1965, **4**, 502.
2. R. A. Walton, *Coord. Chem. Rev.* 1971, **6**, 1.
3. W. J. Baxter and G. Gafner, *Inorg. Chem.* 1972, **11**, 176.
4. E. Gutierrez-Puebla, A. Vegas and S. García-Blanco, *Acta Cryst., Sect. B: Struct. Cryst. Chem.* 1980, **B36**, 145.
5. S. E. Jeffs, R. W. H. Small and I. J. Worral, *Acta Cryst., Sect. C: Cryst. Struct. Commun.* 1984, **C40**, 65, 381.
6. J. Glaser, *Acta Chem. Scand.* 1979, **A33**, 789.
7. M. R. Bermejo and M. Gayoso, *Synth. React. Inorg. Met-Org. Chem.* 1985, **15**, 951.
8. M. I. Fernández, M. R. Berjemo, A. Fernández, E. Solleiro and M. Gayoso, *An. Quím.* 1987, **83B**, 26.
9. M. V. Castaño, A. Sánchez, M. R. Bermejo and M. Gayoso, *An. Quím.* 1983, **79B**, 357.
10. M. R. Berjemo, J. Irisarri and M. Gayoso, *Synth. React. Inorg. Met-Org. Chem.* 1985, **15**, 197.
11. M. R. Bermejo, M. I. Fernández, J. García-Taboada and M. Gayoso, *Synth. React. Inorg. Met-Org. Chem.* 1986, **16**, 327.
12. M. R. Bermejo, E. Solleiro, A. Rodriguez and A. Castiñeiras, *Polyhedron* 1987, **6**, 315.
13. M. R. Bermejo, A. Castiñeiras, M. Gayoso, W. Hiller, U. Englert and J. Strähle, *Z. Naturforsch.* 1984, **39b**, 1159.
14. M. R. Bermejo, F. Botana, M. Gayoso, A. Catiñeiras, W. Hiller and J. Strähle, *Acta Cient. Compost.* 1985, **XXII**, 161.
15. W. Hiller, M. E. García-Fernández, M. R. Bermejo and M. V. Castaño, *Acta Cryst., Sect. C: Cryst. Struct. Commun.* 1986, **C42**, 60.
16. A. Castiñeiras, W. Hiller, M. R. Bermejo and M. Gayoso, *Acta Cryst., Sect. C: Cryst. Struct. Commun.* 1986, **C42**, 1289.
17. A. Castiñeiras, W. J. Hiller, J. Strähle, M. R. Bermejo and M. Gayoso, *An. Quím.* 1986, **82B**, 282.
18. W. Hiller, A. Castiñeiras, M. E. García-Fernández, M. R. Bermejo, J. Bravo and A. Sánchez, *Z. Naturforsch.* 1988, **43b**, 132.
19. M. R. Bermejo, M. T. Lage, M. I. Fernández and A. Castiñeiras, *Synth. React. Inorg. Met-Org. Chem.* 1987, **17**, 79.
20. B. F. G. Johnson and R. A. Walton, *Inorg. Chem.* 1966, **5**, 49.
21. R. A. Walton, *Inorg. Chem.* 1968, **7**, 640, 1927.
22. R. W. Matthews and R. A. Walton, *J. Chem. Soc. (A)* 1968, 1639.
23. R. E. Pearson, *Science* 1956, **151**, 172.
24. V. Ozimec, T. Smith and R. A. Walton, *J. Inorg. Nucl. Chem.* 1967, **39**, 362.
25. J. Irisarri, M. R. Bermejo, M. V. Castaño and M. Gayoso, *Rev. Port. Quím.* 1983, **25**, 174.
26. M. R. Bermejo, G. Botana and M. Gayoso, *Rev. Port. Quím.* 1984, **26**, 113.
27. N. Walker and D. Stuart, *Acta Cryst., Sect. A: Cryst. Phys., Diffr. Theor. Gen. Cryst.* 1983, **A39**, 158.
28. W. H. Zachariasen, *Acta Cryst.* 1963, **16**, 1139.
29. B. A. Frenz, VAXSDP *Structure Determination Package*, Version 2.2. Associates Inc., College Station, Texas U.S.A. and Enraf–Nonius, Delft, Holland (1985).
30. *International Tables for X-Ray Crystallography*, Vol. IV. Kynoch Press, Birmingham, U.K. (1974).
31. F. Blanco, M. V. Castaño, M. R. Bermejo and M. Gayoso, *An. Quím.* 1985, **81B**, 133.
32. W. J. Geary, *Coord. Chem. Rev.* 1971, **7**, 81.
33. K. Henrick, M. McPartlin, R. W. Matthews, G. B. Deacon and R. J. Phillips, *J. Organomet. Chem.* 1980, **193**, 13.
34. S. E. Jeffs, R. W. H. Small and I. J. Worrall, *Acta Cryst., Sect. C: Cryst. Struct. Commun.* 1984, **C40**, 1329.
35. G. Bandoli, G. Bortolozzo, D. A. Clemente, U. Croatto and C. Panattoni, *J. Chem. Soc. (A)* 1970, 2778.
36. D. Thierbach, F. Huber and H. Preut, *Acta Cryst., Sect. B: Cryst. Cryst. Chem.* 1980, **B36**, 974.
37. A. R. Katritzky and J. J. Lagowski, *J. Chem. Soc. (A)* 1961, 43.
38. R. A. Abranovitch and J. B. Davis, *J. Chem. Soc. (B)* 1966, 1132.
39. C. L. Wild, M. Spahis, R. D. Blankenship, J. W. Rogers and R. J. Williams, *Polyhedron* 1983, **2**, 379.
40. H. Shindo, *Chem. Pharm. Bull.* 1956, **4**, 460; H. Shindo, *Chem. Pharm. Bull.* 1958, **6**, 117; H. Shindo, *Chem. Pharm. Bull.* 1959, **7**, 791.
41. N. M. Karayannis, L. L. Pytlewski and C. M. Mikulski, *Coord. Chem. Rev.* 1973, **11**, 93.
42. M. De Bolster and W. Groeneweld, *Rec. Trav. Chim.* 1971, **90**, 477.
43. S. Milicev and D. Hadzi, *Inorg. Chim. Acta* 1977, **21**, 201.
44. K. Tan and M. J. Taylor, *Inorg. Nucl. Chem. Lett.* 1980, **16**, 337.
45. J. R. Masaguer, J. S. Casas, J. Sordo, M. R. Bermejo and M. V. Castaño, *Inorg. Chim. Acta* 1977, **24**, 227.
46. A. J. Carty, *Coord. Chem. Rev.* 1969, **4**, 29.
47. J. R. Hudman, M. Patel and W. R. McWhinnie, *Inorg. Chim. Acta* 1970, **4**, 161.
48. R. A. Walton, *J. Inorg. Nucl. Chem.* 1970, **32**, 2875.
49. K. Arai, T. Chiba and K. Aida, *J. Inorg. Nucl. Chem.* 1981, **43**, 1986.
50. S. E. Jeffs, R. W. Small and I. J. Worrall, *Acta Cryst., Sect. C: Cryst. Struct. Commun.* 1984, **C40**, 1827.

Polyhedron Vol. 7, No. 24, pp. 2569–2573, 1988
Printed in Great Britain

0277–5387/88 $3.00+.00
© 1988 Pergamon Press plc

SYNTHESIS OF SOME *CIS*-DIOXOMOLYBDENUM COMPLEXES AND THEIR USE IN THE EPOXIDATION OF OLEFINS

D. D. AGARWAL* and SAVITA SHRIVASTAVA

School of Studies in Chemistry, Jiwaji University, Gwalior—474011, M.P., India

(*Received* 15 *December* 1987; *accepted after revision* 24 *May* 1988)

Abstract—The *cis*-dioxomolybdenum complexes $MoO_2(L)$ (L = HPD, APAC, AAC, ACEN and APS) have been synthesized and characterized. The epoxidation of olefins has been studied using these molybdenum complexes as catalysts and tert-butylhydroperoxide (TBHP) as oxidant. The studies suggest that these complexes, except [MoO_2(APAC)], did not demetallate during the reaction.

The ability of the cytochrome P-450 enzymes to selectively oxidize alkenes through the activation of molecular oxygen has focussed attention on synthetic metalloporphyrins and their potential as oxidation catalysts.[1–8] Various porphyrin systems have been screened for their ability to catalytically oxidize organic substrates. Various workers[9–11] have reported that molybdenum complexes undergo demetallation but Ledon *et al.*[12] have reported O=Mo(TPP)OMe as a stable catalyst for epoxidation. In the present report we have synthesized and characterized *cis*-dioxomolybdenum complexes using the ligands, 2-hydroxyphenylhydrazonopentane 2,4 dione (HPD), 2-aminophenylacetylacetone (APAC), 2-amino benzoic acid acetylacetone (AAC), acetylacetone ethylenediamine (ACEN) and aminophenyl salicylaldehyde (APS). The complexes so formed are used for the epoxidation of olefins in order to see the possibility of utilizing the non-porphyrin system for epoxidation.

EXPERIMENTAL

All starting alkenes were checked by gas chromatography to ensure that no oxidation products were present. Analytical gas chromatography was done on Perkin–Elmer model 3920 equipped with a flame ionization detector. OV-17 was used as the chromatographic column and the analysis was carried out at 80°C, except in isoprene where a temperature of 35°C was used. Tert-butylhydroperoxide was placed in benzene and estimated by the known procedure.[13] The reference sample of epoxides was prepared by a known procedure.[14] IR spectra were recorded on Beckmann IR-20 spectrophotometer.

Synthesis of the complexes

The ligands HPD, APAC, AAC, ACEN and APS were synthesized by condensing the amine with suitable aldehyde or ketones in absolute alcohol. All the complexes were synthesized[15] by taking both ligand and $MoO_2(acac)_2$ in equimolar ratio (i.e. 0.01 mol each) which were dissolved in ethanol (100 cm^3). The contents were refluxed for 2 h, filtered and the solvent was reduced. On cooling, precipitates were obtained which were filtered, washed and dried *in vacuo*. The melting point and elemental analysis values are given in Table 1.

Procedure for epoxidation

Olefin (0.02 mol), tert-butylhydroperoxide (0.002 mol), catalyst (MoO_2L) (0.0002 mol) and benzene (20 cm^3 as solvent) were placed in a three-necked round-bottomed flask. Dodecane was used as an internal standard. The contents were heated to 70°C using a magnetic stirrer. While carrying out epoxidation of isoprene the temperature was kept at 40°C. The contents were heated for 5 h, then cooled. The catalyst was removed by filtration and the

* Author to whom correspondence should be addressed.

Table 1. Characterization of *cis*-dioxomolybdenum(VI) complexes

S. No.	Complexes	Analyses[a] C	H	N	Colour	Melting point (°C)
1	$MoO_2(C_{11}H_{11}N_2O_3)Me_2SO$	36.7 (36.7)	4.0 (4.0)	6.6 (6.5)	Green	210
2	$MoO_2(C_{13}H_9NO_2)Me_2SO$	43.1 (43.2)	3.6 (3.5)	3.3 (3.3)	Dirty yellow	225
3	$MoO_2(C_{12}H_{18}N_2O_2)$	41.1 (41.1)	5.1 (5.1)	8.0 (8.0)	Ash	190
4	$MoO_2(C_{19}H_{16}N_2O_2)$	49.1 (49.1)	3.4 (3.4)	6.0 (6.0)	Dirty yellow	220
5	$MoO_2(C_{17}H_{16}N_2O_2)$	50.0 (49.9)	3.9 (3.9)	6.8 (6.8)	Black	125

[a] Calculated in parentheses.

tert-butylhydroperoxide (TBHP) was decomposed using aqueous sodium sulphite solution. The contents were extracted with ether and the samples so obtained were dried over anhydrous magnesium sulphate. The products were analysed by G.C.

RESULTS AND DISCUSSION

The analysed data are in agreement with those expected for the dioxomolybdenum complexes. The conductance studies shows that they are non-conducting (Table 1). The magnetic susceptibility values measured by Gouy's method shows that they are diamagnetic.

IR spectra

Spectra in the 4000–250 cm^{-1} range were taken of the solid complexes in KBr discs (Table 2). The $[MoO_2(ACEN)]$ complex shows absorption at 1620 cm^{-1}, assigned to the C=N— stretching, which decreases by 10 cm^{-1} on coordination therefore suggesting its involvement. The absorption bands at 890 and 900 cm^{-1} are assigned to Mo=O. These bands are characteristic bands of *cis*-dioxomolybdenum(VI) complexes. In the IR absorption of the ligand (AAC), the bands at 2699, 1660, 1440 and 1320 cm^{-1} are assigned to ν_{OH} stretching (dimer), $\nu_{C=O}$ frequency of internally hydrogen bonded carboxylic group, ν_{C-O} stretching and OH in-plane bending of the carboxylic group, respectively. All these bands except the one at 1440 cm^{-1} disappear on coordination. The peak at 1620 cm^{-1} is assigned to $\nu_{C=N}$ stretching in the ligands and moves down to 1600 cm^{-1} supporting its involvement in coordination. The band at 940 cm^{-1} has been assigned to Mo=O. In the ligand (HPD) the band at 1640 cm^{-1} is assigned to the $\nu_{C=O}$ group, this band is lowered by 10 cm^{-1} on coordination. The Mo=O absorption bands are observed at 900 and 960 cm^{-1}. The C—O stretching observed in the ligand at 1265 cm^{-1} is shifted to 1285 cm^{-1} on coordination. The ligand APAC spectrum shows bands at 1600 and 1240 cm^{-1} assigned to the $\nu_{C=N}$ and ν_{C-O} stretching of the hydroxyl group. The band at 1660 cm^{-1} moves to 1590 cm^{-1} and the ν_{C-O} band in the complex is

Table 2. IR spectral bands of the *cis*-dioxomolybdenum(VI) complexes

S. No.	Complexes	CH_2 (cm^{-1})	CH (cm^{-1})	CH_3 (cm^{-1})	C=N (cm^{-1})	C=O (cm^{-1})	COOH (cm^{-1})	C—O (cm^{-1})	Mo=O (cm^{-1})
1	$MoO_2(ACEN)$	2960	2910	2860	1600	1510	—	—	890, 900
2	$MoO_2(AAC)$	3000	—	2800	1605	—	1660 1440	—	940
3	$MoO_2(HPD)Me_2SO$	—	—	—	1600	1640	—	1285	900, 960
4	$MoO_2(APAC)$	2930	—	2860	1600	—	—	1260	910

observed at 1260 cm^{-1} suggesting the involvement of these two groups in coordination. The Mo=O absorbs at 910 cm^{-1}.

On the basis of chemical analysis and IR spectral studies the structure assigned to the complexes has been confirmed. The IR spectrum of $[MoO_2(APS)]$ has been discussed elsewhere.[15]

Epoxidation

Epoxidation of cyclohexene with all the catalysts gave cyclohexene oxide in a very good yield. The gas chromatographic analysis shows that the epoxide was the sole product and no cyclohexanone or cyclohexanol was obtained. The two latter products are usually obtained as a result of a free radical pathway. After the reaction the catalysts were separated by filtration, washed, dried and subjected to melting point and IR studies. The m.p. (Table 3) and IR studies suggest that, except for $[MoO_2(APAC)]$, all the other catalysts viz. $[MoO_2(ACEN)]$, $[MoO_2(APS)]$, $[MoO_2(AAC)]$ and $[MoO_2(HPD)]$ withstand the oxidative conditions and the epoxidation follows a heterolytic pathway. All the catalysts have been found to give high yields of cyclohexene oxide. In the case of $[MoO_2(APAC)]$, demetallation of the catalyst takes place. Sheldon[9] has reported that the ligand effect may be observable only during the initial steps of the reaction because of the ligand destruction under the oxidative conditions, thus giving the same rate for the molybdenum catalysed epoxidations independent of the structure of the catalyst. In the present studies all the catalysts, except $[MoO_2(APAC)]$, are stable in the reaction conditions and the ligand effect can be observed with these catalysts.

The epoxidation of isoprene provides an opportunity to compare steric and electronic effects for this epoxidation reaction. $[MoO_2(AAC)]$ has been taken as a representative catalyst (Table 4). Isoprene has two olefinic bonds which can undergo epoxidation, out of the two, one has a methyl group as a substituent. The products (a) and (b) given by isoprene are as shown in eq. (1).

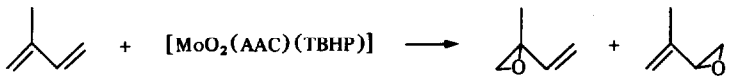

(1)

(a) (b)

The ratio of the two products depends on the nature of the oxidant and the catalyst (Table 4). It has been reported that when epoxidation has been carried out using the $Mo(CO)_6$/TBHP system, product (a) is obtained as a major product.[12] This behaviour is acceptable as the methyl group increases electron density at the olefinic bond therefore making this bond more susceptible to epoxidation (as epoxidation is an electrophilic reaction). Ledon *et al.* have reported that if the [O=Mo(TPP)OMe]/TBHP system is used, the amount of product (b) increases (Table 4) and is a major product,[12] but on using the [O=Mo(TPP)OMe]/Cum–OOH system the major product is (a) (Table 4). These results show that it is the steric behaviour of the ligand and the oxidant which controls the product formation. With the catalysts under investigation it was found that on using the $[MoO_2(AAC)]$/TBHP system (Table 4), the major product was (a), the ratio of (a):(b) was 2.4:1. The formation of (a) as the major product suggests that the $[MoO_2(AAC)]$/TBHP system is electrophilic in nature. The effect of a non-bonded interaction is apparent with the $[MoO_2(AAC)]$/TBHP system as the preference for the methyl substituted double bond has decreased to a 2.4:1 ratio relative to the 4:1 ratio obtained with the $Mo(CO)_6$/TBHP system; the value for the [O=Mo(TPP)(OMe)]/TBHP system is 0.7:1. These observations

Table 3. Characterization of the complexes after epoxidation reaction

S. No.	Complexes	Colour	Melting point (°C)
1	$MoO_2(C_{11}H_{11}N_2O_3)Me_2SO$	Green	210
2	$MoO_2(C_{13}H_9NO_2)Me_2SO$	Brown	225
3	$MoO_2(C_{12}H_{18}N_2O_2)$	Ash	190
4	$MoO_2(C_{17}H_{16}N_2O_2)$	Black	Decomposed
5	$MoO_2(C_{19}H_{16}N_2O_2)$	Pink	222

Table 4. Epoxidation of isoprene

S. No.	Epoxidizing agent	Time (h)	Catalyst	Relative epoxide ratio (a)	(b)	Selectivity of epoxide (%)
1	ACOOH	5	—	5	1	85
2	TBHP	1	$Mo(CO)_6$	4	1	95
3	Cum. OOH	2	O=Mo(TPP)OMe	2.7	1	95
4	TBHP	2	O=Mo(TPP)OMe	0.7	1	95
5	TBHP	2	MoO_2(AAC)	2.4	1	95

suggest that the steric effect due to the ligand of [MoO_2(AAC)] under investigation is responsible for the observed change in selectivity, but the steric effect due to this ligand is less than that observed with the porphyrin ligand where steric factors overweigh the electronic factor.

Effect of pH

The effect of pH was studied by carrying out reaction (i) without buffer, (ii) using 0.10 g of Na_2HPO_4. It was observed that the reaction was very slow and selectivity was poor when Na_2HPO_4 was used. The reaction was considerably fast when no buffer was used. This can be explained on the basis of the reactions shown in eqs (2) and (3).

Basic pH

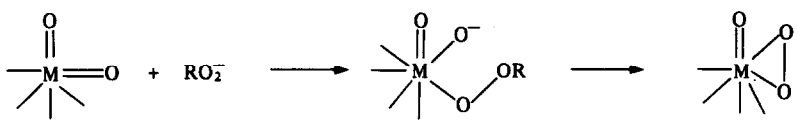

(2)

(a)

Acidic pH

(3)

(b)

This shows that the basic pH of the reaction medium leads to the formation of a peroxo complex (a), which has weaker catalytic activity than the *cis*-dioxomolybdenum complex. A similar effect of pH has been observed with the O=Ti(TPP)/TBHP system.[16]

A mechanism similar to that proposed by Sharpless *et al.*[17] can be proposed for the *cis*-dioxomolybdenum complexes, where firstly the hydroperoxide coordinates to the metal centre and then oxygen atom transfer to the olefin takes place.

REFERENCES

1. Selective catalytic oxidation of hydrocarbons. A critical analysis; Catalytica Associates, Inc, Santa Clara, California, Multiclient Study No. 1979, 1077.
2. P. S. Traylor, D. Dolphin and T. G. Traylor, *J. Chem. Soc., Chem. Commun.* 1984, 279.
3. J. R. Lindsay Smith and P. R. Sleath, *J. Chem. Soc., Perkin Trans. II* 1983, 1165.
4. J. T. Grooves and T. E. Nemo, *J. Am. Chem. Soc.* 1983, **105**, 6243.
5. B. Meunier and B. D. Porter, *Tetrahedron Lett.* 1984, 1895.
6. B. Meunier, E. Guilmet, M. D. Carbalo and R. Poilblane, *J. Am. Chem. Soc.* 1984, **106**, 6668.
7. J. T. Grooves and D. V. Subramanium, *J. Am. Chem. Soc.* 1984, **106**, 1177.
8. D. Mansuay, M. Fontecave and J. F. Bartoli, *J. Chem. Soc., Chem. Commun.* 1983, 253.
9. R. A. Sheldon, *Rec. Trav. Chim. Pay-Bas*, 1973, **92**, 253.

10. P. Forzatti and F. Trifiro, *React. Kinet. Catal. Lett.* 1974, **1**, 367.
11. J. Sobeczek and J. J. Ziolkowski, *Inorg. Chim. Acta* 1976, **19**, 15.
12. H. J. Ledon, P. Durbut and F. Varescon, *J. Am. Chem. Soc.* 1981, **103**, 3601.
13. K. B. Sharpless and T. R. Verhoeven, *Aldrichimice Acta* 1979, **12**, 63.
14. D. Swern (Ed.), *Organic Peroxides*, Vol. II. Wiley-Interscience, New York (1971).
15. J. Topich, *Inorg. Chem.* 1981, **20**, 3704.
16. H. J. Ledon and F. Varescon, *Inorg. Chem.* 1984, **23**, 2735.
17. R. A. Sheldon and J. K. Kochi, *Metal Catalysed Oxidation of Organic Compounds*. Academic Press, New York (1981).

Polyhedron Vol. 7, No. 24, pp. 2575–2581, 1988
Printed in Great Britain

0277–5387/88 $3.00+.00
© 1988 Pergamon Press plc

DINUCLEAR TRANSITION METAL COMPOUNDS OF A DECADENTATE PYRAZOLE-CONTAINING CHELATING LIGAND. X-RAY CRYSTAL STRUCTURE OF $Co_2(tthd)(ClO_4)_4(H_2O)_2(MeOH)_{1.75}$

F. PAAP, W. L. DRIESSEN,* R. A. G. DE GRAAFF and J. REEDIJK

Department of Chemistry, Gorleaus Laboratories, Leiden University, P.O. Box 9502, 2300 RA Leiden, The Netherlands

(*Received* 18 *March* 1988; *accepted* 18 *May* 1988)

Abstract—A potentially decadentate ligand, 1,1,4,7,10,10-hexakis(3,5-dimethyl-1-pyrazolylmethyl)-1,4,7,10-tetraazadecane (tthd), has been synthesized from the reaction of triethylenetetramine with six equivalents of N-hydroxymethyl-3,5-dimethylpyrazole. The tthd ligand forms coordination compounds, $M_2(tthd)(ClO_4)_4(H_2O)_x$, when M is Co, Ni, Cu, Zn and Cd and $x = 4$–8; and $M_2(tthd)(A)_2(ClO_4)_2(H_2O)_x$ when M is Co and Ni, A is NCS or Cl, and $x = 4$–8. The cobalt compound, $Co_2(tthd)(ClO_4)_2(H_2O)_2(MeOH)_{1.75}$, crystallizes in the triclinic space group $P\bar{1}$, $a = 1.959(2)$, $b = 1.5657(3)$, $c = 2.1244(3)$ nm, $\alpha = 105.5(1)$, $\beta = 96.9(1)$, $\gamma = 112.1(1)$. Due to severe disorder of the anions the structure could only be refined to an R_w value of 0.099. The ligand acts as a decadentate, dinucleating ligand. The cobalt ions are distorted octahedrally surrounded by five N-atoms of the tthd ligand and an O-atom of water occupying the sixth coordination place. The other perchlorate compounds have very similar structures, as can be concluded from spectroscopic data.

In the thiocyanate and chloride compounds the anions have replaced the coordinated water molecules, resulting in octahedral Ni compounds. With Co thiocyanate, however, tthd acts as an octadentate ligand, resulting only in five-coordinated compounds.

Several naturally occurring systems such as type III copper proteins[1] and the iron protein, hemerythrin,[2] contain dinuclear metal centres. The oxygen reducing protein in photosystem-II may even contain four manganese atoms in close proximity.[3] Coordination compounds with several dinucleating ligands have been studied as models for these naturally occurring systems.[4–12] Dinucleating systems are also of interest in relation to magnetic properties,[11,13–15] electrochemistry,[16] reactivity[6,10,17,18] and coordination bonding.[19–21]

To investigate the possibility of modelling metalloproteins with relatively simple pyrazole-containing chelating ligands, the ligand 1,1,4,7,10,10-hexakis(3,5-dimethylpyrazole-1-ylmethyl)-1,4,7,10-tetraazadecane, abbreviated tthd, was synthesized[22] and its coordination chemistry towards first-row transition metal ions investigated. The ligand tthd is a potentially decadentate ligand. With its four amine nitrogens and six pyrazole nitrogens the ligand may chelate to two metal ions. Chelation to three or four metal ions cannot be ruled out, though steric factors will restrict the coordination possibilities.

A series of compounds of general formula $M_2(tthd)(ClO_4)_4(solvent)_x$ has been synthesized, together with some mixed-anion compounds (chloride–perchlorate, thiocyanate–perchlorate). A single crystal X-ray analysis of the compound analysing as $Co_2(tthd)(ClO_4)_4(H_2O)_2(MeOH)_x$ has been carried out to investigate the mode of coordination of the tthd ligand.

EXPERIMENTAL

Starting materials

Most solvents, metal salts and starting reagents were commercially available and used without further purification. **Caution:** the compounds described in this article contain perchlorate anions.

* Author to whom correspondence should be addressed.

Although no accidents with perchlorates occurred during the experimental work for this article, it should be pointed out that the use of perchlorates is hazardous because of the possible explosive nature of these compounds. Perchlorates should only be prepared in small amounts and should be handled with adequate care.

The ligand 1,1,4,7,10,10-hexakis(3,5-dimethylpyrazol-1-ylmethyl)-1,4,7,10-tetraazadecane (tthd) was prepared through the reaction of triethylenetetraamine with six equivalents of 1-hydroxymethyl-3,5-dimethylpyrazole in acetonitrile for eight days. After drying with $MgSO_4$ and evaporation of the solvent, the ligand was initially obtained as a yellow oil, which solidified over a period of 3–10 weeks at room temperature. The solid could be recrystallized from a 1 : 1 mixture of toluene and petroleum ether 80/100 and was obtained as a white powder. The purity was checked by NMR and melting point.[22]

Preparation of the compounds

The cobalt, nickel, zinc and copper compounds were synthesized by adding a hot solution of 1.5 mmol of tthd in 15 cm^3 of methanol to a hot solution of 3.0 mmol of the appropriate metal salt in 20 cm^3 of methanol. The cobalt, nickel and zinc compounds separated from the solution as microcrystalline material in several days. The copper compound could be obtained by adding diethyl ether to the solution, after slow evaporation of about 2/3 of the solvent. The cadmium compound was prepared by adding a solution of 1.4 mmol of tthd in 15 cm^3 of hot toluene to a solution of 2.8 mmol of $Cd(ClO_4)_2$ in 15 cm of hot methanol. The compound separated from the solution as a white powder upon standing for several days. Compounds of the formula $M_2(tthd)Cl_2(ClO_4)_2(solvent)_x$ were prepared by adding a mixture of a solution of 3.0 mmol of tthd in 15 cm^3 MeOH and a solution of 3.0 mmol of the appropriate metal perchlorate and 3.0 mmol of the appropriate metal chloride in 15 cm^3 hot methanol. The compounds separated from the solution within a few hours. The compounds $M_2(tthd)(NCS)_2(ClO_4)_2(solvent)_x$ were prepared by adding a hot solution of 3.0 mmol of NH_4NCS in 15 cm^3 methanol to a warm mixture of 3.0 mmol of the appropriate metal perchlorate in 10 cm^3 methanol and 1.5 mmol tthd in 15 cm^3 methanol. The compounds crystallized from the solution upon standing overnight.

Analyses: Found (Calc.) for $Co_2(tthd)(ClO_4)_4(H_2O)_8$: C, 36.2 (36.1); H, 5.7 (5.9); N, 15.3 (16.1); Cl, 10.3 (10.2); Co, 8.9 (8.1). $Zn_2(tthd)(ClO_4)_4(H_2O)_8$: C, 35.9 (35.8); H, 5.6 (5.9); N, 15.6 (15.9); Cl, 10.5 (10.1); Zn, 8.5 (8.9). $Cu_2(tthd)(ClO_4)_4(H_2O)_4$: C, 35.0 (36.2); H, 5.2 (5.4); N, 15.5 (16.1); Cl, 10.9 (10.2); Cu, 10.0 (9.1). $Ni_2(tthd)(ClO_4)_4(H_2O)_6$: C, 36.1 (35.6); H, 5.2 (5.5); N, 15.9 (15.8); Cl, 9.7 (10.0); Ni, 8.0 (8.3). $Ni_2(tthd)Cl_2(ClO_4)_2(H_2O)_8$: C, 38.0 (38.0); H, 5.8 (6.2); N, 17.0 (16.9); Cl, 13.4 (10.7); Ni, 9.1 (8.9). $Ni_2(tthd)(NCS)_2(ClO_4)_2(H_2O)_8$: C, 37.7 (38.5); H, 5.1 (6.0); N, 18.6 (18.4); Cl, 5.8 (5.5); Ni, 8.1 (8.6). $Co_2(tthd)(NCS)_2(ClO_4)_2(H_2O)_4$: C, 40.8 (40.6); H, 4.9 (5.7); N, 19.5 (19.4; Cl, 6.0 (5.5); Co, 9.5 (9.1).

Spectroscopic and instrumental techniques

IR spectra (4000–180 cm^{-1}) were recorded on a Perkin–Elmer PE580 instrument, using KBr pellets and Nujol mulls between NaCl or polyethene discs. Electronic spectra (2000–300 nm) were measured on a Perkin–Elmer UV330 instrument, operating in the diffuse reflectance mode with MgO as a reference. EPR spectra of powdered samples were measured on a Varian E-3 EPR spectrometer using a 9.5 GHz microwave bridge, at ambient and liquid nitrogen temperature. Solutions of methanol were measured as frozen glasses at liquid nitrogen temperature.

The NMR spectrum of the ligand was recorded on a JEOL LNM PS100 instrument, operating at 99.5 MHz with an external lock and using TMS as an internal reference. Elemental analyses were performed at the Microanalytical Laboratory of the University College, Dublin, Republic of Ireland.

Crystal structure determination of a dimeric cobalt compound

Data were collected at ambient temperature on an Enraf–Nonius CAD4 diffractometer for a pink, box-shaped crystal with dimensions, $0.20 \times 0.30 \times 0.50$ mm. Crystals of the compound $Co_2(tthd)(H_2O)_2(ClO_4)_4(solvent)_x$ could be obtained from the reaction mixture. To avoid crystal disintegration, occurring within 1 h after removal from the solvent, the crystal had to be mounted with a drop of mother liquor in a glass capillary, which was then sealed. Details about the data collection and processing and the structure analysis and refinement are given in Table 1.

The positions of the cobalt atoms were located in a Patterson map, the other atom positions were found by the Fourier method AUTOFOUR[23] and difference Fourier analysis. An initial refinement in space group $P\bar{1}$ did not result in a converging model, and the refinement was thereupon carried out in space group $P1$. Atoms which were related to each other by the pseudo centre of symmetry

Table 1. Crystal data and details of measurement and structure analysis and refinement of $[Co_2(tthd)(H_2O)_2][(Co_2(tthd)(MeOH)(H_2O)](ClO_4)_8(H_2O)(MeOH)_{2.5}$

Formula	$C_{43.75}H_{77}Cl_4Co_2N_{16}O_{19.75}$
Molecular weight	1402.86
Crystal system	Triclinic
Space group	$P\bar{1}$
a (nm)	1.1959(2)
b (nm)	1.5657(3)
c (nm)	2.1244(3)
α (°)	105.5(1)
β (°)	96.9(1)
γ (°)	112.1(1)
V (nm^3)	3.4363
Z	2
D_x (g cm^{-3})	1.41
μ(Mo-K_α) (cm^{-1})	7.09
Scan mode	Bisect
Scan range	$2° < \theta < 20°$
Number of independent data collected	6376
Number of data with $I > 2\sigma(I)$	3118
Number of data with $\sin\theta/\lambda > 0.22$	5743
Weighting scheme	$w = 1/\sigma$
R	0.149 (5743 reflections)
	0.103 (3118 reflections)
R_w	0.009 (5743 reflections)
	0.133 (3118 reflections)

were refined with coupled thermal parameters. All atoms of the cations $[Co_2(tthd)(H_2O)_2]^{4+}$ and $[Co_2(tthd)(H_2O)(MeOH)]^{4+}$ were refined anisotropically, as were the two chlorine atoms. All other atoms were refined isotropically. The oxygen atoms of the perchlorate anions were refined with one B value for each set of oxygen atoms.

After initial full-matrix least-squares refinement of the complete model a separate refinement with a diagonally blocked matrix was carried out on the anions and solvent molecules. The perchlorate anions were refined with Waser constraints using a tetrahedral model with a Cl—O distance of 1.39 Å. Six of the eight perchlorates appeared to be disordered and were refined isotropically as ClO_4 groups over two equivalent positions.

After the refinement of the anions and solvent molecules, the cations were refined. To decrease the effect of amorphous scattering, the low order reflections were rejected, leaving 90% of the reflections, which were used for the refinement with a diagonally blocked matrix. The cations were refined anisotropically, and hydrogen atoms were not taken into account. After a final refinement, a correlation matrix was prepared containing the parameters of the cation atoms, which was used for calculation of the geometrical data and estimated standard deviations. The final atomic positional parameters, a list of $F_{obs.}$ and $F_{calc.}$, thermal parameters, non-coordination bond distances and angles are available as supplementary material. Atomic coordinates have been deposited with the Cambridge Crystallographic Data Centre.

RESULTS AND DISCUSSION

Description of the structure of $Co_2(tthd)(H_2O)_2(ClO_4)_4(MeOH)_{1.75}$

The unit cell contains an ion $[Co_2(tthd)(H_2O)_2]^{4+}$ and an ion $[Co_2(tthd)(H_2O)(MeOH)]^{4+}$ in a nearly centrosymmetric configuration with eight perchlorates and several solvent molecules (one water and three methanols with occupancy 0.5 and one methanol with occupancy 1.0) packed around the cations. Hydrogen bridges occur between perchlorates, lattice solvents and coordinated water and methanol molecules.

Coordination bond distances and angles of the cations are given in Table 2. A drawing of the cation $[Co_2(tthd)(H_2O)(MeOH)]^{4+}$, with the atomic numbering, is given in Fig. 1. The other cation is very similar in geometry.

Large deviations from centrosymmetry are found when the perchlorates and the solvent molecules are taken into account. A closer investigation of the

Table 2. Coordination bond lengths (Å) and coordination bond angles (°) of $[Co_2(tthd)(H_2O)_2]^{4+}$ and $[Co_2(tthd)(H_2O)(MeOH)]^{4+}$

Co(1)—N(1)	217(2)	Co(1′)—N(1′)	227(2)
Co(1)—N(12A)	209(2)	Co(1′)—N(12A′)	207(2)
Co(1)—N(12B)	226(2)	Co(1′)—N(12B′)	201(2)
Co(1)—N(4)	236(2)	Co(1′)—N(4′)	223(2)
Co(1)—N(42)	211(2)	Co(1′)—N(42′)	202(2)
Co(1)—O(1)	198(2)	Co(1′)—O(1′)	215(2)
Co(2)—N(10)	212(2)	Co(2′)—N(10′)	237(2)
Co(2)—N(102A)	210(2)	Co(2′)—N(102A′)	208(2)
Co(2)—N(102B)	201(2)	Co(2′)—N(102B′)	226(2)
Co(2)—N(7)	228(2)	Co(2′)—N(7′)	228(2)
Co(2)—N(72)	212(2)	Co(2′)—N(72′)	203(2)
Co(2)—O(2)	205(2)	Co(2′)—O(2′)	214(2)
N(1)—Co(1)—N(4)	80.5(6)	N(1′)—Co(1′)—N(4′)	80.0(6)
N(1)—Co(1)—N(42)	161.4(6)	N(1′)—Co(1′)—N(42′)	153.4(6)
N(1)—Co(1)—N(12A)	78.7(7)	N(1′)—Co(1′)—N(12A′)	84.3(7)
N(1)—Co(1)—N(12B)	74.3(7)	N(1′)—Co(1′)—N(12B′)	77.8(7)
N(1)—Co(1)—O(1)	97.0(8)	N(1′)—Co(1′)—O(1′)	98.8(7)
N(4)—Co(1)—N(42)	82.1(7)	N(4′)—Co(1′)—N(42′)	73.4(6)
N(4)—Co(1)—N(12A)	92.1(7)	N(4′)—Co(1′)—N(12A′)	100.5(6)
N(4)—Co(1)—N(12B)	98.9(7)	N(4′)—Co(1′)—N(12B′)	85.8(7)
N(4)—Co(1)—O(1)	173.1(8)	N(4′)—Co(1′)—O(1′)	174.2(7)
N(42)—Co(1)—N(12A)	109.4(7)	N(42′)—Co(1′)—N(12A′)	101.0(6)
N(42)—Co(1)—N(12B)	98.9(8)	N(42′)—Co(1′)—N(12B′)	99.5(7)
N(42)—Co(1)—O(1)	100.8(8)	N(42′)—Co(1′)—O(1′)	109.2(7)
N(12A)—Co(1)—N(12B)	151.6(7)	N(12A′)—Co(1′)—N(12B′)	159.6(7)
N(12A)—Co(1)—O(1)	81.0(7)	N(12A′)—Co(1′)—O(1′)	84.8(7)
N(12B)—Co(1)—O(1)	94.0(7)	N(12B′)—Co(1′)—O(1′)	88.4(8)
N(7)—Co(2)—N(10)	79.7(7)	N(7′)—Co(2′)—N(10′)	78.1(7)
N(7)—Co(2)—N(72)	81.5(6)	N(7′)—Co(2′)—N(72′)	74.8(6)
N(7)—Co(2)—N(102A)	92.1(6)	N(7′)—Co(2′)—N(102A′)	94.5(6)
N(7)—Co(2)—N(102B)	95.5(8)	N(7′)—Co(2′)—N(102B′)	91.9(7)
N(7)—Co(2)—O(2)	173.9(7)	N(7′)—Co(2′)—O(2′)	173.6(7)
N(10)—Co(2)—N(72)	161.2(7)	N(10′)—Co(2′)—N(72′)	152.7(7)
N(10)—Co(2)—N(102A)	72.8(7)	N(10′)—Co(2′)—N(102A′)	81.6(7)
N(10)—Co(2)—N(102B)	79.4(8)	N(10′)—Co(2′)—N(102B′)	79.9(7)
N(10)—Co(2)—O(2)	104.0(7)	N(10′)—Co(2′)—O(2′)	95.5(7)
N(72)—Co(2)—N(102A)	108.3(8)	N(72′)—Co(2′)—N(102A′)	104.0(8)
N(72)—Co(2)—N(102B)	102.3(8)	N(72′)—Co(2′)—N(102B′)	97.3(8)
N(72)—Co(2)—O(2)	94.7(6)	N(72′)—Co(2′)—O(2′)	111.6(7)
N(102A)—Co(2)—N(102B)	149.3(7)	N(102A′)—Co(2′)—N(102B′)	158.7(7)
N(102A)—Co(2)—O(2)	84.5(7)	N(102A′)—Co(2′)—O(2′)	84.3(7)
N(102B)—Co(2)—O(2)	90.0(9)	N(102B′)—Co(2′)—Co(2′)	87.1(8)

coordinates of the atoms related by pseudo-symmetry, reveals an average deviation from centrosymmetry of 25 pm for the *y*-coordinates. This deviation does not occur for the other coordinates. The small deviation in the *y*-coordinates effectively lowers the crystal symmetry to the triclinic space group $P1$, instead of $P\bar{1}$. The tthd ligand acts as a decadentate, dinucleating ligand to the two cobalt atoms, occupying five coordination positions of an octahedron for each cobalt atom. The sixth position is occupied by a water or methanol oxygen atom, completing the octahedral coordination for the cobalt atoms. The coordination octahedron is quite distorted, with angles varying from 73 to 109°. The N(4)/N(7)—Co—O angles are nearly linear; the other two octahedron axes deviate from linearity, with an average angle of 155°.

The Co—N(pyrazole) distances (average 2.10 Å) are comparable to the distances found in similar compounds,[24,25] as are the Co—N(amine) and

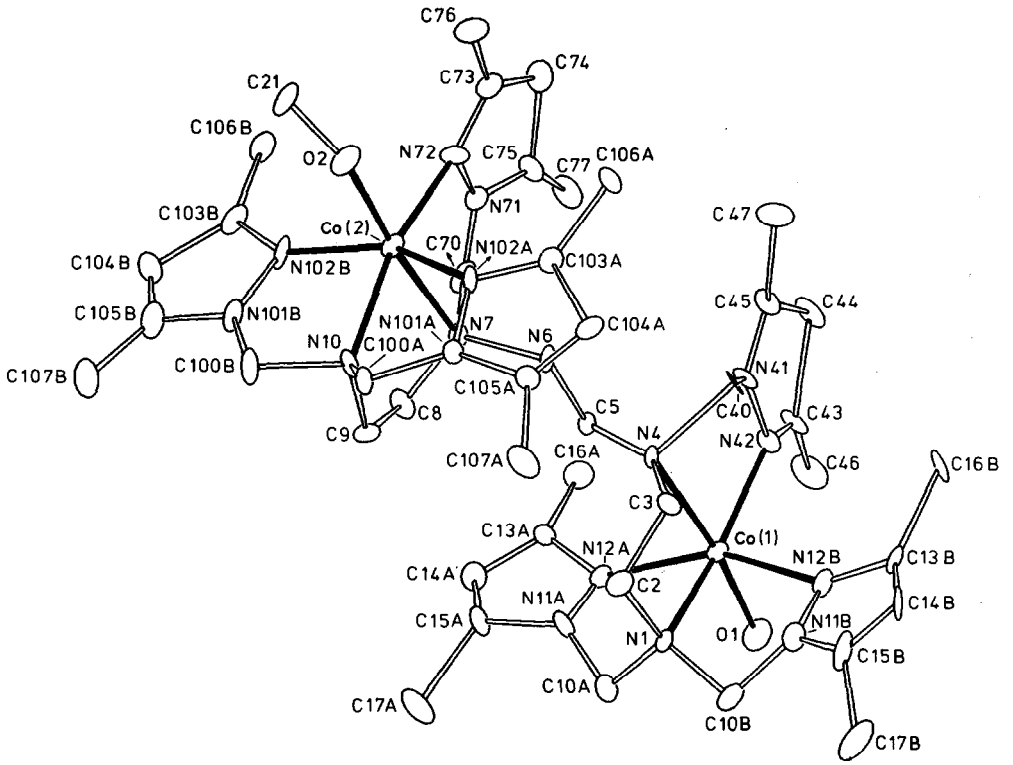

Fig. 1. ORTEP projection of $[Co_2(tthd)(H_2O)(MeOH)]^{4+}$ with atomic numbering and 25% probability ellipsoids.

Co—O distances.[24] The Co—N(4)/N(7) distances are somewhat longer than the other coordination distances, probably due to steric effects caused by the crowding of the methyl groups and the strained ligand conformation.

The pyrazole rings are approximately planar and no stacking occurs between the pyrazole rings. Within the ligand, no unusual features occur, and the average distances and angles can be compared to those found in other pyrazole derivatives.[24,25]

Description of the tthd *compounds*

The IR spectra of the perchlorate compounds are very similar in line shapes and relative intensities throughout the series Co, Ni, Cu, Zn, Cd, indicating a similar ligand conformation for all the compounds. The IR spectra of the compounds $Ni_2(tthd)(NCS)_2(ClO_4)_2$ and $Ni_2(tthd)Cl_2(ClO_4)_2$ are very similar to the IR spectrum of the compound $Ni_2(tthd)(H_2O)_2(ClO_4)_4$, except for the thiocyanate vibrations, indicating a similar ligand conformation for the three compounds. The single thiocyanate vibration at 2080 cm^{-1} is indicative of an N-coordinated thiocyanate ion.[26]

The IR spectra of the compounds $Co_2(tthd)Cl_2(ClO_4)_2$ and $Co_2(tthd)(NCS)_2(ClO_4)_2$ show small differences compared to the perchlorate compounds, besides the thiocyanate vibrations. The similarities are, however, large enough to justify the conclusion that the overall ligand conformation is very similar for these compounds. The single thiocyanate vibration at 2075 cm^{-1} is indicative of an N-coordinated thiocyanate ion.[26]

IR absorptions which can be unambiguously assigned to metal–anion vibrations have not been observed. A combination of low intensity and the presence of ligand vibrations renders it impossible to make positive assignments.

The mixed-anion compounds of cobalt and nickel show a splitting of *ca* 5 cm^{-1} of the pyrazole C—N stretch vibration at 1550 cm^{-1}, probably caused by the inequivalence of pyrazoles (4) and (7) and pyrazoles (1A), (1B), (10A) and (10B). This inequivalence is increased relative to the perchlorate compounds, probably because the coordinated water is replaced by the stronger ligands, chloride and thiocyanate.

Considering the similarities of the IR spectra, it can be concluded that all compounds have structures which very much resemble the structure of the cobalt perchlorate compound. Water (solvent) coordination is occurring in the perchlorate compounds and anion coordination replaces the water coordination in the mixed-anion compounds.

Relevant ligand field spectroscopic data are given in Table 3. The nickel compounds show typical octahedral spectra. The ligand field parameters are

Table 3. Electronic transitions (10^3 cm^{-1}) of the tthd compounds

Compounds[a]	Transitions			
$Ni_2(tthd)(H_2O)_2^{4+}$	10.15	17.5	27.1	
$Ni_2(tthd)(NCS)_2^{2+}$	10.11	16.5	26.0	
$Ni_2(tthd)Cl_2^{2+}$	9.46	14.8	25.8	
$Co_2(tthd)(H_2O)_2^{4+}$	9.41		20.6	
$Co_2(tthd)NCS_2^{2+}$	6.83	13.3	17.2	20.0
$Co_2(tthd)Cl_2^{2+}$	6.46	12.1	17.0	19.1
$Cu_2(tthd)(H_2O)_2^{4+}$	14.9			

[a] Only the cationic part of the molecule is given.

Table 4. ESR data of the tthd compounds

Compound[a]	*g* values (*A* values in Gauss)
$Cu_2(tthd)(H_2O)_2^{4+}$ [b]	2.07
$Zn_2(tthd)(H_2O)_2^{4+}$ [cd]	2.31(125) 2.07
	2.26(150) 2.05

[a] Only the cationic part of the molecule is given.
[b] At 77 K.
[c] Frozen methanol solution at 77 K.
[d] Copper(II) doped compound.

in agreement with the proposed (NiN_5O and distorted NiN_5Cl, NiN_5N') chromophores.[27] The spectrum of the cobalt perchlorate compound is also in agreement with the octahedral structure. The values of the ligand field parameters agree very well with the values of the nickel compound, confirming the structural similarity.

The spectra of the mixed-anion cobalt compounds are typical for five-coordinated compounds.[27–29] The most likely coordination sphere is a combination of the halide or thiocyanate anion with four tthd donor atoms. Considering the distances in the perchlorate compound, the Co—N(4)/N(7) distance is most probably elongated due to the influence of the *trans* coordinated chloride or thiocyanate. Steric effects may also play a role. The cobalt ions thus become square-pyramidally five-coordinated.

The copper compounds show a single ligand field transition, with values expected for six- (or five-) coordinated compounds.[30] Relevant EPR data are given in Table 4. The copper perchlorate compound shows a broad isotropic resonance and a frozen methanol solution shows some axial features, comparable to the spectrum of the copper(II) doped compound $Zn_2(tthd)(H_2O)_2(ClO_4)_4$. These data are in agreement with the proposed distorted octahedral[30] structure.

CONCLUSIONS

The ligand tthd acts as a decadentate, dinucleating ligand towards the metals Co, Ni, Cu, Zn and Cd. Coordination results in a severely distorted coordination octahedron, as is shown by the crystal structure determination of the cobalt perchlorate compound. Water or methanol occupies the sixth coordination position of the octahedron, which is formed by the tthd ligand. In the presence of coordinating anions such as chloride or thiocyanate, the solvent is replaced in the coordination sphere by the anion. This results in a more distorted coordination geometry. IR spectroscopy indicates an (increased) inequivalence of the coordinated pyrazole groups. The ligand field spectra of the cobalt compounds indicate a five-coordinated structure; the tthd ligand apparently acts here as an octadentate ligand, with the amine nitrogens N(4) and N(7) not coordinating to the metal, resulting in a square-pyramidal coordination. The pyrazole containing, chelating ligand pabd,[25] which is derived from aniline, shows a similar effect. The aromatic amine nitrogen can be either coordinating or non-coordinating, depending upon the metal ion and anions. In this ligand, the effect is caused by electronic factors; in the tthd compound steric factors seem to be responsible for this effect.

The tthd ligand imposes a strained structure around the metal ion. This conformational strain causes the structure to be strongly influenced by the choice of the additional ligand and the metal ion.

Acknowledgement—The authors are indebted to Mr S. Gorter for assistance with the data collection.

REFERENCES

1. J. Reedijk, W. L. Driessen and J. van Rijn, in *Biological and Inorganic Copper Chemistry* (Edited by K. D. Karlin and J. Zubieta), p. 143. Adenine Press (1986).
2. R. C. Reem, J. W. Whitakker and A. E. Solomon, *Rev. Port. Quim.* 1985, **27**, 172.
3. C. Critchley and A. M. Sargeson, *FEBS* 1985, **177**, 2.
4. K. Wieghardt, M. Köppen, B. Nuber and J. Weiss, *J. Chem. Soc., Chem. Commun.* 1986, 1530.
5. J. M. Latour, D. Limosin and P. Rey, *J. Chem. Soc., Chem. Commun.* 1985, 464.
6. M. T. Youinou, J. A. Osborn, J. P. Collin and P. Lagrange, *Inorg. Chem.* 1986, **25**, 453.
7. B. Mabad, P. Cassoux, J. P. Tuchagues and D. N. Hendrickson, *Inorg. Chem.* 1986, **25**, 1420.
8. H. P. Berends and D. W. Stephen, *Inorg. Chim. Acta* 1986, **99**, L53.
9. B. Mabad, J. P. Tuchagues, Y. T. Hwang and D. N. Hendrickson, *J. Am. Chem. Soc.* 1985, **107**, 2801.

10. L. Casella and L. Rigoni, *J. Chem. Soc., Chem. Commun.* 1985, 1668.
11. K. Takahashi, Y. Nishida, Y. Maeda and S. Kida, *J. Chem. Soc., Dalton Trans.* 1985, 2375.
12. C. A. McAuliffe, R. V. Parish, S. M. Abu-El-Wafa and R. M. Issa, *Inorg. Chim. Acta* 1986, **115**, 91.
13. L. Rosenberg, L. K. Thompson, E. J. Gabe and F. L. Lee, *J. Chem. Soc., Dalton Trans.* 1986, 625.
14. F. Nepveu, F. J. Bormuth and L. Walz, *J. Chem. Soc., Dalton Trans.* 1986, 1213.
15. O. Kahn, *Angew. Chem.* 1985, **24**, 834; *Struct. Bonding* 1987, **68**, 89.
16. S. K. Mandal, B. Adhikary and K. Nag, *J. Chem. Soc., Dalton Trans.* 1986, 1175.
17. B. Mabad, P. Cassoux, J. P. Tuchagues and D. N. Hendrickson, *Inorg. Chem.* 1986, **25**, 1420.
18. F. M. Ashmawy, C. A. McAuliffe, R. V. Parish and J. Tames, *J. Chem. Soc., Dalton Trans.* 1986, 1391.
19. A. Evers, R. D. Hancock and I. Murase, *Inorg. Chem.* 1986, **25**, 2160.
20. I. Murase, M. Mikuriya, H. Sonoda, Y. Fukuda and S. Kida, *J. Chem. Soc., Dalton Trans.* 1986, 953.
21. L. R. Gahan, K. E. Hart, C. H. L. Kennard, M. A. Kingston, G. Smith and T. C. W. Mak, *Inorg. Chim. Acta* 1986, **116**, 5.
22. W. L. Driessen, *Recl. Trav. Chim. Pays-Bas* 1982, **101**, 441.
23. A. J. Kinneging and R. A. G. de Graaff, *J. Appl. Cryst.* 1984, **17**, 364.
24. G. J. van Driel, W. L. Driessen and J. Reedijk, *Inorg. Chem.* 1985, **24**, 2919.
25. H. L. Blonk, W. L. Driessen and J. Reedijk, *J. Chem. Soc., Dalton Trans.* 1985, 1699.
26. K. Nakamoto, *Infrared and Raman Spectra of Inorganic and Coordination Compounds*, 3rd edn. Wiley Interscience, New York (1978).
27. A. B. P. Lever, *Inorganic Electronic Spectroscopy*, 2nd edn. Elsevier, Amsterdam (1984).
28. M. Ciampolini and N. Nardi, *Inorg. Chem.* 1966, **5**, 41.
29. A. Bencini, C. Benelli and D. Gatteschi, *Inorg. Chem.* 1978, **17**, 3313.
30. B. J. Hathaway and D. E. Billing, *Coord. Chem. Rev.* 1978, **5**, 143.

Polyhedron Vol. 7, No. 24, pp. 2583–2589, 1988
Printed in Great Britain

0277–5387/88 $3.00+.00
© 1988 Pergamon Press plc

COPPER(I) COORDINATION COMPOUNDS WITH TWO BIDENTATE CHELATING PYRAZOLE LIGANDS. X-RAY CRYSTAL STRUCTURES OF DI-μ-CHLORO-BIS[[N,N-BIS(1-PYRAZOLYLMETHYL)AMINOETHANE]COPPER(I)] AND [BIS(N,N-BIS(1-PYRAZOLYLMETHYL)AMINOETHANE]COPPER(I) TRIFLATE

YVON C. M. PENNINGS, WILLEM L. DRIESSEN* and JAN REEDIJK

Department of Chemistry, Gorlaeus Laboratories, Leiden University, P.O. Box 9502, 2300 RA Leiden, The Netherlands

(*Received* 4 *January* 1988; *accepted* 24 *May* 1988)

Abstract—The pyrazole derivatives of aminoethane N,N-bis(3,5-dimethyl-1-pyrazolylmethyl)aminoethane (aebd) and N,N-bis(1-pyrazolylmethyl)aminoethane (aebp) form coordination compounds with copper(I) of stoichiometry [Cu(L)X], with X = Cl, Br, I and SCN, and $[Cu(L)_2X]$, with X = CF_3SO_3 and BF_4. The ligands chelate in a bidentate manner, with only the pyrazole groups coordinating. The crystal structures of two representative examples have been determined: $[Cu(aebp)Cl]_2$ is triclinic, space group $P\bar{1}$, with $a = 8.711(2)$, $b = 9.351(1)$ and $c = 9.528(1)$ Å, $\alpha = 68.57(1)°$, $\beta = 61.47(1)°$ and $\gamma = 77.82(1)°$, and $Z = 2$. Standard least-squares refinement gave $R = 0.029$ ($R_w = 0.038$) for 1804 reflections. $[Cu(aebp)_2]CF_3SO_3$ is monoclinic, space group $P2_1/n$, with $a = 13.352(5)$, $b = 14.663(3)$ and $c = 15.752(4)$ Å, $\beta = 117.49(3)°$, and $Z = 4$. Standard least-squares refinement gave $R = 0.029$ ($R_w = 0.032$) for 1786 reflections. In both cases the copper environment is slightly-distorted tetrahedral. The chloride compound is dimeric with one ligand molecule (Cu—N distances of 2.011(2) and 2.047(2) Å) and two bridging chlorides per copper (Cu—Cl distances of 2.3874(8) and 2.4094(8) Å). With the non-coordinating triflate anion, a monomeric compound with two ligand molecules per copper was obtained (Cu—N distances of 2.018(4), 2.028(4), 2.049(4) and 2.050(4) Å).

Nature seems to prefer (distorted) tetrahedral coordination geometry for copper ions, as for instance in plastocyanin and azurin,[1,2] presumably since a tetrahedral coordination for copper(I) facilitates the regulation of the electrode potential of the active site.

A wide range of pyrazole-containing copper compounds have been studied as models for copper proteins.[3] Copper(II) chelate compounds have been studied extensively, compounds containing Cu^I have obtained less attention probably because they are more difficult to synthesize due to their tendency to disproportionate (especially in aqueous solution)[4] and to undergo oxidation in the presence of air.[5]

In this paper several Cu^I compounds with bis(pyrazole)aminoethane (aebp) and with bis(dimethylpyrazole)aminoethane (aebd) are reported, as well as the crystal structures of two representative compounds.

In earlier reports the syntheses and characterization of coordination compounds of these ligands with copper(II) and other divalent transition metals were described.[6,7] In these compounds the binding mode of the ligands is tridentate, and both pyrazole nitrogens as well as the amine nitrogen coordinate.

EXPERIMENTAL

Starting materials

The syntheses of the ligands N,N-bis(1-pyrazolylmethyl)aminoethane (aebp) and N,N-bis(3,5-

* Author to whom correspondence should be addressed.

dimethyl-1-pyrazolylmethyl)aminoethane (aebd) were performed by a modification of the procedure described by Driessen:[8] N-(hydroxymethyl)pyrazole (0.23 mol), or N-(hydroxymethyl)-3,5-dimethylpyrazole (0.23 mol), respectively, was stirred with aminoethane (0.11 mol) for 40 h at room temperature in 50 cm^3 of acetonitrile. After removal of the organic solvent the colourless oil was dissolved in ether (25 cm^3), washed with a solution of sodium hydroxide (1 N, 5 cm^3) and with water (4×15 cm^3) until it was neutral again.[9] The water was saturated with sodium chloride to improve separation of the two layers and the ether layer was dried with magnesium sulphate. Removal of the solvent by the use of a vacuum rotary evaporator rendered a colourless oil in the case of both ligands. Upon cooling the ligand aebd solidified as a white wax-like solid, (m.p. 38–41°C), contrary to Schoonhoven *et al.*[7] who obtained aebd as a light yellowish oil. The ligand aebp did not solidify and was used as an oil. Characterization of the ligands by IR and NMR spectra showed that they were identical with the compounds reported in the literature.[6,7]

Copper(I) chloride and copper(I) bromide were prepared as solid products by reduction of the respective copper(II) salts with sodium sulphite.[10] Copper(I) tetrafluoroborate was synthesized as the tetrakis acetonitrile complex[11] in an inert N_2 atmosphere with Schlenk equipment: $Cu(H_2O)_6(BF_4)_2$ (0.040 mol) and triethylorthoformiate (15 cm^3) were dissolved in acetonitrile (150 cm^3). The solution was made oxygen-free by repeatedly evacuating and flushing with nitrogen gas. This solution was stirred with copper powder (0.080 mol) for 30 min, and filtration of the suspension resulted in a colourless solution from which a white product crystallized upon evaporation of some of the solvent.

Copper(I) triflate was synthesized as the CO-complex, as reported by Doyle *et al.*[12]

Copper(I) iodide was prepared by the reduction of copper(II) sulphate with sodium thiosulphate in the presence of potassium iodide.[13]

Copper(I) thiocyanate was commercially available, of sufficient purity and used without further treatment.

The solvents used for the syntheses of the coordination compounds were dried over molecular sieves (diethylether: 4 Å, acetonitrile and methanol: 3 Å), made oxygen-free (see above) and stored in a nitrogen atmosphere.

Syntheses of the coordination compounds

All syntheses were performed in a nitrogen atmosphere with Schlenk equipment and under anhydrous conditions. The halogen, thiocyanate and triflate coordination compounds were prepared by warming the appropriate copper(I) salt (5 mmol) in acetonitrile (20 cm^3 for Cl and Br, 70 cm^3 for I, 40 cm^3 for SCN, 15 cm^3 for CF_3SO_3). The ligands aebp or aebd (5 mmol for Cl and Br, 10 mmol for I and SCN, 15 mmol for CF_3SO_3) were dissolved in acetonitrile (5 cm^3) and added to the solution (with iodide and thiocyanate a suspension). In all cases a white (micro)crystalline solid formed after cooling to room temperature. In some cases single crystals suitable for X-ray diffraction were obtained from the filtrate, which was stored at 5°C. With $Cu(CO)CF_3SO_3$ and aebd small amounts of a white powder formed, which proved to be copper dimethylpyrazolate. Apparently decomposition of aebd had occurred.[14,15]

The tetrafluoborate compounds were synthesized as reported by Sorrell.[16] The ligand (10 mmol) in methanol (5 cm^3) was added to the $Cu(CH_3CN)_4BF_4$ complex (5 mmol) in methanol (20 cm^3). The solution was evaporated until it was completely free of solvent (to prevent formation of the acetonitrile compound) and then dissolved again in methanol (20 cm^3) from which it crystallized upon standing for a few days at 5°C. The products were stored in a dry N_2 atmosphere.

Analyses

Metal analyses were carried out complexometrically with EDTA as the complexing agent.[17] Chlorine analyses were carried out potentiometrically with silver nitrate and Ag/H_2SO_4 electrodes. CHN analyses were performed at the Microanalytical Laboratory of the Department of Chemistry at the University College, Dublin, Ireland.

Physical measurements

IR spectra in the 4000–180 cm^{-1} range of the samples pelleted in KBr were recorded on a Perkin–Elmer spectrophotometer, equipped with a PE data station. Proton nuclear magnetic spectra were recorded on a JEOL PS-100 instrument employing a frequency of 99.5 MHz, with TMS (0 ppm) or DMSO (2.49 ppm) as internal standard. X-ray powder diagrams of the compounds were obtained with a Guinier-type camera using Cu-K_α radiation. The samples were protected from atmospheric vapour by adhesive tape.

Data collection and structure refinement

The data collection was carried out at room temperature on a four-circle Enraf–Nonius CAD4

diffractometer with graphite-monochromatized Mo-K_α radiation (λ(Mo-K_α) = 0.71073 Å). The colourless crystals were sealed in glass capillaries. Crystal data and additional details of the data collection and refinement for both complexes are presented in Table 1. Reflections with $I > 2\sigma(I)$ were used in the refinement. Intensities were corrected for Lorentz and polarization effects.

The scanning rate was adjusted to the required precision of $\sigma(I)/I = 0.01$, with a maximum scan time of 120 s reflection^{-1}. The instrument and crystal stability were checked after every 5400 s of radiation time by measuring three reference reflections: no significant changes in the intensities were observed. As soon as the molecular structure was known, an absorption correction was applied for the $[Cu(aebp)Cl]_2$ structure with a Monte-Carlo method as described by de Graaff.[18] Before correction, measurements at different azimuthal positions of two reflections showed a variation of 11.2% in the intensities. As the variation in the intensities for the $[Cu(aebp)_2]CF_3SO_3$ compound was only 4.4%, no absorption correction was performed.

The heavy-atoms were located from Patterson maps. The structures were solved with the computer program *AUTOFOUR*[19] and refined by full-matrix least-squares calculations. The refinement was considered to be complete when the changes in the parameters were smaller than 1/3 of the standard deviation. Scattering factors were taken from ref. 20. The thermal parameters of the hydrogen atoms were kept fixed (4.0 Å^2 for the chloride compound, 5.2 Å^2 for the triflate), and those of the non-hydrogens were refined anisotropically. The function minimized was $\Sigma w(||F_o|-|F_c||)^2$ with $w = \sigma 1/^2(F)$. Selected bond distances and bond angles are given in Table 2. Atomic coordinates, displacement factor coefficients, full lists of bond lengths and angles, and lists of F_o/F_c values have been deposited as supplementary data with the Editor, from whom copies are available on request. Atomic coordinates have also been deposited with the Cambridge Crystallographic Data Centre.

Table 1. Crystal and refinement data

	1	2
Formula	$CuC_{10}H_{15}ClN_5$	$CuC_{21}H_{30}F_3N_{10}O_3S$
f_w	304.26	623.14
a (Å)	8.711(2)	13.352(5)
b (Å)	9.351(1)	14.663(3)
c (Å)	9.528(1)	15.752(4)
α (°)	68.57(1)	90
β (°)	61.47(1)	117.49(3)
γ (°)	77.82(1)	90
V (Å^3)	634.11	2735.61
F(000)	312.77	1289.71
Space group	$P\bar{1}$	$P2_1/n$
Z	2	4
No. of reflections used to determine cell constants	24	24
d (g cm^{-3})	1.593	1.513
Linear abs. coeff. (cm^{-1})	19.235	9.337
Crystal dimensions	0.15 × 0.26 × 0.33	0.22 × 0.33 × 0.47
h, k, l values	$-11 < h < 11$	$-14 < h < 14$
	$0 < k < 16$	$-12 < k < 12$
	$0 < l < 17$	$0 < l < 12$
Scan range (°)	2.0–27.5	2.0–24.0
No. measured data	3085	4430
No. unique data collected	2906	3981
No. data used in refinement	1804	1786
Final R_f[a]	0.029	0.029
Final R_{wf}[b]	0.038	0.032
S	1.0292	1.0999

[a] $R_f = \Sigma(||F_o|-|F_c||)/\Sigma|F_o|$.
[b] $R_{wf} = (\Sigma w(|F_o|-|F_c|)^2/\Sigma wF_o^2)^{1/2}$.

Table 2. Selected interatomic distances (Å) and bond angles (°)

$[Cu(aebp)Cl]_2$		$[Cu(aebp)_2]CF_3SO_3$	
Cu(01)—Cu(01)′	2.9511(7)	Cu(01)—N(12)	2.018(4)
Cu(01)—Cl(02)	2.3874(8)	Cu(02)—N(22)	2.050(4)
Cu(01)—Cl(02)′	2.4094(8)	Cu(01)—N(32)	2.028(4)
Cl(02)—Cl(02)′	3.782(1)	Cu(01)—N(42)	2.049(4)
Cu(01)—N(12)	2.011(2)		
Cu(01)—N(22)	2.047(2)		
Cl(02)—Cu(01)—Cl(02)′	104.07(3)	N(12)—Cu(01)—N(22)	113.4(2)
Cl(02)—Cu(01)—N(12)	109.00(7)	N(12)—Cu(01)—N(32)	111.3(2)
Cl(02)′—Cu(01)—N(12)	116.38(7)	N(12)—Cu(01)—N(42)	112.5(2)
Cl(02)—Cu(01)—N(22)	113.64(7)	N(22)—Cu(01)—N(32)	105.8(2)
Cl(02)′—Cu(01)—N(22)	101.41(6)	N(22)—Cu(01)—N(42)	101.4(2)
N(12)—Cu(01)—N(22)	112.08(9)	N(32)—Cu(01)—N(42)	111.9(2)
Cu(01)—N(12)—N(11)	124.4(2)	Cu(01)—N(12)—N(11)	125.9(4)
Cu(01)—N(12)—C(13)	130.8(2)	Cu(01)—N(12)—C(13)	129.0(4)
Cu(01)—N(22)—N(21)	129.1(2)	Cu(01)—N(22)—N(21)	128.9(3)
Cu(01)—N(22)—C(23)	126.2(2)	Cu(01)—N(22)—C(23)	127.2(4)
		Cu(01)—N(32)—N(31)	125.6(3)
		Cu(01)—N(32)—C(33)	130.4(4)
		Cu(01)—N(42)—N(41)	127.4(3)
		Cu(01)—N(42)—C(43)	125.8(4)

(′) $1-x, 1-y, 1-z$.

RESULTS AND DISCUSSION

General

A listing of spectroscopic characteristics (IR and X-ray powder pattern isomorphism), melting points and analytical data of the new compounds is given in Table 3. Many details in the IR spectra are characteristic for pyrazole derivatives and for the respective anions.[21,22] Several compounds changed colour a few degrees below their melting point, apparently due to oxidation of the Cu^{I} to Cu^{II}. The

Table 3. Spectroscopic and analytical data

	M.p. (°C)	X-ray type	IR type	Cu (%) (calc.)
Cu(aebp)Cl[a,b]	132	A	I	20.9 (20.9)
Cu(aebp)Br	168	A	I	18.1 (18.2)
Cu(aebp)I	177	A	I	33.4 (33.4)
Cu(aebp)SCN	149	B	II	19.6 (19.4)
$Cu(aebp)_2BF_4$	170	C	III	11.3 (11.3)
$[Cu(aebp)_2]CF_3SO_3$[b]	148	D	IV	10.3 (10.2)
Cu(aebd)Cl[a]	133	E	V	17.8 (17.6)
Cu(aebd)Br	141	E	V	15.6 (15.7)
Cu(aebd)I[b]	146	F	VI	14.4 (14.1)
Cu(aebd)SCN	116	G	V′	16.4 (16.6)
$Cu(aebd)_2BF_4$	132	H	VII	9.5 (9.4)

[a] Chlorine contents: Cu(aebp)Cl; 11.8% (calc. 11.6), Cu(aebd)Cl; 9.3% (calc. 9.8).

[b] CHN analyses:

	C (%) (calc.)	H (%) (cal.)	N (%) (calc.)
Cu(aebp)Cl	39.4 (39.5)	5.0 (5.0)	23.4 (23.0)
$[Cu(aebp)_2]CF_3SO_3$	40.0 (40.5)	4.9 (4.8)	22.5 (22.5)
Cu(aebd)I	37.3 (37.2)	5.3 (5.1)	15.8 (15.5)

unusual increase in melting points, in going from chloride to iodide, indicates that the crystal packing of the latter compound is better than that of the chloride compound. Theoretical and experimental values of the copper contents of the compounds were in good agreement.

The NMR signals of the coordination compounds are slightly shifted when compared with those of the free ligand. (NMR data are available as supplementary material.[23]) This indicates that in a DMSO solution the compounds do not dissociate. It is also clear from the spectra that the ligand is still intact.

C,H,N analyses of some representative compounds show a good agreement of the calculated and the measured values. From the Guinier and the IR spectra it is clear that the chloride, bromide and iodide copper(I) aebp compounds are isomorphic. The chloride and bromide copper(I) aebd compounds are also isomorphic. Otherwise, no isomorphism has been observed (see Table 3).

The solutions of the coordination compounds are very sensitive to oxidation by air, while the microcrystalline products slowly change colour when exposed to air. In contrast, the single crystals show no colour change when exposed to the air for several weeks.

Description of the structure of $[Cu(aebp)Cl]_2$

An ORTEP[24] representation of the structure is given in Fig. 1. The copper(I) ion is surrounded by two nitrogens (at 2.011(2) and 2.047(2) Å) and by two chlorides (at 2.3874(8) and 2.4094(8) Å). The compound is dimeric with the chlorides as the bridging atoms. The two nitrogens originate from the pyrazole groups of the ligand, aebp, which utilizes only two of its three possible N-donors. The amine nitrogen–copper distance is too long to be considered as bonding (3.903(2) Å). The geometry around copper is slightly distorted from tetrahedral, with angles ranging from 101.41(6) to 116.38(7)°. The distance between the two chloride atoms is about equal to the Van der Waals distance (3.782(1) Å). The copper–copper distance is 2.9511(7) Å. Several compounds are known of comparable dimeric structures in which the copper(I) atoms are surrounded by two nitrogens and two bridging halogens,[25,26] or by two nitrogens and one bridging halogen.[27]

Description of the structure of $[Cu(aebp)_2]CF_3SO_3$

In the compound, $[Cu(aebp)_2]CF_3SO_3$, the copper(I) ion is surrounded by four nitrogen atoms of two ligand molecules in the range 2.018(4)–2.050(4) Å. These distances can be regarded as normal for this type of compound. An ORTEP[24] representation of the structure is given in Fig. 2. As with $[Cu(aebp)Cl]_2$ only the pyrazole nitrogens contribute to the coordination, the tertiary amine nitrogens are too far away from the copper (3.91 Å) to be considered coordinating. With divalent metals, on the contrary, the ligand is tridentate.[6] The geometry around the copper is slightly distorted tetrahedral, with angles between 101.4(2) and 113.4(2)°. Although the triflate anion is non-coordinating, it is not in disorder as is frequently the case with complex non-coordinating anions.[11] The two pyrazole rings of the ligand are planar (distances to the least-squares plane do not exceed 0.01 Å). The distance of the copper ion to the least-

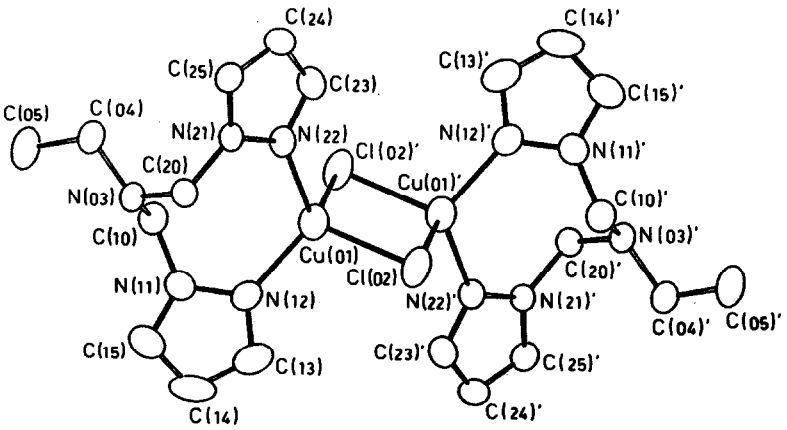

Fig. 1. ORTEP projection[24] with 50% probability vibrational ellipsoids and atomic numbering of $[Cu(aebp)Cl]_2$, hydrogen atoms are omitted.

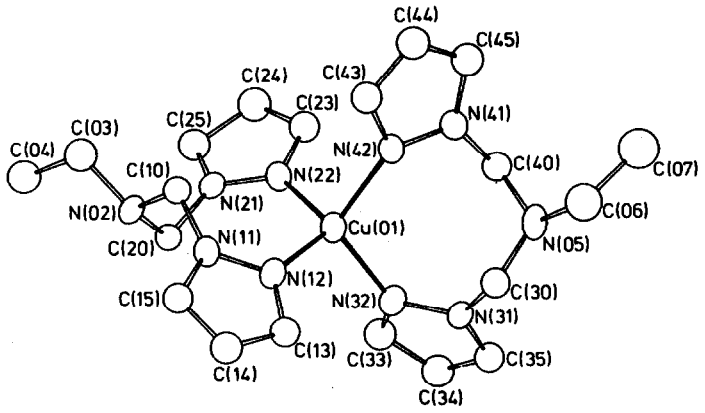

Fig. 2. ORTEP projection[24] with 40% probability vibrational ellipsoids and atomic numbering of the $[Cu(aebp)_2]^+$ cation, hydrogen atoms are omitted.

square planes is 0.13 and 0.05 Å, respectively. The dihedral angle between the pyrazole rings is 140.1(2)°.

Recently the crystal structure[11] of a copper(I) compound with a geometry resembling the present one, i.e. $[Cu(edtp)](BF_4)(CH_3CN)$, in which edtp stands for N,N,N′,N′-tetrakis(1-pyrazolylmethyl)-1,2-diaminoethane was published. Its geometry was also described as almost tetrahedral with copper–nitrogen distances of 2.03 Å and copper–nitrogen angles of 102–115°.

CONCLUSION

The present study has made it clear that the ligands aebp and aebd in all their copper(I) compounds are bidentate, only coordinating through the pyrazole nitrogens. This is in contrast to the coordination to divalent metal ions, in which the amine nitrogen of the ligand is also bound to the metal.

Copper(I) has a preference for a tetrahedral geometry with this type of N-donating ligands. This is in accordance with the preference of nature for a (distorted) tetrahedral coordination geometry in proteins like azurin and plastocyanin.

Acknowledgements—The authors are indebted to Mr S. Gorter and Dr R. A. G. de Graaff for their assistance in the collection and processing of the diffraction data.

Supplementary material available. Listings of fractional coordinates of the atoms of $[Cu(aebp)Cl]_2$ (I) and $[Cu(aebp)_2]CF_3SO_3$ (II), anisotropic thermal parameters of the non-hydrogen atoms of I and II, observed and calculated structure factors of I and II, and bond distances and bond angles of I and II. NMR-data of I, II Cu(aebd)Cl and Cu(aebd)I.

REFERENCES

1. P. M. Colman, H. C. Freeman, J. M. Guss, M. Murata, V. A. Norris, J. A. M. Ramshaw and M. P. Venkatappa, *Nature* 1978, **272**, 319.
2. E. T. Adman, G. W. Canters, H. A. O. Hill and N. A. Kitchen, *FEBS Lett.* 1982, **143**, 287.
3. J. Reedijk, W. L. Driessen and J. van Rijn, *Biological and Inorganic Copper Chemistry* (Edited by K. D. Karlin and J. Zubieta), p. 143. Adenine Press, New York (1986).
4. F. H. Jardine, *Adv. Inorg. Chem. Radiochem.* 1975, **17**, 115.
5. A. D. Zuberbuhler, *Met. Ions Biol. Syst.* 1976, **5**, 325.
6. J. B. J. Veldhuis, W. L. Driessen and J. Reedijk, *J. Chem. Soc., Dalton Trans.* 1986, 537.
7. J. W. F. M. Schoonhoven, W. L. Driessen, J. Reedijk and G. C. Verschoor, *J. Chem. Soc., Dalton Trans.* 1984, 1053.
8. W. L. Driessen, *Recl. Trav. Chim. Pays-Bas* 1982, **101**, 441.
9. E. Bouwman, private communication.
10. R. N. Keller and H. D. Wycoff, *Inorg. Synth.* 1946, **2**, 1.
11. W. L. Driessen, F. B. Hulsbergen, J. Reedijk and G. C. Verschoor, *Transition Met. Chem.* 1985, **10**, 390.
12. D. Doyle, D. A. Eriksen and D. van Engen, *Inorg. Chem.* 1983, **22**, 2892.
13. G. B. Kauffman and R. P. Pinnell, *Inorg. Synth.* 1960, **6**, 3.
14. W. L. Driessen, H. L. Blonk, R. A. G. de Graaff and J. Reedijk, *Acta Cryst., Sect. C* 1987, **C43**, 1516.
15. W. L. Driessen, R. A. G. de Graaff and W. G. R. Wiesmeijer, *Acta Cryst., Sect. C.* 1987, **C43**, 2319.
16. T. N. Sorrell and D. L. Jameson, *J. Am. Chem. Soc.* 1983, **105**, 6013.
17. A. I. Vogel, *Quantitative Inorganic Analyses*. Longmans Green, London (1961).
18. R. A. G. de Graaff, *Acta Cryst., Sect. A.* 1973, **A29**, 298.

19. A. J. Kinneging and R. A. G. de Graaff, *J. Appl. Cryst.* 1984, **17**, 364.
20. *International Table for X-ray Crystallography*, Vol. IV. Kynoch Press, Birmingham, U.K. (1974).
21. S. Trofimenko, *Chem. Rev.* 1982, **72**, 497.
22. J. Reedijk, *Recl. Trav. Chim. Pays-Bas* 1971, **90**, 117.
23. Supplementary material.
24. C. K. Johnson, ORTEP Report ORNL-3794. Oak Ridge National Laboratory, Tennessee (1965).
25. D. A. Haitko and M. F. Garbauskas, *Biological and Inorganic Copper Chemistry* (Edited by K. D. Karlin and J. Zubieta), p. 77. Adenine Press, New York (1985).
26. M. R. Churchill, G. Davies, M. A. El-Sayed, J. A. Fournier, J. Hutchinson and J. A. Zubieta, *Inorg. Chem.* 1984, **23**, 783.
27. W. Clegg, S. R. Acott and C. D. Garner, *J. Chem. Soc., Dalton Trans.* 1984, 2581.

Polyhedron Vol. 7, No. 24, pp. 2591–2595, 1988
Printed in Great Britain

0277–5387/88 $3.00+.00
© 1988 Pergamon Press plc

TRANSITION METAL COORDINATION COMPOUNDS OF A CHELATING IMIDAZOLE–THIOETHER LIGAND. THE X-RAY CRYSTAL STRUCTURE OF (1,6-BIS(4(5)-IMIDAZOLYL)-2,5-DITHIAHEXANE)BIS(NITRATO)COPPER(II)

ELISABETH BOUWMAN, J. CHRISTINE TEN HOVE, WILLEM L. DRIESSEN* and JAN REEDIJK

Department of Chemistry, Gorlaeus Laboratories, Leiden University, P.O. Box 9502, 2300 RA Leiden, The Netherlands

(*Received* 5 *February* 1988; *accepted* 27 *May* 1988)

Abstract—Transition metal coordination compounds with the novel N_2S_2-donor ligand 1,6-bis(4(5)-imidazolyl)-2,5-dithiahexane (abbreviated bhdhx) with general formulae $M(bhdhx)(NO_3)_2$ (M = Co, Ni, Cu) and $M(bhdhx)(H_2O)_2(BF_4)_2$ (M = Cu, Zn) have been isolated. In all compounds the ligand is tetradentate with both thioether sulphurs and imidazole nitrogens coordinating. In all compounds the metal ions are six-coordinated in a distorted octahedral geometry with either nitrates or water molecules as the fifth and sixth ligands. This is confirmed by the ligand field spectra, which agree with a distorted octahedral coordination. The distortion from octahedral, indicated by the ligand field spectrum of the cobalt nitrate compound is such that the S atoms of the ligands must be at a very large distance from the metal ion. A single crystal of $Cu(bhdhx)(NO_3)_2$ was used in a structure determination: orthorhombic space group *Pbcn*, $a = 14.351(5)$, $b = 8.554(3)$, $c = 13.057(4)$ Å, $Z = 4$, and $T = 293$ K. The structure was solved by heavy atom techniques and refined by least-squares methods to a residual R value of 0.033 for 847 significant reflections. The copper ion is at a special position on a two-fold axis, which causes a two-fold symmetry in the ligand. The coordination geometry of the copper atom is distorted octahedral with the two nitrates and the two thioether sulphurs in a *cis* position, and the imidazole nitrogens *trans*. The copper to nitrogen distances are 1.933(4) Å, the copper to sulphur distances are 2.495(1) Å, and the copper to oxygen distances are 2.280(3) Å.

Coordination properties of copper(I) and copper(II) with ligand systems containing nitrogen and sulphur donor atoms as potential coordination sites continue to be of interest as models for the redox active sites in the blue copper proteins.

Recently, several ligands containing both sulphur and nitrogen donor atoms of various nature have been designed and synthesized[1] for the purpose of modelling the active site of (type I) copper proteins. The imidazole group has mostly been substituted by other heterocycles like benzimidazole,[2] pyridine[3] and pyrazole.[4] Instead of a thiol group a thioether group is often introduced, to avoid the too easy reduction of copper(II). So far, coordination compounds with ligands containing both thioether sulphurs and 5-methylimidazol-4-yl have been reported.[5,6]

In the present paper coordination compounds with transition metal ions are described with the related ligand 1,6-bis(4(5)-imidazolyl)-2,5-dithiahexane (bhdhx), which does not have a methyl substituent on the five-position. In the blue copper proteins the histidine residues also contain unsubstituted imidazole groups. The question arises to what extent the methyl group on the five-position of the imidazole influences the coordination behaviour of the ligand and, thereby, the spectroscopic and electronic properties of the resulting coordination complexes. The ligand bhdhx has been prepared earlier by Aoi *et al.*,[7,8] who suggested, on the basis of spectroscopic data, a square-planar coordination

*Author to whom correspondence should be addressed.

of this ligand around the copper(II) ion. To investigate the binding in detail and to prove the chelating nature of the ligand an X-ray structure determination has been performed. Cobalt, nickel and zinc compounds have also been prepared with the ligand bhdhx to allow detailed spectroscopic studies (LF, NMR).

EXPERIMENTAL

Starting materials

The synthesis of the ligand bhdhx has been described in detail elsewhere.[9] The ^{1}H NMR spectrum of the ligand bhdhx (solvent dmso-d_6, internal standard HMDS = Me_3—Si—O—Si—Me_3, hexamethyldisiloxane) showed the following signals: 2.66 ppm (s, 4H, ethane), 3.40 ppm (broad, NH), 3.68 ppm (s, 4H, methylene), 6.90 ppm (s, 2H, 2-imidazole), 7.53 ppm (s, 2H, 5-imidazole). The dihydrochloride salt of the ligand bhdhx showed the following signals (dmso-d_6, internal standard HMS): 2.67 ppm (s, 4H, ethane), 3.84 ppm (s, 4H, methylene), 7.12 ppm (s, 2H, 2-imidazole), 8.00 ppm (s, 2H, 5-imidazole), 9.16 ppm (broad, NH).

All chemicals were commercially available, of sufficient purity, and were used without further treatment.

Synthesis of the complexes

The coordination compounds were prepared by dissolving the appropriate hydrated metal salt (1 mmol) in 5 cm^3 of warm ethanol and adding this solution to a warm solution of the ligand bhdhx (1 mmol) in 25 cm^3 of ethanol. After filtration of the warm reaction mixture, the complexes crystallized on cooling. In some cases evaporation of part of the solvent was necessary before crystallization of the coordination compound occurred. Single crystals were obtained through slow evaporation (room temperature) of the solvent.

Analyses

Metal analyses were carried out complexometrically with EDTA as the complexing agent.[10]

Spectroscopic measurements

IR spectra in the 4000–180 cm^{-1} range of the samples pelleted in KBr were recorded on a Perkin–Elmer 580 spectrophotometer, equipped with a PE data station. Solid-state electronic spectra (28,000–5000 cm^{-1}) were recorded on a Perkin–Elmer 330 spectrophotometer, equipped with a PE data station. Electron paramagnetic resonance spectra of the powdered copper(II) compounds were obtained with a Varian spectrometer at X-band frequency at room temperature and 77 K (liquid nitrogen). NMR spectra were recorded on a JNM-PS-100 NMR spectrometer.

Crystal data

$CuC_{10}H_{14}N_6O_6S_2$, $M_r = 441.92$, orthorhombic, $a = 14.351(5)$, $b = 8.554(3)$, $c = 13.057(4)$ Å, $V = 1603.0$ Å^3 by least-squares refinement of diffractometer angles for 24 reflections, λ(Mo-K_α) = 0.71073 Å, $F(000) = 902.07$, space group *Pbcn*, $Z = 4$, μ(Mo-K_α) = 16.57 cm^{-1}.

Data collection and processing

The data were collected on a four-circle Enraf–Nonius CAD4 diffractometer with graphite monochromatized Mo-K_α radiation: 3079 reflections were measured ($2.0° < \theta < 25.0°$, $-10 < h < 10$, $0 < k < 17$, $0 < l < 15$), of which 1649 were unique, and 847 were considered as observed [$I > 2\sigma(I)$].

Structure analysis and refinement

The structure was solved by direct methods, yielding first the position of the heavy metal, and refined by full-matrix least-squares calculations. The refinement was considered to be complete when the changes in the parameters were smaller than one-third of the standard deviation. Scattering factors were taken from ref. 11.

Hydrogen atoms were located from difference-Fourier maps, except for the hydrogens on the ethylene bridge, which were calculated on a distance of 0.95 Å from their parent atoms. The positional parameters of the hydrogen atoms were coupled to the parent atoms. The thermal parameters of the hydrogen atoms were refined isotropically, coupled with each other, resulting in a final B-value of 5.56 Å^2. The position of the copper ion was kept fixed, because of the two-fold symmetry. The thermal parameters of the non-hydrogens were refined anisotropically. The function minimized was $\Sigma w(||F_o| - |F_c||)^2$ with $w = 1/\sigma^2(F)$. At the final stage the conventional discrepancy index $R_F = \Sigma(||F_o| - |F_c||)/\Sigma|F_o|$ had been reduced to 0.033. The weighted factor $R_w = [\Sigma w(|F_o| - |F_c|)_2/\Sigma w|F_o|^2]^{1/2}$ had been reduced to 0.033. Bond distances and selected bond angles are given in Table 1. The estimated standard deviations in the distances and angles were established using the full correlation matrix. Lists of the atomic posi-

Table 1. Bond lengths (Å) and selected bond angles (°) in $Cu(bhdhx)(NO_3)_2$

Cu(01)—S(04)	2.495(1)
Cu(01)—N(13)	1.933(4)
Cu(01)—O(31)	2.280(3)
S(04)—C(05)	1.801(5)
S(04)—C(10)	1.792(5)
C(05)—C(05′)	1.46(1)
C(10)—C(14)	1.505(6)
N(11)—C(12)	1.324(5)
N(11)—C(15)	1.351(6)
C(12)—N(13)	1.328(5)
N(13)—C(14)	1.376(5)
C(14)—C(15)	1.356(6)
N(3)—O(31)	1.264(5)
N(3)—O(32)	1.245(4)
N(3)—O(33)	1.226(4)
S(04)—Cu(01)—N(13)	83.6(1)
S(04)—Cu(01)—O(31)	99.41(9)
S(04)—Cu(01)—S(04′)	89.88(6)
S(04)—Cu(01)—N(13′)	90.6(1)
S(04)—Cu(01)—O(31′)	169.38(8)
N(13)—Cu(01)—O(31)	95.5(1)
N(13)—Cu(01)—N(13′)	171.8(2)
N(13)—Cu(01)—O(31′)	91.1(1)
O(31)—Cu(01)—O(31′)	71.9(2)

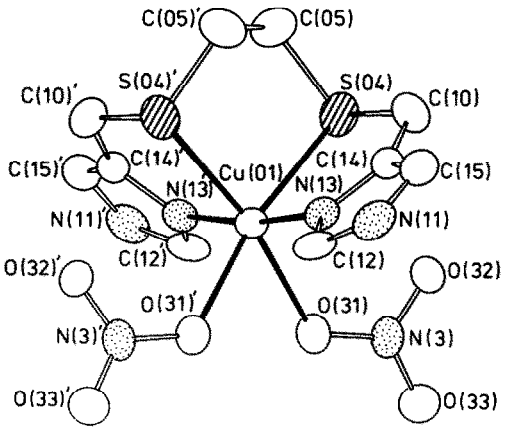

Fig. 1. ORTEP projection of $Cu(bhdhx)(NO_3)_2$ with the atomic labelling. The hydrogen atoms are omitted for clarity. The primed atoms are at the positions $-x$, y, $0.5-z$.

tional and thermal parameters, of bond angles, and of the observed and calculated structure factors are available as supplementary material.[12]

RESULTS AND DISCUSSION

General considerations

A listing of spectroscopic characteristics (ligand field and EPR powder data), IR and X-ray isomorphisms, colours and metal analyses of the transition metal compounds with bhdhx is given in Table 2. Also, some additional C, H, N analyses are given in Table 2. Details of the spectral data will be discussed after the description of the crystal structure.

Description of the structure of $Cu(bhdhx)(NO_3)_2$

An ORTEP[13] projection of the molecular entity $Cu(bhdhx)(NO_3)_2$ is given in Fig. 1. The asymmetric unit consists of half a molecule of $Cu(bhdhx)(NO_3)_2$. The copper ion is lying on a special position on a two-fold axis, which causes a two-fold symmetry in the ligand.

The copper ion is surrounded by two nitrogens, two oxygens and two sulphurs in a distorted octa-

Table 2. Colours, metal contents, IR and X-ray isomorphism, ligand field absorption bands ($\times 10^3$ cm^{-1}) and X-band EPR spectral data of the complexes with bhdhx

Compound (L = bhdhx)	Colour	X-ray, IR type	Metal % exp. (calc.)	LF and EPR data
$Co(L)(NO_3)_2$	brick red	A I	13.0(13.5)	21.2, 17.3, 9.9, 8.3
$Ni(L)(NO_3)_2$[a]	blue	A I	13.1(13.4)	25.4, 15.0, 9.0
$Cu(L)(NO_3)_2$	green	A′ I	14.3(14.4)	15.0, 9.0 $g_\perp$ 2.16, $g_\parallel$ 2.03 (293 K) g_1 2.03, g_2 2.12, g_3 2.19 (77 K)
$Cu(L)(BF_4)_2(H_2O)_2$[b]	green	B II	12.0(12.0)	16.2, 11.4 g_1 2.02, g_2 2.13, g_3 2.20 (293 K)
$Zn(L)(BF_4)_2(H_2O)_2$[c]	white	C III	12.2(12.4)	

C,H,N,O-analyses: found (calc) for: [a] $Ni(L)(NO_3)_2$: C 27.9(27.5), H 3.5(3.2), N 18.1(19.2), O 21.8(22.0). [b] $Cu(L)(H_2O)(BF_4)_2$: C 23.7(23.6), H 3.1(3.2), N 10.7(11.0). [c] $Zn(L)(H_2O)_2(BF_4)_2$: C 22.8(22.6), H 3.4(3.4), N 10.5(10.6).

hedral geometry. The two nitrates are coordinated in a *cis* position. The two sulphur atoms are also *cis* coordinated completing a square-based geometry; the apical positions of the octahedron are occupied by the imidazole nitrogens. The copper to imidazole nitrogen distances are very short, i.e. 1.93 Å and the copper to nitrate oxygen distances are 2.28 Å. The thioether sulphur to copper coordination distances are 2.50 Å. The coordination geometry is therefore compressed octahedral, the axial distances being significantly shorter than the equatorial distances. This compressed geometry is confirmed by the inverted axial EPR spectrum of this copper compound at room temperature (Table 2). The coordination angles around the copper ion deviate significantly from octahedral, the bonding angles lying between 83.6–99.4°. The small coordination angle of 83.6° for the thioether to copper to imidazole nitrogen bond angle must originate from the limited bite of the ligand. Coordination angles that are smaller than ideal, due to the limited ligand bite, have also been encountered with coordination compounds of other imidazole–thioether ligands,[14] and of azole–amine containing ligands e.g. pyrazole–amine containing ligands.[15]

The imidazoles are planar, with deviations from the least-squares planes of less than 0.03 Å. The copper ion is at a distance of 0.09 Å from these least-squares planes. The imidazole planes in the ligand bhdhx are not coplanar, the angle between the two planes is 64.4°. Also, hydrogen bridges are encountered in this crystal structure, between the imidazole–N(11) hydrogen and the nitrate O(32), with an N—O distance of 2.802(5), thereby forming linear chains of $[Cu(bhdhx)(NO_3)_2]$ molecules.

The nitrate compounds

The cobalt, nickel and copper nitrates of bhdhx, $M(bhdhx)(NO_3)_2$, are isostructural (see Table 2). This means there is a $N_2S_2O_2$ chromophore around these metal ions with both nitrate anions coordinated to the metal ions. The ligand field spectrum of the cobalt coordination compound indicates that the coordination geometry of the cobalt ion is quite distorted from octahedral and in fact resembles a somewhat tetrahedral spectrum.[16] Apparently, the cobalt to sulphur distances are too large to be of sufficient influence in the ligand field spectrum. The phenomenon of pseudo-coordination, or semi-coordination has been observed before with bhdhx and related ligands.[17–19] The ligand field spectrum of the nickel compound indicates an averaged octahedral geometry ($Dq = 890\ cm^{-1}$, $B = 900\ cm^{-1}$). The ligand field spectrum of the copper compound agrees with a (distorted) octahedral geometry of the copper ion. The EPR spectrum at room temperature is inverted axial, indicating a compressed geometry. The EPR spectrum at 77 K is rhombic. A zinc nitrate compound could not be obtained, the reaction mixtures yielded oils and amorphous products.

The tetrafluoroborate compounds

No X-ray or IR isomorphism is encountered within the series of tetrafluoroborate compounds given in Table 2. Although the cobalt and nickel compounds with approximate stoichiometry $[M(bhdhx)(H_2O)_2](BF_4)_2 \cdot xH_2O$ with $x = 3$ could be isolated, they did lose variable amounts of lattice solvent; the initial microcrystalline material turned into powder, of which the analytical data (M, C, H, N) could not be fitted. The compounds will therefore not be discussed.

With copper and zinc, the compound $[M(bhdhx)(H_2O)_2](BF_4)_2$ is formed. The zinc compound yielded a single crystal which initially seemed suitable for X-ray determination. The structure showed however much disorder and pseudo-symmetry, which resulted in a very high R value. Attempts to solve the disorder were therefore not undertaken. From the partially solved structure, the coordination environment of the zinc(II) ion could be established as being a distorted octahedron with two water molecules in a *cis* position, the ligand thioether sulphurs also *cis*, and the two imidazole nitrogens *trans*. This coordination environment is very similar to the one depicted in Fig. 1, for the compound $Cu(bhdhx)(NO_3)_2$.

The NMR spectrum of this zinc compound (solvent dmso-d_6, internal standard HMDS) showed the following signals: 2.48 ppm (s, 4H, ethane), 3.70 ppm (s, 4H, methylene), 4.26 ppm (broad, $NH + H_2O$), 7.00 ppm (s, 2H, 2-imidazole), 8.14 ppm (s, 2H, 5-imidazole). These NMR shifts are comparable to the shifts of the hydrochloride salt of bhdhx, rather than to the shifts of the free ligand (see Experimental). The coordinating imidazole-3 nitrogen is now "fixed", which can be compared with the protonated imidazole. The ethane hydrogens are shifted upfield compared to the free ligand, probably because of the coordination of the sulphurs to the zinc ion. The amount of water present in this compound cannot be deduced from the integrals of this NMR spectrum, because of the broad signal, which also comprises the N—H of the imidazole group.

The ligand field spectrum of the copper tetrafluoroborate compound indicates a distorted octahedral geometry; its EPR spectrum is rhombic,

but the low value of g_1 (2.02) clearly indicates a compressed geometry.[20]

CONCLUSION

The present study has made clear that the ligand 1,6-bis(4(5)-imidazolyl)2,5-dithiahexane is a good complexing agent. In all compounds the ligand acts as a tetradentate ligand coordinating through two thioether sulphur atoms and two imidazole nitrogens, although in the cobalt compounds the coordination mode of the sulphur atoms is not well established. The two imidazole nitrogens coordinate in a *trans* position, contrary to the square planar *cis* coordination as proposed by Aoi *et al.*[7] Six-coordination, completed by either two anions or two solvent molecules, is observed in the present compounds.

Acknowledgement—We are indebted to S. Gorter for his assistance in the collection and processing of the diffraction data.

REFERENCES

1. K. D. Karlin and J. Zubieta (Eds), *Copper Coordination Chemistry: Biochemical and Inorganic Perspectives*. Adenine Press, New York (1983)
2. M. J. Schilstra, P. J. M. W. L. Birker, G. C. Verschoor and J. Reedijk, *Inorg. Chem.* 1982, **21**, 2637.
3. K. D. Karlin and J. K. Yandell, *Inorg. Chem.* 1984, **23**, 1184.
4. F. Paap, Ph.D. Thesis, Leiden (1987).
5. J. van Rijn, Ph.D. Thesis, Leiden (1985).
6. E. Bouwman, R. de Gelder, R. A. G. de Graaff, W. L. Driessen and J. Reedijk, *Recl. Trav. Chim. Pays-Bas* 1988, **107**, 163.
7. N. Aoi, G. Matsubayashi and T. Tanaka, *J. Chem. Soc., Dalton Trans.* 1983, 1059.
8. N. Aoi, G. Matsubayashi, T. Tanaka and K. Nakatzu, *Inorg. Chim. Acta* 1984, **85**, 123.
9. E. Bouwman and W. L. Driessen, *Synth. Commun.* 1988, **18**, in press.
10. A. I. Vogel, *Quantitative Inorganic Analyses*. Longmans, Green and Co., London (1961).
11. *International Tables for X-ray Crystallography*, Vol. IV. Kynoch Press, Birmingham (1974).
12. Supplementary Material.
13. C. K. Johnson, ORTEP, Report ORNL-3794. Oak Ridge National Laboratory, Tennessee (1965).
14. J. van Rijn, W. L. Driessen, J. Reedijk and J.-M. Lehn, *Inorg. Chem.* 1984, **23**, 3584.
15. G. J. van Driel, W. L. Driessen and J. Reedijk, *Inorg. Chem.* 1985, **24**, 2919.
16. A. Davidson and E. S. Switkes, *Inorg. Chem.* 1971, **10**, 837.
17. E. Bouwman, A. Burik, J. C. ten Hove, W. L. Driessen and J. Reedijk, *Inorg. Chim. Acta*, in press.
18. J. van Rijn, E. Bouwman, J. R. Empfield, W. L. Driessen and J. Reedijk, in preparation.
19. J. M. M. Smits, R. Janssen, P. T. Beurskens, J. van Rijn and J. Reedijk, *Polyhedron* 1987, **6**, 1843.
20. B. J. Hathaway and D. E. Billing, *Coord. Chem. Rev.* 1970, **5**, 143.

Polyhedron Vol. 7, No. 24, pp. 2597–2600, 1988
Printed in Great Britain

0277–5387/88 $3.00+.00
© 1988 Pergamon Press plc

SYNTHESIS AND PROPERTIES OF SOME DIRUTHENIUM ACETATE COMPOUNDS

F. A. URBANOS, M. C. BARRAL and R. JIMÉNEZ-APARICIO*

Departamento de Química Inorgànica, Facultad de Ciencias Químicas, Universidad Complutense, Ciudad Universitaria, 28040 Madrid, Spain

(*Received* 25 *January* 1988; *accepted* 24 *May* 1988)

Abstract—The compound $[Ru_2(\mu\text{-}O_2CCH_3)_4(THF)_2]BF_4$ (**I**) containing the Ru_2^{5+} unit was prepared by reaction of $Ru_2Cl(\mu\text{-}O_2CCH_3)_4$ with $AgBF_4$ in THF. This compound, in contrast with $Ru_2Cl(\mu\text{-}O_2CCH_3)_4$, is soluble in several polar organic solvents and reacts in THF with $OPPh_3$ and PPh_3 giving $[Ru_2(\mu\text{-}O_2CCH_3)_4(OPPh_3)_2]BF_4 \cdot CH_2Cl_2$ (**II**) and $[Ru(\mu\text{-}O_2CCH_3)(O_2CCH_3)(PPh_3)]_n$ (**III**), respectively. The complex **II** has been also obtained as hexafluorophosphate $[Ru_2(\mu\text{-}O_2CCH_3)_4(OPPh_3)_2]PF_6 \cdot CH_2Cl_2$ (**IV**) by treatment of $Ru_2Cl(\mu\text{-}O_2CCH_3)_4$ with an excess of $NOPF_6$ and PPh_3 in methanol. In this reaction the triphenylphosphine oxide is generated by oxidation of the triphenylphosphine.

Several diruthenium compounds of the type Ru_2ClL_4 (L = carboxylate, amidate, etc.) have been prepared.[1–6] However, very few examples of complexes containing the Ru_2^{4+} [7–9] and Ru_2^{6+} [5,10] units are known.

Thus, Wilkinson *et al.*[7] have obtained diruthenium(II,II) tetracarboxylates $Ru_2(\mu\text{-}O_2CR)_4$ (R = H, Me, CH_2Cl, Et, Ph) by interaction of the reduced "blue solutions" of ruthenium chloride in methanol with alkali–metal carboxylates. The reactivity of these compounds and their adducts towards anionic ligands, donor ligands and oxidizing agents have also been reported. More recently, Drew *et al.*[10] have isolated the complex $Ru_2(\mu\text{-}O_2CCH_3)_4(O_2CCH_3)_2 \cdot H_2O$ by reaction of $Ru_2Cl(\mu\text{-}O_2CCH_3)_4$ with AgO_2CCH_3 in HO_2CCH_3/MeOH; this is the first example of a tetra-μ-carboxylate diruthenium(III,III) compound.

However, the low solubility of $Ru_2Cl(\mu\text{-}O_2CCH_3)_4$ is a problem in the study of the reactivity of the $[Ru_2(\mu\text{-}O_2CCH_3)_4]^+$ unit. Here we report the synthesis and characterization of the complex $[Ru_2(\mu\text{-}O_2CCH_3)_4(THF)_2]BF_4$ (**I**), which is soluble in most common polar organic solvents. We have studied also the reactions of complex **I** with a σ-donor ligand, triphenylphosphine oxide and a σ-donor–π-acceptor ligand, triphenylphosphine.

On the other hand, we have examined the reaction of $Ru_2Cl(\mu\text{-}O_2CCH_3)_4$ with the oxidizing agent, $NOPF_6$, in the presence of PPh_3.

RESULTS AND DISCUSSION

The reaction of $Ru_2Cl(\mu\text{-}O_2CCH_3)_4$ and $AgBF_4$ (1 : 1 mole ratio) in THF, under a dinitrogen atmosphere, leads to the formation of $[Ru_2(\mu\text{-}O_2CCH_3)_4(THF)_2]BF_4$ (**I**) in high yield. The product was obtained as red crystals, is soluble in common polar organic solvents and loses THF in air in short periods of time.

The IR spectrum of **I** in a KBr disc shows strong absorption bands at 1460 and 1400 cm^{-1} assigned to the antisymmetric and the symmetric ν(COO) stretching vibrations, respectively. The separation between these bands may indicate the symmetrical coordination of the carboxylate groups. A strong absorption band at 1070 cm^{-1} is assigned to the vibration of the BF_4^- group; no absorption bands due to the THF ligand were found in this spectrum. However, if the IR spectrum is registered in Nujol mull, a strong absorption at 870 cm^{-1}, due to the coordinated THF, is observed. This facile loss of the weakly coordinated axial THF ligand has been also observed by Wilkinson *et al.*[7] in the complex $Ru_2(\mu\text{-}O_2CCH_3)_4(THF)_2$, but a good analysis could not be obtained.

The reaction of **I** with $OPPh_3$ (1 : 2 mole ratio) in THF or toluene, gives a red solid in high yield. The crystallization of this red solid from di-

* Author to whom correspondence should be addressed.

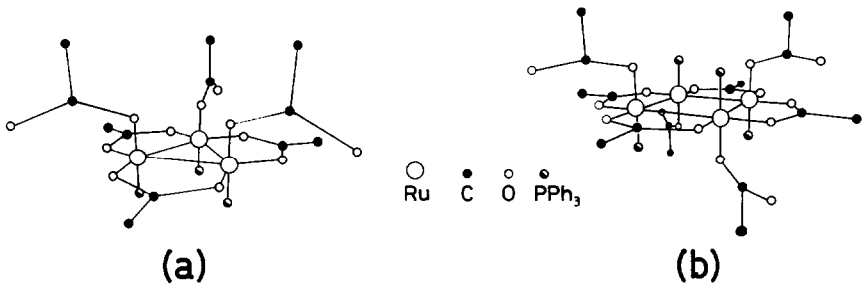

chloromethane–petroleum ether (40–60°C) gives red–brown crystals of $[Ru_2(\mu\text{-}O_2CCH_3)_4(OPPh_3)_2]BF_4 \cdot CH_2Cl_2$ (**II**).

The IR spectrum of **II** exhibits characteristic bands of bridging acetate groups at 1450 and 1400 cm^{-1} corresponding to ν(COO) stretching frequencies; the ν(B—F) stretching of the BF_4^- group appears at 1080 cm^{-1}; the ν(P=O) stretching band of the $OPPh_3$ ligand is observed at 1140 cm^{-1}; this band appears at lower frequencies (*ca* 53 cm^{-1}) than that of the free ligand. The presence of CH_2Cl_2 in this compound shows in the ^1H NMR spectrum (δ = 5.23 ppm, s); the ^1H NMR spectrum of this paramagnetic compound shows the signals corresponding to the CH_3 protons (δ = −5.29 ppm, s) and the C_6H_5 protons (δ = 6.12–5.74 ppm, m) which are shifted to higher fields, similar to other paramagnetic compounds.[11]

Compounds **I** and **II** in acetone solution (~ 10^{-3} M) have conductivities corresponding to those for 1 : 1 electrolytes (Λ_M = 147.94 and 140.63 Ω^{-1} cm^2 mol^{-1}, respectively).

These complexes have the effective magnetic moments per dimer of 4.41 and 4.30 BM, respectively. The magnetic susceptibility measurements at various temperatures (Table 1) indicate that these compounds obey the Curie–Weiss law. These results are similar to those obtained for other carboxylate dimers containing the Ru_2^{5+} unit.[1,12] This is consistent with a $\sigma^2\pi^4\delta^2\pi^{*2}\delta^{*1}$ electronic configuration and three electrons unpaired per dimer.[13]

Complex **I** reacts with triphenylphosphine (1 : 2 mole ratio) to form a violet compound whose elemental analysis is consistent with $[Ru(\mu\text{-}O_2CCH_3)(O_2CCH_3)(PPh_3)]_n$ (**III**). This compound is soluble in polar and non-polar organic solvents such as dichloromethane, THF, toluene, etc.

Complex **III** is diamagnetic. The IR spectrum shows four absorption bands in the carboxyl stretching region at 1470, 1415, 1565 and 1355 cm^{-1} corresponding to bridging and unidentate acetates; this spectrum also shows the bands corresponding to PPh_3 groups. The ^1H NMR spectrum confirms the presence of two inequivalent acetates, showing two singlets for the methyl resonances at 1.74 and 1.69 ppm; the signal corresponding to the aromatic protons appears at 7.20–7.12 ppm.

The $^{31}P\{^1H\}$ NMR spectrum exhibits only one resonance at 35.30 ppm for the PPh_3 ligands, which is consistent with only one type of phosphine in this compound.

The $^{13}C\{^1H\}$ NMR spectrum presents four signals due to acetate groups: two signals appearing at 182.53 and 181.82 ppm are assigned to COO, and two signals appearing at 22.92 and 22.07 ppm are assigned to the CH_3 group. These signals are consistent with bridging and terminal acetate groups. Some resonances corresponding to the phenyl groups appear as pseudoquintuplets at 133.94 and 127.64 ppm; this multiplicity may be due to coupling with three phosphorous atoms.

These spectroscopic data corresponding to complex **III** confirm the stoichiometry $[Ru(\mu\text{-}O_2CCH_3)(O_2CCH_3)(PPh_3)]_n$ and suggest $n \geqslant 3$. Two possible structures, (a) and (b), for this compound are shown above.

Table 1. The magnetic susceptibilities for compounds **I**, **II** and **IV** at various temperatures

					$[Ru_2(\mu\text{-}O_2CCH_3)_4(THF)_2]BF_4$ (**I**)						
T (K)	294.9	288.8	259.5	229.7	199.9	174.9	150.2	125.2	100.4	90.5	85.1
$\chi_M \times 10^3$	8.349	8.124	9.226	10.450	11.680	13.730	16.110	19.280	23.070	25.070	26.720
					$[Ru_2(\mu\text{-}O_2CCH_3)_4(OPPh_3)_2]BF_4 \cdot CH_2Cl_2$ (**II**)						
T (K)	324.9	289.1	288.3	259.8	250.6	229.2	199.7	175.7	169.9	140.1	110.3
$\chi_M \times 10^3$	7.128	7.639	7.995	8.632	9.278	9.232	11.360	12.930	13.290	15.830	19.940
					$[Ru_2(\mu\text{-}O_2CCH_3)_4(OPPh_3)_2]PF_6 \cdot CH_2Cl_2$ (**IV**)						
T (K)	287.9	258.8	230.0	199.0	168.8	140.1	110.1	99.8	90.2	80.3	
$\chi_M \times 10^3$	7.113	8.070	9.198	10.660	18.690	15.240	19.100	20.840	22.940	26.470	

Table 2. Physical and IR spectroscopic properties of the compounds I–IV

Compound	Colour	Analysis (%) Found (Calc.)	Magnetic moment (BM)	Conductivity (Ω^{-1} cm^2 mol^{-1})	IR data (cm^{-1}) ν_a(COO)	ν_s(COO)	(L)
I	red	C 25.1 (28.7) H 4.2 (4.2)	4.41	147.94	1460	1400	870 (THF)
II	red–brown	C 47.0 (46.3) H 3.7 (3.8)	4.30	140.63	1445	1400	1140 (O=P)
III	violet	C 54.0 (54.9) H 4.7 (4.4)	—	—	1470 1565	1415 1355	1100 (PPh_3)
IV	red–brown	C 44.8 (44.1) H 3.7 (3.6)	4.18	125.74	1445	1400	1140 (O=P)

Table 3. NMR data for the compounds II–IV

Compound	^{1}H NMR data (ppm) $\delta(O_2CCH_3)$	δ(L)	$\delta(CH_2Cl_2)$	^{31}P NMR data (ppm)	^{13}C NMR data (ppm) $\delta(O_2CCH_3)$	$\delta(O_2CCH_3)$	δ(L)
II	−5.29(s)	5.93(m)	5.23(s)				
III	1.69(s) 1.74(s)	7.16(m)	—	35.30(s)	22.92(s) 22.07(s)	182.53(s) 181.82(s)	133.94(q) J = 5.15 Hz 131.03(d) J = 44.99 Hz 129.49(s) 127.67(q) J = 5.16 Hz
IV	−5.28(s)	5.91(m)	5.23(s)				

This compound could be generated in a disproportionation reaction similar to that observed by Wilkinson *et al.*[14]

$$2Ru_2^{5+} \rightarrow Ru_2^{4+} + Ru_2^{6+},$$

followed by a reorganization process in the Ru(II)–Ru(II) complex. The disproportionation reaction would also explain why the yield of complex **III** is no more than 50%. The nature of the yellow Ru(III)–Ru(III) complex formed or its transformation products is still uncertain and is under study now.

The $[Ru_2(\mu\text{-}O_2CCH_3)_4(OPPh_3)_2]PF_6 \cdot CH_2Cl_2$ complex (**IV**) has been obtained by reaction of $Ru_2Cl(\mu\text{-}O_2CCH_3)_4$ with $NOPF_6$ and PPh_3 in excess, in methanol, and posterior crystallization in dichloromethane–petroleum ether (40–60°C). The use of $NOPF_6$ in this reaction does not produce the oxidation of the Ru_2^{5+} unit, but the triphenylphosphine is transformed into triphenylphosphine oxide.

The IR, NMR, conductivity and magnetic properties are similar to those of complex **II** described above (see Tables 2 and 3).

EXPERIMENTAL

All reactions were carried out in an inert atmosphere, using standard Schlenk techniques. $Ru_2Cl(\mu\text{-}O_2CCH_3)_4$ was prepared by the literature procedure.[15] $RuCl_3 \cdot 3H_2O$, $NOPF_6$ and $AgBF_4$ were obtained from Johnson Matthey Chemicals Ltd, Ventron and Fluka, respectively. $OPPh_3$ and PPh_3 were obtained from Probus. Solvents were purified and distilled by standard methods. Methanol was used without previous purification.

Elemental microanalysis for C and H were performed by Elemental Microanalysis Ltd, Devon (U.K.). IR spectra in the region 4000–200 cm^{-1} were recorded as KBr discs or Nujol mulls on a Perkin–Elmer 1330 IR spectrophotometer. NMR were recorded on Varian FT-80 or Bruker WM 360 spectrophotometers. Magnetic measurements were made with a magnetometer DSM 5 in the range 85–295 K. Molar conductivities were measured with a Philips PW 9526 digital conductivity meter, using a Philips PW 9512/60 conductivity measuring cell.

Synthesis of $[Ru_2(\mu\text{-}O_2CCH_3)_4(THF)_2]BF_4$ (I)

$Ru_2Cl(\mu\text{-}O_2CCH_3)_4$ (2.00 g, 4.22 mmol) and $AgBF_4$ (0.82 g, 4.22 mmol) were stirred in THF (80 cm^3) for 24 h at room temperature, to give a red solution and a white precipitate of AgCl. The solution was filtered and the precipitate was washed with THF until colourless. The red solution and the combined extracts were reduced to 20 cm^3, and

petroleum ether was added to give a crystalline red solid. Yield 2.14 g, 75.7%.

Synthesis of $[Ru_2(\mu\text{-}O_2CCH_3)_4(OPPh_3)_2]BF_4 \cdot CH_2Cl_2$ **(II)**

To a solution of **I** (0.5 g, 0.75 mmol) in THF (30 cm^3) or to a suspension of **I** (0.5 g, 0.75 mmol) in toluene (30 cm^3), was added $OPPh_3$ (0.42 g, 1.50 mmol). The reaction mixture was stirred at room temperature for 4 h (12 h in toluene). The solvent was removed and the solid was washed with diethyl ether (3×15 cm^3). The red solid was crystallized from dichloromethane–petroleum ether (40–60°C) as red–brown crystals. Yield 0.59 g, 67%.

Synthesis of $[Ru(\mu\text{-}O_2CCH_3)(O_2CCH_3)(PPh_3)]_n$ **(III)**

To a solution of **I** (1 g, 1.49 mmol) in THF (50 cm^3), was added PPh_3 (0.78 g, 2.99 mmol). The solution was stirred at room temperature for 4 h, and changed from red to violet. The solvent was removed to leave a dry residue, which was extracted with toluene (3×20 cm^3). The combined extracts were treated with active C and filtered. The solvent was removed to give a microcrystalline solid which was washed with cold diethyl ether. Yield 0.46 g, 32%.

Synthesis of $[Ru_2(\mu\text{-}O_2CCH_3)_4(OPPh_3)_2]PF_6 \cdot CH_2Cl_2$ **(IV)**

To $Ru_2Cl(\mu\text{-}O_2CCH_3)_4$ (0.5 g, 1.06 mmol) in methanol (30 cm^3), was added an excess of $NOPF_6$ (0.56 g, 3.17 mmol) and PPh_3 (1.39 g, 5.28 mmol). The reaction mixture was stirred at room temperature for 6 h. The solvent was removed to leave a dry residue which was washed with diethyl ether and THF. The orange solid residue was crystallized from dichloromethane–petroleum ether (40–60°C) to give red–brown crystals. Yield 0.82 g, 63%.

Acknowledgements—We are grateful to the Comisión Asesora de Investigación Científica y Técnica (CAICYT) (Spain) for financial support (project PR84-0367). Thanks are due to Dr Sàez and Mr Rojas for their help in obtaining the magnetic measurements.

REFERENCES

1. T. A. Stephenson and G. Wilkinson, *J. Inorg. Nucl. Chem.* 1966, **28**, 2285.
2. A. R. Chakravarty, F. A. Cotton and D. A. Tocher, *Inorg. Chem.* 1985, **24**, 1263.
3. A. R. Chakravarty, F. A. Cotton and D. A. Tocher, *Inorg. Chem.* 1985, **24**, 172.
4. T. Malinski, D. Chang, F. N. Feldmann, J. L. Bear and K. M. Kadish, *Inorg. Chem.* 1983, **22**, 3225.
5. A. R. Chakravarty, F. A. Cotton and D. A. Tocher, *J. Am. Chem. Soc.* 1984, **106**, 6409.
6. A. Bino, F. A. Cotton and T. R. Felthouse, *Inorg. Chem.* 1979, **18**, 2599.
7. A. J. Lindsay, G. Wilkinson, M. Motevalli and M. B. Hursthouse, *J. Chem. Soc., Dalton Trans.* 1985, 2321.
8. A. J. Lindsay, G. Wilkinson, M. Motevalli and M. B. Hursthouse, *J. Chem. Soc., Dalton Trans.* 1987, 2723.
9. M. Berry, C. D. Garner, I. H. Hillier, A. A. MacDowell and W. Clegg, *Inorg. Chim. Acta* 1981, **53**, L61.
10. M. G. B. Drew, P. Higgins and M. McCann, *J. Chem. Soc., Chem. Commun.* 1987, 1385.
11. T. Bheling, G. Wilkinson, T. A. Stephenson, D. A. Tocher and M. D. Walkinshaw, *J. Chem. Soc., Dalton Trans.* 1983, 2109.
12. M. Mukaida, T. Nomura and T. Ishimori, *Bull. Chem. Soc. Jpn.* 1972, **45**, 2143.
13. J. G. Norman Jr, G. E. Renzoni and D. A. Case, *J. Am. Chem. Soc.* 1979, **101**, 5256.
14. R. P. Tooze, G. Wilkinson, M. Motevalli and M. B. Hursthouse, *J. Chem. Soc., Dalton Trans.* 1986, 2711.
15. R. W. Mitchell, A. Spencer and G. Wilkinson, *J. Chem. Soc., Dalton Trans.* 1973, 846.

Polyhedron Vol. 7, No. 24, pp. 2601–2603, 1988
Printed in Great Britain

0277–5387/88 $3.00+.00
© 1988 Pergamon Press plc

EXCHANGE REACTIONS OF DISTIBINES

M. ATEŞ, H. J. BREUNIG* and S. GÜLEÇ

Fachbereich 2, Universität Bremen, Leobenerstraße, D 2800 Bremen 33, F.R.G.

(*Received* 27 *April* 1988; *accepted* 25 *May* 1988)

Abstract—Distibines of the type $R_2SbSbR'_2$ with $R = CH_3$, $R' = C_2H_5$ (**1**), $R = CH_3$, $R' = n\text{-}C_3H_7$ (**2**), $R = CH_3$, $R' = C_6H_5$ (**3**), $R = C_2H_5$, $R' = C_6H_5$ (**4**), $R = n\text{-}C_3H_7$, $R' = C_6H_5$ (**5**), and $R = CH_3$, $R' = 2,4,6\text{-}(CH_3)_2C_6H_2$ (**6**) are formed in equilibria by exchange reactions of the respective distibines of the type R_4Sb_2 and R'_4Sb_2.

Tetramethyldistibine[1–3] is red as a solid, but yellow as a liquid or in solution. Reversible colour changes from orange to yellow are observed when solid tetraethyldistibine is warmed close to the melting point.[1] In contrast, tetra-*n*-propyl-, tetraphenyl-, and tetramesityldistibine are yellow and do not show unusual colour effects. In the course of our investigations of thermochromic distibines[4] we became interested in the colours of compounds of the type $R_2SbSbR'_2$ with different organic substituents R and R′, which may favour thermochromic effects like CH_3 or C_2H_5 or may be indifferent like $n\text{-}C_3H_7$, C_6H_5, or $2,4,6\text{-}(CH_3)_3C_6H_2$ (= Mes). We report now on the syntheses of these asymmetric distibines in equilibrium mixtures with their precursors.

RESULTS AND DISCUSSIONS

Equimolar amounts of tetramethyl- and tetraethyldistibine react as neat liquids at 25°C with rapid exchange of the dialkylantimony moieties forming $Me_2SbSbEt_2$ (**1**) in equilibrium with the parent distibines. Analogous reactions give $Me_2SbSb\textit{n}\text{-}Pr_2$ (**2**), $Me_2SbSbPh_2$ (**3**), $Et_2SbSbPh_2$ (**4**), $n\text{-}Pr_2SbSbPh_2$ (**5**), and $Me_2SbSbMes_2$ (**6**) according to eq. (1).

$$R_2SbSbR_2 + R'_2SbSbR'_2 \rightleftharpoons 2R_2SbSbR'_2 \quad (1)$$

1: $R = CH_3$, $R' = C_2H_5$; **2**: $R = CH_3$, $R' = n\text{-}C_3H_7$; **3**: $R = CH_3$, $R' = C_6H_5$; **4**: $R = C_2H_5$, $R' = C_6H_5$; **5**: $R = n\text{-}C_3H_7$, $R' = C_6H_5$; **6**: $R = CH_3$, $R' = 2,4,6\text{-}(CH_3)_3C_6H_2$.

*Author to whom correspondence should be addressed.

The identification of the products and the determination of their relative concentrations were performed using mass and ^1H NMR spectroscopy. The spectral data are summarized in Table 1. The ^1H NMR spectrum of the equilibrium mixture, which was obtained from equimolar amounts of $(CH_3)_4Sb_2$ and $(C_2H_5)_4Sb_2$ is shown in Fig. 1. The frequencies of the parent distibines were identified by comparison with the spectra of pure samples and by changing the ratio of the components. For the novel mixed distibine **1** we find the expected singlet for the $(CH_3)_2Sb$ protons and a triplet and four quartets of an ABX_3 spin system for the $(C_2H_5)_2Sb$ moiety. This shows that in **1** like in $(C_2H_5)_4Sb_2$, the

Table 1. Spectroscopic data

^1H NMR data (δ, ppm) (C_6D_6)

1: 0.935 Me_2Sb; 1.298 CH_3CSb t; $^3J = 7.4$ Hz; ABX_3 spin system, A: 1.535; B: 1.591 CH_2; $^2J = 12$ Hz. **2**: 0.951 Me_2Sb; 0.945 CH_3CCSb t; $^3J = 7.2$ Hz; 1.5–1.9 CH_2CH_2Sb m. **3**: 0.82 CH_3; 6.95–7.05 m, 7.55–7.62 m C_6H_5. **4**: 1.999 CH_3CSb t; ABX_3 spin system, A: 1.514; B: 1.578 CH_2; $^2J = 12$ Hz; 7.0–7.1 m; 7.65–7.71 m Ph_2Sb. **5**: 0.833 CH_3, $^3J = 7.1$ Hz; 1.30–1.82 CH_2CH_2 m; 7.04–7.11; 7.68–7.72 Ph m. **6**: 0.91 Me_2Sb, 2.10 *p*-CH_3, 2.39 *o*-CH_3, 6.72 C_6H_2. Me_4Sb_2: 0.845; Et_4Sb_2: 1.33 CH_3 t; $^3J = 8$ Hz; ABX_3 spin system, A: 1.60 B: 1.66 CH_2; $^2J = 12$ Hz. $n\text{-}Pr_4Sb_2$: 0.975 CH_3 t, $^3J = 7.2$ Hz; 1.5–1.84 CH_2CH_2 m. Ph_4Sb_2: 6.99–7.03 m; 7.52–7.56 m; Mes_4Sb_2: 2.07 *p*-CH_3, 2.47 *o*-CH_3, 6.66 C_6H_2.

MS data (for ^{121}Sb) m/z (rel. int. %)

1: 330 (85) M^+, 301 (85) M^+—Et, 273 (100) $Me_2Sb_2H^+$. **2**: 358 (40) M^+, 273 (30) $Me_2Sb_2H^+$.

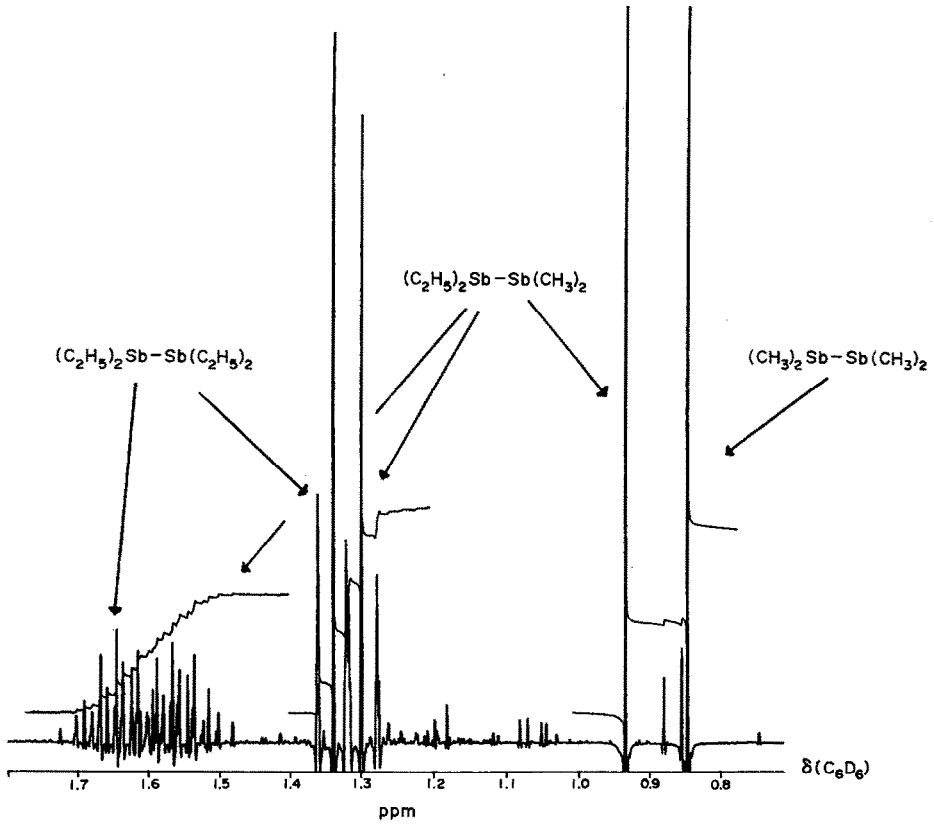

Fig. 1. ^{1}H NMR spectrum of $(CH_3)_2SbSb(C_2H_5)_2$ (**1**) in equilibrium with $(CH_3)_4Sb_2$ and $(C_2H_5)_4Sb_2$.

CH_2 protons are not equivalent and there is no inversion at antimony in these molecules. The ^{1}H NMR data of **1–4** and of the parent distibines are listed in Table 1.

For qualitative analyses of the mixtures, mass spectra have been used in the case of compounds **1** and **2**. The spectra show molecular ions and characteristic fragments of all the compounds including the mixed species. Selected MS data are given in Table 1.

The relative concentrations of the parent and mixed compounds were determined from the integrals of the ^{1}H NMR signals. For $K = [R_2SbSbR'_2]^2/[R_4Sb_2][R'_4Sb_2]$ at 25°C we find $K = 4$ with R = CH_3, R′ = C_2H_5; R = CH_3, R′ = n-C_3H_7; R = n-C_3H_7, R′ = C_6H_5; $K = 7$ with R = C_2H_5, R′ = C_6H_5; $K = 9$ with R = CH_3, R′ = C_6H_5, and $K = 81$ with R = CH_3, R′ = 2,4,6-$(CH_3)_3C_6H_2$. The equilibria with the constant $K = 4$ have a statistical distribution of the R_2Sb or R'_2Sb moieties. This reflects the similarities of the respective bond strengths between these groups. Pauling's concept[5] of ionic covalent resonance energy of AB type molecules may be applied here. Apparently in the case of **1**, **2** and **5** the electronic requirements of the R_2Sb and R'_2Sb groups are as similar as expected. In addition, steric factors should be considered as they may be responsible for the promotion of **3**, **4** and **6** in their respective equilibria. Exchange reactions, where the Pauling postulates[5] are violated, have however been reported for the systems $(CH_3)_4As_2$ with $(C_2H_5)_4As_2$ ($K = 1$) (ref. 6), $(CH_3)_4Sb_2$ with $(CH_3)_4Bi_2$ ($K = 1$, 2) or $(CH_3)_4As_2$ ($K = 0$, 9) (ref. 7) $(CH_3)_4Sb_2$ with $(n$-$C_3H_7)_4Bi_2$ ($K = 0$, 7) (ref. 8). We have no simple explanation for the differences in the equilibrium constants. Most intriguing is the comparison of the diarsine and the analogous distibine system.

Attempts to isolate the mixed compounds **1–4** by distillation or crystallization failed. We could only obtain the parent symmetric distibines. Therefore, the colours of the mixed distibines in a pure state could not be observed. The equilibrium mixtures are yellow liquids at 25°C and form yellow solutions in hydrocarbons. Red solids are obtained, when the mixtures containing **1**, **2**, **3** or **6** are cooled. There are no thermochromic effects in the case of **4** or **5**.

EXPERIMENTAL

All the operations were carried out in an Ar atmosphere. $(CH_3)_4Sb_2$,[9] $(C_2H_5)_4Sb_2$,[9] $(n\text{-}C_3H_7)_4Sb_2$,[10] $(C_6H_5)_4Sb_2$[11] and Mes_4Sb_2[12] were synthesized by previously reported methods. ^1H NMR spectra were recorded on a Bruker 360 MHz FT spectrometer. MS spectra were run on a Varian MAT CH7 A spectrometer.

Syntheses of 1–6

The following mixtures were stirred at room temperature. **1**: 1.17 g of (3.25 mmol) of Et_4Sb_2 with 0.99 g (3.25 mmol) of Me_4Sb_2; 1.42 g (3.94 mmol) of Et_4Sb_2 with 2.47 g (8.13 mmol) of Me_4Sb_2; 0.2 g (0.56 mmol) of Et_4Sb_2 with 0.35 g (1.15 mmol) of Me_4Sb_2; **2**: 1.71 g (4.11 mmol) of $n\text{-}Pr_4Sb_2$ with 1.25 g (4.11 mmol) of Me_4Sb_2; **3**: 0.055 g (0.15 mmol) of Me_4Sb_2 with 0.1 g (0.18 mmol) of Ph_4Sb_2; **4**: 0.51 g (1.43 mmol) of Et_4Sb_2 with 0.78 g (1.41 mmol) of Ph_4Sb_2; **5**: 0.48 g (1.15 mmol) of $n\text{-}Pr_4Sb_2$ with 0.636 g (1.15 mmol) of Ph_4Sb_2; **6**: 0.055 g (0.15 mmol) of Me_4Sb_2 with 0.11 g (0.15 mmol) of Mes_4Sb_2. The equilibrium was controlled by dissolving the mixture in C_6D_6 and recording the NMR spectrum after several minutes.

Acknowledgements—We thank the Deutsche Forschungsgemeinschaft and the Fonds der Chemischen Industrie for financial support.

REFERENCES

1. F. A. Paneth, *Trans. Faraday Soc.* 1934, **30**, 179.
2. A. J. Ashe, III, E. G. Ludwig, J. Oleksyszyn and J. C. Huffman, *Organometallics* 1984, **3**, 337.
3. O. Mundt, H. Riffel, G. Becker and A. Simon, *Z. Naturforsch.* 1984, **39b**, 317.
4. S. Roller, M. Dräger, H. J. Breunig, M. Ateş and S. Güleç, *J. Organometal. Chem.* 1987, **329**, 319.
5. L. Pauling, *J. Am. Chem. Soc.* 1932, **54**, 3570.
6. V. K. Gupta, L. K. Krannich and C. L. Watkins, *Polyhedron* 1987, **6**, 1229.
7. A. J. Ashe and E. G. Ludwig Jr, *J. Organometal. Chem.* 1986, **303**, 197.
8. H. J. Breunig and D. Müller, *Z. Naturforsch.* 1986, **41b**, 1129.
9. H. J. Breunig, V. Breunig-Lyriti and T.-P. Knobloch, *ChemikerZeitung* 1977, **101**, 399.
10. H. J. Breunig and H. Jawad, *Z. Naturforsch.* 1982, **37b**, 1104.
11. H. J. Breunig and T. Severengiz, *Z. Naturforsch.* 1982, **37b**, 395.
12. M. Ateş, H. J. Breunig, A. Soltani-Neshan and M. Tegeler, *Z. Naturforsch.* 1986, **41b**, 321.

Polyhedron Vol. 7, No. 24, pp. 2605–2609, 1988
Printed in Great Britain

0277–5387/88 $3.00+.00
© 1988 Pergamon Press plc

THE REACTION OF *CIS* DIOXOBIS(2,4 PENTANEDIONATO)MOLYBDENUM(VI) AND 2,2′ PYRIDYLBENZOXAZOLE (L), A NOVEL ROUTE TO $\beta[Mo_8O_{26}]^{4-}$

BRIAN PIGGOTT* and SWEE FATT WONG

Inorganic Chemistry Research Laboratory, Chemistry Department, The Hatfield Polytechnic, Hatfield, Herts AL10 9AB, U.K.

and

MICHAEL B. HURSTHOUSE and RICHARD L. SHORT

Department of Chemistry, Queen Mary College, University of London, Mile End Road, London E1 4NS, U.K.

(*Received* 23 *February* 1988; *accepted* 25 *May* 1988)

Abstract—$MoO_2(C_5H_7O_2)_2$, where $C_5H_7O_2$ is 2,4-pentanedione (acac), reacts with 2-2′ pyridylbenzoxazole in acetone to give a product with stoichiometry, $Mo_3C_{24}H_{16}N_6O_{12}$. This product dissolves readily in dimethylformamide to give a brown solution which on standing for several weeks yielded crystals. An X-ray structure determination showed these crystals to contain uncoordinated 2-2′ pyridylbenzoxazole and $[(CH_3)_2NH_2]_4^+[Mo_8O_{26}]^{4-}$.

During the course of our investigations of the ^{95}Mo NMR of Mo^{VI} complexes with N and O donor ligands, $MoO_2(acac)_2$ was reacted with 2-2′ pyridylbenzoxazole (L) and the nature of the products formed is reported here. Instead of forming MoO_2L_2 or $Mo_2O_5L_2$ type complexes as might have been anticipated, a compound of unknown structure was obtained. Attempts to crystallize this compound from dimethylformamide (DMF) for structure determination resulted in the formation of $[(CH_3)_2NH_2]_4^+[Mo_8O_{26}]^{4-}$. This result presents two problems, first, formation of an isopolymolybdate which normally takes place only in acidic solutions and, second, formation of a dimethylammonium ion. Since the solvent used in the crystallization was dimethylformamide this is almost certainly the source of the dimethylamine, which indicates that the above reaction involves its Mo mediated hydrolysis.

*Author to whom correspondence should be addressed.

EXPERIMENTAL

2-2′ Pyridylbenzoxazole was synthesized by the literature method.[1]

Preparation of the compounds

(i) $MoO_2(acac)_2$ (1.63 g, 0.005 mol) was dissolved in acetone (50 cm^3) and to this was added 2-2′ pyridylbenzoxazole (0.98 g, 0.005 mol) in acetone (50 cm^3) with rapid stirring. The grey product, **I**, that very quickly formed was filtered and air-dried. This preparation was carried out three times but the products gave inconsistent analyses.

(ii) Compound **I** was dissolved in DMF, without heating, to give a brown solution which on standing for several weeks produced large chunky crystals. These crystals were suitable for X-ray structure determination. The ^{95}Mo NMR spectrum of this compound in DMF showed a peak at 125 ppm with a line width of 80 Hz and a peak at 23 ppm with a line width of 230 Hz.

(iii) Compound **I** was dissolved in dimethylsulphoxide (DMSO) without heating to give a brown solution which on standing for several weeks gave crystals that contained no molybdenum, and analysed as follows. Found: C, 67.0; H, 4.7; N, 12.9; O (by difference), 15.4. Calc. for $C_{12}H_{10}N_2O_2$: C, 67.3; H, 4.7; N, 13.1; O, 14.9%.

IR spectra were recorded as Nujol mulls on a Pye Unicam SP 300. Mass spectra were recorded on a VG Analytical 70E, with an 11/250 data system, using both electron impact at 70 eV, source temperature 280°C, (sample introduced by direct insertion), and positive fast atom bombardment in a DMSO/glycerol matrix. ^{95}Mo NMR spectra were recorded on a JEOL 90 spectrometer operating at 5.78 MHz. An aqueous 2 M sodium molybdate solution (pH 11) was used as an external chemical shift reference.

X-ray crystallography

The crystal used for X-ray work was sealed in a thin-walled glass capillary. After preliminary photography, unit cell and intensity data were obtained using a CAD4 diffractometer and graphite monochromatized Mo-K_α radiation ($\lambda = 0.71069$ Å) following standard procedures.[2]

The structure was solved by direct methods and refined by full-matrix least-squares; non-hydrogen atoms were assigned anisotropic displacement factor coefficients; hydrogens were included in idealized positions and assigned group isotropic coefficients. Crystallographic data are as follows: $[C_2H_8N]_4^+[Mo_8O_{26}]^{4-}[C_{12}H_8N_2O]_2$, formula weight 1760.4, triclinic, $a = 8.283(8)$, $b = 10.206(1)$, $c = 15.506(3)$ Å, $\alpha = 88.14(1)$, $\beta = 84.29(3)$, $\gamma = 80.59(3)°$, $U = 1287$ Å^3, space group $P\bar{1}$, $Z = 1$, $D_c = 2.27$ g cm^{-3}, μ(Mo-K_α) = 17.9 cm^{-1}, $T = 291$ K. 4517 reflections were recorded, giving 4511 unique and 4198 observed [$I > 1.5\sigma(I)$]. The data were corrected for absorption empirically. 376 parameters, weighting scheme $w = 1/[\sigma^2(F_o) + 0.0003F_o^2]$, final $R = 0.031$, $R_w(= \Sigma w/(\Delta F)^2/\Sigma wF_o^2) = 0.053$. Atomic scattering factors were calculated from data in ref. 3.

Final atomic positional parameters, U_{ij} and U_{iso} values, full lists of bond lengths and angles and tables of F_o/F_c have been deposited as supplementary data with the Editor, from whom copies are available on request. Atomic coordinates have also been deposited with the Cambridge Crystallographic Data Centre.

RESULTS AND DISCUSSION

The Mo, C, H, N and O analyses of compound **I** are inconsistent. The IR spectrum of compound **I** shows two strong bands at 950 and 911 cm^{-1} (Mo=O), and two strong broad bands at 805 and 660 cm^{-1} (Mo—O—Mo).[4]

Several structures can be postulated on the basis of these results and to try and resolve this problem we attempted to recrystallize **I** for an X-ray structure determination. The only common solvents in which **I** dissolved were DMF and DMSO, and these solutions on standing for several weeks produced crystals which were different from **I**. The structure of the crystals from DMF, **II**, is shown in Fig. 1 from which it is seen that L is uncoordinated and the Mo is in the form of the isopolymolybdate ion $[Mo_8O_{26}]^{4-}$, specifically the β isomer, Fig. 2; geometry parameters for this are given in Table 1 and are essentially the same as those

Table 1. Bond lengths (Å) and angles (°) for $[Mo_8O_{26}][NH_2Me_2]_4 \cdot [C_{12}H_8N_2O]_2$

Bond lengths (Å)			
O(2)—Mo(1)	2.337(5)	O(3)—Mo(1)	1.694(5)
O(10)—Mo(1)	1.947(4)	O(11)—Mo(1)	1.746(5)
O(12)—Mo(1)	1.957(4)	O(2)—Mo(2)	2.323(4)
O(4)—Mo(2)	1.699(5)	O(5)—Mo(2)	1.695(5)
O(10)—Mo(2)	2.346(5)	O(13)—Mo(2)	1.917(5)
O(2)—Mo(3)	2.449(4)	O(6)—Mo(3)	1.693(6)
O(7)—Mo(3)	1.691(5)	O(11)—Mo(3)	2.308(5)
O(13)—Mo(3)	1.918(5)	O(14)—Mo(3)	1.940(5)
O(2)—Mo(4)	2.324(4)	O(8)—Mo(4)	1.690(5)
O(9)—Mo(4)	1.700(5)	O(12)—Mo(4)	2.370(5)
O(14)—Mo(4)	1.905(5)		
C(2)—O(1)	1.382(6)	C(9)—O(1)	1.340(6)
C(3)—C(2)	1.388(7)	C(7)—C(2)	1.369(7)
C(4)—C(3)	1.375(8)	C(5)—C(4)	1.375(9)
C(6)—C(5)	1.357(8)	C(7)—C(6)	1.389(7)

Table 1—*continued*

Bond lengths (Å)			
N(8)—C(7)	1.391(6)	C(9)—N(8)	1.339(6)
C(10)—C(9)	1.427(7)	N(11)—C(10)	1.341(6)
C(15)—C(10)	1.402(7)	C(12)—N(11)	1.319(7)
C(13)—C(12)	1.379(7)	C(14)—C(13)	1.384(8)
C(15)—C(14)	1.370(7)		
C(42)—N(41)	1.496(7)	C(43)—N(41)	1.448(8)
C(45)—N(44)	1.441(8)	C(46)—N(44)	1.474(9)
Bond angles (°)			
O(3)—Mo(1)—O(2)	172.7(1)	O(10)—Mo(1)—O(2)	78.2(2)
O(10)—Mo(1)—O(3)	101.7(2)	O(11)—Mo(1)—O(2)	82.2(2)
O(11)—Mo(1)—O(3)	105.0(2)	O(11)—Mo(1)—O(10)	96.5(2)
O(12)—Mo(1)—O(2)	77.6(2)	O(12)—Mo(1)—O(3)	100.2(2)
O(12)—Mo(1)—O(10)	150.7(1)	O(12)—Mo(1)—O(11)	96.3(2)
O(4)—Mo(2)—O(2)	92.4(2)	O(5)—Mo(2)—O(2)	162.0(1)
O(5)—Mo(2)—O(4)	105.5(3)	O(10)—Mo(2)—O(2)	71.2(2)
O(10)—Mo(2)—O(4)	162.6(1)	O(10)—Mo(2)—O(5)	90.8(2)
O(13)—Mo(2)—O(2)	77.3(2)	O(13)—Mo(2)—O(4)	100.4(2)
O(13)—Mo(2)—O(5)	101.1(2)	O(13)—Mo(2)—O(10)	81.9(2)
O(6)—Mo(3)—O(2)	94.5(2)	O(7)—Mo(3)—O(2)	159.7(1)
O(7)—Mo(3)—O(6)	105.7(3)	O(11)—Mo(3)—O(2)	69.7(2)
O(11)—Mo(3)—O(6)	164.2(1)	O(11)—Mo(3)—O(7)	90.0(2)
O(13)—Mo(3)—O(2)	74.1(2)	O(13)—Mo(3)—O(6)	99.0(3)
O(13)—Mo(3)—O(7)	102.0(2)	O(13)—Mo(3)—O(11)	76.9(2)
O(14)—Mo(3)—O(2)	73.6(2)	O(14)—Mo(3)—O(6)	99.4(2)
O(14)—Mo(3)—O(7)	102.6(3)	O(14)—Mo(3)—O(11)	76.9(2)
O(14)—Mo(3)—O(13)	143.8(1)	O(8)—Mo(4)—O(2)	93.2(2)
O(9)—Mo(4)—O(2)	161.3(1)	O(9)—Mo(4)—O(8)	105.3(3)
O(12)—Mo(4)—O(2)	70.4(2)	O(12)—Mo(4)—O(8)	162.3(1)
O(12)—Mo(4)—O(9)	90.9(2)	O(14)—Mo(4)—O(2)	77.2(2)
O(14)—Mo(4)—O(8)	102.9(2)	O(14)—Mo(4)—O(9)	100.7(2)
O(14)—Mo(4)—O(12)	80.5(2)	Mo(2)—O(2)—Mo(1)	98.2(2)
Mo(3)—O(2)—Mo(1)	92.2(2)	Mo(3)—O(2)—Mo(2)	85.9(2)
Mo(4)—O(2)—Mo(1)	99.5(2)	Mo(4)—O(2)—Mo(2)	160.8(1)
Mo(4)—O(2)—Mo(3)	86.0(2)	Mo(2)—O(10)—Mo(1)	109.9(2)
Mo(3)—O(11)—Mo(1)	115.9(2)	Mo(4)—O(12)—Mo(1)	110.2(2)
Mo(3)—O(13)—Mo(2)	116.1(2)	Mo(4)—O(14)—Mo(3)	115.8(3)
C(9)—O(1)—C(2)	105.0(4)	C(3)—C(2)—O(1)	129.5(5)
C(7)—C(2)—O(1)	108.3(4)	C(7)—C(2)—C(3)	122.2(5)
C(4)—C(3)—C(2)	115.0(5)	C(5)—C(4)—C(3)	122.5(6)
C(6)—C(5)—C(4)	122.5(6)	C(7)—C(6)—C(5)	115.7(5)
C(6)—C(7)—C(2)	122.0(5)	N(8)—C(7)—C(2)	108.5(5)
N(8)—C(7)—C(6)	129.5(5)	C(9)—N(8)—C(7)	104.4(4)
N(8)—C(9)—O(1)	113.8(5)	C(10)—C(9)—O(1)	123.3(5)
C(10)—C(9)—N(8)	122.9(5)	N(11)—C(10)—C(9)	116.9(5)
C(15)—C(10)—C(9)	121.0(5)	C(15)—C(10)—N(11)	122.1(5)
C(12)—N(11)—C(10)	117.6(5)	C(13)—C(12)—N(11)	124.1(5)
C(14)—C(13)—C(12)	118.3(5)	C(15)—C(14)—C(13)	118.7(5)
C(14)—C(15)—C(10)	119.0(5)		
C(43)—N(41)—C(42)	112.4(5)	C(46)—N(44)—C(45)	115.2(6)

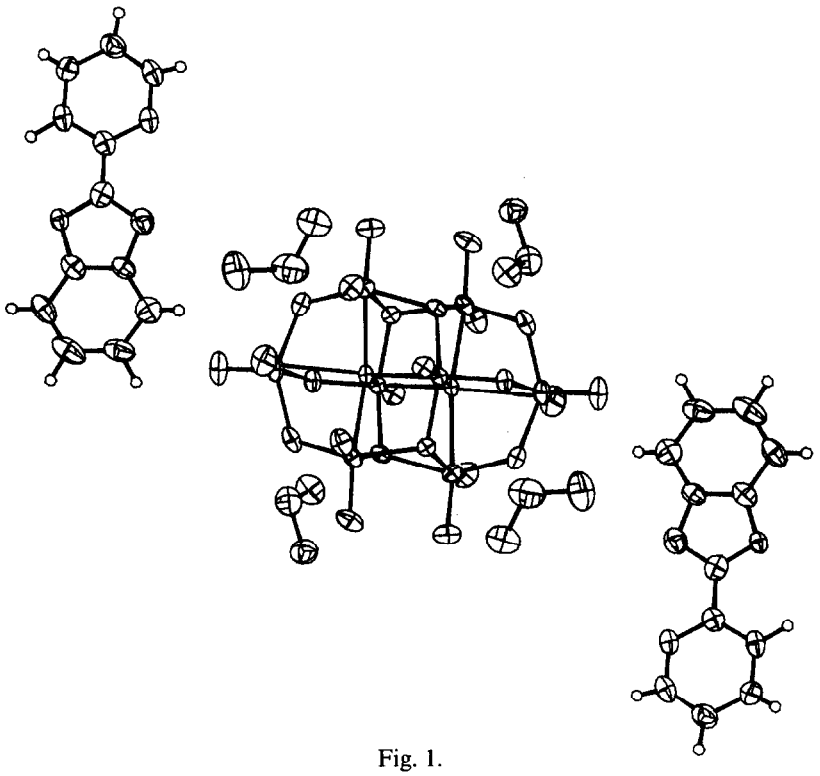

Fig. 1.

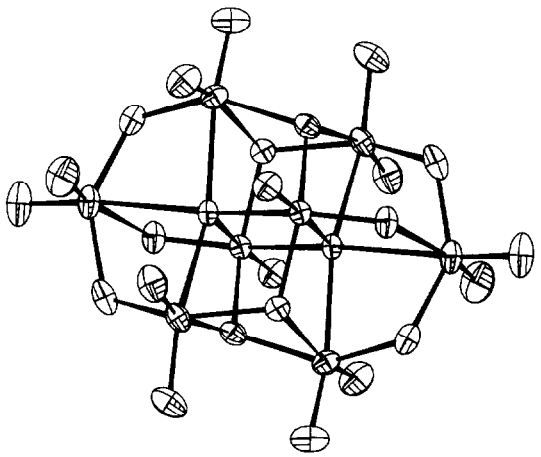

Fig. 2.

discussed previously.[5] The nature of the cation i.e. $(CH_3)_2NH_2^+$ was established unequivocally from its mass spectrum which showed peaks in the FABS at 46 ($Me_2NH_2^+$) and 197 (LH^+).

From a preparative point of view this structure presents two problems. First, it is known that acidification of aqueous sodium molybdate solution to pH 3–4 leads to precipitation of $\alpha[Mo_8O_{26}]^{4-}$ or $\beta[Mo_8O_{26}]^{4-}$ depending on the nature of the cation.[6] However, as can be seen above, the conditions which resulted in the formation of **II** were non-aqueous and certainly non-acidic. The second problem is the source of the dimethylammonium ion. It was initially thought that this, as the free amine, was an impurity in the DMF used but this was ruled out on checking the gas liquid chromatograph of that solvent. Given the lack of structural information for **I**, a mechanism for this reaction is difficult to deduce but a plausible one involves hydrolysis of the DMF. If the solvent coordinates to the molybdenum on dissolution of **I** it would become more susceptible to nucleophilic attack by water molecules which would have been absorbed from the atmosphere. This would give rise to $(CH_3)_2NH$ and possibly formic acid. Acidic conditions are necessary in the condensation of simple molybdenum oxygen species to give large isopolymolybdates to remove the supernumerary oxygen atoms as water molecules, and it is possible that formic acid might provide the appropriate pH.

The DMSO solution produced crystals of **III** that analysed for $C_{12}H_{10}N_2O_2$ and had the highest peak in their mass spectrum at 214. Since **III** corresponds to a compound differing from 2-2′ pyridylbenzoxazole by the elements of water, and its IR spectrum shows bands at 3312 (strong, νNH), 2720 (weak, νOH involved in hydrogen bonding) and 1649 (very strong, νC=O) then it is most probably N-(2-hydroxyphenyl)-2-pyridylcarboxamide,[7] viz. Structure 1.

Acknowledgement—We would like to thank SERC for financial support.

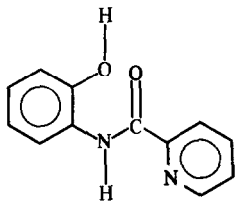

Structure 1.

REFERENCES

1. T. R. Harkins, J. L. Walter, O. E. Harris and H. Freiser, *J. Am. Chem. Soc.* 1956, **78**, 260.
2. R. A. Jones, M. B. Hursthouse, K. M. A. Malik and G. Wilkinson, *J. Am. Chem. Soc.* 1979, **101**, 4128.
3. *International Tables for X-ray Crystallography*, Vol. 4. Kynoch Press, Birmingham (1974).
4. R. N. Hider and C. J. Wilkins, *J. Chem. Soc., Dalton Trans.* 1984, 495.
5. P. Roman, J. M. Gutietrez Zorilla, M. Martinez Ripoll and S. Garcia Blanco, *Polyhedron* 1986, **5**, 1799.
6. W. G. Klemperer and W. Shum, *J. Am. Chem. Soc.* 1976, **98**, 8291.
7. D. Yusupov, S. A. Sarankina, C. A. Ismailova, K. M. Akhmerov and A. B. Kuchkarov, *Dokl. Akad. Naut. UZSSR.* 1983, **5**, 36.

Polyhedron Vol. 7, No. 24, pp. 2611–2614, 1988
Printed in Great Britain

0277–5387/88 $3.00+.00
© 1988 Pergamon Press plc

THE SYNTHESIS, VIBRATIONAL SPECTROSCOPY, AND CRYSTAL AND MOLECULAR STRUCTURE OF $[H_3NCH_2CH_2NH_3][PdBr_6]$

ROBIN J. H. CLARK* and VINCENT B. CROUD†

Christopher Ingold Laboratories, University College London, 20 Gordon Street, London WC1H 0AJ, U.K.

and

HELEN M. DAWES and MICHAEL B. HURSTHOUSE*

Department of Chemistry, Queen Mary College, Mile End Road, London E1N 4NS, U.K.

(*Received* 25 *April* 1988; *accepted* 25 *May* 1988)

Abstract—The complex $[H_3NCH_2CH_2NH_3][PdBr_6]$ has been isolated as well-formed brown crystals. The Raman (single crystal) and FTIR (wax disc) spectra of the complex have been recorded but the band assignments are complicated by extensive factor group splitting and resonance effects. The crystal belongs to space group *Pnnm*, with $Z = 2$, each ion occupying sites of $2/m$ (C_{2h}) symmetry. The $[PdBr_6]^{2-}$ ion is very close to octahedral, the two unique PdBr distances, 2.466(3) and 2.470(3) Å, being equal within experimental error and the BrPdBr angles being $90 \pm 0.8°$. The diammonium cation has an extended, planar, *trans* structure.

Very little information is at hand regarding the $[PdBr_6]^{2-}$ ion apart from the X-ray structural analysis on the rubidium salt, for which the Pd—Br distance is 2.505 Å.[1] The only vibrational data relate to studies carried out over 20 years ago on the potassium salt.[2] We have now succeeded in isolating well-formed crystals of the ethylenediammonium (enH_2^{2+}) salt which were not only suitable for single crystal Raman and for FTIR studies, but also for single crystal X-ray diffraction studies. The X-ray results demonstrate that the $[PdBr_6]^{2-}$ ion is, as expected, close to octahedral symmetry.

EXPERIMENTAL

Preparation of the complex

The complex was prepared by the addition of bromine to an aqueous solution of $Pd(en)(NO_2)_2$ containing both HCl and $NaNO_2$. The solution was warmed slightly and, on being allowed to cool to room temperature, yielded good quality brown crystals of $[H_3NCH_2CH_2NH_3][PdBr_6]$. Found: C, 3.7; H, 1.5; N, 4.5; Br, 72.9%. Calc. for $[H_3NCH_2CH_2NH_3][PdBr_6]$: C, 3.7; H, 1.5; N, 4.3; Br, 73.9%.

Vibrational spectroscopy

The Raman spectra were recorded on a Spex 14018/R6 spectrometer. Exciting radiation was provided by Coherent Radiation model CR12 and CR 3000 K lasers, the powers being kept to < 50 mW. Samples for Raman spectra were in the form of single crystals held at *ca* 80 K with use of a liquid nitrogen and Dewar assembly. Spectra were calibrated by reference to the Rayleigh line.

Grinding the complex with $KClO_4$ or KBr alters the band profiles giving rise to a spectrum more closely resembling that recorded[2] for $K_2[PdBr_6]$. The FTIR spectra were recorded on a Bruker 113V interferometer as a wax disc at *ca* 80 K in the region 600–20 cm^{-1}.

* Authors to whom correspondence should be addressed.
† Present address: Borax Research Ltd., Cox Lane, Chessington, Surrey KT9 1SJ.

X-ray crystallography

All X-ray measurements were made on a crystal of dimensions $0.3 \times 0.25 \times 0.2$ mm using a CAD4 diffractometer operating in the $\omega/2\theta$ scan mode with graphite-monochromated Mo-K_α radiation ($\lambda = 0.71069$ Å) in a manner previously described in detail.[3] The structure was solved using the Patterson search routine of *SHELX* 84[4] developed via difference synthesis and refined by full-matrix least-squares.[5] Details are as follows.

Crystal data. $[C_2N_2H_{10}][PdBr_6]$, $M = 647.9$, orthorhombic, $a = 8.163(2)$, $b = 10.212(3)$, $c = 7.264(1)$ Å, $U = 605.5$ Å^3, space group *Pnnm*, $Z = 2$, $D_c = 3.55$ g cm^{-3}, μ(Mo-K_α) = 208.01 cm^{-1}, $F(000) = 584$, $T = 293$ K.

Data collection. Scan width $w = 0.8 \pm 0.35 \tan\theta$, $1.5 \leqslant \theta \leqslant 30$, $h = -10 \rightarrow 10$, $k = 0 \rightarrow 14$, $l = 0 \rightarrow 11$, scan speed 1.35–6.77° min^{-1}, 961 data collected, 945 unique, 720 observed [$I > 2\sigma(I)$].

Structure refinement. 33 variables, all atoms anisotropic. No hydrogen atoms could be located and attempts to refine those on methylene CH_2 groups in idealized positions were unsuccessful. The weighting scheme $w = [\sigma^2(F_o) + 0.0004F_o^2]$ was applied, and an extinction parameter[5] was refined (value adopted = 0.0036). Final $R = 0.0334$, $R_w = 0.0397$. Scattering factor data were taken from the *International Tables*. Fractional atomic coordinates, U_{ij} coefficients and F_o/F_c tables have been deposited as supplementary data with the Editor, from whom copies are available on request. Atomic coordinates have also been deposited with the Cambridge Crystallographic Data Centre.

RESULTS AND DISCUSSION

Vibrational spectroscopy

Bands observed in the IR and Raman spectra of the $[PdBr_6]^{2-}$ ion as it occurs in $[H_3NCH_2CH_2NH_3][PdBr_6]$ are listed in Table 1. The spectra of ethylenediamine dihydrobromide were also recorded in the region 600–20 cm^{-1}, but no bands found for this compound corresponded with any of those listed in Table 1. The complex, $[H_3NCH_2CH_2NH_3][PdBr_6]$, is strongly absorbing throughout the visible region and so scattering by the cation modes is heavily attenuated by absorption and not subject to resonance Raman effects.

Surprisingly, no Raman bands were detected in the region between the Rayleigh line and those occurring in the 172–198 cm^{-1} region. Weak overtones of the 174–198 cm^{-1} bands could, however, be detected.

The relative intensities of the Raman bands depend somewhat on the wavelength of the exciting line used to gather the data, those at 198.4 and 176.1 cm^{-1} being more intense with red (676.4 nm) excitation while that at 186.3 cm^{-1} is more intense with UV (350.7 nm) excitation (Fig. 1). Resonance effects are thus in evidence, presumably associated with the very broad, intense Br → Pd charge-transfer responsible for the absorption of the ion in the

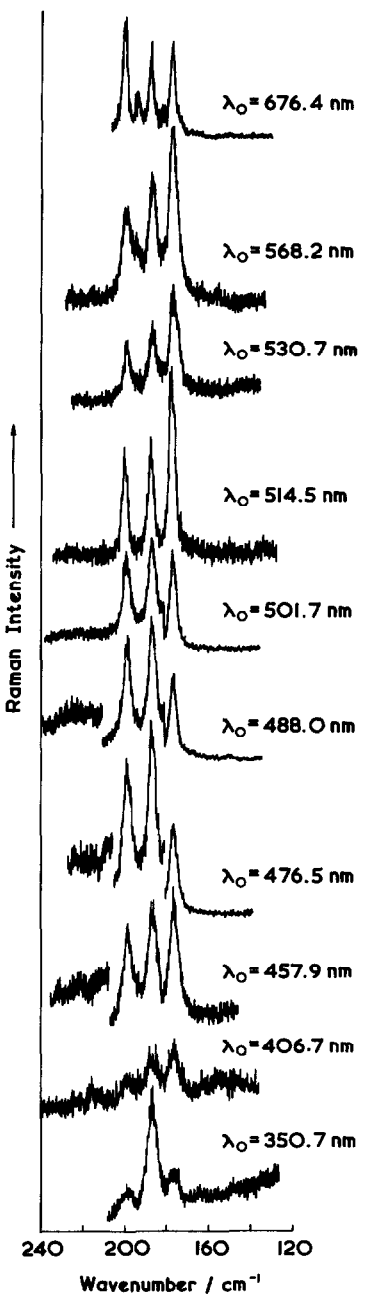

Fig. 1. Raman spectra of $[H_3NCH_2CH_2NH_3][PdBr_6]$ as a single crystal at *ca* 80 K with 676.4, 568.2, 530.7, 514.5, 501.7, 488.0, 476.5, 457.9, 406.7 and 350.7 nm excitation. Slit widths 150/250/150 μm.

Table 1. Wavenumbers and assignments of bands observed in the Raman and FTIR spectra of $[H_3NCH_2CH_2NH_3][PdBr_6]$

FTIR[a]		Raman[b]	
$\tilde{\nu}$ (cm^{-1})	Assignment	$\tilde{\nu}$ (cm^{-1})	Assignment
105 m, 142 m	δ(BrPdBr)		
174 m		172.8 (0.43, sh)	
		176.1 (1)	ν(PdBr)
		186.3 (0.52)	
		192.8 (0.52)	
		198.4 (0.48)	
249 s, 260 vs, 264 sh?, 268 s,sh, 287 m	ν(PdBr)		
306 m			
314 sh	174+142?		

[a] Wax disc at *ca* 80 K.

[b] Single crystal at *ca* 80 K; $\lambda_0 = 676.4$ nm; slits 100/150/100 μm; relative band intensities given in parentheses.

Table 2. Correlation chart for $[PdBr_6]^{2-}$ in $[H_3NCH_2CH_2NH_3][PdBr_6]$

	Point group O_h	Site group[a] C_{2h}	Space group[a] D_{2h}^{12}
ν_1	a_{1g}		
ν_2	e_g	$a_g(4)$	$a_g(4)$, $b_{1g}(4)$
ν_3	t_{1u}	$a_u(4)$	$a_u(4)$, $b_{1u}(4)$
ν_4	t_{1u}	$b_g(2)$	$b_{2g}(2)$, $b_{3g}(2)$
ν_5	t_{2g}	$b_u(5)$	$b_{2u}(5)$, $b_{3u}(5)$
ν_6	t_{2u}		

[a] Correlating about the C_2 axis parallel to c which bisects the BrPdBr angle.

Table 3. Bond lengths (Å) and bond angles (°) for $[H_3NCH_2CH_2NH_3][PdBr_6]$

Bond lengths (Å)			
Br(1)—Pd	2.466(3)	Br(2)—Pd	2.470(3)
N(1)—C(1)	1.493(14)	C(1)—C(1a)	1.430(21)
Bond angles (°)			
Br(1)—Pd—Br(1d)	180.0	Br(1)—Pd—Br(1c)	89.2
Br(1)—Pd—Br(1d)	90.8	Br(1)—Pd—Br(2)	89.3
Br(1)—Pd—Br(2b)	90.7	Br(2)—Pd—Br(2b)	180.0
N(1)—C(1)—C(1a)	112.8		

Key to symmetry operations relating designated atoms to reference atoms at (x, y, z): (a) $1.0-x, -y, 1.0-z$; (b) $1.0-x, 1.0-y, 1.0-z$; (c) $1.0-x, 1.0-y, z$; (d) $x, y, 1.0-z$.

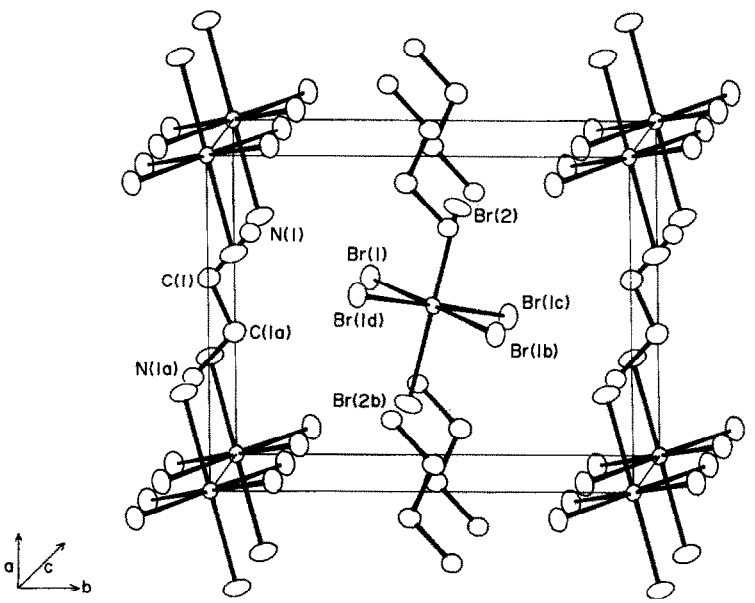

Fig. 2. Unit cell of $[H_3NCH_2CH_2NH_3][PdBr_6]$.

visible region. The 192.8 cm^{-1} band is only evident with 676.4 nm excitation.

Both the Raman and IR spectra of the $[PdBr_6]^{2-}$ ion are more complicated for this salt than for the potassium salt.[2] Indeed, in some spectra, more bands in the PdBr stretching region were detected than would be expected on the basis of site group effects; factor group splittings (Table 2) are strongly evident, probably as a consequence of strong N—H···Br hydrogen bonding within the crystal (*vide infra*). The band assignments given in Table 3 are similar to those given[2] for K_2PdBr_6, viz. $\nu_1(a_{1g})$ 198 cm^{-1}, $\nu_2(e_g)$ 176 cm^{-1}, $\nu_3(t_{1u})$ 253 cm^{-1}, $\nu_4(t_{1u})$ 130 cm^{-1}, $\nu_5(t_{2g})$ 100 cm^{-1}.

X-ray crystallography

A diagram of the unit cell and contents is shown in Fig. 2; bond lengths and angles are given in Table 3. The structure comprises separated $[PdBr_6]^{2-}$ and $[H_3NCH_2CH_2NH_3]^{2+}$ ions, both of which occupy positions of $2/m$ (C_{2h}) symmetry. The $[PdBr_6]^{2-}$ anions have a geometry very close to octahedral, the two unique Pd—Br distances being equal (average 2.468 Å) to within experimental error and the Br—Pd—Br angles deviating by less than 1° from 90°. The diammonium cation has an extended, planar *trans* structure.

The anions are stacked along the *c* axis edge to edge, with Br···Br distances of 3.752 Å. Unfortunately, the hydrogen atoms on the cation could not be located and so it is not possible to define precisely the N—H···Br interactions which are likely to be present. However, the unique nitrogen atom makes a number of contacts which are possible interactions; these are indicated on Fig. 2 and are dimensioned as follows: contact *a* 3.493; *b* 3.501; *c* 3.555; *d* 3.634 (Table 4). It is possible that the $-NH_3^+$ group is disordered so that all of these contacts (and their symmetry equivalents) contain a H-bonding component.

Table 4. Selected non-bonded distances (Å) for $[H_3NCH_2CH_2NH_3][PdBr_6]$

Intramolecular			
Br(2)—Br(1)	3.468	N(1)—Br(1)	3.493
Intermolecular			
Br(2)—Br(1a)	3.511	C(1)—Br(1b)	3.765
Br(1)—Br(1c)	3.462	Br(2)—Br(1c)	3.511
C(1)—Br(1d)	3.765	Br(1)—Br(1e)	3.512
Br(2)—Br(1e)	3.468	N(1)—Br(1e)	3.493
Br(2)—Br(1f)	3.600	C(1)—Br(1g)	3.767
N(1)—Br(1g)	3.555	N(1)—Br(1h)	3.501
N(1)—Br(1i)	3.501	Br(2)—Br(1j)	3.600
C(1)—Br(1k)	3.767	N(1)—Br(1k)	3.555
Br(2)—Br(2l)	3.603	C(1)—Br(2m)	3.889
N(1)—Br(2m)	3.634	N(1)—C(1b)	2.434

Key to symmetry operations relating designated atoms to reference atoms at (x, y, z): (a) $1.0-x, 1.0-y, 1.0-z$; (b) $1.0-x, -y, 1.0-z$; (c) $1.0-x, 1.0-y, z$; (d) $1.0-x, -y, z$; (e) $x, y, 1.0-z$; (f) $0.5-x, 0.5+y, 0.5+z$; (g) $0.5-x, -0.5+y, 0.5+z$; (h) $-0.5+x, 0.5-y, 0.5-z$; (i) $-0.5+x, 0.5-y, 0.5+z$; (j) $0.5-x, 0.5+y, 0.5-z$; (k) $0.5-x, -0.5+y, 0.5-z$; (l) $-x, 1.0-y, 1.0-z$; (m) $0.5-x, -0.5+y, -0.5+z$.

Acknowledgement—The authors thank the S.E.R.C. for financial support.

REFERENCES

1. P. Stoll, Dissertation, ETH, Zurich, Switzerland.
2. P. J. Hendra and P. J. D. Park, *Spectrochim. Acta* 1967, **23A**, 1635.
3. R. A. Jones, M. B. Hursthouse, K. M. A. Malik and G. Wilkinson, *J. Am. Chem. Soc.* 1979, **101**, 4128.
4. G. M. Sheldrick, University of Göttingen, personal communication.
5. G. M. Sheldrick, SHELX 76, University of Cambridge (1976).

Polyhedron Vol. 7, No. 24, pp. 2615–2626, 1988
Printed in Great Britain

0277–5387/88 $3.00+.00
© 1988 Pergamon Press plc

1,2-BIS(DIMETHYL)PHOSPHINOETHANE COMPLEXES OF MOLYBDENUM AND VANADIUM. X-RAY CRYSTAL STRUCTURE OF *TRANS*-[MoCl(η^2-NCMe)(DMPE)$_2$]BPh$_4$, *TRANS*-[Mo(SPh)$_2$(DMPE)$_2$], *TRANS*-[V(NCMe)$_2$(DMPE)$_2$](BPh$_4$)$_2$, *TRANS*-[V(CNBu^t)$_2$(DMPE)$_2$](PF$_6$)$_2$

SIMON J. ANDERSON, FIONNA J. WELLS and GEOFFREY WILKINSON*

Chemistry Department, Imperial College, London SW7 2AY, U.K.

and

BILQUIS HUSSAIN and MICHAEL B. HURSTHOUSE*

Chemistry Department, Queen Mary College, London E1 4NS, U.K.

(*Received* 11 *May* 1988; *accepted* 27 *May* 1988)

Abstract—The replacement of chloride in the complexes, *trans*-[MCl$_2$(dmpe)$_2$], M = Mo and V, dmpe = 1,2-bis(dimethyl)phosphinoethane, by various other ligands has been studied. For Mo, acetonitrile gives the species *trans*-[MoCl(NCMe)(dmpe)$_2$]$^+$, which has isomers with either η^1- or η^2-MeCN; these react with methanol to give the molybdenum(IV) ethylimido complex [MoCl(NEt)(dmpe)$_2$]$^+$. Both Mo and V give [M(NCMe)$_2$(dmpe)$_2$]$^{2+}$ cations.

Other complexes synthesized are *trans*-[MoL$_2$(dmpe)$_2$], L = NEt$_2$, SPh; *trans*-[VL$_2$(dmpe)$_2$], L = CN, SCN, CS$_2$; [VL$_2$(dmpe)$_2$]$^+$, L = EtCN, ^{t}BuNC; [VCl(^{t}BuNC)(dmpe)$_2$]$^+$ and [V(NCMe)$_6$]$^{2+}$.

Nuclear magnetic and electron spin resonance spectra of the compounds are reported and the X-ray crystal structure of four of the compounds listed in the title are described.

We have previously described the synthesis of the acetonitrile complexes, *trans*-[MCl(NCMe)(dmpe)$_2$]$^+$ and *trans*-[M(NCMe)$_2$(dmpe)$_2$]$^{2+}$, M = Cr,[1,2] Fe[3] and Ru,[3] and their reactions with methanol and dihydrogen.

We now describe similar complexes derived from *trans*-[MCl$_2$(dmpe)$_2$], M = Mo[4] and V[5]; these include the molybdenum(II) chloro complex which has isomers with either η^1- or η^2-MeCN. Various vanadium complexes derived from *trans*-[VCl$_2$(dmpe)$_2$] or *trans*-[V(NCMe)$_2$(dmpe)$_2$]$^{2+}$ are also described.

The reactions are summarized in Scheme 1 for molybdenum and Scheme 2 for vanadium. IR and NMR data for the new compounds are given in the Experimental.

RESULTS AND DISCUSSION

Molybdenum compounds

Acetonitrile complexes. The interaction of *trans*-[MoCl$_2$(dmpe)$_2$] with one equivalent of NaBPh$_4$ in refluxing MeCN leads to a red–orange solution from which the complex *trans*-[MoCl(η^1-NCMe)(dmpe)$_2$](BPh$_4$) (1) can be isolated. Recrystallization of this complex from THF gives the isomer *trans*-[MoCl(η^2-MeCN)(dmpe)$_2$](BPh$_4$) (2) as red–brown crystals. A similar reaction using two equivalents of NaBPh$_4$ leads to a red–brown solution from which *trans*-[Mo(NCMe)$_2$(dmpe)$_2$](BPh$_4$)$_2$ (3) can be isolated.

The partially substituted d^4 complexes are both diamagnetic and their ^{1}H NMR spectra show, as well as signals due to dmpe, singlets at 2.1 and 3.2 ppm, assignable to the methyl groups of MeCN, for

* Authors to whom correspondence should be addressed.

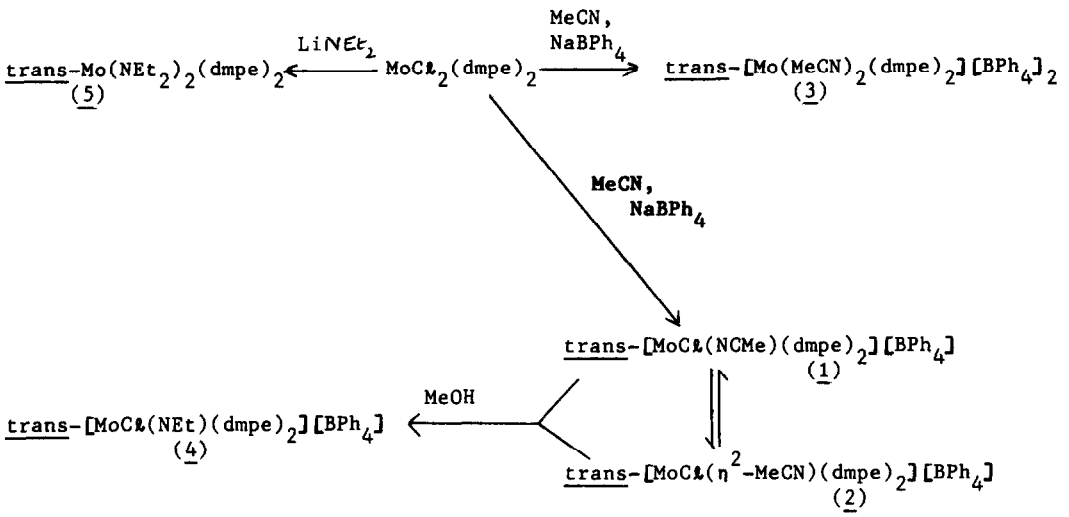

Scheme 1. Reactions of *trans*-[$MoCl_2(dmpe)_2$].

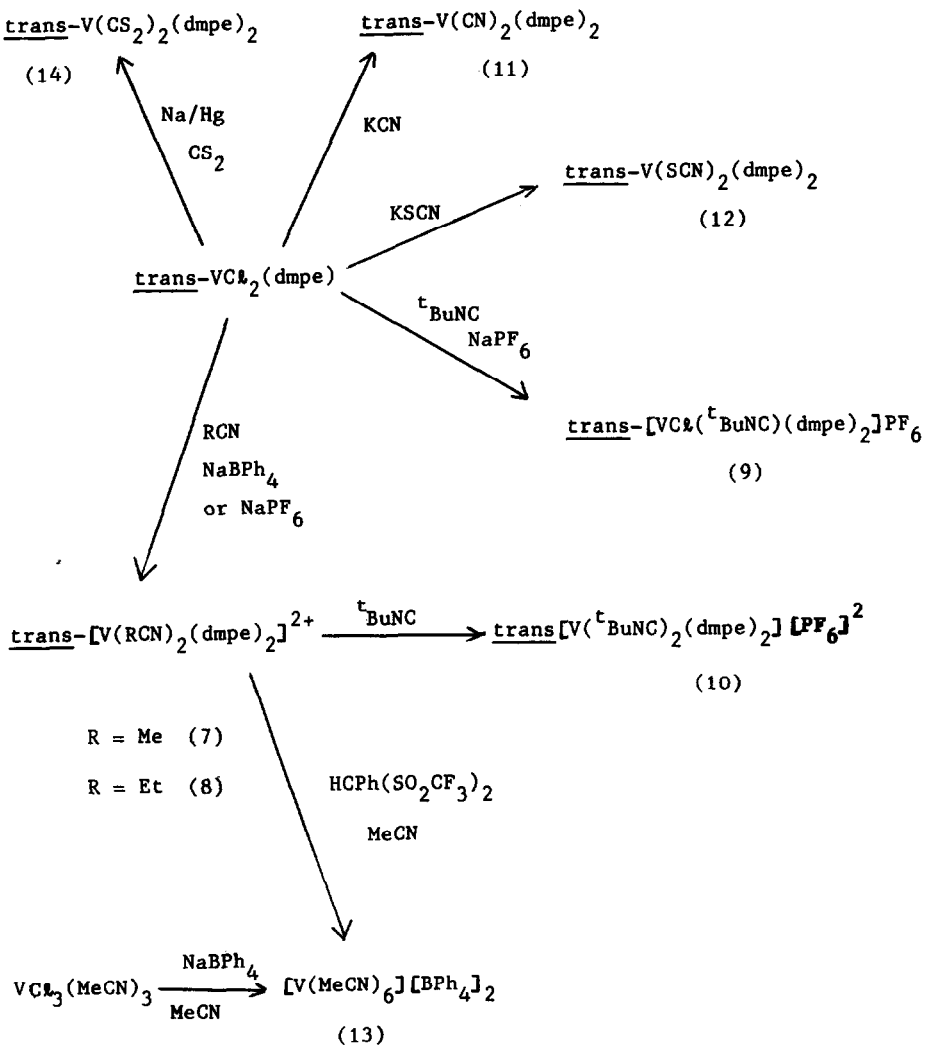

Scheme 2. Reactions of *trans*-[$VCl_2(dmpe)_2$].

1 and **2**, respectively. The $^{31}P\{^1H\}$ spectrum of **1** and **2** show singlets at 33.2 and 35.9 ppm, respectively. The ^{95}Mo NMR spectra show very broad bands at +965 ppm for (**1**) and −25 ppm for (**2**) in accord with the expected increase in shielding of the Mo in the η^2-isomer. The IR spectra of both complexes showed no ν(C≡N) band, but this phenomenon is well known[6] and is not uncommon. The mass spectra of both compounds are similar showing peaks due to the parent ions, while conductivity measurements show both complexes to be 1 : 1 electrolytes.

Although spectroscopic evidence for η^2-bonding has been available for some time, X-ray structural information is available only for $(\eta^5\text{-}C_5H_5)_2Mo(\eta^2\text{-}MeCN)$[7a] and some aryl nitrile complexes, e.g. $(\eta^5\text{-}C_5H_5)(PPh_3)Ir(\eta^2\text{-}NCC_6H_4Cl)$.[7b]

A diagram of the structure of the cation (**2**) is given in Fig. 1, selected bond lengths and angles in Table 1. The structure can be conveniently described as pseudo-octahedral, with the η^2-nitrile ligand occupying one site, *trans* to the chlorine. However, the geometry of the nitrile bonding is such that a metalla-azacyclopropenyl form of bonding is strongly indicated. Thus, the Mo—N and Mo—C bonds in **2** are significantly shorter than in the previously described[7a] η^2-acetonitrile bonded complex, $Cp_2Mo(\eta^2\text{-}NCMe)$. The N—C—Me angle in **2** is 8° smaller than in $Cp_2Mo(\eta^2\text{-}NCMe)$, the value of 130° approaching that expected for sp^2 hydridization at C. However, the N=C bond length in **2** is very similar to that in $Cp_2Mo(\eta^2\text{-}NCMe)$. It is also worth noting that in **2** the Mo—N bond is shorter than the Mo—C bond; the opposite is true in $Cp_2Mo(\eta^2\text{-}NCMe)$.

Adoption of the cyclopropenyl formalism would imply an oxidation state of four for molybdenum

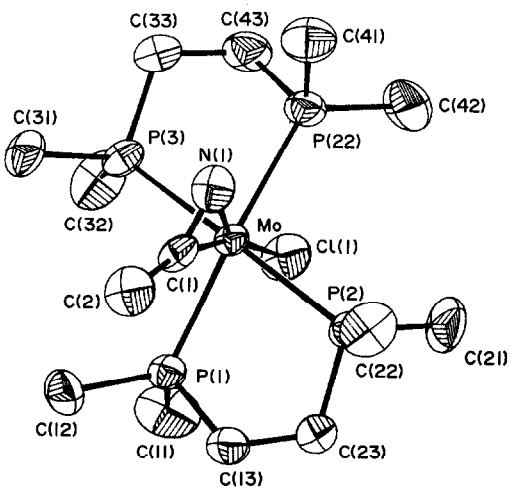

Fig. 1. The structure of $[MoCl(\eta^2\text{-}MeCN)(dmpe)_2]^+$.

which would correlate with the shorter Mo—N, Mo—C bonds in **2**. However, whilst we were able to establish a broad correlation between the metal oxidation state and M—P bond lengths in a number of chromium bis-dimethylphosphinoethane complexes,[1] it seems impossible to have meaningful correlations for molybdenum. A review of a number of MoP_4XY complexes via the Cambridge Crystallographic data base shows a very wide variation of Mo—P distances for the same oxidation state. Indeed for our complex **2**, the Mo—P distances vary, in an apparently arbitrary way, between 2.485–2.523(1) Å.

For *trans*-$[Mo(NCMe)_2(dmpe)_2](BPh_4)_2$ the conductivity, and IR and NMR spectra are in accord with this formulation.

On refluxing either **1** or **2** in methanol a red solution is formed from which can be isolated red prisms of the ethylimido complex of molybdenum(IV), *trans*-$[MoCl(NEt)(dmpe)_2](BPh_4)$ (**4**), which is similar to the chromium analogue;[2] it is a 1 : 1 electrolyte in MeCN and the spectroscopic data are in agreement with this formulation. The formation of the chromium analogue[2] was proposed to proceed *via* an intermediate with a η^2-MeCN group and oxidative addition of methanol as H and OMe followed by hydride transfers leading to N=CHMe and NCH_2Me groups. The same doubtless applies in the present case and the characterization of the η^2-MeCN complex provides substantiation for the first assumption.

Other molybdenum species. Interaction of *trans*-$[MoCl_2(dmpe)_2]$ with two equivalents of $LiNEt_2$ at −78°C in THF yields a bright orange, diamagnetic dialkylamido, *trans*-$[Mo(NEt_2)_2(dmpe)_2]$ (**5**). The ^1H NMR spectrum shows, apart from dmpe, a triplet (δ 0.4 ppm, J_{H-H} = 8 Hz) and a quartet (δ 2.4 ppm, J_{H-H} = 8 Hz) due to the ethyl groups of the NEt_2 group.

Cooper *et al.* reported[4] the synthesis of $Mo(N_2)_2(dmpe)_2$ as an inseparable mixture of *cis* and *trans* isomers. Interaction of this mixture with excess benzenethiol in THF leads to *trans*-$[Mo(SPh)_2(dmpe)_2]$ (**6**) as red cubes. The IR spectrum shows no dinitrogen stretches and a band at 1574 cm^{-1} is due to aromatic stretches. The *trans* structure is confirmed by X-ray crystal structure analysis. A diagram of the molecule, **6**, which has crystallographic $\bar{1}$ symmetry, is given in Fig. 2, selected bond lengths and angles in Table 2. It is interesting to compare the geometry in the coordination sphere with that in the closely related diphenyphosphinoethane complex,[8] $Mo(S^nBu)_2(dppe)_2$, made in a similar way. Thus, in our molecule, **6**, the Mo—S distance is longer than that in the dppe complex, whilst the Mo—P distances

Table 1. Selected bond lengths and angles in [MoCl(η^2-MeCN)(dmpe)$_2$] (**2**)

Bond lengths (Å)			
Cl(1)—Mo(1)	2.487(3)	P(1)—Mo(1)	2.485(3)
P(2)—Mo(1)	2.508(4)	P(3)—Mo(1)	2.523(4)
P(4)—Mo(1)	2.526(4)	N(1)—Mo(1)	1.959(7)
C(1)—Mo(1)	1.981(7)	C(11)—P(1)	1.822(9)
C(12)—P(1)	1.825(7)	C(13)—P(1)	1.834(8)
C(21)—P(2)	1.818(8)	C(22)—P(2)	1.803(8)
C(23)—P(2)	1.828(8)	C(31)—P(3)	1.819(7)
C(32)—P(3)	1.816(7)	C(33)—P(3)	1.825(8)
C(41)—P(4)	1.824(8)	C(42)—P(4)	1.812(8)
C(43)—P(4)	1.843(8)	C(1)—N(1)	1.217(8)
C(2)—C(1)	1.524(10)	C(23)—C(13)	1.493(9)
C(43)—C(33)	1.504(11)		
Bond angles (°)			
P(1)—Mo(1)—Cl(1)	85.2(1)	P(2)—Mo(1)—Cl(1)	83.0(1)
P(2)—Mo(1)—P(1)	80.2(1)	P(3)—Mo(1)—Cl(1)	84.8(1)
P(3)—Mo(1)—P(1)	96.2(1)	P(3)—Mo(1)—P(2)	167.5(1)
P(4)—Mo(1)—Cl(1)	79.1(1)	P(4)—Mo(1)—P(1)	164.1(1)
P(4)—Mo(1)—P(2)	100.0(1)	P(4)—Mo(1)—P(3)	80.1(1)
N(1)—Mo(1)—Cl(1)	158.1(1)	N(1)—Mo(1)—P(1)	116.7(2)
N(1)—Mo(1)—P(2)	99.2(2)	N(1)—Mo(1)—P(3)	93.1(2)
N(1)—Mo(1)—P(4)	79.1(2)	C(1)—Mo(1)—Cl(1)	165.9(2)
C(1)—Mo(1)—P(1)	80.8(3)	C(1)—Mo(1)—P(2)	93.1(2)
C(1)—Mo(1)—P(3)	98.2(2)	C(1)—Mo(1)—P(4)	115.1(3)
C(1)—Mo(1)—N(1)	36.0(2)	C(11)—P(1)—Mo(1)	118.3(3)
C(12)—P(1)—Mo(1)	121.7(3)	C(12)—P(1)—C(11)	100.2(4)
C(13)—P(1)—Mo(1)	106.9(3)	C(13)—P(1)—C(11)	102.1(4)
C(13)—P(1)—C(12)	105.5(4)	C(21)—P(2)—Mo(1)	123.0(3)
C(22)—P(2)—Mo(1)	113.2(3)	C(22)—P(2)—C(21)	103.7(4)
C(23)—P(2)—Mo(1)	108.3(3)	C(23)—P(2)—C(21)	103.2(4)
C(23)—P(2)—C(22)	103.5(4)	C(31)—P(3)—Mo(1)	117.1(3)
C(32)—P(3)—Mo(1)	119.0(3)	C(32)—P(3)—C(31)	103.4(4)
C(33)—P(3)—Mo(1)	107.1(3)	C(33)—P(3)—C(31)	105.4(4)
C(33)—P(3)—C(32)	103.2(4)	C(41)—P(4)—Mo(1)	117.4(3)
C(42)—P(4)—Mo(1)	122.5(3)	C(42)—P(4)—C(41)	102.6(4)
C(43)—P(4)—Mo(1)	105.5(3)	C(43)—P(4)—C(41)	103.0(4)
N(1)—C(1)—Mo(1)	71.1(4)	C(2)—C(1)—Mo(1)	159.2(4)
C(2)—C(1)—N(1)	129.7(6)	C(23)—C(13)—P(1)	111.5(5)
C(13)—C(23)—P(2)	112.6(5)	C(43)—C(33)—P(3)	110.5(5)
C(33)—C(43)—P(4)	110.2(5)		

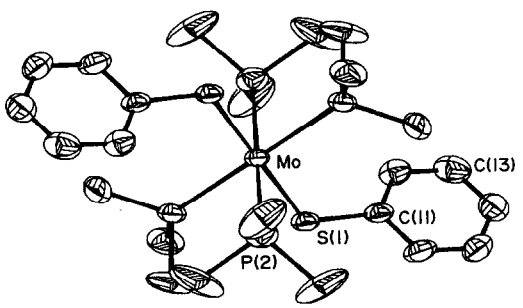

Fig. 2. The structure of *trans*-[Mo(SPh)$_2$(dmpe)$_2$].

are shorter. The changes could reflect the changes in substituent character on both sulphur and phosphorus—electron withdrawing phenyl group for electron releasing alkyl group on the sulphur and vice versa on the phosphines. Also of note is the significant difference between the Mo—P distances in **6**, which are somewhat larger than those in the dppe complex, which could reflect the smoothing out of steric effects. This implies a fairly shallow energy curve for the Mo—P bond strength and highlights the impossibility of making bond length–

Table 2. Selected bond lengths and angles in $[Mo(SPh)_2(dmpe)_2]$ (**6**)

Bond lengths (Å)			
S(1)—Mo(1)	2.380(3)	P(1)—Mo(1)	2.445(3)
P(2)—Mo(1)	2.486(3)	C(11)—S(1)	1.797(5)
C(1)—P(1)	1.821(8)	C(2)—P(1)	1.850(7)
C(3)—P(1)	1.857(8)	C(4)—P(2)	1.855(8)
C(5)—P(2)	1.803(9)	C(6)—P(2)	1.837(10)
C(6)—C(3)	1.452(12)		
Bond angles (°)			
P(1)—Mo(1)—S(1)	82.8(1)	P(2)—Mo(1)—S(1)	86.4(1)
P(2)—Mo(1)—P(1)	79.9(1)	C(11)—S(1)—Mo(1)	123.9(2)
C(1)—P(1)—Mo(1)	124.1(3)	C(2)—P(1)—Mo(1)	118.9(3)
C(2)—P(1)—C(1)	99.1(4)	C(3)—P(1)—Mo(1)	110.5(3)
C(3)—P(1)—C(1)	101.5(4)	C(3)—P(1)—C(2)	98.9(4)
C(4)—P(2)—Mo(1)	120.0(3)	C(5)—P(2)—Mo(1)	119.9(3)
C(5)—P(2)—C(4)	99.3(4)	C(6)—P(2)—Mo(1)	109.4(3)
C(6)—P(2)—C(4)	100.3(5)	C(6)—P(2)—C(5)	105.4(6)
C(12)—C(11)—S(1)	122.3(2)	C(16)—C(11)—S(1)	117.6(2)
C(6)—C(3)—P(1)	113.3(6)	C(3)—C(6)—P(2)	114.3(7)

oxidation state correlations for these Mo complexes, as previously mentioned.

It may be noted that for $(dppe)_2Mo(N_2)_2$ in reaction with bulky thiols, RSH, e.g. R = ^{t}Bu, 2,4,6-$Me_3C_6H_2$ or 2,4,6-$^i Pr_3C_6H_2$, the hydrides $MoH(SR)(dppe)_2$ are obtained[9] suggesting that the bisthiolato compounds are formed by loss of H_2 from such an intermediate on reaction with less bulky thiols.

Vanadium compounds

Nitriles. The interaction of *trans*-$[VCl_2(dmpe)_2]$[5] with two equivalents of $NaBPh_4$ in acetonitrile or propionitrile at room temperature leads to a dark-red solution from which the respective complexes, *trans*-$[V(NCMe)_2(dmpe)_2](BPh_4)_2$ (**7a**) and *trans*-$[V(NCEt)_2(dmpe)_2](BPh_4)_2$ (**8**) can be isolated. The acetonitrile compound can also be isolated as the hexafluorophosphate salt (**7b**) by substituting $NaPF_6$ for $NaBPh_4$. These complexes are all moderately air-sensitive, red, crystalline solids that are paramagnetic, μ_{eff} = 3.4 BM (3e). Both complexes have a weak ν(C≡N) stretch in the IR spectra and are 2:1 electrolytes in MeCN. The *trans*-configuration in **7a** is confirmed by X-ray structure determination.

The structure of compound **7a** comprises two independent centrosymmetric cations and the associated BPh_4 anions. One of the cations shows severe disorder in the conformation of the two dmpe ligands which has hampered attempts to achieve stable refinement (see Experimental). However, the V—N and V—P distances in the poorly defined cation compare satisfactorily with those in the other cation, which has ordering of the dmpe ligands, and so this aspect of the geometry can be discussed with confidence. The diagram of the cation structure shown in Fig. 3 is of the well-behaved unit. Bond lengths and angles for the coordination sphere of both molecules are given in Table 3. Comparisons can be made with a number of structures previously determined. Comparison with the V^0 complex *trans*-$V(CO)_2(dmpe)_2$[10] shows that the V^{II}—P distances are some 0.15 Å longer than the V^0—P distances—a reflection of the stronger V—P π-bonding in the low spin d^5 V^0 system. Comparison with the closely related cationic M^{II} species $[Fe(NCMe)_2(dmpe)_2]^{2+}$ [3] and $[Cr(NCMe)_2(dmpe)_2]^{2+}$ [1] again shows the influence of increasing $d\pi$–$d\pi$ back-bonding with increasing d electron count and spin

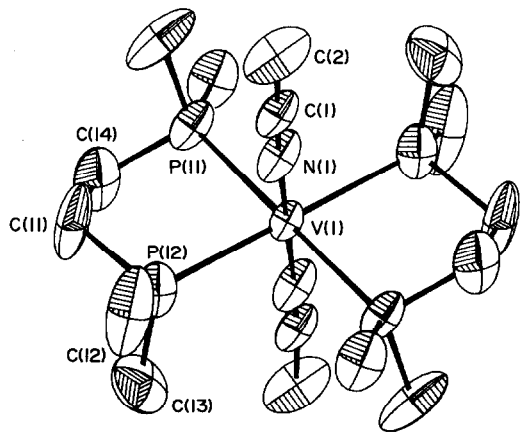

Fig. 3. The structure of *trans*-$[V(NCMe)_2(dmpe)_2]^{2+}$.

Table 3. Selected bond lengths and angles in $[V(NCMe)_2(dmpe)_2]$ (**7a**)

Bond lengths (Å)			
Molecule 1			
P(11)—V(1)	2.522(6)	P(12)—V(1)	2.524(5)
N(1)—V(1)	2.073(11)	C(14)—P(11)	1.859(14)
C(15)—P(11)	1.839(13)	C(16)—P(11)	1.817(16)
C(11)—P(12)	1.893(16)	C(12)—P(12)	1.835(23)
C(13)—P(12)	1.835(15)	C(1)—N(1)	1.147(16)
C(2)—C(1)	1.497(17)	C(14)—C(11)	1.566(24)
Molecule 2			
P(21)—V(2)	2.505(5)	P(22)—V(2)	2.496(6)
N(2)—V(2)	2.080(12)	C(1)—P(21)	1.802(36)
C(2)—P(21)	1.801(10)	C(3)—P(21)	1.803(28)
C(1B)—P(21)	1.800(35)	C(2B)—P(21)	1.800(14)
C(3B)—P(21)	1.800(24)	C(4)—P(22)	1.800(11)
C(5)—P(22)	1.800(26)	C(6)—P(22)	1.800(19)
C(21)—N(2)	1.135(18)	C(22)—C(21)	1.469(20)
Bond angles (°)			
Molecule 1			
P(12)—V(1)—P(11)	80.0(2)	N(1)—V(1)—P(11)	90.2(3)
N(1)—V(1)—P(12)	91.5(3)	C(14)—P(11)—V(1)	107.6(5)
C(15)—P(11)—V(1)	115.8(6)	C(15)—P(11)—C(14)	103.6(7)
C(16)—P(11)—V(1)	122.1(5)	C(16)—P(11)—C(14)	103.5(8)
C(16)—P(11)—C(15)	102.2(6)	C(11)—P(12)—V(1)	108.0(4)
C(12)—P(12)—V(1)	119.3(6)	C(12)—P(12)—C(11)	102.5(8)
C(13)—P(12)—V(1)	116.2(6)	C(13)—P(12)—C(11)	106.3(8)
C(13)—P(12)—C(12)	103.0(8)	C(1)—N(1)—V(1)	172.5(7)
C(2)—C(1)—N(1)	177.2(9)	C(14)—C(11)—P(12)	109.3(9)
C(11)—C(14)—P(11)	107.8(12)		
Molecule 2			
P(22)—V(2)—P(21)	87.1(2)	N(2)—V(2)—P(21)	90.0(3)
N(2)—V(2)—P(22)	89.1(4)	C(1)—P(21)—V(2)	119.2(8)
C(2)—P(21)—V(2)	117.1(12)	C(2)—P(21)—C(1)	108.1(14)
C(3)—P(21)—V(2)	104.0(10)	C(3)—P(21)—C(1)	106.8(19)
C(3)—P(21)—C(2)	99.0(18)	C(1B)—P(21)—V(2)	119.5(7)
C(1B)—P(21)—C(2)	122.5(13)	C(2B)—P(21)—V(2)	106.0(11)
C(2B)—P(21)—C(1B)	95.8(17)	C(3B)—P(21)—V(2)	121.1(9)
C(3B)—P(21)—C(1)	118.7(12)	C(3B)—P(21)—C(1B)	104.5(13)
C(3B)—P(21)—C(2B)	106.2(12)	C(4)—P(22)—V(2)	102.8(9)
C(5)—P(22)—V(2)	126.6(8)	C(5)—P(22)—C(4)	89.3(12)
C(6)—P(22)—V(2)	121.2(7)	C(6)—P(22)—C(4)	92.0(10)
C(6)—P(22)—C(5)	109.9(9)	C(21)—N(2)—V(2)	176.2(7)
C(22)—C(21)—N(2)	179.2(11)	C(3B)—C(2)—C(2B)	121.3(18)
C(4)—C(3)—P(21)	116.2(25)	C(4)—C(3)—C(3B)	102.0(33)
C(2)—C(2B)—C(1)	103.2(18)	C(3)—C(4)—P(22)	120.1(19)

pairing, with the M—P distances decreasing as 2.527(4) (V), 2.380(5) (Cr) and 2.268(4) Å (Fe). The M—N distances show a similar, but slightly larger, change between V and Cr: 2.082(10) to 1.906(6) Å as for M—P distances.

For chromium,[1,2] iron,[11] ruthenium[3] and molybdenum, as noted above, partially substituted cations, $[MCl(NCMe)(dmpe)_2]^+$ can be obtained, but interaction of the vanadium dichloride with one equivalent of $NaBPh_4$ leads only to reduced yields of **7a** or **8**. The bisnitrile complexes did not react with methanol on refluxing.

Isocyanide. The interaction of *trans*-$[VCl_2(dmpe)_2]$ with sodium hexafluorophosphate in refluxing methanol in the presence of ^{t}BuNC leads to a purple solution from which the paramagnetic

(d^3, $\mu_{eff} = 3.6$ BM), *trans*-[VCl('BuNC)(dmpe)$_2$] (PF_6) (**9**), can be isolated as red–purple crystals. The IR spectrum shows a strong band at 2130 cm^{-1} due to ν(C≡N). The disubstituted 'BuNC compound cannot be obtained in high yield by this method, but the interaction of *trans*-[V(NCMe)$_2$(dmpe)$_2$](PF_6)$_2$ with 'BuNC in refluxing methanol gives an orange precipitate, which on recrystallization from acetonitrile yields large prisms of *trans*-[V(CNBu')$_2$(dmpe)$_2$](PF_6)$_2$ (**10**). The *trans*-configuration has been confirmed by an X-ray crystallographic analysis. A diagram of the structure, which lies on a centre of symmetry, is given in Fig. 4, selected bond lengths and angles in Table 4. The important dimensions in the cation show no unusual features. The V—P distances are similar to those in the nitrile complex described above, and the M—C (isonitrile) bond shows no significant multiple bonding.

Cyano and thiocyanato complexes. Treatment of *trans*-[VCl_2(dmpe)$_2$] with two equivalents of KCN and KSCN in acetonitrile leads to the isolation of orange *trans*-[V(CN)$_2$(dmpe)$_2$] (**11**) and red *trans*-[V(NCS)$_2$(dmpe)$_2$] (**12**), respectively. For the cyano complex a strong IR band at 2055 cm^{-1} is assignable as ν(C≡N) while a band at 2060 ν(C≡N) for **12** suggests that the thiocyanato ligands are N-bonded to vanadium. Both compounds are paramagnetic with $\mu_{eff} = 3.7$ BM.

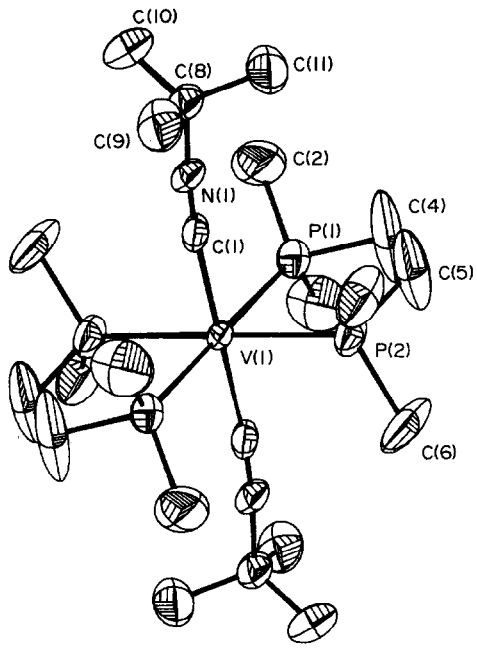

Fig. 4. The structure of *trans*-[V(CNBu')$_2$(dmpe)$_2$]$^{2+}$.

Hexakis(acetonitrile)vanadium(II) *salts.* The interaction of **7** with $HCPh(SO_2CF_3)_2$ in acetonitrile leads to the loss of dmpe and isolation of

Table 4. Selected bond lengths and angles in [V(CNBu')$_2$(dmpe)$_2$] (**10**)

Bond lengths (Å)			
P(1)—V(1)	2.495(4)	P(2)—V(1)	2.502(6)
C(1)—V(1)	2.101(12)	C(2)—P(1)	1.809(16)
C(3)—P(1)	1.781(15)	C(4)—P(1)	1.837(17)
C(5)—P(2)	1.827(15)	C(6)—P(2)	1.829(14)
C(7)—P(2)	1.823(14)	N(1)—C(1)	1.155(11)
C(8)—N(1)	1.483(12)	C(5)—C(4)	1.277(20)
C(9)—C(8)	1.533(17)	C(10)—C(8)	1.482(17)
C(11)—C(8)	1.502(17)		
Bond angles (°)			
P(2)—V(1)—P(1)	80.7(2)	C(1)—V(1)—P(1)	88.8(3)
C(1)—V(1)—P(2)	87.8(3)	C(2)—P(1)—V(1)	119.1(6)
C(3)—P(1)—V(1)	118.4(6)	C(3)—P(1)—C(2)	104.9(9)
C(4)—P(1)—V(1)	106.4(6)	C(4)—P(1)—C(2)	102.9(10)
C(4)—P(1)—C(3)	102.7(11)	C(5)—P(2)—V(1)	107.3(5)
C(6)—P(2)—V(1)	119.0(6)	C(6)—P(2)—C(5)	103.8(9)
C(7)—P(2)—V(1)	119.8(5)	C(7)—P(2)—C(5)	102.8(9)
C(7)—P(2)—C(6)	102.0(7)	N(1)—C(1)—V(1)	174.6(8)
C(8)—N(1)—C(1)	175.0(9)	C(5)—C(4)—P(1)	123.0(12)
C(4)—C(5)—P(2)	121.5(11)	C(9)—C(8)—N(1)	106.5(9)
C(10)—C(8)—N(1)	107.9(10)	C(10)—C(8)—C(9)	111.0(11)
C(11)—C(8)—N(1)	106.2(9)	C(11)—C(8)—C(9)	111.8(11)
C(11)—C(8)—C(10)	113.0(11)		

$[V(CNMe)_6](BPh_4)_2$ (**13**) in a very small yield as green crystals. The IR spectrum shows two bands at 2310 and 2280 cm^{-1} for the symmetric and asymmetric nitrile stretches. The complex is paramagnetic ($\mu_{eff} = 4.0$ BM) and a 1:2 electrolyte in acetonitrile. The complex can be synthesized in much higher yield by the addition of three equivalents of $NaBPh_4$ to an acetonitrile solution of $VCl_3(NCMe)_3$ where MeCN is evidently the reducing agent (cf. ref. 6).

The $[V(NCMe)_6]^{2+}$ ion has previously been inconveniently made as the $[V(CO)_6]^-$ salt by disproportionation of $V(CO)_6$ in MeCN[12] and by reduction of VCl_3 in MeCN by Et_2Zn as the $ZnCl_4^{2-}$ salt.[13]

Carbon disulphide. The reduction of *trans*-$[VCl_2(dmpe)_2]$ in THF by Na/Hg under CO leads to $V(CO)_2(dmpe)_2$.[10] However, reduction under CS_2 leads not to a thiocarbonyl, but to the orange, *trans*-$[V(CS_2)_2(dmpe)_2]$ (**14**). The IR spectrum has strong bands at 1103 and 581 cm^{-1} due to out-of-ring ν(C—S) vibrations of a η^2-coordinated CS_2 group. The latter being slightly lower than the quoted literature range[14] (653–632 cm^{-1}) while the former is similar to that (1141 cm^{-1}) for $(\eta^5\text{-}C_5H_5)_2V(\eta^2\text{-}CS_2)$.[14b]

ESR spectra. The frozen solution spectra of *trans*-$[V(CNBu^t)_2(dmpe)_2](PF_6)_2$ (**10**) has a strong feature at 330 mT together with two weaker features at 160 and 50 mT. The cyanide *trans*-$[V(CN)_2(dmpe)_2]$ (**11**) is similar, with a strong feature at 315 mT and weaker ones at 160 and 810 mT. From *D* vs *B* plots for $S = 3/2$ systems, it appears that the zero-field splitting parameter (*D*) is small in both cases. From the width of the line at $g = 2.00$ an upper limit on *D* is 0.01 cm^{-1}.

The frozen solution spectra of *trans*-$[V(NCS)_2(dmpe)_2]$ (**12**) and *trans*-$[VCl(CNBu^t)(dmpe)_2]^+$ (**9**) are also similar, but different from those of the bisisocyanide and cyanide complexes, **10** and **12**. Two broad low field features at 120 and 280 mT and two weaker features at 520 and 800 mT, appear in the spectrum of the isocyanide **9**, while the thiocyanate **12**, shows similar features at 120, 320, 570 and 815 mT. These spectra can be interpreted using the same plots; the *D* values are larger ($0.3 < D < 0.5$ cm^{-1}) than in the spectra of **10** and **11**.

The spectrum of $[V(NCMe)_6](BPh_4)_2$ (**13**), shows a strong feature at 330 mT—the overlapping of eight equally spaced lines (due to ^{51}V, $I = 7/2$) with *A* (^{51}V) = 0.0073 cm^{-1}. Finally the spectrum of *trans*-$[V(NCMe)_2(dmpe)_2]^{2+}$ (**7**) is more complicated, having a distinctive feature at *ca* 7 mT which indicates that the value of *D* must lie between 0.14–0.16 cm^{-1}.

EXPERIMENTAL

The techniques and instruments used are as described previously.[1,2,10] Molybdenum (^{95}Mo) NMR spectra[15] are referenced to external $NaMoO_4$. Analytical data for new compounds are listed in Table 5.

trans - *Acetonitrile(chloro)bis*[1,2 - *bis(dimethylphosphino)ethane*]*molybdenum*(II)*tetraphenylborate* (**1**)

To $MoCl_2(dmpe)_2$ (0.40 g, 0.85 mmol), in MeCN (50 cm^3), was added an MeCN solution of $NaBPh_4$ (0.30 g, 0.88 mmol). The solution was gently refluxed for 12 h, then cooled and the red–orange solution filtered; reduction in volume and cooling (−20°C) gave a red microcrystalline solid. Yield: 0.30 g, 45%. IR: 3060m, 3040m, 1580m, 1430s, 1415s, 1300m, 1290m, 1260m, 1180w, 1150m, 1140w, 1110sh, 1080m, 1070sh, 1030m, 945sh, 930s, 890m, 865w, 850w, 795m, 745s, 730s, 720sh, 710s, 700s, 670m, 650m, 635, 615m, 605s, 490w, 455w. NMR. ^1H (CD_3CN): 7.25, 6.90 (20, m, BPH_4), 2.10 (3, s, CH_3CN) 1.2–2.0 (32, m, dmpe). $^{31}P\{^1H\}$: 33.2 (s). ^{95}Mo: 965 br.s ($\Delta\nu_{1/2}$ *ca* 12,000 Hz). Mass spectrum: *m/e* 474 (M^+), 433 (M—MeCN), 41 (MeCN). Conductivity (MeCN): $\Lambda_M = 110$ ohm^{-1} cm^2 mol^{-1}.

trans - (η^2 - *Acetonitrile*)(*chloro*)*bis*[1,2 - *bis(dimethylphosphino)ethane*]*molybdenum*(II)*tetraphenylborate* (**2**)

The filtrate from the reaction mixture as above was evaporated and the residue extracted with THF (20 cm^3); reduction in volume and cooling (−20°C) gives brown–orange crystals. Yield: 0.28 g (45%). The same product is obtained if the η^1-MeCN isomer, **1**, is recrystallized from THF. IR: 3040m, 3020m, 1580m, 1430s, 1420s, 1310m, 1295m, 1270m, 1180w, 1150m, 1100br.m, 1070m, 1030m, 950m, 935s, 900m, 850br.m, 800m, 745s, 730s, 705s, 670m, 650m, 635m, 615m, 605s, 460w. NMR. ^1H (C_4D_8O): 7.25, 7.0, 6.85 (20, m, BPh_4), 3.20 (s, 3, CH_3CN); 2.05 (d, 8, PCH_2), 1.65 (d, 24, PMe_2). $^{31}P\{^1H\}$ 35.9(s). ^{95}Mo: −25 ($\Delta\nu_{1/2}$ *ca* 14,000 Hz). Mass spectrum: *m/e* 474 (M^+). Conductivity (MeCN): $\Lambda_M = 120$ ohm^{-1} cm^2 mol^{-1}.

trans - *bis*(*Acetonitrile*)*bis*[1,2 - *bis(dimethylphosphino)ethane*]*molybdenum*(II)*bis*(*tetraphenylborate*) (**3**)

To $MoCl_2(dmpe)_2$ (0.81 g, 1.73 mmol), in MeCN (50 cm^3), was added $NaBPh_4$ (1.19 g, 3.48 mmol).

Table 5. Analytical data for molybdenum and vanadium compounds

Compound	M.p. (°C)	Analysis[a] C	H	N	P	Other
1. $[MoCl(NCMe)(dmpe)_2]BPh_4$	203–205 (dec)	57.4 (57.6)	7.0 (7.0)	1.6 (1.8)	15.8 (15.6)	
2. $[MoCl(\eta^2\text{-}NCMe(dmpe)_2]BPh_4$	195–197 (dec)	57.7 (57.6)	7.1 (7.0)	1.8 (1.8)	15.9 (15.6)	
3. $[Mo(NCMe)_2(dmpe)_2][BPh_4]_2$	219–221 (dec)	68.9 (70.1)	6.5 (6.8)	2.2 (2.4)	10.7 (10.6)	
4. $[MoCl(NEt)(dmpe)_2]BPh_4$	231	58.5 (57.5)	7.3 (7.2)	1.6 (1.7)	15.3 (13.6)	
5. $Mo(NEt_2)_2(dmpe)_2$	172	43.1 (44.4)	8.3 (9.7)	4.8 (5.2)	23.4 (22.9)	
6. $Mo(SPh)_2(dmpe)_2$	214–215	46.0 (46.9)	7.0 (6.9)		19.5 (20.2)	9.4 (S) (10.4)
7. $[V(NCMe)_2(dmpe)_2][BPh_4]_2$	100 (dec)	70.9 (71.7)	7.3 (7.3)	2.6 (2.6)	11.4 (11.6)	
8. $[V(NCEt)_2(dmpe)_2][BPh_4]_2$	160 (dec)	71.9 (72.1)	7.4 (7.5)	2.4 (2.5)	11.4 (11.3)	2.0 (B) (2.0)
9. $[VCl(CNBu^t)(dmpe)_2]PF_6$	150 (dec)	34.8 (33.2)	6.9 (6.7)	2.2 (2.3)	23.7 (25.2)	4.9 (Cl) (5.8)
10. $[V(CNBu^t)_2(dmpe)_2][PF_6]_2$	170 (dec)	32.6 (32.7)	6.3 (6.2)	3.7 (3.5)	23.2 (23.1)	27.6 (F) (28.3)
11. $V(CN)_2(dmpe)_2$	150 (dec)	41.8 (41.7)	8.0 (8.0)	7.0 (7.0)	29.1 (30.8)	
12 $V(SCN)_2(dmpe)_2$	130 (dec)	35.8 (36.0)	6.9 (6.9)	6.3 (6.0)	27.0 (26.6)	3.6 (S) (13.7)
13. $[V(NCME)_6][BPh_4]_2$	196 (dec)	77.6 (77.0)	6.3 (6.2)	9.0 (9.0)		5.7 (V) (5.5)
14. $V(CS)_2(dmpe)_2$	60 (dec)	30.6 (33.4)	6.2 (6.4)		20.8 (24.7)	28.1 (S) (25.5)

[a] Required values in parentheses.

The solution was vigorously refluxed for 18 h, then cooled and the red–brown solution filtered. The solvent was removed *in vacuo* and the residue extracted into hot MeCN (15 cm^3); cooling (−20°C) gave a microcrystalline solid. Yield: 1.23 g, 61%; a further crop can be obtained by concentration of the filtrate and cooling. IR: 3055m, 3035m, 2270w, 1955w, 1895w, 1830w, 1670w, 1580m, 1430s, 1420s, 1300m, 1290m, 1260s, 1185m, 1150m, 1135w, 1100m, 1070w, 1030m, 945s, 930s, 895s, 870w, 845m, 745s, 735s, 710s, 650m, 630m, 620m, 605s. NMR. ^1H (CD_3CN): 7.25, 6.90 (40, m, BPh_4), 2.36 (3, s, CH_3CN) 2.17 (8, d, PCH_2), 1.53 (24, d, PMe_2). $^{31}P\{^1H\}$: 42.0. Conductivity (MeCN): $\Lambda_M = 210$ ohm^{-1} cm^2 mol^{-1}.

trans - (*Chloro*)(*ethylimido*)*bis*[1,2 - *bis*(*dimethylphosphino*)*ethane*]*molybdenum*(IV)*tetraphenylborate* (**4**)

To an MeCN (25 cm^3) solution of **1** or **2** (0.86, 0.74 mmol) was added MeOH (30 cm^3) and the solution was gently refluxed for 4 h, and then cooled. The solvent was removed and the residue extracted with THF (15 cm^3); reduction in volume and cooling (−20°C) gave red crystals. Yield: 0.34 g, 47%; a further crop can be obtained by concentration and cooling. IR: 3055w, 3035w, 1950w, 1880w, 1820w, 1670w, 1580m, 1420s, 1415s, 1305w, 1290m, 1260m, 1250m, 1090m, 1065m, 1030m, 945s, 935s, 895m, 870w, 840m, 800m, 750s, 710s, 645m, 625w, 615s, 475w, 455w. NMR. ^1H (CD_3CN): 7.25, 6.90 (20, m, BPh_4), 2.9 (2, q, J(H—H) = 13 Hz, NCH_2CH_3), 2.0 (8, d, PCH_2) 1.55, 924 (d, PMe_2); 0.9 (3, t, J(H—H) = 13 Hz, NCH_2CH_3) $^{31}P\{^1H\}$: 32.7. Mass spectrum: *m/e* 476 (M^+), 433 (M^+—NEt). Conductivity (MeCN): $\Lambda_M = 78.2$ ohm^{-1} cm^2 mol^{-1}.

trans - *bis*(*Diethylamido*)*bis*[1,2 - *bis*(*dimethylphosphino*)*ethane*]*molybdenum*(II) (**5**)

$MoCl_2(dmpe)_2$ (0.48 g, 1.03 mmol) and $LiNEt_2$ (0.16 g, 2.1 mmol) were cooled to −78°C and THF

($40\ cm^3$) added. After warming to room temperature and refluxing for 6 h, the red solution was cooled, filtered, concentrated and cooled (−20°C) to give orange needles. Yield: 0.33 g, 60%. IR: 1418s, 1317s, 1288s, 1273s, 1135w.br, 1112w.br, 1070w.br, 987m, 935s, 922s, 885s, 831m, 784m, 726s, 695s, 628s, 452m. NMR: ^1H (CD_2Cl_2): 2.45 (4, q, J(H—H) = 8 Hz, NCH_2CH_3) 2.05 (8, s, PCH_2), 1.6 (24, s, PMe_2), 0.4 (6, t, J(H—H) = 8 Hz, NCH_2CH_3).

trans - *bis*(*Phenylthiolato*)*bis*[1,2 - *bis*(*dimethylphosphino*)*ethane*]*molybdenum*(II) (**6**)

To $Mo(N_2)_2(dmpe)_2$ (0.19 g, 0.4 mmol), in THF ($40\ cm^3$), was added a slight excess of PhSH ($0.2\ cm^3$) and the solution was refluxed for 8 h. Evaporation and extraction of the residue into toluene ($30\ cm^3$) followed by reduction in volume and cooling (−20°C) gave dark red cubes. Yield: 0.15 g, 61%. IR: 1580m, 1415m, 1290m, 1275m, 1270m, 1170w, 1150w, 1120w, 1070m, 1060w, 1020m, 935m, 920s, 885m, 845w, 825w, 785w, 740s, 720m, 690s, 640m, 620w, 495m, 450w. NMR: 7.0–7.8 (10H, m, SPh) 0.8–1.5 (32H, m, dmpe). Mass spectrum: m/e 616 (M^+), 539 (M^+—Ph), 466 (M^+—dmpe).

trans - *bis*(*Acetonitrile*)*bis*[1,2 - *bis*(*dimethylphosphino*)*ethane*]*vanadium*(II)*bis*(*tetraphenylborate*) (**7a**)

To *trans*-$VCl_2(dmpe)_2$ (0.5 g, 1.19 mmol), in acetonitrile ($50\ cm^3$), was added $NaBPh_4$ (0.82, 2.4 mmol). After stirring for 24 h, the red solution was filtered, concentrated and cooled to −20°C to yield red prisms. Yield: 1.12 g, 88%. IR: 3060m, 3040m, 2255w, 1580m, 1420s, 1308m, 1292m, 1262m, 1036m, 942s, 930m, 890m, 865w, 845w, 830vw, 800w, 740vs, 615s. Magnetic moment (MeCN, 298 K): $\mu_{eff} = 3.3$ BM. Conductivity (MeCN): $\Lambda_M = 249\ ohm^{-1}\ cm^2\ mol^{-1}$. The cation can be obtained as the corresponding hexafluorophosphate (**7b**) by using $NaPF_6$ in place of $NaBPh_4$.

trans - *bis*(*Propionitrile*)*bis*[1,2 - *bis*(*dimethylphosphino*)*ethane*]*vanadium*(II)*bis*(*tetraphenylborate*) (**8**)

To *trans*-$VCl_2(dmpe)_2$ (0.79 g, 1.87 mmol), in propionitrile ($50\ cm^3$), was added $NaBPh_4$ (1.28 g, 3.74 mmol). The solution was refluxed gently for 24 h and then cooled, filtered and concentrated to −20°C to yield red needles. Yield: 1.54 g, 75%. IR: 3060m, 3040m, 2240, 1580m, 1420s, 1308m, 1292m, 1265m, 945s, 930m, 893w, 870vw, 845vw, 802w, 755s, 736vs, 711vs, 615s. Magnetic moment (solid, 298 K): $\mu_{eff} = 3.4$ BM. Conductivity (EtCN): $\Lambda_M = 183\ ohm^{-1}\ cm^2\ mol^{-1}$.

(*tert* - *Butylisocyanide*)*chlorobis*[1,2 - *bis*(*dimethylphosphino*)*ethane*]*vanadium*(II)*hexafluorophosphate* (**9**)

To *trans*-$VCl_2(dmpe)_2$ (0.39 g, 0.92 mmol) and $NaPF_6$ (0.31 g, 1.85 mmol), in methanol ($50\ cm^3$), was added ^{t}BuNC ($0.25\ cm^3$, 2.21 mmol). After stirring at room temperature for 24 h, the solution was filtered, evaporated and the residue extracted into THF ($50\ cm^3$). The filtrate was concentrated and cooled (−20°C) to give purple–red crystals. Yield: 0.23 g, 41%. IR: 2130vs, 1421s, 1302m, 1284m, 1260m, 1239w, 1190m, 1095m, 1065m, 1020w, 947s, 930s, 892m, 835vs, 735m, 705m, 645m, 561s. Conductivity (MeCN): $\Lambda_M = 114\ ohm^{-1}\ cm^2\ mol^{-1}$. Mass spectrum: m/e 469 (M^+).

trans - *bis*(*tert* - *Butylisocyanide*)*bis*[1,2 - *bis*(*dimethylphosphino*)*ethane*]*vanadium*(II)*bis*(*hexafluorophosphate*) (**10**)

A suspension of *trans*-$[V(MeCN)_2(dmpe)_2][PF_6]_2$ (0.3 g, 0.42 mmol), in methanol ($50\ cm^3$), containing ^{t}BuNC (0.29 M in Et_2O, 0.93 mmol) was refluxed for 24 h. The resulting orange precipitate was collected, washed with Et_2O ($2 \times 20\ cm^3$) and dried *in vacuo*. Yield: 0.27 g, 82%. IR: 2150vs, 1426s, 1311m, 1306w, 1298m, 1260m, 1240m, 1189s, 1095m, 1020m, 952s, 936s, 898m, 875s, 836vs, 745m, 715m, 647w, 565s, 526w, 446w. Magnetic moment (solid, 298 K): $\mu_{eff} = 3.6$ BM. Conductivity (MeCN): $\Lambda_M = 270\ ohm^{-1}\ cm^2\ mol^{-1}$.

trans - *Di*(*cyano*)*bis* - [1,2 - *bis*(*dimethylphosphino*)*ethane*]*vanadium*(II) (**11**)

To *trans*-$VCl_2(dmpe)_2$ (0.38 g, 0.9 mmol), in MeCN ($50\ cm^3$), was added KCN (0.12 g, 0.9 mmol) in $10\ cm^3$ MeOH. The solution was stirred (24 h) then evaporated and the residue extracted into THF ($2 \times 30\ cm^3$). Concentration to *ca* $35\ cm^3$ and then addition of hexane precipitated an orange–yellow solid, which was collected, washed with hexane and dried. Yield: 0.20 g, 55%. IR: 2060s, 1427s, 1301w, 1295w, 1282m, 1262m, 1150w, 1093w, 1020w, 995w, 954vs, 929s, 893m, 840m, 805m, 735s, 707s, 645m. Magnetic moment (MeCN, 298 K): $\mu_{eff} = 3.7$ BM. Mass spectrum: $m/e = 4.6$ (M^+).

trans - *Di(thiocyanato)bis*[1,2 - *bis(dimethylphosphino)ethane*]*vanadium*(II) (**12**)

To *trans*-$VCl_2(dmpe)_2$ (0.29 g, 0.69 mmol), in MeCN (40 cm^3) at −40°C, was added KNCS (0.4 g, 1.44 mol) in MeOH. After stirring at room temperature (24 h), the solvent was removed and the residue extracted into THF (50 cm^3). Subsequent filtration, concentration and cooling to −20°C yielded dark red prisms. Yield: 0.27 g, 85%. IR: 2055vs, 1420s, 1301m, 1287m, 1260m, 1135m, 1083m, 1015w, 990w, 947vs, 928s, 892s, 869m, 838m, 800s, 738s, 705s, 642m, 629w, 480w, 440w. Magnetic moment (solid, 298 K): $\mu_{eff} = 3.7$ BM. Mass spectrum: $m/e = 406$ (M^+).

Hexakis(acetonitrile)vanadium(II)*bis(tetraphenylborate)* (**13**)

(a) To *trans*-$[V(MeCN)_2(dmpe)_2][BPh_4]_2$ (0.31 g, 0.29 mmol), in MeCN (40 cm^3), at −30°C, was added $HCPh(SO_2CF_3)_2$ (0.21 g, 0.59 mmol) in MeCN (20 cm^3). After stirring at room temperature (24 h), the green solution was evaporated and the residue washed with toluene (2 × 20 cm^3) to remove unreacted acid. Subsequent extraction into MeCN, filtration and cooling (−20°C) gave green crystals. Yield: 0.03 g, 10%.

(b) A solution of $VCl_3(MeCN)_3$ (0.78 g, 2.78 mmol) and $NaBPh_4$ (2.90 g, 8.34 mmol), in MeCN (60 cm^3), was stirred at room temperature (24 h), then filtered, concentrated and cooled (−20°C) to give pale green plate-like crystals. Yield: 2.46 g, 95%. IR: 3055m, 2310w, 2280m, 1580w, 1426m, 1299w, 1260s, 1145m, 1095s, 1027s, 845w, 800s, 739m, 726s, 698s, 624w, 615m, 600s, 485w, 462w, 417w. Magnetic moment (solid, 298 K): 4.0 BM. Conductivity (MeCN): $\Lambda_M = 158$ ohm^{-1} cm^2 mol^{-1}.

bis(Carbon disulphide)bis[1,2 - *bis(dimethylphosphino)ethane*]*vanadium*(0) (**14**)

To *trans*-$VCl_2(dmpe)_2$ (0.27 g, 0.64 mmol), in THF (40 cm^3 over sodium amalgam (0.7%, 4 cm^3)

Table 6. Crystal data, details of intensity measurements and structure refinement

Compound	**2**	**6**	**7a**	**10**
Molecular formula	$[C_{14}H_{35}ClMoNP_4]^+$ $[C_{24}H_{20}B]^-$	$C_{24}H_{42}MoP_4S_2$	$[C_{16}H_{33}N_2P_4V]^+$ $2[C_{24}H_{20}B]^-$	$[C_{22}H_{50}N_2P_4V]^+$ $2[F_6P]^-$
Molecular weight	791.91	614.52	1071.72	807.44
Crystal system	Monoclinic	Monoclinic	Triclinic	Monoclinic
a (Å)	15.999(5)	18.854(5)	12.389(3)	10.475(3)
b (Å)	13.182(7)	12.405(2)	12.561(1)	15.714(2)
c (Å)	20.109(5)	13.761(4)	23.798(2)	12.547(3)
Alpha (°)	90	90	90.67(3)	90
Beta (°)	107.40(2)	113.17(3)	104.81(1)	110.29(2)
Gamma (°)	90	90	119.49(3)	90
Volume (Å)	4030.43	2960.20	3074.53	1937.14
Space group	*P*21/*n*	*C*2/*c*	$P\bar{1}$	*P*21/*n*
Z	2	4	2	2
D_c (g cm^{-3})	1.299	1.379	1.157	1.384
Mu	5.10	7.29	2.95	5.64
F(000)	1576	1268	1138	834
h, *k*, *l*, range	−23 → 23 0 → 15 0 → 19	−22 → 22 0 → 16 0 → 16	0 → 13 −13 → 13 −25 → 25	0 → 12 0 → 18 −14 → 14
Total no. of reflections	7701	2860	7660	3750
No. of unique reflections	7076	2606	7660	3406
No. of reflections used ($F > 3\sigma(F)$)	4538	2130	4108	1745
No. of parameters	439	131	541	196
Weighting scheme parameter *g* in $w = 1/[\sigma^2(F)+gF_o^2]$	0.000277	0.000992	0.002114	0.000801
Final *R*	0.0457	0.0425	0.0783	0.0802
Final R_w	0.0441	0.0476	0.0852	0.0834

at −78°C, was added CS_2 (16.6 mmol). After stirring at room temperature (6 h) the solvent was removed and the residue extracted with THF. Subsequent filtration and cooling (−20°C) yielded an orange powder. Yield: 0.14 g, 43%. IR: 1420 m, 1305m, 1289s, 1260w, 1192m, 1103vs, 1050s, 1030s, 946vs, 854s, 800w, 700s, 719s, 700w, 581s. Mass spectrum: m/e = 503 (M^+).

X-ray crystallography

Crystals were sealed under argon in thin-walled glass capillaries. All crystallographic measurements were made using a CAD4 diffractometer, operating in the $\omega/2\theta$ scan mode with graphite monochromated Mo-K_α radiation (λ = 0.71069 Å) as previously described.[16] Experimental details are given in Table 6.

The structures were solved using routine heavy-atom methods and refined by full-matrix least-squares. The refinements of structures **7a** and **9** were affected by high thermal motion or disorder of the PF_6 group in **9** and of the carbon atoms of the dmpe ligands of one of two independent cations in **7a**. These atoms required representation by split sites with some distance constraints, but even this did not completely model the disorder and the final R value obtained is higher than we would prefer. Otherwise all non-hydrogen atoms were refined anisotropically and hydrogens included in idealized positions with group U_{iso} values assigned. Refinement details are summarized in Table 6.

Sources of scattering factor data and computer programs used are as given in ref. 16. All computations were made on a DEC VAX 11/750 computer. Tables of final atomic positional and displacement parameters, full lists of bond lengths and angles, and F_o/F_c values have been deposited as supplementary material with the Editor, from whom copies are available on request. Atomic coordinates have also been deposited with the Cambridge Crystallographic Data Centre.

Acknowledgement—We thank the SERC for studentships (S.J.A. and F. J. W.) and for provision of X-ray facilities.

REFERENCES

1. J. E. Salt, G. Wilkinson, M. Motevalli and M. B. Hursthouse, *J. Chem. Soc., Dalton Trans.* 1986, 1141.
2. A. R. Barron, J. E. Salt, G. Wilkinson, M. Motevalli and M. B. Hursthouse, *J. Chem. Soc., Dalton Trans.* 1987, 2947.
3. A. R. Barron, G. Wilkinson, M. Motevalli and M. B. Hursthouse, *Polyhedron* 1987, **6**, 1089.
4. L. K. Fong, J. R. Fox, B. M. Foxman and N. J. Cooper, *Inorg. Chem.* 1986, **25**, 1880.
5. G. S. Girolami, G. Wilkinson, A. M. R. Galas, M. Thornton-Pett and M. B. Hursthouse, *J. Chem. Soc., Dalton Trans.* 1985, 1339.
6. G. Rouschias and G. Wilkinson, *J. Chem. Soc. (A)* 1968, 489.
7. (a) T. C. Wright, G. Wilkinson, M. Motevalli and M. B. Hursthouse, *J. Chem. Soc., Dalton Trans.* 1986, 2017; (b) P. A. Chetcuti, C. B. Knobler and M. F. Hawthorn, *Organometallics* 1988, **7**, 650.
8. D. C. Povey, R. L. Richards and C. Shortman, *Polyhedron* 1986, **5**, 369.
9. R. A. Henderson, D. L. Hughes, R. L. Richards and C. Shortman, *J. Chem. Soc., Dalton Trans.* 1987, 1115.
10. F. J. Wells, G. Wilkinson, M. Motevalli and M. B. Hursthouse, *Polyhedron* 1987, **6**, 1351.
11. J. M. Bellerby and M. J. Mays, *J. Chem. Soc., Dalton Trans.* 1975, 1281.
12. W. Huber, J. Peterhans and E. Winter, *Chem. Ber.* 1961, **94**, 2572.
13. P. Chandrasekhar and R. H. Bird, *Inorg. Chim. Acta* 1985, **97**, L31.
14. (a) I. S. Butler and A. E. Fenster, *J. Organomet. Chem.* 1974, **66**, 161; (b) M. C. Baird, G. Hartwell and G. Wilkinson, *J. Chem. Soc. (A)* 1968, 348; (c) G. Fachinetti, C. Floriani, A. Chiesi-Villa and C. Guastini, *J. Chem. Soc., Dalton Trans.* 1979, 1612.
15. M. Minelli, J. H. Enemark, R. T. C. Brownlee, M. J. O'Connor and A. G. Wedd, *Coord. Chem. Rev.* 1985, **68**, 169.
16. M. B. Hursthouse, R. A. Jones, K. M. A. Malik and G. Wilkinson, *J. Am. Chem. Soc.* 1979, **101**, 4128.

Polyhedron Vol. 7, No. 24, pp. 2627–2633, 1988
Printed in Great Britain

0277-5387/88 $3.00+.00
© 1988 Pergamon Press plc

COMPLEXES OF RUTHENIUM(II) AND -(III) WITH DIMETHYLSULPHOXIDE—III. BIS-IODO-TETRAKIS-DIMETHYLSULPHOXIDE RUTHENIUM(II) AND SOME OTHER IODO COMPLEXES OF RUTHENIUM(II)

UMA CHARAN SARMA and RAJ K. PODDAR*

Department of Chemistry, North-Eastern Hill University, Bijni Campus, Shillong 793 003, India

(*Received* 12 *January* 1988; *accepted* 27 *May* 1988)

Abstract—The ruthenium(II) complex $[RuI_2(Me_2SO)_4]$ was synthesized and characterized. The Me_2SO ligands are all S-bonded. Reactions of $RuI_2(Me_2SO)_4$ with ligands containing P, N and S donor atoms have been carried out and the complexes obtained were characterized using different physical methods. $[RuI_2L_4]$ (L = CH_3CN, Me_2SO and py), $[RuI_2(CH_3CN)_2(PPh_3)_2]$ and $[RuI_2(CS)(PPh_3)_3]$ have been synthesized using RuI_3 as the source material and characterized as above.

Complexes of ruthenium(II) or -(III) containing iodo groups as one of the coordinating ligands are generally prepared by the metathesis of the corresponding chloro complexes using KI, NaI or HI as the reagent.[1–7] In some cases oxalate or hydrido groups are exchanged using KI, NaI, HI or I_2.[8–12] There are some examples where ruthenium triiodide (either as $RuI_3 \cdot xH_2O$[13–14] or generated *in situ* by treating $RuCl_3 \cdot xH_2O$ with KI/NaI/HI[15–17]) is used as the starting material for the syntheses of ruthenium complexes containing iodo groups. There are no examples where an iodo containing ruthenium complex is used as the precursor for the synthesis of iodo complexes by substituting the coordinated ligand with new ligands. Such examples are known for bromo complexes.[18,19] Some iodo complexes of Ru^{II} containing Me_2SO, CH_3CN or pyridine have now been synthesized and some of the complexes thus obtained were used as precursors for the synthesis of Ru^{II} complexes containing iodide as one of the ligands. $RuI_3 \cdot xH_2O$ was used to synthesize these iodo complexes.

EXPERIMENTAL

Ruthenium trichloride trihydrate was obtained from Aurora–Matthey Ltd, Calcutta. Ruthenium triiodide was prepared by a modification of the reported methods.[20–22] The analysis for iodide was carried out by standard methods[23] after decomposition with a KOH and KNO_3 mixture. Carbon, hydrogen and nitrogen analyses were obtained from CDRI, RSIC, Lucknow. All other physical measurements, viz. IR, UV–vis., ^1H NMR spectra, magnetic and conductivity measurements were carried out as reported earlier.[19,24]

Preparation of ruthenium iodide, $RuI_3 \cdot xH_2O$

To a solution of hydrated ruthenium trichloride (1 g) in water (20 cm^3), hydroiodic acid (5 cm^3) and potassium iodide (5 g) were added. The reaction mixture was stirred at room temperature (for 2 h), when a black compound separated out. The compound was centrifuged, washed 2–3 times with water, then with acetone and dried *in vacuo*. Yield, 1.7 g (85%). It was analysed for its iodide content (Found: 70.5. Calc. for $RuI_3 \cdot 3H_2O$: 70.1%).

(i) *Preparation of* $RuI_2(Me_2SO)_4$

Method A. To a suspension of finely powdered $RuI_3 \cdot xH_2O$ (0.5 g) in acetone (25 cm^3), dimethylsulphoxide (5 cm^3) was added. The mixture was refluxed on a water bath for about 2 h. The colour of the solution changed from black to green and then to brown, and a reddish-brown compound separated out. The compound after centrifugation

* Author to whom correspondence should be addressed.

was washed successively with acetone and ether. It was dried *in vacuo*. Yield, 0.55 g (85%).

Method B. A mixture of $RuI_3 \cdot xH_2O$ (0.5 g) and dimethylsulphoxide (5 cm^3) was refluxed in an oil bath (130–140°C) for 5 min, when a clear solution was obtained. The volume was reduced to 2 cm^3, cooled and acetone was added to it with stirring. The compound which separated after 30 min, was obtained as in method A. Yield, 0.55 g (85%).

(ii) *Preparation of* $RuI_2(py)_4$

A mixture of finely powdered $RuI_3 \cdot xH_2O$ (0.2 g) and pyridine (1 cm^3) was heated on a water bath for about 2 h. A green coloured solution was obtained. A brown crystalline compound separated from the solution, on cooling. It was centrifuged, washed with acetone and ether, and dried *in vacuo*. It was analysed for $RuI_2(py)_4$.

(iii) *Preparation of* $RuI_2(CH_3CN)_4$

A suspension of $RuI_3 \cdot xH_2O$ (0.2 g) in acetonitrile (10 cm^3) was refluxed on a water bath for about 4 h, when a clear solution was obtained. The solution was concentrated and cooled to room temperature, when a reddish-brown crystalline compound separated out. It was centrifuged, washed with ether and dried *in vacuo*. The compound was analysed for $RuI_2(CH_3CN)_4$.

(iv) *Preparation of* $[RuI_2(CH_3CN)_2(PPh_3)_2]$

To a solution of $RuI_3 \cdot xH_2O$ (0.2 g) in acetonitrile (20 cm^3), triphenylphosphine (0.5 g) was added. The mixture was refluxed for 4 h. A yellow solution was obtained which on concentration yielded a yellow crystalline compound. The compound was washed with ether and dried *in vacuo*. It was analysed for the composition, $[RuI_2(CH_3CN)_2(PPh_3)_2]$.

(v) *Preparation of* $[RuI_2(CS)(PPh_3)_3]$

To a suspension of finely powdered $RuI_3 \cdot xH_2O$ (0.2 g) in carbon disulphide (20 cm^3), triphenylphosphine (0.5 g) was added. The mixture was refluxed on a water bath for 2 h. It was kept overnight at room temperature when most of the solvent evaporated and a brownish-red compound separated out. The compound was first washed with water followed by ether and dried *in vacuo*. It was analysed for $[RuI_2(CS)(PPh_3)_3]$.

Reactions of $[RuI_2(Me_2SO)_4]$

(i) *With triphenylphosphine.* To a solution of $[RuI_2(Me_2SO)_4]$ (0.2 g) in methanol (20 cm^3), triphenylphosphine (0.35 g) (molar ratio 1:4) was added. The reaction mixture was refluxed for 5 min and cooled to room temperature, when a dark brown compound crystallized out. It was centrifuged, washed with ether and dried *in vacuo*. The compound was analysed for $[RuI_2(PPh_3)_2(Me_2SO)]$.

$[RuI_2(PPh_3)_2(Me_2SO)]$ was also obtained when a reaction similar to the one above was carried out at room temperature by stirring the reaction mixture for about 1 h.

(ii) *With pyridine.* (a) To a solution of $[RuI_2(Me_2SO)_4]$ (0.2 g) in methanol (10 cm^3), pyridine (1 cm^3) was added and stirred at room temperature for 3 h. A reddish-brown compound separated out, which was centrifuged, washed with ether and dried *in vacuo*. The compound obtained was analysed for $[RuI_2(py)_2(Me_2SO)_2]$.

(b) A reaction similar to (a) was carried out under refluxing conditions of solvent for 2 h and cooled. A dark brown crystalline compound separated. It was washed with ether and dried *in vacuo*. The compound was analysed for $[RuI_2(py)_4]$.

(iii) *With 2,2′-bipyridyl (bipy) or 1,10-phenanthroline (phen).* (a) To a solution of $[RuI_2(Me_2SO)_4]$ (0.2 g) in methanol (20 cm^3), a methanolic solution of 2,2′-bipyridyl or 1,10-phenanthroline (0.2 g in 5 cm^3) was added. The solution was stirred at room temperature for about 3 h. An orange coloured compound separated out in each case, which was washed with acetone and dried *in vacuo*. The compounds had the composition, $[RuI_2(L—L)(Me_2SO)_2]$ (L—L = bipy or phen).

(b) A reaction similar to (a) above using 2,2′-bipyridyl was carried out by refluxing the mixture on a water bath for 3 h. The solution was concentrated and cooled, and the products isolated as in (a) above. It was analysed for $[RuI_2(bipy)_2]$.

(iv) *With acetonitrile.* $[RuI_2(Me_2SO)_4]$ (0.2 g) was dissolved in acetonitrile (20 cm^3). The solution was refluxed for about 1 h, concentrated (2 cm^3) and cooled to room temperature. A yellow crystalline compound separated out which was washed with ether and dried *in vacuo*. The compound had the composition, $[RuI_2(CH_3CN)_3(Me_2SO)]$.

(v) *With sodium diethyldithiocarbamate.* $[RuI_2(Me_2SO)_4]$ (0.2 g) was suspended in toluene (20 cm^3) and sodium diethyldithiocarbamate (0.15 g) was added. The suspension was refluxed for 30 min to give a dark green coloured solution. The solution was concentrated (5 cm^3). Addition of light petroleum ether (b.p. 80–100°C) followed by

cooling in an ice–salt mixture yielded green needle-shaped crystals. The compound had the composition $[Ru(Et_2NCS_2)_2(Me_2SO)_2]$.

RESULTS AND DISCUSSION

The preparation of ruthenium triiodide has been reported either by the metathetic reaction between $RuCl_3 \cdot xH_2O$ and KI in aqueous solution,[20–22] or by the action of HI on RuO_4.[25] We have synthesized $RuI_3 \cdot 3H_2O$ by the metathetic reaction between $RuCl_3 \cdot xH_2O$ and KI in the presence of HI. The compound has $\mu_{eff} = 2.1$ BM at room temperature. The room temperature ESR spectrum shows a broad signal at $g = 2.05$.

$[RuI_2S_4]$ (S = py *or* CH_3CN)

In the literature there are very few reports[13,14] of the use of RuI_3 as a starting compound for the syntheses of Ru^{III} and Ru^{II} iodo compounds. Hence in the present work we have explored the possibility of synthesizing ruthenium iodo compounds using RuI_3 as the source material. RuI_3 is generally insoluble in non-coordinating solvents. Hence, reactions have been carried out using a solvent (S) which coordinates to ruthenium, viz. dimethyl sulphoxide, acetonitrile or pyridine. Normally, when a reaction is carried out between RuI_3 and the solvent (S) under refluxing conditions, products of the composition, RuI_2S_4, are obtained. The solvent, being present in excess, acts both as a coordinating agent and reducing agent (Ru^{III} to Ru^{II}). The compounds, RuI_2S_4 (S = py, MeCN, Me_2SO), are diamagnetic, thereby confirming that the metal(II) ion has a d^6 low spin configuration. Conductivity measurements in acetonitrile or methanol show low molar conductance values (10–15 Ω^{-1} cm^2 mol^{-1}) (Table 1) indicative of iodo groups covalently bonded to ruthenium(II).

The IR spectrum of $RuI_2(py)_4$ shows the presence of all bands due to coordinated pyridine. The spectrum in the far IR region shows bands of medium to weak intensities at 465, 408 and 290 cm^{-1}. The ^1H NMR spectrum (Table 3) in $CDCl_3$ shows triplets at δ 7.03 and 7.63 and a doublet at δ 9.01. The far IR and the ^1H NMR spectra are similar to the one reported for *trans*-$[RuI_2(py)_4]$[9] and hence a *trans* structure for the synthesized $[RuI_2(py)_4]$ is proposed.

An IR spectrum of $[RuI_2(CH_3CN)_4]$ shows a band of medium intensity at 2275 cm^{-1}, besides other bands due to CH_3CN. This band may be assigned to the ν_{CN} of the coordinated CH_3CN group.[26] The presence of only one band around 2275 cm^{-1} indicates that the complex has a *trans* geometry.[26]

Ruthenium(II) *iodo complexes containing* PPh_3 *and other groups*

Reaction of RuI_3 with PPh_3 in a non-coordinating solvent or a weakly coordinating solvent like acetone under refluxing conditions did not result in the formation of the ruthenium iodotriphenylphosphine complex. Reaction of RuI_3, using the melt of PPh_3 as a solvent, at its boiling point did not lead to the coordination of PPh_3, instead RuI_3 separated out, unreacted. However, when RuI_3 was treated with PPh_3, in a coordinating solvent like acetonitrile, a compound of the composition $[RuI_2(CH_3CN)_2(PPh_3)_2]$ was obtained. It is non-conducting and diamagnetic in nature. The IR spectrum shows a band of medium intensity at 2270 cm^{-1} besides other bands due to acetonitrile and PPh_3. One band at 2270 cm^{-1} is characteristic of ν_{CN} of acetonitrile groups coordinated to ruthenium in the *trans* positions.[26] A reaction of RuI_3 with PPh_3 in CS_2 medium resulted in the formation of a compound of the composition $[RuI_2(CS)(PPh_3)_3]$. It is diamagnetic in nature, thereby confirming ruthenium to be in the +2 state. The low value of the molar conductance in CH_3OH (5 Ω^{-1} cm^2 mol^{-1}) is indicative of covalently bonded iodo groups. The IR spectrum shows a band at 1270 cm^{-1}, which could be assigned to ν_{CS} of the thiocarbonyl group.[18]

$[RuI_2(Me_2SO)_4]$

The IR spectrum of $[RuI_2(Me_2SO)_4]$ shows a band at 1079 cm^{-1} (strong), characteristic of ν_{SO} (S-bonded) of the Me_2SO groups. Besides this, bands of medium intensities at 1026, 976 and 930 cm^{-1} are also observed which may be assigned to $\rho_r CH$.[27] The IR spectral pattern in the region 1100–900 cm^{-1} is identical to that of $[RuBr_2(Me_2SO)_4]$,[27] which is reported to have a *trans* geometry, with all S-bonded Me_2SO. This confirms the presence of all Me_2SO groups in an S-bonded fashion. Bora and Singh[14] reported the preparation of $[RuI_2(Me_2SO)_4]$ by a slightly different method and characterized it, using the IR spectrum, as having both S-bonded and O-bonded Me_2SO.

The IR spectrum of $[RuI_2(Me_2SO)_4]$ in the region 600–350 cm^{-1} is similar to that of $[RuCl_3(Me_2SO)_3]^-$, a compound containing all S-bonded Me_2SO groups.[28] It shows a strong absorption at 420 cm^{-1} and a medium band at 383 cm^{-1}. The absorption at 420 cm^{-1} may be due to the combination of ν_{Ru-S} and $\delta_{s(CSO)}$, whereas the 383 cm^{-1} band may be due to $\delta_{a(CSO)}$. Another band at 246 cm^{-1} may tentatively be assigned to ν_{Ru-I}.[29]

Reactions of $[RuI_2(Me_2SO)_4]$

(a) *With triphenylphosphine.* Reaction of $[RuI_2(Me_2SO)_4]$ with PPh_3 at room temperature and under refluxing conditions of methanol gave $[RuI_2(PPh_3)_2(Me_2SO)]$ only. The compound is diamagnetic confirming the oxidation state of Ru as +2. It is non-conducting in nature, confirming the covalent nature of the iodo groups. The IR spectrum of the complex shows all the bands due to PPh_3 and a strong band at 1120 cm^{-1}, which is characteristic of ν_{SO} (S-bonded) of the Me_2SO group. The ^1H NMR spectrum of $[RuI_2(PPh_3)_2(Me_2SO)]$ in $CDCl_3$ at room temperature shows a sharp signal at δ 3.6 and broad signals in the region δ 7.3–7.6. The former one is due to the methyl protons of Me_2SO (S-bonded) and the latter due to the phenyl protons of PPh_3 groups. The ratio of the area under the two signals is 1 : 5 confirming the presence of one Me_2SO and two PPh_3 molecules (6 : 30 protons) in the complex.

(b) *With nitrogen donor ligands.* (i) *Pyridine.* A reaction of $[RuI_2(Me_2SO)_4]$ with pyridine at room temperature leads to the formation of a partially substituted $[RuI_2(py)_2(Me_2SO)_2]$ complex. The IR spectrum shows all the bands due to pyridine and two strong bands at 1070 and 1085 cm^{-1} due to the ν_{SO} (S-bonded) of the Me_2SO molecules. The ^1H NMR spectrum of the complex in $CDCl_3$ shows a sharp signal at δ 3.7 characteristic of the methyl proton of the S-bonded Me_2SO groups. Other signals observed are: a doublet at δ 9.25 and triplets at δ 7.74 and 7.15. The ^1H NMR spectral pattern in the region δ 7.1–9.25 is characteristic of pyridine molecules coordinated in the *trans* position.[9] Furthermore, only one sharp signal at δ 3.7 is indicative that two Me_2SO molecules are also in equivalent environments, which is possible if a *trans* structure is present in $[RuI_2(py)_2(Me_2SO)_2]$. The ratio of the areas of the signals due to the protons of pyridine and Me_2SO is 5 : 6, thereby confirming the presence of equal numbers of pyridine and Me_2SO molecules in the complex. Reactions of $[RuI_2[Me_2SO)_4]$ with pyridine in refluxing methanol leads to a completely substituted product, viz. $[RuI_2(py)_4]$. The IR and ^1H NMR spectra of this compound are superimposable on those of $[RuI_2(py)_4]$ obtained by a reaction of RuI_3 and pyridine, discussed earlier in this work. Hence a *trans* geometry for $[RuI_2(py)_4]$ is proposed.

(ii) *2,2′-bipyridine (bipy) and 1,10-phenanthroline (phen).* Room temperature reaction products of $[RuI_2(Me_2SO)_4]$ with 2,2′-bipyridine and 1,10-phenanthroline have the composition, $[RuI_2(L—L)(Me_2SO)_2]$ (L—L = bipy or phen). The compounds are diamagnetic and have very low molar conductance values, confirming that Ru^{II} complexes contain covalent iodide. The IR spectrum of the bipyridyl containing complex shows strong bands at 1085 and 418 cm^{-1} which could be assigned to ν_{SO} (S-bonded) of the Me_2SO and $\nu_{Ru—S}$, respectively. Similarly, in the case of the phen containing complex, bands at 1105 and 1070 cm^{-1} could be assigned to $\nu_{S=O}$ (S-bonded) of the Me_2SO groups and at 425 cm^{-1} due to $\nu_{Ru—S}$. The ^1H NMR spectrum of the two complexes in CD_3CN, further confirm the composition of the complexes and the bonding mode of Me_2SO groups. The ^1H NMR spectrum of $[RuI_2(bipy)(Me_2SO)_2]$ in CD_3CN shows signals at δ 3.53, 3.42 and 3.37 which are characteristic of the methyl protons of the S-bonded Me_2SO. A doublet at δ 10.1 and a multiplet in the region δ 7.25–8.7 due to the protons of the coordinated bipyridyl group are observed.[30] A doublet at δ 10.1 is due to the two protons present next to the coordinated nitrogen atoms,[30] and multiplets in the region δ 7.25–8.7 are due to the rest of the protons in the bipyridyl. The ratio of the signals around δ 10.1 and around 3.4 is 1 : 6, thereby confirming the presence of two protons from one bipyridyl and 12 protons from the two Me_2SO molecules. The ^1H NMR spectrum of $[RuI_2(phen)(Me_2SO)_2]$ in CD_3CN shows one signal at δ 3.45 which may be assigned to the methyl protons of the S-bonded Me_2SO groups and multiplets in the region δ 7.35–8.3 assigned to the protons due to 1,10-phenanthroline.[31].

Reaction of $[RuI_2(Me_2SO)_4]$ with 2,2′-bipyridine in refluxing methanol led to the formation of $[RuI_2(bipy)_2]$. The compound is the same as that of Fergusson and Harris[32] obtained by the metathesis of $[Ru(bipy)_2Cl_2]$ with iodide. The UV–vis. spectrum of the compound contains absorptions the same as reported previously.[32,33]

(iii) *Acetonitrile.* Reaction of $[RuI_2(Me_2SO)_4]$ with acetonitrile under refluxing conditions substitutes only three of the four Me_2SO molecules leading to the formation of $[RuI_2(CH_3CN)_3(Me_2SO)]$. The IR spectrum of the compound shows two bands of medium intensity at 2310 and 2275 cm^{-1}, assigned to ν_{CN} of coordinated CH_3CN. It shows that at least two of the acetonitrile molecules are bonded in the *cis* position to ruthenium.[26] Two strong bands at 1120 and 1100 cm^{-1} in the complex may be assigned to $\nu_{S=O}$ (S-bonded) of the Me_2SO molecule. The ^1H NMR spectrum of the complex in $CDCl_3$ shows signals at δ 2.5 and 3.55. The signals at δ 2.5 may be assigned to the methyl protons of the coordinated CH_3CN. Protons due to free acetonitrile are observed around δ 2.2. However, upon coordination the acetonitrile methyl protons shift down-

Table 1. Some analytical and physical data of some new Ru^{II}–iodo–Me_2SO complexes

Compounds (colour)	M.p. (°C)	Analysis[a] (%) C	H	N	Molar conductance (Ω^{-1} cm^2 mol^{-1})
$[RuI_2(Me_2SO)_4]$ (Brown)	255–260[b]	14.5 (14.4)	3.7 (3.6)	38.0[c] (38.1)	9[d]
$[RuI_2(CH_3CN)_4]$ (Reddish-brown)	> 250	18.3 (18.5)	2.2 (2.3)	10.8 (10.8)	15[d]
$[RuI_2(py)_2(Me_2SO)_2]$ (Reddish-brown)	210–215[b]	25.0 (25.1)	3.1 (3.3)	4.1 (4.2)	3[e]
$[RuI_2(PPh_3)_2(Me_2SO)]$ (Dark brown)	145–150	47.7 (47.6)	3.5 (3.8)	—	5[f]
$[RuI_2(PPh_3)_2(CH_3CN)_2]$ (Light yellow)	190–195	49.8 (49.9)	3.7 (3.7)	3.2 (3.0)	14[d]
$[RuI_2(CH_3CN)_3(Me_2SO)]$ (Yellow)	160–162	16.9 (17.3)	3.0 (2.7)	7.4 (7.6)	5[f]
$[RuI_2(CS)(PPh_3)_3]$ (Brownish-red)	200–205	55.4 (55.7)	3.6 (3.8)	—	5[d]
$[RuI_2(bipy)(Me_2SO)_2]$ (Orange)	> 250	25.4 (25.2)	3.0 (3.0)	4.0 (4.2)	5[f]
$[RuI_2(phen)(Me_2SO)_2]$ (Orange)	165–170	28.0 (27.7)	3.0 (2.9)	3.8 (4.1)	3[f]

[a] Calculated values are in parentheses.
[b] Decomposes.
[c] % iodide.
[d] In methanol.
[e] In acetonitrile.
[f] In chloroform.
Me_2SO, dimethylsulphoxide; py, pyridine; bipy, 2,2′-bipyridyl; phen, 1,10-phenanthroline.

Table 2. Important IR and UV–vis. bands of some new ruthenium(II) complexes

Compounds	IR bands (cm^{-1})	λ_{max} (nm) (ε)
$[RuI_2(Me_2SO)_4]$	1079s, 1026, 976, 930, 420, 383, 246	480sh (400)[a]
$[RuI_2(CH_3CN)_4]$	2275m	360 (11,000)[b]
$[RuI_2(py)_2(Me_2SO)_2]$	1085s, 1070s	
$[RuI_2(PPh_3)_2(Me_2SO)]$	1120s	
$[RuI_2(PPh_3)_2(CH_3CN)_2]$	2270m	420sh[b]
$[RuI_2(CH_3CN)_3(Me_2SO)]$	2310m, 2275m, 1120s, 1100s	360 (410)[b]
$[RuI_2(CS)(PPh_3)_3]$	1270s	535 (1470)[b] 370sh
$[RuI_2(bipy)(Me_2SO)_2]$	1085s, 418s	375 (3100)[b] 280 (26700) 235 (70600)
$[RuI_2(phen)(Me_2SO)_2]$	1105s, 1070s, 425m	

[a] In CH_3OH.
[b] In CH_3CN.

Table 3. ^{1}H NMR spectral data of some ruthenium(II) complexes[24]

Compound	δ (ppm)	Solvent
$[RuI_2(py)_4]$	7.03t, 7.63t, 9.01d	$CDCl_3$
$[RuI_2(PPh_3)_2(Me_2SO)]$	3.6s, (7.3–7.6)b,m	$CDCl_3$
$[RuI_2(py)_2(Me_2SO)_2]$	3.7s, 7.15t, 7.74t, 9.25d	$CDCl_3$
$[RuI_2(CH_3CN)_3(Me_2SO)]$	2.5, 3.55	$CDCl_3$
$[RuI_2(bipy)(Me_2SO)_2]$	3.37, 3.42, 3.53, (7.25–8.7)m, 10.1d	CD_3CN
$[RuI_2(phen)(Me_2SO)_2]$	3.45s, (7.35–8.3)m	CD_3CN

s, singlets; d, doublets; t, triplets; b, broad; m, multiplets.

field by δ 0.3 (2.5). A signal at δ 3.55 could be assigned to the methyl protons of S-bonded Me_2SO molecules. The ratio of the areas under the two signals is 3:2 thereby confirming the presence of three acetonitrile (9 H) and one Me_2SO (6 H) molecules in the complex.

(iv) *Sodium diethyldithiocarbamate.* The reaction of $[RuI_2(Me_2SO)_4]$ with sodium diethyldithiocarbamate led to the formation of $[Ru(Et_2NCS_2)_2(Me_2SO)_2]$. This compound has been obtained by Evans *et al.*[34] by the reaction of $[RuCl_2(Me_2SO)_4]$ with the ligand. The compound shows a strong band at 1490 cm^{-1} characteristic of ν_{CS} for the bidentate diethyldithiocarbamate groups.[35] Another strong band at 1075 cm^{-1} is due to the ν_{SO} (S-bonded) of the Me_2SO groups.

Electronic spectra

The electronic absorption spectra of all the complexes (Table 2) show some absorptions in the 350–500 nm region. Absorption bands with high ε values (10^3–10^4) are largely due to charge-transfer transitions whereas bands with lower ε values (10^2–10^3) may be of the *d–d* type ($^1A_{1g} \rightarrow {}^1E_g$ or $^1A_2$).[36]

Acknowledgements—One of the authors (U.C.S.) thanks the UGC, New Delhi for the award of a teacher fellowship under the faculty improvement programme. We thank RSIC, NEHU for obtaining IR spectra, UV–vis. spectra and NMR spectra. We also thank RSIC, CDRI, Lucknow for providing analytical data for these compounds and to IACS, Calcutta for measuring room temperature magnetic susceptibilities.

REFERENCES

1. G. T. Morgan and F. H. Burstall, *J. Chem. Soc.* 1936, 41.
2. J. J. Levison and S. D. Robinson, *J. Chem. Soc.* (*A*) 1970, 639.
3. F. P. Dwyer, H. A. Goodwin and E. C. Gyarfas, *Aust. J. Chem.* 1963, **16**, 544.
4. J. G. Hartley and L. M. Venanzi, *J. Chem. Soc.* 1962, 182.
5. R. K. Poddar, U. Agarwala and P. T. Monoharan, *J. Inorg. Nucl. Chem.* 1974, **36**, 2275.
6. M. S. Lupim and B. L. Shaw, *J. Chem. Soc.* (*A*) 1968, 741.
7. B. Bosnich and F. P. Dwyer, *Aust. J. Chem.* 1966, **19**, 2229.
8. D. L. Key, L. F. Larkworthy and J. E. Salmon, *J. Chem. Soc.* (*A*) 1971, 2583.
9. D. W. Raichart and H. Taube, *Inorg. Chem.* 1972, **11**, 999.
10. J. D. Cotton, M. I. Bruce and F. G. A. Stone, *J. Chem. Soc.* (*A*) 1968, 2162.
11. T. Ito, S. Kitazume, A. Yamamoto and S. Ikeda, *J. Am. Chem. Soc.* 1970, **92**, 3011.
12. J. R. Saunders, *J. Chem. Soc., Dalton Trans.* 1972, 1333.
13. R. Colton and R. H. Farthing, *Aust. J. Chem.* 1967, **20**, 1283.
14. T. Bora and M. M. Singh, *Transition Met. Chem.* 1978, **3**, 27.
15. F. P. Dwyer, J. E. Humpoletz and R. S. Nyholm, *J. Proc. R. Soc. N. S. Wales* 1946, **80**, 217.
16. J. Chatt and R. G. Hayter, *J. Chem. Soc.* 1961, 896.
17. R. S. Nyholm and G. J. Sutton, *J. Chem. Soc.* 1958, 561.
18. L. Ruiz-Ramirez and T. A. Stephenson, *J. Chem. Soc., Dalton Trans.* 1973, 1770.
19. U. C. Sarma and R. K. Poddar, *Polyhedron* 1988, **7**, 1737.
20. A. Gutbier and C. Trenkuer, *Z. Anorg. Allg. Chem.* 1905, **45**, 166.
21. F. Krauss and H. Kükenthal, *Z. Anorg. Allg. Chem.* 1924, **137**, 32.
22. S. A. Shchukarev, N. I. Kolbin and A. M. Rayabov, *Russ. J. Inorg. Chem.* 1961, **6**, 517.
23. A. I. Vogel, *Inorganic Quantitative Analysis*, 4th edn, p. 496. ELBS & Longmans, London (1978).
24. U. C. Sarma, K. P. Sarma and R. K. Poddar, *Polyhedron* 1988, **7**, 1727.
25. O. Ruff and E. Vidic, *Z. Anorg. Allg. Chem.* 1924, **136**, 49.
26. R. K. Poddar and U. Agarwala, *J. Inorg. Nucl. Chem.* 1973, **35**, 3769.

27. J. D. Oliver and D. P. Riley, *Inorg. Chem.* 1984, **23**, 156.
28. R. S. McMillan, A. Mercer, B. R. James and J. Trotter, *J. Chem. Soc., Dalton Trans.* 1975, 1006.
29. C. Udovich, J. Takemoto and K. Nakamoto, *J. Coord. Chem.* 1971, **1**, 89.
30. J. D. Birchall, R. D. O'Donoghue and J. R. Wood, *Inorg. Chim. Acta* 1979, **37**, L461.
31. J. D. Miller and R. H. Prince, *J. Chem. Soc.* 1965, 3185.
32. J. E. Fergusson and G. M. Harris, *J. Chem. Soc.* (*A*) 1966, 1293.
33. G. M. Bryant, J. E. Fergusson and H. K. J. Powell, *Aust. J. Chem.* 1971, **24**, 257.
34. I. P. Evans, A. Spencer and G. Wilkinson, *J. Chem. Soc., Dalton Trans.* 1973, 204.
35. C. O'Connor, J. D. Gilbert and G. Wilkinson, *J. Chem. Soc.* (*A*) 1969, 84.
36. A. B. P. Lever, *Inorganic Electronic Spectroscopy*, p. 467. Elsevier, Amsterdam (1984).

Polyhedron Vol. 7, No. 24, pp. 2635–2640, 1988
Printed in Great Britain

0277–5387/88 $3.00+.00
© 1988 Pergamon Press plc

SYNTHESIS AND PROPERTIES OF THE BINUCLEAR VANADIUM(III) AND OXOVANADIUM(IV) CHELATES WITH TETRADENTATE SCHIFF BASES

SAIID A. AMER,* MOHAMED GABER and RAAFAT M. ISSA

Chemistry Department, Faculty of Science, Tanta University, Tanta, Egypt

(*Received* 25 *January* 1988; *accepted after revision* 27 *May* 1988)

Abstract—The complexes of vanadium(III) and oxovanadium(IV) with Schiff bases derived from some aliphatic diamines and 2-hydroxy-1-naphthaldehyde were prepared and characterized by elemental analysis, IR, electronic and EPR spectra. The binuclear V^{III} complexes have the $[V_2(\mu\text{-oxo})(\mu\text{-aquo})]$ core in distorted octahedral environments. The VO^{IV} complexes form monomeric, dimeric or polymeric complexes by ligand bridging. The structures are dependent on the length of the carbon chain linking the imine groups. A complex EPR signal is observed for $[VO(naphbu)]_2$ in chloroform solution at room temperature, its isotropic spectrum exhibits a 15 line hyperfine signal at $g_{av} = 2.014$ and the hyperfine coupling constant is 50 G, suggesting that the centres are weakly coupled. The reactions of the binuclear V^{III} complexes with dioxygen and VO^{IV} complexes with thionylchloride were also studied.

The chemistry of vanadium(IV) is dominated by the stable VO^{2+} ion which forms a wide variety of complexes of the type $[VO(L_4)]$, L_4 = quadridentate or two bidentate ligands.[1–3] The oxovanadium(IV) complexes of Schiff bases derived from 2-hydroxy-1-naphthaldehyde and ethanolamine or propanolamine have antiferromagnetism exchange between V atoms in a binuclear species.[4] Only a few examples are known for oxovanadium(IV) complexes with antiferromagnetic exchange.[5–8] Six-coordinate complexes of the simple V^{4+} ion are uncommon and have been little studied. It was found that direct reaction of vanadyl complexes with thionyl bromide or thionyl chloride readily yielded *trans*-dibromo or dichlorovanadium(IV) complexes, respectively.[9–11]

In the present article the synthesis and characterization of the binuclear vanadium(III) and oxovanadium(IV) complexes of a series of ligands of type **I** are investigated. It is aimed to examine the reaction of the binuclear vanadium(III) complexes with dioxygen and deoxygenation of oxovanadium(IV) complexes.

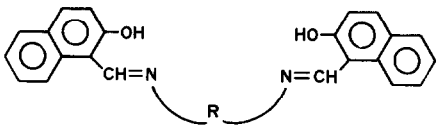

I

	R
H_2-naphen	$(CH_2)_2$
H_2-naphpn	$(CH_2)_3$
H_2-naphbu	$(CH_2)_4$
H_2-naphbtr	$(CH_2)_2$—NH—$(CH_2)_2$
H_2-naphpen	$(CH_2)_5$
H_2-naphdec	$(CH_2)_{10}$

RESULTS AND DISCUSSION

Two types of complexes were isolated $[V_2L_2(O)(H_2O)]$ complexes **1** and **2**, and the [VOL] complexes **3**–**7**, containing dianionic ligands. The complexes are listed in Table 1 together with their analytical data.

IR spectra

The IR spectra, Table 2, show that the characteristic ligand bands ν(C=N) display a shift to lower frequency on complexation. This indicates that the ligand has coordinated as a dianionic tet-

* Author to whom correspondence should be addressed.

Table 1. Analytical data and EPR spectra of V^{III} and VO^{IV} Schiff base complexes

No.	Complex Formula	Colour	M.p. (°C)	Microanalysis results[a] %C	%H	%N	%V	EPR data g-value	A (G)
1	$[V_2(naphen)_2(O)H_2O]$	Green	275	65.6(66.3)	4.0(4.3)	5.8(6.4)	11.6(11.7)	—	—
2	$[V_2(naphpn)_2(O)H_2O]$	Dark green	295	65.9(66.9)	4.4(4.6)	5.6(6.2)	10.4(11.3)	—	—
3	[VO(naphpn)]	Orange	220	69.1(67.1)	4.4(4.5)	6.5(6.3)		2.035	100
4	$[VO(naphbu)]_2$	Olive	250	70.8(67.4)	5.5(4.8)	6.4(6.0)		2.014	50
5	[VO(naphbutra)]	Brown	235	63.9(65.5)	4.8(4.9)	8.8(8.8)		2.017	95
6	[VO(naphpen)]	Green	155	68.2(68.2)	4.9(5.0)	5.7(5.9)	9.0(10.7)	2.016	95
7	[VO(naphdec)]	Green	135	70.7(70.2)	6.1(5.3)	5.4(5.1)	8.6(9.3)	2.015	98

[a] % Found (calc.).

radentate ligand.[12] The spectra of the complexes **1** and **2** show broad bands at 3450 cm^{-1} which are assigned to the —OH stretching vibration of water molecules participating in the coordination sphere. The spectra also exhibit medium intensity bands at 620, 750 and 645 cm^{-1}, respectively; these bands are absent in the spectra of the ligands and can be associated with bridging V—O—V.[13,14] The spectra of the oxovanadium(IV) complexes, **6** and **7**, display a strong band at 970 cm^{-1} assigned to the V=O stretching frequency.[15,16] The spectrum of complex **3** exhibits a medium band at 960 cm^{-1} assigned to ν(V=O). The low value may be attributed to high electron density on the metal due to the chelation of the H_2naphpn ligand. The spectrum of complex **4** displays a strongly split ν(V=O) band at 970 and 950 cm^{-1}; the splitting of the band may be attributed to the interaction between V atoms in the binuclear species. The spectrum of complex **5** comprises a medium band at 3240 cm^{-1} assigned to ν(NH) bonded and the low value of ν(V=O) may be attributed to high electron density on the metal due to the *trans*-NH ligand.[17] Thus the ligand in complex **5** has coordinated as a dianionic pentadentate ligand.

Electronic spectra

Solution electronic spectral data and the solid reflectance spectral data are listed in Table 2. The electronic spectra show, in addition to bands in the UV region due to internal transitions in the ligand, charge-transfer bands at 370–420 nm and *d–d* bands in the visible region at 470–620 nm, which according to the scheme of Ballhausen and Gray[18] ($d_{xy} < d_{xz}$, $d_{yz} < d_{x^2-y^2} < d_{z^2}$) are assigned to $d_{xy} \rightarrow d_{xz}$, d_{yz}, $d_{xy} \rightarrow d_{x^2-y^2}$ and $d_{xy} \rightarrow d_{z^2}$ transitions. Some of these bands are not very well developed, which often gives rise to ambiguity in their assignment. From the data of the reflectance spectra it can be pointed out that

Table 2. IR spectra and electronic absorption spectra of V^{III} and VO^{IV} complexes

Complex	IR spectra cm^{-1} ν_{OH}	$\nu_{C=N}$	$\nu_{V=O}$	V—O—V	Electronic spectra DMF	Reflectance
1	3450	1600(1625)[a]	—	620	380, 405 (CT) 610[B] (*d–d*)	390 (CT) 620[B] (*d–d*)
2	3450	1605(1625)		750,645	380, 425 540, 620	400 (CT) 650[B] (*d–d*)
3	—	1605(1625)	960	—	380, 400, 422 (CT) 530 (*d–d*)	400 (CT) 550 (*d–d*)
4	—	1610(1630)	970,950	—	395, 410 (CT) 550, 490sh (*d–d*)	400 (CT) 550, 600 (*d–d*)
5	—	1610(1630)	920	—	395 (CT) 550, 470sh (*d–d*)	385 (CT) 600 (*d–d*)
6	—	1610(1635)	975	—	390,420 (CT) 540 (*d–d*)	400 (CT) 540, 610 (*d–d*)
7	—	1610(1640)	980	—	390, 420 (CT) 540 (*d-d*)	420 (CT) 540, 630 (*d–d*)

[a] Free ligand values in parentheses.
CT = Charge-transfer transition.
d–d = *d–d* transition; sh = shoulder.

complexes **1**, **2** and **5** have a six-coordinate pseudo-octahedral structure,[13,14] while complexes **3**, **4**, **6** and **7** exhibit a five-coordinate square-pyramidal distribution.[14-16]

EPR spectroscopy

The X-band EPR spectra of the oxovanadium(IV) Schiff base complexes in dilute chloroform solution at room temperature are illustrated in Fig. 1. The isotropic spectra exhibit eight lines arising from interaction of the unpaired electron with a ^{51}V nucleus, except for the spectrum of $[VO(naphbu)]_2$. The monomeric material shows an eight line hyperfine signal at the g values and with the hyperfine splitting constants listed in Table 1. The spectra are characteristic of oxovanadium(IV) complexes.[11,13] The isotropic spectrum of $[VO(naphbu)]_2$ exhibits a 15 line hyperfine signal at $g_{av} = 2.014$ and the hyperfine coupling constant is 50 G. A comparison of the spectra of [VO(naphpn)] and $[VO(naphbu)]_2$ (Fig. 1) illustrates that there are more fine structure features more closely spaced for the dimer than for the monomer. This results from the greater number of possible transitions for a binuclear metal ion than for a mononuclear one.[19]

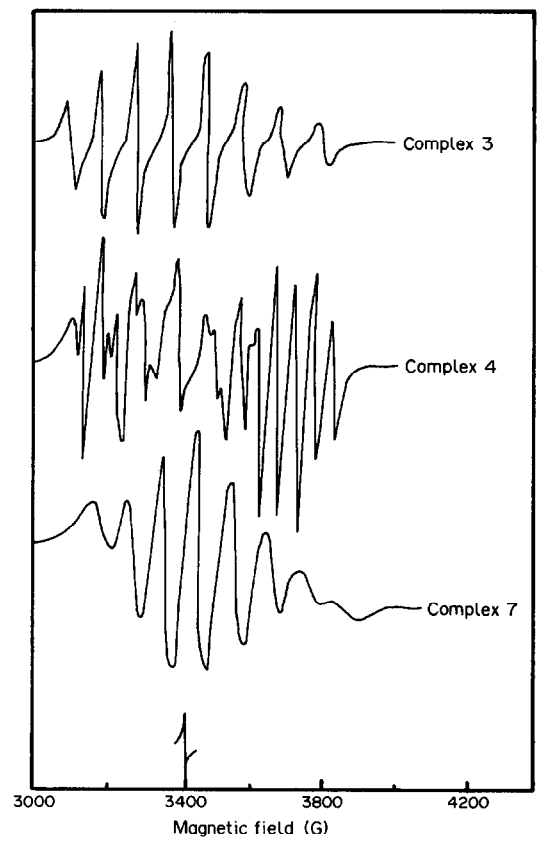

Fig. 1. EPR spectra of the vanadyl complexes in chloroform solution at room temperature.

For systems that have weak coupling between identical nuclei, the hyperfine interval is A/n, where A is the observed single nuclei coupling constant and n is the number of coupled nuclei.[20] Thus, the A value for $[VO(naphbu)]_2$ should be half the value for [VO(naphpn)]. This prediction is observed experimentally in this system ($A = 50$ G, $[VO(naphbu)]_2$; $A = 100$ G [VO(naphpn)]. The spectrum contains groups of approximately 15 lines. The observation of a 15 line spectrum has been attributed to the electron exchange between two ^{51}V nuclei.[21] So, the isotropic spectrum of $[VO(naphbu)]_2$ indicates that the centres are weakly coupled.

Structures

Based on analytical and spectral data one can propose the structures of the types illustrated by **II**–**VI** for the vanadium complexes prepared. It is clear that the structure of the complex seems to be mainly dependent on the length of the methylene chain of the ligand. Increasing the number of methylene carbons between the azomethine groups should relax the structural requirements of the ligand.

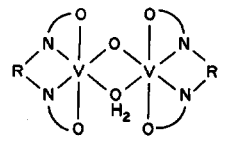

II (complex 1 and 2)

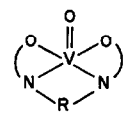

III (complex 3)

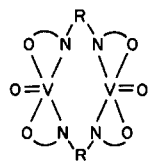

IV (complex 4)

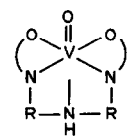

V (complex 5)

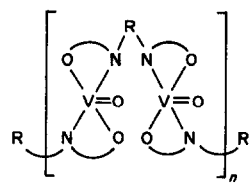

VI (complex 6 and 7)

Reaction of V^{III} complexes with dioxygen

The visible spectral study of the reaction of μ-oxo, μ-aquo-bis [N-N′-propylene bis(naphthylideneiminato)]divanadium(III) (complex **2**)

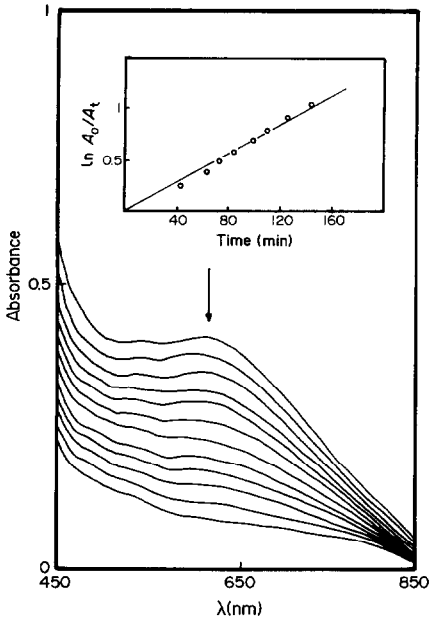

Fig. 2. Repetitive scan for the oxygenation of $[V_2(naphpn)_2(O)H_2O]$ complex (**2**) in DMF at room temperature within 3 h.

and dioxygen in dimethylformamide as a function of time was performed. The spectrum of complex **2** in DMF solution (Fig. 2) is characterized by a band at 630 nm which is attributed to the *d–d* transition of the six-coordinate V^{III} ion. When dioxygen is admitted to the solution the extinction of the band decreases, which eventually disappears. A weak band at 530 nm appears which is assigned to a *d–d* transition within the VO^{2+} ion.[15,16] Bubbling nitrogen through the solution does not regenerate the starting spectrum, denoting that the reaction is irreversible [see eq. (1)].

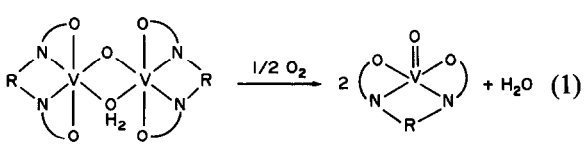

(1)

The rate constant of this reaction has been determined by monitoring the kinetics of the band characterizing the reactant. The decrease of A_0 to A is exponential, and plots of $\ln(A_0-A)/(A_t-A)$ vs time exhibit linearity (Fig. 2) where A_0 and A are the initial and final absorbances of the solution and A_t is the absorbance at varying time throughout the reaction. All absorbance values were recorded at a fixed wavelength. The slope of the plotted line is equal to the reaction rate constant; k observed for oxygenation of complex **2** is $1.2 \times 10^{-4}\ s^{-1}$.

The visible, IR and EPR spectra of the product formed during the absorption of dioxygen are similar to the spectra of the oxovanadium(IV) complex, **3**. It could be concluded that complex **2** is stable in the solid state and oxidized to the VO^{IV} complex in DMF solution.

Deoxygenation of the oxovanadium(IV) *complexes*

The reaction of the oxovanadium(IV) complexes with thionyl chloride in dimethylformamide at room temperature results in a rapid reaction with the colour changing from yellow to dark green. The visible spectral study of the reaction product of [N,N′-propylene bis(naphthlideneiminato)]oxovanadium(IV), complex **3** and thionyl chloride in DMF as a function of time was performed. The visible spectrum of complex **3** in DMF solution (Fig. 3) was characterized by a band at 530 nm which was assigned to the *d–d* transition within the VO^{2+} ion in a five-coordinate square-pyramidal structure. When thionyl chloride was added a rapid reaction occurred with the colour changing from yellow to dark green and the visible spectrum displayed a broad band at 750 nm which was assigned to a *d–d* transition within the V^{4+} ion.[13,14] The band diminishes in extinction and eventually disappears after 2 h indicating that the halogeno complex is unstable and decomposes. The rate constant for the dissociation of the halogeno complex $k_{obs} = 2 \times 10^{-6}\ s^{-1}$ [Fig. 3(a)].

The visible spectral study of the reaction of [N,N′ - butylene - bis(naphthlideneiminato)]oxovanadium(IV) dimer (**4**) and [diethylenetriamine bis (naphthlideneiminato)]oxovanadium(IV), complex **5**, and $SOCl_2$ in DMF as a function of time was performed. The visible spectra [Fig. 3(b)] display three bands at 790, 670 and 420 nm which according to the energy level scheme of Lever,[22] $(d_{xz}, d_{yz}) < d_{xy} < d_{z^2} < d_{x^2-y^2}$ for O_h symmetry with tetragonal distortion, are assigned to $[(d_{xz}, d_{yz}) \rightarrow d_{xy}]$; $[(d_{xz}, d_{yz}) \rightarrow d_{z^2}]$ and $[(d_{xz}, d_{yz}) \rightarrow d_{x^2-y^2}]$ transitions, respectively, of the V^{4+} ion. The spectra show little change indicating that the halogeno complexes are quite stable. The rate constants for formation of the halogeno complex: $k_{obs} = 3.2 \times 10^{-3}\ s^{-1}$, for complex **4** and $k_{obs} = 5 \times 10^{-3}$, for complex **5** [Fig. 3(b)].

The reaction of VO^{IV} complexes with thionyl chloride depends upon the structure of the oxovanadium complex, the presence of a flexible ligand around the vanadyl ion helps chloride to coordinate with the vanadyl ion.

CONCLUSIONS

The binuclear vanadium(III) complexes have a $[V_2(\mu\text{-oxo})(\mu\text{-aquo})]$ core in distorted octahedral

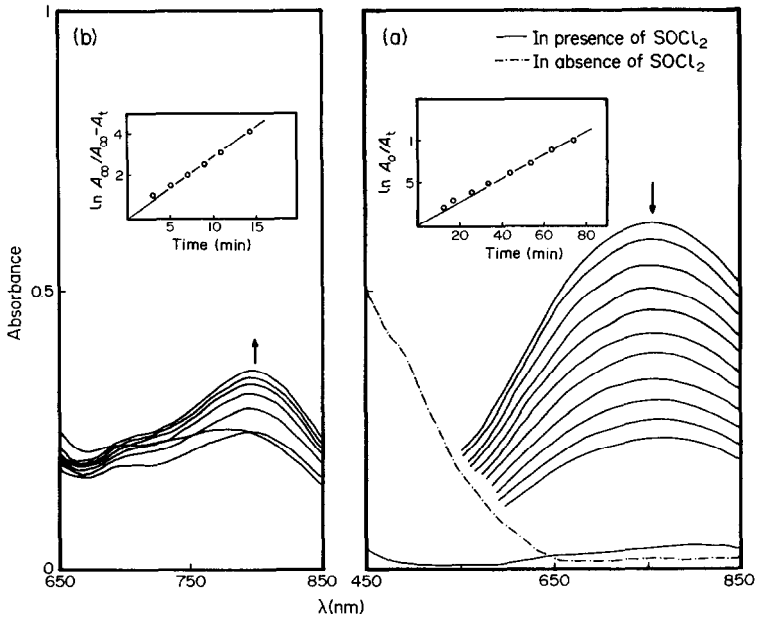

Fig. 3. Electronic absorption spectral sequence of the vanadyl complexes. (a) Decay spectra of [VO(naphpn)], complex **3** within 75 min. (b) Subsequent spectra of [VO(naphbutr)], complex **5** within 18 min.

environments of tetradentate N_2O_2 Schiff base ligands. These complexes are stable in the solid state and oxidized to oxovanadium(IV) in DMF solution. The type of complex formed between $VOCl_2$ and dianonic tetradentate Schiff bases is determined by the length of the carbon chain linking the imine groups and further, that the subsequent reaction with thionyl chloride depends upon the structure of the oxovanadium(IV) complex. Both stable dichloro vanadium(IV) complexes and unstable species have been observed.

EXPERIMENTAL

The ligands, H_2L, (I) were prepared by the standard method.

Preparation of metal complexes

(i) $[V_2L_2(O)H_2O]$ *complexes* **1** *and* **2**. The ligand (0.01 mol) suspended in dioxygen-free hot ethanol (50 cm^3) was mixed with triethylamine (0.02 mol), then vanadium(III) chloride in dioxygen-free ethanol (50 cm^3) was added dropwise to the ligand solution. The mixture was further refluxed with continuous stirring for 1 h under dry dinitrogen. The complex was filtered off, washed with acetone and dried *in vacuo*. The complexes were handled under dry dinitrogen (Yields *ca* 60%).

(ii) [VOL] *complexes* **3**–**7**. The ligand (0.01 mol) suspended in hot ethanol (150 cm^3) was mixed with triethylamine (0.02 mol), then vanadyl chloride in ethanol (50 cm^3) was added dropwise. The mixture was further refluxed for 1 h. The complex was filtered off, washed with acetone and dried *in vacuo* (Yields *ca* 70%).

Physical measurements

The IR spectra were recorded on Perkin–Elmer 598 and 683 IR spectrophotometers; the solid samples were examined as KBr discs. The diffuse-reflectance electronic spectra were measured on an SP 500 spectrophotometer using LiF as a reference. The electronic spectra in dimethylformamide solution were recorded on a Schimadzu 240 UV spectrophotometer. THe EPR X-band spectra were recorded on a varian E9 spectrometer.

REFERENCES

1. D. Bruins and D. L. Weaver, *Inorg. Chem.* 1970, **9**, 130.
2. K. S. Patel and J. C. Bailar, *J. Coord. Chem.* 1973, **3**, 113.

3. M. Mathew, A. J. Carty and G. J. Palenik, *J. Am. Chem. Soc.* 1970, **3**, 113.
4. A. Syamal, *Ind. J. Chem.* 1973, **11**, 363.
5. C. C. Lee, A. Ayamal and L. J. Theriot, *Inorg. Chem.* 1971, **10**, 1669.
6. S. N. Poddar, K. Dey, J. Haldar and S. C. Nathsarkar, *J. Ind. Chem. Soc.* 1970, **47**, 745.
7. Y. Kuge and S. Yamada, *Bull. Chem. Soc. (Japan)* 1970, **43**, 3972.
8. Y. Kuge and S. Yamada, *Bull. Chem. Soc. (Japan)* 1972, **45**, 799.
9. M. Pasquali, F. Marchetti and C. Floriani, *Inorg. Chem.* 1979, **18**, 2401.
10. M. Pasquali, A. Torres-Filho and C. Floriani, *J. Chem. Soc., Chem. Commun.* 1975, 534.
11. A. Jezierski and J. Paynor, *J. Chem. Soc., Dalton Trans.* 1981, 1.
12. K. Yamanouchi and S. Yamada, *Inorg. Chim. Acta* 1975, **12**, 9.
13. J. Selbin, *Coord. Chem. Rev.* 1966, **1**, 393.
14. D. K. Rastogi and P. C. Pachauri, *J. Inorg. Nucl. Chem.* 1977, **39**, 151.
15. J. Selbin, L. H. Holmes and S. P. McGlynn, *J. Inorg. Nucl. Chem.* 1963, **25**, 1359.
16. G. A. Kolawole and K. S. Patel, *J. Chem. Soc., Dalton Trans.* 1981, 1241.
17. F. Cotton and G. Wilkinson, *Advanced Inorganic Chemistry*, p. 716. Wiley Interscience, New York (1980).
18. C. J. Ballhausen and H. B. Gray, *Inorg. Chem.* 1962, **1**, 111.
19. B. Mabad, P. Cassoux, J. P. Tuchagues and D. N. Hendrickson, *Inorg. Chem.* 1986, **25**, 1420.
20. D. P. Kessissaglou, W. Butler and V. Pecoraro, *Inorg. Chem.* 1987, **26**, 495.
21. A. Syamal, *Coord. Chem. Rev.* 1975, **16**, 309.
22. A. B. P. Lever, *Inorganic Electronic Spectroscopy*. Elsevier, Amsterdam (1968).

Polyhedron Vol. 7, No. 24, pp. 2641–2647, 1988
Printed in Great Britain

0277–5387/88 $3.00+.00
© 1988 Pergamon Press plc

TRANSITION METAL COMPLEXES WITH THE THIOSEMICARBAZIDE-BASED LIGANDS—V. SYNTHESIS, CRYSTAL AND MOLECULAR STRUCTURE, AND SPECTRA OF S-METHYL-N(1)-SALICYLIDENE-N(4)-α-METHOXYPICOLYL-ISOTHIOSEMICARBAZIDONICKEL(II)

VUKADIN M. LEOVAC* and VALERIJA I. ČEŠLJEVIĆ

Institute of Chemistry, Faculty of Sciences, V. Vlahovića 2, 21000 Novi Sad, Yugoslavia

and

NIKOLA GALEŠIĆ

"Rudjer Bošković" Institute, PO Box 1016, 41001 Zagreb, Yugoslavia

(*Received* 7 *February* 1988; *accepted* 27 *May* 1988)

Abstract—The reaction of a warm methanolic solution of [Ni(HL)Py]Cl·0.5Py (HL = monoanion of terdentate NNO ligand salicylaldehyde S-methylisothiosemicarbazone) with α-picolinaldehyde yielded the diamagnetic complex NiL (L = dianion of the quadridentate NNNO ligand S-methyl-N(1)-salicylidene-N(4)-α-methoxypicolyl-isothiosemicarbazide). Crystal data: $C_{16}H_{16}N_4NiO_2S$, $M_r = 388.09$, triclinic, space group $P\bar{1}$, $a = 10.218(3)$, $b = 12.020(2)$, $c = 7.525(3)$ Å, $\alpha = 103.67(3)$, $\beta = 107.14(2)$, $\gamma = 103.30(2)°$, $V = 812.2(5)$ Å^3, $Z = 2$, $D_c = 1.58$ g cm^{-3}, $D_m = 1.53$ g cm^{-3}, μ(Cu-K_α) = 30.22 cm^{-1}, final $R = 0.062$ for 2060 observed reflections. With Ni^{II} the ligand forms one six- and two five-membered rings. The Ni coordination environment is slightly distorted square-planar determined from the O atom from salicylaldehyde with the Ni—O bond length of 1.831(4) Å, the N(1) and N(4) atoms from the S-methylisothiosemicarbazide moiety and the N atom from pyridine with the Ni—N bond lengths of 1.835(5), 1.803(5) and 1.908(5) Å, respectively. The compound has been characterized by elemental analysis as well as by IR and electronic spectra.

It has been shown[1,2] that in the presence of VO^{II}, Cu^{II}, Ni^{II} and Fe^{III} ions, salicylaldehyde thiosemicarbazone and its S-alkyl derivatives take part in a condensation reaction with salicylaldehyde yielding complex **I** of the corresponding metal ion and the *in situ* formed "symmetric" quadridentate ONNO ligands, the derivatives of N(1),N(4)-bis(salicylidene)isothiosemicarbazide. The demetallation of the corresponding Ni^{II} complex enabled the isolation of the free ligand, which led to the synthesis of complexes with this class of ligands which could not be prepared by the above template reaction. In this way, the complexes of Zn^{II}, Mn^{II}, Co^{II}, Co^{III} and Cr^{III} were prepared.[3]

Recently,[4] the preparation of the Ni^{II} complex of an "asymmetric" quadridentate ONNO ligand based on S-alkylisothiosemicarbazide, e.g. (acetylacetone S - methyl - N(4) - salicylideneisothiosemicarbazonato)nickel(II) (**II**) was reported. The most interesting observation was that [Ni(HL)Py]Cl·0.5Py (HL = monoanion of salicylaldehyde S-methylisothiosemicarbazone) and acetylacetone did not enter the expected condensation reaction of the coordinated NH_2 group of the fragment =C(—SMe)—NH_2 with acetyleacetone. Instead, a rearrangement of the salicylaldehyde moiety and its binding to the N(4) of the above fragment took place. At the same time, the acetylacetone fragment was bound to the newly liberated N(1) nitrogen.

* Author to whom correspondence should be addressed.

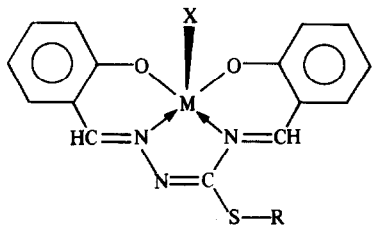

M = Ni(II), Cu(II); X = O
M = V(IV); X = O
M = Fe(III); X = Cl

I

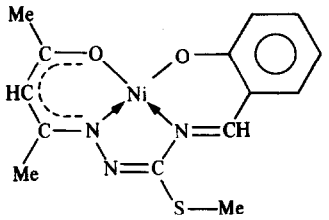

II

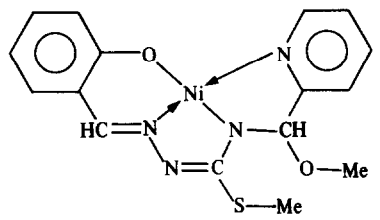

III

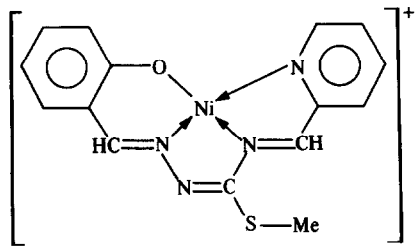

IV

As part of our studies on the synthesis and structure of transition metal complexes with the "asymmetric" quadridentate ligands based on thiosemicarbazide and the reactions of their amide groups, we describe here the synthesis, crystal and molecular structure of an Ni^{II} complex of the unexpected composition, **III**, formed with S-methyl-N(1)-salicylidene-N(4)-α-methoxypicolylisothiosemicarbazide.

EXPERIMENTAL

Chemicals and methods

The starting complex [Ni(HL)Py]Cl·0.5Py was prepared according to the procedure described earlier.[5] The α-picolinaldehyde was puriss grade (Fluka).

Nickel was determined as bis(dimethylglyoximato)nickel(II) after complex decomposition with concentrated nitric and sulphuric acid, whereas C, H and N were determined by standard micro-methods.

The IR (KBr pellet) and electronic spectra ($C = 2.5 \times 10^{-4}$ mol dm^{-3} in EtOH and Py) were recorded on a Perkin–Elmer 457 and a Cary 219 spectrophotometer, respectively.

Determination of the crystal structure

The crystal data are given in the Abstract. The complex crystallizes in the form of deep reddish prismatic rods. D_m was determined by flotation in a mixture of petroleum ether and CCl_4. Intensity data were collected from a crystal defined by the following planes/distances (between opposite faces in mm): ±100/0.046, ±010/0.082, ±001/0.360. A Philips PW 1100 four-circle diffractometer was used with the θ–2θ scanning technique, using a scan width of 1.20° and a scan rate of 0.04 s^{-1}. Unit cell parameters were obtained from least-squares analysis of the setting angles of 16 reflections with $35 \leqslant 2\theta \leqslant 56$. The space group was confirmed as $P\bar{1}$ by the structure determination. Out of 2354 reflections scanned within a hemisphere $\pm h, \pm k, l$ (h, ±11; k, 13, −14; l8) up to $\sin\theta/\lambda = 0.59$ Å^{-1}, 2157 were unique. Three standard reflections ($3\bar{3}1$, $05\bar{1}$, $\bar{1}50$) measured every 2 h showed an average variation of 1%. Corrections were applied for Lorentz and polarization effects and for absorp-

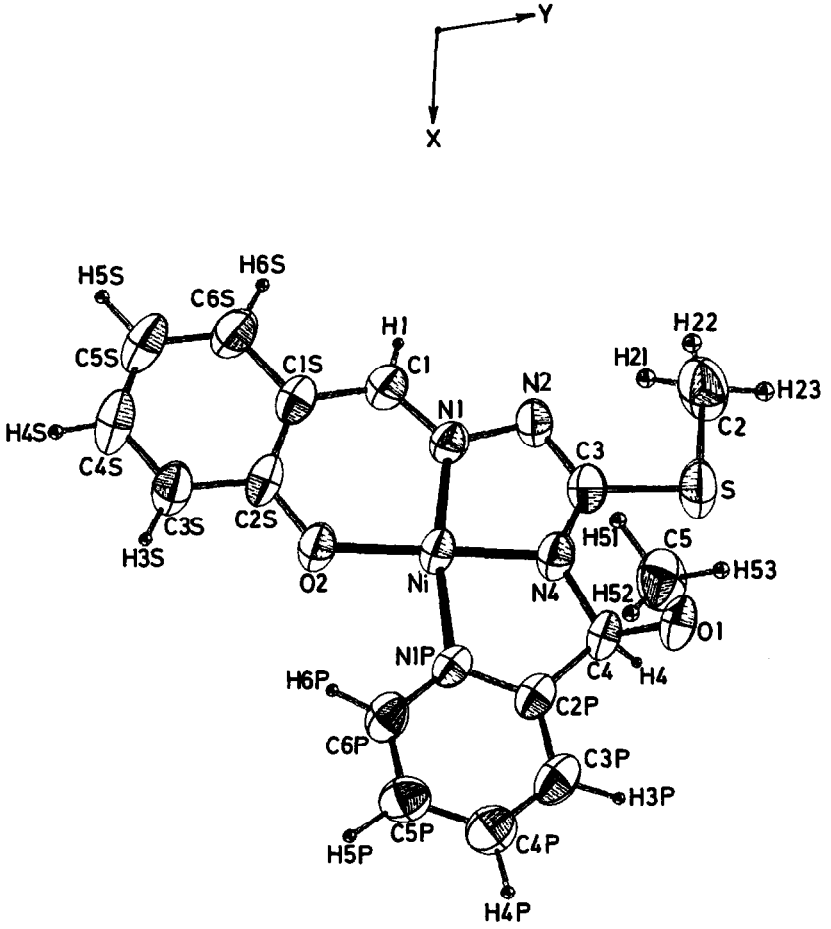

Fig. 1. An ORTEP diagram showing the complex molecule viewed along *c* and the atom numbering.

tion,[6] where transmission factors were from 0.65 to 0.87.

The structure was solved by direct methods.[7] The E map calculated with 342 largest E values ($E \geqslant 1.37$) revealed the position of all non-H atoms with the exception of six C atoms. Subsequent calculations were performed mainly with XRAY76.[8] A difference map revealed the positions of the remaining six C atoms. All H atoms were located from difference maps and theoretical calculations.

Full-matrix least-squares refinement on F was performed for 2060 reflections with $I > 3\sigma(I)$ varying separately and successive coordinates of non-H atoms, their anisotropic temperature factors and coordinates of H atoms (73, 145 and 49 parameters refined, respectively) were determined. Isotropic temperature factors of H atoms were set to be 15% greater than those belonging to corresponding carrier C atoms and were held constant. The function minimized $\Sigma(|F_o|-|F_c|)$ using unit weights gave a final R of 0.062. Goodness-of-fit was 1.22. Parameter shifts were $< 0.10\sigma$ for non-H and $< 0.21\sigma$ for H atoms. The final difference map revealed residuals which were no greater than 0.61 e Å^{-3} except for two irregular maxima of 1.59 and 1.51 e Å^{-3} near the Ni atom. Scattering factors were used from Cromer and Mann[9] for non-H and those of Stewart *et al.*[10] for H atoms; anomalous dispersion factors from Cromer and Liberman were used. All calculations were performed on a Univac 1110 computer at the University Computing Centre in Zagreb.

The complex molecule viewed along *c* with the corresponding atom numbering is shown in Fig. 1. Relevant bond lengths and angles involving non-H atoms are listed in Table 1.*

* Lists of structure factors, positional and temperature parameters, all bond lengths and angles and some mean planes have been deposited as supplementary material with the Editor, from whom copies are available on request. Atomic coordinates have also been deposited with the Cambridge Crystallographic Data Centre.

Table 1. Selected bond lengths (Å) and angles (°) of non-H atoms.

Ni—O(2)	1.831(4)	O(2)—C(2S)	1.320(6)
Ni—N(1)	1.835(5)	N(1)—N(2)	1.409(8)
Ni—N(4)	1.803(5)	N(1)—C(1)	1.274(7)
Ni—N(1P)	1.908(5)	N(2)—C(3)	1.321(7)
S—C(2)	1.803(10)	N(4)—C(3)	1.339(9)
S—C(3)	1.749(7)	N(4)—C(4)	1.443(7)
O(1)—C(4)	1.419(7)	C(1)—C(1S)	1.426(10)
O(1)—C(5)	1.402(12)	C(4)—C(2P)	1.523(10)
O(2)—Ni—N(1)	97.2(2)	Ni—N(4)—C(3)	113.5(3)
O(2)—Ni—N(4)	179.3(3)	Ni—N(4)—C(4)	120.1(5)
O(2)—Ni—N(1P)	95.4(2)	C(3)—N(4)—C(4)	125.2(5)
N(1)—Ni—N(4)	83.0(2)	Ni—N(1P)—C(2P)	114.3(4)
N(1)—Ni—N(1P)	167.3(2)	Ni—N(1P)—C(6P)	125.6(4)
N(4)—Ni—N(1P)	84.3(2)	N(1)—C(1)—C(1S)	125.2(6)
C(2)—S—C(3)	101.8(4)	S—C(3)—N(2)	120.4(5)
C(4)—O(1)—C(5)	116.0(5)	S—C(3)—N(4)	120.3(4)
Ni—O(2)—C(2S)	125.6(4)	N(2)—C(3)—N(4)	119.4(6)
Ni—N(1)—N(2)	115.9(3)	O(1)—C(4)—N(4)	114.7(6)
Ni—N(1)—C(1)	125.7(5)	O(1)—C(4)—C(2P)	112.1(1)
N(2)—N(1)—C(1)	118.4(5)	N(4)—C(4)—C(2P)	104.8(5)
N(1)—N(2)—C(3)	107.6(5)	N(1P)—C(2P)—C(4)	116.3(5)
		C(4)—C(2P)—C(3P)	122.4(5)

Preparation of the complex

0.50 g of [Ni(HL)Py]Cl · 0.5Py[5] was dissolved, by heating, in 10 cm^3 of MeOH to which was then added 1.0 cm^3 of α-picolinaldehyde. The red solution was heated mildly with stirring for about 5 min and left at room temperature for about 5 h. The deep reddish crystals obtained were filtered off and washed with MeOH and Et_2O. Yield: 0.25 g. Found: Ni, 15.0; C, 49.9; H, 4.1; N, 14.3. Calc. for $NiC_{16}H_{16}N_4O_2S$ (M_r = 388.09): Ni, 15.1; C, 49.5; H, 4.2; N, 14.4%.

RESULTS AND DISCUSSION

Synthesis and general properties of the complex

Apart from the synthesis and structure of complex **II**, also reported was the synthesis of complex I [M = Ni(II)][4], which was accomplished by the reaction of [Ni(HL)Py]Cl · 0.5Py (HL = monoanion of salicylaldehyde S-methylisothiosemicarbazone) with salicylaldehyde.

With the aim of obtaining a complex analogous to **I**, which would have the "asymmetric" quadridentate NNNO ligand, S-methyl-N(1)-salicylidene-N(4)-α-picolinylidene-isothiosemicarbazide, we tried out the reaction between a warm methanolic solution of [Ni(HL)Py]Cl · 0.5Py with α-picolinaldehyde. But, instead of complex **IV** of the form NiL*Cl (L* = monoanion of the hypothetic quadridentate ligand) we obtained the NiL complex, **III**, where L = dianion S-methyl-N(1)-salicylidene - N(4) - α - methoxypicolylisothiosemicarbazide which is also a quadridentate NNNO ligand. The formation of the corresponding ligand can be explained by the addition of a molecule of MeOH across the azomethine —CH=N(4)-linkage of the ligand of complex **IV**, formed in the initial stage of the reaction:

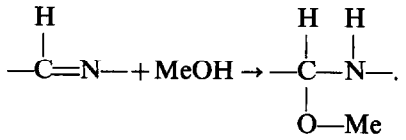

Under the given reaction conditions, the nitrogen atom is deprotonated, which together with deprotonation of the phenolic group yields a dianionic form of the ligand, i.e. leads to formation of the neutral complex NiL. Such behaviour of the azomethine group with respect to alcohols is not unknown. Analogous reactions have been observed in the case of Cu^{II} complexes with the quadridentate ligand NN′-bis(2-pyridylmethylene)ethane-1,2-diamine,[12] as well as in the case of complexes with some quinquedentate macrocyclic (Schiff base) ligands which are derivatives of 2,6-diacetylpyridine and polyfunctional diamines.[13,14] However, the case described here is, to our knowledge, the first

example of such behaviour of the azomethine group in molecules of a great number of various thiosemicarbazone-based ligands and their metal complexes.[15,16]

The complex is stable up to 170°C (when it starts to decompose). It is very soluble in $CHCl_3$ and DMF, less soluble in Me_2CO, MeOH, EtOH and Et_2O, whereas in water it is insoluble.

The molar conductivity ($C = 1 \times 10^{-3}$ mol dm^{-3} in DMF) is close to zero, which suggests the non-electrolyte nature of the complex.

Description of the structure

It is known that thiosemicarbazide and S-methylisothiosemicarbazide groups are bidentate in different ways. In binding to a metal ion both groups use the hydrazine N(1) atom, with the other coordinating atom being S and the amide N(4) atom, respectively.[16–18] In the present structure (Fig. 1) the Ni atom has a slightly distorted square-planar environment. Apart from the N(1) and N(4) atoms from the S-methylisothiosemicarbazide moiety, the pyridine N(1P) atom and the O(2) atom from the salicylaldehyde moiety are involved in coordination. The longest bond length in the coordinating sphere is the Ni—N(1P) bond length of 1.908(5) Å and the shortest is the Ni—N(4) bond length of 1.803(5) Å, involving the N(4) atom with formally negative (−1) electric charge. All these distances are in good agreement with the corresponding values observed in the structures of similar compounds having square-planar coordination around the Ni atom.[4,19–24] The coordinating atoms deviate from their mean plane within ±0.005(6) Å, the Ni atom deviating by 0.015(2) Å. The next closest atom to the Ni atom is the N(1P)^{i} atom [(i) $2-x$, $-y$, $1-z$] at a distance of 3.377(6) Å. The shortest Ni···Ni distance is Ni···Ni^{i} which is 3.739(2) Å.

Most of the complex molecule is generally planar, as the 20 atoms determining the aromatic and chelate rings deviate from their mean plane within ±0.097(7) Å. The benzene and pyridine rings are planar within ±0.008(8) and ±0.013(7) Å, respectively. The interplanar angle between them is 4.7(2)°. The atoms of the six-membered chelate ring adjacent to the benzene ring and the atom of the five-membered chelate ring adjacent to the pyridine ring deviate within ±0.028(7) and 0.024(7) Å from planarity, respectively. Deviations of the atoms of the five-membered chelate ring are somewhat greater being within ±0.051(6) Å from their mean plane.

The bond lengths involving the S-methylisothiosemicarbazide atoms are influenced differently by electron delocalization. The N(1)—N(2) 1.409(8) Å could be considered as a shortened single bond. The N(4)—C(4) bond length of 1.443(7) Å involving the C(sp^3) picoline atom is also greatly shortened. On the other hand, the formally double bond, N(2)—C(3) 1.321(7) Å (there is no peak in the difference map that might indicate the presence of a hydrogen atom in the vicinity of the N(2) atom) and formally single bond, C(3)—N(4) 1.339(9) Å, do not differ significantly, showing strong electron delocalization. A comparison of some different S-methylisothiosemicarbazide and S-methylisothiosemicarbazones metal complexes shows that N(2)—C(3) and C(3)—N(4) bonds could be formally either single or double bonds, respectively [Table 2(a)], or vice versa [Table 2(b)]. The single bonds are, with one exception,[25] always longer than the corresponding adjacent double bonds, although often not significantly. The C—S bond lengths of 1.803(10) and 1.749(7) Å involving C(sp^3) and C(sp^2) atoms, respectively, are as normal.

The methyl group (Me) and the terminal N(4) atom are *trans* with respect to the C(3)—S bond. Most of the complexes listed in Table 2(a) show a *cis* relation, while those in Table 2(b) are mostly *trans*. It means that in both cases the *trans* positions of the S—Me and formally single C(3)—N bonds are preferred. The reasons are probably steric. It is interesting to mention that of the two crystallographically different molecules in the chloro(salicylaldehyde S-methylisothiosemicarbazonato) Cu^{II} complex[29] one shows *cis* and the other a *trans* form.

No intermolecular contacts which were significantly shorter than the sums of atomic van der Waals radii were observed.

IR spectrum

The appearance and positions of the relevant bands in the IR spectrum of the complex confirmed the observed coordination of the ligand. First of all, there are no characteristic bands between 3000–4000 cm^{-1} which indicates the absence of the —NH and —OH groups, i.e. the deprotonation of these groups due to their coordination. (For the sake of the truth, the presence of two weak bands at 3080 and 3020 cm^{-1}, belonging to the ν(CH) aromatic group should be mentioned.) The presence of ν(C—O) bands of medium intensity at 1285 cm^{-1}, which in the spectrum of the non-coordinated salicylaldehyde S-methylisothiosemicarbazone are found at lower energies (1270 cm^{-1}), confirm the coordination of the phenolic oxygen.[37]

A strong band at 1630 cm^{-1} belongs to the ν(—CH=N^{1}—) of the azomethine group whereas

Table 2. Comparison between characteristic bond lengths involving N atoms of the S-methylisothiosemicarbazide moiety. *A*, *B* and *C* represent distances between N(1) and N(2), N(2) and C(3), and C(3) and N(4) atoms, respectively (subscripts s or d denote formally single or double bonds, respectively). The significance Δ/σ of the differences between the *B* and *C* values is expressed as $(|B-C|)/[\sigma^2(B)+\sigma^2(C)]^{1/2}$. The *trans* or *cis* relationships of the terminal N(4) atom and methyl group with regard to the C(3)—S bond are indicated in parentheses next to the corresponding reference number

(a)	A_s	B_s	C_d	Δ/σ	Reference
	1.377(8)	1.371(9)	1.292(9)	6.2	26 (*cis*)
	1.429(12)	1.315(12)	1.284(12)	1.8	17 (*cis*)
	1.392(7)	1.334(8)	1.292(8)	3.7	27 (*trans*)
	1.371(11)	1.343(11)	1.311(13)	1.9	28 (*trans*)
	1.39(1)	1.33(2)	1.30(2)	1.1	29 (*cis*)
	1.39(2)	1.35(2)	1.29(2)	2.1	29 (*trans*)
	1.408(11)	1.352(12)	1.282(12)	4.1	30 (*cis*)
	1.389(12)	1.365(13)	1.305(12)	3.4	30 (*cis*)
	1.44(4)	1.37(4)	1.27(4)	1.8	30 (*cis*)
	1.44(3)	1.34(4)	1.31(4)	0.5	30 (*cis*)
	1.40(1)	1.33(1)	1.34(1)	0.7	25 (*trans*)
	1.387(4)	1.364(6)	1.265(5)	12.7	31 (*cis*)
	1.403(5)	1.337(6)	1.297(6)	4.7	32 (*cis*)
	1.398(5)	1.337(6)	1.299(6)	4.5	32 (*cis*)
(b)	A_s	B_d	C_s	Δ/σ	Reference
	1.405(8)	1.309(9)	1.321(9)	0.9	33 (*cis*)
	1.40(1)	1.30(1)	1.40(1)	7.1	2 (*trans*)
	1.452(12)	1.313(12)	1.344(12)	1.8	18 (*cis*)
	1.393(7)	1.314(8)	1.386(7)	6.8	34 (*trans*)
	1.407(7)	1.281(8)	1.394(7)	10.6	34 (*trans*)
	1.41(1)	1.30(2)	1.40(1)	4.5	35 (*trans*)
	1.382(12)	1.272(12)	1.430(12)	9.3	36 (*trans*)
	1.374(13)	1.324(13)	1.411(12)	4.9	4 (*trans*)
	1.409(8)	1.321(7)	1.339(9)	1.6	This work(*trans*)

another band, which is also strong, at 1600 cm^{-1} corresponds to vibrations of the benzene, i.e. pyridine ring.[38,39] The low-frequency (< 650 cm^{-1}) coordination-sensitive bands belonging to the pyridine ring deformations, observed for the non-coordinated pyridine at 604 (in-plane ring deformation) and 405 cm^{-1} (out-of-plane deformation)[40] are shifted towards higher energies by about 25 and 45 cm^{-1}, respectively, upon coodination. The characteristic ν_{as}(≡C—O—CH_3) band of the ether group appears at 1070 cm^{-1}, while the ν_s of the same group is missing since this group is not active.[38] Finally, the CH bands of —O—CH_3 and —S—CH_3 appear at 2940 (ν_{as}), 2040 (ν_s), and 1460 (δ_{as}) and 1370 cm^{-1} (δ_s).[38]

Electronic spectrum

The position and intensity of the *d–d* transitions at *ca* 26,600 (ε = 1120) amd 26,000 cm^{-1} (ε = 1870) (with a shoulder at 25,000 cm^{-1}) in the spectrum recorded in EtOH and Py, respectively, indicate that the square-planar structure of the complex is also preserved in solution.[41] As the position of the band is practically identical in the two solvents, and no absorption below 24,000 cm^{-1} [42,43] is observed (in both spectra a shoulder appears at about 25,000 cm^{-1}), it can be concluded that the coordination number of Ni^{II} has not been changed even in the presence of Py as a strong electron donor, which points to a strong ligand field of the chelate ligands.

Another support for the square-planar structure of the complex is its diamagnetism and the dark red colour of its solution.

Acknowledgements—The authors thank M. Bruvo MSc (Department for General and Inorganic Chemistry, Faculty of Science, Zagreb) for collecting the diffractometric data. This investigation was supported by the Scientific

Fund of SAP Vojvodina and the Research Council of Croatia.

REFERENCES

1. N. V. Gerbeleu, *Reaktsii na Matritsakh.* Shtiintsa, Kishinev (1980).
2. M. A. Yampol'skaya, S. G. Shova, N. V. Gerbeleu, V. K. Bel'skii and Yu. A. Simonov, *Zh. Neorg. Khim.* 1982, **27**, 2551.
3. V. G. Rusu, N. V. Gerbeleu and M. D. Revenko, *Zh. Neorg. Khim.* 1987, **32**, 2169 and refs therein.
4. V. M. Leovac, V. Divjaković, V. I. Češljević and P. Engel, *Polyhedron* 1987, **6**, 1901.
5. V. M. Leovac, D. M. Petrović, D. Z. Obadović and N. V. Gerbeleu, *Z. Anorg. Allg. Chem.* 1984, **512**, 211.
6. S. Harkema, *ACXR. Absorption Program for Use in Connection with a PW 1100 Diffractometer.* Proceedings of an International Summer School on Crystallographic Computing, Twente, The Netherlands—Working Sessions and Program Market (1978).
7. P. Main, S. J. Fiske, S. E. Hull, L. Lessinger, G. Germain, J.-P. Declercq and M. M. Woolfson, *MULTAN80. A System of Computer Programs for the Automatic Solution of Crystal Structures from X-ray Diffraction Data.* Universities of York, U.K. and Louvain, Belgium (1980).
8. J. M. Stewart, P. A. Machin, C. W. Dickinson, H. L. Ammon, H. Heck and H. Flack, *The XRAY76 System.* Tech. Rep. TR-446. Computer Center, University of Maryland, College Park, Maryland, U.S.A. (1976).
9. D. T. Cromer and J. B. Mann, *Acta Cryst.* 1968, **A24**, 321.
10. R. F. Stewart, E. R. Davidson and W. T. Simpson, *J. Chem. Phys.* 1965, **42**, 3175.
11. D. T. Cromer and D. Liberman, *J. Chem. Phys.* 1970, **53**, 1891.
12. C. M. Harris and E. D. McKenzie, *J. Chem. Soc.* (*A*) 1969, 746.
13. C. Cairns, G. McFall, S. M. Nelson and M. G. B. Drew, *J. Chem. Soc., Dalton Trans.* 1979, 446.
14. D. H. Cook and D. E. Fenton, *Inorg. Chim. Acta* 1977, **25**, 95.
15. S. Padhye and G. B. Kauffman, *Coord. Chem. Rev.* 1985, **63**, 127.
16. M. J. M. Campbell, *Coord. Chem. Rev.* 1975, **15**, 279.
17. V. Divjaković and V. Leovac, III Congresso Italo–Yugoslavo, p. 68. Parma (1979).
18. V. Divjaković, V. M. Leovac and B. Ribár, *Rev. Res. Fac. Sci. Novi Sad* 1983, **13**, 25.
19. E. Gyepes, F. Pavelčik and A. Beno, *Coll. Czech. Chem. Commun.* 1981, **46**, 975.
20. F. S. Stephens and R. S. Vagg, *Inorg. Chim. Acta* 1984, **90**, 17.
21. N. A. Bailey, E. D. McKenzie and J. M. Worthington, *Inorg. Chim. Acta* 1980, **46**, 145.
22. E. Carmona, F. González, M. L. Poveda, J. L. Atwood and R. D. Rogers, *J. Chem. Soc., Dalton Trans.* 1981, 777.
23. M. Mulqi, F. S. Stephens and R. S. Vagg, *Inorg. Chim. Acta* 1981, **52**, 73.
24. F. S. Stephens and R. S. Vagg, *Inorg. Chim. Acta* 1982, **57**, 9.
25. V. Divjaković, V. M. Leovac, B. Ribár, Gy. Argay and A. Kálmán, *Acta Cryst.* 1982, **B38**, 1738.
26. D. Petrović, B. Ribár, S. Carić and V. Leovac, *Z. Krist.* 1979, **150**, 3.
27. D. Petrović, S. Carić, V. Leovac and V. Canić, *Cryst. Struct. Commun.* 1979, **8**, 617.
28. D. Petrović, V. M. Leovac and D. Lazar, *Cryst. Struct. Commun.* 1981, **10**, 823.
29. V. N. Biyushkin, V. I. Gerasimov and N. V. Belov, *Kristallographiya* 1981, **26**, 323.
30. V. Divjaković, B. Ribár, V. M. Leovac and N. V. Gerbeleu, *Z. Krist.* 1981, **154**, 83.
31. V. M. Leovac, V. Divjaković, D. Petrović, G. Argay and A. Kálmán, *Polyhedron* 1983, **2**, 1307.
32. Yu. A. Simonov, V. K. Bel'skii, N. V. Gerbeleu, S. G. Shova and V. B. Arion, *Dokl. Akad. Nauk SSSR* 1985, **282**, 620.
33. B. Ribár, A. Kozmidis-Petrović and V. Leovac, *Cryst. Struct. Commun.* 1980, **9**, 1237.
34. M. A. Yampol'skaya, S. G. Shova, N. V. Gerbeleu, Yu. A. Simonov, V. K. Bel'skii and A. A. Dvorkin, *Zh. Neorg. Khim.* 1983, **28**, 1744.
35. Yu. A. Simonov, M. A. Yampol'skaya, S. G. Shova, V. K. Bel'skii and N. V. Gerbeleu, *Dokl. Akad. Nauk SSSR* 1985, **282**, 895.
36. Yu. A. Simonov, N. V. Gerbeleu, M. D. Revenko, S. G. Shova, V. E. Zavodnik and V. G. Rusu, *Kristalographiya* 1985, **30**, 1090.
37. V. M. Leovac, L. Bjelica and Lj. Jovanović, *Polyhedron* 1985, **4**, 233.
38. K. Nakanishi, *Infrared Absorption Spectroscopy.* Holden-Day, San Francisco (1962).
39. C. M. Harris and E. D. McKenzie, *J. Chem. Soc.* (*A*) 1969, 746.
40. K. Nakamoto, *Infrared and Raman Spectra of Inorganic and Coordination Compounds.* John Wiley, New York (1986).
41. A. B. P. Lever, *Inorganic Electronic Spectroscopy.* Elsevier, Amsterdam (1968).
42. L. Sacconi, P. Nannelli, N. Nardi and U. Campigli, *Inorg. Chem.* 1965, **4**, 943.
43. C. A. Root and D. H. Busch, *Inorg. Chem.* 1968, **7**, 789.

Polyhedron Vol. 7, No. 24, pp. 2649–2653, 1988
Printed in Great Britain

0277–5387/88 $3.00+.00
© 1988 Pergamon Press plc

THE SYNTHESIS OF NOVEL SCHIFF BASE BIS- AND TRIS-CROWN ETHER LIGANDS CONTAINING RECOGNITION SITES FOR ALKALI AND TRANSITION METAL GUEST CATIONS

PAUL D. BEER* and CHRISTOPHER G. CRANE

Department of Chemistry, University of Birmingham, P.O. Box 363, Birmingham B15 2TT, U.K.

(*Received* 29 *February* 1988; *accepted* 27 *May* 1988)

Abstract—New Schiff base bis- and tris-benzo crown ether ligands containing recognition sites for alkali and transition metal guest cations have been prepared. Preliminary coordination studies of these ligands with sodium and copper(I) guest cations have led to the successful isolation of mono- and heteropolymetallic complexes.

The design and synthesis of macropolycyclic molecules containing more than one recognition site for binding several guest species is of considerable current interest in the chemical literature.[1–5] These multi-site receptors may exhibit allosteric properties[5–7] by binding sequentially two or more guest metal cations in close proximity to one another. The resulting polynuclear complexes may facilitate electron transfer studies and serve as models of relevance to biological redox processes. We report here the preparation of a bis-benzo crown ether ligand (**3**) containing a Schiff base dithia linkage and a tris-benzo crown ether (**5**) constructed using a tren bridging moiety.

RESULTS AND DISCUSSION

The condensation of 1,8-diamino-3,6-dithiaoctane (**1**)[8] with two moles of 4-formylbenzo-15-crown-5 (**2**)[9] gave the Schiff base bis-crown ether (**3**) as a white crystalline solid in excellent yields (Scheme 1). The tris-benzo crown ether (**5**) was synthesized by reacting tren (**4**) and three moles of **2** (Scheme 2). Both structures were verified by elemental analysis, mass spectrometry and ^{1}H and ^{13}C NMR spectroscopy (Tables 1–3). The two ligands, **3** and **5**, each contain one recognition site for a transition metal and, respectively, two and three crown ether sites for alkali metal cations.

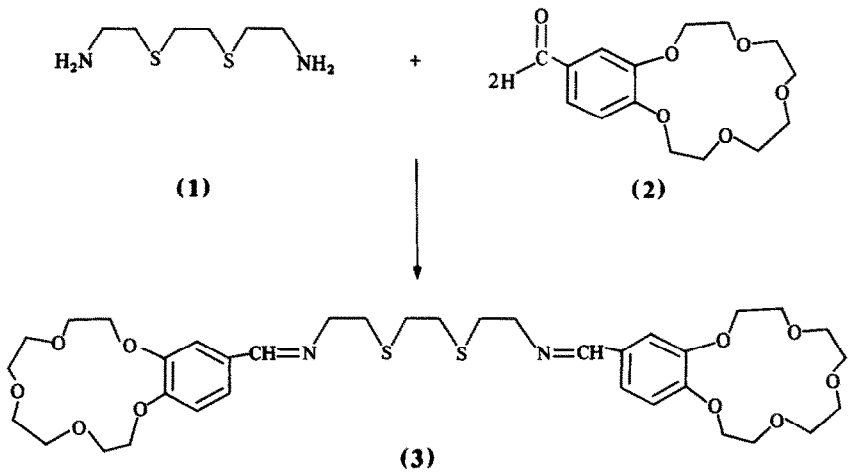

(1) (2) (3)

Scheme 1.

* Author to whom correspondence should be addressed.

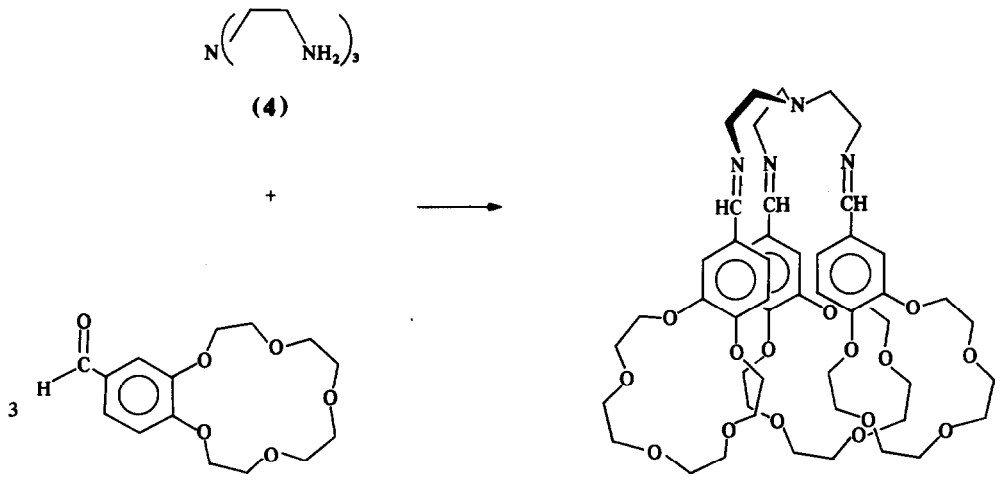

(4) (3) (5)

Scheme 2.

Refluxing **3** with an excess of sodium hexafluorophosphate in acetonitrile led to the successful isolation of a crystalline complex $3 \cdot 2Na^+PF_6^-$. Similarly with **5** and sodium hexafluorophosphate a complex of stoichiometry $5 \cdot 3NaPF_6$ was obtained. These results suggest the respective two and three benzo-15-crown-5 moieties of **3** and **5** are acting independently of one another, each complexing a sodium cation.

The reaction of $Cu^I(CH_3CN)_4PF_6$[10] with both ligands gave the corresponding diamagnetic copper(I) complexes as pale yellow solids. Comparing the respective solution ^{13}C NMR spectra of the ligands and their copper(I) complexes (Tables 2 and 3) reveals that upon complexation, shifts of the NCH_2, SCH_2 and HC=N carbons by up to 4 ppm result. Little change in the positions of the OCH_2 crown absorptions were evident suggesting tetrahedral coordination of the copper(I) cation in both complexes. Subsequent complexation of the copper(I) complexes with sodium gave the respective hetero-polymetallic complexes **6** and **7**, with the copper(I) cation in a tetrahedral coordination environment and the sodium cations bound in the benzo crown ether moieties. The imine stretching frequencies of the free ligands, the corresponding copper(I) and copper(I)–sodium complexes are reported in Table 4. As expected, shifts of the imine stretching frequencies to lower wavenumbers are observed on complexation of copper(I). It is noteworthy that the subsequent binding of sodium at the respective benzo crown ether recognition sites

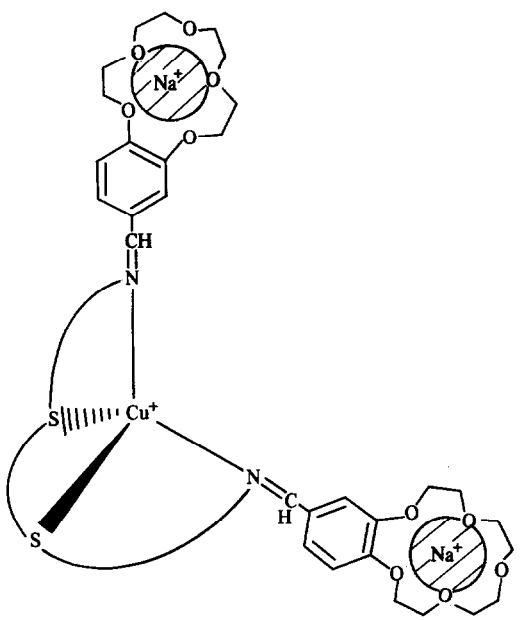

(6)

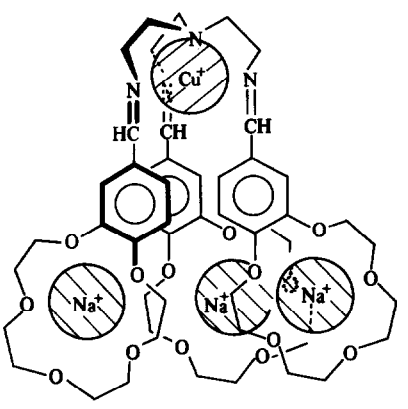

(7)

Table 1. ^{1}H NMR data ($CDCl_3$) of (3) and (5), respectively

	Proton	δ (ppm)	Integration
(3)	Imine	8.15 (s)	2
	Aromatics	7.34–6.82 (m)	6
	Crown-OCH_2, =NCH_2	3.70–4.18 (m)	36
	NCH_2CH_2S	2.83 (t, J = 6 Hz)	4
	SCH_2CH_2S	2.76 (s)	4
(5)	Imine	8.04 (s)	3
	Aromatics	7.29 (s)	3
		6.99 (d, J = 8 Hz)	3
		6.80 (d, J = 8 Hz)	3
	Crown-OC$_2$ =NCH_2	3.60–4.20 (m)	54
	NCH_2	2.91 (t, J = 6 Hz)	6

of both copper(I) complexes induces further shifts to lower wavenumbers of ν(C=N) suggesting the bound alkali metal cations are influencing the electron density at the respective co-bound copper(I) metal centres. Detailed electrochemical studies of these and related polymetallic complexes are in progress to investigate the prospect of tuning the bound transition metal redox centre to certain redox potentials via the binding of one or more Group 1A and Group IIA metal cations at the benzo crown ether moieties.

Table 2. ^{13}C NMR data ($CDCl_3$) of (3) and (3)·Cu^IPF_6

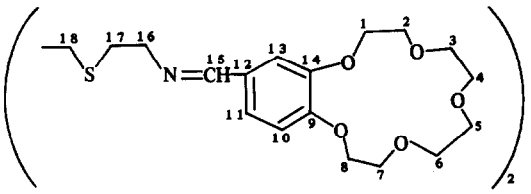

δ (ppm) of (3)	Assignment	(3)·Cu^IPF_6
32.65	C^{18}	32.09
33.10	C^{17}	33.39
61.62	C^{16}	60.15
68.80	Crown-OCH$_2$ (C^1–C^8)	68.50
69.45		69.16
70.43		70.30
71.14		70.88
111.43	C^{10}, C^{13}	112.54
112.73		113.84
123.43	C^{11}	124.18
129.54	C^{12}	126.10
144.34	C^9, C^{14}	148.63
151.59		153.15
161.73	C^{15}	165.80

Table 3. ^{13}C NMR data ($CDCl_3$) of (5) and (5)·Cu^IPF_6

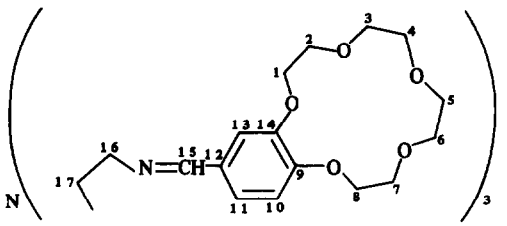

δ (ppm) of (5)	Assignment	δ (ppm) of (5)·Cu^IPF_6
55.93	C^{17}	53.78
59.99	C^{16}	60.87
68.84	Crown-OCH$_2$ (C^1–C^8)	68.77
69.44		69.13
70.43		70.27
71.14		70.95
111.27	C^{10}, C^{13}	112.60
112.76		115.16
123.10	C^{11}	122.16
129.90	C^{12}	126.52
149.25	C^9, C^{14}	149.21
151.29		152.95
161.31	C^{15}	162.84

EXPERIMENTAL

General

^{1}H NMR spectra were recorded at 400 MHz, 270 MHz and ^{13}C NMR spectra at 67.8 and 100 MHz using TMS as internal standard. 1,8-Diamino-3,6-dithiaoctane,[8] 4-formylbenzo-15-crown-5[9] and $Cu^I(CH_3CN)_4PF_6$[10] were prepared according to literature methods. Acetonitrile was dried by distillation from calcium hydride and ethanol by distillation from magnesium ethoxide.

Syntheses

Preparation of **3**. To a stirred solution of 1,8-diamino-3,6-dithiaoctane (**1**) (0.65 g, 3.61 mmol) in dry ethanol (80 cm^3), 4-formylbenzo-15-crown-5 (**2**) (2.14 g, 7.21 mmol) was added in small portions. The resulting mixture was stirred for a further 3 h at ambient temperature and the precipitated white solid product, **3**, was filtered off, washed with

Table 4. Microanalytical and selected IR data

Compound	Analysis[a] (%) C	H	N	C=N frequency[b] (cm^{-1})
(3)	58.5(58.7)	7.1(7.1)	3.5(3.8)	1640
(5)	62.5(62.4)	7.2(7.4)	5.8(5.7)	1640
(3)·2NaPF$_6$	40.0(40.3)	4.9(4.9)	2.9(2.6)	1635
(5)·3NaPF$_6$	41.1(41.3)	5.2(4.9)	4.1(3.8)	1635
(3)·Cu^{I}PF$_6$	45.4(45.7)	5.5(5.5)	3.1(3.0)	1620
(5)·Cu^{I}PF$_6$	51.2(51.5)	5.8(6.1)	4.6(4.7)	1630
[(3)·Cu^{I}2Na]$^{3+}$(PF$_6^-$)$_3$	34.5(33.7)	4.6(4.1)	3.0(2.2)	1615
[(5)·Cu^{I}3Na]$^{4+}$(PF$_6^-$)$_4$	35.7(36.2)	4.6(4.3)	3.7(3.3)	1620

[a] Calculated values given in parentheses.
[b] KBr disc (± 2 cm^{-1}).

diethyl ether and dried *in vacuo*. Yield = 2.39 g, 90%, m.p. 98–99°C. Found: C, 58.5; H, 7.1; N, 3.5. Calc. for $C_{36}H_{52}N_2O_{10}S_2$: C, 58.7; H, 7.1; N, 3.8%. $m/z = 736$.

Preparation of **5**. 4-Formyl benzo-15-crown-5 (**2**) (0.5 g, 1.69 mmol) was dissolved in dry ethanol (50 cm^3) and tren (**4**) (0.082 g, 0.56 mmol) dissolved in ethanol (10 cm^3) added all at once. The resulting homogeneous solution was refluxed for 2 h and allowed to return to ambient temperature overnight. The solvent was removed to leave an oil which was azeotroped with dry toluene (2×20 cm^3). The resulting pale yellow solid was recrystallized from a dichloromethane–hexane mixture. Yield = 0.54 g, 98%, m.p. 83–85°C. Found: C, 62.5; H, 7.2; N, 5.8. Calc. for $C_{51}H_{72}N_4O_{15}$: C, 62.4; H, 7.4; N, 5.7%. $m/z = 980$.

Preparation of (**3**)·2NaPF$_6$. **3** (0.1 g, 0.136 mmol) and NaPF$_6$ (46 mg, 0.27 mmol) were dissolved in dry acetonitrile (30 cm^3) and stirred at room temperature for 2 h. The solvent was removed and the residue washed with hexane. Recrystallization from tetrahydrofuran–hexane gave the product complex. Yield = 70 mg, 48%, m.p. 89–91°C.

Preparation of (**5**)·3NaPF$_6$. **5** (0.1 g, 0.102 mmol) and NaPF$_6$ (51 mg, 0.306 mmol) were dissolved in dry acetonitrile (30 cm^3). The resulting solution was stirred at room temperature for 2 h and the solvent removed *in vacuo*. The residue was washed with heptane to give a white solid. Yield = 74 mg, 50%, m.p. 150–153°C.

Preparation of (**3**)·Cu^{I}PF$_6$. A solution of **3** (0.3 g, 0.41 mmol) and Cu^{I}(CH$_3$CN)$_4$PF$_6$ (0.15 g, 0.41 mmol) in dry acetonitrile (40 cm^3) was refluxed for 2 h. Removal of solvent *in vacuo* gave a pale yellow foaming solid which was recrystallized from acetonitrile. Yield = 0.34 g, 87%, m.p. 90–94°C. Magnetic susceptibility measurements showed the complex to be diamagnetic. ^{1}H NMR ($CDCl_3$): δ 2.96 (s, 4H), 3.70–4.1 (m, 40H), 6.76 (d, $J = 8$ Hz, 2H), 7.48–7.50 (m, 4H), 8.47 (s, 2H).

Preparation of (**5**)·Cu^{I}PF$_6$. A solution of **5** (0.5 g, 0.51 mmol) and Cu^{I}(CH$_3$CN)$_4$PF$_6$ (0.19 g, 0.51 mmol) in dry acetonitrile (60 cm^3) was refluxed for 2 h. Removal of solvent *in vacuo* and washing with ethanol gave a yellow solid. Yield = 0.48 g, 80%, m.p. 201–204°C. Magnetic susceptibility measurements showed the complex to be diamagnetic. ^{1}H NMR ($CDCl_3$): δ 3.08 (s, 6H), 3.64 (s, 6H), 3.70–4.0 (m, 48H), 6.23 (d, $J = 8$ Hz, 3H), 7.39 (s, 3H), 7.87 (d, $J = 8$ Hz, 3H), 8.32 (s, 3H).

Preparation of [(**3**)·Cu^{I}2Na](PF$_6$)$_3$. (**3**)·Cu^{I}PF$_6$ (0.1 g, 0.106 mmol) and NaPF$_6$ (36 mg, 0.22 mmol) were dissolved in dry acetonitrile (30 cm^3) under nitrogen. The resulting solution was stirred at room temperature for 2 h and the solvent removed *in vacuo*. The residue was washed with ethanol and heptane to give a lemon-yellow solid. Yield = 96 mg, 71%, m.p. 188–190°C.

Preparation of [(**5**)·Cu^{I}3Na](PF$_6$)$_4$. (**5**)·Cu^{I}PF$_6$ (0.1 h, 8.4×10^{-2} mmol) was dissolved in dry acetonitrile (30 cm^3) and excess sodium hexafluorophosphate added (0.042 g, 0.25 mmol). The resulting solution was stirred at room temperature for 2 h. Removal of solvent *in vacuo* and washing with ethanol and heptane gave a yellow solid. Yield = 0.084 g, 59%, m.p. 164–166°C.

Acknowledgements—We thank the SERC for financial support and for use of the high field NMR service at the

University of Warwick. We also thank The Research Corporation Trust, L. and D. Blond for additional financial support.

REFERENCES

1. J. C. Chambron and J. P. Sauvage, *Tetrahedron Lett.* 1986, **27**, 865.
2. J. Rebek Jr, J. E. Trend, R. V. Wattley and S. Chakravorti, *J. Am. Chem. Soc.* 1979, **101**, 4333.
3. B. A. Boyce, A. Carroy, J. M. Lehn and D. Parker, *J. Chem. Soc., Chem. Commun.* 1984, 1546.
4. A. D. Hamilton and P. Kazanjian, *Tetrahedron Lett.* 1985, **26**, 5735.
5. P. D. Beer, *J. Chem. Soc., Chem. Commun.* 1986, 1678.
6. J. Rebek Jr, *Acc. Chem. Res.* 1984, **17**, 258.
7. P. D. Beer and A. S. Rothin, *Polyhedron* 1988, 7, 137.
8. F. P. J. Dwyer and F. Lions, *J. Am. Chem. Soc.* 1950, **72**, 1545.
9. E. M. Hyde, B. L. Shaw and I. Shephard, *J. Chem. Soc., Dalton Trans.* 1978, 1696.
10. G. J. Kubas, B. Monzya and A. L. Crubless, *Inorg. Synth.* 1971, **19**, 90.

Polyhedron Vol. 7, No. 24, pp. 2655–2658, 1988
Printed in Great Britain

0277–5387/88 $3.00+.00
© 1988 Pergamon Press plc

INTERACTION OF TITANIUM AND TIN CHLORIDES IN TETRAHYDROFURAN. THE X-RAY CRYSTAL STRUCTURE OF [*TRANS*-$TiCl_2(THF)_4$]$^+$[$SnCl_5(THF)$]$^-$ *

ZOFIA JANAS, PIOTR SOBOTA† and TADEUSZ LIS

Institute of Chemistry, University of Wrocław, 14 Joliot-Curie, 50-383 Wrocław, Poland

(*Received* 19 *February* 1988; *accepted* 27 *May* 1988)

Abstract—The direct reaction between [$TiCl_4(THF)_2$] and $SnCl_2$ in tetrahydrofuran (THF) yields the green paramagnetic salt [*trans*-$TiCl_2(THF)_4$][$SnCl_5(THF)$]. The same compound is also formed in the reaction between [$TiCl_3(THF)_3$] and $SnCl_4$ in THF. Crystals of the title compound are monoclinic with $a = 8.442(4)$, $b = 21.589(9)$, $c = 9.262(5)$ Å, $\beta = 107.91(5)°$, $Z = 2$, space group $P2_1/m$. Both metal ions are in an octahedral environment. The titanium atom in the cation [$TiCl_2(THF)_4$]$^+$ lies on the symmetry centre. The tin atom in [$SnCl_5(THF)$]$^-$ is located on the mirror plane.

Much current research on a super high activity catalyst for the polymerization of olefins is focused on the relationship between different types of surface vacancy on $MgCl_2$ or $TiCl_3$ and polymerization reactivity and selectivity.[1] Attempts to understand the role of $MgCl_2$ as a catalyst support have suffered from the unusual experimental limitations associated with the study of heterogeneous versus homogeneous chemical systems. In solvents having donor properties, e.g. in tetrahydrofuran, the reaction between $MgCl_2$ and $TiCl_4$ proceeds easily. Three different complex compounds, [$Mg(THF)_6$][$TiCl_5(THF)$]$_2$, [$(THF)_4Mg(\mu\text{-}Cl)_2TiCl_4$] and [$Mg_2(\mu\text{-}Cl)_3(THF)_6$][$TiCl_5(THF)$] may be obtained depending upon the molar ratio in which they are combined.[2] The compounds are very good precursors for the ethylene polymerization catalyst.[3] On the other hand, $TiCl_3$ and $MgCl_2$ in THF do not react mutually because, in the simplest sense, the acid–basic properties of $TiCl_3$ and $MgCl_2$ are similar. It was found, however, that $TiCl_3$ reacts with stronger acids than $MgCl_2$ e.g. $ZnCl_2$ to form [*trans*-$TiCl_2(THF)_4$][$ZnCl_3(THF)$].[4]

$$[TiCl_3(THF)_3] + ZnCl_2 \xrightarrow{THF} [\textit{trans}\text{-}TiCl_2(THF)_4][ZnCl_3(THF)]. \quad (1)$$

It was interesting to scrutinize the reaction between $TiCl_4$ and the other main group element chlorides, e.g. tin. The tin compounds were widely applied dozens of years ago, by Montedison Spa as a catalyst for olefin polymerization. For this reason it was interesting to study the synthesis of the tin–titanium compounds i.e. compounds containing two different active centres.

We now report the reaction between tin and titanium chlorides. It was found that $TiCl_4$ with $SnCl_2$ and $TiCl_3$ with $SnCl_4$, in THF, form the same $TiSnCl_7(THF)_5$ compound. The X-ray crystal structure of this compound is described.

EXPERIMENTAL

All manipulations were carried out under N_2 using dried solvents and Schlenk techniques. [$TiCl_4(THF)_2$] and [$TiCl_3(THF)_3$] were obtained by the literature method.[5] Anhydrous $SnCl_4$ and $SnCl_2$ were commercial materials and microanalyses were performed at the University of Wrocław.

Preparation of [*trans*-$TiCl_2(THF)_4$][$SnCl_5(THF)$]

(a) A solution of [$TiCl_4(THF)_2$] (1.43 g, 4.27 mmol) in 30 cm^3 of tetrahydrofuran and 0.41 g (2.13 mmol) of non-aqueous $SnCl_2$ in 20 cm^3 of THF were mixed and left at room temperature. During 12 h the solution changed its colour from orange via green to violet and the green crystals settled

* Dichlorotetrakis(tetrahydrofuran)titanate (IV) pentachloro(tetrahydrofuran)stannate (IV).

† Author to whom correspondence should be addressed.

down. The compound was filtered off under dinitrogen, washed with THF (3×10 cm^3) and dried *in vacuo*. Yield 0.90 g (54%). After condensation of a solution to 15 cm^3, the crystalline $[TiCl_3(THF)_3]$ was isolated from a filtrate. Found: Ti, 6.2; Sn, 15.5; Cl, 32.0. Calc. for $TiSnCl_7(THF)_5$: Ti, 6.2; Sn, 15.3; Cl, 32.0%.

(b) The mixture of $[TiCl_3(THF)_3]$ (1.21 g, 3.25 mmol) and $[SnCl_4(THF)_2]$ (1.31 g, 3.25 mmol) in 50 cm^3 of THF was heated under reflux and N_2 for 6 h and a fine-crystalline blue compound settled down. After cooling the reaction mixture to room temperature the precipitate was filtered off and washed with THF (3×10 cm^3). The yield of 1.6 g (58%) could be increased above 80%, by condensation of the filtrate *in vacuo*. Found: Ti, 5.7; Sn, 14.7; Cl, 29.4. Calc. for $TiSnCl_7(THF)_5$: Ti, 6.2; Sn, 15.3; Cl, 32.0%. The quantitative composition and IR spectrum of the blue crystalline compound is analogous to that of the compound synthesized by method (a).

The crystals for X-ray examination were taken from the post-reaction mixture directly obtained by method (a). The density was measured by flotation in a 1,2-dibromoethane and hexane mixture.

X-ray structure analysis of [*trans*-$TiCl_2(THF)_4$][$SnCl_5(THF)$]

Crystal data. $[TiCl_2(C_4H_8O)_4][SnCl_5(C_4H_8O)]$: $M = 775.4$, monoclinic, $U = 1606$ Å^3, $Z = 2$, $D_c = 1.60$ g cm^{-3}, $D_o = 1.58$ g cm^{-3}, space group $P2_1/m$, Mo-K_α radiation, $\lambda = 0.71069$ Å, $\mu = 16.4$ cm^{-1}.

A specimen ($0.2 < 2R < 0.3$ mm) was cut from a large crystal and sealed in a capillary tube. A Syntex $P2_1$ diffractometer, Mo-K_α radiation and a graphite monochromator were used for the lattice parameters and intensity measurements at $T = 300(2)$ K. Intensities were measured by 2θ–ω scan techniques up to $2\theta = 56°$. The intensity of two standard reflections, which were monitored after every 50 intensity scans, decreased by approximately 5% over the period of data collection. No corrections for crystal decomposition were applied. From 3977 measured reflections, 2317 with $I > 3\sigma(I)$ were used for structure determination. Preliminary examination by Weissenberg photographs showed the space group to be $P2_1$ or $P2_1/m$. The structure was solved by the heavy-atom method. The Sn and Ti atoms were found from a Patterson map, and the centrosymmetric space group $P2_1/m$ was assumed. All other non-H atoms were found from successive difference-Fourier syntheses. Sixteen H atoms were included in geometrically calculated positions. Full-matrix least-squares refinements gave $R = 0.051$ and $R_w = 0.058$. All calculations were made on a NOVA 1200 computer with a locally modified Syntex XTL/XTLE structure determination system.[6] Anomalous dispersion corrections were included for all non-H atoms. The final difference Fourier synthesis showed the highest peak of 0.56 e Å^3 and the maximum Δ/σ was 0.3.*

RESULTS AND DISCUSSION

The addition of $SnCl_2$ to $[TiCl_4(THF)_2]$ at a 1 : 1 molar ratio in tetrahydrofuran results in a colour change of the solution from orange via green to violet and the air-sensitive green crystals formulated as $TiSnCl_7(THF)_5$ precipitated from the solution. After 4 h this was filtered off. A blue known $[TiCl_3(THF)_3]$ compound precipitated from the filtrate overnight.

The IR spectrum of $TiSnCl_7(THF)_5$ presents the stretching ν_{Ti-Cl} and ν_{Sn-Cl} modes at 290 (sh), 303 (vs), 320 (sh) and 390 cm^{-1} (vs), as well as the symmetric and asymmetric ν_{C-O-C} vibrations of the coordinated THF molecules at 838 (vs,br), 927 (vs) and 1038 cm^{-1} (m). The compound is paramagnetic, its magnetic moment is equal to 1.61 BM at room temperature.

$$2[TiCl_4(THF)_2] + SnCl_2 \xrightarrow[293K]{THF} [trans\text{-}TiCl_2(THF)_4][SnCl_5(THF)] + [TiCl_3(THF)_3]. \quad (2)$$

The crystals of $TiSnCl_7(THF)_5$ consist of $[TiCl_2(THF)_4]^+$ cations and $[SnCl_5(THF)]^-$ anions. The selected bond lengths and angles are summarized in Table 1. The structure of the $[TiCl_2(THF)_4]^+$ cation is shown in Fig. 1(a). The titanium atom, which occupies the centre of symmetry, is octahedrally surrounded by two chlorine atoms and four tetrahydrofuran molecules. The Ti—Cl bond length of 2.333(2) Å is comparable to values of 2.366(3) and 2.400(2) Å in [*trans*-$TiCl_2(THF)_4$][$ZnCl_3(THF)$][4] and the [*trans*-$TiCl_2(H_2O)_4]^+$ cation in the $Cs_2TiCl_5 \cdot 4H_2O$ compound,[7] respectively. However, the Ti–water bond length of 2.040(6) Å is somewhat shorter than the Ti—O distances of 2.067(6) and 2.126(5) Å in the compound under investigation.

* Atomic coordinates, displacement factor coefficients, full lists of bond lengths and angles and lists of F_o/F_c values have been deposited as supplementary data with the Editor, from whom copies are available on request. Atomic coordinates have also been deposited with the Cambridge Crystallographic Data Centre.

Table 1. Selected bond lengths (Å) and angles (°) for [*trans*-$TiCl_2(THF)_4$][$SnCl_5(THF)$]

Ti—Cl(1)	2.333(2)	Cl(2)—Sn—Cl(2)′	170.4(1)
Ti—O(1)	2.126(5)	Cl(2)—Sn—Cl(3)	94.8(1)
Ti—O(2)	2.067(6)	Cl(2)—Sn—Cl(4)	89.6(1)
Sn—Cl(2)	2.411(2)	Cl(2)—Sn—Cl(5)	89.8(1)
Sn—Cl(3)	2.382(3)	Cl(3)—Sn—Cl(4)	95.0(1)
Sn—Cl(4)	2.393(4)	Cl(3)—Sn—Cl(5)	92.4(1)
Sn—Cl(5)	2.400(4)	Cl(4)—Sn—Cl(5)	172.6(1)
Sn—O(3)	2.269(8)	O(3)—Sn—Cl(2)	85.2(2)
Cl(1)—Ti—O(1)	90.0(2)	O(3)—Sn—Cl(3)	178.4(2)
Cl(1)—Ti—O(2)	90.9(2)	O(3)—Sn—Cl(4)	86.6(2)
O(1)—Ti—O(2)	90.1(3)	O(3)—Sn—Cl(5)	86.0(2)

The atom marked with a prime is related to this at x, y, z by a mirror plane at $x, 1/y, z$.

In the $[SnCl_5(THF)]^-$ anion the tin atom is surrounded octahedrally by five chlorine atoms and one tetrahydrofuran molecule. The anion is located on a symmetry plane so that the tin atom, three Cl atoms and tetrahydrofuran molecule lie on the former. Since the tetrahydrofuran molecule can not be planar, it is disordered in the crystal. The disorder is based upon the fact, that the carbon C(1) and C(4) atoms bonded to the oxygen atom are statistically positioned on both sides of a symmetry plane [Fig. 1(b)]. Such a type of disorder is possible if the tetrahydrofuran molecules have the skew conformation. The disorder of the tetrahydrofuran molecule may be interpreted also in terms of displacement of the C(1) and C(4) atoms from the mirror plane in the same direction and in this case the tetrahydrofuran molecule should have the envelope conformation. The average Sn—Cl distances are equal, 2.404(11) and 2.382(3) Å for *syn* and *trans* positions, respectively. The geometry of the $[SnCl_5(THF)]^-$ anion could be compared with that of $[TiCl_5(THF)]^-$ and $[HfCl_5(THF)]^-$ anions whose crystal and molecular structure were published earlier.[2,8] The increase of the appropriate Ti—Cl, Sn—Cl, Hf—Cl and metal–oxygen bond distances is understandable in terms of the increased M^{4+} radii (Ti^{4+}, 0.68 Å; Sn^{4+}, 0.71 Å; Hf^{4+}, 0.81 Å) (see Table 2). Electrostatic repulsion between axial and equatorial coordinated chlorine atoms could explain the increase of the angles Cl(3)—Sn—Cl(2,4,5) to an average of 93.9(5)°. A similar phenomenon was observed for $[TiCl_5(THF)]^-$ 94.2(7)° and $[HfCl_5(THF)]^-$ 93.3(1)° anions.[2,8] The structure of the $[ZrCl_5(THF)]^-$ anion was not established.[9]

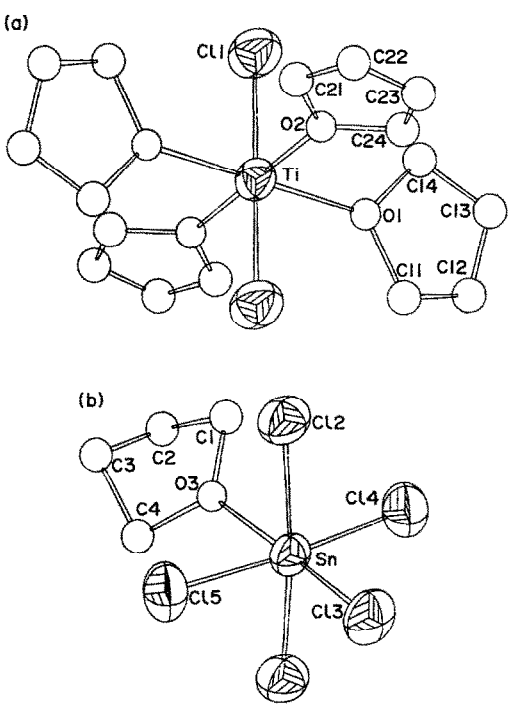

Fig. 1. (a) Structure of the [*trans*-$TiCl_2(THF)_4$]$^+$ cation in the [*trans*-$TiCl_2(THF)_4$][$SnCl_5(THF)$] compound. (b) Structure of the $[SnCl_5(THF)]^-$ anion in the [*trans*-$TiCl_2(THF)_4$][$SnCl_5(THF)$] compound. (The skew conformation of THF is presented.)

It was found that the [*trans*-$TiCl_2(THF)_4$][$SnCl_5(THF)$] compound could be also obtained by direct reaction between $SnCl_4$ and $[TiCl_3(THF)_3]$.

$$[TiCl_3(THF)_3] + SnCl_4 \xrightarrow{THF} [\textit{trans}\text{-}TiCl_2(THF)_4][SnCl_5(THF)]. \quad (3)$$

Thus, it could be believed that reaction (2) is based upon the reduction of $[TiCl_4(THF)_2]$ by $SnCl_2$ to $[TiCl_3(THF)_3]$ and $SnCl_4$ followed by a course similar to that of reaction (3).

The understanding of the unusual role of $MgCl_2$ and other inorganic salts as a supporter required the explanation of why $[TiCl_3(THF)_3]$ reacted with

Table 2. Comparison of bond lengths (Å) in $[MCl_5(THF)]^-$ anions

Compound	M—Cl[a]	M—Cl[b]	M—O	Reference
$[TiCl_5(THF)]^-$	2.307(11)	2.249(3)	2.158(5)	2
$[SnCl_5(THF)]^-$	2.404(11)	2.382(3)	2.269(8)	[c]
$[HfCl_5(THF)]^-$	2.423(4)	2.395(3)	2.218(10)	8

[a] Equatorial.
[b] Axial.
[c] In this paper.

$ZnCl_2$ and $SnCl_4$ [reactions (1)–(3)] but not with $MgCl_2$ and $AlCl_3$.[10] $AlCl_3$ is a more powerful Lewis acid than $ZnCl_2$, nevertheless, it does not form a compound with $[TiCl_3(THF)_3]$. It seems most likely, that the course of the reactions discussed here and similar ones, depends firstly on the equilibria formed in a solution.

$$2[TiCl_3(THF)_3] \rightleftharpoons [TiCl_2(THF)_4]^+ + [TiCl_4(THF)_2]^-. \quad (4)$$

Instead, the acid–base interactions are less important. The $[TiCl_3(THF)_3]$ and inorganic salts undergo ionization in THF, as in reaction (4). The ions in solution react mutually and/or with the substrate $SnCl_4$. The equilibrium attained in solution would depend upon the least soluble species formed in the solution. From the data presented here it follows that the $[MCl_5(THF)]^-$ (M = Ti, Zr, Sn, Hf) type anions form the least soluble compounds with cations, which then settle down in solution and cause the shift of the reaction equilibrium. Instead, in the $[TiCl_3(THF)_3]$, $[MgCl_2(THF)_2]$ or $AlCl_3$ tetrahydrofuran mixture the least soluble compound is $[TiCl_3(THF)_3]$. Catalytic properties of [*trans*-$TiCl_2(THF)_4$][$SnCl_5(THF)$] are the subject of further studies.

Acknowledgement—This work was financially supported by The Polish Academy of Science, Project CPBP 01.12.

REFERENCES

1. P. D. Gavenes, M. Bozzrill, J. W. Kelland and J. M. McMeeking, in *Comprehensive Organometallic Chemistry*, Vol. 3, p. 375. Pergamon Press, Oxford (1982).
2. P. Sobota, J. Utko and T. Lis, *J. Chem. Soc., Dalton Trans.* 1984, **276**, 171.
3. US Pat. No. 4,302,565 and 4,302,566.
4. K. Folting, J. C. Huffman, R. L. Bausemer and K. G. Caulton, *Inorg. Chem.* 1984, **23**, 3286.
5. L. E. Mazner, *Inorg. Synth.* 1982, **21**, 135; K. H. Thiele and W. Schäfer, *Z. Anorg. Allgem. Chem.* 1971, **381**, 205.
6. *Syntex XTL/XTLE Structure Determination System*, Syntex Analytical Instruments, Cupertino (1976).
7. P. J. McCarthy and M. F. Richardson, *Inorg. Chem.* 1983, **22**, 2979.
8. D. Cunningham and J. Flunegan, *J. Chem. Soc., Dalton Trans.* 1979, 162.
9. P. Biagini, F. Calderazzo, G. Pampaloni and P. F. Zanazzi, *Gazz. Chim. Ital.* 1987, **117**, 27.
10. P. Sobota, in *Transition Metal Catalysed Polymerization*, Pergamon Press, New York, in press.

Polyhedron Vol. 7, No. 24, pp. 2659–2665, 1988
Printed in Great Britain

0277–5387/88 $3.00+.00
© 1988 Pergamon Press plc

NEUTRAL AND CATIONIC ORTHOPALLADATED (C⁀N) COMPLEXES (C⁀N = PHENYLAZOPHENYL, DIMETHYLBENZYLAMINE, 8-METHYLQUINOLINE, 2-METHOXY-3-N,N-DIMETHYLAMINOPROPYL)

JUAN FORNIES,* RAFAEL NAVARRO and VIOLETA SICILIA

Departamento de Química Inorgánica, Instituto de Ciencia de Materiales de Aragón, Universidad de Zaragoza-C.S.I.C., 50009 Zaragoza, Spain

(*Received* 11 *April* 1988; *accepted* 27 *May* 1988)

Abstract—By reacting $[Pd(C^N)(\mu\text{-}Cl)]_2$ with $AgClO_4$ in NCMe, the corresponding cationic complexes $[Pd(C^N)(NCMe)_2]ClO_4$ (C⁀N = phenylazophenyl-C^2,N^1; dimethylbenzylamine-C^2,N; 8-methylquinoline-C^8,N) can be obtained. Solutions containing the cations $[Pd(C^N)(S)_2]^+$ are obtained when the reaction is carried out in tetrahydrofuran or acetone (S). The treatment of these solutions with bidentate ligands (L—L) ($Ph_2PCH_2PPh_2$, $Ph_2PNHPPh_2$ or $Ph_2PCH_2PPh_2CHC(O)Ph$) gives the mononuclear $[Pd(C^N)(L—L)]ClO_4$ complexes, with L—L acting as a chelate ligand. On the other hand $[Pd(C^N)(\mu\text{-}Cl)]_2$ reacts with L—L ($Ph_2PCH_2PPh_2$, $Ph_2PNHPPh_2$) yielding $[Pd(C^N)Cl(L—L)]$ with L—L acting as monodentate. The reactions between $[Pd(C^N)(NCMe)_2]ClO_4$ and 2,2′-bipyrimidyl give rise to the formation of the mononuclear $[Pd(C^N)(bipym)]ClO_4$ or binuclear $[Pd_2(C^N)_2(\mu\text{-bipym})](ClO_4)_2$, $[(C^N)Pd(\mu\text{-bipym})Pd(C^{\prime}N^{\prime})](ClO_4)_2$ derivatives. Finally $[Pd(C^N)Cldppm]$ (dppm = $Ph_2PCH_2PPh_2$) react with NaH producing the neutral complexes $[Pd(C^N)(ddppm)]$ (ddppm = $Ph_2PCHPPh_2$) which by reaction with HCl lead again to the starting materials $[Pd(C^N)Cl(dppm)]$.

The synthesis and reactivity of C,N-cyclometallated compounds, which incorporate a N—M—C ring system has attracted considerable recent interest.[1,2] Such complexes represent the interface between classical coordination chemistry and organometallic chemistry. In this paper we report on the reactivity of complexes, $[Pd(\mu\text{-}Cl)(C^N)]_2$, containing C⁀N cyclometallated systems (a)–(d), which render mono- and binuclear palladium(II) derivatives.

(a)

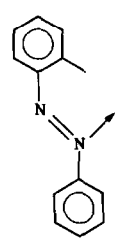

phenylazophenyl - C^2,N^1 (az)

(b)

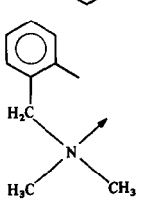

dimethylbenzylamine - C^2,N (dmba)

(c)

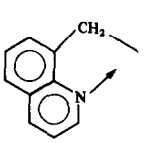

8 - methylquinoline - C^8,N (8 - mq)

(d)

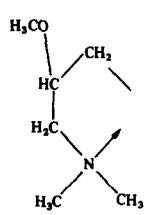

2 - methoxy - 3 - N, N - dimethylaminopropyl (mdmap)

RESULTS AND DISCUSSION

(i) $[Pd(C^N)(S)_2]^+$ *derivatives*

The synthesis of suitable precursors containing two weakly coordinated ligands (S) such as THF (tetrahydrofuran), acetone or NCMe (acetonitrile) have been carried out by halide abstraction from the binuclear $[Pd(C^N)(\mu\text{-}Cl)]_2$ complexes with $AgClO_4$ at room temperature in the solvent S, according to eq. (1)

*Author to whom correspondence should be addressed.

$$[Pd(C\frown N)(\mu\text{-}Cl)]_2 + 2AgClO_4 \xrightarrow{S} 2[Pd(C\frown N)(S)_2]^+ + 2ClO_4^- + 2AgCl \quad (1)$$

C⌒N = az, dmba, 8-mq, mdmap.

For S = NCMe, air and moisture stable solids at room temperature, $[Pd(C\frown N))(NCCH_3)_2]ClO_4$ [C⌒N = az (**1**), dmba (**2**), 8-mq (**3**)], have been obtained; however for S = THF or acetone, precipitation of AgCl takes place, but from the resulting solutions, which probably contain the cations $[Pd(C\frown N)S_2]^+$, we have only isolated oily residues, but not the solid products, although the solutions containing the $[Pd(N\frown C)S_2]^+$ compound have been used as starting materials (see below).

The IR spectra of complexes **1–3** show two bands due to $\nu(C{\equiv}N)$ of the nitrile groups, in agreement with the presence of two mutually *cis*-MeCN groups, shifted to higher energies than those of the free ligand $\nu(C{\equiv}N)$ [MeCN: 2254 cm^{-1};[3] **1**: 2312(s), 2288(s) cm^{-1}; **2**: 2292(s), 2276(s) cm^{-1}; **3**: 2324–2310(m)], in this case both absorptions are split, in keeping with previous observations for other $NCCH_3$ complexes.[3,4] Two absorptions at 1100(vs, br) and 620(s) cm^{-1} are assignable to the ClO_4^- anion.[5]

The ^1H NMR spectra of complexes **1–3** are in agreement with the proposed stoichiometries. The corresponding signals due to the phenylic protons appear in the 8.0–6.8 ppm region. Other relevant signals (δ, ppm) are **1**: 2.17(s, br; 6H) ($NCCH_3$); **2**: 3.92(s, 2H) (Ph—CH_2), 2.83(s, 6H) [$N(CH_3)_2$]; 2.48(s, 3H), 2.30(s, 3H) ($NCCH_3$); **3**: 3.86(s, 2H) (Ph—CH_2—), 2.42(S, 3H), 2.11(s, 3H) ($NCCH_3$).

Complexes **1–3** behave as 1:1 electrolytes in acetone solution ($C \simeq 5 \times 10^{-4}$ M).[6] Not only complexes **1–3** but also the solutions containing $[Pd(N\frown C)S_2]^+$ (S = THF, acetone) can be used as precursors for the preparation of other complexes.

(ii) $[Pd(C\frown N)(L{-}L)]^+$ *derivatives* (L—L = dppm, dppa, bdmp)

The addition of stoichiometric amounts of the ligand L—L (molar ratio 1:1) (L—L = dppm, bis-diphenylphosphinomethane; dppa, bis-diphenylphosphinoamine; bdmp, $PPh_2CH_2PPh_2CHC(O)Ph$, benzoylmethylenediphenylphosphinomethylphosphorane) to THF or acetone solutions containing the $[Pd(C\frown N)(S)_2]^+$ derivatives (S = THF, acetone; C⌒N = az, dmba, 8-mq, mdmap) yield the corresponding $[Pd(C\frown N)(L{-}L)]ClO_4$ compounds [eq. (2)] which are air and moisture stable in solid state and in solution

$$[Pd(C\frown N)_2(S)_2]ClO_4 + L{-}L \rightarrow [Pd(C\frown N)(L{-}L)]ClO_4 + 2S \quad (2)$$

C⌒N = az, L—L = dppm (**4**), dppa (**8**), bdmp (**12**)
C⌒N = dmba, L—L = dppm (**5**), dppa (**9**), bdmp (**13**)
C⌒N = 8-mq, L—L = dppm (**6**), dppa (**10**), bdmp (**14**)
C⌒N = mdmap, L—L = dppm (**7**), dppa (**11**), bdmp (**15**).

These complexes behave as 1:1 electrolytes in acetone solutions ($C \simeq 5 \times 10^{-4}$ M) (see Table 1). Their IR spectra show absorptions at ~ 1100(vs, br) and ~ 620 cm^{-1} assignable to the ClO_4^- (Td) group.[5] Complexes containing dppm (**4–7**) or dppa (**8–11**) show a medium–strong absorption in the 560–535 cm^{-1} range, which indicates that the bidentate P—P ligand is acting as a chelate ligand.[7,8] Complexes **8–11** (L—L = dppa) show no IR absorption assignable to ν(N—H) in the 3500–3100 cm^{-1} region, probably due to the interaction (hydrogen bonds) between N—H and ClO_4 groups.[8] The phospho–ylide complexes (L—L = bdmp) (**12–15**) show an absorption in the 1605–1588 cm^{-1} region due to ν(CO), shifted to high frequencies from the free ylide ligand (ν(CO) 1525 cm^{-1}) [$\Delta\nu = \nu(CO)_{complex} - \nu(CO)_{ylide}$: 75 (**12**), 59 (**13**), 79 (**14**), 53 (**15**) cm^{-1}] thus indicating the coordination of the C ylidic to the metal centre,[9–11] so that the bdmp is acting as a chelate ligand.

The $^{31}P\{^1H\}$ NMR spectra of **4–11** (L—L = dppm, dppa) show the typical pattern of an AB system (see Table 2) in agreement with the presence of two inequivalent P atoms in these complexes. For complexes **12–15** (L—L = bdmp, asymmetric ligand) two isomers can be formed; the $^{31}P\{^1H\}$ NMR spectra of complexes **12**, **13** and **15** show two doublets (an AB system) indicating that in $CDCl_3$ only one isomer is present but the spectrum of complex **14** shows two pairs of doublets (two AB systems) due to the presence of both isomers.

(iii) $[Pd(C\frown N)(bipym)]^+$ *and* $[Pd_2(C\frown N)_2(\mu\text{-}bipym)]^{2+}$ *derivatives*

Complexes $[Pd(C\frown N)(NCMe)_2]ClO_4$ react with bipypm (2,2′-bipyrimidyl) and the nuclearity of the resulting products depends on the molar ratio of Pd/bipym used. For a molar ratio (1:1) the mononuclear complexes where the bipym is acting as a bidentate ligand on a metal centre (mono-bidentate) are mainly obtained, while for a (2:1) ratio the binuclear derivatives containing bipym acting as a bridging ligand between two metal centres (bis-bidentate) are obtained.

Table 1. Analytical results (calculated values in parentheses), molar conductivities ($ohm^{-1}\ cm^2\ mol^{-1}$) and yields

	Complex	Analysis C	H	N	Λ_M	Yield %
1	$[Pd(az)(NCMe)_2]ClO_4$	40.9 (40.9)	3.0 (3.2)	12.4 (11.9)	150	43
2	$[Pd(dmba)(NCMe)_2]ClO_4$	36.5 (36.9)	4.0 (4.3)	9.3 (9.9)	132	92
3	$[Pd(8\text{-}mq)(NCMe)_2]ClO_4$	39.2 (39.1)	3.1 (3.3)	9.2 (9.7)	147	76
4	$[Pd(az)(dppm)]ClO_4$	58.0 (57.6)	4.1 (4.0)	3.6 (3.6)	146	57
5	$[Pd(dmba)(dppm)]ClO_4$	56.2 (56.3)	5.0 (4.7)	1.9 (1.9)	153	92
6	$[Pd(8\text{-}mq)(dppm)]ClO_4$	57.2 (57.4)	4.0 (4.1)	2.0 (1.9)	145	81
7	$[Pd(mdmap)(dppm)]ClO_4$	52.0 (52.7)	4.9 (5.1)	1.4 (2.0)	153	75
8	$[Pd(az)(dppa)]ClO_4$	55.0 (55.9)	4.0 (3.9)	5.8 (5.4)	146	50
9	$[Pd(dmba)(dppa)]ClO_4$	54.0 (54.6)	4.6 (4.6)	3.7 (3.8)	142	75
10	$[Pd(8\text{-}mq)(dppa)]ClO_4$	54.9 (55.7)	4.2 (4.0)	3.8 (3.8)	143	82
11	$[Pd(mdmap)(dppa)]ClO_4$	50.0 (50.9)	4.7 (5.0)	4.0 (3.9)	147	55
12	$[Pd(az)(bdmp)]ClO_4$	60.0 (60.7)	4.6 (4.2)	3.1 (3.1)	156	56
13	$[Pd(dmba)(bdmp)]ClO_4$	59.4 (59.8)	4.9 (4.8)	2.0 (1.7)	149	79
14	$[Pd(8\text{-}mq)(bdmp)]ClO_4$	60.4 (60.7)	4.9 (4.3)	1.5 (1.6)	135	50
15	$[Pd(mdmap)(bdmp)]ClO_4$	57.5 (56.8)	5.5 (5.1)	1.6 (1.7)	150	90
16	$[Pd(dmba)(bipym)]ClO_4$	41.2 (41.0)	3.9 (3.6)	14.1 (14.0)		57
17	$[Pd_2(dmba)_2(\mu\text{-}bipym)](ClO_4)_2$	37.0 (37.2)	3.7 (3.6)	10.0 (10.0)		80
18	$[Pd_2(8\text{-}mq)_2(\mu\text{-}bipym)](ClO_4)_2$	38.8 (39.4)	2.6 (2.6)	10.1 (9.8)		70
19	$[Pd(dmba)(\mu\text{-}bipym)Pd(8\text{-}mq)](ClO_4)_2$	38.0 (38.3)	3.2 (3.1)	10.3 (9.9)		92
20	$[PdCl(dmba)(dppm)]$	61.9 (61.8)	5.0 (5.2)	2.0 (2.1)	11.25	80
21	$[PdCl(8\text{-}mq)(dppm)]$	62.5 (62.9)	4.5 (4.5)	2.1 (2.1)	8.54	82
22	$[PdCl(mdmap)(dppm)]$	57.8 (58.0)	5.8 (5.5)	2.1 (2.2)	11.6	88
23	$[PdCl(8\text{-}mq)(dppa)]$	60.6 (61.0)	5.0 (4.4)	4.0 (4.2)		64
24	$[PdCl(mdmap)(dppa)]$	55.7 (56.0)	6.0 (5.5)	4.3 (4.3)	9.83	66
25	$[Pd(dmba)(dppmp)]$	66.2 (65.4)	5.6 (5.3)	2.0 (2.2)	12.78	56
26	$[Pd(mdmap)(dppmp)]$	61.6 (61.4)	6.3 (5.8)	2.4 (2.3)	20.8	42

Table 2. $^{31}P\{^1H\}$ NMR data (δ in ppm, J in Hz) and some relevant IR data

	P_A	P_B	$^2J(P_A-P_B)$	IR, ν (cm^{-1})
dppm	−21.95			
dppa	43.54			3230[a]
bdmp	14.28	−26.80	63	1525[b]
4	−5.54	−31.60	69	546
5	−1.65	−26.54	52	546
6	−4.57	−26.19	61	542
7	0.83	−22.53	48	540
8	44.41	31.06	71	562
9	47.21	33.80	61	540
10	47.03	37.40	68	552
11	50.31	38.02	60	562
12	36.07	33.45	35	1600[b]
13	31.90	29.91	37	1584[b]
14a	30.81	28.99	41	1604[b]
14b	41.73	12.08	89	
15	32.27	30.57	33	1588[b]
20	33.02	−22.15	80	300[c]
21	28.95	−24.40	62	286[c]
22	30.47	−24.51	59	250[c]
23	70.24	28.75	19	3160,[a] 278[c]
24	69.80	29.15	19	3160,[1] 268[c]
25	−16.07	−30.81	30	894, 868,[d] 562
26	−15.35	−26.54	22	883, 851,[d] 535

[a] (N—H).
[b] ν(C—O).
[c] ν(Pd—Cl).
[d] PPh_2—CH—PPh_2^- ligand.

So, the reaction between $[Pd(dmba)(NCMe)_2]ClO_4$ and bipym (2,2′-bipyrimidyl) (1:1 molar ratio) in CH_2Cl_2 produces the precipitation of $[Pd_2(dmba)_2(\mu\text{-bipym})](ClO_4)_2$ (**17**) (19% yield) and from the resulting mother liquors the mononuclear complex $[Pd(dmba)(bipym)]ClO_4$ (**16**) can be isolated [eq. (3)]

$$[Pd(dmba)(NCMe)_2]ClO_4 + bipym \rightarrow [Pd(dmba)(bipym)]ClO_4 + [Pd_2(dmba)_2(\mu\text{-bipym})](ClO_4)_2. \quad (3)$$

The dinuclear derivatives $[Pd_2(C\widehat{\ }N)_2(\mu\text{-bipym})](ClO_4)_2$ [C^N = dmba (**17**), 8-mq (**18**)] can be obtained by reacting the corresponding $[Pd(C\widehat{\ }N)(NCMe)_2]ClO_4$ and bipym in the molar ratio 2:1. On the other hand the mononuclear $[Pd(dmba)(bipym)]ClO_4$ (**16**), reacts in CH_2Cl_2 with $[Pd(8\text{-mq})(NCMe)_2]ClO_4$ (**3**) yielding the asymmetric binuclear $[(dmba)Pd(\mu\text{-bipym})Pd(8\text{-mq})](ClO_4)_2$ (**19**).

The IR spectra of complexes **16–19** show two strong absorptions at 1100 and 620 cm^{-1} due to the ClO_4^- anion.[5] The mononuclear complex **16** shows two strong absorptions at 1570 and 1550 cm^{-1}, assigned to ring stretching modes of the bipym;[12] the binuclear derivatives, **17–19**, show a strong band near 1570–1580 cm^{-1} and a weak one near 1550–1540 cm^{-1} in keeping with observations previously reported for mono- or binuclear bipym containing complexes.[12] The low solubility of these complexes in usual organic solvents prevents conductivity or NMR studies.

(iv) $[PdCl(C\widehat{\ }N)(L—L)]$ *derivatives*

The binuclear complexes $[Pd(\mu\text{-Cl})(C\widehat{\ }N)]_2$ react with L—L (dppm, dppa) in benzene or THF yielding the corresponding mononuclear derivatives $[PdCl(C\widehat{\ }N)(L—L)]$ [eq. (4)], where the ligand L—L is acting as monodentate

$$[Pd(\mu\text{-Cl})(C\widehat{\ }N)]_2 + 2L—L \rightarrow 2[PdCl(C\widehat{\ }N)(L—L)] \quad (4)$$

C^N = dmba, L—L = dppm (**20**)
C^N = 8-mq, L—L = dppm (**21**), dppa (**23**)
C^N = mdmap, L—L = dppm (**22**), dppa (**24**).

Acetone solutions ($C \simeq 5 \times 10^{-4}$ M) of these complexes are non-conducting. Their IR spectra show an absorption in the 250–300 cm^{-1} region (see Table 2) due to ν(Pd—Cl). No absorptions in the 650–500 cm^{-1} region are observed which indicate that the L—L ligand (L—L = dppm, dppa) is not acting as a chelate ligand.[7,8] Dppa containing complexes (**23**, **24**) show an absorption at 3160 cm^{-1} due to ν(N—H), shifted to lower energies than in the free ligand (3.230 cm^{-1}). The ^{31}P NMR spectra show in all cases two doublets (see Table 2) corresponding to an AB system. By comparison with other palladium or platinum complexes containing mono-coordinated dppm (dppm—P),[7,13,14] positive chemical shift signals are assigned to the coordinated P atom (P_A) and the high negative chemical shift signals are due to the free P atom (P_B).

Signals due to P_A and P_B in the dppa complexes (**23**, **24**) appear in the same range as observed for other palladium or platinum complexes containing monodentate dppa.[8]

(v) [Pd(C^N)(ddppm)] *derivatives* [ddppm = $[Ph_2PCHPPh_2]^-$, C^N = dmba (**25**), mdmap (**26**)]

The reactions between [PdCl(C^N)(dppm)] (C^N = dmba, mdmap) and HNa in THF at room temperature take place with evolution of H_2, deprotonation of the CH_2 group of the dppm ligand and formation of the neutral complexes [Pd(C^N)(ddppm)] C^N = dmba (**25**), mdmap (**26**) according to eq. (5).

$$PdCl(C^N)(dppm—P) + HNa \rightarrow Pd(C^N)(ddppm) + NaCl + H_2. \quad (5)$$

Acetone solutions of complexes **25** and **26** ($C \simeq 5 \times 10^{-4}$ M) are non-conducting. The IR spectra of these complexes do not show absorption in the ν(Pd—Cl) region. Two strong absorptions in the 900–850 cm^{-1} region seem to be characteristic vibrations of the methanide P—CH—P system.

The $^{31}P\{^1H\}$ NMR spectra of complexes **25** and **26** confirm the presence of two inequivalent P atoms (AB system) (See Table 2).

Complexes **25** and **26** react with HCl in CH_2Cl_2 yielding the corresponding PdCl(C^N)(dppm) (**20**, **22**).

EXPERIMENTAL

C, H and N analyses were carried out on a Perkin–Elmer 240B microanalyser. Conductivities were measured with a Philips PW 9501/01 apparatus. IR spectra were recorded (in the 4000–200 cm^{-1} range) on a Perkin–Elmer spectrophotometer using Nujol mulls between polyethylene sheets. ^1H and $^{31}P\{^1H\}$ NMR spectra were recorded on a Varian XL200 (200 MHz for ^1H).

The compounds: $Ph_2PCH_2PPh_2$ (dppm),[15] $Ph_2PNHPPh_2$ (dppa),[16] $Ph_2P—CH_2—PPh_2—CH—C(O)Ph(bdmp)$,[17] $[Pd(\mu\text{-}Cl)_2(az)_2]$,[18] $[Pd_2(\mu\text{-}Cl)_2(dmba)_2]$,[19] $[Pd_2(\mu\text{-}Cl)_2(8\text{-}mq)_2]$,[20] $[Pd_2(\mu\text{-}Cl)_2(mdmap)_2]$[21] were prepared as described elsewhere.

$[Pd(C^N)(NCMe)_2]ClO_4$ (C^N = az (**1**), dmba (**2**), 8-mq (**3**)

To a solution of $[Pd_2(\mu\text{-}Cl)_2(az)_2]$ (0.230 g, 0.362 mmol) in 20 cm^3 of MeCN, $AgClO_4$ (0.149 g, 0.724 mmol) was added. The mixture was stirred (under exclusion of light) for 15 min at room temperature; the AgCl was filtered off and the resulting solution was evaporated to dryness. The residue was treated with ~ 20 cm^3 of *n*-hexane yielding complex **1** (0.279 g, 91% yield). Similar reactions starting from $[Pd_2(\mu\text{-}Cl)_2(dmba)_2]$ or $[Pd_2(\mu\text{-}Cl)_2(8\text{-}mq)_2]$ gave complexes **2** and **3**, respectively.

$[Pd(C^N)(L—L)]ClO_4$ (C^N = az, dmba, 8-mq, mdmap; L—L = dppm, dppa, bdmp (**4–15**)

A typical preparation was as follows: to a suspension of $[Pd(\mu\text{-}Cl)(az)]_2$ (0.200 g, 0.311 mmol) in 20 cm^3 of acetone, $AgClO_4$ (0.129 g, 0.622 mmol) was added and the mixture was refluxed for 30 min. The AgCl formed was eliminated by filtration and then dppm (0.239 g, 0.622 mmol) in 15 cm^3 of benzene was added to the resulting solution. The mixture was stirred at room temperature for 2 h. The solution was evaporated almost to dryness and Et_2O (20 cm^3) was added yielding an orange solid, **4**, 0.272 g, 57% yield.

Complexes **8** and **12** were obtained in a similar way by using dppa or bdmp as L—L ligand, **5**, **9** and **13** were obtained starting from $[Pd(\mu\text{-}Cl)(dmba)]_2$. For complexes **6**, **7**, **10**, **11**, **14** and **15** the procedure was the same but the reactions between the corresponding $[Pd(\mu\text{-}Cl)(C^N)]_2$ derivatives and $AgClO_4$ were carried out in THF. Complexes **10** and **14** are slightly soluble in THF and they precipitate from the THF solution. Yields for the preparation of complexes **4–15** are collected in Table 1.

$[Pd(dmba)(bipym)]ClO_4$ (**16**)

A CH_2Cl_2 (10 cm^3) solution of **2** (0.192 g, 0.459 mmol) was added at room temperature to a CH_2Cl_2

($10\ cm^3$) solution of bipym (0.072 g, 0.459 mmol). A deep yellow solid (**17**), (19% yield) precipitates immediately. The resulting mother liquors after the separation of complex **17** were evaporated to $\sim 3\ cm^3$, and the white solid was washed with *n*-hexane (**16**, 57% yield).

$[Pd_2(C\frown N)_2(\mu\text{-bipym})](ClO_4)_2$ (C⌒N) = dmba (**17**), 8-mq (**18**)

A CH_2Cl_2 ($10\ cm^3$) solution of **2** (0.253 g, 0.6 mmol) was added to a CH_2Cl_2 ($5\ cm^3$) solution of bipym (0.047 g, 0.3 mmol) and the yellow solid was collected by filtration and washed with *n*-hexane (**17**, 80% yield). Working under similar conditions, complex **18**, 70% yield was obtained.

[(dmba)Pd(μ-bipym)Pd(8-mq)]$(ClO_4)_2$ (**19**)

A CH_2Cl_2 ($10\ cm^3$) solution of **3** (0.172 g, 0.4 mmol) was added to a CH_2Cl_2 ($10\ cm^3$) suspension of **16** (0.200 g, 0.4 mmol). The mixture was stirred at room temperature for 30 min. The resulting deep yellow solid which precipitated was washed with *n*-hexane (**19**, 92% yield).

PdCl(C⌒N)(dppm) (C⌒N) = dmba (**20**), 8-mq (**21**), mdmap (**22**)

To a suspension of $[Pd(\mu\text{-Cl})(dmba)]_2$ (0.100 g, 0.181 mmol) in $20\ cm^3$ of benzene, dppm (0.139 g, 0.362 mmol) was added and the mixture was stirred at room temperature for 15 min. The resulting solution was evaporated to $\sim 3\ cm^3$ and $20\ cm^3$ of Et_2O were added, the precipitate was washed with Et_2O (**20**, 80% yield). Complexes **21** and **22** were obtained similarly by using $[Pd(\mu\text{-Cl})(8\text{-mq})]_2$ and $[Pd(\mu\text{-Cl})(mdmap)]_2$, respectively, as starting materials.

[PdCl(C⌒N)(dppa)] (C⌒N) = 8-mq (**23**), mdmap (**24**)

To a suspension of $[Pd(\mu\text{-Cl})(8\text{-mq})]_2$ (0.200 g, 0.352 mmol) in $20\ cm^3$ of THF, dppa (0.271 g, 0.704 mmol) was added and the mixture was stirred at room temperature for 15 min. The resulting white precipitate was collected by filtration and washed with $5\ cm^3$ of THF (**23**, 66% yield). A similar reaction starting from $[Pd(\mu\text{-Cl})(mdmap)]_2$ renders **24**, 66% yield.

Pd(C⌒N)(ddppm) (C⌒N) = dmba (**25**), mdmap (**26**)

To a solution of [PdCl(dmba)(dppm)] (0.330 g, 0.499 mmol) in $20\ cm^3$ of dry THF, HNa (0.2 g) was added under N_2. The mixture was stirred at room temperature for 30 min. The filtered solution was evaporated to dryness and the residue was washed with $15\ cm^3$ of dry Et_2O (**25**, 56% yield). Complex **26** was obtained similarly. Yield 42%.

Reaction of Pd(C⌒N)(ddppm) *with* HCl

To a solution of [Pd(mdmap)(ddppm)] (0.3 g, 0.495 mmol) in $15\ cm^3$ of CH_2Cl_2, $1.2\ cm^3$ of a solution 0.46 mmol of HCl in MeOH (0.556 mmol) were added. The mixture was stirred at room temperature for 5 min, the solution was evaporated to dryness, and the residue was extracted with $\sim 20\ cm^3$ of Et_2O. The resulting solution was evaporated to $\sim 3\ cm^3$ yielding a solid which was identified as [PdCl(mdmap)(dppm)] (**22**, 32% yield).

Acknowledgement—We thank the C.I.C.Y.T. (Spain) for financial support.

REFERENCES

1. I. Omae, Organometallic intramolecular-coordination compounds, *J. Organometal. Chem. Library*, 1986, 18.
2. I. Omae, *Chem. Rev.* 1979, **79**, 287.
3. B. N. Storhoff and H. C. Lewis Jr, *Coord. Chem. Rev.* 1977, **23**, 1.
4. A. D. Hamer and R. A. Walton, *Synth. React. Inorg. Met.-Org. Chem.* 1974, **4**, 573.
5. B. J. Hataway and A. E. Underhill, *J. Chem. Soc.* 1961, 3091.
6. W. J. Geary, *Coord. Chem. Rev.* 1971, **81**, 7.
7. R. Usón, J. Forniés, P. Espinet, R. Navarro and C. Fortuño, *J. Chem. Soc., Dalton Trans.* 1987, 2077.
8. R. Usón, J. Forniés, R. Navarro and J. I. Cebollada, *J. Organometal. Chem.* 1986, **304**, 381.
9. Y. Oosawa, T. Miyamoto, T. Saito and Y. Sasaki, *Chem. Lett.* 1975, 33.
10. H. Koezuka, G. Matsubayashi and T. Tanaka, *Inorg. Chem.* 1974, **13**, 443.
11. R. Usón, J. Forniés, R. Navarro and A. M. Ortega, *J. Organometal. Chem.* 1987, **334**, 389.
12. V. F. Sutcliffe and G. B. Young, *Polyhedron* 1984, **3**, 87.
13. R. C. Langrick, D. M. McEwan, P. G. Pringle and B. L. Shaw, *J. Chem. Soc., Dalton Trans.* 1983, 2487.
14. P. G. Pringle and B. L. Shaw, *J. Chem. Soc., Dalton Trans.* 1984, 849.
15. A. H. Aguiar and J. Beisler, *J. Org. Chem.* 1964, **29**, 1660.
16. H. Noth and L. Meinel, *Z. Anorg. Chem.* 1967, **349**, 225.
17. Y. Oosawa, H. Urabe, T. Saito and Y. Sasaki, *J. Organometal. Chem.* 1976, **122**, 113.

18. A. C. Cope and R. W. Siekman, *J. Am. Chem. Soc.* 1965, **87**, 3272.
19. A. C. Cope and E. C. Friedrich, *J. Am. Chem. Soc.* 1968, **90**, 909.
20. A. C. Deeming and I. P. Rothwell, *J. Organometal. Chem.* 1981, **205**, 117.
21. A. C. Cope, J. M. Kliegman and E. C. Friedrich, *J. Am. Chem. Soc.* 1967, **89**, 287.

Polyhedron Vol. 7, No. 24, pp. 2667–2674, 1988
Printed in Great Britain

0277–5387/88 $3.00+.00
© 1988 Pergamon Press plc

INTERACTION OF IRON(III) TETRASULPHONATED PHTHALOCYANINE WITH CYTOCHROME *c* OXIDASE APOPROTEIN

ŁUCJA OSTROPOLSKA, HELENA PRZYWARSKA-BONIECKA* and HANNA SWIRSKA

Institute of Chemistry, University of Wrocław, Poland

(*Received* 18 *April*, 1988; *accepted* 27 *May* 1988)

Abstract—A complex of bovine cytochrome *c* oxidase protein with iron(III) tetrasulphonated phthalocyanine in place of hemes has been prepared. Its structure and properties have been investigated by difference spectroscopy, electrophoresis, molecular weight estimation, potentiometric measurements and polypeptide fragments examination. The visible absorption spectrum of Fe^{III}–apo-oxidase shows the main intense peak at 657 nm and weaker one at 700 nm. Molecular weight estimation demonstrated that one mole of the complex includes three functional units of MW 130,000 per unit. Spectroscopic examination of dithionite reduced Fe^{III}–apo-oxidase suggests the open crevice structure of the subunits containing iron tetrasulphonated phthalocyanine which is supported by the results of circular dichroism studies. Deep conformational changes of the protein upon displacement of hemes *a* and a_3 are not reversed upon $Fe^{III}L^+$ incorporation into the protein. The molar ratio of the protein to $Fe^{III}L$ in the complex (MW 130,000) was found to be 1:2. In the reduced form $Fe^{III}L$–apo-oxidase reacts with CN^-, N_3^-, imidazole and molecular oxygen. Oxygen binding is irreversible, which indicates that the oxygen adduct is not of the oxyhemoglobin type. Electrophoretic and gel filtration studies of the SDS–urea dissociation products of cytochrome *c* oxidase and its phthalocyanine derivative suggest that $Fe^{III}L$ and hemes *a* and a_3 are located on the same polypeptide fragments of the protein. $Fe^{III}L$–apo-oxidase is reduced by ferrous cytochrome *c* in agreement with their midpoint potentials which are 315.5 and 260 mV, respectively. However, the rate of the reaction of $Fe^{III}L$–apo-oxidase with ferrous cytochrome *c* is markedly lower than that of the native cytochrome *c* oxidase suggesting different mechanisms for this process in both cases.

Cytochrome *c* oxidase is an intrinsic membrane protein, which plays a unique function in the oxygen metabolism and chemical energy conservation. It is responsible for electron transport from cytochrome *c* to O_2 and proton transport through the internal mitochondrial membrane. Approaches to the clarification of the structural bases for the biological function of cytochrome *c* oxidase have generated considerable literature.[1–3]

Bovine cytochrome *c* oxidase consists of at least seven subunits.[2] The functional unit contains four metal centres: two hemes of cytochromes *a* and a_3 and two copper ions. The two heme components of cytochrome *c* oxidase are characterized by their respective ligand binding properties. Cytochrome a_3 binds ligands in both oxidized and reduced states, whereas cytochrome *a* does not bind ligands in either oxidation–reduction state. The heme a_3 is

*Author to whom correspondence should be addressed.

Abbreviations.
L—tetrasulphonated phthalocyanine ligand, $C_{32}H_{12}N_8(SO_3Na)_4$.
$Fe^{III}L$—iron(III) tetrasulphonated phthalocyanine.
$Fe^{III}L$–apo-oxidase—iron(III) phthalocyanine complex with cytochrome *c* oxidase protein.
TCA—trichloroacetic acid.
SDS—Sodium dodecyl sulphate.

closely associated with one of the copper ions and cooperates with them during oxygen reduction.[4-8] The iron ion of heme *a* is in reversible redox equilibrium with the second copper ion and reacts cooperatively with the heme a_3.[9-11] The structure of cytochrome *c* oxidase has been reviewed by Capaldi *et al.*[12] Antonini and co-workers[13-15] have proposed a two-state allosteric model of cytochrome *c* oxidase which accounts for the kinetic behaviour of the enzyme.

The various experimental methods have been applied in the studies on the structure–function relationship of cytochrome *c* oxidase. One of the methods applied in metalloprotein investigations is to study their functional properties after their structural modification. Recently it has been shown that it is possible to substitute heme in hemoproteins by the unnatural porphyrins or other artificial prosthetic groups. Yamanaka and Okunuki[16] have shown that removal of heme d_1 from cytochrome *c* oxidase of *Pseudomonas aeruginosa* results in a concomitant loss of its enzyme activity and that its reconstitution with heme d_1 or another heme group restored partial activity. Hill and Wharton[17] have examined the reconstitution of the *Pseudomonas* cytochrome *c* oxidase apoprotein and have stated that besides heme d_1, only heme *a* yields a product with some oxidase activity. In our previous work we have demonstrated that modification of some hemoproteins by substitution of heme with metal tetrasulphonated phthalocyanines gives complexes with properties resembling those of their natural analogues.[18]

We now report the results of interaction of iron(III) tetrasulphonated phthalocyanine with cytochrome *c* oxidase apoprotein.

EXPERIMENTAL

Materials and methods

Cytochrome *c* oxidase was prepared from beef heart mitochondria according to the method of Yonetani.[19]

Cytochrome *c* apo-oxidase was prepared from oxidase using Teale's acid butanone method with slight modifications.[20,21] The solution of cytochrome *c* oxidase (10 mg cm^{-3}) in 0.02 M potassium phosphate buffer with 1% Tween-80 (pH 7.4) was adjusted at 0°C to pH 3.0 by dropwise additions of 0.1 M HCl and was immediately mixed with an equal volume of ice-cold 2-butanone. The mixture was vigorously shaken for 20 s and allowed to stand at 0°C for 1 min, until the upper layer of butanone, which contained the heme was well separated from the aqueous phase containing the apo-enzyme. The butanone phase was removed and the remaining aqueous phase was treated twice more with 2-butanone and dialysed for 24 h against a 0.02 M potassium phosphate buffer with 0.5% sodium cholate and 1% Tween-80 (pH 7.4). The dialysed solution was centrifuged to remove insoluble material and stored at 0°C.

Pig heart cytochrome *c* was purchased from Biomed, Kraków and purified chromatographically.[22] All the chemicals used in these studies were of analytical purity.

The preparation and purification of iron tetrasulphonated phthalocyanine have been described earlier.[23] Stock solutions were obtained by weighing appropriate amounts of the solid and dissolving it in 100 cm^3 of 0.02 M potassium phosphate buffer, pH 7.4 with 0.5% sodium cholate and 1% Tween-80. Protein concentrations were determined spectrophotometrically with a Specord spectrophotometer. The molar absorptivities used for cytochrome *c* oxidase and apo-oxidase which were determined by dry weight: $\varepsilon_{445} = 8.2 \times 10^4$ M^{-1} cm^{-1} and $\varepsilon_{278} = 1.27 \times 10^5$ M^{-1} cm^{-1}, respectively. Dry products were obtained by dialysis of the protein solution against 0.01 M $KHCO_3$ and lyophilization. Molecular extinction coefficients were calculated for the functional unit of MW 130,000.

The synthesis of $Fe^{III}L$–apo-oxidase was performed by incubation of apoxidase with a four-fold excess of iron tetrasulphonated phthalocyanine in 0.02 M potassium phosphate buffer with 0.5% sodium cholate and 1% Tween-80 at 4°C for three days. The phthalocyanine complex of apo-oxidase was isolated from the reaction mixture chromatographically on Sephadex G-75 column equilibrated with the same buffer. The molar absorptivity of this complex by dry weight for the functional unit was $\varepsilon_{657} = 5.95 \times 10^4$ M^{-1} cm^{-1}. The reduced form of the complex was prepared by addition of a few milligrams of sodium dithionite to the buffered solution and removing the excess of the reductant on a Sephadex G-75 column in the argon atmosphere. Molar absorptivity of the reduced complex was $\varepsilon_{685} = 4.1 \times 10^4$ M^{-1} cm^{-1}.

The molar ratio of $Fe^{III}L$ to apo-oxidase in the $Fe^{III}L$–apo-oxidase complex was determined as follows: 5 cm^3 of a chromatographically purified solution of the complex in a 0.02 M potassium phosphate buffer with 0.5% sodium cholate and 1% Tween-80 ($c = 2.31 \times 10^{-6}$ M) was treated with 10% TCA dropwise to complete precipitation of the protein. The reaction mixture was diluted to 10 cm^3 with the same buffer. Under these conditions

dissociation of the complex occurred with liberation of $Fe^{III}L$. The precipitate was separated by centrifugation and the $Fe^{III}L$ concentration in the solution was estimated spectrophotometrically at 635 nm ($\varepsilon_{635} = 5 \times 10^4\ M^{-1}\ cm^{-1}$). It was found to be 4.5×10^{-6} M. The precipitate was washed with isopropyl ether and dissolved in 1 cm^3 of 1 M NaOH, and the concentration of the apo-oxidase was estimated according to the procedure described by Lowry *et al.*[24] It was found to be 2.21×10^{-6} M. The concentrations of the complex and cytochrome *c* apo-oxidase were calculated per functional unit. The results presented above indicate the molar ratio of apo-oxidase to $Fe^{III}L$ to be 1:2.

Spectrophotometric titration could not be used to determine the stoichiometry of complex formation because of a turbidity of the solutions in the cases where there was a higher excess of the protein.

Absorption spectroscopy

Absorption and difference spectra were obtained using a Cary 15 spectrometer, with a cell compartment, thermostatically controlled at 10°C, or on a Specord spectrophotometer. The measurements were made under equilibrium conditions.

Circular dichroism measurements

Circular dichroism (CD) spectra were recorded using a model ORD/UV-5 Japan Spectropolarimeter with a CD attachment. Samples for CD measurements involved the solutions of $Fe^{III}L$–apo-oxidase in 0.02 M phosphate buffer, pH 7.4, with 0.5% sodium cholate and 1% Tween-80, purified chromatographically. The molar concentrations of the complexes were calculated from the molar absorption coefficients.

Molecular weight estimation

The molecular weight of the complex was determined by gel filtration on a Sephadex G-200 column according to the method of Andrews.[25] The following proteins were used as reference substances: serum albumin (MW 67,000), aldolase (MW 160,000), catalase (MW 240,000), fibrinogen (MW 350,000), ferritin (MW 450,000), urease (MW 480,000) and tyreoglobulin (MW 630,000). The column was equilibrated and eluted with 0.02 M phosphate buffer containing 0.5% sodium cholate and 1% Tween-80. For comparative purposes molecular weights of cytochrome *c* oxidase and apo-oxidase used were determined.

Resolution of $Fe^{III}L$*–apo-oxidase and cytochrome* c *oxidase by electrophoresis in gel containing sodium dodecyl sulphate and urea*

Polyacrylamide gel electrophoresis. The proteins were dissociated by incubation at 37°C for 2 h in 3% SDS and 10 mM β-mercaptoethanol. 100 μg of the reaction mixture was applied to 12.5% polyacrylamide gels (acrylamide–bis-acrylamide 40:1). Samples were electrophoresed following the procedure described by Weber and Osborn.[26]

Gel chromatography on sodium dodecyl sulphate–8M urea. The protein (20 mg) dissolved in 1 cm^3 of buffer containing 0.05 M NaH_2PO_4, 8M urea and 5% SDS (pH 7.2) was incubated at 37°C for 30 min and chromatographed on a Sephadex G-100 column (86 × 2 cm). The column was equilibrated and eluted with this buffer at room temperature according to procedures described by Downer *et al.*[27] Further purification of the isolated fractions was achieved by dialysis against 0.02 M phosphate buffer (pH 7.4).

Oxidation–reducation potential. The oxidation–reduction potential of $Fe^{III}L$–apo-oxidase was studied according to procedures described earlier.[28] The enzymatic reduction of $Fe^{III}L$–apo-oxidase was assayed with Fe^{II} cytochrome *c* as substrate, dissolved in 0.02 M phosphate buffer with 0.5% sodium cholate. All solutions were deoxygenated by argon purging over 2 h. The assay was performed by an anaerobic injection of ferrous cytochrome *c*. (Concentrations: cyt $c = 2.0 \times 10^{-6}$ M, complex $= 2.0 \times 10^{-7}$ M.) The reaction run was followed spectrophotometrically.[29]

RESULTS

The interaction of iron(III) tetrasulphonated phthalocyanine with apo-oxidase was followed by difference spectroscopy. The absorption spectrum of apo-oxidase prepared by Teale's acid butanone method exhibited neither heme *a* nor heme a_3 characteristic bands, indicating dissociation of cytochrome *c* oxidase into hemes *a* and a_3 and protein under such conditions of apo-oxidase preparation.

The difference visible spectrum of the mixture of $Fe^{III}L$ with apo-oxidase in 0.02 M phosphate buffer containing 0.5% sodium cholate and 1% Tween-80 shows the main positive peak at 657 nm in addition to a weak one at 700 nm [Fig. 1(a)]. The negative absorption band appears at 635 nm which corresponds to the non-bonded iron(III) tetrasulphonated phthalocyanine absorptivity. It is evident from this spectrum that apo-oxidase reacts with $Fe^{III}L$ to give a $Fe^{III}L$–apo-oxidase complex.

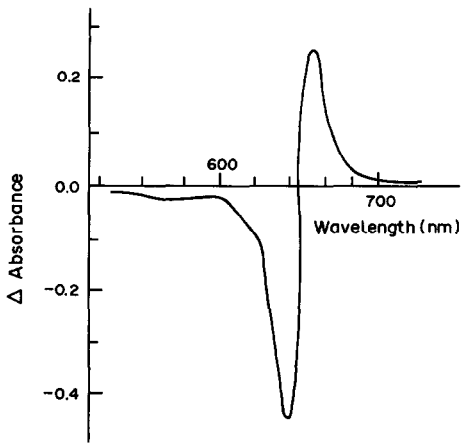

Fig. 1. Difference spectrum of $Fe^{III}L$ + apo-oxidase mixture against the same solutions unmixed. Concentrations: $Fe^{III}L = 1.8 \times 10^{-5}$ M; apo-oxidase = 2.2×10^{-6} M.

The results of gel filtration molecular weight estimation are shown in Fig. 2. The plot of the elution volume (V) against molecular weight indicates the molecular weight of $Fe^{III}L$–apo-oxidase to be about 393,500. This value is comparable with those of bovine cytochrome *c* oxidase (385,000) and apo-oxidase (398,000). The native cytochrome *c* oxidase is a multi-subunit enzyme of MW about 120,000 per functional unit, containing four metal centres: two iron ions of hemes *a* and a_3 together with two copper ions. The molecular weight of the bovine oxidase used in our studies, and its phthalocyanine derivative indicates that one mole of these proteins includes three functional units of MW of about 130,000 per unit. The molar ratio of apo-oxidase to $Fe^{III}L$ in the complex was found to be two moles of $Fe^{III}L$ per functional unit of cytochrome *c* apo-oxidase. This suggests coordination of $Fe^{III}L$ in the heme *a* and a_3 binding sites of the cytochrome *c* oxidase protein.

Properties of the $Fe^{III}L$*–apo-oxidase complex*

The phthalocyanine complex of cytochrome *c* apo-oxidase reduced with an excess of dithionite in anaerobic conditions exhibits a difference spectrum with one negative band at 635 nm and three positive ones at 485, 685 and 740 nm (Fig. 3). The position of the positive band at 685 nm is characteristic for iron(III) tetrasulphonated phthalocyanine complexes. Two other positive bands are suggested to present an intermediate reduction product involving the dithionite–$Fe^{III}L$–apo-oxidase complex with a reduced phthalocyanine ring.

The $Fe^{III}L$–apo-oxidase has no affinity for additional ligands. Reduced with dithionite, however, it combines with cyanide, azide, imidazole and molecular oxygen, as is shown by an increase in intensity of its main absorption band at 685 nm. At the same time the bands at 485 and 740 nm disappear [Fig. 4(a)]. The oxygen adduct is not a reversible ferrous–oxygen complex of the oxyhemoglobin type, it undergoes irreversible autooxidation with degradation of the phthalocyanine ring as shown by the slow decrease in the intensity of its band at 685 nm [Fig. 4(b)].

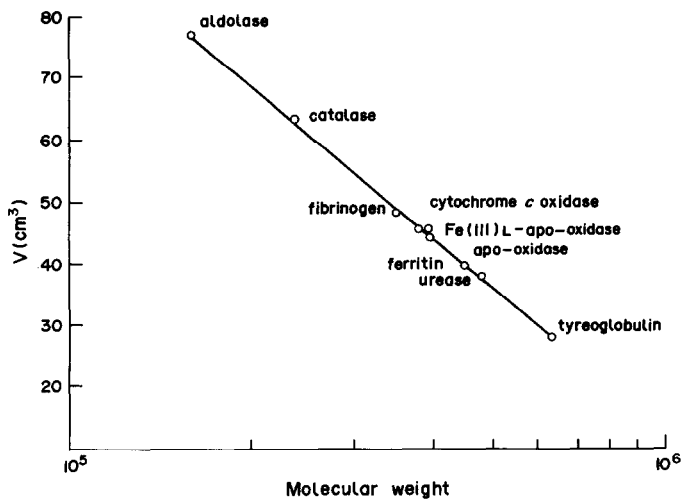

Fig. 2. Gel filtration molecular weight estimation of the iron phthalocyanine complex with apo-oxidase compared to the native cytochrome *c* oxidase and its apoprotein. Column size (86 × 2 cm) equilibrated with 0.02 M phosphate buffer containing 0.5% sodium cholate and 1% Tween-80.

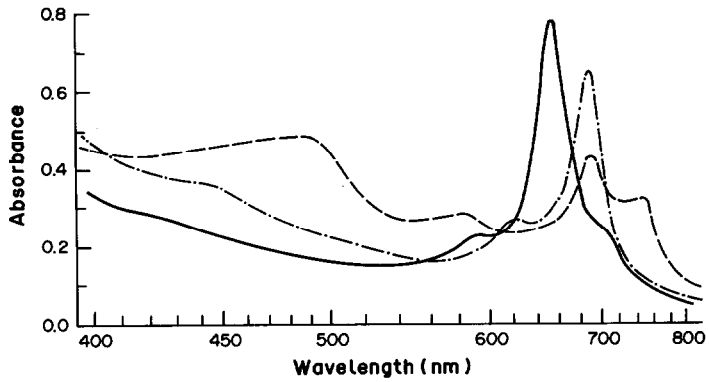

Fig. 3. Absorption spectra of: Fe^{III}–apo-oxidase (——), Fe^{III}L–apo-oxidase reduced with dithionite in argon atmosphere (– – –) and the same solution in oxygen atmosphere 24 h after oxygen saturation (–·–·–). Complex concentration: 2.6×10^{-5} M.

Circular dichroism spectra (CD)

Circular dichroism studies were carried out in the UV region. In Fig. 5 CD spectra of Fe^{III}L–apo-oxidase, cytochrome *c* oxidase and its apoprotein are presented. Fe^{III}L–apo-oxidase exhibits negative CD bands at 208 and 223 nm with ellipticity values of -8.5×10^6 and -10×10^6 deg cm^2 dmol^{-1}, respectively. Apo-oxidase and cytochrome *c* oxidase exhibit negative CD bands at 210 and 220 nm with ellipticity values -9×10^6 and 9.6×10^6 deg cm^2 dmol^{-1} for apo-oxidase, and -54×10^6 and -59×10^6 deg cm^2 dmol^{-1} for cytochrome *c* oxidase. The ellipticity values of apo-oxidase and its

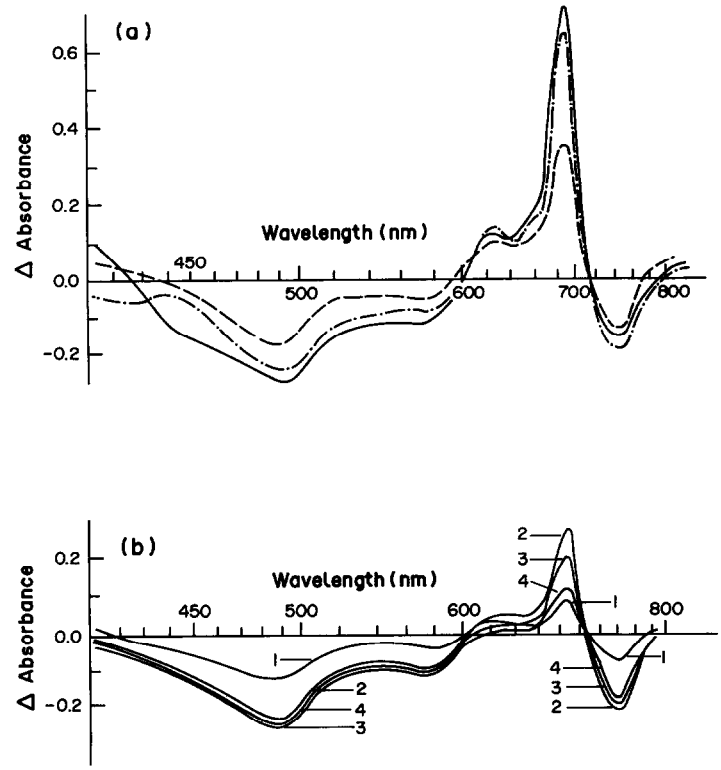

Fig. 4. Difference spectra of dithionite reduced Fe^{III}L–apo-oxidase with additional ligands. (a) Complex+KCN against complex (——), complex+azide (– – –), complex+imidazole (–·–·–), against the same solution of the complex. Complex concentration: 2.7×10^{-5} M. (b) Complex+molecular oxygen against the same solution in argon, recorded in time: (1) after 30 min of the reaction run, (2) after 2 h, (3) after 4 h, (4) after 24 h of the reaction run. Complex concentration: 2.7×10^{-5} M.

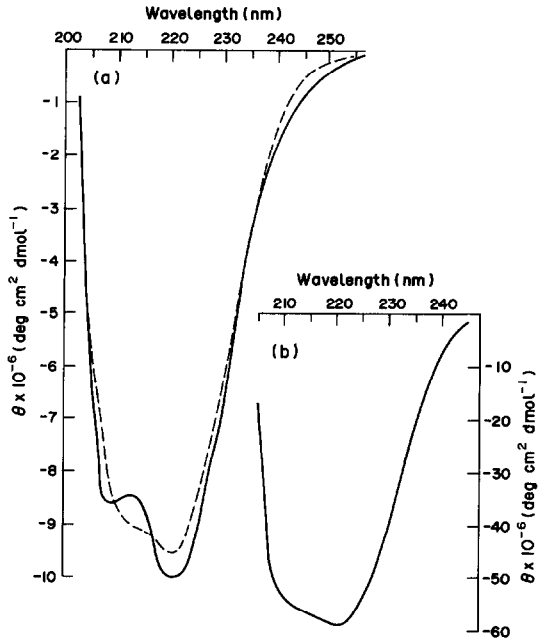

Fig. 5. (a) UV CD spectra of the $Fe^{III}L$–apo-oxidase complex (——) and apo-oxidase (– – –). (b) UV CD spectrum of the bovine cytochrome *c* oxidase.

phthalocyanine complex are comparable which indicates that the ordered structure of the native protein is not reconstituted, due to $Fe^{III}L$ incorporation into cytochrome *c* apoprotein.

Localization of $Fe^{III}L$ *on* $Fe^{III}L$*–apo-oxidase polypeptides*

Bovine cytochrome *c* oxidase incubated with a sodium dodecyl sulphate–urea mixture, under the experimental conditions described above, is dissociated into polypeptide subunits, which on a Sephadex G-100 column give six fractions. The polyacrylamide gel electrophoresis of the reaction mixture, containing urea and sodium dodecyl sulphate shows seven bands with the relative mobilities corresponding to the sequence observed by Capaldi *et al.*[30] [Fig. 6(a)]. In order to obtain information about localization of $Fe^{III}L$ on $Fe^{III}L$–apo-oxidase polypeptide subunits we have performed a similar dissociation of this protein complex. In Fig. 6(b) gel filtration profiles of the dissociation products at 280 and 657 nm are shown. At 280 nm six bands are observed corresponding to the native enzyme polypeptide fractions. They overlap indicating that there is more than one component contributing to each peak. At 657 nm two broad overlapping bands are observed at the "ab" region of the gel filtration profile, together with two lower ones at the "ef" region. Polyacrylamide gel electrophoresis patterns of the top polypeptide fractions containing $Fe^{III}L$, compared with those of the native cytochrome oxidase, have shown that the maximum $Fe^{III}L$ content corresponds to the electrophoretic bands of the native enzyme pattern described as I, V and VII.[30]

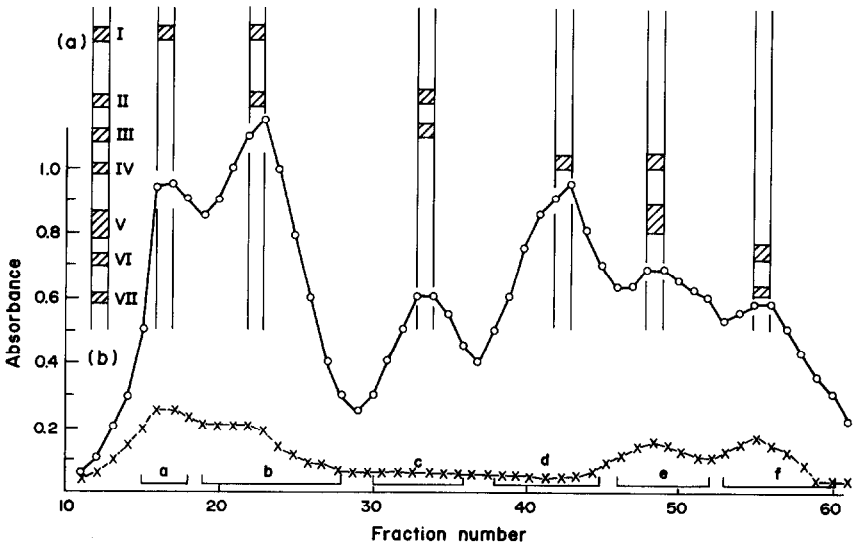

Fig. 6. Elution profiles of dissociated $Fe^{III}L$–apo-oxidase chromatographed on Sephadex G-100 as described in the Experimental, in the presence of SDS–8 M urea. The absorbance profile at 280 nm is indicated by solid line (b). The polypeptide composition of the SDS–urea column fractions is indicated by electrophoretic gels shown above their respective fractions. Cytochrome *c* oxidase electrophoresed in the same way as shown on the left (a). The lower trace (dashed line) is the absorbance profile at 657 nm reflecting the distribution of $Fe^{III}L$ among the different polypeptides.

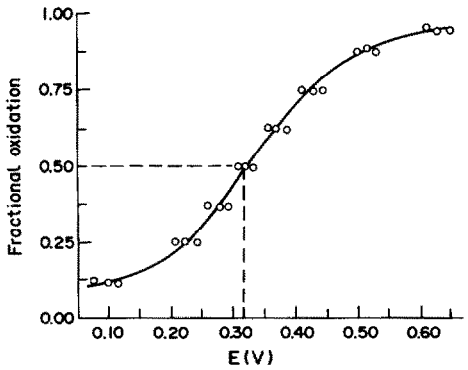

Fig. 7. Oxidation–reduction titration of $Fe^{III}L$–apo-oxidase in 0.02 M phosphate buffer pH 7.4 with 0.5% sodium cholate and 1% Tween-80, with mediators described in text.

The polypeptides corresponding to bands I and V have been suggested to be involved in heme binding.[31] The maximum $Fe^{III}L$ content corresponding to electrophoretic band VII probably results from the slow moving free $Fe^{III}L$ which is partially released from its binding polypeptides by the action of SDS and β-mercaptomethanol.

Oxidation–reduction potential

Figure 7 presents the oxidation–reduction equilibrium curve of the iron phthalocyanine complex with apo-oxidase at 25°C as obtained by the mixture method. Methylene blue was used as mediator. The value of $E_{m,7.4}$ given by the oxidizing titration is +315.5 mV. This value is reproduced in the reducing titration and in the presence of a mixture of the following mediators: $K_3Fe(CN)_6$, methylene blue, thionine and toluene blue. The mid-point potential of $Fe^{III}L$–apo-oxidase indicates that it should oxidize cytochrome *c* ($E_{m,7.4}$ of cytochrome *c* is 260 mV). The appropriate difference spectrum shows that cytochrome *c* does undergo oxidation by this complex (Fig. 8). However, the reaction rate in the case of the phthalocyanine complex is markedly lower than that of the native enzyme. The activity values of this complex and cytochrome *c* oxidase in the reaction with ferrous cytochrome *c* were found to be about 30 and 70 mol min^{-1} mg of the protein, respectively.

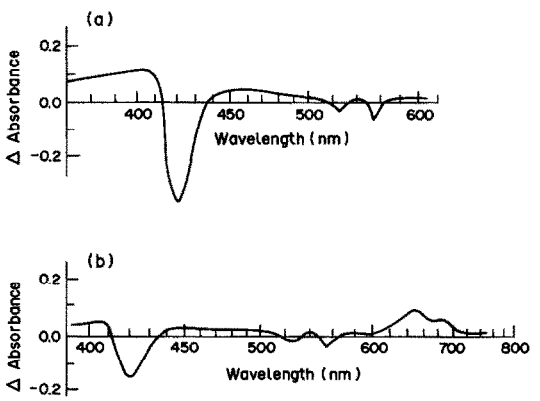

Fig. 8. Difference spectra of the mixtures of the native cytochrome *c* oxidase (a) and $Fe^{III}L$–apo-oxidase (b) with ferrous cytochrome *c* against the same solution of ferrous cytochrome *c*. After 30 min of the reaction run. Concentrations: cytochrome *c* oxidase = $Fe^{III}L$–apo-oxidase = 10^{-7} M; ferrous cytochrome *c* = 3×10^{-6} M.

CONCLUSIONS

Preparation of cytochrome *c* apo-oxidase by Teale's acid butanone method involves dissociation of cytochrome *c* oxidase into heme *a*, heme a_3 and the apoprotein. Removal of the hemes from the protein crevices results in a marked perturbation of its helix structure and complete loss of its enzymic activity.

We have shown that apo-oxidase interacts with iron(III) tetrasulphonated phthalocyanine to give a complex $Fe^{III}L$–apo-oxidase with $Fe^{III}L$ in place of heme *a* and a_3. This complex is characterized by a main intense peak at 657 nm and weaker one at 700 nm. As was shown by molecular weight estimation, one mole of cytochrome *c* oxidase used in our studies, as well as its phthalocyanine complex, contains three functional units of MW 130,000 per unit. The molar ratio of $Fe^{III}L$ to apo-oxidase in the complex was found to be two moles of $Fe^{III}L$ per functional unit of cytochrome *c* apo-oxidase. The iron(III) phthalocyanine complex with apo-oxidase, in anaerobic conditions, undergoes reduction with an excess of dithionite to give $Fe^{III}L$–apo-oxidase. It is suggested by spectroscopic studies that dithionite attacks the phthalocyanine ring to form an intermediate complex, dithionite–$Fe^{III}L$–apo-oxidase, with the reduced phthalocyanine ligand. This suggests an open crevice structure of subunits containing $Fe^{III}L$. Deep conformational changes of cytochrome *c* oxidase upon hemes displacement confirm this. Coordination of apoprotein with $Fe^{III}L$ does not reconstitute an ordered structure of the enzyme.

Iron(III) phthalocyanine coordinated with apo-oxidase has no affinity for additional ligands. However, reduced with dithionite it combines with cyanide, azide, imidazole and molecular oxygen. This is observed by an increase in the intensity of the band at 685 nm. Combination with additional ligands results in the disappearance of the intermediate complex and iron(II) phthalocyanine complex for-

mation. Oxygen binding by $Fe^{III}L$–apo-oxidase is irreversible. The oxygenated complex undergoes slow auto-oxidation with degradation of the phthalocyanine ring, which indicates that it is not a ferrous–oxygen complex of the oxyhemoglobin type.

The results of electrophoretic and chromatographic examination of the SDS–urea dissociation products of $Fe^{III}L$–apo-oxidase, compared to those of the native cytochrome *c* oxidase suggest that $Fe^{III}L$ is located mainly on two polypeptide subunits of the apoprotein, with mobilities corresponding to bands I and V of the native enzyme pattern. The same polypeptide subunits were suggested to be involved in hemes *a* and a_3 binding. These results, supported by the stoichiometry of the $Fe^{III}L$–apo-oxidase complex, which was found to be two moles of $Fe^{III}L$ per mole of apo-oxidase functional unit, suggest coordination of $Fe^{III}L$ in heme *a* and a_3 binding sites on apo-oxidase.

The iron(III) tetrasulphonated phthalocyanine complex with apo-oxidase interacts with ferrous cytochrome *c* causing its oxidation, in agreement with their mid-point potentials which are +315.5 and +260 mV, respectively. However, the rate of this process is markedly lower than that of the reaction of cytochrome *c* oxidase and ferrous cytochrome *c*. This fact can suggest different mechanisms of cytochrome *c* oxidation in both cases. In the case of $Fe^{III}L$–apo-oxidase this process is probably connected with the oxidative properties of $Fe^{III}L$ itself. The activity value of this complex in the reaction with ferrous cytochrome *c* is 30 mol min^{-1} mg of protein, and constitutes 43% of the cytochrome *c* oxidase enzymic activity (70 mol min^{-1} mg of protein).

Finally, we can state that the biological function of cytochrome *c* oxidase requires an exactly defined protein conformation. Removal of heme *a* and a_3 from the protein crevices brings about its irreversible structural perturbations. Coordination of iron tetrasulphonated phthalocyanine in heme binding sites on apo-oxidase does not reconstitute the proper conformation and biological activity of the enzyme, in spite of the close structural similarity between $Fe^{III}L$ and the natural prosthetic groups of cytochrome *c* oxidase.

REFERENCES

1. M. Wikstrom, K. Krab and M. Saraste, *Cytochrome Oxidase: a Synthesis*. Academic Press, London (1981).
2. M. Brunori, E. Antonini and M. T. Wilson, *Metal Ions in Biological Systems* (Edited by H. Sigel), Vol. 13, p. 187. Marcel Dekker, New York (1981).
3. B. G. Malmstrom, *Ann. Rev. Biochem.* 1982, **51**, 21.
4. L. Powers, B. Chance, Y. Ching and P. Angiolillo, *Biophys. J.* 1981, **34**, 465.
5. L. Powers, Y. Ching, B. Chance and B. Muhoberac, *Biophys. J.* 1982, **37**, 403A.
6. G. W. Brudwig, T. N. Stevens, R. N. Morse and S. I. Chan, *Biochemistry* 1981, **20**, 3912.
7. S. Yoshikawa and W. S. Caughey, *J. Biol. Chem.* 1982, **257**, 412.
8. S. Yoshikawa, O. Einarsdottir and W. S. Caughey, *Biophys. J.* 1984, **45**, 372a.
9. D. F. Wilson, J. G. Lindsay and E. S. Brocklehurt, *Biochim. Biophys. Acta* 1972, **256**, 227.
10. T. Tsudzuki and D. F. Wilson, *Arch. Biochem. Biophys.* 1971, **145**, 149.
11. G. T. Babcock, L. E. Vickery and G. Palmer, *J. Biol. Chem.* 1978, **253**, 2400.
12. R. A. Capaldi, F. Malatesta and F. M. Darley-Usmar, *Biochim. Biophys. Acta* 1983, **726**, 125.
13. M. T. Wilson, J. Peterson, E. Antonini, M. Brunori, A. Colosimo and J. Wyman, *Proc. Natl. Ac. Sci. USA* 1981, **78**, 7115.
14. E. Antonini, M. Brunori, A. Colosimo, C. Greenwood and M. T. Wilson, *Proc. Natl. Ac. Sci. USA* 1977, **74**, 3128.
15. M. Brunori, A. Colosimo, G. Rainoni, M. T. Wilson and E. Antonini, *J. Biol. Chem.* 1979, **254**, 10769.
16. T. Yamanaka and K. Okunuki, *Biochem. Z.* 1963, **338**, 62.
17. K. E. Hill and D. C. Wharton, *J. Biol. Chem.* 1978, **253**, 489.
18. H. Przywarska-Boniecka and Ł. Ostropolska, *J. Inorg. Biochem.* 1982, **16**, 183.
19. T. Yonetani, *J. Biol. Chem.* 1961, **236**, 1680.
20. F. W. J. Teale, *Biochim. Biophys. Acta* 1959, **35**, 543.
21. T. Yonetani, *J. Biol. Chem.* 1967, **212**, 5008.
22. W. R. Fischer, H. Taniuchi and C. B. Anfinsen, *J. Biol. Chem.* 1973, **248**, 3188.
23. D. Vonderschmitt, K. Bernauer and S. Fallab, *Helv. Chim. Acta* 1965, **48**, 95.
24. O. H. Lowry, N. J. Rosebrough, A. L. Faar and R. J. Randall, *J. Biol. Chem.* 1951, **193**, 265.
25. P. Andrews, *Biochem. J.* 1964, **91**, 222.
26. K. Weber and M. Osborn, *J. Biol. Chem.* 1969, **244**, 4406.
27. N. W. Downer, N. C. Robinson and R. A. Capaldi, *Biochemistry* 1976, **15**, 2930.
28. L. C. D. Dickinson and I. C. W. Chien, *Biochemistry* 1975, **14**, 3526.
29. T. Yonetani, *J. Biol. Chem.* 1960, **235**, 3138.
30. R. A. Capaldi, R. L. Beer and T. Brencheck, *Biochem. Biophys. Res. Commun.* 1977, **74**, 425.
31. C. A. Yu and L. Yu, *Biochim. Biophys. Acta* 1977, **495**, 248.

Polyhedron Vol. 7, No. 24, pp. 2675–2678, 1988
Printed in Great Britain

0277–5387/88 $3.00+.00
© 1988 Pergamon Press plc

ON THE ELECTRONIC STRUCTURE OF $[W(WS_4)_2]^{2-}$

MOHAMED A. MAKHYOUN

Chemistry Department, Faculty of Science, Alexandria University, Egypt

(*Received* 25 *April* 1988; *accepted* 27 *May* 1988)

Abstract—The ground-state electronic structure of $W_3S_8^{2-}$ has been calculated using the relativistic SCF–MS–X_α method. The results confirm a formal oxidation state of +2 for the central tungsten atom and a +6 oxidation state for the terminal ones. A W—W σ bond is detected within the $7a_{1g}$ molecular orbital leading to a W—W bond order of 1/2. The energy order of the X_α MOs of ligand field interest, localized on the central metal ion, is explained based on the simple angular overlap approach taking into consideration the W—W interactions.

The thioanions, MoS_4^{2-} and WS_4^{2-}, have been often used as bidentate ligands to obtain a variety of metal complexes.[1] From these, a series of complexes of the type $[M(XS_4)_2]^{n-}$ (M = Fe, Co, Ni and Zn; X = Mo or W) has been isolated and characterized.[1-4] The structure of this type of metal complex consists of two XS_4^{2-} anions coordinating as bidentate ligands with the metal (M). A square-planar or tetrahedral arrangement is possible around the central metal. This class of compounds is not only of interest from the theoretical point of view, but also has possible catalytic significance.[1,5]

Szterenberg and Jezowska-Trzebiatowska[6] have applied the parameter-free Fenske–Hall LCAO MO method to the molecular orbital calculations of $[Fe(MoS_4)_2]^{3-}$ and $[Co(MoS_4)_2]^{n-}$ ($n = 2$, 3, 4). The results of such calculations indicate that all molecular orbitals with predominant 3*d* character of the metal (Fe, Co) are found between the occupied orbitals localized on the sulphur ligands and the empty orbitals of 4*d* character of molybdenum. There is a small but positive metal–molybdenum overlap population of the *d*σ type showing a sort of metal–molybdenum bonding.

Bhaduri and Ibers[7] have succeeded in isolating a diamagnetic complex containing the anion $[W(WS_4)_2]^{2-}$, where for the first time, a square-planar geometry around tungsten (central W) is obtained (see Fig. 1).

X-ray determination[7] has indicated that the complex ion has a symmetry approximating D_{2h}, with a tetrahedral coordination around the terminal W atoms (W_t). The central tungsten (W_c) has a square-planar coordination of sulphur atoms with a very slight tetrahedral distortion. The average W_c—W_t bond distance is 2.871 Å, which is shorter than the W—W distance in $W_4S_{12}^{2-}$ [7] by 0.156 Å. Because of this short distance and the expected oxidation state of +2 for W_c, one can anticipate that a sort of W_c—W_t bonding can exist in this complex.

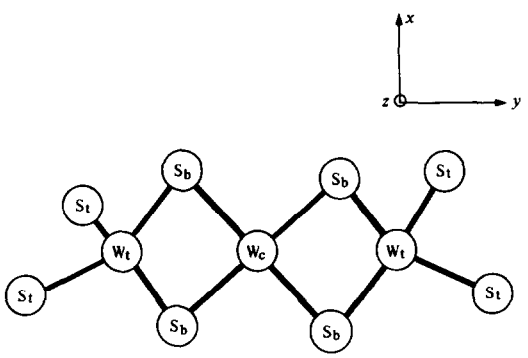

Fig. 1.

By applying the SCF–MS–X_α calculations to the hypothetical complex $W_2Cl_8^{4-}$ Cotton and Kalbacher[8] have shown that there is no qualitative reason why $W_2Cl_8^{4-}$ should not be capable of existence. Their argument is based upon the existence of a strong W—W quadruple bond (similar to the case of $Mo_2Cl_8^{4-}$) as predicted from the MO calculations.

In this work molecular orbital calculations are performed on $W_3S_4^{2-}$, utilizing the relativistic MS–X_α method,[9] to investigate the electronic structure and the possible tungsten–tungsten interactions.

METHOD OF CALCULATIONS

The SCF–X_α scattered wave method, which was developed by Slater and Johnson[10] and updated by Cook and Case[9] is used to determine the ground state electronic structure of $W_3S_8^{2-}$ (a 352 electron system). Because tungsten is a fairly heavy atom ($Z = 74$), a relativistic correction was included within the tungsten and also the sulphur spheres during the SCF calculations, following the procedure of Wood and Boring,[11] which is already incorporated in the QCPE program.[9] The coordinate system of the complex ion was based upon the X-ray structure[6] idealized to D_{2h} symmetry (Table 1), with the W_t—W_c—W_t axis lying along the y axis. Although this coordinate system is not convenient in dealing with the W_c—W_t σ type interaction, it is suitable for discussing the W_cS_4 square-planar structure. The calculations included the use of s-, p-, d- and f-spherical harmonics on the tungsten atoms and s-, p- and d-type harmonics on the sulphur ligands. For the extramolecular region, spherical harmonics up to $l = 4$ were used. The atomic exchange factor α values were taken from the compilation of Schwarz.[12] A weighted average of these atomic values was used for the interatomic and extramolecular regions. The Norman criteria[13] were used in choosing the atomic radii scaled by a factor of 0.88. An external outersphere tangent with the S_t spheres was used, which also served as a Watson sphere on which a charge of +2 is distributed to stabilize the negative anion. A summary of the parameters used in the calculations is given in Table 1.

RESULTS AND DISCUSSION

The following SCF charge distributions are obtained for the two different sets of tungsten atoms in $W_3S_8^{2-}$:

$$W_c^{+0.760}: s^{0.560}, p^{0.471}, d^{4.071}, f^{0.137}$$

$$W_t^{+1.011}: s^{0.546}, p^{0.521}, d^{3.721}, f^{0.201}.$$

Table 1. Parameters used in the X_α calculations

	W_c	W_t	S_b	S_t	Outer sphere
α_i	0.69317	0.69317	0.72475	0.72475	0.70580
R_i	1.3978	1.3357	1.2806	1.3188	5.7758

W_c—S_b 2.344 < S_b—W_c—S_b 99° < S_t—W_t—S_t 111°
W_t—S_b 2.234 < S_b—W_t—S_b 105.8°
W_t—S_t 2.152 < W_c—S_b—W_t 77.6°

Sphere radii and bond distances are in angstroms.

It is observed that although the formal charges of W_c and W_t are +2 (d^4) and +6 (d^0), respectively (this will be confirmed later), they have almost similar orbital populations and close net charges. This can be explained, based upon the Pauling electroneutrality principle,[14] which states that stable complexes are those with structures such that each atom has only a small electric charge, approximating zero. Nevertheless, the source of the above d-orbital population is to some extent different for the two sets of atoms. In the case of W_c, the orbital charge of the d-subshell is mainly due to the electrons occupying two tungsten d-like MOs (namely $7a_{1g}$ and $8a_{1g}$). This also indicates that the formal configuration of W_c can be regarded as $5d^4$, $6p^0$, $6s^0$ (W^{2+}). On the contrary, the d orbital charge observed for W_t is entirely the result of the delocalization of the electrons occupying ligand-like MOs and having small metal d character. (The d-like MOs localized on W_t are unoccupied.) This is in accordance with a formal configuration of $5d^0$, $6s^0$, $6p^0$ (W^{6+}).

The results for the energy eigenvalues of the SCF-ground state of $W_3S_8^{2-}$ and the corresponding orbital charges are given in Table 2. Two types of sulphur atoms are present in $W_3S_8^{2-}$, the bridging set (S_b), and the terminal ones (S_t). We may conclude that since the S_b set of atoms is acting as a bidentate ligand, it should be the one carrying the less negative charge. As a result of this, we observe that (Table 2) the MOs of mainly sulphur (S_b) $3s$ in character ($1a_{1g}$, $1b_{1g}$, $1b_{3u}$ and $1b_{2u}$) are more stable than the corresponding MOs centred on the S_t set ($2a_{1g}$, $2b_{2u}$, $1b_{1u}$ and $1b_{3g}$). The same trend can also be observed for the MOs of predominantly sulphur $3p$ in character. In Fig. 2, a diagram is displayed showing the MOs of ligand field interest centred on W_c and W_t. All the d-like MOs of W_t are empty, whereas two of the MOs localized mainly on W_c are occupied, one of them ($8a_{1g}$) is the HOMO state in $W_3S_8^{2-}$, the LUMO is the $3b_{2g}$ molecular orbital. Note that only four d orbitals are shown in Fig. 2 for W_c. The missing one is the $6b_{1g}$ (d_{xy}), which was not detected by our calculations. This can be attributed to the highly σ antibonding nature of this MO, which is expected to be of energy greater than −0.1 Rydberg. The bonding counterpart of the $6b_{1g}$ MO is presumably the $3b_{1g}$.

Following the angular overlap model (AOM),[15] the energy of the d orbitals in a square-planar geometry like in W_cS_4, can be given as (using the coordinate system of Fig. 1 and ignoring δ bonding contributions): (e_σ and e_π are AOM parameters) d_{z^2} (e_σ), d_{xz}, d_{yz} ($2e_\pi$), $d_{x^2-y^2}$ ($4e_\pi$) and d_{xy} ($3e_\sigma$).

In our case, the situation is slightly different from a square-planar complex MX_4 of axially symmetric

Table 2. Orbital eigenvalues and charge composition in $W_3S_8^{2-}$

Orbital	E (Ryd.)	W_c	W_t	S_b	S_t
$11a_{1g}$	−0.1161	20.1 *d*	14.3 *d*	4.3 *p*+5.5 *d*	
$6b_{3g}$	−0.1200	4.2 *d*	4.0 *p*+19.4 *d*		5.0 *p*+5.0 *d*
$8b_{2u}$	−0.1273		3.6 *p*+19.4 *d*	4.3 *p*	3.6 *p*+3.6 *d*
$10a_{1g}$	−0.1360	20.2 *d*	1.2 *s*+13.1 *d*+3.1 *f*	1.5 *s*	2.1 *p*+4.8 *d*
$5b_{1u}$	−0.1448		5.7 *p*+17.2 *d*	2.4 *d*	4.7 *p*+5.0 *d*
$5b_{3u}$	−0.1830	2.6 *p*	2.0 *p*+21.7 *d*	3.0 *p*+4.6 *d*	2.2 *p*+2.1 *d*
$9a_{1g}$	−0.1869	8.8 *d*	1.6 *p*+23.1 *d*		5.1 *p*+4.2 *d*
$5b_{1g}$	−0.1927	11.0 *d*	1.8 *p*+15.5 *d*	5.8 *p*+4.0 *d*	2.4 *p*
$4b_{2g}$	−0.2405	18.0 *d*	21.2 *d*	3.6 *p*	2.8 *p*+1.8 *d*
$3a_u$	−0.2512		29.1 *d*	2.4 *p*	4.7 *p*+2.3 *d*
$7b_{2u}$	−0.2546	3.2 *f*	28.1 *d*	3.5 *p*	3.9 *p*+1.7 *d*
$5b_{3g}$	−0.3083	71.4 *d*		5.5 *p*	
$3b_{2g}$	−0.3210	53.9 *d*	7.5 *d*	1.9 *p*	3.9 *p*
$8a_{1g}$	−0.3555	18.3 *s*+77.2 *d*			
$7a_{1g}$	−0.4247	44.9 *d*	11.7 *d*	1.4 *p*+2.6 *d*	2.7 *p*
$4b_{3g}$	−0.4687	1.7 *d*			22.9 *p*
$4b_{1u}$	−0.4694			1.4 *p*	22.6 *p*
$2a_u$	−0.4822			12.4 *p*	11.4 *p*
$4b_{3u}$	−0.5050	1.4 *p*	2.0 *p*	2.8 *p*	19.8 *p*
$4b_{1g}$	−0.5056		3.1 *p*	2.8 *p*	20.1 *p*
$2b_{2g}$	−0.5268	12.7 *d*	6.1 *d*	4.7 *p*	13.1 *p*
$6b_{2u}$	−0.5427	3.6 *p*+1.4 *f*	2.7 *p*+2.4 *d*	6.5 *p*	14.3 *p*
$6a_{1g}$	−0.5623		2.0 *p*+9.4 *d*	2.1 *p*	16.0 *p*
$3b_{1u}$	−0.5651	2.4 *p*	2.8 *p*	19.2 *p*	3.4 *p*
$3b_{3g}$	−0.5734	17.2 *d*	2.9 *p*	15.0 *p*	3.8 *p*
$3b_{3u}$	−0.6101	12.0 *p*+1.7 *f*		20.0 *p*	
$1a_u$	−0.6154		16.2 *d*	8.8 *p*	7.1 *p*
$5b_{2u}$	−0.6264	6.1 *p*+2.2 *f*	13.0 *d*	12.2 *p*	2.7 *p*
$3b_{1g}$	−0.6623	12.0 *d*	13.9 *d*	12.3 *p*	
$1b_{2g}$	−0.6426	10.2 *d*	11.0 *d*	12.8 *p*	3.5 *p*
$4b_{2u}$	−0.6939	1.5 *p*	4.4 *s*+8.7 *d*	14.7 *p*	9.5 *p*
$5a_{1g}$	−0.7211		2.9 *s*+11.1 *d*		1.3 *s*+13.6 *p*
$3b_{2u}$	−0.7285		4.6 *s*+9.5 *d*		1.5 *s*+14.3 *p*
$2b_{1u}$	−0.7328		17.2 *d*		12.5 *p*
$2b_{3g}$	−0.7352	1.5 *d*	17.2 *d*		12.0 *p*
$2b_{3u}$	−0.7442		1.3 *p*+15.4 *d*	14.7 *p*	
$2b_{1g}$	−0.7570	25.6 *d*	3.5 *d*	14.6 *p*	
$4a_{1g}$	−0.7738	4.7 *s*+10.6 *d*	5.4 *s*+3.2 *d*	12.7 *p*	1.7 *p*
$3a_{1g}$	−0.8052	9.6 *s*+10.6 *d*	6.7 *d*	14.4 *p*	
$1b_{3g}$	−1.2996		2.0 *p*+4.5 *d*		20.9 *s*
$1b_{1u}$	−1.2998		2.0 *p*+4.5 *d*		20.9 *s*
$2b_{2u}$	−1.3139		1.5 *p*+3.5 *d*	4.9 *s*	16.1 *s*
$2a_{1g}$	−1.3202		2.0 *s*+2.9 *d*		19.7 *s*
$1b_{2u}$	−1.3596	2.0 *p*	4.1 *s*	16.5 *s*	4.6 *s*
$1b_{3u}$	−1.3626	3.2 *p*	2.5 *d*	21.8 *s*	
$1b_{1g}$	−1.3727	7.4 *d*	2.5 *d*	20.7 *s*	
$1a_{1g}$	−1.4123	5.2 *s*+2.5 *d*	2.6 *s*	19.6 *s*	

ligands, because the P_π orbitals of S_b sulphur atoms are engaged in a formation of bridging bonds with the terminal tungsten atoms. This leads to a considerable reduction in the ability of the $d_{x^2-y^2}$ of W_c to participate in $d_\pi - p_\pi$ interactions. In other words, we can anticipate the $d_{x^2-y^2}$ of W_c in $W_3S_8^{2-}$ to be of non-bonding character. By making use of the above argument, we can arrange the energy of the *d* orbitals centred on W_c in the following order (based on the AOM and assuming that $e_\sigma > 2e_\pi$): $d_{x^2-y^2}$ (0) < d_{xy}, d_{yz} ($2e_\pi$) < d_{z^2} (e_σ) < d_{xy} ($3e_\sigma$). This is not the order observed in Fig. 2, but so far we have not considered the possible W—W interactions in this system. The energy order

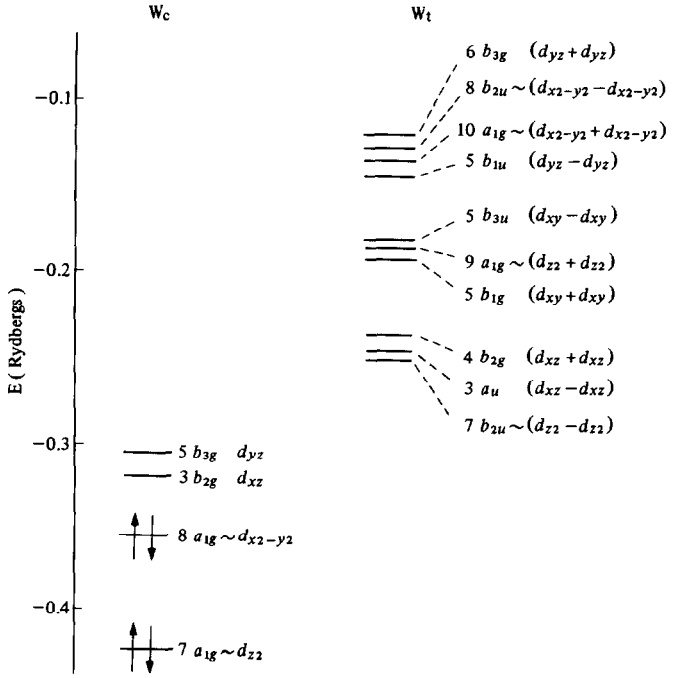

Fig. 2.

of the d orbitals of the central tungsten atom, obtained from the X_α calculations (Fig. 2), can be nicely explained if we adopt the above scheme of energy order based on the AOM approach, taking into consideration the expected stability of the $7a_{1g}$ MO (d_{z^2}), as a result of a d_σ—d_σ bonding between the central tungsten and the terminal set of tungsten atoms. The $7a_{1g}$, is almost the only MO that contains an appreciable W—W bonding interaction in this system. The $8a_{1g}$ MO ($\sim d_{x^2-y^2}$) (see Table 2) is of non-bonding nature and is not expected to contribute to the W_c—W_t bonding. On these grounds, the short W_c—W_t distance can be explained as a result of W—W σ bonding involving mainly the d_{z^2} orbitals on both sides. This sort of interaction is observed predominantly in the $7a_{1g}$ MO, and because the $8a_{1g}$ is of a non-bonding nature and is occupied by two d electrons (on W_c), the expected W_c—W_t bond order will be 1/2.

REFERENCES

1. A. Müller, E. Diemann, R. Jostes and H. Bögge, *Angew. Chem. Int. Ed. Engl.* 1981, **20**, 934.
2. I. Sotofte, *Acta Chem. Scand.* 1976, **A30**, 157.
3. I. Paulat-Böschen, B. Krebs, A. Müller, E. Königere-Ahlborn, H. Donfeld and H. Schulz, *Inorg. Chem.* 1978, **17**, 1440.
4. J. W. McDonald, G. D. Friesen and W. E. Newton, *Inorg. Chim. Acta* 1980, **46**, L79.
5. R. Battaglia, R. Henning and H. Kisch, *Z. Naturforsch.* 1981, **B36**, 396.
6. L. Szterenberg and B. Jezowska-Trzebiatowska, *Inorg. Chim. Acta* 1984, **86**, L29.
7. S. Bhaduri and J. A. Ibers, *Inorg. Chem.* 1986, **25**, 3.
8. F. A. Cotton and B. J. Kalbacher, *Inorg. Chem.* 1977, **16**, 2386.
9. M. Cook and D. A. Case, *Quant. Chem. Prog. Exch.* 1982, **14**, 465.
10. J. C. Slater and K. H. Johnson, *Phys. Rev.* 1972, **B5**, 844.
11. J. H. Wood and A. M. Boring, *Phys. Rev. B: Condens. Matter* 1978, **18**, 2701.
12. K. Schwarz, *Phys. Rev. B: Solid State* 1972, **5**, 2466.
13. J. G. Norman Jr, *J. Chem. Phys.* 1974, **61**, 4360.
14. L. Pauling, *The Nature of the Chemical Bond*, Cornell University Press, New York (1967).
15. M. Gerloch and R. C. Slade, *Ligand-field Parameters*. Cambridge University Press, Cambridge (1973).

Polyhedron Vol. 7, No. 24, pp. 2679–2683, 1988
Printed in Great Britain

0277-5387/88 $3.00+.00
© 1988 Pergamon Press plc

ELECTROCHEMICAL STUDIES ON $Mo_2Cl_4(PR_3)_4$ COMPOUNDS CONTAINING PHOSPHINES OF VARIED BASICITY

DAVID S. HANSELMAN† and THOMAS J. SMITH‡

Department of Chemistry, Kalamazoo College, Kalamazoo, MI 49007, U.S.A.

(*Received* 20 *February* 1988; *accepted after revision* 1 *June* 1988)

Abstract—The electrochemical behaviour of a series of $Mo_2Cl_4(PR_3)_4$ complexes (PR_3 = PMe_3, PEt_3, PPr^n_3, PBu^n_3, PH_2Ph, PMe_2Ph, PEt_2Ph, $PHPh_2$, $PMePh_2$, $PEtPh_2$, $P(OMe)_3$, $P(OMe)Ph_2$) has been examined by cyclic voltammetry in dichloromethane solution. The phosphines were chosen to provide a wide range of Lewis basicity/π acidity as reflected by Tolman's $\bar{\nu}_{CO}$ IR and Bodner's $\Delta\delta_{CO}$ ^{13}C NMR spectral parameters for $Ni(CO)_3(PR_3)$. The Mo_2 compounds undergo either quasi-reversible or irreversible one-electron oxidations except for $P(OMe)_3$ and $P(OMe)Ph_2$ for which no electroactivity was observed before the solvent limit. The anodic peak potentials, $E_{p,a}$, span a range of nearly 700 mV. The half-wave potentials, $E_{1/2}$, for the quasi-reversible couples and $E_{p,a}$ for all were plotted against the IR and NMR values and against the $\delta \rightarrow \delta^*$ transition energies for the Mo_2 species in dichloromethane and in the solid state. For the organometallic spectral parameters excellent linear correlations were obtained while with the electronic spectral data fair correlations resulted. These results indicate that the $Mo_2Cl_4(PR_3)_4$ complexes become more difficult to oxidize as the electron-withdrawing nature of the PR_3 substituents increases and the $\delta \rightarrow \delta^*$ band energy decreases.

Among complexes containing metal–metal quadruple bonds, those of the type $Mo_2X_4(PR_3)_4$, where X = halogen and PR_3 = monodentate phosphine have been particularly useful in understanding this bonding feature. Variation of either halogen or phosphine affords readily accessible series of compounds[1] with which detailed physical studies can be performed, especially when tungsten analogues are also known.[2] Thus, in recent years X-ray crystallography,[3,4] electronic absorption[3–5] and emission,[5,6] vibrational[4] and photoelectron[7] spectroscopies, and theoretical methods (SCF-Xα-SW[7] and Hartree–Fock–Slater[8] techniques) have been applied to these materials. Their redox properties have also been explored beginning with the report of Walton and co-workers on the one-electron oxidations of $Mo_2Cl_4(PR_3)_4$ (R = Et, Pr^n) in dichloromethane solution.[9] More recently, Zietlow *et al.* examined the electrochemical behaviour of seven $Mo_2X_4(PR_3)_4$ species (X = Cl, R = Me, Et, Pr^n, Bu^n; X = Br, R = Me, Et; X = I, R = Me) and found quasi-reversible single-electron oxidations in dichloromethane and both oxidations and reductions in tetrahydrofuran.[10] Similar observations have been reported for $Mo_2Cl_4(PR_3)_4$ by Rothwell and co-workers[11] (R = Me) and by Schrock[2] (R = Bu^n) and their associates. Finally, Gray, Bard and co-workers have also shown that $Mo_2Cl_4(PMe_3)_4$ will exhibit electrogenerated chemiluminescence in THF and acetonitrile.[12]

In this paper we describe an electrochemical investigation of $Mo_2Cl_4(PR_3)_4$ compounds, carried out with the intent of exploring the influence of varying π acidity/Lewis basicity of the PR_3 ligands on redox properties. The species comprising this series are among those we isolated in the solid state in a recent attempt to prepare 20 such complexes.[13] For the 16 we were able to generate, some only in solution, correlations between the transition energy (TE) of the characteristic $\delta \rightarrow \delta^*$ band and literature-derived organometallic spectral parameters which reflect electron-withdrawing propensities of

† Upjohn Summer Research Fellow, 1986.

‡ Author to whom correspondence should be addressed.

the PR_3 ligands were explored. That study also reported the crystal structures of three members of the $Mo_2Cl_4(PR_3)_4$ series (PR_3 = PEt_3, PMe_2Ph, $PHPh_2$). Correlations similar to the previous ones have been obtained with redox potentials resulting from cyclic voltammetry measurements and are reported here.

EXPERIMENTAL

Materials

All $Mo_2Cl_4(PR_3)_4$ compounds were prepared according to previously reported procedures.[13] HPLC-grade dichloromethane (Aldrich) was deoxygenated by purging with nitrogen prior to use. Electrochemical-grade tetra-*n*-butylammonium tetrafluoroborate (TBAB) (Eastman Kodak) was vacuum dried at 100°C for 24 h.

Electrochemistry

All electrochemical measurements were performed using a Bioanalytical Systems CV-27 voltammograph. All studies were carried out at room temperature in dichloromethane containing 0.1 M TBAB as the supporting electrolyte under a nitrogen atmosphere. For cyclic voltammetry (CV) measurements a platinum or glassy carbon disc was used as the working electrode, and a platinum wire served as the auxiliary electrode. Electrode potentials were recorded relative to the silver–silver chloride reference electrode. Constant-potential electrolyses were performed with a Pt gauze working electrode, Pt wire auxiliary electrode, and Ag/AgCl reference.

Linear regression analyses and data plotting were accomplished by use of the Sigma-plot scientific graph system (Jandel Scientific).

RESULTS

Cyclic voltammetry measurements were performed on 12 $Mo_2Cl_4(PR_3)_4$ compounds in dichloromethane solution, and the results for these materials appear in Table 1. All tabulated CV data were obtained using a platinum disc indicating electrode; similar results were observed with a glassy carbon disc as the working electrode for selected complexes. Electrode potentials, measured relative to the silver–silver chloride reference, agree reasonably well with previously reported values allowing for reference electrode and solvent differences.[2,11] Peak-to-peak separations, ΔE_p, for those species displaying a reduction wave on the reverse scan substantially exceed the 59 mV value anticipated for a strictly reversible one-electron (*vide infra*) process, a result due in part to uncompensated solution resistance. However, for the trialkylphosphine species the peak current ratios, $i_{p,c}/i_{p,a}$, are close to unity at higher scan rates (300–600 mV s^{-1}), but they do decrease with decreasing scan rate at slower speeds (50–200 mV s^{-1}). ΔE_p increases with scan rate for all couples for which scan rate dependence was investigated. Thus, for the trialkyl-, dialkylphenyl- and methyldiphenylphosphines, we observed quasi-reversible electron transfer. For $PEtPh_2$, $PHPh_2$ and PH_2Ph totally irreversible behaviour was seen. For $P(OMe)_3$ and $P(OMe)Ph_2$ no CV activity was noted before the solvent limit.

Table 1. Cyclic voltammetry data for $Mo_2Cl_4(PR_3)_4$ compounds in dichloromethane[a]

Phosphine	$E_{p,a}$ (V)	$E_{1/2}$[b] (V)	ΔE_p[b] (mV)	$i_{p,c}/i_{p,a}$
PMe_3	0.67	0.61	122	0.91
PEt_3	0.56	0.50	107	0.97
PPr^n_3	0.53	0.47	129	0.99
PBu^n_3	0.51	0.46	101	0.96
PH_2Ph	1.2[c]	—	—	—
PMe_2Ph	0.72	0.62	189	0.94
PEt_2Ph	0.67	0.60	140	0.76
$PHPh_2$	0.92	—	—	—
$PMePh_2$	0.71	0.66	101	0.66
$PEtPh_2$	0.63	—	—	—
$P(OMe)_3$	—	—	—	—
$P(OMe)Ph_2$	—	—	—	—

[a] All electrode potentials are reported relative to Ag/AgCl reference electrode and at scan rates of 300 mV s^{-1}.

[b] $E_{1/2} = 1/2(E_{p,a} + E_{p,c})$; $\Delta E_p = E_{p,a} - E_{p,c}$.

[c] Near solvent limit.

With each compound the anodic wave in the CV should correspond to a one-electron oxidation.[8] To verify this we carried out constant-potential electrolyses on $Mo_2Cl_4(PPr^n_3)_4$ and $Mo_2Cl_4(PBu^n_3)_4$ in dichloromethane which yielded n values of 1.1 ± 0.1 for both. Similarities in peak shapes and currents for all quasi-reversible systems suggest that this is a general result.

In order to assess the effect of phosphine substituents on the electrochemical behaviour of this series in more detail, we examined possible correlations between electrode potentials and the electronic effects due to the PR_3 ligands. Specifically we used the difference in ^{13}C NMR chemical shift, $\Delta\delta_{CO}$, for CO in $Ni(CO)_4$ and $Ni(CO)_3(PR_3)$ as reported by Bodner *et al.* and the IR CO stretching frequency, $\bar{\nu}_{CO}$, for a series of $Ni(CO)_3(PR_3)$ com-

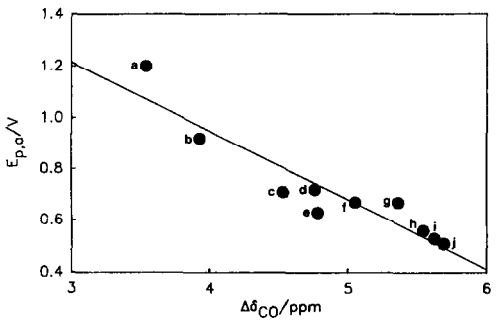

Fig. 1. Plot of $\Delta\delta_{CO}$ vs $E_{p,a}$: (a) PH_2Ph; (b) $PHPh_2$; (c) $PMePh_2$; (d) PMe_2Ph; (e) $PEtPh_2$; (f) PMe_3; (g) PEt_2Ph; (h) PEt_3; (i) PPr^n_3; (j) PBu^n_3.

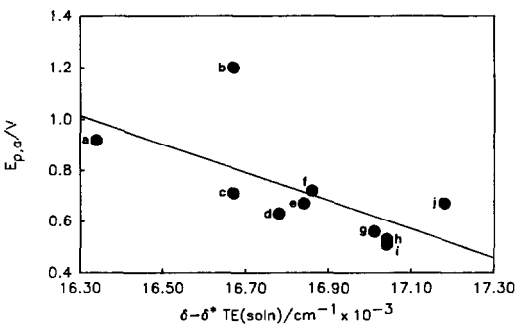

Fig. 3. Plot of $\delta \rightarrow \delta^*$ TE (CH_2Cl_2 solution) vs $E_{p,a}$: (a) $PHPh_2$; (b) PH_2Ph; (c) $PMePh_2$; (d) $PEtPh_2$; (e) PEt_2Ph; (f) PMe_2Ph; (g) PEt_3; (h) PPr^n_3; (i) PBu^n_3; (j) PMe_3.

plexes as gathered by Tolman.[14] The $\Delta\delta_{CO}$ and $\bar{\nu}_{CO}$ numbers are themselves highly correlated (linear correlation coefficient = −0.99). Against these parameters the $Mo_2Cl_4(PR_3)_4$ values for the anodic peak potentials, $E_{p,a}$, for all systems and the half-wave potentials, $E_{1/2}$, for quasi-reversible couples were plotted. Variations in ΔE_p might be expected to introduce some additional scatter in graphs involving $E_{p,a}$, but with only the latter values could the behaviour of the entire series be investigated. Plots of $E_{p,a}$ vs $\Delta\delta_{CO}$ and $\bar{\nu}_{CO}$ are shown in Figs 1 and 2; for both, good linear correlations were obtained ($\Delta\delta_{CO}$, −0.97; ν_{CO}, 0.98). For $E_{1/2}$ vs $\bar{\nu}_{CO}$ (six data points) the scatter (0.99) is indeed less than its $E_{p,a}$ counterpart. However, the $E_{1/2}$ vs $\Delta\delta_{CO}$ plot (seven points) shows slightly increased deviation from linearity (−0.96) relative to $E_{p,a}$ (*vide infra*, rhenium discussion).

Finally we also explored the relationship between $E_{p,a}$ and $E_{1/2}$ and the $^1(\delta \rightarrow \delta^*)$ transition energies for the $Mo_2Cl_4(PR_3)_4$ compounds in dichloromethane and in the solid state.[13] Here the correlation is not nearly so close. However, for both $E_{p,a}$ and $E_{1/2}$ the observed trend is one of generally increasing transition energy (TE) with decreasing potential. The graph of $E_{p,a}$ vs TE(solution) is shown in Fig. 3. The correlation coefficients are: $E_{p,a}$ vs TE(soln), −0.81; $E_{p,a}$ vs TE(ss), −0.73; $E_{1/2}$ vs TE(soln), −0.76; $E_{1/2}$ vs TE(ss), −0.84. For the $E_{p,a}$ plots the point considerably off-line is due to the PH_2Ph complex, while with $E_{1/2}$ values much scatter is seen with the trialkyl-derived complexes. Of the latter, $Mo_2Cl_4(PMe_3)_4$ deviates substantially more than the other compounds.

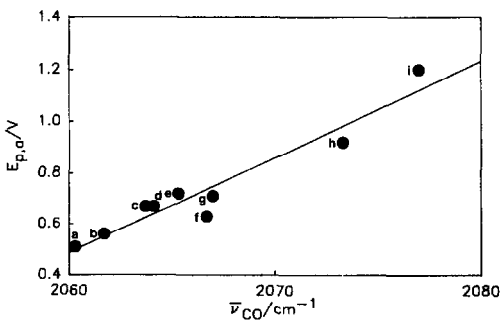

Fig. 2. Plot of $\bar{\nu}_{CO}$ vs $E_{p,a}$: (a) PBu^n_3; (b) PEt_3; (c) PEt_2Ph; (d) PMe_3; (e) PMe_2Ph; (f) $PEtPh_2$; (g) $PMePh_2$; (h) $PHPh_2$; (i) PH_2Ph. No $\bar{\nu}_{CO}$ value was reported for PPr^n_3.[14]

DISCUSSION

The results obtained in this study confirm that $Mo_2Cl_4(PR_3)_4$ compounds undergo quasi-reversible or irreversible one-electron oxidations in dichloromethane and that this behaviour is markedly dependent upon the identity of the phosphine ligand. Indeed the CV anodic peak potentials span a range of nearly 700 mV. The oxidation process involves the loss of a δ-bonding electron:

$$\underset{\sigma^2\pi^4\delta^2}{Mo_2Cl_4(PR_3)_4} \rightarrow \underset{\sigma^2\pi^4\delta^1}{Mo_2Cl_4(PR_3)_4^+} + e^-.$$

The ease of oxidation of the Mo_2^{4+} core is clearly related to the ability of the coordinated phosphine to stabilize or destabilize the resulting Mo_2^{5+} product, as reflected by correlations of the electrode potentials with the organometallic spectral parameters, $\Delta\delta_{CO}$ and $\bar{\nu}_{CO}$. In view of the high correlation of the NMR and IR values for the $Ni(CO)_3(PR_3)$ series, it appears reasonable that they should provide suitable measures of π acidity/Lewis basicity. Not surprisingly then, the most easily oxidized $Mo_2Cl_4(PR_3)_4$ species and those showing essentially reversible electron transfer at rapid scan rates are those containing the electron-releasing tri-

alkylphosphines. In addition, the observation of a steady decrease in $E_{1/2}$ and $E_{p,a}$ with increasing alkyl chain length is in accord with the observations of Gray *et al.*[10] As the alkyl substituents are replaced by phenyl groups and hydrogen atoms, the oxidation becomes more difficult and tends towards total irreversibility. Lastly, for the strongly electron-withdrawing methoxy-substituted ligands, the electron removal is not seen within the solvent oxidation limit.

Although σ-donation effects ($P\sigma \rightarrow Mod\sigma$) undoubtedly play a prominent role in the electronic stabilization of $Mo_2Cl_4(PR_3)_4^+$, particularly with the trialkyl complexes, the pronounced variation of $E_{p,a}$ and $E_{1/2}$ with $\delta \rightarrow \delta^*$TE implicates phosphine interactions with the δ and/or δ^* orbitals. Moreover, Gray *et al.* noted that for the $Mo_2X_4(PMe_3)_4$ triad (X = Cl, Br, I) the ease of oxidation and difficulty of reduction were both in the order Cl < Br < I.[10] This inverse halide order was the opposite to that expected on electronegativity grounds and was attributed to metal(*d*)-to-halide(*d*) back-bonding. We have also observed a similar trend with a series of $Mo_2X_4(LL)_2$ compounds (X = Cl, Br; LL = bidentate phosphine). In the case of the $Mo_2Cl_4(PR_3)_4$ species the oxidation behaviour does follow substituent electronegativity predictions rather closely but for presumably the same reason responsible for the inverse halide order, namely, Mo—P back-bonding. Alternatively, a decrease in Mo effective charge induced by the electron-releasing phosphines would result in expanded Mo 4*d* orbitals and increased δ overlap.[15] This would in turn lead to greater ease of oxidation and blue-shifted $\delta \rightarrow \delta^*$ transitions. While the latter effect could be dominant for the trialkyl phosphines, it would be expected to become less important as PR_3 substituents become more strongly electron withdrawing.

We now turn to the relationship between the electrode potentials and the $\delta \rightarrow \delta^*$ transition energies. The oxidation creates an entity with a metal–metal bond order of 3.5, whereas the spectral process leads to an excited-state species of bond order 3.0:

$$\underset{\sigma^2\pi^4\delta^2}{Mo_2Cl_4(PR_3)_4} \xrightarrow{h\nu} \underset{\sigma^2\pi^4\delta^1(\delta^*)^1}{Mo_2Cl_4(PR_3)_4^*}.$$

It is now clear that the representation of the $\delta \rightarrow \delta^*$ transition as strictly metal-based is an oversimplification. Again, Gray *et al.* have shown that for the series $Mo_2X_4(PMe_3)_4$ (X = Cl, Br, I) this band undergoes substantial shifts in position and intensity upon exchanging halogen atoms.[4] Our own work on the larger set of $Mo_2Cl_4(PR_3)_4$ compounds indicated a similar dependence of the band energy on PR_3.[13] For 16 of these materials we noted linear correlations for plots of $\delta \rightarrow \delta^*$TE obtained from dichloromethane solutions vs $\Delta\delta_{CO}$ (0.923) and vs $\bar{\nu}_{CO}$ (−0.892). The TE/E correlations reported in the present study further substantiate the interaction of the δ and possibly δ^* components and phosphorus-based orbitals. Thus, for example, those complexes most readily oxidized also exhibit the highest energy spectral transition. Although the $^1(\delta \rightarrow \delta^*)$TE does not directly reflect the energy of the δ–δ^* splitting due to electron correlation effects,[16,17] the overall trend does imply a weakening of the δ bond. As the electron-withdrawing power of PR_3 increases as indicated by $\Delta\delta_{CO}$ and $\bar{\nu}_{CO}$, TE decreases, and the compounds become less oxidizable. At the extreme of strongly electronegative substituents examined in our previous study, the $Mo_2Cl_4(PR_3)_4$ species either have fleeting existence in solution, e.g. with $PClPh_2$, or are not observed at all at room temperature, e.g. with $P(OPh)_3$.[13] Presumably phosphines of the latter types cleave the M—M bond of transient $Mo_2Cl_4(PR_3)_4$ or of reactant complexes via interaction with the strong σ and/or π components, since the δ bond may contribute only about 10 kcal mol^{-1} to the total bond energy of the Mo—Mo quadruple bond by two recent estimates.[17,18] However, steric bulk as reflected by the cone angle may also play a role.

The appreciable off-line behaviour in the TE/$E_{p,a}$ plot arises from the PMe_3 and PH_2Ph complexes. We attribute this to variation in the spectral properties rather than the electrode potentials. We previously noted considerable deviation from linearity for both complexes in plots of TE vs $\Delta\delta_{CO}$ and $\bar{\nu}_{CO}$.[13] Both of these ligands contain small substituent groups, and this may influence TE values. It has been suggested that the anomolous emission spectra of $Mo_2Cl_4(PMe_3)_4$ relative to its trialkyl homologues may be due in part to its ability to adopt a staggered configuration in the $^1(\delta\delta^*)$ excited state whereas the larger hydrocarbon chains of the others prevent this rearrangement.[6]

Finally, although our investigations thus far have not allowed us to extend these correlations to reduction processes for the $Mo_2Cl_4(PR_3)_4$ series, and the available data in the literature are restricted to trialkyl species,[10] an isoelectronic set of rhenium(III) compounds does provide this opportunity. Walton *et al.* observed one-electron reductions in CH_2Cl_2 for the $Re_2Cl_6(PR_3)_2$ complexes (PR_3 = PEt_3, PPr^n_3, PBu^n_3, PEt_2Ph, $PMePh_2$, $PEtPh_2$).[19] For these species the reduction products exhibit a $\sigma^2\pi^4\delta^2(\delta^*)^1$ configuration. The phenyl-substituted materials also undergo a second one-

electron reduction. Our plot of their $E_{1/2}$ values for the first reduction vs $\Delta\delta_{CO}$ reveals an essentially linear relationship although the point due to PEt_2Ph is significantly off-line. Curiously, in our $Mo_2/\Delta\delta_{CO}/E_{1/2}$ plot the PEt_2Ph point also deviates somewhat from the best-fit straight line, possibly a reflection of error in the original $\Delta\delta_{CO}$ value. The PEt_2Ph behaviour notwithstanding, the Re correlation clearly indicates the connection between PR_3 electronic effects and ease of reduction. Thus the electron-releasing alkyl groups, in this instance, destabilize the $Re_2Cl_6(PR_3)_2^-$ product whereas phenyl groups lead to net stabilization. These results implicate interaction of Re_2 δ^* and phosphorus-based orbitals.

Acknowledgements—We gratefully acknowledge financial assistance from the Research Corporation, the donors of the Petroleum Research Fund, administered by the American Chemical Society, and the National Science Foundation (Research in Undergraduate Institutions award). D.S.H. acknowledges an Upjohn Summer Research Fellowship awarded by the Upjohn Company. We appreciate the assistance of Prof. Paul Sotherland in the use of the Sigma-plot graphics system.

REFERENCES

1. J. San Filippo, *Inorg. Chem.* 1972, **11**, 3140; J. San Filippo, H. J. Sniadoch and R. L. Grayson, *Inorg. Chem.* 1974, **13**, 2121; H. D. Glicksman, A. D. Hamer, T. J. Smith and R. A. Walton, *Inorg. Chem.* 1976, **15**, 2205.
2. R. R. Schrock, L. G. Sturgeoff and P. R. Sharp, *Inorg. Chem.* 1983, **22**, 2801; R. L. Luck, R. H. Morris and J. F. Sawyer, *Inorg. Chem.* 1987, **26**, 2422.
3. F. A. Cotton, M. W. Extine, T. R. Felthouse, B. W. S. Kolthammer and D. G. Lay, *J. Am. Chem. Soc.* 1981, **103**, 4040; F. A. Cotton and R. Poli, *J. Am. Chem. Soc.* 1986, **108**, 5628; F. A. Cotton and R. Poli, *Inorg. Chem.* 1987, **26**, 3228.
4. M. D. Hopkins, W. P. Schaefer, M. J. Bronikowski, W. H. Woodruff, V. M. Miskowski, R. F. Dallinger and H. B. Gray, *J. Am. Chem. Soc.* 1987, **109**, 408.
5. T. C. Zietlow, M. D. Hopkins and H. B. Gray, *J. Solid State Chem.* 1985, **57**, 112.
6. V. M. Miskowski, R. A. Goldbeck, D. S. Kliger and H. B. Gray, *Inorg. Chem.* 1979, **18**, 86; M. D. Hopkins and H. B. Gray, *J. Am. Chem. Soc.* 1984, **106**, 2468; J. R. Winkler, D. G. Nocera and T. L. Netzel, *J. Am. Chem. Soc.* 1986, **108**, 4451.
7. F. A. Cotton, J. L. Hubbard, D. L. Lichtenberger and I. Shim. *J. Am. Chem. Soc.* 1982, **104**, 679.
8. T. Ziegler, *J. Am. Chem. Soc.* 1984, **106**, 5901.
9. T. C. Zietlow, D. D. Klendworth, T. Nimry, D. J. Salmon and R. A. Walton, *Inorg. Chem.* 1981, **20**, 947.
10. T. C. Zietlow, M. D. Hopkins and H. B. Gray, *J. Am. Chem. Soc.* 1986, **108**, 8266.
11. T. W. Coffindaffer, G. P. Niccolai, D. Powell, I. P. Rothwell and J. C. Huffman, *J. Am. Chem. Soc.* 1985, **107**, 3572.
12. J. Ouyang, T. C. Zietlow, M. D. Hopkins, F.-R. F. Fan, H. B. Gray and A. J. Bard, *J. Phys. Chem.* 1986, **90**, 3841.
13. F. A. Cotton, L. M. Daniels, G. L. Powell, A. J. Kahaian, T. J. Smith and E. Fiore Vogel, *Inorg. Chim. Acta* 1988, **144**, 109.
14. G. M. Bodner, M. P. May and L. E. McKinney, *Inorg. Chem.* 1980, **19**, 1951; C. A. Tolman, *Chem. Rev.* 1977, **77**, 313.
15. We thank a referee for this suggestion.
16. F. L. Campbell, F. A. Cotton and G. L. Powell, *Inorg. Chem.* 1985, **24**, 177.
17. M. D. Hopkins, H. B. Gray and V. M. Miskowski, *Polyhedron* 1987, **6**, 705.
18. J. P. Collman and L. K. Woo, *Proc. Natl. Acad. Sci. U.S.A.* 1984, **81**, 2592.
19. P. Brant, D. J. Salmon and R. A. Walton, *J. Am. Chem. Soc.* 1978, **100**, 4424.

Polyhedron Vol. 7, No. 24, pp. 2685–2694, 1988
Printed in Great Britain

0277–5387/88 $3.00+.00
© 1988 Pergamon Press plc

REACTIONS OF NUCLEOPHILES WITH CYCLOPENTADIENYLIRON COMPLEXED HALOTOLUENES

ROBERT M. MORIARTY,* UDAI S. GILL and YI YIN KU

University of Illinois at Chicago, Department of Chemistry, P.O. Box 4348, Chicago, IL 60680, U.S.A.

(*Received* 26 *March* 1988; *accepted* 1 *June* 1988)

Abstract—η^6-*o*-Chlorotoluene-η^5-cyclopentadienyliron hexafluorophosphate undergoes nucleophilic substitution of the chlorine atom with anions generated (K_2CO_3/DMF) from methyl thioglycolate, diethyl malonate, dimethyl malonate, methyl acetoacetate and 2,4-pentanedione. The compounds prepared were *o*-$CH_3C_6H_4SCH_2CO_2CH_3FeCp^+PF_6^-$, *o*-$CH_3C_6H_4CH(CO_2C_2H_5)_2FeCp^+PF_6^-$, *o*-$CH_3C_6H_4CH(CO_2CH_3)_2FeCp^+PF_6^-$, *o*-$CH_3C_6H_4CH(COCH_3)CO_2CH_3FeCp^+PF_6^-$ and *o*-$CH_3C_6H_4CH_2COCH_3FeCp^+PF_6^-$. Similarly, the reaction of diethyl malonate, dimethyl malonate, methyl acetoacetate anions and methylamine with η^6-2,6-dichlorotoluene-η^5-cyclopentadienyliron hexafluorophosphate yielded monosubstitution of one of the chloro groups. The complexes prepared in this study were η^6-diethyl(3-chloro-2-methyl)phenylmalonate-η^5-cyclopentadienyliron hexafluorophosphate, η^6-dimethyl(3-chloro-2-methyl)phenylmalonate-η^5-cyclopentadienyliron hexafluorophosphate, η^6-methyl(3-chloro-2-methyl)phenylacetoacetate-η^5-cyclopentadienyliron hexafluorophosphate and η^6-3-chloro(2-methyl-N-methyl)aniline-η^5-cyclopentadienyliron hexafluorophosphate. Reaction of η^6-2,6-dichlorotoluene-η^5-cyclopentadienyliron hexafluorophosphate with excess methanol as well as methyl thioglycolate in the presence of K_2CO_3 resulted in disubstitution of both chloro groups to yield new complexes, η^6-2,6-dimethoxytoluene-η^5-cyclopentadienyliron hexafluorophosphate and η^6-methyl[(2-methylphenyl)1,3-dithio] diacetate-η^5-cyclopentadienyliron hexafluorophosphate, respectively. Complexes *o*-$CH_3C_6H_4CH(CO_2C_2H_5)_2FeCp^+PF_6^-$, *o*-$CH_3C_6H_4CH(CO_2CH_3)_2FeCp^+PF_6^-$ and *o*-$CH_3C_6H_4CH_2COCH_3FeCp^+PF_6^-$ react with excess K_2CO_3 and benzyl bromide in refluxing methylene chloride to give 80–90% yields of complexes *o*-$CH_3C_6H_4C(CH_2C_6H_5)(CO_2C_2H_5)_2FeCp^+PF_6^-$, *o*-$CH_3C_6H_4C(CH_2C_6H_5)(CO_2CH_3)_2FeCp^+PF_6^-$ and *o*-$CH_3C_6H_4CH(CH_2C_6H_5)COCH_3FeCp^+PF_6^-$, respectively. Reaction of complex, *o*-$CH_3C_6H_4C(CH_2C_6H_5)(CO_2C_2H_5)_2FeCp^+PF_6^-$ with one molar equivalent of *t*-BuOK followed by acidic work-up gives *o*-$(C_2H_5CO_2CH_2)C_6H_4CH(CO_2C_2H_5)CH_2C_6H_5FeCp^+PF_6^-$. Similarly, reactions of complexes *o*-$CH_3C_6H_4C(CH_2C_6H_5)(CO_2C_2H_5)_2FeCp^+PF_6^-$ and *o*-$CH_3C_6H_4C(CH_2C_6H_5)(CO_2CH_3)_2FeCp^+PF_6^-$ with *t*-BuOK in THF followed by alkylation with methyl iodide gave the new complexes, *o*-$(C_2H_5O_2C(CH_3)CH)C_6H_4CH(CH_2C_6H_5)CO_2C_2H_5FeCp^+PF_6^-$ and *o*-$(CH_3O_2C(CH_3)CH)C_6H_4CH(CH_2C_6H_5)CO_2CH_3FeCp^+PF_6^-$, respectively. Vacuum sublimation of the new complexes, *o*-$CH_3C_6H_4C(CH_2C_6H_5)(CO_2C_2H_5)_2FeCp^+PF_6^-$ and *o*-$(C_2H_5O_2CCH_2)C_6H_4CH(CH_2C_6H_5)CO_2C_2H_5FeCp^+PF_6^-$ gives *o*-$CH_3C_6H_4C(CH_2C_6H_5)(CO_2C_2H_5)_2$ and *o*-$(C_2H_5O_2CCH_2)C_6H_4CH(CH_2C_6H_5)CO_2C_2H_5$, respectively.

The stoichiometric use of $(arene)Cr(CO)_3$ and $[(arene)Fe(Cp)]PF_6$ complexes in organic synthesis allows the selective activation of arenes toward nucleophilic addition, nucleophilic displacement upon a complexed halobenzene and proton abstraction from the benzylic position or methyl of a complexed aryl ring.[1a–f,2a–b] Recently we reported methods for the formation of aryl–carbon bonds[3a–d] based on the chemistry of $CpFe^+$ complexed aryl halides. These complexes undergo aromatic nucleophilic substitution of a chlorine atom with heteroatomic nucleophiles[4a–g] as well

*Author to whom correspondence should be addressed.

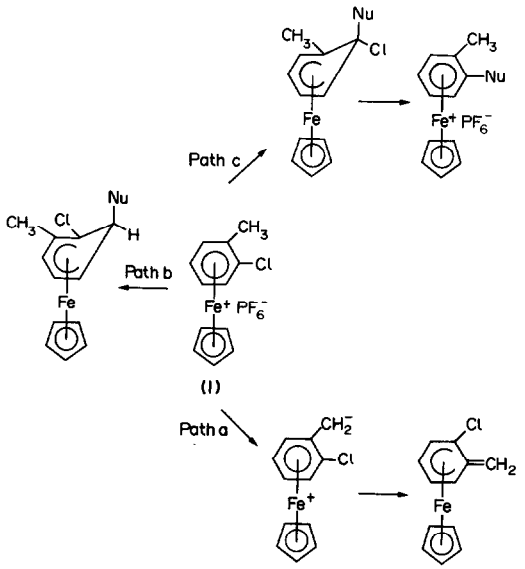

Scheme 1.

as with stabilized enolate anions.[3a–d] Similar S_NAr reactions have also been studied with other metal complexed halobenzenes.[5a–e,*]

Overall, these reactions may be viewed as arylation processes proceeding via nucleophilic substitution reactions using cyclopentadienyliron (CpFe) complexed aryl halides as the source of the aryl group followed by removal of the complexing group (CpFe).[3a–d,7a–c]

As an extension of our initial work,[3a–d] we investigated the S_NAr reactions of η_6-*o*-chlorotoluene-η^5-cyclopentadienyliron hexafluorophosphate (**1**) and η^6-2,6-dichlorotoluene-η^5-cyclopentadienyliron hexafluorophosphate (**2**). These complexes are of particular interest because they can undergo nucleophilic substitution of the chloro group with nucleophiles, as well as deprotonation of the *ortho* methyl group to promote intramolecular annulation. In this paper, we describe the results of our study into this duality of reactions and experiments aimed at sequential arylation, deprotonation and intramolecular cyclization.

Generalized pathways for the reactions of nucleophiles with $CpFe^+$ *complexed halotoluenes*

A priori, three pathways are available for the reaction of nucleophiles with arene complexes of types **1** and **2** (Scheme 1). Methyl deprotonation (path a) does not generally compete in the reactions studied by us, in fact, for heteroatomic nucleophiles (neutral or anionic) displacement[4a–g] of the chlorine atom is the only reaction observed. This latter displacement reaction has not been observed with reactive carbon nucleophiles, in which case ring addition[8a–c] (path b) is especially common. On the other hand, recently, we and others have observed the S_NAr reactions of the $CpFe^+$ complexed aryl halides with stabilized carbanions (path c).[3a–d,7a–c] It is this latter direct displacement which is the main topic of the present study.

RESULTS AND DISCUSSION

Reactions of complexes **1** *and* **2** *with heteronucleophiles*

η^6 - Chlorotoluene - η^5 - cyclopentadienyliron hexafluorophosphate (**1**) has previously been prepared in good yield by ligand exchange reaction between ferrocene and *o*-chlorotoluene[8a] and has been shown to undergo S_NAr reactions with simple alkoxides[7a] and amines.[4b,9] We expected that use of a wider range of nucleophiles might enable the synthesis of more complex organic molecules. The new complex, η^6-2,6-dichlorotoluene-η^5-cyclopentadienyliron hexafluorophosphate (**2**) was made in good yield using the same method as used for **1**.

Our first goal was to establish disubstitution in the case of the dichloro system **2**. As our starting point we pursued the reaction between methyl thioglycolate and complexes **1** and **2**, respectively. Treatment of complex **1** or **2** with excess methyl thioglycolates in the presence of K_2CO_3 in THF/DMF (20 : 1) or DMF gave the corresponding novel mono- and disubstitution toluene complexes, namely, η^6-methyl(*o*-tolyl)thioacetate-η^5-cyclopentadienyliron hexafluorophosphate (**3**) and η^6-methyl[(2 - methylphenyl)1,3 - dithio]diacetate - η^5 - cyclopentadienyliron hexafluorophosphate (**4**), respectively, as orange–yellow crystalline solids (Schemes 2 and 3). Analytical and spectral data are given in the Experimental. Similarly, reaction of complex **2** with methanol in the presence of K_2CO_3 gave the disubstitution product η^6-2,6-dimethoxytoluene-η^5-cyclopentadienyliron hexafluorophosphate (**5**) as yellow plates in excellent yield.

The reaction of complex **2** with an excess of methylamine at room temperature in dichloromethane gave the monosubstitution complex, η^6-3 - chloro - 2 - methyl - N - methylaniline-η^5-cyclopentadienyliron hexafluorophosphate (**6**) as the only product. Failure to achieve disubstitution can

* The order of reactivity of these organometallic aryl halide complexes for S_NAr substitution reaction with methoxide in methanol is $(CO)_3Cr < (CO)_3Mo^+ \ll CpFe^+ < (CO)_3Mn^+$, see ref. 6.

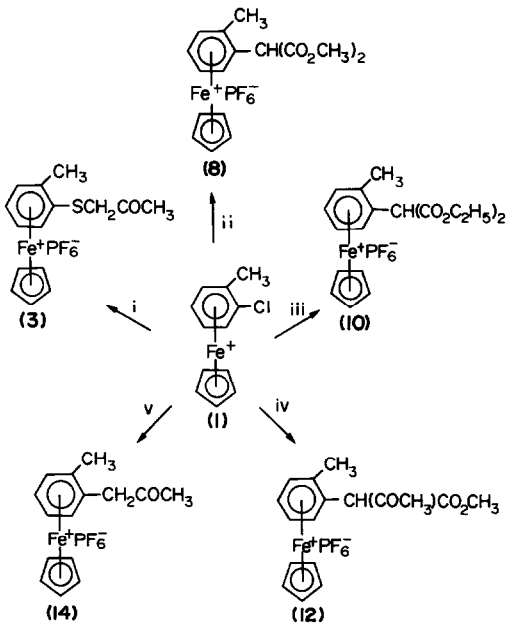

(i) $HSCH_2CO_2CH_3$ (1.5equiv), K_2CO_3 (3equiv), DMF, RT, 15 h; H_3O^+, NH_4PF_6

(ii) $H_2C(CO_2CH_3)_2$ (1.2equiv), K_2CO_3 (3equiv), DMF, RT, 8h; H_3O^+, NH_4PF_6

(iii) $H_2C(CO_2C_2H_5)_2$ (1.2equiv), K_2CO_3 (3equiv), DMF, RT, 8h H_3O^+, NH_4PF_6

(iV) $H_2C(COCH_3)(CO_2CH_3)$ (1.2equiv), K_2CO_3 (3equiv), DMF, RT, 8h; H_3O^+, NH_4PF_6

(V) $H_2C(COCH_3)_2$ (1.2equiv), K_2CO_3 (3equiv), DMF, RT, 8h; H_3O^+, NH_4PF_6

Scheme 2.

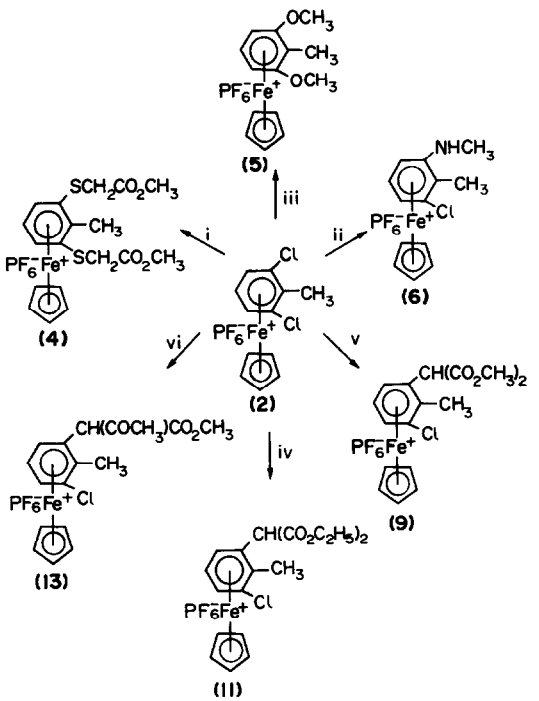

(i) $HSCH_2CO_2CH_3$ (3.0equir), K_2CO_3 (6equir), DMF, RT, 16h; H_3O^+, NH_4PF_6

(ii) H_2NCH_3 (12equiv), CH_2Cl_2, RT, 3h; H_3O^+, NH_4PF_6

(iii) K_2CO_3 (7.2equiv), CH_2OH, 40–50°C, 3h; H_3O^+, NH_4PF_6

(iV) $H_2C(CO_2C_2H_5)$ (1.2equiv), K_2CO_3 (3equiv), RT, 8h; H_3O^+, NH_4PF_6

(V) $H_2C(CO_2CH_3)_2$ (1.2equiv), K_2CO_3 (3equiv), RT, 8h; H_3O^+, NH_4PF_6

(Vi) $H_2C(CO_2CH_3)(CO_2CH_3)$ (1.2equiv), K_2CO_3 (3equiv), RT, 8h; H_3O^+, NH_4PF_6

Scheme 3.

be explained by the circumstance that under the reaction conditions the loss of a proton from the α-position on nitrogen occurs to yield the neutral complex **7**. The formation of cyclohexadienyl complexes of type **7** is well known.[10]

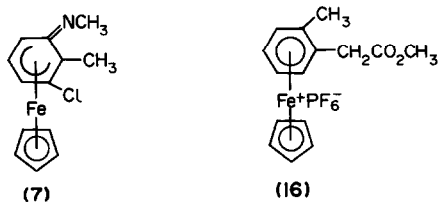

Reactions of complexes **1** *and* **2** *with carbon nucleophiles*

New reactions which lead to the formation of aryl–carbon bonds are of central importance in organic synthesis. From this point of view our attention was directed towards reactions of complexes **1** and **2** with stabilized enolate anions. Complexes **1** and **2** underwent smooth S_NAr reactions with enolate anions derived from dimethyl malonate, diethyl malonate, methyl acetoacetate and 2,4-pentanedione to yield the new substituted toluene complexes **8–14** in excellent yields (Schemes 2 and 3). The spectral properties of these complexes are characteristic. Typically, an η^6-arene complex such as η^6-dimethyl *o*-tolylmalonate-η^5-cyclopentadienyliron hexafluorophosphate (**8**), displays complexed aromatic ring protons in the region δ 6.43–6.52, 1H intensity peak at δ 5.5, Cp at δ 5.2 and two methoxy peaks at δ 4.03 and 3.77 due to methyl ester groups. Similarly η^6-diethyl *o*-tolylmalonate-η^5-cyclopentadienyliron hexafluorophosphate (**10**) showed two sets of quartets and triplets centred at δ 4.5, 4.23 and 1.42, 1.24 due to the ethyl ester groups. Complete NMR spectral data are given in the Experimental. Reaction of 2,4-

pentanedione with complex **1** in the presence of K_2CO_3 in DMF gave directly the corresponding monocarbonyl complex, η^6-*o*-tolylacetone-η^5-cyclopentadienyliron hexafluorophosphate (**14**), which arises from deacetylation of the corresponding β-dicarbonyl complex, *o*-$CH_3C_6H_4CH(COCH_3)_2FeCp^+PF_6^-$ (**15**) during acidic work-up. Analogous deacetylation in this organoiron series has been earlier reported by us and others.[3a–d,7a–c] In the case of η^6-*o*-tolylmethylacetoacetate-η^5-cyclopentadienyliron hexafluorophosphate (**12**) separate treatment with the fluoride anion is required to effect deacylation to yield the ester complex, η^6-*o*-tolylmethylacetate-η^5-cyclopentadienyliron hexafluorophosphate (**16**). These examples show that 2,4-pentanedione and methyl acetoacetate can be used as synthons for $-CH_2COCH_3$ and $-CH_2CO_2CH_3$ groups, respectively. This is important because reaction of $CpFe^+$ complexed aryl halides with enolate anions from acetone and methylacetate give ring addition products rather than substitution.[8b,c] Due to the ease of the above work-up conditions all the nucleophilic substitution reactions were carried our preferentially in the presence of K_2CO_3. Other reaction conditions such as NaH/THF were also found to be effective.

Next we turned our attention to ring annulation using the potential anion from the ring methyl and the adjacent carbonyl group as an anion acceptor in an intramolecular Claisen type process for the complexes η^6-dimethyl *o*-tolylmalonate-η^5-cyclopentadienyliron hexafluorophosphate (**8**) and η^6-diethyl *o*-tolylmalonate-η^5-cyclopentadienyliron hexafluorophosphate (**10**). The desired complexes for this purpose were prepared as follows: treatment of complex **8** with excess K_2CO_3 in CH_2Cl_2, followed by benzylation with benzyl bromide gave the expected benzylated complex **17** in excellent yield. Similar benzylation was accomplished with complexes **10** and **14** to yield new complexes **18** and **19**, respectively. The high resolution ^1H NMR and proton decoupled ^{13}C NMR spectra of complexes **17**, **18** and **19** indicated the formation of a single product with no indication of methyl benzylation.

Next we treated a sample of complex **18** with one molar equivalent of potassium tert-butoxide in THF at room temperature under N_2. The resulting deep red solution on usual acidic work-up gave only the complex **20** in 50% yield. Conversion of **18** → **20** corresponds to a transfer of the carboethoxy group. An intramolecular pathway is depicted in Scheme 4. Obviously group transfer rather than cyclization occurs in **18** → **20** and this result can be understood on the basis of intermediate A (Scheme 4). The course of its decomposition is controlled by ejection of the more stable carbanion rather than the ethoxide anion in the tetrahedral intermediate. The yield of **20** as well as analytical and spectral data are given in the Experimental. Furthermore, complex **21** was obtained in 40–50% yield from reaction between complex **18** and a molar equivalent of potassium tert-butoxide in THF at room temperature followed by alkylation with methyl iodide (6 molar equivalent). Similarly, reaction of complex **17** with potassium tert-butoxide in THF was carried out followed by quenching with methyl iodide to yield the new complex **22**. The yield, analytical and spectral data are given in the Experimental.

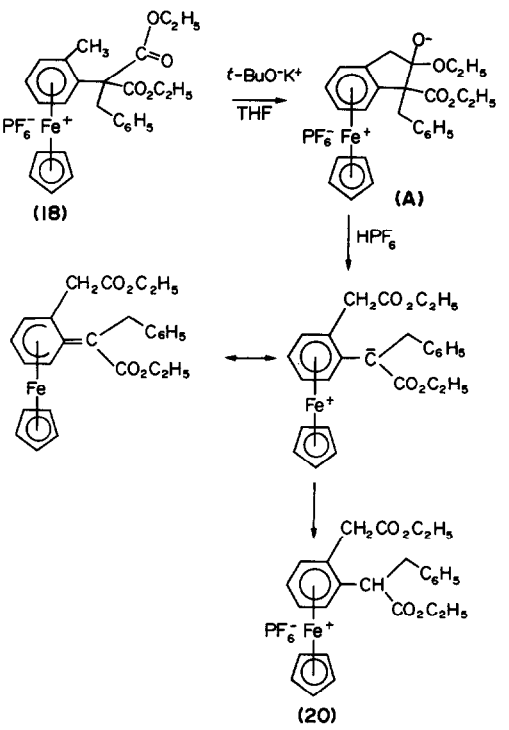

Scheme 4.

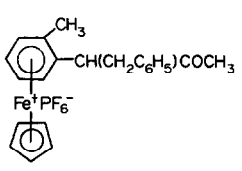

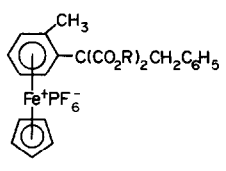

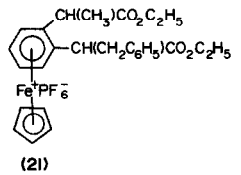

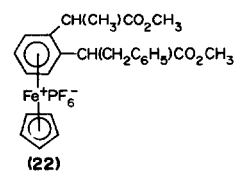

An important feature of the overall synthetic scheme is disengagement of the desired organic ligand from the organometallic complex. Typically, ligand disengagement in the case of *o*-$CH_3C_6H_4C(CH_2C_6H_5)(CO_2C_2H_5)_2FeCp^+PF_6^-$ (**18**) was achieved by vacuum sublimation at 200–220°C (10 mm/Hg) to yield *o*-$CH_3C_6H_4C(CH_2C_6H_5)(CO_2C_2H_5)_2$ in 85% yield. Similarly, ligand disengagement in *o*-$(C_2H_5O_2CCH_2)C_6H_4CH(CH_2C_6H_5)CO_2C_2H_5FeCp^+PF_6^-$ (**20**) gave the free ligand, *o* - $(C_2H_5O_2CCH_2)C_6H_4CH(CH_2C_6H_5)CO_2C_2H_5$ in 80% yield.

CONCLUSIONS

Aromatic nucleophilic substitution reaction upon CpFe complexed *o*-chlorotoluenes provides a method for the introduction of various groups *ortho* to the methyl group. These studies form a basis for further advances in the application of these complexes to the synthesis of substituted arenes. They provide a new class of organometallic complexes with β-oxo functionalities which are difficult to synthesize using Nesmeyanov's ligand exchange method.[8]

EXPERIMENTAL

IR spectra were recorded using the IBM IR 32 and NMR spectra with a Varian EM-360 and Bruker WP-200 and 400 MHz spectrometers. Melting points were determined using a Thomas Hoover Capillary melting point apparatus and are uncorrected. Microanalyses were performed by Microtech Laboratories, Skokie, Illinois. All reactions were performed under a nitrogen atmosphere using standard techniques. Solvents were dried as follows: tetrahydrofuran (THF) from sodium benzophenone; N,N-dimethylformamide (DMF) from molecular sieves (4 Å). K_2CO_3 was obtained from Fisher Scientific Company and was used directly without further purification.

Chlorotoluene complexes

η^6 - *o* - Chlorotoluene - η^5 - cyclopentadienyliron hexafluorophosphate, *o*-$CH_3C_6H_4ClFeCp^+PF_6^-$ (**1**), was prepared by the published procedure,[8a] m.p. 215–217°C, ref. 8a m.p. 219–221°C.

η^6 - 2,6 - *Dichlorotoluene* - η^5 - *cyclopentadienyliron hexafluorophosphate* (**2**)

Ferrocene (18.6 g, 0.1 mol), aluminium chloride (33.3 g, 0.25 mol), aluminium powder (2.7 g, 0.1 mol) and excess 2,6-dichlorotoluene (60 cm^3) were heated at 135–140°C for 5 h under N_2. The reaction mixture was cooled and quenched with ice–water (~ 200 cm^3). The aqueous layer was separated, filtered and washed with ether (3 × 60 cm^3), then it was added to a NH_4PF_6 solution (0.07 mol in 10 cm^3 of H_2O) with stirring and the resulting yellow solid was filtered and washed with ether. After drying, the solid was redissolved in acetone–CH_2Cl_2 (1/4 v/v), dried over $MgSO_4$ and concentrated to a small volume. Addition of ether yielded complex **2** (15 g, 35%): m.p. 206–210°C. ^1H NMR δ (acetone-d_6) 6.84 (1H, d), 6.63 (2H, t), 5.36 (5H, s, *Cp*) and 2.87 (3H, s, Ar*CH*$_3$). An analytical sample was prepared by recrystallization from acetone–ether. Found: C, 34.0; H, 2.5; Cl, 16.2. Calc. for $C_{12}H_{10}Cl_2FePF_6$: C, 33.8; H, 2.4; Cl, 16.6%.

Nucleophilic displacement of a chlorine atom in chlorotoluene complexes **1** *and* **2** *with various nucleophiles*

The general procedure is illustrated by the reactions of complex **1** with $KSCH_2CO_2CH_3$ and $KCH(CO_2C_2H_5)_2$.

Synthesis of η^6*-methyl*(o-*tolyl*)*thioacetate-*η^5*-cyclopentadienyliron hexafluorophosphate* (**3**)

A mixture of complex **1** (784 mg, 2.0 mmol) and methyl thioglycolate (0.27 cm^3, 3.0 mmol) and K_2CO_3 (0.828 mg, 6.0 mmol) in 40 cm^3 of tetrahydrofuran (THF) was stirred at room temperature under N_2 for 16 h. The reaction mixture was quenced with 10 cm^3 of H_2O and 15 cm^3 of 10% HCl and then NH_4PF_6 (0.32 g, 2.0 mmol) was added as a solid. The product was extracted with CH_2Cl_2–CH_3NO_2 (3:1) and dried over $MgSO_4$. The solvent was then removed under reduced pressure using a rotatory evaporator and the residual solid was redissolved in acetone; addition of ether yielded complex **3** (647 mg, 70%): m.p. 119–120°C. ^1H NMR δ (acetone-d_6) 6.57 (1H, d, J = 6 Hz), 6.47 (1H, d, J = 6 Hz), 6.40 (1H, t, J = 6 Hz) and 6.29 (1H, t, J = 6 Hz) aromatics, 5.11 (5 H, s, *Cp*), 4.16 (2H, AB J_{AB} = 16.5 Hz, $CH_2CO_2CH_3$), 3.76 (3H, s, CO_2CH_3) and 2.61 (3H, s, ArCH_3). IR (cm^{-1}, KBr) 1745 (CO). Found: 38.8; H, 3.7. Calc. for $C_{15}H_{17}O_2SFePF_6$: C, 39.0; H, 3.7%.

Synthesis of η^6*-methyl*[(2-*methylphenyl*)1,3-*dithio*]*diacetate-*η^5*-cyclopentadienyliron hexafluorophosphate* (**4**)

Using the same procedure as above and starting with 2.0 mmol of complex **2**, 6.0 mmol of methyl thioglycolate and 12.0 mmol of K_2CO_3, complex **4**

was obtained as a brown–yellow solid in 78% yield: m.p. 115–118°C. ^{1}H NMR δ (acetone-d_6) 6.41–6.56 (3H, m, ArH), 5.12 (5H, s, *Cp*), 4.16 (4H, AB, J_{AB} = 16.5 Hz, $CH_2CO_2CH_3$), 3.75 (6H, s, CO_2CH_3) and 2.75 (3H, s, ArCH_3). IR (cm^{-1}, KBr) 1738 (CO). Found: C, 37.9; H, 3.6. Calc. for $C_{18}H_{21}O_4S_2FePF_6$: C, 38.2; H, 3.7%.

Synthesis of η^6-3-chloro-2-methyl-N-methylaniline-η^5-cyclopentadienyliron hexafluorophosphate (**6**)

A mixture of complex **2** (852 mg, 2.0 mmol) methylamine (2.0 cm^3, 25 mmol) (40% aqueous solution) in 20 cm^3 of methylene chloride (CH_2Cl_2) was stirred at room temperature under N_2. A dark brown solution developed after 5 min and stirring was continued for 3 h. The product was extracted with CH_2Cl_2, the extracts were dried over $MgSO_4$, upon concentration to small volume and addition of ether gave a brown–yellow precipitate of complex **6** (781 mg, 90%): m.p. 162–167°C. ^{1}H NMR δ (acetone-d_6) 6.35 (1H, d, J = 6 Hz), 6.20 (1H, t, J = 6 Hz) and 5.80 (1H, d, J = 7 Hz) aromatics, 5.91 (1H, bs, NH), 4.96 (5H, s, *Cp*), 3.02 (3H, d, J = 5.0 Hz, NCH_3) and 2.55 (3H, s, ArCH_3); IR (cm^{-1}, KBr) 3444 (NH). Found: C, 37.0; H, 3.5; N, 3.3. Calc. for $C_{13}H_{15}ClNFePF_6$: C, 37.0; H, 3.6; N, 3.3%.

Synthesis of η^6-2,6-dimethoxytoluene-η^5-cyclopentadienyliron hexafluorophosphate (**5**)

A mixture of complex **2** (852 mg, 2.0 mmol) and K_2CO_3 (1.0 g, 7.2 mmol) in 20 cm^3 of methanol was heated under reflux for 3 h under N_2. The reaction mixture was cooled and neutralized with 15% HCl. Then methanol was removed using a rotary evaporator and the residue extracted with CH_2Cl_2–CH_3NO_2 (4:1 cm^3) mixtures, the combined extracts were dried over $MgSO_4$ and evaporated to dryness. Crystallization from acetone–ether gave η^6-2,6-dimethoxytoluene-η^5-cyclopentadienyliron hexafluorophosphate (**5**) (672 mg, 80%): m.p. 128–131°C. ^{1}H NMR δ (acetone-d_6) 6.21 (3H, s, ArH), 5.01 (5H, s, Cp), 4.08 (6H, s, ArOCH_3) and 2.36 (3H, s, ArCH_3). Found: C, 40.4; H, 4.1. Calc. for $C_{14}H_{17}O_2FePF_6$: C, 40.2; H, 4.1%.

Synthesis of η^6-diethyl o-tolylmalonate-η^5-cyclopentadienyliron hexafluorophosphate (**10**)

The following procedure is similar to the one used in our earlier work.[3a] A mixture of complex **1** (3.136 g, 8.0 mmol), K_2CO_3 (3.315 g, 24 mmol), diethyl malonate (1.6 ml, 9.6 mmol) and DMF (20 cm^3) was stirred at RT for 8 h under N_2. The red reaction mixture was filtered into a flask containing 10% HCl (30 cm^3). The reaction flask was washed with ethanol (2 × 10 cm^3) and the washings were also filtered. The volatile organic solvent was removed *in vacuo*, and to the remaining yellow solution was added 80 cm^3 of H_2O containing NH_4PF_6 (1.0 g, 7.0 mmol). The yellow solid which precipitated was collected, washed with ether, dried and crystallized from an acetone–ethanol–ether mixture to yield complex **10** (3.3 g, 80%) as a crystalline yellow solid: m.p. 124–127°C. ^{1}H NMR (400 MHz) δ (acetone-d_6) 6.45–6.54 (m, 3H) and 6.41 (d, 1H) aromatics, 5.41 (1H, s, *CH*), 5.18 (5H, s, *Cp*), 4.49 (2H, q, $J \simeq 7$ Hz, CH_2, *endo*), 4.23 (2H, q, $J \simeq 7$ Hz, CH_2, *exo*), 2.57 (3H, s, ArCH_3) and 1.40 (3H, t, $J \simeq 7$ Hz, CH_3, *endo*) 1.22 (3H, t, $J \simeq 7$ Hz, CH_3, *exo*). ^{13}C NMR δ (acetone-d_6) 167.19 and 166.63 (CO's), 103.54, 98.28, 90.75, 88.59 and 87.46 (aromatics), 78.68 (Cp), 63.62 and 63.22 (CO_2CH_2 CH_3's), 54.25 (CH), 18.94 (ArCH_3), 14.24 and 14.11 ($CO_2CH_2CH_3$'s). IR (cm^{-1}, KBr) 1745 and 1734 (CO). Found: C, 44.2; H, 4.6. Calc. for $C_{19}H_{23}O_4FePF_6$: C, 44.2; H, 4.5%.

Synthesis of η^6-diethyl(3-chloro-2-methyl)phenylmalonate-η^5-cyclopentadienyliron hexafluorophosphate (**11**)

Using the process above η^6-2,6-dichlorotoluene-γ^5-cyclopentadienyliron hexafluorophosphate (**2**) gave the monosubstitution complex **11** in 75% yield: m.p. 110–113°C. ^{1}H NMR δ (acetone-d_6) 6.97 (1H, d, J = 6 Hz), 6.59 (1H, t, J = 6 Hz), 6.40 (1H, d, J = 6 Hz) aromatics, 5.56 (1H, s, *CH*), 5.27 (5H, s, *Cp*), 4.47 (2H, q, J = 7 Hz, CH_2CH_3, *endo*), 4.23 (2H, q, J = 7 Hz, CH_2CH_3, *exo*), 2.71 (3H, s, ArCH_3), 1.39 (3H, t, J = 7 Hz, CH_2CH_3, *exo*) and 1.23 (3H, t, J = 7 Hz, *endo*). ^{13}C NMR δ (acetone-d_6) 167.04 and 166.56 (CO's), 109.24, 102.23, 98.48, 89.56, 87.26 and 87.09 (aromatics), 63.89 and 63.42 ($CO_2CH_2CH_3$'s), 55.02 (CH), 16.52 (ArCH_3), 14.21 and 14.14 ($CO_2CH_2CH_3$'s). IR (cm^{-1}, KBr) 1745 and 1730 (CO). Found: C, 41.1; H, 3.9. Calc. for $C_{19}H_{22}O_4ClFePF_6$: C, 41.4; H, 4.0%.

Synthesis of η^6-dimethyl o-tolylmalonate-η^5-cyclopentadienyliron hexafluorophosphate (**8**)

The reaction of dimethyl malonate with complex **1** was carried out according to the procedure described above. After the usual work-up and crystallization from an acetone–ethanol–ether mixture we obtained the desired new substitution product

8 in 85% yield as a yellow crystalline solid: m.p. 115–116°C. ^{1}H NMR δ (acetone-d_6) 6.43–6.52 (4H, m, ArH), 5.46 (1H, s, *CH*), 5.19 (5H, s, *Cp*), 4.03 (3H, s, CO_2CH_3, *endo*), 3.77 (3H, s, CO_2CH_3, *exo*), 2.50 (3H, s, ArCH_3). IR (cm^{-1}, KBr) 1755 and 1739 (CO). Found: C, 41.2; H, 3.9. Calc. for $C_{17}H_{19}O_4FePF_6$: C, 41.8; H, 3.9%.

Synthesis of η^6-dimethyl(3-chloro-2-methyl)phenylmalonate-η^5-cyclopentadienyliron hexafluorophosphate (**9**)

A similar reaction of complex **2** with dimethyl malonate yielded 73% of the new monosubstitution complex **9**: m.p. 119–120°C. ^{1}H NMR δ (acetone-d_6) 6.96 (1H, d, J = 6 Hz), 6.59 (1H, t, J = 6 Hz) and 6.39 (1H, d, J = 6 Hz) aromatics, 5.59 (1H, s, CH), 5.26 (5H, s, Cp), 4.00 (3H, s, CO_2CH_3, *exo*), 3.76 (3H, s, CO_2CH_3, *endo*) and 2.71 (3H, s, ArCH_3). ^{13}C NMR (acetone-d_6) 167.50 and 167.00 (CO's), 109.25, 102.23, 98.42, 89.59, 87.22 and 87.18 (aromatics), 81.02 (Cp), 54.59 (CH), 54.28 and 54.00 (CO_2CH_3's), 16.53 (ArCH_3). IR (cm^{-1}, KBr) 1745 (CO). Found: C, 39.3; H, 3.4. Calc. for $C_{17}H_{18}O_4ClFePF_6$: C, 39.1; H, 3.5%.

Synthesis of η^6-methyl α-o-tolylacetoacetate-η^5-cyclopentadienyliron hexafluorophosphate (**12**)

The reaction between complex **1** and methyl acetoacetate by the above general procedure yielded 78% of complex **12** as a yellow crystalline solid: m.p. 144–146°C. ^{1}H NMR δ (acetone-d_6) 6.2–6.6 (4 H, m, ArH), 5.65 (1H, s, CH), 5.2 (5H, s, Cp), 4.1 (3H, s, CO_2CH_3), 2.55 (3H, s, ArCH_3), 2.40 (3H, s, $COCH_3$). IR (cm^{-1}, KBr) 1754 and 1724 (CO). ^{13}C NMR δ (acetone-d_6) 199.12 ($COCH_3$), 168.27 (CO_2CH_3), 103.31, 98.87, 90.66, 88.41, 87.59 and 87.25 (aromatics), 78.52 (Cp), 60.75 (CH), 54.01 (CO_2CH_3), 29.42 ($COCH_3$), 19.13 (ArCH_3). Found: C, 43.1; H, 4.0. Calc. for $C_{17}H_{19}O_3FePF_6$: C, 43.2; H, 4.0%.

Synthesis of η^6-o-tolylacetone-η^5-cyclopentadienyliron hexafluorophosphate (**14**)

The reaction of complex **1** with 2,4-pentanedione by the general procedure gave complex **14** in 60% yield as a yellow crystalline solid: m.p. 101–103°C. ^{1}H NMR δ (acetone-d_6) 6.31 (4H, bs, ArH), 5.14 (5H, s, *Cp*), 4.56, 4.47, 4.25, 4.16 (2H, AB, $J_{AB} \simeq 18$ Hz, CH_2), 2.46 (3H, s, ArCH_3), 2.30 (3H, s, $COCH_3$). IR (cm^{-1}, KBr) 1722 (CO). Found: C, 43.5; H, 4.1. Calc. for $C_{15}H_{17}OFePF_6$: C, 43.5; H, 4.1%.

Synthesis of η^6-methyl(3-chloro-2-methyl)phenylacetoacetate-η^5-cyclopentadienyliron hexafluorophosphate (**13**)

The reaction between complex **2** and methyl acetoacetate yielded 65% of complex **13** as a yellow powder. ^{1}H NMR δ (acetone-d_6) 6.97 (1H, d, J = 6 Hz), 6.61 (1H, t, J = 6 Hz) and 6.34 (1H, d, J = 6 Hz) aromatics, 5.76 (1H, s, CH), 5.25 (5H, s, Cp), 4.04 (3H, s, CO_2CH_3), 2.68 (3H, s, ArCH_3) and 2.39 (3H, s, $COCH_3$). The product is contaminated with 2% of starting complex **2**.

Synthesis of η^6-(o-tolyl)methylacetate-η^5-cyclopentadienyliron hexafluorophosphate (**16**)

In a three-neck flask purged with nitrogen, was placed complex **12** (944 mg, 2.0 mmol) and tetrabutylammonium fluoride (678 mg, 2.15 mmol). Then 25 cm^3 of degassed CH_2Cl_2 was added via a syringe. The deep red solution was stirred for 5 h at room temperature. A solution of NH_4PF_6 (326 mg, 2.0 mmol) in 10 cm^3 of H_2O was introduced. The product was obtained by extraction with a 6:1 mixture of CH_2Cl_2–CH_3NO_2. The extracts were evaporated to dryness *in vacuo*. The residue was redissolved in a minimum amount of CH_2Cl_2 and passed through a short alumina column (10 cm). The first 50 cm^3 of CH_2Cl_2 extract was discarded. The yellow acetone eluant was concentrated to 2 cm^3 and upon addition of ether, o-$CH_3C_6H_4CH_2CO_2CH_3FeCp^+PF_6^-$ (**16**) (648 mg, 75%) was obtained as a yellow crystalline solid: m.p. 98–100°C. ^{1}H NMR δ (acetone-d_6) 6.41 (4H, s, ArH), 5.17 (5H, s, *Cp*), 4.31, 4.23, 4.05, 3.96 (2H, AB, $J_{AB} \simeq 17$ Hz, CH_2), 3.71 (3H, s, CO_2CH_3) and 2.56 (3H, s, ArCH_3). ^{13}C NMR δ (acetone-d_6) 170.18 (CO), 104.13, 99.52, 90.19, 90.04, 88.02 and 87.53 (aromatics), 78.23 (Cp), 52.63 (CO_2CH_3), 38.21 (CH_2) and 18.80 (ArCH_3). IR (cm^{-1}, KBr) 1748 (CO). Found: C, 41.7; H, 4.1. Calc. for $C_{15}H_{17}O_2FcPF_6$: C, 41.9; H, 4.0%.

General benzylation procedure

Synthesis of o-$CH_3C_6H_4C(CH_2C_6H_5)(CO_2C_2H_5)_2FeCp^+PF_6^-$ (**18**) *from complex* **10**

To a 100 cm^3 two-neck flask equipped with a reflux condenser and containing complex **10** (3.0 g, 5.8 mmol) and K_2CO_3 (3.0 g, 21.7 mmol), was added 25 cm^3 of CH_2Cl_2. The reaction mixture was refluxed under N_2 for 20 min. Then benzyl bromide (1.8 cm^3, 15 mmol) was added and the reaction mixture was refluxed for an additional 8 h. The reaction mixture was filtered to remove solid K_2CO_3

and the solid was washed with CH_2Cl_2 (2 × 15 cm^3). The combined filtrate was concentrated and the pasty material washed with ether (3 × 20 cm^3). The residue was redissolved in CH_2Cl_2 and the resulting solution was washed with H_2O containing NH_4PF_6 (800 mg, 5.0 mmol). The organic layer was separated, dried and concentrated. Addition of ether gave the orange–yellow complex **18** in 90% yield. Further purification of the product by dissolution in acetone followed by addition of ether yielded a crystalline solid: m.p. 118–121°C. ^{1}H NMR δ (acetone-d_6) 7.0–7.24 (3H, m), 6.87–6.91 (2H, m) uncomplexed aromatic, 6.51 (1H, t), 6.89 (1H, d), 6.20 (1H, t), 6.05 (1H, d) complexed aromatic, 5.21 (5H, s, Cp), 4.31–4.52 (4H, m, $CO_2CH_2CH_3$), 3.48, 3.56, 3.91, 3.98 (2H, AB, $J_{AB} \simeq 15$ Hz, $CH_2C_6H_5$), 2.33 (3H, s, $ArCH_3$), 1.32–1.4 (6H, m, $CO_2CH_3CH_3$). ^{13}C NMR δ (acetone-d_6) 169.24 and 168.85 (CO's), 135.58, 131.83, 128.83 and 128.18 (uncomplexed aromatics), 104.10, 102.10, 90.92, 88.80, 88.43 and 86.91 (complexed aromatics), 78.99 (Cp), 63.93 and 63.81 ($CO_2CH_2CH_3$'s), 63.49 (CH), 42.66, ($CH_2C_6H_5$) 20.35, ($ArCH_3$) 14.03 ($CO_2CH_2CH_3$'s). IR (cm^{-1}, KBr) 1716 and 1748 (CO). Found: C, 51.2; H, 4.8. Calc. for $C_{26}H_{29}O_4FePF_6$: C, 51.5; H, 4.8%.

Synthesis of o-$CH_3C_6H_4C(CH_2C_6H_5)(CO_2CH_3)_2$ $FeCp^+PF_6^-$ (**17**) *from complex* **8**

Reaction of complex **8** with benzyl bromide following the above procedure gave a new complex **17** as a yellow crystalline solid in 80–85% yield: m.p. 109–112°C. ^{1}H NMR δ (acetone-d_6) 7.17 (3H, bs) and 6.87 (2H, bs) uncomplexed aromatic, 6.52 (1H, t), 6.42 (1H, d), 6.28 (1H, t), 6.05 (1H, d) complexed aromatic, 5.21 (5H, s, *Cp*), 3.96 (6H, s, CO_2CH_3's), 3.95, 3.88, 3.57, 3.50 (2H, AB, $J_{AB} \simeq 15$ Hz, $CH_2C_6H_5$), 2.29 (3H, $ArCH_3$). ^{13}C NMR δ (acetone-d_6) 169.63, and 169.25 (CO's), 135.46, 131.77, 128.99 and 128.24 (uncomplexed aromatics), 104.03, 102.11, 90.87, 88.75 and 88.41 (complexed aromatics), 79.00 (Cp), 63.34 (CH), 54.28 and 54.2 (CCO_2CH_3's), 42.7 ($CH_2C_6H_5$), 20 ($ArCH_3$). IR (cm^{-1}, KBr) 1743 and 1751 (CO). Found: C, 49.9; H, 4.4. Calc. for $C_{24}H_{25}O_4FePF_6$: C, 49.8; H, 4.4%.

Synthesis of o-$CH_3C_6H_5CH(CH_2C_6H_5)COCH_3$ $FeCp^+PF_6^-$ (**19**) *from complex* **14**

Reaction of complex **14** with benzyl bromide gave complex **19** as a yellow crystalline solid in 80–90% yield: m.p. 144–146°C. ^{1}H NMR δ (acetone-d_6) 7.16–7.25 (3H, m), 7.02–7.08 (2H, m) uncomplexed aromatics, 6.65 (1H, dd, AA'BB'), 6.45 (2H, quintet, AA'BB'), 6.30 (1H, dd, AA'BB') complexed aromatics, 5.04 (5H, s, Cp), 4.64 (1H, ABX quartet, $J_{AX} = 9$ Hz, $J_{BX} = 7$ Hz, $CHCH_2C_6H_5$), 2.96 and 3.43 (2H, ABX, $J_{AB} = 13$ Hz, $J_{BX} = 7$ Hz, $J_{AX} = 9$ Hz, $CHCH_2C_6H_5$), 2.56 (3H, s, $ArCH_3$), 2.30 (3H, s, $COCH_3$). ^{13}C NMR δ (acetone-d_6) 207.92 (CO), 137.97, 130.07, 129.23 and 127.74 (uncomplexed aromatics), 103.76, 102.51, 90.16, 88.07, 87.57 and 87.26 (complexed aromatics), 77.78 (*Cp*), 52.34 (*C*H ($COCH_3$)), 42.67 ($CH_2C_6H_5$), 32.39 ($COCH_3$), 19.39 ($ArCH_3$). IR (cm^{-1}, KBr) 1725 (CO). Found: C, 52.3; H, 4.6. Calc. for $C_{22}H_{23}OFePF_6$: C, 52.4; H, 4.6%.

Synthesis of o-$(C_2H_5CO_2CH_2)C_6H_4CH(CO_2C_2H_5)$ $CH_2C_6H_5FeCp^+PF_6^-$ (**20**) *from complex* **18**

In a 50 cm^3 two-neck flask fitted with a nitrogen inlet was placed complex **18** (600 mg, 1 mmol) and potassium tert-butoxide (112 mg, 1 mmol). Then 25 cm^3 of THF (degassed) was added via syringe. The dark red solution was stirred for 8 h and finally quenched with HPFC (48%). The resulting yellow solution was evaporated *in vacuo* and the residue was extracted with methylene dichloride (3 × 25 cm^3). The combined methylene chloride extracts were dried, concentrated to 5 cm^3 and the addition of ether gave a green–yellow solid of complex **20** in 50% yield. Finally, a nice crystalline product was obtained by recrystallization from acetone–ether: m.p. 158–160°C. ^{1}H NMR (400 MHz) δ (acetone-d_6) 7.20–7.32 (5H, m) uncomplexed aromatics, 6.71 (1H, d) and 6.56–6.58 (3H, m) complexed aromatics, 5.14 (5H, s, *Cp*), 4.40, 4.36, 4.14 and 4.10 (2H, AB, $J_{AB} = 17$ Hz, $—CH_2CO_2C_2H_5$), 4.22–4.32 (5H, m, $—CO_2CH_2CH_3$ and H_x portion of ABX), 3.21 and 3.07 (2H, ABX, $J_{AB} = 13$ Hz, $J_{AX} = 12$ Hz, $J_{BX} = 4$ Hz, $CHCH_2C_6H_5$), 1.26 (3H, t, $J = 7$ Hz, $—CO_2CH_2CH_3$) and 1.18 (3H, t, $J = 7$ Hz, $—CO_2CH_2CH_3$). ^{13}C NMR δ (acetone-d_6) 171.81 and 170.13 (CO's), 138.42, 129.7, 129.35 and 127.9 (uncomplexed aromatics), 104.26, 98.54, 91.15, 88.66, 88.3 and 86.77 (complexed aromatics), 78.57 (Cp), 62.38 ($—CO_2CH_2CH_3$), 48.87 ($—CH_2CO_2C_2H_5$), 42.35 ($—CH_2C_6H_5$), 38.68 ($—CHCH_2C_6H_5$), 14.34 and 14.26 ($—CO_2CH_2CH_3$'s). IR (cm^{-1}, KBr) 1733 and 1722. Found: C, 51.5; H, 4.8. Calc. for $C_{26}H_{29}O_4FePF_6$: C, 51.5; H, 4.8%.

Synthesis of o-$(C_2H_5O_2C(CH_3)CH)C_6H_4CH$ $(CH_2C_6H_5)CO_2C_2H_5FeCp^+PF_6^-$ (**21**) *from complex* **18**

Complex **21** was obtained in 45–60% yield from the reaction between complex **18** and potassium

tert-butoxide, as above, and direct addition of excess methyl iodide (6 molar equivalents): m.p. 176–179°C. ^{1}H NMR (400 MHz) δ (acetone-d_6) 7.32–7.36 (2H, m), 7.25–7.29 (3H, m) uncomplexed aromatics, 6.80 (1H, d) and 6.59–6.67 (3H, m) complexed aromatics, 5.16 (5H, s, *Cp*), 4.55 (1H, q, $J = 7$ Hz, —*CH*CH$_3$), 4.29–4.35 (3H, m, —CO$_2$*CH*$_2$CH$_3$ and H$_x$ portion of ABX), 4.14–4.22 (2H, m, —CO$_2$*CH*$_2$CH$_3$), 3.21 and 2.99 (2H, ABX, $J_{AB} = 13.6$ Hz, $J_{AX} = 11.62$ Hz, $J_{BX} = 3.78$ Hz, CH*CH*$_2$C$_6$H$_5$), 1.91 (3H, d, $J = 7$ Hz, —CH*CH*$_3$), 1.19 (3H, t, $J = 7$ Hz, —CO$_2$CH$_2$*CH*$_3$) and 1.16 (3H, t, $J = 7$ Hz, —CO$_2$CH$_2$*CH*$_3$). ^{13}C NMR δ (acetone-d_6) 172.83 and 171.84 (CO's), 138.31, 129.65, 129.37 and 127.93 (uncomplexed aromatics), 105.2, 103.49, 88.30, 88.11, 986.80 and 86.64 (complexed aromatics), 78.31 (Cp), 62.58 and 62.35 (—CO$_2$*CH*$_2$CH$_3$'s), 48.23 (—*C*HCH$_3$), 42.27 (—*C*H$_2$C$_6$H$_5$), 41.50 (—*C*HCH$_2$C$_6$H$_5$), 17.48 (—CH*CH*$_3$) and 14.22 (—CO$_2$CH$_2$*CH*$_3$). IR (cm^{-1}, KBr) 1733 and 1722 (CO). Found: C, 52.5; H, 4.6. Calc. for $C_{27}H_{28}O_4FePF_6$: C, 52.5; H, 4.6%.

Synthesis of o-(CH$_3$CO$_2$(CH$_3$)CH)C$_6$H$_4$CH(CO$_2$CH$_3$)CH$_2$C$_6$H$_5$FeCp$^+$PF$_6^-$ (**22**) *from complex* **17**

Complex **22** was obtained as a nice yellow solid in 40–50% yield from complex **17**, following the above procedure and quenching the reaction with methyl iodide: m.p. 200–202°C. ^{1}H NMR (400 MHz) δ (acetone-d_6) 7.22–7.35 (5H, m) uncomplexed aromatics, 6.77 (1H, d) and 6.59–6.68 (3H, m) complexed aromatics, 5.16 (5H, s, Cp), 4.57 (1H, q, $J = 7$ Hz, —*CH*CH$_3$), 4.32 (1H, ABX quartet, $J_{AX} = 11.4$ Hz, $J_{BX} = 3.8$ Hz, *CH*CH$_2$C$_6$H$_5$), 3.80 (3H, s, —CO$_2$*CH*$_3$), 3.72 (3H, s, —CO$_2$*CH*$_3$), 3.23 and 2.97 (2H, ABX, $J_{AB} = 13.6$ Hz, $J_{AX} = 11.4$ Hz, $J_{BX} = 3.8$ Hz, CH*CH*$_2$C$_6$H$_5$), and 1.90 (3H, d, $J = 7$ Hz, —CH*CH*$_3$). IR (cm^{-1}, KBr) 1724 and 1740 (CO).

Decomplexation reactions

o - CH$_3$C$_6$H$_4$C(CH$_2$C$_6$H$_5$)(CO$_2$C$_2$H$_5$)$_2$FeCp$^+$PF$_6^-$ (**18**) (300 mg, 0.5 mmol) was placed in a vacuum sublimator. Then the sample was heated at 200°C for 2 h at 10 mm/Hg. The material from the cold finger was eluted with ether. After the removal of ether, the oily residue (133 mg, 85%) was identified, using ^{1}H NMR and ^{13}C NMR spectra, to be diethyl(1-benzyl)(1-tolyl)malonate, *o*-CH$_3$C$_6$H$_4$C(CH$_2$C$_6$H$_5$)(CO$_2$C$_2$H$_5$): ^{1}H NMR (400 MHz) δ (chloroform-d_3) 7.12–7.22 (7H, m) and 6.95–7.03 (2H, dd) aromatic, 4.11–4.22 (4H, m, CO$_2$*CH*$_2$CH$_3$), 3.70 (2H, s, *CH*$_2$C$_6$H$_5$), 2.16 (3H, s, ArC*H*$_3$) and 1.21 (6H, t, CO$_2$CH$_2$*CH*$_3$). ^{13}C NMR (400 MHz) δ (chloroform-d_3) 170.29 (*C*O$_2$C$_2$H$_5$), 137.09, 136.59, 132.00, 130.81, 128.55, 127.56, 127.43, 126.58 and 125.61 (aromatic), 64.58 (*C*(CO$_2$C$_{25}$)$_2$), 61.67 (CO$_2$*CH*$_2$CH$_3$), 41.70 (*CH*$_2$C$_6$H$_5$), 21.00 (Ar*CH*$_3$) and 13.78 (CO$_2$CH$_2$*CH*$_3$).

o - (C$_2$H$_5$O$_2$CCH$_2$)C$_6$H$_4$CH(CH$_2$C$_6$H$_5$)CO$_2$C$_2$H$_5$FeCp$^+$PF$_6^-$ (**20**) (100 mg, 0.165 mmol) was sublimed as described above to yield the free ligand, *o*-(C$_2$H$_5$O$_2$CCH$_2$)C$_6$H$_4$CH(CH$_2$C$_6$H$_5$)(CO$_2$C$_2$H$_5$) (46 mg, 80%). ^{1}H NMR δ (chloroform-d_3) 7.16–7.29 (9H, m, aromatics), 4.11–4.16 (2H, m, CO$_2$*CH*$_2$CH$_3$ and ^{1}H$_X$ portion of ABX), 3.96–4.07 (2H, m, CO$_2$*CH*$_2$CH$_3$), 3.77, 3.73, 3.52 and 3.48 (2H, AB, $J_{AB} = 16$ Hz, *CH*$_2$CO$_2$C$_2$H$_5$), 3.42 and 3.19 (2H, ABX, $J_{AB} = 14$ Hz, $J_{AX} = 8$ Hz, $J_{BX} = 6$ Hz, CH*CH*$_2$C$_6$H$_5$), 1.23 (3H, t, $J = 7$ Hz, CO$_2$CH$_2$*CH*$_3$) and 1.08 (3H, t, $J = 7$ Hz, CO$_2$CH$_2$*CH*$_3$). ^{13}C NMR δ (chloroform-d_3) 173.27 and 171.29 (*C*O$_2$CH$_2$CH$_3$'s), 139.28, 137.92, 132.62, 130.93, 128.99, 128.28, 127.85, 127.50. 127.35 and 126.34 (aromatics), 60.94 and 60.74 (CO$_2$*CH*$_2$CH$_3$), 48.96 (*CH*CO$_2$C$_2$H$_5$), 39.59 (*CH*$_2$C$_6$H$_5$), 38.95 (*CH*$_2$CO$_2$C$_2$H$_5$), 14.14 and 13.96 (CO$_2$CH$_2$*CH*$_3$'s).

Acknowledgement—We thank the Office of Naval Research for support of this work under contract ONR 83K-0306.

REFERENCES

1. For review see: (a) M. F. Semmelhack, G. R. Clark, J. L. Garcia, J. J. Harrison, Y. Thebtaranonth and W. Wulff, *Tetrahedron* 1981, **37**, 3957 and refs therein; (b) M. F. Semmelhack, *NY Acad. Sci.* 1977, **295**, 36; (c) G. Jaouen and J. Meyer, *J. Am. Chem. Soc.* 1975, **97**, 4667; (d) M. Uemura, T. Minami and Y. Hayashi, *J. Chem. Soc., Chem. Commun.* 1984, 1193; (e) A. Meyer and O. Höfer, *J. Am. Chem. Soc.* 1980, **102**, 4410; (f) M. F. Semmelhack and A. Zask, *J. Am. Chem. Soc.* 1983, **105**, 2034.
2. For review see: (a) D. Astruc, *Tetrahedron* 1983, **39**, 4027; (b) R. G. Sutherland, M. Iqbal and A. Piórko, *J. Organometal. Chem.* 1986, **302**, 307.
3. (a) R. M. Moriarty and U. S. Gill, *Organometallics* 1986, **5**, 253; (b) U. S. Gill and R. M. Moriarty, *Synth. React. Inorg. Met.-Org. Chem.* 1986, **16**, 485; (c) U. S. Gill, *Inorg. Chim. Acta*, 1986, **114**, L25; (d) U. S. Gill and R. M. Moriarty, *Synth. React. Inorg. Met.-Org. Chem.* 1986, **16**, 1103.
4. (a) E. I. Sirotkina, A. N. Nesmeyanov and N. A. Vol'kenau, *Izv. Akad. Nauk SSSR, Ser. Khim.* 1969, 1524; (b) C. C. Lee, U. S. Gill, M. Iqbal, C. I. Azogu and R. G. Sutherland, *J. Organometal. Chem.* 1982, **231**, 151; (c) J. F. Helling and W. A. Hendrickson, *J. Organometal. Chem.* 1979, **168**, 87; (d) A. F. Neto and J. Miller, *Ciênc. Cult. (São Paulo)* 1984, **36**, 1765; *Chem. Abstr.* 1985, **102**, 24779m; (e) A. F. Neto and J. Miller, *An. Acad. Brasil Ciênc.* 1982, **54**,

331; (f) C. C. Lee, C. I. Azogu, P. C. Chang and R. G. Sutherland, *J. Organometal. Chem.* 1981, **220**, 181; (g) R. G. Sutherland, A. Piórko, U. S. Gill and C. C. Lee, *J. Heterocyclic Chem.* 1982, **19**, 801.

5. (a) J. F. Bunnett and H. Hermann, *J. Org. Chem.* 1971, **36**, 4081; (b) P. L. Pauson and J. A. Segal, *J. Chem. Soc., Dalton Trans.* 1975, 1677; (c) C. A. Mahaffy and P. L. Pauson, *J. Chem. Res.* 1979, 128(s); C. A. Mahaffy and P. L. Pauson, *J. Chem. Res.* 1979, 1776 (M); (d) A. N. Nesmeyanov, N. A. Vol'kenau, I. N. Bolesova and L. S. Shulpina, *Dokl. Acad. Nauk. SSSR* 1980, **254**, 1408; (e) K. K. Bhasin, W. G. Balkeen and P. L. Pauson, *J. Organometal. Chem.* 1981, **204**, C25.
6. (a) A. C. Knipe, S. J. McGuiness and W. E. Watts, *J. Chem. Soc., Perkin Trans. II* 1981, 193; (b) A. C. Knipe, S. J. McGuiness and W. E. Watts, *J. Chem. Soc., Chem. Commun.* 1979, 842; (c) V. V. Litvak, L. S. Filatova, Y. Yu. Khalikova and V. D. Shteingarts, *Zh. Org. Khim.* 1980, **16**, 336; (d) V. V. Litvak, L. S. Filatova, G. A. Selivanova and V. D. Shteingarts, *Zh. Org. Khim.* 1980, **16**, 342; (e) V. V. Litvak, L. S. Filatova and V. D. Shteingarts, *Zh. Org. Khim.* 1981, **17**, 1285.
7. (a) C. C. Lee, A. S. Abd-El-Aziz, R. L. Chowdhury, A. Piórko and R. G. Sutherland, *Synth. React. Inorg. Met.-Org. Chem.* 1986, **16**, 541; (b) C. C. Lee, A. S. Abd-El-Aziz, R. L. Chowdhury, U. S. Gill, A. Piórko and R. G. Sutherland, *J. Organometal. Chem.* 1986, **315**, 79; (c) R. G. Sutherland, A. S. Abd-El-Aziz, A. Piórko and C. C. Lee, *Synth. Commun.* 1987, **17**, 393.
8. (a) I. U. Khand, P. L. Pauson and W. E. Watts, *J. Chem. Soc. C* 1969, 2024; (b) R. G. Sutherland, R. L. Chowdhury, A. Piórko and C. C. Lee, *J. Chem. Soc., Chem. Commun.* 1985, 1296; (c) R. G. Sutherland, R. L. Chowdhury, A. Piórko and C. C. Lee, *Can. J. Chem.* 1986, **64**, 2031.
9. For a review and leading references see: R. G. Sutherland, *J. Organometal. Chem. Lib.* 1977, 311.
10. (a) J. F. Helling and W. A. Hendrickson, *J. Organometal. Chem.* 1977, 141, 99; (b) C. Moinet and E. Raoult, *J. Organometal. Chem.* 1982, **231**, 245; (c) C. C. Lee, U. S. Gill and R. G. Sutherland, *J. Organometal. Chem.* 1981, **206**, 89.

Polyhedron Vol. 7, No. 24, pp. 2695–2702, 1988
Printed in Great Britain

0277–5387/88 $3.00+.00
© 1988 Pergamon Press plc

BINUCLEAR METHYLPLATINUM AND PHENYLPLATINUM COMPLEXES WITH BIS(DIMETHYLPHOSPHINO)METHANE LIGANDS

NASIM HADJ-BAGHERI and RICHARD J. PUDDEPHATT*

Department of Chemistry, University of Western Ontario, London, Canada N6A 5B7

(*Received* 8 *April* 1988; *accepted* 1 *June* 1988)

Abstract—Reaction of *cis*-$[PtPh_2(SMe_2)_2]$ with $Me_2PCH_2PMe_2$ (dmpm) gave *cis*-$[PtPh_2(dmpm\text{-}P)_2]$ (**1**) or *cis,cis*-$[Pt_2Ph_4(\mu\text{-}dmpm)_2]$ (**2**) and reaction of **1** with $[Pt_2Me_4(\mu\text{-}SMe_2)_2]$ gave *cis,cis*-$[Ph_2Pt(\mu\text{-}dmpm)_2PtMe_2]$ (**3**). Reaction of **1** with *trans*-$[PtClR(SMe_2)_2]$ gave *cis,trans*-$[Ph_2Pt(\mu\text{-}dmpm)_2PtClR]$, R = Me (**5**) or Ph (**6**), and in polar solvents, these isomerized to give $[Ph_2Pt(\mu\text{-}dmpm)_2PtR]^+Cl^-$. When R = Me, further isomerization via the phenyl group transfer gave $[PhMePt(\mu\text{-}dmpm)_2PtPh]^+Cl^-$. Oxidative addition of methyl iodide occurred reversibly at the *cis*-$[PtMe_2P_2]$ unit of **3** to give *cis,fac*-$[Ph_2Pt(\mu\text{-}dmpm)_2PtIMe_3]$ but complex **2** failed to react with MeI. A comparison with similar known complexes of $Ph_2PCH_2PPh_2$ (dppm) is made and differences are attributed primarily to the lower steric hindrance of dmpm.

There has been considerable interest in complexes of general formula $[R_2Pt(\mu\text{-}LL)_2PtR^1_2]$, where R,$R^1$ = alkyl or aryl, and LL = $Ph_2PCH_2PPh_2$ (dppm) or $Me_2PCH_2PMe_2$ (dmpm) or related ligands. We have been interested in the conformational, fluxional and chemical properties of the complexes with R = R^1 = Me,[1–7] while Shaw and co-workers have pioneered routes to the unsymmetrical complexes with R ≠ R^1 using the reagents $[R_2Pt(dppm\text{-}P)_2]$, with monodentate dppm ligands, as intermediates.[8–14] Routes to unsymmetrical complexes, such as $[Ph_2Pt(\mu\text{-}dmpm)_2PtMe_2]$, have now been developed with the aim of studying the relative reactivities of the phenylplatinum and methylplatinum bonds. This work required the synthesis of *cis*-$[PtPh_2(dmpm\text{-}P)_2]$, the first platinum complex with monodentate dmpm ligands, and its properties were also studied. The ligand dmpm has a much greater tendency to form bridged complexes, when compared to the more commonly used ligand dppm,[15] and few complexes with monodentate dmpm ligands have been prepared previously.[16–19] The properties of the unsymmetrical complex $[Ph_2Pt(\mu\text{-}dmpm)_2PtMe_2]$ are compared to those of the symmetrical complexes $[R_2Pt(\mu\text{-}dmpm)_2PtR_2]$, R = Me or Ph.

RESULTS

Synthesis and characterization of cis-$[PtPh_2(dmpm\text{-}P)_2]$ (1), cis,cis-$[Ph_2Pt(\mu\text{-}dmpm)_2PtPh_2]$ (2) *and* cis,cis-$[Ph_2Pt(\mu\text{-}dmpm)_2PtMe_2]$ (3)

Displacement of the dimethylsulphide ligands from *cis*-$[PtPh_2(SMe_2)_2]$ by two equivalents of dmpm gave *cis*-$[PtPh_2(dmpm\text{-}P)_2]$ (**1**) in good yield. The complex was readily characterized by its ^1H and ^{31}P NMR spectra. The ^{31}P NMR spectrum of **1** contained peaks at δ −25.7 ppm, $^1J(PtP)$ = 1717 Hz (coordinated phosphorus) and −58.1 ppm (free phosphorus). The low value of $^1J(PtP)$ is characteristic of a phosphorus *trans* to an alkyl or aryl group[1–14] and proves the *cis* stereochemistry. Two MeP resonances were observed in the ^1H NMR spectrum at room temperature, but four such resonances were observed at low temperature. This is no doubt due to restricted rotation about the PtP bonds at low temperature. The pairs of methyl groups a, b and c, d in structure **1** become equivalent on rotation about the Pt—P bonds. There was no evidence for fluxionality involving exchange of free

* Author to whom correspondence should be addressed.

and coordinated phosphorus atoms of the dmpm-P ligands.[8,10,15]

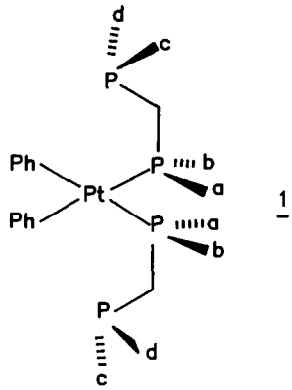

1

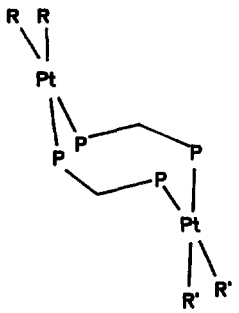

2, R = R' = Ph
3, R = Ph, R' = Me
4, R = R' = Me

The binuclear complex *cis,cis*-$[Pt_2Ph_4(\mu\text{-dmpm})_2]$ (**2**) was prepared by reaction of *cis*-$[PtPh_2(SMe_2)_2]$ with one equivalent of dmpm. The ^{31}P and ^1H NMR data were similar to those for *cis,cis*-$[Pt_2Me_4(\mu\text{-dmpm})_2]$ (**4**) and confirm the structure unambiguously.[3] In particular, the low temperature ^1H NMR spectrum contained only one CH_2P_2 resonance but two *Me*P resonances as expected for the extended chair structure **2**, with non-equivalent PMe^aMe^b groups. This conformation was also found for complex **4**.[3] At room temperature, the two MeP resonances coalesced as inversion of the chair structure occurred [$2 \rightleftharpoons 2'$, eq. (1)]. The activation energy for chair inversion was $\Delta G^\dagger$ (293 K) = 56(±2) kJ mol^{-1}, identical to that found for complex **4**.[3]

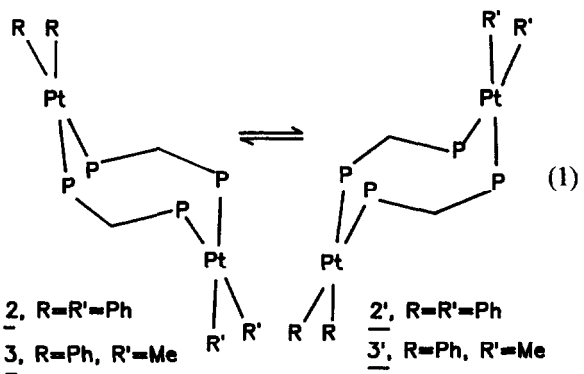

(1)

2, R=R'=Ph
3, R=Ph, R'=Me

2', R=R'=Ph
3', R=Ph, R'=Me

The unsymmetrical complex *cis,cis*-$[Ph_2Pt(\mu\text{-dmpm})_2PtMe_2]$ (**3**) was prepared by reaction of complex **1** with 0.5 equivalent of $[Pt_2Me_4(\mu\text{-}SMe_2)_2]$,[20] with displacement of the weakly bound SMe_2 ligands. As expected, the ^{31}P NMR spectrum of **3** contained two resonances at −23.9 [^1J(PtP) = 1745 Hz] and −25.1 [^1J(PtP) = 1705 Hz] ppm, assigned as phosphorus atoms *trans* to methyl and phenyl. The ^1H NMR spectrum at room temperature contained two *Me*P resonances and a single CH_2P_2 resonance, and each of these resonances split into two at low temperature (Fig. 1). This is exactly what is expected for the extended chair structure **3**, when $R \neq R'$. The activation energy for fluxionality, involving inversion of the chair structure, was $\Delta G^\dagger$ (273 K) = 53(±2) kJ mol^{-1}. These data not only establish the structure and solution conformation of **3**, but also show clearly that no exchange leading to scrambling of methyl and phenyl groups between platinum centres

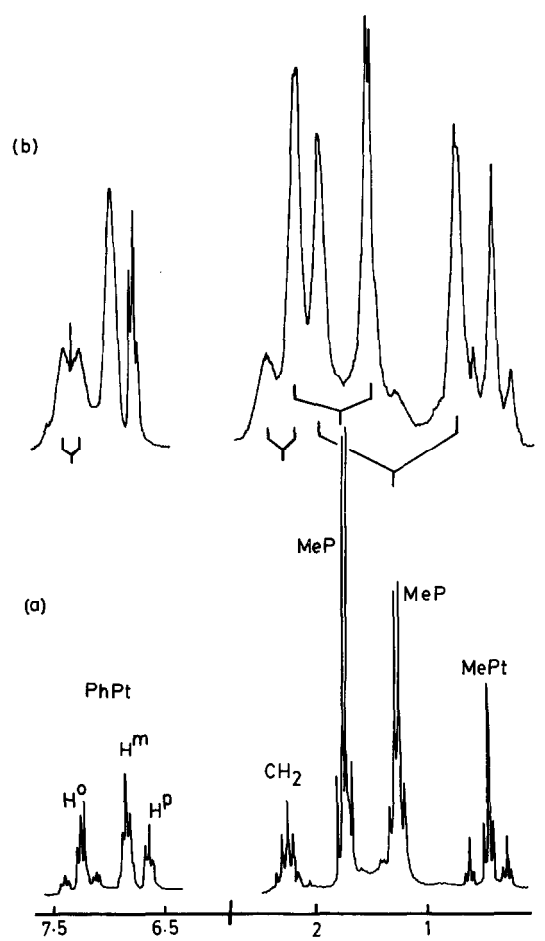

Fig. 1. ^1H NMR spectra (200 MHz) of *cis,cis*-$[Ph_2Pt(\mu\text{-dmpm})_2PtMe_2]$ (**3**); (a) at 20°C, (b) at −50°C.

occurs. Even at 50°C in solution, no change in the ^1H or ^{31}P NMR spectrum was observed.

Complex **1** could be prepared by reaction of the binuclear complex **2** with dmpm, and the reaction is reversible. Thus solutions of **1**, on standing, gave a low intensity resonance in the ^{31}P NMR spectrum due to **2**. Nevertheless, in comparison with analogous dppm complexes,[8-14] **1** is remarkably robust and has no tendency to form the chelate complex $[PtPh_2(dmpm)]$. In addition, whereas free dmpm is very rapidly oxidized by air, complex **1** can be handled in air for brief periods without significant oxidation. Presumably, steric effects retard the reaction of oxygen with the free dimethylphosphino group of **1**.

Synthesis and characterization of cis,trans-$[Ph_2Pt(\mu\text{-dmpm})_2PtClR]$, [**5**, R = Me; **6**, R = Ph], *and* $[Ph_2Pt(\mu\text{-dmpm})_2PtR]^+X^-$, [**7a**, R = Me, X = Cl; **7b**, R = Me, X = PF_6; **8a**, R = Ph, X = Cl; **8b**, R = Ph, X = PF_6]

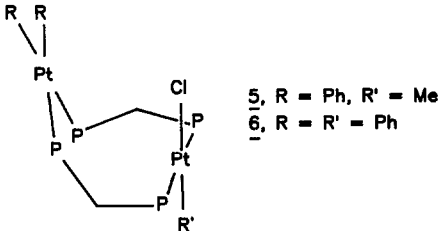

5, R = Ph, R' = Me
6, R = R' = Ph

Complexes **5** and **6** were prepared easily, as pale yellow solids, by reaction of **1** with the corresponding complex *trans*-$[PtClR(SMe_2)_2]$. The ^{31}P NMR spectra of **5** and **6** were very similar and each contained two multiplets, with an apparent triplet structure, arising from the $[AX]_2$ spin system. For example, **5** gave $\delta(P) = -12.2$ ppm, $^1J(PtP) = 2820$ Hz, for the mutually *trans* phosphorus atoms and $\delta(P) = -26.5$ ppm, $^1J(PtP) = 1823$ Hz, for the phosphorus atoms *trans* to the phenyl groups. Thus, the *cis,trans* stereochemistry is firmly established. The observation of two triplets, with the same $^1J(PtP)$ values as above, in the ^{195}Pt NMR spectrum confirmed the skeletal structure. In the ^1H NMR spectra, four MeP resonances were observed for **5** or **6**, with two appearing as apparent doublets (due to the *cis*-PtP_2 fragment) and two as apparent triplets (due to the *trans*-PtP_2 fragment). These are extreme cases of $[A_3X]_2$ spectra (A = CH_3, X = *P*) with low values of $J(XX')$ leading to apparent doublets and high values to apparent triplets and are good indications of *cis*- and *trans*-PtP_2 units, respectively.[21] For complex **5**, the *Me*Pt resonance appeared as the expected triplet, due to $^3J(PH)$ coupling, with ^{195}Pt satellite spectra.

The above spectra were obtained in relatively non-polar solvents (CH_2Cl_2 or acetone), in which the complexes gave almost colourless solutions. When dissolved in methanol or ethanol, the complexes gave intense yellow solutions as the ionic isomers **7a** and **8a** were formed.

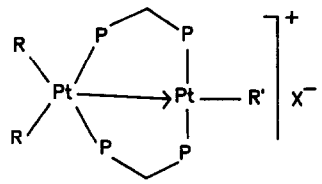

7a, R = Ph, R' = Me, X = Cl
7b, R = Ph, R' = Me, X = PF_6
8a, R = R' = Ph, X = Cl
8b, R = R' = Ph, X = PF_6

If the methanol was evaporated and the products redissolved in a non-polar solvent, the very pale yellow complexes of **5** and **6** were recovered. Hence, the reversible isomerization of eq. (2) is indicated. The cations, **7** and **8**, could be isolated as the hexafluorophosphate salts, **7b** and **8b**, which then retained their intense yellow colour even in non-polar solvents.

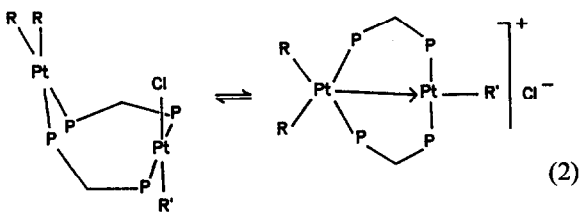

(2)

The structures of **7** and **8** are readily deduced by comparison of their NMR spectra with those of $[Me_2Pt(\mu\text{-dppm})_2PtMe]^+$, which has been characterized crystallographically.[22] As well as the characteristic colour,[9,22] the observation in the ^1H NMR for **7** of a methylplatinum resonance with both coupling constants $^2J(PtCH_3)$ and $^3J(PtPtCH_3)$ well resolved and, in the ^{31}P NMR, a significant decrease in $^1J(PtP)$ for the *cis*-$[Ph_2PtP_2]$ unit compared to **5**, are characteristic of complexes with a donor–acceptor metal–metal bond.[22] In the analogous dppm chemistry, only the cationic complexes analogous to **7** and **8** are formed.[22] We attribute the ability to isolate the neutral complexes, **5** and **6**, to the lower steric effects in the dmpm complexes. It has been found previously that only the ionic $[Pt_2Me_2(\mu\text{-I})(\mu\text{-LL})_2]^+I^-$ is found when LL = dppm but that the neutral $[Pt_2Me_2I_2(\mu\text{-LL})_2]$ is formed when LL = dmpm, and this difference was also attributed to different steric effects of the ligands.[23]

An interesting feature is observed in the chemistry of complex **7**. While complex **5**, like **3**, **6** and **8**, is stable in solution, the NMR spectra of complex **7** decay and new resonances appear after several

hours in solution. We attribute the new resonances to the unsymmetrical complex *cis,trans*-[PhMePt(μ-dppm)$_2$PtPh]$^+$ (**9**) and suggest that it is formed by intramolecular transfer of a phenyl group according to eq. (3), although we have not been able to devise an experiment to prove this hypothesis. The spectral data are fully consistent with the structure **9**, and an intermediate with a Pt$_2$(μ-Ph) group is entirely reasonable by analogy with the known complexes,[24,25] [Pt$_2$(μ-Me){μ-C$_6$H$_4$P(Ph)CH$_2$CH$_2$PPh$_2$}$_2$]$^+$ and [Pt$_2$Me$_2$(μ-C≡CMe)(μ-dppm)$_2$]$^+$. likely mechanism of formation is shown in Scheme 1, and is supported by numerous precedents.[4,5,21,26]

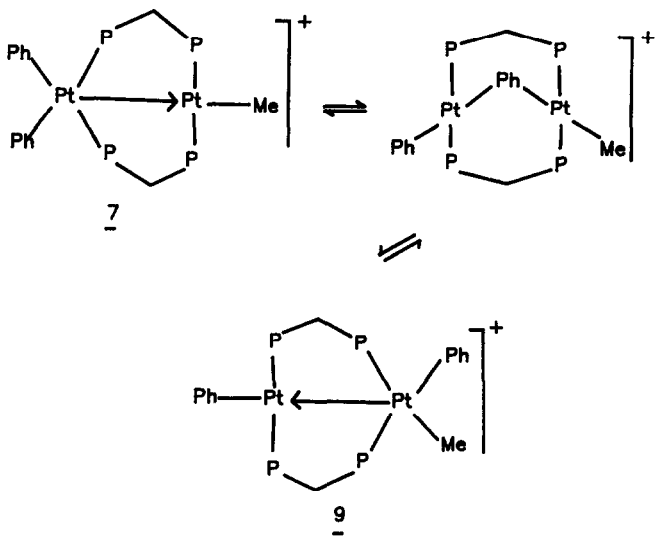

EXPERIMENTAL

NMR spectra were recorded using Varian XL200 or XL300 spectrometers and referenced to Me$_4$Si (^{1}H), H$_3$PO$_4$ (^{31}P) or K$_2$[PtCl$_4$] (^{195}Pt). Complexes [Pt$_2$Me$_4$(μ-SMe$_2$)$_2$] and *trans*-[PtClMe(SMe$_2$)$_2$] were prepared by the literature method.[20]

Reactions of **2** *and* **3** *with iodomethane*

The complex *cis,cis*-[Pt$_2$Me$_4$(μ-dmpm)$_2$] undergoes oxidative addition with MeI to give first [Me$_2$Pt(μ-dmpm)$_2$PtIMe$_3$] and then [Me$_3$Pt(μ-dmpm)$_2$(μ-I)PtMe$_3$]$^+$I$^-$.[4] In contrast, complex **2** failed to react with MeI while complex **3** reacted to give *cis,fac*-[Ph$_2$Pt(μ-dmpm)$_2$PtIMe$_3$] (**10**). Thus no easy oxidative addition at the diphenylplatinum(II) centre occurs in either case. Complex **10** had low thermal stability and readily lost MeI in solution to regenerate complex **3**. Reversible oxidative addition of MeI has previously been observed with *cis,cis*-[Me$_2$Pt(μ-depm)$_2$PtMe$_2$], depm = Et$_2$PCH$_2$PEt$_2$, and was attributed to increased steric hindrance compared with the dmpm analogue.[4]

When complex **10** was heated under reflux with excess MeI, a mixture of two complexes, which were readily separated, was formed. These were identified by the ^{31}P NMR spectra as a less soluble *fac,fac*-Pt(IV),Pt(IV) dimer and as a *trans,fac*-Pt(II),Pt(IV) dimer. From detailed analysis of the ^{1}H NMR spectra and analytical data, these complexes were identified as **11** and **12**, respectively. A

cis-[PtPh$_2$(SMe$_2$)$_2$]

To a suspension of [PtCl$_2$(SMe$_2$)$_2$] (2.0 g, 5.1 mmol, mixture of *cis* and *trans*) in anhydrous diethyl ether (100 cm^3) at 0°C, under an atmosphere of nitrogen, was added dropwise, a solution of PhLi in diethyl ether (2.0 M, 6.5 cm^3). The mixture was stirred continuously during the addition. At the end, a milky white solution was obtained. The diethyl ether layer was separated from the aqueous layer. The aqueous layer was extracted with diethyl ether (60 cm^3). The diethyl ether layer and the extracts were combined and dried over anhydrous MgSO$_4$, and then filtered. Removal of the solvent yielded the product as a white solid. Yield 1.5 g, 3.2 mmol, 62%; m.p. 130°C dec. Found: C, 41.1; H, 4.9. Calc. for C$_{16}$H$_{22}$S$_2$Pt: C, 40.6; H, 4.6%. ^{1}H NMR (in CDCl$_3$): δ (ppm) = 2.1 [s, 6H, ^3J(PtH) = 24 Hz, Me$_2$S], 6.74 [m, 4H, ^3J(HH) = 8 Hz, Ph (*meta*)], 6.9 [d of t, 2H, ^3J(HH) = 7, ^4J(HH) = 2 Hz, Ph (*para*)], 7.3 [d of d, 4H, ^3J(HH) = 8, ^4J(HH) = 2, ^3J(PtH) = 74 Hz, Ph (*ortho*)].

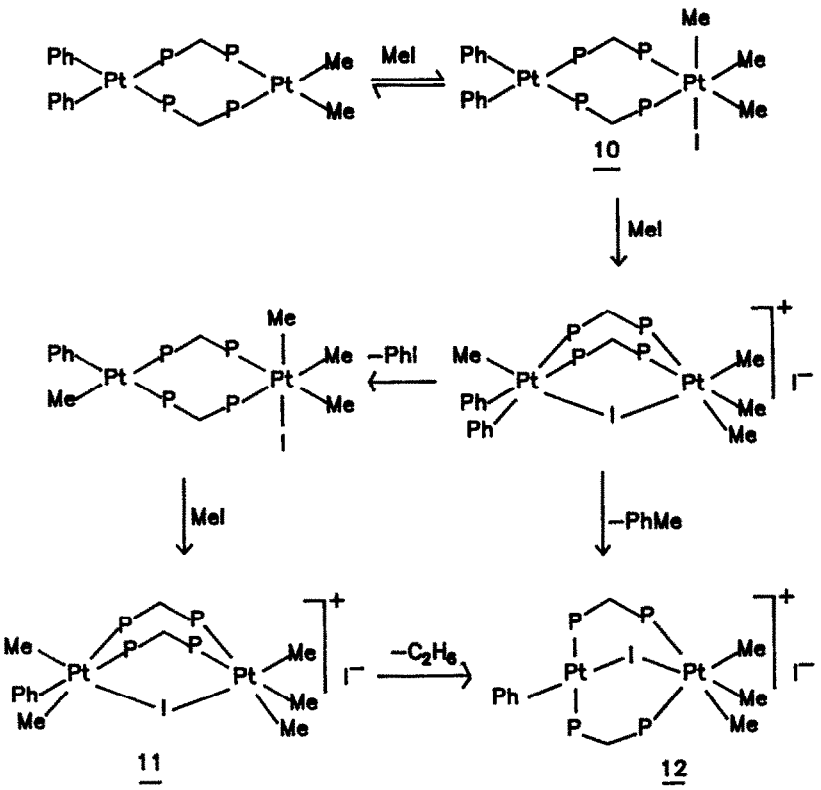

Scheme 1.

trans-[PtClPh(SMe_2)$_2$]

To a solution of *cis*-[$PtPh_2(SMe_2)_2$] (200 mg, 0.42 mmol) in diethyl ether (20 cm^3) was added HCl in diethyl ether (0.2 M, 18.5 cm^3). The mixture was stirred for 1 h at which point the solvent was removed *in vacuo*; the product was washed with pentane (10 cm^3) and dried. Yield 150 mg, 0.35 mmol, 83%; m.p. 92°C dec. Found: C, 27.7; H, 4.1. Calc. for $C_{10}H_{17}ClS_2Pt$: C, 27.8; H, 3.9%. ^1H NMR (in $CDCl_3$): δ (ppm) = 2.3 [s, 6H, ^3J(PtH) = 57 Hz, Me_2S], 6.8–7.3 [m, 10H, Ph].

cis,cis-[$Pt_2Ph_4(\mu$-dmpm)$_2$] (2)

To a solution of *cis*-[$PtPh_2(SMe_2)_2$] (50 mg, 0.11 mmol), in dry CH_2Cl_2 (3 cm^3) under an atmosphere of nitrogen, was added dmpm (20 mg, 0.11 mmol). The mixture was stirred for 0.5 h. Pentane (15 cm^3) was added to precipitate the product. Removal of the solvent and drying *in vacuo* yielded the product as a white microcrystalline solid. Yield 40 mg, 0.04 mmol, 75%; m.p. 145°C dec. Found: C, 41.6; H, 4.9. Calc. for $C_{38}H_{48}P_4Pt_2$: C, 42.1; H, 4.9%. ^1H and $^{31}P\{^1H\}$ NMR (Tables 1 and 2). $^{195}Pt\{^1H\}$ NMR (in $CDCl_3$): δ (ppm) = −4398 [t, ^1J(PtP) = 1682 Hz].

cis-[$PtPh_2(\eta^1$-dmpm)$_2$] (1)

The ligand dmpm (300 mg, 2.2 mmol) was added dropwise to a solution of *cis*-[$PtPh_2(SMe_2)_2$] (500 mg, 1 mmol) in dry CH_2Cl_2 (5 cm^3) under an atmosphere of nitrogen. The mixture was stirred for 1 h. Pentane (15 cm^3) was added to precipitate the product. The solvents were decanted and the white precipitate was further washed with pentane (15 cm^3). Finally, the product was dried. Yield 550 mg, 0.88 mmol, 88%; m.p. 160°C dec. Found: C, 41.5; H, 5.7. Calc. for $C_{22}H_{38}P_4Pt$: C, 42.5; H, 6.1%.

cis,cis-[$Ph_2Pt(\mu$-dmpm)$_2$$PtMe_2$] (3)

To a suspension of complex 1 (440 mg, 0.7 mmol) in CH_2Cl_2 (3 cm^3) was added a solution of [$Pt_2Me_4(\mu$-$SMe_2)_2$] (200 mg, 0.35 mmol) in CH_2Cl_2 (3 cm^3). After stirring for 1/2 h, the volume of the solution was reduced. Addition of pentane (10 cm^3) led to the precipitation of the product. The precipitate was washed several times with pentane (15 cm^3) and dried *in vacuo* to yield the product as a cream coloured microcrystalline solid. Yield 360 mg, 0.43 mmol, 62%; m.p. 143°C dec. Found: C, 41.6; H, 4.9. Calc. for $C_{24}H_{44}P_4Pt_2$: C, 42.1; H, 4.9%.

Table 1. ^{1}H NMR data for complexes **1–8**

Compound	PtMe δ (ppm)	PtMe J(PH) (Hz)	PtMe ^2J(PtH) (Hz)	PMe δ (ppm)	PMe ^2J(PH) (Hz)	PMe ^3J(PtH) (Hz)	P_2CH_2 δ (ppm)	P_2CH_2 ^2J(PH) (Hz)	P_2CH_2 ^3J(PtH) (Hz)
1	—	—	—	1.28 (br s) 1.33 (br s)	—	—	2.31 (m)	8	
1[a]	—	—	—	1.11, 1.31 1.26 ,1.46	—	—	2.4 (m)		
2	—	—	—	1.52 (br m) 0.78, 2.13	—	—	2.31 (m) 2.2, 2.4	12	40
2[a]									
3	0.51 (m)	2	66	1.32 (m) 1.80 (m)	— —	— 16	2.30 (m)	8	40
3[b]	0.54 (m)	—	66	0.82, 2.00 1.60, 2.20	—	—	2.20 (m) 2.40 (m)		
5	1.38 (t)	7	80	1.02 (d) 1.54 (t) 1.71 (t) 1.96 (d)	7 3 3 7	22 24 24 22	2.81 (m)		
6	—	—	—	0.81 (dd) 0.86 (t) 1.70 (t) 2.04 (dd)	7 4 4 7	— — — —	2.84 (m)	8	—
7	1.13 (t)	7	82	1.57 (t) 1.63 (d) 1.69 (t) 1.87 (d)	4 8 4 8	38 14 38 14	2.13 (m)	—	—
8	—	—	—	1.33 (t) 1.40 (t) 1.64 (d) 2.01 (d)	4 4 9 9	— — — —	2.43 (m)	10	—

[a] At −50°C.
[b] At −30°C.

cis,trans-[$Ph_2Pt(\mu$-dmpm$)_2PtClMe$] (**5**)

Complex **1** (100 mg, 0.16 mmol) in CH_2Cl_2 (5 cm^3) was added to a solution of *trans*-[$PtClMe(SMe_2)_2$] (60 mg, 0.16 mmol) in acetone (3 cm^3). The mixture was stirred for 1 h after which time pentane (10 cm^3) was added to precipitate the product. Removal of the solvent and drying *in vacuo* yielded the product as a cream coloured microcrystalline solid. Yield 120 mg, 0.14 mmol, 86%; m.p. 150°C dec. Found: C, 31.5; H, 4.8. Calc. for $C_{23}H_{41}ClP_4Pt_2$: C, 31.8; H, 4.7%.

cis,trans-[$Ph_2Pt(\mu$-dmpm$)_2PtClPh$] (**6**)

trans-[$PtClPh(SMe_2)_2$] (30 mg, 0.06 mmol) in CH_2Cl_2 (3 cm^3) was added to a solution of complex **4** (45 mg, 0.06 mmol) in CH_2Cl_2 (3 cm^3). The mixture was stirred for 1 h. The solvent was removed *in vacuo*; the product was washed with pentane (5 cm^3) and dried. Yield 45 mg, 0.05 mmol, 80%; m.p. 148°C dec. Found: C, 35.8; H, 4.4. Calc. for $C_{28}H_{43}ClP_4Pt_2$: C, 36.2; H, 4.6%. ^{1}H and $^{31}P\{^1H\}$ NMR (Tables 1 and 2). $^{195}Pt\{^1H\}$ NMR (in $CDCl_3$): δ (ppm) = −2055 [t, ^1J(PtP) = 2830 Hz, PtPh], −4370 [t, ^1J(PtP) = 1750 Hz, $PtPh_2$].

[$Ph_2Pt(\mu$-dmpm$)_2PtMe][PF_6$] (**7b**)

The white complex, **5** (50 mg, 0.06 mmol), was dissolved in methanol (3 cm^3) to give a bright yellow solution. To this was added a saturated solution of NH_4PF_6 in methanol (3 cm^3). The mixture was

Table 2. $^{31}P\{^1H\}$ NMR data for complexes **1–8**

Compound	P^a δ (ppm)	P^a $^1J(PtP^b)$ (Hz)	$J(P^aP^b)$ (Hz)	P^b δ (ppm)	P^b $^1J(PtP^b)$ (Hz)
1	−25.7 (m)	1717	61	−58.1	—
2	−26.4 (s)	1682	16, 8	—	—
3	−23.9 (m)	1745	22, 9	−25.1 (m)	1705
5	−12.1 (t)	2820	13	−26.5 (t)	1823
6	−10.9 (t)	2831	8	−25.8 (t)	1750
7	−7.5 (t)	2732	30	−12.5 (t)	1364
8	−11.3 (m)	2732	31	−12.4 (m)	1370

stirred and cooled in an ice bath to initiate crystallization of the product. After a few hours yellow crystals of the product were formed. The product was filtered, washed with water (5 cm^3) and pentane (5 cm^3) and dried *in vacuo*. Yield 40 mg, 0.04 mmol, 66%; m.p. 170°C dec. Found: C, 28.0; H, 4.2. Calc. for $C_{23}H_{41}F_6P_5Pt_2$: C, 28.3; H, 4.2%. ^1H and $^{31}P\{^1H\}$ NMR (Tables 1 and 2). $^{195}Pt\{^1H\}$ NMR (in CD_2Cl_2): δ (ppm) = −2710 [t of t, $^1J(PtP)$ = 2734, $^3J(PtP)$ = 42 Hz, PtMe], −2583 [t of t, $^1J(PtP)$ = 1374, $^3J(PtP)$ = 28 Hz, $PtPh_2$].

$[Ph_2Pt(\mu\text{-dmpm})_2PtPh][PF_6]$ (**8b**)

To a yellow solution of complex **6** (45 mg, 0.05 mmol) in methanol (5 cm^3) was added a saturated solution of NH_4PF_6 in methanol (2 cm^3). The mixture was stirred for 1/2 h and the product was filtered, washed with water (5 cm^3) and pentane (5 cm^3) and dried *in vacuo*. Yield 30 mg, 0.03 mmol, 60%; m.p. 175°C dec. Found: C, 32.0; H, 4.3. Calc. for $C_{28}H_{43}F_6P_5Pt_2$: C, 32.4; H, 4.2%. ^1H and $^{31}P\{^1H\}$ NMR (Tables 1 and 2). $^{195}Pt\{^1H\}$ NMR (in d_6-acetone): δ (ppm) = −2203 [t, $^1J(PtP)$ = 2740 Hz, PtPh], −2247 [t, $^1J(PtP)$ = 1380 Hz, $PtPh_2$].

cis,fac-$[Ph_2Pt(\mu\text{-dmpm})_2PtIMe_3]$ (**10**)

To a solution of complex **3** (90 mg, 0.1 mmol) in CH_2Cl_2 (3 cm^3) was added MeI (1 cm^3) and the mixture was stirred for 1 h. A white precipitate formed during the course of the reaction. This was isolated, washed with pentane (10 cm^3) and dried *in vacuo*. Yield 60 mg, 0.06 mmol, 60%; m.p. 178°C dec. Found: C, 29.3; H, 4.6. Calc. for $C_{25}H_{47}IP_4Pt_2$: C, 30.4; H, 4.7%. ^1H NMR (in $CDCl_3$): δ (ppm) = 0.92 [d of d, 6H, $^2J(PH)$ = 8, $^3J(PtH)$ = 42 Hz, MeP], 1.0 [t, 3H, $^3J(PH)$ = 8, $^2J(PtH)$ = 69 Hz, MePt], 1.13 [d of d, 6H, $^3J(PH)$ = 2, $^3J(PH)$ = 0.5, $^2J(PtH)$ = 56 Hz, MePt], 1.48 [d, 6H, $^2J(PH)$ = 8, $^3J(PtH)$ = 20 Hz, MeP], 1.70 [d, 6H, $^2J(PH)$ = 8 Hz, MeP], 1.86 [d, 6H, $^2J(PH)$ = 8, $^3J(PtH)$ = 22 Hz, MeP], 2.37 [m, 4H, P_2CH_2], 6.68 [m, 2H, Ph (*para*)], 7.04 [m, 4H, Ph (*meta*)], 7.34 [m, 4H, $^3J(PtH)$ = 60 Hz, Ph (*ortho*)]. $^{31}P\{^1H\}$ NMR (in $CDCl_3$): δ (ppm) = −24.5 [s, 2P, $^1J(PtP)$ = 1665 Hz, P^a], −54.7 [s, 2P, $^1J(PtP)$ = 1159 Hz, P^b].

Pyrolysis of **10**

Complex **10** (50 mg, 0.05 mmol) was heated in an oil bath to 160°C. The colour of the solution changed to a slightly darker yellow. Examination of the ^1H NMR spectrum showed the presence of complex **3**.

fac,fac-$[Me_3Pt(\mu\text{-I})(\mu\text{-dmpm})_2PtMe_2Ph][I]$ (**11**) *and* fac,trans-$[Me_3Pt(\mu\text{-I})(\mu\text{-dmpm})_2PtPh][I]$ (**12**)

To a solution of complex **3** (80 mg, 0.08 mmol) in CH_2Cl_2 (3 cm^3) was added MeI (1 cm^3). The mixture was stirred under reflux for 3 h. At this point the reaction mixture consisted of a white precipitate, **11**, and a yellow supernatant, **12**. These fractions were separated, washed with pentane (5 cm^3) and dried *in vacuo*. **11**: Found: C, 27.3; H, 3.6. Calc. for $C_{26}H_{20}I_2P_4Pt_2$: C, 27.6; H, 4.4%. ^1H NMR (in $CDCl_3$): δ (ppm) = 0.94 [m, 6H, $^2J(PtH)$ = 53 Hz, $Me^{a,c}Pt$], 1.03 [t, 3H, $^3J(PH)$ = 8, $^2J(PtH)$ = 72 Hz, Me^bPt], 1.07–1.70 [m, 24H, MeP], 2.4 [m, 4H, P_2CH_2], 6.4 [m, 5H, Ph]. $^{31}P\{^1H\}$ NMR (in $CDCl_3$): δ (ppm) = −41.6 [s, 2P, $^1J(PtP)$ = 1186 Hz, P^a], −45.4 [s, 2P, $^1J(PtP)$ = 1254 Hz, P^b]. **12**: ^1H NMR (in $CDCl_3$): δ (ppm) = 0.99 [br.s, 6H, $^2J(PtH)$ = 53 Hz, MePt], 1.1–1.7 [m, 24H, MeP], 2.6 [m, 4H, P_2CH_2], 6.9–7.3 [m, 5H, Ph]. $^{31}P\{^1H\}$ NMR (in $CDCl_3$): δ (ppm) = −14.5 [t, 2P, $^2J(PP)$ = 7, $^2J(PtP)$ = 2604 Hz, P^a], −43.4 [t, 2P, $^2J(PP)$ = 7, $^1J(PtP)$ = 1192, $^3J(PtP)$ = 136 Hz, P^b].

Acknowledgement—We thank NSERC (Canada) for financial support.

REFERENCES

1. R. J. Puddephatt, M. A. Thomson, Lj. Manojlović-Muir, K. W. Muir, A. A. Frew and M. P. Brown, *J. Chem. Soc., Chem. Commun.* 1981, 805.
2. S. S. M. Ling, R. J. Puddephatt, Lj. Manojlović-Muir and K. W. Muir, *Inorg. Chim. Acta* 1983, **77**, L95.
3. Lj. Manojlović-Muir, K. W. Muir, A. A. Frew, S. S. M. Ling, M. A. Thomson and R. J. Puddephatt, *Organometallics* 1984, **3**, 1637.
4. S. S. M. Ling, I. R. Jobe, Lj. Manojlović-Muir, K. W. Muir and R. J. Puddephatt, *Organometallics* 1985, **4**, 1198.
5. S. S. M. Ling, N. C. Payne and R. J. Puddephatt, *Organometallics* 1985, **4**, 1546.
6. Lj. Manojlović-Muir, I. R. Jobe, B. J. Maya and R. J. Puddephatt, *J. Chem. Soc., Dalton Trans.* 1987, 2117.
7. A. J. McLennan and R. J. Puddephatt, *Organometallics* 1985, **4**, 485.
8. P. G. Pringle and B. L. Shaw, *J. Chem. Soc., Chem. Commun.* 1982, 581.
9. P. G. Pringle and B. L. Shaw, *J. Chem. Soc., Dalton Trans.* 1984, 849.
10. F. S. M. Hassan, D. M. McEwan, P. G. Pringle and B. L. Shaw, *J. Chem. Soc., Dalton Trans.* 1985, 1501.
11. A. T. Hutton, P. G. Pringle and B. L. Shaw, *J. Chem. Soc., Dalton Trans.* 1985, 1677.
12. G. B. Jacobsen and B. L. Shaw, *J. Chem. Soc., Chem. Commun.* 1985, 692.
13. G. B. Jacobsen and B. L. Shaw, *J. Chem. Soc., Dalton Trans.* 1987, 151.
14. C. R. Langrick, D. M. McEwan, P. G. Pringle and B. L. Shaw, *J. Chem. Soc., Dalton Trans.* 1983, 2487.
15. R. J. Puddephatt, *Chem. Soc. Rev.* 1983, 99.
16. R. B. King and K. S. Raghuveer, *Inorg. Chem.* 1984, **23**, 2482.
17. W. K. Wong, K. W. Chiu, G. Wilkinson, M. Motevalli and M. B. Hursthouse, *Polyhedron* 1985, **4**, 1231; W. K. Wong, K. W. Chiu, G. Wilkinson, A. J. Howes, M. Motevalli and M. B. Hursthouse, *Polyhedron* 1985, **4**, 603.
18. M. L. Kullberg and C. P. Kubiak, *Inorg. Chem.* 1986, **25**, 26; F. R. Lemke and C. P. Kubiak, *J. Chem. Soc., Chem. Commun.* 1985, 1729.
19. H. H. Karsch, B. Milewski-Mahrla, J. O. Besenhard, P. Hoffman, P. Stourffert and T. A. Albright, *Inorg. Chem.* 1986, **25**, 3811.
20. J. D. Scott and R. J. Puddephatt, *Organometallics* 1983, **2**, 1643.
21. J. D. Ruddick and B. L. Shaw, *J. Chem. Soc. (A)* 1969, 2801.
22. M. P. Brown, S. J. Cooper, A. A. Frew, Lj. Manojlović-Muir, K. W. Muir, R. J. Puddephatt, K. R. Seddon and M. A. Thomson, *Inorg. Chem.* 1981, **20**, 1500.
23. Lj. Manojlović-Muir, S. S. M. Ling and R. J. Puddephatt, *J. Chem. Soc., Dalton Trans.* 1986, 151.
24. D. P. Arnold, M. A. Bennett, G. M. McLaughlin and G. B. Robertson, *J. Chem. Soc., Chem. Commun.* 1983, 34.
25. A. T. Hutton, B. Shabanzadeh and B. L. Shaw, *J. Chem. Soc., Chem. Commun.* 1984, 549.
26. T. G. Appleton, H. C. Clark and L. E. Manzer, *J. Organomet. Chem.* 1974, **65**, 275.

Polyhedron Vol. 7, No. 24, pp. 2703–2707, 1988
Printed in Great Britain

0277–5387/88 $3.00+.00
© 1988 Pergamon Press plc

THE PREPARATION OF BIMETALLIC COMPLEXES WITH THE LIGAND 1-OXY-2,6-DI[(N,N-BISCARBOXYMETHYL)AMINOMETHYL]-4-CHLOROBENZOL, AND THEIR PHYSICO-CHEMICAL CHARACTERIZATION

G. FAVERO, U. RUSSO, M. VIDALI and B. ZARLI*

Dipartimento di Chimica Inorganica, Metallorganica ed Analitica, Università di Padova, Via Marzolo 1-35131 Padova, Italy

(*Received* 16 *March* 1988; *accepted* 6 *June* 1988)

Abstract—With the binucleating ligand 1-oxy-2,6-di[(N,N-biscarboxymethyl)aminomethyl]-4-chlorobenzol (H_5L) complexes of formulae $FeH_2L \cdot 2H_2O$; $FeH_3L(ClO_4) \cdot H_2O$; $Fe_2L(OH) \cdot 2H_2O$; $M_2HL \cdot nH_2O$ (M = Co, Cu, $n = 2$; M = Ni, $n = 4$); $FeCuL \cdot 3H_2O$; $FeCrL(OH) \cdot 3H_2O$ were prepared and characterized by elemental analysis, IR and electronic spectra and magnetic moment determinations. In addition, thermal analysis data of the complexes and Mössbauer effect spectra of the iron containing complexes are also given and discussed.

Binuclear complexes containing metal centres in close proximity have been the subject of recent investigations because these structural entities can be regarded as models for active sites in metallobiomolecules. Other interesting areas of research on these complexes are the study of intermolecular binding, the possible activation of small molecules between the two metal centres, and the magnetic interactions and multi-electron redox reactions.

In previous works we have reported the preparation of the ligand 1-oxy-2,6-di[(N,N-biscarboxymethyl)aminomethyl]-4-chlorobenzol (Fig. 1) and its mono- and binuclear complexes with *d* and *f* block metal ions.[1,2]

This paper relates the preparation of pure mononuclear chelates and their ineractions with metal salts to yield hetero- and homobinuclear compounds. The thermal decomposition of some of these compounds has been investigated with the view to the possibility of preparing mixed oxides of defined stoichiometry.

EXPERIMENTAL

The ligand 1-oxy-2,6-di[(N,N-biscarboxymethyl) aminomethyl]-4-chlorobenzol (H_5L) was prepared according to the literature method[3] and its purity checked by elemental analysis and physico-chemical measurements.

Preparation of the mononuclear complexes

A methanol solution (20 cm^3) of the appropriate metal perchlorate (1 mmol) was added to a methanol solution (20 cm^3) containing the ter-lithium derivative of the ligand. The mixture was shaken well and heated to boiling, then cooled, reduced to small volume, and ether was added until a precipitate appeared. It was filtered and washed with an ether–methanol (2:1 v/v) mixture. The compound was dried *in vacuo* over silica gel.

Preparation of the homobinuclear complexes

The preparation of the homobinuclear complexes followed previously reported methods.[1]

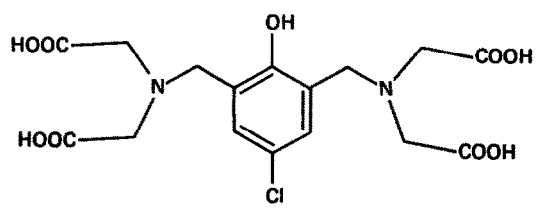

Fig. 1. The ligand 1-oxy-2,6-di[(N,N-biscarboxymethyl) aminomethyl]-4-chlorobenzol.

*Author to whom correspondence should be addressed.

Preparation of the heterobinuclear complexes

The mononuclear chelate (1 mmol) was dissolved in methanol (30 cm^3) and lithium hydroxide (2 mmol) was added. After a clear solution was obtained, the appropriate metal perchlorate (1 mmol) dissolved in methanol (10 cm^3) was added. The resulting mixture was shaken and heated to reflux for 4 h. A precipitate was formed, filtered, washed with methanol and diethyl ether and then dried *in vacuo* over P_4O_{10}.

Chemical and physical measurements

Elemental analyses were performed in the microanalytical laboratory of the Department of Inorganic Chemistry. IR spectra were obtained by a Nicolet 5DSX FTIR spectrophotometer on samples suspended in a KBr matrix or mulled with mineral oil. Electronic spectra were carried out on a Perkin–Elmer Lambda 5 spectrophotometer in Nujol mulls spread on paper.

Magnetic susceptibilities at room temperature were measured by the Faraday method by using an Oxford instrument; the apparatus was calibrated with $Ni(en)_3(ClO_4)_2$.

Weight and energy variations were monitored by a Perkin–Elmer TGS 2 thermobalance and a Perkin–Elmer DSC 4 scanning calorimeter, respectively. The decomposition products were analysed by a VG M16 mass spectrometer with a direct inlet system (DIS).

Mössbauer effect spectra were obtained at 77 K and RT on a conventional constant acceleration spectrometer which utilized a room temperature rhodium matrix cobalt-57 source and was calibrated at RT with a natural abundance α-iron foil. The spectra were fitted to Lorentzian line shapes by using standard least-squares computer minimization techniques. In the fitting procedure, all the parameters were allowed to vary until the very best fit was obtained.

RESULTS AND DISCUSSION

The reaction of the ligand in methanol with iron(III) perchlorate in the molar ratio 1:1 gave the complex $FeH_2L \cdot 2H_2O$ in presence of lithium hydroxide while, without LiOH, the complex $FeH_3L(ClO_4) \cdot H_2O$ has been obtained as a microcrystalline powder. These complexes are soluble in organic coordinating solvents and insoluble in chloroform, methylene chloride and acetonitrile. The IR spectra (in Nujol mulls or KBr pellets) show a broad band ranging from 3600 to 3200 cm^{-1} due to the stretching of coordinated water. The absorption band due to the coordinated carboxylic groups lies at about 1590 cm^{-1} while that of the uncoordinated ones is at 1740 cm^{-1}. The weak band at about 1290 cm^{-1} is assigned to the phenolic C—O group. The iron(III) perchlorate complex shows the characteristic stretching vibrations of the uncoordinated perchlorate anion at 1000 and 625 cm^{-1}. The magnetic moment of $FeH_2L \cdot 2H_2O$ (5.74 BM) is in agreement with an octahedrally surrounded iron(III) in a high-spin state. The electronic spectra of the complexes show a band at about 515 nm confirming an octahedral coordination around the metal ion.

Homo- and heterobimetallic complexes of the type $MM'L \cdot nH_2O$ ($M = M'$ or $M \neq M'$) can also be obtained. The homobimetallic compounds have been prepared by reaction of the free ligand with the metal salt in a 1:2 molar ratio or of the mononuclear chelates with the metal salt in a 1:1 molar ratio.

The elemental analyses of freshly prepared bimetallic complexes are reported in Table 1 along with the Karl–Fisher water analyses. The homobinuclear complexes are soluble in coordinating solvents and insoluble in chloroform, methylene chloride and acetone. The IR spectra of these complexes show a broad band at about 3600–3200 cm^{-1} due to the stretching of the water and bands at about 1590 cm^{-1} are assigned to the coordinated carboxylic groups, while the band at 1740 cm^{-1}, typical of uncoordinated carboxyls, is now absent.

The electronic spectra of copper(II) and cobalt(II) have been discussed elsewhere together with their magnetic moments;[1] the nickel(II) complex shows bands at 630 and 1000 nm typical of a high-spin octahedral nickel(II) ion. Its magnetic moment at room temperature (2.72 BM per atom) is slightly lower than the spin-only value; this decrease can not be surely ascribed to a magnetic interaction between the two metal ions.

The heterobimetallic complexes $FeCuL \cdot 3H_2O$ and $FeCrL(OH) \cdot 3H_2O$ have been prepared in two distinct steps: the preparation of the mononuclear iron(III) compound and then the reaction of this complex with the equimolar amount of the appropriate metal perchlorate. The bimetallic complexes exhibit IR spectra which are different from those of the mononuclear parent compounds. The absorption peak due to the uncoordinated carboxylic groups is absent and a single band at about 1590 cm^{-1} due to the coordinated groups is present. The phenolic C—O stretching mode, which occurs at 1290 cm^{-1} in the mononuclear iron compound, is shifted to 1275 cm^{-1} in the Fe/Cr complex while it lies at the same frequency in the Fe/Cu one indi-

Table 1. Elemental analyses and magnetic moments (BM) of the complexes

Compound	C (%) Calc.	C (%) Found	H (%) Calc.	H (%) Found	N (%) Calc.	N (%) Found	H_2O (%)[a] Calc.	H_2O (%)[a] Found	μ_{eff}[b] (297 K)
Ligand · H_2O	44.0	43.9	4.8	4.9	6.4	6.4	—	—	—
$FeH_2L \cdot 2H_2O$	37.9	37.5	4.8	4.5	5.5	5.4	7.1	7.3	5.74
$FeH_3L(ClO)_4 \cdot H_2O$[c]	32.6	32.6	3.2	3.4	4.7	4.8	3.0	3.2	5.90
$Cu_2HL \cdot 2H_2O$	33.3	33.6	3.3	3.6	4.8	4.9	6.2	6.7	1.66
$Fe_2L(OH) \cdot 2H_2O$	33.2	33.5	3.4	3.6	4.8	5.0	6.2	6.5	4.17
$Co_2HL \cdot 2H_2O$	33.8	33.4	3.4	3.5	4.9	4.7	6.3	6.5	4.40
$Ni_2HL \cdot 4H_2O$	31.9	31.6	3.8	4.1	4.6	4.3	11.9	12.2	2.72
$FeCuL \cdot 3H_2O$	32.7	32.6	3.4	3.3	4.5	4.6	9.2	9.1	—
$FeCrL(OH) \cdot 3H_2O$	32.4	32.3	3.5	3.9	4.7	4.5	9.1	9.3	—

[a] Determined by the Karl–Fisher method.
[b] Values are given per atom.
[c] Cl%: Calc. 12.0; Found 12.3.

cating that in the former complex the phenolic oxygen is involved in the Fe—O—Cr bond.

The electronic spectrum of the Fe/Cu complex is the superimposition of two electronic spectra, in fact it is possible to recognize bands at 514 (Fe) and 740 nm (Cu). So it is probable that the metal ions preserve their coordination geometry without interaction between them. In the spectrum of the Fe/Cr complex the broad band centred at 510 nm is due to the iron(III) ion, comparable to that found in the mononuclear iron complexes reported above.

Mössbauer spectra

The Mössbauer effect spectra of all the iron-containing complexes have been measured at room and liquid nitrogen temperature and two typical spectra are shown in Fig. 2. The resulting spectral and line shape parameters are in Table 2. Each spectrum consists of a single asymmetric quadrupole-split doublet, typical of high-spin iron(III) complexes.[4] The isomer shift range is from 0.48 to 0.57 mm s^{-1} at 77 K; the room temperature values are about 0.1

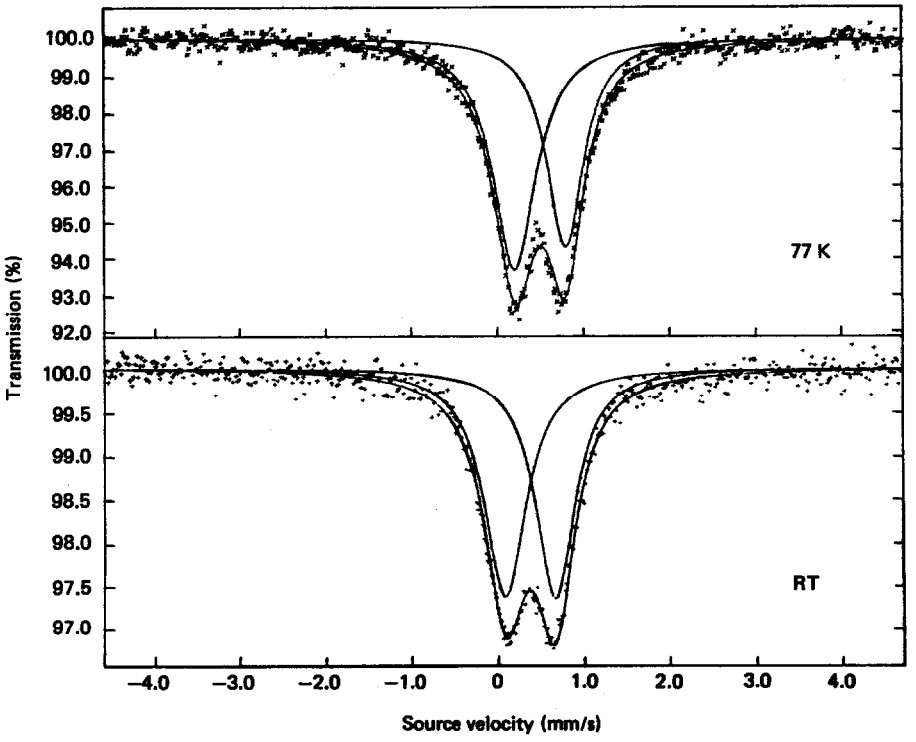

Fig. 2. The Mössbauer spectra of $FeCuL \cdot 3H_2O$ at 77 K and room temperature.

Table 2. Mössbauer parameters for the studied complexes

Compound	T (K)	δ^a (mm/s)	ΔE_Q (mm/s)	Γ^b (mm/s)	Area ratio[c]	E (%)
$FeH_2L \cdot 2H_2O$	RT	0.40	0.73	0.70–0.74	1.17	1.9
	77	0.48	0.68	0.70–0.74	1.13	3.8
$FeH_3L(ClO_4) \cdot H_2O$	RT	—	—	—	—	—
	77	0.52	0.79	0.69–0.72	1.44	2.1
$FeCrL(OH) \cdot 3H_2O$	RT	0.39	0.78	0.52–0.58	1.08	1.8
	77	0.48	0.78	0.57–0.53	1.22	3.1
$Fe_2L(OH) \cdot 2H_2O$	RT	0.39	0.64	0.54–0.57	1.38	1.2
	77	0.49	0.68	0.59–0.57	1.22	2.7
$FeCuL \cdot 3H_2O$	RT	0.39	0.58	0.59–0.54	1.08	0.7
	77	0.51	0.59	0.61–0.51	1.33	1.5

[a] Relative to RT α-iron foil.
[b] Full width at half maximum.
[c] Ratio of the lower energy absorption band to the higher energy absorption band.

mm s^{-1} higher than the low temperature ones, as expected if the second order Doppler shift is considered. All these values are rather insensitive to the presence of a second metal coordinated to the same ligand: in this way a direct metal–metal interaction can be excluded and even the influence of the second metal on the iron *s* electron density, through the ligand donating atoms, is extremely small.

The quadrupole splitting values fall in the range 0.68–0.79 mm s^{-1} at 77 K, typical of high-spin octahedral iron(III) complexes in the $^6A_1$ state. This parameter is highly sensitive to the small distortions induced in the molecule by the second metal and even by the non-coordinated perchlorate anion. So, while the presence of a second iron atom does not change the quadrupole splitting at least at 77 K, the coordination of a copper(II) ion decreases this value to 0.59 mm s^{-1} and coordination of chromium(III) increases it to 0.78 mm s^{-1}. No obvious relation seems to exist between the quadrupole splitting and the ionic or covalent radii of the second metal. Interestingly, the per cent effect decreases from 3.1 to 2.7 and 1.5% on going from chromium to iron and then to copper. The observed asymmetry in the relative area and width of the two quadrupole-split lines is typical of complexes of this type. The most probable origin for this asymmetry could be a temperature dependent spin–spin relaxation effect, which affects one of the nuclear transitions more than the other, resulting in an unequal peak broadening.[5]

Thermal analysis of the complexes

The complexes have been analysed for decomposition steps as reported in the Experimental. The relevant data are reported in Table 3. At least three steps are detectable in the decomposition of the complexes, involving the release of water, carbon dioxide and acetic acid. For a comparison purpose,

Table 3. Heat (kJ per mole of released molecule) and temperature of decomposition (°C) for the ligand and complexes

Release of	(a) Water			(b) Carbon dioxide			(c) Acetic acid		
	moles	temp.	heat	moles	temp.	heat	moles	temp.	heat
$Cu_2HL \cdot 2H_2O$	2.6	100	+57	3.5	250	−21	Traces	360	Very high
$Ni_2HL \cdot 4H_2O$	3.6	130	+64	2.0	335	−15	2.0	385	Very high
$Co_2HL \cdot 2H_2O$	2.0	110	+90	2.0	280	+25	2.0	380	Very high
$Fe_2L(OH) \cdot 2H_2O$	2.2	120	+40	2.0	195	[a]	2.0	230	−217[a]
$FeH_2L \cdot 2H_2O$	1.4	95	+67	2.0	250	−99[a]	2.0	200	[a]
$FeCuL \cdot 3H_2O$	2.0	100	+23	2.0	270	−43	2.0	220	−46
$FeCrL(OH) \cdot 3H_2O$	2.7	115	+67	2.0	320	0	2.0	250	0
$Ligand \cdot H_2O$	1.0	95	+22	4.0	210	−10	Traces	155	Very low

[a] Comprehensive of steps (b) and (c).

the free ligand has also been analysed revealing the same three steps observed for the complexes.

(a) *Release of water.* The ligand and the complexes lose water when heated to 95–130°C. The most strongly bonded water molecules appear to be in the $Co_2HL \cdot 2H_2O$ complex, whereas the most weakly bonded ones are observed in the binuclear $FeCuL \cdot 3H_2O$ and in the free ligand. The dehydration process is accompanied by the absorption of 23–90 kJ per mole of released water, values comparable with the data obtained by us for the process :

$$CuSO_4 \cdot 3H_2O \rightarrow CuSO_4 \cdot H_2O + 2H_2O$$

which involves 75 kJ per mole of water released in the range 90–140°C.

The number of water molecules bonded to the metal atoms, estimated by thermogravity, resulted generally in fair agreement with the analytical data. Values lower than those expected are possibly due to the swiping effect of the gas purging the apparatus, whereas the higher ones should be explained in terms of water absorption by the samples as demonstrated by the successive Karl–Fisher analyses performed.

(b) *Release of carbon dioxide and acetic acid.* The homobinuclear complexes release CO_2 at temperatures between 195–335°C, and acetic acid at sensibly higher temperatures (230–385°C). Instead, the mononuclear and heterobinuclear complexes release, first acetic acid (200–250°C), and then CO_2 (250–320°C). A similar behaviour is also shown by the free ligand, which loses acetic acid at 155°C and CO_2 at 210°C. As one can see from these data, the decomposition temperatures of the complexes are generally higher than those of the free ligand, which is therefore stabilized upon complex formation. The heat balance of the CO_2 releasing decomposition step is slightly negative (−15 to −43 kJ per mole of released CO_2) or positive (+25 kJ for the complex $Co_2HL \cdot 2H_2O$) irrespective if it precedes or follows the acetic acid releasing step. Also, the free ligand displays a similar heat balance (−10 kJ per mole of CO_2). These facts suggest that the balance can be the result of exothermal events connected with intramolecular rearrangements and endothermal ones related to decomposition steps involving the carboxylate groups of the ligand. The influence of the metals bonded to the ligand in the complexes does not appear to be simply related to their electronic properties. The acetic acid releasing decomposition step is generally highly endothermal or moderately exothermal, probably because of a complicated energy balance composed of bond breaking steps accompanied by metal oxides formation.

REFERENCES

1. U. Russo, M. Vidali, B. Zarli, R. Purrello and G. Maccarrone, *Inorg. Chim. Acta* 1986, **120**, 11.
2. B. Zarli, A. Cassol, U. Russo, P. L. Zanonato and M. Vidali, *Polyhedron* 1987, **6**, 1971.
3. G. Schwarzenbach, G. Andreregg and R. Sallmann, *Helv. Chim. Acta* 1952, **35**, 1785.
4. G. J. Long, J. T. Wroblishi, R. V. Thundathil, D. M. Sparlin and E. O. Schlaemper, *J. Am. Chem. Soc.* 1980, **102**, 6040.
5. J. C. Fanning, J. L. Resce, J. C. Lickfield and M. E. Kuton, *Inorg. Chem.* 1985, **24**, 2884.

Polyhedron Vol. 7, No. 24, pp. 2709–2714, 1988
Printed in Great Britain

0277–5387/88 $3.00+.00
© 1988 Pergamon Press plc

LIGAND DEPROTONATION SIGNIFICANCE IN THE FORMATION OF THE MOLYBDATE ION–MALIC ACID COMPLEXES

D. O. MÁRTIRE, M. R. FÉLIZ and A. L. CAPPARELLI*

Instituto de Investigaciones Fisicoquímicas Teóricas y Aplicadas (INIFTA), Facultad de Ciencias Exactas, Universidad Nacional de La Plata, Casilla de Correo 16, Sucursal 4, 1900 La Plata, Argentina

(*Received* 21 *March* 1988; *accepted* 1 *June* 1988)

Abstract—Using the temperature jump technique, the study of the kinetics of the complexing of oxomolybdate anion with malic acid has been carried out in aqueous solutions of pH 7.15–8.5 at ionic strength 0.1 M (KNO_3) and 25°C. A reaction scheme for the formation of 1 : 1 complexes is proposed which accounts for the observed relaxation rates.

The significance of the ligand deprotonation on the complexation reaction of MoO_4^{2-} by a single protonated ligand, i.e.

$$MoO_4^{2-} + LH^n \xrightarrow{k} MoO_3(OH)L^{n-2},$$

(where $n = 1-, 2-$, etc), is analysed on the basis of a simple model. A linear correlation between the $\log k$ and the pK of the monoprotonated ligand (LH) is found for this reaction when the global process is controlled by the proton transfer from the ligand to an oxogroup, i.e.

$$\log k = a - 0.5x pK.$$

It is found that this correlation is satisfied by MoO_4^{2-} and WO_4^{2-}. The experimental slopes for these oxyanions are -0.503 and -0.543 respectively, in agreement with the predictions.

Molybdenum presents several oxidation states, different coordination numbers and the ability to build isopolymeric species—thus making its chemistry very complex.[1] Many metabolic pathways involve this element, those related to the nitrogen fixation in soils being of special interest.[2,3]

In most of these processes, it is supposed that MoO_4^{2-} is the principal species at physiological pH.[2,3] In many aspects, the structural chemistry of MoO_4^{2-} is determined by the oxogroups ligated to Mo; the Mo=O bond is a strong one mainly due to sigma and pi donation from the oxygen atom. At pH higher than 7, Mo(VI) is present principally as MoO_4^{2-} (Td structure). At lower pH, Mo expands its coordination number from 4 to 6.[4,5] In acid media MoO_4^{2-} may be present as MoO_4H^-, its hydrated species or building isopolymolybdates.[6]

Most reactions where Mo(VI) participates seem to be fast enough to be investigated by stopped flow[7–9] or relaxation techniques.[5,10,11]

The chemistry of the interactions between Mo(VI) and hydroxypolycarboxylic acids has been studied mainly from the thermodynamic point of view,[12–19] and there are few kinetic and mechanistic data available on such reactions. As far as we know, only a kinetic study of complexation of Mo(VI) with citric acid has been recently reported.[20]

In this work the interaction between Mo(VI) and L-malic acid (hydroxybutanedioic acid) has been studied to elucidate the kinetics and the mechanisms of these processes with special interst in the rôle played by ligand deprotonation.

EXPERIMENTAL

Reagent grade $Na_2MoO_4 \cdot 2H_2O$ (Merck), L-malic acid (Mallinkrodt), KNO_3 (Carlo Erba), $NaClO_4 \cdot H_2O$ (Merck), and phenol red (Mal-

*Author to whom correspondence should be addressed.

linkrodt) were employed without further purification.

All pH measurements were carried out with a Metrohm AG pH-meter (to ± 0.02 pH units). The instrument was calibrated with appropriate buffer solutions.

Calculations were performed with a Hewlett–Packard 1000-45.

Kinetic measurements

All kinetic measurements were performed using a Messanlagenstudiengessellschaft SB7 A, T-jump equipment. The temperature jump was 5°C and the final temperature 25°C.

The metal concentration was larger than that of the ligand, employing in most conditions a 10:1 relation. The ionic strength was 0.1 M and it was regulated by adding KNO_3. The pH range was 7.15–8.5. Under the present experimental conditions only a 1:1 complex should be formed in agreement with previous thermodynamic studies.[14,15,17–19]

The reaction was followed by measuring the absorbance change at $\lambda = 539$ nm of a pH indicator (phenol red) present in the system at a concentration of 2×10^{-5} M.

Blank experiments were performed. In the absence of metal or ligand no relaxation effect was observed.

RESULTS

Only one relaxation time (τ) was observed under the pH and concentration conditions analysed. The experimental relaxation rates for the Mo(VI)–L-malic acid system are summarized in Table 1.

Each value is the mean of at least five individual measurements and the experimental error (σ) is less than 10%. At a given analytical molybdate concentration ($[MoO_4^{2-}]_0$), a linear dependence of $1/\tau$ on proton concentration is found, the experimental slope being proportional to $[MoO_4^{2-}]_0$. Under our experimental conditions, where the oxyanion concentration is higher than that of the ligand, the dependence of $1/\tau$ on pH and $[MoO_4^{2-}]_0$ is represented by the following empirical equation:

$$1/\tau = 174.4 + 1.22 \times 10^{11}[MoO_4^{2-}]_0 \times [H] \quad s^{-1}. \tag{1}$$

The amplitude of relaxation spectra decreases with increasing pH. At pH higher than 8.3, relaxation spectra are hardly observed.

A similar behaviour has been reported for the Mo(VI)–citrate system.[20]

A complete reaction scheme for the 1:1 complex formation should include several pathways due to the existence of the various protonated forms of reactants, as shown in eq. (2).

$$\begin{array}{lll} & LH^- \rightleftarrows MoO_3(OH)L^{3-} & \text{(a)} \\ MoO_4^{2-} + \uparrow\downarrow & & \\ \Updownarrow & L^{2-} \rightleftarrows MoO_4L^{4-} & \text{(b)} \\ & L^{2-} \rightleftarrows MoO_3(OH)L^{3-} & \text{(c)} \\ MoO_4H^- + \uparrow\downarrow & & \\ & LH^- \rightleftarrows MoO_3(OH)L^{3-} + H^+ & \text{(d)} \end{array}$$

$$InH \rightleftarrows In^- + H^+ \tag{2}$$

Here, L^{2-} and LH^- are the un- and mono-protonated species of ligand; In^- means unprotonated phenol red.

Table 1.

pH	$[MoO_4^{2-}]_0$ ($\times 10^2$ M)	$1/\tau\ \sigma^a$ (s^{-1})	$1/\tau^b$ (s^{-1})
7.15	0.4	232(9)	216.6
7.16	0.8	283(26)	261.0
7.17	0.6	235(13)	236.6
7.22	3.0	540(15)	465.4
7.23	0.4	209(5)	209.0
7.25	0.8	240(12)	244.1
7.28	1.0	282(37)	256.7
7.30	4.0	505(21)	497.1
7.33	1.0	256(22)	247.3
7.35	0.8	253(20)	229.1
7.35	0.4	195(12)	200.1
7.40	0.6	214(9)	209.8
7.40	1.0	251(18)	236.0
7.42	1.0	204(6)	220.5
7.46	0.8	213(5)	216.2
7.46	4.0	233(50)	194.0
7.50	1.0	221(10)	222.7
7.51	1.0	223(28)	221.5
7.52	1.0	233(25)	220.4
7.52	2.5	280(5)	296.7
7.56	1.0	192(6)	216.1
7.56	1.0	219(21)	216.1
7.60	0.4	186(14)	188.2
7.60	1.0	203(13)	212.2
7.60	2.5	284(18)	275.8
7.64	4.0	327(28)	325.2
7.70	1.0	201(5)	204.0
7.77	3.0	287(17)	256.9
7.77	0.8	206(22)	193.8
7.80	2.5	245(4)	237.5
7.81	0.8	206(14)	192.0
7.86	1.0	187(2)	194.3
7.95	4.0	260(22)	247.9
8.00	0.8	193(31)	185.3
8.46	3.0	193(14)	190.2

[a] Experimental.
[b] Calculated.

Under experimental conditions similar to those of this work, only the species $MoO_3(OH)L^{3-}$ has been reported as a 1 : 1 complex.[17-19] Therefore the reaction steps shown in eq. (2) lead to this complex.

As no relaxation spectra are observed at pH > 8.5, where only the unprotonated forms of reactants are present, it can be inferred that reaction (b) does not take place suggesting a proton dependence of the global rate as found experimentally. Furthermore, thermodynamic and spectroscopic studies,[12-15,17] indicate no complex formation at pH higher than 8. Also, other kinetic studies related to Mo(VI) and different chelating agents suggest a non-reactivity between both unprotonated forms of ligand and oxyanion.[8,11,20,21]

Finally, reaction (c) can be discarded considering the concentrations of both reactants to be very small under the experimental conditions. Moreover, its inclusion does not improve the interpretation of the kinetic results. In consequence, eq. (2) reduces to eq. (3).

$$MoO_4^{2-} + LH^- \overset{k_1}{\rightleftharpoons} MoO_3(OH)L^{3-}$$

$$MoO_4H^- + L^{2-} \overset{k_2}{\rightleftharpoons} MoO_3(OH)L^{3-}$$

$$LH^- \rightleftharpoons L^{2-} + H^+ \qquad K_{LH} = 1.94 \times 10^{-5}\ M$$

$$MoO_4H^- \rightleftharpoons MoO_4^{2-} + H^+ \qquad K_{MH} = 1.82 \times 10^{-4}\ M$$

$$InH \rightleftharpoons In^- + H^+ \qquad K_{In} = 1.12 \times 10^{-8}\ M \quad (3)$$

The relaxation rate associated with this mechanism can easily be derived as indicated in the literature.[22] Therefore:

$$1/\tau = k_1 X + k_2 Y + (k_{-,1} + k_{-,2}), \quad (4)$$

or

$$1/\tau = (k_1 + k_2 \times Y/X) \cdot X + (k_{-,1} + k_{-,2}), \quad (4a)$$

with

$$X = [MoO_4^{2-}] \times \frac{(\beta \times [H] \times A) + [LH^-]}{([L^{2-}] + \beta \times K_{LH} \times A)}, \quad (5)$$

$$Y = \frac{[MoO_4H^-] \times (1 - (\beta \times [H] \times A))}{([L^{2-}] + \beta \times K_{LH} \times A)} + \frac{2[L^{2-}] \times ([MoO_4^{2-}] \times [H])}{K_{MH} \times ([L^{2-}] + \beta \times K_{LH} \times A)}, \quad (6)$$

$$A = 1 + [MoO_4^{2-}]/\beta K_{MH},$$

$$\beta = ([In^-] + K_{In} + [H])/(K_{In} + [H]). \quad (7)$$

A simplified expression can be derived considering that $[MoO_4^{2-}]/\beta K_{MH} \ll 1$, $K_{LH} \gg [L]$ and $[MoO_4^{2-}] \approx [MoO_4^{2-}]_0$. With such assumptions, the relation Y/X in eq. (4a) takes the limit value K_{LH}/K_{MH}. Therefore, eq. (4) becomes:

$$1/\tau = (k_1/K_{LH} + k_2/K_{MH}) \cdot [MoO_4^{2-}]_0 \cdot [H^4] + (k_{-,1} + k_{-,2}), \quad (8)$$

which can be compared with eq. (1). This procedure enables us to obtain limit values for the rate constants involved in eq. (3). Therefore:

$$k_1/K_{LH} + k_2/K_{MH} = 1.22 \times 10^{11} M^{-1} s^{-1},$$

$$k_{-,1} + k_{-,2} = 174.4\ s^{-1}, \quad (9)$$

and an approximate value for the equilibrium constant for reaction (1) is:

$$K_1 = 13.6 \times 10^3\ M^{-1}.$$

The above considerations do not enable us to obtain the individual rate constants. However, it can be attained if Y/X is not strictly constant, as really happens for our system. The combination of a non-linear regression routine[23] for solving the polynomial expression for $1/\tau$ and eq. (4a) permit obtaining the individual rate constants k_1, k_2 and $(k_{-,1} + k_{-,2})$. Consisting values for these constants can be calculated accepting that the equilibrium constant K_1 can be handled as a variable parameter within a narrow range of values, i.e. $1.0 \times 10^4 < K_1/M^{-1} < 1.5 \times 10^4$. Outside of this range negative values or $k_{-,1} > 174.5$ are obtained.

The best set of values was selected by considering that the condition $K_2/K_1 = K_{MH}/K_{LH} = 9.33$ must be satisfied. The individual rate constants are:

$$k_1 = (8.3 \pm 1.3) \times 10^5\ M^{-1} s^{-1},$$

$$k_2 = (1.3 \pm 0.5) \times 10^7\ M^{-1} s^{-1},$$

$$k_{-,1} + k_{-,2} = (173.5 \pm 1)\ s^{-1},$$

and $K_1 = 13.3 \times 10^3\ M^{-1}$.

These values were employed for calculating the relaxation rates listed in Table 1.

DISCUSSION

Diebler has studied the reaction between Mo(VI) and 8-hydroxyquinoline[11] and some of its derivative compounds[22] in the pH range 7.5–9.8. Under these conditions, it has been postulated that MoO_4H^- was the unique reactive species.

Kustin *et al.* investigated the reaction of Mo(VI) with catechol.[7] Their results imply that Mo(VI) changes its coordination number from 4 to 6 prior to complexation.

Other studies involving EDTA,[24] 1,2-dihydroxy

anthraquinine-3-sulphonate[25] and catechol derivatives[8] as organic ligands are reported. With the latter and EDTA the participation of MoO_4H^- was considered at pH higher than 7.3.

From ultrasonic studies,[5] a hexacoordinated species was postulated for monoprotonated molybdate. Furthermore, an octahedral complex of $MoO_2(OH)_3H_2O$ has been inferred from NMR studies.[26] This fact led Kustin[8] to admit that complexation itself should be a substitution reaction rather than an addition one.

Tanaka *et al.*[25] working under conditions where one kind of species for metal and ligand are present, showed that the experimental rate is proton dependent. They proposed a nucleophilic attack of the ligand at a face of the tetrahedron of MoO_4^{2-} producing an intermediate where the bond between both reactants is weak, followed by addition of a proton to Mo-oxogroups. Bond formation and configurational changes are the limiting steps of this mechanism.

However, the rate constant k_1 for malic acid is several orders of magnitude higher than for other ligands. This fact can be attributed only to ligand properties.

In Table 2, values of k_1 for different monoprotonated ligands are shown.

Probably, as suggested by Tanaka,[25] the monoprotonated ligand LH^n interacts with the oxyanion attacking at a face of the tetrahedron. According to Tanaka, an external proton would be required to lengthen the Mo—O bond and to strengthen that between Mo and ligand.

However, a simplified model involving the formation of an intramolecular hydrogen bond between the monoprotonated ligand and an oxogroup can be proposed. Thus, we are in the presence of an associative, and in consequence, ligand dependent mechanism. If we denote ABH as the LH^n species, the activated complex would look like that shown in Fig. 1.

As a first approximation, the global activation energy (E) can be written as a sum of two terms: one corresponding to the activation energy of the coordination expansion (E_c) and another to the intramolecular proton transfer (E_t). The last process includes ligand "deprotonation" and molybdate "protonation", the E_t value can be considered proportional to the sum of the activation energies for protonation (E_{mp}) and deprotonation (E_{ld}) of free MoO_4 and LH^n, respectively.* A rough estimation

Table 2. Correlation between pK values and rate constant values corresponding to the reaction step

$$MoO_4^{2-} + LH^n \xrightarrow{k} C$$

Ligand	log k	pK^a
1,2,4-Trihydroxybenzene	1.88[b]	11.82
Pirogallol	2.11[b]	11.64
L-Dopa	2.52[b]	9.78
Epinephrine	2.58[b]	9.90
Oxine	2.61[c]	9.81
Oxine-5-SO3	3.40[c]	8.75
1,2-Dihydroxyanthraquinone-3-sulphonate	4.85[d]	5.32
Citric acid	4.43[e]	5.69
Malic acid	5.92[e]	4.71

[a] pK values were taken from A. Martell and R. M. Smith, *Critical Stability Constants*, Vol. 5, First Supplement. Plenum Press, New York and London (1982).
[b] Taken from ref. 6.
[c] Taken from refs 11 and 22.
[d] Taken from ref. 25.
[e] Reported in this work.

of the proportionality factor would be 0.5. In this way, E_t would be the semi-sum of E_{mp} and E_{ld}. Furthermore, the activation energy for the deprotonation of free ligand is related to the heat of dissociation ΔH by $\Delta H = E_{ld} - E_{lp}$, where E_{lp} is the corresponding activation energy for protonation of the free ligand. Thus:

$$E = E_c + 1/2(E_{mp} + E_{lp}) + 1/2\Delta H. \qquad (10)$$

Because most of the protonation processes are diffusion controlled, E_{lp} could be considered indepedent of ligand nature. Then, for the same oxyanion the first two terms in eq. (10) are constants, that is $E = a + 1/2\Delta H$.

The rate constant is now related to this activation energy through:

$$d \ln k_1/dT = (a + 1/2\Delta H)/RT^2 \qquad (11)$$

because the dissociation constant is related to ΔH

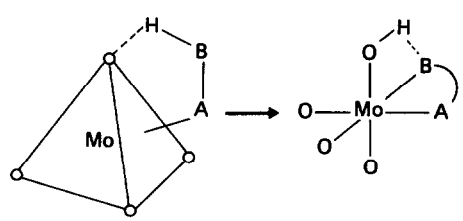

Fig. 1. Activated complex for the reaction between MoO_4^{2-} and a monoprotonated ligand LH^n (where n = 1−, 2−, . . .).

*Similar considerations are found in the literature, especially for substitution reactions in inorganic chemistry and some proton transfer or proton catalysed reactions.[27]

through the Van't Hoff equation:

$$(\mathrm{d}\ln K/\mathrm{d}T) = \Delta H/RT^2 \quad (12)$$

therefore

$$\mathrm{d}\ln k_1/\mathrm{d}T = a/RT + 1/2(\mathrm{d}\ln K/\mathrm{d}T), \quad (13)$$

the integration being straightforward, i.e. $\ln k_1 = b - a/RT + 0.5 \times \ln K$. At constant temperature, we obtain:

$$\log k_1 = \text{const} + 0.5 \log K = \text{const} - 0.5\ \mathrm{p}K. \quad (14)$$

Using available rate constant (k_1) data for reactions between MoO_4^{2-} and monoprotonated ligand species including those reported in this paper, a linear regression between $\log k_1$ and pK, with a slope of -0.503 and a correlation coefficient of 0.98 is obtained, in good agreement with eq. (14). This result is acceptable taking into account the simplicity of the model and the dissimilar origin of the data employed, obtained under very different experimental conditions. In Fig. 2, $\log k_1$ *vs.* pK is shown.

Although a wide range of pK values and rate constants is considered (Fig. 2), this correlation can be accidental. However, a very similar correlation can be found between WO_4^{2-} and some of the ligands indicated in Table 2. Employing Kustin's data,[8] a linear regression can be obtained with a slope of -0.543 and a correlation coefficient of 0.98.

The difference between this correlation and that found in the literature[8] is that the former takes into account the pK values of the LH species consistent with the present model, while the latter is established on basis of the LH_2's pK values.

A kinetic study performed on the Mo(VI)–citric acid system[20] under conditions similar to those of the present study, supports our previous considerations. The complexation reaction shows similar behaviour as observed for the Mo(VI)–malic acid system, i.e. the relaxation rate increases with reactant concentrations and with decreasing pH and the amplitude of the relaxation processes decreases with increasing pH and at pH higher than 8.5, no process is observed. The proposed mechanism is similar to that discussed for Mo(VI)–malic acid. However, another reaction, i.e. $MoO_4H^- + LH^{2-} \rightleftharpoons CH^{3-} \rightleftharpoons C^{4-} + H^+$, is included to account for the potentiometric and enthalpimetric results,[16,17] because of the evident existence of the complex in two different degrees of protonation (C^{4-} and CH^{3-}) in this pH range. For the interaction between MoO_4^{2-} and the monoprotonated citrate, the reported rate constant is:

$$MoO_4^{2-} + LH^{2-} \text{----} C^{4-} \quad k_1 = 2.7 \times 10^4\ M^{-1}\ s^{-1}.$$

In conclusion, the values for the rate constants k_1 obtained for malate, as for citrate, can be justified by the pK values of the monoprotonated ligand. Although some steric hindrances could be present in citric acid, the influence of the ligand deprotonation in both systems should play a significant role.

Let us consider reaction (2) where MoO_4H^- and unprotonated ligand are involved. Rate constant values reported in other systems[8,10] suggest: (a) that these steps are faster than those where MoO_4^{2-} participate (the presence of a proton in MoO_4H^- weakens the Mo—O bond allowing the conformational change) (b) that k_2 values should increase with the basicity of the unprotonated ligand.

Our result for malic acid agrees with the previous consideration and it is consistent with nucleophilic attack of L at MoO_4H^-.

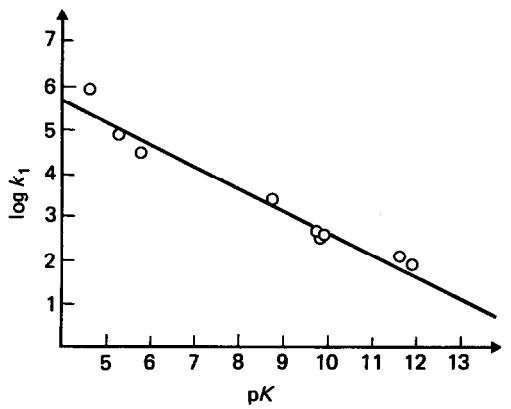

Fig. 2. Correlation between log k and pK values for the reaction of Mo(VI) with several ligands (see Table 2).

Acknowledgements—This work was supported in part by the Consejo Nacional de Investigaciones Cientificas y Tecnicas (CONICET) de la Republica Argentina and Comision de Investigaciones Cientificas de la Provincia de Buenos Aires (CIC). Part of the equipment and the drugs used in the present work were provided by the cooperation agreement between the University of Mainz and the Universidad Nacional de La Plata. The authors are grateful to Dr J. Czarnowski for comments on the manuscript.

REFERENCES

1. F. A. Cotton and G. Wilkinson, *Advanced Inorganic Chemistry*, 3rd Edition. Wiley-Interscience, New York (1972).
2. R. A. D. Wentworth, in *Progress in Inorganic Chemistry* (Edited by J. Lippard), Vol. 22, p. 1. Wiley, New York (1980) and refs cited therein.

3. R. A. D. Wentworth, *Coord. Chem. Rev.* 1976, **18**, 1 and refs cited therein.
4. E. F. C. H. Rohwer and J. J. Cruywagen, *J. S. Afr. Chem. Inst.* 1963, **16**, 26; *ibid* 1969, **17**, 45.
5. D. S. Honig and K. Kustin, *Inorg. Chem.* 1972, **11**, 65.
6. K. H. Von, G. Tytko, G. Baethe, E. R. Hirschfelder, K. Mehnke and D. Stellhorn, *Z. Anorg. Allg. Chem.* 1983, **503**, 43.
7. K. Kustin and S. T. Liu, *J. Am. Chem. Soc.* 1972, **95**, 2487.
8. K. Kustin and K. Gilbert, *J. Am. Chem. Soc.* 1976, **98**, 5502.
9. K. Zare, J. Lagrange and P. Lagrange, *Inorg. Chem.* 1979, **18**, 568.
10. D. S. Honig and K. Kustin, *J. Phys. Chem.* 1972, **76**, 1575.
11. P. F. Knowles and H. Diebler, *Trans. Faraday Soc.* 1968, **64**, 977.
12. M. Cadiot and B. Viossat, *Rev. Chemie Minerale* 1969, **6**, 727.
13. R. A. Chalmers and A. G. Sinclair, *J. Inorg. Nucl. Chem.* 1967, **29**, 2065.
14. A. A. Fedorov, *Zh. Anal. Khim.* 1974, **29**, 891.
15. A. A. Fedorov, *Zh. Obshcs. Khim.* 1975, **45**, 1072.
16. J. J. Cruywagen and R. F. Van der Water, *Polyhedron* 1986, **5**, 521.
17. M. Bartusek, J. Havel and D. Matula, *Coll. Czech. Chem. Commun.* 1986, **51**, 2702.
18. A. Beltran, *J. Inorg. Nucl. Chem.* 1981, **43**, 1337.
19. N. Stolica, in *Standard Potentials in Aqueous Solution* (Edited by A. Bard, R. Parsons and J. Jordan). IUPAC, Marcel Dekker, New York (1985).
20. D. Mártire, M. Féliz and A. Capparelli, *An. Asoc. Qca Arg.* 1987, **76**, 601.
21. H. Diebler and R. Timms, *J. Chem. Soc.* 1971, 273.
22. A. Petrucci, *Ionic Interactions*, Vol. II. Academic Press, New York (1971).
23. P. R. Bevington, *Data Reduction and Error Analysis for Physical Sciences.* McGraw Hill, New York (1969).
24. K. Kustin and D. S. Honig, *J. Am. Chem. Soc.* 1973, **95**, 5525.
25. S. Funashi, Y. Kato, M. Nakayama and M. Tanaka, *Inorg. Chem.* 1980, **20**, 1752.
26. R. R. Vold and R. L. Vold, *J. Mag. Res.* 1975, **19**, 365.
27. T. W. Swaddle, *Coord. Chem. Rev.* 1974, **14**, 217 and refs cited therein.

Polyhedron Vol. 7, No. 24, pp. 2715–2721, 1988
Printed in Great Britain

0277–5387/88 $3.00+.00
© 1988 Pergamon Press plc

TEMPLATE REACTIONS WITH POLYNUCLEAR COMPLEXES. THE REACTION OF $[Mo_2(O_2CCF_3)_4(PR_3)_2]$ (R = Ph, Et) WITH 2-AMINOBENZALDEHYDE

ARVIND SAHAJPAL and PETER THORNTON*

Department of Chemistry, Queen Mary College, Mile End Road, London E1 4NS, U.K.

(*Received* 18 *April* 1988; *accepted* 1 *June* 1988)

Abstract—The binuclear molybdenum(II) complexes $[Mo_2(O_2CCF_3)_4(PR_3)_2]$ (R = Ph, Et) act as templates for the self-condensation of 2-aminobenzaldehyde to give a new class of complexes in which a hydride ion bridges two molybdenum(III) centres, each of which carries a tetradentate macrocyclic ligand (C). The new hydrido complexes $[Mo_2(C)_2(H)(O_2CCF_3)_3(PPh_3)_2]$ (I), $[Mo_2(C)_2(H)_2(O_2CCF_3)_2(PPh_3)_2]$ (II), and $[Mo_2(C)_2(H)_2(O_2CCF_3)_2(PEt_3)_2]_2$ (V) exist in two or more isomeric forms as shown by their IR, ^1H, ^{31}P and ^{19}F NMR spectra. Substitution with thiocyanate, nitrate and tetraphenylborate anions gives the new products $[Mo_2(C)_2(H)(CO)(NCS)_3(PPh_3)_2]$ (III), $[Mo_2(C)_2(H)_2(O_2CCF_3)(NO_3)(PPh_3)_2]$ (IV), $[Mo_2(C)_2(H)(O_2CCF_3)(PPh_3)_2](BPh_4)_2$ (VI) and $[Mo_2(C)_2(H)_2(O_2CCF_3)(PEt_3)_2](BPh_4)$ (VII), which also exist in isomeric forms.

A number of macrocyclic complexes using 2-aminobenzaldehyde and Ni^{II} as the templating metal ion have been prepared by Busch and co-workers.[1] They first prepared complexes of the tetradentate ligand A;† this could then be converted to B by partial base hydrolysis. As the first stage of our investigation into template reactions of binuclear complexes we also reported[2] complexes with ligand B, which in our case was prepared directly from the template reaction between octachlorodimolybdate(II) and 2-aminobenzaldehyde in ethanol. In this, the reaction between the fairly soluble salt $(NH_4)_5[Mo_2Cl_8]Cl \cdot H_2O$ and 2-aminobenzaldehyde gives the molybdenum(IV) product $[Mo_2(B)_2(H_2O)Cl_2]^{2+}2Cl^-$.

As an extension of this work we now report the reaction of 2-aminobenzaldehyde with other Mo_2^{4+} templates $[Mo_2(O_2CCF_3)_4(PR_3)_2]$ (R = Ph, Et). These reactions give a new class of complexes in which a hydride ligand bridges two molybdenum(III) centres each of which carries a tetradentate macrocyclic ligand. Although there are several binuclear molybdenum complexes with one or more bridging hydride ligands[3,4] none have been so far reported with macrocyclic ligands.

RESULTS AND DISCUSSION

The reaction of $[Mo_2(O_2CCF_3)_4(PPh_3)_2]$[5] with 2-aminobenzaldehyde in ethanol gives a variety of binuclear molybdenum complexes (see Scheme 1) containing the tetradentate macrocycle C. When a mixture of these two reactants is heated under reflux for *ca* 3 h in ethanol one obtains the complex $[Mo_2(C)_2(H)(O_2CCF_3)_3(PPh_3)_2]$ (I). The complex is solvated with CH_2Cl_2 (1 mol), which shows in the proton NMR spectrum at δ 5.25 and it exists in possibly two isomeric forms as seen from its IR, ^1H and ^{31}P NMR spectra (see Table 1). The nitrogen analysis for this complex is not satisfactory, but spectroscopic data show that the complex has the stoichiometry indicated above. IR spectra show the presence of both bidentate and monodentate $O_2CCF_3^-$ ligands with antisymmetric CO_2 stretching frequencies at 1605 and 1670 cm^{-1}, respectively. It is possible to differentiate[6] between bidentate and monodentate trifluoroacetate groups because the former absorb at *ca* 1600 cm^{-1} and the latter in the 1600–1700 cm^{-1} range. The C=N stretching frequency for the major isomer is masked

* Author to whom correspondence should be addressed.

† Structures of A, B and C are shown on the following page.

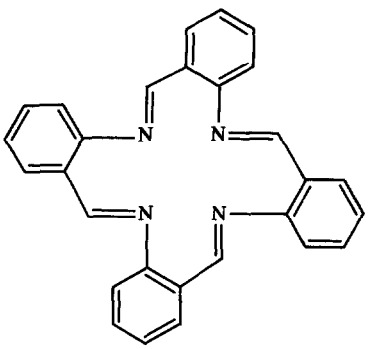

(A)

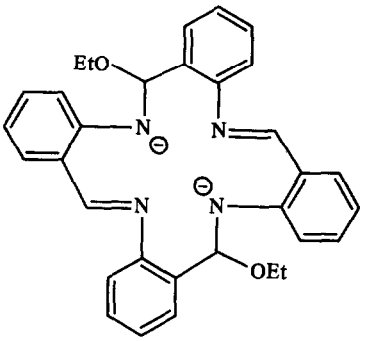

(B)

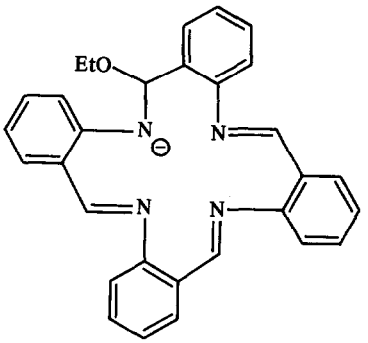

(C)

by the 1605 cm^{-1} band but one can see this at 1602 cm^{-1} in the corresponding thiocyanate complex (see below) where there are no trifluoroacetate groups present; the minor isomer shows a weak band at 1570 cm^{-1} for the C=N stretching frequency. The 80 MHz ^1H NMR spectrum for the methyl protons shows an intense triplet at δ 1.52 and a weak unresolved triplet at δ 1.36 (which is possibly due to virtual coupling with the corresponding methine protons on the macrocycle); the methylene protons show a complex pattern in the region δ (3.8–6.05). The triphenylphosphine ligands are equivalent and show two singlets of different intensities at δ 14.2 and −6.05 for the two isomers in the ^{31}P NMR spectrum.

It was shown by Andersen and co-workers[5] that $[Mo_2(O_2CCF_3)_4(PR_3)_2]$ (R = Ph, Et) exists as isomers in solution with either four or two bridging carboxylate groups and we conclude similar isomerization may occur in the products of our system also. We propose a bridging hydride ligand accompanied by one bridging bidentate and two monodentate trifluoroacetate groups for complex **I**. Hydrides are notoriously difficult to characterize; the principal evidence here for their presence apart from elemental analysis (see Table 2) is the presence of IR bands in the region 1260–1315 cm^{-1} and the complexes' diamagnetism. The IR bands are in a similar region to the ones mentioned by Cotton and Kalbacher[7] for the $[Mo_2X_8H]^{3-}$ ion and have characteristics of temperature dependence already recorded[8] for M—H—M systems. Cotton *et al.* while reinvestigating the structures of the alkali metal salts $[Rb_3Mo_2X_8H]$ and $[Cs_3Mo_2X_8H]$, showed the presence of H atoms using IR spectroscopy and tritium labelling experiments. They had to rely on the IR evidence since there was no high field ^1H NMR data for the M—H—M resonance and the disorder of the μH and μCl atoms made it impossible to locate the position of the bridging hydride ligand by crystallography. The preparation of $[Mo_2Cl_8H]^{3-}$ is one of the few oxidative addition reactions which is known to occur with Mo_2^{4+} compounds and it is favoured under strenuous conditions.[9] Thus $[Mo_2Cl_8]^{4-}$ can be prepared from $[Mo_2(O_2CMe)_4]$ and 12 M HCl at 0°C, but if the temperature is raised to about 60°C one obtains instead the $[Mo_2Cl_8H]^{3-}$ ion (which is considered to arise by protonation of the δ bond). In our case the reaction between $[Mo_2(O_2CCF_3)_4(PR_3)_2]$ (R = Ph, Et) and 2-aminobenzaldehyde is carried out in ethanol at a high temperature and it is likely that a proton is abstracted from the alcohol to give a bridged hydrido species.

Complex **I** could possibly exist in two isomeric

Table 1. IR,[a] ^{1}H NMR[b] and ^{31}P NMR[c] data

Complex	No.	$\nu_{C\equiv N}$ (cm^{-1})	ν_{M-H-M} (cm^{-1})	δ_{CH_3}	δ_{CH_2}	$^{31}P\{^1H\}$ δ (ppm)
$[Mo_2(C)_2(H)(O_2CCF_3)_3(PPh_3)_2]CH_2Cl_2$[d]	I	$\nu_{C\equiv N}$ for major isomer masked by $\nu_{O_2CCF_3}$ at 1605. 1570 (w)—minor isomer	1290, 1315	1.52 (t) 1.36 (weaker unresolved triplet)	3.87–4.84	14.2 (s), −6.05 (m)
$[Mo_2(C)_2(H)_2(O_2CCF_3)_2(PPh_3)_2]$	II	1602 (m) 1570 (w) 1528 (m)	1268, 1288, 1312	1.5 (t), 1.25 (t) 1.2 (t)	3.5–4.75 complex pattern	28.5 (m), 14.2 (s) −6.05 (m)
$[Mo_2(C)_2(H)(CO)(NCS)_3(PPh_3)_2]$	III	1602 (m) 1570 (w)	1290, 1310	1.45 (t) 1.27 (weaker unresolved triplet)	4.02–4.76 complex pattern	14.3 (s), −5.7 (m)
$[Mo_2(C)_2(H)_2(O_2CCF_3)(NO_3)(PPh_3)_2]$	IV	1602 (m) 1570 (w)	1268, 1288, 1312	1.46 (t), 1.26 (t) 1.18 (t)	3.5–4.65 complex pattern	30.5 (m), 14.2 (m), −6.05 (m)
$[Mo_2(C)_2(H)_2(O_2CCF_3)_2(PEt_3)_2]$	V	1602 (m) 1570 (w)	1270, 1290, 1312	0.5–1.5 complex second-order pattern	2.2–4.5 complex pattern	40.1 (s), 40.5 (w)
$[Mo_2(C)_2(H)(O_2CCF_3)(PPh_3)_2](BPh_4)_2$[e]	VI	1602 (m) 1570 (w) 1528 (m)	1290, 1312			
$[Mo_2(C)_2(H)_2(O_2CCF_3)(PEt_3)_2](BPh_4)$[e]	VII	1602 (m) 1570 (w)	1270, 1290, 1315			

[a] IR spectra taken in Nujol; m = medium, w = weak.
[b] NMR spectra run in CD_3CN solution; expressed in δ units relative to Me_4Si (δ 0); t = triplet.
[c] Spectra taken in CD_3CN and referenced to external 85% H_3PO_4 (δ0) negative values being to low frequency.
[d] Dichloromethane solvate δ (ppm) 5.25.
[e] Insufficiently soluble for NMR spectroscopy.

Table 2. Analytical data

Complex	C	H	N	P
$[Mo_2(C)_2H(CO)(NCS)_3(PPh_3)_2]^a$ (III)	65.1	4.6	7.8	3.8
	(65.5)	(4.4)	(8.4)	(3.4)
$[Mo_2(C)_2(H)_2(O_2CCF_3)(NO_3)(PPh_3)_2]$ (IV)	65.1	4.9	6.8	
	(64.9)	(4.5)	(7.0)	
$[Mo(C)_2(H)_2(O_2CCF_3)(PEt_3)_2]$ (V)	56.9	4.9	7.1	3.9
	(57.5)	(5.2)	(7.3)	(4.0)
$[Mo_2(C)_2H(O_2CCF_3)(PPh_3)_2](BPh_4)_2$ (VI)	73.6	5.1	5.2	3.4
	(73.6)	(5.1)	(4.7)	(2.6)
$[Mo_2(C)_2(H)_2(O_2CCF_3)(PEt_3)_2](BPh_4)$ (VII)	66.1	5.6	6.3	3.2
	(66.2)	(5.7)	(6.4)	(3.4)

[a] Sulphur analysis: 4.9 (5.2). Calculated figures in parentheses.

forms as shown in Fig. 1(a) and (b). Another possibility for isomerism is that fewer than four nitrogens of each macrocycle may coordinate to the metal thereby reducing the coordination number below the unexpectedly high value of eight.

The template reaction proceeds differently when the reaction is carried out for a longer period (5 h) with the addition of a slight excess of triphenylphosphine. A small quantity of insoluble brown material separates during this reaction time and the clear solution shows a reddish-brown colour. This gives the dihydrido complex $[Mo_2(C)_2(H)_2(O_2CCF_3)_2(PPh_3)_2]$ (II) which has been characterized by spectroscopic evidence only. The ^1H, ^{31}P NMR and IR data (see Table 1) show that the complex possibly exists in three isomeric forms. The two major isomers show bands of medium intensity for the C≡N stretching frequencies at 1602 and 1528 cm^{-1}; the minor isomer shows a much weaker C≡N stretch at 1570 cm^{-1}. A stronger band for ν_{asym} ($O_2CCF_3^-$) at 1675 cm^{-1} shows that both the trifluoroacetate groups might be monodentate. We did not find reproducible elemental analyses for this complex but the corresponding nitrato complex (see below) has been analysed and it shows similar IR and NMR spectra.

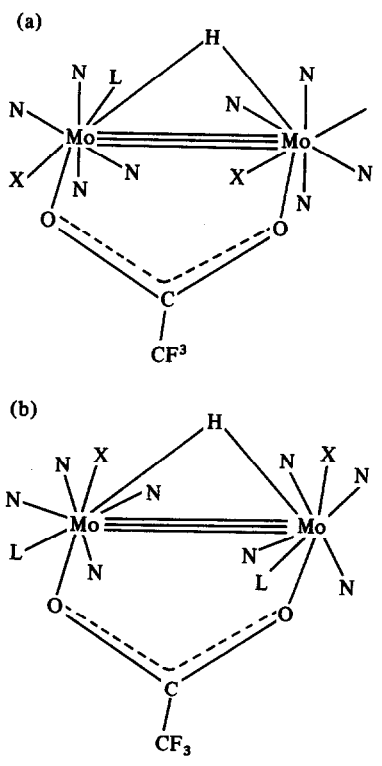

Fig. 1. Isomerism in complex I. L = PPh_3; X = monodentate $O_2CCF_3^-$; N = coordinating atom of macrocyclic ligand C. The monodentate and bridging $O_2CCF_3^-$ ligands are adjacent in isomer (a) and opposite in isomer (b).

Complexes I and II undergo exchange reactions with the thiocyanate and nitrate ion, respectively (see Scheme 1). When I is treated with KNCS in warm ethanol a complex reaction occurs in which the three carboxylate groups are replaced by thiocyanate and a carbonyl group is introduced, which possibly comes from ethanol. This complex, characterized as $[Mo_2(C)_2(H)(CO)(NCS)_3(PPh_3)_2]$ (III), also exists in at least two isomeric forms. The 250 MHz ^1H NMR shows an intense triplet at δ 1.45 and also an unresolved triplet of much lower intensity at δ 1.27 for the methyl protons. The methylene protons show complex multiplets in the region δ (4.02–4.76) and the ^{31}P NMR again shows an intense peak at δ 14.3 and a peak of lower intensity at δ −5.7. Strong bands at 1940 and 2015 cm^{-1} are seen in the IR for the (CO) and (C≡N) groups, respectively, but it is not possible to distinguish between bridging and terminal NCS^- groups from the IR spectrum.[10] The presence of carbonyl is con-

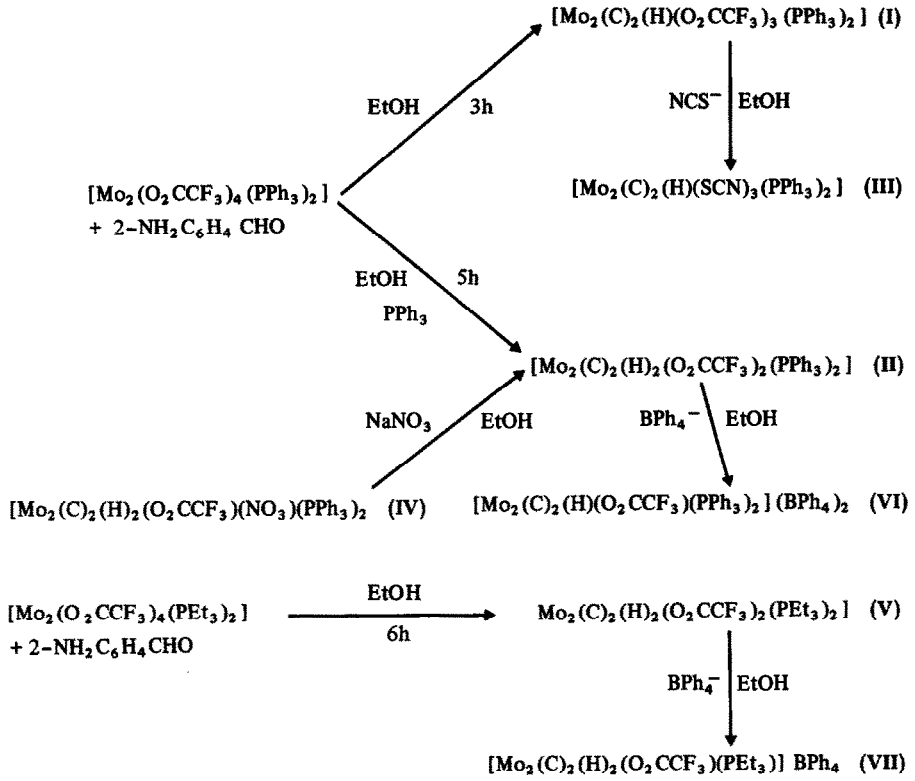

Scheme 1.

firmed by the ^{13}C NMR spectrum, which shows two peaks for the carbonyl groups of the two isomers at δ 196 (stronger) and 195 (weaker).

Treatment of **II** with $NaNO_3$ in ethanol replaces only one of the trifluoroacetate groups to give $[Mo_2(C)_2(H)_2(O_2CCF_3)(NO_3)(PPh_3)_2]$ **(IV)**. The spectroscopic data show that it exists in at least three isomeric forms. The IR spectrum shows a band of medium intensity at 1602 cm^{-1} and a weaker band at 1570 cm^{-1} for the C=N stretch. The ^1H NMR shows three methyl triplets of different intensities at δ 1.46 (strong), 1.18 (weak) and 1.26 (weak) and the ^{31}P NMR also shows three singlets of different intensity at δ 30.5, 14.2 and −6.05.

The template reaction gives $[Mo_2(C)_2(H)_2(O_2CCF_3)_2(PEt_3)_2]$ **(V)** when $[Mo_2(O_2CCF_3)_4(PEt_3)_2]$ is used instead of the corresponding PPh_3 complex and this product is also a mixture of isomeric species. The 250 MHz ^1H NMR spectrum is a second-order spectrum which shows a very complex pattern δ (0.6–1.5) for the methyl protons of the ethoxy group of the macrocycle and the ethyl groups of the triethylphosphine; the methylene protons again show a complex pattern in the region δ (2.2–4.5). The ^{31}P NMR shows peaks of unequal intensity at δ 40.1 and 40.5 for the two isomers and the ^{19}F NMR shows two singlets at δ −75.16 (very strong) and −74.15 (very weak) which implies that the two trifluoroacetate ligands are monodentate in this complex, because monodentate trifluoroacetate groups resonate at *ca* δ −74, whereas bidentate CF_3CO_2 groups resonate at *ca* δ −70.[11–13]

In order to obtain better crystals for X-ray work we performed exchange experiments with the large BPh_4^- anion. Partial replacement of the $O_2CCF_3^-$ ligands in **II** and **V** occurred (see Scheme 1) to give $[Mo_2(C)_2(H)(O_2CCF_3)(PPh_3)_2](BPh_4)_2$ **(VI)** and $[Mo_2(C)_2(H)_2(O_2CCF_3)(PEt_3)_2](BPh_4)$ **(VII)**. The IR spectra (Table 1) show multiple C=N stretching frequencies and Mo—H—Mo bands, but the complexes were insufficiently soluble for NMR spectroscopy. The compounds crystallized as long needles and thin plates, respectively, but neither gave good enough diffraction patterns for X-ray structure determination.

EXPERIMENTAL

^1H, ^{13}C and ^{19}F spectra were recorded at 80 and 250 MHz using Bruker HFX80 and WM 250 spectrometers; ^{31}P NMR were recorded at 90 MHz using a Bruker HFX spectrometer; IR spectra were obtained on Nujol mulls with a Perkin–Elmer 577 grating spectrophotometer; microanalyses (Table

2) were obtained by the microanalysis laboratory, University College, London. 2-Aminobenzaldehyde was prepared from 2-nitrobenzaldehyde[14] and $[Mo_2(O_2CCF_3)_4(PR_3)_2]$ (R = Ph, Et) were prepared by the method of Anderson and coworkers.[5] All reactions were performed under oxygen-free nitrogen.

$[Mo_2(C)_2(H)(O_2CCF_3)_3(PPh_3)_2]$ (I)

A solution of 2-aminobenzaldehyde (2 g, 0.0165 mol) in ethanol (300 cm^3) was refluxed and then cooled to room temperature. $[Mo_2(O_2CCF_3)_4(PPh_3)_2]$ (3.2 g, 0.0027 mol) was then added and the mixture refluxed for *ca* 3 h. The resulting dark brown solution was cooled, filtered and evaporated to dryness to give a dark brown solid, which was washed with *n*-pentane to remove organic by-products, dried and redissolved in excess dichloromethane and filtered. The clear solution was evaporated to dryness and once again washed with *n*-pentane to give a brown microcrystalline product. Yield 2.8 g (52.7%).

$[Mo_2(C)_2(H)_2(O_2CCF_3)_2(PPh_3)_2]$ (II)

A solution of 2-aminobenzaldehyde (2.8 g) in ethanol (400 cm^3) was refluxed and then cooled to room temperature. $[Mo_2(O_2CCF_3)_4(PPh_3)_2]$ (3.25 g, 0.0028 mol) was then added and the mixture heated under reflux for *ca* 10 min. After cooling, PPh_3 (0.5 g) was added and the reaction mixture was refluxed for a further 5 h to give a reddish-brown solution. This was cooled to room temperature, filtered and the solution was evaporated to dryness to give a brown solid, which was washed with *n*-pentane. The product was purified by redissolving the brown solid in excess dichloromethane, filtering and evaporating the clear reddish-brown solution to dryness. The brown microcrystalline solid was finally washed with *n*-pentane and dried *in vacuo*. Yield 2.9 g (55.8%).

$[Mo_2(C)_2(H)(NCS)_2(PPh_3)_2]$ (III)

$[Mo_2(C)_2(H)(O_2CCF_3)_3(PPh_3)_2]$ (1 g, 0.00051 mol) and PPh_3 (0.2 g) were dissolved in ethanol (200 cm^3) and the mixture stirred with gentle heating. Potassium thiocyanate (0.3 g, 0.0031 mol) in hot ethanol was then added to the stirred mixture. This was filtered for another hour to give a dark brown solution, which was filtered and evaporated to dryness to give a reddish-brown solid. This was dissolved in excess dichloromethane, filtered and the solution once again evaporated to dryness. The resulting microcrystalline product was finally washed with *n*-pentane. Yield 0.75 g (79.8 %).

$[Mo_2(C)_2(H)_2(O_2CCF_3)(NO_3)(PPh_3)_2]$ (IV)

$[Mo_2(C)_2(H)_2(O_2CCF_3)_2(PPh_3)_2]$ (1 g, 0.00053 mol) was dissolved in ethanol (200 cm^3) and the light brown solution stirred with gentle heating. Sodium nitrate (0.6 g, 0.007 mol) in hot ethanol was added to the stirred solution. The mixture was stirred for *ca* 90 min, cooled, filtered and the solution evaporated to dryness to give a brown solid. This was dissolved in excess dichloromethane, filtered and the solution once again evaporated to dryness to give a brown microcrystalline solid which was finally washed with *n*-pentane and dried *in vacuo*. Yield 0.8 g (83.3%).

$[Mo_2(C)_2(H)_2(O_2CCF_3)_2(PEt_3)_2]$ (V)

A solution of 2-aminobenzaldehyde (3.2 g, 0.0264 mol) in ethanol (400 cm^3) was refluxed for 5 min and then cooled to room temperature. $[Mo_2(O_2CCF_3)_4(PEt_3)_2]$ (3.4 g, 0.0042 mol) was then added and the mixture was heated under reflux for *ca* 6 h to give a reddish-brown solution, which was cooled to room temperature and filtered. The clear solution was evaporated to dryness to give a brown solid, which was dissolved in excess dichloromethane, filtered and evaporated once again to dryness. The resulting brown solid was washed with *n*-pentane and dried *in vacuo*. Further purification was achieved by dissolving this once again in dichloromethane and evaporating the filtered solution to dryness. Yield 3.5 g (53.8%).

$[Mo_2(C)_2(H)(O_2CCF_3)(PPh_3)_2](BPh_4)_2$ (VI)

$[Mo_2(C)_2(H)_2(O_2CCF_3)_2(PPh_3)_2]$ (0.4 g, 0.00021 mol) was dissolved in ethanol (150 cm^3) and the mixture stirred with gentle heating. Sodium tetraphenylborate (0.1 g, 0.0003 mol) in ethanol was added and the mixture stirred for *ca* 2 h. The resulting light brown solution was cooled and evaporated to dryness to give a light brown solid; this was dissolved in excess dichloromethane, filtered and once again evaporated to dryness to give a brown microcrystalline solid which was finally washed with *n*-pentane and dried *in vacuo*. Yield 0.3 g (60%).

$[Mo_2(C)_2(H)(O_2CCF_3)(PEt_3)_2](BPh_4)$ (VII)

$[Mo_2(C)_2(H)_2(O_2CCF_3)_2(PEt_3)_2]$ (1 g, 0.00065 mol) was dissolved in ethanol (200 cm^3) and the mixture stirred with gentle heating. Sodium tetra-

phenylborate (0.3 g, 0.0009 mol) in ethanol was added and the mixture was stirred for *ca* 2 h. The resulting reddish-brown solution was cooled to room temperature and evaporated to dryness. The light brown microcrystalline solid was finally washed with *n*-pentane and dried *in vacuo*. Yield 0.8 g (69.3%).

Acknowledgement—We thank the University of London Central Research Fund for a grant for chemicals (to A. Sahajpal).

REFERENCES

1. G. A. Melson and D. H. Busch, *J. Am. Chem. Soc.* 1964, **86**, 4834; G. A. Melson and D. H. Busch, *J. Am. Chem. Soc.* 1965, **87**, 1706; L. T. Taylor, F. L. Urbach and D. H. Busch, *J. Am. Chem. Soc.* 1969, **91**, 1072.
2. A. Sahajpal and P. Thornton, *Polyhedron* 1984, **3**, 257.
3. K. W. Chiu, R. A. Jones, A. M. R. Galas, M. B. Hursthouse and G. Wilkinson, *J. Chem. Soc., Dalton Trans.* 1981, 1892.
4. F. A. Cotton and R. A. Walton, *Multiple Bonds between Metal Atoms*, p. 100–103. Wiley, New York (1982).
5. G. S. Girolami, V. V. Mainz and R. A. Andersen, *Inorg. Chem.* 1980, **19**, 805.
6. C. D. Garner and B. Hughes, *Adv. Inorg. Chem.* 1975, **17**, 1.
7. F. A. Cotton and B. J. Kalbacher, *Inorg. Chem.* 1976, **15**, 522.
8. D. S. Moore and S. D. Robinson, *Chem. Soc. Rev.* 1983, **12**, 415.
9. F. A. Cotton, *Chem. Soc. Rev.* 1983, **12**, 35.
10. (a) A. H. Norbury, *Adv. Inorg. Chem. Radiochem.* 1975, **17**, 232; (b) K. Nakamoto, *Infrared and Raman Spectra of Inorganic and Coordination Compounds*, p. 283. Wiley, New York (1981).
11. C. M. Mitchell and F. G. A. Stone, *J. Chem. Soc., Dalton Trans.* 1972, 102.
12. R. B. King and R. N. Kapoor, *J. Organomet. Chem.* 1968, **15**, 457.
13. A. Dobson and S. D. Robinson, *Inorg. Chem.* 1977, **16**, 1321.
14. L. I. Smith and J. W. Opie, *Org. Synth.* 1948, **28**, 11.

Polyhedron Vol. 7, No. 24, pp. 2723–2726, 1988
Printed in Great Britain

0277–5387/88 $3.00+.00
© 1988 Pergamon Press plc

COMPLEXES OF A WATER-SOLUBLE TRIDENTATE SCHIFF BASE LIGAND WITH A NUMBER OF "HARD" METAL IONS

DENNIS F. EVANS* and DAVID A. JAKUBOVIC

Inorganic Chemistry Laboratories, Imperial College, London SW7 2AY, U.K.

(*Received* 18 *May* 1988; *accepted* 1 *June* 1988)

Abstract—2:1 ligand:metal complexes of Al^{III}, Ga^{III}, In^{III}, Sc^{III} and Ge^{IV} with a new tridentate Schiff base ligand, derived from the condensation of salicylaldehyde-5-sulphonate with 2-aminophenol-4-sulphonic acid, have been characterized in aqueous solution by ^1H NMR spectroscopy. Values of pM are reported for the Al^{III}, Ga^{III}, In^{III} and Fe^{III} complexes at pH = 7.4.

Recently we reported some new hexadentate water-soluble Schiff base ligands and their use as sequestrating agents for a variety of metal ions.[1,2] Among these were the biochemically and biomedically interesting Al^{III},[3] Fe^{III},[4] Ga^{III}[5] and In^{III}[6] ions. The pM values (where $pM = -\log_{10}[\text{metal ion}]_{free}$) of the highly water soluble Fe^{III}, Al^{III}, Ga^{III}, In^{III}, Ni^{II} and Zn^{II} complexes were shown to be dependent upon the relative "hardness" or "softness" of the ligands and metal ions, and also the ability of the ligands to accomodate a metal ion of a particular size.[1,2]

Here we describe a new water-soluble tridentate Schiff base, derived from salicylaldehyde-5-sulphonate (sals) and 2-aminophenol-4-sulphonic acid (aps), and its use as a ligand for Al^{III}, Ga^{III}, In^{III}, Fe^{III}, Sc^{III} and Ge^{IV} (see Fig. 1).† This ligand produces an N_2O_4 donor set, in a 2:1 ligand:metal ion octahedral complex, which might favour "harder" metal ions when compared to the N_4O_2 and N_3O_3 donor sets of the previously reported hexadentate ligands.[1,2] To evaluate the binding characteristics of the ligand, pM values were determined for the Al^{III}, Ga^{III}, In^{III} and Fe^{III} complexes at the physiological pH of 7.4.

As observed for the hexadentate Schiff bases[1] the ligand is partially hydrolysed in aqueous solution and so its isolation was not attempted, but instead stoichiometric amounts of the aldehyde and amine were used to generate the ligand *in situ*.

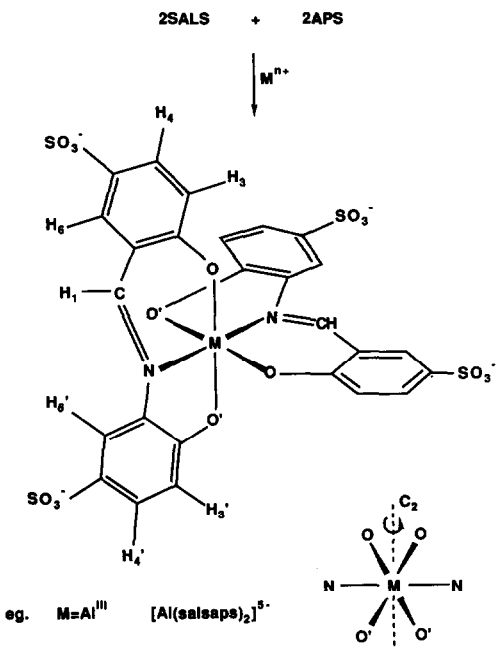

Fig. 1.

EXPERIMENTAL

Sodium salicylaldehyde-5-sulphonate (sals) was prepared as described elsewhere[9] and 2-amino-

*Author to whom correspondence should be addressed.

† For the analogous non-sulphonated, organic soluble, ligand salicylidene-2-aminophenol a solid 2:1 Fe^{III} complex has been reported[7] and also stability constants, in 50% aqueous ethanol, for the Cd^{II} and Mg^{II} complexes.[8]

phenol-4-sulphonic acid (aps) was recrystallized from H_2O (activated charcoal). Both compounds gave satisfactory analyses.

Complete ring deuteriation of 2-aminophenol-4-sulphonic acid. aps (0.4 g) was heated in a sealed glass ampoule, in an Ar atmosphere, with D_2O (5 cm^3) at 160°C for 18 h. After cooling, the grey solid was filtered off, washed with H_2O and dried *in vacuo*. Yield 0.33 g (80%). The ^1H NMR spectrum in $NaOD_{(aq.)}$ showed that all the ring protons had been deuteriated.

^1H NMR spectra were recorded on Bruker WM250FT (250 MHz) and Jeol GSX270 (270 MHz) spectrometers. UV–vis spectra were measured on a Perkin–Elmer 551 spectrophotometer.

Competition reactions between the Schiff base ligand and the various metal ion complexes of N,N,N′,N′-ethylenediaminetetraacetic acid (edta) and N,N,N′,N′,N″-diethylenetriaminepentaacetic acid (dtpa) were performed as described previously.[2] For the Fe^{III} system the reactions were performed in an Ar atmosphere, to prevent oxidation of the aps, and were followed spectrophotometrically with absorbance measurements made at three wavelengths: 570, 590 and 640 nm. ^1H NMR was used to follow the reactions for the Al^{III}, Ga^{III} and In^{III} systems. The Tl^{III}–salsaps system could not be studied due to oxidation of the aps by the Tl^{III}.

The Ge^{IV} complex was prepared by adding a stoichiometric amount of $GeBr_4$ to an acidified solution of the ligand compounds and then slowly increasing the pH, with dilute $KOH_{(aq.)}$, to 7.4.

RESULTS AND DISCUSSION

^1H *NMR spectra*

The ^1H NMR spectrum of salsaps, in D_2O (see Fig. 2), illustrates the partial hydrolysis of the ligand, with the Schiff base in equilibrium with the component aldehyde (sals) and amine (aps). The resultant spectrum is therefore rather complex since all the species produce similar resonance patterns in the same region.

In contrast the spectrum of $[Al(salsaps)_2]^{5-}$ (Fig. 3) shows only one resonance, or set of resonances, for each proton of the ligand. The metal ion is therefore acting as a template for complex formation. The assignment of this spectrum was performed with the use of deuteriated aps to distinguish between the proton resonances of the two rings in the ligand. Coupling constants can also be used to identify the resonances of the two rings, with J_{ortho} and J_{meta} both being larger for the salicylaldehyde ring. A spectrum run on a solution containing a 4 : 1 salsaps : Al^{III} ratio gave separate resonances for the complex and the free tridentate ligand. This proves that the complex is not experiencing intermolecular exchange on an NMR timescale, and from the relative integrals it is clear that the complex has a 2 : 1 salsaps : Al^{III} stoichiometry. A spectrum run on a 1 : 1.5 salsaps : Al^{III} solution yielded a spectrum as for $[Al(salsaps)_2]^{5-}$, with $Al(OH)_3$ precipitating out after a short time.

Similar spectra were recorded for the 2 : 1 salsaps complexes of Ga^{III}, In^{III}, Sc^{III} and Ge^{IV}, with no intermolecular exchange observed (see Table 1).

pM values of the complexes

The values of pM for the salsaps complexes are given in Table 2, together with data from the literature for the edta and saltames complexes (see Fig. 4).

A comparison of the values for the new ligand, salsaps, with its N_2O_4 donor set, and the hexadentate ligand saltames (N_3O_3) shows that the "harder" tridentate ligand forms the more stable complex with the "hardest" metal ion, Al^{III}. It also forms a far more stable complex with the largest ion, In^{III}. This is despite the fact that the hexa-

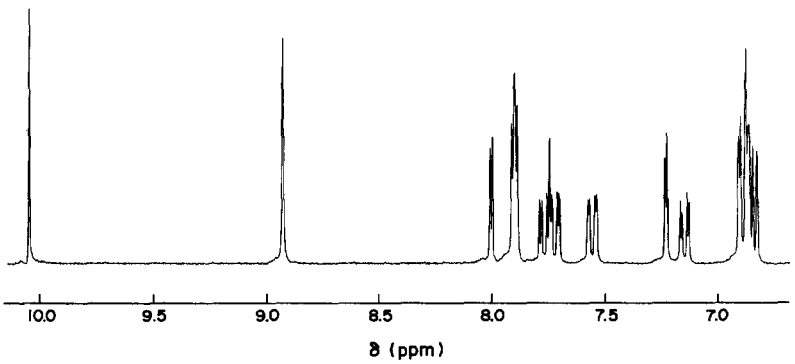

Fig. 2. ^1H NMR spectrum (270 MHz) of 1 : 1 sals : aps in D_2O, pH = 7.4.

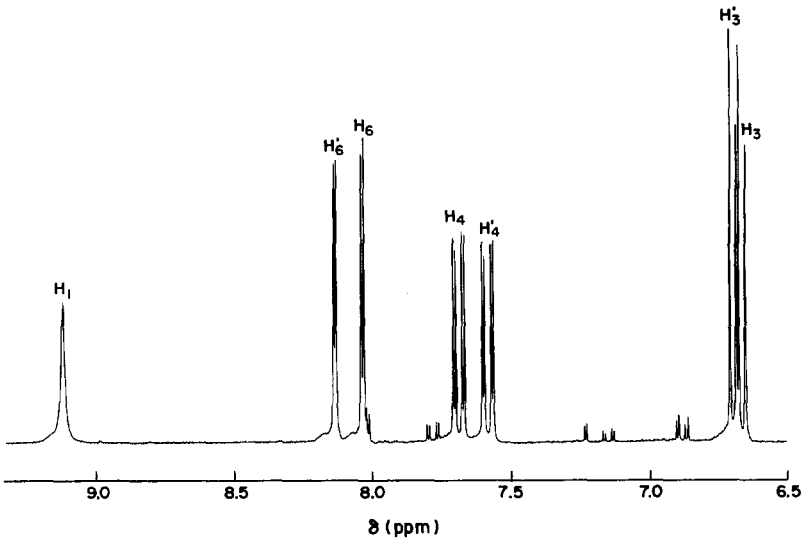

Fig. 3. ^{1}H NMR spectrum (270 MHz) of $[Al^{III}(salsaps)_2]^{5-}$ in D_2O, pH = 7.4, the unassigned peaks of low intensity arise from a slight excess of the ligand.

dentate ligand benefits from the "chelate effect". For a non-dissociating hexadentate ligand pM is independent of ligand concentrations, for a given ligand : metal ratio, whereas for a tridentate ligand pM decreases with increasing dilution. At very low concentrations one might therefore expect the hexadentate Schiff base to form the more stable complexes. (Both Schiff bases will also experience increased ligand hydrolysis at low concentrations, reducing the pM values of their complexes.)

The pM values for the Fe^{III} and Ga^{III} complexes of salsaps are also high, being greater than for edta, but slightly lower than for the saltames complexes. Cyclic voltammetry of an aqueous solution of the Fe^{III} salsaps complex failed to yield a redox potential due either to interference from the solvent bands or irreversibility of the system.

The results discussed here are therefore consistent with those reported previously for a variety of hexadentate Schiff base ligands, with the N_2O_4 donor set favouring "hard" metal ions. It is also clear that the tridentate ligand is more flexible, with respect to metal ion size, than the hexadentate Schiff base saltames.

Table 1. ^{1}H NMR data for the salsaps complexes in D_2O

2 : 1 salsaps : M complex	δ (ppm)						
	H_1	H_3	H'_3	H_4	H'_4	H_6	H'_6
Al^{III}	9.12	6.67	6.69	7.69	7.58	8.04	8.14
Ga^{III}	9.21	6.71	6.77	7.71	7.62	8.05	8.20
In^{III}	9.23	6.81	6.85	7.73	7.62	8.07	8.20
Sc^{III}	9.05	6.62[a] 6.71[a]		7.71	7.52	8.06	
Ge^{IV}	9.23	6.83[a] 6.88[a]		7.87	7.77	8.10	8.30
Free ligand[b]	8.93	6.88	6.91	7.73	7.56	7.91[a] 7.90[a]	

[a] It was not possible to assign these resonances to H or H′ from their coupling constants.

[b] pH = 7.4.

Table 2. pM values for the salsaps, saltames and edta complexes of Al^{III}, Ga^{III}, Fe^{III} and In^{III}

Metal ion	Ionic radius (Å)[a]	pH	pM[b] salsaps	saltames	edta
Al^{III}	0.50	7.40	17.5_8[c]	16.9_3[d]	15.89[e]
Ga^{III}	0.62	7.40	23.3_1[c]	24.6_4[f]	19.35[g]
Fe^{III}	0.60	7.40	25.9_5[h]	$\geqslant 26.2$[i]	23.42[j]
In^{III}	0.81	7.40	22.7_4[c]	17.0_7[k]	23.40[l]

[a] Reference 11.

[b] $pM = -\log_{10}[m^{n+}]_{free}$, at 25°C, where $[ligand]_{total}/[m^{n+}]_{total} = 10$.

[c] $[ligand]_{total} = 0.0078$ M.

[d] $[ligand]_{total} = 0.03$ M, ref. 2.

[e] Reference 12.

[f] $[ligand]_{total} = 0.004$ M, pH = 7.50 and refers to the original pH of the aqueous solution, equilibrium was attained in D_2O, ref. 1.

[g] Calculated from data in refs 12 and 13.

[h] $[ligand]_{total} = 0.003$ M.

[i] $[ligand]_{total} = 0.005$ M and pH = 7.50, ref. 1.

[j] Reference 14.

[k] $[ligand]_{total} = 0.005$ M, ref. 2.

[l] Reference 15.

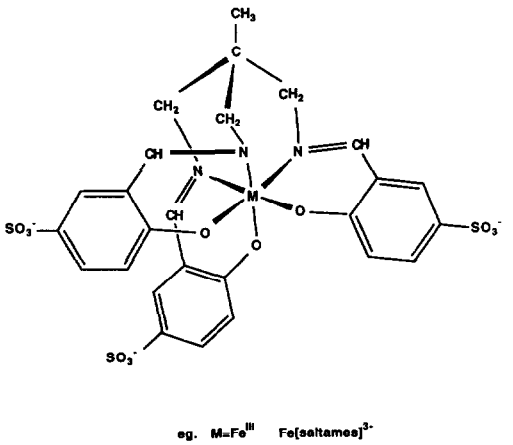

Fig. 4.

The formation of the non-exchanging $[Ge(salsaps)_2]^{4-}$ complex further illustrates the "hard" nature of the salsaps ligand, since the coordination chemistry of Ge^{IV} in aqueous solution largely involves chelating ligands which bind through oxygen only.[10]

Acknowledgement—We thank the S.E.R.C. for a maintenance grant (to D.A.J.).

REFERENCES

1. D. F. Evans and D. A. Jakubovic, *J. Chem. Soc., Dalton Trans.*, in press.
2. D. F. Evans and D. A. Jakubovic, *Polyhedron* 1988, 7, 1881.
3. T. L. Macdonald and R. B. Martin, *Trends Biochem. Sci.* 1988, **13**, 15.
4. A. E. Martell, W. F. Anderson and D. G. Badman, *Development of Iron Chelators for Clinical Use.* Elsevier/North Holland, New York (1986); K. N. Raymond, W. R. Harris, C. J. Carrano and F. L. Weitl, *ACS Symp. Ser.* 1980, **140**, 313.
5. M. A. Green, M. J. Welch and J. C. Huffman, *J. Am. Chem. Soc.* 1980, **106**, 3689.
6. S. M. Moerlein, M. J. Welch, K. N. Raymond and F. L. Weitl, *J. Nucl. Med.* 1981, **22**, 710.
7. E. W. Ainscough, A. N. Brodie, J. E. Plowman, K. L. Brown, A. W. Addison and A. R. Gainsford, *Inorg. Chem.* 1980, **19**, 3655.
8. Z. Holzbecher, *Coll. Czech. Chem. Commun.* 1959, **24**, 3915.
9. M. Botsivali, D. F. Evans, P. H. Missen and M. W. Upton, *J. Chem. Soc., Dalton Trans.* 1985, 1147.
10. P. Pichet and R. L. Benoit, *Inorg. Chem.* 1967, **6**, 1505.
11. L. Pauling, *The Nature of the Chemical Bond*, 3rd edn. Cornell University Press (1960).
12. G. Schwarzenbach, R. Gutt and G. Anderegg, *Helv. Chim. Acta* 1954, **37**, 937.
13. K. Saito and H. Terry, *J. Chem. Soc.* 1956, 4701.
14. G. Anderegg, F. L'Eplattenier and G. Schwarzenbach, *Helv. Chim. Acta* 1963, **46**, 1409.
15. E. Bottari and G. Anderegg, *Helv. Chim. Acta* 1967, **50**, 2349.

Polyhedron Vol. 7, No. 24, pp. 2727–2730, 1988
Printed in Great Britain

0277–5387/88 $3.00+.00
© 1988 Pergamon Press plc

SYNTHESIS AND MOLECULAR STRUCTURE OF THE OPTICALLY ACTIVE ORGANOALUMINIUM DIMER (S)-(−)-(S)-(−)-$[(C_6H_5)CH(CH_3)NHAl(CH_3)_2]_2$

GREGORY H. ROBINSON* and SAMUEL A. SANGOKOYA

Department of Chemistry, Clemson University, Clemson, SC 29634–1905, U.S.A.

and

ROBIN D. ROGERS*

Department of Chemistry, Northern Illinois University, DeKalb, IL 60115, U.S.A.

(*Received* 25 *April* 1988; *accepted* 8 *June* 1988)

Abstract—Reaction of the optically active primary amine (S)-(−)-α-methylbenzylamine with trimethylaluminium in heptane affords the crystalline organoaluminium dimer (S)-(−)-(S)-(−)-$[(C_6H_5)CH(CH_3)NHAl(CH_3)_2]_2$. Isolated as large, colourless, extremely air-sensitive prismatic crystals, the title compound crystallizes in the orthorhombic space group $P2_12_12_1$ with unit cell parameters $a = 8.406(3)$, $b = 15.505(4)$, $c = 17.547(5)$ Å, $V = 2287$ Å^3 and $\rho = 1.03$ g cm^{-3} for $Z = 4$. Least-squares refinement based on 1477 observed reflections converged at $R = 0.056$, $R_w = 0.058$. Methane was eliminated during the course of the reaction due to cleavage of Al—C and N—H bonds resulting in an asymmetric Al_2N_2 fragment at the core of the organoaluminium dimer. The mean Al—C bond distance in the dimethylaluminium units is 1.930(8), while the mean Al—N bond distance is 1.950(5) Å. Specific rotation ($[\alpha]_D^{25}$ in CH_2Cl_2) of the dimer is determined to be −20.6°.

The interaction of aluminium species with primary or secondary amines has both fascinated and intrigued workers in organoaluminium chemistry since Krause and Dittmar reported the synthesis of $(H_3N)Al(p\text{-tolyl})_3$ and $(H_3N)Al(Ph)_3$ almost 60 years ago.[1] The last two decades have witnessed significant activity in the general areas of poly(N-alkyliminoalanes)[2–16] and aluminium–nitrogen oligomers.[17–25] These areas of organoaluminium chemistry are particularly interesting in that their reaction products characteristically possess Al_2N_2 fragments resulting from Al—H/N—H and Al—R/N—H condensations, respectively. Notably, the aluminium–nitrogen oligomers have found utility as catalysts for the polymerization of methyl methacrylate, acetaldehyde and butyraldehyde,[25] while the poly(N-alkyliminoalanes) have demonstrated promise as homogeneous hydrogenation catalysts.[26]

It is particularly significant that optically active amines are absent from the aforementioned organoaluminium complexes. Herein, we report the synthesis and structure of the optically active organoaluminium dimer (S)-(−)-(S)-(−)-$[(C_6H_5)CH(CH_3)NHAl(CH_3)_2]_2$ isolated from reaction of (S)-(−)-α-methylbenzylamine with trimethylaluminium. The title compound represents, to the best of our knowledge, the first examination of condensation products resulting from reaction of aluminium alkyls with optically active amines.

EXPERIMENTAL

Synthesis

Standard Schlenk techniques were employed in conjunction with an inert atmosphere dry box (Vacuum Atmospheres HE-43 Dri-Lab). Heptane was distilled from CaH_2 under an atmosphere of dry argon. Trimethylaluminium and (S)-(−)-α-methyl-

* Authors to whom correspondence should be addressed.

benzylamine, both purchased from Aldrich Chemical Co., were used as received. Single crystal X-ray data were collected on an Enraf–Nonius CAD-4 diffractometer. ^{1}H NMR data were recorded on a JEOL-FX90Q NMR spectrometer. Optical rotation data were recorded on a Horiba Sepa-200 polarimeter.

Inside the dry box a reaction vessel was charged with (S)-(−)-α-methylbenzylamine (7.76 mmol) and dissolved in heptane (20 cm^3). Trimethylaluminium (15.5 mmol) was slowly added via a syringe. The reaction was immediate and quite exothermic. The system was allowed to react at room temperature for several hours. The reaction vessel was subsequently removed from the dry box and heated in an oil bath for 24 h at 120°C. Upon slow cooling to room temperature, colourless, extremely air-sensitive crystals were isolated in quantitative yield (based on the amine); m.p. (dec. 198°C). ^{1}H NMR ($CDCl_3$, TMS external reference): δ −1.33 [s, 3H, Al(CH_3)], −0.96 [s, 3H, Al(CH_3)], −0.91 [s, 3H, Al(CH_3)], −0.57 [s, 3H, Al(CH_3)], 1.34 [d, 3H, C(CH_3)], 1.39 [d, 3H, C(CH_3)], 3.98 [m, 2H, 2CH], 7.24 [m, 10H, aromatic protons]. It is reasonable to have initially anticipated four peaks of comparable intensities for the four Al—CH_3 moieties due to diastereotopic and geometric effects. However, two pairs of peaks of unequal intensities were observed. These peaks and the general pattern of the NMR spectrum are indicative of *cis–trans* isomerism of the title compound in solution.

X-ray structural solution and refinement

A single crystal of the title compound was mounted in a thin-walled glass capillary under an inert atmosphere of argon. Final lattice parameters as determined from a least-squares refinement of $(\sin\theta/\lambda)^2$ values for 24 reflections ($\theta > 20°$) accurately centred on the diffractometer are given in Table 1. Data were collected on an Enraf–Nonius CAD-4 diffractometer by the θ–2θ scan technique. A summary of data collection parameters is given in Table 1. The intensities were corrected for Lorentz polarization effects. Calculations were performed with the SHELX system of computer programs.[27] Structure solution was accomplished by means of the program MULTAN[28] which afforded the location of the Al atoms. The location of these atoms readily revealed the positions of the remaining non-hydrogen atoms. Geometrically constrained hydrogen atoms were included in calculated positions. Hydrogen atoms, located from difference maps, were included in the refinement using fixed thermal parameters. Refinement converged at $R = 0.056$ ($R_w = 0.058$). A final difference map revealed no feature greater than 0.2e$^-$ Å^{-3}.

Table 1. Summary of crystallographic data for (S)-(−)-(S)-(−)-[(C_6H_5)CH(CH_3)NHAl(CH_3)$_2$]$_2$

Formula	$C_{20}H_{32}Al_2N_2$
Formula weight	356.96
Colour; habit	Colourless prisms
Size	0.50 × 0.50 × 0.55 mm
Crystal system	Orthorhombic
Space group	$P2_12_12_1$
a (Å)	8.406(3)
b (Å)	15.505(4)
c (Å)	17.547(5)
Volume (Å^3)	2287
Z (molecules/cell)	4
ρ (calc.)	1.03
Diffractometer	Enraf–Nonius CAD-4
λ(Mo-K_α) (Å)	0.71073
Temperature	20°C
2θ limits	2.0–50.0°
No. of data measured	2292
No. of data observed	1477
Goodness-of-fit	3.3
R	0.056
R_w	0.058

RESULTS AND DISCUSSION

The interactions of aluminium hydride with primary and secondary amines resulting in poly(N-alkyliminoalanes) have been extensively investigated.[2–16] Similarly, aluminium–nitrogen oligomers, prepared from reaction of aluminium alkyls with primary and secondary amines, have been studied by Smith and co-workers.[17–25] For some time now we have been interested in the reaction of organoaluminium species with various macrocyclic amines. Initially our studies concerned the reaction of organoaluminium species with macrocyclic amines such as $(CH_3)_4$[14]aneN$_4$,[29] [14]aneN$_4$[30,31] and [15]aneN$_4$.[32] These reactions resulted in organoaluminium–macrocyclic complexes. Such macrocyclic complexes are significant in that they often serve as precursors to organoaluminium-based host–guest compounds known as liquid clathrates.[33] More recently, we have initiated an investigation of the interactions of aluminium alkyl species with multidentate open chain amines.[34–36]

Optically active amines are noteworthy in their absence from the ensemble of Al—N complexes cited above. Thus, we examined the reaction of trimethylaluminium with the optically active amine (S)-(−)-α-methylbenzylamine; the organoaluminium dimer (S)-(−)-(S)-(−)-[(C_6H_5)CH(CH_3)NHAl(CH_3)$_2$]$_2$ was the only product isolated.

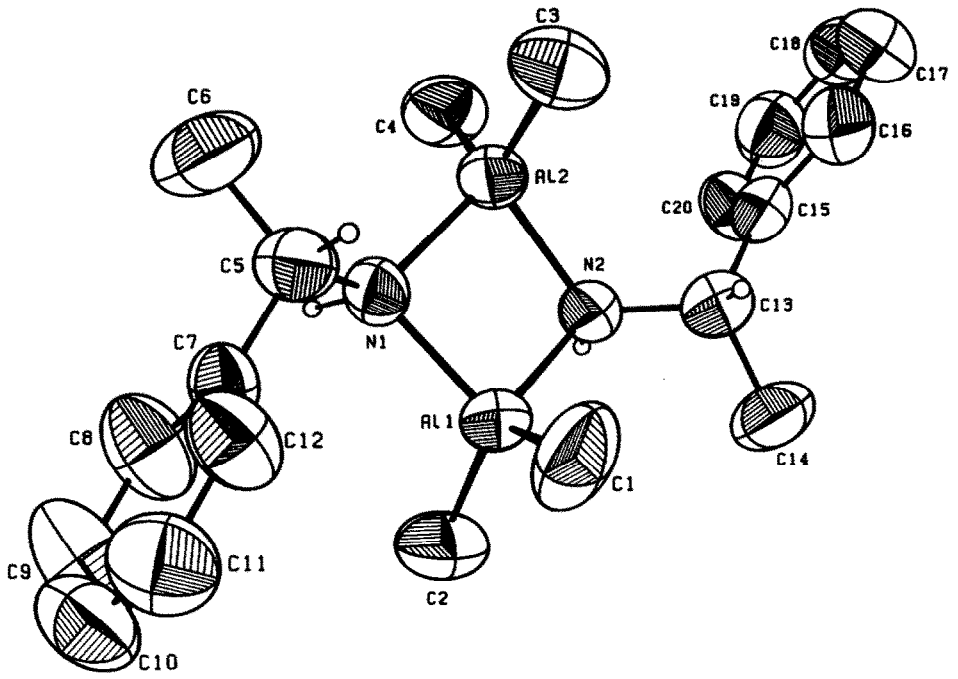

Fig. 1. Molecular structure of (S)-(−)-(S)-(−)-[$(C_6H_5)CH(CH_3)NHAl(CH_3)_2]_2$ showing the atom numbering scheme.

The X-ray crystal structure of (S)-(−)-(S)-(−)-[$(C_6H_5)CH(CH_3)NHAl(CH_3)_2]_2$ is given in Fig. 1; Figure 2, which provides an alternate view of the molecule, indicates that the molecule contains neither a plane of symmetry nor a centre of symmetry. Selected bond distances and angles are given in Table 2. As the chiral carbon atom(s) did not participate in the Al—N condensation, it is reasonable that the title compound retained optical activity. The specific rotation of (S)-(−)-(S)-(−)-[$(C_6H_5)CH(CH_3)NHAl(CH_3)_2]_2$ is determined to be $-20.6°$ $\{[\alpha]_D^{25}(CH_2Cl_2)\}$. This is contrasted with the value of $-39.0°$ $[\alpha]_D^{25}$ for the neat reactant amine.

Several points are worthy of note regarding structure and bonding in (S)-(−)-(S)-(−)-[$(C_6H_5)CH(CH_3)NHAl(CH_3)_2]_2$. During the course of the reaction of trimethylaluminium with (S)-α-methylbenzylamine, one methyl group was cleaved from each of the two $Al(CH_3)_3$ units. Additionally, one aza-hydrogen atom was cleaved from each of the two amine units. Thus, the elimination of methane resulted in the formation of the Al_2N_2 fragment situated at the core of the organoaluminium dimer. Each aluminium and nitrogen atom in the compound is now four-coordinate. The mean Al—N bond distance in the asymmetric Al_2N_2 fragment is 1.950(5) Å. The mean N—Al—N bond angle is

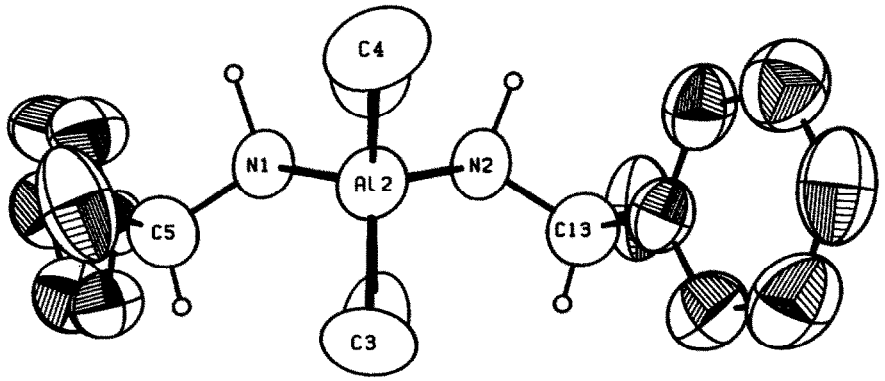

Fig. 2. An alternate view of the (S)-(−)-(S)-(−)-[$(C_6H_5)CH(CH_3)NHAl(CH_3)_2]_2$ molecule.

Table 2. Selected bond distances (Å) and angles (°) for (S)-(−)-(S)-(−)-[$(C_6H_5)CH(CH_3)NHAl(CH_3)_2]_2$[a]

Bond distances			
Al(1)—N(1)	1.944(5)	Al(1)—N(2)	1.956(5)
Al(1)—C(1)	1.953(8)	Al(1)—C(2)	1.937(8)
Al(2)—N(1)	1.952(5)	Al(2)—N(2)	1.947(5)
Al(2)—C(3)	1.910(7)	Al(2)—C(4)	1.920(7)

Bond angles	
N(1)—Al(1)—N(2)	86.2(2)
N(1)—Al(2)—N(2)	86.2(2)
Al(1)—N(1)—Al(2)	92.3(2)
Al(1)—N(2)—Al(2)	92.1(2)

[a] Numbers in parentheses are estimated standard deviations in the least significant digits.

86.2(2)°, while that of the Al—N—Al bond angle is 92.2(2)°. The two methyl carbon atoms, C(6) and C(14), on the two chiral carbon atoms (C(5) and C(13), respectively) are *trans* to each other. From Fig. 2, it is evident that the two aza-hydrogen atoms are in a *cis* orientation with respect to each other as are the hydrogen atoms associated with C(5) and C(13). It is important to note, however, that overall the molecule is in a *trans* orientation.

Acknowledgement—We are grateful to the National Science Foundation for support of this work to G.H.R. (RII-8520554) and for funds to purchase the diffractometer (NIU).

Supplementary material available. Tables of fractional coordinates have been deposited with the Cambridge Crystallographic Data Centre. Complete structural information is available from the Editor.

REFERENCES

1. E. Krause and P. Dittmar, *Ber.* 1930, **63**, 2401.
2. S. Cucinella, T. Salvatori, C. Busetto, G. Perego and A. Mazzei, *J. Organomet. Chem.* 1974, **78**, 185.
3. M. Cesari, G. Perego, G. Del Piero, S. Cucinella and E. Cernia, *J. Organomet. Chem.* 1974, **78**, 203.
4. G. Perego, M. Cesari, G. Del Piero, A. Balducci and E. Cernia, *J. Organomet. Chem.* 1975, **87**, 33.
5. M. Cesari, G. Perego, G. Del Piero, M. Corbellini and A. Immirzi, *J. Organomet. Chem.* 1975, **87**, 43.
6. G. Perego, G. Del Piero, M. Cesari, A. Zazzetta and G. Dozzi, *J. Organomet. Chem.* 1975, **87**, 53.
7. S. Cucinella, G. Dozzi, A. Mazzei and T. Salvatori, *J. Organomet. Chem.* 1975, **90**, 257.
8. S. Cucinella, T. Salvatori, C. Busetto and A. Mazzei, *J. Organomet. Chem.* 1976, **108**, 13.
9. S. Cucinella, G. Dozzi, C. Busetto and A. Mazzei, *J. Organomet. Chem.* 1976, **113**, 233.
10. S. Cucinella, T. Salvatori, C. Busetto and M. Cesari, *J. Organomet. Chem.* 1976, **121**, 137.
11. G. Del Piero, M. Cesari, G. Dozzi and A. Mazzei, *J. Organomet. Chem.* 1977, **129**, 281.
12. G. Del Piero, M. Cesari, G. Perego, S. Cucinella and E. Cernia, *J. Organomet. Chem.* 1977, **129**, 289.
13. C. Busetto, M. Cesari, S. Cucinella and T. Salvatori, *J. Organomet. Chem.* 1977, **132**, 339.
14. G. Del Piero, G. Perego, S. Cucinella, M. Cesari and A. Mazzei, *J. Organomet. Chem.* 1977, **136**, 13.
15. S. Cucinella, G. Dozzi, G. Perego and A. Mazzei, *J. Organomet. Chem.* 1977, **137**, 257.
16. G. Del Piero, M. Cesari, S. Cucinella and A. Mazzei, *J. Organomet. Chem.* 1977, **137**, 265.
17. A. W. Laubengayer, J. D. Smith and G. G. Ehrlich, *J. Am. Chem. Soc.* 1961, **83**, 542.
18. M. Cohen, J. K. Gilbert and J. D. Smith, *J. Chem. Soc.* 1965, 1092.
19. J. K. Gosling and J. D. Smith, *J. Chem. Soc.* 1968, 233.
20. K. Gosling, J. D. Smith and D. H. W. Wharmby, *J. Chem. Soc. A* 1969, 1738.
21. P. B. Hitchcock, J. D. Smith and K. M. Thomas, *J. Chem. Soc., Dalton Trans.* 1976, 1433.
22. G. M. McLaughlin, G. A. Sim and J. D. Smith, *J. Chem. Soc., Dalton Trans.* 1972, 2197.
23. K. J. Alford, A. K. Gosling and J. D. Smith, *J. Chem. Soc., Dalton Trans.* 1972, 2203.
24. S. Amirkhalili, P. B. Hitchcock and J. D. Smith, *J. Chem. Soc., Dalton Trans.* 1979, 1206.
25. S. Amirkhalili, P. B. Hitchcock, A. D. Jenkins, J. Z. Nyathi and J. D. Smith, *J. Chem. Soc., Dalton Trans.* 1981, 377.
26. G. Dozzi, S. Cucinella and A. Mazzei, *J. Organomet. Chem.* 1979, **164**, 1.
27. G. M. Sheldrick, SHELX, a system of computer programs for X-ray structure determination as locally modified (1976).
28. G. Germain, P. Main and M. M. Woolfson, *Acta Cryst., Sect. A:, Cryst. Phys. Diffr., Theor. Gen. Cryst.* 1971, **A27**, 368.
29. G. H. Robinson, H. Zhang and J. L. Atwood, *J. Organomet. Chem.* 1987, **331**, 153.
30. G. H. Robinson, A. D. Rae, C. F. Campana and S. K. Byram, *Organometallics* 1987, **6**, 1227.
31. G. H. Robinson and S. A. Sangokoya, *Organometallics* 1988, **7**, 1453.
32. G. H. Robinson, E. S. Appel, S. A. Sangokoya, H. Zhang and J. L. Atwood, *J. Coord. Chem.* 1988, **17**, 373.
33. J. L. Atwood, *Inclusion Compounds* (Edited by J. L. Atwood, J. E. D. Davies and D. D. MacNicol), Vol. I, pp. 375–405. Academic Press, London (1984).
34. G. H. Robinson and S. A. Sangokoya, *J. Am. Chem. Soc.* 1987, **109**, 6852.
35. G. H. Robinson, F. Moise, W. T. Pennington and S. A. Sangojoya, *J. Cryst. Spect. Res.* 1988, **18**, 387.
36. G. H. Robinson, S. A. Sangokoya, F. Moise and W. T. Pennington, *Organometallics* 1988, **7**, 1887.

Polyhedron Vol. 7, No. 24, pp. 2731–2742, 1988
Printed in Great Britain

0277–5387/88 $3.00+.00
© 1988 Pergamon Press plc

OPTICALLY ACTIVE COORDINATION COMPOUNDS—XLVIII.* SYNTHESIS, RESOLUTION AND INTERCONVERSIONS OF ISOMERS OF TRIS-SALICYLATOCOBALTATE(III)

MIHO FUJITA† and R. D. GILLARD‡

Inorganic Chemistry Research Laboratories, University of Wales, P.O. Box 78, Cardiff CF1 1XL, Wales, U.K.

(*Received* 25 *April* 1988; *accepted* 8 *June* 1988)

Abstract—Stable aqueous solutions of the green ion $[Co(sal)_3]^{3-}$ (sal = dianion, $C_6H_4(\bar{O})(C\bar{O}O)$, of salicylic acid, 2-hydroxybenzoic acid) are obtained from $[Co(NH_3)_5Cl]Cl_2$ and an excess of salicylic acid. Several salts, $[C][Co(sal)_3]$ have been characterized, where $C = [Co(NH_3)_6]^{3+}$ and $[M(en)_3]^{3+}$ (M = Co or Rh, en = 1,2-diaminoethane). By using (+)-$[Rh(en)_3]^{3+}$, optical resolution via less soluble diastereoisomeric salts has been achieved, and isomerization and racemization have been studied. Resolved tris-malonatocobaltate(III) has been used as a model. A novel thermochromism (77–293 K) in solid $\Delta(+)$-$[Rhen_3]\Lambda[Co(sal)_3]$ is described.

Optically active compounds of cobalt(III) with bidentate chelating agents are now common. However, those containing three bidentate six-membered rings are less common. We report here the syntheses and properties of tris-complexes of the salicylate ion with the cobaltic ion.

As before,[2a] we denote salicylic acid (2-hydroxybenzoic acid) by H_2sal, its first conjugate base (deprotonated at the carboxylate function) $Hsal^-$ and its second conjugate base (with both phenolic and carboxylic protons lost) by sal^{-2}.

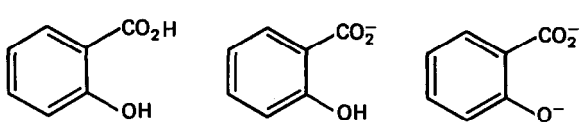

H_2sal $Hsal^-$ sal^{2-}

Salicylates[3] occur widely: many are of great technical utility. Metal salts and compounds are also common and important. Copper salicylate (an intermediate[2b] in the Dow phenol process) has also been useful[4] as an anti-arthritic drug: Hangartner treated 1100 patients during 20 years with "permeton" (12.5 mM sodium salicylate and 0.04 mM copper(II) chloride) and found that 89% had benefitted.

Ferric compounds with salicylate are well known and occur commonly in iron metabolism. For example, many microorganisms produce compounds such as enterochelin[5] containing[6] salicylic acid or 2,3-dihydroxybenzoic acid, and Mycobacteria excrete mycobactins which contain salicylic acid. Similarly, Tait showed[7] that *Micrococcus denitrificans* grown in iron-deficient media excretes iron-chelating derivatives of salicylic acid, e.g. 2-hydroxybenzoyl-N-L-threonyl-N^1,N^8-di-2:3-dihydroxybenzoylspermidine.

However, compounds of salicylates with cobalt (III) are few. Some derivatives with unidentate salicylates *cis*-$[(en)_2(NH_3)Co\{OOC\text{-}C_6H_3(X)OH\}]^{2+}$ (X = H, 5-SO_3^-, 5-Br, 5-NO_2, 3-NO_2), have been made[8] and rates of aquation followed.

Hexakisaquocobalt(III) reacts with salicylate, in acid media, to give a species rather prone to internal redox decompositions, which was thought to be $[Co(Hsal)(H_2O)_4]^{2+}$. (Several mechanistic studies of the related but more accessible $[CoN_4(sal)]^+$ ions have appeared: for example, iodination,[9] mercuration.[10]) In those species $[Co(N)_4(sal)]^+$ (N = NH_3, ½en, etc.) studied, the ligated salicylate

* For part XLVII, see ref. 1.

† Permanent address: Department of Chemistry, Nagoya City University, Mizuho, Nagoya, Japan.

‡ Author to whom correspondence should be addressed.

undergoes ready oxidation with nitric acid, giving a green paramagnetic product. Yamamoto and his colleagues have studied[11] the green paramagnetic species and their analogues extensively.

A similar oxidation of $[Co(en)_2(sal)]^+$ and of analogous $[CoN_4(\text{substituted sal})]^+$ occurs with permanganate, giving chelated oxalate (ethane-1,2-dioate). The mechanism of this extraordinary oxidative ring contraction[2] has been studied in some detail, using optically active complex salts and carbon-labelled salicylatobis-1,2-diaminoethanecobalt(III).

Other recorded properties of salicylates with cobalt are interesting. For example,[12] $[Co(NH_3)_6]^{3+}$, CoA_6^{3+}, is readily extracted into cyclohexanone (K) from aqueous sodium salicylate, NaHsal, NaB, according to

$$CoA_{6(aq)}^{3+} + 3B_{(aq)}^{-} + nK_{aq} \rightleftharpoons [CoA_6B_3K_n]_{org}.$$

The reaction of aquopentamminecobalt(III) chloride with Mordant yellow O gives[13] $[Co(dye)_3]^{6-}$, probably chelated as a salicylate. Nevertheless, the parent tris-salicylatocobalt(III) species have been elusive. An early preparation of the salt $[Co(NH_3)_6][Co(sal)_3]$ could not be repeated[2d] despite a number of careful and independent attempts, and the properties then given do not agree at all with those we now find for the authentic salt. It seems probable that all the substances we have now made are new compounds.

We report here, in detail, (following a short preliminary note[14]) a reliable synthesis of $[Co(sal)_3]^{3-}$, its optical resolution and its isomerization. Its lability towards acid has so far prevented its chemical correlation, by oxidation, to $[Co(C_2O_4)_3]^{3-}$, along the lines of an earlier discovery[2] of the oxidation, eq. (1)

$$(+)\text{-}[Co(en)_2(sal)]^+ \xrightarrow{[O]} (-)\text{-}[Co(en)_2(C_2O_4)]^+. \quad (1)$$

RESULTS AND DISCUSSION

Three factors complicate studies of the optical isomerism of such species as $[Co(sal)_3]^{3-}$. First, the equilibrium constants for ion-pairing with the classical triply charged resolving cations, like $(-)\text{-}[Rhen_3]^{3+}$, may be quite large, and such ion-pairing may select among the anionic complex isomers. Secondly, H_2sal, $Hsal^-$ and sal^{2-} lack a binary element of symmetry relating the two chelating oxygen atoms. So, even for the extremes of composition $[Co(Hsal)_3]$ and $[Co(sal)_3]^{3-}$, there may be facial (1,2,3- or abc) and meridianal (1,2,4- or abd) isomers, each of course racemic. Thirdly, since the ligand may, depending on the pH of its environment, exist as H_2sal, $Hsal^-$ or sal^{2-}, there are further isomeric possibilities, which could be described as tautomerism, where the isomers differ in the relative positions of hydrogen atoms. (i.e. there are three inequivalent phenolic positions in 1,2,4-$[Co(sal)_3]^{3-}$ at which a proton may add to give the three isomers of 1,2,4-$[Co(salH)(sal)_2]^{2-}$, each being racemic).

We avoided the last complication by ensuring that the pH is always high, but the first two have been of concern. We gave weight to the extra geometric isomerism by studying, as a model, the tris-malonatocobaltate(III) anion $[Co(mal)_3]^{3-}$. Here, the complex ion, neglecting any conformational effects in the six-membered rings, has the true symmetry of the D_3 point group.

Further, we have employed throughout, as our chiral influence and resolving agent, the colourless ion, $\Delta(+)\text{-}[Rhen_3]^{3+}$ [or of course its enantiomer $\Lambda(-)$], which shows no strong Cotton effects in the visible region. Our chiroptical spectra above 400 nm therefore comment directly on the cobaltic centres, even in the presence of the resolving agent $(+)\text{-}[Rhen_3]^{3+}$.

Preparation. The alleged preparation[15] of salts of $[Co(sal)_3]^{3-}$ from tris-carbonatocobaltate(III) failed; the product, in our hands, gave a strong thiocyanate test for cobalt(II). A procedure like that used by Pfeiffer[16] for the similar aromatic ligand paeonol $C_9H_{10}O_3$ was used.

$$[Co(NH_3)_5Cl]^{2+} + 3C_9H_{10}O_3 \rightarrow [Co(C_9H_9O_3)_3] + 3H^+ + 5NH_3 + Cl^-.$$

In warm solution, no reaction was seen, but on adding base it became green; chromatography [QAE-Sephadex-A25: elution with 0.1 M NaCl] gave an immobile yellow–green band and two green bands whose spectrum (λ *ca* 570 nm) suggested that they were isomers of $[Co(NH_3)_2(sal)_2]^-$. By adding a solution of $(+)\text{-}[Co(en)_3]Cl_3$ to the reaction mixture and concentrating, green crystals (λ 630 nm) were obtained showing a negative circular dichroism at *ca* 650 nm in KBr disc, DMSO or DMF. Aqueous solutions were unstable.

Following these preliminary indications, a stock solution containing green $[Co(sal)_3]^{3-}$ was made by slow reaction (at 20°C) of pink chloropentamminecobalt(III) chloride with an *excess* of sodium salicylate and hydroxide in water. This solution could be kept at 2°C for several days, although it decomposed readily and rapidly giving cobalt(II) and/or dark precipitates on warming, or on adding acid, or on removing the excess of salicylate.

Several salts with triply charged cations were iso-

Table 1. Salts of the tris-salicylatocobaltate(III) ion

Salt	Formula	Colour	Calculated C	Calculated H	Calculated N	Found C	Found H	Found N
(±)-[Coen$_3$][Co(sal)$_3$]	$C_{27}H_{36}N_6O_9Co_2$	Green[a]	45.9	5.1	11.9	45.4	5.3	11.6
(±)-[Rhen$_3$][Co(sal)$_3$]	$C_{27}H_{36}N_6O_9CoRh$	Green	43.2	4.8	11.2	42.1	4.8	11.9
[Co(NH$_3$)$_6$][Co(sal)$_3$]	$C_{21}H_{30}N_6O_9Co_2$	Green	40.1	4.8	13.4	40.9	5.1	13.4

[a] The description[15] of a substance said to be this salt, made by adding to aqueous [Coen$_3$][NO$_3$]$_3$ a solution of [Co(CO$_3$)$_3$]$^{3-}$ and salicylic acid, then boiling; was "beige". Several samples made in this way here were indeed rose-beige: they had such analyses as C, 33.8; H, 3.6; N, 11.2%, and all contained a lot of cobalt(II).

lated, including those listed in Table 1, with ammines of cobalt(III) and rhodium(III). The properties of the diastereoisomeric salts with the optically active resolving agents, (+)- or (−) tris-ethylenediaminerhodium(III), are given in the Experimental.

Tris-malonatocobaltate(III)

Figure 1 shows the effect on circular dichroism of adding an excess of Λ(+)-[Rhen$_3$]$^{3+}$ to racemic [Co(mal)$_3$]$^{3-}$, (in the presence of a small excess of malonate to inhibit dissociation). Any ion-pairing effects from the excess of malonate here (or salicylate as described later) with the chiral rhodium cation will not affect visible circular dichroism.

The initial spectrum, where there has been no time for racemization, is that of the mixture of 50% Λ and 50% Δ configurations at the cobalt(III) centres. The optical activity arises from the unequal properties of the diastereoisomeric ion-pairs as follows. The four cobaltic species present are (denoting ions by their configuration and chemical symbol of the central element): ΛCo, ΔCo; ΛRhΛCo, and ΛRhΔCo (i.e. each of the two enantiomeric cobalt ions may be either free or ion paired). Further,

$$[\Lambda Co]+[\Lambda RhCo] = [\Delta Co]+[\Lambda Rh\Delta Co].$$

However, because of the selectivity of ion-pairing by ΛRh between ΛCo and ΔCo,

$$[\Lambda Rh\Lambda Co] \neq [\Lambda Rh\Delta Co] \text{ and } [\Lambda Co] \neq [\Delta Co].$$

The observed circular dichroism, the resultant of these four concentrations and their molar differential extinction coefficients, will be non-zero, as observed.

As time passes, the observed circular dichroism spectrum changes. This must be due to a shift in the ΣΔ : ΣΛ from 50 : 50, i.e. to a racemization induced by the selective ion pairing. (The driving force for this slow change is the entropy of mixing, restoring to equality unequal concentrations of free Λ and Δ anions, since the equilibrium constant between them is one, neglecting any small effects of differential solvation transmitted from the dissymmetric but dilute solute.) The rate of this change has been measured, for the particular conditions of Fig. 1, and is kinetically first-order, with a rate constant $k_{obs} = 2 \times 10^{-5}\ s^{-1}$.

The direction of this induction of optical activity

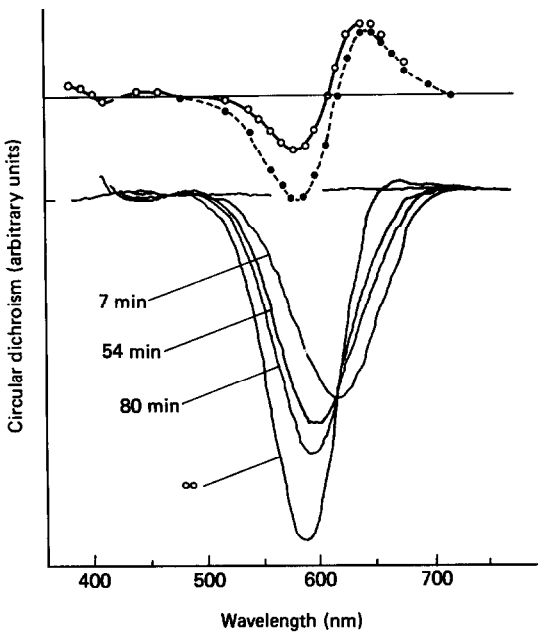

Fig. 1. Selected typical successive circular dichroism spectra for mixed aqueous solutions of tris-malonatocobaltate(III) and Δ-(+)-tris-1,2-diaminoethanerhodium(III) chloride, (lower diagram). Similar zero time changes in the circular dichroism of [Co(mal)$_3$]$^{3-}$ on adding varying excesses of the coloured cation (+)-[Co(en)$_3$]$^{3+}$ are recorded by K. R. Butler and M. R. Snow (*J. Chem. Soc., Dalton Trans* 1976, 251). Upper diagram; -○-○-○-—CD spectrum of resolved Λ[Co(mal)$_3$]$^{3-}$. -●-●-●-—curve obtained by subtracting the original (t = 0) spectrum from the final (t = 430.5 min: shown as ∞) of lower diagram.

is clear from the circular dichroism of the final solution after the removal (by cation exchange) of the inducing agent, (+)-$[Rhen_3]^{3+}$. The residual solution, now containing as chiral species only the tris-malonatocobaltate(III), shows (cf. Fig. 1), the CD spectrum of $\Lambda[Co(mal)_3]^{3-}$. The present spectrum is very similar to that of $\Lambda[Co(mal)_3]^{3-}$ recorded[17] by Douglas following a standard resolution via less soluble diastereoisomers. Under our conditions (excess of malonate, 1.9°C) the $[Co(mal)_3]^{3-}$ shows almost no loss of optical activity during 3 h.

The time variation of circular dichroism of Fig. 1 is entirely consistent with the explanation above. An instant (ion-pairing) selection by (+)-$[Rhen_3]^{3+}$ between the equal concentrations of Δ and $\Lambda[Co(mal)_3]^{3-}$ gives the following distribution of species:

Ion-pairs Δ(+)-$[Rhen_3]\Lambda[Co(mal)_3$
$> \Delta$(+)-$[Rhen_3]\Delta[Comal]_3]$

Anions $\Lambda[Co(mal)_3]^{3-} < \Delta[Co(mal)_3]^{3-}$.

The negative Cotton effect centred at 618 nm is the resultant of these four species in their unequal concentrations.

The total 50 : 50 $\Delta\Lambda$ ratio now shifts slowly* as the cobalt racemizes, and the new concentrations, induced by the chiral (+)-$[Rhen_3]^{3+}$ are (as in the final spectrum of Fig. 1)

Ion-pairs Δ(+)-RhΛCo $\gg \Delta$(+)-RhΔCo

Anions $\Lambda Co = \Delta Co$,

since, overall, the total concentration of ΛCo present is now greater than that of ΔCo.

So, the net change is to increase the concentration of ΛCo at the expense of ΔCo, and (on removing the inducing agent) the spectrum of ΛCo remains. Similarly, the spectrum obtained by subtracting the original ($t = 0$) spectrum of Fig. 1 from the final ($t = 430.5$ min) is very similar to that of authentic $\Lambda[Co(mal)_3]^{3-}$.

This set of observations on the tris-malonato system confirmed the need, in the $[Co(sal)_3]^{3-}$ system, to distinguish carefully between (i) the rapid effects of selective ion-pairing singling out particular chiroptical transitions and giving strong resultant Cotton effects even in a 50Δ : 50Λ overall anionic composition, and (ii) the longer term effects arising from a shift of the configurational equilibrium at the cobalt centre induced (slowly) by the chiral environment provided by the dissymmetric cation.

One final point on the $[Co(mal)_3]^{3-}$ system relates to its circular dichroism. This is shown in Table 2, with that of other CoO_6 chromophores, notably the tris-salicylates studied here. In common with solutions of the oxalato analogue, three Cotton effects are observed beneath the band envelope of the second ligand-field transition (Band II, of parentage $^1A_{1g} \rightarrow {}^1T_{2g}$ in O_h). Years ago, it was pointed out[18] that, since, in D_3 symmetry only two chiroptical absorptions were allowed for Band II, but three extrema are in fact seen, the tris-oxalatocobaltate(III) would seem to contain species of symmetry lower than D_3, such as $[Co(C_2O_4)_2(HC_2O_4)(OH)]^{3-}$. However, there is little other evidence[19] for such hydrolysed ions being present in solution, and, in the absence of the knowledge of the relative band widths† of the individual components of oppositely signed circular dichroism, the structure of $[Co(mal)_3]^{3-}$ under such conditions may be taken as tris-chelated.

Tris-salicylatocobaltates(III)

The racemic ion (containing an unknown ratio of facial and meridianal isomers) was obtained by displacing ammonia and chloride from chloropentakisamminecobalt(III) chloride using an excess of salicylate and enough sodium hydroxide to keep the solution alkaline throughout. The dark green solution gave, on SP-Sephadex (C-25), three bands. The first was dark green and contained the greatest bulk of the cobaltic product, $[Co(sal)_3]^{3-}$. Spectroscopic properties are in Table 2. The visible band of the green solution obeyed the Beer–Lambert law, dilutions being made with sodium salicylate solution.

The second chromatographic band, not char-

* The observation of the common point of $(\Delta\varepsilon,\lambda)$ in successive spectra indicates that a new set of chiroptical transitions is gradually replacing the original, but proves no more than would an isosbestic point, i.e. that the concentrations of *all n* species contributing to absorption at the wavelength of the isodichroic point are linearly related.

† Clearly, if a stronger sharper negative band is superimposed on a broader, weaker positive band (or with signs vice versa for the enantiomer) then the resultant observed circular dichroism may appear with three extrema, + − +, arising from only two electronic transitions. That situation,[20] at present hypothetical, is akin to that which gives rise to the Chartreuse effect in visible spectra. In this context, it is noteworthy that the solid diastereoisomeric salt of the tris-oxalato anion, Λ(−)-$[Rhen_3]$-(−)-$[Co(C_2O_4)_3]$ shows, in a caesium chloride disc, only two peaks near 400 nm (i.e. for Band II), whereas the potassium salt of the same resolved anion $K_3\Lambda(-)[Co(C_2O_4)_3]$ in solution, cf. Table 2, and in a CsCl disc shows three peaks. The suggestion[21] was that the observed spectra arose from two fundamental absorptions of differing breadths.

Table 2. Properties (in *d–d* manifold) of resolved tris chelated anions of cobalt(III) with bidentate oxygen donors, $[Co(O—O)_3]^{3-}$

Anion	Conditions	λ	ε[a]	λ	ε	λ	ε	λ	ε	λ	ε	λ	ε	Angle	Reference
$[Co(CO_3)_3]^{3-}$	(+)-$[Co(en)_3]^{3+}$ salt: KBr disc	620	+												[b]
														ca 70°	[c]
Λ(−)-$[Co(C_2O_4)_3]^{3-}$	K_3 salt: H_2O			602	153					422	204				[d]
														ca 84°	[e]
		617	+3.3					446	+0.26	412	−0.26	366	+0.21		[d]
Δ(+)-$[Co(C_2O_4)_3]^{3-}$	K_3 salt: KBr disc	605	−5							415	+1				[f]
	K_3salt: CsCl disc	605	−10					448	−1	410	+1	370	−2		[f]
Λ(−)-$[Co(C_2O_4)_3]^{3-}$	Δ(−)-$[Rhen_3]^{3+}$ salt: KBr disc	610	+1			555	−3			410	−1.5				[f]
$[Co(mal)_3]^{3-}$	H_2O			606[g]	148					418	142				[h,i,j]
	H_2O			607.5	148					423.5	127				[k]
	H_2O	645	+			583	−	446	+	414	−	380	+		[h]
														ca 93.4°	[l]
$[Co(sal)_3]^{3-}$	H_2O			637	240.6					415	. ~ 500[m]				
		730	+0.1	645	−1.0	583	+0.4	470	−0.2					?	[n]
	Δ(+)-$[Rhen_3]^{3+}$ salt: KBr disc														
	300 K			648	+	~ 520	~ −2	460	−						[h]
	216 K			645	+	~ 520	~ −1	460	−						
	77 K			640	+	~ 520	~ 0	460	−						

[a] Molar extinction coefficient in isotropic absorption if without sign; molar circular dichroism if a signed quantity: disc intensities are relative.

[b] R. D. Gillard, P. R. Mitchell and M. G. Price, *J. Chem. Soc., Dalton Trans.* 1972, 1211.

[c] No structure is yet available for any salt of $[Co(CO_3)_3]^{3-}$: however, for $[Co(NH_3)_4CO_3]Br$, two independent measurements agree with an intrachelate angle of *ca* 70° (C. O. Haagensen and S. E. Rasmussen, *Acta Chem. Scand.* 1963, **17**, 1630; cf. G. A. Barclay and B. F. Hoskins, *J. Chem. Soc.* 1962, 586). Similarly, for $[Co(tn)_2(CO_3)](ClO_4)$ (tn = 1,3-diaminopropane), R. J. Geue and M. R. Snow (*J. Chem. Soc. A* 1971, 2981) found 68.8°.

[d] A. J. McCaffery, S. F. Mason and R. E. Ballard, *J. Chem. Soc.* 1965, 2883.

[e] K. R. Butler and M. R. Snow, *J. Chem. Soc. A* 1971, 565.

[f] Ref. 21.

[g] There is, in many of our solutions containing $[Co(mal)_3]^{3-}$ and an excess of malonate, probably a shoulder at *ca* 520 nm.

[h] This work.

[i] N. C. Kneten and S. T. Spees, *J. Inorg. Nucl. Chem.* 1971, **33**, 2437.

[j] A. G. Sharpe and M. S. Al-Obadie, *J. Inorg. Nucl. Chem.* 1969, **31**, 2963.

[k] Ref. 17.

[l] K. R. Butler and M. R. Snow, (*J. Chem. Soc., Dalton Trans* 1976, 259) give 93.6(8) and 93.5(8) for $(+)_{546}$-$[Coen(mal)_2]^-$.

[m] This is an evident shoulder on a band rising steeply into the UV. The quantities given (which are approximate) are for the resolved band.

[n] Only a few crystal structures of complexed salicylate are available (see ref. 3), and none include a salicylatocobalt(III) moiety.

acterized in detail, had (initially) a clear absorption band at 582 nm, with a molar extinction coefficient of about 160. This (in the presence of an excess of salicylate) slowly became green, with the final spectrum closely resembling that of the $[Co(sal)_3]^{3-}$ from the first band. Our value for the initial extinction coefficient (*ca* 160 at 582 nm) is derived from the 50% increase in maximal visible optical density of the solution, and the known ε_{636} (i.e. 240) of the product. It seems likely, from the absorption at 582 nm (which we take to arise from a $[Co^{III}N_2O_4]$ chromophore) and the slow reaction to form the tris-complex, which we take to be

$$[Co(NH_3)_2(sal)_2]^- + sal^{2-} \rightarrow [Co(sal)_3]^{3-} + 2NH_3,$$

that this band contains one or more isomers of the bis-ammine-bis-salicylatocobaltate(III) ion. Because of the lack of a two-fold symmetry element in salicylate, there are, of course, two *trans*-isomers and three *cis*-isomers: for the *trans*-isomers, with their unique N—Co—N axis, splitting of the lowest energy spin-allowed ligand-field absorption band might be expected, and the band is indeed rather broad. The final spectrum of the aged solution has a rather higher absorbance around 550–560 nm than has the authentic tris-salicylate: this supports the idea that Band II contains some *trans*-$[Co(NH_3)]_2(sal)_2]^-$ (which would absorb around 560–570 nm and would presumably *not* react readily with the excess of salicylate to give the tris-species). The final spectrum would then be due to *ca* 90% of $[Co(sal)_3]^{3-}$ and 10% of isomers of *trans*-$[Co(NH_3)_2(sal)_2]^-$.

The third band on the SP-Sephadex column adsorbed strongly, and did not move readily in the anionic eluant (0.05 M sodium salicylate). However, it was readily eluted with 0.5 M lithium chloride, and had absorption maxima at 502 and 366 nm, typical of a $[Co^{III}N_4O_2]$ chromophore (these bands had maximal extinction coefficients in the ratio $\varepsilon_{502} : \varepsilon_{366} = 1.06 : 1$). We therefore take this (very minor) component to be $[Co(NH_3)_4(sal)]^+$. Its electronic spectrum agrees reasonably well with that[2] of an authentic specimen.

The course of the preparation then seems to be

$$[Co(NH_3)_5Cl]^{2+} \longrightarrow [Co(NH_3)_5(OH)]^{2+}$$

$$\longrightarrow [Co(NH_3)_4(sal)]^+ \text{ (Band III)}$$

$$\downarrow$$

$$[Co(sal)_3]^{3-} \longleftarrow \textit{cis}\text{-}[Co(NH_3)_2(sal)_2]^- \Big\}$$

$$\text{(Band I)} \leftrightarrow\!\!\!\!\times \textit{trans}\text{-}[Co(NH_3)_2(sal)_2]^- \Big\} \text{ (Band II).}$$

We next discuss the striking changes in optical activity when solutions of $[Co(sal)_3]^{3-}$ are treated with the chiral influence of the counter-ion $[Rh(en)_3]^{3+}$. There is no gross change in the nature of the cobaltic chromophore, (CoO_6), as shown by the effective constancy of the electronic spectrum (800–500 nm) after adding tris-ethylenediaminerhodium(III). In a typical experiment, at 1.1°C, the electronic spectrum of $[Co(sal)_3]^{3-}$ (7.52×10^{-4} M) was constant within 1%, in the presence of $[Rhen_3]^{3+}$ (2.52×10^{-2} M) and sodium salicylate (2.0×10^{-3} M), over 260 min.

On leaving solutions originally containing racemic $[Co(sal)_3]^{3-}$ and resolved $[Rhen_3]^{3+}$, as we found for the malonate experiments, there was a very rapid induction of optical activity in the CoO_6 chromophore, followed by a much slower change of this initial circular dichroism to a final spectrum. We describe this in detail later. When the inducing agent, (+)- or (−)-$[Rhen_3]^{3+}$, was removed (by cation-exchange) from these final solutions, the resolved $[Co(sal)_3]^{3-}$ remained. Its circular dichroism spectrum is shown in Fig. 2 and in Table 2. Figure 2 also shows the loss of the Cotton effect for $[Co(sal)_3]^{3-}$ with time. In a typical experiment, at 1.8°C, $k_r = 5.6 \times 10^{-2}\,min^{-1}$. Isodichroic points are observed here on the baseline, showing that no optically active species other than $[Co(sal)_3]^{3-}$ is present in an observable amount (i.e. this is indeed a racemization, rather than a mutarotation or hydrolysis to some other optically stable cobalt complex). The rate constant quoted was measured in the presence of a 27-fold molar excess of $(sal)^{2-}$ over $[Co(sal)_3]^{3-}$. This rate constant is clearly smaller than the true rate constant for uninhibited racemization of $[Co(sal)_3]^{3-}$, which would, in the light of our observations, be optically unstable in neutral solution.

The formation of solid diastereoisomeric salts $[Rhen_3][Co(sal)_3]$ was achieved by using stronger solutions. The circular dichroism spectra are shown in Fig. 3, and listed in Table 2. The circular dichroism spectra of potassium bromide discs were measured for both diastereoisomers, giving essentially enantiomeric spectra, as shown in Fig. 3 (the apparent difference in $|\Delta\varepsilon|$ is merely a comment on the semi-quantitative nature of such spectra: the discs contained equal concentrations of the diastereoisomers).

The spectra of the less soluble diastereoisomer $\Delta(+)$-$[Rhen_3]\Lambda[Cosal_3]$ at three different temperatures are also shown in Fig. 3 (and in Table 2). There is a quite distinct change in the observed spectrum, with the maximal longest wavelength Cotton effect centred at longer wavelengths as the temperature increases. Part of this shift arises from

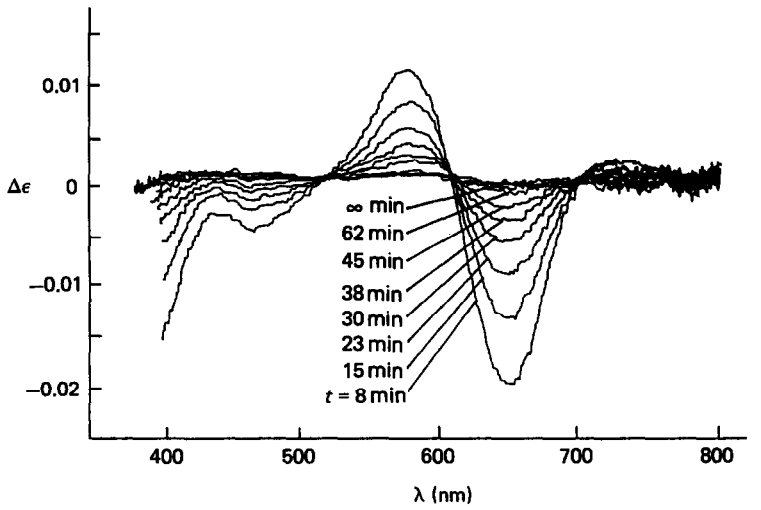

Fig. 2. Circular dichroism spectrum ($t = 0$) of resolved $[Co(sal)_3]^{3-}$ obtained by removing (+)-$[Rhen_3]^{3+}$ and successive stages of racemization, at 1.8°C, giving $k_r = 5.6 \times 10^{-2}$ min^{-1}.

increased positive circular dichroism on the long wavelength edge of the positive band, and part may also be caused by the cancellation of positive circular dichroism below 600 nm, by the appearance at the higher temperatures of a perceptible shoulder of absorption on the negative side at about 520 nm. The relative intensity of the weaker negative band at 460 nm also increases as the temperature increases.

The cause of these striking alterations in Cotton effects is not clear, although the energy involved is so small (taking the onset of the new absorbance as being at 200 K, $kT \simeq 200$ cm^{-1}) that it can hardly represent any structural change (such as isomerization) within the ions making up the solid. Further, since the absorption spectrum shows a very clear minimum at 550 nm, and the "new" band grows at *ca* 520 nm, the transition responsible belongs to Band II of cobalt(III) ($^1T_{2g} \leftarrow {}^1A_{1g}$ of O_h parentage) rather than to Band I (with $^1T_{1g}$ as the corresponding excited state). The observed spectra could arise either from the growth with temperature of a negative Cotton effect at 520 nm or, conceiv-

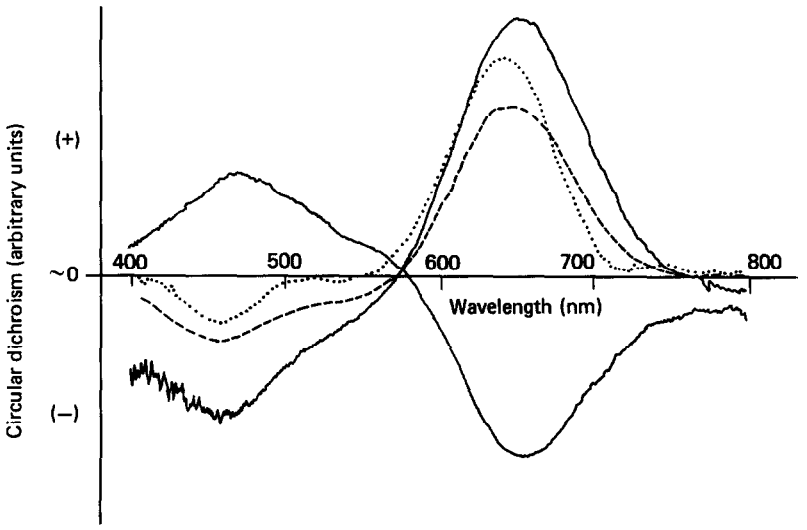

Fig. 3. Circular dichroism spectra (——) of the enantiomeric pair of diastereoisomeric salts Δ-(+)-$[Rh(en)_3][Co(sal)_3]$ (0.7 mg in 140 mg KBr as a pellet of 1 cm diameter) and Λ(−)-$[Rh(en)_3][Co(sal)_3]$ at 298 K, and of the former (0.594 mg in 149.5 mg KBr as a 1 cm pellet) at 77 K (····) and 216 K (– – – –).

ably, by the loss at high temperature of a weak positive Cotton effect at 520 nm (overlapping and, at lower temperature, obscuring the longer wavelength part of a broader, rather stronger, negative band around 500 nm). However, the latter possibility seems remote, since the position of maximal circular dichroism (at 460 nm) is unaffected by the change of temperature.

We are left with the most likely situation that a band with negative circular dichroism is appearing around 520 nm, with essentially no intensity at 77 K, and increasingly measurable intensity at 216 and 293 K. This would, in other contexts, be described as a "hot band" arising from the population of a vibrational level of the electronic ground state. Presumably, the broadening of the stronger Cotton effect (centred at ~ 650 nm) towards its lower energy side on raising the temperature can also be attributed to the influence of "hot bands". However, the major distinction is that, in the case of the higher energy new component around 520 nm, it appears as a discrete shoulder on the strengthening band at 460 nm. If the two were related by being based on the zeroth and first vibrational levels of the same electronic state, their separation is rather too large (*ca* 2500 cm^{-1}, which in itself is not unreasonable as a vibrational frequency, but much greater than for the usual skeletal vibrations of a Co^{III}–O_6 framework). Since the temperature profile of the new band's appearance suggests an energy quantum around 200 cm^{-1}, this obvious explanation based on a hot band may be incorrect. The other likely origin for a change in selection rules within chromophores in a solid structure would lie in a phase transition, and that cannot with present information be dismissed.

We now summarize our results when adding $\Delta(+)$-$[Rhen_3]^{3+}$ to solutions of $[Co(sal)_3]^{3-}$. Equivalent but enantiomorphic spectra are of course obtained with the $(-)$-$[Rhen_3]^{3+}$ ion, but we restrict our description to results obtained with the $(+)$-enantiomer: for convenience, we have inverted spectra which were actually obtained from the $(-)$-species in a few specified cases.

Our kinetic experiments were as follows. The synthetic solution of chromatographically pure $[Co(sal)_3]^{3-}$ (which contained an excess of salicylate ion) showed observable (indeed quite strong) Cotton effects under the 650 nm band as soon as chiral $(+)$-$[Rhen_3]^{3+}$ was added. This "instant" circular dichroism now changes, slowly, as shown in Fig. 4 to a final "equilibrated" spectrum. The rate constants (k_1) for this change under varying conditions, are in Table 3. When the $(+)$-$[Rhen_3]^{3+}$ ion was removed from these equilibrated solutions, solutions containing an excess of one hand of $[Co(sal)_3]^{3-}$ were left (these still of course contained an excess of salicylate ion). The solution now race-

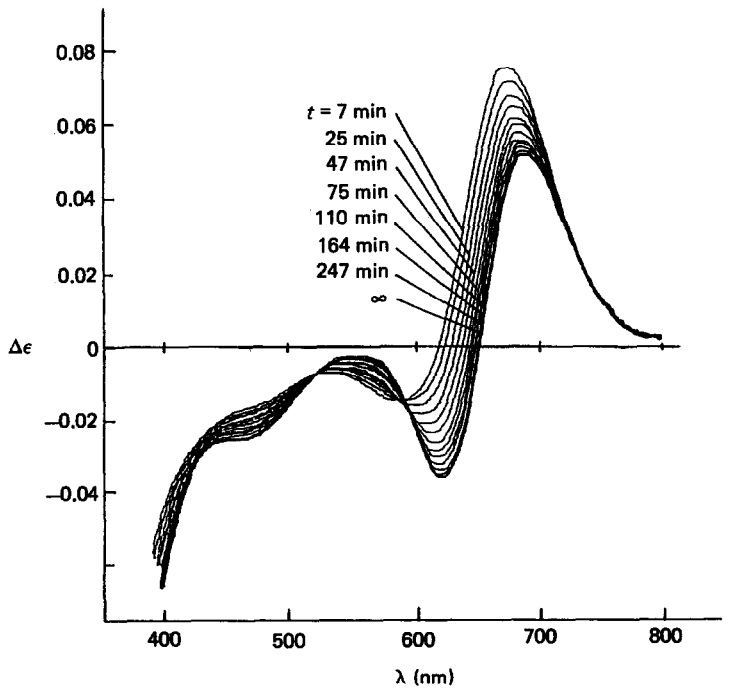

Fig. 4. Successive circular dichroism spectra of a $[Co(sal)_3]^{3-}$ solution treated with Δ-$(+)$-$[Rh(en)_3]Cl_3$ at 1.7°C in water, giving, from measurement at 650 nm, $k = 1.72 \times 10^{-2}$ min^{-1}.

Table 3. Rates of stereochemical change for tris-salicylatocobaltate(III) [k_1 and k_2 in units of min^{-1}]

$[Co(sal)_3^{3-}]$	$[Rhen_3^{3+}]^a$	[Nasal]	k_1	$k_2{}^b$	k_2/k_1	Temperature (°C)
7.34×10^{-4}	2.46×10^{-2}	2.0×10^{-3}	$1.6(4)\times10^{-2}$	$5.0(3)\times10^{-2}$	3.1	2.0
7.34×10^{-4}	2.46×10^{-2}	2.0×10^{-3}	$1.3(8)\times10^{-2}$	$4.4(1)\times10^{-2}$	3.2	1.5
6.96×10^{-4}	1.12×10^{-2}	2.0×10^{-3}	$1.4(5)\times10^{-2}$	$4.3(1)\times10^{-2}$	3.0	1.7
6.75×10^{-4}	1.62×10^{-3}	2.0×10^{-3}	$1.5(4)\times10^{-2}$	[c]		2.0
7.42×10^{-4}	2.44×10^{-2}	2.0×10^{-2}	$1.7(1)\times10^{-2}$	$6.1(4)\times10^{-2}$	3.6	1.7
7.42×10^{-4}	2.44×10^{-2}	2.0×10^{-2}	$1.7(0)\times10^{-2}$	$5.6(0)\times10^{-2}$	3.3	1.8
7.42×10^{-4}	2.44×10^{-2}	2.0×10^{-2}	$1.7(3)\times10^{-2}$	$5.7(0)\times10^{-2}$	3.3	1.8
6.66×10^{-4}	1.67×10^{-3}	2.0×10^{-2}	$1.5(2)\times10^{-2}$	[c]	[c]	2.0
6.66×10^{-4}	3.19×10^{-4}	2.0×10^{-2}	$1.6(8)\times10^{-2}$	[c]	[c]	1.9

[a] As Δ-(+)-$[Rh(en)_3]Cl_3\cdot2.3H_2O$.
[b] Racemization rate, when (+)-$[Rh(en)_3]^{3+}$ removed.
[c] Not measured.

mizes (showing isodichroic points on the base line as in Fig. 2). The rate constants (k_2) for these racemizations are also collected in Table 3.

The most notable fact is that k_1 for each set of conditions is smaller than k_2, so that the rate-determining step of the slow change in optical activity in the presence of (+)-$[Rhen_3]^{3-}$ is not merely racemization. We attribute this difference to a change in populations, not only of enantiometric hand (which would go at least as quickly as the racemization rate: it might conceivably be faster than racemization, since the Δ → Λ change might be accelerated by the stabilization of product by selective ion-pairing, but could hardly be slower), but of populations, not only of enantiomeric hand (which) explanation is supported by the further fact that the successive circular dichroism spectra during k_1 do not quite manifest isodichroic points. If we were merely observing the change from one distribution of a set of species to another distribution of the same set of species, where the initial and final chiroptical spectra intersected (as they do in the present case), then the spectra of all intermediate compositions would pass through the same points of intersection.

Instead of isodichroic points, the successive spectra pass through isodichroic zones, notably between 590–600 nm and between 525–540 nm (in Fig. 4; clearly as external conditions vary, the actual wavelengths of such zones will also change; the argument is unaffected).

There is a rapid rise of optical activity in the CoO_6 chromophore on adding (+)-$[Rhen_3]^{3+}$. The size of this Cotton effect initially produced is larger for larger concentrations of $[Rhen_3]^{3+}$.

Even for the largest excess of (+)-$[Rhen_3]^{3+}$ (2.4×10^{-2} M), we cannot assume complete ion-pairing (which would require an ion-pairing equilibrium constant of about 400). So Δε for the ion-pair is unknown. We deduce the configurations involved in the stereoselective ion-pairing as follows. The initial Δ : Λ distribution for cobalt is 50 : 50. The *final* total Δ : Λ distribution (after equilibrium has been attained in a particular solution) is, taking the positive Cotton effect at 646 nm to arise from the Λ configuration, Λ > Δ. The chiral counter-ion (+)-$[Rhen_3]^{3+}$ has stabilized Λ-$[Co(sal)_3]^{3-}$ relative to its enantiomer. This is supported* by the fact that the less soluble diastereoisomer is (+)-$[Rhen_3]$Λ$[Cosal_3]$.

However, the displacement of equilibrium to the Λ side seems (even in the most favoured case) to be incomplete. Thus, extrapolating the optical activity versus time results back to time zero, we find the maximum value of $\Delta\varepsilon_{646}$ to be 0.32. This seems too

* Though not strongly. The lattice energy of the less soluble diastereoisomer is made up of contributions from interactions not only between single ion-pairs, but also by ion-multiplet effects, unlike the solution cases where we are concerned solely with the 1 : 1 interaction within the sterically complementary solvation sheath (also, of course, handed) made up by the water assembly. However, in practice, for those pairs of 3+ and 3− ions which have been studied in dilute solution, where the resolution has also been achieved by using more concentrated solutions, the stronger selective diastereoisomeric ion-pair gives the less soluble salt.

small to represent an optically pure tris-species,* and we take it that the final solutions (after equilibration and before removal of (+)-$[Rhen_3]^{3+}$) contain at least the following species: {(+)-$[Rhen_3]\cdot\Lambda Cosal_3$} and $\Delta\Lambda[Cosal_3]$.

The circular dichroism found in the lowest energy spin-allowed region for $[Co(sal)_3]^{3-}$ is similar to that for other CoO_6 tris chelates, as shown in Table 2. This is rather remarkable, since the chelate ring angles vary in the range 70–94° from the tris four-membered rings to the tris six-membered rings. The trigonal splitting of the octahedral $^1T_{1g}$ state would be expected to vary widely as these chelate ring angles change, but that is not found. Indeed, as is clear in Table 2, the variation in splitting (and consequently appearance) of the circular dichroism produced by changes of environment for a particular anion, say $[Co(C_2O_4)_3]^{3-}$, is far greater than that in a comparable series containing chelate rings of increasing sizes.

The ions (+)-$[Co(en)_3]^{3+}$ or (−)-$[Rh(en)_3]^{3+}$ of known D [or $\Lambda(C_3)$] configuration have now been used to form diastereoisomeric salts with $[Co(OO)_3]^{3-}$, where $OO = CO_3^{2-}$, $C_2O_4^{2-}$, $C_3H_2O_4^{2-}$ (malonate) and $C_7H_4O_3^{2-}$ (salicylate). It seems likely that the set of anions forming the less soluble diastereoisomers within the D [or $S(C_3)R(C_2$ or $\Lambda]$ $[M(en)_3]^{3+}Rh$) have related configurations. We are working towards establishing the absolute stereochemistry of $[M(sal)_3]^{3-}$ by chemical and crystallographic means.

EXPERIMENTAL

Electronic spectra were measured using a Unicam SP-8000 spectrophotometer. Circular dichroism for solutions generally employed a Dichrographe, and for solids a Jasco instrument.

$[Rh(en)_3]Cl_3\cdot 2.3H_2O$ was prepared and resolved according to the literature.[23]

Preparation of reaction mixture of $[Co(sal)_3]^{3-}$

To a suspension of recrystallized $[CoCl(NH_3)_5Cl_2$ (1.0 g, 0.004 mol) and recrystallized Na(Hsal) (2.9 g, 0.018 mol) in 30 cm^3 of water, 1.0 g of NaOH in 20 cm^3 of water was added and N_2 gas was bubbled into the mixture with constant stirring at room temperature (*ca* 20°C) for about 17 h. The nitrogen helps to drive the reaction by sweeping out ammonia. (If the temperature was raised to *ca* 40°C, the solution turned brown, then gave a grey–brown precipitate.)

During the reaction, the mixture changed from a reddish-pink suspension to brown and then to a greenish-brown solution. A dark green solution was finally obtained after 17 h (or occasionally longer) and filtered. In some cases, the reaction mixture contained a very small amount of greyish-green solid but was usually clear. The clear solution was kept at about 2°C until it was used. Attempts to isolate Na or K (having replaced NaOH by KOH) salts from such reaction mixtures by precipitation failed because addition of alcohol or another organic solvent caused decomposition.

Preparation of $[Rh(en)_3]^{3+}$ *salt with* $[Co(sal)_3]^{3-}$ *from reaction mixture*

The clear solution of $[Co(sal)_3]^{3-}$ was divided into two, and to each half, 0.45 g (0.001 mol) of (+)- or of (−)-$[Rh(en)_3]Cl_3\cdot 3H_2O$ were added. Both solutions were kept ice-cold (*ca* 0°C) overnight (at which point there was no precipitation), then the walls of the vessels were scratched violently with glass rods, to initiate crystallization. After four days, the pale green precipitates were collected and washed with cold water, and dried over P_4O_{10} under reduced pressure. The precipitates were powder-like fine crystals, insoluble in all the many solvents (including water) studied. Yield: (+)-$[Rh(en)_3][Co(sal)_3]$, 0.40 g; (−)-$[Rh(en)_3][Co(sal)_3]$, 0.37 g. Found: C, 41.1; H, 4.8; N, 11.0. Calc. for $[Rh(en)_3][Co(sal)_3]$: C, 43.2; H, 4.8; N, 11.2%.

Purification of $[Co(sal)_3]^{3-}$

The complex ion of $[Co(sal)_3]^{3-}$ in a reaction mixture was purified by a chromatographic method using a column of SP-Sephadex (C-25). A typical procedure is as follows: about 1 cm^3 of cold reaction mixture was poured onto the column (ϕ 2.0 × 16 cm) jacketed with ice-cold water, and a solution of Na(sal) (0.01 M, 0.05 or 0.1 M in other runs) was used for elution. Three bands were observed: two were eluted and one remained adsorbed at the top of the column. This last reddish-pink band was apparently a cationic species. A dark green band which eluted faster was dominant and contains $[Co(sal)_3]^{3-}$. The second band, brownish-green, is fairly small. Separation between the first and second bands was clean.

Isolation of $[Co(sal)_3]^{3-}$ by using anion-

* Even for one containing only six-membered chelate rings, where, as Mathieu pointed out[22] long since, the resultant Cotton effects in the visible region tend to be smaller than for analogous five-membered rings. Notwithstanding this, values of $\Delta\varepsilon$ for $[Co(mal)_3]$ up to 1.5 are recorded.[17]

exchange, for example DEAE- or QAE-Sephadex (A-25) was also attempted, but failed because the adsorbed band was tightly held on the column and gradually decomposed during elution even by Na(sal) solution or $[Rh(en)_3]Cl_3$ solution.

The eluate was collected for each band. The eluate in the first band, which from its absorption spectrum contained $[Co(sal)_3]^{3-}$ was diluted to a suitable concentration with 0.01 M sodium salicylate, such that its absorbance at 636 nm was around 0.8 in a 1.0 cm cell. This solution was used as a stock solution for measurements.

Cobalt analysis in $[Co(sal)_3]^{3-}$ *solution—measurements of the absorption coefficient of* $[Co(sal)_3]^{3-}$

The cobalt content in the stock solution described above was determined in a way similar to a standard colorimetric method[24] using $[CoCl(NH_3)_5]Cl_2$ as standard material. A standard cobalt solution [6.068×10^{-3} M in 0.01 M Na(sal)] was prepared from recrystallized $[CoCl(NH_3)_5]Cl_2$. To 0.5 cm^3, 2.0 cm^3 of $HNO_3 : HCl = 1 : 1$ solution was added, and the mixture was evaporated to dryness by heating. This procedure for decomposition was repeated several times. The residue was washed into a 25 cm^3 volumetric flask with a small quantity of water. The following solutions were added in this order: 1.0 cm^3 of 2% ascorbic acid, 1.0 cm^3 of 2 M $HClO_4$, 5.0 cm^3 of 6 M NH_4SCN and 12.0 cm^3 of acetone. Finally, water (*ca* 5 cm^3) was added up to the mark. The resultant solution was greenish-blue with maximum absorption at 619 nm. Such solutions were prepared from 1.0, 1.5 and 2.0 cm^3 of the standard solution in the same way. Absorbance at 619 nm in a 1.0 cm cell was plotted versus cobalt concentration to give a calibration curve.

Extinction coefficient of $[Co(sal)_3]^{3-}$

The eluate of the first band was analysed several times for cobalt content. The extinction coefficient of $[Co(sal)_3]^{3-}$ at 636 nm was determined as 240.7.

Measurements of circular dichroism (CD) spectra

All CD spectra in solution were measured using a Roussel–Jouan dichrographe III whose cell holder and cell compartment were maintained at about 2°C by iced-water. A typical procedure is: 1 cm^3 of the stock solution of $[Co(sal)_3]^{3-}$ in 0.01 M sal was poured into a 5 cm^3 volumetric flask containing about 3 cm^3 of (+)-$[Rh(en)_3]Cl_3$ solution and ice-cold water was added up to 5.0 cm^3. All solutions, of $[Co(sal)_3]^{3-}$ and (+)-$[Rh(en)_3]^{3+}$ and the mixture were kept in ice-cold water before and during mixture. The mixture was transferred to a 1.0 cm cell and CD spectra were measured (sensitivity, 5×10^{-6} cm) at intervals of about 2°C in the range of wavelengths from 800 to 400 nm.

After equilibration (when appreciable CD change had ceased), the solution was passed through a small PS-Sephadex column (ϕ 1.2 × 5 cm: Na^+ form, equipped with a water jacket, kept cold by iced-water) to remove $[Rh(en)_3]^{3+}$; this quantity of Sephadex (C-25) was quite enough. The CD spectrum of the eluate from the column was measured again under the same conditions as described above other than the sensitivity condition (2×10^{-6} cm^{-1}).

Measurement of CD spectrum in a KBr *disc*

A potassium bromide disc was prepared from 0.781 mg of (+)-$[Rh(en)_3][Co(sal)_3]$ and 141.1 mg of KBr as a pellet with a diameter 1 cm and 0.632 mm thick. For (−)-$[Rh(en)_3][Co(sal)_3]$, 0.515 mg of complex and 145.4 mg of KBr were used to make a pellet 0.664 mm thick. The circular dichroism (CD) spectrum was obtained using a JASCO model J-40. Sensitivities were 5×10^{-4} cm^{-1} and 2×10^{-4} cm^{-1} for (+)- and (−)-$[Rh(en)_3][Co(sal)_3]$, respectively.

Acknowledgements—We wish to thank Dr L. F. Vilas Boas [Ph.D. thesis, UKC (1973)] and Dr Judit Gaal [unpublished work while on leave from Veszprem University, Cardiff (1977)] for preliminary experiments. We also thank Nagoya City University for leave (M.F. 1980–1981 and 1987).

REFERENCES

1. P. S. Cartwright and R. D. Gillard, *Polyhedron* 1988, **7**, 1243.
2. (a) K. Garbett and R. D. Gillard, *J. Chem. Soc. A* 1968, 979, (b) R. D. Gillard, P. R. Mitchell and L. F. Vilas-Boas, *Trans. Met. Chem.* 1977, **2**, 80; (c) R. D. Gillard, J. R. Lyons and P. R. Mitchell, *J. Chem. Soc., Dalton Trans.* 1973, 233; (d) A. G. Beaumont, R. D. Gillard and J. R. Lyons, *J. Chem. Soc. A* 1971, 1361.
3. J. D. Pedrosa de Jesus, in *Comprehensive Coordination Chemistry*, (Edited by G. Wilkinson, R. D. Gillard and J. A. McCleverty), Vol. 2, p. 481. Pergamon Press, Oxford (1987).
4. J. O. Nriagu (Ed.), *Copper in the Environment, Part II, Health Effects*, p. 83. Wiley, New York (1979); F. T. Greenaway, L. J. Norris and J. R. J. Sorenson, *Inorg. Chim. Acta* 1988, **145**, 279 comments on copper(II) complexed by 3,5-di-isopropylsalicylate in this connection.
5. K. O'Brien and F. Gibson, *Biochim. Biophys. Acta* 1970, **215**, 393.

6. J. B. Neilands, *Struct. Bonding* 1972, **11**, 145; J. B. Neilands, in *Metal Ions in Biological Systems* (Edited by S. K. Dhar), p. 23. Plenum Press, New York (1973).
7. G. H. Tait, *Biochem. J.* 1973, **131**, 169.
8. A. C. Dash and B. Mohanty, *J. Inorg. Nucl. Chem.* 1977, **39**, 1139.
9. A. C. Dash, N. Mullick and R. K. Nanda, *Trans. Met. Chem.* 1977, **2**, 222.
10. A. C. Dash, R. K. Nanda and N. Ray, *Ind. J. Chem.* 1982, **214**, 1068.
11. Y. Yamamoto and H. Kudo, *Bull. Chem. Soc. Japan*, 1984, **57**, 287 and refs therein.
12. R. Larsson, *Acta Chem. Scand.* 1962, **16**, 2305.
13. O. Venkataraman, *The Chemistry of the Synthetic Dyes.* Academic Press, New York (1952); in this context, the azosalicylic acids are suitable for chrome dyeing. Among simpler commercial dyes they include Alizarin yellow, Diamond Flavine G, and Eriochrome Flavine A (cf. R. D. Johnson and N. C. Nielson, in *Chemistry of the Coordination Compounds* (Edited by J. C. Bailar), A.C.S. Monograph 131, p. 743. Reinhold, New York (1956) and R. Price in the present ref. 3, **6**, 35).
14. M. Fujita and R. D. Gillard, Abstr. 30th An. Symp. Coord. Chem. Japan. Tokyo (October 1980).
15. H. F. Bauer and W. C. Drinkard, *J. Am. Chem. Soc.* 1960, **82**, 5031.
16. P. Pfeiffer, S. Golther and O. Angern, *Berichte* 1927, **60**, 305.
17. B. E. Douglas, *Inorg. Nucl. Chem. Lett.* 1973, **9**, 1251.
18. A. J. McCaffery and S. F. Mason, *Proc. Chem. Soc.* 1962, 388.
19. R. D. Gillard, S. H. Laurie and P. R. Mitchell, *J. Chem. Soc. A* 1969, 3006.
20. R. D. Gillard, in *Advanced Physical Inorganic Chemistry* (Edited by H. A. O. Hill and P. Day). Wiley, New York (1967)
21. R. D. Gillard, D. J. Shepherd and D. A. Tarr, *J. Chem. Soc., Dalton Trans.* 1976, 594 (Part xxxviii of this series).
22. J-P. Mathieu, *Volume Commem. Victor Henri*, p. 111. Desoer, Liege (1946), cf. R. D. Gillard, *J. Inorg. Nucl. Chem.* 1964, **26**, 657.
23. F. Galsbol, *Inorg. Synth.* 1970, **12**, 269.
24. Z. Marczenko, *Spectrophotometric Determination of Elements*, p. 231. Wiley, New York (1976).

Polyhedron Vol. 7, No. 24, pp. 2743–2752, 1988
Printed in Great Britain

0277–5387/88 $3.00+.00
©1988 Pergamon Press plc

AN IMPROVED SYNTHETIC METHOD AND VIBRATIONAL STUDY OF (PENTAMETHYLCYCLOPENTADIENYL) DICARBONYLRHENIUM DIHALIDES (η^5-C_5Me_5)$Re(CO)_2X_2$ (X = Cl, Br AND I)

GUILLERMO DÍAZ†

Facultad de Ciencias Naturales, Universidad de Playa Ancha, Casillar 34-V, Valparaíso, Chile

and

A. HUGO KLAHN† and CAROLINA MANZUR

Instituto de Química, Universidad Católica de Valparaíso, Casilla 4059, Valparaíso, Chile

(*Received* 1 *February* 1988; *accepted after revision* 8 *June* 1988)

Abstract—An improved synthetic method has been found for the preparation of the pentamethylcyclopentadienyl rhenium dicarbonyldihalide complexes. From the reaction of (η^5-C_5Me_5)$Re(CO)_3$ with Br_2 or I_2 in THF–H_2O a mixture of *cis* and *trans* isomers of (η^5-C_5Me_5)$Re(CO)_2X_2$ X = Br and I is formed. On the other hand, the reaction of [(η^5-C_5Me_5)$Re(CO)_3Cl$][$SbCl_6$] in water gives the *cis*-(η^5-C_5Me_5)$Re(CO)_2Cl_2$ complex. The solid IR spectra of the dicarbonyldihalide complexes are recorded and an assignment of the normal modes in terms of local symmetry is suggested by comparison with those observed in analogous molecules. A normal coordinate analysis performed using a modified general valence force field and considering simplified models, confirms most of the experimental assignments. The set of valence force constants reflects the structure of the isomers under study.

(Pentamethylcyclopentadienyl) dicarbonylrhenium dihalide complexes Cp*$Re(CO)_2X_2$ (Cp* = η^5-C_5Me_5; X = Cl, Br, I) have been known only in recent years.[1] Until now, oxidative addition of halogens (X_2) or hydrogen halides (HX) to the rhenium dinitrogen complex Cp*$Re(CO)_2(N_2)$ has been the more general and convenient method for the preparation of the *cis*-Cp*$Re(CO)_2X_2$ complexes (**I**).[2,3] Further UV-irradiation of the *cis*-isomers, in hexane, transform them into the corresponding *trans*-Cp*$Re(CO)_2X_2$ complexes (**II**).[2,3]

The *trans*-Cp*$Re(CO)_2Cl_2$ complex has also been prepared by reductive carbonylation of the pentamethylcyclopentadienyloxorhenium dichloride Cp*$ReO(Cl_2)$.[4] None of the above methods, however use the commercially available tricarbonyl complex Cp*$Re(CO)_3$, as starting material. Instead, the preparation of the precursors of the dicarbonyldihalide complexes require a multi-step synthesis which necessarily involves a low yield of the products based on the tricarbonyl complex.

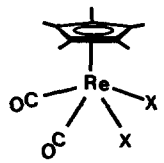

(I)

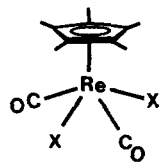

(II)

This prompted us to design a new and more simple route for the synthesis of these complexes directly from the tricarbonyl complex. We hope, that the one-step synthesis of the dicarbonyldihalide complexes will help to develop new synthetic strategies using these potentially important pre-

† Authors to whom correspondence should be addressed.

cursors in organometallic synthesis. In addition, this paper also deals with the IR study of these complexes, from which we expect to characterize the various bands, on the basis of their structural differences. Furthermore, we have carried out a normal coordinate treatment based on a modified general valence force field and taking into account simplified models for these molecules.

The force constant calculation was not carried out with the intention of determining a reliable force field. However, it allows us to make an approximation to the extent of coupling between vibrations. It is also useful in finding out the relative ordering of the vibrational modes.

EXPERIMENTAL

All of the reactions were conducted under nitrogen in Schlenk apparatus connected to a double manifold containing a low vacuum or nitrogen. However, the rhenium dicarbonyldihalide complexes were sufficiently air stable that they could be handled in air without decomposition. IR spectra were measured using Perkin–Elmer model 599 and 621 instruments, in solid state (KBr and polyethylene disc) and in solution (KBr cells). The instruments were calibrated against polystyrene. Commercial $Cp^*Re(CO)_3$ (Strem Chemicals) was used as received. Proton NMR spectra were recorded at 60 MHz on a Varian EM 360. Decomposition points were taken in capillaries and are uncorrected.

Preparation of cis-$Cp^*Re(CO)_2Cl_2$

$Cp^*Re(CO)_3$ (200 mg) was dissolved in 15 cm^3 of $CHCl_3$ at room temperature, and an excess (*ca* 0.3 cm^3) of pure $SbCl_5$ was added by syringe. Immediately, a yellow precipitate of $[Cp^*Re(CO)_3Cl][SbCl_6]$ was formed. The solution was cooled to 0°C and stirred for 1 h. The supernatant slightly yellow solution was pipetted out and discarded. The yellow solid was washed with cold $CHCl_3$ (3×10 cm^3) and then suspended in 20 cm^3 of water and stirred for 3 h. The colour of the solid change from yellow to orange–yellow.

Extraction with CH_2Cl_2, and vacuum evaporation of the solvent yielded a dark red oily solid which was a mixture of $Cp^*Re(CO)_3$ and *cis*-$Cp^*Re(CO)_2Cl_2$ (by IR). The mixture was redissolved in CH_2Cl_2 and dried with Na_2SO_4. The residue, after separation was chromatographed on a silica gel column prepared in petroleum ether (40–60°C). $Cp^*Re(CO)_3$ (30 mg) was washed with petroleum ether and then orange *cis*-$Cp^*Re(CO)_2Cl_2$ (70 mg, 37% yield) was recovered from an orange band which was eluted using $CHCl_3$. Recrystallization from CH_2Cl_2–petroleum ether gave orange microcrystals which decomposed above 180°C without melting. The yellow precipitate of $[Cp^*Re(CO)_3Cl][SbCl_6]$ was identified as follows: IR (CH_2Cl_2), 2130 s and 2075 vs, cm^{-1}. ^1H NMR (acetone-d_6) δ 2.48 s (C_5Me_5).

As a solid and in solution it is air-sensitive. It is insoluble in non-polar organic solvents and slightly soluble in CH_2Cl_2 and chloroform. It dissolves in acetone in which it slowly decomposes giving a blue–green solution from which $Cp^*Re(CO)_3$ and $Cp^*Re(CO)_2Cl_2$ (approximately 4 : 1) were identified by IR as the only carbonyl containing compounds. As a solid it decomposes above 100°C without melting.

Preparation of $Cp^*Re(CO)_2Br_2$ *and separation of its isomers*

The complex $Cp^*Re(CO)_3$ (200 mg) was dissolved in 15 cm^3 of THF, and an excess of Br_2 dissolved in THF was added under stirring to immediately give a dark red solution. To this mixture, 3 cm^3 of water were added and stirred at room temperature for 2 h. THF was pumped off and the residual water pipetted out. The red solid thus formed was dissolved in CH_2Cl_2 and dried with Na_2SO_4. Separation and evaporation of CH_2Cl_2 under vacuum gave a $\sim$ 1 : 1 mixture of *cis*- and *trans*-$Cp^*Re(CO)_2Br_2$ (by IR). The isomeric mixture was chromatographed on a silica gel column prepared in petroleum ether. Elution with CH_2Cl_2–petroleum ether (1 : 1) moved an orange band which yielded the *trans* isomer as an orange solid (66 mg, 25%) which decomposed above 110°C without melting. A red band was next eluted using CH_2Cl_2 which yielded *cis*-$Cp^*Re(CO)_2Br_2$ (78 mg, 29%) as a red solid which decomposed above 180°C without melting.

Preparation of $Cp^*Re(CO)_2I_2$ *and separation of its isomers*

The complex $Cp^*Re(CO)_3$ (200 mg) was dissolved in 15 cm^3 of THF and an excess of I_2 in THF was added under stirring at room temperature. To the resulting dark red solution, 3 cm^3 of 0.1 N aqueous KOH were added and stirred for 3 h at 40°C. THF was pumped off and the aqueous solution pipetted out. The residual wet red solid was washed with 5 cm^3 of water and then dissolved in 20 cm^3 of CH_2Cl_2 and dried with Na_2SO_4. The solution was separated by filtration, the CH_2Cl_2 evaporated until about 2 cm^3 remained and chromatographed on a silica gel column (prepared in

petroleum ether). A CH_2Cl_2–petroleum ether mixture (1 : 1) moved an orange–red band of *trans*-$Cp^*Re(CO)_2I_2$ (25 mg, 8%) which decomposed above 170°C. The *cis* isomer was eluted as a red band using CH_2Cl_2 and recrystallized from CH_2Cl_2–hexane (3 : 1) as red microcrystals which decomposed above 200°C (81 mg, 26%).

Preparation of $[Cp^*Re(CO)_3Br]Br$

The tricarbonyl complex, $Cp^*Re(CO)_3$ (150 mg) was dissolved in 15 cm^3 of chloroform at room temperature. An excess of Br_2 dissolved in $CHCl_3$ was then added. From the resulting orange–red solution a yellow precipitate was slowly formed. By adding petroleum ether the precipitation was near quantitative. The supernatant solution was pipetted out and the solid washed twice with 5 cm^3 of petroleum ether (yield: 190 mg, 90%).

Alternatively, trifluoracetic acid was used as a solvent; however, a poor yield was obtained (*ca* 60%). The compound is air- and temperature-sensitive as a solid and in solution. It is moderately soluble in CH_2Cl_2 and $CHCl_3$ and insoluble in non-polar organic solvents. It dissolves in acetone giving a dark green solution after about 15 min. The IR spectrum indicated the presence of $Cp^*Re(CO)_3$ and $Cp^*Re(CO)_2Br_2$ in solution. As a solid it decomposed above 70°C without melting. IR (CH_2Cl_2) 2130 s and 2070 vs, cm^{-1}. ^1H NMR ($CDCl_3$) δ 2.72 s (C_5Me_5).

RESULTS

(a) *Syntheses*

The reaction between bromine and iodine, and $Cp^*Re(CO)_3$ in THF–H_2O to give the corresponding isomeric mixture of $Cp^*Re(CO)_2X_2$ follows the same pattern as the reaction of $CpRe(CO)_3$ ($Cp = \eta^5$-C_5H_5) and Br_2 trifluoroacetic acid–H_2O which gave the *cis*- and *trans*-$CpRe(CO)_2Br_2$.[5] The two isomers of $Cp^*Re(CO)_2X_2$ could be readily separated by column chromatography and their physical and spectroscopical properties are identical to those reported by Einstein *et al.*[3] We found the THF–H_2O mixture to be the more effective solvent for the preparation of these compounds since in trifluoroacetic acid the reaction of $Cp^*Re(CO)_3$ and Br_2 or I_2 stopped when the cationic complex $[Cp^*Re(CO)_3X]^+$ was formed. Further reaction of the cationic complexes in water also leads to the formation of the dicarbonyldihalide compounds but in low yield (*ca* 10%), with the $Cp^*Re(CO)_3$ being formed among other unidentified products. Despite the low yield observed in the above reactions using the isolated cationic complex $[Cp^*Re(CO)_3X]^+$ (X = Br, I), this route allowed the preparation of the dichloro complex *cis*-$Cp^*Re(CO)_2Cl_2$. The $[Cp^*Re(CO)_3Cl][SbCl_6]$ salt was easily prepared in quantitative yield, from $Cp^*Re(CO)_3$ and $SbCl_5$ in $CHCl_3$. Similarly, the unreported cationic bromo complex $[Cp^*Re(CO)_3Br]^+$ was prepared from the tricarbonyl complex and Br_2 in chloroform or trifluoroacetic acid. The cationic nature of these rhenium compounds was suggested by their IR spectra in solution. The ν(CO) absorptions appear above 2000 cm^{-1} and their intensities and positions are in good agreement with those observed in the cationic complexes $[Cp^*Re(CO)_3I]^+$ [3] and $[CpRe(CO)_3Cl]^+$.[6] The chloro and bromo cationic complexes are yellow, air-sensitive and moderately soluble in polar organic solvents such as $CHCl_3$, CH_2Cl_2 and THF in which they do not survive after 2 h. They react when dissolved in alcohols to produce the alcoxycarbonyl complex, *trans*-$Cp^*Re(CO)_2(COOR)(X)$.[7] The cationic chloro complex was somewhat unstable in acetone solution as demonstrated by the observation of a resonance assigned to $Cp^*Re(CO)_3$, as well as one assigned to $[Cp^*Re(CO)_3Cl]^+$ in the proton NMR spectrum.

(b) *Band assignments*

The observed frequencies and the assignments are listed in Tables 1 and 2. The X-ray data[3] reveals that the overall symmetry of the complexes under study is C_s. However, it is assumed that the vibrational modes for the fragments are almost independent of the rest of the molecule. The concept of "local symmetry"[8–10] has been used in the assignment and interpretation of the spectra. The selection rules are taken to be those for the point group of the fragment. In this sense, the methyl groups were considered as point mass, the Cp* ring was assumed to have D_{5h} symmetry, and the *cis*-$Re(CO)_2X_2$ and *trans*-$Re(CO)_2X_2$ moieties C_s and C_{2v}, respectively. On the other hand, the internal vibrations of the methyl groups can be arranged into the species of the C_{2v} point group. Such an assumption implies that very few combination bands ought to result. In fact, it was not necessary to explain any combination band in this way.

The assignment will be considered, under three headings:

(i) The methyl groups.
(ii) Cp* ring, with methyl groups as point mass.
(iii) The $Re(CO)_2X_2$ groups and the modes involving a movement of the ring against the $Re(CO)_2X_2$ fragments.

Table 1. Observed frequencies in cm^{-1} and assignments for *cis*-Cp*Re(CO)$_2$X$_2$

X = Cl	Br	I	Assignment
2995w, 2970w	2990w, 2970w	2990w, 2965w	$\nu(CH_3)(E)$
2920m	2922m	2920m	$\nu(CH_3)(A_1)$
2010vs	2008ws	2005vs	$\nu(CO)(A'_1)$
1925vs	1932vs	1930vs	$\nu(CO)(A'')$
1500m, 1450	1490m, 1460m	1485, 1463m	$\delta(CH_3)$
1385sh, 1380ms	1385sh, 1380ms	1385sh, 1378ms	$\nu(CC)(E'_1)$
1085w	1080w	1075w	Ring breathing (A'_1)
1030m, 1010m	1030m, 1010m	1030m, 1010m	$\rho(CH_3)$
800w	800w	800w	ν(Ring-Me)
600m	595m	590m, 570vm	δ(ReCO)(A')
540s, 530sh	538s, 530sh	540s, 530sh	δ(ReCO)(A' or A'')
515sh, 500m	510sh, 490m	515sh, 500m, 480	δ(ReCO)(A' or A'')
450w, 420mw	440w, 425mw	450w, 430w	ν(ReC)(A', A'')
370w, 365w	370w, 365w	370w, 365w	Ring-tilt (E_1)
340w	340w	340w	ν(CMe)
315wm			ν(ReCl)
285w	290w	290vw	ν(Cp*Re)
270w, 265vw	270vw, 250vw	270vw, 250vw	γ(CMe)

(i) *Methyl group vibrations.* For all the molecules, bands of medium intensity are observed in the 3000–2000, 1500–1450 and 1050–1000 cm^{-1} regions, which can be ascribed readily to (A_1 and E species) $\nu(CH_3)$, $\delta(CH_3)$, and $\rho(CH_3)$ modes, respectively, by comparison with the established assignments for hexamethylbenzene[11] (methylcyclopentadienyl)manganese tricarbonyl,[12,13] dimethylferrocene[14] and toluene.[15]

(ii) *Ring vibrations.* The expected normal modes for the C_5Me_5 ring with D_{5h} local symmetry are the following: three stretching C—Me vibrations, $\nu CMe(A'_1+E'_1+E'_2)$; three ring vibrations, $\nu CC(A'_1+E'_1+E'_2)$; three out-of-plane CMe bending vibrations, $\delta CMe(A''_1+E'_1+E'_2)$; in-plane ring deformation, $\delta CC(E'_2)$ and out-of-plane ring deformations, $\gamma CC(E'_2)$. However, since the only active species in the IR are the E'_1, the spectra show few bands attributable to ring vibrations. This fact is also observed in the IR spectrum of hexamethylbenzene.[14] Thus, a medium strong band at 1390 cm^{-1} which exhibits a shoulder in the solid state that may be produced by crystal splitting of the degeneracy, is assigned to the CC stretching vibration of the E'_1 species, this normal mode is frequently observed for Cp-derivatives in the 1400–1500 cm^{-1} region.[16,17] Furthermore, a similar assignment is proposed by Parker *et al.*,[13] while Lokshin *et al.*[18] in a vibrational study of Cp*Re(CO)$_3$, have ascribed to this vibration a band at 1420 cm^{-1}. A weak band near 1080 cm^{-1} can be assigned to the A'_1, ring breathing vibration. In this respect, a strong polarized Raman band at 1103 cm^{-1} has been assigned by Lokshin *et al.*[18] to this normal mode, taking into account that similar assignments have been considered for other Cp-derivatives and by comparison with benzene and substituted benzenes. The C—Me stretching (E_1) is placed at 1230 cm^{-1} for Cp—Me by Parker *et al.*[13]

Table 2. Observed frequencies in cm^{-1} and assignments for *trans*-Cp*Re(CO)$_2$X$_2$

X = Br	I	Assignment
2990w, 2980w	3000, 2995w	$\nu(CH_3)(E)$
2925mw	2980mw	$\nu(CH_3)(A_1)$
2020vs	2020vs	$\nu(CO)(A_1)$
1970vs	1970vs	$\nu(CO)(B_2)$
1490m, 1460m	1490m,br, 1440m	$\delta(CH_3)$
1385sh, 1380ms	1390m	$\nu(CC)(E'_1)$
1070w	1080w	Ring breathing (A'_1)
1030m, 1010mw	1030m	$\rho(CH_3)$
800	750m,br	ν(Ring-Me)
620vw	600vw	δ(ReCO)(A_2)
550sh, 535ms	540ms	δ(ReCO)(A_1, B_2, B_1)
490m	500m	δ(ReCO)(A_1, B_2 or B_1)
450w, 400m	460w, 420m	ν(ReC)(A_1 or B_2)
370vw, 360vw	360vw	Ring-tilt (E_1)
340vw	330vw	δ(CMe)
290w	285wv	ν(Cp*Re)
270w, 265w	275vw	γ(CMe)
230w	235vw	δ(CReC)

However, no band is observed by us in that region. A weak band at 800 cm^{-1}, which is also observed in hexamethylbenzene can be tentatively ascribed to that normal mode.

Those vibrations attributed to in-plane δ(CMe) and out-of-plane γ(CMe) bendings are expected in the region below 400 cm^{-1}. In this respect, a weak band at *ca* 350 cm^{-1} can be assigned to δ(CMe) by comparison with the spectrum of $(MeC_5H_4)Mn(CO)_3$[13] and assignments made for toluene[15,19] and dimethylferrocene.[14] The γ(CMe) bending should appear at lower energy, where we have observed weak bands at *ca* 290, 270, 250 and 230 cm^{-1}. However, in this region we also found skeletal modes, so this assignment requires further analysis.

(iii) *Skeletal modes.* Metal–ring vibrations can be ascribed on the basis of C_{5v} symmetry. Three bands (A_1, E_1 and E_2) are expected, but only the A_1Cp*—Re stretch and E_1 ring tilt mode are IR actives.

The A_1 band is reported to be weak and the E_1 band, as a rule, is found at higher frequency than the A_1 bands. Otherwise, it has been noted that the ring-tilt is shifted to higher energy when methyl groups are substituted on the ring. This trend is observed in $MeC_5H_4Mn(CO)_3$[13] and dimethylferrocene.[20] Characteristic absorptions assigned to these normal modes have been observed at 349 and 327 cm^{-1} for $CpRe(CO)_3$,[18] at 372 and 354 cm^{-1} for $CpMn(CO)_3$[21] and at 388 and 354 cm^{-1} for $MeC_5H_4Mn(CO)_3$.[13] On the other hand, these vibrations have been placed at 380 and 360 cm^{-1} for $CpMo(CO)_3I$ and at 370 and 348 cm^{-1} for $CpFe(CO)_2Cl$.[22]

On the basis of the above data and the outlined trends, a weak doublet was assigned to the ring-tilt mode, at *ca* 370 cm^{-1}, whereas the very weak band at *ca* 290 cm^{-1} was tentatively ascribed to the Cp*—Re stretching. The low value of this frequency can be justified by the increased mass of the Cp* ring.

After considering the Cp* ring as a point mass the remaining skeletal vibrations can be classified on the basis of C_s and C_{2v} symmetry for the *cis*-$Re(CO)_2X_2$ and *trans*-$Re(CO)_2X_2$ moieties, respectively. The former group generates 13 vibrational modes ($8A'+5A''$), all allowed in both IR and Raman, including the following normal modes: $\nu CO(A'+A'')$, $\nu ReC(A'+A'')$, $\nu ReX(A'+A'')$, $\delta CReC(A')$, $\delta XReX(A')$, $\delta XReC(A')$ and $\delta ReCO(2A'+2A'')$. When the ring is taken into account four additional modes can be expected, $\delta Cp^*Re(CO)(A'+A'')$ and $\delta Cp^*ReX(A'+A'')$. On the other hand, the *trans*-$Re(CO)_2X_2$ fragment will have 13 vibrational modes ($6A_1+A_2+B_1+5B_2$), only one of them (A_2) is not IR active. The corresponding normal modes are the following: $\nu CO(A_1+B_2)$, $\nu ReC(A_1+B_2)$, $\nu ReX(A_1+B_2)$, $\delta XReX(B_2)$, $\delta CReC(A_1)$, $\delta XReX(A_1)$, $\delta ReCO(A_1+B_2)$, $\delta ReCO(A_2)$ and $\delta ReCO(B_1)$.

The inclusion of the ring in the *trans* moiety will give rise to four additional modes: $\delta Cp^*ReCO(A_1+B_2)$ and $\delta Cp^*ReX(A_1+B_2)$.

CO *stretching modes.* The bands corresponding to these vibrations are the strongest in the spectra of the compounds under investigation. It is recognized that the presence of weaker π-acids, such as halides, should result in an increase in π-bonding to the CO group. This should in turn, lead to larger values for the CO intensities.[23]

The two CO stretching vibrations are found at *ca* 2040 and 1965 cm^{-1} and at 2005 and 1930 cm^{-1} for the *trans*- and *cis*-isomers, respectively. The band observed at higher frequency is assigned to the symmetric species. This will always be the case as it becomes more difficult to stretch one CO bond when the other is also being stretched.

The higher wavenumber of the *trans*-isomer in comparison to the *cis*-isomer can be understood in terms of the increased competition for rhenium *d* electrons between the carbonyl groups when they are mutually *trans*. On the contrary, we would expect a larger increase in the occupancy of the two π-orbitals (antibonding in nature)[24,25] which can receive electron density directly from the halogen, as in the case of the *cis*-complexes. Such an effect results in a weaker CO bond.

The more intense of the two absorptions has the higher frequency for the *cis*-compounds, while the inverse is observed for the *trans*, the relative intensities of the two IR absorptions are dependent upon the angle 2θ between the two CO bonds.[23,26] The angle values thus obtained enable the *cis*- and *trans*-isomers of $Cp^*M(CO)_2X_2$ derivatives to be distinguished.[3] On the other hand, the absorptions reported here are lower than those observed in $CpRe(CO)_2X_2$ by King,[6] in agreement with the fact that these normal modes are influenced by the number of methyl substituents on the aromatic ring. This is because such electron releasing groups increase the degree of $d\pi$–$p\pi$-bonding from the metal to the CO ligands.[13,27]

Re—C *stretching modes.* The stretching M—C modes are usually observed in π-cyclopentadienyl carbonyls[18,22] in the range 450–500 cm^{-1} and are shifted to lower energy in halide derivatives.[22] These bands normally present medium–weak intensities. We have assigned to these normal modes absorptions at *ca* 445 and 423 cm^{-1} and at *ca* 450 and 400 cm^{-1} for the *cis*- and *trans*-complexes,

respectively. In all the cases the band at lower wavenumber is stronger than the one at the higher frequency. This fact is more noticeable in the *trans*-isomers.

The shift of the weaker band in the *cis*-complexes to higher wavenumber can be justified on the basis of π-bonding arguments. Indeed, a CO bonded *trans* to a poorly π-bonding ligand, such as a halide, would be in a more favourable position for participating in strong M—C π-bonding than if it was *trans* to another strongly π-bonding CO. This shift provides for another distinction between the isomers and agrees with the stability of the *cis*-isomers. The distinction between the symmetric and asymmetric species of these normal modes requires either more experimental evidence or theoretical considerations.

ReCO *bending modes*. MCO angle deformations are normally found in the 500–700 cm^{-1} region for compounds of the type $CpM(CO)_3$[13,22] and in other carbonyl complexes.[16,28–30] As with bands corresponding to CO stretching, they shift to lower wavenumbers in halide derivatives.[13,22,31] Moreover, it has been recognized that these bands are stronger and more sensitive to the environment than the ν(CO).[16]

The characteristic absorptions observed in the 500–600 cm^{-1} range reflect the different structures of the *cis*- and *trans*-isomers under study. Thus a medium–strong band found at 590 cm^{-1} for *cis*-$Cp^*Re(CO)_2X_2$ is very weak in the *trans*-isomers. From the selection rules and taking into account the correlation between the species of the distinct local symmetries, this vibration is considered to belong to the A_2 (IR inactive) and A' irreducible representations of the C_{2v} and C_s point groups, respectively. At *ca* 540 cm^{-1} we observed a strong doublet for the *cis*-isomers, which appears as two overlapping bands in the *trans*-complexes. Finally, at *ca* 490 cm^{-1} we find a medium band, which shows different features for the two isomers. In *cis*-$Cp^*Re(CO)_2X_2$ this band is either broad (X = Cl) or it has a shoulder (X = Br, I) while in the *trans*-isomers this vibration is observed as a unique sharp band. The different shape observed for this absorption can be a consequence of crystal effects. The classification of these normal modes into the distinct species of the point groups, can not be done by only IR arguments. Below 320 cm^{-1} the skeletal vibrations occur: ν(ReC), δ(CReC), δ(Cp*ReC), δ(Cp*ReX) and δ(XReX), as well as γ(CMe) and ν(ring-Me), the latter being tentatively placed at 290 cm^{-1}.

The Re—X stretching frequencies should be the strongest of the remaining absorptions. For halopentacarbonyl, Clark and Crosse[32] have assigned to the Re—Cl, Re—Br and Re—I stretching modes, bands observed at 294, 203 and 163 cm^{-1}, respectively. In our study, the only medium band recorded in the low energy region was found at 310 cm^{-1} in the spectra of *cis*-$Cp^*Re(CO)_2Cl_2$.

This rather broad band would contain both the symmetric and asymmetric Re—Cl stretching. Since no band of similar intensity was found for the rest of the molecules, it is expected that the Re—Br and Re—I stretching modes lie outside the limit of the Perkin–Elmer instruments used in this work. A weak doublet near 270 cm^{-1} and a band, also weak, observed at 230 cm^{-1}, cannot be assigned without further theoretical analysis.

(c) *Normal coordinate analysis*

Simplified molecular models. Regarding the complexity of the systems studied, it is desirable to choose simplified models in order to account for most of the doubtful experimental assignments, which are mainly located in the low energy region. Under this premise, these simple models have been taken from the *cis*-$Re(CO)_2X_2$ and *trans*-$Re(CO)_2X_2$ moieties, including the Cp* ring as a point mass.

Structural data and symmetry considerations. The numerical calculation using the GF matrix method,[33] was carried out for the distinct species of the C_s and C_{2v} point groups. The molecular parameters used in the calculation for *cis*-$Cp^*Re(CO)_2I_2$ and *trans*-$Cp^*Re(CO)_2Br_2$ were those found in the X-ray work of Einstein *et al.*[3] These parameters were transferred to *cis*-$Cp^*Re(CO)_2Br_2$ and *trans*-$Cp^*Re(CO)_2I_2$. For *cis*-$Cp^*Re(CO)_2Cl_2$ we used most of the structural data given in ref. 3, with the exception of the Re—Cl bond which was assumed to be equal to the sum of the covalent radii.

Force constants and calculated frequencies. In spite of the simple models considered here, the number of independent force constants to be determined is exceedingly high. For this reason we have performed the calculation using a modified general valence force field approximation (MGVFF), which emphasizes the diagonal elements of the symmetrized F matrix.

The initial values of the valence force constants were chosen considering the trends and extreme values reported in the literature for related molecules.[18,31,32,34–37] Some of these values have been slightly modified to account for the most confident experimental assignments. The final force constants are shown in Table 3. The frequencies calculated from these sets are collected in Tables 4 and 5, where the theoretical assignments of the

Table 3. Internal force constants (mdyn Å^{-1})

trans-Cp*Re(CO)$_2$X$_2$		*cis*-Cp*Re(CO)$_2$X$_2$	
f_{Cp^*Re}	3.300	f_{Cp^*Re}	3.300
f_{ReC}	3.050	f_{ReC}	3.150
$f_{ReC,ReC}$	250	$f_{ReC,ReC}$	−0.050
f_{ReBr}	1.450	f_{ReCl}	1.650
f_{ReBr}	1.350	f_{ReBr}	1.550
$f_{ReX,ReX}$	0.150	f_{ReI}	1.350
f_{CO}	15.650	$f_{ReX,ReX}$	−0.050
$f_{CO,CO}$	0.300	f_{CO}	15.350
$f_{CO,ReCO}$	0.250	$f_{CO,CO}$	0.325
f_{Cp^*ReC}	0.180	$f_{CO,ReCO}$	0.250
f_{Cp^*ReC,Cp^*ReC}	0.25	f_{Cp^*ReC}	0.180
f_{Cp^*ReX}	0.280	f_{Cp^*ReC,Cp^*ReC}	0.025
f_{Cp^*ReX,Cp^*ReX}	0.025	f_{Cp^*ReX}	0.280
f_{CReC}	0.100	f_{Cp^*ReX,Cp^*ReX}	0.025
f_{XReX}	0.300	f_{CReC}	0.100
f_{ReCO}	0.380	f_{XReC}	0.200
$f_{ReCO,ReCO}$	0.025	f_{ReCO}	0.38
$f_{ReCO,ReCO_\perp}$	0.080	$f_{ReCO,ReCO}$	0.025
		$f_{ReCO,ReCO_\perp}$	0.025

Table 4. Calculated vibrational frequencies (cm^{-1}) and PED for the *cis*-Cp*Re(CO)$_2$X$_2$ complexes

A' symmetry	X = Cl	X = Br	X = I	PED[a]
	2011	2008	2010	91% CO+7% ReC
	587	585	583	99% $ReCO_\perp$
	546	543	545	72% ReCO+12% XReC+9% Cp*ReC
	445	446	445	87% ReC+6% CO
	280	283	281	68% Cp*Re+10% ReX+9% XReC
	201	107	200	44% CReC+34% XReC+17% Cp*Re
	210	180	160	70% ReX+8% Cp*Re
	165	150	146	42% Cp*ReX+30% CReC+12% XReC
	139	130	125	45% Cp*ReC+26% Cp*ReX+10% ReX
	115	105	98	87% XReX+8% ReX
	57	53	50	27% Cp*ReC+24% Cp*ReX+28% XReC
A'' symmetry	X = Cl	X = Br	X = I	PED[a]
	1944	1942	1943	90% CO+8% ReC
	540	537	535	99% $ReCO_\perp$
	487	490	485	78% ReCO
	428	430	429	82% ReC+12% ReCO
	301	200	176	81% ReX+12% CpReX
	125	120	110	51% Cp*ReX+28% Cp*ReC+18% ReX
	75	70	65	59% Cp*ReC+36% Cp*ReX

[a] PED Values are very similar for the different *cis*-complexes. We show just those calculated for *cis*-Cp*Re(CO)$_2$I$_2$.

Table 5. Calculated vibrational frequencies (cm^{-1}) and PED for the *trans*-$Cp^*Re(CO)_2X_2$ complexes

A_1 symmetry	X = Br	X = I	PED[a]
	2028	2025	92% CO+7% ReC
	542	550	91% ReCO+8% Cp*ReC
	451	453	85% ReC+6% CO
	285	280	79% Cp*Re+6% ReC+7% XReX
	186	160	83% ReX+7% Cp*Re
	170	167	89% CReC+9% ReX
	126	120	89% XReX+6% Cp*Re
	95	90	50% Cp*ReC+43% Cp*ReX
	71	60	40% Cp*ReC+53% Cp*ReX
A_2 symmetry	598		100% ReCO
B_2 symmetry	1966	1965	92% CO
	530	531	86% ReCO+7% Cp*ReC
	414	412	90% ReC+5% CO
	220	180	82% ReX+13% Cp*ReX
	151	143	52% Cp*ReX+31% CReX+10% Cp*ReC
	96	91	75% Cp*ReC+10% CReX+6% ReX
	60	50	55% CReX+34% Cp*ReX+5% ReX
B_1 symmetry	489		100% ReCO

[a]PED values are very similar for the different *trans*-complexes. We show just those calculated for *trans*-$Cp^*Re^*(CO)_2Br_2$.

vibrations from the Potential Energy Distribution (PED) are also given.

DISCUSSION

The new straightforward method for the preparation of (pentamethylcyclopentadienyl) dicarbonylrhenium dihalide complexes, $Cp^*Re(CO)_2X_2$, directly from the commercially available $Cp^*Re(CO)_3$ shows several advantages compared to other methods described in the literature.[3,4] For instance, this new method involves only one step, higher yields and the formation of the two isomers is obtained simultaneously for X = Br and I. As expected, the decomposition temperatures, the IR, ^1H NMR and mass spectra of these complexes are identical to those reported by Einstein *et al.*[3]

The reaction of $Cp^*Re(CO)_3$ with $SbCl_5$ to give the yellow salt $[Cp^*Re(CO)_3Cl][SbCl_6]$ occurs analogously to the reaction between $CpRe(CO)_3$ and antimony pentachloride described by King.[6] Likewise, the synthesis of the bromo cationic compound $[Cp^*Re(CO)_3Br]^+$ was carried out under similar conditions used for the preparation of the iodo analogue.[2,3]

The formation of the dicarbonyldihalide complexes seems to occur through the cationic complex $[Cp^*Re(CO)_3X]^+$ which in the presence of water (or OH^-) undergoes a nucleophilic attack on one of the coordinated CO groups, as shown in Scheme 1.

A similar nucleophilic attack has been observed in the reaction of these cationic complexes in alcohols where the alcoxycarbonyl complexes were obtained.[7] The decarboxylation of the hydroxycarbonyl complex $Cp^*Re(CO)_2(X)(COOH)$ may form the hydridohalide complex $Cp^*Re(CO)_2(H)(X)$ which can react with the excess of X_2 (or X^-) to give the observed products. Major efforts are actually in progress to establish the mechanism of these reactions.

Within the framework of the simplified models, the MGVFF satisfactorily reproduces the observed frequencies with reasonable force constants, which

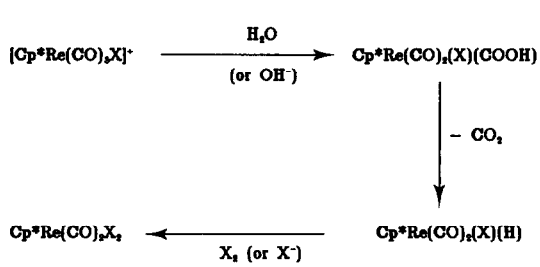

Scheme 1.

reflects the different structures of the molecules. Thus, the decreases of the ReC force constant observed in *trans*-Cp*Re(CO)$_2$X$_2$ in comparison with *cis*-Cp*Re(CO)$_2$X$_2$ is consistent with the lower stability of the former complex.[3] These values are intermediate to those calculated for CpRe(CO)$_3$[18] and W(CO)$_6$[36] complexes. The different values of the f_{CO} obtained for the *cis*- and *trans*-complexes can be attributed to the difference in total 2π CO occupation,[24,25] which indicates that the *trans*-carbonyl ligands have a weaker covalent bond than the *cis*-ligand. Approximate force constants calculated by the classic method of Cotton and Kraihanzel[38] also account for this difference. The larger values of f_{ReC} along with somewhat smaller values of f_{CO} suggest a greater metal–ligand π-bonding for the complexes studied here, when compared with other carbonyl and halocarbonyl metal compounds.

Regarding the Re—X force constants, our values are very similar to those calculated by Clark and Crosse[32] for the series Re(CO)$_5$X, on the basis of a simple model. On the other hand, the Cp*Re force constant used in the present work is the same as that calculated in ref. 18. This value appears to be the only one reported in the literature.

With regard to the bending constants, the most important from a structural point of view, is f_{ReCO}. The one presented here is in good agreement with those reported for the metal–hexacarbonyls.[36,37] This value is also similar to that calculated for Co(CO)$_3$NO.[39]

The remaining force constants are expected to be smaller than 0.5 mdyn Å^{-1} to account for the lower related frequencies. The interaction constants are all rather small, with the exception of $f_{CO,CO}$. This fact has been previously pointed out in ref. 36.

Comparing Tables 4 and 5, and 1 and 2, we can see that the normal coordinate analysis confirms the assignments for ν(CO), δ(ReCO), ν(ReC), ν(Cp*Re) and ν(ReCl), and allows us to distinguish among the distinct symmetry species of these vibrations. Furthermore, the computation was carried out for the skeletal vibrations and the results give an indirect proof for the assignment of a ring-tilt, δ(CMe) and ν(CMe). On the other hand, the calculated frequencies for ν(ReBr) and ν(ReI) are comparable to those reported by Clark and Crosse[32] for Re(CO)$_5$X.

Finally, it is observed that PED presents strong coupling between the low frequency deformation modes, δ(Cp*ReX) and δ(Cp*ReC).

Acknowledgements—A. Hugo Klahn wishes to express his thanks to Prof. Derek Sutton of Simon Fraser University, Canada for his continuing support throughout this work. Guillermo Díaz thanks the Dirección de Investigación, Universidad de Playa Ancha, (Project CNE 11987) and FONDECYT (grant 310). A. Hugo Klahn also acknowledges Universidad Católica de Valparaíso (Project 125.709) and Programa IUPAC/UNESCO de Química en América Latina (contrato 241.759.7).

REFERENCES

1. J. K. Hoyano and W. A. E. Graham, *J. Chem. Soc., Chem. Commun.* 1982, 27.
2. A. H. Klahn, Ph.D. Dissertation, Simon Fraser University (1986).
3. F. W. B. Einstein, A. H. Klahn-Oliva, D. Sutton and K. G. Tyres, *Organometallics* 1986, **5**, 53.
4. W. A. Herman, U. Kusthardt, A. Schafer and E. Herdtweck, *Angew. Chem. Int. Ed. Engl.* 1986, **25**, 817.
5. R. B. King and R. H. Reimann, *Inorg. Chem.* 1976, **15**, 179.
6. R. B. King, *J. Inorg. Nucl. Chem.* 1967, **29**, 2119.
7. A. H. Klahn and C. Manzur, XVIII Congreso Latinoamericano de Química Santiago, Chile (1988).
8. F. A. Cotton, A. D. Liehr and G. Wilkinson, *J. Inorg. Nucl. Chem.* 1955, **1**, 175.
9. H. P. Fritz and J. Manchot, *Spectrochim. Acta* 1962, **18**, 171.
10. R. T. Bailez and E. R. Lippincott, *Spectrochim. Acta* 1958, **10**, 307.
11. N. D. Colthop, L. H. Daly and S. E. Wiberlez, *Introduction to Infrared and Raman Spectroscopy*. Academic Press, New York (1964).
12. D. M. Adams and A. Squire, *J. Organometal. Chem.* 1973, **63**, 381.
13. D. J. Parker and M. H. B. Stiddard, *J. Chem. Soc. A* 1970, 1040.
14. R. T. Bailey and E. R. Lippincott, *Spectrochim. Acta* 1965, **21**, 389.
15. J. K. Wilmshurst and H. J. Bernstein, *Can. J. Chem.* 1957, **35**, 911.
16. I. J. Hyams, R. T. Bailey and E. R. Lippincott, *Spectrochim. Acta* 1967, **23A**, 273.
17. H. P. Fritz, *Adv. Organometal. Chem.* 1964, **1**, 239.
18. B. V. Lokshin, Z. S. Kleemkova and Yu. V. Makarov, *Spectrochim. Acta* 1972, **28A**, 2206.
19. R. H. Silverstein, G. C. Bassler and T. C. Morril, *Spectrometric Identification of Organic Compounds*. John Wiley, New York (1974).
20. N. Fuson, C. Garrión-Lagrange and M. N. Josien, *Spectrochim. Acta* 1960, **16**, 106.
21. D. J. Parker, Ph.D. Thesis, University of London (1968).
22. D. J. Parker, *J. Chem. Soc. A* 1970, 1382.
23. T. L. Brown and D. J. Darensbourg, *Inorg. Chem.* 1967, **6**, 971.
24. M. B. Hall and R. F. Fenske, *Inorg. Chem.* 1972, **11**, 1619.
25. R. F. Fenske and R. L. Dekock, *Inorg. Chem.* 1970, **9**, 1053.
26. W. Beck, A. Melnikott and R. Stahl, *Chem. Ber.* 1966, **99**, 3721.

27. F. Calderazzo, *Inorg. Chem.* 1965, **4**, 223.
28. D. M. Adams, *J. Chem. Soc. A* 1964, 1771.
29. G. Davidson and D. C. Andrews, *J. Chem. Soc., Dalton Trans.* 1972, 126.
30. I. J. Hyams and E. R. Lippincott, *Spectrochim. Acta* 1972, **28A**, 1741.
31. I. J. Hyams, D. Jones and E. R. Lippincott, *J. Chem. Soc. A* 1967, 1987.
32. R. J. H. Clark and B. C. Crosse, *J. Chem. Soc. A* 1969, 224.
33. E. B. Wilson Jr., J. C. Decius and P. C. Cross, *Molecular vibrations*. McGraw–Hill, New York (1955).
34. V. Devarajan and S. J. Cyvin, *Acta Chem. Scand.* 1972, **26**, 1.
35. S. J. Cyvin, J. Brunvoll and L. Schafer, *J. Chem. Phys.* 1971, **54**, 1517.
36. L. H. Jones, R. S. McDowell and M. Goldblatt, *Inorg. Chem.* 1969, **8**, 2349.
37. K. Kawai and H. Murata, *Bull. Chem. Soc. Japan* 1960, **33**, 1008.
38. F. A. Cotton and C. S. Kraihanzel, *J. Am. Chem. Soc.* 1962, **84**, 4432.
39. L. H. Jones, R. S. McDowell and B. I. Swanson, *J. Chem. Phys.* 1973, **58**, 3757.

Polyhedron Vol. 7, No. 24, pp. 2753–2759, 1988
Printed in Great Britain

0277–5387/88 $3.00+.00
© 1988 Pergamon Press plc

KINETICS AND MECHANISM OF THE REACTION BETWEEN SILVER(III) AND THIOUREA IN AQUEOUS ALKALINE MEDIA

LOUIS J. KIRSCHENBAUM* and RAMA K. PANDA†

Department of Chemistry, University of Rhode Island, Kingston, RI 02881, U.S.A.

(*Received* 25 *April* 1988; *accepted* 8 *June* 1988)

Abstract—The tetrahydroxoargentate(III) ion, $Ag(OH)_4^-$, is rapidly reduced by thiourea (tu) in accordance with the three term rate law

$$\text{rate} = \{k_1 + (k_2 + k_3[OH^-])[tu]\}[Ag^{III}]$$

where $k_1 = 1.08\ s^{-1}$, $k_2 = 1.46 \times 10^3\ M^{-1}\ s^{-1}$, and $k_3 = 2.02 \times 10^3\ M^{-2}\ s^{-1}$. The k_1 path occurs via the rate-determining aquation of $Ag(OH)_4^-$ while the other two paths involve axial attack of thiourea on silver. The higher values of k_2 and k_3 compared to the ethylenediamine reaction, which obeys the same rate law, is a reflection of the greater nucleophilicity of tu.

Following the redox reaction, solutions become brown in a reaction that obeys pseudo-first-order kinetics. Similar behaviour is observed when tu is replaced by Na_2S or thioacetamide and when Ag^I reacts with any of these sulphur containing compounds. We attribute this process to the Ag^I promoted formation of sulphide species which eventually precipitate as Ag_2S.

Silver(III) can be stabilized as the $Ag(OH)_4^-$ ion in highly alkaline media.[1] We have studied[2–7] the kinetics of a number of reactions of Ag^{III} and find that a normal pattern of redox reactivity with simple substrates involves nucleophilic attack of the reducing agent on the silver centre which may or may not result in actual replacement of a bound hydroxyl. In some cases,[2,3] we have been able to identify transient Ag^{III}–substrate complexes, and in others, the form of the rate law has led to the conclusion that redox occurs within a five-coordinate intermediate.[4–6] For the systems so far studied, we have noted a qualitative trend in the reactivity which parallels the nucleophilicity of the reducing substrate towards other square planar d^8 transition metal ions.[2]

In the case of the thiosulphate ion, which has a nucleophilic reactivity constant,[8] n_{pt}^0, of 7.34, both four- and five-coordinate intermediates participate in the redox reaction, with substitution occurring only in the hydrolysed silver(III) species.[2] For the much slower reaction of ethylenediamine, $n_{pt}^0 = 3.85$, pre-equilibrium formation of both types of intermediates was also suggested.[4]

Thiourea (tu) has a nucleophilicity towards platinum (7.17) similar to that of thiosulphate as well as the same potential donor atom, sulphur. We have studied the reaction of $Ag(OH)_4^-$ with tu with a view to making comparisons with mechanisms and relative rates. We find that silver(III) is, indeed, rapidly reduced by thiourea. During the course of this work we have observed that, in the strongly basic solution required for Ag^{III} stabilization, the metal reduction product Ag^I mediates the alkaline hydrolysis of thiourea.

EXPERIMENTAL

Solutions of $Ag(OH)_4^-$ were prepared in 1.2 M NaOH by electrolysis of a silver foil anode. The procedure was as previously described[1] except that the platinum wire cathode was replaced by a silver foil; the larger surface area of the cathode eliminates possible problems associated with localized gas evolution. Thiourea (Matheson) solutions were freshly prepared before each run in the appropriate concentration of base to prevent any slow alkaline

*Author to whom correspondence should be addressed.
† On leave from Berhampur University, Berhampur, India.

hydrolysis. $NaClO_4$ solutions for ionic strength adjustment were prepared from $HClO_4$ and low carbonate NaOH. Thioacetamide (tam) and sodium sulphide solutions were freshly prepared from reagent grade solids (Fisher). The $Na_2S \cdot 9H_2O$ was washed before use to remove surface impurities due to air oxidation.

Kinetic experiments were performed by stopped-flow spectrophotometry using an Aminco-Morrow stopped-flow assembly interfaced to a Tandy TRS-80 microcomputer through a Starbuck Data Co. A/D Converter. Disappearance of the silver(III) absorbance (peak at 267 nm) was monitored at 280 nm to minimize background interference due to the substrates. All kinetic data reported here represent the average of at least three replicate runs performed at 25 ± 0.1°C and 1.2 M ionic strength. UV–vis. spectra were recorded on a Cary Model 15 spectrophotometer. Electron paramagnetic resonance (EPR) experiments were performed on a Brucker ER 200 spectrometer after rapid freezing (in liquid N_2) of reaction mixtures.

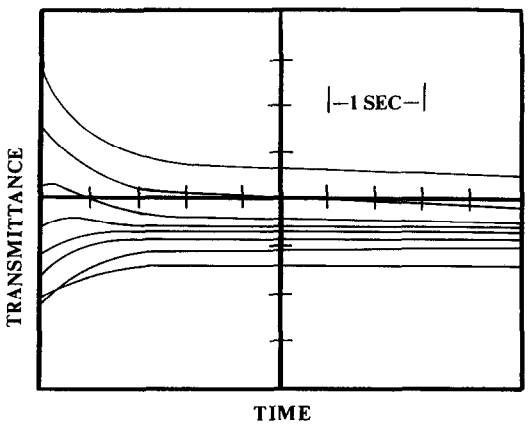

Fig. 1. Stopped-flow traces of the silver(III)–thiourea reaction at various wavelengths. $[Ag(OH)_4^-] = 1.3 \times 10^{-4}$ M, $[tu] = 5 \times 10^{-4}$ M. Monitoring at 10 nm intervals from 350 nm (top curve) to 280 nm (bottom curve after first 200 ms). Transmittance scale is arbitrary and different for each trace. Note distinct biphasic behaviour at intermediate wavelengths. Most experiments were at higher [tu] and, hence, gave greater time separation for the two reactions.

RESULTS

When basic solutions of $Ag(OH)_4^-$ and tu are mixed, the light yellow colour of silver(III) is rapidly converted to a clear brown. The spectrum of the product displays a very broad absorption in the visible which persists for about an hour when $[Ag]_{tot.} \leqslant 2 \times 10^{-4}$ M. At longer times a yellow–brown/black precipitate appears. The brown colour of the product solution is not discharged by acidification (pH ~ 0). Product solutions are EPR silent indicating that the metal is in the +1 oxidation state.

KINETICS OF SILVER(III) REDUCTION BY THIOUREA

Upon mixing in the stopped-flow apparatus, there is a rapid decrease in absorbance in the 260–300 nm region, and a slower absorbance increase at 300–400 nm. The biphasic nature of the overall reaction is demonstrated in Fig. 1. Kinetic data for the two processes were collected at 280 and 350 nm, respectively.

The kinetics of silver(III) disappearance at 280 nm were found to be pseudo-first-order over 4–5 half-lives for the range $1 \times 10^{-5} \leqslant [Ag(OH)_4^-] \leqslant 1.1 \times 10^{-4}$ M with at least a ten-fold excess of the substrate. Average values of the observed rate constant, k_{red} (generally reproducible to within 5%) are listed in Table 1 for $[tu] = 5 \times 10^{-4}$–0.01 M and $[OH^-] = 0.12$–1.2 M. The value of $k_{red.}$ increases with increasing concentrations of both tu and OH^- and obeys the empirical expression given by eq. (1).

$$k_{red.} = A + (B + C[OH^-])[tu]. \quad (1)$$

A non-linear least-squares fit of the data in Table 1 yields the parameters: $A = (1.08 \pm 0.17)\ s^{-1}$, $B = (1.46 \pm 0.04) \times 10^3\ M^{-1}\ s^{-1}$ and $C = (2.02 \pm 0.05) \times 10^3\ M^{-2}\ s^{-1}$. There is good agreement between the experimental and calculated $k_{red.}$ values, when the latter was estimated using the above parameters.

PRODUCT FORMATION

The rate of formation of the coloured product at 350 nm in the silver(III)–tu reaction is also pseudo-first-order, but the observed rate constant $k_{Ag^{III}}$ has a [tu] dependence which reaches a maximum and then decreases at higher concentrations. This behaviour is demonstrated in Fig. 2. The value of $k_{Ag^{III}}$ is independent of the initial $[Ag^{III}]$ and dependent on $[OH^-]$ only in the decreasing portion of the [tu] plot. When the starting reactants are $Ag(OH)_2^-$ and tu, the rate exhibits a similar pattern, but the pseudo-first-order rate constant in this case, k_{Ag^I}, is different from the above-mentioned $k_{Ag^{III}}$ under identical conditions. Table 2 lists representative values for these sets along with those obtained using the other substrates (viz. tam and S^{2-}).

In order to establish the identity and origin of the brown product, a series of comparative experiments were performed with silver(I)* (which has a

* Silver(I) exists as $Ag(OH)_2(OH)_2^-$ in strongly aqueous alkaline solutions.

Table 1. Pseudo-first-order rate constants for the reduction of silver(III) ($k_{red.}$) at 280 nm. 25°C, μ = 1.2 M

[OH⁻] (M)	10^3[L] (M)	$k_{red.}$ (s^{-1})	$k_{red.}$(calc.) (s^{-1})
L = tu			
1.2	0.5	3.07 (3.1)[a]	3.02
	1.0	5.08 (5.0)[a]	4.96
	5.0	21.1	20.5
	10	39.2	39.9
0.6	0.5	2.58	2.42
	1.0	4.2	3.75
	5.0	15.1	14.4
	10	28.0	27.8
0.3	0.5	2.14	2.12
	1.0	2.90	3.24
	5.0	11.4	11.4
	10	22.1	21.7
0.12	0.5	1.63	1.93
	1.0	2.23	2.78
	5.0	8.84	9.59
	10	17.9	18.1
L = tam			
1.2	0.5	155 (154)[a]	
	1.0	260 (263)[a]	

[a] Under deaerated conditions.

Table 2. Pseudo-first-order constants for the 350 nm absorbance increase. 25°C, μ = [OH⁻] = 1.2 M

10^3[L] (M)	$k_{Ag^{III}}$ (s^{-1})	$k_{Ag^{I}}$ (s^{-1})
L = tu		
0.5	1.30	3.30
	1.33[b]	3.32[b]
1.0	(2.11)[a] 2.47	6.35
	2.83[b]	6.32[b]
5.0	(8.62) 8.80	25.1
10	(9.32) 9.60	32.0
50	(1.15) 5.56	2.45
100	(0.30) 1.05	0.73
L = tam		
0.5	1.33	3.32
	1.29[b]	3.20[b]
1.0	2.83	6.32
	3.09[b]	6.56[b]
L = S^{2-}		
0.5	1.35	66.8[c] 3.39
	1.30[b]	66.1[b,c] 3.71[b]
1.0	2.64	123[c] 6.42
	2.80[b]	125[b,c] 6.56[b]

[a] (In parentheses) [OH⁻] = 0.12 M.
[b] Deaerated conditions.
[c] Corresponding to initial absorbance increase.

solubility of about 2×10^{-4} M in 1.2 M NaOH) in place of $Ag(OH)_4^-$ with thioacetamide and sodium sulphide as potential sulphur donors. For all six combinations of the two metal ions with the three substrates, the same product was observed. For the two organic substrates, there was a decrease in the characteristic UV absorbance maxima (233 nm for tu[9,10] and 256 nm for tam) which corresponds to approximately two moles of tu or tam per mole of silver. These spectra show a new band at 228 nm

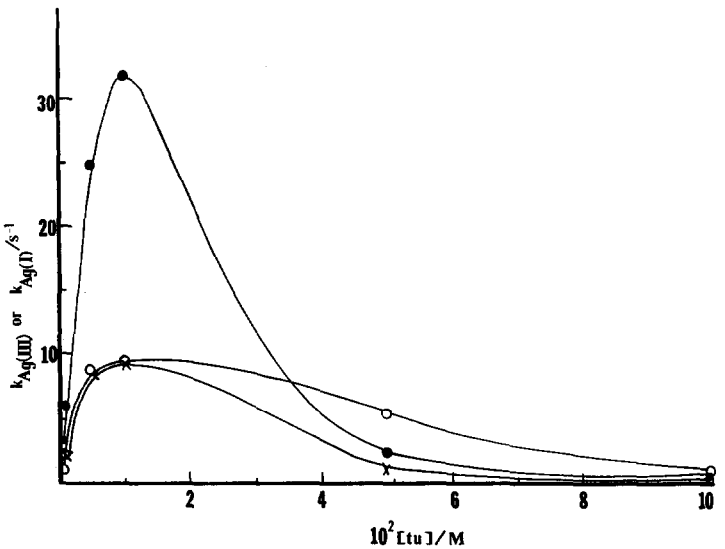

Fig. 2. Observed first-order rate constants for 350 nm absorbance increase. Total silver concentration is $\sim 1 \times 10^{-4}$ M. (×) silver(III) at 0.12 M OH⁻; (○) silver(III) at 1.2 M OH⁻; (●) silver(I) at 1.2 M OH⁻.

which is identical to the peak observed for alkaline solutions of Na_2S.[11,12] In a continuous variations study of the $Ag(OH)_4^-$–tu system, we found only minor spectral changes above a tu : metal ratio of 2 : 1. Thus, in view of the absence of acid–base reversibility, we conclude that the brown product is a colloidal form of silver(I) sulphide or a polymeric precursor. The colloidal nature of the product is consistent with the very broad visible absorbance.

DISCUSSION

The kinetic data for the reduction of Ag^{III} by tu are consistent with a sequence presented in eqs (2)–(5).

$$Ag(OH)_4^- + H_2O \underset{k_{-1}}{\overset{k_1}{\rightleftharpoons}} Ag(OH)_3OH_2 + OH^- \quad (2)$$

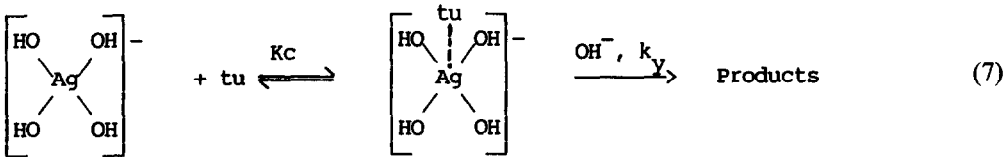

(7)

$$Ag(OH)_4^- + tu \xrightarrow{k_2} \longrightarrow \quad (3)$$

$$Ag(OH)_4^- + tu + OH^- \xrightarrow{k_3} \longrightarrow \quad (4)$$

$$Ag(OH)_3OH_2 + tu \xrightarrow[fast]{k_4} \longrightarrow \quad (5)$$

} products.

A rate law that can be derived from eqs (2)–(5) is as in eq. (6), assuming that $k_1 \ll k_{-1}[OH^-] \ll k_4[tu]$.

$$k_{red.} = k_1 + k_2[tu] + k_3[tu][OH^-]. \quad (6)$$

This is identical to the empirical rate law (1) where $k_1 = A$, $k_2 = B$ and $k_3 = C$.

The mechanism shown envisages that the reduction of Ag^{III} proceeds by the attack of tu, in $[OH^-]$ dependent and independent paths, on the tetrahydroxoargentate(III) and the hydrolysed trihydroxomonoaquaargentate(III) species. The reduction rate is limited (at low [tu] and $[OH^-]$) by the aquation rate constant (k_1). Although the kinetic data for the Ag^{III} reduction have been plausibly explained in terms of the rate law (6) and the reaction sequence (2)–(5), several mechanistic implications need consideration.

The third-order term containing $[OH^-]$ cannot be a termolecular process because the reduction proceeds with considerable ease. The oxidant has been found to exist only as the $Ag(OH)_4^-$ species in alkaline solutions as evidenced from a lack of spectral, kinetic and stoichiometry changes in a wide $[OH^-]$ range (e.g., *ca* 0.1–12 M), and no other species of any stoichiometric significance has been noticed in the absence of other complexing agents.[1] In the present study, therefore, the $[OH^-]$ dependent term cannot be traced to speciation change in the initial reactant $Ag(OH)_4^-$.

For the reduction involving the $Ag(OH)_4^-$, an *inverse* dependence of rate on $[OH^-]$ would be expected if the reaction involved a reversible ligand displacement prior to electron transfer, while a $[OH^-]$ independent would result if the redox was either preceded by a rate-determining ligand (OH^-) replacement or was a simple bimolecular process. Since a distinct $[OH^-]$ dependence has been observed, neither of the above possibilities appears to be important in the k_3 path (*vide infra*). On the other hand, if OH^- interacts with a five-coordinate intermediate to bring about the electron transfer, eq. (7) can be written.

If the magnitude of the formation constant of the five-coordinate intermediate, K_c, is small, then the $[OH^-]$ dependent term of the rate law (6) works out as in eq. (8).

$$k_3 = (k_y K_c)/(1 + K_c[tu]) \sim (k_y K_c) \quad (8)$$

for the reaction conditions employed.

Silver(III) reduction by tu resembles that by ethylenediamine (en) where a rate law identical to eq. (6) was obtained. The average values for en were:[4] $k_1 = 0.6\ s^{-1}$, $k_2 = 32.2\ M^{-1}\ s^{-1}$ and $k_3 = 26.6\ M^{-2}\ s^{-1}$. The rate constant for the aquation of $Ag(OH)_4^-$ (k_1) has been found to be $\sim 1\ s^{-1}$, (i.e. ~ 0.6–$2.5\ s^{-1}$) in several reaction systems.[2–4,6] Since deprotonation of free en would require a value of k_3 above the diffusion-limit, we took the k_3 step as definitive evidence for the reaction taking place within a five-coordinate intermediate while suggesting that the k_1 and k_2 steps involved the formation of a four-coordinate en complex (by "solvent paths"), even though there was no direct evidence for OH^- replacement.[4] In other redox systems involving Ag^{III}, the formation of a true four-coordinate intermediate has since been observed.[2,3]

We note that the ratios of rate constants, k_{tu}/k_{en}, for the two systems are similar (45 and 80, respectively) for both the k_2 and k_3 paths, indicating common mechanisms for both substrates. The larger rates for tu are in line with its higher nucleophilicity. This lends additional credence to the

involvement of an axially bound tu (or en) with subsequent attack by OH^- [eq. (7)] rather than the kinetically equivalent alternative in which first the hydroxyl and then the reductant react in the k_3 path.[4] The involvement of deprotonated thiourea species has been suggested[13] in the electrochemical oxidation of tu at a platinum electrode. However, there seems to be no evidence for stoichiometric amounts of such species.

The similarity of k_1 for the tu and en (as well as other) systems seems a clear indication that the formation of $Ag(OH)_3(H_2O)$ is rate-determining for that path. In the reaction of Ag^{III} with HO_2^-,[6] redox clearly occurs (only) in a five-coordinate intermediate. For the thiosulphate reaction, redox occurs both in four- and five-coordinate intermediates with the latter being especially sensitive to attack by a second $S_2O_3^{2-}$ ion. Oxidation of the azide ion by silver(III) requires substitution of two hydroxyls by the reductant before electron transfer can occur. In light of this diversity of behaviour and the absence of corroborating information, we cannot determine whether or not tu (or en) actually forms a true four-coordinate Ag^{III} complex prior to electron transfer in the k_1 and k_2 paths.

A qualitative comparison of mechanisms of Ag^{III} reduction by several reductants can now be attempted in terms of a general scheme involving the $Ag(OH)_4^-$ species (Scheme 1).

For cases where the electron-transfer step (k_a) is relatively slow, the five-coordinate intermediate may rearrange to a four-coordinate complex with water or OH^- loss prior to electron-transfer by the k_b route. For the azide ion[3] and for the thiosulphate at low ligand concentrations,[2] k_b is rate-determining and, thus, this behaviour is clearly observed. Nitrogen-donor ligands, including anions of polypeptides[14] and dioximes[15] are also oxidized by silver(III) after formation of (characterizable chelate) complexes. $Ag(OH)_4^-$ reactions in which there is strong evidence for the k_a path include HO_2^-,[6] tu and en (third-order path), thiosulphate and arsenite.[5] More studies are being conducted to substantiate this general mechanism of reduction.

Thiourea is known to undergo one-electron transfer(s) to produce the thiourea radical which very rapidly dimerizes to give formamidine disulphide.[9,10,16] The redox potential for the couple,

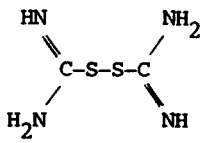

2 tu/formamidine disulphide is reported to be *ca* -0.42 V.[10] That tu is not involved in a one-electron redox mechanism is borne out by the fact that the rate of Ag^{III} reduction by tu is too low when compared to those by other established one-electron reducing agents,[7] such as MnO_4^{2-}, $Fe(CN)_6^{4-}$, $W(CN)_8^{4-}$ and $Mo(CN)_8^{4-}$. The lack of an EPR signal rules out the formation of a discernible, paramagnetic species. Furthermore, the rates of the Ag^{III} reduction (as well as those for the 350 nm absorbance increase) remain unaltered when the reactions are carried out in a deaerated atmosphere (c.f. Tables 1 and 2) suggesting that no stable radical species is formed to participate in radical-induction reactions. Therefore, Ag^{III} appears to be reduced to Ag^I without the production of any discernible Ag^{II} and/or radical intermediates. Although the primary product of oxidation of tu by Ag^{III} could not be detected in the present study (because of the subsequent reactions

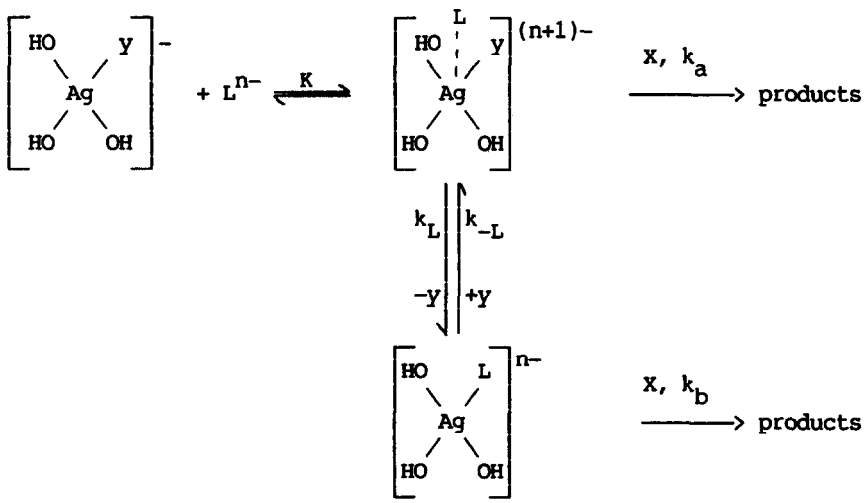

Scheme 1. X = H_2O, OH^- or L^{n-}; y = OH^- or H_2O.

as observed by the 350 nm absorbance increase), formamidine disulphide, which has been identified in many reactions in acid,[9,10] as well as alkaline solutions,[17] is likely to be formed. Formamidine disulphide is also obtained as the primary product of oxidation of thiourea when two-electron oxidants are employed. The loss of two electrons from tu, which normally has a zwiterionic structure results in an electron deficient sulphur centre

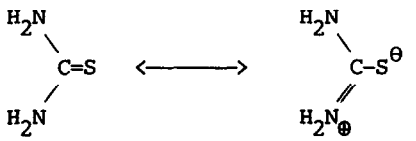

which is very rapidly attacked by another unit of tu to produce the disulphide.[17]

Sulphenic acid, $HOSC(=NH)(NH_2)$, has recently been postulated[18] as an alternative to the disulphide as the two-electron intermediate in the oxidation of tu to sulphate by excess bromine at pH < 2. Under these conditions, the tu sulphur is protonated and this is thought to prevent dimer formation. In contrast, the large excesses of (neutral) tu in our study would favour the formation of formamidine disulphide. Sulphenic acid (or a mixture of products) cannot be ruled out, however, since it could be formed by reaction of the electron deficient sulphur intermediate with hydroxide. The second-order substrate dependence, which supported the formation of tetrathionate in the Ag^{III} thiosulphate reaction,[2] is absent in this case. Although both of the possible products hydrolyse to urea and elemental sulphur,[9,10] the predominant absorbing/scattering species subsequent to redox appear to involve reduced sulphide species.

The production of the brown product, following the reduction of Ag^{III}, that we have taken to be a precursor to solid Ag_2S, has provided some interesting observations which are not fully understood. The kinetics, including $[OH^-]$ dependence, as well as the spectral observations, show qualitative similarities, whether the starting material is Ag^{III} or Ag^{I}, and when tam or the sulphide ion are substituted for tu (Fig. 2). The initial rapid reaction in the case of Ag^{I} and S^{2-} is probably due to the replacement of hydroxyl on $Ag(OH)_2^-$ by one or more S^{2-} units. Silver(I) is known to bring about the hydrolysis of tu (to S^{2-} and urea) in basic solutions.[12b] Indeed, in a recent electrochemical study, thiourea was seen to hydrolyse to Ag_2S at low potential at a silver electrode.[19]

The rate constants in Table 2 are presumably not those for the hydrolysis reaction since the rates are similar even when the reactant is simply the S^{2-} ion. The somewhat lower rates observed in the reactions when the starting reactant is Ag^{III} may reflect an initial interaction between the Ag^{I} product and the oxidized substrate. The observation that an Ag : tu (or Ag : tam) ratio of 1 : 2 (rather than 1 : 0.5) is required for saturation of the 350 nm absorbance may indicate that two sulphur units are bound to each silver in a precursor to the final Ag_2S product.

Finally, the very fact that the observed kinetics are first-order in absorbance increase suggests that the rate is controlled by a homogeneous rather than a heterogeneous process. Kinetic studies of rapid nucleation from homogeneous solutions are scarce and not well understood. Thus, we are unable to make a detailed mechanistic analysis of the formation of colloidal silver sulphide.

Acknowledgements—We wish to thank the Donors of the Petroleum Research Fund, administered by the American Chemical Society for support of this research. We are grateful to Berhampur University, India for extending study leave to Rama K. Panda.

REFERENCES

1. (a) G. L. Cohen and G. Atkinson, *J. Electrochem. Soc.* 1968, **115**, 1236; (b) L. J. Kirschenbaum, J. H. Ambrus and G. Atkinson, *Inorg. Chem.* 1973, **12**, 2832.
2. J. D. Rush and L. J. Kirschenbaum, *Inorg. Chem.* 1985, **24**, 744.
3. E. T. Borish and L. J. Kirschenbaum, *Inorg. Chem.* 1984, **23**, 2355.
4. L. J. Kirschenbaum, *J. Inorg. Nucl. Chem.* 1976, **38**, 881.
5. L. J. Kirschenbaum and J. D. Rush, *Inorg. Chem.* 1983, **22**, 3304.
6. E. T. Borish and L. J. Kirschenbaum, *J. Chem. Soc., Dalton Trans.* 1983, 769.
7. (a) L. J. Kirschenbaum, E. T. Borish and J. D. Rush, *Israel J. Chem.* 1985, **25**, 159; (b) E. T. Borish, L. J. Kirschenbaum and E. Mentasti, *J. Chem. Soc., Dalton Trans.* 1985, 1789.
8. F. Basolo and R. G. Pearson, *Mechanisms of Inorganic Reactions*, 2nd edn, Chap. 5. John Wiley, New York (1967).
9. M. Hoffmann and J. O. Edwards, *Inorg. Chem.* 1977, **16**, 3333. Tu has a maximum at 235 nm in aqueous acid solutions. We have observed the thiourea absorption band at 233 nm in aqueous neutral and alkaline solutions.
10. J. D. Lydon and R. C. Thompson, *Inorg. Chem.* 1986, **25**, 3694.
11. J. H. Karchmer (Ed.), *The Analytical Chemistry of Sulfur and its Compounds*, Part II. Wiley Interscience, New York (1972), (a) Chap. 1 by H. V. Drushel 'Sulfides'; (b) Chap. 10 by P. Raizman and Q. E. Thompson.

12. K. Y. Chen and J. C. Morris, *Environ. Sci. Tech.* 1972, **6**, 529.
13. T. C. Franklin and M. Iwunze, *Electroanal. Chem.* 1980, **108**, 97.
14. L. J. Kirschenbaum and J. D. Rush, *J. Am. Chem. Soc.* 1984, **106**, 1003.
15. L. J. Kirschenbaum, R. K. Panda, E. T. Borish and E. Mentasti, submitted to *Inorg. Chem.*
16. L. Catalini, *MTP (Med. Tech. Publ. Co.) Int. Rev. Sci.; Inorg. Chem. Ser. One* 1972, **9**, 269.
17. J. L. Walter, J. A. Ryan and T. J. Lane, *J. Am. Chem. Soc.* 1956, **78**, 5560.
18. R. H. Simoyi and I. R. Epstein, *J. Phys. Chem.* 1987, **91**, 5124.
19. M. Hepel and S. Bruckenstein, *Electrochim. Acta* 1987, **32**, 41.

Polyhedron Vol. 7, No. 24, pp. 2761–2767, 1988
Printed in Great Britain

0277–5387/88 $3.00+.00
© 1988 Pergamon Press plc

COMPLEXES OF MACROCYCLIC POLYETHERS WITH SOME POTASSIUM MONOETHYL BENZENEAZOPHOSPHONATES

Lj. TUŠEK-BOŽIĆ* and M. ĆURIĆ

Department of Physical Chemistry, Rudjer Bošković Institute, Croatia, Zagreb, Yugoslavia

(*Received* 26 *April* 1988; *accepted* 13 *June* 1988)

Abstract—Complexes of the potassium monoethyl ester of [α-(4-benzeneazoanilino)-N-benzyl]phosphonic acid, [α-(4-benzeneazoanilino)-N-4-hydroxybenzyl]phosphonic acid and [α-(4-benzeneazoanilino)-N-4-methoxybenzyl]phosphonic acid with dibenzo-18-crown-6 and dibenzo-24-crown-8 have been studied. The new complexes were identified and characterized on the basis of elemental and thermogravimetric analysis, conductivity measurements, and UV, IR and ^{1}H NMR spectra. The results obtained were compared with those obtained for the corresponding sodium monoalkyl benzeneazophosphonate complexes. It has been observed that the formation of salt complexes is controlled by a combination of factors, including the metal cation size in relation to the polyether hole, size and charge density of the anion, as well as the choice of the reaction solvent.

Much interest has been directed towards the chemical and biological applications of the macrocyclic polyethers as a result of their ability to form complexes with alkali metals, especially sodium and potassium. Macrocyclic polyethers resemble the biologically important transport agents, such as the more complex naturally occurring macrocyclic antibiotics, which are known to make cell membranes selectively permeable to alkali cations.[1,2] The rate of cation transport is significantly influenced by the nature of the anion which accompanied the cation–macrocyclic polyether complex.[3] Therefore, increasing interest has been developed in obtaining information on complex formation with salts of organic anions because of their relevance to natural systems. The chelating anions mostly used were those derived from nitrophenols and nitro-, hydroxy- and aminobenzoic acids.[4–9]

We recently reported investigations which dealt with macrocyclic polyether complexes with sodium salts of monoalkyl esters of some benzeneazophosphonic acids.[10,11] In this paper we extend this study to the potassium complexes. A series of new complexes between potassium monoethyl benzeneazophosphonates (KX_1–KX_3) and dibenzo-18-crown-6 (DB18C6) and dibenzo-24-crown-8 (DB24C8) have been synthesized and characterized.

Salt	R
KX_1	H
KX_2	OH
KX_3	OMe

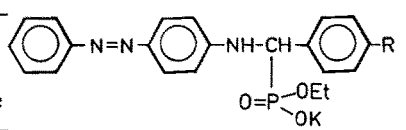

EXPERIMENTAL

Materials

Dibenzo-18-crown-6 (DB18C6, the trivial name for 6,7,9,10,17,18,20,21-octahydrodibenzo [b,k] [1,4,7,10,13,16] hexaoxacyclooctadecin) and dibenzo-24-crown-8 (DB24C8, the trivial name for 6,7,9,10,12,13,20,21,23,24,26,27 - dodecahydrodi - benzo [b,n] [1,4,7,10,13,16,19,22] octaoxacyclotetracosin) prepared as previously described,[12] were purified by repeated recrystallizations from the appropriate solvents, DB18C6 from acetone and DB24C8 from methanol.

Monoethyl esters of [α-(4-benzeneazoanilino(-N-benzyl]phosphonic acid,[13] [α-(4-benzeneazoanilino)-N-4-hydroxybenzyl]phosphonic acid[14] and [α-

*Author to whom correspondence should be addressed.

(4-benzeneazoanilino)-N-4-methoxybenzyl]phosphonic acid[14] required for the preparation of the corresponding potassium salts were prepared and purified according to the literature cited.

Analytical grade solvents were used for the preparation of the salt complexes. The purification of methanol was carried out by the published method[15] in order to obtain a solvent suitable for conductance measurements.

Preparation of potassium salts

Potassium salts of monoethyl benzeneazophosphonates (KX_1–KX_3) were prepared by mixing an equimolar amount of the monoethyl ester and potassium hydroxide in absolute ethanol at the ambient temperature for 4–6 h. After evaporation of the solvent, the yellow–orange potassium salts were isolated and recrystallized twice from absolute ethanol. Although all the potassium monoethyl benzeneazophosphonates were hygroscopic compounds, after drying *in vacuo* by heating to about 50°C for 8 h they were obtained anhydrous.

Preparation of complexes

Reactions were in general carried out by dissolving an equimolar amount of macrocyclic polyether and the potassium salt of the monoethyl ester of benzeneazophosphonic acid in acetonitrile or ethanol and boiling under reflux for 3–6 h with vigorous stirring. The clear hot solution was filtered and allowed to stand at room temperature. The complex was gradually formed by removal of solvent. The crystalline precipitate was filtered off, and recrystallized from the reaction solvent. The complexes obtained were hygroscopic compounds as were the free potassium benzeneazophosphonates, but after drying under high vacuum for several hours at 50°C they became anhydrous.

Physical measurements and analysis

Melting points were determined using hot-stage (0–360°C) microscopy and are uncorrected. UV spectra were obtained in methanolic solutions with a Perkin–Elmer 124 spectrophotometer. IR spectra were recorded on KBr pellets and Nujol mulls in the region 4000–200 cm^{-1} using a Perkin–Elmer 580B spectrophotometer. ^1H NMR spectra were obtained with a JEOL FX90Q Fourier transform NMR spectrometer in deuterochloroform solutions with tetramethylsilane as the internal standard using a sweep width of 1200 Hz. Conductivity measurements were performed in methanol using a CD 7A Tacussel conductivity bridge. The solutions were thermostated at 25∓0.02°C in a double water bath and stirred by means of a magnetic stirrer. The procedure of measuring and calculation of equivalent conductance at infinite dilution and ion-pair dissociation constants of free potassium salts and their complexes was the same as described elsewhere,[9] using the expanded form of the Fuoss–Hsia conductance equation.

Chemical analyses were obtained from the Microanalytical Laboratory of the Institute Rudjer Bošković. Thermogravimetric analyses were carried out with a Cahn RG electromicro balance applying a heating rate of 2°C min^{-1} in an atmosphere of static air.

RESULTS AND DISCUSSION

Physical propeties, analytical and conductance data of potassium monoethyl benzeneazophosphonates and their complexes with DB18C6 and DB24C8 are given in Table 1. Their spectral data are summarized in Tables 2 and 3. The potassium salts ($\mathbf{KX_1}$–$\mathbf{KX_3}$) as new compounds were prepared from the monoethyl benzeneazophosphonates by reaction with potassium hydroxide, which was a more convenient synthesis than that used for the preparation of the corresponding sodium salts by the alkaline hydrolysis of diethyl benzeneazophosphonates.[13,14] Potassium benzeneazophosphonates have substantially lower melting points than the corresponding sodium salts and are much more soluble in common organic solvents. It was shown that when the solubility of the alkali metal salt is reduced, as in the case of sodium benzeneazophosphonates,[10] the role of solvent becomes a more important factor in complexation with macrocyclic polyethers. Thus, in the reaction of DB18C6 and DB24C8 with all potassium benzeneazophosphonates, the complexes are obtained from acetonitrile in good yields, whereas with the sodium salts, in some cases only the unreacted starting materials crystallize on cooling the reaction mixture. Furthermore, those sodium salt complexes obtained from acetonitrile, decompose when recrystallized. In contrast, all potassium salt complexes could be recrystallized from the reaction solvent. The failure to isolate the metal salt complexes from alcoholic solutions can be attributed to the strong hydrogen bonding between the anion or cation and the synthesis media.

DB18C6 and DB24C8 form 1:1 complexes both with sodium and potassium salts. The potassium ion (ionic diameter 2.66 Å) and, of course, the smaller sodium ion should fit well into the hole of the 18-membered polyether ring (2.6–3.2 Å diameter)[16] with the anion and solvent molecules

Table 1. Analytical and physical data of potassium benzeneazophosphonates and their complexes with macrocyclic polyethers

Compound	Reaction solvent	M.p. (°C)	Found (calc.) (%) C	H	N	P	K	Limiting conductance[a] (Ω^{-1} cm^2 mol^{-1})
KX_1	EtOH	184–186	58.0	4.8	9.8	7.3	8.9	103.8
			(58.2)	(4.9)	(9.7)	(7.1)	(9.0)	(97.7)
K(DB18C6)X_1	MeCN	139–141	61.8	5.9	5.1	3.7	4.8	68.1
			(62.0)	(5.7)	(5.3)	(3.9)	(4.9)	(65.8)
K(DB24C8)X_1	MeCN	89–90	61.5	6.2	4.6	3.4	4.5	74.2
			(61.3)	(6.1)	(4.8)	(3.5)	(4.4)	(72.4)
KX_2	EtOH	140–142	55.9	4.9	9.2	6.6	8.9	102.5
			(56.1)	(4.7)	(9.3)	(6.9)	(8.7)	(96.4)
K(DB18C6)X_2	EtOH, MeCN	125–127	61.0	5.7	5.0	3.8	4.6	66.4.
			(60.8)	(5.6)	(5.2)	(3.8)	(4.8)	(64.8)
K(DB24C8)X_2	EtOH, MeCN	100–102	60.2	6.1	4.4	3.2	4.1	72.1
			(60.2)	(5.9)	(4.7)	(3.4)	(4.0)	(70.2)
KX_3	EtOH	156–157	57.3	5.2	9.2	6.4	8.3	101.1
			(57.0)	(5.0)	(9.1)	(6.7)	(8.4)	(95.6)
K(DB18C6)X_3	MeCN	126–127	61.0	5.9	5.0	3.6	4.8	65.1
			(61.2)	(5.7)	(5.1)	(3.8)	(4.7)	(63.7)
K(DB24C8)X_3	MeCN	89–90	60.3	6.1	4.5	3.1	4.4	70.4
			(60.6)	(6.2)	(4.6)	(3.4)	(4.3)	(68.8)

[a] In methanol at 25°C. Data for the corresponding sodium compounds are given in parentheses for comparison.

Table 2. Selected UV and IR data of the novel compounds

Compound	UV data[a] λ_{max}(log ε)	νOH, νNH	IR data (cm^{-1})[b] ν_{as}Ar—O—CH_2 ν_{as}P=O, $\nu_{as}PO_2^-$	$\nu_{as}CH_2$—O—CH_2 δC—O—(P)	$\nu_{sym}PO_2^-$ νP—O—(C)	$\omega\tau CH_2$ ν aliph. C—C
KX_1	260 (3.67)	3380m br	1241vs	1156m	1082s	948m
				1142s	1051s	924w
K(DB18C6)X_1	269 (4.11)	3380w	1252vs	1130vs	1091s	959s
	277sh (4.02)	3230m	1219s	1105s	1060vs	948s
K(DB24C8)X_1	269 (4.10)	3320w br	1261vs	1140vs	1080s	942m
	274sh (4.07)		1228s	1130sh	1054s	928m
				1108s		
KX_2	260sh (3.88)	3372m br	1253s	1140sh	1074vs	957m
			1242sh	1131s	1068s	
					1054s	
K(DB18C6)X_2	271 (4.11)	3380w br	1253vs	1130vs	1067s	959m
	277sh (4.06)		1218s		1054s	948s
K(DB24C8)X_2	271 (4.13)	3384w br	1260vs	1140vs	1070sh	941m
	280sh (4.02)		1228s	1130s	1053s	928m
				1107s		
KX_3	264sh (3.86)	3382m br	1249s	1157m	1075s	948m
			1221s	1142s	1046s	
K(DB18C6)X_3	270 (4.17)	3380w br	1254vs	1130vs	1068sh	960m
	277sh (4.12)		1219s		1057s	948s
K(DB24C8)X_3	270 (4.05)	3320m br	1260s	1136s	1076s	942m
			1228s	1107s	1052s	928m

[a] In methanol, 250–300 nm region.
[b] KBr pellets.

Table 3. ^{1}H NMR data of the potassium salts and their complexes

Compound	Chemical shift δ in ppm (J in Hz)[1]
KX_1	1.10 (t, 3H, $J = 7$, CH_3); 3.71 (m, 2H, $POCH_2$); 4.64 (d, 1H, $J = 22.5$, PCH); 6.62–8.01 (m, 15H, ArH+NH)
$K(DB18C6)X_1$	1.10 (t, 3H, $J = 7$, CH_3); 3.78 (m, 2H, $POCH_2$); 4.05 (s, 16H, four OCH_2CH_2O); 4.68 (d br, 1H, $J = 22$, PCH); 5.86 (s br, 1H, NH); 6.46–7.98 (m, 14H, anion ArH); 6.83, 6.87 (two s, 8H, crown ArH)
$K(DB24C8)X_1$[b]	1.03 (t, 3H, $J = 7$, CH_3); overlapping 3.69 (s, 10H, $POCH_2$+four H_3 —OCH_2); 3.80 (m, 8H, four H_2 —OCH_2); 4.15 (m, 8H, four H_1 —OCH_2); 4.66 (d, 1H, $J = 22$, PCH); 5.98 (s br, 1H, NH); 6.54–7.91 (m, 14H, anion ArH); 6.87 (s, 8H, crown ArH)
KX_2	1.08 (t, 3H, $J = 7$, CH_3); 3.73 (m, 2H, $POCH_2$); 4.66 (d, 1H, $J = 22$, PCH); 6.64–8.02 (m, 15H, ArH+NH+OH)
$K(DB18C6)X_2$	1.10 (t, 3H, $J = 7$, CH_3); 3.80 (m, 2H, $POCH_2$); 3.94 (s, 16H, four OCH_2CH_2O); 4.51 (d br, 1H, $J = 22$, PCH); 5.77 (s br, 1H, NH); 6.34–7.84 (m, 14H, anion ArH+OH); 6.77, 6.81 (two s, 8H, crown ArH)
$K(DB24C8)X_2$[b]	1.04 (t, 3H, $J = 7$, CH_3); overlapping 3.70 (s, 10H, $POCH_2$+four H_3 —OCH_2); 3.80 (m, 8H, four H_2 —OCH_2); 4.10 (m, 8H, four H_1 —OCH_2); 4.58 (d br, 1H, $J = 22$, PCH); 6.01 (s br, 1H, NH); 6.48–7.84 (m, 14H, anion ArH+OH); 6.87 (s, 8H, crown ArH)
KX_3	1.07 (t, 3H, $J = 7$, CH_3); 3.63 (s, 3H, OCH_3); 3.71 (m, 2H, $POCH_2$); 4.66 (d, 1H, $J = 22$, PCH); 6.65–7.95 (m, 14H, ArH+NH)
$K(DB18C6)X_3$	1.11 (t, 3H, $J = 7$, CH_3); 3.51 (s, 3H, OCH_3); 3.75 (m, 2H, $POCH_2$); 4.07 (s, 16H, four OCH_2CH_2O); 4.68 (d br, 1H, $J = 21$, PCH); 5.84 (s br, 1H, NH); 6.41–7.85 (m, 13H, anion ArH); 6.85, 6.87 (two s, 8H, crown ArH)
$K(DB24C8)X_3$[b]	1.02 (t, 3H, $J = 7$, CH_3); 3.56 (s, 3H, OCH_3); overlapping 3.68 (s, 10H, $POCH_2$+four H_3 —OCH_2); 3.79 (m, 8H, four H_2 —OCH_2); 4.08 (m, 8H, four H_1 —OCH_2); 4.64 (d, 1H, $J = 22$, PCH); 6.05 (s br, 1H, NH); 6.59–7.98 (m, 13H, anion ArH); 6.85 (s, 8H, crown ArH)

[a] In $CDCl_3$, abbreviations: s, singlet; d, doublet; t, triplet; m, multiplet; br, broad signal.
[b] Polyether protons are designated by the number of the carbon to which they are attached (H_{1-3}, see Fig. 3).

having the possibilities of interacting with the metal ion from the axial directions. DB24C8 (hole diameter about 4.7 Å)[16] produces 1:1 complexes with potassium benzeneazophosphonates from a 1:1 as well as a 1:2 reaction mixture. Previous studies have shown that DB24C8 can also form bimetallic complexes with sodium and potassium ions with respect to the nature of the counter anion.[4,5,17] The 24-membered polyether ring is very flexible and may complex the metal cation by partially wrapping around it with a change in conformation either by expelling the conjugate anion and the solvent molecules from the cation coordination sphere,[18,19] or leaving space for coordination with the anion.[20] The metal–ligand interactions are of the ion–dipole type and in the complex the charge of the metal ions is extensively delocalized. When some degree of charge-transfer between the metal cation and anion is possible, as in the case of benzeneazophosphonates, the more stable complexes are formed.

A detailed conductance study is one of the approaches to elucidate the interaction forces which act in solution between the macrocyclic polyether and an alkali salt. The equivalent conductance dependence on the concentration of potassium monoethyl benzeneazophosphonates and their complexes in methanol is presented in Fig. 1. It was shown that the potassium salts and their complexes are completely dissociated in a methanolic solution. The values obtained for the equivalent conductance at infinite dilution (Λ_0) are summarized in Table 1 together with the data of the corresponding sodium compounds which are included for the sake of comparison. The great differences between the Λ_0 values of the free alkali metal salts and their complexes imply that the polyether complexation considerably increases the size of the cation. Additional interaction of the complexed cation with solvent molecules, which becomes possible after the anion is removed, may cause a further decrease in the mobility of the complexes. Alkali metal cations are known to be extensively solvated in methanol.[21] A larger solvation effect is expected for the smaller sodium ion than for the potassium ion, and consequently, a lower mobility is obtained for the sodium salts and their complexes with respect to the potassium analogues. The gradation in Λ_0 values of DB18C6 and DB24C8 complexes reflects different final sizes of the solvodynamic cation–polyether units. The fact, that the total drop in the equivalent

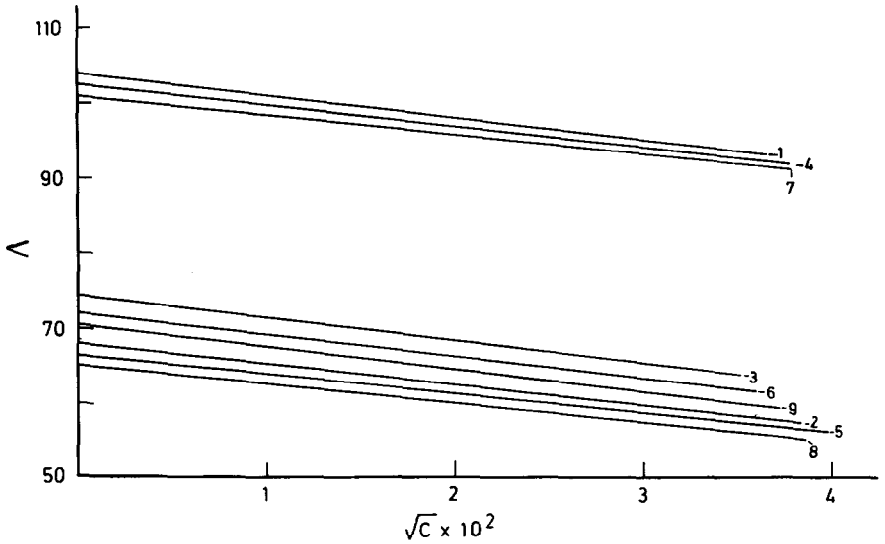

Fig. 1. The conductivity of potassium salts and their complexes at 25°C against the concentration$^{1/2}$. (1) KX_1, (2) K(DB18C6)X_1, (3) K(DB24C8)X_1, (4) KX_2, (5) K(DB18C6)X_2, (6) K(DB24C8)X_2, (7) KX_3, (8) K(DB18C6)X_3, (9) K(DB24C8)X_3.

conductance for DB18C6 complexes (~ 36%) is greater than for the corresponding DB24C8 complexes (~ 30%), can be explained by the weaker solvation of the latter complexes. The results obtained lead us to suppose that the conduction process is not only conditioned by the size of the complexes which are formed, but also by competitive interactions caused by the solvent and the macrocyclic polyether on the cation, and by the relative sizes of the cation and the hole of the polyether compound.

Spectral studies

UV spectra. The UV spectra of the complexes dissolved in methanol show some spectral changes in the 280 nm region, where intraligand transition occurs, compared to the free ligand spectra. DB18C6 and DB24C8 have, in methanol, a characteristic absorption at 274 nm ($\log \varepsilon = 3.72$) and 276 nm ($\log \varepsilon = 3.64$), respectively.[12] In the spectra of the complexes a slight hypsochromic shift of this band is noticed, as well as the appearance of a new peak not clearly separated from the main one.

Potassium salts and their macrocyclic polyether complexes give an absorption at 396 nm ($\log \varepsilon \sim 4.4$) assigned to conjugation of the azo groups with aromatic rings (π–π^* transition), which remains unchanged upon complex formation, suggesting essentially the same ion-pair structure for salts and their complexes. From the conductivity data it was shown that both, the potassium salts and their polyether complexes, are fully dissociated in a methanolic solution.

IR spectra. No significant differences are observed between the IR spectra of sodium and potassium monoethyl benzeneazophosphonates and their complexes, respectively. The frequencies associated with the characteristic functional groups are presented in Table 2. In free potassium salts the ionized PO_2^- group exists along with the P=O group as these compounds show multiple bands in the region 1260–1175 cm^{-1}. This absorption has been ascribed to the P=O stretching and to the asymmetric stretching vibrations of the PO_2^- group. Symmetric vibration of the ionized PO_2^- group is found between 1100–1070 cm^{-1}. Furthermore, potassium salts absorb in the region 1160–1125 cm^{-1} and between 1070–1000 cm^{-1}. The former bands could be assigned to the C—O—(P) and the latter to the P—O—(C) vibration. The absorption in the region 982–940 cm^{-1} is considered to arise from the ethyl C—C vibrations. As free macrocyclic polyethers give a series of complex bands between 1260–900 cm^{-1} arising from various modes of vibration of ether and methylene groups, the spectra of the complexes of potassium salts with macrocyclic polyethers are too complex to allow the precise assignment of the absorption bands. However, the spectrum of the solid complex distinctively differed from that of a physical mixture of the constituents. Considerable changes may be noticed in the region 1000–900 cm^{-1} which contains bands arising from various deformation modes of vibration of the methylene groups. While free DB18C6 has two bands at 987 and 932 cm^{-1}, its complexes are characterized by a strong band around 960 cm^{-1} and a medium one at 948 cm^{-1}. Free DB24C8 has two

strong bands at 958 and 920 cm^{-1}, and a medium one at 936 cm^{-1} associated with these vibrations. In the spectra of its complexes two medium bands appear around 942 and 928 cm^{-1}.

^1H *NMR spectra.* All potassium salts and their complexes are sufficiently soluble in chloroform for recording and studying ^1H NMR spectra. Free potassium salts have a triplet for the methyl protons and a multiplet for the methylene protons of the $POCH_2CH_3$ group. The absorption of the methylene protons is complex because of the coupling between the CH_2 and CH_3 protons and the spin–spin splitting by the phosphorus. The proton of the benzylic CH group appears as a doublet due to the spin–spin interaction with the phosphorus. The NH proton as well as the phenolic OH proton are overlapped by the aromatic protons. In the spectra of the complexes there are no substantial chemical shift differences of these absorptions. Only the NH proton is found as a broad singlet at δ 5.5–6.0 ppm. More significant differences were observed on comparing the spectra of the complexes with the spectra of the free macrocyclic polyethers.

DB18C6 has two multiplets at about δ 4.11 ppm for the methylene protons of the polyether ring and a singlet at δ 6.92 ppm for the aromatic protons.[12] The ether multiplet is typical for the XCH_2CH_2Y fragment with the rapid rotamer conversion.[22] In the complexes, the polyether ring protons are shifted upfield by 5–14 Hz and are found as a single absorption. On the other hand the aromatic protons appear as two singlets at lower field ($\Delta\delta = 5-14$ Hz).

Free DB24C8 has three sets of resonant signals, at δ 4.16 ppm for H_1, at δ 3.89 for H_2 and at δ 3.83 ppm for H_3 methylene protons of the polyether ring. The aromatic protons appear as a singlet at 6.88 ppm.[12] The complex spectrum in the ether region is attributed to the chemical non-equivalent ether fragments (Fig. 2). While the chemical shift of the aromatic protons is essentially unchanged upon complex formation, the ether protons show chemical shift differences between the complexed and non-complexed macrocyclic polyether. In the complexes, the so-called "outer" $ArOCH_2$ methylene protons (H_1) are shifted upfield by 4–6 Hz and the so-called "inner" CH_2OCH_2 protons (H_2 and H_3) are shifted upfield by 8–13 Hz. All potassium complexes show very similar spectral characteristics regardless of which benzeneazophosphonate anion is used. The binding of potassium to DB24C8 induces the same general spectral patterns observed for the sodium

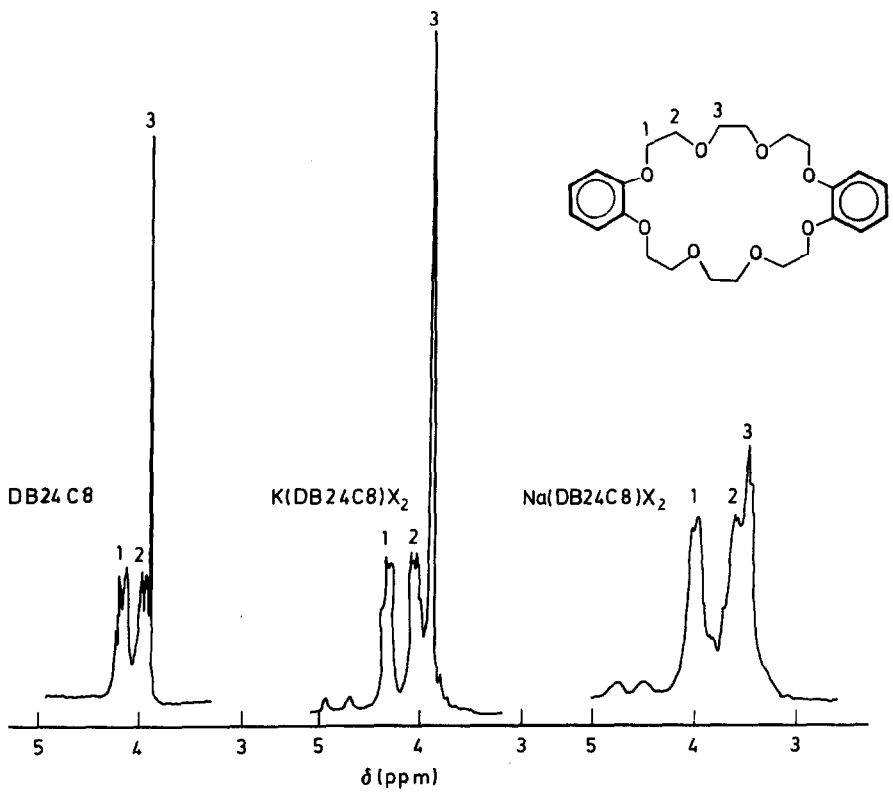

Fig. 2. ^1H NMR spectra of the ether region of DB24C8 and its complexes with KX_2 and NaX_2 in $CDCl_3$. Shifts are relative to TMS.

complexation, indicating the same conformation of these complexes, although there is a greater anion dependence in the sodium complexes. The variation of observed shift with the anion is attributed to ion pairing. Sodium salt complexes show less ion-pair dissociation than the corresponding potassium complexes in chloroform solution, and therefore, in the sodium complexes the anion has a more important role in the resulting chemical shift of the polyether ring protons. The slight broadening of the polyether absorptions observed in sodium benzeneazophosphonate complexes confirms this assumptions (see Fig. 2).[10]

Obviously, the complexes which formed were found to depend not only on the size of the cation and the polyether cavity, but also on the choice of anion and solvent.

Acknowledgement—Financial support by the Foundation for Scientic Research of SR Croatia is gratefully acknowledged.

REFERENCES

1. G. Eisenman, S. M. Ciani and G. Szabo, *J. Memb. Biol.* 1968, **1**, 294.
2. J. D. Lamb, J. J. Christensen, S. R. Izatt, K. Bedke, M. S. Astin and R. M. Izatt, *J. Am. Chem. Soc.* 1980, **102**, 3399.
3. H. Tsukube, *J. Chem. Soc., Perkin Trans. I* 1982, 2359.
4. N. S. Poonia and M. R. Truter, *J. Chem. Soc., Dalton Trans.* 1973, 2062.
5. N. S. Poonia, B. P. Yaday and V. W. Bhaywart, *Inorg. Nucl. Chem. Lett.* 1977, **13**, 119; N. S. Poonia, *J. Am. Chem. Soc.* 1974, **94**, 1012.
6. Lj. Tušek, H. Meider-Goričan and P. R. Danesi, *Z. Naturforsch.* 1976, **31B**, 330.
7. R. Sinta, P. S. Rose and J. Smid, *J. Am. Chem. Soc.* 1983, **105**, 4337.
8. E. Buncel, H. S. Shin, R. A. B. Bannard, J. G. Purdon and B. G. Cox, *Talanta* 1984, **31**, 585.
9. Lj. Tušek-Božić and B. Božić, *Electrochim. Acta* 1985, **30**, 789; Lj. Tušek-Božić and B. Božić, *Croat. Chem. Acta* 1984, **57**, 119.
10. Lj. Tušek-Božić and D. Sevdić, *Polyhedron* 1985, **4**, 1959; Lj. Tušek-Božić and D. Sevdić, 1986, **5**, 877.
11. Lj. Tušek-Božić, *J. Solution Chem*, in press.
12. C. J. Pedersen, *J. Am. Chem. Soc.* 1967, **89**, 7017.
13. V. Jagodić and Lj. Tušek, *J. Org. Chem.* 1972, **37**, 1222.
14. Lj. Tušek and V. Jagodić, *Croat. Chem. Acta* 1977, **49**, 829.
15. R. L. Kay, C. Zawoyski and D. F. Evans, *J. Phys. Chem.* 1965, **69**, 4208.
16. C. J. Pedersen, *J. Am. Chem. Soc.* 1970, **92**, 386.
17. M. Mercer and M. R. Truter, *J. Chem. Soc., Dalton Trans.* 1973, 2469.
18. H. D. H. Stöver, A. Delville and S. Detellier, *J. Am. Chem. Soc.* 1985, **107**, 4167.
19. M. Bisnaire, C. Detellier and D. Nadon, *Can. J. Chem.* 1982, **60**, 3071.
20. A. Rodrique, J. W. Bovenkamp, B. V. Lacroix, R. A. B. Bannard and G. W. Buchanan, *Can. J. Chem.* 1986, **64**, 808.
21. R. L. Kay, B. J. Hales and G. P. Cunningham, *J. Phys. Chem.* 1967, **71**, 3925.
22. D. Live and S. I. Chan, *J. Am. Chem. Soc.* 1976, **98**, 3769.

Polyhedron Vol. 7, No. 24, pp. 2769–2772, 1988
Printed in Great Britain

0277–5387/88 $3.00+.00
© 1988 Pergamon Press plc

SYNTHESIS AND SPECTROSCOPIC PROPERTIES OF THE NOVEL CATIONIC ALKYNE COMPLEXES $[WI(CO)(NCMe)L_2(\eta^2\text{-}RC_2R)][BF_4]$ (L = PEt_3 OR PMe_2Ph; R = Me OR Ph)

PAUL K. BAKER,* ELAINE M. ARMSTRONG and KEVIN R. FLOWER

Department of Chemistry, University College of North Wales, Bangor, Gwynedd LL57 2UW, U.K.

(*Received* 14 *December* 1987; *accepted* 16 *June* 1988)

Abstract—The complexes $[WI_2(CO)L_2(\eta^2\text{-}RC_2R)]$ (L = PEt_3 or PMe_2Ph; R = Me or Ph) react with an equimolar quantity of $Ag[BF_4]$ in acetonitrile at room temperature to give good yields of the new purple cationic alkyne complexes $[WI(CO)(NCMe)L_2(\eta^2\text{-}RC_2R)][BF_4]$. ^{31}P NMR spectroscopy indicates that the phosphines are *trans* to each other in these compounds. ^{13}C NMR spectroscopy suggests that the alkyne ligands are donating four electrons to the tungsten in these complexes.

There has been considerable recent interest in alkyne complexes of molybdenum(II) and tungsten(II) mainly due to the ability of the alkyne ligand to utilize both sets of filled perpendicular $p\pi$ orbitals when coordinated to the metal.[1–6] Cationic alkyne complexes of molybdenum(II) have also received particular attention due to the increased susceptibility of the alkyne ligand to nucleophilic attack when coordinated to the metal.[7] Although a wide variety of cationic alkyne complexes of molybdenum(II) and tungsten(II) containing cyclopentadienyl or indenyl as attached ligands have been reported,[7–9] very few cationic alkyne complexes of molybdenum(II) or tungsten(II) containing halides as attached ligands have been described. Some examples include the isonitrile complexes $[MX(CNR)_4(\eta^2\text{-}RNHC_2NHR)]^+$ reported by Lippard and co-workers.[10] In this paper we wish to describe the preparation and spectral properties of the new cationic alkyne complexes $[WI(CO)(NCMe)L_2(\eta^2\text{-}RC_2R)][BF_4]$ (L = PEt_3 or PMe_2Ph; R = Me or Ph).

EXPERIMENTAL

All preparations were carried out under an atmosphere of dry nitrogen using standard Schlenk line techniques. CH_2Cl_2 was dried and distilled before use.

The complexes $[WI_2(CO)L_2(\eta^2\text{-}RC_2R)]$ (L = PEt_3 or PMe_2Ph; R = Me or Ph) were prepared by the literature method,[11] $[W(CO)_6]$, RC_2R etc. were all purchased from commercial sources.

^1H and ^{13}C NMR spectra were recorded on a Jeol FX 60 MHz spectrometer (all spectra were calibrated against tetramethylsilane). ^{31}P NMR spectra were recorded on a Bruker WH-400 MHz spectrometer at the University of Warwick (all spectra were calibrated against 85% H_3PO_4). IR spectra were recorded on a Perkin–Elmer 197 IR spectrophotometer. Elemental analyses for C, H and N were recorded on a Carlo–Erba Elemental Analyser MOD 1106 (using helium as a carrier gas).

$[WI(CO)(NCMe)(PEt_3)_2(\eta^2\text{-}MeC_2Me)][BF_4]$ (1)

To $[WI_2(CO)(PEt_3)_2(\eta^2\text{-}MeC_2Me)]$ (0.922 g, 1.22 mmol) dissolved in NCMe (15 cm^3), with continuous stirring under a stream of dry nitrogen, was added $Ag[BF_4]$ (0.23 g, 1.22 mmol). After stirring for 20 h the solvent was removed *in vacuo*. The crude product was then redissolved in CH_2Cl_2 (15 cm^3) and filtered to remove AgI. The solvent was then reduced *in vacuo* to 4 cm^3 and dropwise addition of Et_2O caused precipitation of the purple cationic complex $[WI(CO)(NCMe)(PEt_3)_2(\eta^2\text{-}MeC_2Me)][BF_4]$, (yield 0.68 g, 73%), which was recrystallized from CH_2Cl_2–Et_2O.

A similar reaction of $[WI_2(CO)(PMe_2Ph)_2(\eta^2\text{-}MeC_2Me)]$ with $Ag[BF_4]$ in acetonitrile afforded the analogous cationic complex $[WI(CO)(NCMe)$

*Author to whom correspondence should be addressed.

Table 1. Physical and analytical[a] data for the complexes $[WI(CO)(NCMe)L_2(\eta^2\text{-}RC_2R)][BF_4]$

Complex	Colour	Yield (%)	C	H	N
(1) $[WI(CO)(NCMe)(PEt_3)_2(\eta^2\text{-}MeC_2Me)][BF_4]$	Purple	73	29.9 (30.1)	4.9 (5.2)	1.6 (1.8)
(2) $[WI(CO)(NCMe)(PMe_2Ph)_2(\eta^2\text{-}MeC_2Me)][BF_4]$	Purple	68	34.9 (34.6)	4.0 (3.9)	1.5 (1.8)
(3) $[WI(CO)(NCMe)(PEt_3)_2(\eta^2\text{-}PhC_2Ph)][BF_4]$	Purple	70	39.2 (39.5)	4.9 (4.9)	1.4 (1.6)
(4) $[WI(CO)(NCMe)(PMe_2Ph)_2(\eta^2\text{-}PhC_2Ph)][BF_4]$	Purple	63	43.3 (43.0)	3.7 (3.8)	1.5 (1.5)

[a] Calculated values in parentheses.

$(PMe_2Ph)_2(\eta^2\text{-}MeC_2Me)][BF_4]$ **(2)** (see Table 1 for colour and yield).

$[WI(CO)(NCMe)(PEt_3)_2(\eta^2\text{-}PhC_2Ph)][BF_4]$ **(3)**

To $[WI_2(CO)(PEt_3)_2(\eta^2\text{-}PhC_2Ph)]$ (0.75 g, 0.851 mmol) dissolved in NCMe (15 cm^3), with continuous stirring under a stream of dry nitrogen, was added $Ag[BF_4]$ (0.165 g, 0.851 mmol). After stirring for 20 h the solvent was removed *in vacuo*. The crude product was then redissolved in CH_2Cl_2 (15 cm^3) and filtered to remove AgI. The solvent volume was then reduced *in vacuo* to 4 cm^3 and dropwise addition of Et_2O caused precipitation of the purple cationic complex $[WI(CO)(NCMe)(PEt_3)_2(\eta^2\text{-}PhC_2Ph)][BF_4]$, (yield 0.53 g, 70%) which was recrystallized from CH_2Cl_2–Et_2O.

A similar reaction of $[WI_2(CO)(PMe_2Ph)_2(\eta^2\text{-}PhC_2Ph)]$ with $Ag[BF_4]$ afforded the analogous cationic complex $[WI(CO)(NCMe)(PMe_2Ph)_2(\eta^2\text{-}PhC_2Ph)][BF_4]$ **(4)** (see Table 1 for colour and yield).

RESULTS AND DISCUSSION

Equimolar quantities of $[WI_2(CO)L_2(\eta^2\text{-}RC_2R)]$ (L = PEt_3 or PMe_2Ph; R = Me or Ph) and $Ag[BF_4]$ react in acetonitrile at room temperature to give good yields of the purple cationic alkyne complexes $[WI(CO)(NCMe)L_2(\eta^2\text{-}RC_2R)][BF_4]$ by iodide abstraction [eq. (1)].

$$[WI_2(CO)L_2(\eta^2\text{-}RC_2R)] + Ag[BF_4] \xrightarrow{NCMe} [WI(CO)(NCMe)L_2(\eta^2\text{-}RC_2R)][BF_4] + AgI. \quad (1)$$

All the new complexes **(1–4)** have been fully characterized by elemental analysis (C, H and N) (Table 1), IR spectroscopy (Table 2), and ^1H, ^{13}C and ^{31}P NMR spectroscopy (Tables 3, 4 and 5). The complexes are all very soluble in NCMe, CH_2Cl_2 and $CHCl_3$ and as expected they are insoluble in Et_2O and hydrocarbon solvents. The compounds are stable when stored under nitrogen, however, they slowly decompose when exposed to air in solution.

In view of the X-ray crystal structure of the phenylacetylene complex, $[MoBr_2(CO)(PEt_3)_2(\eta^2\text{-}PhC_2H)]$, reported by Templeton and coworkers,[12] it is likely that the iodide will be substituted by the acetonitrile ligand opposite to the stronger *trans*-directing ligand i.e. carbon monoxide, in our closely related diiodide compounds

Table 2. IR data[a] for the complexes $[WI(CO)(NCMe)L_2(\eta^2\text{-}RC_2R)][BF_4]$

Complex	ν(CO) (cm^{-1})	ν(CN) (cm^{-1})	ν(C≡C) (cm^{-1})
(1)	1950(s)	2375(w) 2350(w)	1660(w)
(2)	1950(s)	2370(w) 2345(w)	1650(w)
(3)	1980(s)	2355(w) 2335(w)	1640(w)
(4)	1980(s)	2350(w) 2330(w)	1635(w)

[a] Spectra recorded as $CHCl_3$ films between NaCl plates; s, strong; w, weak.

Table 3. ^1H NMR data[a] for the complexes $[WI(CO)(NCMe)L_2(\eta^2\text{-}RC_2R)][BF_4]$

Complex	^1H (δ) (ppm)
(1)	2.96 (s, 6H, ≡C—*Me*); 1.99 (s, 3H, NC*Me*); 1.68 (bm, 12H, CH_2); 0.97 (bm, 18H, CH_3)
(2)	7.34 (s, 10H, *Ph*); 2.83 (s, 6H, ≡C—*Me*); 2.02 (s, 3H, NC*Me*); 1.8 (m, 12H, CH_3)
(3)	7.73 (s, 10H, *Ph*); 3.0 (s, 3H, NC*Me*); 1.84 (m, 12H, CH_2); 0.96 (m, 18H, CH_3)
(4)	7.53 (s, 20H, *Ph*); 2.04 (s, 3H, NC*Me*); 1.77 (m, 12H, CH_3)

[a]Spectra run in $CDCl_3$ (+25°C) referenced to Me_4Si: s, singlet; bm, broad multiplet; m, multiplet.

Table 4. ^{13}C NMR data[a] for the complexes $[WI(CO)(NCMe)L_2(\eta^2\text{-}RC_2R)][BF_4]$

Complex	^{13}C (δ) (ppm)
(1)	221.6 (s, *C*≡*C*); 217.95 (*C*≡O); 19.23 (m, CH_2); 7.67 (s, CH_3); 4.16 (s, Me*C*N)
(2)	226.9 (s, *C*≡*C*); 220.1 (s, *C*≡O); 130.2, 129.3, 128.9, 128.6, 128.3 (m, Ph); 123.6 (s, *C*≡N); 15.72 (m, CH_3); 3.38 (s, Me*C*N)
(3)	220.5 (s, *C*≡*C*); 204.6 (s, *C*≡O); 132.0, 131.5, 130.3, 129.6, 128.1 (m, Ph); 125.9 (s, *C*≡N); 19.36 (m, CH_2); 7.8 (s, CH_3); 4.4 (s, Me*C*N)
(4)	219.1 (s, *C*≡*C*); 206.6 (s, *C*≡O); 132.0, 131.1, 130.4, 129.4, 129.2, 128.7, 127.9 (m, Ph); 124.5 (s, Me*C*N); 17.28 (m, CH_3); 3.63 (s, Me*C*N)

[a]Spectra run in $CDCl_3$ (+25°C) referenced to Me_4Si: s, singlet; m, multiplet.

$[WI_2(CO)L_2(\eta^2\text{-}RC_2R)]$.[11] The ^{31}P NMR spectrum of $[WI(CO)(NCMe)(PEt_3)_2(\eta^2\text{-}MeC_2Me)][BF_4]$ **(1)** shows a single resonance δ −5.02 (J_{WP} = 523.92 Hz), similarly single resonances are observed for compounds **2–4**. This indicates a *trans*-arrangement of the phosphine ligands attached to the metal in these compounds. Hence the proposed structure for **1–4** is shown in Fig. 1. Several unsuccessful attempts were made to grow crystals for X-ray crystallography of compounds **1–4**.

The IR spectra (Table 2) of **1–4**, as expected, all show a single carbonyl band at 1950 cm^{-1} for the but-2-yne complexes and at 1980 cm^{-1} for the diphenylacetylene compounds. These values are relatively low for a cationic complex, however, as suggested above it is likely that the carbonyl ligand is *trans* to the acetonitrile which is a good σ-donor ligand (Fig. 1). The IR spectra also show weak asymmetric doublets at, for example, 2375 and 2350 for **1** which is assigned to coordinated acetonitrile. The increase in ν(C≡N) upon coordination to the metal is due to a coupling of the C—N and N–metal stretching vibrations and to an increased C—N force constant which is in accord with the acetonitrile functioning purely as a σ donor ligand.[13] The alkyne (C≡C) stretching bands are at a lower wavenumber than for the free alkyne, which is expected since electron density is being donated into the π^*-orbitals of the coordinated alkyne from the filled metal orbitals. A broad band centred at ≈ 1050 cm^{-1} ν(BF) is observed for all the complexes **1–4** which confirms the ionic nature of these complexes.

The but-2-yne resonances in the ^1H NMR spectra of **1** and **2** both show a single methyl resonance at room temperature which indicates that the but-2-yne ligand is rotating very rapidly (faster than the NMR time scale) at room temperature. Attempts were made to measure the barrier to but-2-yne rotation of **1** and **2**. However the but-2-yne resonances remained as singlets down to −60°C, suggesting a low barrier to but-2-yne rotation for complexes **1** and **2**.

The ^{13}C NMR spectra of complexes **1–4** all show

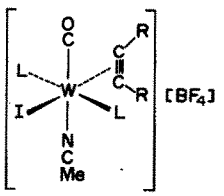

Fig. 1. Proposed structure of $[WI(CO)(NCMe)L_2(\eta^2\text{-}RC_2R)][BF_4]$.

Table 5. ^{31}P NMR data[a] for the complexes $[WI(CO)(NCMe)L_2(\eta^2\text{-}RC_2R)][BF_4]$

Complex	^{31}P (δ) (ppm)
(1)	−5.02 (s J_{WP} = 523.92 Hz)
(2)	−22.52 (s J_{WP} = 540.89 Hz)
(3)	−5.81 (s J_{WP} = 514.82 Hz)
(4)	−23.71 (s J_{WP} = 533.46 Hz)

[a]Spectra run in $CDCl_3$ (+25°C) referenced to 85% H_3PO_4.

alkyne carbon resonances above 200 ppm. Although it is difficult to distinguish, without carrying out labelling studies, between C≡O and C≡C resonances (Table 4) we have assigned the alkyne contact carbons as the lower field resonances which have often been previously reported.[4] Templeton and Ward[14] have correlated the number of electrons donated by an alkyne ligand to the metal and the alkyne contact carbon chemical shift. The values for complexes **1–4** described in this paper are between 219.1 and 226.9 ppm which indicates that the alkynes are donating four electrons to the tungsten in these compounds. The highly coloured nature of these compounds has been previously observed with "four-electron" monoalkyne complexes of molybdenum(II) and tungsten(II).[4,11,12]

The cationic alkyne complexes $[WI(CO)(NCMe)L_2(\eta^2\text{-}RC_2R)][BF_4]$ are highly reactive and we are currently exploring the chemistry of these compounds with a diverse range of neutral and anionic reagents; in particular, reaction with reducing agents in view of the wide range of chemistry reported by Green and co-workers[7] on the related cyclopentadienyl or indenyl system $[MoLL'(\eta^2\text{-}RC_2R')(\eta^5\text{-}C_5H_5 \text{ or } C_9H_7)][BF_4]$.

Acknowledgements—We wish to thank Dr O. W. Howarth for running the ^{31}P NMR spectra of complexes **1–4** at the University of Warwick and we thank the SERC for support.

REFERENCES

1. P. S. Braterman, J. L. Davidson and D. W. A. Sharp, *J. Chem. Soc., Dalton Trans.* 1976, 241.
2. K. Tatsumi, R. Hoffmann and J. L. Templeton, *Inorg. Chem.* 1982, **21**, 466.
3. M. Kamata, K. Hirotsu, T. Higuchi, M. Kido, K. Tatsumi, T. Yoshida and S. Otsuka, *Inorg. Chem.* 1983, **22**, 2416.
4. S. R. Allen, P. K. Baker, S. G. Barnes, M. Green, L. Trollope, L. M. Muir and K. W. Muir, *J. Chem. Soc., Dalton Trans.* 1981, 873.
5. K. A. Mead, H. Morgan and P. Woodward, *J. Chem. Soc., Dalton Trans.* 1983, 271.
6. J. L. Davidson, *J. Chem. Soc., Dalton Trans.* 1983, 1667.
7. M. Green, *J. Organomet. Chem.* 1986, **300**, 93 and refs cited therein.
8. M. Bottrill and M. Green, *J. Chem. Soc., Dalton Trans.* 1977, 2365.
9. P. L. Watson and R. G. Bergman, *J. Am. Chem. Soc.* 1980, **102**, 2698.
10. C. M. Giandomenico, C. T. Lam and S. J. Lippard, *J. Am. Chem. Soc.* 1982, **104**, 1263.
11. E. M. Armstrong, P. K. Baker, M. Harman and M. B. Hursthouse, *J. Chem. Soc., Dalton Trans.*, in press.
12. P. B. Winston, S. J. N. Burgmayer, T. L. Tonker and J. L. Templeton, *Organometallics* 1986, **5**, 1707.
13. P. C. Ford and R. E. Clarke, *J. Chem. Soc., Chem. Commun.* 1968, 1109.
14. J. L. Templeton and B. C. Ward, *J. Am. Chem. Soc.* 1980, **102**, 3288.

SUBJECT INDEX

A

Acetates and acetato complexes
  cobalt(II), 1603
  cobalt(III), 2103
  copper(II), 39,1533,1869
  molybdenum(II), 2111
  molybdenum(III), 255
  molybdenum(III,IV), 2181
  nickel(II), 1603
  palladium(II), 1003,1619
  rhodium(II), 461
  ruthenium(II), 1621
  tungsten(III), 255
  uranium(VI), 205,647
  vanadium(I), 1351
Acetic acid, solubilization of
  gold, 483
Acetonitrile complexes
  cobalt(III), 1875
  iron(II), 1089
  molybenum(II), 2081
  rhenium(II,III), 1483
  ruthenium(II), 1089
  tungsten(II), 2081
  vanadium(I), 1351
2-Acetylpyridine complexes
  platinum(IV), 319
  rhenium(I), 593
  tin(IV), 393
2-Acetylpyridine thiosemicarbazone complexes, copper(II), 39
Actinides, pyrazolone complexes, 2099
Acyl complexes, rhenium(I), 593
Adenine, adenosine complexes
  ruthenium(III), 387
Adenosine mono-, di-, triphosphate complexes, aluminium, 2095
Alamine 336, in solvent extraction of palladium, 1125
Alanine complexes
  cobalt(III), 947
  copper(II), 1669
  iron(III), 969
Alanylprolyl peptide complexes
  copper(II), 45
Alcohol complexes
  copper(II), 881,1319
  nickel(II), 1457
  rhenium(V), 1647
Alcoholamine complexes
  nickel(II), 1279
Aldehyde complexes
  tin(IV), 393
Aldol reaction, copper(II) complexes, 1473
Aliquat 336, in solvent extration of palladium, 1125
Alkenes
  hydrogenation catalysis, iridium(I), rhodium(I) complexes, 1329
  reactions with metal - metal bonds, 763
Alkene complexes
  lanthanides(0), 826
  zirconium(III), 645
Alkoxides and alkoxo complexes
  aluminium, 1791
  indium(III), 507
  molybdenum(III), 255,1677
  tungsten(III), 255,1677,1747
  tungsten(VI), 163,1551,1657
Alkyls
  bismuth(III), 1593
  indium(III), 507
  iron, 2067
  lanthanides(II), 815
  molybdenum, 2067
  molybdenum(III), 255
  niobium(V), 2019
  platinum(IV), 319,549,1157,1261
  rhenium(V), 1169
  rhenium(VII), 1599
  tantalum(V), 2019
  tin(IV), 383,393,587,1037,1639
  titanium(IV), 2019
  tungsten, 2067
  tungsten(III), 255
  tungsten(VI), 1839
Alkylamides
  molybdenum(III), 255,1677
  tungsten(III), 255,1677
O,O′-Alkylenedithiophosphates
  titanium(IV), 1681
Alkylidyne complex
  rhenium(VII), 1599
Alkylimido complexes
  rhenium(V), 1169
  tungsten(VI), 1657
4-(Alkylmercaptomethyl)imidazole complexes, copper(II), 943
N-Alkylphenothiazine complexes
  molybdenum(IV), 465
Alkynes
  reactions with metal - metal

bonds, 763,783
reduction by organolanthanides(II), 822
Alkyne complexes
lanthanides(0), 826
Alkynides, lanthanides(II), 815
Allogon, nickel(II) diphosphine nitrate complex, 1223
Aluminium
adenosine phosphate complexes, 2095
alkoxide, 1791
bromide oxo tungsten(VI) complex, 1839
catecholate diketonate, 525
chloride complexes, 975
cysteine nitrilotriacetate thiourea complexes on cellulose, 1197
magnesium hydroxide, 1587
magnesium oxide, 1791
Schiff base siloxy thiolate compounds, 1097
trimethyl, reactions with phosphazenes, 132
Americium(III) pyrazolone complexes, 2099
Amide complexes
cobalt(II), 1235
cobalt(III), 1875
copper(II), 1053,1399,1669
iron(I), 1497
ruthenium(III), 1009
tin(IV), 1037
uranium(VI), 647
vanadium, 1445
vanadium(IV), 841
Amidinate complex
iridium(III), 1625
Amidophosphazene complexes
iridium(I), rhodium(I), 1999
Amine complexes
borane, 1183
Co(II), Ir(I),(III), 921
iron(II), 1089
molybdenum(0), 1523
molybdenum(IV), 465
nickel(II), 921,1279
palladium(II), 921
platinum(II), 85,225,921
rhodium(I),(III), 921
ruthenium(II), 1089
tungsten(VI), 163,1657
zinc, 1111
Aminoacid complexes
on cellulose, 1197
aluminium, cadmium, calcium, 1197
cobalt(II), 633,1197,2037,2053
cobalt(III), 105,651,947
copper(II), 633,845,1197,1669, 2037,2053
iron(III), 969,1197
magnesium, 1197
manganese(II), 2037,2053
mercury, 1197
nickel(II), 633
palladium(II), 1391
zinc, 633,1197
Aminoalkylphenothiazine complexes
molybdenum(IV), 465
Aminoarsines, reactions with diarsines, 1229
Aminodicarboxylate, tin(IV), 1639
2-Aminomethylpyridine complexes
borane, 1183
2-Aminophenoxides
molybdenum(0), 1523
molybdenum(VI), 275
tungsten(VI), 275
Aminophosphine complexes, 2009
Aminopolycarboxylate complexes
beryllium, 1364
on cellulose, 1197
cobalt(III), 1571
copper(II), europium(III), iron(III), lanthanum, lithium, 1971
palladium(II), 571
platinum(II), 571
ruthenium(III), 603
Aminopolyphosphonate complex
manganese(II), 403
2-Aminopyridine complexes
borane, 1183
2-Aminopyrimidine complexes
borane, 1183
copper(II), 855
2-Aminothiophenoxides
bismuth(III), 1593
molybdenum(0), 1533
Ammines
chromium(III), 1153,1239
cobalt(III), 1337,1343,1347, 1563,1571,1929
iridium(III), 1347
iron(II),(III), 1191
molybdenum(VI), 275
palladium(II), 79,225
platinum(II), 85,225
rhodium(III), 1347
ruthenium(II), 159
ruthenium(II,III), 1711
tungsten(VI), 275
Angular overlap parameters
cobalt(III) aminoacid complexes, 947
ruthenium(II) dipyridyl complexes, 1621
Aniline complexes
palladium(II), 1059
platinum(II), 85
Aniline-2-carboxylate complexes
molybdenum(VI), 275
tungsten(VI), 275
4-Anisyl, tellurium(IV), 219
Antimony(III)
dithiocarbamate phenyl compounds, 411
Antimony(V)
carboxylate phenyl compounds, 1161
dithiocarbamate phenyl compounds, 411
organo compounds, book review, 660
Arabinose compounds
tin(IV), 383
Arene complexes
chromium(I), 2151
ruthenium(II), 473
Arginine complexes
copper(II), 1669
Arsenate, calcium, 1049
Arsenic complexes
cobalt, nickel, 1491

Arsenic(III) alkyl dialkylamido compounds, 1229
Arsenic(V) hydroxyapatite, 1049
Arsine complexes
gold(I), 1255
iridium(III), 921,1255
manganese(II), 1699
palladium(II), 921,1619
Pt(II), Rh(I), 921
rhodium(III), 921,1255
ruthenium(II), 1255,1383
Arsine oxide complexes
iron(II), 1325
Aryls
antimony(III), 411
antimony(V), 411,1161
bismuth(III), 1593
lanthanides(II), 817
palladium(II), 1003
phosphorus(III), 915
rhenium(V), 1169
silicon, 435
tellurium(IV), 219
tin(IV), 393,397,587,1037
titanium(IV), 2019
Arylimido complexes
chromium(IV), iron(III), 2191
tungsten(VI), 163
Arylphosphido complexes
lithium, 987
Asparagine complexes
iron(III), 969
Azide complexes
ruthenium(II), 1621
vanadium(I), 1351
Azine complexes, cobalt(II), 1075
Azobenzene, reduction by organo-lanthanides(II), 822
Azole complexes
cadmium, 1477
cerium(IV), 285
cobalt(II), 1477,1843,1993
cobalt(III), 1347,1563
copper(II), 943,1149
iridium(III), 1347
mercury, 1209
nickel(II), 1457,1477,1843
platinum(II), 85,341
rhodium(III), 1347
ruthenium(III), 1009
uranium(VI), 285
vanadium(IV), 455
zinc, 1209,1477

B

Bamboo, use in solubilising gold and silver, 483
Barium
crown amine-ether carboxylate complexes, 29
crown ether complexes, 535
phosphinedicarboxylate water complex, 1407
Benzaldehyde semicarbazone, thio-semicarbazone complexes, aluminium, 1097
Benzene-1,2-dioxydiacetates
Ca,Co,Mg,Mn,Ni,Zn, 871
1,2-Benzenediselenolate
bismuth(III), 1593
1,2-Benzeneditellurolate
hafnium(IV), 1923
1,2-Benzenedithiolate
bismuth(III), 1593
Benzo-18-crown-6 complex
hydrogen ion, 1469
Benzoate
indium(III), 507
7,8-Benzoquinoline complexes
palladium(II), 1243
1-Benzoylacetonates
iron(II),(III), 1421
2-Benzoylpyridine complexes
tin(IV), 393
Benzyls
rhenium(V), 1169
tin(IV), 1037
titanium(IV), 2019
(Benzylthio)acetates
cadmium, zinc, 881
Beryllium
aminopolycarboxylates, 1364
hydroxide iminodiacetate complexes, 303
Bicarbonate complexes
ruthenium(II), 1621
Bicyclo[2.2.1]-hepta-2,5-diene complexes, rhodium(I), 1427
Biphenyl complex
chromium(I), 2151
Bipyrimidine complexes
lanthanides, 175
palladium(II), rhodium(I), 1427
1,1'-Bis(aminomethyl)ferrocene, 1243
1,6-Bis(benzimidazol-2-yl)-2,5-dioxahexane complex, copper(II), 1149
1,7-Bis(benzimadozol-2-yl)-2,6-dithiaheptane complexes, cobalt(II), nickel(II), 1843
1,6-Bis(benzimadozol-2-yl)-2,5-dithiahexane complexes, cobalt(II), nickel(II), 1843
Bis(dimethylarsino)sulphide complexes, Au(I), Rh(III), Ru(II), 1255
1,2-Bis(dimethylphosphino)ethane complexes,
iron(II), 1089
mercury, 655
molybdenum(III), 255
molybdenum(IV), 1741
ruthenium(II), 1089
tungsten(III), 255
vanadium(0),(I), 1351
1,4-Bis(diphenylarsine oxide)butane complexes, iron(II), 1325
1,2-Bis(diphenylarsine oxide)ethane complexes, iron(II), 1325
Bis(2-diphenylarsinoethyl)benzylamine complexes, 921
1,4-Bis(diphenylphosphine oxide)-butane complexes, iron(II), 1325
1,2-Bis(diphenylphosphine oxide)-ethane complexes, iron(II), 1325
1,6-Bis(diphenylphosphine oxide)-hexane complexes, iron(II), 1325
2,3-Bis(diphenylphosphino)butane complexes
molybdenum(II), 715
rhenium(III), 715

1,2-Bis(diphenylphosphino)ethane complexes
manganese(I), 1879
molybdenum(II), 715
palladium(II), 1261
platinum(II), 1261
rhenium(II),(II,III),(IV), 1483
ruthenium(0), 1709
1,2-Bis(diphenylphosphino)ethane-diselenide complexes, tellurium(IV), 219
1,2-Bis(diphenylphosphino)ethene complexes,
osmium(II), 1131
rhenium(II), 907,1483
rhenium(II,III), 1483
rhenium(III), 907,1925
rhenium(IV), 1483
ruthenium(II), 1131
Bis(diphenylphosphino)ether complexes, molybdenum(II), 1103
Bis(2-diphenylphosphino)ethylamine complexes, Ir(III),Pd(II), Pt(II), Rh(I),(III), 1727
Bis(2-diphenylphosphinoethyl)benzylamine complexes, 921
1,2-Bis(diphenylphosphino)ethyne complexes, rhenium(III), 1925
1,1′-Bis(diphenylphosphino)ferrocene complexes, ruthenium(II), 473
Bis(diphenylphosphino)methane complexes
iridium(I), 111
manganese(I), 111,1879
mercury, 655
molybdenum(II), 95,261,1103
rhodium(I), 111
ruthenium(II), 473
tungsten(II), 1135
Bis(diphenylphosphinomethyl)dimethylsilane complex, nickel(II), 1223
1,2-Bis(diphenylphosphino)propane complexes
mercury, 655
molybdenum(II), 715
Bis[di-(4-tolyl)phosphino]ether complexes, molybdenum(II), 1103
1,1′-Bis(3-methyl-5-oxo-2-aza-3-hexenyl)ferrocene, 1243
Bis(methylseleno)methane complexes, chromium(0), tungsten(0), 1785
Bis(methylthio)methane complexes chromium(0), tungsten(0), 1785
Bismuth(III)
aminothiophenoxide bromide diselenolate dithiolate methyl phenyl complexes, 1593
chloride iron(0) complex, 2031
Bis(pentane-2,4-dione)ethylenediimine complexes
cobalt(III), 995
1,7-Bis(2-pyridyl)-2,6-dithiaheptane complexes, copper(II), 943
1,6-Bis(2-pyridyl)-2,5-dithiahexane complexes, copper(II), 943
1,8-Bis(2-pyridyl)-3,6-dithiaoctane complexes, copper(II), 943
2,3-Bis(2-pyridyl)pyrazine complexes, Cr(0),Mo(0),W(0), 1673
Bis(salicylaldehyde)ethylenediimine complexes, cobalt(III), 995
Biuret complexes
vanadium(IV), 841
Book reviews
antimony(V) organo compounds, 660
carbosilanes, 659
clusters, 347
copper organo compounds, 1716
organometallic chemistry, 1716, 2035
periodic table, 659
structural methods, 1715
tin(IV) organo compounds, 660
titanium organo compounds, 660
Borane, reactions with amines, pyridines, pyrimidines in water, 1183
Boranes, electron diffraction, 1849
Borane anions, polyhedral, 619, 2129
Borate esters, spiro type, 2119
Borohydride complexes, 1936
uranium(III), 189
Boron
carbohydrate complexes, 1415
in heteropolymolybdate, 519
Bromate, reaction with diaminoazobenzene, 2137
Bromate complexes
ruthenium(II), 1621
Bromides and bromo complexes
aluminium, 1839
bismuth(III), 1593
cobalt(II), 921,1075
cobalt(III), 1563,1571
copper(II), 1149,1399
iridium(I), 111
iron(II), 1325
lanthanum, 1021
manganese(I), 111,1879
manganese(II), 1075
mercury, 543
molybdenum(0), 1781
molybdenum(II), 715,729,1103
nickel(II), 921,1075,1407
palladium(II), 225,1003,1065
platinum(II), 85,225,1065
platinum(IV), 319,1261
rhenium(I), 593,1255
rhenium(II), 729,1483
rhenium(II,III), 1483
rhenium(III), 715,907
rhenium(IV), 1483
rhenium(V), 1169
rhodium(I), 111,1503
rhodium(III), 1885
ruthenium(II), 1383,1621
selenium(II), 849
thallium(III), 315
tungsten(0), 1781
tungsten(II), 729
tungsten(VI), 1839
vanadium(IV), 455
zinc, 1075
zirconium(III), 645
2-Bromobenzoate
chromium(III), 1153
9-Bromo-1,2-dicarba-closo-decaborane(11), 1559
Bromophenylhydrazine, 1577

4-Bromothiophenoxide, iron, 1445
α-Bromovalerate, copper(II), 1203
2,3-Butanediol, catalytic hydrogenation, 2187
Butanethiolates, iron, 2085
Butaperazine complexes
molybdenum(IV), 465
i-,n-,s-Butoxides
copper(II), zirconium(IV), 427
t-Butoxides
copper(II), 427
indium, 507
molybdenum(III), 255
tungsten(III), 255
tungsten(VI), 1551
zirconium(IV), 427
Butyls
indium(III), 507
tin(IV), 383,587,1037
t-Butylamine complexes
tungsten(VI), 163,1657
4-t-Butylbenzoate complexes
rhodium(II), 461
n-Butyl(cyanoethyl)dithiocarbamate, antimony(III), 411
t-Butylidyne complexes
molybdenum(III), 255
tungsten(III), 255
t-Butylimido complexes
rhenium(V), 1169
tungsten(VI), 1657
t-Butylisocyanide complexes
tungsten(VI) 1657
t-Butylthiolate, iron(-I), 1147
Butyrate, rhodium(II), 461
N-iso-Butyroyl-L-lysine complexes
Co,Cu,Ni,Zn, 633

C

Cadmium
carboxylate thioether water complex, 881
chloride hydrazone complexes, 1075
chloride Schiff base complex, 1319
crown amine - ether carboxylate complexes, 29
cysteine nitrilotriacetate thiourea complexes on cellulose, 1197
glycylglycine imidazole pyridoxamine complexes, 1477
hydroxycarboxylates, 1517
nitrilotri(methylenephosphonate)complexes, 1247
phosphine oxide quinoline complexes, 963
Schiff base thiolate complexes, 1653
Caesium
crown ether complexes, 417
Calcium
arsenate hydroxide, 1049
catecholdicarboxylate water complexes, 871
crown amine - ether carboxylate complexes, 29
crown ether complexes, 535
cysteine nitrilotriacetate thiourea complexes on cellulose, 1197
Californium(III) pyrazolone complexes, 2099
Carbaboranes
electrophilic substitutions, 1981
halogenation, 1737
PE spectra, 1559
Carbazol-9-yl complexes
Eu(II), Yb(II), 1143
Carbohydrate compounds
boron, 1415
tin(IV), 383
Carbonate complexes
cobalt(III), 651,1343
ruthenium(II), 1621
Carbon monoxide, reduction by organolanthanides(II), 821
Carbonyl complexes
chromium(0), 503,1673,1785
chromium(I), 759
iridium(I), 111,1999
iridium(III), 1727
iron, 1445,2067
iron(0), 1959,2031
iron(-II), 1273
iron(II), 1703
manganese(I), 111,1879
molybdenum, 2067
molybdenum(0), 503,1673,1781, 1797
molybdenum(I), 759
molybdenum(II), 95,261,1103, 2081
palladium(0), 1987
platinum(II), 85
rhenium(I), 593,1255
rhodium(I), 111,1427,1987,2073
ruthenium(II), 837,1255,1851, 2009
ruthenium(III), 2009
tungsten, 2067
tungsten(0), 337,503,1673,1781, 1785,1797
tungsten(I), 759
tungsten(II), 1135,2081
vanadium(0),(I), 1351
Carborane - phosphazenes, 131,146
Carbosilanes, book review, 659
Carboxylate complexes
antimony(V), 1161
barium, 29
cadmium, 29,881
calcium, 29
chromium(III), 1153
cobalt(II), 29,1603
cobalt(III), 2103
copper(II), 29,39,53,855,881, 1203,1533,1869
indium(III), 507
iron(II), 29,53
iron(III), 2155
lead, lithium, 29
magnesium, 29
manganese(II), 29,1699
molybdenum(0), 1523
molybdenum(II), 1523,2111
molybdenum(III), 255,1523
molybdenum(III,IV), 2181
molybdenum(VI), 273
nickel(II), 29,1603
palladium(II), 1003,1619
potassium, 29
rhodium(II), 461

ruthenium(II), 1621
sodium, strontium, 29
tellurium(IV), 219
thallium(I), 401
tin(IV), 397,587
tungsten(III), 255
tungsten(VI), 273
uranium(VI), 647
vanadium(I), 1351
zinc, 29,53,881
2-Carboxylatoquinoline complexes
Mo(VI), W(VI), 273
Catecholamine, 25
Catecholate complexes
aluminium, 525
copper(II), 53,845
Fe(II), Zn, 53
Catecholdicarboxylates, 871
CD spectra
chromium(III) diimine complexes, 105
cobalt(III) aminoacid complexes, 105
cobalt(III) diketonates, 583
cobalt(III) substitutions, 651
copper(II) peptide complexes, 45
molybdenum(II), rhenium(III) diphosphine halide complexes, 715
Cellulose, functionalised for metal complex formation, 1197
Cerium(III)
bipyrimidine nitrate complexes, 175
Cerium(IV)
azole nitrate sulphate complexes, 285
heteropolytungstate, 519
Chirality,
chromium(III) diimine, cobalt(III) aminoacid complexes, 105
quadruply bonded complexes, 715
Chloride, reaction with
iridium(III) complex, 101
Chlorides and chloro complexes
aluminium, 975
bismuth(III), 2031
cadmium, 1075,1319
chromium(III), 1239
chromium(VI), 1721,2145
cobalt(II), 897,921,1075,1843
cobalt(III), 1337,1563,1875
copper(II), 39,897
europium(III), 175
gold(I), 1255
gold(III), 2077
holmium, 175
iridium(I), 111,2009
iridium(III), 921,1509,1727, 1885,2009
iron, 1445
iron(II), 1089,1325
iron(III), 969
lanthanum, 175,1021
lead(II), 563
magnesium, 975
manganese(I), 111
manganese(II), 897,1075,1699
mercury, 543,1075,1781
molybdenum(0), 1781
molybdenum(II), 715,729,2081, 2111
molybdenum(IV), 1741
molybdenum(V), 668
nickel(II), 897,921,1075,1407, 1457,1843,2009
niobium(V), 668
osmium(II), 1131
osmium(II,III), 1439
osmium(IV), 1695
palladium(II), 225,319,447,571, 921,1003,1059,1065,1391,1427, 1727,1797,2009
platinum(II), 85,225,571,921, 1065,1295,1727,1797,1803
platinum(IV), 319,1261
rhenium(-I), 1577
rhenium(I), 1255,2073
rhenium(II), 729,907,1483
rhenium(II,III), 1483
rhenium(III), 715,907,1925
rhenium(IV), 1483,1647
rhenium(V), 668,1169,1647
rhenium(VI), 1647
rhodium(I), 111,1427,2009,2027
rhodium(III), 921,1009,1255, 1727,1885,2009
ruthenium(II), 473,837,1089, 1131,1255,1383,1621,1851,2009
ruthenium(II,III), 1711
ruthenium(III), 1009,1875,2009
selenium(II), 849
silver(I), 1695
tantalum(III),(IV), 741
tantalum(V), 1765
tellurium(IV), 219
thallium(I), 1721
thallium(III), 479
tin(II), 71
tin(IV), 393,1037
titanium(IV), 1681
tungsten(II), 729,2081
tungsten(III), 729
tungsten(V), 668
tungsten(VI), 163,1657
uranium(VI), 285,647
vanadium(II), 1433
vanadium(IV), 455
vanadium(V), 1807
ytterbium, yttrium, 175
zinc, 1075,1111
zirconium(III), 645
Chloroacetate complexes
cobalt(II), nickel(II), 1603
9-Chloro-1,2[&1,7]-dicarba-closo-decaborane(11), 1559
4-Chlorophenylimide complexes
iron(III), 2191
Chlorophosphazenes, cyclic, 125
4-Chloropyridine-N-oxide complexes, thallium(III), 315
4-Chlorothiophenoxide, iron, 1445
Chlorpromazine complexes
molybdenum(IV), 465
Chromate, reaction with
diaminoazobenzene, 2137
Chromium(0)
carbonyl complexes, 503
carbonyl diimine complexes,1673
carbonyl selenoether thioether complexes, 1785
phosphazene complexes, 138
phosphorus cluster complexes, 364,369,373

Chromium(I) biphenyl complex, 2151
Chromium(II)
heteronuclear metal - mtal bonds, 793
oxidation by molybdenum(III), 1975
phosphazene complexes, 140,143
Chromium(III)
ammine carboxylate complexes, 1153
ammine chloride water complexes, 1239
dehydroacetic acid complex, 1235
diimine complexes, 105
porphyrin water complex, 1361
Chromium(IV)
arylimido porphyrin complex, 2191
Chromium(VI)
chloride oxo complex, 2145
reaction with thallium(I), 1721
CNDO/2 calculations, transition metal complexes, 1215
Cobalt
metallaboranes, 1937,1942,1953
phosphorus cluster complex, 371
triphosphine tripnictide/-chalcogenide complexes, 1491
Cobalt(0)
phosphinoalkyne complexes, 151
phosphorus cluster complexes, 355,373,376,379
Cobalt(0,I)
phosphorus cluster complex, 360
Cobalt(I)
phosphazene complexes, 142
phosphite mercury(I) complexes, 543
phosphorus cluster complex, 356,359,363,366,372,378
Cobalt(II)
amide dehydroacetic acid complex, 1235
amine halide phosphine complexes, 921
aminoacid complexes, 633,2037, 2053
aminophosphine chloride complexes, 2009
azine halide hydrazone thiocyanate complexes, 1075
azole chloride thioether complexes, 1843
azole phenoxide complex, 1993
carboxylate diamine water heterobinuclear complexes, 1603
catecholdicarboxylate water complexes, 871
crown amine - ether carboxylate complexes, 29
cyanide complexes, 1909
cysteine nitrilotriacetate thiourea complexes on cellulose, 1197
diaminoazobenzene complex, 2137
dioxygen porphyrin pyridine complex, 1071
glycylglycine imidazole pyridoxamine complexes, 1477
heterobinuclear complexes, 897
in heteropolytungstate, 1513
hydroxycarboxylates, 1517
oxime Schiff base complexes, 205
phosphazene complexes, 137,142
phthalocyanines, 1463
pyrimidine Schiff base complexes, 2103
salicylaldiine Schiff base complexes, 1319
sulphite complexes, 1717
water complex in borane - amine reactions, 1183
Cobalt(III)
acetate pyrimidine Schiff base complexes, 2103
acetonitrile chloride dimethylformamide macrocyclic tetramine sulphonate complexes, 1875
aminoacid complexes, 105,947
ammine carbonate complexes, 1343
ammine bromide complex, 1571
ammine chloride sulphoxide water complexes, 1337
ammine cyanide water iron(III) complex, 1929
ammine water complex, 1571
carbonate ethylenediamine glycine oxalate complexes, 651
diamine hydroxoaqua nitrite thiocyanate complexes, 181
diketonates, 583
ethylenediaminetetraacetate complex, 1571
halide nitrite pseudohalide complexes, 1563
in heteropolymolybdates, 1343
ketoimine pyridine salicylaldimine complexes, 995
Cone packing model, lanthanide complexes, 1041
Coordination saturation lanthanide complexes, 1041
Copper
organo compounds, book review, 1716
Copper(I)
organo compounds, reactions with phosphazenes, 131
phosphorus cluster complexes, 377
Copper(II)
alkoxide zirconium compounds, 427
amide aminoacid dioxane pyridine salicylaldimine sulphoxide water complexes, 1669
amide bromide complexes, 1399
amide diamine pyridine triamine complexes, 1053
aminoacid complexes, 633,2037, 2053
aminoacid catecholate phenanthroline complexes, 845
aminopolycarboxylate phenoxide water heterobinuclear complexes, 1971
azole bromide ether complex, 1149

azole pyridine thioether complexes, 943
bromovalerate, 1203
carboxylate catecholate complexes, 53
carboxylate ethanol complexes, 881
carboxylate ether pyrimidine water complexes, 855
carboxylate terpyridine water complexes, 1533
carboxylate water complexes, 1869
crown amine - ether carboxylate complexes, 29
cysteine nitrilotriacetate thiourea complexes on cellulose, 1197
dehydroacetic acid complex, 1235
diaminoazobenzene complex, 2137
diketonate, triketonate complexes, 1473
ethanol salicylaldimine Schiff base water complex, 1319
heterobinuclear complexes, 897
heteropolymolybdates, 213
hydroxycarboxylates, 1517
ketoimine macrocycle polyamine pyridine Schiff base complexes, 2169
macrocyclic Schiff base complexes, 289
macrocyclic tetramine complexes, 1291
nitrilotri(methylenephosphonate)complexes, 1247
nitrosoalkylhydroxylamine complexes, 1375
nitrosoresorcinol complexes, 1033
oxime Schiff base complexes, 205
peptide complexes, 45
phosphazene complexes, 136
phthalocyanines, 1463
pyridine thiosemicarbazone complexes, 39
salicylaldoxime complexes, 197
tetrasalicylaldimine complexes, 513

15-Crown-5 in halophosphine synthesis, 1295

Crown amine - ether complexes
Ba,Ca,Cd,Co,Cu,Fe,K,Li,Mg,Mn, Na,Ni,Pb,Sr,Zn, 29

Crown ether complexes
Ba,Ca, 535
caesium, 417
hydrogen ion, 1469
potassium, 417,577
silver, 535
sodium, 417
strontium, 435
uranium(III),(VI), 189

Curium(III) pyrazolone complexes, 2099

Curtius rearrangement, siloxane synthesis, 435

Cyanide complexes
cobalt(II), 1909
cobalt(III), 1563,1929
iron(0), 1191
iron(II), 159
iron(III), 1929
manganese(II), 1909
molybdenum(IV), 269
nickel(II), 1407
palladium(II), 79
ruthenium(II), 1383,1621
tungsten(V), 641
vanadium(I), 1351

4-Cyanopyridine complexes
iron(II), 159

4-Cyanopyridine-N-oxide complexes
thallium(III), 315

Cyclam complexes
cobalt(III), ruthenium(III), 1875

Cyclic voltammetry
chromium(0) carbonyl diimine complexes, 1673
cobalt(II) pyrimidine Schiff base complexes, 2103
cobalt(III) ammine imidazole complexes, 1347
cobalt(III) Schiff base complexes, 995
copper(II) macrocyclic tetramine complexes, 1291
ferrocene ketoimine palladium(II) complex, 1243
heterobinuclear complexes, 897, 1243
iridium(III) ammine imidazole complexes, 1347
iron thio thiophenoxide molybdenum(VI) complex, 1445
iron(II),(III) diketonates, 1421
molybdenum(0) carbonyl diimine complexes, 1673
molybdenum(VI) disulphide thio iron complex, 1445
nickel(II) dithiolate complexes, 863
osmium(II,III) chloride oxopyridine complex, 1439
rhenium(I) acylpyridine bromide carbonyl complexes, 593
rhenium(II),(II,III) diphosphine halide nitrile complexes, 1483
rhenium(III) diphosphine halide complexes, 907,1925
rhenium(V) chloride oxo phenoxide salicylaldimine complexes, 1647
rhodium(III) ammine imidazole complexes, 1347
ruthenium(II) chloride cymene diphosphine dipyridyl pyrazine complexes, 473
ruthenium(III) ethylenediaminetetraacetate mercaptopyridine complexes, 603
tungsten(0) carbonyl diimine complexes, 1673

Cyclobutyldithiocarbamate antimony(III), 411

Cycloheptatrienyl complexes thallium(III), 479

Cyclohexaphosphate, 531

Cyclohexoxide tungsten(III), 1747

Cyclohexyl, tin(IV), 587

Cyclohexylthioglycolate complexes
thallium(I), 397
Cyclometallated complexes
palladium(II), 1003,1243,1619
Cyclometallathiazine complexes
platinum(II), 2165
1,5-Cyclooctadiene complexes
iridium(I), 1329
rhodium(I), 1329,1427
Cyclooctaphosphate, 531
Cyclooctatetraene complexes
lanthanides(0), 829
lanthanides(II), 808
Cyclopentadienyl complexes
chromium(I), 759
hafnium(IV), 1923
iron(0), 2031
iron(II), 1243,1703
lanthanides(II), 808,818
molybdenum, 2067
molydenum(I), 759
rhenium(VII), 1165
rhodium(III), 1255
ruthenium(II), 1383
tungsten, 2067
tungsten(I), 759
Cyclopentadienyl(diphenyl)phosphine, cyclopentadienylphosphine, 1797
Cyclopentyldithiocarbamate
antimony(III), 411
Cyclopolyphosphates, 531,1863
Cyclotetraphosphine, 1295
p-Cymene complexes
ruthenium(II), 473
Cysteine, reaction with
molybdenum(IV) complexes, 465
Cysteine complexes, on cellulose, 1197
Cysteinesulphinate complex
cobalt(III), 105
Cytidine, cytosine complexes
ruthenium(III), 387

D

Dehydroacetic acid complexes
Cr(III), Co(II), Cu(II) Ni(II), 1235
1,4-Diacetylbenzenebishydrazone complexes, Cd,Hg,Mn,Ni,Zn, 1075
1,3-Diacetyl-2-hydroxy-5-methylbenzene complexes, 897
Diamagnetic anisotropy, metal - metal bonds, 1677
Diamine complexes
cobalt(II), 1603
cobalt(III), 181,651
copper(II), 1053
lithium, 987
molybdenum(III), 255
nickel(II), 1603
palladium(II), 225
platinum(II), 225
ruthenium(II), 837,1621
tungsten(III), 255
tungsten(VI), 1657
uranium(VI), 205
Diaminoazobenzene complexes, 2137
1,2-Diaminocyclohexanetetraacetate complexes, palladium(II), platinum(II), 571
1,2-Diaminopropane complexes
copper(II), 1053
1,2-Diaminopropanetetraacetate complexes, palladium(II), platinum(II), 571
Diarsines, reactions with
aminoarsines, 1229
Diarsine complexes
rhenium(I), 1255
Diazabutadienes, complexes and reactions with $PdCl_2$, 1059
Diazadiphosphacyclopentanones, 1823
Diazenide complexes
rhenium(-I), 1577
Diazoalkanes, reactions with
metal - metal bonds, 768
Dibenzo-13-crown-10 complexes
Ag,Ba,Ca,Sr, 535
Dibenzo-21-crown-7 complexes
hydrogen ion, 1469
Dibenzo-30-crown-8 complexes
hydrogen ion, 1469
Dibenzo-30-crown-10 complexes
potassium, 577
Dibenzoylmethanides
iron(II),(III), 1421
Dibenzyldithiocarbamates
antimony(III), 411
Di-i,n-butyldithiocarbamates
antimony(III), 411
2,6-Di-t-butyl-4-methylphenoxides
europium(II), 1143
ytterbium(II), 1143
2,6-Di-t-butylphenol, oxidation catalysed by cobalt(II) complexes, 2103
2,6-Di-t-butylphenoxide
tantalum(V), 1765
Di-i,n,t-butylsulphoxide complexes,
nickel(II), 1313
uranium(VI), 1913
1,2[&1,7]-Dicarba-closo-decaborane(12), 1559
4,5-Dicarba-arachno-heptaborane-(13), 1737
10,10-Dicarboxyethyl-1,4,8,12-tetraazacyclopentadecane complexes, copper(II), 1291
Dicarboxylates
cobalt(III), 651
palladium(II), 447
Dichloroacetates, cobalt(II), nickel(II), 1603
Dichloromethane, solvent for cyclic voltammetry, 1421
1,1-Dicyanoethene-2,2-diselenolate complexes, technetium(V), 1547
1,2-Dicyanoethene-1,2-dithiolate
bismuth(III), 1593
Dicyclohexyl-27-crown-9 complexes
hydrogen ion, 1469
Dicyclohexyl-30-crown-10 complexes, hydrogen ion, 1469
Didecylsulphoxide complexes
uranium(VI), 1913
Dielectric constant
vanadium(V) chloride oxo pyridylthiourea complexes, 1807
Diels - Alder addition, cyclopentadienylphosphine, 1797
Diene complexes

iridium(I), 1329,1999
rhodium(I), 1329,1427,1999
2-Diethylaminoethanol complexes
nickel(II), 1279
Diethyldithiocarbamates
antimony(III),(V), 411
iron(I), 1497
molybdenum(II), 1523
ruthenium(II), 1383
Diethyldithiophosphate
titanium(IV), 1681
tungsten(IV), 1115
Diethylenetriamine complexes
copper(II), 1053
Diethylether complexes
tantalum(V), 1765
Di-2-ethylhexyldithiocarbamates
antimony(III), 411
Diethyl malonate, reaction with
copper(II) tetramine complex,
1291
Differential pulse electrochemistry, copper(II) tetrasalicylaldimine complexes, 513
Difluoro-(2-methoxyphenyl)phosphine complexes, Pt(II), 1295
1,4-Diformylbenzenebishydrazone
complexes, Cd,Hg,Mn,Ni,Zn, 1075
Diglycolate, tin(IV), 1639
Diheptylsulphoxide, dihexylsulphoxide complexes,
uranium(VI), 1913
3,4-Dihydroxycinnamic acid
complexes, Cu,Fe,Zn, 53
Dihydroxyethyldithiocarbamates
antimony(III), 411
2,3-Dihydroxynaphthalene
complexes, copper(II), 845
Diimine complexes
chromium(0), 1673
chromium(III), 105
copper(II), 845
manganese(I), 1879
molybdenum(0), 1673,1781
neodymium(III), 957
palladium(II), 1427
praseodymium(III), 957
rhodium(I), 1427,2187
ruthenium(II), 1383,1621
ruthenium(III), 651,1009
sodium, 1833
tungsten(0), 1673,1781
tungsten(VI), 1657
4,4′-Diisocyanobiphenyl complex
rhodium(I), 2027
Diketonates
aluminium, 525
cobalt(III), 583
copper(II), 1473
indium(III), 507
iron(II),(III), 1421
magnesium, 1791
manganese(III), 2003
nickel(II), 497
ruthenium(II), 1383,1621
Dimethoxybenzoates
copper(II), 1869
1,4-Di(4′-methoxy)phenyl-2,3-dimethyl-1,4-diazabutadiene
complex, palladium(II), 1059
Dimethylamides
molybdenum(III), tungsten(III),
255
2-Dimethylaminoethanol complexes
nickel(II), 1279
2-Dimethylarsinobenzoate
manganese(II), 1699
Dimethylbarbituric acid complexes
cobalt(II),(III), 2103
N,N-Dimethylbenzylamine complexes
palladium(II), 1243
2,3-Dimethylbutanediolates
molybdenum(III), 1677
tungsten(III), 1677
5,5′-Dimethyl-2,2′-dipyridyl
complexes, chromium(III), 105
4,4-Dimethyl-1,2-diselenacyclopentane complex,
rhenium(I), 2073
Dimethyldithiocarbamates
nickel(II), 497
Dimethyldithiophosphate
iron(I), 1497
N,N′-Dimethylethylenediamide
complexes, molybdenum(III),
tungsten(III), 1677
N,N′-Dimethylethylenediamine
complexes, molybdenum(III),
tungsten(III), 255
1,1′-Dimethylferrocene, 943
Dimethylformamide, solvent for
crown ether complexes, 535
Dimethylformamide complexes
cobalt(II), 1235
cobalt(III), 1875
copper(II), 1053,1399
iron(I), 1497
ruthenium(III), 1009
uranium(VI), 647
vanadium, 1445
Dimethyl(methylthio)arsine
complexes, Au(I), Rh(III),
Ru(II), 1255
Dimethyl(phenyl)phosphine
complexes,
palladium(II), 1541
platinum(II), 1541,2165
rhenium(V), 1647
Dimethylsulphoxide, solvent
crown ether complexes, 535
cyclic voltammetry, 1421
Dimethylsulphoxide complexes
cobalt(III), 1337
copper(II), 1669
nickel(II), 1313
tin(IV), 1037
2,5-Dimethylthiophenoxide
rhenium(-I), 1577
Dimethylthiourea complexes
ruthenium(II), 837
2,4-Dinitrosoresorcinol complexes
copper(II), 1033
Dinonylnaphthalenesulphonate
complexes, mercury, zinc, 1209
Dinonylsulphoxide complexes
uranium(VI), 1913
Di-n-octylphosphinate complexes
nickel(II), 1251
Dioctylsulphoxide complexes
uranium(VI), 1913
Dioxane complexes
copper(II), 1669
Dioxygen complexes
cobalt(II), 1071
Di-i-pentylsulphoxide complexes
uranium(VI), 1913

Diphenoxy(phenyl)phosphine
complexes, rhodium(I), 1503
2-Diphenylarsinobenzoate
manganese(II), 1699
1,4-Diphenyl-2,3-dimethyl-1,4-di-
azabutadiene, 1059
Diphenyl(methoxy)phosphine
complexes, rhodium(I), 1503
Diphenyl(methyl)phosphine
complexes,
palladium(II), 1541
platinum(II), 1541,2165
tungsten(VI), 1657
Diphenyl(nitro)formazones, 13
2,6-Diphenylphenoxides
Nb(V),Ta(V),Ti(IV), 2019
Diphenyl(phenoxy)phosphine
complexes, rhodium(I), 1503
Diphenylphosphide complexes
lithium, 987
Diphenylphosphine complexes
manganese(I), 1879
(2-Diphenylphosphinoethyl)benzyl-
amine complexes, Co,Ir,Ni,Pd,
Rh,Ru, 2009
Diphenyl(i-propoxy)phosphine
complexes, rhodium(I), 1503
Diphenylthiocarbazone, 13
Diphenylthiocarbazone complexes
molybdenum(0), 1523
Diphosphine complexes
dimeric, review, 729
iridium(I), 111
iron(II), 1089
manganese(I), 111,1879
mercury, 655
molybdenum(0), 1797
molybdenum(II), 95,715,729,1103
molybdenum(III), 255
molybdenum(IV), 1741
nickel(II), 1223
osmium(II), 1131
palladium(II), 1261,1797
platinum(II), 1261,1797
rhenium(II), 729,907,1483
rhenium(II,III), 1483
rhenium(III), 715,907,1925
rhenium(IV), 1483
rhodium(I), 111
ruthenium(0), 1709
ruthenium(II), 473,1089,1131
tungsten(0), 1797
tungsten(II), 729,1135
tungsten(III), 255,729
vanadium(0),(I), 1351
Diphosphinoamine complexes
Ir(III),Pd(II),Pt(II),
Rh(I),(III), 1727
Diphosphoxane complexes
molybdenum(II), 1103
Dipropyldithiocarbamates
antimony(III), 411
Di-i-propyldithiophosphates
titanium(IV), 1681
2,6-Di-i-propylphenoxide
tantalum(V), 1765
Di-n-propylsulphoxide complexes
nickel(II), 1313
2,2′-Dipyridyl, reactions with
molybdenum(IV) complexes, 465
2,2′-Dipyridyl complexes
chromium(III), 105
manganese(I), 1879
molybdenum(0), 1781
rhodium(I), 2187
ruthenium(II), 1383,1571,1621
ruthenium(III), 651
tungsten(0), 1781
tungsten(VI), 1657
4,4′-Dipyridyl complexes
ruthenium(II), 473
Diselenide complex
rhenium(I), 2073
Diselenolate complexes
bismuth(III), 1593
technetium(V), 1547
Disulphide complexes
molybdenum(VI), 1445
Disulphurdinitride $[S_2N_2^{2-}]$
complexes, palladium(II),
platinum(II), 1541
Ditellurolene complex
hafnium(IV), 1923
Dithiocarbamates
antimony(III),(V), 411
iron(I), 1497
molybdenum(II), 1523
nickel(II), 497
ruthenium(II), 1383
Dithioformate complex
ruthenium(II), 1851
Dithiolate complexes
bismuth(III), 1593
nickel(II), 627,863
Dithiophosphates
iron(I), 1497
titanium(IV), 1681
tungsten(IV), 1115
Dithizone, 13
2-Di-4′-tolylarsinobenzoate
manganese(II), 1699
N,N′-Di-4-tolylformamidinate
iridium(II), 1625
Diundecylsulphoxide complexes
uranium(VI), 1913
Dodecanoates, iron(III), 2155
Dopamine complexes
copper(II), 845
DTA
aluminium magnesium hydroxide,
1587
arsenic(V) hydroxyapatite, 1049
copper(II) carboxylate
terpyridine water complexes,
1533
gold(III) chloride complex,
2077
indium(III) dibutyl compounds,
507
iron(II) cyanide pyrazine
pyridine complexes, 1757
molybdenum(IV) aminoalkylpheno-
thiazine oxo complexes, 465
molybdenum(VI) oxo
salicylaldimine complex, 1635
phthalocyanines, 1463
silver(I,III) oxide, 1309
spinel formation, 1791
tin(IV) methyl polycarboxylate
complexes, 1639
vanadium(IV) azole halide
nitrate pyridine sulphate
complexes, 455
vanadium(IV) biuret oxo
sulphate complexes, 841

E

Edge - shared octahedral dimeric structures, 667
Electric conductance
cerium(IV) azole nitrate complex, 285
copper(II) amide bromide complexes, 1399
copper(II) ethanol salicylaldimine Schiff base water complexes, 1319
gold(III) chloride complex, 2077
iridium(I) aminophosphine chloride complexes, 2009
iridium(I) carbonyl diphosphine halide manganese(I) complexes, 111
iridium(I) diene phosphine phosphine sulphide complexes, 1329
iridium(III) aminophosphine chloride complexes, 2009
iron(II) amine chloride diphosphine nitrile phosphine complexes, 1089
iron(III) aminoacid chloride hydroxide complexes, 969
lanthanide bipyrimidine chloride nitrate complexes, 175
manganese(I) carbonyl diphosphine halide iridium(I) rhodium(I) complexes, 111
molybdenum(VI) amine carboxylate oxo peroxide water complex, 275
nickel(II), palladium(II) aminophosphine chloride complexes, 2009
rhenium(II),(II,III) diphosphine halide nitrile complexes, 1483
rhenium(IV) chloride oxo phenoxide salicylaldimine complexes, 1647
rhodium(I) aminophosphine chloride complexes, 2009
rhodium(I) carbonyl chloride diene diimine palladium(II) complexes, 1427
rhodium(I) carbonyl diphosphine halide manganese(I) complexes, 111
rhodium(I) diene phosphine phosphine sulphide complexes, 1329
rhodium(III) aminophosphine chloride complexes, 2009
ruthenium(II) amine chloride diphosphine nitrile phosphine complexes, 1089
ruthenium(II) aminophosphine carbonyl chloride complexes, 2009
ruthenium(III) aminophosphine chloride complexes, 2009
titanium(IV) chloride dithiophosphates, 1681
vanadium(IV) azole halide nitrate pyridine sulphonate complexes, 455
Electric conductance (solid state)
indium - tin - oxide films, 507
rhodium(I) chloride diisocyanide polymeric complex, 2027
vanadium(V) chloride oxo pyridylthiourea complex, 1807
Electronic spectra
aluminium Schiff base complexes, 1097
chromium(0) carbonyl complexes, 503
chromium(0) carbonyl diimine complexes, 1673
chromium(III) diimine complexes, 105
chromium(IV) arylimido porphyrin complex, 2191
chromium(VI) chloride oxo complex, 2145
cobalt(II) amine halide phosphine complexes, 921
cobalt(II) aminophosphine chloride complexes, 2009
cobalt(II) azine halide hydrazone thiocyanate complexes, 1075
cobalt(II) azole chloride thioether complexes, 1843
cobalt(II) azole phenoxide complexes, 1993
cobalt(II) carboxylate diamine water heterobinuclear complexes, 1603
cobalt(II) dioxygen porphyrin pyridine complex, 1071
cobalt(II) heterobinuclear complexes, 897
cobalt(II) pyrimidine Schiff base complexes, 2103
cobalt(II) salicylaldimine Schiff base complexes, 1319
cobalt(III) aminoacid complexes, 105,947
cobalt(III) ammine halide nitrite pseudohalide water complexes, 1563
cobalt(III) diketonates, 583
cobalt(III) macrocyclic complexes, 1875
copper(II) amide bromide complexes, 1399
copper(II) amide diamine pyridine triamine complexes, 1053
copper(II) aminoacid catecholate phenanthroline complexes, 845
copper(II) aminopolycarboxylate phenoxide water heterobinuclear complexes, 1971
copper(II) bromovaleratre, 1203
copper(II) carboxylate terpyridine water complexes, 1533
copper(II) carboxylate water complexes, 1869
copper(II) heterobinuclear complexes, 897
copper(II) macrocyclic Schiff base complexes, 289
copper(II) nitrosoalkylhydrox-

ylamine complexes, 1364
copper(II) peptide complexes, 45
copper(II) salicylaldimine Schiff base complexes, 1319
copper(II) tetrasalicylaldimine complexes, 513
copper(II) zirconium(IV) alkoxides, 427
diaminoazobenzene, 2137
gold(III) chloride complex, 2077
heteropolymolybdates, 213,519
heteropolytungstates, 213,519
iron carbonyl thio heteropolynuclear complexes, 1445
iron(0) cyanide complex, 1191
iron(II) ammine thiocyanate, 1191
iron(II) arsine oxide halide phosphine oxide thiocyanate water complexes, 1325
iron(II) cyanide pyrazine pyridine complexes, 1757
iron(II) cyanide pyridine ruthenium(II) complex, 159
iron(III) aminoacid chloride hydroxide complexes, 969
iron(III) aminopolycarboxylate phenoxide water heterobinuclear complexes, 1971
isopolymolybdates, 519
isopolytungstates, 519
lanthanide(II) carbazolyl ether indolyl phenoxide complexes, 1143
lanthanide(III) bipyrimidine chloride nitrate complexes, 175
lead(II) nitrate thione complex, 2177
Magnus salts, 225
manganese(II) heterobinuclear complexes, 897
metal - metal bonds, 695,705, 715,723,1439
molybdenum(0) carbonyl complexes, 503
molybdenum(0) carbonyl diimine complexes, 1673
molydenum(0) dinitrosyl complexes, 1523
molybdenum(II) chloride binuclear complex, 1975
molybdenum(II) diphosphine halide complexes, 715
molybdenum(II) dithiocarbamate nitrosyl picolinate complexes, 1523
molybdenum(III) chloride hydride binuclear complex, 1975
molybdenum(IV) aminoalkylphenothiazine oxo complexes, 465
molybdenum(VI) disulphide thio iron complexes, 1445
molybdenum(VI) oxo salicylaldimine complex, 1635
nickel(II) amine halide phosphine complexes, 921
nickel(II) aminophosphine chloride complexes, 2009
nickel(II) azole chloride thioether complexes, 1843
nickel(II) carboxylate diamine water heterobinuclear complexes, 1603
nickel(II) diaminotetrazole complexes, 1457
nickel(II) diphosphine nitrate complexes, 1223
nickel(II) dithiolate complexes, 863
nickel(II) halide hydrazone thiocyanate complexes, 1075
nickel(II) heterobinuclear complexes, 897
nickel(II) ketoimine salicylaldimine thiosemicarbazide complexes, 1901
nickel(II) macrocyclic Schiff base complexes, 289
nickel(II) naphthylideneaminoacid complexes, 1017
nickel(II) nitrate sulphoxide complexes, 1313
nickel(II) nitrogen - sulphur complex, 939
nickel(II) perthiocarbonate tetrasulphide complexes, 627
nickel(II) salicylaldimine Schiff base complexes, 1319
nickel(II) Schiff base thiolate complexes, 1653
osmium(II,III) chloride oxopyridine complex, 1439
palladium(II) amine arsine chloride phosphine complexes, 921
palladium(II) aminoacid chloride thioether complexes, 1391
palladium(II) chloride dicarboxylate thioether complexes, 447
palladium(II) diphosphinoamine complexes, 1727
palladium(II,IV) ammine diamine halide complexes, 225
phthalocyanine complexes, 1463
platinum(II) amine arsine chloride phosphine complexes, 921
platinum(II) diphosphinoamine complexes, 1727
platinum(II,IV) ammine diamine halide complexes, 225
platinum(II) carbonyl halide complexes, 85
praseodymium macrocycle semicarbazone thiosemicarbazone water complexes, 1611
rhenium(I) acylpyridine bromide carbonyl complexes, 593
rhenium(II),(II,III) diphosphine halide nitrile complexes, 1483
rhenium(III) diphosphine halide complexes, 715,907,1925
rhodium(I) chloride diisocyanide polymeric complex, 2027
rhodium(I) diphosphinoamine complexes, 1727
rhodium(II) carboxylate macrocyclic complexes, 461

rhodium(III) amine arsine chloride phosphine complexes, 921
rhodium(III) diphosphinoamine complexes, 1727
rhodium(III) pentasulphide $[S_5]^{2-}$ complex, 1775
ruthenium(II) ammonia nitrile iron(II) complex, 159
ruthenium(II) cyclopentadienyl complexes, 1383
ruthenium(III) edta mercapto-pyridine complexes, 603
ruthenium(III) mercaptoquinazo-linone complexes, 1009
ruthenium(III) nucleoside perchlorate purine pyrimidine complexes, 387
technetium(V) diselenolate oxo complex, 1547
thiocarbazones, 13
tin(IV) phenyl trifluoroacetate, 397
tungsten(0) carbonyl complexes, 503
tungsten(0) carbonyl diimine complexes, 1673
tungsten(IV) dithiophosphate thio compound, 1115
tungsten(VI) thio iron complexes, 1445
uranium(VI) dioxo acetate diamine nitrate oxime Schiff base complexes, 205
vanadium amide thio iron complexes, 1445
vanadium(IV) azole halide nitrate pyridine sulphonate complexes, 455
vanadium(IV) biuret oxo sulphate complexes, 841
vanadium(V) chloride oxo pyridylthiourea complexes, 1807

Electron diffraction, boranes, 1999

Electron microscopy
aluminium magnesium hydroxide, 1587
arsenic(V) hydroxyapatite, 1049
iron(II) cyanide pyrazine pyridine complexes pyrolysis, 1757
silver(I,III) oxide, 1309
spinel formation, 1791

Enthalpy of activation
fluxional rearrangements, 549, 1261
hydrogen peroxide decomposition by manganese(II) complex, 403
substitutions, chromium(III) porphyrin complexes, 1361
substitutions, ruthenium(III) edta complexes, 603

Enthalpy of formation
alkali metal crown ether complexes, 417
cobalt(II) aminoacid complexes, 2037,2053
cobalt(II) dioxygen porphyrin pyridine complex, 1071
copper(II) aminoacid complexes, 2037,2053
hydrogen ion crown ether complexes, 1469
thallium(I) cyclohexylthioglycolate compounds, 401
triorganotin chloride solvates, 1037

Enthalpy of solution
arsenic(V) hydroxyapatite, 1049

Entropy of activation
chromium(I) arene complex reduction, 2151
fluxional rearrangements, 563, 1147,1261
hydrogen peroxide decomposition by manganese(II) complex, 403
substitutions, chromium(III) porphyrin complexes, 1361
substitutions, ruthenium(III) edta complexes, 603

Entropy of formation
cobalt(II) aminoacid complexes, 2037,2053
cobalt(II) dioxygen porphyrin pyridine complex, 1071
copper(II) aminoacid complexes, 2037,2053
thallium(I) cyclohexylthioglycolate compounds, 401
triorganotin chloride solvates, 1037

Erythritol complexes, boron, 1415

Erythrose compounds
tin(IV), 383

ESR spectra
cobalt(II) pyrimidine Schiff base complexes, 2103
copper(II) aminoacid salicylaldimine complexes, 1669
copper(II) carboxylate terpyridine water complexes, 1533
copper(II) carboxylate water complexes, 1869
copper(II) diamine triamine complexes, 1053
copper(II) peptide complexes, 45
copper(II) pyridine thiosemicarbazone complexes, 39
copper(II) tetrasalicylaldimine complexes, 513
copper(II) zirconium(IV) alkoxides, 427
iron(-I) nitrite nitrosyl complex, 2091
iron carbonyl nitrene nitroso polynuclear radical anions, 1959
iron nitrosyl thiolate thiomolybdate thiophenoxide complexes, 2085
iron(I) amide dithioanion nitrosyl pyridine quinoline-thiolate complexes, 1497
iron(III) aminoacid chloride hydroxide complexes, 969
iron(III) nitrosyl oxo Schiff base complexes, 295
manganese(II) arsine carboxylate chloride water complexes, 1699
molybdenum(V) methyl oxo complexes, 1081
nickel(II) dithiolate

complexes, 627
rhenium(II,III) diphosphine halide nitrile complexes, 1483
rhodium(I) chloride diisocyanide polymeric complex, 2027
ruthenium(I,II) chloride cymene dipyridyl pyrazine complexes, 473
ruthenium(III) mercaptoquinazolinone complexes, 1009
tungsten(V) methyl oxo complexes, 1081
vanadium(IV) azole halide nitrate pyridine sulphonate complexes, 455
Ethane-1,2-dithiolates
nickel(II), 863
Ethenethiolate, iron, 2085
Ethanol complexes
copper(II), 881,1319
nickel(II), 1457
Ethanolamine complexes
nickel(II), 1279
Ethene complexes
zirconium(III), 645
Ether complexes
copper(II), 855,1149,1669
europium(II), 1143
lithium, magnesium, 1081
molybdenum(II), 2111
molybdenum(III,IV),(V), 2181
platinum(IV), 549
tantalum(V), 1765
vanadium(II), 1433
ytterbium(II), 1143
Ethoxides and ethoxo complexes
copper(II), 427
tungsten(VI), 163,1657
zirconium(IV), 427
Ethylamine complexes
iron(II), ruthenium(II), 1089
2-(Ethylamino)ethanol complexes
nickel(II), 1279
Ethylenebis(isonitrosoacetylacetoneimine) complexes, Co(II), Cu(II),U(VI), 205
Ethylenebis(salicylaldimine) complex, molybdenum(VI), 1635
Ethylenediamine complexes
cobalt(III), 181,651
copper(II), 1053
palladium(II), 225
platinum(II), 225
ruthenium(II), 837,1621
uranium(VI), 205
Ethylenediaminetetraacetate complexes,
cobalt(III), 1571
palladium(II), platinum(II), 571
ruthenium(III), 603
Ethylenediaminetetra(methylenephosphonate) complex, manganese(II), 403
2-Ethylhexanoate
indium(III), 507
N-Ethyliminodiacetate complexes
beryllium, 303
Ethyltetramethylcyclopentadienyl
rhenium(VII), 1165
Europium(II)
carbazolyl ether indolyl phenoxide complexes, 1143
organometallics, 807
Europium(III)
aminopolycarboxylate nitrate phenoxide water heterobinuclear complexes, 1971
bipyrimidine chloride nitrate complexes, 175
pyrazolone complexes, 2095
EXAFS
uranium(III) borohydride crown ether complexes, 189
uranium(VI) dioxo crown ether complex, 189

F

Ferraboranes, 1937,1941,1946
Ferrocene, 943
Ferrocene derivatives, 1243
Fluorescence spectra
rhenium(I) acylpyridine bromide carbonyl complexes, 593
Fluorides and fluoro complexes
rhenium(V), 1169
ruthenium(II), 1621
2-Fluorobenzoate
chromium(III), 1153
Fluorophosphazenes, cyclic, 123; polymeric, 132
6-Fluoro-2-oxopyridine complexes
osmium(II,III), 1439
Fluxional behaviour
hafnium(IV) cyclopentadienyl ditellurolene complex, 1923
iron(-I) nitrosyl thiolates, 1147
molybdenum(II) carbonyl diphosphine diphosphoxane halide complexes, 1103
palladium(II), platinum(II), (IV) thiolate - bridged complexes, 1261
platinum(IV) tridentate complexes, 549
selenoether, thioether complexes, 1785
Formaldehyde, reaction with
copper(II) tetramine complex, 1291
Formates
copper(II), 1533
ruthenium(II), 1621
Formation constants
actinide pyrazolone complexes, 2009
alkali metal crown ether complexes, 417,577
alkaline earth crown ether complexes, 535
aluminium adenosine phosphate complexes, 2095
beryllium aminopolycarboxylates, 1364
beryllium hydroxide iminodiacetate complexes, 303
boron oligosaccharide complexes, 1415
cadmium glycylglycine imidazole pyridoxamine complexes, 1477
cellulose - attached complexes, 1197

chromium(VI) chloride oxo complex, 2145
cobalt(II) aminoacid complexes, 633,2037,2053
cobalt(II) azole phenoxide complexes, 1993
cobalt(II) cyanide complexes, 1909
cobalt(II) dioxygen porphyrin pyridine complex, 1071
cobalt(II) glycylglycine imidazole pyridoxamine complexes, 1477
cobalt(II) sulphite complexes, 1717
cobalt(III) ammine chloride sulphoxide water complex, 1337
copper(II) amide bromide complexes, 1399
copper(II) aminoacid complexes, 633,2037,2053
copper(II) bromovalerate, 1203
copper(II) carboxylate catecholate complexes, 53
copper(II) peptide complexes, 45
crown amine-ether carboxylate complexes, 29
hydroxynaphthalenecarboxylates, 1517
iron(II) carboxylate catecholate complexes, 53
iron(III) carboxylates, 2155
lanthanide pyrazolone complexes, 2099
lanthanum hydroxide complexes, 1283
manganese(II) aminoacid complexes, 2037,2053
manganese(II) cyanide complexes, 1909
nickel(II) aminoacid complexes, 633
nickel(II) ethanolamine complexes, 1279
nickel(II) glycylglycine imidazole pyridoxamine complexes, 1477
nickel(II) halide phosphinedicarboxylate pseudohalide complexes, 1407
nickel(II) mercaptocarboxylate complexes, 613
nickel(II) phosphinate complexes, 1251
nitrilotri(methylenephosphonate) complexes, 1247
palladium(II) chloride dicarboxylate thioether complexes, 447
palladium(II) vitamin B_6 complexes, 329
potassium crown ether thiocyanate complexes, 577
silver crown ether complexes, 535
thallium(I) cyclohexylthioglycolate complexes, 401
tin(IV) triorgano chloride solvates, 1037
zinc aminoacid complexes, 633
zinc carboxylate catecholate complexes, 53
zinc glycylglycine imidazole pyridoxamine complexes, 1477
zinc mercaptocarboxylate complexes, 613
2-Formylpyridine thiosemicarbazone complexes, copper(II), 39
Free energy of activation
fluxionality, hafnium(IV) cyclopentadienyl ditellurolene complex, 1923
fluxionality, selenoether, thioether complexes, 1785
fluxionality, thiolate - bridged complexes, 1261
fluxionality, tridentate complexes, 549
Free energy of formation
thallium(I) cyclohexylthioglycolate complexes, 401
tin(IV) triorgano chloride solvates, 1037
Free energy of solution, arsenic(V) hydroxyapatites, 1049
Fructose compounds
boron, 1415
tin(IV), 383
2-Furoate, tin(IV), 587

G

Galactose compounds
boron, 1415
tin(IV), 383
Germanes, 441
Germanium in heteropolyanions, 519
Glucose compounds
boron, 1415
tin(IV), 383
Glycine complexes
cobalt(III), 651,947
Glycolates
phosphorus(III), 915
technetium(V), 1707
Glycylglycine complexes
Cd,Co,Ni,Zn, 1477
Gold
metallaboranes, 1952
solubilization, Chinese method, 483
Gold(I)
arsine chloride complexes, 1255
Gold(III)
diaminoazobenzene complex, 2137
Graham π-parameter, 503
Grignard reagents, reactions with phosphazenes, 125
Guanine, guanosine complexes
ruthenium(III), 387

H

Hafnium(IV) cyclopentadienyl ditellurolene complex, 1923
Hartree - Fock calculations
aluminium magnesium chloride complexes, 975
Heterobinuclear complexes
cobalt(II)-nickel(II), 1603
cobalt(III)-iron(III), 1929

palladium(II)-rhodium(I), 1427
Heteropolymolybdates
cobalt(III), 1343
copper(II), 213
manganese(II), 213
nickel(II), 213
phosphorus(v), 1681
topology, 309
tungsten(V), vanadium(V), 1813
zinc, 213
Heteropolytungstates
cobalt(II), 931,1513
molybdenum(V), 1813
nickel(II), 213
phosphorus(V), 931
topology, 309
vanadium(V), 1813
Heteropolyvanadates
molybdenum(VI), tungsten(VI), 1813
Hexamethylenetetramine complexes
zinc, 1111
Hexamethylphosphoramide complexes
tin(IV), 1037
uranium(VI), 647
Hexaphosphine complex
platinum(II), 1803
HFS calculations, metal-metal bonds, 685
High pressure reaction,
cobalt(II) dioxygen porphyrin pyridine complex, 1071
Histidine, reactions with
molybdenum(IV) complexes, 465
Histidine complexes
copper(II), 1669
iron(III), 969
mercury, zinc, 1209
Holmium
bipyrimidine chloride nitrate complexes, 175
HPLC, phosphates, 1863
Hydrazide complexes
rhenium(VII), 1577
Hydrazone complexes
cadmium, 1075
lanthanum, 1021
manganese(II), mercury, nickel(II), zinc, 1075
Hydrides and hydrido complexes
iridium(III), 1727
manganese(I), 111
platinum(II), 341
rhodium(I), 111,2187
rhodium(III), 345
tantalum(III),(IV), 741
Hydrogen
reaction with nitrile complexes, 1089
transfer, catalysis by rhodium(I) complexes, 1427
Hydrogen ion, reaction with crown ethers, 1469
Hydrogen dinitrate anion, 1885
Hydrogen peroxide
decomposition by Mn(II), 403
Hydrolysis
chromium(III) ammine carboxylate complexes, 1153
cyclopolyphosphates, 531,1863
Hydroxides and hydroxo complexes
aluminium, 1587
beryllium, 303
calcium, 1049
iron(III), 969
lanthanum, 1283
magnesium, 1587
tin(IV), 1639
Hydroxoaqua ($H_3O_2^-$) complexes
cobalt(III), 181
Hydroxyapatite, arsenic(V), 1049
1-(2′-Hydroxybenzyl)-2-(2′-hydroxyphenyl)-benzimidazole complexes, Ce(IV), U(VI), 285
Hydroxycarboxylates
Cd,Co,Cu,Ni,Zn, 1517
Hydroxyethyl(methyl)dithiocarbamate, antimony(III), 411
2-Hydroxy-3-formyl-5-methyl-1-benzal ketones, 1473
Hydroxylamine, oxidation, 641
2-Hydroxy-5-methylbenzene-1,3-dicarbaldehyde complexes, 897, 1473
3-Hydroxy-2-naphthalenecarboxylates, Cd,Co,Cu,Ni,Zn, 1517
N-(2-Hydroxyphenyl)salicylideneiminate complexes, rhenium(IV), (V),(VI), 1647
8-Hydroxyquinoline complex,
manganese(III), 2003
2-Hydroxy-1,3-xylyl-15-crown-4 complexes, Cs, K, Na, 417
2-Hydroxy-1,3-xylyl-18-crown-5 complexes, Cs, K, Na, 417
Hypoxanthine complexes
ruthenium(III), 387

I

Imidazole complexes
cadmium, cobalt(II), 1477
cobalt(III), iridium(III), 1347
mercury, 1209
nickel(II), 1477
platinum(II), 85
rhodium(III), 1347
ruthenium(III), 1009
zinc, 1209,1477
Iminodiacetate complexes
beryllium, 303
tin(IV), 1639
Indium - tin - oxide films, 507
Indium(III)
alkoxide butyl carboxylate diketonate phenoxide compounds, 507
Indolyl compounds
europium(II), ytterbium(II), 1143
Inosine complexes
ruthenium(III), 387
Interfacial tensions, solvent
extraction, copper(II) salicylaldoximes, 197
Iodate, reaction with
diaminoazobenzene, 2137
Iodate complexes
ruthenium(II), 1621
Iodides and iodo complexes
cobalt(III), 1563
gold, 483
mercury, 543
molybdenum(0), 1781
molybdenum(II), 261,729,1103
molybdenum(III,IV),(V), 2181

nickel(II), 921
platinum(IV), 319
rhenium(I), 1255
rhenium(II), 729
rhenium(V), 1169
ruthenium(II), 1383
thallium(III), 315
tungsten(0), 1781
tungsten(II), 729,1135
9-Iodo-1,2[&1,7]-dicarba-closo-decaborane(11), 1559
IR spectra
acyl compounds, 593
aldehyde complexes, 393
alkoxides, 163,427,2161
alkyls, 383,587,1081,1639
amide complexes, 1009
amidophosphazene, 1999
amine complexes, 85,461,465, 1053
aminoacid complexes, 845
aminopolycarboxylates, 603,1971
ammines, 85,159,1347
arsenate, 1049
arsine complexes, 921,1383
arsine oxide complexes, 1325
arsine oxide protonation, 2077
aryls, 587
arylimides, 163,2191
azole complexes, 85,285,1009, 1347
binucleating ligand, 897
biuret complexes, 841
bromides, 85,315,921,1021,1065, 1075,1325,1885
bipyrimidine complexes, 175
carbazolyls, 1143
carbohydrate complexes, 383
carbonyls, 85,95,111,261,593, 837,1103,1135,1255,1273,1351, 1427,1445,1673,1703,1781, 1851,1879,1987,1999,2009, 2031,2081
carboxylates, 275,461,587,1017, 1161,1351,1639,1699,2111
catecholates, 845
chlorides, 85,163,907,921,975, 1003,1021,1059,1065,1075, 1295,1325,1383,1427,1483, 1647,1657,1681,1699,1727, 1807,1885,2009,2111
cyanide complexes, 79,1191, 1383,1563,1757
cyclam complexes, 1875
cyclometallated complexes, 1003
cyclometallathiazine complexes, 2165
cyclopentadienyl complexes, 1383
dehydroacetic acid complexes, 1235
diazabutadiene complexes, 1059
diazenide complexes, 1577
diimine complexes, 845,1383, 1427
diketonates, 1383
diphosphoxane complexes, 1103
diselenolate complexes, 1547
dithiocarbamates, 411,1383,1523
dithiocarboxylates, 1851
dithiolates, 627
dithiophosphates, 1681
dithizone complexes, 1523
ether complexes, 1081,1639
fluorophosphine complex, 1295
heteropolymolybdates, 213
heteropolytungstates, 213
hydrazide complexes, 1577
hydrazone complexes, 1021,1075
hydrides, 341,741,1727
hydroxides, 1049,1587,1639
iminodiacetate, 1639
indolyls, 1143
iodides, 315
isocyanatophenylsiloxanes, 435
ketone complexes, 393,1021,1611
lactones, 423
mercaptoquinazolinone complexes, 1009
nitrates, 175,285,455,1021, 1223,1313,1885,1971
nitrile complexes, 159,1089, 1483
nitro (organic) compound, 1291
nitrosyls, 1523
nucleoside complexes, 387
organotrithiophosphate complexes, 539
oxime complexes, 205
oxo complexes, 205,275,285, 455,465,841,891,1081,1547, 1635,1647,1707,1807,1913
oxoquinoline complexes, 275
perchlorates, 387,1053,1383, 1427
peroxide complexes, 275
perthiocarbonate, 627
phenoxides, 1097,1143,1971
phosphine complexes, 921,1223, 1987
phosphinedicarboxylates, 1407
phosphine oxide complexes, 1325,1913
phosphine selenide complexes, 219
phosphine sulphide complexes, 1329
phthalocyanines, 1463
picolinates, 1523
purine complexes, 387
pyrazolone complexes, 1913
pyridine complexes, 85,393,479, 603,1021,1383,1885
pyridine-N-oxide complexes, 85, 315
pyridylthiourea complexes, 1807
pyrimidine complexes, 387,2103
quinone oxime complexes, 1509
salicylaldimines, 275,1319,1901
Schiff base complexes, 513, 1003,1021,1097,1319,1611, 1635,1653,1901,2103
semicarbazone complexes, 1611
siloxy compounds, 1097
stibine complexes, 1383
sulphates, 285,455,841
sulphonates, 1875
sulphoxide complexes, 1313,1913
tetrafluoroborates, 1383
tetraphenylborates, 1383
tetrasulphido complexes, 627
thiazyl compounds, 2161
thiocyanates, 455,1075,1191, 1273,1325,1383
thiodiacetic acid complexes, 1065

thioether complexes, 1065
thiolates, 603,1097,1653
thione complexes, 603,2177
thiosemicarbazone complexes, 39,1611
thiourea complexes, 837,2081
tropolonates, 891
uracil complexes, 2103
water complexes, 465,897,1325, 1603,1699,1971
Iridium(0)
phosphorus cluster complexes, 355,359,367,376,379
Iridium(I)
amidophosphazene carbonyl diene phosphine complexes, 1999
amine phosphine complexes, 921
aminophosphine chloride complexes, 2009
carbonyl diphosphine halide manganese(I) complexes, 111
Iridium(II)
amidinate complex, 1625
Iridium(III)
amine arsine chloride phosphine complexes, 921
aminophosphine chloride complexes, 2009
ammine imidazole complexes, 1347
carbonyl chloride diphosphino-amine hydride complex, 1727
chloride pyridine quinone-oxime complexes, 1509
diene phosphine phosphine-sulphide complexes, 1329
halide pyridine complexes, 1885
tropolonates, 891
water complex, 101
Iron
alkyl carbonyl phosphine heterobinuclear complexes, 2067
carbonyl chloride thio thiophenoxide heterometallic complexes, 1445
carbonyl nitrene nitroso polynuclear radical anions, 1959
metallaboranes, 1937,1941,1946
nitrosyl thio complexes, 2091
nitrosyl thiolate thiomolybdate thiophenoxide complexes, 2085
Iron(-II)
carbonyl mercury complex, 1273
Iron(-I)
nitrite nitrosyl complex, 2091
nitrosyl thiolates, 1147
Iron(0)
carbonyls, 1959
carbonyl cyclopentadienyl bismuth(III) complex, 2031
cyanide complex, 1191
phosphazene complexes, 142
phosphorus cluster complexes, 352,366,373,379
Iron(0,I,I)
phosphazene complexes, 141
Iron(I)
amide dithioanion nitrosyl pyridine quinolinethiolate complexes, 1497
phosphazene complexes, 141
Iron(II)
amine chloride diphosphine nitrile phosphine complexes, 1089
ammine thiocyanate complexes, 1191
arsine oxide halide phosphine oxide thiocyanate water complexes, 1325
carbonyl cyclopentadienyl thio-semicarbazide thiosemicarbazone complexes, 1703
carboxylate catecholate complexes, 53
crown amine - ether carboxylate complexes, 29
cyanide pyrazine pyridine complexes, 1757
cyanide pyridine ruthenium(II) complex, 159
diketonates, 1421
nitrilotri(methylenephosphonate) complexes, 1247
phosphazene complexes, 138,143
phosphazene porphyrin complexes, 144
phosphazenocyclopentadienyls, 147
pyridine quinone-oxime complexes, 1027
sulphate, 483
Iron(III)
aminoacid chloride hydroxide complexes, 969
aminopolycarboxylate phenoxide water heterobinuclear complexes, 1971
ammine thiocyanate complexes, 1191
arylimido salicylaldimine complexes, 2191
carboxylate complexes, 2155
cyanide cobalt(III) complex, 1929
cysteine nitrilotriacetate thiourea complexes on cellulose, 1197
diketonates, 1421
nitrosoalkylhydroxylamine complexes, 1375
nitrosyl oxo Schiff base complexes, 295
phosphazene porphyrin complexes, 144
Irving, H.M.N.H., tribute, 1; bibliography, 3
4-Isocyanatophenylsiloxanes, 435
Isocyanide complexes
rhodium(I), 2027
tungsten(VI), 1657
Isonicotinamide, isonicotinate complexes, iron(II), 1757
Isopolyanions
isopropanol oxidation catalysis, 1919
topology, 309
Isoprenaline, 25
Isopropanol oxidation, 1919

J

Jaeger complexes, nickel(II), 423

K

Kerosene, in solvent extraction
of palladium(II), 1125
Ketoimine complexes
cobalt(III), 995
copper(II), 2169
nickel(II), 1901,2169
palladium(II), 1243
Ketone complexes
lanthanum, 1021
tin(IV), 393
Kinetic studies
complex formation, heterobinuclear by pyrolysis, 1929
complex formation, palladium(II) - sulphur aminoacids, 1391
complex formation, palladium(II) - vitamin B_6, 329
fluxionality, tridentate complexes, 549
hydrolysis, chromium(III) ammine carboxylates, 1153
hydrolysis, cobalt(III) sulphonate complexes, 1875
hydrolysis, cyclopolyphosphates, 531,1863
oxidative addition, HCl to $[Mo_2Cl_8]^{4-}$, 1975
photoaquation, molybdenum(IV) cyanide complex, 269
photolysis, tungsten(0) carbonyl phosphine piperidine complex, 337
radiolysis, germanes, 441
redox, chromium(VI) - thallium(I), 1721
redox, copper(II) azole pyridine thioether complexes - ferrocenes, 943
redox, cobalt(III), rhodium(III) complexes - vanadyl, 1347
redox, NH_2OH - $[W(CN)_8]^{3-}$, 641
solvent extraction, copper(II) salicylaldimines, 197
spinel formation, 1791
substitution, chromium(III) porphyrin water complex, 1361
substitution, cobalt(III) aminopolycarboxylate ammine bromide complexes, 1571
substitution, ruthenium(III) aminopolycarboxylate complexes, 603

L

Lacquer, in solubilization of gold and silver, 483
Lactones, on macrocyclic complexes, 423
Lactose, lactulose complexes, boron, 1415
Lanthanides(II)
carbazolyl ether indolyl phenoxide complexes, 1143
Lanthanides(III)
aminopolycarboxylate nitrate phenoxide water heterobinuclear complexes, 1971
bipyrimidine chloride nitrate complexes, 175
coordination saturation, 1041
low oxidation states, organometallics, review, 803
nitrate complexes, 489
pyrazolone complexes, 2099
Lanthanum
aminopolycarboxylate nitrate phenoxide water heterobinuclear complexes, 1971
bipyrimidine chloride complexes, 175
halide macrocyclic nitrate complexes, 1021
hydroxide complexes, 1283
Lattice energies, magnesium chlorides, 975
Lawesson's reagent, 539
Lead(II)
chloride complexes, 563
crown amine - ether carboxylate complex, 29
cysteine nitrilotriacetate thiourea complexes on cellulose, 1197
nitrate thione complex, 2177
nitrilotri(methylenephosphonate) complexes, 1247
Leucine complexes
iron(III), 969
Ligand synthesis
aminopolycarboxylate, 1364
bis(ketoimine)ferrocene, 1243
diketonate, 1473
hydrazones, 1075
Jaeger complexes, 423
macrocyclic Schiff bases, 289
macrocyclic tetramines, 1291
salicylaldimine Schiff bases, 1319
triketonate, 1473
Lithium
alkyls, aryls, reactions with phosphazenes, 123,130,133,143
amine diphenylphosphide complexes, 987
aminopolycarboxylate phenoxide water heterobinuclear complexes, 1971
carboranes, reactions with phosphazenes, 131
crown amine - ether carboxylate complex, 29
ether oxo rhenium(V) compound, 1081
metallocenes, reactions with phosphazenes, 147
Lutetium(III) pyrazolone complexes, 2099

M

Macrocyclic complexes
cobalt(III), 1875
copper(II), 289,1291,2169
lanthanum, 1021
nickel(II), 289,423,2169
potassium, 1161
praseodymium(III), 1611
rhodium(II), 461
rubidium, 1161

ruthenium(III), 1875
sodium, 1161
Magnesium
aluminium hydroxide, 1587
aluminium oxide, 1791
catecholdicarboxylate water complexes, 871
chloride complexes, 975
crown amine-ether carboxylate complexes, 29
cysteine nitrilotriacetate thiourea complexes on cellulose, 1197
diaminoazobenzene complex, 2137
diethyl, reactions with phosphazenes, 132
ether oxo molybdenum(V) tungsten(V) compounds, 1081
Grignards, reactions with phosphazenes, 132
heteropolymolybdates, 213
Magnetic moments
chromium(III) dehydroacetic acid complexes, 1235
chromium(IV) arylimido porphyrin complex, 2191
cobalt(II) amide dehydroacetic acid complexes, 1235
cobalt(II) amine halide phosphine complexes, 921
cobalt(II) azine halide hydrazone thiocyanate complexes, 1075
cobalt(II) carboxylate diamine water heterobinuclear complexes, 1603
cobalt(II) heterobinuclear complexes, 897
cobalt(II) phthalocyanines, 1463
cobalt(II) pyrimidine Schiff base complexes, 2103
cobalt(II) salicylaldimine Schiff base complexes, 1319
copper(II) aminopolycarboxylate phenoxide water heterobinuclear complexes, 1971
copper(II) dehydroacetic acid complexes, 1235
copper(II) ethanol salicylaldimine Schiff base complexes, 1319
copper(II) heterobinuclear complexes, 897
copper(II) nitrosoalkylhydroxylamine complexes, 1375
copper(II) nitrosoresorcinol complexes, 1033
copper(II) oxime Schiff base complexes, 205
cobalt(II) phthalocyanines, 1463
copper(II) zirconium(IV) alkoxides, 427
iron(II) ammine thiocyanate complex, 1191
iron(II) arsine oxide halide phosphine oxide thiocyanate water complexes, 1325
iron(II) pyridine quinone - oxime complexes, 1027
iron(III) aminoacid chloride hydroxide complexes, 969
iron(III) aminopolycarboxylate phenoxide water heterobinuclear complexes, 1971
iron(III) arylimido salicylaldimine complexes, 2191
iron(III) nitrosoalkylhydroxylamine complexes, 1375
iron(III) nitrosyl oxo Schiff base complexes, 295
manganese(II) arsine carboxylate chloride water complexes, 1699
manganese(II) halide hydrazone complexes, 1075
manganese(II) heterobinuclear complexes, 897
molybdenum(0) dinitrosyl complexes, 1523
molybdenum(II) nitrosyl picolinate complex, 1523
molybdenum(III,IV),(V) acetate ether iodide oxo complexes, 2181
nickel(II) carboxylate diamine water heterobinuclear complexes, 1603
nickel(II) dehydroacetic acid complexes, 1235
nickel(II) diaminetetrazole complexes, 1457
nickel(II) diphosphine nitrate complex, 1223
nickel(II) halide hydrazine thiocyanate complexes, 1075
nickel(II) heterobinuclear complexes, 897
nickel(II) nitrate sulphoxide complexes, 1313
nickel(II) perthiocaronate tetrasulphide complexes, 627
nickel(II) salicylaldimine Schiff base complexes, 1319
osmium(II,III) chloride oxopyridine complex, 1439
praseodymium macrocyclic semicarbazone thiosemicarbazone water complexes, 1611
pyridine thiosemicarbazone complexes, 39
rhenium(III) chloride diphosphine complexes, 907
rhenium(IV),(VI) chloride oxo phenoxide salicylaldimine complexes, 1647
ruthenium(III) mercaptoquinazolinone complexes, 1009
vanadium(0) carbonyl diphosphine complexes, 1351
vanadium(IV) azole halide nitrate pyridine sulphate complexes, 455
Magnus salts, 225
Manganese metallaboranes, 1942
Manganese(I)
bromide carbonyl diimine diphosphine perchlorate phosphine complexes, 1879
carbonyl diphosphine halide hydride iridium(I) rhodium(I) complexes, 111
phosphorus cluster complexes, 368,375,379

Manganese(II)
aminoacid complexes, 2037,2053
aminopolyphosphonate complex, 403
arsine carboxylate chloride water complexes, 1699
catecholdicarboxylate water complexes, 871
crown amine-ether carboxylate complexes, 29
cyanide complexes, 1909
halide hydrazone complexes, 1075
heterobinuclear complexes, 897
phosphazene complexes, 138
Manganese(III) diketonate hydroxyquinoline complexes, 2003
Manganese(III),(IV) in H_2O_2 decomposition, 403
Mannose complexes, boron, 1415
Mass spectra
bismuth(III) aminothiophenoxide methyl phenyl compounds, 1593
cobalt, triphosphine tripnictide/-chalcogenide complexes, 1491
hafnium cyclopentadienyl ditellurolene complex, 1923
nickel triphosphine tripnictide/-chalcogenide complexes, 1491
phthalocyanines, 1463
rhenium(I) carbonyl chloride diarsine complex, 1255
rhenium(VII) alkyl alkylidyne chloride complex, 1599
spiroborates, 2119
tin(IV) phenyl trifluoroacetate, 397
MCD spectra
heteropolymolybdates, 213
heteropolytungstates, 213
Melezitose complexes, boron, 1415
1-l-Menthyloxy-3-acylacetone complexes, cobalt(III), 583
Mepazine, methotrimeprazine complexes, molybdenum(IV), 465
Mercaptoacetic acid derivatives, antimony(V) complexes, 1161
Mercaptocarboxylate complexes
antimony(V), 1161
nickel(II), zinc, 613
N-(2-Mercaptoethyl)salicylaldimine complexes, aluminium, 1097
N-(2-Mercaptophenyl)benzaldimine complexes, aluminium, 1097
2-Mercapto-3-phenyl-4-quinazolinone complexes, rhodium(III), ruthenium(III), 1009
N-(2-Mercaptophenyl)salicylaldimine complexes, aluminium, 1097
3-Mercaptopropionic acid derivatives, antimony(V) complexes, 1161
2-Mercaptopyridine complexes
ruthenium(II), 837
ruthenium(III), 603
Mercury
azole sulphonate complexes, 1209
chloride hydrazone complexes, 1075
chloride molybdenum(0), tungsten(0) complexes, 1781
in cobalt(III) substitutions, 1337
cysteine nitrilotriacetate thiourea complexes on cellulose, 1197
diaminoazobenzene complex, 2137
diphosphine complexes, 655
halide cobalt(I) complex, 543
thiocyanate iron(-II) complex, 1273
Metal - metal bonds
carbonyl cyclopentadienyl compounds, review, 759
diamagnetic anisotropy, 1677
edge - shared octahedra, 667
electronic spectra, 695, 705, 715,723
heteronuclear quadruple, review, 793
molecular orbitals, 679,685, 695,705,741
molybdenum(III), tungsten(III), 1677
Metallaboranes, review, 1935
Methanethiolates
iron, 2085
palladium(II), 1261
platinum(II),(IV), 1261
Methanol, solvent for crown ether complexes, 535
Methanol complexes
rhenium(V), 1647
Methionine complexes
iron(III), 969
palladium(II), 1391
Methoxides
copper(II), zirconium(IV), 427
2-Methoxybenzoate, copper(II), 1869
5-Methoxynaphthoquinone oxime complexes, iron(II), 1027
4-Methoxypyridine-N-oxide complexes, thallium(III), 315
2-Methoxy-1,3-xylyl-15-crown-4 complexes, alkali metals, 417
2-Methoxy-1,3-xylyl-18-crown-5 complexes, alkali metals, 417
Methyls
bismuth(III), 1593
molybdenum(V), 1081
niobium(V), 2019
platinum(IV), 319,549,1157,1261
rhenium(V), 1081,1169
silicon, 435
tantalum(V), 2019
tin(IV), 393,587,1639
titanium(IV), 2019
tungsten(V), 1081
9-Methyladenine complexes
borane, 1183
Methylamine complexes
palladium(II), 225
2-(Methylamino)ethanol complexes
nickel(II), 1279
Methylbenzylamine, Schiff base, complexes, platinum(IV), 319
2-Methyl-2-(4-chlorophenoxy)propionate complexes, copper(II), 855
Methylcyclopentadienyl, iron(0), 2031

S-Methylcysteine complexes
palladium(II), 1391
Methyldithiocarbamate
molybdenum(II), 1523
N-Methylformamide complexes
copper(II), 1669
2-Methylimidazole complexes
mercury, zinc, 1209
1-Methylimidazoline-2(3H)-thione
complex, lead(II), 2177
N-Methyliminodiacetate complexes,
beryllium, 303
4-(5′-Methyl-3′-isoxazolylazo)-
resorcinol complex, cobalt(II),
1993
Methyl-C-nitrilotriacetate
beryllium, 1364
2-Methyl-2-nitrosopropane, 1959
2-Methyl-4-nitrosoresorcinol
complexes, copper(II), 1033
10-Methyl-10-nitro-1,4,8,12-
tetraazacyclopentadecane
complexes, copper(II), 1291
3-Methyl-2,4-pentanedionates
iron(II),(III), 1421
2-Methyl-2-phenoxypropionate
complexes, copper(II), 855
Methyl(phenyl)hydrazide complexes
rhenium(VII), 1577
2-Methyl-2[&3]-(phenylthio)pro-
pionate complexes, copper(II),
881
Methylphosphinediacetates
barium, nickel(II), 1407
3-Methylpyridine complexes
ruthenium(III), 1009
4-Methyl-N-8-quinolinylbenzene-
sulphonamide complexes,
cadmium, 963
3-Methyltetrahydrofuran complexes
vanadium(II), 1433
Methylthiourea complexes
ruthenium(II), 837
Micelle complexes
mercury, zinc, 1209
Millet wine, in silver
solubilization, 483
MNDO calculations, carbaboranes,
1559
Moessbauer spectra
iron(II) pyridine quinone -
oxime complexes, 1027
iron(III) aminoacid chloride
hydroxide complexes, 969
iron(III) nitrosyl oxo Schiff
base complexes, 295
tin(IV) alkyl aryl
carboxylates, 587
tin(IV) alkyl carbohydrate
compounds, 383
tin(IV) methyl polycarboxylate
complexes, 1639
Molecular orbitals
aluminium magnesium chloride
complexes, 975
carbaboranes, 1559
lithium phosphide, 987
metal - metal bonds, 679,685,
695,705,741,760
transition metal complexes,
1215
Molybdenum
alkyl carbonyl cyclopentadienyl
iron complexes, 2067
Molybdenum(0)
amine diphenylthiocarbazone
nitrosyl phenoxide picolinate
thiophenoxide complexes, 1523
carbonyl complexes, 503
carbonyl diimine complexes,
1673
carbonyl diimine halide mercury
complexes, 1781
carbonyl diphosphine complex,
1797
phosphazene complexes, 138,146
phosphorus cluster complexes,
366,373
Molybdenum(I)
phosphorus cluster complexes,
357,362,371,379
Molybdenum(II)
acetate chloride ether
phosphine complex, 2111
acetonitrile carbonyl chloride
thiourea complexes, 2081
carbonyl diphosphine
diphosphoxane halide
complexes, 1103
carbonyl diphosphine
thiocyanate complex, 95
carbonyl iodide phosphine
complex, 261
chloride binuclear complex,
1975
diphosphine halide complexes,
715,729
dithiocarbamate nitrosyl
picolinate complexes, 1523
heteronuclear metal - metal
bonds, 793
phosphazene complexes, 140,143
Molybdenum(III)
acetate alkoxides alkyls
alkylamide alkylidyne diamine
diphosphine pyridine
complexes, 255
alkoxides, alkylamides, metal -
metal bonds, 1677
chloride hydride binuclear
complex, 1975
picolinate, 1523
Molybdenum(III,IV) acetate ether
iodide oxo complex, 2181
Molybdenum(IV)
aminoalkylphenothiazine oxo
complexes, 465
chloride diphosphine thio
complex, 1741
cyanide complex, 269
Molybdenum(V)
chloride, 668
ether iodide oxo complex, 2181
methyl oxo magnesium compound,
1081
Molybdenum(VI)
amine carboxylate oxo
oxyquinoline peroxide
phenoxide pyridine
salicylaldimine water
complexes, 275
cyclopentadienyl halide oxo
complexes, non-formation, 281
disulphide thio iron complexes,
1445
heteropolyanions, 213,519,1343,

1681,1813
as heteropolyion, 1813
isopolyanions, 519
oxo salicylaldimine complexes, 1611
oxo tropolonate complexes, 891
thio iron complexes, 2085
Mu jing fruit, in silver solubilization, 483

N

Naphthoquinone oxime complexes
iridium(III), 1509
iron(II), 1027
rhodium(III), 1509
Naphthylideneaminoacid complexes
nickel(II), 1017
3-(2-Naphthyl)-2-mercaptopropenoic acid complexes, Ni,Zn, 613
Neodymium(III)
phenanthroline pyrazolone complexes, 957
ternary oxide, 668
Neutron diffraction
aluminium magnesium chlorides, 975
Nickel, metallaboranes, 1939
Nickel(0)
phosphorus cluster compounds, 354,363
Nickel(I)
phosphorus cluster compound, 355,359,376,378
Nickel(II)
alcoholamine complexes, 1279
amine azole ethanol halide thiocyanate water complexes, 1457
amine halide phosphine complexes, 921
aminoacid complexes, 633
aminophosphine chloride complexes, 2009
azole chloride thioether complexes, 1843
carboxylate diamine water heterobinuclear complexes, 1603
catecholdicarboxylate water complexes, 871
crown amine carboxylate ether complexes, 29
cysteine nitrilotriacetate thiourea complexes on cellulose, 1197
dehydroacetic acid complex, 1235
diaminoazobenzene complex, 2137
diketonate, 497
diphosphine nitrate complex, 1223
dithiocarbamate, 497
dithiolate complexes, 863
dithiolate perthiocarbonate tetrasulphide complexes, 627
glycylglycine imidazole pyridoxamine complexes, 1477
halide hydrazone thiocyanate complexes, 1075
halide phosphinedicarboxylate pseudohalide complexes, 1407
heterobinuclear complexes, 897
heteropolymolybdates, 213
heteropolytungstates, 213
hydroxycarboxylates, 1517
ketoimine macrocyclic polyamine pyridine Schiff base complexes, 2169
ketoimine salicylaldimine thiosemicarbazide complexes, 1901
macrocyclic complexes, 285,423
mercaptocarboxylate complexes, 613
naphthylideneaminoacid complexes, 1017
nitrate sulphoxide complexes, 1313
nitrilotri(methylenephosphonate) complexes, 1247
nitrogen - sulphur complex, 939
phosphazene complexes, 137
phosphinate complexes, 1251
phthalocyanines, 1463
salicylaldimine Schiff base complexes, 1319
Schiff base thiolate complexes, 1653
triphosphine trichalcogenide/-pnictide complexes, 1491
Nicotinamide, nicotinate complexes, iron(II), 1757
Niobium(V)
alkyl phenoxides, 2019
chloride, 668
Nitrate complexes
cerium(III), 175
cerium(IV), 285
europium, 175,1971
holmium, 175
lanthanides, 175,285,489,1021, 1971
lanthanum, 1021,1971
lead(II), 2177
nickel(II), 1223,1313
uranium(VI), 205,285
vanadium(IV), 455
yttrium, 175
Nitrene complexes, iron, 1959
Nitrile complexes
cobalt(III), 1875
iron(II), 1089
molybdenum(II), 2081
rhenium(II,III), 1483
ruthenium(II), 159,1089
tungsten(II), 2081
vanadium(I), 1351
Nitriloacetatedipropionate, nitrilodiacetatepropionate complexes, beryllium, 1364
Nitrilotriacetate complexes
beryllium, 1364
on cellulose, 1197
Nitrilotri(methylenephosphonate) complexes, 1247
Nitrilotripropionate complexes
beryllium, 1364
Nitrite,
reaction with diaminoazobenzene, 2137
in solubilization of silver, 483
Nitrite complexes
cobalt(III), 181,1563
iron(-I), 2091

ruthenium(II), 1621
Nitroalkanes, reaction with iron carbonyls, 1959
2-Nitrobenzoate, chromium(III), 1153
Nitrocyclohexane, sodium salt, 1959
Nitroethane, reaction with copper(II) tetramine complex, 1291
Nitrogen - sulphur complex nickel(II), 939
Nitromethane, sodium salt, 1959
5-Nitro-1,10-phenanthroline complexes, copper(II), 845
4-Nitropyridine complexes thallium(III), 315
Nitrosoalkanes, reaction with iron carbonyls, 1959
N-Nitroso-N-alkylhydroxylamine complexes, copper(II), iron(III), 1375
Nitrosoresorcinols, complexes copper(II), 1033
Nitrosyls
iron, 1959,2085,2091
iron(-I), 1147,2091
iron(I), 1497
iron(III), 295
molybdenum(0),(II), 1523
rhenium(I), 1503
NMR(^{1}H) spectra
acyl complexes, 593
aldehyde complexes, 393
alkoxides, 163,1657,1747,2161
alkyls, 319,549,587,1081,1261, 1593,1599,1839,2019
alkylamide, 1657
alkylidyne complex, 1599
alkylidyne-vinyl complex, 2067
amide complexes, 1875
amine complexes, 837,1089,1657
aminophosphine complexes, 2009
aminopolycarboxylates, 571
ammines, 85,1347
aniline complexes, 85
anisyls, 219
arsine complexes, 1255,1383
arsine oxide protonation, 2077
aryls, 397,587
arylimides, 163
azole complexes, 1209,1347
bipyrimidine complexes, 175
carbaborane, 1737
carboxylates, 2111
catecholate, 525
cyclam complexes, 1875
cyclometallated complexes, 1003
cyclopentadienyls, 1243,1383, 1923,2031
cymene complexes, 473
diarsine complexes, 1255
diazadiphosphacyclopentanones, 1823
diene complexes, 1329,1427
diimine complexes, 1657
diketonates, 525,583,1383,2003
diphosphine complexes, 111, 1131,1261,1709,1797
diphosphinoamine complexes, 921,1727
dipyridyl complexes, 473
ditellurolene complex, 1923
dithiocarbamates, 411,1383
dithiocarboxylate, 1851
dithiolates, 863
dithiophosphates, 1115,1681
ether complexes, 549,1765,2111
fluxional complexes, 549
glycolate, 1707
hydride complexes, 741,1727
hydroxyquinoline complexes, 2003
imidazole complexes, 85
ketoimine complexes, 1243,2169
ketone complexes, 393
lactones, 423
lanthanide complexes, 1611
macrocyclic complexes, 1611, 1875,2169
metallaboranes, 1958
micelle complexes, 1209
nitrile complexes, 1089,1875
phenoxides, 1765
phosphines, 1295
phosphine complexes, 163,741, 921,1295,1329,1383,1657,1709, 1879,2067,2111
phosphinedicarboxylates, 1407
phosphine oxide complexes, 1913
phosphine selenide complexes, 219
phosphine sulphide complexes, 1329
picoline complexes, 1657
pinacolate, 1747
purine complexes, 387
pyrazine complexes, 85,473
pyrazolone complexes, 1913
pyridine complexes, 85,393
pyridylthiourea complexes, 1807
pyrimidine complexes, 387
Schiff base complexes, 319, 1003,1097,1635,1653,2169
selenoether complexes, 549,1785
siloxanes, 435
siloxyl complexes, 1097
spiroborates, 2119
stibine complexes, 1383
sulphonate complexes, 1209
sulphoxide complexes, 1913
tetraalkylammonium salts, 163
thiazyl compounds, 2161
thiocarbazones, 13
thioether complexes, 549,1785
thiolates, 1147,1261,1653
thione complex, 2177
thiophenoxide, 1445
thiourea complexes, 837
tropolonates, 891
NMR(^{7}Li) spectra
diphenylphosphide complexes, 987
NMR(^{10}B) spectra
carbaboranes, 1981
NMR(^{11}B) spectra
carbaboranes, 1737,1981
metallaboranes, 1956
NMR(^{13}C) spectra
alkoxides, 163,1657
alkyls, 319,1081,2019
alkylamides, 1657
alkylidne-vinyl complex, 2067
amine complexes, 1657
aminoacid complex, 105
aminopolycarboxylates, 571

aryls, 2019
arylimides, 163
carbaborane, 1737
carbonyls, 2031,2067,2081
carboxylate, 2111
catecholate, 525
cyclopentadienyls, 1243,2031
diarsine complexes, 1255
diimine complexes, 1657,1673
diketonate, 525
diphosphine complexes, 1797
diphosphinoamine complexes, 1727
dithiocarbamates, 411
dithiophosphates, 1115,1681
ether complexes, 1745,2111
glycolate, 1707
ketoimine complexes, 1243,2169
macrocyclic complexes, 2169
phenoxides, 1745
phosphine complexes, 163,1657, 2067,2111
picoline complexes, 1657
pyridine complexes, 319,479
pyridinium salt, 479
Schiff base complexes, 319,2169
spiroborates, 2119
tetraalkylammonium salts, 163, 489
tropolonates, 891
NMR(^{14}N) spectra
aminoacid complexes, 2037,2053
nitrate complexes, 489
tetraalkylammonium salts, 489
NMR(^{15}N) spectra
nitrosyls, 1147,2091
NMR(^{17}O) spectra
aminoacid complexes, 2037,2053
heteropolyanions, 1813
NMR(^{19}F) spectra
fluorophosphines & complexes, 1295
NMR(^{31}P) spectra
aminophosphine complexes, 2009
diazadiphosphacyclopentanones, 1823
diphenylphosphido complexes, 987
diphosphine complexes, 95,111, 473,655,1103,1261,1351,1483, 1709,1797,1879
diphosphinoamine complexes, 921,1727
diphosphoxane complexes, 1103
dithiophosphates, 1115,1681
phosphines, 1295
phosphine complexes, 261,539, 741,921,1089,1295,1329,1541, 1709,1879,2165
phosphine selenide complexes, 219
phosphine sulphide complexes, 1329
phosphorus cluster complexes, 359,370,379
NMR(^{39}K) spectra
potassium crown ether thiocyanate complex, 577
NMR(^{51}V) spectra
heteropolyvanadates, 1813
vanadium(I) carbonyl diphosphine complexes, 1351
NMR(^{95}Mo) spectra
heteropolymolybdates, 1813
molybdenum(III) alkylidyne complexes, 255
molybdenum(III) binuclear complexes, 255
NMR(^{119}Sn) spectra
triorganotin chloride solvates, 1037
NMR(^{183}W) spectra
tungsten(III) alkylidyne complexes, 255
tungsten(III) binuclear complexes, 255
NMR(^{195}Pt) spectra
platinum(II) diphosphine thiolate platinum(IV) complex, 1261
platinum(IV) chloride methyl thiolate platinum(II) complex, 1261
NMR(^{199}Hg) spectra
mercury diphosphine complexes, 655
NMR(NOE) spectra
catecholate, diketonate, 525
NMR(2D) spectra
carbaboranes, 1737,1981
2,5-Norbornadiene complexes
iridium(I), rhodium(I), 1329
Nuclear waste, extraction of
palladium from, 1125
Nucleophiles, reactions with
metal - metal bonds, 760
Nucleoside complexes
ruthenium(III), 387

O

Octyls, tin(IV), 383
Oligosaccharide complexes,
boron, 1415
Organoantimony(V) compounds, book review, 660
Organocopper compounds, book review, 1716
Organolanthanides, review, 803
Organometallic chemistry, book reviews, 1716,2035
Organometallic oxides, review, 1165
Organophosphorus compounds
reactions with metal - metal bonds, 762
Organosulphur compounds
reactions with metal - metal bonds, 761
Organotin(IV) compounds, book review, 660
Organotitanium(IV) compounds, book review, 660
Organotrithiophosphate complexes
platinum(II), 539
Ornithine complexes
copper(II), 1669
Osmium metallacarboranes, 1944
Osmium(II)
chloride diphosphine complexes, 1131
Osmium(II,III)
chloride oxopyridine complex, 1439
Osmium(III)
tropolonates, 891

Osmium(IV)
chloride silver(I) complex, 1695
Osmium(VI)
oxo tropolonate complexes, 891
Oxalates and oxalato complexes
cobalt(III), 651
ruthenium(II), 1621
Oxides
aluminium, magnesium, 1791
neodymium(III), rhenium(V), 668
silver(I,III), 1309
Oxime complexes
cobalt(II), 205
copper(II), 197,205
iridium(III), rhodium(III), 1509
uranium(VI), 205
Oxo complexes
aluminium, 1839
chromium(VI), 2145
iron(III), 295
lithium, magnesium, 1081
molybdenum(III,IV), 2181
molybdenum(IV), 465
molybdenum(V), 2181
molybdenum(VI), 275,891,1635
osmium(VI), 891
rhenium(IV), 1647
rhenium(V), 1081,1577,1647
rhenium(VI), 1647
rhenium(VII), 1165,1577
silicon, 435
tantalum(V), 1765
technetium(V), 1547,1707
tungsten(V), 1081
tungsten(VI), 275,891,1839
uranium(VI), 189,205,285,647, 1319,1913
vanadium(IV), 841
vanadium(V), 1807
N-(2-Oxophenyl)salicylaldimine complex, molybdenum(VI), 275
Oxopyridine complexes
osmium(II),(III), 1439
8-Oxoquinoline complexes
Mo(VI), W(VI), 275

P

Palladium, extraction from nuclear waste, 1125
Palladium(0)
carbonyl phosphine complex, 1987
phosphorus cluster complexes, 354,379
phosphorus cluster complex, 355,360,376,379
Palladium(II)
acetate halide phosphine Schiff base cyclometallated complexes, 1003
acetate arsine phosphine cyclometallated compounds, 1619
amine arsine chloride phosphine complexes, 921
aminoacid chloride thioether complexes, 1391
aminophosphine chloride complexes, 2009
aminopolycarboxylate chloride complexes, 571
ammine cyanide complexes, 79
aniline chloride complex, 1059
chloride dicarboxylate thioether complexes, 447
chloride diimine complexes, 1427
chloride diphosphine complex, 1797
chloride diphosphinoamine complex, 1727
chloride vitamin B_6 complexes, 329
cyclometallated ketoimine iron(II) complexes, 1243
diaminodiazobenzene complex, 2137
diphosphine thiolate platinum(IV) complex, 1261
halide thiodiacetic acid complexes, 1065
phosphazene complexes, 137
phosphine $S_2N_2^{2-}$ complexes, 1541
Palladium(II,IV)
ammonia diamine halide complexes, 225
PE spectra, carbaboranes, 1559
nido-Pentaborane(9), 1849
arachno-Pentaborane(11), 1849
Pentachloride dimers, 668
Pentamethylcyclopentadienyls
iron(0), 2031
lanthanides(II), 811,818
rhenium(VII), 1165
rhodium(III), 1255
tungsten, 2067
1,1,4,7,7-Pentamethyl-1,4,7-triazaheptane complexes, lithium, 987
2,4-Pentanedione, reaction with ferrocene derivative, 1243
2,4-Pentanedionates
aluminium, 525
indium(III), 507
iron(II),(III), 1421
magnesium, 1791
manganese(III), 2003
ruthenium(II), 1383,1621
n-Pentanethiolate, iron, 2085
Pentasulphide $[S_5]^{3-}$ complex
rhodium(III), 1775
neo-Pentoxides
molybdenum(III), 255
tungsten(III), 255
neo-Pentyls
molybdenum(III), 255
rhenium(V), 1169
tungsten(III), 255
tungsten(VI), 1839
Peptide complexes
cadmium, cobalt(II), 1477
copper(II), 45
nickel(II), zinc, 1477
Perazine complexes
molybdenum(IV), 465
Perchlorates and complexes
manganese(I), 1879
ruthenium(III), 387
Periodic table, book review, 659
Permanganate, reaction with diaminodiazobenzene, 2137
Peroxo complexes

molybdenum(VI), tungsten(VI), 275
Perthiocarbonate [CS_4^{2-}] complexes, nickel(II), 627
1,10-Phenanthroline, reactions with molybdenum(IV) complexes, 465
1,10-Phenanthroline complexes
chromium(III), 105
copper(II), 845
europium(II), 1143
manganese(I), 1879
molybdenum(0), 1781
neodymium(III), 957
praseodymium(III), 957
ruthenium(II), 1383
ruthenium(III), 1009
sodium, 1833
tungsten(0), 1781
ytterbium(II), 1143
Phenoxides
aluminium, 525
cobalt(II), 897,1993
copper(II), 897,1971
europium(III), 1971
indium(III), 507
iridium(III), 1509
iron(III), 1971
lanthanum, 1971
lithium, 1971
manganese(II), 897
molybdenum(0), 1523
molybdenum(II), 261
nickel(II), 897
niobium(V), 2019
rhenium(IV),(V),(VI), 1647
rhodium(III), 1509
sodium, 1833
tantalum(V), 1765,2019
titanium(IV), 2019
tungsten(VI), 163
Phenyls
antimony(III), 411
antimony(V), 411,1161
bismuth(III), 1593
rhenium(V), 1169
silicon, 435
tellurium(IV), 219
tin(IV), 393,397,587,1037
titanium(IV), 2019
Phenylalanine complexes
copper(II), 845
iron(III), 969
N-Phenyl-(β-amino-4-methylstyryl)diphenylphospha-1λ^5-azene) complexes, Ir(I),Rh(I), 1999
o-Phenylenebissalicylideneiminate complexes, iron(III), 295
Phenylimido complexes
iron(III), 2191
tungsten(VI), 163
2-Phenyl-indol-1-yl compounds
Eu(II), Yb(II), 1143
1-Phenyl-3-methyl-4-acetyl-5-pyrazolone complexes, uranium(VI), 1913
1-Phenyl-3-methyl-4-benzoyl-5-pyrazolone complexes, neodymium(III), 957
praseodymium(III), 957
1-Phenyl-3-methyl-4-trifluoroacetylpyrazolone complexes, actinides(III), lanthanides, 2099
3-Phenyl-2,4-pentanedionates
iron(II),(III), 1421
Phenylphosphonate complexes
vanadium(I), 1351
Phosphazenes, organometallic chemistry, review, 119
Phosphazene - phosphines, 144
Phosphinate complexes
nickel(II), 1251
Phosphine complexes
cobalt(II), 921
iridium(I), 921,1329,1999
iridium(III), 921
iron, 2067
iron(II), 1089
manganese(I), 1879
molybdenum(II), 261,2111
nickel(II), 921
palladium(0), 1987
palladium(II), 921,1003,1541, 1619
platinum(II), 341,539,891,921, 1295,1541,2165
rhenium(-I), 1577
rhenium(V), 1169,1647
rhodium(I), 921,1329,1503,1727, 1999,2187
rhodium(III), 921
ruthenium(0), 1709
ruthenium(II), 1089,1383,1851
silver(I), 1695
tantalum(III),(IV), 741
tungsten(0), 337
tungsten(II), 1135
tungsten(VI), 163,1657
uranium(VI), 647
zirconium(III), 645
Phosphinedicarboxylates
barium, nickel(II), 1407
Phosphine oxide complexes
cadmium, 963
iron(II), 1325
uranium(VI), 647,1913
Phosphine selenide complexes
tellurium(IV), 219
Phosphine sulphide complexes
iridium(I), rhodium(I), 1329
Phosphite [organo] complexes
cobalt(I), 543
rhodium(I), 1503
Phosphonate complexes
vanadium(I), 1351
Phosphorane, 1295
Phosphorus
atoms and clusters in complexes, review, 351
cluster complexes, cobalt, nickel, 1491
P - P bond formation, 1823
Phosphorus(III)
aryl glycol silyl compounds, 915
aryl halogen compounds, 1295
Phosphorus(V)
in heteropolyanions, 519,931, 1681
Photoaquation, molybdenum(IV) cyanide complex, 269
Photocatalysis, $[Ru(dipy)_3]^{2+}$ in cobalt(III) substitutions, 1571
Photoelectron spectra
carbaboranes, 1559

metal - metal bonds, 685
Photolysis, tungsten(0) carbonyl phosphine piperidine complex, 337
Phthalocyanines, Co,Cu,Ni,Zn, 1463
Picolinate complexes
molybdenum(0),(II),(III), 1523
molybdenum(VI), 275
tungsten(VI), 275
4-Picoline complexes
iridium(III), 1885
rhodium(III), 1885
ruthenium(II), 1383
tungsten(VI), 1657
2-[&3,4]Picoline-N-oxide complexes, thallium(III), 315
Picrate complex, sodium, 1833

Pinacolate, tungsten(III), 1747
Piperidine complexes
ruthenium(II), 837
tungsten(0), 337
Platinum
detection with $SnCl_2$, 71
Platinum(0)
phosphorus cluster complexes, 378
Platinum(I)
phosphorus cluster complex, 355,360,376,379
Platinum(II)
amine ammonia azole carbonyl halide pyrazine pyridine pyridine-N-oxide complexes, 85
amine arsine chloride phosphine complexes, 921
azole hydride phosphine complex, 341
chloride diphosphine complex, 1797
chloride diphosphinoamine complexes, 1727
chloride hexaphosphine complex, 1803
chloride phosphine complexes, 1295
cyclometallathiazine phosphine complexes, 2165
diphosphine thiolate platinum(IV) complex, 1261
halide thiodiacetic acid complexes, 1065
organotrithiophosphate phosphine complex, 539
phosphazene complexes, 137
phosphine $S_2N_2^{2-}$ complexes, 1541
phosphine tropolonate complexes, 891
Platinum(II,IV)
ammonia diamine halide complexes, 225
Platinum(IV)
aminopolycarboxylate chloride complexes, 571
ether methyl selenoether thioether complexes, 549
halide methyl pyridine Schiff base complexes, 319
halide methyl thiolate palladium(II) platinum(II) complexes, 1261
methyl thiolate, 1157
Polarization
vanadium(V) chloride oxo pyridylthiourea complexes, 1807
Polarography
chromium(I) biphenyl complex, 2151
cobalt(III) Schiff base complexes, 995
copper(II) tetrasalicylaldimine complexes, 513
thallium(I) cyclohexylthioglycolate complexes, 401
Polyhedral borane anions, 619, 2129
Polymerization, cobalt(III) cyanide complexes, 1563
Poly(N-methacroyl-L-lysine complexes, Co,Cu,Ni,Zn, 633
Polyphosphates, 531,1863
Polyurethane foams, absorption of Pt(Rh)/Sn complex, 71
Porphyrin complexes
chromium(III), 1361
chromium(IV), 2191
cobalt(II), 1071
Potassium
crown amine - ether carboxylate complexes, 29
crown ether complexes, 417
crown ether thiocyanate complex, 577
macrocyclic complexes, 1161
nitrate, 483
Potentiometric titrations
acyl-lysine complexes, 633
crown amine - ether carboxylate complexes, 29
heteropolyanion formation, 1813
lanthanum hydroxide complexes, 1283
Praseodymium(III)
macrocyclic semicarbazone thiosemicarbazone water complexes, 1611
phenanthroline pyrazolone complexes, 957
Proline complexes
cobalt(II), copper(II), 2037
iron(III), 969
manganese(II), 2037
Prolylalanyl peptide complexes
copper(II), 45
Prolylprolylglycine complexes
copper(II), 45
Promethazine complexes
molybdenum(IV), 465
i[&n]-Propanethiolate, iron, 2085
Propane-2-ol, catalytic hydrogenation, 2187
Propene-3-ol, oxidation, 275
Propericiazine complexes
molybdenum(IV), 465
Propionate complexes
copper(II), 1533
indium(III), 507
rhodium(II), 461
vanadium(I), 1351
Propionitrile complexes
iron(II), 1089
Propionylpromazine complexes

molybdenum(IV), 465
i-Propoxides
aluminium, 1791
copper(II), 427
molybdenum(III), 255
tungsten(III), 255
tungsten(VI), 1551
zirconium(IV), 427
n-Propoxides
copper(II), zirconium(IV), 427
n-Propyls
tin(IV), 587
N-Propyliminodiacetate complexes
beryllium, 303
Purine complexes
ruthenium(III), 387
Pyrazinamide complexes
iron(II), 1757
Pyrazine complexes
iron(II), 1757
platinum(II), 85
ruthenium(II), 473
Pyrazolone complexes
actinides(III), lanthanides, 2099
neodymium(III), 957
praseodymium(III), 957
uranium(VI), 1913
Pyridine complexes
borane, 1183
cobalt(II), 1071
cobalt(III), 995
copper(II), 39,943,1053,1669, 2169
iridium(III), 1509,1885
iron(I), 1497
iron(II), 159,1027,1757
lanthanum, 1021
molybdenum(0),(II), 1523
molybdenum(III), 255,1523
molybdenum(VI), 275
nickel(II), 2169
platinum(II), 85
platinum(IV), 319
rhenium(I), 593
rhodium(III), 1885
ruthenium(II), 837,1383
ruthenium(III), 603,1009
thallium(III), 479
tin(IV), 393,1037
tungsten(III), 255
tungsten(VI), 275,1657
vanadium(IV), 455
vanadium(V), 1807
2-Pyridinecarboxaldehyde complexes,
platinum(IV), 319
tin(IV), 393
Pyridine-N-oxide complexes
platinum(II), 85
thallium(III), 315
Pyridoxal-5′-phosphate complexes
palladium(II), 329
Pyridoxamine complexes
Cd,Co,Ni,Zn, 1477
Pyridoxamine phosphate complexes
palladium(II), 329
2-(2′-Pyridyl)benzimidazole complexes, vanadium(IV), 455
2-Pyridylcarbonylmethylide complexes, rhenium(I), 593
4-Pyridylcyanide complex
ruthenium(II), 159
Pyridylthiourea complexes
vanadium(V), 1807
Pyrimidine complexes
borane, 1183
cobalt(II),(III), 2103
copper(II), 855
ruthenium(III), 387
Pyrolysis, indium(III) dibutyl compounds, 507
Pyrrole-2-carboxylate complexes
tin(IV), 587
Pyrrolyldithiocarbamate
molybdenum(II), 1523

Q

Quinoline complexes, cadmium, 963
8-Quinolinethiolate complexes
iron(I), 1497
Quinone oxime complexes
iron(II), 1027

R

γ-Radiolysis, germane, 441
Raffinose complexes, boron, 1415
Raman spectra
aminopolycarboxylates, 603
bromides, 543,849,1065
chlorides, 543,849,1059,1065
Co/Hg complexes, 543
cyanide complexes, 79
diazabutadiene complexes, 1059
heteropolymolybdate, 1681
iodides, 543
metal - metal bond, 2027
oxo complexes, 891
phosphite complexes, 543
pyridine complexes, 603
thiodiacetic acid, thioether complexes, 1065
thiolate, thione complexes, 603
tin(IV) binuclear complex, 397
Rhamnose compounds, tin(IV), 383
Rhenium(-I)
chloride diazenide phosphine thiophenoxide complexes, 1577
Rhenium(I)
acylpyridine bromide carbonyl complexes, 593
carbonyl chloride diselenide complex, 2073
carbonyl diarsine halide complexes, 1255
phosphorus cluster complexes 373
Rhenium(II)
diphosphine halide complexes, 729,907,1483
Rhenium(II,III)
diphosphine halide nitrile complexes, 1483
Rhenium(III)
chloride diphosphine complexes, 1925
diphosphine halide complexes, 715,907,1483
Rhenium(IV)
chloride oxo phenoxide salicylaldimine complex, 1647
Rhenium(V)
alkyl alkylimido aryl

cyclopentadienyl halide oxo compounds, 1169
chloride, 668
chloride methanol oxo phenoxide phosphine salicylaldimine complexes, 1647
methyl oxo lithium complex, 1081
oxo thiophenoxide complex, 1577
ternary oxide, 668
Rhenium(VI)
chloride oxo phenoxide salicylaldimine complex, 1647
Rhenium(VII)
alkyl alkylidyne chloride complex, 1599
hydrazide oxo thiophenoxide complex, 1577
trioxo(pentamethylcyclopentadienyl), review, 1165
Rhodium
phosphorus cluster complexes 370
Rhodium(0)
phosphorus cluster complex 355,359,376,379
Rhodium(I)
amidophosphazene phosphine complexes, 1999
amine arsine phosphine complexes, 921
aminophosphine chloride complexes, 2009
bromide nitrosyl phosphine phosphite complexes, 1503
carbonyl chloride diene diimine palladium(II) complexes, 1427
carbonyl diphosphine halide hydride manganese(I) complexes, 111
chloride diisocyanide polymeric complex, 2027
chloride phosphine complexes, 2187
diene phosphine phosphine-sulphide complexes, 1329
diphosphinoamine phosphine complex, 1727
dipyridyl complexes, 2187
hydride phosphine complexes, 2187
phosphorus cluster complex 352,363
Rhodium(II)
carboxylate macrocyclic tetramine thioether triamine complexes, 461
phosphazene complexes, 142
phosphazenocarborane complexes, 146
Rhodium(III)
amine arsine chloride phosphine complexes, 921
aminophosphine chloride complexes, 2009
ammine imidazole cobalt(III) complexes, 1347
arsine chloride cyclopentadienyl complexes, 1255
chloride diphosphinoamine complex, 1727
chloride mercaptoquinazolinone complexes, 1009
halide pyridine complexes, 1885
hydride complex on polymer, 345
pentasulphide [S_5^{2-}] complex, 1775
quinone-oxime complexes, 1509
Ribose compounds, tin(IV), 383
Rubidium
macrocyclic complexes, 1161
Ruthenium
metallaboranes, 1941,1950
Ruthenium(0)
diphosphine phosphine complex, 1709
phosphazene complexes, 141
Ruthenium(I,II), formation in Ru(II) dimer complexes
electroreduction, 473
Ruthenium(II)
amine chloride diphosphine nitrile phosphine complexes, 1089
aminophosphine carbonyl chloride complexes, 2009
ammine nitrile iron(II) complex, 159
arsine carbonyl chloride complexes, 1255
arsine cyclopentadienyl diimine diketonate dithiocarbamate halide phosphine pseudohalide pyridine stibine complexes, 1383
carbonyl chloride diamine piperidine pyridine thiol thiourea urea complexes, 837
carbonyl chloride dithioformate phosphine complex, 1851
chloride cymene diphosphine dipyridyl pyrazine complexes, 473
chloride diphosphine complexes, 1131
dipyridyl complexes, 1571,1621
phosphazene complexes, 139,143
phosphazenocyclopentadienyl complexes, 147
Ruthenium(II,III)
ammine chloride complex, 1711
Ruthenium(III)
amide azole chloride mercaptoquinazolinone phenanthroline pyridine water complexes, 1009
chloride macrocyclic tetramine sulphonate complexes, 1875
aminophosphine carbonyl chloride complexes, 2009
dipyridyl complexes, 651
ethylenediaminetetraacetate mercaptopyridine complexes, 603
nucleoside perchlorate purine pyrimidine complexes, 387

S

$S_2N_2H^-$ complexes
nickel(II), 939
Pd(II), Pt(II), 1541
S_3N^- complexes, platinum(II), 2165

$S_3N_8^-$ salt, 1541
Saccharose complexes, boron, 1415
Salicylaldimine complexes
  aluminium, 1097
  cadmium, cobalt(II), 1319
  cobalt(III), 995
  copper(II), 513,1319,1669
  iron(III), 2191
  molybdenum(VI), 275,1635
  nickel(II), 1319,1901
  rhenium(IV),(V),(VI), 1647
  uranium(VI), zinc, 1319
Salicylaldoxime complexes
  copper(II), 197
Samarium(II) organometallics, 807
Schiff base complexes
  aluminium, 1097
  cadmium, 1319,1653
  cobalt(II), 205,1319,2103
  cobalt(III), 2103
  copper(II), 205,289,1319,2169
  iron(III), 295,2191
  nickel(II), 289,1017,1319,1653, 2169
  palladium(II), 1003
  platinum(IV), 319
  praseodymium(III), 1611
  uranium(VI), 205,1319
  zinc, 1319,1653
Selenium complexes
  cobalt, nickel, 1491
Selenium(II) halide complexes, 849
Selenoether complexes
  chromium(0), 1785
  platinum(IV), 549
  tungsten(0), 1785
Semicarbazone complexes
  aluminium, 1097
  praseodymium(III), 1611
Serine complexes
  copper(II), 1669
Silicon
  aryl methyl oxo compounds, 435
  in heteropolyanions, 519
Siloxanes, 435
Siloxy compounds, aluminium, 1097
Silver(I)
  chloride phosphine osmium(IV) complex, 1695
  crown ether complexes, 535
  diaminoazobenzene complex, 2137
  nitrate complex, 1885
  solubilization, Chinese method, 483
Silver(I,III) oxide, 1309
Silyl, phosphorus(III), 915
Sodium
  crown amine - ether carboxylate complex, 29
  crown ether complexes, 417
  macrocyclic complexes, 1161
  organo compounds, reactions with phosphazenes, 132
  phenanthroline picrate complex, 1833
Solubility product
  arsenic(V) hydroxyapatite, 1049
Solvation, cobalt(III) ammine chloride sulphoxide water complexes, 1337
Solvent extraction
  actinide(III) pyrazolone complexes, 2099
  alkali metal macrocyclic complexes, 1161
  cadmium phosphine oxide quinoline complexes, 963
  copper(II) bromovalerate, 1203
  copper(II) macrocyclic complexes, 289
  copper(II) salicylaldoximes, 197
  iron(III) carboxylates, 2155
  lanthanide phenanthroline pyrazolone complexes, 957
  lanthanide pyrazolone complexes, 2099
  lead(II) chloride complexes, 563
  mercury azole sulphonate complexes, 1209
  nickel(II) diketonate, dithiocarbamate, 497
  nickel(II) macrocyclic complexes, 289
  nickel(II) phosphinate complexes, 1251
  palladium(II) diaminoazobenzene complex, 2137
  palladium(II) - tributyl phosphate, 1125
  uranium(VI) dioxo acetate chloride phosphine complexes, 647
  zinc azole sulphonate complexes, 1209
Sorbose compounds, tin(IV), 383
Spectrophotometric titrations
  cobalt(II) azole phenoxide complexes, 1993
Spiroborate complexes, 2119
Stibine complexes
  ruthenium(II), 1383
"Strati-bis" complexes
  copper(II), 513
Strontium
  crown amine - ether carboxylate complex, 29
  crown ether complexes, 535
Structural methods, book review, 1715
Substitutions
  iridium(III), 101
Sulphamate complexes
  vanadium(I), 1351
Sulphate complexes
  cerium(IV), uranium(VI), 285
  vanadium(IV), 455,841
Sulphite complexes
  cobalt(II), 1717
  ruthenium(II), 1621
Sulphonate complexes
  cobalt(III), 1875
  mercury, 1209
  ruthenium(III), 1875
  zinc, 1209
Sulphoxide complexes
  cobalt(III), 1337
  copper(II), 1669
  nickel(II), 1313
  tin(IV), 1037
  uranium(VI), 1913
Sulphur complexes
  cobalt, nickel, 1491
Sulphur - nitrogen complex
  nickel(II), 939

T

Tantalum(III),(IV)
chloride hydride phosphine complexes, 741
Tantalum(V)
alkyl phenoxides, 2019
chloride ether oxo phenoxide complexes, 1765
Tautomerism, thiocarbazones, 13
Technetium(V)
diselenolate oxo complex, 1547
glycolate oxo complex, 1707
Tellurium(IV)
aryl carboxylate chloride phosphine-selenide complexes, 219
Terbium(III) pyrazolone complexes, 2099
Terpyridine complexes
copper(II), 1533
Tetrabenzo-18-crown-6 complexes
hydrogen ion, 1469
Tetrabutylammonium salts, 489
Tetrachloro-1,2-benzoquinone, 1823
Tetracyanobiimidazole complexes
platinum(II), 341
Tetrafluorobenzobarrelene complexes, rhodium(I), 1427
Tetrahydrofuran complexes
europium(II), 1143
lithium, magnesium, 1081
molybdenum(II), 2111
molybdenum(III,IV),(V), 2181
vanadium(II), 1433
ytterbium(II), 1143
Tetrakis(2-benzimidazolylmethyl)-diaminoethane complexes, nickel(II), 1457
Tetrakis(methylthio)methane complex, chromium(0), 1785
1,2,3,4-Tetrakis(salicylideneamino)-2,3-bis(phenylbutane) complexes, copper(II), 513
Tetrakis(4-trimethylammoniumphenyl)porphyrin complex, chromium(III), 1361
Tetramethyldiphosphine disulphide complexes, Ir(I), Rh(I), 1329
Tetramethylethylenediamine complexes,
cobalt(II), 1603
lithium, 987
nickel(II), 1603
tungsten(VI), 1657
2,2,6,6-Tetramethyl-3,5-heptanedionates. iron(II),(III), 1421
Tetramethylthiourea complexes
molybdenum(II), 2081
ruthenium(II), 837
tungsten(II), 2081
Tetramine complexes
cobalt(III), 1875
copper(II), 1291
rhodium(II), 461
ruthenium(III), 1875
Tetraminophthalocyanines
Co,Cu,Ni,Zn, 1463
Tetraphenylporphyrin complexes
chromium(IV), 2191
cobalt(II), 1071
Tetrapropylammonium salts, 489
Tetrasulphide [S_4^{2-}] complexes
nickel(II), 627
TGA
aluminium magnesium hydroxide, 1587
arsenic(V) hydroxyapatite, 1049
copper(II) carboxylate terpyridine water complexes, 1533
copper(II) carboxylate water complexes, 1869
copper(II) nitrosoresorcinol *complexes*, 1033
gold(III) chloride complex, 2077
indium(III) dibutyl compounds, 507
iron(II) cyanide pyrazine pyridine complexes, 1757
iron(III) aminoacid chloride hydroxide complexes, 969
molybdenum(IV) aminoalkylphenothiazine oxo complexes, 465
molybdenum(VI) oxo salicylaldimine complex, 1635
phthalocyanine complexes, 1463
silver(I,III) oxide, 1309
spinel formation, 1791
tin(IV) dicarboxylate methyl complexes, 1639
vanadium(IV) azole halide nitrate pyridine sulphate complexes, 455
vanadium(IV) biuret oxo sulphate complexes, 841
Thallium(I)
cyclohexylthioglycolate complexes, 401
Thallium(III)
chloride cycloheptatrienyl complex, non-formation, 479
chloride pyridine complex, 479
halide pyridine-N-oxide complexes, 315
reaction with chromium(VI), 1721
Thenoyltrifluoroacetonate
nickel(II), 497
Thio compounds
molybdenum(IV), 1741
molybdenum(VI), 1445,2085
tungsten(IV), 1115
tungsten(VI), 1445,1551
vanadium(V), 1445
Thiocarbazone, 13
Thiocyanate, reaction with chromium(III) complex, 1361
Thiocyanate complexes
cobalt(II), 1075
cobalt(III), 181
copper(II), 39
iron(II), 1191,1325
iron(III), 1191
mercury, 1273
molybdenum(II), 95
nickel(II), 1075,1407
potassium, 577
ruthenium(II), 1383,1621
zinc, 1075
Thiodiacetic acid complexes
Pd(II), Pt(II), 1065
Thiodiglycolate, tin(IV), 1639
3,3′-Thiodipropionic acid

complexes, palladium(II), 447
Thioether complexes
cadmium, 881
chromium(0), 1785
cobalt(II), 1843
copper(II), 943
nickel(II), 1843
palladium(II), 447,1065,1391
platinum(II), 1065
platinum(IV), 549
rhodium(II), 461
tungsten(0), 1785
Thiol complexes
ruthenium(II), 837
Thiolates
aluminium, 1097
cadmium, 1653
iron, 2085
iron(-I), 1147
nickel(II), 1653
Pd(II), Pt(II), 1261
platinum(IV), 1157,1261
ruthenium(III), 603
thallium(I), 401
zinc, 1653
Thiomolybdate, iron, 2085
Thione complexes
lead(II), 2177
ruthenium(III), 603
2-Thiophenacetate, tin(IV), 587
Thiophenoxides
iron, 1445,2085
molybdenum(0), 1523
platinum(IV), 1157
rhenium(-I),(V),(VII), 1577
Thiosemicarbazide complexes
iron(II), 1703
nickel(II), 1901
Thiosemicarbazone complexes
aluminium, 1097
copper(II), 39
iron(II), 1703
praseodymium(III), 1611
Thiourea complexes
on cellulose, 1197
molybdenum(II), 2081
ruthenium(II), 837
tungsten(II), 2081
vanadium(V), 1807
Thulium(III) pyrazolone complexes, 2099
Thymidine, thymine complexes
ruthenium(III), 387
Tin(II)
chloride, detection of Pt by, 71
Tin(IV)
aldehyde chloride ketone methyl phenyl pyridine complexes, 393
alkyl amide aryl chloride pyridine sulphoxide complexes, 1037
alkyl aryl carboxylates, 587
alkyl carbohydrate compounds, 383
amine dicarboxylate ether hydroxide methyl complexes, 1639
chloride ruthenium(II) complex, 1383
dibutyl oxide, 507
organo compounds, book review 660
phenyl trifluoroacetates, 397
Titanium(IV)
alkyl phenoxides, 2019
chloride dithiophosphates, 1681
organo compounds, book review, 660
phosphazene complexes, 137
4-Tolylimide complexes
chromium(IV), iron(III), 2191
Topology, hetero- and isopolyanions, 309
Triamine complexes
copper(II), 1053
lithium, 987
rhodium(II), 461
Tribenzo-18-crown-6 complexes
hydrogen ion, 1469
2,4,6-Tri-t-butylphenyl phosphorus(III), 915
Tri-n-butylphosphate, solvent extraction of palladium(II), 1125
Tri-n-butylphosphate complexes
cadmium, 963
uranium(VI), 1913
Tributylphosphine oxide complexes
uranium(VI), 647
Tributylphosphine selenide complexes, tellurium(IV), 219
Tributylphosphite complexes
uranium(VI), 647
Trichloroacetate
cobalt(II), 1603
Trichlorostannate complexes
ruthenium(III), 1383
Tridodecylammonium salts, 563
Triethylenetetramine complexes
copper(II), 1291
Triethylphosphine complexes
palladium(II), 1541
platinum(II), 1541,2165
zirconium(III), 645
Triethylphosphine sulphide complexes, Ir(I), Rh(I), 1329
Trifluoroacetate complexes
nickel(II), 1603
tellurium(IV), 219
tin(IV), 397
vanadium(I), 1351
Trifluoromethylsulphonate complexes, cobalt(III), ruthenium(III), 1875
1,1,1-Trifluoro-2,4-pentanedionates, iron(II),(III), 1421
Trihexylammonium salts, 563
Triketonate complexes
copper(II), 1473
Trimethylacetate complexes
rhodium(II), 461
Trimethylphosphine complexes
iron(II), 1089
molybdenum(II), 2111
palladium(0), 1987
rhenium(V), 1169
ruthenium(0), 1709
ruthenium(II), 1089
tantalum(III),(IV), 741
tungsten(II), 1135
tungsten(VI), 163,1657
Trimethylphosphine sulphide complexes, Ir(I), Rh(I), 1329
Trimethylsiloxide

aluminium, 1097
Trimethylsilyl
phosphorus(III), 915
Trimethylsilylmethyls
molybdenum(III), 255
rhenium(VII), 1599
titanium(IV), 2019
tungsten(III), 255
Trimethylsilylmethylidynes
molybdenum(III), 255
rhenium(VII), 1599
tungsten(III), 255
Trioctylammonium salts, 563
Tri-n-octylphosphine oxide
complexes
cadmium, 963
uranium(VI), 1913
1,4,10-Trioxa-7,13-diazacyclopentadecane-N,N'-diacetate
complexes, 29
Triphenylarsine complexes
ruthenium(II), 1383
Triphenylarsine oxide, 275,2077
Triphenylphosphine, reaction with
molybdenum nitrosyl complexes, 1523
Triphenylphosphine complexes
iridium(I), 921,1329,1999
palladium(II), 1003,1541
platinum(II), 341,539,891,2165
rhenium(-I), 1577
rhodium(I), 921,1329,1727,1999, 2187
ruthenium(II), 1383,1851
silver(I), 1695
tungsten(0), 337
Triphenylphosphine oxide, 275
Triphenylphosphine oxide
complexes, uranium(VI), 647
Triphenylphosphine selenide
complexes, tellurium(IV), 219
Triphenylphosphine sulphide
complexes, Ir(I), Rh(I), 1329
Triphenylphosphite complexes
cobalt(I), 543
Triphenylstibine complexes
ruthenium(II), 1383
Triphosphine complexes
cobalt, nickel, 1491
Tripnictide/-chalcogenide
complexes, cobalt, nickel, 1491
Tri-i-propylphosphine complexes
rhodium(I), 2187
Tris(diphenylphosphinomethyl)ethane complexes, cobalt, nickel, 1491
Tris(methylthio)methane complexes
chromium(0), tungsten(0), 1785
Trithiazyltrialkoxides, 2161
Tri(4-tolyl)phosphine selenide
complexes, tellurium(IV), 219
Tropolonates, Ir,Mo,Os,Pt,W, 891
Tryptophan complexes
copper(II), 1669
iron(III), 969
Tungsten
alkyl carbonyl cyclopentadienyl iron complexes, 2067
metallacarbaboranes, 1943
Tungsten(0)
carbonyl complexes, 503
carbonyl diimine complexes, 1673
carbonyl diimine halide mercury complexes, 1781
carbonyl diphosphine complex, 1797
carbonyl phosphine complex, 337
carbonyl selenoether thioether complexes, 1785
phosphazene complexes, 138,146
phosphorus cluster complexes, 366,373
Tungsten(I)
phosphorus cluster complex, 368
Tungsten(II)
acetonitrile carbonyl chloride thiourea complexes, 2081
carbonyl diphosphine iodide phosphine complexes, 1135
diphosphine halide complexes, 729
heteronuclear metal - metal bonds, 793
phosphazene complexes, 140,143
Tungsten(III)
acetate alkoxide alkyl alkylamide alkylidyne diamine diphosphine pyridine complexes, 255
alkoxide dimers, reactions with alkynes, review, 783
alkoxide,alkylamide dimers, 1677
alkoxide, pinacolate, 1747
phosphorus cluster complex, 363
Tungsten(IV)
dithiophosphate thio compound, 1115
Tungsten(V)
chloride, 668
cyanide complex, 641
methyl oxo magnesium compound, 1081
Tungsten(VI)
alkoxide alkylimide amine chloride diamine dipyridyl isocyanide oxo phosphine pyridine complexes, 1657
alkoxide amine arylimide chloride phosphine complexes, 163
alkoxide thio complexes, 1551
alkyl bromide oxo aluminium complex, 1839
amine carboxylate oxo oxyquinoline peroxide phenoxide pyridine water complexes, 275
cyclopentadienyl halide oxo complexes, non-formation, 281
heteropolyanions, 213,519,931, 1513,1813
as heteropolyanion, 1813
isopolyanions, 519,1919
oxo tropolonate complexes, 891
thio iron complexes, 1445
Tyrosine complexes
copper(II), 845,1669

U

Uracil complexes
cobalt(II),(III), 2103
ruthenium(III), 387

Uranium(III)
borohydride crown ether complexes, 189
Uranium(VI)
dioxo acetate amide chloride phosphine phosphine-oxide complexes, 647
dioxo acetate azole chloride nitrate sulphate complexes, 285
dioxo acetate diamine nitrate oxime Schiff base complexes, 205
dioxo crown ether complex, 189
dioxo phosphine oxide pyrazolone sulphoxide complexes, 1913
dioxo salicylaldimine Schiff base complex, 1319
Uridine complexes
ruthenium(III), 387

V

Valine complexes, iron(III), 969
Vanadium(0) carbonyl diphosphine complex, 1351
Vanadium(I) acetonitrile azide carbonyl carboxylate chloride cyanide diphosphine phosphonate sulphamate complexes, 1351
Vanadium(II) chloride ether complexes, 1433
Vanadium(IV)
azole halide nitrate pyridine sulphate complexes, 475
biuret oxo sulphate complexes, 841
Vanadium(V)
amide thio iron complexes, 1445
chloride oxo pyridylthiourea complexes, 1807
diaminoazobenzene complex, 2137
heteropolyvanadates, 1813
in heteropolyanions, 519,1813
Vitamin B_6 complexes
palladium(II), 329
Volume of activation
chromium(III) substitutions, 1361

W

Water complexes
barium, 1407
cadmium, 881
chromium(III), 1239,1361
cobalt(II), 897,931,1603
cobalt(III), 1337,1563
copper(II), 855,897,1319,1533, 1669,1869,1971
europium(III), 1971
iron(II), 1325
iron(III), 1971
lanthanum, lithium, 1971
manganese(II), 897,1699
molybdenum(IV), 465
molybdenum(VI), 275
nickel(II), 897,1457,1603
praseodymium(III), 1611
ruthenium(III), 1009
tungsten(VI), 275
zinc, 881,1111
Wheat sauce, in solubilisation of silver, 483

X

Xα calculations, metal - metal bonds, 685,695,741
Xanthate complexes
iron(I), 1497
X-ray crystal structures
aluminium bromide oxo tungsten(VI) complex, 1839
barium phosphinedicarboxylate water complex, 1407
bismuth(III) chloride iron(0) complex, 2031
cadmium carboxylate water complex, 881
catecholdicarboxylate water complexes, 871
chromium(III) ammine chloride water complex, 1239
cobalt(I) phosphite mercury(I) complex, 543
cobalt(II) amide dehydroacetic acid complex, 1235
cobalt(II) carboxylate diamine water nickel(II) complex, 1603
cobalt(II) heteropolytungstate water complex, 931
cobalt(III) acetate pyrimidine Schiff base complex, 2103
cobalt(III) diamine hydroxoaqua nitrite thiocyanate complexes, 181
copper(II) azole bromide ether complex, 1149
copper(II) carboxylate ether pyrimidine water complexes, 855
copper(II) carboxylate terpyridine water complexes, 1533
copper(II) carboxylate water complex, 881
copper(II) nitrosoalkylhydoxylamine complex, 1375
cyclotetraphosphine, 1295
diazadiphosphacyclopentanones, 1823
heteropolytungstate, 931
iridium(II) amidinate complex, 1625
iridium(III) chloride pyridine quinone-oxime complex, 1509
iron molybdenum(VI) carbonyl thio complex, 1445
iron(0) carbonyl cyclopentadienyl bismuth(III) complex, 2031
iron(II) carbonyl mercurithiocyanate complex, 1273
iron(II) diphosphine nitrile complexes, 1089
iron(III) nitrosoalkylhydroxylamine complex, 1375
isoprenaline, 25
lead(II) nitrate thione complex, 2177
lithium amine diphenylphosphide complexes, 987
magnesium ether oxo tungsten(V) compound, 1081
Magnus salts, 225

molybdenum(0) nitrosyl picolinate, 1523
molybdenum(II) acetate chloride phosphine complex, 2111
molybdenum(II) carbonyl diphosphine thiocyanate complex, 95
molybdenum(II) carbonyl diphosphoxane halide complexes, 1103
molybdenum(II) carbonyl iodide phosphine complex, 261
molybdenum(III,IV) acetate ether iodide oxo complex, 2181
molybdenum(IV) chloride diphosphine thio complex, 1741
molybdenum(V) ether iodide oxo complex, 2181
molybdenum(VI) oxo tropolonate complexes, 891
nickel(II) azole chloride thioether complexes, 1843
nickel(II) carboxylate diamine water cobalt(II) complex, 1603
nickel(II) diaminetetrazole complexes, 1457
nickel(II) diphosphine nitrate complex, 1223
nickel(II) dithiolate complex, 863
nickel(II) ketoimine salicylaldimine thiosemicarbazide complexes, 1901
nickel(II) phosphinedicarboxylate complex, 1407
osmium(II) chloride diphosphine complexes, 1131
osmium(II,III) chloride oxopyridine complex, 1439
osmium(IV) chloride silver(I) complex, 1695
palladium(0) carbonyl phosphine complex, 1987
palladium(II) aniline chloride complex, 1059
phosphorus(III) aryl glycol silyl compounds, 915
platinum(II) azole hydride phosphine complex, 341
platinum(II) chloride hexaphosphine complex, 1803
platinum(II) chloride phosphine complex, 1295
platinum(II) cyclometallathiazine phosphine complexes, 2165
platinum(II) diphosphine thiolate platinum(IV) complex, 1261
platinum(II) organotrithiophosphate phosphine complex, 539
platinum(IV) chloride methyl thiolate platinum(II) complex, 1261
platinum(IV) methyl thiolate, 1157
rhenium(-I) chloride diazenide phosphine thiophenoxide complexes, 1577
rhenium(I) carbonyl chloride diselenide complex, 2073
rhenium(II) chloride diphosphine complex, 907
rhenium(V) alkyl halide oxo phosphine complexes, 1169
rhenium(V) oxo thiophenoxide complex, 1577
rhenium(VII) alkyl alkylidyne chloride complex, 1599
rhenium(VII) cyclopentadienyl oxo compound, 1165
rhenium(VII) hydrazide oxo thiophenoxide complex, 1577
rhodium(I) bromide nitrosyl phosphine phosphite complexes, 1503
rhodium(III) pentasulphide complex, 1775
ruthenium(II) carbonyl chloride dithioformate phosphine complex, 1851
ruthenium(II) chloride diphosphine complexes, 1131
ruthenium(II,III) ammine chloride complex, 1711
$S_3N_8^-$ salt, 1541
silver(I) chloride phosphine osmium(IV) complex, 1695
sodium phenanthroline picrate complex, 1833
tantalum(III),(IV) chloride hydride phosphine complexes, 741
tantalum(V) chloride oxo phenoxide complexes, 1765
technetium(V) diselenolate oxo complex, 1547
titanium(IV) alkyl aryl phenoxides, 2019
trithiazyltrialkoxides, 2161
tungsten(II) carbonyl diphosphine iodide complex, 1135
tungsten(III) alkoxide, pinacolate, 1747
tungsten(IV) dithiophosphate thio compound, 1115
tungsten(V) methyl oxo magnesium compound, 1081
tungsten(VI) alkoxide arylimide chloride complex, 163
tungsten(VI) alkoxide thio complexes, 1551
tungsten(VI) alkyl bromide oxo aluminium complex, 1839
uranium(III) borohydride crown ether complex, 189
uranium(VI) dioxo acetate amide chloride complex, 647
vanadium(0) carbonyl diphosphine complex, 1351
vanadium(I) carbonyl carboylate diphosphine nitrile complex, 1351
vanadium(II) chloride ether complexes, 1433
zinc carboxylate water complex, 881
zinc chloride hexamethylenetetramine water complex, 1111
zirconium(III) alkene halide phosphine complexes, 645
X-ray diffraction
aluminium magnesium hydroxide,

1587
arsenic(V) hydroxyapatite, 1049
heterobinuclear complexes, 897
hydrogen dinitrate anion salts, 1885
iron(III) nitrosyl oxo Schiff base complexes, 295
metallophthalocyanines, 1463
rhodium(I) chloride diisocyanide polymeric complex, 2027
silver(I) nitrate complexes, 1885
spinel formation, 1791

Y

Ylides, 593
Ytterbium(II)
carbazolyl ether indolyl phenoxide complexes, 1143
organometallics, 807
Ytterbium(III)
bipyrimidine chloride complexes, 175
Yttrium
bipyrimidine chloride nitrate complexes, 175

Z

Zinc
aminoacid complexes, 633
azole sulphonate complexes, 1209
biochemistry, review, 61
carboxylate catecholate complexes, 53
carboxylate water complex, 881
catecholdicarboxylate water complexes, 871
chloride hexamethylenetetramine water complexes, 1111
crown amine-ether carboxylate complexes, 29
cysteine nitrilotriacetate thiourea complexes on cellulose, 1197
glycylglycine imidazole pyridoxamine complexes, 1477
halide hydrazone thiocyanate complexes, 1075
heteropolymolybdates, 213
hydroxycarboxylates, 1517
mercaptocarboxylate complexes, 613
nitrilotri(methylenephosphonate) complexes, 1247
organo compounds, reactions with phosphazenes, 133
phosphazene complexes, 138
phthalocyanines, 1463
salicylaldimine Schiff base complexes, 1319
Schiff base thiolate complexes, 1653
Zirconium(III)
alkene halide phosphine complexes, 645
Zirconium(IV)
alkoxide copper(II) compounds, 427

Printed in Great Britain at Aberdeen University Press

AUTHOR INDEX

Abe, Y. 2135
Abel, E. W. 1169, 1321, 1329, 1855
Abram, U. 285
Adams, H. 1861
Adams, R. D. 967, 1071, 1543, 2251, 2263
Agarwal, D. D. 2569
Aguilar, M. 5
Akbar Ali, M. 2183
Al-Tahir, A. B. 219
Albrecht, I. 2307
Alegret, S. 5
Allison, J. 1559
Almond, M. J. 629
Alobaidi, N. 235, 1931
Alvarez, D. Jr 1285
Ama, T. 353
Ambwani, B. 1939
Amer, S. A. 2635
Anderson, S. J. 2615
Andrews, D. G. 827
Ang, K. P. 695
Angelova, O. 1273
Ansari, M. A. 471
Aravamudan, G. 1267
Arce, A. J. 979
Arif, A. M. 561, 2091
Arliguie, T. 2031
Armentrout, P. B. 1573
Armstrong, E. M. 63, 245, 2769
Arnold, D. P. 2225
Arriortua, M. I. 1383
Askham, F. R. 1785
Ates, M. 2601
Atwood, J. L. 1693, 2083
Avsar, E. 213
Ayoko, G. A. 11
Azam, K. A. 1793

Babaeva, V. P. 345
Babin, J. E. 967, 1071, 2263
Babkov, A. V. 1203
Baerends, E. J. 1625
Baghlaf, A. O. 219
Bahl, B. K. 2175
Bahsoun, A. A. 2035
Bailey, N. A. 1861
Baird, M. C. 1965
Baker, P. K. 63, 245, 2719, 2769
Bakir, M. 1279
Bala, S. 2465
Bancroft, D. P. 615
Bandy, J. A. 1819
Bandyopadhyay, D. 1135
Baralt, O. 2411
Barr, D. 665, 2119
Barral, M. C. 2597
Barron, A. R. 77, 2091
Bartecki, A. 601
Bashall, A. P. 2221
Basnet, R. B. 147
Basset, J.-M. 2399
Bassner, S. L. 791
Basson, S. S. 2193
Bastida, R. 2503
Basumatary, J. K. 635
Bates, P. A. 1401, 1793, 1855
Battezzati, L. 597
Bayeul, D. 303
Beardwood, P. 1911
Beck, A. 2387
Beck, W. 2255
Beckett, M. A. 1169, 1855
Beer, P. D. 137, 2649
Beltran, D. 1383
Ben Hadda, T. 575
Bender, R. 2271
Benfield, R. E. 2549
Bennett, R. 2233
Benzi, P. 597
Bercaw, J. E. 759, 1409, 1441, 2053
Bergman, R. G. 1429
Bermejo, M. R. 2561
Berry, D. H. 759
Berthon, G. 2487
Besteiro, J. C. 87
Bhardwaj, R. 709
Bilgrien, C. J. 1453
Bitterwolf, T. E. 409, 1377
Block, E. 1397
Bock, H. 2429
Bolos, C. 2233
Bontchev, P. R. 1273
Bookham, J. L. 129, 239
Bott, S. G. 2083
Bottomley, L. A. 589
Boumezioud, M. 513
Bouwman, E. 2591
Bradley, D. C. 1289, 1791, 2049
Braga, D. 2549

Bratsch, S. G. 1677
Braunstein, P. 2271
Breunig, H. J. 2601
Breysse, M. 2405
Brito, F. 1187
Brown, M. P. 1147
Brown, P. R. 1819
Brown, S. J. 2009
Brownstein, S. 97
Bruce, D. W. 1861
Bryndza, H. E. 1441
Buckner, S. W. 1583
Buiten, J. 585
Bukietynska, K. 641
Bulls, A. R. 1409
Bursten, B. E. 943
Busch, D. H. 2243
Buschmann, H-J. 721
Butler, A. R. 1197

Calderazzo, F. 2039, 2246
Calsy-Harrison, A. M. 1197
Campagna, S. 207
Campbell, M. J. M. 1719
Canich, J. A. M. 737
Cantrell, K. J. 573
Capparelli, A. L. 2709
Carmona, E. 163, 1767, 1831
Cartwright, P. S. 1243, 1801, 2143
Carty, A. J. 1045, 2285
Casabo, J. 43
Casals, I. 2509
Casas, J. S. 2487
Casassas, E. 689, 1335
Casey, C. P. 881
Castiglioni, M. 597
Castineiras, A. 2503, 2561
Caulton, K. G. 1285, 2171
Cayton, R. H. 943
Celap, M. B. 1153
Cesljevic, V. I. 2641
Chadha, R. K. 1121
Chakravarty, A. R. 685
Chakravorti, M. C. 1135
Chandrasekaran, J. 471
Charalambous, J. 2233, 2235
Chaudret, B. 2031
Chauhan, V. 623
Chawla, S. K. 1939
Chen, Y-J. 1891
Cheng, Z. 369
Cherkas, A. A. 1045
Chesnut, R. W. 753
Chidambaram, Sp. 1267
Chisholm, M. H. 399, 757, 903, 919, 1015, 1991, 2515
Chmielewski, P. 25, 337
Choi, K. Y. 203
Choplin, A. 2399
Christophersen, M. J. N. 2521
Chudzynska, H. 1289
Ciavatta, L. 1355, 1773
Cieslak-Golonka, M. 601
Cinquantini, A. 195
Clark, D. L. 903
Clark, D. T. 2297
Clark, G. R. 117, 297
Clark, H. C. 1349
Clark, R. J. H. 2611
Clegg, W. 2239
Colbran, S. B. 1759
Cole-Hamilton, D. J. 1945
Colson, S. F. 417, 1919
Compton, N. A. 2239
Connor, J. A. 161
Conroy, B. K. 903
Constable, E. C. 2531
Contreras, R. 679, 2095
Cooley, N. A. 1965
Cornell, R. M. 385
Costa Pessoa, J. 1245
Costamagna, J. 489
Cotton, F. A. 83, 87, 463, 615, 737, 1311, 1667, 1673, 2201
Cotton, S. 169
Cowley, A. H. 77, 1317, 1901, 1909
Cox, J. 731
Crane, C. G. 2649
Croud, V. B. 2611
Cruywagen, J. J. 547
Curic, M. 2761
Curtis, M. D. 2411
Cusumano, M. 207

D'Agostino, M. F. 807
D'Ornelas, L. 2399
Dance, I. G. 2205
Dance, J. M. 543
Daniels, L. M. 1667
Dao, C. N. 2495
Das, B. K. 685
Davies, A. G. 1225, 1789
Davis, R. 425
Davison, A. 1981
Dawes, H. M. 651, 2049, 2611
De Meric De Bellefon, C. 2271
De Sanctis, Y. 979

De Wet, H. F. 547
Deacon, G. B. 249
Decock-Le Reverend, B. 1089
Deeming, A. J. 651, 979, 1401, 1793
Dennis, C. R. 2193
Dhillon, R. 1861
Dhubhghaill, O. N. 17, 187
Dias, A. R. 1531
Diaz, C. 673
Diaz, G. 2743
Dickens, P. G. 243
Dickson, R. S. 859
Diemann, E. 2405
Diez, J. 37
Dikshit, S. K. 623
Dillon, K. B. 1725
Dodd, A. 2235
Doherty, N. M. 837
Domaille, P. J. 1441
Dominguez, S. 1187
Donia, A. M. 2149
Downs, A. J. 629
Drago, R. S. 1453
Drdakova, E. 669
Drew, M. G. B. 245, 2229
Driessen, W. L. 2575, 2583, 2591
Drozdzynski, J. 167
Drummond, D. K. 1693
Duatti, A. 195
Dunmur, D. A. 1861
Duraj, S. A. 737
Durrant, J. L. A. 425
Dymek, C. J. Jr 1139

Earley, J. E. 1393
Edwards, A. J. 79, 103
Eilmes, J. 2197
Einarsrud, M.-A. 1139
Eisenstein, O. 405
El-Amouri, H. 2035
El-Ezaby, M. S. 747
El-Saied, F. A. 2149
Elsevier, C. J. 2521
Eltzner, W. 2405
Erim, F. B. 213
Erker, G. 2451
Errington, R. J. 2239
Esteve, C. 229
Evans, D. F. 1881, 2723
Evans, W. J. 1693
Everhart, M. 1393

Faktor, M. M. 1289
Falagan, S. 37
Falvello, L. R. 615
Favero, G. 2703
Fawcett, J. 2015
Feinstein-Jaffe, I. 741
Felix, M. S. B. 1793
Feliz, M. R. 2709
Feng, L. 393
Feng, Q. 291
Ferguson, G. 17, 187, 1349
Fernandez, A. 2561
Fernandez-G., J. M. 2159
Fernandez-Vincent, C. 679
Ferrao, M. L. C. C. H. 421
Filella, M. 331
Finke, R. G. 1469, 1499
Fitzpatrick, N. J. 223
Florido, A. 5
Flower, K. R. 2769
Flumignan, E. 2477
Fogg, D. E. 2285
Folting, K. 2171
Fong, L. K. 1441
Fonrodona, G. 689, 1335
Forghieri, F. 1231
Fornies, J. 2659
Fox, S. G. 349
Francois, M. A. 489
Fraser, S. G. 245
Freiser, B. S. 1583
Frigo, D. M. 587, 1289, 2247
Fronczek, F. R. 1785
Fryzuk, M. D. 1001
Fujita, M. 2731
Fung, A. S. 2421

Gaber, M. 2635
Galesic, N. 2641
Galindo, A. 1767, 1831
Gallagher, M. 2307
Gamasa, P. 37
Gang, Z. 393, 1101
Garcia Bugarin, M. 2487
Garcia Montelongo, F. 495
Garcia, J. 229
Garcia, M. A. 1067
Garcia, M. E. 2487
Garcia, R. 43
Garg, B. S. 147
Garralda, M. A. 1067
Garriga, N. 331
Garvey, R. G. 523
Gates, B. C. 2421
Gayoso, M. 2561
Gencheva, G. 1273

Geoffroy, G. L. 791, 2331
Georgiadis, R. 1573
Gholivand, M. B. 1227
Gibson, J. F. 1911
Gibson, V. C. 579, 2217, 2221
Gielen, M. 363
Gill, U. S. 2685
Gillard, R. D. 349, 1175, 1243, 1245, 1801, 2143, 2731
Gimeno, J. 37
Giolando, D. M. 1317, 1909
Giovanoli, R. 385
Girolami, G. S. 2001
Giuffrida, A. 207
Giuliani, A. M. 1211
Gladysz, J. A. 2209
Glidewell, C. 1197, 1371
Glowiak, T. 2495
Gonzalez, A. A. 1491
Gonzalez, V. 495
Gonzalez-Duarte, P. 2509
Goodfellow, R. 505
Goodgame, D. M. L. 1299, 1807
Goodgame, M. 1869
Gorce, J-N. 589
Graaff, R. A. G. de 2575
Graddon, D. P. 2129
Granifo, J. 489
Gray, H. B. 2246
Greaves, S. J. 1973
Green, M. L. H. 1819
Griffith, G. A. 2015
Griffith, W. P. 1305, 1973
Gromov, D. V. 345
Gruehn, R. 2393
Grzybkowski, W. 535, 2473
Guczi, L. 2387
Guglielmo, G. 207
Guilard, R. 303
Guille-Photin, C. 1767
Gulec, S. 2601
Gungor, M. 1827
Gupta, H. K. 623
Gupta, V. D. 483
Gutierrez, E. 1831
Gutierrez, M. D. 659

Hadj-Bagheri, N. 2695
Hahn, E. 2307
Hall, L. A. 2155
Halpern, J. 1483
Hammond, C. E. 399, 2515
Hamor, T. A. 1931
Hampden-Smith, M. J. 187, 1349, 1991
Han, S. H. 2331
Hanselman, D. S. 2679
Hanusa, T. P. 725
Harding, M. M. 1147
Hare, P. M. 1819
Harrison, J. F. 1559
Hassan, M. M. 747
Hay, B. P. 1469, 1499
Hay, C. M. 987
Hayat, L. J. 747
Heaton, D. E. 1901
Hefner, J. G. 561
Henderson, D. E. 369
Herdtweck, E. 2027
Hermanek, S. 669
Hernandez-Padilla, M. 1187
Herrera, J. V. 1187
Herrmann, G. 2341
Herrmann, W. A. 2027
Hey, E. 2083
Heyen, B. J. 1207
Hidai, M. 2369
Higuchi, T. 2213
Hiller, W. 2503, 2561
Hirotsu, K. 2213
Hiskia, A. 477
Hoff, C. D. 1429, 1491
Hoggard, P. E. 523
Holmes, J. M. 2531
Horton, A. D. 987, 1841
Horvath, I. T. 2345
House, D. A. 1159
Housecroft, C. E. 1759
Hove, J. C. T. 2591
Howes, A. J. 235, 1931
Hsu, L.-Y. 2399
Huffman, J. C. 399, 753, 903, 919, 1991, 2171, 2515
Hughes, L. A. 1693
Hunt, S. E. 1861
Hursthouse, M. B. 235, 323, 651, 1079, 1289, 1363, 1401, 1781, 1793, 1855, 1919, 1931, 2049, 2087, 2605, 2611, 2615
Huskowska, G. E. 2495
Hussain, B. 1079, 1289, 1363, 2615
Hussain, I. 1869

Ibarlucea, L. 1067
Ichida, H. 1131
Ichikawa, M. 2351
Inamoto, N. 2213

Indrasenan, P. 143
Irish, B. 97
Ishaq, M. 219
Issa, R. M. 2635
Iuliano, M. 1773
Izquierdo, A. 331

Jakubovic, D. A. 1881, 2723
Janas, Z. 2655
Janiak, C. 2307
Janke, C. J. 315
Jankowska, E. 439
Jardine, F. H. 1827
Jean, Y. 405
Jeffery, J. C. 775
Jeffery, T. L. 629
Jelinek, T. 669
Jemmis, E. D. 871
Jenkins, S. M. 859
Jensen, C. M. 1035
Jesih, A. 1217
Jezierski, A. 25
Jezowska-Trzebiatowska, B. 337
Jimenez-Aparicio, R. 2597
Jishan, X. 393
Johnson, B. F. G. 1107, 1759, 2549
Johnson, I. L. 1371
Johnston, R. L. 2437
Jones, C. J. 79, 235, 1931
Jones, R. 647
Jones, R. A. 77, 561, 1317, 1901, 1909
Jun, M.-J. 529
Jung, J.-S. 529
Juranic, N. 1153

Kabli, R. A. 219
Kaden, L. 285
Kaesz, H. D. 1035, 1891
Kaitner, B. 1349
Kalck, P. 2441
Kaminsky, W. 2375
Kang, H. 1397
Kapoor, P. 2175
Kapoor, P. N. 1389
Kapoor, R. 2175
Karim, M. 1401
Kashanian, S. 1227
Kasprzyk, S. P. 1053
Kaur, P. 2175
Kawa, H. 2023
Kee, T. P. 579, 2217, 2221
Keggan, C. E. 1147
Keister, J. B. 847
Kelley, M. J. 2421
Kelly, P. F. 419, 1925
Kennedy, R. J. 161
Khan, M. A. 49, 425
Khandelwal, B. L. 635
Khoo, C. S. 2129
Kibala, P. A. 83
Kidd, K. B. 1901
Kikukawa, M. 2135
Kim, C. H. 529
Kim, H-S. 967
King, R. B. 1813
Kirschenbaum, L. J. 2753
Kiss, T. 1089
Kitagawa, S. 463, 1673
Klaebe, A. 679
Klahn, A. H. 2743
Klapotke, Th. 1221
Klein, N. 605
Klein, S. I. 2165
Klinszporn, L. 535
Kneuper, H-J. 961
Knobler, C. B. 1891
Knox, S. A. R. 837
Koenig, T. W. 1499
Kolax, C. 2307
Kolinski, R. A. 1053
Konings, M. S. 881
Koo, B-K. 1397
Korste, L. 605
Koschmieder, S. U. 561
Krampe, W. 581
Krannich, L. K. 2553
Kreibig, U. 605
Ku, Y. Y. 2685
Kuhns, J. D. 2543
Kumar, R. 49, 1121
Kuncheria, B. 143
Kwik, W. L. 695

Labinger, J. A. 2246
Lacroix, M. 2405
Lagow, R. J. 2023
Lagrange, P. 513
Lahuerta, P. 87, 1311
Lalinde, E. 1861
Lancashire, R. J. 1245
Lane, K. R. 1609
Lappert, M. F. 2083
Laschi, F. 195
Latorre, J. 1311
Lawrance, G. A. 1263
Lawrence, S. A. 741

Le Bozec, H. 575
Leclercq, C. 2405
Lecomte, C. 303
Lee, K-W. 523
Lee, K. E. 2209
Legendziewicz, J. 2495
Legros, J. P. 229, 307
Leipoldt, J. G. 2193
Leovac, V. M. 2641
Levine, L. J. 725
Lewandos, G. S. 837
Lewis, J. 1759
Lezama, L. 1383
Lima, J. F. de 1687
Lindsay, A. J. 1239
Lis, T. 2655
Lisowski, J. 337
Liu, S. 401, 1129, 1397
Llusar, R. 87
Loebel, J. 2307
Longley, C. J. 1079
Look, P. 505
Lopez de la Vega, R. 1491
Lopez, R. 659
Lorenz, B. 285
Lota, J. S. 2233
Lott, K. A. K. 741
Luks, E. 439
Lundquist, E. G. 2171
Lutar, K. 1217
Lutfullah 705

Ma, H. 1095
MacConnachie, P. T. F. 1965
Macaskova, L. 1745
Macias, A. 2503
Macicek, J. 1273
Macpherson, K. A. 837
Madaeni, S. 1227
Maggs, A. A. 1861
Magon, L. 195
Maharaj, D. I. 2155
Maitlis, P. M. 827, 1861
Majumder, S. M. M. H. 2183
Makhyoun, M. A. 2675
Malinar, M. J. 1153
Manhas, B. S. 2465
Manley, B. C. 2023
Manning, T. M. 1263
Manriquez, J. M. 1409
Manzur, C. 2743
Marafie, H. M. 747
Marchant, N. S. 919
Marchi, A. 195
Marder, S. R. 881
Marin, J. M. 1831
Marks, T. J. 1405, 1517
Marques Netto, A. 2165
Martin, J. D. 1991
Martin, R. L. 2243
Martinho Simoes, J. A. 1531
Martire, D. O. 2709
Masana, A. 715
Masters, A. F. 2009
Matondo, S. O. C. 2235
Matsubayashi, G.-E. 379
Matsuzaka, H. 2369
Matusz, M. 83, 2201
Mavridis, A. 1559
Mays, M. J. 987
McCabe, D. J. 2411
McCleverty, J. A. 103, 235, 449, 1931
McCormick, M. J. 725
McDermott, G. 1239
McDevitt, M. R. 2421
McDowell, D. 2229
McFarlane, H. C. E. 1875
McFarlane, W. 129, 239, 1875
McGlinchey, M. J. 807, 2297
McPartlin, M. 2221, 2235
McWhinnie, W. R. 635
Mederos, A. 1187
Melnik, M. 1745
Mesa, J. L. 1383
Miguel, D. 443
Milgrom, L. R. 57
Mingos, D. M. P. 2437
Miravitlles, C. 2509
Mitchell, S. H. 1175
Mitewa, M. 1273
Molins, E. 2509
Monge, A. 1831
Mont, W-W. du 1317
Moodley, K. G. 1991
Moriarty, R. M. 2685
Morikawa, M. 2135
Morris, R. H. 2031
Morris, R. J. 2001
Morrison, E. C. 1719
Moss, M. A. J. 79
Motevalli, M. 1363, 1919
Mridha, M. A. U. 2183
Mrozinski, J. 1053, 1745
Mukerjee, S. L. 1491
Mul, W. P. 2521
Muller, A. 2405
Muller, F. 2521

Mulvey, R. E. 665, 2119
Murakami Iha, N. Y. 1687
Murray, M. 505

Nadal, LL. 715
Nagase, S. 2213
Nakamura, S. 155
Nasim, M. 2189
Navarro, R. 2659
Nehete, D. T. 709
Nekrasov, Yu. S. 345
Nelson, J. 2229
Nettle, A. 2095
Newton, J. 2087
Ngoan, D. C. 2495
Nguyen, M. T. 223
Nicholls, D. 1147
Nicholson, T. 171
Nickel, S. 2307
Nielson, A. J. 67, 117, 297
Niitsu, T. 2213
Nikrahi, A. 1227
Nisbet, M. P. 1725
Nolan, S. P. 1429, 1491
Norman, N. C. 2239
Nunn, C. M. 77, 1317, 1901, 1909

O'Leary, M. A. 1263
Odagaki, Y. 2213
Okey, J. N. 1869
Olatunji, M. A. 11
Olby, B. G. 1781
Olmstead, M. M. 609
Ontiveros, C. D. 1015
Orpen, A. G. 837
Orr, R. 1861
Orrell, K. G. 1169, 1321, 1329
Osborn, J. A. 2035
Ostropolska, L. 2667
Owen, S. M. 253, 1759
Oye, H. A. 1139
Ozeki, T. 1131

Paap, F. 2575
Paciello, R. A. 1441
Page, P. R. 2087
Palacios, M. S. 543
Palamidis, E. 2307
Pampaloni, G. 2039
Panda, R. K. 2753
Pande, L. M. 2189
Pandey, K. K. 709
Papaconstantinou, E. 477
Papavassiliou, M. 581
Park, C. H. 203
Parkin, G. 2053
Pathirana, N. D. 2235
Paxton, K. 1931
Paz-Sandoval, M. A. 679
Peacock, R. D. 2015
Pearlstein, R. M. 1981
Pelizzi, G. 2039
Penner-Hahn, J. E. 2411
Pennings, Y. C. M. 2583
Penny, D. J. 243
Perez Pont, Mª L. 495
Perkins, P. G. 2119
Perrier, R. E. 2297
Perumareddi, J. R. 1705
Peters, K. 2095
Peters, K. S. 1619
Piers, W. E. 1001
Piggott, B. 323, 2605
Pilarczyk, M. 535
Pitombo, L. R. M. 2477
Pizarro, J. L. 1383
Plesek, J. 669
Poddar, R. K. 1727, 1737, 2627
Poe, A. J. 1939
Polm, L. H. 2521
Pomp, C. 2537
Ponec, V. 2383
Pons, J. 43
Popov, A. I. 1341
Porto, R. 1355, 1773
Powell, G. L. 1207
Powell, H. R. 2049, 2235
Powell, R. D. 1305
Power, J. M. 1317, 1909
Power, P. P. 609
Prakash, D. 1
Prasad, B. V. 871
Preti, C. 1231
Proud, G. P. 651
Przywarska-Boniecka, H. 2667
Puddephatt, R. J. 767, 2695
Purcell, T. G. 647

Qureshi, K. B. 1321, 1329

Raczko, M. 601
Radecka-Paryzek, W. 439
Radivojsa, P. N. 1153
Rahman, A. Abd. 1147
Rahman, S. A. 219
Raithby, P. R. 987, 1759
Rama Rao, E. 29

Randall, L. H. 1045
Ravenek, W. 1625
Reed, D. 17, 665
Reedijk, J. 2575, 2583, 2591
Reeve, R. N. 1725
Rewari, S. 709
Rheingold, A. L. 791
Rhinebarger, R. R. 1341
Ribeiro da Silva, M. A. V. 421
Ricevuto, V. 207
Rickard, C. E. F. 117, 297
Robinson, G. H. 2727
Robinson, S. D. 417, 1781, 1919
Rodger, A. 1107
Rogers, R. D. 2727
Rogers, V. 1719
Rojo, T. 1383
Romero, M. A. 659
Rosales, M. J. 2159
Rossi, R. 195
Roth, W. J. 737
Rothin, A. S. 137
Rothwell, I. P. 753
Ruegger, H. 1349
Ruhl, B. L. 17
Ruiz, C. 1831
Russell, D. R. 2015
Russo, U. 2703

Sabat, M. 1517
Saez, I. M. 827
Sahajpal, A. 2715
Sailor, M. J. 955
Salas, J. M. 659
Saltzman, S. J. 369
Sanau, M. 87, 1311
Sanchez, L. 163, 1767
Sanchez, Mª J. 495
Sancho, A. 307
Sangokoya, S. A. 2727
Santana, B. 495
Santos Barbieri, R. 2165
Sarkar, S. 471
Sarma, K. P. 1727
Sarma, U. C. 1727, 1737, 2627
Sasaki, Y. 1131
Saum, S. E. 1785
Savage, P. D. 1079
Saxena, A. K. 2189
Scheller, D. 285
Schmid, G. 605, 2321
Schmidt, G. F. 2341
Schmutzler, R. 505
Schnering, H. G. von 2095
Schock, L. E. 1517
Schomburg, D. 505
Schonauer, D. 605
Schrock, R. R. 1841
Schumann, H. 2307
Schwank, J. 2411
Schwotzer, W. 87, 615, 1311
Scotti, M. 2095
Senglet, N. 303
Seshasayee, M. 1267
Seyam, A. M. 1517
Shamsipur, M. 1227
Shapley, J. R. 961
Sharma, H. K. 1389
Shaw, A. 579, 2217
Sheppard, R. N. 57
Shibanova, T. A. 1267
Shore, S. G. 2399
Short, R. L. 1781, 2605
Shrimal, A. K. 1639
Shrivastava, S. 2569
Shriver, D. F. 955
Sicilia, V. 2659
Siddiqi, Z. A. 705
Sik, V. 1169, 1321, 1329
Sillanpaa, E. R. J. 1801, 2143
Simonov, V. I. 1267
Simpson, N. J. 1945
Singh, A. K. 635
Singh, H. B. 1169
Singh, K. 151
Singh, R. P. 147, 483
Singh, R. V. 151
Singh, S. P. 1
Singh, S. R. 147
Sipachev, V. A. 345
Skapski, A. C. 1305
Skelton, B. W. 859
Slawin, A. M. Z. 57, 1925
Sloan, O. D. 329
Smith, F. E. 2183
Smith, G. P. 1605
Smith, L. M. 1289
Smith, T. J. 2679
Snaith, R. 665, 2119
Sobota, P. 2655
Sola, J. 2509
Solana, I. 87
Sordo, J. 2487
Sorensen, P. E. 1197
Sorrell, R. M. 2221
Soto, L. 229, 307
Sovago, I. 1089
Spalding, T. R. 17, 187

Speier, G. 609
Squires, R. R. 1609
Srivastava, D. K. 483, 2553
Srivastava, S. 1063
Srivastava, S. C. 1639
Stahl, K. A. 1991
Stam, C. H. 2521
Stanley, G. G. 1785
Steffan, U. 443
Steffey, B. D. 753
Steiger, R. 2375
Stephenson, D. 1169
Stephenson, N. 2243
Steudel, R. 581
Stibr, B. 669
Stone, F. G. A. 443
Stoutland, P. O. 1429
Strahle, J. 2561
Strzelecki, H. 2473
Styring, P. 1861
Suarez-Varela, J. 229
Subramaniam, V. 523
Sudha, N. 1169
Suss-Fink, G. 2341
Sutin, K. A. 2297
Suzuki, N. 155
Swirska, H. 2667
Syngollitou-Kourakou, A. S. 557

Taira, Z. 353
Takats, J. 931
Tam, W. 1441
Tanaka, T. 379
Tandon, J. P. 151
Taqui Khan, M. M. 29, 1063
Tasi, M. 1071, 2263
Tassi, L. 1231
Tauler, R. 1335
Tay, A. W. N. 695
Teixidor, F. 43
Teo, B. K. 2317
Tewari, S. K. 709
Thiel, W. R. 2027
Thomas, N. C. 731
Thompson, A. M. 1159
Thompson, L. 2411
Thompson, M. E. 1409
Thomson, S. K. 1953
Thornton, P. 323, 329, 2715
Thuy, P. N. 641
Tinsley, P. W. 315
Toma, H. E. 1687
Tondre, C. 513
Tooley, P. A. 2421
Tortorelli, L. J. 315, 1751
Toscano, R. A. 2159
Tosi, G. 1231
Tossidis, I. A. 557
Toyota, K. 2213
Trotta, E. 1211
Tschinke, V. 1625
Tuck, D. G. 49, 1121
Tuong, T. D. 249
Tuseev, N. I. 345
Tusek-Bozic, Lj. 2761
Tyeklar, Z. 609

Uden, P. C. 369
Urbanos, F. A. 2597
Urch, D. S. 671
Uribe, G. 679

Vaida, V. 1619
Valderrama, M. 2095
Valiente, M. 5, 715
Valkonen, J. 1801, 2143
Vargas, M. E. 489
Varnagy, K. 1089
Vasca, E. 1355
Vender, M. 2009
Venturi, M. 597
Versluis, L. 1625
Vidal, C. F. 2503
Vidali, M. 2703
Vidyasagar, K. 1667
Vilas Boas, L. F. 1245
Villax, I. 2087
Vitali, F. 2039
Vogt, A. 337
Vollhardt, K. P. C. 1023
Volpe, P. 597
Vrieze, K. 2521
Vrinat, M. 2405
Vucelic, D. 1153
Vucic, M. 1153

Waki, H. 291
Walborsky, E. C. 1023
Waldo, G. 2411
Walker, N. P. C. 323
Walton, R. A. 1279
Watkins, C. L. 2553
Wayland, B. B. 1545
Weller, M. T. 243
Wells, F. J. 2615
Went, M. J. 775
Werner, H. 2095

Westmoreland, D. L. 77
Wheatley, J. D. 1827
White, A. H. 859
Wieghardt, K. 2245, 2537
Wilkes, J. S. 1139
Wilkinson, G. 1079, 1239, 1363, 2615
Williams, D. J. 57, 647, 1299, 1807, 1925
Williams, D. R. 501
Williams, R. A. 725
Winpenny, R. E. P. 1299, 1807
Wlodarczyk, A. 103, 449
Wolfe, T. A. 1071
Wong, A. C. C. 1363
Wong, S. F. 2605
Woods, C. 315, 1751
Woollins, J. D. 419, 647, 1925
Wragg, M. S. 1861
Wyk, A. J. van 2193

Yagasaki, A. 1131
Yamamoto, A. 2245
Yamazaki, S. 353
Yang, G. K. 1619
Ye, Z. 1095
Yeh, W-Y. 961
Yokoyama, K. 379
Yongxiang, M. 393, 1101
Yoshifuji, M. 2213
Young, G. B. 1953
Yu, Y. 1095
Yun, S. S. 203
Yutronic, N. 673

Zaidan, A. 219
Zaidi, S. A. A. 705
Zanello, P. 195
Zaric, S. 1153
Zarli, B. 2703
Zemva, B. 1217
Zhang, H. 1693
Zhang, K. 1491
Ziegler, T. 1625
Zubieta, J. 171, 401, 1129, 1397

Printed in Great Britain at Aberdeen University Press